Samuel Chackalamannil, David Rotella, Simon Ward

Comprehensive Medicinal Chemistry III

About the pagination of this eBook

This eBook contains a multi-volume set.

To navigate this eBook by page number, you will need to use the volume number and the page number, separated by punctuation or a space.

Refer to the Cumulative Index and match the page reference style exactly in the Go box at the bottom of the screen.

COMPREHENSIVE MEDICINAL CHEMISTRY III

This page intentionally left blank

COMPREHENSIVE MEDICINAL CHEMISTRY III

EDITORS-IN-CHIEF

Samuel Chackalamannil
Rutgers University, Piscataway, NJ, United States

David Rotella
Montclair State University, Montclair, NJ, United States

Simon E. Ward
University of Sussex, Brighton, United Kingdom

VOLUME 1

GENERAL PERSPECTIVE - THE FUTURE OF DRUG DISCOVERY

VOLUME EDITORS

Ana Martinez
Centro de Investigaciones Biologicas-CSIC, Madrid, Spain

Carmen Gil
Centro de Investigaciones Biologicas-CSIC, Madrid, Spain

ELSEVIER

Elsevier
Radarweg 29, PO Box 211, 1000 AE Amsterdam, The Netherlands
The Boulevard, Langford Lane, Kidlington, Oxford OX5 1GB, United Kingdom
50 Hampshire Street, 5th Floor, Cambridge, MA 02139, United States

Copyright © 2017 Elsevier Ltd. All rights reserved

No part of this publication may be reproduced or transmitted in any form or by any means, electronic or mechanical, including photocopying, recording, or any information storage and retrieval system, without permission in writing from the publisher. Details on how to seek permission, further information about the Publisher's permissions policies and our arrangements with organizations such as the Copyright Clearance Center and the Copyright Licensing Agency, can be found at our website: www.elsevier.com/permissions.

This book and the individual contributions contained in it are protected under copyright by the Publisher (other than as may be noted herein).

Notices
Knowledge and best practice in this field are constantly changing. As new research and experience broaden our understanding, changes in research methods, professional practices, or medical treatment may become necessary.

Practitioners and researchers may always rely on their own experience and knowledge in evaluating and using any information, methods, compounds, or experiments described herein. In using such information or methods they should be mindful of their own safety and the safety of others, including parties for whom they have a professional responsibility.

To the fullest extent of the law, neither the Publisher nor the authors, contributors, or editors, assume any liability for any injury and/or damage to persons or property as a matter of products liability, negligence or otherwise, or from any use or operation of any methods, products, instructions, or ideas contained in the material herein.

Library of Congress Cataloging-in-Publication Data
A catalog record for this book is available from the Library of Congress

British Library Cataloguing-in-Publication Data
A catalogue record for this book is available from the British Library

ISBN 978-0-12-803200-8

For information on all publications visit our website at
http://store.elsevier.com

Working together
to grow libraries in
developing countries
www.elsevier.com • www.bookaid.org

Publisher: Oliver Walter
Acquisition Editor: Rachel Gerlis
Content Project Manager: Gemma Tomalin
Associate Content Project Manager: Marise Willis
Designer: Mark Rogers

Printed and bound in the United Kingdom

PREFACE

Previous editions of *Comprehensive Medicinal Chemistry*, published in 1990 and 2006, provided an integrated reference source that encompassed all major aspects of drug discovery research. The third edition follows this tradition and considerably expands its scope and content.

The trailblazing scientific discoveries of the 21st century have brought new opportunities for drug discovery research. The discipline of medicinal chemistry continues to evolve as it adapts to these new opportunities and strives to solve new challenges. Covered in the new edition are not only the breakthrough therapies of the past decade in cancer, hepatitis C, heart failure, dyslipidemia, cystic fibrosis, multiple sclerosis, HIV, etc., but also extensive discussion of new business models in drug discovery research, shifting industry demographics, emerging technologies, *in silico* drug discovery tools, experimental ADME and toxicology, and biologics medicine. The tone of this edition is prospective in which contributors identify outstanding issues and paths forward in their area of expertise. The aim is to provide drug discovery scientists in industry, government, academia, and research organizations with a contemporary global perspective on the field that includes a look ahead in selected areas.

The eight individual volumes fulfill these objectives and include extensive discussion of biomolecular therapeutics, drug targeting and delivery, development of chemical biology tools, data collection and analysis, *in silico* models as predictors for biological properties, identification/validation of new targets, approaches to quantify target engagement, new methods for synthesis of drug candidates such as green chemistry, development of novel scaffolds for drug discovery, and the role of regulatory agencies in drug discovery.

The individual volume editors have done an outstanding job to identify topics and contributors to meet these goals and we thank them for their hardwork and diligence. In volume 1, Ana Martinez and Carmen Gil recruited an international group of contributors who provide chapters on the emerging role of organizations other than traditional pharmaceutical companies in drug discovery, the evolving science of chemical biology, and new organic chemistry contributions to the discipline. In volume 2, Helmut Buschmann, Norbert Handler, and Andrea Wolkerstorfer have accomplished a seemingly impossible task and attracted world-leading experts across the wide field of drug discovery enabling technologies, covering contemporary thinking in a wide range of key disciplines that enable modern medicinal chemistry and drug discovery and development. The computational enabling technologies are the focus of volume 3, in which Andy Davis and Colin Edge have assembled chapters covering both ligand-based and protein structure–based advances as well as exciting new methodologies and case studies exploiting these. Alan Wilson identified experts in the fields of pharmacokinetics and toxicology who describe a wide range of contemporary advances in prediction and analysis of pharmaceutical properties and drug safety in volume 4. In volume 5, Ian Collins, Louis Lombardo, and Will Watkins have assembled leading experts to discuss high impact drug discovery accomplishments over the past decade in cancer chemotherapeutics, immunology and inflammation, and infectious diseases therapeutic areas. Ved Srivastava edited volume 6 on biologic medicines, a significant and rapidly evolving area where medicinal chemistry plays an important role. The chapters in this volume provide timely information on not only protein-based drugs, such as monoclonal antibodies and therapeutic proteins, but also peptides and nucleic acid–based therapeutics. Volume 7, edited by Adrian Hall, Santhosh Neelamkavil, and Rob Jones, presents a detailed account of the major advances in CNS, metabolic, and cardiovascular fields over the past decade and the promising new opportunities. Joerg Holenz edited volume 8 that presents case histories of successful drug discovery and strategic differentiation that have resulted in commercialized drugs and candidates in advanced clinical trials.

We are truly grateful to the publishing team at Elsevier that includes Gemma Tomalin, Rachel Gerlis, Marise Willis, and Sean Simms for their assistance and support throughout the process. With their expertise, this project became what we believe is a noteworthy and valuable resource for the discipline of medicinal chemistry. We look forward to the response and feedback of our colleagues who will use this information in their own work.

Samuel Chackalamannil, David P. Rotella, and Simon E. Ward

EDITORS-IN-CHIEF: BIOGRAPHIES

Dr. Samuel Chackalamannil

Dr. Chackalamannil obtained his PhD in chemistry from Yale University in 1984 and subsequently worked in drug discovery research at Schering-Plough Corporation and Merck Research Laboratories, where he was a distinguished fellow when he left in 2011. Since then, he has been teaching at Ernest Mario School of Pharmacy, Rutgers University, New Jersey.

Dr. Chackalamannil has significant accomplishments in the discovery of new medicines. He led the discovery of vorapaxar (Zontivity®), an FDA-approved antiplatelet drug for the prevention of heart attack and stroke. His group also discovered a PDE-5 inhibitor clinical candidate dasantafil and an adenosine A2a antagonist clinical candidate for the treatment of Parkinson's disease. Altogether, he was responsible for the discovery of nine development candidates in cardiovascular, central nervous system, and metabolic disease areas.

Dr. Chackalamannil is a coinventor of 62 allowed US patents and numerous patent applications worldwide. He has published 81 peer-reviewed articles and has coauthored a book. He has also given numerous lectures at international meetings and academic institutions.

Dr. Chackalamannil is a two-time recipient of the Thomas Alva Edison Award for Emerging Technology Patent and a two-time recipient of the Presidential Award for Discovery at Schering-Plough Research Institute. He has chaired several sessions at American Chemical Society national meetings and Gordon Research Conference on Medicinal Chemistry and was an organizer for Chemistry as a Life Science Symposium.

Dr. David Rotella

Dr. Rotella earned a PhD in medicinal chemistry from The Ohio State University and carried out postdoctoral research in organic chemistry at Penn State University. He joined the faculty at Montclair State University in July 2011 as the Margaret and Herman Sokol Professor of medicinal chemistry after a successful career in the pharmaceutical industry. He is an expert in the discovery and optimization of small molecule drug candidates for use in metabolic, cardiovascular, cancer, and central nervous system diseases. His current research is focused on discovering new lead compounds for use in parasitic and central nervous system diseases. He has coedited the seventh edition of *Burger's Medicinal Chemistry* and is a senior editor for the Royal Society of Chemistry's Drug Discovery book series. He has authored over 40 peer-reviewed articles, is an inventor on 8 issued US patents, and has contributed 10 book chapters.

Simon E. Ward

Simon Ward has an MA in natural sciences and PhD in synthetic organic chemistry from Cambridge University, UK. He has a wide-ranging experience of drug discovery in both large and small companies (GlaxoSmithKline, Knoll Pharmaceuticals, Vernalis, Chiroscience, BioCrea) and specialist experience of discovering and developing drugs for central nervous system indications. He has led multidisciplinary project teams and medicinal chemistry groups from target identification through to early clinical studies, delivering multiple clinical development candidates across indications. He is a fellow of the Royal Society of Chemistry. He is currently a professor of medicinal chemistry at the University of Sussex, UK, and the director of the Sussex Drug Discovery Centre, which he established within the University of Sussex in 2010.

This page intentionally left blank

CONTRIBUTORS TO VOLUME 1

M Abou-Gharbia
Moulder Center for Drug Discovery Research, Temple University School of Pharmacy, Philadelphia, PA, United States

D Baglieri
University of Messina, Messina, Italy

E J Barreiro
Laboratório de Avaliação e Síntese de Substâncias Bioativas (LASSBio, www.lassbio.icb.ufrj.br), Instituto de Ciências Biomédicas da Universidade Federal do Rio de Janeiro, RJ, Brasil

M K Bayliss
GSK Medicines Research Centre, Stevenage, SG1 2NY, Hertfordshire, United Kingdom

A Bender
Centre for Molecular Informatics, Cambridge, United Kingdom

J Benningshof
Mercachem, Nijmegen, The Netherlands

A Bhat
Ipsen Bioscience, Inc., Cambridge, MA, United States

B E Blass
Moulder Center for Drug Discovery Research, Temple University School of Pharmacy, Philadelphia, PA, United States

M L Bolognesi
Department of Pharmacy and Biotechnology, Alma Mater Studiorum, University of Bologna, Bologna

N J Brandon
AstraZeneca Neuroscience Innovative Medicines and Early Development Biotech Unit, Waltham, MA, United States

D L Browne
Cardiff University, Cardiff, United Kingdom

J N Burrows
Medicines for Malaria Venture (MMV), Geneva, Switzerland

D Cavalla
Numedicus Limited, Cambridge, United Kingdom

F Cesaroni
University of Messina, Messina, Italy

H Céster Schlaak
Integral BioConsulting, Las Rozas, Spain

W E Childers
Moulder Center for Drug Discovery Research, Temple University School of Pharmacy, Philadelphia, PA, United States

A Cross
AstraZeneca Neuroscience Innovative Medicines and Early Development Biotech Unit, Waltham, MA, United States

A Crupi
University of Messina, Messina, Italy

S G Davies
University of Oxford, Oxford, United Kingdom

I J P de Esch
Vrije Universiteit Amsterdam, Amsterdam, The Netherlands

C de Graaf
Vrije Universiteit Amsterdam, Amsterdam, The Netherlands

J M de la Fuente
Instituto de Ciencia de Materiales de Aragón, CSIC-Universidad de Zaragoza

F Giordanetto
Taros Chemicals GmbH & Co. KG, Dortmund, Germany

A Gissi
European Chemicals Agency (ECHA), Helsinki, Finland

V Grazú
Instituto de Ciencia de Materiales de Aragón, CSIC-Universidad de Zaragoza

L Gutiérrez
Instituto Universitario de Nanociencia de Aragón (INA), Universidad de Zaragoza, Zaragoza, Spain

S J Haggarty
Massachusetts General Hospital and Harvard Medical School, Boston, MA, United States

M M Hann
GSK Medicines Research Centre, Stevenage, SG1 2NY, Hertfordshire, United Kingdom

R Hooft van Huijsduijnen
Medicines for Malaria Venture (MMV), Geneva, Switzerland

J L Howard
Cardiff University, Cardiff, United Kingdom

P Jones
University of Dundee, Dundee, Scotland, United Kingdom

K Jozwiak
Medical University of Lublin, Lublin, Poland

G K Kanev
Vrije Universiteit Amsterdam, Amsterdam, The Netherlands

P D Kennewell
University of Oxford, Oxford, United Kingdom

A J Kooistra
Vrije Universiteit Amsterdam, Amsterdam, The Netherlands

A R Leach
GSK Medicines Research Centre, Stevenage, SG1 2NY, Hertfordshire, United Kingdom; and The European Bioinformatics Institute (EMBL-EBI), Wellcome Genome Campus, CB10 1SD, United Kingdom

L M Lima
Laboratório de Avaliação e Síntese de Substâncias Bioativas (LASSBio, www.lassbio.icb.ufrj.br), Instituto de Ciências Biomédicas da Universidade Federal do Rio de Janeiro, RJ, Brasil

G F Mangiatordi
Università degli Studi di Bari Aldo Moro, Bari, Italy

A Mascaraque
IIQ, CSIC—Universidad de Sevilla, Seville, Spain

G Müller
Mercachem, Nijmegen, The Netherlands

J Nakhle
Ipsen Innovation, Les Ulis, France

A Nelson
University of Leeds, Leeds, United Kingdom

T Netzeva
European Chemicals Agency (ECHA), Helsinki, Finland

O Nicolotti
Università degli Studi di Bari Aldo Moro, Bari, Italy

E Oerton
Centre for Molecular Informatics, Cambridge, United Kingdom

A Pannifer
University of Dundee, Dundee, Scotland, United Kingdom

J Pardo
Department Microbiology, Preventive Medicine and Public Health, Universidad de Zaragoza, Zaragoza, Spain; and Immune Effector Cells Group, Aragón Health Research Institute (IIS Aragón), Biomedical Research Centre of Aragón (CIBA), Universidad de Zaragoza, Zaragoza, Spain

M Pérez-Hernández
Department Microbiology, Preventive Medicine and Public Health, Universidad de Zaragoza, Zaragoza, Spain; and Immune Effector Cells Group, Aragón Health Research Institute (IIS Aragón), Biomedical Research Centre of Aragón (CIBA), Universidad de Zaragoza, Zaragoza, Spain

A Rajasekaran
KMCH College of Pharmacy, Coimbatore, India

J Rojo
IIQ, CSIC—Universidad de Sevilla, Seville, Spain

A J Russell
University of Oxford, Oxford, United Kingdom

F Sanz
Universitat Pompeu Fabra, Barcelona, Spain

C Schotten
Cardiff University, Cardiff, United Kingdom

L Silpa
University of Oxford, Oxford, United Kingdom

M C Silva
Massachusetts General Hospital and Harvard Medical School, Boston, MA, United States

S B Singh
Vitae Pharmaceuticals, West Office Center Drive, Fort Washington, PA, United States

M Snape
AMO Pharma Ltd, Surrey, United Kingdom

T Sobański
European Chemicals Agency (ECHA), Helsinki, Finland

A Sousa-Herves
IIQ, CSIC—Universidad de Sevilla, Seville, Spain

G Stepien
Instituto Universitario de Nanociencia de Aragón (INA), Universidad de Zaragoza, Zaragoza, Spain

P Thirumurugan
Medical University of Lublin, Lublin, Poland

C M Tice
Vitae Pharmaceuticals, West Office Center Drive, Fort Washington, PA, United States

M R Tranfaglia
FRAXA Research Foundation, Newburyport, MA, United States

N Tsomaia
Ipsen Bioscience, Inc., Cambridge, MA, United States

D Tzalis
Taros Chemicals GmbH & Co. KG, Dortmund, Germany

M Ufret
Ipsen Bioscience, Inc., Cambridge, MA, United States

A M Vaiserman
Institute of Gerontology, Kiev, Ukraine

S van Boeckel
Pivot Park Screening Center, Oss, The Netherlands

T N C Wells
Medicines for Malaria Venture (MMV), Geneva, Switzerland

R Westwood
University of Oxford, Oxford, United Kingdom

G M Wynne
University of Oxford, Oxford, United Kingdom

Y Zheng
Vitae Pharmaceuticals, West Office Center Drive, Fort Washington, PA, United States

This page intentionally left blank

CONTENTS OF ALL VOLUMES

Preface *v*

Editors-in-Chief: Biographies *vii*

Contributors to Volume 1 *ix*

Editorial Board *xxiii*

General Perspective—The Future of Medicinal Chemistry *xxv*

VOLUME 1: GENERAL PERSPECTIVE - THE FUTURE OF DRUG DISCOVERY

1.01 Academic Drug Discovery Centers: Key Players in the Future of the Pharmaceutical Industry 1
M Abou-Gharbia, B E Blass, and W E Childers

1.02 Drug Repurposing Review 11
D Cavalla, E Oerton, and A Bender

1.03 Human iPSC Models in Drug Discovery: Opportunities and Challenges 48
M C Silva, A Cross, N J Brandon, and S.J. Haggarty

1.04 From Imaging Agents to Theranostic Drugs in Alzheimer's Disease 74
M L Bolognesi

1.05 Nutraceuticals 107
A Rajasekaran

1.06 Continuous Flow Processing as a Tool for Medicinal Chemical Synthesis 135
D L Browne, J L Howard, and C Schotten

1.07 Beyond Bioisosterism: New Concepts in Drug Discovery 186
L M Lima and E J Barreiro

1.08 Spirocyclic Scaffolds in Drug Discovery 211
C M Tice, Y Zheng, and S B Singh

1.09 Nanotechnology in Drug Discovery and Development 264
L Gutiérrez, G Stepien, L Gutiérrez, M Pérez-Hernández, J Pardo, J Pardo, V Grazú, and J M de la Fuente

1.10 Click Chemistry in Medicinal Chemistry for Comprehensive Medicinal Chemistry III 296
P Thirumurugan and K Jozwiak

1.11 Future of Medicinal Chemistry: Next-Generation Therapeutics 326
N Tsomaia, M Ufret, A Bhat, and J Nakhle

1.12 Anti-Aging Drugs 349
A M Vaiserman

1.13 Regenerative Medicine 379
S G Davies, P D Kennewell, A J Russell, L Silpa, R Westwood, and G M Wynne

1.14 Data Integration and Sharing Supporting Drug R&D 436
F Sanz

1.15 Structural Chemogenomics Databases to Navigate Protein–Ligand Interaction Space 444
G K Kanev, A J Kooistra, I J P de Esch, and C de Graaf

1.16 Nontest Methods for REACH Legislation 472
A Gissi, G F Mangiatordi, T Sobański, T Netzeva, and O Nicolotti

1.17 New Models of Drug Discovery and Development for Neglected Disease Populations 491
T N C Wells, R Hooft van Huijsduijnen, and J N Burrows

1.18 European Lead Factory 505
F Giordanetto, P Jones, A Nelson, J Benningshof, G Müller, A Pannifer, S van Boeckel, and D Tzalis

1.19 Closing Distances Between Academia and Market 520
F Cesaroni, D Baglieri, and A Crupi

1.20 Present and Future Challenges and Opportunities for Intellectual Property in an Open Landscape: Open Labs and the Internet 529
H Céster Schlaak

1.21 Ethics in Drug Discovery 540
M Snape

1.22 The Rise of Rare Disease Foundations: How Patient Associations Can Drive the Drug Discovery Process 549
M R Tranfaglia

1.23 Contemporary Considerations for Discovering a Successful Medicine 560
M M Hann, M K Bayliss, and A R Leach

1.24 Perspectives of Carbohydrates in Drug Discovery 577
J Rojo, A Sousa-Herves, and A Mascaraque

VOLUME 2: DRUG DISCOVERY TECHNOLOGIES

2.01 Drug Discovery Technologies: Current and Future Trends 1
M C Noe and M-C Peakman

2.02 Hit and Lead Generation Strategies 33
P Ettmayer, R Schnitzer, A Bergner, and H Nar

2.03 Multiobjective Optimization of Biological and Physical Properties in Drug Discovery 64
M P Gleeson and D Montanari

2.04 Predictive Toxicology: Latest Scientific Developments and Their Application in Safety Assessment 94
D Armstrong, S Li, W Frieauff, H-J Martus, J Reilly, D Mikhailov, S Whitebread, and L Urban

2.05 Privileged Structures and Motifs (Synthetic and Natural Scaffolds) 116
A M Jones

2.06 High-Throughput Crystallography and Its Applications in Drug Discovery 153
H Nar, D Fiegen, S Hörer, A Pautsch, and D Reinert

2.07 Kinetics, Thermodynamics, and Ligand Efficiency Metrics in Drug Discovery 180
G A Holdgate

2.08 Fragment-Based Drug Design: Strategic Advances and Lessons Learned 212
H Chen, X Zhou, Y Gao, H Chen, and J Zhou

2.09 Computational Models to Predict Toxicological Endpoints in Drug Discovery and Strategies for Data Integration 233
A Brigo and W Muster

2.10 Overview of Drug Polypharmacology and Multitargeted Molecular Design 259
R Chaudhari, Z Tan, and S Zhang

2.11 Allosteric Modulators 276
S Lu and J Zhang

2.12 Novel Therapeutics Targeting Epigenetics 297
P M Woster

2.13 Small-Molecule Inhibitors of Protein−Protein Interactions 329
Z Liu, H Chen, E A Wold, and J Zhou

2.14 Next Generation Sequencing Technologies 354
R Rajesh Singh

2.15 Cellular Imaging in Drug Discovery: Imaging and Informatics for Complex Cell Biology 362
Z Li, M E Cvijic, and L Zhang

2.16 3D High-Content Screening of Organoids for Drug Discovery 388
L Li and D V LaBarbera

2.17 Label-Free Screening Technologies 416
Y Fang

2.18 Systems Biology: Methods and Applications 434
B Titz, A Knorr, A Sewer, F Martin, N V Ivanov, M Talikka, I Gonzalez Suarez, M C Peitsch, and J Hoeng

2.19 Systems Chemical Biology: Integrating Medicinal Chemistry and Systems Biology for Drug Discovery 481
R-S Wang and J Loscalzo

2.20 Translational Aspects in Drug Discovery 495
L Detalle, K Vanheusden, M L Sargentini-Maier, and T Stöhr

2.21 Companion Diagnostics: From Biomarkers to Diagnostics 530
J T Jørgensen and K B Nielsen

VOLUME 3: IN SILICO DRUG DISCOVERY TOOLS

3.01 Perspective on Calculations of Binding Free Energies 1
H Yoon and A Warshel

3.02 Advances in Molecular Simulation 14
M Aldeghi and P C Biggin

3.03 Recent Progress in Free Energy Methods 34
G Saladino, C Estarellas, and F L Gervasio

3.04 Molecular Dynamics, Quantum Mechanics, and Combined Quantum Mechanics/Molecular Mechanics Methods for Drug Discovery and Development 51
E J M Lang and A J Mulholland

3.05 Progress in the Understanding of Traditional and Nontraditional Molecular Interactions 67
Robin Taylor

3.06 Using 3D Structural Information in Computational Design 101
A M Davis and C M Edge

3.07 Protein Structure Prediction and Homology Modeling 120
A R Leach and P J Thomas

3.08 Modeling and Design for Membrane Protein Targets 145
M Congreve, A Bortolato, G Brown, and R M Cooke

3.09 2/3D Pharmacophore Definitions and Their Application 189
R A Lewis and F Sirockin

3.10 Matched Molecular Pair Analysis 221
A G Leach, I Lukac, J M Zarnecka, A G Dossetter, and E J Griffen

3.11 Lessons and Successes in the Use of Molecular Fields 253
P Tosco and M Mackey

3.12 Molecular Docking—A Solved Problem? 297
J Cole, E Davis, G Jones, and C R Sage

3.13 Modeling Protein Flexibility in Molecular Docking 319
C Yan and X Zou

3.14 Chemical Data Formats, Fingerprints, and Other Molecular Descriptions for Database Analysis and Searching 329
D Bajusz, A Rácz, and K Héberger

3.15 Quantitative Structure–Activity Relationships 379
A M Davis

3.16 Empirical and Physics-Based Calculations of Physical–Chemical Properties 393
E L Ratkova, Y A Abramov, I I Baskin, D J Livingstone, M V Fedorov, M Withnall, and I V Tetko

3.17 Predicting Target and Chemical Druggability 429
T I Oprea and C Hasselgren

3.18 Data Analysis and Visualization Tools 440
C J Swain

3.19 Examples of SAR-Centric Patent Mining Using Open Resources 464
C Southan

3.20 An Introduction to Systems Biology and Quantitative Systems Pharmacology 488
B C Gomes

VOLUME 4: EXPERIMENTAL ADME AND TOXICOLOGY

4.01 Role of ADME/PK in Drug Discovery, Safety Assessment, and Clinical Development 1
R E White

4.02 ADME Optimization in Drug Discovery 34
D F McGinnity and K Grime

4.03 Drug-Metabolizing Enzyme Systems I 45
H Yamazaki

4.04 Human PK Prediction and Modeling 51
T H Grasela, V Lukacova, D N Morris, R D Clark, K A Andrews, and M B Bolger

4.05 PBPK Modeling to Estimate Metabolite Formation From First-Pass Organs: Intestine and Liver 83
Qi Joy Yang and K Sandy Pang

4.06 Drug Classification and Drug Disposition Prediction 102
C M Hosey and L Z Benet

4.07 Genetically Humanized Animal Models 130
K Samuelsson, N Scheer, I Wilson, C R Wolf, and C J Henderson

4.08 A Comprehensive Overview of the Current Status and Application of Predictive ADMET: Introduction and Overview 150
T Hartung

4.09 *In Silico* Tools and their Application 156
G J Myatt, L D Beilke, and K P Cross

4.10 Use of Stem Cells in Toxicology 177
P Matz, L-S Spitzhorn, J Otte, M-A Kawala, J Woestmann, H Yigit, W Wruck, and J Adjaye

4.11 Genetic Toxicology 195
Sudheer Beedanagari

4.12 Drug-Induced Liver Disease 204
A K Daly

4.13 Drug-Induced Liver Injury: Mechanism-Informed Prediction in Drug Development 217
C Goldring, R Weaver, B Kramer, U Klingmueller, A Oppelt, B Van der Water, J Commandeur, A Guillouzo, D Naisbitt, N French, N Kitteringham, C Pridgeon, P Knolle, J Sidaway, R Sison-Young, L Kamalian, A Mercer, L Faulkner, R Pieters, M Ingelman-Sundberg, and B Kevin Park

4.14 The Future of Carcinogenicity Testing 239
A Pandiri, R Kovi, C Alden, and R Sills

4.15 Emerging Translatable Safety Biomarkers 255
J Tarrant

4.16 Toxicity Prediction—Regulatory Perspective 285
J P Hanig and W Slikker

VOLUME 5: CANCER, IMMUNOLOGY AND INFLAMMATION, AND INFECTIOUS DISEASE

5.01 Cancer Biology and the Principles of Targeted Cancer Drug Discovery 1
P Hillmann, D Schmitz, J Mestan, S D′ Alonzo, and D Fabbro

5.02 Selective Kinase Inhibitors in Cancer 39
A A Mortlock, D M Wilson, J G Kettle, F W Goldberg, and K M Foote

5.03 Covalent Kinase Inhibitors for Cancer 76
Timothy D Owens and Yan Lou

5.04 Targeting DNA Damage Response Pathways in Cancer 104
Ganiy Opeyemi Abdulrahman, and N J Curtin

5.05 Targeting the Androgen Receptor Signaling Axis 134
H Li, P Rennie, and A Cherkasov

5.06 Protein–Protein Interaction Inhibitors in Cancer 154
I R Hardcastle

5.07 Targeting Protein Synthesis, Folding, and Degradation Pathways in Cancer 202
A Elisa Pasqua, B Wilding, M D Cheeseman, and K Jones

5.08 Inhibitors of Epigenetic Regulation in Cancer 281
D Harvey and M Foley

5.09 Targeting Promoter Quadruplex Nucleic Acids for Cancer Therapy 308
A Paulo, C C Castillo, and S Neidle

5.10 Targeting Pre-mRNA Processing in Cancer 341
T R Webb and S Stamm

5.11 Cancer Immunotherapy—An Emerging Field That Bridges Oncology and Immunology Research 357
J L Adams, K J Duffy, M L Moore, and J Yang

5.12 Evolution of Small-Molecule Immunology Research—Changes Since CMC II 395
T G Murali Dhar and A J Dyckman

5.13 Small Molecule Immunosuppressants in Inflammatory Disease 420
R Fleischmann

5.14 Therapeutic Approaches to MS and Other Neurodegenerative Diseases 439
L P Kotra and J Park

5.15 Lupus and Lupus Overlap Diseases: Emerging Therapies 474
V C Kyttaris

5.16 Small-Molecule Drugs for the Treatment of Inflammatory Bowel Disease 495
L R Fitzpatrick and T Woldemariam

5.17 Recent Epidemiological Changes in Infectious Diseases 511
M J Pucci, C Callebaut, A Cathcart, and K Bush

5.18 Direct-Acting Antiviral Agents for the Treatment of Hepatitis C Virus Infection 553
N A Meanwell

5.19 New Antiretrovirals for HIV and Antivirals for HBV 628
S E Lazerwith, D Siegel, R M McFadden, M R Mish, and W C Tse

5.20 Antiviral Drugs for Acute Infections 665
K L Powell, E Thomas, and G S Cockerill

5.21 New Drugs and Emerging Leads in Antibacterial Drug Discovery 682
D G Brown

5.22 Antifungal Chemistry Review 703
M Birch and G Sibley

5.23 Antiparasitic Agents 717
R T Jacobs

VOLUME 6: BIOLOGICS MEDICINE

6.01 Peptide-Based Cancer Vaccines and Therapeutics for Solid Tumors Overexpressing HER-1, HER-2, HER-3, VEGF and IGF-1R 1
P T P Kaumaya and T Bekaii-Saab

6.02 Cancer Immunotherapy 32
R Ajina, D AlDeghaither, S Jablonski, and L M Weiner

6.03 Strategy and Tactics for Designing Analogs: Biochemical Characterization of the Large Molecules 66
J-M Ahn, K Kassees, T-K Lee, B Manandhar, and A M Yousif

6.04 Chimeric Somatostatin—Dopamine Compounds (Dopastatins) for the Treatment of Neuroendocrine Disease 116
J Hill, S Kim, N Tsomaia, J Z Dong, and M Culler

6.05 Basic Principles of Formulation for Biotherapeutics: Approaches to Alternative Drug Delivery 131
L Otvos, Jr.

6.06 Orally Delivered Peptides for Treatment of Inflammatory Bowel Disease 157
M L Smythe

6.07 Evolution of mAb Downstream Process Platforms 171
A A Shukla, L Wolfe, and C Norman

6.08 Emerging Bioanalytical Methods for the Bioanalysis of Biotherapeutics 180
B Gorovits and R Pillutla

6.09 Analytical and Formulation Development Road Map for Protein Therapeutics 198
M P Ramprasad

6.10 Recent Advances in Medicinal Chemistry of Antisense Oligonucleotides 216
K R Ito and S Obika

6.11 Manufacturing of Oligonucleotides 233
E Paredes, V Aduda, K L Ackley, and H Cramer

6.12 Current Progress and Future Prospects in Nucleic Acid Based Therapeutics 280
M Takahashi, S-p Han, L J Scherer, S Yoon, and J J Rossi

VOLUME 7: CNS, PAIN, METABOLIC SYNDROME, CARDIOVASCULAR, TISSUE FIBROSIS AND URINARY INCONTINENCE

7.01 Recent Advances and Future Directions in the Treatment of Epilepsy 1
T Kurokawa, Y Kazuta, and T Watanabe

7.02 Progress and Challenges in the Development of PET Ligands to Aid CNS Drug Discovery 20
J Mercier, L Provins, and J Hannestad

7.03 Progress in the Discovery of Ca Channel Blockers for the Treatment of Pain 65
P Beswick

7.04 Sodium Channel Blockers for the Treatment of Pain 131
D R Witty, D T MacPherson, and G M P Giblin

7.05 CGRP Receptor Antagonists for the Treatment of Migraine 176
G M Dubowchik and I M Bell

7.06 Orexin Receptor Antagonists 225
B T Shireman and M A Letavic

7.07 Targeting γ-Secretase for the Treatment of Alzheimer's Disease 280
A Hall and A I Velter

7.08 Targeting β-Secretase (BACE) for the Treatment of Alzheimer's Disease 326
A Hall and H J M Gijsen

7.09 Targeting Phosphodiesterases in the CNS 384
J Kehler

7.10 Inhibiting Kinases in the CNS 408
H Tsui, Q Zeng, K Chen, and X Zhang

7.11 Modulating AMPA Receptors for the Treatment of CNS Disorders 447
Tristan Reuillon, Simon E Ward, and Paul Beswick

7.12 GLP-1 Receptor Agonists for the Treatment of Diabetes and Obesity 481
A Palani, Y-Y Zhou, M Halleck, and P Carrington

7.13 Sodium–Glucose Cotransporters 491
G Bebernitz

7.14 DPP-4 Inhibitors 512
T Biftu and R SinhaRoy

7.15 Advances in Antiplatelet Agents 556
E A Meyer, E Caroff, and M A Riederer

7.16 Advances in Anticoagulants 600
M L Quan, P W Glunz, and J M Smallheer

7.17 Treatments for Heart Failure 628
W Michael Seganish, J J Lynch, Jr. and S Sorota

7.18 Advances in Hypercholesterolemia 663
A Pirillo, G D Norata, and A L Catapano

7.19 Drug Discovery in Tissue Fibrosis 694
S Pinto, M Hoek, Y Huang, P Costet, L Ma, and J E Imbriglio

7.20 β_3-AR Agonists for the Treatment of Overactive Bladder 714
S D Edmondson

VOLUME 8: CASE HISTORIES IN RECENT DRUG DISCOVERY

8.01 Medicinal Chemistry Case History: Osimertinib (AZD9291) 1
R A Ward and M R V Finlay

8.02 Trametinib 33
H Kawasaki and T Yamaguchi

8.03 Discovery of the Hypoxia-Activated Prodrug SN30000 58
M P Hay, K O Hicks, and W R Wilson

8.04 The Discovery of First-in-Class Inhibitors of the Nedd8-Activating Enzyme (NAE) and the Ubiquitin-Activating Enzyme (UAE) 95
J Ciavarri and S Langston

8.05 The Discovery of p97 Inhibitors 113
D J Wustrow, D J Anderson, M Rolfe, and H-J Zhou

8.06 Discovery of AMG 337: Using Structure Guided Scaffold Hybridization to Optimize Physicochemical Properties and Target Coverage of a MET Kinase Inhibitor 138
A A Boezio, E A Peterson, and J-C Harmange

8.07 Discovery of AZD0156: The First Potent and Selective Inhibitor of ATM Kinase for Clinical Evaluation 161
K G Pike

8.08 Tepotinib 178
O Schadt and A Blaukat

8.09 Verubecestat 204
A W Stamford, J N Cumming, J D Scott, and C O Strickland

8.10 The Discovery of Macitentan—A Standard Medicinal Chemistry Program? 252
M H Bolli, C Boss, J Gatfield, M Iglarz, and A Treiber

8.11 Case Histories: Anacetrapib 284
A Ali and J Duffy

8.12 Discovery of ROMK Inhibitor MK-7145: A Novel Mechanism Diuretic 308
Alexander Pasternak

8.13 Fragment-Based Discovery of AZD2716: A Novel, Potent Secreted Phospholipase A_2 ($sPLA_2$) Inhibitor for the Treatment of Coronary Artery Disease 339
F Giordanetto and D Pettersen

8.14 Canagliflozin 349
S Nomura

8.15 The Discovery and Development of *Seletalisib*: A Potent and Selective PI3Kδ Inhibitor for Inflammatory Diseases 366
D C Brookings

8.16 Medicinal Chemistry Case History: Structure-Based Drug Design of Oral and Inhaled p38 MAP Kinase Inhibitors as Clinical Candidates 408
L Xing and J Mathias

8.17 Are Two Better Than One in Rheumatoid Arthritis? Development of Dual p38α MAPK/PDE-4 Inhibitors for Treatment of TNFα-Driven Diseases 431
W Albrecht, S M Bauer, and S A Laufer

8.18 The Discovery of Potent and Selective Nonsteroidal Glucocorticoid Receptor Modulators AZD5423 and AZD7594, for the Inhaled Treatment of Respiratory Diseases 450
P Sjö, T Hansson, and K Edman

8.19 The Discovery of the MCH-1 Receptor Antagonist NGD-4715 for the Potential Treatment of Obesity 488
J Tarrant, K J Hodgetts, B L Chenard, J E Krause, and D Doller

8.20 Case History: AN5568 (SCYX-7158) 516
Y-K Zhang, Y R Freund, and R T Jacobs

8.21 KAE609 (Cipargamin): Discovery of Spiroindolone Antimalarials 529
B K S Yeung

8.22 Medicinal Chemistry Case History: Discovery of the Dihydroorate Dehydrogenase Inhibitor DSM265 as an Antimalarial Drug Candidate 544
M A Phillips, P K Rathod, T Rueckle, D Matthews, J N Burrows, and S A Charman

8.23 Harvoni: A Combination Therapy for Curing HCV 558
M J Sofia and J O Link

8.24 Discovery of Boceprevir and Narlaprevir: Ketoamide-Derived HCV NS3 Serine Protease Inhibitors for the Treatment of Chronic Hepatitis C 583
S Venkatraman

Index 609

EDITORIAL BOARD

EDITORS-IN-CHIEF

Samuel Chackalamannil
Rutgers University, Piscataway, NJ, United States

David Rotella
Montclair State University, Montclair, NJ, United States

Simon E. Ward
University of Sussex, Brighton, United Kingdom

VOLUME 1
GENERAL PERSPECTIVE - THE FUTURE OF DRUG DISCOVERY

VOLUME EDITORS

Ana Martinez
Centro de Investigaciones Biologicas-CSIC, Madrid, Spain

Carmen Gil
Centro de Investigaciones Biologicas-CSIC, Madrid, Spain

VOLUME 2
DRUG DISCOVERY TECHNOLOGIES

VOLUME EDITORS

Helmut Buschmann
Savira Pharmaceuticals GmbH, Vienna, Austria

Norbert Handler
Savira Pharmaceuticals GmbH, Vienna, Austria

Andrea Wolkerstorfer
Baxalta Innovations GmbH — Now part of Shire, Vienna, Austria

VOLUME 3
IN SILICO DRUG DISCOVERY TOOLS

VOLUME EDITORS

Andrew M. Davis
AstraZeneca R&D Gothenburg, Gothenburg, Sweden

Colin Edge
GlaxoSmithKline Medicines Research Centre, Stevenage, United Kingdom

VOLUME 4
EXPERIMENTAL ADME AND TOXICOLOGY

VOLUME EDITOR

Alan G. E. Wilson
Lexicon Pharmaceuticals, The Woodlands, TX, United States

VOLUME 5
CANCER, IMMUNOLOGY AND INFLAMMATION, AND INFECTIOUS DISEASE

VOLUME EDITORS

Ian Collins
The Institute of Cancer Research, London, United Kingdom

William Watkins
Gilead Sciences, Foster City, CA, United States

Louis J. Lombardo
Bristol-Myers Squibb Research and Development, Princeton, NJ, United States

VOLUME 6
BIOLOGICS MEDICINE

VOLUME EDITOR

Ved Srivastava
Intarcia Therapeutics, Durham, NC, United States

VOLUME 7
CNS, PAIN, METABOLIC SYNDROME, CARDIOVASCULAR, TISSUE FIBROSIS AND URINARY INCONTINENCE

VOLUME EDITORS

Adrian Hall
UCB BioPharma SPRL, Brussels, Belgium

Santhosh Neelamkavil
Merck Research Laboratories, Kenilworth, NJ, United States

Rob Jones
BlackThorn Therapeutics, San Francisco, CA, United States

VOLUME 8
CASE HISTORIES IN RECENT DRUG DISCOVERY

VOLUME EDITOR

Joerg Holenz
R&D Neurosciences TAU, GSK, PA, United States

GENERAL PERSPECTIVE—THE FUTURE OF MEDICINAL CHEMISTRY

Introduction

This first volume of the third edition of *Comprehensive Medicinal Chemistry* is entitled "The Future of Medicinal Chemistry" with the aim to describe not only a full perspective of our field in these first years of the 21st century but also the most relevant changes that will impact it without any doubt in the next future. The volume contains 24 chapters addressing our changing landscape and practice of drug discovery, the important role of academic laboratories and small companies in this task, the new methodologies for drug discovery and drug synthesis, the role of public–private collaboration sectors, the importance of intellectual property coverage and the interaction with patients associations, and how to effectively measure the value of new drugs, among others. Written by a combination of notable academic and industry experts working in the field, this volume tries to show how the dynamic environment of the 21st century has brought and will bring new challenges and opportunities for the drug discovery and development process. Hopefully, researchers working together will be able to offer patients and society better and safer drugs that enhance the quality of life.

This general perspective of the future of medicinal chemistry intends to be an essential and professional reference to this important field for students and researchers in chemistry, biochemistry, pharmaceutical sciences, and drug discovery. Also the book will be essential reading for scientists at all levels who wish to improve their scientific horizon.

We would like to sincerely thank all the contributors for their time, professional work, and enthusiasm while preparing this book. We also hope that all researchers working in the exciting world of drug discovery enjoy and create new ideas while reading this volume.

Ana Martinez and Carmen Gil
Volume Editors

This page intentionally left blank

PERMISSION ACKNOWLEDGMENTS

The following material is reproduced with kind permission of Taylor & Francis

Scheme 2 Cellular Imaging in Drug Discovery: Biomolecular Imaging and Informatics (HCS, HCA, HCI)
Figure 2 Past Present Future
Figure 5 Past Present Future
Figure 6 Past Present Future
www.taylorandfrancisgroup.com

The following material is reproduced with kind permission of Oxford University press

Table 1 Targeting G-quadruplex Nucleic Acids for Cancer Therapy
Table 2 Targeting G-quadruplex Nucleic Acids for Cancer Therapy
Figure 1 Protein Structure Prediction and Homology Modelling
www.oup.com

The following material is reproduced with kind permission of American Association for the Advancement of Science

Figure 3b,c Cellular Imaging in Drug Discovery: Biomolecular Imaging and Informatics (HCS, HCA, HCI)
www.aaas.org

The following material is reproduced with kind permission of Nature Publishing Group

Table 4 Use of Stem Cells in Toxicology
Table 6 Use of Stem Cells in Toxicology
Figure 17 Strategy and Tactics for Designing Analogs; Biochemical Characterization of the Large Molecules
Figure 30 Strategy and Tactics for Designing Analogs; Biochemical Characterization of the Large Molecules
Figure 2 Cellular Imaging in Drug Discovery: Biomolecular Imaging and Informatics (HCS, HCA, HCI)
Figure 3a Cellular Imaging in Drug Discovery: Biomolecular Imaging and Informatics (HCS, HCA, HCI)
Figure 4 Cellular Imaging in Drug Discovery: Biomolecular Imaging and Informatics (HCS, HCA, HCI)
Figure 5a Cellular Imaging in Drug Discovery: Biomolecular Imaging and Informatics (HCS, HCA, HCI)
Figure 9a Cellular Imaging in Drug Discovery: Biomolecular Imaging and Informatics (HCS, HCA, HCI)
Figure 20 Epigenetics: Novel Therapeutics Targeting Epigenetics
Figure 1 UCB5857
Figure 6 Empirical and Physics Based Calculations of Physical Properties
Figure 4 Progress and Challenges in the Development if PET Ligands to Aid CNS Drug Discovery
http://www.nature.com

1.01 Academic Drug Discovery Centers: Key Players in the Future of the Pharmaceutical Industry

M Abou-Gharbia, BE Blass, and WE Childers, Moulder Center for Drug Discovery Research, Temple University School of Pharmacy, Philadelphia, PA, United States

© 2017 Elsevier Ltd. All rights reserved.

1.01.1	**Pharmaceutical Industry Challenges: Productivity, Cost, Politics, and Patent Expirations**	2
1.01.2	**The Bayh–Dole Act of 1980: A Catalyst for Academic Drug Discovery**	2
1.01.2.1	The Role of Academic Drug Discovery Centers	3
1.01.2.2	Academic Drug Discovery Center Structure and Function	3
1.01.2.3	Founder Focused Academic Drug Discovery Centers	6
1.01.2.4	Research Coordination Academic Drug Discovery Centers	6
1.01.2.5	Fully Integrated Academic Drug Discovery Centers	7
1.01.2.6	US Academic Drug Discovery Centers	7
1.01.2.7	Risks and Rewards of Academic Drug Discovery Centers	7
1.01.3	**Concluding Remarks**	8
References		9

There can be no question that the pharmaceutical industry has played a major role in improving the lives of patients across the globe through the development of novel therapeutics. People suffering with cardiovascular diseases, cancer, and even HIV/AIDS have dramatically improved prospects thanks in large part to the pharmaceutical industry. The identification and commercialization of multi-billion dollar drugs such as Lipitor (Atorvastatin),[1] Gleevac (Imatinib),[2] Plavix (Clopidogrel),[3] and Singulair (Monteluclast),[4] (**Fig. 1**) provided the pharmaceutical industry with unprecedented levels of cash flow to support on-going operations, as well as the search for cures to additional, unmet medical conditions. By 2010, these four drugs alone had combined annual sales of nearly $31 billion.[5] The industry that started with Paul Ehrlich[6] at the beginning of the 20th century reached a high point by the 1990s. In 1996, 53 new molecular entities were approved by the FDA,[7] and new technologies such as high through-put screening,[8] chemical library synthesis,[9] genome sequencing,[10] and biotechnology[11] appeared to provide a runway for even greater success.

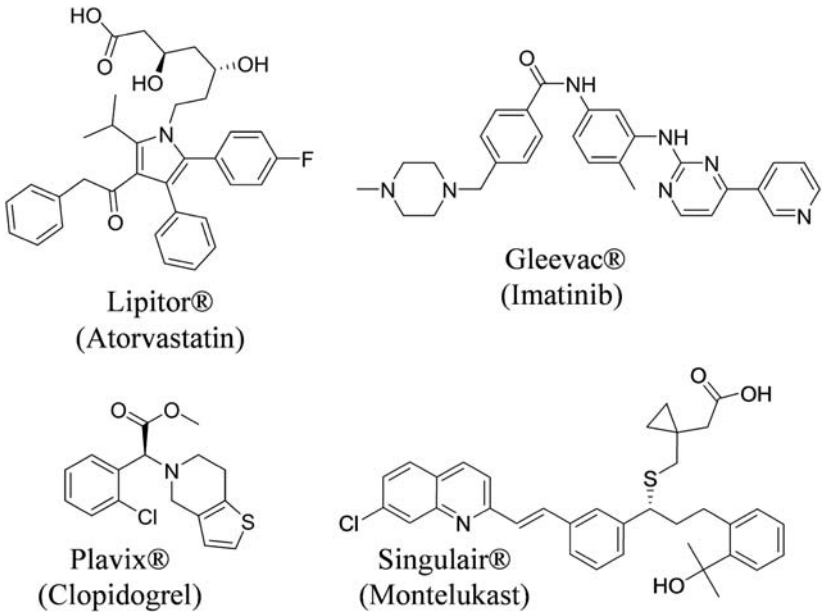

Fig. 1 Representative multi-billion dollar drugs.

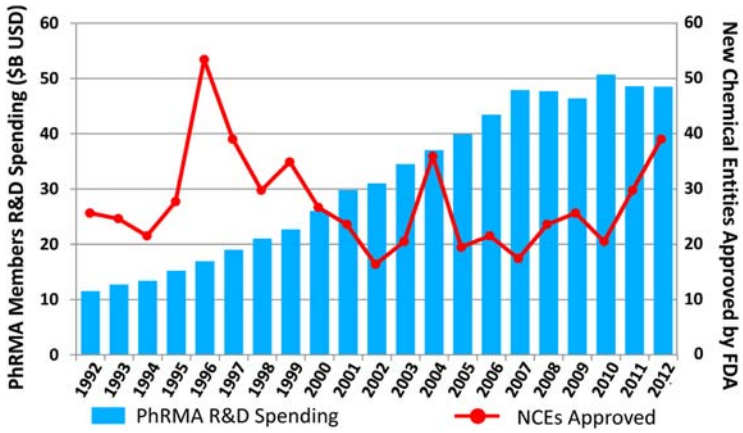

Fig. 2 US R&D expenditures and NCE approvals.

1.01.1 Pharmaceutical Industry Challenges: Productivity, Cost, Politics, and Patent Expirations

Over the past 30 years, however, the pharmaceutical industry has struggled to realize the lofty visions that were set for it in the 1980s and 1990s. The high water mark of the 1996 class of FDA approved drugs was followed by nearly 20 years of lower than expected productivity as measured by new drug approvals, a dramatic rise in the cost of research (Fig. 2),[7] increased competition from generic drug companies, and greater focus on the overall cost of health care. Between 1997 and 2011, the number of new molecule achieving FDA approval hovered at 26, while the cost of research sky rocketed. In 1996, research and development expenditures were approximately $17 billion, but by 2012 these costs were just under $50 billion. Similarly, the cost of a single FDA approval increased at an alarming rate. In 1987, a Tufts Center for the Study of Drug Development analysis concluded these costs at $231 million, but by 2010 the cost estimate had reached $1.75 billion, over 7.5 times the cost in 1987.[12] Generic drug companies have also added to the strain on the pharmaceutical industry, as the number of Abbreviated New Drug Application (ANDA) challenges to branded companies' patents has increased by over 450%.[13] Many brand companies sought to mitigate the potential impact of generic drugs by increasing their efforts in biologics (e.g., antibodies, protein therapeutics, etc.), as the pathway to generic biologic (biosimilars) represented uncharted territory. This changed, however, with passage of the Biologics Price Competition and Innovation (BPCI) Act in 2009 and the Patient Protection and Affordable Care Act in 2010.[14] This legislation codified a regulatory pathway for biosimilars, and the first biosimilar, Zarxio, a biosimilar version of Amgen's Neuogen), was approved by the FDA in Mar. 2015.[15]

The twin forces of politics and patent expirations have also increased over the last 30 years. Politicians and public figures routinely site the pharmaceutical industry as a leading cause of increased health care cost without recognizing the enormous benefits of the "wonder drugs" provided by the industry. This has led to wide spread questioning of pricing practices and the "profit before patient" view of the pharmaceutical industry. The atmosphere is mistrust of the pharmaceutical industry lead numerous insurance companies to refuse to pay for new, important medications. Payment for Advair (fluticasone propionate/salmeterol), an important new drug for asthma and chronic obstructive pulmonary disease (COPD) met stiff resistance in 2014.[16] In a similar manner, the high price of Harvoni (ledipasvir/sofobovir), a single pill fixed dose combination medicine capable of eradicating hepatitis C, has lead numerous health insurance companies to deny coverage.[17] The overall cost benefit of curing hepatitis C in 12 weeks and preventing liver damage that could ultimately result in liver transplant was lost in the chorus of calls for decreased drug prices. At the same time, the expected jump in innovation as a result of technological advances failed to materialize, creating a significant patent cliff for the pharmaceutical industry. Nearly $70 billion in branded pharmaceuticals lost patent protection in 2010–12,[18] and an estimated $290 billion of branded product sales are at risk between 2012 and 2018 as a result of patent expiration.[5]

All of these factors forced the pharmaceutical industry to undertake significant structural changes. Mergers and acquisitions, layoffs, and out-sourcing of research became common place in an industry that had previously been nearly immune to these activities. During the 2000–09 time period, over 1345 merger and acquisition deals valued at over $690 billion were consummated.[19] Over 300,000 pharmaceutical jobs were eliminated as a result of these activities,[20] and this substantial decrease in internal resources forced the pharmaceutical industry to abandon its staunchly held position that all R&D efforts should be done internally. Pharmaceutical companies began to increase their emphasis on "externally driven" research programs. Contract research organizations (CROs) and contract manufacturing organizations (CMOs) became an integral part of the pharmaceutical industry and flourished, but at the same time, a new player entered the drug discovery and development landscape, the academic drug discovery center.

1.01.2 The Bayh–Dole Act of 1980: A Catalyst for Academic Drug Discovery

There is no doubt that academic institutions have played, and will continue to play, a major role in the study of disease pathology and the identification of potential therapeutic targets. Prior to 1980, however, academic institutions rarely took part in the

commercially focused drug discovery arena. The vast majority of academic research was, and continues to be funded by federal research grants, and prior to 1980, patents developed using federal funds could only be licensed to commercial entities on a nonexclusive basis. Success in the pharmaceutical industry is predicated upon product exclusivity, and as a result, the industry had little interest in cooperating with academic institutions. This changed dramatically with the passage of the Bayh–Dole act of 1980, also referred to as the Patent and Trademark Law Amendment Act. Under this new law, universities and colleges were free to provide exclusive licenses to patents that were developed using federal funding.[21] In effect, the provisions of this law open the door to increased collaboration between the pharmaceutical industry and the academic world.

Over the next 35 years, as the pharmaceutical industry was contracting its scientific workforce, academic institution began building expertise in drug discovery. Not surprisingly, initial efforts took place in isolated academic laboratories, and some in the academic community were leery of partnering with commercial organizations. Lack of industrial experience also hampered early efforts, but as industrial scientists were laid off from commercial organizations, some took positions in academic institutions, providing real world experience to academic research. By 2001, 12 academic drug discovery centers had been established in the United States, and by 2013 there were over 100 centers in the United States and numerous academic drug discovery centers across the globe (**Table 1**).[22] These centers act as a source of novel science that bolsters the pharmaceutical industry's efforts to identify novel therapies for patients in need, while also providing academic scientists with the opportunity to move their research into the commercial realm, where it could provide real world benefits. This chapter provides an overview of the role academic drug discovery centers play in the modern pharmaceutical industry landscape, the resources and commitment required for a successful academic center, and representative success stories.

1.01.2.1 The Role of Academic Drug Discovery Centers

In general, academic drug discovery centers align their resources and programs to fulfill two important missions. First, these centers act as training grounds for the next generation of drug discovery scientists. While it is possible for young scientists interested in careers in the pharmaceutical industry to gain employment through a traditional single discipline educational path, this route does not provide the breadth of experience necessary for success in the pharmaceutical industry. Academic drug discovery centers, on the other hand, offer students the opportunity to engage in multidisciplinary programs focused on the identification of novel therapeutics. Students become experts in their chosen field of study, while also engaging in team based programs similar to those that occur in the pharmaceutical industry. This is especially true in fully integrated academic drug discovery centers (see below).

The second and equally important mission of the academic drug discovery center is to move academic science beyond the laboratory and into the commercial world. As noted earlier, the pharmaceutical industry's ability to innovate has decreased over the last 35 years as a result of mergers, layoffs, and numerous other factors. Over that same time period, the academic community has continued to be a source of innovation. In fact, one could argue that the innovative capacity of the academic community has increased as many highly qualified scientists made the transition from the industrial community into the academic arena.

The pharmaceutical industry has recognized the potential of the combination of cutting edge academic research and entrepreneurially minded academic scientists (especially those with previous industrial careers) and has expanded its effort to engage academic drug discovery centers. In some cases, these interactions are in the form of traditional sponsored research programs, but other forms of collaborations have been established. The California Institute for Biomedical Research (Calibr), for example, was established by Merck in 2012 as an independent, nonprofit academic institute dedicated to advancing the discoveries of academic scientists from around the world.[23] Pfizer established similar institutions in multiple locations. The "Centers for Therapeutic Innovation" (CTIs) in Boston, New York, San Diego, and San Francisco were opened by Pfizer with the expressed intent of collaborating with academic scientists.[24] Eli Lilly and GlaxoSmithKline have taken a more hands-off approach by establishing programs designed to provide academic scientist with access to their resources. The "Open Innovation Drug Discovery Program" at Eli Lilly provides academic scientists with access to a suite of established *in vitro* screening assays of interest to the company. Data is provided free of charge and academic scientists have the opportunity to engage the company to explore opportunities to move the program forward together or they can move forward on their own.[25] GlaxoSmithKline's "Discovery Fast Track Challenge"[26] and "Discovery Partnerships with Academia (DPAc),"[27] on the other hand, are more akin to the traditional grant submission process. Academic scientists submit proposals that are examined by a GlaxoSmithKline's review board to determine if the proposal is in line with the company's interests and meets their scientific standards. Irrespective of the form of the interaction, it is clear that the pharmaceutical industry has recognized the growing importance of academic drug discovery centers, and it is highly likely that these new organizations will continue to play an important role in the identification of novel therapeutics.

1.01.2.2 Academic Drug Discovery Center Structure and Function

The concept of structure dictating function that has long been recognized in biology also applies to the world of academic drug discovery centers. The capabilities and capacities of individual academic drug discovery centers are dictated by the overall organizational structure and support systems. While these features are certainly subject to change over time as centers evolve, there are essentially three types of centers that have appeared over the last 35 years: (1) those that are based on the founders expertise and research focus, (2) those that focus on coordinating the research efforts of outside groups, and (3) integrated centers whose operations are akin to a small biotech company. Each of these scenarios has benefits and weaknesses that merit further exploration.

Table 1 Academic drug discovery centers and resources

Name	*Affiliation*	*Location*
ACRF Drug Discovery Centre	Children's Cancer Institute Australia for Medical Research	Sydney, Australia
ACRF Rational Drug Discovery Centre	St Vincent's Institute for Medical Research	Victoria, Australia
Alabama Drug Discovery Alliance	University of Alabama, Birmingham	Birmingham, AL, USA
BIO5 Oro Valley	University of Arizona	Oro Valley, AZ, USA
BioDistrict New Orleans	Tulane University Health Science Center, LSU Health Science Center, Xavier University of Louisiana, Louisiana Cancer Research Consortium	New Orleans, LA, USA
Blavatnik Biomedical Accelerator at Harvard University	Harvard University	Cambridge, MA, USA
Brain Science Institute	Johns Hopkins University	Baltimore, MD, USA
BRITE	North Carolina Central University	Durham, NC, USA
Broad Institute	Harvard University and Massachusetts Institute of Technology	Cambridge, MA, USA
Bryan Alzheimer's Disease Drug Discovery Program	Duke University	Durham, NC, USA
California Center for Antiviral Drug Discovery	University of California, Irvine, Los Angeles, and San Francisco	Irvine, CA, USA
Cellular Screening Center	The University of Chicago	Chicago, IL, USA
Center for Advancement of Drug Research and Evaluation	Western University of Health Sciences	Pomona, CA, USA
Center for Diagnostics and Therapeutics	Georgia State University	Atlanta, GA, USA
Center for Drug Design	University of Minnesota	Minneapolis, MN, USA
Center for Drug Design and Development	University of Toledo	Toledo, OH, USA
Center for Experimental Drugs and Diagnostics	Massachusetts General Hospital Harvard Medical School	Cambridge, MA, USA
Center for Innovative Drug Discovery	University of Texas San Antonio, University of Texas Health Science Center San Antonio	San Antonio, TX, USA
Center for Integrative Chemical Biology and Drug Discovery	University of North Carolina Eshelman School of Pharmacy	Chapel Hill, NC, USA
Center for Investigational Therapeutics	University of Utah Huntsman Cancer Institute	Salt Lake City, UT, USA
Center for Molecular Innovation and Drug Discovery	Northwestern University	Evanston, IL, USA
Center for Pharmaceutical Research and Innovation	University of Kentucky College of Pharmacy	Lexington, KY, USA
Center for Protein Therapeutics	University at Buffalo School of Pharmacy and Pharmaceutical Sciences	Amherst, NY, USA
Center for the Discovery of New Medicines	University of Michigan	Ann Arbor, MI, USA
Center for Therapeutic Innovation	University of Miami	Miami, FL, USA
Center For World Health and Medicine	Saint Louis University	Saint Louis, MO, USA
Center of Excellence in Pharmacokinetics and Pharmacodynamics	University at Buffalo School of Pharmacy and Pharmaceutical Sciences	Amherst, NY, USA
Centre of Applied Medical Research	Foundation for Applied Medical Research, University of Navarra, University Hospital of the University of Navarra	Pamplona, Spain
Chemical Biology Consortium Sweden	Karolinska Institute	Stockholm, Sweden
Collaborative Engagement in Novel Therapeutic Research and Enterprise	University of Illinois	Chicago, IL, USA
Colorado Center for Drug Discovery	Colorado State University	Fort Collins, CO, USA
Conrad Prebys Center for Chemical Genomics	Sanford-Burnham Medical Research Institute	La Jolla, CA, USA
Dana-Farber Cancer Institute Medicinal Chemistry Core	Dana-Farber Cancer Institute	Boston, MA, USA
Department of Chemical Biology and Therapeutics	St Jude Children's Research Hospital	Memphis, TN, USA
Drug Discovery Core at the Medical University of South Carolina	Medical University of South Carolina	Charleston, SC, USA
Drug Discovery, Development and Delivery Core	Penn State College of Medicine	Hershey, PA, USA
Emory Chemical Biology Discovery Center	Emory University	Atlanta, GA, USA
Eskitis Institute for Drug Discovery	Griffith University	Brisbane, QLD, Australia
Experimental Therapeutics Institute	Icahn School of Medicine at Mount Sinai	New York, NY, USA
Florida Center of Excellence for Drug Discovery and Innovation	University of South Florida	Tampa, FL, USA
Harvard NeuroDiscovery Center Laboratory for Drug Discovery	Brigham and Women's Hospital, Harvard Medical School	Cambridge, MA, USA
Health Research Institute of Santiago de Compostela	University of Santiago de Compostela	Santiago de Compostela, Spain
High-Throughput Screening Resource Center	The Rockefeller University, Weill Cornell Medical College	New York, NY, USA
ICCB-Longwood Screening Facility	Harvard Medical School	Boston, MA, USA
Institute for Neurotherapeutics Discovery	University of California, Davis	Sacramento, CA, USA
Institute for Structural Biology and Drug Discovery	Virginia Commonwealth University	Richmond, VA, USA

Table 1 Academic drug discovery centers and resources—cont'd

Name	*Affiliation*	*Location*
Institute for Therapeutics Discovery and Development	University of Minnesota College of Pharmacy	Minneapolis, MN, USA
Institute for Tuberculosis Research	University of Illinois at Chicago	Chicago, IL, USA
Institute of Chemical Biology and Drug Discovery	Stony Brook University, State University of New York	Stony Brook, NY, USA
Integrated Initiative in Global Health	Northeastern University	Boston, MA, USA
KU Specialized Chemistry Center	University of Kansas	Lawrence, KS, USA
Laboratory for Neglected Disease Drug Discovery	Northeastern University	Boston, MA, USA
Lieber Institute Drug Discovery Division	Johns Hopkins University School of Medicine	Baltimore, MD, USA
LIMR Chemical Genomics Center	Lankenau Institute for Medical Research	Wynnewood, PA, USA
LSUHSC Neuroscience Center of Excellence	Louisiana State University Health Sciences Center, New Orleans School of Medicine	New Orleans, LA, USA
Michigan High Throughput Screening Center	Kalamazoo Valley Community College	Kalamazoo, MI, USA
Milwaukee Institute for Drug Discovery	University of Wisconsin-Milwaukee	Milwaukee, WI, USA
Moffitt Cancer Center Drug Discovery	H. Lee Moffitt Cancer Center and Research Institute	Tampa, FL, USA
Moulder Center for Drug Discovery Research	Temple University School of Pharmacy	Philadelphia, PA, USA
MRC Protein Phosphorylation and Ubiquitylation Unit	The University of Dundee	Dundee, UK
MSU Drug Discovery Center	Michigan State University	East Lansing, MI, USA
MUSC Drug Discovery Center	Medical University of South Carolina	Charleston, SC, USA
National Center for Natural Products Research	University of Mississippi	University, MS, USA
National Institute of Mental Health Psychoactive Drug Screening Program	University of North Carolina Chapel Hill Medical School	Chapel Hill, NC, USA
New York State Center of Excellence in Bioinformatics and Life Sciences Translational Pharmacology Research Core	University at Buffalo School of Pharmacy and Pharmaceutical Sciences	Buffalo, NY, USA
NJ Center for Science Technology and Mathematics	Kean University	Union, NJ, USA
Oregon Translational Research and Development Institute	Oregon Bioscience Association, Oregon Health and Science University, Portland State University, Oregon State University	Portland, OR, USA
Penn Center for Molecular Discovery	University of Pennsylvania	Philadelphia, PA, USA
PharmaCenter Bonn	University of Bonn	Bonn, Germany
Platform of Chemical Biology & ADME of Strasbourg	University of Strasbourg	Illkirch, France
Purdue University Center For Drug Discovery	Purdue Univeristy	West Lafayette, IN, USA
Research Institute for Medicines	University of Lisbon	Lisbon, Portugal
Rockefeller University Center for Clinical and Translational Science Therapeutic Discovery and Development Program	Rockefeller University	New York, NY, USA
Rutgers University Biomedical Research Consortium	Rutgers University	New Brunswick, NJ, USA
Sanford-Burnham Medical Research Institute at Lake Nona	University of Florida, Harbor Branch Institute Oceanographic Institute at Florida Atlantic University	Orlando, FL, USA
SciLifeLab Drug Discovery and Development Platform	Karolinska Institute, Uppsala University, Stockholm University, KTH Royal Institute of Technology	Stockholm, Sweden
Small Molecule Discovery Center	University of California San Francisco	San Francisco, CA, USA
Sokol Institute of Pharmaceutical Life Sciences	Montclair State University	Montclair, NJ, USA
SPARK Translational Research Program	Stanford University School of Medicine	Stanford, CA, USA
Stanford Behavioral and Functional Neuroscience Laboratory	Stanford University School of Medicine	Stanford, CA, USA
Stanford High-Throughput Bioscience Center	Stanford University School of Medicine	Stanford, CA, USA
Texas A&M Natural Products LINCHPIN Laboratory	Texas A&M University	College Station, TX, USA
Texas Screening Alliance for Cancer Therapeutics	Texas A&M Health Science Center Baylor College of Medicine University of Texas at Austin Rice University MD Anderson Cancer Center The Methodist Hospital Research Institute	Houston, TX, USA
The Institute of Cancer Research London	The Institute of Cancer Research	London, UK
Translational Neuroscience Center at Boston Children's Hospital	Boston Children's Hospital, Harvard Medical School	Boston, MA, USA
UCLA Molecular Screening Shared Resource	University of California, Los Angeles	Los Angeles, CA, USA
UCSD Drug Discovery Institute	University of California, San Diego	San Diego, CA, USA
UI Centre for Drug Discovery	University of Illinois at Chicago	Chicago, IL, USA
University of Colorado Denver High Throughput and High Content Screening Core	University of Colorado Skaggs School of Pharmacy and Pharmaceutical Sciences	Aurora, CO, USA
University of Georgia Center for Drug Discovery	University of Georgia	Athens, GA, USA

(Continued)

Table 1 Academic drug discovery centers and resources—cont'd

Name	*Affiliation*	*Location*
University of Iowa Pharmaceuticals	University of Iowa	Iowa City, IA, USA
University of Kansas High-Throughput Screening Laboratory	University of Kansas, Lawrence University of Kansas Medical Center	Lawrence, KS, USA
University of New Mexico Center for Molecular Discovery	University of New Mexico	Albuquerque, NM, USA
University of New Mexico Clinical and Translational Science Center	University of New Mexico Health Sciences Center	Albuquerque, NM, USA
University of North Texas Health Science Center Preclincal Services	University of North Texas Health Science Center	Fort Worth, TX, USA
University of Sussex Translational Drug Discovery Group	University of Sussex	East Sussex, UK
University of Wisconsin Small Molecule Screening and Synthesis Facility	University of Wisconsin Madison	Madison, WI, USA
UNMC Drug Discovery Institute	University of Nebraska Medical Center	Omaha, NE, USA
UTMB Center for Addiction Research/Innovations in Molecular Therapeutics	The University of Texas Medical Branch, University of Houston, MD Anderson, University of Texas Health Science Center at Houston, University of Texas at Austin	Galveston, TX, USA
Vanderbilt Center for Neuroscience Drug Discovery	Vanderbilt University Medical Center	Nashville, TN, USA
Vanderbilt High-throughput Screening Facility	Vanderbilt University, Vanderbilt University Medical Center	Nashville, TN, USA
Vanderbilt Institute of Chemical Biology	Vanderbilt University, Vanderbilt University Medical Center	Nashville, TN, USA
Virginia Tech Center for Drug Discovery	Virginia Tech	Blacksburg, VA, USA
Yale Center for Molecular Discovery	Yale University	West Haven, CT, USA

1.01.2.3 Founder Focused Academic Drug Discovery Centers

In many cases, academic drug discovery centers are heavily focused on a particular area of biology or specific disease states that are in line with the founding member's research interests. This sharp focus provides the organization with an exceptionally high level of expertise in their particular field of interest and allows for concentration of resources. Many of the early academic drug discovery centers were founded using this strategic platform, as they were almost always built on preexisting expertise of established, often tenured, academic scientists. This format was especially popular with the first academic drug discovery centers. In the early days of these ventures (just after the passage of the Bayh–Dole act of 1980) many were skeptical that academic institutions could produce commercially viable therapeutics. By focusing on preexisting expertise, these centers were able to leverage their capabilities to attract grant funding to support their programs.

While this approach can and has been successful, it suffers from the inherent limitation of expertise to a particular disease focus, thereby limiting funding opportunities. In addition, operations of this type often require outside collaboration in order to move programs forward. Biology driven centers, for example, often lack internal medicinal chemistry support, *in vitro* ADME expertise, and other functions required for the successful identification of novel therapeutics. These centers tend to be smaller operations with limited foot prints and infrastructure (faculty and staff of five or fewer), but can be successful in driving academic research into the commercial world through collaborative efforts. The California Center for Antiviral Drug Discovery, for example, was founded in 2010 to take advantage of the founder's in depth knowledge of RNA viruses. Similarly, the Center for Protein Therapeutics at the University of Buffalo's School of Pharmacy and Pharmaceutical Science open its door in 2008 as part of an effort to build on in house expertise in protein science. This organization has attracted sponsorships and funding from numerous industrial partners such as Novartis, Amgen, and Roche.

1.01.2.4 Research Coordination Academic Drug Discovery Centers

The research coordination approach is an alternative to research driven operations. In this scenario, the center is focused on building bridges between research groups within an academic institution and identifying potential external collaborators for on-going research activities within the larger organization. Program management, especially when external resources are required, and technology transfer expertise are key drivers of these operations. They are usually staffed by one to three people who act as contact points, have limited research budgets, and have a portfolio of programs that is heavily dependent on the interest of the faculty of the parent organization. An attractive feature of this scenario is the relatively low cost of entry. A single person or small group of individuals with industrial experience and a network of contacts can run a center of this type without requiring a significant investment in research infrastructure and scientific support staff. The success of this endeavor, however, is predicated upon the willingness of academicians at the parent university/college to work with the center, as the center itself is not a research driven resource.

While this approach can be successful and is attractive to academic institutions unwilling or unable to commitment substantial funds to academic drug discovery, it is clearly limited in scope and capabilities. The Drug Discovery, Development, and Delivery Core (D4 Core) in Hershey, PA, for example, is associated with Penn State College of Medicine was founded in 2002. Currently, this organization has three employees and collaborates with numerous on-site and off-site groups in an effort to pursue drug discovery programs.

1.01.2.5 Fully Integrated Academic Drug Discovery Centers

In some instances, universities have elected to establish independent drug discovery centers that more closely resemble a small to mid-size biotech company than an academic research laboratory. These operations generally consist of several tenured or tenure track faculty members and supporting staff scientists whose collective experience and expertise encompasses the key facets of drug discovery science (e.g., medicinal chemistry, *in vitro* screening science, *in vivo* pharmacokinetics, *in vivo* pharmacology, formulations science, etc.). Significant pharmaceutical industry experience is often available within these centers, as they have attracted numerous scientists who were caught up in the merger and acquisition feeding frenzy of the last 20 years. Research infrastructure and enabling technologies (e.g., high throughput screening laboratories, laboratory animal facilities, chemical screening libraries, *in vitro* ADME screening etc.) is established as part of the on-going operation, and in many cases substantial funding is made available by the parent university to support early stage research (that which is not quite ready for external grant funding).

While these centers have the advantage of direct access to what amounts to a fully integrated drug discovery operation, there is a substantial cost to creating and maintaining this type of organization that is often out of reach of many institutions. As a result, there are only a handful of academic drug discovery centers that qualify as fully integrated. Several of them started out as founder focused centers that built on their success, but this is not always the case. Some of these centers engage in contract research programs to maintain funding for nontenured faculty and staff members that are critical to the day-to-day operation in periods, as grant funds are often insufficient to cover these costs. Still others are benefactors of successful alumni interested in building the research reputation of their alma mater. Irrespective of the source of funding, there can be no doubt that this class of academic drug discovery center is an expensive endeavor, but it is achievable. Prominent examples of successful, fully integrated academic drug discovery centers include the Emory Institute for Drug Development,[28] the Yale Center for Molecular Discovery,[29] the Vanderbilt Center for Neuroscience Drug Discovery (VCNDD),[30] Northeastern University's Center of Drug Discovery (CDD),[31] and the Moulder Center for Drug Discovery Research (MCDDR).[32]

1.01.2.6 US Academic Drug Discovery Centers

In an effort to gain a better understanding of the academic drug discovery landscape in the United States, Frey et al.[33] conducted a survey of 56 academic drug discovery centers. Like their industrial counterparts, academic drug discovery centers maintain an active interest in cancer and infectious disease. Over 85% of centers surveyed reported active programs focused on the identification of novel anticancer agents, while 71% reported an interest in discovering novel treatments for infectious disease. Orphan diseases and maladies primarily found in less developed nations also comprised a significant portion of academic drug discovery centers research portfolios with 36% and 30% of centers reporting active efforts in these areas respectively. Not surprisingly, target selections tended to be higher risk in nature, as only 18% of disease modification targets under investigation were clinically validated. In addition, nearly 50% of targeted biochemical pathways had little or no validation in the literature.

With regard to capabilities, expertise, and funding, Frey's survey demonstrated a wide variation in all of these factors. While almost all of the centers (93%) reported the capacity to run *in vitro* cell based primary assays, less than half (42%) had the capacity to perform pharmacokinetic and metabolism studies on potential lead compounds. Target identification and hit to lead medicinal chemistry capacity was noted at the majority of academic drug discovery centers (77% and 72% respectively), but just over half (51%) reported the ability to perform *in vivo* efficacy studies. Only a handful of centers reported that they could perform all functions of early to mid-stage drug discovery work. This situation is likely the result of funding limitations. While some centers reported annual budget in excess of $10 million, the majority of centers' annual operating expenses were much smaller (>$2 million), some as low as $25,000 per year. Experience gaps may also be a limiting factor. More than half of the responding institutions reported that <25% of their staff scientists had industrial drug discovery experience, and <40% had tenure track faculty members focused on drug discovery.

1.01.2.7 Risks and Rewards of Academic Drug Discovery Centers

While one of the goals of an academic drug discovery center is to provide academic scientists with a method of making their research appealing to an industrial partner, any discussion of this potential value proposition would be incomplete without considering the impact of the second goal of these centers, the training of the next generation of scientists. There should be no illusions regarding the fact the primary goals of the academic institutions and industrial organizations are not the same. At the end of the day, an academic institution's primary operating mandate is to educate its students and help them start their professional lives. As a result of this and the "publish or perish" mentality embedded within many universities, there is often significant pressure to publish results rapidly. In order to mitigate the risk of premature public disclosure of potentially commercially viable research results, academic drug discovery centers often work in close collaboration with university technology transfer offices. Strategically filed patent applications

can protect the intellectual property developed in academic laboratories, while still providing academicians with the opportunity to publish important scientific findings. Importantly, academicians who file provisional patent applications are bound by the same time limitations as any other patent applicant, and failure to meet a patent deadline can have a negative impact on potential patent rights. In addition, although many technology transfer departments will support the cost of a provisional application, the cost of patent cooperation treaty (PCT) and national stage applications can become prohibitively expensive even in the largest academic institutions. As a result, great care must be taken in deciding when, how and if a patent application is warranted.

Irrespective of this risk, there are a number of clinically important therapeutic agents that originated from the academic community. Prezista (Darunavir, **3a**), an important HIV protease inhibitor marketed by Janssen Therapeutics, for example, was discovered by Professor Arun K. Ghosh and his colleagues at the University of Illinois, Chicago.[34] In a similar fashion, Gilead Sciences' nucleoside reverse transcriptase inhibitor HIV therapy Emtriva (Emtricitabine, **3b**) was not originally identified in the pharmaceutical industry. This key drug was first identified by Professor Dennis Liotta's research team at Emory University and the identification of a number of important clinical compounds makes it clear that acadscovery R.[35] The importance of this therapeutic agent is highlighted by its inclusion in the World Health Organization's List of Essential Medicines. Similar recognition is paid to Ziagen (abacavir), an HIV reverse transcription inhibitor originally discovered in the laboratory of Robert Vince at the University of Minnesota and marketed by GSK. Additional success stories include Professor Edward C. Taylor's identification of Alimta (Pemetrexed, **3c**) an anticancer agent marketed by Eli Lilly,[36] Zolinza (vorinostat), the first marketed histone deacetylase inhibitor discovered by Columbia professor Ronald Breslow and Sloan Kettering researcher Paul Marks and Lyrica (Pregabalin, **3d**), a fibromyalgia therapy that produced sales of $3.7 billion in 2011, which was originally identified by Professor Richard Silverman's group at Northwestern University.[37] The financial rewards to the academic institutions and scientists credited with the inventions can be substantial. The discovery and commercialization of Lyrica (Pregabalin), for example, netted Northwestern University and its staff a one-time payment of $700 million, as well as annual licensing fees for the compound.[38]

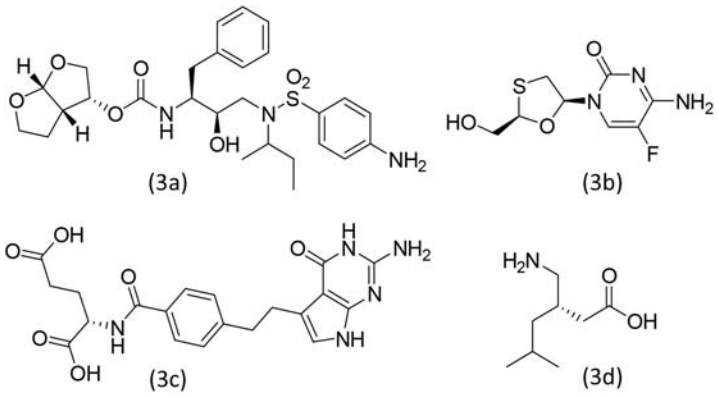

Fig. 3 Prezista (Darunavir) (**3a**), Emtriva (Emtricitabine) (**3b**), Alimta (Pemetrexed) (**3c**), in CAS database.ct as drawn. It is consistent with the structure Lyrica (Pregabalin) (**3d**).

The development of Kyprolis (Carfilzomib (**4c**), Fig. 4) is another interesting success story that began in an academic facility. In the late 1990s, Craig Crews and his colleagues at Yale were investigating the properties of Epoxomicin (**4a**), a microbially derived antitumor compound, and related analogs with the hope of determining a mechanism(s) of action. Their work eventually led to the conclusion that this class of compounds inhibits the proteasome. They also produced an analog designated YU-101 (**4b**), a viable drug discovery lead compound that was licensed to a spin-off company, Proteolix, in Dec. 2003. This company rose over $18 Million in financing to support the eventual identification and early clinical study of Kyprolis(Carfilzomib, **4c**). In late 2009, the company was acquired by Onyx Pharmaceuticals in a deal that included an initial upfront payment of $276 million. Additional payments based on milestones brought the value to over $535 million.[39] The drug was approved by the FDA for the treatment of multiple myeloma in Jun. 2012. A little more than 1 year later, in Aug. of 2013, Amgen bought Onyx for $10.4 billion.[40] Although exact dollar figures have not been disclosed, it is likely that Dr. Crews, his colleagues, and Yale received financial rewards at each of these events.

1.01.3 Concluding Remarks

The long term impact of academic drug discovery centers and academic/industry partnerships on the pharmaceutical industry is likely to be positive and long lasting. The opportunity to commercialize academic research with the potential to earn hundreds

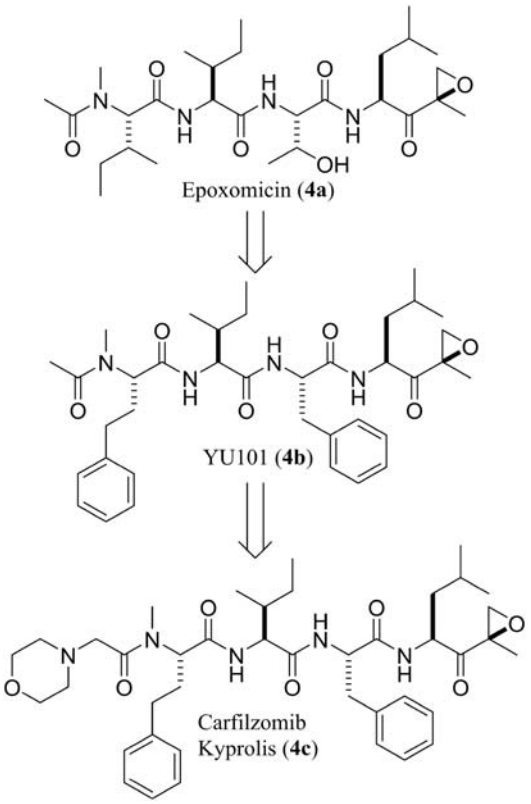

Fig. 4 Identification of Kyprolis (Carfilzomib).

of millions of dollars is a strong, attractive feature that many universities will not ignore. At the same time, the opportunity to better prepare their students to work in the pharmaceutical industry is a highly valuable asset in the competitive job market of the 21st century. Academic drug discovery centers and academic/industry partnerships provide the pharmaceutical industry with two things it needs in constant supply in order to thrive, novel scientific avenues for potential therapeutics and well trained scientists entering the work force to discover the next generation of "wonder drugs."

See also: 1.23. Contemporary Considerations for Discovering a Successful Medicine.

References

1. Roth, B. D. Preparation of Anticholesteremic (R-(R*R*))-2-(4-Fluorophenyl)-β, γ-Dihydroxy-5-(1-Methylethyl-3-Phenyl-4(Phenylamino)Carbonyl)-1H-Pyrrolyl-1-Heptanoic acid, its Lactone Form and Salts Thereof. **1991**, EP409281.
2. (a) Zimmermann, J.; Buchdunger, E.; Mett, H.; Meyer, T.; Lydon, N. B. Potent and Selective Inhibitors of the ABL-Kinase: Phenylaminopyrimidine (PAP) Derivatives. *Bioorg. Med. Chem. Lett.* **1997,** *7* (2), 187–192; (b) Druker, B. J.; Lydon, N. B. Lessons Learned from the Development of an Abl Tyrosine Kinase Inhibitor for Chronic Myelogenous Leukemia. *J. Clin. Investig.* **2000,** *105* (1), 3–7.
3. Springthorpe, B.; Bailey, A.; Barton, P.; Birkinshaw, T. N.; Bonnert, R. V.; Brown, R. C.; Chapman, D.; Dixon, J.; Guile, S. D.; Humphries, R. G.; Hunt, S. F.; Ince, F.; Ingall, A. H.; Kirk, I. P.; Leeson, P. D.; Leff, P.; Lewis, J.; Martin, B. P.; McGinnity, D. F.; Mortimore, M. P.; Paine, S. W.; Pairaudeau, G.; Patel, A.; Rigby, A. J.; Riley, R. J.; Teobald, B. J.; Tomlinson, W.; Webborn, P. J. H.; Willis, P. A. From ATP to AZD6140: The Discovery of an Orally Active Reversible P2Y12 Receptor Antagonist for the Prevention of Thrombosis. *Bioorg. Med. Chem. Lett.* **2007,** *17* (21), 6013–6018.
4. Labelle, M.; Belley, M.; Gareau, Y.; Gauthier, J. Y.; Guay, D.; Gordon, R.; Grossman, S. G.; Jones, T. R.; Leblanc, Y. Discovery of MK-0476, a Potent and Orally Active Leukotriene D4 Receptor Antagonist Devoid of Peroxisomal Enzyme Induction. *Bioorg. Med. Chem. Lett.* **1995,** *5* (3), 283–288.
5. EvaluatePharma. *World Preview 2018: Embracing the Patent Cliff,* 2012. http://info.evaluatepharma.com/WP2018_ELS_LP.htm.
6. (a) Bosch, F.; Rosich, L. The Contributions of Paul Ehrlich to Pharmacology: A Tribute on the Occasion of the Centenary of His Nobel Prize. *Pharmacology* **2008,** *82,* 171–179; (b) Drews, J. Drug Discovery: A Historical Perspective. *Science* **2000,** *287,* 1960–1964.
7. http://www.phrma.org/.
8. High-Throughput Screening in Drug Discovery, Hüser, J. (Ed.); Mannhold, R.; Kubinyi, H.; Folkers, G. (Series Eds.); Wiley-VCH, 2006.
9. Rankovic, Z.; Morphy, R. *Lead Generation Approaches in Drug Discovery;* John Wiley & Sons Inc.: Hoboken, NJ, 2010.
10. Ng, P. C.; Kirkness, E. F. Whole Genome Sequencing. *Methods Mol. Biol.* **2010,** *628,* 215–226.
11. Blass, B. E. *Basic Principles of Drug Discovery and Development;* Academic Press: Waltham, MA, 2015, pp 59–66. Chapter 2.
12. Paul, S. M.; Mytelka, D. S.; Dunwiddie, C. T.; Persinger, C. C.; Munos, B. H.; Lindborg, S. R.; Schacht, A. L. How to Improve R&D productivity: The Pharmaceutical Industry's Grand Challenge. *Nat. Rev. Drug Discov.* **2010,** *9,* 203–214.

13. Barry, C.; Arad, R.; Johnston, A.; Parent, A.; Ansell, L.; Arnold, M. *2012 patent litigation study;* PricewaterhouseCoopers, 2012. http://www.pwc.com/us/en/forensic-services/publications/2012-patent-litigation-study.jhtml.
14. *Public Law 111–148*. March 23; United States Government Printing Office: Washington, DC, 2010. https://www.gpo.gov/fdsys/granule/PLAW-111publ148/PLAW-111publ148/content-detail.html.
15. FDA. *FDA approves first biosimilar product Zarxio*. March 6., 2015 http://www.fda.gov/newsevents/newsroom/pressannouncements/ucm436648.htm.
16. Merck Kitamura, M. Glaxo's Advair Loses U.S. Market Share to Astra, Bloomberg.com February 4, 2014. http://www.bloomberg.com/news/articles/2014-02-04/glaxo-s-advair-loses-u-s-market-share-as-breo-sales-rise.
17. (a) Pfeifer, S. *Woman Sues Anthem Blue Cross for Refusing to Cover Hepatitis C Drug*. May 18; The Los Angeles Times, 2015. http://www.latimes.com/business/la-fi-anthem-blue-cross-harvoni-lawsuit-20150518-story.html; (b) Aleccia, J. *Lawsuit Targets Medicaid policy that Limits Spendy Hepatitis C Drugs*. February 17.; The Seattle Times, 2016 http://www.seattletimes.com/seattle-news/health/lawsuit-targets-medicaid-policy-that-limits-spendy-hep-c-drugs/; (c) Millman, J. *A New Lawsuit Claims $84,000 is Way Too Much for This Lifesaving Drug*. December 11.; The Washington Post, 2014. https://www.washingtonpost.com/news/wonk/wp/2014/12/11/a-new-lawsuit-claims-84000-is-way-too-much-for-this-lifesaving-drug/.
18. Davis, P. J. *Beyond the Patent Cliff – Signs of Recovery in Biopharma's New Normal;* Accenture Life Sciences, 2012. http://www.accenture.com/SiteCollectionDocuments/PDF/Accenture-Life-Sciences-Beyond-The-Patent-Cliff-Signs-Of-Recovery-in-Biopharmas-New-Normal.pdf.
19. (a) Stone, K. Big Pharma's Merger Mania. About.com; http://pharma.about.com/od/BigPharma/tp/Big-Pharmas-Merger-Mania.htm. (b) Deal Search Online Home Page, Irving Levin Associates, Inc.; http://www.levinassociates.com/dealsearch/.
20. (a) Lamattina, J. The Impact of Mergers on Pharmaceutical R&D. *Nat. Rev. Drug Discov.* **2011,** *10,* 559–560; (b) Firestone, R. Lessons From 54 Years of Pharmaceutical Research. *Nat. Rev. Drug Discov.* **2011,** *10,* 963; (c) Munos, B. Lessons From 60 Years of Pharmaceutical Innovation. *Nat. Rev. Drug Discov.* **2009,** *8,* 959–968; (d) Comanor, W.; Scherer, F. *Mergers and Innovation in the Pharmaceutical Industry*. Harvard Kennedy School Faculty Research Working Paper Series., 2011 https://research.hks.harvard.edu/publications/workingpapers/citation.aspx?PubId=8053&type=FN&PersonId=219.
21. Technology Transfer, Administration of the Bayh-Dole Act by Research Universities. U.S. Government Accounting Office (GAO) Report to Congressional Committees. May 7, 1978.
22. Slusher, B. S.; Conn, P. J.; Frye, S.; Glicksman, M.; Arkin, M. Bringing Together the Academic Drug Discovery Community. *Nat. Rev. Drug Discov.* **2013,** *12* (11), 811–812.
23. http://www.calibr.org/index.htm.
24. http://www.pfizer.com/research/rd_partnering/centers_for_therapeutic_innovation.
25. https://openinnovation.lilly.com/dd/about-open-innovation/how-does-open-innovation-work.html.
26. http://openinnovation.gsk.com/na/index.php.
27. http://www.dpac.gsk.com/.
28. http://eidd.emory.edu/.
29. http://ycmd.yale.edu/.
30. http://www.vcndd.com/.
31. http://www.cdd.neu.edu/.
32. http://moulder.temple.edu.
33. Frye, S.; Crosby, M.; Edwards, T.; Juliano, R. US Academic Drug Discovery. *Nat. Rev. Drug Discov.* **2011,** *10,* 409–410.
34. (a) Ghosh, A. K.; Kincaid, J. F.; Cho, W.; Walters, D. E.; Krishnan, K.; Hussain, K. A.; Koo, Y.; Cho, H.; Rudall, C.; Holland, L.; Buthod, J. Potent HIV Protease Inhibitors Incorporating High-Affinity P2-Ligands and (R)-[(hydroxyethyl)Amino]sulfonamide Isostere. *Bioorg. Med. Chem. Lett.* **1998,** *8* (6), 687–690; (b) Vazquez, M. L.; Mueller, R. A.; Talley, J. J.; Getman, D. P.; Decrescenzo, G. A.; Freskos, J. N.; Bertenshaw, D. E.; Heintz, Robert M. Hydroxyethylamino Sulfonamides Useful as Retroviral Protease Inhibitors WO 9506030 A1, **1995**.
35. (a) Schinazi, R. F.; McMillan, A.; Cannon, D.; Mathis, R.; Lloyd, R. M.; Peck, A.; Sommadossi, J. P.; St Clair, M.; Wilson, J.; Furman, P. A. Selective Inhibition of Human Immunodeficiency Viruses by Racemates and Enantiomers of Cis-5-Fluoro-1-[2-(Hydroxymethyl)-1,3-Oxathiolan-5-yl]Cytosine. *Antimicrob. Agents Chemother.* **1992,** *36* (11), 2423–2431; (b) Frick, L. W.; Lambe, C. U.; St. John, L.; Taylor, L. C.; Nelson, D. J. Pharmacokinetics, Oral Bioavailability, and Metabolism in Mice and Cynomolgus Monkeys of (2′R,5′S)-cis-5-fluoro-1-[2-(hydroxymethyl)-1,3-oxathiolan-5-yl] cytosine, An Agent Active Against Human Immunodeficiency Virus and Human Hepatitis B Virus. *Antimicrob. Agents Chemother.* **1994,** *38* (12), 2722–2729.
36. (a) Taylor, E. C.; Patel, H. H. Synthesis of Pyrazolo[3,4-d]Pyrimidine Analogs of the Potent Antitumor Agent N-[4-[2-(2-Amino-4(3H)-Oxo-7H-Pyrrolo[2,3-d]Pyrimidin-5-yl)Ethyl] Benzoyl]-L-Glutamic Acid (LY231514). *Tetrahedron* **1992,** *48* (37), 8089–8100; (b) Taylor, E. C.; Kuhnt, D. G.; Shih, C.; Grindey, G. B. Preparation of N-[Pyrrolo[2,3-d] Pyrimidin-3-Ylacyl]Glutamates as Neoplasm Inhibitors. US5248775, **1993**.
37. (a) Taylor, C. P.; Vartanian, M. G.; Yuen, P. W.; Bigge, C.; Suman-Chauhan, N.; Hill, D. R. Potent and Stereospecific Anticonvulsant Activity of 3-isobutyl GABA Relates to *in vitro* Binding at a Novel Site Labeled by Tritiated Gabapentin. *Epilepsy Res.* **1993,** *14* (1), 11–15; (b) Silverman, R. B.; Andruszkiewicz, R.; Yuen, P. W.; Sobieray, D. M.; Franklin, L. C.; Schwindt, M. A. Preparation of GABA and L-Glutamic Acid Analogs for Antiseizure Treatment. WO 9323383A1, **1993**.
38. Wang, A. L. *Northwestern University Leads Nation in Tech Transfer Revenue;* Crain's Chicago Business: Chicago, IL, 2012.
39. Halford, B. Carfilzomib: From Discovery To Drug: How an Academic Pursuit to Understand Epoxomicin Became the Cancer Treatment Carfilzomib. *Chem. Eng. News* **2012,** *90* (35), 34–35.
40. Cimilluca, D.; Rockoff, J. D.; Walker, J. Amgen Strikes $10.4 Billion Deal for Onyx. *Wall Street J.* **2013**.

1.02 Drug Repurposing Review

D Cavalla, Numedicus Limited, Cambridge, United Kingdom
E Oerton and A Bender, Centre for Molecular Informatics, Cambridge, United Kingdom

© 2017 Elsevier Ltd. All rights reserved.

1.02.1 Historical Perspective 11
1.02.2 Successes: From Chance Clinical Findings to Determinate Strategy 12
1.02.3 Advantages and Disadvantages of Drug Repurposing 14
1.02.3.1 Attritional Risk 16
1.02.3.2 Cost 16
1.02.3.3 Time 16
1.02.3.4 Disadvantages 16
1.02.3.5 Off-Label Medicine 17
1.02.4 Variants 18
1.02.4.1 Repurposing of Generic Drugs 18
1.02.4.2 Public/Private Partnerships for Repurposing of Abandoned Assets 19
1.02.4.3 Off-Target Versus On-Target 19
1.02.4.4 Rare Diseases 20
1.02.5 Approaches to the Identification of Drug Repurposing Candidates 21
1.02.5.1 Experimental Approaches 21
1.02.5.1.1 Target-association screening 21
1.02.5.2.2 Phenotypic screening 21
1.02.5.2 Knowledge-Based Approaches 23
1.02.5.2.1 Literature-based 23
1.02.5.1.2 Ontologies 24
1.02.5.3 Retrospective Analysis 25
1.02.6 Data Mining Approaches for the Prediction of Drug Repurposing Opportunities 27
1.02.6.1 Data Types 27
1.02.6.2 Data Processing 27
1.02.6.3 Resources 28
1.02.6.4 Validation 29
1.02.6.5 Structure–Target Data Mining 29
1.02.6.5.1 Chemical structure methods 29
1.02.6.5.2 Protein structure methods 30
1.02.6.5.3 Molecular docking and binding site similarity 30
1.02.6.5.4 Drug–target interaction profiles 30
1.02.6.6 Effects-Based Data Mining 31
1.02.6.6.1 Genome-based 33
1.02.6.6.2 Transcriptome-based 34
1.02.6.6.3 Proteome-based 34
1.02.6.6.4 Phenome-based 35
1.02.6.7 Integrated Approaches 38
1.02.6.8 Practical Considerations 40
1.02.7 Beyond Repurposing: Tailoring an Existing Drug for a New Use 41
1.02.8 Conclusion 43
References 43

1.02.1 Historical Perspective

The use to which a medicine could be put has long been of great interest to the practicing doctor, yet (at least until recently) it has not been a primary concern for the medicinal chemist. This review will explore why multiple uses of a drug should be advantageously considered earlier and more thoroughly in the discovery phase of new medicines and the consequences of this approach for medicinal chemistry.

From the earliest times of healthcare, doctors have applied the contents of their medicine cabinet for more than one use. Traditional folk medicines are often proposed for the treatment of a bewilderingly wide range of purposes. The clinician always has been

and still remains central to the discovery of new uses for existing drugs; they approach the issue using the "relatedness principle," whereby a drug might be useful for a related condition to the one for which it is conventionally used. A survey of new therapeutic uses for new molecular entity drugs approved in 1998 revealed 143 examples, of which 57% were discovered by practicing clinicians independent of either pharmaceutical company or university research.[1] This figure demonstrates the special position that clinicians occupy in being able to identify new therapeutic applications for the pharmacopeia and suggests further that there are many more applications we do not currently know about.

As distinct from the historical interest in new use for existing medicines, the modern strategy of drug repurposing suggests that a deliberate search for the ideal indication for a new drug would be a useful exercise before first-in-man studies are performed; it thereby extends our conventional view of medicinal chemistry, which largely takes into account only the chemical and biological properties of a new medicine. Repurposing involves a three-dimensional evaluation of a drug, including its chemistry, its medical use, and the biological target through which the utility is derived.[2] This approach diverges from the traditional discovery approach taken during most of the last century, which follows an investigation of a particular disease-related target. Instead, drug repurposing starts with the drug, follows all the biology around the drug's activities, and ends with the identification of a number of new diseases it might be useful for.

The field of drug repurposing has been confused by its nomenclature: other terms include drug repositioning, reprofiling, and therapeutic switching. It is not clear whether these terms relate to subtly different aspects of essentially the same process, which has been generally described as "the … concept of branching the development of an active pharmaceutical ingredient, at any stage of the life cycle and regardless of the success or misfortune it has encountered so far, to serve a therapeutic purpose that is significantly different from the originally intended one."[3]

In its different guises, drug repurposing may involve the identification for a new indication of a developmental compound, a launched proprietary product, or a generic drug. Repurposing may involve a change of dose, change of route of administration, change of formulation, or none of these, in which case it may represent more of a product line extension. The developmental, regulatory, and commercial aspects (including in particular patent protection) of each of these alternatives differ substantially from each other. The change of indication may involve further optimization of the active principle, and it is this sense that drug repurposing may be of most relevance to the medicinal chemist, although strictly speaking this departs from pure repurposing. This hybrid strategy can benefit from many of the advantages of drug repurposing and indeed in some senses go beyond these advantages. The reasons why this may occur and its consequences are dealt with at the end of this article.

1.02.2 Successes: From Chance Clinical Findings to Determinate Strategy

The historical origins of drug repurposing in clinical practice are one of the main reasons for its current acclaim. In other words, as success in pharmaceutical R&D becomes ever more challenging, investigators have been attracted to this strategy because of the case histories demonstrating benefits for both patients and manufacturers based on products with secondary uses. Many of these findings were serendipitous, but they have revealed more than just another use for an existing drug. The frequency of these experiences has also taught us that one biomolecule is often involved in many different diseases, and it is this pleiotropy that makes repurposing (of a modulator of such biomolecule) a promising strategy.

The use of thalidomide (Fig. 1) in leprosy is a marvelous example. Thalidomide was originally approved for the treatment of insomnia and morning sickness during pregnancy, but banned by the WHO (World Health Organization) for its teratogenicity

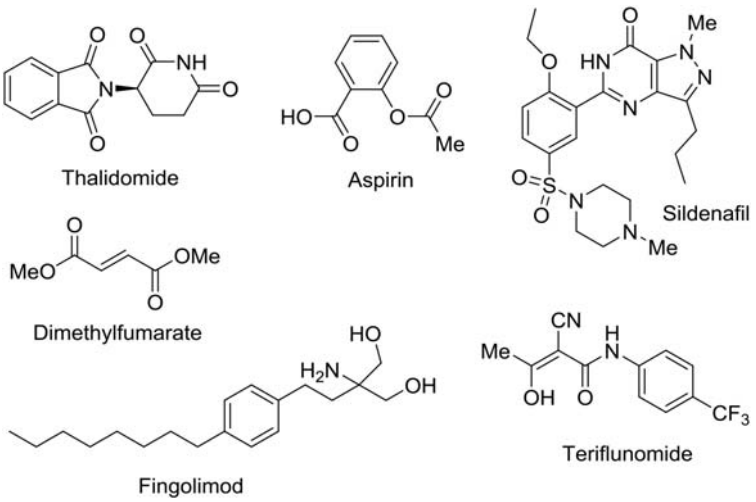

Fig. 1 Chemical structures of compounds mentioned in this section. Clockwise from top left: thalidomide, aspirin, sildenafil, teriflunomide, fingolimod, and dimethyl fumarate.

in 1962 and withdrawn from the market in Europe and Canada. It was almost universally believed that that would be the end of its medical life.

But in 1964, a critically ill patient with erythema nodosum leprosum (ENL), a complication of multibacillary leprosy, was referred to Dr. Jacob Sheskin, who was at the Hadassah University in Jerusalem. The patient was originally from Morocco and was being treated by the University Hospital of Marseilles, France. Leprosy (Hansen's disease) is a chronic, infectious human disease caused by a similar bacillus to that that causes tuberculosis.

Sheskin's patient was on the verge of death for months, he had not slept for more than 2 or 3 h in any diurnal period due to the pain of his condition, and although he had no drug to treat leprosy, the doctor administered thalidomide because he thought that its indication for insomnia would allow his patient to sleep better. In fact, it did much more than that. One day after administering two pills of thalidomide, the patient slept for about 20 h without waking. After 2 days, the pain, which had been so severe, had disappeared almost entirely. After another 3 days, Sheskin decided to withdraw treatment, and the condition rapidly worsened.

To confirm his findings, Sheskin traveled to Venezuela, where leprosy was endemic and thalidomide was still available, where he ended up treating 173 patients in clinical trials in which over 90% were symptomatically cured. The development was taken up by the US pharmaceutical company Celgene, and thalidomide was finally approved in 1997 by the Food and Drug Administration (FDA) for treatment of ENL; it was also subsequently approved for multiple myeloma. Please confirm that the approved product is a single enantiomer of thalidomide. The other stereoisomer is the one leading to the toxicity.

There are many examples of secondary uses for existing drugs, but the case of thalidomide represents the most remarkable. If a product that is the byword for pharmaceutical poison can induce almost a Lazarus-like effect in a life-threatening disease and then become approved for such use, surely there are effectively no existing drugs for which an alternative use cannot be posited. The constraint in this analysis is revealed by the following thought experiment: if thalidomide can be approved for these serious conditions despite its appalling safety record in the context of the original indications, it must equally be the case that an existing drug, deemed safe in an original serious indication, is not necessarily acceptably "safe" in a less serious secondary indication. The product needs to be subject to a new regulatory review and a new safety/efficacy assessment, in the context of this new indication. Thus, it is difficult to countenance the new use of, say, an existing cancer chemotherapeutic for a condition any less severe than cancer (unless there are ameliorating factors such as a lower dose, for instance).

An argument often proposed against drug repurposing is that after a product has been used for a number of years, its effects in patients will have been well appreciated and its utility thoroughly assessed: nothing new remains to be discovered. The flaw in this contention is clearly revealed by the story of aspirin. Aspirin (**Fig. 1**) derives from the bark of the willow tree, the use of which to relieve headaches, pains, and fevers was known to Hippocrates (http://inventors.about.com/library/inventors/blaspirin.htm). Its isolated form was discovered in the early 19th century, and Bayer Aspirin first appeared on the market in 1899. Much later, in the 1960s, the British pharmacologist and Nobel Laureate John Vane discovered that aspirin could disrupt a pathway needed for platelet aggregation.[4] Further studies in the 1980s showed that this effect could be used for the prevention of heart attacks and stroke. Nowadays, low-dose aspirin is used widely for this effect. Beyond cardiovascular properties, there was suspicion that the same pathway could be involved in cancer. A further 30 years was required for the amalgamation of this clinical evidence, so that, in December 2010, important clinical information was reported supporting the benefit of aspirin in preventing colorectal and other cancers.[5] It is now over 100 years since aspirin was first commercialized as a painkiller, showing how long it can take for therapeutic uses to be discovered even with a well-known drug. Even the work on colorectal cancer, based on data from 25,000 patients, is published with the caveat that "further research is needed." The main reason for this very long time interval is the lack of commercial incentive to develop a generic drug for a new indication, since generic substitution removes any commercial exclusivity that might reward a successful innovator. Clinical trials of aspirin in cancer are currently being financed from the public purse, and this takes much longer than if commercial investment were available.

A deterministic approach to the identification of new indications for developmental drugs started to become widespread following the approval of the use of sildenafil for erectile dysfunction in 1998. The commercial success of this product introduction by a large pharmaceutical company and the prospective identification and pursuit of a secondary indication of an incompletely developed drug attracted significant interest in drug repurposing as a strategy.

The discovery of sildenafil (**Fig. 1**) began in 1985 with chemists at Pfizer searching for inhibitors of cGMP phosphodiesterase type 5 (PDE5) enzyme as novel antihypertensives. Test compounds that were shown to inhibit PDE5 activity resulted in vasodilation and platelet inhibition, and the project was shifted toward the therapy of angina. Human trials began in Wales, which were disappointing for their primary end point, but some patients reported the unexpected side effect of penile erections, which ultimately led to the development of sildenafil (Viagra™) as a treatment for erectile dysfunction. Some time later, the role of PDE5 in pulmonary hypertension became better understood, and sildenafil was repurposed for a second time for this condition. Pulmonary hypertension is a general term for a disease process resulting in a progressive increase in pressure in the vessels supplying the lungs, particularly the pulmonary artery. Different from and much more serious than general hypertension, it can be idiopathic, familial, or secondary to a variety of conditions such as rheumatoid arthritis (RA) and Human Immunodeficiency Virus (HIV). Patients with the disease often present with signs and symptoms of right-sided heart failure, including shortness of breath, dizziness, fainting, and leg swelling. It is a life-threatening disease, unlike erectile dysfunction, and left untreated can be fatal with a median survival of 2–3 years from time of diagnosis. In its idiopathic form, pulmonary arterial hypertension is a rare disease with an incidence of about 2–3 million per year; other forms, however, are far more common.

Sildenafil relaxes the arterial wall, leading to decreased pulmonary arterial resistance and pressure. This, in turn, reduces the workload of the right ventricle of the heart and improves symptoms of right-sided heart failure. Pfizer conducted three trials on

sildenafil in pulmonary arterial hypertension, the largest being an international multicenter, randomized, blinded, controlled study involving 278 patients with the disease. Based on the results showing improvements in exercise capacity, the company submitted an additional registration for sildenafil to the FDA, and it was approved for this indication in 2005. The dose of sildenafil required to treat pulmonary hypertension was as low as one-fifth of the dose for erectile dysfunction.

Finally, an example of a determinate development of product for a new use in modern times came to fruition in 2013, when a compound we had known for 200 years was approved both in Europe and in the United States for the treatment of relapsing multiple sclerosis. The product manufacturer was the large biotech company Biogen Idec, who had licensed it from a small German company called Fumapharm.

The product, codenamed BG-12, is more commonly called dimethyl fumarate (**Fig. 1**), known since the early days of organic chemistry and first synthesized as early as 1819. It was therefore nearly two centuries later that the use in multiple sclerosis was approved. For at least 150 years, dimethyl fumarate was considered only as an organic chemical rather than as a pharmaceutical, without plausible beneficial therapeutic effects. It was used for a long while as a mold inhibitor, for incorporation in leather items such as sofas during storage. However, it is also an allergic sensitizer at very low concentrations (down to 1 part per million), producing extensive, pronounced eczema that is difficult to treat. In 2007, 60 Finnish users of leather sofas that had been manufactured with dimethyl fumarate in them were given serious rashes, and as a consequence, the importation of products containing dimethyl fumarate was banned in the European Union in 2009.

Prior to consideration for the treatment for multiple sclerosis, dimethyl fumarate (and other fumarate esters) had been used for the treatment of psoriasis, and a product called Fumaderm™ had been approved in Germany for this use since 1994. Biogen was interested in this product as a substrate for wider use in conditions related to the licensed indication. The pathophysiology of psoriasis is based on various immune and inflammatory mechanisms that are shared with other conditions, and therefore, Biogen undertook a basic investigation of the biochemical pharmacology underpinning the product. They discovered that dimethyl fumarate's mechanism of action involves upregulation of nuclear factor (erythroid-derived 2)-like 2 (Nrf2) and subsequent induction of an antioxidant response. It does this by modifying the cysteine groups of a protein called KEAP-1, which tethers Nrf2 in the cytoplasm. Once modified by fumarate, the KEAP-1/Nrf2 complex dissociates, and Nrf2 migrates to the nucleus, where it activates various antioxidant pathways. With such an understanding in hand, Biogen chose to develop dimethyl fumarate for multiple sclerosis (MS).

While Fumaderm™ was a popular product for psoriasis within Germany, its use was geographically constrained. Once licensed to Biogen Idec, a much larger development resource was allocated to the much longer term studies necessary for multiple sclerosis. They sponsored two main trials to prove the efficacy of the product involving 1200 and 1430 patients with relapsing remitting MS, conducted over 2 years.

The result of this effort was the regulatory approval of an oral product, Tecfidera™, containing a slightly different composition of fumarate esters at a higher dose than Fumaderm™. Many of the existing products for MS require intramuscular or subcutaneous injection, and the oral delivery of Tecfidera™ offers distinct advantages; in addition, compared with other oral MS products, it poses a lower risk of cardiac adverse events relative to fingolimod (**Fig. 1**) and a lower risk of liver toxicity compared with teriflunomide (**Fig. 1**). It is now approved in both the United States and Europe and has recently been allocated 10 years of regulatory exclusivity in the latter territory. This is a remarkable story of the introduction of a valuable new therapeutic option in a very serious disease that has lain unappreciated for nearly 200 years. It proves that major improvements in therapy can derive from evaluating existing compounds in ways that had not hitherto been anticipated. From the patient's perspective, drug repurposing offers huge benefits.

An extensive list of 74 drug repurposing examples of drugs that have been approved or orphan-designated for a secondary use is to be found at http://drugrepurposing.info/index.php.

1.02.3 Advantages and Disadvantages of Drug Repurposing

The 505(b)(2) process is a regulatory pathway applicable in the United States that applies to drugs that have already been approved with small modifications to the product, for instance, either as a new formulation or in terms of a new use. It stands in comparison with the 505(b)(1) pathway that applies to new chemical entities. The proportion of FDA approvals based on the 505(b)(2) regulatory pathway has been increasing markedly in recent years. In 2014, there were 41 FDA approvals via this pathway, surpassing the 505(b)(1) route that registered 35 approvals.[6] Not all of the 505(b)(2) approvals relate to drug repurposing. Another, slightly earlier statistic provides that 20% of the 84 new marketed drug products in 2013 derive specifically from repurposing.[7] It has been estimated that repurposed drugs now generate $250 billion per annum, constituting around 25% of annual revenue for the pharmaceutical industry.[8,9] Some of the most prominent commercial examples are shown in **Table 1**. The last row in the table represents a structural variant of the famous repurposing example, thalidomide, a strategy that is dealt with at the end of the article. These commercial successes have fuelled a growing appreciation of the repurposing strategy.

Differentiated as a modern prospective strategy of R&D, compared with the historical one reliant on clinical serendipity, drug repurposing started to be used widely in the first few years of the new millennium. There are a number of reasons for this, most prominent among them being an attempt to solve the poor, and declining, drug R&D productivity in the pharmaceutical industry over the past 2–3 decades. It has been estimated that it may cost more than USD 1800 million to develop a new drug de novo. In addition, due to regulatory requirements regarding safety, efficacy, and quality, the time required has been estimated to be 10–17 years.[10] Because of the cost, time, and risk of failure, the expected value of a drug discovery program at its inception has been

Table 1 Commercial successes of drug repurposing

Generic name	*Brand name*	*Structure*	*Original indication*	*New indication (year)*	*Company*	*Peak annual sales ($bn)*
Gemcitabine	Gemzar	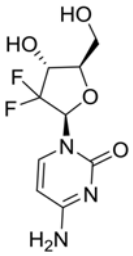	Antiviral	Cancers (breast, ovarian, lung, and pancreatic) (various)	Lilly	1.72
Raloxifene	Evista	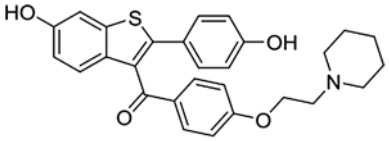	Osteoporosis	Breast cancer (2007)	Lilly	1.09[a]
Finasteride	Proscar	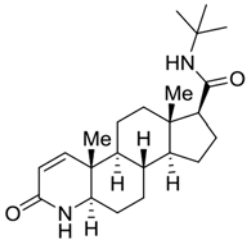	Benign prostatic hypertrophy (1992)		Merck	0.74
	Propecia			Male pattern baldness (1997)	Merck	0.43
Sildenafil	Viagra	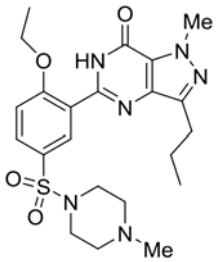	Angina	Erectile dysfunction (1998)	Pfizer	2.05
	Revatio		Angina/erectile dysfunction	Pulmonary hypertension (2005)	Pfizer	0.53
Rituximab	Rituxan		Various cancers	Rheumatoid arthritis, Wegener granulomatosis, and microscopic polyangiitis (MPA) (2004)	Biogen and Roche	1.2
Dimethyl fumarate	Tecfidera	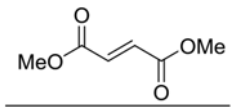	Psoriasis	Multiple sclerosis (2013)	Biogen	2.91
Thalidomide	Thalidomid	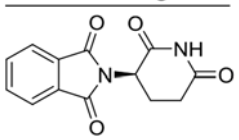	Antinausea and insomnia	Leprosy (1998) Multiple myeloma (2006)	Celgene Celgene	0.54
Lenalidomide	Revlimid	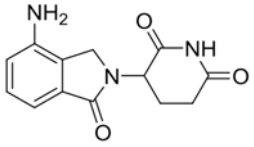	Structural analog of thalidomide	Multiple myeloma, myelodysplastic syndrome, and mantle cell lymphoma (2006)	Celgene	4.28

[a]Peak annual sales includes both osteoporosis and breast cancer numbers.

estimated as less than zero for a small-molecule drug discovery campaign. According to an analysis from 2009, the estimated net present value for an average small molecule is -$65 million with an internal rate of return (IRR) of 7.5%.[11]

1.02.3.1 Attritional Risk

Approximately 10 drug candidates need to enter into human investigation in order to produce one new molecular entity product launch,[12] and before that, many thousands of molecular library members may need to be screened, structurally optimized, and tested for animal toxicology studies in order for the preclinical candidates themselves to enter first-in-human studies. A reduced risk of R&D failure is therefore to be expected if one starts with a product that has already been through at least part of the process of development. A report by Thomson Reuters suggests improved success rates of around 25% for drug repurposing projects relative to the 10% or so for conventional new drugs.[13]

Most of the risk of failure is associated with uncertain efficacy, but it is also worth pointing out that safety is a relative concept and is not assured for the new indication, even for a well-known approved drug. While it is true that repurposed developments can (normally) take advantage of preexisting data, this does not mean that acceptable safety for the new product is unequivocally established. The safety of a chemotherapeutic agent is quite different from that of a new treatment for insomnia, as pointed out in the discussion around thalidomide. It is actually not easy to repurpose chemotherapeutic drugs because there are scant examples within that class that would be acceptable for another use.[14] Furthermore, certain therapeutic areas have been highlighted by regulatory agencies for detailed examination of safety hazards: a good example is that of new antidiabetic drugs, which are required to undergo extensive safety assessments because of the greater risk of adverse cardiovascular events among diabetic patients. There are also risks in situations where the route of administration is changed in the new development (for instance, in changing from oral to inhaled administration). Therefore, the risks of safety being a reason for discontinuing a repurposing development are reduced, but not eliminated.

1.02.3.2 Cost

The normal regulatory approval process for a pharmaceutical product based on a new chemical entity is discussed earlier.[10] This headline figure ($1.8bn) includes the costs of partly pursuing programs that are ultimately unsuccessful as well as a component associated with the cost of the capital deployed while funds are allocated to these failures. Compared with the cost of a new molecule entirely, new product development costs for drug-repurposed products are limited to the mid- and later stages of clinical development. It has been estimated that these costs amount to around $300 million, assuming that the drug repurposing candidate has to undergo phase II and phase III clinical trials.[15] This figure is predicated on the model proposed by Paul et al., but still represents an approximately 84% saving, compared with the cost of a de novo drug R&D program referred to earlier.

Part of the reason for this dramatic difference in cost is due to the reduction in attrition resulting from better success rates for repurposing projects. Although the bulk of the development costs for a new chemical entity program is also encountered in repurposing projects, the reduced expenditure on failed programs and the associated costs of capital give rise to this substantial cost saving for the repurposing strategy.

1.02.3.3 Time

Relative to the conventional approach, the evaluation of efficacy in a human setting is dramatically brought forward in repurposing programs. New chemical entity projects require years of research and discovery before the utility is even investigated, with substantial expenditure of time and money in the preclinical development phase. Aside from the economic impact, the benefit for the patient is dramatic, with much reduced times for new product innovation and associated improvements in healthcare. The fractional improvement in time taken to proof-of-concept studies is especially dramatic for repurposing relative to NCE discovery. As shown in **Fig. 2**, the time required for preclinical activities can be shrunk to 1–3.5 years compared with the normal expected duration of 4 and 9 years.[16]

Beyond discovery, the formulation of new development plans and their undertaking, market analyses, intellectual property (IP), and regulatory diligence are still required.[16] The time requirements for later drug development and regulatory approval for a repurposed drug program are often comparable with those for traditional R&D,[17,18] so that overall, the drug development cycle for a repositioned drug is expected to require between 3 and 12 years compared with the traditional 10–17 years.

1.02.3.4 Disadvantages

One of the features of drug repurposing that is of substantial advantage is the ability to obtain the so-called "method-of-use" patents framed around the discovery of the secondary use of a compound. Under international patent law, new pharmaceutical uses differ from new uses of other things in their ability to be protected. Such patents are valid in most countries including the major pharmaceutical markets, though "the 'mere' identification of a new use" of a drug in India remains a significant exception. These patents last for the same period as conventional "composition of matter" patents. In some cases, they can be sufficient in themselves to protect a marketed repurposed product; however, they are seen as weaker and more easily challenged.

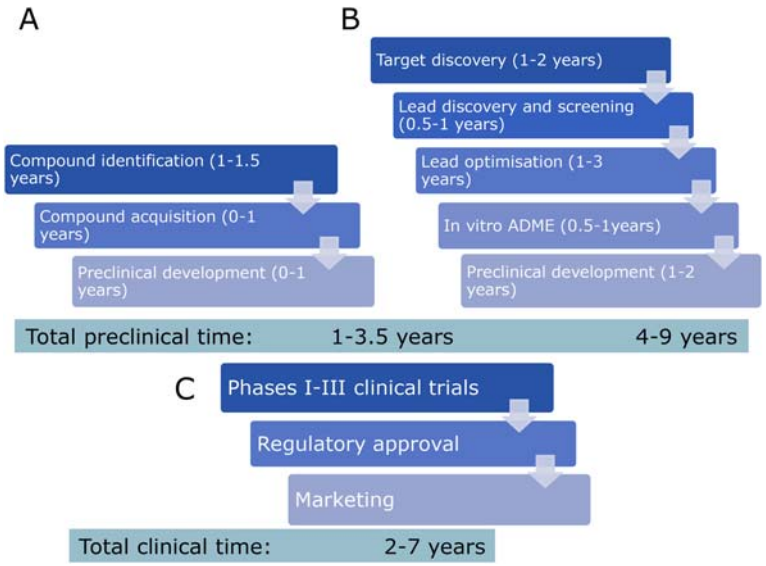

Fig. 2 Comparison of the processes and times for preclinical development of drug repurposing projects (A) with conventional new chemical entity projects (B). The processes and times for clinical development of both types of project are similar (C).

The weakness derives from the greater difficulty for a patent holder in controlling utilization in parallel conditions. For instance, the patent that protected the use of sildenafil for the treatment of erectile dysfunction did not cover its use in pulmonary hypertension, which was the third purpose (taking the original anticipated use in angina as the first) for which the drug was used. This was not a problem for the marketing company, since Pfizer had both indications—erectile dysfunction and pulmonary hypertension—under its control, but could have been a problem if two companies shared the franchise for sildenafil in two separate indications.

The second problem, that of litigatory challenge, is also exemplified with sildenafil, since Pfizer filed a patent both on the compound itself and on its use in erectile dysfunction. After Viagra was approved and it became clear that the use of selective PDE5 inhibitors in this condition would become a major market success, other companies discovered and developed compounds of similar mechanism for the same purpose. However, Pfizer's method-of-use patent claimed not only just sildenafil but also other "selective cGMP phosphodiesterase inhibitors" for erectile dysfunction, and while this patent was in force, it prevented the marketing of these competitors' products. A huge process of patent litigation ensued, which resulted in the invalidation of Pfizer's European patent and restriction of its rights under the US patent 6,469,012 (though the company retained protection for sildenafil itself for the treatment of erectile dysfunction).[19] The challenge was based primarily on an issue of obviousness, that is, whether the effects of sildenafil (and similar compounds) would have been predictable based on prior art publications. Given the breadth of scientific literature that can be cited, this is an issue for any method-of-use patent.

The second major disadvantage of drug repurposing is a commercial one, related to the potential substitution of a repurposed product, often by a generic competitor. Off-label generic substitution can markedly limit the commercial opportunity for a repurposed drug, as is most eminently demonstrated with the use of aspirin referred to earlier. Again, sildenafil also clearly exemplifies this issue, because, in the United States, generic versions that are intended for the treatment of pulmonary hypertension can be used "off-label" for the treatment of erectile dysfunction, although multiple pills are required. Though legally, Pfizer has a monopoly on the sale of products containing sildenafil for erectile dysfunction under the method-of-use patent US 6,469,012, it is a difficult area to police, and some generic substitution occurs. This situation arises from the freedom of a medical practitioner to prescribe a product that, according to his or her professional judgment, best suits the medical needs of the patient. This commercial factor may limit the development of a significant proportion of drug repurposing candidates, and pharmaceutical companies may be quite wary of drug repurposing projects that might suffer from generic substitution due to insufficient market potential.[20]

The repurposing drugs in oncology (ReDO) project is an international collaboration initiated by a diverse group of researchers, clinicians, and patient advocates all working in the not-for-profit sector, seeking new and effective cancer treatments based on existing drugs.[21] From the retrospective evidence listed earlier, there are many examples of drugs used for other purposes that have been associated with reduced rates of cancer incidence. These would make good candidates for investigation for their anticancer properties, at least for their effects in cancer prevention or reoccurrence. However, the process of acquisition of further data and regulatory approval of a specific anticancer product based on these generic substances is very unlikely to be compensated by a preferentially priced product. In this sense, the very existence of generic products acts in opposition to repurposed drug innovation.

1.02.3.5 Off-Label Medicine

When a new medicine is brought to market, the regulatory agencies judge its fitness for use according to a very specific set of conditions, the so-called product label, within which a pharmaceutical company may legally promote the product. This judgment is based

on a careful assessment of the safety and efficacy of the medicine when used under these restricted conditions. However, once approved, a medical practitioner may vary the use of the product outside the regulatory stipulations so long as, in his or her judgment, its prescription is in the interests of the patient. The variation may relate to the medical use, the type of patient, the dose, or the length of time that the medicine is administered.

Off-label prescriptions are written commonly for pediatric use and for certain therapeutic areas such as oncological and psychiatric situations. In all, they are estimated to amount for 20% of pharmaceutical prescriptions.[22] However, around 73–79% of off-label uses lack any, or any good, scientific support.[23,24] A good example of this is the use of antibiotics for viral infections, a form of off-label use that has contributed to the increasing threat from bacterial resistance. In addition to issues related to efficacy, off-label use is associated with two to three times the rate of adverse events, including serious adverse events. In summary, there are less evidence for efficacy and evidence for poorer safety. National acceptance of off-label use varies, with German practitioners restricted to being able to write such prescriptions for serious conditions where there are no alternative approved treatments. A slightly less stringent set of professional rules apply in the United Kingdom, though it is not clear how strictly these rules are followed. In the United States, doctors are comparatively much less bounded, with the FDA prevented by statute from interfering in medical practice and the American Medical Association unwilling to limit the professional freedom of their members to make their own prescription choices. Some of those in support of such freedoms even argue against a requirement for doctors to tell their patients when a product is not labeled for their patient's condition.

Despite the lack of evidential support, and the greater risks of side effects, the freedom to prescribe off-label is a right coveted by practitioners, with some justification. Historically, the successful identification of ancillary medical uses often derives from this freedom, and in rare diseases, for instance, where there are only approved treatments for around 5% of the known conditions, there is often no alternative. The remarkable discovery of the efficacy of thalidomide in leprosy is certainly owed to this freedom, and in this case, many people with leprosy would have suffered and in some cases died if this unlikely treatment had not been discovered to be useful.

Nevertheless, the decision to prescribe in an off-label fashion does not normally lead to a proper evaluation of the results of that prescription, in the same way as would occur in a clinical trial. The freedom to prescribe off-label medicine is generally limited by the lack of an associated onus to collect and report the consequences of such a prescription. The practice is unregulated by the FDA, and it is characterized by poorer safety and efficacy statistics. The use of antipsychotics in dementia patients is one example among many where there are no therapeutic benefit and a greater risk of stroke as a result of the practice. In the United Kingdom, there was a report commissioned into the associated patient harm that estimated 1800 excess deaths per year.[25] In another case, the agent NovoSeven (factor VIIa) was approved for certain forms of hemophilia or congenital deficiencies in the coagulant protein, but the proportion of unregulated prescriptions reached alarming proportions, rising to up to 98% off-label use, and ultimately no clinical benefit in most of these uses, where again excess deaths arose.[26] Similarly, epoetin alfa, an erythropoietin-stimulating agent, was originally approved for patients with anemia in end-stage kidney disease and (later) with HIV. However, it was prescribed much more broadly than these two orphan-designated uses implied, and the market quickly expanded to include nearly all kidney dialysis patients and ultimately many more patients with anemia, not just the very serious cases for which the product was approved. With time, the doses that were used also increased, until in 2006, where the sales of the product Epogen reached $5.6bn. Thereafter, safety concerns were raised because in the less serious cases, and at the higher doses, the safety of the product compared unfavorably with the benefit.[27] Ultimately, the FDA required new warnings to be added to the product label, and since then, sales have dropped off. The drug was also associated with performance enhancement, most notably of the cyclist Lance Armstrong. There are therefore multiple facets of erythropoietin, from the approved lifesaving antianemic product in rare blood conditions to off-label use in general improvement of "well-being and happiness" in much more common and milder cases of anemia to a drug that can be used to cheat in sport.

Off-label medicine is a gray area in which the interests of the patient are often subservient to those of pharmaceutical companies, reimbursement authorities, and doctors. Absent a commercial reward, pharmaceutical companies often choose to pursue alternative avenues of R&D, on the basis of a more assured commercial return, rather than because such alternatives are inevitably likely to deliver better healthcare. Increasingly, the new products deriving from such pharmaceutical R&D present a serious challenge to reimbursement authorities.

1.02.4 Variants

There are a number of different variants of the drug repurposing strategy. Most of these variants differ by virtue of the characteristics of the starting point for the repurposing activity. Each of these variants gives rise to different commercial challenges, patent opportunities, and possible routes to regulatory approval.

1.02.4.1 Repurposing of Generic Drugs

In the simplest case, old, generic drugs without patent protection are used: there are 1527 new molecular entities that have been approved by the FDA since its inception in 1938–2011.[28] Repurposing opportunities that use strictly the same generic drug, in the same formulation and same route of administration, are likely to be encumbered by generic substitution as was demonstrated by the example of aspirin referred to earlier. On the other hand, a number of repurposing developments have been initiated for

different doses, formulations, or routes of administration. In such circumstances, the original preclinical toxicology package may need to be modified or bridged to reflect the new circumstances. In addition, there may be new safety requirements that supersede the regulations in place at the time of the first approval, so that the original toxicology data need to be updated. The process toward clinical testing will therefore need to be carefully assessed on a case-by-case basis. The onus of additional preclinical toxicology is particularly evident for inhaled drug repositioning, where the formulation of a respiratory product and its preclinical toxicology is quite an expensive and time-consuming process.

1.02.4.2 Public/Private Partnerships for Repurposing of Abandoned Assets

The problem of substitution for repurposed generic drugs, coupled with the awareness of the unrealized commercial value in discontinued developments, has engendered an interest in repurposing of programs oriented toward products that have been partially but not fully developed. In such cases, the repurposed product, on success, would represent the only product based on this active ingredient on the market. Some years ago, the opportunity from stalled candidate drugs that have passed phase I but not phase II or III clinical trials was identified as representing a vast pool of repositioning substrates.[29] However, gaining access to collections of failed drugs and the necessary data to progress into clinical trials is typically hard due to intellectual property and confidentiality issues.[30]

A collaborative approach involving a public/private partnership was first broached in the United Kingdom, between the Medical Research Council (MRC) and a single industrial partner, AstraZeneca. The program was called the "Mechanisms for Human Diseases Initiative" and was based on a library of 22 midstage stalled developmental compounds contributed by the pharmaceutical company. At around the same time, in the United States, the NIH convened a round table of leading representatives from academia, government, and private sector R&D to explore new uses for abandoned and approved therapeutics, where pharmaceutical companies would create a pool of compounds for further investigation. This led, in 2012, to the NIH establishing the NCATS (National Center for Advancing Translational Sciences) institute and implementing an initiative called "Discovering New Therapeutic Uses for Existing Molecules." In both cases, the essential model was the deployment of partially developed compounds from industry and financial support from public funds to develop these assets for new uses. A similar collaboration was entered into in 2012 by the Broad Institute and Roche, the latter contributing a collection of 300 compounds with various indications in hopes of identifying alternative uses for the drugs using the research institute's screening technologies.[31]

From the governmental perspective, the advantage lay in the ability to access to high-quality developmental compounds. The MRC and NIH deployed part of their national government-allocated budgets and set up translational grant schemes for which academic investigators would compete; industry contributed their partly developed compounds and associated data. From the industry perspective, this permitted stalled assets with little or no accountancy value to be worked in an efficient manner through a drug repurposing strategy. The value from the remaining patent life in a stalled asset, or from working in an area of chemical space adjacent to the industrial partner's preexisting chemical knowledge, meant that the outcome from successful repositioning by the academic partner might be taken forward with alacrity.

Another unanticipated benefit of the schemes was the use of crowdsourcing to identify new opportunities for these compounds. In the NIH/NCATS scheme, examination of the submissions showed that 15 of the 16 compounds that received five or more applications had been proposed for at least three different indications. The diversity of the proposed developments emanating from one compound supports the potential of repurposing for new therapeutic outcomes.[32] More pertinently, the recent publication of human evidence that the NKB antagonist AZD4901 is a potent suppressor of follicle development and estradiol secretion in women, with potential therefore in polycystic ovarian syndrome, is one of the first reports in support of this kind of partnership between industry and academia.[33]

Other, similar examples of industry–academia partnerships forged with a drug repurposing remit in mind include those between Pfizer and Washington University (St. Louis)[34] and also in Taiwan, with the National Research Program for Biopharmaceuticals (NRPB).[35]

1.02.4.3 Off-Target Versus On-Target

In addition to the stage of development, another dimension in repurposing revolves around whether the mechanism underpinning the new indication is the same or different from that implicated in the original indication. The difference is more than academic in impact.

Most repurposing involves the identification of a new indication for an existing compound working through the original mechanism or target. This is called "on-target" repurposing.[36] The principle is that new biology has connected the old drug to a new indication via the same pathway or protein interaction as is responsible for the original indication. Sildenafil's use in erectile dysfunction and in pulmonary hypertension involves this principle: both indications are effected through inhibition of cGMP PDE5.

Sometimes, however, repurposing involves a new mechanism entirely. The use of doxycycline (**Fig. 3**) for the treatment of periodontitis is such an example. "Off-target" repurposing of this type is rarer because the compound was normally optimized for a mechanism in the original discovery campaign, so it is unlikely to be an optimal compound for another mechanism. In the case of doxycycline, its original antibacterial activity is due to inhibition of protein synthesis by preventing the attachment of aminoacyl-tRNA to the ribosomal acceptor (A) site.[37] Surprisingly, doxycycline also has more potent effects against matrix metalloproteinases and specifically via its effect on collagenase and gelatinase in preventing the infiltration of polymorphonuclear cells

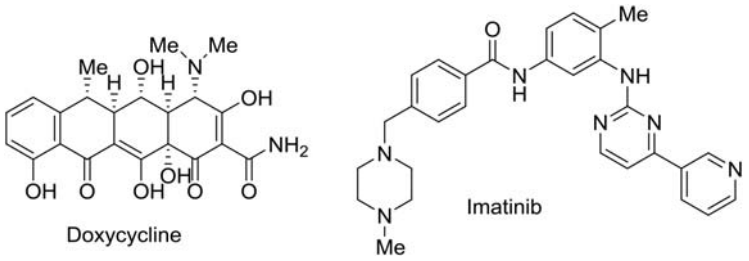

Fig. 3 Chemical structures of compounds mentioned in this section. Left: doxycycline. Right: imatinib.

into gingival tissue of patients affected with periodontitis.[38] The therapeutic benefit of doxycycline in this condition is observed at sub-antibacterial doses, a factor that was crucial in the regulatory approval of the product, since the FDA wanted to avoid the chronic exposure of patients to an effective antibiotic, because of the potential for resistant bacteria to be produced.

Many existing drugs have multiple protein targets to which they bind; some of these targets are currently known, but many more are not. Recent studies have evaluated the extent of polypharmacology by analyzing all known drug–target interactions. A human pharmacology interaction network connecting proteins that share one or more chemical binders has been created.[39] In their database of 276,122 active compounds, 35% hit more than one target. In a second study, Mestres and coworkers integrated seven drug–target interaction databases and found that, on average, each drug interacted with six different targets.[40] However, not only does off-target repurposing require that the repurposing substrate acts at a secondary target but also it does so within a window of therapeutically acceptable dosing. It is, as a result, much rarer than on-target repurposing.

Tyrosine kinase inhibitors are a highly promiscuous therapeutic class of marketed drugs in terms of the number of enzymes they inhibit. These drugs normally bind competitively to the ATP-active site, and there are over 500 similar ATP-binding sites in the human protein kinome.[41] One of the first marketed tyrosine kinase inhibitors was imatinib (**Fig. 3**), which was first introduced for the treatment of chronic myelogenous leukemia (CML). This condition begins in the often asymptomatic chronic phase and over the course of several years progresses through an accelerated phase and ultimately to a blast crisis, by which time it is associated with a very high mortality rate. From diagnosis, the median survival period is just over 5 years. Imatinib is an inhibitor of the tyrosine kinase bcr-abl, and this enzyme is involved in a specific genetic abnormality associated with CML. While imatinib was originally heralded as a breakthrough of a new generation of selective kinase inhibitors, it later became clear that it is also an inhibitor of two other tyrosine kinases through which it produces a useful therapeutic effect. The first of these is PDGF-R, inhibition of which is responsible for use in dermatofibrosarcoma. The second is c-kit; mutations in both c-kit and PDGF-R are central but independent events in gastrointestinal stromal tumor (GIST), and inhibition of both these enzymes proposed to underlie imatinib's benefit in this condition.[42]

1.02.4.4 Rare Diseases

Drug repurposing is a particularly attractive approach for rare diseases, and the term "rare-purposing" has even been trademarked by the company Healx Ltd, which is focused entirely on this strategy. This is so for both scientific and commercial reasons. Scientifically, these diseases are often poorly characterized in their pathophysiology and lack a clear understanding of the biological pathways necessary to interdict or compounds to interdict them with. In silico techniques for predictive repurposing (which are described in more detail in the next section) offer a relatively quick method of identifying testable hypotheses that may be translated into the clinic. In addition, from a commercial perspective, there are specific regulatory measures that are meant to encourage research into rare diseases, and these measures can provide commercial exclusivity in situations where repurposed products cannot be protected by patent or that patent is weak.

From the perspective of unmet medical need, a huge opportunity exists: there are over 7000 rare diseases. Over 95% of these lack an FDA-approved therapeutic agent.[43] Rare diseases are often equated with "orphan" diseases because they lack an approved therapeutic treatment, and various forms of regulatory legislation have been enacted in the major pharmaceutical markets to incentivize the development of drugs for this type of condition.

In the United States, a rare disease is defined as one that affects less than 200,000 persons.[44] The Orphan Drug Act (ODA) was enacted there because the economics for developing a drug for a rare disease, where the costs of R&D can only be amortized over a relatively small number of patients, were unfavorable. As a result of this act, which allocates additional market exclusivity in such situations, over 300 drugs and biological products for rare diseases have been approved by the US FDA since 1983 (compared with fewer than 10 such products in the decade prior to 1983). Orphan products represented 30% of products approved for the first time by the FDA in the 5-year period from 2004 to 2008.[45] Today, the rare disease market is growing rapidly and becomes attractive for pharmaceutical R&D. Despite the small patient populations, significant market sizes can be expected because of high prices. As an example, the drug Soliris (eculizumab) from Alexion Pharmaceuticals is priced at over $500 k per patient per year and recorded sales of over $1bn in 2013.

Table 2 Legislation in major pharmaceutical markets offering commercial incentives for orphan drug developments

	United States	*Japan*	*Australia*	*European Union*
Legislation date	1983	1993	1997/98	2000
Prevalence	Fewer than 200,000 (6.25 per 10,000)	Fewer than 50,000 (4 per 10,000)	Fewer than 2000 (1.1 per 10,000)	Fewer than 5 per 10,000
Market exclusivity	7 years	Reexamination period extended from 4 to 10 years	None	10 years
Fee waiver	Yes	No	Yes	At least partial

The US legislation enables fast-track FDA approval, marketing protection, tax incentives, and funding for clinical research in rare diseases. In particular, once a drug is approved, a generic version in that indication cannot be approved for 7 years (in addition to normal patent protection). The developer may also receive tax concessions, grants, and waiver of regulatory fees. As an indicator of the success of the ODA, similar legislation is now in place in Singapore, Japan, Europe, and Australia, with each jurisdiction having a slightly different definition of an orphan indication and applicable commercial incentive (see **Table 2**). For instance, whereas in the United States, an orphan designation may apply if the prevalence is less than 200,000 (approximately 6.25 in 10,000); in Europe, the corresponding figure is 5 in 10,000 (corresponding to approximately 250,000 patients in the EU28).

The regulatory protection in rare diseases is particularly important given the relative weakness of patent protection for repurposed generic products, which is often confined to "method of use"-type intellectual property. Thus, there is much repurposing activity in this area. A comparison of the FDA approval database with those drugs that have received orphan drug designation revealed 236 that were "promising" for the treatment of a rare disease, though not yet approved for marketing for that condition.[45]

1.02.5 Approaches to the Identification of Drug Repurposing Candidates

1.02.5.1 Experimental Approaches

Experimental screening in drug repurposing involves the parallel testing of compounds against one or more targets or phenotypes in large pharmacological assays. This large-scale approach works on the principle that the greater the number of compounds that are screened, the greater the number of repositioning candidates that should be generated[46]; the most promising candidates can then be progressed to more focused experimental testing. Even if the number of positive hits as a percentage of total compounds screened remains low, the relatively low cost of this initial screening makes this an effective repurposing approach. There are two main approaches to screening in drug repurposing: target-association screening and phenotype-based screening.[30]

1.02.5.1.1 Target-association screening

Target-association approaches aim to associate a target with a disease or drug, measured via in vitro assays in either a one-drug many-target approach (for instance, identifying previously unknown off-targets of a drug) or a one-target many-drug approach. An example of the former is the identification of new targets for the kinase inhibitor gefitinib.[47] In this study, HeLa cellular extracts were washed over immobilized gefitinib (**Table 3**) to determine binding affinity, resulting in the identification of more than 20 new gefitinib targets that were then validated in cellular assays. One of these new targets was the protein kinase RICK. Pretreatment of cells with gefitinib was found to reduce RICK activity by up to half; however, while RICK is known to be involved in immune response, it is not clear to what extent its inhibition would be of therapeutic benefit. This illustrates how the one-drug many-target approach can lead to an "orphan target" problem.

A one-target many-drug approach therefore begins with identification of a disease-relevant target and then attempts to find drugs that modulate its activity. One study targeted the migratory factor AceMIF, inhibition of which could be used to prevent or treat infection by the blood-feeding hookworm parasite[48] (**Table 3**). A high-throughput screening approach was used to assess almost 1000 FDA-approved drugs for AceMIF inhibition. Putative inhibitors identified by the screen were assessed in further in vitro tests, identifying six compounds as AceMIF-specific inhibitors, half of which demonstrated hookworm toxicity in an ex vivo assay. Interestingly, some of these compounds had known antihelminthic activity through other mechanisms: pyrantel pamoate, for example, is known to cause paralysis in parasitic worms through inhibition of parasite cholinesterase. This suggests that AceMIF inhibition may be an additional mechanism of action of pyrantel pamoate. As well as identifying drug repurposing candidates, then, target-based screening can also help to elucidate the ways in which existing compounds work.

1.02.5.2.2 Phenotypic screening

The second type of screening is phenotypic screening. Phenotypic screens are end point-driven, requiring no prior reasoning about targets or disease biology. This can serve as both advantage and disadvantage—on the one hand, such approaches are less hypothesis-driven[49] and can broaden the search space by preventing excessive focus on currently known biology ("looking for one's keys under the streetlight"[49]), increasing the potential for discovery of completely new biology: various examples of its success

Table 3 Overview of drug repurposing candidates from selected experimental approaches

Selected candidates—target/indication	*Structure*	*References*
Gefitinib—RICK (receptor-interacting serine/threonine-protein kinase 2)	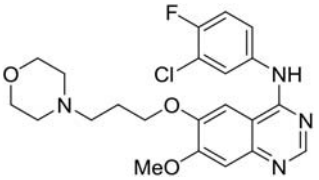	47
Furosemide—hookworm infection	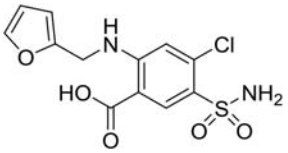	48
Pyrantel pamoate—hookworm infection	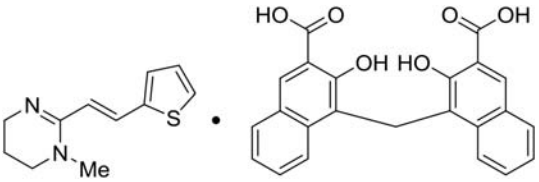	48
Sodium meclofenamate—hookworm infection	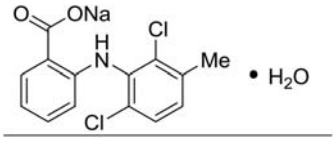	48
Apomorphine—tobacco dependence	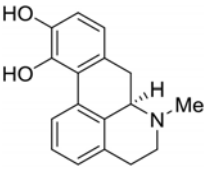	53
Topiramate—tobacco dependence	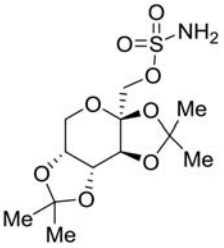	53

are shown in **Table 3**. On the other hand, if a promising candidate is discovered through this end point-driven approach, it may then be required to elucidate its mechanism (for instance, via target identification), which can be a costly and time-consuming process.[50]

Phenotype-based screens can be cell-based (in vitro) or in vivo assays. Cell-based screens allow high-throughput, automated phenotypic analysis, such as that developed by Recursion Pharmaceuticals, in which a phenotypic fingerprint ("phenoprint") of human disease is identified via machine learning methods from thousands of cellular models of genetic disease. These phenoprints can be assessed following drug treatment using automated image analysis techniques, allowing the testing of thousands of drugs in parallel. This platform can be applied to any of an estimated 4500 diseases with a loss-of-function mutation component, with promising applications in the genetic diseases Rett syndrome, Diamond–Blackfan anemia, and cerebral cavernous malformation.[51]

A key advantage of phenotypic screens over target-based screens is their ability to capture biological complexity that cannot be represented in reductionist target-based approaches.[52] Extending this idea further, in vivo phenotypic screens progress directly to screening drugs in animal models of disease. For example, a repurposing study in a zebra fish model of tobacco dependence[53] ran a focused screen of 39 drugs (chosen based on their side effect and contraindication profiles). Six of these medicines, including topiramate and apomorphine (**Table 3**), were found to inhibit the nicotine response in the zebra fish model. The complexity of using animal models means that in vivo screening tends to be lower-throughput and more specialized than what is possible with cellular assays. However, larger-scale in vivo screens are possible: the phenotypic screening platform developed by Melior Discovery uses 40 animal models representing 14 disease areas across a broad range of disease types, from neurological and neurodegenerative diseases to pain, which can be evaluated in parallel. Melior claims that their platform allows compounds to be tested

across the full range of disease models in roughly 10 weeks. Such higher-throughput phenotypic screening has the potential to significantly increase the speed of the early drug discovery process by testing in multiple diseases at once for fast identification of "interesting" versus noninteresting drug candidates.

The disadvantages of phenotypic screening include the risks of missing potentially relevant compounds due to poor absorption, distribution, metabolism, and excretion (ADME) properties or alternatively of identifying "false-positive" candidates (or rejecting candidates that are false-negatives) in a disease model of limited relevance to the human condition.[50] Although target-based screening has received more attention than phenotypic screening in recent decades, phenotypic screening has overtaken target-based screening in the identification of new drugs, with 28 first-in-class small molecules identified through phenotypic screening compared with 17 identified through a target-based approach in the period of 1999–2008.[54] By reducing the need for a strong target hypothesis, phenotypic screens represent a form of "systematic serendipity," enabling the potential for discovery outside of what is predictable from current pharmaceutical knowledge.

1.02.5.2 Knowledge-Based Approaches

There exists a huge body of knowledge about drugs and disease that is qualitative, rather than quantitative, in nature. This knowledge is distributed across various resources such as the biomedical and chemical literature or captured in clinical records. Humans are able to understand and make inferences from diverse sources of information, but this understanding is limited by a problem of scale: the sum total of human knowledge on drug and disease is far too big for any one individual to comprehend. By collecting this information and parsing it into a form that can be "understood" (or mined) by a computer, knowledge-based approaches aim to bring to light new associations between drugs and disease.

1.02.5.2.1 Literature-based

Literature-based discovery treats large sets of scientific literature as a vast system of interconnections between research parameters and navigates through these interconnections to reveal indirect relationships among seemingly unconnected biomedical entities such as genes, signaling pathways, physiological processes, and diseases. In addition to being used to uncover candidates for drug repurposing, it may also be used to describe the basic molecular mechanisms underlying a disease, to better understand the biological effects of a drug, or to evaluate its benefit/risk profile.

In order to achieve this, literature-based approaches make use of the chemical, biological, and clinical knowledge that is held in natural language format ("natural language" refers to any human language as opposed to a language designed to be understood by a computer). Literature mining aims to extract relevant entities from text sources (in this case, scientific literature, clinical trial reports, electronic health records, etc.) and determine the logical relations between entities.

The general principle is that if A is related to B and B is related to C, then it is plausibly true that A is related to C. Interestingly, from a patent perspective, not only is the inference of C to A novel, but also it may in certain circumstances be nonobvious. This type of process is described in Fig. 4. Beginning with an object of interest, A, other objects B can be tentatively related to it within the literature by identifying the co-occurrence of A and B objects within PubMed or MEDLINE records (titles and abstracts). Each B object can then be queried to identify other objects, C, that co-occurred with them in the literature, such as if they occur together in the same sentence. Each of these new objects, C, which are not themselves A or B objects, is related to A only implicitly. In other words, they have no documented relationship with A, but they share one or more second-order relationships with A. This large list of implicitly related objects will contain potential discoveries of new relationships.

However, because of their abundance, it is necessary to prioritize and rank these objects in some manner. For instance, concepts can be expressed as single words or phrases, while the strength of relationships between A and C can be stratified using the number of intermediate concepts B. Spurious links are filtered out by mining a large number of papers, where the "noise" of false associations (e.g., resulting from co-occurrence in a list) is rendered statistically insignificant by the use of a large number of sources.[55] Alternatively, more complex natural language processing approaches can be applied to uncover the semantic relationships present in the text, allowing a deeper understanding of the association between concepts. A review of the alternative methods to link concepts and rank the relationships has been published by Deftereos et al.[56]

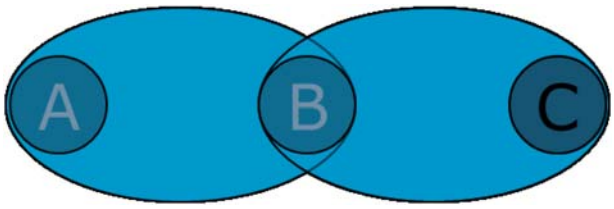

Fig. 4 Swanson's ABC model. Concept A is related to concept B, as reported in one set of papers (indicated by the ellipse on the left), while B is related to C according to another set of papers (indicated by the ellipse on the right). Although A is not known to be directly related to C, one can infer an indirect relation through B. A, B, and C can stand for drugs, targets, diseases, pathways, or any other concept of relevance for the problem to be addressed.

An example of the first approach ("co-occurrence") is the drug–disease knowledge graph created by Gramatica et al.,[55] who combined text mining with graph theory to discover indirect associations spread across three million PubMed extracts. A link is based on the co-occurrence of two concepts in a sentence, with the significance of the link being defined by the number of co-occurrences between the two (the amount of evidence for the association) and the length of the path between them. Longer paths allow for the representation of indirect mechanisms, but long paths also introduce the possibility of spurious connections between concepts. Their graph can link concepts including diseases, drugs, genes, proteins, and biological processes, allowing inference of the mechanism of action of drugs and diseases. Their network linked the tyrosine kinase inhibitor imatinib (approved for use in hyperproliferative disorders including GISTs, mastocytosis, and several leukemias) with Creutzfeldt–Jakob disease (CJD). Through explicit representation of these biological concepts, the system can provide a clear biological rationale for this suggestion: the path imatinib → c-Abl → > apoptosis → CJD indicates that imatinib could work through inhibition of the apoptotic effect of the kinase c-Abl, which has been experimentally linked to CJD. Other methods based on co-occurrence include the natural language approach developed by Weeber et al.[57] and the LitLinker system developed by Yetisgen-Yildiz et al.,[58] which identifies MeSH terms in MEDLINE papers that are closely related to the starting and target concepts, which are then refined to remove synonymous or noninteresting concepts by analyzing word probability distributions. This approach led to the identification of endocannabinoids as potential agents for Alzheimer's disease, α-amino-3-hydroxy-5-methyl-4-isoxazolepropionic acid (AMPA) receptor ligands for migraine, and secretin agonists for schizophrenia.

A more complex literature mining approach was used by Xu et al.,[59] who created a phenotypic measure of disease similarity based on the extent of shared symptoms between two diseases. Over 120,000 disease–symptom associations were extracted from 21 million MEDLINE citations using syntactic patterns such as "*symptom* in *disease*" or "*symptom* associated with *disease*." By learning these syntactic patterns from the literature, spurious or negative associations can be more easily filtered out. Through the creation of a large machine-understandable disease–phenotype database, the authors were able to demonstrate that the number of shared drugs between two diseases showed a positive correlation with the number of shared symptoms. This literature-based correlation was stronger than the correlation obtained from the shared symptoms listed in an existing knowledge base (the Unified Medical Language System). Having demonstrated that shared symptoms between two diseases may also indicate the potential for shared drugs, the authors are now developing a system to use these literature-mined disease–symptom associations for drug repurposing.

1.02.5.1.2 Ontologies

A common problem when working with natural language sources in computational applications is the problem of synonymy, where multiple terms may be used to refer to the same or similar concepts such as the use of generic versus brand names of drugs or the use of the term "dementia" to refer to the symptoms of Alzheimer's or Parkinson's disease. One way in which this can be overcome is by linking to ontologies. Ontologies seek to represent real-world domains in a standardized manner, organizing concepts from natural language in a common system of naming and interrelationships. By specifying relationships between entities—such as "is-a," "has-a," or "part-of"—ontologies can uncover implicit structures in existing resources and make these structures explicitly machine-understandable, aiding the discovery of new associations between diseases and drugs.

A specialized ontology for chemical biology and chemogenomics, Chem2Bio2OWL,[60] has been used in drug repurposing to add semantic annotations to a drug–target interaction network.[61] The network, built from drug and target similarity data and drug–target interaction data, was annotated with "path patterns": for example, "drug *binds* target *binds* drug *binds* target." Paths considered to be significant were used to build a drug similarity network, in which clusters of drugs with different indications could represent repurposing opportunities—for example, the migraine treatment butalbital was clustered with nine insomnia drugs, which the authors suggest is due to its depressant action as a barbiturate. The authors caution, however, that because their method does not yet distinguish between activation and inhibition of a target, drug pairs in the network may represent opposite indications, that is, adverse drug effects.

One problem presented by the use of ontologies is that of a proliferation of ontologies, in which several ontologies seek to represent the same or similar domains, yet use slightly different representations, leading to incompatibility between different sources. Qu et al.[62] created a disease–drug correlation ontology through integration of existing ontologies, standardizing the vocabulary used to relate these terms across different resources. These included MeSH, SNOMED CT, and the NCI thesaurus, which describe disease-associated concepts; GO, which provides a standardized vocabulary for genes and gene products; and the ATC (Anatomic Therapeutic Chemical) classification system, which provides a classification system for drugs. Drug and disease information was compiled from sources such as DrugBank and OMIM and enriched with knowledge from other sources such as GO and KEGG pathways through the retrieval of existing relationships (*is-a* and *has-a*) in these sources. Graph-theoretical approaches were then applied in order to discover significant and interesting links. The authors applied their method to generate a pharmacome–diseasome graph for systemic lupus erythematosus (SLE), ranking tamoxifen as a highly promising candidate for treatment of SLE. Other examples are shown in **Table 4**.

Existing approaches have shown the utility of knowledge-based methods for drug repurposing through extracting information from existing ontologies, from integrating between databases, and from the literature. However, there are still many data sources yet to be exploited, including clinical trial reports, electronic health records, insurance claims, and patients' self-reported effects. These methods have already been used for the detection of adverse drug reaction events and could in the future be extended to detect beneficial drug effects that could lead to repurposing opportunities.[63]

Table 4 Overview of drug repurposing candidates from selected knowledge-based approaches

Selected candidates—target/indication	*Structure*	*Validation*	*References*
Aviptadil—sarcoidosis		Literature support	55
Imatinib—Creutzfeldt–Jakob disease	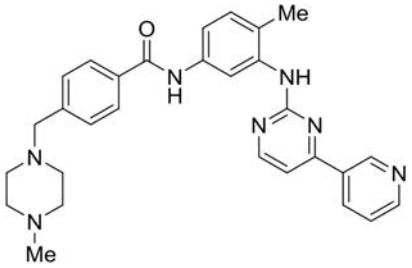	Literature support	55
Tamoxifen—systemic lupus erythematosus	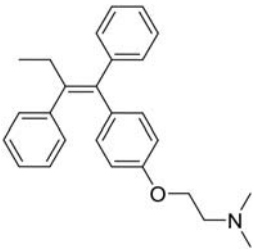	Literature support for predicted mechanism of action	62

1.02.5.3 Retrospective Analysis

When used in a clinical situation, the co-occurrence of diseases other than those indicated for the prescribed medicine can give clues about other potential applications for the product. Retrospective analysis may occur in any setting; a post hoc analysis can be conducted on the experience of using a drug in the real world, but it may also be conducted on clinical trial data. Such data have the additional advantage of better control and randomization of patients. Retrospective analysis represents a method of uncovering additional uses for a drug that only becomes evident from analysis of the data for an end point that was not anticipated at the time the trial was planned.

Cancer is a particularly common example, which may be identified as a secondary indication, because its frequency of occurrence is almost always recorded as a potential side effect in patients on any prescribed or investigational medication, in order to alert patients and regulatory agencies of a potential carcinogenic effect. Thus, by comparing the incidence of cancer for a cohort of patients when treated with a particular drug, as against a suitable control group, we might identify the potential for this drug as an anticancer agent, in other words, the opposite of a carcinogenic effect. It is important to differentiate the effect from this analysis as a cancer-preventative agent with its utility as a cancer-curative agent, and secondly, the retrospective identification of an association is not proof positive from a prospective viewpoint. But these two issues aside, this type of study is of significant power in drug repurposing.[64]

A survey of retrospective evidence in a variety of possible secondary indications is shown in **Table 5**.

In the field of cancer, some of the retrospective findings of prevention have been extended to prospective clinical trials. Metformin has been studied in a prospective trial for its effect against proliferation in breast cancer, with some benefit attributed.[126]

Caution should be exercised in extrapolating from a retrospective association to a prospective causal relationship, as revealed by the example of the use of HMG-CoA reductase inhibitors (statins) in sepsis. In this case, rosuvastatin was not associated with an improvement in 60-day mortality in sepsis-associated acute respiratory distress syndrome (ARDS),[127] despite the various epidemiological associations of reduced mortality in statin users with sepsis. The difference between the two results can be attributed to the need for long-term dosing with statins for the production of their benefits against vascular leak, through inhibition of RhoA prenylation, an off-target effect of these drugs. A clinical benefit of statins in an emergency situation involving sepsis would require a much more immediate effect than can be produced by this mechanism.

Table 5 Retrospective associations suggesting drug repurposing utility

Mechanism (where known) or drug	*Indication*	*References*
5-HT uptake inhibitor	Myocardial infarction	65
ACE inhibitor	Alzheimer's disease	66
	Cachexia	67
	Immune downregulation	68
Acetylcholinesterase inhibitor	Autism	69
Angiotensin II (AT1) antagonists	Alzheimer's disease	70
Beta-adrenergic antagonist	Alzheimer's disease	66
	Cancer	71
	Cancer metastasis; cancer, breast	72
	Cancer, liver	73
	Cancer, lung	74
	Cancer, ovarian	75
	Cancer, prostate	76
	Melanoma	77
	Osteoporosis	78
Calcium channel blockers	Alzheimer's disease	79
	Cancer, lung	80
Gefitinib	Asthma	81
Glibenclamide	Sepsis	82
HMG-CoA reductase inhibitor	Age-related macular degeneration	83
	Alzheimer's disease	84
	Asthma	85
	Bacterial diseases	86
	Burn injury	87
	Cancer	Esophageal,[88] liver,[89] prostate[90]
	Cataracts	91
ACE inhibitor, HMG-CoA reductase inhibitor	COPD	92
HMG-CoA reductase inhibitor	Depression	93
	Epilepsy	94
	Glaucoma	95
	Influenza, COPD	96
	Osteoporosis	97
	Periodontitis	98
	Pneumonia	99
	Rheumatoid arthritis	100
	Sepsis	101
	Transplant rejection	102
Hydroxychloroquine	Diabetes (type II)	103
Ibuprofen	Parkinson's disease	104
Metformin	Alzheimer's disease	105
	Cancer	Bladder,[106,107] colorectal,[54,108] endometrial,[109] liver,[110] lung,[111] pancreatic,[112] prostate[113]
NSAIDs	Cancer, colorectal	114
Na^+/K^+ ATPase inhibitor (digoxin)	Cancer	Lung,[115] prostate[116]
PPAR gamma agonists	Cancer, colorectal; cancer, liver	117
	Psoriasis	118
Quinolone antibiotic	Cancer	119
SERM (selective estrogen receptor modulator)	Kidney disease, chronic (renal failure)	120
TNF antagonist	Cancer	121
	Diabetes (type II)	122
	Kawasaki disease	123
	Stroke	124
	Systemic vasculitis	123
Tricyclic antidepressants	Cancer	125

An interesting example of retrospective analysis leading to a clinically effective agent is in the area of cachexia. Cachexia is a wasting disease, formally defined as the loss of more than 5% of body weight over a period of less than 12 months, normally in association with a chronic disease. It occurs commonly with not only cancer but also chronic heart failure, kidney disease, and chronic obstructive pulmonary disease (COPD). A reexamination of various clinical trials of therapeutic agents for chronic heart failure, specifically those of angiotensin converting enzyme (ACE) inhibitors[67] and beta blockers,[128] looked at weight as a marker

for cachexia. Both these classes of drug have been formally investigated for the treatment of chronic heart failure. Weight is of course routinely measured in any clinical trial protocol, so the reanalysis could be done without the need for additional measurements. In the case of the beta blockers, a stratification exercise to delineate the mechanistic basis indicated the involvement of beta-1 and beta-2 adrenergic as well as 5-HT1A receptors for optimal activity and identification of S-pindolol as a preferred agent (which possesses all three of these activities) with greater efficacy than other similar agents, including its racemate.[129,130] Interestingly, in the subsequent ACT-ONE clinical trial, at therapeutic doses that do not decrease blood pressure, the product not only is highly effective for alleviation of catabolism but also promotes anabolism and improves functional ability in cancer cachectic patients.[131]

1.02.6 Data Mining Approaches for the Prediction of Drug Repurposing Opportunities

Data mining approaches to drug repurposing take advantage of preexisting data in order to form drug repurposing hypotheses without the need to perform any new experiments. This in silico repurposing takes advantages of the ever-increasing amount of (often publicly accessible) data on drugs, targets, and disease. This section will review examples of these methods and show how they transform biological and chemical data into biologically plausible hypotheses for drug repurposing.

At their core, all data mining repurposing methods (here also referred to as "computational repurposing") share the same basic approach: some process is applied to chemical, biological, and/or pharmacological data in order to form hypotheses about drugs and disease in those different spaces. The ability to derive novel hypotheses (chiefly candidates for repurposing but also hypotheses concerning the mechanism of action of a drug or drug–target interactions) depends both on the input data and on the processing that is applied to that data.

1.02.6.1 Data Types

Computational drug repurposing methods can be broadly classified as either *structure–target-* or *effects*-based, depending on the data type(s) used. Structure–target repurposing is based on the chemical or three-dimensional structures of drugs and their biological targets and the interactions between them. These approaches tend to be drawn from the chemical biology and cheminformatics areas. On the other hand, effects-based repurposing looks at the biological effects of drugs and disease on the body. Effects-based methods use data relating to molecular activity and phenotype, such as -omics or side effect data, to measure the action of a drug or disease on the body without necessarily needing to make explicit its precise mechanism. Repurposing examples in this section have been grouped according to these categories, which will be described in more detail in the relevant section.

1.02.6.2 Data Processing

Given a particular type (or types) of input data, a computational repurposing method generally applies an algorithmic process in order to form new associations or predictions that will be the basis of repurposing hypotheses. Although the choice of algorithm may be influenced by the data used (not only the type of data as described in the previous section but also the size of the dataset and its quality), repurposing algorithms can be broadly classified into three categories independently of the data type:

- *Similarity-based*: Similarity-based approaches work on the assumption that structurally similar drugs bind to similar targets and can be repositioned to treat similar diseases (i.e., diseases with shared disease biology). Similarity-based approaches are appealing in drug repurposing because they are intuitively clear: the rationale behind repurposing suggestions can be easily understood when the suggestion is derived from the similarity between two given drugs or diseases. However, the success of these approaches depends on the strength of the similarity assumption—for instance, a minor structural difference between two otherwise identical drugs could be crucial to the drug effect, or there could be important differences in drug–disease response that are not captured by the chosen similarity metric.
- *Activity-based*: Activity-based methods aim to find some representation of the mechanism or mode of action of a drug or disease effect (e.g., through drug–target interaction or effects on gene expression) and use this information to form new drug–disease associations. These methods are often associated with a reductionist, structure–target-based viewpoint but can also use a more holistic systems biology representation of activity, such as determination of perturbed biological pathways from gene expression data.
- *Misclassification-based*: "Misclassification" here relates to the machine learning task of classification: given data on an item belonging to one of several classes, predict which class the item belongs to. In drug repurposing, the task is often to determine which therapeutic class(es) a drug belongs to. For a classifier with sufficiently high accuracy, misclassifications could be interpreted as repurposing suggestions. The drawback of this method is that it is a "black box" approach—classifiers often use hundreds of features (features are some element of the input data, such as the absence or presence of a particular structural element of a drug), and the way in which classifiers make decisions from these features means that it can be difficult to discover why the drug has been assigned to a particular class. Further, in the drug repurposing task, it could be impossible to measure the true rate of error of a classifier and therefore to discriminate between classifications that are valuable repurposing suggestions and those that are simply errors resulting from model artifacts. Prior biological rationale, or experimental validation, is required to distinguish between the two.

These categories may not be clearly delimited, and one type of approach may form the basis for another, for example, some machine learning approaches use drug–disease similarity or activity as input data and some similarity-based methods use activity as a similarity measure. Further, a huge variety of methods are used within each general type of approach, examples of which will be discussed later in this section.

1.02.6.3 Resources

A key advantage of data mining methods is that they can distill down vast amounts of data into useful hypotheses. For a human, too much data can be overwhelming and hamper our ability to detect any useful signal (the "needle in a haystack" problem), whereas data mining methods often perform better the more data they have as input. The methods presented in this section use upward of hundreds of disease or drug cases, from which hundreds of thousands of associations may be formed. Where do all these data come from? Most computational repurposing methods use data stored in publicly accessible databases or repositories. Each repository is specialized for a different data type or purpose, and methods making use of several different data types may have to integrate data from different repositories, which is not always trivial. **Table 6** details some of the data sources used in the examples in this section.

A data mining method can only ever be as good as the data it uses—the term "garbage in, garbage out" certainly applies here—and the quality of data stored in biological, chemical, and pharmacological data repositories can be variable. Firstly, there are the inaccuracies present in the data itself: data may be noisy, imprecise, biased, or (for data that are not a directly measurable quantity) a model prediction with an associated level of uncertainty. Then, there are the problems inherent in the use of large datasets: due to the volume of data being stored, most data repositories involve automatic annotation to a greater or lesser extent and may be based on literature mining or automatic extraction techniques, all of which introduce some potential for error. Alternatively, the data may rely on a community curation model (such as that used by Wikipedia), with data submitted by individual users with varying degrees of external moderation. Manually curated resources do exist, although these tend to be smaller and more specialized, and of course are subject to human error. Consideration of input quality is therefore essential in algorithm design. Depending on the approach used, however, it may be possible to "average out" any inaccuracies contained in individual entries by the use of large datasets (see, e.g.,

Table 6 Selected data sources used in data mining drug repurposing

Name	*Description*	*Examples of use*	*Size as of 2015*
Drug and target data			
DrugBank http://www.drugbank.ca/	Links drugs (chemical and pharmacological information) to targets (sequence, structure, and pathway information)	20,62,132–134	7759 drugs 4300 proteins
STITCH http://stitch.embl.de/	Chemical–protein interaction database	135,136	300,000 small molecules and 2.6 million proteins from 1133 organisms
Therapeutic Target Database http://bidd.nus.edu.sg/group/cjttd/	Provides information about drug targets and their associated drugs, diseases, and pathways	137	2025 targets 17,816 drugs
MATADOR http://matador.embl.de/	A manually annotated list of drug–target interactions	136	–
Genomic and transcriptomic data			
PharmGKB https://www.pharmgkb.org/	Collates information about the impact of genetic variation on drug response	132,136,138	–
OMIM http://www.omim.org/	Details human genes and genetic disorders and their associated phenotypes	62,139	8000 phenotypes 15,000 genes
Gene Expression Omnibus http://www.ncbi.nlm.nih.gov/geo/	Repository of gene expression studies with associated analysis tools	133,140,141	61,804 experiment series
Connectivity Map https://www.broadinstitute.org/cmap/	Gene expression data from cultured human cell lines treated with small-molecule perturbagens including FDA-approved drugs	140,142–146	1309 small-molecule perturbagens
Other biological data			
NCBI Biosystems	A database of biological pathways linked to other entities in the NCBI system (molecular and chemical data and associated literature)	147	–
KEGG http://www.genome.jp/kegg/	A collection of bioinformatics databases including pathway maps, genes and proteins, compounds, diseases, and drugs, together with shared analysis tools	133 148 140,149	–
SIDER http://sideeffects.embl.de/	Associates marketed drugs with indications and side effect information extracted from packaging labels	133,149–151	1430 drugs 5880 side effects 140,064 drug–side effect pairs

Gramatica et al.[55]), and for many data mining algorithms, it is preferable to use large volumes of "mostly accurate" data than to use smaller amounts of verified data.

1.02.6.4 Validation

If experimental repurposing methods represent in vivo or in vitro repurposing, data mining methods can be thought of as "in silico" repurposing. Just as the in vivo effect of a drug may not perfectly reflect its properties in vitro, its effect as predicted in silico is still further removed from its true activity in a living system, and some method of validation is required to determine how much confidence we should place in these predictions before progressing suggested repurposing candidates to experimental testing. An in silico measure of performance is also required for model selection (to determine which parameters give the best performance) and for training of classifiers in machine learning methods. These performance measures can be loosely categorized into three types:

- *Prediction of existing associations*: Many machine learning-based methods measure predictive performance by the ability to predict (or rather reproduce) the existing associations (to diseases, targets, or other drugs) of drugs, for example, by predicting drug class or drug indication. This ties into the misclassification approach—the better the performance of a method at predicting existing associations, the more confidence we can have in its "errors" (according to existing labels) as potential repurposing candidates.
- *Literature support*: If a suggested drug and indication (or drug and target) are mentioned together in the biomedical literature, this provides a form of confirmation for the prediction. Validation from literature support can be done in two ways. The first is selective support, where a thorough literature search (often manual) is performed for the most promising repurposing candidates in order to discover more about the repurposing rationale before making a recommendation. Alternatively, a large-scale literature mining approach (often automated) can be used, enabling measurement of literature support for all the repurposing candidates to measure the overall performance of the method. Of course, simple co-occurrence of two terms in an abstract or publication does not imply a recommendation for drug repurposing—the two could be in a negative relation to each other (see section "**Knowledge-based approaches**" for a discussion of issues related to automated literature mining methods)—but literature support provides a simple way to measure which suggestions are supported by biological or pharmacological reasoning.
- *Clinical trial support*: If a drug has entered clinical trials for use in a particular disease, this provides an even stronger validation for the repurposing suggestion. Clinical trial support does not necessarily imply that a drug is effective in a disease—entering a clinical trial does not mean the drug has passed the trial!—but it does mean that the recommendation of the predictive method is at least plausible, and the recommendation to reposition can be considered correct.

All of these methods rely on prior knowledge for validation. In some senses, however, this prior knowledge could be considered not validation but invalidation—a method that perfectly predicts all previously known associations of a drug without making any errors (misclassifications according to existing labels) would score highly for accuracy, but is of no use for drug repurposing. Further, when using known associations for validation, it is unclear whether any additionally predicted associations are valuable repurposing suggestions or simply classification errors. This raises the question of whether it is suitable to use the ability to predict what is already known as a proxy to measure the ability to predict what is currently unknown, that is, the ability to make novel and clinically useful repurposing suggestions. Prior knowledge can only measure performance within already explored pharmacological space,[152] and its use as a surrogate outcome may penalize more "exploratory" methods that are less accurate in predicting known drug indications but may come up with a wider range of plausible novel suggestions. While this type of trade-off is a common issue in prediction tasks, the balance must be determined according to the desired outcomes of the system (prediction of useful new repurposing candidates) and should not be biased by the evaluation task. With these limitations in mind, experimental validation of promising repurposing candidates remains the best way to test the practical utility of a computational repurposing method.

1.02.6.5 Structure–Target Data Mining

Structure–target repurposing methods use the structure of drugs and their biological targets, and the known interactions between them, to suggest new associations for drugs. The basis of most structure–target methods is polypharmacology—the binding of drugs to multiple targets. Polypharmacology is increasingly recognized as an important paradigm in the development of new therapeutics, in terms of drugs that can modulate multiple targets at once (in contrast with the highly selective "magic bullet" approach).[153] In structure–target repurposing, polypharmacology generally refers to the association of drugs with new targets distinct from the target involved in the original indication of the drug. This can be achieved through transferring drug–target associations between similar drugs or, vice versa, between target molecules sharing similar ligand-binding sites. However, the polypharmacological profile of a drug (the range of targets with which it interacts or the "interactome") can also be used—for example, as input to a classifier-based approach—to predict new disease indications, bypassing target prediction entirely. This section will describe some of the different approaches used to reposition drugs through their structure and interaction information.

1.02.6.5.1 Chemical structure methods

To find new indications for a drug, it would seem most straightforward to start with its chemical structure—intuitively, we would expect structurally similar molecules to bind to similar targets. SuperPred[154] uses the chemical similarity of drug compounds, including similarity of structural fingerprints (measured by the Tanimoto coefficient, which describes the ratio of the shared structural elements to the total number of structural elements present in both molecules) and of physicochemical properties ("rule of

five" properties[155]), to predict their biological effect (ATC class) and similarity to existing drugs. The system was used to identify drugs with structural similarity to the antihypertensive drug enalapril and found six drugs with Tanimoto coefficient >0.8 (indicating a high number of shared substructures), all of which had literature support for a clinically similar effect. The extent to which structurally similar drugs share similar activities is controversial, however, and it has been stated that there is only a 30% chance that molecules with a Tanimoto coefficient of Daylight fingerprints >0.85 share binding activity and that "similar compounds do not necessarily interact with the target macromolecule in similar ways."[156] Efforts have been made to overcome this by grouping drugs by their targets: one method developed by Keiser et al.[157] represented drug targets by their set of known binding ligands and determined the structural similarity of drugs to each set to predict new targets, including the action of fluoxetine (Prozac) as a beta-1 agonist. Twenty-three out of 30 predictions were experimentally confirmed. However, due to more general problems with the use of chemical structure data—including statistical biases inherent in the most commonly used measure of structural similarity, the Tanimoto coefficient,[158] and the limitation of the search space to drugs structurally similar to the starting set—recent repurposing methods have tended to include chemical structure as a component of integrated methods involving multiple data sources, rather than use chemical structure as the sole predictor.

1.02.6.5.2 Protein structure methods

Rather than using chemical structures to represent the binding capabilities of a drug, the problem can be approached from the opposite direction: using the biological structure of a protein to represent the ligand-binding capabilities of a drug target. Protein structure-based repurposing therefore works through target-to-multiple drug association, rather than through the drug-to-multiple target associations of chemical structure methods. Protein structural similarity has been used to identify treatments for the neglected tropical disease schistosomiasis.[136] Drug–target interaction databases (including DrugBank, the Therapeutic Target Database, PharmGKB, STITCH, and the manually annotated MATADOR database) were interrogated with schistosome protein sequences, searching for homology to known human drug targets to predict interactions with known drugs. As well as six drugs already known to be active against *Schistosoma*, their method identified 115 other drugs inside this schistosomicidal compound space. The authors suggest that all 115 drugs in this active compound space are viable drug repositioning candidates, although it is unlikely that all of these candidates will be suitable for repositioning: this issue relates to the sensitivity–specificity trade-off, which will be discussed later in this section.

One issue with protein structure-based repurposing is that the flexibility of protein–ligand binding means that similar compounds can bind to targets in very different ways, and so structural similarity does not always guarantee similarity of drug binding.[159] One study[160] compared the use of drug-based (chemical structure) similarity and target-based (protein target genomic sequence) similarity for the prediction of novel drug–target interactions and found both to be inferior to a method based on prediction from known interactions. Indeed, it has been shown that pharmacological effects are more closely correlated with drug–target interactions than structural similarity.[161] The next section will describe methods that use drug–target interactions as a starting point for repurposing.

1.02.6.5.3 Molecular docking and binding site similarity

Rather than looking at the structures of drugs or their targets in isolation (as with the methods discussed earlier), it is possible to use the interactions between the two to predict new drug–target associations. Molecular docking models the physical interaction between a ligand (i.e., a drug) and its target (or set of targets)[162] in order to predict binding affinities, measuring the strength of associations between drugs and their protein targets. Molecular docking is important in drug design (see Ref. 163 for a review), and many docking models have been developed (e.g., TarFisDock,[164] BioDrugScreen,[165] and DOCK[166]). The last of these programs, DOCK, was originally developed in 1982 and has been used in a number of drug discovery and repurposing programs, notably in the identification of the antipsychotic agent haloperidol as a highly selective inhibitor of HIV-1 and HIV-2 proteases.[167] This could be considered as one of the earliest examples of computational drug repurposing, although it was technically more of a computational screening approach, using DOCK to assess the binding potential of each of 10,000 molecules in the Cambridge Crystallographic Database to HIV-1 protease.

Molecular docking has also been combined with structural similarity of ligand-binding sites in a drug repurposing study for drug-resistant tuberculosis.[168] Binding-site similarity methods are related to the protein structure methods described earlier, but use the structure of binding sites rather than that of the whole protein. This is a more specific measure of structural similarity than whole-protein structure, as the presence of similar ligand-binding sites enables otherwise structurally different proteins to bind the same drug.[169] This combined approach first finds off-targets of a drug by searching the proteome for molecules with similar ligand-binding sites and then uses molecular docking to evaluate physical interaction of candidates from the first step. This method suggested the antiparkinsonian drug entacapone as a lead compound for the treatment of drug-resistant tuberculosis, but the general idea could also be applied in other disease contexts. Having identified a lead compound, the knowledge of its primary and off-targets can then be used to further optimize the compound for efficacy, selectivity, and ADME properties through selective optimization of side activities.[170]

1.02.6.5.4 Drug–target interaction profiles

Drug–target interaction profiles are a natural extension of molecular docking methods in the drug repositioning task. While molecular docking methods use drug–target interactions to find significant associations of a drug or target of interest, drug–target interaction data can also be combined over multiple drugs and/or targets, forming an "interaction profile" showing binding patterns on

a larger scale. Similarity between interaction profiles can be used for repurposing, on the basis that drugs with similar binding patterns may have similar therapeutic effects.[137,171]

One example of how such an interaction profile can be used in drug repurposing is drug–protein interaction-based repurposing,[135] which is based on drug–protein interactions from STITCH. This method determines the drug–protein interaction profile of drugs indicated for a particular therapeutic effect—essentially a binary drug–protein matrix where 1 represents an interaction (binding, activation, or inhibition) of a drug with a protein and 0 represents no interaction. This matrix was used in a supervised machine learning approach to identify drugs with similar interaction profiles and determine the possibility of their having the same therapeutic effect. Predictions included nitrendipine and nimodipine for hypertension and dexamethasone for malaria (dexamethasone has been anecdotally reported to be beneficial in cerebral malaria, but a literature search later revealed that clinical trials did not show significant effect). Another example of interaction profile similarity methods in drug repurposing is drug repositioning and adverse reactions via chemical–protein interactome (DRAR-CPI),[172] a tool for the prediction of new drug indications (or adverse effects) of a submitted molecule. DRAR-CPI generates a molecule interaction profile (termed the "interactome") and checks for similarity to that of drugs in the library interactome, based on interaction of 254 small molecules with 385 human proteins. Interactome similarity indicated links between a group of antipsychotics and a group of anti-infectives (which are supported by studies showing the antimicrobial effects of the antipsychotics prochlorperazine and chlorpromazine), implying potential for repurposing of others in the same group.

Interaction profile methods can also be combined with molecular docking in order to incorporate binding affinity scores in the interaction profiles. This method has been applied to identify therapeutic targets in Alzheimer's disease (AD),[137] creating an interactome of 10 known AD drugs and 47 randomly chosen "control" (non-AD) drugs docked against 401 human proteins. Proteins that tended to be targeted by the AD drugs but not by the control drugs were therefore assumed to be implicated in AD. As well as the known AD target acetylcholinesterase, the docking-based interactome revealed that two other target families thought to be involved in AD—estrogen receptor, the ligands of which have reported neuroprotective and anti-inflammatory effects, and histone deacetylase—may have already been targeted by existing AD drugs. As well as new drug targets, the similarity of the AD drug interactomes indicates that interactome similarity could be used to reveal drugs sharing therapeutic effects in a multitarget approach to drug repurposing.

Many recent drug repurposing methods have used drug–target interaction data as one component of an integrated approach, often forming the chemical/structural component of methods that attempt to integrate both biological and chemical data types. One such method integrates chemical and protein structural similarity with known drug–target interactions from DrugBank to create a "consensus response score"—a quantitative measure of the association between a drug and its protein target.[173] Using a drug similarity network based on the consensus response scores, new indications were predicted for 185 drugs, of which 72% were supported by literature. Integrated approaches such as this have become popular in computational drug repurposing in recent years and will be discussed in more detail later in this section. Further examples of specific structure–target predictions are shown in **Table 7**.

When considering drug–target interaction-based repurposing methods, it is useful to consider the topology of the network—what the "interaction space" looks like. In a drug–target network linking FDA-approved drugs with their targets, it was found that highly connected nodes were connected to each other at a higher degree than would be expected by chance. This indicates that many drugs target a small number of highly targeted proteins, leading to "follow-on" drugs,[174] which indeed has been a frequent strategy employed in the pharmaceutical industry in recent decades. Conversely, many proteins can be targeted by a small number of drugs. For example, antipsychotics or other drugs acting on the central nervous system are a class that is frequently suggested for repurposing to new indications.[167,172,175] Why should this class come up so frequently? Due to the polygenic nature of central nervous system (CNS) disorders, the most effective therapeutics are those that interact with multiple targets.[176] These drugs may therefore be among the most highly connected in drug–target interaction space, which would lead to a higher rate of repurposing suggestions within this class. On the other hand, CNS-active compounds frequently rely on a fine balance of quantitative activities against these multiple targets, and it is not obvious whether this balance is sufficiently captured yet in computational drug repurposing approaches. Finally, it is worth bearing in mind that drug–target interaction methods only take into account those proteins that are known to be drug targets and therefore cover only a fraction of the entire human protein space,[137] limiting the potential for discovery of drugs that act *via* novel disease-associated targets.

There are a few considerations specific to structure–target repurposing that result from the "reductionist" nature of structure–target methods, namely, that they look at individual aspects of drugs in the system, rather than examining the entire response of an organism. This has its advantages—structure–target methods can provide a neat biological rationale through an explicit mechanism of action, rather than the "black box" of effects-based methods—but by considering only structure and binding, structure–target methods fail to consider the broader systemic effect of drug administration in a biological system. There is a gap between measured structure–target data and the eventual in vivo effect[177] resulting from, for example, metabolism of compounds in the body and unidentified off-target effects. Further data mining approaches to drug repurposing take a more holistic systems biology view of drugs and disease. These "effects-based" methods will be discussed in the next section.

1.02.6.6 Effects-Based Data Mining

Effects-based repurposing methods use biological data to analyze the ways in which a drug or disease perturbs a biological system, providing a systems-level view of drug treatment. These methods are situated along the whole spectrum of biological data

Table 7 Overview of drug repurposing candidates from selected structure–target approaches

Selected candidates—target/indication	*Structure*	*Validation*	*References*
Fluoxetine—β_1 receptor agonist	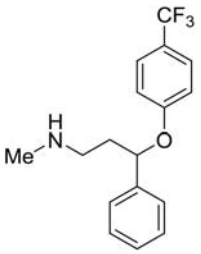	Experimental validation	157
Ifenprodil—5-HT transporter inhibitor	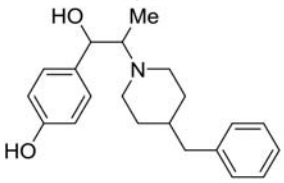	Experimental validation	157
Delavirdine—histamine H_4 receptor agonist	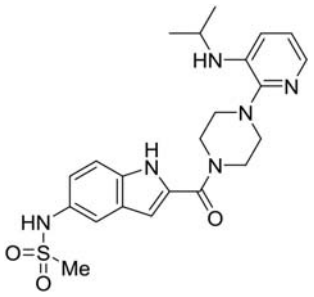	Experimental validation	157
Aprindine—schistosomicidal agent	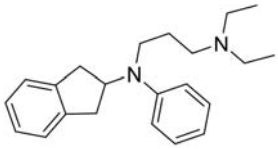	Ability to predict known schistosomicidal drugs	136
Clotrimazole—schistosomicidal agent	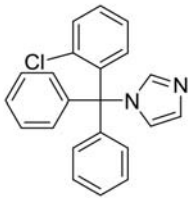	Ability to predict known schistosomicidal drugs	136
Griseofulvin—schistosomicidal agent	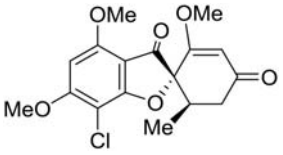	Ability to predict known schistosomicidal drugs	136
Cinnarizine—schistosomicidal agent	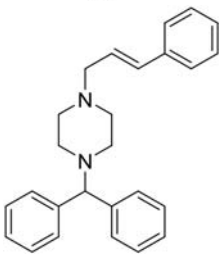	Ability to predict known schistosomicidal drugs	136
Nimodipine—hypertension	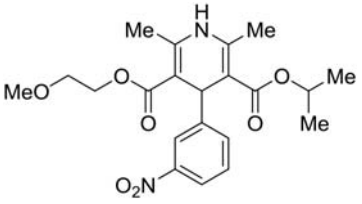	Literature support	135

Table 7 Overview of drug repurposing candidates from selected structure–target approaches—cont'd

Selected candidates—target/indication	*Structure*	*Validation*	*References*
Verapamil—HIV	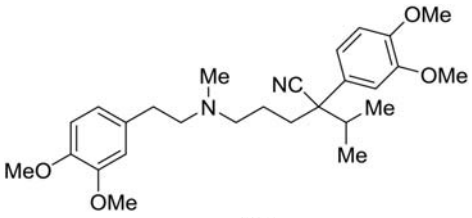	Literature support	135
Dexamethasone—HIV	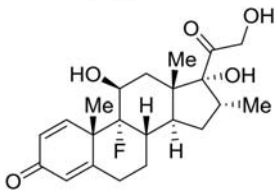	Literature support	135
Entacapone—drug-resistant tuberculosis	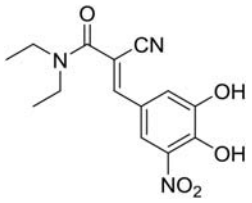	Experimental validation	168

(collectively known as -omics), from gene–drug associations (the genome) to drug effects on gene expression (the transcriptome) and the translation into proteins (the proteome) to the eventual range of outcomes of the drug effect (the phenome), each of which can be considered a biological consequence of the one preceding. -Omics data as a readout of a biological system aim to capture a drug or disease effect on multiple components of the system at once. Quantifying drug–disease effect in this way allows comparison between drug and disease that takes the response of the biological system into account and in turn can help to formulate new repurposing hypotheses.

1.02.6.6.1 Genome-based

As modern molecular biology is increasingly able to identify disease–gene and gene–drug relationships, genome-based repurposing aims to reveal the "hidden link" between the two in order to predict novel disease–drug associations. Known drug–gene relationships are listed in databases including the Pharmacogenomics Knowledge Base (PharmGKB, https://www.pharmgkb.org/), which contains drug–gene links derived from co-occurrence in literature, and STITCH (http://stitch.embl.de/), which contains drug–protein (i.e., translated gene) associations based on literature mining. Databases such as OMIM (http://omim.org/) list known disease–gene associations, or predicted associations can be derived from, for example, comparison of mutant phenotypes, as listed in PhenomeNet.[138] The challenge is then to link disease–gene and gene–drug relationships to predict novel, relevant disease–drug relationships. Genome-based methods can be considered as an example of target-to-multiple disease repurposing (the primary target of a drug is involved in multiple diseases),[178] in contrast to the drug-to-multiple target or target-to-multiple drug methods associated with structure–target repurposing.

Many disease–gene relationships have been established through genome-wide association studies (GWAS), which aim to link genetic variants to phenotypic traits using large population studies. Computational drug repurposing methods can combine the results of several GWAS, increasing their power to detect disease–gene associations and creating an informed basis for drug repurposing. One meta-analysis of GWAS in RA identified candidate genes for RA risk and found that these risk genes were enriched for the drug targets of approved RA drugs.[179] This suggested that drugs approved for other indications that targeted RA risk genes could be repurposed for RA treatment—for example, the risk genes CDK6 and CDK4 are targets of approved cancer drugs, one of which (flavopiridol) the authors note has been shown to improve RA symptoms in animal trials. Further, the authors point out that previously approved RA drugs, such as rituximab, were initially developed for cancer treatment, suggesting that repurposing from cancer to RA therapy is biologically plausible.

Other methods for disease–gene association discovery include RNAi screening, which allows identification of loss-of-function mutations associated with particular phenotypic outcomes. A recent RNAi screen[175] identified genes that were modifiers of the proteostasis network involved in the genetic disease alpha-1-antitrypsin deficiency (ATD). Drug–target association databases were then searched to find FDA-approved drugs that targeted these gene products, identifying the antipsychotic fluspirilene, which was shown to be effective against ATD in a mammalian cell line. While genome-based approaches are intuitively appealing due to the apparent simplicity of the drug–gene–disease relationship, it is worth considering that the relationship between a gene and its associated gene

product (i.e., protein) as a drug target is not always clear-cut due to the biological distance between genotype and phenotype, involving, for example, splice variants, posttranslational modifications of the protein, and other factors. The next section will cover an intermediate step between the two: the transcriptome.

1.02.6.6.2 Transcriptome-based

Transcriptome-based repurposing methods can be viewed as an attempt to bridge the genotype–phenotype gap by moving closer to the phenotype of a disease. The transcriptome provides a quantitative measure of the effects of a drug on a biological system, revealing "hidden" information about the effects of a drug[180] that may not be clinically observable or predictable from structure or target information. There are many publicly available gene expression resources, from repositories such as the NCBI's Gene Expression Omnibus (GEO, http://www.ncbi.nlm.nih.gov/geo/) and EMBL-EBI's ArrayExpress (http://www.ebi.ac.uk/arrayexpress/) to curated resources such as GeneSigDB (http://www.genesigdb.org/genesigdb/), which aims to summarize the expression content of published gene expression studies. The release of the Broad Institute's Connectivity Map (CMap, https://www.broadinstitute.org/cmap/) in 2006 provided a valuable source of information about drug transcriptional response, measuring gene expression of cultured human cells following treatment with 1309 small molecules including FDA-approved drugs. The aim of this project was to show the "connectivity" between transcriptional signatures (sets of genes that are significantly up- or downregulated) induced by drug compounds and those of disease—for instance, a high correlation between the signatures of thiazolidinediones and a published gene signature for obesity predicts the observed adverse effect of weight gain resulting from use of thiazolidinediones.

Several transcriptome-based drug repurposing methods have followed the same reasoning in the opposite direction—if positively correlated signatures can predict adverse effects, can a negative correlation of drug and disease signatures predict treatments? Several repurposing studies have been developed around this inverse signature methodology, including that of Sirota et al.,[142] which tested for "oppositeness" of gene expression signatures of disease to drug-induced signatures from CMap using an enrichment-based method, gene set enrichment analysis (GSEA).[181] GSEA tests whether significantly regulated genes in a disease signature fall near the top or the bottom of the ranked list of genes changed in response to drugs. If the genes upregulated in a disease condition are strongly downregulated by drug treatment, this indicates that the drug could be a plausible treatment option for this disease. Their approach was experimentally validated by testing the use of cimetidine as a treatment for lung adenocarcinoma. This group then applied this approach to focus on particular diseases, for example, small-cell lung cancer[182] and inflammatory bowel disease (IBD)[183]; other studies have refined the inverse signature approach to predict treatments for colorectal cancer,[184] skeletal muscle atrophy,[144] leukemia, and breast and prostate cancers.[140]

Information about drug transcriptomic effects can also be used to reveal similarities between the biological effects of drugs. The drug similarity network created by Iorio et al.[180] used CMap transcriptional data, observing that drugs with similar transcriptomic profiles perturb the same biological pathways and therefore may share similar mechanisms of action. Using this approach, they discovered that fasudil—a vasodilator that was thought to have a well-characterized mechanism of action—additionally acts as a promoter of cellular autophagy. Fasudil showed high transcriptional similarity to a known enhancer of cellular autophagy, 2-deoxy-D-glucose (2DOG), and this activity was confirmed in vitro, suggesting its potential repurposing to neurodegenerative disorders. Combining the drug similarity with the inverse signature approach, Hu and Agarwal[143] created a disease–drug network using gene expression signatures from GEO and drug signatures from CMap. Negatively correlated disease and drug signatures were considered as repurposing candidates, including antimalarials for the treatment of Crohn's disease; the network also included disease–disease connections revealing molecular-level relationships between diseases and drug–drug connections that could illuminate drug targets or mechanisms of action.

Although gene expression data have been widely used in computational drug repurposing methods, they suffer from context effects dependent on cell line or species.[149] Providing more specific measurements across parameters including drug dosage and cell type, the Library of Integrated Network-Based Cellular Signatures (LINCS) is being developed as a large-scale successor to CMap. The LINCS will cover over 20,000 compounds (of which ~1300 are FDA-approved drugs) tested in multiple cell lines. While the LINCS will be a valuable resource for transcriptomics-based drug repurposing, it cannot alleviate the problem of noise inherent in the use of gene expression data. As well as biological noise caused by cell cycle stage, transcriptional bursts, and interindividual variation,[64] there is also technical noise caused by imperfect measurement of the amount of RNA present in a given sample. One way to minimize the effect of noise is to map gene expression data onto a higher-level biological space—that of pathways. Converting molecular data to a systems-level representation of pathway enrichment or depletion can strengthen the (sometimes subtle) signals present in the transcriptomic data to give a clearer picture of the drug or disease effect. In one approach, Pan et al.[147] mapped the protein and gene targets (determined from gene expression) of drugs to pathways contained in the NCBI BioSystems database (http://www.ncbi.nlm.nih.gov/biosystems/). As well as revealing the mechanisms of action involved in known drug treatments, some drugs were linked to pathways responsible for other diseases—such as the association of glioblastoma to gefitinib or small-cell lung cancer to celecoxib—suggesting their possible association in a drug repurposing approach.

1.02.6.6.3 Proteome-based

The emergence of newer -omics technologies such as proteomics provides alternative ways to measure the effects of drugs or disease in the body. According to the central dogma of molecular biology, the proteome is a closer molecular approximation to the phenotype than either the genome or the transcriptome, and it is therefore a practically relevant biological space to explore for drug repurposing. Proteomics is less well established than transcriptomics and there is less data available, so repurposing studies using

proteomics tend to focus on specific diseases, rather than the more general multidisease approaches that are possible with transcriptomics. Zhang et al.[145] integrated the results of multiple GWAS, proteomics, and metabolomics studies to create a diabetes metabolite–protein network. The network was searched for potential antidiabetic protein targets with known drug interactions, which were therefore considered to be candidates for repurposing. They then used CMap to compare the gene expression patterns of the repurposing candidates with those of known antidiabetic drugs and to drugs with diabetes-like adverse effects. Four COX2 inhibitors (diflunisal, nabumetone, niflumic acid, and valdecoxib) were proposed for the treatment of type 1 diabetes and two drugs (phenoxybenzamine and idazoxan) targeting ADRA2A (alpha-2A adrenergic receptor) for type 2 diabetes. Note that this is technically repurposing via a meta-analysis of -omics studies rather than a proteomics-based repurposing method; however, this demonstrates the utility of these different data types for drug repurposing alongside more established transcriptomics and genomics techniques.

1.02.6.6.4 Phenome-based

At the opposite end of the scale of molecular biology, the human phenome—which in this context represents the range of drug end points, with regard to both disease progression and side effects—can be a valuable source of information for repurposing, representing in some sense the most relevant measure of drug action. Phenome-based repurposing is a black box model of drug effects, assuming no knowledge about the mechanism of action of a drug. Unlike the genome or transcriptome, the phenome is easily observable in the clinic and—although subject to variation through each clinician's particular classification of observations—does not suffer to the same extent from the problem of noise and measurement error. However, phenomic data present their own problems in terms of appropriate standardization of qualitative observations, and many efforts are under way to create ontologies (Disease Ontology, International classification of disease (ICD), Medical Subject Headings (MeSH)) that standardize the medical language of diseases and side effects.

The phenotypic effects of drugs include their therapeutic effects (their indications), as well as their adverse effects. Chiang and Butte[185] used drug indications (including off-label uses) to link diseases in a guilt-by-association approach—if two diseases share a number of similar therapies, those indicated for either disease but not the other may then be candidates for repurposing. Indeed, they found that drug indications suggested by this method were 12 times more likely to be under evaluation in clinical trials than nonsuggested drugs. Another method used phenome information from SIDER (see **Table 8**) to build a latent variable model based on the interconnectivity of indications and side effects, which was able to generate probabilistic alternative indications for drugs.[150] In this Bayesian model, the phenotypes (drug indications and side effects) represent an observed outcome of drug treatment, and the molecular mechanisms through which drugs exert their action represent hidden variables from which new links between drugs and phenotypes can be inferred. The predictions were validated against literature support—the repurposing of thalidomide to

Table 8 Overview of drug repurposing candidates from selected effects-based approaches

Selected candidates—target/ indication	*Structure*	*Validation*	*References*
Flavopiridol—rheumatoid arthritis	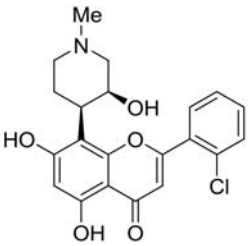	Literature support	179
Wortmannin—α1-antitrypsin deficiency	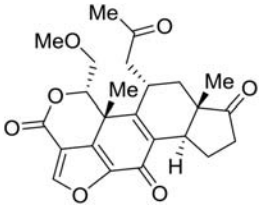	In vivo validation	175
Fluspirilene—α1-antitrypsin deficiency	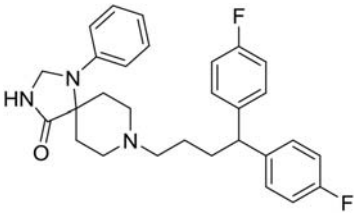	In vivo validation	175

(Continued)

Table 8 Overview of drug repurposing candidates from selected effects-based approaches—cont'd

Selected candidates—target/ indication	*Structure*	*Validation*	*References*
Fluoxetine—α1-antitrypsin deficiency	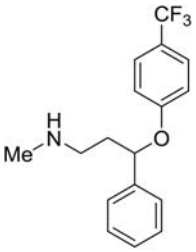	In vivo validation	175
Amiodarone—α1-antitrypsin deficiency	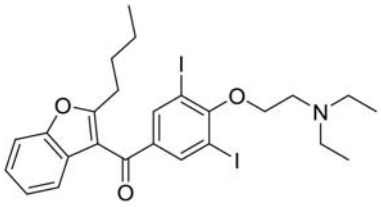	In vivo validation	175
Cimetidine—lung adenocarcinoma	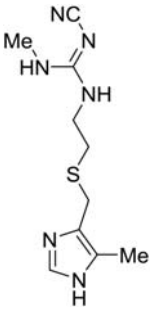	In vitro and in vivo validation	142
Citalopram—colorectal cancer	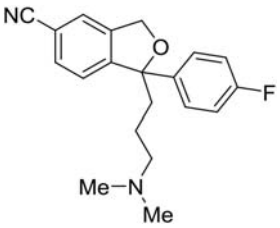	In vitro and in vivo validation	184
Troglitazone—colorectal cancer	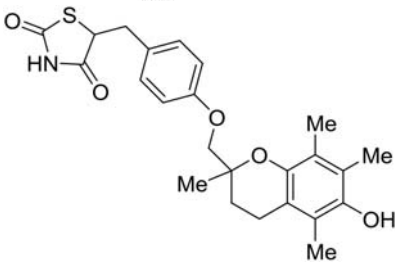	In vitro and in vivo validation	184
Enilconazole—colorectal cancer	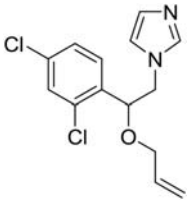	In vitro and in vivo validation	184
Tamoxifen—atopy	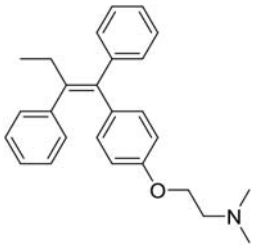	Literature support	143

Table 8 Overview of drug repurposing candidates from selected effects-based approaches—cont'd

Selected candidates—target/ indication	*Structure*	*Validation*	*References*
Rapamycin—Huntington's disease	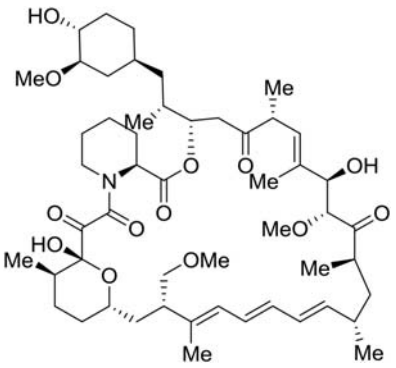	Literature support	143
Gefitinib—glioblastoma	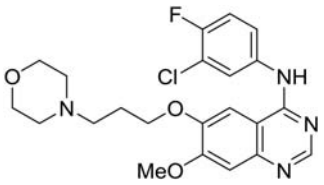	Literature support	147
Celecoxib—small-cell lung cancer	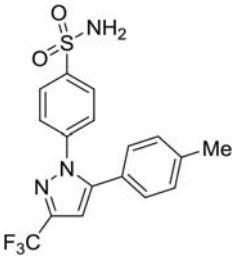	Literature support	147
Atazanavir—HIV	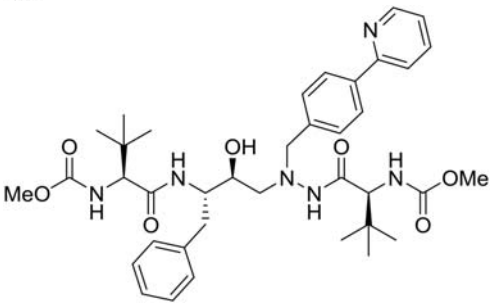	Literature support	150
Aripiprazole—dementia	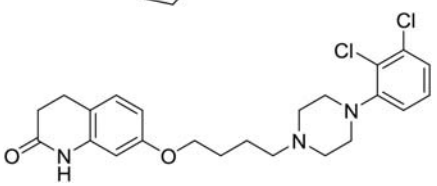	Literature support	150
Itraconazole—meningitis	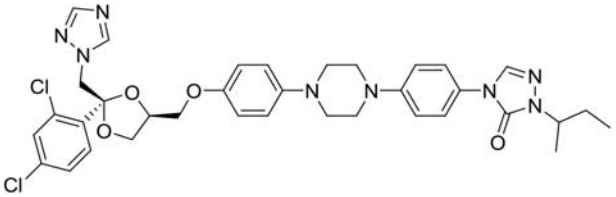	Literature support	150
Mefenamic acid—rheumatoid arthritis	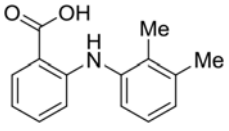	Literature support	150

multiple myeloma, as discussed earlier in this article, was among the candidates proposed by their method. However, another well-known example of repurposing—the antidepressant bupropion (Wellbutrin™) for smoking cessation—was used to illustrate a limitation of their method: the indication "smoking cessation" is not included in the SIDER database and therefore cannot be predicted. This is a more general point about data mining methods—the space in which predictions can be made is necessarily constrained by the data source, meaning that less well-explored areas of pharmacological space may be missed by these methods. This is particularly problematic in the case of rare or orphan diseases.

Side effects are another aspect of the phenome that can be mined for drug repurposing. Campillos et al.[186] used drug side effects to infer drug targets, working from the assumption that two drugs causing similar effects in the body must share a target. By inferring targets from side effects alone, the authors were able to discover associations between chemically dissimilar drugs or drugs with no known targets. They experimentally tested 20 "unexpected" predictions (associations between dissimilar drugs from different therapeutic areas) and confirmed binding to predicted targets in 13 of these drugs, indicating a link between the Alzheimer's treatment donepezil (which has previously been proposed as a treatment of depression) and the antidepressant venlafaxine. Following the success of this approach, the group developed the Side Effect Resource (SIDER) database,[187] which connects drugs to indications and side effect terms. This has been used to develop further side effects-based repurposing methods, such as the large side effect similarity network constructed by Ye et al.,[151] which covered 2183 drugs across nearly 6500 side effects.

Part of the power of effects-based approaches comes from their ability to integrate information about the effects of disease as well as drugs. By combining these different domains, these methods aim to reveal new knowledge that would not be apparent from looking at either domain alone. Extending this concept further, knowledge-based approaches aim to gather information from many different sources in order to form new links between diverse concepts.

1.02.6.7 Integrated Approaches

Integrated approaches combine both effects-based and structure–target methods. By combining these two different data spaces, it is hoped that more can be revealed than from examining either space alone. Luo et al.[172] compared their target-based drug associations with effects-based predictions based on gene expression data and found a high agreement rate of 74%, suggesting that these different approaches are complementary and concordant. High agreement between two data sources strengthens the predictive "signal" against the noise of spurious or false associations: when multiple data sources are used, the common core of agreement can be considered high-confidence predictions, while predictions that are not unanimously supported by all data types could be considered the more "interesting" or less obvious predictions. This section describes examples of data integration, as well as issues relating to data choice and data filtering: examples of the methods used are shown in **Table 9**.

An initial example of this is the classifier-based approach developed by Napolitano et al.[146] This study integrated different types of drug information to quantify drug similarity: similarity of chemical structures, distance of target proteins in a protein–protein interaction network, and transcriptomic effects from CMap. Using machine learning methods, a classifier was created to predict the ATC codes (a classification according to anatomical system and therapeutic effect) of drugs given information on these three features. The method is based on the interpretation of misclassifications as putative drug indications. With classification performance (accuracy) of 78% on prediction of ATC codes, novel misclassifications could therefore be new leads for drug repurposing. An example of a "known misclassification" (i.e., a misclassification that has clinical support) is the diuretic spironolactone, which was predicted to be in the ATC class "sex hormones and modulators of the genital system": spironolactone has known antiandrogenic effects and is sometimes prescribed off-label for hirsutism and other androgenic disorders. One consideration of this method, however, is that it is only able to predict broad therapeutic classes rather than specific uses. While this might be sufficient for some classes—for example, the class "beta blocking agents" indicates a mechanism of action—in some cases, this broad description will not provide enough information to inform a repurposing hypothesis. The description of spironolactone as a "modulator of the genital system," for instance, is not specific enough to be useful in drug repurposing.

Table 9 Data types used by integrated methods

Drug indication	*Phenotypic features of disease*	*Chemical structure*	*Protein sequence similarity*	*Drug–target interaction*	*Disease-related genes*	*Closeness of drug–disease-related genes in a PPI network*	*Side effects*	*Other molecular features of disease, for example, pathway and environmental factors*	*Gene expression following drug treatment*	*References*
X	X	X	X	X						134
	X	X	X		X	X	X			133
X	X				X		X	X		148
		X				X			X	146
		X	X				X			139
				X					X	147

Rather than the narrowness of predicted categories, the description "specific" in a classification context usually refers to the ability of the test to discriminate negative results in a binary classification task (the proportion of predicted negatives that are true-negatives). Specificity is the converse of sensitivity, which is a measure of the proportion of positive results correctly identified—in this case, the proportion of drugs predicted to belong to a therapeutic class that actually belong to that class. In a high-specificity classifier, misclassifications can be more confidently predicted as potential candidates for repurposing. The balance between sensitivity and specificity is given by the "area under the receiver operating curve" (AUC), which plots the true-positive rate against the false-positive rate and is used to measure classifier performance in the following studies.

Recent integrated approaches have included information about disease as well as drug information. One of the first studies to include both of these domains was the PREDICT system developed by Gottlieb et al.,[133] which extended the "guilt-by-association" concept of association transfer. PREDICT works from the assumption that drug–disease associations can be "transferred" between sufficiently similar diseases and drugs. The measures used for drug similarity include chemical structure, drug side effects, and various measures of similarity of their protein targets (similarity of genetic sequence, closeness in a PPI network, and semantic similarity of gene targets). Two different types of disease similarity measures were included: phenotypic, using medical terms from MeSH and HPO, and gene signature-based, using gene expression signatures from GEO and similarity of disease-related genes (as for protein target similarity in the preceding text). Known disease–drug associations allow a classifier to learn the relative contribution of each drug–drug and disease–disease similarity measure to the strength of the drug–disease association; the classifier then balances information from each similarity measure in order to predict new associations. The PREDICT system is particularly notable for its high predictive ability, achieving an AUC of 0.9 in predicting known drug indications using the phenotypic disease similarity measure (rising to 0.93 using the signature-based method) and finding significant overlap of predictions with drugs being tested in clinical trials. Examples of predictions supported by previous studies include the immunosuppressive azathioprine for treatment of the inflammatory disorder familial Mediterranean fever and the use of the dopamine receptor agonist cabergoline to improve migraine symptoms. The authors suggest that their gene signature-based measures of similarity, where a disease is represented purely by its gene expression profile, could be also used for personalized medicine applications.

Also making use of similarity information, the PreDR method[139] integrated drug–drug and disease–disease similarity, using "structure, activity, and phenotype data" (chemical similarity, protein target sequence similarity, and side effects data) for drug similarity and using phenotype data from OMIM for disease similarity. Each type of drug data was found to be predictive individually (with AUC of 0.83, 0.89, and 0.89, respectively); however, data fusion (integrating the three data types) was shown to improve the prediction of drug–disease associations, achieving an AUC of 0.9 and an overall accuracy of 0.82. This seems intuitively clear, but in machine learning, more information does not always lead to better performance: for example, the features may not be fully independent of one another, which can be the case when integrating different biological or pharmacological measurements of the same event. For example, chemical structure affects drug–target interaction, and phenotypically similar diseases share related disease genes, and this relationship between features could potentially affect classification performance.

Whereas these approaches aimed to infer disease–drug associations from measures of disease and drug similarity, more recent approaches have integrated drug–disease associations as another feature from which to infer novel associations (see **Table 10**). The heterogeneous network model developed by Wang et al.[134] represents diseases, drugs, and targets as nodes in a "three-layer graph." Each layer of the graph is constructed from associations between diseases, drugs, and targets (measured by phenotypic, chemical structure, and target sequence similarity, respectively), and connections between the layers are constructed from disease–drug and drug–target interactions from DrugBank. The strength of association between a disease and a drug is computed by an "iterative updating" algorithm, in which the association strengths depend on the other associations in the network. As with PreDR, the authors were interested in the contribution of each data type to the overall accuracy of the method, in this case examining the contribution of target nodes to their initial drug–disease network. Drug target information was found to improve the performance of the network (AUC 0.92 for the target information compared with 0.84 for the drug–disease-only network). The method was able to make predictions even for diseases with few currently available treatments: for non-small-cell lung cancer, which has only one currently known drug treatment, the top three predictions (cisplatin, carboplatin, and temozolomide) were all supported by previous studies.

Through the integration of different types of data, these approaches have aimed to minimize the drawbacks of each individual type. As the data integration approach has grown in popularity, several databases have been developed to aid integrated drug repurposing by collating data from different sources, including PROMISCUOUS[188] and PharmDB.[189] As well as being a function of the explosion of -omics and cheminformatics data resources in recent years, this is part of a general trend toward data fusion approaches in informatics. By combining data on both the biological (gene expression, pathway disruption, and side effects) and chemical (drug structure and target binding) aspects of drug action, we can reach a more holistic view of a drug's effect. The methods covered here have not yet explored all of the potential sources of information on drug effect. Other spaces that could be exploited for drug repurposing could include, for instance, the metabolome: indeed, metabolic networks have been used in a systems biology approach to model the systemic perturbations caused by a drug in order to predict its off-targets.[190] As mentioned earlier, when combining multiple data sources, the contribution of each individual source must be assessed for its contribution to the performance of the method. The utility of different information sources for repurposing prediction tasks could even help to inform the way we think about drug design and lead optimization.

Table 10 Overview of drug repurposing candidates from selected integrated approaches

Selected candidates—target/indication	*Structure*	*Validation*	*References*
Azathioprine—familial Mediterranean fever	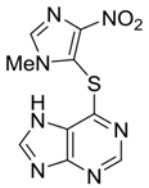	Literature support	133
Cabergoline—migraine	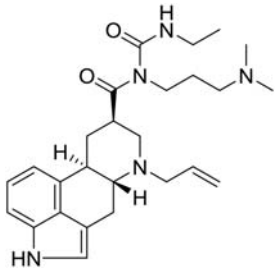	Literature support	133
Carboplatin—non-small-cell lung cancer	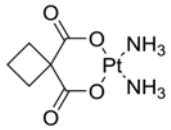	Literature support	134
Temozolomide—non-small-cell lung cancer	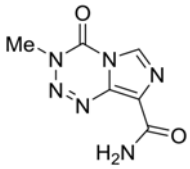	Literature support	134

1.02.6.8 Practical Considerations

Despite the range of different data types and different approaches used in computational drug repurposing, these methods all share common drawbacks that must be considered carefully before making the jump to large-scale experimental validation or thinking about clinical applications. These include the following:

- *Quality of input data*: All of the data sources discussed here suffer to some extent from the problems of missing, incomplete, inaccurate, or erroneous data, especially molecular biology data types (such as gene expression and proteomics data) that are particularly prone to noise and data sources that are generated from computational modeling or prediction (such as molecular docking or disease-related genes) that contain more potential for error. Further, there is a trade-off that must be made between data quality and the number of data points that can be used in a model. While it is generally true that filtering poor quality data will improve performance, overstringent filtering criteria (especially for particularly noise-prone data) may result in such a reduction in the number of available data points that it actually becomes detrimental to performance.
- *Broad versus focused approaches*: Many computational repurposing methods aim to be broad in scope—they aim to suggest drugs for a range of diseases from different disease areas. Although broad-ranging methods are more widely applicable and can be viewed as more challenging and therefore conceptually more interesting, it could also be argued that single-disease studies have more practical utility. More focused approaches (such as the diabetes,[145] schistosomiasis,[136] and RA[179] studies discussed earlier) benefit from increased clinical and commercial focus (see later) and therefore may be more amenable to clinical translation. Another approach is to develop the general method on a large scale and then refine it for specific diseases, such as the work of the Dudley group on "inverse signature" drug repurposing, which was demonstrated to work with a set of 100 diseases from GEO[142] and then used to predict candidate treatments for small-cell lung cancer[182] and inflammatory bowel disease.[183]
- *Experimental validation of hypotheses*: Where authors have experimentally evaluated their repurposing suggestions, this is a good proof of principle of their method, but it is clearly a big step to make between demonstrating a desired effect in in vitro tests and demonstrating efficacy in the clinic. Although repositioned drugs have a slight advantage over novel drugs in that their pharmacokinetic properties have already been determined, the new indication may require a different dosage or delivery method in order to be effective. A case in point is the discovery of the antipsychotic haloperidol as a highly selective inhibitor of HIV-1 and HIV-2 proteases via a molecular docking approach[167] (discussed in more detail earlier). Although haloperidol appeared to be an effective anti-HIV agent, the concentration required to function as an inhibitor was more than 1000 times than that normally given in its use as an antipsychotic, at which dosage it would be highly toxic. In this case, haloperidol was proposed as a useful

lead candidate for drug development; however, this shows the importance of experimental validation even for highly promising candidates.

- *Need for clinical and commercial awareness*: Although computational methods can suggest repurposing candidates, they cannot yet replace expert clinical knowledge. For example, the graph-based method developed by Gramatica et al.[55] suggested the peptide CNP (C-type natriuretic peptide) for treatment of sarcoidosis, even providing a biologically sound mechanism of action through which this treatment would work. However, CNP can in some cases act as a vasodilator and thus could not be considered as a treatment option for sarcoidosis due to its potential to cause serious adverse effects. Similarly, although a repurposing candidate may be biologically plausible and supported by experimental validation, there are still commercial and economic factors to consider when assessing candidates, such as market size versus cost, competitors, and intellectual property issues[20] as discussed earlier in this article.

Data mining approaches to drug repurposing use biological, chemical, pharmacological, and clinical data to reveal new associations between drugs and disease. Benefiting from recent advances in computational data science, including machine learning, natural language understanding, and big data processing, as well as the expansion of large biochemical databases holding diverse drug and disease data types, computational methods can form a valuable first step in drug repurposing efforts. While computational repurposing must always be complemented by experimental validation and human expertise, its strength lies in its ability to take data and, through application of computational analysis, create valuable information that can lead to new repurposing hypotheses. Of course, the value of this information depends on the translation of computational predictions to clinical reality.

1.02.7 Beyond Repurposing: Tailoring an Existing Drug for a New Use

Drug repurposing starts from a compound that has progressed into development; thus, it has been optimized for the original indication for which it was intended; however, in the new indication, the drug is not necessarily optimized. This is certainly the case if the repurposing involves a new target (off-target repurposing), since the basic medicinal chemical optimization will not have been done for this situation. It will also arise when the new indication involves polypharmacological activities, since in this situation also, the balance of pharmacological activities will probably not be right for the new indication. Additionally, the structure–activity relationships that pertained to the original indication may not pertain to the new indication. But even when the target is the same, the pharmacokinetic parameters that were optimized for the original indication may not be right for the new indication. For instance, if the new use requires CNS penetration, whereas the original use was peripheral in basis, there may be a good reason to change the molecule to better suit it for CNS distribution.

In circumstances such as these, and others, a certain amount of structural variation may be required to identify the ideal drug for the new indication. Hybrid projects involving a new use and a new molecule may reduce some of the salient advantages of drug repurposing. Clearly, even with a small chemical change, the opportunity to avert the entire preclinical development stage of the R&D process is lost. In addition, there is a certain amount of drug design and medicinal chemistry optimization to be performed. Set against these disadvantages, the repurposing component has allowed a reduced requirement for discovery chemistry while simultaneously granting a greater degree of novelty in the product by virtue of its twin differentiating characteristics (i.e., both a new molecule and a new indication).[2] The most advantageous strategic balance to be struck between a certain amount of molecular optimization and the alternative product development based entirely on the preexisting molecule for a new use will vary on a case-by-case basis. Additional factors that may influence that choice include the need for reformulation for development in the new use; for instance, in repurposing an oral product for an inhaled use, a substantial formulation and bridging toxicology package will need to be put in place. Repurposing in such cases involves a significant amount of preclinical development.

In Table 11, we see various examples of this strategy. In most of these cases, the new drug derived from a project that originated with the discovery of a new use for the parent drug. For example, gabapentin was originally developed for epilepsy, but after its approval, it became clear that the drug was useful in neuropathic pain. Initially, Pfizer tried to promote it for the secondary use without obtaining regulatory approval, but after significant fines were levied by the FDA for off-label promotion, the company developed a new, but closely related, product (pregabalin) for neuropathic pain. In the case of thalidomide, this is approved for the treatment of leprosy and multiple myeloma, whereas its structural variant lenalidomide is approved for the treatment of multiple myeloma and myelodysplastic syndromes; in addition, it is suggested to have a better side effect profile.

The case of raloxifene, a selective estrogen receptor modulator, is interesting: the story originated with tamoxifen, a drug for the treatment of breast cancer. The initial idea was to find a related drug that would treat breast cancer in patients resistant to tamoxifen. However, early trials were unsuccessful, and Lilly changed tack, choosing instead to develop raloxifene for osteoporosis. Once this tamoxifen analog was on the market, it became clear from retrospective studies that raloxifene did in fact prevent the reoccurrence of malignancy in women with breast cancer; it was later approved for this condition too. Thus, the project had come full circle, from abandonment in the cure of breast cancer to use in its prevention.[26] Finally, one of the most remarkable drug repurposing examples involves the use of prostanoid FP receptor agonists for eyelash lengthening and thickening. Originally, the drug latanoprost was developed as an ophthalmic solution for the treatment of glaucoma, but it was noticed to act as an eyelash growth stimulator, as a side effect, in patients. Rather than develop latanoprost itself for this new indication, Allergan chose to develop the analog bimatoprost to increase the length, thickness, and darkness of eyelashes, and the product Latisse™ was ultimately approved as a cosmetic rather than a pharmaceutical.

Table 11 Examples of new drugs for a secondary use closely related to parents that work for a primary use

Original drug	*Original indication*	*Structure*	*New drug*	*New indication*	*Structure*
Gabapentin	Epilepsy	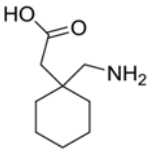	Pregabalin	Neuropathic pain	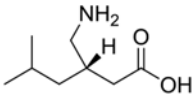
			Gabapentin enacarbil	Restless leg syndrome	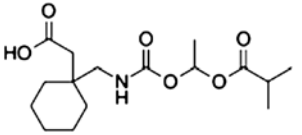
Thalidomide	Leprosy, multiple myeloma	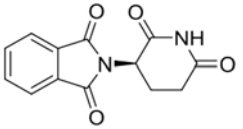	Lenalidomide	Myelodysplastic syndromes	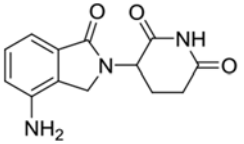
Flupirtine	Epilepsy	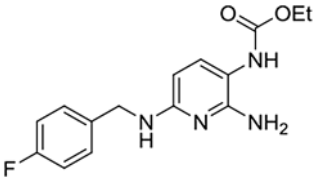	Ezogabine	Neuropathic pain	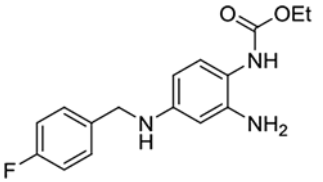
Leflunomide	Rheumatoid arthritis	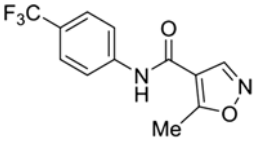	Teriflunomide (metabolite of leflunomide)	Multiple sclerosis	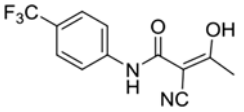
Tamoxifen	Breast cancer	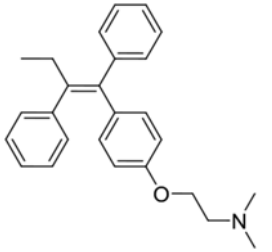	Raloxifene	Osteoporosis	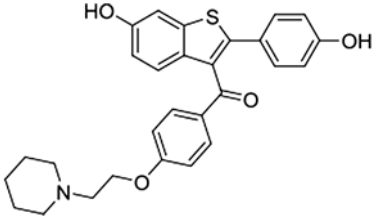
Latanoprost	Glaucoma	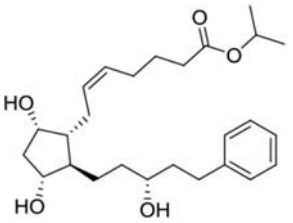	Bimatoprost	To increase the length, thickness, and darkness of eyelashes	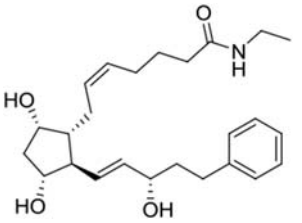

1.02.8 Conclusion

The use of previously discovered drugs for new indications has the potential to revolutionize modern medicine. By exploiting existing pharmacological space, drug repurposing can significantly decrease risk, time, and cost compared with what is possible in de novo drug development. Although drug repurposing has existed in some form for as long as humans have practiced medicine, in recent years, efforts to systematize the traditionally serendipitous route to drug repurposing have led to the development of methods to identify potential drug repurposing candidates at the preclinical stage. These developments have benefited from advances in experimental and computational science, as well as from efforts toward increased sharing and open accessibility of data and pharmacological knowledge. As well as the potential productivity gains for a pharmaceutical industry that is often acknowledged to be undergoing a decline in R&D output, repurposing offers an avenue for the development of drugs for rare and orphan diseases that would otherwise be neglected due to economic factors.

References

1. DeMonaco, H. J.; Ali, A.; von Hippel, E. The Major Role of Clinicians in the Discovery of Off-Label Drug Therapies. *Pharmacother. J. Hum. Pharmacol. Drug Ther.* **2006,** *26,* 323–332.
2. Cavalla, D. APT Drug R&D: The Right Active Ingredient in the Right Presentation for the Right Therapeutic Use. *Nat. Rev. Drug Discov.* **2009,** *8,* 849–853.
3. Mucke, H. A. M. A New Journal for the Drug Repurposing Community. *Drug Repurposing, Rescue, Repositioning* **2014,** *1,* 3–4.
4. Vane, J. R. Inhibition of Prostaglandin Synthesis as a Mechanism of Action for Aspirin-Like Drugs. *Nat. New Biol.* **1971,** *231,* 232–235.
5. Rothwell, P. M.; Fowkes, F. G. R; Belch, J. F.; Ogawa, H.; Warlow, C. P.; Meade, T. W. Effect of Daily Aspirin on Long-Term Risk of Death Due to Cancer: Analysis of Individual Patient Data from Randomised Trials. *Lancet* **2011,** *377,* 31–41.
6. 2014 505(b)(2) NDA Approvals The 505(b)(2) Blog. http://camargopharma.com/2015/01/2014-505b2-nda-approvals/ (accessed 20 July 2016).
7. Graul, A. I.; Cruces, E.; Stringer, M. The Year's New Drugs & Biologics, 2013: Part I. *Drugs Today (Barc.)* **2014,** *50,* 51–100.
8. Naylor, S.; Kauppi, D. M.; Schonfeld, J. M. Therapeutic Drug Repurposing, Repositioning and Rescue Part II: Business Review. Spring 15. *Drug Discov. World* **2015**, *16,* 57–62.
9. Tobinick, E. L. The Value of Drug Repositioning in the Current Pharmaceutical Market. *Drug News Perspect.* **2009,** *22,* 119–125.
10. Paul, S. M.; Mytelka, D. S.; Dunwiddie, C. T.; Persinger, C. C.; Munos, B. H.; Lindborg, S. R.; Schacht, A. L. How to Improve R&D Productivity: The Pharmaceutical Industry's Grand Challenge. *Nat. Rev. Drug Discov.* **2010,** *9,* 203–214.
11. David, E.; Tramontin, T.; Zemmel, R. Pharmaceutical R&D: The Road to Positive Returns. *Nat. Rev. Drug Discov.* **2009,** *8,* 609–610.
12. DiMasi, J. A.; Grabowski, H. G. The Cost of Biopharmaceutical R&D: Is Biotech Different? *Manage. Decis. Econ.* **2007,** *28,* 469–479.
13. Thayer, A. Drug Repurposing. *Chem. Eng. News* **2012,** *90* (40).
14. Oprea, T. I.; Mestres, J. Drug Repurposing: Far Beyond New Targets for Old Drugs. *AAPS J.* **2012,** *14,* 759–763.
15. Naylor, S.; Kauppi, D. M.; Schonfeld, J. M. Therapeutic Drug Repurposing, Repositioning and Rescue Part III Market Exclusivity Using Intellectual Property and Regulatory Pathways. *Drug Discov. World* **2015**, *16,* 62–69.
16. Ashburn, T. T.; Thor, K. B. Drug Repositioning: Identifying and Developing New Uses for Existing Drugs. *Nat. Rev. Drug Discov.* **2004,** *3,* 673–683.
17. Li, J.; Zheng, S.; Chen, B.; Butte, A. J.; Swamidass, S. J.; Lu, Z. A Survey of Current Trends in Computational Drug Repositioning. *Brief. Bioinform.* **2015,** *17* (1), 2–12.
18. DiMasi, J. A. Innovating by Developing New Uses of Already-Approved Drugs: Trends in the Marketing Approval of Supplemental Indications. *Clin. Ther.* **2013,** *35,* 808–818.
19. Sildenafil. *Wikipedia, Free Encycl.* (2015, September). https://en.wikipedia.org/wiki/Sildenafil (accessed 18 March 2016).
20. Rastegar-Mojarad, M.; Ye, Z.; Kolesar, J. M.; Hebbring, S. J.; Lin, S. M. Opportunities for Drug Repositioning from Phenome-Wide Association Studies. *Nat. Biotechnol.* **2015,** *33,* 342–345.
21. Pantziarka, P.; Bouche, G.; Meheus, L.; Sukhatme, V.; Sukhatme, V. P.; Vikas, P. The Repurposing Drugs in Oncology (ReDO) Project. *Ecancermedicalscience* **2014,** *8,* 442.
22. Cavalla, D. *Off-Label Prescribing: Justifying Unapproved Medicine;* Wiley-Blackwell: London, 2015.
23. Eguale, T.; Buckeridge, D. L.; Winslade, N. E.; Benedetti, A.; Hanley, J. A.; Tamblyn, R. Drug, Patient, and Physician Characteristics Associated with Off-Label Prescribing in Primary Care. *Arch. Intern. Med.* **2012,** *172,* 781–788.
24. Radley, D. C.; Finkelstein, S. N.; Stafford, R. S. Off-Label Prescribing Among Office-Based Physicians. *Arch. Intern. Med.* **2006,** *166,* 1021–1026.
25. Banerjee, S. *The Use of Antipsychotic Medication for People with Dementia: Time for Action;* Department of Health: London, 2009, 7.
26. Yank, V.; Tuohy, C. V.; Logan, A. C.; Bravata, D. M.; Staudenmayer, K.; Eisenhut, R.; Sundaram, V.; McMahon, D.; Olkin, I.; McDonald, K. M.; Owens, D. K.; Stafford, R. S. Systematic Review: Benefits and Harms of In-Hospital Use of Recombinant Factor VIIa for Off-Label Indications. *Ann. Intern. Med.* **2011,** *154,* 529–540.
27. Mesgarpour, B.; Heidinger, B. H.; Schwameis, M.; Kienbacher, C.; Walsh, C.; Schmitz, S.; Herkner, H. Safety of Off-Label Erythropoiesis Stimulating Agents in Critically Ill Patients: A Meta-Analysis. *Intensive Care Med.* **2013,** *39,* 1896–1908.
28. Summary of NDA Approvals & Receipts, 1938 to the Present. WebContent. http://www.fda.gov/aboutfda/whatwedo/history/productregulation/summaryofndaapprovalsreceipts1938tothepresent/default.htm (accessed 18 March 2016).
29. Tartaglia, L. A. Complementary New Approaches Enable Repositioning of Failed Drug Candidates. *Expert Opin. Investig. Drugs* **2006,** *15,* 1295–1298.
30. Li, Y. Y.; Jones, S. J. Drug Repositioning for Personalized Medicine. *Genome Med.* **2012,** *4,* 27.
31. Roche, Broad Institute Seek New Uses for Old Drugs | GEN News Highlights (2012). http://www.genengnews.com/gen-news-highlights/roche-broad-institute-seek-new-uses-for-old-drugs/81247689/ (accessed 18 March 2016).
32. Colvis, C. M.; Austin, C. P. The NIH-Industry New Therapeutic Uses Pilot Program: Demonstrating the Power of Crowdsourcing. *Assay Drug Dev. Technol.* **2015,** *13,* 297–298.
33. Skorupskaite, K.; George, J.; Anderson, R. A. Role of a Neurokinin B Receptor Antagonist in the Regulation of Ovarian Function in Healthy Women. *Lancet (London, England)* **2015,** *385* (Suppl.), S92.
34. Pfizer Announce Groundbreaking Research Collaboration. FirstWordPharma. Washington University. http://www.firstwordpharma.com/node/648995 (accessed 18 Mar 2016).
35. AstraZeneca — AstraZeneca Announces "Open Innovation" Research Collaboration with Taiwan's Research Program for Biopharmaceuticals. FirstWordPharma. http://www.firstwordpharma.com/node/1147366 (accessed 18 March 2016).
36. Li, Y. Y.; Jones, S. J. Drug Repositioning for Personalized Medicine. *Genome Med.* **2012,** *4,* 27.
37. Chopra, I.; Roberts, M. Tetracycline Antibiotics: Mode of Action, Applications, Molecular Biology, and Epidemiology of Bacterial Resistance. *Microbiol. Mol. Biol. Rev.* **2001,** *65,* 232–260.
38. Golub, L. M.; Sorsa, T.; Lee, H. M.; Ciancio, S.; Sorbi, D.; Ramamurthy, N. S.; Gruber, B.; Salo, T.; Konttinen, Y. T. Doxycycline Inhibits Neutrophil (PMN)-Type Matrix Metalloproteinases in Human Adult Periodontitis Gingiva. *J. Clin. Periodontol.* **1995,** *22,* 100–109.
39. Paolini, G. V.; Shapland, R. H. B; van Hoorn, W. P.; Mason, J. S.; Hopkins, A. L. Global Mapping of Pharmacological Space. *Nat. Biotechnol.* **2006,** *24,* 805–815.

40. Mestres, J.; Gregori-Puigjané, E.; Valverde, S.; Solé, R. V. The Topology of Drug-Target Interaction Networks: Implicit Dependence on Drug Properties and Target Families. *Mol. Biosyst.* **2009,** *5,* 1051–1057.
41. Manning, G.; Whyte, D. B.; Martinez, R.; Hunter, T.; Sudarsanam, S. The Protein Kinase Complement of the Human Genome. *Science* **2002,** *298,* 1912–1934.
42. Lasota, J.; Miettinen, M. KIT and PDGFRA Mutations in Gastrointestinal Stromal Tumors (GISTs). *Semin. Diagn. Pathol.* **2006,** *23,* 91–102.
43. RARE Diseases: Facts and Statistics. *Glob. Genes.* http://globalgenes.org/rare-diseases-facts-statistics/ (accessed 23 Sep 2015).
44. Sardana, D.; Zhu, C.; Zhang, M.; Gudivada, R. C.; Yang, L.; Jegga, A. G. Drug Repositioning for Orphan Diseases. *Brief. Bioinform.* **2011,** *12,* 346–356.
45. Xu, K.; Coté, T. R. Database Identifies FDA-Approved Drugs with Potential to Be Repurposed for Treatment of Orphan Diseases. *Brief. Bioinform.* **2011,** *12,* 341–345.
46. Carnero, A. High Throughput Screening in Drug Discovery. *Clin. Transl. Oncol.* **2006,** *8,* 482–490.
47. Brehmer, D.; Greff, Z.; Godl, K.; Blencke, S.; Kurtenbach, A.; Weber, M.; Müller, S.; Klebl, B.; Cotten, M.; Kéri, G.; Wissing, J.; Daub, H. Cellular Targets of Gefitinib. *Cancer Res.* **2005,** *65,* 379–382.
48. Cho, Y.; Vermeire, J. J.; Merkel, J. S.; Leng, L.; Du, X.; Bucala, R.; Cappello, M.; Lolis, E. Drug Repositioning and Pharmacophore Identification in the Discovery of Hookworm MIF Inhibitors. *Chem. Biol.* **2011,** *18,* 1089–1101.
49. Reaume, A. G. Drug Repurposing Through Nonhypothesis Driven Phenotypic Screening. *Drug Discov. Today Ther. Strateg.* **2011,** *8,* 85–88.
50. Zheng, W.; Thorne, N.; McKew, J. C. Phenotypic Screens as a Renewed Approach for Drug Discovery. *Drug Discov. Today* **2013,** *18,* 1067–1073.
51. Gibson, C. C.; Zhu, W.; Davis, C. T.; Bowman-Kirigin, J. A.; Chan, A. C.; Ling, J.; Walker, A. E.; Goitre, L.; Monache, S. D.; Retta, S. F.; Shiu, Y.-T. E.; Grossmann, A. H.; Thomas, K. R.; Donato, A. J.; Lesniewski, L. A.; Whitehead, K. J.; Li, D. Y. Strategy for Identifying Repurposed Drugs for the Treatment of Cerebral Cavernous Malformation. *Circulation* **2014,** *131* (3), 289–299.
52. Kotz, J. Phenotypic Screening, Take Two. *Sci. Bus. Exch.* **2012,** *5,* 1–3.
53. Cousin, M. A.; Ebbert, J. O.; Wiinamaki, A. R.; Urban, M. D.; Argue, D. P.; Ekker, S. C.; Klee, E. W. Larval Zebrafish Model for FDA-Approved Drug Repositioning for Tobacco Dependence Treatment. *PLoS One* **2014,** *9,* e90467.
54. Swinney, D. C.; Anthony, J. How Were New Medicines Discovered? *Nat. Rev. Drug Discov.* **2011,** *10,* 507–519.
55. Gramatica, R.; Di Matteo, T.; Giorgetti, S.; Barbiani, M.; Bevec, D.; Aste, T. Graph Theory Enables Drug Repurposing – How a Mathematical Model Can Drive the Discovery of Hidden Mechanisms of Action. *PLoS One* **2014,** *9,* 1–10.
56. Deftereos, S. N.; Andronis, C.; Friedla, E. J.; Persidis, A.; Persidis, A. Drug Repurposing and Adverse Event Prediction Using High-Throughput Literature Analysis. *Wiley Interdiscip. Rev. Syst. Biol. Med.* **2011,** *3,* 323–334.
57. Weeber, M.; Klein, H.; de Jong-van den Berg, L. T. W; Vos, R. Using Concepts in Literature-Based Discovery: Simulating Swanson's Raynaud–Fish Oil and Migraine–Magnesium Discoveries. *J. Am. Soc. Inf. Sci. Technol.* **2001,** *52,* 548–557.
58. Yetisgen-Yildiz, M.; Pratt, W. Using Statistical and Knowledge-Based Approaches for Literature-Based Discovery. *J. Biomed. Inform.* **2006,** *39,* 600–611.
59. Xu, R.; Li, L.; Wang, Q. Towards Building a Disease-Phenotype Knowledge Base: Extracting Disease-Manifestation Relationship from Literature. *Bioinformatics* **2013,** *29,* 2186–2194.
60. Chen, B.; Ding, Y.; Wild, D. J. Improving Integrative Searching of Systems Chemical Biology Data Using Semantic Annotation. *J. Cheminform.* **2012,** *4,* 6.
61. Chen, B.; Ding, Y.; Wild, D. J. Assessing Drug Target Association Using Semantic Linked Data. *PLoS Comput. Biol.* **2012,** *8.*
62. Qu, X. A.; Gudivada, R. C.; Jegga, A. G.; Neumann, E. K.; Aronow, B. J. Inferring Novel Disease Indications for Known Drugs by Semantically Linking Drug Action and Disease Mechanism Relationships. *BMC Bioinform.* **2009,** *10,* S4.
63. Hurle, M. R.; Yang, L.; Xie, Q.; Rajpal, D. K.; Sanseau, P.; Agarwal, P. Computational Drug Repositioning: From Data to Therapeutics. *Clin. Pharmacol. Ther.* **2013,** *93,* 335–341.
64. Raser, J. M.; O'Shea, E. K. Noise in Gene Expression: Origins, Consequences, and Control. *Science* **2005,** *309,* 2010–2013.
65. Kimmel, S. E.; Schelleman, H.; Berlin, J. A.; Oslin, D. W.; Weinstein, R. B.; Kinman, J. L.; Sauer, W. H.; Lewis, J. D. The Effect of Selective Serotonin Re-uptake Inhibitors on the Risk of Myocardial Infarction in a Cohort of Patients with Depression. *Br. J. Clin. Pharmacol.* **2011,** *72,* 514–517.
66. Wagner, G.; Icks, A.; Abholz, H.-H.; Schröder-Bernhardi, D.; Rathmann, W.; Kostev, K. Antihypertensive Treatment and Risk of Dementia: A Retrospective Database Study. *Int. J. Clin. Pharmacol. Ther.* **2012,** *50,* 195–201.
67. Anker, S. D.; Negassa, A.; Coats, A. J. S; Afzal, R.; Poole-Wilson, P. A.; Cohn, J. N.; Yusuf, S. Prognostic Importance of Weight Loss in Chronic Heart Failure and the Effect of Treatment with Angiotensin-Converting-Enzyme Inhibitors: An Observational Study. *Lancet* **2003,** *361,* 1077–1083.
68. Gage, J. R.; Fonarow, G.; Hamilton, M.; Widawski, M.; Martínez-Maza, O.; Vredevoe, D. L. Beta Blocker and Angiotensin-Converting Enzyme Inhibitor Therapy Is Associated with Decreased Th1/Th2 Cytokine Ratios and Inflammatory Cytokine Production in Patients with Chronic Heart Failure. *Neuroimmunomodulation* **2004,** *11,* 173–180.
69. Hardan, A. Y.; Handen, B. L. A Retrospective Open Trial of Adjunctive Donepezil in Children and Adolescents with Autistic Disorder. *J. Child Adolesc. Psychopharmacol.* **2002,** *12,* 237–241.
70. Hajjar, I.; Brown, L.; Mack, W. J.; Chui, H. Impact of Angiotensin Receptor Blockers on Alzheimer's Disease Neuropathology in a Large Brain Autopsy Series. *Arch. Neurol.* **2012,** *69,* 1632–1638.
71. Cole, S. W.; Sood, A. K. Molecular Pathways: Beta-Adrenergic Signaling in Cancer. *Clin. Cancer Res.* **2012,** *18,* 1201–1206.
72. Powe, D. G.; Voss, M. J.; Zänker, K. S.; Habashy, H. O.; Green, A. R.; Ellis, I. O.; Entschladen, F. Beta-Blocker Drug Therapy Reduces Secondary Cancer Formation in Breast Cancer and Improves Cancer Specific Survival. *Oncotarget* **2010,** *1,* 628–638.
73. Nkontchou, G.; Aout, M.; Mahmoudi, A.; Roulot, D.; Bourcier, V.; Grando-Lemaire, V.; Ganne-Carrie, N.; Trinchet, J.-C.; Vicaut, E.; Beaugrand, M. Effect of Long-Term Propranolol Treatment on Hepatocellular Carcinoma Incidence in Patients with HCV-Associated Cirrhosis. *Cancer Prev. Res.* **2012,** *5,* 1007–1014.
74. Lin, C.-S.; Lin, W.-S.; Lin, C.-L.; Kao, C.-H. Carvedilol Use Is Associated with Reduced Cancer Risk: A Nationwide Population-Based Cohort Study. *Int. J. Cardiol.* **2015,** *184,* 9–13.
75. Watkins, J. L.; Thaker, P. H.; Nick, A. M.; Ramondetta, L. M.; Kumar, S.; Urbauer, D. L.; Matsuo, K.; Squires, K. C.; Coleman, R. L.; Lutgendorf, S. K.; Ramirez, P. T.; Sood, A. K. Clinical Impact of Selective and Nonselective Beta-Blockers on Survival in Patients with Ovarian Cancer. *Cancer* **2015,** *121,* 3444–3451.
76. Kaapu, K. J.; Ahti, J.; Tammela, T. L. J; Auvinen, A.; Murtola, T. J. Sotalol, But Not Digoxin Is Associated with Decreased Prostate Cancer Risk: A Population-Based Case-Control Study. *Int. J. Cancer* **2015,** *137* (5), 1187–1195.
77. Lemeshow, S.; Sørensen, H. T.; Phillips, G.; Yang, E. V.; Antonsen, S.; Riis, A. H.; Lesinski, G. B.; Jackson, R.; Glaser, R. β-Blockers and Survival Among Danish Patients with Malignant Melanoma: A Population-Based Cohort Study. *Cancer Epidemiol. Biomarkers Prev.* **2011,** *20,* 2273–2279. A *Publ. Am. Assoc. Cancer Res.* cosponsored by *Am. Soc. Prev. Oncol.*
78. Bonnet, N.; Pierroz, D. D.; Ferrari, S. L. Adrenergic Control of Bone Remodeling and Its Implications for the Treatment of Osteoporosis. *J. Musculoskelet. Neuronal Interact.* **2008,** *8,* 94–104.
79. Yasar, S.; Xia, J.; Yao, W.; Furberg, C. D.; Xue, Q.-L.; Mercado, C. I.; Fitzpatrick, A. L.; Fried, L. P.; Kawas, C. H.; Sink, K. M.; Williamson, J. D.; DeKosky, S. T.; Carlson, M. C.; Investigators, F. the G. E. of M. (GEM) S. Antihypertensive Drugs Decrease Risk of Alzheimer Disease Ginkgo Evaluation of Memory Study. *Neurology* **2013,** *81,* 896–903.
80. Zacharski, L. R.; Moritz, T. E.; Haakenson, C. M.; O'Donnell, J. F.; Ballard, H. S.; Johnson, G. J.; Ringenberg, Q. S.; Schilsky, R. L.; Spaulding, M. B.; Tornyos, K. Chronic Calcium Antagonist Use in Carcinoma of the Lung and Colon: A Retrospective Cohort Observational Study. *Cancer Invest.* **1990,** *8,* 451–458.
81. Hur, G. Y.; Lee, S. Y.; Lee, S. H.; Kim, S. J.; Lee, K. J.; Jung, J. Y.; Lee, E. J.; Kang, E. H.; Jung, K. H.; Lee, S. Y.; Kim, J. H.; Shin, C.; Shim, J. J.; In, K. H.; Kang, K. H.; Yoo, S. H. Potential Use of an Anticancer Drug Gefinitib, an EGFR Inhibitor, on Allergic Airway Inflammation. *Exp. Mol. Med.* **2007,** *39,* 367–375.

82. Koh, G. C. K. W.; Maude, R. R.; Schreiber, M. F.; Limmathurotsakul, D.; Wiersinga, W. J.; Wuthiekanun, V.; Lee, S. J.; Mahavanakul, W.; Chaowagul, W.; Chierakul, W.; White, N. J.; van der Poll, T.; Day, N. P. J.; Dougan, G.; Peacock, S. J. Glyburide Is Anti-inflammatory and Associated with Reduced Mortality in Melioidosis. *Clin. Infect. Dis.* **2011,** *52,* 717–725.
83. McGwin, G.; Owsley, C.; Curcio, C. A.; Crain, R. J. The Association Between Statin Use and Age Related Maculopathy. *Br. J. Ophthalmol.* **2003,** *87,* 1121–1125.
84. Caballero, J.; Nahata, M. Do Statins Slow Down Alzheimer's Disease? A Review. *J. Clin. Pharm. Ther.* **2004,** *29,* 209–213.
85. Huang, C.-C.; Chan, W.-L.; Chen, Y.-C.; Chen, T.-J.; Chou, K.-T.; Lin, S.-J.; Chen, J.-W.; Leu, H.-B. Statin Use in Patients with Asthma: A Nationwide Population-Based Study. *Eur. J. Clin. Invest.* **2011,** *41,* 507–512.
86. Donnino, M. W.; Cocchi, M. N.; Howell, M.; Clardy, P.; Talmor, D.; Cataldo, L.; Chase, M.; Al-Marshad, A.; Ngo, L.; Shapiro, N. I. Statin Therapy Is Associated with Decreased Mortality in Patients with Infection. *Acad. Emerg. Med.* **2009,** *16,* 230–234.
87. Fogerty, M. D.; Efron, D.; Morandi, A.; Guy, J. S.; Abumrad, N. N.; Barbul, A. Effect of Preinjury Statin Use on Mortality and Septic Shock in Elderly Burn Patients. *J. Trauma* **2010,** *69,* 99–103.
88. Hippisley-Cox, J.; Coupland, C. Unintended Effects of Statins in Men and Women in England and Wales: Population Based Cohort Study Using the QResearch Database. *BMJ* **2010,** *340,* c2197.
89. Tsan, Y.-T.; Lee, C.-H.; Ho, W.-C.; Lin, M.-H.; Wang, J.-D.; Chen, P.-C. Statins and the Risk of Hepatocellular Carcinoma in Patients with Hepatitis C Virus Infection. *J. Clin. Oncol. Off. J. Am. Soc. Clin. Oncol.* **2013,** *31,* 1514–1521.
90. Marcella, S. W.; David, A.; Ohman-Strickland, P. A.; Carson, J.; Rhoads, G. G. Statin Use and Fatal Prostate Cancer. *Cancer* **2012,** *118,* 4046–4052.
91. Fong, D. S.; Poon, K.-Y. T. Recent Statin Use and Cataract Surgery. *Am. J. Ophthalmol.* **2012,** *153. 222–228.e1.*
92. Mortensen, E. M.; Copeland, L. A.; Pugh, M. J. V; Restrepo, M. I.; de Molina, R. M.; Nakashima, B.; Anzueto, A. Impact of Statins and ACE Inhibitors on Mortality After COPD Exacerbations. *Respir. Res.* **2009,** *10,* 45.
93. Otte, C.; Zhao, S.; Whooley, M. A. Statin Use and Risk of Depression in Patients with Coronary Heart Disease: Longitudinal Data from the Heart and Soul Study. *J. Clin. Psychiatry* **2012,** *73,* 610–615.
94. Etminan, M.; Samii, A.; Brophy, J. M. Statin Use and Risk of Epilepsy. *Neurology* **2010,** *75,* 1496–1500.
95. Leung, D. Y. L.; Li, F. C. H.; Kwong, Y. Y. Y.; Tham, C. C. Y.; Chi, S. C. C.; Lam, D. S. C. Simvastatin and Disease Stabilization in Normal Tension Glaucoma: A Cohort Study. *Ophthalmology* **2010,** *117,* 471–476.
96. Frost, F. J.; Petersen, H.; Tollestrup, K.; Skipper, B. Influenza and COPD Mortality Protection as Pleiotropic, Dose-Dependent Effects of Statins. *Chest* **2007,** *131,* 1006–1012.
97. Scranton, R. E.; Young, M.; Lawler, E.; Solomon, D.; Gagnon, D.; Gaziano, J. M. Statin Use and Fracture Risk: Study of a US Veterans Population. *Arch. Intern. Med.* **2005,** *165,* 2007–2012.
98. Cunha-Cruz, J.; Saver, B.; Maupome, G.; Hujoel, P. P. Statin Use and Tooth Loss in Chronic Periodontitis Patients. *J. Periodontol.* **2006,** *77,* 1061–1066.
99. Vinogradova, Y.; Coupland, C.; Hippisley-Cox, J. Risk of Pneumonia in Patients Taking Statins: Population-Based Nested Case-Control Study. *Br. J. Gen. Pract.* **2011,** *61,* e742–e748.
100. Chodick, G.; Amital, H.; Shalem, Y.; Kokia, E.; Heymann, A. D.; Porath, A.; Shalev, V. Persistence with Statins and Onset of Rheumatoid Arthritis: A Population-Based Cohort Study. *PLoS Med.* **2010,** *7,* e1000336.
101. Gupta, R.; Plantinga, L. C.; Fink, N. E.; Melamed, M. L.; Coresh, J.; Fox, C. S.; Levin, N. W.; Powe, N. R. Statin Use and Sepsis Events [Corrected] in Patients with Chronic Kidney Disease. *J. Am. Med. Assoc.* **2007,** *297,* 1455–1464.
102. Li, Y.; Gottlieb, J.; Ma, D.; Kuehn, C.; Strueber, M.; Welte, T.; Simon, A. R.; Warnecke, G.; Haverich, A. Graft-Protective Effects of the HMG-CoA Reductase Inhibitor Pravastatin After Lung Transplantation—A Propensity Score Analysis with 23 Years of Follow-up. *Transplantation* **2011,** *92,* 486–492.
103. Wasko, M. M.; Hubert, H. B.; Lingala, V.; et al. Hydroxychloroquine and Risk of Diabetes in Patients with Rheumatoid Arthritis. *JAMA* **2007,** *298,* 187–193.
104. Chen, H.; Jacobs, E.; Schwarzschild, M. A.; McCullough, M. L.; Calle, E. E.; Thun, M. J.; Ascherio, A. Nonsteroidal Anti-inflammatory Drug Use and the Risk for Parkinson's Disease. *Ann. Neurol.* **2005,** *58,* 963–967.
105. Hsu, C.-C.; Wahlqvist, M. L.; Lee, M.-S.; Tsai, H.-N. Incidence of Dementia Is Increased in Type 2 Diabetes and Reduced by the Use of Sulfonylureas and Metformin. *J. Alzheimer's Dis.* **2011,** *24,* 485–493.
106. Rieken, M.; Xylinas, E.; Kluth, L.; Crivelli, J. J.; Chrystal, J.; Faison, T.; Lotan, Y.; Karakiewicz, P. I.; Fajkovic, H.; Babjuk, M.; Kautzky-Willer, A.; Bachmann, A.; Scherr, D. S.; Shariat, S. F. Association of Diabetes Mellitus and Metformin Use with Oncological Outcomes of Patients with Non-Muscle-Invasive Bladder Cancer. *BJU Int.* **2013,** *112,* 1105–1112.
107. Rieken, M.; Xylinas, E.; Kluth, L.; Crivelli, J. J.; Chrystal, J.; Faison, T.; Lotan, Y.; Karakiewicz, P. I.; Sun, M.; Fajkovic, H.; Babjuk, M.; Bachmann, A.; Scherr, D. S.; Shariat, S. F. Effect of Diabetes Mellitus and Metformin Use on Oncologic Outcomes of Patients Treated with Radical Cystectomy for Urothelial Carcinoma. *Urol. Oncol.* **2014,** *32. 49.e7–14.*
108. Tseng, C.-H. Diabetes, Metformin Use, and Colon Cancer: A Population-Based Cohort Study in Taiwan. *Eur. J. Endocrinol.* **2012,** *167,* 409–416.
109. Ko, E. M.; Walter, P.; Jackson, A.; Clark, L.; Franasiak, J.; Bolac, C.; Havrilesky, L. J.; Secord, A. A.; Moore, D. T.; Gehrig, P. A.; Bae-Jump, V. Metformin Is Associated with Improved Survival in Endometrial Cancer. *Gynecol. Oncol.* **2014,** *132,* 438–442.
110. Pollak, M.; Gonzalez-Angulo, A. M. Metformin and Hepatic Carcinogenesis. *Cancer Prev. Res. (Phila.)* **2012,** *5,* 500–502.
111. Lai, S.-W.; Liao, K.-F.; Chen, P.-C.; Tsai, P.-Y.; Hsieh, D. P. H; Chen, C.-C. Antidiabetes Drugs Correlate with Decreased Risk of Lung Cancer: A Population-Based Observation in Taiwan. *Clin. Lung Cancer* **2012,** *13,* 143–148.
112. Wang, Z.; Lai, S.-T.; Xie, L.; Zhao, J.-D.; Ma, N.-Y.; Zhu, J.; Ren, Z.-G.; Jiang, G.-L. Metformin Is Associated with Reduced Risk of Pancreatic Cancer in Patients with Type 2 Diabetes Mellitus: A Systematic Review and Meta-Analysis. *Diabetes Res. Clin. Pract.* **2014,** *106,* 19–26.
113. Yu, H.; Yin, L.; Jiang, X.; Sun, X.; Wu, J.; Tian, H.; Gao, X.; He, X. Effect of Metformin on Cancer Risk and Treatment Outcome of Prostate Cancer: A Meta-Analysis of Epidemiological Observational Studies. *PLoS One* **2014,** *9*, e116327.
114. Johnson, C. C.; Jankowski, M.; Rolnick, S.; Yood, M. U.; Alford, S. H. Influence of NSAID Use Among Colorectal Cancer Survivors on Cancer Outcomes. *Am. J. Clin. Oncol.* **2014**. Epub 2014 Dec 10.
115. Lip, S.; Carlin, C.; McCallum, L.; Touyz, R. H.; Dominiczak, A. F.; Padmanabhan, S. LB01.03: Incidence and Prognosis of Cancer Associated with Digoxin and Common Antihypertensive Drugs. *J. Hypertens.* **2015,** *33* (Suppl. 1), e45.
116. Platz, E. A.; Yegnasubramanian, S.; Liu, J. O.; Chong, C. R.; Shim, J. S.; Kenfield, S. A.; Stampfer, M. J.; Willett, W. C.; Giovannucci, E.; Nelson, W. G. A Novel Two-Stage, Transdisciplinary Study Identifies Digoxin as a Possible Drug for Prostate Cancer Treatment. *Cancer Discov.* **2011,** *1* (1), 68.
117. Chang, C.-H.; Lin, J.-W.; Wu, L.-C.; Lai, M.-S.; Chuang, L.-M.; Chan, K. A. Association of Thiazolidinediones with Liver Cancer and Colorectal Cancer in Type 2 Diabetes Mellitus. *Hepatology* **2012,** *55,* 1462–1472.
118. Brauchli, Y. B.; Jick, S. S.; Curtin, F.; Meier, C. R. Association Between Use of Thiazolidinediones or Other Oral Antidiabetics and Psoriasis: A Population Based Case-Control Study. *J. Am. Acad. Dermatol.* **2008,** *58,* 421–429.
119. Paul, M.; Gafter-Gvili, A.; Fraser, A.; Leibovici, L. The Anti-cancer Effects of Quinolone Antibiotics? *Eur. J. Clin. Microbiol. Infect. Dis.* **2007,** *26,* 825–831.
120. Melamed, M. L.; Blackwell, T.; Neugarten, J.; Arnsten, J. H.; Ensrud, K. E.; Ishani, A.; Cummings, S. R.; Silbiger, S. R. Raloxifene, a Selective Estrogen Receptor Modulator, Is Renoprotective: A Post-Hoc Analysis. *Kidney Int.* **2011,** *79,* 241–249.
121. Wu, C.-Y.; Chen, D.-Y.; Shen, J.-L.; Ho, H. J.; Chen, C.-C.; Kuo, K. N.; Liu, H.-N.; Chang, Y.-T.; Chen, Y.-J. The Risk of Cancer in Patients with Rheumatoid Arthritis Taking Tumor Necrosis Factor Antagonists: A Nationwide Cohort Study. *Arthritis Res. Ther.* **2014,** *16,* 449.

122. Gupta-Ganguli, M.; Cox, K.; Means, B.; Gerling, I.; Solomon, S. S. Does Therapy with Anti-TNF-α Improve Glucose Tolerance and Control in Patients with Type 2 Diabetes? *Diabetes Care* **2011,** *34,* e121.
123. Son, M. B.; Gauvreau, K.; Burns, J. C.; Corinaldesi, E.; Tremoulet, A. H.; Watson, V. E.; Baker, A.; Fulton, D. R.; Sundel, R. P.; Newburger, J. W. Infliximab for Intravenous Immunoglobulin Resistance in Kawasaki Disease: A Retrospective Study. *J. Pediatr.* **2011,** *158. 644–649.e1*.
124. Westlake, S. L.; Colebatch, A. N.; Baird, J.; Curzen, N.; Kiely, P.; Quinn, M.; Choy, E.; Ostor, A. J. K.; Edwards, C. J. Tumour Necrosis Factor Antagonists and the Risk of Cardiovascular Disease in Patients with Rheumatoid Arthritis: A Systematic Literature Review. *Rheumatology (Oxford)* **2011,** *50,* 518–531.
125. Walker, A. J.; Card, T.; Bates, T. E.; Muir, K. Tricyclic Antidepressants and the Incidence of Certain Cancers: A Study Using the GPRD. *Br. J. Cancer* **2011,** *104,* 193–197.
126. DeCensi, A.; Puntoni, M.; Guerrieri-Gonzaga, A.; Cazzaniga, M.; Serrano, D.; Lazzeroni, M.; Vingiani, A.; Gentilini, O.; Petrera, M.; Viale, G.; Cuzick, J.; Bonanni, B.; Pruneri, G. Effect of Metformin on Breast Ductal Carcinoma In Situ Proliferation in a Randomized Presurgical Trial. *Cancer Prev. Res. (Phila)* **2015,** *8* (10), 888–894.
127. National Heart, Lung, and Blood Institute ARDS Clinical Trials Network; Truwit, J. D.; Bernard, G. R.; Steingrub, J.; Matthay, M. A.; Liu, K. D.; Albertson, T. E.; Brower, R. G.; Shanholtz, C.; Rock, P.; Douglas, I. S.; deBoisblanc, B. P.; Hough, C. L.; Hite, R. D.; Thompson, B. T. Rosuvastatin for Sepsis-Associated Acute Respiratory Distress Syndrome. *N. Engl. J. Med.* **2014,** *370,* 2191–2200.
128. Lainscak, M.; Keber, I.; Anker, S. D. Body Composition Changes in Patients with Systolic Heart Failure Treated with Beta Blockers: A Pilot Study. *Int. J. Cardiol.* **2006,** *106,* 319–322.
129. Cavalla, D. Treatment of Cachexia. Patent EP2094254 B1, filed December 5, 2007, and issued June 22, 2011.
130. Pötsch, M.; Tschirner, A.; Palus, S.; Beadle, J.; Coats, A. J. S; Anker, S. D.; Springer, J. MT-102, a New "Anabolic Catabolic Transforming Agent", Improves Heart Function in a Rat Model of Cancer Cachexia. Abstracts of the 6th Cachexia Conference, Milan, Italy, December 8–10, 2011 (Part 2). *J. Cachexia Sarcopenia Muscle* **2012,** *3,* 51–68.
131. Beadle, J.; Coats, A.; Fuang, H.; Prabhash, K.; von Haehling, S.; Brown, R.; Anker, S. D. Survival and Quality of Life Data from the ACT ONE Randomised, Double-Blind, Placebo-Controlled, Phase II Study of Espindolol for the Treatment and Prevention of Cachexia in Patients with Stage III/IV Non-small Cell Lung Cancer or Colorectal Cancer. *Ann. Oncol.* **2014,** *25,* iv146–iv164.
132. Grover, M. P.; Ballouz, S.; Mohanasundaram, K. A.; George, R. A.; Sherman, C. D.; Crowley, T. M.; Wouters, M. A. Identification of Novel Therapeutics for Complex Diseases from Genome-Wide Association Data. *BMC Med. Genomics* **2014,** *7,* S8.
133. Gottlieb, A.; Stein, G. Y.; Ruppin, E.; Sharan, R. PREDICT: A Method for Inferring Novel Drug Indications with Application to Personalized Medicine. *Mol. Syst. Biol.* **2011,** *7,* 496.
134. Wang, W.; Yang, S.; Zhang, X.; Li, J. Drug Repositioning by Integrating Target Information Through a Heterogeneous Network Model. *Bioinformatics* **2014,** *30,* 1–8.
135. Liu, R.; Singh, N.; Tawa, G. J.; Wallqvist, A.; Reifman, J. Exploiting Large-Scale Drug-Protein Interaction Information for Computational Drug Repurposing. *BMC Bioinform.* **2014,** *15,* 210.
136. Neves, B. J.; Braga, R. C.; Bezerra, J. C. B; Cravo, P. V. L; Andrade, C. H. In Silico Repositioning-Chemogenomics Strategy Identifies New Drugs with Potential Activity Against Multiple Life Stages of Schistosoma mansoni. *PLoS Negl. Trop. Dis.* **2015,** *9*, e3435.
137. Yang, L.; Chen, J.; Shi, L.; Hudock, M. P.; Wang, K.; He, L. Identifying Unexpected Therapeutic Targets via Chemical-Protein Interactome. *PLoS One* **2010,** *5*, e9568.
138. Hoehndorf, R.; Schofield, P. N.; Gkoutos, G. V. PhenomeNET: A Whole-Phenome Approach to Disease Gene Discovery. *Nucleic Acids Res.* **2011,** *39*, e119.
139. Wang, Y.; Chen, S.; Deng, N.; Wang, Y. Drug Repositioning by Kernel-Based Integration of Molecular Structure, Molecular Activity, and Phenotype Data. *PLoS One* **2013,** *8*, e78518.
140. Shigemizu, D.; Hu, Z.; Hung, J. H.; Huang, C. L.; Wang, Y.; DeLisi, C. Using Functional Signatures to Identify Repositioned Drugs for Breast, Myelogenous Leukemia and Prostate Cancer. *PLoS Comput. Biol.* **2012,** *8,* 1–9.
141. Dudley, J. T.; Deshpande, T.; Butte, A. J. Exploiting Drug-Disease Relationships for Computational Drug Repositioning. *Brief. Bioinform.* **2011,** *12* (4), 303–311.
142. Sirota, M.; Dudley, J. T.; Kim, J.; Chiang, A. P.; Morgan, A. A.; Sweet-Cordero, A.; Sage, J.; Butte, A. J. Discovery and Preclinical Validation of Drug Indications Using Compendia of Public Gene Expression Data. *Sci. Transl. Med.* **2011,** *3,* 96ra77.
143. Hu, G.; Agarwal, P. Human Disease-Drug Network Based on Genomic Expression Profiles. *PLoS One* **2009,** *4* (8), e6536.
144. Kunkel, S. D.; Suneja, M.; Ebert, S. M.; Bongers, K. S.; Fox, D. K.; Malmberg, S. E.; Alipour, F.; Shields, R. K.; Christopher, M. mRNA Expression Signatures of Human Skeletal Muscle Atrophy Identify a Natural Compound That Increases Muscle Mass. *Cell Metab.* **2012,** *13,* 627–638.
145. Zhang, M.; Luo, H.; Xi, Z.; Rogaeva, E. Drug Repositioning for Diabetes Based on "Omics" Data Mining. *PLoS One* **2015,** *10,* e0126082.
146. Napolitano, F.; Zhao, Y.; Moreira, V. M.; Tagliaferri, R.; Kere, J.; D'Amato, M.; Greco, D. Drug Repositioning: A Machine-Learning Approach Through Data Integration. *J. Cheminform.* **2013,** *5,* 30.
147. Pan, Y.; Cheng, T.; Wang, Y.; Bryant, S. H. Pathway Analysis for Drug Repositioning Based on Public Database Mining. *J. Chem. Inf. Model.* **2014,** *54,* 407–418.
148. Iwata, H.; Sawada, R.; Mizutani, S.; Yamanishi, Y. Systematic Drug Repositioning for a Wide Range of Diseases with Integrative Analyses of Phenotypic and Molecular Data. *J. Chem. Inf. Model.* **2014,** *55* (2), 446–459.
149. Iskar, M.; Zeller, G.; Blattmann, P.; Campillos, M.; Kuhn, M.; Kaminska, K. H.; Runz, H.; Gavin, A.-C.; Pepperkok, R.; van Noort, V.; Bork, P. Characterization of Drug-Induced Transcriptional Modules: Towards Drug Repositioning and Functional Understanding. *Mol. Syst. Biol.* **2013,** *9,* 662.
150. Bisgin, H.; Liu, Z.; Fang, H.; Kelly, R.; Xu, X.; Tong, W. A Phenome-Guided Drug Repositioning Through a Latent Variable Model. *BMC Bioinform.* **2014,** *15,* 267.
151. Ye, H.; Liu, Q.; Wei, J. Construction of Drug Network Based on Side Effects and Its Application for Drug Repositioning. *PLoS One* **2014,** *9*, e87864.
152. Cavalla, D. Predictive Methods in Drug Repurposing: Gold Mine or Just a Bigger Haystack? *Drug Discov. Today* **2013,** *18,* 523–532.
153. Anighoro, A.; Bajorath, J.; Rastelli, G. Polypharmacology: Challenges and Opportunities in Drug Discovery. *J. Med. Chem.* **2014,** *57,* 7874–7887.
154. Dunkel, M.; Günther, S.; Ahmed, J.; Wittig, B.; Preissner, R. SuperPred: Drug Classification and Target Prediction. *Nucleic Acids Res.* **2008,** *36,* W55–W59.
155. Lipinski, C. A.; Lombardo, F.; Dominy, B. W.; Feeney, P. J. Experimental and Computational Approaches to Estimate Solubility and Permeability in Drug Discovery and Development Settings. *Adv. Drug Deliv. Rev.* **2001,** *46,* 3–26.
156. Martin, Y. C.; Kofron, J. L.; Traphagen, L. M. Do structurally Similar Molecules Have Similar Biological Activity? *J. Med. Chem.* **2002,** *45,* 4350–4358.
157. Keiser, M. J.; Setola, V.; Irwin, J. J.; Laggner, C.; Abbas, A. I.; Hufeisen, S. J.; Jensen, N. H.; Kuijer, M. B.; Matos, R. C.; Tran, T. B.; Whaley, R.; Glennon, R. A.; Hert, J.; Thomas, K. L. H.; Edwards, D. D.; Shoichet, B. K.; Roth, B. L. Predicting New Molecular Targets for Known Drugs. *Nature* **2009,** *462,* 175–181.
158. Godden, J. W.; Xue, L.; Bajorath, J. Combinatorial Preferences Affect Molecular Similarity/Diversity Calculations Using Binary Fingerprints and Tanimoto Coefficients. *J. Chem. Inf. Model.* **2000,** *40,* 163–166.
159. Kubinyi, H. Similarity and Dissimilarity: A Medicinal Chemist's View. *Perspect. Drug Discov. Des.* ***1998****, 9–11*, 225–252.
160. Cheng, F.; Liu, C.; Jiang, J.; Lu, W.; Li, W.; Liu, G.; Zhou, W.; Huang, J.; Tang, Y. Prediction of Drug-Target Interactions and Drug Repositioning via Network-Based Inference. *PLoS Comput. Biol.* **2012,** *8,* e1002503.
161. Yamanishi, Y.; Kotera, M.; Kanehisa, M.; Goto, S. Drug-Target Interaction Prediction from Chemical, Genomic and Pharmacological Data in an Integrated Framework. *Bioinformatics* **2010,** *26,* 246–254.
162. Ekins, S.; Mestres, J.; Testa, B. In Silico Pharmacology for Drug Discovery: Methods for Virtual Ligand Screening and Profiling. *Br. J. Pharmacol.* **2007,** *152,* 9–20.
163. Kitchen, D. B.; Decornez, H.; Furr, J. R.; Bajorath, J. Docking and Scoring in Virtual Screening for Drug Discovery: Methods and Applications. *Nat. Rev. Drug Discov.* **2004,** *3,* 935–949.
164. Li, H.; Gao, Z.; Kang, L.; Zhang, H.; Yang, K.; Yu, K.; Luo, X.; Zhu, W.; Chen, K.; Shen, J.; Wang, X.; Jiang, H. TarFisDock: A Web Server for Identifying Drug Targets with Docking Approach. *Nucleic Acids Res.* **2006,** *34,* W219–W224.
165. Li, L.; Bum-Erdene, K.; Baenziger, P. H.; Rosen, J. J.; Hemmert, J. R.; Nellis, J. A.; Pierce, M. E.; Meroueh, S. O. BioDrugScreen: A Computational Drug Design Resource for Ranking Molecules Docked to the Human Proteome. *Nucleic Acids Res.* **2010,** *38,* D765–D773.

166. Ewing, T. J.; Makino, S.; Skillman, A. G.; Kuntz, I. D. DOCK 4.0: Search Strategies for Automated Molecular Docking of Flexible Molecule Databases. *J. Comput. Aided Mol. Des.* **2001,** *15,* 411–428.
167. DesJarlais, R. L.; Seibel, G. L.; Kuntz, I. D.; Furth, P. S.; Alvarez, J. C.; Ortiz de Montellano, P. R.; DeCamp, D. L.; Babe, L. M.; Craik, C. S. Structure-Based Design of Nonpeptide Inhibitors Specific for the Human Immunodeficiency Virus 1 Protease. *Proc. Natl. Acad. Sci.* **1990,** *87,* 6644–6648.
168. Kinnings, S. L.; Liu, N.; Buchmeier, N.; Tonge, P. J.; Xie, L.; Bourne, P. E. Drug Discovery Using Chemical Systems Biology: Repositioning the Safe Medicine Comtan to Treat Multi-drug and Extensively Drug Resistant Tuberculosis. *PLoS Comput. Biol.* **2009,** *5*, e1000423.
169. Haupt, V. J.; Schroeder, M. Old Friends in New Guise: Repositioning of Known Drugs with Structural Bioinformatics. *Brief. Bioinform.* **2011,** *12,* 312–326.
170. Wermuth, C. G. Selective Optimization of Side Activities: The SOSA Approach. *Drug Discov. Today* **2006,** *11,* 160–164.
171. Simon, Z.; Peragovics, A.; Vigh-Smeller, M.; Csukly, G.; Tombor, L.; Yang, Z.; Zahoránszky-Kohalmi, G.; Végner, L.; Jelinek, B.; Hári, P.; Hetényi, C.; Bitter, I.; Czobor, P.; Málnási-Csizmadia, A. Drug Effect Prediction by Polypharmacology-Based Interaction Profiling. *J. Chem. Inf. Model.* **2012,** *52,* 134–145.
172. Luo, H.; Chen, J.; Shi, L.; Mikailov, M.; Zhu, H.; Wang, K.; He, L.; Yang, L. DRAR-CPI: A Server for Identifying Drug Repositioning Potential and Adverse Drug Reactions via the Chemical-Protein Interactome. *Nucleic Acids Res.* **2011,** *39,* W492–W498.
173. Tan, F.; Yang, R.; Xu, X.; Chen, X.; Wang, Y.; Ma, H.; Liu, X.; Wu, X.; Chen, Y.; Liu, L.; Jia, X. Drug Repositioning by Applying "Expression Profiles" Generated by Integrating Chemical Structure Similarity and Gene Semantic Similarity. *Mol. Biosyst.* **2014,** *10,* 1126–1138.
174. Yildirim, M. A.; Goh, K.-I.; Cusick, M. E.; Barabási, A.-L.; Vidal, M. Drug-Target Network. *Nat. Biotechnol.* **2007,** *25,* 1119–1126.
175. O'Reilly, L. P.; Long, O. S.; Cobanoglu, M. C.; Benson, J. A.; Luke, C. J.; Miedel, M. T.; Hale, P.; Perlmutter, D. H.; Bahar, I.; Silverman, G. A.; Pak, S. C. A Genome-Wide RNAi Screen Identifies Potential Drug Targets in a *C. elegans* Model of α1-Antitrypsin Deficiency. *Hum. Mol Genet.* **2014,** *23* (19), 5123–5132.
176. Roth, B. L.; Sheffler, D. J.; Kroeze, W. K. Magic Shotguns Versus Magic Bullets: Selectively Non-selective Drugs for Mood Disorders and Schizophrenia. *Nat. Rev. Drug Discov.* **2004,** *3,* 353–359.
177. Segall, M. D.; Champness, E. J. The Challenges of Making Decisions Using Uncertain Data. *J. Comput. Aided Mol. Des.* **2015,** *29* (9), 809–816.
178. Anighoro, A.; Bajorath, J.; Rastelli, G. Polypharmacology: Challenges and Opportunities in Drug Discovery. *J. Med. Chem.* **2014,** *57,* 7874–7887.
179. Okada, Y.; Wu, D.; Trynka, G.; Raj, T.; Terao, C.; Ikari, K.; Kochi, Y.; Ohmura, K.; Suzuki, A.; Yoshida, S.; Graham, R. R.; Manoharan, A.; Ortmann, W.; Bhangale, T.; Denny, J. C.; Carroll, R. J.; Eyler, A. E.; Greenberg, J. D.; Kremer, J. M.; Pappas, D. A.; Jiang, L.; Yin, J.; Ye, L.; Su, D.-F.; Yang, J.; Xie, G.; Keystone, E.; Westra, H.-J.; Esko, T.; Metspalu, A.; Zhou, X.; Gupta, N.; Mirel, D.; Stahl, E. A.; Diogo, D.; Cui, J.; Liao, K.; Guo, M. H.; Myouzen, K.; Kawaguchi, T.; Coenen, M. J. H; van Riel, P. L. C. M.; van de Laar, M. A. F. J.; Guchelaar, H.-J.; Huizinga, T. W. J; Dieudé, P.; Mariette, X.; Bridges, S. L.; Zhernakova, A.; Toes, R. E. M; Tak, P. P.; Miceli-Richard, C.; Bang, S.-Y.; Lee, H.-S.; Martin, J.; Gonzalez-Gay, M. A.; Rodriguez-Rodriguez, L.; Rantapää-Dahlqvist, S.; Arlestig, L.; Choi, H. K.; Kamatani, Y.; Galan, P.; Lathrop, M.; Eyre, S.; Bowes, J.; Barton, A.; de Vries, N.; Moreland, L. W.; Criswell, L. A.; Karlson, E. W.; Taniguchi, A.; Yamada, R.; Kubo, M.; Liu, J. S.; Bae, S.-C.; Worthington, J.; Padyukov, L.; Klareskog, L.; Gregersen, P. K.; Raychaudhuri, S.; Stranger, B. E.; De Jager, P. L.; Franke, L.; Visscher, P. M.; Brown, M. A.; Yamanaka, H.; Mimori, T.; Takahashi, A.; Xu, H.; Behrens, T. W.; Siminovitch, K. A.; Momohara, S.; Matsuda, F.; Yamamoto, K.; Plenge, R. M. Genetics of Rheumatoid Arthritis Contributes to Biology and Drug Discovery. *Nature* **2014,** *506,* 376–381.
180. Iorio, F.; Bosotti, R.; Scacheri, E.; Belcastro, V.; Mithbaokar, P.; Ferriero, R.; Murino, L.; Tagliaferri, R.; Brunetti-Pierri, N.; Isacchi, A.; di Bernardo, D. Discovery of Drug Mode of Action and Drug Repositioning from Transcriptional Responses. *Proc. Natl. Acad. Sci. U. S. A.* **2010,** *107,* 14621–14626.
181. Subramanian, A.; Tamayo, P.; Mootha, V. K.; Mukherjee, S.; Ebert, B. L.; Gillette, M. A.; Paulovich, A.; Pomeroy, S. L.; Golub, T. R.; Lander, E. S.; Mesirov, J. P. Gene Set Enrichment Analysis: A Knowledge-Based Approach for Interpreting Genome-Wide Expression Profiles. *Proc. Natl. Acad. Sci.* **2005,** *102,* 15545–15550.
182. Jahchan, N. S.; Dudley, J. T.; Mazur, P. K.; Flores, N.; Yang, D.; Palmerton, A.; Zmoos, A.-F.; Vaka, D.; Tran, K. Q. T; Zhou, M.; Krasinska, K.; Riess, J. W.; Neal, J. W.; Khatri, P.; Park, K. S.; Butte, A. J.; Sage, J. A Drug Repositioning Approach Identifies Tricyclic Antidepressants as Inhibitors of Small Cell Lung Cancer and Other Neuroendocrine Tumors. *Cancer Discov.* **2013,** *3* (12), 1364–1377.
183. Dudley, J. T.; Sirota, M.; Shenoy, M.; Pai, R. K.; Roedder, S.; Chiang, A. P.; Morgan, A. A.; Sarwal, M. M.; Pasricha, P. J.; Butte, A. J. Computational Repositioning of the Anticonvulsant Topiramate for Inflammatory Bowel Disease. *Sci. Transl. Med.* **2011,** *3,* 96ra76.
184. van Noort, V.; Schölch, S.; Iskar, M.; Zeller, G.; Ostertag, K.; Schweitzer, C.; Werner, K.; Weitz, J.; Koch, M.; Bork, P. Novel Drug Candidates for the Treatment of Metastatic Colorectal Cancer Through Global Inverse Gene-Expression Profiling. *Cancer Res.* **2014,** *74,* 5690–5699.
185. Chiang, A. P.; Butte, A. J. Systematic Evaluation of Drug-Disease Relationships to Identify Leads for Novel Drug Uses. *Clin. Pharmacol. Ther.* **2009,** *86,* 507–510.
186. Campillos, M.; Kuhn, M.; Gavin, A.-C.; Jensen, L. J.; Bork, P. Drug Target Identification Using Side-Effect Similarity. *Science* **2008,** *321,* 263–266.
187. Kuhn, M.; Campillos, M.; Letunic, I.; Jensen, L. J.; Bork, P. A Side Effect Resource to Capture Phenotypic Effects of Drugs. *Mol. Syst. Biol.* **2010,** *6,* 343.
188. von Eichborn, J.; Murgueitio, M. S.; Dunkel, M.; Koerner, S.; Bourne, P. E.; Preissner, R. PROMISCUOUS: A Database for Network-Based Drug-Repositioning. *Nucleic Acids Res.* **2011,** *39,* D1060–D1066.
189. Lee, H. S.; Bae, T.; Lee, J.-H.; Kim, D. G.; Oh, Y. S.; Jang, Y.; Kim, J.-T.; Lee, J.-J.; Innocenti, A.; Supuran, C. T.; Chen, L.; Rho, K.; Kim, S. Rational Drug Repositioning Guided by an Integrated Pharmacological Network of Protein, Disease and Drug. *BMC Syst. Biol.* **2012,** *6,* 80.
190. Chang, R. L.; Xie, L.; Xie, L.; Bourne, P. E.; Palsson, B.Ø. Drug Off-Target Effects Predicted Using Structural Analysis in the Context of a Metabolic Network Model. *PLoS Comput. Biol.* **2010,** *6*, e1000938.

1.03 Human iPSC Models in Drug Discovery: Opportunities and Challenges

MC Silva, Massachusetts General Hospital and Harvard Medical School, Boston, MA, United States
A Cross and NJ Brandon, AstraZeneca Neuroscience Innovative Medicines and Early Development Biotech Unit, Waltham, MA, United States
SJ Haggarty, Massachusetts General Hospital and Harvard Medical School, Boston, MA, United States

© 2017 Elsevier Ltd. All rights reserved.

1.03.1 Introduction 48
1.03.1.1 Historical and Technological Advances 48
1.03.1.2 Human Biology Context 49
1.03.2 iPSCs ex vivo Disease Models 49
1.03.2.1 Human iPSC-Derived Cell Models to Study Disease in Cellular- and Genomic-Relevant Contexts 50
1.03.2.1.1 Patient iPSC differentiation into disease-relevant cell types 51
1.03.2.1.2 Assessing disease mechanisms in complex genetic disorders 56
1.03.2.2 Integrative and Translational Research of Human Disease Etiology 57
1.03.2.2.1 Phenotyping pipelines in preclinical studies 57
1.03.2.2.2 Integrative approaches across cell models and patient clinicopathological data 59
1.03.2.3 Human iPSC Models as Potential Preclinical Alternatives to Animal Models 60
1.03.3 Potential Roles for iPSC Models in Drug Development Pipeline 61
1.03.3.1 Examples of CNS-Focused iPSC Drug-Discovery Screening 61
1.03.3.1.1 Psychiatric disorder model screening 61
1.03.3.1.2 Neurodegenerative disorder model screening 62
1.03.3.1.3 Pain and sensory neuron disease model screening 63
1.03.3.2 Quantitative Cellular Pharmacology 63
1.03.3.2.1 Advances Enabling Novel Assay Development and Target Validation 63
1.03.3.2.2 Toxicology and Drug Metabolism 64
1.03.4 Patient Stratification and Disease Diagnosis 64
1.03.4.1 iPSCs to Predict Drug Responders and Nonresponders 64
1.03.4.2 Role of iPSC Disease Models in Clinical Diagnosis and Prognosis 65
1.03.5 Challenges and Concluding Remarks 66
References 66

1.03.1 Introduction

1.03.1.1 Historical and Technological Advances

Progress in the field of stem cell research has the potential to be transformative for translational medicine. Human embryonic stem cells (hESCs) and induced pluripotent stem cells (iPSCs) have the capacity for self-renewal in culture and are able, in theory, to differentiate into any cell type of the body, provided that appropriate culture conditions are developed.[1–5] Given these properties and physiological similarities to human cells in situ, stem cell culture has shown great promise as an ex vivo system for studying human development and, most importantly, human disease. An urgent need for better clinicotherapeutic outcomes has directed interest to the use of these physiologically relevant human cells in the drug-discovery process, including early testing of efficacy and toxicity of promising therapeutics, and as a valuable source of specialized cells for regenerative medicine.[6–8]

Pioneers in this field, Yamanaka and colleagues, demonstrated in 2006 that human somatic cells, such as dermal fibroblasts from a skin biopsy, could be reprogrammed into iPSC through the retrovirus-mediated transduction of cells with four transcription factors (Oct3/4, Sox2, c-Myc, and Klf4), now commonly referred to as "Yamanaka factors."[2,3,5] This discovery granted the investigators Dr. Shinya Yamanaka and Dr. John Gurdon the 2012 Nobel Prize in Physiology/Medicine for the discovery that mature cells can be reprogrammed to become pluripotent. With subsequent and continued efforts by several other groups, remarkable improvements in reprogramming strategies, robustness, and iPSC differentiation throughput have been developed with innovations continuing at a rapid pace.[9–17] While the pioneering work by Yamanaka and colleagues relied on the delivery of transcription factors using retroviruses that integrated in the host-cell genome of skin fibroblasts, subsequent innovations have allowed for higher efficiency reprogramming and for additional types of somatic cells, including blood, hair cells, and endothelial cells (e.g., from urine) to be successfully reprogrammed.[18] Beyond increasing efficiency, one significant improvement has been the implementation of integration-free reprogramming methods that do not permanently insert any transgene into the genome (so-called scarless reprogramming), circumventing concerns of mutagenesis or damage to the host-cell genome, and relying on DNA plasmid-based methods and nonintegrating Sendai virus.[9,11,12,19] Thereafter, integration-free mRNA-based transcription factors, micro-RNAs (miRNA), and small molecule-based reprogramming cocktails were successfully developed[13,15] and together have made it feasible to routinely make human iPSCs.

Another area of remarkable advance focuses on direct differentiation of somatic cells into specific cell types such as cardiomyocytes,[20,21] hepatocytes,[22] intestinal and pancreatic cells,[23,24] microglia,[25–27] and neurons.[28–34] In the latter case, variations in induced neurons (iN) protocols involving different transcription factor combinations have shown the potential to further yield defined neuronal subtypes, such as dopaminergic or GABAergic neurons.[35] By eliminating the need to first generate iPSCs, direct reprogramming and differentiation into a specific cell type have the potential to have important, although not yet well established, advantages, including shortening the time frame to obtain the cultured cells of interest. Another significant advantage might be reducing disruption in epigenetic marks associated with iPSC generation, which will be relevant for using these cells as models of human disease. Still, technical restrictions, such as output of relatively small number of cells, are a limiting factor for routine or large-scale studies. This may be resolved with newer approaches, such as generation of induced progenitor cells that retain a replicative capacity allowing expansion of the number of cells from the initial somatic cell population. For example, induced neural progenitor cells (iNPCs)[36] can, similar to NPCs derived from iPSCs,[37,38] be stably kept in culture in proliferative state, differentiated into almost a limitless quantity of neurons with ease while recapitulating key aspects of brain neurogenesis, and allow for long-term differentiation (months).[39–41]

As advantages of certain technologies over others become more evident, continued efforts focus on standardizing and refining the robustness of iPSC models for use in human disease modeling and drug discovery is critical. In parallel, the creation of large cohorts of human iPSCs (e.g., NYSCF Research Institute Stem Cell Repository, StemBANCC, HipSci Consortium, Stem Cells Network DPUK Cohorts) will further accelerate the robustness of findings across different disease models and assay end-points.[42–44]

1.03.1.2 Human Biology Context

Drug screening performed in a variety of human cell lines has contributed significantly to therapeutics progress, particularly in the area of oncology where patient-derived cell lines have been used extensively. But now, patient-specific iPSCs derived models, that recapitulate key aspects of human disease "in a dish," may offer a more relevant, robust, scalable, and cost-effective model of human disease physiology, and an attractive system for drug discovery,[45–47] even though the use of these cells still presents challenges at the level of throughput and capacity for full maturation.

In the context of central nervous system (CNS) disorders, where access to physiologically active and relevant disease-affected cells is extremely limiting, iPSC-derived in vitro culture of specific cell types, such as human neurons and glial cells, is transformative.[35,48] Together with implementation of state-of-the-art phenotyping approaches, including quantitative biochemistry, functional genomics, proteomics, and perhaps most notably, high-throughput (HTS) and high-content (HCS) chemical screening for drug discovery,[6] the potential for understanding and treating human disease is unprecedented, creating a paradigm shift in translational research.[48–50] Focus on patient-specific iPSC-derived neuronal cell models to study molecular and cellular pathophysiological mechanisms has also benefited from growing small molecule and oligonucleotide-based libraries that allow probing gene, protein and molecular pathways' function, and detection of early disease-specific alterations toward identification of disease biomarkers and therapeutic targets. A broad review of human iPSC-derived CNS disease models can be found in expertise literature.[35,48,51–60]

Contrary to traditional approaches, where animal and immortalized cell models are relied upon for drug screening, efficacy readouts, toxicity assessment, and mode-of-action (MOA) studies, and where the "human context" is often only implemented later at the clinical trial phase, patient iPSC-derived models fundamentally introduce the "human context" early in the discovery pipeline. Ultimately, a comprehensive understanding of disease mechanisms, coupled with small-molecule screening, offers unprecedented opportunities for drug discovery, including early testing of drug-target engagement, efficacy against the human target, and toxicity, in a human cell-type and disease-relevant context, at a preclinical trial phase (**Fig. 1**). Such strategies have the potential to increase the probability of success and, perhaps, lower the costs of drug discovery and repurposing.

While many quantifiable phenotypes in human iPSC-derived culture systems may prove adaptable to screening formats, addressing the question of which in vitro phenotypes are ultimately relevant to disease pathophysiology and should be the focus of drug development requires careful consideration.[48,61] Integrative research approaches, across cellular models of the same or related disorders, and in concert with clinicopathological patient data, can offer unique opportunities in recognizing disease-relevant phenotypes, understanding disease in a broader context (e.g., common aspects of neuronal death among related neurodegenerative diseases), and identifying biomarkers and therapeutic targets (**Fig. 2**).

Here, we will focus first on the latest advances in human disease iPSC-derived models, disease etiology phenotyping pipelines, and the potential for preclinical diagnostics. Then, we will address strategies to identify therapeutic targets, HTS/HCS approaches for drug discovery, and drug efficacy and toxicity testing. A number of key challenges will also be discussed, including optimization for cost-effective large-scale culture of iPSCs and iPSC-derived neuronal cultures, standardization of differentiation protocols, throughput and automation of phenotypic assays, and the urgent need for scaling iPSC-derived cellular models to larger patient cohorts with routine integration of clinicopathological information.

1.03.2 iPSCs ex vivo Disease Models

While stem cells are highly relevant for many areas of active therapeutic development and regenerative medicine, a tremendous effort has been directed toward the development of human iPSC-derived models of diseases affecting tissues and cell types that cannot be accessed noninvasively or are of a limited nature in terms of availability. This is particularly the case for neurodegenerative

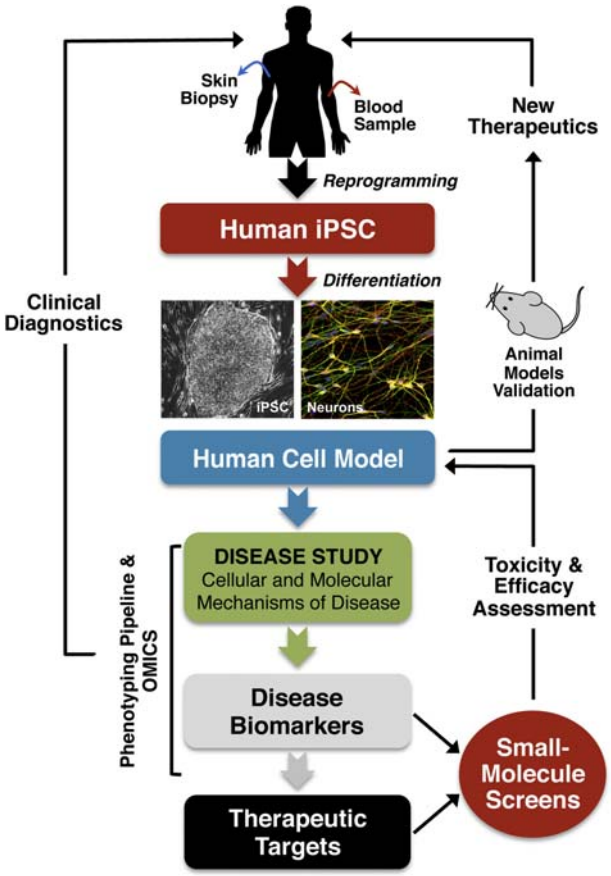

Fig. 1 Human iPSC in drug discovery. iPSC-based models of human disease focus on endogenous physiologically relevant proteins and molecular pathways, with the genetic context associated with disease. Coupled with extensive phenotypic analysis and validation across an increasing number of cell lines, iPSC-derived cells can have an important role in clinical diagnostics and interpretation of genetic variation. Most remarkably, iPSC-derived cell models show increasing potential for small-molecule screening and secondary testing of novel therapeutics' efficacy, toxicity, and mode of action, in a human context and in advance of animal testing and human clinical trials.

and psychiatric disorders where access to living brain tissue is severely limited, and there is a need to investigate the physiology and response of specific cell types to therapeutic agents. Thus, patient iPSC-derived neurons that represent unique ex vivo models of human neuronal networks present the opportunity to investigate disease-relevant genes and proteins at endogenous physiologically relevant levels and in the context of the genomic background associated with disease.[45,62] For these reasons, below we will use the CNS as a case study to point out the value of human iPSC models for ex vivo disease modeling, with similar rationale existing for studies of other diseases and cell types.

1.03.2.1 Human iPSC-Derived Cell Models to Study Disease in Cellular- and Genomic-Relevant Contexts

Traditional approaches for studying pathophysiological mechanisms of human disorders have relied on animal and immortalized cell lines disease models, through overexpression of human transgenes predicted to be causal to disease, in a particular cell type amenable to phenotypic measurements. Although these have been instrumental in initial screening efforts and progression of candidate therapeutics through preclinical efficacy and safety tests, and in elucidating disease mechanisms, these model systems have had poor success in translation to human patient-relevant findings, and ultimately in the registration of new drugs, particularly in the area of CNS disorders.[45,63] This is thought to be partly the result of a concerning disconnect between phenotypic findings and drug pharmacological properties in isolated recombinant model systems versus the actual "native" human system. The physiological and genomic inaccuracy of many disease models might be a fundamental reason for the hindered identification of validated therapeutic targets and the cause of high-cost, failed clinical trials. Justly, research of many diseases was negatively affected by the unavailability and inaccessibility to appropriate cell types, that is, human tissue affected by the disease, carrying the disease-associated genomic background and pathology-relevant altered proteins and biochemical pathways. This translational disconnect has the potential to be overcome by human iPSC-based model systems and screens. Human stem cell-derived neurons allow access to physiologically relevant cell types and protein complexes without the need for overexpression of heterologous genes, representing a reliable system to investigate molecular and cellular disease mechanisms.[35,45,48–50]

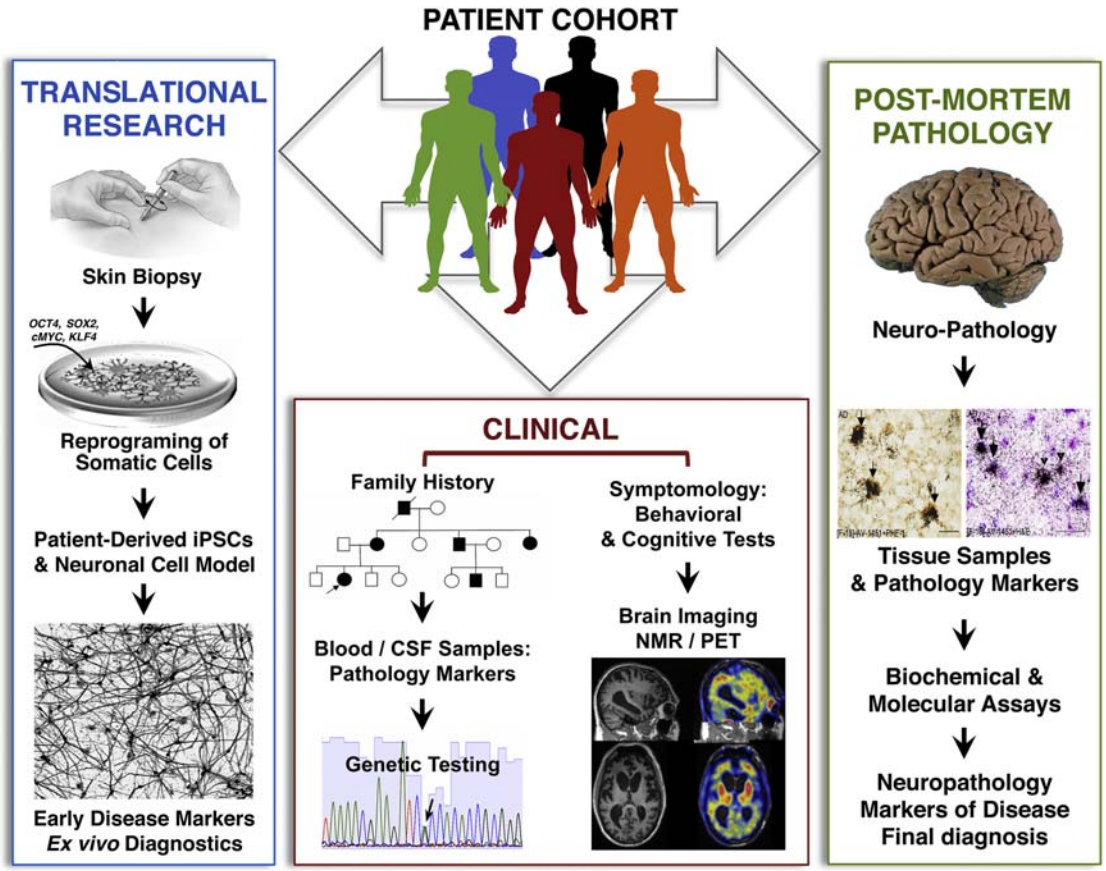

Fig. 2 Translational research integrative approaches: patient cohort-based iPSC-derived cellular models (left), rich and longitudinal clinical phenotyping information (middle), and postmortem pathology data (right). Patient-specific iPSC-derived cell models are a critical tool in the study of early disease molecular and cellular mechanisms. Results interpretation in the context of clinicopathological data allows discerning the most relevant phenotypes, identification of biomarkers with relevance for preclinical and clinical diagnostics, as well as therapeutics development. Brain imaging offers guidance regarding areas of the brain and neuronal circuitries affected by disease, neuronal atrophy, and death, for further studies; NMR (nuclear magnetic resonance) and PET (positron emission tomography) images (Adapted from Ghetti, B.; Oblak, A. L.; Boeve, B. F.; Johnson, K. A.; Dickerson, B. C.; Goedert, M. Invited Review: Frontotemporal Dementia Caused by Microtubule-Associated Protein tau Gene (MAPT) Mutations: A Chameleon for Neuropathology and Neuroimaging. *Neuropathol. Appl. Neurobiol.* **2015**, *41* (1), 24–46). Postmortem pathology data (Adapted from Marquie, M.; Normandin, M. D.; Vanderburg, C. R.; Costantino, I. M.; Bien, E. A.; Rycyna, L. G.; Klunk, W. E.; Mathis, C. A.; Ikonomovic, M. D.; Debnath, M. L.; Vasdev, N.; Dickerson, B. C.; Gomperts, S. N.; Growdon, J. H.; Johnson, K. A.; Frosch, M. P.; Hyman, B. T.; Gomez-Isla, T. Validating Novel Tau Positron Emission Tomography Tracer [F-18]-AV-1451 (T807) on Postmortem Brain Tissue. *Ann. Neurol.* **2015**, *78* (5), 787–800) is relevant to validate the ultimate progression of disease, to ensure that the right processes are being targeted for therapeutics.

1.03.2.1.1 Patient iPSC differentiation into disease-relevant cell types

A major obstacle in developing accurate models of human disease has been, in many cases, the inaccessibility to disease-relevant human tissue, especially if it requires routine patient's sample collection (e.g., biopsy). Even in cases where tissue is available, terminally differentiated cells such as neurons cannot be maintained in culture, prohibiting the possibility of experimental reproducibility and scalable studies. Conversely, readily accessible tissues such as lymphocytes do not necessarily recapitulate all the signaling and molecular pathways that are affected by CNS disorders. With implementation of iPSC technologies, the ability to use genetic and cellular "accurate" human-derived models to investigate the step-by-step molecular and cellular events associated with disease has started to show great impact on the understanding of particular types of neurological diseases. Patient-specific iPSCs and differentiated cells effectively model a human disease genome and proteome in a format amenable to ex vivo investigation, with access to otherwise difficult or impossible-to-obtain living cell types of the human nervous system. Methodology advances in the production of scalable cultures of iPSC-derived specific cell types, including NPCs and neurons,[35–38] represent a significant step forward in the development of platforms for phenotypic HTS-compatible assays, for testing genotype–phenotype correlations in complex genetic disorders, and to support integrated approaches to human chemical neurobiology. Most remarkably, patient iPSCs-derived neuronal cells recapitulate key aspects of human disease ex vivo.

In the context of *psychiatric disorders*, development of effective therapies is one of the greatest 21st century challenges in medicine, affecting millions of individuals worldwide.[64] A major contributory factor is that the causes of mental illnesses are complex and heterogeneous in nature and still not well understood. While risk for common disorders such as bipolar disorder, major depression,

schizophrenia, and autism is clearly polygenic in nature, there is also potential for contribution of both epigenetic variation and environmental factors to disease susceptibility (Fig. 3).[50,65–67] This polygenicity renders it very difficult to create genetically accurate models of psychiatric disorders in animals. Not only do they often lack neuroanatomical regions, and therefore circuitry thought to contribute to pathology, but comparison between mouse and human model systems has exposed real challenges on extrapolation of phenotypes.[50,68] For these disorders, not only access to physiologically active and relevant CNS cell types for research is practically impossible, the precise identity and location of such cells that play a causal role in disease pathogenesis remains, in many cases, unclear. Thus, patient iPSC-derived in vitro NPCs, neurons, and glial cells have paved a new era in psychiatric research since they capture the complex genetic architecture of polygenic susceptibility and allow access to a diversity of neuronal and glial subtypes.[48,50]

Multiple hESC- and iPSC-derived cellular models have been generated for distinct monogenic and polygenic psychiatric disorders, where epigenetic, chemical, proteomic, and signaling pathways dysregulation can be assessed and measured in a cell-specific manner, increasingly providing a powerful means to dissect the underlying disease biology.[39,48,50,69–72] There are now a growing number of human iPSCs models of monogenic psychiatric disorders such as fragile X syndrome[39,73] and Rett syndrome,[74–76] along with a smaller number of human iPSCs models for the polygenic psychiatric disorders schizophrenia[77,78] and bipolar disorder.[79–82] But human iPSC-derived models only demonstrated applicability for modeling psychiatric disorders when reports of cellular phenotypes started to emerge. These include electrophysiological and signaling defects, aberrant neuronal differentiation patterns, and alterations in protein expression in differentiated neurons.[51] For Rett syndrome, a severe childhood onset, neurodevelopmental disorder due to mutations principally in the *MECP2* gene, different iPSC-derived neuronal models have collectively revealed a number of potentially disease-relevant phenotypes, including changes in soma size, glutamatergic synaptic deficits, and altered gene transcription.[83–85] Schizophrenia iPSC-derived NPCs exhibit elevated levels of reactive oxygen species,[77] consistent with proteomic analysis of patients' brain tissue that also revealed disruption of mitochondrial function and oxidative stress.[86] Simultaneously, these models have provided the foundation for developing phenotypic assays suitable for functional genomic and chemical screens.[50] The value of these human in vitro cell models is further corroborated by phenotypic responsiveness to pharmacological agents, and therefore translational potential, including rescue of abnormal calcium signaling with the voltage-dependent L-type calcium channel antagonist nimodipine and rescue of neuronal differentiation patterns by roscovitine in the case of Timothy syndrome, a multisystemic disorder with cardiac, developmental, and autistic features[48,87]; rescue of glutamatergic synapses by the insulin-like growth factor 1 in Rett syndrome cultured neurons[76,88]; and rescue of gene expression abnormalities and connectivity differences in schizophrenia iPSC-derived neurons with the tricyclic dibenzoxazepine antipsychotic loxapine.[77] Meanwhile, targeted small-molecule screens for modulators of pathways affected in psychiatric diseases are beginning to emerge (Table 1). WNT pathway dysregulation has been associated with both psychiatric and neurodegenerative diseases, and a screen by Zhao et al. led

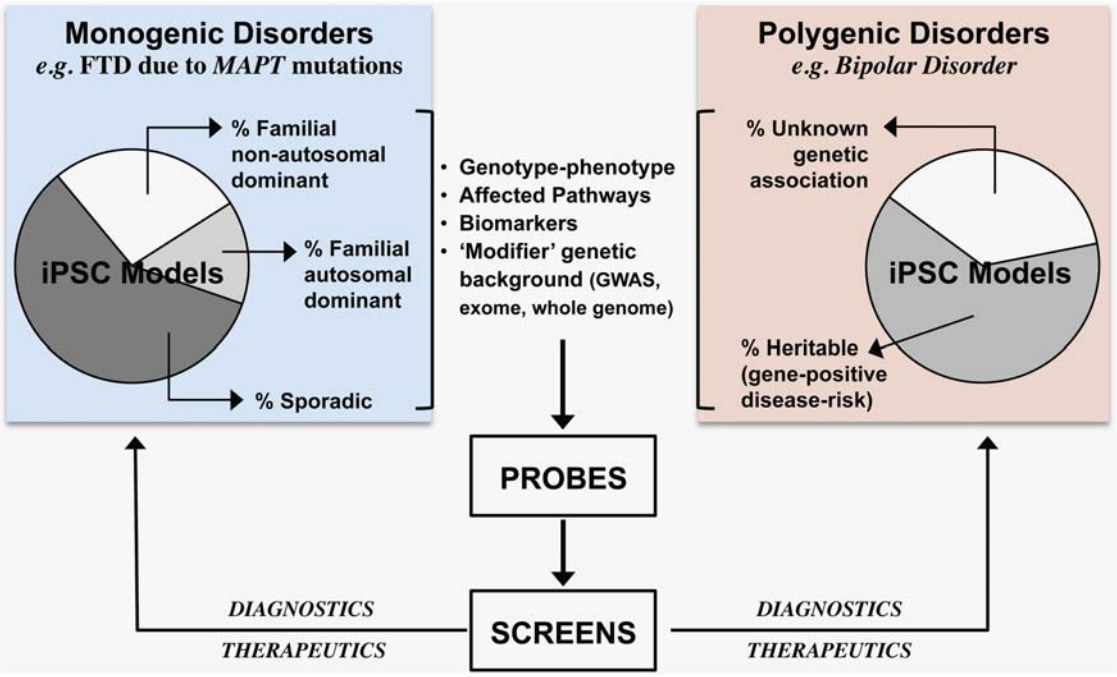

Fig. 3 Genetic variability among CNS disorders (simplified schematic). Patient iPSC-derived models capture the disease-associated genetic variability and allow the study of molecular and cellular phenotypes in a disease-relevant genomic background. Common phenotypes across diseases, independent of heritability class, may reveal the most relevant phenotypes to pursue for biomarker ID and small-molecule screening, with the goal of finding chemical therapeutics effective for a larger number of diseases, that is, by targeting and correcting the "common aspects" of pathogenesis.

Table 1 Examples of low- and high-throughput screens performed leading to lead compounds across stem cell biology and disease areas

Model	*Screening strategy*	*Library size/type*	*Positive hits/lead structure*	*Reference*
ESCs self-renewal (regenerative medicine)	mESCs, Oct4-GFP reporter assay. HTS 384-well plate format	50,000 Compounds	17 Hits Lead class: 3,4-dihydropyrimido[4,5-d] pyrimidines	Chen et al. (2006)[246]
ESC survival[a] (regenerative medicine)	hESC survival in vitro	Candidate approach: caspase inhibitors, growth factors, trophic factors, and kinase inhibitors	ROCK inhibitor Y-27632, most potent inhibitor of apoptosis	Watanabe et al. (2007)[247]
ESC proliferation and differentiation (regenerative medicine)	hESC self-renewal or differentiation. HTS/HCS 384-well plate format, automated laser-scanning confocal microscopy. OCT4/NANOG markers	2880 Small molecules (biologically active and structurally diverse compounds including 748 marketed drugs)	22 Hits: activators of proliferation (THEA, SNM, GTFX, FBP); differentiation inducers (tretinoin, retinoic acid, SLG, CYM, SRM)	Desbordes et al. (2008)[248]
ESC fate (regenerative medicine)	hESC fate regulators, HTS/HCS	1040 Compounds (two commercial libraries)	17 Promoters of differentiation (steroids), 5 promoters of viability (e.g., pinacidil)	Barbaric et al. (2010)[249]
AMPA glutamatergic neuronal potentiation	ESC-derived neurons (mouse and human). Fluorimetric imaging plate reader (FLiPR) Assay	2.4 Million compound library	37 Hits, 7 correspond to two novel molecular series (CE-382349)	McNeish et al. [89]
SMA, motor neuron survival	Rescue of protein survival of motor neuron (SMN) expression. Image-based (antibody-based) HTS/HCS 384-well plate format	3500 Bioactive compounds: LOPAC1280 Collection, Spectrum Collection, Prestwick Chemical Library, and custom set of 289 chemicals	188 Hits validated in SMA patient fibroblasts Mainly RTK-PI3K-AKT-GSK-3 signaling cascade modulator compounds	Makhortova et al. (2011)[250]
Schizophrenia[a]	Patient iPSC-derived neurons. Improved neuronal connectivity (synaptic markers and electrophysiology) in vitro	5 Candidate compounds: Clozapine, loxapine, Olanzapine, Risperidone, and Thioridazine	Loxapine	Brennand et al. [77]
WNT/β-catenin signaling, neuropsychiatric diseases	WNT-reporter assay in iPSC-derived NPCs, HTS 384-well plate format	1500 Compounds (FDA-approved and known bioactives)	45 Hits increased WNT activity (e.g., Riluzole, Trifluridine, Kaempferol, FG7142)	Zhao et al. [40]
ALS motor neurons[a]	Familial and sporadic ALS-TDP-43 patient iPSC-derived motor neurons. Rescue of phenotypes	4 Candidate compounds: trichostatin A, spliceostatin A, anacardic acid, and garcinol	Anacardic acid	Egawa et al. [90]
Familial dysautonomia	Familial dysautonomia patient-derived iPSC neural-crest precursors: rescue of expression of *IKBKAP* gene	6912 Small molecules	8 Hits Lead molecule: SKF-86466	Lee et al. [91]
AD neurons[a]	Suppression of Aβ oligomers-induced cellular stress in familial and sporadic AD patient-derived neurons (ER and oxidative stress phenotypes rescue)	3 Candidate compounds: BSI (β-secretase inhibitor IV), DHA (docosahexaenoic acid), ibenzoylmethane (DBM14-26), NSC23766	BSI, DHA	Kondo et al. [92]
NCS proliferation and viability	iPSC-derived neural stem cell (NCS), proliferation, and viability modulators. CompacT SelecT cell culture robotic platform HTS micro-well plate format	1000 Compounds	5 Potentiators of proliferation and viability (e.g., Cdk-2 modulator)	McLaren et al. (2013)[251]
ALS-SOD1 motor neurons	mESC-derived motor neurons, ALS model with mutant SOD1, survival screen. HTS 384-well plate format.	5000 Small molecules (known drugs, bioactives, and annotated chemicals) × 3 concentrations	Lead: kenpaullone Other hits: MMP inhibitor 1,10-phenanthroline monohydrate; CP55940; MDL 28170; A 77636, 3-Tropanylindole-3-carboxylate methiodide, FPL-64176, Tyrphostin A9	Yang et al. [93]

(Continued)

Table 1 Examples of low- and high-throughput screens performed leading to lead compounds across stem cell biology and disease areas—cont'd

Model	*Screening strategy*	*Library size/type*	*Positive hits/lead structure*	*Reference*
Sporadic ALS	Sporadic ALS patients' iPSC-derived motor neurons. HCS for inhibitors of TDP-43 aggregation (custom-built automated screening system with robotics and automated confocal microscopy)	1757 Bioactive compounds	Four classes of compounds: cyclin-dependent kinase inhibitors, c-Jun N-terminal kinase inhibitors (JNK), Triptolide, and FDA-approved cardiac glycosides, Digoxin, Lanatoside C, and Proscillaridin A	Burkhardt et al. [94]
PD dopaminergic neurons[a]	Neuroprotection of iPSC-derived dopaminergic neurons, by MTT viability assay and PD-rotenone toxicity model. Low-throughput assay, 96-well plate format	44 Compounds	16 Hits (e.g., indomethacin, nicotine, EGCG, resveratrol, taurine, lpoic acid)	Peng et al. (2013)[252]
AD/Aβ neuronal toxicity[a]	Human iPSC-derived forebrain neurons exposed to Aβ1-42 aggregates (insult). HTS for blocking Aβ1-42 toxicity, cell viability assay, and electrophysiology	"Several hundred compounds" from a GSK proprietary compounds library	19 Hits (including Cdk2 inhibitor)	Xu et al. (2013)[253]
Drug-induced arrhythmia[a] (drug development/ toxicology)	Human iPSC-derived cardiomyocytes model for drug-induced arrhythmia. Microelectrode array recordings of beating embryoid bodies exposed to a panel of drugs. Drug toxicology	Candidate approach: drugs prescribed for atrial fibrillation and ventricular tachycardia; other ion channel blockers (e.g., sotalol, quinidine, nifedipine, verapamil)	–	Navarrete et al. (2013)[254]
Cardiotoxicity[a] (drug development/toxicology)	Human iPSC-derived cardiomyocytes from patients with hereditary cardiac disorders to model genotype-dependent cardiac drug toxicity	Candidate approach: cisapride, nicorandil, alfuzosin, verapamil	–	Liang et al. (2013)[255]
Tumorigenesis and safety of hPSC-based treatments	Elimination of hPSCs while preserving progenitor and differentiated cells. HTS in 384-well format, automatic assessment of cell viability	52,000 Small molecules	15 Pluripotent cell-specific inhibitors (PluriSIns); most selective compound, PluriSIn #1 (SCD1 inhibitor) induces ER stress, protein synthesis attenuation, and apoptosis	Ben-David et al. (2013)[256]
Liver disease	Alpha-1 antitrypsin (AAT)-deficiency patient iPSC-derived hepatocytes. AAT expression rescue. IF-based HTS	3131 Clinical compounds (John Hopkins Drug Library)	5 Confirmed hits in multiple lines: carbamazepine, glipizide, lithium, valproic acid, thiamine	Choi et al. (2013)[257]
ALS motor neurons[a]	Familial and sporadic ALS patient iPSC-derived motor neurons electrophysiology (hyperexcitability phenotype)	Candidate approach (Kv7/KCNQ channel activity regulators)	Retigabine (antiepileptic drug)	Wainger et al. [95]
Fragile X syndrome	Rescue of *FMR1* gene expression, in Fragile X patient iPSC-derived neural cells. FRET assay for FMRP detection. HTS 1536-well plate format	5000 Bioactive compounds	6 Compounds	Kumari et al. [96]
Fragile X syndrome	Rescue of *FMR1* gene expression in patient iPSC-derived NPCs. HCS/HTS 384-well plate format	50,000 Compounds	790 Active compounds	Kaufmann et al. [97]
WNT/β-catenin signaling; neuropsychiatric diseases	WNT-reporter assay in iPSC-derived NPCs HTS	300,000 Compounds (NIH-supported Molecular Libraries Program)	Multiple scaffolds	S.J. Haggarty (personal communication)

[a]Small-scale, proof-of-concept studies.
HTS, high-throughput screen; HCS, high-content screen; hESC, human embryonic stem cells; mESC, mouse embryonic stem cells; iPSC, induced pluripotent stem cells.

to the identification of a number of both known and novel small-molecule regulators of WNT signaling in human NPCs, including selective mGLUR1 (metabotropic glutamate receptor 1) antagonists and the FDA-approved drug riluzole (Rilutek).[40] Even though these are examples of targeted studies, the value of psychiatric patient iPSC-derived cell models for small-molecule screening has been established, with the additional potential for follow-up mechanistic studies of the MOA of pharmacological agents in human cells, at a preclinical phase.

Neurodegenerative diseases are another group of heterogeneous devastating illnesses. Symptomatic treatments are available for some diseases, but no effective disease-modifying therapies have been registered. The unmet medical need grows exponentially with the aging population, with prevention and/or timely diagnosis at the forefront of current research.[98,99] These disorders can be familial or sporadic (**Fig. 3**), with onset in adult life and chronic progressive course, leading eventually, to a fatal outcome.[98,100] A main feature is the age-dependent focal and progressive loss of neuronal structure and function, characteristically associated with the presence of aberrant protein inclusions in the affected neurons, leading to neuronal death, astrogliosis, and spongiosis.[100–103] Protein aggregation can result from a mutation in a disease-related gene, leading to expression and accumulation of aberrant misfolded proteins in the cell or, in the absence of genetic alterations, it is thought to be a result of environmental stresses (e.g., head trauma injury) and aging.[100,104] From a disease evolution point of view, it is thought that neuronal cells accumulate aberrant proteins to a certain degree, until a large amount of damage has been sustained, giving place to a progressive proteostasis and cellular "collapse," starting with cells most vulnerable to the protein-mediated toxicity, toward a more global state that affects different functional systems along disease progression.[99,100,104,105] In addition, one of the most interesting but also debated theories today is the so-called protein spreading hypothesis of many neurodegenerative disorders where misfolded/aggregated proteins propagate between neighboring neurons and glial cells.[106–109] This hypothesis is thought to underlie the progression or "staging" of many disorders such as Parkinson's and Alzheimer's disease (AD) across brain regions. Despite the shared features of abnormal protein accumulation, and possibly propagation, leading to neuronal toxicity and death, the correlations between genetics, clinicopathology, and diagnosis are, in some cases, intricate, as revealed by genomic sequencing studies of cohorts of patients.[110–112] Such studies have shown that a given gene or mutation is not necessarily predictive of a single disease.[99,100,102,113,114] In some cases clinicopathological phenotypes can be somewhat predicted by the underlying genetic landscape, for example, polyglutamine expansions in the huntingtin (*HTT*) gene in Huntington's disease (HD)[115] or α-synuclein mutations in Parkinson's disease (PD).[116,117] However, in other cases, such as AD, frontotemporal lobar degeneration (FTLD) and other tauopathies, or amyotrophic lateral sclerosis (ALS), genotyping-based diagnosis is not straightforward as symptoms and associated clinicopathological findings are not always related to the same cytological and postmortem phenotypes.[99,102,114,118–122] Overall, disease variability among individuals of the same genotype and even among individuals with the same exact gene mutation remains poorly understood.

Another key issue, in addition to genotype–phenotype variability, is that of selective vulnerability. The biological mechanisms of neurodegeneration are highly associated with what is referred to as "focal" neuronal death, which means only a select group of neurons are affected in specific regions of the brain, within a tissue that ubiquitously expresses the same disease-associated gene mutation(s), while neurons immediately proximal remain unaffected.[123] Consider the specific examples: AD is associated with the selective damage of neural circuits involved in cognition and memory, including the neocortex, hippocampus, amygdala, basal forebrain cholinergic system, and brainstem monoaminergic nuclei[124]; FTLD affects mainly the frontal, insular, cingulate, and anterior temporal cortex, leading to changes in behavior, personality, and/or language, with relative preservation of memory[101,119,125]; whereas ALS shows a selective involvement of lower motor and pyramidal neurons, leading to muscle atrophy and spastic paralysis. Moreover, within the mentioned neuronal circuits, specific forms of disease can be associated with a strict loss of neuronal subtypes, as is the case of frontoinsular von Economo neurons and fork cell loss in FTLD subtypes.[126,127] The basis for this selective vulnerability, at a specific time in life, is still difficult to address experimentally, but it will require discerning what molecular networks are dysregulated in disease, to determine what predisposes preferentially specific neurons to death, in response to cell stress accumulation.

The identification of gene mutations associated with neurodegeneration prompted investigators to establish in vitro and animal model systems to examine cellular and molecular abnormalities in a genotype–phenotype dependent manner. Transgenic mice expressing human disease-causing gene mutations recapitulate many features of disease and have proved to be very useful in investigating biochemical alterations and pathogenic mechanisms in neural tissues, the evolution of pathology with aging, and in testing potential therapeutic agents.[98] Simpler organisms like the nematode *Caenorhabditis elegans* and the fruit fly *Drosophila melanogaster* also took an important role in the study of the molecular basis of human diseases, offering rapid transgenic model generation, the possibility for genome-wide screens and study of genetic interactions with cellular phenotypes.[98,100,128] Mounting evidence from model systems, together with emerging clinical research and diagnostic tools, such as PET (positron emission tomography) imaging that can detect brain alterations ahead of symptomology onset, and biomarker studies in AD (cerebral spinal fluid (CSF) levels of tau), have revealed that many disease-related cellular and biochemical alterations occur at a presymptomatic stage, turning attention toward the period in the disease when treatment will ultimately prove critical (**Fig. 2**).[129–134] Although postmortem protein inclusions are well accepted as pathological features of neurodegeneration, there has been great controversy about the role of aggregation in the disease process. A growing body of evidence has demonstrated that events preceding the formation of inclusion bodies, including abnormal disease-protein monomers and small assemblies of oligomeric species, might be the actual trigger for neuronal toxicity.[100,104,135] Therefore, a better understanding of the early biochemistry and biophysics of protein conformational change, species formed, and aberrant interaction with cellular components/pathways is indispensable to unravel the cellular toxic events, as well as cellular protective mechanisms that could be exploited from a therapeutics development perspective. Furthermore,

approaches to study the propagation of misfolded proteins are very important and could identify new therapeutic pathways or processes to prevent the spread of toxic protein species.

Patient or gene (mutation)-positive iPSCs are now used to generate cellular models to study early molecular and cellular mechanisms of disease, in a human disease-relevant cell context.[35,47] Notably, lineage-converted cells are able to recapitulate disease phenotypes and provide insight into disease mechanisms. As an example, induced motor neurons derived from ALS patients have been shown to have hyperexcitability due to SOD1 (A4V) mutations,[95] as well as rapid degeneration in culture relative to control neurons.[136] In iPSC-derived neuronal models of tauopathy, multiple groups have reported aberrant tau accumulation and insolubility, posttranslational modifications (PTMs), and subcellular mislocalization as early markers of pathogenesis.[41,92,137–140] Consequences of the early protein accumulation include altered proteostasis pathways, upregulation of stress markers, and increased neuronal vulnerability to cell death. In particular, disruption of protein clearance and endosomal–lysosomal pathways (proteasome and autophagy), endoplasmic reticulum (ER) stress unfolded protein response (UPR), mitochondrial dysfunction, and oxidative stress are strong models for tau-mediated toxicity and neurodegeneration (also seen in AD cases[92]). Consistent with these findings, human studies have identified protein clearance pathway components as CSF markers of neurodegeneration, and mounting evidence shows UPR, mitochondrial dysfunction, and oxidative stress associated with early stages of tauopathy and AD sporadic cases,[92,137,138,141,142] highly reinforcing the validity of iPSC-based cell models in the identification of disease biomarkers.[143] Moreover, overlap in stress markers (e.g., oxidative stress, disruption of protein clearance) and shared increased susceptibility to stress in tauopathy and PD patient-derived neurons, together with clinicopathological information, start to provide larger insight into common processes of neurodegeneration,[144] also supporting the proposition that the onset of cellular pathology occurs earlier than clinical manifestations. In addition, iPSC-derived neurons have also been used to study the spreading hypothesis as related to specific tau species.[139] Finally, increasing advances in iPSC differentiation into defined neuronal subtypes, representative of affected and nonaffected cell types in disease, will allow to probe cell-specific vulnerability to disease proteins, which will be much more challenging than solving gene-phenotype associations.[145]

It is also important to acknowledge that, although not the focus of this article, continued improvement in iPSC methodologies and tissue-specific differentiation have benefited other areas of medical research such as genetic *cardiovascular disease*[146,147] (**Table 1**). Human iPSC-derived cardiomyocyte cells, vascular endothelial cells, and smooth muscle cells that recapitulate key aspects of cardiovascular disease have enabled large-scale chemical and functional genomics screening.[20] Moreover, the potential to derive cardiomyocyte cells is also of great relevance to assess the risk of new therapeutics and dosing optimization, independently of targeted disease, with respect to arrhythmic risk, cardiotoxicity, and myopathy, through plasma markers measurements and cell-specific alterations of molecular and signaling properties.[20]

Overall, findings across human iPSC-derived models of disease are starting to provide more insight into disease mechanisms, guidance for the identification of early disease-relevant phenotypes and potential therapeutic targets, as well as new diagnostic tools, also leading to the development of promising pharmaceutical screens for novel therapeutic agents.

1.03.2.1.2 Assessing disease mechanisms in complex genetic disorders

Understanding the genetic basis of complex human disorders has followed the development of state-of-the-art genomic tools. Remarkable advances in next-generation sequencing (NGS)[111] and genome-wide association studies (GWAS) have led to the identification of disease-causing gene mutations, in addition to gene loci and rare variants that confer either higher or lower risk for disease.[148] For cases where a particular gene or mutation can be directly associated with clinical outcome, the development of animal and cellular models has been somewhat straightforward by simply overexpressing the human gene mutation, and then measuring molecular alterations, cellular phenotypes, and animal behavior. This effort becomes remarkably more complex when the goal is to model diseases that are sporadic, that do not have a clear genetic link or are associated with risk genes, or diseases that are polygenic.[77,92,149,150] Since patient iPSC-derived cells take into account patients' genomic background and allow the generation of both familial and sporadic forms of disease models, there is not a need to have a priori knowledge of the genetic "cause" to create a useful model of a human disease. Moreover, molecular, biochemical, and cellular phenotypes are explored in each patient's own genomic background that through clinicopathological data can be determined to be permissive to the disease state. This is particularly important, as the majority of neurological diseases are sporadic or rare monogenic forms, rendering animal models quite ineffectual. Still, to determine which phenotypes are disease-relevant, and beyond individual inherent variability, it is necessary to study multiple stem cell clones, from multiple patients, and compare phenotypes against multiple healthy individuals. Again, the broader disease relevance of a given phenotype can only be demonstrated by examining cells from patients with different mutations in disease-causing genes, as well as in a large number of sporadic cases (**Fig. 3**).

Advances in genomic tools have contributed to a greater understanding of the genetic architecture of psychiatric diseases,[149] revealing common variants at a large number of loci, but with each variant only having a small contribution to disease risk, that is, a polygenic component (**Fig. 3**). The small contribution of individual common risk variants, together with the rarity of large-effect loci or mutations (Mendelian), mean that accurate conclusions for genetic contribution to disease can only be obtained through large clinical cohorts, specially if the goal is to define causal or contributory role for *de novo* mutations or rare variants.[50,149,151] Moreover, the large heterogeneity and polygenicity in psychiatric disorders makes modeling extremely complex, specifically with respect to connecting the multiplicity of molecular, cellular, and circuit dysfunctions to complex human behavior. Despite the limitations in developing "accurate" model systems of human psychiatric disorders, mouse models of the few large-effect loci or Mendelian risk genes of disease have been developed and contributed significantly to the field, but successful translation has been limited in terms of fundamentally new mechanisms-of-action therapeutics with disease-modifying potential, rather

than affecting only symptomatic aspects.[152,153] As already mentioned, with patient iPSC-derived cell models and increasing access to larger cohorts of psychiatric patients, it will be possible, and potentially more successful, to focus on common phenotypes across models, and disease-modifying or corrective therapeutics. To date, the studies examining monogenic forms of psychiatric disease via patient iPSC-derived neuronal models are encouraging, even though still representative of a small sample size (for representative work see Refs. [39,48,50,51,69,71,76,77,81,83,87]).

For neurodegenerative diseases, the genetic landscape is somewhat different. Diseases are usually associated with a main gene(s) and protein(s), accounting for a percentage of sporadic cases and a percentage of familial cases (Fig. 3). These percentages represent different values for diseases such as Frontotemporal Dementia (FTD), ALS, and PD, whereas HD, for instance, is inherited in a fully autosomal dominant manner.[99,102,114–116,119] Although the principal genes and proteins associated with each disease are thought to account for the vast majority of pathological phenotypes, the underlying genetics do not always match the same pathology. Therefore, efforts to elucidate the link between genetic variation, proteinopathy and neurodegeneration, are critical for finding disease-modifying therapies. In many cases, NGS and GWAS have led to the identification of not only disease-causing gene mutations but also gene loci and rare variants that confer higher or lower risk for disease vulnerability, starting to explain some phenotypic variability and clinicopathological data among individuals with the same gene mutation, emphasizing the concept of modifier genetic background.[119,148,154,155] Also here, patient iPSC models offer the opportunity to study disease etiology in two important ways. First, patient-derived cells offer the "most accurate" cell environment, with disease-relevant genes and proteins expressed at physiological relevant levels, and in the appropriate cellular context, to study molecular and cellular early events leading to neurodegeneration. This aspect is particularly significant when assessing protein accumulation- and aggregation-mediated toxicity, as these are highly dependent on concentration and cell type. Second, with increasing throughput in gene editing technologies (e.g., clustered regularly interspaced short palindromic repeats or CRISPR/Cas9[156]), it is now possible to determine, across otherwise isogenic cellular backgrounds, single gene mutation contribution to cellular phenotypes with relevance for disease.[157,158] When applied to large-scale and integrative research pipelines, these approaches can reveal the most relevant targets for therapeutics (Fig. 3).

1.03.2.2 Integrative and Translational Research of Human Disease Etiology

The era of iPSC-derived cellular models of human disease brought the potential to introduce the human context into the earliest stages of CNS drug discovery. However, investigative approaches usually focus on identifying in vitro phenotypes associated with genetic variation in disease, and then identifying candidate pharmacological agents that rescue these phenotypes in that specific cell model.[48] The challenge is in identifying the most relevant phenotype(s), that is, the determination of a "disease-relevant phenotype," to allow successful pharmacological investigation. A step forward might involve the development of standardized functional and phenotypic cellular assays, which can be run in a pipeline format for iPSC-derived cell models characterization and categorization, with downstream implementation of these same assays in the validation of pharmacological agents (Fig. 4). Observation of similar phenotypes across models of psychiatric and neurodegenerative disorders is promising, but true progress will involve integrative approaches guided by complementary information emerging from biomarker, clinical, and postmortem studies of human disease biology. In this regard, patient clinical cohorts that are extensively and longitudinally phenotyped by a variety of clinical and psychometric assessments, quantitative structural, functional, and molecular neuroimaging measurements, fluid biomarker sampling, and neuropathological analysis, offer a rich clinical-imaging-pathologic phenotype dataset context in which to interpret results from iPSC models. Finally, genomic approaches for patient stratification (NGS and GWAS) may also provide insights into clinical phenotypic variation, contributing to more complete understanding of the genetic architecture and pathways of disease mechanisms (Figs. 2 and 3).

1.03.2.2.1 Phenotyping pipelines in preclinical studies

Human iPSC-derived cell models hold the capability of supporting screening for disease-specific phenotypes and targets, and identifying initial hit structures for therapeutic development.[50] Even so, iPSC-derivation of expandable, self-renewing NPCs, which provide large-scale and consistent sampling of human neurons compatible with large-scale, HTS, has only recently become possible[40,48,97] (Table 1). By allowing a more precise understanding of genotype–phenotype relationship in disease-relevant human cell types, the use of human iPSC- and NPC-derived models in tandem with emerging genome engineering approaches provides a previously "missing link" between basic research and translational efforts. Nonetheless, given the complexity and diversity of biological processes involved in cellular phenotypic assays, it is unlikely that traditional approaches to drug discovery will be successful. In fact, cellular phenotypic assays need to replicate the disease phenotype to such an extent to confidently predict the translation of a given compound to clinically relevant features of illness. This presents challenges, given the relative immature nature of the differentiated cell types from iPSCs and lack of more tissue-like organization, which will be discussed later.

The main point of this section is to overview phenotypic methodologies that have been developed to characterize cellular models of human disease, including cutting-edge, single-cell level resolution, high-content automated imaging for network-targeted chemical genomics, and genotype and cell-type selective vulnerability in CNS disorders. Although harder to implement than to conceptualize, when coordinated in the format of a pipeline and consistently employed in the characterization of patient iPSC-derived neuronal models, standardized assays may help overcome technical issues of variability among same disease cellular models, leading to cumulative evidence of the "real" molecular and cellular disease alterations (Fig. 4). Such effort can also determine, across differently generated models and disease-related models, which are the phenotypes most relevant to a certain disease

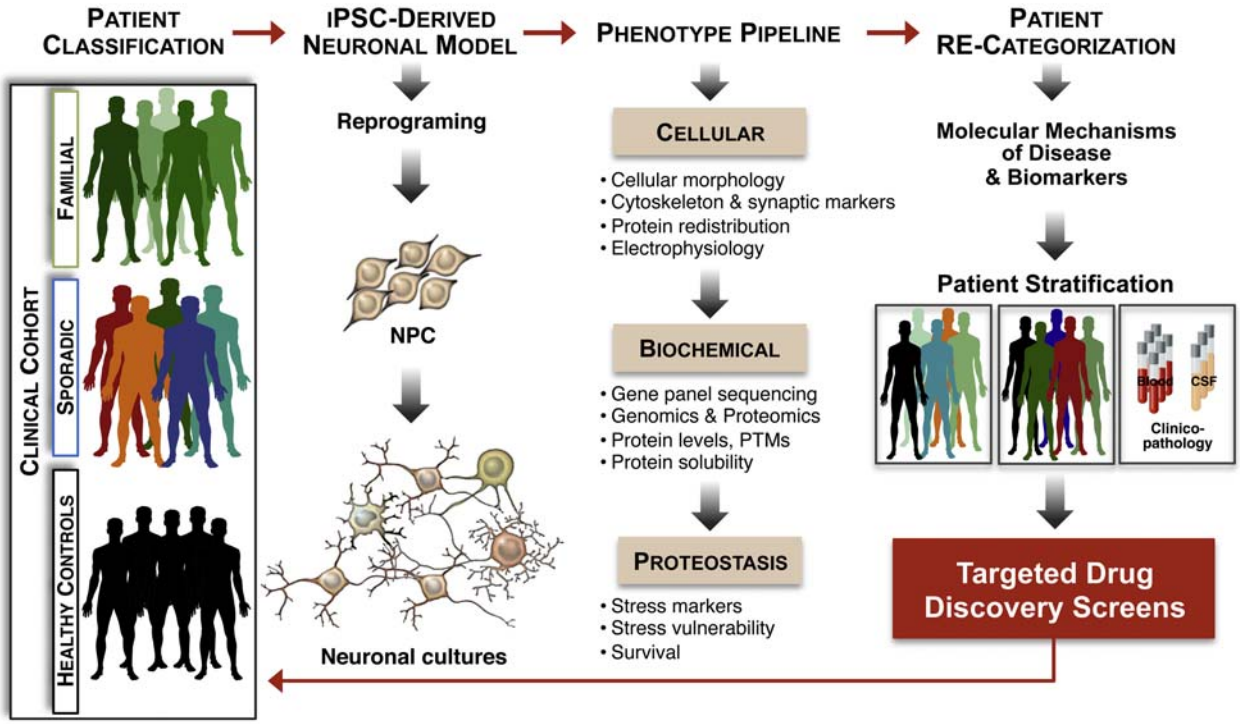

Fig. 4 Clinical cohort-based iPSC-derived cell banking approaches, with development and integration of standardized phenotypic pipelines, for determining molecular mechanisms of disease. Patient stratification based on clinical, genetic, and phenotypic data, for determination of drug screening targets and therapeutic trials in defined subpopulations.

category (e.g., cell stress pathways activated upstream of protein aggregation in neurodegeneration models), and therefore, which are the targets with highest potential for a positive therapeutic outcome (e.g., prevention of cell death in neurodegeneration). Phenotyping pipelines, in concert with clinical assessment and imaging, can ultimately represent valuable preclinical/presymptomatic diagnostic tools. We address here advances in genomic, biochemical, and cellular assays that can be employed toward a scalable platform of preclinical disease evaluation.

1.03.2.2.1.1 Genomics

Remarkable developments in NGS, whole exome sequencing, and GWAS have allowed for high-throughput sequencing of human genomic regions with considerable ease.[102,110–112,155] This has led to the identification of common genetic variants, as well as rare variants (<1% frequency in the population) and high-risk variants segregating with multifactorial, complex genetic disorders.[110,154,159] While the underlying genetics do not necessarily map directly onto specific pathologies, continued efforts to elucidate the link between genetic variability and disease phenotypes are critical to the development of disease-modifying therapies. Currently, sequencing efforts across larger patient cohorts start to offer important interpretive guidance in the mapping of pathways and cellular components with relevance to neuronal integrity, homeostasis, and functionality. As sequence data become available, integration with longitudinal clinical phenotypes, patient iPSC model research and postmortem neuropathology, can guide functional studies toward discovery of disease mechanisms and pathogenicity, and ultimately identification of promising therapeutic targets. Data integration across cohort datasets may also contribute to the development of a gene-panel-based diagnostics. Given the advances in genomics on a population level with efforts to assemble large (>1 million person) cohorts of fully sequenced subjects,[160] perhaps best exemplified by the Precision Medicine Initiative led by the FDA (see https://www.nih.gov/precision-medicine-initiative-cohort-program), one concept that has received much recent attention is the notion of using "experiments of nature" in the form of allelic variants of genes to provide correlative support of whether modulating a specific target will have the desired effect on human physiology and disease biology.[161–163] In certain cases, an allelic series can be identified that supports the directionally of what a therapeutic is desired to do (i.e., loss of function or gain of function), as well as specific structural elements of target that may drive specific physiological outcomes.[161] These observations then set the stage for efforts to identify a therapeutic modality that can mimic the effect of the genetic perturbation. Here, being able to directly measure the biochemical and cellular consequence of specific mutations and allelic series using patient-derived or engineered iPSC models holds tremendous promise for elucidating translatable, pharmacodynamic markers of target modulation; moreover, doing so with human iPSC models allows the potential to simultaneously develop appropriate screening system for drug discovery as discussed later.

1.03.2.2.1.2 Biochemical and cellular phenotypes

In cell models of human diseases where a gene and protein(s) have been associated with pathogenicity, biochemical profiling of patient iPSC-derived cell cultures has relied on techniques, such as quantitative measurement of gene (qRT-PCR) and protein expression (Western blotting), analysis of protein PTMs of relevance to disease mechanisms, and detection of protein species of reduced solubility and increased molecular weight, thought to contribute to disease but still through an unknown mechanisms and unclear timeline. Then, high-resolution, high-content microscopy can reveal a range of quantifiable phenotypes in patient iPSC-derived cells, including developmental/differentiation patterns, expression and subcellular localization of functional markers, as well as (mis)localization of molecules and proteins that are relevant for disease. This is well illustrated by multiple recently described iPSC-derived neuronal models.[35,39,58,138–140,150,157,164,165] Although cultures of specific "purified" cell types are a goal for dissecting disease cell-specific vulnerability, more "mixed" type cultures also allow, with proper cell-type markers, to dissect differential phenotypes within a population of neurons, without losing possible noncell autonomous mechanisms of disease etiology (e.g., glia contribution to neuronal death in ALS[93]). For cell models of psychiatric diseases, with unknown genetics or polygenicity, patient-derived neuronal cultures still allow access to measures of signaling pathway markers, and genotype–phenotype relationships through pathway-selective reporter genes,[40] high-content imaging,[39] and multiplexed gene expression and proteomic profiling assays.[50,166–168] Another remarkable technique uses multielectrode array technology that measures spontaneous bursting activity and evoked action potentials in stem cell-derived neuronal cultures, to capture information processing in an in vitro functional network,[169,170] with crucial relevance in monitoring pharmacological agents effect on network electrical and synaptic activity in studies with patient-derived neurons. Finally, state-of-art genome engineering technologies, such as the CRISPR/Cas9 system,[156] allow correcting or introducing disease mutations in otherwise isogenic iPSC lines, providing a rigorous test of genotype–phenotype correlations.[157,158,171] These tools also complement interpretation of the functional significance of rare genetic variants, as well as probing specificity and target-dependent rescue of phenotypes by any pharmaceutical agent.

1.03.2.2.1.3 Proteomics

Expanding on antibody-based approaches, quantitative methodologies for protein analysis using high-resolution, mass spectrometry (MS) assays have emerged as powerful phenotyping tools for iPSC-derived cells.[172–174] For example, in the case of neurodegenerative disorders involving dysregulation of tau, the FLEXITau MS assay generates MS profiles to detect differences in disease-relevant proteins, in this case tau, from patient iPSC-derived neurons, offering absolute quantification of levels, PTMs associated with neuropathology, and expression ratios between mutant and nonmutant proteins (in heterozygous patients), far surpassing accuracy of any other method.[41,173] Similar approaches with postmortem brain tissue can reveal disease-specific patterns of protein biochemistry (bar-coding), aiding in disease categorization at the preclinical stage with iPSC-derived neurons, and possibly accelerating diagnostics.[173,175]

1.03.2.2.1.4 Proteomic networks and disease nodes

Besides individual protein analysis, implementation of quantitative global proteomic MS profiling of patient iPSC-derived cells, over longitudinal culture periods, has the potential to reveal the dynamic dysregulation of protein networks, directly reveal which nodes in the network are more affected in disease, and identifying the most common alterations across similar diseases. Combined proteomic and pharmacological profiling of patient iPSC-derived neuronal models is an innovative approach to discover network-targeting chemical probes that unveil genotype-specific vulnerability in patient-only cells. That is, to dissect causality and direct link between disease-network nodes and neuropathology, pharmacological tools have the potential to perturb biological pathways in a temporally conditional manner to confirm altered vulnerability, contributing to the dissection of molecular pathways affected in disease. Based on recent studies with neurodegenerative iPSC-derived models,[41,137–140,157,176] patient-derived neurons do reveal dysregulation of specific proteostasis pathways. When further disrupted, by adding pathway-specific "insults," disease neurons' viability dramatically decreases, corroborating pathway involvement in disease and the validity of this research approach.[41,92,164] Development of neuronal stress probes toolboxes might be an efficient and cost-effective manner of validating large sets of proteomic data, to reveal molecular targets in disease.

Overall, phenotypic, disease-specific assays screened against focused libraries allow the entire proteome to be interrogated in a human cell context, to discover candidate therapeutic targets and representing a powerful paradigm shift in drug discovery (**Fig. 4**).

1.03.2.2.2 Integrative approaches across cell models and patient clinicopathological data

With the increasing applicability for iPSC-derived models of disease, it has become critical to quality control the emerging data. If robust disease-relevant cellular phenotypes can routinely be assessed in patient-derived in vitro cell models, it might just become feasible to use these biochemical imaging and physiological "pipelines" as new diagnostic tools for preclinical assessment and guidance of clinical trials.[133,134] Undoubtedly, these efforts will require integrative approaches for data interpretation in the context of clinicopathological data (**Figs. 2** and **4**).

A growing effort has been putting resources into increasing volunteer-based patient cohorts and building patient-iPSC line banks (e.g., NYSCF Research Institute Stem Cell Repository, StemBANCC, HipSci Consortium, Stem Cells Network DPUK Cohorts),[42–44] in order to work with individuals who have been extensively phenotyped by sophisticated clinical, psychometric assessments and imaging.[42,177] In a number of cases, these cohorts include quantitative neuroimaging measurements, fluid biomarker sampling, and, in many cases, patients who have agreed to brain donation. This rich set of clinical data will provide an invaluable context

in which to interpret findings from the iPSC model experiments (Fig. 2). Conversely, emerging disease biomarkers related to specific pathophysiological processes have been corroborated by various biomarker-autopsy correlation studies. Examples include increased uptake of amyloid-specific tracers associated with postmortem fibrillar Aβ deposits in AD patients; increase in tau and phospho-tau burden associated with neurofibrillary tau tangle burden at autopsy of AD and FTD cases; and specific brain areas atrophy on live patients' MRI (magnetic resonance imaging) correlated with neuron loss and tau immunostaining burden at autopsy in AD and FTD. For neurodegenerative tauopathies, ante-mortem MRI and PET scans increasingly report on disruption of brain morphology, (hypo)metabolism, and increased uptake of tau PET tracers often overlapping and correlated with tau inclusions burden at autopsy.[120,133,134,178–180] These promising results represent remarkably powerful methods of diagnosis, even presymptom onset, in living patients. Together with longitudinal clinical follow-up and postmortem neuropathology, this sets the stage for comparison and validation of data from patient iPSC-derived neuronal models that also report on early disruption of molecular pathways and cellular events preonset of disease (Fig. 2). Such integrative approaches have the power to elucidate genotype–phenotype variation and anatomical specificity among diseases, offering powerful guidance for phenotypic rescuing therapeutic targets, and clinical trials design.

Conceptually, testing experimental therapeutics in patient-specific iPSC models provides a powerful proof-of-concept for correlating physiologically relevant models of human disease to preexisting disease biomarkers (e.g., AD[133,134]), establishing the role of iPSC-based models in drug discovery, driven by human disease biology at each step of the process.

1.03.2.3 Human iPSC Models as Potential Preclinical Alternatives to Animal Models

Despite large investments in drug-discovery research, the overall success rate of pharmaceutical drug development for many diseases remains low. This has been debated furiously over the past decade and reviewed extensively elsewhere (e.g., [181]). Within AstraZeneca for example, there has been extensive study of the success rate of programs and implementation of the so-called 5R-criteria to increase the probability of success at each stage of the drug-discovery process.[182] Historically, the primary explanations for the high failure rate of drugs in the clinic were due to toxicology and safety issues but, thanks to the implementation of additional assays for toxicological screening and rigorous optimization of the properties of a molecule earlier in the drug-discovery process, this has become less of a problem. Instead, efficacy of the new therapeutic in the patient is now the main issue. Prominent explanations for this include the use of inappropriate screening assays which do not fully represent the disease state of the target, especially in neuroscience, the (mis)use of animal models, and the wrong patients being selected for the trial, which together contribute to the large gap in translation from bench to clinic.[152,153,183] Traditional drug-discovery approaches use biochemical (in vitro) and animal or human immortalized cell culture models (ex vivo or in cellulo) for initial screening of small-molecule libraries. Animal models are then employed for in vivo testing of drug delivery to target organs and cells, drug efficacy, and toxicity. The "human context" has typically only been implemented late in the discovery process, often during clinical trials, after lead compounds have been identified and thoroughly tested in animal models. Approaches using human stem cell disease models represent a paradigm shift that introduces the "human context" early in the drug-discovery pipeline. It also contributes to "personalized therapeutics/precision medicine" development as increasing patient-specific disease understanding can help select the correct patients for a trial and also predict treatment response (Fig. 4).[20,49,147,184,185]

In the case of CNS disorders, although rodent and human nervous systems share a number of evolutionary conserved properties, there are also critical differences in terms of neurogenesis and neural patterning that are critical when studying human diseases. Moreover, specific types of neurons that are affected in disease (e.g., von Economo neurons in FTD) are found only in humans and other large mammals and not in rodents, clearly highlighting the potential advantage of human iPSC-derived neuronal cultures if appropriate differentiation protocols can be created.[62,127,186–188] Additionally, many aspects of gene epigenetic regulation, particularly relevant in polygenic psychiatric diseases, are unique to the human genome and cannot be adequately investigated in nonhuman systems.[189,190] Finally, the immortalization process of animal or human cells to derive stable cell lines (e.g., HeLa, HEK293, and SH-SY5Y cells) interferes with the normal mechanisms of cell differentiation, and therefore the use of nonimmortalized, iPSC-differentiated cells allows access to a more physiologically relevant state with "human cell context."[48,50]

Replacement of animal-based studies has been strongly pursued also in toxicology studies, which are required to determine the effect of a substance on a tissue/organ at a particular concentration. This allows the determination of safety margins when selecting doses for human trials of a new therapeutic. Studies that convert in vitro results, generated at the tissue, cell, or subcellular level, into dose–response or potency information relating to an organism, that is, the human body (in vitro to in vivo extrapolation), have relied on stem-cell-derived generation of three-dimensional (3D) cultures that closely resemble human tissues/organs in silico, for not only disease studies but also toxicology studies.[191–193] Moreover, early in vitro toxicity testing using iPSC and differentiated specific cell types, such as hepatocytes, cardiomyocytes, neurons, or intestinal tissue, will serve as a cost-effective alternative to traditional in vivo testing (Table 1).[6,194]

Recent examples of successful FDA-approved drug discovery, in disease areas where animal models were deemed inadequate to accurately test efficacy (e.g., Kalydeco for cystic fibrosis[195]), combined with the uncertainties of modeling psychiatric disorders in animals,[153] provide strong motivation to pursue human stem cell-based drug discovery. Large-scale chemical screens in human iPSC models, which provide direct readouts of pathogenicity in vitro and an acceleration of the screening procedure relative to animal models, can lead to the identification of lead compounds that modulate disease-specific molecular processes, in a human cellular context (Table 1). However, the reality might as well be that due to the complexity of disease mechanisms in whole organisms, only a small percentage of initially promising small chemicals may qualify for application in humans. In other words, with

potential for increasing translational pharmacology and accelerate the overall drug development process, these ex-vivo systems may be a powerful step to determine efficacy prior to commencing clinical trials,[147] but it is probable that maximum drug-discovery success could lie within a cooperation between human iPSC-derived cell models and posterior animal testing. At present, validation of drug candidates identified via iPSC chemical screens does not obviate the relevance provided by downstream characterization and validation in animal models (Fig. 1).

1.03.3 Potential Roles for iPSC Models in Drug Development Pipeline

Though human patient-derived iPSC models provide ideal disease-relevant context in which to identify modifying agents of disease-related phenotypes, these can only truly contribute to drug screening if these stem cell-based cultures can be adapted for HTS-compatible formats. Moving beyond the testing of individual drugs, as described in a number of published studies to date, large-scale, HTS has only recently begun to be performed with stem-cell-derived cells. As summarized by the examples from CNS disorders and others in Table 1, gathered evidence so far indicates strong potential for screens to be performed at multiple stages of human cell development with stem cell models.

Two key, interrelated concepts when contemplating the use of human iPSC models in the context of drug screening are: (1) the disease biology supporting the relevance of a particular ex vivo cellular phenotype and (2) the translatability of the phenotypes being measured. These are not concepts unique to the use of human iPSC models but are nonetheless important to address considering the still nascent stage of the use of iPSC models in drug discovery.

In the case of disease relevance, while many cellular phenotypes could in principle be used to support drug-discovery efforts, demonstration of the relevance and specificity of a particular phenotype to the underling disease biology often requires data integration at multiple levels and knowledge that, for many diseases, is presently unknown. For example, since there are only symptomatic treatments of most psychiatric disorders, definitive knowledge of a disease-modifying pathway does not currently exist (but optimistically will in the future). Ultimately, the demonstration of the relevance of the particular phenotype and novel mechanism is only achievable through first-in-human clinical trials. Here, while conceptually powerful, even genetic data for the effect of gain- and loss-of-function mutations in an allelic series providing strong correlative validation of a particular target still requires demonstration that a therapeutic agent can mimic the effect of a protective allele or reverse the effect of a deleterious allele.

In the case of translatability of the phenotypes being measured, a critical question is whether a particular molecular mechanism modulated ex vivo will have the same biological effects when modulated in an in vivo context. With the use of patient-derived models the feasibility of the translation of the specific molecular marker being analyzed, be it an antibody or specific mRNA transcript, is more straightforward than redeveloping probes to measure the human homolog of a rodent or other model system. In many cases, new therapeutic modalities that are being developed will likely benefit from being optimized in the context of human biology. This includes antibodies that target protein–protein interactions, antisense oligonucleotides, and most of all gene editing using CRISPR/Cas9 and related technologies.

1.03.3.1 Examples of CNS-Focused iPSC Drug-Discovery Screening

With the two concepts of disease relevance and translatability in mind, below we summarize specific examples using cases of CNS and peripheral nervous system disorders to highlight ongoing technical approaches to novel therapeutic discovery using human iPSC models.

Landmark studies have highlighted important methodological considerations for investigation of CNS disorders with iPSCs, in particular as we consider these cells for HTS where the assays need to be relevant, robust, and reproducible to enable the more classical design-test-iterate process of early drug discovery.[77] Fortunately, parallel advances in automated microscopy and high-content imaging technologies now allow single-cell and subcellular level analysis of phenotypes with increased throughput in image acquisition, adaptable to iPSC-derived neuronal cell cultures.[196–198] Also, increased sophistication and throughput of computational methods for analysis of large imaging files with elevated number of parameters enables automated quantification of a diverse range of cellular features.[196,199] Furthermore, advances have been made in the generation of robust means to derive NPCs and adapt their use for HTS/HCS, functional genomics, and proteomics.[200–202]

1.03.3.1.1 Psychiatric disorder model screening

One of the first, and still largest scale that has been publicly disclosed, phenotypic screens relevant to multiple psychiatric and degenerative disorders is that of McNeish et al.[89] that aimed to identify novel classes of AMPA (alpha-amino-3-hydroxy-5-methyl-4-isoxazole propionic acid) glutamate receptor potentiators, involving both mouse and human stem cell-derived neuronal cultures subject to a calcium influx assay performed with a fluorimetric imaging plate reader (FLIPR) assay (Table 1). Given the importance of glutamatergic neurotransmission to multiple areas of nervous system plasticity and the challenge of faithfully accessing the biology of ion channels that are composed of multiple subunits and regulator subunits, this work reflects the potential for disease biology-relevant chemical screening with stem cell-derived neurons. That the throughput achieved enabled screening of over 2 million compounds further demonstrates the scalability of such assays.

Rather than targeting a specific neurotransmitter system, but with the goal of identifying novel proneurogenic compounds, McLaren et al.[172] reported on a screen of ~1000 compounds for their ability to enhance proliferation and/or viability of human

iPSC-derived NPCs using a bioluminescence-based assay (Table 1). The compounds identified from this screen hold potential both as research tools to aid in the expansion of NPC to large-scale necessary for HTS and leads for developing proneurogenic compounds that may be relevant to a range of psychiatric and degenerative disorders.

As an example of screening for small molecules that directly target a genetic cause of a psychiatric disorder, HTS for compounds capable of restoring expression of the silenced *FMR1* gene encoding the Fragile X mental retardation protein (FMRP) that causes Fragile X syndrome has recently been reported. Using a homogenous, time-resolved fluorescence resonance energy transfer (FRET) assay to measure FMRP levels in a high-density, 1536-well plate format the first of these from Kumari et al.[96] reported the identification of six structurally diverse compounds out of 5000 screened that were capable of enhancing FMRP expression. As an alternative screening methodology, using high-content imaging, Kaufmann et al.[97] screened over 50,000 compounds yielding a small number of compounds (structures not reported) also capable of reactivating FMRP expression (Table 1). While in both cases the level of FMRP expression obtained was fairly modest and may not be sufficient to rescue neurodevelopmental phenotypes and ultimately be effective in vivo,[39] nonetheless the success of these screening efforts demonstrate the feasibility of screening for additional FMRP enhancers using a range of methodologies as is now underway in both academic laboratories and industry.

An alternative approach to discovering therapeutic targets for psychiatric disorders than the focus on a specific target like an ion channel or gene expression states, as in the case of FXS screens, has been to use phenotypic assays to target the function of entire pathways. For example, the WNT signaling pathway is a key regulator of the nervous system development and plasticity and is modulated by a number of clinically used drugs, including the mood stabilizers lithium and valproate.[203] Dysregulation of WNT signaling has been implicated in the etiology of multiple psychiatric disorders, most notably autism spectrum disorders where strong genetic evidence implicates disruption of the function of genes such as *CHD8* encoding a chromatin remodeling enzyme involved in WNT signaling, and *CTNNB1* encoding β-catenin that interacts with CHD8 complexes.[204] On the basis of these findings, the discovery of novel targets for CNS-selective modulation of WNT/GSK3 signaling has the potential to be relevant for a range of disorders. To this end, Zhao et al. recently described a small-molecule screen for modulators of the WNT/β-catenin signaling pathway in human iPSC-derived NPCs, based on a stably integrated HTS-compatible, luciferase-based WNT pathway reporter system[40,48] (Table 1). After development and optimization for a 384-well plate format, this assay was used to screen a collection of ~1500 compounds from a library of US Food and Drug Administration (FDA)-approved drugs and known bioactive compounds, leading to the identification of a number of both known and novel small-molecule regulators of WNT signaling in human NPCs, including enhancers of lithium. Further optimization of this assay to an automated format has enabled screening of over 300,000 compounds for novel activators and inhibitors of WNT signaling demonstrating the feasibility to perform large-scale screens with human iPSC-derived cells in pathway-directed assays.

1.03.3.1.2 Neurodegenerative disorder model screening

One of the greatest opportunities afforded by human iPSC technology relates to the opportunity to investigate the early steps of disease pathogenesis. For this reason, and owing to the fact that in many cases the relevant cell types affected by the disease pathophysiology are often better understood than in psychiatric disorders, the use of iPSC models for drug discovery in neurodegenerative disorders has begun to see significant attention.

For example, aberrant tau accumulation and PTMs along with dysregulation of proteostasis pathways have now been reported in the context of iPSC models of tauopathies.[41,137–140,157,205] Additional examples of disease-relevant phenotypes have also been reported in iPSC models of multiple other genetic forms of neurodegeneration, including ALS,[90,206] AD,[92,150,207,208] and PD.[209–211] Collectively these observations set the stage for advancing therapeutic screens based upon specific disease hypotheses that are beginning to be realized. For example, Silva et al.[41] demonstrated the ability of mTORC1 inhibition, upon rapamycin treatment, to cause tau clearance through autophagy and rescue the enhanced stress vulnerability of iPSC-derived neurons with an A152T tau variant associated with FTD. Another example of rescuing FTD patient iPSC-derived neuronal phenotypes with pharmacological agents is the demonstration by Lee et al., in the context of a premature stop mutation (S116X) in the *GRN* gene-encoding progranulin (PGRN), that 1-[2-(2-tert-butyl-5-methylphenoxy)-ethyl]-3-methylpiperidine (MPEP) decreases Sortilin (SORT1) expression and rescues extracellular PGRN secretion.[212] Using iPSC-derived cortical neurons from PGRN-FTD subjects with the same mutation, Almeida et al.[164] provided proof-of-concept that *GRN* mRNA and PGRN protein levels can be upregulated through treatment with suberoylanilide hydroxamic acid, a histone deacetylase inhibitor. Taken together, these data provide concrete examples for the potential of FTD iPSC-derived models for novel target discovery.

In the context of the motor neuron disorder ALS, Egawa et al.[90] generated molecularly defined motor neuron subtypes from a panel of familial ALS patients' iPSCs with mutations (Q343R, M337V, G298S) in the Tar DNA-binding protein-43 (TDP-43), which caused aberrant, insoluble, cytosolic aggregates of TDP-43 along with aberrant neurite outgrowth. Screening a small collection of four compounds revealed that anacardic acid, a compound with histone acetyltransferase inhibitory activity among other effects, rescued abnormal ALS motor neuron phenotypes. Based on results from an initial large-scale screen of motor neurons from control and mutant SOD1 (G93A) mouse ESCs (Table 1), Yang et al.[93] demonstrated that the multikinase inhibitor kenpaullone prolonged survival of human iPSC-derived motor neurons with both SOD1 (L144F) and TDP-43 (M337V) mutations, while a second compound that interestingly failed clinical trials in ALS, dexpramipexole, was inactive, and a third compound, olesoxime, that also failed ALS clinical trails was only able to mildly rescue SOD1 (L144F) but not TDP-43 (M337V) survival. Instead of a survival phenotype in ALS, Burkhardt et al.[94] turned to a high-content chemical screen of over 1700 compounds based upon TDP-43 aggregate detection in iPSC-derived motor neuron cultures from sporadic ALS patients (Table 1). This screen led to the identification of the FDA-approved, cardiac glycosides drugs, including digoxin, lanatoside C, and proscillaridin A, two inhibitors of

cyclin-dependent kinase (CDK) inhibitors (flavopiridol, Cdk1/2 inhibitor III), four c-Jun N-terminal kinase (JNK) inhibitors (Incedis-01, BP-11767, NSN01, NSN02), and the natural product triptolide, all capable of reducing TDP-43 aggregates through mechanisms not yet well understood.

Of further note, while not a HTS *per se*, a notable example of the use of iPSC for potential novel therapeutic discovery is the work of Wainger et al. in the context of ALS that identified a hyperexcitable phenotype in ALS patient iPSC-derived motor neuron subtypes, which could be reversed by the existing antiepileptic drug retigabine (ezogabine; Potiga).[95] Here the use of detailed electrophysiology drove the selection of a pharmacological agent for subsequent clinical investigation.

1.03.3.1.3 Pain and sensory neuron disease model screening

Outside of the CNS, pioneering work from the laboratory of Dr. Lorenz Studer and colleagues demonstrated the ability of conduct a screen of over 6000 small molecules in patient-derived neural crest precursor cells for the ability to rescue expression of the *IKBKAP* gene that is disrupted in the rare neurogenetic disorder familial dysautonomia.[91] This screen led to identification of multiple agents targeting cAMP/protein kinase A activity and phosphorylation of the transcription factor CREB that plays a key role in gene transcription and neuroplasticity. Additionally, studies from Pfizer on iPSC-derived peripheral sensory neurons from patients with inherited erythromelalgia, caused by gain-of-function mutations in the *SCN9A* gene encoding the sodium channel Nav1.7, have also demonstrated the utility of iPSC models for drug discovery in the area of pain disorders.[213] Here, the clinical severity presented by patients could be correlated with ex vivo hyperexcitability of neurons, and this altered electrophysiological phenotype could be suppressed by Nav1.7 antagonists providing proof-of-concept of the therapeutic target for a sensory neuron disorder.

1.03.3.2 Quantitative Cellular Pharmacology

Besides the discovery of novel biologically active agents through HTS, another valuable use for human iPSC models in drug discovery is their use in quantitative cellular pharmacology. Here, the notion is to be able to rigorously assess target engagement in a physiologically and disease relevant cellular system, in order to define pharmacodynamic markers that are essential for successful translational studies.[162]

The contemporary approach to identifying lead molecules for drug discovery is based on selecting a target, establishing an in vitro screening assay and then identifying a molecule that interacts with that target, oftentimes through HTS. In many cases, in order to support high-throughput screening platforms, isolated recombinant proteins or even fragments of proteins are used for the screening assay. It is well recognized that isolated proteins or a protein fragment is far removed from the native drug target in a relevant cellular context, and from the molecular and physicochemical environment in which it resides. There are many examples of this disconnect between the pharmacological properties of drugs in these recombinant test systems when compared to the effects of drugs in native systems. The studies of Dr. Peter Sorger and colleagues exemplify this disconnect where drugs acting on components of the PI3K/AKT/mTOR pathway show discrepant dose–response curves and unusual pharmacological properties in native systems compared to activities of recombinant system.[214] Moreover, studies by McDonald and coworkers have shown that AKT signaling complexes associated with the plasma membrane are regulated by drugs such as PI3K inhibitors with high potency, whereas complexes in the nuclear compartment are not.[215] Human iPSC-derived neurons or glia potentially provide access to the native target in physiologically relevant protein complexes without the need for overexpression in a cellular context that may not model the native context appropriately. As such, iPSC-based screening assays promise to provide a more relevant approach as either a primary or secondary screening platform for the identification and characterization of CNS active drugs, particularly with advances in high-throughput generation of cultures of defined neuronal subtypes.[200,202]

These considerations are particularly relevant to CNS targets, many of which are cell-surface receptors or ion channels, often within large protein/lipid complexes, highly regulated by cellular activity and sensitive to the depolarization state of the cell. An interesting example is provided by the NMDA receptor, which is a heteropentameric ligand-gated ion channel of high interest as a target for the treatment of several neuropsychiatric disorders. Recombinant NMDA receptor complexes are extremely difficult to stably express in cell lines suitable for drug screening, at least in part due to their high calcium conductance. Human iPSC-derived neurons can express functional NMDA receptors that can be characterized electrophysiologically and are amenable to quantitative pharmacological assessment. Zhang et al.[216] have shown that the NMDA receptor currents in iPSC-derived neurons are consistent with GRIN2B-containing receptors and are specifically phosphorylated by FYN kinase, providing a platform for screening novel modulators of receptor function. Human stem cells can also provide a platform for the expression of recombinant human targets. For example, using the pluripotent cell line NTERA-2, ionotropic GABA and glycine receptors were successfully expressed as stable cell lines.[217] These receptors have been studied in recombinant systems at the screening level; however, these engineered systems lack the relevant neuronal environment and are limited by the restricted number of receptor subunits that can be coexpressed. Expression in a human iPSC-derived cell system combined with fluorescence imaging provides a potential high-content system amenable to quantitative pharmacological analysis and more closely modeling the native system.

1.03.3.2.1 Advances Enabling Novel Assay Development and Target Validation

Although only a limited number of large-scale screens for novel therapeutic agents have been performed to date (**Table 1**), a number of technical and conceptual advances on the horizon make it highly likely that the number of therapeutic screening efforts utilizing

human iPSC models will continue to expand. These efforts will expand from the beginning of the drug-discovery process involving the identification of novel targets and lead compounds, all the way through the optimization of development candidates for in vivo studies in humans.

A major driver for these efforts is likely to entail the use of CRISPR/Cas9 and related genome-editing techniques for the creation of isogenic cell models to aid in the understanding of genotype–phenotype correlations and the basic function of genes.[218,219] Here, matched sets of isogenic controls will reduce the sample size needed to associate a particular phenotype with a specific genetic alteration. However, the potential for clonal variation and off-target effects of genome-editing process still ideally requires that multiple clones be analyzed.[49] In addition to editing of the genome, adaptations of the CRISPR/Cas9 system are also enabling site-specific modulation of both the epigenome, through recruitment of epigenetic regulatory enzymes, and transcriptional regulation through the fusion of Cas9 to either transcriptional repressor domains for CRISPR inhibition (CRISPRi) or transcriptional activators domains for CRISPR activation (CRISPRa).[220,221] These functional genomic and epigenomic tools, in conjunction with patient-derived iPSC models, hold much promise for creation of innovative tools to assist in therapeutic target identification and validation. The future creation of a complete collection of human iPSC gene knockout (or overexpression) lines using genome-editing techniques will rapidly advance the systematic comparison of genotypes–phenotypes and aid in the performance of "synthetic lethal" and other functional genomic screens currently only possible in model organisms or through pooled CRISPR/Cas screening approaches that are emerging.[222]

Techniques of genome editing also enable the creation of innovative assays for use in drug screening by "tagging" promoters for the creation of endogenous reporter genes or reporter proteins without the need to express them as transgenes, enabling the investigation of physiologically relevant protein complexes with minimized risk of altering their composition and stoichiometry. For example, iPSC lineage-specific reporters for MAP2 (neural lineage specific) or GFAP (astrocyte lineage specific) gene expression have been generated through the targeting of NanoLuc-HaloTag construct to the 3′-prime end of genes of interest to allow normal levels of expression of the endogenous genes with facile detection of protein expression in both live cells for kinetic studies and fixed cells through the luciferase or HaloTag reporters.[223] The near future is bound to provide a suite of molecular and cellular tools for rapid and inexpensive generation of HTS-compatible assays in human iPSC models customized for each disease area.

1.03.3.2.2 Toxicology and Drug Metabolism

There has been considerable effort to establish iPSC-derived cellular models to inform on potential toxicity of drug candidates.[20–34,49,224,225] While a comprehensive review of this area is beyond the scope of the current article, there are a number of applications that are particularly relevant to CNS drug discovery. Through a combination of the nature of many CNS drug targets and the requirement to produce compounds with physicochemical properties consistent with brain exposure, cardiotoxicity has been a major problem in CNS drug discovery. Most approaches to this problem have studied the electrophysiological responses to drugs in iPSC-derived cardiomyocytes.[20,21,231] The use of human iPSC-derived cardiomyocytes in this context provides several major advantages, namely, the expression of a near full repertoire of cardiac ion channels modulating cardiac function and the ability to derive cells from risk genotypes for screening. Patient iPSC-derived cardiomyocytes are increasingly used to evaluate cardiac risk across genotypes and specific syndromes including long QT syndrome and various cardiomyopathies. Recent studies by AstraZeneca using a range of 51 cardiotoxic compounds demonstrated 70% specificity and greater than 85% sensitivity of the screening method for predicting risk, similar to data produced by other investigators.

In addition to cardiomyocytes, iPSC-derived hepatocytes[22,232] and hematopoietic cells have also been used extensively for ex vivo toxicity testing.[49,224] Human hepatocytes and liver microsomal preparations are the mainstay of ex vivo systems used to generate primary predictions of drug metabolism in humans. These methods are now, or could well be, supplemented by several novel iPSC-based methods.[22,193] The potential to induce the expression of drug-metabolizing enzymes, particularly cytochrome P450s, in the liver and intestine can be modeled in iPSC-derived hepatocytes and enterocytes,[226] and a variety of methods have been employed to derive iPSC-derived cell systems for studying drug transport and diffusion,[227] including models of the blood–brain barrier.[225]

1.03.4 Patient Stratification and Disease Diagnosis

Once patient-specific iPSCs were demonstrated as feasible by Yamanaka and colleagues, the concept of "clinical trials in a dish" was immediately recognized as a potential strategy for the identification of subpopulations of patients with a particular disease that may respond to a particular therapeutic agent[49] (**Fig. 4**). Furthermore, patient-specific iPSC generation has also been recognized as a potential means to generate cellular signatures in response to diverse pharmacological or functional genomic perturbations to create diagnostic subgroups of patients.[48,49,228] Together, these concepts have important implications for the future of medicine that have been referred to, appropriately so if they can come to fruition, as "game changing."[49]

1.03.4.1 iPSCs to Predict Drug Responders and Nonresponders

The realization of using iPSC-derived cellular models for patient stratification requires overcoming the dual obstacles of the generation of sufficiently large patient cohort-derived iPSCs to be able to identify responders and nonresponders, and the development of

molecular or cellular biomarkers that have sufficient predictive power and accuracy to translate between ex vivo assays and in vivo treatment of diseases. For diseases where efficacy in the clinic is poorly predicted by existing animal models due to poor evolutionarily conserved biology, for example where causal genetic variation is located in noncoding regions of the genome, or where tissues like the brain are highly elaborated comparing rodents to humans, this strategy may provide an alternative path forward to gain confidence in efficacy. Furthermore, by identifying ex vivo responders based upon the response of patient-specific iPSCs models prior to a Phase II trial, the actual clinical trial itself could be performed with subjects predicted to respond to the drug, based on their specific iPSC-based results. Theoretically, this would increase the power of studies to detect drug efficacy in smaller patient populations and minimize the negative effects of exposing patients to ineffective treatments. While this has yet to be achieved, conceptually the cost and timeline of generation of such a cohort is relatively insignificant compared to the costs and setbacks of a failed Phase II or Phase III trial.

Additionally, such ex vivo patient iPSC-derived cellular responses could be used in advance of patient treatment for already approved drugs where patient response is suboptimal. For example, being able to predict which subjects respond to the mood stabilizer lithium on the basis of iPSC-derived neuronal cell assays in which patients are classified into responder and nonresponder subjects could greatly improve the standard of care in bipolar disorder since roughly half of patients do not respond to this treatment. In the case of lithium, to date such approaches have only been performed retrospectively with the observation of a correlation between clinical response and the ability to suppress a hyperexcitability phenotype in hippocampal-like neurons in lithium responders- and not nonresponders-derived iPSC models.[82] Besides performing such studies prospectively, the sample size analyzed will need to be scaled appropriately to represent the heterogeneity of the disorder. This approach could also be used, for example, to dissect the relationship between gene epigenetic status and drug response (e.g., *FMR1* methylation status and mGluR5 antagonist response in Fragile X syndrome).[229] Most important, assuming faithful recapitulation of the gene epigenetic status in vitro and in vivo in the brain, pretesting of compounds in patient iPSC-derived neuronal cells may help improve prediction of clinical response.

With time, the systematic generation of ex vivo response data in large cohorts for different classes of existing medicines, as well as novel experimental therapeutics, may ultimately allow the discovery of predictive rules for future development of medicines when performed in conjunction with generating full genome sequences and tracking of individuals longitudinally using electronic health records. At the same time, by focusing on the response of individual patients, the use of patient-specific iPSC models and ex vivo drug response provides a practical realization of the concepts of personalized and precision medicine.[160]

Overall, the prediction of whether patients will respond to a particular pharmacological agent based upon ex vivo analysis of iPSC-derived cellular phenotypes, alone or in combination with genetic information, has the potential to impact how modern preclinical studies and clinical trials are performed (**Fig. 4**). While current regulatory policies prevent the replacement of standard clinical trials with an "iPSC clinical trial," it may be feasible in the future to establish such a framework if sufficient prospective predictions of drug response and efficacy are obtained for challenging disorders.[49] Such studies would not obviate the need for careful safety and toxicology studies, which themselves are beginning to benefit from using patient-specific iPSC models,[230] as mentioned earlier for cardiotoxicity,[231] hepatoxicity,[232] and neurotoxicity,[231,233] creating new avenues to demonstrate the efficacy of medicines with the potential for eliminating ineffective ones earlier on in the development process.

1.03.4.2 Role of iPSC Disease Models in Clinical Diagnosis and Prognosis

While the fundamental basis of most current medicine is the treatment of disease symptoms once they manifest, the future of medicine will ideally focus on the development of highly effective, disease-modifying and preventative treatments, along with diagnostic methods that allow the identification of high-risk individuals. This will enable treatment to be initiated early, potentially at a time when it can be most effective, specifically for neurodegenerative disorders where prevention of neuronal cell death is crucial. While molecular and genetic diagnoses for certain disorders are increasingly possible given the availability of specific molecular assays, along with advances in human genome sequencing, many diseases lack precise molecular biomarkers and are polygenic in nature rendering a strict genetic diagnosis not feasible at present. For these collective reasons, beyond the prediction of whether patients will respond to a particular pharmacological agent based upon ex vivo analysis of iPSC-derived cellular phenotypes, there is increasing interest in the concept of generating ex vivo drug-response signatures to diagnose patients and group them into subgroups with the ultimate goal of being able to provide a prognosis (**Fig. 4**).

One strategy being employed to advance this concept is that of using a panel of cellular stressors to reveal susceptibility to disease pathophysiology. For example, using iPSC-derived neuronal models of tauopathy Silva et al.[41] has observed that coupled to dysregulation of tau and enhanced stress-inducible markers, neurons from FTD subjects show increased cell vulnerability to a panel of proteotoxic, excitotoxic, and mitochondrial stressor compounds. This enhanced neuronal vulnerability of neurons to stressors could be rescued upon CRISPR/Cas9-mediated targeting of the *MAPT* locus to knockout tau, demonstrating the causal link to a known pathogenic factor. Since the majority of cases of FTD are sporadic in nature and lack mutations in tau, the application of this panel of cell stressor could conceivably reveal if FTD cases without tau mutations show similar susceptibility. This diagnostic grouping of patients could then be used to predict mechanisms of tau-mediated pathogenesis in cases of sporadic FTD. Beyond assays of cellular viability, the generation of transcriptional signatures using multiplexed gene expression-based screening and proteomic signatures has tremendous potential as drug-response signatures if applied across cohorts of iPSC models.[166–168]

All said, it is still too early to determine whether iPSC models will have a major impact on diagnosis and prognosis of a particular disease. Certainly, iPSCs can be used to analyze the response of a particular cell to a therapeutic, but whether this would predict

a long-term beneficial effect in a human is not known. In terms of diagnosis it is possible that studies of iPSCs could play a role in tandem with other technologies, such as PET-imaging, peripheral blood, or cerebrospinal fluid analysis, to identify patients at very early stages of the disease and then monitor appropriate biomarkers in response to treatment (Fig. 4).

1.03.5 Challenges and Concluding Remarks

On account of a persistent disconnect between phenotypic-driven drug pharmacology from in vitro cellular models or in vivo animal models, and drug efficacy in human trials, the quest for optimized preclinical biological model systems, better predictive of clinical outcome, is a present and urgent challenge in drug discovery. Integral to this quest is the capacity of working with the *bona fide* human disease-relevant cells or tissue.[234,235]

While human iPSC-derived cellular models present promising avenues for pharmacological probes and drug discovery, there are still a number of limitations and challenges.[236] One general limitation is the fact that postmitotic cell types obtained through the directed differentiation of iPSCs are still relatively immature, based on a number of gene expression and physiological markers. This issue is particularly relevant for tissues with limited replicative turnover of cells, for example, the CNS where many cell types in the brain mature over an individual's lifetime. Possible strategies to circumvent this aspect and promote faster maturation and aging of, for example, neural cells in culture are being addressed.[36,237] Additionally, efforts to create 3D cultures of "organoids" with more physiological arrangements of cells into tissue-like structures are gaining traction.[238–240] Certainly assays relying on longer culturing periods and more complex architectures are likely to better capture features of mature cell types, but at the cost of diminished feasibility and scalability. Despite progress in identifying the developmental course of specific cell types, for example, neurons, glia,[241] and pancreatic β-cells,[242] reducing these to practical techniques for drug-discovery efforts still presents challenges.

At present, there is still a lack of robust methodology for reproducible, large-scale production of disease-relevant specific cell types, but current efforts are focused on promoting culture compatibility with HTS modalities, including high-content imaging, multidimensional signature-based screening, and in vitro network activity with multielectrode arrays.[6] These technologies are in active and remarkable development, as is the utility of patient-specific stem models.[35,50,62,90,209,243] Another simple, if very relevant and practical, limitation in human stem cell research for drug-discovery purposes is the relative high cost of cell culture media and supplements, along with the expertise required to reliably generate robust cultures. Together with low scalability for iPSC differentiation, many publications tend to describe and characterize only a minimum number of case and control lines, which can always be susceptible to artifacts introduced by subtle differences in cell line generation, and limited representation of genetically heterogeneous patient populations, particularly for complex, polygenic disorders. Then, it becomes critical for initial findings in small numbers of lines to be replicated in larger cohorts and in multiple lines from individual subjects, with efforts for data integration across genotypes, cell lines, and clinicopathological data, which is currently being addressed with urgency (Figs. 2 and 4).

Another point for consideration has to do with patient-derived cellular models that address mainly cell-autonomous aspects of disease, exploring phenotypes in individual cultured cells regardless of their *milieu*, and without a clear definition of their developmental stage. The concerning aspect is neglecting potentially relevant aspects of the tissue of interest that can certainly influence the outcome of therapeutic interventions. For example, cell-to-cell interactions among neuronal subtypes and glia, synaptic transmission between neurons, and the existence of complex neural networks that creates a circuitry known to be critical to high-order brain function and plasticity are challenging to faithfully mimic with ex vivo cellular models.[187,244] Nonetheless, even if a disease is most apparent at the network level, it does not necessarily follow that deficits will not be observed at the individual cell level. Along these lines, mixed cell populations that result from standard differentiation protocols that were initially considered a limitation might instead represent an opportunity to interrogate multiple cell types simultaneously without losing possible cell nonautonomous mechanisms of disease etiology. Complementary validation of phenotypes with other systems, premortem patient clinical data and postmortem disease pathology, should circumvent many of these concerns (Fig. 2).

In conclusion, in order to improve usefulness of human iPSC modeling for drug-discovery efforts, it is of prime importance to focus on standardization of protocols for iPSCs generation and differentiation,[245] define standards of disease phenotyping in terms of intra- and inter-individual variation, and include strict quality control parameters. The main driving force for advancing human iPSC-derived models in drug discovery will continue to be the concrete demonstration that these cellular systems can: (1) be effectively used to understand the molecular and cellular mechanisms of disease, and possibly the basis for selective cellular vulnerability seen in many diseases and (2) be employed in functional cellular and biochemical assays toward discovery of the next-generation therapeutic agents for the treatment and ultimately prevention of a myriad of human diseases.

References

1. Reubinoff, B. E.; Pera, M. F.; Fong, C. Y.; Trounson, A.; Bongso, A. Embryonic Stem Cell Lines From Human Blastocysts: Somatic Differentiation In Vitro. *Nat. Biotechnol.* **2000,** *18* (4), 399–404.
2. Takahashi, K.; Tanabe, K.; Ohnuki, M.; Narita, M.; Ichisaka, T.; Tomoda, K.; Yamanaka, S. Induction of Pluripotent Stem Cells From Adult Human Fibroblasts by Defined Factors. *Cell* **2007,** *131* (5), 861–872.
3. Takahashi, K.; Yamanaka, S. Induction of Pluripotent Stem Cells From Mouse Embryonic and Adult Fibroblast Cultures by Defined Factors. *Cell* **2006,** *126* (4), 663–676.

4. Thomson, J. A.; Itskovitz-Eldor, J.; Shapiro, S. S.; Waknitz, M. A.; Swiergiel, J. J.; Marshall, V. S.; Jones, J. M. Embryonic Stem Cell Lines Derived From Human Blastocysts. *Science* **1998,** *282* (5391), 1145–1147.
5. Yu, J.; Vodyanik, M. A.; Smuga-Otto, K.; Antosiewicz-Bourget, J.; Frane, J. L.; Tian, S.; Nie, J.; Jonsdottir, G. A.; Ruotti, V.; Stewart, R.; Slukvin, I. I.; Thomson, J. A. Induced Pluripotent Stem Cell Lines Derived From Human Somatic Cells. *Science* **2007,** *318* (5858), 1917–1920.
6. Desbordes, S. C.; Studer, L. Adapting Human Pluripotent Stem Cells to High-Throughput and High-Content Screening. *Nat. Protoc.* **2013,** *8* (1), 111–130.
7. Eglen, R.; Reisine, T. Primary Cells and Stem Cells in Drug Discovery: Emerging Tools for High-Throughput Screening. *Assay Drug Dev. Technol.* **2011,** *9* (2), 108–124.
8. Jensen, J.; Hyllner, J.; Bjorquist, P. Human Embryonic Stem Cell Technologies and Drug Discovery. *J. Cell. Physiol.* **2009,** *219* (3), 513–519.
9. Fusaki, N.; Ban, H.; Nishiyama, A.; Saeki, K.; Hasegawa, M. Efficient Induction of Transgene-Free Human Pluripotent Stem Cells Using a Vector Based on Sendai Virus, an RNA Virus That Does Not Integrate Into the Host Genome. *Proc. Jpn. Acad. Ser. B Phys. Biol. Sci.* **2009,** *85* (8), 348–362.
10. Okita, K.; Ichisaka, T.; Yamanaka, S. Generation of Germline-Competent Induced Pluripotent Stem Cells. *Nature* **2007,** *448* (7151), 313–317.
11. Okita, K.; Nakagawa, M.; Hyenjong, H.; Ichisaka, T.; Yamanaka, S. Generation of Mouse Induced Pluripotent Stem Cells Without Viral Vectors. *Science* **2008,** *322* (5903), 949–953.
12. Stadtfeld, M.; Nagaya, M.; Utikal, J.; Weir, G.; Hochedlinger, K. Induced Pluripotent Stem Cells Generated Without Viral Integration. *Science* **2008,** *322* (5903), 945–949.
13. Warren, L.; Manos, P. D.; Ahfeldt, T.; Loh, Y. H.; Li, H.; Lau, F.; Ebina, W.; Mandal, P. K.; Smith, Z. D.; Meissner, A.; Daley, G. Q.; Brack, A. S.; Collins, J. J.; Cowan, C.; Schlaeger, T. M.; Rossi, D. J. Highly Efficient Reprogramming to Pluripotency and Directed Differentiation of Human Cells With Synthetic Modified mRNA. *Cell Stem Cell* **2010,** *7* (5), 618–630.
14. Xu, J.; Du, Y.; Deng, H. Direct Lineage Reprogramming: Strategies, Mechanisms, and Applications. *Cell Stem Cell* **2015,** *16* (2), 119–134.
15. Yu, J.; Hu, K.; Smuga-Otto, K.; Tian, S.; Stewart, R.; Slukvin, I. I.; Thomson, J. A. Human Induced Pluripotent Stem Cells Free of Vector and Transgene Sequences. *Science* **2009,** *324* (5928), 797–801.
16. Williams, L. A.; Davis-Dusenbery, B. N.; Eggan, K. C. SnapShot: Directed Differentiation of Pluripotent Stem Cells. *Cell* **2012,** *149* (5), 1174–1174 e1.
17. Zhang, Y.; Pak, C.; Han, Y.; Ahlenius, H.; Zhang, Z.; Chanda, S.; Marro, S.; Patzke, C.; Acuna, C.; Covy, J.; Xu, W.; Yang, N.; Danko, T.; Chen, L.; Wernig, M.; Sudhof, T. C. Rapid Single-Step Induction of Functional Neurons From Human Pluripotent Stem Cells. *Neuron* **2013,** *78* (5), 785–798.
18. Raab, S.; Klingenstein, M.; Liebau, S.; Linta, L. A Comparative View on Human Somatic Cell Sources for iPSC Generation. *Stem Cells Int.* **2014,** *2014,* 768391.
19. Okita, K.; Matsumura, Y.; Sato, Y.; Okada, A.; Morizane, A.; Okamoto, S.; Hong, H.; Nakagawa, M.; Tanabe, K.; Tezuka, K.; Shibata, T.; Kunisada, T.; Takahashi, M.; Takahashi, J.; Saji, H.; Yamanaka, S. A More Efficient Method to Generate Integration-Free Human iPS Cells. *Nat. Methods* **2011,** *8* (5), 409–412.
20. Del Alamo, J. C.; Lemons, D.; Serrano, R.; Savchenko, A.; Cerignoli, F.; Bodmer, R.; Mercola, M. High Throughput Physiological Screening of iPSC-Derived Cardiomyocytes for Drug Development. *Biochim. Biophys. Acta* **2016,** *1863* (7 Pt B), 1717–1727.
21. Ieda, M.; Fu, J. D.; Delgado-Olguin, P.; Vedantham, V.; Hayashi, Y.; Bruneau, B. G.; Srivastava, D. Direct Reprogramming of Fibroblasts into Functional Cardiomyocytes by Defined Factors. *Cell* **2010,** *142* (3), 375–386.
22. Du, Y.; Wang, J.; Jia, J.; Song, N.; Xiang, C.; Xu, J.; Hou, Z.; Su, X.; Liu, B.; Jiang, T.; Zhao, D.; Sun, Y.; Shu, J.; Guo, Q.; Yin, M.; Sun, D.; Lu, S.; Shi, Y.; Deng, H. Human Hepatocytes With Drug Metabolic Function Induced from Fibroblasts by Lineage Reprogramming. *Cell Stem Cell* **2014,** *14* (3), 394–403.
23. Phillips, B. W.; Hentze, H.; Rust, W. L.; Chen, Q. P.; Chipperfield, H.; Tan, E. K.; Abraham, S.; Sadasivam, A.; Soong, P. L.; Wang, S. T.; Lim, R.; Sun, W.; Colman, A.; Dunn, N. R. Directed Differentiation of Human Embryonic Stem Cells into the Pancreatic Endocrine Lineage. *Stem Cells Dev.* **2007,** *16* (4), 561–578.
24. Spence, J. R.; Mayhew, C. N.; Rankin, S. A.; Kuhar, M. F.; Vallance, J. E.; Tolle, K.; Hoskins, E. E.; Kalinichenko, V. V.; Wells, S. I.; Zorn, A. M.; Shroyer, N. F.; Wells, J. M. Directed Differentiation of Human Pluripotent Stem Cells Into Intestinal Tissue In Vitro. *Nature* **2011,** *470* (7332), 105–109.
25. Heneka, M.; Andreasson, K. I.; Bachstetter, A. D.; Colonna, M.; Ginhoux, F.; Holmes, C.; Lamb, B.; Landreth, G.; Lee, D. C.; Low, D.; Lynch, M. A.; Monsonego, A.; O'Banion, M. K.; Pekny, M.; Puschmann, T.; Russek-Blum, N.; Sandusky, L. A.; Selenica, M. B.; Takata, K.; Teeling, J.; Town, T.; Van Eldik, L. J.; Schulz, J. B. Targeting Innate Immunity for Neurodegenerative Disorders of the Central Nervous System. *J. Neurochem.* **2016,** *138,* 653–693.
26. Fagan, T. Induced Microglia Make Debut at Keystone Symposium CONFERENCE COVERAGE SERIES Keystone Symposia. http://www.alzforum.org/news/conference-coverage/induced-microglia-make-debut-keystone-symposium.
27. Chen, W.; Abud, E. A.; Yeung, S. T.; Lakatos, A.; Nassi, T.; Wang, J.; Blum, D.; Buee, L.; Poon, W. W.; Blurton-Jones, M. Increased Tauopathy Drives Microglia-Mediated Clearance of Beta-Amyloid. *Acta Neuropathol. Commun.* **2016,** *4* (1), 63.
28. Ambasudhan, R.; Talantova, M.; Coleman, R.; Yuan, X.; Zhu, S.; Lipton, S. A.; Ding, S. Direct Reprogramming of Adult Human Fibroblasts to Functional Neurons Under Defined Conditions. *Cell Stem Cell* **2011,** *9* (2), 113–118.
29. Hu, W.; Qiu, B.; Guan, W.; Wang, Q.; Wang, M.; Li, W.; Gao, L.; Shen, L.; Huang, Y.; Xie, G.; Zhao, H.; Jin, Y.; Tang, B.; Yu, Y.; Zhao, J.; Pei, G. Direct Conversion of Normal and Alzheimer's Disease Human Fibroblasts into Neuronal Cells by Small Molecules. *Cell Stem Cell* **2015,** *17* (2), 204–212.
30. Li, W.; Sun, W.; Zhang, Y.; Wei, W.; Ambasudhan, R.; Xia, P.; Talantova, M.; Lin, T.; Kim, J.; Wang, X.; Kim, W. R.; Lipton, S. A.; Zhang, K.; Ding, S. Rapid Induction and Long-Term Self-Renewal of Primitive Neural Precursors From Human Embryonic Stem Cells by Small Molecule Inhibitors. *Proc. Natl. Acad. Sci. U. S. A.* **2011,** *108* (20), 8299–8304.
31. Pang, Z. P.; Yang, N.; Vierbuchen, T.; Ostermeier, A.; Fuentes, D. R.; Yang, T. Q.; Citri, A.; Sebastiano, V.; Marro, S.; Sudhof, T. C.; Wernig, M. Induction of Human Neuronal Cells by Defined Transcription Factors. *Nature* **2011,** *476* (7359), 220–223.
32. Son, E. Y.; Ichida, J. K.; Wainger, B. J.; Toma, J. S.; Rafuse, V. F.; Woolf, C. J.; Eggan, K. Conversion of Mouse and Human Fibroblasts into Functional Spinal Motor Neurons. *Cell Stem Cell* **2011,** *9* (3), 205–218.
33. Tsunemoto, R. K.; Eade, K. T.; Blanchard, J. W.; Baldwin, K. K. Forward Engineering Neuronal Diversity Using Direct Reprogramming. *EMBO J.* **2015,** *34* (11), 1445–1455.
34. Yoo, A. S.; Sun, A. X.; Li, L.; Shcheglovitov, A.; Portmann, T.; Li, Y.; Lee-Messer, C.; Dolmetsch, R. E.; Tsien, R. W.; Crabtree, G. R. MicroRNA-Mediated Conversion of Human Fibroblasts to Neurons. *Nature* **2011,** *476* (7359), 228–231.
35. Ichida, J. K.; Kiskinis, E. Probing Disorders of the Nervous System Using Reprogramming Approaches. *EMBO J.* **2015,** *34* (11), 1456–1477.
36. Lee, J. H.; Mitchell, R. R.; McNicol, J. D.; Shapovalova, Z.; Laronde, S.; Tanasijevic, B.; Milsom, C.; Casado, F.; Fiebig-Comyn, A.; Collins, T. J.; Singh, K. K.; Bhatia, M. Single Transcription Factor Conversion of Human Blood Fate to NPCs with CNS and PNS Developmental Capacity. *Cell Rep.* **2015,** *11* (9), 1367–1376.
37. Chambers, S. M.; Fasano, C. A.; Papapetrou, E. P.; Tomishima, M.; Sadelain, M.; Studer, L. Highly Efficient Neural Conversion of Human ES and iPS Cells by Dual Inhibition of SMAD Signaling. *Nat. Biotechnol.* **2009,** *27* (3), 275–280.
38. Nemati, S.; Hatami, M.; Kiani, S.; Hemmesi, K.; Gourabi, H.; Masoudi, N.; Alaei, S.; Baharvand, H. Long-Term Self-Renewable Feeder-Free Human Induced Pluripotent Stem Cell-Derived Neural Progenitors. *Stem Cells Dev.* **2011,** *20* (3), 503–514.
39. Sheridan, S. D.; Theriault, K. M.; Reis, S. A.; Zhou, F.; Madison, J. M.; Daheron, L.; Loring, J. F.; Haggarty, S. J. Epigenetic Characterization of the FMR1 Gene and Aberrant Neurodevelopment in Human Induced Pluripotent Stem Cell Models of Fragile X Syndrome. *PLoS One* **2011,** *6* (10). e26203.
40. Zhao, W. N.; Cheng, C.; Theriault, K. M.; Sheridan, S. D.; Tsai, L. H.; Haggarty, S. J. A High-Throughput Screen for Wnt/beta-Catenin Signaling Pathway Modulators in Human iPSC-Derived Neural Progenitors. *J. Biomol. Screen.* **2012,** *17* (9), 1252–1263.
41. Silva, M. C.; Cheng, C.; Mair, W.; Almeida, S.; Fong, H.; Biswas, M. H. U.; Zhang, Z.; Huang, Y.; Temple, S.; Coppola, G.; Geschwind, D. H.; Karydas, A.; Miller, B. L.; Kosik, K. S.; Gao, F. B.; Steen, J. A.; Haggarty, S. J. Human iPSC-Derived Neuronal Model of Tau-A152T Frontotemporal Dementia Reveals Tau-Mediated Mechanisms of Neuronal Vulnerability. *Stem Cell Rep.* **2016,** *7* (3), 325–340.
42. Soares, F. A.; Sheldon, M.; Rao, M.; Mummery, C.; Vallier, L. International Coordination of Large-Scale Human Induced Pluripotent Stem Cell Initiatives: Wellcome Trust and ISSCR Workshops White Paper. *Stem Cell Rep.* **2014,** *3* (6), 931–939.

43. Leha, A.; Moens, N.; Meleckyte, R.; Culley, O. J.; Gervasio, M. K.; Kerz, M.; Reimer, A.; Cain, S. A.; Streeter, I.; Folarin, A.; Stegle, O.; Kielty, C. M.; HipSci, C.; Durbin, R.; Watt, F. M.; Danovi, D. A High-Content Platform to Characterise Human Induced Pluripotent Stem Cell Lines. *Methods* **2016,** *96,* 85–96.
44. Morrison, M.; Klein, C.; Clemann, N.; Collier, D. A.; Hardy, J.; Heisserer, B.; Cader, M. Z.; Graf, M.; Kaye, J. StemBANCC: Governing Access to Material and Data in a Large Stem Cell Research Consortium. *Stem Cell Rev.* **2015,** *11* (5), 681–687.
45. Dolmetsch, R.; Geschwind, D. H. The Human Brain in a Dish: The Promise of iPSC-Derived Neurons. *Cell* **2011,** *145* (6), 831–834.
46. Sayed, N.; Liu, C.; Wu, J. C. Translation of Human-Induced Pluripotent Stem Cells: From Clinical Trial in a Dish to Precision Medicine. *J. Am. Coll. Cardiol.* **2016,** *67* (18), 2161–2176.
47. Wan, W.; Cao, L.; Kalionis, B.; Xia, S.; Tai, X. Applications of Induced Pluripotent Stem Cells in Studying the Neurodegenerative Diseases. *Stem Cells Int.* **2015,** *2015,* 382530.
48. Haggarty, S. J.; Silva, M. C.; Cross, A.; Brandon, N. J.; Perlis, R. H. Advancing Drug Discovery for Neuropsychiatric Disorders Using Patient-Specific Stem Cell Models. *Mol. Cell. Neurosci.* **2016,** *73,* 104–115.
49. Inoue, H.; Nagata, N.; Kurokawa, H.; Yamanaka, S. iPS Cells: A Game Changer for Future Medicine. *EMBO J.* **2014,** *33* (5), 409–417.
50. Haggarty, S. J.; Perlis, R. H. Translation: Screening for Novel Therapeutics With Disease-Relevant Cell Types Derived From Human Stem Cell Models. *Biol. Psychiatry* **2014,** *75* (12), 952–960.
51. Brennand, K. J.; Gage, F. H. Modeling Psychiatric Disorders Through Reprogramming. *Dis. Model. Mech.* **2012,** *5* (1), 26–32.
52. Brennand, K. J.; Marchetto, M. C.; Benvenisty, N.; Brustle, O.; Ebert, A.; Izpisua Belmonte, J. C.; Kaykas, A.; Lancaster, M. A.; Livesey, F. J.; McConnell, M. J.; McKay, R. D.; Morrow, E. M.; Muotri, A. R.; Panchision, D. M.; Rubin, L. L.; Sawa, A.; Soldner, F.; Song, H.; Studer, L.; Temple, S.; Vaccarino, F. M.; Wu, J.; Vanderhaeghen, P.; Gage, F. H.; Jaenisch, R. Creating Patient-Specific Neural Cells for the In Vitro Study of Brain Disorders. *Stem Cell Rep.* **2015,** *5* (6), 933–945.
53. Freedman, B. S. Modeling Kidney Disease with iPS Cells. *Biomark. Insights* **2015,** *10* (Suppl. 1), 153–169.
54. Jaworska, E.; Kozlowska, E.; Switonski, P. M.; Krzyzosiak, W. J. Modeling Simple Repeat Expansion Diseases With iPSC Technology. *Cell. Mol. Life Sci.* **2016,** *73* (21), 4085–4100.
55. Lee, S.; Huang, E. J. Modeling ALS and FTD with iPSC-Derived Neurons. *Brain Res.* **2015;** http://dx.doi.org/10.1016/j.brainres.2015.10.003.
56. Liu, L.; Huang, J. S.; Han, C.; Zhang, G. X.; Xu, X. Y.; Shen, Y.; Li, J.; Jiang, H. Y.; Lin, Z. C.; Xiong, N.; Wang, T. Induced Pluripotent Stem Cells in Huntington's Disease: Disease Modeling and the Potential for Cell-Based Therapy. *Mol. Neurobiol.* **2015;** http://dx.doi.org/10.1007/s12035-015-9601-8.
57. Marchetto, M. C.; Winner, B.; Gage, F. H. Pluripotent Stem Cells in Neurodegenerative and Neurodevelopmental Diseases. *Hum. Mol. Genet.* **2010,** *19* (R1), R71–R76.
58. Mattis, V. B.; Svendsen, C. N. Modeling Huntingtons Disease With Patient-Derived Neurons. *Brain Res.* **2015;** http://dx.doi.org/10.1016/j.brainres.2015.10.001.
59. Spitalieri, P.; Talarico, V. R.; Murdocca, M.; Novelli, G.; Sangiuolo, F. Human Induced Pluripotent Stem Cells for Monogenic Disease Modelling and Therapy. *World J. Stem Cells* **2016,** *8* (4), 118–135.
60. Torrent, R.; De Angelis Rigotti, F.; Dell'Era, P.; Memo, M.; Raya, A.; Consiglio, A. Using iPS Cells Toward the Understanding of Parkinson's Disease. *J. Clin. Med.* **2015,** *4* (4), 548–566.
61. Zeltner, N.; Studer, L. Pluripotent Stem Cell-Based Disease Modeling: Current Hurdles and Future Promise. *Curr. Opin. Cell Biol.* **2015,** *37,* 102–110.
62. Shi, Y.; Kirwan, P.; Smith, J.; Robinson, H. P.; Livesey, F. J. Human Cerebral Cortex Development From Pluripotent Stem Cells to Functional Excitatory Synapses. *Nat. Neurosci.* **2012,** *15* (3), 477–486. S1.
63. Dragunow, M. The Adult Human Brain in Preclinical Drug Development. *Nat. Rev. Drug Discov.* **2008,** *7* (8), 659–666.
64. Kessler, R. C.; Aguilar-Gaxiola, S.; Alonso, J.; Chatterji, S.; Lee, S.; Ormel, J.; Ustun, T. B.; Wang, P. S. The Global Burden of Mental Disorders: An Update From the WHO World Mental Health (WMH) Surveys. *Epidemiol. Psichiatr. Soc.* **2009,** *18* (1), 23–33.
65. Fass, D. M.; Schroeder, F. A.; Perlis, R. H.; Haggarty, S. J. Epigenetic Mechanisms in Mood Disorders: Targeting Neuroplasticity. *Neuroscience* **2014,** *264,* 112–130.
66. Hyman, S. E. Revolution Stalled. *Sci. Transl. Med.* **2012,** *4* (155), 155cm11.
67. Sullivan, P. F.; Daly, M. J.; O'Donovan, M. Genetic Architectures of Psychiatric Disorders: The Emerging Picture and Its Implications. *Nat. Rev. Genet.* **2012,** *13* (8), 537–551.
68. Seok, J.; Warren, H. S.; Cuenca, A. G.; Mindrinos, M. N.; Baker, H. V.; Xu, W.; Richards, D. R.; McDonald-Smith, G. P.; Gao, H.; Hennessy, L.; Finnerty, C. C.; Lopez, C. M.; Honari, S.; Moore, E. E.; Minei, J. P.; Cuschieri, J.; Bankey, P. E.; Johnson, J. L.; Sperry, J.; Nathens, A. B..; Billiar, T. R.; West, M. A.; Jeschke, M. G.; Klein, M. B.; Gamelli, R. L.; Gibran, N. S.; Brownstein, B. H.; Miller-Graziano, C.; Calvano, S. E.; Mason, P. H.; Cobb, J. P.; Rahme, L. G.; Lowry, S. F.; Maier, R. V.; Moldawer, L. L.; Herndon, D. N.; Davis, R. W.; Xiao, W.; Tompkins, R. G.; Inflammation and Host Response to Injury Large Scale Collaborative Research Program. Genomic Responses in Mouse Models Poorly Mimic Human Inflammatory Diseases. *Proc. Natl. Acad. Sci. U. S. A.* **2013,** *110* (9), 3507–3512.
69. Bhattacharyya, A.; Zhao, X. Human Pluripotent Stem Cell Models of Fragile X Syndrome. *Mol. Cell. Neurosci.* **2016,** *73,* 43–51.
70. Doers, M. E.; Musser, M. T.; Nichol, R.; Berndt, E. R.; Baker, M.; Gomez, T. M.; Zhang, S. C.; Abbeduto, L.; Bhattacharyya, A. iPSC-Derived Forebrain Neurons From FXS Individuals Show Defects in Initial Neurite Outgrowth. *Stem Cells Dev.* **2014,** *23* (15), 1777–1787.
71. Telias, M.; Kuznitsov-Yanovsky, L.; Segal, M.; Ben-Yosef, D. Functional Deficiencies in Fragile X Neurons Derived From Human Embryonic Stem Cells. *J. Neurosci.* **2015,** *35* (46), 15295–15306.
72. Telias, M.; Segal, M.; Ben-Yosef, D. Neural Differentiation of Fragile X Human Embryonic Stem Cells Reveals Abnormal Patterns of Development Despite Successful Neurogenesis. *Dev. Biol.* **2013,** *374* (1), 32–45.
73. Urbach, A.; Bar-Nur, O.; Daley, G. Q.; Benvenisty, N. Differential Modeling of Fragile X Syndrome by Human Embryonic Stem Cells and Induced Pluripotent Stem Cells. *Cell Stem Cell* **2010,** *6* (5), 407–411.
74. Ananiev, G.; Williams, E. C.; Li, H.; Chang, Q. Isogenic Pairs of Wild Type and Mutant Induced Pluripotent Stem Cell (iPSC) Lines From Rett Syndrome Patients as in vitro Disease Model. *PLoS One* **2011,** *6* (9). e25255.
75. Cheung, A. Y.; Horvath, L. M.; Carrel, L.; Ellis, J. X-chromosome Inactivation in Rett Syndrome Human Induced Pluripotent Stem Cells. *Front. Psych.* **2012,** *3,* 24.
76. Marchetto, M. C.; Carromeu, C.; Acab, A.; Yu, D.; Yeo, G. W.; Mu, Y.; Chen, G.; Gage, F. H.; Muotri, A. R. A Model for Neural Development and Treatment of Rett Syndrome Using Human Induced Pluripotent Stem Cells. *Cell* **2010,** *143* (4), 527–539.
77. Brennand, K. J.; Simone, A.; Jou, J.; Gelboin-Burkhart, C.; Tran, N.; Sangar, S.; Li, Y.; Mu, Y.; Chen, G.; Yu, D.; McCarthy, S.; Sebat, J.; Gage, F. H. Modelling Schizophrenia Using Human Induced Pluripotent Stem Cells. *Nature* **2011,** *473* (7346), 221–225.
78. Chiang, C. H.; Su, Y.; Wen, Z.; Yoritomo, N.; Ross, C. A.; Margolis, R. L.; Song, H.; Ming, G. L. Integration-Free Induced Pluripotent Stem Cells Derived From Schizophrenia Patients With a DISC1 Mutation. *Mol. Psychiatry* **2011,** *16* (4), 358–360.
79. Bavamian, S.; Mellios, N.; Lalonde, J.; Fass, D. M.; Wang, J.; Sheridan, S. D.; Madison, J. M.; Zhou, F.; Rueckert, E. H.; Barker, D.; Perlis, R. H.; Sur, M.; Haggarty, S. J. Dysregulation of miR-34a Links Neuronal Development to Genetic Risk Factors for Bipolar Disorder. *Mol. Psychiatry* **2015,** *20* (5), 573–584.
80. Chen, H. M.; DeLong, C. J.; Bame, M.; Rajapakse, I.; Herron, T. J.; Mclnnis, M. G.; O'Shea, K. S. Transcripts Involved in Calcium Signaling and Telencephalic Neuronal Fate are Altered in Induced Pluripotent Stem Cells From Bipolar Disorder Patients. *Transl. Psychiatry* **2014,** *4.* e375.
81. Madison, J. M.; Zhou, F.; Nigam, A.; Hussain, A.; Barker, D. D.; Nehme, R.; van der Ven, K.; Hsu, J.; Wolf, P.; Fleishman, M.; O'Dushlaine, C.; Rose, S.; Chambert, K.; Lau, F. H.; Ahfeldt, T.; Rueckert, E. H.; Sheridan, S. D.; Fass, D. M.; Nemesh, J.; Mullen, T. E.; Daheron, L.; McCarroll, S.; Sklar, P.; Perlis, R. H.; Haggarty, S. J. Characterization of Bipolar Disorder Patient-Specific Induced Pluripotent Stem Cells From a Family Reveals Neurodevelopmental and mRNA Expression Abnormalities. *Mol. Psychiatry* **2015,** *20* (6), 703–717.
82. Mertens, J.; Wang, Q. W.; Kim, Y.; Yu, D. X.; Pham, S.; Yang, B.; Zheng, Y.; Diffenderfer, K. E.; Zhang, J.; Soltani, S.; Eames, T.; Schafer, S. T.; Boyer, L.; Marchetto, M. C.; Nurnberger, J. I.; Calabrese, J. R.; Odegaard, K. J.; McCarthy, M. J.; Zandi, P. P.; Alda, M.; Nievergelt, C. M.; ; Pharmacogenomics of Bipolar Disorder Study.; Mi, S.; Brennand, K. J.; Kelsoe, J. R.; Gage, F. H.; Yao, J. Differential Responses to Lithium in Hyperexcitable Neurons From Patients With Bipolar Disorder. *Nature* **2015,** *527* (7576), 95–99.

83. Farra, N.; Zhang, W. B.; Pasceri, P.; Eubanks, J. H.; Salter, M. W.; Ellis, J. Rett Syndrome Induced Pluripotent Stem Cell-Derived Neurons Reveal Novel Neurophysiological Alterations. *Mol. Psychiatry* **2012,** *17* (12), 1261–1271.
84. Kim, K. Y.; Hysolli, E.; Park, I. H. Neuronal Maturation Defect in Induced Pluripotent Stem Cells From Patients With Rett Syndrome. *Proc. Natl. Acad. Sci. U. S. A.* **2011,** *108* (34), 14169–14174.
85. Squillaro, T.; Alessio, N.; Cipollaro, M.; Melone, M. A.; Hayek, G.; Renieri, A.; Giordano, A.; Galderisi, U. Reduced Expression of MECP2 Affects Cell Commitment and Maintenance in Neurons by Triggering Senescence: New Perspective for Rett Syndrome. *Mol. Biol. Cell* **2012,** *23* (8), 1435–1445.
86. Prabakaran, S.; Swatton, J. E.; Ryan, M. M.; Huffaker, S. J.; Huang, J. T.; Griffin, J. L.; Wayland, M.; Freeman, T.; Dudbridge, F.; Lilley, K. S.; Karp, N. A.; Hester, S.; Tkachev, D.; Mimmack, M. L.; Yolken, R. H.; Webster, M. J.; Torrey, E. F.; Bahn, S. Mitochondrial Dysfunction in Schizophrenia: Evidence for Compromised Brain Metabolism and Oxidative Stress. *Mol. Psychiatry* **2004,** *9* (7), 684–697, 643.
87. Pasca, S. P.; Portmann, T.; Voineagu, I.; Yazawa, M.; Shcheglovitov, A.; Pasca, A. M.; Cord, B.; Palmer, T. D.; Chikahisa, S.; Nishino, S.; Bernstein, J. A.; Hallmayer, J.; Geschwind, D. H.; Dolmetsch, R. E. Using iPSC-Derived Neurons to Uncover Cellular Phenotypes Associated With Timothy Syndrome. *Nat. Med.* **2011,** *17* (12), 1657–1662.
88. Pini, G.; Scusa, M. F.; Benincasa, A.; Bottiglioni, I.; Congiu, L.; Vadhatpour, C.; Romanelli, A. M.; Gemo, I.; Puccetti, C.; McNamara, R.; O'Leary, S.; Corvin, A.; Gill, M.; Tropea, D. Repeated Insulin-Like Growth Factor 1 Treatment in a Patient With Rett Syndrome: A Single Case Study. *Front. Pediatr.* **2014,** *2,* 52.
89. McNeish, J.; Roach, M.; Hambor, J.; Mather, R. J.; Weibley, L.; Lazzaro, J.; Gazard, J.; Schwarz, J.; Volkmann, R.; Machacek, D.; Stice, S.; Zawadzke, L.; O'Donnell, C.; Hurst, R. High-Throughput Screening in Embryonic Stem Cell-Derived Neurons Identifies Potentiators of Alpha-Amino-3-Hydroxyl-5-Methyl-4-Isoxazolepropionate-Type Glutamate Receptors. *J. Biol. Chem.* **2010,** *285* (22), 17209–17217.
90. Egawa, N.; Kitaoka, S.; Tsukita, K.; Naitoh, M.; Takahashi, K.; Yamamoto, T.; Adachi, F.; Kondo, T.; Okita, K.; Asaka, I.; Aoi, T.; Watanabe, A.; Yamada, Y.; Morizane, A.; Takahashi, J.; Ayaki, T.; Ito, H.; Yoshikawa, K.; Yamawaki, S.; Suzuki, S.; Watanabe, D.; Hioki, H.; Kaneko, T.; Makioka, K.; Okamoto, K.; Takuma, H.; Tamaoka, A.; Hasegawa, K.; Nonaka, T.; Hasegawa, M.; Kawata, A.; Yoshida, M.; Nakahata, T.; Takahashi, R.; Marchetto, M. C.; Gage, F. H.; Yamanaka, S.; Inoue, H. Drug Screening for ALS Using Patient-Specific Induced Pluripotent Stem Cells. *Sci. Transl. Med.* **2012,** *4* (145), 145ra104.
91. Lee, G.; Ramirez, C. N.; Kim, H.; Zeltner, N.; Liu, B.; Radu, C.; Bhinder, B.; Kim, Y. J.; Choi, I. Y.; Mukherjee-Clavin, B.; Djaballah, H.; Studer, L. Large-Scale Screening Using Familial Dysautonomia Induced Pluripotent Stem Cells Identifies Compounds That Rescue IKBKAP Expression. *Nat. Biotechnol.* **2012,** *30* (12), 1244–1248.
92. Kondo, T.; Asai, M.; Tsukita, K.; Kutoku, Y.; Ohsawa, Y.; Sunada, Y.; Imamura, K.; Egawa, N.; Yahata, N.; Okita, K.; Takahashi, K.; Asaka, I.; Aoi, T.; Watanabe, A.; Watanabe, K.; Kadoya, C.; Nakano, R.; Watanabe, D.; Maruyama, K.; Hori, O.; Hibino, S.; Choshi, T.; Nakahata, T.; Hioki, H.; Kaneko, T.; Naitoh, M.; Yoshikawa, K.; Yamawaki, S.; Suzuki, S.; Hata, R.; Ueno, S.; Seki, T.; Kobayashi, K.; Toda, T.; Murakami, K.; Irie, K.; Klein, W. L.; Mori, H.; Asada, T.; Takahashi, R.; Iwata, N.; Yamanaka, S.; Inoue, H. Modeling Alzheimer's Disease With iPSCs Reveals Stress Phenotypes Associated With Intracellular Abeta and Differential Drug Responsiveness. *Cell Stem Cell* **2013,** *12* (4), 487–496.
93. Yang, Y. M.; Gupta, S. K.; Kim, K. J.; Powers, B. E.; Cerqueira, A.; Wainger, B. J.; Ngo, H. D.; Rosowski, K. A.; Schein, P. A.; Ackeifi, C. A.; Arvanites, A. C.; Davidow, L. S.; Woolf, C. J.; Rubin, L. L. A Small Molecule Screen in Stem-Cell-Derived Motor Neurons Identifies a Kinase Inhibitor as a Candidate Therapeutic for ALS. *Cell Stem Cell* **2013,** *12* (6), 713–726.
94. Burkhardt, M. F.; Martinez, F. J.; Wright, S.; Ramos, C.; Volfson, D.; Mason, M.; Garnes, J.; Dang, V.; Lievers, J.; Shoukat-Mumtaz, U.; Martinez, R.; Gai, H.; Blake, R.; Vaisberg, E.; Grskovic, M.; Johnson, C.; Irion, S.; Bright, J.; Cooper, B.; Nguyen, L.; Griswold-Prenner, I.; Javaherian, A. A Cellular Model for Sporadic ALS Using Patient-Derived Induced Pluripotent Stem Cells. *Mol. Cell. Neurosci.* **2013,** *56,* 355–364.
95. Wainger, B. J.; Kiskinis, E.; Mellin, C.; Wiskow, O.; Han, S. S.; Sandoe, J.; Perez, N. P.; Williams, L. A.; Lee, S.; Boulting, G.; Berry, J. D.; Brown, R. H., Jr.; Cudkowicz, M. E.; Bean, B. P.; Eggan, K.; Woolf, C. J. Intrinsic Membrane Hyperexcitability of Amyotrophic Lateral Sclerosis Patient-Derived Motor Neurons. *Cell Rep.* **2014,** *7* (1), 1–11.
96. Kumari, D.; Swaroop, M.; Southall, N.; Huang, W.; Zheng, W.; Usdin, K. High-Throughput Screening to Identify Compounds That Increase Fragile X Mental Retardation Protein Expression in Neural Stem Cells Differentiated From Fragile X Syndrome Patient-Derived Induced Pluripotent Stem Cells. *Stem Cells Transl. Med.* **2015,** *4* (7), 800–808.
97. Kaufmann, M.; Schuffenhauer, A.; Fruh, I.; Klein, J.; Thiemeyer, A.; Rigo, P.; Gomez-Mancilla, B.; Heidinger-Millot, V.; Bouwmeester, T.; Schopfer, U.; Mueller, M.; Fodor, B. D.; Cobos-Correa, A. High-Throughput Screening Using iPSC-Derived Neuronal Progenitors to Identify Compounds Counteracting Epigenetic Gene Silencing in Fragile X Syndrome. *J. Biomol. Screen.* **2015,** *20* (9), 1101–1111.
98. Price, D. L.; Sisodia, S. S.; Borchelt, D. R. Genetic Neurodegenerative Diseases: The Human Illness and Transgenic Models. *Science* **1998,** *282* (5391), 1079–1083.
99. Hardy, J.; Gwinn-Hardy, K. Genetic Classification of Primary Neurodegenerative Disease. *Science* **1998,** *282* (5391), 1075–1079.
100. Ross, C. A.; Poirier, M. A. Opinion: What is the Role of Protein Aggregation in Neurodegeneration? *Nat. Rev. Mol. Cell Biol.* **2005,** *6* (11), 891–898.
101. Neumann, M.; Kovacs, G. G.; Mackenzie, I. R. A. Neuropathology of Frontotemporal Dementia and Related Disorders. In *Hodges' Frontotemporal Dementia;* Dickerson, B. C., Ed., 2nd ed.;; 2015; pp 165–184.
102. Rademakers, R.; Neumann, M.; Mackenzie, I. R. Advances in Understanding the Molecular Basis of Frontotemporal Dementia. *Nat. Rev. Neurol.* **2012,** *8* (8), 423–434.
103. Skovronsky, D. M.; Lee, V. M.; Trojanowski, J. Q. Neurodegenerative Diseases: New Concepts of Pathogenesis and Their Therapeutic Implications. *Annu. Rev. Pathol.* **2006,** *1,* 151–170.
104. Powers, E. T.; Morimoto, R. I.; Dillin, A.; Kelly, J. W.; Balch, W. E. Biological and Chemical Approaches to Diseases of Proteostasis Deficiency. *Annu. Rev. Biochem.* **2009,** *78,* 959–991.
105. Balch, W. E.; Morimoto, R. I.; Dillin, A.; Kelly, J. W. Adapting Proteostasis for Disease Intervention. *Science* **2008,** *319* (5865), 916–919.
106. Aguzzi, A.; Lakkaraju, A. K. Cell Biology of Prions and Prionoids: A Status Report. *Trends Cell Biol.* **2016,** *26* (1), 40–51.
107. Lim, J.; Yue, Z. Neuronal Aggregates: Formation, Clearance, and Spreading. *Dev. Cell* **2015,** *32* (4), 491–501.
108. Prusiner, S. B. Biology and Genetics of Prions Causing Neurodegeneration. *Annu. Rev. Genet.* **2013,** *47,* 601–623.
109. Walsh, D. M.; Selkoe, D. J. A Critical Appraisal of the Pathogenic Protein Spread Hypothesis of Neurodegeneration. *Nat. Rev. Neurosci.* **2016,** *17* (4), 251–260.
110. Jin, S. C.; Pastor, P.; Cooper, B.; Cervantes, S.; Benitez, B. A.; Razquin, C.; Goate, A.; Cruchaga, C. Pooled-DNA Sequencing Identifies Novel Causative Variants in PSEN1, GRN and MAPT in a Clinical Early-Onset and Familial Alzheimer's Disease Ibero-American Cohort. *Alzheimers Res. Ther.* **2012,** *4* (4), 34–43.
111. Metzker, M. L. Sequencing Technologies—The Next Generation. *Nat. Rev. Genet.* **2010,** *11* (1), 31–46.
112. Tsuji, S. Genetics of Neurodegenerative Diseases: Insights From High-Throughput Resequencing. *Hum. Mol. Genet.* **2010,** *19* (R1), R65–R70.
113. Josephs, K. A.; Hodges, J. R.; Snowden, J. S.; Mackenzie, I. R.; Neumann, M.; Mann, D. M.; Dickson, D. W. Neuropathological Background of Phenotypical Variability in Frontotemporal Dementia. *Acta Neuropathol.* **2011,** *122* (2), 137–153.
114. Cruts, M.; Theuns, J.; Van Broeckhoven, C. Locus-Specific Mutation Databases for Neurodegenerative Brain Diseases. *Hum. Mutat.* **2012,** *33* (9), 1340–1344.
115. Ross, C. A.; Aylward, E. H.; Wild, E. J.; Langbehn, D. R.; Long, J. D.; Warner, J. H.; Scahill, R. I.; Leavitt, B. R.; Stout, J. C.; Paulsen, J. S.; Reilmann, R.; Unschuld, P. G.; Wexler, A.; Margolis, R. L.; Tabrizi, S. J. Huntington Disease: Natural History, Biomarkers and Prospects for Therapeutics. *Nat. Rev. Neurol.* **2014,** *10* (4), 204–216.
116. Polymeropoulos, M. H.; Lavedan, C.; Leroy, E.; Ide, S. E.; Dehejia, A.; Dutra, A.; Pike, B.; Root, H.; Rubenstein, J.; Boyer, R.; Stenroos, E. S.; Chandrasekharappa, S.; Athanassiadou, A.; Papapetropoulos, T.; Johnson, W. G.; Lazzarini, A. M.; Duvoisin, R. C.; Di Iorio, G.; Golbe, L. I.; Nussbaum, R. L. Mutation in the Alpha-Synuclein Gene Identified in Families With Parkinson's Disease. *Science* **1997,** *276* (5321), 2045–2047.
117. Spillantini, M. G.; Crowther, R. A.; Jakes, R.; Hasegawa, M.; Goedert, M. Alpha-Synuclein in Filamentous Inclusions of Lewy Bodies From Parkinson's Disease and Dementia With Lewy Bodies. *Proc. Natl. Acad. Sci. U. S. A.* **1998,** *95* (11), 6469–6473.
118. Herrup, K. The Case for Rejecting the Amyloid Cascade Hypothesis. *Nat. Neurosci.* **2015,** *18* (6), 794–799.
119. Cruts, M.; Van Broeckhoven, C. *Genetics of Frontotemporal Dementia and Related Disorders,* 2nd ed.;, 2015.
120. Ghetti, B.; Oblak, A. L.; Boeve, B. F.; Johnson, K. A.; Dickerson, B. C.; Goedert, M. Invited Review: Frontotemporal Dementia Caused by Microtubule-Associated Protein tau Gene (MAPT) Mutations: A Chameleon for Neuropathology and Neuroimaging. *Neuropathol. Appl. Neurobiol.* **2015,** *41* (1), 24–46.

121. Rohrer, J. D.; Guerreiro, R.; Vandrovcova, J.; Uphill, J.; Reiman, D.; Beck, J.; Isaacs, A. M.; Authier, A.; Ferrari, R.; Fox, N. C.; Mackenzie, I. R.; Warren, J. D.; de Silva, R.; Holton, J.; Revesz, T.; Hardy, J.; Mead, S.; Rossor, M. N. The Heritability and Genetics of Frontotemporal Lobar Degeneration. *Neurology* **2009,** *73* (18), 1451–1456.
122. Yu, C. E.; Bird, T. D.; Bekris, L. M.; Montine, T. J.; Leverenz, J. B.; Steinbart, E.; Galloway, N. M.; Feldman, H.; Woltjer, R.; Miller, C. A.; Wood, E. M.; Grossman, M.; McCluskey, L.; Clark, C. M.; Neumann, M.; Danek, A.; Galasko, D. R.; Arnold, S. E.; Chen-Plotkin, A.; Karydas, A.; Miller, B. L.; Trojanowski, J. Q.; Lee, V. M.; Schellenberg, G. D.; Van Deerlin, V. M. The Spectrum of Mutations in Progranulin: A Collaborative Study Screening 545 Cases of Neurodegeneration. *Arch. Neurol.* **2010,** *67* (2), 161–170.
123. Bang, J.; Spina, S.; Miller, B. L. Frontotemporal Dementia. *Lancet* **2015,** *386* (10004), 1672–1682.
124. Morrison, J. H.; Hof, P. R. Life and Death of Neurons in the Aging Brain. *Science* **1997,** *278* (5337), 412–419.
125. Goedert, M.; Ghetti, B.; Spillantini, M. G. Frontotemporal Dementia: Implications for Understanding Alzheimer Disease. *Cold Spring Harb. Perspect. Med.* **2012,** *2* (2), a006254.
126. Kim, E. J.; Sidhu, M.; Gaus, S. E.; Huang, E. J.; Hof, P. R.; Miller, B. L.; DeArmond, S. J.; Seeley, W. W. Selective Frontoinsular von Economo Neuron and Fork Cell Loss in Early Behavioral Variant Frontotemporal Dementia. *Cereb. Cortex* **2012,** *22* (2), 251–259.
127. Seeley, W. W. Selective Functional, Regional, and Neuronal Vulnerability in Frontotemporal Dementia. *Curr. Opin. Neurol.* **2008,** *21* (6), 701–707.
128. Feany, M. B. Studying Human Neurodegenerative Diseases in Flies and Worms. *J. Neuropathol. Exp. Neurol.* **2000,** *59* (10), 847–856.
129. Chien, D. T.; Szardenings, A. K.; Bahri, S.; Walsh, J. C.; Mu, F.; Xia, C.; Shankle, W. R.; Lerner, A. J.; Su, M. Y.; Elizarov, A.; Kolb, H. C. Early Clinical PET Imaging Results With the Novel PHF-tau Radioligand [F18]-T808. *J. Alzheimers Dis.* **2014,** *38* (1), 171–184.
130. Dani, M.; Brooks, D. J.; Edison, P. Tau Imaging in Neurodegenerative Diseases. *Eur. J. Nucl. Med. Mol. Imaging* **2016,** *43* (6), 1139–1150.
131. Maruyama, M.; Shimada, H.; Suhara, T.; Shinotoh, H.; Ji, B.; Maeda, J.; Zhang, M. R.; Trojanowski, J. Q.; Lee, V. M.; Ono, M.; Masamoto, K.; Takano, H.; Sahara, N.; Iwata, N.; Okamura, N.; Furumoto, S.; Kudo, Y.; Chang, Q.; Saido, T. C.; Takashima, A.; Lewis, J.; Jang, M. K.; Aoki, I.; Ito, H.; Higuchi, M. Imaging of tau Pathology in a Tauopathy Mouse Model and in Alzheimer Patients Compared to Normal Controls. *Neuron* **2013,** *79* (6), 1094–1108.
132. Cheng, H. C.; Ulane, C. M.; Burke, R. E. Clinical Progression in Parkinson Disease and the Neurobiology of Axons. *Ann. Neurol.* **2010,** *67* (6), 715–725.
133. Jack, C. R., Jr.; Holtzman, D. M. Biomarker Modeling of Alzheimer's Disease. *Neuron* **2013,** *80* (6), 1347–1358.
134. Jack, C. R., Jr.; Knopman, D. S.; Jagust, W. J.; Petersen, R. C.; Weiner, M. W.; Aisen, P. S.; Shaw, L. M.; Vemuri, P.; Wiste, H. J.; Weigand, S. D.; Lesnick, T. G.; Pankratz, V. S.; Donohue, M. C.; Trojanowski, J. Q. Tracking Pathophysiological Processes in Alzheimer's Disease: An Updated Hypothetical Model of Dynamic Biomarkers. *Lancet Neurol.* **2013,** *12* (2), 207–216.
135. Kirkitadze, M. D.; Bitan, G.; Teplow, D. B. Paradigm Shifts in Alzheimer's Disease and Other Neurodegenerative Disorders: The Emerging Role of Oligomeric Assemblies. *J. Neurosci. Res.* **2002,** *69* (5), 567–577.
136. Wen, X.; Tan, W.; Westergard, T.; Krishnamurthy, K.; Markandaiah, S. S.; Shi, Y.; Lin, S.; Shneider, N. A.; Monaghan, J.; Pandey, U. B.; Pasinelli, P.; Ichida, J. K.; Trotti, D. Antisense Proline-Arginine RAN Dipeptides Linked to C9ORF72-ALS/FTD Form Toxic Nuclear Aggregates That Initiate In Vitro and In Vivo Neuronal Death. *Neuron* **2014,** *84* (6), 1213–1225.
137. Ehrlich, M.; Hallmann, A. L.; Reinhardt, P.; Arauzo-Bravo, M. J.; Korr, S.; Ropke, A.; Psathaki, O. E.; Ehling, P.; Meuth, S. G.; Oblak, A. L.; Murrell, J. R.; Ghetti, B.; Zaehres, H.; Scholer, H. R.; Sterneckert, J.; Kuhlmann, T.; Hargus, G. Distinct Neurodegenerative Changes in an Induced Pluripotent Stem Cell Model of Frontotemporal Dementia Linked to Mutant TAU Protein. *Stem Cell Rep.* **2015,** *5* (1), 83–96.
138. Iovino, M.; Agathou, S.; Gonzalez-Rueda, A.; Del Castillo Velasco-Herrera, M.; Borroni, B.; Alberici, A.; Lynch, T.; O'Dowd, S.; Geti, I.; Gaffney, D.; Vallier, L.; Paulsen, O.; Karadottir, R. T.; Spillantini, M. G. Early Maturation and Distinct tau Pathology in Induced Pluripotent Stem Cell-Derived Neurons From Patients With MAPT Mutations. *Brain* **2015,** *138* (Pt 11), 3345–3359.
139. Usenovic, M.; Niroomand, S.; Drolet, R. E.; Yao, L.; Gaspar, R. C.; Hatcher, N. G.; Schachter, J.; Renger, J. J.; Parmentier-Batteur, S. Internalized Tau Oligomers Cause Neurodegeneration by Inducing Accumulation of Pathogenic Tau in Human Neurons Derived From Induced Pluripotent Stem Cells. *J. Neurosci.* **2015,** *35* (42), 14234–14250.
140. Wren, M. C.; Zhao, J.; Liu, C. C.; Murray, M. E.; Atagi, Y.; Davis, M. D.; Fu, Y.; Okano, H. J.; Ogaki, K.; Strongosky, A. J.; Tacik, P.; Rademakers, R.; Ross, O. A.; Dickson, D. W.; Wszolek, Z. K.; Kanekiyo, T.; Bu, G. Frontotemporal Dementia-Associated N279K tau Mutant Disrupts Subcellular Vesicle Trafficking and Induces Cellular Stress in iPSC-Derived Neural Stem Cells. *Mol. Neurodegener.* **2015,** *10,* 46.
141. Abisambra, J. F.; Jinwal, U. K.; Blair, L. J.; O'Leary, J. C., 3rd; Li, Q.; Brady, S.; Wang, L.; Guidi, C. E.; Zhang, B.; Nordhues, B. A.; Cockman, M.; Suntharalingham, A.; Li, P.; Jin, Y.; Atkins, C. A.; Dickey, C. A. Tau Accumulation Activates the Unfolded Protein Response by Impairing Endoplasmic Reticulum-Associated Degradation. *J. Neurosci.* **2013,** *33* (22), 9498–9507.
142. Stoveken, B. J. Tau Pathology as a Cause and Consequence of the UPR. *J. Neurosci.* **2013,** *33* (36), 14285–14287.
143. Heywood, W. E.; Galimberti, D.; Bliss, E.; Sirka, E.; Paterson, R. W.; Magdalinou, N. K.; Carecchio, M.; Reid, E.; Heslegrave, A.; Fenoglio, C.; Scarpini, E.; Schott, J. M.; Fox, N. C.; Hardy, J.; Bahtia, K.; Heales, S.; Sebire, N. J.; Zetterburg, H.; Mills, K. Identification of Novel CSF Biomarkers for Neurodegeneration and Their Validation by a High-Throughput Multiplexed Targeted Proteomic Assay. *Mol. Neurodegener.* **2015,** *10* (1), 64.
144. Nguyen, H. N.; Byers, B.; Cord, B.; Shcheglovitov, A.; Byrne, J.; Gujar, P.; Kee, K.; Schule, B.; Dolmetsch, R. E.; Langston, W.; Palmer, T. D.; Pera, R. R. LRRK2 Mutant iPSC-Derived DA Neurons Demonstrate Increased Susceptibility to Oxidative Stress. *Cell Stem Cell* **2011,** *8* (3), 267–280.
145. Zhou, J.; Seeley, W. W. Network Dysfunction in Alzheimer's Disease and Frontotemporal Dementia: Implications for Psychiatry. *Biol. Psychiatry* **2014,** *75* (7), 565–573.
146. Willems, E.; Spiering, S.; Davidovics, H.; Lanier, M.; Xia, Z.; Dawson, M.; Cashman, J.; Mercola, M. Small-Molecule Inhibitors of the Wnt Pathway Potently Promote Cardiomyocytes From Human Embryonic Stem Cell-Derived Mesoderm. *Circ. Res.* **2011,** *109* (4), 360–364.
147. Ebert, A. D.; Liang, P.; Wu, J. C. Induced Pluripotent Stem Cells as a Disease Modeling and Drug Screening Platform. *J. Cardiovasc. Pharmacol.* **2012,** *60* (4), 408–416.
148. Hudry, E.; Dashkoff, J.; Roe, A. D.; Takeda, S.; Koffie, R. M.; Hashimoto, T.; Scheel, M.; Spires-Jones, T.; Arbel-Ornath, M.; Betensky, R.; Davidson, B. L.; Hyman, B. T. Gene Transfer of Human Apoe Isoforms Results in Differential Modulation of Amyloid Deposition and Neurotoxicity in Mouse Brain. *Sci. Transl. Med.* **2013,** *5* (212), 212ra161.
149. Geschwind, D. H.; Flint, J. Genetics and Genomics of Psychiatric Disease. *Science* **2015,** *349* (6255), 1489–1494.
150. Israel, M. A.; Yuan, S. H.; Bardy, C.; Reyna, S. M.; Mu, Y.; Herrera, C.; Hefferan, M. P.; Van Gorp, S.; Nazor, K. L.; Boscolo, F. S.; Carson, C. T.; Laurent, L. C.; Marsala, M.; Gage, F. H.; Remes, A. M.; Koo, E. H.; Goldstein, L. S. Probing Sporadic and Familial Alzheimer's Disease Using Induced Pluripotent Stem Cells. *Nature* **2012,** *482* (7384), 216–220.
151. Schizophrenia Working Group of the Psychiatric Genomics Consortium. Biological Insights From 108 Schizophrenia-Associated Genetic Loci. *Nature* **2014,** *511* (7510), 421–427.
152. Nestler, E. J.; Hyman, S. E. Animal Models of Neuropsychiatric Disorders. *Nat. Neurosci.* **2010,** *13* (10), 1161–1169.
153. Kaiser, T.; Feng, G. Modeling Psychiatric Disorders for Developing Effective Treatments. *Nat. Med.* **2015,** *21* (9), 979–988.
154. Steele, J. C.; Guella, I.; Szu-Tu, C.; Lin, M. K.; Thompson, C.; Evans, D. M.; Sherman, H. E.; Vilarino-Guell, C.; Gwinn, K.; Morris, H.; Dickson, D. W.; Farrer, M. J. Defining Neurodegeneration on Guam by Targeted Genomic Sequencing. *Ann. Neurol.* **2015,** *77,* 458–468.
155. Vilarino-Guell, C.; Rajput, A.; Milnerwood, A. J.; Shah, B.; Szu-Tu, C.; Trinh, J.; Yu, I.; Encarnacion, M.; Munsie, L. N.; Tapia, L.; Gustavsson, E. K.; Chou, P.; Tatarnikov, I.; Evans, D. M.; Pishotta, F. T.; Volta, M.; Beccano-Kelly, D.; Thompson, C.; Lin, M. K.; Sherman, H. E.; Han, H. J.; Guenther, B. L.; Wasserman, W. W.; Bernard, V.; Ross, C. J.; Appel-Cresswell, S.; Stoessl, A. J.; Robinson, C. A.; Dickson, D. W.; Ross, O. A.; Wszolek, Z. K.; Aasly, J. O.; Wu, R. M.; Hentati, F.; Gibson, R. A.; McPherson, P. S.; Girard, M.; Rajput, M.; Rajput, A. H.; Farrer, M. J. DNAJC13 Mutations in Parkinson Disease. *Hum. Mol. Genet.* **2014,** *23* (7), 1794–1801.
156. Mali, P.; Yang, L.; Esvelt, K. M.; Aach, J.; Guell, M.; DiCarlo, J. E.; Norville, J. E.; Church, G. M. RNA-Guided Human Genome Engineering via Cas9. *Science* **2013,** *339* (6121), 823–826.

157. Fong, H.; Wang, C.; Knoferle, J.; Walker, D.; Balestra, M. E.; Tong, L. M.; Leung, L.; Ring, K. L.; Seeley, W. W.; Karydas, A.; Kshirsagar, M. A.; Boxer, A. L.; Kosik, K. S.; Miller, B. L.; Huang, Y. Genetic Correction of Tauopathy Phenotypes in Neurons Derived From Human Induced Pluripotent Stem Cells. *Stem Cell Rep.* **2013,** *1* (3), 226–234.
158. Kiskinis, E.; Sandoe, J.; Williams, L. A.; Boulting, G. L.; Moccia, R.; Wainger, B. J.; Han, S.; Peng, T.; Thams, S.; Mikkilineni, S.; Mellin, C.; Merkle, F. T.; Davis-Dusenbery, B. N.; Ziller, M.; Oakley, D.; Ichida, J.; Di Costanzo, S.; Atwater, N.; Maeder, M. L.; Goodwin, M. J.; Nemesh, J.; Handsaker, R. E.; Paull, D.; Noggle, S.; McCarroll, S. A.; Joung, J. K.; Woolf, C. J.; Brown, R. H.; Eggan, K. Pathways Disrupted in Human ALS Motor Neurons Identified Through Genetic Correction of Mutant SOD1. *Cell Stem Cell* **2014,** *14* (6), 781–795.
159. Hyde, C. L.; Nagle, M. W.; Tian, C.; Chen, X.; Paciga, S. A.; Wendland, J. R.; Tung, J. Y.; Hinds, D. A.; Perlis, R. H.; Winslow, A. R. Identification of 15 Genetic Loci Associated With Risk of Major Depression in Individuals of European Descent. *Nat. Genet.* **2016,** *48,* 1031–1036.
160. Collins, F. S.; Varmus, H. A new Initiative on Precision Medicine. *N. Engl. J. Med.* **2015,** *372* (9), 793–795.
161. Plenge, R. M.; Scolnick, E. M.; Altshuler, D. Validating Therapeutic Targets Through Human Genetics. *Nat. Rev. Drug Discov.* **2013,** *12* (8), 581–594.
162. Plenge, R. M. Disciplined Approach to Drug Discovery and Early Development. *Sci. Transl. Med.* **2016,** *8* (349), 349ps15.
163. Kathiresan, S. Developing Medicines That Mimic the Natural Successes of the Human Genome: Lessons From NPC1L1, HMGCR, PCSK9, APOC3, and CETP. *J. Am. Coll. Cardiol.* **2015,** *65* (15), 1562–1566.
164. Almeida, S.; Zhang, Z.; Coppola, G.; Mao, W.; Futai, K.; Karydas, A.; Geschwind, M. D.; Tartaglia, M. C.; Gao, F.; Gianni, D.; Sena-Esteves, M.; Geschwind, D. H.; Miller, B. L.; Farese, R. V., Jr.; Gao, F. B. Induced Pluripotent Stem Cell Models of Progranulin-Deficient Frontotemporal Dementia Uncover Specific Reversible Neuronal Defects. *Cell Rep.* **2012,** *2* (4), 789–798.
165. Bilican, B.; Serio, A.; Barmada, S. J.; Nishimura, A. L.; Sullivan, G. J.; Carrasco, M.; Phatnani, H. P.; Puddifoot, C. A.; Story, D.; Fletcher, J.; Park, I. H.; Friedman, B. A.; Daley, G. Q.; Wyllie, D. J.; Hardingham, G. E.; Wilmut, I.; Finkbeiner, S.; Maniatis, T.; Shaw, C. E.; Chandran, S. Mutant Induced Pluripotent Stem Cell Lines Recapitulate Aspects of TDP-43 Proteinopathies and Reveal Cell-Specific Vulnerability. *Proc. Natl. Acad. Sci. U. S. A.* **2012,** *109* (15), 5803–5808.
166. Lamb, J.; Crawford, E. D.; Peck, D.; Modell, J. W.; Blat, I. C.; Wrobel, M. J.; Lerner, J.; Brunet, J. P.; Subramanian, A.; Ross, K. N.; Reich, M.; Hieronymus, H.; Wei, G.; Armstrong, S. A.; Haggarty, S. J.; Clemons, P. A.; Wei, R.; Carr, S. A.; Lander, E. S.; Golub, T. R. The Connectivity Map: Using Gene-Expression Signatures to Connect Small Molecules, Genes, and Disease. *Science* **2006,** *313* (5795), 1929–1935.
167. Abelin, J. G.; Patel, J.; Lu, X.; Feeney, C. M.; Fagbami, L.; Creech, A. L.; Hu, R.; Lam, D.; Davison, D.; Pino, L.; Qiao, J. W.; Kuhn, E.; Officer, A.; Li, J.; Abbatiello, S.; Subramanian, A.; Sidman, R.; Snyder, E.; Carr, S. A.; Jaffe, J. D. Reduced-Representation Phosphosignatures Measured by Quantitative Targeted MS Capture Cellular States and Enable Large-Scale Comparison of Drug-Induced Phenotypes. *Mol. Cell. Proteomics* **2016,** *15* (5), 1622–1641.
168. Peck, D.; Crawford, E. D.; Ross, K. N.; Stegmaier, K.; Golub, T. R.; Lamb, J. A Method for High-Throughput Gene Expression Signature Analysis. *Genome Biol.* **2006,** *7* (7), R61.
169. Ban, J.; Bonifazi, P.; Pinato, G.; Broccard, F. D.; Studer, L.; Torre, V.; Ruaro, M. E. Embryonic Stem Cell-Derived Neurons Form Functional Networks In Vitro. *Stem Cells* **2007,** *25* (3), 738–749.
170. Heikkila, T. J.; Yla-Outinen, L.; Tanskanen, J. M.; Lappalainen, R. S.; Skottman, H.; Suuronen, R.; Mikkonen, J. E.; Hyttinen, J. A.; Narkilahti, S. Human Embryonic Stem Cell-Derived Neuronal Cells Form Spontaneously Active Neuronal Networks In Vitro. *Exp. Neurol.* **2009,** *218* (1), 109–116.
171. Raitano, S.; Ordovas, L.; De Muynck, L.; Guo, W.; Espuny-Camacho, I.; Geraerts, M.; Khurana, S.; Vanuytsel, K.; Toth, B. I.; Voets, T.; Vandenberghe, R.; Cathomen, T.; Van Den Bosch, L.; Vanderhaeghen, P.; Van Damme, P.; Verfaillie, C. M. Restoration of Progranulin Expression Rescues Cortical Neuron Generation in an Induced Pluripotent Stem Cell Model of Frontotemporal Dementia. *Stem Cell Rep.* **2015,** *4* (1), 16–24.
172. MacLean, B.; Tomazela, D. M.; Shulman, N.; Chambers, M.; Finney, G. L.; Frewen, B.; Kern, R.; Tabb, D. L.; Liebler, D. C.; MacCoss, M. J. Skyline: An Open Source Document Editor for Creating and Analyzing Targeted Proteomics Experiments. *Bioinformatics* **2010,** *26* (7), 966–968.
173. Mair, W.; Muntel, J.; Tepper, K.; Tang, S.; Biernat, J.; Seeley, W. W.; Kosik, K. S.; Mandelkow, E.; Steen, H.; Steen, J. A. FLEXITau: Quantifying Post-Translational Modifications of Tau Protein in vitro and in Human Disease. *Anal. Chem.* **2016,** *88,* 3704–3714.
174. Singh, S.; Springer, M.; Steen, J.; Kirschner, M. W.; Steen, H. FLEXIQuant: A Novel Tool for the Absolute Quantification of Proteins, and the Simultaneous Identification and Quantification of Potentially Modified Peptides. *J. Proteome Res.* **2009,** *8* (5), 2201–2210.
175. Sanders, D. W.; Kaufman, S. K.; DeVos, S. L.; Sharma, A. M.; Mirbaha, H.; Li, A.; Barker, S. J.; Foley, A. C.; Thorpe, J. R.; Serpell, L. C.; Miller, T. M.; Grinberg, L. T.; Seeley, W. W.; Diamond, M. I. Distinct Tau Prion Strains Propagate in Cells and Mice and Define Different Tauopathies. *Neuron* **2014,** *82* (6), 1271–1288.
176. Mertens, J.; Stuber, K.; Poppe, D.; Doerr, J.; Ladewig, J.; Brustle, O.; Koch, P. Embryonic Stem Cell-Based Modeling of Tau Pathology in Human Neurons. *Am. J. Pathol.* **2013,** *182* (5), 1769–1779.
177. Wray, S.; Self, M.; Lewis, P. A.; Taanman, J. W.; Ryan, N. S.; Mahoney, C. J.; Liang, Y.; Devine, M. J.; Sheerin, U. M.; Houlden, H.; Morris, H. R.; Healy, D.; Marti-Masso, J. F.; Preza, E.; Barker, S.; Sutherland, M.; Corriveau, R. A.; D'Andrea, M.; Schapira, A. H.; Uitti, R. J.; Guttman, M.; Opala, G.; Jasinska-Myga, B.; Puschmann, A.; Nilsson, C.; Espay, A. J.; Slawek, J.; Gutmann, L.; Boeve, B. F.; Boylan, K.; Stoessl, A. J.; Ross, O. A.; Maragakis, N. J.; Van Gerpen, J.; Gerstenhaber, M.; Gwinn, K.; Dawson, T. M.; Isacson, O.; Marder, K. S.; Clark, L. N.; Przedborski, S. E.; Finkbeiner, S.; Rothstein, J. D.; Wszolek, Z. K.; Rossor, M. N.; Hardy, J. Creation of an Open-Access, Mutation-Defined Fibroblast Resource for Neurological Disease Research. *PLoS One* **2012,** *7* (8). e43099.
178. Marquie, M.; Normandin, M. D.; Vanderburg, C. R.; Costantino, I. M.; Bien, E. A.; Rycyna, L. G.; Klunk, W. E.; Mathis, C. A.; Ikonomovic, M. D.; Debnath, M. L.; Vasdev, N.; Dickerson, B. C.; Gomperts, S. N.; Growdon, J. H.; Johnson, K. A.; Frosch, M. P.; Hyman, B. T.; Gomez-Isla, T. Validating Novel Tau Positron Emission Tomography Tracer [F-18]-AV-1451 (T807) on Postmortem Brain Tissue. *Ann. Neurol.* **2015,** *78* (5), 787–800.
179. Chhatwal, J. P.; Schultz, A. P.; Marshall, G. A.; Boot, B.; Gomez-Isla, T.; Dumurgier, J.; LaPoint, M.; Scherzer, C.; Roe, A. D.; Hyman, B. T.; Sperling, R. A.; Johnson, K. A. Temporal T807 Binding Correlates With CSF tau and Phospho-tau in Normal Elderly. *Neurology* **2016,** *87,* 920–926.
180. Murray, M. E.; Przybelski, S. A.; Lesnick, T. G.; Liesinger, A. M.; Spychalla, A.; Zhang, B.; Gunter, J. L.; Parisi, J. E.; Boeve, B. F.; Knopman, D. S.; Petersen, R. C.; Jack, C. R., Jr.; Dickson, D. W.; Kantarci, K. Early Alzheimer's Disease Neuropathology Detected by Proton MR Spectroscopy. *J. Neurosci.* **2014,** *34* (49), 16247–16255.
181. Waring, M. J.; Arrowsmith, J.; Leach, A. R.; Leeson, P. D.; Mandrell, S.; Owen, R. M.; Pairaudeau, G.; Pennie, W. D.; Pickett, S. D.; Wang, J.; Wallace, O.; Weir, A. An Analysis of the Attrition of Drug Candidates From Four Major Pharmaceutical Companies. *Nat. Rev. Drug Discov.* **2015,** *14* (7), 475–486.
182. Cook, D.; Brown, D.; Alexander, R.; March, R.; Morgan, P.; Satterthwaite, G.; Pangalos, M. N. Lessons Learned From the Fate of AstraZeneca's Drug Pipeline: A Five-Dimensional Framework. *Nat. Rev. Drug Discov.* **2014,** *13* (6), 419–431.
183. Lloyd, K. C.; Robinson, P. N.; MacRae, C. A. Animal-Based Studies Will be Essential for Precision Medicine. *Sci. Transl. Med.* **2016,** *8* (352), 352.
184. Perlis, R. H. Translating Biomarkers to Clinical Practice. *Mol. Psychiatry* **2011,** *16* (11), 1076–1087.
185. Perlis, R. H.; Uher, R.; Ostacher, M.; Goldberg, J. F.; Trivedi, M. H.; Rush, A. J.; Fava, M. Association Between Bipolar Spectrum Features and Treatment Outcomes in Outpatients With Major Depressive Disorder. *Arch. Gen. Psychiatry* **2011,** *68* (4), 351–360.
186. Allman, J. M.; Tetreault, N. A.; Hakeem, A. Y.; Manaye, K. F.; Semendeferi, K.; Erwin, J. M.; Park, S.; Goubert, V.; Hof, P. R. The von Economo Neurons in the Frontoinsular and Anterior Cingulate Cortex. *Ann. N. Y. Acad. Sci.* **2011,** *1225,* 59–71.
187. Hansen, D. V.; Rubenstein, J. L.; Kriegstein, A. R. Deriving Excitatory Neurons of the Neocortex From Pluripotent Stem Cells. *Neuron* **2011,** *70* (4), 645–660.
188. Mariani, J.; Simonini, M. V.; Palejev, D.; Tomasini, L.; Coppola, G.; Szekely, A. M.; Horvath, T. L.; Vaccarino, F. M. Modeling Human Cortical Development In Vitro Using Induced Pluripotent Stem Cells. *Proc. Natl. Acad. Sci. U. S. A.* **2012,** *109* (31), 12770–12775.

189. Djebali, S.; Davis, C. A.; Merkel, A.; Dobin, A.; Lassmann, T.; Mortazavi, A.; Tanzer, A.; Lagarde, J.; Lin, W.; Schlesinger, F.; Xue, C.; Marinov, G. K.; Khatun, J.; Williams, B. A.; Zaleski, C.; Rozowsky, J.; Roder, M.; Kokocinski, F.; Abdelhamid, R. F.; Alioto, T.; Antoshechkin, I.; Baer, M. T.; Bar, N. S.; Batut, P.; Bell, K.; Bell, I.; Chakrabortty, S.; Chen, X.; Chrast, J.; Curado, J.; Derrien, T.; Drenkow, J.; Dumais, E.; Dumais, J.; Duttagupta, R.; Falconnet, E.; Fastuca, M.; Fejes-Toth, K.; Ferreira, P.; Foissac, S.; Fullwood, M. J.; Gao, H.; Gonzalez, D.; Gordon, A.; Gunawardena, H.; Howald, C.; Jha, S.; Johnson, R.; Kapranov, P.; King, B.; Kingswood, C.; Luo, O. J.; Park, E.; Persaud, K.; Preall, J. B.; Ribeca, P.; Risk, B.; Robyr, D.; Sammeth, M.; Schaffer, L.; See, L. H.; Shahab, A.; Skancke, J.; Suzuki, A. M.; Takahashi, H.; Tilgner, H.; Trout, D.; Walters, N.; Wang, H.; Wrobel, J.; Yu, Y.; Ruan, X.; Hayashizaki, Y.; Harrow, J.; Gerstein, M.; Hubbard, T.; Reymond, A.; Antonarakis, S. E.; Hannon, G.; Giddings, M. C.; Ruan, Y.; Wold, B.; Carninci, P.; Guigo, R.; Gingeras, T. R. Landscape of Transcription in Human Cells. *Nature* **2012,** *489* (7414), 101–108.
190. Lee, J. T. Epigenetic Regulation by Long Noncoding RNAs. *Science* **2012,** *338* (6113), 1435–1439.
191. Choi, S. H.; Kim, Y. H.; Hebisch, M.; Sliwinski, C.; Lee, S.; D'Avanzo, C.; Chen, H.; Hooli, B.; Asselin, C.; Muffat, J.; Klee, J. B.; Zhang, C.; Wainger, B. J.; Peitz, M.; Kovacs, D. M.; Woolf, C. J.; Wagner, S. L.; Tanzi, R. E.; Kim, D. Y. A Three-Dimensional Human Neural Cell Culture Model of Alzheimer's Disease. *Nature* **2014,** *515* (7526), 274–278.
192. Coecke, S.; Pelkonen, O.; Leite, S. B.; Bernauer, U.; Bessems, J. G.; Bois, F. Y.; Gundert-Remy, U.; Loizou, G.; Testai, E.; Zaldivar, J. M. Toxicokinetics as a Key to the Integrated Toxicity Risk Assessment Based Primarily on Non-Animal Approaches. *Toxicol. In Vitro* **2013,** *27* (5), 1570–1577.
193. Leite, S. B.; Wilk-Zasadna, I.; Zaldivar, J. M.; Airola, E.; Reis-Fernandes, M. A.; Mennecozzi, M.; Guguen-Guillouzo, C.; Chesne, C.; Guillou, C.; Alves, P. M.; Coecke, S. Three-Dimensional HepaRG Model as an Attractive Tool for Toxicity Testing. *Toxicol. Sci.* **2012,** *130* (1), 106–116.
194. Adler, S.; Pellizzer, C.; Hareng, L.; Hartung, T.; Bremer, S. First Steps in Establishing a Developmental Toxicity Test Method Based on Human Embryonic Stem Cells. *Toxicol. In Vitro* **2008,** *22* (1), 200–211.
195. Hadida, S.; Van Goor, F.; Zhou, J.; Arumugam, V.; McCartney, J.; Hazlewood, A.; Decker, C.; Negulescu, P.; Grootenhuis, P. D. Discovery of N-(2,4-di-Tert-Butyl-5-Hydroxyphenyl)-4-oxo-1,4-Dihydroquinoline-3-Carboxamide (VX-770, Ivacaftor), a Potent and Orally Bioavailable CFTR Potentiator. *J. Med. Chem.* **2014,** *57* (23), 9776–9795.
196. Boutros, M.; Heigwer, F.; Laufer, C. Microscopy-Based High-Content Screening. *Cell* **2015,** *163* (6), 1314–1325.
197. Sirenko, O.; Hesley, J.; Rusyn, I.; Cromwell, E. F. High-Content High-Throughput Assays for Characterizing the Viability and Morphology of Human iPSC-Derived Neuronal Cultures. *Assay Drug Dev. Technol.* **2014,** *12* (9–10), 536–547.
198. Wheeler, H. E.; Wing, C.; Delaney, S. M.; Komatsu, M.; Dolan, M. E. Modeling Chemotherapeutic Neurotoxicity With Human Induced Pluripotent Stem Cell-Derived Neuronal Cells. *PLoS One* **2015,** *10* (2). e0118020.
199. Finkbeiner, S.; Frumkin, M.; Kassner, P. D. Cell-Based Screening: Extracting Meaning From Complex Data. *Neuron* **2015,** *86* (1), 160–174.
200. Ho, S. M.; Hartley, B. J.; Tcw, J.; Beaumont, M.; Stafford, K.; Slesinger, P. A.; Brennand, K. J. Rapid Ngn2-Induction of Excitatory Neurons From hiPSC-Derived Neural Progenitor Cells. *Methods* **2016,** *101,* 113–124.
201. Martinez, R.; Hsu, S.; Ezerskiy, L. A.; Shu, H. J.; Mennerick, S.; Goate, A. M.; Karch, C. M. Efficient Production, Banking and Terminal Differentiation of Neural Progenitor Cells From Human Induced Pluripotent Stem Cells. (in press).
202. Cheng, C.; Fass, D.; Folz-Donahue, K.; MacDonald, M.; Haggarty, S. J. Highly Expandable Human iPSC-Derived Neural Progenitor Cells (NPC) and Neurons for Central Nervous System Disease Modeling and High-Throughput Screening. Current Protocols. (in press).
203. Okerlund, N. D.; Cheyette, B. N. Synaptic Wnt Signaling-a Contributor to Major Psychiatric Disorders? *J. Neurodev. Disord.* **2011,** *3* (2), 162–174.
204. O'Roak, B. J.; Vives, L.; Fu, W.; Egertson, J. D.; Stanaway, I. B.; Phelps, I. G.; Carvill, G.; Kumar, A.; Lee, C.; Ankenman, K.; Munson, J.; Hiatt, J. B.; Turner, E. H.; Levy, R.; O'Day, D. R.; Krumm, N.; Coe, B. P.; Martin, B. K.; Borenstein, E.; Nickerson, D. A.; Mefford, H. C.; Doherty, D.; Akey, J. M.; Bernier, R.; Eichler, E. E.; Shendure, J. Multiplex Targeted Sequencing Identifies Recurrently Mutated Genes in Autism Spectrum Disorders. *Science* **2012,** *338* (6114), 1619–1622.
205. Silva, M. C.; Cheng, C.; Reis, S.; Lucente, D.; Dickerson, B.; Consortium, T.; Haggarty, S. J. Tauopathy: Discovery of Small Molecule Modulators of Tau Phenotypes in Human iPSC-Derived Neuronal Models of Frontotemporal Degeneration. Society for Neuroscience, Annual Meeting, Chicago, IL.
206. Dimos, J. T.; Rodolfa, K. T.; Niakan, K. K.; Weisenthal, L. M.; Mitsumoto, H.; Chung, W.; Croft, G. F.; Saphier, G.; Leibel, R.; Goland, R.; Wichterle, H.; Henderson, C. E.; Eggan, K. Induced Pluripotent Stem Cells Generated From Patients With ALS Can Be Differentiated Into Motor Neurons. *Science* **2008,** *321* (5893), 1218–1221.
207. Shi, Y.; Kirwan, P.; Smith, J.; MacLean, G.; Orkin, S. H.; Livesey, F. J. A Human Stem Cell Model of Early Alzheimer's Disease Pathology in Down Syndrome. *Sci. Transl. Med.* **2012,** *4* (124), 124ra29.
208. Muratore, C. R.; Rice, H. C.; Srikanth, P.; Callahan, D. G.; Shin, T.; Benjamin, L. N.; Walsh, D. M.; Selkoe, D. J.; Young-Pearse, T. L. The Familial Alzheimer's Disease APPV717I Mutation Alters APP Processing and Tau Expression in iPSC-Derived Neurons. *Hum. Mol. Genet.* **2014,** *23* (13), 3523–3536.
209. Cooper, O.; Seo, H.; Andrabi, S.; Guardia-Laguarta, C.; Graziotto, J.; Sundberg, M.; McLean, J. R.; Carrillo-Reid, L.; Xie, Z.; Osborn, T.; Hargus, G.; Deleidi, M.; Lawson, T.; Bogetofte, H.; Perez-Torres, E.; Clark, L.; Moskowitz, C.; Mazzulli, J.; Chen, L.; Volpicelli-Daley, L.; Romero, N.; Jiang, H.; Uitti, R. J.; Huang, Z.; Opala, G.; Scarffe, L. A.; Dawson, V. L.; Klein, C.; Feng, J.; Ross, O. A.; Trojanowski, J. Q.; Lee, V. M.; Marder, K.; Surmeier, D. J.; Wszolek, Z. K.; Przedborski, S.; Krainc, D.; Dawson, T. M.; Isacson, O. Pharmacological Rescue of Mitochondrial Deficits in iPSC-Derived Neural Cells From Patients With Familial Parkinson's Disease. *Sci. Transl. Med.* **2012,** *4* (141), 141ra90.
210. Woodard, C. M.; Campos, B. A.; Kuo, S. H.; Nirenberg, M. J.; Nestor, M. W.; Zimmer, M.; Mosharov, E. V.; Sulzer, D.; Zhou, H.; Paull, D.; Clark, L.; Schadt, E. E.; Sardi, S. P.; Rubin, L.; Eggan, K.; Brock, M.; Lipnick, S.; Rao, M.; Chang, S.; Li, A.; Noggle, S. A. iPSC-Derived Dopamine Neurons Reveal Differences Between Monozygotic Twins Discordant for Parkinson's Disease. *Cell Rep.* **2014,** *9* (4), 1173–1182.
211. Flierl, A.; Oliveira, L. M.; Falomir-Lockhart, L. J.; Mak, S. K.; Hesley, J.; Soldner, F.; Arndt-Jovin, D. J.; Jaenisch, R.; Langston, J. W.; Jovin, T. M.; Schule, B. Higher Vulnerability and Stress Sensitivity of Neuronal Precursor Cells Carrying an Alpha-Synuclein Gene Triplication. *PLoS One* **2014,** *9* (11). e112413.
212. Lee, W. C.; Almeida, S.; Prudencio, M.; Caulfield, T. R.; Zhang, Y. J.; Tay, W. M.; Bauer, P. O.; Chew, J.; Sasaguri, H.; Jansen-West, K. R.; Gendron, T. F.; Stetler, C. T.; Finch, N.; Mackenzie, I. R.; Rademakers, R.; Gao, F. B.; Petrucelli, L. Targeted Manipulation of the Sortilin-Progranulin Axis Rescues Progranulin Haploinsufficiency. *Hum. Mol. Genet.* **2014,** *23* (6), 1467–1478.
213. Cao, L.; McDonnell, A.; Nitzsche, A.; Alexandrou, A.; Saintot, P. P.; Loucif, A. J.; Brown, A. R.; Young, G.; Mis, M.; Randall, A.; Waxman, S. G.; Stanley, P.; Kirby, S.; Tarabar, S.; Gutteridge, A.; Butt, R.; McKernan, R. M.; Whiting, P.; Ali, Z.; Bilsland, J.; Stevens, E. B. Pharmacological Reversal of a Pain Phenotype in iPSC-Derived Sensory Neurons and Patients With Inherited Erythromelalgia. *Sci. Transl. Med.* **2016,** *8* (335), 335ra56.
214. Fallahi-Sichani, M.; Honarnejad, S.; Heiser, L. M.; Gray, J. W.; Sorger, P. K. Metrics Other Than Potency Reveal Systematic Variation in Responses to Cancer Drugs. *Nat. Chem. Biol.* **2013,** *9* (11), 708–714.
215. MacDonald, M. L.; Westwick, J. K. Exploiting Network Biology to Improve Drug Discovery. *Methods Mol. Biol.* **2007,** *356,* 221–232.
216. Zhang, W. B.; Ross, P. J.; Tu, Y.; Wang, Y.; Beggs, S.; Sengar, A. S.; Ellis, J.; Salter, M. W. Fyn Kinase Regulates GluN2B Subunit-Dominant NMDA Receptors in Human Induced Pluripotent Stem Cell-Derived Neurons. *Sci. Rep.* **2016,** *6,* 23837.
217. Kuenzel, K.; Friedrich, O.; Gilbert, D. F. A Recombinant Human Pluripotent Stem Cell Line Stably Expressing Halide-Sensitive YFP-I152L for GABAAR and GlyR-Targeted High-Throughput Drug Screening and Toxicity Testing. *Front. Mol. Neurosci.* **2016,** *9,* 51.
218. Doudna, J. A.; Charpentier, E. Genome Editing. The New Frontier of Genome Engineering With CRISPR-Cas9. *Science* **2014,** *346* (6213), 1258096.
219. Hsu, P. D.; Lander, E. S.; Zhang, F. Development and Applications of CRISPR-Cas9 for Genome Engineering. *Cell* **2014,** *157* (6), 1262–1278.
220. Dominguez, A. A.; Lim, W. A.; Qi, L. S. Beyond Editing: Repurposing CRISPR-Cas9 for Precision Genome Regulation and Interrogation. *Nat. Rev. Mol. Cell Biol.* **2016,** *17* (1), 5–15.
221. Thakore, P. I.; Black, J. B.; Hilton, I. B.; Gersbach, C. A. Editing the Epigenome: Technologies for Programmable Transcription and Epigenetic Modulation. *Nat. Methods* **2016,** *13* (2), 127–137.
222. Miles, L. A.; Garippa, R. J.; Poirier, J. T. Design, Execution, and Analysis of Pooled in vitro CRISPR/Cas9 Screens. *FEBS J.* **2016,** *283,* 3170–3180.

223. Pei, Y.; Sierra, G.; Sivapatham, R.; Swistowski, A.; Rao, M. S.; Zeng, X. A Platform for Rapid Generation of Single and Multiplexed Reporters in Human iPSC Lines. *Sci. Rep.* **2015,** *5,* 9205.
224. Ko, H. C.; Gelb, B. D. Concise Review: Drug Discovery in the Age of the Induced Pluripotent Stem Cell. *Stem Cells Transl. Med.* **2014,** *3* (4), 500–509.
225. Aday, S.; Cecchelli, R.; Hallier-Vanuxeem, D.; Dehouck, M. P.; Ferreira, L. Stem Cell-Based Human Blood–brain Barrier Models for Drug Discovery and Delivery. *Trends Biotechnol.* **2016,** *34* (5), 382–393.
226. Negoro, R.; Takayama, K.; Nagamoto, Y.; Sakurai, F.; Tachibana, M.; Mizuguchi, H. Modeling of Drug-Mediated CYP3A4 Induction by Using Human iPS Cell-Derived Enterocyte-Like Cells. *Biochem. Biophys. Res. Commun.* **2016,** *472* (4), 631–636.
227. Kodama, N.; Iwao, T.; Katano, T.; Ohta, K.; Yuasa, H.; Matsunaga, T. Characteristic Analysis of Intestinal Transport in Enterocyte-Like Cells Differentiated From Human Induced Pluripotent Stem Cells. *Drug Metab. Dispos.* **2016,** *44* (10). http://dx.doi.org/10.1124/dmd.116.069336.
228. Watmuff, B.; Berkovitch, S. S.; Huang, J. H.; Iaconelli, J.; Toffel, S.; Karmacharya, R. Disease Signatures for Schizophrenia and Bipolar Disorder Using Patient-Derived Induced Pluripotent Stem Cells. *Mol. Cell. Neurosci.* **2016,** *73,* 96–103.
229. Jacquemont, S.; Curie, A.; des Portes, V.; Torrioli, M. G.; Berry-Kravis, E.; Hagerman, R. J.; Ramos, F. J.; Cornish, K.; He, Y.; Paulding, C.; Neri, G.; Chen, F.; Hadjikhani, N.; Martinet, D.; Meyer, J.; Beckmann, J. S.; Delange, K.; Brun, A.; Bussy, G.; Gasparini, F.; Hilse, T.; Floesser, A.; Branson, J.; Bilbe, G.; Johns, D.; Gomez-Mancilla, B. Epigenetic Modification of the FMR1 Gene in Fragile X Syndrome is Associated With Differential Response to the mGluR5 Antagonist AFQ056. *Sci. Transl. Med.* **2011,** *3* (64), 64ra1.
230. Shinde, V.; Sureshkumar, P.; Sotiriadou, I.; Hescheler, J.; Sachinidis, A. Human Embryonic and Induced Pluripotent Stem Cell Based Toxicity Testing Models: Future Applications in New Drug Discovery. *Curr. Med. Chem.* **2016;** http://dx.doi.org/10.2174/0929867323666160627113436.
231. Deshmukh, R. S.; Kovacs, K. A.; Dinnyes, A. Drug Discovery Models and Toxicity Testing Using Embryonic and Induced Pluripotent Stem-Cell-Derived Cardiac and Neuronal Cells. *Stem Cells Int.* **2012,** *2012,* 379569.
232. Medine, C. N.; Lucendo-Villarin, B.; Storck, C.; Wang, F.; Szkolnicka, D.; Khan, F.; Pernagallo, S.; Black, J. R.; Marriage, H. M.; Ross, J. A.; Bradley, M.; Iredale, J. P.; Flint, O.; Hay, D. C. Developing High-Fidelity Hepatotoxicity Models From Pluripotent Stem Cells. *Stem Cells Transl. Med.* **2013,** *2* (7), 505–509.
233. Pei, Y.; Peng, J.; Behl, M.; Sipes, N. S.; Shockley, K. R.; Rao, M. S.; Tice, R. R.; Zeng, X. Comparative Neurotoxicity Screening in Human iPSC-Derived Neural Stem Cells, Neurons and Astrocytes. *Brain Res.* **2016,** *1638* (Pt A), 57–73.
234. Heilker, R.; Traub, S.; Reinhardt, P.; Scholer, H. R.; Sterneckert, J. iPS Cell Derived Neuronal Cells for Drug Discovery. *Trends Pharmacol. Sci.* **2014,** *35* (10), 510–519.
235. Inoue, H.; Yamanaka, S. The Use of Induced Pluripotent Stem Cells in Drug Development. *Clin. Pharmacol. Ther.* **2011,** *89* (5), 655–661.
236. Sandoe, J.; Eggan, K. Opportunities and Challenges of Pluripotent Stem Cell Neurodegenerative Disease Models. *Nat. Neurosci.* **2013,** *16* (7), 780–789.
237. Miller, J. D.; Ganat, Y. M.; Kishinevsky, S.; Bowman, R. L.; Liu, B.; Tu, E. Y.; Mandal, P. K.; Vera, E.; Shim, J. W.; Kriks, S.; Taldone, T.; Fusaki, N.; Tomishima, M. J.; Krainc, D.; Milner, T. A.; Rossi, D. J.; Studer, L. Human iPSC-Based Modeling of Late-Onset Disease via Progerin-Induced Aging. *Cell Stem Cell* **2013,** *13* (6), 691–705.
238. Jo, J.; Xiao, Y.; Sun, A. X.; Cukuroglu, E.; Tran, H. D.; Goke, J.; Tan, Z. Y.; Saw, T. Y.; Tan, C. P.; Lokman, H.; Lee, Y.; Kim, D.; Ko, H. S.; Kim, S. O.; Park, J. H.; Cho, N. J.; Hyde, T. M.; Kleinman, J. E.; Shin, J. H.; Weinberger, D. R.; Tan, E. K.; Je, H. S.; Ng, H. H. Midbrain-Like Organoids From Human Pluripotent Stem Cells Contain Functional Dopaminergic and Neuromelanin-Producing Neurons. *Cell Stem Cell* **2016,** *19* (2), 248–257.
239. Qian, X.; Nguyen, H. N.; Song, M. M.; Hadiono, C.; Ogden, S. C.; Hammack, C.; Yao, B.; Hamersky, G. R.; Jacob, F.; Zhong, C.; Yoon, K. J.; Jeang, W.; Lin, L.; Li, Y.; Thakor, J.; Berg, D. A.; Zhang, C.; Kang, E.; Chickering, M.; Nauen, D.; Ho, C. Y.; Wen, Z.; Christian, K. M.; Shi, P. Y.; Maher, B. J.; Wu, H.; Jin, P.; Tang, H.; Song, H.; Ming, G. L. Brain-Region-Specific Organoids Using Mini-bioreactors for Modeling ZIKV Exposure. *Cell* **2016,** *165* (5), 1238–1254.
240. Clevers, H. Modeling Development and Disease With Organoids. *Cell* **2016,** *165* (7), 1586–1597.
241. Lui, J. H.; Hansen, D. V.; Kriegstein, A. R. Development and Evolution of the Human Neocortex. *Cell* **2011,** *146* (1), 18–36.
242. Pagliuca, F. W.; Millman, J. R.; Gurtler, M.; Segel, M.; Van Dervort, A.; Ryu, J. H.; Peterson, Q. P.; Greiner, D.; Melton, D. A. Generation of Functional Human Pancreatic Beta Cells In Vitro. *Cell* **2014,** *159* (2), 428–439.
243. Espuny-Camacho, I.; Michelsen, K. A.; Gall, D.; Linaro, D.; Hasche, A.; Bonnefont, J.; Bali, C.; Orduz, D.; Bilheu, A.; Herpoel, A.; Lambert, N.; Gaspard, N.; Peron, S.; Schiffmann, S. N.; Giugliano, M.; Gaillard, A.; Vanderhaeghen, P. Pyramidal Neurons Derived From Human Pluripotent Stem Cells Integrate Efficiently into Mouse Brain Circuits In Vivo. *Neuron* **2013,** *77* (3), 440–456.
244. Arguello, P. A.; Gogos, J. A. Genetic and Cognitive Windows Into Circuit Mechanisms of Psychiatric Disease. *Trends Neurosci.* **2012,** *35* (1), 3–13.
245. Paull, D.; Sevilla, A.; Zhou, H.; Hahn, A. K.; Kim, H.; Napolitano, C.; Tsankov, A.; Shang, L.; Krumholz, K.; Jagadeesan, P.; Woodard, C. M.; Sun, B.; Vilboux, T.; Zimmer, M.; Forero, E.; Moroziewicz, D. N.; Martinez, H.; Malicdan, M. C.; Weiss, K. A.; Vensand, L. B.; Dusenberry, C. R.; Polus, H.; Sy, K. T.; Kahler, D. J.; Gahl, W. A.; Solomon, S. L.; Chang, S.; Meissner, A.; Eggan, K.; Noggle, S. A. Automated, High-Throughput Derivation, Characterization and Differentiation of Induced Pluripotent Stem Cells. *Nat. Methods* **2015,** *12* (9), 885–892.
246. Chen, S.; Do, J. T.; Zhang, Q.; Yao, S.; Yan, F.; Peters, E. C.; Scholer, H. R.; Schultz, P. G.; Ding, S. Self-Renewal of Embryonic Stem Cells by a Small Molecule. *Proc. Natl. Acad. Sci. U. S. A.* **2006,** *103* (46), 17266–17271.
247. Watanabe, K.; Ueno, M.; Kamiya, D.; Nishiyama, A.; Matsumura, M.; Wataya, T.; Takahashi, J. B.; Nishikawa, S.; Nishikawa, S.; Muguruma, K.; Sasai, Y. A ROCK Inhibitor Permits Survival of Dissociated Human Embryonic Stem Cells. *Nat. Biotechnol.* **2007,** *25* (6), 681–686.
248. Desbordes, S. C.; Placantonakis, D. G.; Ciro, A.; Socci, N. D.; Lee, G.; Djaballah, H.; Studer, L. High-Throughput Screening Assay for the Identification of Compounds Regulating Self-Renewal and Differentiation in Human Embryonic Stem Cells. *Cell Stem Cell* **2008,** *2* (6), 602–612.
249. Barbaric, I.; Gokhale, P. J.; Andrews, P. W. High-Content Screening of Small Compounds on Human Embryonic Stem Cells. *Biochem. Soc. Trans.* **2010,** *38* (4), 1046–1050.
250. Makhortova, N. R.; Hayhurst, M.; Cerqueira, A.; Sinor-Anderson, A. D.; Zhao, W. N.; Heiser, P. W.; Arvanites, A. C.; Davidow, L. S.; Waldon, Z. O.; Steen, J. A.; Lam, K.; Ngo, H. D.; Rubin, L. L. A Screen for Regulators of Survival of Motor Neuron Protein Levels. *Nat. Chem. Biol.* **2011,** *7* (8), 544–552.
251. McLaren, D.; Gorba, T.; Marguerie de Rotrou, A.; Pillai, G.; Chappell, C.; Stacey, A.; Lingard, S.; Falk, A.; Smith, A.; Koch, P.; Brustle, O.; Vickers, R.; Tinsley, J.; Flanders, D.; Bello, P.; Craig, S. Automated Large-Scale Culture and Medium-Throughput Chemical Screen for Modulators of Proliferation and Viability of Human Induced Pluripotent Stem Cell-Derived Neuroepithelial-Like Stem Cells. *J. Biomol. Screen* **2013,** *18* (3), 258–268.
252. Peng, J.; Liu, Q.; Rao, M. S.; Zeng, X. Using Human Pluripotent Stem Cell-Derived Dopaminergic Neurons to Evaluate Candidate Parkinson's Disease Therapeutic Agents in MPP+ and Rotenone Models. *J. Biomol. Screen* **2013,** *18* (5), 522--533.
253. Xu, X.; Lei, Y.; Luo, J.; Wang, J.; Zhang, S.; Yang, X. J.; Sun, M.; Nuwaysir, E.; Fan, G.; Zhao, J.; Lei, L.; Zhong, Z. Prevention of Beta-Amyloid Induced Toxicity in Human iPS Cell-Derived Neurons by Inhibition of Cyclin-Dependent Kinases and Associated Cell Cycle Events. *Stem Cell Res* **2013,** *10* (2), 213–227.
254. Navarrete, E. G.; Liang, P.; Lan, F.; Sanchez-Freire, V.; Simmons, C.; Gong, T.; Sharma, A.; Burridge, P. W.; Patlolla, B.; Lee, A. S.; Wu, H.; Beygui, R. E.; Wu, S. M.; Robbins, R. C.; Bers, D. M.; Wu, J. C. Screening Drug-Induced Arrhythmia [Corrected] Using Human Induced Pluripotent Stem Cell-Derived Cardiomyocytes and Low-Impedance Microelectrode Arrays. *Circulation* **2013,** *128* (11 Suppl 1), S3–13.
255. Liang, P.; Lan, F.; Lee, A. S.; Gong, T.; Sanchez-Freire, V.; Wang, Y.; Diecke, S.; Sallam, K.; Knowles, J. W.; Wang, P. J.; Nguyen, P. K.; Bers, D. M.; Robbins, R. C.; Wu, J. C. Drug Screening Using a Library of Human Induced Pluripotent Stem Cell-Derived Cardiomyocytes Reveals Disease-Specific Patterns of Cardiotoxicity. *Circulation* **2013,** *127* (16), 1677–1691.
256. Ben-David, U.; Gan, Q. F.; Golan-Lev, T.; Arora, P.; Yanuka, O.; Oren, Y. S.; Leikin-Frenkel, A.; Graf, M.; Garippa, R.; Boehringer, M.; Gromo, G.; Benvenisty, N. Selective Elimination of Human Pluripotent Stem Cells by an Oleate Synthesis Inhibitor Discovered in a High-Throughput Screen. *Cell Stem Cell* **2013,** *12* (2), 167–179.
257. Choi, S. M.; Kim, Y.; Shim, J. S.; Park, J. T.; Wang, R. H.; Leach, S. D.; Liu, J. O.; Deng, C.; Ye, Z.; Jang, Y. Y. Efficient Drug Screening and Gene Correction for Treating Liver Disease Using Patient-Specific Stem Cells. *Hepatology* **2013,** *57* (6), 2458–2468.

1.04 From Imaging Agents to Theranostic Drugs in Alzheimer's Disease

ML Bolognesi, Department of Pharmacy and Biotechnology, Alma Mater Studiorum, University of Bologna, Bologna

© 2017 Elsevier Ltd. All rights reserved.

1.04.1	**Overview of Alzheimer's Disease (AD) Therapy and Diagnosis**	74
1.04.2	**Diagnosis of AD**	75
1.04.2.1	SPs and NFTs as Biomarkers for AD Diagnosis	76
1.04.2.1.1	Background to the concept of AD biomarkers	76
1.04.2.1.2	Amyloid hypothesis supports Aβ as an AD biomarker	77
1.04.2.1.3	Tau hypothesis supports tau as an AD biomarker	77
1.04.2.1.4	Current perspectives	78
1.04.3	**Development of PET Tracers for AD Diagnosis**	79
1.04.3.1	PET Tracers Approved for Aβ Plaque Imaging	79
1.04.3.1.1	Aβ PET tracers derived from Thioflavin T	80
1.04.3.1.2	Aβ PET tracers derived from CR	82
1.04.3.2	PET Tracers for Aβ Plaque Imaging Evaluated in Human Subjects	83
1.04.3.2.1	Aβ single-photon emission computed tomography (SPECT) tracers	84
1.04.3.3	PET Tracers for NFT Imaging	84
1.04.3.3.1	Quinoline- and benzimidazole-derived tau PET tracers	85
1.04.3.3.2	Benzothiazole-derived tau PET tracers	86
1.04.3.3.3	Benzoimidazopyrimidine- and pyridoindole-derived tau PET tracers	87
1.04.4	**Development of Fluorescent Probes as Innovative Imaging Agents for AD Diagnosis**	87
1.04.4.1	Thioflavin T and CR as Starting Points for the Development of Fluorescent Imaging Agents	88
1.04.4.2	First Fluorescent Probes Used for in vivo Aβ Plaque Imaging	89
1.04.4.2.1	NIAD-4 and derivatives	89
1.04.4.2.2	AOI987	90
1.04.4.2.3	THK-265	90
1.04.4.3	Recent Development of Fluorescent Probes for In vivo Aβ Plaque Imaging	90
1.04.4.3.1	Photoswitchable fluorescent probes	92
1.04.4.4	Fluorescent Probes Used for In vivo NFT Imaging	92
1.04.4.5	Fluorescent Probes Used for Amyloid Imaging in the Retina and Olfactory Epithelium	94
1.04.5	**Curcumin as a Versatile Scaffold for the Development of Diagnostic and Therapeutic Agents for AD**	94
1.04.6	**Development of Theranostics against AD**	96
1.04.6.1	Theranostic Small Molecules for AD	97
1.04.6.1.1	BTA-1, BSB, and PE154 as theranostic precursors	98
1.04.6.1.2	SLOH as a theranostic small molecule	98
1.04.6.1.3	G8 as a theranostic small molecule	99
1.04.6.1.4	PiB-C as a theranostic small molecule	100
1.04.6.1.5	CRANAD-28 as a theranostic small molecule	100
1.04.6.1.6	TBT as a theranostic small molecule	100
1.04.6.2	Theranostic Nanomedicine for AD	101
1.04.7	**Conclusions**	101
References		102

1.04.1 Overview of Alzheimer's Disease (AD) Therapy and Diagnosis

Although we savor the promise of a new era of personalized medicine, much of today's drug prescribing is still "trial and error," with a success rate after treatment that is consequently modest. This approach, in addition to the serious medical consequences for the individual patients, has undoubted economic consequences for the healthcare system and the society as a whole. For most serious chronic diseases, early diagnosis and early intervention are two important aspects that are tightly intertwined. The lesson we learned in the cancer field is that an incorrect or delayed treatment decision may result in pathology dissemination with no or very low chances of cure and can even culminate in death. Even worse, for infectious diseases, delay in the recognition of infectiousness facilitates increased transmission.

The same awareness is being acquired in the field of Alzheimer's disease (AD). AD is a major public health problem affecting nearly 35 million patients worldwide with numbers projected to rise to 115.4 million by 2050. In 2013, an estimated 44.35 million people were living with dementia worldwide, predicted to be 75.62 million by 2030, and 135.46 million by 2050.[1] In addition,

with the rise in aging population in the developing countries, the proportion of patients with neurodegenerative diseases is also surging. The prevalence of AD ranges from 6.44% in south India to 4.86% in Shanghai, China to 3.92% in Sri Lanka, for populations above 65 years.[1] These challenges are exacerbated by the lack of effective treatments and by the fact that there is no widely available gold standard for diagnosis.

At present, no effective cure or prophylaxis exists for AD. Four cholinesterase (ChE) inhibitors (tacrine, rivastigmine, donepezil, and galantamine, in Fig. 1) and the *N*-methyl-D-aspartate (NMDA) antagonist memantine (Fig. 1) are the only drugs approved by the US Food and Drug Administration (FDA) and European Medicines Agency (EMA) for AD treatment. The ChE inhibitors were developed on the basis of the cholinergic hypothesis, which correlates the clinically observed cholinergic dysfunction (ie, marked degeneration of cholinergic neurons, loss of cholinergic transmission, and changes in ChE and choline acetyltransferase activity in the cerebral cortex and hippocampus) with the pathology. Memantine is an antagonist of glutamate NMDA receptors (NMDAR) with a peculiar mechanism of action: it preferentially blocks excessive extrasynaptic NMDAR activity while largely sparing the normal synaptic one.[2]

Unfortunately, both drug classes provide only symptomatic treatment, are modestly effective and offer limited temporary benefit, and do not alter the course of the disease.[2] Thus, a number of novel strategies aimed to modify the disease process have been developed. The major developments in this direction of the last two decades are the amyloid-β (Aβ)- and tau-based treatments, which could hold the key to curing AD in the near future. However, reduction of cognitive and functional decline and cortical neurodegeneration, through small molecules or immune-based therapeutics directed toward Aβ, has had little success so far. After focusing on anti-Aβ approaches for many years, the pharmaceutical industry is making major investments in programs designed to discover tau-based therapeutics. Progress has been limited, however, and few such drugs are in clinical development. Several other drugs with different mechanisms of action have been thoroughly investigated in preclinical studies, but most of them have failed to produce any result in the clinical scenario. This makes AD one of the most unsuccessful therapeutic areas of drug discovery,[3] but it also is of great opportunity.[4]

In the battle against this devastating disorder, the tremendous difficulty in developing effective drugs has been attributed to three main factors. First, despite significant advances in understanding the pathological and pathophysiological determinants of AD, such as Aβ, tau, neuroinflammation, oxidative stress, and synaptic dysfunction, we still lack a detailed understanding of the causal roles of these phenomena and the interactions between them. As a result, many potential targets have been identified but not yet validated, so we lack precise knowledge of those that can give rise to disease-modifying treatments.[5] Second, as with all drugs targeting the central nervous system (CNS), AD drugs must cross the blood–brain barrier (BBB) and reach their targets at a concentration sufficient to achieve the desired effect. Indeed, an estimated 98% of systemically administered small molecules do not possess the physicochemical properties required for optimal brain exposure.[6] Third, as for any chronic disease treatment for elderly people with multiple comorbidities and concomitant treatments, these drugs must not be toxic or prone to developing drug–drug interaction.[7]

Ideally, any pharmacological treatment should be timely and rely on an in-depth understanding of the disease biology and the drug's mechanism of action. Better understanding of the disease molecular roots, therefore, is essential, and early diagnosis combined with a comprehensive management strategy initiated early in the course of the cognitive decline will likely be the most effective method of controlling the progression of AD.[8] We are far from being there yet, but recent advances in molecular medicine and molecular diagnostics have given us sufficient confidence about the prospects of personalized medicine in AD.[9]

1.04.2 Diagnosis of AD

Currently, premortem diagnosis of AD relies on clinically documenting decline in memory, cognition, and function over time. However, pathology has already caused severe brain damage in individuals who are diagnosed in this way, as neurodegeneration is estimated to start 20–30 years before the first clinical symptoms become apparent.[10]

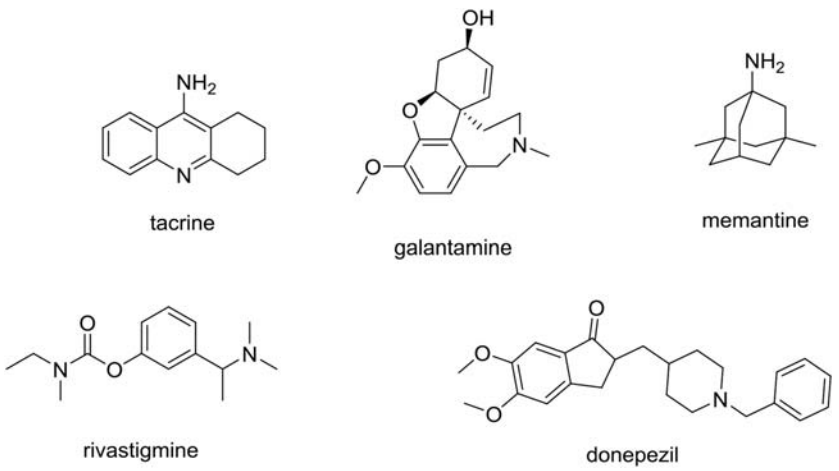

Fig. 1 Chemical structures of drugs approved for AD.

In addition, it is only by actually looking at the affected brain that a pathologist can be able to see exactly what occurred in specific areas and correlate it with the clinical picture of AD. The pathological diagnosis following biopsy or autopsy is thus the only definitive diagnosis of that patient's disease. Considering that brain biopsy is an invasive procedure with evident risk to the patient and also considering that there is currently no cure for AD, brain biopsy is very rarely performed because the risk outweighs the value. Thus, a definitive diagnosis of AD requires both clinically demonstrated dementia and the identification of the two pathological hallmarks of the disease, that is, senile plaques (SPs) and neurofibrillary tangles (NFTs), at autopsy.

In this scenario, researchers have been intensely working to find an easy and accurate way to diagnose AD before the clinical symptoms are evident. In other words, they have been looking for appropriate biomarkers. According to the Glossary provided by FDA, a biomarker is "a characteristic that is objectively measured and evaluated as an indicator of normal biological processes, pathogenic processes, or pharmacologic responses to a therapeutic intervention."[11] In the years, several biomarkers have been identified such as serum low-density lipoprotein for cardiovascular diseases, fasting blood glucose level for diabetes, and, more recently, p53 gene and matrix metalloproteinase for cancer. In AD, a number of biomarkers, indicating the presence of pathology and AD-associated neuronal injury in vivo, have been developed. These biomarkers have strong potential not only for clinical use in etiologic determination, predictive prognosis, and monitoring disease progression but also for serving as an outcome measures in disease-modifying therapeutic trials.[12]

1.04.2.1 SPs and NFTs as Biomarkers for AD Diagnosis

Generally speaking, biomarkers can be broadly classified as "diagnostic" biomarkers, used to guide patient selection, and "pharmacodynamic" biomarkers to evaluate target engagement and drug's mechanism of action. Indeed, "diagnostic" biomarkers are indispensable in clinics for distinguishing individuals with prodromal signs of AD from healthy aging adults. Such biomarkers would be also ideal for differentiating AD from other types of dementia, such as mild cognitive impairment (MCI), or mixed forms of dementia, such as vascular dementia (VaD), frontotemporal lobe dementia, or Lewy body dementia. This is important because treatment for these diseases might differ. In parallel, "pharmacodynamic" biomarkers are considered vital at a preclinical level to confirm that a therapeutic agent will reach its intended target and have the desired biological effect. Thus, scientists have also committed to developing "pharmacodynamic" biomarkers to support AD clinical trials.

1.04.2.1.1 Background to the concept of AD biomarkers

There are currently no universally validated biomarkers for AD, but several potential candidates have been identified and began evaluating in preclinical and clinical models.

Biomarkers have been described using several modalities, including magnetic resonance imaging (MRI) scans of brain volume, imaging of cerebral Aβ deposition, studies of cerebral metabolism with fluoro-deoxy-D-glucose (FDG), genotyping of genetic polymorphisms known to be associated with disease risk, and quantification of specific proteins (total tau, phosphorylated tau, and the 42-amino acid form of Aβ ($A\beta_{42}$)) in the cerebrospinal fluid (CSF) or in the plasma.[13]

The best-established method for the detection and tracking of AD pathology relies on structural MRI measurements of regional and whole-brain atrophy. Several studies had demonstrated that structural MRI estimates of tissue damage or loss in characteristically vulnerable brain regions, such as hippocampus and entorhinal cortex, are predictive of progression of MCI to AD. Additionally, the clinical utility of MRI in differentiating AD from other pathologies, such as VaD or non-Alzheimer neurodegeneration, has been widely recognized. However, it has been pointed out that MRI evaluation is based on the assessment of volume change, which is a nonspecific, late feature in disease progression.[14]

Positron emission tomography (PET) is now well established for clinical use in neurodegenerative disorders. Measurements of cerebral glucose metabolism, by using [^{18}F]FDG PET, are of unequivocal value in early diagnosis, differential diagnosis, and the evaluation of drug treatment. In AD patients, neurodegeneration is accompanied by synaptic dysfunction, which is denoted by decreased [^{18}F]FDG uptake on PET scan. Studies consistently find increasing decline in the regional cerebral metabolic rate for glucose in the parietal and temporal cortex in clinically affected patients and in the frontal cortex and whole brain as the pathology becomes more severe.[14]

The search of risk genes that can help in diagnosis is also a very active field: at the moment, investigators have pinpointed three genes (amyloid precursor protein (*APP*), presenilin 1 (*PS1*, also known as *PSEN1*), and presenilin 2 (*PS2*, also known as *PSEN2*)) with rare variations that cause AD and several others that increase risk but do not guarantee that a person will develop the disease. Genetic testing for allele 4 of apolipoprotein E (*APOE-e4*), the strongest risk gene, is included in some clinical trials to identify participants at high risk for the disease. However, as diagnosis unaccompanied by cures is of questionable value, APOE-e4 testing is not currently recommended outside research settings. Nevertheless, it is conceivable that as more effective treatments are developed, genetic profiling will become a solid risk assessment tool for wider use.[10]

Since Alois Alzheimer's seminal report in 1907,[15] the scientific community has considered the defining and main pathological hallmarks of the disease to be extracellular Aβ deposits in SP and intracellular NFT, consisting of paired helical filaments (PHFs) of abnormally hyperphosphorylated tau protein. Of the possible AD biomarkers, SP and NFT are pathological hallmarks that should precede clinical symptoms by several years.[16] This peculiar feature makes in vivo imaging of Aβ and tau particularly suitable for diagnosing patients at risk and detecting AD before dementia occurs, that is, at an MCI stage.

1.04.2.1.2 Amyloid hypothesis supports Aβ as an AD biomarker

According to the "amyloid cascade hypothesis,"[17] the generation of Aβ would happen from the consecutive proteolysis of a large transmembrane protein, the APP, and it would aggregate or deposit in extracellular insoluble SP. β-Secretase produces the NH_2-terminus of Aβ, cleaving APP to provide a soluble version (β-APPs) and a 99-residue COOH-terminal fragment (C99) that remains membrane bound (Fig. 2). Alternatively, α-secretase cuts within the Aβ region to produce α-APPs and an 83-residue COOH-terminal fragment (C83). Both C99 and C83 are substrates for a second proteolytic enzyme, γ-secretase, which performs an unusual cut within the transmembrane domain to produce the amyloidogenic peptide Aβ from C99 and the not amyloidogenic one (p3) from C83 (Fig. 2). Proteolysis by γ-secretase is heterogeneous: most of the Aβ species produced is a 40-residue peptide ($Aβ_{40}$), whereas a small proportion is a 42-residue COOH-terminal variant ($Aβ_{42}$).[18]

The longer and more hydrophobic $Aβ_{42}$ is much more prone to fibril formation than $Aβ_{40}$, and even though $Aβ_{42}$ is a minor form of Aβ, it is the major Aβ species found in SP. In addition to $Aβ_{40}$ and $Aβ_{42}$, another isoform exists, the 38-residue peptide, whose levels in the CSF of AD patients resulted particularly elevated. Experimental evidences consolidated the "amyloid hypothesis"[17] showing that the amount of fibrillogenic Aβ is increased by the vast majority of mutations causing familial AD and that Aβ impairs neuronal functions in a variety of experimental models.[17] These Aβ peptides display an intrinsic tendency to aggregation: soluble Aβ is thought to undergo a conformational change to high β-sheet content, which renders it prone to aggregate into soluble oligomers, larger insoluble fibrils, and finally plaques. In this process, the fibrillogenic $Aβ_{42}$ isoform triggers the misfolding of other Aβ species. Currently, the nature of the neurotoxic Aβ species is very difficult to define because monomers, soluble oligomers, insoluble oligomers, and insoluble amyloid fibrils are expected to exist and accumulate in dynamic equilibrium in the brain. Initially, only Aβ deposited in plaques was assumed to be neurotoxic, but more recent findings suggest that soluble oligomers (amyloid β-derived diffusible ligands or ADDLs) might be the central players. The most widely held view is that aggregation of Aβ peptide in oligomers initiates the vicious cycle that ultimately leads to neuronal death and to the disruption of memory and cognitive functions that characterize AD.[19] This knowledge has been translated into anti-Aβ therapeutic strategies with putative disease-modifying effects, which are being tested in ongoing clinical trials.[20]

1.04.2.1.3 Tau hypothesis supports tau as an AD biomarker

NFTs are fibrillar aggregates constituted mainly by PHFs of the abnormal hyperphosphorylated form of tau protein. Tau is a neuronal microtubule-associated protein, which is involved in microtubule stabilization, and plays an important physiological

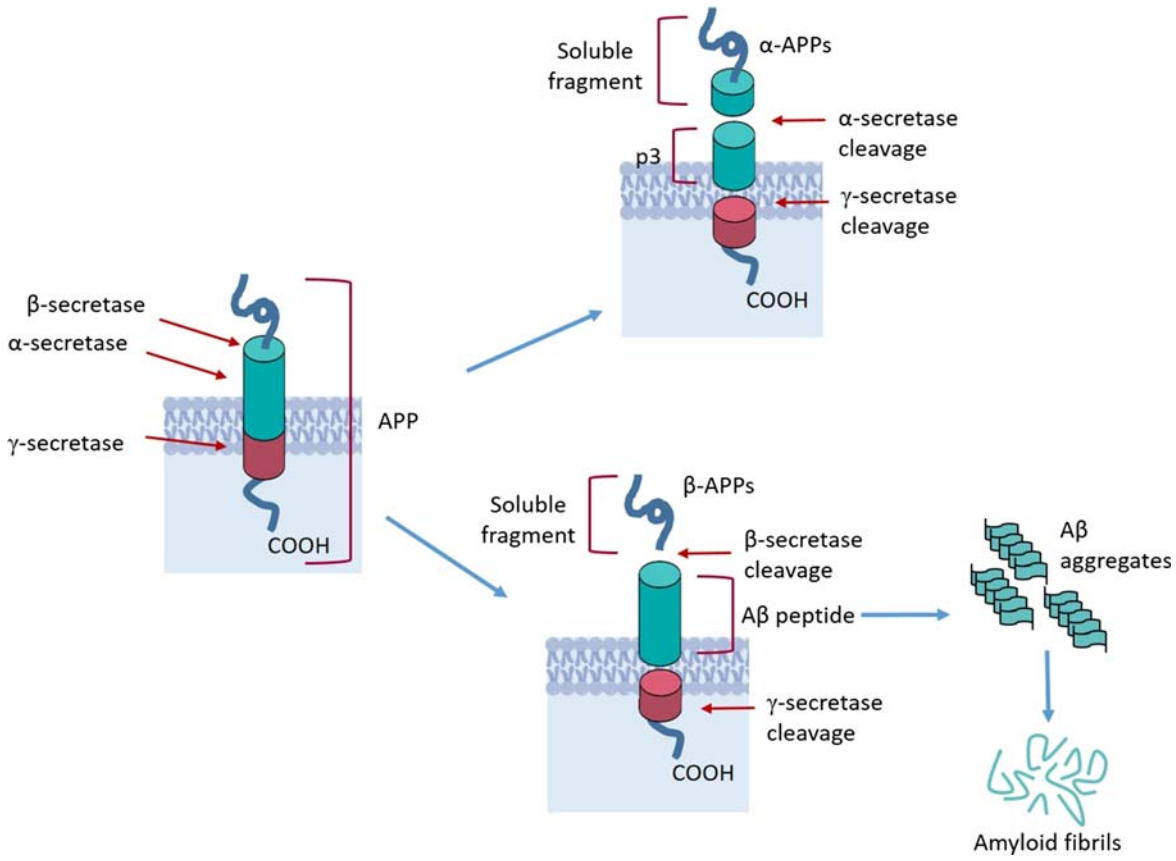

Fig. 2 Schematic depiction of the amyloid cascade.

role in microtubule dynamics and axonal transport. Tau functions can be regulated by its phosphorylation state at ~40 phosphorylatable sites, including serines, threonines, and tyrosines.[21] Tau is abnormally phosphorylated in the brain of AD patients, and there are strong evidences supporting that tau hyperphosphorylation is an early event in the development of neurofibrillary pathology. Tau hyperphosphorylation within the microtubule-binding domain results in its reduced ability to bind and stabilize microtubule assembly, leading to the disruption of axonal transport and ultimately to accelerate synaptic loss and cell death (Fig. 3). Dephosphorylation of tau isolated from NFT restores its ability to bind neuronal microtubules, indicating that the mechanisms regulating phosphorylation/dephosphorylation kinetics are perturbed in AD.[21]

Several kinases have been shown to be capable of phosphorylating tau in vitro, including proline-directed kinases such as mitogen-activated protein kinase 1 (also known as ERK2), glycogen synthase kinase-3 (GSK-3), and cyclin-dependent kinase 5 (CDK5), and non-proline-directed enzymes such as casein kinase 1, protein kinase A, and MAP/microtubule affinity-regulating kinase 1.[22] Recent studies have demonstrated that the majority of tau protein phosphorylation sites can be modified by GSK-3. Furthermore, overexpression of GSK-3 results in tau hyperphosphorylation and disrupted microtubules in transgenic (Tg) mice, suggesting a major role for this kinase enzyme as a validated therapeutic target for AD.[23]

In the hyperphosphorylated form, tau loses its affinity to microtubules and begins to self-assemble, resulting in the formation of PHF and straight filaments, which evolve to NFT.

1.04.2.1.4 Current perspectives

Importantly, the tremendous advances in molecular imaging have allowed us to image the autoptic biomarkers proposed by Dr. Alzheimer in living human brain. With the commercial availability of appropriate tracers, it is nowadays possible to visualize Aβ deposition noninvasively directly in AD patients.[24] The possibility of using amyloid as a biomarker allows, in turn, for the identification of preclinical cases as candidates for early intervention. It also allows for the effectiveness of antiamyloid therapy to be followed in individual patients.[24]

Although Aβ aggregates have been clearly associated with AD pathology,[17] there is still an active discussion as to whether their presence closely correlates with disease progression and severity. If it is not a universally validated biomarker, it has been unequivocally demonstrated that Aβ deposits accumulate in the brain of individuals at risk of developing AD. Consequently, Aβ imaging has not been approved for the diagnosis of AD or for staging disease progression but rather as a diagnostic method for the exclusion of AD in subjects that are cognitively impaired and Aβ PET-negative. Particularly, a negative amyloid scan substantially decreases the odds of having AD and can impact clinical decision-making or treatment. Conversely, in at-risk subjects, a positive amyloid scan is associated with a threefold greater risk of converting to dementia. Currently, it is being evaluated as a diagnostic tool for defining the preclinical stages of AD.[25]

In contrast to SP, the density and neocortical spread of NFT correlate with progressive neuronal degeneration and cognitive impairment,[26] thus potentially making imaging of NFT a more desirable biomarker for AD. Mounting evidence support the central role of tau in the pathogenesis of AD, delineating this protein as both a diagnostic and a therapeutic target.[27] For instance, imaging NFT may allow the early detection of disease, possibly even before the onset of cognitive symptoms, and presymptomatic staging. PET imaging of NFT, especially when done in conjunction with Aβ diagnosis, may also provide a means for distinguishing between AD and non-AD dementias: the presence of NFT and the absence of Aβ would provide support for the latter diagnosis, while the presence of both NFT and Aβ would support the former. In addition, as already pointed out for Aβ, it may allow to investigate the effect of disease-modifying therapies on tau aggregation.

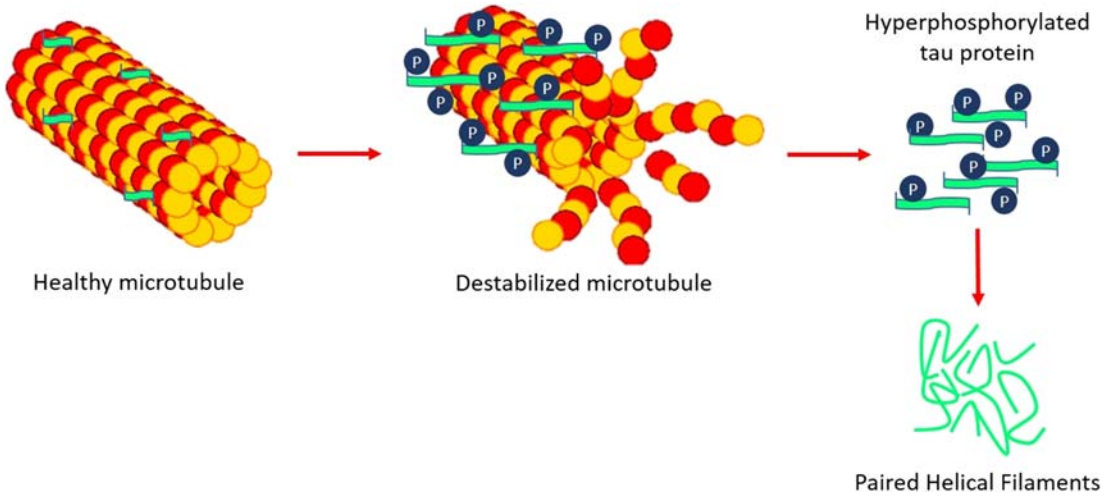

Fig. 3 Schematic depiction of tau cascade.

1.04.3 Development of PET Tracers for AD Diagnosis

Considering the strong premise that imaging of Aβ and tau might advance personalized medicine concepts in AD, provide clinical diagnosis, and ultimately lead to a cure, several small-molecule imaging probes directed to these two biomarkers have been developed and will be discussed in the following. Basically, they belong to two main classes, each of which will be reviewed in this article: PET radiotracers and fluorescent probes (see Section "Development of Fluorescent Probes as Innovative Imaging Agents for AD Diagnosis"). Thanks to their recent approval, PET radiotracers are more promising in terms of their translational applications. However, fluorescent probes hold tremendous capacity for enhancing the delivery of diagnostic procedures and, at the same time, promoting the development of truly innovative therapeutic and diagnostic tools.

PET scan with its widespread applications has emerged as an essential tool in the detection, staging, treatment monitoring, and identification of recurrent disease in a large number of maladies. At the same time, the application of PET had proved beneficial in accelerating drug discovery and development in several therapeutic areas.[28] PET is an imaging technique based on the visualization and quantification of positron-emitting radionuclides. The emitted positrons annihilate nearby electrons, thus generating two low-energy photons (511 keV), which are detected by detectors inserted in PET scanners. Examples of routinely used positron-emitting radionuclides are ^{11}C, ^{13}N, ^{15}O, ^{18}F, ^{44}Sc, ^{62}Cu, ^{64}Cu, ^{68}Ga, ^{72}As, ^{74}As, ^{76}Br, ^{82}Rb, ^{86}Y, ^{89}Zr, and ^{124}I.[29] The short-lived ^{11}C and ^{18}F are ideal for molecular imaging purposes. Given the exquisite sensitivity of PET scanners and the excellent tissue-penetrating properties of photons, radionuclide concentrations in the (sub)picomolar range generally suffice to produce high signal-to-noise ratios and provide useful images and quantitative information. Therefore, PET is routinely used in the clinics.[29]

PET imaging plays also a unique role in drug development because of its ability to quantify drug properties in vivo. The advantages of PET are that, by employing radiotracer principles, it is capable of quantitatively measuring a variety of in vivo processes without perturbing the biochemistry of systems that are easily saturable or operate at low capacity, such as receptors and enzymes.[30] For these reasons, PET is nowadays a key molecular imaging technique that has revolutionized the ability to image molecular processes in the brain.[31]

1.04.3.1 PET Tracers Approved for Aβ Plaque Imaging

Starting from 2000, in vivo imaging of brain amyloid using PET scanning has been extensively used in research studies of dementia.[32] With the passage of time, this methodology has moved rapidly from highly selected centers of excellence to full commercialization with three fluorinated Aβ PET tracers (florbetapir (**1**), Eli Lilly's Amyvid™; flutemetamol (**2**), GE Healthcare's Vizamyl™; florbetaben (**3**), Piramal's Neuraceq™ in Fig. 4) on the market as for 2016.[33] This has allowed wider distribution, with the technique now being available in many countries for clinical practice. All three Aβ imaging ligands have been tested in well-conducted, blinded clinical trials, and all have demonstrated a robust correlation with brain Aβ load, particularly with SP, though they also bind to Aβ in other districts (eg, in blood vessels). It should be emphasized that it is currently unclear whether one of these imaging agents has advantages over the others; they adopt different methods for analyzing and reading scans (flutemetamol uses color and florbetaben and florbetapir provide grayscale images), and they have slightly different tracer kinetics in terms of how scan time relates to time of injection.[32]

As matter of fact, the clinical development of Aβ neuroimaging marks an important step change in our ability to characterize and assess patients with MCI and dementia. Currently, there are clinical situations where it promises to play a crucial role to enhancing diagnostic accuracy. However, the real innovation of Aβ imaging is likely to be not only about improving diagnostics but also about appropriately selecting patients at an early AD stage for disease-modifying therapies once these become available. In addition, as

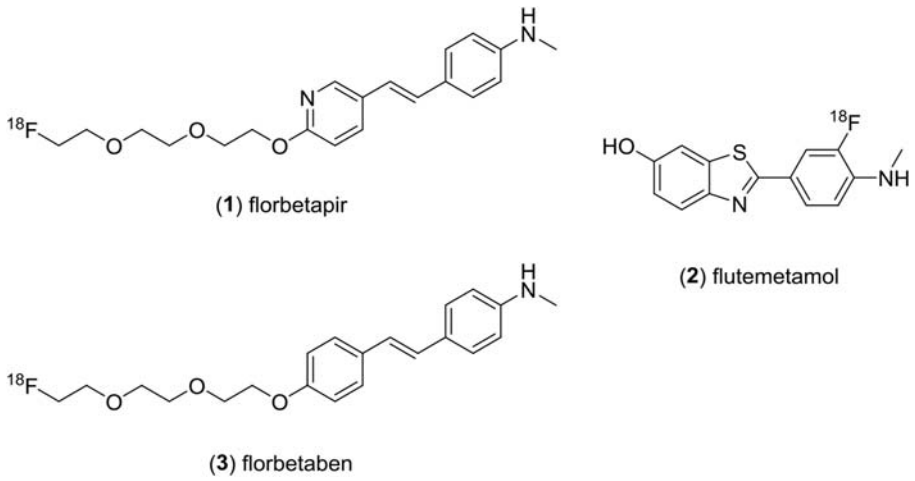

Fig. 4 Chemical structures of PET tracers approved for AD.

part of a wider biological profiling of a complex disease, it promises to drive forward new ways of understanding and classifying dementia.[32]

Motivated by the potential relevance of PET tracers in AD, great medicinal chemistry development has taken place.[34] The last few years have witnessed a great improvement in concepts and methodologies for the design and synthesis of such agents. Learning from the first examples (see the illuminating interview to the brain PET scan pioneer, Louis Sokoloff[35]), today we have set some fundamental prerequisites for a successful radiopharmaceutical directed to Aβ. First, it should effectively bind and image Aβ cerebral deposits. This means that its amount in a given brain area must be quantitatively associated with the amount of Aβ in that area, and there must be a sufficiently high signal-to-noise ratio.[36] Another important consideration is that all currently available imaging agents target fibrillar Aβ in a β-sheet conformation. As already pointed out, Aβ oligomeric species may be a key initiator for AD pathogenic pathways. Although the possibility that these agents bind to Aβ oligomers in a β-sheet conformation after reaching a necessary size (trimer or tetramer) cannot be ruled out, the in vivo signal is not directly representative of these species. This is because of their lower concentration with respect to insoluble Aβ plaques. However, on the basis of the equilibrium existing between monomers, small oligomers, fibrillar Aβ aggregates, and plaques, a relationship exists between the Aβ PET signal and oligomer concentration.[37] In addition to these basic considerations, in general, a PET small-molecule tracer must fulfill a wide range of requirements summarized in **Table 1**.

With specific regard to CNS-directed PET tracers, BBB permeability is an even more crucial issue, as poor BBB permeability remains one of the most frequent causes of failure of promising CNS tracers.[31] Although Lipinski's rule of five[38] for oral availability are applicable for the case of CNS PET tracers,[31] a specific prediction model has been recently developed.[39] This model encompasses calculated distribution coefficients (log *D*) at pH 7.4, molecular weight, topological polar surface area, number of hydrogen bond donors, and protonation constant pK_a of the most basic center. To this respect, it has been verified that low lipophilicity of the tracer reduces BBB permeability, whereas very high lipophilicity results in excessive nonspecific binding, imparting high background signal, which makes the quantitation of the specific binding signal challenging. Furthermore, unspecific binding increases the radiation burden to the patient.[31]

It should be also remarked that brain uptake of PET tracers can also be limited by the presence of several efflux transporters located in the BBB. One of the most relevant is P-glycoprotein (P-gp), situated at the luminal side of brain capillary endothelium, where it functions as an active Adenosine triphosphate (ATP-driven) efflux pump for a wide range of xenobiotics. Hence, brain levels of CNS tracers that are substrates of P-gp might be considerably low, resulting, in turn, in variability of tracer uptake and binding. A number of studies, both in vitro and in vivo, have been performed recently to examine possible interactions of established radiotracers and P-gp.[31]

1.04.3.1.1 Aβ PET tracers derived from Thioflavin T

In this very active area of research, the histopathologic dyes Thioflavin T (ThT, **4**, in **Fig. 5**) and Congo red (CR, **5**, in **Fig. 6**) have provided the structural inspiration for the development of many tracers aimed at the detection of Aβ in living patients. The two dyes show common molecular features that are optimal for Aβ recognition: they are relatively planar, hydrophobic aromatic molecules that can interact with the cross-β-sheet structure found in all amyloid fibrils.

Different from receptors and enzymes, Aβ aggregates are cavity-less proteins that lack a designated binding domain or a substrate binding site. This presents considerable challenges to the development of small-molecule probes. Fibrillar Aβ adopts a cross-β-sheet structure with highly ordered monomers aggregated on the basis of hydrogen bonding, π–π stacking of aromatic residues, and electrostatic interactions (mainly involving glutamate-lysine). $Aβ_{40}$ contains hydrophobic portions both in the middle (residues 17–21) and at the C terminus (residues 30–40). The parallel orientation of β-sheet structures generates small channels and hydrophobic pockets that extend along the length of the filament to which aromatic molecules can intercalate and bind via π–π interactions. Thus, molecules that are known to interact with Aβ plaques all share common structural motifs in that they have planar π aromatic systems. It is thought that their binding involves the molecule entering a hydrophobic pocket or channel and binding via a combination of hydrophobic and π–π interactions. It is likely that there is more than one such binding site on Aβ plaques.[40]

In light of this, it was soon clear that benzothiazole ThT (**4**) could serve as a valuable starting point when searching for new molecules with potential clinical application. It suffers, though, from two major shortcomings: first, ThT has a permanent positive charge, which hampers BBB permeation. Second, its binding affinity to fibrils is quite low. Thus, an optimization campaign was launched in the search for more lipophilic and potent derivatives. Structure–activity relation (SAR) studies on ThT structure revealed that the similar aromatic, planar benzofuran, imidazo-pyridine, benzoxazole, or imidazole scaffolds retained a similar binding

Table 1 Requirements for an ideal PET tracer

- MW < 500
- High target/nontarget binding affinity ratio
- Rapid blood clearance
- Favorable transport between blood and target tissue
- Low peripheral metabolism
- Rapid clearance from nontarget tissues (liver, kidney, and intestine)
- Ideal physical and biological half-life

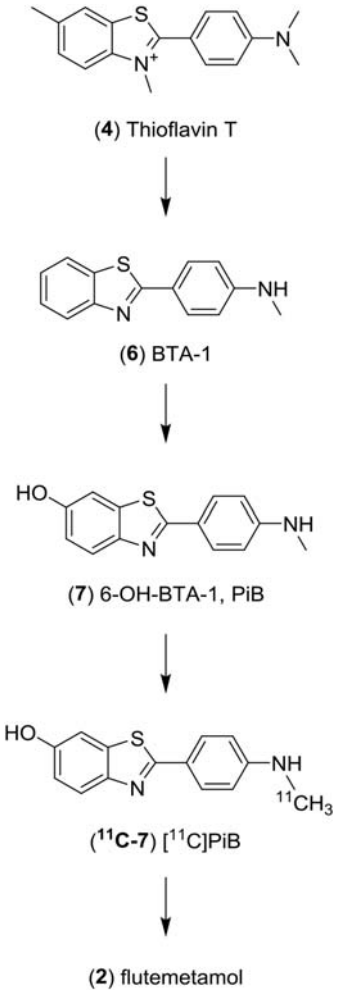

Fig. 5 Thioflavin T (**4**) and its derivatives developed as PET tracers.

profile. Additionally, the aniline could be substituted with other flat, rigid moieties (eg, stilbene) without significantly negative effects. Insertion of a planar styrene group between the benzothiazole and the aniline is also well tolerated, while some substitutions, such as bithiophenes, even increase affinity.[9]

Among the several investigated chemical classes of ThT derivatives, benzothiazole aniline (abbreviated as BTA) represents the most widely explored one. To note, these compounds emanated from academic research.[41] Well aware that such a benzothiazolium salt would never cross the BBB, a team based at the University of Pittsburgh modified ThT structure by a simple demethylation (methyl groups in positions 3 and 6) of the benzothiazole ring and of the aniline nitrogen. In 2001, Klunk et al. reported that this neutral ThT analog, named BTA-1, (**6**, Fig. 5) possessed very good brain entry and a higher affinity for Aβ deposits in AD brain.[42] A further SAR campaign identified a hydroxylated derivative (*N*-methyl-2-(4′-methylaminophenyl)-6-hydroxybenzothiazole, 6-OH-BTA-1, **7**) (Fig. 5) with clearance properties that were ideal for a PET radiotracer. Preclinical studies showed that it bound to AD brain with an affinity in the single-digit nanomolar range and, more importantly, entered the brain rapidly and cleared rapidly as well.[43] Therefore, the [^{11}C]-labeled *N*-methyl-2-(4′-methylaminophenyl)-6-hydroxybenzothiazole ([^{11}C]-**7**) was selected for the first human trial of a ThT-derived imaging agent. For simplicity, [^{11}C]-**7** was given the code of [^{11}C]PiB "Pittsburgh Compound-B," the acronym by which it is universally recognized. Thanks to its favorable profile, [^{11}C]PiB has become the benchmark PET Aβ agent, already adopted for the direct visualization of brain SP in thousands of AD patients.

Unfortunately, the 20-min radioactive decay half-life of ^{11}C limits the use of [^{11}C]-**7** to major organizations with an on-site cyclotron facility and ^{11}C radiochemistry infrastructure, making the access restricted and with costs prohibitive for routine clinical use.[44] To overcome these limitations, several tracers labeled with ^{18}F ($t_{1/2}$ of 110 min)—which allow the centralized production and regional distribution, as currently practiced worldwide in the supply of [^{18}F]FDG for clinical use—were developed.[45] This shift from an ^{11}C- to ^{18}F-labeled tracer was expected to significantly enhance the impact of amyloid imaging on research and clinical diagnosis.

Under the proposition of circumventing the aforementioned limitations and allowing a broader application of [^{11}C]PiB, an [^{18}F]-fluorinated derivative was developed. H-to-F substitution of the hydrogen atom in position 3′ of the aniline ring afforded

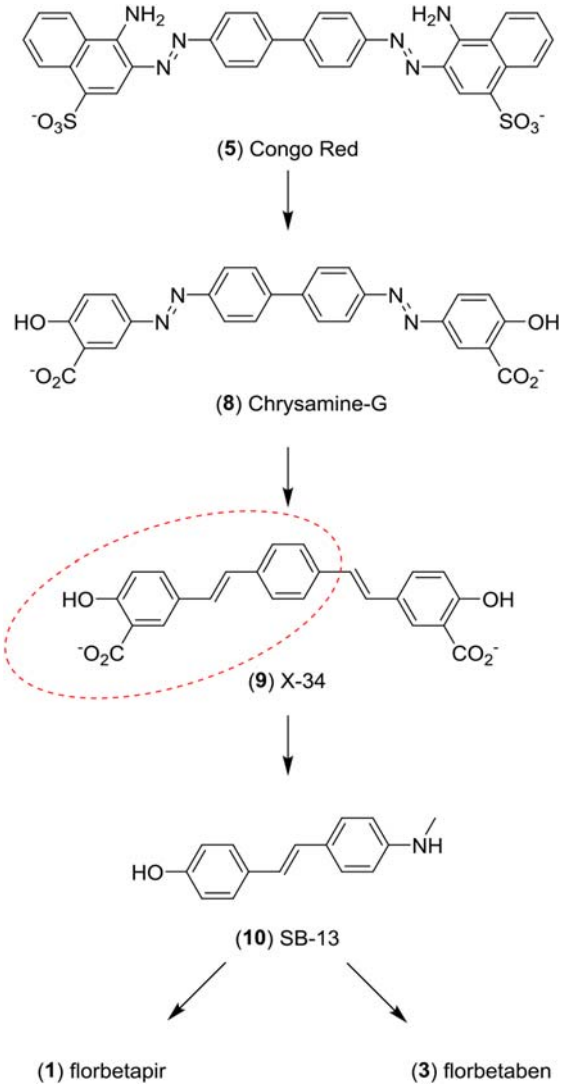

Fig. 6 Congo red (**5**) and its derivatives developed as PET tracers.

[^{18}F]3′F-PiB, also known as flutemetamol (**2**).[41] This compound, also developed at the University of Pittsburgh Medical Center, showed patterns of binding and distribution, in in vivo PET studies, comparable to that of [^{11}C]PiB. After successful completion of clinical trials, in 2014, flutemetamol received marketing authorization from the EMA for imaging of Aβ plaques in suspected AD.

1.04.3.1.2 Aβ PET tracers derived from CR

CR (**5**, in Fig. 6) is another dye widely used for histopathologic staining of SP. More than 100 years after its discovery, CR is still of fundamental importance from a diagnostic point of view. CR staining of fixed tissue and the detection of apple-green birefringence when examined under polarized light remain essential for the diagnosis of amyloidosis.[46] As for the case of ThT (**4**), CR (**5**) served as a starting point for the development of AD PET tracers. To decrease its molecular weight and to increase the metabolic stability and lipophilicity, derivatives of salicylic acid, for example, Chrysamine-G (**8**, in Fig. 6), and divinylbenzene compounds such as X-34 (**9**, in Fig. 6) were developed.[47] Although these compounds showed high log *D* values, they failed to exhibit good brain uptake in preclinical studies.

To enhance BBB permeation, the carboxylic and hydroxyl moieties were removed, and the molecular weight was further reduced, yielding trans-stilbene derivatives as promising lead structures. A cooperative effort between research groups of the University of Pennsylvania and the company Avid Radiopharmaceuticals was set to further optimize the stilbene structure. This intensive effort ultimately resulted in the development of florbetaben (**3**).[48] In 2005, a series of fluoropegylated stilbene derivatives was successfully prepared and tested.[49] Of these, a low-molecular-weight and neutral stilbene derivative, SB-13 (**10**, Fig. 6), demonstrated excellent binding affinity and labeling of SP.[50] A preliminary PET human study with [^{11}C]-SB-13 revealed excellent differential increased uptake and retention in the frontal cortex of AD patients, when compared to control subjects. Notwithstanding these remarkable

preliminary results, no further clinical studies were undertaken, probably due to the technical limitation associated with ^{11}C. However, these data stimulated the search for SB-13 derivatives to be labeled with ^{18}F. In details, by adding three PEG units to the stilbene, a more appropriate lipophilicity was obtained, without loss of specificity. In addition, PEG was shown to be an efficient and effective prosthetic group for ^{18}F labeling. The isosteric replacement of a phenyl ring with a pyridine provided the new classes of styrylpyridines, whose optimized compound was florbetapir (**1**). Both fluorinated tracers, florbetaben and florbetapir, received FDA approval for the estimation of Aβ plaque density in the human brain by means of PET.[31]

1.04.3.2 PET Tracers for Aβ Plaque Imaging Evaluated in Human Subjects

Despite the availability of already three marketed agents, the development of PET amyloid tracers is still attracting considerable attention. Several reviews discussing the status and advances of this class of PET imaging agents have been recently published, to whom the reader is directed for a more comprehensive description.[47,51] The examples reported in the succeeding text are thus intended to provide updates of the progress made in clinical trials.

Interesting Aβ tracers directly derived from the BTA class are [^{11}C]AZD2184 (**11**, in Fig. 7) and [^{18}F]AZD4694 (or [^{18}F]NAV4694, **12**). Their development was motivated by considering that the marketed ^{18}F-labeled tracers have greater nonspecific white matter binding than [^{11}C]PiB and some have even lower cortical binding in AD patients. These characteristics make scan visual interpretation more challenging (particularly for the detection of low levels of cortical SP) and increase the level of expertise required for accurate and consistent scan interpretation in clinical practice.[52] Thus, the guiding hypothesis was that lower lipophilicity (log *D*) than that of previously developed radioligands would translate into lower nonspecific binding. On this bases, the analog of [^{11}C]PiB containing a 2-pyridinyl group instead of 2-phenyl, AZD2184, was synthesized. It displayed a high affinity for Aβ fibrils in vitro. In vivo autoradiography studies showed that [^{11}C]AZD2184 (**11**) exhibits a higher signal-to-background ratio in postmortem brain sections from AD patients, which parallel the reduction of log *D* (1.8 for AZD2184 vs. 2.8 for PiB).[53] The benzofuran isosteres of BTAs have generally showed quite higher binding affinity to Aβ fibrils, together with favorable log *D* and half-life values. [^{18}F]NAV4694 (**12**) is a fluorinated benzofuran derivative with a wider dynamic range than [^{11}C]PiB possibly due to high affinity. Additionally, the ratio between cerebellum and white matter was significantly higher for **12**, which suggests lower nonspecific binding than [^{11}C]PiB. Competition study showed that **12** cannot be fully displaced by [^{11}C]PiB, which suggests binding in early forms of amyloid. Collectively, these robust in vitro and in vivo properties support the unique binding of **12** and highlight its potential for early diagnosis in AD.[54] Indeed, a phase 3 clinical trial to evaluate the efficacy and safety of [^{18}F]NAV4694 (**12**) for detection of cerebral Aβ when compared with postmortem histopathology will end in Dec. 2016.[55] In parallel, a third compound, AZD2995 (**13**), with an even lower log *D* (1.3) than that of AZD2184 (1.8) has been developed. Its development allowed researcher at AstraZeneca to postulate that the specific binding to Aβ plaques is dependent upon the compound ability to form hydrogen bonds with Aβ. They also pointed out that for BTA congeners, the presence of a hydrogen bond donor both on the left-hand and right-hand side of the molecule is essential for the specific binding to brain SP. The preclinical profile of **13** in relation to the reference ligand PiB suggests that the corresponding ^{11}C-labeled compound may enable PET visualization of Aβ deposits in the living human brain, with a higher sensitivity than the currently used PET ligands.[56]

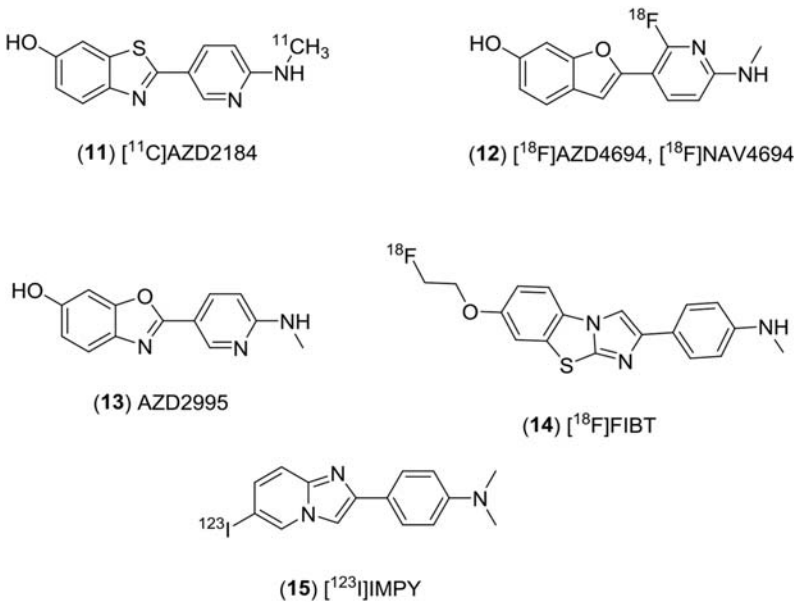

Fig. 7 Chemical structures of **11**–**15**, developed as Aβ PET/SPECT tracers.

Imidazo[2,1-b]benzothiazoles (IBTs) are another promising novel class of Aβ PET ligands. Their good in vivo imaging properties have previously been shown in preclinical studies. Among IBTs, fluorinated [^{18}F]FIBT (**14**) has been selected for further characterization and advancement toward use in humans. [^{18}F]FIBT characteristics have been analyzed in relation to PiB, as reference ligand.[57]

1.04.3.2.1 Aβ single-photon emission computed tomography (SPECT) tracers

To give a more comprehensive view of the subject, the parallel development of SPECT radiotracers should be mentioned. Compared with PET, SPECT has greater accessibility, lower cost, and greater availability as a routine diagnostic method due to the use of easily generated radioisotopes with longer half-lives (eg, [^{125}I], $t_{1/2}$ of 60.1 days, [^{123}I], $t_{1/2}$ of 13.2 h, and [^{99m}Tc], $t_{1/2}$ of 6.0 h). Although several radioiodinated or ^{99m}Tc-labeled probes for Aβ plaques have been described, unfavorable pharmacokinetic properties, such as low brain uptake and slow washout, have prevented their use in AD patients.[58] 6-Iodo-2-(4′-dimethylamino)phenyl-imidazo[1,2-*a*]pyridine (IMPY) is the first SPECT imaging agent to be tested in clinical studies. Although [^{123}I]IMPY (**15**, in Fig. 7) showed excellent features as an Aβ imaging probe in preclinical studies, the preliminary clinical data displayed a low signal-to-noise ratio, possibly due to an excessive lipophilicity and low stability in vivo.[58] Consequently, there is no current SPECT imaging probe useful for the clinical diagnosis of AD.

1.04.3.3 PET Tracers for NFT Imaging

As discussed earlier, the last two decades have been focused on developing numerous Aβ ligands for the noninvasive detection of Aβ deposition in the brain. However, several findings increasingly suggest the progression of tau pathology as a more reliable biomarker. Indeed, a large number of postmortem studies show that the number of NFT in the brain is highly associated with cognitive impairment, and tau deregulation is a key mediator of neurodegeneration.[59] Thus, a selective and specific tau imaging agent will be crucial to achieve a more comprehensive understanding of AD pathophysiology. Moreover, tau imaging could confirm the various stages of tau deposition and assist in the early and differential diagnosis of AD, especially with references to other non-AD tauopathies.[59] In this perspective, tau PET imaging would help not only in the diagnosis but also in the development of anti-tau therapeutics by supporting subject enrollment and evaluation of drug efficacy in clinical trials. As for 2016, approved PET radiotracers are not available. Conversely, tau is widely detected in postmortem histochemistry examination by using two gold standard methods that are AT8 anti-tau antibody and Gallyas silver staining.[59]

Developing imaging agents for tau pathology requires to overcome several obstacles. Similar to Aβ, tau PET tracers should be small, lipophilic, and nontoxic molecules that readily cross the BBB. Ideally, a CNS PET ligand should not form BBB permeable radioactive metabolites and exhibit low nonspecific binding (to avoid low signal-to-noise ratio due to undesired binding). In contrast to Aβ, because most tau aggregates are intracellular, a tau radiotracer ought to cross the cell membrane to reach its target. Moreover, six different isoforms of tau exist, and different combinations of these isoforms resulted in different clinical phenotypes. The wide spectrum of posttranslational modifications at which tau aggregates are subjected (such as phosphorylation, nitration, acetylation, glycosylation, truncation, prolyl isomerization, glycation, and ubiquitination) further complicates the situation.[59,60] Another obstacle in the development of specific tau imaging agents is the coexistence, in AD brains, of Aβ and other misfolded proteins that share the same β-sheet secondary structure. In particular, Aβ and tau proteins colocalize in gray matter areas, and α-synuclein-containing aggregates are sometimes abundant in AD patients' brains. The situation is further complicated by the much lower brain concentrations of tau than Aβ. Depending on the brain region, the concentration of tau is 5–20 times lower, requiring a radiotracer with high Aβ/tau selectivity.[61] Thus, binding affinity is another very important property for an in vivo tau radioligand. Although in vitro studies showed that based on affinity, a 3- to 30-fold selectivity is sufficient, simulation studies suggested that a 20- to 50-fold selectivity for tau over Aβ is required to image tau aggregates in vivo.[61] Finally, and as for any PET candidate, tau radiotracers must be synthetically accessible through quick and efficient processes.[60]

Since Aβ plaques, NFT, and other amyloid aggregates share a similar β-sheet structure, it is not surprising that structural similarities exist between imaging agents for both species. In particular, as the structural diversity of tau protein and its aggregates, as well as their posttranslational modifications, makes impossible studying potential binding sites for a PET ligand, ligand discovery is mainly based on compound screening approaches.[60] These approaches exploit competitive in vitro assays using synthetic tau aggregates or postmortem AD human brain homogenates or sections. Notably, screening campaigns based on synthetic tau aggregates have not been very successful, while assays based on native proteins have yielded the most promising candidates. The reason of such difference could be derived by the fact that synthetic tau aggregates do not have similar hyperphosphorylated or glycated or ubiquitinated residues as the native ones.[60]

From a peculiar medicinal chemistry standpoint, it should be emphasized that few papers describing tau ligands discuss SAR around the different chemotypes.[61] Even, no one provide any robust conclusion about the molecular features required to achieve NFT selectivity over SP.[60] For this reason, the majority of the examples deals with nonselective candidates. The first described potential PET tracer for Aβ and tau was the naphthalene derivative [^{18}F]-FDDNP (2-[1-[6-[*N*-(2[^{18}F]-fluoroethyl)-*N*-methylamino]naphthalen-2-yl]ethylidene]malononitrile, **16**, in Fig. 8), synthesized and characterized by Barrio et al. back in 1999.[62] Importantly, [^{18}F]-FDDNP was used to obtain the first human PET images of AD brain in an 82-year-old woman.[63] However, in vitro evaluation of [^{18}F]-FDDNP at concentrations correspondent to those used for the PET scan showed limited binding to both Aβ and NFT. Thus, its low binding affinity and lack of selectivity hindered further optimization. In light of this, researchers turned their attention to novel probes with higher selectivity.

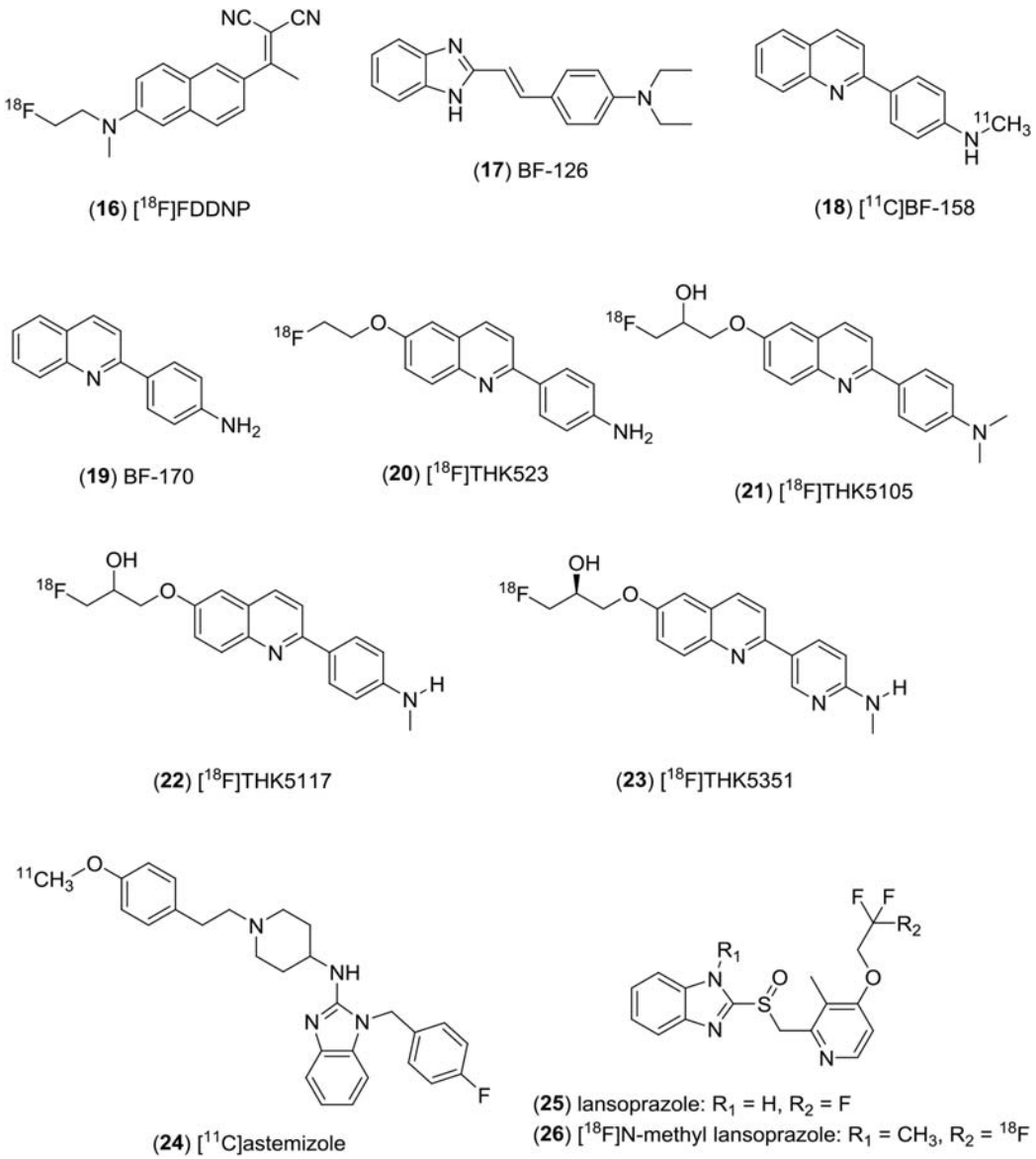

Fig. 8 Chemical structures of **16**–**26**, developed as tau PET tracers.

1.04.3.3.1 Quinoline- and benzimidazole-derived tau PET tracers

One of the earliest ligand screening campaigns for PET tracers targeting specifically tau aggregates was performed in 2005 by Okamura's group.[64] After testing more than 2000 small molecules, they discovered quinolines and benzimidazoles as lead structures. In particular, they proposed the benzimidazole BF-126 (**17**) and the quinolines BF-158 (**18**) and BF-170 (**19**) as candidate probes.[64]

Structurally, BF-126 (**17**) is very similar to [^{11}C]PiB, with the substitution of the benzothiazole ring with a benzimidazole and the insertion of a carbon–carbon double bond spacer between the planar aromatic bicyclic ring and the aniline substituent at position 2. The aniline moiety is present also in the quinoline derivatives **18** and **19**, which do not possess any spacer. Quinolines **18** and **19** emerged as better tau ligands than **17** in terms of binding affinity. Thus, **18** was radiolabeled with ^{11}C for in vitro autoradiographic studies. However, the short half-life of ^{11}C limited its further clinical application.[65]

This led to the synthesis of the first-generation THK series, obtained by labeling quinoline tau ligands derivatives with ^{18}F. In 2011, Fodero-Tavoletti's group reported the identification of [^{18}F]THK523 (6-(2-[^{18}F]fluoroethoxy)-2-(4-aminophenyl)quinolone, **20**).[66] The introduction of an alkyl ether at the position 6 of the quinoline ring allowed the introduction of ^{18}F and at the same time improved affinity and selectivity toward tau.[60] Indeed, in vitro studies showed that [^{18}F]THK523 (**20**) binds selectively to PHF-tau, but it is not able to bind non-AD tau aggregates.[59] Then, after the evaluation of its ability to cross the BBB, [^{18}F]THK523 was tested in vivo in a tau Tg mouse model, confirming its capability to successfully label tau deposits.[67] On these bases, [^{18}F]THK523 was tested in human subjects.[68] In vivo PET imaging showed higher cortical retention in AD patients compared with healthy controls,

and the probe distribution was in agreement with the reported PHF histopathologic brain distribution in AD autoptic specimens. However, a too high retention in white matter precluded the assessment of tau pathology by visual inspection of PET scans.

Thus, the optimization of the alkyl chain at the position 6 of the quinoline afforded a second-generation THK series, reported by Okamura's group in 2013.[69] The two corresponding tertiary and secondary anilines, [^{18}F]THK5105 (1-([2-[4-(dimethylamino)phenyl]quinolin-6-yl]oxy)-3-[^{18}F]fluoropropan-2-ol, **21**) and [^{18}F]THK5117 (1-([2-[4-(methylamino)phenyl]quinolin-6-yl]oxy)-3-[^{18}F]fluoropropan-2-ol, **22**), demonstrated higher binding affinity for tau aggregates than for Aβ plaques in in vitro studies and in AD brain sections. They also showed a more favorable pharmacokinetics than **20**, with no defluorination in vivo. From a chemical point of view, the presence of the secondary alcohol in **21** and **22** introduces a polar moiety, which might be responsible of the observed higher selectivity.[60] Furthermore, the clearance of these derivatives from normal brain was faster than that of **20**, suggesting **21** and **22** suitable candidates for clinical application. First-in-human PET studies with [^{18}F]THK5105 (**21**) revealed its ability to differentiate between AD patients and healthy controls. However, a still slow kinetics and clearance prevented its further investigation. Although [^{18}F]THK5117 (**22**) showed faster kinetics and better signal-to-noise ratio, it was later realized that both probes showed substantial white matter binding, which may lead to misinterpretation of the PET scans. To bypass this shortage, in 2015, the same group developed the single S-enantiomer [^{18}F]THK5351 ((*S*)-1-(fluoro-[^{18}F])-3-((2-(6-(methylamino)pyridin-3-yl)quinolin-6-yl)oxy)propan-2-ol, **23**),[70] by replacing the benzene ring of **22** with a pyridine. Indeed, as observed with Aβ PET tracers, pyridine derivatives show reduced lipophilicity, which correlates with the amount of nonspecific binding.[71] In addition, it is well-known that enantiomers show differences in biological properties, such as affinity for a given target and metabolism.[72] Thus, fast pharmacokinetics, high contrast, and low white matter retention of **23** allowed sensitive detection of tau aggregates in humans.[70]

Two benzimidazole drugs, astemizole (**24**, in Fig. 8) and lansoprazole (**25**), have been found to bind PHF in a repurposing-based approach.[73] However, **24** displayed no selectivity for NFT over SP, together with a low brain uptake and clearance. Although **25** also showed low affinity toward PHF, several of its radioactive derivatives were synthesized and preliminary tested in mice and nonhuman primates. In particular, [^{18}F]*N*-methyl lansoprazole (**26**) has been proposed as a candidate for progression into clinical trials. However, human studies with this tracer have not been reported so far.

1.04.3.3.2 Benzothiazole-derived tau PET tracers

Another screening campaign aimed to identify novel tau-selective probes was performed in 2007 by Kuret and colleagues. The screening of a library of more than 70,000 compounds[74] identified phenyldiazenyl benzothiazole (PDB) derivative **27** (Fig. 9) as novel lead structure. In light of this, Ono and colleagues, in 2011, developed radioiodinated SPECT PDB derivatives by replacing the methoxy group of **27** with a ^{125}I.[75] Among them, [^{125}I]PDB-3 ((E)-4-((6-[^{125}I]-iodobenzo[*d*]thiazol-2-yl)diazenyl)-*N*,*N*-dimethylaniline, **28**) showed high and selective binding affinity for tau aggregates in vitro. However, **28** exhibited poor pharmacokinetics in healthy mice. Therefore, the same group synthesized the PET derivative [^{18}F]FPPDB ((E)-4-((6-(2-(2-(2-[^{18}F]-fluoroethoxy)ethoxy)ethoxy)benzo[*d*]thiazol-2-yl)diazenyl)-*N*,*N*-dimethylaniline, **29**).[76] Interestingly, **29**, which carries the same prosthetic group of florbetapir (**1**) and florbetaben (**3**), showed higher brain uptake and faster clearance than SPECT tracer **28**. Unfortunately, a lower selectivity between tau and Aβ aggregates was found.

More recently, Higuchi and colleagues developed the benzothiazole-derived probes phenyl/pyridinylbutadienyl-benzothiazoles/benzothiazoliums (PBBs).[77] These compounds derived from the stretching of the core structure of ThT (**4**), with two C=C double bond inserts between aniline (or aminopyridine) and benzothiazole (or benzothiazolium) groups. All the synthesized PBBs were able to intensely label NFT and SP in AD brain sections. Thanks to encouraging preliminary data, three potential probes were radiolabeled to conduct PET assays in Tg mice model of tau pathology. [^{11}C]PBB3 (2-[4-(4-methylaminophenyl)-1,3-butadienyl]-benzothiazol-5,6-diol, **30**) yielded the best visualization of NFT and was then selected for exploratory in vivo PET imaging studies in AD patients. **30** showed minimal nonspecific binding and seems able to monitor the temporospatial spreading of tau pathology

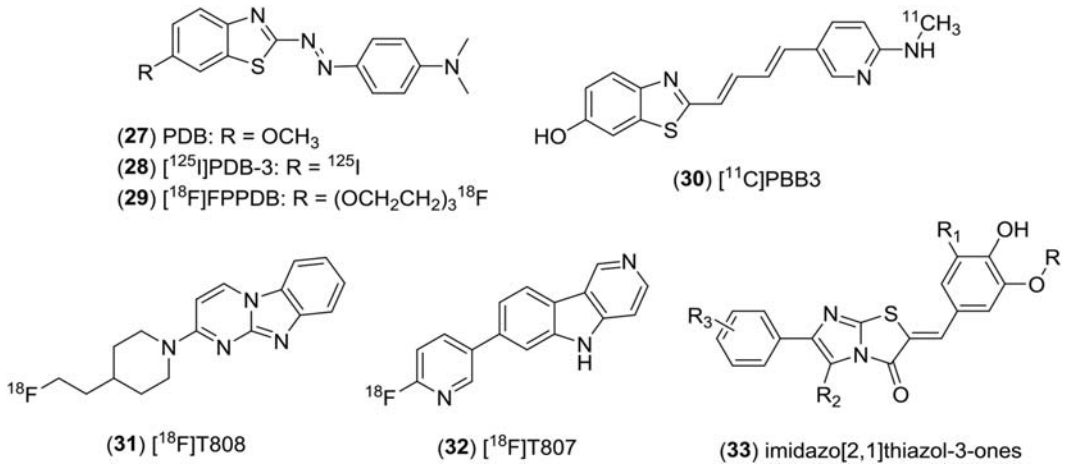

Fig. 9 Chemical structures of **27**–**33**, developed as tau PET tracers.

from the limbic system to neocortical areas, as AD progresses. Moreover, **30** is able to visualize tau deposits also in non-AD tauopathies, emerging as a very promising tool not only in AD diagnosis but also for the differential diagnosis of different neurological conditions.

1.04.3.3.3 Benzoimidazopyrimidine- and pyridoindole-derived tau PET tracers

In 2007, Kolb and coworkers tested over 900 compounds using autoradiographic assays on human brain tissue sections, discovering a novel chemotype, that is, benzo[4,5]imidazo[1,2-a]pyrimidines. Thus, they developed the novel tau PET imaging probe candidate [^{18}F]T808 (2-(4-(2-[^{18}F]fluoroethyl)piperidin-1-yl)benzo[4,5]imidazo[1,2-a]pyrimidine, **31**).[78] **31** rapidly crossed the BBB, followed by rapid clearance, suggesting minimal nonspecific binding in mice. Successively, they developed the related class of 5*H*-pyrido[4,3-b]indoles.[79] After several rounds of optimization, [^{18}F]T807 (7-(6-[^{18}F]fluoropyridin-3-yl)-5*H*-pyrido[4,3-b]indole, **32**) was identified as a favorable tau PET imaging probe.[79] In vitro autoradiography in AD brain sections suggested that **32** binds NFT of human AD brains with high specificity and weak or no interaction with Aβ. On the basis of their encouraging profiles, **31** and **32** have been advanced to clinical tests.

First-in-human PET studies with **32** in AD patients, MCI patients, and healthy participants have shown that its cortical retention matches the known distribution of PHF in the brain. These results were confirmed by postmortem studies showing a strong association of tau pathology with dementia severity. Human studies in three healthy controls and eight AD patients showed better kinetics for **31** than **32**, but substantial defluorination was observed in some cases. A large multicenter study of **32** (renamed as [^{18}F]AV1451) is ongoing, which is expected to validate these initial findings.

Finally, a recent patent application from Hoffmann-La Roche claims imidazo[2,1]thiazol-3-one derivatives (with general structure **33**, in Fig. 9) as potent and exceptionally selective tau aggregate ligands.[80] From a chemical point of view, it is interesting to note the characteristic structure of these molecules, with the highly polar phenolic terminus on one side and a lipophilic aromatic terminus on the opposite side. Indeed, previous studies with these kinds of amphiphilic molecules had suggested that it may be possible to increase potency and selectivity against amyloid aggregates by incorporating lipophilic and hydrophilic features in the same structure.[81] However, it is not possible to estimate the full potential of these molecules, since the affinity and selectivity in human AD brain have not been disclosed yet. These molecules might be included in a recently registered clinical phase 1 study titled "Evaluation of [^{11}C]RO6924963, [^{11}C]RO6931643, and [^{18}F]RO6958948 as tracers for PET imaging of tau in healthy and Alzheimer's disease participants," which, however, does not unveil the chemical structures of the target compounds.[60]

1.04.4 Development of Fluorescent Probes as Innovative Imaging Agents for AD Diagnosis

In addition to radiation-based imaging techniques such as PET and SPECT, optical imaging is one of the most attractive modalities in research and clinical practice, which possesses the advantages of ease of operation, rapid detection, and no exposure to radiation. Although fluorescence microscopy has proved to be one of the most powerful tools in biology and accesses a variety of molecular probes, until the very recent years its application to the intact animal has been limited to imaging few hundred micrometers below the surface. The rest of the animal has eluded investigation at the microscopic level without excising tissue or performing extensive surgery. Therefore, the current ability to perform minimally invasive deep in vivo fluorescence imaging in intact animal studies has represented a breakthrough.

Briefly, when an organic flurophore absorbs light, the molecule will transit from its ground state (S_0) to a higher energy level excited state (S_2). In the excited state, the electrons rapidly, in a few picoseconds, relax to the lowest available energy state (S_1), through a process called internal conversion. Once in this state and after a lag period of several nanoseconds (the fluorescence lifetime), the electrons will relax back to ground state S_0, releasing their stored energy in an emitted photon at a wavelength corresponding to the energy difference of the two energy states ($S_1 \rightarrow S_0$). Because of this relationship, the absorbance and emission spectra are usually mirror images of each other. The energy of emission is lower than that of excitation, which results in a longer wavelength than the excitation light. The difference between the excitation and the emission energy (wavelength) is termed the Stokes shift. The fluorescence quantum yield (QY) is the ratio of photons absorbed to photons emitted. In other words, the QY reflects the probability of the excited state being deactivated by fluorescence rather than by another, nonradiative mechanism.[82]

The so-called "push–pull" organic fluorophores constitute a blueprint in the search for new fluorescent probes for imaging application. They are small molecules in which a π-conjugated bridge (with various lengths and structures) is end-capped with a donor (D) and an acceptor (A) moiety (Fig. 10). The peculiar optical properties of such molecules are due to intramolecular charge transfer. A typical arrangement of these fluorophores is a D–π–A system with strong electron- donating groups ($-NH_2$, $-NR_2$, or –OR) as D and strong electron-withdrawing groups ($-NO_2$ or –CN) as A. These molecules exhibit various degrees of flexibility in

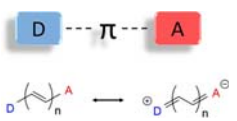

Fig. 10 Typical architecture of a push–pull fluorophore.

the ground and excited state that might be correlated with the fluorescence processes. For a more detailed discussion, please see Staderini et al.[83]

1.04.4.1 Thioflavin T and CR as Starting Points for the Development of Fluorescent Imaging Agents

ThT (**4**, in Fig. 5) is a cationic benzothiazole fluorescent dye widely used to detect Aβ fibrils ex vivo in AD autoptic tissues and to monitor fibril formation in vitro.[84] Structurally, it has a hydrophobic end with a dimethylaminophenyl group, linked to a benzothiazolium containing the polar N and S atoms. Vassar and Culling[85] were the first to unveil the diagnostic potential of ThT, which was shown to detect amyloid in the kidney with high specificity.[85] Following these pioneering studies, considerable advances in understanding the ThT fluorescent response upon binding to Aβ species have been made. ThT is currently universally recognized as a "smart" Aβ probe, thanks to a peculiar fluorescence profile: (i) Its absorption maximum and fluorescence spectrum undergo a redshift when bound, and (ii) the fluorescence emission at 480 nm upon excitation at 440 nm is proportional to the quantity of amyloid fibrils present. This property can be exploited to follow time courses of fibrillation, and such kinetic studies give valuable insight into the underlying molecular mechanisms. Moreover, reduction in ThT fluorescence is often taken to be an indication of the inhibition of the self-assembly process. This behavior was conveniently exploited by LeVine to set up a versatile, inexpensive assay for monitoring fibril formation, which is still the most widely used method for monitoring Aβ aggregation in vitro, and assess the inhibitory potency of newly developed aggregation inhibitors.[86] However, extreme care should be taken when comparing fibril formation under different conditions, since several factors may affect the fluorescence intensity, such as fibrils and ThT concentration and ionic strength. A large number of studies were aimed to correlate the ThT fluorescent behavior with its binding mode with Aβ, but a high-resolution molecular characterization has been hampered by the insolubility and heterogeneous nature of the amyloid fibrils.[87] However, experiments (notably solid-state nuclear magnetic resonance) have provided high-resolution structures of Aβ fibrillar aggregates that can be used in conjunction with computational modeling to probe detailed binding interactions with amyloid dyes. Despite that and the fact that the reported models are somewhat conflicting, two effects occurring upon interaction have been proposed: (1) steric and electronic stabilization (via charge transfer) of the ground-state charge distribution and (2) restriction in the rotational freedom of the carbon–carbon bond between the benzothiazolium and aniline rings in its electronically excited state.[87]

Similarly, staining of amyloid fibrils with the dye CR (**5**, in Fig. 6) has been used since the beginning of the 1920s.[88] CR is a linear and amphiphilic molecule, with a hydrophilic portion encompassing two amino groups and a negatively charged sulfate group (at neutral pH) and a hydrophobic portion consisting of a central biphenyl core, along with a diazo group with two flanking naphthalene rings. Upon binding to amyloid fibrils, CR gives a characteristic apple-green birefringence when examined between crossed polarizer and analyzer, while a distinctive shift in absorbance maximum from 490 to 540 nm is observed.[87] It has been recently proposed that the birefringence might be due to the anisotropic orientation of the CR dipoles resulting from the spatial ordering of these molecules in the grooves along the amyloid fibril axis. The fluorescent enhancement of the bound CR, in turn, should be associated with the torsional restriction of this molecule upon binding. CR is most often applied in diagnosis of amyloid in ex vivo tissue sections using polarization microscopy, although light microscopy and fluorescence microscopy have also been exploited. Although it has been used for the in vitro quantification of Aβ binding by using absorption spectroscopy,[87] CR lacks sensitivity at low Aβ fibril concentration compared to ThT. Furthermore, CR is not well suited for Aβ aggregation inhibitory assays, since it interferes with protein misfolding processes and aggregation.[87]

Following the wide use of ThT and CR in histopathology, the first evidence of the possibility of a fluorescence staining directly in mouse models of AD was provided by Hyman et al. in 2001.[89] The revolutionary goal of this study was to develop a novel imaging approach, using in vivo multiphoton microscopy and the Thioflavin S (ThS, **34**, in Fig. 11) dye, to image SPs in PDAPP Tg mice (APP Tg mice with V717F (Indiana) mutation). Importantly, another aim of this work consisted in exploiting the developed approach for monitoring the effects of an antibody directed to Aβ. Although Thioflavin S (**34**) was effectively able to visualize plaques using this technique, it must be administered topically (direct application to the pial surface) because it does not cross the BBB. It is clear that the lack of a systemic administration prevented its use as in vivo imaging agent in humans.[89]

To overcome this critical limitation, Klunk and colleagues started a broad analog search and synthesis program to obtain more lipophilic, less ionized derivatives of CR. Indeed, this molecule is too highly charged to enter the brain in significant quantities. The analog Chrysamine-G (**8**, in Fig. 6), obtained through the replacement of the sulfonate group by a less ionizable carboxylic group, was tested for the ability to bind to Aβ in vitro and permeate the brain of normal mice.[90] Despite the initial positive results obtained in vitro and in vivo, it was soon realized that the potential of **8** as an in vivo probe was hampered by the still marginal brain entry of this relatively large, acidic compound. On these bases, they started an intense optimization campaign centered on CR and **8**. A systematic series of structural modifications of the pharmacophoric functions resulted in the promising fluorescent probe methoxy-X04 (**35**, Fig. 11).[91] Compared to the parent compounds, **35** has a significantly reduced molecular weight of 344 Da, a value that falls into the optimal range for brain entry. The carboxylic acid groups found in **8** were replaced by the weakly acidic phenols, which, with a pK_a of 10.82, would be uncharged at physiological pH. Furthermore, the log *P* of **35** is 2.6, higher than that of the less lipophilic Chrysamine-G (log *P* 1.8) and significantly higher than that of the charged CR (log $P - 0.18$). After confirming that **35** retained a binding affinity for Aβ fibrils ($K_d = 26.8$ nM) very similar to that of Chrysamine-G ($K_d = 25.3$ nM), it was successfully used to stain plaques, tangles, and cerebrovascular amyloid in postmortem sections of AD brain with good specificity. More importantly, using multiphoton microscopy to obtain high-resolution fluorescent images from the brains of living PS1/APP mice, individual plaques could be distinguished after a single intravenous injection of **35**.[91] In a separate study, **35** has been successfully

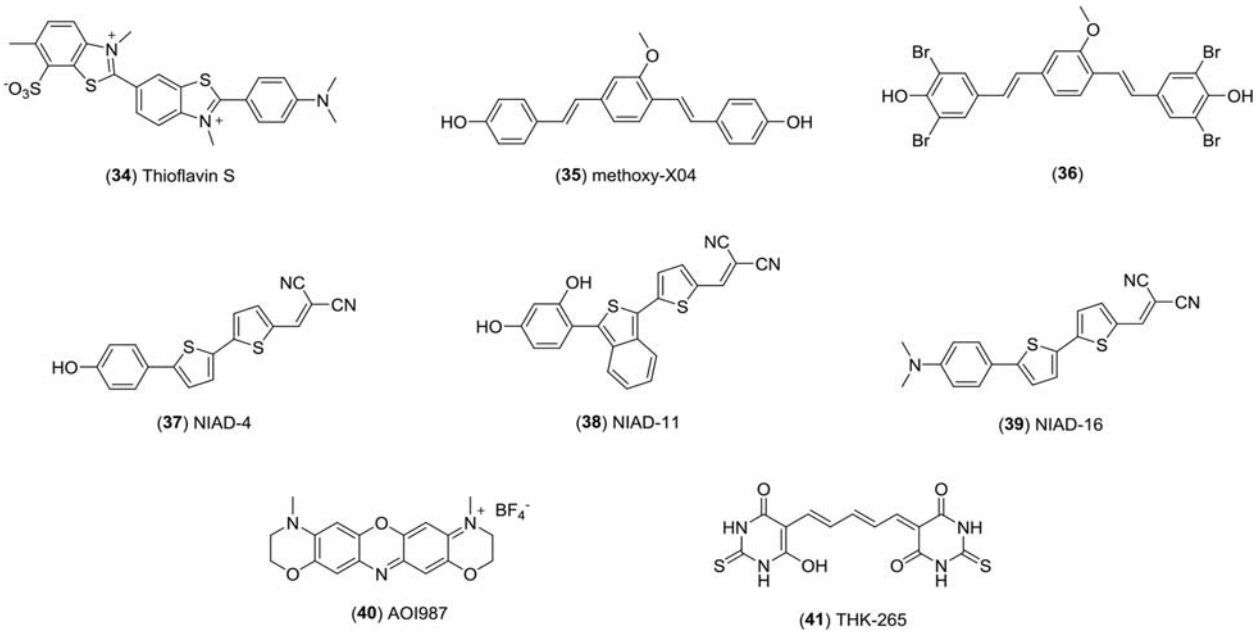

Fig. 11 Chemical structures of **34–41**, developed as Aβ fluorescent probes.

exploited to chart the entire kinetics of growth of a single plaque in Tg2576 mice. It revealed a plateau and/or a sigmoid-shaped progression of Aβ accumulation, confirming previous studies in humans performed with PiB.[92] Despite being a well-established dye, **35** suffers of a slow elimination in vivo. Thus, it has been the starting point for further medicinal chemistry activities by the group of Schmidt. The derivatizations performed resulted in new fluorescent sensors with improved binding properties to NFT and SP, as demonstrated in histochemical staining experiments on human brain tissue and by a Thiazine red displacement assay in vitro.[93] One of these derivatives, **36** (Fig. 11), showed a 24-fold higher affinity for NFT compared to Aβ plaques and thus holds potential to be profiled as a tau-selective fluorescent probe in vivo.

1.04.4.2 First Fluorescent Probes Used for in vivo Aβ Plaque Imaging

As already highlighted, the permanent charge or the ionizable nature of the first developed fluorescent agents hindered their BBB crossing. Besides, the heterogeneous complexes of lipids and proteins in brain tissue are also excitable in the 400–550 nm range, and their emission spectra (550–750 nm) are broad and overlap those of many commonly used dyes. Consequently, researchers moved to the development of neutral probes with a longer emission wavelength, in the near-infrared (NIR) region (650–900 nm).

Thus, in addition to the fundamental prerequisite of BBB permeability, it was increasingly clear that the design of fluorescent dyes for in vivo applications needed to incorporate several other important criteria including (1) a suitable wavelength interval of absorption and emission (NIR range), (2) the ability to rapidly enter the brain after intravenous injection, and (3) specific labeling of the Aβ deposits with concomitant rapid clearing of the unbound dye. Another unique advantage of fluorescence optical imaging is the possibility to attain substantial differences in the photo-physical/optical properties between the bound and unbound forms of the tracer. This would allow a significant increase in imaging contrast, which cannot be exploited with techniques based on radioligands.[94]

1.04.4.2.1 NIAD-4 and derivatives

These concepts inspired the rational design of NIAD-4 (**37**, in Fig. 11) by Swager and coworkers in 2005.[95] They merged the pharmacokinetic requirements with an electronic structure design to produce a compound possessing a suitable spectral range of the absorption and emission bands, with the explicit aim of developing a fluorescent probe to be used in vivo. They employed the typical push–pull architecture with terminal D and A moieties interconnected by a highly polarizable linker. Particularly, **37**, carrying a dithienyl-ethenyl π-conjugated bridge between D and A was purposely designed as one of the simplest possible structures (molecular weight of 334 Da). **37** showed excellent binding affinity ($K_d = 10$ nM) and a dramatic enhancement of the fluorescence intensity (about 400-fold) when labeling Aβ aggregates. Binding studies with fibrillar proteins revealed that **37** binds to the same site as BTA-1 (**6**). The reported affinity is much higher than that of ThT ($K_d = 580$ nM) and not dissimilar to that of high-affinity compounds like PiB (**7**) ($K_d = 4.3$ nM). The increased fluorescence intensity was explained by considering the reduced free rotation of aromatic rings in the excited state. In vivo two-photon imaging experiments in Tg mice demonstrated that **37** readily crossed the BBB after intravenous injection and labeled Aβ plaques in brain and cerebrovascular amyloid angiopathy on blood vessels.[95] In a more recent study, **37** showed a broader pH tolerance than ThT in monitoring Aβ formation, especially under acidic condition.[64]

Although **37** has the undoubted merit of being one of the first rationally designed Aβ probes achieving emission wavelength over 600 nm upon binding with Aβ aggregates, the maximum (603 nm) does not fall within the optimal NIR range of 650–900 nm. Studies with this probe still required the use of the invasive cranial window technique to perform in vivo fluorescence imaging, which is impractical in the clinical setting. To achieve longer emissions, the same group subsequently developed a further series of NIAD-4 analogs, including NIAD-11 (**38**) and NIAD-16 (**39**, in Fig. 11).[96] In details, in **38**, a new push–pull-type NIR fluorophore containing isothianaphthene subunits was synthesized, whereas **39** was obtained by replacing the terminal hydroxyl group of NIAD-4 with a dimethylamino group. As expected, this modification resulted in a bathochromic shift of the emission maximum ($\lambda_{em} = 720$ nm). Thanks to these positive properties, **39** distinguished vascular and nonvascular Aβ plaques through fluorescence lifetime imaging in APP Tg mice.[97]

1.04.4.2.2 AOI987

The pharmaceutical industry naturally was very interested in the development of fluorescent probes. In 2005, researchers at Novartis had defined a target product profile for such new fluorescent probes, which included the following key elements: a low-molecular weight (< 500 Da) and high lipophilicity (log *P* between 1 and 4) to be able to cross the BBB in sufficient amounts for detection and a specific binding to amyloid aggregates without degradation.[98] Moreover, they clearly stated that fluorescence emission maxima should lie in the NIR range, that is, between $650 < \lambda < 900$ nm. Among a series of properly synthesized analogs, the oxazine dye AOI987 (**40**, in Fig. 11) fulfilled all the requirements for selective in vivo Aβ staining. The compound readily penetrated the BBB and bound to Aβ fibrils with a K_d of 220 nM. More importantly, the fluorescence properties were promising, with absorption and emission maxima at 650 and 670 nm, respectively, and a high QY of 41%, an important prerequisite for high sensitivity. Although the researchers could not define the interaction at a molecular level, they proposed intercalation of the planar oxazine with the β-sheet structure of Aβ fibrils as a plausible model. Undoubtedly, the most striking achievement of their study was that they could develop **40** as the first fluorescent Aβ probe for noninvasive NIR detection. Experiments using NIR fluorescence (NIRF) imaging demonstrated that SP could be imaged in living APP23 mice with intact cranium and BBB, after intravenous administration of **40**. For the first time, they were able to quantify the Aβ load by spatial integration of fluorescence intensities, analogous to the quantification of receptor densities in classic receptor neuroimaging studies. In vivo results were confirmed by ex vivo measurements on mouse brains, immediately after acquiring the final in vivo NIRF image. Fluorescence microscopy further confirmed selective in vivo staining of SP in APP23 mice, whereas the brain sections of wild-type animals showed no fluorescence signal. As clearly highlighted by the authors, the noninvasiveness of NIRF imaging with **40** allowed repeated measurements over the lifetime of a mouse, providing an ideal tool for monitoring disease progression in AD animal models and assessing the efficacy of potential AD treatments.[98] Although **40** was reported as an efficient NIR probe for detecting and monitoring SP in a noninvasive way, it still presents two shortcomings, such as a small Stokes shift (25 nm) and moderate binding ($K_d = 220$ nM).

1.04.4.2.3 THK-265

A more recent example is represented by the thiopental dimer THK-265 (**41**, in Fig. 11), which, differently from the previously discussed rational examples, was discovered by screening a large pool of commercial NIRF dye for their binding toward Aβ aggregates.[99] Since the dye exhibited a low toxicity and a good brain uptake, together with optimal optical properties and amyloid affinity, its capability of visualizing Aβ plaques was explored in vivo. Its usefulness as an efficient imaging probe was verified in the APP mouse model, where it provided good discrimination between amyloid deposits in the brain and other nonpathological tissues.[99] When compared with **40**, **41** showed a higher QY and a higher absorption coefficient, together with a higher binding affinity toward Aβ ($K_d = 97$ nM). Building on these promising results and the fact that this molecule is commercially available, Schmidt et al. developed a systematic protocol for staging disease progression by using **41** as NIR probe to evaluate different Aβ aggregation levels in mice of different ages. The intensity of the NIRF signal correlated well with the plaque burden, indicating its utility for direct monitoring of Aβ aggregation progression. Importantly, this study opens up the possibility for efficient, presymptomatic monitoring of Aβ deposition in the aging brain in AD patients.[100]

1.04.4.3 Recent Development of Fluorescent Probes for In vivo Aβ Plaque Imaging

Since these first applications, an impressive development of new NIR fluorescent agents has taken place in recent years, which parallels the enormous technological advances in the optical imaging instrumentations and techniques. In principle, molecular fluorescence-based imaging avoids some technical difficulties of other modalities, such as the use of X-ray in CT and the facility requirements of PET probes (a local cyclotron for generating short-lived positron-emitting radionuclides and a synthetic unit to produce radiolabeled agents).[101] However, as previously discussed, conventional fluorescence methods, such as two-photon fluorescence microscopy and fluorescence molecular tomography (FMT), required craniotomy, cranial windows, and skull thinning. This is due to tissue absorption and light scattering, and scattering is the most significant attenuation factor. Current developments on the hardware and reconstruction algorithms have improved signal localization and quantification by introducing FMT approaches combined with other modalities. The development of optoacoustic tomography is going to allow imaging of physiological and molecular markers at higher resolution.[102] These innovations will further advance the scope of imaging in the area of medicine and biology and certainly have an impact on the drug discovery process. As for the most sophisticated and in vivo effective techniques, resolution and tissue penetration have been significantly improved by combining FMT with CT[103] or MRI[104] (see Refs.[105] and [106] for a more detailed description). As a further implementation, the optical imaging pioneer Ntziachristos recently developed

multispectral optoacoustic tomography (MSOT).[107] MSOT is a high-tech method wherein ultrasound waves are generated in response to the absorption of transient light within the tissue. The feasibility of this approach for the functional imaging of the human brain through the intact skull and scalp has been successfully validated in living mice with glioblastoma, by exploiting the FDA-approved NIR dye indocyanine green.[108]

The impressive technological innovations in fluorescent imaging have stimulated tremendous research efforts to develop novel agents with truly translational potential to be used for in vivo imaging of Aβ plaques. The past experience in the field taught researchers that pharmacokinetic, biophysical, and imaging properties should be simultaneously considered when designing NIR agents. The most comprehensive description of the target requirements has been provided by the group of Moore, who have identified the following requirements for a high-quality probe: (1) specificity to Aβ plaques; (2) reasonable lipophilicity (log *P* between 1 and 3); (3) molecular weight less than 600 Da; (4) emission wavelength > 650 nm and a large Stokes shift; (5) high-affinity binding; (6) high QY; (7) low-affinity binding with bovine serum albumin (BSA); (8) reasonable stability in blood; (9) straightforward synthesis; (10) and, most importantly, upon binding to Aβ plaques, its ability to significantly change its fluorescence properties (ie, fluorescence intensity, fluorescence lifetime, emission wavelength, and QY).[109] Obviously, the simultaneous presence of all these features in a single molecule is not easy, highlighting that the development of these probes is not an easy task to medicinal chemists.

In spite of these challenges, many promising fluorescent imaging probes have been published together with several more recent reviews of a wider scope.[83,94,110] Herein, we focus on very recent (2014–16) examples of fluorescent imaging agents designed to bind Aβ plaques or tau aggregates. Importantly, all the selected agents have demonstrated some utility in in vivo imaging applications. We will show how they substantiate the feasibility of the fluorescent imaging in advancing clinical diagnosis of AD.

The recent work of Cui and colleagues brilliantly exemplifies an iterative design process for achieving NIRF Aβ probes.[111] Starting from a small set of NIR probes based on D (*N*,*N*′-dimethylaniline)-π-A (dicyanomethylene group) architecture, the promising derivative DANIR 2c (**42**, in Fig. 12) was selected as a suitable candidate. **42** displayed high affinity for Aβ plaques and delivered good performances in APPswe/PSEN1 Tg mice in vivo and in fluorescent staining of brain sections from an AD patient. However, its emission wavelength was only 625 nm when bound to Aβ aggregates. To improve **42**'s fluorescence properties, the group

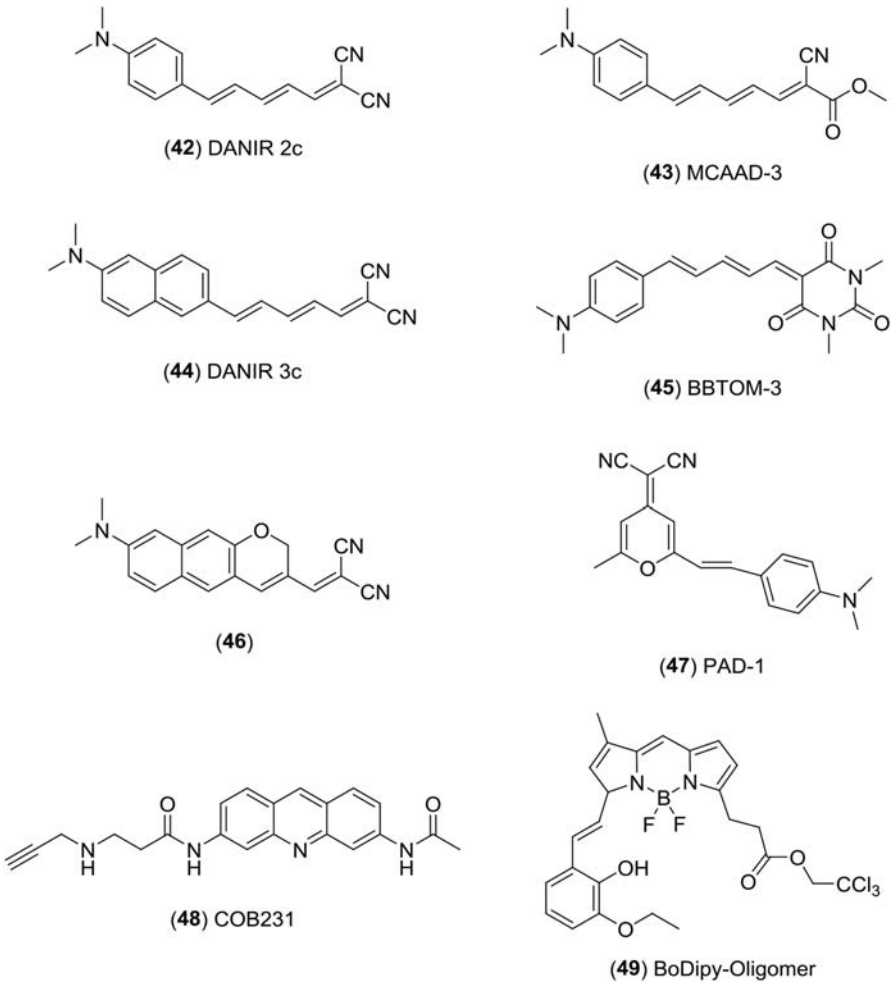

Fig. 12 Chemical structures of **42**–**49**, developed as Aβ fluorescent probes in vivo.

synthesized another set of DANIR-derived probes with different acceptor moieties.[112] The selected NIR probe MCAAD-3 (**43**, in Fig. 12) satisfied most requirements for detecting Aβ plaques in vitro and in vivo. However, it suffered from a low QY. Accordingly, the group recently developed an additional set of DANIR-derived probes by replacing the benzene donor group with a naphthalene ring.[113] Of these probes, DANIR 3c (**44**, in Fig. 12) showed excellent fluorescent properties ($\lambda_{em} > 650$ nm and high QY) and displayed high sensitivity and high affinities to Aβ aggregates. In vivo NIR imaging revealed that **44** is a brain-permeating probe, which efficiently differentiated between Tg and wild-type mice and fluorescently stained Aβ aggregates from an AD patient.

As a further improvement, the same authors reasoned that a coplanar geometry of a probe is a crucial feature for Aβ binding. In addition to this, the emission maximum of **43** and **44** upon binding to SP is below 650 nm, which is not within the NIR optical window. Thus, they envisioned the planar barbituric acid moiety of THK265 (**41**) as a more planar, stronger acceptor to obtain a higher affinity and longer emission wavelength. Indeed, BBTOM-3 (**45**) showed a remarkable binding affinity ($K_d = 13.7$ nM), which was higher than that of **42** ($K_d = 36.9$ nM) and **43** ($K_d = 106$ nM). These results corroborate the initial idea that the planar barbituric acid acceptor moiety (A) makes a significant contribution to the binding affinity. The probe displayed also higher emission wavelength and larger Stokes shift, thus further confirming the rational design applied. Importantly, in pharmacokinetic studies in mice, **45** displayed approximately 20-fold higher brain uptake than parent compound **41**. After confirming the specific binding on brain slices from APPswe/PSEN1 Tg mice and AD patients, in vivo studies were undertaken. As expected, higher fluorescence signals were observed in the brains of the AD mice than in the WT after intravenous injection of **45**.[114]

Kim et al. designed a cyclic analog of **42** and **46** (Fig. 12), as part of a project to develop two-photon fluorophores that can be excited and emit at longer wavelength region ($\lambda_{ex} \sim 900$ nm; $\lambda_{em} \geq 650$ nm), minimizing autofluorescence.[115] The benzo[g]chromene derivative **46** has all the features required for the in vivo imaging of Aβ plaques in the 5XFAD mouse model. Moreover, the fluorescence staining performances are greatly improved with respect to **42** (thanks to the additional conjugation and rigidified structure), particularly upon binding with Aβ aggregates.

Recently, researchers reported the recurrence of a similar acceptor–donor architecture, a chemically different dicyanomethylene-4H-pyran-based dye, namely, PAD-1 (**47**, in Fig. 12).[116] **47** has been described as "smart," thanks to its ability to detect Aβ fibrils in living APP/PS1 Tg mice with a marked turn-on effect.

The proflavine COB231 (**48**, in Fig. 12)[117] was recently identified by exploiting the intrinsic fluorescence of the acridine scaffold. Interestingly, **48** has been evaluated on postmortem human and mice brain slices and in vivo in triple-Tg mice (3xTg-AD), showing a specific labeling of SP over NFT. The originality of **48** is its clickable function, which could be extremely useful for further applications.

A notable and newly discovered fluorescent probe is the oligomer-specific BODIPY-Oligomer (BD-Oligo, **49**, in Fig. 12), which was developed through a diversity-oriented fluorescent library approach and high-content imaging-based screening.[118] This probe allows dynamic oligomer monitoring during in vitro fibrillogenesis and shows Aβ oligomer staining in APP/PS1 AD mice. To date, 49 is the only amyloid probe that discriminates between Aβ monomers, oligomers, and fibrils, raising the possibility of early diagnosis of AD through detecting soluble oligomers.

1.04.4.3.1 Photoswitchable fluorescent probes

As an emerging alternative to the probes described earlier, photoswitchable fluorescent probes constitute a powerful tool for optical imaging.[119] Conventional fluorescent probes are easily photobleached and therefore can only respond irreversibly to one event. Conversely, photoswitchable fluorophore can be reversibly cycled between bright and dark states multiple times. These probes are able to achieve a resolution of ~50 nm or better and limit background interference while maintaining the high molecular specificity and cell compatibility compared to the conventional fluorophores.

The first application of switchable derivatives for Aβ imaging has been recently published by Yi et al.[120] The authors connected an aminonaphthalene-2-cyanoacrylate (ANCA) fragment,[121] which is a well-known Aβ-targeting motif, with diarylethene (DAE) units through a short polyether chain. DAE units, which can reversibly photocyclise upon irradiation with UV and visible light, are promising candidate fluorescent switch systems because of their fast response, excellent thermal stability, and outstanding fatigue resistance. Two interesting probes, T1 (**50**, in Fig. 13) and its corresponding bivalent derivative T2 (**51**), have been characterized as high-affinity probes for Aβ aggregates with a strong increase of fluorescence intensity upon binding and remarkable antiphotobleaching, both in vitro and in tissues. Particularly, **51** showed reversible changes upon switching irradiation of UV and visible light, validating its photoswitchable properties. The associated color change is attributable to the different electrical structures corresponding to the open-ring and closed-ring isomers, which allowed selective staining of Aβ aggregates in brain sections of APP/PS1 Tg mice. Indeed, when **51** is irradiated with 405 nm for 150 s, it specifically highlights Aβ deposits, and the fluorescence of the irradiated deposits was turned off, depending on changing between its open and closed states. Interestingly, the fluorescence of the Aβ deposits could be recovered by irradiating with 633 nm. Although it has not been applied in vivo yet, these encouraging results may provide a new perspective for in vivo high-resolution fluorescence imaging.

1.04.4.4 Fluorescent Probes Used for In vivo NFT Imaging

Despite the previously discussed recent evidence supporting tau pathology as a more reliable AD biomarker, only a few fluorescent probes for NFT have been reported to date. This could be likely due to the fact that most of tau tangles are present inside of the neurons, whereas Aβ has an extracellular localization. Consequently, tau has been less accessible, and fewer fluorescent probes with respect to Aβ have been discovered.[122]

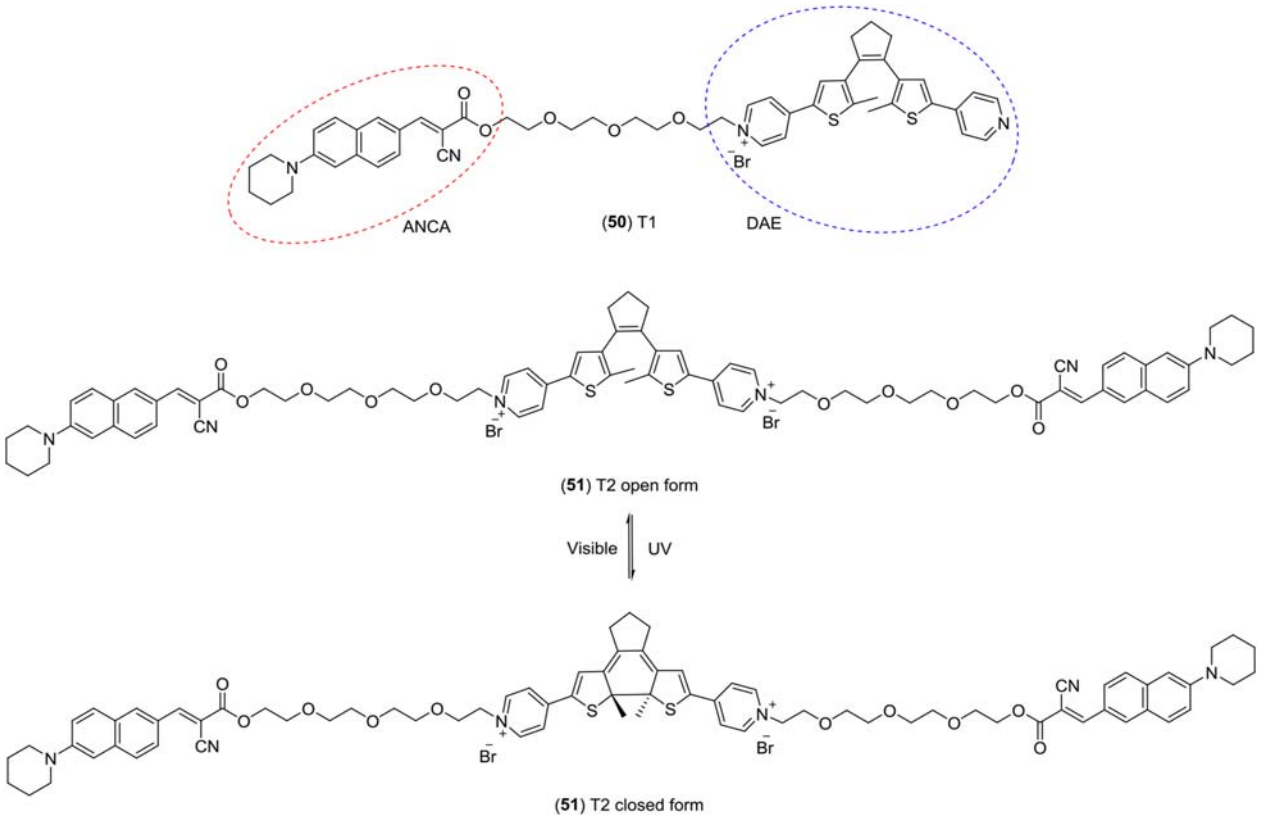

Fig. 13 Chemical structures of **50** and **51** and the photochromism of **51**.

Thus, there is an urgent need for tau imaging tools to complement Aβ imaging tracers that now are widely used. The majority of Aβ imaging agents used for clinical PET studies do not bind to tau lesions. In addition, several candidate tau probes do not bind to tau inclusions in non-AD tauopathy brains without plaque deposition. Therefore, currently, tau aggregates can be clinically characterized only in AD patients with combined Aβ and tau amyloids.

In 2013, Higuchi and colleagues realized that the lipophilicity of β-sheet ligands is associated with their selectivity for tau versus Aβ. The core dimensions of these molecules are major determinants of their reactivity toward a broad spectrum of tau aggregates in different tauopathies.[77] Moreover, these researchers found that affinity for non-AD tau inclusions of different molecules could be attributed to a core structure with a specific extent ranging from 13 to 19 Å. They therefore developed a series of fluorescent and BBB-penetrant compounds, named PBBs (see Section "**Benzothiazole-derived tau PET tracers**"), capable of detecting tau aggregates in AD and non-AD tauopathies. Based on promising in vitro and ex vivo human data, PBB3 (**52**, in **Fig. 14**), with a relatively low log *P*, was characterized through in vivo fluorescence and two-photon laser scanning microscopy imaging. Intravenous administration of **52** in PS19 mice resulted in its rapid transfer to the CNS extracellular matrix and subsequently to the cytoplasm of neurons, where it could bind to intracellular tau inclusions. On the basis of the encouraging preliminary data using this nonlabeled fluorescent compound, some of the synthesized probes were radiolabeled to conduct autoradiographic and PET assays. As discussed earlier, one of these probes, [^{11}C]PBB3 (**30**), was one of the first reported human PET tau imaging tracers.

It has already been highlighted that to precisely monitor the progression of AD, it is desirable to visualize Aβ and tau protein deposits separately. Recently, multispectral fluorescence imaging (MSFI) has been widely used for preclinical applications in microscopy. Moreover, an important application of MSFI is the identification of different protein aggregates, thanks to the fact that some fluorescent compounds show different Stokes shift of the wavelength to various protein fibrils.

Okamura and colleagues, in 2005, found that the previously mentioned benzimidazole derivative BF-126 (**17**) (see Section "**Quinoline- and benzimidazole-derived tau PET tracers**") emitted a different color of fluorescence when bound to Aβ and tau protein.[64] This finding suggested that a single fluorescent probe could differentiate deposits of these two proteins using MSFI technique. Moreover, SAR studies indicated that the backbone of benzimidazole was crucial to show distinctive fluorescence spectra when bound to PHF. Based on this, in 2014, the same group developed a novel fluorescent probe, BF-188 (2-[[4-(4-methylamino)phenyl]-1,3-butadienyl]benzimidazole, **53**, in **Fig. 14**), that can selectively detect Aβ and tau deposits in a wavelength-dependent manner. MSFI imaging with **53** clearly distinguish PHF from Aβ in AD brain sections. Moreover, this molecule shows sufficient brain uptake and rapid washout in normal mice. Thus, they suggested that **53** can potentially be used for selective in vivo imaging of tau and Aβ deposits in AD brain.[123]

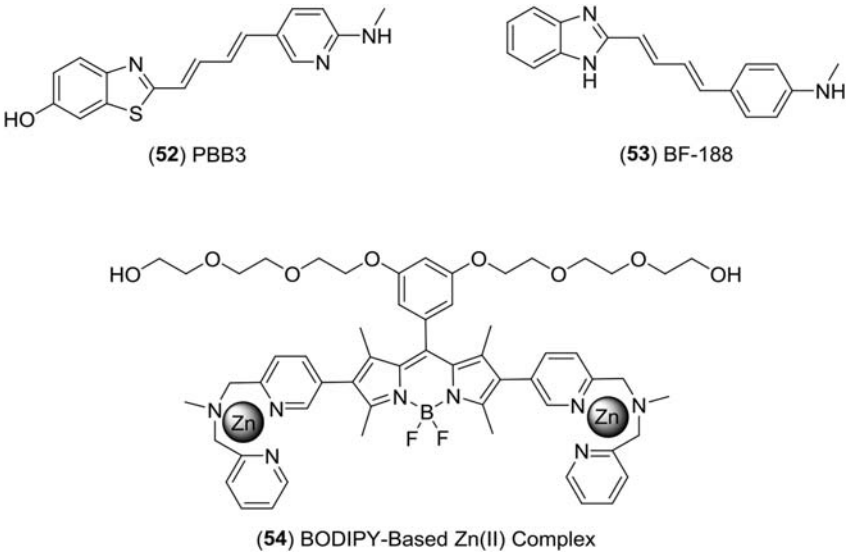

Fig. 14 Chemical structures of **52–54**, developed as tau fluorescent probes.

Despite not encompassing a typical "small-molecule" structure and therefore beyond the scope of this book chapter, the reader should be aware that several coordination complexes have been developed as fluorescent tau imaging agents. As a prototypical example, Ojida et al. reported a well-designed fluorescent BODIPY-based Zn(II) complex (**54**) for selectively detecting hyperphosphorylated tau proteins in brain sections of AD patients.[124] In this book chapter, we did not discuss further these references.

1.04.4.5 Fluorescent Probes Used for Amyloid Imaging in the Retina and Olfactory Epithelium

Another possible approach to a noninvasive NIR optical imaging in AD could rely on the use of neural tissues that are not shielded by the skull. Indeed, while most AD-related pathology occurs in the brain of AD patients and Tg mouse, many pathological hallmarks have been detected in the eye, which is certainly more accessible for imaging than the brain. It is widely accepted that there is high homology between the retinal and cerebral vasculatures and nerve cells and fibers of the retina form a sensory extension of the brain.[125] Thus, the retina could provide a unique opportunity for early diagnosis of AD in animal models and humans by exploiting NIR imaging. By using an advanced optical imaging microscope designed to examine the retina in live rodents, Koronyo-Hamaoui and colleagues were able to in vivo detect the curcumin (**55**, in Fig. 15) fluorescent signal from retinal Aβ in AD mice and visualize individual plaques at an unprecedentedly high resolution.[126] Unfortunately, the same findings were not replicated by Schon and colleagues, who examined postmortem retinas of patients who had suffered from AD. While they could detect hyperphosphorylated tau in Tg mice retina, they did not observe any fibrillar tau or Aβ aggregates in the retina of AD patients.[127] Thus, given the current uncertainties and controversies on the issues related to performance and validation of Aβ deposition in the retina as a biomarker for early detection of AD,[128] further studies are warranted.

The olfactory epithelium, being also an extension of the brain, has emerged as an alternative target for NIR imaging. The lack of a BBB between the nose and brain indicates that the nasal cavity might enable small molecules to access the brain and the CNS by pathways involving the olfactory epithelium and bulb. Therefore, the human olfactory system could be conducive to the diagnosis and treatment of brain disorders, such as AD. While engaged in the development of fluorescent pyrazine, pyrimidine, and pyridazine derivatives for an in vitro and in vivo tau-based diagnosis of AD, Schmidt and colleagues discovered an AD-related deposition of tau aggregates in Bowman's glands of the olfactory epithelium of AD patients. This allowed the authors to propose its use for an endoscopic diagnosis of AD in the olfactory system at very high resolution. The advantages of such a method compared with those of the imaging techniques based on radiotracers, which, as already emphasized, require elaborate infrastructure and on-site radiochemical synthesis of suitable tracers, are apparent. It is interesting to note that the presence of NFT was confirmed by staining, whereas no Aβ deposits could be observed in this region.[129] Whether or not the severity of tau accumulation in Bowman's glands correlates to AD pathology is still a matter of debate. However, this observation has shown potential for the noninvasive diagnosis of AD via changes in the olfactory epithelium in the early stages of disease. Along the same line, the same group developed a series of trimethine cyanine dyes, which were shown to act as efficacious fluorescent probes for the detection of tau deposits in olfactory epithelium tissue. Other concomitant interesting properties, such as good aqueous solubility and negligible cytotoxicity, suggest that these probes hold potential for in vivo applications.[130]

1.04.5 Curcumin as a Versatile Scaffold for the Development of Diagnostic and Therapeutic Agents for AD

Curcumin (**55**, in Fig. 15), the principal curcuminoid of the curry Indian spice, is a brightly colored powder that has been consumed daily for thousands of years in India, Asia, and the Middle East. Similar to many other herbal remedies, people first used **55** as a food

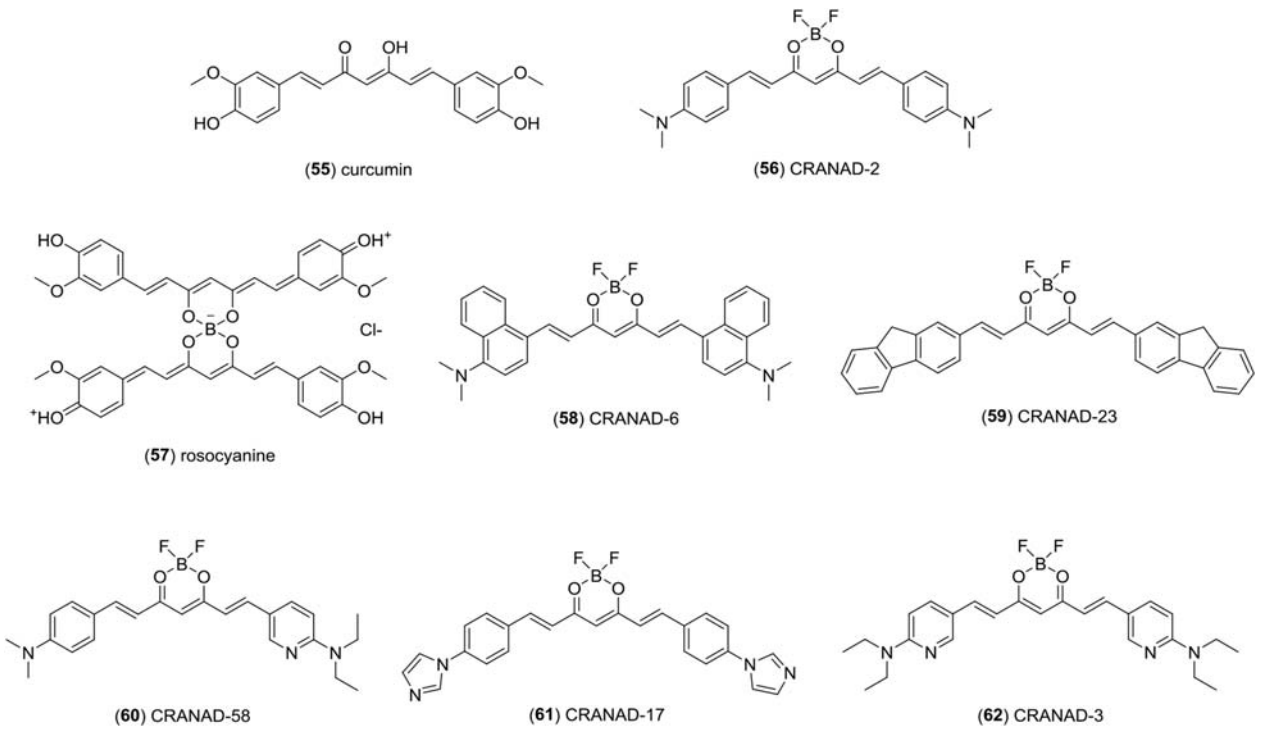

Fig. 15 Chemical structures of curcumin and its derivatives **56–62**, developed as diagnostic and therapeutic agents for AD.

additive and later discovered its several biological properties. **55** is known for its antitumor, antioxidant, antiarthritic, and antiinflammatory properties. Furthermore, it represents a promising tool for delaying or preventing the progression of AD and, at the same time, a promising histological staining reagent for SP.[131] On this basis, Backsai et al. first demonstrated that **55** both labels (by two-photon imaging) and disrupts amyloid plaques in vivo, exerting a neuroprotective effect in an APP–tau Tg mouse model. Indeed, Choe et al. suggested **55** as a potential PET probe for amyloid imaging, thanks to a high-affinity binding for Aβ aggregates ($K_d = 0.20$ nM).[132]

In light of this promising profile, Moore's group started to actively work on this scaffold with the aim of synthesizing new curcumin-derived NIR probes for Aβ. In fact, **55** itself is not an optimal in vivo probe because of its short emission wavelength, limited access to the BBB, and rapid metabolism.

In 2009, they reported the design and synthesis of the first curcumin-based NIR probe, CRANAD-2 (**56**, in Fig. 15).[109]

The rationale behind the design of **56** was based on three considerations. First, it is notorious that **55** reacts with boric acid to form the red-colored compound rosocyanine (**57**), which consists of two curcumins connected by a borate ring. The observed color change from yellow (curcumin) to red (rosocyanine) may be ascribed to the introduction of a boron atom ($\pi \rightarrow \pi^*$ from oxygen to empty orbital of boron) into the rosocyanine fragment. Thus, the authors hypothesized that the redshift benefit of boron incorporation could be used to design boron-containing curcumin derivatives with emission in the desired NIR range. Second, although 2,2-difluoro-1,3,2-dioxaborines are known compounds and their fluorescence properties have been characterized, the fluorescence change caused by difluoroboronate incorporation into diketone remained unexplored. Nevertheless, Moore and Ran noticed that the introduction of difluoroboronate ring into dipyrromethene systems affords the well-documented redshifted BODIPY dyes. Therefore, it was reasonable to speculate that by incorporating a difluoroboronate moiety into **55**, it would generate an appropriate redshift. Finally, *N*,*N*′-dimethyl group is well known as the best absorption redshift pushing group for *para*-substituted aromatic ring. Thus, they modified **55** by replacing the phenolic hydroxyl groups with *N*,*N*′-dimethyl ones, to enable redshifted absorption and, consequently, an additional redshift in emission.[109]

As rationally designed, **56** was able to satisfy all the requirements for a NIR agent for the detection of Aβ plaques both in vitro and in vivo. **56** showed high affinity for Aβ aggregates, a reasonable log *P* value (log $P = 3$), stability in serum, and a weak interaction with BSA. Moreover, after intravenous injection in Tg mice, a significantly higher signal than that from control mice was observed. Thus, **56** could be considered a "smart" probe because it displayed a significant fluorescence intensity increase, an emission blueshift, a lifetime change, and QY improvement upon interacting with insoluble Aβ aggregates. However, **56** lacked the capability of detecting soluble Aβ species.

In order to further optimize **56**, Moore and Ran synthesized several derivatives (eg, CRANAD-6, **58**, and CRANAD-23, **59**) but with no success in terms of fluorescent property improvement.[133] Finally, a longer π conjugation system was exploited for the design of CRANAD-58 (**60**, in Fig. 15). As expected, **60** displayed excitation and emission into the NIR region, and significant fluorescence property changes upon mixing with both soluble and insoluble Aβ species in vitro. In vivo NIR imaging revealed that **60** was capable of differentiating Tg and wild-type mice as young as 4 months old, the age that lacks apparently visible Aβ plaques, and

Aβ is likely in its soluble forms. Thus, the authors suggested that incorporation of PET isotopes into the CRANAD-58 (**60**) molecule could be feasible for the next translational studies.[133]

Moreover, in the same work, the authors took advantages of **55**'s ability to attenuate the $A\beta_{42}$-cross-linking induced by copper. This led to the synthesis of a new derivative, CRANAD-17 (**61**). It is well known that copper coordinates with two imidazoles on His13 and His14 of $A\beta_{42}$ to induce cross-linking with the Tyr position. Thus, **61** was used as an anchoring moiety to drive the compound to the vicinity of His13 and His14, whereas imidazole rings were incorporated to compete with His13/His14 for copper binding. As expected, SDS-PAGE gel and western blot indicated that **61** was capable of inhibiting $A\beta_{42}$ cross-linking induced by copper.[133]

These results corroborate the tremendous potential of the curcumin scaffold as a "privileged" fragment toward the development of small molecules able to both image and inhibit Aβ. In this respect, Moore and Ran demonstrated that the "diagnostic" analog CRANAD-3 (**62**) could be used as an NIRF imaging probe to monitor the Aβ-lowering effectiveness of "therapeutic" CRANAD-17 (**61**).[134]

NIRF imaging is generally more suitable than PET imaging for animal studies, thanks to its low cost, simple operation, and easy data analysis. As previously discussed, **56** was not able to detect soluble Aβ species, which are considered the most neurotoxic species and thus, potentially, could act as biomarkers for presymptomatic stages of AD. Then, the same authors synthesized CRANAD-3 (**62**, in Fig. 15), by the replacement of the two phenyl rings of **56** with pyridyls to introduce the possibility of hydrogen bonding between the engaged Aβ fragment and the nitrogen atoms of the pyridines. **62** displayed an emission peak at 730 nm and showed excellent fluorescence response toward soluble Aβ species. Moreover, in vivo two-photon microscopic imaging and NIRF imaging indicated that **62** is able to penetrate the BBB and specifically labels Aβ aggregates. Based on this encouraging data, first, the authors investigated the ability of **62** to monitor the therapeutic effectiveness of the curcumin derivative **61** and the drug candidate LY2811376, a well-characterized BACE-1 inhibitor. As expected, the fluorescence signal of **61** from APP/PS1 mice after LY2811376 treatment was 33% lower than the signal from the same mice before treatment. Second, they performed a preliminary in vivo therapeutic treatment of APP/PS1 mice with **61** for 6 months. CRANAD-17 is an imidazole-containing curcumin analog developed by the same group in 2013, which is able to reduce copper-induced Aβ cross-linking. After 6 months of treatment, NIRF imaging with **62** indicated that the **61**-treated group showed NIRF signals 25% lower than the signal from the nontreated one. For the first time, an NIR probe was effectively used to monitor AD therapy, and thus, **62** could be considered as one of the first companion diagnostics for AD, that is, an NIRF imaging probe able to monitor the Aβ-lowering effectiveness of therapeutics.[135]

1.04.6 Development of Theranostics against AD

In addition to the "pure" diagnostic role, molecular imaging has potential to move drug discovery toward more effective, individualized interventions. As therapies become directed at specific molecular pathways, personalizing treatments to the "molecular profile" of individual patients will be essential. In this respect, optical imaging should be critical to determine the type and required dose of drug for successful treatment. Imaging can guide customized therapy by envisaging an initial treatment regimen and suggesting a modification in therapeutic plan based on patient response. It will also allow monitoring of side effects during treatment and mapping drug delivery to diseased and normal tissues with the aim of minimizing off-target toxicity in normal tissue.[102]

In traditional approaches, imaging probes and drugs are pursued separately, which is time-consuming and expensive. Key challenges to the pharmaceutical industry today are the ballooning R&D cost and declining productivity driven to a large extent by the ever-increasing need to prove clinical efficacy and cost-effectiveness of new drugs. The need to satisfy these demands before drug approval results in an increasing development time and thereby also in a decrease of the window of opportunity afforded by the drug's patent life. To overcome these disadvantages, developing agents that have potentials for both therapy and imaging is highly desirable.[136] These agents have already been developed at research level with the name of "theranostics": their judicious application to the clinics has the potential to positively impact these challenges, reducing risk and costs, accelerating drug approval, and, ultimately, enhancing medical and commercial success.[136]

The term "theranostics" was first coined by the US consultant John Funkhouser in a press release from the company Cardiovascular Diagnostics in 1998, to describe a material that allows the combined diagnosis, treatment, and follow-up of disease.[137] The advent of theranostics has been in line with ongoing efforts to develop more specific, individualized therapies for various diseases and to combine diagnostic and therapeutic capabilities into a single agent. The use of theranostics is also strongly supported by the fact that most incurable diseases are immensely heterogeneous, and all existing treatments are effective for only limited patient subpopulations and at selective stages of disease development. The great anticipation of theranostics is that the fusion of diagnosis and therapy could provide therapeutic protocols likely to offer improved prognoses.[138] This is because it allows to stratify those patients most likely to respond to a targeted therapy in accordance with their "molecular profile" at a given time-point or, conversely, those patients for whom the risk of adverse effects is higher.

Since its first definition in 1998, the concept of theranosis has expanded, being nowadays quite broad in its meaning. In its most traditional sense of "diagnostics-guided therapy," it can be exemplified by the classical management of type 2 diabetes, whereby glucose blood levels are measured to determine the timing of the treatment and which patients will benefit from the insulin-based therapy. Another classical example relates to radioisotopic forms of sodium iodide, which represents the first molecule used for both diagnosis and therapy, depending on the emission of the chosen isotope. In particular, application of the theranostic approach to thyroid cancers and appropriate cases of thyrotoxicosis involves the possibility of accurate dosimetry with the positron-emitting ^{124}I, so that the appropriate amount of ^{131}I can be administered to destroy the pathological tissue.[139] A more recent

application deals with a test designed to stratify patients with BRAF-mutant unresectable or metastatic melanoma who may be suitable for treatment with a BRAF inhibitor. In this sense, detecting BRAF mutation is equivalent to measuring blood glucose in that it allows identifying which patients would benefit from vemurafenib, a small-molecule inhibitor targeted to mutant BRAF. In both the diabetes and melanoma examples, the diagnostic tool and the therapeutic agent are completely different because they share no molecular components. On the other hand, these two examples differ at least in one regard: while glucose levels represent a "non-targeted" biomarker of the disease state (the true drug's therapeutic target being insulin receptor), detection of BRAF mutation underpins the very presence of the target against which the targeted drug has an inhibitory effect. In fact, the mutated BRAF constitutes both a therapeutic target and a disease biomarker, that is a "targeted" biomarker. In another incarnation of a targeted biomarker, the same agent could be employed in both diagnostic and therapeutic strategies. In this instance, the diagnostic and the therapeutic agents do share at least one molecular component. Following the very elegant definition provided by O'Shannessy and colleagues in 2014, they can be named as "leveraged theranostics." Hence, as schematically depicted in **Fig. 16**, we can describe at least three different theranostic classes: non-targeted, targeted, and leveraged.[140]

1.04.6.1 Theranostic Small Molecules for AD

Despite their recent emergence, a plethora of theranostics are being developed in cancer research.[141] However, although CNS still does not nearly match oncology in either diagnostic or therapeutic prospects owing to a poorer understanding of the disease's molecular roots, theranostic approaches against neurodegeneration begin to be intensively pursued.[142] An analysis of the literature reveals that most of the reported examples deal with theranostics directed to Aβ. As discussed earlier, Dr. Alzheimer identified the amyloid aggregates already a century ago as the postmortem neuropathologic hallmarks of the disease, and more recently, they have been selected as an effective biomarker for clinical diagnosis. At the same time, on the basis of the amyloid hypothesis, amyloid aggregates have been considered as a potential therapeutic target for drug discovery endeavors. Indeed, during the last two decades, tremendous effort has been devoted to the design of small drug-like molecules and antibodies capable of inhibiting Aβ aggregation and deposition. Thus, in the years, Aβ has been undoubtedly regarded from a double diagnostic and therapeutic perspective. This has provided the logical foundation for the development of fluorescent probes able to image Aβ deposition and, at the same time, to provide therapeutic strategies. In other words, such molecules could act as truly targeted or leveraged theranostics against AD.

Interestingly, to these two different categories correspond different design strategies to obtaining them. In particular, the reported lead generation strategy is a rational approach that relies on framework combination. As enunciated in the field of multitarget drugs by Morphy and Rankovic,[143] the framework combination is a medicinal chemistry strategy based on the integration of two molecular frameworks into a new single molecule. They use the terms linking, fusing, and merging, depending upon the extent to which the two starting frameworks are amalgamated. At one end of the spectrum, there are conjugated ligands, which contain separate pharmacophoric moieties connected by a linker. At the other end of the spectrum, there are ligands in which the two pharmacophores overlap or are highly integrated (fusing and merging). Whereas ligands designed by conjugating two distinct pharmacophores are more likely to have high molecular weight and less likely to have oral and CNS drug-like properties, the fused or overlapped compounds are likely to have lower molecular weight and potentially superior drug-like properties. In addition to such rational framework combination, a completely unbiased method could be followed, that is, a screening approach. Despite being less commonly found in the literature, this encompasses compound classes that are already known to be effective Aβ sensors, which are screened for their therapeutic potential and vice versa.[135]

Although huge development is taking place in the field of AD theranostics, it was not until 2012 that the first examples appeared in the literature. To this respect, it should be emphasized that the precision of current bibliographic searches can be undermined by the fact that other terms, such as "multifunctional" and "bifunctional" fluorophores, other than theranostics have been used by some authors. Actually, the literature contains examples where the aim of developing theranostics has not been consciously planned. However, as the reported small molecules are able to simultaneously imaging and inhibiting Aβ peptides aggregates, we can consider them as truly theranostic agents.

Fig. 16 Possible strategies to pursue theranostic approaches. *BM*, biomarker; *Dx*, diagnostic; *Rx*, therapeutic.

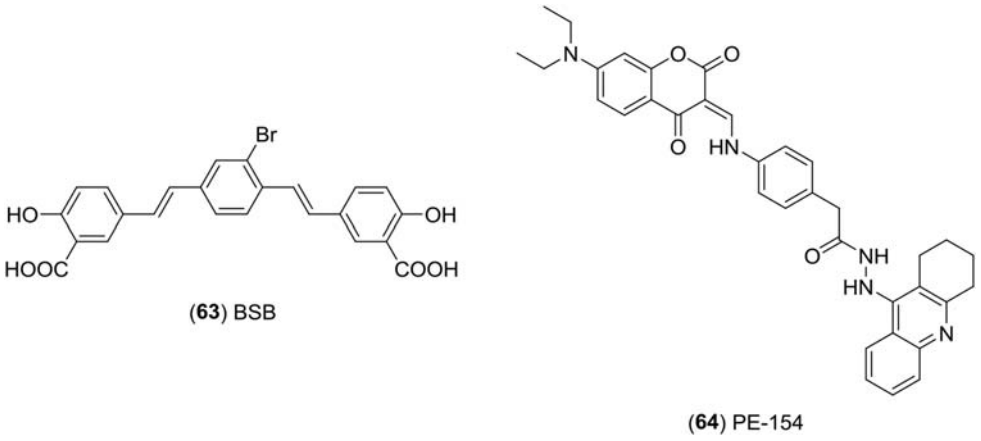

Fig. 17 Chemical structures of **63** and **64**, developed as theranostic precursors.

1.04.6.1.1 BTA-1, BSB, and PE154 as theranostic precursors

This is the case of a very pioneering study published by Ishikawa et al. in 2004.[144] ThT derivative BTA-1 (**6**, in Fig. 5) or CR derivative BSB (**63**, in Fig. 17), known to image Aβ plaques, fluorescently labeled prion plaques in the brain of patients affected by Gerstmann–Sträussler–Scheinker disease, a type of human prion disease. At the same time, both of them were found capable of inhibiting amyloid prion in brain tissues and displaying remarkable antiprion activity in ScN2a cell models ($IC_{50}=4$ nM for **6** and 1.4 μM for **63**).[144] **6** and **63** are therefore examples of potential antiprion theranostic compounds discovered through a screening approach. Despite this promising in vitro potential, neither compound was effective in vivo. Intravenous injection of **63** prolonged significantly but slightly the incubation periods of prion-infected Tga20 mice. However, no significant survival prolongation was observed. Consequently, both BTA-1 (**6**) and BSB (**63**) might be theranostic candidates against prion diseases, but it is likely that these compounds have poor permeability into the brain.[145] A comment is deserved about the capacity of a diagnostic/therapeutic agent to be active toward more than one neurodegenerative diseases. Indeed, neurodegenerative diseases, which encompass highly prevalent disorders such as AD and Parkinson's disease, and other less common ones, such as Huntington's disease, spinocerebellar ataxias, amyotrophic lateral sclerosis, and prion diseases, share several common features. In spite of peculiar clinical manifestation, all neurodegenerative disorders share the presence of cerebral deposits of misfolded protein aggregates. These deposits are a typical disease signature, and, although in each one the main protein component is different, they have similar morphological, structural, and staining characteristics. Compelling evidence suggests that in all these diseases, the accumulation of misfolded protein aggregates is the triggering factor in the pathology and leads to neurodegeneration. If such findings pose interesting questions about the possibility of common strategies for monitoring the amyloid aggregation process and for therapeutic intervention, from a diagnostic point of view, specificity would be mandatory for a differential diagnosis.

Another early example of theranostics was reported by Gütschow and coworkers already in 2009.[146] It deals with the generation of a theranostic small molecule against AD, developed starting from dual binding site acetylcholinesterase (AChE) inhibitors. This class of promising molecules was inspired by the discovery that AChE is one of the several proteins associated with amyloid plaque deposits. It has become increasingly clear that AChE, similar to other chaperone proteins, accelerates the assembly of Aβ peptide into amyloid fibrils.[147] The peripheral anionic site (PAS) of AChE has been identified as responsible for this proaggregating activity. This has provided the rationale for the development of dual inhibitors of AChE, that is, molecules that target the active site of the enzyme and the PAS. Such inhibitors should effectively prevent the aggregation of Aβ into toxic fibrils. Thus, in order to investigate the interplay between fibrils and AChE, Gütschow and colleagues developed a high-affinity, fluorescent ChE inhibitor,[146] PE154 (**64**, in Fig. 17).[148] This molecule originated from previously established heterodimeric ChE inhibitors, with the fluorogenic moiety deriving from the 7-aminocoumarin skeleton. Moreover, the planar electron-rich aromatic system of 7-aminocoumarin was anticipated as a useful interaction partner for Trp286.[149] Detailed in vitro kinetic analysis revealed that PE154 is a picomolar inhibitor of AChE. When characterizing **64**'s fluorescence properties (excitation peak at 405 nm and emission peak at 517 nm), a strong enhancement in fluorescence intensity in the presence of the target protein AChE was observed. Then, competition experiments with drug donepezil provide additional evidence for the binding mode of **64** within the enzyme gorge. The effective properties of **64** as a histological dye toward SP were revealed by confocal laser scanning microscopy in brain tissue sections of triple-Tg mice and an autoptic AD case. This was the first successful report of SP labeling by using a fluorescent, high-affinity AChE inhibitor. However, the authors could not precisely define whether **64** binds to AChE inside the plaques or to the amyloid structure itself.

1.04.6.1.2 SLOH as a theranostic small molecule

Carbazole-based cyanine fluorophores are highly sensitive fluorescent probes for double-stranded DNA and two-photon absorption dyes for two-photon excited bioimaging.[150] Moreover, monocyanine fluorophores were found to bind to Aβ peptide with concomitant strong fluorescence enhancement (>80-fold). On these bases, Li and Wong, in 2012, developed novel molecules

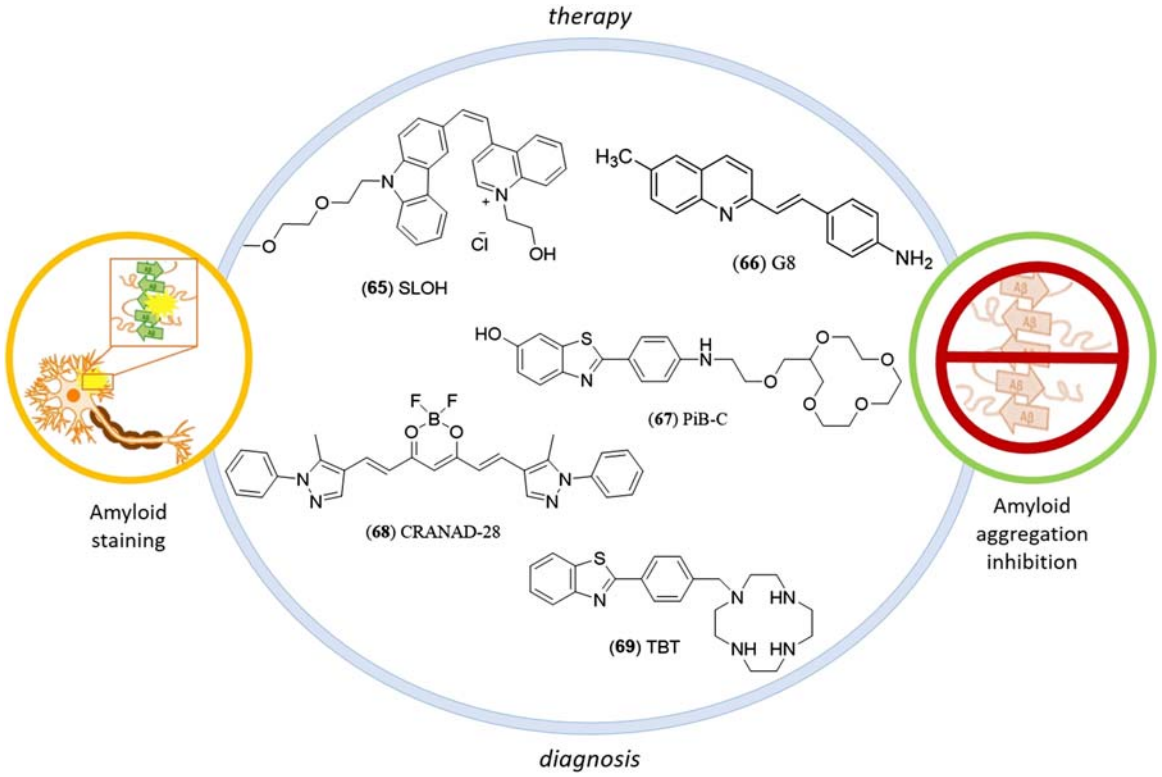

Fig. 18 Theranostic profile of **65**–**69**.

able to directly image and inhibit Aβ fibrillogenesis,[151] thanks to this dual activity they called "bifunctional." Thus, the carbazole scaffold was variously functionalized with the aim of optimizing critical functional properties such as Aβ-binding, cytotoxicity, and BBB permeability. The conducted SAR studies led to the discovery of a new promising compound, namely SLOH (**65**, in Fig. 18). As regards the diagnostic properties, in addition to an optimal intrinsic fluorescence, **65** showed a strong and progressive increase in fluorescence intensity, concomitant with a blueshift of the emission maximum, upon Aβ binding. Importantly, the fluorescence enhancement was much stronger for Aβ fibrils than for Aβ peptide. As regards the therapeutic properties, the authors demonstrated the ability of **65** to inhibit Aβ aggregation, by disrupting both the nucleation and elongation processes. The molecular mechanism of the inhibitory action was also corroborated by a circular dichroism study. A low toxicity together with a strong neuroprotective effect of SLOH toward the Aβ-induced cytotoxicity in SH-SY5Y cell line and mouse primary cortical cells further corroborated its potential. A preliminary in vivo proof of principle was obtained, as the authors demonstrated **65**'s abilities to enter the brain of live Tg mice and to specifically target Aβ plaques. In light of this profile, **65** emerges as a truly theranostic agent for AD.

1.04.6.1.3 G8 as a theranostic small molecule

The very first small molecule proposed as theranostic agent was styrylquinoline G8 (**66**, in Fig. 18), developed by Bolognesi and coworkers.[152] In 2013, they developed a small molecule able to potentially diagnose, deliver therapy, and monitor response to therapy in AD and prion diseases. The starting point of their work was the finding that several styryl derivatives, developed to improve the CNS properties of CR, were employed as AD imaging agents in vivo (see Section "**Aβ PET tracers derived from CR**"). Later, in 2012, styryl-1H-indole and styrylquinoline derivatives were reported as SPECT imaging probes to detect Aβ plaques. Thus, styryl moiety appears as a crucial framework for the ability of small molecules to label and interfere with pathological fibrillar aggregates, while the quinoline moiety is considered a privileged scaffold, displaying good pharmacokinetic properties and a high degree of drug-likeness. In light of this, they synthesized and evaluated (E)-6-methyl-4′-amino-2-styrylquinoline (**66**) as a theranostic agent able to potentially diagnose, deliver therapy, and monitor response to therapy in AD and prion diseases. As their goal was to develop a NIR fluorescent molecule, an amino group was purposely introduced to have an electron-releasing substituent conjugated with the quinoline nitrogen. After the characterization of its fluorescence properties, the authors evaluated **66**'s potential as a dual therapeutic/diagnostic agent. An antiaggregating property in the micromolar range, measured by a ThT-based fluorometric assay, suggested its ability as a moderate inhibitor of the Aβ fibrilization process. More importantly, a strong hypsochromic shift of the emission maximum (from 528 to 490 nm), concomitant with a hyperchromic effect upon Aβ binding, highlighted its potential as an amyloid sensor. Purposely addressed displacement studies suggested that **66** may have a primary high-affinity binding site distinct from ThT and a secondary low-affinity binding site in common with ThT. To substantiate **66**'s theranostic potential at a disease level, a cell-based model of prion diseases was exploited (ScGT1 cells). Fluorescent spots associated to prion fibrils were observed in infected

ScGT1 cells treated with **66**, using a ThS filter, which is within the NIR optical window. At the same time, when assessing the therapeutic antiprion potential in the same cell model, **66** showed a very low toxicity together with a remarkable activity: an EC_{50} of 0.5 μM, which makes it a very potent antiprion drug candidate. In addition, **66** exhibited BBB permeability *in* vitro (PAMPA test), demonstrating its value as CNS-directed agent. Thus, after the findings that **66** is able to stain and modulate both Aβ and prion protein, the authors proposed G8 as a promising theranostic tool to diagnose, deliver targeted therapy, and monitor response to therapy not only in AD but also in prion diseases.[152]

1.04.6.1.4 PiB-C as a theranostic small molecule

In 2014, Moore, Ran, and colleagues[153] exploited a novel approach to inhibit Aβ aggregation through a noncovalent modification at its surface. It is known that crown ethers can form stable complexes with protonated amines through the formation of hydrogen bonds. Moreover, it was reported that positively charged Aβ fibrils and protofibrils are highly cytotoxic and neutralization of the charges could reduce neuronal toxicity. Thus, the authors hypothesized that crown ethers could form noncovalent complexes with Aβ peptides through the formation of hydrogen bonds with protonated amino acids, such as arginine 5 (R5), lysines 16 and 28 (K16 and K28), and histidines 13 and 14 (H13 and H14). To note, previous studies suggested that K16 forms intersheet salt bridges and K28 form intrapeptide salt bridges with aspartate-23, all leading to the stabilization of the misfolded peptides. Thus, it was highly reasonable that breaking down these interactions should attenuate Aβ aggregation process. As a preliminary support to their hypothesis, the researchers verified the antiaggregating ability of a crown ether. 12-Crown-4 ether was chosen over other analogs, due to its low-molecular weight (beneficial for BBB penetration), its effective ability to form complexes with charged amino acids, and its negligible disturbance of physiological ion homeostasis. Both ThT testing and dot blotting indicated that this molecule could efficiently inhibit Aβ aggregation, albeit not in a specific way. Thus, to achieve a targeted effect, the authors planned to link the 12-crown-4 ether moiety with PiB (**7**), the widely used Aβ PET ligand. The new conjugate, called PiB-C (**67**, in Fig. 18), was then synthesized by attaching the 12-crown-4 ether moiety to the amino group of PiB. PiB-C showed an Aβ-aggregation inhibitory effect, as indicated by ThT testing and dot blotting, even stronger than PiB, suggesting the critical contribution of the crown ether moiety to the inhibitory effect. Then, the capability of **67** to reduce Aβ toxicity in SH-SY5Y cells was assessed, in comparison with 12-crown-4 ether. Both molecules lowered the toxicity of Aβ, while PiB did not, demonstrating that the neuroprotective ability of **67** was not originated from PiB. Finally, the authors tested the ability of **67** to specifically interact with Aβ plaques in a biologically relevant environment in vitro and in vivo, using two-photon imaging. As expected, PiB-C could clearly label plaques in APP/PS1 mouse brains not only ex vivo but also in vivo. Thus, the double merit of this study is the proposal of a novel strategy to attenuate Aβ aggregation and the development of the new theranostic agent PiB-C.

1.04.6.1.5 CRANAD-28 as a theranostic small molecule

Another theranostic agent, the curcumin-based CRANAD-28 (**68**, in Fig. 18), was proposed in 2014 by the same authors.[154] Previously, they had developed curcumin analogs able to detect soluble and insoluble Aβ (see Section "Curcumin as a Versatile Scaffold for the Development of Diagnostic and Therapeutic Agents for AD"), but some of them were endowed with low QY. To overcome this limitation, they hypothesized that the replacement of phenyl rings of curcumin with pyrazoles could increase the probe's brightness. This is because the inductive electron-withdrawing effect of one of the nitrogens of pyrazole could lead to a low tendency of electron delocalization in the system, which decreases tautomerization and increases QY. On the other hand, in a previous study, the authors had showed that similar curcumin analogs containing an imidazole ring could interfere with the coordination of copper and thus attenuate Aβ cross-linking (see Section "Curcumin as a Versatile Scaffold for the Development of Diagnostic and Therapeutic Agents for AD").

On this logical basis, they synthesized **68**, where the pyrazole could interfere with the copper coordination, and the phenyl substitution at the N-1 position could further reduce tautomerization and, in turn, improve QY. Thanks to the rationale design, **68** exhibited encouraging fluorescence properties in terms of optical range (excitation peak at 498 nm and emission peak at 578) and QY. Thus, the authors separately evaluated its diagnostic and therapeutic activities. Interestingly, its fluorescence intensity was quenched by Aβ, supportive of a direct interaction. This initial result was confirmed by ex vivo brain slice studies, where **68** provided an excellent contrast for SP. Then, after a positive evaluation of the BBB penetration, the capability of CRANAD-28 for the two-photon imaging of Aβ plaques was effectively validated in APP/PS1 mice. In parallel, western blotting analysis showed that **68** could significantly inhibit natural and copper-induced Aβ cross-linking. Thus, the authors were able to demonstrate the truly theranostic potential of **68**, as a two-photon imaging probe and as an inhibitor of Aβ cross-linking. The great novelty of **68**, although its emission maximum is not within the NIR region, is that it was the first theranostic agent to be successfully tested in an in vivo mouse model. Thus, CRANAD-28 marks an important stage in the search of novel molecules that may contribute to AD diagnosis and therapy in the future.

1.04.6.1.6 TBT as a theranostic small molecule

A more recently proposed theranostic small molecule is TBT (**69**, in Fig. 18), developed in 2015 by Yang, Wang, and colleagues.[155] The rationale behind their study was that metal chelators act as potential therapeutics for AD by reducing metal-induced Aβ aggregation and consequent neurotoxicity and counterbalance metal ion dyshomeostasis. Indeed, metal dyshomeostasis is a contributing cause of AD and of several other neurodegenerative diseases. Particularly, abnormal concentrations of Cu^{2+} and Zn^{2+} have been detected in the neocortex of AD patients, especially associated with Aβ deposits.[156] Interestingly, binding sites for both metal ions have been identified on Aβ oligomers, where they are thought to critically mediate amyloid toxicity.[157] On these bases, the authors

hypothesized that proper modification of chelators with sensing functions would be a promising strategy for developing dual-functional chelators, acting simultaneously as probes and inhibitors of metal-induced Aβ aggregation. To this aim, they developed the novel fluorescent chelator **69**. **69** was designed by following a linking strategy, as it is composed of a metal chelating 1,4,7,10-tetraazacyclododecane (cyclen) group and the Aβ-targeting 2-phenylbenzothiazole group. Indeed, cyclen was selected for its high modulatory efficacy toward metal-induced Aβ aggregation while 2-phenylbenzothiazole as the neutral ThT derivative with a well-known Aβ binding affinity. **69** can tightly bind to Zn^{2+} or Cu^{2+} via coordination interactions between the cyclen group and the metal ions. Moreover, this molecule also exhibited high selectivity for Cu^{2+} and Zn^{2+} over other biologically relevant metal ions. The synergistic effect of the two starting moieties was clearly evident from the profile shown by **69** in the ThT fluorescence competition assay. Additionally, molecular docking analysis suggested that TBT competes with ThT due to overlapping binding sites in Aβ. Then, after confirming that **69** specifically inhibits Zn^{2+}- and Cu^{2+}-induced $Aβ_{40}$ aggregation, the authors were able to monitor the disaggregation of $Aβ_{40}$ aggregates in brain homogenates of APPswe/PSEN1 Tg mice, by using TBT fluorescence behavior. In this respect, **69** is capable of targeting and disaggregating metal-associated Aβ aggregates and self-monitoring the disaggregation by fluorescence decrease even in the brain homogenates of AD mice. All these results, together with TBT's specificity, neuroprotectivity, efficient BBB permeability, and rapid washout, highlighted the potential of this fluorescent chelator as a theranostic tool for AD. However, it is important to highlight that in vivo studies are essential to evaluate the effective applicability of TBT as a theranostic agent in AD.

1.04.6.2 Theranostic Nanomedicine for AD

Although beyond the scope of this book chapter, which is devoted to diagnostic and theranostic small molecules, it should be noted that nanomedicines have been the first theranostics to be developed. In the last two decades, several approaches based on nanoparticles (NPs) ranging in size 1–1000 nm have been successfully brought to the clinic to treat cancer, pain, and infectious diseases. These therapies successfully exploit the general ability of NPs to deliver drugs more precisely, to improve their solubility, to prevent degradation, to increase their therapeutic index, and to reduce the immune response. NPs designed specifically for biomedical applications so far are of different types, mainly liposomes, solid lipid NPs, albumin NPs, polymeric NPs and magnetic NPs, dendrimers, nanogels, and quantum dots. These NPs, in addition to positive features such as biological stability and biocompatibility, have the intrinsic versatility of allowing incorporation of several biological or drug molecules.[158] In spite of these positive features, when referring to the specific development of nanomaterials for CNS applications, a major therapeutic challenge is that they must penetrate the brain, protected by the BBB. The mechanism of uptake and retention of a nanoparticulate system in brain delivery can be through various possibilities: (i) retention of particulate formulation in the blood capillaries of the brain, which, when adsorbed, creates a concentration gradient across the endothelial cells; (ii) suitable surfactant coating, possibly inhibiting the efflux mechanism and allowing the drug to be retained at the site of action; (iii) diffusion of the drug that can be enhanced by opening the tight junction of the endothelial cells; and (iv) release of the drug (normally by endocytosis). Drug delivery is also possible by all of the aforementioned processes.[159] On this ground, researchers have begun to intensively pursue theranostic approaches against neurodegeneration.[160] Some selected examples are provided in the succeeding text. These are only intended to give readers the flavor of the approach and direct them to the original literature or more thorough reviews with several recent reports on the potential applications of theranostic NPs in AD.[161]

Interestingly, a nanotechnological approach has been applied to overcome the low BBB uptake of potential theranostic small-molecule PE154 (**64**). Härtig and coworkers developed carboxylated poly(glycidyl methacrylate) and core-shell polystyrene-block-poly(*n*-butyl cyanoacrylate) NPs both loaded with PE154.[148] Although NPs were directly injected in the hippocampus of triple-Tg AD mice, their clear ability to target Aβ deposits with high specificity was confirmed. This in vivo study provided also the proof of principle of Aβ targeting by using PE154, after its release from NPs in vivo. In addition, the authors consciously considered the possibility of developing a theranostic approach for AD.[162]

Among the various NPs used in AD-related disease research, magnetic iron oxide NPs are particularly promising because of their high biocompatibility, distinctive magnetic properties, relative nontoxicity, biodegradability, and capacity for use as multimodal contrast agents.[163] In this context, Huang et al. developed a biomimetic approach based on superparamagnetic iron oxide glyconanoparticles to inhibit and detect Aβ fibrilization.[164] They build on the finding that carbohydrates, such as gangliosides, have been shown to play significant roles in amyloid aggregation initiation. The binding of Aβ by the glyconanoparticles was demonstrated through several techniques and its detection both in vitro and ex vivo by MRI. Furthermore, the glyconanoparticles were not only nontoxic to SH-SY5Y cells but also greatly reduced Aβ-induced cytotoxicity, highlighting the potential of these NPs for the dual detection and imaging of Aβ.[164] Another theranostic application of Aβ-directed iron NPs is exemplified by the work of Margel et al. These authors reported in 2013 the immobilization of the specific anti-Aβ monoclonal antibody BAM10 to NIR fluorescent maghemite ($γ$-Fe_2O_3) NPs, with the explicit aim of inhibiting Aβ fibrillation kinetics and of detecting Aβ fibrils. Indeed, the developed NP significantly hindered Aβ fibrillation process, such as Aβ-induced cytotoxicity to PC-12 cells. Furthermore, they enabled specific detection of Aβ fibrils ex vivo by fluorescence imaging.[165]

1.04.7 Conclusions

As can be seen from the discussed examples, in the last 20 years, an active and considerable progress has been made in the development and application of tracers for SP and NFT imaging in AD. As amyloid PET has entered into clinical use, we have clearly

understood the potential diagnostic benefits of this tool. The possibility to directly visualize in vivo Aβ deposition, previously only possible at autopsy, undoubtedly represents a major step forward. Equally important is the possibility that PET may facilitate the development of new treatments and of accurate and reliable assessments for diagnosis and for evaluations of the effectiveness of proposed treatments. As an easier and cheaper alternative to PET tracers, fluorescent probes have gained tremendous attention for imaging of both Aβ and tau aggregates. Furthermore, fluorescence imaging has given impetus to the development of theranostics, which combine therapeutic and diagnostic properties in a single chemical entity. In this book chapter, we focused on theranostic small molecules and their applications in AD imaging. The different strategies applied for the design of these molecules were discussed along with the in vitro and in vivo results. Currently, there is no registered theranostics available in the market for AD imaging. This is because there are still many crucial issues that need to be addressed, and their translational potential has been only marginally investigated. Although no one knows if theranostics will reach the clinics, there are already valid argument that these unconventional tools might increase our overall understanding of AD and could be critical for both finding and personalizing its treatment.

References

1. Alzheimer's Disease International, Policy Brief for Heads of Government: The Global Impact of Dementia 2013–2050. https://http://www.alz.co.uk/research/GlobalImpactDementia2013.pdf (accessed 9 February 2016).
2. Anand, R.; Gill, K. D.; Mahdi, A. A. Therapeutics of Alzheimer's Disease: Past, Present and Future. *Neuropharmacology* **2014,** *76,* 27–50. Pt A.
3. Cummings, J. L.; Morstorf, T.; Zhong, K. Alzheimer's Disease Drug-Development Pipeline: Few Candidates, Frequent Failures. *Alzheimers Res. Ther.* **2014,** *6* (4), 37.
4. Schulze, U.; Ringel, M. What Matters Most in Commercial Success: First-In-Class or Best-In-Class? *Nat. Rev. Drug Discov.* **2013,** *12* (6), 419–420.
5. Pankevich, D. E.; Altevogt, B. M.; Dunlop, J.; Gage, F. H.; Hyman, S. E. Improving and Accelerating Drug Development for Nervous System Disorders. *Neuron* **2014,** *84* (3), 546–553.
6. Rankovic, Z. CNS Drug Design: Balancing Physicochemical Properties for Optimal Brain Exposure. *J. Med. Chem.* **2015,** *58* (6), 2584–2608.
7. Bolognesi, M. L.; Legname, G. Approaches for Discovering Anti-Prion Compounds: Lessons Learned and Challenges Ahead. *Expert Opin. Drug Discov.* **2015,** *10* (4), 389–397.
8. Becker, R. E.; Greig, N. H.; Giacobini, E.; Schneider, L. S.; Ferrucci, L. A New Roadmap for Drug Development for Alzheimer's Disease. *Nat. Rev. Drug Discov.* **2014,** *13* (2), 156.
9. Bolognesi, M. L. Amyloid Chemical Probes and Theranostics: Steps Toward Personalized Medicine in Neurodegenerative Diseases. In *Medicinal Chemistry Approaches to Personalized Medicine;* Wiley-VCH Verlag GmbH & Co. KGaA: Weinheim, Germany, 2013; pp 211–226.
10. Alzheimer's and Dementia Testing for Earlier Diagnosis. http://www.alz.org/research/science/earlier_alzheimers_diagnosis.asp—Biomarkers (accessed 9 February 2016).
11. DDT Glossary. http://www.fda.gov/Drugs/DevelopmentApprovalProcess/DrugDevelopmentToolsQualificationProgram/ucm284395.htm (accessed 9 February 2016).
12. McEvoy, L. K.; Brewer, J. B. Biomarkers for the Clinical Evaluation of the Cognitively Impaired Elderly: Amyloid Is Not Enough. *Imaging Med.* **2012,** *4* (3), 343–357.
13. Blennow, K.; Hampel, H.; Weiner, M.; Zetterberg, H. Cerebrospinal Fluid and Plasma Biomarkers in Alzheimer Disease. *Nat. Rev. Neurol.* **2010,** *6* (3), 131–144.
14. Reiman, E. M.; Jagust, W. J. Brain Imaging in the Study of Alzheimer's Disease. *NeuroImage* **2012,** *61* (2), 505–516.
15. Alzheimer, A. Über eine eigenartige Erkrankung der Hirnrinde. *Allg. Zschr. Psychiatr. Psych. gerichtl. Med.* **1907,** *64,* 146–148.
16. Pike, K. E.; Savage, G.; Villemagne, V. L.; Ng, S.; Moss, S. A.; Maruff, P.; Mathis, C. A.; Klunk, W. E.; Masters, C. L.; Rowe, C. C. Beta-Amyloid Imaging and Memory in Non-Demented Individuals: Evidence for Preclinical Alzheimer's Disease. *Brain* **2007,** *130* (Pt 11), 2837–2844.
17. Hardy, J.; Selkoe, D. J. The Amyloid Hypothesis of Alzheimer's Disease: Progress and Problems on the Road to Therapeutics. *Science* **2002,** *297* (5580), 353–356.
18. Haass, C.; Kaether, C.; Thinakaran, G.; Sisodia, S. Trafficking and Proteolytic Processing of APP. *Cold Spring Harb. Perspect. Med.* **2012,** *2* (5), a006270.
19. Mucke, L.; Selkoe, D. J. Neurotoxicity of Amyloid Beta-Protein: Synaptic and Network Dysfunction. *Cold Spring Harb. Perspect. Med.* **2012,** *2* (7), a006338.
20. Karran, E.; Mercken, M.; De Strooper, B. The Amyloid Cascade Hypothesis for Alzheimer's Disease: An Appraisal for the Development of Therapeutics. *Nat. Rev. Drug Discov.* **2011,** *10* (9), 698–712.
21. Iqbal, K.; Liu, F.; Gong, C. X. Tau and Neurodegenerative Disease: The Story So Far. *Nat. Rev. Neurol.* **2016,** *12* (1), 15–27.
22. Dolan, P. J.; Johnson, G. V. The Role of Tau Kinases in Alzheimer's Disease. *Curr. Opin. Drug Discov. Devel.* **2010,** *13* (5), 595–603.
23. Martinez, A.; Perez, D. I.; Gil, C. Lessons Learnt From Glycogen Synthase Kinase 3 Inhibitors Development for Alzheimer's Disease. *Curr. Top. Med. Chem.* **2013,** *13* (15), 1808–1819.
24. Moyer, B. R.; Barrett, J. A. Biomarkers and Imaging: Physics and Chemistry for Noninvasive Analyses. *Bioanalysis* **2009,** *1* (2), 321–356.
25. Sperling, R. A.; Aisen, P. S.; Beckett, L. A.; Bennett, D. A.; Craft, S.; Fagan, A. M.; Iwatsubo, T.; Jack, C. R., Jr.; Kaye, J.; Montine, T. J.; Park, D. C.; Reiman, E. M.; Rowe, C. C.; Siemers, E.; Stern, Y.; Yaffe, K.; Carrillo, M. C.; Thies, B.; Morrison-Bogorad, M.; Wagster, M. V.; Phelps, C. H. Toward Defining the Preclinical Stages of Alzheimer's Disease: Recommendations From the National Institute on Aging-Alzheimer's Association Workgroups on Diagnostic Guidelines for Alzheimer's Disease. *Alzheimers Dement.* **2011,** *7* (3), 280–292.
26. Villemagne, V. L.; Furumoto, S.; Fodero-Tavoletti, M.; Harada, R.; Mulligan, R. S.; Kudo, Y.; Masters, C. L.; Yanai, K.; Rowe, C. C.; Okamura, N. The Challenges of Tau Imaging. *Future Neurol.* **2012,** *7* (4), 409–421.
27. Medeiros, R.; Baglietto-Vargas, D.; LaFerla, F. M. The Role of Tau in Alzheimer's Disease and Related Disorders. *CNS Neurosci. Ther.* **2011,** *17* (5), 514–524.
28. Rudin, M.; Weissleder, R. Molecular Imaging in Drug Discovery and Development. *Nat. Rev. Drug Discov.* **2003,** *2* (2), 123–131.
29. Kunjachan, S.; Ehling, J.; Storm, G.; Kiessling, F.; Lammers, T. Noninvasive Imaging of Nanomedicines and Nanotheranostics: Principles, Progress, and Prospects. *Chem. Rev.* **2015,** *115* (19), 10907–10937.
30. Zhang, L.; Villalobos, A. Recent Advances in the Development of PET and SPECT Tracers for Brain Imaging. *Annu. Rep. Med. Chem.* **2012,** *47,* 105–119.
31. (a) Mier, W.; Mier, D. Advantages in Functional Imaging of the Brain. *Front. Hum. Neurosci.* **2015,** *9,* 249; (b) Piel, M.; Vernaleken, I.; Rosch, F. Positron Emission Tomography in CNS Drug Discovery and Drug Monitoring. *J. Med. Chem.* **2014,** *57* (22), 9232–9258.
32. O'Brien, J. T.; Herholz, K. Amyloid Imaging for Dementia in Clinical Practice. *BMC Med.* **2015,** *13,* 163.
33. Approved Amyloid Imaging Agents Work About Equally Well. http://www.alzforum.org/news/research-news/approved-amyloid-imaging-agents-work-about-equally-well (accessed 9 February 2016).
34. Kung, H. F.; Choi, S. R.; Qu, W.; Zhang, W.; Skovronsky, D. 18F Stilbenes and Styrylpyridines for PET Imaging of A Beta Plaques in Alzheimer's Disease: A Miniperspective. *J. Med. Chem.* **2010,** *53* (3), 933–941.
35. Archival Interview—Louis Sokoloff. https://http://www.sfn.org/About/History-of-Neuroscience/Autobiographical-Videos-of-Prominent-Neuroscientists/Louis-Sokoloff (accessed 9 February 2016).
36. Klunk, W. E.; Mathis, C. A. The Future of Amyloid-Beta Imaging: A Tale of Radionuclides and Tracer Proliferation. *Curr. Opin. Neurol.* **2008,** *21* (6), 683–687.

37. Johnson, K. A.; Fox, N. C.; Sperling, R. A.; Klunk, W. E. Brain Imaging in Alzheimer Disease. *Cold Spring Harb. Perspect. Med.* **2012,** *2* (4), a006213.
38. Lipinski, C. A. Lead- and Drug-Like Compounds: The Rule-of-Five Revolution. *Drug Discov. Today Technol.* **2004,** *1* (4), 337–341.
39. Zhang, L.; Villalobos, A.; Beck, E. M.; Bocan, T.; Chappie, T. A.; Chen, L.; Grimwood, S.; Heck, S. D.; Helal, C. J.; Hou, X.; Humphrey, J. M.; Lu, J.; Skaddan, M. B.; McCarthy, T. J.; Verhoest, P. R.; Wager, T. T.; Zasadny, K. Design and Selection Parameters to Accelerate the Discovery of Novel Central Nervous System Positron Emission Tomography (PET) Ligands and Their Application in the Development of a Novel Phosphodiesterase 2A PET Ligand. *J. Med. Chem.* **2013,** *56* (11), 4568–4579.
40. Hickey, J. L.; Donnelly, P. S. Diagnostic Imaging of Alzheimer's Disease With Copper and Technetium Complexes. *Coord. Chem. Rev.* **2012,** *256* (19–20), 2367–2380.
41. Huryn, D. M.; Resnick, L. O.; Wipf, P. Contributions of Academic Laboratories to the Discovery and Development of Chemical Biology Tools. *J. Med. Chem.* **2013,** *56* (18), 7161–7176.
42. Klunk, W. E.; Wang, Y. M.; Huang, G. F.; Debnath, M. L.; Holt, D. P.; Mathis, C. A. Uncharged Thioflavin-T Derivatives Bind to Amyloid-Beta Protein With High Affinity and Readily Enter the Brain. *Life Sci.* **2001,** *69* (13), 1471–1484.
43. Klunk, W. E.; Engler, H.; Nordberg, A.; Wang, Y. M.; Blomqvist, G.; Holt, D. P.; Bergstrom, M.; Savitcheva, I.; Huang, G. F.; Estrada, S.; Ausen, B.; Debnath, M. L.; Barletta, J.; Price, J. C.; Sandell, J.; Lopresti, B. J.; Wall, A.; Koivisto, P.; Antoni, G.; Mathis, C. A.; Langstrom, B. Imaging Brain Amyloid in Alzheimer's Disease With Pittsburgh Compound-B. *Ann. Neurol.* **2004,** *55* (3), 306–319.
44. Nordberg, A. The Use of Amyloid Imaging in Clinical Praxis: A Critical Review. *Clin. Transl. Imaging* **2015,** *3* (1), 7–11.
45. Villemagne, V. L.; Rowe, C. C. Amyloid PET Ligands for Dementia. *PET Clin.* **2010,** *5* (1), 33–53.
46. Steensma, D. P. "Congo" Red: Out of Africa? *Arch. Pathol. Lab. Med.* **2001,** *125* (2), 250–252.
47. Mathis, C. A.; Mason, N. S.; Lopresti, B. J.; Klunk, W. E. Development of Positron Emission Tomography Beta-Amyloid Plaque Imaging Agents. *Semin. Nucl. Med.* **2012,** *42* (6), 423–432.
48. Barthel, H.; Sabri, O. Florbetaben to Trace Amyloid-Beta in the Alzheimer Brain by Means of PET. *J. Alzheimers Dis.* **2011,** *26* (Suppl 3), 117–121.
49. Zhang, W.; Oya, S.; Kung, M. P.; Hou, C.; Maier, D. L.; Kung, H. F. F-18 Stilbenes as PET Imaging Agents for Detecting Beta-Amyloid Plaques in the Brain. *J. Med. Chem.* **2005,** *48* (19), 5980–5988.
50. Ono, M.; Wilson, A.; Nobrega, J.; Westaway, D.; Verhoeff, P.; Zhuang, Z. P.; Kung, M. P.; Kung, H. F. 11C-Labeled Stilbene Derivatives as Abeta-Aggregate-Specific PET Imaging Agents for Alzheimer's Disease. *Nucl. Med. Biol.* **2003,** *30* (6), 565–571.
51. (a) Eckroat, T. J.; Mayhoub, A. S.; Garneau-Tsodikova, S. Amyloid-Beta Probes: Review of Structure-Activity and Brain-Kinetics Relationships. *Beilstein J. Org. Chem.* **2013,** *9,* 1012–1044; (b) Zhu, L.; Ploessl, K.; Kung, H. F. PET/SPECT Imaging Agents for Neurodegenerative Diseases. *Chem. Soc. Rev.* **2014,** *43* (19), 6683–6691; (c) Tu, P.; Fu, H.; Cui, M. Compounds for Imaging Amyloid-Beta Deposits in an Alzheimer's Brain: A Patent Review. *Expert Opin. Ther. Pat.* **2015,** *25* (4), 413–423.
52. Rowe, C. C.; Pejoska, S.; Mulligan, R. S.; Jones, G.; Chan, J. G.; Svensson, S.; Cselenyi, Z.; Masters, C. L.; Villemagne, V. L. Head-to-Head Comparison of 11C-PiB and 18F-AZD4694 (NAV4694) for Beta-Amyloid Imaging in Aging and Dementia. *J. Nucl. Med.* **2013,** *54* (6), 880–886.
53. Johnson, A. E.; Jeppsson, F.; Sandell, J.; Wensbo, D.; Neelissen, J. A.; Jureus, A.; Strom, P.; Norman, H.; Farde, L.; Svensson, S. P. AZD2184: A Radioligand for Sensitive Detection of Beta-Amyloid Deposits. *J. Neurochem.* **2009,** *108* (5), 1177–1186.
54. Zimmer, E. R.; Leuzy, A.; Aliaga, A.; Cheewakriengkrai, L.; Mohades, S.; Schilling, L. P.; Benedet, A. L.; Schirrmacher, E. S.; Soucy, J.-P.; Guiot, M.-C.; Reininger, C.; Gauthier, S.; Rosa-Neto, P. In Vitro Properties of [18F]NAV4694: Dynamic Range, Displacement, and White-Matter Binding. *Alzheimers Dement.* **2014,** *10* (4), P23–P24.
55. PET Imaging Agent [18F]NAV4694 for Detecting Cerebral Beta-Amyloid. https://http://www.nia.nih.gov/alzheimers/clinical-trials/pet-imaging-agent-18fnav4694-detecting-cerebral-beta-amyloid (accessed 9 February 2016).
56. Swahn, B. M.; Wensbo, D.; Sandell, J.; Sohn, D.; Slivo, C.; Pyring, D.; Malmstrom, J.; Arzel, E.; Vallin, M.; Bergh, M.; Jeppsson, F.; Johnson, A. E.; Jureus, A.; Neelissen, J.; Svensson, S. Synthesis and Evaluation of 2-Pyridylbenzothiazole, 2-Pyridylbenzoxazole and 2-Pyridylbenzofuran Derivatives as 11C-PET Imaging Agents for Beta-Amyloid Plaques. *Bioorg. Med. Chem. Lett.* **2010,** *20* (6), 1976–1980.
57. Yousefi, B. H.; Manook, A.; Grimmer, T.; Arzberger, T.; von Reutern, B.; Henriksen, G.; Drzezga, A.; Forster, S.; Schwaiger, M.; Wester, H. J. Characterization and First Human Investigation of FIBT, a Novel Fluorinated Abeta Plaque Neuroimaging PET Radioligand. *ACS Chem. Neurosci.* **2015,** *6* (3), 428–437.
58. Ono, M.; Saji, H. SPECT Imaging Agents for Detecting Cerebral Beta-Amyloid Plaques. *Int. J. Mol. Imaging* **2011,** *2011,* 543267.
59. (a) Harada, R.; Okamura, N.; Furumoto, S.; Tago, T.; Yanai, K.; Arai, H.; Kudo, Y. Characteristics of Tau and Its Ligands in PET Imaging. *Biomolecules* **2016,** *6* (1), 7; (b) Villemagne, V. L.; Fodero-Tavoletti, M. T.; Masters, C. L.; Rowe, C. C. Tau Imaging: Early Progress and Future Directions. *Lancet Neurol.* **2015,** *14* (1), 114–124.
60. Ariza, M.; Kolb, H. C.; Moechars, D.; Rombouts, F.; Andres, J. I. Tau Positron Emission Tomography (PET) Imaging: Past, Present, and Future. *J. Med. Chem.* **2015,** *58* (11), 4365–4382.
61. Villemagne, V. L.; Okamura, N. In Vivo Tau Imaging: Obstacles and Progress. *Alzheimers Dement.* **2014,** *10* (3 Suppl), S254–S264.
62. Barrio, J. R.; Huang, S.-C.; Cole, G.; Satyamurthy, N.; Petric, A.; Phelps, M. E. PET Imaging of Tangles and Plaques in Alzheimer Disease With a Highly Hydrophobic Probe. *J. Labelled Comp. Radiopharm.* **1999,** *42,* S194–S195.
63. Agdeppa, E. D.; Kepe, V.; Liu, J.; Flores-Torres, S.; Satyamurthy, N.; Petric, A.; Cole, G. M.; Small, G. W.; Huang, S. C.; Barrio, J. R. Binding Characteristics of Radiofluorinated 6-Dialkylamino-2-Naphthylethylidene Derivatives as Positron Emission Tomography Imaging Probes for Beta-Amyloid Plaques in Alzheimer's Disease. *J. Neurosci.* **2001,** *21* (24), RC189.
64. Okamura, N.; Suemoto, T.; Furumoto, S.; Suzuki, M.; Shimadzu, H.; Akatsu, H.; Yamamoto, T.; Fujiwara, H.; Nemoto, M.; Maruyama, M.; Arai, H.; Yanai, K.; Sawada, T.; Kudo, Y. Quinoline and Benzimidazole Derivatives: Candidate Probes for in vivo Imaging of Tau Pathology in Alzheimer's Disease. *J. Neurosci.* **2005,** *25* (47), 10857–10862.
65. Watanabe, H.; Ono, M.; Saji, H. Novel PET/SPECT Probes for Imaging of Tau in Alzheimer's Disease. *Sci. World J.* **2015,** *2015,* 124192.
66. Fodero-Tavoletti, M. T.; Okamura, N.; Furumoto, S.; Mulligan, R. S.; Connor, A. R.; McLean, C. A.; Cao, D.; Rigopoulos, A.; Cartwright, G. A.; O'Keefe, G.; Gong, S.; Adlard, P. A.; Barnham, K. J.; Rowe, C. C.; Masters, C. L.; Kudo, Y.; Cappai, R.; Yanai, K.; Villemagne, V. L. 18F-THK523: A Novel in vivo Tau Imaging Ligand for Alzheimer's Disease. *Brain* **2011,** *134* (Pt 4), 1089–1100.
67. Harada, R.; Okamura, N.; Furumoto, S.; Tago, T.; Maruyama, M.; Higuchi, M.; Yoshikawa, T.; Arai, H.; Iwata, R.; Kudo, Y.; Yanai, K. Comparison of the Binding Characteristics of [18F]THK-523 and Other Amyloid Imaging Tracers to Alzheimer's Disease Pathology. *Eur. J. Nucl. Med. Mol. Imaging* **2013,** *40* (1), 125–132.
68. Villemagne, V. L.; Furumoto, S.; Fodero-Tavoletti, M. T.; Mulligan, R. S.; Hodges, J.; Harada, R.; Yates, P.; Piguet, O.; Pejoska, S.; Dore, V.; Yanai, K.; Masters, C. L.; Kudo, Y.; Rowe, C. C.; Okamura, N. In Vivo Evaluation of a Novel Tau Imaging Tracer for Alzheimer's Disease. *Eur. J. Nucl. Med. Mol. Imaging* **2014,** *41* (5), 816–826.
69. Okamura, N.; Furumoto, S.; Harada, R.; Tago, T.; Yoshikawa, T.; Fodero-Tavoletti, M.; Mulligan, R. S.; Villemagne, V. L.; Akatsu, H.; Yamamoto, T.; Arai, H.; Iwata, R.; Yanai, K.; Kudo, Y. Novel 18F-Labeled Arylquinoline Derivatives for Noninvasive Imaging of Tau Pathology in Alzheimer Disease. *J. Nucl. Med.* **2013,** *54* (8), 1420–1427.
70. Harada, R.; Okamura, N.; Furumoto, S.; Furukawa, K.; Ishiki, A.; Tomita, N.; Tago, T.; Hiraoka, K.; Watanuki, S.; Shidahara, M.; Miyake, M.; Ishikawa, Y.; Matsuda, R.; Inami, A.; Yoshikawa, T.; Funaki, Y.; Iwata, R.; Tashiro, M.; Yanai, K.; Arai, H.; Kudo, Y. 18F-THK5351: A Novel PET Radiotracer for Imaging Neurofibrillary Pathology in Alzheimer Disease. *J. Nucl. Med.* **2016,** *57* (2), 208–214.
71. Forsberg, A.; Jureus, A.; Cselenyi, Z.; Eriksdotter, M.; Freund-Levi, Y.; Jeppsson, F.; Swahn, B. M.; Sandell, J.; Julin, P.; Schou, M.; Andersson, J.; Johnstrom, P.; Varnas, K.; Halldin, C.; Farde, L.; Svensson, S. Low Background and High Contrast PET Imaging of Amyloid-Beta With [11C]AZD2995 and [11C]AZD2184 in Alzheimer's Disease Patients. *Eur. J. Nucl. Med. Mol. Imaging* **2013,** *40* (4), 580–593.
72. Ariëns, E. J. Promiscuity in Pharmacology. *Trends Pharmacol. Sci.* **1988,** *9* (7), 235.
73. Rojo, L. E.; Alzate-Morales, J.; Saavedra, I. N.; Davies, P.; Maccioni, R. B. Selective Interaction of Lansoprazole and Astemizole With Tau Polymers: Potential New Clinical Use in Diagnosis of Alzheimer's Disease. *J. Alzheimers Dis.* **2010,** *19* (2), 573–589.
74. Honson, N. S.; Johnson, R. L.; Huang, W.; Inglese, J.; Austin, C. P.; Kuret, J. Differentiating Alzheimer Disease-Associated Aggregates With Small Molecules. *Neurobiol. Dis.* **2007,** *28* (3), 251–260.

75. Matsumura, K.; Ono, M.; Hayashi, S.; Kimura, H.; Okamoto, Y.; Ihara, M.; Takahashi, R.; Mori, H.; Saji, H. Phenyldiazenyl Benzothiazole Derivatives as Probes for in vivo Imaging of Neurofibrillary Tangles in Alzheimer's Disease Brains. *Med. Chem. Commun.* **2011,** *2* (7), 596–600.
76. Matsumura, K.; Ono, M.; Kimura, H.; Ueda, M.; Nakamoto, Y.; Togashi, K.; Okamoto, Y.; Ihara, M.; Takahashi, R.; Saji, H. 18F-Labeled Phenyldiazenyl Benzothiazole for in vivo Imaging of Neurofibrillary Tangles in Alzheimer's Disease Brains. *ACS Med. Chem. Lett.* **2012,** *3* (1), 58–62.
77. Maruyama, M.; Shimada, H.; Suhara, T.; Shinotoh, H.; Ji, B.; Maeda, J.; Zhang, M. R.; Trojanowski, J. Q.; Lee, V. M. Y.; Ono, M.; Masamoto, K.; Takano, H.; Sahara, N.; Iwata, N.; Okamura, N.; Furumoto, S.; Kudo, Y.; Chang, Q.; Saido, T. C.; Takashima, A.; Lewis, J.; Jang, M. K.; Aoki, I.; Ito, H.; Higuchi, M. Imaging of Tau Pathology in a Tauopathy Mouse Model and in Alzheimer Patients Compared to Normal Controls. *Neuron* **2013,** *79* (6), 1094–1108.
78. Zhang, W.; Arteaga, J.; Cashion, D. K.; Chen, G.; Gangadharmath, U.; Gomez, L. F.; Kasi, D.; Lam, C.; Liang, Q.; Liu, C.; Mocharla, V. P.; Mu, F.; Sinha, A.; Szardenings, A. K.; Wang, E.; Walsh, J. C.; Xia, C.; Yu, C.; Zhao, T.; Kolb, H. C. A Highly Selective and Specific PET Tracer for Imaging of Tau Pathologies. *J. Alzheimers Dis.* **2012,** *31* (3), 601–612.
79. Xia, C.-F.; Arteaga, J.; Chen, G.; Gangadharmath, U.; Gomez, L. F.; Kasi, D.; Lam, C.; Liang, Q.; Liu, C.; Mocharla, V. P.; Mu, F.; Sinha, A.; Su, H.; Szardenings, A. K.; Walsh, J. C.; Wang, E.; Yu, C.; Zhang, W.; Zhao, T.; Kolb, H. C. [18F]T807, a Novel Tau Positron Emission Tomography Imaging Agent for Alzheimer's Disease. *Alzheimers Dement.* **2013,** *9* (6), 666–676.
80. Gobbi, L.; Knust, H.; Koblet, A. Imidazo[2,1]thiazol-3-One Derivatives Useful as Diagnostic Agents for Alzheimer's Disease. *ACS Med. Chem. Lett.* **2014,** *5,* 619–620.
81. Taghavi, A.; Nasir, S.; Pickhardt, M.; Heyny-von Haussen, R.; Mall, G.; Mandelkow, E.; Mandelkow, E. M.; Schmidt, B. *N*'-Benzylidene-benzohydrazides as Novel and Selective Tau-PHF Ligands. *J. Alzheimers Dis.* **2011,** *27* (4), 835–843.
82. Nolting, D. D.; Gore, J. C.; Pham, W. Near-Infrared Dyes: Probe Development and Applications in Optical Molecular Imaging. *Curr. Org. Synth.* **2011,** *8* (4), 521–534.
83. Staderini, M.; Martin, M. A.; Bolognesi, M. L.; Menendez, J. C. Imaging of Beta-Amyloid Plaques by Near Infrared Fluorescent Tracers: A New Frontier for Chemical Neuroscience. *Chem. Soc. Rev.* **2015,** *44* (7), 1807–1819.
84. Khurana, R.; Coleman, C.; Ionescu-Zanetti, C.; Carter, S. A.; Krishna, V.; Grover, R. K.; Roy, R.; Singh, S. Mechanism of Thioflavin T Binding to Amyloid Fibrils. *J. Struct. Biol.* **2005,** *151* (3), 229–238.
85. Vassar, P. S.; Culling, C. F. Fluorescent Stains, With Special Reference to Amyloid and Connective Tissues. *Arch. Pathol.* **1959,** *68,* 487–498.
86. LeVine, H., III; Scholten, J. D. Screening for Pharmacologic Inhibitors of Amyloid Fibril Formation. *Methods Enzymol.* **1999,** *309,* 467–476.
87. Groenning, M. Binding Mode of Thioflavin T and Other Molecular Probes in the Context of Amyloid Fibrils-Current Status. *J. Chem. Biol.* **2010,** *3* (1), 1–18.
88. Howie, A. J.; Brewer, D. B. Optical Properties of Amyloid Stained by Congo Red: History and Mechanisms. *Micron* **2009,** *40* (3), 285–301.
89. Bacskai, B. J.; Kajdasz, S. T.; Christie, R. H.; Carter, C.; Games, D.; Seubert, P.; Schenk, D.; Hyman, B. T. Imaging of Amyloid-Beta Deposits in Brains of Living Mice Permits Direct Observation of Clearance of Plaques With Immunotherapy. *Nat. Med.* **2001,** *7* (3), 369–372.
90. Klunk, W. E.; Debnath, M. L.; Pettegrew, J. W. Chrysamine-G Binding to Alzheimer and Control Brain: Autopsy Study of a New Amyloid Probe. *Neurobiol. Aging* **1995,** *16* (4), 541–548.
91. Klunk, W. E.; Bacskai, B. J.; Mathis, C. A.; Kajdasz, S. T.; McLellan, M. E.; Frosch, M. P.; Debnath, M. L.; Holt, D. P.; Wang, Y.; Hyman, B. T. Imaging Abeta Plaques in Living Transgenic Mice With Multiphoton Microscopy and Methoxy-X04, a Systemically Administered Congo Red Derivative. *J. Neuropathol. Exp. Neurol.* **2002,** *61* (9), 797–805.
92. Burgold, S.; Filser, S.; Dorostkar, M. M.; Schmidt, B.; Herms, J. In Vivo Imaging Reveals Sigmoidal Growth Kinetic of Beta-Amyloid Plaques. *Acta Neuropathol. Commun.* **2014,** *2,* 30.
93. Bolander, A.; Kieser, D.; Scholz, C.; Haussen, R. H. V.; Mall, G.; Goetschy, V.; Czech, C.; Schmidt, B. Synthesis of Methoxy-X04 Derivatives and Their Evaluation in Alzheimer's Disease Pathology. *Neurodegener. Dis.* **2014,** *13* (4), 209–213.
94. Tong, H. J.; Lou, K. Y.; Wang, W. Near-Infrared Fluorescent Probes for Imaging of Amyloid Plaques in Alzheimer's Disease. *Acta Pharm. Sin. B* **2015,** *5* (1), 25–33.
95. Nesterov, E. E.; Skoch, J.; Hyman, B. T.; Klunk, W. E.; Bacskai, B. J.; Swager, T. M. In Vivo Optical Imaging of Amyloid Aggregates in Brain: Design of Fluorescent Markers. *Angew. Chem. Int. Ed. Engl.* **2005,** *44* (34), 5452–5456.
96. Meek, S. T.; Nesterov, E. E.; Swager, T. M. Near-Infrared Fluorophores Containing Benzo[C]Heterocycle Subunits. *Org. Lett.* **2008,** *10* (14), 2991–2993.
97. Raymond, S. B.; Skoch, J.; Hills, I. D.; Nesterov, E. E.; Swager, T. M.; Bacskai, B. J. Smart Optical Probes for Near-Infrared Fluorescence Imaging of Alzheimer's Disease Pathology. *Eur. J. Nucl. Med. Mol. Imaging* **2008,** *35* (Suppl. 1), S93–S98.
98. Hintersteiner, M.; Enz, A.; Frey, P.; Jaton, A. L.; Kinzy, W.; Kneuer, R.; Neumann, U.; Rudin, M.; Staufenbiel, M.; Stoeckli, M.; Wiederhold, K. H.; Gremlich, H. U. In Vivo Detection of Amyloid-Beta Deposits by Near-Infrared Imaging Using an Oxazine-Derivative Probe. *Nat. Biotechnol.* **2005,** *23* (5), 577–583.
99. Okamura, N.; Mori, M.; Furumoto, S.; Yoshikawa, T.; Harada, R.; Ito, S.; Fujikawa, Y.; Arai, H.; Yanai, K.; Kudo, Y. In Vivo Detection of Amyloid Plaques in the Mouse Brain Using the Near-Infrared Fluorescence Probe THK-265. *J. Alzheimers Dis.* **2011,** *23* (1), 37–48.
100. Schmidt, A.; Pahnke, J. Efficient Near-Infrared in vivo Imaging of Amyoid-Beta Deposits in Alzheimer's Disease Mouse Models. *J. Alzheimers Dis.* **2012,** *30* (3), 651–664.
101. Weissleder, R.; Nahrendorf, M. Advancing Biomedical Imaging. *Proc. Natl. Acad. Sci. U. S. A.* **2015,** *112* (47), 14424–14428.
102. Krucker, T.; Sandanaraj, B. S. Optical Imaging for the New Grammar of Drug Discovery. *Philos. Trans. A Math. Phys. Eng. Sci.* **2011,** *369* (1955), 4651–4665.
103. Ale, A.; Ermolayev, V.; Herzog, E.; Cohrs, C.; de Angelis, M. H.; Ntziachristos, V. FMT-XCT: in vivo Animal Studies With Hybrid Fluorescence Molecular Tomography-X-Ray Computed Tomography. *Nat. Methods* **2012,** *9* (6), 615–620.
104. McCann, C. M.; Waterman, P.; Figueiredo, J. L.; Aikawa, E.; Weissleder, R.; Chen, J. W. Combined Magnetic Resonance and Fluorescence Imaging of the Living Mouse Brain Reveals Glioma Response to Chemotherapy. *NeuroImage* **2009,** *45* (2), 360–369.
105. Ntziachristos, V. Going Deeper Than Microscopy: The Optical Imaging Frontier in Biology. *Nat. Methods* **2010,** *7* (8), 603–614.
106. Razansky, D.; Deliolanis, N. C.; Vinegoni, C.; Ntziachristos, V. Deep Tissue Optical and Optoacoustic Molecular Imaging Technologies for Pre-Clinical Research and Drug Discovery. *Curr. Pharm. Biotechnol.* **2012,** *13* (4), 504–522.
107. Taruttis, A.; Ntziachristos, V. Advances in Real-Time Multispectral Optoacoustic Imaging and Its Applications. *Nat. Photon.* **2015,** *9* (4), 219–227.
108. Burton, N. C.; Patel, M.; Morscher, S.; Driessen, W. H.; Claussen, J.; Beziere, N.; Jetzfellner, T.; Taruttis, A.; Razansky, D.; Bednar, B.; Ntziachristos, V. Multispectral Opto-Acoustic Tomography (MSOT) of the Brain and Glioblastoma Characterization. *NeuroImage* **2013,** *65,* 522–528.
109. Ran, C.; Xu, X.; Raymond, S. B.; Ferrara, B. J.; Neal, K.; Bacskai, B. J.; Medarova, Z.; Moore, A. Design, Synthesis, and Testing of Difluoroboron-Derivatized Curcumins as Near-Infrared Probes for in vivo Detection of Amyloid-Beta Deposits. *J. Am. Chem. Soc.* **2009,** *131* (42), 15257–15261.
110. Ono, M.; Saji, H. Recent Advances in Molecular Imaging Probes for [Small Beta]-Amyloid Plaques. *MedChemComm* **2015,** *6* (3), 391–402.
111. Cui, M. C.; Ono, M.; Watanabe, H.; Kimura, H.; Liu, B. L.; Saji, H. Smart Near-Infrared Fluorescence Probes With Donor-Acceptor Structure for in vivo Detection of Beta-Amyloid Deposits. *J. Am. Chem. Soc.* **2014,** *136* (9), 3388–3394.
112. Fu, H.; Cui, M.; Tu, P.; Pan, Z.; Liu, B. Evaluation of Molecules Based on the Electron Donor-Acceptor Architecture as Near-Infrared Beta-Amyloidal-Targeting Probes. *Chem. Commun.* **2014,** *50* (80), 11875–11878.
113. Fu, H. L.; Cui, M. C.; Zhao, L.; Tu, P. Y.; Zhou, K. X.; Dai, J. P.; Liu, B. L. Highly Sensitive Near-Infrared Fluorophores for in vivo Detection of Amyloid-Beta Plaques in Alzheimer's Disease. *J. Med. Chem.* **2015,** *58* (17), 6972–6983.
114. Zhou, K.; Fu, H.; Feng, L.; Cui, M.; Dai, J.; Liu, B. The Synthesis and Evaluation of Near-Infrared Probes With Barbituric Acid Acceptors for in vivo Detection of Amyloid Plaques. *Chem. Commun.* **2015,** *51* (58), 11665–11668.
115. Kim, D.; Moon, H.; Baik, S. H.; Singha, S.; Jun, Y. W.; Wang, T.; Kim, K. H.; Park, B. S.; Jung, J.; Mook-Jung, I.; Ahn, K. H. Two-Photon Absorbing Dyes With Minimal Autofluorescence in Tissue Imaging: Application to in vivo Imaging of Amyloid-Beta Plaques With a Negligible Background Signal. *J. Am. Chem. Soc.* **2015,** *137* (21), 6781–6789.

116. Cheng, Y.; Zhu, B.; Deng, Y.; Zhang, Z. In Vivo Detection of Cerebral Amyloid Fibrils With Smart Dicynomethylene-4H-pyran-Based Fluorescence Probe. *Anal. Chem.* **2015,** *87* (9), 4781–4787.
117. Garin, D.; Virgone-Carlotta, A.; Gozel, B.; Oukhatar, F.; Perret, P.; Marti-Battle, D.; Touret, M.; Millet, P.; Dubois-Dauphin, M.; Meyronet, D.; Streichenberger, N.; Laferla, F. M.; Demeunynck, M.; Chierici, S.; Sallanon, M. M.; Ghezzi, C. COB231 Targets Amyloid Plaques in Post-Mortem Human Brain Tissue and in an Alzheimer Mouse Model. *J. Neurochem.* **2015,** *132* (5), 609–618.
118. Teoh, C. L.; Su, D. D.; Sahu, S.; Yun, S. W.; Drummond, E.; Prelli, F.; Lim, S.; Cho, S.; Ham, S.; Wisniewski, T.; Chang, Y. T. Chemical Fluorescent Probe for Detection of A beta Oligomers. *J. Am. Chem. Soc.* **2015,** *137* (42), 13503–13509.
119. Chozinski, T. J.; Gagnon, L. A.; Vaughan, J. C. Twinkle, Twinkle Little Star: Photoswitchable Fluorophores for Super-Resolution Imaging. *FEBS Lett.* **2014,** *588* (19), 3603–3612.
120. Lv, G.; Cui, B.; Lan, H.; Wen, Y.; Sun, A.; Yi, T. Diarylethene Based Fluorescent Switchable Probes for the Detection of Amyloid-Beta Pathology in Alzheimer's Disease. *Chem. Commun.* **2015,** *51* (1), 125–128.
121. Chang, W. M.; Dakanali, M.; Capule, C. C.; Sigurdson, C. J.; Yang, J.; T'heodorakis, E. A. ANCA: A Family of Fluorescent Probes That Bind and Stain Amyloid Plaques in Human Tissue. *ACS Chem. Neurosci.* **2011,** *2* (5), 249–255.
122. Zhang, X.; Ran, C. Dual Functional Small Molecule Probes as Fluorophore and Ligand for Misfolding Proteins. *Curr. Org. Chem.* **2013,** *17* (6).
123. Harada, R.; Okamura, N.; Furumoto, S.; Yoshikawa, T.; Arai, H.; Yanai, K.; Kudo, Y. Use of a Benzimidazole Derivative BF-188 in Fluorescence Multispectral Imaging for Selective Visualization of Tau Protein Fibrils in the Alzheimer's Disease Brain. *Mol. Imaging Biol.* **2014,** *16* (1), 580–593.
124. Ojida, A.; Sakamoto, T.; Inoue, M. A.; Fujishima, S. H.; Lippens, G.; Hamachi, I. Fluorescent BODIPY-Based Zn(II) Complex as a Molecular Probe for Selective Detection of Neurofibrillary Tangles in the Brains of Alzheimer's Disease Patients. *J. Am. Chem. Soc.* **2009,** *131* (18), 6543–6548.
125. Frost, S.; Martins, R. N.; Kanagasingam, Y. Ocular Biomarkers for Early Detection of Alzheimer's Disease. *J. Alzheimers Dis.* **2010,** *22* (1), 1–16.
126. Koronyo, Y.; Salumbides, B. C.; Black, K. L.; Koronyo-Hamaoui, M. Alzheimer's Disease in the Retina: Imaging Retinal Abeta Plaques for Early Diagnosis and Therapy Assessment. *Neurodegener. Dis.* **2012,** *10* (1–4), 285–293.
127. Schon, C.; Hoffmann, N. A.; Ochs, S. M.; Burgold, S.; Filser, S.; Steinbach, S.; Seeliger, M. W.; Arzberger, T.; Goedert, M.; Kretzschmar, H. A.; Schmidt, B.; Herms, J. Long-Term in vivo Imaging of Fibrillar Tau in the Retina of P301S Transgenic Mice. *PLoS One* **2012,** *7* (12), e53547.
128. Ho, C. Y.; Troncoso, J. C.; Knox, D.; Stark, W.; Eberhart, C. G. Beta-Amyloid, Phospho-Tau and Alpha-Synuclein Deposits Similar to Those in the Brain Are Not Identified in the Eyes of Alzheimer's and Parkinson's Disease Patients. *Brain Pathol.* **2014,** *24* (1), 25–32.
129. Bolander, A.; Kieser, D.; Voss, C.; Bauer, S.; Schon, C.; Burgold, S.; Bittner, T.; Holzer, J.; Heyny-von Haussen, R.; Mall, G.; Goetschy, V.; Czech, C.; Knust, H.; Berger, R.; Herms, J.; Hilger, I.; Schmidt, B. Bis(arylvinyl)pyrazines, —pyrimidines, and -pyridazines as Imaging Agents for Tau Fibrils and Beta-Amyloid Plaques in Alzheimer's Disease Models. *J. Med. Chem.* **2012,** *55* (21), 9170–9180.
130. Gu, J.; Anumala, U. R.; Heyny-von Haußen, R.; Hölzer, J.; Goetschy-Meyer, V.; Mall, G.; Hilger, I.; Czech, C.; Schmidt, B. Design, Synthesis and Biological Evaluation of Trimethine Cyanine Dyes as Fluorescent Probes for the Detection of Tau Fibrils in Alzheimer's Disease Brain and Olfactory Epithelium. *ChemMedChem* **2013,** *8* (6), 891–897.
131. Yang, F.; Lim, G. P.; Begum, A. N.; Ubeda, O. J.; Simmons, M. R.; Ambegaokar, S. S.; Chen, P. P.; Kayed, R.; Glabe, C. G.; Frautschy, S. A.; Cole, G. M. Curcumin Inhibits Formation of Amyloid Beta Oligomers and Fibrils, Binds Plaques, and Reduces Amyloid In Vivo. *J. Biol. Chem.* **2005,** *280* (7), 5892–5901.
132. Ryu, E. K.; Choe, Y. S.; Lee, K.-H.; Choi, Y.; Kim, B.-T. Curcumin and Dehydrozingerone Derivatives: Synthesis, Radiolabeling, and Evaluation for β-Amyloid Plaque Imaging. *J. Med. Chem.* **2006,** *49* (20), 6111–6119.
133. Zhang, X.; Tian, Y.; Li, Z.; Tian, X.; Sun, H.; Liu, H.; Moore, A.; Ran, C. Design and Synthesis of Curcumin Analogues for in vivo Fluorescence Imaging and Inhibiting Copper-Induced Cross-Linking of Amyloid Beta Species in Alzheimer's Disease. *J. Am. Chem. Soc.* **2013,** *135* (44), 16397–16409.
134. Zhang, X.; Tian, Y.; Zhang, C.; Tian, X.; Ross, A. W.; Moir, R. D.; Sun, H.; Tanzi, R. E.; Moore, A.; Ran, C. Near-Infrared Fluorescence Molecular Imaging of Amyloid Beta Species and Monitoring Therapy in Animal Models of Alzheimer's Disease. *Proc. Natl. Acad. Sci. U.S.A.* **2015,** *112* (31), 9734–9739.
135. Bolognesi, M. L.; Gandini, A.; Prati, F.; Uliassi, E. From Companion Diagnostics to Theranostics: A New Avenue for Alzheimer's Disease? *J. Med. Chem.* **2016**. submitted.
136. THERANOSTICS an emerging tool in drug discovery and commercialisation. Fall 02. http://www.ddw-online.com/personalised-medicine/p148484-theranostics-an-emerging-tool-in-drug-discovery-and-commercialisation-fall-02.html (accessed 9 February 2016).
137. Kelkar, S. S.; Reineke, T. M. Theranostics: Combining Imaging and Therapy. *Bioconjug. Chem.* **2011,** *22* (10), 1879–1903.
138. Xie, J.; Lee, S.; Chen, X. Nanoparticle-Based Theranostic Agents. *Adv. Drug Deliv. Rev.* **2010,** *62* (11), 1064–1079.
139. Silberstein, E. B. Radioiodine: The Classic Theranostic Agent. *Semin. Nucl. Med.* **2012,** *42* (3), 164–170.
140. Nicolaides, N. C.; O'Shannessy, D. J.; Albone, E.; Grasso, L. Co-Development of Diagnostic Vectors to Support Targeted Therapies and Theranostics: Essential Tools in Personalized Cancer Therapy. *Front. Oncol.* **2014,** *4,* 141.
141. Kojima, R.; Aubel, D.; Fussenegger, M. Novel Theranostic Agents for Next-Generation Personalized Medicine: Small Molecules, Nanoparticles, and Engineered Mammalian Cells. *Curr. Opin. Chem. Biol.* **2015,** *28,* 29–38.
142. Prati, F.; Bolognesi, M. L. Chapter Thirteen—Tackling Neurodegeneration With Multi-Target and Theranostic Small Molecules. In 2015 *Medicinal Chemistry Reviews*; Manoj, C. D., Ed.; Vol. 50, American Chemical Society; Washington, DC, 2015; pp 347–356.
143. Morphy, R.; Rankovic, Z. Designing Multiple Ligands—Medicinal Chemistry Strategies and Challenges. *Curr. Pharm. Design* **2009,** *15* (6), 587–600.
144. Ishikawa, K.; Doh-ura, K.; Kudo, Y.; Nishida, N.; Murakami-Kubo, I.; Ando, Y.; Sawada, T.; Iwaki, T. Amyloid Imaging Probes Are Useful for Detection of Prion Plaques and Treatment of Transmissible Spongiform Encephalopathies. *J. Gen. Virol.* **2004,** *85* (Pt 6), 1785–1790.
145. Teruya, K.; Doh-ura, K. Amyloid-Binding Compounds and Their Anti-Prion Potency. *Curr. Top. Med. Chem.* **2013,** *13* (19), 2522–2532.
146. Elsinghorst, P. W.; Hartig, W.; Goldhammer, S.; Grosche, J.; Gutschow, M. A Gorge-Spanning, High-Affinity Cholinesterase Inhibitor to Explore Beta-Amyloid Plaques. *Org. Biomol. Chem.* **2009,** *7* (19), 3940–3946.
147. Inestrosa, N. C.; Alvarez, A.; Perez, C. A.; Moreno, R. D.; Vicente, M.; Linker, C.; Casanueva, O. I.; Soto, C.; Garrido, J. Acetylcholinesterase Accelerates Assembly of Amyloid-Beta-Peptides Into Alzheimer's Fibrils: Possible Role of the Peripheral Site of the Enzyme. *Neuron* **1996,** *16* (4), 881–891.
148. Hartig, W.; Kacza, J.; Paulke, B. R.; Grosche, J.; Bauer, U.; Hoffmann, A.; Elsinghorst, P. W.; Gutschow, M. In Vivo Labelling of Hippocampal Beta-Amyloid in Triple-Transgenic Mice With a Fluorescent Acetylcholinesterase Inhibitor Released From Nanoparticles. *Eur. J. Neurosci.* **2010,** *31* (1), 99–109.
149. Munoz-Torrero, D.; Camps, P. Dimeric and Hybrid Anti-Alzheimer Drug Candidates. *Curr. Med. Chem.* **2006,** *13* (4), 399–422.
150. Feng, X. J.; Wu, P. L.; Bolze, F.; Leung, H. W.; Li, K. F.; Mak, N. K.; Kwong, D. W.; Nicoud, J. F.; Cheah, K. W.; Wong, M. S. Cyanines as New Fluorescent Probes for DNA Detection and Two-Photon Excited Bioimaging. *Org. Lett.* **2010,** *12* (10), 2194–2197.
151. Yang, W.; Wong, Y.; Ng, O. T.; Bai, L. P.; Kwong, D. W.; Ke, Y.; Jiang, Z. H.; Li, H. W.; Yung, K. K.; Wong, M. S. Inhibition of Beta-Amyloid Peptide Aggregation by Multifunctional Carbazole-Based Fluorophores. *Angew. Chem. Int. Ed. Engl.* **2012,** *51* (8), 1804–1810.
152. Staderini, M.; Aulic, S.; Bartolini, M.; Tran, H. N.; Gonzalez-Ruiz, V.; Perez, D. I.; Cabezas, N.; Martinez, A.; Martin, M. A.; Andrisano, V.; Legname, G.; Menendez, J. C.; Bolognesi, M. L. A Fluorescent Styrylquinoline With Combined Therapeutic and Diagnostic Activities Against Alzheimer's and Prion Diseases. *ACS Med. Chem. Lett.* **2013,** *4* (2), 225–229.
153. Tian, Y. L.; Zhang, X. L.; Li, Y. Y.; Shoup, T. M.; Teng, X.; Elmaleh, D. R.; Moore, A.; Ran, C. Z. Crown Ethers Attenuate Aggregation of Amyloid Beta of Alzheimer's Disease. *Chem. Commun.* **2014,** *50* (99), 15792–15795.
154. Zhang, X. L.; Tian, Y. L.; Yuan, P.; Li, Y. Y.; Yaseen, M. A.; Grutzendler, J.; Moore, A.; Ran, C. Z. A Bifunctional Curcumin Analogue for Two-Photon Imaging and Inhibiting Crosslinking of Amyloid Beta in Alzheimer's Disease. *Chem. Commun.* **2014,** *50* (78), 11550–11553.

155. Yang, T.; Wang, X.; Zhang, C.; Ma, X.; Wang, K.; Wang, Y.; Luo, J.; Yang, L.; Yao, C.; Wang, X. Specific Self-Monitoring of Metal-Associated Amyloid-Beta Peptide Disaggregation by a Fluorescent Chelator. *Chem. Commun. (Camb.)* **2015,** *52,* 2245–2248.
156. White, A. R.; Faller, P.; Atwood, C. S.; Zatta, P. Metals and Alzheimer's Disease. *Int. J. Alzheimers Dis.* **2011,** *2011,* 659424.
157. Savelieff, M. G.; Lee, S.; Liu, Y.; Lim, M. H. Untangling Amyloid-Beta, Tau, and Metals in Alzheimer's Disease. *ACS Chem. Biol.* **2013,** *8* (5), 856–865.
158. Wilson, C. M.; Magnaudeix, A.; Naves, T.; Vincent, F.; Lalloue, F.; Jauberteau, M. O. The Ins and Outs of Nanoparticle Technology in Neurodegenerative Diseases and Cancer. *Curr. Drug Metab.* **2015,** *16* (8), 609–632.
159. Dilnawaz, F.; Sahoo, S. K. Therapeutic Approaches of Magnetic Nanoparticles for the Central Nervous System. *Drug Discov. Today* **2015,** *20* (10), 1256–1264.
160. Aulic, S.; Bolognesi, M. L.; Legname, G. Small-Molecule Theranostic Probes: A Promising Future in Neurodegenerative Diseases. *Int. J. Cell Biol.* **2013,** *2013,* 150952.
161. (a) Andrieux, K.; Couvreur, P. Nanomedicine as a Promising Approach for the Treatment and Diagnosis of Brain Diseases: The Example of Alzheimer's Disease. *Ann. Pharm. Fr.* **2013,** *71* (4), 225–233; (b) Amiri, H.; Saeidi, K.; Borhani, P.; Manafirad, A.; Ghavami, M.; Zerbi, V. Alzheimer's Disease: Pathophysiology and Applications of Magnetic Nanoparticles as MRI Theranostic Agents. *ACS Chem. Neurosci.* **2013,** *4* (11), 1417–1429; (c) Ruozi, B.; Belletti, D.; Pederzoli, F.; Veratti, P.; Forni, F.; Vandelli, M. A.; Tosi, G. Nanotechnology and Alzheimer's Disease: What Has Been Done And What To Do. *Curr. Med. Chem.* **2014,** *21* (36), 4169–4185.
162. Brambilla, D.; Le Droumaguet, B.; Nicolas, J.; Hashemi, S. H.; Wu, L. P.; Moghimi, S. M.; Couvreur, P.; Andrieux, K. Nanotechnologies for Alzheimer's Disease: Diagnosis, Therapy, and Safety Issues. *Nanomedicine* **2011,** *7* (5), 521–540.
163. Busquets, M. A.; Sabate, R.; Estelrich, J. Potential Applications of Magnetic Particles to Detect and Treat Alzheimer's Disease. *Nanoscale Res. Lett.* **2014,** *9* (1), 538.
164. Kouyoumdjian, H.; Zhu, D. C.; El-Dakdouki, M. H.; Lorenz, K.; Chen, J.; Li, W.; Huang, X. Glyconanoparticle Aided Detection of Beta-Amyloid by Magnetic Resonance Imaging and Attenuation of Beta-Amyloid Induced Cytotoxicity. *ACS Chem. Neurosci.* **2013,** *4* (4), 575–584.
165. Skaat, H.; Corem-Slakmon, E.; Grinberg, I.; Last, D.; Goez, D.; Mardor, Y.; Margel, S. Antibody-Conjugated, Dual-Modal, Near-Infrared Fluorescent Iron Oxide Nanoparticles for Antiamyloidgenic Activity and Specific Detection of Amyloid-Beta Fibrils. *Int. J. Nanomedicine* **2013,** *8,* 4063–4076.

1.05 Nutraceuticals

A Rajasekaran, KMCH College of Pharmacy, Coimbatore, India

© 2017 Elsevier Ltd. All rights reserved.

1.05.1	**Introduction**	108
1.05.2	**Rational for the Use of Nutraceuticals**	109
1.05.3	**Different Terminologies**	109
1.05.3.1	Nutraceuticals	109
1.05.3.2	Functional Foods	109
1.05.3.3	Dietary Supplement	109
1.05.3.4	Medical Foods	109
1.05.3.5	Designer Foods	110
1.05.3.6	Phytochemicals	110
1.05.4	**Classification of Nutraceuticals**	110
1.05.4.1	Classification by Natural Food Source	110
1.05.4.2	Classification by Chemical Nature	110
1.05.4.3	Classification by Pharmacological Action	110
1.05.5	**Vitamins as Nutraceuticals**	110
1.05.5.1	Water Insoluble Vitamins	110
1.05.5.2	Water Soluble Vitamins	111
1.05.6	**Minerals as Nutraceuticals**	114
1.05.6.1	Essential Macrominerals	114
1.05.6.1.1	Calcium	114
1.05.6.1.2	Magnesium	116
1.05.6.1.3	Phosphorus	116
1.05.6.1.4	Potassium	116
1.05.6.1.5	Sodium	116
1.05.6.1.6	Sulfur	117
1.05.6.2	Essential Trace Minerals/Microminerals	117
1.05.6.2.1	Chromium	117
1.05.6.2.2	Cobalt	117
1.05.6.2.3	Copper	117
1.05.6.2.4	Fluoride	117
1.05.6.2.5	Iodine	117
1.05.6.2.6	Iron	117
1.05.6.2.7	Manganese	117
1.05.6.2.8	Molybdenum	117
1.05.6.2.9	Selenium	117
1.05.6.2.10	Zinc	118
1.05.7	**Phytochemicals as Nutraceuticals**	118
1.05.7.1	Carotenoids	118
1.05.7.2	Phenolics	119
1.05.7.3	Organosulfur Compounds	121
1.05.8	**Plants as Nutraceuticals**	121
1.05.9	**Microbes as Nutraceuticals**	123
1.05.9.1	Probiotics	123
1.05.9.2	Prebiotics	123
1.05.10	**Health Benefits of Nutraceuticals**	124
1.05.10.1	Nutraceuticals in CVDs	125
1.05.10.1.1	Polyunsaturated fatty acids	125
1.05.10.1.2	Dietary fibers	126
1.05.10.1.3	Flavonoids	126
1.05.10.1.4	Plant sterols	126
1.05.10.1.5	Policosanol	126
1.05.10.1.6	Vegetables in prevention of CVDs	126
1.05.10.1.7	Coenzyme Q10	127
1.05.10.1.8	Potassium	127
1.05.10.1.9	Fermented red yeast rice	127

1.05.10.2	Nutraceuticals in Cancer Prevention	127
1.05.10.2.1	Minerals in cancer management	129
1.05.10.2.2	Vitamins in cancer management	129
1.05.10.3	Nutraceuticals in Diabetes	129
1.05.10.4	Nutraceuticals in Obesity	129
1.05.10.5	Nutraceuticals in Chronic Inflammatory Disorders	130
1.05.10.5.1	Glucosamine	130
1.05.10.5.2	Chondroitin	130
1.05.10.5.3	Methylsulfonylmethane	130
1.05.10.5.4	*S*-Adenosyl methionine	131
1.05.10.5.5	Pomegranate	131
1.05.10.6	Nutraceuticals for Parkinson's Disease	131
1.05.10.7	Nutraceuticals for Alzheimer's Disease	131
1.05.11	**Conclusion**	132
References		132

Abbreviations

AA Arachidonic acid
ALA Alpha linolenic acid
ATP Adenosine triphosphate
COX Cyclooxygenase
CVD Cardiovascular diseases
DHA Docosahexaenoic acid
DMSO Dimethyl sulfoxide
DNA Deoxyribonucleic acid
EFA Essential fatty acids
EPA Eicosapentanoicacid
GLA Gamma linolenic acid
GSK Glycogensynthasekinase
HDL High density lipoprotein
HMEC Human mammary epithelial cells
HMG CoA Hydroxy-methyl-glutaryl-coenzyme A
IU International units
LDL Low density lipoprotein
MCF-7 Michigan cancer foundation-7
NF-kB Nuclear factor kappa-light-chain-enhancer of activated B cells
PUFA Poly unsaturated fatty acids
RA Rheumatoid arthritis
TGS Triglycerides

1.05.1 Introduction

Nutraceuticals, including functional food, received considerable interest because of their presumed safety and potential nutritional and therapeutic effects in the form of food. It was presumed before 1990 that nutraceuticals are natural foods that provide energy for daily requirement in the body. Later it was realized that nutraceuticals may have beneficial effects on different nutritional disorders.[1] Nutrients are substances that have health-promoting as well as health-protective activity and they can be classified into two types, namely, macronutrients and micronutrients. Macronutrients include protein, carbohydrate, lipid or fat, and crude fiber. Micronutrients include different minerals, vitamins, antioxidants, etc.

According to a survey, diet was rated and considered to be more highly preferred by consumers than exercise or hereditary factors for achieving good health.[2] Further, numerous epidemiological studies suggest that the risks for many chronic diseases are diet related, and hence appropriate use of nutraceuticals can significantly decrease the diet-related chronic diseases, such as heart disease, cancer, stroke, and diabetes. Thus, pharmaceutical and nutritional companies have shown keen interest in bringing these products into the market because they possess potential nutritional value and multiple therapeutic properties. Some popular nutraceuticals include carotenoids, curcumin, gingerol, glucosamine, ginseng, lycopene, folic acid, cod liver oil, omega-3 eggs, calcium-enriched orange juice, green tea, etc. Majority of the nutraceuticals are claimed to possess multiple therapeutic benefits, though substantial evidence about their unwanted effects is lacking for the nutraceuticals.

Hippocrates (460–370 BC) correctly emphasized, "Let food be your medicine and medicine be your food." Currently there is an increased global interest due to the recognition that "nutraceuticals" play a major role in health enhancement. The term "nutraceutical" was coined by combining the terms "nutrition" and "pharmaceutical" in 1989 by Dr. Stephen De Felice, Chairman of the Foundation for Innovation in Medicine.[3] "Nutraceutical" is a marketing term developed for nutritional supplement that is sold with the intent to treat or prevent disease and thus has no regulatory definition.[4] Such products may include isolated nutrients, dietary supplements, and diets to genetically engineered "designer" foods, functional foods, herbal products, and processed foods such as cereals, soups, and beverages.

1.05.2 Rational for the Use of Nutraceuticals

- Regular consumption of synthetic drugs for the treatment of various diseases may cause serious side effects/organ failure whereas the nutraceuticals from natural source is safe.
- Daily intake of food consumed by many people does not have enough fiber, carbohydrate, protein, and the right amounts of vitamins and minerals to maintain good health. Rapidly increasing chronic diseases like cardiovascular diseases (CVDs), cancer, diabetes, and obesity leading to death is mainly due to suboptimal diet quality. Reports suggest that mortality is increasing every year mainly due to insufficient intake of fruits, nuts/seeds, whole grains, vegetables, seafoods, as well as minerals. Thus, nutraceuticals are considered as sources of health promotion.[5]
- Disease treatment by allopathic/modern medicine is highly expensive.
- Drugs derived from plants can be used for treatment or prevention of disease, whereas the food derived from plants enact as nutraceutical by preventing the disease and by eliciting health benefits.

1.05.3 Different Terminologies

There are different terminologies and definitions used by different countries with respect to nutraceuticals as "functional foods," "dietary supplements," "designer foods," "medical foods," "pharmafoods," and "phytochemicals," and there is a thin line of difference between these terminologies in their interchangeable usage by different people on different occasions.

1.05.3.1 Nutraceuticals

Nutrition is the science of how living organisms obtain and use food required for growth and health. De Felice defined "nutraceutical" as a food or part of a food that provides medical or health benefits, encompassing prevention and treatment of diseases.[6] "Pharmaceuticals" may be considered as drugs used mainly to treat diseases, while "nutraceuticals" are those that are intended to prevent diseases. The distinction between pharmaceuticals and nutraceuticals is cute, but superficial and erroneous. Pharmaceuticals are substances that may have patent protection as a result of extensive testing to conform to the specifications of respective governments. Both pharmaceuticals and nutrients can cure and prevent disease(s) but only pharmaceuticals have governmental sanction. Examples of nutraceuticals include fortified dairy products (milk as such is a nutrient and its product casein is a pharmaceutical), citrus fruits (orange juice is nutrient and its constituent ascorbic acid is a pharmaceutical), lutein-containing multivitamin tablets, fish oil capsules, herb extracts, glucosamine, and chondroitin sulfate pills.

1.05.3.2 Functional Foods

Nutraceuticals, sometimes referred to as "functional foods," have caused heated debate because they blur the traditional dividing line between food and medicine. When food is being cooked or prepared using "scientific intelligence" with or without the knowledge of how or why it is being used, then the food is called as "functional food." Thus, functional food provides the body with the required amount of vitamins, fats, proteins, and carbohydrates necessary for healthy survival. When functional food aids in the prevention and/or treatment of disease(s)/disorder(s) other than deficiency conditions like anemia, it is called a "nutraceutical." Tomato fruit packed with a specific type of compound that helps to remove toxic compounds from our body and prevent damage to vital organs like the heart, kidney, lungs, and brain is a typical example of functional food. Other examples of functional foods include soybean, fish, oat meal, cereal bran (wheat, rice), and tea (green and black). Government of Canada for national public health defines functional foods as, "food that is similar in appearance to, or may be, a conventional food that is consumed as part of a usual diet, and is demonstrated to have physiological benefits and/or reduce the risk of chronic disease beyond basic nutritional functions, i.e. they may contain bioactive compounds." The Institute of Medicine's Food and Nutrition Board defined functional foods as, "any food or food ingredient that may provide a health benefit beyond the traditional nutrients it contains."

Functional foods included a wide variety of foods and food components believed to improve overall health and well-being, reduce the risk of specific diseases, or minimize the effects of other health concerns.

1.05.3.3 Dietary Supplement

The US dietary supplement health and education act (DSHEA) of 1994 defines "dietary supplement" as a product (other than tobacco) that is intended to supplement the diet that bears or contains one or more ingredients, like vitamin, mineral, a herb, an amino acid, or a concentrate, metabolite, constituent, extract, or combinations of these.

1.05.3.4 Medical Foods

"Medical foods" are a specific category of therapeutic agents that are intended for the nutritional management of a specific disease. An example of medical foods is formulations intended to manage patients with inborn errors in amino acid metabolism. Newer medical foods are designed to manage hyperhomocysteinemia, pancreatic exocrine insufficiency, inflammatory conditions, cancer, and other diseases.

1.05.3.5 Designer Foods

"Designer food" refers to the food that is designed to have some health benefits other than its traditional nutritional value. "Fortified food is the synonym for designer food," which refers to the food fortified or enriched with nutrient content already present in it or other complementary nutrient. The term was introduced in Japan in 1980s for referring to processed food containing nutrients of some additional health benefits apart from its own nutritional value,[7] whereas in China, designer food (referred to as health foods) is their traditional medicine. The addition of docosahexaenoic acid (DHA) to health drinks for improving brain and visual development and the use of probiotics and nucleotides to enhance immune response and sports nutrition are important examples of designer food.

1.05.3.6 Phytochemicals

Phytochemicals have been used for more than 5000 years in China, Greece, and India for the treatment and prevention of various diseases. Phytochemicals (also called phytonutrients) are the constituents present in plants that may help in reducing the risk of developing certain diseases. For example, consuming tomatoes and garlic that contains phytochemicals lycopene and allicin may reduce the risk of cancer. Consuming grapes that contain resveratrol may reduce the risk of CVDs.

1.05.4 Classification of Nutraceuticals

Nutraceuticals can be classified on the basis of their food sources, chemical nature, and based on the pharmacological action.

Based on natural food source
Based on chemical nature
Based on pharmacological action

1.05.4.1 Classification by Natural Food Source

On the basis of natural food source it is classified as the products obtained from plants, animals, minerals, or microbial sources (Table 1).

1.05.4.2 Classification by Chemical Nature

Based on chemical constitution nutraceuticals can be classified (Fig. 1) into six types, namely, isoprenoid derivatives, phenolic substances, amino acid-based substances, carbohydrates and derivatives, fatty acids and structural lipids, and minerals.

1.05.4.3 Classification by Pharmacological Action

Nutraceuticals can be grouped based on their pharmacological benefits as detailed in Table 2.

Nutraceuticals can also be categorized as traditional nutraceuticals and nontraditional nutraceuticals. Traditional nutraceuticals are natural foods that contain several natural components that deliver benefits beyond basic nutrition, such as lycopene in tomatoes, omega-3 fatty acids in salmon, resveratrol in grapes, or saponins in soy beans. Nontraditional nutraceuticals are artificial foods prepared by adding bioactive components for well-being of humans. It can be subdivided into fortified and recombinant nutraceuticals. Fortified nutraceuticals are the food with agricultural breeding or with added nutrients. Orange juice with calcium, cereals with added vitamins or minerals, flour with added folic acid, and milk with cholecalciferol are some of the examples of fortified nutraceuticals. Energy-providing foods such as bread, alcohol, fermented starch, yogurt, cheese, vinegar, and others that are produced with the help of biotechnology are called recombinant nutraceuticals.

1.05.5 Vitamins as Nutraceuticals

Vitamins are the complex substances of organic origin, which in small quantities are necessary for the maintenance of human and animal life. Fat soluble vitamins A, D, E, and K (Fig. 2) can be stored in the body, whereas the water soluble vitamins (Fig. 3) cannot be stored in the body because they are eliminated through the body fluids like urine and transpiration. Important health benefits of water soluble and water insoluble vitamins are detailed further.

1.05.5.1 Water Insoluble Vitamins

Vitamin A (**1**) exists in several forms, namely, in alcohol form as retinol; in aldehyde form as retinal; in acid form as retinoic acid, where all these forms are known as retinoids. Vitamin A, which is rich in carrots and green vegetables, is essential for growth and

Table 1 Natural food source of nutraceuticals

	Nutraceuticals	*Source*
Plants	Antioxidant vitamins (vitamin C, vitamin E)	Citrus fruits, wheat germ oil, cotton seed oil, peanut oil
	Curcumin	Turmeric
	Dietary fibers	Fruits, barley, oats, lignin, cellulose, pectin
	Lycopene	Tomatoes
	Flavonoids	Grapes
	Isoflavonoids	Soybeans
	Polyunsaturated fatty acids	Flaxseed (*L. usitatissimum*), walnuts, canola oil, soybeans
Animals	Carnitine	Heart, skeletal muscles
	Glucosamine	Bovine
	Methylsulfonylmethane	Meat, milk
Minerals	Calcium	Leafy greens, milk, yogurt, cheese, creams, okra
	Chromium	*Aloe vera*, barley, black pepper, brewer's yeast, broccoli, eggs, mushrooms, green beans, legumes, oats, onions, potatoes, rye, green chili spices, spirulina, tomatoes, whole grains
	Cobalt	Green leafy vegetables, broccoli, nuts, fish, organ meats, oysters, spinach, whole grains
	Copper	Almonds, apples, apricots, beetroot, berries, buckwheat, caraway seeds, cashew nuts, cherries, dates, dried beans, drumstick leaves, egg yolk, fennel, berries, grapes, guava, kiwi fruit, lamb, legumes, lemons, mango, millet, mushrooms, nuts, oats, pears, peas, plums, potatoes, pumpkin, radish, raisins, shellfish, spinach, spirulina, spring onions, strawberries, tea, walnuts, whole grains, yams
	Iron	Meat, fish, poultry
	Iodine	Beetroot, citrus fruits, egg yolk, fish liver oils, garlic, halibut, pears, pineapples, prawns, sea salt, shellfish, spirulina, strawberries, turnip greens, yogurt
	Magnesium	Dark leafy greens, nuts, seeds, fish, beans, whole grains, yogurt, banana, dry fruits
	Manganese	Legumes, cereals, green leafy vegetables, tea
	Phosphorous	Milk, meat, nuts, fish, beans, whole grains
	Potassium	Avocado, potato, sweet potato, tomato, mushroom
	Zinc	Apples, beef, caraway, cherries, chicory, cucumber, drumstick leaves, egg yolk, fennel, flaxseed, garlic, green tea, legumes, melon, milk, mulberries, mushrooms, oats, oysters, peanuts, peas, pine nuts, pork, poultry, prawns, shellfish, spirulina, sweet potato, tapioca, watermelon seeds, whole grains
Microbes	Probiotics	*Lactobacilli*, *Streptococci*, *Bifidobacteria*
	Prebiotics	Oligofructose, inulin, galactooligosaccharide, lactulose

development, maintenance of healthy vision, skin, and mucous membranes. Being an antioxidant it may aid in the prevention and treatment of certain cancers[8] and in the treatment of certain skin disorders.[9]

There are two major forms of vitamin D, namely, vitamin D_2 (**2**), found in plants and better known as ergocalciferol or calciferol, and vitamin D_3 (**3**), found in animal tissues and often referred to as cholecalciferol. Vitamin D is essential for formation of bones and teeth, and helps the body in absorption of calcium. It is essential for the prevention of autoimmune diseases, heart diseases, diabetes, hypertension, and cancer.[10,11] The recommended daily intake of vitamin D is 200 IU for children and adults up to 50 years old, 400 IU for people of 51–70 years old, and 600 IU for people over 70 years old.

Vitamin E (**4**) helps to form blood cells, muscles, nerve tissue, boosts the immune system, and protects oxidation of polyunsaturated fatty acids (PUFAs). It is involved in the maintenance of membrane stability and immune function, inhibition of cancer cell growth and differentiation, free radical scavenging, inhibition of deoxyribonucleic acid (DNA), ribonucleic acid, and protein synthesis in cancer cells.

Vitamin K (**5**) is essential for blood clotting and plays a major role in the prevention of osteoporosis,[12] vascular calcification, and CVD.

1.05.5.2 Water Soluble Vitamins

Daily intake of B-complex vitamins is recommended to combat high level of homocysteine, a known risk factor for heart diseases. B-complex vitamins are generally recommended to those who use caffeine, alcohol, excessive sugar, or oral birth pills in their diet, since they are water soluble and easily excreted from the body.

Vitamin B_1, or thiamine, (**6**) plays an important role in the treatment of Alzheimer's disease, congestive heart failure, and cancer.

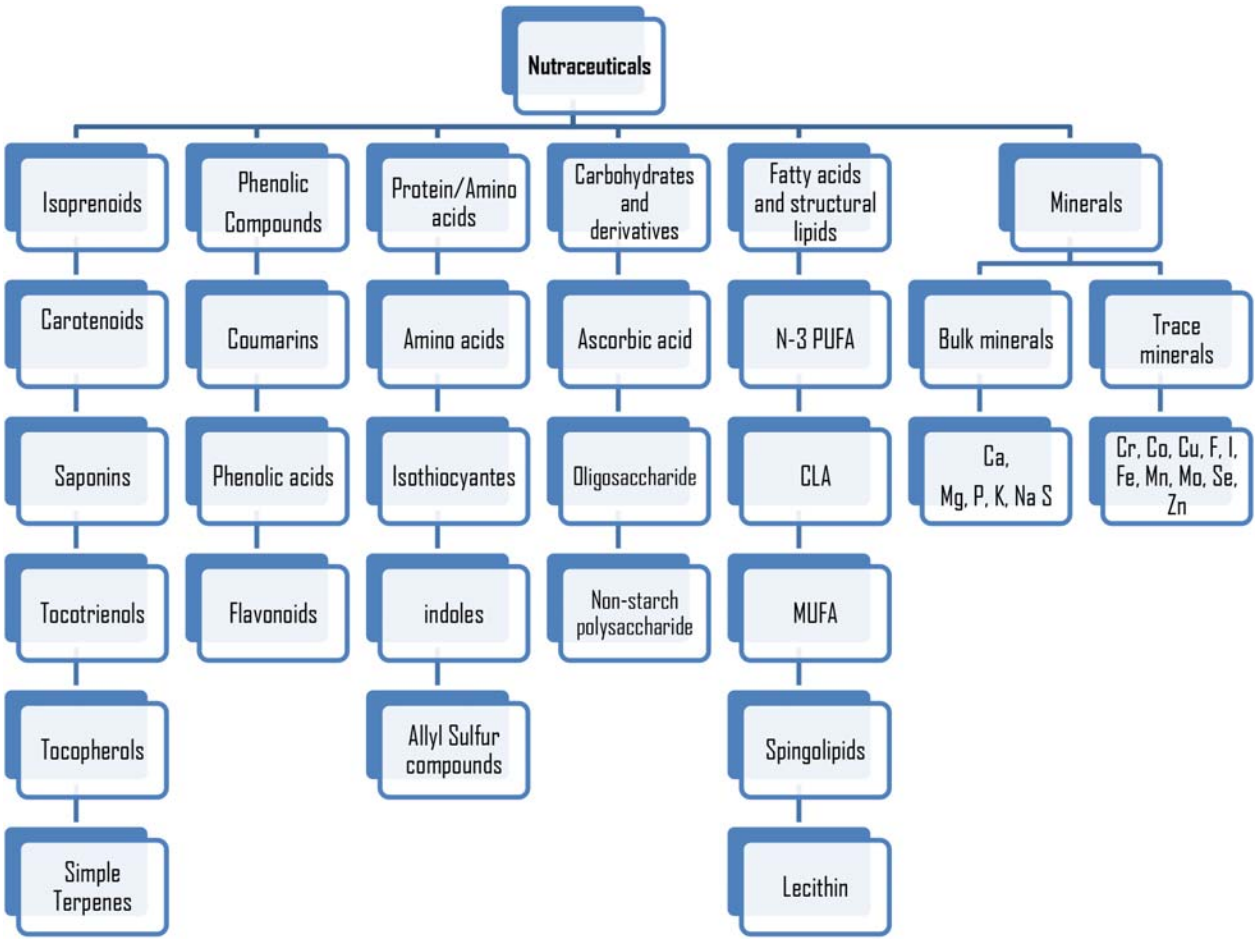

Fig. 1 Classification of nutraceuticals based on chemical nature.

Table 2 Pharmacological action of various nutraceuticals

Pharmacological action	*Nutraceuticals*
Anti-Alzheimer	β-Carotene, curcumin, lutein, lycopene
Antiarthritic	Glucosamine, chondroitin methylsulfonylmethane
Anticancer	Curcumin, selenium present in fruits and vegetables
Antidiabetic	Ethyl esters of omega-3 fatty acids (docosahexaenoic lipoic acid), dietary fibers
Antioxidant	Ascorbic acid, lycopene, tocopherol
Anti-Parkinson's	Ascorbic acid, creatine
Eye health	Lutein, zeaxanthin
Lipid-lowering agent	Polyunsaturated fatty acids
Inhibition of LDL oxidation	Niacin, green tea, resveratrol, garlic, policosanol, sesame
Reduction of total and LDL cholesterol	Plant sterols, flaxseed, garlic, dietary fiber, soy protein
HMG-CoA reductase inhibition	Red yeast rice, green tea, garlic, omega-3-fatty acids, plant sterols
Reduction of triglycerides	Niacin, red yeast rice, orange juice, flaxseed, resveratrol
Increase in total HDL	Niacin, pomegranate, curcumin
Prevention of cardiovascular diseases	Omega-3 poly unsaturated fatty acids, vitamins, minerals, polyphenols, dietary fibers, flavonoids present in onion, vegetables, grapes, red wine, apples, and cherries
Weight loss	Ephedrine, caffeine, ma huang-guarana, chitosan, green tea, 5-hydroxytryptophan, glucomannan, fenugreek, conjugated linoleic acid, capsaicin, *M. charantia*

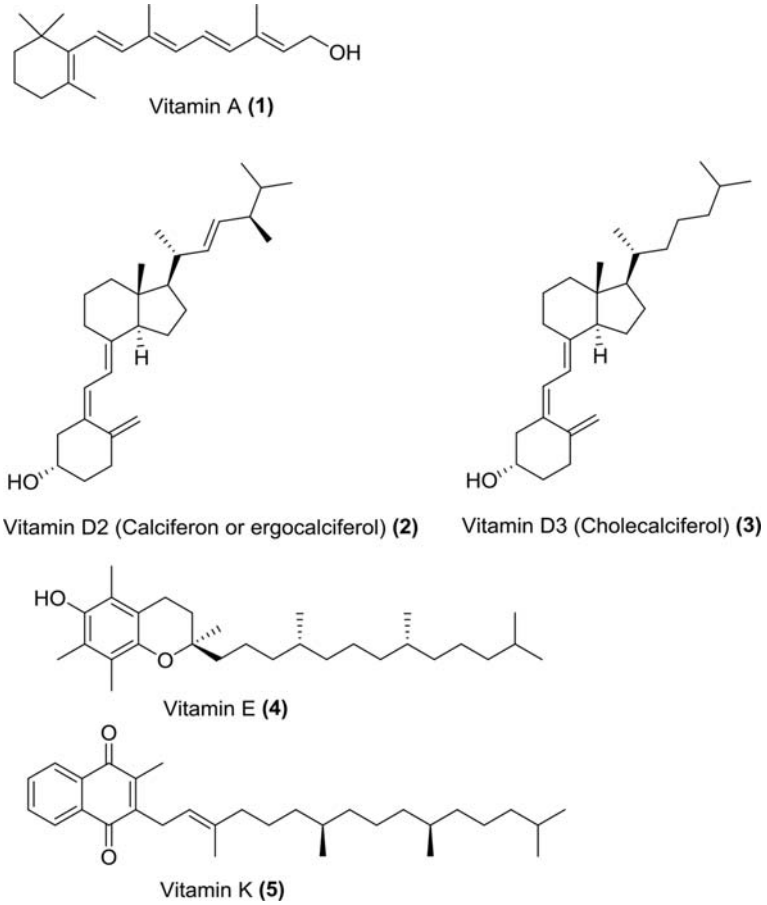

Fig. 2 Chemical structures of water insoluble vitamins.

Riboflavin-5-phosphate is a cofactor for vitamin B_2 (**7**), which is beneficial for people who lack the enzyme to convert vitamin B_2 because of nutritional factors or disease condition. Riboflavin helps in preventing cataracts[13] and is used as a prophylaxis in migraine headaches.

Niacinamide deficiency may cause neurological and skin problems. The major dietary sources of niacin are peanuts, ragi, pulses, soyabean, etc. Niacin(**8**) (vitamin B_3) is chemoprotective[14] and prevents insulin-dependent diabetes mellitus[15] and helps to prevent high cholesterol and CVDs.[16]

Pantothenic acid (vitamin B_5) (**9**) plays an important role in the degradation of fatty acids, and production of sterols and steroid hormones. Dextrorotatory isomer D-pantothenic acid (yellow) is found to possess biological activity and since it is highly unstable in acid, alkali, and in high temperature, it is given in the stable form of calcium pantothenate (white). It is present in peanut butter, almonds, cheese, and lobster. Supplementation of pantothenic acid helps in healing wounds and lowering cholesterol/triglycerides levels.[17]

Vitamin B_6 (pyridoxine) (**10**) is crucial for glucose production, hormone modulation, and neurotransmitter synthesis. Pyrodoxal 5-phosphate is considered as an active form of vitamin B_6, which helps in preventing CVD (by lowering the levels of homocysteine), improving immune and cognitive functions, and reducing the formation of kidney stones.

Biotin (vitamin H or B_7) (**11**) plays an important role in the prevention of diabetes, high cholesterol, and hair loss.[18]

Vitamin B_9 is also called folic acid (**12**), and is important in the prevention of heart diseases (regulates homocysteine levels),[19] colorectal and breast cancer,[20,21] Alzheimer's disease, and cognitive impairment.[22]

Vitamin B_{12} helps in the prevention of CVD,[23] cancer,[24] Alzheimer's disease, and dementia.[25]

Vitamin C (**13**) is required for the growth and repair of tissues in all parts of our body. Vitamin C is essential for the healing of wound and for the repair and maintenance of cartilage, bones, and teeth. Vitamin C deficiency can lead to dry and splitting hair, gingivitis, rough, dry, scaly skin, decrease in wound-healing rate, scurvy, easy bruising, nose bleeds, swollen and painful joints, anemia, etc. Vitamin C combats cancer by promoting collagen synthesis and thus prevents tumors from invading other tissues. Vitamin C, a natural antioxidant, prevents the oxidative DNA damage and also inactivates nuclear factor kappa-light-chain-enhancer of activated B cells (NF-kB) in endothelial cells during the inflammation process and hence can inhibit tumor promotion.[26] As body does not manufacture vitamin C, it is important to include plenty of vitamin C-containing foods in daily diet.

Health benefits, source, and deficiency diseases of all water soluble and water insoluble vitamins are provided in **Table 3**.

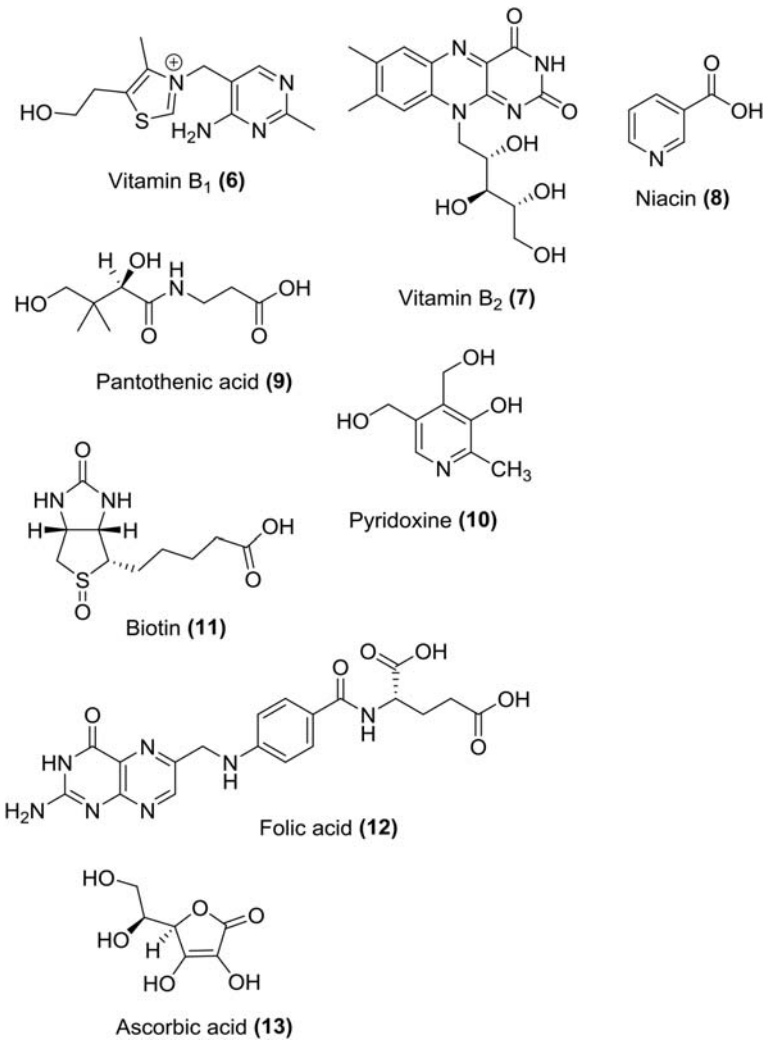

Fig. 3 Chemical structures of water soluble vitamins.

1.05.6 Minerals as Nutraceuticals

Dietary minerals are inorganic elements essential for life, present in the soil and water, which are absorbed by plants. Human body requires some minerals that are essential for normal functioning called as essential minerals, which can be divided into macrominerals (major minerals) and microminerals (trace minerals). The essential six bulk or macrominerals required in relatively large amounts include calcium, magnesium, phosphorus, potassium, sodium, sulfur, and the minerals needed only in very small amounts include chromium, cobalt, copper, fluoride, iodine, iron, manganese, molybdenum, selenium, and zinc.[27] These minerals are essential because they are critical for the production of vitamins, enzymes, and hormones in the body, as well as for the proper blood circulation, fluid regulation, nerve transmission, muscle contraction, cellular integrity, and energy production. These minerals work synergistically with each other and with other nutrients, and minimize the cause of a disease.

1.05.6.1 Essential Macrominerals

1.05.6.1.1 Calcium

The human body needs calcium more than any other mineral, as 99% of the quantity in the body is used for building strong bones and teeth and the remaining 1% is used by the blood, muscles, and nerves. Calcium also plays a role in many other vital physiological activities, including blood clotting, nerve conduction, muscle contraction, regulation of enzyme activity, cell membrane function, and blood pressure regulation. It is present in fruits like blackberries, blackcurrants, dates, grapefruit, mulberries, orange, pomegranate, leafy greens, milk, yogurt, cheese, and okra.

Table 3 Health benefits of vitamins

Vitamins	Source		Deficiency disease	Health benefits
	Plants	Others		
Vitamin A	*Amaranthus* sp. *Brassica oleraceae* *Cucurbita pepo* *Daucus carota* *Pisum sativum* *Spinacia oleracea*	Fish liver oil, milk, cheese, butter	Night blindness, xerophthalmia, keratomalacia	Essential for growth, prevention and treatment of certain cancer, improvement in vision
Vitamin D (calciferol) (also called sunshine vitamin)	*Beta vulgaris* *Cucurbita moschata*, *C. pepo* *Pastinaca sativa* *Solanum tuberosum* *Spirulina maxima*	Fish liver oil, wheat germ oil, egg yolk, milk, butter, mushrooms	Rickets in children osteomalacia in adults	Essential for formation of bones and teeth, helps body to absorb and use calcium, prevents colon cancer
Vitamin E (tocopherol)	*B. vulgaris C. moschata*, *C. pepo* *P. sativa S. tuberosum* *Spirulina maxima*	Wheat germ oil, cotton seed oil, peanut oil, soy bean oil	Sterility, degenerative changes in muscle, aging of skin	Antioxidant, helps to form blood cells, muscles, lung, and nerve tissue, improves immune system
Vitamin K	*Asparagus officinalis* *B. oleraceae* *Cucumis sativus* *D. carota* *P. sativum* *S. oleracea*	Meats, cheese, eggs	Hemorrhagic condition	Essential for clotting of blood, regulates calcium level, and activates proteins involved in bone health
Vitamin B_1 (thiamine)	*Ipomoea batatas* *P. sativum* *P. sativa S. tuberosum*	Cereals, pulses, nuts, yeast	Beriberi, corneal opacity	Essential for functioning of heart, muscles, and nervous system
Vitamin B_2 (riboflavin)	*Amaranthus* sp. *C. pepo* *P. sativum*	Whole grains, milk, eggs	Photophobia, dry itchy eyes, depression, memory loss, fatigue	Essential for growth and reproduction
Vitamin B_3 (niacin)	*C. pepo* *P. sativum* *Glycine max*	Liver, meat, yeast	Chick dermatitis	Helps in functioning of digestive system
Vitamin B_5 (pantothenic acid)	*B. oleraceae*, *Phaseolus vulgaris* *P. sativum* *G. max*	Milk, yeast eggs, whole fish, chicken, grain cereals	Fatigue, insomnia, depression, vomiting, stomach pain	Helps in lowering cholesterol level
Vitamin B_6 (pyridoxine)	*Amaranthus* sp. *B. oleraceae*, *Capsicum annum* *P. sativum* *S. tuberosum*	Rice polishing, yeast, egg, milk	Pellagra, depression, mental confusion, anemia, nausea, glossitis	Plays role in creation of antibodies in immune system, maintains normal nerve function
Vitamin B_7 (Vitamin H or biotin)	*Allium cepa* *B. oleraceae*, *C. sativus* *D. carota* *Juglans regia* *Prunus dulcis*	Egg yolk, peanuts, yeast bread, whole-wheat cheese, cheddar pork, salmon	Anemia, anorexia dermatitis, conjunctivitis	Helps body to metabolize proteins and process glucose

(Continued)

Table 3 Health benefits of vitamins—cont'd

Vitamins	Source		Deficiency disease	Health benefits
	Plants	*Others*		
Vitamin B_9 (folic acid)	*Brassica rapa* *B. oleraceae*, *Phaseolus lunatus* *P. vulgaris*	Chicken giblets, kidney, egg yolk, wheat flour, whole grain breads	Macrocylic anemia	Helps in producing RBC, protects against heart disease by lowering homocysteine, maintains normal brain function
Vitamin C (ascorbic acid)	*Amaranthus* sp. *C. annum* *B. oleraceae*, *P. sativum* Citrus fruits, berries	Milk, egg	Scurvy	Powerful antioxidant plays important role in preventing the body from oxidative damage

1.05.6.1.2 Magnesium

Magnesium is present abundantly in the intracellular fluid of our body and it functions as an important cofactor for more than 300 enzymes in the body. It is important for all energy-dependent transport systems like glycolysis, oxidative energy metabolism, and biosynthetic reactions. It maintains normal muscle and nerve function, keeps heart rhythm steady, lowers hypertension, and reduces the incidence of heart disease. Green leafy vegetables mainly spinach, nuts, avocados, whole grains, legumes, soy beans, and chocolate contain magnesium. Maximum recommended daily intake from supplements is 420 mg day^{-1} for men and 320 mg day^{-1} for women.

1.05.6.1.3 Phosphorus

Phosphorus combined with calcium is necessary to create the calcium–phosphorus balance necessary for the growth of bones and teeth and for the formation of nerve cells. This mineral is also essential for the assimilation of carbohydrates and fats. Being an important component of nucleic acids, it plays vital role in building cellular structure of every cell in the body. In addition, the metabolism of lipids relies on phosphorus and it is an essential component of lipid-containing structures such as cell membranes and nervous system structures. In addition to its role in forming the mineral matrix of bone, phosphorus is an essential component of numerous other life-critical compounds including adenosine triphosphate (ATP).

1.05.6.1.4 Potassium

Potassium is essential to the life of every cell of a living being and is the most widely distributed in all tissues. It plays an important role as a catalyst in energy metabolism and in the synthesis of glycogen and protein. Potassium is most concentrated in the intracellular fluids (117 g) of the body compared with extracellular (3 g) fluids. The gradient, or the difference in concentration within the cell compared with the plasma, is essential in the generation of the electrical impulses in the body that allow muscles and the brain to function. Potassium is necessary for growth, electrical activity of the heart, maintaining normal blood pressure, and muscle function including the heart and nerve impulse transmission. It protects bone mineral density and reduces the formation of kidney stones. Potassium is rich in bananas, cherries, dates, grapefruit, guavas, pomegranates, watermelons, French beans, avocados, potatoes, pumpkins, and sweet potatoes.

Potassium helps

- to overcome fatigue and aids in clear thinking by sending oxygen to the brain
- to regulate body fluids that prevent dehydration
- kidneys to detoxify blood and acts as an alkalizing agent in keeping a proper acid–alkaline balance in the blood and tissues
- in the secretion of hormones and prevent female disorders by stimulating the endocrine hormone production
- in production of sperm in males

1.05.6.1.5 Sodium

Sodium chloride, the chemical name for common salt, which contains 39% of sodium, is an element that never occurs in free form in nature. It is found in an associated form with many minerals especially in plentiful amounts with chlorine. The body of a healthy person weighing about 65 kg contains 256 g of sodium chloride. Of this the major part, just over half, is in the extracellular fluid. About 96 g is in the bone and less than 32 g in the cells. Sodium is the most abundant chemical in the extracellular fluid of the body. It acts with other electrolytes, especially potassium, in the intracellular fluid, to regulate the osmotic pressure and maintain a proper water balance within the body. It is a major factor in maintaining acid–base equilibrium, in transmitting nerve impulses, and in relaxing muscles. It is also required for glucose absorption and for the transport of other nutrients across cell membranes. It

promotes a clear brain, resulting in a better disposition and less mental fatigue. Because of its influence on calcium, sodium can also help dissolve any stones forming within the body. It is also essential for the production of hydrochloric acid in the stomach and plays a part in many other glandular secretions.

1.05.6.1.6 Sulfur

Sulfur in the human body is present in the two sulfur-containing amino acids, methionine and cysteine, or in the double form of the latter known as cystine. The main purpose of sulfur is to dissolve in waste materials. It helps to eject some of the waste and poisons like heavy metals from the system.

1.05.6.2 Essential Trace Minerals/Microminerals

1.05.6.2.1 Chromium

It is an essential trace element required for normal function of insulin and regulation of glucose metabolism. It stimulates the production of proteins in the body, raises immunity against infections, and suppresses the feeling of hunger. It also plays a role in the production of high-density lipoprotein (HDL) cholesterol in liver. With an increase in age the level in chromium decreases, which is one of the factor for developing type 2 diabetes.

1.05.6.2.2 Cobalt

Cobalt is a component of vitamin B_{12}, a nutritional factor necessary for the formation of red blood cells and thus preventing anemia. The presence of this mineral in foods helps the synthesis of hemoglobin and the absorption of iron from food. Vitamin B_{12} with cobalt helps in the production of DNA, choline, and red blood cells, promotes a healthy nervous system, and lowers blood pressure.

1.05.6.2.3 Copper

Copper plays an important role in the conversion of iron to hemoglobin. Copper helps in the synthesis of other proteins and enzymes, supports the functioning of the nervous system, stimulates the growth of red blood cells, and is necessary for the correct functioning of brain cells. It also helps in the maintenance and development of bones, tendons, and connective tissues. Copper, together with zinc, improves the absorption of vitamin D, which in turn aids in the absorption of calcium. It is present in almonds, caraway seeds, cashew nuts, cherries, dates, drumstick leaves, egg yolk, berries, grapes, guava, kiwifruit, mushrooms, nuts, potatoes, and strawberries.

1.05.6.2.4 Fluoride

Fluoride is important for the development of bones and teeth, and helps in the prevention of dental caries and in the treatment of osteoporosis.[28] Fluoridated water, tea, canned salmon, and mackerel are the sources of fluoride.

1.05.6.2.5 Iodine

Table salt is the main source for iodine. Iodine is highly essential to synthesize two vital hormones, thyroxine (T4) and tri-iodothyronine (T3), important for the normal development, growth, and metabolism.

1.05.6.2.6 Iron

Iron rich in green vegetables, lentils, and soybeans is essential for producing hemoglobin (a substance in red blood cells) as the deficiency of the same will cause iron-deficiency anemia. It is essential to carry oxygen to body tissues. Consuming vitamin C together with iron-containing meals can increase or optimize iron absorption. Iron is also a part of myoglobin, which helps muscles to store oxygen.

1.05.6.2.7 Manganese

Manganese is present in trace amounts in the body in bones, liver, kidneys, and pancreas. Legumes, cereals, green leafy vegetables, tea, brown rice, beans, pineapple, raspberries, strawberries, cinnamon, squash, and turmeric are some of the foods that contain rich and high concentration of manganese. Manganese helps the body to form cartilage, bones, and blood clotting factors. Manganese is necessary for normal brain and nerve function and plays essential role in fat and carbohydrate metabolism, calcium absorption, and blood sugar regulation. It is an important cofactor in the key enzymes of glucose metabolism.

1.05.6.2.8 Molybdenum

Molybdenum is a component of several enzymes that plays an important role in sulfur metabolism. It is present in milk and helps in prevention of osteoporosis. Sources of molybdenum include whole grains, beans, and dairy products.

1.05.6.2.9 Selenium

Selenium presents in broccoli, asparagus, red wine, dietary fiber, pepper, peas, soya beans, mushroom, cloves, fenugreek, and ginger reported to decrease the risk of colon cancer. Fruits like banana, lychee, apple, watermelon, mango, guava, and pomegranate also contain selenium. The concentration of selenium in fruits and vegetables depends on the content of selenium in the soil in the region where these foodstuffs are grown.[29] Fish and Brazil nuts are rich in selenium, but it exists in cereals, wheat, and most

vegetables as selenomethionine, showing higher bioavailability than the form found in dairy products and meat. It is an essential component of glutathione peroxidase, which is involved in the reduction of hydroperoxidases. Selenium is required in very little amount of 70 mcg for male and 55 mcg for female to protect their health.

1.05.6.2.10 Zinc

The human body's need for zinc is small but its role in growth and well-being is enormous. Zinc is the healing mineral and part of the enzymes that helps the body to metabolize protein, carbohydrate, and alcohol. It also aids in building bones and healing wounds. Around two grams of zinc is available in the body where it is highly concentrated in the hair, skin, eyes, nails, and testes. Zinc is a cofactor in many enzymes that regulates growth and development, sperm generation, digestion, and nucleic acid synthesis. It plays an essential role in guarding against diseases and infections and is also required to transport vitamin A to the retina. Low levels of zinc can be observed in those who drink alcohol, as alcohol decreases zinc absorption and increases urinary secretion of zinc. Low zinc levels can cause liver deterioration and diminished functioning of the reproductive organs, immune system, and skin. Zinc is present in vegetables, namely, French beans, okra, peas, potatoes, pumpkins, and in fruits, namely, blackberries, dates, pomegranates, and raspberries.

1.05.7 Phytochemicals as Nutraceuticals

Presently, the use of phytochemicals is increasing due to its nutritional and medical importance supported by scientific data. Phytochemicals play an important role in human health as antioxidants and help in preventing various diseases like cancer, CVDs, diabetes, and inflammatory disorders. The major phytochemicals commonly used as nutraceuticals are carotenoids, phenolic compounds, and organosulfur compounds (Table 4).

1.05.7.1 Carotenoids

Carotenoids are biosynthesized by plants and microbes, but not by animals, and hence must obtain them from their food. There are 600 carotenoids reported from nature, where 40 were used in human diet and 14 found blood. It is present in yellow (pumpkin), orange (carrots), and red colored (tomatoes, papaya, watermelon, pink guava, and pink grape fruit) fruits and vegetables. Carotenoids can be classified into two major classes based on their structural elements; carotenes, constituted by carbon and hydrogen (eg, lycopene(**14**), α-carotene(**15**), and β-carotene(**16**)), and xanthophylls, constituted by carbon, hydrogen, and additionally oxygen (hydroxyl, methoxy, carboxyl, keto, or epoxy groups) (eg, lutein(**17**), zeaxanthin(**18**), β-cryptoxanthin(**19**), astaxanthin(**20**), and

Table 4 Sources and health benefits of phytochemicals used as nutraceuticals

Category	*Phytochemicals*	*Source*	*Health benefits*
Alkaloid	Piperine	Pepper	Stomachic
Carotenoids	Zeaxanthin	Wolfberry, carrot, celery, lettuce	Eye health
	α-Carotene and β-carotene	Carrots, pumpkin, orange, apricots, cantaloupe and sweet potato	Prevention of cancer
	Lutein	Spinach, red pepper, mango, papaya, peach	Protection from colon cancer
	Lycopene	Tomatoes, watermelon, papaya, apricot, pink guava, pink grape fruit	Lowers the risk of cancer and atherosclerosis
Glycoside	Withaferin, Withanolides	*Withania somnifera*	Immunomodulator and protects from cancer
Organosulfur compounds	Sulforanes, glucosinloates	Cruciferous vegetables, broccoli, cabbage, cauliflower, radish	Reduce the risk of prostate and colon cancer
	Allicin	Garlic, onion	Antioxidant and prevention of cancer
Phenolics	Anthocyanins	Berry, grape, maize, blackberry, orange	Antioxidant, antiinflammatory
	Rutin	Asparagus, buckwheat, citrus fruits	Strengthen capillary walls
	Catechins	Tea	Antioxidant
	Curcumin	Turmeric	Antioxidant, anticancer
	Quercetin	Tea, onion, grape, buckwheat	Antioxidant, vasodilator
	Resveratrol	Grape, groundnut, blueberry, red wine	Prevents aging, cancer, diabetes, heart disease
	Silymarin	Milk thistle (*Silybum marianum*)	Protect UV induced cancer and hepatoprotective
Phytosterol	Stigmosterol	Soya bean	Prevents arthritis and cancer
Polyunsaturated fatty acids	α-Linoleic acid	Flaxseed	Prevention of cancer and CVD
Terpenes	Zingiberine	Ginger	Carminative, prevents dizziness

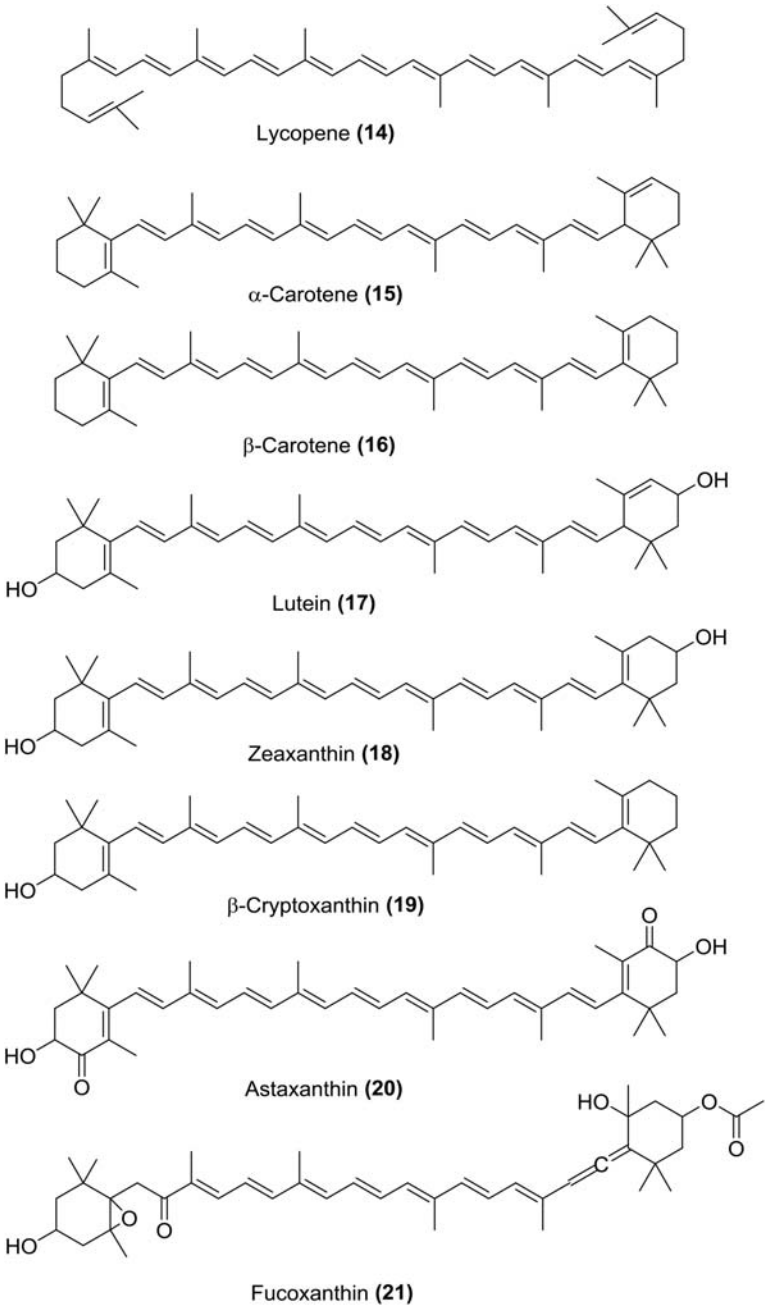

Fig.4 Chemical structures of some important carotenoids.

fucoxanthin(**21**)) (Fig. 4).[30] Among the different types, carotene that contains six-membered rings at the end is found to be active compared with the carotene containing the five-membered rings. Carotenoids are important for human health, as they exert protective effects against serious disorders like cancer,[31] heart diseases,[32,33] and degenerative eye diseases.[34]

Protective effect of carotenoids against cancer is mainly due to the presence of multiple conjugated double bonds which reduces the reactive oxygen species.

1.05.7.2 Phenolics

Phenolics are the most abundant antioxidants in the human diet, and they modulate the activity of a wide range of enzymes and cell receptors. More than 4000 polyphenols have been identified in many plant foods, including vegetables, grains, nuts, cereals, oilseeds (rapeseed, canola, flaxseed, and olive seeds), legumes (barley, corn, nuts, oats, beans, pulses), spices, chocolate, tea, and

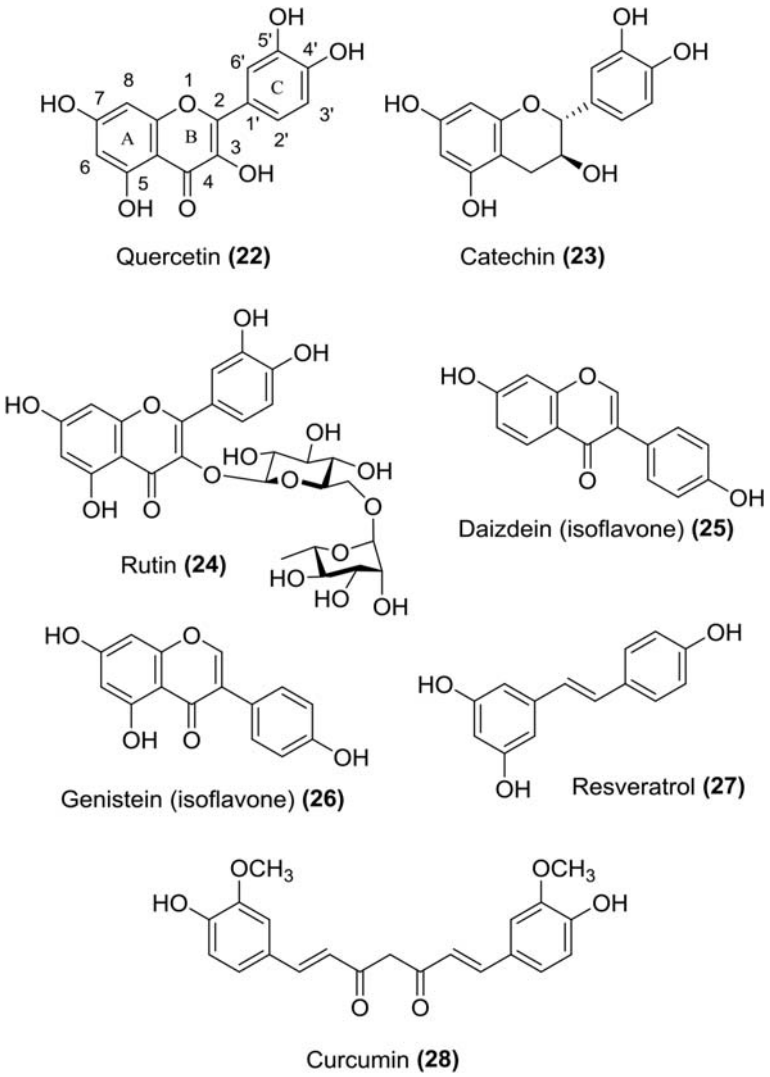

Fig. 5 Chemical structures of some important phenolic nutraceuticals.

beverages (fruit juices, tea, coffee, cocoa, beer, and wine).[35] Fruits such as apple, grape, pear, cherry, and various berries are rich sources of polyphenols.

Plants and food contain large variety of phenolic derivatives as phenolic acids, flavonoids, stilbenes, coumarins, tannins, lignans, and lignins. Dietary fruits rich in polyphenolic compounds reduce the incidence of cancer by inhibiting certain enzymes that promote cell proliferation or promote activities of enzymes that induce cell death.

Phenolic acids like gallic acid and caffeic acid, the derivatives of hydroxy benzoic acids and hydroxy cinnamic acids, helps in preventing the cancer due to its potent antioxidant properties. Caffeic acid in the form of caffeoyl esters is common in apples, pears, grapes, and gallic acid. Grain-derived products are especially significant in human diet as they have higher concentration of phenolic acids in the outer layers of kernel that constitute the bran. Ferulic acid, a phenolic acid present in oats, sweet corn, and tomatoes is a potent antioxidant, helps to reduce blood pressure and protect skin.

Flavonoids are the largest class of polyphenols with a common carbon skeleton of diphenyl propane (C6–C3–C6) representing two benzene rings connected through three carbon atoms. Flavonoids are classified into flavonols (isorhamnetin, kaempferol, myricetin, quercetin(**22**)), flavanols (catechin (**23**), gallocatechin, epicatechin, epicatechin gallate, epigallocatechin), flavones (apigenin, chrysin, luteolin, rutin (**24**)), isoflavones (biochanin A, daidzein (**25**), daidzin, formononetin, genistein (**26**), glycitein) (Fig. 5), flavononols (astilbin, engeletin, genistin, taxifolin), flavonones (eriodictyol, hesperidin, isosakuranetin, naringenin, naringin, taxifolin), anthocyanidins (cyanidin, delphinidin, epigenidin, malvidin, pelargonidin, peonidin, petunidin), and chalcones (butein, okanin) based on the structural variations in the number and positions of OH groups or the presence of ketonic group in the middle ring.[36] Catechins (flavanol) and anthocyanins are collectively known as flavans as they do not have carbonyl group at third position.

Buckwheat (*Fagopyrum esculentum*), rich source of rutin and quercetin (flavonols), also present in high levels in onion, berries, and apples reported to exert protection against inflammation and cancer.[37] Ortho dihydroxy substitution in B ring, double bond between 2 and 3 positions, and carbonyl group in C ring are essential for quercetin to render potent antioxidant activity.[38]

Flavonol and kaempferol are widely distributed in common fruits such as apples and tomatoes, which help in protecting against cancer, inflammation, and bacterial infections.

Flavones like apigenin and luteolin are abundantly present in common fruits such as grapefruit, plant-derived beverages, and vegetables such as parsley, onions, oranges, tea, chamomile, wheat sprouts, and in peppermint, aid in preventing the cancer due to its potential antioxidant, antiinflammatory, and antitumor properties.[39]

The chief flavonoid constituents of green tea are flavanols (catechin (**23**), epicatechin, catechingallate, and epigallocatechin gallate), flavonols (quercetin (**22**), kaempferol, and their glycosides), flavones (vitexin, isovitexin), and phenolic acids (gallic acid, chlorogenic acid), which are able to reduce the risk of cancer, CVD, and inflammations.[40]

Citrus fruits are major sources of flavonones where hesperidin, which is found in abundance (120–250 mg L^{-1}) in orange juice, is a natural free radical agent that gives nutritional tune to the cardiovascular system.

Isoflavones rich in soy help in reducing body weight, improving glucose metabolism, and promoting heart health.

Polymerization of flavonoids into large molecules called tannins include the proanthocyanidins (or condensed tannins) and the hydrolysable tannins. They act as antioxidant by accepting free radicals, but the antioxidant activity depends on their chemical structure.

Resveratrol (**27**), a nonflavonoid polyphenol/stilbene derivative (3,4,5′-trihydroxy-*trans*-stilbene) rich in peanuts, grapes, red/white wine, blueberries, cranberries, cocoa, and dark chocolate, helps in protecting the heart and circulatory system, lowering cholesterol, and protecting against clots, which can cause heart attacks and stroke.

Nonflavonoid polyphenol, curcumin (**28**), chemically known as 1,7-bis(4-hydroxy-3-methoxyphenyl)-1,6-heptadiene-3,5-dione, is an active component of the plant *Curcuma longa* (Zingiberaceae), is responsible for the yellow color, and is known to possess multiple pharmacological effects. It is used in the treatment of inflammatory ailments, obesity, and other metabolic diseases. Its immunomodulatory properties including antioxidant, antiinflammatory, and antitumor properties are well documented.[41] Curcumin interacts directly with cyclooxygenase-2 (COX-2), DNA polymerase, lipoxygenase, glycogen synthase kinase-3b, and cytokines (tumor necrosis factor-α).

Protective roles of flavonoids in human health include heart diseases,[42] eye diseases,[43] diabetes,[44] and neurodegenerative diseases, like Alzheimer's or Parkinson's.[45] The other potential health benefits of flavonoids include antifungal,[46] antibacterial,[47] and antiallergic[48] activity.

Flavonoids also exert a positive effect on the prevention and/or treatment of different types of cancer, namely ovarian, colon, lung, laryngeal, prostate, pancreatic, esophageal, breast, leukemia, renal cell carcinoma, and hepatocellular carcinoma.

1.05.7.3 Organosulfur Compounds

Glucosinloates are nitrogen- and sulfur-containing compounds present in cruciferous vegetables, cress, horse radish, rucola, and mustards, which provide protection against carcinogenesis. Glucoraphanin, the glucosinolates of sulforaphane present in all the cruciferous vegetables like broccoli, cabbage, and cauliflower, is responsible for cancer preventive activity.[49] Studies revealed that broccoli sprouts combined with glucoraphanin powder synergistically enhanced the bioavailability of sulforaphane and proved that regular intake of designer broccoli sprouts enriched with glucoraphanin powder reduces the risk of cancer compared with glucoraphanin powder or sprouts alone.[50]

Mustard, like broccoli and cabbage, belongs to *Brassica* family and is native to Europe having potential benefits against cancer due to the presence of phytonutrient glucosinolate. Among the three varieties of mustard seeds namely black mustard (*Brassica nigra*), white mustard (*Brassica alba*), and brown mustard (*Brassica juncea*), black variety is most popular for its aroma and flavor (due to the presence of sinalbin) and hence it is preferred in cooking. Mustard seed contains minerals such as calcium, magnesium, phosphorus, potassium, selenium, vitamin A, vitamin K, folic acid, and dietary fiber. Mustard oil helps in reducing the levels of glycosylated proteins, serum glucose, aids in reducing lipid peroxidation, and stimulates glucose metabolism.

Garlic and onion belong to allium family reported to contain high amount of sulfur compounds. Garlic is one of the very commonly used ingredient in many cuisines worldwide that contains allicin, alliin, diallyl disulfides (organosulfur compounds), minerals, and vitamins, which help in preventing the various diseases such as cancer, CVDs, obesity, and type 2 diabetes.[51] Onion is an important condiment and vegetable used in every kitchen in the world that contains large amount of sulfur compounds (cepaenes and thiosulfinates), flavonoids (quercetin), vitamins, minerals (calcium, chromium), and dietary fiber. Antioxidant, antitumor, and immune enhancing properties of onions may be due to the presence of flavonoids. High amount of sulfur compounds in onion stimulate the action of amino acids to nervous system, reduce symptoms associated with diabetes mellitus, inhibit platelet aggregation (involved in thrombosis), and prevent inflammatory processes associated with asthma.[52]

1.05.8 Plants as Nutraceuticals

Medicinal plants are being used by indigenous people for many years for the prevention and treatment of various diseases (**Table 5**). Plants synthesize primary metabolites and secondary metabolites, where the primary metabolites like carbohydrates, lipids, and

Table 5 List of medicinal plants used as nutraceuticals

Name of the medicinal plant	*Botanical name*	*Activity claimed*
Amla	*Emblica offficinalis*	Antioxidant, antiinflammatory, diuretic, stomachic, digestive, prevents peptic ulcer
A. vera	*Aloe barbadensis*	Antiinflammatory, emollient, wound healing
Ajowan fruits	*Trachyspermum ammi*	Source of thymol
Aswagantha	*W. somnifera*	Nerve tonic
Bael	*Aegle marmelos*	Chronic diarrhea
Bahera	*Terminalia belerica*	Antidiarrheal, antidiabetic
Baical skullcap	*Scutellaria baicalensis*	Antimicrobial
Bitter guard (Karela)	*M. charantia*	Antidiabetic
Black gram	*Vigna mungo*	Source of proteins, lowers the risk of CVD, helps in maintaining body weight
Boswellia	*Boswellia serrata*	Antiarthritic
Bottle guard	*Lagenaria siceraria*	Reduces total cholesterol, triglycerides (TGS), and low density lipoproteins (LDL) levels. Helps in digestion and reliving constipation
Brahmi	*Centella asiatica*	Brain tonic, improves concentration, and alertness
Coriander	*Coriandrum sativum*	Digestive, stimulant, and flavoring agent
Caraway	*Carum carvi*	Aromatic, carminative
Cardamom	*Elettaria cardamomum*	Carminative
Chamomile	*Matricaria recutita*	Antiinflammatory, spasmolytic, antimicrobial, and wound healing
Cinnamon	*Cinnamomum zeylanicum*	Flavoring agent
Chaulai	*Amaranthus hybridus*	Helps in preventing CVD
Curry leaf	*Murraya koenigii*	Antioxidant, anti tumor, anti inflammatory, anti hyperglycemic, hypoglycemic, and hypolipidemic
Dill	*Anethum graveolens*	Carminatives
Drumstick	*Moringa oleifera*	Antiepileptic, antiinflammatory, antiulcer, antispasmodic, diuretic, antihypertensive, cholesterol lowering, antioxidant, antidiabetic, hepatoprotective, antibacterial, and antifungal
Echinacea	*Echinacea purpurea*	Act as an immune stimulant and treatment of cold and flu symptoms
Ephedra	*Ephedra sinica*	Helps in reducing bronchial edema
Fennel	*Foeniculum vulgare*	Carminative, aromatic, and stimulant
Fenugreek	*Trigonella foenum*	Lowers TGS, total cholesterol, and LDL
Ginger	*Zingiber officinale*	Carminative, antiemetic, treatment of dizziness
Ginseng	*Panax ginseng*	Adaptogen
Green tea	*C. sinensis*	Antioxidant, reduces risk of CVD, enhances humoral and cell mediated immunity
Garlic	*A. sativum*	Prevents atherosclerosis, hypercholesterolemia, high blood pressure
Kalmegh	*Andrographis paniculata*	Protects against all infections including virus
Kidney bean	*P. vulgaris*	Diuretic and flushes out the toxins from the body hypoglycemia
Liquorice	*Glycyrrhiza glabra*	Expectorant, peptic ulcer
Mentha	*Mentha piperita*	Carminative, stimulant, and counter-irritant
Mushrooms	*Boletus* sp.	Helps in preventing CVD, anticancer, antidiabetic property
Mustard	*B. nigra*, *B. juncea*	Helps in prevention of cancer
Myrobalan	*Terminalia chebula*	Digestive, stomachic, laxative
Pepper	*Piper nigrum*	Digestive, stomachic
Pipal	*Piper longum*	Carminative
Neem	*Azadirachta indica*	Antiseptic, ulcers, boils
Nutmeg	*Myristica fragrans*	Carminatives
Oats	*Avena sativa*	Lower cholesterol
Okra	*Abelmoschus esculentus*	Helps in increasing sperm count
Onion	*A. cepa*	Antioxidant, helps in preventing heart disease and cancer
Rasna	*Alpinia officinarum*	Carminatives
Red pepper	*C. annum*	Antiarthritic and antioxidant
Senna	*Cassia angustifolia*	Laxative
Shatavari	*Asparagus* sp.	Tonic and astringent

Table 5 List of medicinal plants used as nutraceuticals—cont'd

Name of the medicinal plant	*Botanical name*	*Activity claimed*
Suran	*Amorphophallus companulatus*	Prevent gastric troubles and rheumatic pain
Suwa	*Anethum graveolens*	Flatulent colic, ulcers
Tea leaves	*C. sinensis*	Antioxidant, helps in prevention of cancer and CVD
Tulsi	*Ocimum sanctum*	Expectorant
Turmeric	*C. longa*	Antiinflammatory agents
Vaj	*Acorus calamus*	Antispasmodic and carminative
Vasaka	*Adhatoda vasica*	Expectorant
Vidang	*Embelia ribes*	Anthelmintic
Wild marygold	*Tagetes minuta*	Antimicrobial

amino acids involve in the growth of the plants. The low molecular weight secondary metabolites have no recognized contribution in the growth of plants but provide health benefits to humans. But the major challenge in herbal nutraceuticals is meeting the requirements of stability as most herbs need low humidity conditions due to their hygroscopic nature.

1.05.9 Microbes as Nutraceuticals

1.05.9.1 Probiotics

Probiotics are live microorganisms such as *Lactobacillis* sp. (*L. acidophilus*, *L. plantarum*, *L. casei subspecies rhamnosus*, *L. brevis*, *L. delbreuckii subspecies bulgaricus*), *Bifidobacteria* sp. (*B. adolescentis*, *B. bifidum*, *B. longum*, *B. infanti*, and *B. breve*), and *Streptococcus thermophilus* present in human body and provides various health benefits on ingestion (World Health Organization). Probiotics inhibit the growth of bad bacteria and help in producing vitamins especially vitamin K and ensure that the immune system works properly. These probiotics are commercially available as spores or in lyophilized forms or in the form of probiotic fortified fermented dairy products. *Lactobacilli* sp. are naturally found in fermented foods like sauerkraut and yogurt. Probiotics are potential in the treatment pediatric antibiotic-associated diarrhea, acute upper respiratory tract infections, chronic and acute enteric infections, and their associated diarrheal complexes.[53] Daily dietary intake of probiotics reduces the incidence and severity of acute and chronic infection, prevents and reduces the recurrence of cancers and incidence of several atopic conditions,[54] and increases the level of liver aminotransferases in patients with nonalcoholic fatty liver disease.[55] Probiotics like *Lactobacillus bulcaricus* help in preventing colon cancer by blocking the breakdown of enzymes β-glucuronidase. They produce lactic acid that lowers the pH of intestine and inhibits harmful bacteria such as *Clostridium*, *Salmonella*, *Shigella*, *E. coli*, and *Helicobacter pylori*. Probiotics decreases the production of a variety of toxic or carcinogenic metabolites and aids in absorption of minerals, especially calcium and magnesium, due to increased intestinal acidity. Calcium and magnesium in turn enhances the dietary nutrition utilization. Probiotics also aids in production of β-D-galactosidase enzymes (that break down lactose) and antimicrobial substances acidophilin, bacteriocin, etc. Some *Lactobacillus* sp. able to break down the bile in the gut, thus inhibiting its reabsorption and lowers the blood cholesterol. Probiotic bacteria ferment dietary fiber to produce short-chain fatty acids, mainly acetates, propionate, and butyrates that increase blood flow to the colon and act as metabolic fuel for the intestinal cells.

Chronic gastritis leading to peptic ulcer is one of the major concern in the long-term infection of *H. pylori*. Treatment of *H. pylori* infection involves expensive therapeutic interventions, which lead to the development of unpleasant side effects and antibiotic resistance.[56] Therefore, the use of food-based products such as probiotics may be a cost-effective way to manage symptoms associated with *H. pylori* infection. The gastric mucosal barrier represents a first line of defense against pathogenic bacteria and the intake of probiotics strengthens this barrier by producing antimicrobial substances, competing with *H. pylori* for adhesion receptors, stimulating mucin production, and stabilizing the gut mucosal barrier. *H. pylori* is known to suppress *MUCI* and *MUC5A* gene expression where probiotics like *L. plantarum* and *L. rhamnosus* can increase the expression of *MUC2* and *MUC3* genes and cause subsequent extracellular secretion of mucin.[57] This property mediates the ability of these strains to restore the mucosal permeability of gastric mucosa or inhibit the adherence of pathogenic bacteria. In addition to antimicrobial effect of lactic acid produced relatively in large amounts by lactobacilli (probiotic), lowering of the pH could inhibit the *H. pylori*[58]; the possible mechanisms by which probiotic bacteria *L. reuteri* inhibits the binding of *H. pylori* to specific glycolipid receptors asialo-GMI and sulfatide.[59]

1.05.9.2 Prebiotics

A prebiotic is a nondigestible component which beneficially affects the host by selectively stimulating the growth and/or activity of one or a limited number of colonic bacteria, thereby improving the health of the host. Prebiotics are called as "colonic food" as they are not digested or absorbed in the stomach and small intestine but gets fermented once they reach the large intestine. Once it enters the colon it become a substrate for the endogenous bacteria and indirectly provides energy and metabolic substrates to the host. Inulin is an example of prebiotic, also known as raftiline, found in several foods such as wheat, onion, garlic, fruits, and vegetables.

Fig. 6 Nutraceuticals used in prevention for various diseases.

Prebiotics are partially soluble in water where it forms slightly thickened product that has a bland neutral taste without any flavor and can contribute to body and mouth feel of food products. Other examples of prebiotics include oligofructose, garlic, onions, chicory root, asparagus, lactulose, whole wheat, rye, and barley. Potential health benefits of prebiotics include increasing the absorption of certain minerals such as calcium, magnesium, and iron, reducing the risk of colon cancer, reduction in cholesterol and blood lipids, and prevention of gastrointestinal tract infections. It helps in increasing the growth of *Bifidobacteria*, which in turn renders beneficial effects by producing nutrients such as B-group vitamins, folic acid, and digestive enzymes, reduces food intolerance by utilizing residual nutrients from the upper gut, and reduces the liver toxins like blood amines and ammonia, by using them as fuels. It alters the colonic microflora toward a healthier composition or selectively stimulates the growth and/or activity of intestinal bacteria associated with health and well-being. Presence of high levels of milk proteins (disulfide bridges) is believed to stimulate the growth of *Bifidobacterium* species, which are known to suppress growth of pathogenic bacteria in the colon. It favors the immune system, improves resistance against infection, and lessens the chances of type 2 diabetes and osteoporosis. Foods containing the combination of probiotics (bacteria) and prebiotics (saccharides) are referred to as synbiotics.

1.05.10 Health Benefits of Nutraceuticals

The use of nutraceuticals, as an attempt to accomplish desirable therapeutic outcomes with reduced side effects, as compared with other therapeutic agents has met with great monetary success. Consumption of plant-based foods, nuts, whole grains, cereals, and marine foods plays a vital role in disease prevention and health promotion.

Some popular nutraceuticals include glucosamine, chondroitin, methylsulfone and *S*-adenosyl methionine (for arthritis), lutein (for macular degeneration), ginseng (for cold), echinacea (antiimmune), folic acid, cod liver oil capsules, etc. The most popular functional food and beverage products include omega-3 eggs, omega-3 enriched yogurts, calcium-enriched orange juice, and green tea, to mention a few. Majority of the nutraceuticals do possess multiple therapeutic benefits; however, in the present article, much effort has been devoted to decentralize them based on their disease-specific major indication.

Nutraceuticals are claimed to possess physiological benefit or protection (Fig. 6) against the following diseases:

CVD
Cancer

Diabetes
Obesity
Chronic inflammatory disorders
Parkinson's disease
Alzheimer's disease

1.05.10.1 Nutraceuticals in CVDs

CVD is the name for the group of disorders of the heart and blood vessels that include hypertension (high blood pressure), coronary heart disease (heart attack), cerebrovascular disease (stroke), heart failure (heart muscle weakness leads to decreased or insufficient flow of oxygen rich blood flow to various organs of the body), and peripheral vascular disease. It was reported that low intake of fruits and vegetables is associated with a high mortality in CVD.[60] Many research studies have identified a protective role for a diet rich in fruits and vegetables against CVD.[61] Nutraceuticals in the form of antioxidants, dietary fibers, omega-3 PUFAs (n-3 PUFAs), vitamins, and minerals are recommended together with physical exercise for the prevention and treatment of CVD. It has been demonstrated that molecules like polyphenols present in grapes and in wine alter cellular metabolism and signaling, which is consistent with reducing arterial disease.[62]

1.05.10.1.1 Polyunsaturated fatty acids

Fatty acids can be categorized as saturated fatty acid, monounsaturated fatty acid, and PUFA. Saturated fatty acids usually contain 14 or more linearly arranged carbon atoms without any double bonds or unsaturation, and these fatty acids are found mostly as triglycerides in edible oils and fats. Monounsaturated fatty acids like oleic acid contain only one double bond, whereas PUFA contain multiple unsaturated double bonds found mostly in fish and plant oils, for example, linoleic acid, eicosapentaenoic acid (EPA), DHA, α-linolenic acid (ALA), and γ-linolenic acid (GLA). EPA, DHA, and ALA are called omega-3 fatty acids or n-3 PUFAs as the double bonds are located at the third carbon atom from its terminal. Linoleic and GLA are called as omega-6 or n-6 PUFAs as they have their first double bond at sixth carbon. Human body is able to synthesize fatty acids except these two omega-3 and omega-6 fatty acids and hence a diet balanced in omega-3 and omega-6 fatty acids is essential for human beings.[63] Long chain omega-3-PUFAs are of great interest because of their effectiveness in prevention of coronary heart disease, hypertension, diabetes, autoimmune disorders, and cancer and are essential for maintenance and development of normal growth, especially for the brain.

1.05.10.1.1.1 Omega-3 fatty acids

Omega-3 fatty acids are unsaturated fatty acids found in green leafy vegetables, vegetable oils, nuts, and fish oil. Tuna or white fish like sole, snapper, and cod contain less amount of DHA and EPA compared to oily fish like salmon, mackerel, and bluefish. Increase in heart failure risk may be possible by eating fried fish as frying destroys the omega fatty acids and increases the trans-fat content. The simplest omega-3 fatty acid is linolenic acid, which has potential health benefits in CVD and in inflammatory disorders. The most common omega-3 fatty acids found in the diet include long chain PUFA, EPA, and DHA. Dietary consumption of omega-3 fatty acid reduces the incidence of CVD, osteoarthritis,[64] and rheumatoid arthritis (RA).[65] Designer diet-based approach will be effective for increasing omega-3 fatty acid.[66]

Omega-3 fatty acids are proved to be beneficial in various disorders such as CVD, hypertension, autoimmune, allergic, and neurological disorders, and it is also essential for normal functioning of the human physiology not only in normal adult but also in pregnant and lactating women. Supplementation with omega-3 fatty acid along with nonsteroidal antiinflammatory drugs (NSAIDs) in juvenile idiopathic arthritis was proved to be effective as it reduces the daily requirements of NSAIDs and the risk of related side effects due to NSAIDs.

Caston and Leeson[67] also reported that it is possible to increase the concentration of omega-3 fatty acid in a hen's egg by adding flaxseed or fish oil in its diet. In the year 2006, Bourre and Galea[68] produced designer egg fortified with omega-3 fatty acid by feeding hens with linseed, minerals, vitamins, and lutein. The nutritional value of 100 g of these eggs contains six times more of the omega-3 fatty acid ALA, three times more DHA, three times more vitamin D, four times more folic acid, six times more vitamin E, six times more lutein and zeaxanthin, 2.5 times more iodine, and four times more selenium. These eggs also contain a little amount of cholesterol and, like standard eggs, are rich in B complex vitamins, vitamin A, phosphorus, and proteins. The consumption of these eggs improved the blood concentration of omega-3 fatty acids, HDL cholesterol, and triglycerides.[69]

DHA is one of the major components present in brain, retina, and testes. Major source of DHA is fish oils and marine algae. Daily dose of 2.5 g is recommended for cardiovascular and eye health.

Dietary supplementation of flaxseed oil (from flax plant *Linum usitatissimum*) that contains 50% ALA, which is an essential omega-3 fatty acid, helps in lowering blood pressure. Candlenut, hemp seed, pumpkin seed, canola, walnut, and soyabean are the other dietary sources of ALA. Recommended dose of this essential fatty acid (EFA) is 1–2 g day^{-1}.

Cardioprotective effects of omega-3 fatty acids include reduction in plasma levels of triglycerides and bad lipoproteins, inhibition of thromboxane A2 synthesis, improved endothelial function, up- and downregulation of genes involved in the synthesis of proteins, prevention of arrhythmias, decrease in plasma homocysteine levels, and increase in nitric oxide (vasodilator) production.

1.05.10.1.1.2 Omega-6 fatty acids

Linoleic acid and arachidonic acid (AA) are the Omega-6 fatty acids that have been found to possess cancer protective properties. The human body converts linoleic acid into GLA, and the latter get converted into AA. EPA synthesized from omega-3 fatty acid and GLA synthesized from omega-6 fatty acid have important roles in the maintenance of good health.

Appropriate balance of these two types of fatty acids, omega-3 and omega-6, should be maintained as these two work together to promote health. EFA deficiency and omega 6/3 imbalance are linked with serious health conditions, such as heart attacks, cancer, insulin resistance, asthma, lupus, schizophrenia, depression, postpartum depression, stroke, obesity, diabetes, arthritis, attention deficit hyperactivity disorder, and Alzheimer's disease.

1.05.10.1.2 Dietary fibers

Dietary fiber is defined as nondigestable carbohydrates and lignin that are intrinsic and intact in plants as an essential nutrient required for proper digestion of foods and proper functioning of the digestive tract. Diets deficient in fiber content may cause constipation, increase in blood glucose, and increase in cholesterol levels. Dietary fiber can be divided into two categories based on solubility and viscosity, where the health benefits are based on these physical attributes. Dietary fiber can be classified as soluble and insoluble based on the chemical properties.[70] Soluble dietary fibers include β-glucans, pectins, gums, barley, and hemicelluloses, which are rich in fruits, oats, barley, and beans. Insoluble dietary fibers include celluloses, some hemicelluloses, and lignins. Research report suggests that consumption of dietary fiber may prevent CVD, diabetes, obesity, lower triglycerides, and blood cholesterol levels. Oat fiber has the tendency to lower plasma cholesterol and low density lipoprotein (LDL) cholesterol. The probable mechanism behind the lipid-lowering effect of water soluble fibers like pectin is that it decreases the uptake of bile acids in the intestine. Readily soluble dietary fibers present in mustard seeds help to improve digestion in the body and make the bowel movements better, thus improving the overall metabolism of the body.

1.05.10.1.3 Flavonoids

Flavonoids are widely distributed in onion, cruciferous vegetables, black grapes, red wine, grapefruits, apples, cherries, and berries. Flavonoids in plants available as flavones (containing the flavonoid apigenin found in chamomile), flavanones (hesperidin-citrus fruits; silybin-milk thistle), and flavonols (tea: quercetin, kaempferol, and rutin grapefruit; rutin buckwheat; ginkgo flavone glycosides—ginkgo) play a major role in curing the CVDs.[71,72]

Flavonoids in regularly consumed foods may reduce the risk of death from coronary heart disease. It protects the vascular system and strengthens the tiny capillaries that carry oxygen and essential nutrients to all cells. Flavonoids exert health benefits by blocking angiotensin-converting enzyme, preventing platelet aggregation, and blocking the enzyme cyclooxygenase.

Hesperidin, a flavanone glycoside classified as a citrus bioflavonoid, is present in high amounts in lemon and orange peels. In combination with a flavone glycoside called diosmin, it is used for the treatment of venous insufficiency and hemorrhoids.

Resveratrol (**27**) occurs naturally in grapes, mulberries, white hellebore, and in peanut butter. It is a constituent of red wine and considered to be responsible for "French Paradox," that is, the observation that people from Southern France suffer a relatively low incidence of ischemic heart disease, although they eat diet rich in saturated fats.[73] It is proven to prevent CVD and cancer in a dose of 15–200 mg day^{-1}.

Proanthocyanidins that are the polyphenolic derivatives that contribute colors to various fruits like plums, grapes, blackberry, cranberry, and cherries have been proved to have protective action against many cardiovascular risk factors.

1.05.10.1.4 Plant sterols

Phytosterols in diet have the potential to reduce the morbidity and mortality of CVD.[74] The most abundant plant sterols include sitosterol, campesterol, and stigmasterol with typical daily intakes ranging from 150 to 400 mg day^{-1}. Plant sterols called as phytosterols, present in green and yellow vegetables nuts, seeds, legume, fruits, and grains in significant amounts, compete with dietary cholesterol due to biochemical similarity, thereby blocking the uptake as well as facilitating its excretion from the body. Statins may be combined with plant phytosterols for additional reduction of LDL cholesterol.

1.05.10.1.5 Policosanol

Policosanol (octacosanol, $CH_3(CH_2)_{26}CH_2OH$), a naturally occurring long chain aliphatic alcohol with 28 carbons, is obtained from superficial waxy layers of fruits, leaves, and epidermis of many plants reported to possess lipid-lowering effect (reduced LDL cholesterol) similar to that of statins, and increasing HDL cholesterol.[75] The recommended dose of policosanol tablet or capsule is 100 mg day^{-1}.

1.05.10.1.6 Vegetables in prevention of CVDs

1.05.10.1.6.1 Garlic

Garlic (*Allium sativum*) belongs to the family Liliaceae and is used as a spice, food, and folklore medicine for more than 5000 years. It contains sulfur compounds (allicin, alliin, allyl sulfides), terpenes (linalool, α-phellandrene, citral, geraniol), and high levels of phosphorous, calcium, iron, selenium, germanium, vitamins like riboflavin, thiamine, nicotinic acid, and vitamin C. Cholesterol in blood and tissues derived from diet or from endogenous synthesis has long been implicated as a significant risk factor in CVD. Allicin, an active constituent present in garlic, reported to have lipid-lowering activity with 9–12% reduction in total

cholesterol level.[76] Garlic blocks the synthesis of cholesterol by acting on the enzyme hydroxy-methyl-glutaryl-coenzyme A (HMG-CoA) reductase, thereby reducing the risk of CVD.

1.05.10.1.6.2 Onion

Consumption of onion with food increases the beneficial HDL cholesterol, lowers total blood cholesterol, triglycerides, reduces blood pressure, thins the blood, and keeps blood free from clots.

1.05.10.1.6.3 Ginger

Ginger, the rhizome of *Zingiber officinalis*, one of the most widely used species of the ginger family, is a common condiment for various foods and beverages. Ginger has a long history of medicinal use dating back 2500 years. Pungent constituents present in ginger and other zingiberaceous plants have potent antioxidant and antiinflammatory activities and also exhibit cancer preventive activity.

1.05.10.1.7 Coenzyme Q10

It is an endogenously synthesized lipid soluble antioxidant and is synonymically called as ubiquinone or ubidecarone. It is present in fish, chicken, cereals, and in spinach. Clinical studies confirmed supplementation of food with Coenzyme Q10, which helps in the prevention of congestive heart failure, hypertension, and myopathy related to statin therapy.[77] It is not only recommended for cardiovascular health but also for cancer prevention with a daily dose of 100–360 mg.

1.05.10.1.8 Potassium

Potassium is the third most abundant mineral in the body. Its primary function is to maintain muscle health, to control the electrical activity of the heart, and to maintain the acid–base balance. Dietary intake of potassium lowers blood pressure, and reduces the risk of coronary heart disease, stroke, and cardiac arrhythmias.

1.05.10.1.9 Fermented red yeast rice

Folk medicine in various countries like China, Japan, and India has the tradition of using fermented food for its health benefits, which includes red yeast rice. In Chinese traditional medicine, red yeast rice has been used as a medicine for digestion and revitalization.[78] Monacolin K (also known as lovastatin) present in monascus (*Monascus purpureus*) fermented red rice reported to inhibit the synthesis of cholesterol.[79–81]

Optimal nutrition, vitamins, antioxidants, minerals, weight reduction, exercise, cessation of smoking, restriction of alcohol and caffeine plus other lifestyle modifications can prevent, delay the onset, reduce the severity, and control CVDs.

1.05.10.2 Nutraceuticals in Cancer Prevention

Oxygen is most important for humans and animals to sustain life, but their metabolic products cause cancer. During the production of cell energy, mitochondria utilize almost 95% of oxygen and throw off unpaired electron called as free radicals. When these unpaired electrons get near the DNA molecules they grab electron (from nitrogen) to balance themselves. This causes damage to DNA molecules, which affects the function of normal cells and when they divide they form new cells causing cancer.

Consumption of regular and large amount of alcohol, smoking, modern lifestyles, change in dietary constituents, high meat consumption, and limited physical activity led to an increasing mortality rate for cancer worldwide. Nutraceuticals were examined for cancer therapy as the synthetic anticancer drugs may often cause adverse effects to the normal organs.[82,83]

Nutraceuticals containing glucosinolates, carotenoids, polyphenolic compounds, and vitamins possess antioxidant property and thus help in preventing the cancer (**Fig. 7**).

Glucosinolates are found in cruciferous vegetables including the *Brassica* crops Brussels sprouts, broccoli, cauliflower, cabbage, watercress, oilseed rape, and mustard are powerful activators of liver detoxification enzymes.[84] Glucosinolates and their hydrolysis products, including indoles and isothiocyanates (−N═C═S), and high intake of cruciferous vegetables have been associated with lower risk of lung and colorectal cancer. They also regulate white blood cells and cytokines. White blood cells are the scavengers of the immune system and cytokines act as "messengers," coordinating the activities of all immune cells. Bio-transformation products of glucosinolates include isothiocyanates, dithiolthiones, and sulforaphane. They block the enzymes that promote tumor growth, particularly in the breast, liver, colon, lung, stomach, and esophagus.

Diets rich with carotenoids like α-carotene, β-carotene, lycopene, lutein, cryptoxanthin, and lycopene present in tomatoes, watermelon, papaya, apricot, pink guava, and pink grape fruit have beneficial effects in human health, such as lowering the risk of cancer and enhancement of immune system function. Due to its potent antioxidant property, carotene helps in cancer prevention (induce apoptosis and inhibit cell cycle progression in cancer cells) and the recommended daily dose is 10–40 mg. Around 40% of human diets we consume constitute of fruits and vegetables are the major source of carotenoids. Thus, consumption of plant-based diets rich in a variety of vegetables (broccoli, carrots, arugula, pumpkins, sweet potatoes, squash, tomatoes, watercress) and fruits (apricots, cantaloupes, mangos, papayas, peaches, persimmons, and legumes) decrease the overall cancer rates to 20%.[85]

Polyphenolic compounds such as anthocyanins and flavonoids in red grape wine were proved to have inhibitory effect on breast cancer cells. A study by Hakimuddin et al.[86] supported the fact that red wine polyphenolic fractions have anticancer property against breast cancer cell lines (Michigan cancer foundation-7, MCF-7) and the authors also reported relatively low cytotoxicity toward

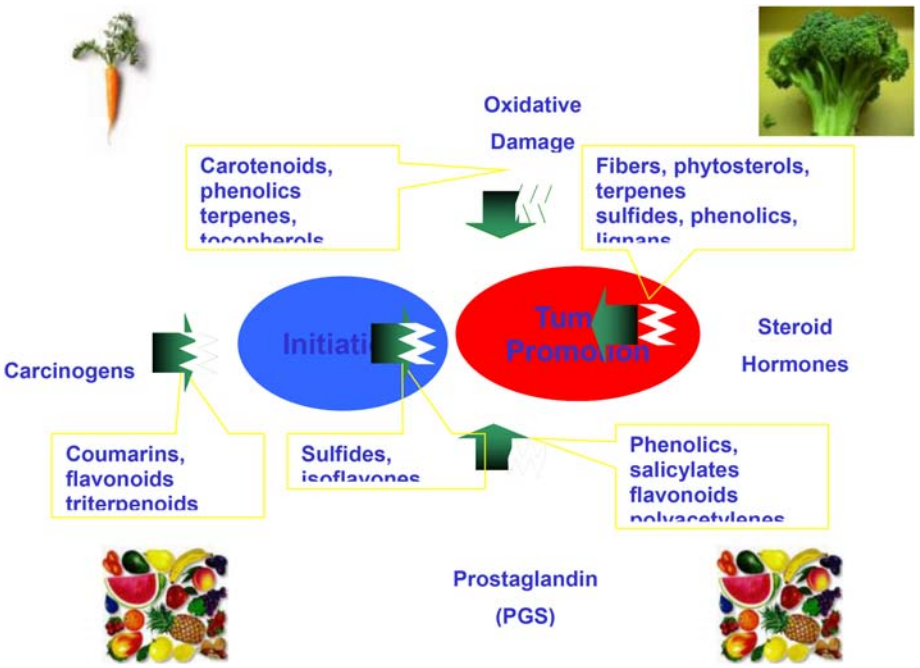

Fig. 7 Role of nutraceuticals in cancer.

normal human mammary epithelial cells (HMEC) and a nontumorigenic MCF-10A cells, which is contrast to the authentic flavonoids such as quercetin, naringenin, and catechin, which inhibited the growth of HMEC much more than that of MCF-7 cancer cells. The polyphenols induced calcium release by disrupting mitochondrial function through membrane damage, which results in selective cytotoxicity toward MCF-7 cells. Apart from its anticancer activity, the polyphenolic fractions showed discrete antioxidant action on cancer cell lines.[87] These studies suggested that consumption of wine, or other polyphenol-rich foods and beverages, could have a beneficial antiproliferative effect on breast cancer cell growth.

Onions, rich in powerful antioxidant, namely, quercetin, prevent the damage of DNA by free radicals, decrease cancer tumor initiation, promote healing of stomach ulcers, and inhibit the proliferation of breast, ovarian, and colon cancer.[88]

Soy isoflavone occurs in nature in glycoside form. Genistein is the major isoflavone present along with other iso flavones, daidzein and glycitein. Recommended dose of 30–50 mg day^{-1} is given for cancer prevention.

Tea is consumed as beverage in almost all the countries in the world. The studies also showed beneficiary effect of tea in reducing the risk of a variety of illnesses such as cancer and coronary heart disease. Tea plant *Camellia sinensis* is cultivated globally, which contains rich source of polyphenols including epigallocatechin 3-gallate. Tea can be of three types namely green tea, black tea, and Oolang tea. Green tea is an unfermented tea that contains high amount of polyphenols like catechin, gallocatechin, epicatechin, epigallocatechin, epicatechin gallate, and epigallocatechin gallate. Worldwide 78% of black tea, 20% of green tea, and 2% of Oolang tea are manufactured and are being consumed by western countries, Asian countries, and in southern China, respectively. Black and Oolang tea are the partially and completely fermented form of tea. Both black tea and green tea were proved to have potential in preventing lung, stomach, esophagus, duodenum, pancreas, liver, colon,[89] and skin cancers and have preventive effect on atherosclerosis, coronary heart disease, high blood cholesterol concentration, and high blood pressure. The health benefits of polyphenols from tea were extended by combining them with other food in the form of designer food.[90] A recommended dose of 5–100 mg day^{-1} is used for cancer prevention.

Phytochemicals (−)-epigallocatechin-3-gallate from green tea, curcumin from turmeric, sulforaphane from broccoli, genistein from soy isoflavone, and lycopene from tomatoes have the potential in prevention of breast cancer.

Triptolide, a diterpene triepoxide isolated from the roots of the Chineseherb *Tripterygium wilfordii*, helps in prevention of cancer.

Ellagic acid, a nonflavonoid polyphenol present in strawberries, raspberry, cranberries, grapes, walnuts, pomegranates, soybean, cabbage, ginger, licorice root, and umbelliferous vegetables, has protective property against cancer.

Allicin, chemically called as cysteine thiosulfinate, is an important constituent present in garlic to reduce the risk of cancer by inducing carcinogen detoxification, inhibiting tumor cell proliferation, scavenging free radicals, inhibiting DNA adduct formation, and inducing cell cycle arrest and apoptosis.

Pectin is a soluble fiber found abundant in citrus fruits, particularly in the peel, and prevents prostate cancer metastasis by inhibiting the cancer cells from adhering to other cells in the body. Naturally occurring phenolic acid derivatives such as ferulic, caffeic, gallic acids, and curcumin are reported to possess anticancer activity.

1.05.10.2.1 Minerals in cancer management

Selenium is an important mineral that has cancer preventive effects. It induces P450 enzyme present in liver that detoxify the cancerogenic molecules. Selenium appears to exert its cancer chemopreventive effects through induction of cell cycle arrest and apoptosis and reduction of angiogenesis.[91] Selenium is present in the active site of many enzymes including thioredoxin, which catalyze the oxidation–reduction reactions thereby causing apoptosis.

Manganese present in trace amounts in the body is an essential component of the antioxidant enzyme superoxide dismutase, which helps to fight against free radicals and prevent heart disease and cancer.

1.05.10.2.2 Vitamins in cancer management

Vitamin C (**13**), an essential nutrient in the human diet and a free radical scavenger, helps in the remedy for gastric cancer. It is important for the development of immune cell system and mobilizes these specialized cells to fight against cancer. The reported mechanism of prevention of cancer by vitamin C is induction of apoptosis through cell cycle arrest, activation of the apoptosis factors, and interference with iron uptake in cells. Vitamin D_3 (**3**) has been shown to reduce the incidence of colon cancer.[92] Vitamins E (**4**) being a powerful antioxidant has been suggested to prevent lung cancer. Since folic acid plays an integral role in DNA methylation and DNA synthesis, it may possess cancer protective effect.

1.05.10.3 Nutraceuticals in Diabetes

Diabetes is a metabolic disorder, where the body is unable to utilize carbohydrate due to lack of insulin, a hormone naturally produced by the beta cells of the islets of langerhans in pancreas. Number of people affected by type 2 diabetes is increasing in every country and this fast-growing metabolic disorder is expected to affect 592 million worldwide by 2035. Apart from pharmaceuticals and lifestyle changes, nutraceuticals played a major role in prevention and management of diabetes. Researchers have proved that cinnamon, garlic, onion, ginseng, *Gymnema sylvestre*, fenugreek, bitter melon, and mushroom such as *Pleurotus obstreatus* have specific health benefits against diabetes.[93,94] The probable beneficial antidiabetic effects of these functional foods may be due to their decreased glucose production in liver, decrease in intestinal glucose absorption, increase in insulin production, and increase in peripheral glucose uptake. Among diabetes, type 2 diabetes is growing rapidly worldwide and nuts enriched with omega-3 fatty acid and cinnamon are potential functional foods for the treatment of type 2 diabetes. Omega-3 fatty acids have been suggested to reduce glucose tolerance in patients predisposed to diabetes.

Diabetic complications due to harmful glucose metabolites may be reduced by diet supplementation of diet with DHA. EFAs during pregnancy are recommended for women with gestational diabetes mellitus.[95]

Lipoic acid (thioctic acid), a naturally occurring dithiol compound and essential cofactor for mitochondrial bioenergetic enzymes, is an important micronutrient with antioxidant properties that can alleviate the pain associated by this diabetic neuropathy.[96]

Leaf extract of *Psidium guajava* (guava) prevents the protein glycation, thereby strongly protects against the complications of diabetes. Gutierres et al.[97] reported that curcumin supplemented with yogurt prevent diabetes.

Fiber-rich foods reported to increase insulin action by increasing insulin receptor binding and by decreasing the rate of absorption of sugar from blood thereby maintaining sugar level in the body. High fiber content cherries believed to have antidiabetic action primarily due to the antioxidant properties and blood glucose reducing properties of anthocyanins and quercetin present in the fruit. Diabetes and associated symptoms are believed to be regulated by the cherries by poor glucose utilization. Fenugreek, a good diabetes-reversing herb because of its high-soluble fiber content, helps to lower blood sugar levels by slowing the digestion and absorption of carbohydrates. Fenugreek contains 4-hydroxyisoleucine and galactomann that helps in increasing insulin production and slowing down the absorption of blood sugar levels respectively.

Supplementation of diet with vanadium decreases fasting blood glucose levels, glycated hemoglobin levels, and cholesterol levels at a dose of 45–150 mcg day^{-1}.

Aqueous extract of *M. purpureus* fermented rice is also reported for antidiabetic activity in streptozotocin induced diabetic rats.[98]

1.05.10.4 Nutraceuticals in Obesity

Obesity is due to excessive consumption of high-fat and energy-rich foods, which leads to the formation of fatty plaques on the inner surface of the arteries that restrict the flow of blood to various parts of the body. The absence of blood circulation in some organs can cause harmful consequences such as angina pectoris, heart attack, cardiac arrest, transient ischemic attack, and stroke. In addition, obesity is accompanied by other complications such as diabetes, fatty liver, cholesterol gallstones, sleep apnea, osteoarthritis respiratory disorders, insulin resistance (diabetes), osteoarthritis, renal dysfunction, cancer, and reduced fertility.[99]

The very high prevalence of more than 50% obese population globally is in need of nutraceutical in addition to continuous and regular physical exercise in its prevention and treatment. Rapid rise in obesity rates is due to excessive consumption of energy-rich foods. Nutraceuticals like conjugated linoleic acid, capsaicin, *Momordica charantia*, and *Psyllium* fiber possess potential antiobese properties.[100] Increase in body weight and fat can be considerably reduced in obese individuals by taking nutraceuticals like ephedrine, ma huang-guarana, chitosan, green tea, glucomannan, fenugreek, and vitamin C in the dietary supplement.

Intake of dietary fibers with meals is important to control obesity where it may decrease body weight, body fat, and body mass index.[101] Dietary fiber reduces the caloric density of foods by physical dilution and by entrapment of nutrients, which reduces the

rate of digestion and absorption (bioavailability) of nutrients, especially glucose and lipids. Glucomannan is a natural gel forming fiber obtained from *Amorphopallus konjac* tubers chemically called beta 1,4-linked D-glucose and D-mannose having high viscosity promote weight loss and is effective in the prevention/treatment of overweight and obesity. Soluble fibers that form viscous hydrated masses suppress appetite better than the less viscous fibers. The high viscosity prolongs the presence of nutrients in the small intestine, downregulates release of appetite stimulating hormones, and leads to reduced appetite. Buckwheat seed proteins have beneficial role in obesity and constipation acting similar to natural fibers present in food.[102]

Supplemenation of food with omega-3 fatty acid has been shown to involve in weight loss, decreased appetite, modulation of lipogenic gene expression, and tissue metabolism.

Curcumin (diferuloylmethane) is a useful phytochemical that attenuates obesity-induced inflammation and obesity-related metabolic complications and weight loss at a dose of 400 mg day^{-1}.

5-Hydroxytryptophan and green tea extract may promote weight loss, while the former decreases appetite, the later increases the energy expenditure.[103]

Studies revealed that two carotenoids namely fucoxanthin and astaxanthin may have significant effect in reduction of body weight.

1.05.10.5 Nutraceuticals in Chronic Inflammatory Disorders

Arthritis is one of the very common inflammatory disorders occurring in elderly population. It was reported that more than 1% of world population is affected by arthritis. It is characterized by pain, swelling, and stiffness in joints due to synovial inflammation and hyperplasia, autoantibody production, cartilage, and bone destruction. Among 100 types of arthritis, rheumatoid and osteoarthritis are most common types of arthritis. Nutrient supplement with glucosamine (**29**), chondroitin (**30**), methylsulfonylmethane (**31**), and *S*-adenosyl methionine (**32**) proved that it can alleviate diseased condition of RA (Fig. 8).

1.05.10.5.1 Glucosamine

It is present in cartilage, tendon, and ligament tissue in humans. Normal diet does not contain this glucosamine and must be synthesized by body and the ability of this synthesis decreases with age. For arthritic treatment, it is given as an oral dose of 1500 mg day^{-1} in sulfate or hydrochloride or *n*-acetyl forms.

1.05.10.5.2 Chondroitin

Chondroitin is a glycoaminoglycan made up of alternative sequences of differently sulfonated units of uronic acid and *N*-acetyl galactosamine. It is a substance that occurs naturally in the body and lubricates joints and maintains healthy cartilage tissue. It can be commercially obtained only from animal sources like bovine, pigs, and chicken cartilage. Daily recommended dose of 1200–1500 mg day^{-1} is orally given for arthritis.

1.05.10.5.3 Methylsulfonylmethane

It is derivative of DMSO, also called as dimethyl sulfone or methyl sulfone. It is present in meat, milk, and in asparagus. It is recommended for healthy joints up to a dose of 2 g day^{-1} available in the form of cream, tablets, capsules, and powders.

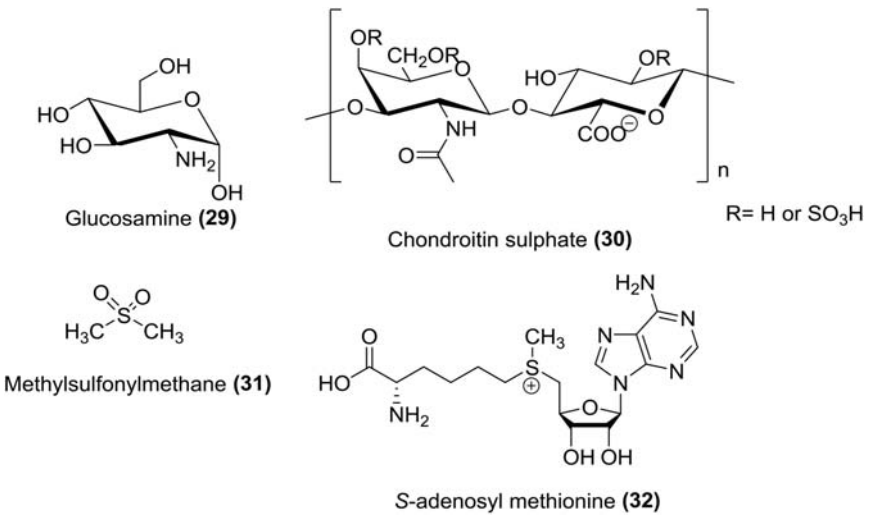

Fig. 8 Chemical structures of some nutraceuticals used in inflammatory disorders.

1.05.10.5.4 S-Adenosyl methionine

S-Adenosyl methionine synthatase is the enzyme responsible for the production of *S*-adenosyl methionine from methionine and ATP. *S*-adenosyl methionine is involved in transmethylation, translation, and aminopropylation reaction. The recommended daily dose of *S*-adenosyl methionine for joints and mental health is in the range of 200–1200 mg.

1.05.10.5.5 Pomegranate

High content of soluble polyphenols, hydrolyzable tannins, anthocyanins, and punicalagins in pomegranate fruit proved to have preventive effect on inflammation, arthritis, and pain.[104] Antiinflammatory activity was reported to exhibit by inhibiting the activity of NF-kB, COX-2, and Prostaglandin E2.[105]

1.05.10.6 Nutraceuticals for Parkinson's Disease

Parkinson's disease is a brain disorder that results from nerve damage in certain regions of the brain causing muscle rigidity, tremor, and akinesia,[106] usually occurring in mid to late adult life. Dopamine-rich foods like meat, milk products, fish, beans, nuts, soy products, and dopamine quinine, a naturally occurring form of dopamine present in banana are recommended for the prevention of Parkinson's disease. Canadian researchers indicated that vitamin E in food may be protective against Parkinson's disease.[107] Creatine is a nitrogenous organic acid produced in liver from amino acids L-arginine, glycine, and L-methionine that helps to supply energy to cells. Researchers have suggested that nutraceuticals such as creatine, glutathione, vitamins C and D, coenzyme Q10, polyphenols, stilbenes, and phytoestrogens prevent or delay the progression of Parkinson's disease (Fig. 9).

1.05.10.7 Nutraceuticals for Alzheimer's Disease

Alzheimer's disease is the first most common aging-related disorder in the world. It is characterized by progressive dementia with memory loss as the major clinical manifestation. Several lines of evidence strongly suggest that oxidative stress is etiologically related to a number of neurodegenerative disorders including Alzheimer's disease. Nutraceutical antioxidants, like β-carotene, curcumin, lutein, lycopene, turmerin etc., may exert positive effects on specific diseases by neutralizing the negative effects, oxidative

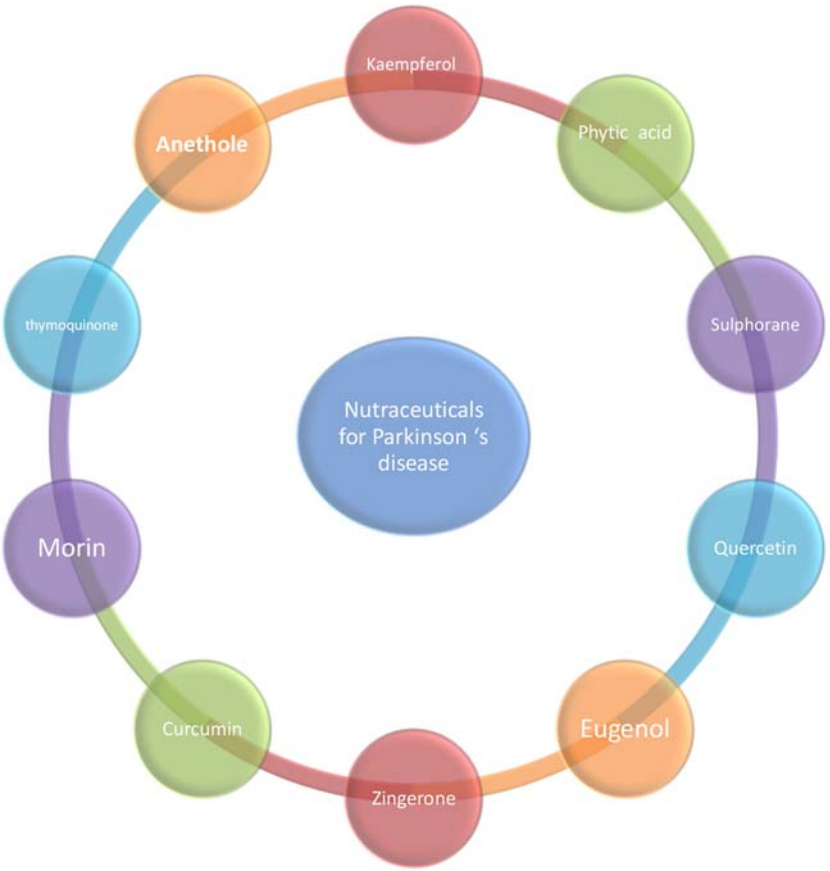

Fig. 9 Nutraceuticals in prevention of Parkinson's disease.

stress, mitochondrial dysfunction, and various forms of neural degeneration. Oleic acid, a monounsaturated fatty acid, has also been proposed to have a potential role in decreasing brain-related disorders such as dementia and Alzheimer's disease. DHA is essential for the maintenance of normal brain function in infants and adults and hence decrease in DHA level may have onset of Alzheimer's disease. Epigallocatechcin-3-gallate, an important constituent of green tea, is suggested as a potential agent for Alzheimer's disease as it has the ability to inhibit aggregation of amyloid-β, which is a major pathogenic factor in the development and severity of the disease. A great deal of research has pointed to deleterious roles of metal ions in the development of Alzheimer's disease, by the augmentation of oxidative stress by metal ion. The growing trend in nutraceutical intake is a result of the belief that they postpone the development of dementias such as Alzheimer's disease.

1.05.11 Conclusion

Nutraceuticals present in a healthy diet provide energy and nutrient supplements to body, which are required for maintaining optimal health. Low intake of vegetables fruits, minerals, and vitamins clearly indicated for the cause of development of various diseases. Antioxidants, dietary fibers, with recommended daily requirement of proteins, vitamins, and minerals together with physical exercise can prevent and treat these diseases. Poor lifestyle habits, consumption of junk food, and low physical activity led to a number of diseases related to nutritional deficiencies. Thus to conclude, optimal nutrition with proper intake of nutraceuticals in maintaining health to combat against acute and chronic diseases due to nutritional disorders will promote optimal health, longevity, and quality of life. However, their success in prevention of diseases and maintaining health mainly depends on purity, efficacy, and safety of nutraceuticals. Assessment of efficacy of nutraceuticals is essential and it is the measure of its ability to improve health and well-being. Assessment of safety can be based on the type of nutraceuticals, that is, if raw materials of nutraceuticals are traditional foods (yogurt, oat meal, and tea), then toxicity study may not be required as they are recognized as safe foods. If the raw materials of nutraceuticals are not traditional, then safety data for genotoxicity, carcinogenicity, teratogenicity, and 90-day toxicity study is required.

References

1. Sharma, R. Nutraceuticals and Nutraceutical Supplementation Criteria in Cancer: A Literature Survey. *Open Nutraceuticals J.* **2009,** *2,* 92–106.
2. Manisha, P.; Rohit, K. V.; Shubhini, A. S. Nutraceuticals: New Era of Medicine and Health. *Asian J. Pharm. Clin. Res.* **2010,** *3,* 11–15.
3. Brower, V. Nutraceuticals: Poised for a Healthy Slice of the Healthcare Market? *Nat. Biotechnol.* **1998,** *16,* 728–731.
4. Zeisel, S. H. Regulation of Nutraceuticals. *Science* **1999,** *285,* 185–186.
5. Das, L.; Bhaumik, E.; Raychaudhuri, U.; Chakraborty, R. Role of Nutraceuticals in Human Health. *J. Food Sci. Technol.* **2012,** *49,* 173–183.
6. De Felice, S. L. The Nutraceutical Revolution, Its Impact on Food Industry. *Trends Food Sci. Technol.* **1995,** *6,* 59–61.
7. Arai, S. Studies on Functional Foods in Japan. *Biosci. Biotechnol. Biochem.* **1996,** *60,* 9–15.
8. Prakash, P.; Krinsky, N. I.; Russell, R. M. Retinoids, Carotenoids, and Human Breast Cancer Cell Cultures: A Review of Differential Effects. *Nutr. Rev.* **2000,** *58* (6), 170–176.
9. Heller, E. H.; Shiffman, N. J. Synthetic Retinoids in Dermatology. *Can. Med. Assoc. J.* **1985,** *132* (10), 1129–1136.
10. Guyton, K. Z.; Kensler, T. W.; Posner, G. H. Vitamin D and Vitamin D Analogs as Cancer Chemopreventive Agents. *Nutr. Rev.* **2003,** *61* (7), 227–238.
11. Holick, M. F. Vitamin D: Importance in the Prevention of Cancers, Type 1 Diabetes, Heart Disease, and Osteoporosis. *Am. J. Clin. Nutr.* **2004,** *79* (3), 362–371.
12. Vermeer, C.; Knapen, M. H.; Schurgers, L. J. Vitamin K and Metabolic Bone Disease. *J. Clin. Pathol.* **1998,** *51* (6), 424–426.
13. Kuzniarz, M.; Mitchell, P.; Cumming, R. G.; Flood, V. M. Use of Vitamin Supplements and Cataract: The Blue Mountains Eye Study. *Am J. Ophthalmol.* **2001,** *132* (1), 19–26.
14. Premkumar, V. G.; Yuvaraj, S.; Vijayasarathy, K.; Gangadaran, S. G.; Sachdanandam, P. Effect of Coenzyme Q10, Riboflavin and Niacin on Serum CEA and CA 15–3 Levels in Breast Cancer Patients Undergoing Tamoxifen Therapy. *Biol. Pharm. Bull.* **2007,** *30* (2), 367–370.
15. Hannan, F.; Davoren, P. Use of Nicotinic Acid in the Management of Recurrent Hypoglycemic Episodes in Diabetes. *Diabetes Care* **2001,** *24* (7), 1301.
16. Canner, P. L.; Berge, K. G.; Wenger, N. K.; Stamler, J.; Friedman, L.; Prineas, R. J.; Friedewald, W. Fifteen Year Mortality in Coronary Drug Project Patients: Long-Term Benefit With Niacin. *J. Am. Coll. Cardiol.* **1986,** *8* (6), 1245–1255.
17. Naruta, E.; Buko, V. Hypolipidemic Effect of Pantothenic Acid Derivatives in Mice With Hypothalamic Obesity Induced by Aurothioglucose. *Exp. Toxicol. Pathol.* **2001,** *53* (5), 393–398.
18. Charles, B. M.; Hosking, G.; Green, A.; Pollitt, R.; Bartlett, K.; Taitz, L. S. Biotin-Responsive Alopecia and Developmental Regression. *Lancet* **1979,** *2* (8134), 118–120.
19. Shirodaria, C.; Antoniades, C.; Lee, J.; Jackson, C. E.; Robson, M. D.; Francis, J. M.; Moat, S. J.; Ratnatunga, C.; Pillai, R.; Refsum, H.; Neubauer, S.; Channon, K. M. Global Improvement of Vascular Function and Redox State With Low-Dose Folic Acid. Implications for Folate Therapy in Patients With Coronary Artery Disease. *Circulation* **2007,** *115,* 2262–2270.
20. Kune, G.; Watson, L. Colorectal Cancer Protective Effects and the Dietary Micronutrients Folate, Methionine, Vitamins B6, B12, C, E, Selenium and Lycopene. *Nutr. Cancer* **2006,** *56* (1), 11–21.
21. Lajous, M.; Romieu, I.; Sabia, S.; Boutron-Ruault, M. C.; Clavel-Chapelon, F. Folate, Vitamin B12 and Postmenopausal Breast Cancer in a Prospective Study of French Women. *Cancer Causes Control* **2006,** *17* (9), 1209–1213.
22. Tettamanti, M.; Garri, M. T.; Nobili, A.; Riva, E.; Lucca, U. Low Folate and the Risk of Cognitive and Functional Deficits in the Very Old: The Monzino 80-Plus Study. *J. Am. Coll. Nutr.* **2006,** *25* (6), 502–508.
23. Quinlivan, E. P.; McPartlin, J.; McNulty, H.; Ward, M.; Strain, J. J.; Weir, D. G.; Scott, J. M. Importance of Both Folic Acid and Vitamin B12 in Reduction of Risk of Vascular Disease. *Lancet* **2002,** *359* (9302), 227–228.
24. Donaldson, M. S. Nutrition and Cancer: A Review of the Evidence for an Anti-Cancer Diet. *Nutr. J.* **2004,** *3,* 19.
25. Clarke, R.; Smith, A. D.; Jobst, K. A.; Refsum, H.; Sutton, L.; Ueland, P. M. Folate, Vitamin B12, and Serum Total Homocysteine Levelsin Confirmed Alzheimer Disease. *Arch. Neurol.* **1998,** *55* (11), 1449–1455.
26. Lee, K. W.; Lee, H. J.; Surh, Y. J.; Lee, C. Y. Vitamin C and Cancer Chemoprevention: Reappraisal. *Am. J. Clin. Nutr.* **2003,** *78* (6), 1074–1078.
27. Lieberman, S.; Brunning, N. *Real Vitamin and Mineral Book;* Penguin Books: New York, 2003.

28. Riggs, B. L.; Hodgson, S. F.; O'Fallon, W. M.; Chao, E. Y.; Wahner, H. W.; Muhs, J. M.; Cedel, S. L.; Melton, L. J. Effect of Fluoride Treatment on the Fracture Rate in Postmenopausal Women With Osteoporosis. *N. Engl. J. Med.* **1990,** *322* (12), 802–809.
29. Ferguson, L. R.; Philpott, M.; Karunasinghe, N. Dietary Cancer and Prevention Using Antimutagens. *Toxicology* **2004,** *198* (2004), 147–159.
30. De Quiros, A. R. B.; Costa, H. S. Analysis of Carotenoids in Vegetable and Plasma Samples: A Review. *J. Food Compos. Anal.* **2006,** *19,* 97–111.
31. Kantoff, P. Prevention, Complementary Therapies, and New Scientific Developments in the Field of Prostate Cancer. *Rev. Urol.* **2006,** *8* (2), S9–S14.
32. Lonn, E. M.; Yusuf, S. Clinical Evidence: Emerging Approaches in Preventing Cardiovascular Disease. *West. J. Med.* **1999,** *171* (4), 247–252.
33. Sesso, H. D.; Liu, S.; Gaziano, J. M.; Buring, J. E. Dietary Lycopene, Tomato-Based Food Products and Cardiovascular Disease in Women. *J. Nutr.* **2003,** *133,* 2336–2341.
34. Mozaffarieh, M.; Sacu, S.; Wedrich, A. The Role of the Carotenoids, Lutein and Zeaxanthin, in Protecting Against Age-Related Macular Degeneration: A Review Based on Controversial Evidence. *Nutr. J.* **2003,** *2,* 20.
35. Scalbert, A.; Manach, C.; Morand, C.; Remesy, C. Dietary Polyphenols and the Prevention of Diseases. *Crit. Rev. Food Sci. Nutr.* **2005,** *45,* 287–306.
36. Beecher, G. R. Overview of Dietary Flavonoids: Nomenclature, Occurrence and Intake. *J. Nutr.* **2003,** *133,* 3248S–3254S.
37. Singh, B. N.; Singh, B. R.; Singh, R. L.; Prakash, D.; Singh, D. P.; Sharma, B. K.; Upadhyay, G.; Singh, H. B. Polyphenolics From Various Extracts/Fractions of Red Onion (*Allium cepa*) Peel With Potential Antioxidant and Antimutagenic Activities. *Food Chem. Toxicol.* **2009,** *47,* 1161–1167.
38. Rice-Evans, C. A.; Miller, J. M.; Paganga, G. Structure-Antioxidant Activity Relationship of Flavonoids and Phenolic Acids. *Free Radic. Biol. Med.* **1999,** *20,* 935–936.
39. Shukla, S.; Gupta, S. Apigenin: A Promising Molecule for Cancer Prevention. *Pharm. Res.* **2010,** *27* (6), 962–978.
40. Aneja, R.; Hake, P. W.; Burroughs, T. J.; Denenberg, A. G.; Wong, H. R.; Zingarelli, B. Epigallowcatechin, a Green Tea Polyphenol, Attenuates Myocardial Ischemia Reperfusion Injury in Rats. *Mol. Med.* **2004,** *10,* 1–6.
41. Gao, X.; Kuo, J.; Jiang, H.; Deeb, D.; Liu, Y.; Divine, G.; Chapman, R. A.; Dulchavsky, S. A.; Gautam, S. C. Immuno-Modulatory Activity of Curcumin: Suppression of Lymphocyte Proliferation, Development of Cell-Mediated Cytotoxicity and Cytokine Production *In Vitro. Biochem. Pharmacol.* **2004,** *68,* 51–61.
42. Mursu, J.; Nurmi, T.; Tuomainen, T. P.; Ruusunen, A.; Salonen, J. T.; Voutilainen, S. The Intake of Flavonoids and Carotid Atherosclerosis: The Kuopio Ischaemic Heart Disease Risk Factor Study. *Br. J. Nutr.* **2007,** *98* (4), 814–818.
43. Zhang, B.; Osborne, N. N. Oxidative-Induced Retinal Degeneration Is Attenuated by Epigallocatechin Gallate. *Brain Res.* **2006,** *1124* (1), 176–187.
44. Li, T.; Liu, J.; Zhang, X.; Ji, G. Antidiabetic Activity of Lipophilic (−) Epigallocatechin-3-gallate Derivative Under Its Role of Alphaglucosidase Inhibition. *Biomed. Pharmacother.* **2007,** *61* (1), 91–96.
45. Mandel, S.; Amit, T.; Reznichenko, L.; Weinreb, O.; Youdim, M. B. Green Tea Catechins as Brain-Permeable, Natural Iron Chelators Antioxidants for the Treatment of Neurodegenerative Disorders. Review. *Mol. Nutr. Food Res.* **2006,** *50* (2), 229–234.
46. Friedman, M. Overview of Antibacterial, Antitoxin, Antiviral, and Antifungal Activities of Tea Flavonoids and Teas. *Mol. Nutr. Food Res.* **2007,** *51* (1), 116–134.
47. Tim Cushnie, T. P.; Lamb, A. J. Antimicrobial Activity of Flavonoids. *Int. J. Antimicrob. Agents* **2005,** *26,* 343–356.
48. Kawai, M.; Hirano, T.; Higa, S.; Arimitsu, J.; Maruta, M.; Kuwahara, Y.; Ohkawara, T.; Hagihara, K.; Yamadori, T.; Shima, Y.; Ogata, A.; Kawase, I.; Tanaka, T. Flavonoids and Related Compounds as Anti-Allergic Substances. *Allergol. Int.* **2007,** *56* (2), 113–123.
49. Traka, M.; Meithein, R. Glucosinolates Isothiocyantes and Human Health. *Phytochem. Rev.* **2009,** *8,* 269–282.
50. Cramer, J. M.; Teran-Garcia, M.; Jeffery, E. H. Enhancing Sulforaphane Absorption and Excretion in Healthy Men Through the Combined Consumption of Fresh Broccoli Sprouts and a Glucoraphanin-Rich Powder. *Br. J. Nutr.* **2011,** *13,* 1–6.
51. Touloupakis, E.; Ghanotakis, D. F. Nutraceutical Use of Garlic Sulfur-Containing Compounds. *Adv. Exp. Med. Biol.* **2010,** *698,* 110–121.
52. Augusti, K. Therapeutic Values of Onion and Garlic. *Indian J. Exp. Biol.* **1996,** *34,* 634–640.
53. Sleator, R. D. Probiotics—A Viable Therapeutic Alternative for Enteric Infections Especially in the Developing World. *Discov. Med.* **2010,** *10* (51), 119–124.
54. Sleator, R. D.; Hill, C. New Frontiers in Probiotic Research. *Lett. Appl. Microbiol.* **2008,** *46* (2), 143–147.
55. Aller, R.; De Luis, D. A.; Izaola, O.; Conde, R.; Gonzalez Sagrado, M.; Primo, D.; De La Fuente, B.; Gonzalez, J. Effect of a Probiotic on Liver Aminotransferases in Nonalcoholic Fatty Liver Disease Patients: A Double Blind Randomized Clinical Trial. *Eur. Rev. Med. Pharmacol. Sci.* **2011,** *15* (9), 1090–1095.
56. Megraud, F. H. Pylori Antibiotic Resistance: Prevalence, Importance, and Advances in Testing. *Gut* **2004,** *53,* 1374–1384.
57. Mack, D. R.; Ahrne, S.; Hyde, L.; Wei, S.; Hollingsworth, M. A. Extracellular MUC3 Mucin Secretion Follows Adherence of *Lactobacillus* Strains to Intestinal Epithelial Cells In Vitro. *Gut* **2003,** *52,* 827–833.
58. Aiba, Y.; Suzuki, N.; Kabir, A. M.; Takagi, A.; Koga, Y. Lactic Acid-Mediated Suppression of *Helicobacter pylori* by the Oral Administration of *Lactobacillus salivarius* as a Probiotic in a Genotobiotic Murine Model. *Am. J. Gastroenterol.* **1998,** *93,* 2097–2101.
59. Mukai, T.; Asasaka, T.; Sato, E.; Mori, K.; Matsumoto, M.; Ohori, H. Inhibition of Binding of *Helicobacter pylori* to the Glycolipid Receptors by Probiotic *Lactobacillus reuteri*. *FEMS Immunol. Med. Microbiol.* **2002,** *32,* 105–110.
60. Rissanen, T. H.; Voutilainen, S.; Virtanen, J. K.; Venho, B.; Vanharanta, M.; Mursu, J.; Salonen, J. T. Low Intake of Fruits, Berries and Vegetables Is Associated With Excess Mortality in Men: The Kuopio Ischaemic Heart Disease Risk Factor (KIHD) Study. *J. Nutr.* **2003,** *13,* 199–204.
61. Hu, F. B.; Willett, W. C. Optimal Diets for Prevention of Coronary Heart Disease. *JAMA* **2002,** *288,* 2569–2578.
62. German, J. B.; Walzem, R. L. The Health Benefits of Wine. *Ann. Rev. Nutr.* **2000,** *20,* 561–593.
63. Hargis, P. S.; Van Elswyk, M. E. Manipulating the Fatty Acid Composition of Poultry Meat and Eggs for the Health Conscious Consumer. *World's Poultry Sci. J.* **1993,** *49,* 251–264.
64. Roush, J. K.; Dodd, C. E.; Fritsch, D. A.; Allen, T. A.; Jewell, D. E.; Schoenherr, W. D.; Richardson, D. C.; Leventhal, P. S.; Hahn, K. A. Multicenter Veterinary Practice Assessment of the Effects of Omega-3 Fatty Acids on Osteoarthritis in Dogs. *J. Am. Vet. Med. Assoc.* **2010,** *236* (1), 59–66.
65. Kjeldsen-Kragh, J.; Lund, J. A.; Riise, T.; Finnanger, B.; Haaland, K.; Finstad, R.; Mikkelsen, K.; Førre, O. Dietary Omega-3 Fatty Acid Supplementation and Naproxen Treatment in Patients With Rheumatoid Arthritis. *J. Rheumatol.* **1992,** *19* (10), 1531–1536.
66. Kris-Etherton, P. M.; Harris, W. S.; Appel, L. J. Fish Consumption, Fish Oil, Omega-3 Fatty Acids and Cardiovascular Disease. *Circulation* **2002,** *106,* 2747–2757.
67. Caston, L.; Leeson, S. Research Note: Dietary Flaxseed and Egg Composition. *Poultry Sci.* **1990,** *69,* 1617–1620.
68. Bourre, J. M.; Galea, F. An Important Source of Omega-3 Fatty Acids, Vitamins D and E, Carotenoids, Iodine and Selenium: A New Natural Multi-Enriched Egg. *J. Nutr. Health Ageing* **2006,** *10* (5), 371–376.
69. Surai, P. F.; Sparks, N. H. C. Designer Eggs: From Improvement of Egg Composition to Functional Food. *Trends Food Sci. Technol.* **2001,** *2* (1), 7–16.
70. Anderson, J.; Baird, P.; Davis, R.; Ferreri, S.; Knudtson, M.; Korayn, A. Health Benefits of Dietary Fiber. *Nutr. Rev.* **2009,** *67* (4), 188–205.
71. Cook, N. C.; Samman, S. Flavonoids—Chemistry, Metabolism, Cardioprotective Effects, and Dietary Sources. *J. Nutr. Biochem.* **1996,** *7,* 66–76.
72. Hollman, P. C. H.; Feskens, E. J.; Katan, M. B. Tea Flavonols in Cardiovascular Disease and Cancer Epidemiology. *Proc. Soc. Exp. Biol. Med.* **1999,** *220,* 198–202.
73. Ferrieres, J. The French Paradox: Lessons for Other Countries. *Heart* **2004,** *90,* 107–111.
74. Dutta, P. C. *Phytosterols as Functional Food Components and Nutraceuticals;* Marcel Dekker: Edinburgh, 2003.
75. Berthold, I. G.; Berthhold, H. K. Policosanol: Clinical Pharmacology and Therapeutic Significance of a New Lipid-Lowering Agent. *Am. Heart J.* **2002,** *143,* 356–365.
76. Silagy, C.; Neil, A. Garlic as a Lipid Lowering Agent: A Meta-Analysis. *J. R. Coll. Physicians Lond.* **1994,** *28,* 39–45.
77. McMurray, J. J. V.; Dunselman, P.; Wedel, H.; Cleland, J. G. F.; Lindberg, M.; Hjalmarson, A.; Kjekshus, J.; Waagstein, F.; Apetrei, E.; Barrios, V. Coenzyme Q10, Rosuvastatin, and Clinical Outcomes in Heart Failure. *J. Am. Coll. Cardiol.* **2010,** *56,* 1196–1204.
78. Heber, D.; Yip, I.; Ashley, J. M.; Elashoff, D. A.; Elashoff, R. M.; Go, V. L. Cholesterol-Lowering Effects of a Proprietary Chinese Red-Yeast Rice Dietary Supplement. *Am. J. Clin. Nutr.* **1999,** *69,* 231–236.
79. Endo, A. Monacolin K, a New Hypocholesterolemic Agent Produced by a *Monascus* Species. *J. Antibiot.* **1979,** *32,* 852–854.

80. Rajasekaran, A.; Kalaivani, M. Hypolipidemic and Antioxidant Activity of Aqueous Extract of *Monascus purpureus* Fermented Indian Rice in High Cholesterol Diet Fed Rats. *Turk. J. Med. Sci.* **2011,** *41* (1), 25–32.
81. Kalaivani, M.; Sabitha, R.; Kalaiselvan, V.; Rajasekaran, A. Health Benefits and Clinical Impact of Major Nutrient, Red Yeast Rice: A Review. *Food Bioprocess Technol.* **2010,** *3* (3), 333.
82. Margovich, M. J.; Morris, J.; Brown, V.; Ellis, J.; Logothetis, B.; Weber, R. Nutraceutical Use in Late-Stage Cancer. *Cancer Metastasis Rev.* **2010,** *29,* 503–510.
83. Davenport, D. J.; Roudebush, P. The Use of Nutraceuticals in Cancer Therapy. *NAVC Proc. Small Animal-Oncol.* **2006,** *20,* 7–11.
84. Fenwick, G. R.; Heaney, R. K. Glucosinolates and Their Break-Down Products in Cruciferous Crops, Foods and Feeding Stuffs. *Food Chem.* **1983,** *11,* 249–271.
85. Basu, H. N.; Vecchio, A. J. D.; Flider, F.; Orthoefer, F. T. Nutritional and Potential Disease Prevention Properties of Carotenoids. *J.A.O.C.S.* **2001,** *78* (7), 665–675.
86. Hakimuddin, F.; Paliyath, G.; Meckling, K. Selective Cytotoxicity of a Red Grape Wine Flavonoid Fraction Against MCF-7 Cells. *Breast Cancer Res. Treat.* **2004,** *85* (1), 65–79.
87. Damianaki, A.; Bakogeorgou, E.; Kampa, M.; Notas, G.; Hatzoglou, A.; Panagiotou, S.; Gemetzi, C.; Kouroumalis, E.; Martin, P. M.; Castanas, E. Potent Inhibitory Action of Red Wine Polyphenols on Human Breast Cancer Cells. *J. Cell. Biochem.* **2000,** *78* (3), 429–441.
88. Potter, J. D. Colorectal Cancer: Molecules and Populations. *J. Natl. Cancer Inst.* **1999,** *91,* 916–932.
89. Weisburger, J. H.; Rivenson, A.; Aliaga, C.; Reinhardt, J.; Kelloff, G. J.; Boone, C. W.; Steele, V. E.; Balentine, D. A.; Pittman, B.; Zang, E. Effect of Tea Extracts, Polyphenols, and Epigallocatechin Gallate on Azoxymethane-Induced Colon Cancer. *Proc. Soc. Exp. Biol. Med.* **1998,** *217* (1), 104–108.
90. Mukhtar, H.; Ahmad, N. Tea Polyphenols: Prevention of Cancer and Optimizing Health. *Am. J. Clin. Nutr.* **2000,** *71* (6), 1698S–1702S.
91. Jiang, C.; Ganther, H.; Lu, J. Monomethyl Selenium-Specific Inhibition of MMP-2 and VEGF Expression: Implications for Angiogenic Switch Regulation. *Mol. Carcinog.* **2000,** *29,* 236–250.
92. Grant, W. B.; Garland, C. F. Evidence Supporting the Role of Vitamin D in Reducing the Risk of Cancer. *J. Intern. Med.* **2002,** *252,* 178–179.
93. Ballali, S.; Lanciai, F. Functional Food and Diabetes: A Natural Way in Diabetes Prevention? *Int. J. Food Sci. Nutr.* **2012,** *63* (1), 51–61.
94. Jayasuriya, W. J.; Wanigatunge, C. A.; Fernando, G. H.; Abeytunga, D. T.; Suresh, T. S. Hypoglycaemic Activity of Culinary *Pleurotus ostreatus* and *P. Cystidiosus* Mushrooms in Healthy Volunteers and Type 2 Diabetic Patients on Diet Control and the Possible Mechanisms of Action. *Phytother. Res.* **2015,** *29* (2), 303–309.
95. Thomas, B.; Ghebremeskel, K.; Lowy, C.; Crawford, M.; Bridget Offley-Shore, R. N. Nutrient Intake of Women With and Without Gestational Diabetes With a Specific Focus on Fatty Acids. *Nutrition* **2006,** *22,* 230–236.
96. Coleman, M. D.; Eason, R. C.; Bailey, C. J. The Therapeutic Use of Lipoic Acid in Diabetes: A Current Perspective. *Environ. Toxicol. Pharmacol.* **2001,** *10,* 167–172.
97. Gutierres, V. O.; Pinheiro, C. M.; Assis, R. P.; Vendramini, R. C.; Pepato, M. T.; Brunetti, I. L. Curcumin-Supplemented Yoghurt Improves Physiological and Biochemical Markers of Experimental Diabetes. *Br. J. Nutr.* **2011,** *9,* 1–9.
98. Rajasekaran, A.; Kalaivani, M. Anti-Diabetic Activity of Aqueous Extract of *Monascus purpureus* Fermented Rice in High Cholesterol Diet Fed-Streptozotocin-Induced Diabetic Rats. *Asian J. Sci. Res.* **2009,** *4,* 180–189.
99. Caterson, I. D.; Gill, T. P. Obesity: Epidemiology and Possible Prevention. *Best Pract. Res. Clin. Endocrinol. Metab.* **2002,** *16,* 595–610.
100. Kasbia, G. S. Functional Foods and Nutraceuticals in the Management of Obesity. *Nutr. Food Sci.* **2005,** *35,* 344–351.
101. Slavin, J. L. Dietary Fiber and Body Weight. *Nutrition* **2005,** *21* (3), 411–418.
102. Si-quan, L.; Zhang, Q. H. Advances in the Development of Functional Foods From Buckwheat. *Crit. Rev. Food Sci. Nutr.* **2001,** *41,* 451–464.
103. Bell, S. J.; Goodrick, G. K. A Functional Food Product for the Management of Weight. *Crit. Rev. Food Sci. Nutr.* **2002,** *42,* 163–178.
104. Seeram, N. P.; Adams, L. S.; Henning, S. M.; Niu, Y.; Zhang, Y.; Nair, M. G.; Heber, D. In Vitro Antiproliferative, Apoptotic and Antioxidant Activities of Punicalagin, Ellagic Acid and a Total Pomegranate Tannin Extract are Enhanced in Combination With Other Polyphenols as Found in Pomegranate Juice. *J. Nutr. Biochem.* **2005,** *16,* 360–367.
105. Rasheed, Z.; Akhtar, N.; Haqqi, T. M. Pomegranate Extract Inhibits the Interleukin-1beta-Induced Activation of MKK-3, p38alpha-MAPK and Transcription Factor RUNX-2 in Human Osteoarthritis Chondrocytes. *Arthritis Res. Ther.* **2010,** *12,* R195.
106. Losso, J. N. Targeting Excessive Angiogenesis With Functional Foods and Nutraceuticals. *Trends Food Sci. Technol.* **2003,** *14,* 455–468.
107. Latif, S.; Anwar, F.; Ashraf, M.; Gilani, A. H. *Moringa oleifera*: A Food Plant With Multiple Medicinal Uses. *Phytother. Res.* **2007,** *21,* 17–25.

1.06 Continuous Flow Processing as a Tool for Medicinal Chemical Synthesis

DL Browne, JL Howard, and C Schotten, Cardiff University, Cardiff, United Kingdom

© 2017 Elsevier Ltd. All rights reserved.

1.06.1	**Introduction**	135
1.06.2	**Fragments and Heterocycles**	136
1.06.2.1	Hazardous Gases	136
1.06.2.2	Diazonium Salts	139
1.06.2.3	Azides	140
1.06.2.4	Nitration	142
1.06.2.5	Oxidation	143
1.06.2.6	Reduction	143
1.06.2.7	Organometallic Reagents	145
1.06.2.8	Cyclocondensation	148
1.06.2.9	Cross-Coupling Reactions	150
1.06.2.10	Nucleophilic Substitution	151
1.06.2.11	Cycloaddition	151
1.06.2.12	Photochemistry	153
1.06.2.13	Miscellaneous	154
1.06.3	**Library Preparation and Automated Processes**	157
1.06.4	**Reaction Monitoring and Self-Optimizing Systems**	162
1.06.5	**Multistep Flow Processes**	166
1.06.6	**Conclusion and Outlook**	180
References		183

1.06.1 Introduction

Continuous flow processing as applied to the synthesis of fine chemicals is a burgeoning field of research. Specifically, this chemical processing technique has thus far been most closely aligned to the pharmaceutical industry.[1]

There are likely several reasons for this, not the least of which is the ongoing relationship between organic chemists in academia and industrialists in drug discovery and development. The issues and problems sometimes encountered when operating standard round-bottom flask, or "batch" reactions are familiar to all practitioners of synthesis. Indeed these problems typically compound themselves as scales are increased, such as during the early stages of a long natural product synthesis or in the pilot and process scaling for further drug development. A well-optimized and designed flow synthesis machine can negate many of the problems associated with scale-up. This is particularly the case for variation in reaction outcomes and reliability, especially if such results are born of poor control of mixing, heat-transfer, rates of addition, and timing. Essentially flow chemical techniques offer a tighter control on the important reaction parameters that synthetic chemists do not always consider, control, and/or monitor. Moreover, it achieves this through the very method itself, that is, it does not leave room for operator variation. Herein we shall provide a snapshot of some relevant examples of continuous flow processing for medicinal chemistry applications. Our account is by no means exhaustive, and we preemptively apologize for the many excellent examples that we have not incorporated into this overview. We have tried to provide comprehensive referencing to relevant review articles and would refer readers to those for more detailed overviews of more specific areas of interest. This article is designed to provide some initial theory on flow concepts and equipment before presenting a survey of examples as divided up in the subchapters.

Why use continuous flow processing? There are a few key considerations one should be aware of when deciding whether to use flow processing techniques. Unlike a traditional batch reactor where scale is dependent on the volume of the reactor, for a flow process scale is dependent on the length of time for which the process is run. Essentially once the flow process is started, product will be produced at a continuous rate and emerge from the reactor over time. Any point along the flow path represents a unique time point in the reaction process. Conversely for batch—the whole vessel experiences the same time point for the reaction as a bulk from start to finish. This imparts quite profound consequences on how one can start to think about a flow system in terms of space and time. Directly born from this consideration is the notion that continuous flow is inherently safer than batch. For example, if a reaction proceeds through the intermediacy of a hazardous or unstable species then in the flow reactor this will correspond to a single section of the reactor circuit and therefore a subsection of the whole inventory. Essentially, if an incident occurs, then only a small portion of the total inventory will represent the hazard, whereas in the analogous batch reactor the whole reaction vessel will represent the hazard. Incidents caused by these hazards could occur when mixing is insufficient, reaction exotherms are not dissipated, and runaway processes take hold. This brings us to the second inherent safety benefit of flow processing, improved surface area to volume ratios (SA:V). The improved SA:V means that previously uncontrolled exotherms can now be controlled as the heat

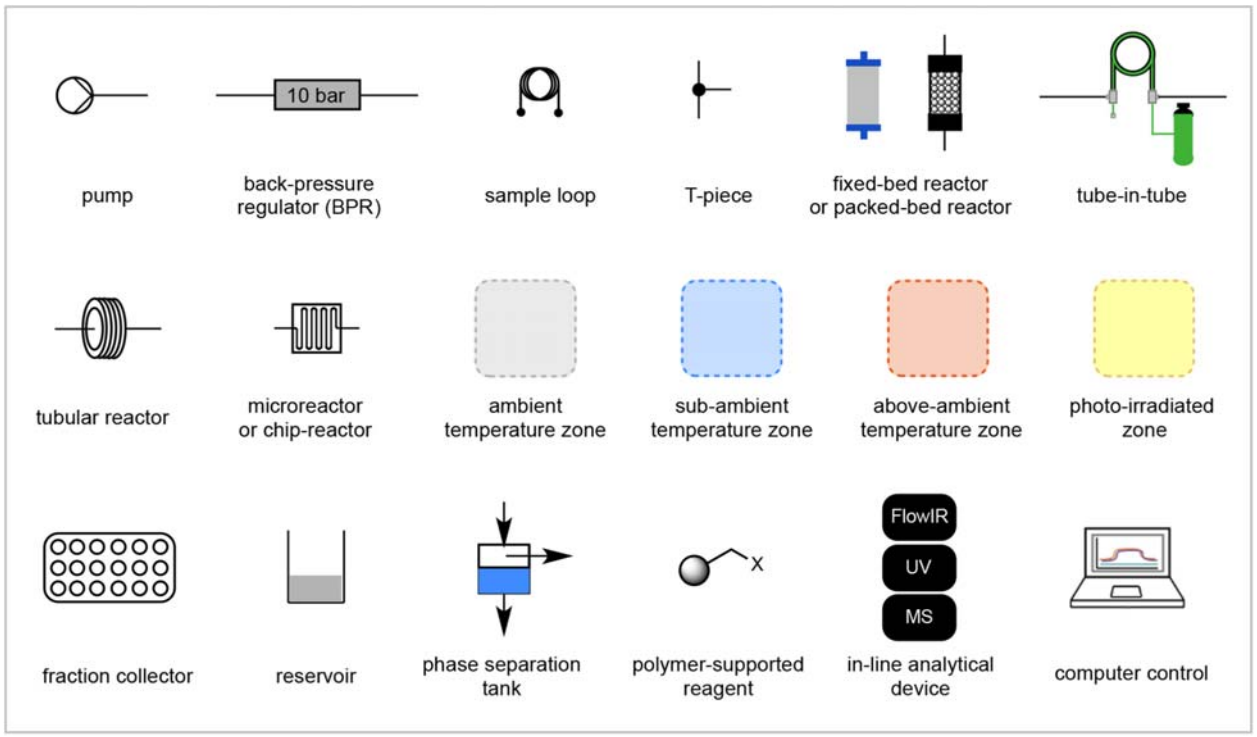

Scheme 1 Key of flow components.

generated can be dissipated much more effectively so that thermal runaways are less likely. Conversely the flowing streams can be heated much more rapidly. Heating of reaction streams represents another benefit for flow processing. Not only can materials be heated more rapidly and hazards minimized, but streams can be pressurized and therefore superheated, known as hypothermal conditions. This is simply achieved by adding a back pressure regulator to the system and heating past the standard boiling point. Notably, unlike microwave reactors, pressurized flow systems have no free headspace which can often remove more volatile components from reaction streams or present a hazard themselves. Additional benefits of a flow setup comprise the ability to multistep, daisy-chain, or telescope reactions or chemical processes together. This can allow the avoidance of isolating unstable compounds by advancing them rapidly to the next synthetic step. Rather than running into another reaction, flow processes can also be intercepted for reaction quenching and inline purification. Indeed, designing continuous processes that greatly streamline the separation and purification parts is where significant time and cost savings can be made at scale.

Throughout this article we will provide schematic diagrams that depict the assembled flow components required to make some of the molecules described. Scheme 1 provides a summary of some of the more commonly occurring components that will be used in this article.

1.06.2 Fragments and Heterocycles

Continuous flow processing is effective across a range of scales. The ability to scale up from a segmented discovery setup producing tens of milligrams to a pilot process capable of producing multikilograms per day makes it an important technology for incorporation into medicinal chemistry programs. One machine could produce a diverse variety of fragments and heterocycles incorporating hazardous reagents or high temperatures and then be easily reconfigured to churn out any single one of interest. Owing to this versatility, continuous flow processing of new or stalwart fragments and heterocycles has achieved much attention. In this section we will provide a snapshot overview of some of the capabilities offered by this synergy.

1.06.2.1 Hazardous Gases

The use of reactive gases in a direct chemical transformation is often the most efficient pathway with respect to atom economy. However, it can be highly restricted depending on the hazards of the gas and the pressure involved. Using continuous flow methods has the prospect of allowing much easier handling of gases from a practical point of view. In addition, the mass transfer of gas into the solution is improved, compared to batch reactors, due to the larger surface area. This enables new reaction pathways where otherwise the reaction would not work or be too dangerous using traditional batch methods.[2] There are several ways to introduce

gases to a continuous reaction. The easiest is to simply merge a stream of gas with a stream of the other reactants in solution. Depending on the pressure and flow rate this then leads either to a homogeneous solution with all the gas dissolved or to segmented flow conditions. Another method is the introduction of special reactors such as a falling film or a tube-in-tube reactor. In the falling film reactor the liquid is dispersed over a surface in the reactor to form a thin layer creating a large surface area. The gas is then flowed through from the other side. The tube-in-tube reactor consists of an outer and an inner tube.[3] A original inner-tubing material is the semipermeable membrane Teflon (AF-2400) that enables gas transport from one side to the other. Typically the outer tube is pressurized with the desired gas, while the reaction mixture is pumped through the inner tube. The gas transfer into the solution is thereby dependent on the pressure differential of the gas across the membrane and the flow rate of the liquid. Much work has been reported on the use of tube-in-tube reactors, and we do not wish to reproduce excellent overviews here.[2,3] Instead we have picked just a few examples to highlight the utility of this technology.

The introduction of fluorine atoms into organic molecules is of pharmaceutical and agrochemical interest. However, the most efficient method, direct fluorination using hazardous fluorine gas, is incredibly exothermic and represents a significant safety issue in handling large excesses of fluorine gas. Continuous flow processing offers the prospect of addressing both of these drawbacks.[4] The enhanced safety in handling the gas and the increased reaction and temperature control due to the large SA:V enables the direct use of fluorine gas. One example of direct fluorination to form 4-fluoropyrazoles has been introduced by Sandford and coworkers.[5] The reactor employed has been designed by Chambers and Spink[6] for the introduction of elemental fluorine and is fabricated from nickel-based materials. Sandford and coworkers fluorinated a 1,3-diketone that then cyclized with a hydrazine to give the desired pyrazole derivate (**Scheme 2**). This is the first example of a multistep flow process involving direct fluorination with fluorine gas, or at least 10% F_2 in N_2. Notably such pyrazoles could be prepared by use of selectfluor in the initial 1,3-dicarbonyl steps, but the present method would be much more appropriate at scale from a cost of goods perspective.

Stevens and coworkers introduced a continuous process that would generate and consume HCN in situ but avoid release of the hazardous gas in large quantities.[7] The setup consists of two streams (**Scheme 3**), first, 2-formylbenzoic acid and acetic acid and second, KCN and aniline. These streams are combined and mixed in a microreactor. By separating the cyanide and acid components the hydrogen cyanide is only formed in the reactor and then consumed directly. The aniline and the formylbenzoic acid form an imine followed by addition of the cyanide. This can then ring close and tautomerize to form the product. Interestingly, they introduced a stream of inert immiscible fluorous solvent, Fluorinert, to carry precipitate formed during the reaction through the reactor.

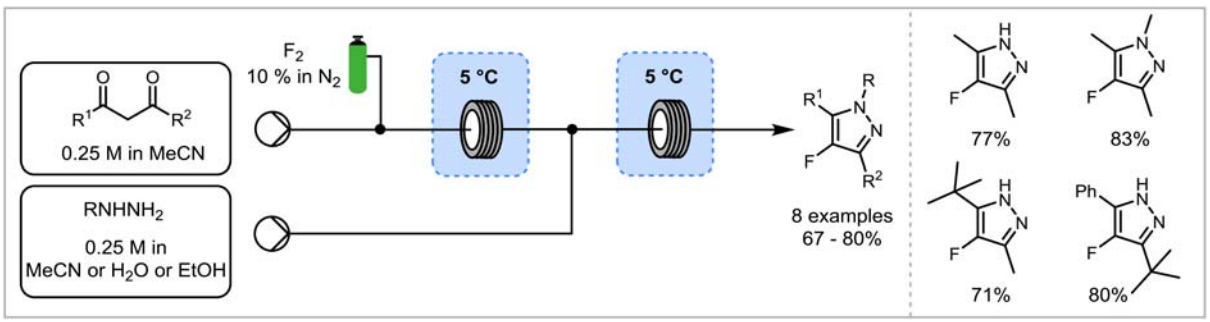

Scheme 2 Fluorination in flow using F_2 gas.[5]

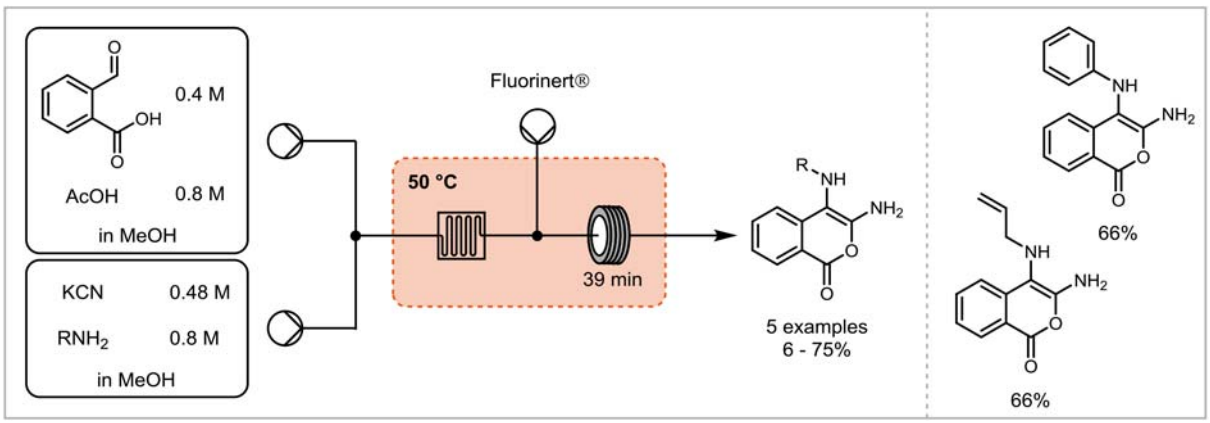

Scheme 3 Flow synthesis of 3,4-diamino-1H-isochromen-1-ones using HCN.[7]

Kappe and coworkers used the tube-in-tube reactor to introduce in situ prepared diazomethane into a reaction.[8] Diazomethane is a C_1 building block that can be used for methylation or acylation. However, due to its hazards, its use is usually avoided. Incorporating its generation into a continuous flow process allows improved safety as it is generated and consumed in situ. Since the first report of its in situ generation from Diazald (*N*-methyl-*N*-nitroso-*p*-toluenesulfonamide) in flow by Struempel and coworkers,[9] many other examples and precursors have been demonstrated, such as the base induced decomposition of MNU (*N*-methyl-*N*-nitrosourea) by Maggini and coworkers.[10] Kappe and coworkers generated diazomethane in a tube-in-tube reactor from *N*-methyl-*N*-nitroso-*p*-toluenesulfonamide (Diazald®) and potassium hydroxide in the inner tube and then performed the reaction in the outer tube. This allowed the safe use of anhydrous diazomethane. After finding an appropriate solvent system they performed methylation and acylation reactions. In a subsequent paper this technique was then applied to a multistep reaction to target an intermediate of the antiretroviral agent Atazanavir (**Scheme 4**).[11] First a Cbz-protected amino acid is activated to form an activated species. In a condensation with diazomethane an α-diazo ketone is formed that is then transformed into the α-halo ketone product in a hydrohalogenation reaction.

Martin et al. investigated the formation of diazoketones from acyl chlorides using different diazomethane precursors (**Scheme 5**).[12] They found that the less hazardous $TMSCH_2N_2$ gave better results than Diazald. The concept was demonstrated by synthesizing nine

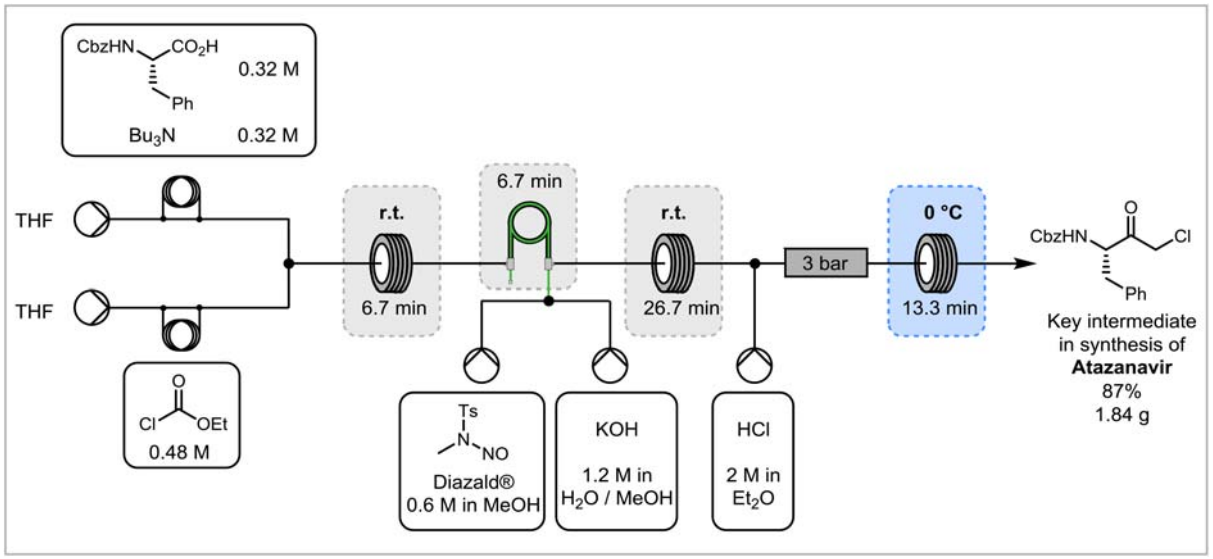

Scheme 4 Flow synthesis of a key intermediate using diazomethane.[11]

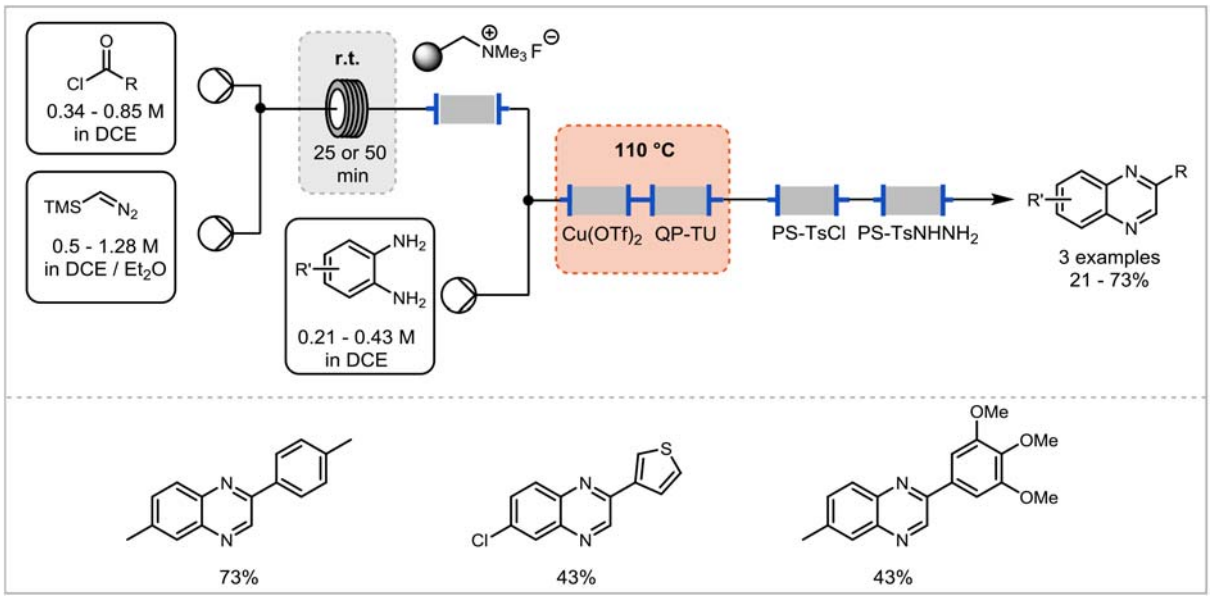

Scheme 5 Flow synthesis of quinoxalines.[12]

different diazoketones (46–98% yield). These diazoketones can then be further converted into different products. They investigated the conversion of phenylenediamines into quinoxalines. From the isolated diazoketones they were able to synthesize 21 different quinoxalines (30–96% yield) including a protein kinase inhibitor. They were also able to demonstrate a telescoped flow process where the quinoxaline was synthesized from the acid chloride via generation and use of the diazoketone (3 examples, 21–73%).

1.06.2.2 Diazonium Salts

Diazonium salts and diazo compounds are important intermediates in organic chemistry given their versatility and wide availability of the required starting materials. However, these nitrogen-rich compounds can lose nitrogen gas if not controlled appropriately. Thermal runaways are dangerous not only because of the heat given off but also because a large volume of gas is evolved causing a pressure build up. One way to control this is to prepare and consume them in situ using flow methods.[13] In this way the temperature is controlled very efficiently, and only a small amount of these hazardous intermediates are present at one time. Flow procedures offer the ability to produce and consume hazardous materials, such as diazonium salts, in situ so that only small quantities of reactive intermediate are present at any one time. This, and the enhanced temperature control, enables safer reaction performance, so many reactions involving diazonium salts and diazo compounds are reported under continuous flow conditions.

Diazonium salts are usually formed by treating an amine, usually an aromatic aniline, with a nitrite source. Those can then perform various other reactions where the diazonium group is replaced either in a nucleophilic substitution (e.g., Balz–Schiemann reaction) or in a radical mechanism (e.g., Sandmeyer reaction) or intercepted by a nucleophile (e.g., to form a triazene).

Malet-Sanz et al. demonstrated the use of diazonium salts prepared in situ in a copper-free iododeamination (Scheme 6).[14] In contrast to the Sandmeyer reaction this does not require a copper catalyst, as the reaction is performed in neutral conditions proceeding via a triazene intermediate to form radical intermediates. To stabilize the radicals acetonitrile was chosen and molecular iodine acted as the iodine source. The reaction proceeds smoothly, and the application to 13 examples was demonstrated, including those that are sterically demanding and electron-rich, albeit observing generally lower yields with these substrates.

Malet-Sanz et al. also adapted their method to the preparation of arylsulfonyl chlorides in a Meerwein chlorosulfo-de-diazotisation reaction (Scheme 7).[15] The challenge for this reaction setup was the incompatibility of the original reaction conditions with the flow setup due to precipitates and corrosive starting materials. Therefore they substituted the water-soluble nitrite source

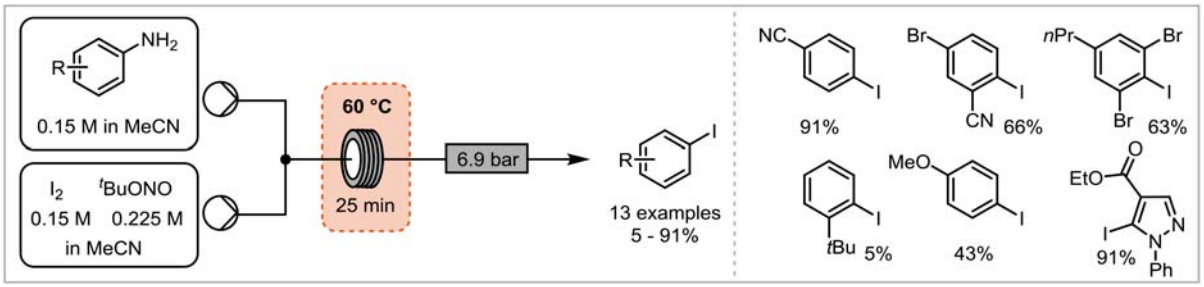

Scheme 6 Copper-free iododeamination of diazonium salts in flow.[14]

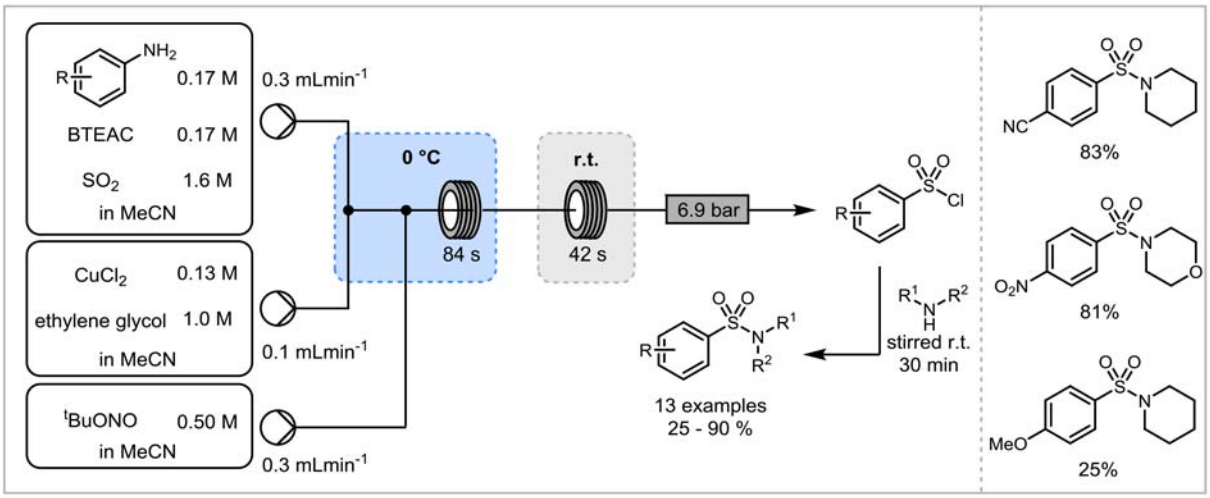

Scheme 7 Synthesis of aryl sulfonyl chlorides from diazonium salts in flow.[15]

$NaNO_2$, with *t*-BuONO which is soluble in most organic solvents and also does not need the aid of an acid. The delivery of the copper catalyst, which aids the halogen transfer, was investigated, and a homogeneous solution with ethylene glycol as a cosolvent was found to be optimal. This stream was combined with a stream of the aniline, benzyltriethylammonium chloride, and SO_2. Precipitation of a triazene by-product was observed for some examples under neutral conditions. To avoid the formation of the triazene in the first place, the order of reactant streams was changed adding the nitrite last. Using this procedure they were able to generate 13 examples of arylsulfonyl chlorides.

Wirth and coworkers introduced a biphasic, fluorous segmented approach to the diazonium-type Heck–Matsuda reaction in flow (**Scheme 8**).[16] They accelerated the reaction by using segmented flow conditions to enhance micromixing. The aniline stream is thereby segmented by an inert phase before combination with *t*-BuONO for diazotation. The diazonium salt is then intercepted by an alkene in a Heck–Matsuda coupling reaction to form the desired trans stilbene products.

1.06.2.3 Azides

Similar to diazonium salts and diazo compounds, azides are highly versatile yet hazardous materials due to the possible loss of nitrogen gas.[17] Ley and coworkers performed a Curtius rearrangement in flow to safely handle acyl azides. The acyl azides are thereby produced in situ from diphenylphosphoryl azide (DPPA) and the corresponding acid. After reaction with a nucleophile the resultant isocyanate is trapped on a solid support (**Scheme 9**).[18] This enables the inline purification of the product mixture. Using this method they were able to produce 25 g of material, demonstrating the suitability of flow processes to larger scale syntheses.

Jensen and coworkers demonstrated a multistep continuous flow synthesis of carbamates also making use of the Curtius rearrangement (**Scheme 10**).[19] Streams of the acid chloride and sodium azide were combined to form the organic azide. Liquid–liquid phase separation was realized in a microseparator before the reaction mixture was heated where upon nitrogen gas was liberated to form an isocyanate that was then intercepted by an alcohol to afford a variety of carbamate products.

Noël, Hessel, and coworkers performed a catalyst-free Huisgen cycloaddition to synthesize a Rufinamide precursor featuring the triazole heterocyclic moiety (**Scheme 11**).[20] Several dipolarophiles are known to perform this reaction; however these are highly toxic and flammable. Noël and Hessel utilized a greener and less expensive dipolarophile, (*E*)-methyl 3-methoxyacrylate, that

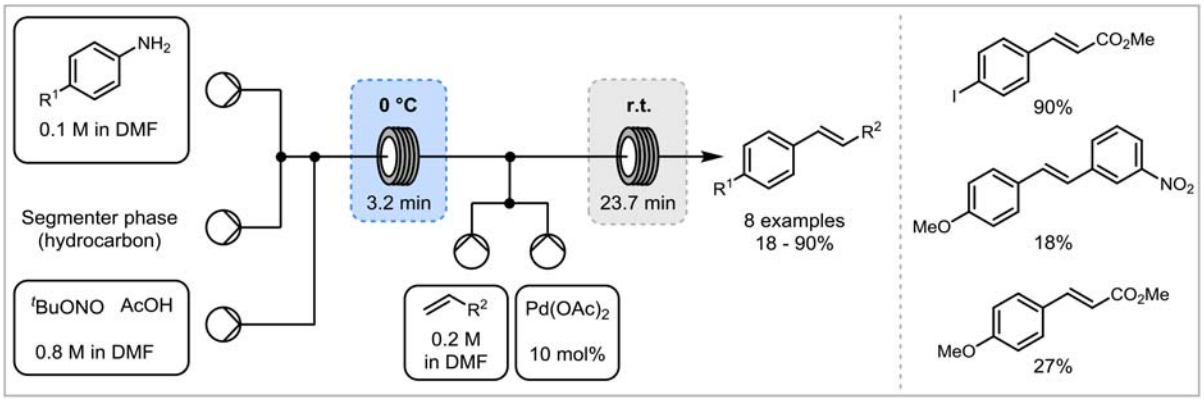

Scheme 8 Heck–Matsuda reaction under segmented flow.[16]

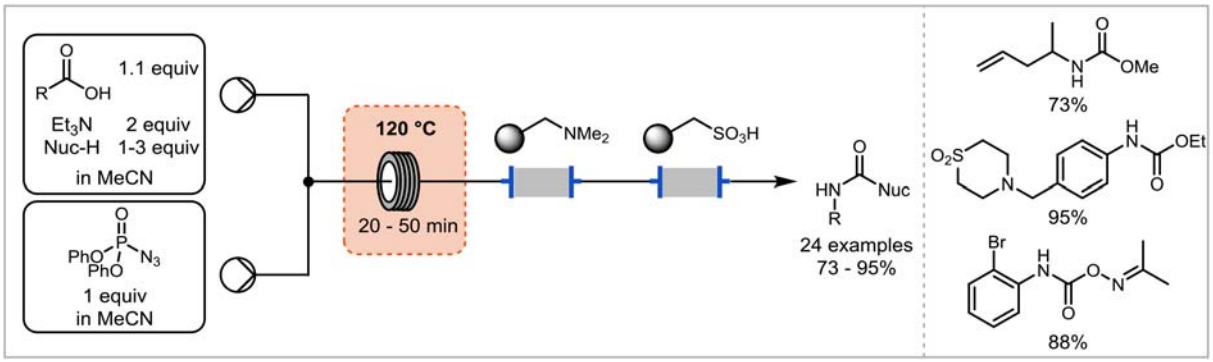

Scheme 9 Curtius arrangement in flow.[18]

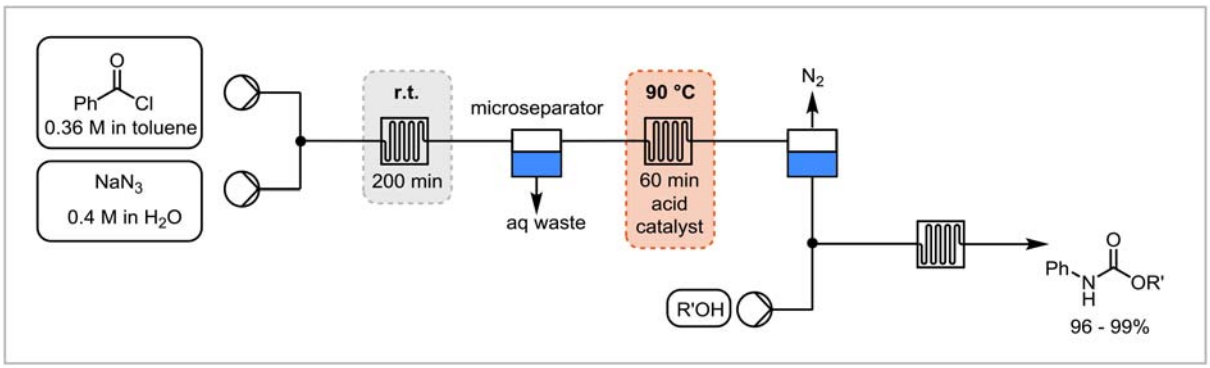

Scheme 10 Synthesis of carbamates via a Curtius rearrangement in flow.[19]

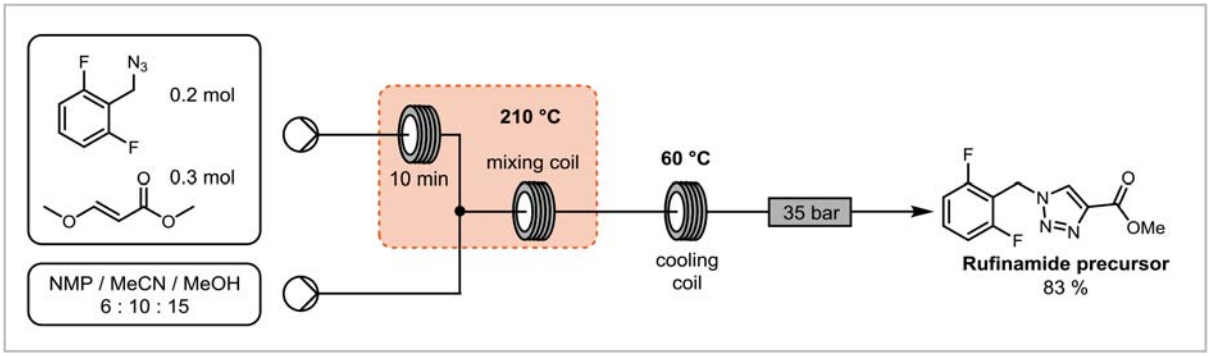

Scheme 11 Flow synthesis of a Rufinamide precursor.[20]

does not require transition metal catalysis. They premixed the neat starting materials, a benzyl azide and their dipolarophile, and passed them through a heated reactor coil. However, they had to take into account that azides readily decompose at elevated temperatures. After investigating the behavior at different temperatures, they found that 210°C and 10 min residence time gave optimal results. This permitted a decrease in the reaction time from 28 h at 135°C in batch to 10 min at 210°C in flow. Interestingly, the reaction worked under solvent-free conditions with a corresponding increase in reaction rate. However, dilution was needed to dissolve the product and prevent precipitation. The reaction proceeded smoothly and gave 83% yield of the Rufinamide precursor after purification.

Roberge, Kappe, and coworkers introduced a process to prepare tetrazoles from nitriles and the toxic and explosive hydrazoic acid (Scheme 12).[21] The hydrazoic acid is generated and consumed in situ by mixing an aqueous sodium azide solution with a solution of acetic acid and nitrile in N-methyl-2-pyrrolidone (NMP). The tetrazole is then formed by reaction with the nitrile. By increasing the reaction temperature to over 200°C, process intensification with decreased reaction times was demonstrated.

Roberge, Kappe, and coworkers used TMS azide to ring-open oxazolines followed by reduction to the amino amide (Scheme 13).[22] The oxazoline reagent stream and the neat $TMSN_3$ stream were merged prior to heating. The heating-induced ring opening at the C-5 before the azide was reduced in an H-cube to give the amino amide. Thereby the ring is opened by the in situ formed HN_3 gas by solvolysis of $TMSN_3$ with MeOH).

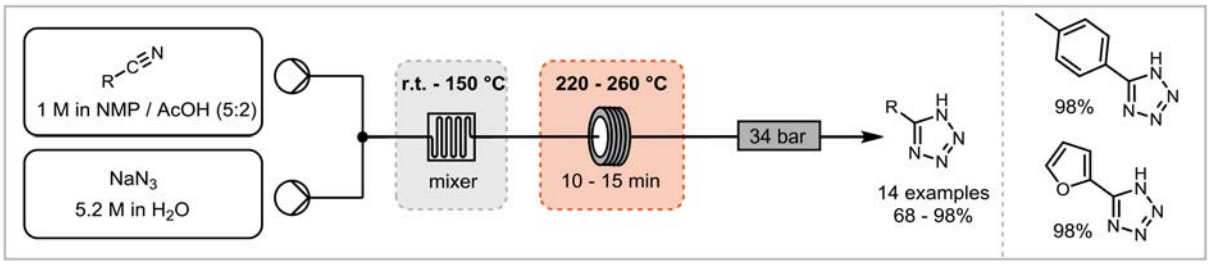

Scheme 12 Synthesis of tetrazoles in flow.[21]

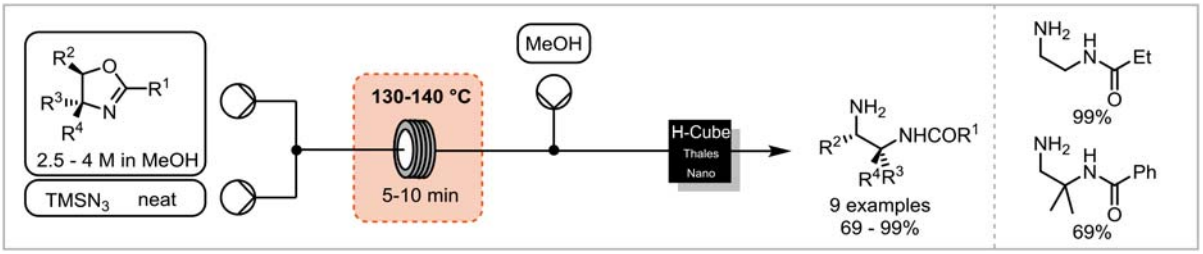

Scheme 13 Ring opening of oxazolines with hydrazoic acid in flow.[22]

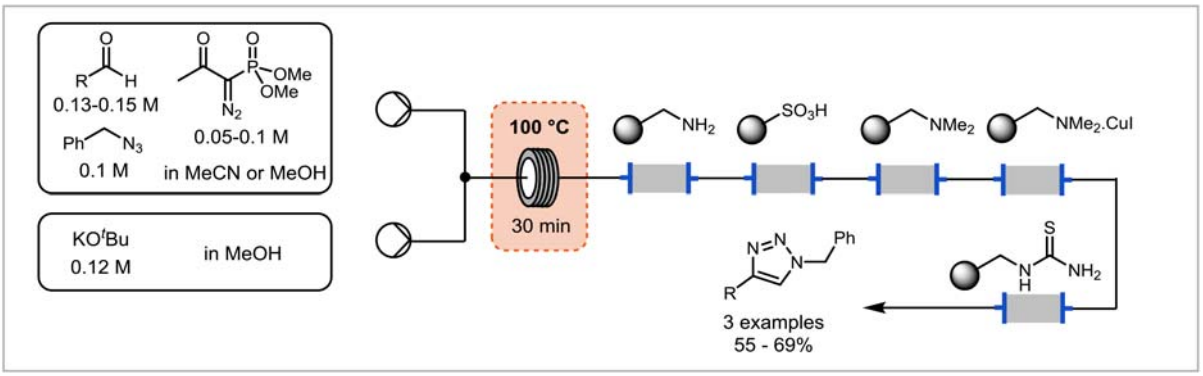

Scheme 14 Flow synthesis of triazoles.[23]

Another method making use of azides has been introduced by Ley and coworkers in their synthesis of triazoles (Scheme 14).[23] Their work focused on avoiding conventional work-up procedures but instead using immobilized reagents and scavenging methods. They used the Bestmann–Ohira reagent, dimethyl (1-diazo-2-oxopropyl)phosphonate, with KO*t*Bu to generate a diazomethyl phosphonate in situ which then formed a terminal acetylene from an aldehyde. The clean product was obtained after passing it through the first three of the packed cartridges. In a telescoped process an azide was mixed into the reagent streams and reacted with the acetylene in a copper-catalyzed cycloaddition to form the desired triazole. The reaction setup could be further modified to also first oxidize an alcohol to the corresponding aldehyde starting material.

Seeberger and coworkers used an azido acrylate to synthesize indoles in a Hemetsberger–Knittel reaction via an aziridine intermediate (Scheme 15).[24] The azido acrylate starting material was prepared in a Knoevenagel condensation beforehand. In the flow reactor it was then thermolytically cleaved to give a nitrene that is then in equilibrium with the aziridine. Importantly, in only 21 min they could produce a precursor for a DAAO inhibitor on an 8.5 g scale.

1.06.2.4 Nitration

Nitration reactions can be very hazardous when performed on large scales in batch. They release large amounts of heat, and multiple nitration can be problematic. The products can also be highly explosive. However, the ability to control exotherms in flow allows improved selectivity and safety. As such, there have been many nitration reactions performed using continuous flow.[25]

The improved safety is exemplified in the synthesis of triaminophloroglucinol, by Kappe and coworkers.[26] They start from inexpensive phloroglucinol and subject it to nitrating conditions (Scheme 16). An ultrasound bath was used to prevent blocking of the reactor by precipitation of the high energy compound trinitrophloroglucinol. The nitro groups on this explosive intermediate were directly hydrogenated to amines using hydrogen generated from the H-Cube over a PtO_2 catalyst.

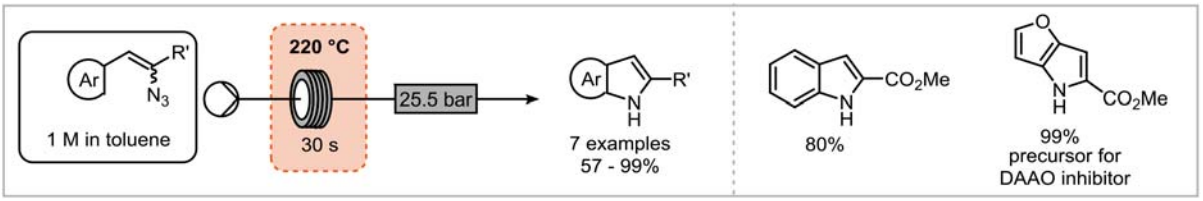

Scheme 15 Synthesis of indoles in flow via aziridines.[24]

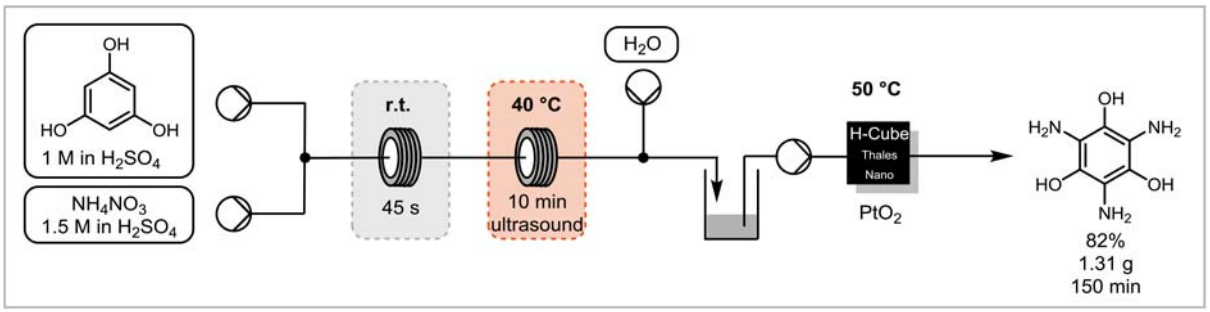

Scheme 16 Synthesis of triaminophloroglucinol in flow.[26]

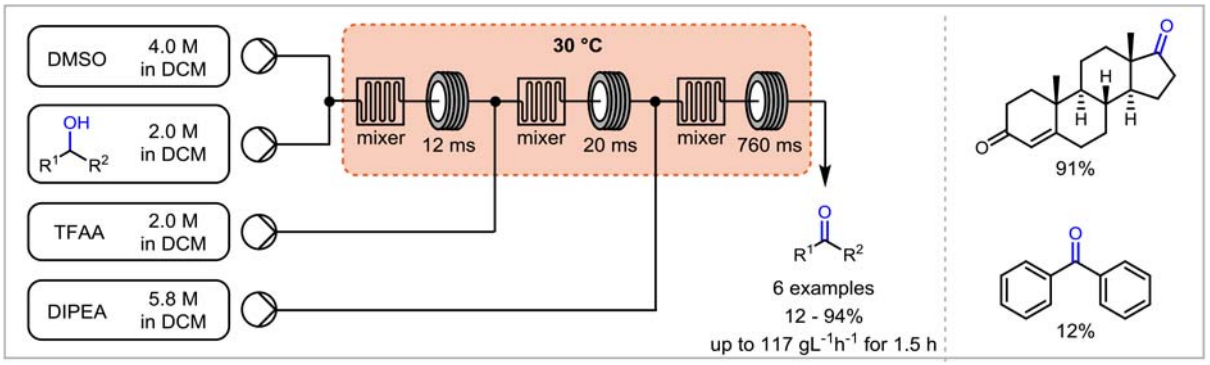

Scheme 17 Swern oxidation in flow.[29]

1.06.2.5 Oxidation

Typical oxidation reactions make use of hazardous oxidizing agents, are often exothermic, and have the potential to form explosive mixtures. Selectivity can also be an issue, especially where overoxidation is possible, or there are multiple potential sites for oxidation. Using flow processes can solve some of these issues, and indeed there are several examples which address these.[27]

The Swern oxidation is a key method for the selective transformation of alcohols to aldehydes, avoiding overoxidation to carboxylic acids. In batch, it is normally necessary to use cryogenic temperatures to avoid side reactions, such as the Pummerer rearrangement. There have been several examples of the Swern oxidation in flow, allowing it to proceed at room temperature with very short reaction times and minimal side product formation.[28] **Scheme 17** shows one example, where trifluoroacetic anhydride was used to activate the DMSO and then oxidize alcohols in less than 1 s at 30°C.[29] The exact order of addition was found to be important to minimize side product formation. The authors have also demonstrated the ability to scale up this method.

The selective oxidation of alcohols to aldehydes has also been achieved in flow using controlled delivery of oxygen gas (**Scheme 18**).[30] A solution of the alcohol meets a stream of O_2 and passed through a cartridge packed with a Ruthenium catalyst at 90°C. Several alcohols were selectively oxidized using this method and often leading to high yields of the corresponding aldehyde.

1.06.2.6 Reduction

Several of the key issues of oxidation are also present in reduction reactions. Problems of selectivity due to the possibility of overreduction or reduction at different sites exist. Hydrogenation is commonly performed in flow, especially after the introduction of the

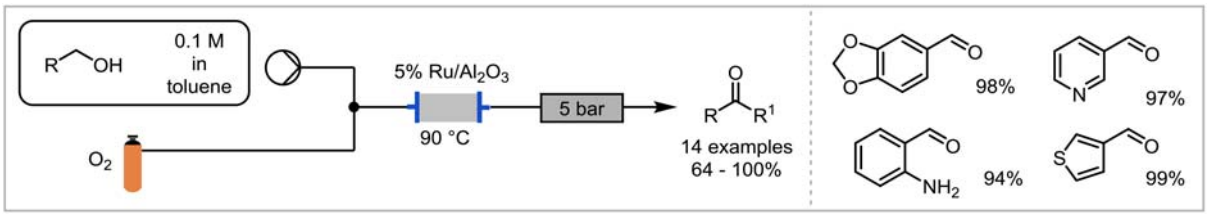

Scheme 18 Selective oxidation of alcohols in flow using O_2 gas.[30]

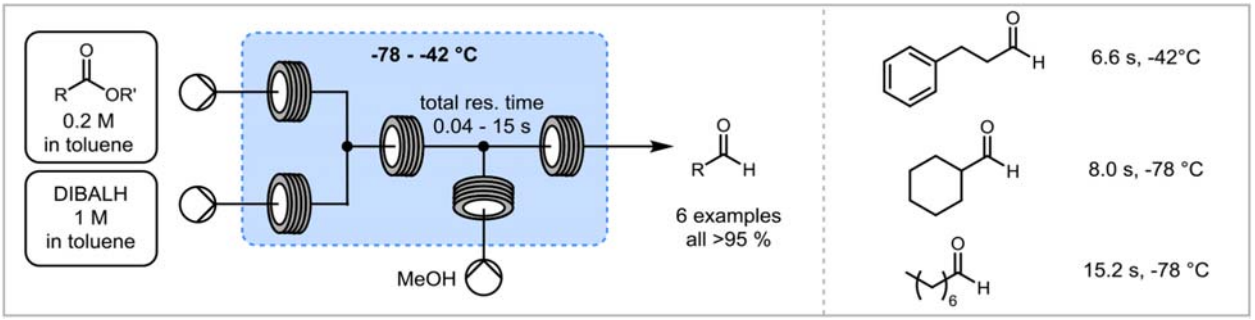

Scheme 19 Selective reduction of esters to aldehydes in flow.[33]

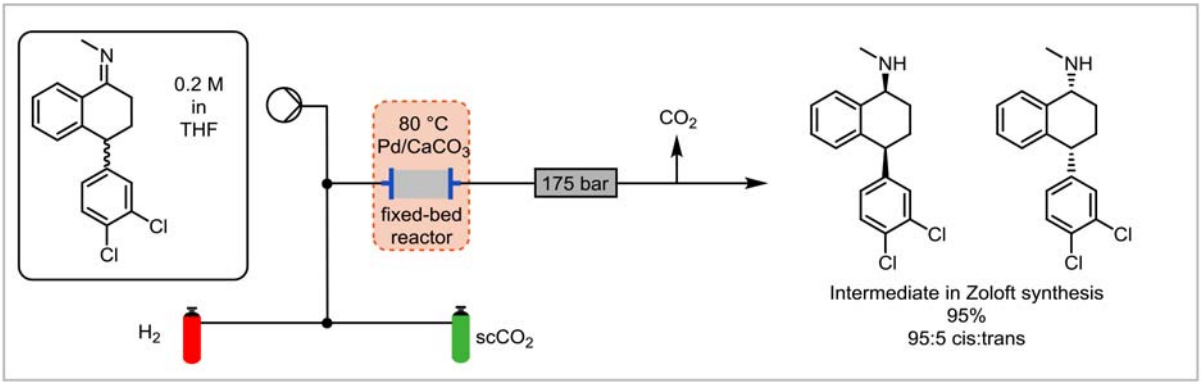

Scheme 20 Hydrogenation of an imine in flow to produce a key intermediate.[34]

H-Cube, which safely generates H_2 gas by in situ electrolysis of water. There are many examples of hydrogenation under flow conditions.[31] Other reductions have also been achieved in flow, some of which are presented later.

The reduction of esters using diisobutylaluminium hydride (DIBALH) to obtain only the aldehyde, without overreduction to the alcohol, is a challenge. However, using flow processes can improve the selectivity.[32] A report by Webb and Jamison demonstrates that this selective reduction can be achieved in 15 s (Scheme 19).[33] Solutions of DIBALH and the ester were precooled and then allowed to mix and react. A stream of methanol was added to dilute and quench the mixture. This process was found to be extremely selective in forming the aldehyde, with six examples of over 95% yield.

In order to make an intermediate required in the synthesis of the antidepressant Zoloft a continuous flow hydrogenation of an imine was reported by Clark, Poliakoff, and Wells (Scheme 20).[34] Notably, the reaction was performed in supercritical carbon dioxide, which improves the heat transfer properties of the system. A stream of the imine was mixed with hydrogen gas in supercritical carbon dioxide and heated at 80°C over $Pd/CaCO_3$ catalyst. Notably, an improved chemoselectivity was observed in the supercritical carbon dioxide due to prevention of hot-spots on the catalyst bed. The desired product was isolated with excellent yield and diastereomeric ratio.

Jensen and coworkers performed the Wolff–Kishner reduction of ketones and aldehydes (Scheme 21).[35] Initially the carbonyl reacts with hydrazine to form a hydrazone which on treatment with base affords the desired reaction. This requires very harsh reaction conditions, heating the carbonyl with hydrazine and strong base to high temperature. In this case 200°C was used, allowing the reaction time to be decreased in comparison to traditional batch conditions. The use of a resilient silicon carbide microreactor was required in order to achieve these conditions.

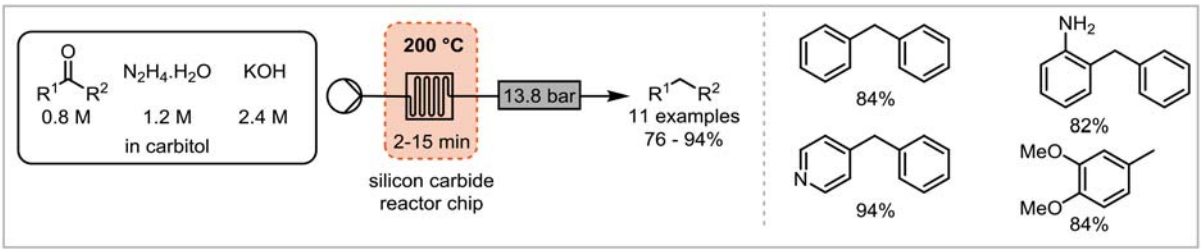

Scheme 21 Wolff–Kishner reduction of ketones in flow.[35]

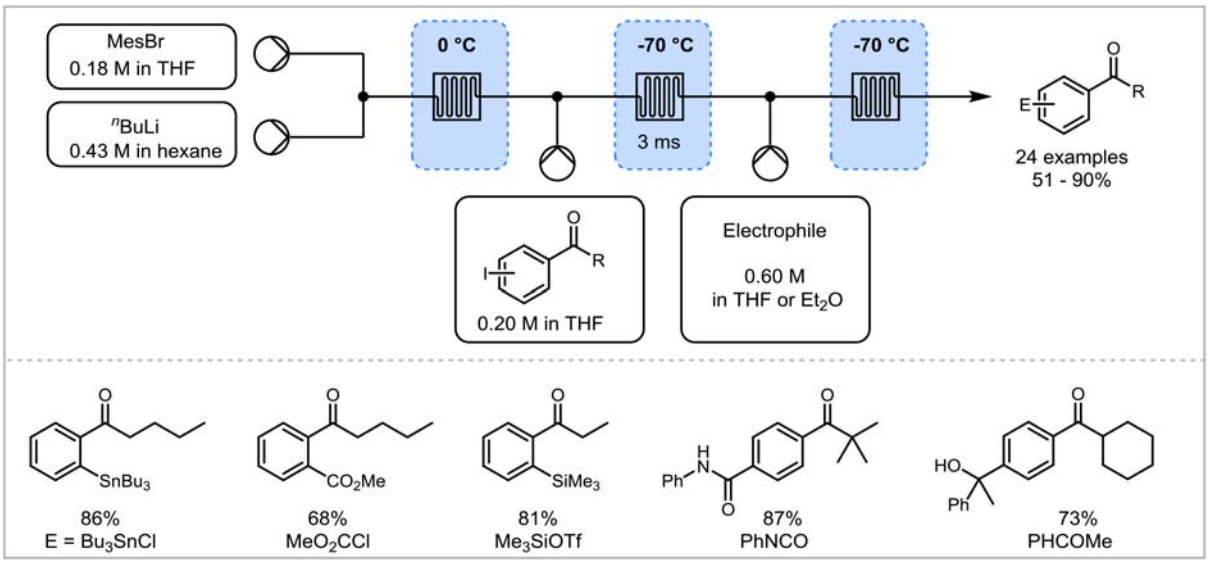

Scheme 22 Lithium halogen exchange followed then interception by an electrophile in flow.[37]

1.06.2.7 Organometallic Reagents

The use of organometallic reagents, such as Grignard reagents, is extremely important in the synthesis of many compounds. These methods are widespread during syntheses due to their versatility. However, there are several issues associated with the use of organometallic reagents. Organometallic reactions in general are exothermic, and the ability to dissipate heat quickly in flow, due to the large SA:V associated with flow reactors, is desirable. This is especially valid when preparing such reagents on large scales. Organometallic reagents are often air and water sensitive, and problems with solubility and precipitates are often encountered due to insoluble by-products, such as magnesium salts after a Grignard reaction. However, these problems can be overcome by the use of peristaltic pumps, which are able to process slurries or the addition of diluting streams to dissolve potentially insoluble materials. Owing to this, the pumps and other hardware used need to be suitable for handling such corrosive materials. There are now many examples of using organometallic reagents in flow including the use of "flash chemistry," pioneered by Yoshida.[36]

Flash chemistry involves using extremely short reaction times in order to prevent reactive intermediates from decomposing, and it has particular applications to organometallic reactions. In this example, an aryl lithium species is intercepted by an external electrophile despite an intramolecular carbonyl being present (Scheme 22).[37] The lithiating species, mesityl lithium, was generated from *n*-butyllithium and mesityl bromide. A stream of aryl iodide was added, and a lithium iodide exchange takes place to form the lithiated intermediate. This reaction takes place at $-70°C$ with a residence time of only 3 ms required to avoid decomposition. This lithiated intermediate was then directly intercepted by a stream of an external electrophile. A range of electrophiles and aryl iodides were successfully transformed using this method.

The preparation of aryl magnesium reagents in flow and subsequent reaction with carbonyls has been demonstrated by Ley, Knochel, and coworkers (Scheme 23).[38] A stream of the aryl bromide was combined with a stream of *i*-PrMgCl·LiCl in order to achieve

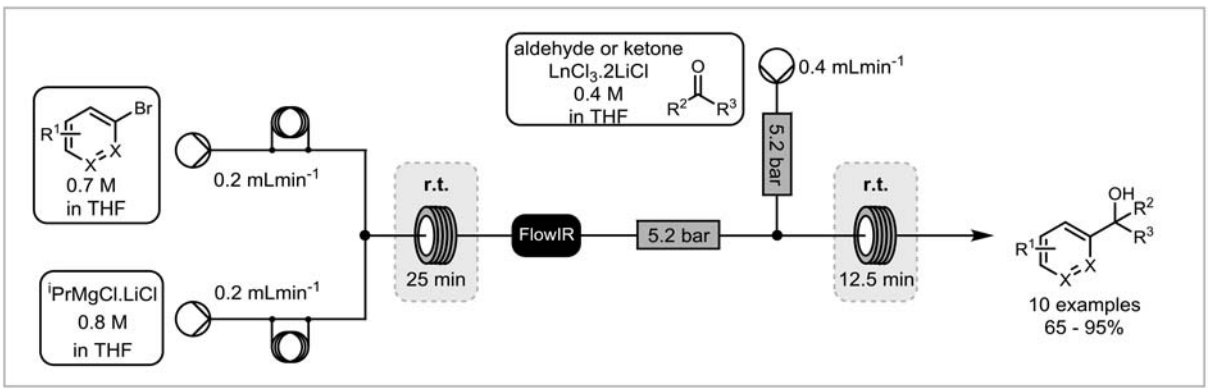

Scheme 23 Preparation of Grignard reagent and subsequent reaction in flow.[38]

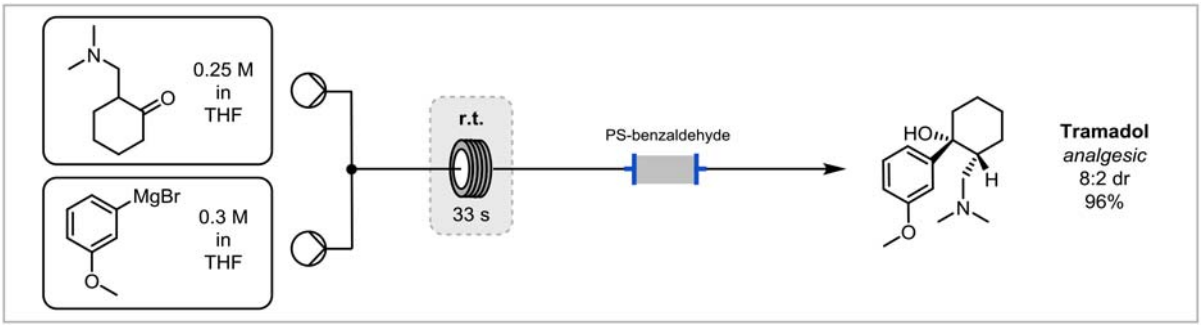

Scheme 24 Preparation of tramadol in flow via a Grignard reaction.[39]

the magnesium/halogen exchange. The mixture was passed through a reactor coil at room temperature for 25 min, and the output was monitored by inline IR to continuously monitor correct Grignard formation via concentration monitoring. The peaks observed due to THF coordination with the aryl magnesium species were used to determine the concentration of active Grignard reagent present. The formation of the protonated species and the homocoupled product were also monitored using characteristic bands in the fingerprint region after calibration. The aryl magnesium formed was then reacted with a range of aldehydes and ketones successfully demonstrating the preparation, monitoring, and reaction of these species in flow.

The flow synthesis of the analgesic, Tramadol, was reported by Rencurosi and coworkers in 2010 (Scheme 24).[39] A Grignard reaction was performed under flow conditions, achieving a high yield with a residence time of only 33 s at room temperature. The streams of ketone and Grignard reagent were combined and passed through a reactor coil. The exiting stream then passed through a scavenger column of polymer-supported benzaldehyde to remove any remaining unreacted Grignard reagent. Tramadol was afforded in excellent yield.

Grignard reagents have also been used in flow to synthesize functionalized phenol fragments (Scheme 25).[40] Initially, the relevant nucleophile was deprotonated by the Grignard reagent. This stream was then combined with a stream of the 1,2-dihalobenzene and heated to allow benzyne formation via magnesium halide exchange followed by elimination. The benzyne was then intercepted by the nucleophile resulting in the formation of an arylmagnesium intermediate. The input of air then oxidized the arylmagnesium species to the desired ortho-functionalized phenol. The overall setup provides a convenient method to prepare a diverse array of ortho functionalized phenols, as demonstrated by the eight examples reported.

Another commonly used organometallic reagent is lithium diisopropylamide (LDA). In scaling up the synthesis of a promising reflux inhibitor, Pontén and coworkers used a flow procedure to generate LDA in situ (Scheme 26).[41] Instead of the −78°C required in batch, they were able to generate LDA after 13 s at 35°C in a flow reactor coil. The stream of LDA was then combined with the stream of *N*-Boc glycine methyl ester and methyl phosphinate. The mixture was directed through a heated reactor to afford 400 g of the protected product.

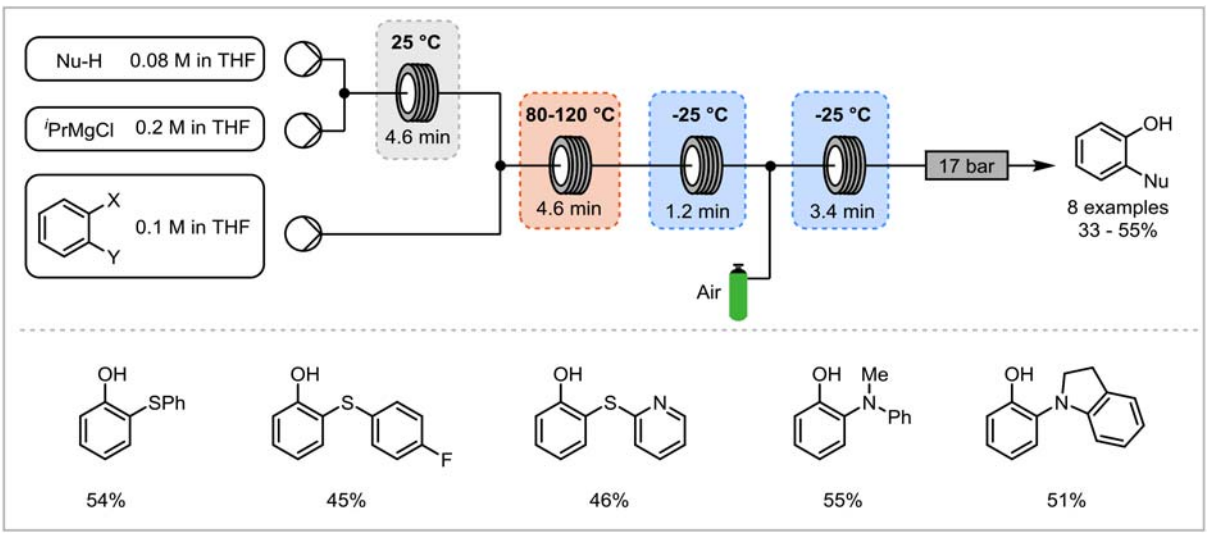

Scheme 25 Synthesis of ortho-functionalized phenols in flow via benzyne formation.[40]

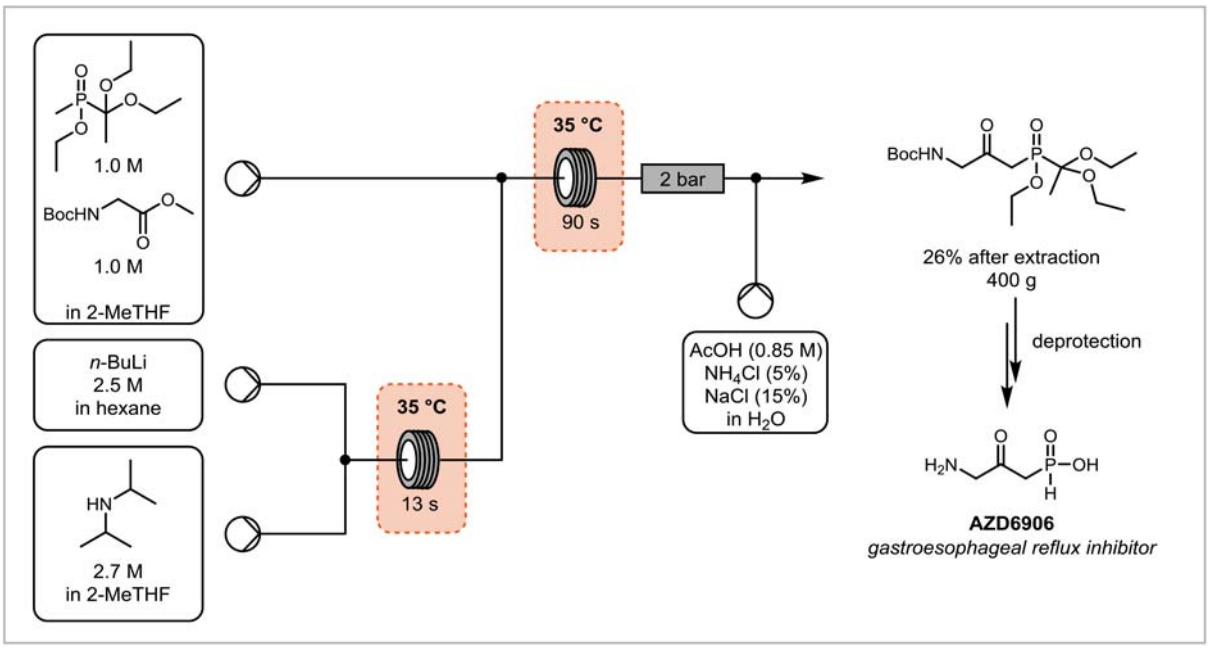

Scheme 26 Formation and use of LDA in flow.[41]

Organolithium species are also often used as strong bases. While synthesizing benzodiazepines in flow, Baxendale and coworkers used butyllithium to deprotonate an amine nucleophile in order to achieve an S_NAr reaction (Scheme 27).[42] The three streams were all precooled before combining at the T-piece and heating to 115°C in the reactor. An inline extraction was then performed, followed by passing the organic layer through a column of alumina to remove any trace water. A stream of methanol was added to dilute the mixture, and the nitro group was reduced to the aniline, which underwent an intramolecular cyclization. This was performed using the H-Cube to generate hydrogen gas with a PtO_2 catalyst. Several benzodiazepines were synthesized continuously by this method.

The continuous lithiation of alkynes and subsequent carboxylation with CO_2 has been studied by Kappe and coworkers (Scheme 28).[43] A stream of LiHMDS was combined with a stream of alkyne to form a lithiated species. Gaseous carbon dioxide was then introduced, and the mixture quenched with water forming the carboxylated product after a total residence time of only 23.5 s. This was successfully applied to the synthesis of 14 different carboxylated alkynes.

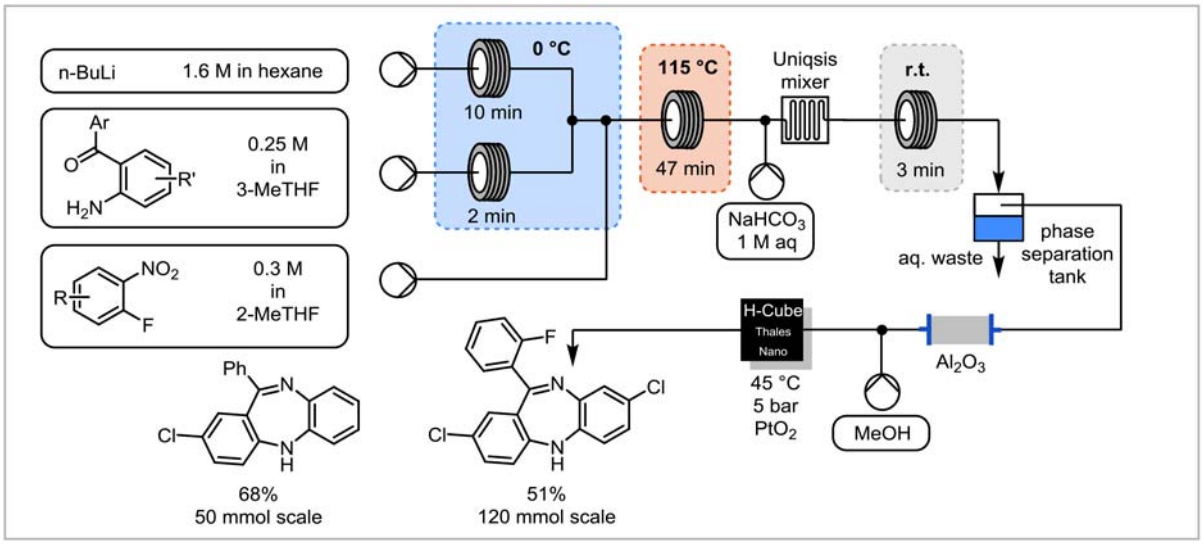

Scheme 27 Flow synthesis of benzodiazepines.[42]

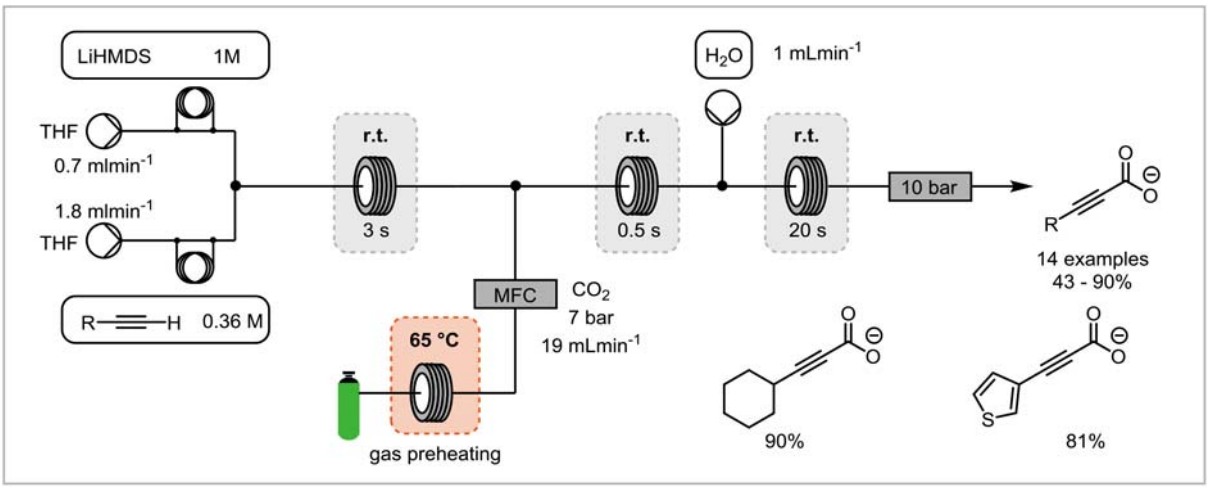

Scheme 28 Lithiation of alkynes and subsequent trapping with carbon dioxide in flow.[43]

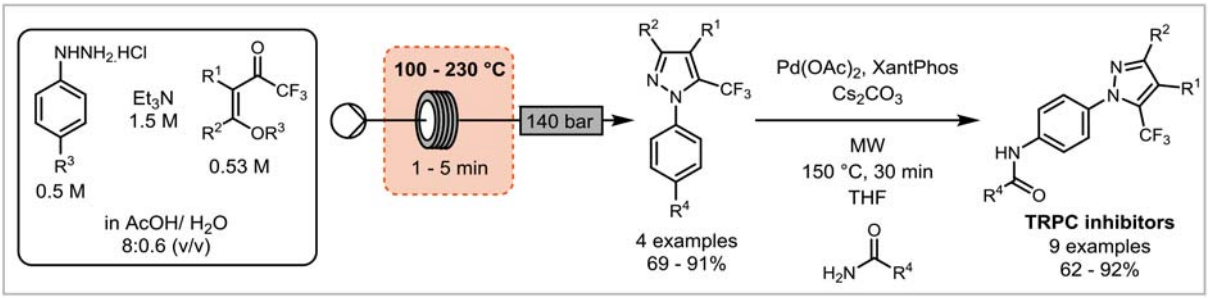

Scheme 29 Synthesis of pyrazoles in flow as an intermediate for TRPC inhibitors.[44]

1.06.2.8 Cyclocondensation

Cyclocondensation reactions are the key method by which heterocycles are synthesized, and there have been several key demonstrations of such reactions under continuous flow conditions. Although no focused review exists for this topic examples are numerous and we will provide an overview of only a few of these here.

In their work synthesizing pyrazoles under high temperature and pressure flow conditions, Kappe and coworkers went on to synthesize nine different inhibitors of canonical transient receptor potential channels (Scheme 29).[44] The use of high temperatures allowed the condensation of hydrazines with enones which then enabled the fast synthesis of several pyrazoles. Subsequent palladium-catalyzed Buchwald–Hartwig amidation under microwave conditions afforded a range of bioactive TRPC inhibitors in good yields.

Another application of high temperature flow conditions for heterocycle formation is reported by Herath and Cosford.[45] Microreactors were used to perform a Hantzsch pyrrole synthesis using the HBr generated to directly hydrolyze the ester to the 3-carboxylic acid (Scheme 30). It was also possible to further react the pyrrole-3-carboxylic acid derivatives directly with amines to synthesize the amide. This method was used in the synthesis of two cannabinoid receptor subtype 1 inverse agonists.

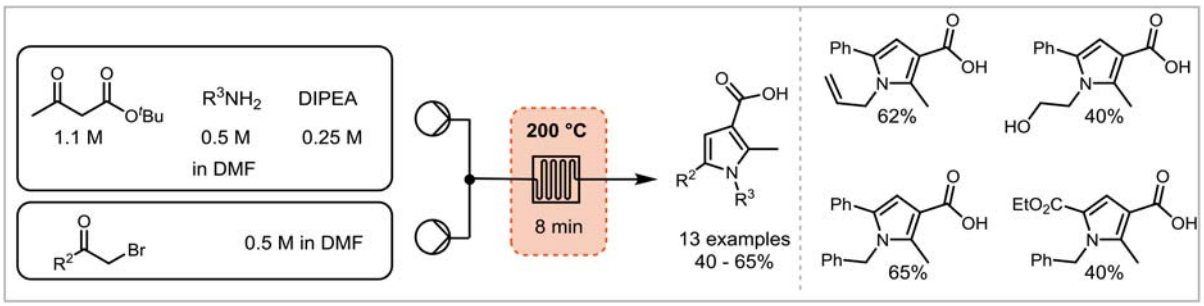

Scheme 30 Hantzsch pyrrole synthesis in flow.[45]

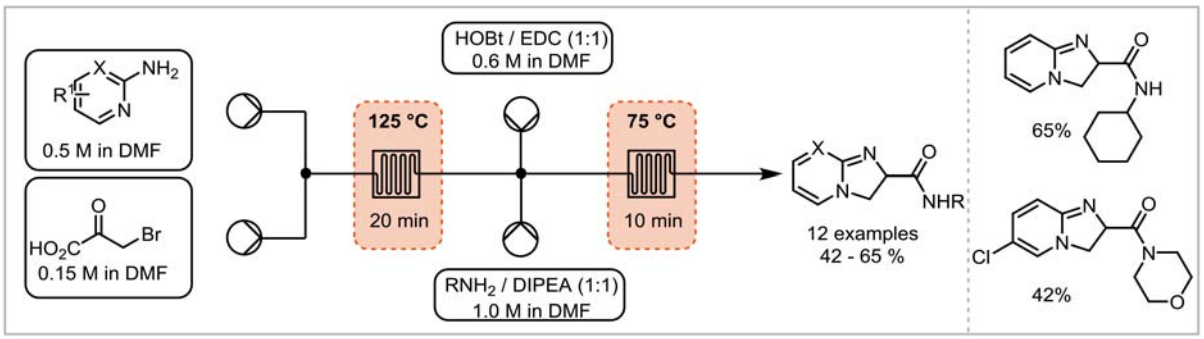

Scheme 31 Imidazole synthesis in flow.[46]

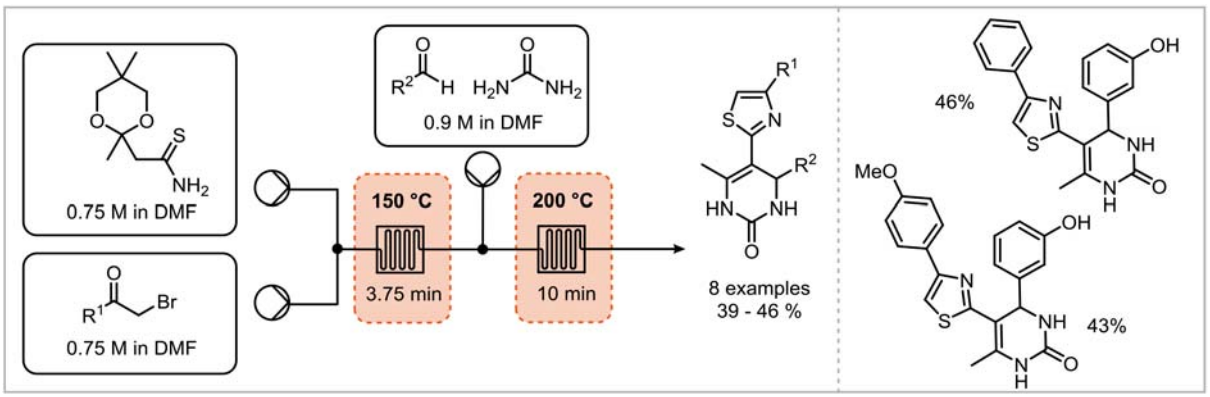

Scheme 32 Flow synthesis of thiazoles.[47]

Cosford and coworkers also reported the two-step synthesis of imidazoles using microreactors (Scheme 31).[46] Initially, condensation of bromopyruvic acid with 2-aminopyridines was performed to yield the imidazo[1,2-a]pyridine-2-carboxylic acid. The acid was directly transformed to the amide by addition of a stream of the required amine with N,N-diisopropylethylamine (DIPEA) and a stream of hydroxybenzotriazole (HOBt) and 1-ethyl-3-(3-dimethylaminopropyl)carbodiimide (EDC). This leads to the successful multistep flow synthesis of several imidazo[1,2-a] heterocycles, including a key intermediate for the synthesis of AB530, an FLT3 kinase inhibitor.

A further report from Cosford and coworkers demonstrates the synthesis of thiazoles making use of high temperature microreactors in a two-step synthesis (Scheme 32).[47] Initially, the condensation of an α-bromoketone with a thioamide gives the β-ketothiazole by the Hantzsch thiazole synthesis. A stream of aldehyde and urea was then combined with the main stream and heated for 10 min yielding the dihydropyrimidinone via the Biginelli reaction, catalyzed by HBr from the first step.

Kappe and coworkers report a synthesis of 7-ethyltryptophol, a key intermediate in the synthesis of several pharmaceutically active molecules (Scheme 33).[48] The synthesis involved heating a stream of hydrazine hydrochloride with dihydrofuran in a Fischer-indole synthesis. After carefully analyzing the formation of side products to determine optimal reaction conditions, 7-ethyltryptophol was isolated in 39% yield.

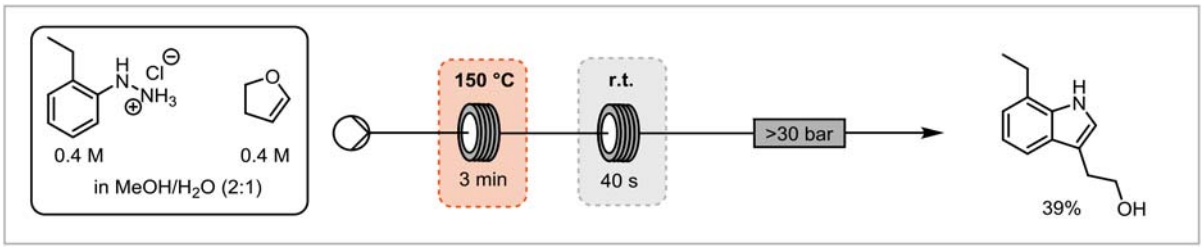

Scheme 33 Flow synthesis of 7-ethyltryptophol.[48]

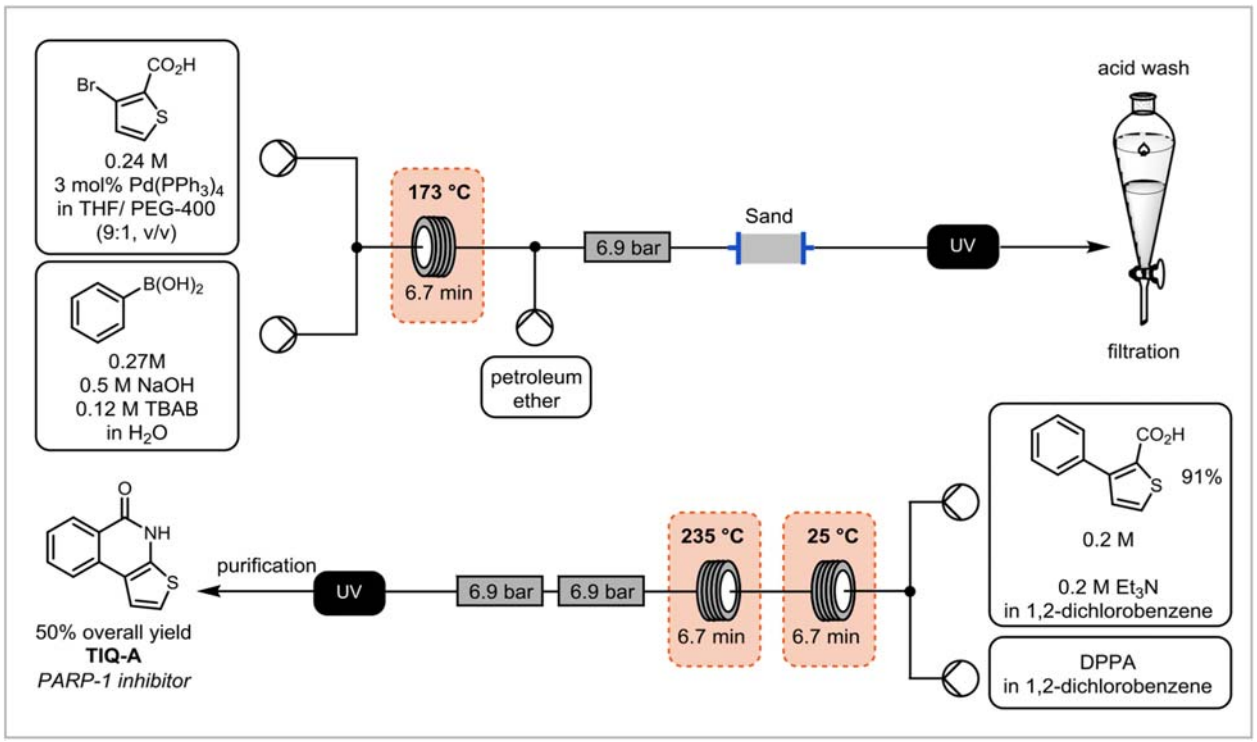

Scheme 34 Two-step flow synthesis of a PARP-1 inhibitor.[50]

1.06.2.9 Cross-Coupling Reactions

There are many examples of cross-coupling reactions being performed in flow, some of which are presented here.[49] These reactions often form vital key steps during the syntheses of target molecules. In general, catalysts can be homogeneous or heterogeneous, with homogeneous catalysts often serving to mediate more challenging coupling reactions due to an enhanced understanding of their properties.

In their synthesis of a PARP-1 inhibitor, Gioiello and coworkers used a Suzuki coupling reaction in the first step (**Scheme 34**).[50] Initially, a stream of the bromothiophene and palladium catalyst was combined with a stream of the boronic acid before entering a heated reactor coil for 6.7 min residence time. After extraction, the coupled product was isolated in excellent yield. Following reaction with a stream of diphenylphosphorylazide and reaction at 25°C, the acyl azide was then heated to 235°C in order to achieve cyclization. The resulting thieno[2,3-c]isoquinolin-5(4H)-one scaffold was isolated with good overall yield.

The palladium-catalyzed C–N coupling of aryl chlorides with hydrazines has been demonstrated by Buchwald and coworkers (**Scheme 35**).[51] Initially, the aryl hydrazine is made by coupling hydrazine with an aryl chloride at room temperature, with sonication required to prevent blocking of the microreactor. It was discovered that BrettPhos was an appropriate ligand for the monoarylation of hydrazine. The aryl hydrazine was then combined with a stream of aldehyde or 1,3-diketone and subjected to 60°C for a residence time of 6 min to afford the corresponding hydrazine or pyrazole products.

The two-step synthesis of benzotriazoles in flow, as reported by Chen and Buchwald, also makes use of a C–N coupling (**Scheme 36**).[52] The initial coupling of an amine to an aryl chloride was performed either by an S_NAr reaction, which was efficient for aryl chlorides with electron withdrawing substituents, or by palladium-catalyzed C–N coupling for other substrates. This stream was then subjected to hydrogenation conditions over Pd/C to reduce the nitro group. Diazotization and subsequent cyclization to the benzotriazole were conducted at room temperature using sodium nitrite under acidic conditions. This method proved versatile for a number of substrates and avoided the issues associated with the use of benzyne and azides.

The Heck aminocarbonylation reaction of aryl iodides has been reported by Ryu and coworkers.[53] The decomposition of formic acid was used to generate CO gas in situ, which was then passed through a tube-in-tube reactor (**Scheme 37**). The aryl iodide and amine substrates, along with the palladium catalyst and ligands, were passed through the tube-in-tube reactor, where it came into contact with the CO for 2.7 h at 80°C to yield the amide fragments.

The Sonogashira coupling reaction was used as a key step in the flow synthesis of 3-aminoindolizines, reported by James and coworkers.[54] In this work, a bromopyridine was coupled with an alkyne, and the resulting alkynylpyridine cyclized by a copper-catalyzed cycloisomerization reaction to yield the aminoindolizine product (**Scheme 38**). In the flow setup, this reaction sequence was realized by simply heating a stream of all reagents to 180°C for 5–10 min. This method allowed the fast synthesis of 31 examples of 3-aminoindolizines, which are a key substructure in many drugs.

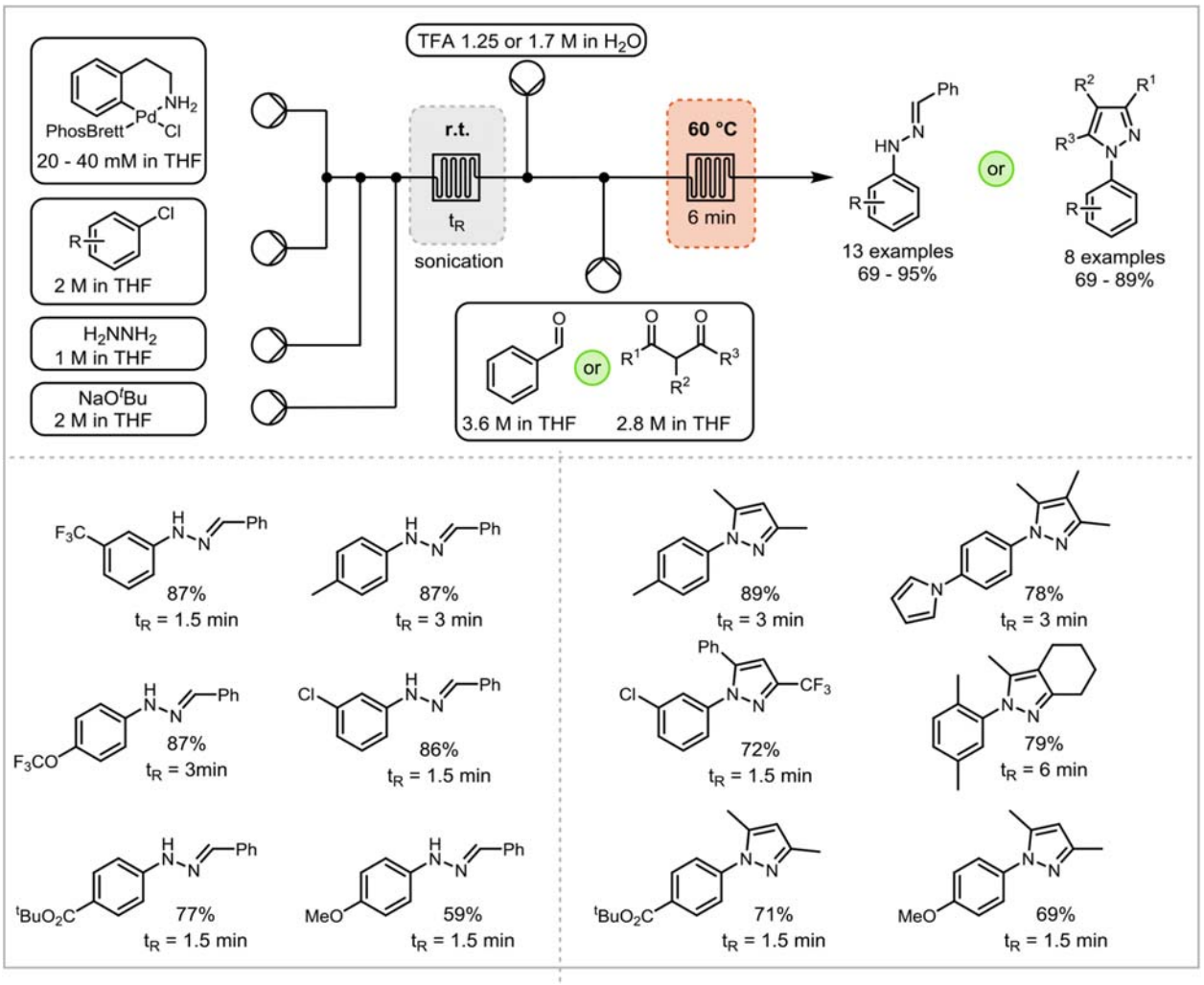

Scheme 35 Flow synthesis of hydrazines and pyrazoles.[51]

1.06.2.10 Nucleophilic Substitution

Nucleophilic substitution, including nucleophilic aromatic substitution, is a key reaction in synthesis. Indeed, there are many reports of these reactions in flow. The lack of a headspace void in flow reactors means that mutagenic alkylating agents can be used more conveniently at high temperatures as they can be contained in solution phase.

The two-step synthesis of the proton pump inhibitor, Lansoprazole, has been performed using microreactors by Gangula and coworkers (Scheme 39).[55] The first step is the nucleophilic substitution of a pyridyl chloride by a thiol to yield the thioether, which was then oxidized to the sulfoxide. Both steps were performed at very high flow rates in microreactors so that the residence times were very low. This avoided overoxidation to the sulfone and presumably allowed improved dissipation of an exotherm, thus enabling the rapid synthesis of three benzimidazole drugs.

The nucleophilic ring opening of epoxides by an amine was conducted by Jamison and coworkers during their synthesis of metoprolol.[56] A stream of *i*-propylamine was combined with a stream of an epoxide and heated in a microreactor at 240°C (Scheme 40). The first ring opening afforded the secondary amine intermediate, which attacks another epoxide leading to the tertiary amine, metoprolol, as the final product in 91% yield. It was found that control over chemo-selectivity, that is, mono- or disubstitution could be conveniently controlled by taking advantage of plug flow characteristics.

1.06.2.11 Cycloaddition

Cycloaddition reactions are important in the synthesis of heterocycles and have been used in flow to synthesize a range of nonaromatic heterocycles including particular attention to pyrrolidines. In 2010, Ley and coworkers reported the 1,3-dipolar cycloaddition of nonstabilized azomethine ylides with nitroalkenes.[57] Trifluoroacetic acid (TFA) was required to generate the dipole, so a solution of the alkene and TFA was flowed through a T-piece, where it was combined with a stream of the azomethine ylide

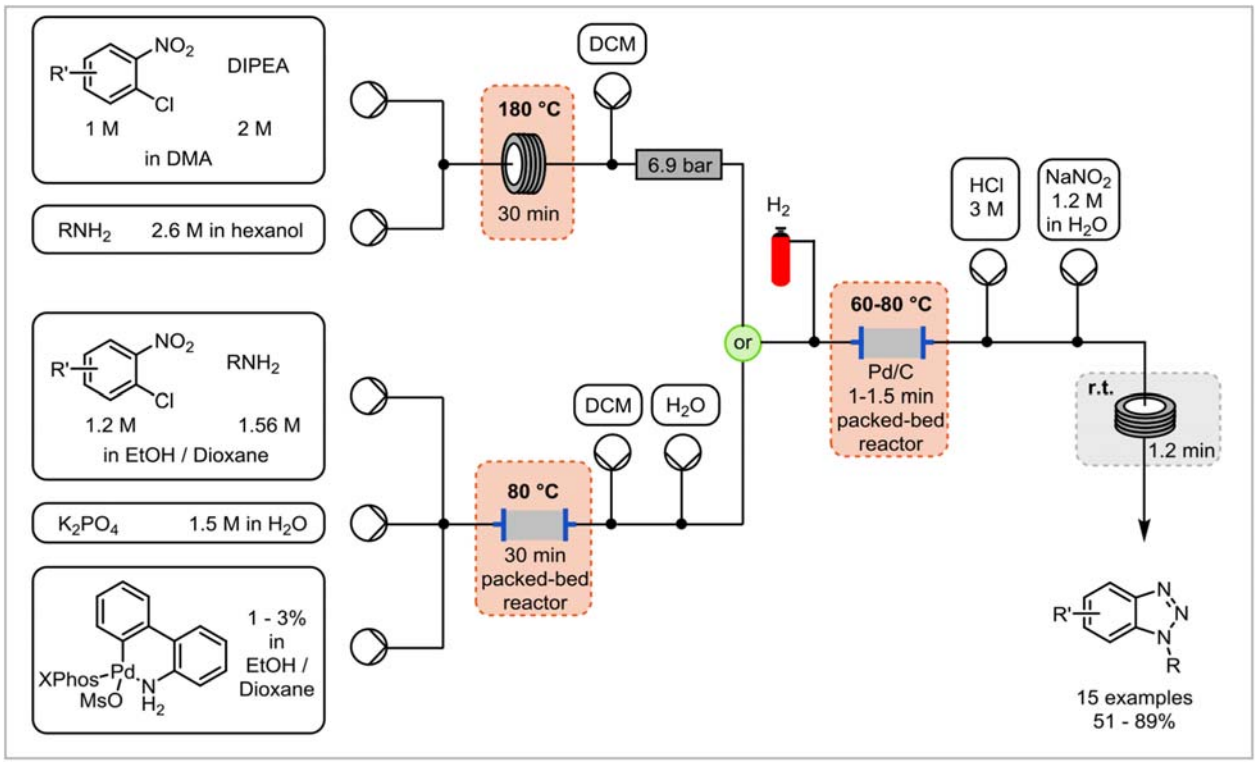

Scheme 36 Benzotriazole synthesis via C–N coupling in flow.[52]

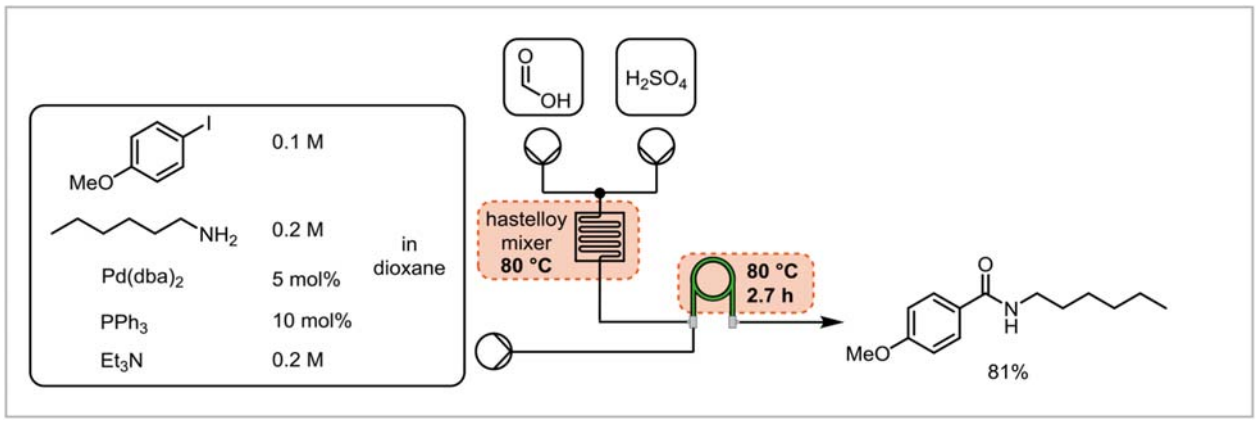

Scheme 37 Aminocarbonylation in flow.[53]

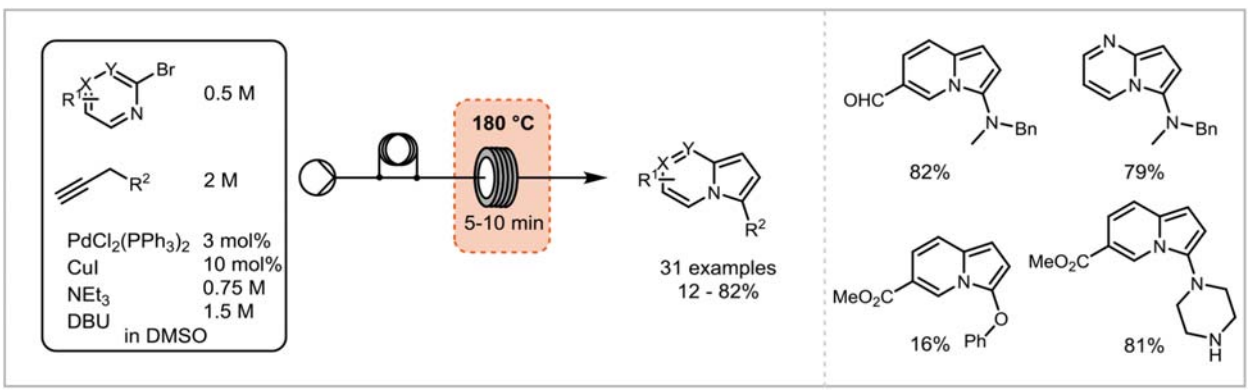

Scheme 38 Synthesis of 3-aminoindolizines in flow.[54]

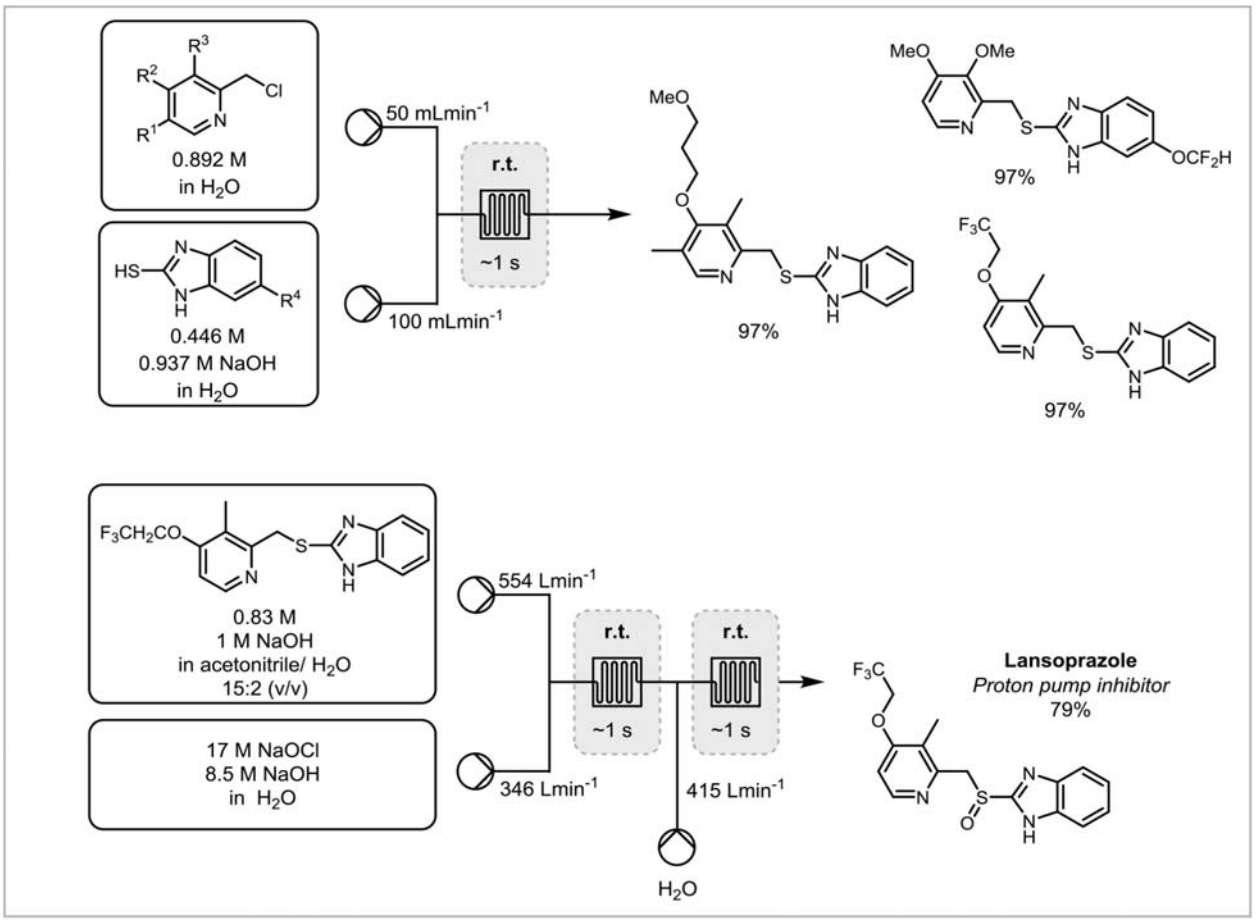

Scheme 39 Synthesis of lansoprazole in flow.[55]

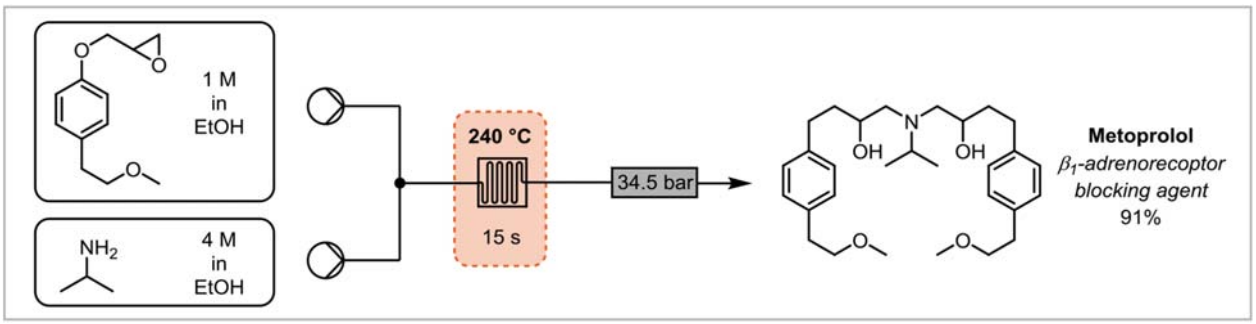

Scheme 40 Flow synthesis of metoprolol.[56]

precursor (Scheme 41). The combined stream was then passed through a heated reactor coil and subsequent scavenger columns in order to remove any unreacted alkene. By using this method, 10 different examples of pyrrolidine scaffolds were synthesized in good yields.

A similar cycloaddition reaction has also been reported in flow by Fray and coworkers.[58] The same azomethine ylide precursor was used to synthesize the pyrrolidine ring. Using different alkene substrates, they were able to perform the reaction at 70°C for 10 min (Scheme 42).

1.06.2.12 Photochemistry

Flow chemistry offers advantages over batch methods in the area of photochemistry. This is due to the Beer–Lambert law, whereby the intensity of light decreases nonlinearly with penetration depth. Therefore, the shape of traditional batch reactors is inefficient and

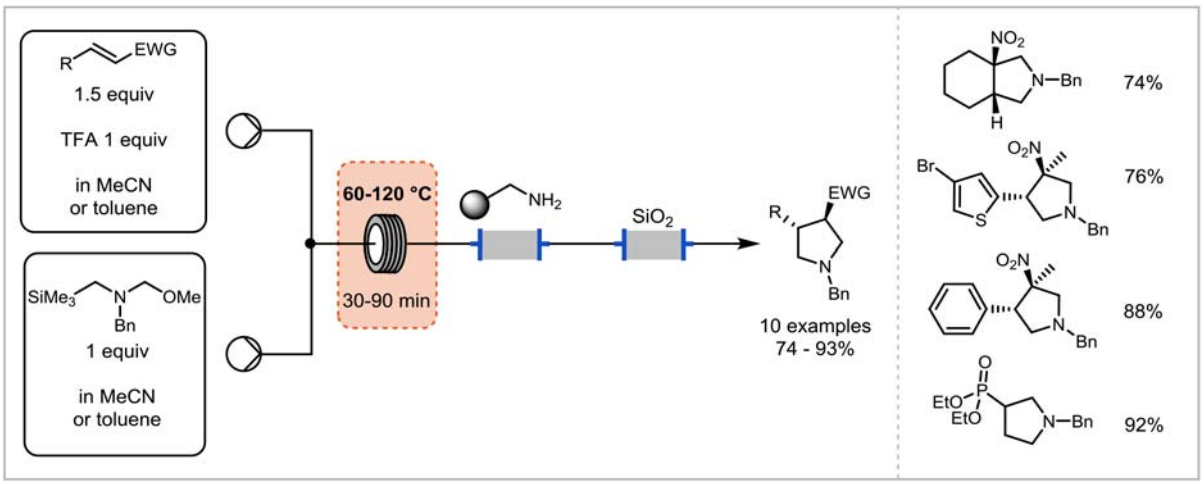

Scheme 41 Ley's pyrrolidine synthesis in flow.[57]

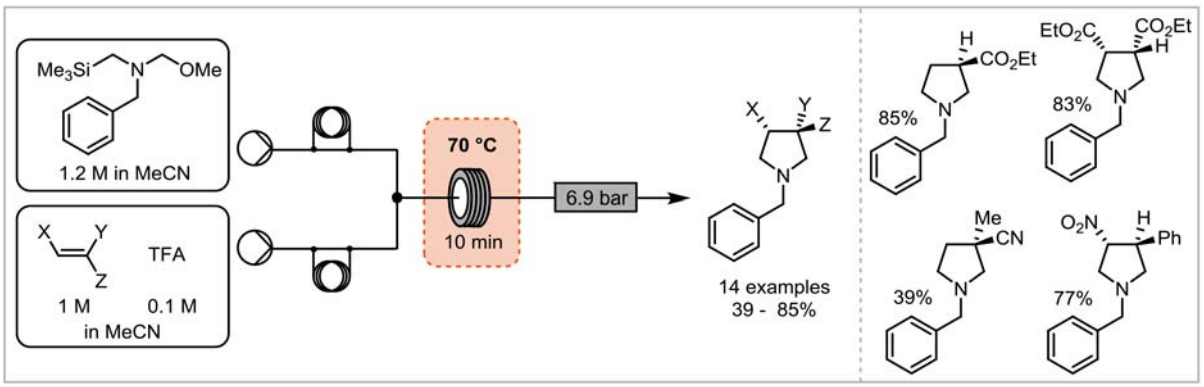

Scheme 42 Fray's pyrrolidine synthesis in flow.[58]

unreliable for photochemical reactions, as the edge receives full irradiation, and the center of the reactor much less. The large SA:V of continuous flow tubular reactors allows a much greater control of the intensity of light that enters the reaction mixture. As such, there are many examples of light-induced transformations performed in flow conditions, some of which are highlighted here.[59]

Two methods, both thermal and photochemical, for the synthesis of 2H-azirines have been compared by Kirschning and coworkers.[60] The vinyl azide starting material was subjected to either inductive heating or irradiation by a mercury lamp. It was observed that the yield was higher under photochemical conditions, so a one-step process to form a range of dihydropyrroles was developed. In this process, the azirine ring opens photochemically to generate the nitrile ylides, which undergo [3 + 2]-cycloaddition with alkene dipolarophiles (Scheme 43). Eight examples of dihydropyrroles were synthesized using this method.

Several carbazole analogues of the antiinflammatory drug Carprofen were synthesized by Collins and coworkers.[61] The use of photochemistry was required to perform the cyclodehydrogenation of diphenylamine derivatives using an I_2/propylene oxide oxidant system (Scheme 44).

Ryu and coworkers have applied photochemistry in flow to the functionalization of cycloalkanes, in this case chlorination using sulfuryl chloride (Scheme 45).[62] They were able to successfully chlorinate different ring sizes of alkanes with reasonable yields. The accurate control of light exposure, molar ratios, and reaction times by using a flow setup allowed good control of the selectivity.

The use of photoreactors has been applied to the generation of nitrenes by Seeberger and coworkers.[63] They report the preparation of 3H-azepinones by the photolysis of aryl azides (Scheme 46). This forms the nitrene which, in the presence of water, rearranges to give the 3H-azepinone. The azepinone scaffold is present in some pharmaceutically active compounds, and some examples are γ-secretase inhibitors for the treatment of Alzheimer's disease.

1.06.2.13 Miscellaneous

Due to the high SA:V of flow reactors, the heat exchange is more efficient than in batch. This can allow exothermic reactions to be safely controlled and can also allow more control over heating than in batch processes. Polomski and coworkers demonstrated the

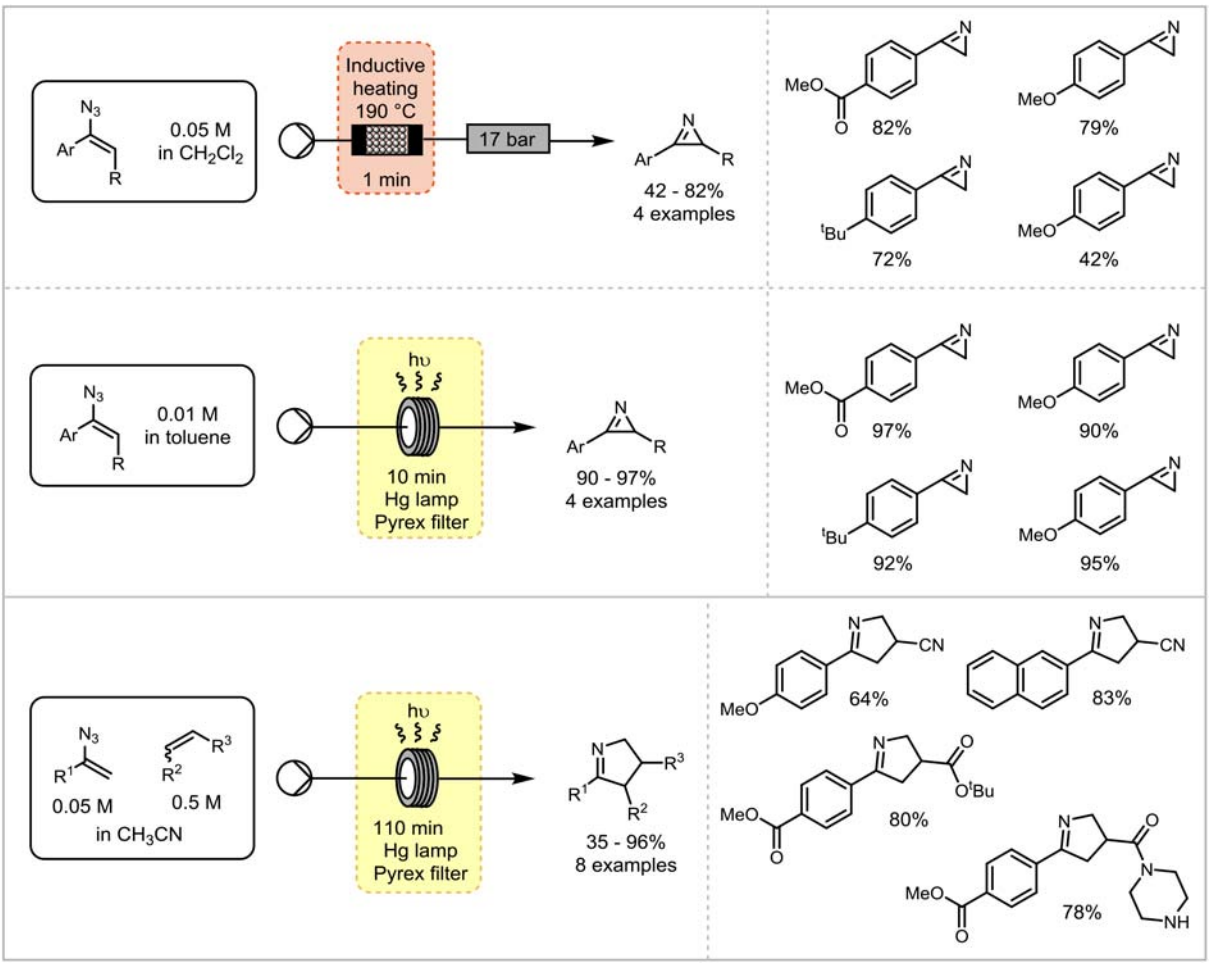

Scheme 43 Flow synthesis of azirines and subsequent cycloaddition.[60]

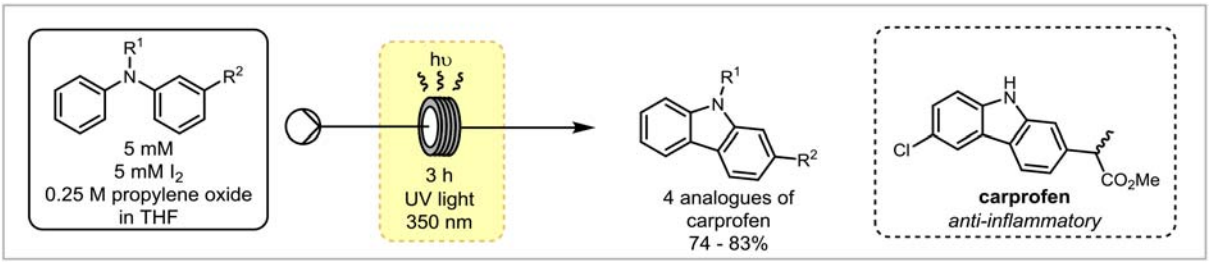

Scheme 44 Flow synthesis of carprofen using a photochemical reactor.[61]

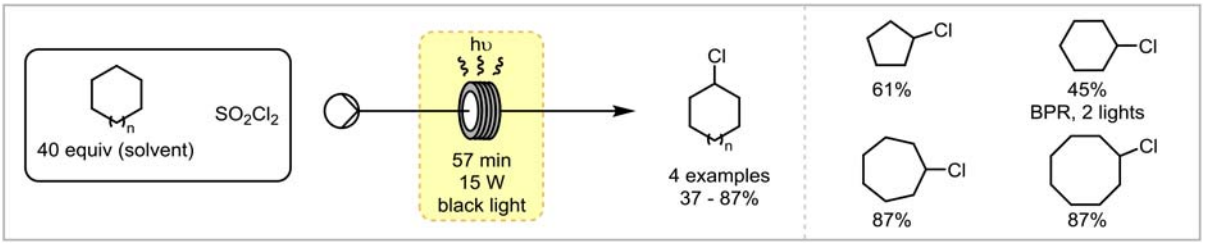

Scheme 45 Photochemical monochlorination of alkanes.[62]

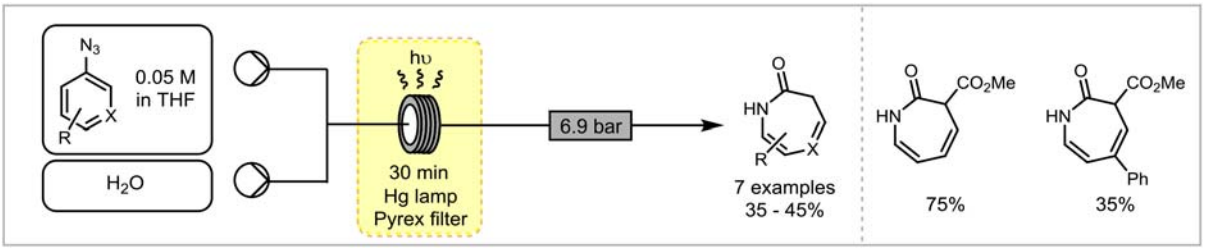

Scheme 46 Flow photolysis of aryl azides.[63]

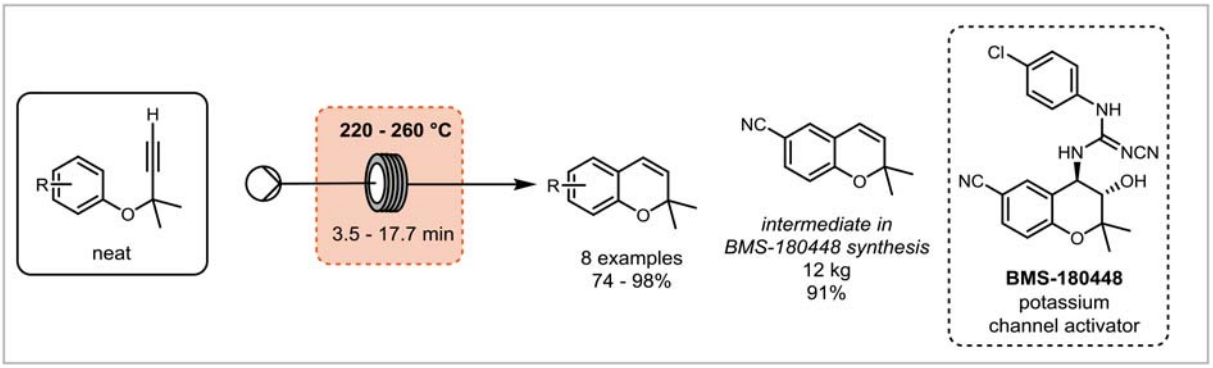

Scheme 47 Large-scale Claisen rearrangement in flow to control the exotherm.[64]

use of a flow process to carefully control the temperature during a Claisen rearrangement (Scheme 47).[64] Heating is required to initiate the reaction, but the overall process is exothermic which can lead to thermal runaways. This makes accurate temperature control, especially on a large scale, challenging. In addition to safety concerns, poor temperature control in batch can lead to degradation. In the flow setup, a neat stream of the precursor was heated accurately in a reactor coil, causing the Claisen rearrangement to occur selectively and in high yields. This setup was able to deliver a large quantity (12 kg) of a key intermediate in the synthesis of a potassium channel activator. This demonstrates the ease of scaling up reactions when performed in flow conditions compared to batch.

The use of high temperatures and pressures is possible in flow conditions by incorporating a back-pressure regulator (BPR) and is often easier than the same process in batch. In batch it is necessary to manufacture vessels capable of operating at high pressures, which is especially difficult and expensive on large scales. In flow, scale-up can involve simply running the system for a longer period of time, or increasing the internal diameter and mixing of the flow tubes. Kappe and coworkers report the high temperature and pressure pyrolysis of Meldrum's acid derivatives (Scheme 48).[65] After loss of CO_2 and acetone, the intermediate ketene undergoes electrocyclization to afford the oxazinone product with 80% yield.

The formation of C–O bonds via C–H activation, disclosed by Kappe and coworkers in 2012, is the first example of C–H activation under continuous flow conditions.[66] They adopted a copper-catalyzed procedure, using tert-butyl hydroperoxide (TBHP) as the terminal oxidant. A stream of ether, the catalyst, and the 2-carbonyl-substituted phenol were combined with a stream of TBHP, passed through a mixer, and then allowed to react at 130°C for 20 min (Scheme 49). The desired acetals were then obtained, demonstrating successful C–H activation.

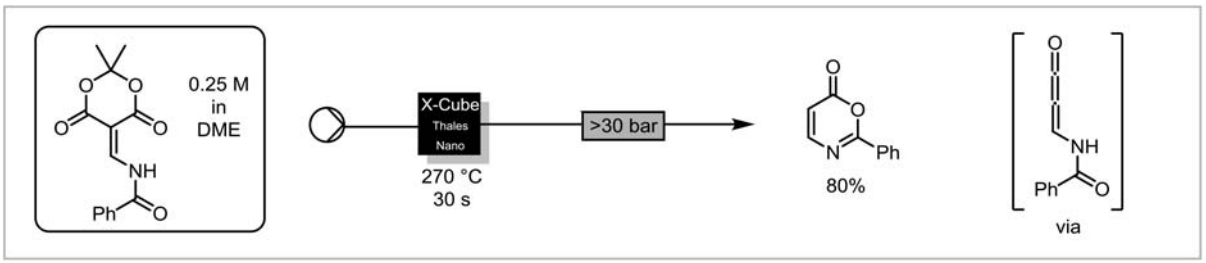

Scheme 48 Flow pyrolysis of Meldrum's acid derivatives.[65]

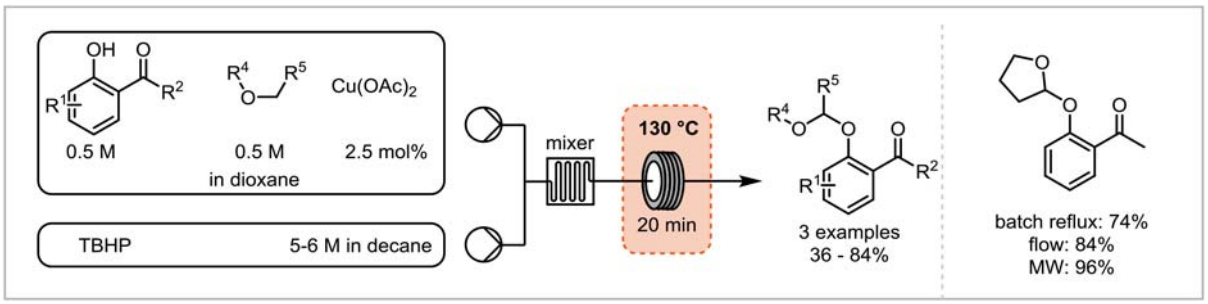

Scheme 49 C–H activation in flow.[66]

The application of flow chemistry to the synthesis of a range of fragments and heterocycles interesting for pharmaceutical industry has been described briefly. Particular attention is paid to reactivity that can be challenging in batch such as the safe handling of hazardous gases and reagents. This can make it possible to scale-up syntheses to pilot plant scale which would otherwise be challenging.

1.06.3 Library Preparation and Automated Processes

Continuous flow systems are well suited to the synthesis of large libraries of similar compounds. Once good conditions are found for a transformation, it is often straightforward to introduce many different substrates to one reaction setup in order to make many related molecules. This ability is especially relevant to drug-discovery processes, where libraries of potentially bioactive molecules have to be synthesized and screened in order to find a successful "hit." Usually an array of different starting materials is used, leading to more complex products. This process can involve several steps, and it is possible to integrate biological screening into the system. This process can be fully automated in order to improve efficiency and decrease human interaction.

Petersen et al. used a multistep synthesis to rapidly synthesize receptor ligands such as chemokine receptor CCR8 from three building blocks on-demand (Scheme 50).[67] In the first step a diamine, which is mono Cbz protected, reacts with an isocyanate to form a disubstituted urea derivative. Excess isocyanate was scavenged using a solid-supported trisamine before the second amine was deprotected by hydrogenation. This amine was alkylated with a benzyl bromide derivative on solid-supported *N*-methylmorpholine. Excess benzyl bromide was removed on solid-supported trisamine to yield the desired product. This method allows easy access to a library based around the *N*-benzyl-piperazine-urea scaffold, which is present in a number of ligands for receptors, enzymes, and ion channels.

Ley and coworkers developed a process that made use of the "catch–react–release" method to access a library of 2-aminopyrimidines which are precursors to Imatinib (Scheme 51).[68] This method usually decreases downstream processing and delivers clean products directly. This process is comparable to batch mode solid-supported reactions. The starting material, an

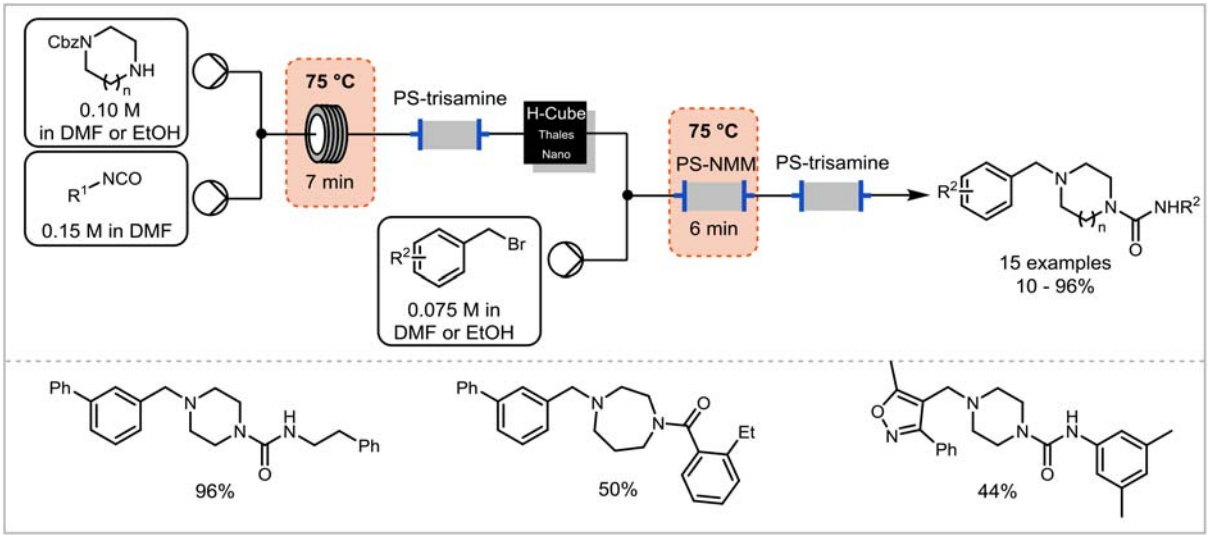

Scheme 50 Synthesis of receptor ligands on demand.[67]

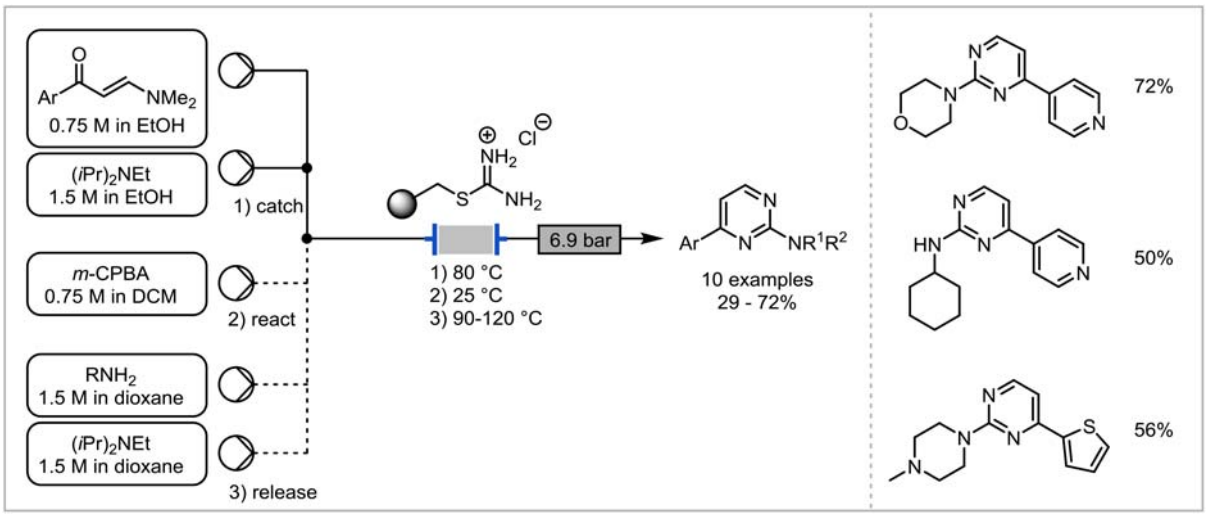

Scheme 51 Use of "Catch–react–release" method in the synthesis of 2-aminopyrimidines.[68]

enaminone in this case, was pumped through the system and caught on a solid support, an isothiouronium chloride-functionalized monolith. Then a valve was switched to deliver the next reagent and perform the subsequent reaction. Ley and coworkers first performed an oxidative activation with meta-chloroperoxybenzoic acid (m-CPBA) before switching to a primary amine input to release the final product. The "catch–react–release" method enables a high throughput of substrates by reducing downstream processes, in this case solvent changes and by-product removal.

A modular reaction approach to not only synthesize one but three different classes of substrates has been developed by Seeberger and coworkers.[69] Five different reaction modules have been developed: module 1 (oxidation with (2,2,6,6-tetramethylpiperidin-1-yl)oxyl (TEMPO) or bleach), module 2 (olefination with triethylphosphonoacetate and *t*BuOK or methyl cyanoacetate and piperidine), module 3 (Michael addition with $MeNO_2$ and tetra-n-butylammonium fluoride (TBAF)), module 4 (hydrogenation using the H-cube with either Pd/C or Raney Ni), and module 5 (saponification with LiOH). Depending on the starting materials, order of the modules and reagent choice different substrates can be targeted (Scheme 52). In all cases a secondary alcohol was oxidized to a ketone in module 1 before olefination in module 2. Depending on the reagent used either a Knoevenagel condensation to yield an α-nitrile ester (**2a**) or a Horner–Wadsworth–Emmons reaction to yield an α,β-unsaturated ester could be performed (**2b**). Both of these intermediates can then either underwent Michael addition in module 3 or hydrogenation in module 4. Michael addition of nitromethane in module 3 led to γ-nitroesters which could be either transformed to γ-lactams via hydrogenation in module 4 or to γ-amino acids initially via hydrolysis in module 5 and then hydrogenation in module 4. Intermediate **2** can also undergo hydrogenation in module 4 directly to give β-amino acids after hydrolysis in module 5. The authors demonstrated how powerful this modular approach can be, as three different classes of substrates, γ-lactams, γ-amino acids, and β-amino acids, can be approached using the same equipment.

Ley, Baxendale, and coworkers combined several enabling technologies to quickly synthesize a library of imidazolepyridines, a family of casein kinase I inhibitors (Scheme 53).[70] The process has four reaction steps incorporating continuous flow processing with solid-supported reagents, scavenging resins, and autosamplers under fully automated software control. In the first step an organolithium base mediated the addition of a methylated aromatic to an ester. Delivering the organolithium base at scale proved to be a challenge due to its hazards and incompatibility with the seals in high pressure pumps. This was addressed by introducing a "dual sample injection loop" where one sample loop was used to deliver the base while the other was being loaded automatically. The second step was an α-bromination using an immobilized perbromide species to give the monobrominated ketone selectively. This proved to be a more convenient method than using bromine directly as standard flow equipment could be used. In the third step the imidazopyridazine core was generated in a cyclocondensation. Reaction temperature, residence times, and reagent ratios were screened automatically using the Vapourtec Flow Commander software. In the last step structural diversity was achieved by displacing the chlorine substituent with an array of amines using an autosampler at high temperature and pressure using a back pressure regulator. This gave 20 examples of imidazopyridazines in four steps and is a good demonstration of the capability of automated flow processing.

Once a library of compounds have been synthesized, they then have to be screened for biological activity. Baxendale, Ley, and coworkers synthesized a library of substrates, here $GABA_A$ agonists with an imidazo[1,2-a] pyridine structure, and biologically evaluated them in line (Scheme 54).[71] In this case, inline frontal affinity chromatography was used, demonstrating a seamless chemistry–biology interface. The multistep synthesis consisted of three steps. The first step is an immobilized-acid catalyzed condensation between ethyl glyoxylate and acetophenone derivatives leading to unsaturated ketones that cyclize in the presence of aminopyridine derivatives. Incorporating a back pressure regulator enabled superheating of the solvent and therefore a faster

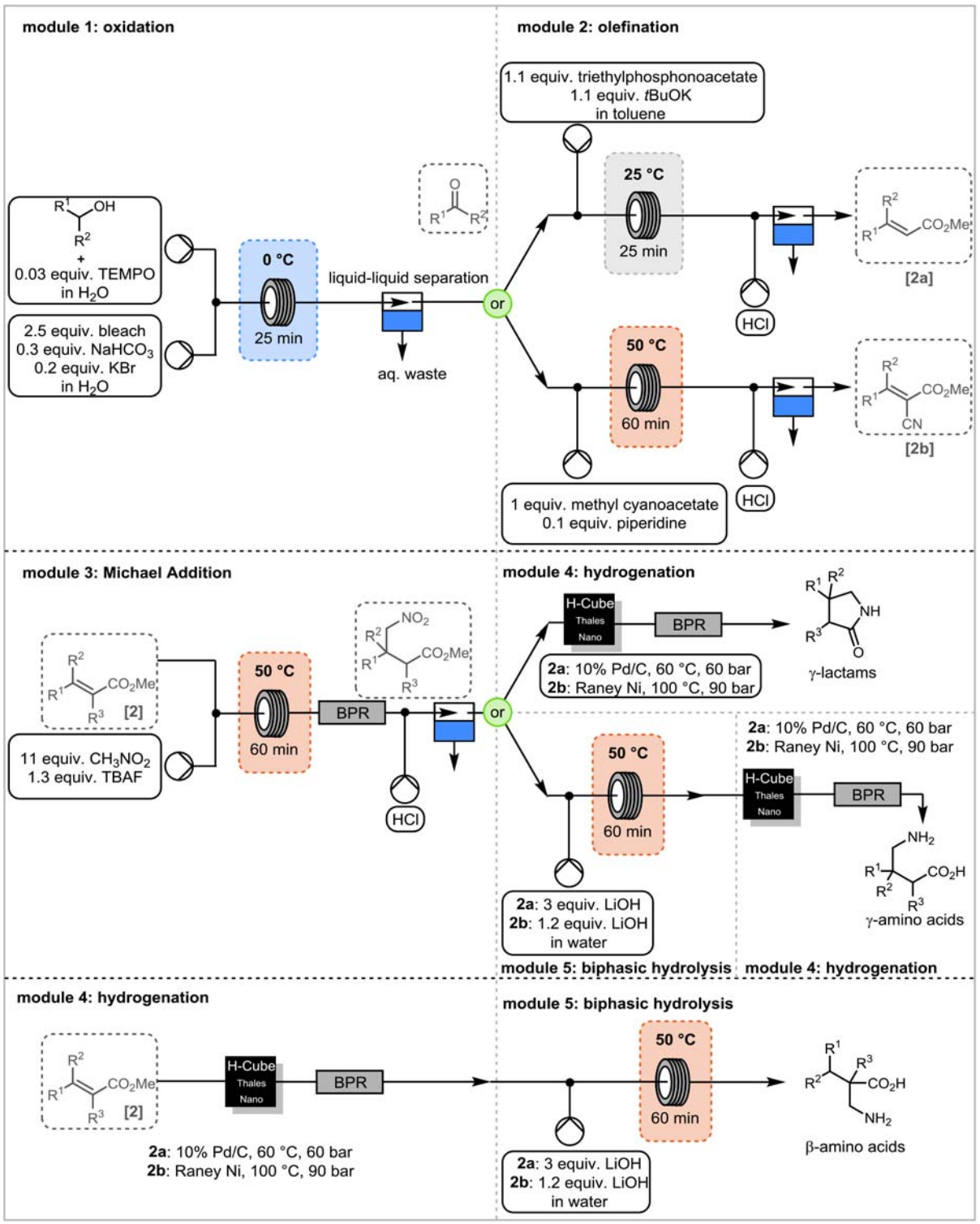

Scheme 52 Synthesis of different classes of compounds using the same five modules.[69]

reaction. Excess aminopyridine was captured on a supported acid resin and could be removed by injecting ammonia in methanol. Column chromatography was then performed to obtain a pure product. For the last step two different reactions were performed as a point to introduce structural diversity on the imidazo pyridine scaffold. The ester could either be transformed into the amide by high temperature amidation, or to the acid by rapid saponification at high temperature. Autosamplers were used to synthesize a library of products, including Zolpidem and Alpidem, that were then tested for biological activity by inline frontal affinity chromatography.

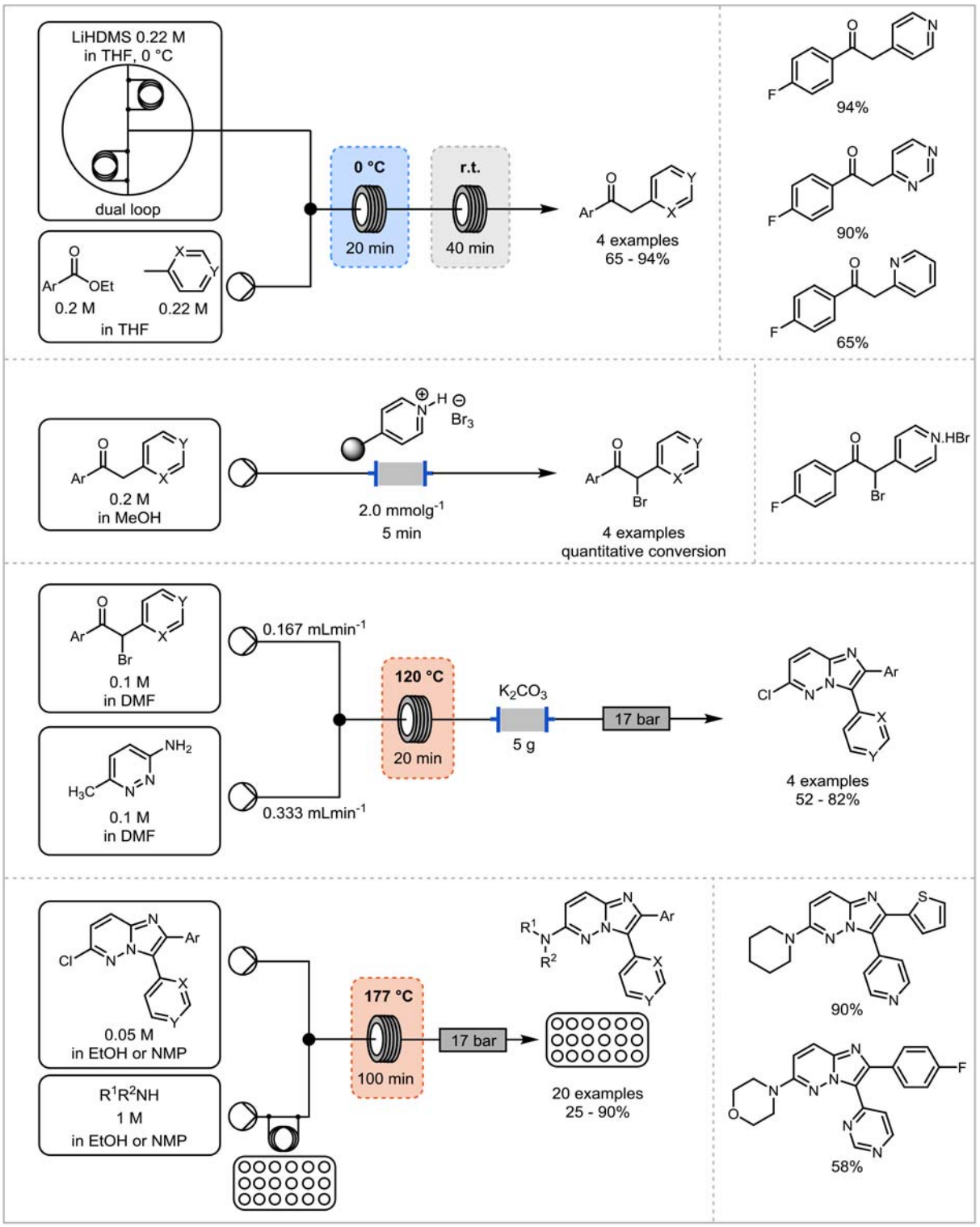

Scheme 53 Synthesis of a library of imidazopyridazines using autosamplers.[70]

A joint collaboration between Cyclofluidic, Sandexis, and Accelerys has resulted in a closed-loop process with a feedback algorithm. This system is capable of synthesizing and evaluating the biological activity of an array of compounds and then choosing the next compound to synthesize (Scheme 55).[72] Two fragments were cross coupled using a Sonogashira reaction in a relatively straightforward reaction setup, purified and analyzed via LC–MS. The product was diluted and then further probed in a bioassay

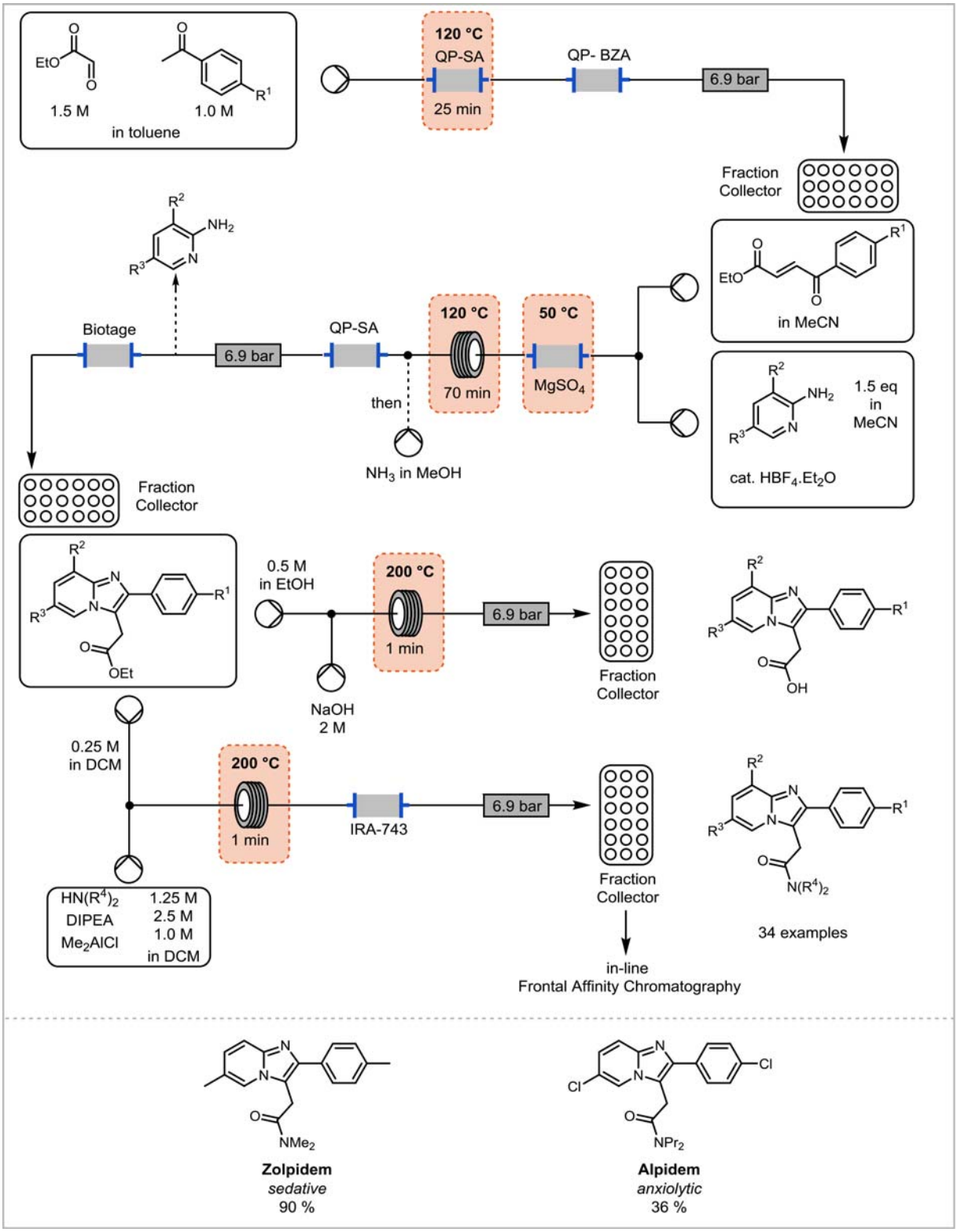

Scheme 54 Automated synthesis of a library of $GABA_A$ agonists and evaluation of biological activity in line.[71]

to investigate the biological activity. This information was fed into an activity prediction algorithm (Random-Forest regression) which would then determine the next set of starting materials. In this manner 21 compounds were synthesized and evaluated as AbI kinase inhibitors with a novel template being identified.

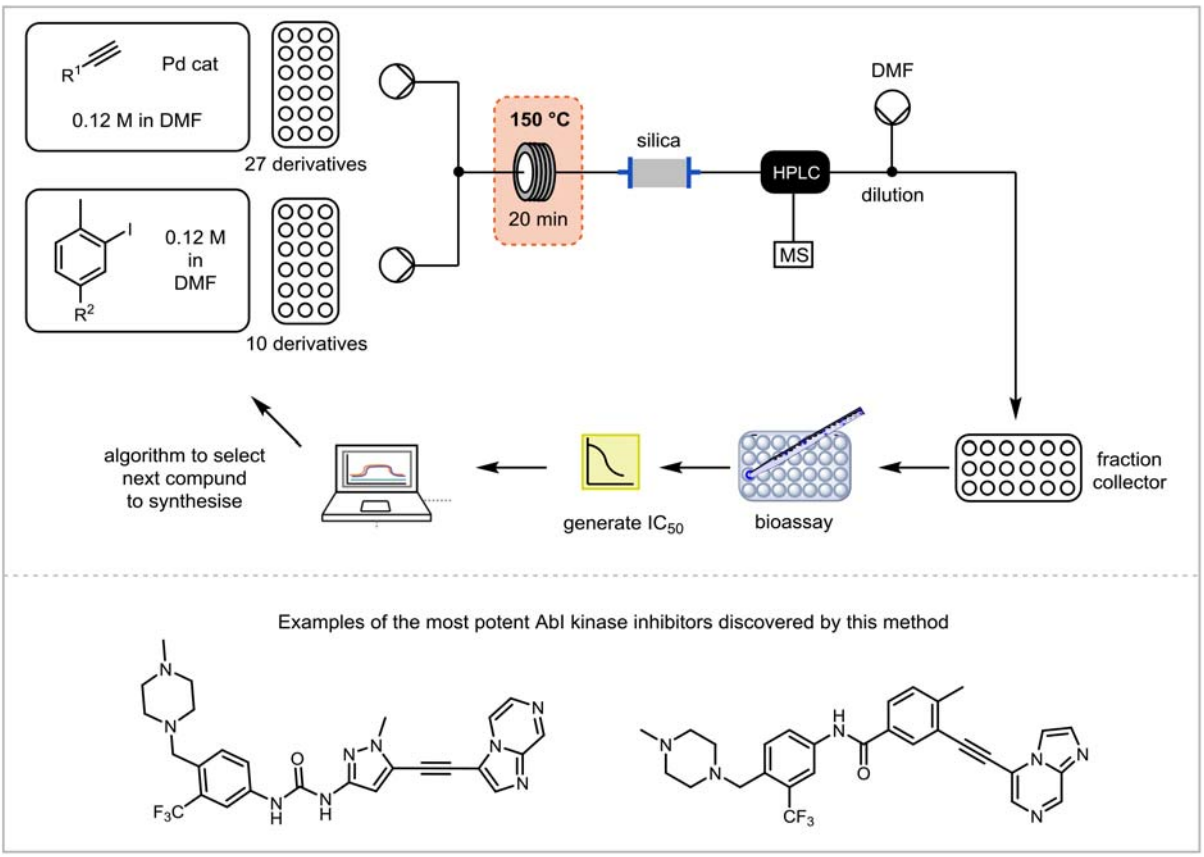

Scheme 55 Automated synthesis of a library of compounds by the Sonogashira reaction and inline determination of biological activity. By computer control using an algorithm, new leads could be found using this automated feedback loop.[72]

The ability of flow processing to easily generate libraries of compounds has the prospect of leading to a more streamlined drug-discovery approach. The addition of automation leads to further improvement in efficiency, especially when combined with biological screening. The final example presented here adds another level of automation to this process by choosing substrates using an algorithm. Such automated feedback loops can also be used to optimize reaction conditions, be it for yield, cost, or even towards sustainable metrics.

1.06.4 Reaction Monitoring and Self-Optimizing Systems

With the increased availability of inline analysis systems, such as the flow IR cell, monitoring of complex features of reactions as they proceed are becoming more and more attractive. Many standard techniques for offline analysis have now been adapted to inline analysis, with IR, HPLC, GC, mass spectrometry, and NMR available. These monitoring tools allow fast characterization of a reaction mixture and can be used to measure consumption of starting materials, formation of desired products and side products, as well as monitoring hazardous intermediates to prevent dangerous build up.

Automated systems have been used to decrease manual handling steps, such as automatically shutting down a system or switching pumps and valves on and off without requiring the operator to be present. When automated systems are combined with real-time data from inline monitoring and simple algorithms, they can be designed to perform tasks without input from an operator. These tasks vary from simple, such as switching a pump on or off depending on the height of liquid in a reservoir, to performing many experiments in order to optimize reactions automatically.[73] This technology offers the prospect of an enormous reduction in workload to chemists, transferring the burden of reaction optimization to computer algorithms.

Such self-optimizing systems generally follow the same basic steps in order to find optimum conditions for a reaction. An initial set of reaction conditions is chosen, applied to the reaction setup and the data from inline monitoring used by an algorithm to find a new set of conditions. This process is repeated without any manual interaction until optimized conditions are obtained. A few examples for automated self-optimizing systems using different inline monitoring techniques are presented here.

In 2010, Ley and coworkers demonstrated the ability to use inline IR monitoring and automated control to ensure a key reagent was introduced at the correct time during a multistep flow synthesis of a δ-opioid receptor agonist (Scheme 56).[74] Initially, the

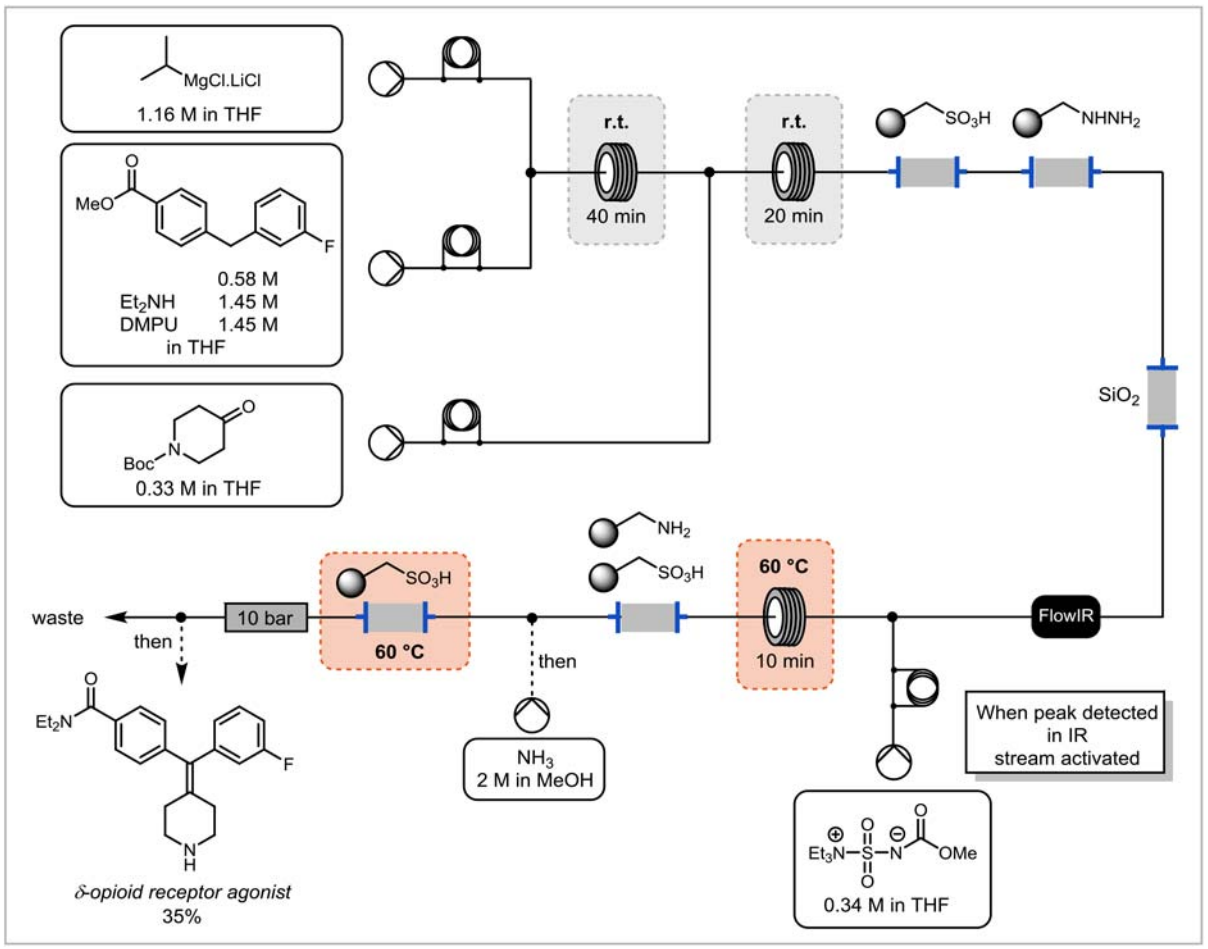

Scheme 56 Inline IR used to automatically introduce a reagent at the correct time during the flow synthesis of a δ-opioid receptor agonist.[74]

methyl ester is converted to the amide with dimethylamine, using a Grignard reagent as a base. At room temperature, the diarylmethyl proton was removed so that the diarylmethylcarbanion was directly intercepted with a Boc-protected piperidone. This addition could be accurately timed by the strong color of the deprotonated diarylmethyl species. After passing through scavenger columns to remove excess amine, piperidone, and magnesium salts, the stream was directed through an inline ReactIR flow cell. The stream of the Burgess reagent could then be automatically and accurately switched on when the intermediate was being detected in the ReactIR cell. The stream was subsequently heated to 60°C to achieve dehydration, and excess Burgess reagent and by-products were scavenged. The dehydrated product was then directed through a heated column of sulfinic acid, causing Boc deprotection and catching the product. The product was then released by passing a solution of ammonia through the column, yielding the target δ-opioid receptor agonist in 35% overall yield.

The use of IR as an inline monitoring tool is one of the most facile, as spectrometers are compact, and once a characteristic peak has been identified, it can be used to measure concentrations of one component in mixtures of several compounds. As such, there are several examples using IR in self-optimizing systems. Another example, reported by Jensen and coworkers, demonstrates the power of self-optimizing systems to find the conditions required to make different products in an aminocarbonylation reaction (Scheme 57).[75] This reaction takes place under biphasic conditions, with a liquid phase containing the aryl halide substrate and palladium catalyst, and a gaseous phase of CO, taking advantage of good mixing under the segmented flow regime. The two products observed had characteristic, nonoverlapping amide absorptions in the IR spectrum, so the yield of each in the reaction solution could be determined easily. A thorough kinetic study could be performed with minimal operator intervention, and it was found that the selectivity could be controlled by changing temperature and pressure.

Another demonstration of IR monitoring in self-optimization is reported by the Ley group performing an Appel reaction (Scheme 58).[76] This example takes the idea of reduced operator input even further and allows the system to be controlled from anywhere in the world over the Internet.[77] The setup comprised separate streams of alcohol, CBr_4, solvent, and triphenylphosphine. These streams are combined, passed through a reactor coil and then through an inline IR spectrometer. The peaks due to the alcohol starting material and triphenylphosphine oxide by-product could be monitored and tracked simultaneously. The flow rate of each stream and the temperature of the reactor coil could be controlled remotely over the Internet. This permitted the automatic

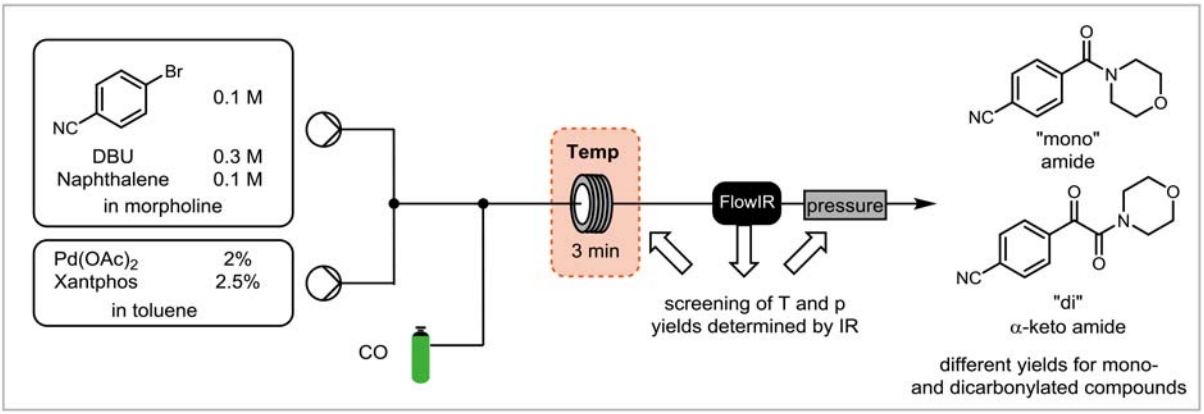

Scheme 57 Automated investigation of the effect of temperature and pressure on selectivity in an aminocarbonylation reaction.[75]

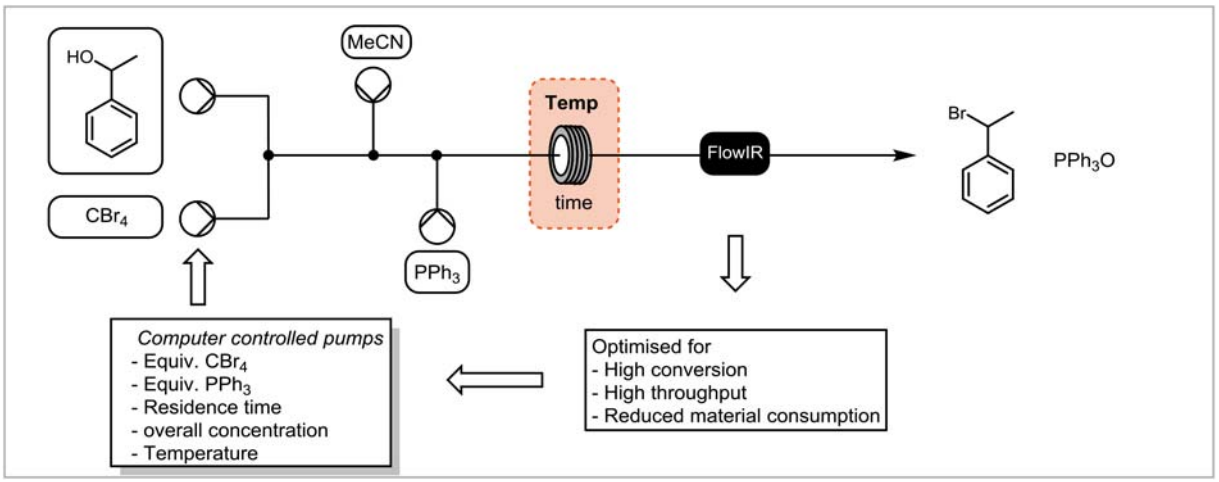

Scheme 58 Self-optimization of an Appel reaction.[76]

optimization algorithm to vary five different parameters. The reaction was optimized for throughput, conversion, and consumption. A simple algorithm can then automatically find conditions that lead to a process with high conversion, high throughput, and low material consumption. A yield of 92% was achieved with productivity of 1.9 g h^{-1} after 30 iterations.

An alternative inline analysis method is liquid or gas chromatography which can be performed online. The reaction outlet is connected to a valve which samples a small slug of the flowing stream and relays it into an offline spectrometer. An example of self-optimization using this online chromatography is reported by Poliakoff and coworkers (Scheme 59).[78] The methylation of an aliphatic alcohol with dimethyl carbonate in super critical carbon dioxide was investigated. The setup comprised of a stream containing both of the starting reagents which was combined with super critical carbon dioxide and subjected to heating. A valve could then inject samples automatically to perform GLC to determine yield. The temperature, system pressure, and CO_2 flow rate were computer controlled. This reaction can yield two different products, both the methyl ether and carbonate. Optimal conditions to form each product were found using the super modified simplex (SMSIM) algorithm, taking approximately 35 h for each optimization.

Inline mass spectrometry is a sensitive technique allowing very small scale reactions to be optimized. This is useful when trying to avoid the use of large quantities of reagents for optimization or if very hazardous intermediates are produced. Ley and coworkers demonstrate the use of inline mass spectrometry to find optimal conditions to minimize the amount of hazardous intermediate exiting the system (Scheme 60).[79] In this setup, a stream of anthranilic acid meets a stream of furan and *tert*-butyl nitrite to form a hazardous diazonium salt. The combined stream is then heated, eliminating N_2 and CO_2 from the diazonium salt to form benzyne. Benzyne then undergoes a Diels–Alder reaction with furan yielding the desired product. After the reactor coil, the stream is diverted to a mass spectrometer where the products were analyzed. Several side products were identified, and the temperature and residence times were optimized to ensure that all diazonium salt is consumed before the stream exits the reactor. This approach also maximized selectivity for the desired product.

An example of optimizing reactions by inline HPLC was reported by Ahmed-Omer and Sanderson during their multistep synthesis of Fluoxetine, an antidepressant (Scheme 61).[80] They demonstrated the use of online HPLC during the enantioselective

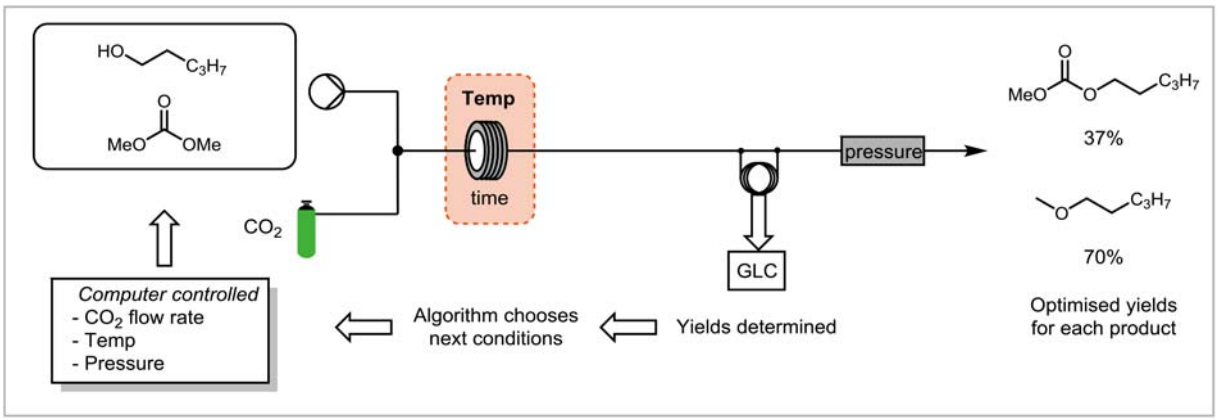

Scheme 59 Self-optimization using online chromatography.[78]

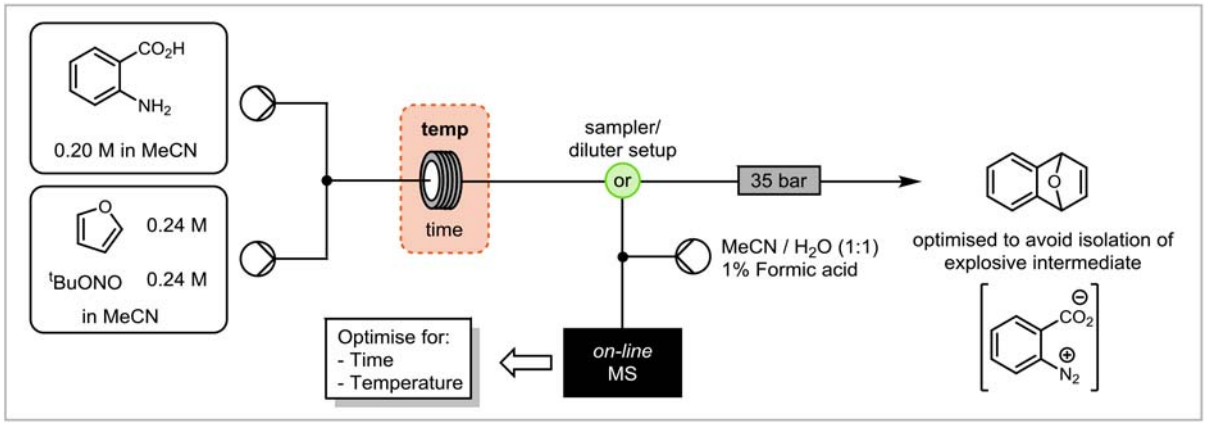

Scheme 60 Optimization using online mass spectrometry.[79]

reduction of a benzylic ketone. The ketone stream was combined with a stream of the diethylaniline borane reducing agent and a chiral oxazaborolidine catalyst before the combined stream passed through two reactor coils with different temperatures. A UV detector was used to determine when the reaction mixture had reached the end of the system, and a fraction collector allowed samples to be taken for HPLC. The residence time, temperature, stoichiometry, and total concentration were varied in order to optimize the yield and enantiomeric excess. Using this method, the enantiomeric excess was increased from 72% to 92%. After demonstrating the use of their method they optimized each step required for the synthesis of (±)-Fluoxetine in the same way. In the first step, a stream of the 3-chloro-1-phenyl-propan-1-one was combined with a stream of BH_3.THF and passed through a reactor coil at room temperature for 5 min to yield the racemic secondary alcohol. Subsequent nucleophilic substitution by methylamine was achieved after 10 min at 140°C, yielding the secondary amine in 89% yield after optimization. The arylation of the benzylic alcohol was achieved by a Mitsunobu reaction first generating the phosphonium, betaine in situ from streams of diisopropyl azodicarboxylate (DIAD) and PBu_3, followed by the addition of streams of the phenol and benzylic alcohol. Optimal conditions of 5 min and 70°C gave the antidepressant Fluoxetine in 86% yield.

Clearly, the use of reaction monitoring in tandem with automation and computer control to optimize reactions has the potential to speed up the optimization process dramatically. When correctly applied, it can relieve the operator from repetitive work and run experiments continuously without input required. However, it is important to choose parameters and algorithms carefully. Finite numerical parameters are most straightforward such as temperature, pressure, and flow rates. Parameters such as solvents and ligands are more difficult to use in such systems. The problem is twofold: First, numerical values should be assigned to particular attributes, such as dielectric constants, boiling point, or binding affinity. Second, a greater infrastructure is necessary to deliver a variety of solvents, ligands, or additives to the automated reactor system. This would typically consist of an autosampling liquid handling robot but may also use robotic weighing, measuring, and diluting processes. Automatic, self-optimization is a relatively new technique enabled by the increased availability of inline monitoring techniques with the prospect of optimizing ever more complex processes with minimal human input.

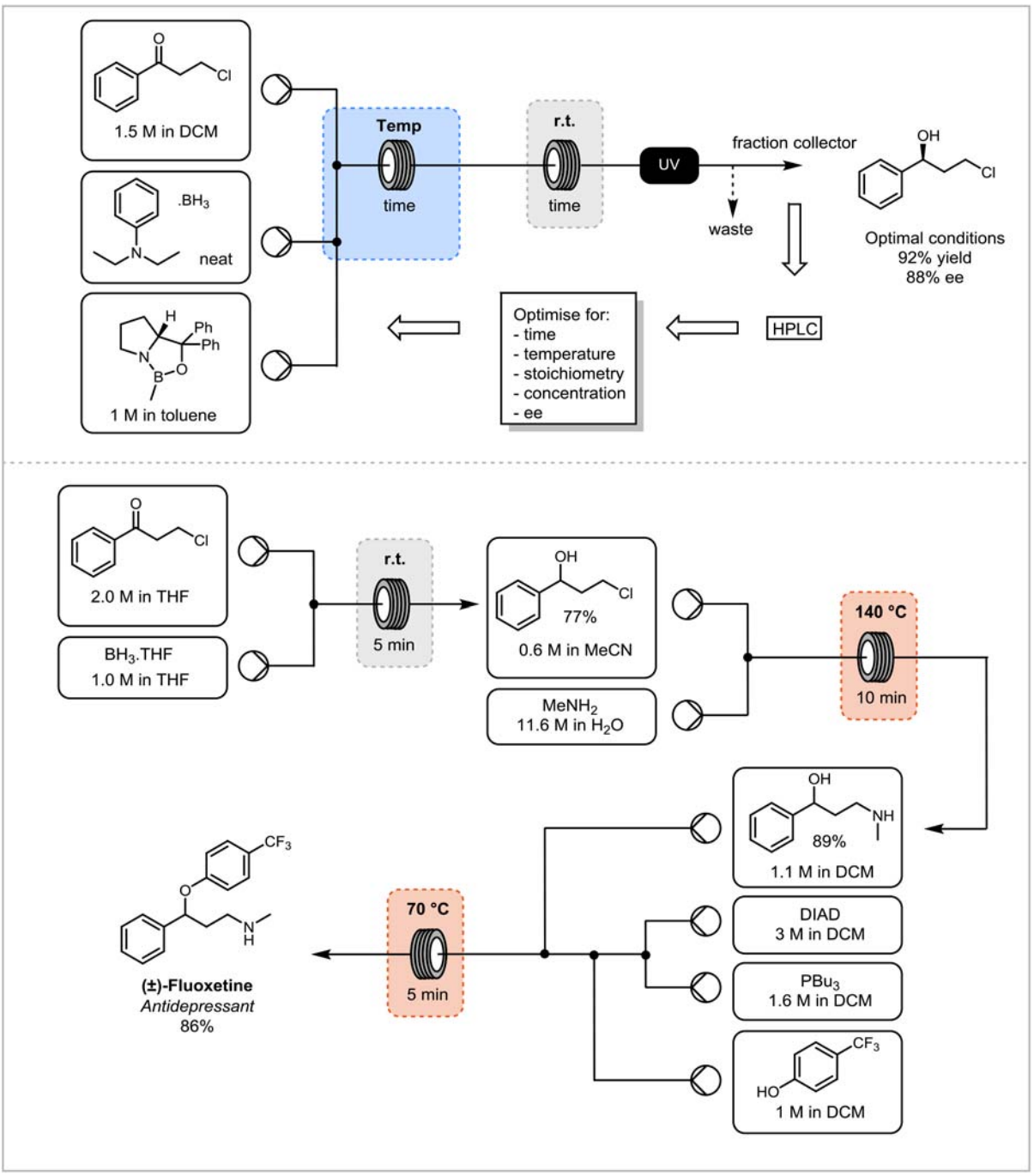

Scheme 61 Flow synthesis of Fluoxetine making use of HPLC for optimization.[80]

1.06.5 Multistep Flow Processes

Multistep or telescoped flow synthesis involves directly chaining together multiple reaction steps to form one continuous flow system in order to achieve the synthesis of a target molecule. The finalized process can be a thing of beauty and a form of art where consecutive reaction steps are designed to operate in a flow manner, whereby solvent compatibility, flow rates, coil temperatures, system pH levels, and longevity of operation all need to work in tandem. If all of these attributes are satisfied then this can lead to machines capable of reliably and monotonously performing the same reaction processes. Indeed, it was perhaps owing to the intricacy and elegance of one of the first reports on multistep flow synthesis, targeting the alkaloid natural product Oxomaritidine, that the utility and importance of flow chemistry to this chemical sector was realized.[81]

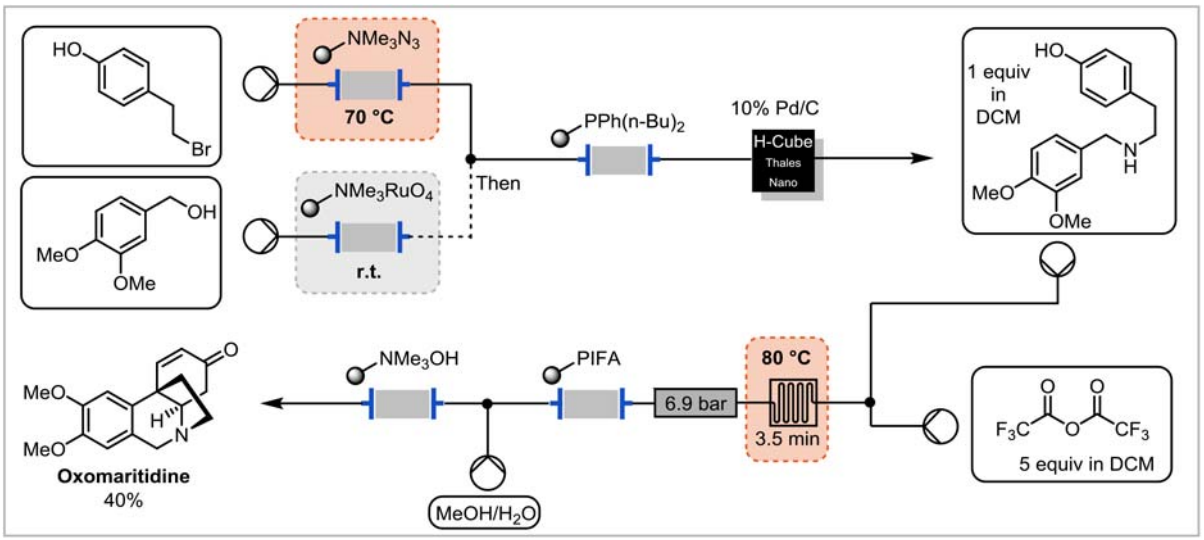

Scheme 62 Continuous flow multistep synthesis of Oxomaritidine.[81]

In 2006, Ley et al. reported the end-to-end preparation of Oxomaritidine using continuous flow technologies and polymer-supported reagents. Many of the principles of polymer-supported reagents that were investigated and understood in the decade prior to this report were key to realizing the continuous flow route. Cartridge charging and loading with reagents along with "catch–react–release" protocols were developed for flow systems for the first time in this synthesis. As shown in **Scheme 62** the alkyl bromide material was first passed through an ion-exchange resin supporting azide anions which effected an S_N2 displacement. The resulting azide species was then caught on a polymer-supported phosphine as an iminophosphorane ready to react in a subsequent step. In tandem to this, a benzylic alcohol substrate underwent Ley oxidation to the corresponding aldehyde, mediated by a PS-RuO_4. The aldehyde then passed through the iminophosphorane column to react in an aza-Wittig process and release the resulting imine from the support (leaving behind the phosphine oxide). The imine was immediately reduced over a palladium on charcoal cartridge to the secondary amine. This material was then collected so as to reset the flow rates and then pumped into a microfluidic chip with (trifluoroacetic anhydride) TFAA in order to acylate the amine prior to oxidation of the phenol moiety using hypervalent iodine (again on polymer support). This reaction resulted in concomitant C–C bond formation between the two aromatic rings. Finally the N-protecting group was removed, allowing conjugate addition of the amine to the quinone in order to furnish Oxomaritidine in an overall 40% yield. This process still stands as one of the more complex examples reported to date. However, more importantly, it paved the way and perhaps inspired others to explore the area of multistep flow approaches. Here, a snapshot of some developments is reported, where we pay particular attention to those attributes that are aligned with a modern medicinal chemistry research laboratory.

The nonsteroidal antiinflammatory drug Ibuprofen has been the center of attention for several flow syntheses to date.[82] However, the report by McQuade and coworkers in 2009 marks the first multistep approach where all three synthetic steps were run in a continuous process (**Scheme 63**). In the first step a triflic acid-mediated Friedel–Crafts acylation reaction was conducted in a microreactor chip. It was noted that $AlCl_3$ was a viable mediator of this reaction but was not compatible with further processes downstream, an important consideration in establishing a telescoped flow process. The second step, a 1,2 aryl migration, was effected with phenyliodine diacetate (PIDA) in the presence of trimethylorthoformate to deliver the methyl ester which was saponified in the final reactor with potassium hydroxide. Notably the synthesis by this route was complete in 10 min, and it was noted that scale-up could be made with appropriate consideration of pumps, mixers, and reactor channel dimensions. From the three microchip process a 51% yield of Ibuprofen was recovered after recrystallization.

Following the first report of a photochemical flow reaction in 2005 by Booker-Milburn and Berry,[83] 2012 saw the first report of the use of such a processing technology to trigger a reaction cascade toward the antimalarial artemisinin(**Scheme 64**).[84] Here, a stream of dihydroartemisinic acid in DCM is combined with oxygen and a porphyrin-based photosensitizer before passing through a region of tubing exposed to UV irradiation from a mercury lamp. This process results in a photochemical singlet-oxygen ene reaction where the resultant peroxy-ene species then undergoes Hock cleavage in the presence of trifluoroacetic acid (delivered as another stream) to afford artemisinin in 39% yield following column chromatography. Since this report there have been several improvements to the technique toward artemisinin.

There has also been a drive to move away from artemisinin-derived antimalarial compounds due to resistant strains developing. As such, the endoperoxide antimalarial OZ439 was identified as a potent compound toward malaria, including artemisinin-resistant strains. The preparation of this compound has been neatly developed in flow (**Scheme 65**).[85] The reaction sequence commences with the partial, but selective hydrogenation of the bisphenol starting material over a palladium on charcoal catalyst. The resulting phenol ketone material is acylated continuously before feeding the ketone into an ozonolysis reaction with the

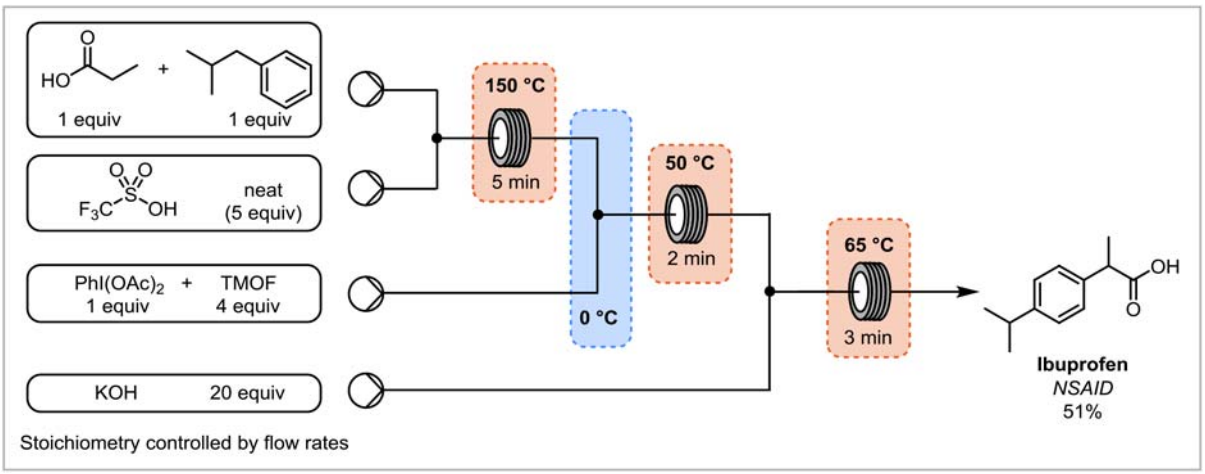

Scheme 63 Continuous flow multistep synthesis of Ibuprofen.[82a]

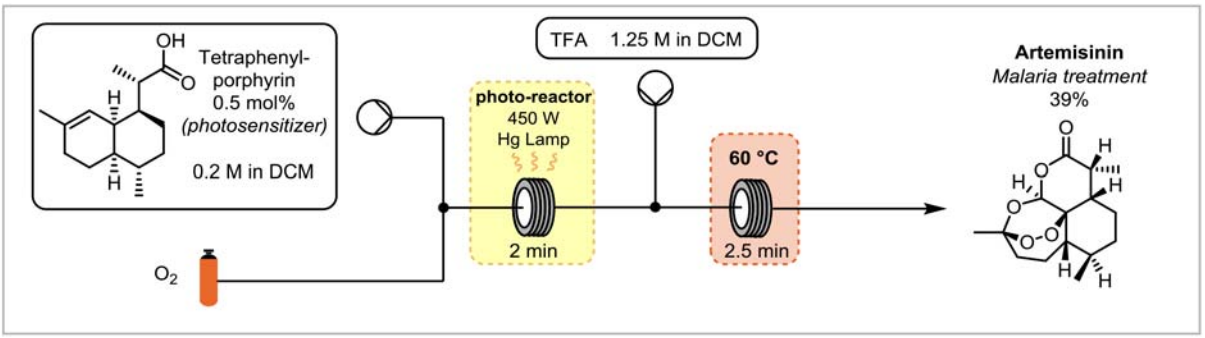

Scheme 64 Continuous flow photochemical synthesis artemisinin.[84a]

adamantane-derived oxime. Initially ozonolysis of the oxime generates the adamantyl oxido-oxonium which then traps the ketone as a secondary ozonide or endoperoxide. The product is then further elaborated offline.

As an alternative to photo irradiation, electromagnetic induction can be harnessed for synthesis through inductive heating.

Inductive heating is a phenomenon observed when a rapidly alternating magnetic field is passed through a magnetic, conductive, or superparamagnetic material. The application of this heating technique in continuous flow synthesis has been explored by Kirschning.[86] In general the technique involves the introduction of a column packed with magnetic materials into an induction loop. The flowing stream then passes over the inductively heated particles as it passes through the column.

The method is well suited to reactions at high temperatures and short reaction times although more controlled processes have also been demonstrated. In 2013, the technique was used in the multistep synthesis of the schizophrenia and bipolar disorder therapeutic Olanzapine (Zyprexa).[87] The synthesis commences with a Buchwald–Hartwig coupling of 2-iodo-nitrobenzene with an aminothiophene, using Xantphos as ligand (Scheme 66). It was found optimal to introduce the base for this reaction via a second stream. Inline aqueous extraction of the base was necessary prior to the next step which was a reduction of the nitro group over palladium on charcoal. The product amino nitrile was then cyclized in the presence of acid in the third continuous step where correct solvent choice and acid concentration were critical to the success of the cyclization to the benzodiazepine core. With optimal conditions this material could be isolated in 98% yield. The final step required Lewis acid-mediated trans amination, whereby preparation of a silica/titanium material facilitated the desired reaction. This solid material was homogenized with "Magsilica," a magnetic material, and loaded into the inductive coil so that effective heating could take place to deliver Olanzapine in 83% yield. Inductive heating has also been used in the multistep synthesis of Amitriptyline.[88]

Amitriptyline is on the WHO model list of Essential Medicines and has been used to treat a range of disorders such as depression, migraines, neuropathic pain, fibromyalgia, and nocturnal enuresis. The Kirschning flow synthesis of this important transtherapeutic compound commences with a Wurtz coupling of aryl lithium species generated in situ by the treatment of the bisbromo starting material with butyllithium (Scheme 67). Use of a gas permeable AF-2400 tube-in-tube reactor is then critical for the introduction of carbon dioxide as an electrophile for the preparation of the dibenzosuberone core. For the second phase of the synthesis dibenzosuberone was then mixed with the appropriate Grignard reagent under flow conditions, where room temperature was sufficient to dissipate the exotherm of the organometallic reaction. The output of this reactor was then quenched and kept mobile (by

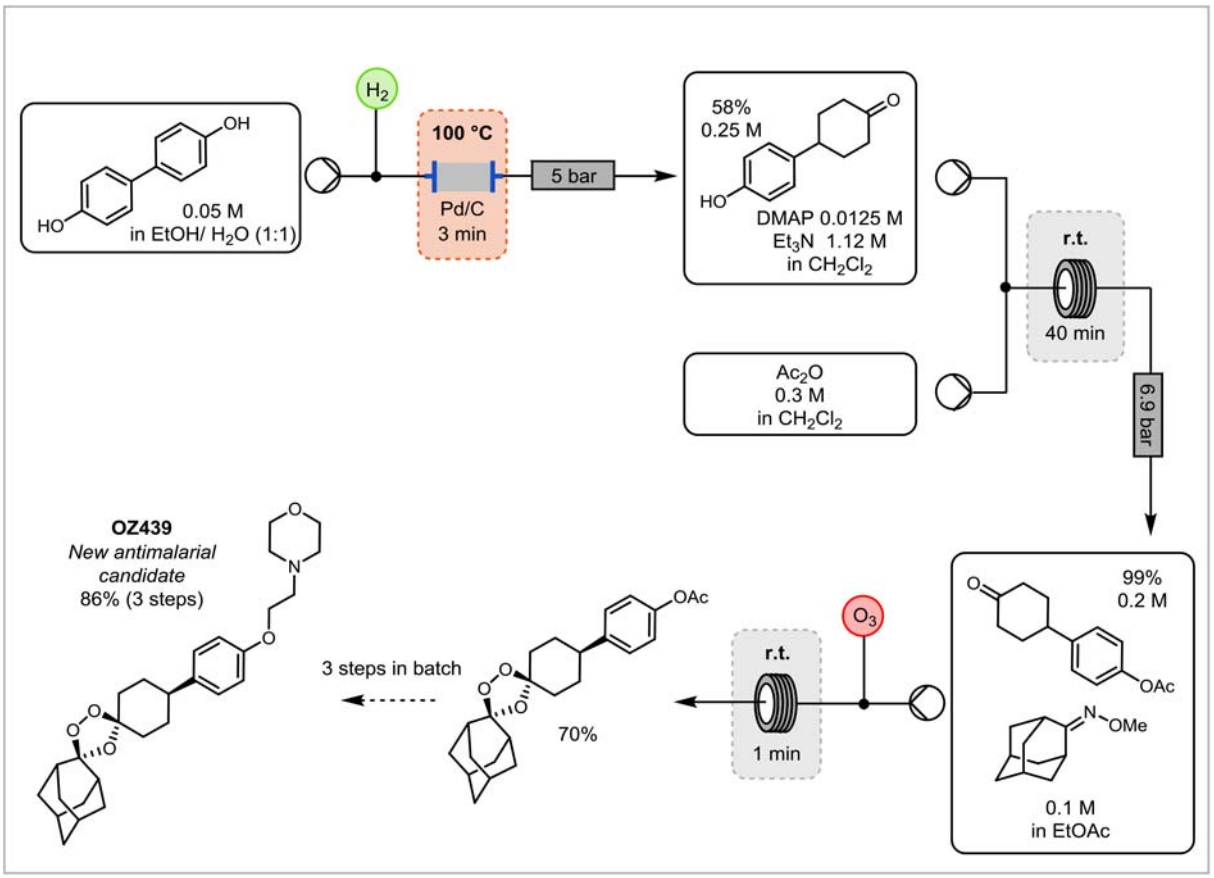

Scheme 65 Continuous flow synthesis of endoperoxide antimalarial OZ439.[85]

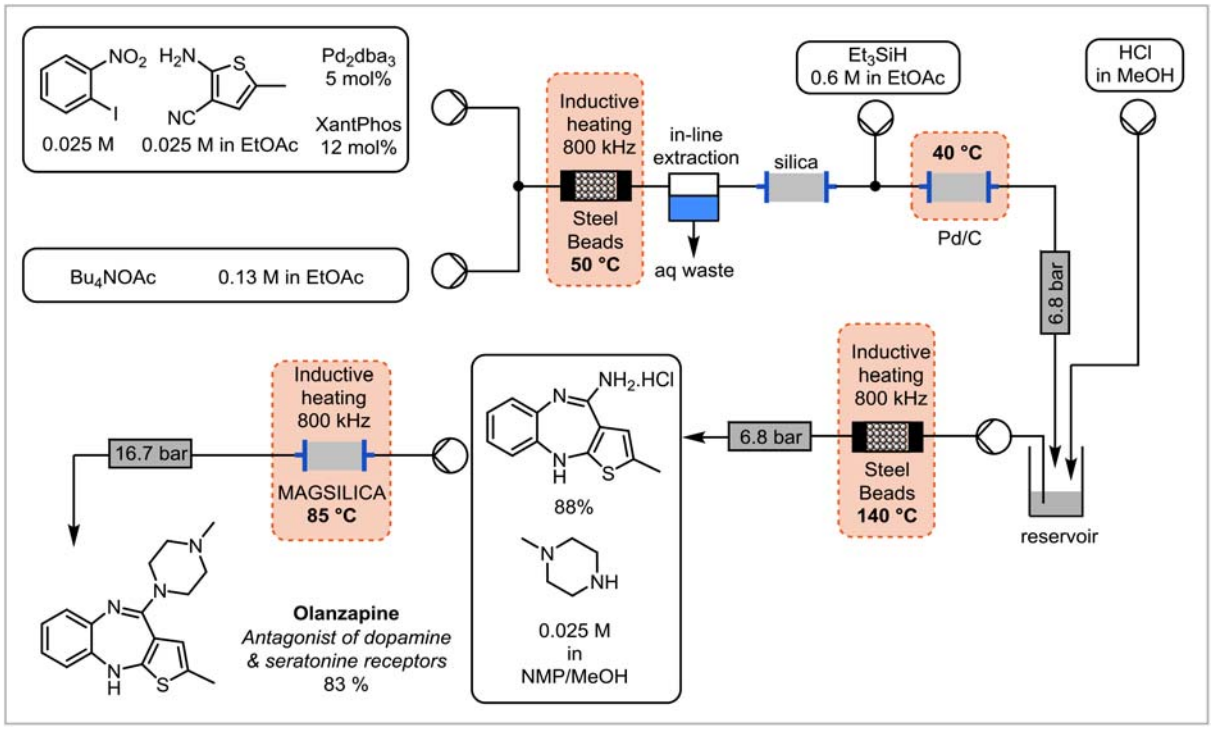

Scheme 66 Continuous flow multistep synthesis of Olanzapine.[87]

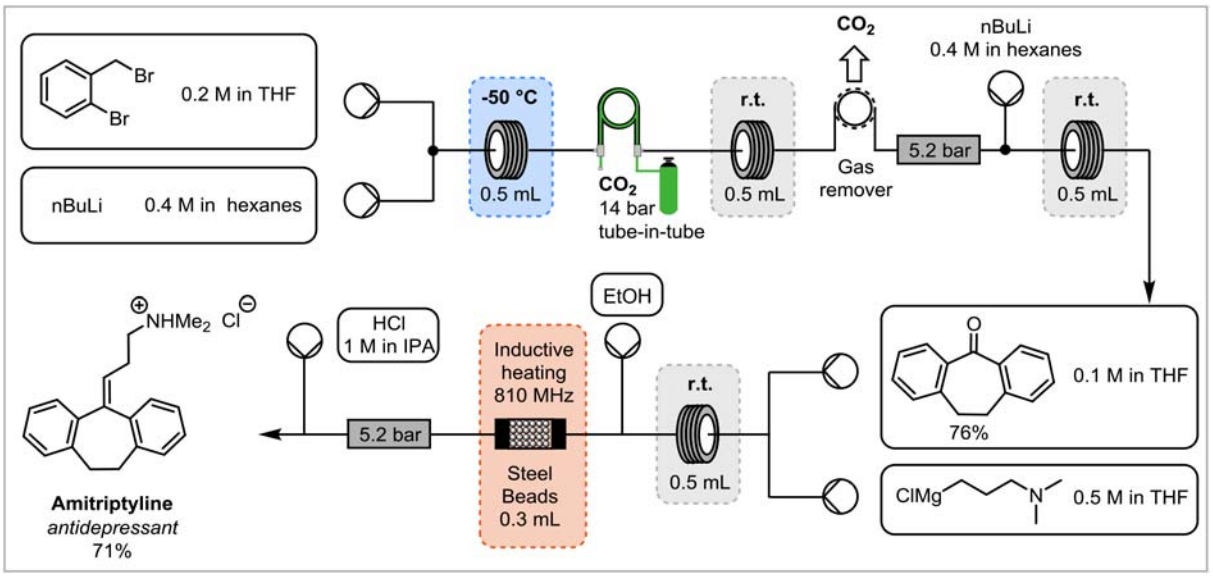

Scheme 67 Continuous flow multistep synthesis of Amitriptyline.[88]

dissolution of potentially problematic magnesium salts) by addition of a stream of ethanol before passing into a high-frequency inductive heating zone to promote the elimination of a tertiary alcohol. Final addition of HCl enabled precipitation and isolation of Amitriptyline·HCl in 71% yield.

Continuous processing of organometallics has been problematic at the early scale-up phase due to pumping issues, where single-shot syringe pumps and HPLC systems can run into problems. In a report aimed at addressing this shortfall by using peristaltic pumping technology Ley and coworkers demonstrate the end-to-end synthesis of Tamoxifen.[89]

In 2013, Tamoxifen was announced as a preventative treatment measure in the United Kingdom for females at risk of breast cancer, where a 5-year prescription reduces the risk by one-third and protection could last for 20 years. The multistep continuous flow synthesis of this important chemical commenced with a lithium-halogen exchange reaction of bromobenzene starting material (Scheme 68). The freshly formed organometallic was then intercepted with a stream containing a ketone electrophile and passage through a reaction coil at 30°C before interception with trifluoroacetic anhydride to generate the active alcohol leaving group. At this stage the combined flow rates and productivity are relatively high (compared to the previously described methods in this

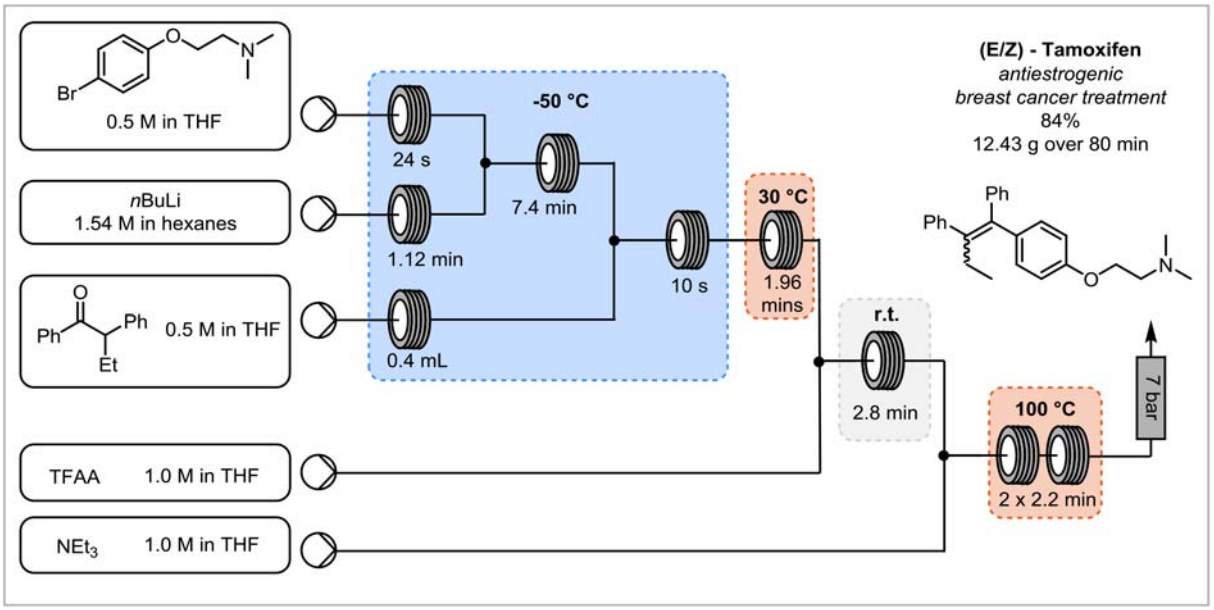

Scheme 68 Continuous flow multistep synthesis of *E*/*Z*-Tamoxifen.[89]

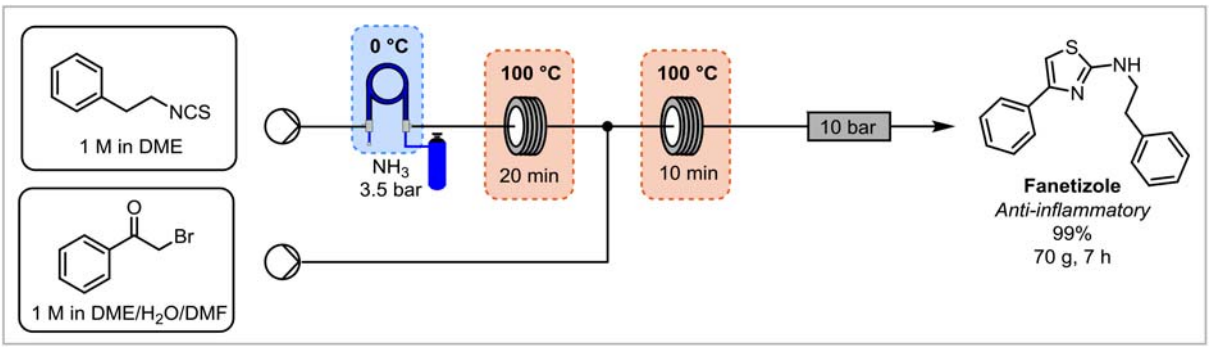

Scheme 69 Continuous flow multistep synthesis of Fanetizole.[90]

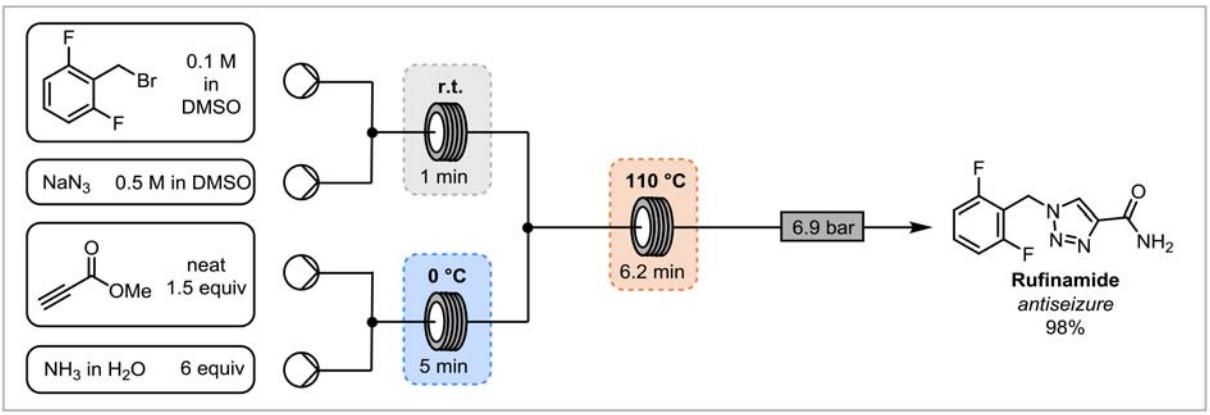

Scheme 70 Continuous flow multistep synthesis of Rufinamide.[91a]

section), and thus the reactor coils used must have a larger volume to provide sufficient residence time. This increases the pressure-drop across the system and would be a problem for pumps with low pressure resistance. Regardless, addition of a stream of triethylamine to the trifluoroacetate material and passage through a 20 mL coil at 100°C was enough to deliver the necessary elimination reaction and afford *E*/*Z*-Tamoxifen in 84% yield. Running this system for an 80 min period produced 12.43 g of material, enough for 900 doses of formulated active pharmaceutical ingredient (API).

Ley has also demonstrated the synthesis of the antiinflammatory compound Fanetizole, incorporating the use of gaseous ammonia through an AF-2400 tube-in-tube reactor (**Scheme 69**).[90] Here the flow system was designed so that colorimetric titration could be used for the determination of ammonia concentration under a range of solvents, pressures, temperatures, and flow rates. It was demonstrated that these could be prepared on demand and remain at reliable accuracy for extended periods. With this setup established, equistoichiometric amounts of ammonia were introduced to an isothiocyanate stream passing through the tube-in-tube reactor. This ammonia-enriched solution was then passed through a heated coil for formation of the thiourea before introduction of an alpha bromo ketone and heating again in a second coil. The desired product Fanetazole then precipitated as a pure solid upon standing, giving 99% yield at a productivity of 70 g delivered over 7 h.

The anticonvulsant drug Rufinamide has also succumbed to flow synthesis and was delivered in short order by Jamison et al. using a three-stage continuous process (**Scheme 70**).[20,91] Combination of the requisite benzyl bromide with sodium azide rapidly delivered the 1,3-dipole, whereas the other component for the click reaction was prepared inline by reaction of excess aqueous ammonia with neat methyl propiolate. Combining the alkynylamide with the azide in standard perfluoroalkoxy (PFA) tubing afforded a 3:1 mixture of triazole regioisomers in low yield. Crucially, it was found that by fabricating the final reactor coil from copper tubing allowed the cycloaddition reaction to progress in both greatly improved yield and selectivity for the desired regioisomer (20:1).

The sartan drugs are angiotensin receptor blockers, used for the treatment of hypertension. Telmisartan represents a recent example to come off patent and features a carboxylic acid as a bioisostere to the tetrazole motif which is common to most other sartans. Indeed, continuous flow preparations of tetrazoles using azide chemistry have been the focus of several flow chemical projects where process safety was a key driving force. In this case however, Gupton and Belecki et al. start their multistep process with the N-alkylation of the trifluoroboronate bearing benzimidazole with the biaryl carboxylate (**Scheme 71**).[92] This was found to proceed at 100°C with a 20 min residence time. The output of the alkylation reactor was then met with a stream of potassium hydroxide for ester saponification. The final step pumped the carboxylic acid material and *N*-methyl benzimidazole through

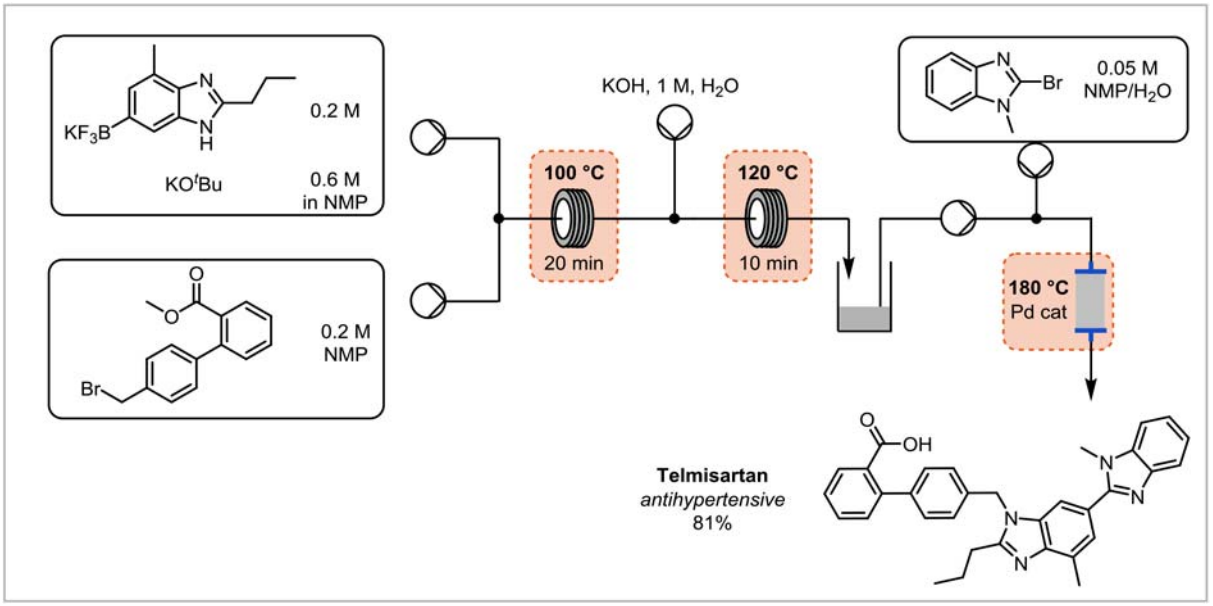

Scheme 71 Continuous flow multistep synthesis of Telmisartan.[92]

a cartridge containing SiliaCat DPP-Pd to effect Suzuki cross-coupling at 180°C, the final production rate here corresponding to 1 mg min^{-1}.

Vildagliptin is an orally active antidiabetic drug featuring an adamantanol ring system. Novartis have reported an integrated batch and flow process for the synthesis of this compound where the key Vilsmeier reagent is generated safely inline (Scheme 72).[93] The process first commences with a batch acylation of L-proline amide. Upon completion, this material was then pumped out of the reaction pot into a well-monitored flow circuit at 26 mL min^{-1}. Meanwhile dimethylformamide (DMF) was pumped into a mixer and reactor with $POCl_3$ to generate the Vilsmeier reagent which then passes out to the second reactor to effect dehydration of the amide to nitrile. The cyano product was then deposited into a batch reactor ready for alkylation with the amino adamantanol. The overall process was conducted at large scale with the use of pressure sensors, mass flow controllers, and integrated emergency action software controllers. Such controllers permit the machinery to shutdown automatically upon deviation from previously defined conditions.

(*S*)-Rolipram is an important antiinflammatory drug and a member of the GABA series of compounds. Kobayashi and coworkers have demonstrated a succinct asymmetric flow approach to this target compound (Scheme 73).[94] Initially they combined a stream of nitromethane and the appropriate aldehyde before passing this through a basic silica bed to mediate a condensation reaction. The

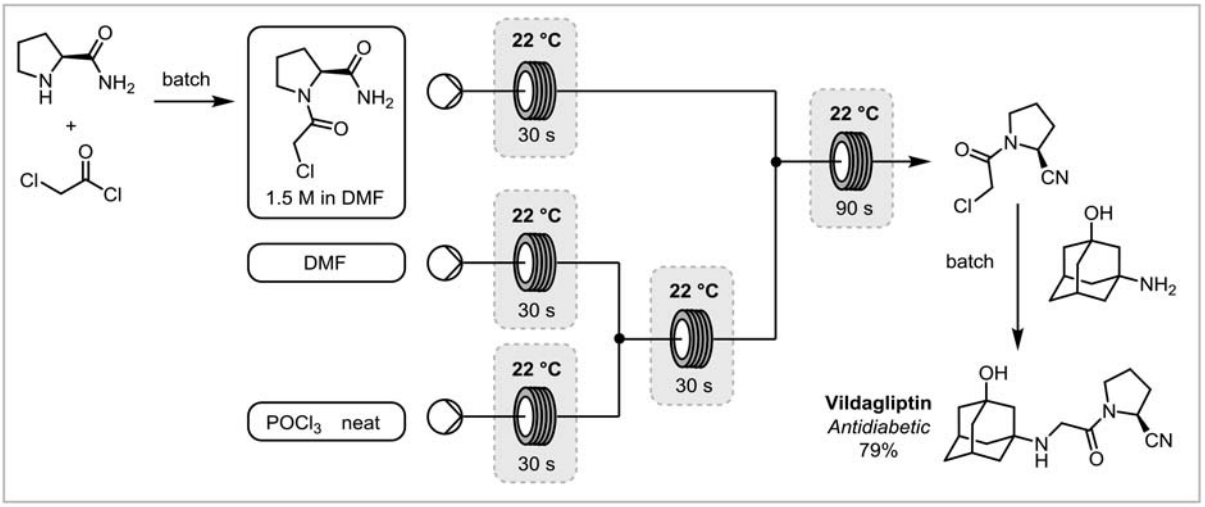

Scheme 72 Continuous flow multistep and batch hybrid synthesis of Vildagliptin.[93]

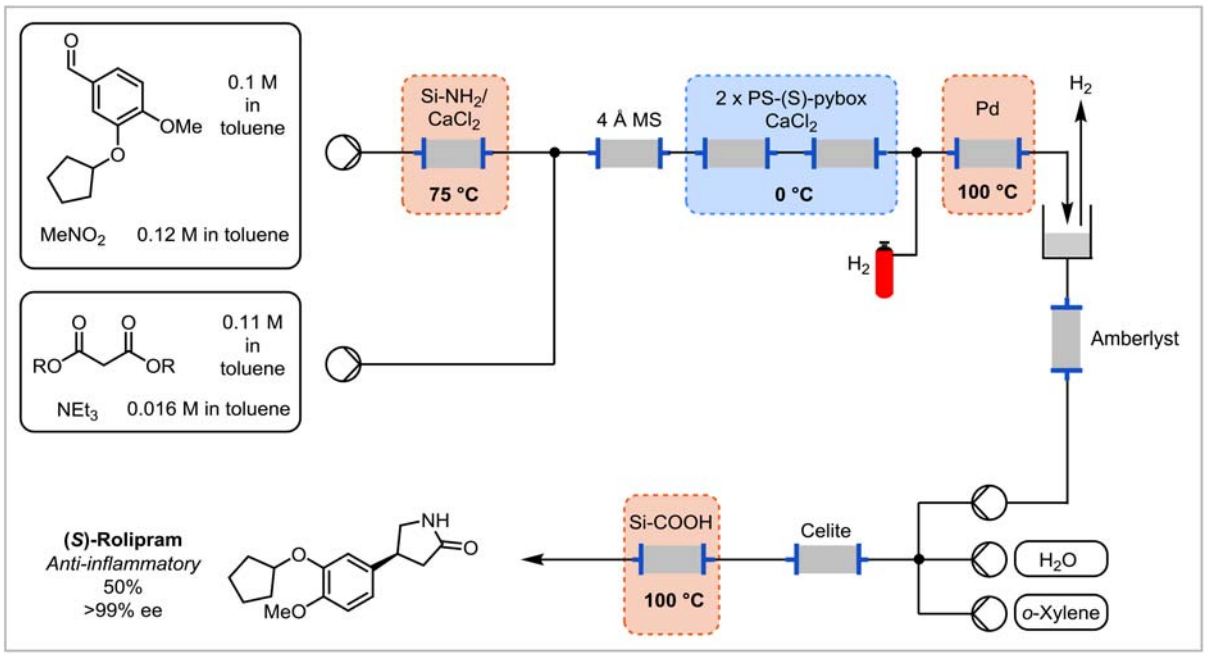

Scheme 73 Continuous flow multistep synthesis of Rolipram.[94]

resulting nitroalkene was then intercepted with a malonate, where a chiral Lewis acid in the form of polymer-supported PyBox-ligated calcium chloride induced an asymmetric conjugate addition reaction. The resulting adduct then underwent nitro group reduction and concomitant cyclization to give the γ-lactam product. In the final step, this material decarboxylates following initial ester hydrolysis to deliver (*S*)-Rolipram in 50% isolated yield and >99% *ee*.

Celebrex, a pyrazole-based antiinflammatory used for the treatment of arthritis, has also been prepared under multistep continuous processing (Scheme 74).[95] In this instance the method hinged on the use of vitamin C for the reduction of diazonium salts as a preferred strategy to the use of tin (II) chloride. This was deemed favorable as it reduces the downstream processing needed to wash away toxic tin residues. The requisite aniline is first diazotized before intercepting with the vitamin C reducing agent. This hydrazine adduct is then combined with a 1,3-dicarbonyl and under acidic conditions passed through a heated coil resulting in cleavage of the hydrazine adduct and cyclocondensation to provide the pyrazole structure. Inline flow IR was used here to monitor

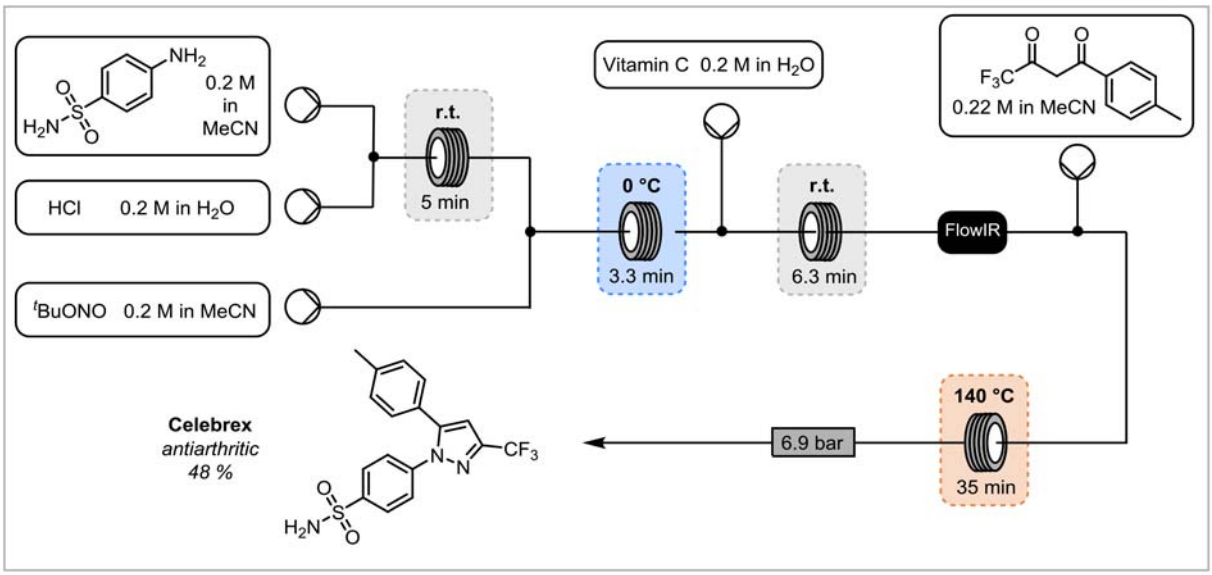

Scheme 74 Continuous flow multistep synthesis of Celebrex.[95]

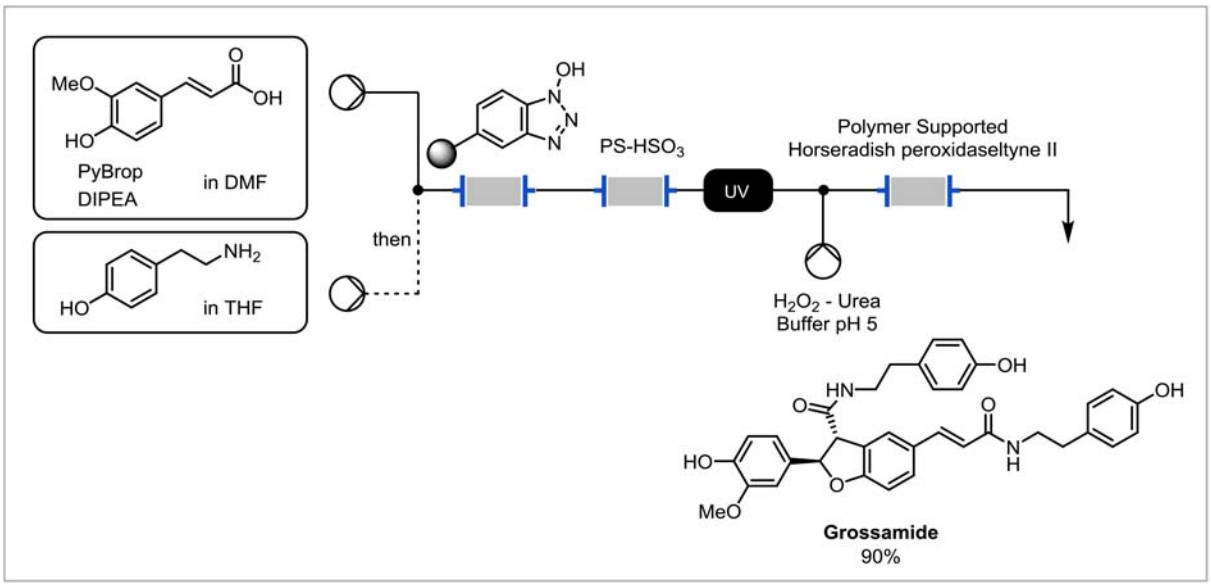

Scheme 75 Continuous flow multistep synthesis of Grossamide.[96]

the presence and concentration of the formed adduct but also to check that all of the diazonium salt had been consumed. The overall process afforded Celebrex in 48% yield and in high purity following a simple aqueous extraction.

Inline monitoring is now used frequently for flow processes, but perhaps the first example in the context of multistep organic synthesis was in 2006 when applied to the synthesis of Grossamide (Scheme 75).[96] Grossamide was prepared using a catch–react–release approach and also exemplifies the first biocatalyzed flow reaction. The synthetic approach starts by passing a solution of carboxylic acid, DIPEA and PyBroP over a polymer-supported HOBt. This then catches the carboxylic acid in the form of its activated ester. A switching valve then triggers to draw from a stock of amine that then passes through and reacts with the activated carboxylate and thus releasing it as an amide. Any unused amine is then subsequently caught on a PS-acid resin, while the amide product passes through an inline UV cell. The cell triggers the rest of the system, namely, the pumping of a pH 5 buffer solution to aid the biocatalyzed oxidative dimerization to afford Grossamide in 90% yield.

The catch–react–release and UV combination have also been incorporated into the multistep synthesis of the leukemia treatment Imatinib and related analogues (Scheme 76).[97] This time an acid chloride was caught on a polymer supported 4-dimethylaminopyridine (PS-DMAP) as an active amide. This caught carboxylate then underwent the same type of react and release with an aniline nucleophile. The amide product proceeds to a UV-triggered fraction collector ready for the next step. The following steps consist of alkylation at a piperidine nitrogen and a Buchwald–Hartwig cross-coupling. Finally the whole system features inline scavengers and purification with just one automated chromatography step at the end to remove ligands and excess reagents. The overall yield of the process was 32% for Imatinib, with similar yields for a range of prepared analogues.

Capecitibine and indeed 5′-deoxyribonucleosides in general represent a potent compound class, particularly as antiviral and antitumor agents. Jamison and Shen reported a telescoped process for the three-step preparation of these compounds making use of an organic Brønsted acid-catalyzed C—N bond formation through the silyl-Hilbert–Johnson reaction (Scheme 77).[98] The initial reaction step joins a stream containing the 5′-deoxyribose donor and 5 mol% of a pyridinium catalyst with a stream of the silylated pyrimidinone. These combined streams then passed through a heated microfluidic reactor chip to mediate the key bond formation before combination with another stream to form the desired amide in a second reactor chip. Finally, merging with a stream of sodium hydroxide results in global deprotection to furnish Capecitabine in 72% overall yield. Importantly, this method was readily adopted for the preparation of Doxifluoridine and Galocitabine.

The Jamison group has also reported the continuous synthesis of diphenylhydramine, the API of Benadryl, an antihistamine drug (Scheme 78).[99] Remarkably this synthesis demonstrates the processing of a molten ammonium salt without any blockage of the reactor tubing. The salt was generated in situ by reaction of neat *N*-*N*-dimethylaminoethanol with neat chlorodiphenylmethane. These two streams were combined and then heated at 175°C with a residence time of 16 min. Upon exiting the reactor, the neat molten tertiary amine hydrochloride salt was diluted first with aqueous sodium hydroxide and then by hexane before passage through a liquid–liquid phase separating device. The final API product was then secured in 93% yield by addition of HCl to induce crystallization.

The processing of neat reagents was also a key part of the preparation of Aliskiren (Scheme 79).[100] A Novartis-MIT collaboration has resulted in a multistep process for the preparation, separation, crystallization, drying, and formulation of the final Aliskiren product. The process starts with an acid-catalyzed ring opening amide formation where all three channels were pumped neat through a heated tubular reactor. Following this, the stream is diluted and undergoes liquid–liquid extraction. The organic phase,

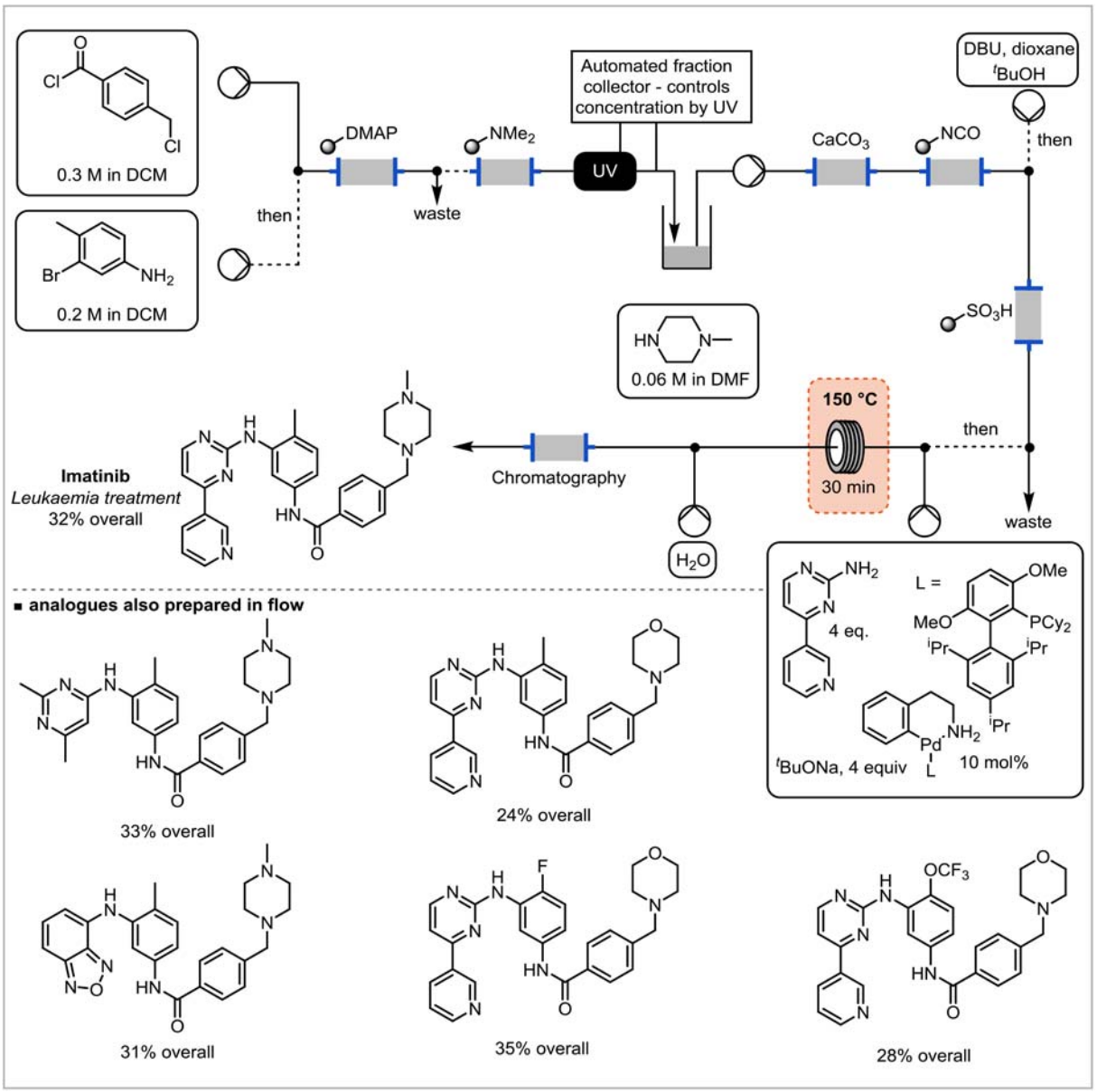

Scheme 76 Continuous flow multistep synthesis of Imatinib and analogues.[97]

now containing the desired product and remaining starting material, passed into a crystallizing chamber where heptane was added to induce crystallization of the product. The precipitate was then filtered, washed, and automatically diluted to the correct concentration for the following Boc deprotection step. After deprotection, NaOH was added to neutralize, and a liquid–liquid phase separation follows this.

Further addition of ethyl acetate to the resulting organic stream caused precipitation of remaining NaCl, which was removed using a microfilter. In the second crystallization pot, fumaric acid was added to the API material and promoted crystallization as the hemi-fumarate salt. Again the crystals were filtered, washed, and diluted appropriately (again in an automated fashion), before addition of silica which behaves as a glidant material. The slurry was then continuously dried and conveyed through a rotating heated drum with the final drying phase in a vacuum drier. This solid material, which at this point contained 5000 ppm ethyl acetate, passed through a heated extruder in combination with PEG. The extruded mixture was then molded into tablets six at a time. Clearly this is an excellent and exciting demonstration of the capabilities and goes to show that downstream processing is actually where the bulk of time and energy is spent. Achieving regulatory sign-off on such manufacturing processes is a current focus to help bring this technology to the market place.

The same collaborative research team has very recently demonstrated a compact, modular API manufacturing approach. The plug-and-play modules were connected in four different configurations, permitting the multistep synthesis, purification, real-

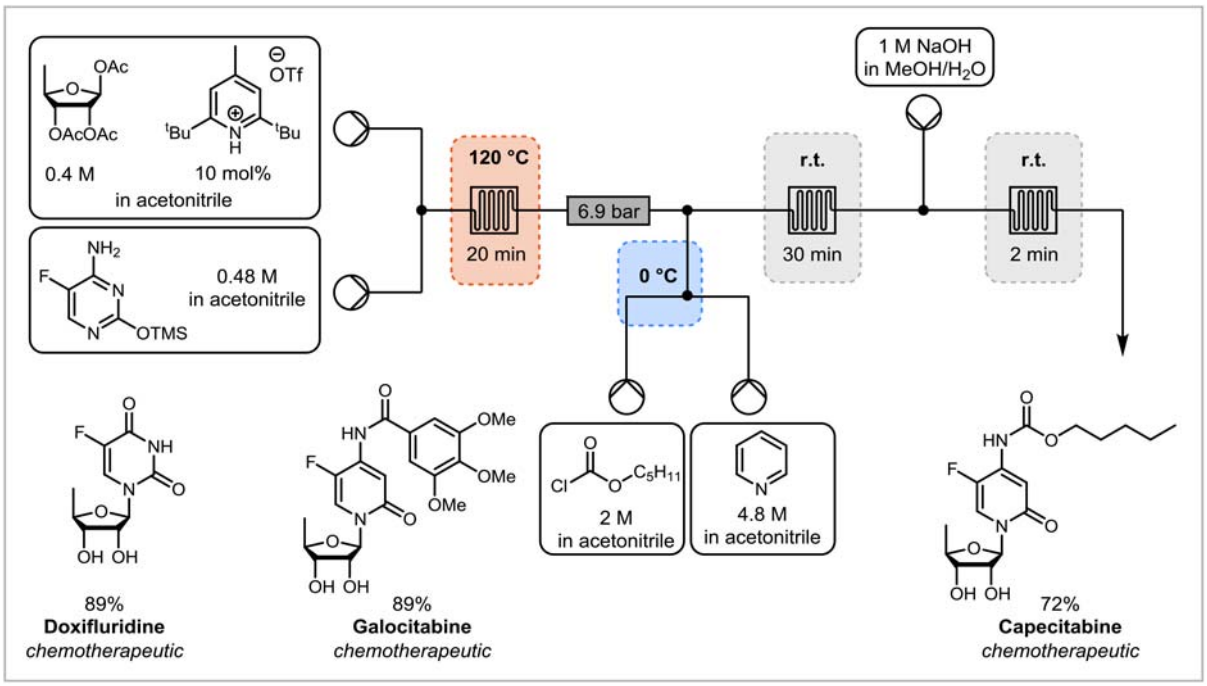

Scheme 77 Continuous flow multistep synthesis of Capecitabine.[98]

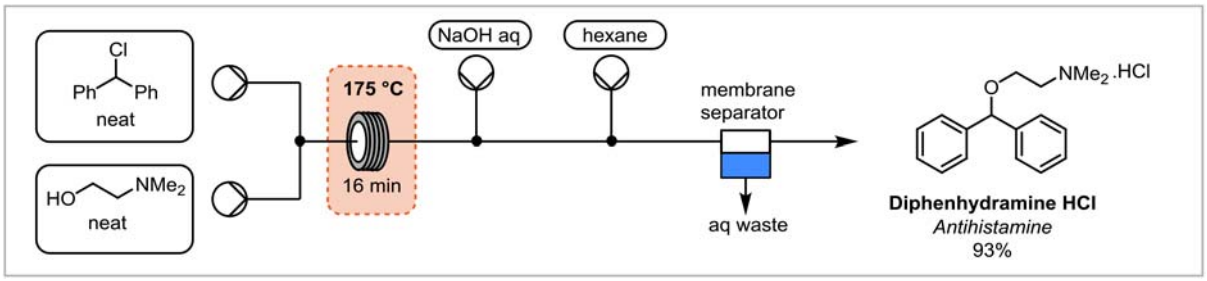

Scheme 78 Continuous flow multistep synthesis of diphenylhydramine.[99]

time monitoring, crystallization, and formulation of four different drug products (Schemes 80 and 81). By connecting a reactor module to a liquid–liquid extractive workup and subsequent charcoal filtration, Diphenhydramine could be crystallized as the hydrochloride salt in the first module. The synthesis of Lidocaine also took place in four modules. This time two reactor modules were required prior to liquid–liquid extraction and crystallization.

For the synthesis of Diazepam a total of six modules were daisy-chained together. In the first two reactor modules the Diazepam was synthesized. This was followed by liquid–liquid extraction (module 3), charcoal-bed filtration (module 4), acidification and extraction (module 5), and final crystallization (module 6) to provide the CNS depressant. Finally, a total of seven modules were used to prepare Fluoxetine. A similar configuration was used to that of Diazepam but now with a liquid–liquid extraction module between the initial two reactor modules. Overall the compact, reconfigurable device for the on-demand synthesis of health-care products is a very exciting prospect. One could imagine these devices serving to support remote or third-world populations.

Efavirenz is an antiretroviral used for the treatment of HIV. It features a trifluoromethyl group, which was discovered through SAR to modulate binding affinity through altering the pK_a of the carbamate H-bond donor. In the continuous flow multistep synthesis of this compound the CF_3 was introduced as an acyl electrophile (Scheme 82).[102] Treatment of 1,4-dichlorobenzene with butyllithium resulted in directed-ortho-metallation at the 2 position before quenching with the morpholino-CF_3-amide to give the desired fluorinated building block in 87% yield. This trifluoroketone then became the electrophile for a lithiated alkyne. The alkynyl alcohol next underwent an impressive O−C and N−C bond formation by passage through a column packed with sodium cyanate. The first step here presumably being attack of the alcohol on the cyanate followed by a ring closing S_NAr process. Overall, Efavirenz was delivered in 45% yield through this process.

Perhaps the most elaborate and intricate continuous flow synthesis to date is that designed for Merclinertant, a neurotensin receptor 1 antagonist (Schemes 83–85).[104] The synthesis features the flow preparation of two fragments followed by their unison

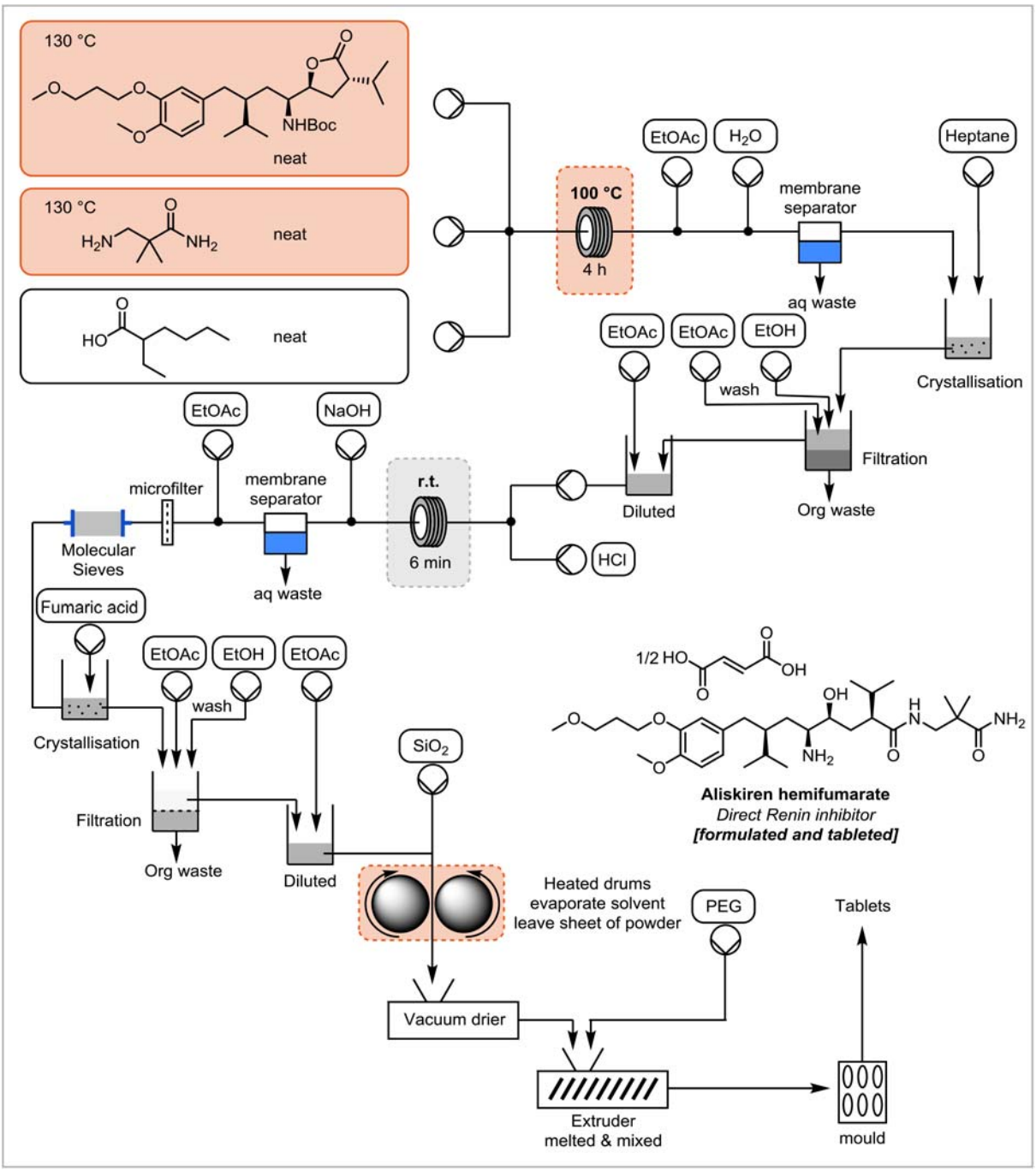

Scheme 79 Continuous flow multistep synthesis included drug formulation of Aliskiren.[100]

also under flow conditions. The synthesis of the pyrazole fragment commences with the O-acylation of 1,3-cyclohexadione (Scheme 83). This then passed through a column-containing polymer-supported DMAP which induced an O to C acyl migration. The formed tricarbonyl was then treated with iodine to promote iodination, elimination, and aromatization. The resulting trisubstituted diphenol compound was then methylated using dimethyl carbonate prior to undergoing a Claisen condensation with diethyl oxalate. The resultant 1,3,4-tricarbonyl was then transformed into the pyrazole product with a quinolone hydrazine under acidic conditions. Here liquid–liquid phase separation was used for the inline purification of the pyrazole product. To complete the fragment the ethyl ester was saponified at high temperature.

The adamantyl fragment was also prepared continuously (Scheme 84). Starting from the parent adamantanone, ethylmagnesium bromide was added. The formed propargyl alcohol then participated in an acid-induced Ritter reaction followed by a 5-

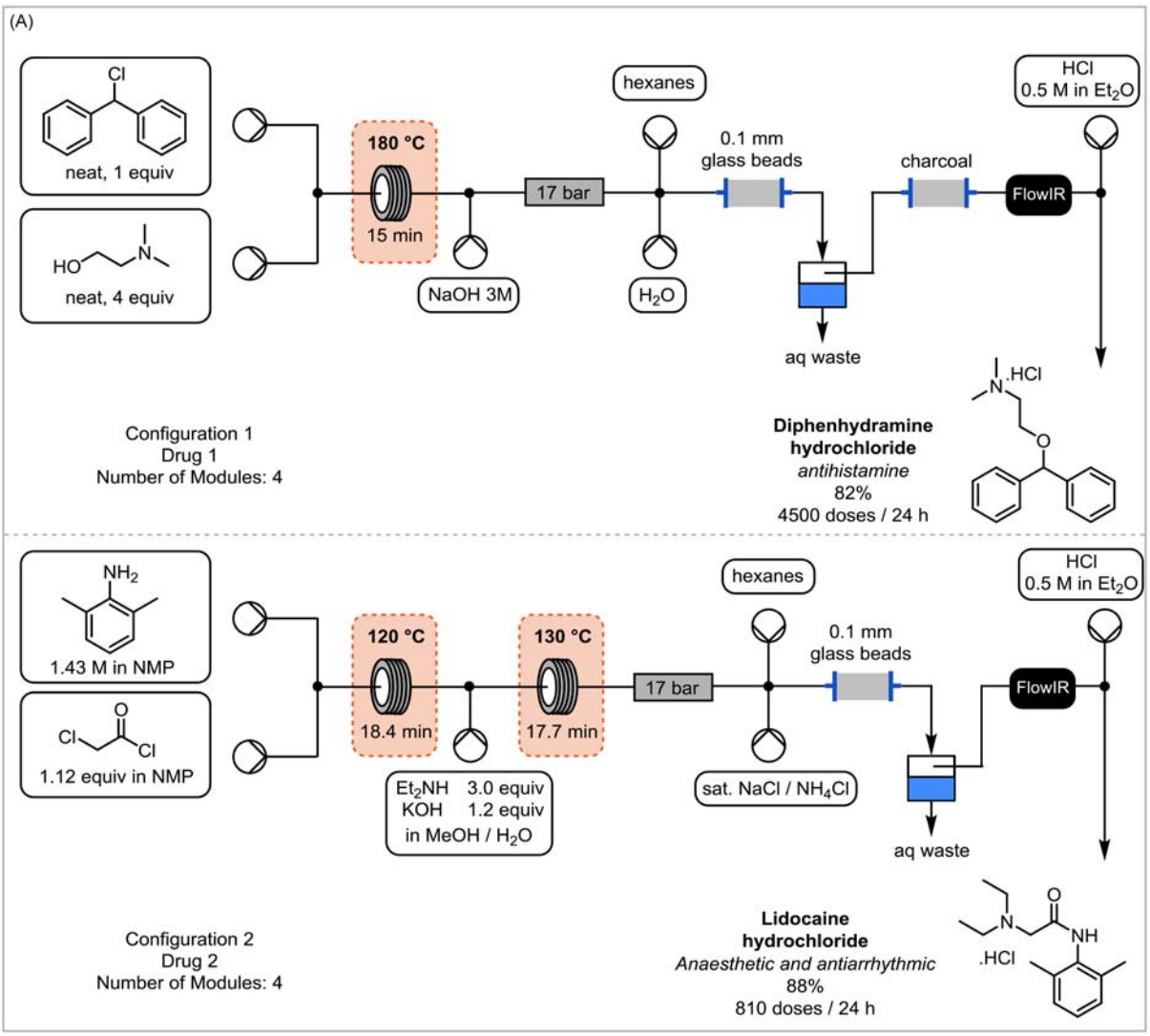

Scheme 80 Modular approach for the production of Diphenhydramine and Lidocaine.

exo-dig cyclization. The spirocyclic product then undergoes ozonoylsis of the exo-double bond before ring opening to provide the 2-aminoadamantane-2carboxylic acid fragment.

Fragment unison took place through the use of in situ generated phosgene (Scheme 85). Several precautions were put into place to ensure the controlled generation of this material, namely, the use of triphosgene, a more stable equivalent available in solid form. Second, inline flow-IR monitoring was used to monitor phosgene concentration. In the event, passage of triphosgene, DIPEA, and the pyrazole carboxylic acid fragment through a heated initiation coil resulted in the formation of the activated acid. This activated species was then intercepted with the amino adamantane to afford the Boc-protected material. Deprotection was carried out in batch by simply stirring the advanced intermediate over quadrapure (polymer supported) sulfuric acid for 18 h.

This machine-assisted synthesis of Merclinertant demonstrates several of the key considerations required in the planning of a multistep flow process. While other processes described within this section demonstrate some of these aspects, the synthesis of Merclinertant highlights many of them all in one example. Some of these considerations can be quite subtle to those unfamiliar with the practicalities of flow chemical processing.

Resetting of flow rates is a critical practice. As a multistep process moves to higher complexity more streams will be added to the flow circuitry. With more streams comes a higher cumulative flow rate and subsequently, residence times in typical reactor coil sizes (1, 2, 5, 10, and 20 mL) rapidly become shorter. In addition, long lengths of narrow bore tubing can cause "pressure drops" that can be problematic. A common solution to this problem then is to put a break in the flow circuit where the material can be dropped into a reservoir and repumped out to the next stage. This resetting process can be seen in many flow chemistry examples, especially when a continuous process is reported, that is, not using single-shot syringe pumps.

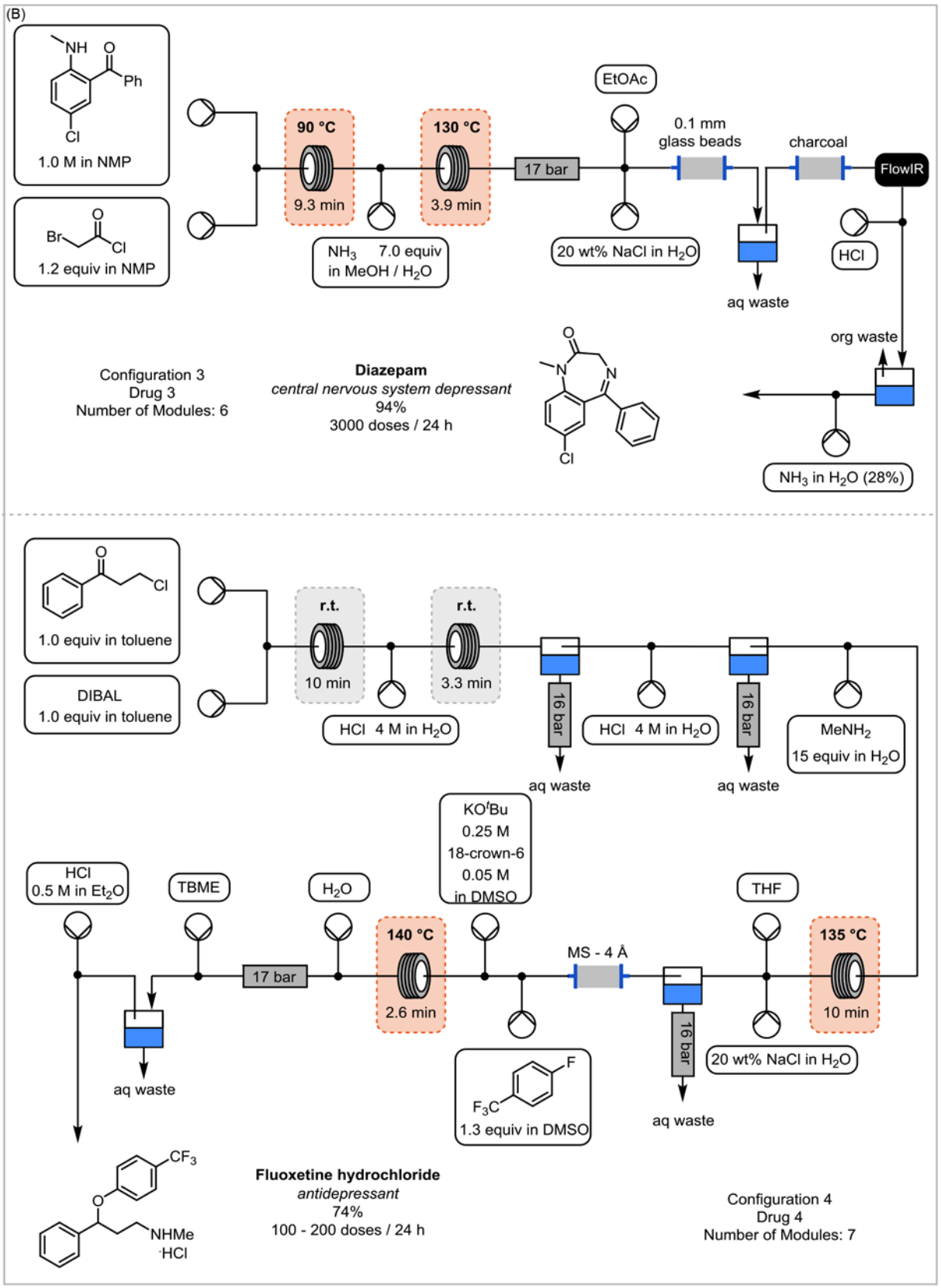

Scheme 81 Modular approach for the production of Diazepam and Fluoxetine hydrochloride.[101]

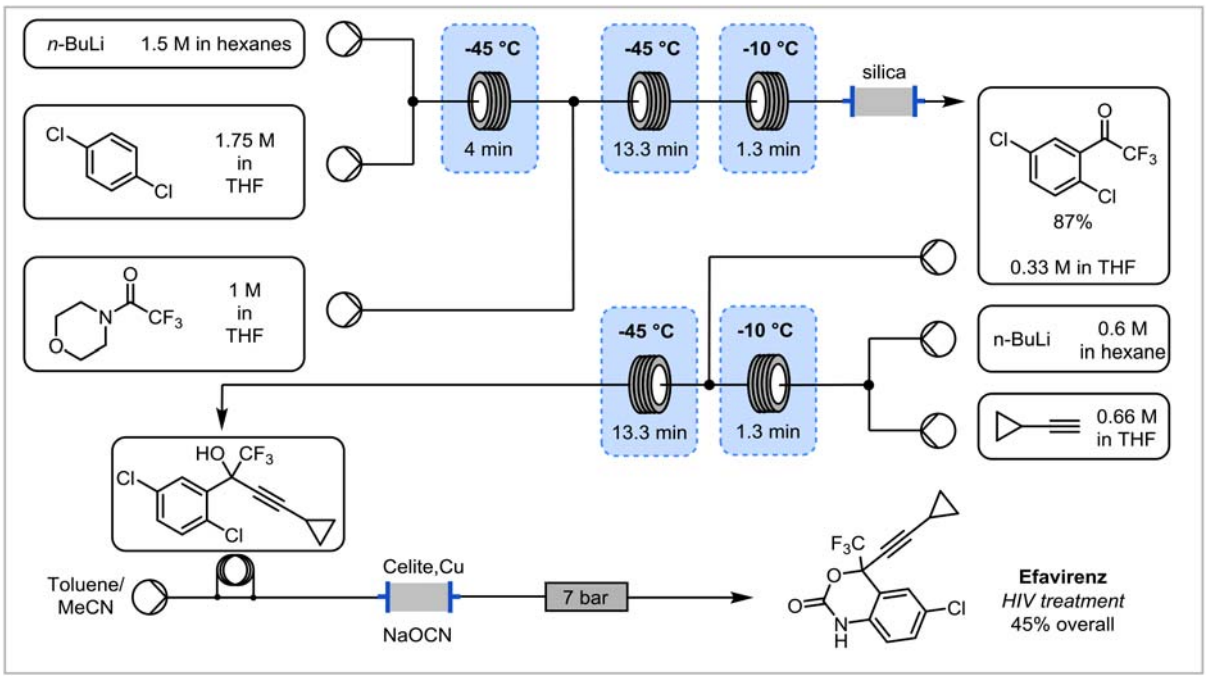

Scheme 82 Continuous flow multistep synthesis of Efavirenz.[102]

Solvent changes or compatibility planning is another key consideration. Usually the latter is the most demonstrated, where a common solvent is found that is viable for all steps. In instances where this is not possible then solvent switching modules can be used in order to change from one solvent to another.[105] This practice is still far from widespread at the discovery and early pilot flow scales.

Inline purification through scavenging cartridges, or now, more commonly liquid–liquid extraction is also a critical part of a complex synthesis process. By-products or surplus reagents from one step can negatively affect the subsequent one, and therefore careful planning is needed to ensure that these can be removed.

In addition, attention should be paid to the possibility of forming solid particulates that can block the reactor entirely—this can be catastrophic for the process if the pumps are not pressure respondent.[106] However, with all of these considered several exciting and challenging targets have already been accomplished, and it is clear that the attention is now focused on true manufacturing processes using this exciting technology.

1.06.6 Conclusion and Outlook

We hope to have provided an overview of the capabilities afforded by running reactions in continuous flow mode. While we are not advocating a straight swap of flow for batch (in fact, quite the opposite), we are certainly excited by many of the developments and would advocate careful consideration of flow as an alternative technique to batch. These developments have been driven by open-minded individuals, willing to explore the potential benefits of the technique. Such individuals have either been chemists stepping into the area of chemical engineering or vice versa. Certainly the most impressive feats stem from collaboration between the two disciplines. It is clearly important to encourage more frequent collaborations of this nature in the future.

In this article we have provided an introduction to the key drivers for adopting flow, at least those drivers directly relevant to the synthesis and isolation of compounds. We then provided a survey of some of the hazardous chemistry reported before moving on to more elaborate setups that can make and screen compounds, optimize reactions and even synthesize, purify, and formulate tablets. For the latter parts of this article, computer control and statistical modeling have been important to the synthesis process. This trend will likely continue, as machines become smarter and more effective at helping humans perform mundane tasks. It is tempting and even worrying to predict a future where machines make man obsolete in the laboratory. In reality, this is still far from the horizon! Machines, or more specifically, computer control units operating on algorithms, require a reliable set of input data, without which the predictive power and modeling will likely always be "hit-and-miss." Due to nonstandardization of reported data and even a lack of understanding of some seemingly simple reactions, it is unlikely that we will provide sufficiently good input data to the machines in the near future. Machines can however play a critical supporting role though. They can conduct repetitive measuring and manipulation task with far greater accuracy, reproducibility, and even stamina. Machines can work 24/7! Embracing machines to aid us

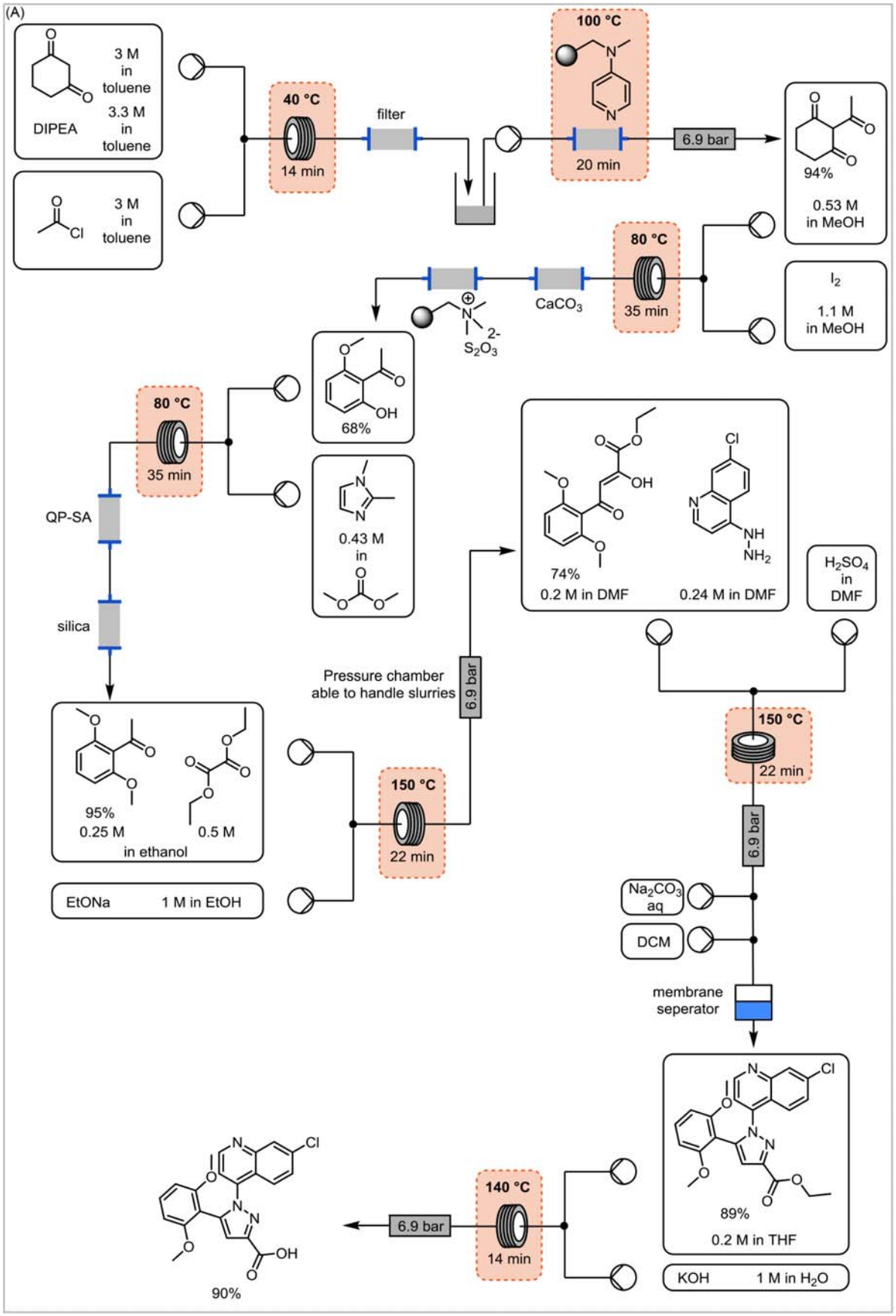

Scheme 83 Multistep flow synthesis of the pyrazole fragment.

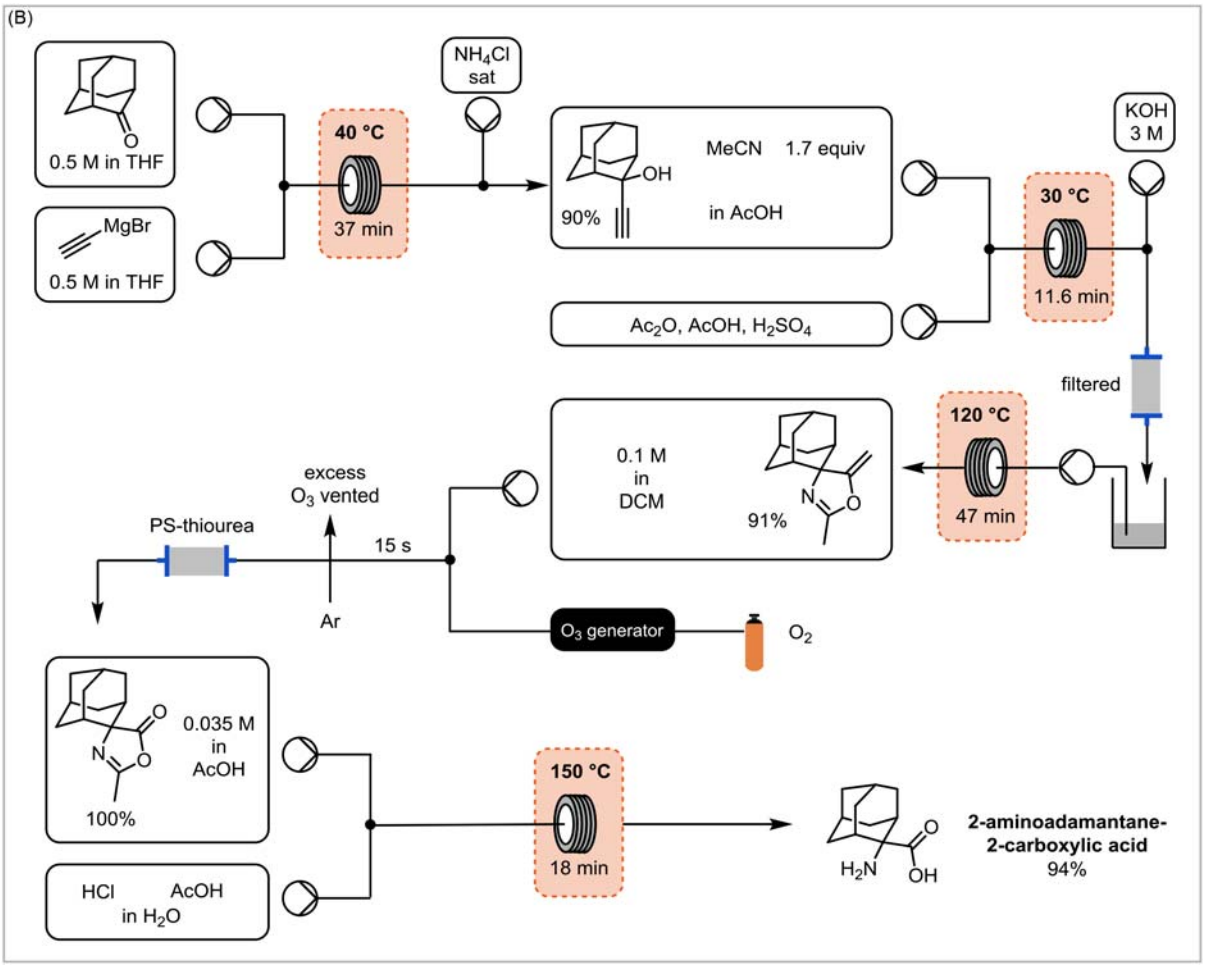

Scheme 84 Continuous flow multistep synthesis of adamantyl fragment.[103]

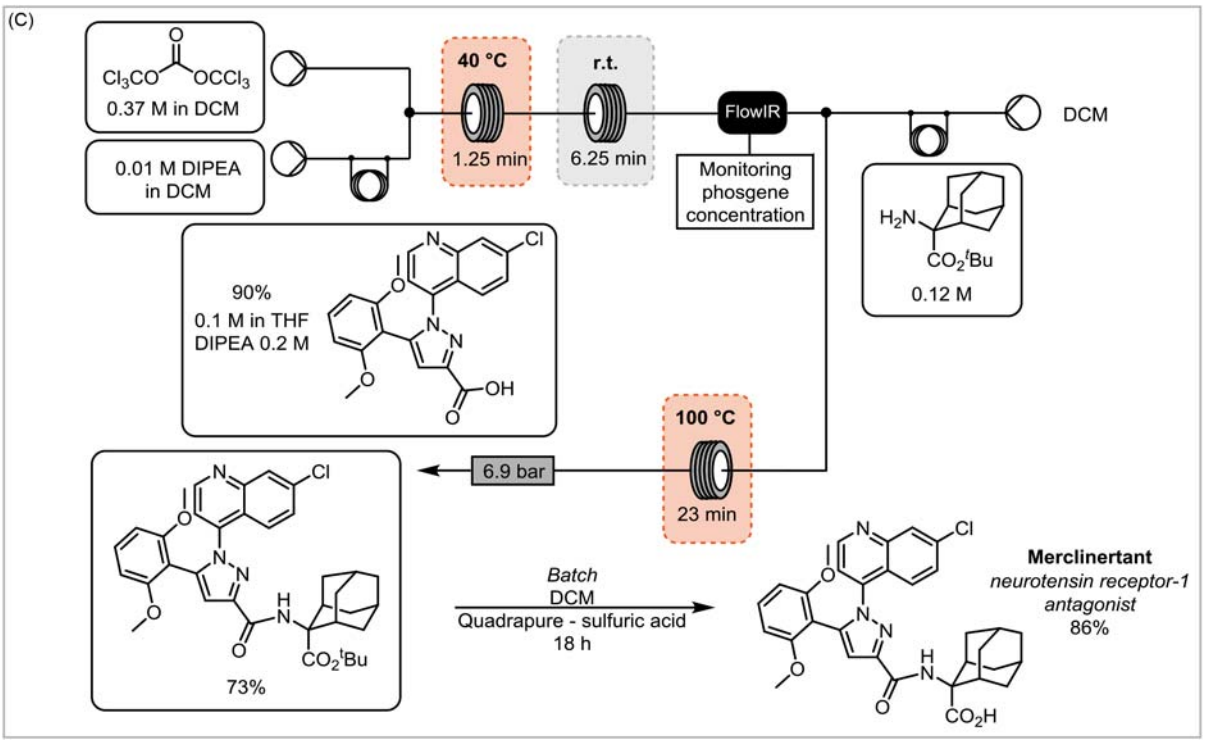

Scheme 85 Continuous flow multistep synthesis of Merclinertant.[104]

with such tasks will free us up with more time to fulfill tasks that machines cannot (yet) do, such as designing and planning syntheses and processes.

So where next for flow chemistry? Clearly the technique has utility and longevity with industry, but as it is "just" a technique it likely has to become more inventive to maintain ongoing academic development. Certainly continuous flow photochemistry and electrochemical methods have a productive overlap that will continue to develop. For traditional thermal methods, the challenges are now to discover new reactions and reactivity through this technique; "flash" chemistry seems to be an area that can deliver on this front.[107] Adoption and application to other areas of chemistry such as supramolecular materials, inorganic complexes, polymer synthesis, and nanoparticle preparation will provide interest for academics in the years to come.

Another important question is where do the students come from with flow experience to then become industrial chemists? Certainly the active research groups in this area can continue to supply some students—but can they meet the demand, especially as more companies and chemical sectors adopt flow practice? Should flow chemistry be taught at the undergraduate level or should it be taught once employees arrive at a company? Can the setting-up and running of an experiment in flow be carried out by a technician, or technical service? Our experience would suggest that this is not the case; there are always some useful observations made by running processes in flow. Certainly, once you have enough experience you can begin to think in a flow processing mind-set and this can take you in directions that you would perhaps otherwise not consider. We hope that this brief article on the topic has served to whet your creative appetite to flow processing for organic synthesis.

References

1. (a) Gutmann, B.; Cantillo, D.; Kappe, C. O. *Angew. Chem. Int. Ed.* **2015,** *54,* 6688–6728; (b) Baumann, M.; Baxendale, I. R. *Beilstein J. Org. Chem.* **2015,** *11,* 1194–1219; (c) Pastre, J. C.; Browne, D. L.; Ley, S. V. *Chem. Soc. Rev.* **2013,** *42,* 8849–8869; (d) Wegner, J.; Ceylan, S.; Kirschning, A. *Chem. Commun.* **2011,** *47,* 4583–4592; (e) Webb, D.; Jamison, T. F. *Chem. Sci.* **2010,** *1,* 675–680; (f) Porta, R.; Benaglia, M.; Puglisi, A. *Org. Process. Res. Dev.* **2015,** *20,* 2–25; (g) Stouten, S. C.; Noël, T.; Wang, Q.; Hessel, V. *Aust. J. Chem.* **2013,** *66,* 121–130; (h) Movsisyan, M.; Delbeke, E. I. P.; Berton, J. K. E. T.; Battilocchio, C.; Ley, S. V.; Stevens, C. V. *Chem. Soc. Rev.* **2016,** *45,* 4892–4928.
2. Mallia, C. J.; Baxendale, I. R. *Org. Process. Res. Dev.* **2016,** *20,* 327–360.
3. Brzozowski, M.; O'Brien, M.; Ley, S. V.; Polyzos, A. *Acc. Chem. Res.* **2015,** *48,* 349–362.
4. McPake, C. B.; Sandford, G. *Org. Process. Res. Dev.* **2012,** *16,* 844–851.
5. Breen, J. R.; Sandford, G.; Yufit, D. S.; Howard, J. A. K.; Fray, J.; Patel, B. *Beilstein J. Org. Chem.* **2011,** *7,* 1048–1054.
6. Chambers, R.; Spink, R. H. *Chem. Commun.* **1999,** 883–884.
7. Acke, D. R.; Stevens, C. V. *Green Chem.* **2007,** *9,* 386–390.
8. Mastronardi, F.; Gutmann, B.; Kappe, C. O. *Org. Lett.* **2013,** *15,* 5590–5593.
9. Struempel, M.; Ondruschka, B.; Daute, R.; Stark, A. *Green Chem.* **2008,** *10,* 41–43.
10. Rossi, E.; Woehl, P.; Maggini, M. *Org. Process. Res. Dev.* **2011,** *16,* 1146–1149.
11. Pinho, V. D.; Gutmann, B.; Miranda, L. S.; de Souza, R. O.; Kappe, C. O. *J. Org. Chem.* **2014,** *79,* 1555–1562.
12. Martin, L. J.; Marzinzik, A. L.; Ley, S. V.; Baxendale, I. R. *Org. Lett.* **2010,** *13,* 320–323.
13. (a) Müller, S. T. R.; Wirth, T. *ChemSusChem* **2015,** *8,* 245–250; (b) Deadman, B. J.; Collins, S. G.; Maguire, A. R. *Chem. Eur. J.* **2015,** *21,* 2298–2308; (c) O'Brien, A. G.; Levesque, F.; Suzuki, Y.; Seeberger, P. H. *Chim. Oggi Chem. Today* **2011,** *29,* 57–60.
14. Malet-Sanz, L.; Madrzak, J.; Holvey, R. S.; Underwood, T. *Tetrahedron Lett.* **2009,** *50,* 7263–7267.
15. Malet-Sanz, L.; Madrzak, J.; Ley, S. V.; Baxendale, I. R. *Org. Biomol. Chem.* **2010,** *8,* 5324–5332.
16. Ahmed-Omer, B.; Barrow, D. A.; Wirth, T. *Tetrahedron Lett.* **2009,** *50,* 3352–3355.
17. Bräse, S.; Gil, C.; Knepper, K.; Zimmermann, V. *Angew. Chem. Int. Ed.* **2005,** *44,* 5188–5240.
18. Baumann, M.; Baxendale, I. R.; Ley, S. V.; Nikbin, N.; Smith, C. D.; Tierney, J. P. *Org. Biomol. Chem.* **2008,** *6,* 1577–1586.
19. Sahoo, H. R.; Kralj, J. G.; Jensen, K. F. *Angew. Chem.* **2007,** *119,* 5806–5810.
20. Borukhova, S.; Noël, T.; Metten, B.; de Vos, E.; Hessel, V. *ChemSusChem* **2013,** *6,* 2220–2225.
21. Gutmann, B.; Roduit, J. P.; Roberge, D.; Kappe, C. O. *Angew. Chem. Int. Ed.* **2010,** *49,* 7101–7105.
22. Gutmann, B.; Roduit, J. P.; Roberge, D.; Kappe, C. O. *Chem. Eur. J.* **2011,** *17,* 13146–13150.
23. Baxendale, I. R.; Ley, S. V.; Mansfield, A. C.; Smith, C. D. *Angew. Chem. Int. Ed.* **2009,** *48,* 4017–4021.
24. O'Brien, A. G.; Lévesque, F.; Seeberger, P. H. *Chem. Commun.* **2011,** *47,* 2688–2690.
25. Kulkarni, A. A. *Beilstein J. Org. Chem.* **2014,** *10,* 405–424.
26. Cantillo, D.; Damm, M.; Dallinger, D.; Bauser, M.; Berger, M.; Kappe, C. O. *Org. Process. Res. Dev.* **2014,** *18,* 1360–1366.
27. Gemoets, H. P.; Su, Y.; Shang, M.; Hessel, V.; Luque, R.; Noël, T. *Chem. Soc. Rev.* **2016,** *45,* 83–117.
28. (a) Kawaguchi, T.; Miyata, H.; Ataka, K.; Mae, K.; Yoshida, J.i. *Angew. Chem. Int. Ed.* **2005,** *44,* 2413–2416; (b) McConnell, J. R.; Hitt, J. E.; Daugs, E. D.; Rey, T. A. *Org. Process. Res. Dev.* **2008,** *12,* 940–945.
29. van der Linden, J. J.; Hilberink, P. W.; Kronenburg, C. M.; Kemperman, G. J. *Org. Process. Res. Dev.* **2008,** *12,* 911–920.
30. Zotova, N.; Hellgardt, K.; Kelsall, G. H.; Jessiman, A. S.; Hii, K. K. M. *Green Chem.* **2010,** *12,* 2157–2163.
31. (a) Cossar, P. J.; Hizartzidis, L.; Simone, M. I.; McCluskey, A.; Gordon, C. P. *Org. Biomol. Chem.* **2015,** *13,* 7119–7130; (b) Irfan, M.; Glasnov, T. N.; Kappe, C. O. *ChemSusChem* **2011,** *4,* 300–316.
32. Webb, D.; Jamison, T. F. *Org. Lett.* **2012,** *14,* 2465–2467.
33. Webb, D.; Jamison, T. F. *Org. Lett.* **2011,** *14,* 568–571.
34. Clark, P.; Poliakoff, M.; Wells, A. *Adv. Synth. Catal.* **2007,** *349,* 2655–2659.
35. Newman, S. G.; Gu, L.; Lesniak, C.; Victor, G.; Meschke, F.; Abahmane, L.; Jensen, K. F. *Green Chem.* **2014,** *16,* 176–180.
36. (a) Yoshida, J.-i.. *Flash Chemistry: Fast Organic Synthesis in Microsystems;* Wiley: Chichester, UK, 2008; (b) Yoshida, J.i.; Nagaki, A.; Yamada, T. *Chem. Eur. J.* **2008,** *14,* 7450–7459.
37. Kim, H.; Nagaki, A.; Yoshida, J.-i. *Nat. Commun.* **2011,** *2,* 264.
38. Brodmann, T.; Koos, P.; Metzger, A.; Knochel, P.; Ley, S. V. *Org. Process. Res. Dev.* **2012,** *16,* 1102–1113.
39. Riva, E.; Gagliardi, S.; Martinelli, M.; Passarella, D.; Vigo, D.; Rencurosi, A. *Tetrahedron* **2010,** *66,* 3242–3247.
40. He, Z.; Jamison, T. F. *Angew. Chem. Int. Ed.* **2014,** *53,* 3353–3357.

41. Gustafsson, T.; Sörensen, H.; Pontén, F. *Org. Process. Res. Dev.* **2012,** *16,* 925–929.
42. Baumann, M.; Baxendale, I. R.; Hornung, C. H.; Ley, S. V.; Rojo, M. V.; Roper, K. A. *Molecules* **2014,** *19,* 9736–9759.
43. Pieber, B.; Glasnov, T.; Kappe, C. *RSC Adv.* **2014,** *4,* 13430–13433.
44. Obermayer, D.; Glasnov, T. N.; Kappe, C. O. *J. Org. Chem.* **2011,** *76,* 6657–6669.
45. Herath, A.; Cosford, N. D. *Org. Lett.* **2010,** *12,* 5182–5185.
46. Herath, A.; Dahl, R.; Cosford, N. D. *Org. Lett.* **2009,** *12,* 412–415.
47. Pagano, N.; Herath, A.; Cosford, N. D. *J. Flow Chem.* **2012,** *1,* 28–31.
48. Gutmann, B.; Gottsponer, M.; Elsner, P.; Cantillo, D.; Roberge, D. M.; Kappe, C. O. *Org. Process. Res. Dev.* **2013,** *17,* 294–302.
49. (a) Noël, T.; Buchwald, S. L. *Chem. Soc. Rev.* **2011,** *40,* 5010–5029; (b) Reynolds, W. R.; Plucinski, P.; Frost, C. G. *Catal. Sci. Technol.* **2014,** *4,* 948–954.
50. Filipponi, P.; Ostacolo, C.; Novellino, E.; Pellicciari, R.; Gioiello, A. *Org. Process. Res. Dev.* **2014,** *18,* 1345–1353.
51. DeAngelis, A.; Wang, D. H.; Buchwald, S. L. *Angew. Chem. Int. Ed.* **2013,** *52,* 3434–3437.
52. Chen, M.; Buchwald, S. L. *Angew. Chem. Int. Ed.* **2013,** *52,* 4247–4250.
53. Brancour, C.; Fukuyama, T.; Mukai, Y.; Skrydstrup, T.; Ryu, I. *Org. Lett.* **2013,** *15,* 2794–2797.
54. Lange, P. P.; Bogdan, A. R.; James, K. *Adv. Synth. Catal.* **2012,** *354,* 2373–2379.
55. Reddy, G. S.; Reddy, N. S.; Manudhane, K.; Rama Krishna, M. V.; Ramachandra, K. J. S.; Gangula, S. *Org. Process. Res. Dev.* **2013,** *17,* 1272–1276.
56. Bedore, M. W.; Zaborenko, N.; Jensen, K. F.; Jamison, T. F. *Org. Process. Res. Dev.* **2010,** *14,* 432–440.
57. Baumann, M.; Baxendale, I. R.; Ley, S. V. *Synlett* **2010**, (5), 749–752.
58. Grafton, M.; Mansfield, A. C.; Fray, M. J. *Tetrahedron Lett.* **2010,** *51,* 1026–1029.
59. (a) Elliott, L. D.; Knowles, J. P.; Koovits, P. J.; Maskill, K. G.; Ralph, M. J.; Lejeune, G.; Edwards, L. J.; Robinson, R. I.; Clemens, I. R.; Cox, B.; Pascoe, D. D.; Koch, G.; Eberle, M.; Berry, M. B.; Booker-Milburn, K. I. *Chem. Eur. J.* **2014,** *20,* 15226–15232; (b) Su, Y.; Straathof, N. J.; Hessel, V.; Noël, T. *Chem. Eur. J.* **2014,** *20,* 10562–10589; (c) Cambié, D.; Bottecchia, C.; Straathof, N. J.; Hessel, V.; Noël, T. *Chem. Rev.* **2016;** http://dx.doi.org/10.1021/acs.chemrev.5b00707.
60. Cludius-Brandt, S.; Kupracz, L.; Kirschning, A. *Beilstein J. Org. Chem.* **2013,** *9,* 1745–1750.
61. Caron, A.; Hernandez-Perez, A. C.; Collins, S. K. *Org. Process. Res. Dev.* **2014,** *18,* 1571–1574.
62. Matsubara, H.; Hino, Y.; Tokizane, M.; Ryu, I. *Chem. Eng. J.* **2011,** *167,* 567–571.
63. Bou-Hamdan, F. R.; Lévesque, F.; O'Brien, A. G.; Seeberger, P. H. *Beilstein J. Org. Chem.* **2011,** *7,* 1124–1129.
64. Bogaert-Alvarez, R. J.; Demena, P.; Kodersha, G.; Polomski, R. E.; Soundararajan, N.; Wang, S. S. *Org. Process. Res. Dev.* **2001,** *5,* 636–645.
65. Cantillo, D.; Sheibani, H.; Kappe, C. O. *J. Org. Chem.* **2012,** *77,* 2463–2473.
66. Kumar, G. S.; Pieber, B.; Reddy, K. R.; Kappe, C. O. *Chem. Eur. J.* **2012,** *18,* 6124–6128.
67. Petersen, T. P.; Ritzén, A.; Ulven, T. *Org. Lett.* **2009,** *11,* 5134–5137.
68. Ingham, R. J.; Riva, E.; Nikbin, N.; Baxendale, I. R.; Ley, S. V. *Org. Lett.* **2012,** *14,* 3920–3923.
69. Ghislieri, D.; Gilmore, K.; Seeberger, P. H. *Angew. Chem. Int. Ed.* **2015,** *54,* 678–682.
70. Venturoni, F.; Nikbin, N.; Ley, S. V.; Baxendale, I. R. *Org. Biomol. Chem.* **2010,** *8,* 1798–1806.
71. Guetzoyan, L.; Nikbin, N.; Baxendale, I. R.; Ley, S. V. *Chem. Sci.* **2013,** *4,* 764–769.
72. Desai, B.; Dixon, K.; Farrant, E.; Feng, Q.; Gibson, K. R.; van Hoorn, W. P.; Mills, J.; Morgan, T.; Parry, D. M.; Ramjee, M. K. *J. Med. Chem.* **2013,** *56,* 3033–3047.
73. (a) Fabry, D. C.; Sugiono, E.; Rueping, M. *Isr. J. Chem.* **2014,** *54,* 341–350; (b) Fabry, D. C.; Sugiono, E.; Rueping, M. *React. Chem. Eng.* **2016,** *1,* 129–133.
74. Qian, Z.; Baxendale, I. R.; Ley, S. V. *Chem. Eur. J.* **2010,** *16,* 12342–12348.
75. Moore, J. S.; Smith, C. D.; Jensen, K. F. *React. Chem. Eng.* **2016,** *1,* 272–279.
76. Fitzpatrick, D. E.; Battilocchio, C.; Ley, S. V. *Org. Process. Res. Dev.* **2016,** *20,* 386–394.
77. Skilton, R. A.; Bourne, R. A.; Amara, Z.; Horvath, R.; Jin, J.; Scully, M. J.; Streng, E.; Tang, S. L. Y.; Summers, P. A.; Wang, J.; Perez, E.; Asfaw, N.; Aydos, G. L. P.; Dupont, J.; Comak, G.; George, M. W.; Poliakoff, M. *Nat. Chem.* **2015,** *7,* 1–5.
78. Parrott, A. J.; Bourne, R. A.; Akien, G. R.; Irvine, D. J.; Poliakoff, M. *Angew. Chem. Int. Ed.* **2011,** *50,* 3788–3792.
79. Browne, D. L.; Wright, S.; Deadman, B. J.; Dunnage, S.; Baxendale, I. R.; Turner, R. M.; Ley, S. V. *Rapid Commun. Mass Spectrom.* **2012,** *26,* 1999–2010.
80. Ahmed-Omer, B.; Sanderson, A. J. *Org. Biomol. Chem.* **2011,** *9,* 3854–3862.
81. Baxendale, I. R.; Deeley, J.; Griffiths-Jones, C. M.; Ley, S. V.; Saaby, S.; Tranmer, G. K. *Chem. Commun.* **2006,** 2566–2568.
82. (a) Bogdan, A. R.; Poe, S. L.; Kubis, D. C.; Broadwater, S. J.; McQuade, D. T. *Angew. Chem. Int. Ed.* **2009,** *48,* 8547–8550; (b) Snead, D. R.; Jamison, T. F. *Angew. Chem.* **2015,** *127,* 997–1001; (c) Baumann, M.; Baxendale, I. R. *React. Chem. Eng.* **2016,** *1,* 147–150.
83. Hook, B. D.; Dohle, W.; Hirst, P. R.; Pickworth, M.; Berry, M. B.; Booker-Milburn, K. I. *J. Org. Chem.* **2005,** *70,* 7558–7564.
84. (a) Lévesque, F.; Seeberge, P. H. *Angew. Chem. Int. Ed.* **2012,** *51,* 1706–1709; (b) Kopetzki, D.; Lévesque, F.; Seeberger, P. H. *Chem. Eur. J.* **2013,** *19,* 5450–5456; (c) Gilmore, K.; Kopetzki, D.; Lee, J. W.; Horváth, Z.; McQuade, D. T.; Seidel-Morgenstern, A.; Seeberger, P. H. *Chem. Commun.* **2014,** *50,* 12652–12655; (d) Fan, X.; Sans, V.; Yaseneva, P.; Plaza, D. D.; Williams, J.; Lapkin, A. *Org. Process. Res. Dev.* **2012,** *16,* 1039–1042; (e) Riva, E.; Rencurosi, A.; Gagliardi, S.; Passarella, D.; Martinelli, M. *Chem. Eur. J.* **2011,** *17,* 6221–6226; (f) Pieber, B.; Glasnov, T.; Kappe, C. O. *Chem. Eur. J.* **2015,** *21,* 4368–4376; (g) Amara, Z.; Bellamy, J. F.; Horvath, R.; Miller, S. J.; Beeby, A.; Burgard, A.; Rossen, K.; Poliakoff, M.; George, M. W. *Nat. Chem.* **2015,** *7,* 489–495.
85. Lau, S.-H.; Galván, A.; Merchant, R. R.; Battilocchio, C.; Souto, J. A.; Berry, M. B.; Ley, S. V. *Org. Lett.* **2015,** *17,* 3218–3221.
86. (a) Ceylan, S.; Coutable, L.; Wegner, J.; Kirschning, A. *Chem. Eur. J.* **2011,** *17,* 1884–1893; (b) Kirschning, A.; Kupracz, L.; Hartwig, J. *Chem. Lett.* **2012,** *41,* 562–570; (c) Ceylan, S.; Friese, C.; Lammel, C.; Mazac, K.; Kirschning, A. *Angew. Chem. Int. Ed.* **2008,** *47,* 8950–8953.
87. Hartwig, J.; Ceylan, S.; Kupracz, L.; Coutable, L.; Kirschning, A. *Angew. Chem. Int. Ed.* **2013,** *52,* 9813–9817.
88. Kupracz, L.; Kirschning, A. *Adv. Synth. Catal.* **2013,** *355,* 3375–3380.
89. Murray, P. R.; Browne, D. L.; Pastre, J. C.; Butters, C.; Guthrie, D.; Ley, S. V. *Org. Process. Res. Dev.* **2013,** *17,* 1192–1208.
90. Pastre, J. C.; Browne, D. L.; O'Brien, M.; Ley, S. V. *Org. Process. Res. Dev.* **2013,** *17,* 1183–1191.
91. (a) Zhang, P.; Russell, M. G.; Jamison, T. F. *Org. Process. Res. Dev.* **2014,** *18,* 1567–1570; (b) Ott, D.; Borukhova, S.; Hessel, V. *Green Chem.* **2016,** *18,* 1096–1116; (c) Borukhova, S.; Noel, T.; Metten, B.; de Vos, E.; Hessel, V. *Green Chem.* **2016**.
92. Martin, A. D.; Siamaki, A. R.; Belecki, K.; Gupton, B. F. *J. Flow Chem.* **2015,** *5,* 145–147.
93. Sedelmeier, J.r.; Ley, S. V.; Baxendale, I. R.; Baumann, M. *Org. Lett.* **2010,** *12,* 3618–3621.
94. Tsubogo, T.; Oyamada, H.; Kobayashi, S. *Nature* **2015,** *520,* 329–332.
95. Poh, J.-S.; Browne, D. L.; Ley, S. V. *React. Chem. Eng.* **2016,** *1,* 101–105.
96. Baxendale, I. R.; Griffiths-Jones, C. M.; Ley, S. V.; Tranmer, G. K. *Synlett* **2006**, (3), 427–430.
97. Hopkin, M. D.; Baxendale, I. R.; Ley, S. V. *Chem. Commun.* **2010,** *46,* 2450–2452.
98. Shen, B.; Jamison, T. F. *Org. Lett.* **2012,** *14,* 3348–3351.
99. Snead, D. R.; Jamison, T. F. *Chem. Sci.* **2013,** *4,* 2822–2827.
100. Mascia, S.; Heider, P. L.; Zhang, H.; Lakerveld, R.; Benyahia, B.; Barton, P. I.; Braatz, R. D.; Cooney, C. L.; Evans, J.; Jamison, T. F. *Angew. Chem. Int. Ed.* **2013,** *52,* 12359–12363.
101. Adamo, A.; Beingessner, R. L.; Behnam, M.; Chen, J.; Jamison, T. F.; Jensen, K. F.; Monbaliu, J.-C. M.; Myerson, A. S.; Revalor, E. M.; Snead, D. R.; Stelzer, T.; Weeranoppanant, N.; Wong, S. Y.; Zhang, P. *Science* **2016,** *352,* 61–67.

102. Correia, C. A.; Gilmore, K.; McQuade, D. T.; Seeberger, P. H. *Angew. Chem. Int. Ed.* **2015,** *54,* 4945–4948.
103. Battilocchio, C.; Baxendale, I. R.; Biava, M.; Kitching, M. O.; Ley, S. V. *Org. Process. Res. Dev.* **2012,** *16,* 798–810.
104. Battilocchio, C.; Deadman, B. J.; Nikbin, N.; Kitching, M. O.; Baxendale, I. R.; Ley, S. V. *Chem. Eur. J.* **2013,** *19,* 7917–7930.
105. (a) Deadman, B. J.; Battilocchio, C.; Sliwinski, E.; Ley, S. V. *Green Chem.* **2013,** *15,* 2050–2055; (b) Hartman, R. L.; Sahoo, H. R.; Yen, B. C.; Jensen, K. F. *Lab Chip* **2009,** *9,* 1843–1849.
106. Hartman, R. L. *Org. Process. Res. Dev.* **2012,** *16,* 870–887.
107. Kim, H.; Min, K.-I.; Inoue, K.; Im, D. J.; Kim, D.-P.; Yoshida, J.-i. *Science* **2016,** *352,* 691–694.

1.07 Beyond Bioisosterism: New Concepts in Drug Discovery

LM Lima and EJ Barreiro, Laboratório de Avaliação e Síntese de Substâncias Bioativas (LASSBio, www.lassbio.icb.ufrj.br), Instituto de Ciências Biomédicas da Universidade Federal do Rio de Janeiro, RJ, Brasil

© 2017 Elsevier Ltd. All rights reserved.

1.07.1	Introduction	186
1.07.2	Bioisosterism in Nature	187
1.07.3	Functional Bioisosterism	188
1.07.4	Functional Bioisosteres of Esters and Amides	194
1.07.5	Retroisosterism	195
1.07.6	Ring Closure or Anelation and Ring Opening	196
1.07.7	Classical Bioisosterism	200
1.07.8	Ring Bioisosterism	202
1.07.9	Final Remarks	207
References		208

1.07.1 Introduction

The concept of *bioisosterism* refers to frameworks, fragments, atoms, and groups presented in the structures of bioactive compounds that have similar molecular volume, shape, electronic distribution, and physical–chemical properties. It is a molecular modification strategy, based on the replacement of interchangeable molecular fragment(s) (atoms, functional groups, subunits) having similar steric–electronic profile and comparable physical–chemical properties.[1–6]

Bioisosterism is a key strategy in medicinal chemistry aiming to promote molecular modifications in a starting structure (i.e., hit, lead, prototype), in order to improve pharmacokinetic (PK), pharmacodynamic (PD), and toxicological profiles. It is considered also strategic to circumvent intellectual properties issues. In summary, bioisosterism is applied by medicinal chemists to remove unwanted side effects or toxicity, to improve ADME, and to enhance selectivity and potency by a target bioreceptor. In a few cases, the motivation for the use of bioisosterism concept results from the need to overcome patent barriers, being mainly used in the search for novel structural analogues of an innovative drug.[7–10]

A basic principle in medicinal chemistry is that structurally similar compounds have similar physicochemical properties and similar biological activities. This principle is the core for the application of bioisosterism. Consequently, any bioisosteric replacement must consider steric and size attributes, electronic characteristics, comparative solubility, and hydrophobic effects between the elected interchangeable groups or fragments.

However, success by application of bioisosterism requires some knowledge of the structure activity relationships in the parent molecule. In this context, the understanding of pharmacophoric and auxophoric contributions of each of the molecular subunits that comprise the structure of a hit, a lead, or a prototype, is important. Similarly, the metabolic inactivation pathways, as well as the main structural factors determining the physical–chemical properties that regulate their bioavailability and their adverse side effects, direct or not, must be known.

Bioisosterism resulted from the use of the principle of isosterism, developed by Langmuir in 1919, studying the chemical behavior and reactivity of certain atoms and groups with the same number of valence electrons, therefore isoelectronic (e.g., N_2 and CO).[1]

In 1951, Friedman introduced the term bioisosterism to describe the influence of isosteric replacements upon biological activity. He established the concept that if a compound fits the broadest definition for isosteres and has the same type of biological activity, then it can be considered a bioisostere.[11]

Bioisosterism, in its first applications as a molecular modification strategy, has been benefited by the hydride displacement law, an empirical rule formulated by Grimm in 1925.[12] It states that the addition of a hydrogen atom with a pair of electrons (i.e., hydride) to an atom, produces a pseudoatom presenting the same physical properties as those present in the column immediately behind on the Periodic Table of the Elements for the initial atom (**Fig. 1**). In accordance with Grimm's hydride displacement law, any atom belonging to groups IVA, VA, VIA, and VIIA on the periodic table change their properties by adding a hydride, becoming isoelectronic pseudoatoms.

Further work by Erlenmeyer and Hinsberg broadened the principle of isosterism, defining it as atoms, ions, or molecules in which the peripheral layers of electrons can be considered identical.[13]

In 1970, Alfred Burger classified and subdivided *bioisosterism* into two categories: classic and nonclassic.[14] The classic bioisosterism includes atoms, groups, and radicals having peripheral layers of electrons with same valence. They are arranged in mono-, di-, tri-, or tetravalent atoms or groups (**Table 1**). This classification also covers the rings equivalents concept. The nonclassical bioisosterism is the most challenging type of isosteric relationship (**Table 2**). It includes the strategies of retroisosterism, ring opening, ring closure or annelation, and equivalent functional groups.[4–6,9] Another unique contribution of Burger had been the

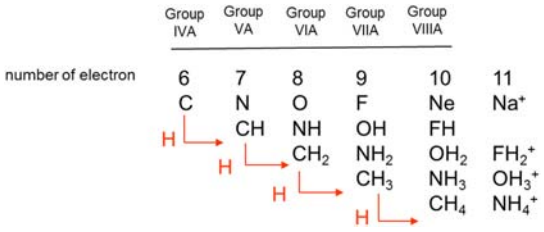

Fig. 1 Grimm's hydride displacement law.

Table 1 Classic bioisosteric groups and atoms

Monovalent	*Divalent*	*Trivalent*	*Tetravalent*
F, OH, NH_2, CH_3, OR	$-CH_2-$	$-CH-$	$=C=$
Cl, SH, PH_2, SiR_3, SR	$-O-$	$=N-$	$=Si=$
Brx	$-S-$	$=P-$	$=N^+=$
I	$-Se-$	$=As-$	$=P^+=$
	$-Te-$	$=Sb-$	$=As^+=$
			$=Sb^+=$

Table 2 Nonclassic biososteres

$-CO-$	$-COOH$	$-SO_2NH_2$	$-H$	$-CONH-$	$-COOR-$	$-CONH_2$
$-CO_2-$	$-SO_3H$	$-PO(OH)NH_2$	$-F$	$-NHCO-$	$-ROCO-$	$-CSNH_2$
$-SO-$	Tetrazole					
$-SO_2NR-$	$-SO_2NHR$		$-OH$		$-$Cathecol	
$-CON-$	3-Hydroxy-isoxazole		$-CH_2OH$		$-$Benzimidazole	
$-CH(CN)-$	3-Hydroxy chromene		$-NHCONH_2$			
R–S–R′	$=N-$		$-NH-CS-NH_2$			$-C_5H_4N$
(R–O–R′)						
R–N(CN)–R′	$-C(CN)=$		$-NH-C(=CHNO_2)-NH_2$			$-C_6H_5$
R–C(CN)(CN)–R′						$-C_4H_4N$
	$-$Halogen					C_4H_4S
	$-CF_3$					
	$-CN$					
	$-N(CN)_2$					
	$-C(CN)_3$					

assumption that to be a bioisostere, compounds need to affect biochemically associated systems as agonists or antagonist. Consequently, for the first time, the bioisosterism concept was not related to similar activity, but with the ability to be recognized by a same bioreceptor.[15]

The Main Factors to be Considered in Terms of a Planned Bioisosteric Substitution Include:

1. Molecular size and volume, electronic distribution of atoms, and considerations on the degree of hybridization, polarity, bond angles and distances, and inductive and mesomeric effects;
2. Lipid and aqueous solubility;
3. Chemical reactivity of the interchangeable isosteric groups or atoms or subunits, anticipating their main changes in the biotransformation process, including those related to the formation of eventual toxic metabolites;
4. Conformational factors, including the differentiating in the ability to form inter- and/or intramolecular H-bonding.

In the following, we will discuss in this article some selected examples of both nonclassical and classical bioisosterism, in order to give an idea of the versatility of this molecular modification strategy, used by medicinal chemists in the steps of ligand design, planning of a congeneric series, lead optimization, and as key tool in the identification of new drugs that are authentic therapeutic copies or me-too.[16]

1.07.2 Bioisosterism in Nature

Bioisosterism is a common phenomenon found in nature as a form of increasing chemical diversity (Fig. 2). The comparison between the structures of serine (1) and cysteine (2) or tyrosine (3) versus hystidine (4) is a nice example to illustrate isosterism

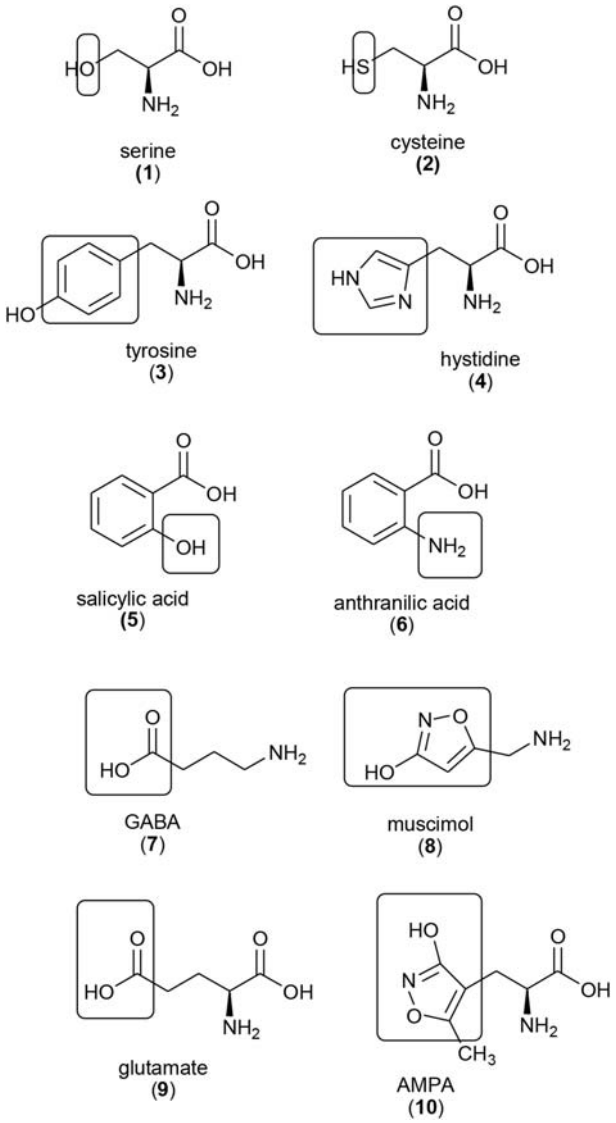

Fig. 2 Examples of classic and nonclassic bioisosterism in nature.

of divalent group (O × S) and equivalent rings, respectively, widely distributed in nature. Salicylic acid (**5**) and anthranilic acid (**6**) are examples of monovalent bioisosteres (OH × NH_2), which boosted the design of important nonsteroidal antiinflammatory drugs. Examples of nonclassic bioisosterism can also be found in nature, as exemplified by the functional group isosterism between GABA (gamma-aminobutyric acid, **7**) and muscinol (**8**), or between neurotransmitters glutamate (**9**) and AMPA (alfa-amino-3-hydroxy-5-methyl-4-isoxazolepropionic acid, **10**) (Fig. 2).

1.07.3 Functional Bioisosterism

Starting from a peptide-based molecule (**11**) identified as cathepsin K inhibitor with poor metabolic stability, Gauthier and coworkers [17] proposed the bioisosteric replacement of amide function by a trifluoroethylamine subunit, resulting in the design of compound **12** (Fig. 3). This peptide-mimetic derivative (**12**) showed great inhibitory potency against cathepsin K, with improved selectivity profile (cathepsin K versus cathepsin B) and better metabolic stability (Fig. 3). Further optimizations resulted in the discovery of odanacatib (**13**) indicated for the treatment of osteoporosis.

A classical example of functional bioisosterism is the interchangeable relationship between the OH group of phenol subunity and sulfonamide. Larsen and Lish,[18] looking for new compounds able to modulate the catecholamines receptors proposed the replacement of OH-phenolic, presented in the structure of adrenaline simplified analogue **15**, by the NH–SO_2CH_3 group. This structural modification resulted in a phenylmethylsulfonamide fragment (**16**) with a strong structural similarity with

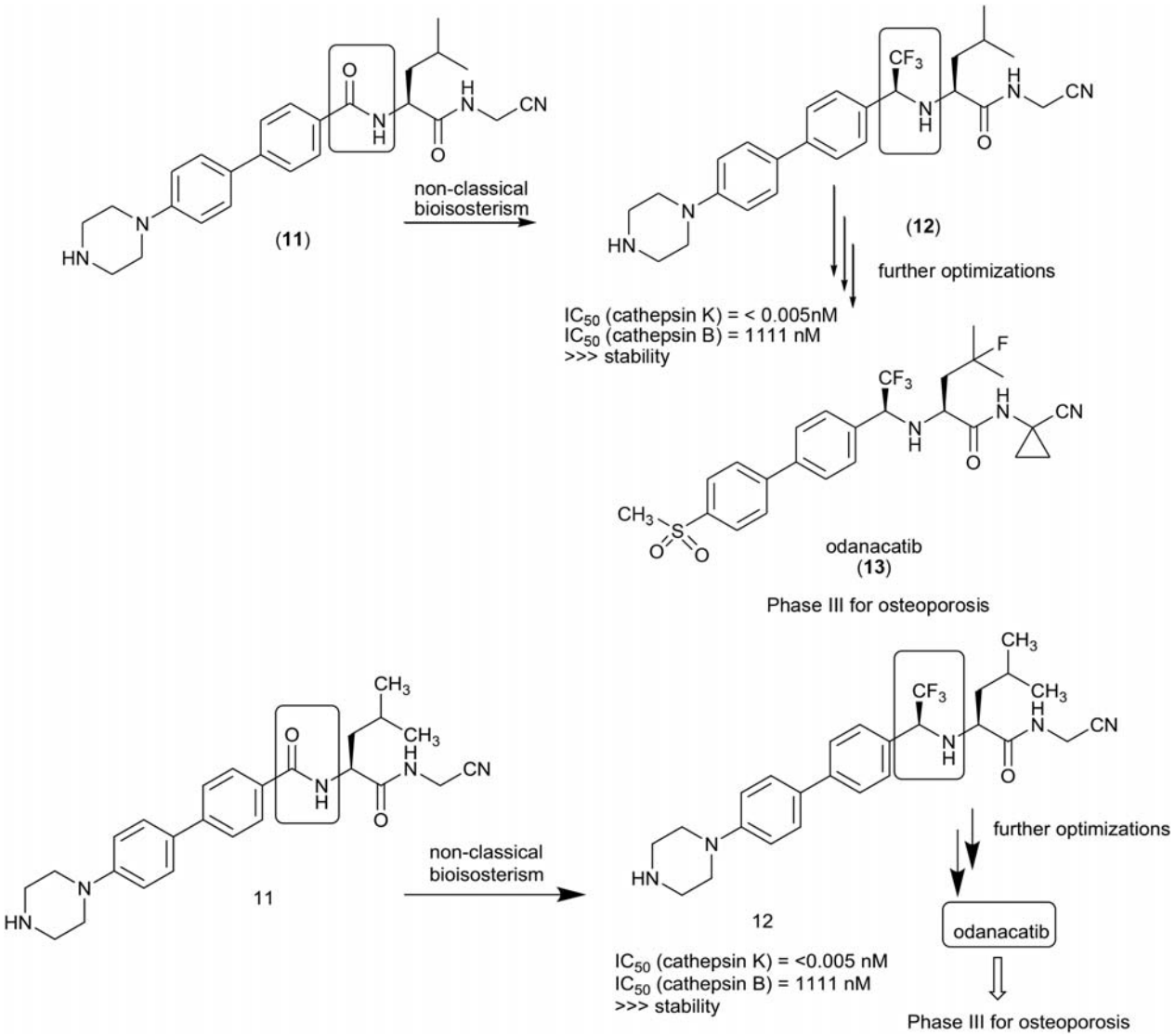

Fig. 3 Nonclassic bioisosteric relationship between the amide (**11**) and trifluoroethylamine (**12**) subunits in the genesis of cathepsin K inhibitors.

adrenaline (**14**) and **15**. Despite the differences considering steric and size attributes, the phenol and arylsulfonamide share similar acidity, due to the similarity between the pK_a of the **OH**-phenol and **NH**-sulfonamide function, that is, 9.1 and 9.6, respectively. Therefore, for catecholamine receptors both fragments are considered interchangeable and constitute a nice example of functional bioisosterism (Fig. 4).

More recently, the same bioisosteric replacement was proposed by Lin and coworkers.[19] The exchange of phenol group (**17**) by an arylsulfonamide (**18**) resulted in a bioisoster fourfold more potent than the parent prototype, acting as an antagonist of gonadotropin hormone receptors (Fig. 5).

An interesting example of nonclassical bioisosterism involving the phenol function, more specifically the 2,6-difluorophenol, was described by Demopoulos from the University of Thessaloniki, Greece. This author and coworkers,[20] searching for new aldose reductase inhibitors had previously indentified the carboxylic acid derivative **19**. From this lead compound and aiming to improve lipophilicity, the authors proposed the replacement of carboxylic acid by a more lipophilic bioisosteric fragment. Therefore, the acetic acid subunit (**19**) was replaced by a 2,6-difluorophenol, resulting in compound **20**, that has been shown to be five times more potent as aldose reductase inhibitor and almost threefold more lipophilic (Fig. 6).

The same parent prototype (**19**) was optimized by Papastavrou and coworkers,[21] with the introduction of 1-hydroxypyrazole ring (**21**) as new acetic acid nonclassical bioisostere (Fig. 7). This interchangeable isosteric replacement resulted in an equipotent inhibitor of aldehyde dehydrogenase (ALDH)-2 and in an expressive increased in the inhibition of ALDH-1. Advantages pointed out in favor of 1-hydroxypyrazole ring (**20**) as an isostere of carboxylic acid (**18**) are that it has less acidic property (pK_a 6.98 versus pK_a 4.37) and higher lipophilicity, resulting in greater potential to permeate more freely through biological barriers.

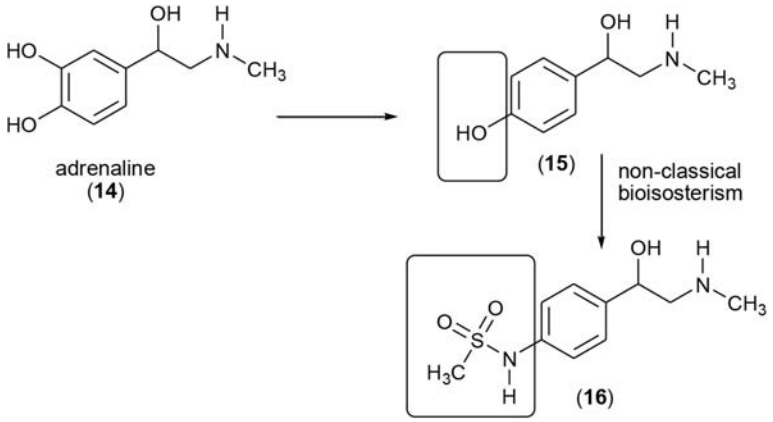

Fig. 4 Nonclassic bioisosteric relationship between the phenol (**15**) and phenylsulfonamide (**16**) in the genesis of adrenaline (**14**) analogues.

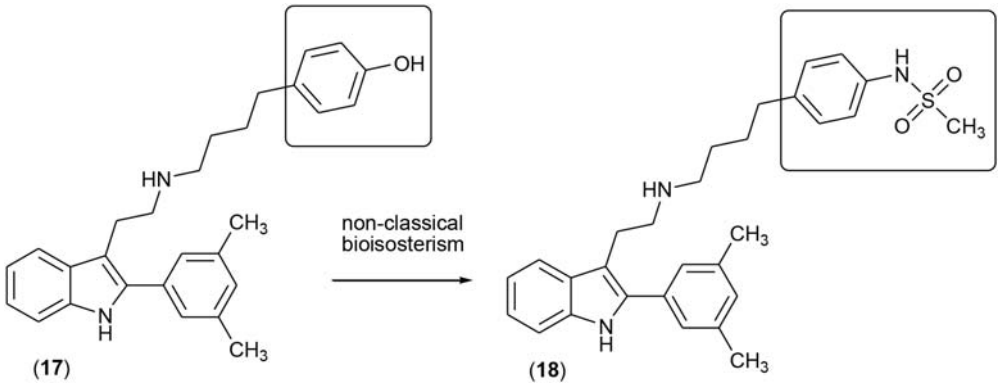

Fig. 5 Example of functional bioisosterism between PhOH (**17**) and $PhNHSO_2CH_3$ (**18**).

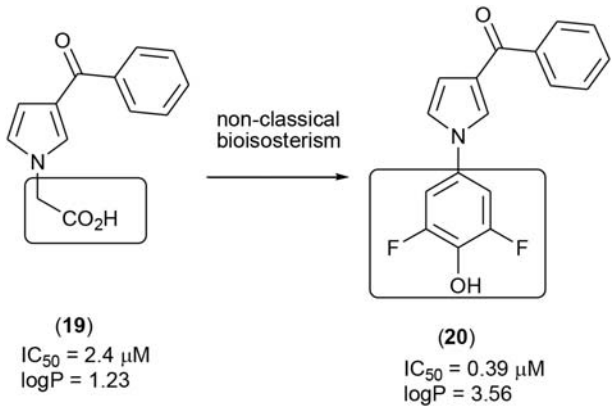

Fig. 6 Example of functional bioisosterism between the carboxylic acid group (**19**) and 2,6-difluorophenol subunit (**20**).

Other important examples of carboxylic acid bioisostere can be represented by the 3-hydroxy-1,2-oxazol-4-yl (**10**), 4-hydroxy-1,2,3-oxadiazol-5-yl (**22**), and 4-hydroxy-1,2,3-tiadiazol-5-yl moieties (**23**). These moieties can be found in the structures of AMPA (**10**) and TDPA (**23**), maintaining a nonclassical boisosteric relationship with carboxylic acid presented in glutamate (**9**), the agonist of ionotropic glutamate receptors (Fig. 8).[22]

Sulfonic and phosphonic acids are considered common carboxylic acid isosteres, and this kind of nonclassical bioisosterism can be identified in nature comparing the structures of the amino acids beta-alanine (**24**), taurine (**25**), and ciliatine (**26**). The same bioisosteric relationship can be also identified comparing the structures of baclofen (**27**), an agonist of $GABA_b$ receptors used as antispastic agent, and saclofen (**28**) and phaclofen (**29**), both identified as a $GABA_b$ antagonists (Fig. 9).[23]

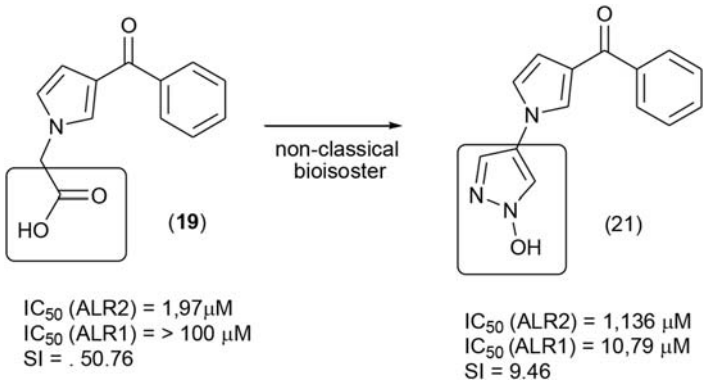

Fig. 7 Example of functional bioisosterism between the carboxylic acid (**19**) and 1-hydroxypyrazole ring (**21**).

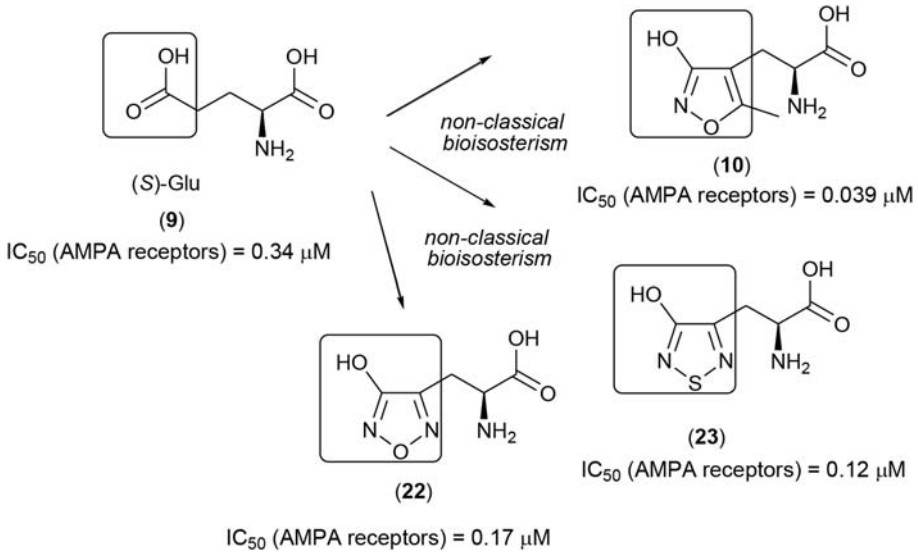

Fig. 8 The nonclassical bioisosterism of functional groups involving a carboxylic acid (**9**) and the 3-hydroxy-1,2-oxazol-4-yl (**10**), 4-hydroxy-1,2,3-oxadiazol-5-yl (**22**), and 4-hydroxy-1,2,3-thiadiazol-5-yl (**23**) moieties.

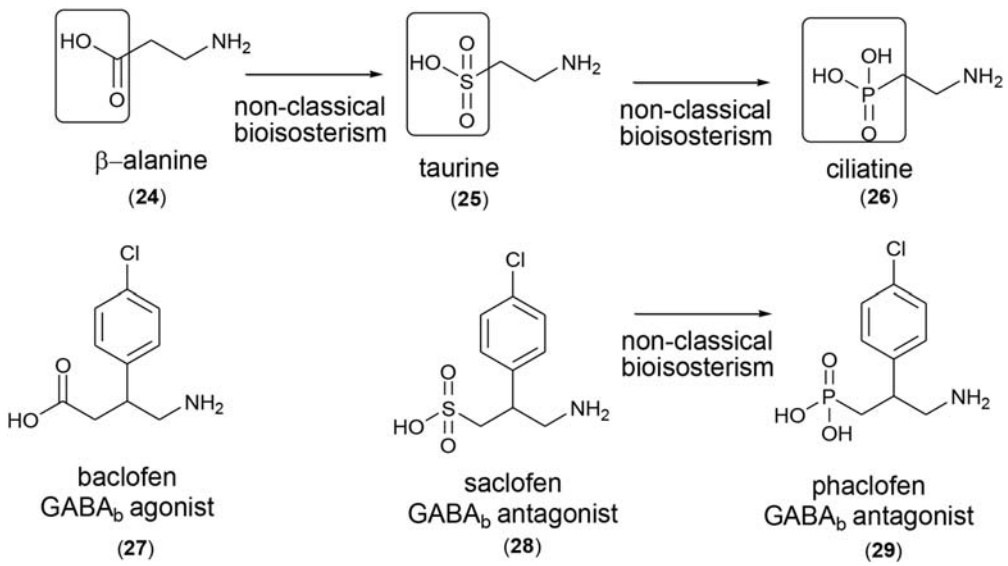

Fig. 9 Examples of nonclassical bioisosterism between carboxylic, sulfonic, and phosphonic acids subunits.

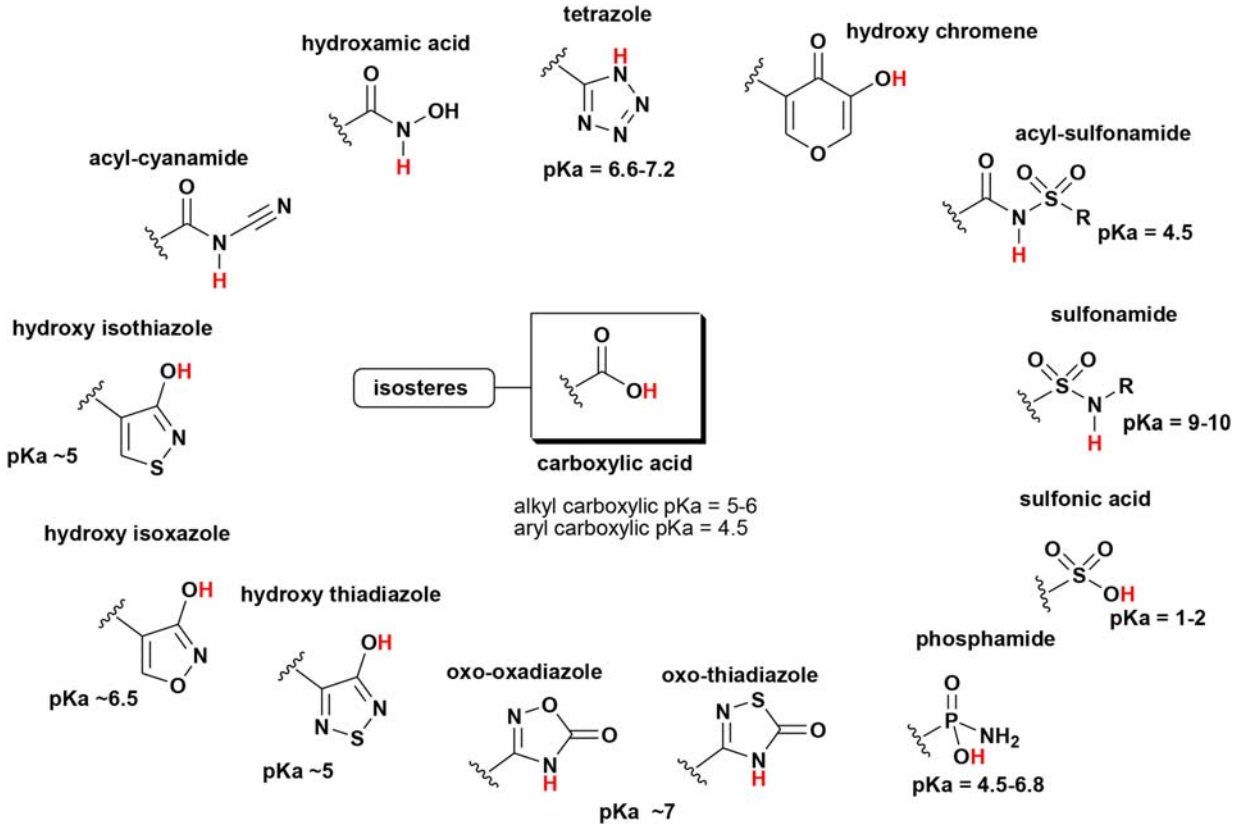

Fig. 10 Examples of carboxylic acid bioisosteres having different pK_a.

In fact, many examples of carboxylic acid bioisosteres have been previously described in the literature.[5,9,24] Fig. 10 illustrates the most common fragments or groups considered interchangeable with carboxylic acid, maintaining a nonclassical bioisosteric relationship with this important functional group in medicinal chemistry.

Others examples of functional bioisosterism can be discussed. An interesting one was reported by Koller and coworkers.[25] The authors described aromatic **N** versus aromatic **F** bioisosterism and their applicability to replace natural bases of nucleic acid structures, generating nonpolar nucleoside isosteres (Fig. 11).

Another example can be demonstrated by the work performed by Sheng and coworkers.[26] Searching for new antifungal agents, the authors proposed the replacement of **O** atom, present in the phenoxyalkylpiperazine side chain contained in the structure of fluconazole analogue **33**, by a triazolone ring (**34**). From these studies, a new nonclassical bioisosteric relationship was established, being demonstrated that the replacement of oxygen by triazolone could improve the water solubility without a loss of hydrogen bonding interaction with CYP51 (Fig. 12).

Guanidine (**35**) is a privileged molecular subunit, having frequently a low oral bioavailability, mainly due its high basicity. The proposal of replacement of the hydrogen atom linked to imine framework by monovalent electron withdrawing groups, such as cyano, nitro, acyl, and sulfonyl (i.e., **36**–**39**), have been demonstrated to be a great strategy to modulate guanidine basicity, resulting in the obtention of new scaffolds maintaining a functional bioisosterim relationship (Fig. 13).

Dmitriev and Ragulin[27] reported a curious potential functional bioisosterism. In order to prepare pseudo dipeptides, having structural similarity with certain fragments of β-amyloid peptides, the authors proposed the design of phosphinic acid oligopeptides (**41** and **43**) as a nonclassical isostere of amide subunit, and then synthesized peptidomimetics analogues of Arg-Glu (**40**) and Gly-Leu (**42**) (Fig. 14).

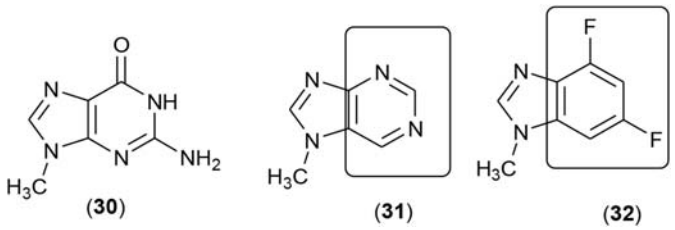

Fig. 11 Nonclassical bioisosteric relationship between aromatic-fluorine (**32**) and aromatic-nitrogen (**31**).

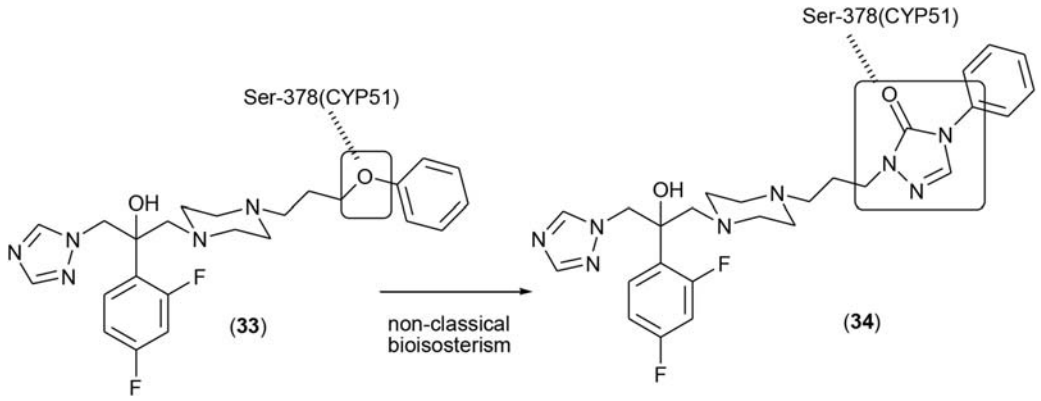

Fig. 12 Nonclassical bioisosteric replacement of oxygen atom (**33**) by a triazolone ring (**34**).

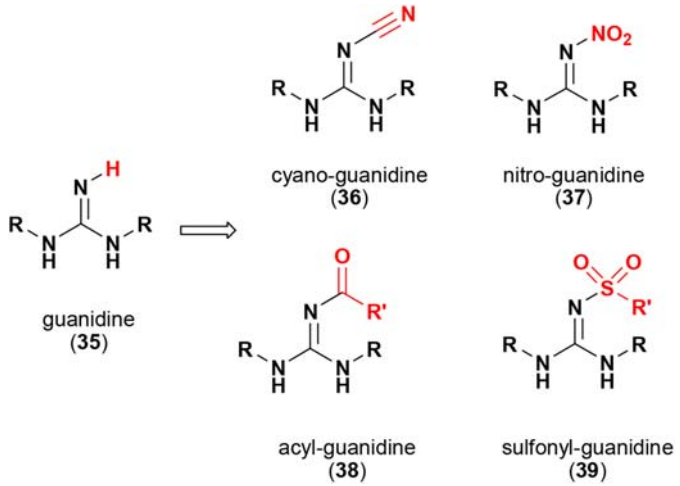

Fig. 13 Isosteres of the substituted guanidine fragment.

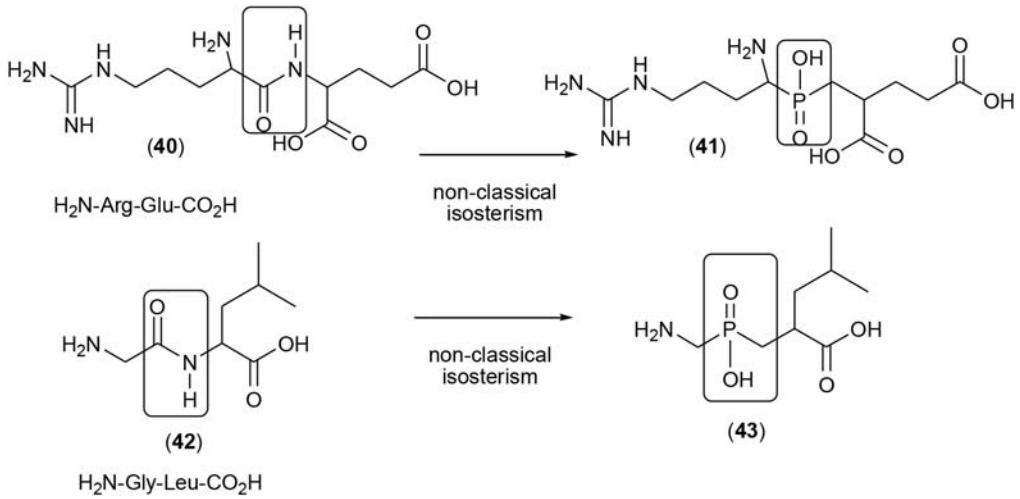

Fig. 14 Structures of dipeptides Arg-Glu (**40**) and Gly-Leu (**42**) and their phosphinic acidic pseudo peptides (**41** and **43**).

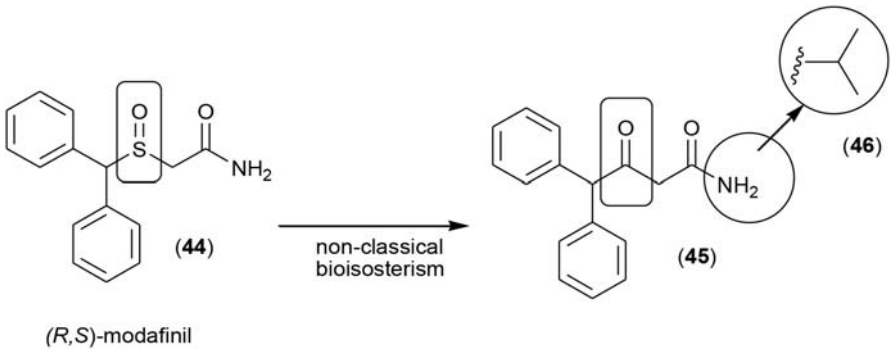

Fig. 15 Structures of (*R,S*)-modafinil (**44**) and its achiral nonclassical bioisosteres **45** and **46.**

A common functional bioisosterism is represented by **C═O × S═O** groups. Modafinil (**44**) is a chiral sulfoxide drug used in the treatment of excessive sleepiness caused by narcolepsy, sleep disorder, and obstructive sleep apnea. Aiming to design nonasymmetric modafinil analogues, Risi and coworkers[28] proposed the isosteric replacement of sulfoxide function by a carbonyl group. Evaluation of the comparative effect on the spontaneous and the electrically evoked tritiated serotonin efflux from rat cortical slices showed a loss of activity for compound **45**, which was restored modifying the primary amide (**45**) into the corresponding *N*-isopropyl derivative **46** (Fig. 15).

1.07.4 Functional Bioisosteres of Esters and Amides

Countless chemotypes or frameworks are isosteres of ester and amide functions.[9,29] The use of this type of bioisosterism is performed, basically, to circumvent metabolic instability of these functional groups, which are vulnerable to hydrolysis catalyzed by different enzymes (e.g., esterases, amidases, carboxyesterases, lipases) widely distributed in humans.

The oxazole ring, present in compound **47**, was introduced as nonclassical bioisostere of the ester group presented in the structure of prototype **48** (Fig. 16). This bioisosteric replacement has advantages like the increase in log*P* values and the enhancement in plasma metabolic stability.[30] Similarly, the pyrrole nucleus (e.g., **50**, Fig. 16) can work as functional and stable amide isostere (e.g., **49**, Fig. 16).[31]

Starting from a series of pyrimidinylthioacetanilides identified as HIV-1 nonnucleoside reverse transcriptase inhibitors, Li and coworkers[32] proposed the nonclassical bioisosteric replacement of amide functionality by a 1,2,3-triazole ring (Fig. 17). The results indicated that despite a better metabolic stability compound **52** was 10-fold less active than the amide prototype **51**.

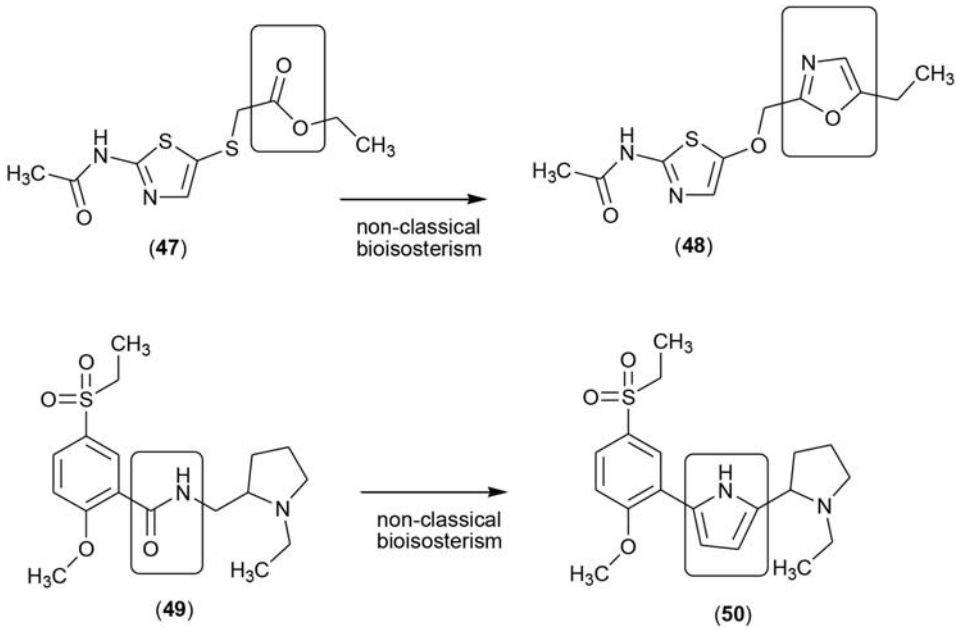

Fig. 16 Functional isosteres of esters and amides.

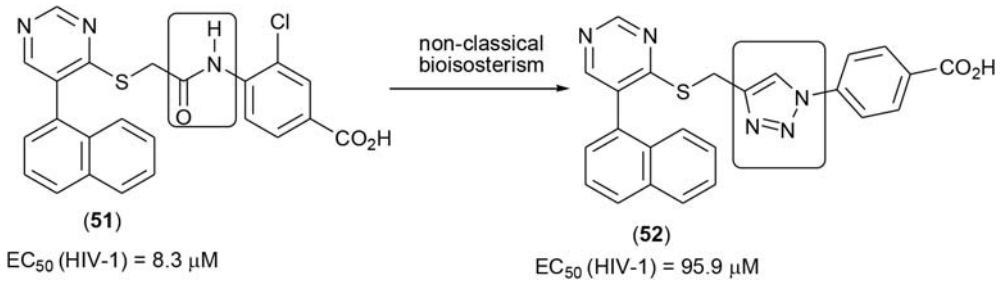

Fig. 17 Structures of pyrimidinylthioacetanilide **51**, an inhibitor of HIV-1 nonnucleoside reverse transcriptase, and its nonclassical bioisoster **52.**

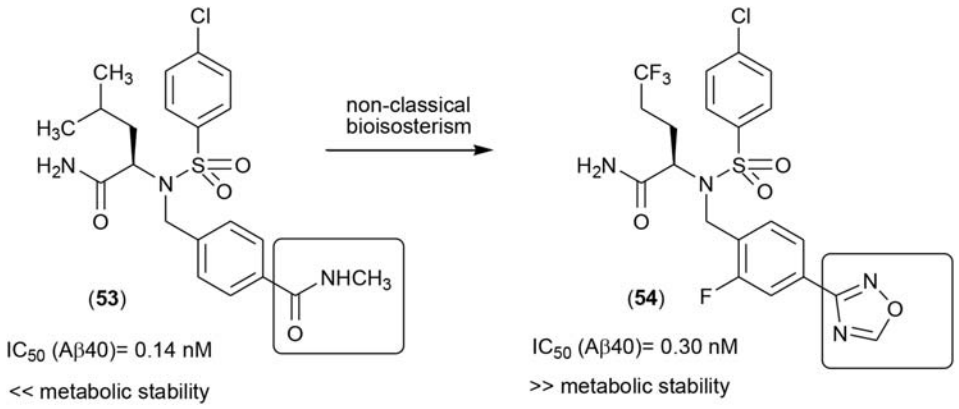

Fig. 18 Inhibitor of γ-secretase **53** and its nonclassical bioisoster **54.**

Aiming to develop a potent and selective γ-secretase inhibitor for the treatment of Alzheimer's disease, Gillman and coworkers[33] previously identified the *N*-methyl-substituted benzenecarboxamide **53**, which showed poor in vitro microsomal stability, indicating the potential for rapid clearance in vivo. In an effort to improve brain penetration and metabolic stability, the authors proposed the nonclassical bioisosterism replacement of the amide function for a 1,2,4-oxadiazole ring, resulting in a compound more lipophilic (**54**) than the parent prototype **53** (Fig. 18). They also demonstrate that the new bioisostere **54** was a potent inhibitor of γ-secretase, presenting good PK profile in rats and dogs.

1.07.5 Retroisosterism

Retroisosterism or reversal of functional groups is a type of nonclassical bioisosterism that is commonly used to improve stability. Retropeptides, for instance, are normally more resistant to enzymatic attacks. From the prototype thiorphan (**55**), a potent inhibitor of neutral endopeptidase (NEP), an enzyme responsible for the hydrolysis of vasoactive peptides, including the natriuretic peptides, angiotensin II, and endothelin-1, the retro-thiorphan (**56**) was designed and prepared (Fig. 19). The reversal of amide position in

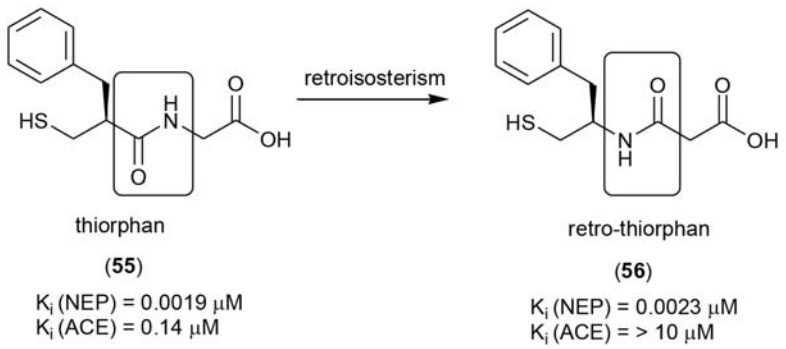

Fig. 19 Retroisosteres of amides: thiorphan (**55**) and retro-thiorphan (**56**).

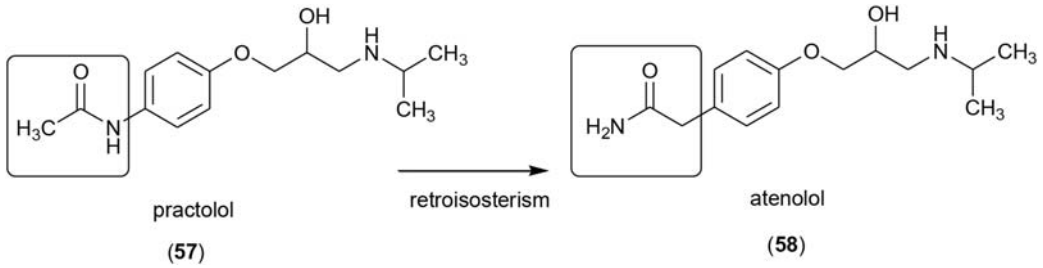

Fig. 20 Retroisosteres of amides: practolol and atenolol.

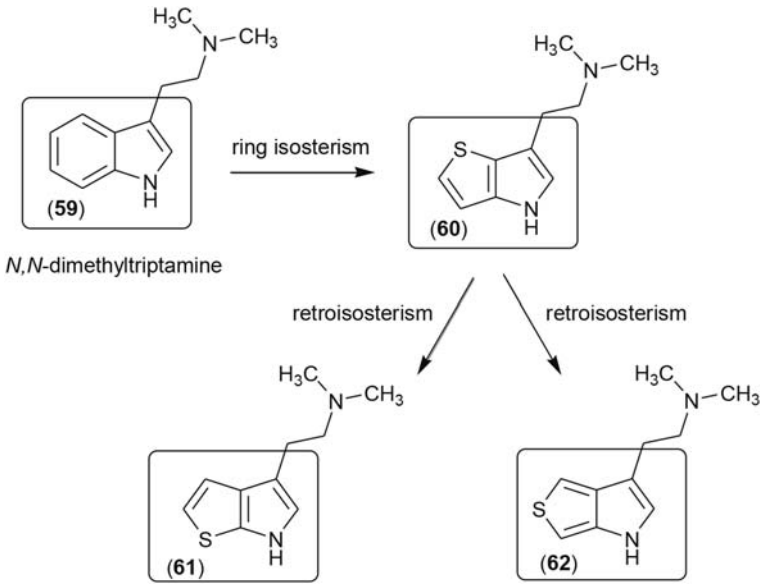

Fig. 21 Retroisosteres of the thienopyrrole system, a classical bioisostere of indole ring.

these peptides (**55** and **56**) resulted in an equipotent inhibition of NEP. However, their effect on the activity of angiotensin-converting enzyme (ACE) was quite different. Retro-thiorphan (**56**) was 71-fold less active against ACE. These results indicated that the retroisosterism strategy was crucial for the selection against NEP and ACE metalloproteins.[34]

Nonpeptidic compounds, as exemplified by the drugs practolol (**57**) and atenolol (**58**), can keep a retroisostere relationship. In fact, atenolol (**58**) differs from practolol (**57**) only for the reversal position of amide subunity (Fig. 20). However, atenolol is a cardioselective β-blocker with fewer side effects than the isomer practolol.[35]

Starting with the prototype *N*,*N*-dimethyltryptamine (**59**), Blair and coworkers[36] proposed initially the classical ring isosterism of the indole system and the 4*H*-thieno[3,2-*b*]pyrrole nucleus (**60**). Following the possibility of two regioisomers of thienopyrrole system, the authors proposed the design of the retroisosteres 6*H*-thieno[2,3-*b*]pyrrole (**61**) and 1*H*-thieno[3,4-*b*]pyrrole (**62**). The results demonstrated that with the exception of the 1*H*-thieno[3,4-*b*]pyrrole (**62**), unstable and hard to synthesize, the other heterocyclic isomeric systems are authentic bioisosteres of the indole nucleus, presenting affinity and selectivity for the serotonin receptors similar to prototype **59** (Fig. 21).

Aiming the discovery of new acetylcholinesterase (AChE) inhibitors, as potential anti-Alzheimer candidate, Barreiro and coworkers[37] designed a novel scaffold from molecular modification of the structure of tacrine (**63**), one of the first therapeutic resources available for the treatment of Alzheimer disease (AD). Starting from tacrine (**63**), the authors proposed the bioisosteric replacement of quinoline ring by the 1-phenyl-1*H*-pyrazolo[3,4-*b*]pyridine system, resulting in compound **64**, that was considerably less active in inhibiting the AChE than the prototype tacrine. Further modification, based on retroisosterism, resulted in compound **65**, presenting the nucleus 1-phenyl-1*H*-pyrazolo[4,3-*b*]pyridine, which was more potent than compound **64**, having a better selective index (AChE vs. BChE) than tacrine (Fig. 22).

1.07.6 Ring Closure or Anelation and Ring Opening

Among the nonclassical bioisosterism strategies, the anelation or ring closure procedure is worth mentioning. Normally this strategy aims to restrict conformational possibilities, creating a more rigid structure that can be better recognized by a hypothetic receptor, if

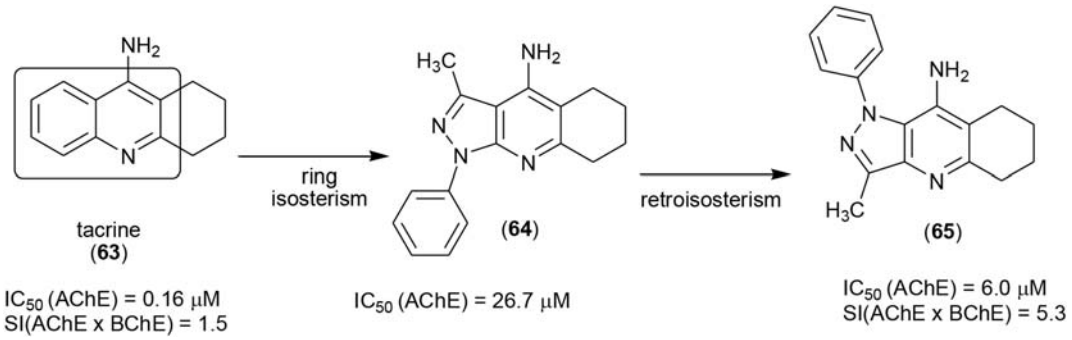

Fig. 22 Classic ring isostere (**64**) and nonclassical retroisostere (**65**) of tacrine (**63**).

it mimics the bioactive conformation, contributing in this case for the enhancement of affinity. Recently, Capparelli and coworkers[38] described the efforts to optimize the activity of the lead-compound MC113 (**66**). This compound was described as a promising inhibitor of P-glycoprotein (P-gp), with good selectivity toward P-gp versus multidrug resistance associated protein 1 (MRP1). Various elongated spacers, between the biphenyl fragment and pyrazine nucleus, were introduced in the structure of MC113. The *O*-butyl spacer resulted in an oxa-homologous derivative **67**, which displayed good potency toward the target protein. Further, aiming to investigate the role of flexibility, conformationally constrained analogues were designed, applying the anelation strategy, resulting in the chromene derivative **68**. This compound was significantly less potent than the parent compound **67**, and was inactive toward MRP1 (Fig. 23). These results indicated that the flexibility could be a requirement to improve P-gp activity and the conformational restriction imposed for compound **68** impairs the recognition by the target protein.

A successful application of ring closure strategy can be exemplified by the discovery of frovatriptan (**71**). This drug was designed by molecular modification on the structure of 5-carboxamidotriptamine (**69**), an analogue of the natural agonist of serotonin receptors. This compound presented soft lability to metabolic oxidation catalyzed by monoaminoxidases, and showed low selectivity against the different isoforms of 5-hydroxytryptamine (5-HT) receptors. Therefore, a lead optimization step was realized and planned based on the application of ring closure procedure, resulting in compound BRL-56905 (**70**).[39] This compound

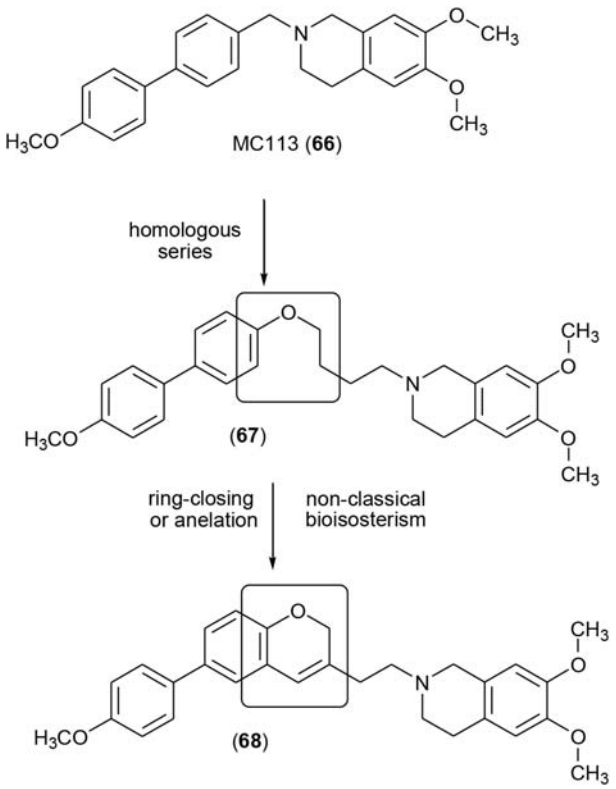

Fig. 23 Structures of MC113, the homologous **67**, and the conformationally constrained analogue **68**.

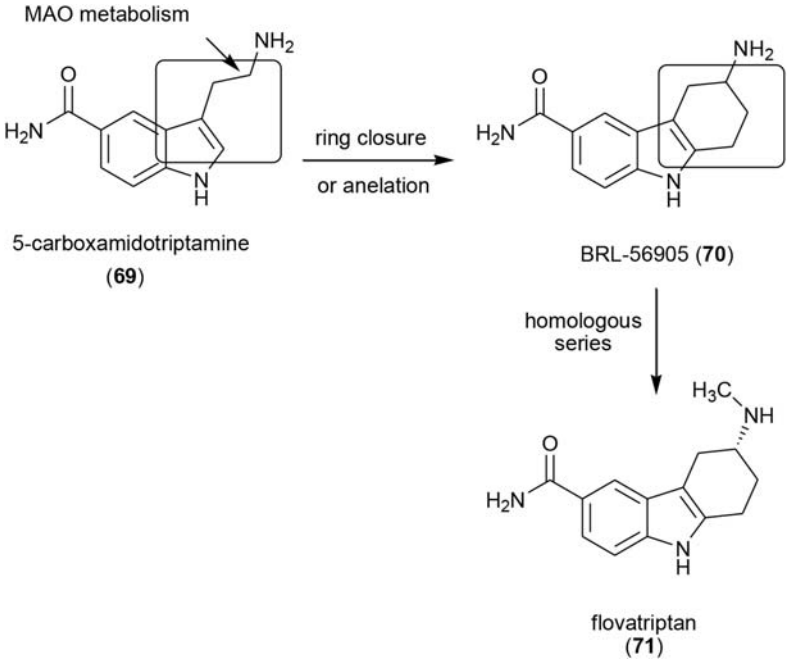

Fig. 24 Genesis of flovatriptan (**71**) and BRL-56905 (**70**) by application of ring closure strategy in the structure of the prototype 5-carboxamidotriptamine (**69**).

presented higher affinity to the 5-HT_{1A} receptors than to the 5-HT_{1D}, and showed remarkable selectivity when compared to the initial prototype **69**. Its metabolic stability was optimized after the introduction of methyl group linked to the amine subunit, resulting in the structure of flovatriptan (**71**), indicated for the treatment of migraine (Fig. 24).

Searching for selective agonists of dopaminergic receptors subtype 2 (D_2), useful in the treatment of Parkinson's disease, schizophrenia and other psychiatric illnesses, compound **72** containing a metabolically labile phenol function, was structurally modified in order to improve its PK profile. Therefore, the tricyclic compounds **73** and **74** were designed by ring closure strategy, eliminating the site of conjugation with phase II metabolizing enzymes, but keeping the heteroatom with unpaired electron, able to be recognized by the target receptor through H-bond interactions. These cyclic analogues presented affinity for D2 receptors and were active by in vivo administration, characterizing themselves as novel nonclassic bioisosteres of OH-phenol (Fig. 25).[40]

The conformational restriction induced by a ring closure procedure is one of the useful approaches to guide biologically active conformations. However, if the restricted structure does not reach the bioactive conformation, the ring closure strategy will result in inactive compounds. To solve that problem, the opposite strategy, namely ring opening, can be employed, restoring the necessary flexibility to interact with bioreceptors in an adequate conformation.

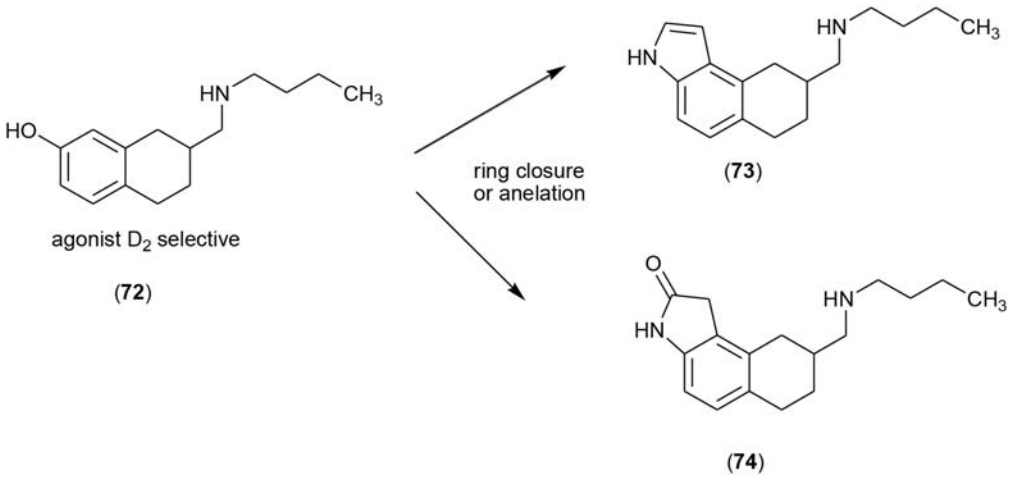

Fig. 25 Structure of the phenol derivative **72** and its bioisosteres **73** and **74.**

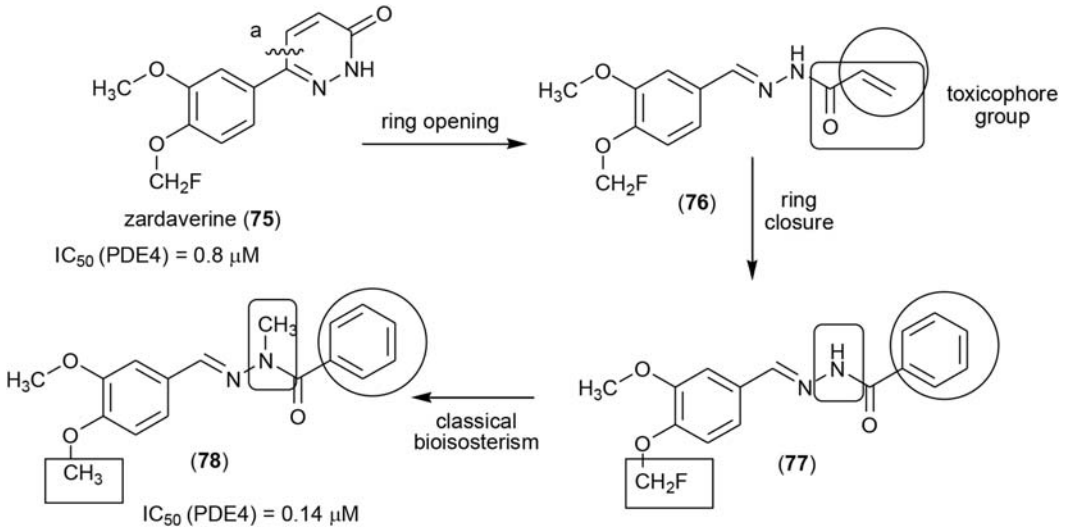

Fig. 26 New PDE4 inhibitor designed from molecular modifications on structure of zardaverine.

Looking for new drug candidate to treat asthma, Kummerle and coworkers[41] selected zardaverine (75) as a prototype for molecular modification. This conformationally restricted prototype was modified applying the principle of ring opening strategy, resulting in the cleavage of the pyridazinone ring (Fig. 26). The opened structure **76** was modified in order to eliminate the toxicophoric profile of α,β-unsaturated carbonyl subunit. Further modifications based on classical bioisosteric replacements resulted in the identification of compound **78**, which was more potent than zardaverine in the inhibition of PDE4.

The analysis of the possible conformers of compound **78** revealed three main conformational possibilities represented by conformers **78a**, **78b**, and **78c**. They differ from the relative orientation between C═O and N−CH_3 and CH═N and NCH_3, as depicted in Fig. 27. Docking studies indicated that conformers **78a**, **78b**, and **78c** are almost isoenergetic and could result in stable complex with the target protein (i.e., PDE4). Aiming to define the bioactive conformation, the authors proposed the design of restricted analogues of conformers **78a** and **78b**, freezing the conformations identified by in silico approach. As illustrated in

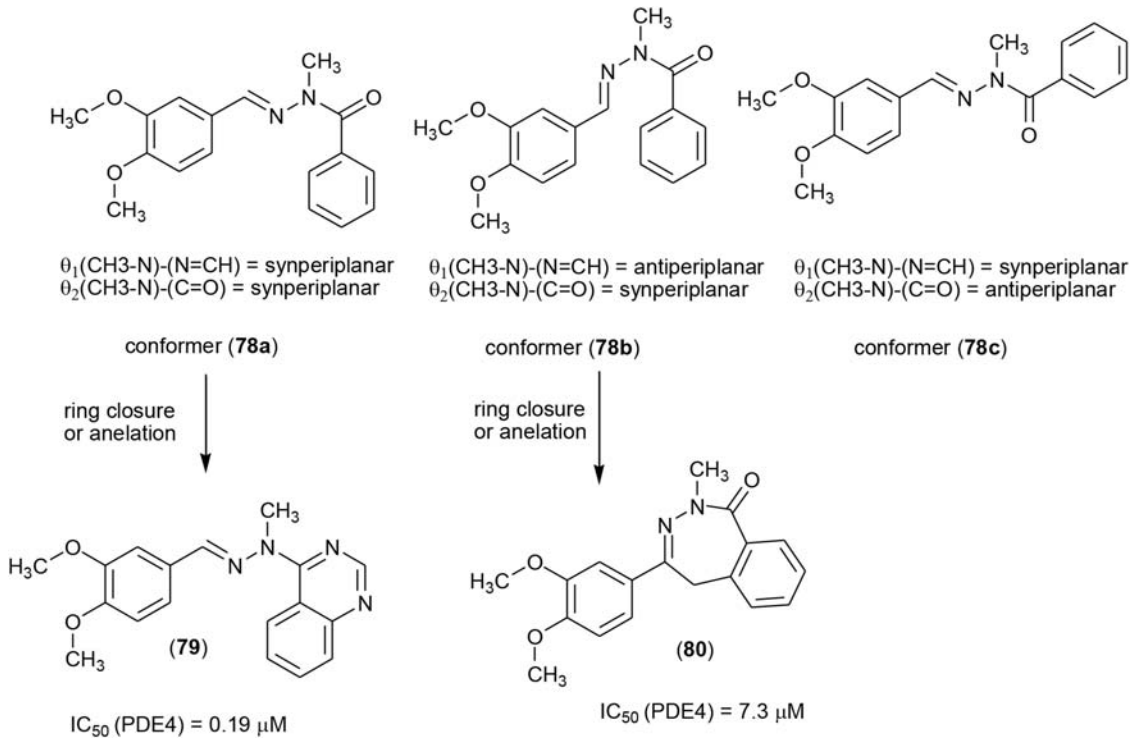

Fig. 27 Design of conformationally restricted analogues **79** and **80** inspired in the different conformers of compound **78.**

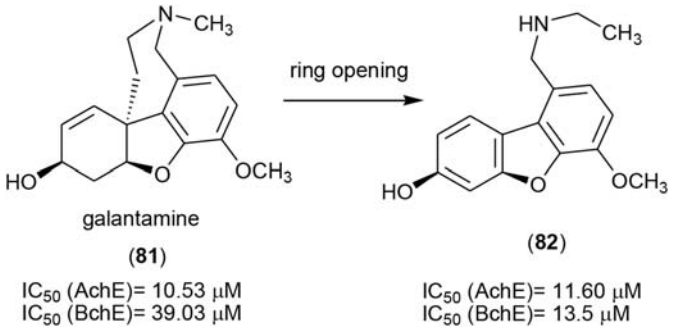

Fig. 28 Nonclassical bioisostere of galantamine (**81**) by opening ring strategy (**82**).

Fig. 27, the frozen analogues **79** and **80** showed different potency in inhibit PDE4 activity, being the quinazoline **79**, 38-fold more potent than benzodiazepinone **80**. These results suggest that the biologically active conformation should be the one represented by conformers **78a**.[41]

Galantamine (**81**) is a natural acetilchoniesterase inhibitor approved drug to treat AD, which is also an allosteric modulator of nicotinic receptors. Based on the hypothesis that the benzofuran fragment and the nitrogen atom of amine group are the pharmacophores responsible for galantamine activity, while the other parts of the structure are auxophoric units, Fang and coworkers[42] proposed the simplification of complex congested quaternary carbon followed by a ring opening strategy on the seven-member azepine ring, generating acyclic amine galantamine analogue **82** (Fig. 28). This compound, having a higher degree of conformational freedom in the amine side chain, was demonstrated to be equipotent to the parent drug.

1.07.7 Classical Bioisosterism

Searching for PDE4D selective inhibitors that could exert pro-cognitive effects with reduced emetic potential, Brullo and coworkers[43] investigated the role of classical bioisosteric replacement of the 3-methoxy group with a 3-difluoromethoxy unit in the PDE4D inhibition activity, and realized the comparison between their blood brain barrier crossing ability (Fig. 29). Authors demonstrated that the 3-difluoromethoxy isostere was the best compound in terms of selectivity and safety, despite having a lower PDE4D inhibitory activity. This isostere (**84**) also enhanced the intracellular cyclic adenosine monophosphate levels more than its nonfluorinated analogue **83**, suggesting that due to the fluorine substitution, it can better cross the cell membrane. This hypothesis was confirmed by preliminary tests, which demonstrated that 3-difluoromethoxy isostere **84** showed a better BBB penetration, its brain/plasma ratio being 20% higher in comparison with its nonfluorinated analogue **83**.

An interesting example of divalent classical bioisosterism between **CH_2/O** was reported in a series of carboxylic acid lipophilic derivatives that work as partial agonists over the PGI_2 receptor (IP2), which are effective as antiplatelet agent. The series originated with the discovery of octimibate (**85**) that was structurally modified to generate compound **86**. This compound was subject of further optimization allowing the identification of the bioisosteres **87** and **88** (BMY-42393), a molecule optimized as a partial IP2 agonist (Fig. 30).[44,45]

The use of this type of bioisosterism has been successfully employed when the cyclic oxygen atom of prostacyclin (PGI_2; **89**), involved in the enol ether function, responsible for the extreme chemical lability of this icosanoid, was substituted by a methylene group providing a stable bioisostere active as agonist of prostacyclin receptors. Further modifications, at ω-side chain of eicosanoid skeleton, resulted in the discovery of iloprost (**90**) (Fig. 31). Cicaprost (**91**) is a me-too drug designed by bioisoteric replacement of **CH_2** by **O**. This exchange in C-3 of α-side chain of cicaprost (**91**) was planned aiming to prevent β-oxidation, an usual metabolic reaction involved in the inactivation of prostanoids and their analogues (Fig. 31).[45,46]

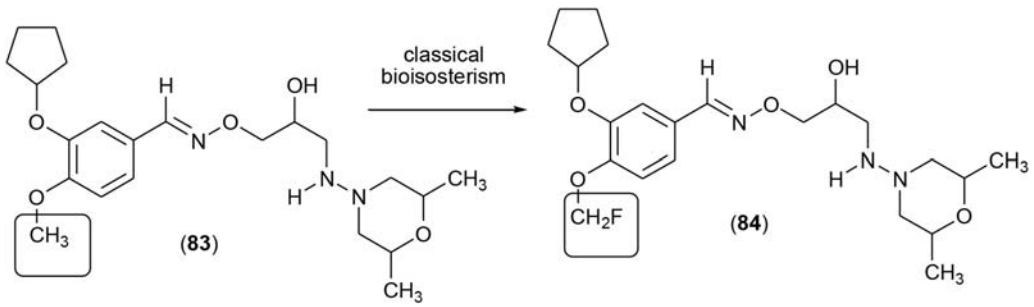

Fig. 29 Structures of classical bioisosteres containing the 3-methoxy versus 3-difluoromethoxy isosterism.

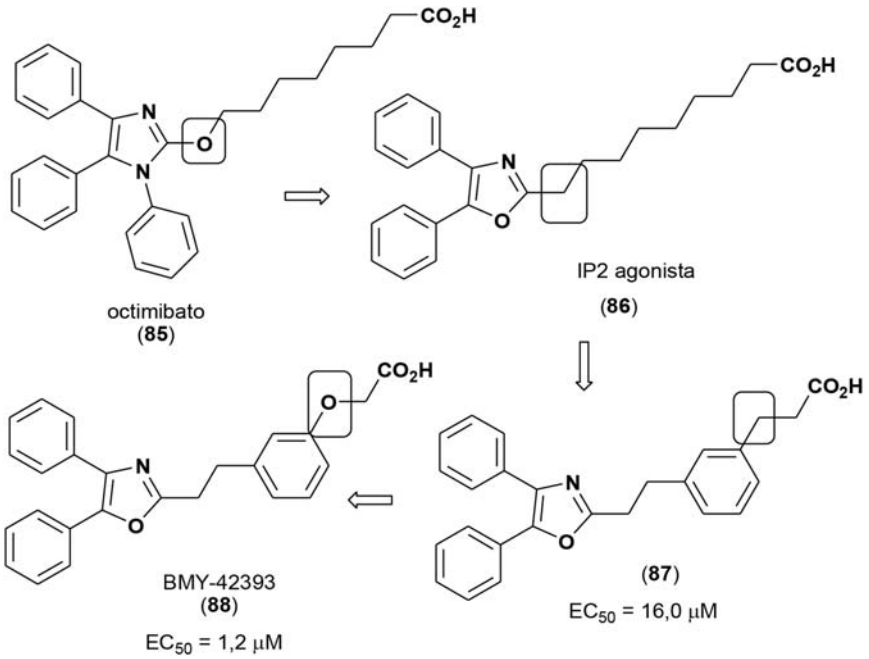

Fig. 30 Classic bioisosterism of divalent group CH_2/O.

Regarding the classical bioisoster of the divalent group, Faustino and coworkers[47] described the characterization of the structure and properties of 6-selenoguanine (**93**), and studied the impact of its introduction in DNA. The 6-selenoguanine was obtained by the isosteric replacement of oxygen atom of carbonyl function presented in guanine (**92**) by a selenium atom (Fig. 32). This seleno-derivative showed promising nanotechnological properties and a unique capability to modulate the equilibrium between different forms of DNA, opening interesting possibilities in antigene-based therapies.

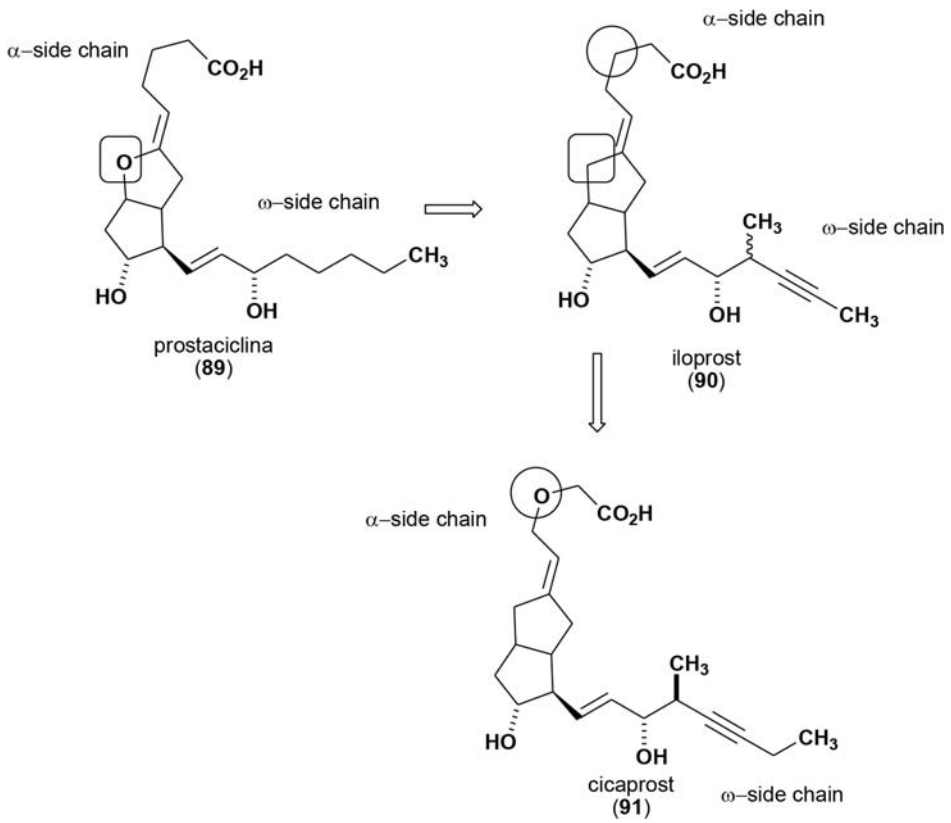

Fig. 31 Classic functional bioisosterism —O—/—CH_2— in prostanoids and analogues.

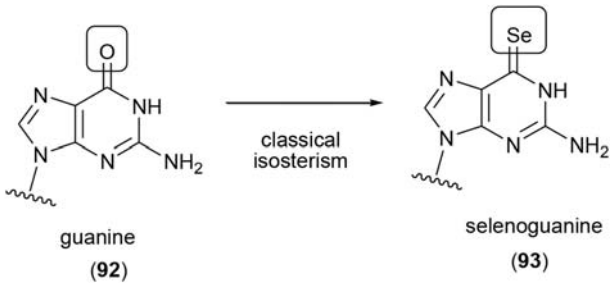

Fig. 32 Structures of the nucleobases guanine (**92**) and its classical isostere selenoguanine (**93**).

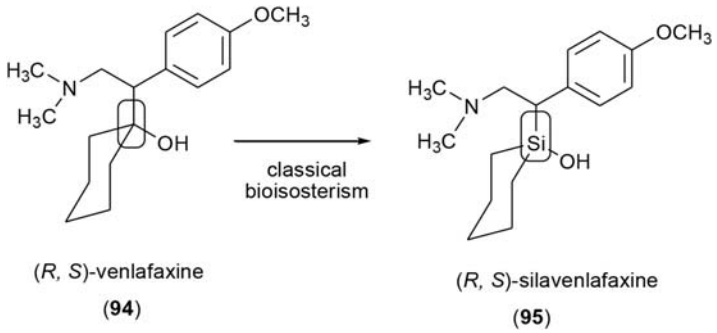

Fig. 33 Structures of (*R,S*)-venlafaxine (**94**) and its classical bioisoster (*R,S*)-silavenlafaxine (**95**).

Considering the classical bioisosterism of tetravalent groups, the isosteric replacement of carbon atom by silicon has gained prominence in the literature. Among the benefits of silicon in medicinal chemistry, the possibility to create a novel chemical space favoring intellectual properties opportunity is remarkable. Furthermore, the replacement of **C** by **Si** can modify in vitro potency and selectivity, alter rate of metabolism, improve in vivo half-life, enhance tissue distribution, and so on.[48] Several silicon bioisosteres of classical drugs have been developed. Daiss and coworkers[49] reported the impact of sila-substitution on the activities of the venlafaxine enantiomers, a potent and selective serotonin reuptake inhibitor (SSRI). The replacement of quaternary carbon of venlafaxine (**94**) by a silicon atom resulted in the respective silavenlafaxine isostere (**95**) (Fig. 33). The comparison between the pharmacological activities of venlafaxine enantiomers and its sila-isostere showed a great difference in their selectivity profile in inhibiting serotonin reuptake and/or noradrenaline and dopamine transporter.

The **C** versus **Si** isosterism was also applied in order to obtain a new active haloperidol analogue. Haloperidol (**96**) is an antipsychotic drug developed by Paul Janssen, which mechanism of action involves blockage of dopamine (D2) receptors in the brain. Therefore, the sila-haloperidol (**97**) was designed, synthesized, and evaluated against recombinant human dopamine receptors (D1, D2, D4, and D5), using radioligand binding experiments. The **C**/**Si** bioisosteres displayed similar potency at D1, D4, and D5 receptors. However, sila-haloperidol (**97**) was 4.7-fold more potent at D2 receptor than haloperidol (**96**) (Fig. 34). Moreover, sila-analogue (**97**) was speculated to be safer than haloperidol, since silicon–carbon double bond is not stable under physiologic conditions and therefore, cannot undergo water elimination to form sila-HPTP (**100**). HPTP (**98**) is considered a key intermediate in the bioactivation of haloperidol (**96**) in the pyridinium-type metabolite (HPP^+, **99**) that has been implicated in the irreversible Parkinsonism-like side effects induced by haloperidol (Fig. 34).[50]

1.07.8 Ring Bioisosterism

Fig. 35 shows classic aromatic ring bioisosterism from the phenyl ring, with 6 electrons π, circled by equivalent isosteric systems represented by several rings of six or five atoms, such as pyridine, pyrazine, pyrimidine, pyrrol, pyrazol, imidazole, thiazole, oxazole, thiophene, furan, and so on. Surrounding this circle are depicted isosteric rings with 10 π, electrons including naphthyl, quinolyl, quinoxalyl, etc. Tricyclic, linear, or angular systems, with 14 π, electrons complete the brief of possible equivalent rings that could be used applying the ring bioisosterism strategy.

Related to the indole system (**A**),[51] illustrated in Fig. 36, it is possible to identify based on the ring bioisosterism, eight equivalent rings (**B–I**) that fulfill the principle of isosterism and, therefore, could be used in an interchangeable way.

Among the myriad of interchangeable rings based on classical isosterism, five-membered heterocycles are noteworthy (Fig. 37). As mentioned in the selected examples previously mentioned, these heterocycles can be considered isosteres of amide and ester moieties with greater metabolic stability. However, for scaffold hopping or lead optimization, special attention should be paid

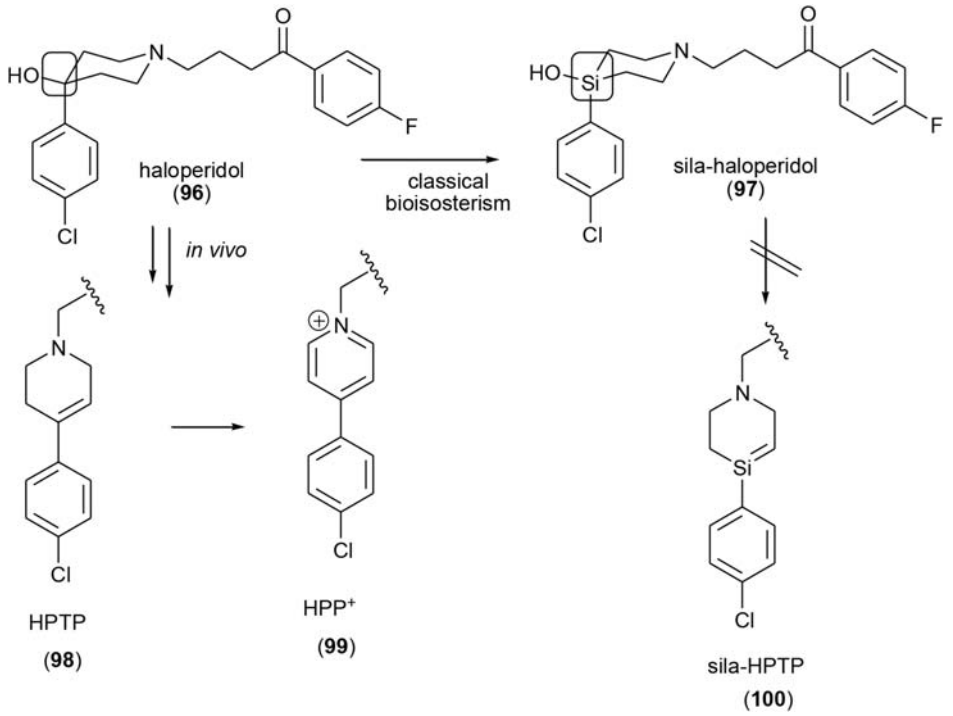

Fig. 34 Structures of haloperidol (**96**) and its sila-bioisostere **97**. Indication of the formation of toxic metabolite HPP^+ from the intermediate HPTP and the inability to form similar intermediate (i.e., sila-HPTP) from the sila-haloperidol isostere.

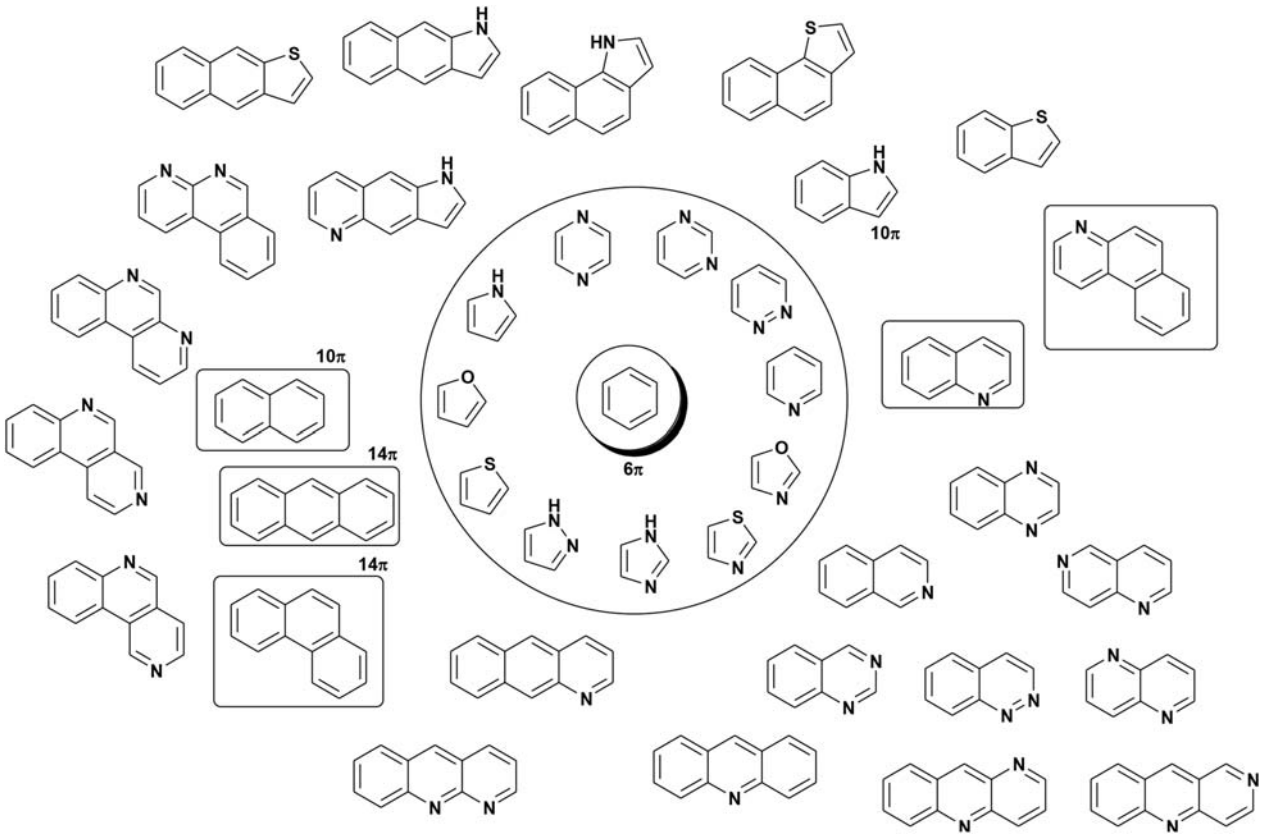

Fig. 35 Classic aromatic ring isosteres.

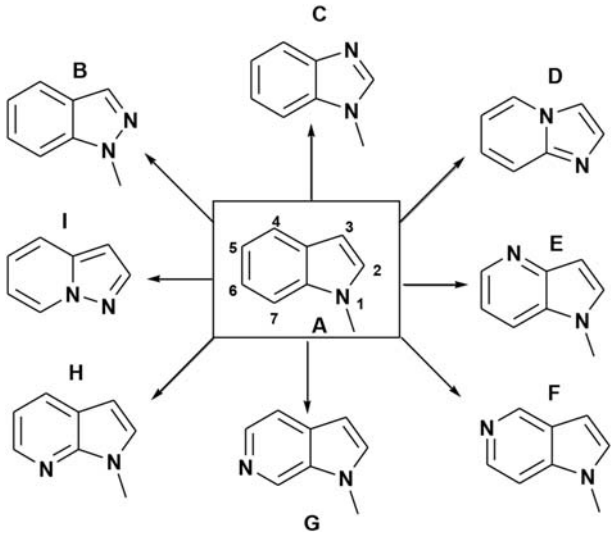

Fig. 36 Indole ring isosteres (**A**).

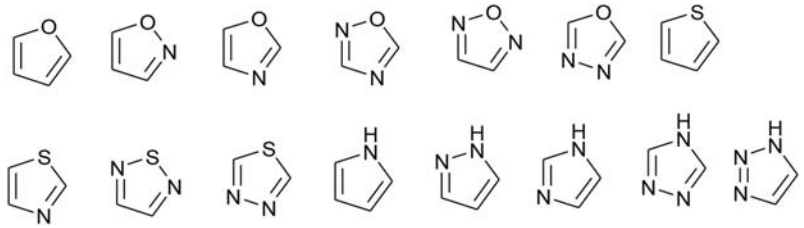

Fig. 37 Examples of five-member ring bioisosteres.

to the unique properties of S-containing heterocycles. It is important to keep in mind that the replacement of O by S atom in a heterocycle will not necessarily result in a bioisosterically equivalent compound. A nice example can be demonstrated by the attempt to replace 1,3-thiazole ring by 1,3-oxazole nucleus aiming to identify new VEGFR2 (vascular endothelial growth factor receptor subtype 2) inhibitors (Fig. 38). Authors demonstrated that the ability of the S atom to engage in donating $n_o \rightarrow \sigma^*$ interaction with the lone pairs of neighboring heteroatoms can lead to conformational and steric effects that are unique of S-containing heterocycles, restraining the capability to identify bioisosteric equivalents.[52]

Ring bioisosterism was used by Francisco and coworkers[53] in an attempt to identify new structural analogues of rimonabant, an antagonist of cannabinoid receptors, approved for obesity control, and withdrawn by Sanofi–Aventis in Jan. 2009. Authors proposed the isosteric replacement of pyrazole ring by 1,3-thiazole and 1,2,4-triazole systems (Fig. 39).[54,55]

An special example of ring bioisosterism was first described by Edwards and coworkers,[56] who described the discovery of ferrocenyl-penicillins and ferrocenyl-cephalosporins designed by replacement of phenyl ring by ferrocene organometallic system. Based on this initial work, and on the demonstration that ferrocene group possesses aromatic properties, and also considering the cytotoxic activity of the ferrocenium cation (Fc+•), which is easily formed by oxidation in biological media, Top and

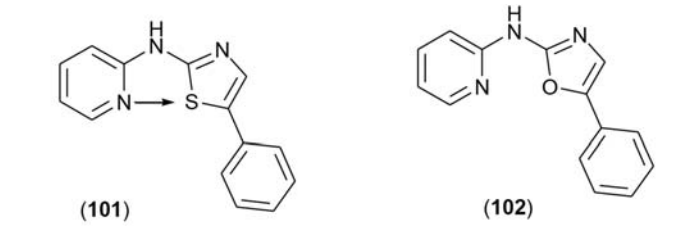

Fig. 38 Structures and IC_{50} values of thiazole versus oxazole isosteres against VEGFR-2, demonstrating the stabilizing of N → S interaction that cannot mimic by the oxazole ring.

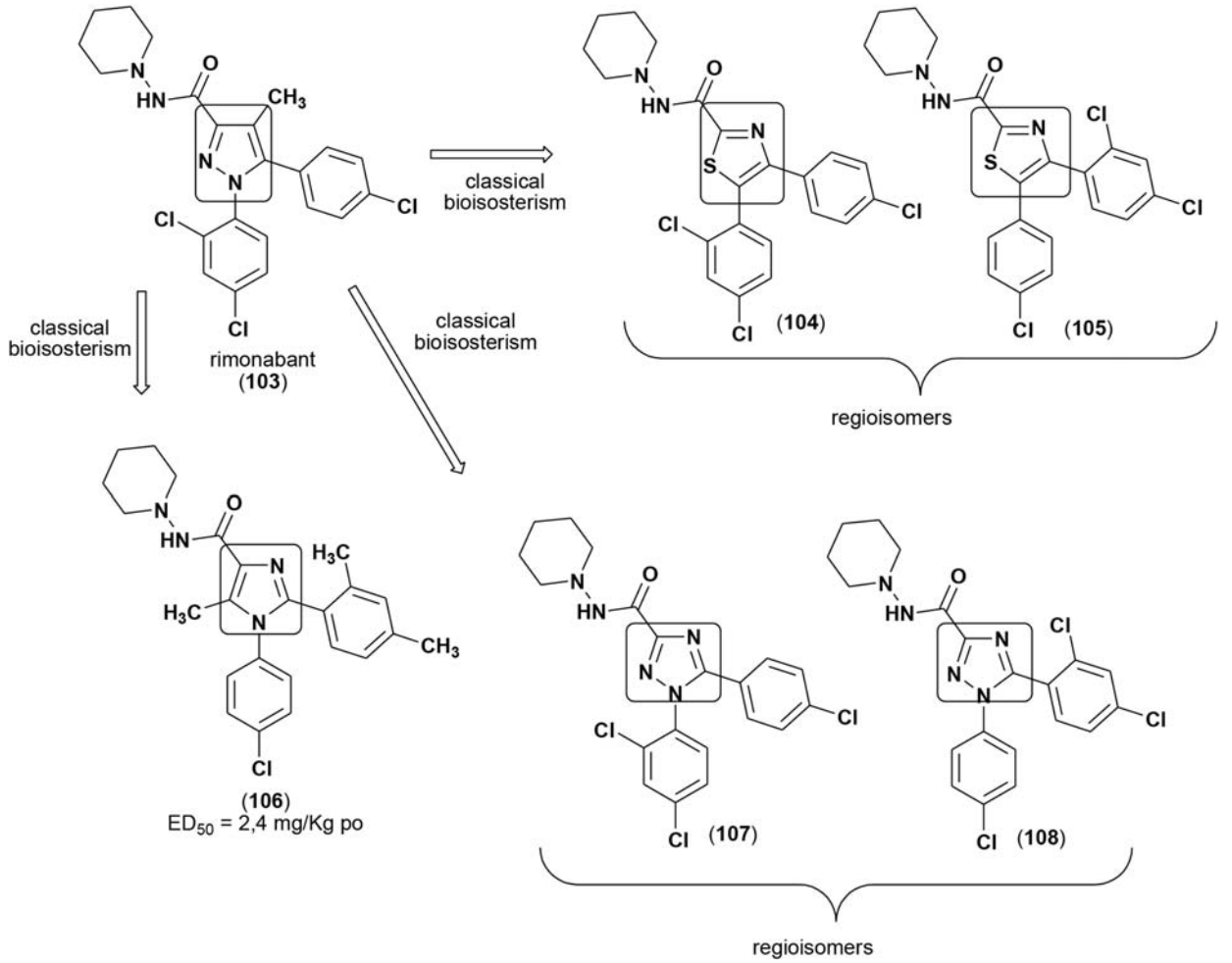

Fig. 39 Five ring bioisosteres with CB_1 antagonist properties.

coworkers[57] proposed the replacement of phenyl ring, presented in tamoxifen (**109**) and its active metabolite (i.e., endoxifen, **110**), by an aromatic ferrocenyl substituent (Fig. 40). This approach resulted in the discovery of ferrocifen (**111**), a new selective estrogen receptor modulator with similar antitumor activity as tamoxifen.

More recently, the same type of ring isosterism was explored in an attempt to optimize the antimicrobial activity of bisacodyl (**112**), a drug originally used as a laxative agent. From this molecular modification strategy, a series of bisacodyl-ferrocene (e.g., **113**) were designed and prepared, being identified as compounds with optimized antimicrobial activity (Fig. 41).[58]

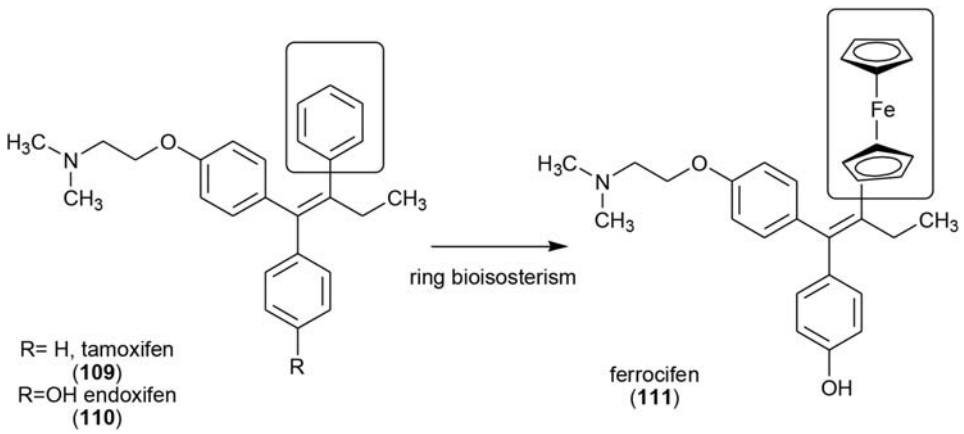

Fig. 40 Ring bioisosterism between tamoxifen (**109**), endoxifen (**110**), and ferrocifen (**111**).

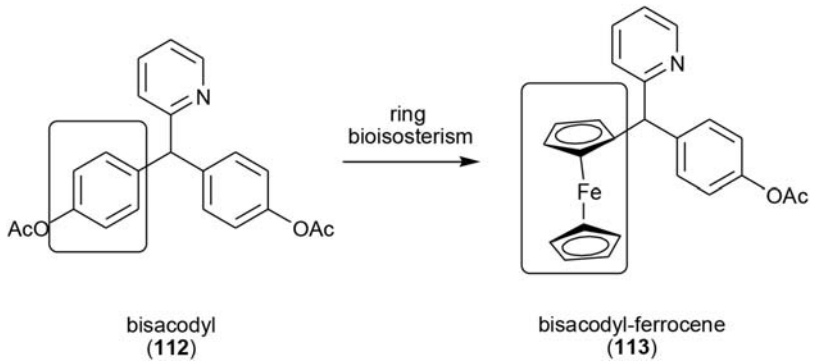

Fig. 41 Ring bioisosterism between bisacodyl (**112**) and its ferrocene analogue **113.**

Ring bisosterism is the most popular molecular modification strategy used by researchers in pharmaceutical industry and academia to discover new me-too drugs. Many examples could be used to fulfill this statement. Nevertheless, just a few examples will be discussed in this article.

Piroxicam (**114**) can be considered the prototype of first-generation nonsteroidal antiinflammatory drug belonging to oxicam class. The replacement of phenyl ring by a thiophene system resulted in the discovery of tenoxicam (**115**), while the same ring bioisosterism strategy applied on the pyridine moiety of pyroxicam resulted in the identification of isoxicam (**116**, Fig. 42).[59,60]

Regarding the class of phosphodiesterase 5 (PDE5) inhibitors, sildenafil (**117**), approved for the treatment of erectile dysfunction, is the innovative drug that was used as prototype for molecular modification resulting in me-too drugs, such as vardenafil (**118**). The 1*H*-pyrazolo[4,3-*d*]pyrimidin-5-yl nucleus presented in sildenafil (**117**) had demonstrated to be a classical bioisoster of 3,5,6,8-tetrazabicyclo[4.3.0]nona-3,7,9-trien-2-one ring in **118** (Fig. 43).[61] It should be pointed out that moving the nitrogen atom in vardenafil (**118**) permits an interaction with the enzyme that is not present in sildenafil (**117**). This contributes to the improved potency of vardenafil.

Fluoxetine (**119**) is a SSRI that represents an innovative drug to treat major depressive disorder and obsessive–compulsive disorder. Applying two consecutive bioisosteric replacements, based on the exchange of phenyl ring by a naphtyl subunit and by a thiophene moiety, duloxetine (**120**) was discovered (Fig. 44).[62] This me-too drug has the same therapeutic indication as fluoxetine.

The structural similarity existing between COX-2 inhibitors, celecoxib (**121**) and etoricoxib (**122**), is detected in the light of bioisosterism. Comparing both structures easily identified the presence of a terphenyl type system, formed by a central heterocyclic ring, such as a pyrazole in celecoxib and a pyridine in etoricoxibe. Exchange between phenyl unit and pyridine ring represents the

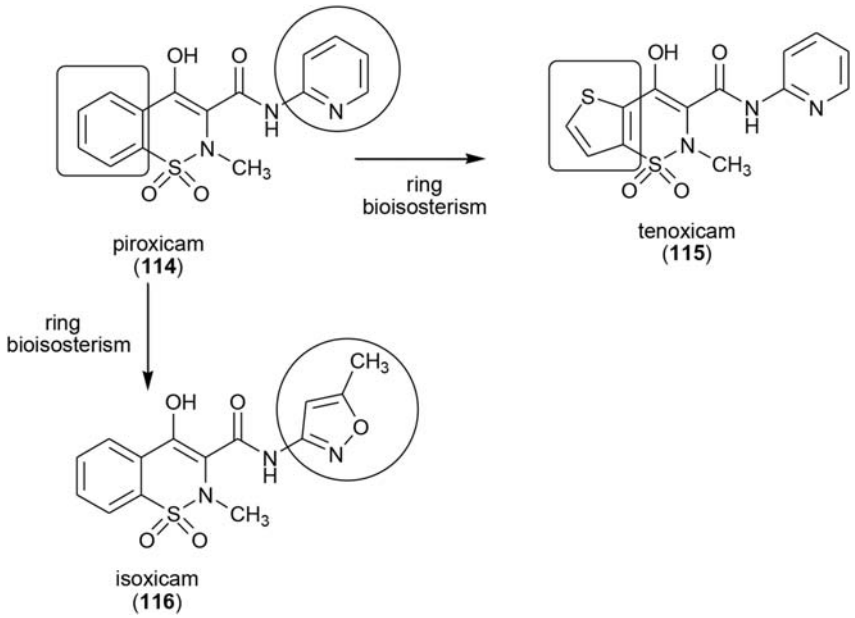

Fig. 42 Bioisosterism of rings and discovery of me-too antiinflammatory of the oxicam class: piroxicam (**114**), tenoxicam (**115**), and isoxicam (**116**).

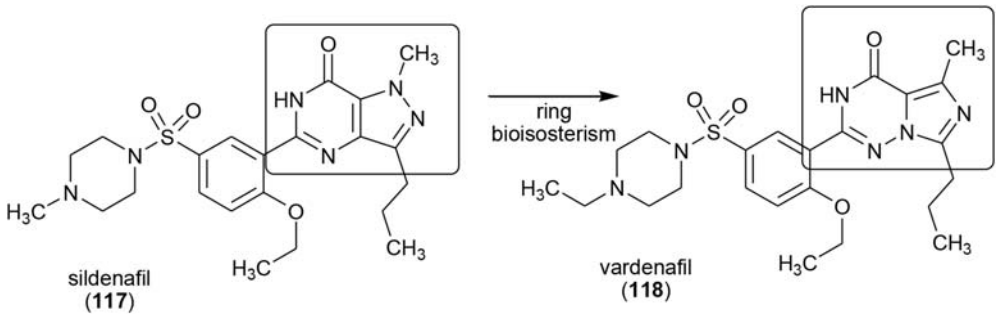

Fig. 43 Ring bioisosterism between sildenafil (**117**) and vardenafil (**118**).

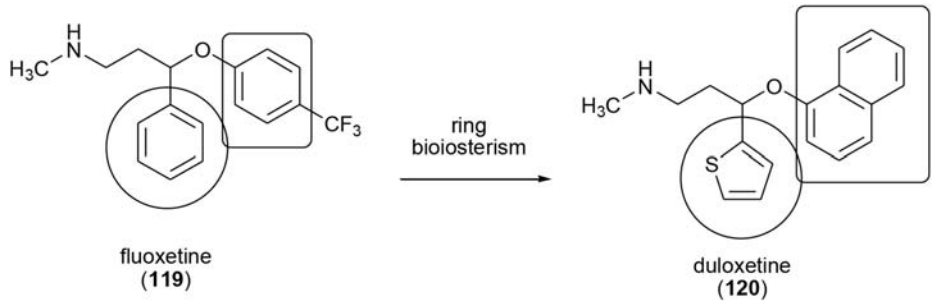

Fig. 44 Ring bioisosterism between fluoxetine (**119**) and duloxetine (**120**).

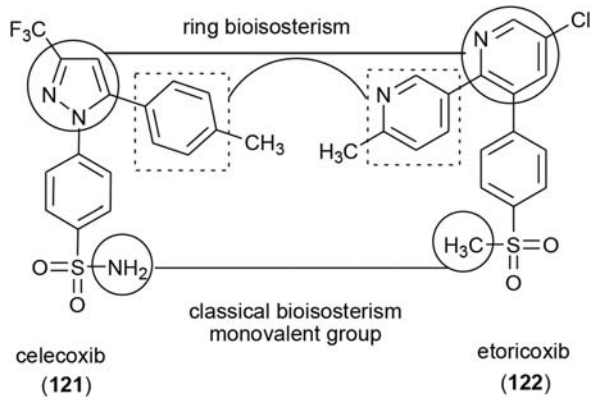

Fig. 45 Bioisosteric relationships between selective COX-2 inhibitors celecoxib (**121**) and etoricoxib (122).

second molecular modification introduced in celecoxib structure based on ring bioisosterism. The replacement of the CH_3 group by a NH_2, both monovalent groups, allowed the design of methylsulfone subunit from a sulfonamide fragment. Therefore, etoricoxib (**122**) can be considered a me-too antiinflammatory drug planned by three consecutive application of classical bioisosterism (Fig. 45).[63]

1.07.9 Final Remarks

The use of *bioisosterism*, as illustrated so far in this article, is an important tool in *Medicinal Chemistry* in order to design new compounds by the application of ligand-based drug design or even structure-based drug design strategies. It is also an amazing approach to optimize the pharmadynamic or PK properties of a previous hit or lead compound. Many researchers in academia and mainly in pharmaceutical companies use bioisosterism as a key strategy to construct a congeneric series, to enlarge chemical space, and to circumvent intellectual property issues.

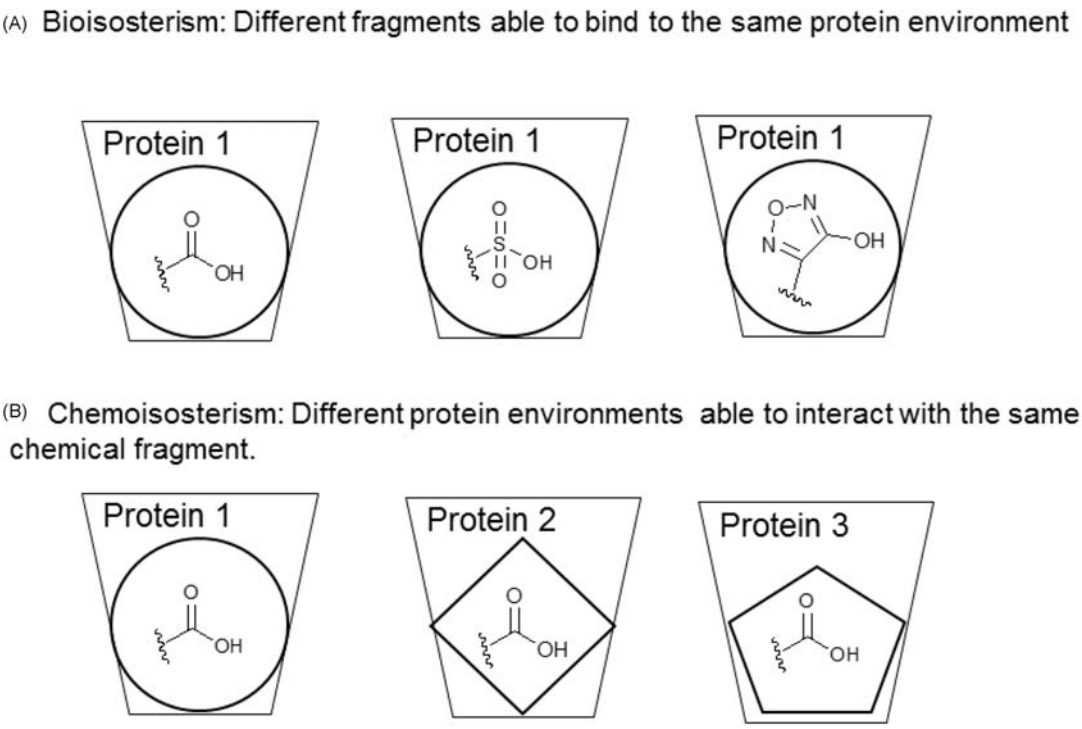

Fig. 46 Schematic definition of bioisosterism (A) and chemoisosterism (B). Adapted from Jalencas, X., Mestres, J. J. *Chem. Inf. Model.* **2013**, *53*, 279; Jalencas, X., Mestres, J. *Med. Chem. Commun.* **2013**, *4*, 80.

As previously mentioned, any bioisosteric replacement must consider steric or size attributes, electronic features, solubility, and hydrophobic effects. Therefore, many theoretical descriptors can be used to characterize properties of groups or fragments or subunits considered interchangeables, indicating if these groups are or not appropriate for a bioisosteric replacement.

Although it is possible to use two dimensional descriptors and chemical intuition to guide bioisosteric replacement, the use of in silico approaches is becoming more common. These approaches can use QSAR strategies, pharmacophore searching, and databases for bioisosteres. Several molecular representations and similarity metrics are available to help the identification of three-dimensional molecular similarities, using measures of 3D shape and electrostatic distribution, facilitating the search for new bioisosteric relationships.[10,64–67]

It is noteworthy that bioisosterism looks at the interaction between chemical fragments or subunits or functional groups and protein environments from the perspective of the latter. However, the assumption that binding sites of different proteins can share a high degree of electronic and steric similarities, easily detected between members of the same protein family, was responsible for the emergence of the concept of chemoisosterism. Chemoisosterism is defined as the property by which different protein environments, sharing similar cavity shapes and features, can tolerate the interaction with the same chemical fragment. Therefore, the understanding of the degree of chemoisosterism among protein environments can help medicinal chemists to make assumptions about potential cross-pharmacology between different protein targets, as well as into the selectivity of bioactive small molecules and its further implications to toxicity and adverse reactions.[68,69] The schematic comparative definition of bioisosterism and chemoisosterism can be easily comprehended by the illustration exemplified in Fig. 46. Combination of both concepts can help medicinal chemists not only to diversify the chemical space for a specific target, but also to anticipate on-target and off-target effects for a specific bioisosteric fragments.

The bioisosterism is a very useful technique used in scaffold hopping strategy,[70] assisting the medicinal chemists to design and discover structurally novel compounds, starting from lead molecules by modifying the molecular backbone of the template, and increasing the chemical space of new chemical entity candidates.

See also: 2.05. Privileged Structures and Motifs (Synthetic and Natural Scaffolds).

References

1. Langmuir, I. J. Isomorphism, Isosterism and Covalence. *Am. Chem. Soc.* **1919,** *41*, 1543.
2. Thornber, C. W. Isosterism and molecular modification in drug design. *Chem. Soc. Rev.* **1979,** *8*, 563.
3. Lipinski, C. A. Bioisosterism in drug design. *Annu. Rep. Med. Chem.* **1986,** *21*, 283.

4. Patani, G. A.; LaVoie, E. J. Bioisosterism: A Rational Approach in Drug Design. *Chem. Rev.* **1996,** *96,* 3147.
5. Lima, L. M.; Barreiro, E. J. Bioisosterism: a useful strategy for molecular modification and drug design. *Curr. Med. Chem.* **2005,** *12,* 23.
6. Burger, A. Isosterism and bioisosterism in drug design. *Prog. Drug Res.* **1991,** *37,* 287.
7. Olesen, P. H. The use of bioisosteric groups in lead optimization. *Curr. Opin. Drug Discov. Devel.* **2001,** *4,* 471.
8. Langdon, S. R.; Ertl, P.; Brown, N. Bioisosteric replacement and scaffold hopping in lead generation and optimization. *Mol. Inf.* **2010,** *29,* 366.
9. Meanwell, N. A. Synopsis of some recent tactical application of bioisosteres in drug design. *J. Med. Chem.* **2011,** *54,* 2529.
10. Brown, N. *Bioisosteres in Medicinal Chemistry;* Weinheim: Wiley-VCH Verlag, 2012.
11. Friedman, H. L. First Symposium on Chemical–biological Correlation, May 26–27, 1950, NAS-NRS Publication No. 206, Washington, D.C., 1951, pp. 295–362.
12. Grimm, H. G. Structure and Size of the Non-metallic Hydrides. *Zeitsc. Elektrochem.* **1925,** *31,* 474.
13. Erlenmeyer, H.; Leo, M. Über Pseudoatome. *Helv. Chim. Acta* **1932,** *15,* 1171.
14. Burger, A. *A Guide to the Chemical Basis of Drug Design;* Wiley: New York, 1983.
15. Burger, A. *Medicinal Chemistry,* 3rd ed.; Wiley: New York, 1970. p.127.
16. Fischer, J.; Ganellin, C. R. *Analogue-Based Drug Discovery;* Wiley-VCH Verlag GmbH & Co: Weinheim, 2006.
17. Gauthier, J. Y.; Chauret, N.; Cromlish, W.; Desmarais, S.; Duong, L. T.; Falgueyret, J.-P.; Kimmel, D. B.; Lamontagne, S.; Léger, S.; LeRiche, T.; Li, C. S.; Massé, F.; McKay, D. J.; Nicoll-Griffith, D. A.; Oballa, R. M.; Palmer, J. T.; Percival, M. D.; Riendeau, D.; Robichaud, J.; Rodan, G. A.; Rodan, S. B.; et al. The discovery of odanacatib (MK-0822), a selective inhibitor of cathepsin K. *Bioorg. Med. Chem. Lett.* **2008,** *18,* 923.
18. Larsen, A. A.; Lish, P. M. A New Bio-isostere : Alkylsulphonamidophenethanolamines. *Nature* **1964,** *203,* 1283.
19. Lin, P.; Marino, P. D.; Lo, J.-L.; Yang, Y. T.; Cheng, K.; Smith, R. G.; Fisher, M. H.; Wyvratt, M. J.; Goulet, M. T. 2-(3,5-Dimethylphenyl)tryptamine Derivatives that Bind to the GnRH Receptor. *Bioorg. Med. Chem. Lett.* **2001,** *11,* 1073.
20. Nicolaou, I.; Zika, C.; Demopoulos, V. J. [1-(3,5-difluoro-4-hydroxyphenyl)-1H-pyrrol-3-yl]phenylmethanone as a bioisostere of a carboxylic acid aldose reductase inhibitor. *J. Med. Chem.* **2004,** *47,* 2706.
21. Papastavrou, N.; Chatzopoulou, M.; Pegklidou, K.; Nicolaou, I. 1-Hydroxypyrazole as a bioisostere of the acetic acid moiety in a series of aldose reductase inhibitors. *Bioorg. Med. Chem.* **2013,** *21,* 4951.
22. Lolli, M. L.; Giordano, C.; Pickerin, D. S.; Rolando, B.; Hansen, K. B.; Foti, A.; Contreras-Sanz, A.; Amir, A.; Fruttero, R.; Gasco, A.; Nielsen, B.; Johansen, T. N. 4-hydroxy-1,2,5-oxadiazol-3-yl moiety as bioisoster of the carboxy function. Synthesis, ionization constants, and molecular pharmacological characterization at ionotropic glutamate receptors of compounds related to glutamate and its homologues. *J. Med. Chem.* **2010,** *53,* 4110.
23. Macchiarulo, A.; Pellicciari, R. Exploring the other side of biologically relevant chemical space: insights into carboxylic, sulfonic and phosphonic acid bioisosteric relationships. *J. Mol. Graphics Modell.* **2007,** *26,* 728.
24. Tosco, P.; Lolli, M. L. Hydroxy-1,2,5-oxadiazolyl moiety as bioisoster of the carboxy function. A computational study on gamma-aminobutyric acid (GABA) related compounds. *J. Mol. Model* **2008,** *14,* 279.
25. Koller, A. N.; Bozilovic, J.; Engels, J. W.; Gohlke, H. Aromatic N versus aromatic F: bioisosterism discovered in RNA base pairing interactions leads to a novel class of universal base analogs. *Nucleic Acids Res.* **2010,** *38,* 3133.
26. Sheng, C.; Che, X.; Wang, W.; Wang, S.; Cao, Y.; Miao, Z.; Yao, J.; Zhang, W. Design and synthesis of novel triazole antifungal derivatives by structure-based bioisosterism. *Eur. J. Med. Chem.* **2011,** *46,* 5276.
27. Dmitriev, M. E.; Ragulin, V. V. Synthesis of phosphorus isosters of β-amyloid peptides fragment. *Russ. J. Gen. Chem.* **2015,** *85,* 2091.
28. De Risi, C.; Ferraro, L.; Pollini, G. P.; Tanganelli, S.; Valente, F.; Veronese, A. C. Efficient synthesis and biological evaluation of two modafinil analogues. *Bioorg. Med. Chem.* **2008,** *16,* 9904.
29. Kier, L. B.; Hall, L. H. Bioisosterism: quantitation of structure and property effects. *Chem. Biodivers.* **2004,** *1,* 138.
30. Kim, K. S.; Kimball, S. D.; Misra, R. N.; Rawlins, D. B.; Hunt, J. T.; Xiao, H. Y.; Lu, S.; Qian, L.; Han, W. C.; Shan, W.; Mitt, T.; Cai, Z. W.; Poss, M. A.; Zhu, H.; Sack, J. S.; Tokarski, J. S.; Chang, C. Y.; Pavletich, N.; Kamath, A.; Humphreys, W. G.; Marathe, P.; Bursuker, I.; Kellar, K. A.; Roongta, U.; Batorsky, R.; Mulheron, J. G.; Bol, D.; Fairchild, C. R.; Lee, F. Y.; Webster, K. R. J. Discovery of Aminothiazole Inhibitors of Cyclin-Dependent Kinase 2: Synthesis, X-ray Crystallographic Analysis, and Biological Activities. *Med. Chem.* **2002,** *45,* 3905.
31. Van-Wijngaarden, I.; Kruse, C. G.; Van-Hes, R.; Van-der-Heyden, J. A. M.; Tulp, M. T. M. 2-Phenylpyrroles as conformationally restricted benzamide analogs. A new class of potential antipsychotics. 1. *J. Med. Chem.* **1987,** *30,* 2099.
32. Li, X.; Lu, X.; Chen, W.; Liu, H.; Zhan, P.; Pannecouque, C.; Balzarini, J.; De Clercq, E.; Liu, X. Arylazolyl(azinyl)thioacetanilides. Part 16: Structure-based bioisosterism design, synthesis and biological evaluation of novel pyrimidinylthioacetanilides as potent HIV-1 inhibitors. *Bioorg. Med. Chem.* **2014,** *22,* 5290.
33. Gillman, K. W.; Starrett, J. E.; Parker, M. F.; Xie, K.; Bronson, J. J.; Marcin, L. R.; McElhone, K. E.; Bergstrom, C. P.; Mate, R. A.; Williams, R.; Meredith, J. E.; Burton, C. R.; Barten, D. M.; Toyn, J. H.; Roberts, S. B.; Lentz, K. A.; Houston, J. G.; Zaczek, R.; Albright, C. F.; Decicco, C. P.; Macor, J. E.; Olson, R. E. Discovery and Evaluation of BMS-708163, a Potent, Selective and Orally Bioavailable γ-Secretase Inhibitor. *ACS Med. Chem. Lett.* **2010,** *1,* 120.
34. Roderick, S. L.; Fournie-Zaluski, M. C.; Roques, B. P.; Matthews, B. W. Thiorphan and retro-thiorphan display equivalent interactions when bound to crystalline thermolysin. *Biochemistry* **1989,** *28,* 1493.
35. Ciapetti, P., Giethlen, B. *The Practice of Medicinal Chemistry*; 3rd ed.; C. G. Wermuth, ed.; Academic Press, Cambridge, MA; 2008; p. 322.
36. Blair, J. B.; Marona-Lewicka, D.; Kanthasamy, A.; Lucaites, V. L.; Nelson, D. L.; Nichols, D. E. Thieno[3,2-b]- and Thieno[2,3-b]pyrrole Bioisosteric Analogues of the Hallucinogen and Serotonin Agonist N,N-Dimethyltryptamine. *J. Med. Chem.* **1999,** *42,* 1106.
37. Barreiro, E. J.; Camara, C. A.; Verli, H.; Brazil-Más, L.; Castro, N. G.; Cintra, W. M.; Aracava, Y.; Rodrigues, C. R.; Fraga, C. A. M. Design, Synthesis, and Pharmacological Profile of Novel Fused Pyrazolo[4,3-d]pyridine and Pyrazolo[3,4-b][1,8]naphthyridine Isosteres: A New Class of Potent and Selective Acetylcholinesterase Inhibitors. *J. Med. Chem.* **2003,** *46,* 1144.
38. Capparelli, E.; Zinzi, L.; Cantore, M.; Contino, M.; Perrone, M. G.; Luurtsema, G.; Berardi, F.; Perrone, R.; Colabufo, N. A. SAR Studies on Tetrahydroisoquinoline Derivatives: The Role of Flexibility and Bioisosterism To Raise Potency and Selectivity toward P-glycoprotein. *J. Med. Chem.* **2014,** *57,* 9983.
39. King, F. D.; Brown, A. M.; Gaster, L. M.; Kaumann, A. J.; Medhurst, A. D.; Parker, S. G.; Parsons, A. A.; Patch, T. L.; Raval, P. (.+-.)-3-Amino-6-carboxamido-1,2,3,4-tetrahydrocarbazole: a conformationally restricted analog of 5-carboxamidotryptamine with selectivity for the serotonin 5-HT1D receptor. *J. Med. Chem.* **1993,** *36,* 1918.
40. Mewshaw, R. E.; Zhao, R.; Shi, X.; Marquis, K.; Brennan, J. A.; Mazandarani, H.; Coupet, J.; Andree, T. H. New Generation Dopaminergic Agents. Part 8: Heterocyclic Bioisosteres that Exploit the 7-OH-2-(aminomethyl)chroman D2 Template. *Bioorg. Med. Chem. Lett.* **2002,** *12,* 271.
41. Kummerle, A. E.; Schmitt, M.; Cardozo, S. V. S.; Lugnier, C.; Villa, P.; Lopes, A. B.; Romeiro, N. C.; Justiniano, H.; Martins, M. A.; Fraga, C. A. M.; Bourguignon, J.-J.; Barreiro, E. J. Design, Synthesis, and Pharmacological Evaluation of N-Acylhydrazones and Novel Conformationally Constrained Compounds as Selective and Potent Orally Active Phosphodiesterase-4 Inhibitors. *J. Med. Chem.* **2012,** *55,* 7525.
42. Fang, L.; Fang, X.; Gou, S.; Lupp, A.; Lenhardt, I.; Sun, Y.; Huang, Z.; Chen, Y.; Zhang, Y.; Fleck, C. Design, synthesis and biological evaluation of D-ring opened galantamine analogs as multifunctional anti-Alzheimer agents. *Eur. J. Med. Chem.* **2014,** *76,* 376.
43. Brullo, C.; Massa, M.; Villa, C.; Ricciarelli, R.; Rivera, D.; Pronzato, M. A.; Fedele, E.; Barocelli, E.; Bertoni, S.; Flammini, L.; Bruno, O. Synthesis, biological activities and pharmacokinetic properties of new fluorinated derivatives of selective PDE4D inhibitors. *Bioorg. Med. Chem.* **2015,** *23,* 3426.
44. Merritt, J. E.; Hallam, T. J.; Brown, A. M.; Boyfield, I.; Cooper, D. G.; Hickey, D. M.; Jaxa-Chamiec, A. A.; Kaumann, A. J.; Keen, M.; Kelly, E. Octimibate, a potent non-prostanoid inhibitor of platelet aggregation, acts via the prostacyclin receptor. *Br. J. Pharmacol.* **1991,** *102,* 251.

45. Skuballa, W.; Schillinger, E.; Sturtzbechet, C-St; Vorbruggen, H. Prostaglandin analogs. Part 9. Synthesis of a new chemically and metabolically stable prostacyclin analog with high and long-lasting oral activity. *J. Med. Chem.* **1986,** *29,* 313.
46. Skuballa, W.; Vorbrüggen, H. A new route to 6a-carbacyclin. Synthesis of a stable, biologically potent prostacyclin analogue. *Angew. Chem. Int. Ed. Engl.* **1981,** *20,* 1046.
47. Faustino, I.; Curutchet, C.; Luque, F. J.; Orozco, M. The DNA-forming properties of 6-selenoguanine. *Phys. Chem. Chem. Phys.* **2014,** *16,* 1101.
48. Showell, G. A.; Mills, J. S. Chemistry challenges in lead optimization: silicon isosteres in drug discovery. *Drug Discov. Today* **2003,** *8,* 551.
49. Daiss, J. O.; Burschka, C.; Mills, J. S.; Montana, J. G.; Showell, G. A.; Warneck, J. B. H.; Tacke, R. Sila-venlafaxine, a Sila-Analogue of the Serotonin/Noradrenaline Reuptake Inhibitor Venlafaxine: Synthesis, Crystal Structure Analysis, and Pharmacological Characterization. *Organometallics* **2006,** *25,* 1188.
50. Tacke, R.; Heinrich, T.; Bertermann, R.; Burschka, C.; Hamacher, A.; Kassack, M. U. Sila-haloperidol: A Silicon Analogue of the Dopamine (D2) Receptor Antagonist Haloperidol. *Organometallics* **2004,** *23,* 4468.
51. Alves, F. R. S.; Barreiro, E. J.; Fraga, C. A. M. From nature to drug discovery: the indole scaffold as a privileged structurel. *Mini Rev. Med. Chem.* **2009,** *9,* 782.
52. Dudkin, V. Y. Bioisosteric equivalence of five-membered heterocycles. *Chem. Heterocycl. Compd.* **2012,** *48,* 27.
53. Francisco, M. E. Y.; Seltzman, H. H.; Gilliam, A. F.; Mitchell, R. A.; Rider, S. L.; Pertwee, R. G.; Stevenson, L. A.; Thomas, B. F. Synthesis and Structure−Activity Relationships of Amide and Hydrazide Analogues of the Cannabinoid CB1 Receptor Antagonist N-(Piperidinyl)- 5-(4-chlorophenyl)-1-(2,4-dichlorophenyl)-4-methyl-1H-pyrazole-3-carboxamide (SR141716). *J. Med. Chem.* **2002,** *45,* 2708.
54. Katoch-Rouse, R.; Pavlova, O. A.; Caulder, T.; Hoffman, A. F.; Mukhin, A. G.; Horti, A. G. Synthesis, Structure−Activity Relationship, and Evaluation of SR141716 Analogues: Development of Central Cannabinoid Receptor Ligands with Lower Lipophilicity. *J. Med. Chem.* **2003,** *46,* 642.
55. Lange, J. H. M.; van Stuivenberg, H. H.; Coolen, H. A. K. C.; Adolfs, T. J. P.; McCreary, A. C.; Keizer, H. G.; Wala, H. C.; Veerman, W.; Borst, A. J. M.; de Looff, W.; Verveer, P. C.; Kruse, C. G. Bioisosteric Replacements of the Pyrazole Moiety of Rimonabant: Synthesis, Biological Properties, and Molecular Modeling Investigations of Thiazoles, Triazoles, and Imidazoles as Potent and Selective CB1 Cannabinoid Receptor Antagonists. *J. Med. Chem.* **2005,** *48,* 1823.
56. Edwards, E. I.; Epton, R.; Marr, G. A new class of semi-synthetic antibiotics: ferrocenyl-penicillins and -cephalosporins. *J. Organomet. Chem.* **1976,** *107,* 351.
57. Top, S.; Tang, J.; Vessières, A.; Carrez, D.; Provot, C.; Jaouen, G. Ferrocenyl hydroxytamoxifen: a prototype for a new range of oestradiol receptor site-directed cytotoxics. *Chem. Commun.* **1996,** 955.
58. Görmen, M.; Veitía, M. S.-I.; Trigui, F.; El Arbib, M.; Ferrouda, C. Ferrocenyl analogues of bisacodyl: Synthesis and antimicrobial activity. *J. Organomet. Chem.* **2015,** *794,* 274.
59. Binder, D.; Hromatka, O.; Geissler, F.; Schmied, K.; Noe, C. R.; Burri, K.; Pfister, R.; Strub, K.; Zeller, P. Analogues and derivatives of tenoxicam. 1. Synthesis and antiinflammatory activity of analogues with different residues on the ring nitrogen and the amide nitrogen. *J. Med. Chem.* **1987,** *30,* 687.
60. DiPasquale, G.; Rassaert, C.; Richter, R.; Welaj, P.; Gingold, J.; Singer, R. The anti-inflammatory properties of isoxicam (4-hydroxy-2methyl-N-(5-methyl-3isoxolyl-2H-1,2-benzothiazine-3-carboxamide 1,1-dioxide). *Agents Actions* **1975,** *5,* 256.
61. Stark, S.; Sachse, R.; Liedl, T.; Hensen, J.; Rohde, G.; Wensing, G.; Horstmann, R.; Schrott, K. M. Vardenafil increases penile rigidity and tumescence in men with erectile dysfunction after a single oral dose. *Eur. Urol.* **2001,** *40,* 181.
62. Wong, D. T.; Robertson, D. W.; Bymaster, F. P.; Krushinski, J. H.; Reid, L. R. LY227942, an inhibitor of serotonin and norepinephrine uptake: biochemical pharmacology of a potential antidepressant drug. *Life Sci.* **1988,** *43,* 2049.
63. Chauret, N.; Yergey, J. A.; Brideau, C.; Friesen, R. W.; Mancini, J.; Riendeau, D.; Silva, J.; Styhler, A.; Trimble, L. A.; Nicoll-Griffith, D. A. In vitro metabolism considerations, including activity testing of metabolites, in the discovery and selection of the COX-2 inhibitor etoricoxib (MK-0663). *Bioorg. Med. Chem. Lett.* **2001,** *11,* 1059.
64. Jaouen, G.; Top, S.; Vessières, A.; Leclercq, G.; McGlinchey, M. J. The first organometallic selective estrogen receptor modulators (SERMs) and their relevance to breast cancer. *Curr. Med. Chem.* **2004,** *11,* 2505.
65. Jaouen, G.; Vessières, A.; Top, S. Ferrocifen type anti cancer drugs. *Chem. Soc. Rev.* **2015,** *44,* 8802.
66. Jennings, A.; Tennant, M. Selection of Molecules Based on Shape and Electrostatic Similarity: Proof of Concept of "Electroforms". *J. Chem. Inf. Model.* **2007,** *47,* 1829.
67. Papadatos, G.; Brown, N. In silico applications of bioisosterism in contemporary medicinal chemistry practice. *Comput. Mol. Sci.* **2013,** *3,* 339.
68. Jalencas, X.; Mestres, J. Identification of Similar Binding Sites to Detect Distant Polypharmacology. *Mol. Inf.* **2013,** *32,* 976.
69. Jalencas, X., Mestres, J. *J. Chem. Inf. Model.*, **2013**, *53*, 279; Jalencas, X.; Mestres, J. On the origins of drug polypharmacology. *Med. Chem. Commun.*, **2013**, *4*, 80.
70. Braese, S. ed. *Privileged Scaffolds in Medicinal Chemistry: Design, Synthesis, Evaluation, RSC Drug Discovery series*, Thurston, D. (Editor-in-Chief), Rotella, D., Martinez, A., Fox, D. (Series Editors), RSC Publishing, London; 2016; pp. 1–15.

1.08 Spirocyclic Scaffolds in Drug Discovery

CM Tice, Y Zheng, and SB Singh, Vitae Pharmaceuticals, West Office Center Drive, Fort Washington, PA, United States

© 2017 Elsevier Ltd. All rights reserved.

1.08.1	**Introduction**	211
1.08.2	**Conformational Analysis of Spirocycles**	213
1.08.2.1	Overview of Conformational Analysis of Spirocyclic Scaffolds	213
1.08.2.2	Spiro[2.*n*] Ring Systems	214
1.08.2.3	Spiro[3.*n*] Ring Systems	214
1.08.2.4	Spiro[4.4] Ring Systems	214
1.08.2.5	Spiro[4.5] Ring Systems	215
1.08.2.5.1	Isolated ring systems	215
1.08.2.5.2	Benzo-fused ring systems	215
1.08.2.6	Spiro[5.5] Ring Systems	216
1.08.2.6.1	Isolated ring systems	216
1.08.2.6.2	Benzo-fused spiro[5.5] ring systems	218
1.08.2.7	Spiro[*m*.6] Ring Systems	218
1.08.3	**Medicinal Chemistry of Spirocycles**	220
1.08.3.1	Spiro[2.*n*] Ring Systems	220
1.08.3.1.1	Spiro[2.2] ring systems	220
1.08.3.1.2	Spiro[2.3] ring systems	220
1.08.3.1.3	Spiro[2.4] ring systems	221
1.08.3.1.4	Spiro[2.5] ring systems	223
1.08.3.1.5	Spiro[2.$\geq$6] ring systems	225
1.08.3.2	Spiro[3.*n*] Ring Systems	225
1.08.3.2.1	Spiro[3.3] ring systems	225
1.08.3.2.2	Spiro[3.4] ring systems	225
1.08.3.2.3	Spiro[3.5] ring systems	226
1.08.3.3	Spiro[4.*n*] Ring Systems	229
1.08.3.3.1	Spiro[4.4] ring systems	229
1.08.3.3.2	Spiro[4.5] ring systems	235
1.08.3.3.3	Spiro[4.6] ring systems	243
1.08.3.4	Spiro[5.*n*] Ring Systems	245
1.08.3.4.1	Spiro[5.5] ring systems	245
1.08.3.4.2	Spiro[5.6] ring systems	252
1.08.3.5	Polyspirocycles	253
1.08.3.6	Noncarbon Spiro Atom	253
1.08.4	**Conclusions**	253
References		254
Relevant Websites		263

1.08.1 Introduction

Spirocycles are ring systems in which two rings share a single atom known as the spiro atom. Most often, the spiro atom is an sp^3 hybridized carbon atom, although ring systems are known in which the spiro atom is another element, such as a quaternized sp^3 nitrogen.

The nomenclature of spirocycles was originally proposed by von Baeyer.[1] The structures in **Fig. 1** will serve as illustration. The C_{10} molecule **1**, in which a cyclohexane and a cyclopentane share a single atom, is named as spiro[4.5]decane. The numbers within the square brackets indicate the numbers of atoms in chains joining the spiro atom, with the shorter chain listed first. The spiro atom is numbered as position 5 in this case and numbering then continues around the larger ring. Replacement of the carbon atom at position 2 in **1** gives the amine **2**, which is named 2-azaspiro[4.5]decane. Similarly replacement of the carbon atom at position 8 in **2** with oxygen gives aminoether **3** which is named 8-oxa-2-azaspiro[4.5]decane. This review is organized on the basis of formal nomenclature; however, in practice, **2** would often be described as a spiropyrrolidine and this type of informal nomenclature will also be employed.

Spirocycles are well represented among natural products and have attracted the interest of the synthetic community. Seven examples, selected for their structural diversity and biological activity, are depicted in **Fig. 2**. Spiroepoxide fumagillin (**4**) possesses

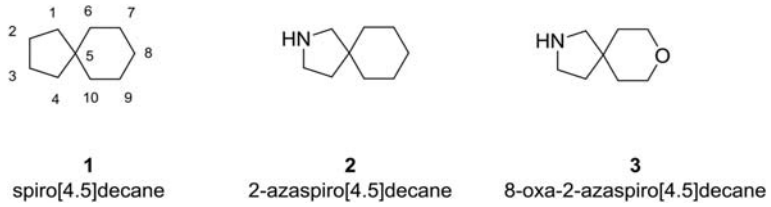

Fig. 1 Nomenclature of spirocycles.

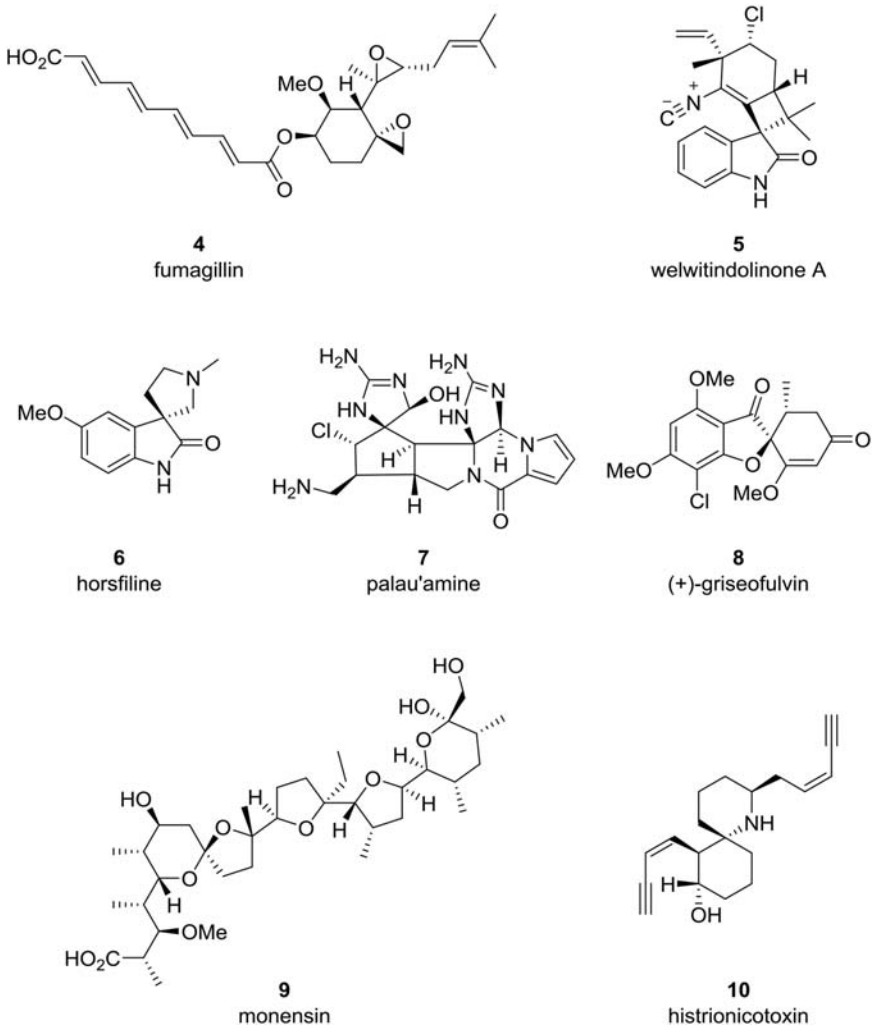

Fig. 2 Selected spirocyclic natural products.

antiangiogenic and amebicidal activity and has been a starting point for medicinal chemistry.[2] Welwitindolinone A (**5**)[3] and horsfiline (**6**)[4] both incorporate spiroindolinone groups, a ring system that has been of considerable interest to medicinal chemists.[5] Palau'amine (**7**)[6] has cytotoxic, antibiotic, and immunosuppressive activity and is reported to inhibit the human 20*S* proteasome.[7] (+)-Griseofulvin (**8**) is an orally bioavailable antifungal drug used in man.[8] The polyether monensin (**9**) is a spiroketal antibiotic used in animal husbandry.[9] Histrionicotoxin (**10**) inhibits nicotinic acetyl choline receptors.[10]

Spirocycles have also captured the imagination of medicinal chemists. Their ability to project substituents in all three dimensions on a generally rigid framework makes them attractive scaffolds for drug discovery and, in fact, some of them have been considered to be privileged structures.[11] In many cases, spirocycles have a high fraction of sp^3 carbons (Fsp3) and can be expected to be more water soluble, and thus more druglike, than aromatic systems of similar molecular weight (MW) and carbon content.[12,13] In addition, spirocycles may offer advantages in terms of patentability.

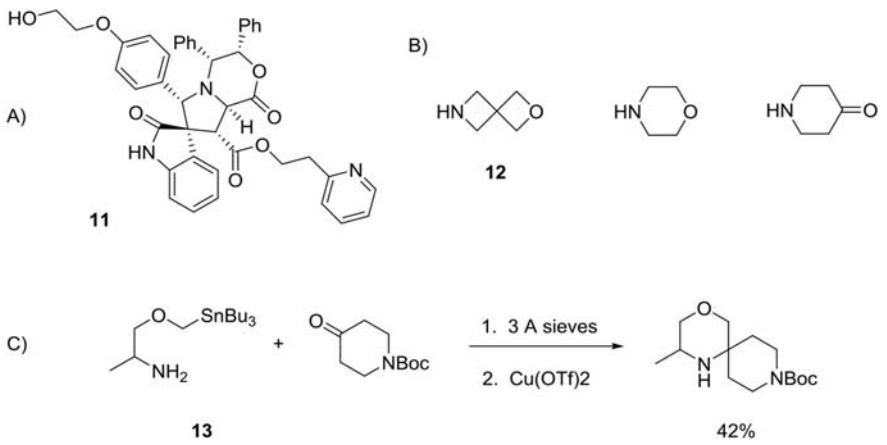

Fig. 3 (A) Biologically active spirocycle discovered using DOS. (B) Spirooxetane. (C) Spirocycle synthesis using SnAP chemistry.

The ability of certain spirocycles, particularly spirocyclic lactams to mimic β-turns in peptides and proteins, may provide a partial explanation for their privileged status.[14] A number of spirocyclic systems have been synthesized and evaluated as β-turn mimetics.[15–21]

Diversity-oriented synthesis (DOS) aims to produce libraries of natural product-like molecules for biological screening.[22] Given their prevalence among natural products and status as privileged substructures,[11,23] it is unsurprising that spirocycles have been exploited in DOS.[24–27] For example, Schreiber's group described the discovery of spirooxindole **11** (Fig. 3A) which synergizes the activity of the actin polymerase inhibitor latrunculin B with an EC_{50} of 550 nM.[28] Spirocycles have also found to use as acaricides[29] and fungicides.[30]

The synthetic literature related to spirocycles is vast. A crude search for the term "spiro" using SciFinder, and limited to the year 2014, retrieved the following numbers of articles from leading organic chemistry journals: *Org. Lett*. 55, *Tetrahedron Lett*. 51, *Tetrahedron* 39, *Eur. J. Org. Chem*. 33, *J. Org. Chem*. 30, *Org. Biomol. Chem*. 21, and *Synthesis* 20. There can be no doubt that development of methods for synthesis of spirocycles continues to interest organic chemists. Various aspects of the synthesis of spirocycles have been reviewed.[31–42] While the synthesis of spirocycles is outside the scope of this article, two recent developments can be highlighted. Firstly, a body of work from the Carreira group describing the preparation of spirocycles including four-membered rings mirrors the general increase in interest in rings of this size in drug discovery.[43–46] For example, spirooxetane **12** was considered as a potential bioisostere of morpholine and 4-oxopiperidine (Fig. 3B).[44] Secondly, the Bode group has recently described bifunctional SnAP reagents, for example, **13**, a number of which are now commercially available, capable of converting cyclic ketones to spirocycles in one pot (Fig. 3C).[47,48] An ongoing challenge to the synthetic community is the control of stereochemistry at multiple positions on spirocyclic scaffolds, allowing full advantage to be taken of the three-dimensional nature of these ring systems.

The focus of this article will be on the conformational analysis of spirocycles, an understanding of which is essential to structure-based drug design involving spirocycles, and selected examples of the deployment of spirocycles in drugs and drug discovery.[49] Both topics are organized based on the International Union of Pure and Applied Chemistry (IUPAC) nomenclature of spirocycles. Due to space limitations it was necessary to exclude many interesting reports of spirocycles in medicinal chemistry.

1.08.2 Conformational Analysis of Spirocycles

1.08.2.1 Overview of Conformational Analysis of Spirocyclic Scaffolds

Spiro ring fusion has been increasingly used to restrict molecular conformation. Smaller spiro structures are rigid with limited or no conformational flexibility. Spirocyclic scaffolds containing a large ring system (larger than seven-membered) are generally highly flexible unless otherwise constrained. Therefore, for drug discovery purposes, we are usually interested in spirocyclic scaffolds that contain rings smaller than eight-membered ring, for example, spiro[*m*.*n*] where $m \leq n$ and *m* and *n* are between 2 and 6.

Apart from spiroketals,[31,50] conformational preferences for spirocyclic systems are generally less well studied than nonspiro ring systems and experimental energetic information is often scarce. Recently, we found that the hybrid density functional theory at the B3LYP/6-31G* level of theory is capable of accurately describing the conformational preferences of geminal disubstituted cyclohexanes. Conceptually spiro scaffolds are just a special case of geminal disubstituted systems. Given the scarcity of experimental energetic information regarding inherent conformational preferences of spirocyclic scaffolds in general, we investigated the conformational preferences of various commonly used spiro[4.5] and spiro[5.5]-ring systems using the B3LYP/6-31G* level of theory. Comparison with available experimental data is made whenever available. In general, the conformational preference of spirocyclic scaffolds can be predicted based on the *A*-values of the corresponding geminal disubstituted cyclohexanes.

1.08.2.2 Spiro[2.*n*] Ring Systems

Spiro[2.2]pentane (where $n=2$), the smallest spirocyclic prototype molecule with two three-membered rings fused together through a spiroatom, is completely rigid. The conformational flexibility of spiro[2.*n*] ring systems, where $n>2$, is determined by the larger ring due to the rigidity of the three-membered ring (Fig. 4). For instance, spiro[2.5]octane (**14**) has similar ring inversion barrier (10.5 kcal mol^{-1}) to cyclohexane itself (10.2 kcal mol^{-1}).[51] Even in this case, the presence of the spirocyclopropane ring can sometimes induce unusual conformational effect, for example, the axial predominance in spiro[2.5]octan-4-ol derivatives. A small spiro ring fusion is generally introduced to improve structural novelty and patentability if presented peripherally in a molecule, in such cases the small ring can often be replaced by geminal dimethyl without losing much binding potency.

1.08.2.3 Spiro[3.*n*] Ring Systems

A four-membered ring can be either planar or puckered. Unsubstituted cyclobutane and azetidine prefer a wing-shaped conformation with small inversion barriers of 1.45 and 1.26 kcal mol^{-1}, respectively, while oxetane is essentially planar.[52] When two four-membered rings are fused together to form a spiro[3.3] system, the two four-membered rings can be either planar or puckered depending on the nature of the rings and their substitution patterns. Both cyclobutane rings of spiro[3.3]heptane containing molecules are normally puckered (eg, CSD code: SPHBAH).[53] Oxetane is planar while azetidine can be either planar or puckered depending on the substituent on N and also protonation state (eg, CSD codes EMUDAS, NUQSEY, AKUQUT). Overall, spiro[3.3] systems do not exhibit a great deal of conformational flexibility.

As with three-membered rings, when a four-membered ring is fused to a larger ring to form a spiro scaffold, the conformational flexibility of the resulting system is determined mainly by the larger ring due to limited conformational flexibility of the four-membered ring (Fig. 5).

1.08.2.4 Spiro[4.4] Ring Systems

Cyclopentane has two low energy conformations: the envelope conformation with four atoms coplanar and the half-chair conformation with three atoms coplanar (Fig. 6). The envelope conformation is about 0.5 kcal mol^{-1} lower in energy than the half-chair conformation with a very small interconversion (pseudorotational) barrier between them; the inversion barrier for the envelope conformation is <5.0 kcal mol^{-1}.[54] For methylcyclopentane, the pseudorotational barrier increases to 3.4 kcal mol^{-1} and in the most stable conformation the methyl group prefers to be equatorial at the flap of the envelope by 0.9 kcal mol^{-1}.[54] Thus in a spiro[4.4] system, the two five-membered rings in principle can be either in half-chair or envelope conformations. Similarly, tetrahydrofuran is puckered with the C_2-symmetrical T form (the envelope conformation with a flap oxygen) being the lowest in energy. Both pseudorotational and inversion barriers are small (0.22 cal mol^{-1} and 4.15 mol^{-1}, respectively).[55]

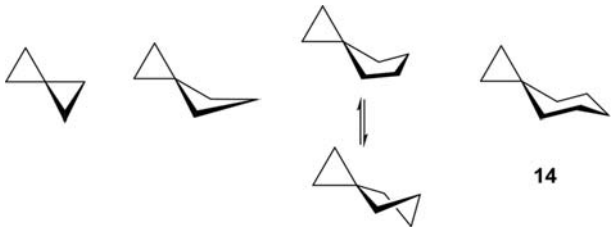

Fig. 4 Conformations of spiro[2.2]pentane, spiro[2.3]hexane, spiro[2.4]heptane, and spiro[2.5]octane.

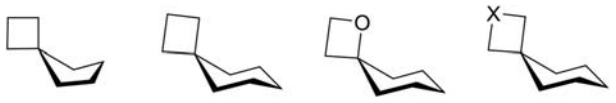

Fig. 5 Low energy conformations of spiro[3.4] and spiro[3.5] ring systems.

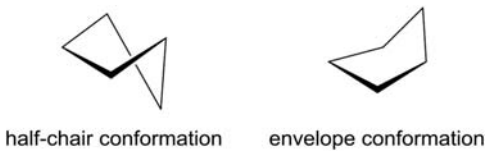

Fig. 6 Low energy conformations of cyclopentane.

Table 1 Energy differences of spiro[4.5]decane conformers

15eq 15ax 16eq 16ax

	X	$\Delta E\ X_{ax} - X_{eq}$ (kcal mol^{-1})[a]		R	$\Delta E\ N_{ax} - N_{eq}$ (kcal mol^{-1})
15a	CH_2	0	**16a**	H	−0.17
15b	O	−0.68 (−0.4 to −0.5[b])	**16b**	Me	3.11
15c	C=O	0.29			
15d	NH	−0.07			
15e	NH_2^+	−0.15			

[a]Calculated at the B3LYP/6-31G* level of theory.
[b]Experimental value at 35°C.

Also, pyrrolidine is found to undergo rapid pseudorotation with the N–H equatorial envelope conformer being the lowest in energy.[56] There are over 2400 structures in CSD that contain spiro[4.4] scaffolds.[53]

1.08.2.5 Spiro[4.5] Ring Systems

1.08.2.5.1 Isolated ring systems

For spiro[4.5]decane, the conformation of the five-membered ring can in principle be in either the envelope or the half-chair conformation, whilst the six-membered ring would be in the chair conformation. Again, the conformational flexibility of such a spiro system is mainly determined by the six-membered ring. Owing to symmetry, the two low energy conformations of spiro[4.5]decane (**15a**) are equivalent in energy (Table 1). However, the equilibrium between axial and equatorial conformers can be perturbed by changing the nature of X. In 1-oxaspiro[4.5]decane (**15b**), the oxygen prefers to be in the axial position as shown both experimentally[57] and theoretically.[58] In keto compound **15c**, the carbonyl slightly prefers to be in the equatorial position. In amine **15d**, there is little preference for axial versus equatorial; however, the protonated form **15e** shows a slight preference to adopt the axial position.

For spiro lactam **16a**, the axial conformation of the nitrogen is slightly favored (Table 1), however, the presence of an *N*-alkyl group in this conformation (eg, **16b**) would result severe steric clashes between the *N*-alkyl group and the two axial C–Hs at positions 7 and 9. As a result, the equatorial conformation is preferred. A conformational switch of this type can be very useful in controlling ligand conformation in drug design.

Similarly, when both heteroatoms and unsaturation were introduced into the five-membered ring system as in **17** and **18**, the preference of an ether oxygen over a methylene group to adopt the axial configuration still persists according to our calculations at the B3LYP/6-31G* level of theory (Table 2). Even though experimental energetics are not available for these systems, experimental data are available for analogous systems **19** and **20**. In these cases the theoretical results are higher but nonetheless in general agreement with the experimental observations.[59]

Introducing a heteroatom into the six-membered ring of a spiro[4.5] ring system also influences conformational preferences as reported for some spiropiperidine NK2 receptor antagonists.[60]

1.08.2.5.2 Benzo-fused ring systems

For spiro[4.5] systems, the five-membered ring is often fused to an aromatic ring. A ring fusion of this type is expected to affect the conformational preference of the resulting spiro scaffolds. There are two ways to fuse a phenyl ring with the five-membered ring of the spiro[4.5] scaffolds: 1,2 or 2,3-fusion (Tables 3 and 4).

Some examples with a benzo fusion in the 1,2-position are shown in Table 3. For 1,2-phenyl fusion, the phenyl moiety generally prefers to be in the equatorial position. The exception is the lactam **21f** in which the phenyl moiety is predicted to be in the axial position, in agreement with small molecule X-ray crystal structure (CSD code: EBAXIQ, Table 3). However, the magnitude of this conformational preference can be manipulated by introducing a polar group at Z such as oxygen (**21g**) or amine (**21h**).

For 2,3-benzo fusion, the two conformations of the parent compound **22a** are equal in energy due to symmetry (Table 4). The conformational preferences of these systems are usually similar to that of the corresponding unfused scaffolds (**22b** vs. **15b**, **22c** vs. **15c**, **22d** vs. **15d**).

Table 2 Energy differences of spiro[4.5]decane conformers with multiple heteroatoms

	$\Delta E_{axial\text{-}equatorial}$ (kcal mol^{-1})	
	Experimental	*Calculated B3LYP/6-31G**
17eq ⇌ **17ax**		−0.54
18eq ⇌ **18ax**		−0.55
19eq ⇌ **19ax**	−0.27	−0.48
20eq ⇌ **20ax**	0.40	0.88

Table 3 Energy differences of benzo-fused spiro[4.5]decane conformers

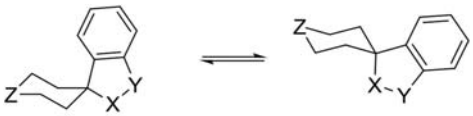
21eq ⇌ **21ax**

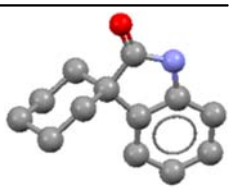
21f eq
CSD code: EBAXIQ

	X	*Y*	*Z*	$\Delta E\ X_{ax} - X_{eq}$ (kcal mol^{-1})
21a	CH_2	CH_2	CH_2	−1.78
21b	O	CH_2	CH_2	−2.23
21c	NH	C=O	CH_2	−1.73
21d	NH	C=O	NH_2^+	−1.31
21e	NH	C=O	O	−1.75
21f	C=O	NH	CH_2	0.94
21g	C=O	NH	O	−1.24
21h	C=O	NH	NH_2^+	−5.86

N-Alkylation appears to be a general conformational switch and can be of great value in controlling ligand conformation in drug design. For the spiroindoxyl ring system (**16a** vs. **16b** in Table 1, 22d vs. **22e** in Table 4), it has been demonstrated N-methylation is sufficient to flip the conformation of the six-membered ring.[61]

1.08.2.6 Spiro[5.5] Ring Systems

1.08.2.6.1 Isolated ring systems

In spiro[5.5] ring systems, since the four atoms attached to the spiroatom can be in either axial or equatorial positions, there are four combinations: eaea, aeea, aeae, and eaae. For the prototypic spiro[5.5]undecane (**23**), those four conformations are energetically

Table 4 Energy differences of benzo-fused spiro[4.5]decane conformers

22eq **22ax**

	X	*Y*	$\Delta E\ X_{ax} - X_{eq}$ (kcal mol^{-1})
22a	CH_2	CH_2	0
22b	O	CH_2	−0.64
22c	C=O	CH_2	0.75
22d	NH	CH_2	−0.05
22e	NMe	CH_2	3.9
22f	NH	C=O	−0.37

equivalent (Fig. 7). Interestingly, introducing a spiro ring fusion also introduces an axial chirality,[62] for example, the top two conformations are mirror images, and so are the bottom two. In the case of **23**, they interconvert rapidly and are inseparable.[62]

Changing one of the four atoms attached to the spiroatom of **23** into an oxygen atom results in 1-oxaspiro[5.5]undecane **24** where the two chair conformations are no longer energetically equivalent (Table 5). Both experimental and theoretical investigations of chair conformations demonstrated that the oxygen prefers to be in the axial position by 0.9[50] and 1.3 kcal mol^{-1}, respectively. Introducing a second oxygen atom attached to the spiroatom results in two possible structures **25** and **26**. If the two oxygen atoms are in the same ring (**25**, Table 5), the two conformations are equal in energy due to symmetry. Alternatively, if they are in different rings, the resulting spiroketal 1,7-dioxaspiro[5.5]undecane (**26**, Table 6) has three conformational possibilities: both oxygens in axial positions (**26aa**), one oxygen in an axial and one in an equatorial position (**26ea**), or both oxygen atoms in equatorial positions (**26ee**). Experimentally, it has been demonstrated that only the diaxial conformation **26aa** exists at room temperature,[50] indicating that the other conformations must be at least 2 kcal mol^{-1} higher in energy. Both previous[63] and current theoretical calculations are generally in agreement with the experiment, but the magnitudes of the calculated energy differences regarding the higher energy conformations are significantly different from those estimated by Deslongchamps and coworkers based on steric and anomeric considerations.[50]

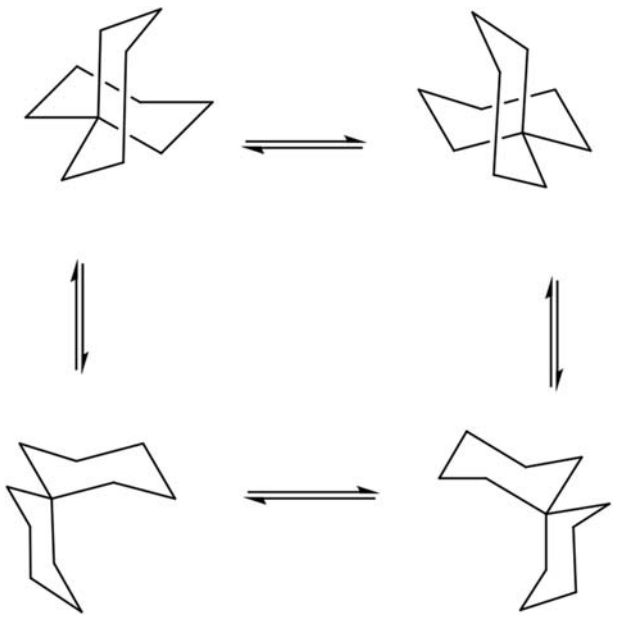

Fig. 7 Spiro[5.5]undecane (**23**) conformations.

Table 5 Calculated energy differences of 1-oxa- and 1,5-dioxaspiro[5.5]undecane conformers

	$\Delta E_{axial\text{-}equatorial}$ (kcal mol^{-1})	
	Experimental	*Calculated (B3LYP/6-31G*)*
24eq **24ax**	−0.9	−1.3
25eq **25ax**	0	–

Table 6 Calculated energy differences of 1,7-dioxaspiro[5.5]undecane conformers

26ee **26ae** **26aa**

	E_{ee} (kcal mol^{-1})	E_{ae} (kcal mol^{-1})	E_{aa} (kcal mol^{-1})
Calculated (B3LYP/6-31G*)	8.40	3.92	0
DMSO, theoretical[a]	4.52	2.62	0
Estimated[b]	4.8	2.4	0

[a]Data from Ref.[63].
[b]Data from Ref.[50].

The conformational preference of spiro[5.5] ring systems can also be modulated by the presence of additional polar group or introducing substituent on the rings. Some examples are shown in Table 7. The influence of a protonated basic amine is particularly striking (**29c**, **30c**). Therefore, there is great conformational variation in spiro[5.5] systems.

1.08.2.6.2 Benzo-fused spiro[5.5] ring systems

As with spiro[4.5] ring systems, there are two ways to fuse a phenyl ring to one of the six-membered rings: 1,2-fusion and 2,3-fusion. As discussed above in the case of spiro[4.5] systems, the conformational preferences for 2,3-fusion are similar to the unfused system. Only the 1,2-fusion is considered here and, as in the spiro[4.5] systems, the phenyl moiety prefers to be in the equatorial position (Table 8).

1.08.2.7 Spiro[*m*.6] Ring Systems

Cycloheptane has several low energy conformations: chair, twist chair, boat, and twist boat.[64–66] The twist chair conformation is the most stable one and undergoes pseudorotation via the chair conformation as the transition state. Similarly, the twist boat also undergoes pseudorotation via the boat conformer as transition state with little energy barrier[64] or vice versa depending on the level of theory used in the theoretical investigations.[65] The inherent flexibility of seven-membered ring can be constrained by introducing unsaturation, one or more heteroatom, bridging, benzo fusion, or a combination of these elements. The well-known seven-membered scaffolds in drugs include benzodiazepines and azepinones. For spiro[*m*.6] scaffolds, if *m* is smaller than 5, the conformational flexibility is mainly determined by the seven-membered ring unless the seven-membered ring is highly constrained. For spiro[5.6] systems, both rings can significantly impact the conformational flexibility. Two structures (NUVYUY and RENCIY) from CSD are shown as examples in Fig. 8.

Table 7 Calculated conformational energy differences in spiro[5.5] ring systems

27eq 27ax

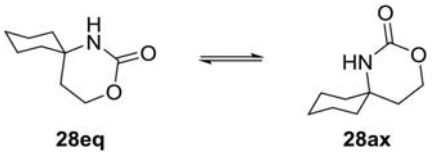

28eq 28ax

	X	$\Delta E\ X_{ax} - X_{eq}$ (kcal mol^{-1})
27a	CH_2	0
27b	O	−1.3
27c	C=O	−0.74

	$\Delta E\ N_{ax} - N_{eq}$ (kcal mol^{-1})
28a	−0.19

29eq 29ax

30eq 30ax

	X	*ΔE $O_{ax} - O_{eq}$ (kcal mol^{-1})*
29a	CH_2	−1.30 (−0.9[a])
29b	O	−1.54
29c	NH_2^+	−4.69

	X	*ΔE $O_{ax} - O_{eq}$ (kcal mol^{-1})*
30a	CH_2	−1.30
30b	O	0.13
30c	NH_2^+	−6.08

[a]Experimentally determined.

Table 8 Calculated conformational energy differences of benzo-fused spiro[5.5] ring systems

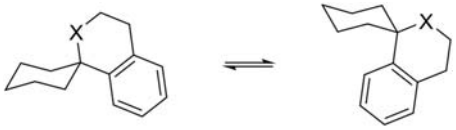

31ax 31eq

	X	*ΔE $X_{ax} - X_{eq}$ (kcal mol^{-1})*
31a	CH_2	−3.38
31b	O	−4.48
31c	NH	−4.89
31e	C=O	−1.70

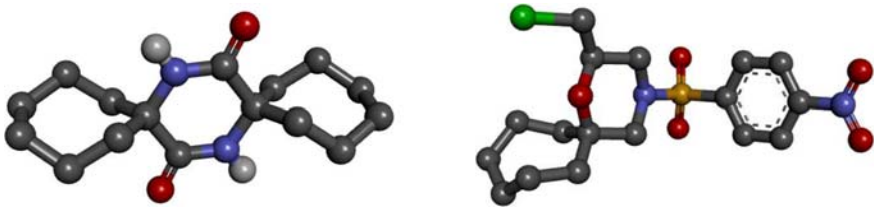

Fig. 8 X-ray structures of spiro[5.6] compounds.

Fig. 9 General structures of spiro[2.*n*] ring systems.

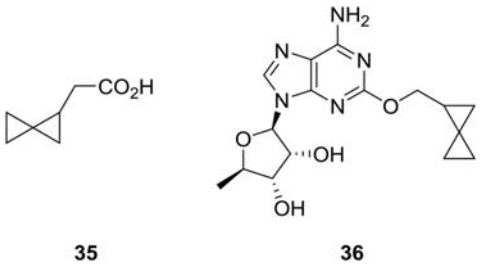

Fig. 10 Spiro[2.2]pentanes.

1.08.3 Medicinal Chemistry of Spirocycles

1.08.3.1 Spiro[2.*n*] Ring Systems

Spiro[2.*n*] ring systems include spirocyclopropanes (**32**, Fig. 9), spiroepoxides (**33**), and spiroaziridines (**34**). Cyclopropanes, including spirocyclopropanes, offer the attraction of increased stability to cytochrome P450 (CYP) mediated oxidation as compared to an isosteric geminal dimethyl group.[67] Spiroepoxides (**33**), on the other hand, are reactive to nucleophiles and have enjoyed application as covalent inhibitors. Spiroaziridines (**34**) have rarely been employed in medicinal chemistry.

1.08.3.1.1 Spiro[2.2] ring systems

Spiro[2.2]pentanes have seen occasional use in drug discovery. Spiropentane acetic acid **35** (Fig. 10) is an inhibitor of medium-chain acyl-CoA dehydrogenase with in vivo activity in rat when injected intraperitoneally at 80 mg kg^{-1}.[68] 2-Alkoxyadenosine analog **36** is a potent inhibitor ($IC_{50} = 40$ nM) of bacterial NAD^+-dependent DNA ligase; however, the spirocycle does not impart in vivo stability in this case.[69,70] Replacement of the spiro[2.2]pentylmethyl group with *trans*-4-(trifluoromethyl)cyclohexyl reduced clearance from 96 to 27 mL min^{-1} kg^{-1}.[71]

1.08.3.1.2 Spiro[2.3] ring systems

All carbon spiro[2.3]hexanes have occasionally been employed in medicinal chemistry.[72,73] For example, **37** (Fig. 11) is a positive allosteric modulator of the $mGlu_5$ receptor, a target with possible relevance in the treatment of schizophrenia, with an EC_{50} value of 3.9 nM and 95% efficacy.[72]

Two spirocyclic β-lactams have been reported. Spirocyclopropane **38** inhibits β-lactamases TEM-1 and AmpC with IC_{50} values of 0.65 and 0.02 μM, respectively. It is proposed to be a mechanism-based irreversible inhibitor.[74] Spiroepoxide **39** has antibacterial activity and, in addition, has been shown to irreversibly inhibit β-lactamase I with concomitant covalent modification of the protein.[75]

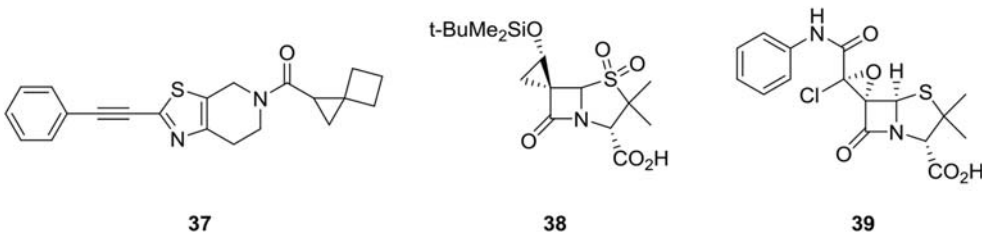

Fig. 11 Spiro[2.3] ring systems.

Table 9 Anti-hepatitis C virus spirocyclopropane ledipasvir

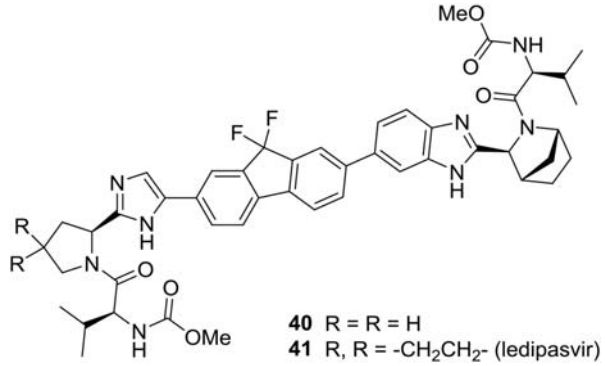

40 R = R = H
41 R, R = -CH_2CH_2- (ledipasvir)

	40	*41*
EC_{50} Gt1a (nM)	0.056	0.031
EC_{50} Gt1b (nM)	0.004	0.004
Protein binding shift	14×	6.7×
IV CL rat/dog/cyno (L $h^{-1}kg^{-1}$)[a]		0.43/0.13/0.17
IV $t_{1/2}$ rat/dog/cyno (h)[b]		4.7/7.4/10.3
F rat/dog/cyno (%)[c]		33/53/41

[a]Clearance.
[b]$t_{1/2}$ = Half-life.
[c]F = Oral bioavailability.

1.08.3.1.3 Spiro[2.4] ring systems

Compound **40** (Table 9) is a hepatitis C virus (HCV) nonstructural protein 5A (NS5A) inhibitor and was discovered by structure activity relationship (SAR) investigations, including desymmetrization, around dimeric inhibitors of this protein such as daclatasvir. The spirocyclopropane was introduced into **40** in the final optimization of the compound and afforded the drug **41** (ledipasvir) which is now approved for HCV treatment as one component of Harvoni®.[76] This subtle change imparted a small improvement genotype 1a (GT1a) replicon potency and a decrease in protein binding shift. The compound has low clearance, good bioavailability, and long half lives in three species. In healthy volunteers, a single 3 mg kg^{-1} oral dose of **41** had a $t_{1/2}$ of 45 and a 24 h trough concentration of 2.5 nM, 12-fold above the plasma protein-adjusted EC_{50}.

The limited oral bioavailability of the nociceptin/orphanin FQ (ORL1) receptor antagonist **42** was ascribed to its poor metabolic stability (Table 10).[77] An intensive scan of replacements for the essential cyclooctyl hydrophobe identified the spirocyclic bicycle

Table 10 Spirocyclopropane nociceptin/orphanin FQ (ORL1) receptor antagonist

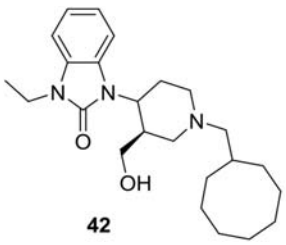

42

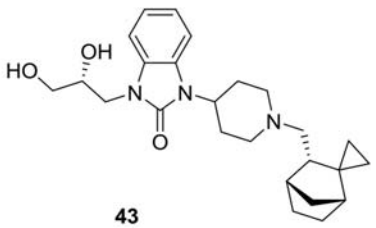

43

	ORL1 IC_{50} (nM)	*Rat* F *(%)*	*RLM*[a,b]	*HLM*[c]
42	2.3	7	0	0
43	2.3	33	70	53

[a]% Remaining at t = 30 min.
[b]*RLM*, rat liver microsomes.
[c]HLM, human liver microsomes.

shown on the right-hand side of **40** as the optimum group. Combination of this group with incorporation of a diol on the left hand side and deletion of the hydroxymethyl group provided clinical candidate **43**.

Polo-like kinase 4 (PLK4) is a kinase involved in the mitotic cycle and is viewed as a potential anticancer target. A lead from screening was subjected to iterative structure-based design, synthesis, and bioassay against PLK4 leading to the discovery of compound **44** (**Table 11**).[78] To overcome configurational instability of the double bond exocyclic to the indolinone ring, the authors replaced the double bond with a spirocyclopropane to give **45**.[79] This change maintained in vitro potency against PLK4 and growth inhibition against two cancer cell lines, MCF-7 and MDA-MB-468. In addition, water solubility, free fraction, and stability in human liver microsomes were increased, while CYP3A4 inhibition was decreased. Further optimization provided **46** which has a GI_{50} value of less than 1 nM against MCF-7 cells and was shown to be orally bioavailable in mice. Oral dosing of **46** at 25 mg kg^{-1} once a day (q.d.) for 21 days resulted in 76% inhibition of tumor growth in a mouse MDA-MB-468 breast cancer xenograft model. Replacement of the dimethylamino group in **46** with 2,6-dimethyl-4-morpholino gave the clinical candidate **47** (CFI-400945).[80,81] In addition to maintaining cellular potency, this compound demonstrated a 35× higher mouse plasma area under the curve (AUC) than **45** when both compounds were dosed at 25 mg kg^{-1} per os (PO).

Compound **48** (AM-1638) is a full agonist of GPR40, a G-protein-coupled receptor (GPCR) target involved in regulation in insulin secretion, with an EC_{50} value of 160 nM (**Fig. 12**). Efforts to constrain the conformation of the phenylpropanoic acid region led to the identification of spirocycle **49** (AM-5262) which possesses improved potency (EC_{50} = 81 nM) and is a full agonist.[82] In addition **49** is more selective than **48** against a panel of 101 GPCRs, ion channels, transporters, and enzymes and has lower clearance in rat. In HF/STZ type II diabetic mice, **49** dosed at 30 mg kg^{-1} provided similarly efficacy in an oral glucose tolerance test to 60 mg kg^{-1} of **48**.

Table 11 Spirocyclopropane polo-like kinase 4 (PLK4) inhibitors

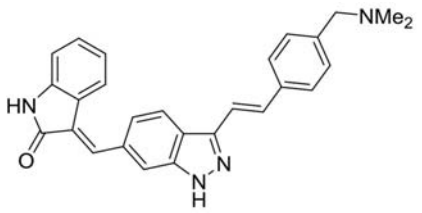

44

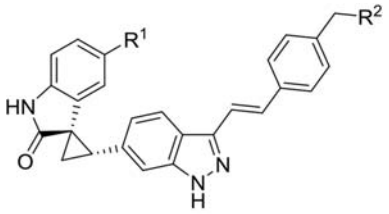

45 R^1 = H, R^2 = NMe_2

46 R^1 = OMe, R^2 = NMe_2

47 R^1 = OMe, R^2 = 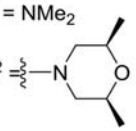 (CFI-400945)

Cpd	*PLK4 IC_{50} (nM)*	*MCF-7 GI_{50} (nM)*	*MDA-MB-468 GI_{50} (nM)*	*Water solubility (μg mL^{-1})*	*PPB[a] (%)*	*HLM $t_{1/2}$[b] (min)*
44	4	7	12	<0.1	98.4	40
45	2	<10	<10	1.7	94.7	>60
46	1	<1	10	–	–	–
47	3	8	6			>60

[a]*PPB*, plasma protein binding.
[b]*HLM*, human liver microsome.

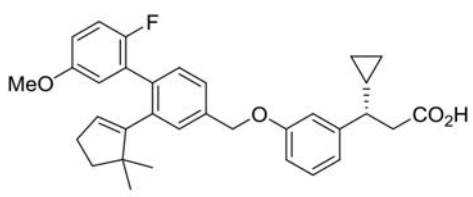

48 (AM-1638)

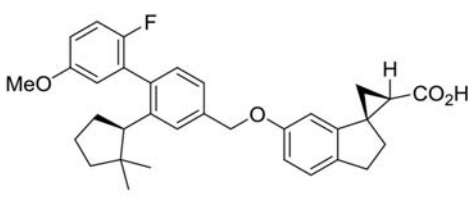

49 (AM-5262)

Fig. 12 Spirocyclopropane GPR40 agonists.

Table 12 Spirocyclopropane agonist of human metabotropic glutamate 2 (hmGlu2) and 3 (hmGlu3)

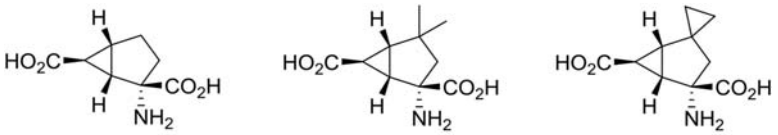

50 **51** **52**

	hmGlu2 K_i *(nM)*	*hmGlu3* K_i *(nM)*	*hmGLu2* EC_{50} *(nM/%)*	*hmGLu3* EC_{50} *(nM/%)*
50	72	107	7/100	28/100
51	2760	2000	600/92	>25,000/–
52	260	177	8/99	62/88

Compound **50** is a dual agonist of the human metabotropic glutamate 2 (hmGlu2) and 3 (hmGlu3) receptors (Table 12).[83] Geminal dimethyl analog **51** exhibits reduced ability to displace a radiolabeled ligand from receptor preparations, and retains weak agonist activity against hmGlu2 but is inactive as an agonist on hmGlu3. Spirocyclopropane is often deployed as an isostere of the geminal dimethyl group; however, in this instance **52** (LY2934747) retains dual agonist activity, albeit with reduced potency on hmGlu3 compared to **50**.

Spirocyclopropane **53** is highly selective for cyclooxygenase type 2 inhibition over COX-1 and is active in vivo upon oral administration at 30 mg kg^{-1} in three rat assays (Fig. 13).[84] Earlier SAR indicated that the corresponding spirocyclobutyl series was less active in vivo.

Spirocyclic analogs of carbanucleosides have been explored as antivirals by several groups.[85–87] For example, **54** is 4× more potent than the standard compound 2′-*C*-methylcytidine in the HCV RNA replicon Huh7 assay.[87]

Aziridines have not received much attention from medicinal chemists. Steroid derivatives **55a** and **55b** provide rare examples of spiroaziridines.[88] The two compounds are inhibitors of human 17α-hydroxylase/C_{17-20} lyase, a heme containing enzyme, with IC_{50} values of 339 and 372 nM respectively. Related nonspirocyclic compounds were more potent inhibitors.

1.08.3.1.4 Spiro[2.5] ring systems

The spiroepoxide natural product fumagillin (**4**, Figs. 2 and 14) is a covalent inhibitor of methionine aminopeptidase-2 (MetAP-2).[89,90] Several biological activities, resulting from inhibition of MetAP-2 by **4** and its semisynthetic analogs, with potential clinical application have been reported. For example, **56** (TNP-470, AGM-1470) inhibits the growth of tumors in animal models due to its antiangiogenic activity and reached Phase 2 clinical trials.[91,92] Compound **56** also exhibits antiparasitic activity.[93] Carbamate **57** (PPI-2458) resulted from an effort to improve the poor oral bioavailability of **56** and reduce its central nervous system (CNS) penetration (Table 13).[94] In addition to demonstrating improved inhibition of MetAP-2 and more potent inhibition of the growth of human umbilical vein endothelial cells (HUVEC), compound **57** was 9% orally bioavailable in rat and none of the animals displayed CNS toxicity and when dosed at 60 mg kg^{-1} day^{-1} IV for 14 days. More recently another analog, **58** (ZGN-433, beloranib) for the treatment of obesity has completed Phase 2 (Fig. 14).[95]

The natural product FR901464 (**59**) and its *O*-methyl derivative spliceostatin A (**60**) have been shown to bind to the SF3b subunit of the spliceosome and disrupt its functioning (Fig. 15).[96] Compounds with this mode of action are of interest in oncology.

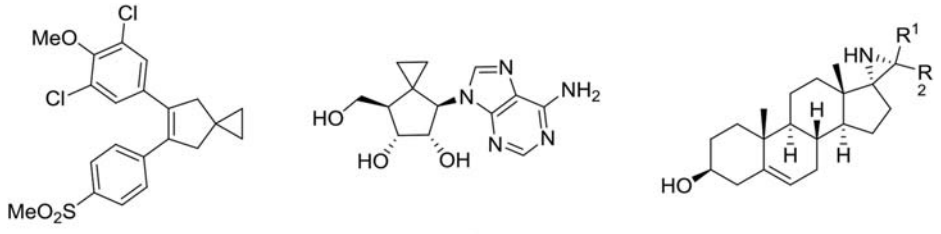

53
COX-2 IC_{50} 6 nM
COX-1 IC_{50} >100 μM

54

55a R^1 = H, R^2 = Me
55b R^1 = Me, R^2 = H

Fig. 13 Selected spiro[2.4] compounds.

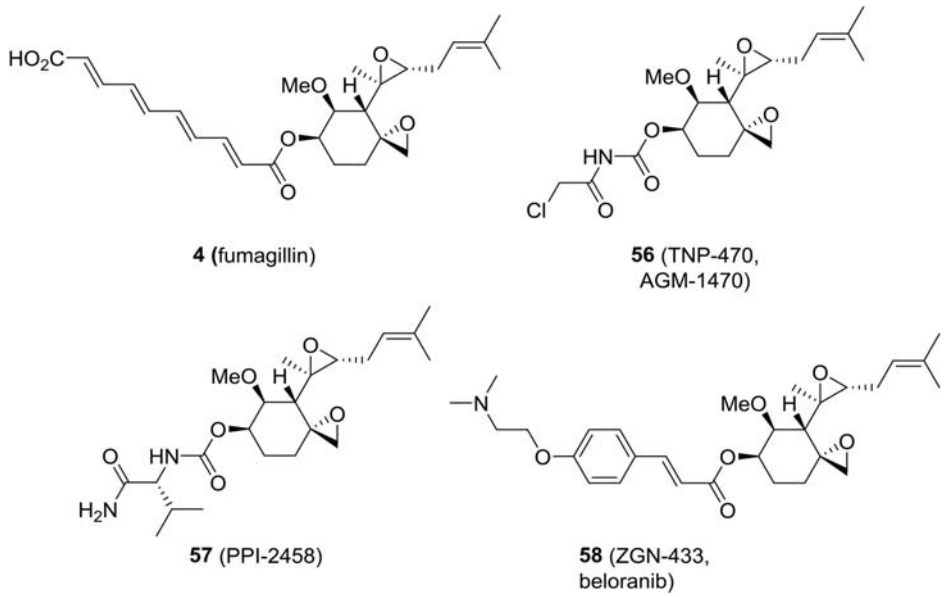

Fig. 14 Fumagillin analogs.

A group at St. Jude Children's Research Hospital has prepared a series of analogs, including **61**, termed sudemycins, with fewer stereocenters.[97] Further optimization of **61** led to carbamate sudemycin D6 (**62**) which displayed cytotoxic activity against several tumor cell lines (SK-MEL-2: $IC_{50} = 39$ nM; HeLa: $IC_{50} = 50$ nM).[98]

Orally bioavailable γ-amino acid pregabalin (**63**) is approved for treatment of neuropathic pain (Fig. 16). It binds to the α_2-δ subunit of voltage-gated calcium channels with a K_i of 19 nM. Spirocyclic β-amino acid **64** binds with a K_i of 13 nM. Like **63**, **64** protected DBA/2 mice from audiogenically induced tonic seizures when 30 μg was injected into the cerebral ventricles; however, **64** was not effective when dosed orally at 30 mg kg^{-1}.[99] Unlike **63**, **64** is not a substrate for active transport into the CNS by the system L transporter.

Table 13 Optimization of TNP-470

	MetAP-2[a] *(% activity)*[b]	*Growth inhibition of HUVEC*[c] *IC_{50} (nM)*	*Rats showing CNS toxicity at 60 mg kg^{-1} for 14 days (%)*
56	4	0.25	100
57	2.8	0.095	0

[a]MetAP2, methionine aminopeptidase-2.
[b]% Activity remaining after treatment with 400 nM of compound for 8 h.
[c]*HUVEC*, human umbilical vein endothelial cells.

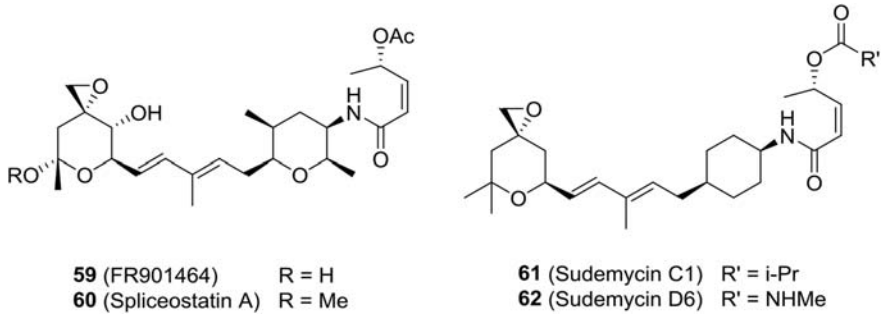

Fig. 15 Spiroepoxide spliceosome inhibitors.

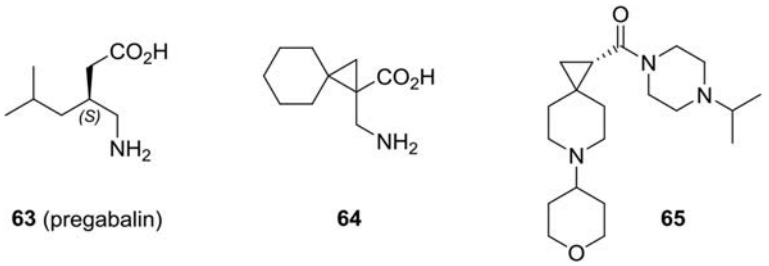

Fig. 16 Selected spiro[2.5] compounds.

Exploration of a 6-azaspiro[2.5]octane core resulted in the discovery of selective histamine-3 receptor (H_3R) antagonist **65**.[100] The compound has a receptor binding K_i of 0.8 nM and a cellular IC_{50} of 8.3 nM. The compound is highly selective for H_3R over other biogenic amine receptors, including H_1R, H_2R, and H_4R. It has oral bioavailability of 99% in rat, a brain to plasma ratio of 3.

1.08.3.1.5 Spiro[2.≥6] ring systems

Dual inhibitors of angiotensin converting enzyme (ACE) and neutral endopeptidase (NEP) are expected to possess superior antihypertensive activity. Geminal dimethyl compound **66a** exhibits double digit nanomolar inhibition of both ACE and NEP (Table 14). The subtle change brought about by constraining the two methyl groups to give spirocyclopropane **66b** maintains ACE potency, but leads to a 6× loss in NEP potency.[101]

1.08.3.2 Spiro[3.*n*] Ring Systems

With the important exception of β-lactams, four-membered rings have been exploited in medicinal chemistry to a lesser extent than three-, five-, and six-membered rings. Similarly, four-membered rings are less numerous in spirocycles, although this situation has begun to change driven by improved methods for their synthesis.[44–46]

1.08.3.2.1 Spiro[3.3] ring systems

2-Oxa-6-azaspiro[3.3]heptane and 2,6-diazaspiro[3.3]heptane have been proposed as isosteres of morpholine and piperazine, respectively,[44,46,102] and they have increasingly appeared in the medicinal chemistry literature in these roles. Three examples follow. Replacement of the morpholine ring in leucine rich repeat kinase 2 inhibitor **67** with 2-oxa-6-azaspiro[3.3]heptane gave **68** (Fig. 17A) which suffered a drastic loss in potency.[103] By contrast, replacement of the piperazine ring in ketohexokinase inhibitor **69** with 2,6-diazaspiro[3.3]heptane provided **70** with slightly improved potency (Fig. 17B).[104] In a series of stearoyl CoA desaturase (SCD) inhibitors, piperazine and 2,6-diazaspiro[3.3]heptane analogs **71** and **72** had comparable potency (Fig. 17C).[105]

1.08.3.2.2 Spiro[3.4] ring systems

Compound **73** inhibits epidermal growth factor receptor (EGFR) kinase with an IC_{50} of 15 nM and is cytotoxic to HCC827 cells, a cell line which contains an EGFR-activating mutation, with an IC_{50} of 28 nM (Fig. 18).[106] In addition, the compound has 34 μg mL^{-1} water solubility. Compound **74**, and its analogs, employs a spirocycle to fill the S2 pocket[107] of HCV protease, in place of the substituted pyrrolidine present in boceprevir and telaprevir.[108] Compound **74** has an EC_{50} of 800 nM against the HCV replicon in Huh7 cells. Cytotoxicity discouraged further exploration of this series.

Table 14 Dual angiotensin converting enzyme (ACE) and neutral endopeptidase (NEP) inhibitors

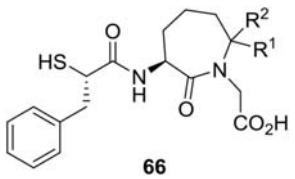

66

	R^1	R^2	*ACE IC_{50} (nM)*	*NEP IC_{50} (nM)*
66a	Me	Me	12	63
66b		$-CH_2CH_2-$	9.6	377

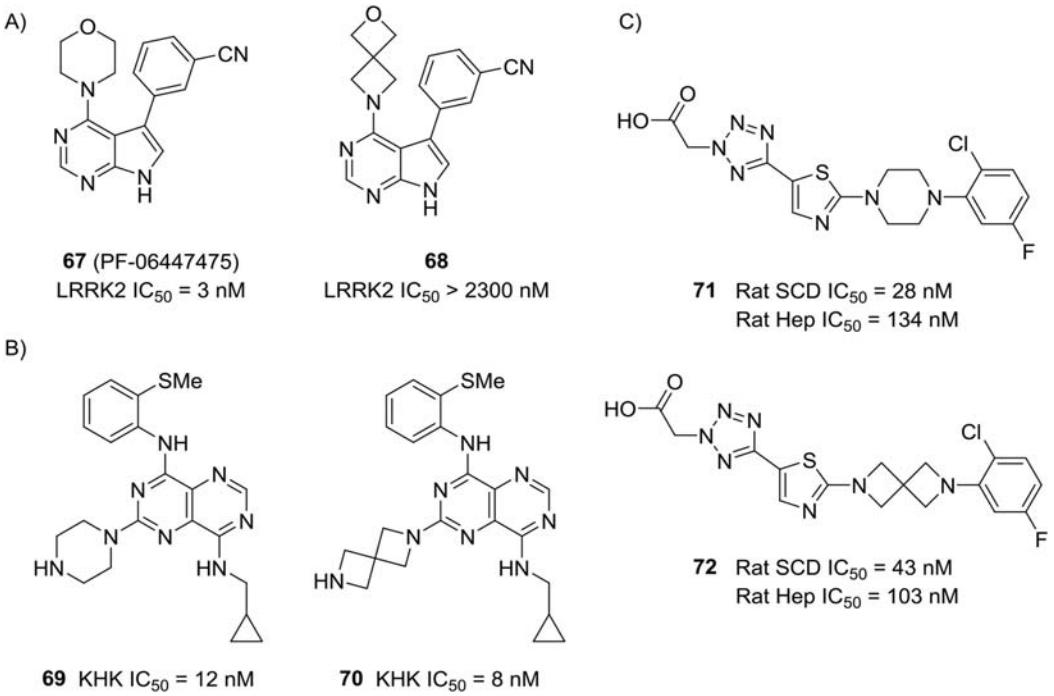

Fig. 17 Examples of the use of spiro[3.3] ring systems.

The prodrug sofosbuvir (**75**) is marketed for the treatment of HCV (Table 15). Two groups have reported analogs of sofosbuvir in which the methyl and fluoro substituents at the 2′ position are replaced with a spirooxetane.[109,110] Both groups initially explored cytidine analogs **76a** and found weak activity in the replicon assay. Conversion to the phosphoramidate prodrugs **76b**[109] and **76c**[110] led to approximately 4× improvements in potency. The uridine analog **77a** is inactive in the replicon assay; however, the derived triphosphate **77b** weakly inhibited NS5B polymerase ($IC_{50} = 39$ μM) and phosphoramidate prodrug **77c** was active in the replicon assay. Replacement of the uracil moiety with 6-methoxypurine and the methyl ester with an *n*-butyl ester afforded **78b** with submicromolar activity in the replicon assay.[109]

1.08.3.2.3 Spiro[3.5] ring systems

Urea **79** (PF-04457845) is a covalent inhibitor of fatty acid amide hydrolase (FAAH) which is orally efficacious at 1 mg kg^{-1} the complete Freunds adjuvant (CFA) rat model of pain and was nominated as a clinical candidate (Table 16).[111] The aminopyridazine moiety functions as a leaving group in **79**. A library synthesis approach was adopted in an effort to replace the methylenepiperidine core with various spirocycles. Compound **80** was identified as the most promising compound from an initial 126-member library constructed from 3 left hand tail groups, 14 spirocyclic cores, and 3 aminoheterocycle leaving groups.[112] Additional rounds of library synthesis were undertaken with the goal of optimizing potency, restoring oral bioavailability, and moving parameters such as MW into optimal ranges for CNS drugs. These goals were met with the discovery of a second clinical candidate **81** (PF-04862853) with MW <400 and a minimum effective dose of 0.3 mg kg^{-1} in the CFA model.[113]

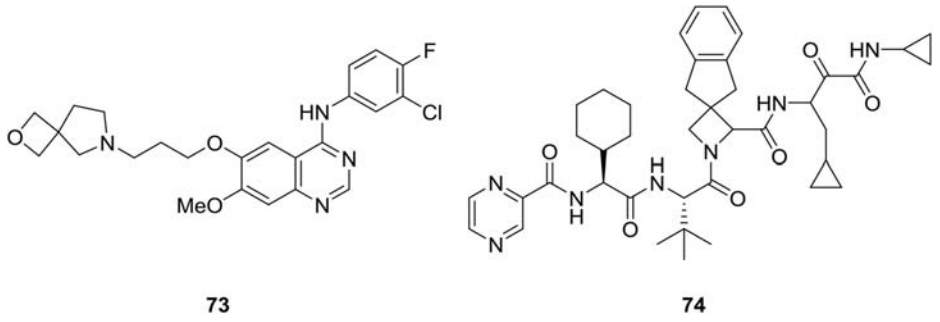

Fig. 18 Selected spiro[3.4] compounds.

Table 15 Spirocyclic nucleoside antivirals

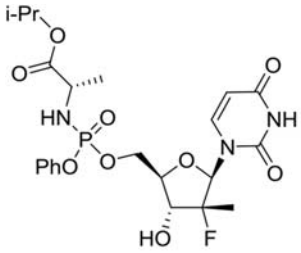

75 (sofosbuvir)

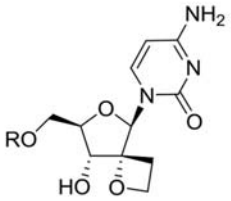

76a R = H

76b R =

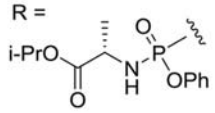

76c R =

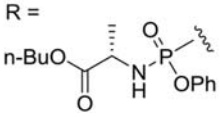

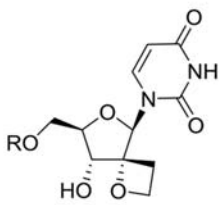

77a R = H
77b R = triphosphate
77c R =

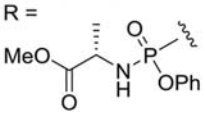

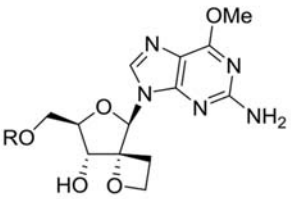

78a R = H

78b R =

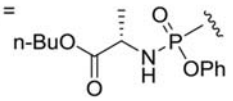

	HCV replicon EC_{50} (μM)	*Cytotoxicity CC_{50} (μM)*
76a	57[a]/17[b]	>100[a]/>98[b]
76b	17[a]	>100[a]
76c	4[b]	>98[b]
77a	>100[a]	>100[a]
77b	39	
77c	17[a]	>100[a]
78a	>100[a]	
78b	0.27[a]	>20[a]

[a]Data from Ref.[109].
[b]Data from Ref.[110].

Table 16 Spirocyclic covalent inhibitors of fatty acid amide hydrolase (FAAH)

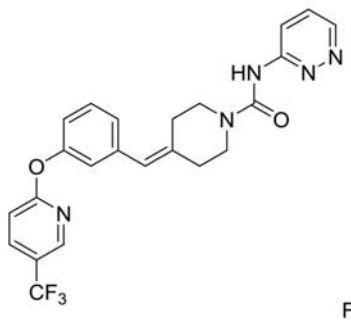

79 (PF-04457845)

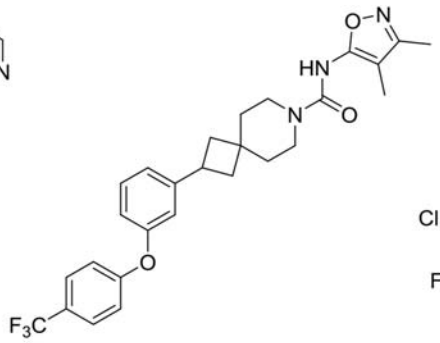

80

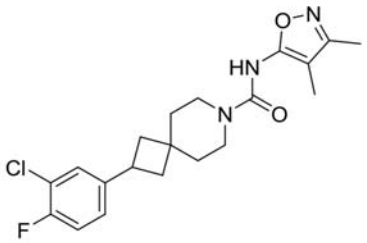

81 (PF-04862853)

	MW	*hFAAH k_{inact}/K_i ($M\ s^{-1}$)*	*CFA minimum effective dose ($mg\ kg^{-1}$)*
79	453	40,300	0.1 (PO)
80	500	1760	>10 (IP)
81	392	4190	0.3 (PO)

Table 17 Spirocyclic ghrelin receptor inverse agonists

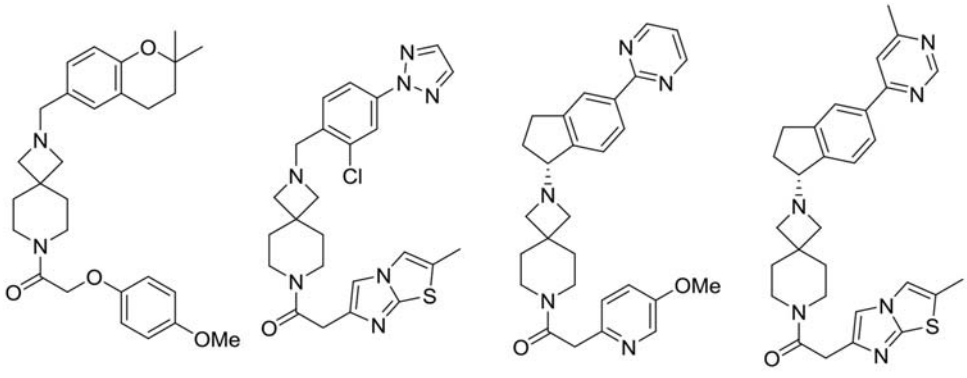

82 **83** **84** **85** (PF-5190457)

	Binding IC_{50} (nM)	*Receptor K_i (nM/%)*	*M2[a] K_i (nM)*	*M2[a] pK_b (nM)*
82	211	408/−22		–
83	5	7/−35	269	
84	30	25/−42	14,450	660
85	4	7/−29		1950

[a] *M2*, human muscarinic acetyl choline M2 receptor.

High throughput screening (HTS) identified spiroazetidine **82** as an inverse agonist of the ghrelin receptor (Table 17). Inverse agonists of this receptor are anticipated to have beneficial effects on body weight and glucose homeostasis. Optimization of the two end groups for potency and improved druglike properties led to **83**.[114] Significant off-target pharmacology of **83** on the human muscarinic acetyl choline M2 receptor was uncovered. Constraining the benzyl substituent on the azetidine nitrogen into an (*R*)-indanyl group reduced binding to the M2 receptor, for example, **84**.[115] Further optimization for potency and M2 selectivity identified the favorable properties of the 6-methyl-4-pyrimidinyl group and led to the discovery of the clinical candidate **85** (PF-5190457).[116] In cultured human whole islets, 1 μM of **85** stimulated insulin secretion more effectively than 11.2 mM glucose.

A group at Amgen has reported on a series of hydroxyethylamine beta-site amyloid precursor protein cleaving enzyme 1 (BACE1) inhibitors that incorporate a spirocyclobutane (Table 18). The genesis of the spirocyclic component, which occupies

Table 18 Spirocyclobutyl beta-site amyloid precursor protein cleaving enzyme 1 (BACE1) inhibitors

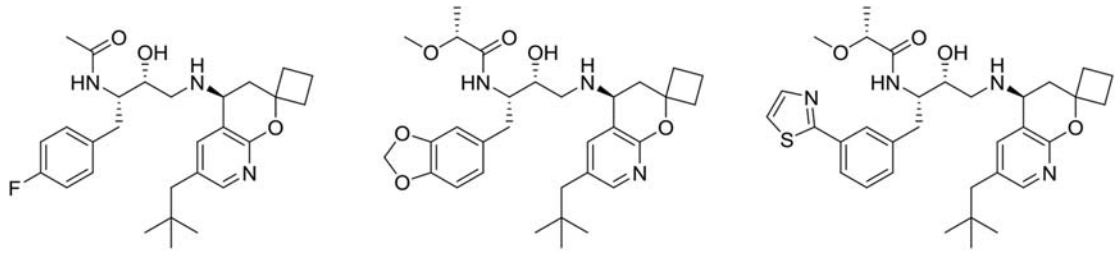

86 **87** **88**

Cpd	*BACE1 IC_{50} (nm)*	*Cell IC_{50} (nM)*	*Rat efflux ratio*	*%F[a]*	*PO dose (mg kg^{-1})*	*Brain Aβ reduction[b] (%)*
86	5	12	43	39	100	32
87	17	26	6	>100	30	44
88	6	10	1.7	>100	30	59

[a] *F*, oral bioavailaibility.
[b] *Aβ*, amyloid beta.

Table 19 Spirocyclic checkpoint kinase 1 (ChK1) inhibitor

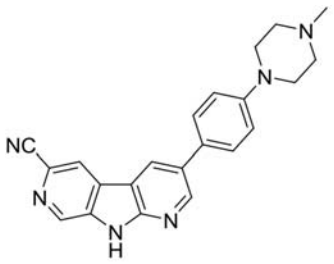

89

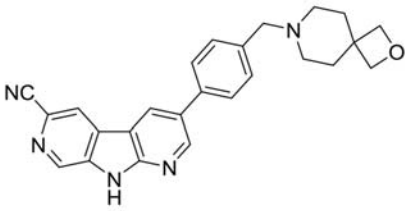

90

Cpd	*ChK1 IC_{50} (nM)*	*ChK1 cellular EC_{50} (nM)*	*AChE IC_{50} (nM)*
89	1.3	98	18
90	2.5	73	2420

the S1′ and S2′ pockets[107] of the enzyme, has not been reported. Compound **86** demonstrated a 32% reduction in brain β-amyloid (Aβ) level, when dosed at 100 mg kg^{-1} PO to rats.[117] The disappointing in vivo efficacy was ascribed to suboptimal pharmacokinetics and poor CNS penetration. Furthermore, **86** is subject to permeability glycoprotein (PGP) mediated efflux, limiting drug levels in brain. Incorporation of a 3,4-methylenedioxy substituent on the benzyl group in place of 4-fluoro imparted potent CYP3A4 inhibition and, as a result, reduced clearance in liver microsomes. Combination of this change with replacement of the acetamide by a methoxypropionamide provided **87** which is slightly less potent than **86** but has reduced PGP efflux and improved bioavailability.[118,119] Compound **87** demonstrated a 44% reduction in brain Aβ level, when dosed at 30 mg kg^{-1} PO to rats, but unfortunately, caused drug-induced tachycardia in dog. A further round of optimization led to thiazole substituted analog **88** with improved potency and a lower rat efflux ratio.[120] This compound retained CYP3A4 inhibitory activity, resulting again in high oral bioavailability and further improved brain Aβ reduction.

Diazacarbazole **89** is a potent, orally bioavailable inhibitor of checkpoint kinase 1. In the course of profiling for off-target activities, **89** was found to be a potent acetyl cholinesterase (AChE) inhibitor (Table 19).[121] An X-ray structure of **89** bound to ChK1 and a model of **89** bound to AChE were employed to guide analog synthesis toward more selective compounds. Spirooxetane **90** demonstrated improved Chk1 cellular activity and a $>125\times$ reduction in inhibition of AChE compared to **89**. Four cycles of treatment of HT-29 xenograft mice with gemcitabine, followed 24 h later by PO administration of 50 mg kg^{-1} of **90**, resulted in complete inhibition of tumor growth.

1.08.3.3 Spiro[4.*n*] Ring Systems

1.08.3.3.1 Spiro[4.4] ring systems

First reported in 1959, spironolactone (**91**) is an antagonist of aldosterone, the major endogenous ligand of the mineralocorticoid receptor (MR) (Fig. 19). Its use in the clinic as an antihypertensive is limited by side effects including gynecomastia, hyperkalemia, and menstrual irregularities, resulting from its lack of selectivity for MR over the androgen and progesterone receptors (AR and PR, respectively). Efforts to improve the selectivity of **91** resulted in the discovery of eplerenone (**92**) which binds to MR with $20\times$ reduced potency than **91**, to AR with $12\times$ reduced potency and to PR with $>140\times$ reduced potency.[122,123] Despite its reduced

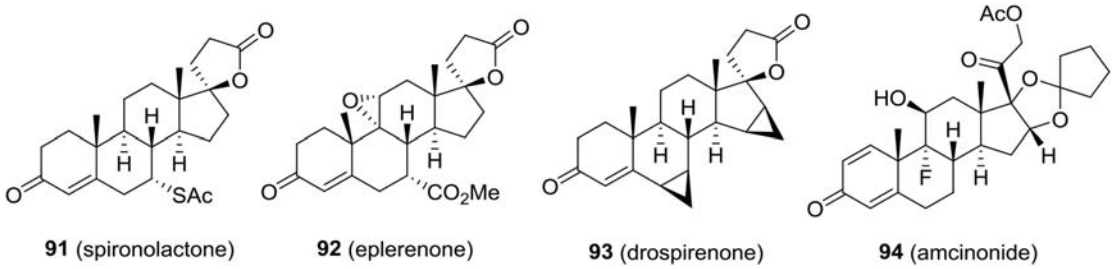

91 (spironolactone) **92** (eplerenone) **93** (drospirenone) **94** (amcinonide)

Fig. 19 Spirocyclic mineralocorticoid receptor antagonists and amcinonide.

Table 20 Losartan analogs

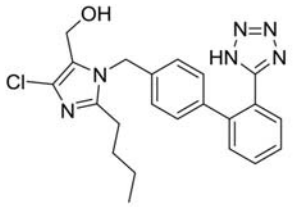

95 (losartan)

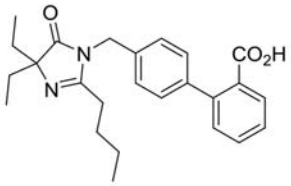

96

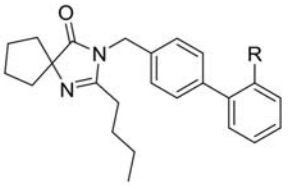

97a R = CO_2H
97b R = 5-tetrazolyl
(irbesartan)

Cpd	*ATII binding IC_{50} (nM)*	*Rabbit aortic ring IC_{50} (nM)*
95	14	25
96	56	270
97a	10	63
97b	1.3	4

binding to MR in vitro, **92** is a more potent aldosterone antagonist in vivo and exhibits reduced antiandrogenic and progestagenic effects. Drospirenone (**93**) is an analog of **91** which has been optimized for PR antagonism, although it retains antimineralocorticoid activity comparable to that of progesterone.[124] Compound **93** is used clinically, in combination with ethinylestradiol, as an oral contraceptive.

Spiroketal amcinonide (**94**) is a topical corticosteroid used for treatment of atopic dermatitis and allergic contact dermatitis.[125]

Researchers at Sanofi hypothesized that an imidazolin-4-one ring could replace the hydroxymethylimidazole moiety in the antihypertensive angiotensin II receptor blocker losartan (**95**, Table 20).[126] Analogs with a single substituent at the 5-position proved to be unstable, so 5,5-disubstituted analogs were investigated. Spirocycle **97a** was more potent than the isosteric 5,5-diethyl analog **93**. Reintroduction of the tetrazole ring gave irbesartan (**97b**) which is a clinically used antihypertensive.

Enalapril (**98a**) is prescribed for the treatment of hypertension (Table 21). It is a prodrug of the active dicarboxylic acid inhibitor enalaprilat **98b**. Incorporation of a spirocyclic amino acid into **98a**, in place of proline gave spirapril **99a**.[127] Both ester **99a** and diacid **99b** were more potent than **98a** and **98b** in vivo. Compound **99a** is marketed as an antihypertensive.

Telcagepant (**100**) is a calcitonin gene-related peptide (CGRP) receptor antagonist which entered clinical trials for the treatment of acute migraine (Fig. 20, Table 22).[128] Development was terminated when elevated levels of the liver enzyme alanine transaminase were found in treated patients. Dealkylation of the azabenzimidazolinone ring from the 4-position of the piperidine ring is a major metabolic pathway of telcagepant, contributing to its rapid first pass metabolism in rhesus.[129] Replacement of this linkage with a suitable spirocycle, incorporating the key cyclic CONH moiety from telcagepant, was expected to block this pathway

Table 21 Spirocyclic angiotensin converting enzyme (ACE) inhibitors

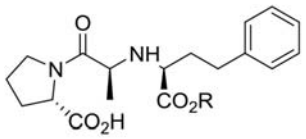

98a (enalapril)
98b (enalaprilat)

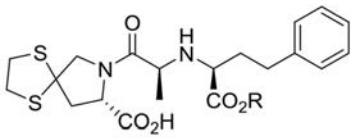

99a (spirapril)
99b (spiraprilat)

Cpd	*R*	*In vitro ACE IC_{50} (nM)*	*In vivo ACE ID_{50} ($\mu g\ kg^{-1}$)*
98a	Et	1273	57
98b	H	3	15
99a	Et	67	16
99b	H	1	8

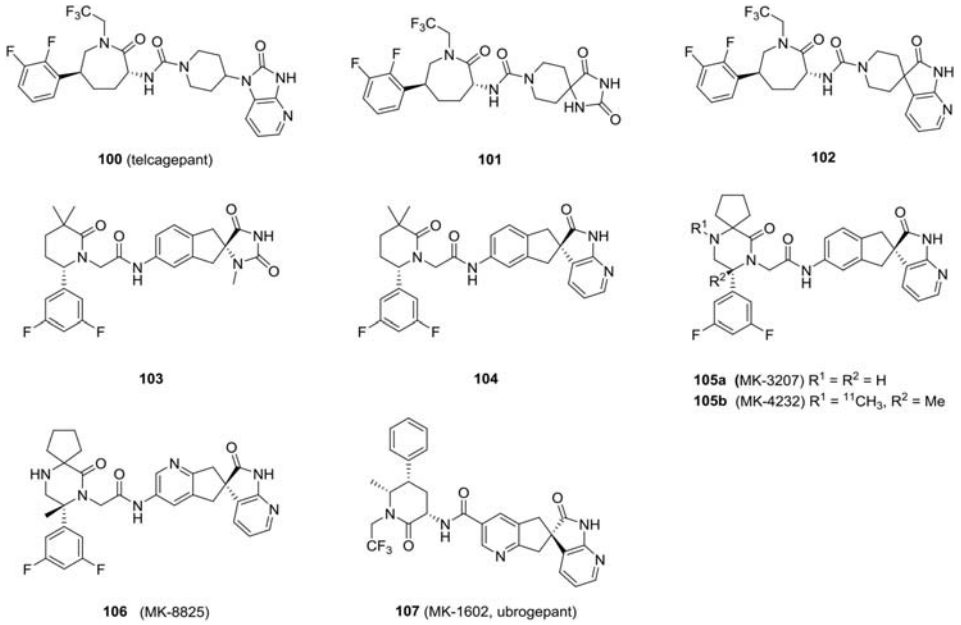

Fig. 20 Calcitonin gene-related peptide (CGRP) receptor antagonist structures.

Table 22 Calcitonin gene-related peptide (CGRP) receptor antagonist biological data

	CGRP K_i *(nM)*	*cAMP* IC_{50}[a] *(nM)*	*HS cAMP* IC_{50}[b] *(nM)*	*Rat* F[c] *(%)*
100	0.8	2	11	
101	46	94	122	
102	1.7	3.3	11	35
103	0.23			
104	0.035	0.16	0.35	12
105a	0.021	0.12	0.17	74
105b	0.046	0.1	0.39	
106	0.047	0.23	0.34	28

[a]Inhibition of CGRP-induced cAMP production in HEK293 cells.
[b]Inhibition of CGRP-induced cAMP production in HEK293 cells in the presence of 50% human serum.
[c]*F*, oral bioavailability.

while maintaining receptor potency. Scientists at Merck reported a survey of spirocycles which identified spirohydantoin **101** and spiroazaoxindole **102** as compounds with potential for optimization.[130] Replacement of the left hand portion of **101** with other groups lead to compound **103** which is more potent in vitro than telcagepant.[131] Replacement of the hydantoin with an azaoxindole gave **104** which, as expected based on the earlier work,[132] gained potency. The oral bioavailability of compound **104** was limited in rat (12%) and nil in rhesus (0%).[133] Introduction of an NH in the lactam ring and tying back the geminal dimethyl substituents into a spirocyclopentane provided **105a** (MK-3207) with excellent in vitro potency and improved oral bioavailability in both rat (74%) and rhesus (9%).[133] Further modifications afforded ^{11}C PET ligand **105b** (MK-4232)[134] and **106** (MK-8825).[135] The structure of ubrogepant (**107**), a second clinical candidate, has been revealed, but the details of its discovery have yet to be published.[136] Interestingly, the configuration of the spirocycle in **107** is inverted relative to **105a** and **106**. Presumably this is a function of the attachment point of the left hand portion of the molecule as described for earlier compounds.[137]

Compound **108** is potent inhibitor of the zinc metalloproteinase tumor necrosis factor-α-converting enzyme (TACE), albeit with substantially reduced potency in a whole blood assay (WBA) measuring inhibition of TNF-α release (Table 23).[138] Molecular modeling indicated that the 4-position of the cyclopentane ring of **105** is solvent exposed. Spiroketal **109** was equipotent to **108** in binding but was 20× more potent in the WBA.[139] The acid labile dioxolane ring precluded further development of **109**. Spirotetrahydrofurans **110** and **111** both bound tightly to TACE and demonstrated ~4× improved potency in the WBA compared to **108**.[139] Compound **110** retained the same level of oral bioavailability of **108** in a dog.

Based on examination of crystal structures of the mouse double minute 2 homolog (MDM2) protein, also known as E3 ubiquitin-protein ligase, bound to p53 tumor suppressor, Wang and coworkers designed and synthesized densely functionalized spirooxindole **112** as an inhibitor of this protein–protein interaction (Fig. 21, Table 24).[140] Initial optimization led to compound

Table 23 Tumor necrosis factor-α-converting enzyme (TACE) inhibitors

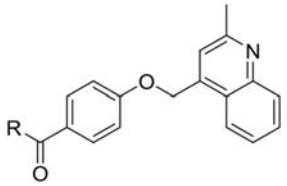

	108	***109***	***110***	***111***
R	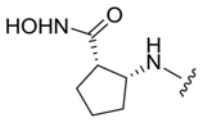	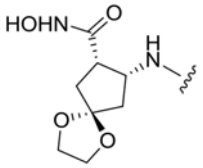	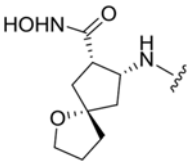	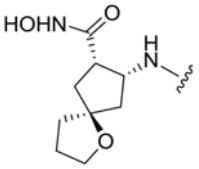
pTACE IC_{50} (nM)	1.0	1.0	1.0	1.0
WBA[a] IC_{50} (nM)	475	24	108	143
F[b] rat			31%	35%
F[b] dog	68%		68%	

[a] *WBA*, whole blood assay.
[b] *F*, oral bioavailability.

113 (MI-63) with an in vitro K_i of 3 nM but low oral bioavailability in rat.[141,142] A successful campaign to improve pharmacokinetic (PK) properties identified **114** (MI-219), albeit with a 3.5 × loss in MDM2 binding.[142] A careful study of the stability of the isomers of **115** showed that, under aqueous conditions, retro Mannich opening of the pyrrolidine ring followed by reclosure of the pyrrolidine ring resulted in the formation of all four stereosiomers.[143] Furthermore, the isomer with the syn arrangement of the 2-neopentyl and 4-halophenyl groups (depicted in **115**) is more potent than the anti arrangement (depicted in **114**). Although both **114** and **115** inhibit growth of SJSA-1 osteosarcoma cells in vitro, in the SJSA-1 xenograft model in mice, both compounds required >200 mg kg^{-1} PO doses to inhibit tumor growth and did not achieve complete tumor regression. PK properties were

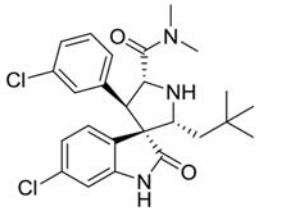

112

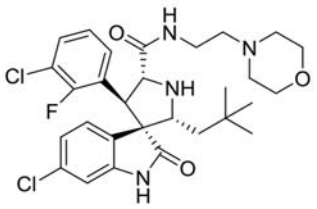

113 (MI-63)

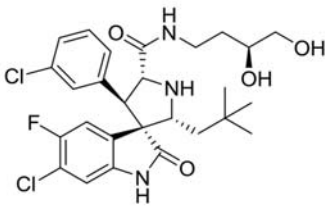

114 (MI-219)

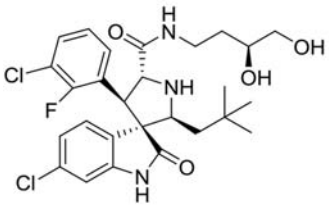

115

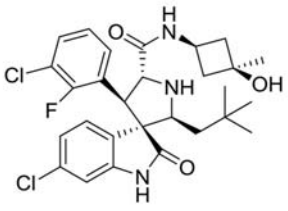

116 (MI-888)

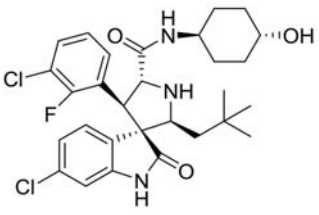

117 (MI-77301, SAR405838)

Fig. 21 Structures of spirocyclic compounds inhibitors of the MDM2-p53 protein–protein interaction.

Table 24 Biological data of MDM2-p53 protein–protein interaction inhibitors

	112	*113*	*114*	*115*	*116*	*117*
MDM2 K_i (nM)	86	3	13	0.86	0.44	0.88
SJSA cell IC_{50} (μM)		0.5	0.7	0.25	0.08	0.09
PO Dose (mg kg^{-1})		25	25	25	25	
C_{max} (μg L^{-1})		248	3751	675	1726	
$AUC_{(0-t)}$ (μg $L^{-1} h^{-1}$)		321	7677	2138	14,874	
$t_{1/2}$[a] (h)		1.3	1.4	3.4	3.2	
F[b] rat (%)		10	65			

[a] $t_{1/2}$, half-life.
[b] F, oral bioavailability.

targeted for further improvement.[144] The side chain 1,2-diol was identified as the major site of metabolism. Removal of one hydroxyl groups and conformational constraint led to aminocyclobutanol derivative **116** (MI-888) and aminocyclohexanol derivative **117**. Compound **116** demonstrated improved potency and PK properties. In SJSA xenograft mice, 30 mg kg^{-1} day^{-1} of both **116** and **117** delivered by oral gavage for 2 weeks inhibited tumor growth, while 100 mg kg^{-1} day^{-1} provided complete tumor regression. Compound **117** was shown to be configurationally stable under conditions that earlier compounds such as **112** and **115** isomerized. This compound has been extensively characterized in cancer cell lines and xenograft models, and entered Phase I clinical trials in 2012, however no results have been reported.[145–147]

Separately, a group at Hoffmann-La Roche hybridized a nonspirocyclic compound MDM2-p53 protein–protein interaction inhibitor they had discovered[148] with **116** to afford **118** (RO8894)[149] and its pyridine and thiophene analogs, **119** (RO2468) and **120** (RO5353), respectively (Table 25).[150] In a homogeneous time resolved fluorescence (HTRF) binding assay, all three compounds bound to MDM2 with single-digit nanomolar affinity and all three had average IC_{50} values of $\leq$20 nM against a panel of three p53 cancer cell lines. Compounds **118** and **120** showed very high oral bioavailability in mice. Compound **118** achieved tumor regression in SJSA xenograft mice when dosed once a day PO at 6.25 mg kg^{-1} for 30 days, while compounds **119** and **120** achieved the same effect at 10 mg kg^{-1} PO once a day.

Spirothiazolidine **121**,[151] designed from MI-219, was further optimized for potency in two cell lines, MCF-7 human breast adenocarcinoma and HT29 human colon carcinoma, to give **122** (Fig. 22).[152]

Table 25 MDM2-p53 protein–protein interaction inhibitors from Roche

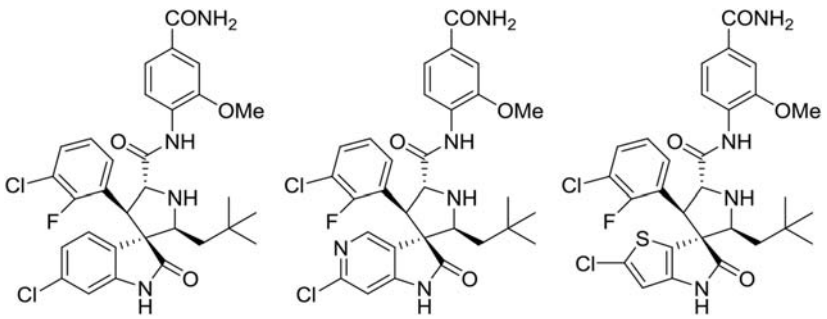

118 (RO8894) **119** (RO2468) **120** (RO5353)

	118	*119*	*120*
HTRF[a] IC_{50} (nM)	5	6	7
MTT IC_{50} (nM)	20	15	7
PO dose (mg kg^{-1})	25	5	10
PO DNAUC[b](ug h mL^{-1} mg^{-1} kg^{-1})	3.7	4.2	1.5
CL (mL min^{-1} kg^{-1})	5.8	1.8	9.9
$t_{1/2}$ (h)	7.1	3.0	3.0
F mouse (%)	92	46	92

[a] *HTRF*, homogeneous time resolved fluorescence.
[b] *DNAUC*, dose normalized area under the curve.

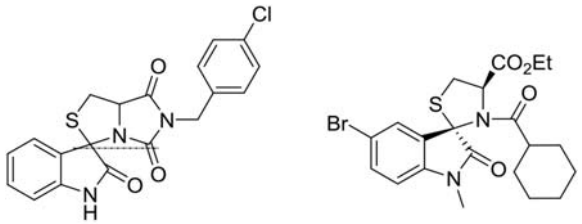

121

MCF-7 IC_{50} = 1200 nM

HT29 IC_{50} = 1600 nM

122

MCF-7 IC_{50} = 40 nM

HT29 IC_{50} = 70 nM

Fig. 22 MDM2-p53 protein–protein interaction inhibitors from the University of Naples.

Borrowing some features from an earlier series of fused hydantoin antagonists of leukocyte function associated antigen-1 (LFA-1),[153] scientists at Bristol-Myers-Squibb discovered spirocyclic hydantoin **123** (Table 26).[154] This compound was shown to be orally bioavailable in mouse and dog, and, at 10 mg kg^{-1}, it significantly blocked eosinophil accumulation in airways in the mouse ovalbumin lung inflammation model. Compound **123** was advanced into the clinic. Examination of an X-ray crystal structure of **123** bound to LFA-1 indicated that the thiophene carboxylic acid group projected into solvent and does not interact with the protein. Replacement of this group with a pyridine carboxylic acid directly attached to the pyrrolidine nitrogen to give **124** allowed formation of an additional hydrogen bond with the protein and a concomitant 7× increase in binding potency a HUVEC: T-cell binding assay.[155] In addition, **124** was ~4× more potent than **123** in blocking human T-cell activation in a mixed lymphocyte reaction assay and in a human IL-2 whole blood ex-vivo assay. Compound **124** was also advanced into clinical trials.

γ-Secretase inhibitors have been explored as potential therapeutic agents for Alzheimer's disease. Initial optimization of an HTS hit led to butanesulfonamide **125** with an IC_{50} of 610 nM in SHSY5Y cells (Table 27).[156] Replacement of the butyl group in **125** with a trifluoroethylamino group gave 4× more potent sulfamide **126**.[157] Constraining the sulfamide into a spirocycle to give **127** provided a further 8× boost in potency. Following SAR developed in the original sulfonamide lead series, a piperidinoallyl group was appended to **127** to give **128**, which achieved subnanomolar potency. This compound reduced brain Aβ(40) in transgenic APP-YAC mice with an ED_{50} of 17 mg kg^{-1} when dosed orally. Further optimization of **1** targeted the allyl linker and resulted in compound **129** which has ≥35% oral bioavailability in rat, dog, and rhesus and an ED_{50} of 1 mg kg^{-1} in APP-YAC assay.[158]

Table 26 Leukocyte function associated antigen-1 (LFA-1) antagonists

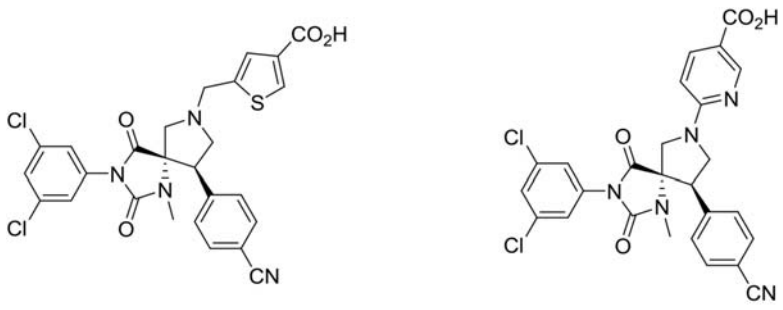

123 (BMS-587101)

124 (BMS-688521)

	123	***124***
HUVEC/T-cell[a] IC_{50}	18 nM	2.5 nM
MLR[b] IC_{50}	280 nM	60 nM
Human IL-2 mRNA IC_{50}	276 nM	65 nM
F (mouse)	41%	50%
F (dog)	100%	48%

[a] *HUVEC/T-cell*, human umbilical vein endothelial cell T-cell adhesion assay.
[b] *MLR*, mixed lymphocyte reaction assay.

Table 27 γ-Secretase inhibitors

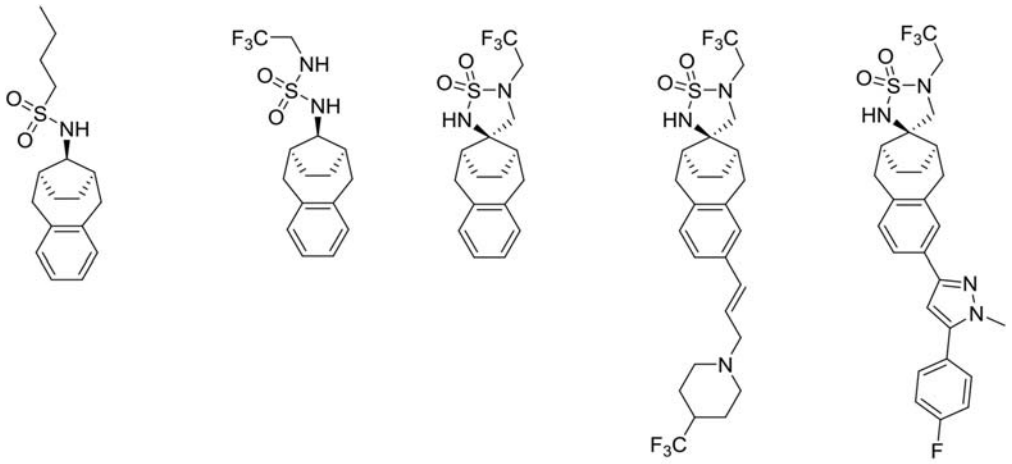

125 **126** **127** **128** **129**

	125	*126*	*127*	*128*	*129*
SHSY5Y IC_{50}	610 nM	134 nM	17 nM	0.24 nM	0.06 nM
APP-YAC ED_{50}				17 mg kg^{-1}	1 mg kg^{-1}

1.08.3.3.2 Spiro[4.5] ring systems

Investigation of the psychosedative activity of a series of *N*-(4-phenyl-1-piperazinylalkyl) cyclic imides, using animal models, showed that the spirocycle **130b** had superior properties to the geminal dimethyl analog **130a** (Fig. 23).[159] Replacement of the phenyl ring with a pyrimidine and lengthening of the alkylene linker led to the discovery of buspirone (**131**), prescribed for the treatment of anxiety.[160] Compound **131** is a member of the azapirone class of drugs and is a partial agonist of the serotonin 5-HT_{1A} receptor and an antagonist of the dopamine D_2, D_3, and D_4 receptors. It has been a starting point for drug discovery efforts aimed at improving on its receptor selectivity[161,162] and identifying compounds with broader therapeutic uses.[163] Alnespirone (**132**)[161] and tiospirone (**133**)[163] are two prominent analogs which retain the spirocyclic imide ring system.

Spiperone (**135**) was discovered in the early 1960s by C. Janssen and P. A. Janssen and is a typical antipsychotic (Table 28).[164,165] It is the only spirocyclic member of the butyrophenone class of drugs. Benperidol (**134**), another member of this class, can be considered as a nonspirocyclic analog of **132**. Spiperone is an antagonist of the dopamine D_2, serotonin 5-$HT_{1A,}$ and 5-HT_{2A}

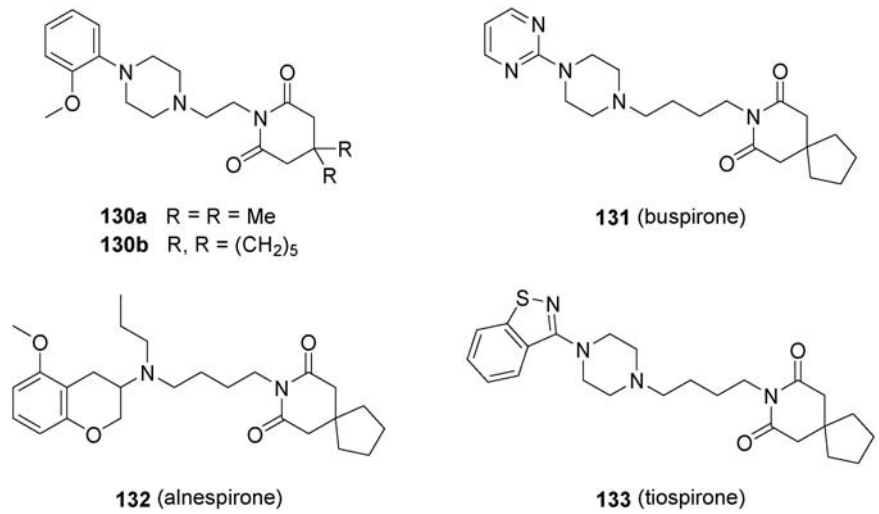

130a R = R = Me
130b R, R = $(CH_2)_5$

131 (buspirone)

132 (alnespirone)

133 (tiospirone)

Fig. 23 Spirocyclic central nervous system drugs.

Table 28 Spiperone and selected analogs

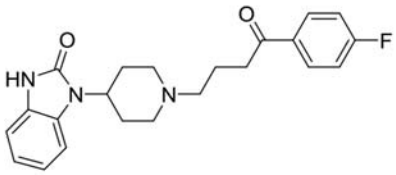

134 (benperidol)

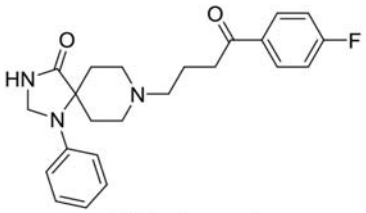

135 (spiperone)

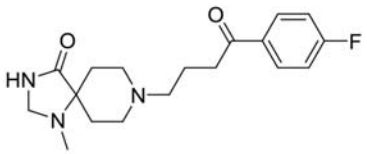

136

Cpd	K_i (nM)	
	5-HT_{2A}	5-HT_{1A}	D_2
135	1.8	58	0.5
136	23	>10,000	220

receptors. Efforts continue to identify more selective analogs.[166,167] For example, the *N*-methyl analog **136** experiences a 12× reduction in binding to 5-HT_{2A} but much greater losses in binding to 5-HT_{1A} (>170×) and D_2 (440×).

Fluspirilene (**137**, Table 29) is a typical antipsychotic, injected for the treatment of schizophrenia, which was first disclosed in the same patent as **135** (Table 28).[164] Compound **137** is primarily a dopamine D_2 and serotonin 5-HT_{2A} antagonist. Its pharmacology has been compared to 11 other antipsychotics.[168]

Enilospirone (**138**) was discovered as one member of genus of compounds that increased motility in mice (Fig. 24).[169] The compound has been of interest to enhance performance in long duration tasks.[170] At higher doses it causes sleep disturbances.[171] Fenspiride (**139**) is an antitussive.[172] Guanadrel (**140**) is a postganglionic adrenergic blocking agent prescribed as antihypertensive.[173] It functions as a partial agonist of the sodium-dependent noradrenaline transporter. Compared to the nonspirocyclic analog guanethidine (**141**), **140** has a more desirable clinical profile, exhibiting a rapid onset of action and a shorter half-life in the body.[174] The neurokinin 1 (NK1) receptor antagonist rolapitant (**142**) was approved for the treatment of delayed phase chemotherapy-induced nausea and vomiting in 2015.[175]

Selective inhibitors of sodium glucose cotransporter 2 (SGLT2) have been targeted for the treatment of diabetes. Using a pharmacophore query based on the structures of known hSGLT2 inhibitors including **143** (Table 30), researchers at Chugai identified a series spirocyclic *C*-aryl glucosides which they optimized into the highly isoform-selective clinical candidate tofogliflozin (**144**).[176]

Table 29 Fluspirilene biological data

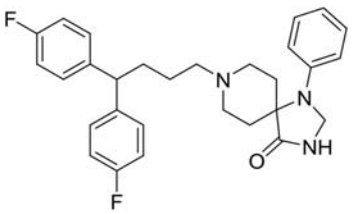

137 (fluspirilene)

	Rat receptor K_i *(nM)*	*Human receptor* K_i *(nM)*
5-HT_{1A}	110	56
5-HT_{1B}	>5000	
5-HT_{2A}	3.5	9.5
5-HT_{2B}	1830	–
D_1	450	–
D_2	1.5	–
D_{2L}	–	0.67
D_{2S}	–	1.2
D_3	1.1	3.9

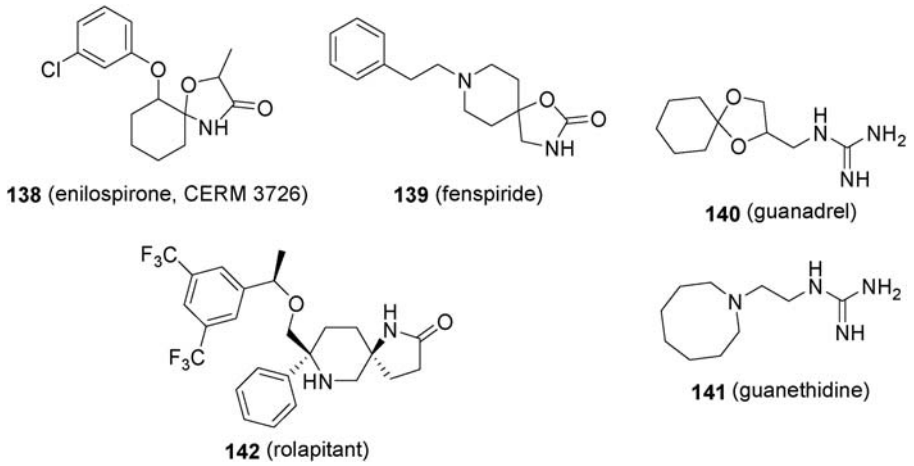

Fig. 24 Selected spiro[4.5] drugs.

Table 30 Human sodium/glucose cotransporter 2 (hSGLT2) inhibitors

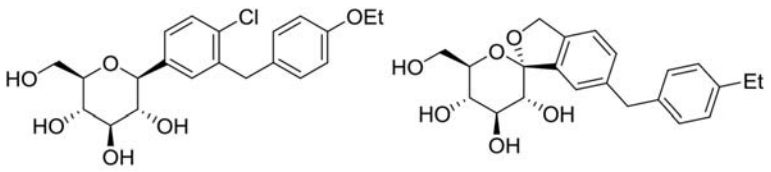

	hSGLT2 IC_{50} (nM)	*hSGLT1 IC_{50} (nM)*	*Selectivity*
143	1.3	800	615
144	2.9	8444	2912

Patchett and coworkers at Merck have described the discovery and optimization of spirocycle growth hormone (GH) secretagogues which mimic the effect of the endogenous peptide hormone ghrelin. Screening a collection of compounds prepared during earlier receptor projects uncovered spiropiperidine **145** with an EC_{50} of 300 nM for GH release in a rat pituitary cells (Fig. 25, Table 31).[177] Derivitization of the spirocyclic core led to the discovery of **146** with an EC_{50} of 50 nM as a mixture of four isomers. Concern that the strongly basic quinuclidine ($pK_a = 11$) would hinder oral absorption, prompted a quest for replacements which identified α-aminoisobutyramide. Compound **147** with an EC_{50} of 14 nM is a single isomer.[178] A 2 mg kg^{-1} PO dose of this compound increased GH levels by $\geq 4\times$ in beagle dogs. Incorporation of polar groups at the benzylic position of the spiroindane provided further potency increases as shown by **148a–c**.[179,180] Combination of a polar group at this position with replacement of the indolylmethyl group with a benzyloxymethyl group[181] led to the discovery of clinical candidate **149** (MK-0677) with an EC_{50} of 1.3 nM in the rat pituitary assay and full response in the dog model at 0.25 mg kg^{-1} PO.[177] Additional work afforded ester **150a**, a potent compound with a short half-life in vivo,[182] and amide **150b** with a subnanomolar EC_{50} value and full efficacy in the dog model at 0.06 mg kg^{-1} PO.[183]

Spiropiperidines have also proved to be effective ligands at other GPCRs with endogenous peptide ligands. Compound **151** binds to the oxytocin receptor with a K_i of 780 nM and is $>100\times$ selective over the vasopressin V_1 and V_2 receptors (Fig. 26).[184] Compound **152** binds to human somatostatin receptor subtype2 (sst_2) with a K_i of 1.6 nM and $>1000\times$ selectivity over sst_1, sst_3, sst_4, and sst_5.[185] Compound **153** binds to the tachykinin NK2 receptor with a K_i of 1.25 nM and is an antagonist in vivo.[60]

Weakly basic aminoheterocycles emerged as the favored head group to interact with the catalytic dyad Asp 32 and Asp 228 in beta-site amyloid precursor protein cleaving enzyme (BACE, β-secretase) inhibitors.[186–188] Several research groups have deployed the aminoheterocycle as one ring of a spirocyclic system. Workers at Amgen focused on the 2-aminooxazoline moiety which has a favorable pK_a (Fig. 27, Table 32).[189] Early analogs such as **154** achieved only micromolar potency. Guided by X-ray crystallography, the two phenyl rings were constrained with an ether linkage to form a spirocyclic xanthene core which was optimized to

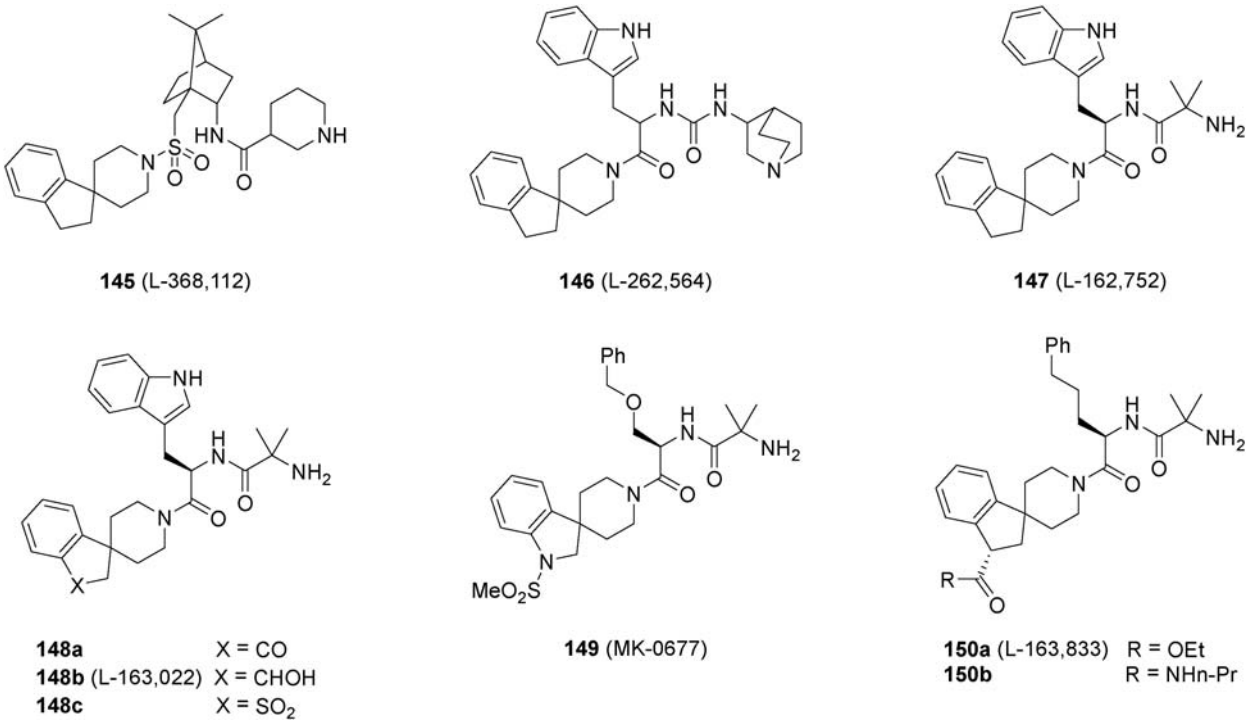

Fig. 25 Spirocyclic ghrelin agonists.

Table 31 Biological data of spirocyclic ghrelin agonists

		Dog GH release	
	Rat pituitary EC_{50} (nM)	*PO dose (mg kg^{-1})*	*Responders*
145	300		
146	50		
147	14	2.0	2/2
148a	1.2	1.0	2/2
148b	0.6	1.0	2/2
148c	2.1		
149	1.3	0.25	8/8
150a	1.0	0.25	5/8
150b	0.15	0.06	6/6

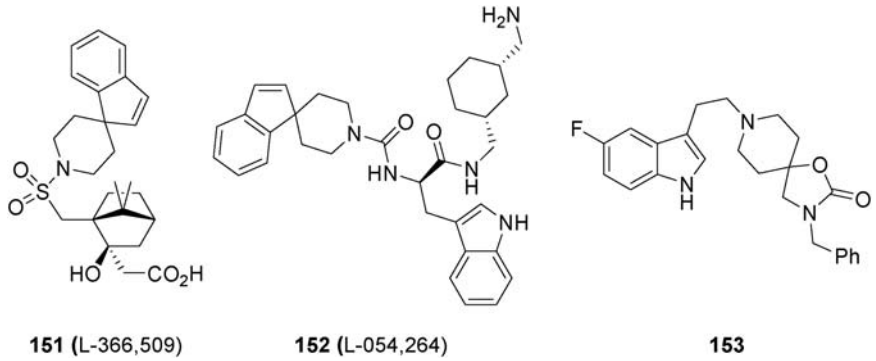

Fig. 26 Spiro[4.5] G-protein-coupled receptor (GPCR) ligands.

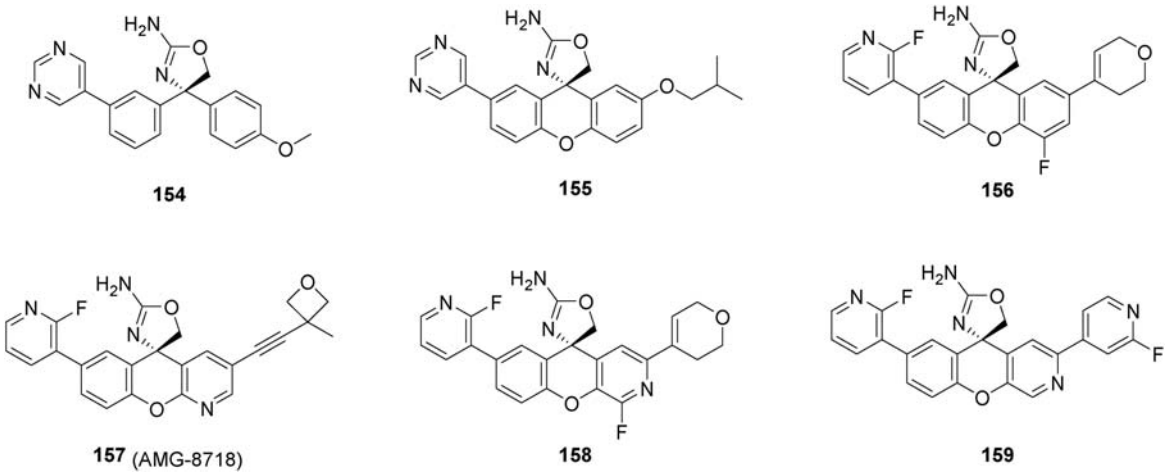

Fig. 27 Spirocyclic 2-aminooxazoline beta-site amyloid precursor protein cleaving enzyme (BACE) inhibitors from Amgen.

Table 32 Biological data of spirocyclic 2-aminooxazoline beta-site amyloid precursor protein cleaving enzyme (BACE) inhibitors from Amgen

Cpd	*BACE IC_{50} (nM)*	*BACE cellular IC_{50} (nM)*	*hERG (μM)*	*Aβ reduction in rat CSF (%)*	*Aβ reduction in rat brain (%)*
154	11,400	13,000			
155	8	36	1.84	76[a]	45[a]
156	0.3	4	3.3	78[b]	67[b]
157	0.7	4	>10	69[b]	48[b]
158	0.3	4	>15	74[c]	75[c]
159	0.9	21	>10	74[b]	65[b]

[a]Four hours after a single 30 mg kg^{-1} PO dose.
[b]Four hours after a single 10 mg kg^{-1} PO dose.
[c]Four hours after a single 3 mg kg^{-1} PO dose.

afford **155** with a >1000× increase in potency in vitro and a 350× increase in cellular potency, while maintaining properties expected to lead to CNS penetration. The oral bioavailability of **155** was 31% in rat and, following a single 30 mg kg^{-1} oral dose, it reduced $Aβ_{40}$ levels in brain and cerebrospinal fluid (CSF) by 76% and 45%, respectively. However, **155** was a low single-digit micromolar human ether-a-go-go-related gene (hERG) inhibitor. Several follow-up compounds (**156–159**), all of which incorporate a 2-fluoro-3-pyridyl moiety to fill the S3 pocket,[107] retain on-target potency while reducing the hERG liability.[190–193] Significant reductions in both rat CSF and brain Aβ levels were reported for these compounds following single oral doses of 30 mg kg^{-1} or lower; notably **158** achieved >70% reduction in both compartments at 3 mg kg^{-1}.

A collaborative effort at Array Biopharma and Genentech started with the racemic spirocyclic acyl guanidine **160** (Table 33).[194] Guided by X-ray crystallography, the bromine atom in **160** was replaced with a pyrimidine ring to give **161** which experienced

Table 33 Spirocyclic beta-site amyloid precursor protein cleaving enzyme 1 (BACE1) inhibitors

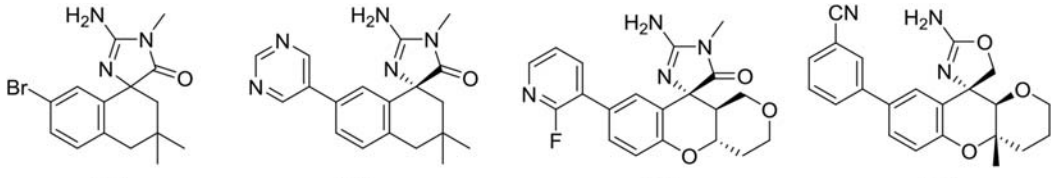

Cpd No.	*BACE IC_{50} (nM)*	*BACE cellular IC_{50} (nM)*	*CatD IC_{50} (nM)*	*Papp ($\times 10^{-6}$ cm s^{-1})*	*h PGP ER*	*Rat CSF Aβ reduction (%)*
160	37,000	–	97,740		3.4	
161	48	27	5166	5.4	53	17[a]
162	10	5	840	9	67	40[a]
163	45	39	58,000	19	3.4	63[a]

[a]Sixty milligram per kilogram PO, t=3 h.

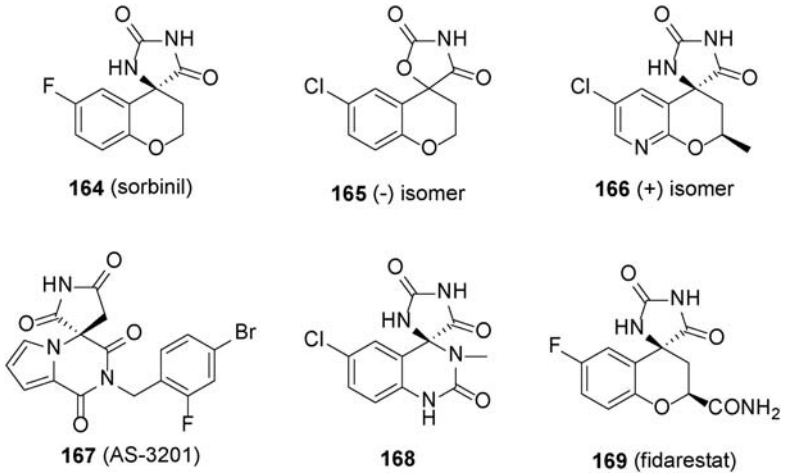

Fig. 28 Spirocyclic aldose reductase inhibitors.

a 770 × increase in potency against BACE1 but only an 18 × increase against the important off-target aspartyl protease, cathepsin D (CatD). Despite being a PGP substrate, a single 60 mg kg^{-1} PO dose of **161** to rat reduced the CSF Aβ level by 17% after 3 h. Several modifications, including replacement of the pyrimidine ring with 2-fluoro-3-pyridyl group and the geminal dimethyl substituents with a fused tetrahydropyran ring provided **162** with improved BACE potency, both in the in vitro enzyme assay and in the cell, but decreased CatD selectivity.[195] Compound **162** was also subject to PGP-mediated efflux but nonetheless effectively reduced CSF Aβ levels in guinea pig, rat, and cynomolgus monkey. Further SAR investigation, including replacement of the aspartate binding motif, afforded **163** with BACE potency comparable to **161** but greater CatD selectivity and reduced PGP efflux.[196]

Aldose reductase (AldR) catalyzes the formation of sorbitol which is implicated in the development of diabetic complications. The spirohydantoin sorbinil (**164**) was discovered by a group working at Pfizer and the absolute configuration of the active enantiomer was determined (Fig. 28, Table 34).[197–199] The (−) isomer of spirooxazolidinone **165** was a more potent binder to calf lens AldR than sorbinil but was less effective in an in vivo model that measured sorbitol levels in the sciatic nerve of streptozotocin induced diabetic rats.[200] Aza analog **166** was also a more potent binder but was less potent in the in vivo streptozocinized rat assay, possibly due to reduced metabolic stability.[201] On the other hand, the in vitro potency of spirosuccinimide **167** from Dainippon is reflected in its in vivo efficacy.[202]

Compound **168**, a more polar compound than **164**, is 10 × more potent in vitro than sorbinil; however, the effectiveness of the two compounds at inhibiting polyol accumulation in sciatic nerve is comparable, while **168** is much less effective at reducing polyol accumulation in lens (Table 35).[203] These results suggest that **168** does not penetrate the lens.

Fidarestat (**169**), a carbamoyl analog of **164**, is a 200 × more potent inhibitor of human AldR than **164** and its selectivity over the related enzyme aldehyde reductase is much improved (Table 36).[204] In addition, **169** is 8 × more potent in the streptozocinized rat

Table 34 Aldose reductase assay data of spirocyclic compounds

	Lens AldR IC_{50} (nM)	*Human placenta AldR IC_{50} (nM)*	*In vivo STZ rat ED_{50} (mg kg^{-1})*
164	260[a]	170	0.25
165[b]	100[a]		1.5–2.5
166		7.5	0.5
167	15[c]		0.18

[a]Calf.
[b](−) Isomer.
[c]Pig.

Table 35 Aldose reductase assay data of spirocyclic derivatives

	Male rabbit lens AldR IC_{50} (nM)	*Inhibition of polyol accumulation in rat sciatic nerve 15 mg kg^{-1} (%)*	*Inhibition of polyol accumulation in rat lens 15 mg kg^{-1} (%)*
164	250	90	69
168	22	86	6

Table 36 Aldose reductase assay data of fidarestat

	Rat lens AldR IC_{50} (nM)	*Human AldR IC_{50} (nM)*	*Human erythrocyte AHR IC_{50} (nM)*	*AHR/AldR selectivity*	*In vivo STZ rat ED_{50} (mg kg^{-1})*
164	250	2000	5400	2.7×	8.5
169	20	9	1200	133×	1.0

Table 37 ATP-sensitive potassium channel openers

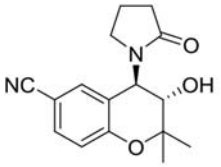

170 (chromakalim)

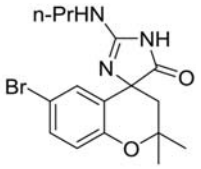

171

	Membrane polarization at 0.1 μM (%)	*Δ MAP at 0.01 mg kg^{-1} (mm Hg)*	*Δ HR at 0.01 mg kg^{-1} (bpm)*
170	<5	−14.7	+33.8
171	28	−25.6	+44.9

model. The origins of potency and selectivity of **169** have been studied by X-ray crystallography.[205–208] Compound **169** progressed to Phase 3 clinical trials.[209,210]

Chromakalim (**170**) acts on cell membrane adenosine triphosphate (ATP)-sensitive potassium channels, opening them and resulting in vasodilation (Table 37). Spirocycle **171** more effectively caused membrane hyperpolarization at 0.1 μM and caused a greater decrease in mean arterial pressure (MAP) and a greater increase in heart rate (HR) when dosed at 0.01 mg kg^{-1} IV.[211] Subsequently, the same authors demonstrated that potency resides in the (S) isomer of **171**.[212]

Conformational restriction of patented cholesterylester transfer protein (CETP) inhibitor **172** by introduction of an ether spirocycle, to give **173**, improved its potency and reduced its liphophilicity (Table 38).[213] Introduction of a second ether provided **174** with a further increase in potency and decrease in clogP. Compound **174** is orally bioavailable and dose dependently inhibited plasma CETP activity in hCETP transgenic mice, leading to a 74% increase in high density lipoprotein (HDL)-cholesterol after 5 days at the 10 mg kg^{-1} dose.

Matrix metalloproteinases (MMPs) contribute to thrombus dissolution; thus, inhibitors of MMPs have potential as for the prevention and treatment of hemorrhage. Using the X-ray structures of two known inhibitors, **175** and **176** bound to MMP13 and MMP3, respectively, spirocyclic lead **177a** was designed (Table 39). Further optimization led to the discovery of the preclinical candidate **177b**.[214] The detailed pharmacology of **177b** has been published.[215]

k Opioid agonists are expected to be potent analgesics without the undesired side effects such as respiratory depression and inhibition of gastrointestinal motility that result from the μ opioid receptor. Methoxycyclohexane **178** was the most potent of several analogs in which the position and stereochemistry of the methoxy group was varied (Table 40).[216] The methoxy group was

Table 38 Spirocyclic cholesterylester transfer protein (CETP) inhibitors

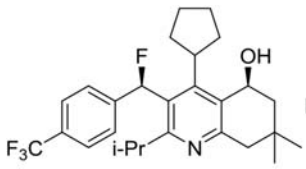

172

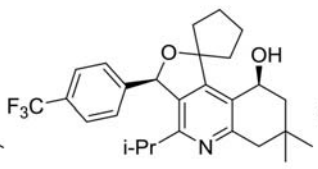

173

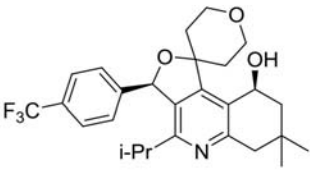

174

Cpd	*hCETP IC_{50} (nM)*	*clogP*
172	247	7.6
173	51	5.8
174	18	4.6

Table 39 Spirocyclic matrix metalloproteinases (MMP) inhibitors

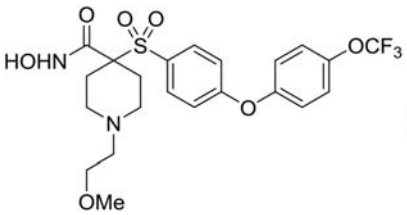

175 (SC-78080)

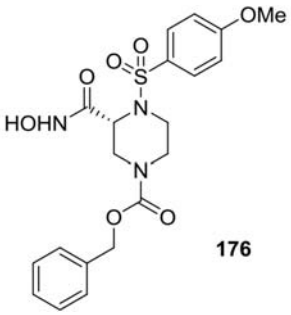

176

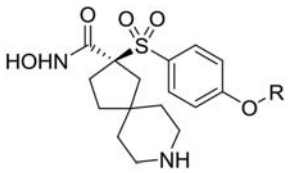

177a R = Me
177b R = 4-MeNHCOC$_6$H$_4$

Cpd	*MMP3 IC_{50} (nM)*	*MMP10 IC_{50} (nM)*
177a	96	84
177b	15	12

Table 40 Spirocyclic k opioid agonists

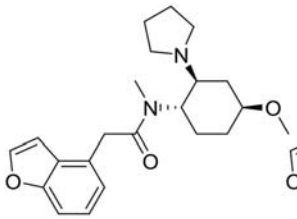

178

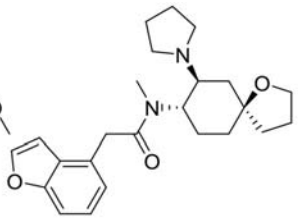

179 (enadoline)

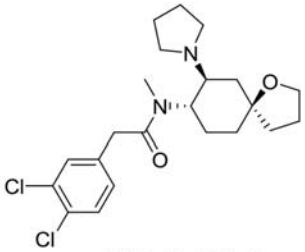

180 (spiradoline)

	k opioid K_i (nM)	*μ opioid K_i (nM)*	*μ/k selectivity*	*Rat paw pressure MPE_{50} (mg kg^{-1})*
178	7	3300	465	0.07
179	0.8	1260	1520	0.024
180	8	83	11	0.4

constrained into a spiro tetrahydrofuran to give enadoline (**179**), which was both more potent against the μ receptor and more selective over the k receptor. In addition, when dosed IV, **179** is 25× more potent than morphine in the rat paw pressure assay. The closely related compound spiradoline (**180**)[217] was less selective and less effective in the rat paw pressure assay.

Rigid analogs of acetyl choline have been explored as acetyl choline receptor agonists. Cevimeline (**181**, Fig. 28) is a muscarinic M1 and M3 agonist used clinically for treatment of dry mouth (Fig. 29).[218,219] On the other hand, spirocarbamate **182**, another conformationally constrained ACh analog, binds to the nicotinic acetyl choline receptor α7 (nAChRα7) with triple digit nanomolar potency but is selective over other subtypes and is orally bioavailable in rat (Table 41).[220] Substitution of the carbamate NH with a chlorothiophene afforded **183** which was almost 40× more potent than **182** against nAChRα7 but retained 200× selectivity against the α4β2 subtype and oral bioavailability in rat.[221] CYP2D6 inhibition by **183** was associated with the chlorothiophene

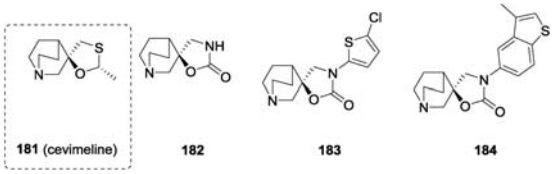

181 (cevimeline) **182** **183** **184**

Fig. 29 Spirocyclic acetyl choline receptor modulators.

Table 41 Spirocyclic nicotinic acetyl choline receptor (nAChR) modulators

Cpd	*nAChRα7 K_i (nM)*	*nAChRα4β2 K_i (nM)*	*nAChRα1β2γδ K_i (nM)*	*CYP2D6 IC_{50} (nM)*	*Rat F 10 mg kg^{-1} PO dose (%)*
182	340	>10,000	>10,000		103
183	9	1800	>10,000	2000	108
184	3	>10,000		>30,000	10

moiety. Replacement with a 3-methyl-5-benzothiophenyl group provided **184** with further increased on-target potency but without the CYP2D6 liability.[222] The oral bioavailability of **184** was low in rat but higher in monkey, 83% after a 10 mg kg^{-1} PO dose.

Piperidinopyridine **185** was uncovered in a high throughput screen of 63,040 compounds against the wingless-related integration site (WNT) pathway (**Table 42**).[223] Its favorable physical properties (MW = 274, alogP = 1.6, water solubility >1 mg mL^{-1}) made it an attractive starting point for optimization. Since the biochemical target of **185** is unknown, ligand-based methods were applied to its optimization. Replacement of the piperidine carboxamide with a spirolactam and introduction of a two ring system in place of one chlorine led to the discovery of **186**. This compound had low oral bioavailability and was an inhibitor of CYP3A4 (IC_{50} = 2100 nM). Replacement of the morpholine ring with an *N*-methyl pyrazole gave **187** with improved oral bioavailability in rat and reduced CYP3A4 inhibition. Compound **187** demonstrated a 37% reduction in tumor weight when dosed at 70 mg kg^{-1} bid for 9 days to COLO205-F1756 xenograft mice.

CC chemokine receptor 2 (CCR2) antagonists have been studied for the treatment of inflammatory diseases. An HTS campaign at Merck uncovered α-aminoamide **188** originally prepared during their NK1 program (**Fig. 30**).[224] Replacement of the dimethylamine with a spirocyclic piperidine gave **189** with a 9× improvement in binding and functional activity in a chemotaxis assay (**Table 43**). This compound was, however, more potent against NK1 (IC_{50} = 50 nM) and CC chemokine receptor 5 (CCR5) (IC_{50} = 30 nM) than CCR2. Substitution of the spirocycle with a methyl group and replacement of the 4-fluorophenyl with cyclopropyl gave **190** with improved CCR2 binding, functional activity in a Ca^{2+} flux assay and diminished binding to CCR5 (38% inhibition at 1 μM).[225] Replacement of the flexible linker with a cyclopentane provided **191a** and **191b** with subnanomolar activity in the two functional assays.[226,227] Compound **191a** displayed ~500× selectivity over CCR5. Both **191a** and **191b** had rat oral bioavailability >15%.

Two groups have reported spirocyclic inhibitors of mast tryptase (**Table 44**). Researchers at Sanofi discovered compound **192**; however, this compound was rapidly metabolized by semicarbazide sensitive amine oxidase (SSAO).[228] Consideration of the mechanism of SSAO suggested that reducing the electrostatic potential around the benzylamine would decrease the rate of metabolism by SSAO. This line of thought resulted in the discovery of **193** which was equipotent against β-tryptase and considerably more stable upon incubation with SSAO. It was also stable to rat and human liver microsomes (<20% metabolized at t = 20 min) and was not a hERG blocker. A group at Johnson & Johnson subsequently disclosed **194**, a spirocyclic analog of **192**.[229] Compound **194** is stable in human liver microsomes ($t_{1/2}$ > 100 min), 100% orally bioavailable in rat and was efficacious when dosed PO at 20 mg kg^{-1} bid for 4 days in a guinea pig model of asthma.

1.08.3.3.3 Spiro[4.6] ring systems

Dual antagonist of the histamine H_1 and serotonine 5-HT_{2A} receptors have potential for the treatment of insomnia. Structural modification of mianserin (**195a**) and mirtazapine (**195b**) led to the discovery of **196** with promising dual antagonist activity

Table 42 WNT pathway blockers

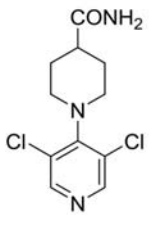

185

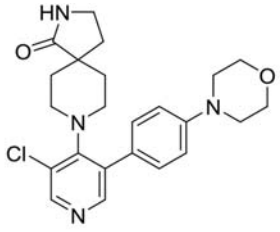

186

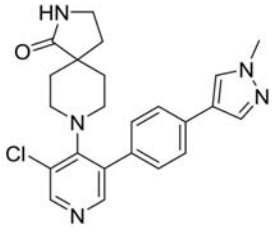

187

Cpd	*WNT IC_{50} (nM)*	*HLM (% metabolized after 30 min)*	*h Clint (μL min^{-1} kg^{-1})*	*CYP3A4 IC_{50} (nM)*	*%F rat*
185	1760	22		7000	
186	30	20	115	2100	8
187	5		84	11,400	88

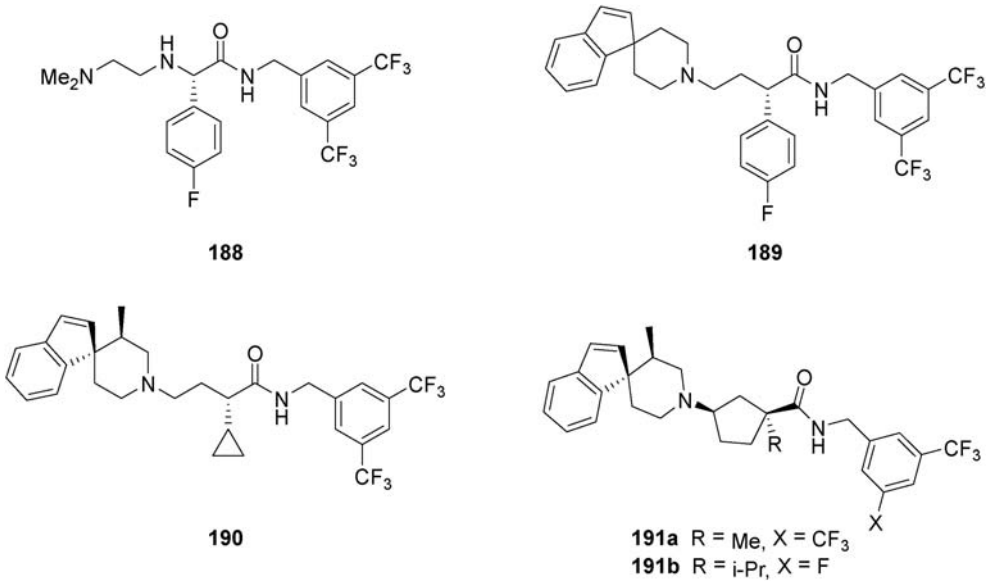

Fig. 30 Development of spirocyclic chemokine receptor 2 (CCR2) antagonists.

Table 43 Spirocyclic chemokine receptor 2 (CCR2) antagonists

	CHO hCCR2 IC_{50} (nM)	*Monocyte hCCR2 IC_{50} (nM)*	*Chemotaxis IC_{50} (nM)*	*Ca^{2+} flux IC_{50} (nM)*
188	720			
189	80		176	
190	14	4		4
191a		1.3	0.45	
191b	3.1		0.15	0.71

against H_1 and 5-HT_{2A} receptors (Table 45).[230] In addition to lacking selectivity toward 5-HT_{2B} and 5-HT_{2C} receptors, the compound suffered from significant off-target activity against cytochrome P450 2D6 (CYP2D6) and hERG potassium channels. Replacement of the dimethylamino group with an azetidine carboxylic acid to give **197** maintained on-target potency but eliminated the CYP2D6 and hERG liabilities.[231] Despite its zwitterionic character, compound **197** was orally bioavailable (Rat $F = 54\%$) and penetrated the CNS. A 3 mg kg^{-1} PO dose of **197** resulted in a statistically significant increase in total sleep time.

Table 44 Mast tryptase inhibitors

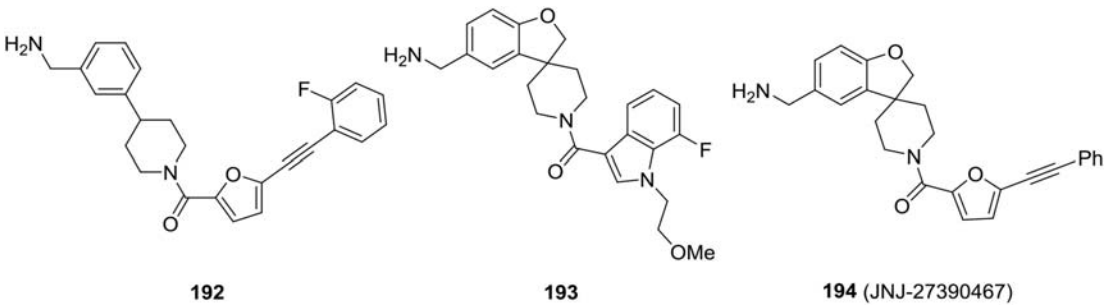

	β-tryptase K_i (nM)	*SSAO stability (% remaining at t = 20 min)*
192	16	8
193	15	89
194	4	

Table 45 Histamine (H_1) and serotonine (5-HT_{2A}) dual antagonists

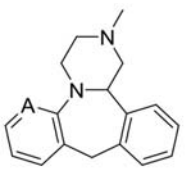

195a (mianserin) A = CH
195b (mirtazapine) A = N

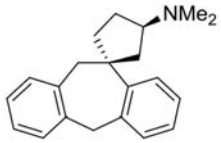

196

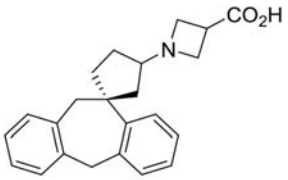

197

	H_1 IC_{50} (nM)	*5-HT_{2A} IC_{50} (nM)*	*5-HT_{2B} IC_{50} (nM)*	*5-HT_{2C} IC_{50} (nM)*	*2D6 IC_{50} (nM)*	*hERG IC_{50} (nM)*
195a	0.3	3	4	0.8		
195b	0.2	79	158	13		
196	4	13	16	8	<100	7950
197	6	16	79	6	>10,000	>50,000

Table 46 Spirocyclic endomorphin-2 mimetics

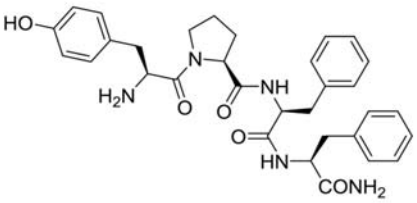

198 (endomorphin-2)

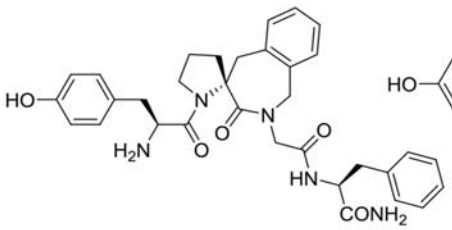

199

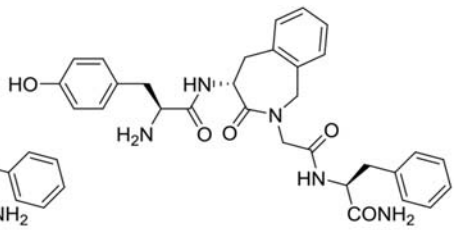

200

	μ opioid K_i (nM)	*δ opioid K_i (nM)*	*Agonist IC_{50} (nM)*[a]
198	10	–	17
199	29	>10,000	50
200	2245	2965	–

[a]Mouse vas deferens preparation.

Endomorphin-2 (**198**) is an endogenous opioid peptide with affinity for the μ-opioid receptor (Table 46). Compound **199** is an example of successful replacement of a dipeptide with a spirocycle which has been shown to be a β-turn mimetic.[14,232] Compound **199** suffered a 3× loss in binding potency but retained μ selectivity and functional activity as an agonist. Compound **200**, a non-spirocyclic analog of **199** which is not expected to adopt a β-turn conformation, was almost 1000× less potent in binding.

1.08.3.4 Spiro[5.*n*] Ring Systems

1.08.3.4.1 Spiro[5.5] ring systems

Selective monohydrogenation of the spiroketal natural product 5-*O*-demthylavermectin A_{1a} (**201**) affords compound 22,23-dihydroavermectin B_{1a} (**202**), the major component of ivermectin, an antihelminthic used in both human and animal health (Fig. 31).[233]

Artemisinin (**203**) is an important antimalarial drug (Fig. 32).[234] The peroxide moiety is essential for its biological activity. Spirocycles incorporating the 1,2,4-trioxane ring have been explored as one avenue in the effort to discover analogs with superior properties. The adamantane **204** (CDRI 97/98), discovered at the Central Drug Research Institute in India, has entered Phase 1 clinical trials.[235] Compound **205**, recently described by the same group, is orally active against multidrug resistant *Plasmodium yoelii nigerensis* in mice at a dose of 24 mg kg^{-1} for 4 days.[236]

Selective agonists of the δ opioid receptor have shown efficacy in animal models of pain. Compound **206a**, with a K_i of 500 nM against the δ receptor, was discovered by screening a proprietary library (Table 47).[237] Deletion of the 4-chlorobenzylsulfonyl group

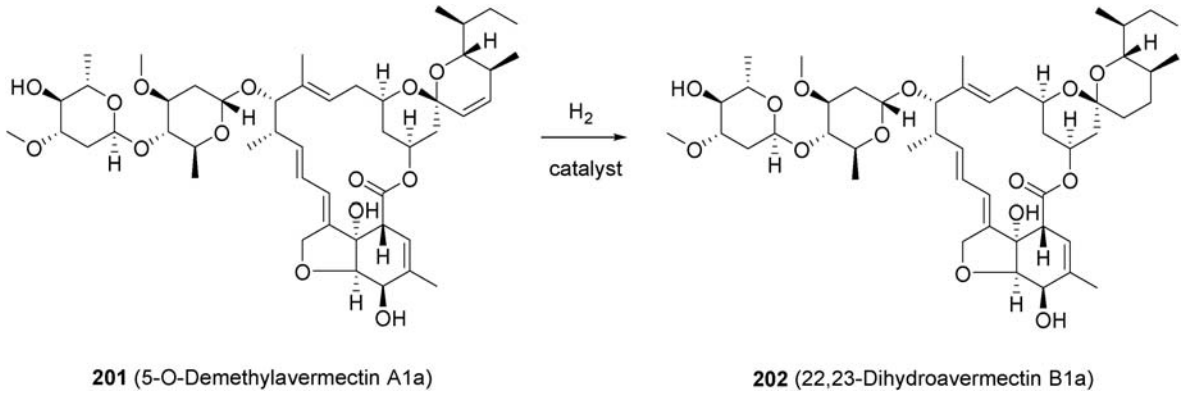

201 (5-O-Demethylavermectin A1a) **202** (22,23-Dihydroavermectin B1a)

Fig. 31 Preparation of the major component of ivermectin.

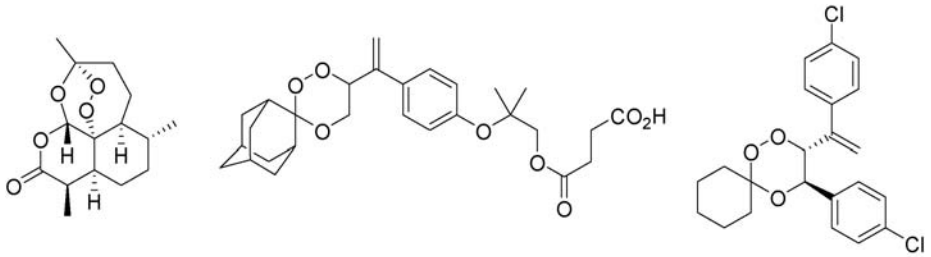

203 (artemisinin) **204** (CDRI 97/98) **205**

Fig. 32 Antimalarial trioxanes.

to give **206b** provided a 3× increase in potency, while introduction of the double bond in **207** imparted a further 2× potency improvement. While **207** demonstrated promising selectivity over the μ and k opioid receptors, it had a hERG liability. Exploration of substituent SAR around the pendant benzene ring led to the discovery of *N,N*-diethylamide **208a** with improved potency against the δ receptor, retention of isoform selectivity, and a reduced hERG liability. Introduction of a hydroxyl group on the fused benzene ring provided **208b** (ADL5859) with subnanomolar potency, excellent receptor isoform selectivity, and a much improved hERG

Table 47 Selective δ opioid receptor agonists

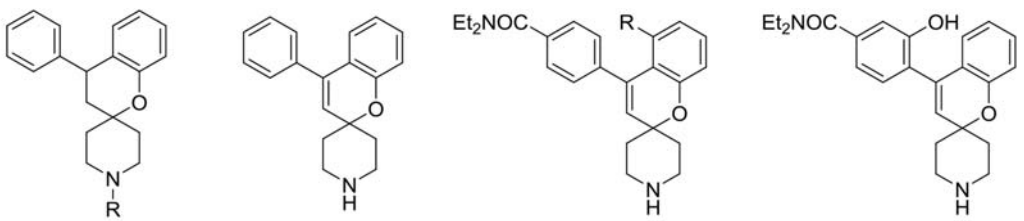

206a R = 4-ClC$_6$H$_4$CH$_2$SO$_2$ **206b** R = H **207** **208a** R = H **208b** (ADL5859) R = OH **209** (ADL5747)

Cpd	*δ* K_i *(nM)*	*δ* EC_{50} *(nM)*	*μ inhibition at 10 μM (%)*	*k inhibition at 10 μM (%)*	*hERG* IC_{50} *(nM)*
206a	500				
206b	160				
207	71	380	42	(K_i = 3400 nM)	680
208a	1.8	19	32	29	7900
208b	0.84	20	32	37	78,000
209	2.7	94	18	25	56,700

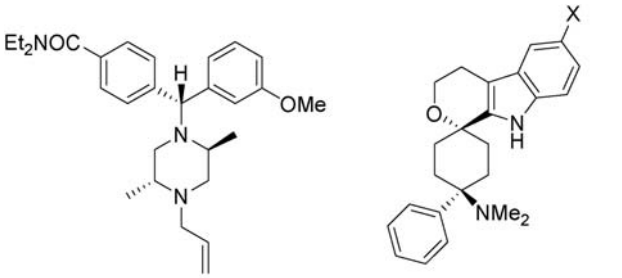

210 **211a** X= H
211b X = F (cebranopadol)

Fig. 33 δ Opioid receptor agonist and dual nociceptin/orphanin FQ peptide (NOP) and μ opioid receptor agonists.

IC_{50}. Compound **208b** was orally bioavailable (rat $F=33\%$) and efficacious in the rat Freund's complete adjuvant (FCAdj) mechanical hyperalgesia assay with an ED_{50} of 1.4 mg kg^{-1} when dosed PO. This compound was well tolerated in a Phase I safety study and was advanced into a Phase II proof of concept study. An alternative optimization of **208a** gave **209** (ADL5747) which is less potent than **208b** in vitro but has an improved ED_{50} of 0.03 mg kg^{-1} in the fluorescent cytoprint assay (FCA).[238] The oral bioavailability of **209** was 38% in rat and it was free of significant off-target liabilities, including against hERG. Compound **209** was advanced into Phase 1 clinical trials. Unlike the nonspirocyclic δ opioid receptor agonist **210** (Fig. 33), neither **208b** nor **209** causes convulsions in mice.

Spirocycle **211a** binds potently to, and is a full agonist of, both the nociceptin/orphanin FQ peptide (NOP) and μ opioid receptors; however, it has poor PK properties (rat $F=4\%$).[239] The fluoro derivative **211b** (cebranopadol) has much improved oral bioavailability (rat $F=23\%$) and has advanced to Phase 2 for the treatment of pain.[240]

Ligands of the σ receptor have been explored for treatment of various neurological disorders. Spiropipideridines have been a prominent class among ligands for this receptor. Compound **212** was first reported by Merck as a 5 nM ligand (Fig. 34, Table 48).[242] Subsequently, two isoforms of the receptor were discovered and **212** was shown to be selective for σ_1.[241] Introduction of a sulfur into the spirocycle and transposition of the fused benzene ring afforded spipethiane (**213**) with improved σ_1 selectivity.[243] This compound also has $>20{,}000\times$ selectivity over the dopamine D_2 receptor. Further advances in σ_1 selectivity were achieved by the group led by Wunsch with compounds **214a**, **214b**, and **215**.[244–246] On the other hand, a group at Lundbeck introduced an ether linkage into the spirocycle and replaced the benzyl substituent with a larger group to give **216a** which is σ_2

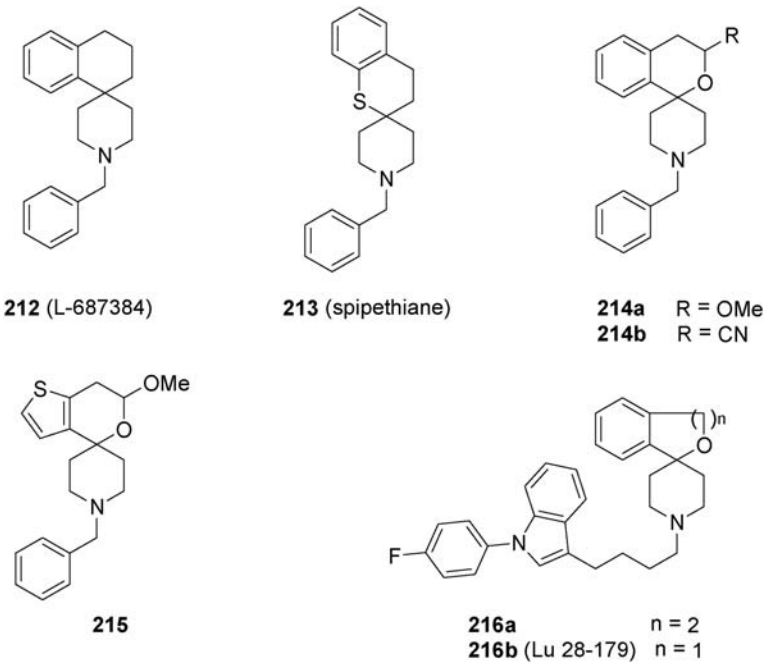

212 (L-687384) **213** (spipethiane) **214a** R = OMe
214b R = CN

215 **216a** n = 2
216b (Lu 28-179) n = 1

Fig. 34 σ Receptor ligands.

Table 48 σ Receptor bioassay data of some spirocyclic derivatives

	$\sigma_1 K_i$ (nM)	$\sigma_2 K_i$ (nM)	σ_2/σ_1 selectivity
212	0.26[a]	12[a]	46
213	0.5	416	832
214a	1.3	3500	2708
214b	1.5	1590	1030
215	0.3	1260	3940
216a	53[a]	0.9[a]	0.017
216b	17[a]	0.12[a]	0.007

[a] IC_{50}.[241]

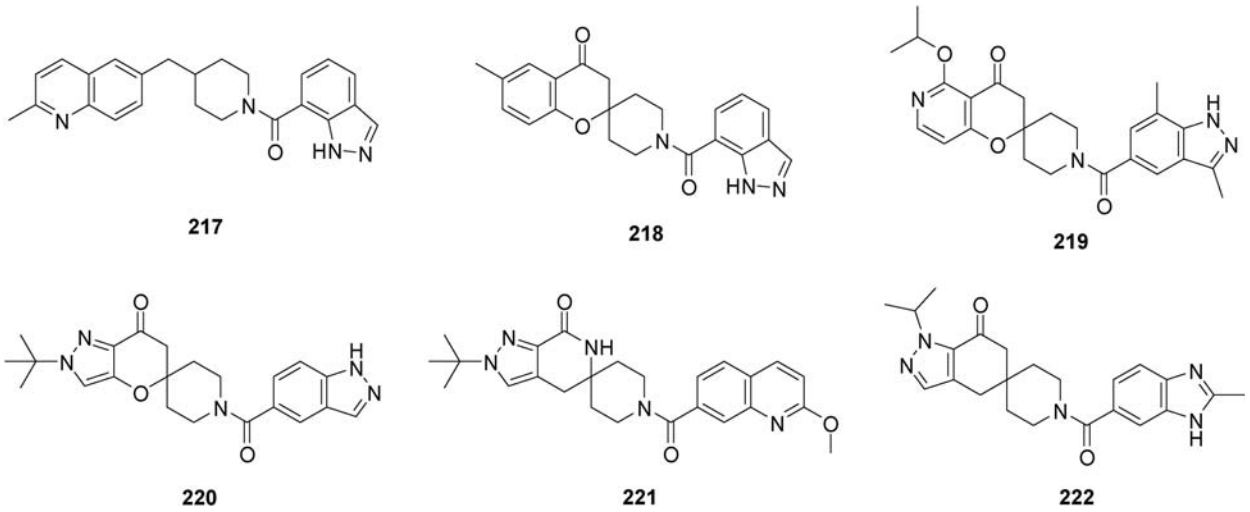

Fig. 35 Acetyl CoA carboxylase inhibitors.

selective. Reducing the cyclic ether from a six- to a five-membered ring provided **216b** with further increased σ_2 potency and selectivity.[241]

Dual inhibitors of acetyl CoA carboxylase isozymes 1 and 2 (ACC1 and ACC2) are expected to decrease fatty acid synthesis in liver and adipose tissue while increasing fatty acid oxidation in liver and muscle, leading to increased energy expenditure, reduced adiposity, and improved insulin sensitivity. Initial follow up of an HTS hit led to compound **217** (Fig. 35, Table 49).[247] The quinoline moiety was replaced with a spirochromanone to afford **218** with ca. 5× improved potency on both isozymes. Further optimization of both chromanone and indazole rings gave **219** which was more potent and orally bioavailable in rat (F=8-52% depending on the formulation). In an effort to reduce lipophilicity, the pyridine ring was replaced with a pyrazole to give **220** which retained potency.[248] The ketone in **220** was observed to undergo reduction in vivo in some species. To avoid this problem, spirolactams, including **221**, were explored.[249] Compound **221** has a clean CYP profile, 71% oral bioavailability in rat, and had an ED_{50} of 1.3 mg kg^{-1} for inhibition of incorporation of ^{14}C acetate into lipids in rats. In an alternative approach, the alkyl substituent on the pyrazole was moved so as to sterically block the ketone.[250] This, combined with other changes, led to **222** which was 40% bioavailable and had an ED_{50} of 7.8 mg kg^{-1} for inhibition of incorporation of ^{14}C acetate into lipids in rats.

Table 49 Biological data of acetyl CoA carboxylase (ACC) inhibitors

	rACC1 IC_{50} (nM)	hACC1 IC_{50} (nM)	hACC2 IC_{50} (nM)	HLM[a] stability (mL min^{-1} kg^{-1})
217	3380			
218	634		641	
219	12		20	
220	17	19	11	<8
221		10	4	<8
222	24	27	33	<5

[a] *HLM*, human liver microsome.

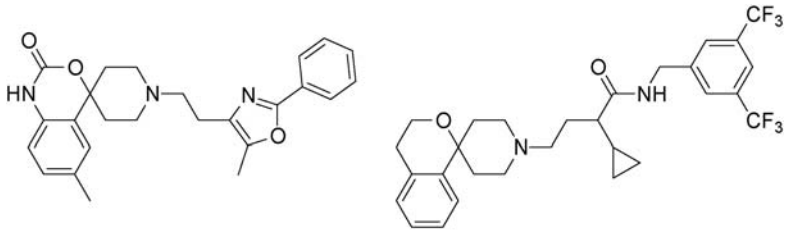

223 (RS-504393) **224**

Fig. 36 Spirocyclic chemokine receptors 2 (CCR2) ligands.

Phase I clinical studies demonstrated that **222** has PK properties suitable for once a day dosing and increased whole-body fatty acid utilization.

The CCR2 and CCR5, respectively, have both been addressed with spirocycles. Compound **223** from Roche was one of the first ligands of CCR2 to be described, with IC_{50} values of 89 and 330 nM in binding and functional assays (**Fig. 36**).[251] However, it lacked any selectivity over the human α1a receptor (IC_{50} = 72 nM). Compound **224** is structurally related to CCR2 antagonists described above (**Fig. 30**), and had an IC_{50} of 17 nM in a Ca^{2+} flux assay.[252]

CCR5 is the target site of the antiretroviral drug maraviroc. A group working at Ono Pharmaceuticals employed a library synthesis approach predicated on the privileged status of spirocycles as GPCR ligands[11] to discover **225a** (**Table 50**).[253] The poor oral bioavailability of **225a** was improved by introduction of a carboxylic acid to give **225b**, despite reduced rat liver microsome (RLM) stability.[254,255] Separately it was found that the methylene group connecting the diketopiperazine to the cyclohexane ring was a major site of metabolic hydroxylation.[256] One of the stereoisomeric metabolites, compound **226a**, had good potency.[257] Combination of the carboxylic acid and hydroxyl moieties provided the clinical candidate aplaviroc (**226b**) which progressed to Phase 2 when liver toxicity was encountered.[257,258]

Concurrently, a group working at Roche also disclosed spirocyclic CCR5 antagonists (**Table 51**).[259] Compound **227** has good oral bioavailability in rat, is highly selective over CCR1, CCR2, CCR3, CCR4, CCR6, and CXCR4 (IC_{50} values > 50 μM), and has a clean CYP profile. Interestingly, little difference in the antiviral activities of the enantiomers of **227** was observed. Hybridization of **227** with CCR5 antagonists from other companies, including Ono,[257,258] led to oxazinones **228** with comparable potency.[260] Although the oral bioavailability of **228** in rat was only 10%, it was significantly better in dog (85%) and monkey (42%). The 4-aminopiperidine moiety in **228** was replaced with an azabicycle to give **229** which also demonstrated good antiviral activity.[261]

The orexin system plays a key role in the regulation of sleep and wake.[262] Two related spirolactams, **230** and **231**, were reported as orexin receptor antagonists by workers at Novartis and Aurigene (**Table 52**).[263] While **230** was significantly more potent at both receptor isoforms than **231**, it lacked significant oral bioavailability in mouse. Compound **231** was more selective toward hOX_2R and had much improved oral bioavailability. When dosed orally to mice at 50 mg kg^{-1}, compound **231** clearly increased sleep

Table 50 Chemokine receptors 5 (CCR5) blockers

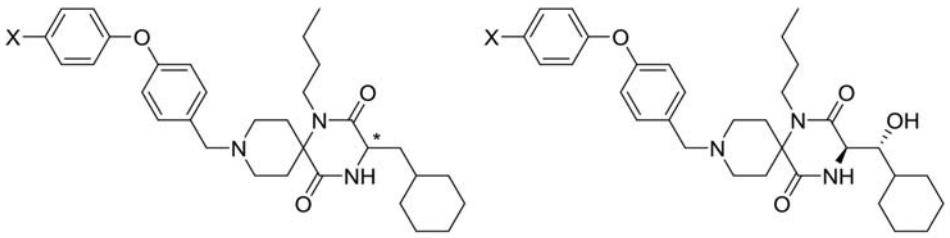

225a X = H, * = RS
225b X = CO_2H, * = S

226a X = H
226b (aplaviroc) X = CO_2H

	X	*	*CCR5 Ca^{2+} assay IC_{50} (nM)*	*RLM stability* t = *15 min (% remaining)*	*Rat* F *(%)*
225a	H	RS	28	33	2
225b	CO_2H	S	13	22	34
226a	H	–	53	18	
226b	CO_2H	–	34	39	23

Table 51 Spirocyclic compounds as CCR5 blockers

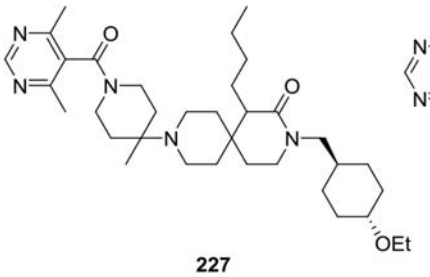

227

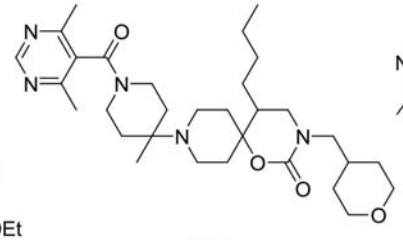

228

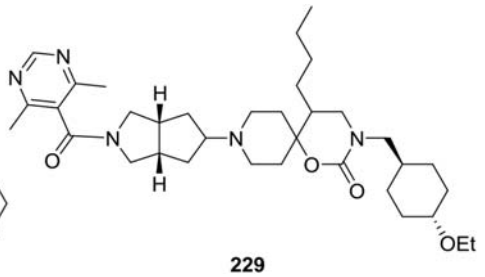

229

	CCR5 binding IC_{50} (nM)	*Anti-HIV IC_{50} (nM)*	*Rat* F[a] *(%)*
227	30	5	66
228	25	6	10
229	34	4	

[a] *F*, oral bioavailability.

Table 52 Orexin receptor antagonists

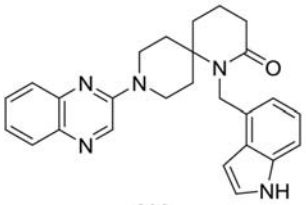

230

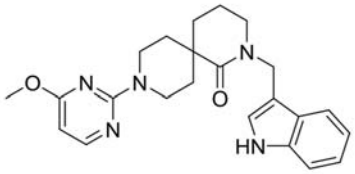

231

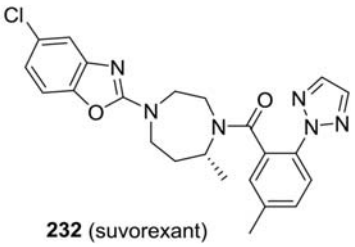

232 (suvorexant)

	hOX_1R K_i (nM)	*hOX_2R K_i (nM)*	*Selectivity*	*Mouse* F *(%)*
230	9	0.5	18	5
231	512	14	36	47
232	2	9	0.2	

time; however, the detailed effect of the compound on sleep architecture differed from that of the suvorexant (**232**) which has modest OX_1R selectivity.

Stearoyl CoA desaturase-1 (SCD1) inhibitor **233**[264] was optimized by replacement of a benzoyl group with a spirocycle to give **234** with significantly improved potency in vitro and in cells (Table 53).[265] Replacement of the $CONHCH_2CH(OH)$ linker with an oxadiazolylmethyl group gave **235a** and **235b**.[266] Both these compounds made further potency gains in the cellular assay and the latter compound had excellent oral bioavailability. Compound **235b** also demonstrated potent, dose-dependent reduction of the plasma desaturation index upon oral administration for 7 days.

A number of spirocyclic barbituric acid derivatives have been studied as bacterial DNA gyrase inhibitors with potential antibacterial utility. PNU-286607 (**236**) was discovered at Pharmacia by whole cell HTS (Table 54).[267] The compound has excellent oral bioavailability in mice and was efficacious against methicilin-resistant *S. aureus* UC9213 in mice ($ED_{50} = 19.5$ mg kg^{-1}; *cf* ciprofloxacin $ED_{50} = 10$ mg kg^{-1}). Scientists at AstraZeneca modified the structure by incorporation of a fused isoxazole ring to give **(−)-237** and subsequently ETX0914 (**238**) which has been advanced as a clinical candidate for treatment of uncomplicated gonorrhea.[268,269]

Compound **239** (MRK-560) is a γ-secretase modulator with selectivity for presenilin-1 (PS-1) over presenilin-2 (PS-2), which may result in an improved therapeutic window (Table 55).[270,271] Extensive investigation around **239** led to the discovery of the unusual spirocyclic phosphonate **(−)-240** which displayed similar or improved potency, and selectivity toward PS-1.[272] This compound possessed a clean hERG and CYP profile, notably demonstrating a much reduced CYP2C9 liability compared to MRK-560. A single 10 mg kg^{-1} PO dose of **(−)-240** reduced Aβ levels in rat plasma, CSF, and brain by 69%, 45%, and 39% respectively after 6 h.

(*S*)-(−)-**241**, an activator of mitochondrial ATP-sensitive potassium channel, displayed similar cardioprotective effect to diazoxide when preadministered IP at 40 mg kg^{-1} to Langendorff perfused rat hearts (Fig. 37).[273,274]

Table 53 Spiro[5.5] compounds as stearoyl CoA desaturase-1 (SCD1) inhibitors

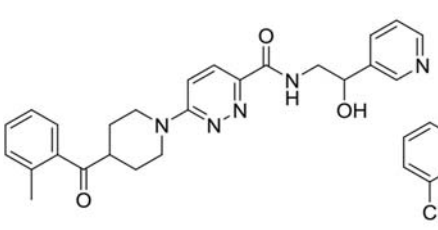

233

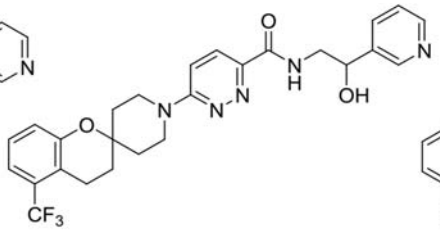

234

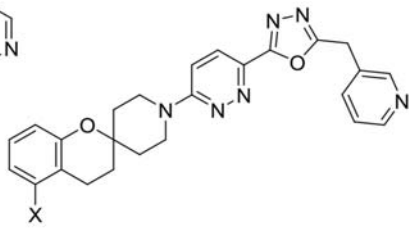

235a X = CF_3
235b X = F

	hSCD-1 IC_{50} (nM)	*Cellular IC_{50} (nM)*	*Mouse* F *(%)*
233	28	43	68
234	0.3	3	67
235a	0.03	0.8	–
235b	0.3	0.7	>95

Table 54 DNA gyrase inhibitors

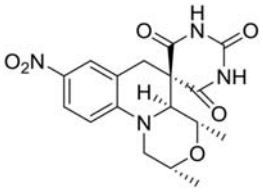

236 (PNU-286607)

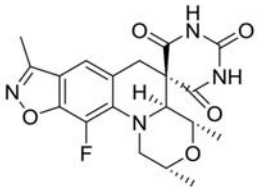

(-)-237

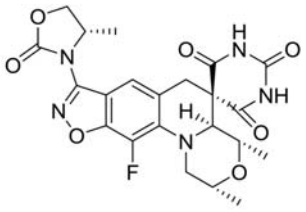

238 (ETX0914)

	E. coli *IC_{50} (nM)*	*Rat* F *(%)*	*Mouse* F *(%)*
236	9000		95
(−)-237	290	71	58
238	170	31	

Table 55 γ-Secretase inhibitors

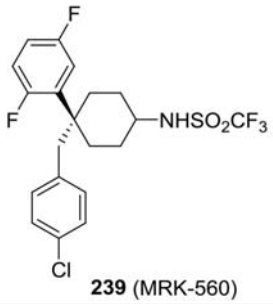

239 (MRK-560)

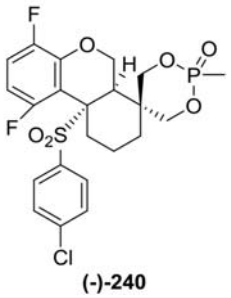

(-)-240

	Membrane Aβ40 IC_{50} (nM)	*Cell Aβ40/Aβ42 IC_{50} (nM)*	*Selectivity PS-2/PS-1*	*CYP2C9 IC_{50} (nM)*
239	14	15/5	37	<300
(−)-240	10	3/5	33	>20,000

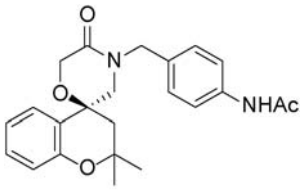

(S)-(-)-241

Fig. 37 ATP-sensitive potassium channel activator.

Table 56 Inhibitors of the apoptosis protein XIAP

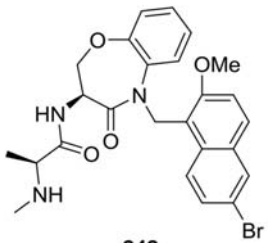

242

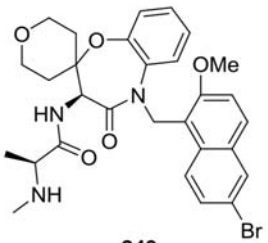

243

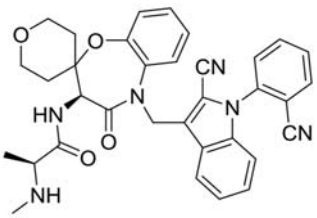

244

	BIR2 IC_{50} (nM)	*BIR3 IC_{50} (nM)*	*Rat blood stability (% remaining at t = 4 h)*	*Rat iv CL (mL min^{-1} kg^{-1})*
242	101	>54,000	7	521
243	65	23,500	88	60
244	39	3060		41

1.08.3.4.2 Spiro[5.6] ring systems

The X-linked inhibitor of apoptosis protein (XIAP) is often overexpressed in cancer cells and is an oncology target. Optimization of a screening hit afforded benzoxazepinone **242**, a selective inhibitor of the BIR2 domain of XIAP (Table 56).[275] Compound **242** was rapidly cleared in vivo by amide hydrolysis. Stability in rat blood was found to correlate with in vivo stability. Installation of a bulky spirotetrahydrofuran ring to give **243** improved both potency and rat blood stability. The napthalene system in **243** was shown to be subject to oxidative metabolism. Replacement with an *N*-phenylindole afforded **244** with further improved potency and reduced clearance.

Inhibitors of SCD1 have been investigated for the treatment of obesity and insulin resistance; however, significant on-target side effects have been observed, including alopecia and partial eye-closure. A group at Merck identified spirobenzoxazepine **245a** as an HTS hit (Table 57). Optimization for potency provided **245b** and **246**. The hypothesis that a liver-selective compound would result

Table 57 Spiro[5.6] derivatives as stearoyl-CoA desaturase (SCD1) inhibitors

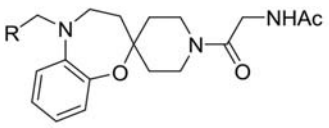

245a R = isobutyl
245b R = 4-t-Bu-phenyl

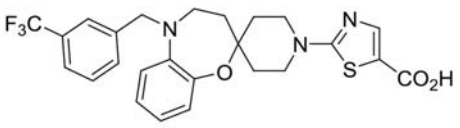

246

	SCD1 IC_{50} (nM)	*AUC[a] (ng g^{-1} h^{-1})*	*Liver/plasma*
245a	6400		
245b	17	3464	17
246	8	2308	56

[a]*AUC*, area under the curve.

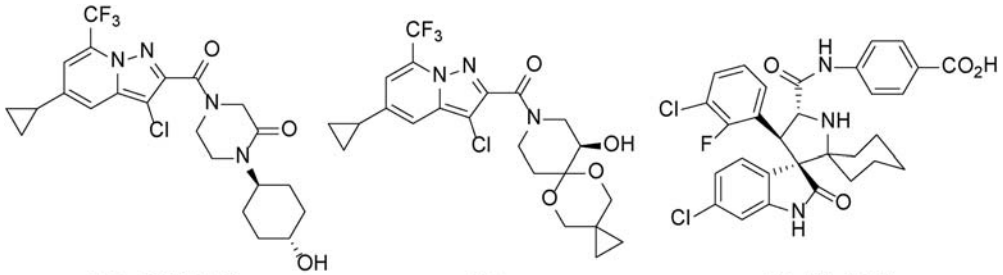

Fig. 38 Polyspirocycles.

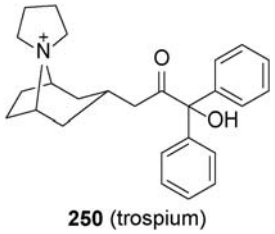

Fig. 39 Trospium.

in reduced side effects led to the prioritization of **246**. In vivo testing suggested that a further improvement in liver selectivity would be required to eliminate side effects.[276]

1.08.3.5 Polyspirocycles

Polyspirocycles have received some attention from medicinal chemists (Fig. 38). GSK8853 (**247**) inhibits the NS4B protein and is a clinical candidate for treatment of HCV.[277] Related compound **248**, endowed with a three ring spirocycle, displays comparable in vitro potencies against HCV 1a and 1b.[278] Compound **249** is a potent inhibitor of the MDM2–p53 interaction ($K_i = 0.16$ nM) and is related to compounds discussed above (Fig. 21).[279]

1.08.3.6 Noncarbon Spiro Atom

Trospium chloride (**250**) is a muscarinic M1 antagonist used clinically for the treatment of overactive bladder (Fig. 39).[280]

1.08.4 Conclusions

Spirocycles have been employed by medicinal chemists for over 50 years.[164,281] Spirocycles have been incorporated into molecules that address enzymes, receptors, ion channels, and protein–protein interactions. Targets for which spirocycles have been intensively exploited include HCV NS5B polymerase, grehlin receptor,[282] CGRP,[283] the MDM2-p53 protein–protein interaction,[147] γ-secretase,[284] β-secretase,[285] AR, the σ receptor, and acetyl CoA carboxylase (ACC).[286]

Unsurprisingly, the majority of the spirocyclic ring systems exploited in drug discovery are composed of five-, six-, and to a lesser degree three-membered rings. Spirocycles incorporating four-membered rings have seen more use in recent years as methods for their synthesis have been published.[46] Spirocycles have been introduced on the periphery of molecules[76] and as the central core.[176] Many of the early examples of spirocycles in drug discovery were piperidines in which C4 was the spiroatom.[161,164,172,177] These have the advantage of not necessarily introducing a chiral center into the molecule. However, to fully take advantage of the ability of spirocycles to project functional groups in a wide variety of directions, a sound understanding of conformational preferences of spirocycles and the ability to control stereochemistry at multiple positions around the spirocyclic nucleus are necessary.

A large body of literature describing the synthesis of spirocycles exists and continues to grow as evidenced by continuing publications describing the synthesis of spirocycles in journals focused on organic chemistry. Molecules with new spirocyclic ring systems and different substitution patterns will be added to screening collections. Furthermore, the synthesis of spirocyclic molecules emerging from structure-based drug design is more likely to be undertaken when literature precedent is available. In addition, the increased availability of spirocyclic scaffolds from chemical suppliers will facilitate compound and library synthesis.

Table 58 Spirocyclic drugs on the market and in clinical trials[a]

Identifier (cpd. no.)	*Target*	*Disease*
Marketed drugs		
Amcinonide (**94**)	–	Atopic dermatitis
Buspirone (**131**)	5-HT_{1A}, D_4, etc.	Anxiety
Cevimeline (**181**)	M1, M3	Dry mouth
22,23-Dihydroavermectin B_{1a} (**202**)	GluCl	Helminth infection
Drospirenone (**93**)	PR	Birth control[b]
Eplerenone (**92**)	MR	Hypertension
Fenspiride (**139**)	–	Cough
Fluspirilene (**137**)	5-HT_{2A}, D_2, etc.	Schizophrenia
Guanadrel (**140**)	NET	Hypertension
Irbesartan (**97b**)	AT II	Hypertension
Ledipasvir (**41**)	HVC NS5A	Hepatitis C[c]
Rolapitant (**142**)	NK1	Nausea/emesis
Spiperone (**135**)	5-HT_{2A}, etc.	Schizophrenia
Spirapril (**99a**)	ACE	Hypertension[d]
Spironolactone (**91**)	MR	Hypertension
Tofogliflozin (**144**)	SGLT2	Diabetes
Trospium (**250**)	M1	Overactive bladder
Phase 3		
Beloranib (**58**)	MetAP-2	Obesity[e]
Fidarestat (**169**)	Aldose reductase	Diabetes
Phase 2		
ADL5859 (**208b**)	δ Opioid receptor	Pain
ADL5747 (**209**)	δ Opioid receptor	Pain
Aplaviroc (**226b**)	CCR5	HIV
BMS-587101 (**123**)	LFA-1	Immunological disorders
Cebranopadol (**211b**)	NOP and μ opioid receptors	Pain
ETX0914 (**238**)	DNA gyrase	Gonorrhea
TNP-470, AGM-1470 (**56**)	MetAP-2	Cancer
Ubrogepant (**107**)	CGRP	Migraine
Phase 1		
CFI-400945 (**47**)	PLK4	Cancer
PF-04862853 (**81**)	FAAH	Pain
MI-77301/SAR405838 (**117**)	MDM2-p53	Cancer
BMS-688521 (**124**)	LFA-1	Immunological disorders
CDRI 97/98 (**204**)	–	Malaria
- (222)	ACC1/ACC2	Diabetes

[a]Highest phase of clinical trials reached.
[b]In combination with ethinylestradiol.
[c]Marketed in combination with sofosbuvir (**75**) as Harvoni®.
[d]Prodrug.
[e]Trial halted Dec. 2015.

In the quest for drug candidates with improved physical properties, the reduced aromatic character of spirocycles also renders them more attractive molecular fragments than aryl–aryl coupling products that have been a mainstay in medicinal chemistry over the last 20+ years. It seems certain that spirocycles are not only in some marketed drugs (Table 58) but also they will play a leading role in the future of drug discovery.

References

1. von Baeyer, A. Systematik und Nomenclatur bicyclischer Kohlenwasserstoffe. *Ber. Dtsch. Chem. Ges.* **1900,** *33,* 3771–3775.
2. Gamba-Sanchez, D. Fumagillin and Structurally Related Molecules as Source of New Drugs. *Mini-Rev. Org. Chem.* **2012,** *9,* 126–142.
3. Stratmann, K.; Moore, R. E.; Bonjouklian, R.; Deeter, J. B.; Patterson, G. M. L.; Shaffer, S.; Smith, C. D.; Smitka, T. A. Welwitindolinones, Unusual Alkaloids From the Blue-Green Algae *Hapalosiphon welwitschii* and *Westiella intricata*. Relationship to Fischer Indoles and Hapalinodoles. *J. Am. Chem. Soc.* **1994,** *116,* 9935–9942.
4. Jossang, A.; Jossang, P.; Hadi, H. A.; Sevenet, T.; Bodo, B. Horsfiline, an Oxindole Alkaloid From *Horsfieldia superba*. *J. Org. Chem.* **1991,** *56,* 6527–6530.
5. Galliford, C. V.; Scheidt, K. A. Pyrrolidinyl-Spirooxindole Natural Products as Inspirations for the Development of Potential Therapeutic Agents. *Angew. Chem. Int. Ed.* **2007,** *46,* 8748–8758.
6. Kinnel, R. B.; Gehrken, H. P.; Scheuer, P. J. Palau'amine: A Cytotoxic and Immunosuppressive Hexacyclic Bisguanidine Antibiotic From the Sponge *Stylotella agminata*. *J. Am. Chem. Soc.* **1993,** *115,* 3376–3377.

7. Lansdell, T. A.; Hewlett, N. M.; Skoumbourdis, A. P.; Fodor, M. D.; Seiple, I. B.; Su, S.; Baran, P. S.; Feldman, K. S.; Tepe, J. J. Palau'amine and Related Oroidin Alkaloids Dibromophakellin and Dibromophakellstatin Inhibit the Human 20*S* Proteasome. *J. Nat. Prod.* **2012,** *75,* 980–985.
8. Petersen, A. B.; Roennest, M. H.; Larsen, T. O.; Clausen, M. H. The Chemistry of Griseofulvin. *Chem. Rev.* **2014,** *114,* 12088–12107.
9. Lowicki, D.; Huczynski, A. Structure and Antimicrobial Properties of Monensin A and Its Derivatives: Summary of the Achievements. *Biomed. Res. Int.* **2013,** *742149*, 14 pp.
10. Aronstam, R. S.; King, C. T., Jr.; Albuquerque, E. X.; Daly, J. W.; Feigl, D. M. Binding of [3*H*]perhydrohistrionicotoxin and [3*H*]phencyclidine to the Nicotinic Receptor-Ion Channel Complex of *Torpedo electroplax.* Inhibition by Histrionicotoxins and Derivatives. *Biochem. Pharmacol.* **1985,** *34,* 3037–3047.
11. Patchett, A. A.; Nargund, R. P. Privileged Structures — An Update. In *Annual Reports in Medicinal Chemistry;* Doherty, A. M., Ed.; vol. 35; Academic Press: San Diego, 2000; pp 289–298. Chapter 26.
12. Lovering, F.; Bikker, J.; Humblet, C. Escape from Flatland: Increasing Saturation as an Approach to Improving Clinical Success. *J. Med. Chem.* **2009,** *52,* 6752–6756.
13. Ritchie, T. J.; MacDonald, S. J. F.; Young, R. J.; Pickett, S. D. The Impact of Aromatic Ring Count on Compound Developability: Further Insights by Examining Carbo- and Hetero-Aromatic and -Aliphatic Ring Types. *Drug Discov. Today* **2011,** *16,* 164–171.
14. Ross, N. T.; Katt, W. P.; Hamilton, A. D. Synthetic Mimetics of Protein Secondary Structure Domains. *Philos. Trans. R. Soc. A* **2010,** *368,* 989–1008.
15. Hinds, M. G.; Welsh, J. H.; Brennand, D. M.; Fisher, J.; Glennie, M. J.; Richards, N. G. J.; Turner, D. L.; Robinson, J. A. Synthesis, Conformational Properties, and Antibody Recognition of Peptides Containing β-Turn Mimetics Based on α-Alkylproline Derivatives. *J. Med. Chem.* **1991,** *34,* 1777–1789.
16. Paul, P. K. C.; Burney, P. A.; Campbell, M. M.; Osguthorpe, D. J. Design of a Natural Cis Peptide and Bond Motif to Form Type VI β-Turn Mimetic. *Bioorg. Med. Chem. Lett.* **1992,** *2,* 141–144.
17. Fernandez, M. M.; Diez, A.; Rubiralta, M.; Montenegro, E.; Casamitjana, N.; Kogan, M. J.; Giralt, E. Spirolactams as Conformationally Restricted Pseudopeptides: Synthesis and Conformational Analysis. *J. Org. Chem.* **2002,** *67,* 7587–7599.
18. Bittermann, H.; Gmeiner, P. Chirospecific Synthesis of Spirocyclic β-Lactams and Their Characterization as Potent Type II β-Turn Inducing Peptide Mimetics. *J. Org. Chem.* **2006,** *71,* 97–102.
19. Lomlim, L.; Einsiedel, J.; Heinemann, F. W.; Meyer, K.; Gmeiner, P. Proline Derived Spirobarbiturates as Highly Effective β-Turn Mimetics Incorporating Polar and Functionalizable Constraint Elements. *J. Org. Chem.* **2008,** *73,* 3608–3611.
20. Lesma, G.; Cecchi, R.; Cagnotto, A.; Gobbi, M.; Meneghetti, F.; Musolino, M.; Sacchetti, A.; Silvani, A. Tetrahydro-β-carboline-Based Spirocyclic Lactam as Type II' β-Turn: Application to the Synthesis and Biological Evaluation of Somatostatin Mimetics. *J. Org. Chem.* **2013,** *78,* 2600–2610.
21. Damour, D.; Barreau, M.; Blanchard, J.-C.; Burgevin, M.-C.; Doble, A.; Pantel, G.; Labaudiniere, R.; Mignani, S. Synthesis and Binding Affinities of Novel Spirocyclic Lactam Peptidomimetics of Somatostatin. *Chem. Lett.* **1998,** 943–944.
22. Thomas, G. L.; Wyatt, E. E.; Spring, D. R. Enriching Chemical Space With Diversity-Oriented Synthesis. *Curr. Opin. Drug Discovery Dev.* **2006,** *9,* 700–712.
23. Ortholand, J.-Y. Towards Privileged, Natural-Like Spiro Compounds. *sp2* **2007,** *6* (32), 34.
24. Wipf, P.; Stephenson, C. R. J.; Walczak, M. A. A. Diversity-Oriented Synthesis of Azaspirocycles. *Org. Lett.* **2004,** *6,* 3009–3012.
25. Dhara, K.; Midya, G. C.; Dash, J. A Diversity-Oriented Approach to Spirocyclic and Fused Hydantoins via Olefin Metathesis. *J. Org. Chem.* **2012,** *77,* 8071–8082.
26. Kang, F.-A.; Sui, Z. A Diversity-Oriented-Synthesis Protocol for Scaffold Discovery Based on a General Synthetic Route to Spirocycles. *Tetrahedron Lett.* **2011,** *52,* 4204–4206.
27. Hung, A. W.; Ramek, A.; Wang, Y.; Kaya, T.; Wilson, J. A.; Clemons, P. A.; Young, D. W. Route to Three-Dimensional Fragments Using Diversity-Oriented Synthesis. *Proc. Natl. Acad. Sci. U. S. A.* **2011,** *108,* 6799–6804.
28. Lo, M. M. C.; Neumann, C. S.; Nagayama, S.; Perlstein, E. O.; Schreiber, S. L. A Library of Spirooxindoles Based on a Stereoselective Three-Component Coupling Reaction. *J. Am. Chem. Soc.* **2004,** *126,* 16077–16086.
29. Bretschneider, T.; Benet-buchholz, J.; Fischer, R.; Nauen, R. Spirodiclofen and Spiromesifen — Novel Acaricidal and Insecticidal Tetronic Acid Derivatives With a New Mode of Action. *Chimia* **2003,** *57,* 697–701.
30. Kramer, W.; Weissmuller, J.; Gau, W.; Etzel, W.; Stelzer, U. KWG 4168 (Spiroxamine). Chemistry and Stereochemistry. *Pflanzenschutz-Nachr. Bayer (Ger. Ed.)* **1997,** *50,* 5–14.
31. Perron, F.; Albizati, K. F. Chemistry of Spiroketals. *Chem. Rev.* **1989,** *89,* 1617–1661.
32. Sannigrahi, M. Stereocontrolled Synthesis of Spirocyclics. *Tetrahedron* **1999,** *55,* 9007–9071.
33. Dake, G. Recent Approaches to the Construction of 1-Azaspiro[4.5]decanes and Related 1-Azaspirocycles. *Tetrahedron* **2006,** *62,* 3467–3492.
34. Trost, B. M.; Brennan, M. K. Asymmetric Syntheses of Oxindole and Indole Spirocyclic Alkaloid Natural Products. *Synthesis* **2009,** 3003–3025.
35. Rosenberg, S.; Leino, R. Synthesis of Spirocyclic Ethers. *Synthesis* **2009,** *16,* 2651–2673.
36. Kotha, S.; Deb, A. C.; Lahiri, K.; Manivannan, E. Selected Synthetic Strategies to Spirocyclics. *Synthesis* **2009,** 165–193.
37. Marti, C.; Carreira, E. M. Construction of Spiro[Pyrrolidine-3,3′-Oxindoles] — Recent Applications to the Synthesis of Oxindole Alkaloids. *Eur. J. Org. Chem.* **2003,** *2003,* 2209–2219.
38. Ball-Jones, N. R.; Badillo, J. J.; Franz, A. K. Strategies for the Enantioselective Synthesis of Spirooxindoles. *Org. Biomol. Chem.* **2012,** *10,* 5165–5181.
39. Undheim, K. Stereoselective Reactions in Preparation of Chiral α-Heteraspiro[*m.n*]alkanes. *Synthesis* **2015,** *47,* 2497–2522.
40. Smith, L. K.; Baxendale, I. R. Total Syntheses of Natural Products Containing Spirocarbocycles. *Org. Biomol. Chem.* **2015,** *13,* 9907–9933.
41. Awan, S. I.; Werz, D. B. Syntheses of 1,2-Annulated and 1-Spiroannulated Carbohydrate Derivatives: Recent Developments. *Bioorg. Med. Chem.* **2012,** *20,* 1846–1856.
42. Bari, S.; Bhalla, A. Spirocyclic β-Lactams. Synthesis and Biological Evaluation of Novel Heterocycles. *Top. Heterocycl. Chem.* **2010,** *22,* 49–99.
43. Wuitschik, G.; Carreira, E. M.; Wagner, B.; Fischer, H.; Parrilla, I.; Schuler, F.; Rogers-Evans, M.; Muller, K. Oxetanes in Drug Discovery: Structural and Synthetic Insights. *J. Med. Chem.* **2010,** *53,* 3227–3246.
44. Wuitschik, G.; Rogers-Evans, M.; Buckl, A.; Bernasconi, M.; Marki, M.; Godel, T.; Fischer, H.; Wagner, B.; Parrilla, I.; Schuler, F.; Schneider, J.; Alker, A.; Schweizer, W. B.; Muller, K.; Carreira, E. M. Spirocyclic Oxetanes: Synthesis and Properties. *Angew. Chem. Int. Ed.* **2008,** *47,* 4512–4515.
45. Burkhard, J. A.; Wagner, B.; Fischer, H.; Schuler, F.; Müller, K.; Carreira, E. M. Synthesis of Azaspirocycles and Their Evaluation in Drug Discovery. *Angew. Chem. Int. Ed.* **2010,** *49,* 3524–3527.
46. Carreira, E. M.; Fessard, T. C. Four-Membered Ring-Containing Spirocycles: Synthetic Strategies and Opportunities. *Chem. Rev.* **2014,** *114,* 8257–8322.
47. Geoghegan, K.; Bode, J. W. Bespoke SnAP Reagents for the Synthesis of C-Substituted Spirocyclic and Bicyclic Saturated N-Heterocycles. *Org. Lett.* **2015,** *17,* 1934–1937.
48. Siau, W.-Y.; Bode, J. W. One-Step Synthesis of Saturated Spirocyclic N-Heterocycles With Stannyl Amine Protocol (SnAP) Reagents and Ketones. *J. Am. Chem. Soc.* **2014,** *136,* 17726–17729.
49. Zheng, Y.; Tice, C. M.; Singh, S. B. The Use of Spirocyclic Scaffolds in Drug Discovery. *Bioorg. Med. Chem. Lett.* **2014,** *24,* 3673–3682.
50. Deslongchamps, P.; Pothier, N. Conformational Analysis of 1-Oxaspiro[5.5]undecanes. A Powerful Probe for the Endo and the Exo Anomeric Effects in Acetals. *Can. J. Chem.* **1990,** *68,* 597–603.
51. Lambert, J. B.; Gosnell, J. L.; Bailey, D. S. Conformational Effect of the Spiro Linkage Between Three- and Six-Membered Rings. *J. Org. Chem.* **1972,** *37,* 2814–2817.
52. Legon, A. C. Equilibrium Conformations of Four- and Five-Membered Cyclic Molecules in the Gas Phase: Determination and Classification. *Chem. Rev.* **1980,** *80,* 231–262.
53. Allen, F. The Cambridge Structural Database: A Quarter of a Million Crystal Structures and Rising. *Acta Crystallogr. B* **2002,** *58,* 380–388.
54. Eliel, E. L.; Wilen, S. H.; Mander, L. N. *Stereochemistry of Organic Compounds;* Wiley & Sons: New York, 1994; p. 1267.
55. Wu, A.; Cremer, D. Extension of the Karplus Relationship for NMR Spin-Spin Coupling Constants to Nonplanar Ring Systems: Pseudorotation of Tetrahydrofuran. *Int. J. Mol. Sci.* **2003,** *4,* 158–192.

56. Carballeira, L.; Pérez-Juste, I.; Van Alsenoy, C. Theoretical Study of Pyrrolidine: Revised Conformational Energies and Vibrational Assignments. *J. Phys. Chem. A* **2002,** *106,* 3873–3884.
57. Picard, P.; Moulines, J. Conformational Study in the 1-Oxaspiro[4.5]decane Series. *Tetrahedron Lett.* **1970,** *20,* 5133–5136.
58. Rablen, P. R.; Paquette, L. A.; Borden, W. T. Why Doesn't All-trans-1,2,3,4,5,6-Hexaspiro(THF)cyclohexane Complex Metal Ions? *J. Org. Chem.* **2000,** *65,* 9180–9185.
59. Angiolini, L.; Duke, R. P.; Jones, R. A. Y.; Katritzky, A. R. Conformational Analysis of Saturated Heterocycles. XLV. *N*-Alkyldihydro-1,3,5-dithiazines and *N*-Alkyltetrahydro-1,3,5-thiadiazines. *J. Chem. Soc. Perkin Trans.* **1972,** *2,* 674–680.
60. Smith, P. W.; Cooper, A. W. J.; Bell, R.; Beresford, I. J. M.; Gore, P. M.; McElroy, A. B..; Pritchard, J. M.; Saez, V.; Taylor, N. R. New Spiropiperidines as Potent and Selective Non-Peptide Tachykinin NK2 Receptor Antagonists. *J. Med. Chem.* **1995,** *38,* 3772–3779.
61. Sulsky, R.; Gougoutas, J. Z.; DiMarco, J.; Biller, S. A. Conformational Switching and the Synthesis of Spiro[2*H*-indol]-3(1*H*)-ones by Radical Cyclization. *J. Org. Chem.* **1999,** *64,* 5504–5510.
62. Dodziuk, H. Conformation Analysis of Spiranes by the Force-Field Method. Part 1. Chirality and Diastereoisomerism of Spiro-Compounds: Spiro[5.5]undecane and Derivatives. *J. Chem. Soc. Perkin Trans.* **1986,** *2,* 249–251.
63. Weldon, A. J.; Tschumper, G. S. Energetics of Oxaspirocycle Prototypes: 1,7-Dioxaspiro[5.5]undecane and 1,7,9-Trioxadispiro[5.1.5.3]hexadecane. *J. Org. Chem.* **2006,** *71,* 9212–9216.
64. Bocian, D. F.; Strauss, H. L. Conformational Structure and Energy of Cycloheptane and Some Related Oxepanes. *J. Am. Chem. Soc.* **1977,** *99,* 2876–2882.
65. Entrena, A.; Campos, J.; Gomez, J. A.; Gallo, M. A.; Espinosa, A. A New Systematization of the Conformational Behavior of Seven-Membered Rings. Isoclinal Anomeric and Related Orientations. *J. Org. Chem.* **1997,** *62,* 337–349.
66. Wiberg, K. B. The C7−C10 Cycloalkanes Revisited. *J. Org. Chem.* **2003,** *68,* 9322–9329.
67. Exner, K.; von Rague Schleyer, P. Theoretical Bond Energies: A Critical Evaluation. *J. Phys. Chem. A* **2001,** *105,* 3407–3416.
68. Tserng, K. Y.; Jin, S. J.; Hoppel, C. L. Spiropentaneacetic Acid as a Specific Inhibitor of Medium-Chain Acyl-CoA Dehydrogenase. *Biochemistry* **1991,** *30,* 10755–10760.
69. Stokes, S. S.; Huynh, H.; Gowravaram, M.; Albert, R.; Cavero-Tomas, M.; Chen, B.; Harang, J.; Loch, J. T., III; Lu, M.; Mullen, G. B.; Zhao, S.; Liu, C.-F.; Mills, S. D. Discovery of Bacterial NAD+-Dependent DNA Ligase Inhibitors: Optimization of Antibacterial Activity. *Bioorg. Med. Chem. Lett.* **2011,** *21,* 4556–4560.
70. Mills, S. D.; Eakin, A. E.; Buurman, E. T.; Newman, J. V.; Gao, N.; Huynh, H.; Johnson, K. D.; Lahiri, S.; Shapiro, A. B..; Walkup, G. K.; Yang, W.; Stokes, S. S. Novel Bacterial NAD+-Dependent DNA Ligase Inhibitors With Broad-Spectrum Activity and Antibacterial Efficacy In Vivo. *Antimicrob. Agents Chemother.* **2011,** *55,* 1088–1096.
71. Stokes, S. S.; Gowravaram, M.; Huynh, H.; Lu, M.; Mullen, G. B.; Chen, B.; Albert, R.; O'Shea, T. J.; Rooney, M. T.; Hu, H.; Newman, J. V.; Mills, S. D. Discovery of Bacterial NAD+-Dependent DNA Ligase Inhibitors: Improvements in Clearance of Adenosine Series. *Bioorg. Med. Chem. Lett.* **2012,** *22,* 85–89.
72. Packiarajan, M.; Grenon, M.; Zorn, S.; Hopper, A. T.; White, A. D.; Chandrasena, G.; Pu, X.; Brodbeck, R. M.; Robichaud, A. J. Fused Thiazolyl Alkynes as Potent mGlu5 Receptor Positive Allosteric Modulators. *Bioorg. Med. Chem. Lett.* **2013,** *23,* 4037–4043.
73. Qin, J.; Rao, A.; Chen, X.; Zhu, X.; Liu, Z.; Huang, X.; Degrado, S.; Huang, Y.; Xiao, D.; Aslanian, R.; Cheewatrakoolpong, B.; Zhang, H.; Greenfeder, S.; Farley, C.; Cook, J.; Kurowski, S.; Li, Q.; van Heek, M.; Chintala, M.; Wang, G.; Hsieh, Y.; Li, F.; Palani, A. Discovery of a Potent Nicotinic Acid Receptor Agonist for the Treatment of Dyslipidemia. *ACS Med. Chem. Lett.* **2011,** *2,* 171–176.
74. Sandanayaka, V. P.; Prashad, A. S.; Yang, Y.; Williamson, R. T.; Lin, Y. I.; Mansour, T. S. Spirocyclopropyl β-Lactams as Mechanism-Based Inhibitors of Serine β-Lactamases. Synthesis by Rhodium-Catalyzed Cyclopropanation of 6-Diazopenicillanate Sulfone. *J. Med. Chem.* **2003,** *46,* 2569–2571.
75. Gledhill, L.; Williams, P.; Bycroft, B. W. Irreversible Inactivation of β-Lactamase I From *Bacillus cereus* by Chlorinated 6-spiroepoxypenicillins. *Biochem. J.* **1991,** *276,* 801–807.
76. Link, J. O.; Taylor, J. G.; Xu, L.; Mitchell, M.; Guo, H.; Liu, H.; Kato, D.; Kirschberg, T.; Sun, J.; Squires, N.; Parrish, J.; Keller, T.; Yang, Z.-Y.; Yang, C.; Matles, M.; Wang, Y.; Wang, K.; Cheng, G.; Tian, Y.; Mogalian, E.; Mondou, E.; Cornpropst, M.; Perry, J.; Desai, M. C. Discovery of Ledipasvir (GS-5885): A Potent, Once-Daily Oral NS5A Inhibitor for the Treatment of Hepatitis C Virus Infection. *J. Med. Chem.* **2014,** *57,* 2033–2046.
77. Satoh, A.; Sagara, T.; Sakoh, H.; Hashimoto, M.; Nakashima, H.; Kato, T.; Goto, Y.; Mizutani, S.; Azuma-Kanoh, T.; Tani, T.; Okuda, S.; Okamoto, O.; Ozaki, S.; Iwasawa, Y.; Ohta, H.; Kawamoto, H. Identification of an Orally Active Opioid Receptor-Like 1 (ORL1) Receptor Antagonist 4-{3-[(2*R*)-2,3-Dihydroxypropyl]-2-oxo-2,3-dihydro-1*H*-benzimidazol-1-yl}-1-[(1*S*,3*S*,4*R*)-spiro[bicyclo[2.2.1]heptane-2,1′-Cyclopropan]-3-ylmethyl]piperidine as Clinical Candidate. *J. Med. Chem.* **2009,** *52,* 4091–4094.
78. Laufer, R.; Forrest, B.; Li, S.-W.; Liu, Y.; Sampson, P.; Edwards, L.; Lang, Y.; Awrey, D. E.; Mao, G.; Plotnikova, O.; Leung, G.; Hodgson, R.; Beletskaya, I.; Mason, J. M.; Luo, X.; Wei, X.; Yao, Y.; Feher, M.; Ban, F.; Kiarash, R.; Green, E.; Mak, T. W.; Pan, G.; Pauls, H. W. The Discovery of PLK4 Inhibitors: (E)-3-((1H-Indazol-6-yl)methylene) indolin-2-ones as Novel Antiproliferative Agents. *J. Med. Chem.* **2013,** *56,* 6069–6087.
79. Sampson, P. B.; Liu, Y.; Patel, N. K.; Feher, M.; Forrest, B.; Li, S.-W.; Edwards, L.; Laufer, R.; Lang, Y.; Ban, F.; Awrey, D. E.; Mao, G.; Plotnikova, O.; Leung, G.; Hodgson, R.; Mason, J.; Wei, X.; Kiarash, R.; Green, E.; Qiu, W.; Chirgadze, N. Y.; Mak, T. W.; Pan, G.; Pauls, H. W. The Discovery of Polo-Like Kinase 4 Inhibitors: Design and Optimization of Spiro[cyclopropane-1,3′[3*H*]indol]-2′(1′*H*)-ones as Orally Bioavailable Antitumor Agents. *J. Med. Chem.* **2015,** *58,* 130–146.
80. Sampson, P. B.; Liu, Y.; Forrest, B.; Cumming, G.; Li, S.-W.; Patel, N. K.; Edwards, L.; Laufer, R.; Feher, M.; Ban, F.; Awrey, D. E.; Mao, G.; Plotnikova, O.; Hodgson, R.; Beletskaya, I.; Mason, J. M.; Luo, X.; Nadeem, V.; Wei, X.; Kiarash, R.; Madeira, B.; Huang, P.; Mak, T. W.; Pan, G.; Pauls, H. W. The Discovery of Polo-Like Kinase 4 Inhibitors: Identification of (1R,2S)-2-(3-((E)-4-(((cis)-2,6-Dimethylmorpholino)methyl)styryl)-1H-indazol-6-yl)-5′-methoxyspiro[cyclopropane-1,3′-indolin]-2′-one (CFI-400945) as a Potent, Orally Active Antitumor Agent. *J. Med. Chem.* **2015,** *58,* 147–169.
81. Mason, J. M.; Lin, D. C.-C.; Wei, X.; Che, Y.; Yao, Y.; Kiarash, R.; Cescon, D. W.; Fletcher, G. C.; Awrey, D. E.; Bray, M. R.; Pan, G.; Mak, T. W. Functional Characterization of CFI-400945, a Polo-Like Kinase 4 Inhibitor, as a Potential Anticancer Agent. *Cancer Cell* **2014,** *26,* 163–176.
82. Wang, Y.; Liu, J.; Dransfield, P. J.; Zhu, L.; Wang, Z.; Du, X.; Jiao, X.; Su, Y.; Li, A.-r.; Brown, S. P.; Kasparian, A.; Vimolratana, M.; Yu, M.; Pattaropong, V.; Houze, J. B.; Swaminath, G.; Tran, T.; Nguyen, K.; Guo, Q.; Zhang, J.; Zhuang, R.; Li, F.; Miao, L.; Bartberger, M. D.; Correll, T. L.; Chow, D.; Wong, S.; Luo, J.; Lin, D. C. H.; Medina, J. C. Discovery and Optimization of Potent GPR40 Full Agonists Containing Tricyclic Spirocycles. *ACS Med. Chem. Lett.* **2013,** *4,* 551–555.
83. Monn, J. A.; Prieto, L.; Taboada, L.; Pedregal, C.; Hao, J.; Reinhard, M. R.; Henry, S. S.; Goldsmith, P. J.; Beadle, C. D.; Walton, L.; Man, T.; Rudyk, H.; Clark, B.; Tupper, D.; Baker, S. R.; Lamas, C.; Montero, C.; Marcos, A.; Blanco, J.; Bures, M.; Clawson, D. K.; Atwell, S.; Lu, F.; Wang, J.; Russell, M.; Heinz, B. A.; Wang, X.; Carter, J. H.; Xiang, C.; Catlow, J. T.; Swanson, S.; Sanger, H.; Broad, L. M.; Johnson, M. P.; Knopp, K. L.; Simmons, R. M. A.; Johnson, B. G.; Shaw, D. B.; McKinzie, D. L. Synthesis and Pharmacological Characterization of C4-Disubstituted Analogs of 1S,2S,5R,6S-2-Aminobicyclo[3.1.0]hexane-2,6-Dicarboxylate: Identification of a Potent, Selective Metabotropic Glutamate Receptor Agonist and Determination of Agonist-Bound Human mGlu2 and mGlu3 Amino Terminal Domain Structures. *J. Med. Chem.* **2015,** *58,* 1776–1794.
84. Huang, H.-C.; Li, J. J.; Garland, D. J.; Chamberlain, T. S.; Reinhard, E. J.; Manning, R. E.; Seibert, K.; Koboldt, C. M.; Gregory, S. A.; Anderson, G. D.; Veenhuizen, A. W.; Zhang, Y.; Perkins, W. E.; Burton, E. G.; Cogburn, J. N.; Isakson, P. C.; Reitz, D. B. Diarylspiro[2.4]heptenes as Orally Active, Highly Selective Cyclooxygenase-2 Inhibitors: Synthesis and Structure−Activity Relationships. *J. Med. Chem.* **1996,** *39,* 253–266.
85. Liu, L. J.; Kim, E.; Hong, J. H. Synthesis of Novel 6′-Spirocyclopropyl-5′-Norcarbocyclic Adenosine Phosphonic Acid Analogs as Potent Anti-Hiv Agents. *Nucleosides Nucleotides Nucleic Acids* **2011,** *30,* 784–797.
86. Oh, C. H.; Kim, E.; Hong, J. H. Design and Synthesis of Novel Carbocyclic Versions of 2′-spirocyclopropyl Ribonucleosides as Potent Anti-HCV Agents. *Nucleosides Nucleotides Nucleic Acids* **2011,** *30,* 423–439.
87. Gadthula, S.; Rawal, R. K.; Sharon, A.; Wu, D.; Korba, B.; Chu, C. K. Synthesis and Antiviral Activity of Cyclopropyl-Spiro-Carbocyclic Adenosine, (4R,5S,6R,7R)-4-(6-Amino-9H-Purin-9-yl)-7-(Hydroxymethyl)spiro[2.4]heptane-5,6-Diol Against Hepatitis C Virus. *Bioorg. Med. Chem. Lett.* **2011,** *21,* 3982–3985.

88. Ling, Y.-Z.; Li, J.-S.; Kato, K.; Liu, Y.; Wang, X.; Klus, G. T.; Marat, K.; Nnane, I. P.; Brodie, A. M. H. Synthesis and in vitro Activity of Some Epimeric 20α-Hydroxy, 20-Oxime and Aziridine Pregnene Derivatives as Inhibitors of Human 17α-Hydroxylase/C17,20-Lyase and 5α-Reductase. *Bioorg. Med. Chem.* **1998,** *6,* 1683–1693.
89. Griffith, E. C.; Su, Z.; Turk, B. E.; Chen, S.; Chang, Y.-H.; Wu, Z.; Biemann, K.; Liu, J. O. Methionine Aminopeptidase (Type 2) is the Common Target for Angiogenesis Inhibitors AGM-1470 and Ovalicin. *Chem. Biol.* **1997,** *4,* 461–471.
90. Liu, S.; Widom, J.; Kemp, C. W.; Crews, C. M.; Clardy, J. Structure of Human Methionine Aminopeptidase-2 Complexed With Fumagillin. *Science* **1998,** *282,* 1324–1327.
91. Ingber, D.; Fujita, T.; Kishimoto, S.; Sudo, K.; Kanamaru, T.; Brem, H.; Folkman, J. Synthetic Analogs of Fumagillin that Inhibit Angiogenesis and Suppress Tumor Growth. *Nature (London)* **1990,** *348,* 555–557.
92. Castronovo, V.; Belotti, D. TNP-470 (AGM-1470): Mechanisms of Action and Early Clinical Development. *Eur. J. Cancer* **1996,** *32A,* 2520–2527.
93. Arico-Muendel, C.; Centrella, P. A.; Contonio, B. D.; Morgan, B. A.; O'Donovan, G.; Paradise, C. L.; Skinner, S. R.; Sluboski, B.; Svendsen, J. L.; White, K. F.; Debnath, A.; Gut, J.; Wilson, N.; McKerrow, J. H.; DeRisi, J. L.; Rosenthal, P. J.; Chiang, P. K. Antiparasitic Activities of Novel, Orally Available Fumagillin Analogs. *Bioorg. Med. Chem. Lett.* **2009,** *19,* 5128–5131.
94. Arico-Muendel, C. C.; Benjamin, D. R.; Caiazzo, T. M.; Centrella, P. A.; Contonio, B. D.; Cook, C. M.; Doyle, E. G.; Hannig, G.; Labenski, M. T.; Searle, L. L.; Lind, K.; Morgan, B. A.; Olson, G.; Paradise, C. L.; Self, C.; Skinner, S. R.; Sluboski, B.; Svendsen, J. L.; Thompson, C. D.; Westlin, W.; White, K. F. Carbamate Analogues of Fumagillin as Potent, Targeted Inhibitors of Methionine Aminopeptidase-2. *J. Med. Chem.* **2009,** *52,* 8047–8056.
95. Kim, D. D.; Krishnarajah, J.; Lillioja, S.; de Looze, F.; Marjason, J.; Proietto, J.; Shakib, S.; Stuckey, B. G. A.; Vath, J. E.; Hughes, T. E. Efficacy and Safety of Beloranib for Weight Loss in Obese Adults: A Randomized Controlled Trial. *Diabetes, Obes. Metab.* **2015,** *17,* 566–572.
96. Kaida, D.; Motoyoshi, H.; Tashiro, E.; Nojima, T.; Hagiwara, M.; Ishigami, K.; Watanabe, H.; Kitahara, T.; Yoshida, T.; Nakajima, H.; Tani, T.; Horinouchi, S.; Yoshida, M. Spliceostatin A Targets SF3b and Inhibits Both Splicing and Nuclear Retention of Pre-mRNA. *Nat. Chem. Biol.* **2007,** *3,* 576–583.
97. Fan, L.; Lagisetti, C.; Edwards, C. C.; Webb, T. R.; Potter, P. M. Sudemycins, Novel Small Molecule Analogues of FR901464, Induce Alternative Gene Splicing. *ACS Chem. Biol.* **2011,** *6,* 582–589.
98. Lagisetti, C.; Palacios, G.; Goronga, T.; Freeman, B.; Caufield, W.; Webb, T. R. Optimization of Antitumor Modulators of Pre-mRNA Splicing. *J. Med. Chem.* **2013,** *56,* 10033–10044.
99. Schwarz, J. B.; Gibbons, S. E.; Graham, S. R.; Colbry, N. L.; Guzzo, P. R.; Le, V.-D.; Vartanian, M. G.; Kinsora, J. J.; Lotarski, S. M.; Li, Z.; Dickerson, M. R.; Su, T.-Z.; Weber, M. L.; El-Kattan, A.; Thorpe, A. J.; Donevan, S. D.; Taylor, C. P.; Wustrow, D. J. Novel Cyclopropyl B-Amino Acid Analogues of Pregabalin and Gabapentin That Target the α2-δ Protein. *J. Med. Chem.* **2005,** *48,* 3026–3035.
100. Brown, D. G.; Bernstein, P. R.; Griffin, A.; Wesolowski, S.; Labrecque, D.; Tremblay, M. C.; Sylvester, M.; Mauger, R.; Edwards, P. D.; Throner, S. R.; Folmer, J. J.; Cacciola, J.; Scott, C.; Lazor, L. A.; Pourashraf, M.; Santhakumar, V.; Potts, W. M.; Sydserff, S.; Giguère, P.; Lévesque, C.; Dasser, M.; Groblewski, T. Discovery of Spirofused Piperazine and Diazepane Amides as Selective Histamine-3 Antagonists With in vivo Efficacy in a Mouse Model of Cognition. *J. Med. Chem.* **2014,** *57,* 733–758.
101. Robl, J. A.; Sulsky, R.; Sieber-McMaster, E.; Ryono, D. E.; Cimarusti, M. P.; Simpkins, L. M.; Karanewsky, D. S.; Chao, S.; Asaad, M. M.; Seymour, A. A.; Fox, M.; Smith, P. L.; Trippodo, N. C. Vasopeptidase Inhibitors: Incorporation of Geminal and Spirocyclic Substituted Azepinones in Mercaptoacyl Dipeptides. *J. Med. Chem.* **1999,** *42,* 305–311.
102. Burkhard, J.; Carreira, E. M. 2,6-Diazaspiro[3.3]heptanes: Synthesis and Application in Pd-Catalyzed Aryl Amination Reactions. *Org. Lett.* **2008,** *10,* 3525–3526.
103. Henderson, J. L.; Kormos, B. L.; Hayward, M. M.; Coffman, K. J.; Jasti, J.; Kurumbail, R. G.; Wager, T. T.; Verhoest, P. R.; Noell, G. S.; Chen, Y.; Needle, E.; Berger, Z.; Steyn, S. J.; Houle, C.; Hirst, W. D.; Galatsis, P. Discovery and Preclinical Profiling of 3-[4-(Morpholin-4-yl)-7H-Pyrrolo[2,3-d]pyrimidin-5-yl]benzonitrile (PF-06447475), a Highly Potent, Selective, Brain Penetrant, and in vivo Active LRRK2 Kinase Inhibitor. *J. Med. Chem.* **2015,** *58,* 419–432.
104. Maryanoff, B. E.; O'Neill, J. C.; McComsey, D. F.; Yabut, S. C.; Luci, D. K.; Jordan, A. D.; Masucci, J. A.; Jones, W. J.; Abad, M. C.; Gibbs, A. C.; Petrounia, I. Inhibitors of Ketohexokinase: Discovery of Pyrimidinopyrimidines With Specific Substitution That Complements the ATP-Binding Site. *ACS Med. Chem. Lett.* **2011,** *2,* 538–543.
105. Lachance, N.; Gareau, Y.; Guiral, S.; Huang, Z.; Isabel, E.; Leclerc, J.-P.; Leger, S.; Martins, E.; Nadeau, C.; Oballa, R. M.; Ouellet, S. G.; Powell, D. A.; Ramtohul, Y. K.; Tranmer, G. K.; Trinh, T.; Wang, H.; Zhang, L. Discovery of Potent and Liver-Targeted Stearoyl-CoA Desaturase (SCD) Inhibitors in a Bispyrrolidine Series. *Bioorg. Med. Chem. Lett.* **2012,** *22,* 980–984.
106. Zhao, F.; Lin, Z.; Wang, F.; Zhao, W.; Dong, X. Four-Membered Heterocycles-Containing 4-Anilino-quinazoline Derivatives as Epidermal Growth Factor Receptor (EGFR) Kinase Inhibitors. *Bioorg. Med. Chem. Lett.* **2013,** *23,* 5385–5388.
107. Schechter, I.; Berger, A. On the Size of the Active Site in Proteases. I. Papain. *Biochem. Biophys. Res. Commun.* **1967,** *27,* 157–162.
108. Bondada, L.; Rondla, R.; Pradere, U.; Liu, P.; Li, C.; Bobeck, D.; McBrayer, T.; Tharnish, P.; Courcambeck, J.; Halfon, P.; Whitaker, T.; Amblard, F.; Coats, S. J.; Schinazi, R. F. Azetidines and Spiro Azetidines as Novel P2 Units in Hepatitis C Virus NS3 Protease Inhibitors. *Bioorg. Med. Chem. Lett.* **2013,** *23,* 6325–6330.
109. Du, J.; Chun, B.-K.; Mosley, R. T.; Bansal, S.; Bao, H.; Espiritu, C.; Lam, A. M.; Murakami, E.; Niu, C.; Micolochick Steuer, H. M.; Furman, P. A.; Sofia, M. J. Use of 2′-Spirocyclic Ethers in HCV Nucleoside Design. *J. Med. Chem.* **2014,** *57,* 1826–1835.
110. Jonckers, T. H. M.; Vandyck, K.; Vandekerckhove, L.; Hu, L.; Tahri, A.; Van Hoof, S.; Lin, T.-I.; Vijgen, L.; Berke, J. M.; Lachau-Durand, S.; Stoops, B.; Leclercq, L.; Fanning, G.; Samuelsson, B.; Nilsson, M.; Rosenquist, Å.; Simmen, K.; Raboisson, P. Nucleotide Prodrugs of 2′-Deoxy-2′-Spirooxetane Ribonucleosides as Novel Inhibitors of the HCV NS5B Polymerase. *J. Med. Chem.* **2014,** *57,* 1836–1844.
111. Johnson, D. S.; Stiff, C.; Lazerwith, S. E.; Kesten, S. R.; Fay, L. K.; Morris, M.; Beidler, D.; Liimatta, M. B.; Smith, S. E.; Dudley, D. T.; Sadagopan, N.; Bhattachar, S. N.; Kesten, S. J.; Nomanbhoy, T. K.; Cravatt, B. F.; Ahn, K. Discovery of PF-04457845: A Highly Potent, Orally Bioavailable, and Selective Urea FAAH Inhibitor. *ACS Med. Chem. Lett.* **2011,** *2,* 91–96.
112. Meyers, M. J.; Long, S. A.; Pelc, M. J.; Wang, J. L.; Bowen, S. J.; Walker, M. C.; Schweitzer, B. A.; Madsen, H. M.; Tenbrink, R. E.; McDonald, J.; Smith, S. E.; Foltin, S.; Beidler, D.; Thorarensen, A. Discovery of Novel Spirocyclic Inhibitors of Fatty acid Amide Hydrolase (FAAH). Part 1: Identification of 7-Azaspiro[3.5]nonane and 1-Oxa-8-Azaspiro[4.5]decane as Lead Scaffolds. *Bioorg. Med. Chem. Lett.* **2011,** *21,* 6538–6544.
113. Meyers, M. J.; Long, S. A.; Pelc, M. J.; Wang, J. L.; Bowen, S. J.; Schweitzer, B. A.; Wilcox, M. V.; McDonald, J.; Smith, S. E.; Foltin, S.; Rumsey, J.; Yang, Y.-S.; Walker, M. C.; Kamtekar, S.; Beidler, D.; Thorarensen, A. Discovery of Novel Spirocyclic Inhibitors of Fatty acid Amide Hydrolase (FAAH). Part 2. Discovery of 7-Azaspiro[3.5] nonane Urea PF-04862853, an Orally Efficacious Inhibitor of Fatty acid Amide Hydrolase (FAAH) for Pain. *Bioorg. Med. Chem. Lett.* **2011,** *21,* 6545–6553.
114. Kung, D. W.; Coffey, S. B.; Jones, R. M.; Cabral, S.; Jiao, W.; Fichtner, M.; Carpino, P. A.; Rose, C. R.; Hank, R. F.; Lopaze, M. G.; Swartz, R.; Chen, H.; Hendsch, Z.; Posner, B.; Wielis, C. F.; Manning, B.; Dubins, J.; Stock, I. A.; Varma, S.; Campbell, M.; DeBartola, D.; Kosa-Maines, R.; Steyn, S. J.; McClure, K. F. Identification of Spirocyclic Piperidine-Azetidine Inverse Agonists of the Ghrelin Receptor. *Bioorg. Med. Chem. Lett.* **2012,** *22,* 4281–4287.
115. McClure, K. F.; Jackson, M.; Cameron, K. O.; Kung, D. W.; Perry, D. A.; Orr, S. T. M.; Zhang, Y.; Kohrt, J.; Tu, M.; Gao, H.; Fernando, D.; Jones, R.; Erasga, N.; Wang, G.; Polivkova, J.; Jiao, W.; Swartz, R.; Ueno, H.; Bhattacharya, S. K.; Stock, I. A.; Varma, S.; Bagdasarian, V.; Perez, S.; Kelly-Sullivan, D.; Wang, R.; Kong, J.; Cornelius, P.; Michael, L.; Lee, E.; Janssen, A.; Steyn, S. J.; Lapham, K.; Goosen, T. Identification of Potent, Selective, CNS-Targeted Inverse Agonists of the Ghrelin Receptor. *Bioorg. Med. Chem. Lett.* **2013,** *23,* 5410–5414.
116. Bhattacharya, S. K.; Andrews, K.; Beveridge, R.; Cameron, K. O.; Chen, C.; Dunn, M.; Fernando, D.; Gao, H.; Hepworth, D.; Jackson, V. M.; Khot, V.; Kong, J.; Kosa, R. E.; Lapham, K.; Loria, P. M.; Londregan, A. T.; McClure, K. F.; Orr, S. T. M.; Patel, J.; Rose, C.; Saenz, J.; Stock, I. A.; Storer, G.; VanVolkenburg, M.; Vrieze, D.; Wang, G.; Xiao, J.; Zhang, Y. Discovery of PF-5190457, a Potent, Selective, and Orally Bioavailable Ghrelin Receptor Inverse Agonist Clinical Candidate. *ACS Med. Chem. Lett.* **2014,** *5,* 474–479.

117. Kaller, M. R.; Harried, S. S.; Albrecht, B.; Amarante, P.; Babu-Khan, S.; Bartberger, M. D.; Brown, J.; Brown, R.; Chen, K.; Cheng, Y.; Citron, M.; Croghan, M. D.; Graceffa, R.; Hickman, D.; Judd, T.; Kriemen, C.; La, D.; Li, V.; Lopez, P.; Luo, Y.; Masse, C.; Monenschein, H.; Nguyen, T.; Pennington, L. D.; Miguel, T. S.; Sickmier, E. A.; Wahl, R. C.; Weiss, M. M.; Wen, P. H.; Williamson, T.; Wood, S.; Xue, M.; Yang, B.; Zhang, J.; Patel, V.; Zhong, W.; Hitchcock, S. A Potent and Orally Efficacious, Hydroxyethylamine-Based Inhibitor of β-Secretase. *ACS Med. Chem. Lett.* **2012,** *3,* 886–891.
118. Wood, S.; Wen, P. H.; Zhang, J.; Zhu, L.; Luo, Y.; Babu-Khan, S.; Chen, K.; Pham, R.; Esmay, J.; Dineen, T. A.; Kaller, M. R.; Weiss, M. M.; Hitchcock, S. A.; Citron, M.; Zhong, W.; Hickman, D.; Williamson, T. Establishing the Relationship Between in vitro Potency, Pharmacokinetic, and Pharmacodynamic Parameters in a Series of Orally Available, Hydroxyethylamine-Derived β-Secretase Inhibitors. *J. Pharmacol. Exp. Ther.* **2012,** *343,* 460–467.
119. Weiss, M. M.; Williamson, T.; Babu-Khan, S.; Bartberger, M. D.; Brown, J.; Chen, K.; Cheng, Y.; Citron, M.; Croghan, M. D.; Dineen, T. A.; Esmay, J.; Graceffa, R. F.; Harried, S. S.; Hickman, D.; Hitchcock, S. A.; Horne, D. B.; Huang, H.; Imbeah-Ampiah, R.; Judd, T.; Kaller, M. R.; Kreiman, C. R.; La, D. S.; Li, V.; Lopez, P.; Louie, S.; Monenschein, H.; Nguyen, T. T.; Pennington, L. D.; Rattan, C.; San Miguel, T.; Sickmier, E. A.; Wahl, R. C.; Wen, P. H.; Wood, S.; Xue, Q.; Yang, B. H.; Patel, V. F.; Zhong, W. Design and Preparation of a Potent Series of Hydroxyethylamine Containing β-Secretase Inhibitors That Demonstrate Robust Reduction of Central β-Amyloid. *J. Med. Chem.* **2012,** *55,* 9009–9024.
120. Dineen, T. A.; Weiss, M. M.; Williamson, T.; Acton, P.; Babu-Khan, S.; Bartberger, M. D.; Brown, J.; Chen, K.; Cheng, Y.; Citron, M.; Croghan, M. D.; Dunn, R. T.; Esmay, J.; Graceffa, R. F.; Harried, S. S.; Hickman, D.; Hitchcock, S. A.; Horne, D. B.; Huang, H.; Imbeah-Ampiah, R.; Judd, T.; Kaller, M. R.; Kreiman, C. R.; La, D. S.; Li, V.; Lopez, P.; Louie, S.; Monenschein, H.; Nguyen, T. T.; Pennington, L. D.; San Miguel, T.; Sickmier, E. A.; Vargas, H. M.; Wahl, R. C.; Wen, P. H.; Whittington, D. A.; Wood, S.; Xue, Q.; Yang, B. H.; Patel, V. F.; Zhong, W. Design and Synthesis of Potent, Orally Efficacious Hydroxyethylamine Derived β-Site Amyloid Precursor Protein Cleaving Enzyme (BACE1) Inhibitors. *J. Med. Chem.* **2012,** *55,* 9025–9044.
121. Gazzard, L.; Williams, K.; Chen, H.; Axford, L.; Blackwood, E.; Burton, B.; Chapman, K.; Crackett, P.; Drobnick, J.; Ellwood, C.; Epler, J.; Flagella, M.; Gancia, E.; Gill, M.; Goodacre, S.; Halladay, J.; Hewitt, J.; Hunt, H.; Kintz, S.; Lyssikatos, J.; Macleod, C.; Major, S.; Médard, G.; Narukulla, R.; Ramiscal, J.; Schmidt, S.; Seward, E.; Wiesmann, C.; Wu, P.; Yee, S.; Yen, I.; Malek, S. Mitigation of Acetylcholine Esterase Activity in the 1,7-Diazacarbazole Series of Inhibitors of Checkpoint Kinase 1. *J. Med. Chem.* **2015,** *58,* 5053–5074.
122. de Gasparo, M.; Joss, U.; Ramjoué, H. P.; Whitebread, S. E.; Haenni, H.; Schenkel, L.; Kraehenbuehl, C.; Biollaz, M.; Grob, J.; Schmidlin, J. Three New Epoxy-Spirolactone Derivatives: Characterization in vivo and In Vitro. *J. Pharmacol. Exp. Ther.* **1987,** *240,* 650–656.
123. Grob, J.; Boillaz, M.; Schmidlin, J.; Wehrli, H.; Wieland, P.; Fuhrer, H.; Rihs, G.; Joss, U.; Gasparo, M. D.; Haenni, H.; Ramjoué, H. P.; Whitebread, S. E.; Kalvoda, J. Steroidal, Aldosterone Antagonists: Increased Selectivity of 9α,11-Epoxy Derivatives. *Helv. Chim. Acta* **1987,** *80,* 566–585.
124. Krattenmacher, R. Drospirenone: Pharmacology and Pharmacokinetics of a Unique Progestogen. *Contraception* **2000,** *62,* 29–38.
125. Wepierre, J.; Bogaievsky, Y. Comparative Pharmacological Activity of Triamcinolone Acetonide and of a New Topical Steroid: Amcinonide, after Percutaneous or Oral Administration (Author's Transl). *J. Pharmacol.* **1980,** *11,* 449–462.
126. Bernhart, C. A.; Perreaut, P. M.; Ferrari, B. P.; Muneaux, Y. A.; Assens, J. L. A.; Clement, J.; Haudricourt, F.; Muneaux, C. F.; Taillades, J. E.; Vignal, M.-A.; Gougat, J.; Guiraudou, P. R.; Lacour, C. A.; Roccon, A.; Cazaubon, C. F.; Breliere, J.-C.; Le Fur, G.; Nisato, D. A New Series of Imidazolones: Highly Specific and Potent Nonpeptide AT1 Angiotensin II Receptor Antagonists. *J. Med. Chem.* **1993,** *36,* 3371–3380.
127. Smith, E. M.; Swiss, G. F.; Neustadt, B. R.; McNamara, P.; Gold, E. H.; Sybertz, E. J.; Baum, T. Angiotensin Converting Enzyme Inhibitors: Spirapril and Related Compounds. *J. Med. Chem.* **1989,** *32,* 1600–1666.
128. Hopkins, C. R. ACS Chemical Neuroscience Molecule Spotlight on Telcagepant (MK-0974). *ACS Chem. Neurosci.* **2011,** *2,* 334–335.
129. Roller, S.; Cui, D.; Laspina, C.; Miller-Stein, C.; Rowe, J.; Wong, B.; Prueksaritanont, T. Preclinical Pharmacokinetics of MK-0974, an Orally Active Calcitonin-Gene Related Peptide (CGRP)-Receptor Antagonist, Mechanism of Dose Dependency and Species Differences. *Xenobiotica* **2009,** *39,* 33–45.
130. Burgey, C. S.; Potteiger, C. M.; Deng, J. Z.; Mosser, S. D.; Salvatore, C. A.; Yu, S.; Roller, S.; Kane, S. A.; Vacca, J. P.; Williams, T. M. Optimization of Azepanone Calcitonin Gene-Related Peptide (CGRP) Receptor Antagonists: Development of Novel Spiropiperidines. *Bioorg. Med. Chem. Lett.* **2009,** *19,* 6368–6372.
131. Wood, M. R.; Schirripa, K. M.; Kim, J. J.; Quigley, A. G.; Stump, C. A.; Bell, I. M.; Bednar, R. A.; Fay, J. F.; Bruno, J. G.; Moore, E. L.; Mosser, S. D.; Roller, S.; Salvatore, C. A.; Kane, S. A.; Vacca, J. P.; Selnick, H. G. Novel CGRP Receptor Antagonists Through a Design Strategy of Target Simplification With Addition of Molecular Flexibility. *Bioorg. Med. Chem. Lett.* **2009,** *19,* 5787–5790.
132. Stump, C. A.; Bell, I. M.; Bednar, R. A.; Bruno, J. G.; Fay, J. F.; Gallicchio, S. N.; Johnston, V. K.; Moore, E. L.; Mosser, S. D.; Quigley, A. G.; Salvatore, C. A.; Theberge, C. R.; Blair Zartman, C.; Zhang, X.-F.; Kane, S. A.; Graham, S. L.; Vacca, J. P.; Williams, T. M. The Discovery of Highly Potent CGRP Receptor Antagonists. *Bioorg. Med. Chem. Lett.* **2009,** *19,* 214–217.
133. Bell, I. M.; Gallicchio, S. N.; Wood, M. R.; Quigley, A. G.; Stump, C. A.; Zartman, C. B.; Fay, J. F.; Li, C.-C.; Lynch, J. J.; Moore, E. L.; Mosser, S. D.; Prueksaritanont, T.; Regan, C. P.; Roller, S.; Salvatore, C. A.; Kane, S. A.; Vacca, J. P.; Selnick, H. G. Discovery of MK-3207: A Highly Potent, Orally Bioavailable CGRP Receptor Antagonist. *ACS Med. Chem. Lett.* **2010,** *1,* 24–29.
134. Bell, I. M.; Gallicchio, S. N.; Stump, C. A.; Bruno, J. G.; Fan, H.; Gantert, L. T.; Hostetler, E. D.; Kemmerer, A. L.; McWherter, M.; Moore, E. L.; Mosser, S. D.; Purcell, M. L.; Riffel, K.; Salvatore, C. A.; Sanabria-Bohorquez, S.; Staas, D. D.; White, R. B.; Williams, M.; Zartman, C. B.; Cook, J. J.; Hargreaves, R. J.; Kane, S. A.; Graham, S. L.; Selnick, H. G. [11C]MK-4232: The First Positron Emission Tomography Tracer for the Calcitonin Gene-Related Peptide Receptor. *ACS Med. Chem. Lett.* **2013,** *4,* 863–868.
135. Bell, I. M.; Stump, C. A.; Gallicchio, S. N.; Staas, D. D.; Zartman, C. B.; Moore, E. L.; Sain, N.; Urban, M.; Bruno, J. G.; Calamari, A.; Kemmerer, A. L.; Mosser, S. D.; Fandozzi, C.; White, R. B.; Zrada, M. M.; Selnick, H. G.; Graham, S. L.; Vacca, J. P.; Kane, S. A.; Salvatore, C. A. MK-8825: A Potent and Selective CGRP Receptor Antagonist With Good Oral Activity in Rats. *Bioorg. Med. Chem. Lett.* **2012,** *22,* 3941–3945.
136. Bell, I. M.; Fraley, M. E.; Gallicchio, S. N.; Ginnetti, A.; Mitchell, H. J.; Paone, D. V.; Staas, D. D.; Wang, C.; Zartman, C. B.; Stevenson, H. E. Preparation of Piperidinonylcarboxamideazaindane Derivatives for Use as CGRP Receptor Antagonists. WO2012064910A1.
137. Wood, M. R.; Schirripa, K. M.; Kim, J. J.; Bednar, R. A.; Fay, J. F.; Bruno, J. G.; Moore, E. L.; Mosser, S. D.; Roller, S.; Salvatore, C. A.; Vacca, J. P.; Selnick, H. G. Novel CGRP Receptor Antagonists From Central Amide Replacements Causing a Reversal of Preferred Chirality. *Bioorg. Med. Chem. Lett.* **2010,** *20,* 6827–6830.
138. Duan, J. J. W.; Chen, L.; Lu, Z.; Xue, C.-B.; Liu, R.-Q.; Covington, M. B.; Qian, M.; Wasserman, Z. R.; Vaddi, K.; Christ, D. D.; Trzaskos, J. M.; Newton, R. C.; Decicco, C. P. Discovery of β-Benzamido Hydroxamic Acids as Potent, Selective, and Orally Bioavailable TACE Inhibitors. *Bioorg. Med. Chem. Lett.* **2008,** *18,* 241–246.
139. Ott, G. R.; Asakawa, N.; Lu, Z.; Liu, R.-Q.; Covington, M. B.; Vaddi, K.; Qian, M.; Newton, R. C.; Christ, D. D.; Traskos, J. M.; Decicco, C. P.; Duan, J. J. W. α,β-Cyclic-β-Benzamido Hydroxamic acids: Novel Templates for the Design, Synthesis, and Evaluation of Selective Inhibitors of TNF-α Converting Enzyme (TACE). *Bioorg. Med. Chem. Lett.* **2008,** *18,* 694–699.
140. Ding, K.; Lu, Y.; Nikolovska-Coleska, Z.; Qiu, S.; Ding, Y.; Gao, W.; Stuckey, J.; Krajewski, K.; Roller, P. P.; Tomita, Y.; Parrish, D. A.; Deschamps, J. R.; Wang, S. Structure-Based Design of Potent Non-Peptide MDM2 Inhibitors. *J. Am. Chem. Soc.* **2005,** *127,* 10130–10131.
141. Ding, K.; Lu, Y.; Nikolovska-Coleska, Z.; Wang, G.; Qiu, S.; Shangary, S.; Gao, W.; Qin, D.; Stuckey, J.; Krajewski, K.; Roller, P. P.; Wang, S. Structure-Based Design of Spiro-oxindoles as Potent, Specific Small-Molecule Inhibitors of the MDM2−p53 Interaction. *J. Med. Chem.* **2006,** *49,* 3432–3435.
142. Yu, S.; Qin, D.; Shangary, S.; Chen, J.; Wang, G.; Ding, K.; McEachern, D.; Qiu, S.; Nikolovska-Coleska, Z.; Miller, R.; Kang, S.; Yang, D.; Wang, S. Potent and Orally Active Small-Molecule Inhibitors of the MDM2-p53 Interaction. *J. Med. Chem.* **2009,** *52,* 7970–7973.
143. Zhao, Y.; Liu, L.; Sun, W.; Lu, J.; McEachern, D.; Li, X.; Yu, S.; Bernard, D.; Ochsenbein, P.; Ferey, V.; Carry, J.-C.; Deschamps, J. R.; Sun, D.; Wang, S. Diastereomeric Spirooxindoles as Highly Potent and Efficacious MDM2 Inhibitors. *J. Am. Chem. Soc.* **2013,** *135,* 7223–7234.
144. Zhao, Y.; Yu, S.; Sun, W.; Liu, L.; Lu, J.; McEachern, D.; Shargary, S.; Bernard, D.; Li, X.; Zhao, T.; Zou, P.; Sun, D.; Wang, S. A Potent Small-Molecule Inhibitor of the MDM2–p53 Interaction (MI-888) Achieved Complete and Durable Tumor Regression in Mice. *J. Med. Chem.* **2013,** *56,* 5553–5561.

145. Wang, S.; Sun, W.; Zhao, Y.; McEachern, D.; Meaux, I.; Barrière, C.; Stuckey, J. A.; Meagher, J. L.; Bai, L.; Liu, L.; Hoffman-Luca, C. G.; Lu, J.; Shangary, S.; Yu, S.; Bernard, D.; Aguilar, A.; Dos-Santos, O.; Besret, L.; Guerif, S.; Pannier, P.; Gorge-Bernat, D.; Debussche, L. SAR405838: An Optimized Inhibitor of MDM2–p53 Interaction That Induces Complete and Durable Tumor Regression. *Cancer Res.* **2014,** *74,* 5855–5865.
146. Carry, J.-C.; Garcia-Echeverria, C. Inhibitors of the p53/hdm2 Protein–Protein Interaction — Path to the Clinic. *Bioorg. Med. Chem. Lett.* **2013,** *23,* 2480–2485.
147. Zhao, Y.; Aguilar, A.; Bernard, D.; Wang, S. Small-Molecule Inhibitors of the MDM2-p53 Protein–Protein Interaction (MDM2 Inhibitors) in Clinical Trials for Cancer Treatment. *J. Med. Chem.* **2015,** *58,* 1038–1052.
148. Ding, Q.; Zhang, Z.; Liu, J.-J.; Jiang, N.; Zhang, J.; Ross, T. M.; Chu, X.-J.; Bartkovitz, D.; Podlaski, F.; Janson, C.; Tovar, C.; Filipovic, Z. M.; Higgins, B.; Glenn, K.; Packman, K.; Vassilev, L. T.; Graves, B. Discovery of RG7388, a Potent and Selective p53–MDM2 Inhibitor in Clinical Development. *J. Med. Chem.* **2013,** *56,* 5979–5983.
149. Zhang, Z.; Ding, Q.; Liu, J.-J.; Zhang, J.; Jiang, N.; Chu, X.-J.; Bartkovitz, D.; Luk, K.-C.; Janson, C.; Tovar, C.; Filipovic, Z. M.; Higgins, B.; Glenn, K.; Packman, K.; Vassilev, L. T.; Graves, B. Discovery of Potent and Selective Spiroindolinone MDM2 Inhibitor, RO8994, for Cancer Therapy. *Bioorg. Med. Chem.* **2014,** *22,* 4001–4009.
150. Zhang, Z.; Chu, X.-J.; Liu, J.-J.; Ding, Q.; Zhang, J.; Bartkovitz, D.; Jiang, N.; Karnachi, P.; So, S.-S.; Tovar, C.; Filipovic, Z. M.; Higgins, B.; Glenn, K.; Packman, K.; Vassilev, L.; Graves, B. Discovery of Potent and Orally Active p53-MDM2 Inhibitors RO5353 and RO2468 for Potential Clinical Development. *ACS Med. Chem. Lett.* **2014,** *5,* 124–127.
151. Gomez-Monterrey, I.; Bertamino, A.; Porta, A.; Carotenuto, A.; Musella, S.; Aquino, C.; Granata, I.; Sala, M.; Brancaccio, D.; Picone, D.; Ercole, C.; Stiuso, P.; Campiglia, P.; Grieco, P.; Ianelli, P.; Maresca, B.; Novellino, E. Identification of the Spiro(oxindole-3,3′-Thiazolidine)-Based Derivatives as Potential p53 Activity Modulators. *J. Med. Chem.* **2010,** *53,* 8319–8329.
152. Bertamino, A.; Soprano, M.; Musella, S.; Rusciano, M. R.; Sala, M.; Vernieri, E.; Di Sarno, V.; Limatola, A.; Carotenuto, A.; Cosconati, S.; Grieco, P.; Novellino, E.; Illario, M.; Campiglia, P.; Gomez-Monterrey, I. Synthesis, In Vitro, and in Cell Studies of a New Series of [Indoline-3,2′-Thiazolidine]-Based p53 Modulators. *J. Med. Chem.* **2013,** *56,* 5407–5421.
153. Potin, D.; Launay, M.; Nicolai, E.; Fabreguette, M.; Malabre, P.; Caussade, F.; Besse, D.; Skala, S.; Stetsko, D. K.; Todderud, G.; Beno, B. R.; Cheney, D. L.; Chang, C. J.; Sheriff, S.; Hollenbaugh, D. L.; Barrish, J. C.; Iwanowicz, E. J.; Suchard, S. J.; Dhar, T. G. M. De novo Design, Synthesis, and in vitro Activity of LFA-1 Antagonists Based on a Bicyclic[5.5]hydantoin Scaffold. *Bioorg. Med. Chem. Lett.* **2005,** *15,* 1161–1164.
154. Potin, D.; Launay, M.; Monatlik, F.; Malabre, P.; Fabreguettes, M.; Fouquet, A.; Maillet, M.; Nicolai, E.; Dorgeret, L.; Chevallier, F.; Besse, D.; Dufort, M.; Caussade, F.; Ahmad, S. Z.; Stetsko, D. K.; Skala, S.; Davis, P. M.; Balimane, P.; Patel, K.; Yang, Z.; Marathe, P.; Postelneck, J.; Townsend, R. M.; Goldfarb, V.; Sheriff, S.; Einspahr, H.; Kish, K.; Malley, M. F.; DiMarco, J. D.; Gougoutas, J. Z.; Kadiyala, P.; Cheney, D. L.; Tejwani, R. W.; Murphy, D. K.; McIntyre, K. W.; Yang, X.; Chao, S.; Leith, L.; Xiao, Z.; Mathur, A.; Chen, B.-C.; Wu, D.-R.; Traeger, S. C.; McKinnon, M.; Barrish, J. C.; Robl, J. A.; Iwanowicz, E. J.; Suchard, S. J.; Dhar, T. G. M. Discovery and Development of 5-[(5S,9R)-9-(4-Cyanophenyl)-3-(3,5-Dichlorophenyl)-1- Methyl-2,4-Dioxo-1,3,7-Triazaspiro[4.4]non-7-yl-Methyl]-3-Thiophenecarboxylic Acid (BMS-587101)A Small Molecule Antagonist of Leukocyte Function Associated Antigen-1†. *J. Med. Chem.* **2006,** *49,* 6946–6949.
155. Watterson, S. H.; Xiao, Z.; Dodd, D. S.; Tortolani, D. R.; Vaccaro, W.; Potin, D.; Launay, M.; Stetsko, D. K.; Skala, S.; Davis, P. M.; Lee, D.; Yang, X.; McIntyre, K. W.; Balimane, P.; Patel, K.; Yang, Z.; Marathe, P.; Kadiyala, P.; Tebben, A. J.; Sheriff, S.; Chang, C. Y.; Ziemba, T.; Zhang, H.; Chen, B.-C.; DelMonte, A. J.; Aranibar, N.; McKinnon, M.; Barrish, J. C.; Suchard, S. J.; Murali Dhar, T. G. Small Molecule Antagonist of Leukocyte Function Associated Antigen-1 (LFA-1): Structure−Activity Relationships Leading to the Identification of 6-((5S,9R)-9-(4-Cyanophenyl)-3-(3,5-Dichlorophenyl)-1-Methyl-2,4-Dioxo-1,3,7-Triazaspiro[4.4]nonan-7-yl)nicotinic Acid (BMS-688521). *J. Med. Chem.* **2010,** *53,* 3814–3830.
156. Lewis, S. J.; Smith, A. L.; Neduvelil, J. G.; Stevenson, G. I.; Lindon, M. J.; Jones, A. B..; Shearman, M. S.; Beher, D.; Clarke, E.; Best, J. D.; Peachey, J. E.; Harrison, T.; Castro, J. L. A Novel Series of Potent γ-Secretase Inhibitors Based on a Benzobicyclo[4.2.1]nonane Core. *Bioorg. Med. Chem. Lett.* **2005,** *15,* 373–378.
157. Sparey, T.; Beher, D.; Best, J.; Biba, M.; Castro, J. L.; Clarke, E.; Hannam, J.; Harrison, T.; Lewis, H.; Madin, A.; Shearman, M.; Sohal, B.; Tsou, N.; Welch, C.; Wrigley, J. Cyclic Sulfamide γ-Secretase Inhibitors. *Bioorg. Med. Chem. Lett.* **2005,** *15,* 4212–4216.
158. Keown, L. E.; Collins, I.; Cooper, L. C.; Harrison, T.; Madin, A.; Mistry, J.; Reilly, M.; Shaimi, M.; Welch, C. J.; Clarke, E. E.; Lewis, H. D.; Wrigley, J. D. J.; Best, J. D.; Murray, F.; Shearman, M. S. Novel Orally Bioavailable γ-Secretase Inhibitors With Excellent in vivo Activity. *J. Med. Chem.* **2009,** *52,* 3441–3444.
159. Wu, Y.-H.; Smith, K. R.; Rayburn, J. W.; Kissel, J. W. Psychosedative Agents. N-(4-Phenyl-1-Piperazinylalkyl)-Substituted Cyclic Imides. *J. Med. Chem.* **1969,** *12,* 876–881.
160. Wu, Y.-H.; Rayburn, J. W.; Allen, L. E.; Ferguson, H. C.; Kissel, J. W. Psychosedative Agents. 2. 8-(4-Substituted 1-Piperazinylalkyl)-8-Azaspiro[4.5]decane-7,9-diones. *J. Med. Chem.* **1972,** *15,* 477–479.
161. Podona, T.; Guardiola-Lemaitre, B.; Caignard, D.-H.; Adam, G.; Pfeiffer, B.; Renard, P.; Guillaumet, G. 3,4-Dihydro-3-Amino-2H-1-Benzopyran Derivatives as 5-HT1A Receptor Ligands and Potential Anxiolytic Agents. 1. Synthesis and Structure-Activity Relationship Studies. *J. Med. Chem.* **1994,** *37,* 1779–1793.
162. Hibert, M. F.; Gittos, M. W.; Middlemiss, D. N.; Mir, A. K.; Fozard, J. R. Graphics Computer-Aided Receptor Mapping as a Predictive Tool for Drug Design: Development of Potent, Selective, and Stereospecific Ligands for the 5-HT1A Receptor. *J. Med. Chem.* **1988,** *31,* 1087–1093.
163. Yevich, J. P.; New, J. S.; Smith, D. W.; Lobeck, W. G.; Catt, J. D.; Minielli, J. L.; Eison, M. S.; Taylor, D. P.; Riblet, L. A.; Temple, D. L., Jr. Synthesis and Biological Evaluation of 1-(1,2-Benzisothiazol-3-yl)- and (1,2-Benzisoxazol-3-yl)piperazine Derivatives as Potential Antipsychotic Agents. *J. Med. Chem.* **1986,** *29,* 359–369.
164. Janssen, C. Substituted 4-oxo-1,3,8-triazaspiro[4.5]decanes. BE633914.
165. Janssen, P.A.J.; Janssen, C. 2,4,8-Triazaspiro[4.5]dec-2-enes. US3155669.
166. Mach, R. H.; Jackson, J. R.; Luedtke, R. R.; Ivins, K. J.; Molinoff, P. B.; Ehrenkaufer, R. L. Effect of *N*-Alkylation on the Affinities of Analogs of Spiperone for Dopamine D2 and Serotonin 5-HT2 Receptors. *J. Med. Chem.* **1992,** *35,* 423–430.
167. Metwally, K. A.; Dukat, M.; Egan, C. T.; Smith, C.; DuPre, A.; Gauthier, C. B.; Herrick-Davis, K.; Teitler, M.; Glennon, R. A. Spiperone: Influence of Spiro Ring Substituents on 5-HT2A Serotonin Receptor Binding. *J. Med. Chem.* **1998,** *41,* 5084–5093.
168. Schotte, A.; Janssen, P. F. M.; Gommeren, W.; Luyte, W. H. M. L.; Van Gompel, P.; Lesage, A. S.; De Loore, K.; Leysen, J. E. Risperidone Compared With New and Reference Antipsychotic Drugs: in vitro and in vivo Receptor Binding. *Psychopharmacology (Berlin)* **1996,** *124,* 57–73.
169. Mauvernay, R. Y.; Busch, N.; Moleyre, J.; Simond, J.; Monteil, A. 6-Aryloxy-2-Oxo-1-Azaoxa(or -thia)spiro[4,5]decanes. DE2542154A1.
170. Caille, E. J.; Bassano, J. L.; Lacoste, J. P.; Poulain, P. H. Étude de la molécule 3726 CERM au niveau du processus hypnique, de l'activité cérébrale en état de veille et dela disponsibilité au reveil. *Psychol. Méd.* **1978,** *10,* 1823–1837.
171. Nicholson, A. N.; Stone, B. M. 6-(3-Chloro)-Phenoxy-2-Methyl-1-Oxa-4-Azospiro-[4,5]decan-3-One (CERM 3726) and Sleep of Healthy Men. *Psychopharmacology (Berlin)* **1982,** *76,* 157–159.
172. Regnier, G.; Canevari, R.; Le Douarec, J. C.; Laubie, M.; Duhault, J. 2-Oxazolidinones. II. Synthesis and Pharmacological Properties of 1,3,8-Oxadiazaspiro [4,5]decan-2-One. *Chim. Ther.* **1969,** *4,* 185–194.
173. Hardie, W. R.; Aaron, J. E. 1,3-Dioxolan-4-yl-Alkyl Guanidines. US 3,547,951.
174. Dunn, M. I.; Dunlap, J. L. Guanadrel. A New Antihypertensive Drug. *JAMA* **1981,** *245,* 1639–1642.
175. Olver, I. Role of Rolapitant in Chemotherapy-Induced Emesis. *Lancet Oncol.* **2015,** *16,* 1006–1007.
176. Ohtake, Y.; Sato, T.; Kobayashi, T.; Nishimoto, M.; Taka, N.; Takano, K.; Yamamoto, K.; Ohmori, M.; Yamaguchi, M.; Takami, K.; Yeu, S.-Y.; Ahn, K.-H.; Matsuoka, H.; Morikawa, K.; Suzuki, M.; Hagita, H.; Ozawa, K.; Yamaguchi, K.; Kato, M.; Ikeda, S. Discovery of Tofogliflozin, a Novel *C*-Arylglucoside With an O-Spiroketal Ring System, as a Highly Selective Sodium Glucose Cotransporter 2 (SGLT2) Inhibitor for the Treatment of Type 2 Diabetes. *J. Med. Chem.* **2012,** *55,* 7828–7840.
177. Patchett, A. A.; Nargund, R. P.; Tata, J. R.; Chen, M. H.; Barakat, K. J.; Johnston, D. B. R.; Cheng, K.; Chan, W. W.-S.; Butler, B.; Hickey, G.; Jacks, T. M.; Schleim, K. D.; Pong, S. S.; Chaung, L.-Y. P.; Chen, H. Y.; Frazier, E.; Leung, K. H.; Chiu, S.-H. L.; Smith, R. G. Design and Biological Activities of L-163,191 (MK-0677): A Potent, Orally Active Growth Hormone Secretagogue. *Proc. Natl. Acad. Sci. U. S. A.* **1995,** *92,* 7001–7005.

178. Chen, M.-H.; Steiner, M. G.; Patchett, A. A.; Cheng, K.; Wei, L.; Chan, W. W. S.; Butler, B.; Jacks, T. M.; Smith, R. G. Analogs of the Orally Active Growth Hormone Secretagogue L-162,752. *Bioorg. Med. Chem. Lett.* **1996,** *6,* 2163–2168.
179. Tata, J. R.; Nargund, R. P.; Murphy, M. M.; Johnston, D. B. R.; Patchett, A. A.; Cheng, K.; Wei, L.; Chan, W. W. S.; Butler, B.; Jacks, T. M.; Hickey, G.; Smith, R. G. The Synthesis and Activity of Spiroindane Growth Hormone Secretagogues. *Bioorg. Med. Chem. Lett.* **1997,** *7,* 663–668.
180. Chen, M.-H.; Pollard, P. P.; Patchett, A. A. Synthesis and Biological Activities of Spiroheterocyclic Growth Hormone Secretagogues. *Bioorg. Med. Chem. Lett.* **1999,** *9,* 1261–1266.
181. Nargund, R. P.; Chen, M.-H.; Johnston, D. B. R.; Barakat, K. J.; Tata, J. R.; Cheng, K.; Jacks, T. M.; Chan, W. W. S.; Wei, L.; Butler, B. R.; Hickey, G. J.; Smith, R. G.; Patchett, A. A. Peptidomimetic Growth Hormone Secretagogues: Synthesis and Biological Activities of Analogs Varied at the Indole Nucleus of the Prototypical Spiropiperidine L-162,752. *Bioorg. Med. Chem. Lett.* **1996,** *6,* 1731–1736.
182. Tata, J. R.; Lu, Z.; Jacks, T. M.; Schleim, K. D.; Cheng, K.; Wei, L.; Chan, W. W. S.; Butler, B.; Tsou, N.; Leung, K.; Chiu, S. H. L.; Hickey, G.; Smith, R. G.; Patchett, A. A. The Design and Synthesis of Orally Active Short Duration Spiroindane Growth Hormone Secretagogues. *Bioorg. Med. Chem. Lett.* **1997,** *7,* 2319–2324.
183. Lu, Z.; Tata, J. R.; Cheng, K.; Wei, L.; Chan, W. W. S.; Butler, B.; Schleim, K. D.; Jacks, T. M.; Hickey, G.; Patchett, A. A. Highly Potent Growth Hormone Secretagogues. *Bioorg. Med. Chem. Lett.* **2007,** *17,* 3657–3659.
184. Evans, B. E.; Leighton, J. L.; Rittle, K. E.; Gilbert, K. F.; Lundell, G. F.; Gould, N. P.; Hobbs, D. W.; DiPardo, R. M.; Veber, D. F.; Pettibone, D. J.; Clineschmidt, B. V.; Anderson, P. S.; Freidinger, R. M. Orally Active, Nonpeptide Oxytocin Antagonists. *J. Med. Chem.* **1992,** *35,* 3919–3927.
185. Yang, L.; Guo, L.; Pasternak, A.; Mosley, R.; Rohrer, S.; Birzin, E.; Foor, F.; Cheng, K.; Schaeffer, J.; Patchett, A. A. Spiro[1H-Indene-1,4′-Piperidine] Derivatives As Potent and Selective Non-Peptide Human Somatostatin Receptor Subtype 2 (sst2) Agonists. *J. Med. Chem.* **1998,** *41,* 2175–2179.
186. Congreve, M.; Aharony, D.; Albert, J.; Callaghan, O.; Campbell, J.; Carr, R. A. E.; Chessari, G.; Cowan, S.; Edwards, P. D.; Frederickson, M.; McMenamin, R.; Murray, C. W.; Patel, S.; Wallis, N. Application of Fragment Screening by X-ray Crystallography to the Discovery of Aminopyridines as Inhibitors of β-Secretase. *J. Med. Chem.* **2007,** *50,* 1124–1132.
187. Baxter, E. W.; Conway, K. A.; Kennis, L.; Bischoff, F.; Mercken, M. H.; De Winter, H. L.; Reynolds, C. H.; Tounge, B. A.; Luo, C.; Scott, M. K.; Huang, Y.; Braeken, M.; Pieters, S. M. A.; Berthelot, D. J. C.; Masure, S.; Bruinzeel, W. D.; Jordan, A. D.; Parker, M. H.; Boyd, R. E.; Qu, J.; Alexander, R. S.; Brenneman, D. E.; Reitz, A. B.. 2-Amino-3,4-Dihydroquinazolines as Inhibitors of BACE-1 (β-Site APP Cleaving Enzyme): Use of Structure Based Design to Convert a Micromolar Hit into a Nanomolar Lead. *J. Med. Chem.* **2007,** *50,* 4261–4264.
188. Oehlrich, D.; Prokopcova, H.; Gijsen, H. J. M. The Evolution of Amidine-Based Brain Penetrant BACE1 Inhibitors. *Bioorg. Med. Chem. Lett.* **2014,** *24,* 2033–2045.
189. Huang, H.; La, D. S.; Cheng, A. C.; Whittington, D. A.; Patel, V. F.; Chen, K.; Dineen, T. A.; Epstein, O.; Graceffa, R.; Hickman, D.; Kiang, Y. H.; Louie, S.; Luo, Y.; Wahl, R. C.; Wen, P. H.; Wood, S.; Fremeau, R. T. Structure- and Property-Based Design of Aminooxazoline Xanthenes as Selective, Orally Efficacious, and CNS Penetrable BACE Inhibitors for the Treatment of Alzheimer's Disease. *J. Med. Chem.* **2012,** *55,* 9156–9169.
190. Epstein, O.; Bryan, M. C.; Cheng, A. C.; Derakhchan, K.; Dineen, T. A.; Hickman, D.; Hua, Z.; Human, J. B.; Kreiman, C.; Marx, I. E.; Weiss, M. M.; Wahl, R. C.; Wen, P. H.; Whittington, D. A.; Wood, S.; Zheng, X. M.; Fremeau, R. T.; White, R. D.; Patel, V. F. Lead Optimization and Modulation of hERG Activity in a Series of Aminooxazoline Xanthene β-Site Amyloid Precursor Protein Cleaving Enzyme (BACE1) Inhibitors. *J. Med. Chem.* **2014,** *57,* 9796–9810.
191. Dineen, T. A.; Chen, K.; Cheng, A. C.; Derakhchan, K.; Epstein, O.; Esmay, J.; Hickman, D.; Kreiman, C. E.; Marx, I. E.; Wahl, R. C.; Wen, P. H.; Weiss, M. M.; Whittington, D. A.; Wood, S.; Fremeau, R. T.; White, R. D.; Patel, V. F. Inhibitors of β-Site Amyloid Precursor Protein Cleaving Enzyme (BACE1): Identification of (S)-7-(2-Fluoropyridin-3-yl)-3-((3-Methyloxetan-3-yl)ethynyl)-5′H-Spiro[chromeno[2,3-b]pyridine-5,4′-Oxazol]-2′-Amine (AMG-8718). *J. Med. Chem.* **2014,** *57,* 9811–9831.
192. Cheng, Y.; Brown, J.; Judd, T. C.; Lopez, P.; Qian, W.; Powers, T. S.; Chen, J. J.; Bartberger, M. D.; Chen, K.; Dunn, R. T.; Epstein, O.; Fremeau, R. T.; Harried, S.; Hickman, D.; Hitchcock, S. A.; Luo, Y.; Minatti, A. E.; Patel, V. F.; Vargas, H. M.; Wahl, R. C.; Weiss, M. M.; Wen, P. H.; White, R. D.; Whittington, D. A.; Zheng, X. M.; Wood, S. An Orally Available BACE1 Inhibitor That Affords Robust CNS Aβ Reduction Without Cardiovascular Liabilities. *ACS Med. Chem. Lett.* **2015,** *6,* 210–215.
193. Chen, J. J.; Liu, Q.; Yuan, C.; Gore, V.; Lopez, P.; Ma, V.; Amegadzie, A.; Qian, W.; Judd, T. C.; Minatti, A. E.; Brown, J.; Cheng, Y.; Xue, M.; Zhong, W.; Dineen, T. A.; Epstein, O.; Human, J.; Kreiman, C.; Marx, I.; Weiss, M. M.; Hitchcock, S. A.; Powers, T. S.; Chen, K.; Wen, P. H.; Whittington, D. A.; Cheng, A. C.; Bartberger, M. D.; Hickman, D.; Werner, J. A.; Vargas, H. M.; Everds, N. E.; Vonderfecht, S. L.; Dunn, R. T., II; Wood, S.; Fremeau, R. T., Jr.; White, R. D.; Patel, V. F. Development of 2-Aminooxazoline 3-Azaxanthenes as Orally Efficacious β-Secretase Inhibitors for the Potential Treatment of Alzheimer's Disease. *Bioorg. Med. Chem. Lett.* **2015,** *25,* 767–774.
194. Hunt, K. W.; Cook, A. W.; Watts, R. J.; Clark, C. T.; Vigers, G.; Smith, D.; Metcalf, A. T.; Gunawardana, I. W.; Burkard, M.; Cox, A. A.; Geck Do, M. K.; Dutcher, D.; Thomas, A. A.; Rana, S.; Kallan, N. C.; DeLisle, R. K.; Rizzi, J. P.; Regal, K.; Sammond, D.; Groneberg, R.; Siu, M.; Purkey, H.; Lyssikatos, J. P.; Marlow, A.; Liu, X.; Tang, T. P. Spirocyclic β-Site Amyloid Precursor Protein Cleaving Enzyme 1 (BACE1) Inhibitors: From Hit to Lowering of Cerebrospinal Fluid (CSF) Amyloid β in a Higher Species. *J. Med. Chem.* **2013,** *56,* 3379–3403.
195. Thomas, A. A.; Hunt, K. W.; Volgraf, M.; Watts, R. J.; Liu, X.; Vigers, G.; Smith, D.; Sammond, D.; Tang, T. P.; Rhodes, S. P.; Metcalf, A. T.; Brown, K. D.; Otten, J. N.; Burkard, M.; Cox, A. A.; Do, M. K. G.; Dutcher, D.; Rana, S.; DeLisle, R. K.; Regal, K.; Wright, A. D.; Groneberg, R.; Scearce-Levie, K.; Siu, M.; Purkey, H. E.; Lyssikatos, J. P.; Gunawardana, I. W. Discovery of 7-Tetrahydropyran-2-yl Chromans: β-Site Amyloid Precursor Protein Cleaving Enzyme 1 (BACE1) Inhibitors That Reduce Amyloid β-Protein (Aβ) in the Central Nervous System. *J. Med. Chem.* **2014,** *57,* 878–902.
196. Thomas, A. A.; Hunt, K. W.; Newhouse, B.; Watts, R. J.; Liu, X.; Vigers, G.; Smith, D.; Rhodes, S. P.; Brown, K. D.; Otten, J. N.; Burkard, M.; Cox, A. A.; Geck Do, M. K.; Dutcher, D.; Rana, S.; DeLisle, R. K.; Regal, K.; Wright, A. D.; Groneberg, R.; Liao, J.; Scearce-Levie, K.; Siu, M.; Purkey, H. E.; Lyssikatos, J. P. 8-Tetrahydropyran-2-yl Chromans: Highly Selective Beta-Site Amyloid Precursor Protein Cleaving Enzyme 1 (BACE1) Inhibitors. *J. Med. Chem.* **2014,** *57,* 10112–10129.
197. Peterson, M. J.; Sarges, R.; Aldinger, C. E.; MacDonald, D. P. CP-45,634: A Novel Aldose Reductase Inhibitor That Inhibits Polyol Pathway Activity in Diabetic and Galactosemic Rats. *Metabolism* **1979,** *28,* 456–461.
198. Sarges, R.; Bordner, J.; Dominy, B. W.; Peterson, M. J.; Whipple, E. B. Synthesis, Absolute Configuration and Conformation of the Aldose Reductase Inhibitor Sorbinil. *J. Med. Chem.* **1985,** *28,* 1716–1720.
199. Sarges, R.; Schnur, R. C.; Belletire, J. L.; Peterson, M. J. Spiro Hydantoin Aldose Reductase Inhibitors. *J. Med. Chem.* **1988,** *31,* 230–243.
200. Schnur, R. C.; Sarges, R.; Peterson, M. J. Spiro Oxazolidinedione Aldose Reductase Inhibitors. *J. Med. Chem.* **1982,** *25,* 1451–1454.
201. Sarges, R.; Goldstein, S. W.; Welch, W. M.; Swindell, A. C.; Siegel, T. W.; Beyer, T. A. Spiro Hydantoin Aldose Reductase Inhibitors Derived From 8-Aza-4-Chromanones. *J. Med. Chem.* **1990,** *33,* 1859–1865.
202. Negoro, T.; Murata, M.; Ueda, S.; Fujitani, B.; Ono, Y.; Kuromiya, A.; Komiya, M.; Suzuki, K.; Matsumoto, J.-i. Novel, Highly Potent Aldose Reductase Inhibitors: (R)-(−)-2-(4-Bromo-2-Fluorobenzyl)-1,2,3,4-Tetrahydropyrrolo[1,2-a]pyrazine- 4-Spiro-3′-Pyrrolidine-1,2′,3,5′-Tetrone (AS-3201) and Its Congeners. *J. Med. Chem.* **1998,** *41,* 4118–4129.
203. Yamagishi, M.; Yamada, Y.; Ozaki, K.; Asao, M.; Shimizu, R.; Suzuki, M.; Matsumoto, M.; Matsuoka, Y.; Matsumoto, K. Biological Activities and Quantitative Structure-Activity Relationships of Spiro[imidazolidine-4,4′(1′H)-quinazoline]-2,2′,5(3′H)-Triones as Aldose Reductase Inhibitors. *J. Med. Chem.* **1992,** *35,* 2085–2094.
204. Mizuno, K.; Yamaguchi, T.; Inoue, A.; Tomiya, N.; Unno, R.; Miura, K.; Usui, T.; Matsumoto, Y.; Kondo, Y.; Yoshina, S.; Kondo, Y.; Sato, M.; Matsubara, A.; Kato, N.; Nakano, K.; Shirai, M.; Inoue, T.; Awaya, J.; Asaeda, N.; Hayasaka, I.; Koide, M.; Hibi, C.; Ban, M.; Sawai, K.; Kurono, M. Profile of a New Aldose Reductase Inhibitor, (2S,4S)-6-Fluoro-2′,5′-Dioxospiro[chroman-4,4′-Imidazolidine]-2-Carboxamide. *Excerpta Med.* **1990,** *913,* 89–96.
205. Oka, M.; Matsumoto, Y.; Sugiyama, S.; Tsuruta, N.; Matsushima, M. A Potent Aldose Reductase Inhibitor, (2S,4S)-6-Fluoro-2′,5′-Dioxospiro[chroman-4,4′-Imidazolidine]-2-Carboxamide (Fidarestat): Its Absolute Configuration and Interactions With the Aldose Reductase by X-ray Crystallography. *J. Med. Chem.* **2000,** *43,* 2479–2483.
206. El-Kabbani, O.; Carbone, V.; Darmanin, C.; Oka, M.; Mitschler, A.; Podjarny, A.; Schulze-Briese, C.; Chung, R. P. T. Structure of Aldehyde Reductase Holoenzyme in Complex With the Potent Aldose Reductase Inhibitor Fidarestat: Implications for Inhibitor Binding and Selectivity. *J. Med. Chem.* **2005,** *48,* 5536–5542.

207. El-Kabbani, O.; Darmanin, C.; Oka, M.; Schulze-Briese, C.; Tomizaki, T.; Hazemann, I.; Mitschler, A.; Podjarny, A. High-Resolution Structures of Human Aldose Reductase Holoenzyme in Complex With Stereoisomers of the Potent Inhibitor Fidarestat: Stereospecific Interaction Between the Enzyme and a Cyclic Imide Type Inhibitor. *J. Med. Chem.* **2004,** *47,* 4530–4537.
208. Petrova, T.; Steuber, H.; Hazemann, I.; Cousido-Siah, A.; Mitschler, A.; Chung, R.; Oka, M.; Klebe, G.; El-Kabbani, O.; Joachimiak, A.; Podjarny, A. Factorizing Selectivity Determinants of Inhibitor Binding Toward Aldose and Aldehyde Reductases: Structural and Thermodynamic Properties of the Aldose Reductase Mutant Leu300Pro-Fidarestat Complex. *J. Med. Chem.* **2005,** *48,* 5659–5665.
209. Hotta, N.; Toyota, T.; Matsuoka, K.; Shigeta, Y.; Kikkawa, R.; Kaneko, T.; Takahashi, A.; Sugimura, K.; Koike, Y.; Ishii, J.; Sakamoto, N. Clinical Efficacy of Fidarestat, a Novel Aldose Reductase Inhibitor, for Diabetic Peripheral Neuropathy: A 52-Week Multicenter Placebo-Controlled Double-Blind Parallel Group Study. *Diabetes Care* **2001,** *24,* 1776–1782.
210. Mealy, N.; Castaner, J. SNK-860. Symptomatic Antidiabetic Aldose Reductase Inhibitor. *Drugs Future* **1996,** *21,* 261–265.
211. Gadwood, R. C.; Kamdar, B. V.; Dubray, L. A. C.; Wolfe, M. L.; Smith, M. P.; Watt, W.; Mizsak, S. A.; Groppi, V. E. Synthesis and Biological Activity of Spirocyclic Benzopyran Imidazolone Potassium Channel Openers. *J. Med. Chem.* **1993,** *36,* 1480–1487.
212. Gadwood, R. C.; Thomasco, L. M.; Groppi, V. E.; Burnett, B. A.; Humphrey, S. J.; Smith, M. P.; Watt, W. Chiral Spirocyclic Benzopyran Potassium Channel Openers: Evidence for the Active Conformation of Levcromakalim. *Bioorg. Med. Chem. Lett.* **1995,** *5,* 2101–2104.
213. Trieselmann, T.; Wagner, H.; Fuchs, K.; Hamprecht, D.; Berta, D.; Cremonesi, P.; Streicher, R.; Luippold, G.; Volz, A.; Markert, M.; Nar, H. Potent Cholesteryl Ester Transfer Protein Inhibitors of Reduced Lipophilicity: 1,1′-Spiro-Substituted Hexahydrofuroquinoline Derivatives. *J. Med. Chem.* **2014,** *57,* 8766–8776.
214. Orbe, J.; Sánchez-Arias, J. A.; Rabal, O.; Rodríguez, J. A.; Salicio, A.; Ugarte, A.; Belzunce, M.; Xu, M.; Wu, W.; Tan, H.; Ma, H.; Páramo, J. A.; Oyarzabal, J. Design, Synthesis, and Biological Evaluation of Novel Matrix Metalloproteinase Inhibitors as Potent Antihemorrhagic Agents: From Hit Identification to an Optimized Lead. *J. Org. Chem.* **2015,** *58,* 2465–2488.
215. Orbe, J.; Rodríguez, J. A.; Sánchez-Arias, J. A.; Salicio, A.; Belzunce, M.; Ugarte, A.; Chang, H. C. Y.; Rabal, O.; Oyarzabal, J.; Páramo, J. A. Discovery and Safety Profiling of a Potent Preclinical Candidate, (4-[4-[[(3R)-3-(Hydroxycarbamoyl)-8-Azaspiro[4.5]decan-3-yl]sulfonyl]phenoxy]-*N*-Methylbenzamide) (CM-352), for the Prevention and Treatment of Hemorrhage. *J. Med. Chem.* **2015,** *58,* 2941–2957.
216. Halfpenny, P. R.; Horwell, D. C.; Hughes, J.; Hunter, J. C.; Rees, D. C. Highly Selective k-Opioid Analgesics. 3. Synthesis and Structure-Activity Relationships of Novel *N*-[2-(1-pyrrolidinyl)-4- or -5-Substituted Cyclohexyl]arylacetamide Derivatives. *J. Med. Chem.* **1990,** *33,* 286–291.
217. Vonvoigtlander, P. F.; Lahti, R. A.; Ludens, J. H. U-50,488: A Selective and Structurally Novel Non-Mu (kappa) Opioid Agonist. *J. Pharmacol. Exp. Ther.* **1983,** *224,* 7–12.
218. Fisher, A.; Gurwitz, D.; Barak, D.; Haring, R.; Karton, I.; Brandeis, R.; Pittel, Z.; Marciano, D.; Meshulam, H.; Vogel, Z.; Heldman, E. Rigid Analogs of Acetylcholine Can be M1-Selective Agonists: Implications for a Rational Treatment Strategy in Alzheimer's Disease. *Bioorg. Med. Chem. Lett.* **1992,** *2,* 839–844.
219. Shapiro, G.; Floersheim, P.; Amstutz, R.; Boddeke, H.; Bolliger, G.; Cottens, S.; Enz, A.; Gmelin, G.; Gull, P.; Supavilai, P. Muscarinic Agonist SAR of Azaspirodioxolanes. *Bioorg. Med. Chem. Lett.* **1992,** *2,* 815–820.
220. Mullen, G.; Napier, J.; Balestra, M.; DeCory, T.; Hale, G.; Macor, J.; Mack, R.; Loch, J.; Wu, E.; Kover, A.; Verhoest, P.; Sampognaro, A.; Phillips, E.; Zhu, Y.; Murray, R.; Griffith, R.; Blosser, J.; Gurley, D.; Machulskis, A.; Zongrone, J.; Rosen, A.; Gordon, J. (−)-Spiro[1-Azabicyclo[2.2.2]octane-3,5′-Oxazolidin-2′-One], a Conformationally Restricted Analogue of Acetylcholine, Is a Highly Selective Full Agonist at the α7 Nicotinic Acetylcholine Receptor. *J. Med. Chem.* **2000,** *43,* 4045–4050.
221. Tatsumi, R.; Fujio, M.; Satoh, H.; Katayama, J.; Takanashi, S.-i.; Hashimoto, K.; Tanaka, H. Discovery of the α7 Nicotinic Acetylcholine Receptor Agonists. (R)-3′-(5-Chlorothiophen-2-yl)spiro-1-Azabicyclo[2.2.2]octane-3,5′-[1′,3′]oxazolidin-2′-One as a Novel, Potent, Selective, and Orally Bioavailable Ligand. *J. Med. Chem.* **2005,** *48,* 2678–2686.
222. Tatsumi, R.; Fujio, M.; Takanashi, S.-i.; Numata, A.; Katayama, J.; Satoh, H.; Shiigi, Y.; Maeda, J.-i.; Kuriyama, M.; Horikawa, T.; Murozono, T.; Hashimoto, K.; Tanaka, H. (*R*)-3′-(3-Methylbenzo[b]thiophen-5-yl)spiro[1-Azabicyclo[2,2,2]octane-3,5′-oxazolidin]-2′-One, a Novel and Potent α7 Nicotinic Acetylcholine Receptor Partial Agonist Displays Cognitive Enhancing Properties. *J. Med. Chem.* **2006,** *49,* 4374–4383.
223. Mallinger, A.; Crumpler, S.; Pichowicz, M.; Waalboer, D.; Stubbs, M.; Adeniji-Popoola, O.; Wood, B.; Smith, E.; Thai, C.; Henley, A. T.; Georgi, K.; Court, W.; Hobbs, S.; Box, G.; Ortiz-Ruiz, M.-J.; Valenti, M.; De Haven Brandon, A.; TePoele, R.; Leuthner, B.; Workman, P.; Aherne, W.; Poeschke, O.; Dale, T.; Wienke, D.; Esdar, C.; Rohdich, F.; Raynaud, F.; Clarke, P. A.; Eccles, S. A.; Stieber, F.; Schiemann, K.; Blagg, J. Discovery of Potent, Orally Bioavailable, Small-Molecule Inhibitors of WNT Signaling From a Cell-Based Pathway Screen. *J. Med. Chem.* **2015,** *58,* 1717–1735.
224. Pasternak, A.; Marino, D.; Vicario, P. P.; Ayala, J. M.; Cascierri, M. A.; Parsons, W.; Mills, S. G.; MacCoss, M.; Yang, L. Novel, Orally Bioavailable γ-Aminoamide CC Chemokine Receptor 2 (CCR2) Antagonists. *J. Med. Chem.* **2006,** *49,* 4801–4804.
225. Butora, G.; Morriello, G. J.; Kothandaraman, S.; Guiadeen, D.; Pasternak, A.; Parsons, W. H.; MacCoss, M.; Vicario, P. P.; Cascieri, M. A.; Yang, L. 4-Amino-2-Alkyl-Butyramides as Small Molecule CCR2 Antagonists With Favorable Pharmacokinetic Properties. *Bioorg. Med. Chem. Lett.* **2006,** *16,* 4715–4722.
226. Yang, L.; Butora, G.; Jiao, R. X.; Pasternak, A.; Zhou, C.; Parsons, W. H.; Mills, S. G.; Vicario, P. P.; Ayala, J. M.; Cascieri, M. A.; MacCoss, M. Discovery of 3-Piperidinyl-1-Cyclopentanecarboxamide as a Novel Scaffold for Highly Potent CC Chemokine Receptor 2 Antagonists. *J. Med. Chem.* **2007,** *50,* 2609–2611.
227. Butora, G.; Jiao, R.; Parsons, W. H.; Vicario, P. P.; Jin, H.; Ayala, J. M.; Cascieri, M. A.; Yang, L. 3-Amino-1-Alkyl-Cyclopentane Carboxamides as Small Molecule Antagonists of the Human and Murine CC Chemokine Receptor 2. *Bioorg. Med. Chem. Lett.* **2007,** *17,* 3636–3641.
228. Liang, G.; Choi-Sledeski, Y. M.; Poli, G. B.; Chen, X.; Minnich, A.; Wang, Q.; Tsay, J.; Sides, K.; Vaz, R. J. Structure-Based Design, Synthesis, and Profiling of a [Small Beta]-Tryptase Inhibitor With a Spiro-piperidineamide Scaffold, Benzylamine P1 Group, and a Substituted Indole P4 Group. *MedChemComm* **2011,** *2,* 794–799.
229. Costanzo, M. J.; Yabut, S. C.; Zhang, H.-C.; White, K. B.; de Garavilla, L.; Wang, Y.; Minor, L. K.; Tounge, B. A.; Barnakov, A. N.; Lewandowski, F.; Milligan, C.; Spurlino, J. C.; Abraham, W. M.; Boswell-Smith, V.; Page, C. P.; Maryanoff, B. E. Potent, Nonpeptide Inhibitors of Human Mast Cell Tryptase. Synthesis and Biological Evaluation of Novel Spirocyclic Piperidine Amide Derivatives. *Bioorg. Med. Chem. Lett.* **2008,** *18,* 2114–2121.
230. Castiglioni, E.; Di Fabio, R.; Togninelli, A.; Brough, S.; Brown, F.; Cin, M. D.; Gianotti, M.; Marchioro, C.; Merlo, G.; Spinosa, R.; Wigglesworth, M. J.; Botta, M. Towards the Discovery of New Hypnotic Agents: Synthesis and Preliminary Pharmacological Evaluation of a Novel Class of Dibenzo[*a,d*]cycloheptene Derivatives. *ChemMedChem* **2010,** *5,* 1843–1846.
231. Gianotti, M.; Botta, M.; Brough, S.; Carletti, R.; Castiglioni, E.; Corti, C.; Dal-Cin, M.; Delle Fratte, S.; Korajac, D.; Lovric, M.; Merlo, G.; Mesic, M.; Pavone, F.; Piccoli, L.; Rast, S.; Roscic, M.; Sava, A.; Smehil, M.; Stasi, L.; Togninelli, A.; Wigglesworth, M. J. Novel Spirotetracyclic Zwitterionic Dual H1/5-HT2A Receptor Antagonists for the Treatment of Sleep Disorders. *J. Med. Chem.* **2010,** *53,* 7778–7795.
232. Tomboly, C.; Ballet, S.; Feytens, D.; Kover, K. E.; Borics, A.; Lovas, S.; Al-Khrasani, M.; Furst, Z.; Toth, G.; Benyhe, S.; Tourwe, D. Endomorphin-2 With a β-Turn Backbone Constraint Retains the Potent μ-Opioid Receptor Agonist Properties. *J. Med. Chem.* **2008,** *51,* 173–177.
233. Chabala, J. C.; Mrozik, H.; Tolman, R. L.; Eskola, P.; Lusi, A.; Peterson, L. H.; Woods, M. F.; Fisher, M. H.; Campbell, W. C. Ivermectin, a New Broad-Spectrum Antiparasitic Agent. *J. Med. Chem.* **1980,** *23,* 1134–1136.
234. Tu, Y. The Discovery of Artemisinin (qinghaosu) and Gifts From Chinese Medicine. *Nat. Med. (N. Y., NY, U. S.)* **2011,** *17,* 1217–1220.
235. Wells, T. N. C.; van Huijsduijnen, R. H.; Van Voorhis, W. C. Malaria Medicines: A Glass Half Full? *Nat. Rev. Drug Discov.* **2015,** *14,* 424–442.
236. Maurya, R.; Soni, A.; Anand, D.; Ravi, M.; Raju, K. S. R.; Taneja, I.; Naikade, N. K.; Puri, S. K.; Wahajuddin; Kanojiya, S.; Yadav, P. P. Synthesis and Antimalarial Activity of 3,3-Spiroanellated 5,6-Disubstituted 1,2,4-Trioxanes. *ACS Med. Chem. Lett.* **2013,** *4,* 165–169.
237. Le Bourdonnec, B.; Windh, R. T.; Ajello, C. W.; Leister, L. K.; Gu, M.; Chu, G.-H.; Tuthill, P. A.; Barker, W. M.; Koblish, M.; Wiant, D. D.; Graczyk, T. M.; Belanger, S.; Cassel, J. A.; Feschenko, M. S.; Brogdon, B. L.; Smith, S. A.; Christ, D. D.; Derelanko, M. J.; Kutz, S.; Little, P. J.; DeHaven, R. N.; DeHaven-Hudkins, D. L.; Dolle, R. E. Potent, Orally Bioavailable Delta Opioid Receptor Agonists for the Treatment of Pain: Discovery of *N,N*-Diethyl-4-(5-Hydroxyspiro[chromene-2,4′-Piperidine]-4-yl)benzamide (ADL5859). *J. Med. Chem.* **2008,** *51,* 5893–5896.

238. Le Bourdonnec, B.; Windh, R. T.; Leister, L. K.; Zhou, Q. J.; Ajello, C. W.; Gu, M.; Chu, G.-H.; Tuthill, P. A.; Barker, W. M.; Koblish, M.; Wiant, D. D.; Graczyk, T. M.; Belanger, S.; Cassel, J. A.; Feschenko, M. S.; Brogdon, B. L.; Smith, S. A.; Derelanko, M. J.; Kutz, S.; Little, P. J.; DeHaven, R. N.; DeHaven-Hudkins, D. L.; Dolle, R. E. Spirocyclic Delta Opioid Receptor Agonists for the Treatment of Pain: Discovery of *N,N*-Diethyl-3-Hydroxy-4-(spiro[chromene-2,4′-Piperidine]-4-yl) Benzamide (ADL5747). *J. Med. Chem.* **2009,** *52,* 5685–5702.
239. Schunk, S.; Linz, K.; Frormann, S.; Hinze, C.; Oberbörsch, S.; Sundermann, B.; Zemolka, S.; Englberger, W.; Germann, T.; Christoph, T.; Kögel, B.-Y.; Schröder, W.; Harlfinger, S.; Saunders, D.; Kless, A.; Schick, H.; Sonnenschein, H. Discovery of Spiro[cyclohexane-Dihydropyrano[3,4-b]indole]-Amines as Potent NOP and Opioid Receptor Agonists. *ACS Med. Chem. Lett.* **2014,** *5,* 851–856.
240. Schunk, S.; Linz, K.; Hinze, C.; Frormann, S.; Oberboersch, S.; Sundermann, B.; Zemolka, S.; Englberger, W.; Germann, T.; Christoph, T.; Koegel, B.-Y.; Schroeder, W.; Harlfinger, S.; Saunders, D.; Kless, A.; Schick, H.; Sonnenschein, H. Discovery of a Potent Analgesic NOP and Opioid Receptor Agonist: Cebranopadol. *ACS Med. Chem. Lett.* **2014,** *5,* 857–862.
241. Moltzen, E. K.; Perregaard, J.; Meier, E. Sigma Ligands With Subnanomolar Affinity and Preference for the.sigma.2 Binding Site. 2. Spiro-Joined Benzofuran, Isobenzofuran, and Benzopyran Piperidines. *J. Med. Chem.* **1995,** *38,* 2009–2017.
242. Chambers, M. S.; Baker, R.; Billington, D. C.; Knight, A. K.; Middlemiss, D. N.; Wong, E. H. F. Spiropiperidines as High-Affinity, Selective Sigma Ligands. *J. Med. Chem.* **1992,** *35,* 2033–2039.
243. Quaglia, W.; Giannella, M.; Piergentili, A.; Pigini, M.; Brasili, L.; Di Toro, R.; Rossetti, L.; Spampinato, S.; Melchiorre, C. 1′-Benzyl-3,4-Dihydrospiro[2H-1-Benzothiopyran-2,4′-Piperidine] (Spipethiane), a Potent and Highly Selective σ1 Ligand. *J. Med. Chem.* **1998,** *41,* 1557–1560.
244. Maier, C. A.; Wünsch, B. Novel Spiropiperidines as Highly Potent and Subtype Selective σ-Receptor Ligands. Part 1. *J. Med. Chem.* **2002,** *45,* 438–448.
245. Maier, C. A.; Wünsch, B. Novel σ Receptor Ligands. Part 2. SAR of Spiro[[2]benzopyran-1,4′-Piperidines] and Spiro[[2]benzofuran-1,4′-Piperidines] With Carbon Substituents in Position 3. *J. Med. Chem.* **2002,** *45,* 4923–4930.
246. Oberdorf, C.; Schepmann, D.; Vela, J. M.; Diaz, J. L.; Holenz, J.; Wünsch, B. Thiophene Bioisosteres of Spirocyclic σ Receptor Ligands. 1. N-Substituted Spiro[piperidine-4,4′-Thieno[3,2-c]pyrans]. *J. Med. Chem.* **2008,** *51,* 6531–6537.
247. Corbett, J. W.; Freeman-Cook, K. D.; Elliott, R.; Vajdos, F.; Rajamohan, F.; Kohls, D.; Marr, E.; Zhang, H.; Tong, L.; Tu, M.; Murdande, S.; Doran, S. D.; Houser, J. A.; Song, W.; Jones, C. J.; Coffey, S. B.; Buzon, L.; Minich, M. L.; Dirico, K. J.; Tapley, S.; Kirk McPherson, R.; Sugarman, E.; James Harwood, H., Jr.; Esler, W. Discovery of Small Molecule Isozyme Non-Specific Inhibitors of Mammalian Acetyl-CoA Carboxylase 1 and 2. *Bioorg. Med. Chem. Lett.* **2010,** *20,* 2383–2388.
248. Freeman-Cook, K. D.; Amor, P.; Bader, S.; Buzon, L. M.; Coffey, S. B.; Corbett, J. W.; Dirico, K. J.; Doran, S. D.; Elliott, R. L.; Esler, W.; Guzman-Perez, A.; Henegar, K. E.; Houser, J. A.; Jones, C. S.; Limberakis, C.; Loomis, K.; McPherson, K.; Murdande, S.; Nelson, K. L.; Phillion, D.; Pierce, B. S.; Song, W.; Sugarman, E.; Tapley, S.; Tu, M.; Zhao, Z. Maximizing Lipophilic Efficiency: The Use of Free-Wilson Analysis in the Design of Inhibitors of Acetyl-CoA Carboxylase. *J. Med. Chem.* **2012,** *55,* 935–942.
249. Griffith, D. A.; Dow, R. L.; Huard, K.; Edmonds, D. J.; Bagley, S. W.; Polivkova, J.; Zeng, D.; Garcia-Irizarry, C. N.; Southers, J. A.; Esler, W.; Amor, P.; Loomis, K.; McPherson, K.; Bahnck, K. B.; Préville, C.; Banks, T.; Moore, D. E.; Mathiowetz, A. M.; Menhaji-Klotz, E.; Smith, A. C.; Doran, S. D.; Beebe, D. A.; Dunn, M. F. Spirolactam-Based Acetyl-CoA Carboxylase Inhibitors: Toward Improved Metabolic Stability of a Chromanone Lead Structure. *J. Med. Chem.* **2013,** *56,* 7110–7119.
250. Griffith, D. A.; Kung, D. W.; Esler, W. P.; Amor, P. A.; Bagley, S. W.; Beysen, C.; Carvajal-Gonzalez, S.; Doran, S. D.; Limberakis, C.; Mathiowetz, A. M.; McPherson, K.; Price, D. A.; Ravussin, E.; Sonnenberg, G. E.; Southers, J. A.; Sweet, L. J.; Turner, S. M.; Vajdos, F. F. Decreasing the Rate of Metabolic Ketone Reduction in the Discovery of a Clinical Acetyl-CoA Carboxylase Inhibitor for the Treatment of Diabetes. *J. Med. Chem.* **2014,** *57,* 10512–10526.
251. Mirzadegan, T.; Diehl, F.; Ebi, B.; Bhakta, S.; Polsky, I.; McCarley, D.; Mulkins, M.; Weatherhead, G. S.; Lapierre, J.-M.; Dankwardt, J.; Morgans, D.; Wilhelm, R.; Jarnagin, K. Identification of the Binding Site for a Novel Class of CCR2b Chemokine Receptor Antagonists: Binding to a Common Chemokine Receptor Motif Within the Helical Bundle. *J. Biol. Chem.* **2000,** *275,* 25562–25571.
252. Strunz, A. K.; Zweemer, A. J. M.; Weiss, C.; Schepmann, D.; Junker, A.; Heitman, L. H.; Koch, M.; Wuensch, B. Synthesis and Biological Evaluation of Spirocyclic Antagonists of CCR2 (Chemokine CC Receptor Subtype 2). *Bioorg. Med. Chem.* **2015,** *23,* 4034–4049.
253. Habashita, H.; Kokubo, M.; Hamano, S.-i.; Hamanaka, N.; Toda, M.; Shibayama, S.; Tada, H.; Sagawa, K.; Fukushima, D.; Maeda, K.; Mitsuya, H. Design, Synthesis, and Biological Evaluation of the Combinatorial Library With a New Spirodiketopiperazine Scaffold. Discovery of Novel Potent and Selective Low-Molecular-Weight CCR5 Antagonists. *J. Med. Chem.* **2006,** *49,* 4140–4152.
254. Nishizawa, R.; Nishiyama, T.; Hisaichi, K.; Hirai, K.; Habashita, H.; Takaoka, Y.; Tada, H.; Sagawa, K.; Shibayama, S.; Maeda, K.; Mitsuya, H.; Nakai, H.; Fukushima, D.; Toda, M. Spirodiketopiperazine-Based CCR5 Antagonists: Improvement of Their Pharmacokinetic Profiles. *Bioorg. Med. Chem. Lett.* **2010,** *20,* 763–766.
255. Nishizawa, R.; Nishiyama, T.; Hisaichi, K.; Hirai, K.; Habashita, H.; Takaoka, Y.; Tada, H.; Sagawa, K.; Shibayama, S.; Maeda, K.; Mitsuya, H.; Nakai, H.; Fukushima, D.; Toda, M. Discovery of Orally Available Spirodiketopiperazine-Based CCR5 Antagonists. *Bioorg. Med. Chem.* **2010,** *18,* 5208–5223.
256. Nishizawa, R.; Nishiyama, T.; Hisaichi, K.; Matsunaga, N.; Minamoto, C.; Habashita, H.; Takaoka, Y.; Toda, M.; Shibayama, S.; Tada, H.; Sagawa, K.; Fukushima, D.; Maeda, K.; Mitsuya, H. Spirodiketopiperazine-Based CCR5 Antagonists: Lead Optimization From Biologically Active Metabolite. *Bioorg. Med. Chem. Lett.* **2007,** *17,* 727–731.
257. Nishizawa, R.; Nishiyama, T.; Hisaichi, K.; Minamoto, C.; Murota, M.; Takaoka, Y.; Nakai, H.; Tada, H.; Sagawa, K.; Shibayama, S.; Fukushima, D.; Maeda, K.; Mitsuya, H. Discovery of 4-[4-({(3R)-1-Butyl-3-[(R)-Cyclohexyl(hydroxy)methyl]-2,5-Dioxo-1,4,9-Triazaspiro[5.5]undec-9-yl}methyl)phenoxy]benzoic Acid hydrochloride: A Highly Potent Orally Available CCR5 Selective Antagonist. *Bioorg. Med. Chem.* **2011,** *19,* 4028–4042.
258. Nishizawa, R.; Nishiyama, T.; Hisaichi, K.; Minamoto, C.; Matsunaga, N.; Takaoka, Y.; Nakai, H.; Jenkinson, S.; Kazmierski, W. M.; Tada, H.; Sagawa, K.; Shibayama, S.; Fukushima, D.; Maeda, K.; Mitsuya, H. Spirodiketopiperazine-Based CCR5 Antagonist: Discovery of an Antiretroviral Drug Candidate. *Bioorg. Med. Chem. Lett.* **2011,** *21,* 1141–1145.
259. Yang, H.; Lin, X.-F.; Padilla, F.; Gabriel, S. D.; Heilek, G.; Ji, C.; Sankuratri, S.; deRosier, A.; Berry, P.; Rotstein, D. M. Discovery of a Potent, Selective and Orally Bioavailable 3,9-Diazaspiro[5.5]undeca-2-One CCR5 Antagonist. *Bioorg. Med. Chem. Lett.* **2009,** *19,* 209–213.
260. Rotstein, D. M.; Gabriel, S. D.; Makra, F.; Filonova, L.; Gleason, S.; Brotherton-Pleiss, C.; Setti, L. Q.; Trejo-Martin, A.; Lee, E. K.; Sankuratri, S.; Ji, C.; de Rosier, A.; Dioszegi, M.; Heilek, G.; Jekle, A.; Berry, P.; Weller, P.; Mau, C.-I. Spiropiperidine CCR5 Antagonists. *Bioorg. Med. Chem. Lett.* **2009,** *19,* 5401–5406.
261. Lemoine, R. C.; Petersen, A. C.; Setti, L.; Chen, L.; Wanner, J.; Jekle, A.; Heilek, G.; de Rosier, A.; Ji, C.; Rotstein, D. M. Evaluation of a 4-Aminopiperidine Replacement in Several Series of CCR5 Antagonists. *Bioorg. Med. Chem. Lett.* **2010,** *20,* 1830–1833.
262. Roecker, A. J.; Cox, C. D.; Coleman, P. J. Orexin Receptor Antagonists: New Therapeutic Agents for the Treatment of Insomnia. *J. Med. Chem.* **2016,** *59,* 504–530.
263. Betschart, C.; Hintermann, S.; Behnke, D.; Cotesta, S.; Fendt, M.; Gee, C. E.; Jacobson, L. H.; Laue, G.; Ofner, S.; Chaudhari, V.; Badiger, S.; Pandit, C.; Wagner, J.; Hoyer, D. Identification of a Novel Series of Orexin Receptor Antagonists With a Distinct Effect on Sleep Architecture for the Treatment of Insomnia. *J. Med. Chem.* **2013,** *56,* 7590–7607.
264. Uto, Y.; Ogata, T.; Kiyotsuka, Y.; Ueno, Y.; Miyazawa, Y.; Kurata, H.; Deguchi, T.; Watanabe, N.; Konishi, M.; Okuyama, R.; Kurikawa, N.; Takagi, T.; Wakimoto, S.; Ohsumi, J. Novel Benzoylpiperidine-Based Stearoyl-CoA Desaturase-1 Inhibitors: Identification of 6-[4-(2-Methylbenzoyl)piperidin-1-yl]pyridazine-3-Carboxylic Acid (2-Hydroxy-2-Pyridin-3-ylethyl)amide and Its Plasma Triglyceride-Lowering Effects in Zucker Fatty Rats. *Bioorg. Med. Chem. Lett.* **2010,** *20,* 341–345.
265. Uto, Y.; Kiyotsuka, Y.; Ueno, Y.; Miyazawa, Y.; Kurata, H.; Ogata, T.; Deguchi, T.; Yamada, M.; Watanabe, N.; Konishi, M.; Kurikawa, N.; Takagi, T.; Wakimoto, S.; Kono, K.; Ohsumi, J. Novel Spiropiperidine-Based Stearoyl-CoA Desaturase-1 Inhibitors: Identification of 1′-{6-[5-(Pyridin-3-ylmethyl)-1,3,4-Oxadiazol-2-yl]pyridazin-3-yl}-5-(Trifluoromethyl)-3,4-dihydrospiro[chromene-2,4′-Piperidine]. *Bioorg. Med. Chem. Lett.* **2010,** *20,* 746–754.
266. Uto, Y.; Ueno, Y.; Kiyotsuka, Y.; Miyazawa, Y.; Kurata, H.; Ogata, T.; Yamada, M.; Deguchi, T.; Konishi, M.; Takagi, T.; Wakimoto, S.; Ohsumi, J. Synthesis and Evaluation of Novel Stearoyl-CoA Desaturase 1 Inhibitors: 1′-{6-[5-(Pyridin-3-ylmethyl)-1,3,4-oxadiazol-2-yl]pyridazin-3-yl}-3,4-Dihydrospiro[chromene-2,4′-Piperidine] Analogs. *Eur. J. Med. Chem.* **2010,** *45,* 4788–4796.

267. Miller, A. A.; Bundy, G. L.; Mott, J. E.; Skepner, J. E.; Boyle, T. P.; Harris, D. W.; Hromockyj, A. E.; Marotti, K. R.; Zurenko, G. E.; Munzner, J. B.; Sweeney, M. T.; Bammert, G. F.; Hamel, J. C.; Ford, C. W.; Zhong, W.-Z.; Graber, D. R.; Martin, G. E.; Han, F.; Dolak, L. A.; Seest, E. P.; Ruble, J. C.; Kamilar, G. M.; Palmer, J. R.; Banitt, L. S.; Hurd, A. R.; Barbachyn, M. R. Discovery and Characterization of QPT-1, the Progenitor of a New Class of Bacterial Topoisomerase Inhibitors. *Antimicrob. Agents Chemother.* **2008,** *52,* 2806–2812.
268. Basarab, G. S.; Brassil, P.; Doig, P.; Galullo, V.; Haimes, H. B.; Kern, G.; Kutschke, A.; McNulty, J.; Schuck, V. J. A.; Stone, G.; Gowravaram, M. Novel DNA Gyrase Inhibiting Spiropyrimidinetriones With a Benzisoxazole Scaffold: SAR and in vivo Characterization. *J. Med. Chem.* **2014,** *57,* 9078–9095.
269. Basarab, G. S.; Doig, P.; Galullo, V.; Kern, G.; Kimzey, A.; Kutschke, A.; Newman, J. P.; Morningstar, M.; Mueller, J.; Otterson, L.; Vishwanathan, K.; Zhou, F.; Gowravaram, M. Discovery of Novel DNA Gyrase Inhibiting Spiropyrimidinetriones: Benzisoxazole Fusion With N-Linked Oxazolidinone Substituents Leading to a Clinical Candidate (ETX0914). *J. Med. Chem.* **2015,** *58,* 6264–6282.
270. Best, J. D.; Smith, D. W.; Reilly, M. A.; O'Donnell, R.; Lewis, H. D.; Ellis, S.; Wilkie, N.; Rosahl, T. W.; Laroque, P. A.; Boussiquet-Leroux, C.; Churcher, I.; Atack, J. R.; Harrison, T.; Shearman, M. S. The Novel γ Secretase Inhibitor *N*-[Cis-4-[(4-Chlorophenyl)sulfonyl]-4-(2,5-Difluorophenyl)cyclohexyl]-1,1,1-Trifluoromethanesulfonamide (MRK-560) Reduces Amyloid Plaque Deposition Without Evidence of Notch-Related Pathology in the Tg2576 Mouse. *J. Pharmacol. Exp. Ther.* **2007,** *320,* 552–558.
271. Churcher, I.; Beher, D.; Best, J. D.; Castro, J. L.; Clarke, E. E.; Gentry, A.; Harrison, T.; Hitzel, L.; Kay, E.; Kerrad, S.; Lewis, H. D.; Morentin-Gutierrez, P.; Mortishire-Smith, R.; Oakley, P. J.; Reilly, M.; Shaw, D. E.; Shearman, M. S.; Teall, M. R.; Williams, S.; Wrigley, J. D. J. 4-Substituted Cyclohexyl Sulfones as Potent, Orally Active γ-Secretase Inhibitors. *Bioorg. Med. Chem. Lett.* **2006,** *16,* 280–284.
272. Zhao, Z.; Pissarnitski, D. A.; Josien, H.; Wu, W.-L.; Xu, R.; Li, H.; Clader, J.; Burnett, D. A.; Terracina, G.; Hyde, L.; Lee, J.; Song, L.; Zhang, L. Discovery of a Novel, Potent Spirocyclic Series of γ-Secretase Inhibitors. *J. Med. Chem.* **2015,** *58,* 8806–8817.
273. Breschi, M. C.; Calderone, V.; Digiacomo, M.; Manganaro, M.; Martelli, A.; Minutolo, F.; Rapposelli, S.; Testai, L.; Tonelli, F.; Balsamo, A. Spirocyclic Benzopyran-Based Derivatives as New Anti-ischemic Activators of Mitochondrial ATP-Sensitive Potassium Channel. *J. Med. Chem.* **2008,** *51,* 6945–6954.
274. Rapposelli, S.; Calderone, V.; Cirilli, R.; Digiacomo, M.; Faggi, C.; La Torre, F.; Manganaro, M.; Martelli, A.; Testai, L. Enantioselectivity in Cardioprotection Induced by (*S*)-(−)-2,2-Dimethyl-*N*-(4′-Acetamido-Benzyl)-4-Spiromorpholone-Chromane. *J. Med. Chem.* **2009,** *52,* 1477–1480.
275. Donnell, A. F.; Michoud, C.; Rupert, K. C.; Han, X.; Aguilar, D.; Frank, K. B.; Fretland, A. J.; Gao, L.; Goggin, B.; Hogg, J. H.; Hong, K.; Janson, C. A.; Kester, R. F.; Kong, N.; Le, K.; Li, S.; Liang, W.; Lombardo, L. J.; Lou, Y.; Lukacs, C. M.; Mischke, S.; Moliterni, J. A.; Polonskaia, A.; Schutt, A. D.; Solis, D. S.; Specian, A.; Taylor, R. T.; Weisel, M.; Remiszewski, S. W. Benzazepinones and Benzoxazepinones as Antagonists of Inhibitor of Apoptosis Proteins (IAPs) Selective for the Second Baculovirus IAP Repeat (BIR2) Domain. *J. Med. Chem.* **2013,** *56,* 7772–7787.
276. Deng, Y.; Yang, Z.; Shipps, G. W.; Lo, S.-M.; West, R.; Hwa, J.; Zheng, S.; Farley, C.; Lachowicz, J.; van Heek, M.; Bass, A. S.; Sinha, D. P.; Mahon, C. R.; Cartwright, M. E. Discovery of Liver-Targeted Inhibitors of Stearoyl-CoA Desaturase (SCD1). *Bioorg. Med. Chem. Lett.* **2013,** *23,* 791–796.
277. Pouliot, J. J.; Thomson, M.; Xie, M.; Horton, J.; Johnson, J.; Krull, D.; Mathis, A.; Morikawa, Y.; Parks, D.; Peterson, R.; Shimada, T.; Thomas, E.; Vamathevan, J.; Van Horn, S.; Xiong, Z.; Hamatake, R.; Peat, A. J. Preclinical Characterization and in vivo Efficacy of GSK8853, a Small-Molecule Inhibitor of the Hepatitis C Virus NS4B Protein. *Antimicrob. Agents Chemother.* **2015,** *59,* 6539–6550.
278. Tai, V. W. F.; Garrido, D.; Price, D. J.; Maynard, A.; Pouliot, J. J.; Xiong, Z.; Seal, J. W.; Creech, K. L.; Kryn, L. H.; Baughman, T. M.; Peat, A. J. Design and Synthesis of Spirocyclic Compounds as HCV Replication Inhibitors by Targeting Viral NS4B Protein. *Bioorg. Med. Chem. Lett.* **2014,** *24,* 2288–2294.
279. Aguilar, A.; Sun, W.; Liu, L.; Lu, J.; McEachern, D.; Bernard, D.; Deschamps, J. R.; Wang, S. Design of Chemically Stable, Potent, and Efficacious MDM2 Inhibitors That Exploit the Retro-Mannich Ring-Opening-Cyclization Reaction Mechanism in Spiro-oxindoles. *J. Med. Chem.* **2014,** *57,* 10486–10498.
280. Michel, M. C.; Oelke, M.; Zinner, N. Novel Muscarinic Antagonists to Treat Incontinence and/or Overactive Bladder. *Drug Discov. Today Ther. Strateg.* **2005,** *2,* 1–6.
281. Cella, J. A.; Tweit, R. C. Steroidal Aldosterone Blockers. II. *J. Org. Chem.* **1959,** *24,* 1109–1110.
282. Moulin, A.; Ryan, J.; Martinez, J.; Fehrentz, J.-A. Recent Developments in Ghrelin Receptor Ligands. *ChemMedChem* **2007,** *2,* 1242–1259.
283. Bell, I. M. Calcitonin Gene-Related Peptide Receptor Antagonists: New Therapeutic Agents for Migraine. *J. Med. Chem.* **2014,** *57,* 7838–7858.
284. Hall, A.; Patel, T. R. γ-Secretase Modulators: Current Status and Future Directions. *Prog. Med. Chem.* **2014,** *53,* 101–145.
285. Probst, G.; Xu, Y.-z. Small-Molecule BACE1 Inhibitors: A Patent Literature Review (2006–2011). *Expert Opin. Ther. Pat.* **2012,** *22,* 511–540.
286. Abramson, H. N. The Lipogenesis Pathway as a Cancer Target. *J. Med. Chem.* **2011,** *54,* 5615–5638.

Relevant Websites

287. http://www.chem.qmul.ac.uk/iupac/spiro/ - Nomenclature of spiro compounds.
288. http://www.sigmaaldrich.com/chemistry/chemistry-products.html?TablePage=119773947, http://www.spirochem.com/new-products/, http://synthonix.com/index.php/buy-online/s-t/spiro-compounds.html/ - Spiro building blocks.
289. http://www.mdpi.com/journal/molecules/special_issues/spiro_compounds - Special issue on Spiro compounds.

1.09 Nanotechnology in Drug Discovery and Development

L Gutiérrez and G Stepien, Instituto Universitario de Nanociencia de Aragón (INA), Universidad de Zaragoza, Zaragoza, Spain
L Gutiérrez, Department of Analytical Chemistry, Universidad de Zaragoza, Zaragoza, Spain
M Pérez-Hernández and J Pardo, Department Microbiology, Preventive Medicine and Public Health, Universidad de Zaragoza, Zaragoza, Spain; and Immune Effector Cells Group, Aragón Health Research Institute (IIS Aragón), Biomedical Research Centre of Aragón (CIBA), Universidad de Zaragoza, Zaragoza, Spain
J Pardo, Aragón I+D Foundation (ARAID), Government of Aragon, Zaragoza, Spain
V Grazú and JM de la Fuente, Instituto de Ciencia de Materiales de Aragón, CSIC-Universidad de Zaragoza

© 2017 Elsevier Ltd. All rights reserved.

1.09.1 Introduction 265
1.09.2 Nanomaterials 265
1.09.2.1 Description 265
1.09.2.1.1 Liposomes 266
1.09.2.1.2 Polymeric nanoparticles 266
1.09.2.1.3 Gold nanoparticles 266
1.09.2.1.4 Magnetic nanoparticles 266
1.09.2.1.5 Silica nanoparticles 267
1.09.2.1.6 Quantum dots 267
1.09.2.2 Advantages of Nanomaterials in Medicine 267
1.09.2.3 Actual Research Trends 268
1.09.3 Biodistribution 272
1.09.3.1 *In vivo* Optical Imaging 272
1.09.3.2 *In vivo* Positron Emission Tomography 274
1.09.3.3 *In vivo* Magnetic Resonance Imaging 275
1.09.3.4 *In vivo* Magnetic Particles Imaging 275
1.09.3.5 *Ex vivo* Light Microscopy 276
1.09.3.6 *Ex vivo* Fluorescent Microscopy 276
1.09.3.6.1 Autoradiography 276
1.09.3.7 Transmission Electron Microscopy 276
1.09.3.8 Elemental Analysis 277
1.09.3.9 Magnetometry 277
1.09.3.10 Conclusions 278
1.09.4 Toxicity 278
1.09.4.1 Proliferation Assays 278
1.09.4.1.1 MTT 278
1.09.4.1.2 Alamar blue assay 279
1.09.4.1.3 Clonogenic assay 279
1.09.4.1.4 Cell division assay 280
1.09.4.1.5 EdU proliferation assay 280
1.09.4.2 Cell Membrane Permeability 281
1.09.4.2.1 Trypan blue 281
1.09.4.2.2 Fluorescein diacetate 281
1.09.4.2.3 Calcein acetoxymethyl 281
1.09.4.2.4 DNA intercalating fluorescent agents 282
1.09.4.2.5 Lactate dehydrogenaze enzyme 282
1.09.4.3 Cell Death Mechanisms 282
1.09.4.3.1 Annexin-V 282
1.09.4.3.2 ROS generation 283
1.09.4.3.3 Loss of mitochondrial membrane potential 283
1.09.4.3.4 Cell morphology 284
1.09.4.4 Instrumentation for Detection of Fluorescent Probes 284
1.09.4.5 General Considerations for the Presence of NPs 284
1.09.5 Future Challenges 284
1.09.5.1 Development of New Materials 285
1.09.5.2 Green Nanoscience 285

1.09.5.3 Circular Economy 285
1.09.5.4 Biodegradable Products 285
1.09.5.5 Development of New Applications 286
1.09.5.6 Transference to Industry 286
References 286

1.09.1 Introduction

The definition of nanotechnology varies depending on the source, or even field, but in general it comprises the production, characterization and understanding of the novel properties of materials at the nanometer scale to be used in the design of new systems. The development of nanotechnology in the past few decades has resulted in an explosion of materials, properties and applications able to revolutionize our world. Just a few examples that have resulted in Nobel prizes are the design of the scanning tunnelling microscope (1986, G. Binning and H. Rohrer), the discovery of fullerenes (1996, R. F. Curl, H. W. Kroto and R. E. Smalley) or graphene (2010, A. Geim and K. Novoselov) and the development of super-resolved fluorescence microscopy (2014, E. Betzig, S. W. Hell and W. E. Moerner).

Definitely, nanotechnology is changing our approach to develop new materials and applications, not only in the frame of health, as it would be further discussed later in this chapter, but also in areas that seem so distant as electronics,[1–3] energy,[4] construction and building materials,[5] environmental remediation,[6] sensors,[7] food industry[8] or orthopedic implants.[9]

Nanotechnology will have an impact in the health sector in several different ways. One would be related to the development of nanomaterials with new properties, other associated to the characterization of biological processes and finally other related to the improvement of imaging techniques.

In this book chapter we will focus on the use of nanomaterials in the frame of drug development. In general, nanomaterials can have different physicochemical properties than their bulk counterparts, therefore, resulting in products with new properties, not like those of conventionally-manufactured products. The development of new materials aims at fruitfully succeeding at challenges from conventional medicine as: the use of poorly water-soluble compounds encapsulated in water soluble matrices, the targeted delivery of drugs to specific tissues minimizing the dose required and the impact in other body areas, the delivery of several drugs for combined therapy or the possibility of theranostics, combined diagnosis and treatment.

One of the interesting advantages of using nanomaterials in medicine is related to the same size that these structures have in comparison with biological structures vital to the cell, such as proteins.[10]

In this book chapter we will focus on four different aspects related to the application of nanotechnology to drug development. The first section is devoted to give an overview of the different nanomaterials being used in health treatments. This section aims to provide a general description of the wide variety of compositions being tested, associated at the same time to an extreme range of different properties and possible different applications. The second section is a discussion on the different challenges that the development of nanomaterials for health treatment are facing, ranging from the synthesis of the compound and scale-up for their transference to industry production, theoretical studies to envisage the properties of new possible materials, environmental and geopolitical risks and the difficulties associated to the approval of new drugs by regulatory agencies. The last two sections are devoted to the study of the biodistribution and toxicity of new nanomaterials for health treatment. Regarding the approval by regulatory agencies, these two concerns, drug biodistribution and toxicity, need to be evaluated before any new nanomaterial is transformed into a commercially viable product. Biodistribution studies can be performed *in vivo* and *ex vivo* using a wide variety of techniques. Not all the techniques are appropriated for all the different nanomaterials given the wide variety of properties that they present. We have performed a classification based on the different characterization techniques, indicating which method is adequate for each kind of compound. We have also described a wide variety of toxicological studies that can be performed to assure the safe use of the new developed materials, however, still there is a lack of standardized protocols in the frame of nanomaterials, therefore resulting in difficulties comparing results from different research groups. In the last section of this book chapter we present a detailed description of the approaches to evaluate the toxicity of nanomaterials *in vitro* used in the frame of drug development.

1.09.2 Nanomaterials

1.09.2.1 Description

The European Union Commission Recommendation of 18 October 2011 (2011/696/UE) on the definition of nanomaterial provides de following description "Nanomaterial means a natural, incidental or manufactured material containing particles, in an unbound state or as an aggregate or as an agglomerate and where, for 50% or more of the particles in the number size distribution, one or more external dimensions is in the size range 1–100 nm. (…)."[11]

This definition includes materials so diverse as quantum dots (QD), dendrimers or graphene. Therefore, subsequent classification strategies have tried to order them according to the number of dimensions on the nanometric range. Depending on the shape,

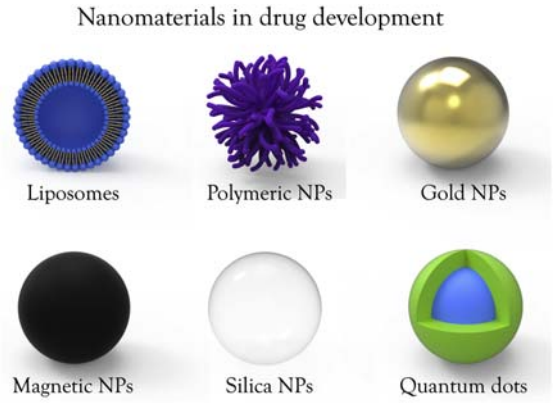

Fig. 1 Most commonly used materials in drug development: liposomes, polymer particles, gold nanoparticles, magnetic nanoparticles, silica nanoparticles, and quantum dots.

nanomaterials could be classified as: 0D, where the three dimensions are below 100 nm, such as nanoparticles or fullerenes, 1D, where one of the three dimensions is above 100 nm, such as nanotubes or nanowires or 2D, where two of the three dimensions are above 100 nm, such as sheets, discs or graphene.[12]

In the case of nanomaterials for biomedical applications, and especially in the frame of drug development, most of the nanomaterials that have been developed or are under clinical studies correspond to 0D compounds where all the dimensions are below 100 nm. In what follows, a brief description of liposomes, polymer particles, gold nanoparticles (AuNPs), magnetic nanoparticles (MNPs), silica nanoparticles and QD, the most commonly used materials in drug development, is provided (**Fig. 1**).

1.09.2.1.1 Liposomes

Liposomes are spherical structures composed of a bilayer of lipids. Their composition makes them good candidates for biomedical applications given their relatively biocompatible and biodegradable properties. Due to their bilayer structure, liposomes can encapsulate drugs either in the phospholipid bilayer or in the entrapped aqueous volume.[13]

Advantages of these materials include, among others, the possibility of carrying hydrophilic or hydrophobic drugs enhancing their solubility, protecting the drug from premature degradation, or improve the selectivity to deliver drugs in targeted tissues.[14]

All these properties have resulted in several nanoformulations based on lyposomes being approved by the FDA (US Food and Drug Administration) and currently available commercially.[14]

1.09.2.1.2 Polymeric nanoparticles

There are a wide variety of materials being used for the synthesis of polymeric nanoparticles, resulting in an infinite diversity of chemical composition and properties. Examples of different compositions include polymer from synthetic origin such as polylactic acid (PLA), polyglycolide (PLG), polylactide-co-glycolide (PLGA), polycyanoacrylate (PCA), polycaprolactone (PCL) or polyalkylcyanoacrylate (PACA) and polymers from biological origin such as chitosan, albumin, gelatin or sodium alginate.[15]

From all these different compositions, some of them, such as PLGA, have been approved by FDA for its use in humans, opening the way to the encapsulations of several drugs for therapeutic use.[16] An example of this would be the encapsulation of Gentamicin by collagen.[17]

Among the advantages of polymeric materials are: the possibility to carry different molecules internally or externally, the release of their cargo under different stimuli such as pH, or temperature and their biodegradability.

1.09.2.1.3 Gold nanoparticles

AuNPs are good candidates for drug delivery applications for several reasons. First, gold is inert, therefore it presents reduced toxicity risks associated to other heavy metals. AuNPs are easily synthetised and their surface easily modified through thiol linkages.[18] Finally, AuNPs optical properties arising from the localized surface plasmon resonance could trigger drug release at remote places.[18]

Gold nanoformulations have not yet been approved by FDA but are already in clinical trials.[19]

1.09.2.1.4 Magnetic nanoparticles

Although magnetic materials for biomedical applications could include a wide variety of compositions including elements such as Co, Fe or Ni in different alloys or forming part of oxides, in the practice, most of the work is being performed using two iron oxides (maghemite or magnetite)[20] specially due to their low toxicity,[21] and the capacity of the body iron metabolism to transform iron released from the particles into ferritin,[22] allowing the recycling of this metal within the body.

Their interest relies in their magnetic properties, being able to: (i) modify local magnetic fields, for example to be used as contrast agents for Magnetic Resonance Imaging (MRI), (ii) act as heat mediators in alternating magnetic fields for magnetic hyperthermia,

or (iii) concentrate in an specific location by the presence of an external magnetic field, to be used as drug delivery systems.[23] MNPs have been already approved by FDA as MRI contrast agents.[19]

1.09.2.1.5 Silica nanoparticles

Silica, an oxide of silicon, has received a wide attention from the research community in the frame of drug transport given its mesoporous structure at the nanoscale that provides large pore volumes to transport different drugs.[24] Advantages of this material include the easy control of their particle size, resistance to temperature and pH, control over the pore size resulting in large pore volumes and an easily functionalized surface.[25]

1.09.2.1.6 Quantum dots

QD are fluorescent nanoparticles composed of semiconductor materials typically in the size range between 2 and 10 nm.[26] QD have unique optical properties that make them especially relevant for imaging techniques. Therefore, linking drugs to these materials becomes an interesting approach to perform both imaging and treatment at the same time. For biomedical applications, particles with a core of CdSe or CdTe, coated by a layer of ZnS have been tested, however, an extra coating layer is required for *in vivo* applications.[26] The main drawback of these materials is related to their toxicity, as the use of heavy metals for *in vivo* applications may have important long-term effects.

1.09.2.2 Advantages of Nanomaterials in Medicine

The use of nanomaterials in medicine offers several advantages over conventional therapeutic treatments (Fig. 2). First, their use allows the possibility to *improve delivery of various therapeutic agents* including drugs, nucleic acids, etc. This is because nanocarriers can: (i) encapsulate poorly soluble drugs; (ii) protect the therapeutic molecules from being degraded in the body before reaching their target; (iii) modify their blood circulation and tissue distribution profile; (iv) enhance the absorption of drugs into the target tissue and target cells by combining passive and active targeting mechanisms; (v) allow for better control over the timing and spatial distribution of drugs to the tissue; and (iv) prevent drugs from interacting with normal cells, thus avoiding usual side effects of conventional administered drugs.[27] Besides, due to their high surface area *it is possible to allocate several therapeutic molecules in a single nanocarrier*. This facilitates the combination of active pharmaceutical ingredients (API), which is commonly practiced in several diseases. Particularly in cancer treatment this could potentially offer synergistic effects to promote the efficacy of therapies, while limiting the risk of resistance. When multiple APIs are administered separately, each one acts according to its own distinct pharmacokinetic and pharmacodynamics properties. Thus, it is not easy to synchronize that each target cells or tissues receive optimal levels of each of them. Conversely, if multiple APIs are combined in a single nanocarrier, the spatiotemporal exposure of each drug can be controlled more precisely.[28]

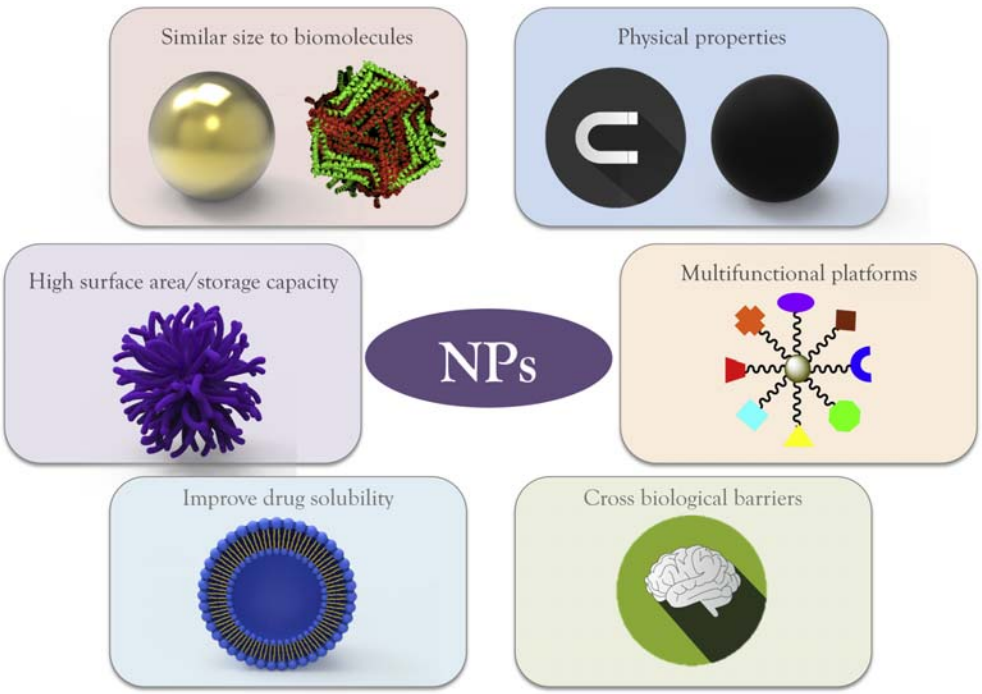

Fig. 2 Key features of nanocarriers for their use in medicine.

Additionally, *inorganic nanoparticles exhibit unique physical properties* due to their nanometer size making them ideal for a host of novel applications in the field of disease therapeutics.[29] For example, as a result of their intrinsic superparamagnetic character, MNPs are valuable in medicine as efficient transversal relaxation (T2) MRI contrast agents. Besides, under the influence of an alternating magnetic field (AMF) they can release localized heat that could be used to trigger drug delivery or destroy cells by ablation. Like magnetic ones, AuNPs could also be efficient agents for targeted cell ablation and remotely controlled drug release due to heat generation in response to light irradiation. In addition, this efficient conversion of light to heat is able to create higher levels of photoacoustic signals and thus AuNPs could also be used as contrast enhancement agents for photoacoustic tomography (PAT). Other applications of AuNPs, due to their physical properties, that could also be combined with the already mentioned include their use as contrast enhancers for computed tomography (CT) and X-ray absorbers for cancer therapy. This clearly shows that the use of a nanoparticle or the combination of different ones in what is named as hybrid nanoparticles has a huge potential for the development of all-in-one nanocarriers. Thus the use of only one type of nanocarrier not only acknowledges for the combined use of different therapies but also different imaging technologies to obtain from structural information to functional imaging.[30] Although nanomedicines at present are in an early stage of development, nanotechnology clearly has a great potential to achieve an overall impact on the medical field with significant advances in patient screening, diagnosis, staging, treatment, and monitoring.

In spite of these advantages for their use in therapy and promising preclinical efficacy results of monotherapy nanomedicines, the overall success rate for drugs moving through clinical trials to FDA approval is near one to ten. This rate is even lower than that from earlier years, that was 1 in 5 to 1 in 6.[31] The discrepancy between preclinical data and clinical outcomes could be explained because until 2010 the main driver of nanotechnology was scientific discovery growing from curiosity-driven research.[32] Consequently, it was not usually taken into account issues of great importance to improve the chances of success after clinical trials during the design of nanodrugs. Among these issues are: proposed clinical use, route of administration, likely dose, and frequency of dosing.[33] Other causes are low accumulation of the NPs in the target tissue due to less pronounced enhanced permeability and retention (EPR) effect, the heterogeneity of human tumors as well as the intrinsic/acquired drug resistance to monotherapy over the treatment course.[34] However, during this new decade it is expected that this tendency will change achieving a real impact of nanomaterials on the improvement of healthcare accelerated by an application-driven research.

Currently, there are several nanotechnology-enabled diagnostic and therapeutic agents undergoing clinical trials, and only few nanodrugs approved by the FDA.[19] Examples of already FDA approved nanoformulations are liposome encapsulated drugs (Doxil,[35] DaunoXone[36]), microemulsions (Cyclosporine[37]), albumin-bound nanoparticles (Abraxane[38]), products using nanocrystal technology (Rapamune[39]) and iron oxides nanoparticles for MRI (Feridex[40]). Other nanoformulations still under study but already in clinical trials are based on AuNPs, gold nanoshells or polymeric micelles.[19] In addition, other nanoformulations have also been approved for other uses, such as silver nanoparticles for antibacterial wound dressing,[41] silica and zirconium nanoparticles as dental composites (3 M ESPE Filtek),[42] liposomes in cosmetics,[43] or titanium dioxide and zinc dioxide nanoparticles for sunscreens (**Table 1**).[44]

1.09.2.3 Actual Research Trends

As it was mentioned, until 2010 most of the nanoparticles that were developed for therapy applications had a relatively simple design, were focused basically on cancer monotherapy and accumulated on the target site mostly by passive targeting mechanisms. However, since then, research focused on the development of more sophisticated high-quality nanomedicines by rational design. What clearly shows that research efforts in the field are growing exponentially is that from the 35.000 articles on "nanoparticles + therapy" reported in Pubmed until February 2016, more than 80% were published since 2010. In order to improve the success of nanomedicines during clinical trials, several key topics have been and are still focus of on-going research: (i) targeted drug release triggered by external *stimuli*; (ii) development of smart nanomedicines able to temporary adapt to changing environments; (iii) multi-biofunctionalization of nanoparticles; and (iv) development of hybrid nanomedicines.

The development of *"smart" nanomaterials able to deliver a therapeutic agent due to environmental causes or remote stimulus* allows to achieve a more precise control, not only temporary but also spatially, of the release of drugs.[45] Several strategies have been reported in order to trigger the target-specific release of the drug such as the use of acidic pH in the tumors, the low pH of endosomes/lysosomes, the intracellular redox potential, the presence of tumor specific proteolytic enzymes, etc.[46,47] Alternative approaches employ physicochemical properties of nanoparticles to develop remote actuation tools for controlled drug delivery. One of these approaches is the use of alternating magnetic field (AMF) to trigger cell death or the release of drugs from MNPs due to heat generation. More recently, it was also shown the effects that a phenomena named as magneto–mechanical has on biomacromolecules, biomembranes, subcellular structures and cells which can be observed using super-low and low AMF in the absence of heating.[48,49] This phenomenon could also be used alone or in combination with hyperthermia for therapy. Another approach for remotely triggered therapy is the use of near-infrared activated plasmonic nanomaterials. The photothermal response of this nanocarriers can be exploited not only for *in vivo* diagnosis (optoacoustic imaging) but also for therapy (drug delivery and photothermal ablation therapy). Besides, playing with the irradiation conditions, it is possible to control the mechanism of cell death from necrosis to apoptosis.[50]

Besides achieving the triggered delivery of drugs, a step forward in the development of high-quality smart nanomedicines is to make them responsive to changing surroundings. Namely to design *nanoparticles able to temporarily adapt* their size, shape, surface chemistry, wettability, adhesive properties, etc. This not only could be used for triggering the release of the therapeutic cargo but

Table 1 Summarizes key characteristics of selected examples of organic and inorganic nanodrugs that were already approved or are still under clinical trials

Nanodrug	*Composition*	*Manufacturer*	*Mechanism of local accumulation*	*Used for*	*Characteristics*	*Disadvantages*	*FDA approval date/ clinical trial status*
Doxyl	Pegylated lyposomal doxorrubicin	Orthobiotech, Schering-Plough	Passive targeting	Ovarian/breast cancer; AIDS-related Kaposi's sarcoma	(i) Enhanced circulation time (4 days) (ii) Improved pharmacokinetic profile	(i)10- to 20-fold more expensive than doxorubicin (ii) skin reactions/ hypersensitivity (iii) more secondary effects than Myiocet	November 1995
Myocet	Non-pegylated lyposomal doxorrubicin	Elan Pharmaceuticals/ Sopherion	Passive targeting	Metastatic breast cancer	(i) different in terms of the lipid composition, size, loading method than Doxyl (ii) enhanced plasma half life (16–50 h) (iii) different tissue distribution profile than Doxyl (iv) different dosing and safety profiles than Doxyl.		2000 in Canada and Europe
ThermoDox	Thermosensitive liposomal doxorrubicin	Celsion Corporation	Passive targeting	Hepatocellular carcinoma	(i) Release their cargo when local tissue temperatures are increased to 39–42°C by application of radiofrequency (ii) allows local concentration of the drug 25-fold more than IV doxorubicin, and up to several times than other liposomal doxorubicin formulations		In clinical phase III
Abraxane	Albumin-bound Paclitaxel nanospheres of 130 nm (Nab). Nab paclitaxel in combination with gemcitabine	Abraxis Bioscience, Astrazeneca Celgene	Glycoprotein 60-mediated endothelial cell transcytosis of Nab and accumulation in the area of tumor by albumin binding to SPARC (secreted protein, acidic and rich in cysteine)	Various cancers Metastatic pancreatic cancer	(i) More effective than paclitaxel at treating tumors because a higher dosage can be delivered (ii) Decrease in side effects from solvent related hypersensitivity reactions (iii) Decrease time of administration (iv) Less toxic than paclitaxel (v) Predictable and linear pharmacokinetics	More expensive than free paclitaxel formulations (Taxol or Onxal)	Jan.–05 Sep. 2013
Aurimmune (CYT-6091)	Tumor necoris factor (TNF-α) bound to colloidal Gold nanoparticles	Cytimmune Sciences	Active vectorization in order to disrupt tumor blood vessels and enable follow-on chemotherapy to penetrate the tumor and kill the cancer cells inside	Head and Neck cancer	Better tolerated and at lower doses causes greater tumor regression than TNF itself		In clinical pahse II

also could help to overcome several biological barriers that could impair therapeutic effectiveness.[51,52] For example, it is well known that nanoparticles with sizes ranging from 100 nm or higher are the ones with best accumulation and retention rates in tumors due to EPR effect. However, recent *in vivo* studies show that particles with less than 100 nm could penetrate better poorly permeable tumors.[53] To solve this limitation, researchers have designed NPs that circulate as large particles and their size is reduced once they reach the tumor.[54] Different stimuli could be used to gain control over extracellular particle transport: (i) internal *stimuli* due specific microenvironment of tumors (low pH, presence of proteases, hypoxia, etc.)[55] or (ii) external *stimuli* (ultrasounds, light, magnetic field, etc.).[56,57] Not only it is possible to gain control over particle size but also over their cellular uptake. In this sense it was already validated *in vivo* a higher uptake by tumor cells of NPs whose surface chemistry could be temporary controlled.[58] This is achieved by masking ligands for targeting or cell internalization by non-ionic hydrophilic polymers during NPs circulation to avoid non-specific interactions with immune cells and normal tissues. This protective layer is linked to the nanocarrier surface by a stimulus sensitive linker. This way, unmasking and promotion of a selective interaction of nanocarriers with tumor cells could be triggered only when they reach target sites. The same internal and/or external stimuli already mentioned could trigger this exposure of cell-interactive ligands.[59–62]

In order to improve the therapeutic effectiveness, another milestone to be reached is the design of *nanomedicines functionalized with different biomolecules*. This allows introducing different bio-capabilities to the nanomaterial such as active targeting, the ability of overcoming several biological barriers, etc.[63] However, the development of appropriate multi bio-functionalization strategies is a big challenge due to the wide variety of nanomaterials and biomolecules available for this purpose.

The biomolecules to be joined to the surface of the nanomaterial could vary significantly in terms of size, chemical composition, 3D complexity, location of its biological active site, and so forth. If properly designed, an oriented functionalization strategy could be a powerful tool to improve the stability, activity, specificity and selectivity of the attached biomolecule, which results in more bioactive materials and in substantial improvements of its subsequent biotechnological or biomedical (biosensing, therapy, theranosis, etc.) application.[64–67] However, a conjugation chemistry that works well with a specific biomolecule could not be adequate for another one. Besides, the wide variety of available nanomaterials shows large differences in terms of size, shape, surface area, net charge, density of reactive groups, colloidal stability, etc. Thus, no universal methodologies exist and the optimization of the most adequate functionalization strategy for each particular combination of nanomaterial and biomolecules is required. Proof of this difficulty is the low number of articles on the topic, as indexed by ISI Web of Knowledge® (keywords combination: biofunctionalization + nanoparticles and multifunctionalization + nanoparticles) (**Fig. 3**).

The importance of selecting an adequate multifunctionalization strategy was highlighted recently by de la Fuente *et al.*[68] Their objective was to develop an optimal multifunctional AuNP to achieve optimal effectiveness of RNA interference for cancer therapy. In this sense, they developed a library of NPs using different bio-functionalization strategies in order to find not only the optimal conjugation methodology but also the optimal combination among different biomolecules (siRNA, biofunctional spacers, cell penetrating peptides as membrane translocating agents and a fluorophore).[68] However, with only one of the obtained nanoconjugates (siRNA/RGD-AuNPs) successful targeting in the lung was achieved using a lung cancer syngeneic orthotopic murine model following direct intratracheal delivery. In this model, significant c-Myc oncogene down regulation followed by tumor growth inhibition and prolonged survival of lung tumor-bearing mice was attained.[69]

Another complementary line of research to bridge the gap between preclinical animal tests and clinical human trial, is *the development of hybrid nanocarriers* composed of at least two different nanomaterials. This kind of nanocarriers allows combining the advantages of purely inorganic and organic nanoparticles. Besides, they also possess unique advantages for imaging and therapeutic applications.[34] For example, it is possible to design nanoparticles with superior pharmacokinetics, multi-stage delivery systems, enhance EPR accumulation and with a combination of therapies in the same nanosystem (eg, co-delivery of chemotherapeutics and biologics plus photothermal ablation, etc.).[70] Besides, accommodating multiple therapies into one single nanocarrier has

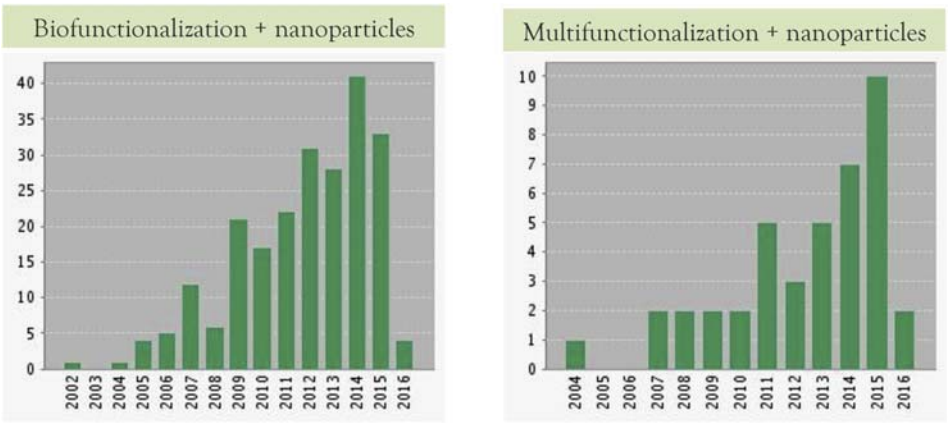

Fig. 3 Number of published articles per year at ISI Web of Knowledge® using biofunctionalization&nanoparticles or multifunctionalization&nanoparticles as keywords.

several advantages, including reduced manufacturing cost, improved patient compliance, and easy-to-monitor release, pharmacokinetics, and biodistribution of different drugs. Although optimized formulations of these complex nanocarries are expected to have a bright future in nanomedicine, the potential safety of each component and/or metabolite that might arise as a result of their *in vivo* degradation or metabolic fate must be studied in detail.

Another step forward in order to revolutionize nanomedicine-based therapy is to *extend research to other diseases than cancer*. Although, still most published articles are focused on cancer therapy, an increasing number of articles are focused on the treatment of other diseases. This is the case of the use of *nanocarriers for Human Immunodeficiency Virus (HIV) infections*. While HIV infections are reducing in incidence since the introduction of Highly Active Anti-retroviral Therapy (HAART), there still remain a number of challenges such as fighting the existence of virus reservoirs, drug resistance and anatomical barriers to antiretroviral therapy. In this sense, the experience acquired during the development of smart nanocarriers for cancer chemotherapy is being used for the design of smart antiretroviral nanocarriers.[71,72] Other application of nanocarriers is their use for *treatment of hepatic diseases* including other pathologies such as hepatic fibrosis and microbial infections in addition to hepatocellular carcinoma.[73] Their prevalence is rising due to the inability to deliver enough concentration of therapeutics and/or contribution to undesirable side effects of standard medication. Therefore this is another field where nanocarriers could have a great potential for improving the delivery of drugs in a more specific manner and by simultaneously minimizing side effects. Nanocarriers have also a potential role in the *early detection and treatment of different neurodegenerative disorders* such as amyotrophic lateral sclerosis,[74] Alzheimer's disease (AD),[75,76] Parkinson's disease (PD)[77–79] and Huntington's disease (HD).[80,81] To date, the blood–brain barrier (BBB) remains one of the reasons for the lack of success in the development of treatments as it prevents the penetration of therapeutic agents and diagnostic tools. It is estimated that more than 98% of small molecular weight drugs and practically 100% of large molecular weight drugs (mainly peptides and proteins) developed for Central Nervous System (CNS) pathologies do not readily gain access to the brain extracellular fluid from the blood. BBB is characterized by tight junctions between endothelial cells, by the absence of fenestrations and low occurrence of pinocytic activity. Transcytosis is the only way for NPs and macromolecules to be captured on one side of the endothelial's BBB cells (bloodstream), drawn across the cell and be ejected on the other side (brain extracellular fluid) or be degraded within lysosomes leading to the drug being released into the brain tissue. There are several transcellular routes that include passive diffusion, carrier-mediated transport (CMT), receptor-mediated endocytosis (RME) and adsorptive-endocytosis (AME).[82] Due to the size limit of passive diffusion, most nanocarriers cannot enter by diffusion. A popular approach to achieve the transcellular passage of NP-linked drugs is to functionalize the NPs with biomolecules that are transported into the brain by the carriers expressed in the brain microvessel endothelial cells. In this sense, more than 20 carrier-mediated transporter proteins have been identified in cerebral capillaries of BBB. Due to their high transport capacity, the most popular carriers used for NP transport are those for large aminoacids (e.g., LAT1) and glucose (e.g., GLUT1).[83] Although these transporter are primarily involved in molecular translocation of relatively small molecules, there are several examples on the bibliography using glucose-modified NPs in order to cross BBB.[84,85] In this sense, a recent example shows how glucose-modified paclitaxel-loaded polymeric nanoparticles, due to their transport via GLUT1, were successfully employed in the treatment of intracranial glioma in mice.[86] However, much more examples could be found in the bibliography targeting receptors that internalize ligands by means of vesicular transport. This is because such transport can readily accommodate nanoparticles with a size of 100–200 nm. Among the most used ligands for the functionalization of NPs in order to reach their translocation by RME are: transferrin, insulin, low-density-lipoproteins (LDL), leptin, thiamine, glutathione, encephalin.[87] Conversely, the concept of adsorptive-mediated transcytosis through the BBB was originally described to occur for cationic proteins (e.g., serum albumin) that can bind the endothelial cell surface but also cross the BBB. This mechanism, applied to NPs, is based on the proper functionalization of their surface with positive charges or positively charged biomolecules (e.g., TAT peptide, albumin, etc.) allowing electrostatic interaction with the negative charges on endothelial cells.[88]

Nanocarriers have been investigated for the development of new effective *antimicrobial therapies for gastrointestinal diseases*.[89] This has a huge impact in developing countries because most of the population lives below the poverty line, making infectious diseases the major cause of morbidity and mortality. The currently available antibiotics or anti-retroviral drugs are specific to certain types of infections and have several limitation such as increasing emergence of antibiotic resistance, high production costs, significant side effects, limited accessibility and adherence of the patient to the treatment. Due to the already mentioned intrinsic features of the use of nanocarriers in therapy, they might be promising to overcome these problems specifically by oral administration of NPs. For example, their incorporation in food or beverages products could be an easy administration of therapeutics with high rates of acceptance and adherence of patients. The use of nanocarriers in the *diagnosis and* as *immunotherapeutic platforms in autoimmune diseases* is also a current field of research. A big advantage of nanomaterials for this application is that they have a natural tendency to accumulate in inflamed tissues, through vascular leakage, macrophage uptake or their active targeting by specific receptors or ligands.[90,91] Another challenging field of application of nanotherapeutics is the *treatment in ocular diseases*. Topical treatment of them is a current challenge as ocular drug bioavailability is less than 5%. This is because to reach the targeted ocular structures drugs applied directly onto the eye need to bypass different biological barriers. The use of nanocarriers to increase ocular drug bioavailability has started in the 80s with the use of liposomes. However, it was during the last decade that this field of research has grown substantially and other type of carriers others than liposomes have been explored including polymeric nanoparticles [chitosan, gelatin, poly-(lactic-co-glycolic acid), hyaluronic acid, etc], nanocapsules, dendrimers, and nanocrystals, etc. Namely, the most important milestones achieved so far are: (i) to show that nanocarriers for this administration route could associate with a wide variety of different drugs, (ii) increase of their residence time onto the ocular surface, (iii) reduction of degradation of labile drugs, and (iv) increase drug bioavailability by improving their interaction with the corneal and conjunctival epithelia.[92] Other interesting

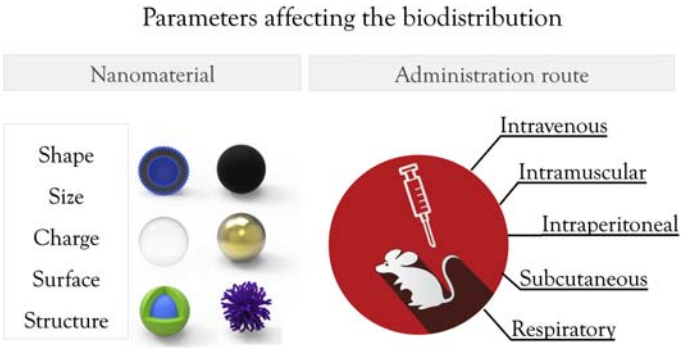

Fig. 4 Parameters that affect the biodistribution of different nanomedicines, classified depending on the physicochemical properties and the administration route.

new field of research is the *improvement of diabetes mellitus treatment* by achieving oral delivery of insulin. The current insulin therapy is via subcutaneous injection, which often fails to mimic glucose homeostasis that occurs in normal individuals. Oral delivery is the most convenient administration route. However, insulin oral delivery is a challenge due to its rapid enzymatic degradation in the gastrointestinal tract (GI), the physiological barrier that represents epithelial cells of GI and the physicochemical properties of insulin that has a large molecular size and tends to aggregate above 100 mM. Nanocarriers have immense potential for the effective oral delivery of insulin and thus different type of nanoparticulate carriers are being currently engineered for this application such as polymeric nanoparticles and micelles.[93] Although some of them have been already through preclinical animal stage testing, there are still many challenges to overcome such as studying the toxicity of these materials administered on a chronic basis.

Among others diseases in which nanocarriers could have a potential to improve their treatment are respiratory diseases,[94,95] Cowel bowel disease,[96] wound healing and skin regeneration,[97] malaria,[98] leishmaniasis,[99] haemophilia, cardiovascular diseases, and rheumatoid arthritis.[100]

1.09.3 Biodistribution

Understanding the *in vivo* biodistribution and degradation pathways of new nanomaterials is fundamental to ensure their safe implementation for biomedical applications. This knowledge would also allow the optimization of the dose required for each treatment.

Several parameters influence the biodistribution of nanomedicines, namely, the physicochemical properties of these compounds, such as shape, size or surface modifications among others or the administration route (Fig. 4). Even the anesthesia used during particle administration may significantly change nanoparticles biodistribution.[101]

This section focuses, not on the parameters affecting the biodistribution, but on the different techniques that are currently being employed to track the biodistribution of different nanomaterials, paying special attention to the advantages and limitations of each technique. Classification of the different techniques has been performed according to the possible use of each approach either *in vivo* or *ex vivo* (Fig. 5).

1.09.3.1 *In vivo* Optical Imaging

Since the fluorescence in the visible light is only applicable for thin tissue samples, the fluorescence based techniques for *in vivo* imaging and therefore possible biodistribution characterization drive into the small spectrum window of the NIR (near infrared) region (650–950 nm). In this NIR window, because of the minimal adsorption of water, hemoglobin and lipids, as well as low autofluorescence and tissue scatter, light penetration is maximal. The depth penetration, normally described as >1 cm, depends highly on imagined tissue type.[102] However it can be increased due to the new microscopy imaging techniques.[103,104] The fluorophores used for NPs labeling must fulfill several requirements, like high brightness and photostability, large Stokes shift, high fluorescence quantum yields (high sensitivity), resistance to degradation in biological systems. Also, they should present preferably low toxicity level. So far only one fluorophore, indocyanine green (ICG), has been accepted by US FDA commission for clinical trials.[105] Because of its several limitations also some derivatives of the ICG are considered.[106] Nevertheless, another polymethines, especially Cy5.5 or Cy7 are one of the most popular organic fluorophores used for NIR imaging.[107,108] Moreover, ultimately several new NIR probes with improved properties have also been described.[109–113]

In vivo biodistribution of several types of NPs can be followed through optical imaging studies. One of the most popular choices for fluorescence imaging applications are QD. This popularity is supported by excellent optic properties, such as narrow and tuneable emissions bands, broad excitation spectra, high fluorescence quantum yields and high resistance to

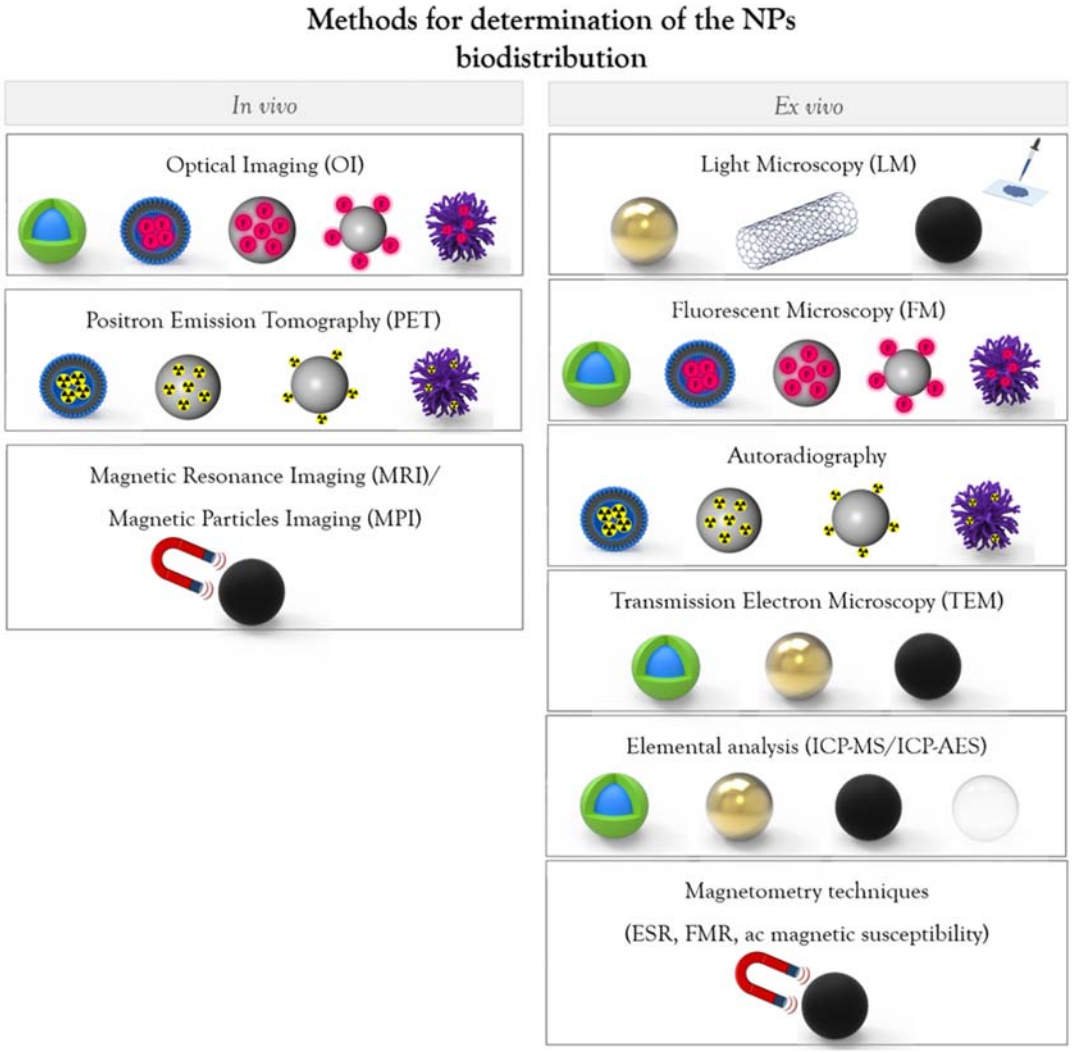

Fig. 5 Methods for the in vivo and ex vivo evaluation of nanomaterials in biomedicine, including the type of material that could be characterized by each technique, as described in **Fig.1**. Gray Nanoparticles are designated as general NPs (including silica, gold or magnetic NPs, and QD).

photobleaching.[114–116] In a single assay with only one excitation source, different colors of QD can be applied enabling multiplexing and simultaneous visualization of different targets.[117] However, the potentially high toxicity of QD resulting from heavy metal ions release[118] limits drastically their potential application in clinical imaging or at least hamper it in case of polymer protected QD as little is known about the mechanism of metabolism or clearance from living organism of this described as stably protected and essentially nontoxic particles.[119,120]

Apart from QD, a wide range of polymer or inorganic matrix- based particles loaded with organic NIR dyes can be localized *in vivo* through optical imaging.[121] However, the combination of several factors makes NIR dye-doped NPs suitable for optical imaging applications, such as brightness of the system resulting inter alia from the efficient fluorophore linking/immobilization strategy.[122]

Dye doped NPs can be fabricated by embedding the fluorophore inside typically the core-shell structured NPs either covalently or noncovalently (mainly: dye-doped silica NPs[123–126]; dye-doped calcium phosphate NPs; dye-containing lipoprotein NPs) or by coupling the fluorophore to the shell/surface of NP (mainly: silica NPs, metallic NPs).

The first case seems to be especially attractive for imaging application for several reasons. High payload of dye molecules per nanoparticle enhance the fluorescence and embedding a fluorophore within the NPs matrix prevents its possible leaching from the particles which can be triggered by the proteins and lipophilic cellular microenvironment and therefore give a false signal. Moreover enclosing dyes within NPs provides its photostability and biocompatibility and the fluorophore high water solubility and toxicity is no more a problematic question, since appropriate surface modification can provide hydrophilicity, stability and multi functionality of the NP.

Within the NIR dye-containing nanoparticles, dye-doped silica NPs seems to be excellent choice for bioapplications, mainly because amorphous silica appears to be a biocompatible and nontoxic material and the surface hydroxyl groups can be easily modified using a conventional silane-based chemistry.[127] What is more, the silica matrix is optically transparent that allows excitation

and emission light to pass through efficiently.[128,129] The *in vivo* biodistribution studies have been performed on a variety of silica NPs (inter alia on ICG-doped mesoporous silica NPs,[130] (red-F)-labeled amorphous silica particles,[131] Ru-BPY doped PEG-Silica NPs[132,133]).

Calcium phosphate (CP) NPs (CPNPs) is another interesting class of inorganic materials which can be doped with fluorophores and therefore show promising properties for animal imaging.[134] Since CP is generally regarded as safe by FDA, it has been widely used to synthesize a novel and no viral systems for targeted drugs or genes effective delivery.[135,136] Also ICG-doped and PEGylated CPNPs has been designed for accumulation studies in breast adenocarcinoma xenografts.[137]

High biocompatibility, biodegradability, payload capacity and nonimmunogenicity make lipoprotein NPs ideal to be used in biomedical fields. Lipoproteins nanocarriers of NIR probes have been reported, enabling *in vivo* validation of the LDL rerouting principle and providing *in vivo* application of enhanced cancer optical imaging in live animals.[138]

Apart from inorganic particles, also organic polymers have been applied for engineering NIR-containing NPs. Optical imaging of intravenously administrated poly-lactide-co-glycolide (PLGA) NPs conjugated with NIR probe (DY-675) and a simil-opioid glycopeptide (g7) showed brain localization.[139] In another approach, NIR-emissive polymersomes were generated through self-assembly of amphiphilic diblock copolymers and conjugated multi(porphyrin) based NIR fluorophores.[140]

In addition to QD and NIR-doped NPs, several nanosized probes can be used as fluorescence imaging agents, where carbon nanotubes (CNTs) are one of them. Although special attention is focused on CNTs mechanical, thermal and electronic properties in terms of electronic devices, their potential application in biomedical imaging began to be explored after discovery of fluorescent semiconducting CNTs. Single-walled nanotubes (SWNTs) present unique features, like emission in the region of 1000–1400 nm (still suitable for optical imaging), photostability, large Stokes shifts and large surface area facilitating functionalization of a large amounts of targeting ligands or drugs.[141]

Coatings and surface modifications of metallic NPs can serve not only to improve their biocompatibility and functionality properties but also to render the fluorescence. Attaching a fluorophore to the NP can be made by depositing additional coatings carrying fluorophore or by immobilizing a fluorophore on the NP surface. The first one can be achieved by the layer-by –layer (LbL) technique,[142] although the *in vivo* stability of the deposited layer remains a problematic issue.[143,144] On the other hand, rich NPs surface chemistry is ideal for straightforward functionalization with desired biomolecules including fluorophores.[145] Although the design of fluorescent NPs especially of small diameters is challenging because multiple fluorophores on the surface of a NP quench each other if they are located within the energy-transfer distance.[146] Moreover, the properties of fluorophore–NP conjugates strongly depend on the efficiency of the fluorophore-linking strategy, the type of immobilization and stability of the fluorophore or even polymer/shell coupled with fluorophore upon *in vivo* administration and cell internalization.[122,147]

1.09.3.2 *In vivo* Positron Emission Tomography

Positron emission tomography (PET) is another imagine technique which enables *in vivo* localization of those NPs which are chelated or incorporated with isotopes without the need for external excitation.[102] This technique relies on recording high energy gamma rays from positron emitting isotope.[148] It characterizes with the highest sensitivity of all imagine modalities and has no tissue penetration limits[149] although the anatomical resolution is rather poor because of spatial resolution limitations.[150] PET, despite being approved by FDA as a clinical molecular imaging technique, exposes living tissues to strongly ionizing radiation and moreover is extremely expensive (positron-emitting isotopes can be generated mostly with a cyclotron or less commonly with a generator source). Nevertheless it is still considered as a highly popular imaging technique potentially improved upon NPs help.

Various isotopes for NPs labeling can be purchased from PET radiopharmacies, which exist through the world and can provide common PET traces on a daily basis.[151] One crucial factor that should be considered in NPs radiolabeling is the radionuclide physical half-life ($T½$). For biodistribution study in a short time frame after NPs administration, short-lived radionuclides such as fluorine-18 ($T½ = 109.7$ min), gallium-68 ($T½ = 67.7$ min) or interestingly even nitrogen-13 ($T½ = 9.97$ min) can be applied. On the contrary, prolonged time frame scanning can be obtained using longer-lived radionuclides, namely copper-64 ($T½ = 12.7$ h), bromine-76 ($T½ = 16.2$ h), iodine-124 ($T½ = 4.1$ d), and arsenic-74 ($T½ = 17.8$ d). Once selected, the radionuclide can be conjugated directly on the NPs surface via different labeling methods. Also it can be indirectly attached through a simple hydrocarbon chain, a peptide, or a polyethylene glycol unit linker to the NP core.[152,153] A vast number or organic as well as inorganic radiolabeled NPs has been successfully traced *in vivo*, among them gold NPs,[154,155] iron oxide NPs,[156,157] aluminum oxide NPs,[158] QD,[159] rare earth containing NPs,[160] silica NPs,[161–163] polymers,[164,165] liposomes.[166] However, because of the poor PET imaging resolution, most of the mentioned biodistribution studies have been supported by incorporation of other imaging modalities and creation of multimodaling approach. Commonly PET technique is combined with computed tomography (CT),[167] NIRF agents (within silica NPs[161]; *International Patent WO 2010/030120* or QD[168]) or MRI (in conjugation with iron oxide NPs[156]). Especially the PET/MRI approach is considered as a powerful combination as both sensitivity and anatomical resolution can be obtained in simultaneous acquisition.[169,170]

Finally for PET application, one more aspect has to be taken into account. Namely, labeling with more than one radioisotope is not possible as all positron emitters lead to 511-keV gamma rays so there is no distinction between them. However this drawback can be overcome by applying another nuclear imaging technique named single photon emission computed tomography (SPECT).[171] For SPECT different radioisotopes such as technetium-99m ($T½ = 6$ h), iodine-123 ($T½ = 13$ h), indium-111 ($T½ = 2.8$ days) or iodine-131 ($T½ = 8$ h) are used. As in this technique single photon emitters decay under the emission of gamma

rays with energies between 100 and 300 keV, various isotopes with different gamma rays energies can be used simultaneously. Despite of the possibility of numerous radionuclides multiplexing, in an order of magnitude this technique is less sensitive than PET (sensitivity lower of about two/three orders of magnitude)[148] and therefore as PET this technique is more often applied together with other imaging modalities such as NIRF or MRI.[169]

1.09.3.3 *In vivo* Magnetic Resonance Imaging

MRI is a non-destructive method applicable for MNPs tracking *in vivo*. This technique is based on the physical phenomenon of protons relaxation in a static magnetic field after excitation pulse application.[172] The magnetic resonance image is generated by monitoring the local variation in relaxation corresponding to image contrast, which results from proton density as well as chemical and physical nature of the specimen tissue. Two different relaxation mechanisms can be distinguished: longitudinal relaxation (T_1-recovery) and transverse relaxation (T_2-decay).[173] MRI per se provides physiological and pathological information about living tissue, however for the enhancement and quantification of physiological information, MRI contrast agents are broadly used and now constitute an integral part of MRI studies.[174] Therefore NPs which are able to increase the T1 signal or reduce the T2 signal, in other words act respectively as a positive or negative contrast agents, can be detected by MRI. The effectiveness of contrasting the MR image by MNPs can be described by its relaxivity, which is the proportionality constant of the measured rate of relaxation, or R1 (1/T1) and R2 (1/T2), over a range of contrast agent concentrations.[102] Its value depends on the NPs magnetic properties, but also on experimental conditions (field strength, temperature, the medium in which the measurements are performed). MRI special advantage over other techniques in NPs *in vivo* tracking is high spatial resolution (micrometers) and tissue penetration depth (NPs can be detected everywhere in the body), however its main drawback is poor sensitivity, high cost and complexity.[148]

Among MNPs that can be traced by MRI, iron oxide NPs (IONPs) and Gd(III)-doped NPs are the most popular ones. Particularly IONPs receive special attention as they are presently being employed in a variety of biomedical applications, inter alia because of the unique magnetic properties they present. Specially NPs with superparamagnetic properties are extremely attractive, as they show fast response to applied magnetic fields with negligible remanence (residual magnetism) and coercivity (the field required to bring the magnetization to zero) what prevents agglomerates formation at room temperature.[175] Superparamagnetic IONPs have been deeply investigated for *in vivo* applications as contrast agents for liver disease diagnosis,[176] lymph-node imaging, angiography and blood-pool imaging.[177] However, the efficiency of IONPs as contrast agents, and therefore the possibility of their *in vivo* tracking depends on many physicochemical characteristics of NPs,[178] where size dependent effect of magnetism is just one of them.[179] One of the biggest drawbacks of IONPs detection via MRI is related to the contrast they generate. As they act as negative imaging agents the produced dark signal can be confused with pathological alternations. Additionally the high susceptibility of IONPs can provoke magnetic field distortion on neighboring normal tissue called susceptibility artifact of "blooming effect." As a result dark images are generated with no background around the lesions.[180] To overcome this limitation various solutions have been proposed,[181–183] although they do not eliminate signal loss or magnetic susceptibility artifacts.

Apart from NPs with a core fully based on iron oxide, systems with other magnetic cores can also be detected by MRI. Alloy-based nanomaterials with high relaxivities are one of them. For instance compounds known as ferrites where one of the Fe ions in an iron oxide has been replaced with a different atom such as Mn, Zn, Co, Ni present high saturation magnetisation and increased relaxation rates, making them good candidates for T2 contrast agents.[184] Particularly Mn-ferrites have been described as highly suitable for MRI imaging.[185]

Another type of nanomaterials that can be visualized by MRI are those incorporated with Gd(III). Gd(III) is the most known example of paramagnetic material which provides bright, positive contrast in MRI. In various reports attachment of Gd(III) complexes to nanostructures based on silica,[186,187] TiO_2,[188] gold,[189] dendrimer,[190] nanodiamond,[191] polymer[192] etc. has been described. The high yield MRI contrast in the case of Gd(III)-doped NPs is provided mostly because of high payload of gadolinium ions and a slow tumbling motion of particles.[102] Moreover, Gd- based NPs gadolinium oxide (Gd_2O_3), gadolinium fluoride (GdF_3), and gadolinium phosphate ($GdPO_4$) have been investigated as MRI contrast agents, although uniformly sized Gd NPs have not yet been obtained.[180]

Other nanomaterials with potential recognition *in vivo* via MRI include gold-iron oxide (Au-Fe_3O_4) NPs, metallic ion NPs, porous hollow Fe_3O_4 NPs and Fe-based alloy nanoparticles, such as iron–cobalt (FeCo) and iron–platinum (FePt) NPs.

1.09.3.4 *In vivo* Magnetic Particles Imaging

As one of the MRI major drawback using MNPs acting as T2 contrast agents is the difficulty in tracking them in tissues with naturally low MRI signals (specially in lungs) a novel imaging modality has recently been proposed. Magnetic Particle Imaging (MPI), introduced in 2005,[193] is based on a direct imaging of the SPIONs intense magnetization in contrast to MRI which indirectly detects the MNPs via the nearby proton relaxation.[194] As a result, MPI identifies only MNPs and not diamagnetic tissue (with zero MPI signal) giving a bright contrast with no obscuring background. As the signal strength is proportional to the MNPs amount, direct measurement of MNPs concentration at certain location is possible. Although for now only a few prototypes of small animal MPI scanners have been constructed, the interest in this new imaging modality is substantial as its utility for *in vivo* MNPs tracking superior over MRI has recently been demonstrated.[195]

1.09.3.5 *Ex vivo* Light Microscopy

Light microscopic evaluation of histological sections is probably the oldest and the most common technique that can be applied for simultaneous toxopathological assessment and visualization of certain NPs types. It requires organ preparation in form of 3–8 μm thickness formalin-fixed and paraffin embedded (FFPE) or more recently cryosectioned tissue samples but at the same time it is sensitive, efficient and cost-effective. However, because of the light microscopy limited resolution to 200–500 nm, single NPs cannot be observed even at the highest microscopic magnification. Therefore only NPs which form aggregates of a major than the resolution limit size and are able to attenuate a visible light can be detected by light microscopy.[196] After a general hematoxylin and eosin (HE) staining[197] that produces blue/violet and pink staining of baso- and acidophilic substances respectively, dark deposits of NPs clusters can be easily detected. Several types of NPs have been successfully detected in HE-stained tissue sections. For example, IONPs forming brown aggregates have been found in glioblastoma sections[198] or in prostate cancer cells[199] in patients after intratumoral injections. Likewise, gold NPs presence in brain of adult albino rat has been detected in HE sections after oral administration.[200] In other studies, tissue sections confirmed CNTs or titanium dioxide deposition in bronchioloalveolar lungs region[201] and on superficial stratum corneum layers of skin[202], respectively.

Depending on the NPs properties, these compounds can be visualized by light microscopic evaluation using specific stains. One of the most popular is Prussian blue staining, commonly used for identifying iron ions in tissue sections.[203–205] The main drawback is that this procedure does not differentiate endogenous iron present in the tissue from the administrated one.[206] To overcome poor sensitivity obtained with traditional Prussian blue staining, an alternative method has been proposed for visualization unlabeled MNPs which employs their intrinsic peroxidase-mimicking activity.[207] Another histological stain named Alcian blue has been successfully applied for negative charged sulfate group detection of dendritic polyglycerol sulfate (dPGS) NPs in Kupffer cells of mice liver.[208] In another approach gold-labeled CNTs have been visualized through light microscopy by silver enhancement method.[209]

1.09.3.6 *Ex vivo* Fluorescent Microscopy

Biodistribution of fluorescently labeled NPs can be determined also *ex vivo* by fluorescent microscopy examination of tissue sections.[210–212] This approach provides resolution similar to that of bright field light microscopy[213] and therefore fluorescently labeled NPs can only be detected if densely packed. Notwithstanding this method enables tracking NPs with much higher spatial and temporal resolution than the one obtained by *in vivo* whole body imaging. For better understanding the NPs localization usually additional approaches are applied, like concurrent counterstain of nuclei with the blue fluorescent dye 4′,6-diamidino-2-phenylindole (DAPI), merging images of fluorescence microscopy and bright field microscopy or immunofluorescent labeling of marker proteins.[214] Moreover, in the last case, the co-localization resolution can be reinforced by employing confocal laser scanning microscopy which enables optical sectioning of the slide for serial 2D and 3D reconstructions of tissues or single cells.[215] Furthermore, recently interesting technique named intravital fluorescence multiphoton imaging has emerged for studying the *in vivo* behavior of fluorescent nanomaterials.[216,217]

As described in the optical imaging section, various NPs classes can be labeled with a wide range of fluorophores and therefore be detected in tissue sections by fluorescence microscopy examination, although the conjugation strategy, in terms of fluorophore stability, has a crucial meaning for signal veracity.[122] As for the bright field light microscopy, the tissue for fluorescent microscopy examination is prepared in the same form of thin sections. Theoretically not only NIR fluorophores can be used for NPs labeling and further detection. However because of the low tissue background autofluorescence in NIR region,[218] using long wavelength fluorophores is still preferable.

1.09.3.6.1 Autoradiography

Distribution of radiolabeled NPs (described in PET section) can also be detected in organs and tissues *ex vivo* by so called whole body autoradiography (WBA) technique.[219] In a standard WBA procedure the whole animal body after the sacrifice is frozen and cryo-sliced into 30–50 μm sections so the radioactivity can be evaluated in different body parts.[220] Phosphor imaging technology permits also semi-quantification of the radiolabeled material with a resolution at organ/suborgan level. Tissues of interest selected from previous WBA imaging can be further applied for another related technique with cellular/subcellular resolution called microautoradiography (MARG)[221] or light microscope autoradiography (LMA).[208] Commonly it requires mounting thin tissue sections onto photographic emulsion coated glass slides and sample examination under light microscopy. As the same tissue can also be stained with HE, pathological examination is possible in the context of autoradiographic NPs signal.[208] Besides, autoradiography can also be adjusted for electron microscopy analysis.[222]

Although mostly used in pharmacology for studying molecules distribution,[223] quantitative WBA and MARG/LMA have been applied for biodistribution examination of several radiolabeled NPs, among others lipid NPs,[224] lyposomes,[225,226] polymer NPs,[208,227] or silver NPs.[228]

1.09.3.7 Transmission Electron Microscopy

Significantly higher resolution than light microscopy can be provided by transmission electron microscopy (TEM). Therefore detailed information of subcellular structures and the precise localization, distribution and morphology of even single NPs inside cells can be obtained.[229] However certain electron density of NPs is required for their unambiguous visualization. For example

organic NPs which characterizes low tissue contrast normally require other visualization techniques.[208] Nevertheless tissue localization of various types of electron dense inorganic NPs have been successfully characterized by TEM, among them titanium dioxide NPs,[202,230] silica NPs,[211] silver NPs,[231] gold NPs,[232] magnetic NPs,[233,234] or QD.[235] NPs with insufficient electron density for TEM detection, can by labeled for example by synthesizing NP around a gold core or covalent binding of colloidal gold.[209] Importantly, it has to be taken into account that standard staining with lead citrate and uranyl acetate for TEM imaging can caused artifacts misinterpreted as NPs. In this context very often supplementary technical refinement is employed. Energy dispersive X-ray (EDX) analysis and electron energy loss spectroscopy (EELS) are techniques which enable qualitative elemental analysis of an electron microscope sample and therefore unambiguous differentiation of NPs from tissue artifacts.[196,232,236] Additionally another tool offered by TEM, namely electron beam diffraction has demonstrated its high utility in MNPs differentiation from ferritin intracellular iron storing protein.[234]

Apart from laborious and costly specimen preparation for TEM, the analytical throughput of samples is one of the major technical difficulties as only small tissue volume of 1–10 μm^3 is usually analyzed. As low NPs doses are administrated *in vivo*, far fewer NPs are accumulated within each cell and far fewer exposed cells are present in exposed tissues.[214] Therefore individual NPs observation in ultra-thin sections of tiny volume tissue samples is sometimes unattainable. To overcome this limitation a scanning transmission electron microscopy (STEM) approach has recently been proposed. In this approach, dark and bright field images were recorded together with control of the image contrast settings to analyse 243,000 μm^3 of liver tissue in a single setting.[237] Moreover, in terms of limited information from selected regions of TEM sample, new method called X-ray scanning analytical microscopy (XSAM) has emerged as an alternative. This non-destructive technique based on the analysis of energy-dispersed fluorescent X-rays in air has been applied for iron elemental mapping in whole mice.[238]

Overall TEM analysis can be most useful for tracking detailed NPs sub-cellular localization as an addition to a series of other detection tools rather than first choice high-throughput imaging technique.[239]

1.09.3.8 Elemental Analysis

Accurate quantification of NPs made of materials natively not found in the body can be obtained by elemental analysis with spectroscopic methods such as inductively coupled plasma-atomic emission spectroscopy (ICP-AES) or inductively coupled plasma-mass spectrometry (ICP-MS). Elemental analysis is a destructive method which requires acidic sample digestion before dilution and analysis which is rather expensive. However, a huge benefit of this technique over other detection methods is its high precision and the possibility of tracing even small amounts of internalized NPs as its detection limits reaches sub-ppb.[240,241] Additionally, in some cases it is possible to convert the mass concentration obtained from elemental analysis into NPs number, as it has been demonstrated for Au NPs.[242] Elemental analysis has been applied for detection of many NPs types in tissues/organs/biological fluids samples, such as QD,[243–245] titanium NPs,[246] Au NPs,[242,247,248] Ag NPs,[249,250] silica NPs,[211,251] or IONPs.[252,253] Importantly in case of IONPs, this technique does not differentiate between iron originated from NPs and endogenous one (in form of transferrin, ferritin or haemoglobin).[254] Therefore magnetometry techniques are considered a better alternative to elemental analysis or optical approaches for magnetic NPs quantification.[255]

As this analysis does not provide any spatial information about NPs localization it is normally preceded by visualization approaches. Moreover, it has to be mentioned that elemental analysis is unable to differentiate between metal species, and therefore does not distinguish elements confined within the nanomaterial from ions leached from the nanostructure.[229]

1.09.3.9 Magnetometry

Alternative to the elemental analysis, magnetometry techniques can provide quantitative and selective determination of MNPs in cells or tissues based on their magnetic properties. Among them, Electron Spin Resonance (ESR), Ferromagnetic Resonance (FMR) and ac (alternating current) magnetic susceptibility are the most popular ones.

ESR is a spectroscopy technique used for studying chemical species with unpaired electrons (including paramagnetic, ferri-/ferromagnetic and anti-ferromagnetic materials)[256] and therefore applicable for MNPs detection. Although ESR is more sensitive for MNPs than for endogenous iron containing proteins,[257] the proper differentiation between them is unattainable as it has been shown in case of superparamagnetic ferrofluids which contribute to the same resonance signal in the EPR spectra as Fe^{3+} ferritin ions.[258] The sample preparation is destructive but this method provides very high quantification sensitivity (ie, nM Fe g^{-1} tissue). Hence ESR served as a robust MNPs detection techniques in several studies.[257,259,260]

FMR is another spectroscopic technique basically consisted in EPR. However in this case dynamics of magnetization of unpaired electrons collectively coupled in a ferro- or ferrimagnetic lattice is followed instead of detecting resonance of individual electron spins.[261] Although not extensively applied its quantitatively and selectivity in *ex vivo* MNPs biodistribution studies have been confirmed.[234,262]

AC magnetic susceptibility is a technique based on the ac magnetic field application and the following recording of the resulting magnetization.[263] Normally the experiment is performed from cryogenic up to room temperatures what enables differentiation of MNPs with even not fully homogenous size and importantly the discrimination between tissue endogenous iron and exogenously delivered MNPs.[264] Besides, MNPs quantification is possible after incorporation into the protocol a collection of precisely prepared standards.[233] In terms of long term biodistribution studies the utility of ac magnetic susceptibility for the evaluation of MNPs transformation over time has been confirmed.[265] Because of its high sensitivity (order of 1 μg Fe g^{-1} dry tissue)[264] and selectivity

superior over traditional MNPs detection methods,[255] ac magnetic susceptibility has been applied in a variety of biodistribution studies.[22,233,234,265,266]

Magnetic measurements are sensitive, specific for transition metals and provide information about MNPs biodistribution from a substantial portion of tissue/organ sample. However as the measurements assess the bulk magnetic properties of the sample no information about the MNPs localization is obtained.[267] Therefore they are normally combined with other visualization approaches.

1.09.3.10 Conclusions

The variety and availability of detection methods for NPs biodistribution studies enable more and more comprehensive understanding of effects caused by NPs delivered *in vivo*. However a single technique is often deficient for unraveling all the questions regarding the NPs biodistribution within a body. Therefore for obtaining reliable information on NPs biodistribution a combination of different detection methods is recommended. *In vivo* approaches provide a non-invasive molecular imaging of NPs whose limited resolution can be overcome by following *ex vivo* studies of dissected organs/tissues. Successively, quantitative determination and subcellular NPs localization can be obtained by employing elemental analysis and electron microscopy studies, respectively. Moreover, in case of MNPs, magnetometry techniques seem to perfectly address the overtime MNPs transformation issues.

1.09.4 Toxicity

Nanoparticles exposure is not limited to NPs developed for biomedical applications; they are present in multiple consumer products such as cosmetic, processed foods, electronic items, etc. That is why, in parallel to investigations concerning the synthesis of new nanomaterials, testing the interactions of these materials with the living world is mandatory for the secure development of nanotechnology.

The special physicochemical properties of nanoparticles (NPs) that show great promise for biomedical applications, may also affect cellular physiology including viability and other critical functions. Apart from specific aspects of each type of NPs such as composition, charge and shape,[268] there are common features that may produce similar mechanisms by which they affect cellular homeostasis or viability.[269] The size of the NPs itself (nano) appears to cause several adverse effects. First of all, because they can reach places where larger particles cannot enter such as placental[270] or hematoencephalic barrier in some cases,[271] enter into cells and be accumulated in endosomes (increasing the local concentration) or in the nucleus.[272] Additionally the high surface/volume ratio increases the surface area available for interaction with signaling pathways or cellular components such as proteins and lipids.[273]

Despite the high number of toxicological studies, the impact assessment of NPs use remains unclear, because the results reported in the literature are ambiguous and the great variety in types of NPs, incubation conditions, assay or cells used, make impossible to compare between different studies.[269] To increase the understanding on this topic standardized protocols to be able to compare different studies are needed.

The toxicity of NPs includes short-term consequences such as loss of cell viability inducing cell death or /and long-term effects such as decreasing cell survival or cell proliferation, inhibiting growth due to cell cycle arrest or senescence, or even they may interfere in cell signaling pathways altering cell activity. Besides the great number of toxicological studies carried out *in vitro*, reliable results are only the ones obtained using different types of cells (different origin), a wide range of concentrations, incubation conditions and all sorts of assays that cover all the aspects that may be affected by NPs. In order to select the appropriate tests, it is important to understand what they really measure and their limitations. In this section we discuss the most popular and interesting assays currently used to determine toxicity *in vitro*.

1.09.4.1 Proliferation Assays

There are a variety of tests used to analyze the proliferation status of the cell. However, common tests that study the NPs effect on cell proliferation only provide evidence of a proliferation decrement if it is caused due to distortion of cell metabolism activity or cell division, besides NPs may affect cell proliferation for many other different reasons.

1.09.4.1.1 MTT

The MTT assay was the first rapid colorimetric assay developed for cell viability high screening in a 96-well format. This assay measures the reduction of yellow MTT (3-(4,5-dimethylthiazol-2-yl)-2,5-diphenyltetrazolium bromide) to an insoluble blue formazan product by mitochondrial succinate dehydrogenase.[274]

The MTT substrate is added to cells in culture, usually at a final concentration of 0.2–0.5 mg/mL, and incubated for 1–4 h. Then, the cells and formazan product are solubilized with an organic solvent (eg, isopropanol, DMSO, etc.) and absorbance at 570 nm is measured using a multiwell scanning spectrophotometer.[275]

When cells die they lose their ability to convert MTT into formazan, thus, color formation presumably serves as a marker of the viable cells. The MTT assay was developed as a non-radioactive alternative to tritiated thymidine incorporation into DNA for measuring cell proliferation[274] and has been widely used in academic labs for economic reasons and because of their degree of

precision and rapidity, no washing steps are needed. It is very useful for screening a large number of samples at the same time, as the first step to select the range of concentrations (LD50) and the most effective drugs. However, it has some problems and limitations.

Problems: Despite the fact this method was designed for proliferation and cytotoxicity assays, it measures the activity of a mitochondrial enzyme and the signal generated is dependent on the level of cell metabolism.[276] MTT reduction assays are often erroneously described as cell proliferation assay without the use of proper controls to confirm effects on metabolism.[277] Culture conditions may affect the metabolism and consequently the rate of MTT reduction into formazan. For example, in adherent cells metabolism may be reduced when growth is inhibited by contact in a confluence cell culture situation. On the other hand the metabolism may be increased when components of the NPs can be utilized by the cell as nutrients (Fe_3O_4, lipids, carbohydrates, etc.). Other adverse culture conditions are an altered pH or depletion of essential nutrients such as glucose.[278]

As a colorimetric assay, some substances can interfere with absorbance readings, enhancing the signal generating false results. The interference can be produced by the NPs,[279,280] the color of ligands or some medium compounds such as phenol red, which can be reduced using an acid solubilizing solution that changes the color of phenol red to yellow color that may have less interference.[281]

This test is not valid for some NPs (Carbon) because of interactions or absorption of the formazan product used in this assay.[282] This assay measures the product of a reduction reaction (formazan), so, reducing compounds such as paclitaxel, cisplatin, coenzyme A, DTT, or ascorbic acid, among others, may reduce MTT non-enzymatically[283–287] and the high levels of reactive oxygen species (ROS) produced by NPs incubation may alter redox equilibrium of the cell[288] increasing the absorbance values in assay wells independently of cell viability. The assay method must be considered as an endpoint assay because the formazan crystals can harm cells during exocytosis resulting cytotoxic.[289]

Improvements/tricks: Suspected chemical interference of NP should be confirmed by measuring absorbance values from control wells containing culture medium, MTT and various concentrations of the NPs without cells. A variety of formazan solubilizing methods (DMSO, SDS, organic solvents, acidified isopropanol, etc.) have been used to stabilize the color, avoid evaporation, and reduce interference by culture medium components.[290–292] It is possible to change maximum absorbance at other length in order to avoid interference using new tetrazolium compounds as substrates for the MTT assay, such as MTS[293] (absorbance maximum at 490–500 nm).

The amount of signal generated is dependent not only on the number of viable cells and their metabolic activity but also on several parameters including: the concentration of MTT and the incubation time. These parameters should be considered when optimizing the assay conditions to generate a sufficient amount of product that can be detected above background.

1.09.4.1.2 Alamar blue assay

This assay is similar to MTT; it measures the ability of metabolically active cells to convert resazurin (blue) to the molecule resorufin (bright red fluorescence) that can be measured in a plate reader on a fluorescence spectrophotometer (560ex/590em), on a UV–vis spectrophotometer (570 nm) or by flow cytometry.[294]

Problems: The enzymes that mediate the reduction are not well known, they may be mitochondrial or cytosolic and microsomal enzymes.[295] The extensive reduction of Alamar Blue may led to a final nonfluorescent product (hydroresorufin), and hence an underestimation of cellular activity. This test is similar to MTT, so do the problems. The differences for Alamar Blue assay are the higher sensitivity and the non-toxic reactants.[296] However, it has been observed a interference of the carbon NP itself in the fluorescence reading due to a quenching effect.[297]

1.09.4.1.3 Clonogenic assay

The clonogenic assay measures the capability of a single cell to form a colony (Fig. 6). It is a widely used experimental approach to test for the effects of drugs/genes on the growth and proliferative characteristics of cells *in vitro*. After incubation with NPs, the number of cells in each sample are counted and diluted to seed 100 cells per well. Depending on the size of the formed colonies, a 6-well plate or petri dishes (3–5 replicates of each) can be used. The incubation period varies from 1 to 3 weeks depending on the cell line, and it must be equivalent to at least 6 cell divisions to form sufficiently large clones to be visible with the naked eye. The colonies should be fixed, stained and counted.

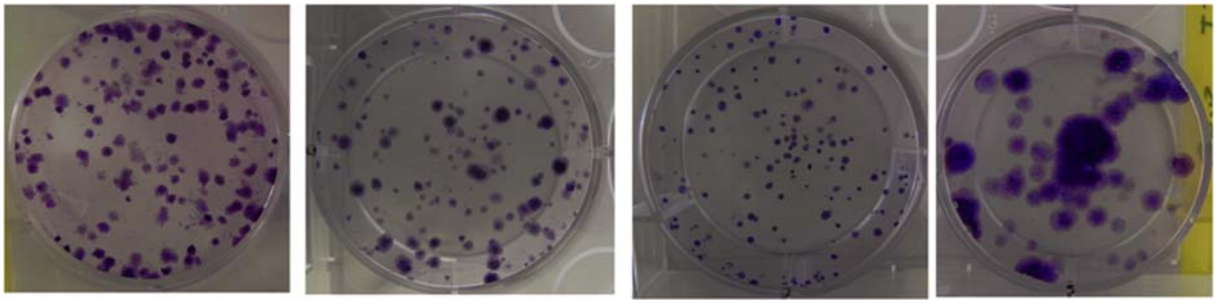

Fig. 6 Difference in the form of the colonies between cell lines. From left to right A549, B16, MiaPaca and MEF cells.

Problems: This assay is the gold standard to analyze cell viability but has the disadvantage that it is limited to adherent cells, additionally not all adherent cells are able to form colonies *in vitro* at low cell density where cell-to-cell contacts and self-produced growth factors are limited. On the other hand this assay is time-consuming and labor-intensive and shows high intra-individual variability because accurate quantification depends on the ability of the operator to visualize and count cell colonies precisely. Additionally, some colonies may be lost during staining and washing steps.

How to solve these problems: In order to reduce operator fatigue, the counting can be done using a stereomicroscope, and to reduce intra-individual variability it can be automatized using a digital imaging software or Image J.[298,299] Cells with low adherence may be grown in collagen matrix, however, some dyes stain collagen (eg, metilen blue), so different staining methods have been developed to reduce background. The most popular dye to direct counting is crystal violet and ethydium bromide which can be used with a UV illuminator.[300]

The major advantage of this method is the low interference of the NPs with the assay reactives, because the only possible interference is with the staining agent, which is used only to visualize automatically colonies or to take images, so the intensity is not important and the colonies can be counted without the necessity of be stained.

1.09.4.1.4 Cell division assay

This assay measures proliferation using flow cytometry. It consists on the incorporation of a fluorescent compound (CFSE) into cells for labeling and tracing them through successive divisions (Fig. 7). Cells are incubated with CFDA-SE (carboxyfluorescein diacetate succinimidyl ester), which diffuses into the cell where it is cleaved into CFSE, a highly fluorescent derivative that is retained in the cell. With each division the fluorescence results in the half and it can be monitored up to 8 divisions before the fluorescence decreases to background levels. In order have a reference value, a control of undivided cells is needed.[301,302]

Problems and solutions: This cell division assay is faster (2–7 days) and less labor-intensive than the clonogenic assay and allows researchers to analyze cell proliferation with other cell-live techniques such as multiparametric analysis, cell sorting, or immunophenotyping. However is more expensive and a flow cytometer is required. High concentration of CFSE is cytotoxic, so a titration of CFSE to obtain an optimal staining concentration is needed. Other fluorescent labels at different ex/em maximum have been developed, such as cell trace violet, yellow or far red to avoid interference with NPs or their ligands.[303]

1.09.4.1.5 EdU proliferation assay

5-ethynyl-2′-deoxyuridine (EdU) is a nucleoside analog dye-labeled which is incorporated into proliferating cells in their DNA during its synthesis, dyeing the cells with a bright fluorescent label that can be detected by flow cytometry or fluorescence microscopy and it can be used in cell cultures or tissues.

The original protocol was developed in the late 1950s and used ^{3}H-thymidine.[304] Due to the inconvenience of the radioactivity and poor sensitivity of this method, it was overtaken by more sensitive, nonradioactive methods, in particular by 5-bromo-2′-deoxyuridine, referred to as (BrdU).[305] The EdU assay is an alternative to traditional BrdU methods for detecting and quantitating newly synthesized DNA.[306] EdU assay is fast and reliable, it also can be used for detection s-phase cell cycle. This method can be performed with other dyes or antibodies even to detect intracellular antigens.

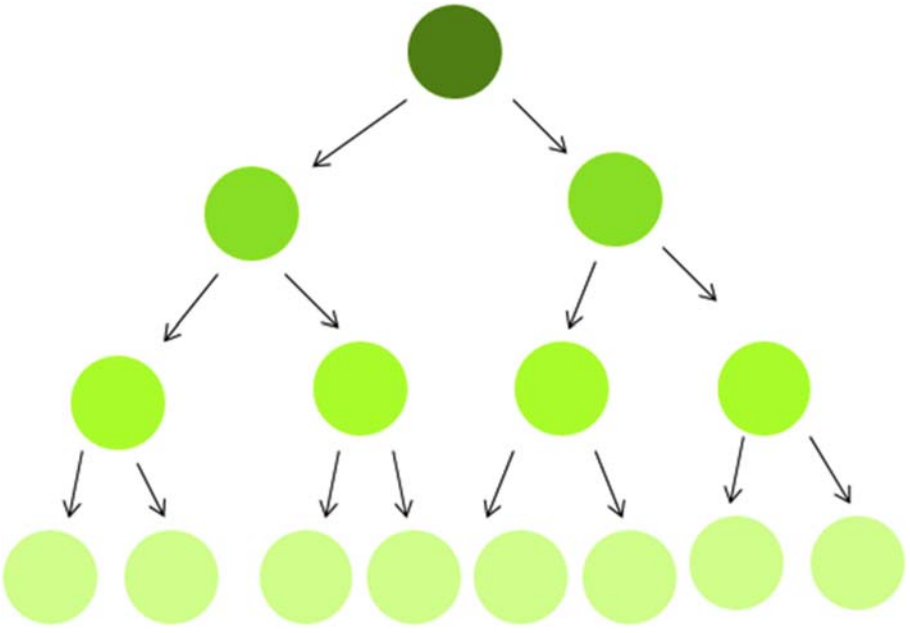

Fig. 7 Cell division assay: The fluorescence is half-decreased in each division.

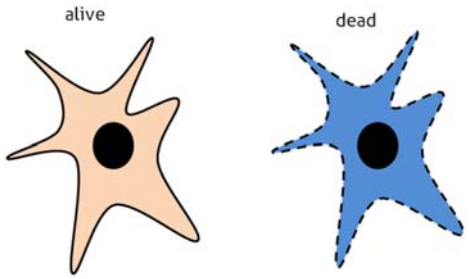

Fig. 8 Schematic representation of Tripan blue staining dead cells.

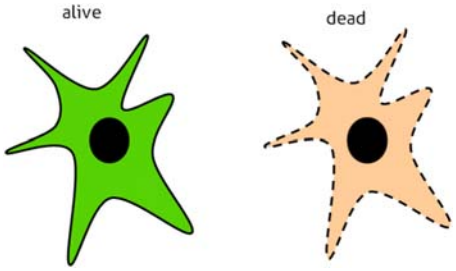

Fig. 9 Schematic representation of fluorescein diacetate staining alive cells.

1.09.4.2 Cell Membrane Permeability

One of the aspects to consider a cell dead is the loss of its membrane integrity. These methods are based on the principle that live cells prevent the entrance of certain dyes because they have intact membrane whereas dead cells are stained or vice versa. Usually the protocols consist on the incubation of the cells with the dye and further visualization.

Problems: The major limitation of these assays is that they cannot distinguish between healthy cells and the cells that are actually dying (in early stage) but still with the intact membrane or alive but losing cell functions, so the results may be underestimated.

1.09.4.2.1 Trypan blue

It is a widely used assay for staining dead cells. Trypan blue enters dead cells and stains their cytoplasm in blue (Fig. 8). Cell viability is determined by counting the unstained/stained cells with a microscope or other instruments. This method is easy and cheap and can be performed in all laboratories, because the only instrument needed is a light microscope.

1.09.4.2.2 Fluorescein diacetate

This compound freely penetrates intact cells where it is hydrolyzed to fluorescein (green), which is retained in the cell due to its polarity. In this method, the cytosol of live cells is stained green and can be detected using a fluorescence microscope or flow cytometer (Fig. 9).

1.09.4.2.3 Calcein acetoxymethyl

Calcein acetoxymethyl (Calcein-AM) is a substrate that passively crosses the cell membrane and in the cytosol is hydrolyzed by the enzyme esterase to a polar green-fluorescent product (calcein) that is retained into cells with intact membrane (Fig. 10). This

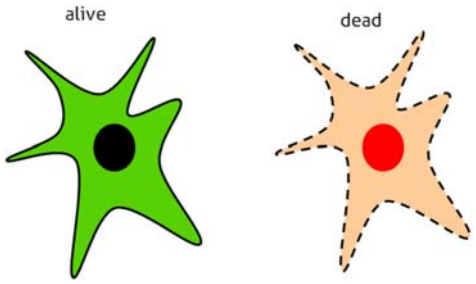

Fig. 10 Schematic representation of a combination of Calcein-AM (staining live cells) and a DNA intercalating agent (staining nucleus of dead cells).

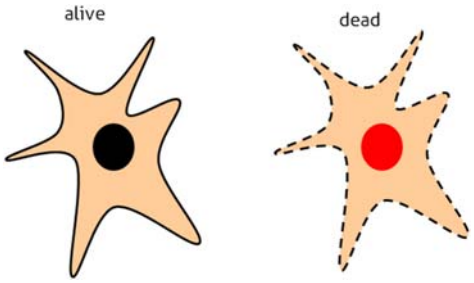

Fig. 11 Schematic representation of intercalating DNA agents staining nucleus of dead cells.

method not only analyses cell membrane integrity but also esterase activity. The fluorophore calcein displays good retention characteristics (several hours after fixation) and low pH sensitivity. This dye is usually used with ethidium homodimer-1 in commercial kits. The test is simple, fast and can be performed using a fluorescence microscope, flow cytometer or fluorescence microplate reader.

1.09.4.2.4 DNA intercalating fluorescent agents

Ethidium bromide, propidium iodine (PI) and 7- amino-actinomycin D (7-AAD) are three red fluorescent dyes that intercalate into DNA of membrane-damaged cells (Fig. 11). Ethidium bromide is considered carcinogenic, that is the reason why it is currently less used. PI and 7-AAD are both excited at 488 nm but the emission range(625 nm for PI and 655 nm for 7-AAD 655 nm), makes the difference, PI has significant spectral overlap with the fluorophore PE (Phycoerythrin) whereas 7-AAD no. Thus, 7-AAD is favorite in multiparameter staining experiments.

1.09.4.2.5 Lactate dehydrogenaze enzyme

The intracellular cytosolic enzyme lactate dehydrogenaze (LDH) can be released to the extracellular media by membrane-damaged cells. LDH activity measured in the culture medium can be used as an indicator of cell membrane integrity. LDH catalyzes the reduction of NAD+ to NADH by oxidation of lactate to piruvate. The formed NADH can be quantified with a second reaction where 2-(p-iodophenyl)-3-(p-nitrophenyll-5-tetrazolium) (p-INT) salt is reduced to a red formazan product in the presence of diaphorase or phenazine methosulfate (PMS) (Fig. 12). The colored product absorbs at 490–520 nm and can be detected spectrophotometrically, with a microplate reader for a large number of samples.[307]

Problem: The serum present in culture medium has considerable LDH-activity and phenol red indicator absorbs at 490 nm causing a significant decrease in sensitivity, thus serum and phenol red should be used also as a control to set up the base line (background). However, the main drawback is that some NPs (CdSe, Au and silicon) can inhibit the activity of LDH.[308]

1.09.4.3 Cell Death Mechanisms

1.09.4.3.1 Annexin-V

Apoptosis is a cell death mechanism characterized by keeping the plasma membrane intact. During apoptosis, phosphatidylserine (PS), a phospholipid usually found in the inner side of the plasma membrane, is translocated to the outer side resulting in its accessibility to annexin-V. This method consists on the incubation of cells with annexin-V joined to a fluorophore to detect apoptotic cell death by flow cytometry.[309]

Problems: When the membrane is damaged (necrotic cells), annexin-V can bind PS in the inner side, therefore in order to distinguish between necrotic and apoptotic cells the experiment should be carried out additionally with 7-AAD or PI (Fig. 13).

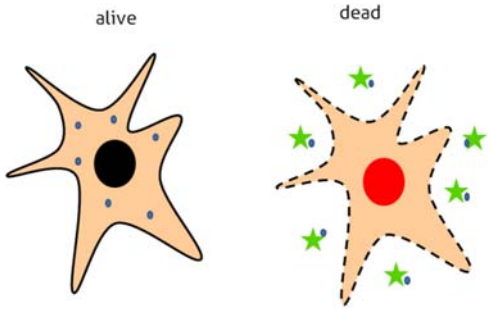

Fig. 12 Schematic representation of LDH activity detection in dead cells.

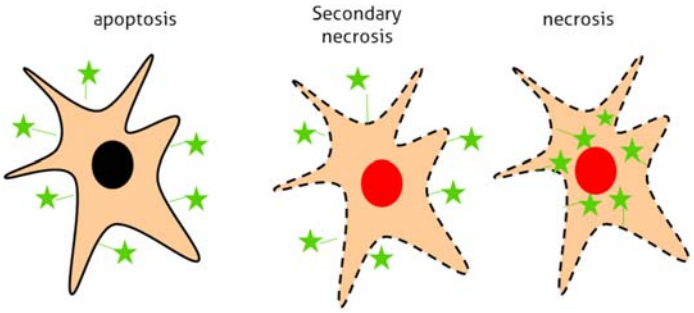

Fig. 13 Schematic representation of Annexin-V staining. In green annexine-V and in red PI/7AAD staining. An apoptotic cell is only stained with annexine-V, however a necrotic cell can be stained by both, because annexine-V not only can bind to PS in the outer side of the plasma membrane but also can enter into the cell and bind the inner PS.

1.09.4.3.2 ROS generation

Upon exposure to NPs, the most common cellular response involves the generation of ROS,[310,311] which has been described as one of the most relevant cytotoxic aspects caused by the internalization of NPs inside the cell.[312,313] ROS encompasses a number of reactive molecules and free radicals derived from molecular oxygen including superoxide ($O_2^{\bullet -}$), hydroperoxy radical ($HOO^{\bullet}$), hydroxyl radical ($OH^{\bullet}$), nitric oxide ($NO^{\bullet}$), hydrogen peroxide (H_2O_2), and peroxynitrite ($ONOO^-$).

The methods used to determine ROS consist on the use of oxidizable dyes that react with different intracellular ROS. The most widely used are fluorometric assays that offer very good sensitivity. Among them the most popular are dihydroethidium (2-HE) and derives forms of 2′-7′-dichlorofluorescein (DCF) such as H_2DCF-DA. 2-HE is oxidized specifically by superoxide anions and the product (red) intercalates with DNA.However, derives forms of 2′-7′-dichlorofluorescein, are oxidized by a wide range of ROS producing DCF (530 nm emission).[314] The fluorescent products can be detected using fluorescence microscopy, flow cytometry or a microplate reader. Some studies have also used oxidized colored compounds or other chemiluminescent substances.[315–317]

Problems: ROS production can be tolerated up to certain levels without side effects because most cells have defense mechanisms to reduce them, such as glutathione redox system.[318] The level of toleration depends on the cell type and it is not well defined.[319] Usually low and transient ROS increase can be tolerated by most cell types,[311] however, when the amount of ROS is excessive and persists over a long period of time, results in cell damage.[320–322] That is the reason why ROS generation results should be considered carefully. In order to analyse whether the effects are transient or long-lasting, ROS levels should be measured at different time points after NPs exposure and other parameters to determine their toxicity such as cell death or proliferation assays should also be determined. Besides, ROS generation assay does not indicate directly cell damage induced by NPs exposure, it is useful to determine the mechanism of a possible toxic effect. The major drawback of this method is that some NPs interfere with the assay.[323–325]

1.09.4.3.3 Loss of mitochondrial membrane potential

Several types of NPs target mitochondria[326,327] so, it is important to study its state. The mitochondrial membrane potential ($\Delta\psi_m$) is a signal of cell health, it provides the charge gradient required for ATP production, Ca^{2+} sequestration and regulates ROS production.[328,329] Loss of mitochondrial membrane potential is a signal of bioenergetic stress and may result in the release of apoptotic factors leading to cell death.

The mitochondrial perturbation can be measured using fluorescent probes [eg, tetramethylrhodamine ethyl ester (TMRE), Rhodamine 123 (Rhod123) and $DiOC_6(3)$ (3,3′-dihexyloxacarbocyanine iodide)].[330,331] These dyes are typically lipophilic positive charged compounds that accumulate into the mitochondrial membrane matrix space according to the Nernst equation (the more negative the mitochondria is charged the more accumulation of the probe).[332] When the mitochondria lost the differential of membrane potential the dye cannot be retained and the fluorescence decrease (**Fig. 14**). Fluorescent probe accumulation in mitochondria is analyzed by optical or confocal microscopy, flow cytometry, or fluorescent plate reader.

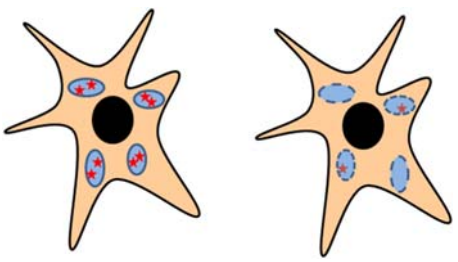

Fig. 14 Schematic representation of mitochondrial potential staining. The mitochondrias are simply represented in blue, the loss of mitochondrial potential in discontinuous line and the fluorescent probe in red.

Problems: High dye concentrations (50–100 nM to several micro molar) form aggregates into the mitochondria quenching some of the fluorescent emissions and once the dye is release, the fluorescence is unquenched increasing the fluorescent signal.[333]

1.09.4.3.4 Cell morphology

NPs occupy an intracellular volume usually inside endosomes or may be attached to the cell membrane. This can alter cellular morphology affecting the structure of cytoskeleton network.[334–337] The NPs effects on cytoskeletal deformations remains uninvestigated, however, as the cytoskeleton participates in cell division, intracellular signaling, exocytosis and endocytosis pathways, among others, NPs may affect them and the elastic and adherent properties of the cell.

On the other hand, the possible adverse effects may be transient, due to the fact the NPs concentration inside the cell decrease each division because they may be divided into both resultant cells and also released from the cell. It is important to evaluate NPs endocytic pathway and intracellular time-dependent location as well as assess the maximal cellular loading capacity without effects. The effect of NPs on cytoskeletal organization can be measured using different techniques:

- *Immunofluorescence analysis of cytoskeleton organization* using fluorescence (confocal/normal) microscopy. Cells are incubated with fluorophore conjugated phalloidin for F-actin and anti-tubulin antibodies for b-tubulin[336] and the results are compared to the control. The major drawback in this assay is the interpretation of the results; it is difficult to detect small differences that cannot be quantified.
- *Cell adhesion assay*[336]: Cells are seeded and sometimes stained with coomassie and the number of adhered cells are counted and refereed to the control.

1.09.4.4 Instrumentation for Detection of Fluorescent Probes

The majority of the fluorescent probes used to analyze cytotoxicity induced by NPs can be detected using different instruments with advantages and disadvantages each one:

- *Fluorescent microscopy*: The results are visual, easy to comprehend and using confocal microscopy, the intracellular location of the labeling can be determined. It is possible to quantify the number of cells affected and even the fluorescence intensity using image treatment software. However, it presents photooxidation problems because light exposure is difficult to control and may not be the same in all samples, for that reason quantifying is not reliable. It is the most-laboring and time-consuming technique.
- *Microplate spectrophotometry*: The advantage respect from fluorescence microscopy is that the photooxidation is the same in all samples, thus the results are comparable and the quantification is accurate. It is the quickest, easiest and less-laboring method, but it is less sensitive and exposure time cannot be modified. Additionally, the value obtained is the mean of the complete well and the results should be done respect to a control.
- *Flow cytometry*: Flow cytometer analyses cells individually and rapidly, the photooxidation is the same in all samples, and therefore quantification is reliable. The fluorescence measurement can be correlated with other aspects of the cells such as size and complexity or granularity and can be performed in the combination of multiparametric experiments.[50,338,339] Thanks to the advances in laser and fluorochrome technology it is possible to detect up to 18 colors at the same time. Nowadays there are more complex cytometers, which recover specific cells after measurement (sorters) or with a camera enclosed acting as a microscope which allows to differentiate between extra and intracellular labeling.

1.09.4.5 General Considerations for the Presence of NPs

The evaluation of nanomaterial safety is not standardized yet, thus, literature is full of conflicting reports, which show different degrees of toxicity with similar nanoparticles.

The NPs themselves may interfere with analytical techniques (fluorescence/absorbance, assay components or reactives, etc.).[340] They can bind to proteins and dyes[341,342] and alter the produced signal affecting their structure and/or function. The consequence can be an enhancement or a reduction in their absorbance or fluorescence. Carbon nanoparticles present the highest levels of interference with the cytotoxic assays because of their absorption ability,[297,343,344] however ionic nanoparticles also interfere with cytotoxic assays[323,325,345]

That is why the use of accurate controls (assay components, analyte and NPs) is needed in order to confirm whether the NPs interfere in the assay. It is becoming evident that these assays have to be standardized and optimized for NPs to avoid misleading results.

A multiparametric study is essential to obtain as much information as possible about the most of the aspects that may be affected by the presence of NPs.

1.09.5 Future Challenges

In spite of the good results already being obtained by nanoformulations for drug delivery and the improvement that these materials provide in comparison with the as-prepared drugs, there is always room for improvement. In this section we present a series of ideas

regarding trends that should be fulfilled in the long-term research associated to nanomaterials for drug delivery. Despite the inherent complexity associated to such a wide variety of nanomaterials being used in the drug industry, it is possible to define general future development trends for all of them.

1.09.5.1 Development of New Materials

It is important to continue developing new materials, synthetic or semi-synthetic with new properties, exploring alternative synthesis routes as the production by biological systems[346] or genetically modified cell factories.[347] Novel materials, which in principle would be used for non-biomedical applications, such as graphene, whose electrical properties led to an explosion of interest in high speed electronics,[348] are recently being tested for biomedical applications[349] such as carriers for anticancer drugs.[350] Regarding the development of new materials or structures, it will be of great importance to predict the advantages of new alternatives by theoretical approaches. Theoretical simulations will identify the properties of new materials, allowing an easier development of new materials. Currently, computational methods are being used to estimate solubility for drug development.[351] These methods allow the evaluation of physico-chemical properties of drugs before entering pre-clinical stages and Phase I safety evaluation. The analysis helps in the prediction of which compounds may fail in these stages, saving time and money in these expensive stages. Similar computational and mathematical tools should be developed for the evaluation of emerging nanomaterials in drug development. However, in many cases, these theoretical approaches are more difficult to achieve than in normal drugs, given the complexity of the new nanomaterials. Theoretical approaches would be able to predict, for example, the magnetic properties of nanoparticles in the frame of cancer treatment.[352,353] More sophisticated approaches should also focus on the interactions with the biological systems.[354]

1.09.5.2 Green Nanoscience

It is also necessary to pay attention to synthesis methods, trying to generate the less amount possible of waste products and approaching Green Chemistry routes.[355] Not just in the production of nanomaterials, but specially for those to be used in biomedical applications and the development of new drugs, we should make an effort to design materials and processes minimizing the hazards throughout the material's life cycle and approaching to a green nanoscience.[356] Synthesis routes should be improved to produce well-defined materials, with reproducible purity profiles, avoiding the use of hazardous materials and minimizing waste products.[356] Some examples of this are the production of silver nanoparticles with antimicrobial activity using leaf extract of *Mimusops elengi*,[357] or the production of AuNPs for drug delivery using water extracts of *Eclipta Alba* leaves.[358] The leaf extract reduces metal ion into metal nanoparticles, avoiding the use of stabilizing agent to prevent agglomeration and requiring less energy consumption than other chemical approaches.

1.09.5.3 Circular Economy

Although this is not commonly something scientists focus on, we should also think of using materials whose essential elements are guaranteed from a geopolitical perspective (Circular economy). Many new nanomaterials being studied in the frame of drug development, such as silver, gold or MNPs and QD, contain metals. Given their extensive utilization in a wide variety of applications and the increased consumer demand from a growing population worldwide, concerns over the security of supply and accessibility of these valuable elements has been raised.

According to a recent study on "Criticality of metals and metalloids,"[359] metals that are present in several nanomaterials for drug development are under different risks associated to imbalances between metal supply and demand in global markets. For example, Selenium, Cadmium and Indium, used as part of QD and Silver, used in the preparation of silver nanoparticles would have a high supply risk, as these metals have small geological resources relative to their current demands.[359] Gold, has high risk in environmental implications given the impacts related to its extraction and processing.[359] Lead, also part of some quantum dot formulations, has high risk to vulnerability to supply restriction, which is related to the degree to which suitable substitutes are unavailable.[359]

1.09.5.4 Biodegradable Products

One of the future challenges would be the production of biodegradable materials that could be degraded by the organism of metabolized and incorporated within the normal metabolic routes. Biodegradable materials would also allow the sustained drug release over a period of time within the target site. There are already several known polymers, both from synthetic or natural origin, with biocompatible properties and whose resorbability is achieved through natural pathways. Biodegradable synthetic polymers that form nanoparticles for drug delivery include, among others, poly(lactic acid) (PLA), poly(glycolic acid) (PGA), and their copolymers, poly(lactide-co-glycolide) (PLGA).[360] Other materials such as porous silicon nanoparticles self-destruct in short periods of time with no evidence of toxicity,[361] therefore releasing drugs in more efficient periods of time than other biodegradable polymers that take longer to degrade.[362] Biodegradable polymers of natural origin include, among others, collagen, that has been used to encapsulate gentamicin and is commercially available,[17] albumin,[363] hyaluronic acid[364] or chitosan.[365] Regarding the use of metal-containing nanoparticles such as silver, gold or MNPs and QD, it should be noted that the human

body has the mechanisms to transfer iron from MNPs into safe storage through normal metabolic routes,[22] however the mechanisms for assimilation or excretion of other metals are not so clear yet.

1.09.5.5 Development of New Applications

We should also investigate new applications with existing materials. A clear example of this would be the new applications being developed using MNPs. These materials have been widely studied as heat generators for cancer treatment by magnetic hyperthermia,[353,366] drug delivery systems[266] or contrast agents for MRI[367,368] and MPI.[369–371] Recently, novel applications of these materials include their use in wound healing,[372,373] stroke treatment,[374] regenerative medicine,[375] transient opening of the blood brain barrier,[376] tissue engineering,[377] non-invasive diagnosis of Alzheimer Disease using MRI,[378] diabetes treatment,[379] or parasite diagnosis.[380]

1.09.5.6 Transference to Industry

Once that the nanotechnology's *discovery* phase,[356] in which new properties, transformations of matter, devices, and applications was the main focus, has passed, the next step is the transference of all the knowledge acquired in the development of new nanomaterials to the industry. Reaching a commercial product involves the production of bigger amounts of materials, prioritizing processes whose scale up is possible, easy and economically viable. Retaining the nanomaterial quality obtained in the small batches usually produced in research laboratories is not easy once the production levels must be reached. Scaling up processes is usually associated with an increase in the inhomogeneities associated, for example, to the reagents concentration or temperature reached. All these inhomogeneities lead to a loose of control of the final product.

In order to solve this, reactions using continuous flow could have an advantage when compared with the use of big volume synthesis approaches. Some examples of continuous flow production have already been described for liposomes,[381] silver nanoparticles,[382] AuNPs[383] or MNPs.[384] The production of materials in larger scales is also associated with new safety concerns. Waste products should be reduced and safety of the material in the frame of the whole society and the environment should be assessed. All these developments should then be performed minimizing the adverse impact of nanomaterials in the environment, especially in biological systems.

Apart from the large scale production, the fundamental step for the obtention of commercially viable products is the approval by regulatory agencies. FDA is the regulatory agency of the US in charge, among other roles, of the regulation and supervision of new developed drugs. New drugs, especially those using nanotechnology developments, should be evaluated and approved by FDA confirming not only their low risk profile but also their benefit. Knowledge of the nanoformulations biocompatibility, biodistribution and production reliability are fundamental for their successful translation into commercially viable products. One of the main hurdles that new developments face is the lack of information concerning the fate of these materials once they have performed their purpose. However, the complex nature of some of the formulations, comprising several different parts such as an inorganic core and the surface coating, comprising a biocompatible molecule and optional bio-conjugates, makes more and more complicated to analyze the biodistribution and degradation of the different parts and also of the whole nanoformulation.[385] It has recently been pointed out that these complex structures should be seen as inorganic/organic/biological nanohybrids with complex distribution and degradation pathways.[385] It could be concluded that although more complex nanoformulations may have better performance than simple ones, it would be much easier for the simple nanoformulations to reach the clinical practice due to regulatory issues.

References

1. Peng, Q.; Dearden, A. K.; Crean, J.; Han, L.; Liu, S.; Wen, X.; De, S. New Materials Graphyne, Graphdiyne, Graphone, and Graphane: Review of Properties, Synthesis, and Application in Nanotechnology. *Nanotechnol. Sci. Appl.* **2014,** *7,* 1–29.
2. Forshaw, M.; Stadler, R.; Crawley, D.; Nikolić, K. A Short Review of Nanoelectronic Architectures. *Nanotechnology* **2004,** *15,* S220.
3. Schwierz, F. Graphene Transistors. *Nat. Nanotechnol.* **2010,** *5,* 487–496.
4. Serrano, E.; Rus, G.; García-Martínez, J. Nanotechnology for Sustainable Energy. *Renew. Sustain. Energy Rev.* **2009,** *13,* 2373–2384.
5. Sanchez, F.; Sobolev, K. Nanotechnology in Concrete—A Review. *Construct. Build Mater.* **2010,** *24,* 2060–2071.
6. Karn, B.; Kuiken, T.; Otto, M. Nanotechnology and In Situ Remediation: A Review of the Benefits and Potential Risks. *Environ. Health Perspect.* **2009,** *117,* 1823–1831.
7. Vaddiraju, S.; Tomazos, I.; Burgess, D. J.; Jain, F. C.; Papadimitrakopoulos, F. Emerging Synergy Between Nanotechnology and Implantable Biosensors: A Review. *Biosens. Bioelectron.* **2010,** *25,* 1553–1565.
8. Weiss, J.; Takhistov, P.; McClements, D. J. Functional Materials in Food Nanotechnology. *J. Food Sci.* **2006,** *71,* R107–R116.
9. Park, G. E.; Webster, T. J. A Review of Nanotechnology for the Development of Better Orthopedic Implants. *J. Biomed. Nanotechnol.* **2005,** *1,* 18–29.
10. Whitesides, G. M. The 'Right' Size in Nanobiotechnology. *Nat. Biotechnol.* **2003,** *21,* 1161–1165.
11. Potocnik, J. Commission Recommendation of 18 October 2011 on the Definition of Nanomaterial (2011/696/EU). *Off. J. Eur. Union* **2011,** *275,* 38–40.
12. Pokropivny, V. V.; Skorokhod, V. V. Classification of Nanostructures by Dimensionality and Concept of Surface Forms Engineering in Nanomaterial Science. *Mater. Sci. Eng. C* **2007,** *27,* 990–993.
13. Sharma, A.; Sharma, U. S. Liposomes in Drug Delivery: Progress and Limitations. *Int. J. Pharm.* **1997,** *154,* 123–140.
14. Allen, T. M.; Cullis, P. R. Drug Delivery Systems: Entering the Mainstream. *Science* **2004,** *303,* 1818–1822.
15. Soppimath, K. S.; Aminabhavi, T. M.; Kulkarni, A. R.; Rudzinski, W. E. Biodegradable Polymeric Nanoparticles as Drug Delivery Devices. *J. Control. Release* **2001,** *70,* 1–20.
16. Kumari, A.; Yadav, S. K.; Yadav, S. C. Biodegradable Polymeric Nanoparticles Based Drug Delivery Systems. *Colloids Surf. B* **2010,** *75,* 1–18.

17. Friberg, Ö.; Dahlin, L.-G.; Källman, J.; Kihlström, E.; Söderquist, B.; Svedjeholm, R. Collagen-Gentamicin Implant for Prevention of Sternal Wound Infection; Long-Term Follow-up of Effectiveness. *Interact. Cardiovasc. Thorac. Surg.* **2009,** *9,* 454–458.
18. Ghosh, P.; Han, G.; De, M.; Kim, C. K.; Rotello, V. M. Gold Nanoparticles in Delivery Applications. *Adv. Drug Deliv. Rev.* **2008,** *60,* 1307–1315.
19. Pillai, G. Nanomedicines for Cancer Therapy: An Update of FDA Approved and Those Under Various Stages of Development. *SOJ Pharm. Pharm. Sci.* **2014,** *1,* 13.
20. Gutierrez, L.; Costo, R.; Gruttner, C.; Westphal, F.; Gehrke, N.; Heinke, D.; Fornara, A.; Pankhurst, Q. A.; Johansson, C.; Veintemillas-Verdaguer, S.; Morales, M. P. Synthesis Methods to Prepare Single- and Multi-Core Iron Oxide Nanoparticles for Biomedical Applications. *Dalton Trans.* **2015,** *44,* 2943–2952.
21. Ruiz, A.; Mancebo, A.; Beola, L.; Sosa, I.; Gutierrez, L. Dose–Response Bioconversion and Toxicity Analysis of Magnetite Nanoparticles. *IEEE Magn. Lett.* **2016,** *7,* 1–5, 1502205.
22. Ruiz, A.; Gutierrez, L.; Caceres-Velez, P. R.; Santos, D.; Chaves, S. B.; Fascineli, M. L.; Garcia, M. P.; Azevedo, R. B.; Morales, M. P. Biotransformation of Magnetic Nanoparticles as a Function of Coating in a Rat Model. *Nanoscale* **2015,** *7,* 16321–16329.
23. Colombo, M.; Carregal-Romero, S.; Casula, M. F.; Gutiérrez, L.; Morales, M. P.; Böhm, I. B.; Heverhagen, J. T.; Prosperi, D.; Parak, W. J. Biological Applications of Magnetic Nanoparticles. *Chem. Soc. Rev.* **2012,** *41,* 4306–4334.
24. Yang, P.; Gai, S.; Lin, J. Functionalized Mesoporous Silica Materials for Controlled Drug Delivery. *Chem. Soc. Rev.* **2012,** *41,* 3679–3698.
25. Slowing, I. I.; Vivero-Escoto, J. L.; Wu, C.-W.; Lin, V. S. Y. Mesoporous Silica Nanoparticles as Controlled Release Drug Delivery and Gene Transfection Carriers. *Adv. Drug Deliv. Rev.* **2008,** *60,* 1278–1288.
26. Zrazhevskiy, P.; Sena, M.; Gao, X. Designing Multifunctional Quantum Dots for Bioimaging, Detection, and Drug Delivery. *Chem. Soc. Rev.* **2010,** *39,* 4326–4354.
27. Grazu, V.; Moros, M.; Sánchez-Espinel, C. Nanocarriers as Nanomedicines: Design Concepts and Recent Advances. *Nanobiotechnology* **2012,** *4,* 337–385.
28. Bertrand, N.; Wu, J.; Xu, X.; Kamaly, N.; Farokhzad, O. C. Cancer Nanotechnology: The Impact of Passive and Active Targeting in the Era of Modern Cancer Biology. *Adv. Drug Deliv. Rev.* **2014,** *66,* 2–25.
29. Lohse, S. E.; Murphy, C. J. Applications of Colloidal Inorganic Nanoparticles: From Medicine to Energy. *J. Am. Chem. Soc.* **2012,** *134,* 15607–15620.
30. Mahajan, A.; Goh, V.; Basu, S.; Vaish, R.; Weeks, A. J.; Thakur, M. H.; Cook, G. J. Bench to Bedside Molecular Functional Imaging in Translational Cancer Medicine: To Image or to Imagine? *Clin. Radiol.* **2015,** *70,* 1060–1082.
31. Hay, M.; Thomas, D. W.; Craighead, J. L.; Economides, C.; Rosenthal, J. Clinical Development Success Rates for Investigational Drugs. *Nat. Biotechnol.* **2014,** *32,* 40–51.
32. Roco, M. C.; Mirkin, C. A.; Hersam, M. C. Nanotechnology Research Directions for Societal Needs in 2020: Summary of International Study. *J. Nanopart. Res.* **2011,** *13,* 897–919.
33. Duncan, R.; Gaspar, R. Nanomedicine(s) Under the Microscope. *Mol. Pharm.* **2011,** *8,* 2101–2141.
34. He, C.; Lu, J.; Lin, W. Hybrid Nanoparticles for Combination Therapy of Cancer. *J. Control. Release* **2015,** *219,* 224–236.
35. Barenholz, Y. C. Doxil®—The First FDA-Approved Nano-Drug: Lessons Learned. *J. Control. Release* **2012,** *160,* 117–134.
36. Fox, J. L. FDA Advisors Okay NeXstar's DaunoXome. *Nat. Biotechnol.* **1995,** *13,* 635–636.
37. Mihatsch, M. J.; Kyo, M.; Morozumi, K.; Yamaguchi, Y.; Nickeleit, V.; Ryffel, B. The Side-Effects of Ciclosporine-A and Tacrolimus. *Clin. Nephrol.* **1998,** *49,* 356–363.
38. Harries, M.; Ellis, P.; Harper, P. Nanoparticle Albumin-Bound Paclitaxel for Metastatic Breast Cancer. *J. Clin. Oncol.* **2005,** *23,* 7768–7771.
39. Camardo, J. The Rapamune era of Immunosuppression 2003: The Journey From the Laboratory to Clinical Transplantation. *Transplant. Proc.* **2003,** *35,* S18–S24.
40. Clement, O.; Siauve, N.; Cuénod, C.-A.; Frija, G. Liver Imaging With Ferumoxides (Feridex(R)): Fundamentals, Controversies, and Practical Aspects. *Top. Magn. Reson. Imaging* **1998,** *9,* 167–182.
41. Hayman, M. L. The Emerging Product and Patent Landscape for Nanosilver Containing Medical Devices. *Nanotechnol. Law Bus.* **2009,** *6,* 148–158.
42. Ogle, O. E.; Byles, N. Nanotechnology in Dentistry Today. *West Indian Med. J.* **2014,** *63,* 344–348.
43. Mu, L.; Sprando, R. L. Application of Nanotechnology in Cosmetics. *Pharm. Res.* **2010,** *27,* 1746–1749.
44. Sambandan, D. R.; Ratner, D. Sunscreens: An Overview and Update. *J. Am. Acad. Dermatol.* **2011,** *64,* 748–758.
45. Núñez-Lozano, R.; Cano, M.; Pimentel, B.; de la Cueva-Méndez, G. 'Smartening' Anticancer Therapeutic Nanosystems Using Biomolecules. *Curr. Opin. Biotechnol.* **2015,** *35,* 135–140.
46. Ganta, S.; Devalapally, H.; Shahiwala, A.; Amiji, M. A Review of Stimuli-Responsive Nanocarriers for Drug and Gene Delivery. *J. Control. Release* **2008,** *126,* 187–204.
47. Lu, Y.; Sun, W.; Gu, Z. Stimuli-Responsive Nanomaterials for Therapeutic Protein Delivery. *J. Control. Release* **2014,** *194,* 1–19.
48. Golovin, Y. I.; Gribanovsky, S. L.; Golovin, D. Y.; Klyachko, N. L.; Majouga, A. G.; Master, A. M.; Sokolsky, M.; Kabanov, A. V. Towards Nanomedicines of the Future: Remote Magneto-Mechanical Actuation of Nanomedicines by Alternating Magnetic Fields. *J. Control. Release* **2015,** *219,* 43–60.
49. Moros, M.; Ambrosone, A.; Stepien, G.; Fabozzi, F.; Marchesano, V.; Castaldi, A.; Tino, A.; de la Fuente, J. M.; Tortiglione, C. Deciphering Intracellular Events Triggered by Mild Magnetic Hyperthermia in vitro and In Vivo. *Nanomedicine* **2015,** *10,* 2167–2183.
50. Pérez-Hernández, M.; del Pino, P.; Mitchell, S. G.; Moros, M.; Stepien, G.; Pelaz, B.; Parak, W. J.; Gálvez, E. M.; Pardo, J.; de la Fuente, J. M. Dissecting the Molecular Mechanism of Apoptosis During Photothermal Therapy Using Gold Nanoprisms. *ACS Nano* **2015,** *9,* 52–61.
51. Abouelmagd, S. A.; Hyun, H.; Yeo, Y. Extracellularly Activatable Nanocarriers for Drug Delivery to Tumors. *Expert Opin. Drug Deliv.* **2014,** *11,* 1601–1618.
52. Yoo, J.-W.; Doshi, N.; Mitragotri, S. Adaptive Micro and Nanoparticles: Temporal Control Over Carrier Properties to Facilitate Drug Delivery. *Adv. Drug Deliv. Rev.* **2011,** *63,* 1247–1256.
53. Cabral, H.; Matsumoto, Y.; Mizuno, K.; Chen, Q.; Murakami, M.; Kimura, M.; Terada, Y.; Kano, M. R.; Miyazono, K.; Uesaka, M.; Nishiyama, N.; Kataoka, K. Accumulation of Sub-100 nm Polymeric Micelles in Poorly Permeable Tumours Depends on Size. *Nat. Nanotechnol.* **2011,** *6,* 815–823.
54. Stocke, N. A.; Arnold, S. M.; Zach Hilt, J. Responsive Hydrogel Nanoparticles for Pulmonary Delivery. *J. Drug Delivery Sci. Technol.* **2015,** *29,* 143–151.
55. Wong, C.; Stylianopoulos, T.; Cui, J.; Martin, J.; Chauhan, V. P.; Jiang, W.; Popović, Z.; Jain, R. K.; Bawendi, M. G.; Fukumura, D. Multistage Nanoparticle Delivery System for Deep Penetration Into Tumor Tissue. *Proc. Natl. Acad. Sci.* **2011,** *108,* 2426–2431.
56. Chen, Y.-C.; Liao, L.-C.; Lu, P.-L.; Lo, C.-L.; Tsai, H.-C.; Huang, C.-Y.; Wei, K.-C.; Yen, T.-C.; Hsiue, G.-H. The Accumulation of Dual pH and Temperature Responsive Micelles in Tumors. *Biomaterials* **2012,** *33,* 4576–4588.
57. Tong, R.; Hemmati, H. D.; Langer, R.; Kohane, D. S. Photoswitchable Nanoparticles for Triggered Tissue Penetration and Drug Delivery. *J. Am. Chem. Soc.* **2012,** *134,* 8848–8855.
58. McNeeley, K. M.; Karathanasis, E.; Annapragada, A. V.; Bellamkonda, R. V. Masking and Triggered Unmasking of Targeting Ligands on Nanocarriers to Improve Drug Delivery to Brain Tumors. *Biomaterials* **2009,** *30,* 3986–3995.
59. Carlisle, R.; Choi, J.; Bazan-Peregrino, M.; Laga, R.; Subr, V.; Kostka, L.; Ulbrich, K.; Coussios, C.-C.; Seymour, L. W. Enhanced Tumor Uptake and Penetration of Virotherapy Using Polymer Stealthing and Focused Ultrasound. *J. Natl. Cancer Inst.* **2013,** *105* (22), 1701–1710, 20.
60. Lee, E. S.; Gao, Z.; Kim, D.; Park, K.; Kwon, I. C.; Bae, Y. H. Super pH-Sensitive Multifunctional Polymeric Micelle for Tumor pHe Specific TAT Exposure and Multidrug Resistance. *J. Control. Release* **2008,** *129,* 228–236.
61. Tang, Z.; Lim, C.-K.; Palafox-Hernandez, J. P.; Drew, K. L. M.; Li, Y.; Swihart, M. T.; Prasad, P. N.; Walsh, T. R.; Knecht, M. R. Triggering Nanoparticle Surface Ligand Rearrangement via External Stimuli: Light-Based Actuation of Biointerfaces. *Nanoscale* **2015,** *7,* 13638–13645.
62. Yao, L.; Daniels, J.; Moshnikova, A.; Kuznetsov, S.; Ahmed, A.; Engelman, D. M.; Reshetnyak, Y. K.; Andreev, O. A. pHLIP Peptide Targets Nanogold Particles to Tumors. *Proc. Natl. Acad. Sci.* **2013,** *110,* 465–470.
63. Fratila, R. M.; Mitchell, S. G.; del Pino, P.; Grazu, V.; de la Fuente, J. M. Strategies for the Biofunctionalization of Gold and Iron Oxide Nanoparticles. *Langmuir* **2014,** *30,* 15057–15071.

64. Fernández-Lorente, G.; Lopez-Gallego, F.; Bolivar, J. M.; Rocha-Martin, J.; Moreno-Perez, S.; Guisan, J. M. Immobilization of Proteins on Highly Activated Glyoxyl Supports: Dramatic Increase of the Enzyme Stability via Multipoint Immobilization on Pre-Existing Carriers. *Curr. Org. Chem.* **2015,** *19,* 1719–1731.
65. Parolo, C.; de la Escosura-Muñiz, A.; Polo, E.; Grazú, V.; de la Fuente, J. M.; Merkoçi, A. Design, Preparation, and Evaluation of a Fixed-Orientation Antibody/Gold-Nanoparticle Conjugate as an Immunosensing Label. *ACS Appl. Mater. Interfaces* **2013,** *5,* 10753–10759.
66. Puertas, S.; de Gracia Villa, M.; Mendoza, E.; Jiménez-Jorquera, C.; de la Fuente, J. M.; Fernández-Sánchez, C.; Grazú, V. Improving Immunosensor Performance Through Oriented Immobilization of Antibodies on Carbon Nanotube Composite Surfaces. *Biosens. Bioelectron.* **2013,** *43,* 274–280.
67. Puertas, S.; Moros, M.; Fernández-Pacheco, R.; Ibarra, M. R.; Grazú, V.; de la Fuente, J. M. Designing Novel Nano-Immunoassays: Antibody Orientation Versus Sensitivity. *J. Phys. D Appl. Phys.* **2010,** *43,* 474012.
68. Conde, J.; Ambrosone, A.; Sanz, V.; Hernandez, Y.; Marchesano, V.; Tian, F.; Child, H.; Berry, C. C.; Ibarra, M. R.; Baptista, P. V.; Tortiglione, C.; de la Fuente, J. M. Design of Multifunctional Gold Nanoparticles for in vitro and in vivo Gene Silencing. *ACS Nano* **2012,** *6,* 8316–8324.
69. Conde, J.; Tian, F.; Hernández, Y.; Bao, C.; Cui, D.; Janssen, K.-P.; Ibarra, M. R.; Baptista, P. V.; Stoeger, T.; de la Fuente, J. M. In Vivo Tumor Targeting via Nanoparticle-Mediated Therapeutic siRNA Coupled to Inflammatory Response in Lung Cancer Mouse Models. *Biomaterials* **2013,** *34,* 7744–7753.
70. Wang, D.; Xu, Z.; Yu, H.; Chen, X.; Feng, B.; Cui, Z.; Lin, B.; Yin, Q.; Zhang, Z.; Chen, C.; Wang, J.; Zhang, W.; Li, Y. Treatment of Metastatic Breast Cancer by Combination of Chemotherapy and Photothermal Ablation Using Doxorubicin-Loaded DNA Wrapped Gold Nanorods. *Biomaterials* **2014,** *35,* 8374–8384.
71. Adhikary, R. R.; More, P.; Banerjee, R. Smart Nanoparticles as Targeting Platforms for HIV Infections. *Nanoscale* **2015,** *7,* 7520–7534.
72. Ramana, L. N.; Anand, A. R.; Sethuraman, S.; Krishnan, U. M. Targeting Strategies for Delivery of Anti-HIV Drugs. *J. Control. Release* **2014,** *192,* 271–283.
73. Reddy, L. H.; Couvreur, P. Nanotechnology for Therapy and Imaging of Liver Diseases. *J. Hepatol.* **2011,** *55,* 1461–1466.
74. Mazibuko, Z.; Choonara, Y. E.; Kumar, P.; Du Toit, L. C.; Modi, G.; Naidoo, D.; Pillay, V. A Review of the Potential Role of Nano-Enabled Drug Delivery Technologies in Amyotrophic Lateral Sclerosis: Lessons Learned from Other Neurodegenerative Disorders. *J. Pharm. Sci.* **2015,** *104,* 1213–1229.
75. Kogan, M. J.; Bastus, N. G.; Amigo, R.; Grillo-Bosch, D.; Araya, E.; Turiel, A.; Labarta, A.; Giralt, E.; Puntes, V. F. Nanoparticle-Mediated Local and Remote Manipulation of Protein Aggregation. *Nano Lett.* **2006,** *6,* 110–115.
76. Neely, A.; Perry, C.; Varisli, B.; Singh, A. K.; Arbneshi, T.; Senapati, D.; Kalluri, J. R.; Ray, P. C. Ultrasensitive and Highly Selective Detection of Alzheimer's Disease Biomarker Using Two-Photon Rayleigh Scattering Properties of Gold Nanoparticle. *ACS Nano* **2009,** *3,* 2834–2840.
77. Hu, K.; Shi, Y.; Jiang, W.; Han, J.; Huang, S.; Jiang, X. Lactoferrin Conjugated PEG-PLGA Nanoparticles for Brain Delivery: Preparation, Characterization and Efficacy in Parkinson's Disease. *Int. J. Pharm.* **2011,** *415,* 273–283.
78. Wen, Z.; Yan, Z.; Hu, K.; Pang, Z.; Cheng, X.; Guo, L.; Zhang, Q.; Jiang, X.; Fang, L.; Lai, R. Odorranalectin-Conjugated Nanoparticles: Preparation, Brain Delivery and Pharmacodynamic Study on Parkinson's Disease Following Intranasal Administration. *J. Control. Release* **2011,** *151,* 131–138.
79. Newland, B.; Newland, H.; Werner, C.; Rosser, A.; Wang, W. Prospects for Polymer Therapeutics in Parkinson's Disease and Other Neurodegenerative Disorders. *Prog. Polym. Sci.* **2015,** *44,* 79–112.
80. Godinho, B. M. D. C.; Ogier, J. R.; Darcy, R.; O'Driscoll, C. M.; Cryan, J. F. Self-Assembling Modified β-Cyclodextrin Nanoparticles as Neuronal siRNA Delivery Vectors: Focus on Huntington's Disease. *Mol. Pharm.* **2013,** *10,* 640–649.
81. Stachowiak, E. K.; Roy, I.; Lee, Y.-W.; Capacchietti, M.; Aletta, J. M.; Prasad, P. N.; Stachowiak, M. K. Targeting Novel Integrative Nuclear FGFR1 Signaling by Nanoparticle-Mediated Gene Transfer Stimulates Neurogenesis in the Adult Brain. *Integr. Biol.* **2009,** *1,* 394–403.
82. Denora, N.; Trapani, A.; Laquintana, V.; Lopedota, A.; Trapani, G. Recent Advances in Medicinal Chemistry and Pharmaceutical Technology—Strategies for Drug Delivery to the Brain. *Curr. Top. Med. Chem.* **2009,** *9,* 182–196.
83. Ohtsuki, S.; Terasaki, T. Contribution of Carrier-Mediated Transport Systems to the Blood–Brain Barrier as a Supporting and Protecting Interface for the Brain; Importance for CNS Drug Discovery and Development. *Pharm. Res.* **2007,** *24,* 1745–1758.
84. Gromnicova, R.; Davies, H. A.; Sreekanthreddy, P.; Romero, I. A.; Lund, T.; Roitt, I. M.; Phillips, J. B.; Male, D. K. Glucose-Coated Gold Nanoparticles Transfer Across Human Brain Endothelium and Enter Astrocytes In Vitro. *PLoS One* **2013,** *8,* e81043.
85. Gromnicova, R.; Yilmaz, C. U.; Orhan, N.; Kaya, M.; Davies, H.; Williams, P.; Romero, I. A.; Sharrack, B.; Male, D. Localization and Mobility of Glucose-Coated Gold Nanoparticles Within the Brain. *Nanomedicine* **2016,** *11,* 617–625.
86. Jiang, X.; Xin, H.; Ren, Q.; Gu, J.; Zhu, L.; Du, F.; Feng, C.; Xie, Y.; Sha, X.; Fang, X. Nanoparticles of 2-Deoxy-D-Glucose Functionalized Poly (Ethylene Glycol)-co-Poly (Trimethylene Carbonate) for Dual-Targeted Drug Delivery in Glioma Treatment. *Biomaterials* **2014,** *35,* 518–529.
87. Georgieva, J. V.; Hoekstra, D.; Zuhorn, I. S. Smuggling Drugs Into the Brain: An Overview of Ligands Targeting Transcytosis for Drug Delivery Across the Blood–Brain Barrier. *Pharmaceutics* **2014,** *6,* 557–583.
88. Masserini, M. Nanoparticles for Brain Drug Delivery. *ISRN Biochem.* **2013,** *2013,* 238428.
89. Madureira, A. R.; Pereira, A.; Pintado, M. Current State on the Development of Nanoparticles for Use Against Bacterial Gastrointestinal Pathogens. Focus on Chitosan Nanoparticles Loaded With Phenolic Compounds. *Carbohydr. Polym.* **2015,** *130,* 429–439.
90. Serra, P.; Santamaria, P. Nanoparticle-Based Autoimmune Disease Therapy. *Clin. Immunol.* **2015,** *160,* 3–13.
91. Clemente-Casares, X.; Santamaria, P. Nanomedicine in Autoimmunity. *Immunol. Lett.* **2014,** *158,* 167–174.
92. Reimondez-Troitiño, S.; Csaba, N.; Alonso, M. J.; de la Fuente, M. Nanotherapies for the Treatment of Ocular Diseases. *Eur. J. Pharm. Biopharm.* **2015,** *95* (Pt B), 279–293.
93. Alai, M. S.; Lin, W. J.; Pingale, S. S. Application of Polymeric Nanoparticles and Micelles in Insulin Oral Delivery. *J. Food Drug Anal.* **2015,** *23,* 351–358.
94. Pham, D.-D.; Fattal, E.; Tsapis, N. Pulmonary Drug Delivery Systems for Tuberculosis Treatment. *Int. J. Pharm.* **2015,** *478,* 517–529.
95. Di Gioia, S.; Trapani, A.; Castellani, S.; Carbone, A.; Belgiovine, G.; Craparo, E. F.; Puglisi, G.; Cavallaro, G.; Trapani, G.; Conese, M. Nanocomplexes for Gene Therapy of Respiratory Diseases: Targeting and Overcoming the Mucus Barrier. *Pulm. Pharmacol. Ther.* **2015,** *34,* 8–24.
96. Hua, S.; Marks, E.; Schneider, J. J.; Keely, S. Advances in Oral Nano-Delivery Systems for Colon Targeted Drug Delivery in Inflammatory Bowel Disease: Selective Targeting to Diseased Versus Healthy Tissue. *Nanomed.: Nanotechnol., Biol. Med.* **2015,** *11,* 1117–1132.
97. Gainza, G.; Villullas, S.; Pedraz, J. L.; Hernandez, R. M.; Igartua, M. Advances in Drug Delivery Systems (DDSs) to Release Growth Factors for Wound Healing and Skin Regeneration. *Nanomedicine* **2015,** *11,* 1551–1573.
98. Aditya, N. P.; Vathsala, P. G.; Vieira, V.; Murthy, R. S. R.; Souto, E. B. Advances in Nanomedicines for Malaria Treatment. *Adv. Colloid Interface Sci.* **2013,** *201–202,* 1–17.
99. Gutierrez, V.; Seabra, A. B.; Reguera, R. M.; Khandare, J.; Calderon, M. New Approaches From Nanomedicine for Treating Leishmaniasis. *Chem. Soc. Rev.* **2016,** *45,* 152–168.
100. Lee, H.; Lee, M.-Y.; Bhang, S. H.; Kim, B.-S.; Kim, Y. S.; Ju, J. H.; Kim, K. S.; Hahn, S. K. Hyaluronate–Gold Nanoparticle/Tocilizumab Complex for the Treatment of Rheumatoid Arthritis. *ACS Nano* **2014,** *8,* 4790–4798.
101. Gutierrez, L.; Mejias, R.; Lazaro, F. J.; Serna, C. J.; Barber, D. F.; Morales, M. P. Effect of Anesthesia on Magnetic Nanoparticle Biodistribution After Intravenous Injection. *IEEE Trans. Magn.* **2013,** *49,* 398–401.
102. Hahn, M. A.; Singh, A. K.; Sharma, P.; Brown, S. C.; Moudgil, B. M. Nanoparticles as Contrast Agents for In-Vivo Bioimaging: Current Status and Future Perspectives. *Anal. Bioanal. Chem.* **2011,** *399,* 3–27.
103. Ntziachristos, V. Going Deeper Than Microscopy: The Optical Imaging Frontier in Biology. *Nat. Methods* **2010,** *7,* 603–614.
104. Peng, H.-S.; Chiu, D. T. Soft Fluorescent Nanomaterials for Biological and Biomedical Imaging. *Chem. Soc. Rev.* **2015,** *44,* 4699–4722.
105. Ntziachristos, V.; Yodh, A. G.; Schnall, M.; Chance, B. Concurrent MRI and Diffuse Optical Tomography of Breast After Indocyanine Green Enhancement. *Proc. Natl. Acad. Sci. U. S. A.* **2000,** *97,* 2767–2772.

106. Licha, K.; Riefke, B.; Ntziachristos, V.; Becker, A.; Chance, B.; Semmler, W. Hydrophilic Cyanine Dyes as Contrast Agents for Near-Infrared Tumor Imaging: Synthesis, Photophysical Properties and Spectroscopic in vivo Characterization. *Photochem. Photobiol.* **2000,** *72,* 392–398.
107. Sima, P. D.; Kanofsky, J. R. Cyanine Dyes as Protectors of K562 Cells From Photosensitized Cell Damage. *Photochem. Photobiol.* **2000,** *71,* 413–421.
108. Yi, X.; Wang, F.; Qin, W.; Yang, X.; Yuan, J. Near-Infrared Fluorescent Probes in Cancer Imaging and Therapy: An Emerging Field. *Int. J. Nanomedicine* **2014,** *9,* 1347–1365.
109. He, X.; Wang, K.; Cheng, Z. In Vivo Near-Infrared Fluorescence Imaging of Cancer With Nanoparticle-Based Probes. *Wiley Interdiscip. Rev. Nanomed. Nanobiotechnol.* **2010,** *2,* 349–366.
110. Hintersteiner, M.; Enz, A.; Frey, P.; Jaton, A.-L.; Kinzy, W.; Kneuer, R.; Neumann, U.; Rudin, M.; Staufenbiel, M.; Stoeckli, M.; Wiederhold, K.-H.; Gremlich, H.-U. In Vivo Detection of Amyloid-Beta Deposits by Near-Infrared Imaging Using an Oxazine-Derivative Probe. *Nat. Biotechnol.* **2005,** *23,* 577–583.
111. Pauli, J.; Brehm, R.; Spieles, M.; Kaiser, W. A.; Hilger, I.; Resch-Genger, U. Novel Fluorophores as Building Blocks for Optical Probes for in vivo Near Infrared Fluorescence (NIRF) Imaging. *J. Fluoresc.* **2010,** *20,* 681–693.
112. Pauli, J.; Vag, T.; Haag, R.; Spieles, M.; Wenzel, M.; Kaiser, W. A.; Resch-Genger, U.; Hilger, I. An in vitro Characterization Study of New Near Infrared Dyes for Molecular Imaging. *Eur. J. Med. Chem.* **2009,** *44,* 3496–3503.
113. Rohand, T.; Qin, W.; Boens, N.; Dehaen, W. Palladium-Catalyzed Coupling Reactions for the Functionalization of BODIPY Dyes With Fluorescence Spanning the Visible Spectrum. *Eur. J. Org. Chem.* **2006,** *2006* (20), 4658–4663.
114. Gao, J.; Chen, K.; Xie, R.; Xie, J.; Lee, S.; Cheng, Z.; Peng, X.; Chen, X. Ultrasmall Near-Infrared Non-Cadmium Quantum Dots for in vivo Tumor Imaging. *Small* **2010,** *6,* 256–261.
115. Tavares, A. J.; Chong, L.; Petryayeva, E.; Algar, W. R.; Krull, U. J. Quantum Dots as Contrast Agents for in vivo Tumor Imaging: Progress and Issues. *Anal. Bioanal. Chem.* **2011,** *399,* 2331–2342.
116. Zheng, J.; Nicovich, P. R.; Dickson, R. M. Highly Fluorescent Noble Metal Quantum Dots. *Annu. Rev. Phys. Chem.* **2008,** *22,* 4109.
117. Kobayashi, H.; Hama, Y.; Koyama, Y.; Barrett, T.; Regino, C. A. S.; Urano, Y.; Choyke, P. L. Simultaneous Multicolor Imaging of Five Different Lymphatic Basins Using Quantum Dots. *Nano Lett.* **2007,** *7,* 1711–1716.
118. Derfus, A. M.; Chan, W. C. W.; Bhatia, S. N. Probing the Cytotoxicity of Semiconductor Quantum Dots. *Nano Lett.* **2004,** *4,* 11–18.
119. Ballou, B.; Lagerholm, B. C.; Ernst, L. A.; Bruchez, M. P.; Waggoner, A. S. Support Info3: Noninvasive Imaging of Quantum Dots in Mice. *Bioconjug. Chem.* **2004,** *15,* 79–86.
120. Gao, X.; Cui, Y.; Levenson, R. M.; Chung, L. W. K.; Nie, S. In Vivo Cancer Targeting and Imaging With Semiconductor Quantum Dots. *Nat. Biotechnol.* **2004,** *22,* 969–976.
121. Santra, S.; Zhang, P.; Wang, K.; Tapec, R.; Tan, W. Conjugation of Biomolecules With Luminophore-Doped Silica Nanoparticles for Photostable Biomarkers. *Anal. Chem.* **2001,** *73,* 4988–4993.
122. Menendez-Miranda, M.; Costa-Fernández, J. M.; Encinar, J. R.; Parak, W. J.; Carrillo-Carrion, C. Determination of the Ratio of Fluorophore/Nanoparticle for Fluorescence-Labelled Nanoparticles. *Analyst* **2016,** *141* (4), 1266–1272.
123. Trenkmann, I.; Bok, S.; Korampally, V.; Gangopadhyay, S.; Graaf, H.; von Borczyskowski C. Counting Single Rhodamine 6G Dye Molecules in Organosilicate Nanoparticles. Chem Phys . **2012**, 406(*8*), 41–46.
124. Montalti, M.; Prodi, L.; Rampazzo, E.; Zaccheroni, N. Dye-Doped Silica Nanoparticles as Luminescent Organized Systems for Nanomedicine. *Chem. Soc. Rev.* **2014,** *43,* 4243–4268.
125. Sokolov, I.; Naik, S. Novel Fluorescent Silica Nanoparticles: Towards Ultrabright Silica Nanoparticles. *Small* **2008,** *4,* 934–939.
126. Wang, L.; Tan, W. Multicolor FRET Silica Nanoparticles by Single Wavelength Excitation. *Nano Lett.* **2006,** *6,* 84–88.
127. Halas, N. J. Nanoscience Under Glass: The Versatile Chemistry of Silica Nanostructures. *ACS Nano* **2008,** *2,* 179–183.
128. Santra, S.; Malhotra, A. Fluorescent Nanoparticle Probes for Imaging of Cancer. *Wiley Interdiscip. Rev. Nanomed. Nanobiotechnol.* **2011,** *3,* 501–510.
129. Sharma, P.; Brown, S.; Walter, G.; Santra, S.; Moudgil, B. Nanoparticles for Bioimaging. *Adv. Colloid Interface Sci.* **2006,** *123–126,* 471–485.
130. Lee, C. H.; Cheng, S. H.; Wang, Y. J.; Chen, Y. C.; Chen, N. T.; Souris, J.; Chen, C. T.; Mou, C. Y.; Yang, C. S.; Lo, L. W. Near-Infrared Mesoporous Silica Nanoparticles for Optical Imaging: Characterization and in vivo Biodistribution. *Adv. Funct. Mater.* **2009,** *19,* 215–222.
131. Nabeshi, H.; Yoshikawa, T.; Matsuyama, K.; Nakazato, Y.; Matsuo, K.; Arimori, A.; Isobe, M.; Tochigi, S.; Kondoh, S.; Hirai, T.; Akase, T.; Yamashita, T.; Yamashita, K.; Yoshida, T.; Nagano, K.; Abe, Y.; Yoshioka, Y.; Kamada, H.; Imazawa, T.; Itoh, N.; Nakagawa, S.; Mayumi, T.; Tsunoda, S. I.; Tsutsumi, Y. Systemic Distribution, Nuclear Entry and Cytotoxicity of Amorphous Nanosilica Following Topical Application. *Biomaterials* **2011,** *32,* 2713–2724.
132. He, X.; Nie, H.; Wang, K.; Tan, W.; Wu, X.; Zhang, P. In Vivo Study of Biodistribution and Urinary Excretion of Surface-Modified Silica Nanoparticles in vivo Study of Biodistribution and Urinary Excretion of Surface-Modified Silica Nanoparticles. *Anal. Chem.* **2008,** *80,* 9597–9603.
133. Lu, J.; Liong, M.; Li, Z.; Zink, J. I.; Tamanoi, F. Biocompatibility, Biodistribution, and Drug-Delivery Efficiency of Mesoporous Silica Nanoparticles for Cancer Therapy in Animals. *Small* **2010,** *6,* 1794–1805.
134. Morgan, T. T.; Muddana, H. S.; Altinoğlu, E.İ.; Rouse, S. M.; Tabaković, A.; Tabouillot, T.; Russin, T. J.; Shanmugavelandy, S. S.; Butler, P. J.; Eklund, P. C.; Yun, J. K.; Kester, M.; Adair, J. H. Encapsulation of Organic Molecules in Calcium Phosphate Nanocomposite Particles for Intracellular Imaging and Drug Delivery. *Nano Lett.* **2008,** *8,* 4108–4115.
135. Bisht, S.; Bhakta, G.; Mitra, S.; Maitra, A. pDNA Loaded Calcium Phosphate Nanoparticles: Highly Efficient Non-Viral Vector for Gene Delivery. *Int. J. Pharm.* **2005,** *288,* 157–168.
136. Gatzeva-topalova, P. Z.; Warner, L. R.; Pardi, A.; Carlos, M., Structure and flexibility of the complete periplasmic domain of BamA: the protein insertion machine of the outer membrane. *Structure* **2010**, 10;*18*(11), 1492–1501.
137. Russin, T. J.; Kaiser, J. M.; Barth, B. M.; Eklund, P. C.; Kester, M.; Adair, J. H., Near-infrared emitting fluorophore-doped calcium phosphate nanoparticles for in vivo imaging of human breast cancer. *ACS Nano.* **2008**, 28;*2*(10), 2075–2084.
138. Chen, J.; Corbin, I. R.; Li, H.; Cao, W.; Glickson, J. D.; Zheng, G., Ligand Conjugated Low-Density Lipoprotein Nanoparticles for Enhanced Optical Cancer Imaging in Vivo. J. Am. Chem. Soc. **2007**, *129*(18), 5798–5799.
139. Tosi, G.; Bondioli, L.; Ruozi, B.; Badiali, L.; Severini, G. M.; Biffi, S.; De Vita, A.; Bortot, B.; Dolcetta, D.; Forni, F.; Vandelli, M. A. NIR-Labeled Nanoparticles Engineered for Brain Targeting: in vivo Optical Imaging Application and Fluorescent Microscopy Evidences. *J. Neural Transm.* **2011,** *118,* 145–153.
140. Ghoroghchian, P. P.; Frail, P. R.; Susumu, K.; Blessington, D.; Brannan, A. K.; Bates, F. S.; Chance, B.; Hammer, D. A.; Therien, M. J. Near-Infrared-Emissive Polymersomes: Self-Assembled Soft Matter for in vivo Optical Imaging. *Proc. Natl. Acad. Sci. U. S. A.* **2005,** *102,* 2922–2927.
141. Zhang, X.; Bloch, S.; Akers, W.; Achilefu, S. Near-Infrared Molecular Probes for in vivo Imaging. *Curr. Protoc. Cytom. 60*, 12.27.1–12.27.20. © 2012 by John Wiley & Sons, Inc.
142. Morton, S. W.; Poon, Z.; Hammond, P. T. The Architecture and Biological Performance of Drug-Loaded LbL Nanoparticles. *Biomaterials* **2013,** *34,* 5328–5335.
143. Costa, R. R.; Mano, J. F. Polyelectrolyte Multilayered Assemblies in Biomedical Technologies. *Chem. Soc. Rev.* **2014,** *43,* 3453–3479.
144. Poon, Z.; Lee, J. B.; Morton, S. W.; Hammond, P. T., Controlling In Vivo Stability and Biodistribution in Electrostatically Assembled Nanoparticles for Systemic Delivery. Nano letters **2011**,*11*(5), 2096–2103.
145. Maldonado, C. R.; Salassa, L.; Gomez-Blanco, N.; Mareque-Rivas, J. C. Nano-Functionalization of Metal Complexes for Molecular Imaging and Anticancer Therapy. *Coord. Chem. Rev.* **2013,** *257,* 2668–2688.
146. Sun, G.; Berezin, M. Y.; Fan, J.; Lee, H.; Ma, J.; Zhang, K.; Wooley, K. L.; Achilefu, S. Bright Fluorescent Nanoparticles for Developing Potential Optical Imaging Contrast Agents. *Nanoscale* **2010,** *2,* 548–558.
147. Kreyling, W. G.; Abdelmonem, A. M.; Ali, Z.; Alves, F.; Geiser, M.; Haberl, N.; Hartmann, R.; Hirn, S.; de Aberasturi, D. J.; Kantner, K.; Khadem-Saba, G.; Montenegro, J.-M.; Rejman, J.; Rojo, T.; de Larramendi, I. R.; Ufartes, R.; Wenk, A.; Parak, W. J. In Vivo Integrity of Polymer-Coated Gold Nanoparticles. *Nat. Nanotechnol.* **2015,** *10,* 619–623.

148. Massoud, T. F.; Massoud, T. F.; Gambhir, S. S.; Gambhir, S. S. Molecular Imaging in Living Subjects: Seeing Fundamental Biological Processes in a New Light. *Genes Dev.* **2003,** *17* (5), 545–580.
149. Morales-avila, E.; Ferro-flores, G.; Ocampo-GarcÚa, B. E.; de MarÚa RamÚrez, F. Radiolabeled Nanoparticles for Molecular Imaging, Molecular Imaging. In *Tech;* Schaller, B., Ed.; 2012; http://dx.doi.org/10.5772/31109. http://www.intechopen.com/books/molecular-imaging/radiolabeled-nanoparticles-for-molecular-imaging. Available from:.
150. Debbage, P.; Jaschke, W. Molecular Imaging With Nanoparticles: Giant Roles for Dwarf Actors. *Histochem. Cell Biol.* **2008,** *130,* 845–875.
151. Gambhir, S. S. Molecular Imaging of Cancer With Positron Emission Tomography. *Nat. Rev. Cancer* **2002,** *2,* 683–693.
152. Stockhofe, K.; Postema, J. M.; Schieferstein, H.; Ross, T. L. Radiolabeling of Nanoparticles and Polymers for PET Imaging. *Pharmaceuticals* **2014,** *7,* 392–418.
153. Xing, Y.; Zhao, J.; Conti, P. S.; Chen, K. Radiolabeled Nanoparticles for Multimodality Tumor Imaging. *Theranostics* **2014,** *4,* 290–306.
154. Guerrero, S.; Herance, J. R.; Rojas, S.; Mena, J. F.; Gispert, J. D.; Acosta, G. A.; Albericio, F.; Kogan, M. J. Synthesis and in vivo Evaluation of the Biodistribution of a 18 F-Labeled Conjugate Gold-Nanoparticle-Peptide With Potential Biomedical Application. *Bioconjug. Chem.* **2012,** *23,* 399–408.
155. Unak, G.; Ozkaya, F.; Ilker Medine, E.; Kozgus, O.; Sakarya, S.; Bekis, R.; Unak, P.; Timur, S. Gold Nanoparticle Probes: Design and in vitro Applications in Cancer Cell Culture. *Colloids Surf. B* **2012,** *90,* 217–226.
156. Xie, J.; Chen, K.; Huang, J.; Lee, S.; Wang, J.; Gao, J.; Li, X.; Chen, X. PET/NIRF/MRI Triple Functional Iron Oxide Nanoparticles. *Biomaterials* **2010,** *31,* 3016–3022.
157. Yang, X.; Hong, H.; Grailer, J. J.; Rowland, I. J.; Javadi, A.; Hurley, S. A.; Xiao, Y.; Yang, Y.; Zhang, Y.; Nickles, R. J.; Cai, W.; Steeber, D. A.; Gong, S. cRGD-Functionalized, DOX-Conjugated, and 64Cu-Labeled Superparamagnetic Iron Oxide Nanoparticles for Targeted Anticancer Drug Delivery and PET/MR Imaging. *Biomaterials* **2011,** *32,* 4151–4160.
158. Perez-Campana, C.; Gomez-Vallejo, V.; Martin, A.; San Sebastian, E.; Moya, S. E.; Reese, T.; Ziolo, R. F.; Llop, J. Tracing Nanoparticles In Vivo: A new General Synthesis of Positron Emitting Metal Oxide Nanoparticles by Proton Beam Activation. *Analyst* **2012,** *137,* 4902–4906.
159. Ducongé, F.; Pons, T.; Pestourie, C.; Hérin, L.; Thézé, B.; Gombert, K.; Mahler, B.; Hinnen, F.; Kühnast, B.; Dollé, F.; Dubertret, B.; Tavitian, B. Fluorine-18-Labeled Phospholipid Quantum Dot Micelles for in vivo Multimodal Imaging From Whole Body to Cellular Scales. *Bioconjug. Chem.* **2008,** *19,* 1921–1926.
160. Liu, Q.; Sun, Y.; Li, C.; Zhou, J.; Li, C.; Yang, T.; Zhang, X.; Yi, T.; Wu, D.; Li, F. 18 F-Labeled Magnetic-Upconversion Nanophosphors via Rare-Earth Cation-Assisted Ligand Assembly. *ACS Nano* **2011,** *5,* 3146–3157.
161. Kumar, R.; Roy, I.; Ohulchanskky, T.; Vathy, L. In Vivo Biodistribution and Clearance Studies Using Multimodal Organically Modified Silica Nanoparticles. *ACS Nano* **2010,** *4,* 699–708.
162. Lee, S. B.; Kim, H. L.; Jeong, H.-J.; Lim, S. T.; Sohn, M.-H.; Kim, D. W. Mesoporous Silica Nanoparticle Pretargeting for PET Imaging Based on a Rapid Bioorthogonal Reaction in a Living Body. *Angew. Chem. Int. Ed.* **2013,** *52,* 10549–10552.
163. Sarparanta, M.; Bimbo, L. M.; Rytkönen, J.; Mäkilä, E.; Laaksonen, T. J.; Laaksonen, P.; Nyman, M.; Salonen, J.; Linder, M. B.; Hirvonen, J.; Santos, H. A.; Airaksinen, A. J. Intravenous Delivery of Hydrophobin-Functionalized Porous Silicon Nanoparticles: Stability, Plasma Protein Adsorption and Biodistribution. *Mol. Pharm.* **2012,** *9,* 654–663.
164. Fukukawa, K.-I.; Rossin, R.; Hagooly, A.; Pressly, E. D.; Hunt, J. N.; Messmore, B. W.; Wooley, K. L.; Welch, M. J.; Hawker, C. J. Synthesis and Characterization of Core–Shell Star Copolymers for in vivo PET Imaging Applications. *Biomacromolecules* **2008,** *9,* 1329–1339.
165. Herth, M. M.; Barz, M.; Moderegger, D.; Allmeroth, M.; Jahn, M.; Thews, O.; Zentel, R.; Rösch, F. Radioactive Labeling of Defined HPMA-Based Polymeric Structures Using [18 F]FETos for in vivo Imaging by Positron Emission Tomography. *Biomacromolecules* **2009,** *10,* 1697–1703.
166. Petersen, A. L.; Binderup, T.; Rasmussen, P.; Henriksen, J. R.; Elema, D. R.; Kjær, A.; Andresen, T. L. 64Cu Loaded Liposomes as Positron Emission Tomography Imaging Agents. *Biomaterials* **2011,** *32,* 2334–2341.
167. Devaraj, N. K.; Keliher, E. J.; Thurber, G. M.; Nahrendorf, M.; Weissleder, R. 18 F Labeled Nanoparticles for in vivo PET-CT Imaging. *Bioconjug. Chem.* **2009,** *20,* 397–401.
168. Chen, K.; Li, Z.-B.; Wang, H.; Cai, W.; Chen, X. Dual-Modality Optical and Positron Emission Tomography Imaging of Vascular Endothelial Growth Factor Receptor on Tumor Vasculature Using Quantum Dots. *Eur. J. Nucl. Med. Mol. Imaging* **2008,** *35,* 2235–2244.
169. Cherry, S. R.; Louie, A. Y.; Jacobs, R. E. The Integration of Positron Emission Tomography With Magnetic Resonance Imaging. *Proc. IEEE* **2008,** *96,* 416–438.
170. Pichler, B.; Wehrl, H. PET/MRI: The Next Generation of Multi-Modality Imaging? *Semin. Nucl. Med.* **2009,** *38,* 199–208.
171. Rosenthal, M. S.; Cullom, J.; Hawkins, W.; Moore, S. C.; Tsui, B. M.; Yester, M. Quantitative SPECT Imaging: A Review and Recommendations by the Focus Committee of the Society of Nuclear Medicine Computer and Instrumentation Council. *J. Nucl. Med.* **1995,** *36,* 1489–1513.
172. Bruns, O. T.; Ittrich, H.; Peldschus, K.; Kaul, M. G.; Tromsdorf, U. I.; Lauterwasser, J.; Nikolic, M. S.; Mollwitz, B.; Merkel, M.; Bigall, N. C.; Sapra, S.; Reimer, R.; Hohenberg, H.; Weller, H.; Eychmüller, A.; Adam, G.; Beisiegel, U.; Heeren, J. Real-Time Magnetic Resonance Imaging and Quantification of Lipoprotein Metabolism in vivo Using Nanocrystals. *Nat. Nanotechnol.* **2009,** *4,* 193–201.
173. Sun, C.; Lee, J.; Zhang, M. Magnetic Nanoparticles in MR Imaging and Drug Delivery. *Adv. Drug Deliv. Rev.* **2008,** *60,* 1252–1265.
174. Sosnovik, D. E.; Nahrendorf, M.; Weissleder, R. Magnetic Nanoparticles for MR Imaging: Agents, Techniques and Cardiovascular Applications. *Basic Res. Cardiol.* **2008,** *103,* 122–130.
175. Lu, A. H.; Salabas, E. L.; Schüth, F. Magnetic Nanoparticles: Synthesis, Protection, Functionalization, and Application. *Angew. Chem. Int. Ed.* **2007,** *46,* 1222–1244.
176. Wang, Y.-X. J. Superparamagnetic Iron Oxide Based MRI Contrast Agents: Current Status of Clinical Application. *Quant. Imaging Med. Surg.* **2011,** *1,* 35–40.
177. Corot, C.; Robert, P.; Idée, J. M.; Port, M. Recent Advances in Iron Oxide Nanocrystal Technology for Medical Imaging. *Adv. Drug Deliv. Rev.* **2006,** *58,* 1471–1504.
178. Issa, B.; Obaidat, I. M.; Albiss, B. A.; Haik, Y. Magnetic Nanoparticles: Surface Effects and Properties Related to Biomedicine Applications. *Int. J. Mol. Sci.* **2013,** *14,* 21266–21305.
179. Jun, Y. W.; Lee, J. H.; Cheon, J. Chemical Design of Nanoparticle Probes for High-Performance Magnetic Resonance Imaging. *Angew. Chem. Int. Ed.* **2008,** *47,* 5122–5135.
180. Na, H. B.; Song, I. C.; Hyeon, T. Inorganic Nanoparticles for MRI Contrast Agents. *Adv. Mater.* **2009,** *21,* 2133–2148.
181. Cunningham, C. H.; Arai, T.; Yang, P. C.; McConnell, M. V.; Pauly, J. M.; Conolly, S. M. Positive Contrast Magnetic Resonance Imaging of Cells Labeled With Magnetic Nanoparticles. *Magn. Reson. Med.* **2005,** *53,* 999–1005.
182. Huang, J.; Zhong, X.; Wang, L.; Yang, L.; Mao, H. Improving the Magnetic Resonance Imaging Contrast and Detection Methods With Engineered Magnetic Nanoparticles. *Theranostics* **2012,** *2,* 86–102.
183. Stuber, M.; Gilson, W. D.; Schär, M.; Kedziorek, D. A.; Hofmann, L. V.; Shah, S.; Vonken, E. J.; Bulte, J. W. M.; Kraitchman, D. L. Positive Contrast Visualization of Iron Oxide-Labeled Stem Cells Using Inversion-Recovery With ON-Resonant Water Suppression (IRON). *Magn. Reson. Med.* **2007,** *58,* 1072–1077.
184. Busquets, M. A.; Estelrich, J.; Sánchez-Martín, M. J. Nanoparticles in Magnetic Resonance Imaging: From Simple to Dual Contrast Agents. *Int. J. Nanomedicine* **2015,** *140,* 1727–1741.
185. Yang, H.; Zhang, C.; Shi, X.; Hu, H.; Du, X.; Fang, Y.; Ma, Y.; Wu, H.; Yang, S. Water-Soluble Superparamagnetic Manganese Ferrite Nanoparticles for Magnetic Resonance Imaging. *Biomaterials* **2010,** *31,* 3667–3673.
186. Kobayashi, Y.; Imai, J.; Nagao, D.; Takeda, M.; Ohuchi, N.; Kasuya, A.; Konno, M. Preparation of Multilayered Silica-Gd-Silica Core-Shell Particles and Their Magnetic Resonance Images. *Colloids Surf. A Physicochem. Eng. Asp.* **2007,** *308,* 14–19.
187. Taylor, K. M. L.; Kim, J. S.; Rieter, W. J.; An, H.; Lin, W.; Lin, W. Mesoporous Silica Nanospheres as Highly Efficient MRI Contrast Agents. *J. Am. Chem. Soc.* **2008,** *130,* 2154–2155.
188. Xu, J.; Ao, Y.; Fu, D.; Yuan, C. Synthesis of Gd-Doped TiO2 Nanoparticles Under Mild Condition and Their Photocatalytic Activity. *Colloids Surf. A Physicochem. Eng. Asp.* **2009,** *334,* 107–111.
189. Song, Y.; Xu, X.; MacRenaris, K. W.; Zhang, X.-Q.; Mirkin, C. A.; Meade, T. J. Multimodal Gadolinium-Enriched DNA-Gold Nanoparticle Conjugates for Cellular Imaging. *Angew. Chem.* **2009,** *121,* 9307–9311.
190. Kobayashi, H.; Brechbiel, M. W. Nano-Sized MRI Contrast Agents With Dendrimer Cores. *Adv. Drug Deliv. Rev.* **2005,** *57,* 2271–2286.

191. Manus, L. M.; Mastarone, D. J.; Waters, E. A.; Zhang, X. Q.; Schultz-Sikma, E. A.; MacRenaris, K. W.; Ho, D.; Meade, T. J. Gd(III)-Nanodiamond Conjugates for MRI Contrast Enhancement. *Nano Lett.* **2010,** *10,* 484–489.
192. Sitharaman, B.; Van Der Zande, M.; Ananta, J. S.; Shi, X.; Veltien, A.; Walboomers, X. F.; Wilson, L. J.; Mikos, A. G.; Heerschap, A.; Jansen, J. A. Magnetic Resonance Imaging Studies on Gadonanotube-Reinforced Biodegradable Polymer Nanocomposites. *J. Biomed. Mater. Res. A* **2010,** *93,* 1454–1462.
193. Gleich, B.; Weizenecker, J. Tomographic Imaging Using the Nonlinear Response of Magnetic Particles. *Nature* **2005,** *435,* 1214–1217.
194. Zheng, B.; Vazin, T.; Goodwill, P. W.; Conway, A.; Verma, A.; Saritas, E. U.; Schaffer, D.; Conolly, S. M. Magnetic Particle Imaging Tracks the Long-Term Fate of in vivo Neural Cell Implants With High Image Contrast. *Sci. Rep.* **2015,** *5,* 14055.
195. Arami, H.; Khandhar, A. P.; Tomitaka, A.; Yu, E.; Goodwill, P. W.; Conolly, S. M.; Krishnan, K. M. In Vivo Multimodal Magnetic Particle Imaging (MPI) With Tailored Magneto/Optical Contrast Agents. *Biomaterials* **2015,** *52,* 251–261.
196. Lehmbecker, A.; Rittinghausen, S.; Rohn, K.; Baumgärtner, W.; Schaudien, D. Nanoparticles and Pop-off Technique for Electron Microscopy: A Known Technique for a New Purpose. *Toxicol. Pathol.* **2014,** *42,* 1041–1046.
197. Avwioro, G. Histochemical Uses of Haematoxylin—A Review. *JPCS* **2011,** *1,* 24–34.
198. van Landeghem, F. K. H.; Maier-Hauff, K.; Jordan, A.; Hoffmann, K. T.; Gneveckow, U.; Scholz, R.; Thiesen, B.; Brück, W.; von Deimling, A. Post-Mortem Studies in Glioblastoma Patients Treated With Thermotherapy Using Magnetic Nanoparticles. *Biomaterials* **2009,** *30,* 52–57.
199. Johannsen, M.; Gneveckow, U.; Taymoorian, K.; Thiesen, B.; Waldöfner, N.; Scholz, R.; Jung, K.; Jordan, A.; Wust, P.; Loening, S. A. Morbidity and Quality of Life During Thermotherapy Using Magnetic Nanoparticles in Locally Recurrent Prostate Cancer: Results of a Prospective Phase I Trial. *Int. J. Hyperthermia* **2007,** *23,* 315–323.
200. El-Drieny, E. A. E. A.; Sarhan, N. I.; Bayomy, N. A.; Elsherbeni, S. A. E.; Momtaz, R.; Mohamed, H. E.-D. Histological and Immunohistochemical Study of the Effect of Gold Nanoparticles on the Brain of Adult Male Albino Rat. *J. Microsc. Ultrastruct.* **2015,** *3,* 181–190.
201. Porter, D. W.; Hubbs, A. F.; Mercer, R. R.; Wu, N.; Wolfarth, M. G.; Sriram, K.; Leonard, S.; Battelli, L.; Schwegler-Berry, D.; Friend, S.; Andrew, M.; Chen, B. T.; Tsuruoka, S.; Endo, M.; Castranova, V. Mouse Pulmonary Dose- and Time Course-Responses Induced by Exposure to Multi-Walled Carbon Nanotubes. *Toxicology* **2010,** *269,* 136–147.
202. Adachi, K.; Yamada, N.; Yamamoto, K.; Yoshida, Y.; Yamamoto, O. In Vivo Effect of Industrial Titanium Dioxide Nanoparticles Experimentally Exposed to Hairless Rat Skin. *Nanotoxicology* **2010,** *4,* 296–306.
203. Chen, P. Y.; Liu, H. L.; Hua, M. Y.; Yang, H. W.; Huang, C. Y.; Chu, P. C.; Lyu, L. A.; Tseng, I. C.; Feng, L. Y.; Tsai, H. C.; Chen, S. M.; Lu, Y. J.; Wang, J. J.; Yen, T. C.; Ma, Y. H.; Wu, T.; Chen, J. P.; Chuang, J. I.; Shin, J. W.; Hsueh, C.; Wei, K. C. Novel Magnetic/Ultrasound Focusing System Enhances Nanoparticle Drug Delivery for Glioma Treatment. *Neuro Oncol.* **2010,** *12,* 1050–1060.
204. Hsieh, W.-J.; Liang, C.-J.; Chieh, J.-J.; Wang, S.-H.; Lai, I. R.; Chen, J.-H.; Chang, F.-H.; Tseng, W.-K.; Yang, S.-Y.; Wu, C.-C.; Chen, Y.-L. In Vivo Tumor Targeting and Imaging With Anti-Vascular Endothelial Growth Factor Antibody-Conjugated Dextran-Coated Iron Oxide Nanoparticles. *Int. J. Nanomedicine* **2012,** *7,* 2833–2842.
205. Lee, M. J. E.; Veiseh, O.; Bhattarai, N.; Sun, C.; Hansen, S. J.; Ditzler, S.; Knoblaugh, S.; Lee, D.; Ellenbogen, R.; Zhang, M.; Olson, J. M. Rapid Pharmacokinetic and Biodistribution Studies Using Cholorotoxin-Conjugated Iron Oxide Nanoparticles: A Novel Non-Radioactive Method. *PLoS One* **2010,** *5,* 1–8.
206. Scharlach, C.; Kratz, H.; Wiekhorst, F.; Warmuth, C.; Schnorr, J.; Genter, G.; Ebert, M.; Mueller, S.; Schellenberger, E. Synthesis of Acid-Stabilized Iron Oxide Nanoparticles and Comparison for Targeting Atherosclerotic Plaques: Evaluation by MRI, Quantitative MPS, and TEM Alternative to Ambiguous Prussian Blue Iron Staining. *Nanomed.: Nanotechnol., Biol. Med.* **2015,** *11,* 1–11.
207. Liang, M.; Yan, X., Ex Vivo Detection of Iron Oxide Magnetic Nanoparticles in Mice Using Their Intrinsic Peroxidase-Mimicking Activity. *Mol. Pharmaceutics*, **2012**, *9*(7), 1983–1989.
208. Holzhausen, C.; Gröger, D.; Mundhenk, L.; Welker, P.; Haag, R.; Gruber, A. D. Tissue and Cellular Localization of Nanoparticles Using 35S Labeling and Light Microscopic Autoradiography. *Nanomed.: Nanotechnol., Biol. Med.* **2013,** *9,* 465–468.
209. Mercer, R. R.; Scabilloni, J.; Wang, L.; Kisin, E.; Murray, A. R.; Schwegler-Berry, D.; Shvedova, A. A.; Castranova, V. Alteration of Deposition Pattern and Pulmonary Response as a Result of Improved Dispersion of Aspirated Single-Walled Carbon Nanotubes in a Mouse Model. *Am. J. Physiol. Lung Cell. Mol. Physiol.* **2008,** *294,* L87–L97.
210. Cho, M.; Cho, W. S.; Choi, M.; Kim, S. J.; Han, B. S.; Kim, S. H.; Kim, H. O.; Sheen, Y. Y.; Jeong, J. The Impact of Size on Tissue Distribution and Elimination by Single Intravenous Injection of Silica Nanoparticles. *Toxicol. Lett.* **2009,** *189,* 177–183.
211. Fu, C.; Liu, T.; Li, L.; Liu, H.; Chen, D.; Tang, F. The Absorption, Distribution, Excretion and Toxicity of Mesoporous Silica Nanoparticles in Mice Following Different Exposure Routes. *Biomaterials* **2013,** *34,* 2565–2575.
212. Roger, M.; Clavreul, A.; Venier-Julienne, M.-C.; Passirani, C.; Sindji, L.; Schiller, P.; Montero-Menei, C.; Menei, P. Mesenchymal Stem Cells as Cellular Vehicles for Delivery of Nanoparticles to Brain Tumors. *Biomaterials* **2010,** *31,* 8393–8401.
213. Kner, P.; Chhun, B. B.; Griffis, E. R.; Winoto, L.; Gustafsson, M. G. L. Super-Resolution Video Microscopy of Live Cells by Structured Illumination. *Nat. Methods* **2009,** *6,* 339–342.
214. Hubbs, A. F.; Mercer, R. R.; Benkovic, S. A.; Harkema, J.; Sriram, K.; Schwegler-Berry, D.; Goravanahally, M. P.; Nurkiewicz, T. R.; Castranova, V.; Sargent, L. M. Nanotoxicology—A Pathologist's Perspective. *Toxicol. Pathol.* **2011,** *39,* 301–324.
215. van Schooneveld, M. M.; Vucic, E.; Koole, R.; Zhou, Y.; Stocks, J.; Cormode, D. P.; Tang, C. Y.; Gordon, R. E.; Nicolay, K.; Meijerink, A.; Fayad, Z. A.; Mulder, W. J. M. Improved Biocompatibility and Pharmacokinetics of Silica Nanoparticles by Means of a Lipid Coating: A Multimodality Investigation. *Nano Lett.* **2008,** *8,* 2517–2525.
216. Cheng, S.-H.; Li, F.-C.; Souris, J. S.; Yang, C.-S.; Tseng, F.-G.; Lee, H.-S.; Chen, C.-T.; Dong, C.-Y.; Lo, L.-W. Visualizing Dynamics of Sub-Hepatic Distribution of Nanoparticles Using Intravital Multiphoton Fluorescence Microscopy. *ACS Nano* **2012,** *6,* 4122–4131.
217. Smith, B. R.; Cheng, Z.; De, A.; Rosenberg, J.; Gambhir, S. S. Dynamic Visualization of RGD-Quantum Dot Binding to Tumor Neovasculature and Extravasation in Multiple Living Mouse Models Using Intravital Microscopy. *Small* **2010,** *6,* 2222–2229.
218. Monici, M. Cell and Tissue Autofluorescence Research and Diagnostic Applications. *Biotechnol. Annu. Rev.* **2005,** *11,* 227–256. Elsevier.
219. Solon, E. G., Autoradiography: High-Resolution Molecular Imaging in Pharmaceutical Discovery and Development. *Expert Opin Drug Discov.* **2007**, *2*(4), 503–514.
220. Payan, J. P.; Binet, S.; Beydon, D.; Ferrari, E. Bio-Distribution Study of 1,2-Diethylbenzene and Its Main Metabolites by Whole-Body Autoradiography and Tissue Homogenates. *Arch. Toxicol.* **2008,** *82,* 591–600.
221. Nagata, T., Techniques and Application of Microscopic Radioautography. *Histol Histopathol.* **1997**, *12*(4), 1091–1124.
222. Caro, L. G.; van Tubergen, R. P. High-Resolution Autoradiography: I. Methods. *J. Cell Biol.* **1962,** *15,* 173–188.
223. Solon, E. G. Use of Radioactive Compounds and Autoradiography to Determine Drug Tissue Distribution. *Chem. Res. Toxicol.* **2012,** *25,* 543–555.
224. Shi, B.; Abrams, M. Technologies for Investigating the Physiological Barriers to Efficient Lipid Nanoparticle-siRNA Delivery. *J. Histochem. Cytochem.* **2013,** *61,* 407–420.
225. Huang, F.-Y. J.; Lee, T.-W.; Kao, C.-H. K.; Chang, C.-H.; Zhang, X.; Lee, W.-Y.; Chen, W.-J.; Wang, S.-C.; Lo, J.-M. Imaging, Autoradiography, and Biodistribution of 188 Re-Labeled PEGylated Nanoliposome in Orthotopic Glioma Bearing Rat Model. *Cancer Biother. Radiopharm.* **2011,** *26,* 717–725.
226. Lee, W. C.; Hwang, J. J.; Tseng, Y. L.; Wang, H. E.; Chang, Y. F.; Lu, Y. C.; Ting, G.; Whang-Peng, J.; Wang, S. J. Therapeutic Efficacy Evaluation of 111in-VNB-Liposome on Human Colorectal Adenocarcinoma HT-29/luc Mouse Xenografts. *Nucl. Instrum. Methods Phys. Res., Sect. A* **2006,** *569,* 497–504.
227. Al-Hallak, M. H. D. K.; Sarfraz, M. K.; Azarmi, S.; Roa, W. H.; Finlay, W. H.; Rouleau, C.; Löbenberg, R. Distribution of Effervescent Inhalable Nanoparticles After Pulmonary Delivery: An in vivo Study. *Ther. Deliv.* **2012,** *3,* 725–734.
228. Al-Sid-Cheikh, M.; Rouleau, C.; Pelletier, E. Tissue Distribution and Kinetics of Dissolved and Nanoparticulate Silver in Iceland Scallop (Chlamys Islandica). *Mar. Environ. Res.* **2013,** *86,* 21–28.
229. Marquis, B. J.; Love, S. A.; Braun, K. L.; Haynes, C. L. Analytical Methods to Assess Nanoparticle Toxicity. *Analyst* **2009,** *134,* 425–439.
230. Wu, J.; Liu, W.; Xue, C.; Zhou, S.; Lan, F.; Bi, L.; Xu, H.; Yang, X.; Zeng, F. D. Toxicity and Penetration of TiO2 Nanoparticles in Hairless Mice and Porcine Skin After Subchronic Dermal Exposure. *Toxicol. Lett.* **2009,** *191,* 1–8.

231. Samberg, M. E.; Oldenburg, S. J.; Monteiro-Riviere, N. A. Evaluation of Silver Nanoparticle Toxicity in Skin in vivo and kerAtinocytes In Vitro. *Environ. Health Perspect.* **2010,** *118,* 407–413.
232. Wang, L.; Li, Y. F.; Zhou, L.; Liu, Y.; Meng, L.; Zhang, K.; Wu, X.; Zhang, L.; Li, B.; Chen, C. Characterization of Gold Nanorods in vivo by Integrated Analytical Techniques: Their Uptake, Retention, and Chemical Forms. *Anal. Bioanal. Chem.* **2010,** *396,* 1105–1114.
233. Gutiérrez, L.; Mejías, R.; Barber, D. F.; Veintemillas-Verdaguer, S.; Serna, C. J.; Lázaro, F. J.; Morales, M. P. Ac Magnetic Susceptibility Study of in vivo Nanoparticle Biodistribution. *J. Phys. D Appl. Phys.* **2011,** *44,* 255002.
234. Levy, M.; Luciani, N.; Alloyeau, D.; Elgrabli, D.; Deveaux, V.; Pechoux, C.; Chat, S.; Wang, G.; Vats, N.; Gendron, F. O.; Factor, C. C.; Lotersztajn, S.; Luciani, A.; Wilhelm, C.; Gazeau, F. Long Term in vivo Biotransformation of Iron Oxide Nanoparticles. *Biomaterials* **2011,** *32,* 3988–3999.
235. Mortensen, L. J.; Oberdo, G.; Pentland, A. P.; Delouise, L. A. In Vivo Skin Penetration of Quantum Dot Nanoparticles in the Murine Model the Effect of UVR. *Nano Lett.* **2008,** *8* (9), 2779–2787.
236. Asharani, P. V.; Lian Wu, Y.; Gong, Z.; Valiyaveettil, S. Toxicity of Silver Nanoparticles in Zebrafish Models. *Nanotechnology* **2008,** *19,* 255102.
237. Kempen, P. J.; Thakor, A. S.; Zavaleta, C.; Gambhir, S. S.; Sinclair, R. A Scanning Transmission Electron Microscopy (STEM) Approach to Analyzing Large Volumes of Tissue to Detect Nanoparticles. *Microsc. Microanal.* **2013,** *19,* 1290–1297.
238. Abe, S.; Kida, I.; Esaki, M.; Akasaka, T.; Uo, M.; Hosono, T.; Sato, Y.; Jeyadevan, B.; Kuboki, Y.; Morita, M.; Tohji, K.; Watari, F. Biodistribution Imaging of Magnetic Particles in Mice: X-ray Scanning Analytical Microscopy and Magnetic Resonance Imaging. *Bio-Med. Mater. Eng.* **2009,** *19,* 213–220.
239. Ostrowski, A.; Nordmeyer, D.; Boreham, A.; Holzhausen, C.; Mundhenk, L.; Graf, C.; Meinke, M. C.; Vogt, A.; Hadam, S.; Lademann, J.; Ruhl, E.; Alexiev, U.; Gruber, A. D. Overview About the Localization of Nanoparticles in Tissue and Cellular Context by Different Imaging Techniques. *Beilstein J. Nanotechnol.* **2015,** *6,* 263–280.
240. Subramanian, K. S. Determination of Metals in Biofluids and Tissues: Sample Preparation Methods for Atomic Spectroscopic Techniques. *Spectrochim. Acta B At. Spectrosc.* **1996,** *51,* 291–319.
241. Szpunar, J. Bio-Inorganic Speciation Analysis by Hyphenated Techniques. *Analyst* **2000,** *125,* 963–988.
242. Chithrani, B. D.; Ghazani, A. A.; Chan, W. C. W. Determining the Size and Shape Dependence of Gold Nanoparticle Uptake Into Mammalian Cells. *Nano Lett.* **2006,** *6,* 662–668.
243. Chu, M.; Wu, Q.; Wang, J.; Hou, S.; Miao, Y.; Peng, J.; Sun, Y. In Vitro and in vivo Transdermal Delivery Capacity of Quantum Dots Through Mouse Skin. *Nanotechnology* **2007,** *18,* 455103.
244. Fischer, H. C.; Liu, L.; Pang, K. S.; Chan, W. C. W. Pharmacokinetics of Nanoscale Quantum Dots: in vivo Distribution, Sequestration, and Clearance in the Rat. *Adv. Funct. Mater.* **2006,** *16,* 1299–1305.
245. Yang, R. S. H.; Chang, L. W.; Wu, J. P.; Tsai, M. H.; Wang, H. J.; Kuo, Y. C.; Yeh, T. K.; Yang, C. S.; Lin, P. Persistent Tissue Kinetics and Redistribution of Nanoparticles, Quantum Dot 705, in Mice: ICP-MS Quantitative Assessment. *Environ. Health Perspect.* **2007,** *115,* 1339–1343.
246. van Ravenzwaay, B.; Landsiedel, R.; Fabian, E.; Burkhardt, S.; Strauss, V.; Ma-Hock, L. Comparing Fate and Effects of Three Particles of Different Surface Properties: Nano-TiO2, pigmentary TiO2 and Quartz. *Toxicol. Lett.* **2009,** *186,* 152–159.
247. Balasubramanian, S. K.; Jittiwat, J.; Manikandan, J.; Ong, C.-N.; Yu, L. E.; Ong, W.-Y. Biodistribution of Gold Nanoparticles and Gene Expression Changes in the Liver and Spleen After Intravenous Administration in Rats. *Biomaterials* **2010,** *31,* 2034–2042.
248. Sonavane, G.; Tomoda, K.; Makino, K. Biodistribution of Colloidal Gold Nanoparticles After Intravenous Administration: Effect of Particle Size. *Colloids Surf. B* **2008,** *66,* 274–280.
249. Garza-Ocañas, L.; Ferrer, D. A.; Burt, J.; Diaz-Torres, L. A.; Ramírez Cabrera, M.; Rodríguez, V. T.; Luján Rangel, R.; Romanovicz, D.; Jose-Yacaman, M. Biodistribution and Long-Term Fate of Silver Nanoparticles Functionalized With Bovine Serum Albumin in Rats. *Metallomics* **2010,** *2,* 204–210.
250. Tang, J.; Xiong, L.; Wang, S.; Wang, J.; Liu, L.; Li, J.; Yuan, F.; Xi, T. Distribution, Translocation and Accumulation of Silver Nanoparticles in Rats. *J. Nanosci. Nanotechnol.* **2009,** *9,* 4924–4932.
251. Lu, J.; Li, Z.; Zink, J. I.; Tamanoi, F. In Vivo Tumor Suppression Efficacy of Mesoporous Silica Nanoparticles-Based Drug-Delivery System: Enhanced Efficacy by Folate Modification. *Nanomed.: Nanotechnol., Biol. Med.* **2012,** *8,* 212–220.
252. Chen, H.; Wang, L.; Yeh, J.; Wu, X.; Cao, Z.; Wang, Y. A.; Zhang, M.; Yang, L.; Mao, H. Reducing Non-Specific Binding and Uptake of Nanoparticles and Improving Cell Targeting With an Antifouling PEO-b-PγMPS Copolymer Coating. *Biomaterials* **2010,** *31,* 5397–5407.
253. Jain, T. K.; Reddy, M. K.; Morales, M. A.; Leslie-Pelecky, D. L.; Labhasetwar, V. Biodistribution, Clearance, and Biocompatibility of Iron Oxide Magnetic Nanoparticles in Rats. *Mol. Pharm.* **2008,** *5,* 316–327.
254. Patil, U.; Adireddy, S.; Jaiswal, A.; Mandava, S.; Lee, B.; Chrisey, D. In Vitro/In Vivo Toxicity Evaluation and Quantification of Iron Oxide Nanoparticles. *Int. J. Mol. Sci.* **2015,** *16,* 24417–24450.
255. Maurizi, L.; Sakulkhu, U.; Gramoun, A.; Vallee, J.-P.; Hofmann, H. A Fast and Reproducible Method to Quantify Magnetic Nanoparticle Biodistribution. *Analyst* **2014,** *139,* 1184–1191.
256. lawska-Waniewska, A.; Mosiniewicz-Szablewska, E.; Nedelko, N.; Gałązka-Friedman, J.; Friedman, A. Magnetic Studies of Iron-Entities in Human Tissues. *J. Magn. Magn. Mater.* **2004,** *272–276,* 2417–2419.
257. Chertok, B.; Cole, A. J.; David, A. E.; Yang, V. C. Comparison of Electron Spin Resonance Spectroscopy and Inductively-Coupled Plasma Optical Emission Spectroscopy for Biodistribution Analysis of Iron-Oxide Nanoparticles. *Mol. Pharm.* **2010,** *7,* 375–385.
258. Gamarra, L. F.; Pontuschka, W. M.; Amaro, E.; Costa-Filho, A. J.; Brito, G. E. S.; Vieira, E. D.; Carneiro, S. M.; Escriba, D. M.; Falleiros, A. M. F.; Salvador, V. L. Kinetics of Elimination and Distribution in Blood and Liver of Biocompatible Ferrofluids Based on Fe3O4 Nanoparticles: An EPR and XRF Study. *Mater. Sci. Eng. C* **2008,** *28,* 519–525.
259. Chertok, B.; Moffat, B. A.; David, A. E.; Yu, F.; Bergemann, C.; Ross, B. D.; Yang, V. C. Iron Oxide Nanoparticles as a Drug Delivery Vehicle for MRI Monitored Magnetic Targeting of Brain Tumors. *Biomaterials* **2009,** *29,* 487–496.
260. Schleich, N.; Po, C.; Jacobs, D.; Ucakar, B.; Gallez, B.; Danhier, F.; Préat, V. R. Comparison of Active, Passive and Magnetic Targeting to Tumors of Multifunctional Paclitaxel/SPIO-Loaded Nanoparticles for Tumor Imaging and Therapy. *J. Control. Release* **2014,** *194,* 82–91.
261. Wilhelm, C.; Gazeau, F.; Bacri, J. C. Magnetophoresis and Ferromagnetic Resonance of Magnetically Labeled Cells. *Eur. Biophys. J.* **2002,** *31,* 118–125.
262. Gamarra, L. F.; daCosta-Filho, A. J.; Mamani, J. B.; de Cassia Ruiz, R.; Pavon, L. F.; Sibov, T. T.; Vieira, E. D.; Silva, A. C.; Pontuschka, W. M.; Amaro, E., Jr. Ferromagnetic Resonance for the Quantification of Superparamagnetic Iron Oxide Nanoparticles in Biological Materials. *Int. J. Nanomedicine* **2010,** *5,* 203–211.
263. Gutiérrez, L.; Morales, M. P.; Lázaro, F. J. Prospects for Magnetic Nanoparticles in Systemic Administration: Synthesis and Quantitative Detection. *PCCP* **2014,** *16,* 4456–4464.
264. López, A.; Gutiérrez, L.; Lázaro, F. J. The Role of Dipolar Interaction in the Quantitative Determination of Particulate Magnetic Carriers in Biological Tissues. *Phys. Med. Biol.* **2007,** *52,* 5043–5056.
265. Mejías, R.; Gutiérrez, L.; Salas, G.; Pérez-Yagüe, S.; Zotes, T. M.; Lázaro, F. J.; Morales, M. P.; Barber, D. F. Long Term Biotransformation and Toxicity of Dimercaptosuccinic Acid-Coated Magnetic Nanoparticles Support Their Use in Biomedical Applications. *J. Control. Release* **2013,** *171,* 225–233.
266. Mejías, R.; Pérez-Yagüe, S.; Gutiérrez, L.; Cabrera, L. I.; Spada, R.; Acedo, P.; Serna, C. J.; Lázaro, F. J.; Villanueva, T.; Morales, M. D. P.; Barber, D. F. Dimercaptosuccinic Acid-Coated Magnetite Nanoparticles for Magnetically Guided in vivo Delivery of Interferon Gamma for Cancer Immunotherapy. *Biomaterials* **2011,** *32,* 2938–2952.
267. Hurley, K. R.; Ring, H. L.; Kang, H.; Klein, N. D.; Haynes, C. L. Characterization of Magnetic Nanoparticles in Biological Matrices. *Anal. Chem.* **2015,** *87,* 11611–11619.
268. Tian, F.; Clift, M. J.; Casey, A.; Del Pino, P.; Pelaz, B.; Conde, J.; Byrne, H. J.; Rothen-Rutishauser, B.; Estrada, G.; de la Fuente, J. M.; Stoeger, T. Investigating the Role of Shape on the Biological Impact of Gold Nanoparticles In Vitro. *Nanomedicine (Lond.)* **2015,** *10,* 2643–2657.

269. Soenen, S. J.; Himmelreich, U.; Nuytten, N.; de Cuyper, M. Cytotoxic Effects of Iron Oxide Nanoparticles and Implications for Safety in Cell Labelling. *Biomaterials* **2011,** *32,* 195–205.
270. Chu, M.; Wu, Q.; Yang, H.; Yuan, R.; Hou, S.; Yang, Y.; Zou, Y.; Xu, S.; Xu, K.; Ji, A.; Sheng, L. Transfer of Quantum dots From Pregnant Mice to Pups Across the Placental Barrier. *Small* **2010,** *6,* 670–678.
271. Kong, S. D.; Lee, J.; Ramachandran, S.; Eliceiri, B. P.; Shubayev, V. I.; Lal, R.; Jin, S. Magnetic Targeting of Nanoparticles Across the Intact Blood–Brain Barrier. *J. Control. Release* **2012,** *164,* 49–57.
272. Gu, Y. J.; Cheng, J.; Lin, C. C.; Lam, Y. W.; Cheng, S. H.; Wong, W. T. Nuclear Penetration of Surface Functionalized Gold Nanoparticles. *Toxicol. Appl. Pharmacol.* **2009,** *237,* 196–204.
273. Verma, A.; Stellacci, F. Effect of Surface Properties on Nanoparticle-Cell Interactions. *Small* **2010,** *6,* 12–21.
274. Mosmann, T. Rapid Colorimetric Assay for Cellular Growth and Survival: Application to Proliferation and Cytotoxicity Assays. *J. Immunol. Methods* **1983,** *65,* 55–63.
275. Riss, T. L.; Moravec, R. A.; Niles, A. L.; et al. Cell Viability Assays. In *Assay Guidance Manual;* Sittampalam, G. S., Coussens, N. P., Nelson, H., Eds.; Eli Lilly & Company and the National Center for Advancing Translational Sciences: Bethesda (MD), 2004. http://www.ncbi.nlm.nih.gov/books/NBK144065/. Available from:.
276. Berridge, M. V.; Tan, A. S. Characterization of the Cellular Reduction of 3-(4,5-Dimethylthiazol-2-yl)-2,5-Diphenyltetrazolium Bromide (MTT): Subcellular Localization, Substrate Dependence, and Involvement of Mitochondrial Electron Transport in MTT Reduction. *Arch. Biochem. Biophys.* **1993,** *303,* 474–482.
277. Huyck, L.; Ampe, C.; Van Troys, M. The XTT Cell Proliferation Assay Applied to Cell Layers Embedded in Three-Dimensional Matrix. *Assay Drug Dev. Technol.* **2012,** *10,* 382–392.
278. Marshall, N. J.; Goodwin, C. J.; Holt, S. J. A Critical Assessment of the Use of Microculture Tetrazolium Assays to Measure Cell Growth and Function. *Growth Regul.* **1995,** *5,* 69–84.
279. Zhang, C.; Wangler, B.; Morgenstern, B.; Zentgraf, H.; Eisenhut, M.; Untenecker, H.; Kruger, R.; Huss, R.; Seliger, C.; Semmler, W.; Kiessling, F. Silica- and Alkoxysilane-Coated Ultrasmall Superparamagnetic Iron Oxide Particles: A Promising Tool to Label Cells for Magnetic Resonance Imaging. *Langmuir* **2007,** *23,* 1427–1434.
280. Belyanskaya, L.; Manser, P.; Spohn, P.; Bruinink, A.; Wick, P. The Reliability and Limits of the MTT Reduction Assay for Carbon Nanotubes-Cell Interaction. *Carbon* **2007,** *45,* 2643–2648.
281. Plumb, J. A.; Milroy, R.; Kaye, S. B. Effects of the pH Dependence of 3-(4,5-Dimethylthiazol-2-yl)-2,5-Diphenyl-tetrazolium Bromide-Formazan Absorption on Chemosensitivity Determined by a Novel Tetrazolium-Based Assay. *Cancer Res.* **1989,** *49,* 4435–4440.
282. Monteiro-Riviere, N. A.; Inman, A. O.; Zhang, L. W. Limitations and Relative Utility of Screening Assays to Assess Engineered Nanoparticle Toxicity in a Human Cell Line. *Toxicol. Appl. Pharmacol.* **2009,** *234,* 222–235.
283. Ulukaya, E.; Colakogullari, M.; Wood, E. J. Interference by Anti-Cancer Chemotherapeutic Agents in the MTT-Tumor Chemosensitivity Assay. *Chemotherapy* **2004,** *50,* 43–50.
284. Chakrabarti, R.; Kundu, S.; Kumar, S. Vitamin A as an Enzyme that Catalyzes the Reduction of MTT to Formazan by Vitamin C. *J. Cell. Biochem.* **2000,** *80,* 133–138.
285. Bernas, T.; Dobrucki, J. Mitochondrial and Nonmitochondrial Reduction of MTT: Interaction of MTT With TMRE, JC-1, and NAO Mitochondrial Fluorescent Probes. *Cytometry* **2002,** *47,* 236–242.
286. Pagliacci, M. C.; Spinozzi, F.; Migliorati, G.; Fumi, G.; Smacchia, M.; Grignani, F.; Riccardi, C.; Nicoletti, I. Genistein Inhibits Tumour Cell Growth in vitro but Enhances Mitochondrial Reduction of Tetrazolium Salts: A Further Pitfall in the Use of the MTT Assay for Evaluating Cell Growth and Survival. *Eur. J. Cancer* **1993,** *29A,* 1573–1577.
287. Collier, A. C.; Pritsos, C. A. The Mitochondrial Uncoupler Dicumarol Disrupts the MTT Assay. *Biochem. Pharmacol.* **2003,** *66,* 281–287.
288. Soenen, S. J.; Brisson, A. R.; De Cuyper, M. Addressing the Problem of Cationic Lipid-Mediated Toxicity: The Magnetoliposome Model. *Biomaterials* **2009,** *30,* 3691–3701.
289. Lu, L.; Zhang, L.; Wai, M. S.; Yew, D. T.; Xu, J. Exocytosis of MTT Formazan Could Exacerbate Cell Injury. *Toxicol. In Vitro* **2012,** *26,* 636–644.
290. Tada, H.; Shiho, O.; Kuroshima, K.; Koyama, M.; Tsukamoto, K. An Improved Colorimetric Assay for Interleukin 2. *J. Immunol. Methods* **1986,** *93,* 157–165.
291. Hansen, M. B.; Nielsen, S. E.; Berg, K. Re-Examination and Further Development of a Precise and Rapid Dye Method for Measuring Cell Growth/Cell Kill. *J. Immunol. Methods* **1989,** *119,* 203–210.
292. Denizot, F.; Lang, R. Rapid Colorimetric Assay for Cell Growth and Survival. Modifications to the Tetrazolium Dye Procedure Giving Improved Sensitivity and Reliability. *J. Immunol. Methods* **1986,** *89,* 271–277.
293. Cory, A. H.; Owen, T. C.; Barltrop, J. A.; Cory, J. G. Use of an Aqueous Soluble Tetrazolium/Formazan Assay for Cell Growth Assays in Culture. *Cancer Commun.* **1991,** *3,* 207–212.
294. Vidal-Aroca, F.; Meng, A.; Minz, T.; Page, M. G.; Dreier, J. Use of Resazurin to Detect Mefloquine as an Efflux-Pump Inhibitor in Pseudomonas Aeruginosa and Escherichia Coli. *J. Microbiol. Methods* **2009,** *79,* 232–237.
295. O'Brien, J.; Wilson, I.; Orton, T.; Pognan, F. Investigation of the Alamar Blue (resazurin) Fluorescent Dye for the Assessment of Mammalian Cell Cytotoxicity. *FEBS J.* **2000,** *267,* 5421–5426.
296. Hamid, R.; Rotshteyn, Y.; Rabadi, L.; Parikh, R.; Bullock, P. Comparison of Alamar Blue and MTT Assays for High Through-Put Screening. *Toxicol. In Vitro* **2004,** *18,* 703–710.
297. Casey, A. H. E.; Davoren, M.; Lyng, F. M.; Byrne, H. J.; et al. Spectroscopic Analysis Confirms the Interactions Between Single Walled Carbon Nanotubes and Various Dyes Commonly Used to Assess Cytotoxicity. *Carbon* **2007,** *45,* 1425–1432.
298. Rafehi, H.; Orlowski, C.; Georgiadis, G. T.; Ververis, K.; El-Osta, A.; Karagiannis, T. C. Clonogenic Assay: Adherent Cells. *Journal of Visualized Experiments: JoVE.* **2011 2011**, (49). http://dx.doi.org/10.3791/2573, 2573.
299. Salmon, S. E.; Young, L.; Lebowitz, J.; Thomson, S.; Einsphar, J.; Tong, T.; Moon, T. E. Evaluation of an Automated Image Analysis System for Counting Human Tumor Colonies. *Int. J. Cell Cloning* **1984,** *2,* 142–160.
300. Guda, K.; Natale, L.; Markowitz, S. D. An Improved Method for Staining Cell Colonies in Clonogenic Assays. *Cytotechnology* **2007,** *54,* 85–88.
301. Parish, C. R.; Glidden, M. H.; Quah, B. J.; Warren, H. S. Use of the Intracellular Fluorescent dye CFSE to Monitor Lymphocyte Migration and Proliferation. In *Current Protocols in Immunology;* Coligan, J. E.; et al., Eds.; 2009. Chapter 4, Unit4 9.
302. Lyons, A. B. Analysing Cell Division in vivo and in vitro Using Flow Cytometric Measurement of CFSE Dye Dilution. *J. Immunol. Methods* **2000,** *243,* 147–154.
303. Filby, A.; Day, W.; Purewal, S.; Martinez-Martin, N. The Analysis of Cell Cycle, Proliferation, and Asymmetric Cell Division by Imaging Flow Cytometry. In *Imaging Flow Cytometry: Methods and Protocols.* In Barteneva, S. N., Vorobjev, A. I., Eds.; Springer New York: New York, NY, 2016; pp 71–95.
304. Hughes, W. L.; Bond, V. P.; Brecher, G.; Cronkite, E. P.; Painter, R. B.; Quastler, H.; Sherman, F. G. Cellular Proliferation in the Mouse as Revealed by Autoradiography With Tritiated Thymidine. *Proc. Natl. Acad. Sci. U. S. A.* **1958,** *44,* 476–483.
305. Gratzner, H. G. Monoclonal Antibody to 5-Bromo- and 5-Iododeoxyuridine: A New Reagent for Detection of DNA Replication. *Science* **1982,** *218,* 474–475.
306. Salic, A.; Mitchison, T. J. A Chemical Method for Fast and Sensitive Detection of DNA Synthesis In Vivo. *Proc. Natl. Acad. Sci. U. S. A.* **2008,** *105,* 2415–2420.
307. Decker, T.; Lohmann-Matthes, M. L. A Quick and Simple Method for the Quantitation of Lactate Dehydrogenase Release in Measurements of Cellular Cytotoxicity and Tumor Necrosis Factor (TNF) Activity. *J. Immunol. Methods* **1988,** *115,* 61–69.
308. Maccormack, T. J.; Clark, R. J.; Dang, M. K.; Ma, G.; Kelly, J. A.; Veinot, J. G.; Goss, G. G. Inhibition of Enzyme Activity by Nanomaterials: Potential Mechanisms and Implications for Nanotoxicity Testing. *Nanotoxicology* **2012,** *6,* 514–525.
309. Ozdemir, O. Flow Cytometric Cell-Mediated Cytotoxicity Assay. *J. Immunol. Methods* **2007,** *318,* 158–159. author reply 160–1.
310. Pisanic, T.; Jin, S.; Shubayev, V. *Iron Oxide Magnetic Nanoparticle Nanotoxicity: Incidence and Mechanisms, in Nanotoxicity;* John Wiley & Sons: Chichester, UK, 2009.
311. Stroh, A.; Zimmer, C.; Gutzeit, C.; Jakstadt, M.; Marschinke, F.; Jung, T.; Pilgrimm, H.; Grune, T. Iron Oxide Particles for Molecular Magnetic Resonance Imaging Cause Transient Oxidative Stress in Rat Macrophages. *Free Radic. Biol. Med.* **2004,** *36,* 976–984.
312. Nel, A.; Xia, T.; Madler, L.; Li, N. Toxic Potential of Materials at the Nanolevel. *Science* **2006,** *311,* 622–627.

313. Nel, A. E.; Madler, L.; Velegol, D.; Xia, T.; Hoek, E. M.; Somasundaran, P.; Klaessig, F.; Castranova, V.; Thompson, M. Understanding Biophysicochemical Interactions at the Nano-Bio Interface. *Nat. Mater.* **2009,** *8,* 543–557.
314. Wang, H.; Joseph, J. A. Quantifying Cellular Oxidative Stress by Dichlorofluorescein Assay Using Microplate Reader. *Free Radic. Biol. Med.* **1999,** *27,* 612–616.
315. Kobayashi, H.; Gil-Guzman, E.; Mahran, A. M.; Rakesh; Nelson, D. R.; Thomas, A. J., Jr.; Agarwa, A. Quality Control of Reactive Oxygen Species Measurement by Luminol-Dependent Chemiluminescence Assay. *J. Androl.* **2001,** *22,* 568–574.
316. Sekiya, M.; Umezawa, K.; Sato, A.; Citterio, D.; Suzuki, K. A Novel Luciferin-Based Bright Chemiluminescent Probe for the Detection of Reactive Oxygen Species. *Chem. Commun. (Camb.)* **2009,** *21,* 3047–3049.
317. Uy, B.; McGlashan, S. R.; Shaikh, S. B. Measurement of Reactive Oxygen Species in the Culture Media using Acridan Lumigen PS-3 Assay. *J. Biomol. Tech.* **2011,** *22,* 95–107.
318. Halliwell, B. Biochemistry of Oxidative Stress. *Biochem. Soc. Trans.* **2007,** *35,* 1147–1150.
319. Diaz, B.; Sanchez-Espinel, C.; Arruebo, M.; Faro, J.; de Miguel, E.; Magadan, S.; Yague, C.; Fernandez-Pacheco, R.; Ibarra, M. R.; Santamaria, J.; Gonzalez-Fernandez, A. Assessing Methods for Blood Cell Cytotoxic Responses to Inorganic Nanoparticles and Nanoparticle Aggregates. *Small* **2008,** *4,* 2025–2034.
320. Le Bras, M.; Clement, M. V.; Pervaiz, S.; Brenner, C. Reactive Oxygen Species and the Mitochondrial Signaling Pathway of Cell Death. *Histol. Histopathol.* **2005,** *20,* 205–219.
321. Wiseman, H.; Halliwell, B. Damage to DNA by Reactive Oxygen and Nitrogen Species: Role in Inflammatory Disease and Progression to Cancer. *Biochem. J.* **1996,** *313* (Pt 1), 17–29.
322. Shaikh, S.; Nicholson, L. F. Advanced Glycation End Products Induce in vitro Cross-Linking of Alpha-Synuclein and Accelerate the Process of Intracellular Inclusion Body Formation. *J. Neurosci. Res.* **2008,** *86,* 2071–2082.
323. Kroll, A.; Pillukat, M. H.; Hahn, D.; Schnekenburger, J. Interference of Engineered Nanoparticles With in vitro Toxicity Assays. *Arch. Toxicol.* **2012,** *86,* 1123–1136.
324. Aueviriyavit, S.; Phummiratch, D.; Maniratanachote, R. Mechanistic Study on the Biological Effects of Silver and Gold Nanoparticles in Caco-2 Cells-Induction of the Nrf2/HO-1 Pathway by High Concentrations of Silver Nanoparticles. *Toxicol. Lett.* **2014,** *224,* 73–83.
325. Doak, S. H.; Griffiths, S. M.; Manshian, B.; Singh, N.; Williams, P. M.; Brown, A. P.; Jenkins, G. J. Confounding Experimental Considerations in Nanogenotoxicology. *Mutagenesis* **2009,** *24,* 285–293.
326. Oberdorster, G.; Oberdorster, E.; Oberdorster, J. Nanotoxicology: An Emerging Discipline Evolving From Studies of Ultrafine Particles. *Environ. Health Perspect.* **2005,** *113,* 823–839.
327. Xiao, G. G.; Wang, M.; Li, N.; Loo, J. A.; Nel, A. E. Use of Proteomics to Demonstrate a Hierarchical Oxidative Stress Response to Diesel Exhaust Particle Chemicals in a Macrophage Cell Line. *J. Biol. Chem.* **2003,** *278,* 50781–50790.
328. Nicholls, D. G.; Ward, M. W. Mitochondrial Membrane Potential and Neuronal Glutamate Excitotoxicity: Mortality and Millivolts. *Trends Neurosci.* **2000,** *23,* 166–174.
329. Szabadkai, G.; Duchen, M. R. Mitochondria: the Hub of Cellular Ca2+ Signaling. *Physiology (Bethesda)* **2008,** *23,* 84–94.
330. Johnson, L. V.; Walsh, M. L.; Bockus, B. J.; Chen, L. B. Monitoring of Relative Mitochondrial Membrane Potential in Living Cells by Fluorescence Microscopy. *J. Cell Biol.* **1981,** *88,* 526–535.
331. Lemasters, J. J.; Ramshesh, V. K. Imaging of Mitochondrial Polarization and Depolarization With Cationic Fluorophores. *Methods Cell Biol.* **2007,** *80,* 283–295.
332. Ehrenberg, B.; Montana, V.; Wei, M. D.; Wuskell, J. P.; Loew, L. M. Membrane Potential can be Determined in Individual Cells From the Nernstian Distribution of Cationic Dyes. *Biophys. J.* **1988,** *53,* 785–794.
333. Duchen, M. R. Mitochondria in Health and Disease: Perspectives on a New Mitochondrial Biology. *Mol. Aspects Med.* **2004,** *25,* 365–451.
334. Soenen, S. J.; Illyes, E.; Vercauteren, D.; Braeckmans, K.; Majer, Z.; De Smedt, S. C.; De Cuyper, M. The Role of Nanoparticle Concentration-Dependent Induction of Cellular Stress in the Internalization of Non-Toxic Cationic Magnetoliposomes. *Biomaterials* **2009,** *30,* 6803–6813.
335. Soenen, S. J.; Nuytten, N.; De Meyer, S. F.; De Smedt, S. C.; De Cuyper, M. High Intracellular Iron Oxide Nanoparticle Concentrations Affect Cellular Cytoskeleton and Focal Adhesion Kinase-Mediated Signaling. *Small* **2010,** *6,* 832–842.
336. Gupta, A. K.; Gupta, M. Cytotoxicity Suppression and Cellular Uptake Enhancement of Surface Modified Magnetic Nanoparticles. *Biomaterials* **2005,** *26,* 1565–1573.
337. Wu, X.; Tan, Y.; Mao, H.; Zhang, M. Toxic Effects of Iron Oxide Nanoparticles on Human Umbilical Vein Endothelial Cells. *Int. J. Nanomedicine* **2010,** *5,* 385–399.
338. Maecker, H. T. Multiparameter Flow Cytometry Monitoring of T Cell Responses. *Methods Mol. Biol.* **2009,** *485,* 375–391.
339. Bolton, D. L.; Roederer, M. Flow Cytometry and the Future of Vaccine Development. *Expert Rev. Vaccines* **2009,** *8,* 779–789.
340. Ong, K. J.; MacCormack, T. J.; Clark, R. J.; Ede, J. D.; Ortega, V. A.; Felix, L. C.; Dang, M. K.; Ma, G.; Fenniri, H.; Veinot, J. G.; Goss, G. G. Widespread Nanoparticle-Assay Interference: Implications for Nanotoxicity Testing. *PLoS One* **2014,** *9,* e90650.
341. Asuri, P.; Bale, S. S.; Karajanagi, S. S.; Kane, R. S. The Protein-Nanomaterial Interface. *Curr. Opin. Biotechnol.* **2006,** *17,* 562–568.
342. Casey, A.; Herzog, E.; Lyng, F. M.; Byrne, H. J.; Chambers, G.; Davoren, M. Single Walled Carbon Nanotubes Induce Indirect Cytotoxicity by Medium Depletion in A549 Lung Cells. *Toxicol. Lett.* **2008,** *179,* 78–84.
343. Holder, A. L.; Goth-Goldstein, R.; Lucas, D.; Koshland, C. P. Particle-Induced Artifacts in the MTT and LDH Viability Assays. *Chem. Res. Toxicol.* **2012,** *25,* 1885–1892.
344. Davoren, M.; Herzog, E.; Casey, A.; Cottineau, B.; Chambers, G.; Byrne, H. J.; Lyng, F. M. In Vitro Toxicity Evaluation of Single Walled Carbon Nanotubes on Human A549 Lung Cells. *Toxicol. In Vitro* **2007,** *21,* 438–448.
345. Pfaller, T.; Colognato, R.; Nelissen, I.; Favilli, F.; Casals, E.; Ooms, D.; Leppens, H.; Ponti, J.; Stritzinger, R.; Puntes, V.; Boraschi, D.; Duschl, A.; Oostingh, G. J. The Suitability of Different Cellular in vitro Immunotoxicity and Genotoxicity Methods for the Analysis of Nanoparticle-Induced Events. *Nanotoxicology* **2010,** *4,* 52–72.
346. Leszczak, V.; Place, L. W.; Franz, N.; Popat, K. C.; Kipper, M. J. Nanostructured Biomaterials From Electrospun Demineralized Bone Matrix: A Survey of Processing and Crosslinking Strategies. *ACS Appl. Mater. Interfaces* **2014,** *6,* 9328–9337.
347. Meneksedag-Erol, D.; Tang, T.; Uludağ, H. Molecular Modeling of Polynucleotide Complexes. *Biomaterials* **2014,** *35,* 7068–7076.
348. Allen, M. J.; Tung, V. C.; Kaner, R. B. Honeycomb Carbon: A Review of Graphene. *Chem. Rev.* **2010,** *110,* 132–145.
349. Shen, H.; Zhang, L.; Liu, M.; Zhang, Z. Biomedical Applications of Graphene. *Theranostics* **2012,** *2,* 283–294.
350. Zhang, L.; Xia, J.; Zhao, Q.; Liu, L.; Zhang, Z. Functional Graphene Oxide as a Nanocarrier for Controlled Loading and Targeted Delivery of Mixed Anticancer Drugs. *Small* **2010,** *6,* 537–544.
351. Lipinski, C. A.; Lombardo, F.; Dominy, B. W.; Feeney, P. J. Experimental and Computational Approaches to Estimate Solubility and Permeability in Drug Discovery and Development Settings. *Adv. Drug Deliv. Rev.* **2012,** *64* (Suppl), 4–17.
352. Conde-Leboran, I.; Baldomir, D.; Martinez-Boubeta, C.; Chubykalo-Fesenko, O.; del Puerto Morales, M.; Salas, G.; Cabrera, D.; Camarero, J.; Teran, F. J.; Serantes, D. A Single Picture Explains Diversity of Hyperthermia Response of Magnetic Nanoparticles. *J. Phys. Chem. C* **2015,** *119,* 15698–15706.
353. Carrey, J.; Mehdaoui, B.; Respaud, M. Simple Models for Dynamic Hysteresis Loop Calculations of Magnetic Single-Domain Nanoparticles: Application to Magnetic Hyperthermia Optimization. *J. Appl. Phys.* **2011,** *109,* 083921.
354. Kitano, H. A Robustness-Based Approach to Systems-Oriented Drug Design. *Nat. Rev. Drug Discov.* **2007,** *5,* 202–210.
355. Anastas, P. T.; Eghbali, N. Green Chemistry: Principles and Practice. *Chem. Soc. Rev.* **2010,** *39* (1), 301–312.
356. Hutchison, J. E. Greener Nanoscience: A Proactive Approach to Advancing Applications and Reducing Implications of Nanotechnology. *ACS Nano* **2008,** *2,* 395–402.
357. Prakash, P.; Gnanaprakasam, P.; Emmanuel, R.; Arokiyaraj, S.; Saravanan, M. Green Synthesis of Silver Nanoparticles from Leaf Extract of Mimusops Elengi, Linn. For Enhanced Antibacterial Activity Against Multi Drug Resistant Clinical Isolates. *Colloids Surf. B* **2013,** *108,* 255–259.
358. Sudip, M.; Sushma, V.; Sujata, P.; Ayan Kumar, B.; Manika Pal, B.; Bojja, S.; Chitta Ranjan, P. Green Chemistry Approach for the Synthesis and Stabilization of Biocompatible Gold Nanoparticles and Their Potential Applications in Cancer Therapy. *Nanotechnology* **2012,** *23,* 455103.

359. Graedel, T. E.; Harper, E. M.; Nassar, N. T.; Nuss, P.; Reck, B. K. Criticality of Metals and Metalloids. *Proc. Natl. Acad. Sci.* **2015,** *112,* 4257–4262.
360. Hans, M. L.; Lowman, A. M. Biodegradable Nanoparticles for Drug Delivery and Targeting. *Curr. Opin. Solid State Mater. Sci.* **2002,** *6,* 319–327.
361. Park, J.-H.; Gu, L.; von Maltzahn, G.; Ruoslahti, E.; Bhatia, S. N.; Sailor, M. J. Biodegradable Luminescent Porous Silicon Nanoparticles for in vivo Applications. *Nat. Mater.* **2009,** *8,* 331–336.
362. Ferrari, M. Cancer Nanotechnology: Opportunities and Challenges. *Nat. Rev. Cancer* **2005,** *5,* 161–171.
363. Prinsen, B. H. C. M. T.; de Sain-van der Velden, M. G. M. Albumin Turnover: Experimental Approach and Its Application in Health and Renal Diseases. *Clin. Chim. Acta* **2004,** *347,* 1–14.
364. Hunt, D. R.; Jovanovic, S. A.; Wikesjö, U. M.; Wozney, J. M.; Bernard, G. W. Hyaluronan Supports Recombinant Human Bone Morphogenetic Protein-2 Induced Bone Reconstruction of Advanced Alveolar Ridge Defects in Dogs. A Pilot Study. *J. Periodontol.* **2001,** *72,* 651–658.
365. De Matteis, L.; Mitchell, S. G.; de la Fuente, J. M. Supramolecular Antimicrobial Capsules Assembled From Polyoxometalates and Chitosan. *J. Mater. Chem. B* **2014,** *2,* 7114–7117.
366. Jordan, A.; Scholz, R.; Wust, P.; Fähling, H.; Roland, F. Magnetic Fluid Hyperthermia (MFH): Cancer Treatment With AC Magnetic Field Induced Excitation of Biocompatible Superparamagnetic Nanoparticles. *J. Magn. Magn. Mater.* **1999,** *201,* 413–419.
367. Rosen, J. E.; Chan, L.; Shieh, D.-B.; Gu, F. X. Iron Oxide Nanoparticles for Targeted Cancer Imaging and Diagnostics. *Nanomedicine* **2012,** *8,* 275–290.
368. Hilger, I.; Kaiser, W. A. Iron Oxide-Based Nanostructures for MRI and Magnetic Hyperthermia. *Nanomedicine* **2012,** *7,* 1443–1459.
369. Eberbeck, D.; Dennis, C. L.; Huls, N. F.; Krycka, K. L.; Gruttner, C.; Westphal, F. Multicore Magnetic Nanoparticles for Magnetic Particle Imaging. *IEEE Trans. Magn.* **2013,** *49,* 269–274.
370. Gehrke, N.; Briel, A.; Ludwig, F.; Remmer, H.; Wawrzik, T.; Wellert, S. New Perspectives for MPI: A Toolbox for Tracer Research. In *Magnetic Particle Imaging,* 140, Buzug, T. M., Borgert, J., Eds.; Springer Berlin Heidelberg: Berlin Heidelberg, 2012; pp 99–103.
371. Khandhar, A. P.; Ferguson, R. M.; Arami, H.; Krishnan, K. M. Monodisperse Magnetite Nanoparticle Tracers for in vivo Magnetic Particle Imaging. *Biomaterials* **2013,** *34,* 3837–3845.
372. Bradshaw, M.; Clemons, T.; Ho, D.; Gutierrez, L.; Lazaro, F.; House, M.; St Pierre, T. G.; Fear, M.; Wood, F.; Iyer, S. Manipulating Directional Cell Motility Using Intracellular Superparamagnetic Nanoparticles. *Nanoscale* **2015,** *7,* 4884–4889.
373. Meddahi-Pellé, A.; Legrand, A.; Marcellan, A.; Louedec, L.; Letourneur, D.; Leibler, L. Organ Repair, Hemostasis, and in vivo Bonding of Medical Devices by Aqueous Solutions of Nanoparticles. *Angew. Chem. Int. Ed.* **2014,** *53,* 6369–6373.
374. Bonnecaze, R.; Clements, M. Magnetically Driven Flows of Suspensions of Rods to Deliver Clot-Busting Drugs to Dead-end Arteries. *Bull. Am. Phys. Soc.* **2014,** *59.* D9.7.
375. Gao, Y.; Lim, J.; Teoh, S.-H.; Xu, C. Emerging Translational Research on Magnetic Nanoparticles for Regenerative Medicine. *Chem. Soc. Rev.* **2015,** *44,* 6306–6329.
376. Tabatabaei, S. N.; Girouard, H.; Carret, A.-S.; Martel, S. Remote Control of the Permeability of the Blood–Brain Barrier by Magnetic Heating of Nanoparticles: A Proof of Concept for Brain Drug Delivery. *J. Control. Release* **2015,** *206,* 49–57.
377. Sasaki, T.; Iwasaki, N.; Kohno, K.; Kishimoto, M.; Majima, T.; Nishimura, S.-I.; Minami, A. Magnetic Nanoparticles for Improving Cell Invasion in Tissue Engineering. *J. Biomed. Mater. Res. A* **2008,** *86A,* 969–978.
378. Cheng, K. K.; Chan, P. S.; Fan, S.; Kwan, S. M.; Yeung, K. L.; Wáng, Y.-X. J.; Chow, A. H. L.; Wu, E. X.; Baum, L. Curcumin-Conjugated Magnetic Nanoparticles for Detecting Amyloid Plaques in Alzheimer's Disease Mice Using Magnetic Resonance Imaging (MRI). *Biomaterials* **2015,** *44,* 155–172.
379. Tsai, S.; Shameli, A.; Yamanouchi, J.; Clemente-Casares, X.; Wang, J.; Serra, P.; Yang, Y.; Medarova, Z.; Moore, A.; Santamaria, P. Reversal of Autoimmunity by Boosting Memory-like Autoregulatory T Cells. *Immunity* **2010,** *32,* 568–580.
380. Candido, R. R. F.; Favero, V.; Duke, M.; Karl, S.; Gutiérrez, L.; Woodward, R. C.; Graeff-Teixeira, C.; Jones, M. K.; St. Pierre, T. G. The Affinity of Magnetic Microspheres for Schistosoma Eggs. *Int. J. Parasitol.* **2015,** *45,* 43–50.
381. Jahn, A.; Reiner, J. E.; Vreeland, W. N.; DeVoe, D. L.; Locascio, L. E.; Gaitan, M. Preparation of Nanoparticles by Continuous-Flow Microfluidics. *J. Nanopart. Res.* **2008,** *10,* 925–934.
382. Horikoshi, S.; Abe, H.; Torigoe, K.; Abe, M.; Serpone, N. Access to Small Size Distributions of Nanoparticles by Microwave-Assisted Synthesis. Formation of Ag Nanoparticles in Aqueous Carboxymethylcellulose Solutions in Batch and Continuous-Flow Reactors. *Nanoscale* **2010,** *2,* 1441–1447.
383. Wagner, J.; Köhler, J. M. Continuous Synthesis of Gold Nanoparticles in a Microreactor. *Nano Lett.* **2005,** *5,* 685–691.
384. Chin, S. F.; Iyer, K. S.; Raston, C. L.; Saunders, M. Size Selective Synthesis of Superparamagnetic Nanoparticles in Thin Fluids under Continuous Flow Conditions. *Adv. Funct. Mater.* **2008,** *18,* 922–927.
385. Feliu, N.; Docter, D.; Heine, M.; del Pino, P.; Ashraf, S.; Kolosnjaj-Tabi, J.; Macchiarini, P.; Nielsen, P.; Alloyeau, D.; Gazeau, F.; Stauber, R. H.; Parak, W. J. In Vivo Degeneration and the Fate of Inorganic Nanoparticles. *Chem. Soc. Rev.* **2016,** *45* (9), 2440–2457.

1.10 Click Chemistry in Medicinal Chemistry for Comprehensive Medicinal Chemistry III

P Thirumurugan and K Jozwiak, Medical University of Lublin, Lublin, Poland

© 2017 Elsevier Ltd. All rights reserved.

1.10.1	**Introduction**	296
1.10.2	**Anticancer Agents Generated via Click Chemistry Reaction**	298
1.10.3	**Antiproliferative Agents Synthesized Using Click Chemistry**	304
1.10.4	**Antiviral and Other Lead Small Molecules Synthesized From Click Chemistry**	305
1.10.5	**Click Chemistry in Receptor–Ligand-Binding Studies**	309
1.10.5.1	Agonist	309
1.10.5.2	Antagonist	311
1.10.5.3	Selective Binding Ligands	314
1.10.6	**In Situ Click Chemistry**	317
1.10.6.1	Screening and Identification of Biotin Protein Ligase (BPL) Inhibitors	318
1.10.6.2	Probing the Binding Site of Abl Tyrosine Kinase	318
1.10.6.3	Antibody-Like Protein-Capture Agents	318
1.10.7	**Conclusion and Future Directions**	322
References		322
Relevant Websites		324
History of Click chemistry		324
Click chemistry—synthetic point of view		324
Finn, Fokin, and Sharpless are suggested as possible Nobel Prize winners for "the development of modular click chemistry"		324
Click hot topics		324
Click Chemistry Tools / Bioconjugate Technologies		324
Click chemistry for drug discovery		325

1.10.1 Introduction

Creating novel drug candidates with improved biological properties and diminished adverse effect for treating human disease such as AIDS and cancer is one of the most important challenges faced by contemporary medicinal chemists.[1–4] Synthetic chemists and biologists initiated the process by taking a lead structure and then finding functional analogs exhibiting the preferred biological activities. Then, medicinal chemist used their experience and chemical insights to eventually choose a functional analog for further development.[5,6] Conventional methods of drug discovery are now being implemented by approaches made possible by identifying the molecular processes involved in disease. In this view, drug design begins with attempting to identify a molecular target (typically a receptor or protein in the body) followed by identification of molecules that affect the function of that target. Making these lead structures without side products and purification is synthetically demanding.[6,7] Click chemistry describes a set of powerful, highly reliable, and selective reactions to generate substances quickly and reliably by joining small units together through heteroatom links (C–X–C).[8–10] Click chemistry in drug design has many advantages and key features of click chemistry can be summarized as follows:[11]

Click reactions progress quickly at low or room temperatures in compatible eco-friendly solvent medium such as water and water-miscible solvents such as THF, methanol, ethanol, DMF, and DMSO and are suitable for microscale solution-phase parallel synthesis without the need for protecting group manipulations. As a result, click chemistry enables the rapid and reliable screening of large library of functional analogs with almost complete chemo-selectivity with broad functional group tolerance.[10,11] The orthogonality of the azide and alkyne functionalities to a diverse range of functional groups and reaction conditions allows the assembly of reactants decorated with diverse unprotected functionalities. The development of new methods for click synthesis is still of interest due to the importance of this function in drug discovery. Several existing methodologies such as copper and ruthenium salt catalyzed describe the regioselective formation of the 1,4-disubstituted triazole unit; efforts also have been made at developing methodologies for the exclusive formation of the 1,5-disubstituted regioisomers that are important in medicinal chemistry (**Fig. 1A**).[12,13] The triazole product is an effective pharmacophore. The 1,2,3-triazole structural motif generated in the click reaction is much more than just a passive linker unit and is considered to be a safe bioequivalent surrogate for amide, which is a widely employed functional group in drug design.[14] The 1,2,3-triazole moiety has several advantages:[14] (i) Its chemical robustness is favorable for adoption in drug discovery programs; (ii) it has a moderate dipole moment (5 debye) and the two H-bond acceptors at N_2 and N_3 can interact with biomolecular targets via enhanced H-bonding interactions, dipole interactions, or pi–pi stacking interactions as shown **Fig. 1A**; (iii) the 1,2,3-triazole offers high chemical stability in biological environments,

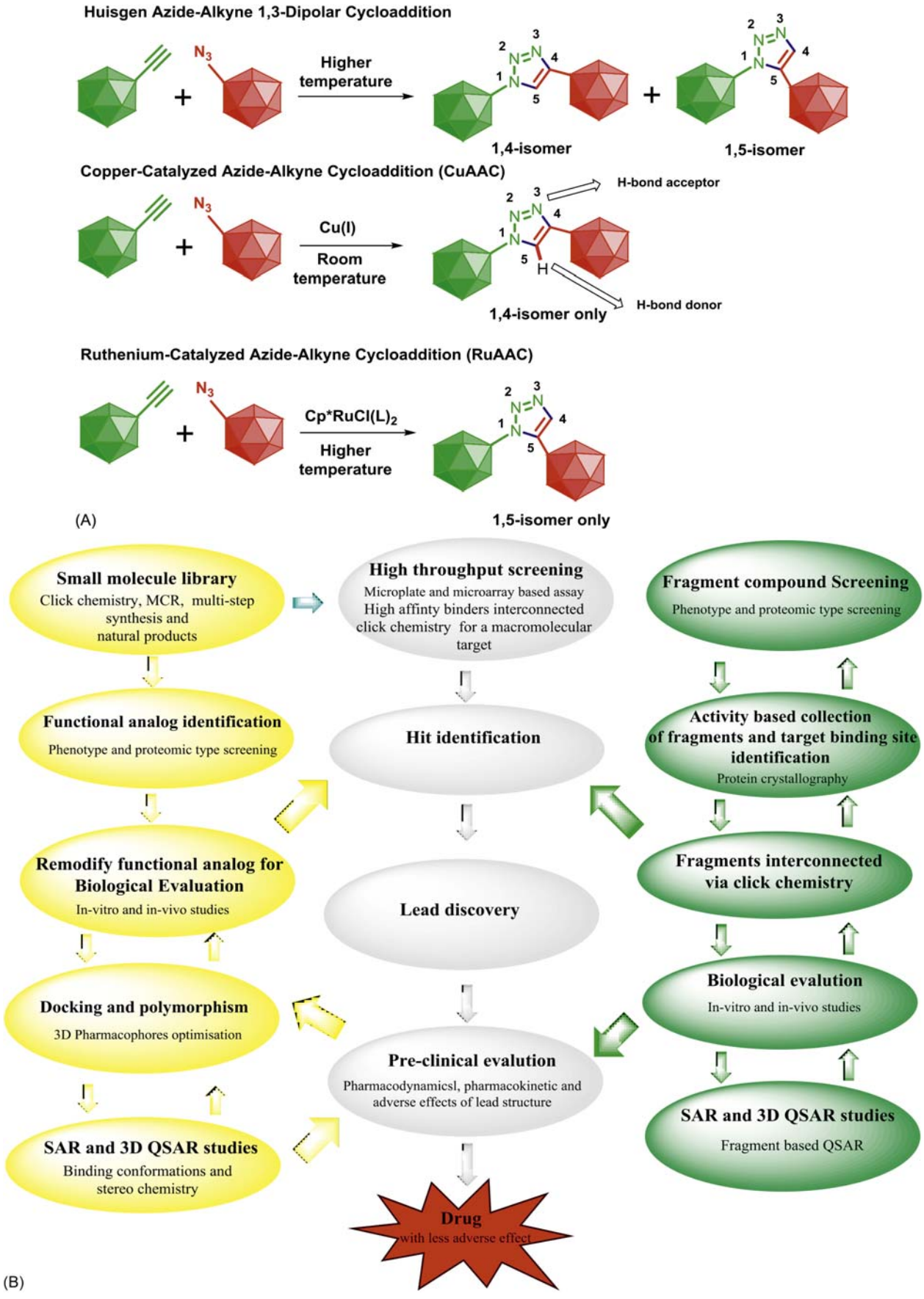

Fig. 1 (A) Schematic representation of (i) Huisgen 1,3-dipolar cycloaddition at higher temperature and (ii) copper (I) salt-catalyzed click reaction at room temperature and (iii) ruthenium-catalyzed azide–alkyne cycloaddition for exclusive formation of 1,5-isomer. (B) Drug discovery process workflow chart: click chemistry employed for various stages of drug candidate development. FBDD, SAR, and QSAR studies are essential elements of drug discovery process. *FBDD*, fragment-based drug design; *QSAR*, quantitative SAR; *SAR*, structure–activity relationship.

including acidic and basic milieus and oxidative and reductive conditions.[15] X-ray crystal structures of protein–triazole complexes are available, which is helpful for drug design, and the pharmacokinetic profile of this moiety has been investigated.[15] Equally important, 1,4-triazoles are metabolically inert, whereas 1,5-triazoles can be metabolized to N-oxides, which are reactive intermediates. Further, 1,4-disubstituted triazoles have a negligible inhibitory effect on the cytochrome P450 family of metabolizing enzymes, compared with the 1,5-isomers, and this is favorable for avoiding drug–drug interactions.[16] These attributes make 1,4-triazole suitable for use either as a potent pharmacophore that can directly participate in drug–receptor interactions or as a nonlabile covalent spacer between discrete N-1 and C-4 or C-5 substituents while maintaining excellent chemical and metabolic stability.[17–19] The triazole analogs are found in a number of biologically active compounds especially anti-HIV, antibiotic, antiviral, and antimicrobial activities.[14,20–22]

A drug discovery process contains several steps that include various chemical and biological screening. Present drug discovery depends on massive screening of chemical libraries against various extracellular and intracellular molecular targets to find novel chemotypes with the desired mode of action. How click chemistry can be effectively applied to drug discovery process is described in Fig. 1B.

1.10.2 Anticancer Agents Generated via Click Chemistry Reaction

Target-based approach in drug discovery is most appealing in contemporary pharmaceutical research, which requires that two key issues should be addressed well for drug development:[23,24] (i) biological targets with an activity that has a causative role in either the onset or progression of a human disease must be identified and (ii) therapeutic agents that appropriately modulate the activity of these targets in humans with limited or no adverse effects must be developed.[25] Conventional drug discovery processes such as high-throughput screening, combinatorial chemistry, and the sequencing of the human genome were remedies for the problems facing the pharmaceutical companies. The utilization of these technologies is well established at most modern pharmaceutical industries; however, the return on investment in terms of marketed products has not met expectations in the early 1990s. Due to severe commercial pressure to increase discovery productivity, medicinal chemists started using advent screening technology such as fragment-based methods for drug development process. Fragment-based drug design (FBDD) is an important tool for lead identification in drug discovery that has emerged in the past decade.[26,27] FBDD is focused on screening smaller numbers of compounds (typically 1000 chemical library) in the hopes of finding low-affinity fragments (with K_d values in the high micromolar to millimolar range). By contrast, conventional screening attempts to evaluate as many compounds as technologically possible (typically 100,000 or more) in the hopes of finding relatively potent drug leads (with K_d values ideally less than 1 μM).

The fragmentation of molecules leads to smaller pieces or even into discrete functional groups (e.g., carboxylate, amine, and alcohol) has been used for some time to simplify the computational analysis of ligand binding and to map out different pharmacophoric elements required for high-affinity binding.[28] The proper optimization of each unique interaction in the binding site and subsequent incorporation into a single molecular entity should produce a compound with a binding affinity that is the sum of the individual interactions.[29]

The efficiency of fragment-based methods can be improved by a combination of other conventional drug discovery techniques with FBDD. The impact of combined drug discovery methods has made in progressing new medicines into clinic.[29] Several enzymes have multiple binding pockets; yet conventional inhibitor development generally focuses primarily on the active site. However, in some cases, the secondary/allosteric binding sites confer selectivity as well as potency. Within this context, click chemistry, due to its highly modular and efficient reaction nature, has been identified as one of the most practical methods toward fragment-based inhibitor assembly where $N+M$ combinations of inhibitor fragments lead to the generation of $N \times M$ potential bidentate inhibitors. Identified small fragments joined together easily without affecting active site using click chemistry reaction or other conventional chemical reactions. Ligands with multiple binding pockets generated via FBDD can be used to selectively inhibit the over expressed protein or enzyme.[17,20]

Click chemistry is an ideal reaction to connect the prodrugs without affecting pharmacological activities. Some of click chemistry reaction-generated drug candidates that reached to clinical trials are shown in Fig. 2. Click-FBDD-based drug screening allows for more efficient lead identification and lead optimization procedures in medicinal chemistry. In this connection, it is easy to predict the usefulness of this reaction in fragment-based ligand design. Triazole peptidomimetic fragments could act as building blocks to be used in fragment-based approaches for drug discovery, thereby rendering this technique feasible in drug discovery. Hence, we go through here some of the lead drug-like molecules generated via click chemistry reaction described in the literature as novel drug development toward many incurable diseases like anticancer, antiviral, and anti-TB.[17,20] Some of triazole derivatives shown in Fig. 2 are under clinical trials for cancer therapy. Radicicol triazole (i) is a promising heat shock protein 90 (Hsp90)-based anticancer agent prepared from synthetically modified natural product of radicicol (dienone of cycloproparadicicol replaced with a triazole).[30] The conformational constraints of **r**eceptor-**a**ssociated **p**rotein 1 are important for binding to the Hsp90 N-terminal domain, and triazole analogs showed a significant drop-in activity compared to radicicol itself, and interestingly, radicicol triazole inhibits Kasumi-1 leukemia cells (IC_{50} value of 620 nM).[30] Letrozole (ii) and anastrozole (iii) are nonsteroidal aromatase inhibitors for the treatment of hormonally responsive breast cancer after surgery.[31] Both drugs work by inhibiting the synthesis of estrogen primarily in the body. This helps to starve cancer cells by depriving them of estrogen. Carboxyamidotriazole (iv) is an orally active potential antineoplastic agent, and it binds non-voltage-operated calcium channels, blocking both Ca^{2+} influx into cells and Ca^{2+} release from intracellular stores, resulting in the disruption of calcium channel-mediated signal transduction.[32]

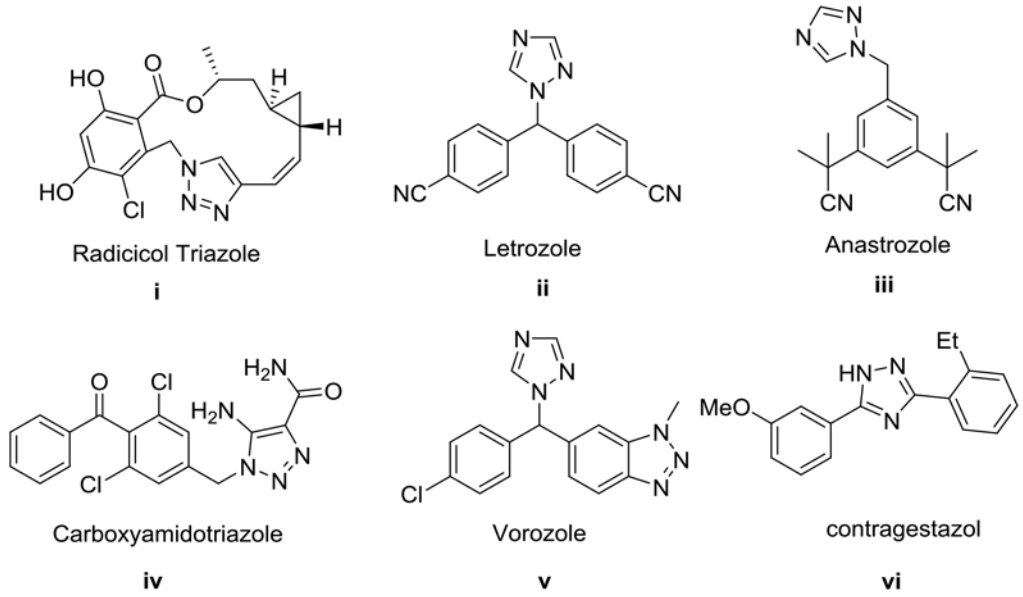

Fig. 2 Triazole-based analogs under clinical trials as cancer therapy agents.

Carboxyamidotriazole derivative also may inhibit tumor cell growth, invasion, and metastasis. Vorozole (v) is an imidazole-based specific, selective, and potent aromatase inhibitor and useful for postmenopausal patients with advanced breast cancer.[33] Vorozole is a triazole derivative, which binds to the cytochrome P450 moiety of aromatase, thus causing reversible inhibition of the enzyme. Plasma estradiol levels are reduced by about 90% in postmenopausal women treated with vorozole. Phase II clinical studies found vorozole to be an effective agent for the treatment of postmenopausal women with advanced breast cancer, achieving objective responses in up to 35% of patients. In two large phase III studies, vorozole 2.5 mg day^{-1} demonstrated favorable clinical efficacy compared with aminoglutethimide and megestrol. Vorozole improved patients' quality of life to a greater extent than aminoglutethimide.[34] Contragestazol is a nonhormonal antifertility agent and displayed a high activity on arresting early pregnancy in animals. Recently, contragestazol also exhibited outstanding effect on the suppression of ovarian cancer cell growth in human cell tumor models.[35]

A collection of triazole-dithiocarbamate derivatives were synthesized and evaluated for anticancer activity against four human tumor cell lines (MGC-803, MCF-7, PC-3, and EC-109). Most of the synthesized compounds exhibited moderate to potent activity against MGC-803 and MCF-7. The synthesized triazole analogs showed excellent broad-spectrum anticancer activity with IC_{50} values ranging from 0.73 to 11.61 μM (MGC-803, MCF-7, PC-3, and EC-109 cell lines). Particularly, compound **1** (Fig. 3) was more potent than 5-fluorouracil against all tested human cancer cell lines. Flow cytometry analysis demonstrated that treatment of MGC-803 with 3c led to cell cycle arrest at G2/M phase accompanied by an increase in apoptotic cell death after 12 h.[36]

Girard and his coworkers recently prepared mono- and bis-triazole derivatives from propiolic acid. All mono- and bis-alkyne triazole compounds were tested in vitro for their cytotoxic activity using B16 melanoma cells. Compound **2** ($IC_{50} = 0.28$ μM; Fig. 3) showed nanomolar level of cytotoxic activity using B16 melanoma cells.[37]

Kumar and Kalivendi et al. prepared a series of podophyllotoxin derivatives by using azide–alkyne click chemistry. Podophyllotoxin derivatives were evaluated for their cytotoxicity against a panel of four human cancer cell lines and their IC_{50} values were found to be in the range of 2.4– 29.06 μM. The cytotoxicity exhibited by the majority of tested compounds was found to be comparable and often more effective than doxorubicin, and compound **3** (Fig. 3) exhibited good cytotoxicity on A-549 cell lines.[38]

Triazole derivatives of epipodophyllotoxin–chalcone were generated toward the development of better anticancer agents. These hybrids consist of structurally different but functionally similar topoisomerase-II inhibitors, which were conjugated together through click chemistry. Evaluation of the anticancer activity of these synthesized conjugates against a panel of six human cancer cell lines proved their potential cytotoxicity. Among evaluated compounds, compound **4** (Fig. 3) was found to be the most potent, especially selective against SW-620 and SKN-SH cell lines.[39]

Bertrand and coworkers recently reported the synthesis of clickable pH-responsive pH-mediated release of histone deacetylase inhibitors. HDACi are an important class of molecules belonging to the epigenetic modulators used for innovative cancer strategies. The behavior of these prodrugs was determined by a bioluminescence resonance energy transfer assay in living tumor cells. Innovative type of clickable prodrug (5; Fig. 3) entered cancer cells and showed restored antiproliferative properties attributed to the effective release of the HDAC inhibitors. A correlation between kinetic studies, dose responses, and biological activities was obtained, making such clickable prodrug good candidates for new strategies in epigenetic-oriented anticancer therapies.[40]

A series of triazole-linked osthol derivatives were synthesized using click chemistry approach. All the derivatives were subjected to 3-(4,5-dimethylthiazol-yl)-diphenyl tetrazolium bromide (MTT) cytotoxicity screening against a panel of seven different human

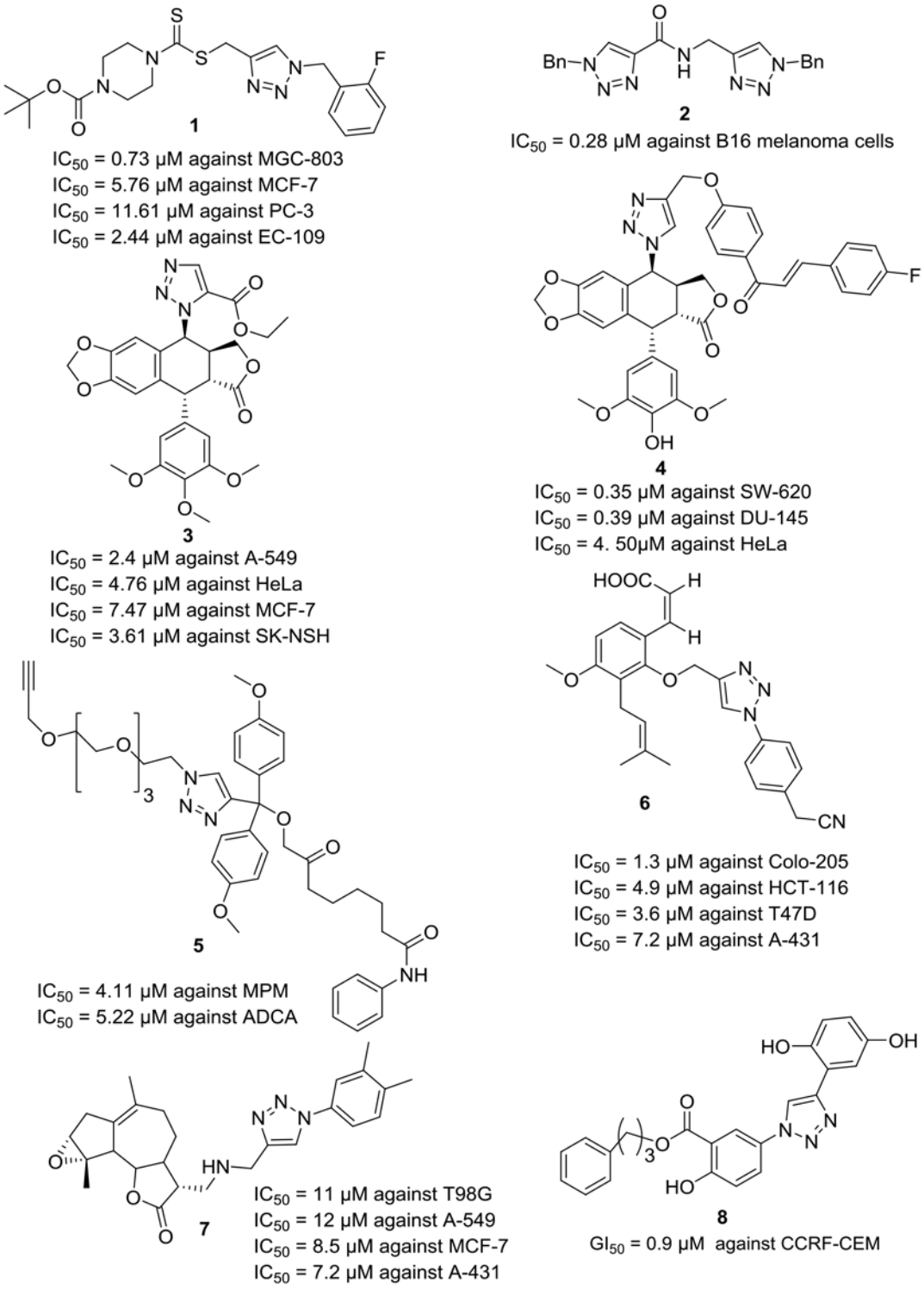

Fig. 3 Potent click functional triazole generated for anticancer activity with low IC_{50}.

cancer cell lines, viz., colon (colo-205 and HCT-116), breast (T47D), lung (NCIH322 and A549), prostate (PC-3), and skin (A-431) to check their cytotoxic potential. Interestingly, among the tested molecules, most of the analogs displayed better cytotoxic activity than the parent osthol. Of the synthesized triazoles, compound 6 (Fig. 3) showed the best activity with IC_{50} of 1.3, 4.9, 3.6, 41.0, 35.2, 26.4, and 7.2 μM against colon (Colo-205 and HCT-116), breast (T47D), lung (NCI-H322 and A549), prostate (PC-3), and skin (A-431) cancer lines, respectively. Compound **6** induced potent apoptotic effects in Colo-205 cells. The population of

apoptotic cells increased from 11.4% in case of negative control to 24.1% at 25 μM of **6**. Compound **6** also induced a remarkable decrease in mitochondrial membrane potential (LJm) leading to apoptosis of cancer cells used.[41]

Bhat and his coworkers synthesized a series of 1,4-disubstituted 1,2,3-triazoles of Ludartin for their behavior against a panel of five human cancerous cell lines. Sulforhodamine B cytotoxicity screening of the resulting products against a panel of five human cancerous cell lines revealed that few of the analogs display promising broad-spectrum cytotoxic effect. Among all synthesized compounds, only **7** (Fig. 3) displayed the best cytotoxic effect with IC_{50} values of 12, 11, 38, 39, and 8.5 μM but less than the standard Ludartin (1) with IC_{50} values of 6.3, 7.4, 7.5, 6.9, and 0.5 μM against human neuroblastoma (T98G), lung (A-549), prostate (PC-3), colon (HCT-116), and breast (MCF-7) cancer cell lines, respectively.[42]

Click-based approach for rapid synthesis of lavendustin triazoles is used by Ryu and his coworkers. Lavendustin substituents were varied to investigate chemical space and the auxophoric $-CH_2-NH-$ was altered to a 1,2,3-triazole for rapid click conjugation. Lavendustin triazoles were evaluated against HCT116 colon cancer and CCRF-CEM leukemia cell lines. Among 28 analogs, compound **8** (Fig. 3) inhibited CCRF-CEM leukemia cell growth with the GI_{50} value of 0.9 μM.[43]

Phenyl-substituted berberine triazolyls was generated using click cycloaddition. The synthesized berberine triazolyl compounds were evaluated for anticancer activity against a panel of three human cancer cell lines, including MCF-7 (breast), SW-1990 (pancreatic), and SMMC-7721 (liver) and the noncancerous human umbilical vein endothelial cell (HUVEC) cell lines. The screening results indicated that most of the compounds displayed notable anticancer activities against the MCF-7 cells compared with berberine. Triazole analog **9** (Fig. 4) showed potent inhibitory activity against the SW-1990 and SMMC-7721 cell lines, with half-maximal inhibitory concentration (IC_{50}) values of 8.54 ± 1.97 μM and 11.87 ± 1.83 μM, respectively. Compound **10** exhibited the most potent inhibitory activity against the MCF-7 cell line, with an IC_{50} value of 12.57 ± 1.96 μM. Compound **9** and compound **10** (Fig. 4) exhibited low cytotoxicity in the HUVEC cell line, with IC_{50} values of 25.49 ± 3.24 μM and 30.47 ± 3.47 μM, respectively.[44]

A series of 2-pyridone triazole derivatives evaluated their antitumor activities in vitro. The bioassays showed that most of the synthesized compounds exerted inhibitory effects on six human cancer cell lines to various extents. Especially, compound **11** (Fig. 4) showed good antitumor activities (IC_{50} values of A549, HeLa, and SW480 cancer cell lines were 0.86, 0.54, and 0.21 μM, respectively).[45]

Ursolic phenyl triazolyl derivatives were synthesized via click chemistry and the synthetic compounds were evaluated for anticancer activity against a panel of four human cancer cell lines including A-549 (lung), MCF-7 (breast), HCT-116 (colon), THP-1 (leukemia), and normal human epithelial cell line (FR-2) using sulforhodamine B assay. The pharmacological results showed that most of the compounds displayed high level of antitumor activities against the tested cancer cell lines compared with ursolic acid. Compound **12** (Fig. 4) was found to be the most potent compound among the synthesized compounds.[46]

A library of podophyllotoxin 4β-[(4-alkyl)-1,2,3-triazol-1-yl] derivatives were synthesized by employing click chemistry approach and evaluated for cytotoxicity against a panel of human cancer cell lines (SF-295, A-549, PC-3, Hep-2, HCT-15, and MCF-7). Majority of the compounds proved more potent than etoposide, and selected compounds **13** and **14** (Fig. 4) exhibited significant anticancer activity with IC_{50} values in the range of 0.001–1 μM. DNA fragmentation and flow-cytometric results reveal that 4β-[(4-alkyl)-1,2,3-triazol-1-yl] podophyllotoxin derivatives induce dose-dependent apoptosis. Docking experiments showed a good correlation between their calculated interaction energies with the topoisomerase II and the observed IC_{50} values of all these compounds.[47]

Click chemistry employed for the synthesis of novel heat shock protein 90 (Hsp90)-based anticancer agent, triazole-cyclopropradicicol derivative. Preliminary biological evaluations revealed triazole-cyclopropradicicol 15 (Fig. 4) potent inhibitor of Hsp90, with $IC_{50} = 400$ nM. Triazole-cyclopropradicicol 15 also displayed significant in vitro inhibitory activity against the leukemia cell line Kasumi-1 ($IC_{50} = 650$ nM).[48]

Chang and his coworkers employed click chemistry for the synthesis of a library of carbohydrate–cyclopamine derivatives with various structural motifs for exploring the desired activity. From this initial library, we have observed one derivative that exhibits improved activity against lung cancer cell as compared to cyclopamine. Compound **16** (Fig. 4) expressed potent activity against lung cancer cell lines with IC_{50} value of 33 μM.[49]

A library of 1,2,3-triazole-pyrrolo[2,1-c][1,4]benzodiazepines functional derivatives were synthesized by employing "click" chemistry. These molecules exhibited promising DNA-binding affinity and evaluated for their in vitro anticancer activity in selected human cancer cell lines of breast (Zr-75-1 and MCF7), oral (KB, DWD, and Gurav), ovary (A2780), colon (Colo205), lung (A549), prostate (PC3), and cervix (SiHa) by using the sulforhodamine B (SRB) method. Especially, compound **17** (Fig. 5) showed good inhibition against various cancer cells like oral, ovarian, colon, lung, prostate, and cervical.[50]

Benzo-macrolactone derivatives were prepared by click chemistry reaction and evaluated as inhibitors of Hsp90, an emerging target for novel cancer therapeutic agents. The synthesis of resorcylic acid macrolactone analogs of the natural product radicicol was described in the literature in which the key steps are the acylation and ring opening of a homophthalic anhydride to give an isocoumarin, followed by a ring-closing metathesis to form the macrolactone. The novel triazole-macrocyclic lactones were evaluated for Hsp90 inhibition in two Hsp90 binding assays: the fluorescence-polarization (FP) assay and the TR-FRET assay. Their growth inhibitory potency in HCT116 human colon cancer cell line, as measured by the SRB assay, was also determined. Compound **18** (Fig. 5) showed good inhibition of Hsp90 in the FP assay in the series.[51]

Click chemistry was employed for the synthesis of a series of triazole-containing novobiocin analogs. The antiproliferative effects of these compounds were evaluated against two breast cancer cell lines (SKBr-3 and MCF-7) and manifested activities similar to their amide-containing counterparts. In addition, Hsp90-dependent client protein degradation was observed via western blot

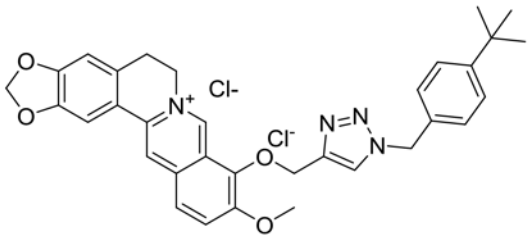

9

IC_{50} = 8.54 μM against SW-190
IC_{50} = 11.87 μM against SMMC-7721
IC_{50} = 25.49 μM against HUVEC

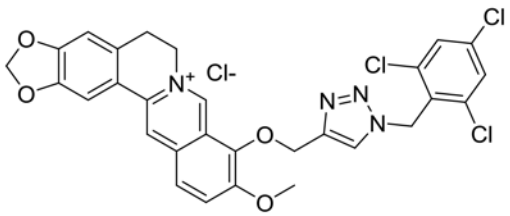

10

IC_{50} = 12.57 μM against MCF-7
IC_{50} = 30.47 μM against HUVEC

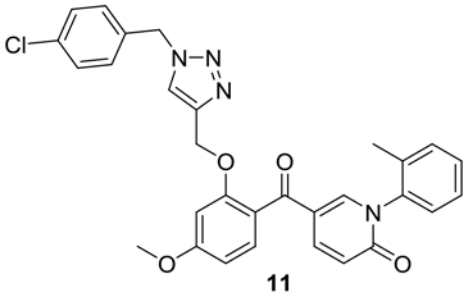

11

IC_{50} = 0.86 μM against A549
IC_{50} = 0.54 μM against HeLa
IC_{50} = 0.21 μM against SW480

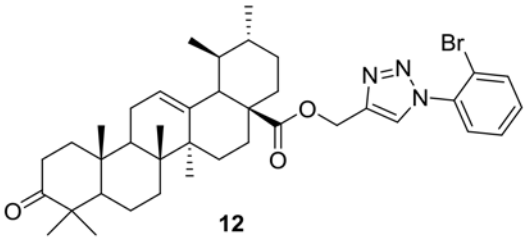

12

IC_{50} = 2.89 μM against A549
IC_{50} = <0.1 μM against MCF-7
IC_{50} = <0.1 μM against HP-1

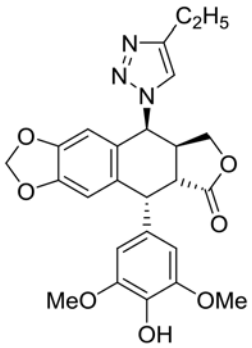

13

IC_{50} = 0.06 μM against PC-3
IC_{50} = 0.05 μM against Hep-2
IC_{50} = 0.04 μM against MCF-7

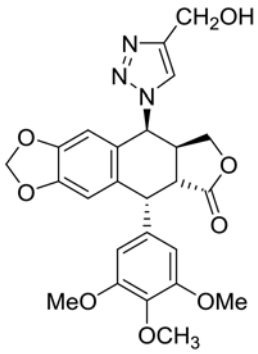

14

IC_{50} = 0.06 μM against PC-3
IC_{50} = 0.06 μM against Hep-2
IC_{50} = 0.01 μM against MCF-7

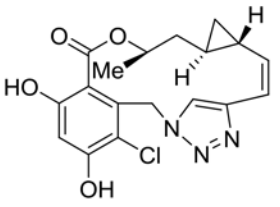

15

IC_{50} = 400 nM against Hsp90
IC_{50} = 650 nM against Kasumi-1 leukemia

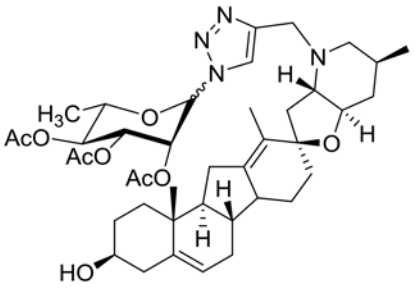

16

IC_{50} = 33 μM against A549

Fig. 4 Potent click triazole analogs generated for anticancer activity.

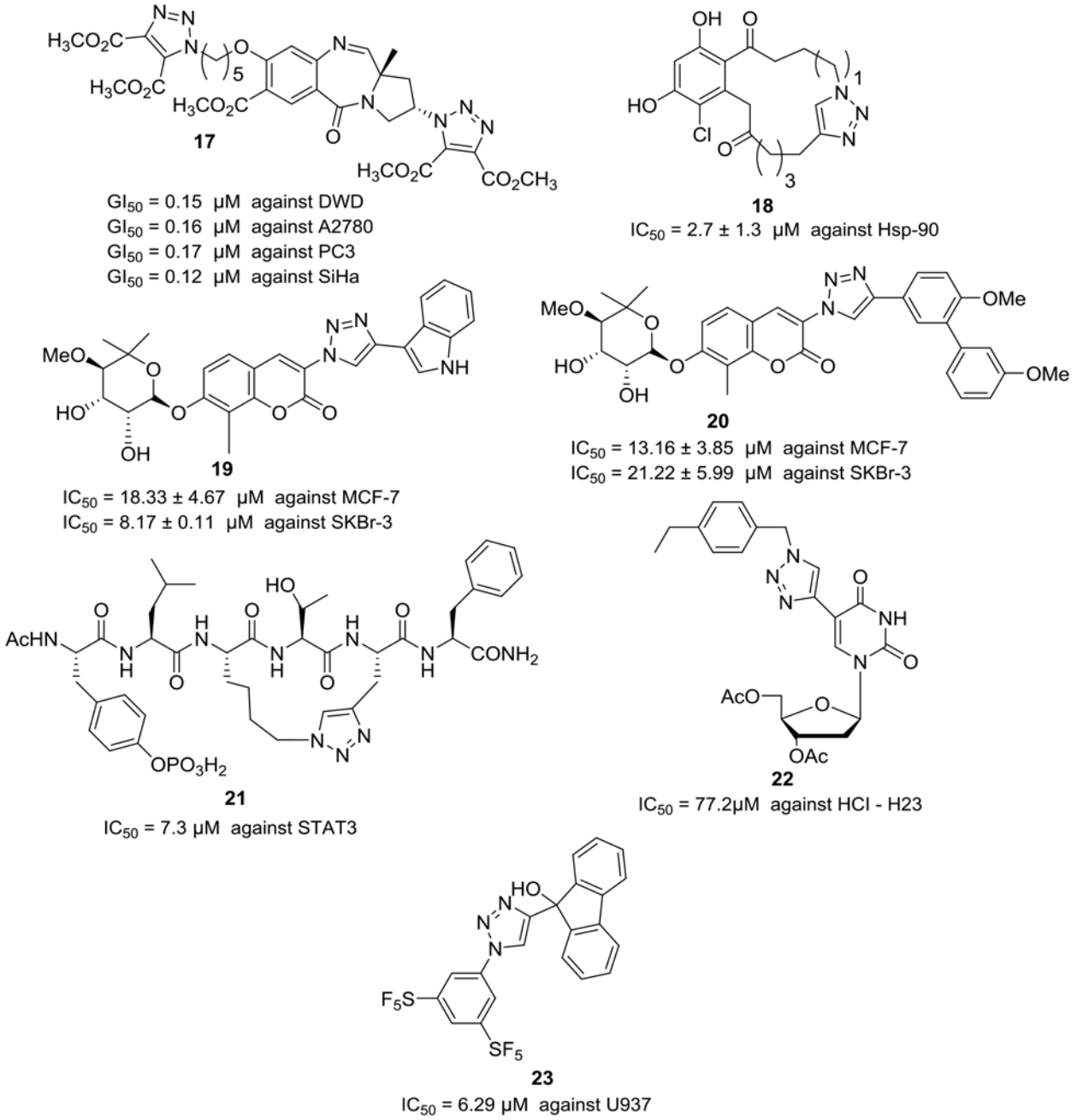

Fig. 5 Potent anticancer lead structures generated via click chemistry reactions.

analyses, supporting a common mode of Hsp90 inhibition for both structural classes. Compounds **19** and **20** showed most potent inhibition against SKBr-3 and MCF-7 among homologous series (Fig. 5).[52]

STAT3 (signal transducers and activators of transcription 3) is a promising molecular target for design of new anticancer drugs. Wang and coworkers reported the synthesis of conformationally constrained macrocyclic peptidomimetic analogs via click chemistry. Compound **21** (Fig. 5) was revealed to bind to STAT3 with a K_i value of 7.3 μM in a competitive fluorescence-polarization-based binding assay, representing a promising initial lead compound.[53]

Kim et al. employed click chemistry for the synthesis of C5-modified nucleosides from 5-iodo-2′-deoxyuridine and their activity against six types of human cancer cell lines (HCT15, MM231, NCI-H23, NUGC-3, PC-3, and ACHN). Researchers synthesized several azides from benzylic bromides and their click reactions with 5-ethynyl-2′-deoxyuridine provided triazole derivatives anticancer development. Compound **22** (Fig. 5) revealed good inhibition against lung cancer lines (NCI-H23) with $IC_{50} = 77.2$ μM.[54]

Pentafluorosulfanyl-containing 1,4-disubstituted 1,2,3-triazoles were synthesized by click reaction in good yields, and their biological activities were evaluated against human leukemic monocyte lymphoma U937 cells. An analogous fluorenol-substituted triazole (**23**; Fig. 5) exhibited promising cytotoxic effects against U937 cells, with an IC_{50} value of 6.29 μM.[55]

1.10.3 Antiproliferative Agents Synthesized Using Click Chemistry

Sekhar and coworkers recently prepared a series of novel 6-(4-((substituted-1*H*-1,2,3-triazol-4-yl)methyl) piperazin-1-yl)phenanthridine derivatives using click chemistry reaction and evaluated them as antiproliferative agents against four cancer cell lines by MTT assay. Among the synthesized triazole derivatives, **24** and **25** (Fig. 6) showed good activity against all the test cell lines. In particular, **24** ($IC_{50}=9.73$ μM) exhibited excellent activity against THP1 cancer cell line, and **25** ($IC_{50}=7.22$ μM) emerged as more active compound than the standard drug etoposide against HL60 cancer cell line.[56]

A series of salinomycin or monensin and cinchona alkaloid derivatives were obtained by click chemistry of respective N-propargyl amides of salinomycin or monensin with four different cinchona alkaloid-derived azides. In vitro antiproliferative activity of these conjugates evaluated against three cancer cell lines (LoVo, LoVo/DX, and HepG2) showed that four of the compounds exhibited high antiproliferative activity (IC_{50} below 3.00 μM, compound **26**; Fig. 6) and appeared to be less toxic and more selective against normal cells than two standard anticancer drugs.[57]

Pertino and his coworkers prepared dehydroabietic acid (DHA) triazole derivatives using click chemistry. The antiproliferative activity of the new DHA triazole derivatives was assessed toward human cell lines, namely, normal lung fibroblast (MRC-5), gastric epithelial adenocarcinoma (AGS), lung cancer (SK-MES-1), and bladder carcinoma (J82) cells. Better antiproliferative effect was found for compound **27** (Fig. 6), with an IC_{50} of 6.1 μM and selectivity on SK-MES-1 cells.[58]

A series of 1,2,3-triazoleedithiocarbamate urea triazoles were synthesized and their antiproliferative activities against four selected human cancer cell lines were evaluated. The results showed that the synthesized triazole derivatives exhibited potent activity in selected human cancer cell lines. Among them, compounds **28** and **29** showed broad spectrum of anticancer activity with IC_{50} values ranging from 1.62 to 20.84 μM and 0.76 to 13.55 μM, respectively. Interestingly, compounds **28** and **29** (Fig. 6), being very potent against MGC-803 cells, exhibited no significant cytotoxicity against normal human embryonic kidney cells at up to 55 and 70 mM, respectively.[59]

Nagarapu and his coworkers recently reported a series of novel 1,2,3-triazole-1,4-benzoxazine hybrids synthesized via click chemistry approach and evaluated for antiproliferative activity against four cancer cell lines such as HeLa (cervical), MIAPACA (pancreatic), MDA-MB-231 (breast), and IMR32 (neuroblastoma). Compound **30** (Fig. 6) exhibited antiproliferative activity with GI_{50} values ranging from 0.1 to 1.1 μM, respectively, against all cell lines, like HeLa, MDA-MB-231, MIAPACA, and IMR32, whereas compound **31** (Fig. 6) showed significant activity against MDA-MB-231 and IMR32 with GI_{50} values ranging from 1.1 and 1.4 μM.[60]

8-Hydroxyquinoline derivatives were synthesized with good yields by performing copper-catalyzed Huisgen 1,3-dipolar cycloaddition between an 8-O-alkylated-quinoline containing a terminal alkyne and various aromatic azides. These compounds were evaluated in vitro for their antiproliferative activity on various cancer cell types. Among the halogenated derivatives, the chlorinated ones showed the best overall activity, with **32** (Fig. 6) showing the lowest MG MID GI_{50} value of 0.7. Protected sugar triazole derivative **33** (Fig. 7) was the most active against and highly selective for ovarian cancer cells (OVCAR-03, $GI_{50}<0.25$ μg mL^{-1}), showing greater activity against these cells than doxorubicin.[61]

Bis-prolinamide pyridine derivatives were generated via click chemistry by Dash and coworkers. Pyridine analog (compound **34**; Fig. 7) showed better *c*-KIT1 G-quadruplex binding ligand than the benzene-substituted bis-prolinamide derivatives, suggesting that H-bonding plays a key role in controlling the conformation of the pyridyl ligand for the selective recognition. The FID assay revealed that the pyridyl ligand (compound **34**; Fig. 7) binds with high affinity to *c*-KIT1 and displays moderate to high *c*-KIT1 specificity over c-MYC, h-TELO, and c-KIT2 quadruplexes. In addition, the pyridyl ligand effectively inhibited the cell growth and induced cell death of HepG2 cancer cells.[62]

Functionalized flavone–triazole–tetrahydropyran conjugates were generated via click reactions by Ahmed and coworkers, and these flavone–triazoles were screened in vitro for their antiproliferative activity against three human cancer cell lines (MDA-MB 231, KCL22, and HeLa). Compounds **35** (IC_{50} 0.61 μM; Fig. 7) and **36** (IC_{50} 0.70 μM; Fig. 7) exhibited antiproliferative activity better than the reference drugs against the KCL22 cells and MDA-MB 231 cells, respectively.[63]

A series of estrone derivatives substituted 16α-triazolyl on ring D were synthesized by click chemistry and investigated for their antiproliferative action on human adherent cell lines. Estrone derivatives (compound **37**, Fig. 7) exhibited in vitro potencies comparable to that of the clinically utilized reference agent cisplatin.[64]

Steroidal 15β,17β-triazole alcohol derivatives were generated via click chemistry and these synthetic steroidal triazoles tested for antiproliferative activity. Structures **38** and **39** showed good antiproliferative activity with MCF-7, HeLa, and A431 cell lines among tested series of steroidal triazoles.[65]

Hu and his coworkers reported the synthesis of indole N-hydroxyarylamide alkyl substituted triazole, and their in vitro biological activities were examined. Most of triazole derivatives showed promising anticancer activities; particularly compound **40** shown in Fig. 7 had a significant HDACs inhibitory and antiproliferative activities comparable to or slightly stronger than SAHA against human carcinoma cells. Furthermore, compound **40** exhibited much better selectivity for HDAC1 over HDAC6 and HDAC8 than SAHA. In addition, compound **40** also could dose-dependently induce cancer cell cycling arrest at G0/G1 phase and promote the expression of the acetylation for histone H3 and tubulin in vitro.[66]

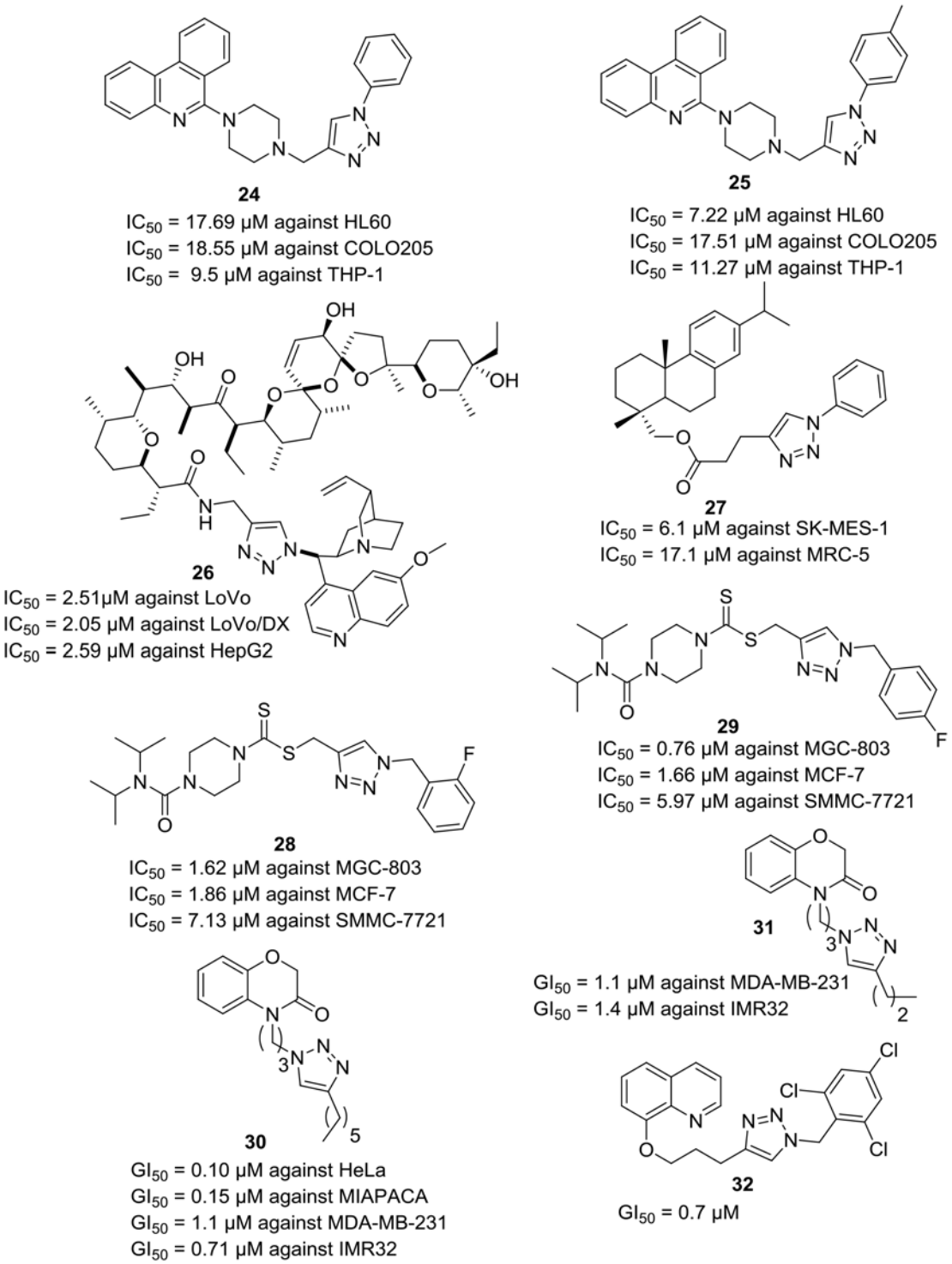

Fig. 6 Click triazole lead structures generated for antiproliferative agents (IC_{50} is the drug concentration causing 50% inhibition of the desired activity and GI_{50} is the concentration for 50% of maximal inhibition of cell proliferation and should be used for cytostatic (as opposed to cytotoxic) agents).

1.10.4 Antiviral and Other Lead Small Molecules Synthesized From Click Chemistry

A library of 2′-deoxy-2′-fluoro-4′-triazole cytidine nucleosides were synthesized via click chemistry by Song and coworkers. These nucleoside analogs exhibited potent anti-HIV-1 activity with no cytotoxicity observed at the highest tested concentration up to 25 μM. Among them, compounds **41** and **42** (Fig. 8) exhibited extremely potent antiviral activity and thus had a great potential for further development as novel nucleoside reverse transcriptase inhibitors (NRTIs) for the treatment of HIV-1 infection.[67]

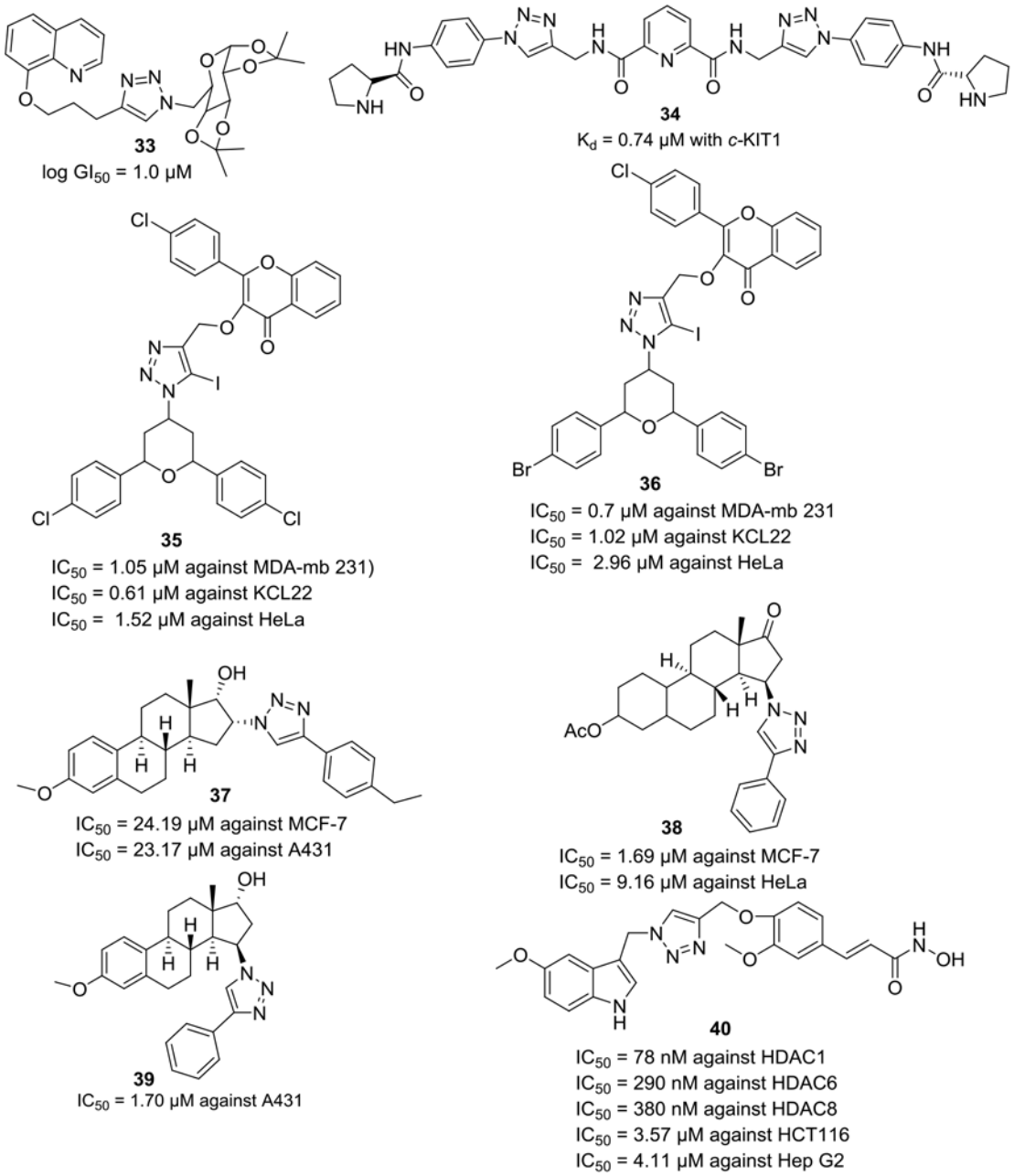

Fig. 7 Lead chemical structures with antiproliferative agents generated via click chemistry reaction.

A library of rupestonic acid triazole derivatives were generated using click chemistry, and these compounds were subjected for in vitro activities against various strains of influenza A virus (H1N1, oseltamivir-resistant H1N1, and H3N2) and influenza B virus. The results showed that most of structures were active against the H1N1 strain of influenza A virus. The screening results showed that **43** and **44** (Fig. 8) were better than ribavirin in inhibiting plaque formation, in good accordance with their anti-influenza B activities.[61]

A series of naphthalene-1,4-dione substituted triazoles were generated via click reaction and screened against broad spectrum of viruses. The screening results of identified compound **45** showed good inhibition against five viruses such as West Nile virus (WNV), dengue virus type 2 (DENV-2), Western equine encephalitis virus (WEEV), vesicular stomatitis virus (VSV), and yellow fever virus (YFV).[68]

Sugar derivatives of ristocetin from azido-ristocetin aglycon and various propargyl glycosides were prepared for employing click chemistry. Triazole sugar derivatives were found active against gram-positive bacteria and showed favorable antiviral activity against the H1N1 subtype of influenza A virus. Compound **46** (Fig. 8) showed good inhibition activity against H1N1 subtype of influenza A virus with EC_{50} value of 4.0 μM.[69]

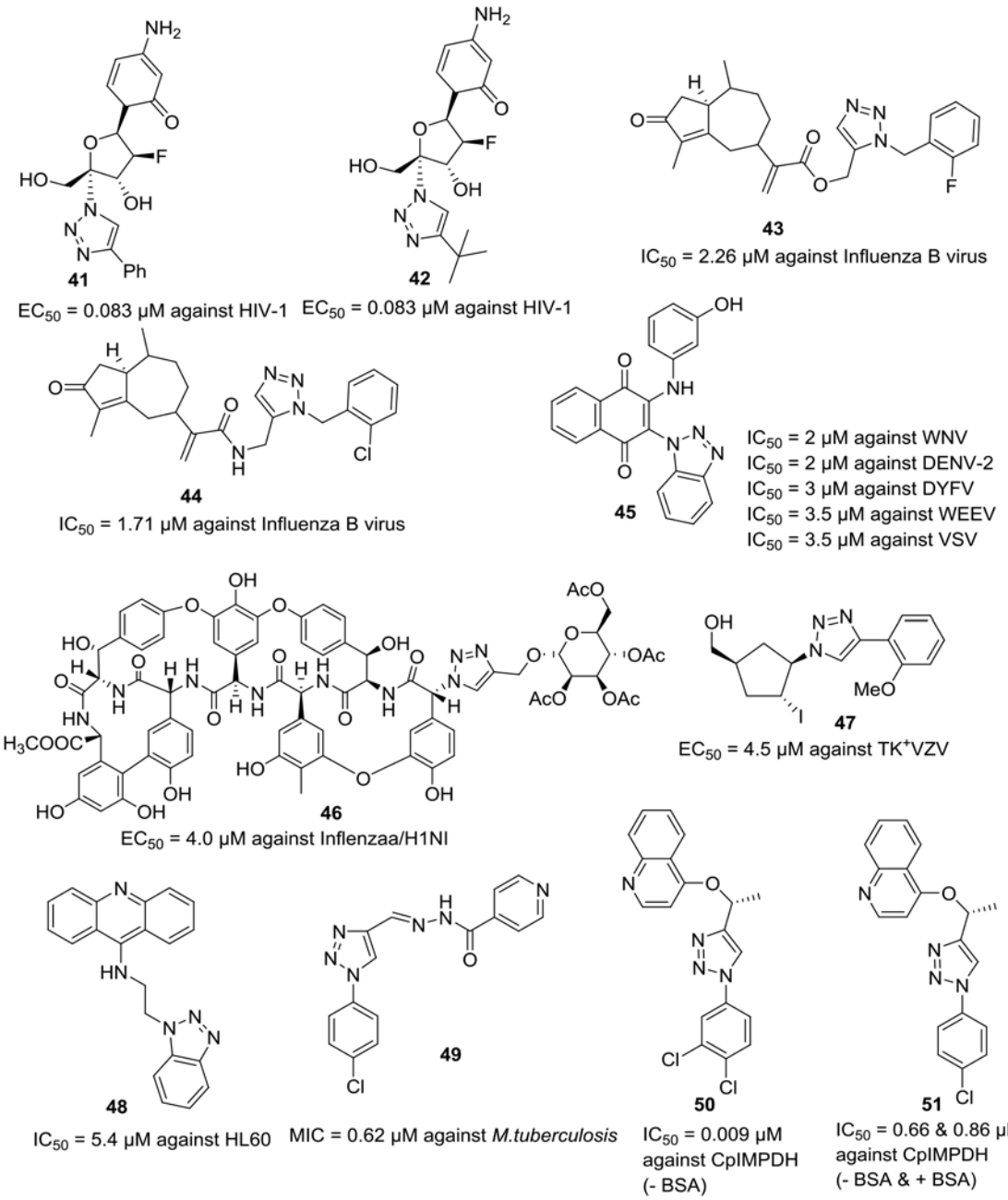

Fig. 8 Chemical lead structures of antiviral, antibacterial, and some other drugs synthesized via click chemistry.

A series of racemic 4-aryl-1,2,3-triazolo-2′,3′-dideoxy-2′-iodocarbanucleosides and 4-aryl-1,2,3-triazolo-2′,3′-dideoxy-2′,3′-didehydrocarbanucleosides were prepared using click chemistry reaction by Caamaño et al. These compounds were evaluated for their inhibitory activities against cytomegalovirus (CMV Davis strain) and varicella-zoster virus (TK^+VZV, thymidine kinase-positive strain, and TK^-VZV, thymidine kinase-deficient strain) in human embryonic lung (HEL) cells. Compound **47** (Fig. 8) exhibited specific inhibitory potential against TK^+VZV ($EC_{50} = 4.5\ \mu g\ mL^{-1}$).[70]

DNA intercalators have found great utility as antitumor agents, from natural products such as doxorubicin and actinomycin D to synthetic agents such as mitoxantrone and amsacrine. Amsacrine is an acridine that binds to DNA and inhibits the enzyme topoisomerase. A small set of 9-aminoacridine-3- and 4-carboxamides were synthesized efficiently using the benzyne/azide click chemistry. The synthesis of threading intercalators was bound to DNA with reasonable affinity and had up to low micromolar antitumor activity. Compound **48** (Fig. 8) revealed good antitumor activity with HL60 cell line.[71]

4-Substituted N-phenyl-1,2,3-triazole derivatives were prepared using click chemistry reported by Boechat and coworkers. The phenyl triazole derivatives were screened in vitro for antimicrobial activity against *Mycobacterium tuberculosis* strain H37Rv

(ATCC 27294) using the Alamar Blue susceptibility test. The activity was expressed as the minimum inhibitory concentration (MIC) in $\mu g\,mL^{-1}$ (μM). Derivatives of isoniazid (INH), (*E*)-N′-[(1-aryl)-1*H*-1,2,3-triazole-4-yl)methylene] isonicotinoyl hydrazides (**49**; Fig. 8), exhibited significant activity with MIC values ranging from 2.5 to 0.62 $\mu g\,mL^{-1}$. In addition, they displayed low cytotoxicity against liver cells (hepatoma HepG2) and kidney cells (BGM), thereby providing a high therapeutic index.[72]

A library of 1,2,3-triazole-containing ether cryptosporidium parvum inosine 5′-monophosphate dehydrogenase (CpIMPDH) inhibitors were prepared using click chemistry by Cuny et al. Compounds **50** and **51** (Fig. 8) showed most potent CpIMPDH inhibitors among the tested compounds. These 1,2,3-triazole CpIMPDH inhibitors are used as potential therapeutics for treating cryptosporidiosis.[73]

A series of 1,2,3-triazolylsterols were prepared from pregnenolone through reductive amination and azide–alkyne click chemistry by Labadie et al. Triazolyl sterols were screened in vitro against different parasites and compound **52** (Fig. 9) showed low micromolar IC_{50} value against *Leishmania donovani*.[74]

Synthetic mimics of triazole peptide linkers were prepared using click chemistry. An enhancement antimicrobial activity against *Staphylococcus aureus* and *Escherichia coli* was observed when these triazole peptide linkers were administered in the presence of mouse serum. Compound **53** (Fig. 9) had minimum inhibitory concentrations (MICs) of 0.39 and 6.25 $\mu g\,mL^{-1}$, respectively, and an HC50 of 693 $\mu g\,mL^{-1}$.[75]

A series of benzene-substituted triazole amides were prepared via click chemistry and these compounds were tested for their antiepileptic activity. Epilepsy is a neurological disorder characterized by unprovoked seizures affecting at least 50 million people worldwide. There is a continuing demand for new anticonvulsant agents as it has not been possible to control every kind of seizure with the currently available antiepileptic drugs. Compound **54** (Fig. 9) exhibiting antiepileptic activity was generated via click chemistry.[76]

Click chemistry employed for interconnecting lead functional analogs of antibiotics in order to improve the pharmacokinetic properties. Compound **55** showed good antibacterial activity with improved efficiency.[77] Among the best-known examples of triazole-containing structures is tazobactam, a β-lactamase inhibitor that is marketed in combination with the broad-spectrum antibiotic piperacillin. Tazobactam (**56**) and related triazole-containing compounds (**57**, **58**, and **59**; Fig. 9) turned out to be potent β-lactamase inhibitors with higher potency than clavulanic acid and sulbactam, and the triazole ring appears to play a pivotal role for its potency.[77]

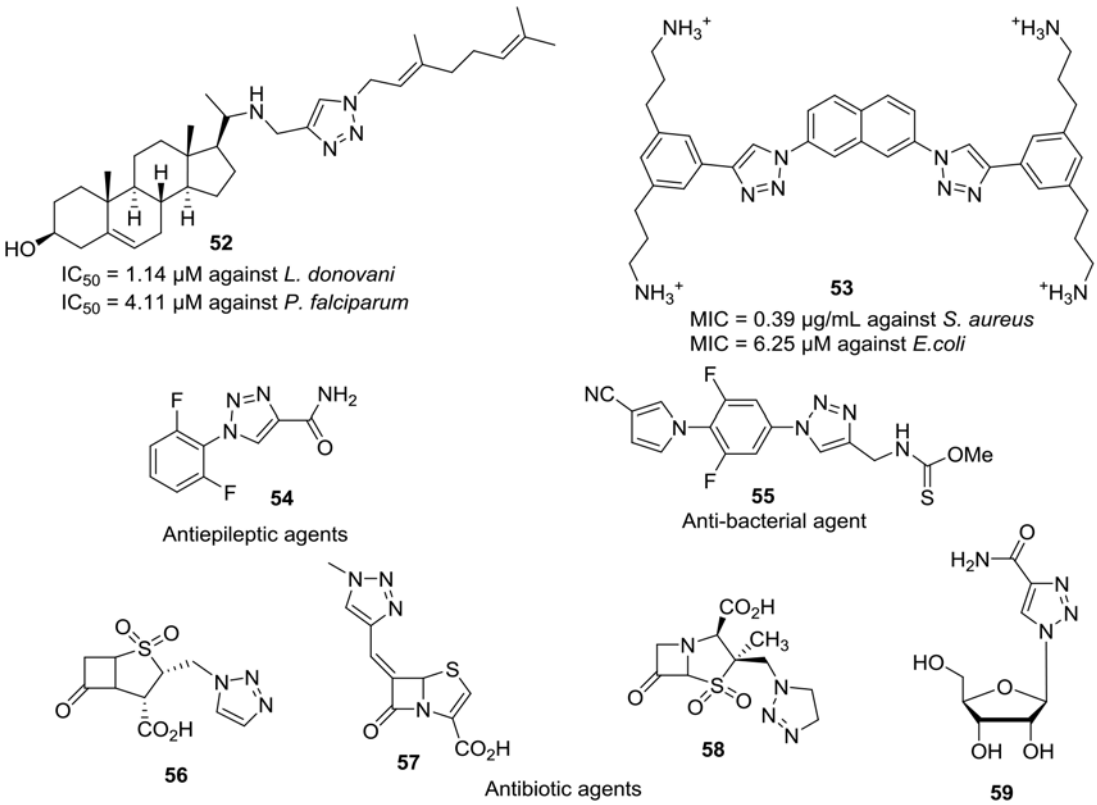

Fig. 9 Chemical lead analogs of antimicrobial, antibiotic, and some other drugs constructed via click chemistry.

1.10.5 Click Chemistry in Receptor–Ligand-Binding Studies

Receptor–ligand interactions play an important role in biological systems and their studies form an important part of contemporary drug development. Cells are activated by the binding of specific ligand molecules to cell-surface receptors. The interaction between the ligand and the receptor is characterized by association and dissociation rate constants and by processing of the ligand–receptor complex what may involve internalization, recycling, and ligand degradation steps. All of these processes may contribute to the means by which the ligand–receptor interaction ultimately generates the signals necessary for cellular responses.[78]

Receptors that couple to G-proteins communicate signals from a large number of hormones, neurotransmitters, chemokines, and autocrine and paracrine factors. G-proteins play a significant role in signaling pathways.[79] It regulates important cellular components, such as metabolic enzymes, ion channels, and the transcriptional machinery. The resulting alterations in cellular behavior and function are manifested in many critical systemic functions, including embryonic development, learning and memory, and organismal homeostasis. These results are in the propagation of regulated activities through increasingly complex layers of organization to serve as the basis of integration at the systemic level. Among the many receptors, GPCRs in humans are all potentially very important drug targets.[80,81]

Several research groups employed click chemistry reaction for the development of selective agonist and antagonist and efficient binding ligand synthesis for various GPCR receptors–ligand binding. These developments of the new agonist and antagonist and efficient binding ligands are very useful in the new drug discovery for the uncured diseases. Here, we are outlining some of the effective synthetic triazole generated via click chemistry used triazole for selective agonist and antagonist and efficient binding ligand development.[20]

1.10.5.1 Agonist

A series of N-arylpiperazinylmethyl triazoles were synthesized, and they were evaluated for dopamine and serotonin receptor binding. A brief library of triazoles substituted fluoroalkyl, fluoroalkoxy, fluoroalkoxyphenyl, and deoxyfluoroglucosyl derivatives was tested for D4 receptor affinity and selectivity. The D4 receptor affinity and selectivity tuned by altering the chemical moiety attached to the triazole unit. Among the screened triazole derivatives, fluoroethoxyphenyl triazole derivative **60** (Fig. 10) showed weak partial agonism at D4 with an binding affinity (K_i) of 14 nM.[82]

Gmeiner et al. reported aminomethyl-substituted biaryls bearing a triazole moiety synthesized and investigated for dopamine and serotonin receptor binding. SAR experiments on dopaminergic arylazole derivatives lead to highly active D4 partial agonist showing substantial 5-HT_{1A} binding as well. N-arylpiperazine triazole derivative **61** (Fig. 10) showed good high affinity for the D_4R ($K_i = 2.7$ nM) besides being moderately selective over the D_2 and D_3 receptor subtypes.[83]

Click chemistry was employed for the peptide–peptide conjugate ligand synthesis for full activator of corticotropin-releasing factor type 1 receptor (CRF1R) using a high-throughput approach. An acetylene-tagged peptide library was synthesized and conjugated to an azide-modified high-affinity carrier peptide derived from the CRF C-terminus using copper-catalyzed dipolar cycloaddition. The resulting conjugates reconstituted potent agonists and were tested in situ for the activation of the CRF1 receptor in a cell-based assay. Compound **62** (Fig. 10) showed good activation and binding affinity toward CRF1 receptor. Unnatural amino acid peptide–peptide analogs also were synthesized using click chemistry, and these conjugates showed good binding affinity and activation with CRF1 receptor with IC_{50} values of 1.6 ± 1.0 nM. By the use of this approach, researchers (i) defined the minimal sequence motif that is required for full receptor activation, (ii) identified the critical functional groups and structure–activity relationships, (iii) developed an optimized, highly modified peptide probe with high potency ($EC_{50} = 4$ nM) that is specific for the activation domain of the receptor, and (iv) probed the behavioral role of CRF receptors in living mice.[84]

A series of 1,4-disubstituted 1,2,3-triazoles were generated and tested for their ability to increase oleic acid oxidation in human myotubes using a high-throughput multiwell assay. Compounds **63** (Fig. 10) exhibited potent agonist activities with peroxisome proliferator-activated receptors (PPAR). Compound **63** exhibited dual agonist effects for both PPARα and PPARδ in a luciferase-based assay.[85]

1-Aryl-3-benzazepine arylpiperazinyl functional analogs were synthesized by combining a D1 receptor agonistic pharmacophore and a $5HT_{1A}$ receptor pharmacophore through click reaction. Compound **64** (Fig. 10) showed the highest affinity at the $5HT_{1A}$ receptor with K_i value of 85 nM. Functional assays indicated that compound **64** showed full agonistic activity with 5-HT_{1A} receptor.[86]

The cytokine macrophage migration inhibitory factor (MIF) is involved in inflammation and cell proliferation via pathways initiated by its binding to the transmembrane receptor cluster of differentiation 74 (CD74). MIF also promotes 5′ AMP-activated protein kinase (AMPK) activation with potential benefits for response to myocardial infarction and ischemia–reperfusion. Jorgensen et al. reported the synthesis of agonists for MIF–CD74 receptors using click chemistry. The three compounds (**65a**, **65b**, **and 65c**; Fig. 10) showed full agonist effect with MIF–CD74 receptor.[87]

Adenosine receptors (ARs) regulate the release of neurotransmitters in the central nervous system. ARs are G protein-coupled receptors (GPCRs) and found in myocytes, astrocytes, neurons, neutrophils, eosinophils, and other cell types. Both A_3AR agonists and antagonists are proposed for the treatment of cancer and inflammatory diseases. Click chemistry was employed for the synthesis of 2-dialkynyl derivatives of (N)-methanocarba-triazole nucleosides for A_3 adenosine receptor-selective agonist development. Most potent and selective novel compound was a 1-adamantyl derivative **66** ($K_i = 6.5$ nM; Fig. 10), which suggested the existence of

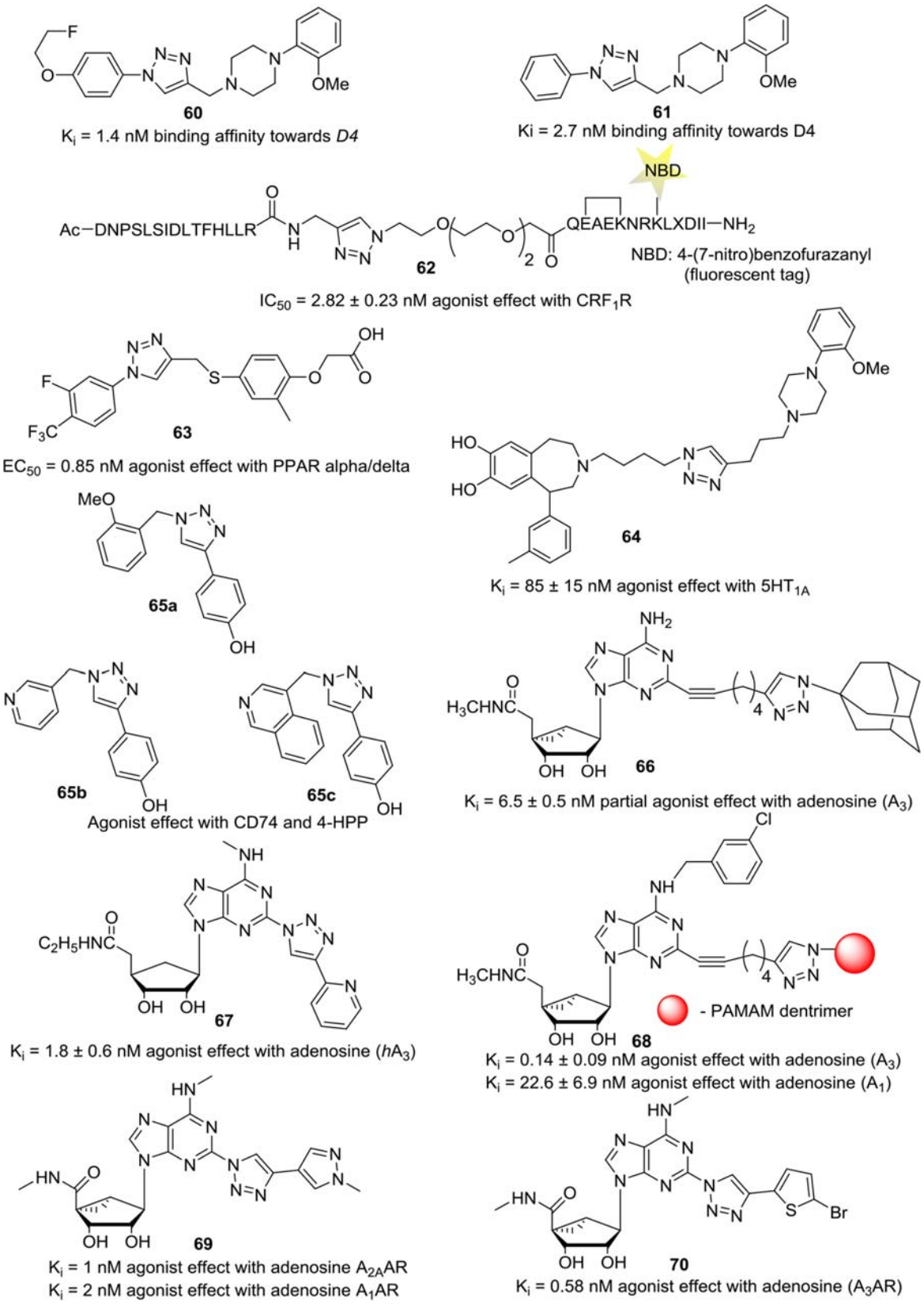

Fig. 10 Chemical lead functional analogs with agonistic effect on various receptors generated by click chemistry.

a hydrophobic binding pocket in this region of the receptor. Curiously, compound **66** proved to be a partial agonist of the A_3AR with only 27.8% of the maximal efficacy in comparison with 5′-N-ethylcarboxamidoadenosine.[88]

Two series of 2-(1,2,3-triazolyl)adenosine derivatives were prepared via click chemistry, and the binding affinity at the human A_1, A_2, and A_3ARs (adenosine receptors) and relative efficacy at the A_3AR of these compounds were determined. Some triazol-1-yl analogs showed A_3AR affinity in the low nanomolar range, with a high ratio of A_3/A_2A selectivity and a moderate-to-high A_3/A_1 ratio. The 5′-OH ethyluronamide analogs showed increased A_3AR affinity and behaved as full agonists, that is, compound **67** (Fig. 10), with 910-fold A_3/A_1 selectivity.[89]

Polyamidoamine (PAMAM) dendrimer triazole conjugate series was prepared using click chemistry reaction from alkyne of a 2-octadiynyl nucleoside and azide-derivatized G4 (fourth-generation) PAMAM dendrimers. A_3AR activation was preserved in these multivalent conjugates, which bound with apparent K_i of 0.1–0.3 nM. A bifunctional conjugate **68** (Fig. 10) activated both A_3 and A_1 with selectivity in comparison with other AR receptors.[90]

Aryltriazole derivatives of (N)-methanocarba adenosine 5′-uronamides were prepared toward adenosine receptor binding reported by Jacobson et al.[86] Derivatives of selective A_3AR agonists containing a triazole linker in place of an ethynyl group, a preferred substitution as predicted using molecular modeling, were prepared and shown to parallel the ethynyl series in receptor affinity and selectivity, due to its ability to fit a narrow cleft in the receptor. The triazole analogs with various N6 and C2-aryltriazolyl substitutions were synthesized and characterized in binding (K_i at hA3AR 0.3–12 nM) and in vivo to demonstrate efficacy in controlling chronic neuropathic pain. Especially, compound **69** showed agonistic effect with A_2AR and A_1AR receptors, whereas compound **70** (Fig. 10) showed selective agonism to the A_3AR receptor.[91]

1.10.5.2 Antagonist

A series of N-arylpiperazinylmethyl triazolyl derivatives synthesized and these compounds were tested for their preferential affinity for the D4 receptor. Fluoropropoxyphenyl homologue **71** turned out to act as a neutral D4 antagonist ($K_i = 5.1$ nM). Compound **71** (Fig. 11) revealed an excellent balance between D4 receptor affinity and subtype selectivity, providing lead candidates for the development of ^{18}F-labeled radioligands for D4 receptor imaging studies by positron emission tomography (PET).[82]

The $P2Y_{14}$ receptor (purinergic receptor P2Y, G-protein-coupled, 14 ($P2Y_{14}R$)), one of eight P2Y G protein-coupled receptors (GPCR), is involved in inflammatory, endocrine, and hypoxic processes and is an attractive pharmaceutical target. The newly synthesized compound series was consistent with the structural insights gained from $P2Y_{12}R$-based homology modeling and docking at this closely related receptor. The resulting $P2Y_{14}R$ model with its ECLs (extracellular loops) defined conformationally allows prediction of specific interactions with antagonist analogs. Chain-elongated alkynyl or amino derivatives for click coupling were synthesized, and their antagonist activities were measured in *h*$P2Y_{14}R$-expressing CHO cells. Moreover, a new Alexa Fluor 488 (AF488)-containing derivative **72** (MRS4174, $K_i = 80$ pM; Fig. 11) exhibited high affinity, as compared to 13 nM for the alkyne precursor.[92]

Click chemistry has been employed for the synthesis of cyclopeptidic second mitochondria-derived activator of caspase (Smac) mimetics by Wang et al.[88] Two compounds bind to X-linked inhibitor of apoptosis protein (XIAP) and cIAP-1/cIAP-2 with low nanomolar affinities and restore the activities of caspase-9 and caspase-3/caspase-7 inhibited by inhibitors of apoptosis proteins (XIAP). Especially, compound **73** (Fig. 11) potently inhibits cancer cell growth and is five to eight times more potent than the initial lead compound.[93]

Endothelin (ET) receptors play an important role in the expression and function of abnormal in cardiovascular diseases, tumor progression, and tumor metastasis. Michel et al.[89] explored click chemistry for the synthesis of high-affinity ET_A-selective receptor ligands with clogD values ranging from 1.50 to 3.90, which allow systematic investigations of pharmacokinetic properties and metabolic stability. Compound **74** (Fig. 11) showed good selectivity toward ET_B/ET_A.[94]

Labeled molecular probes are powerful pharmacological tools to study and characterize ligand–receptor interactions. Click chemistry was used as a tool to facilitate the access to labeled novel pirenzepine derivatives. The incorporation of a fluorophore (lissamine rhodamine B), a nonfluorescent dye (Patent Blue VF), or biotin into a muscarinic antagonist pirenzepine scaffold was done by using click chemistry. The affinity of the compounds for the *human* M1 muscarinic receptor fused to enhanced green fluorescent protein (EGFP) was checked under classical radioligand and FRET binding assays. Pirenzepine triazole (**75**; Fig. 11) displayed a nanomolar affinity for the M1 receptor. In addition, both dye-labeled derivatives behave as potent acceptors of energy from excited EGFP with a very high quenching efficiency.[95]

1-Phenyl-1*H*-1,2,3-triazoles were prepared via click chemistry for selective antagonist development for β3 over α1β2γ2 GABA receptors by Ozoe and his coworkers. Among screened triazole analogs, the 4-n-propyl-5-chloromethyl analog of triazole (**76**; Fig. 11) showed antagonist affinity for both β3 and α1β2γ2 receptors with K_i values of 42 ± 5 nM, respectively.[96]

Dopamine D2 receptor homodimers are the promising target proteins for the discovery of a typical antipsychotics. To investigate and control GPCR, dimerization may be provided by the exploration and characterization of bivalent ligands, which can act as molecular probes simultaneously binding two adjacent binding sites of a dimer. The synthesis of bivalent D_2 receptor ligands was performed, incorporating the 1,4-disubstituted aromatic piperidines/piperazines (1,4-DAPs) and triazolyl-linked spacer elements. Radioligand-binding assays revealed that the bivalent ligands exhibited a distinct binding profile compared with monovalent ligand. Bivalent ligands **77** and **78** (Fig. 11) revealed a most potent binding affinity toward the D_2 receptors.[97]

Substituted aryl-1,2,3-triazoles were synthesized using click chemistry for binding of the cytokine macrophage migration inhibitory factor (MIF) to its receptor CD74. Especially, compound **79** (Fig. 11) showed antagonist effect with CD74 receptor.[87]

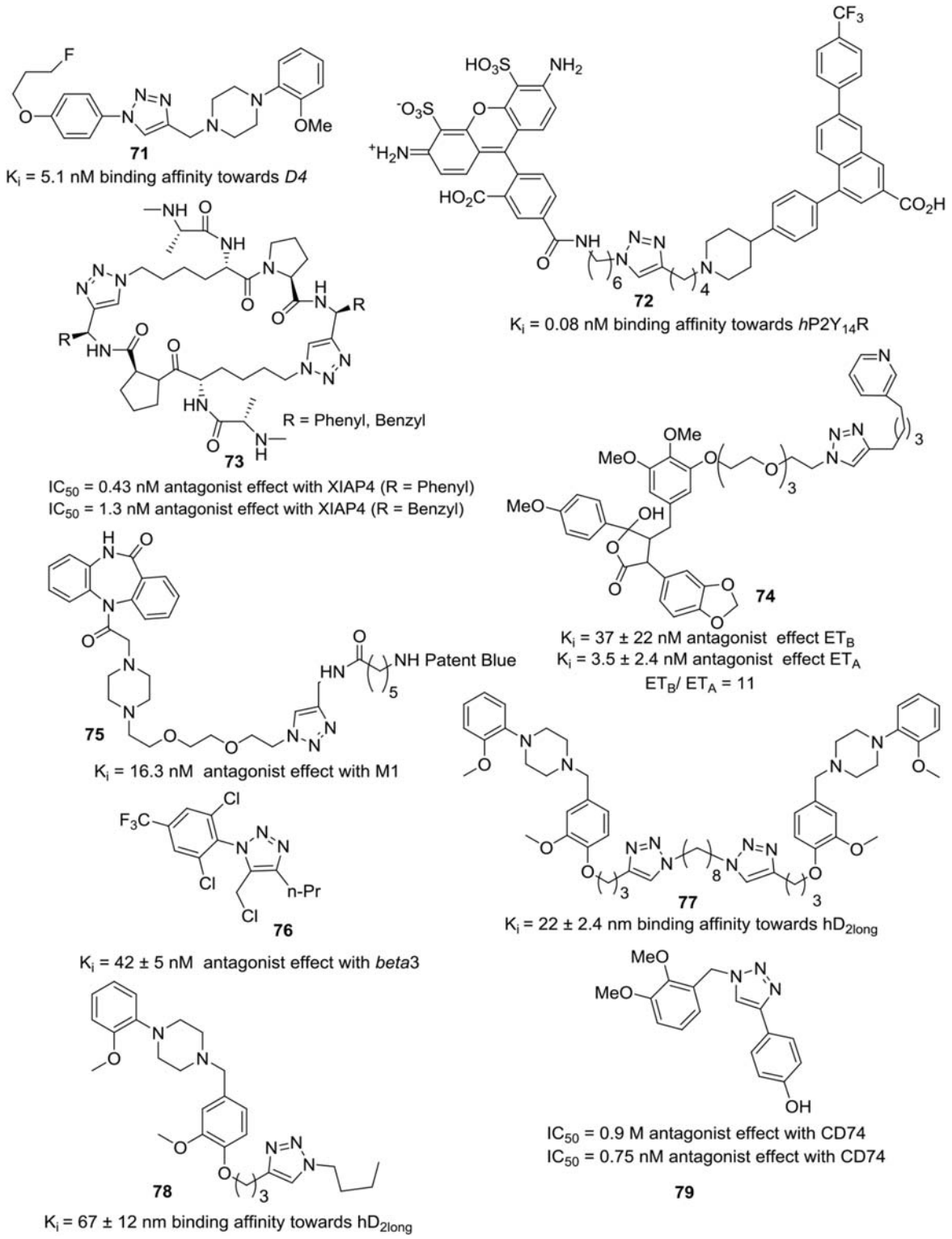

Fig. 11 Lead chemical triazole functional derivatives with antagonistic effect on various G-protein-coupled receptors synthesized via click chemistry.

1,1′-Substituted ferrocene triazole derivatives were generated via click chemistry for the development of novel antagonist for dopamine receptor by Gmeiner and his coworkers. 1,1′-Substituted ferrocene triazoles were used for the fine-tuning of biological activity and for the attachment of linker units generating bivalent GPCR ligands. Receptor binding assay was evaluated by radioligand displacement experiments, revealing super-affinity with sub- to single-digit nanomolar K_i values for particular test

compounds. As a neutral antagonist at the dopamine receptors D_3 and D_4 and a potent partial agonist at the D_2 subtype (intrinsic activity = 57%, EC_{50} = 2.5 nM), the bifunctional ferrocene **80** (Fig. 12) revealed a unique activity profile.[98]

Peptide triazole functional derivatives were constructed via click reaction of both aryl and alkyl acetylenes with an internally incorporated azidoproline derived from the parent peptide. These triazole conjugates were found to exhibit several orders of magnitude increase in both affinity for HIV-1 gp120 and inhibition potencies at both the CD4 and coreceptor binding sites of gp120. Structural factors in the added triazole grouping were responsible for the increased binding affinity and antiviral activity of the dual inhibitor conjugates. Peptide conjugate potencies were measured in both kinetic and cell infection assays. High affinity was sterically specific, being exhibited by the *cis*- but not the *trans*-triazole. Aromatic, hydrophobic, and steric features in the residue side chain are important for increased affinity and inhibition (compound **81**; Fig. 12).[99]

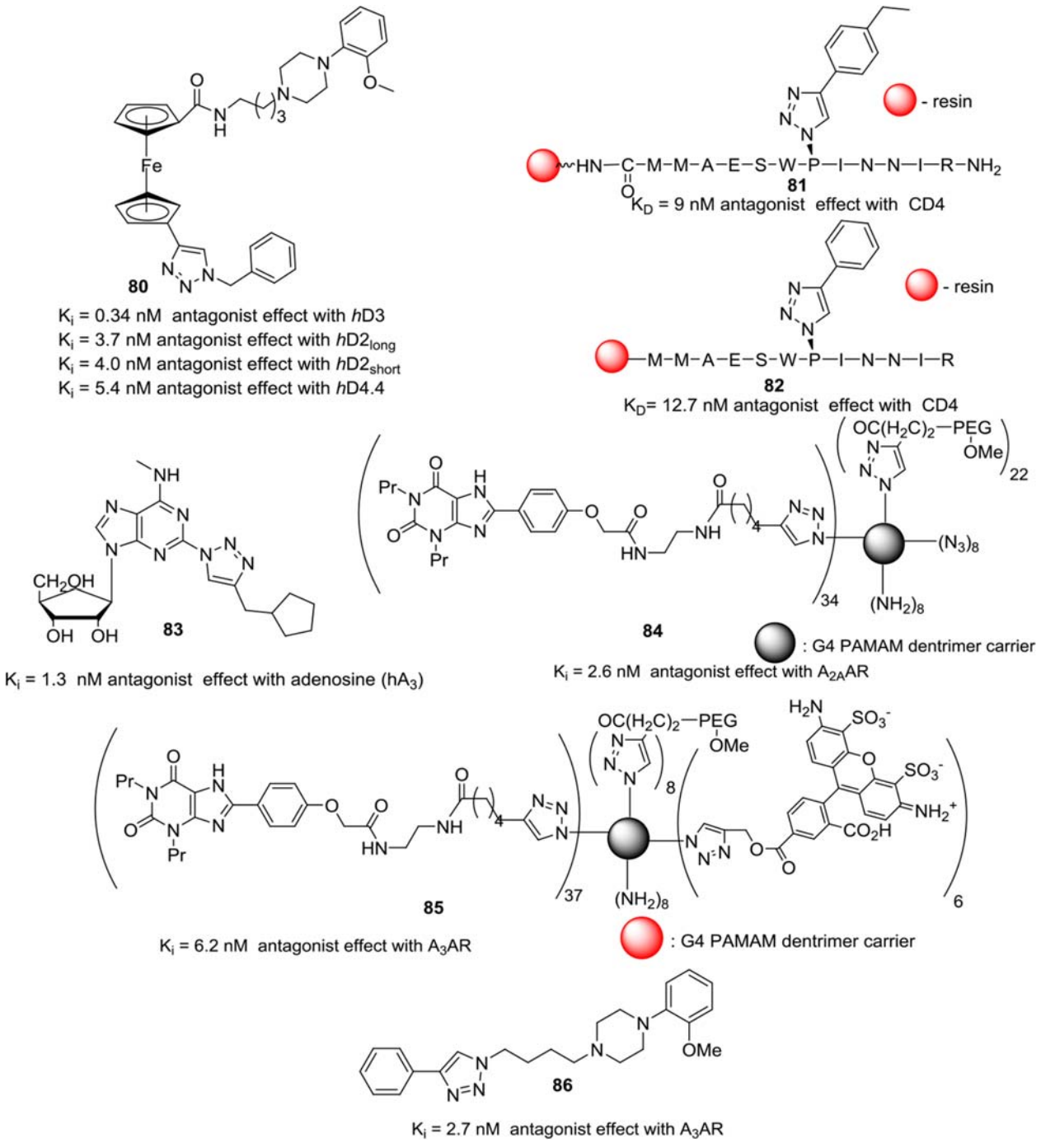

Fig. 12 Click triazole functional analogs generated for antagonist effect on various receptors.

Click chemistry was employed for the synthesis of high-affinity dual antagonist for HIV-1 envelope glycoprotein gp120 by Chaiken and his coworkers. The peptide analog **82** (Fig. 12) of (2*S*,4*S*)-4-(4-phenyl-1*H*-1,2,3-triazol-1-yl)pyrrolidine-2-carboxylic acid at residue position 6 was binding to gp120 with an affinity two orders of magnitude greater than that of the parent peptide and strongly inhibits the interaction of gp120 with both CD4.[100]

2-(1,2,3-Triazolyl)adenosine derivatives were prepared via click chemistry, and their binding affinity of the human A_1, A_2, and A_3ARs (adenosine receptors) and relative efficacy at the A_3AR were examined. 2-Triazole analogs with an unmodified ribose moiety **83** (Fig. 12) showed good antagonist activity at the A_3AR.[89]

GPCR ligand–dendrimer (GLiDe) conjugates were prepared for a potent adenosine receptor (AR) antagonist for treating Parkinson's disease, asthma, and other diseases by Jacobson and his coworkers. Xanthine amine congener (XAC) was appended with an alkyne group on an extended C8 substituent for coupling by Cu(I)-catalyzed click chemistry with azide-derivatized G4 PAMAM dendrimers to form triazoles. These conjugates also contained triazole-linked PEG groups for increasing water solubility and optionally prosthetic groups for spectroscopic characterization and affinity labeling. Human AR binding affinity increased progressively with the degree of xanthine substitution to reach K_i values in the nanomolar range. The order of affinity of each conjugate was hA$_2$AR > hA$_3$AR > hA$_1$AR, while the corresponding monomer was ranked hA$_2$AR > hA$_1$AR ≥ hA$_3$AR. The antagonist activity of the most potent conjugate **84** (34 xanthines per dendrimer; Fig. 12) was examined at the G_i-coupled A_2AR, and it showed significant binding affinity toward A_2AR at low nanomolar concentration. The conjugate **85** (Fig. 12) showed most potent antagonist activity toward A_3AR with K_i value of 6.2 ± 0.9 nM.[101]

A series of 1,4-disubstituted triazoles were synthesized via click chemistry by Carro et al. 1,4-Disubstituted triazoles derivatives were evaluated as potential ligands on several subtypes of dopamine receptors in in vitro competition assays, showing high affinity for dopamine D_3 receptors, lower affinity for D_2 and D_4, and no affinity for the D_1 receptors. Triazole derivative **86** (Fig. 12) displayed the maximum affinity toward D_3 receptor with a K_i value of 2.7 nM, selectivity over D_2 (70-fold) and D_4 (200-fold), and behavior as a competitive antagonist in the low nanomolar range.[102]

1.10.5.3 Selective Binding Ligands

A series of 4-phenylpiperazines triazole derivatives were generated via click chemistry to explore the triazole as a bioisosteric substitution for the amide linker commonly found in this chemical class of D_3R (dopamine D_3 receptor)-selective ligands. Several 1,2,3-triazole-synthesized compounds had high (K_i = 1–10 nM) affinity for D_3R and >80-fold selectivity for D_3R over D_2R. Compounds **80**, **81**, and **82** (Fig. 13) showed good affinity toward D_2R, D_3R, and D_4R, respectively.[103]

Integrin receptors consist of heterodimeric glycoproteins involved in cell–cell and cell–extracellular matrix adhesion and signal transduction. Many integrins, which are glycoproteins, contain the arginine–glycine–aspartic acid (RGDa) tripeptide sequence, found in a series of peptide-based ligands such as vitronectin, fibronectin, and osteopontin. Regarding RGD-dependent integrins, $\alpha_v\beta_3$ and $\alpha_v\beta_5$ receptors have received increasing attention as therapeutic targets, as they are expressed in various cell types and are involved in inflammatory and tumor-related processes. $\alpha_v\beta_3$ integrin expression is upregulated in many solid tumors and contributes to the mechanisms involved in tumor growth and metastatic dissemination. During the progression from a benign melanocytic disease to a metastatic malignant melanoma, melanocytes undergo a series of changes in the expression of cell-surface molecules, including $\alpha_v\beta_3$ integrin. Guarna and his coworkers employed click chemistry for the discovery of triazole-based arginine–glycine–aspartate (RGD) mimetics, which showed binding affinity properties toward $\alpha_v\beta_3/\alpha_v\beta_5$ integrins. Biological assays showed compound **83** (Fig. 13) capable of binding $\alpha_v\beta_3$ integrin with nanomolar affinity according to a two-site model, and molecular modeling studies revealed a peculiar π-stacking interaction between the triazole ring and Tyr178 side chain. Accordingly, compound **83** inhibited the adhesion of integrin-expressing human melanoma cells to RGD-containing proteins of the extracellular matrix, such as vitronectin, fibronectin, and osteopontin, and also angiogenesis in vitro and in vivo experimental models. The relevant biological effects exerted by compound **83** suggest its potential application as an antiangiogenic agent in the diagnosis and therapy of tumors where $\alpha_v\beta_3$ integrin expression is upregulated.[104]

Neurotensin (NT) is a secreted tridecapeptide, which is widely distributed throughout the central nervous system, and function as a neurotransmitter or a neuromodulator. NT binds to the neurotensin receptor (NTR) where of three different subtypes, NTR1, NTR2, and NTR3, are characterized. NTR1 and NTR2 belong to the family of G-protein-coupled receptors, and their internalization mechanism via receptor-mediated endocytosis is well described by Mazella and Vincent. NTRs as promising target for cancer diagnosis and therapy were well reported in the literature. Wuest and coworkers employed click chemistry for the synthesis of neurotensin-containing peptide heterodimer analogs. Neurotensin-containing peptide dimer analogs were used in an in vitro binding assay to determine binding affinity toward the neurotensin receptor-1 (NTR1). The determined IC_{50} values of 0.7 μM indicated only very low binding affinity of the neurotensin (compound **84**; Fig. 13)-containing peptide heterodimer toward the NTR1.[105]

1,4-Substituted triazole-based peptidomimetics were prepared for binding affinity toward somatostatin receptor (SSTR). Stereoisomeric peptidomimetics were synthesized by click chemistry, using the ligand TBTA (tris-(benzyltriazolylmethyl)amine) to suppress competing homodimer formation (compound **85**; Fig. 13). NMR analysis showed that all compounds existed in a single conformation on the NMR timescale. The compounds exhibited diverse selectivity against the five human SSTR subtypes 1–5. In an attempt to define the three-dimensional pharmacophoric requirements for receptor binding, the most potent human SSTR subtype 4 peptidomimetic was overlaid with all the other peptidomimetics. Three ligand groups were thus identified: selective ligands, broad-spectrum binders, and low-affinity ligands.[106]

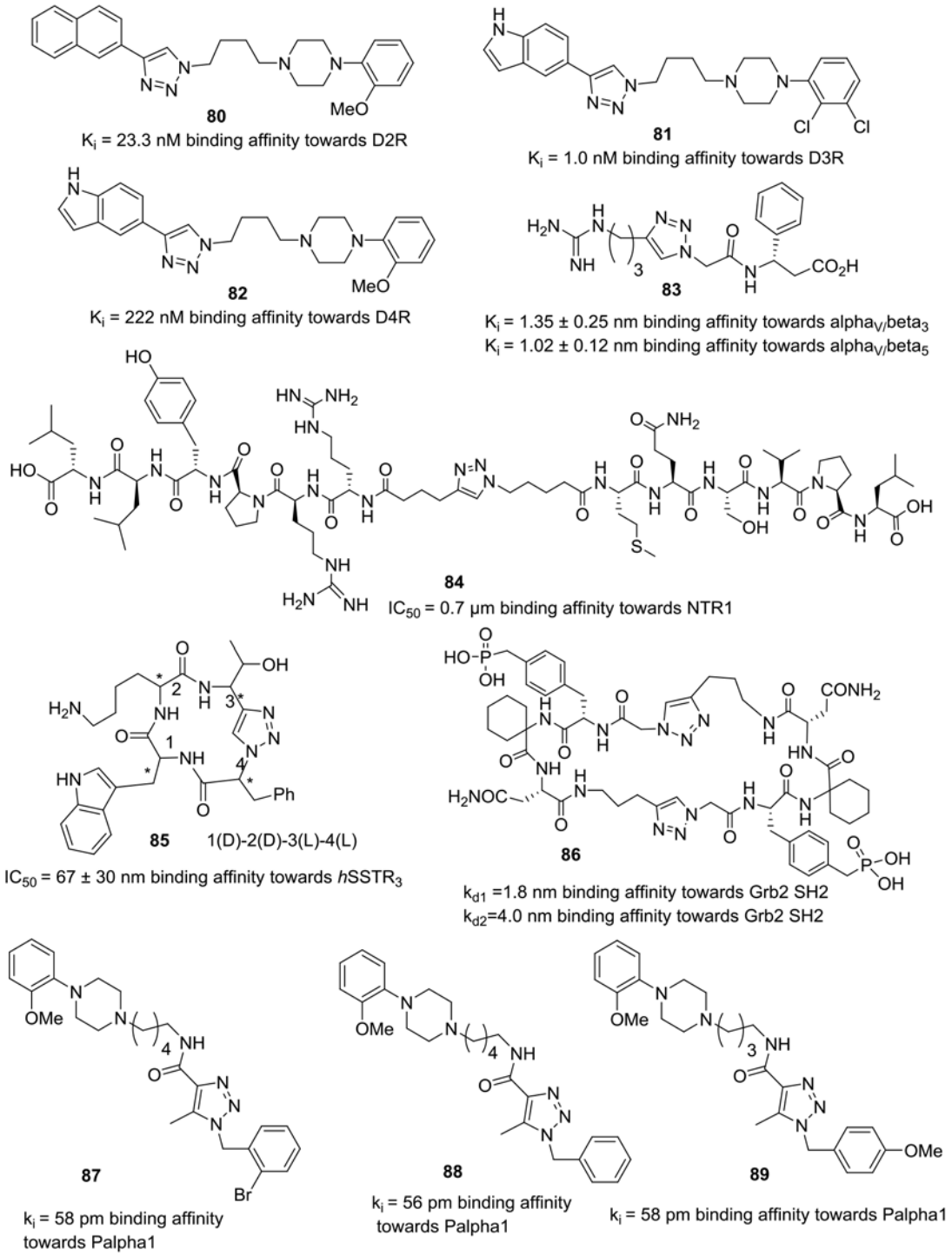

Fig. 13 Triazole lead structures of receptor-selective binding ligands explored via click chemistry.

Growth factor receptor-bound protein 2 (Grb2) is a SH2/SH3 domain-containing adaptor protein that links growth factor receptor tyrosine kinases to the Ras signaling pathway. For Grb2 SH2 domains, where open-chain "pTyr-Xxx-Asn" sequences are preferentially recognized in type-I β-turn conformations, induction of turn geometries through macrocyclization using ring-closing olefin metathesis2 (RCM) has resulted in a number of potent binding inhibitors. Burke and his workers employed click chemistry for the synthesis of triazole-containing macrocycles based on the Grb2 SH2 domain-binding motif, "Pmp-Ac6c-Asn," where Pmp and Ac6c stand for 4-phosphonomethylphenylalanine and α-amino cyclohexane carboxylic acid, respectively.

In Grb2 SH2, domain-binding assays revealed that compound **86** (Fig. 13) showed most binding affinity toward Grb2 SH2 of the series.[107]

Parallel solid-supported synthesis of formyl aryloxymethyltriazole (FAMT) resins was prepared using click chemistry by Gmeiner and his research group. A library of test compounds revealing three points of diversity were generated by a four-step BAL-based strategy including reductive amination, acylation, 1,3-dipolar cycloaddition, and TFA-induced cleavage. The target compounds were screened for neuroreceptor binding employing eight different GPCRs, whereas high-affinity dopamine D_3 and α1-receptor binders were identified. The library members **87**, **88**, and **89** (Fig. 13) revealed K_i values for the α1 receptor in the medium picomolar range.[108]

α-Amino-3-hydroxy-5-methyl-4-isoxazolepropionic acid receptors (AMPAs) are hetero-tetrameric combinations of GluR1–4 subunits that provide the major fast excitatory inputs in the CNS. Regulation of AMPA receptor number at the postsynaptic membrane contributes to changes in synapse strength and to synaptic plasticity. Such regulation requires a synaptic infrastructure that controls the trafficking and localization of receptors, such as through the interaction of receptors with synaptic scaffolding proteins. The central nervous system glutamate receptors are an important target for drug discovery. Abell and his coworkers reported synthesis and glutamate receptor activity of 1,4- and 1,5-disubstituted 1,2,3-triazolyl amino acid glutamate homologues. In vitro screening indicated selective binding for **90** (Fig. 14) at AMPA receptors of the series with IC_{50} value of 49 μM.[109]

Pharmacological effects of cannabinoid and endogenous cannabinoid ligands are mediated by two subtypes of transmembrane G-protein-coupled receptors: CB1 and CB2. CB1 receptors are expressed in the central nervous system (CNS) with high density in the cerebellum, hippocampus, and striatum. CB1 receptors are found in some peripheral tissues (the urinary bladder, testis, and ileum) as well. CB2 receptors are predominantly located in the immune system (tonsils, spleen, and immune cells) with very low concentration in the CNS. CB1 agonists have potential therapeutic applications in developing drugs for pain, nausea, glaucoma, stroke, cancer, and neurological disorders such as multiple sclerosis and Parkinson's disease. The potential applications of CB1

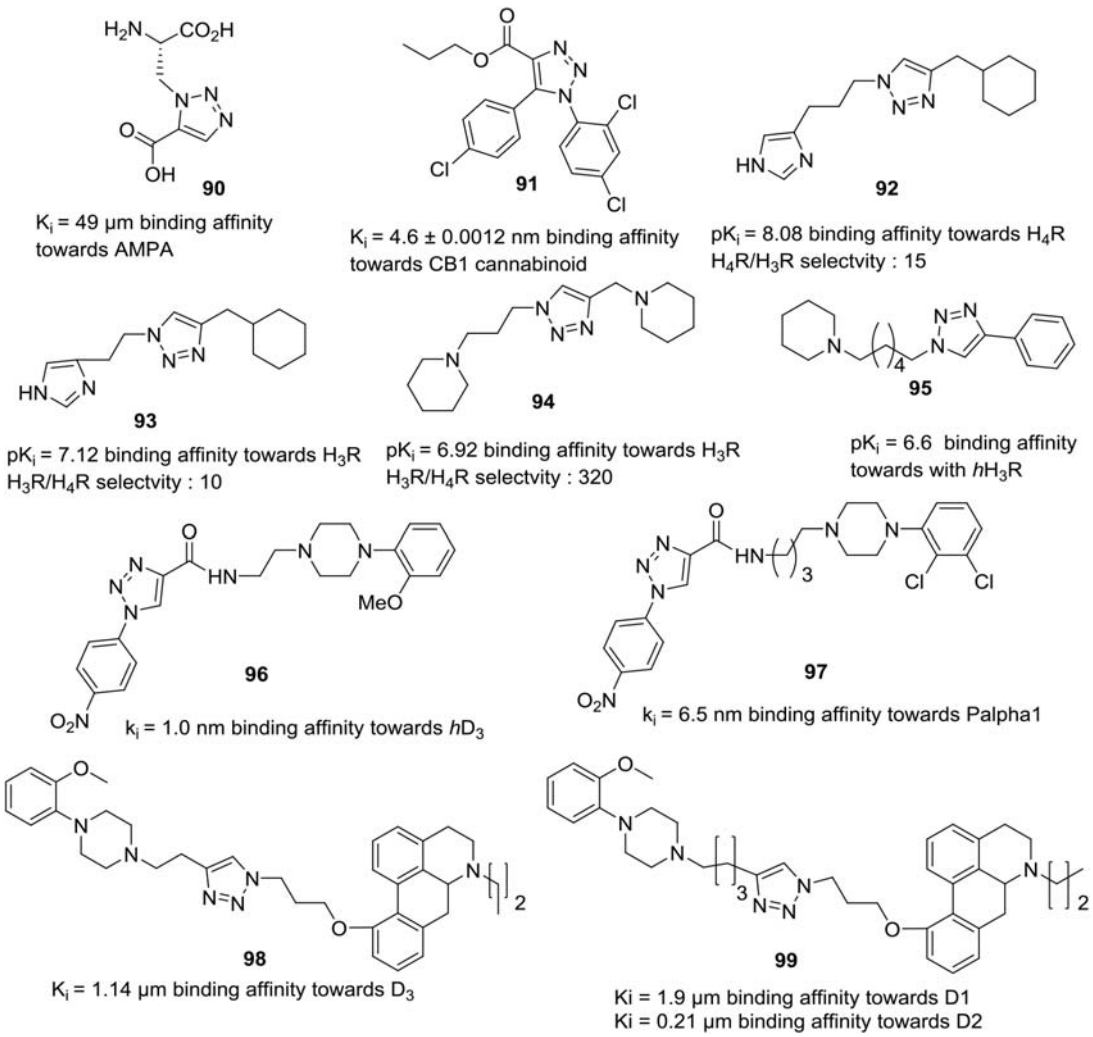

Fig. 14 Chemical triazole lead structures of receptor-selective binding ligands generated via click chemistry.

antagonists include the therapeutic treatment of obesity and related metabolic disorders as well as medications for drug addiction. Trudell and his workers employed click chemistry for the synthesis of a series of 4-alkoxycarbonyl-1,5-diaryl-1,2,3-triazoles and evaluated as a novel class of potent cannabinoid receptor ligands. The *n*-propyl ester **91** ($K_i = 4.6$ nM, Fig. 14) exhibited the most potent binding affinity toward cannabinoid receptor of the series.[110]

The histamine H_3 (H_3R) and H_4 (H_4R) receptors attract considerable interest from the medicinal chemistry community. It is playing an important role in inflammation and immune responses with possible applications in diseases such as inflammatory bowel disease, allergic asthma, and pruritus. Wijtmans and his coworkers employed click chemistry to assemble diverse triazole compounds containing a peripheral imidazole group. The imidazole ring posed some problems in the click chemistry putatively due to Cu(II) coordination, but Boc protection of the imidazole and removal of oxygen from the reaction mixture provided effective strategies. Pharmacological studies of triazole scaffold proved remarkably sensitive H_4R affinities. With subtle changes in aliphatic group, **92** and **93** (Fig. 14) were obtained, which boosted high H_4R affinity ($pK_i = 8.08$ and 7.12) and a good H_4R/H_3R selectivity of 15 and 10 noteworthy for a monosubstituted imidazole compound. In contrast, a replacement of both peripheral groups by piperidines led to compound **94** (Fig. 14) with good H_3R affinity ($pK_i = 6.92$) and excellent H_3R/H_4R selectivity (320).[111]

Human histamine H_3 receptors (hH$_3$R) in the central nervous system (CNS) are auto- and heteroreceptors modulating the synthesis and the release of histamine as well as the liberation of various other neurotransmitters. Hence, histaminergic neurons, which spread from the tuberomamillary nucleus into most parts of the brain, influence the neurotransmitter balance in the respective compartments in dependence of colocalized neurons. Central functions like vigilance, attention, and learning are affected. Modulation of this neuronal interplay by hH$_3$R antagonists/inverse agonists might be an effective approach in the therapy of neuronal diseases, for example, cognitive impairment, sleep/wake disorders, epilepsy, and obesity. The diversity of potential indications gives a hint of the complexity of hH$_3$R modulation. Stark and his coworker employed click chemistry for the synthesis of human histamine H_3 receptor (hH3R) binding ligands using ω-piperidinylalkayl azide derivatives. Compound **95** (Fig. 14) showed the most binding affinity toward hH3R within this series, showing receptor binding affinity in the nano- and subnanomolar concentration range.[112]

Dopamine (DA) D_3 receptor belongs to the D_2-like subfamily of dopamine receptors, including D_2, D_3, and D_4, functionally distinct from the D_1-like subfamily (D_1 and D_5). D_3 receptor is implicated in a variety of brain functions and proposed as a promising therapeutic target for a number of neurological and psychiatric disorders, including schizophrenia, depression, drug abuse, Parkinson's disease, and restless leg syndrome. Gmeiner et al. successfully applied click chemistry for a parallel synthesis of dopaminergic phenyltriazoles utilizing the triazolylmethylcatechol (TMC) resin. A focused model library of 20 test compounds revealing three points of diversity was generated by a three-step SPOS approach. Product purification was performed employing a solid-supported carboxylic acid anhydride as a scavenger. GPCR-ligand-binding screening revealed dopamine D_3 ligand (**96**, Fig. 14) with K_i values in the single-digit nanomolar range. Also compound **97** showed good binding affinity toward Pα1 with K_i value of 6.5 nM.[113]

Click chemistry was employed for the synthesis of a series of aporphine analogs from appropriate precursors and aryl piperazines. These compounds displayed good to high affinity at the D_3 receptor and low or no affinity at the D_1 and D_2 receptors. Compound **98** (Fig. 14) showed good affinity at the D_3 receptor and low affinity at the D_1 and D_2 receptors with $K_i = 1.14$ nM against D_3 receptor. Compound **99** (Fig. 14) was identified as the most potent at the D_1 and D_2 receptors among our newly synthesized analogs with K_i values of 1.9 and 0.21 μM against D_1 and D_2 receptor, respectively.[114]

1.10.6 In Situ Click Chemistry

Modern medicinal chemists mainly are applying fragment-based approaches to find lead molecules more efficiently to facilitate the drug discovery process.[6,115] The conventional approach used by medicinal chemists in drug discovery consists of the synthesis of a collection of compounds and subsequent biological screening. The procedure would be shortened and optimized if the biological target could actively choose its best ligand. Indeed, the target would act as the ideal template to generate the perfect hit. In this specific context, it is therefore possible to envisage that, at room temperature, an enzyme could bring azide and alkyne containing molecules in close proximity so as to overcome the high energetic barrier allowing the click chemistry reaction to occur in room temperature catalyzed by an enzyme. In this manner, only compounds that fit correctly into the active site of the enzyme should react to give new potent ligands of the enzyme. The schematic pictorial representation of in situ click chemistry[116–119] of enzyme inhibitor is shown in Fig. 15.

Several reports have appeared in which fragment-like monomers are allowed to react together in the presence of target protein. In certain cases, the rate of formation of a few possible products from a potentially large number is dramatically accelerated by sequestering the two components inside a host structure due to the appropriate orientation of the fragments. The resulting compounds always have good potency because they are preselected to be good binders. This approach has been effectively applied to the click triazole-forming reaction of azides and acetylenes, because the reactive partners appear to snap together when properly oriented.[120]

Many examples of the in situ click chemistry concept are present in the literature and have been reviewed in details in our review article in 2013.[20] Some of the recent updates are described in the succeeding text. In principle, the "click chemistry" approach to drug design is applicable to almost any target. If it is possible to use a pure enzyme, the function of which can be measured easily, then the techniques are easier to apply. However, Finn stresses, "the in situ approach has the virtue of being potentially useful when

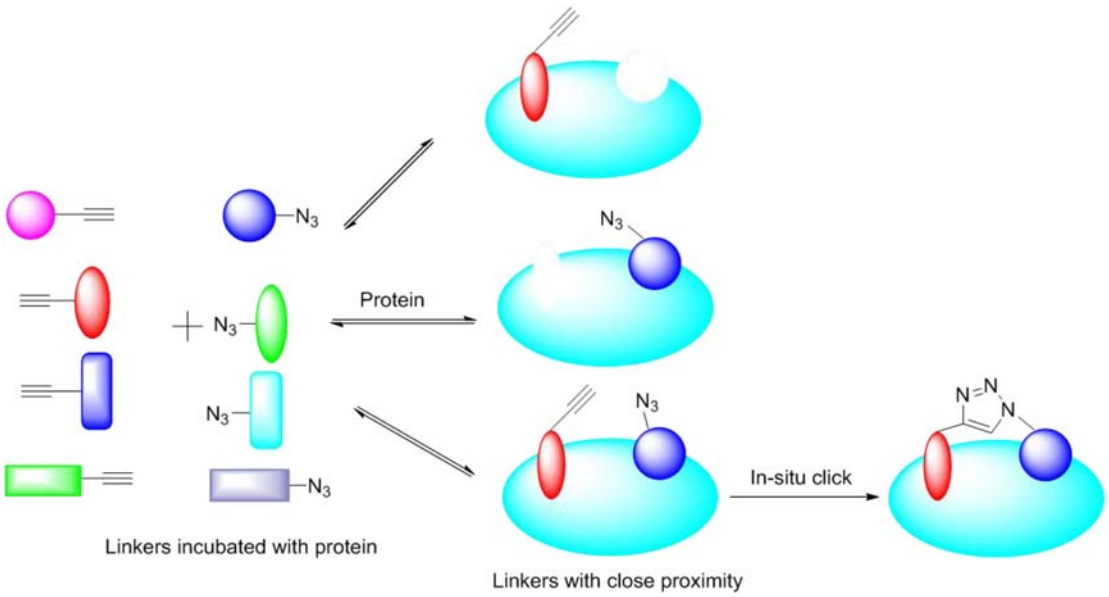

Fig. 15 Schematic diagram of the development of enzyme inhibitors using in situ click chemistry strategy.

these conditions were met. If everything works perfectly, one can even imagine administering a set of pieces of a drug to a patient and having the drug assembled itself at the desired site (e.g., a tumor tissue) in response to the specific nature of the target." Further development work with enzyme inhibitors is now in progress in many research groups, on a variety of diseases including AIDS, cancer, anthrax, and Huntington's disease.[116]

1.10.6.1 Screening and Identification of Biotin Protein Ligase (BPL) Inhibitors

In situ click chemistry was employed for screening and to probe the binding sites of biotin protein ligase inhibitors by Abell. This technique is the elegant approach for identifying enzyme inhibitors, where the target enzyme is used to select the appropriate combination of azide and alkyne analogs from a library. Once bound in the active site, they assemble via click chemistry reaction into the corresponding triazole-based inhibitor. BPL is the clinically important bacterial pathogen *Staphylococcus aureus* (Sa). The function of BPL is to catalyze the stepwise formation of biotinyl-50-AMP from biotin and ATP. Biotinyl-50-AMP then enables biotinylation of enzymes central to fatty acid biosynthesis and the tricarboxylic acid cycle. The triazoles are prepared by click of biotin alkyne and adenosine azide fragments. A leaky mutant (SaBPL-R122G) of wild-type SaBPL was used to enhance the turnover rate for the reaction of biotin alkyne with an azide to give a triazole. That allowed the enzyme to select the optimum triazole-based inhibitor using a library of such azides in a single experiment, with improved efficiency and sensitivity of detection, difficulties which could restrict the general utility of a multicomponent in situ click approach to ligand optimization. The leaky mutant had a 40-fold enhanced rate of product dissociation relative to the target enzyme (SaBPL). Particularly, compound **101** (Fig. 16) indented in this library-based experiment was the most potent inhibitor. Enhancing the efficiency of a target enzyme is an important approach for improving the utility of multicomponent in situ click beyond the few examples reported to date.[121]

1.10.6.2 Probing the Binding Site of Abl Tyrosine Kinase

Passarella and his coworker successfully applied in situ click chemistry for ligand-binding site of Abl and the ability of this enzyme to form its inhibitor. The selection of coupling analogs was incubated with the enzyme based on the structure of "hits" originating from docking studies and/or high-throughput screens. For example, many of the known inhibitors of tyrosine kinase could be dissected in frameworks and properly functionalized with azide/alkyne moieties to be used as libraries of building blocks for in situ click reaction, in the presence of any available tyrosine kinase. The detection of the Abl-bound compounds is favored by HR-ESI-MS. Especially, compound **102** (Fig. 17) bound with Abl was detected by HR-MS at lower concentration of azide (0.25 μM), alkyne (0.25 μM), and Abl (0.0185 μM). This detection method will open the way for the preparation and in-depth biological evaluation of selective molecules as lead structures.[122]

1.10.6.3 Antibody-Like Protein-Capture Agents

Antibody-based capture agents are important novel method to detect most proteins. A good antibody displays high affinity and selectivity for its related protein, though antibodies are often costly and they may appear unstable toward chemical and biochemical

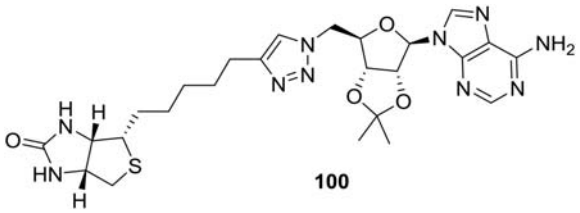

100

K_d= 0.11 μm binding affinity *Se*BPL(wild-type)
K_d= 9.83 μm binding affinity *Se*BPL(R122G)

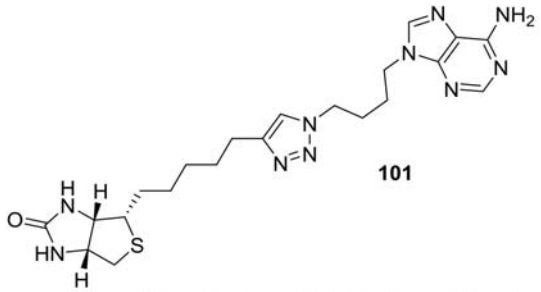

101

K_d= 0.06 μm binding affinity *Se*BPL(wild-type)
K_d= 2.96 μm binding affinity *Se*BPL(R122G)

Fig. 16 Lead triazole analogs of biotin protein ligase (BPL) inhibitors generated using in situ click chemistry.

processes. Several alternative protein-capture agents, including oligonucleotide aptamers and phage-display peptides, were reported, each of which had advantages as well as significant limitations.[123]

Agnew and coworkers first developed a triligand capture agent against bovine carbonic anhydrase II (bCAII).[124] In situ click chemistry approach was applied for the building of multiligand protein-capture agents and triligand capture agent screened against *human* bovine carbonic anhydrase II (h(b)CAII). Bead-based combinatorial synthesis of oligopeptides was employed for attaching alkyne group at the terminal of each library analog. Hexapeptide anchor sequence was confirmed from beads bound the protein most strongly, followed by Edman sequencing. The anchor ligand exhibited a weak affinity ($K_D \approx 500$ mM) against bCAII. The anchor compound was then incubated with bCAII and a second D-amino acid peptide library bearing azido-amino acids of variable side-chain length. After two screens, a consensus 2° peptide was identified and conjugated to the anchor peptide by the click reaction to yield a biligand with significantly improved affinity ($K_D = 3$ mM) as determined using surface plasmon resonance. The process was repeated to generate a high-affinity triligand (**103**) as measured by SPR techniques ($K_D \approx 45$ and 64 nM) that could function as a drop-in antibody replacement in immunoblotting experiments. Importantly, the triligand was formed on-bead only in the presence of bCAII or human carbonic anhydrase II (hCAII). Recent years, two more triligands (**104** and **105**; $K_d = 0.5–5$ μM; Fig. 18) were developed for human carbonic anhydrase II inhibitors.[125] Similarly triligand (**106**, Fig. 19) was developed by Millward and coworkers for prostate-specific antigen-binding peptides (anti-PSA triligand with cyclic anchor peptide) generated via click reaction from modification cyclic peptide reported in the literature.[125]

Iterative in situ click chemistry was applied to generate Akt-specific branched peptide triligand (**107**; Fig. 19) with mid-nanomolar affinity for protein kinase B (Akt1). Each peptide module in the branched structure made unique contributions to affinity and/or specificity resulting in a 200 nM affinity ligand that efficiently immunoprecipitated Akt from cancer cell lysates and labels Akt in fixed cells. The resulting branched triligand was found to inhibit the catalytic activity of Akt1 without directly binding to the ATP or peptide substrate pockets, suggesting an allosteric mode of inhibition. The triligand immunoprecipitated Akt from OVCAR3 ovarian cancer cell lysates and a fluorescent variant was used to image membrane-localized Akt in cell culture after stimulation with insulin and EGF. In both cases, the triligand compared favorably with commercial monoclonal antibodies.[126]

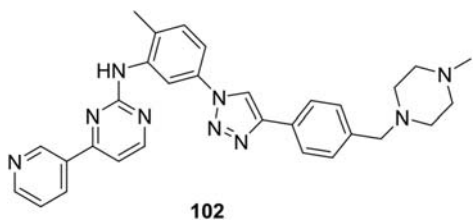

102

Fig. 17 Lead triazole analogs of Abl tyrosine kinase inhibitors generated using in situ click chemistry.

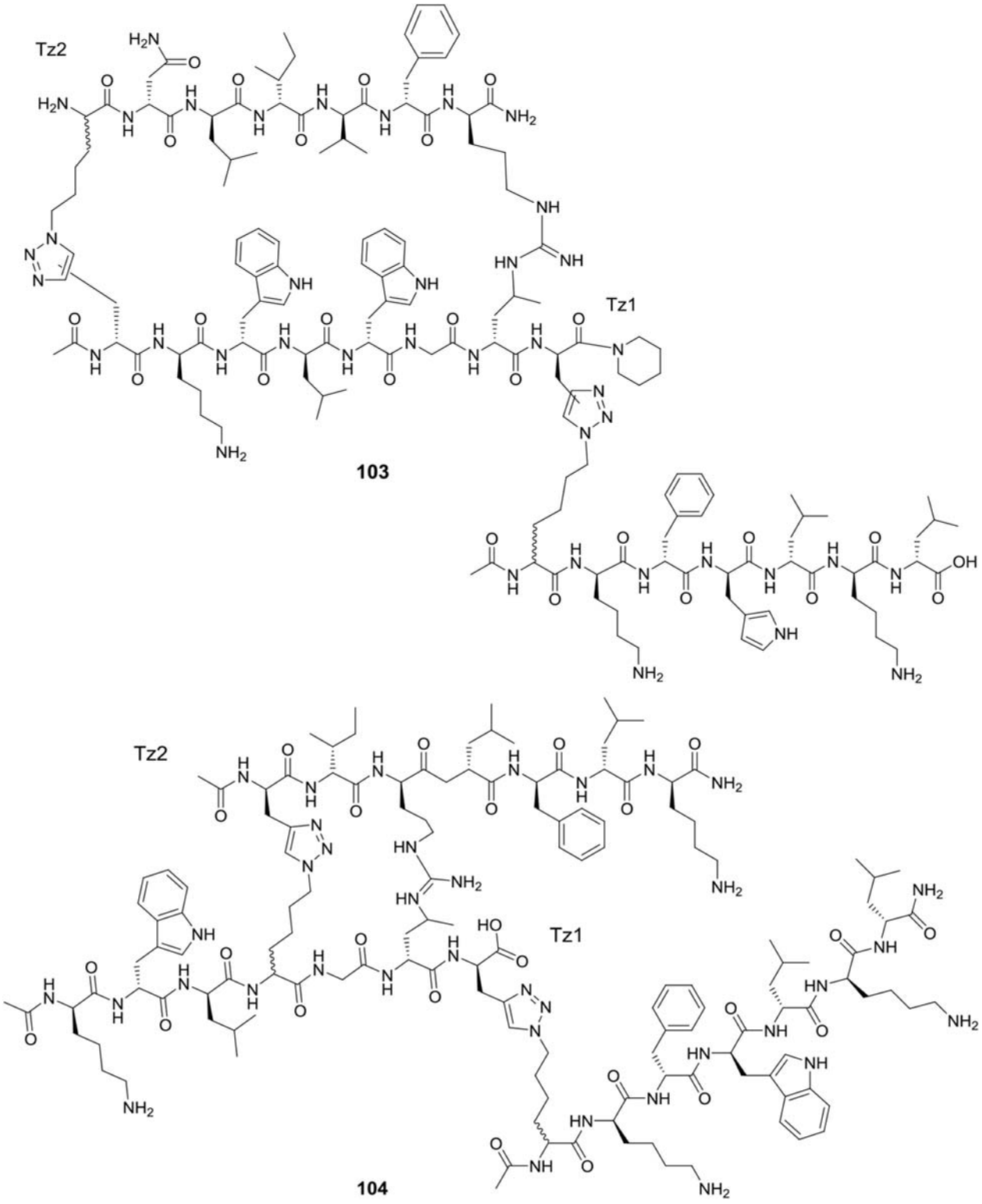

Fig. 18 Lead triazole analogs of carbonic anhydrase II inhibitors generated using in situ click chemistry.

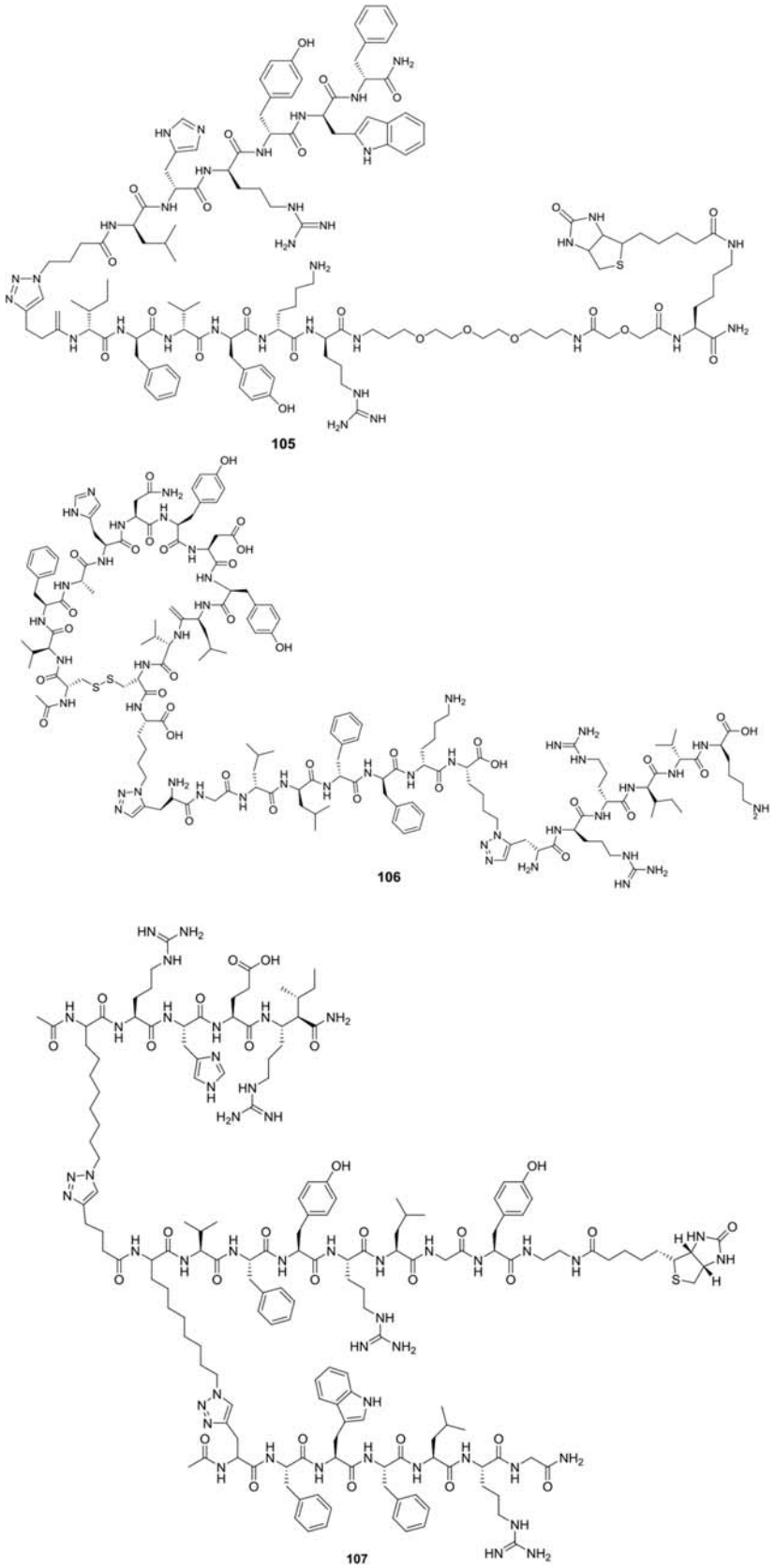

Fig. 19 Lead triazole analogs of carbonic anhydrase II, anti-PSA triligand, and protein kinase B inhibitors generated using in situ click chemistry.

1.10.7 Conclusion and Future Directions

In this article, we provided an overview in medicinal science applications for the researchers that intend effective utilization of click chemistry. Innovative and more efficient chemical reactions (click chemistry) and methodologies, which may override the laborious protection/deprotection and purification steps in conventional total synthesis, could revolutionize the next-generation chemical and biological research. We have demonstrated from this article that click chemistry is one of the powerful tools for the construction of heteroatom links for chemistry and biology in drug development and investigation of biological system. The copper(I)-catalyzed 1,2,3-triazole-forming reaction between azides and terminal alkynes has become the gold standard reaction due to its reliability, specificity, and biocompatibility. Research in drug development in this click chemistry field is still increasing exponentially. We have discussed the use of click chemistry in the area of the synthesis of agents with anticancer activity, antiproliferative, antiviral, antimicrobial, etc., and have intended to demonstrate the diversity of applications of this chemical strategy in the area of drug discovery. Lead triazole functional analogs are used for anticancer agents, antiproliferative, antiviral, and antimicrobial development. On the other hand, click chemistry has been effectively applied for the development of agonists, antagonist, and selective ligand in receptor–ligand-binding studies for drug development in the field of medicinal chemistry. Lead triazole structures were used in the literature for various receptor–ligand-binding studies for effective drug development. Additionally, in situ click chemistry ingenious strategies are effectively applied into new ways of generating extremely potent inhibitors against certain enzymes. Especially, in situ click chemistry is used for protein ligase, Abl tyrosine kinase, carbonic anhydrase II, and protein kinase B (Akt1) potent enzyme inhibitor development.

In contemporary drug discovery research, click chemistry is playing important role for generating drug-like candidates to understand biochemical pathways and access the information of the drug-binding sites in the receptor site in the cell membrane. Click chemistry can be applied in several areas and is rapidly increasing with possibilities of exciting discoveries on the horizon. Apart from the general areas of materials science, nanoscience, and bioconjugation, the concept has already made huge impact in drug discovery. A constant drive toward simpler chemical reactions such as click reaction with a wide scope is in progress. Due to the simplicity of click reactions, biochemists and molecular biologists are able to make complex molecular systems without much bothering about the synthetic chemistry. Click chemistry in the future will reach the level of ready-made chemistry like many kits available in the market to make it easy to use. On the other hand, click chemistry reaction is used to site-specific functionalization biological macromolecules (protein, DNA, glycans, lipids, and cell surfaces) and living systems (virus nanoparticles, bacterial-like microorganism, and zebrafish embryos) under physiological conditions. These click modified bimolecular assemblies can be effectively used in target-based drug delivery in the future. Click activity or affinity-based protein profiling methods facilitate the detection of many disease applicable enzymes and careful pharmacological probes to perturb and characterize these proteins in cells. Activity-based proteomics can provide insight into the metabolic and signaling pathways that support illuminate new strategies for disease diagnosis and treatment.

References

1. Shen, B. *Cell* **2015,** *163,* 1297–1300.
2. Copeland, R. A. *Evaluation of Enzyme Inhibitors in Drug Discovery: A Guide for Medicinal Chemists and Pharmacologists;* John Wiley & Sons: Hoboken, New Jersey, 2013.
3. Nussinov, R.; Tsai, C.-J. *Cell* **2013,** *153,* 293–305.
4. Patrick, G. L. *An Introduction to Medicinal Chemistry;* Oxford University Press: Oxford, 2013.
5. Lipinski, C. A.; Lombardo, F.; Dominy, B. W.; Feeney, P. J. *Adv. Drug Deliv. Rev.* **2012,** *64,* 4–17.
6. Hopkins, A. L.; Keserü, G. M.; Leeson, P. D.; Rees, D. C.; Reynolds, C. H. *Nat. Rev. Drug Discov.* **2014,** *13,* 105–121.
7. Jhoti, H.; Williams, G.; Rees, D. C.; Murray, C. W. *Nat. Rev. Drug Discov.* **2013,** *12,* 644.
8. Kolb, H. C.; Finn, M.; Sharpless, K. B. *Angew. Chem. Int. Ed.* **2001,** *40,* 2004–2021.
9. Kolb, H. C.; Sharpless, K. B. *Drug Discov. Today* **2003,** *8,* 1128–1137.
10. Rostovtsev, V. V.; Green, L. G.; Fokin, V. V.; Sharpless, K. B. *Angew. Chem.* **2002,** *114,* 2708–2711.
11. Finn, M. G.; Fokin, V. V. *Chem. Soc. Rev.* **2010,** *39,* 1231–1232.
12. Kappe, C. O.; Van der Eycken, E. *Chem. Soc. Rev.* **2010,** *39,* 1280–1290.
13. Moorhouse, A. D.; Moses, J. E. *ChemMedChem* **2008,** *3,* 715–723.
14. Hou, J.; Liu, X.; Shen, J.; Zhao, G.; Wang, P. G. *Expert Opin. Drug Discovery* **2012,** *7,* 489–501.
15. Musumeci, F.; Schenone, S.; Desogus, A.; Nieddu, E.; Deodato, D.; Botta, L. *Curr. Med. Chem.* **2015,** *22,* 2022–2050.
16. Agalave, S. G.; Maujan, S. R.; Pore, V. S. *Chem. Asian J.* **2011,** *6,* 2696–2718.
17. Wang, X.; Huang, B.; Liu, X.; Zhan, P. *Drug Discov. Today* **2015,** *21,* 118–132.
18. Hein, C.; Liu, X.-M.; Wang, D. *Pharm. Res.* **2008,** *25,* 2216–2230.
19. Holub, J. M.; Kirshenbaum, K. *Chem. Soc. Rev.* **2010,** *39,* 1325–1337.
20. Thirumurugan, P.; Matosiuk, D.; Jozwiak, K. *Chem. Rev.* **2013,** *113,* 4905–4979.
21. Kalesh, K. A.; Yang, P.-Y.; Srinivasan, R.; Yao, S. Q. *QSAR Comb. Sci.* **2007,** *26,* 1135–1144.
22. Kalesh, K. A.; Shi, H.; Ge, J.; Yao, S. Q. *Org. Biomol. Chem.* **2010,** *8,* 1749–1762.
23. Yang, Y.; Adelstein, S. J.; Kassis, A. I. *Drug Discov. Today* **2012,** *17,* S16–S23.
24. Swinney, D. C.; Anthony, J. *Nat. Rev. Drug Discov.* **2011,** *10,* 507–519.
25. Niphakis, M. J.; Cravatt, B. F. *Annu. Rev. Biochem.* **2014,** *83,* 341–377.
26. Erlanson, D. A. *In Fragment-Based Drug Discovery and X-Ray Crystallography;* Springer: Berlin, 2012, 1–32.
27. Murray, C. W.; Verdonk, M. L.; Rees, D. C. *Trends Pharmacol. Sci.* **2012,** *33,* 224–232.
28. Howard, S.; Abell, C. *Fragment-Based Drug Discovery;* Royal Society of Chemistry: Cambridge, UK, 2015.

29. Murray, C. W.; Rees, D. C. *Angew. Chem. Int. Ed.* **2015**.
30. Eggenweiler, H.M.; Wolf, M.; Buchstaller, H.P.; Sirrenberg, C., Triazole derivative as an HSP 90 inhibitor. U.S. Patent US 8816070 B2 / PCT/EP2007/010775, 2014.
31. Geisler, J.; Haynes, B.; Anker, G.; Dowsett, M.; Lønning, P. E. J. *Clin. Oncol.* **2002,** *20,* 751–757.
32. Hussain, M. M.; Kotz, H.; Minasian, L.; Premkumar, A.; Sarosy, G.; Reed, E.; Zhai, S.; Steinberg, S. M.; Raggio, M.; Oliver, V. K. J. *Clin. Oncol.* **2003,** *21,* 4356–4363.
33. Harper-Wynne, C. L.; Sacks, N. P.; Shenton, K.; MacNeill, F. A.; Sauven, P.; Laidlaw, I. J.; Rayter, Z.; Miall, S.; Howes, A.; Salter, J. J. *Clin. Oncol.* **2002,** *20,* 1026–1035.
34. Goss, P.; Winer, E.; Tannock, I. J. *Clin. Oncol.* **1999,** *17,* 52.
35. Yang, B.; He, Q.-j.; Zhu, D.-y.; Lou, Y.-j.; Fang, R.-y. *Cancer Chemother. Pharmacol.* **2006,** *57,* 268–273.
36. Duan, Y.-C.; Ma, Y.-C.; Zhang, E.; Shi, X.-J.; Wang, M.-M.; Ye, X.-W.; Liu, H.-M. *Eur. J. Med. Chem.* **2013,** *62,* 11–19.
37. Elamari, H.; Slimi, R.; Chabot, G. G.; Quentin, L.; Scherman, D.; Girard, C. *Eur. J. Med. Chem.* **2013,** *60,* 360–364.
38. Hyder, I.; Yedlapudi, D.; Kalivendi, S. V.; Khazir, J.; Ismail, T.; Nalla, N.; Miryala, S.; Sampath Kumar, H. M. *Bioorg. Med. Chem. Lett.* **2015,** *25,* 2860–2863.
39. Banday, A. H.; Kulkarni, V. V.; Hruby, V. J. *Med. Chem. Commun.* **2015,** *6,* 94–104.
40. Delatouche, R.; Denis, I.; Grinda, M.; Bahhaj, F. E.; Baucher, E.; Collette, F.; Héroguez, V.; Grégoire, M.; Blanquart, C.; Bertrand, P. *Eur. J. Pharm. Biopharm.* **2013,** *85,* 862–872.
41. Farooq, S.; Shakeelm, u. R.; Hussain, A.; Hamid, A.; Qurishi, M. A.; Koul, S. *Eur. J. Med. Chem.* **2014,** *84,* 545–554.
42. Lone, S. H.; Bhat, K. A.; Majeed, R.; Hamid, A.; Khuroo, M. A. *Bioorg. Med. Chem. Lett.* **2014,** *24,* 1047–1051.
43. Yoon, J.; Ryu, J.-S. *Bioorg. Med. Chem. Lett.* **2010,** *20,* 3930–3935.
44. Jin, X.; Yan, T.-H.; Yan, L.; Li, Q.; Wang, R.-L.; Hu, Z.-L.; Jiang, Y.-Y.; Sun, Q.-Y.; Cao, Y.-B. *Drug Des. Dev. Ther.* **2014,** *8,* 1047.
45. Lv, Z.; Zhang, Y.; Zhang, M.; Chen, H.; Sun, Z.; Geng, D.; Niu, C.; Li, K. *Eur. J. Med. Chem.* **2013,** *67,* 447–453.
46. Rashid, S.; Dar, B. A.; Majeed, R.; Hamid, A.; Bhat, B. A. *Eur. J. Med. Chem.* **2013,** *66,* 238–245.
47. Reddy, D. M.; Srinivas, J.; Chashoo, G.; Saxena, A. K.; Sampath Kumar, H. M. *Eur. J. Med. Chem.* **2011,** *46,* 1983–1991.
48. Lei, X.; Danishefsky, S. J. *Adv. Synth. Catal.* **2008,** *350,* 1677–1681.
49. Zhang, J.; Garrossian, M.; Gardner, D.; Garrossian, A.; Chang, Y.-T.; Kim, Y. K.; Chang, C.-W. T. *Bioorg. Med. Chem. Lett.* **2008,** *18,* 1359–1363.
50. Kamal, A.; Shankaraiah, N.; Devaiah, V.; Laxma Reddy, K.; Juvekar, A.; Sen, S.; Kurian, N.; Zingde, S. *Bioorg. Med. Chem. Lett.* **2008,** *18,* 1468–1473.
51. Day, J. E. H.; Sharp, S. Y.; Rowlands, M. G.; Aherne, W.; Workman, P.; Moody, C. J. *Chem. Eur. J.* **2010,** *16,* 2758–2763.
52. Peterson, L. B.; Blagg, B. S. J. *Bioorg. Med. Chem. Lett.* **2010,** *20,* 3957–3960.
53. Chen, J.; Nikolovska-Coleska, Z.; Yang, C.-Y.; Gomez, C.; Gao, W.; Krajewski, K.; Jiang, S.; Roller, P.; Wang, S. *Bioorg. Med. Chem. Lett.* **2007,** *17,* 3939–3942.
54. Lee, Y.-S.; Park, S. M.; Kim, H. M.; Park, S.-K.; Lee, K.; Lee, C. W.; Kim, B. H. *Bioorg. Med. Chem. Lett.* **2009,** *19,* 4688–4691.
55. Yang, Y. D.; Tokunaga, E.; Akiyama, H.; Saito, N.; Shibata, N. *ChemMedChem* **2014,** *9,* 913–917.
56. Nagesh, H.; Suresh, N.; Prakash, G.; Gupta, S.; Rao, J.; Sekhar, K. *Med. Chem. Res.* **2015,** *24,* 523–532.
57. Skiera, I.; Antoszczak, M.; Trynda, J.; Wietrzyk, J.; Boratyński, P.; Kacprzak, K.; Huczyński, A. *Chem. Biol. Drug Des.* **2015,** *86,* 911–917.
58. Pertino, M. W.; Verdugo, V.; Theoduloz, C.; Schmeda-Hirschmann, G. *Molecules* **2014,** *19,* 2523–2535.
59. Duan, Y.-C.; Zheng, Y.-C.; Li, X.-C.; Wang, M.-M.; Ye, X.-W.; Guan, Y.-Y.; Liu, G.-Z.; Zheng, J.-X.; Liu, H.-M. *Eur. J. Med. Chem.* **2013,** *64,* 99–110.
60. Bollu, R.; Palem, J. D.; Bantu, R.; Guguloth, V.; Nagarapu, L.; Polepalli, S.; Jain, N. *Eur. J. Med. Chem.* **2015,** *89,* 138–146.
61. de O Freitas, L. B.; Borgati, T. F.; De Freitas, R. P.; Ruiz, A. L. T. G.; Marchetti, G. M.; de Carvalho, J. E.; da Cunha, E. F. F.; Ramalho, T. C. *Eur. J. Med. Chem.* **2014,** *84,* 595–604.
62. Chauhan, A.; Paladhi, S.; Debnath, M.; Mandal, S.; Das, R. N.; Bhowmik, S.; Dash, J. *Bioorg. Med. Chem.* **2014,** *22,* 4422–4429.
63. Ahmed, N.; Konduru, N. K.; Ahmad, S.; Owais, M. *Eur. J. Med. Chem.* **2014,** *82,* 552–564.
64. Molnár, J.; Frank, É.; Minorics, R.; Kádár, Z.; Ocsovszki, I.; Schönecker, B.; Wölfling, J.; Zupkó, I. *PLoS One* **2015,** *10,* e0118104.
65. Kádár, Z.; Molnár, J.; Schneider, G.; Zupkó, I.; Frank, É. *Bioorg. Med. Chem.* **2012,** *20,* 1396–1402.
66. You, T.; Chen, K.; Wang, F.-H.; Li, P.-H.; Li, L.-Y.; Wu, Z.-H.; Ni, K.-H.; Zheng, Z.-Q. *Chin. Chem. Lett.* **2014,** *25,* 474–478.
67. Wu, J.; Yu, W.; Fu, L.; He, W.; Wang, Y.; Chai, B.; Song, C.; Chang, J. *Eur. J. Med. Chem.* **2013,** *63,* 739–745.
68. Puig-Basagoiti, F.; Qing, M.; Dong, H.; Zhang, B.; Zou, G.; Yuan, Z.; Shi, P.-Y. *Antiviral Res.* **2009,** *83,* 71–79.
69. Pintér, G.; Bereczki, I.; Batta, G.; Ötvös, R.; Sztaricskai, F.; Rőth, E.; Ostorházi, E.; Rozgonyi, F.; Naesens, L.; Szarvas, M.; Boda, Z.; Herczegh, P. *Bioorg. Med. Chem. Lett.* **2010,** *20,* 2713–2717.
70. Perez-Castro, I.; Caamano, O.; Fernandez, F.; Garcia, M. D.; Lopez, C.; Clercq, E. D. *Org. Biomol. Chem.* **2007,** *5,* 3805–3813.
71. Howell, L. A.; Howman, A.; O'Connell, M. A.; Mueller, A.; Searcey, M. *Bioorg. Med. Chem. Lett.* **2009,** *19,* 5880–5883.
72. Boechat, N.; Ferreira, V. F.; Ferreira, S. B.; Ferreira, M.d. L. G.; da Silva, F.d. C.; Bastos, M. M.; Costa, M.d. S; Lourenço, M. C. S.; Pinto, A. C.; Krettli, A. U.; Aguiar, A. C.; Teixeira, B. M.; da Silva, N. V.; Martins, P. R. C.; Bezerra, F. A. F. M.; Camilo, A. L. S.; da Silva, G. P.; Costa, C. C. P. *J. Med. Chem.* **2011,** *54,* 5988–5999.
73. Maurya, S. K.; Gollapalli, D. R.; Kirubakaran, S.; Zhang, M.; Johnson, C. R.; Benjamin, N. N.; Hedstrom, L.; Cuny, G. D. J. *Med. Chem.* **2009,** *52,* 4623–4630.
74. Porta, E. O.; Carvalho, P. B.; Avery, M. A.; Tekwani, B. L.; Labadie, G. R. *Steroids* **2014,** *79,* 28–36.
75. Fu, T.-h.; Li, Y.; Thaker, H. D.; Scott, R. W.; Tew, G. N. *ACS Med. Chem. Lett.* **2013,** *4,* 841–845.
76. Kharb, R.; Sharma, P. C.; Yar, M. S. J. *Enzyme Inhib. Med. Chem.* **2011,** *26,* 1–21.
77. Tron, G. C.; Pirali, T.; Billington, R. A.; Canonico, P. L.; Sorba, G.; Genazzani, A. A. *Med. Res. Rev.* **2008,** *28,* 278–308.
78. Hulme, E. C.; Trevethick, M. A. *Br. J. Pharmacol.* **2010,** *161,* 1219–1237.
79. Gether, U.; Kobilka, B. K. J. *Biol. Chem.* **1998,** *273,* 17979–17982.
80. Ye, S.; Huber, T.; Vogel, R.; Sakmar, T. P. *Nat. Chem. Biol.* **2009,** *5,* 397–399.
81. Sakmar, T. P. *Nat. Chem. Biol.* **2011,** *7,* 500–501.
82. Banerjee, A.; Maschauer, S.; Hübner, H.; Gmeiner, P.; Prante, O. *Bioorg. Med. Chem. Lett.* **2013,** *23,* 6079–6082.
83. Löber, S.; Hübner, H.; Gmeiner, P. *Bioorg. Med. Chem. Lett.* **2006,** *16,* 2955–2959.
84. Devigny, C.; Perez-Balderas, F.; Hoogeland, B.; Cuboni, S.; Wachtel, R.; Mauch, C. P.; Webb, K. J.; Deussing, J. M.; Hausch, F. J. *Am. Chem. Soc.* **2011,** *133,* 8927–8933.
85. Ciocoiu, C. C.; Nikolić, N.; Nguyen, H. H.; Thoresen, G. H.; Aasen, A. J.; Hansen, T. V. *Eur. J. Med. Chem.* **2010,** *45,* 3047–3055.
86. Zhang, J.; Zhang, H.; Cai, W.; Yu, L.; Zhen, X.; Zhang, A. *Bioorg. Med. Chem.* **2009,** *17,* 4873–4880.
87. Jorgensen, W. L.; Gandavadi, S.; Du, X.; Hare, A. A.; Trofimov, A.; Leng, L.; Bucala, R. *Bioorg. Med. Chem. Lett.* **2010,** *20,* 7033–7036.
88. Tosh, D. K.; Chinn, M.; Yoo, L. S.; Kang, D. W.; Luecke, H.; Gao, Z.-G.; Jacobson, K. A. *Bioorg. Med. Chem.* **2010,** *18,* 508–517.
89. Cosyn, L.; Palaniappan, K. K.; Kim, S.-K.; Duong, H. T.; Gao, Z.-G.; Jacobson, K. A.; Van Calenbergh, S. J. *Med. Chem.* **2006,** *49,* 7373–7383.
90. Tosh, D. K.; Yoo, L. S.; Chinn, M.; Hong, K.; Kilbey, S. M.; Barrett, M. O.; Fricks, I. P.; Harden, T. K.; Gao, Z.-G.; Jacobson, K. A. *Bioconjugate Chem.* **2010,** *21,* 372–384.
91. Tosh, D. K.; Paoletta, S.; Chen, Z.; Crane, S.; Lloyd, J.; Gao, Z.-G.; Gizewski, E. T.; Auchampach, J. A.; Salvemini, D.; Jacobson, K. A. *Med. Chem. Commun.* **2015,** *6,* 555–563.
92. Kiselev, E.; Barrett, M. O.; Katritch, V.; Paoletta, S.; Weitzer, C. D.; Brown, K. A.; Hammes, E.; Yin, A. L.; Zhao, Q.; Stevens, R. C.; Harden, T. K.; Jacobson, K. A. *ACS Chem. Biol.* **2014,** *9,* 2833–2842.
93. Sun, H.; Liu, L.; Lu, J.; Qiu, S.; Yang, C.-Y.; Yi, H.; Wang, S. *Bioorg. Med. Chem. Lett.* **2010,** *20,* 3043–3046.
94. Michel, K.; Büther, K.; Law, M. P.; Wagner, S.; Schober, O.; Hermann, S.; Schäfers, M.; Riemann, B.; Höltke, C.; Kopka, K. J. *Med. Chem.* **2011,** *54,* 939–948.
95. Bonnet, D.; Ilien, B.; Galzi, J.-L.; Riché, S.; Antheaune, C.; Hibert, M. *Bioconjugate Chem.* **2006,** *17,* 1618–1623.

96. Alam, M. S.; Huang, J.; Ozoe, F.; Matsumura, F.; Ozoe, Y. *Bioorg. Med. Chem.* **2007,** *15,* 5090–5104.
97. Kühhorn, J.; Hübner, H.; Gmeiner, P. J. *Med. Chem.* **2011,** *54,* 4896–4903.
98. Huber, D.; Hübner, H.; Gmeiner, P. J. *Med. Chem.* **2009,** *52,* 6860–6870.
99. Gopi, H.; Umashankara, M.; Pirrone, V.; LaLonde, J.; Madani, N.; Tuzer, F.; Baxter, S.; Zentner, I.; Cocklin, S.; Jawanda, N.; Miller, S. R.; Schön, A.; Klein, J. C.; Freire, E.; Krebs, F. C.; Smith, A. B.; Sodroski, J.; Chaiken, I. J. *Med. Chem.* **2008,** *51,* 2638–2647.
100. Gopi, H. N.; Tirupula, K. C.; Baxter, S.; Ajith, S.; Chaiken, I. M. *ChemMedChem* **2006,** *1,* 54–57.
101. Kecskés, A.; Tosh, D. K.; Wei, Q.; Gao, Z.-G.; Jacobson, K. A. *Bioconjugate Chem.* **2011,** *22,* 1115–1127.
102. Insua, I.; Alvarado, M.; Masaguer, C. F.; Iglesias, A.; Brea, J.; Loza, M. I.; Carro, L. *Bioorg. Med. Chem. Lett.* **2013,** *23,* 5586–5591.
103. Keck, T. M.; Banala, A. K.; Slack, R. D.; Burzynski, C.; Bonifazi, A.; Okunola-Bakare, O. M.; Moore, M.; Deschamps, J. R.; Rais, R.; Slusher, B. S.; Newman, A. H. *Bioorg. Med. Chem.* **2015,** *23,* 4000–4012.
104. Trabocchi, A.; Menchi, G.; Cini, N.; Bianchini, F.; Raspanti, S.; Bottoncetti, A.; Pupi, A.; Calorini, L.; Guarna, A. J. *Med. Chem.* **2010,** *53,* 7119–7128.
105. Richter, S.; Ramenda, T.; Bergmann, R.; Kniess, T.; Steinbach, J.; Pietzsch, J.; Wuest, F. *Bioorg. Med. Chem. Lett.* **2010,** *20,* 3306–3309.
106. Beierle, J. M.; Horne, W. S.; Van Maarseveen, J. H.; Waser, B.; Reubi, J. C.; Ghadiri, M. R. *Angew. Chem. Int. Ed.* **2009,** *48,* 4725–4729.
107. Choi, W. J.; Shi, Z.-D.; Worthy, K. M.; Bindu, L.; Karki, R. G.; Nicklaus, M. C.; Fisher, R. J.; Burke, T. R., Jr. *Bioorg. Med. Chem. Lett.* **2006,** *16,* 5265–5269.
108. Loaiza, P. R.; Löber, S.; Hübner, H.; Gmeiner, P. J. *Comb. Chem.* **2006,** *8,* 252–261.
109. Stanley, N. J.; Pedersen, D. S.; Nielsen, B.; Kvist, T.; Mathiesen, J. M.; Bräuner-Osborne, H.; Taylor, D. K.; Abell, A. D. *Bioorg. Med. Chem. Lett.* **2010,** *20,* 7512–7515.
110. Shu, H.; Izenwasser, S.; Wade, D.; Stevens, E. D.; Trudell, M. L. *Bioorg. Med. Chem. Lett.* **2009,** *19,* 891–893.
111. Wijtmans, M.; de Graaf, C.; de Kloe, G.; Istyastono, E. P.; Smit, J.; Lim, H.; Boonnak, R.; Nijmeijer, S.; Smits, R. A.; Jongejan, A.; Zuiderveld, O.; de Esch, I. J. P.; Leurs, R. J. *Med. Chem.* **2011,** *54,* 1693–1703.
112. Sander, K.; Kottke, T.; Hoffend, C.; Walter, M.; Weizel, L.; Camelin, J.-C.; Ligneau, X.; Schneider, E. H.; Seifert, R.; Schwartz, J.-C.; Stark, H. *Org. Lett.* **2010,** *12,* 2578–2581.
113. Loaiza, P. R.; Löber, S.; Hübner, H.; Gmeiner, P. *Bioorg. Med. Chem.* **2009,** *17,* 5482–5487.
114. Ye, N.; Wu, Q.; Zhu, L.; Zheng, L.; Gao, B.; Zhen, X.; Zhang, A. *Bioorg. Med. Chem.* **2011,** *19,* 1999–2008.
115. Baker, M. *Nat. Rev. Drug Discov.* **2013,** *12,* 5–7.
116. Mamidyala, S. K.; Finn, M. *Chem. Soc. Rev.* **2010,** *39,* 1252–1261.
117. Lewis, W. G.; Green, L. G.; Grynszpan, F.; Radić, Z.; Carlier, P. R.; Taylor, P.; Finn, M. G.; Sharpless, K. B. *Angew. Chem.* **2002,** *114,* 1095–1099.
118. Whiting, M.; Muldoon, J.; Lin, Y.-C.; Silverman, S. M.; Lindstrom, W.; Olson, A. J.; Kolb, H. C.; Finn, M. G.; Sharpless, K. B.; Elder, J. H.; Fokin, V. V. *Angew. Chem. Int. Ed.* **2006,** *45,* 1435–1439.
119. Manetsch, R.; Krasinski, A.; Radic, Z.; Raushel, J.; Taylor, P.; Sharpless, K. B.; Kolb, H. C. J. *Am. Chem. Soc.* **2004,** *126,* 12809–12818.
120. Whiting, M.; Muldoon, J.; Lin, Y. C.; Silverman, S. M.; Lindstrom, W.; Olson, A. J.; Kolb, H. C.; Finn, M.; Sharpless, K. B.; Elder, J. H. *Angew. Chem. Int. Ed.* **2006,** *45,* 1435–1439.
121. Tieu, W.; SoaresdaCosta, T. P.; Yap, M. Y.; Keeling, K. L.; Wilce, M. C. J.; Wallace, J. C.; Booker, G. W.; Polyak, S. W.; Abell, A. D. *Chem. Sci.* **2013,** *4,* 3533–3537.
122. Peruzzotti, C.; Borrelli, S.; Ventura, M.; Pantano, R.; Fumagalli, G.; Christodoulou, M. S.; Monticelli, D.; Luzzani, M.; Fallacara, A. L.; Tintori, C.; Botta, M.; Passarella, D. *ACS Med. Chem. Lett.* **2013,** *4,* 274–277.
123. Lee, S. S.; Lim, J.; Tan, S.; Cha, J.; Yeo, S. Y.; Agnew, H. D.; Heath, J. R. *Anal. Chem.* **2010,** *82,* 672–679.
124. Agnew, H. D.; Rohde, R. D.; Millward, S. W.; Nag, A.; Yeo, W.-S.; Hein, J. E.; Pitram, S. M.; Tariq, A. A.; Burns, V. M.; Krom, R. J.; Fokin, V. V.; Sharpless, K. B.; Heath, J. R. *Angew. Chem. Int. Ed.* **2009,** *48,* 4944–4948.
125. Millward, S. W.; Agnew, H. D.; Lai, B.; Lee, S. S.; Lim, J.; Nag, A.; Pitram, S.; Rohde, R.; Heath, J. R. *Integr. Biol.* **2013,** *5,* 87–95.
126. Millward, S. W.; Henning, R. K.; Kwong, G. A.; Pitram, S.; Agnew, H. D.; Deyle, K. M.; Nag, A.; Hein, J.; Lee, S. S.; Lim, J.; Pfeilsticker, J. A.; Sharpless, K. B.; Heath, J. R. J. *Am. Chem. Soc.* **2011,** *133,* 18280–18288.

Relevant Websites

History of Click chemistry

[127]. https://en.wikipedia.org/wiki/Click_chemistry.

Click chemistry—synthetic point of view

[128]. http://www.organic-chemistry.org/namedreactions/click-chemistry.shtm.

Finn, Fokin, and Sharpless are suggested as possible Nobel Prize winners for "the development of modular click chemistry"

[129]. http://www.scripps.edu/newsandviews/e_20111107/sharpless.html.
[130]. http://sciencewatch.com/nobel/predictions/modular-click-chemistry.

Click hot topics

[131]. http://www.wiley-vch.de/util/hottopics/clickchem/.
[132]. http://pubs.rsc.org/en/journals/journalissues/cs#!issueid=cs039004&type=current.
[133]. http://pubs.rsc.org/en/content/articlelanding/2010/cs/c003740k#!divAbstract.

Click Chemistry Tools / Bioconjugate Technologies

[134]. http://clickchemistrytools.com/.
[135]. https://www.thermofisher.com/ae/en/home/life-science/cell-analysis/labeling-chemistry/click-chemistry-labeling-and-detection/click-chemistry-tools-for-biological-assays.html.
[136]. http://www.sigmaaldrich.com/chemistry/chemical-synthesis/technology-spotlights/click.html.

Click chemistry for drug discovery

[137]. http://www.sciencedirect.com/science/article/pii/S1359644603029337.
[138]. http://eu.wiley.com/WileyCDA/WileyTitle/productCd-3527608605.html.
[139]. http://pubs.acs.org/doi/abs/10.1021/cr200409f.
[140]. http://europepmc.org/abstract/med/21954075.

1.11 Future of Medicinal Chemistry: Next-Generation Therapeutics

N Tsomaia, M Ufret, and A Bhat, Ipsen Bioscience, Inc., Cambridge, MA, United States
J Nakhle, Ipsen Innovation, Les Ulis, France

© 2017 Elsevier Ltd. All rights reserved.

1.11.1	**Introduction**	326
1.11.2	**Expanding Druggable Target Space**	328
1.11.2.1	PPIs and Their Modulators	328
1.11.2.1.1	Macrocycles	329
1.11.2.1.2	Biological selection of backbone-modified macrocyclic peptides	330
1.11.2.1.3	Stable peptide frameworks for therapeutic applications	331
1.11.2.2	Immune Targets and Vaccines	332
1.11.2.3	Oligonucleotides and Oligonucleotide Drugs	334
1.11.3	**Targeted Delivery of Next-Generation Therapeutics**	335
1.11.3.1	CPPs as Delivery Vectors	336
1.11.3.1.1	Cellular uptake pathways for drug delivery with CPPs	336
1.11.3.1.2	Molecular determinants of cell-permeability	337
1.11.3.1.3	Enhancing endosomal escape of biologic drugs	338
1.11.3.2	Targeting Specific Tissues	339
1.11.3.2.1	Delivery of therapeutics across the blood–brain barrier	340
1.11.3.2.2	Targeting the pituitary	341
1.11.3.2.3	Targeted delivery to the liver	341
1.11.3.2.4	Targeting the pancreas	342
1.11.3.3	Targeting Tumors	342
1.11.3.3.1	Antibody–drug conjugates	342
1.11.3.3.2	GPCRs as targeting vectors	343
1.11.4	**Concluding Remarks**	343
References		344
Relevant Websites		348

Abbreviations

ASGPR Asialoglycoprotein receptor
AZL Azobenzene linchpin
BBB Blood–brain barrier
BoNT Botulinum neurotoxin
CPPs Cell-penetrating peptides
CSA Cyclosporin A
GalNAc *N*-Acetylgalactosamine
GHRH Growth hormone-releasing hormone
GPCRs G-protein-coupled receptors
KDC Knottin peptide–drug conjugate
mAbs Monoclonal antibodies
NRPSs Nonribosomal peptide synthetases
PAMPA Parallel artificial membrane permeability assay
PPI Protein–protein interaction
RMT Receptor-mediated transcytosis
SAR Structure activity relationship
SFTI Sunflower trypsin inhibitors
siRNA Small-interfering RNA
TSIs Targeted secretion inhibitors

1.11.1 Introduction

The practice of modern medicinal chemistry can be described as forced Darwinian evolution in chemical space. It is marked by iterative cycles of chemical modifications to organic molecules, followed by the biological testing of these compounds. Successive iterations of synthesis and biological testing gradually build up a picture of "structure–activity relationships" (SAR) that reveal how structural changes impact the biological properties of organic compounds. SAR studies are the navigational tools that help guide the medicinal chemist across the chemical landscape. They identify the promising chemical structures that have the right blend of chemical, physical, and biological properties for human clinical testing with the eventual goal that one of these compounds becomes an approved "drug." It is inherently implied in this paradigm that in order to practice their craft and generate useful SAR data, medicinal chemists have the ability to manipulate chemical structures in a controlled and defined manner. Thus, not

surprisingly, the practice of medicinal chemistry has evolved in conjunction with advances in modern organic synthesis, molecular modeling, and analytical chemistry, which has given chemists tools for precise structural manipulations in heterocyclic organic molecules. Over the past century, low molecular weight heterocyclic compounds that can be orally administered have been the dominant class of molecules in pharmaceutical pipelines. In contrast, despite delivering significant clinical and medical benefits, drugs made of relatively larger, more complex compositions such as peptides, antibiotics, naturally derived proteins, and serums have not been a major focus of pharmaceutical industry. These molecular modalities have been at the periphery, or even outside the scope, of the traditional medicinal chemist's remit.

However, the pharmaceutical landscape started to shift over the last 40 years due to advances in molecular biology and recombinant protein expression. These technologies, along with protein purification and characterization tools, gave birth to the biotechnology industry and ushered in the era of engineered protein drugs. Early biotech companies such as Genentech, Celltech, Hybritech, MedImmune, Biogen, Amgen, Genzyme, and Genetics Institute, to name a few, were pioneers on this new frontier. In contrast to orally delivered and synthetically produced small molecules, these companies were developing high molecular weight protein drugs that could not be delivered orally, but rather as injectables. In 1982, the US FDA approved the first recombinant protein therapeutic, human insulin. Since then, biologics have been steadily growing as a successful class of drugs, delivering medications such as human growth hormone (GH), interferons, and engineered antibodies. While the acceptance of biologics as drugs was slow in the beginning, the pharmaceutical industry has seen an accelerated shift over the past decade toward embracing them.

Biologic drugs represent a tremendous investment value for the industry as they provide highly differentiated therapeutic options for difficult-to-treat diseases that can command higher prices. Unlike small molecules, it is not trivial to create "generic" versions of biologics, since they are made by living organisms and are characterized by inherent batch to batch variability. In addition, their development involves significantly more complex manufacturing and chemistry, manufacturing, and controls components compared to small molecules, and once approved, they are granted an extended regulatory exclusivity period. Historically, this has provided financial and commercial incentives for developers of biologic drugs. In 2015, there were 7 biologics among the top 10 selling drugs (**Table 1**).

According to a recent report from the Tufts Center for Study of Drug Development, clinical trials of biologic drugs have risen by over 155% from 355 in 2001 to more than 900 in 2012.[2] The worldwide sales have increased from $36 billion in the early 2000s, to $165 billion by 2013, and it is projected that the overall worldwide sales from biologic drugs will exceed $300 billion by 2020.

In order to lower costs for biologic drugs, under the Affordable Care Act, the FDA has required fewer clinical and preclinical data submissions for biosimilars, products that are highly similar to an original biologic. In 2015, the FDA approved the first biosimilar product in the United States—zarxio™ (Sandoz)—which is used for boosting white blood cells in cancer patients, and is a less expensive version of neupogen (Amgen). Shortly after, the FDA-approved Celltrion's Inflectra™ (infliximab), which is a biosimilar molecule of the original product Remicade® (infliximab). Inflectra™ is now the first biosimilar monoclonal antibody (mAb) therapy approved in the United States (see listed Websites 1 and 2 for reference).

Today, there are more than 50 biosimilars in the development pipeline. It is expected that these generic-like products will enter the market in the near future. Nonetheless, there are still a number of regulatory hurdles in place that prevent approved biosimilars from immediate access as a substitute. Most importantly, due to growing patient needs, innovators will keep delivering creative solutions and make differentiated and enhanced products. This will continue to challenge "me-too" alternatives and "biosimilar" products.

The advent of biologic drugs has also coincided with a bleak period of productivity for small molecule drugs. The promise of technology-focused initiatives such as high-throughput screening (HTS), genome mapping, computer-aided drug design, and combinatorial chemistry has resulted in a significant increase in investments and input costs for R&D programs. A number of excellent articles have dissected the various causes for the productivity decline in drug discovery focused on small molecule medicinal chemistry.[3–8] These reviews drive home the point that the technology-driven, target-focused, reductionist approaches have been

Table 1 Top 10 products[1]

Trade name	*Type*	*Marketer*	*Medical use*	*Estimated 2015 sales ($ billions)*	*Change from 2014 (%)*
Humira®	Antibody	AbbVie, Eisai	Inflammation	14.2	13
Harvoni®	Small molecule	Gilead Sciences	Hepatitis C	13.9	554
Enbrel®	Protein	Amgen, Pfizer, Takeda	Inflammation	8.7	−2
Remicade®	Antibody	Janssen, Merck & Co.	Inflammation	8.3	−10
Rituxan®	Antibody	Roche	Cancer	7	3
Lantus®	Peptide	Sanofi	Diabetes	6.9	2
Avastin®	Antibody	Roche, Chugai	Cancer	6.6	4
Herceptin®	Antibody	Roche	Cancer	6.5	5
Januvia®/Janumet®	Small molecule	Merck & Co.	Diabetes	6.2	3
Seretide®	Small molecule	GlaxoSmithKline	Asthma	5.7	−11

Foreign currencies converted at current exchange rates.
Company data, stock analysis, and C&EN estimates.

a letdown in drug discovery research and recommend strategies that rely more on phenotypic screening and predictive animal models as a way out of the productivity crisis; but, these approaches come with challenges of their own.

The rise of biologics coupled with the poor productivity of small molecule discovery programs has significantly altered the role of medicinal chemists as the drivers of innovation and value creation for the early stage R&D in biopharma industry. The synthesis of organic molecules is regarded as a commodity that is readily purchased in cheaper overseas markets such as China or India. At the same time, the spotlight has shifted to molecular biologists and protein engineers, who can help design and create highly lucrative biologic drugs. In 2002, Paul Earhardt authored a forward-looking, exhaustive review titled *Medicinal Chemistry in the New Millennium: A Glance Into the Future.*[9] The review presented a picture of how the practice of medicinal chemistry would evolve in 21st century and predicted a number of trends and strategies that would be adopted by medicinal chemists. However, the discussion almost exclusively focused on orally administered small molecules as the singular modality of operation for medicinal chemists. Yet, by the end of the first decade since the publication of that review, it is evident that this view is no longer relevant.

The shift toward biologic drugs has also increased the acceptance and representation of injectable drugs in development pipelines. Novel formulation technologies, reduced dosing frequencies, smaller injection volumes, and friendly delivery devices have dramatically improved patient compliance and thus enabled greater acceptance of these nontraditional modalities. Alternative routes of administration have the potential to become convenient and cost-effective delivery systems, hence allowing for the development of next-generation biologic drugs. Thus the chemists, to a certain degree, have been liberated from the high barrier to design molecules that need to be orally administered. The increased acceptance of the nonoral delivery modalities will continue to open new areas of opportunities for drug design.

A detailed discussion of the drug design and optimization strategies of the various modalities is too broad of a topic and is beyond the scope of this discussion. However, herein we attempt to present the drug design opportunities at these interfaces not from a modality or a product perspective, but rather from a solutions perspective. In other words, the motivation to design new classes of therapeutics beyond small molecules is driven by the promise of (a) expanding druggable target space, and (b) targeted delivery of next-generation drugs. Each of these areas is discussed here with a view toward the future (rather than an exhaustive review of the literature) and it is important to recognize that there are number of programs or examples that will overlap significantly between these topics.

1.11.2 Expanding Druggable Target Space

The practice of drug discovery is at an interesting crossroads. The completion of the Human Genome Project in 2001 coupled with recent advances in computational tools, data science, chemical biology, proteomics, and analytical methods gave us unprecedented insights into human physiology and disease biology. We have gained a greater understanding of molecular mechanisms for human diseases, and this knowledge has opened up possibilities for new therapeutic treatments. Synthetic small molecules, which have been the main source of leads in drug discovery pipelines,[10,11] successfully address traditional targets such as G-protein-coupled receptors (GPCRs), nuclear receptors, kinases, and voltage-gated or ligand-gated ion channels[12]; but the vast majority of the proteins encoded in the human genome remain "undruggable." The emerging biological target space has triggered the need for complex synthetic drug modalities that can effectively modulate intracellular protein–protein interactions (PPIs), the immune system, or manipulate gene function at the RNA level. The following section briefly describes newer targets spaces, opportunities for new modalities, and how new design approaches can impact them.

1.11.2.1 PPIs and Their Modulators

The interactions between two proteins represent a fundamental step in driving signaling pathways and cellular processes both inside and outside the cell. The modulation of such PPIs, in turn, provides significant opportunities to control dysregulated proteins in a disease state. For example, intracellular PPIs play a key role during tumor progression. They link oncogenic networks that trigger a cascade of events fostering tumor growth, invasion, and metastasis.[13] The central role of PPI networks, the so-called interactome, is a vast source of new therapeutic targets in drug discovery. Some examples include an amplified c-myc interaction with Max that regulates tumor cell proliferation, differentiation, and apoptosis,[14] and the interaction of the protein eIF4E with eIF4G to increase mRNA translation and to promote tumorigenesis.[15] Recent studies have shown the importance of specific PPIs in a number of different diseases such as multiple sclerosis and Alzheimers.[16] At present, more than 14,000 PPIs have been characterized in humans.[17] PPI interfaces are characterized by relatively featureless and large interaction surfaces of $\sim$1000–2000 A^2 which make it difficult for small molecule drugs to effectively target them.[18–24] Small molecules are better suited for protein targets that present deep cavities and hydrophobic grooves of $\sim$300–500 A^2. The work in the PPI field has led to a better understanding of various types of interactions based on their complexity. Furthermore, the realization that only a small number of residues, referred to as hot spots, are likely to contribute the majority of the binding energy has also helped drive progress; advances in screening technologies, and a combination of computational and biophysical tools, have helped identify a number of successful synthetic PPI modulators.[18–23] Venetoclax or ABT-199 is an orally active, potent, and selective PPI inhibitor of BCL-2, with proapoptotic activity. It was approved in 2016 for treatment of patients with chronic lymphocytic leukemia ith 17p deletion. The development of ABT-199 is the culmination of over a decade's worth of work, and demonstrates the ability of fragment-based screening, structural biology, and focused medicinal chemistry, in delivering a successful PPI inhibitor. In spite of the success with Venetoclax, the challenge with PPI targets still

looms large in the coming years. It will demand innovation in the screening, designing, and delivery of suitable chemical matter, which will likely be outside the rule-of-five (Ro5) space.

Peptides, proteins, and antibodies, all of which offer larger interaction surface areas, are better suited as PPI inhibitors. They have the ability to mimic protein fragments and functional motifs at PPI interfaces. These modalities demonstrate exquisite potency and an exceptional ability for highly selective targeting, which leads to a lower risk of toxicity and side effects. In the 1980s, production of fully human therapeutic mAbs facilitated the transformation of mAbs into the most successful drugs among protein-based therapies. Today, most biologic drugs in development pipelines are antibody-based proteins, and there are a number of blockbuster mAb drugs on the market that target extracellular proteins.[25]

However, as their large size restricts their diffusion across the cell membrane, it is a challenge for proteins and antibodies to address biological PPI targets in the intracellular space. Peptides and macrocycles are alternative classes of molecules that are uniquely suited to impact PPI targets in the intracellular space. These classes of compounds have the ability to modulate targets with extended binding interfaces. The challenges and the opportunities for medicinal chemists lie in their ability to design these molecules so that they (a) effectively permeate the cell membrane, (b) access the intracellular compartments, and (c) devise new ways of identifying viable hits as starting points for chemical optimization efforts.

1.11.2.1.1 Macrocycles

1.11.2.1.1.1 Synthetic macrocycles

Natural products which feature a macrocycle, that is, a ring system made of 12 or more atoms, have been successfully developed as drugs. There is evidence that macrocyclic structures that are not Ro5 compliant can nevertheless demonstrate good physicochemical properties and permeability comparable to smaller molecules. Thus, they can be viable chemical matter for targeting intracellular PPIs and even be developed as orally bioavailable drugs. The current compound collections that are screened to identify initial hits are biased by binding pockets of traditional targets, and they sample a narrow range of the chemical space and physicochemical properties. Consequently, they do not effectively complement PPI interfaces. There are a number of new technologies that create macrocyclic libraries of "beyond Ro5 compounds" to allow for the fast and extensive search of chemical space for hit identification.[26,27] Screening libraries can be generated using synthetic platforms that utilize amphoteric reagents for small peptidomimetic macrocycles,[28,29] macrocyclic template chemistry,[30] chemical linkage of peptides onto scaffolds,[31] and DNA-programmed chemistry.[32] In addition, advances in diversity-oriented synthesis strategies have enabled a generation of screening libraries of complex natural-product-like macrocycles. A better understanding of the chemical space of PPI inhibitors will help to create new and focused chemical libraries that could ensure more successful HTS in the future.[33,34]

1.11.2.1.1.2 Peptide macrocycles

Peptide macrocycles are uniquely positioned to target PPIs for drug development. The effective modulation of these challenging therapeutic targets often requires structurally complex ligands. Such complexity has been successfully afforded by antibodies and proteins. However, large biologics cannot efficiently cross the cellular membrane, thus placing the intracellular target space beyond their reach. Peptide-based macrocycles are the smallest biomolecules that have the molecular complexity to effectively recognize the large interaction surfaces of challenging biological targets. These modalities are amenable to biological display tools such as phage and mRNA libraries. In addition, well-established cyclization and medicinal chemistry strategies can be employed to improve selectivity, potency, stability, and the permeability of peptide macrocycles, making them an attractive class of molecules outside of the Ro5 space.

It is well established that many naturally occurring cyclic peptides penetrate the cell by passive membrane diffusion, the most prominent example of which is the orally administered drug cyclosporin A (CSA). The permeability mechanism of natural cyclic peptide products originates from their remarkable chemical diversity, as many of them are biosynthesized via nonribosomal peptide synthetases (NRPSs) and are often modified by "tailoring" NRPS enzymes. This class of compounds incorporates features such as nonproteinogenic amino acids, depsipeptide linkages, *N*-methylation, thiazole/oxazole rings, and backbone cyclization. These diverse structural elements enable the tuning of the pharmacokinetic properties of macrocycles, while ensuring their effective target engagement. Specifically, macrocyclization increases the enzymatic stability of a peptide as compared with their linear precursors—partly by eliminating charged N- and C-termini, and partly due to the fact that conformationally distorted cyclic structures do not usually fit into endopeptidase recognition sites. In addition, cyclization preorganizes peptides, significantly reducing entropic penalty upon binding, which can translate into improved target affinity and specificity. The delineation of the structural features that govern and fine-tune cell-permeability is more challenging. A number of studies have shown that the conformational flexibility of macrocycles is one of the key facilitating factors for passive membrane permeability. Using simple model systems, it was previously demonstrated that the formation of internal hydrogen bonds in nonpolar media correlates with passive diffusion.[35–39] To further elucidate the determinants of passive cellular permeability, 62 systematically modified cyclic hexapeptides were studied via Caco-2 and parallel artificial membrane permeability (PAMPA) assays.[40] The study correlated cell-permeability with experimentally measured physicochemical properties, such as lipophilicity and solvent interactions. The authors proposed an "island of permeability" to understand the peptide features contributing to cellular uptake. The developed model was supported by molecular dynamics simulations, which related experimental observations to predicted three-dimensional (3D) structures.

In the most recent study, Jacobson and Lokey elucidated the passive membrane diffusion of 39 cyclic peptide natural products using a PAMPA assay. Additionally, they applied a computational algorithm to predict the passive permeability of the same peptides based on their known or predicted 3D structures. The study highlighted a few conformational and structural features that were

common characteristics of permeable cyclic peptides. Consistent with previous findings, they emphasized the importance of peptide conformation with respect to cellular permeation. Specifically, *N*-methylation patterns, modified backbone stereochemistry, and stabilized structures with intramolecular hydrogen bonding were frequently observed. Furthermore, depsipeptide linkages and thiazole/oxazole rings were highlighted as new strategies to eliminate or tie-up backbone amide NH groups. Interestingly, the structure-based in silico model was successful in predicting permeation for only those molecules where experimental 3D structures were known. This fact emphasizes that structure determination methods, such as NMR and X-ray crystallography, are essential sources of experimental data because it remains challenging to accurately predict relevant 3D conformations of macrocyclic molecules. The study also reported a number of new chemical scaffolds that demonstrated passive membrane permeability. These results highlight that peptides derived from natural sources could be used as the basis for structural information to guide the design of compounds with drug-like properties. However, the challenge remains in understanding, at a molecular level, what makes macrocyclic peptides cell-permeable.

In the past, backbone-modified macrocyclic peptides were mainly isolated form living organisms. The discovery and development of such ligands required the synthesis of large macrocyclic libraries with diverse backbone modifications, which was a challenge for synthetic chemists. Today, advances in biological selection technologies, coupled with creative synthetic approaches, allow us to pursue the systematic exploration of the macrocyclic peptide chemical space for drug discovery. In the following section, we will highlight a few ongoing developments in the field.

1.11.2.1.2 Biological selection of backbone-modified macrocyclic peptides

It is not trivial to conduct a fast and extensive search of the backbone-modified macrocyclic peptide space for hit identification. While various synthetic platforms can generate diverse macrocycles, biological selection methods remain powerful alternatives for peptide library generation and screening. The selection techniques (e.g., phage-, ribosome-, yeast-, mRNA-display) allow for fast and cost-effective screening of very large libraries (10^9–10^{13} compounds) with the amplification of target-bound peptide sequences during iterative selection rounds. In recent years, the selection methods that produce ribosomally synthesized macrocyclic peptides have been able to generate functional diversity beyond proteinogenic amino acids by integrating synthetic groups in the displayed peptides. They usually exploit two different approaches for posttranslational peptide cyclization and chemical modification. One of them employs the selective cross-linking of natural amino acid side chains with chemical reagents. This approach constrains the linear peptide library via a synthetic linker, yielding a genetically encoded library of peptide derivatives. A remarkable number of macrocyclization chemistries have been successfully integrated with phage- and mRNA-displayed libraries.[41] Using this methodology, genetically encoded linear peptides have been converted to cyclic and bicyclic derivatives that carry various nonproteinogenic recognition moieties and functional groups.[42,43] In the most recent study, the Derda group proposed an elegant posttranslational modification of phage-displayed peptides.[44] The synthetic approach was inspired by the cyclization chemistry that utilizes 1,3-dichloroacetone, recently described by Dawson and coworkers to enhance helical secondary structures.[45] The Derda group reported phage-displayed libraries of macrocylic glycopeptides for selection of ligands for glycan-binding proteins. However, the approach could incorporate any known inhibitor, enzyme substrate, or small molecule to generate displayed libraries of macrocyclic peptide-fragment conjugates. A detailed overview of the novel strategies for cyclization of phage libraries displayed on the pIII protein of M13 phage libraries is depicted in **Fig. 1**.

In vitro selection of hybrid peptide–drug conjugates has been performed on mRNA-display libraries as well.[48] Other studies have demonstrated that high-diversity mRNA-displayed peptides can be covalently cyclized, as illustrated via the posttranslational cross-linking of the N-terminal amine and the ε-amine of a lysine side chain.[49] One of the limitations of this approach is the fact that only one chemical modification is possible per displayed library, which makes it difficult to find an optimal combination of chemical linker and peptide sequence. In their latest publication, the Derda group introduced a method of "silent barcodes" to trace the identities of multiple synthetic linkers within a mixed modified library.[50] The approach can be extended to other in vitro display technologies, such as mRNA or T7-phage.

Alternatively, to incorporate nonproteinogenic groups in the peptide chain, genetic code reprogramming is used. An mRNA-display generates large libraries ($>10^{13}$) of peptides that are covalently linked with their corresponding mRNAs.[51] The unique feature of this technology is that, when coupled with the customized in vitro translation systems, it is capable of incorporating nonnatural building blocks in macrocyclic peptides. Namely, in the reconstituted in vitro translation system protein synthesis using recombinant elements,[52–54] natural amino acids can be replaced with chemically similar and tRNA-synthetase compatible nonnatural residues. Alternatively, the flexible in vitro translation[55,56] approach relies on "flexizyme," an engineered flexible ribozyme that does not recognize the side chain or the amino group of the activated amino acid, and therefore is able to charge a wide variety of nonproteinogenic building blocks.[57]

While the selection methods described earlier can produce large lists of potential binders, it remains a challenge to rank the peptide affinities in a high-throughput manner. To address this issue, the Roberts group developed a novel approach by combining next-generation DNA sequencing and mRNA display.[58] Specifically, their high-throughput sequencing kinetics method could determine the K_{on} and K_{off} rates for thousands of ligands simultaneously without synthesizing and purifying individual peptides. A few years ago, the same group reported a two-step selection process that simultaneously selected for protease resistance and target binding.[59] These scientific advances offer a powerful technology platform with the potential to discover macrocyclic ligands with drug-like properties for a wide variety of therapeutic targets. Based on a report from 2014, 68 macrocyclic drugs on the market were almost equally distributed between two classes of compounds—cyclic peptides and macrolides; all peptides were delivered parenterally, except for CSA.[60] It is promising that, in clinical trials, cyclic peptides represented the largest group of macrocycles,

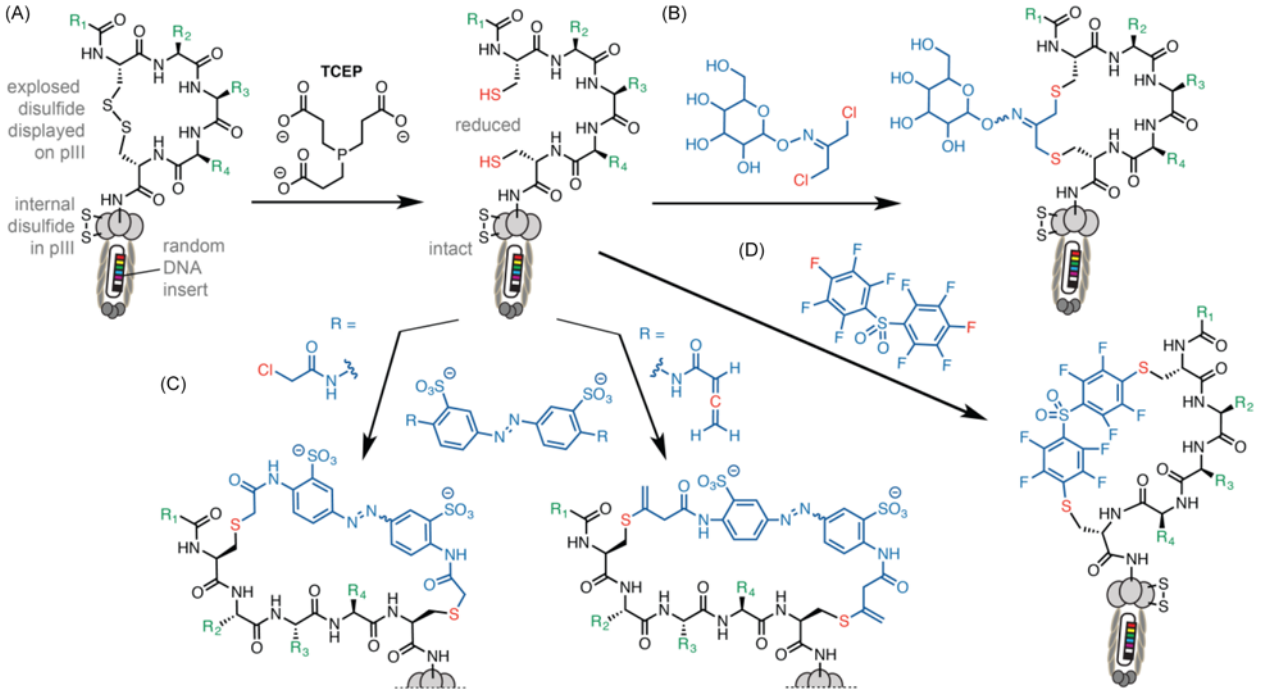

Fig. 1 Overview of the strategies for cyclization of phage libraries displayed on pIII protein of M13 phage libraries produced from commercially available vector M13KE (New England Biolabs). (A) The most critical step is regioselective reduction of phage-displayed disulfides. The bulky hydrophilic reducing agent (tris(2-carboxyethyl)phosphine) (TCEP) affords this reduction while leaving the disulfide bonds inside protein pIII intact.[42] (B) Reduced thiols can be alkylated using various dichlorooximes[44]; for example, dichlorooxime displaying a monosaccharide yields a cyclic glycopeptide. This reaction occurs specifically on displayed thiols and not on the internal thiols or any nucleophiles on phage. (C) Libraries of macrocycles that change conformation reversibly in response to light can be produced by cross-linking the thiols with light-responsive azobenzene linchpin (AZL). Bis(allenamide) AZL (left)[46] is ~30 times more reactive than bis(chloroacetamie) AZL (right).[42] (D) Modification of phage libraries by decafluorodiphenylsulfone yields libraries of macrocycles that contain hydrophobic "perfluoro-staple."[47] This figure is a courtesy of the Derda Group.

with three orally administered candidates.[60] Current research shows that CSA is not a unique example in demonstrating passive permeability in the macrocyclic peptide chemical space; there have been a number of non-CSA scaffolds reported with drug-like passive membrane transport.[37,40,61] Yet, it remains to be seen if we can discover and develop new peptides into orally bioavailable drugs. The challenge to understand how to find and validate successful cell-permeable macrocyclic inhibitors for intracellular targets with desired in vivo activities still remains. Correlating structural features with permeability and bioavailability will be an important driver in this field; it will help design macrocyclic structures that are well suited for targeting intracellular PPIs that remain out of the reach of antibody or protein therapeutics.

1.11.2.1.3 Stable peptide frameworks for therapeutic applications

Chemically constraining peptide secondary structures to their biologically active conformations is a well-established approach in peptidic drug design. Carefully mimicking and/or stabilizing specific structural elements at PPI recognition interfaces has become the main strategy for the rational design of synthetic ligands which selectively modulate PPIs.[62] A number of computational methods were developed to find druggable pockets on protein targets,[62a] or to identify the residues and/or peptide segments that have the highest impact on binding interactions. Recently published algorithms allow for a systematic search of the Protein Data Bank database using customizable parameters[63] to find α-helix-,[64,65] β-strands-, or loop-mediated PPI interfaces.[63] Validated in silico tools are routinely used to select peptide fragments that are viable starting points for PPI inhibitor design.[66] Numerous synthetic approaches have been developed for peptide stabilization; this stabilization mimics specific secondary structures and confers chemical/enzymatic stability, as well as increased potency and selectivity.[67,67a] These methodologies have delivered a number of successful PPI inhibitors with remarkable in vitro and in vivo bioactivities when it comes to extracellular targets. However, reaching the desired in vivo efficacy is still a challenge when targeting intracellular PPIs, since designing cell-permeability rationally within an active molecule is not a straightforward task.

Disulfide-rich peptides with well-defined 3D frameworks are a fascinating class of molecules with tremendous potential for therapeutic applications (Fig. 2). Sunflower trypsin inhibitors (SFTI), Θ-defensins, and cyclotides are peptide families of various size and complexity that naturally incorporate not only disulfide bonds, but also head-to-tail cyclization. These molecules are characterized by exceptional stability and low toxicity. Their loop regions, which are important for molecular recognition, are very tolerant to sequence substitutions. This allows for the grafting of various bioactive peptides into their stable frameworks, making them

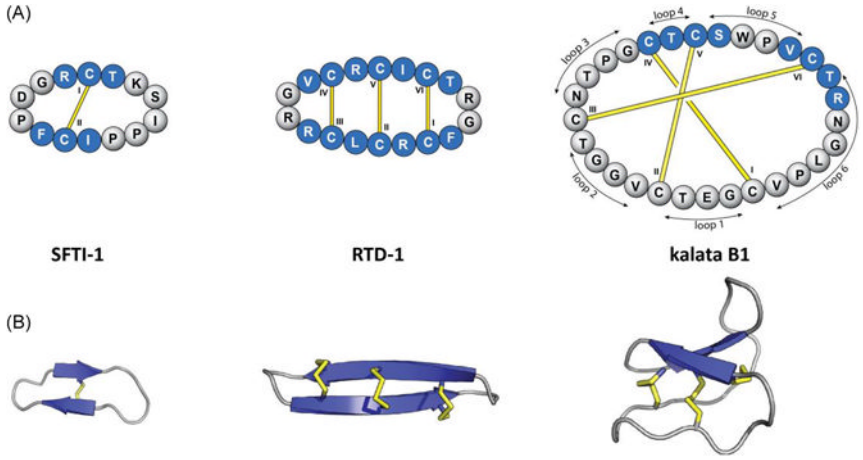

Fig. 2 Sequences and structures of three disulfide-rich peptide families, represented by SFTI-1 (PDB ID: 1JBL), RTD-1 (PDB ID: 2LYF), and kalata B1 (PDB ID: 1NB1). (A) β-Sheets are depicted in *blue* and disulfide bonds in *yellow*. For the disulfide connectivity, cysteine residues are identified using roman numerals. The sequences are drawn in a clockwise direction for each peptide. (B) Secondary structures of the three disulfide cyclic peptides, showing β-sheets as *arrows*. The structure of RTD-1 has been flipped 180 degrees in the horizontal plane to better show the disulfide connectivity.[68]

attractive scaffolds for drug development applications. Grafting an active peptide epitope into a well-defined 3D scaffold potentially reduces binding entropy and harnesses the intrinsic stability of the framework. Since the discovery of disulfide-rich molecular frameworks, an immense amount of research has been done on these molecules by David Craik and his team, as well as others.[68,69]

A number of successful examples have been reported for engineered cyclotides—the largest known family of cyclic peptides found in nature. This class of molecules is ribosomally produced in plants; they are defined by head-to-tail cyclized backbone and a cyclic cystine knot motif that confers exceptional thermal, chemical, and proteolytic stability. In a recent study, engineered cyclotides were designed for the treatment of multiple sclerosis.[70] Namely, a peptide epitope with the immunoregulatory function (from myelin oligodendrocyte glycoprotein) was grafted into the kalata B1 scaffold (loop 5). The results obtained in a mouse model suggest that an engineered cyclotide could be used as a stable vaccine to treat immune-mediated diseases. In another study, Craik et al. showed that cyclotides kalata B1 and MCoTI-II, as well as trypsin inhibitor SFTI-I, cross the cellular membrane by various mechanisms, hence identifying a new class of cyclic cell-penetrating peptides (CPPs).[71,72] Recently, Camarero and coworkers reported that grafted cyclotide could efficiently modulate intracellular PPI.[73] Specifically, engineered cell-permeable MCoTI-II could antagonize the interaction between the transcription factor p53, and its binding oncogenic proteins, HDM2 or HDMX, in vitro and in vivo. These findings extend the potential realm of application for disulfide-rich cyclic peptide scaffolds for intracellular targeting.

Knottins are another interesting family of disulfide-rich peptides found in fungi, plants, and animals. They possess a cystine knot core, but no head-to-tail cyclization. Native and engineered knottins are studied for diagnostic and therapeutic applications. Their engineered frameworks were shown to be effective modulators of various therapeutic targets. Several knottins have already reached clinical trials. The first FDA-approved knottin on the market is a synthetic version of the MVIIA conotoxin that originates from the cone snail venom. The peptide was approved for intrathecal use to treat chronic pain under the generic name Ziconotide (distributed as Prialt®).

Another native knottin chlorotoxin, derived from scorpion venom, was found to preferentially bind malignant glioma cells when conjugated to a near-infrared dye. The chlorotoxin is being developed in the clinic as "tumor paint"—an optical imaging contrast agent to help surgeons differentiate between cancerous and healthy tissues during surgery.[74]

In the most recent study, the Cochran group synthesized and studied a series of knottin peptide–drug conjugates (KDC) (**Fig. 3A**). The results demonstrated that the KDC could deliver gemcitabine to malignant cells, which express tumor-associated integrins.[75] The evidence shows that this knottin–drug conjugate binds to tumor cells with low nanomolar affinity, is internalized by an integrin-mediated mechanism, and acts as a highly potent inhibitor of several malignant cell lines as the drug payload is released intracellularly. The same team has previously labeled knottins with various tags including fluorescent small molecules, radioisotopes, and ultrasound contrast reagents (**Fig. 2B**). They demonstrated that labeled knottins can be used for the in vivo imaging of tumors in mice.

Due to their small size, knottins allow for easy synthesis and have the potential for better tumor penetration.[76] If cell- and tissue-specific targeting is tuned effectively, these peptide-small molecule constructs can potentially overcome the limitations of antibody–drug conjugates (ADCs).

1.11.2.2 Immune Targets and Vaccines

Targeting of the immune system with vaccines for treating infectious diseases is probably one of the most successful medical innovations to date. Prophylactic vaccines have helped us combat and eliminate the morbidity associated with several deadly infectious

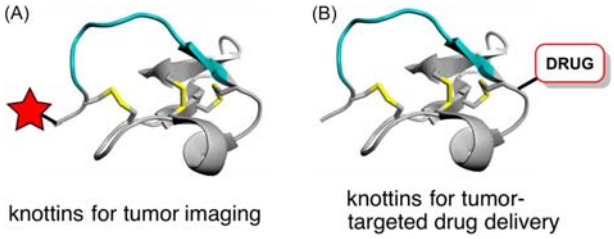

Fig. 3 (A) Knottins labeled with fluorescent small molecules, radioisotopes, or ultrasound contrast reagents for tumor-imaging. (B) Knottin peptide–drug conjugates (KDCs) for tumor-targeted drug delivery. Reproduced with permission from Cox, N.; Kintzing, J. R.; Smith, M.; Grant, G. A.; Cochran, J. R. Integrin-Targeting Knottin Peptide-Drug Conjugates Are Potent Inhibitors of Tumor Cell Proliferation. *Angew. Chem. Int. Ed. Engl.* **2016**, *55*, 9894–9897. Copyright Wiley-VCH Verlag GmbH & Co. KGaA.

diseases such as diphtheria, smallpox, polio, measles, mumps, and rubella. Vaccines were traditionally made from attenuated live organisms (bacteria or viruses) or whole inactivated pathogens.[77] For example, the bacillus Calmette-Guérin vaccine is an attenuated form of the *Mycobacterium bovis*. This vaccine, initially used against tuberculosis, is widely used today in the treatment of non-muscle invasive bladder cancer due to its ability to enhance tumor immune responses.[78] The early generations of vaccines involved the creation of inactivated or attenuated pathogens, or toxoids from pathogens, as therapeutic agents. However, these strategies carry a number of challenges, including the risk of infection, the reversion of the virulence induced by mutations, undesirable reactions to the vaccine components, and the inability to develop effective vaccines against pathogens that are difficult to grow in cultures or ones that present hypervariable antigens. The variability between batches and strains, the heterogeneity in vaccine mixtures, and the strict conditions in manufacturing, storage, and handling[79] create additional development and production challenges, not to mention that the development process can be slow and time-consuming. In response to these challenges, the field has moved on to the concept of "subunit" vaccines, where specific portions or subunits of antigens are used as immunostimulatory agents. One of the limitations of subunit vaccines is that they are not as immunogenic as those with whole pathogens.

One way of boosting immunogenicity of subunit vaccines is to use them in conjunction with "adjuvants" which serve to boost host immune responses. There are two types of adjuvants, namely immune potentiators that stimulate the immune system, and delivery systems that deliver and present antigens to the immune system in an effective manner. In 2014, the NIH reported that better adjuvants are needed, and committed up to $70 million over the next 5 years to new adjuvant research.[80] The field of adjuvant research presents some interesting opportunities for chemical design approaches, as highlighted by a recent study that demonstrated that the efficacy of vaccines can be improved through the proper design and modulation of physicochemical properties, and through the formulation of polymer carriers of toll-like receptor agonists, which are a form of vaccine adjuvants.

In order to improve immunogenicity, subunit antigens have been chemically conjugated to protein carriers such as the tetanus toxin, diphtheria toxin, or CRM197, a nontoxic variant of diphtheria toxin. Bioconjugate vaccine strategies have been fundamental to the development of highly successful vaccines such as Prevnar-13, Menactra, Menomune, and HibTiter. These were created by conjugating bacterial polysaccharides to immunogenic carrier proteins. The evolution of conjugation strategies and its impact on therapeutic practice is evident in the development of Prevnar, Synflorix, and Prevnar-13, which are conjugate vaccines of cell capsule sugars from 7, 10, and 13 serotypes, respectively. The field of generating antigen conjugates, where the antigens are displayed in specific repetitive arrays on various polymers and carrier proteins, is a growing area of research and promises the opportunity to create more effective and potent vaccines. Another advancement in the vaccine field is the concept of reverse vaccinology and structural vaccinology, wherein the combination of human immunology, structural biology, and bioinformatics is applied rigorously to identify antigenic epitopes. The rational design of vaccines is challenging and requires crystallographic analyses and computational modeling, along with a good understanding of immune biology, to effectively help advance the development of synthetic vaccines.[81,82] There is a growing effort to create homogeneous molecular vaccines. For example, using genetic code expansion methods (including the amber suppression technique or the rare sense codon reassignment), peptide or protein engineering can be done in a manner that allows for the break of self-tolerance.[83,84] These approaches will allow for the preparation of highly immunogenic synthetic vaccines without the need for carrier protein bioconjugations.

The success with prophylactic vaccines and the advances in knowledge-based immunogen design and conjugation strategies have created opportunities for deploying "therapeutic vaccines." Therapeutic vaccines are intended to activate the immune system to recognize and combat existing infections or diseased cells. Much of the work in the therapeutic vaccine space to date has focused on trying to harness the immune system to recognize and eliminate cancer cells. Dendreon's Provenge (Sipuleucel-T) became the first FDA-approved therapeutic vaccine when it received approval for treatment of metastatic prostate cancer in 2010. Since then, there have been others: a cholesterol-lowering vaccine that targets pcsk9, antinicotine vaccines to aid in smoking cessation, and anti-cocaine vaccines for treating cocaine addiction. There are multiple cancer vaccines currently in clinical trials for a range of different solid tumors. Carbohydrates, proteins, peptides, glycopeptides, and glycolipids have been used as antigens in these approaches. For example, recent progress has been made in the field of peptide vaccination to mimic T-cell epitopes and to trigger an effective engagement of the immune system, particularly in combinatory regimens.[85,86] As a result, a large number of peptide vaccinations for solid tumors are currently in clinical trials, such as those targeting HER2, IDO, and IDH1. The design of such peptides takes advantage of the new immunoinformatic tools that combine both computational and experimental epitope mapping for optimal

immunogenicity prediction.[87–89] Yet, the peptide vaccination field is still experiencing some difficulties, such as the delivery route, the low intrinsic immunogenicity of individual peptides, the ability to predict the immune response of a pool of epitopes, and also the need to mimic both linear and conformational B-cell epitopes.[90] Answering these questions will be an exciting challenge to be met in the effort to broadly increase the use of peptide vaccination in cancer therapy and in combinatory regimens in the coming years.

In addition to vaccines, the field of immunooncology has seen an explosive growth, as strategies to activate patients' immune system by blocking immunosuppressive checkpoints in the tumor microenvironment have been successful in the clinic.[91] The FDA-approved anti-CTLA4 and anti-PD1 antibodies for the treatment of melanoma greatly improved the overall survival of patients.[92,93] There are growing opportunities for small molecules to become important players in the immunooncology space. Similarly, peptides, macrocycles, or tumor-directing bispecific constructs and conjugates could also present interesting opportunities for medicinal chemistry approaches in this field.

1.11.2.3 Oligonucleotides and Oligonucleotide Drugs

The number of small molecules or natural products which target and interact with nucleic acids are relatively limited. They include a few cytotoxic chemotherapeutic agents that target DNA, a few aminoglycoside and macrolide antibiotics that target bacterial RNA, and antimetabolites, which interfere with DNA synthesis and are used as anticancer and antiviral agents.[94] Over the last two decades, there has been a tremendous explosion in the understanding of RNA biology. This has led to surprising insights into the structure, function, and mechanism of how RNA molecules control and regulate various cellular processes. RNA can be broadly grouped into molecules that are directly involved in translating and coding for proteins, exemplified by mRNA and the noncoding RNAs that do not directly encode proteins but regulate gene expression through indirect mechanisms. The increased understanding of the role that RNA plays in cellular processes and its role in disease biology has opened up the RNA field as an exciting therapeutic target. RNA targeting is an attractive approach for protein targets that are inaccessible to small molecules, proteins, and peptides, and it has the potential to significantly expand the universe of druggable targets.[95] Antisense oligonucleotides (ASOs) represent a broad class of oligonucleotide (ONT) drugs that bind a target RNA and modulate its function by interfering with its translation, or by causing a degradation of target RNA. There are two main types of ASOs, namely RNAse H-dependent ASOs and small-interfering RNAs (siRNAs). RNAse H-dependent ASOs are single-stranded ONTs that bind target mRNAs and reduce gene expression by sterically blocking the ribosomes and RNAse H-mediated cleavage of the mRNA. siRNAs, on the other hand, are double-stranded RNAs which inhibit gene expression by causing the destruction of the target RNA via RNAse Argonaute 2. In addition to mRNA, other RNA targets that are of great interest include micro RNA (miRNA), exon skipping RNAs, and long noncoding RNAs.

There are tremendous opportunities for medicinal chemistry in the RNA field. It has been clearly demonstrated that it is possible to modulate the potency, stability, toxicity, biodistribution, and pharmacokinetic behavior of ONTs through chemical design and structural modifications. SAR studies can be built around the design of a specific ONT sequence and combinations of specific structural modifications in the nucleobase, sugar, or the phosphodiester linkages. ONT drugs need to be taken up in cells in order to be active. There are opportunities for chemists to modify the physicochemical properties of ONT, as well as to design and develop such formulation and delivery vehicles that increase cellular uptake, as well as target the delivery of ONTs to specific tissues. Over the last 13 years, two single-stranded ASO drugs (fomivirsen and mipomersen) have reached the market. Fomivirsen was developed in 1998 to block the translation of viral mRNAs in immunocompromised patients with cytomegalovirus retinitis, but was discontinued due to low demand.[96] Mipomersen was approved by the FDA in 2013 to inhibit apolipoprotein B mRNA in patients with familial hypercholesterolemia, a rare genetic disorder that leads to excessive levels of low-density lipoprotein cholesterol.[97] More than 30 ASOs are currently at various stages of clinical development in efforts to reduce the overexpression of genes associated with cancer, diabetes, cardiovascular, and inflammatory disorders, and other rare diseases.[98] For example, mongersen, an oral SMAD7 ASO, targets SMAD7 overexpression leading to Crohn's disease-related inflammation.[99] Other examples include oblimersen, an intravenous infusion of bcl-2 antisense oligodeoxynucleotide in Phase 1 clinial trials for patients with solid tumors,[100] and BL-7040, an orally available synthetic ONT in development for the treatment of inflammatory bowel disease.[101] To date, half of these studies correspond to the development of ONT therapeutics targeting hepatocyte-expressed genes in the liver (an organ that plays a major role in metabolism and secretion of carrier proteins, coagulation factors, hormones, and apolipoproteins).[102] In addition, it has been shown that phosphorothioate-modified ASOs accumulate in the liver, rendering it an attractive space for this class of drugs.[103] However, a broader clinical translation of ONT therapeutics is still hampered by their challenging delivery.

Alternatively, nonnucleotide small molecules that selectively target specific RNAs were also developed. For instance, some antibiotics, such as aminoglycosides and tetracyclines, are able to target RNA structures in the ribosome (rRNA) of bacteria, and thereby alter their growth.[104] Synthetic small molecules were also used to target DM1, a mutated gene in the context of myotonic dystrophies.[105] Increasing the affinity of synthetic small molecules to RNA could be achieved by rendering them positively charged, allowing them to bind strongly to negative-charged RNA. It remains challenging, however, to optimize the physicochemical properties of small molecules, such as hydrophobicity and aromaticity, to make them more selective to specific RNAs.

Nonetheless, RNAi-based biologic therapies can provide greater target specificity than small molecules and they can also target intracellular proteins that are difficult to reach with mAbs. Significant efforts are underway for modulating their tissue distribution and toxicity profile. For instance, siRNAs can be covalently conjugated with *N*-acetylgalactosamine (GalNAc), a ligand for the asialoglycoprotein receptor (ASGPR) which is expressed on the cell surface of hepatocytes, allowing a specific delivery of RNAi to target tissues.[106] siRNAs can also be complexed with peptides designed to penetrate tumors and pass through the tumor cell membranes.

Table 2 Injectable programs in Phase 2 and Phase 3 clinical trials by molecule type[109]

Modality	*Phase 3 (%)*	*Phase 2 (%)*
Injectable programs—molecule type by phase		
Antibody	23	19
Carbohydrate	1	2
Cell therapy	5	10
Gene therapy	3	5
Oligonucleotide	1	3
Peptide	10	12
Polymer	1	<1
Protein	21	17
siRNA	1	2
Small molecule	25	22
Other/undefined	9	7
Total	477	1103

PharmaCycle products and pipeline module.

For instance, siRNAs targeting the ID4 oncogene, coupled with specific tumor peptides containing cyclic nonapeptide LyP-1 (CGNKRTRGC) and capable of tumor-homing and penetration, were shown to be effective in treating ovarian tumors in mice.[107] siRNAs could be also wrapped in lipopeptide nanoparticles (NP), which have been shown to offer 100 times the potency of naked design, and would thereby allow lower doses of ONT molecules as well as a better toxicity profile in rodents and primates.[108] Further investigations around the delivery of RNAi biologic therapies could help broaden their use in cancer therapy and beyond.

1.11.3 Targeted Delivery of Next-Generation Therapeutics

Significant advances have been made in the discovery of highly potent and selective biologic drugs in the past few decades. This progress, in combination with the decline in small molecule discovery programs, has led to an increased acceptance of injectable drugs. Not surprisingly, all 7 biologics from the top 10 selling drugs (see **Table 1**) are injectables. Moreover, the majority of the developing pipeline for injectables consists of various biologics, including siRNA, peptide, protein, and antibody therapeutics (**Table 2**).[109] mAbs, for example, are routinely administered via intravenous or subcutaneous injection. Given the long-circulating half-life of most mAbs, weekly, monthly, or even less frequent injections is adequate to get the desired exposure with these therapeutic agents. Thus, injectables in patient friendly formats can significantly improve compliance and potentially bypass the problem of poor oral bioavailability for biologics. Yet, achieving adequate exposure and distribution of peptide, protein, and ONT-based therapeutics remains a key issue in drug development, as these molecules often exhibit a short plasma half-life and low cellular uptake. The short exposure/PK profile is generally due to proteolysis and poor metabolic stability,[110] while the low cellular uptake is associated with the large molecular weight and physicochemical properties of biologics. A wide range of methodologies are continuously being explored to overcome these challenges, leading to the development of novel formulations and delivery technologies.

To create peptide/protein drugs that have longer duration of action, improved PK profile, and more compliant dosing regimens, the bioconjugation to polymeric carriers has been used routinely.[111–116] The most advanced bioconjugation technology is PEGylation, with the first PEGylated molecule, Adagen®, having been approved by the FDA in 1990. Since then, more than 10 PEGylated biologics have been approved by the FDA, with a similar number going through clinical trials.[116] Bioconjugation to other carriers such as antibodies, Fc-fragments, sialic acid polymers, lipids, and polypeptide fragments continues to be investigated as an alternative to the PEGylation strategy. Other technologies being explored include lentiviral particles (e.g., MS2-chimeric retrovirus-like particles),[117] lipid-based technologies (e.g., liposomes, Saint-PhD)[118,119] NP (e.g., Nanocin),[120] supercharged proteins (e.g., β-defensin-3),[121] inactivated toxins (e.g., anthrax toxin),[122] and CPPs (e.g., PepFects).[123,124] These strategies may help to improve the bioavailability of different types of biologics (DNA, RNA, peptide, protein, vaccines) by preventing proteolytic and enzymatic degradation, or by increasing their cellular uptake via different mechanisms of cell entry, including direct membrane translocation and endosomal entry/escape.

Another aspect, as important as the PK profile and cellular uptake, is the delivery of drugs specifically to cells of interest. When a therapeutic agent affects healthy tissue, patients may experience side effects which limit the dose of the drug. One way to improve the efficacy and tolerability of therapeutics is to alter their biodistribution by selectively delivering them into diseased cells. Targeted delivery is a strategy that is used to achieve cell-specific drug delivery via receptor-mediated endocytosis or transcytosis. Receptor-mediated endocytosis is the key mechanism that facilitates internalization of the receptor–ligand complexes. Receptor-mediated transcytosis (RMT) is defined as transporting macromolecular cargo from one side of the cell to the other within

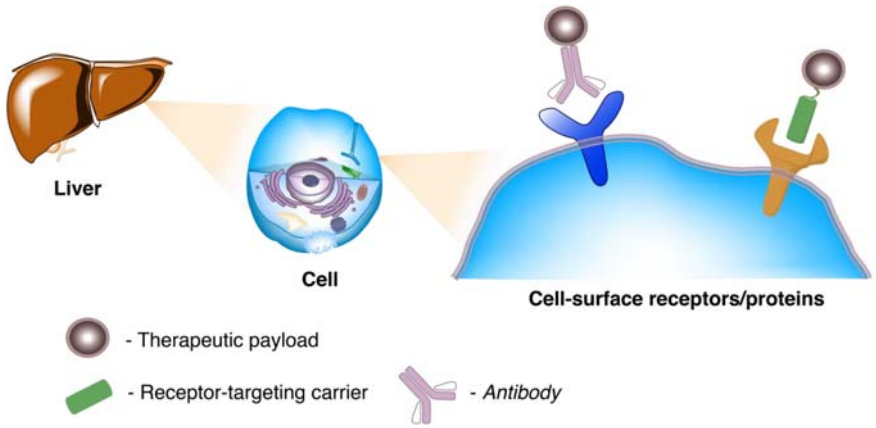

Fig. 4 Cartoon diagram illustrating targeted drug delivery to liver.

membrane-bound carriers(s).[125] Receptor-mediated endocytosis is the key mechanism that facilitates internalization of the receptor–ligand complexes. The approach takes advantage of cell-surface receptors or proteins that are overexpressed in different tissue types, malignant cells, or tumor microenvironments. Ligands, which bind to these proteins, act as targeting agents and transport conjugated therapeutics to the specific cells. Cytotoxic dugs, imaging agents, radionuclides, and miRNAs are some examples of therapeutic cargos that have been successfully delivered by this approach. The receptor-targeting moieties, as shown in Fig. 4, include antibodies and their derivatives, peptides, carbohydrates, aptamers, and nonantibody proteins.

In this section, we discuss current research in efforts to deliver biotherapeutics to the intracellular space. Initially, we review CPP-mediated delivery of drugs, their cellular uptake mechanisms, and the design principles that guide peptide cell-permeability. In subsequent sections, we highlight recent developments and challenges in those targeted therapies that utilize transcytosis or endocytosis, the internalization mechanism of overexpressed receptors, to deliver bioconjugates to the site of action.

1.11.3.1 CPPs as Delivery Vectors

Living cells tightly and selectively control the translocation of various molecules through the plasma membrane by utilizing ion channels, carrier proteins, or their innate endocytic uptake mechanism. However, it is known that chemically intractable proteins, which represent a vast majority (>80%) of the human proteome, reside in the intracellular space.[126] Therefore, it is essential that we find a way to efficiently deliver bioactive molecules into the cytosol and nucleus of the cell. Most small, hydrophobic organic molecules easily cross lipid bilayers by passive diffusion or carrier-mediated transport. However, as published data suggest, small molecule drugs can only target about 10% of the druggable genome.[127] For biologic drugs, on the other hand, cell-permeability is a major hurdle that impedes the realization of their full potential as pharmaceuticals. In fact, the vast majority of proteins cannot penetrate the cell.

Peptides have an inherent advantage over large biologics in crossing the cellular membrane. CPPs, also referred to as protein-transduction domains, are a specific class of molecules that are typically less than 30 amino acids long and can permeate the phospholipid bilayer without significant toxicity. CPPs can be derived from natural proteins, large combinatorial libraries of plasmid or phage displays, phylomers, as well as from de novo synthesis. A number of excellent reviews have described and classified known CPPs based on their origin and physicochemical properties.[128–130]

CPPs are used for a number of applications such as: (1) elucidating the mechanism of cell entry; (2) acting as vectors to transport various attached cargos, including small RNA/DNA, antibodies, and NP; and (3) designing functional cell-permeable peptides by incorporating bioactive motifs within the CPP sequence. The design rules, however, of grafting active domains remain elusive and difficult to distill. Currently, one of the most popular approaches for the intracellular delivery of biologic drugs in vivo is their fusion to CPPs, as are described in recent reviews.[129–131] Other approaches have also been studied and reported, including the conjugation of biologics to receptor ligands, cell-penetrating proteins, and lipid NP.

1.11.3.1.1 Cellular uptake pathways for drug delivery with CPPs

In the past, understanding the mechanism for the cellular uptake of CPPs has been a topic of debate as earlier experiments reported contradictory results. This was due, partly, to the unrecognized artifacts of flow cytometry and fluorescence microscopy of fixed cells. It was not trivial to distinguish between fluorescent groups that are bound to the cell surface and those that are taken up by the cell.[132] Furthermore, while labeling CPPs fluorescently is one of the most convenient ways to monitor cellular uptake, it was demonstrated that the addition of a hydrophobic fluorescent dye could in fact alter the cellular interaction mechanism.[133] Another common practice to study various routes of endocytosis is the use of chemical inhibitors. However, these methods have limitations, and they are often highly dependent on the specific cell line used.[132] Therefore, the experimental results should be interpreted

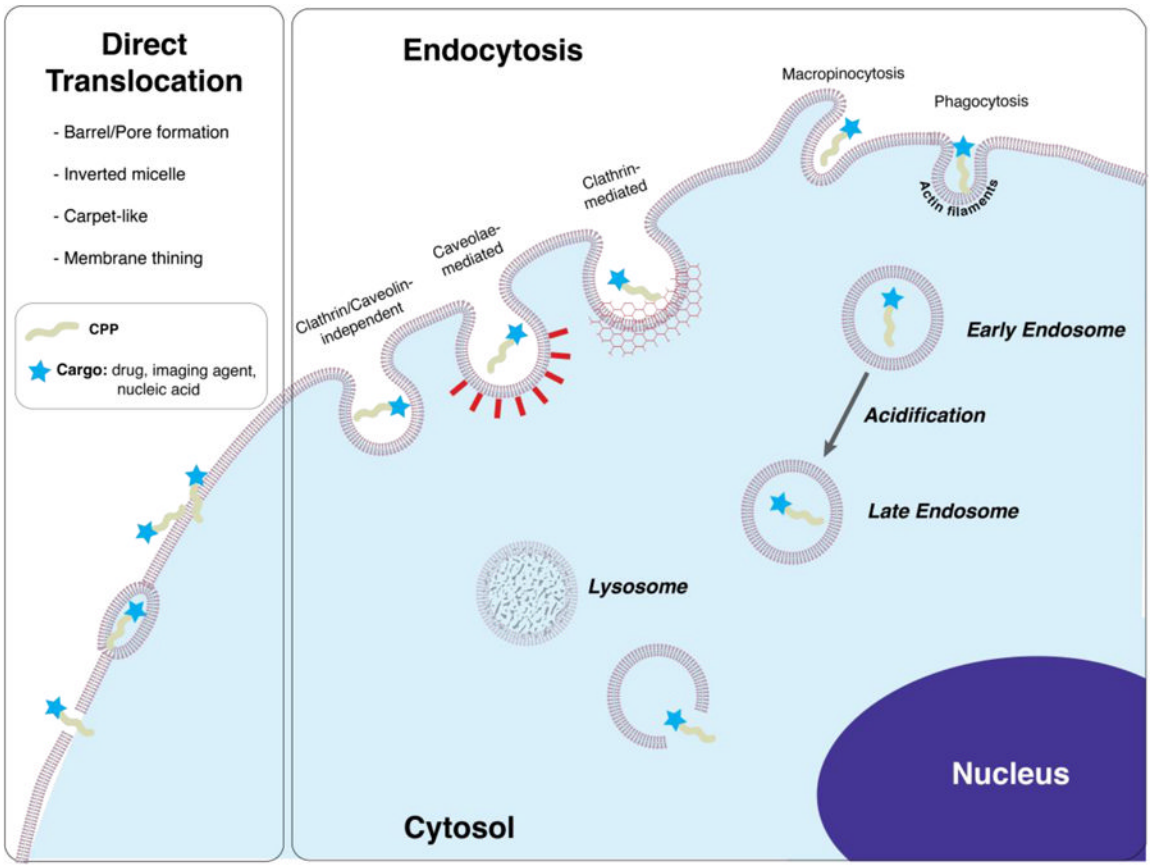

Fig. 5 Entry pathways of cell-permeable peptides.

carefully. Based on accumulated data and experience, subsequent studies of the permeability mechanism were better able to differentiate between cellular binding, cellular endocytic uptake, and direct translocation.[131,134] It was consequently recognized that the uptake mechanism depends on the CPP sequence, its concentration, the physicochemical nature of the attached cargo, the type of cell line, the incubation time, and the temperature. It has been reported that each CPP could utilize more than one uptake mechanism depending on the conditions. In addition, endocytosis and direct translocation could occur at the same time. These considerations make it difficult to describe the complex process of cellular uptake with a common set of rules.

For arginine-rich CPPs, direct translocation is the primary mechanism at low CPP concentrations, which is a receptor-independent route of cell entry. Above 2 μM, this mechanism is replaced by endocytosis, and at concentrations higher than 10 μM, rapid cytoplasmic entry takes place via transduction.[135]

Fig. 5 provides a summary of major cellular uptake mechanisms, such as direct translocation and endocytosis. The latter includes different mechanistic pathways such as macropinocytosis, clathrin- or dynamin-dependent uptake, and caveolae/lipid raft-mediated endocytosis. A number of review papers delve into the subject in more detail.[136–139]

1.11.3.1.2 Molecular determinants of cell-permeability

Despite extensive research conducted within the past decade, the general requirements of the structure–transport relationship for cellular permeability of peptides are not well understood. Nevertheless, it is widely recognized that the internalization pathway is chosen depending on the character and the strength of the initial interaction of a CPP with the plasma membrane.[140] The initial step in cellular uptake often involves the electrostatic interaction between positively charged peptides and negatively charged phospholipids or the proteoglycans on the cell surface. While this step is not required for cellular entry, the number and nature of positively charged groups can have a tremendous effect. Experimental data have demonstrated that the uptake rate is higher for those CPP sequences that contain arginine instead of lysine. This phenomenon is attributed to the unique ability of guanidinium headgroups to form bidentate hydrogen bonds with negatively charged groups on the cell surface.[137,141] Interestingly, as described in a recent review by Lonn and Dowdy,[142] efficient transduction of TAT (peptide responsible for the uptake of transactivator protein) can occur in cell lines that are deficient in glycosaminoglycans and sialic acids. However, enzymatic removal of cell-surface proteins completely abrogates TAT-mediated transport. The data suggest that interaction with cell-surface proteins is an important step for initiation of macropinocytotic TAT uptake.[143]

Furthermore, hydrophobic side chains—especially aromatic groups—are also believed to enhance the translocation ability of CPPs, as they strongly influence peptide–lipid interaction. It has been shown that intracellular localization and the efficiency of oligoarginine-based CPPs could be tuned via the introduction of tryptophan residues.[144] Specifically, the number and distribution of tryptophans has affected the cellular uptake mechanism as CPP analogs were internalized via endocytic and/or nonendocytic pathways.

The correlation between the secondary structure of peptides and their ability to permeate the cell remains unclear. While most CPPs are unstructured in aqueous solution, many adopt a range of conformations (α-helix, β-strand, β-turn) during their interaction with various lipid environments and membrane mimetics.[145] This variability in their structure could be detected within the same peptide sequence due to different cellular environments and experimental conditions. One commonly observed feature is amphipathicity, which leads to the classification of CPPs in three structural classes: primary amphipathic, secondary amphipathic, and nonamphipathic. Specific peptide sequences and their uptake mechanisms are well documented in recently published comprehensive reviews.[146,147]

Various structural elements are found in secondary amphipathic peptides, including polyproline II, β-sheets, and α-helices. One of the common motifs, the amphipathic α-helix, has a hydrophobic patch on one face. However, the other faces of helical CPPs vary between cationic, anionic, or polar.[128] Hence, when it comes to efficient cellular entry, the general rules and requirements for secondary structure elements are difficult to delineate. Evidence suggests that helix stabilization often results in more efficient membrane translocation.[148] In a recent study, an arginine-based peptide was elegantly designed into an α-helical shape by incorporating novel nonproteinogenic amino acids.[149] When intracellular uptake was examined, the data showed that stable α-helical structures entered cells more efficiently than the corresponding nonhelical arginine nonapeptide (R_9). Nonetheless, helicity is not generally necessary to achieve efficient cellular uptake, as different peptide conformations can trigger different uptake mechanisms. A number of studies have found that cyclization could also enhance cell-permeability of arginine-rich CPPs.[148] In contrast, Medina et al. recently reported a constitutively disordered, arginine-rich peptide, CLIP6, which directly translocates through the cell membrane without folding. CLIP6 demonstrated an exclusively nonendosomal cell entry mechanism, and avoided lytic conformation due to its disordered state.[150] Hence, conformational flexibility might be the most important feature of CPPs when interacting with various lipids, because peptides can adapt their structure to specific environments and determine their route of entry.[137] More importantly, experimental evidence obtained so far suggests that each cellular uptake mechanism might have its own structure–transport relationship.[135] However, without a full understanding of the molecular interactions that trigger efficient internalization of peptides, it remains a pervasive challenge to rationally design and tune cell-permeability.

1.11.3.1.3 Enhancing endosomal escape of biologic drugs

Endocytic trafficking is one of the major challenges that limit the intracellular delivery of therapeutic agents. While some advances have been made, novel methodologies are developed continuously to improve the efficient cytosolic entry of biologic drugs.

At high concentrations (>10 M), some CPPs have been shown to predominantly penetrate the cellular membrane via direct transduction.[135] However, it is generally believed that most positively charged CPP sequences, which bind to the cell surface, enter the cell by at least one of the endocytic mechanisms that form endocytic vesicles. As a result, the CPP-cargo conjugate is predominantly entrapped in the endosomes, and eventually it either becomes enzymatically degraded in the lysosomes or recycled back to the cell surface. Therefore, a large fraction of biological agents does not reach intracellular target proteins in vivo. Consequently, a high concentration of an active compound is required for efficient cytosolic delivery and for the desired biological efficacy on intracellular targets.

It has been shown that certain types of proteins are also able to deliver attached cargos (proteins, peptides, and nucleic acids) into mammalian cells. An example is a class of superpositively charged proteins such as +36 GFP.[151] These proteins have demonstrated effective intracellular delivery of conjugated cargo, but a significant fraction of them remains trapped in endosomes.

Endosomal release has been studied extensively in recent years to address the problem of endosomal localization of biologics. New technologies have enabled the identification of a number of mechanisms, including pore formation, the pH-buffering effect, conformational change, and the photochemical disruption of the endosomal membrane. Based on this knowledge, various chemical agents have been designed and tested to achieve the safe and efficient release of therapeutics into the cytosol. Some important considerations for the escape agent include low immunogenicity and toxicity, as well as affordable manufacturing cost for large-scale production. Furthermore, the endosomal escape properties of the agent should not depend drastically on the nature of the attached cargo. We will highlight a few examples in this article, while more detailed reviews on this topic can be found in recent publications.[152,153]

One of the strategies used to achieve efficient cytosolic delivery is based on the discovery of peptide sequences that can facilitate the early endosomal escape of conjugated cargo molecules. A recent study demonstrated the successful use of such peptides to enhance the endosomal escape of protein cargos fused to +36 GFP.[154] In order to find endosomolytic peptide sequences, authors cleverly screened a panel of known antimicrobial peptides which disrupt microbial membranes without mammalian cell toxicity. One of the key challenges in testing such peptides is the lack of general assays that can differentiate between proteins that are trapped inside the endosomes, from proteins that have been released into the cytosol. It is usually necessary to assemble multiple independent assays, and to combine the results with mutational studies. As a result of these efforts, a 13-residue peptide called aurein 1.2 was discovered. This peptide was able to significantly enhance the cytosolic delivery of proteins and their cargos in cell culture and in vivo. It was shown that aurein 1.2 facilitates endosomal escape in a cargo-independent manner.

A recent study has reported the discovery of rationally designed miniature proteins with arginine residues at various positions on the helical surface of the hairpin fold.[155] These miniproteins reach the cytosol through rapid internalization, followed by early endosomal release. A similar uptake pathway was detected for a novel cyclic amphipathic peptide, cFΦR4, which enters cells through multiple endocytic mechanisms and promotes an early endosomal release of its cargo.[156] cFΦR4 is one of the most active transporter peptides known today that delivers active biologics directly into the cytoplasm. However, the exact mechanism of endosomal escape remains to be determined.

Other strategies that can improve endosomal escape efficiency include the proton-sponge effect, multivalent CPPs, and those that mimic the mechanisms of enveloped viruses releasing viral capsid into the cytoplasm.[142] While some progress has been made with these strategies, the endosomal entrapment remains one of the major hurdles of CPP-mediated delivery of biologic drugs.

1.11.3.2 Targeting Specific Tissues

Targeting tumor cell-specific receptors is an approach widely used to deliver ligand-conjugated therapeutic payloads to malignant cells. When ligand binds to a cell-surface receptor, receptor-mediated endocytosis takes place triggering innate internalization of the receptor–ligand complex within clathrin-coated vesicles (Fig. 6). This process is usually preceded by downstream signaling. Often, the ligand dissociates from the receptor in the acidic environment of the late endosome. Subsequently, the receptor can be either recycled to the membrane for another round of signaling/internalization, or transferred to the lysosomes, along with the ligand, for degradation. The fate of the ligand internalized via receptor-mediated endocytosis tends to be degradation via the lysosomes. Therefore, endocytic escape is required if the drug needs to reach its biological target inside the cell. While the therapeutic effect of a ligand-conjugated payload depends on the potency of the payload, the drug should also be metabolically stable, and there should not be any loss due to its excretion. In addition, it is important to estimate the minimal level (or absolute number) of receptor expression that is necessary to deliver the sufficient amount of a drug, as well as the ratio of receptor expression in diseased versus healthy tissue, and the rate of internalization and recycling.

Ligands that internalize via receptor-mediated endocytosis include hormones, growth factors, small molecules, toxins, lectins, viruses, antibodies, and serum transport proteins.

The main criterion for the selection of a receptor is its distribution pattern. The higher the receptor upregulation level on malignant relative to normal cells, the better the specificity of targeted delivery and the lower the toxic side effects from the exposure of healthy cells to the drug. While a high overexpression ratio (tumor vs. normal) is required, many receptor-targeted therapeutics in

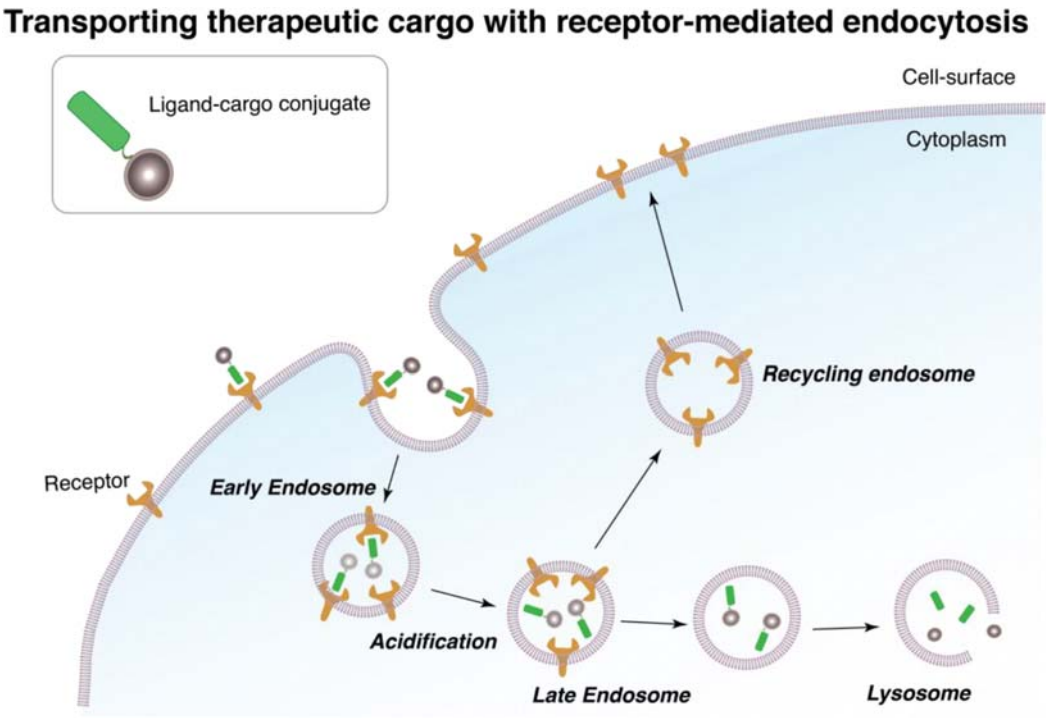

Fig. 6 Schematic representation of receptor-mediated endocytosis: a ligand in the extracellular space binds to its target receptor and triggers signaling/internalization of the receptor–ligand complex. Common compartments during the intracellular trafficking are shown: early endosome, late endosome where dissociation of the receptor–ligand may happen, recycling of receptors to the cell surface, and releasing the attached payload into the cytoplasm.

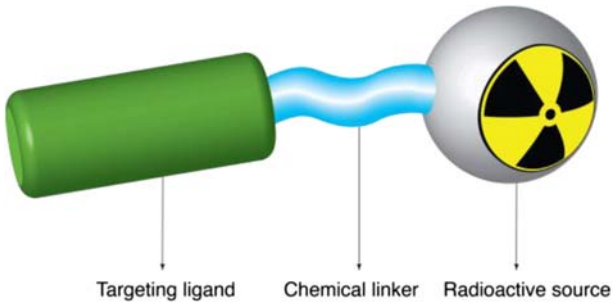

Fig. 7 A schematic representation of a conjugate with a radioactive source as a therapeutic, diagnostic, or imaging agent.

the clinic only show a two- or threefold difference in receptor upregulation, which is still an improvement in comparison to non-targeted therapy.[157] One factor that amplifies specificity of targeted delivery besides the overexpression ratio is the receptor recycling rate, which is usually greater in malignant cells and translates into increased drug transport.

It is important to note that receptor internalization is not always a necessary step in achieving the desired therapeutic effect. For example, cell-surface receptor antagonists are generally not internalized via endocytosis. Yet, they have successfully delivered drugs to tumor-specific receptors. For example, radiolabeled receptor-binding somatostatin analogs are used in peptide receptor radionuclide therapy for the treatment of neuroendocrine tumors (NETs). These antagonists have shifted the paradigm by demonstrating more favorable pharmacokinetics and better tumor visualization than agonists did. Subsequently, gastrin-releasing peptide receptor targeting antagonists showed better PK profiles and fewer side effects, showing promise in early clinical trials for prostate cancer imaging.[158]

In radionuclide therapy, a radioactive source is covalently attached or chelated to a targeting ligand via a chemical linker (**Fig. 7**), sometimes referred to as "PK modifier." The physicochemical properties of the linker dramatically influence the PK, biodistribution, tumor uptake, and rate and route of conjugate excretion, while the effectiveness of the therapy depends on the expression of the targeted receptor and the nature of the radionuclide.

Recent years have seen a tremendous growth of biological data generation. The input provided by bioinformaticians in analyzing these data creates great potential for the discovery of new clinical targets. The profiling of proteins or receptors for ectopic expression and overexpression in tumor/disease tissues, with little or no expression in healthy tissues, provides new opportunities for the development of therapeutics that can target malignant cells, reducing side effects and improving the therapeutic index.

In this section, we highlight a few examples of how the distribution of cell-surface receptors and proteins has been used for the specific targeting of pathologic cells. We emphasize cases that involve crossing various biological barriers in order to deliver therapeutic cargos to the brain, pituitary gland, liver, pancreas, and to tumor tissues.

1.11.3.2.1 Delivery of therapeutics across the blood–brain barrier

Treating neurological disorders such as Alzheimer's, Parkinson's, strokes, lysosomal storage disorders, schizophrenia, depression, and brain tumors require the transport of a drug through the blood–brain barrier (BBB).[159] There are tremendous unmet patient needs when it comes to central nervous system disorders, as crossing the BBB remains a significant hurdle for delivering biotherapeutics. The BBB is a protective barrier that separates the brain from circulating blood, allowing water and other essential molecules in, while excluding macromolecules and potential neurotoxins from entering the extracellular fluid of the brain. For biologics, the main physiological entry mechanism into the brain is RMT. There are a number of known receptors associated with RMT, including the transferrin receptor (TfR), insulin receptor, lipoprotein receptor, and the diphtheria toxin receptor.[160] The ligands that bind to these cell-surface receptors have been frequently used for targeted cargo delivery across the BBB. A specific example of this is the delivery of protein drugs fused to a mAb of the TfR.

The TfR transports iron-bound Tf into the brain. When the Tf–TfR complex is formed, the process of endocytosis is initiated. When the complex reaches the late endosome's acidic environment, iron dissociates and the Tf–TfR gets recycled back into the plasma membrane of the brain endothelial cells.

The transferrin receptor monoclonal antibody (TfRMAb) has been used as a shuttle to deliver therapeutics into the brain. The TfRMAb binds an epitope within the extracellular domain (ECD) of TfR1 with low affinity and gets internalized via RMT at a similar rate as transferrin itself.[159] Importantly, the TfRMAb-binding epitope is spatially removed from the endogenous Tf binding site, therefore it does not interfere with the transport of iron into the brain.[159,161]

Several examples in the literature illustrate how TfRMAb can be engineered as a fusion protein to successfully deliver therapeutic antibodies,[162,163] neurotrophins (the glial-derived neurotrophic factor and erythropoietin), decoy receptors (ECD of the type II TNFR), and lysosomal enzymes (iduronidase (IDUA)), and iduronate 2-sufatase. The TfRMAb has also been engineered as a fusion protein with avidin to allow the delivery of a biotinylated β-amyloid peptide radiopharmaceutical used for the imaging of amyloid plaques in the brain of patients with Alzheimer's disease. In all of these examples, the TfRMAb was engineered to retain its binding affinity to the TfR1 as well as the activity of the therapeutic protein.[159] If clinical trials prove successful, this approach can be applied to almost any class of recombinant protein to produce a BBB-penetrating IgG-therapeutic fusion for the delivery of biologics into the brain.

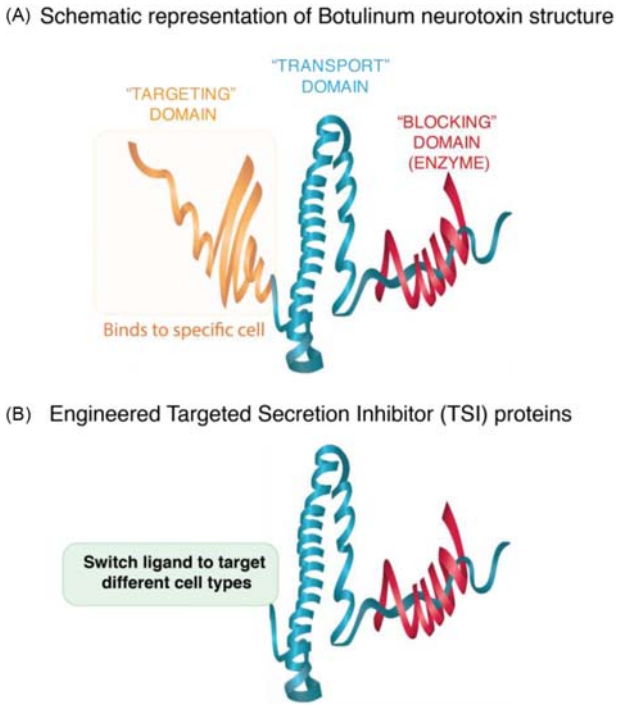

Fig. 8 Schematic representation of BoNT and TSI proteins. Adapted from Foster, K.; Chaddock, J. A. Targeted Secretion Inhibitors-Innovative Protein Therapeutics. *Toxins* **2010**, *2*, 2795–2815.

1.11.3.2.2 Targeting the pituitary

Acromegaly is a disease resulting from excess GH secretion, nearly always originating from a benign tumor of the somatotroph cells in the pituitary gland. A targeted secretion inhibitor (TSI), a botulinum neurotoxin (BoNT) engineered protein, was developed to treat acromegaly. It specifically targets the GH-releasing hormone (GHRH) receptor, which is overexpressed on somatotroph cells.

BoNT is a highly effective therapeutic drug due to its specificity and duration of action in targeting the neuromuscular junction. It contains three domains: a neuronal targeting domain (H_C), a translocation domain (H_N), and an enzymatic domain (LC). It is the enzymatic domain of BoNT that carries out the therapeutic action inside the cell and causes neuroparalysis (Fig. 8).[164] This enzymatic domain targets SNAREs (soluble *N*-ethylmaleimide-sensitive factor-attachment protein receptors), the polypeptides responsible for vesicle fusion to the membrane that causes neurotransmitter release.[165,166]

TSIs are engineered proteins where the neuronal cell-targeting domain (H_C) of BoNT is replaced with a peptide or protein that targets a specific cell-surface receptor, while retaining the enzymatic (LC) and translocation (H_N) domains. A detailed description of the research has been reviewed.[167]

For the treatment of acromegaly, the targeting domain of BoNT was replaced by the GHRH peptide, which binds the GHRH receptor. This TSI construct showed in vitro and in vivo efficacy, as GH secretion inhibition was observed with cleavage of the SNARE of interest, in this case the vesicle-associated membrane protein, which is associated with GH release.[168–170] While the studies explored thus far show promising in vivo efficacy results, a safety window for systemic administration of TSIs is still to be determined. Delivering TSIs to nontarget tissues that have a marginal expression of the targeted receptor remains a concern. However, due to the fact that the TSIs act on specific SNAREs, in order to observe a toxin effect, nontargeted tissues would have to contain the targeted SNAREs.

If this approach proves successful, the engineered TSIs could lead to a new class of biologics for the treatment of disorders that are characterized by overproduction of a particular hormone or neurotransmitter, such as endocrine secretory disorders, neuropathic pain, or overactive bladder.[158]

1.11.3.2.3 Targeted delivery to the liver

Gene silencing has been developed as a therapeutic treatment for many infectious, metabolic, and genetic diseases such as hemophilia, hepatitis, and transthyretin (TTR)-related amyloidosis, which are controlled by processes of the liver. Due to its potential for treating a variety of diseases, including cancer, gene silencing has generated a lot of interest in the field since the discovery of siRNA in 1999.[171] There are, however, many challenges in developing siRNA therapeutics, some of which include poor in vivo stability, efficient delivery to the desired tissue to avoid off-target effects, and intracellular delivery. Some of these challenges have been addressed with the use of NP, which protect ONTs from proteases and facilitate the intracellular delivery of these negatively charged molecules.

Kupffer cells, which form part of the reticuloendothelial system, are responsible for a large uptake of NP by the liver. The use of lipid NP has proven efficient for a few treatments, but the development of targeted delivery to hepatocytes has improved the therapeutic potential of siRNAs. Targeting the liver can be achieved through the ASGPR, which is expressed on hepatocytes. The ASGPR facilitates the uptake and clearance of glycoproteins with terminal galactose and GalNAc via clathrin-mediated endocytosis (as shown in Fig. 5).[172–174] Multivalency presentation can yield ligands that bind in the low nanomolar range, depending on their valency and spatial orientation.[175]

Galactose-modified cationic liposomes have been used to deliver siRNA to the liver via binding to the ASGPR.[174] Liposomes containing a higher ratio of the galactose-modified lipid showed increased uptake of the siRNA by HuH-7 cells, a hepatocellular carcinoma cell line. Gene silencing was demonstrated in this cell line with a twofold higher suppression of hVEGF-A protein expression over nongalactosylated cationic liposomes. Five and sixty minutes post administration of the galactose-modified cationic liposomes, enhanced transfer to hepatocytes was demonstrated in mice, with a higher content of ^{3}H-labeled siRNA found in the liver. The enhanced siRNA accumulation in the liver was eliminated by pretreating mice with asialofetuin, an ASPGR ligand, providing evidence that the higher uptake was due to the ASGPR. Other reports have also demonstrated targeted delivery of siRNA or oligodeoxynucleotides to the liver via liposomes containing galactosylated cholesterol derivatives.[176,177]

A similar concept was used by Jiang et al. to demonstrate in vivo gene silencing.[172] siRNA was encapsulated in cationic liposome NP and the surface of the NP was decorated with a galactose-modified PEGylated lipid to produce galactose-modified liposome nanoparticles (Gal-LipoNP). Fas siRNA was successfully delivered to the livers of mice in a ConA-induced fulminant hepatitis model, in which liver injury was induced at the predetermined peak time of gene silencing. Gene silencing peaked at ~90% 3 days after tail-vein administration of the Gal-LipoNP/Fas siRNA complex. However, the effect was still observed on the seventh day postadministration, with ~50% gene silencing. Administration of LipoNP/Fas siRNA (particles not modified with galactose) yielded only ~25% gene silencing 24 h postinjection.

In vivo gene silencing in the liver has been demonstrated by Alnylam Pharmaceuticals. Direct conjugation of triantennary GalNAc ligands to stabilized siRNA has led to the development of various drug candidates. The enhanced stabilization chemistry is used to prepare the siRNA–GalNAc conjugates which deliver compounds via subcutaneous administration with improved tissue-specific delivery and efficacy relative to intravenous administration.[175] Alnylam's most advanced product utilizing this technology, revusiran (ALN-TTRsc), is currently in Phase 3 clinical trials to evaluate its efficacy and safety in patients with TTR-mediated familial amyloidotic cardiomyopathy.

GalNAc has also been used by Arrowhead Research Corporation to facilitate in vivo delivery of siRNA to the liver for the treatment of hepatitis B virus (HBV). However, in this case, the GalNAc is conjugated to a melittin-like peptide (NAG-MLP) instead of being conjugated to the siRNA. This conjugate is coadministered with a cholesterol-conjugated siRNA (chol-siRNA) targeting HBV.[178] The product, ARC-520, is currently in Phase 2b clinical trials for the treatment of chronic HBV. The drug consists of two vials, one of which contains the NAG-MLP that targets hepatocytes and promotes endosomal escape; the second vial contains two chol-siRNAs for broader genotype coverage, and is coadministered intravenously.

1.11.3.2.4 Targeting the pancreas

Vesicular monoamine transporter-2 (VMAT-2) is a tissue-specific marker that is expressed in the brain and endocrine tissues. (+)-Dihydrotetrabenazine (DTBZ) is a selective ligand for VMAT-2 that is used for pancreatic beta cell imaging in rodent and human studies. Wu et al. took advantage of the tissue specificity of DTBZ to deliver specific payloads to pancreatic cells. Aminopyrazines (AP), known to have stimulatory and proliferative effects on pancreatic beta cells, were conjugated to DBTZ. This was done in a manner that allowed the conjugates to retain both the binding affinity for VMAT-2 and proliferative effects on beta cells. Tissue distribution studies in rodents revealed that the concentration of DTBZ-AP conjugates were 15-, 2- and 5-fold higher in the pancreas, liver, and kidney, respectively, than in the plasma. The clearance rate of the conjugate was similar to DTBZ. The conjugate demonstrated a much higher volume of distribution at steady state compared to DTBZ, resulting in a significantly increased half-life for the conjugates and a prolonged duration of exposure in the target tissue. This early stage study demonstrated the enhanced delivery of a beta cell proliferating agent to the pancreas by conjugating with a validated imaging agent. However, more work needs to be done to translate the potential of this approach into a clinical application.[179]

1.11.3.3 Targeting Tumors

1.11.3.3.1 Antibody–drug conjugates

Bioconjugation has made it possible to bring together the precise targeting and the long half-lives of mAbs with the cell killing power of highly potent toxins. This has created a new class of drugs called antibody drug conjugates, also known as ADCs. The approval of two ADCs, namely brentuximab vedotin (SGN-35, Adcetris) for Hodgkin's and anaplastic large cell lymphoma, and trastuzumab emtansine (T-DM1, Kadcyla) for HER2^{+} breast cancer, has validated the ADC concept and triggered intensive R&D efforts in all aspects of ADC research.[180] ADCs have created tremendous excitement in the oncology-targeted mAb space; at present, there are over 90 different ADCs in preclinical and over 50 in clinical development for the treatment of both solid and liquid tumors.

An ADC consists of a mAb and a cytotoxic payload that are connected via a chemical linker that result in a molecule that is greater than the sum of its parts. The combination with a cytotoxic agent can significantly enhance the potency and tumor killing potential (increased efficacy) of a mAb. Similarly, the combination with a targeted antibody can increase selective delivery of cytotoxic agent to the tumor cells, while minimizing the exposure to normal, tissue resulting in improved safety and tolerability. The choice of the

linker and conjugation chemistry has a major impact on the efficacy, disposition, and toxicity of ADCs. The chemistry for making the first generation ADCs has been dictated by the limitations of working with proteins. For example, trastuzumab emtansine[181] and brentuximab vedotin[182] were generated by conjugating cytotoxic drugs to native (exposed) lysine or cysteine residues in the antibody backbones. These early conventional conjugations were not site-selective and resulted in highly heterogeneous drug products composed of number of distinct molecular species, differing both in the number and location of conjugation sites.[183,184] This high level of heterogeneity complicates the interpretation of preclinical data as well as the analytical characterization of the ADC molecules. Studies have demonstrated that different molecular species within the same ADC product can have different stability,[185] pharmacokinetic,[186] and efficacy profiles.

In an attempt to reduce ADC heterogeneity and improve product profiles, site-specific conjugation of payloads to proteins has been an intense area of research. New site-specific conjugation technologies have used protein antibody engineering to build unnatural anchoring elements in the antibody sequences followed by an orthogonal conjugation chemistry to selectively attach payloads to these anchors. In addition, there are a few methods that have been able to reduce product heterogeneity by controlled and selective conjugations to native cysteines or lysines. The methods that rely on protein engineering have an inherent advantage as they offer the opportunity to find the optimal site of conjugation for a given antibody and toxin combination. These methods take advantage of protein engineering to move the conjugation site across any region of the antibody and enable a true exploration of the impact of conjugation site on the biological properties of ADCs. The work with the site-specific ADCs has definitively shown that the site of conjugation has a major impact on the pharmacological properties of an ADC and is a critical parameter in the design of ADCs. There are tremendous opportunities for continued medicinal chemistry design inputs in evolving these methods and developing SAR with appropriate linkers and toxins.

In addition to ADCs cytotoxic conjugates, polymers, NP, protein fragments, peptides, and small molecules are also actively being pursued with the goal of selective delivery of therapeutic agents to tumor cells. The potential advantage of using nonantibody carriers could include improved tumor penetration, ease of manufacturing, access to novel targets, and potential differentiation with regards to dosing schedules and toxicities. The lessons learned in the design and development of ADCs and similar conjugates can be applied to the broader field of conjugates for targeted delivery to other tissues, and will continue to be a fertile arena of research for trained chemists.

1.11.3.3.2 GPCRs as targeting vectors

GPCRs are the largest family of cell membrane receptors with ~900 members, and are characterized by their seven transmembrane domains. This family of receptors can be subcategorized into different classes depending on their structure and function. Most GPCRs are internalized via clathrin-dependent endocytosis upon agonist binding/stimulation, although it has been demonstrated that some receptor families are constitutively internalized via clathrin-independent endocytosis. Following internalization, the receptor can be either recycled back to the plasma membrane for another round of signal transduction, or transported to the lysosomes for degradation.[187–190]

GPCRs control a wide variety of physiological and pathological processes. Their signaling pathways are implicated in the pathophysiology of various diseases, including tumor growth and metastasis, infectious diseases, and metabolic, immunological, and neurodegenerative disorders. A large proportion of clinically approved drugs, between 30% and 40%, target GPCRs as ligands modulating their signaling pathways. GPCR endogenous ligands include cations, neurotransmitters, lipids, peptide hormones, and glycoproteins.[187]

The overexpressed receptors can also be used as targeting vectors to bring cytotoxic drugs specifically to cancer cells, thus reducing side effects caused by systemic administration. Some examples of this include the Peptide–drug conjugates Zoptrex™ (AEZS-108), a luteinizing hormone-releasing hormone (LHRH)–doxorubicin conjugate, and AEZS-138, a LHRH–disorazol Z conjugate. AEZS-108 has completed Phase 2 trials for the treatment of ovarian cancer and prostate cancer with positive results, and is undergoing Phase 3 trials for endometrial cancer. AEZS-138 is still in preclinical studies and has shown positive results against various tumor cell lines. Both of these conjugates target the LHRH receptor, which is overexpressed in various tumor tissues; the receptor is not commonly found on normal tissue, with the exception of the pituitary gland.

Following the same approach, there is increasing interest in taking advantage of GPCR overexpression for imaging and therapy of different types of tumors. The approach involves attaching the appropriate radionuclide (diagnostic or therapy purposes) to specific ligands that target overexpressed receptors. OctreoScan, an octreotide analog labeled with ^{111}In which targets the somatostatin receptor, was approved in 1994 for SPECT imaging of NETs and other neoplasms expressing somatostatin receptors. More recently, it was demonstrated that antagonists targeting somatostatin receptor 2 (SSTR2) and SSTR3 have higher uptake and longer retention than the somatostatin agonists.[191] A Phase 1/2 trial has completed for OPS202, a ^{68}Ga-labeled SSTR2 antagonist being developed by Ipsen for the detection of NETs; a Phase 1/2 trial is planned for the therapeutic analog labeled with ^{177}Lu (OPS201) for the treatment of gastroenteropancreatic NETs.

1.11.4 Concluding Remarks

A detailed knowledge of gene–protein pathway networks in the human body is essential for biomedical research. Emerging biological target spaces, such as PPIs, the immune system, or RNA/DNA, are opening new opportunities for drug discovery. Designing next-generation therapeutics to modulate these targets demands an understanding of their mechanisms on a molecular level.

To date, the Human Genome Project has identified 20,687 protein-coding genes.[192] However, the experimentally determined map of proteins and peptides that are expressed by the genome does not yet exist. It is still not clear which human genes are translated into proteins, what the expression patterns in specific cell types are, or what the PPI network looks like. With the development of new analytical and bioinformatics technologies, systematic mapping of the human proteome will continue.[193] In the coming years, its integration with genomic data will provide a better insight into human disease biology, which is essential for more informed target selection, derisking, and validation in the early stages of drug discovery.

Understanding various biological barriers and designing molecular transporters or therapeutics that are able to cross these barriers is one of the key challenges of postgenomic drug discovery.

Powerful therapeutic tools, such as siRNA or cytotoxic agents, require cell-specific delivery. Receptor-mediated targeting for imaging and therapy of different types of tumors can reduce unwanted side effects. However, an understanding of the overexpression patterns and the distribution of protein targets in malignant and normal tissues is essential for cell selectivity.

The chemical modalities in today's drug development are becoming increasingly complex. The modular nature of peptide and protein chemistry opens up opportunities to create multifunctional molecular modalities with diverse properties, such as peptide-antibodies or peptide–small molecule conjugates. Due to this complexity, the traditional medicinal chemist's skills are no longer sufficient to guide chemistry efforts in the pharmaceutical industry. In order to design innovative conjugates, multifunctional ligands, novel delivery systems, an understanding of structural biology, molecular modeling, and bioinformatics has become as essential for medicinal chemists as skills in synthetic chemistry. Drug development is a multidisciplinary field with a multiparametric design space. This development is advanced by a continuous chain of decisions which constantly balance risks and benefits. Consequently, it has become imperative for chemists and biologists to think across the aisles. Those who are able to stand at the crossroads of this multidisciplinary vision will reap the benefits of the promise held by next-generation therapeutics.

References

1. Thayer, A. M. Cover Stories: 2015 Pharma Year In Review: Leading Drugs Under Fire. *Chem. Eng. News* **2015,** *93,* 19.
2. (2013) Biotech Products in Big Pharma Pipeines Have Grown Dramatically. Tufts CSDD Impact Report 15.
3. Williams, M. Productivity Shortfalls in Drug Discovery: Contributions From the Preclinical Sciences? *J. Pharmacol. Exp. Ther.* **2011,** *336,* 3–8.
4. Swinney, D. C.; Anthony, J. How Were New Medicines Discovered? *Nat. Rev. Drug Discov.* **2011,** *10,* 507–519.
5. Scannell, J. W.; Blanckley, A.; Boldon, H.; Warrington, B. Diagnosing the Decline in Pharmaceutical R&D Efficiency. *Nat. Rev. Drug Discov.* **2012,** *11,* 191–200.
6. Scannell, J. W.; Bosley, J. When Quality Beats Quantity: Decision Theory, Drug Discovery, and the Reproducibility Crisis. *PLoS One* **2016,** *11,* e0147215.
7. Munos, B. Lessons From 60 Years of Pharmaceutical Innovation. *Nat. Rev. Drug Discov.* **2009,** *8,* 959–968.
8. Owens, P. K.; Raddad, E.; Miller, J. W.; Stille, J. R.; Olovich, K. G.; Smith, N. V.; Jones, R. S.; Scherer, J. C. A Decade of Innovation in Pharmaceutical R&D: The Chorus Model. *Nat. Rev. Drug Discov.* **2015,** *14,* 17–28.
9. Earhardt, P. Medicinal Chemistry in the New Millennium. *Pure Appl. Chem.* **2002,** *74,* 703–785.
10. Barker, A.; Kettle, J. G.; Nowak, T.; Pease, J. E. Expanding Medicinal Chemistry Space. *Drug Discov. Today* **2013,** *18,* 298–304.
11. Hopkins, A. L.; Groom, C. R. The Druggable Genome. *Nat. Rev. Drug Discov.* **2002,** *1,* 727–730.
12. Bauer, R. A.; Wurst, J. M.; Tan, D. S. Expanding the Range of 'Druggable' Targets With Natural Product-Based Libraries: An Academic Perspective. *Curr. Opin. Chem. Biol.* **2010,** *14,* 308–314.
13. Ivanov, A. A.; Khuri, F. R.; Fu, H. Targeting Protein–Protein Interactions as an Anticancer Strategy. *Trends Pharmacol. Sci.* **2013,** *34,* 393–400.
14. Chen, B. J.; Wu, Y. L.; Tanaka, Y.; Zhang, W. Small Molecules Targeting c-Myc Oncogene: Promising Anti-Cancer Therapeutics. *Int. J. Biol. Sci.* **2014,** *10,* 1084–1096.
15. Siddiqui, N.; Sonenberg, N. Signalling to eIF4E in Cancer. *Biochem. Soc. Trans.* **2015,** *43,* 763–772.
16. Goni, J.; Esteban, F. J.; de Mendizabal, N. V.; Sepulcre, J.; Ardanza-Trevijano, S.; Agirrezabal, I.; Villoslada, P. A Computational Analysis of Protein-Protein Interaction Networks in Neurodegenerative Diseases. *BMC Syst. Biol.* **2008,** *2,* 52.
17. Rolland, T.; Tasan, M.; Charloteaux, B.; Pevzner, S. J.; Zhong, Q.; Sahni, N.; Yi, S.; Lemmens, I.; Fontanillo, C.; Mosca, R.; Kamburov, A.; Ghiassian, S. D.; Yang, X.; Ghamsari, L.; Balcha, D.; Begg, B. E.; Braun, P.; Brehme, M.; Broly, M. P.; Carvunis, A. R.; Convery-Zupan, D.; Corominas, R.; Coulombe-Huntington, J.; Dann, E.; Dreze, M.; Dricot, A.; Fan, C.; Franzosa, E.; Gebreab, F.; Gutierrez, B. J.; Hardy, M. F.; Jin, M.; Kang, S.; Kiros, R.; Lin, G. N.; Luck, K.; MacWilliams, A.; Menche, J.; Murray, R. R.; Palagi, A.; Poulin, M. M.; Rambout, X.; Rasla, J.; Reichert, P.; Romero, V.; Ruyssinck, E.; Sahalie, J. M.; Scholz, A.; Shah, A. A.; Sharma, A.; Shen, Y.; Spirohn, K.; Tam, S.; Tejeda, A. O.; Trigg, S. A.; Twizere, J. C.; Vega, K.; Walsh, J.; Cusick, M. E.; Xia, Y.; Barabasi, A. L.; Iakoucheva, L. M.; Aloy, P.; De Las Rivas, J.; Tavernier, J.; Calderwood, M. A.; Hill, D. E.; Hao, T.; Roth, F. P.; Vidal, M. A Proteome-Scale Map of the Human Interactome Network. *Cell* **2014,** *159,* 1212–1226.
18. Tse, C.; Shoemaker, A. R.; Adickes, J.; Anderson, M. G.; Chen, J.; Jin, S.; Johnson, E. F.; Marsh, K. C.; Mitten, M. J.; Nimmer, P.; Roberts, L.; Tahir, S. K.; Xiao, Y.; Yang, X.; Zhang, H.; Fesik, S.; Rosenberg, S. H.; Elmore, S. W. ABT-263: A Potent and Orally Bioavailable Bcl-2 Family Inhibitor. *Cancer Res.* **2008,** *68,* 3421–3428.
19. Vassilev, L. T.; Vu, B. T.; Graves, B.; Carvajal, D.; Podlaski, F.; Filipovic, Z.; Kong, N.; Kammlott, U.; Lukacs, C.; Klein, C.; Fotouhi, N.; Liu, E. A. In Vivo Activation of the p53 Pathway by Small-Molecule Antagonists of MDM2. *Science* **2004,** *303,* 844–848.
20. Zhao, Y.; Yu, S.; Sun, W.; Liu, L.; Lu, J.; McEachern, D.; Shargary, S.; Bernard, D.; Li, X.; Zhao, T.; Zou, P.; Sun, D.; Wang, S. A Potent Small-Molecule Inhibitor of the MDM2-p53 Interaction (MI-888) Achieved Complete and Durable Tumor Regression in Mice. *J. Med. Chem.* **2013,** *56,* 5553–5561.
21. Leao, M.; Pereira, C.; Bisio, A.; Ciribilli, Y.; Paiva, A. M.; Machado, N.; Palmeira, A.; Fernandes, M. X.; Sousa, E.; Pinto, M.; Inga, A.; Saraiva, L. Discovery of a New Small-Molecule Inhibitor of p53-MDM2 Interaction Using a Yeast-Based Approach. *Biochem. Pharmacol.* **2013,** *85,* 1234–1245.
22. Thanos, C. D.; DeLano, W. L.; Wells, J. A. Hot-Spot Mimicry of a Cytokine Receptor by a Small Molecule. *Proc. Natl. Acad. Sci. U. S. A.* **2006,** *103,* 15422–15427.
23. Nero, T. L.; Morton, C. J.; Holien, J. K.; Wielens, J.; Parker, M. W. Oncogenic Protein Interfaces: Small Molecules, Big Challenges. *Nat. Rev. Cancer* **2014,** *14* (4), 248–262.
24. Wojcik, P.; Berlicki, L. Peptide-Based Inhibitors of Protein-Protein Interactions. *Bioorg. Med. Chem. Lett.* **2016,** *26,* 707–713.
25. Leader, B.; Baca, Q. J.; Golan, D. E. Protein Therapeutics: A Summary and Pharmacological Classification. *Nat. Rev. Drug Discov.* **2008,** *7,* 21–39.
26. Terrett, N. K. Methods for the Synthesis of Macrocycle Libraries for Drug Discovery. *Drug Discov. Today Technol.* **2010,** *7,* e97–e104.
27. Mallinson, J.; Collins, I. Macrocycles in New Drug Discovery. *Future Med. Chem.* **2012,** *4,* 1409–1438.
28. Hili, R.; Rai, V.; Yudin, A. K. Macrocyclization of Linear Peptides Enabled by Amphoteric Molecules. *J. Am. Chem. Soc.* **2010,** *132* (9), 2889–2891.
29. Roxin, A.; Chen, J.; Scully, C. C.; Rotstein, B. H.; Yudin, A. K.; Zheng, G. Conformational Modulation of in vitro Activity of Cyclic RGD Peptides Via Aziridine Aldehyde-Driven Macrocyclization Chemistry. *Bioconjug. Chem.* **2012,** *23,* 1387–1395.

30. Marsault, E.; Hoveyda, H. R.; Gagnon, R.; Peterson, M. L.; Vezina, M.; Saint-Louis, C.; Landry, A.; Pinault, J. F.; Ouellet, L.; Beauchemin, S.; Beaubien, S.; Mathieu, A.; Benakli, K.; Wang, Z.; Brassard, M.; Lonergan, D.; Bilodeau, F.; Ramaseshan, M.; Fortin, N.; Lan, R.; Li, S.; Galaud, F.; Plourde, V.; Champagne, M.; Doucet, A.; Bherer, P.; Gauthier, M.; Olsen, G.; Villeneuve, G.; Bhat, S.; Foucher, L.; Fortin, D.; Peng, X.; Bernard, S.; Drouin, A.; Deziel, R.; Berthiaume, G.; Dory, Y. L.; Fraser, G. L.; Deslongchamps, P. Efficient Parallel Synthesis of Macrocyclic Peptidomimetics. *Bioorg. Med. Chem. Lett.* **2008,** *18,* 4731–4735.
31. Timmerman, P.; Beld, J.; Puijk, W. C.; Meloen, R. H. Rapid and Quantitative Cyclization of Multiple Peptide Loops Onto Synthetic Scaffolds for Structural Mimicry of Protein Surfaces. *Chembiochem* **2005,** *6,* 821–824.
32. Gartner, Z. J.; Tse, B. N.; Grubina, R.; Doyon, J. B.; Snyder, T. M.; Liu, D. R. DNA-Templated Organic Synthesis and Selection of a Library of Macrocycles. *Science* **2004,** *305,* 1601–1605.
33. Sperandio, O.; Reynes, C. H.; Camproux, A. C.; Villoutreix, B. O. Rationalizing the Chemical Space of Protein–Protein Interaction Inhibitors. *Drug Discov. Today* **2010,** *15,* 220–229.
34. Tsomaia, N. Peptide Therapeutics: Targeting the Undruggable Space. *Eur. J. Med. Chem.* **2015,** *94,* 459–470.
35. White, T. R.; Renzelman, C. M.; Rand, A. C.; Rezai, T.; McEwen, C. M.; Gelev, V. M.; Turner, R. A.; Linington, R. G.; Leung, S. S.; Kalgutkar, A. S.; Bauman, J. N.; Zhang, Y.; Liras, S.; Price, D. A.; Mathiowetz, A. M.; Jacobson, M. P.; Lokey, R. S. On-Resin *N*-Methylation of Cyclic Peptides for Discovery of Orally Bioavailable Scaffolds. *Nat. Chem. Biol.* **2011,** *7,* 810–817.
36. Chatterjee, J.; Mierke, D.; Kessler, H. N-Methylated Cyclic Pentaalanine Peptides as Template Structures. *J. Am. Chem. Soc.* **2006,** *128,* 15164–15172.
37. Beck, J. G.; Chatterjee, J.; Laufer, B.; Kiran, M. U.; Frank, A. O.; Neubauer, S.; Ovadia, O.; Greenberg, S.; Gilon, C.; Hoffman, A.; Kessler, H. Intestinal Permeability of Cyclic Peptides: Common Key Backbone Motifs Identified. *J. Am. Chem. Soc.* **2012,** *134,* 12125–12133.
38. Rezai, T.; Yu, B.; Millhauser, G. L.; Jacobson, M. P.; Lokey, R. S. Testing the Conformational Hypothesis of Passive Membrane Permeability Using Synthetic Cyclic Peptide Diastereomers. *J. Am. Chem. Soc.* **2006,** *128,* 2510–2511.
39. Rezai, T.; Bock, J. E.; Zhou, M. V.; Kalyanaraman, C.; Lokey, R. S.; Jacobson, M. P. Conformational Flexibility, Internal Hydrogen Bonding, and Passive Membrane Permeability: Successful In Silico Prediction of the Relative Permeabilities of Cyclic Peptides. *J. Am. Chem. Soc.* **2006,** *128,* 14073–14080.
40. Wang, C. K.; Northfield, S. E.; Swedberg, J. E.; Colless, B.; Chaousis, S.; Price, D. A.; Liras, S.; Craik, D. J. Exploring Experimental and Computational Markers of Cyclic Peptides: Charting Islands of Permeability. *Eur. J. Med. Chem.* **2015,** *97,* 202–213.
41. Chen, S.; Touati, J.; Heinis, C. Tracking Chemical Reactions on the Surface of Filamentous Phage Using Mass Spectrometry. *Chem. Commun. (Camb.)* **2014,** *50,* 5267–5269.
42. Jafari, M. R.; Deng, L.; Kitov, P. I.; Ng, S.; Matochko, W. L.; Tjhung, K. F.; Zeberoff, A.; Elias, A.; Klassen, J. S.; Derda, R. Discovery of Light-Responsive Ligands Through Screening of a Light-Responsive Genetically Encoded Library. *ACS Chem. Biol.* **2014,** *9,* 443–450.
43. Heinis, C.; Rutherford, T.; Freund, S.; Winter, G. Phage-Encoded Combinatorial Chemical Libraries Based on Bicyclic Peptides. *Nat. Chem. Biol.* **2009,** *5,* 502–507.
44. Ng, S.; Derda, R. Phage-Displayed Macrocyclic Glycopeptide Libraries. *Org. Biomol. Chem.* **2016,** *14,* 5539–5545.
45. Assem, N.; Ferreira, D. J.; Wolan, D. W.; Dawson, P. E. Acetone-Linked Peptides: A Convergent Approach for Peptide Macrocyclization and Labeling. *Angew. Chem. Int. Ed.* **2015,** *54,* 8665–8668.
46. Jafari, M. R.; Lakusta, J.; Lundgren, R. J.; Derda, R. Allene Functionalized Azobenzene Linker Enables Rapid and Light-Responsive Peptide Macrocyclization. *Bioconjug. Chem.* **2016,** *27,* 509–514.
47. Kalhor-Monfared, S.; Jafari, M. R.; Patterson, J. T.; Kitov, P. I.; Dwyer, J. J.; Nuss, J. M.; Derda, R. Rapid Biocompatible Macrocyclization of Peptides With Decafluoro-Diphenylsulfone. *Chem. Sci.* **2016,** *7,* 3785–3790.
48. Li, S.; Roberts, R. W. A Novel Strategy for In Vitro Selection of Peptide-Drug Conjugates. *Chem. Biol.* **2003,** *10,* 233–239.
49. Millward, S. W.; Takahashi, T. T.; Roberts, R. W. A General Route for Post-Translational Cyclization of mRNA Display Libraries. *J. Am. Chem. Soc.* **2005,** *127,* 14142–14143.
50. Tjhung, K. F.; Kitov, P. I.; Ng, S.; Kitova, E. N.; Deng, L.; Klassen, J. S.; Derda, R. Silent Encoding of Chemical Post-Translational Modifications in Phage-Displayed Libraries. *J. Am. Chem. Soc.* **2016,** *138,* 32–35.
51. Roberts, R. W.; Szostak, J. W. RNA-Peptide Fusions for the In Vitro Selection of Peptides and Proteins. *Proc. Natl. Acad. Sci. U. S. A.* **1997,** *94,* 12297–12302.
52. Josephson, K.; Hartman, M. C. T.; Szostak, J. W. Ribosomal Synthesis of Unnatural Peptides. *J. Am. Chem. Soc.* **2005,** *127,* 11727–11735.
53. Hartman, M. C. T.; Josephson, K.; Lin, C. W.; Szostak, J. W. An Expanded Set of Amino Acid Analogs for the Ribosomal Translation of Unnatural Peptides. *PLoS One* **2007,** *2,* e972.
54. Shimizu, Y.; Inoue, A.; Tomari, Y.; Suzuki, T.; Yokogawa, T.; Nishikawa, K.; Ueda, T. Cell-Free Translation Reconstituted With Purified Components. *Nat. Biotechnol.* **2001,** *19,* 751–755.
55. Murakami, H.; Ohta, A.; Ashigai, H.; Suga, H. A Highly Flexible tRNA Acylation Method for Nonnatural Polypeptide Synthesis. *Nat. Methods* **2006,** *3,* 357–359.
56. Goto, Y.; Katoh, T.; Suga, H. Flexizymes for Genetic Code Reprogramming. *Nat. Protoc.* **2011,** *6,* 779–790.
57. Morimoto, J.; Hayashi, Y.; Iwasaki, K.; Suga, H. Flexizymes: Their Evolutionary History and the Origin of Catalytic Function. *Acc. Chem. Res.* **2011,** *44,* 1359–1368.
58. Jalali-Yazdi, F.; Lai, L. H.; Takahashi, T. T.; Roberts, R. W. High-Throughput Measurement of Binding Kinetics by mRNA Display and Next-Generation Sequencing. *Angew. Chem. Int. Ed.* **2016,** *55,* 4007–4010.
59. Howell, S. M.; Fiacco, S. V.; Takahashi, T. T.; Jalali-Yazdi, F.; Millward, S. W.; Hu, B.; Wang, P.; Roberts, R. W. Serum Stable Natural Peptides Designed by mRNA Display. *Sci. Rep.* **2014,** *4,* 6008.
60. Giordanetto, F.; Kihlberg, J. Macrocyclic Drugs and Clinical Candidates: What Can Medicinal Chemists Learn From Their Properties? *J. Med. Chem.* **2013,** *57* (2), 278–295.
61. Hewitt, W. M.; Leung, S. S.; Pye, C. R.; Ponkey, A. R.; Bednarek, M.; Jacobson, M. P.; Lokey, R. S. Cell-Permeable Cyclic Peptides From Synthetic Libraries Inspired by Natural Products. *J. Am. Chem. Soc.* **2015,** *137,* 715–721.
62. de Vega, M. J.; Martín-Martínez, M.; González-Muñiz, R. Modulation of Protein-Protein Interactions by Stabilizing/Mimicking Protein Secondary Structure Elements. *Curr. Top. Med. Chem.* **2007,** *7,* 33–62.
62a. Diller, D. J.; Swanson, J.; Bayden, A. S.; Jarosinski, M.; Audie, J. Rational, Computer-Enabled Peptide Drug Design: Principles, Methods, Applications and Future Directions. *Future Med. Chem.* **2015,** *7,* 2173–2193.
63. Gavenonis, J.; Sheneman, B. A.; Siegert, T. R.; Eshelman, M. R.; Kritzer, J. A. Comprehensive Analysis of Loops at Protein–Protein Interfaces for Macrocycle Design. *Nat. Chem. Biol.* **2014,** *10,* 716–722.
64. Jochim, A. L.; Arora, P. S. Assessment of Helical Interfaces in Protein–Protein Interactions. *Mol. Biosyst.* **2009,** *5,* 924–926.
65. Raj, M.; Bullock, B. N.; Arora, P. S. Plucking the High Hanging Fruit: A Systematic Approach for Targeting Protein–Protein Interactions. *Bioorg. Med. Chem.* **2013,** *21,* 4051–4057.
66. Miller, S. E.; Watkins, A. M.; Kallenbach, N. R.; Arora, P. S. Effects of Side Chains in Helix Nucleation Differ From Helix Propagation. *Proc. Natl. Acad. Sci. U. S. A.* **2014,** *111* (18), 6636–6641.
67. Hill, T. A.; Shepherd, N. E.; Diness, F.; Fairlie, D. P. Constraining Cyclic Peptides to Mimic Protein Structure Motifs. *Angew. Chem. Int. Ed. Engl.* **2014,** *53,* 13020–13041.
67a. Bird, G. H.; Gavathiotis, E.; LaBelle, J. L.; Katz, S. G.; Walensky, L. D. Distinct BimBH3 (BimSAHB) Stapled Peptides for Structural and Cellular Studies. *ACS Chem. Biol.* **2014,** *9,* 831–837.
68. Northfield, S. E.; Wang, C. K.; Schroeder, C. I.; Durek, T.; Kan, M. W.; Swedberg, J. E.; Craik, D. J. Disulfide-Rich Macrocyclic Peptides as Templates in Drug Design. *Eur. J. Med. Chem.* **2014,** *77,* 248–257. http://dx.doi.org/10.1016/j.ejmech.2014.07.083.
69. Getz, J. A.; Cheneval, O.; Craik, D. J.; Daugherty, P. S. Design of a Cyclotide Antagonist of Neuropilin-1 and -2 That Potently Inhibits Endothelial Cell Migration. *ACS Chem. Biol.* **2013,** *8,* 1147–1154.

70. Wang, C. K.; Gruber, C. W.; Cemazar, M.; Siatskas, C.; Tagore, P.; Payne, N.; Sun, G.; Wang, S.; Bernard, C. C.; Craik, D. J. Molecular Grafting Onto a Stable Framework Yields Novel Cyclic Peptides for the Treatment of Multiple Sclerosis. *ACS Chem. Biol.* **2014,** *9,* 156–163.
71. Schroeder, C. I.; Swedberg, J. E.; Craik, D. J. Recent Progress Towards Pharmaceutical Applications of Disulfide-Rich Cyclic Peptides. *Curr. Protein Pept. Sci.* **2013,** *14,* 532–552.
72. Cascales, L.; Henriques, S. T.; Kerr, M. C.; Huang, Y. H.; Sweet, M. J.; Daly, N. L.; Craik, D. J. Identification and Characterization of a New Family of Cell-Penetrating Peptides: Cyclic Cell-Penetrating Peptides. *J. Biol. Chem.* **2011,** *286,* 36932–36943.
73. Ji, Y.; Majumder, S.; Millard, M.; Borra, R.; Bi, T.; Elnagar, A. Y.; Neamati, N.; Shekhtman, A.; Camarero, J. A. In Vivo Activation of the p53 Tumor Suppressor Pathway by an Engineered Cyclotide. *J. Am. Chem. Soc.* **2013,** *135,* 11623–11633.
74. Moore, S. J.; Leung, C. L.; Cochran, J. R. Knottins: Disulfide-Bonded Therapeutic and Diagnostic Peptides. *Drug Discov. Today Technol.* **2012,** *9,* e3–e11.
75. Veiseh, M.; Gabikian, P.; Bahrami, S. B.; Veiseh, O.; Zhang, M.; Hackman, R. C.; Ravanpay, A. C.; Stroud, M. R.; Kusuma, Y.; Hansen, S. J.; Kwok, D.; Munoz, N. M.; Sze, R. W.; Grady, W. M.; Greenberg, N. M.; Ellenbogen, R. G.; Olson, J. M. Tumor Paint: A Chlorotoxin:Cy5.5 Bioconjugate for Intraoperative Visualization of Cancer Foci. *Cancer Res.* **2007,** *67,* 6882–6888.
76. Cox, N.; Kintzing, J. R.; Smith, M.; Grant, G. A.; Cochran, J. R. Integrin-Targeting Knottin Peptide-Drug Conjugates Are Potent Inhibitors of Tumor Cell Proliferation. *Angew. Chem. Int. Ed. Engl.* **2016,** *55* (34), 9894–9897.
77. De Gregorio, E.; Rappuoli, R. From Empiricism to Rational Design: A Personal Perspective of the Evolution of Vaccine Development. *Nat. Rev. Immunol.* **2014,** *14,* 505–514.
78. Ingersoll, M. A.; Albert, M. L. From Infection to Immunotherapy: Host Immune Responses to Bacteria at the Bladder Mucosa. *Mucosal Immunol.* **2013,** *6,* 1041–1053.
79. Jones, L. H. Recent Advances in the Molecular Design of Synthetic Vaccines. *Nat. Chem.* **2015,** *7,* 952–960.
80. Parmley, S. Boosting Adjuvants. *SciBX* **2014,** *7.* http://dx.doi.org/10.1038/scibx.2014.1281.
81. Malito, E.; Carfi, A.; Bottomley, M. J. Protein Crystallography in Vaccine Research and Development. *Int. J. Mol. Sci.* **2015,** *16,* 13106–13140.
82. Riley, T. P.; Singh, N. K.; Pierce, B. G.; Weng, Z.; Baker, B. M. Computational Modeling of T Cell Receptor Complexes. *Methods Mol. Biol.* **2016,** *1414,* 319–340.
83. Wals, K.; Ovaa, H. Unnatural Amino Acid Incorporation in *E. Coli*: Current and Future Applications in the Design of Therapeutic Proteins. *Front. Chem.* **2014,** *2*, 15.
84. Zeng, Y.; Wang, W.; Liu, W. R. Towards Reassigning the Rare AGG Codon in *Escherichia Coli*. *Chembiochem* **2014,** *15,* 1750–1754.
85. Talebian Yazdi, M.; Keene, K. R.; Hiemstra, P. S.; van der Burg, S. H. Recent Progress in Peptide Vaccination in Cancer With a Focus on Nonsmall-Cell Lung Cancer. *Expert Rev. Vaccines* **2014,** *13,* 87–116.
86. Temizoz, B.; Kuroda, E.; Ishii, K. J. Vaccine Adjuvants as Potential Cancer Immunotherapeutics. *Int. Immunol.* **2016,** *28* (7), 329–338.
87. Flower, D. R. Designing Immunogenic Peptides. *Nat. Chem. Biol.* **2013,** *9,* 749–753.
88. Peters, B.; Bui, H. H.; Frankild, S.; Nielson, M.; Lundegaard, C.; Kostem, E.; Basch, D.; Lamberth, K.; Harndahl, M.; Fleri, W.; Wilson, S. S.; Sidney, J.; Lund, O.; Buus, S.; Sette, A. A Community Resource Benchmarking Predictions of Peptide Binding to MHC-I Molecules. *PLoS Comput. Biol.* **2006,** *2*, e65.
89. Lin, H. H.; Zhang, G. L.; Tongchusak, S.; Reinherz, E. L.; Brusic, V. Evaluation of MHC-II Peptide Binding Prediction Servers: Applications for Vaccine Research. *BMC Bioinformatics* **2008,** *9* (Suppl. 12), S22.
90. Reche, P.; Flower, D. R.; Fridkis-Hareli, M.; Hoshino, Y. Peptide-Based Immunotherapeutics and Vaccines 2015. *J. Immunol. Res.* **2015,** *2015,* 349049.
91. Adams, J. L.; Smothers, J.; Srinivasan, R.; Hoos, A. Big Opportunities for Small Molecules in Immuno-Oncology. *Nat. Rev. Drug Discov.* **2015,** *14,* 603–622.
92. Buchbinder, E. I.; Desai, A. CTLA-4 and PD-1 Pathways: Similarities, Differences, and Implications of Their Inhibition. *Am. J. Clin. Oncol.* **2016,** *39,* 98–106.
93. Yun, S.; Vincelette, N. D.; Green, M. R.; Wahner Hendrickson, A. E.; Abraham, I. Targeting Immune Checkpoints in Unresectable Metastatic Cutaneous Melanoma: A Systematic Review and Meta-Analysis of Anti-CTLA-4 and Anti-PD-1 Agents Trials. *Cancer Med.* **2016,** *5* (7), 1481–1491.
94. Puigvert, J. C.; Sanjiv, K.; Helleday, T. Targeting DNA Repair, DNA Metabolism and Replication Stress as Anti-Cancer Strategies. *FEBS J.* **2016,** *283,* 232–245.
95. Gogtay, N. J.; Sridharan, K. Therapeutic Nucleic Acids: Current Clinical Status. *Br. J. Clin. Pharmacol.* **2016,** *82* (3), 659–672.
96. Andrei, G.; De Clercq, E.; Snoeck, R. Drug Targets in Cytomegalovirus Infection. *Infect. Disord. Drug Targets* **2009,** *9,* 201–222.
97. Patel, R. S.; Scopelliti, E. M.; Savelloni, J. Therapeutic Management of Familial Hypercholesterolemia: Current and Emerging Drug Therapies. *Pharmacotherapy* **2015,** *35,* 1189–1203.
98. Prakash, T. P.; Graham, M. J.; Yu, J.; Carty, R.; Low, A.; Chappell, A.; Schmidt, K.; Zhao, C.; Aghajan, M.; Murray, H. F.; Riney, S.; Booten, S. L.; Murray, S. F.; Gaus, H.; Crosby, J.; Lima, W. F.; Guo, S.; Monia, B. P.; Swayze, E. E.; Seth, P. P. Targeted Delivery of Antisense Oligonucleotides to Hepatocytes Using Triantennary *N*-Acetyl Galactosamine Improves Potency 10-Fold in Mice. *Nucleic Acids Res.* **2014,** *42,* 8796–8807.
99. Monteleone, G.; Di Sabatino, A.; Ardizzone, S.; Pallone, F.; Usiskin, K.; Zhan, X.; Rossiter, G.; Neurath, M. F. Impact of Patient Characteristics on the Clinical Efficacy of Mongersen (GED-0301), an Oral Smad7 Antisense Oligonucleotide, in Active Crohn's Disease. *Aliment. Pharmacol. Ther.* **2016,** *43,* 717–724.
100. Scarfo, L.; Ghia, P. Reprogramming Cell Death: BCL2 Family Inhibition in Hematological Malignancies. *Immunol. Lett.* **2013,** *155,* 36–39.
101. Gilboa-Geffen, A.; Wolf, Y.; Hanin, G.; Melamed-Book, N.; Pick, M.; Bennett, E. R.; Greenberg, D. S.; Lester, S.; Rischmueller, M.; Soreq, H. Activation of the Alternative NFkappaB Pathway Improves Disease Symptoms in a Model of Sjogren's Syndrome. *PLoS One* **2011,** *6*, e28727.
102. Sehgal, A.; Vaishnaw, A.; Fitzgerald, K. Liver as a Target for Oligonucleotide Therapeutics. *J. Hepatol.* **2013,** *59,* 1354–1359.
103. Geary, R. S. Antisense Oligonucleotide Pharmacokinetics and Metabolism. *Expert Opin. Drug Metab. Toxicol.* **2009,** *5,* 381–391.
104. Hong, W.; Zeng, J.; Xie, J. Antibiotic Drugs Targeting Bacterial RNAs. *Acta Pharm. Sin. B* **2014,** *4,* 258–265.
105. Ofori, L. O.; Hoskins, J.; Nakamori, M.; Thornton, C. A.; Miller, B. L. From Dynamic Combinatorial 'Hit' to Lead: In Vitro and In Vivo Activity of Compounds Targeting the Pathogenic RNAs That Cause Myotonic Dystrophy. *Nucleic Acids Res.* **2012,** *40,* 6380–6390.
106. Matsuda, S.; Keiser, K.; Nair, J. K.; Charisse, K.; Manoharan, R. M.; Kretschmer, P.; Peng, C. G.; V Kel'in, A.; Kandasamy, P.; Willoughby, J. L.; Liebow, A.; Querbes, W.; Yucius, K.; Nguyen, T.; Milstein, S.; Maier, M. A.; Rajeev, K. G.; Manoharan, M. siRNA Conjugates Carrying Sequentially Assembled Trivalent *N*-Acetylgalactosamine Linked Through Nucleosides Elicit Robust Gene Silencing In Vivo in Hepatocytes. *ACS Chem. Biol.* **2015,** *10,* 1181–1187.
107. Ren, Y.; Cheung, H. W.; von Maltzhan, G.; Agrawal, A.; Cowley, G. S.; Weir, B. A.; Boehm, J. S.; Tamayo, P.; Karst, A. M.; Liu, J. F.; Hirsch, M. S.; Mesirov, J. P.; Drapkin, R.; Root, D. E.; Lo, J.; Fogal, V.; Ruoslahti, E.; Hahn, W. C.; Bhatia, S. N. Targeted Tumor-Penetrating siRNA Nanocomplexes for Credentialing the Ovarian Cancer Oncogene ID4. *Sci. Transl. Med.* **2012,** *4*, 147ra112.
108. Dong, Y.; Love, K. T.; Dorkin, J. R.; Sirirungruang, S.; Zhang, Y.; Chen, D.; Bogorad, R. L.; Yin, H.; Chen, Y.; Vegas, A. J.; Alabi, C. A.; Sahay, G.; Olejnik, K. T.; Wang, W.; Schroeder, A.; Lytton-Jean, A. K.; Siegwart, D. J.; Akinc, A.; Barnes, C.; Barros, S. A.; Carioto, M.; Fitzgerald, K.; Hettinger, J.; Kumar, V.; Novobrantseva, T. I.; Qin, J.; Querbes, W.; Koteliansky, V.; Langer, R.; Anderson, D. G. Lipopeptide Nanoparticles for Potent and Selective siRNA Delivery in Rodents and Nonhuman Primates. *Proc. Natl. Acad. Sci. U. S. A.* **2014,** *111,* 3955–3960.
109. Kararli, T.; Sedo, K.; Bossart, J. *Injectables: The New Oral?* PharmaCircle LLC, 2016, 46–48. http://www.pharmacircle.com/rc/.
110. Skalko-Basnet, N. Biologics: The Role of Delivery Systems in Improved Therapy. *Biologics: Targets and Therapy* **2014,** *8,* 107–114.
111. Shah, T. Bioconjugates: The Adaptable Challenge. *Biopharm. Int.* **2013,** *26* (1), 34–38.
112. Chen, C.; Constantinou, A.; Chester, K. A.; Vyas, B.; Canis, K.; Haslam, S. M.; Dell, A.; Epenetos, A. A.; Deonarain, M. P. Glycoengineering Approach to Half-Life Extension of Recombinant Biotherapeutics. *Bioconjug. Chem.* **2012,** *23,* 1524–1533.
113. Liebner, R.; Mathaes, R.; Meyer, M.; Hey, T.; Winter, G.; Besheer, A. Protein HESylation for Half-Life Extension: Synthesis, Characterization and Pharmacokinetics of HESylated Anakinra. *Eur. J. Pharm. Biopharm.* **2014,** *87,* 378–385.
114. Podust, V. N.; Balan, S.; Sim, B. C.; Coyle, M. P.; Ernst, U.; Peters, R. T.; Schellenberger, V. Extension of In Vivo Half-Life of Biologically Active Molecules by XTEN Protein Polymers. *J. Control. Release* **2015,** *240,* 52–66.
115. Podust, V. N.; Sim, B. C.; Kothari, D.; Henthorn, L.; Gu, C.; Wang, C. W.; McLaughlin, B.; Schellenberger, V. Extension of In Vivo Half-Life of Biologically Active Peptides via Chemical Conjugation to XTEN Protein Polymer. *Protein Eng. Des. Sel.* **2013,** *26,* 743–753.

116. Swierczewska, M.; Lee, K. C.; Lee, S. What Is the Future of PEGylated Therapies? *Expert Opin. Emerg. Drugs* **2015,** *20,* 531–536.
117. Prel, A.; Caval, V.; Gayon, R.; Ravassard, P.; Duthoit, C.; Payen, E.; Maouche-Chretien, L.; Creneguy, A.; Nguyen, T. H.; Martin, N.; Piver, E.; Sevrain, R.; Lamouroux, L.; Leboulch, P.; Deschaseaux, F.; Bouille, P.; Sensebe, L.; Pages, J. C. Highly Efficient In Vitro and In Vivo Delivery of Functional RNAs Using New Versatile MS2-Chimeric Retrovirus-Like Particles. *Mol. Therapy Methods Clin. Dev.* **2015,** *2,* 15039.
118. Sercombe, L.; Veerati, T.; Moheimani, F.; Wu, S. Y.; Sood, A. K.; Hua, S. Advances and Challenges of Liposome Assisted Drug Delivery. *Front. Pharmacol.* **2015,** *6,* 286.
119. van der Gun, B. T.; Monami, A.; Laarmann, S.; Rasko, T.; Slaska-Kiss, K.; Weinhold, E.; Wasserkort, R.; de Leij, L. F.; Ruiters, M. H.; Kiss, A.; McLaughlin, P. M. Serum Insensitive, Intranuclear Protein Delivery by the Multipurpose Cationic Lipid SAINT-2. *J. Control. Release* **2007,** *123,* 228–238.
120. Khan, I.; Khan, M.; Umar, M. N.; Oh, D. H. Nanobiotechnology and Its Applications in Drug Delivery System: A Review. *IET Nanobiotechnol.* **2015,** *9,* 396–400.
121. Cronican, J. J.; Beier, K. T.; Davis, T. N.; Tseng, J. C.; Li, W.; Thompson, D. B.; Shih, A. F.; May, E. M.; Cepko, C. L.; Kung, A. L.; Zhou, Q.; Liu, D. R. A Class of Human Proteins That Deliver Functional Proteins Into Mammalian Cells in vitro and In Vivo. *Chem. Biol.* **2011,** *18,* 833–838.
122. Liao, X.; Rabideau, A. E.; Pentelute, B. L. Delivery of Antibody Mimics Into Mammalian Cells via Anthrax Toxin Protective Antigen. *Chembiochem* **2014,** *15,* 2458–2466.
123. Arukuusk, P.; Parnaste, L.; Hallbrink, M.; Langel, U. PepFects and NickFects for the Intracellular Delivery of Nucleic Acids. *Methods Mol. Biol.* **2015,** *1324,* 303–315.
124. Kurrikoff, K.; Gestin, M.; Langel, U. Recent In Vivo Advances in Cell-Penetrating Peptide-Assisted Drug Delivery. *Exp. Opin. Drug Deliv.* **2016,** *13,* 373–387.
125. Tuma, P. L.; Hubbard, A. L. *Transcytosis* **2003,** *83,* 871–932.
126. Verdine Gregory, L. Drugging the "Undruggable". *Harvey Lect.* **2010,** *102,* 1–15.
127. Verdine, G. L. Drugging the "Undruggable". In *The Harvey Lectures, Series 102;* Wiley: Hoboken, NJ, 2010; pp 1–16.
128. Milletti, F. Cell-Penetrating Peptides: Classes, Origin, and Current Landscape. *Drug Discov. Today* **2012,** *17,* 850–860.
129. Wang, F.; Wang, Y.; Zhang, X.; Zhang, W.; Guo, S.; Jin, F. Recent Progress of Cell-Penetrating Peptides as New Carriers for Intracellular Cargo Delivery. *J. Control. Release* **2013,** *174C,* 126–136.
130. Durzynska, J.; Przysiecka, L.; Nawrot, R.; Barylski, J.; Nowicki, G.; Warowicka, A.; Musidlak, O.; Gondzicka-Jozefiak, A. Viral and Other Cell-Penetrating Peptides as Vectors of Therapeutic Agents in Medicine. *J. Pharmacol. Exp. Ther.* **2015,** *354,* 32–42.
131. Ramsey, J. D.; Flynn, N. H. Cell-Penetrating Peptides Transport Therapeutics Into Cells. *Pharmacol. Ther.* **2015,** *154,* 78–86.
132. Iversen, T.-G.; Skotland, T.; Sandvig, K. Endocytosis and Intracellular Transport of Nanoparticles: Present Knowledge and Need for Future Studies. *Nano Today* **2011,** *6,* 176–185.
133. Szeto, H. H.; Schiller, P. W.; Zhao, K.; Luo, G. Fluorescent Dyes Alter Intracellular Targeting and Function of Cell-Penetrating Tetrapeptides. *FASEB J.* **2005,** *19,* 118–120. http://dx.doi.org/10.1096/fj.1004-1982fje.
134. Skotland, T.; Iversen, T. G.; Torgersen, M. L.; Sandvig, K. Cell-Penetrating Peptides: Possibilities and Challenges for Drug Delivery in vitro and In Vivo. *Molecules* **2015,** *20,* 13313–13323.
135. Brock, R. The Uptake of Arginine-Rich Cell-Penetrating Peptides: Putting the Puzzle Together. *Bioconjug. Chem.* **2014,** *25,* 863–868.
136. Sandvig, K.; Pust, S.; Skotland, T.; van Deurs, B. Clathrin-Independent Endocytosis: Mechanisms and Function. *Curr. Opin. Cell Biol.* **2011,** *23,* 413–420.
137. Bechara, C.; Sagan, S. Cell-Penetrating Peptides: 20 Years Later, Where Do We Stand? *FEBS Lett.* **2013,** *587,* 1693–1702.
138. Schmid, S. L.; Sorkin, A.; Zerial, M. Endocytosis: Past, Present, and Future. *Cold Spring Harb. Perspect. Biol.* **2014,** *6,* a022509.
139. Rizzuti, M.; Nizzardo, M.; Zanetta, C.; Ramirez, A.; Corti, S. Therapeutic Applications of the Cell-Penetrating HIV-1 Tat Peptide. *Drug Discov. Today* **2015,** *20,* 76–85.
140. Loughran, S. P.; McCrudden, C. M.; McCarthy, H. O. Designer Peptide Delivery Systems for Gene Therapy. *Eur. J. Nanomed.* **2015,** *7,* 85–96.
141. Sakai, N.; Matile, S. Anion-Mediated Transfer of Polyarginine Across Liquid and Bilayer Membranes. *J. Am. Chem. Soc.* **2003,** *125,* 14348–14356.
142. Lonn, P.; Dowdy, S. F. Cationic PTD/CPP-Mediated Macromolecular Delivery: Charging into the Cell. *Exp. Opin. Drug Deliv.* **2015,** *12* (10), 1627–1636.
143. Gump, J. M.; June, R. K.; Dowdy, S. F. Revised Role of Glycosaminoglycans in TAT Protein Transduction Domain-Mediated Cellular Transduction. *J. Biol. Chem.* **2009,** *285,* 1500–1507.
144. Rydberg, H. A.; Matson, M.; Amand, H. L.; Esbjorner, E. K.; Norden, B. Effects of Tryptophan Content and Backbone Spacing on the Uptake Efficiency of Cell-Penetrating Peptides. *Biochemistry* **2012,** *51,* 5531–5539.
145. Eiriksdottir, E.; Konate, K.; Langel, U.; Divita, G.; Deshayes, S. Secondary Structure of Cell-Penetrating Peptides Controls Membrane Interaction and Insertion. *Biochim. Biophys. Acta* **2010,** *1798,* 1119–1128.
146. Reissmann, S. Cell Penetration: Scope and Limitations by the Application of Cell-Penetrating Peptides. *J. Pept. Sci.* **2014,** *20,* 760–784.
147. Zaro, J. L.; Shen, W.-C. Cationic and Amphipathic Cell-Penetrating Peptides (CPPs): Their Structures and in vivo Studies in Drug Delivery. *Front. Chem. Sci. Eng.* **2015,** *9,* 407–427.
148. Lattig-Tunnemann, G.; Prinz, M.; Hoffmann, D.; Behlke, J.; Palm-Apergi, C.; Morano, I.; Herce, H. D.; Cardoso, M. C. Backbone Rigidity and Static Presentation of Guanidinium Groups Increases Cellular Uptake of Arginine-Rich Cell-Penetrating Peptides. *Nat. Commun.* **2011,** *2,* 453.
149. Yamashita, H.; Oba, M.; Misawa, T.; Tanaka, M.; Hattori, T.; Naito, M.; Kurihara, M.; Demizu, Y. A Helix-Stabilized Cell-Penetrating Peptide as an Intracellular Delivery Tool. *Chembiochem* **2015,** *17* (2), 137–140.
150. Medina, S. H.; Miller, S. E.; Keim, A. I.; Gorka, A. P.; Schnermann, M. J.; Schneider, J. P. An Intrinsically Disordered Peptide Facilitates Non-Endosomal Cell Entry. *Angew. Chem. Int. Ed. Engl.* **2016,** *55* (10), 3369–3372.
151. Cronican, J. J.; Thompson, D. B.; Beier, K. T.; McNaughton, B. R.; Cepko, C. L.; Liu, D. R. Potent Delivery of Functional Proteins Into Mammalian Cells In Vitro and in vivo Using a Supercharged Protein. *ACS Chem. Biol.* **2010,** *5,* 747–752.
152. Martens, T. F.; Remaut, K.; Demeester, J.; De Smedt, S. C.; Braeckmans, K. Intracellular Delivery of Nanomaterials: How to Catch Endosomal Escape in the Act. *Nano Today* **2014,** *9,* 344–364.
153. Varkouhi, A. K.; Scholte, M.; Storm, G.; Haisma, H. J. Endosomal Escape Pathways for Delivery of Biologicals. *J. Control. Release* **2011,** *151,* 220–228.
154. Li, M.; Tao, Y.; Shu, Y.; LaRochelle, J. R.; Steinauer, A.; Thompson, D.; Schepartz, A.; Chen, Z. Y.; Liu, D. R. Discovery and Characterization of a Peptide That Enhances Endosomal Escape of Delivered Proteins In Vitro and In Vivo. *J. Am. Chem. Soc.* **2015,** *137,* 14084–14093.
155. Appelbaum, J. S.; LaRochelle, J. R.; Smith, B. A.; Balkin, D. M.; Holub, J. M.; Schepartz, A. Arginine Topology Controls Escape of Minimally Cationic Proteins From Early Endosomes to the Cytoplasm. *Chem. Biol.* **2012,** *19,* 819–830.
156. Qian, Z.; LaRochelle, J. R.; Jiang, B.; Lian, W.; Hard, R. L.; Selner, N. G.; Luechapanichkul, R.; Barrios, A. M.; Pei, D. Early Endosomal Escape of a Cyclic Cell-Penetrating Peptide Allows Effective Cytosolic Cargo Delivery. *Biochemistry* **2014,** *53,* 4034–4046.
157. Srinivasarao, M.; Galliford, C. V.; Low, P. S. Principles in the Design of Ligand-Targeted Cancer Therapeutics and Imaging Agents. *Nat. Rev. Drug Discov.* **2015,** *14,* 203–219.
158. Chatalic, K. L.; Kwekkeboom, D. J.; de Jong, M. Radiopeptides for Imaging and Therapy: A Radiant Future. *J. Nucl. Med.* **2015,** *56,* 1809–1812.
159. Pardridge, W. M. Blood-Brain Barrier Drug Delivery of IgG Fusion Proteins With a Transferrin Receptor Monoclonal Antibody. *Exp. Opin. Drug Deliv.* **2015,** *12,* 207–222.
160. Pulicherla, K. K.; Verma, M. K. Targeting Therapeutics Across the Blood Brain Barrier (BBB), Prerequisite Towards Thrombolytic Therapy for Cerebrovascular Disorders—An Overview and Advancements. *AAPS PharmSciTech* **2015,** *16,* 223–233.
161. Bien-Ly, N.; Yu, Y. J.; Bumbaca, D.; Elstrott, J.; Boswell, C. A.; Zhang, Y.; Luk, W.; Lu, Y.; Dennis, M. S.; Weimer, R. M.; Chung, I.; Watts, R. J. Transferrin Receptor (TfR) Trafficking Determines Brain Uptake of TfR Antibody Affinity Variants. *J. Exp. Med.* **2014,** *211,* 233–244.
162. Yu, Y. J.; Zhang, Y.; Kenrick, M.; Hoyte, K.; Luk, W.; Lu, Y.; Atwal, J.; Elliott, J. M.; Prabhu, S.; Watts, R. J.; Dennis, M. S. Boosting Brain Uptake of a Therapeutic Antibody by Reducing Its Affinity for Transcytosis Target. *Sci. Transl. Med.* **2011,** *3* (84), 84ra44.
163. Couch, J. A.; Yu, Y. J.; Zhang, Y.; Tarrant, J. M.; Fuji, R. N.; Meilandt, W. J.; Solanoy, H.; Tong, R. K.; Hoyte, K.; Luk, W.; Lu, Y.; Gadkar, K.; Prabhu, S.; Ordonia, B. A.; Nguyen, Q.; Lin, Y.; Lin, Z.; Balazs, M.; Scearce-Levie, K.; Ernst, J. A.; Dennis, M. S.; Watts, R. J. Addressing Safety Liabilities of TfR Bispecific Antibodies That Cross the Blood–Brain Barrier. *Sci. Transl. Med.* **2013,** *5,* 183ra157.

164. Foster, K.; Chaddock, J. A. Targeted Secretion Inhibitors-Innovative Protein Therapeutics. *Toxins* **2010,** *2,* 2795–2815.
165. Mahrhold, S.; Strotmeier, J.; Garcia-Rodriguez, C.; Lou, J.; Marks, J. D.; Rummel, A.; Binz, T. Identification of the SV2 Protein Receptor-Binding Site of Botulinum Neurotoxin Type E. *Biochem. J.* **2013,** *453,* 37–47.
166. Keith, F.; John, C. Targeted Secretion Inhibitors-Innovative Protein Therapeutics. *Toxins (Basel)* **2010,** *2,* 2795–2815.
167. Stancombe, P. R.; Masuyer, G.; Birch-Machin, I.; Beard, M.; Foster, K. A.; Chaddock, J. A.; Acharya, K. R. Engineering Botulinum Neurotoxin Domains for Activation by Toxin Light Chain. *FEBS J.* **2012,** *279,* 515–523.
168. Garcia, E. A.; Trivellin, G.; Aflorei, E. D.; Powell, M.; Grieve, J.; Alusi, G.; Pobereskin, L.; Shariati, B.; Cudlip, S.; Roncaroli, F.; Mendoza, N.; Grossman, A. B.; Harper, E. A.; Korbonits, M. Characterization of SNARE Proteins in Human Pituitary Adenomas: Targeted Secretion Inhibitors as a New Strategy for the Treatment of Acromegaly? *J. Clin. Endocrinol. Metab.* **2013,** *98,* E1918–E1926.
169. Leggett, J.; Harper, E.; Waite, E.; Marks, P.; Martinez, A.; Lightman, S. GHRH Receptor-Targeted Botulinum Neurotoxin Selectively Inhibits Pulsatile GH Secretion in Male Rats. *Endocrinology* **2013,** *154,* 3305–3318.
170. Somm, E.; Bonnet, N.; Zizzari, P.; Tolle, V.; Toulotte, A.; Jones, R.; Epelbaum, J.; Martinez, A.; Huppi, P. S.; Aubert, M. L. Comparative Inhibition of the GH/IGF-I Axis Obtained With Either the Targeted Secretion Inhibitor SXN101959 or the Somatostatin Analog Octreotide in Growing Male Rats. *Endocrinology* **2013,** *154,* 4237–4248.
171. Hamilton, A. J.; Baulcombe, D. C. A Species of Small Antisense RNA in Posttranscriptional Gene Silencing in Plants. *Science* **1999,** *286,* 950–952.
172. Jiang, N.; Zhang, X.; Zheng, X.; Chen, D.; Siu, K.; Wang, H.; Ichim, T. E.; Quan, D.; McAlister, V.; Chen, G.; Min, W. P. A Novel In Vivo siRNA Delivery System Specifically Targeting Liver Cells for Protection of ConA-Induced Fulminant Hepatitis. *PLoS One* **2012,** *7,* e44138.
173. Lorenzer, C.; Dirin, M.; Winkler, A. M.; Baumann, V.; Winkler, J. Going Beyond the Liver: Progress and Challenges of Targeted Delivery of siRNA Therapeutics. *J. Control. Release* **2015,** *203,* 1–15.
174. Sonoke, S.; Ueda, T.; Fujiwara, K.; Kuwabara, K.; Yano, J. Galactose-Modified Cationic Liposomes as a Liver-Targeting Delivery System for Small Interfering RNA. *Biol. Pharm. Bull.* **2011,** *34,* 1338–1342.
175. Nair, J. K.; Willoughby, J. L.; Chan, A.; Charisse, K.; Alam, M. R.; Wang, Q.; Hoekstra, M.; Kandasamy, P.; Kel'in, A. V.; Milstein, S.; Taneja, N.; O'Shea, J.; Shaikh, S.; Zhang, L.; van der Sluis, R. J.; Jung, M. E.; Akinc, A.; Hutabarat, R.; Kuchimanchi, S.; Fitzgerald, K.; Zimmermann, T.; van Berkel, T. J.; Maier, M. A.; Rajeev, K. G.; Manoharan, M. Multivalent *N*-Acetylgalactosamine-Conjugated siRNA Localizes in Hepatocytes and Elicits Robust RNAi-Mediated Gene Silencing. *J. Am. Chem. Soc.* **2014,** *136,* 16958–16961.
176. Sato, A.; Takagi, M.; Shimamoto, A.; Kawakami, S.; Hashida, M. Small Interfering RNA Delivery to the Liver by Intravenous Administration of Galactosylated Cationic Liposomes in Mice. *Biomaterials* **2007,** *28,* 1434–1442.
177. Wang, S. L.; Yu, F. B.; Jiang, T. Y.; Sun, C. S.; Wang, T.; Zhang, J. H. Design and Synthesis of Novel Galactosylated Polymers for Liposomes as Gene Drug Carriers Targeting the Hepatic Asialoglycoprotein Receptor. *J. Drug Target.* **2008,** *16,* 233–242.
178. Wooddell, C. I.; Rozema, D. B.; Hossbach, M.; John, M.; Hamilton, H. L.; Chu, Q.; Hegge, J. O.; Klein, J. J.; Wakefield, D. H.; Oropeza, C. E.; Deckert, J.; Roehl, I.; Jahn-Hofmann, K.; Hadwiger, P.; Vornlocher, H. P.; McLachlan, A.; Lewis, D. L. Hepatocyte-Targeted RNAi Therapeutics for the Treatment of Chronic Hepatitis B Virus Infection. *Mol. Ther.* **2013,** *21,* 973–985.
179. Hao, X.; Jin, Q.; Va, P.; Li, C.; Shen, W.; Laffitte, B.; Wu, J. Pancreas-Specific Delivery of b-Cell Proliferating Small Molecules. *ChemMedChem* **2016,** *11,* 1129–1132.
180. Sievers, E. L.; Senter, P. D. Antibody-Drug Conjugates in Cancer Therapy. *Annu. Rev. Med.* **2013,** *64,* 15–29.
181. Lewis Phillips, G. D.; Li, G.; Dugger, D. L.; Crocker, L. M.; Parsons, K. L.; Mai, E.; Blättler, W. A.; Lambert, J. M.; Chari, R. V. J.; Lutz, R. J.; Wong, W. L. T.; Jacobson, F. S.; Koeppen, H.; Schwall, R. H.; Kenkare-Mitra, S. R.; Spencer, S. D.; Sliwkowski, M. X. Targeting HER2-Positive Breast Cancer With Trastuzumab-DM1, an Antibody-Cytotoxic Drug Conjugate. *Cancer Res.* **2008,** *68,* 9280.
182. Senter, P. D.; Sievers, E. L. The Discovery and Development of Brentuximab Vedotin for Use in Relapsed Hodgkin Lymphoma and Systemic Anaplastic Large Cell Lymphoma. *Nat. Biotechnol.* **2012,** *30,* 631–637.
183. Wang, L.; Amphlett, G.; Blättler, W. A.; Lambert, J. M.; Zhang, W. Structural Characterization of the Maytansinoid-Monoclonal Antibody Immunoconjugate, huN901–DM1, by Mass Spectrometry. *Protein Sci.* **2005,** *14,* 2436–2446.
184. Sun, M. M. C.; Beam, K. S.; Cerveny, C. G.; Hamblett, K. J.; Blackmore, R. S.; Torgov, M. Y.; Handley, F. G. M.; Ihle, N. C.; Senter, P. D.; Alley, S. C. Reduction–Alkylation Strategies for the Modification of Specific Monoclonal Antibody Disulfides. *Bioconjug. Chem.* **2005,** *16,* 1282–1290.
185. Hamblett, K. J.; Senter, P. D.; Chace, D. F.; Sun, M. M. C.; Lenox, J.; Cerveny, C. G.; Kissler, K. M.; Bernhardt, S. X.; Kopcha, A. K.; Zabinski, R. F.; Meyer, D. L.; Francisco, J. A. Effects of Drug Loading on the Antitumor Activity of a Monoclonal Antibody Drug Conjugate. *Clin. Cancer Res.* **2004,** *10,* 7063.
186. Shen, B.-Q.; Xu, K.; Liu, L.; Raab, H.; Bhakta, S.; Kenrick, M.; Parsons-Reponte, K. L.; Tien, J.; Yu, S.-F.; Mai, E.; Li, D.; Tibbitts, J.; Baudys, J.; Saad, O. M.; Scales, S. J.; McDonald, P. J.; Hass, P. E.; Eigenbrot, C.; Nguyen, T.; Solis, W. A.; Fuji, R. N.; Flagella, K. M.; Patel, D.; Spencer, S. D.; Khawli, L. A.; Ebens, A.; Wong, W. L.; Vandlen, R.; Kaur, S.; Sliwkowski, M. X.; Scheller, R. H.; Polakis, P.; Junutula, J. R. Conjugation Site Modulates the In Vivo Stability and Therapeutic Activity of Antibody-Drug Conjugates. *Nat. Biotechnol.* **2012,** *30,* 184–189.
187. Heng, B. C.; Aubel, D.; Fussenegger, M. An Overview of the Diverse Roles of G-Protein Coupled Receptors (GPCRs) in the Pathophysiology of Various Human Diseases. *Biotechnol. Adv.* **2013,** *31,* 1676–1694.
188. Drake, M. T.; Shenoy, S. K.; Lefkowitz, R. J. Trafficking of G Protein-Coupled Receptors. *Circ. Res.* **2006,** *99,* 570–582.
189. Scarselli, M.; Donaldson, J. G. Constitutive Internalization of G Protein-Coupled Receptors and G Proteins via Clathrin-Independent Endocytosis. *J. Biol. Chem.* **2009,** *284,* 3577–3585.
190. van Koppen, C. J.; Jakobs, K. H. Arrestin-Independent Internalization of G Protein-Coupled Receptors. *Mol. Pharmacol.* **2004,** *66,* 365–367.
191. Ginj, M.; Zhang, H.; Waser, B.; Cescato, R.; Wild, D.; Wang, X.; Erchegyi, J.; Rivier, J.; Macke, H. R.; Reubi, J. C. Radiolabeled Somatostatin Receptor Antagonists Are Preferable to Agonists for in vivo Peptide Receptor Targeting of Tumors. *Proc. Natl. Acad. Sci. U. S. A.* **2006,** *103,* 16436–16441.
192. Kim, M.-S.; Pinto, S. M.; Getnet, D.; Nirujogi, R. S.; Manda, S. S.; Chaerkady, R.; Madugundu, A. K.; Kelkar, D. S.; Isserlin, R.; Jain, S.; Thomas, J. K.; Muthusamy, B.; Leal-Rojas, P.; Kumar, P.; Sahasrabuddhe, N. A.; Balakrishnan, L.; Advani, J.; George, B.; Renuse, S.; Selvan, L. D. N.; Patil, A. H.; Nanjappa, V.; Radhakrishnan, A.; Prasad, S.; Subbannayya, T.; Raju, R.; Kumar, M.; Sreenivasamurthy, S. K.; Marimuthu, A.; Sathe, G. J.; Chavan, S.; Datta, K. K.; Subbannayya, Y.; Sahu, A.; Yelamanchi, S. D.; Jayaram, S.; Rajagopalan, P.; Sharma, J.; Murthy, K. R.; Syed, N.; Goel, R.; Khan, A. A.; Ahmad, S.; Dey, G.; Mudgal, K.; Chatterjee, A.; Huang, T.-C.; Zhong, J.; Wu, X.; Shaw, P. G.; Freed, D.; Zahari, M. S.; Mukherjee, K. K.; Shankar, S.; Mahadevan, A.; Lam, H.; Mitchell, C. J.; Shankar, S. K.; Satishchandra, P.; Schroeder, J. T.; Sirdeshmukh, R.; Maitra, A.; Leach, S. D.; Drake, C. G.; Halushka, M. K.; Prasad, T. S. K.; Hruban, R. H.; Kerr, C. L.; Bader, G. D.; Iacobuzio-Donahue, C. A.; Gowda, H.; Pandey, A. A Draft Map of the Human Proteome. *Nature* **2014,** *509,* 575–581.
193. Wilhelm, M.; Schlegl, J.; Hahne, H.; Gholami, A. M.; Lieberenz, M.; Savitski, M. M.; Ziegler, E.; Butzmann, L.; Gessulat, S.; Marx, H.; Mathieson, T.; Lemeer, S.; Schnatbaum, K.; Reimer, U.; Wenschuh, H.; Mollenhauer, M.; Slotta-Huspenina, J.; Boese, J.-H.; Bantscheff, M.; Gerstmair, A.; Faerber, F.; Kuster, B. Mass-Spectrometry-Based Draft of the Human Proteome. *Nature* **2014,** *509,* 582–587.

Relevant Websites

https://www.novartis.com/news/media-releases/sandoz-launches-zarxiotm-filgrastim-sndz-first-biosimilar-united-states.

http://www.pfizer.com/news/press-release/press-release-detail/fda_approves_inflectra_biosimilar_infliximab_the_first_u_s_biosimilar_monoclonal_antibody_for_all_eligible_indications.

1.12 Anti-Aging Drugs

AM Vaiserman, Institute of Gerontology, Kiev, Ukraine

© 2017 Elsevier Ltd. All rights reserved.

1.12.1	**Introduction**	349
1.12.2	**Antioxidants**	351
1.12.2.1	Oxidative Damage Theory of Aging: Conceptual Basis and Clinical Expectations	351
1.12.2.2	Life Extension by Antioxidants	352
1.12.2.3	Antioxidant Supplementation: Contradictions, Controversies and Paradoxes	355
1.12.3	**Pharmacological Interventions Mimicking Calorie Restriction**	357
1.12.3.1	Inhibitors of Glycolytic Metabolism	358
1.12.3.2	Inhibitors of GH/IGF-1 Pathway	359
1.12.3.3	Sirtuin-Activating Compounds	359
1.12.3.3.1	Resveratrol	360
1.12.3.3.2	Synthetic activators of sirtuins	361
1.12.3.4	Pharmacological Inhibition of mTOR Pathway	361
1.12.3.4.1	Rapamycin	362
1.12.3.5	AMPK Pathway	363
1.12.3.5.1	Metformin	363
1.12.4	**Autophagy**	365
1.12.4.1	Pharmacological Induction of Autophagy	366
1.12.5	**Melatonin**	367
1.12.6	**Perspective and conclusion**	368
Acknowledgments		370
References		370
Relevant websites		378

1.12.1 Introduction

Average human longevity has dramatically increased in the course of humanity's history.[1] The most drastic changes have occurred in the last century when implementation of vaccination, disinfectants and antibiotics led to a substantial reduction of infectious diseases as a cause of death. The continuing decline in mortality over the last decades among the elderly is most probably owing to the preventative factors, such as improved diets, as well as a reduction in smoking and exercise.[2] Kennedy and Pennypacker noted in their recent paper that if current demographic trends continue then 20% percent of the global population of 9 billion will be over the age of 60 by 2050.[3] As a consequence, most modern nations undergo rapid population aging. Although the life expectancy has enhanced dramatically in modern generations, this process has not been accompanied by an equivalent increase in healthy life expectancy.[4] Since aging is a major risk factor in most chronic diseases, the prevalence of age-associated disorders, such as neurodegenerative disease, type 2 diabetes, cardiovascular disease, osteoporosis and cancer, rises considerably with the increasing average age in populations of developed countries, representing a great socio-economic challenge. It has been estimated that in the U.S., there will be more than 30 million people over the age of 80 by 2050; half of them will suffer from different forms of dementia, and at least 3 million of all adults in the U.S. will be diagnosed with Parkinson's disease.[5] The expected increase in these and other age-related conditions will have substantial consequences for future society including increased financial and psychological burden for families and greater pressure on government health care programs and entitlement budgets.[6,7] Eric Le Bourg recently pointed that 'the increased proportion of elderly people in the population of developed countries — the so-called demographic aging — explains a part of the now observed enormous interest of country leaders and lay public for aging matters, and thus for biogerontology research'.[8]

Life span extension research has traditionally raised concerns that it may lead to increasing the size of the elderly population and, thereby, to the high prevalence of aging-associated chronic pathologies. Numerous experimental studies have, however, showed that extension of life span is usually accompanied by delayed or reduced morbidity including cardiovascular disease, neurodegeneration, and tumors.[9] There is also evidence from human epidemiological studies which is consistent with these findings from animal models. For example, it has been found that centenarians, in particular those who live in so-called 'Blue Zones' (five regions in Europe, Latin America, Asia and the U.S. with unusually high concentrations of centenarians), not only exhibit exceptional longevity, but also often remain free from disability and chronic disease until very advanced ages.[10]

For the last decades, the primary strategy in gerontology and geriatric research has been the compression of morbidity. This strategy claims that we may limit morbidity to a shorter period closer to the natural end of life, thus reducing the burden of illness and disability, by delaying the age of onset of major age-related chronic diseases.[11] Geroscience, a novel field within biological aging

research, is centered on healthspan extension.[12] Extending healthspan is a critical component of achieving optimal longevity, defined as living long, but with good health and quality of life, including improved functioning, productivity and independence. The efforts to increase healthspan are currently focused on slowing the basic biological processes of aging such as cellular senescence, mitochondrial dysfunction, age-related decline of stress resistance, dysregulated cellular energy sensing/growth pathways, impaired proteostasis, deteriorated stem cell function/bioavailability, as well as inflammation/oxidative stress.[11–14] All these processes interfere with the normal physiological cellular signaling pathways, demanding compensatory adjustments with aging to maintain homeostasis. A good example is intensification of insulin secretion by the beta cells of the pancreas in order to counteract the peripheral insulin resistance. Another example is the recruitment of additional neural circuits in prefrontal regions of the brain to maintain cognitive functioning in the face of pathological neural changes. At a certain stage, however, these compensatory mechanisms become exhausted and the effects of aging are manifested, thereby increasing the risk for functional decline and the development and progression of chronic diseases.[15]

Research on life extension is a part of a larger investigation field widely known as 'anti-aging medicine'. Emerging in the beginning of 1990s as a new speciality in medical practice, anti-aging medicine became the increasingly discussed and debated topic over the past years.[16] The main goal of anti-aging medicine is to prolong both a healthspan and life span by specific regimes of exercise and dieting, as well as by advanced biomedical interventions aimed at slowing, stopping or reversing the aging process.[17,18] The major assumption underlying anti-aging research is that age-related senescence can be considered as a pathophysiological phenomenon that can be prevented or even reversed,[19] and modern anti-aging medicine promotes biomedical technologies that have the potential to delay or postpone this process.[2] Traditionally, aging is considered to be 'natural' and therefore inevitable. However, in the view of many authors, the idea that aging is indefeasible part of human nature is quite questionable.[20] In accordance with many modern evolutionary theories of aging, it has emerged as a by-product of evolutionary processes and does not have a specific function.[21] If aging is really not an intrinsic, irrevocable component of life, then it could be manipulated similarly to other processes which are generally deemed to be unnatural or pathological.[20] The rapid progress in understanding the mechanisms underlying aging and longevity over the last decades and first successful pharmacological interventions to extend healthy life span in various model organisms now indicate that the process of aging is malleable.

There are two main tasks in biogerontology research. The first one is life extension and the second one is prevention of age-associated pathologies. Since numerous studies indicate that many genetic pathways determining aging and longevity are highly conserved across species, it can be suggested that life-extending treatments which are effective in invertebrates might also be effective for vertebrates including humans. Therefore, a number of experiments in this field were performed on invertebrate model systems, including the nematode *Caenorhabditis elegans*, the fruit fly *Drosophila melanogaster*, and the yeast *Saccharomyces cerevisiae*. The main advantage of using such short-lived models is that they allow quickly evaluate the effects of such treatments on the pathways involved in the aging process. Moreover, these models seem suitable because there are organisms whose genomes have been fully sequenced and annotated. Rodent models are also widespread in anti-aging studies because they are relatively inexpensive, easy to maintain and manage, and may be used to investigating such important areas in aging research as behavior, cognition and memory. Studies on life span extension in nonhuman primates are of interest as well because they may be successfully used for better comprehension of the aging process in human beings. However, without denying the importance of such studies, it should be noted that the extension of longevity per se, not accompanied by a decrease of the risk of age-associated pathologies, would certainly not be adequate.

The development of pharmacological agents targeting aging-related functional declines and pathological manifestations ('anti-aging drugs') is now in the spotlight in geroscience. Over the last 20 years, an exponential growth of research in the field of geriatric pharmacology, including the study of prospective anti-aging drugs, is observed.[22] The first step in the drug development process involves the selection of druggable targets.[23] The situation when gene targets are determined by the study of genetic variations linked to either gain-of-function or loss-of-function phenotypes, is especially useful because these targets may be considered as those which had been reliably validated.[24] Over the past two decades, a number of genes have been identified that play an unequivocal role in the control of aging and longevity,[25–27] and all of these genes represent attractive drug targets. Currently, many pharmacological agents targeting the putative mechanisms of aging mentioned above are under development. Another way for anti-aging drug discovery is evaluating the pharmacological agents already approved by the FDA and other regulatory agencies for the treatment of particular conditions associated with aging, such as beta-blockers, metformin, statins, renin-angiotensin-aldosterone system inhibitors, thiazolidinediones, as well as anti-inflammatory medications.[11] These classes of drugs are commonly used in the treatment of patients with chronic medical illnesses and their efficacy and safety has been proven in many clinical trials. They have been also shown to improve physiological functioning, health, and well-being in middle to old age patients with chronic disorders.[28] Such agents are presently not used in treatment of age-related physiological dysfunctions in the absence of clinical manifestation of disease. However, these medications might theoretically be redirected to treating or preventing conditions or syndromes typically associated with aging. Therefore, the longevity dividend, that is an idea that extending healthy life by slowing aging may prove to be the most efficient way to combat the fatal and disabling diseases that plague us today, [29,30] can provide an opportunity to revitalize the drug development pipeline. By delaying the aging process per se, it likely would be possible to delay or prevent all age-associated pathologies rather than to overcome them one by one, which is the current approach of the disease-based paradigm of drug development. Furthermore, delaying the progression of a particular age-related chronic disorder, for example, cardio-vascular disease, will apparently have only a modest effect on the population life expectancy because comorbidity, for example, cancer, will to a great extent substitute the reduction in mortality risk caused by preventing the targeted pathology. The main idea of geroscience is that delaying the clinical manifestation of all of age-associated diseases as a group by inhibiting the basic

aging mechanisms can be far more effective than preventing the individual chronic disorders.[31] A recent analysis conducted by Goldman et al.[32] demonstrated that substantial socio-economic benefits might be derived from this approach in comparison with current public health strategy targeted to prevention of particular diseases. According to this analysis, the economic impact of delaying aging and increasing healthspan in the U.S. is estimated at ~$7 trillion dollars over the next 50 years. Hence, it is evident that discovery of new drug targets based on biogerontological research represents an incredible opportunity for the pharmaceutical and healthcare industries.[33]

1.12.2 Antioxidants

The free radical theory of aging (now more commonly termed the oxidative damage theory of aging) first postulated by Denham Harman in 1956,[34] was historically perhaps the most influential theory of aging. It was one of the earliest concepts to try to explain the basic cause of age-related functional decline and aging-associated pathologies. This theory suggests that free radicals and other reactive oxygen species (ROS), formed unavoidably in the course of normal metabolism in mitochondria as undesirable side products of the oxidative energy metabolism, and arising due to the action of adverse exogenous factors, can damage various biomolecules, and accumulation of these damages is the proximal cause of aging and age-associated diseases.[34] As a consequence, it is supposed that life span is determined by the rate at which these damages occur (Fig. 1).

1.12.2.1 Oxidative Damage Theory of Aging: Conceptual Basis and Clinical Expectations

It has been well established since the free radical theory of aging was first formulated that advanced ages are linked to elevated production of free radicals and other ROS including superoxide anion ($O_2\cdot^-$), hydroxy (HO·), peroxy (ROO·), alkoxy (RO·), and hydroperoxy (HOO·) radicals, mostly from mitochondria, and with increased markers of oxidative injury, such as carbonylated proteins, lipoperoxides, and oxidized DNA.[35–38] Under physiological conditions, excess ROS in the body are eliminated by endogenous antioxidative defense systems, including, among others, superoxide dismutase (SOD), enzyme detoxifying superoxide radical ($O_2\cdot^-$), catalase (CAT) and glutathione peroxidase both involved in the detoxification of peroxides, and glutathione reductase involved in the regeneration of glutathione (Fig. 2).

Together, these antioxidant systems allow keep the cellular equilibrium between oxidation and antioxidation processes. However, the endogenous antioxidant systems may be insufficient, especially in conditions of chronic oxidative stress, that generally accompany aging and degenerative age-associated disorders.[35] In such conditions, exogenous antioxidant compounds may play a substantial role in maintaining the homeostatic balance in living organisms. They include, among others, vitamin E, vitamin C, beta-carotene and other carotenoids, lipoic acid, glutathione, coenzyme Q10, flavonoids, phenols, polyphenols, phytoestrogens, as well as several minerals such as zinc, selenium and manganese. Therefore, there is continuous demand for exogenous antioxidant compounds in order to prevent the oxidative damage of biomolecules under the conditions of a disequilibrium redox state in favor of oxidation. However, high doses of such agents can be toxic due to their prooxidative effects at high concentrations or their potential to react with beneficial concentrations of ROS normally occurring at physiological conditions and required for effective cellular functioning.[36]

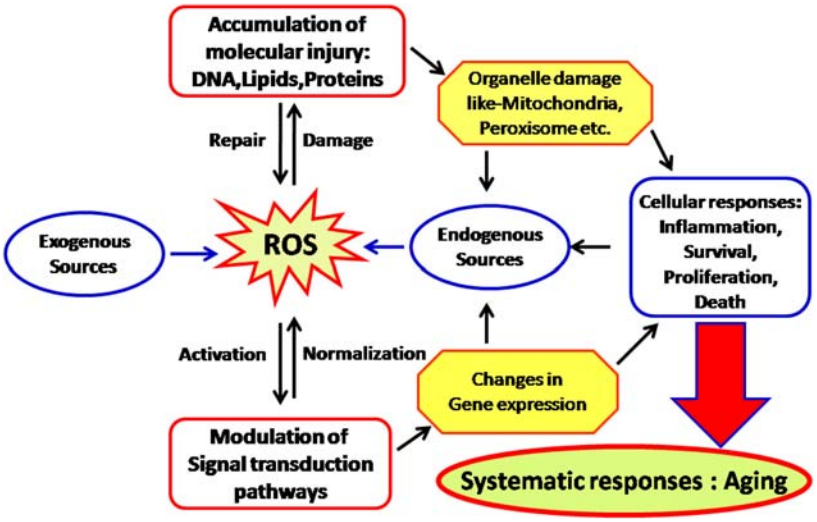

Fig. 1 Reactive oxygen species (ROS) generated by endogenous as well as exogenous sources, cause damage and accumulation of proteins, lipids and DNAs, when defensive (repair) mechanisms of body become weak. These ROS also modulate the signal transduction pathways. These disturbances cause organelle damage, changes in gene expression followed by altered cellular responses which ultimately results into aging (The figure is reproduced with permission of the copyright holders from Pandey and Rizvi[35]).

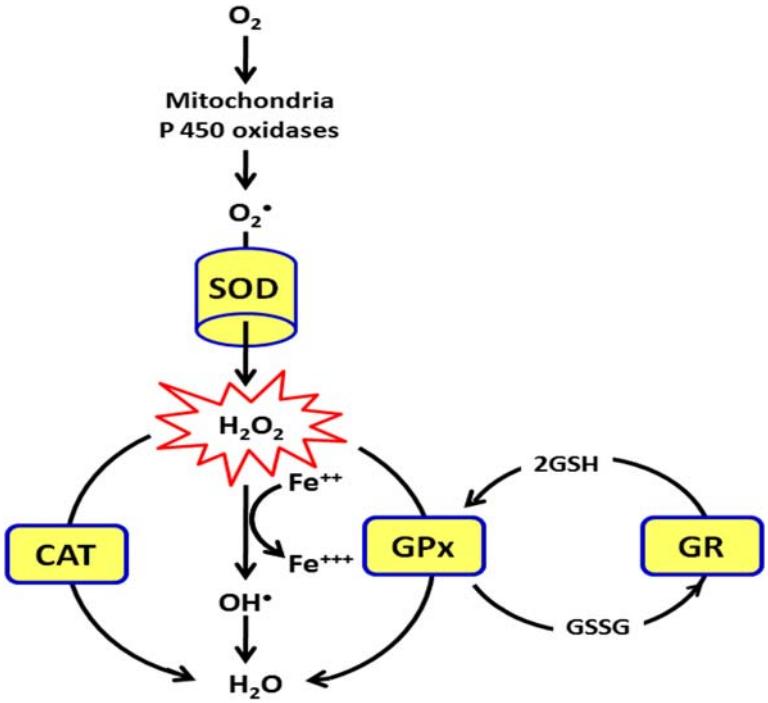

Fig. 2 Superoxide dismutase (SOD), glutathione peroxidase (GPx), glutathione reductase (GR) and catalase (CAT) are the main endogenous enzymatic defense systems of all aerobic cells. They give protection by directly scavenging superoxide radicals and hydrogen peroxide, converting them to less reactive species. SOD catalyzes the dismutation of superoxide radical ($\bullet O_2$) to hydrogen peroxide (H_2O_2). Although H_2O_2 is not a radical, it is rapidly converted by fenton reaction into $\bullet OH$ radical which is very reactive. GPx neutralizes hydrogen peroxide by taking hydrogens from two glutathione (GSH) molecules resulting in two H_2O and one *glutathione disulfide* (GSSG). GR then regenerates GSH from *GSSG*. CAT the important part of enzymatic defense, neutralizes H_2O_2 into H2O (The figure is reproduced with permission of the copyright holders from Pandey and Rizvi[35]).

If the oxidative damage theory of aging is true and if aging is really due to free radical reactions, it should be possible to extend the organismal life span by activation of antioxidant defence. Based on this assumption, a number of studies in various experimental models have attempted to delay aging and prolong longevity using dietary supplementation with natural or synthetic antioxidants or by manipulating the antioxidant genes.[39,40] A large number of studies have been performed to investigate whether supplementation with antioxidants, especially vitamins C and E, may extend the life span of different model animals. Vitamin C, also referred to as ascorbic acid, L-ascorbic acid and ascorbate, is the major hydrophilic (water-soluble) antioxidant. In cell membranes, it may rapidly reduce the α-tocopheroxyl radicals and level of low-density lipoprotein (LDL) to regenerate α-tocopherol and to inhibit the generation of free radicals.[41] Vitamin E (α-tocopherol) is the main hydrophobic (fat-soluble) antioxidant in cell membranes and circulating lipoproteins. The antioxidant function of vitamin E is strongly supported by regeneration promoted by vitamin C. Vitamin E is known to prevent atherosclerosis due to the reduction of oxidative stress and inhibition of LDL oxidation.[42] In addition to vitamins, other substances such as melatonin,[43] ubiquinone (coenzyme Q)[44] and lipoic acid[45] also considered to be efficient efficient antioxidants.

It is believed by many researchers now that development of novel means of delivery of antioxidants into cells or construction of novel antioxidant compounds may open new perspectives for modulation of aging and healthspan extension. Since mitochondria are the main source of ROS in the cell, mitochondrially targeted antioxidants might be more effective than traditional ones.[46] The most demonstrative indications favoring this conclusion originate from recent discoveries of in vivo effects of mitochondria-targeted antioxidants including MitoQ and plastoquinone (SkQs).[47] Chemical structures of main antioxidant substances are presented in Fig. 3.

1.12.2.2 Life Extension by Antioxidants

Findings on the effects of antioxidant supplementation on life span of experimental organisms such as the fruit fly, *Drosophila melanogaster*, the nematode worm, *Caenorhabditis elegans*, and rodents are summarized in Table 1.

As it is seen from the Table 1, supplementation with substances having antioxidant properties resulted in controversial effects on life span of different model organisms. In most cases, it caused life extension accompanied by reduced age-associated oxidative stress,[93–96,98] increased antioxidant enzymes activity,[77,79,80] enhanced stress resistance,[58–61,64,66,69,70] increased reproductive activity,[54,85] and modulated expression of aging-related genes.[78,81,83–86] In several studies, however, the life span and fertility were unchanged or even decreased.[55,65,87,88,92,95] Furthermore, in some cases the life-extending capacity of substances with potent

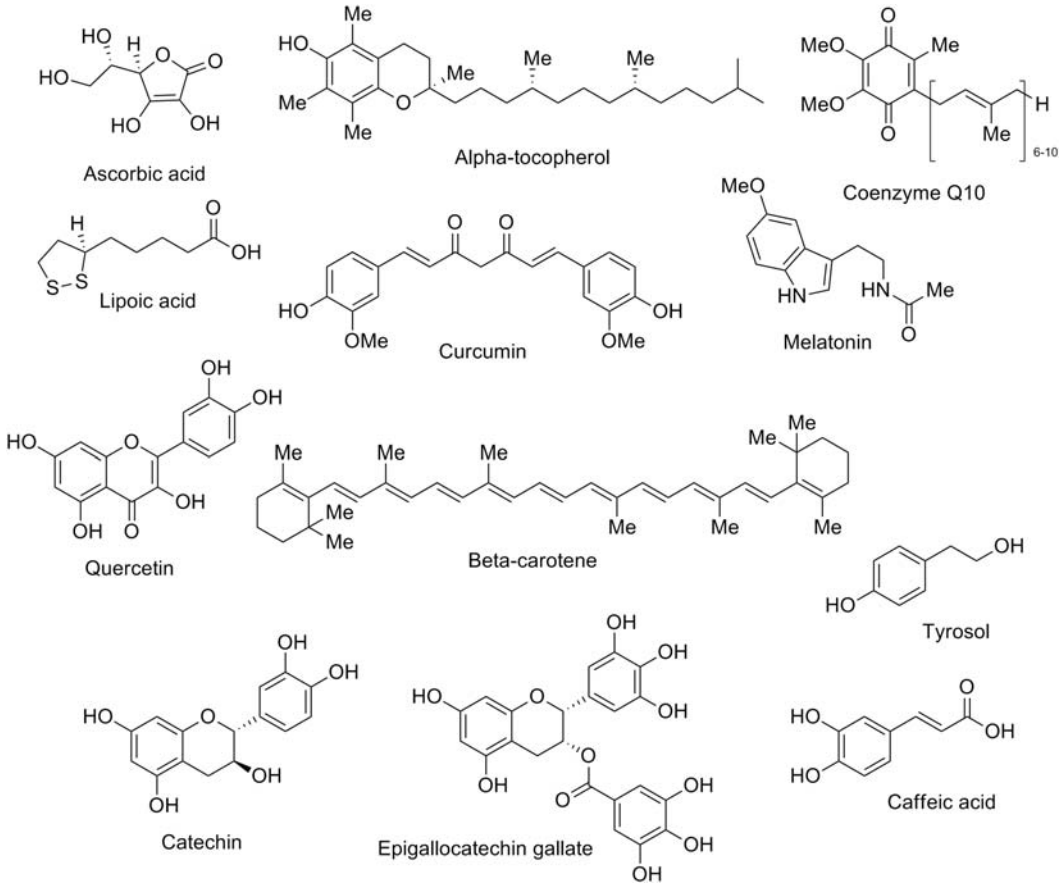

Fig. 3 Main antioxidant substances.

Table 1 Summary of the effects of substances having antioxidant properties on the life span and associated functional traits of model organisms

Experimental del/Agent	*Effects observed*	*Reference*
Rotifer		
Vitamin E	Extended pre-reproductive stage	Sawada et al.[48]
Indolepropionamide	Increased life span	Poeggeler et al.[49]
Caenorhabditis elegans		
Vitamin E; CoQ	Increased life span; reduced superoxide anion levels	Ishii et al.[50]
Vitamin E	Increased life span; delayed reproduction	Harrington and Harley[51]
Polydatin, a natural resveratrol glycoside	Increase of mean life span by 31% and 62% under normal and acute stress conditions, respectively	Wen et al.[52]
Curcumin	Increased life span	Liao et al.[53]
Quercetin, a major flavonoid in the human diet	Increased life span; increased reproductive capacity; enlarged body size	Surco-Laos et al.[54]
Quercetin-3-O-glucoside	Increase of mean life span by 23% by low concentrations, decrease of life span by high concentrations	Dueñas et al.[55]
Flavonoids myricetin, quercetin, kaempferol, naringenin	Increased life span in wild-type worms	Grünz et al.[56]
Caffeic acid; rosmarinic acid	Increased life span; reduced body size; altered lipid metabolism; delayed reproduction	Pietsch et al.[57]
Flavanol catechin	Increased life span; enhanced stress resistance; reduced body length	Saul et al.[58]
Epigallocatechin gallate	Increased life span; enhanced stress resistance	Abbas and Wink[59]
Epigallocatechin gallate	Increased life span under stress conditions; no effect under normal conditions	Zhang et al.[60]
Ferulsinaic acid	Increased life span; improved resistance for heat and oxidative stresses; attenuated lipid peroxidation	Sayed[61]
EUK-8 and EUK-134, SOD/CAT mimetics	Increased mean life span of wild-type worms by 44%, and prematurely aging worms by 67%	Melov et al.[62]
Tyrosol, an olive oil phenol	Increased life span	Cañuelo et al.[63]

(Continued)

Table 1 Summary of the effects of substances having antioxidant properties on the life span and associated functional traits of model organisms—cont'd

Experimental del/Agent	*Effects observed*	*Reference*
KPG-7, herb mixture complex	Increased life span; protection against oxidative stress	Moriwaki et al.[64]
EUK-8	Dose-dependent reduction of life span and fertility	Keaney and Gems[65]
Ginkgo biloba extract, EGb 761	Increased life span; increased stress resistance	Wu et al.[66]
Royal jelly	Increased life span	Honda et al.[67]
Platinum nanoparticles (nano-Pt), a SOD/CAT mimetic	Increased life span; reduced accumulation of lipofuscin and ROS induced by paraquat	Kim et al.[68]
N-acetyl-L-cysteine	Increased life span; increased resistance to oxidative, UV and heat stresses	Oh et al.[69]
Extract from Acanthopanax sessiliflorus	Increased life span; increased resistance to heat shock and UV irradiation; reduced oxidative DNA damage	Park et al.[70]
Drosophila melanogaster		
Lipoic acid and resveratrol	Increased life span	Bauer et al.[71]
Melatonin	Increased life span	Izmaylov and Obukhova[72]
EUK-8 and EUK-134; MitoQ	Increased life span in SOD-deficient flies; no effect in wild type flies	Magwere et al.[73]
SkQ1	Increased life span	Krementsova et al.[74]
Epitalon	Increase of mean life span by 11–16%	Khavinson et al.[75]
Carnosine, S,S-Trolox-carnosine, STC	20% increase of male mean life span, no effect on females; increase of male mean life span by 16%, female by 36%	Stvolinsky et al.[76]
Curcumin	Increased life span; enhanced SOD activity	Suckow and Suckow[77]
Curcumin	Increased life span; reduced oxidative stress; improved locomotion; modulated expression of aging-related genes	Lee et al.[78]
Curcumin	Increased life span; increased SOD activity; reduced accumulation of malondialdehyde and lipid peroxidation	Shen et al.[79]
Aloe vera extract	Increased life span; increased antioxidant enzymes activity; increased locomotor activity	Chandrashekara and Shakarad [80]
Black rice extract	Increase of mean life span by 14%; up-regulation of SOD1, SOD2, CAT and Rpn11, and down-regulation of Mth genes	Zuo et al.[81]
Cocoa	Increased life span; metal-chelating effects	Bahadorani and Hilliker[82]
Blueberry extract	Increased life span; up-regulation of SOD, CAT and Rpn11, and down-regulation of Mth genes	Peng et al.[83]
Cranberry anthocyanin extract	Increase of mean life span by 10%; up-regulation of SOD1 and down-regulation of MTH, InR, TOR and PEPCK genes	Wang et al.[84]
Cranberry extract	Increased life span; increased reproduction; higher expression of oxidative stress and heat shock response genes	Wang et al.[85]
Sesamin, a major lignan in sesame oil	Increase of mean life span; up -regulation of SOD1, SOD2, CAT and Rpn11 genes; attenuation of neurodegeneration	Zuo et al.[86]
Musca domestica		
EUK-8 and EUK-134	No effect on life span under normoxic conditions; shortened life span under hyperoxic conditions	Bayne and Sohal[87]
Mus musculus		
Vitamin E	Increased median life span in C57BL/6 mice by 15%; anti-cancer effect via inducing the P21 signalling pathway	Banks et al.[88]
Vitamin E	No effect on life span	Morley and Trainor[89]
Vitamin E	Increase in mean but not maximum life span; lower fatal tumour incidence	Blackett and Hall[90]
Tetrahydrocurcumin; polyphenol from green tea	Increased survival in male C57BL/6 mice	Kitani et al.[91]
Commercial nutraceutical combinations	No or detrimental effect on life span	Spindler et al.[92]
Carboxyfullerene, SOD mimetic	Increased life span; reduced age-associated oxidative stress; rescued age-related cognitive impairment	Quick et al.[93]
Royal jelly	Increase of mean life span of C3H/HeJ mice by 25%, no effect on maximum life span; reduced oxidative damage	Inoue et al.[94]
Alpha-lipoic acid	Decreased life span in senescent prone SAMP8 mice; reduced oxidative stress and improved memory in old mice	Farr et al.[95]
Melatonin	Increased life span; normalized redox status of the mitochondria and increased ATP levels in SAMP8 mice	Rodríguez et al.[96]
SkQ1	Increased life span; prevented age-dependent disappearance of estrous cycles; retardation of age-linked immune decline	Anisimov et al.[97]
Rattus norvegicus		
Epigallocatechin gallate	Increased life span; reduced liver and kidney damage; improved age-associated inflammation and oxidative stress	Niu et al.[98]

antioxidant activity have been manifested in superoxide dismutase (SOD)-deficient mutants with compromised antioxidant defence[73] or in normal animals under stress conditions,[60] but were not shown if wild-type animals reared in normal conditions were investigated. In addition, antioxidant compounds have commonly been shown to be able to affect the mean life span but they were failed to show consistent effects in extending a maximum life span of wild-type animals,[90,94] suggesting that these effects could be caused by reduction of mortality owing to the prevention or delay of age-related diseases rather than due to the interference with the aging process per se. Generally, life-extending effects have been observed so far in species that are evolutionarily distant from mammals. All of the life-extending strategies used, however, did not induce a similar extension of the longevity in mammals, where more complex control systems are likely working over the aging process, probably requiring more elaborate and specific interventions.

1.12.2.3 Antioxidant Supplementation: Contradictions, Controversies and Paradoxes

Taken together, the findings from research of antioxidant compounds suggest that the mechanisms underlying the effects of these agents are complex and interacting in ways that are difficult to address experimentally. Theoretically, the effects of supplementation with exogenous antioxidants may be explained by mechanisms other than antioxidant activity of itself. It is known that endogenous and exogenous antioxidants act interactively (e.g., synergistically) to maintain or re-establish the redox homeostasis.[36] In some cases, the effects of substances with potent antioxidant capabilities could be related not with their own antioxidant action, but with induction of endogenous antioxidant mechanisms; the intake of high levels of exogenous antioxidants can, however, suppress the synthesis of endogenous antioxidants as well.[40] This is an important point as a fine-tuned balance between oxidative and anti-oxidative processes is critical in maintaining healthy biological systems.[36] The excessive supplementation of antioxidants may lead to destroying the delicate control mechanisms of homeostasis resulting in deterioration of health status and life shortening.[99] Since it is difficult to assess the quantity and quality of food consumed by experimental organisms, it may be suggested that the intake of high amounts of antioxidants can modulate their feeding behavior and thus lead to malnutrition or even starvation.[100] If so, it can be assumed that life-extending effects of exogenous antioxidants might be explained, at least partly, by the mechanism of calorie restriction (CR). Indeed, it is well known that severe lowering of calorie intake may dramatically slow the rate of aging and delay the onset of various age-related disorders such as type 2 diabetes, cardiovascular disease, cancer, and neurodegenerative disease in a number of experimental models (see the respective subsection below). Moreower, the life-extending effects of antioxidants and other substances may be a by-product of other, rather deleterious, effects such as decreased rate of development, lower weight, and reduced level of metabolic rate.[100] This is all the more true that most compounds having anti-oxidant properties are multi-functional: the mechanisms that are operative or dominant in a particular situation are dependent on the certain biological conditions and thus these conditions can affect the kinetics and hence the antioxidant activity. For example, ascorbic acid can act, depending on particular conditions, not only as an antioxidant, but also as an oxygen scavenger, a metal chelating agent, and a reducing agent.[101] Similarly, although curcumin demonstrates superior antioxidant activity, its life-extending properties may be caused by its indirect antioxidant action, namely, induction of exogenous antioxidant enzymes, or by interference with various cellular signaling pathways such as inflammatory cytokines, growth factors and their receptors, adhesion molecules, apoptosis-associated and cell-cycle proteins, several transcription factors including NF-kappaB (a major transcription factor for inflammatory responses), activator protein 1 (AP-1) and signal transducer and activator transcription factor as well as with several longevity-associated enzymes like mitogen-activated protein kinase (MAPK), mammalian target of rapamycin (mTOR), and protein kinase B (Akt).[40]

Another important point is that antioxidants show contradictory behaviors in differing biological environments, depending on their concentration and the nature of neighbouring molecules, they may act as pro-oxidants.[102] In addition, whereas high concentrations of ROS are hazardous for all living beings and damage all major cellular constituents, numerous evidence have been reported that at proper cellular concentrations they play a significant role as regulatory mediators in various signaling processes such as signal transduction from membrane receptors and control of gene expression, as well as in cell cycle regulation, cellular proliferation and differentiation, and autophagy stimulation.[103,104] Therefore, the intake of high doses of exogenous antioxidants can result in the disruption of the pro/antioxidant balance and to adverse health effects. Moreover, the life-extending effects induced by antioxidants can also be explained by the hormesis phenomenon, that is, a dose–response relationship characterized by low-dose stimulation and high-dose inhibition.[105] Similarly to the hormesis-inducing compounds (hormetins), antioxidants act in some concentration range, and their high concentrations are generally toxic to most organisms. Paradoxically, the effect of longevity hormesis can be mediated by increased formation of ROS.[40,103] According to the concept of mitochondrial hormesis ('mitohormesis'), whereas high levels of ROS generated in the mitochondria may cause cellular damage and promote aging, their moderate levels can induce an adaptive response and thus improve the systemic defense mechanisms. This hypothesis postulates that ROS act as essential signaling molecules to promote healthspan and longevity, and that intake of exogenous antioxidants can be useless or even harmful.[106]

On the basis of these facts, Bouayed and Bohn[36] pointed in their review that supplementation with exogenous antioxidants can lead to the double-edged effects depending on their concentrations: physiologic doses cause beneficial effects while high doses lead to harmful effects. The schematic presentation of these ideas is reproduced from the article by Bouayed and Bohn[36] in Fig.4.

Given all these contradictions, it is no wonder that conflicting data are reported on the health effects of long-term dietary antioxidant supplementation in human populations. It has been indicated in a number of investigations that oxidative damage is substantially involved in the pathogenesis of many aging-associated disorders including neurodegenerative Alzheimer's and

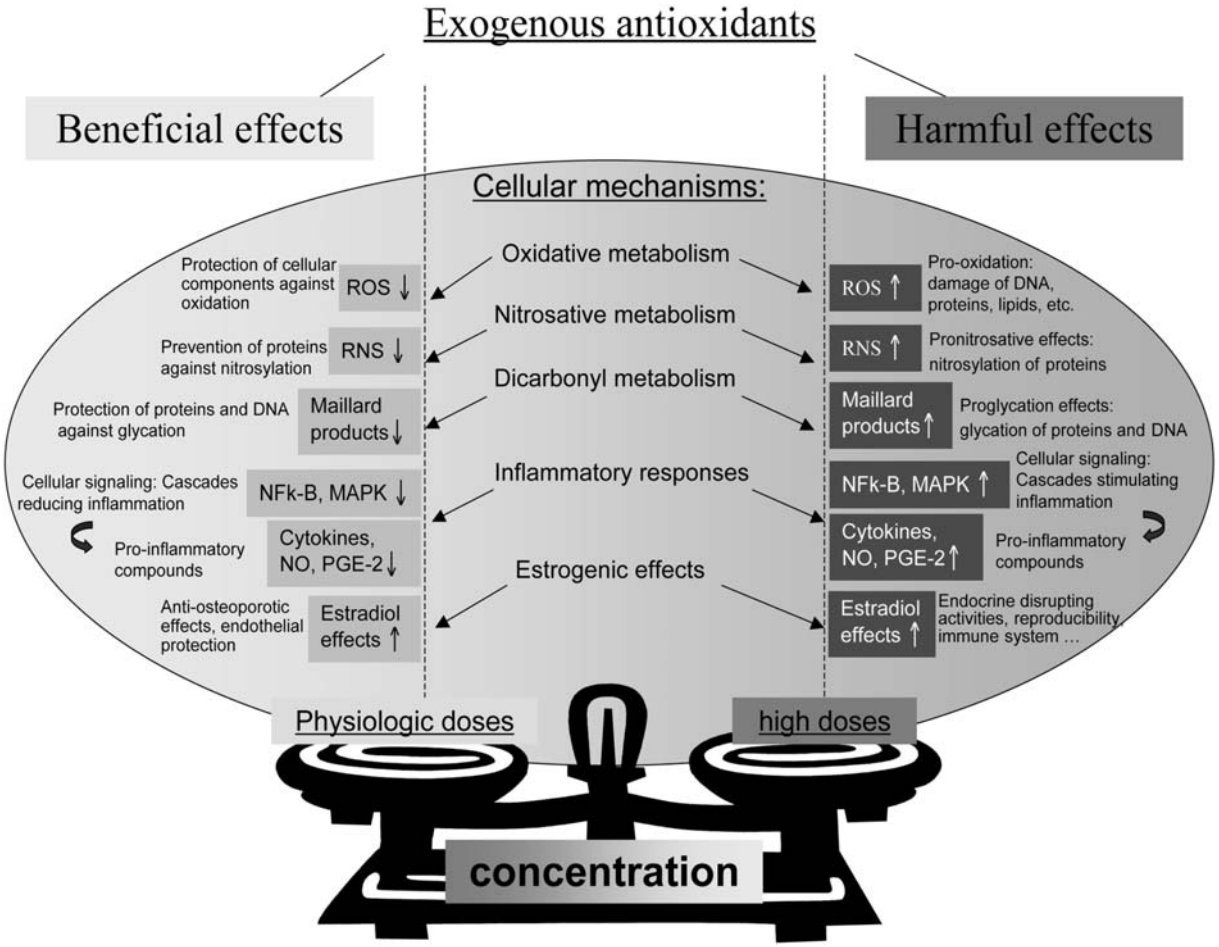

Fig. 4 Double-edged effects of exogenous antioxidants on cellular responses including oxidative, nitrosative and dicarbonyl metabolisms and other pathways such as inflammatory processes depending potentially on their concentrations: physiologic doses leading to beneficial effects whereas high doses may result in harmful effects. Specifically, 'beneficial or harmful effects of natural compounds may also occur independently from their (anti-) oxidative properties e.g., as a result of the activation of particular cellular pathways including inflammatory processes, nitrogen and dicarbonyl metabolisms for which a close relation exists. Indeed, inflammation, nitrosative stress (resulting from excessive production of reactive nitrogen species) and carbonyl stress (resulting from excessive accumulation of reactive dicarbonyl compounds) may exacerbate or provoke oxidative stress and vice versa. Besides the biphasic effects of antioxidants on oxidative metabolism, it has also been reported that natural compounds can display double-edged effects on inflammatory reactions… Other activities of natural compounds might result in beneficial as well as harmful effects such as due to the estrogen-like activity of isoflavones, as they are able to bind to ß-estradiol receptors. Independently of their antioxidant activity, polyphenols are also able to exert modulatory effects in cells, resulting in outcomes depending on the activated pathways among others, e.g., by interacting with intracellular signaling cascades [e.g., the nuclear factor kappa B (NFkB) and the mitogen-activated protein kinase (MAPK)] or by binding to the ATP-binding sites of a large number of proteins, including mitochondrial ATPase, calcium plasma membrane ATPase, protein kinase A, protein kinase C and topoisomerase. It also has been revealed that some antioxidants (e.g., quercetin and naringenin) are able to inhibit certain cytochrome P450 enzymes (CYP1A1 and CYP3A4, respectively) involved in the bioactivation of chemical carcinogens, constituting another proposed chemopreventive mechanism of polyphenols against cancer development including lung cancer. In addition, it has been demonstrated that polyphenols (e.g., chlorogenic acid, EGCG and rutin) at pharmacological (non-nutritional) doses could interact with GABAA receptors or modulate neurotransmitters (e.g., serotonin and noradrenaline), resulting in interesting pharmacologic properties on the central nervous system including anti-anxiety and antidepressant activities.. The figure is reproduced with permission of the copyright holders from Bouayed, J.; Bohn, T., Exogenous antioxidants – Double-edged swords in cellular redox state: Health beneficial effects at physiologic doses versus deleterious effects at high doses, Oxid Med Cell Longev 3 (4) (2010) 228–237.

Parkinson's diseases,[107,108] type 2 diabetes,[109] atherosclerosis and other cardiovascular complications,[110–112] as well as sarcopenia[113] and osteoporosis.[114] Some authors therefore suggest that enhancing the antioxidant defense system in relevant organs can be useful in reducing the oxidative stress and the impact of age-related pathologies. In animal models, it has been really demonstrated that dietary supplementation with exogenous antioxidants may attenuate the development and progression of various age-related disorders, including amyotrophic lateral sclerosis, Parkinson disease, and heart failure.[115–120] Application of that idea for human beings has, however, turned out to be rather problematic. Most controlled clinical trials failed to demonstrate any clinical benefits of antioxidant-based therapies for aging-associated diseases such as cardiovascular disease,[121,122] stroke[123]

and type 2 diabetes.[124,125] This controversy may be linked to the excessive intake of antioxidants or with insufficient bioavailability of the antioxidants in the relevant organs to reduce the oxidative damage.[126]

The excessive levels of exogenous antioxidants may interfere with endogenous cellular signaling mechanisms and thus can be harmful.[127] Indeed, in a large-scale study the use of multivitamins more than seven times per week was shown to be linked to a substantial increase of prostate cancer risk when compared to never users.[128] Supplementation with antioxidants (vitamin C and E combined) precluded the health-promoting effects of exercise in humans.[129] In a large trial of beta-carotene conducted among heavy smoking men in Finland who were at high risk for developing lung cancer, a significant increase in lung cancer diagnoses among those taking the supplement compared to those taking a placebo has been revealed.[130] In another trial among heavy smokers and people exposed to asbestos, an increased incidence of lung cancer and elevated risk of death from lung cancer, cardiovascular disease, and any cause were found in both smokers and workers exposed to asbestos who took the combination of beta carotene and vitamin A.[131] In meta-analyses of observational studies and randomized controlled trials conducted in well-nourished and healthy populations, antioxidant supplementation has been repeatedly associated with undesirable consequences for the health and all-cause mortality.[132–135]

Taken together, these findings indicate that antioxidant intake may not always be advantageous to human health.[136] The paradoxical situation when oxygen radicals and other ROS are involved in various human diseases, but supplementation with large doses of dietary antioxidants to human individuals has resulted, in most cases, in little or no preventative or therapeutic effect, is commonly referred to the term 'antioxidant paradox'. The manipulation of level of endogenous antioxidants (eg, by supplying mild pro-oxidants) seems a more useful approach to prevention and treatment of disorders in which ROS play an important role than the consumption of large doses of exogenous dietary antioxidants.[137] From this, Bast and Haenen[138] have recently concluded that 'initial excitement regarding the potential health benefits of antioxidants has diminished. Currently, it is even claimed that antioxidants increase mortality. The antioxidant pendulum appears to swing from healthy to toxic and from general panacea to insignificant ingredient. Owing to the polarity of views towards antioxidants, nutritional recommendation ranges from advice to increase antioxidant status in plasma to the notion that it is a useless measurement.

In summary, while benefits of supplementation with exogenous antioxidants seem obvious in case of increased oxidative stress and endogenous antioxidant deficiency, additional studies are required to determine the potential risks and benefits associated with intake of antioxidants by healthy persons.

1.12.3 Pharmacological Interventions Mimicking Calorie Restriction

The raised doubts about the effectiveness of antioxidant treatments have currently led to an increased interest in alternative anti-aging therapies. Among them, calorie restriction (CR)-based therapeutic strategies seem to be the most promising now. CR is defined as a restriction of food intake without malnutrition in organisms normally fed ad libitum.[139] Presently, CR, a diet providing all the essential nutrients and vitamins but having significantly (30%–70%) lower amount of calories, is accepted as a well-known and established experimental procedure for life extension, although some authors suggest that the restriction of specific nutrients including protein and particular amino acids such as methionine may play a crucial role.[140] It is well known, since the pioneering work of McCay and co-workers, that CR may promote longevity and slow aging. In this study, it has been found that rats subjected to 40 % CR had up to 50 % longer median and maximum life span than animals fed a standard diet.[141] From that time, a number of studies have demonstrated that CR may retard aging or extend life span in many experimental models including yeast, worms, insects and rodents.[142–144] More recently, evidence was obtained that CR may lead to a delayed onset of various age-related disorders in non-human primates such as rhesus monkeys.[145–147] Specifically, prolonged CR resulted in lowered body fat, decelerated rate of muscle loss with age, lowered incidence of cancer, cardio-vascular disease and type 2 diabetes, as well as in improved insulin sensitivity and glucose tolerance. In addition, in conditions of CR the age-related and all-cause mortality of monkeys was substantially reduced.[148] In recent years, accumulating data indicate that moderate CR with qualitatively adequate diet can cause a powerful protective effect against inflammation, hypertension, obesity, type 2 diabetes, and cardio-vascular disease, and also reduce the metabolic risk factors linked to cancer in humans.[149,150] However, although CR has been established to clearly reduce risk factors linked to aging in humans, it is still a matter of debate whether CR can result in increase of human life expectancy.

The important point is that since the human maximum longevity is substantially greater relative to that of closely related non-human primate species, it is likely that humans have acquired genetic variations mimicking the effects of CR. By testing this assumption, Rizza et al.[151] have compared the transcriptome differences between humans and other primates, with the transcriptome changes observed in mice subjected to CR. Findings from this research show that evolution of human life span is likely independent of CR-induced mechanisms of life extension. Based on these and other findings, it can be assumed that application of CR can be a promising direction to the human life extension.[152]

Converging lines of evidence indicate that beneficial effects of CR are mediated by the same pathways which are also involved in the control of tissue repair, immunity, appetite, thermoregulation, and metabolism. [153] Importantly, these effects of CR likely result not from passive metabolic changes, but rather from processes that are highly regulated and depend on the activation of specific effectors.[154] Major nutrient-sensing pathways linked with regulation of the life span by CR are the insulin/insulin-like growth factor signaling (IIS), the adenosine monophosphate (AMP)-activated protein kinase (AMPK) and mTOR pathways, as well as sirtuins, especially SIRT1. These signaling pathways also represent important regulators of cell growth and proliferation, mitochondrial

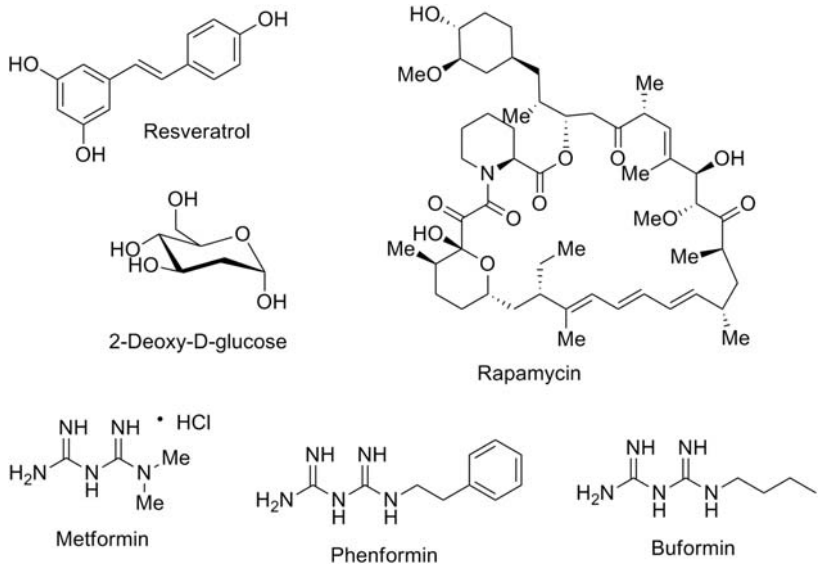

Fig. 5 Chemical agents able to mimick calorie restriction.

function, autophagy, and survival. In addition, the nutrient-sensing pathways involved in CR are known to be regulated by cross talk with one another.

To produce the beneficial effects on healthspan and life span reported in experimental conditions, the long-term CR is necessary. It can be obviously problematic for most modern people. When discussing the clinical trials initiated to assess the therapeutic potential of CR in humans, Ingram et al.[152] stressed that 'even if results from these studies could eventually substantiate CR as an effective pro-longevity strategy for humans, the utility of this intervention would be hampered because of the degree and length of restriction required.' These challenges have generated interest in developing alternatives to CR, which may provide pro-healthspan and pro-longevity benefits of CR without the significant reduction in the long-term food intake. Such agents are referred to as CR mimetics. Ingram et al.[152] defined the characteristic properties of CR mimetics as follows: (1) inducing the hormonal, metabolic and physiological effects similar to those of CR; 2) activation of the stress response pathways like the CR; 3) life span extension and reducing the incidence or delaying the onset of age-associated disorders.

The signaling pathways mediating the effects of CR and most promising pharmacological agents modulating these pathways, such as resveratrol, rapamycin and metformin (Fig. 5), are described in detail in the subsections below.

1.12.3.1 Inhibitors of Glycolytic Metabolism

Hyperglycemia and hyperinsulinemia are widespread in advanced ages. The age-related metabolic disorders such as type 2 diabetes, which are commonly accompanied by disturbance in insulin signaling and glucose homeostasis, are known to produce various aging-like phenotypes such as cancer and other age-associated disorders. Untreated diabetes patients typically have elevated glucose levels and they are more susceptible to certain diseases, such as neurological degeneration, kidney problems, heart disease, vascular and microvascular damage, impaired wound healing and cataracts, which typically occur in most non-diabetics much later in life.[155,156] Hyperglycemia-induced oxidative stress is known to promote the generation of advanced glycosylation end products (AGEs), thereby substantially affecting the rate of aging.[155] The accumulation of AGEs has been shown to be accelerated in diabetes patients and it was suggested to be a credible biomarker for both aging and 'metabolic memory' (the persistence of deleterious effects of prior hyperglycaemia on the initiation and progression of diabetic vasculopathies even after glucose normalization).[157,158] Moreover, hyperinsulinemia, a marker of insulin resistance which is also known to increase with age, is an important causal factor in the pathogenesis of cancer.[159]

CR has been repeatedly shown to reduce the levels of glucose and insulin, and to improve the insulin sensitivity.[160] Therefore, the inhibition of particular enzymes within the glycolytic pathway is assumed to be promising strategy to produce CR-like anti-aging effects.[161] The first candidate agent in this pharmacological category is 2-deoxy-D-glucose, an analog of glucose having a hydrogen atom instead of a hydroxyl group at its C2 position, which may be taken up by cells through the glucose transporters.[162] Within the cell, 2-deoxy-D-glucose is converted to 2-deoxyglucose 6-phosphate by hexokinase in the first step of glycolysis. 2-deoxyglucose 6-phosphate can in turn inhibit phosphoglucose isomerase at the second step of glycolysis and imped processing of glucose to fructose 6-phosphate. Due to these properties, 2-deoxy-D-glucose was applied for decades to affect glycolysis in a variety of organisms from bacteria to mammals, and it was repeatedly shown to have therapeutic benefits for treating epilepsy, viral infection and cancer.[163] This preparation is considered to be particularly promising in anti-cancer therapies. Indeed, since cancerous cells exhibit enhanced glycolysis and use this metabolic pathway for generation of ATP as a main source of their energy supply, the elevated

dependence of cancerous cells on glycolytic pathway for ATP generation provides a biochemical basis for the development of therapeutic strategies to preferentially kill malignant cells by the pharmacological inhibition of glycolysis.[164,165] This drug was also shown to recapitulate several aspects of the CR phenotype such as reduced levels of circulating insulin and body temperature in short-term rodent trials, while obvious toxic effects of 2-deoxy-D-glucose have been demonstrated in one chronic feeding study conducted up to now. In this research, a remarkable CR-like phenotype was revealed in rats treated with this drug, such as reduced food intake and decreased weight gain. These changes, however, were accompanied by cardiac vacuolization and increased mortality in treated animals.[162] Thus, the potential toxicity of 2-deoxy-D-glucose leads to serious challenges in the CR-based therapeutic application of this medication.

1.12.3.2 Inhibitors of GH/IGF-1 Pathway

Among the signaling pathways associated with CR, insulin/insulin-like growth factor-1 (IGF-1) pathway is known to play an important and evolutionary conserved role in the regulation of longevity. There is plenty of research evidence to suggest that CR, as well as protein and amino acid restriction and intermittent fasting, may extend the mammalian life span via modulation of IGF-1 signaling.[166] Accumulating evidence from animal models indicates that reduction in the level of IGF-1 may result in life extension. Particular polymorphic variants of the IGF-1 receptor gene have been shown to be related to the human life span,[167,168] in particular, to the exceptional longevity of centenarians.[169] In addition, low circulating IGF-I bioactivity was shown to be associated with longevity of the exceptionally long-lived individuals,[170] and their offspring.[171]

Remarkably, the long-lived growth hormone (GH) receptor knockout Laron dwarf mice (GHR−/−) were shown to be insulin sensitive despite obesity, and were also found to have significantly reduced IGF-1 levels and decreased risks for diabetes and cancer.[172,173] Similarly, Laron syndrome patients who have low IGF1 levels despite normal or increased levels of GH, have been shown to be protected from cancer and diabetes.[174,175] As a consequence, it can be assumed that treatments targeted at lowering IGF-1 levels could be a promising pharmaceutical strategy for healthspan extension.

Recently, several pharmacological inhibitors of the GH/IGF-1 axis have been proposed for the treatment in patients with acromegaly.[176] Such agents include, for examole, analogues of somatostatin which can reduce the serum levels of GH by suppression of GH secretion by pituitary somatotrophs, thus resulting in reduced serum IGF-1 levels. Although such therapy may potentially lead to adverse effects because these substances are known to suppress secretion of several hormones including the insulin, unfavorable consequences such as anorexia, diarrhea and gallstones, were observed only in 20–50% treated acromegalic patients. Another drug from this pharmacological class to be approved for treating acromegaly is the antagonist of the GH receptor, pegvisomant, which is known to inhibit GH secretion and also inhibit GH action by binding to and blocking the GH receptor.[177,178] In patients treated with pegvisomant, a dose-dependent decrease of IGF-1 levels (up to 90%) has been demonstrated.[177,179] Thereby, since pegvisomant can cause advantageous effects on glucose metabolism by reducing the serum IGF-1 and increasing the insulin sensitivity, it is believed to be a promising agent for health- and life span extension. However, even though no substantial harmful effects of pegvisomant have been observed in the long-term research by van der Lely et al.,[180] further studies are needed to prove its safety. Modulation of IGF-1 availability may be another mode to inhibit IGF-1 action. For this purpose, pharmacological agents modulating the pregnancy-associated plasma protein-A (PAPP-A), a zinc metalloproteinase that enhances the local bioavailability of the IGFs, may be developed. Indeed, it has been reported that PAPP-A knockout mice have significantly extended healthy life span, suggesting an important role of PAPP-A in aging and age-related disease.[181,182] Healthspan-promoting effects of such preparations, however, have not been studied yet and will likely be the subject of future research.

1.12.3.3 Sirtuin-Activating Compounds

Sirtuins, also known as Silent Information Regulators (SIRs), are nicotinamide adenine dinucleotide (NAD+)–dependent protein deacetylases which are thought to play a fundamental role in epigenetic regulation of gene expression by mediating the assembly and maintenance of the silenced chromatin. Sir2, a NAD+−dependent class III histone deacetylase, has been initially identified as a molecule with potent anti-aging properties in yeast studies.[183] Subsequently, Sir2 has been shown to be implicated in control of life span in yeast, the nematode *Caenorhabditis elegans*, and the fruit fly *Drosophila*. In mammals, SIRT1, a homologue of Sir2, has been revealed to act as anti-aging molecule in the context of CR.[184] SIRT1 has been repeatedly found to regulate various biological processes such as gene silencing, mitochondrial biogenesis, stress resistance, inflammation, glucose and lipid metabolism, cell survival, apoptosis and autophagy.[185,186] The important role of SIRT1 in the effects of CR has been revealed in SIRT1 transgenic mice that manifest a CR-like phenotype, exhibiting decreased levels of insulin, fasting glucose blood cholesterol, adipokines, and greater glucose tolerance than the control animals.[187] In addition, in a controlled intervention trial conducted in healthy humans, with measurements before and after the intervention, it has been found that 25 % reduction in calorie intake during six months caused overexpression of peroxisome proliferator-activated receptor (PPAR)-γ coactivator-1α (PGC-1α) and SIRT1 in the skeletal muscle, accompanied by enhanced mitochondrial function and decreased levels of the oxidative stress, body temperature, metabolic rate, visceral fat mass and insulin resistance in non-obese young adults.[188] However, in several studies in yeast, nematodes and *Drosophila*, CR was shown to be able to extend life span in the absence of Sir2.[189–191] Therefore, the importance of sirtuins, particularly SIRT1, in CR-related life extension is still unclear. However, since the activation of SIRT1 is known to decelerate the progression of age-associated diseases and conditions thus extending healthspan, SIRT1 is a potential target for CR mimetics.[192] In addition, the control of SIRT1 activity is closely linked to that of the AMPK, which regulates lipid, cholesterol

and glucose metabolism in specialized metabolic tissues, such as liver, muscle and adipose tissue, and is one of the central regulators of metabolism in eukaryotes.[193] AMPK is known to be activated in conditions where nutrients are limited and promotes oxidative metabolism. It is also known that AMPK can be activated by increasing NAD+ production, and activation of SIRT1 leads to increased AMPK activation via the deacetylation of liver kinase B1 (LKB1), which is the major upstream AMPK kinase.[194,195]

1.12.3.3.1 Resveratrol

Large-scale screening of compounds which are capable of activating SIRs led to the discovery of 18 small molecules demonstrating such properties.[196] Among them, resveratrol, which is a naturally occurring polyphenolic phytoalexin present mostly in grape skins and red wine, but also in peanuts and berries, has been studied most extensively.[197] The investigation of this chemical initially started through the "French paradox" which describes improved cardiovascular outcomes despite a high-fat diet characteristic of Mediterranean countries, including France.[198] In experimental studies, administration of resveratrol in doses of 100–1000 1000 μM mu;M resulted in life extension of short-lived models, such as yeast, worms, fruit flies, and honey bee (for a summary of these studies, see **Table 2**).

The resveratrol-induced life extension in these model organisms was shown to be dependent on the functional Sir2, and was not observed when nutrients were restricted.[199] Resveratrol has been also demonstrated to prolong the life span and retard the onset of age-related markers in short-lived vertebrates such as fish.[200,201] In mice model, resveratrol exerted the beneficial effects on life span and metabolism in high-fat diet-induced obese animals.[202] In mice fed a standard diet, resveratrol delayed age-related deterioration and mimicked transcriptional aspects of dietary restriction without extending life span.[203] In mammals, resveratrol also exhibited the ability to protect against a variety of age-related diseases including Alzheimer's disease, type 2 diabetes and cancer.[208] In obese male patients, 30 days of resveratrol supplementation (150 mg per day) resulted in CR-like effects manifested in prevention of obesity-associated metabolic dysregulation by activating the AMPK/SIRT1 pathway in the skeletal muscle.[209] In addition, resveratrol caused enhanced intramyocellular lipid levels and decreased circulating glucose, intrahepatic lipid content, alanine-aminotransferase, triglycerides and inflammatory markers. More recently, 30-day supplementation with the same dose of resveratrol led to a significantly decreased adipocyte size, with a shift toward a reduction in the proportion of large adipocytes and an increase in the proportion of small adipocytes.[210] Today, resveratrol is one of the most popular dietary supplements on the market. In the U.S., two-thirds of people who consume multiple dietary supplements, consume resveratrol.[211] It should, however, be noted that, despite the high expectations placed on resveratrol as a promising anti-aging drug, some challenges are associated with its application. In recent commentary published in Ann NY Acad Sci, Vang has stressed that: '(1) many different cellular effects are observed for resveratrol, but it is not known whether they arise from one point of action (or a few) or whether resveratrol is non-specific in its action; (2) the health-promotion effect of dietary resveratrol is likely a combinatory effect of various bioactive components in the mixture (diet); (3) the known cell biological response to resveratrol is presently based on exposure to short-term high levels, and better in vitro analyses have to be developed; (4) the actual level of resveratrol and resveratrol metabolites present in vitro

Table 2 Summary of the effects of resveratrol on the life span and associated functional traits of model organisms

Model organism	*Effects observed*	*Reference*
Saccharomyces cerevisiae	Extension of replicative life span by 70%	Howitz et al.[204]
Caenorhabditis elegans	9-18 % increase in mean life span; transcriptional induction of a family of genes encoding prion-like glutamine/asparagine-rich proteins involved in endoplasmic reticulum stress response to unfolded proteins	Viswanathan et al.[205]
	10-14 % increase in mean life span without reducing fecundity	Wood et al.[199]
Drosophila melanogaster	29 % increase in mean life span, 20–22 % increase in maximum life span without reducing fecundity	Wood et al.[199]
	10-17 % increase in mean life span	Bauer et al.[71]
	10-15 % increase in mean life span; downregulation of genes in aging-related pathways, including antioxidant peroxiredoxins, insulin-like peptides involved in insulin-like signaling and several downstream genes in Jun-kinase signaling involved in oxidative stress response	Wang et al.[206]
Apis mellifera	33-38 % increase in mean life span; ingestion of fewer quantities of food under ad libitum feeding conditions	Rascón et al.[207]
Nothobranchius furzeri	33-56 % increase in median life span, 27–59 % increase in maximum life span; delaying the age-dependent decay of locomotor activity and cognitive performances and reducing the expression of neurofibrillary degeneration in the brain	Valenzano et al.[200]
Nothobranchius guentheri	19 % increase in mean life span, 28 % increase in maximum life span; enhanced cognitive ability and locomotor activity; protection from neurodegeneration; reduced rate of lipofuscin formation	Yu and Li[201]
Mus musculus	31% reduced risk of death from the high calorie diet until the 114 weeks of age; increased insulin sensitivity, reduced insulin-like growth factor-1 levels, increased AMPK and peroxisome proliferator-activated receptor-gamma coactivator 1alpha activity, increased mitochondrial number, improved motor function	Baur et al.[202]
	No effect on life span, but a marked reduction in signs of aging, including reduced albuminuria, decreased inflammation, and apoptosis in the vascular endothelium, increased aortic elasticity, greater motor coordination, reduced cataract formation, and preserved bone mineral density	Pearson et al.[203]

and in vivo during experiments may be over- and underestimated, respectively, because resveratrol is not very soluble in water; and (5) only a few small clinical studies have been published to date, focusing on the therapeutic effects of resveratrol.' [212]

1.12.3.3.2 Synthetic activators of sirtuins

Over the last decade, several synthetic activators of SIRT1 such as SRT1460, SRT1720, SRT2104 and SRT2183 (Fig. 6) have been synthesized by a biotechnology company Sirtris Pharmaceuticals. The most studied among them is SRT1720, a specific SIRT1 activator that has been shown previously to cause life extension and amelioration of metabolic impairments in mice fed a high-fat diet.[213] More recently, it has been found that SRT1720 supplementation can result in life span extension and delayed onset of age-associated metabolic diseases in mice fed a standard diet.[214] In a mice model, SRT1720 has been also demonstrated to be able to reverse the adverse age-related changes such as excessive superoxide production, vascular endothelial dysfunction and inflammation.[215] Recently, beneficial effects of another SIRT1 activator, SRT2104, on bone and muscle mass, as well as on survival of male mice have been revealed.[216]

1.12.3.4 Pharmacological Inhibition of mTOR Pathway

The mechanistic (also known as mammalian) target of the rapamycin (mTOR) pathway is another nutrient-sensing pathway playing an important role in mediating the beneficial effects of CR on the rate of aging and longevity.[217] mTOR is a serine/threonine protein kinase that is evolutionarily conserved in all species. It has been repeatedly found to be involved in the processes of cell growth, metabolism and regulation of energy homeostasis.[218] Within the cell, mTOR exists as a part of two distinct multiprotein complexes called mTOR complex 1 (mTORC1) and mTOR complex 2 (mTORC2).[219] mTORC1 is controlled by numerous signals including amino acids, growth factors and cellular energy and is known to regulate various important cellular processes such as transcription, translation and autophagy.[220] There is ample evidence to indicate that mTORC1 is the main mTOR complex involved in regulating longevity.[221] In the presence of sufficient nutrients, growth factors and energy availability, mTOR switches off autophagy and stress resistance, and switches on cell growth pathways, including translation and ribosomal biogenesis.[222] Since the rate of protein synthesis is known to inversely correlate with longevity,[223] inhibition of protein synthesis mediated by reducing mTOR pathway activity may likely be involved in the life-extending effects across species.[222]

The observation that mTOR is activated by particular amino acids can provide a causal mechanism for the recent findings that decrease in the proportion of protein in the diet, rather than CR per se, can cause a longevity-promoting effect in different experimental models.[224–226] In addition, mTOR signaling is known to play a crucial role in mediating aging and age-related metabolic disorders, such as obesity, type 2 diabetes and cancer.[227] Therefore, mTOR is believed to be a leading target for the pharmacological interventions to modulate the nutrient response pathway and to slow aging. Inhibition of this pathway was repeatedly shown to

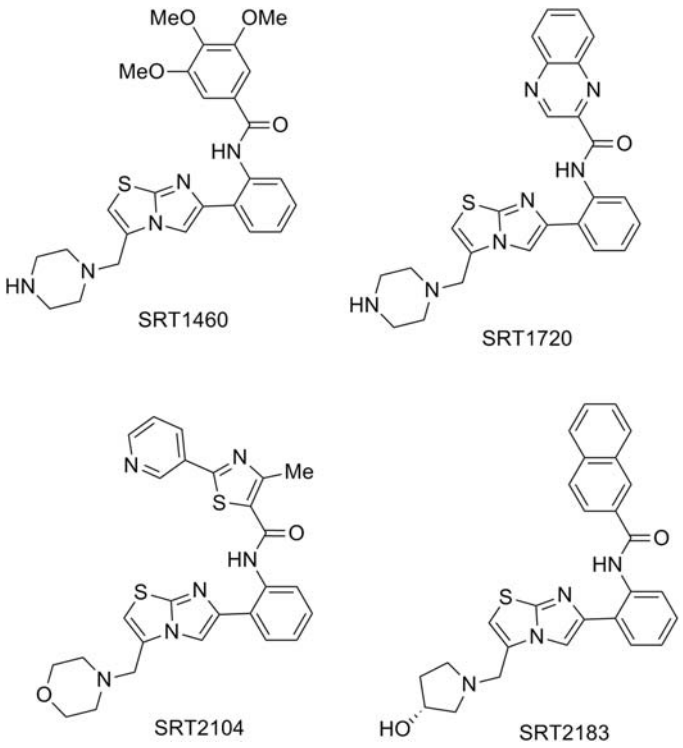

Fig. 6 Sirtuins activators.

confer protection against a growing list of age-related pathologies and to extend life span in a wide spectrum of model organisms.[228] Genetic inhibition of mTOR signaling resulted in life extension in worms,[229,230] fruit flies,[231] and mice.[232] Recently, it has been shown in the gene expression analysis of mTOR pathway, that this pathway not only plays a role in the regulation of aging in animal models, but also in human health and longevity.[233]

1.12.3.4.1 Rapamycin

A commonly used inhibitor of mTOR is rapamycin. It is a natural compound produced by bacteria *Streptomyces hygroscopicus* that was first found in an Easter Island soil sample around 1970. This substance was initially developed as an antifungal agent but was subsequently demonstrated to have significant regulatory effects on many important biological processes including cell growth, proliferation, and inflammation via its inhibitory action on mTOR.[234] Since rapamycin was found to inhibit the immune response, it has been subsequently adopted as a standard therapy to prevent graft rejection in transplant recipients and to treat autoimmune disorders.[235] Currently, rapamycin is approved by FDA for use as an immunosuppressant following transplant surgery and for the treatment of renal cell carcinoma.[234] Due to these properties, rapamycin is suggested to be the most promising anti-aging agent now.[236] Life-extending properties of rapamycin were investigated in several studies conducted in yeast, worms, fruit flies and mice.[221] Supplementation with rapamycin, mostly in doses of 14 ppm ($\sim$2.24 mg kg^{-1}/day) to 42 ppm ($\sim$6.72 mg kg^{-1}/day), lead to significant increase of both mean and maximum life span in these experimental models. A brief summary of these studies is presented in the **Table 3**. Therapy with rapamycin has been also demonstrated to delay variety of aging-associated changes in mice, including liver degeneration, tendon stiffening, accumulation of subcellular alterations in the myocardium, endometrial hyperplasia, and decline in physical activity.[250] In addition, it proved to be effective against other age-related pathological conditions such as retinopathy,[251] cardiac hypertrophy,[252] neurodegenerative disorders,[253] cognitive decline,[254] and loss of stem cell function.[255]

On the basis of the data obtained, it is suggested that potential mechanisms of life extension by rapamycin include antitumor effects,[256,257] induction of autophagy,[258] stem cell guidance,[259] as well as immune-modulating and anti-inflammatory activity.[260] Moreover, the reduction of the rate of protein synthesis can likely mediate the life-extending effects of rapamycin because of decrease of the overall translation rate can prevent the accumulation of damaged or misfolded proteins which could in turn affect longevity.[261] In addition, mTOR is known to be negatively regulated by other nutrient-sensing pathways such as the AMPK and SIRT1 pathways.[262]

Although chronic treatment with rapamycin is known to inhibit both mTORC1 and mTORC2, the life-extending effects of rapamycin are believed to be mediated by the inhibition of TORC1 activity. At the same time, suppression of mTORC2 by rapamycin may lead to impaired glucose homeostasis and insulin resistance owing to unfavorable effects on hepatic gluconeogenesis.[232] Potentially detrimental side effects of chronic rapamycin administration, including hyperglycemia, glucose intolerance and insulin resistance, have been demonstrated in several rodent studies.[263,264] The substantial side effects of rapamycin were also shown in

Table 3 Summary of the effects of rapamycin on the life span and associated functional traits of model organisms

Model organism	*Effects observed*	*Reference*
Saccharomyces cerevisiae	Extension of chronological life span up to 54%	Powers et al.[237]
	15% increase in replicative life span	Medvedik et al.[238]
	19% increase in replicative life span	Ha and Huh [239]
Cenorhabditis elegans	19 % increase in mean life span	Robida-Stubbs et al.[240]
Drosophila melanogaster	Extension of female life span up to 17% and 23% (median and maximum, respectively) on rich media and up to 54% and 36% during starvation; increased resistance to starvation and paraquat stress	Bjedov et al.[241]
	Standard diet: increase in the male mean life span on 6% and increase in the female mean life span on 26%;	Sun et al.[242]
	Low-calorie diet: decrease in the male mean life span on 12% and increase in the male mean life span on 57%	
Mus musculus	14% increase in 90% mortality for female and 9% for male genetically heterogeneous mice fed rapamycin beginning at 600 days of age heterogeneous mice	Harrison et al.[243]
	Increased mean life span (male: 10%; female: 18%) in genetically heterogeneous mice fed rapamycin from the age of 9 months; attenuating age-associated decline in spontaneous activity in males but not in females	Miller et al.[244]
	Increase of mean life span of genetically heterogeneous mice by 23% (males) to 26% (females)	Miller et al.[245]
	11% increased maximum life span in females, prevention of age-related weight gain, decreased rate of aging and suppressed carcinogenesis in transgenic HER-2/neucancer-prone mice	Anisimov et al.[246]
	8% increased maximum life span, inhibited age-related weight gain, decreased aging rate, and delayed spontaneous cancer in inbred females	Anisimov et al.[247]
	Improved survival of C57BL/6 mice after the late-life rapamycin feeding; reduced total and resting metabolic rate during the light (inactive) phase.	Zhang et al.[248]
	Increased median life span in male C57BL/6J mice	Neff et al.[249]

humans from clinical trials with cancer patients in which it has been used as a monotherapy.[265] Side effects of rapamycin in humans include metabolic changes, such as hyperlipidemia, decreased insulin sensitivity, glucose intolerance, hypertension and an increased incidence of new-onset diabetes,[234] as well as diarrhoea, anaemia, nausea or vomiting, thrombocytopenia, skin rash, stomatitis and malignancies (lymphoma and skin cancers).[234, 266,267] The rapamycin-induced metabolic defects were demonstrated, however, to be fully reversible. In both lean and obese mice, these effects have been shown to be almost completely lost within a few weeks of cessation of rapamycin treatment, indicating that chronic treatment with rapamycin does not induce permanent impairments in glucose metabolism.[268]

The important point is that treatment with rapamycin starting late in life is sufficient to extend life span, and, moreover, that transient late-life treatments can yield similar benefits.[221] Indeed, the findings from mice studies suggest that rapamycin supplementation initiated late in life (20 months of age) is nearly as effective as beginning at 9 months of age.[243,244] Late-life transient rapamycin intervention was also shown to reverse the age-associated heart dysfunction, and it also led to the beneficial behavioral, skeletal, and motor changes in 24-month-old female C57BL/6J mice.[269] The opportunity for the benefits of a mid- or late-life rapamycin therapy seems crucially important since mid- or late-life interventions are preferable when considering potential translation of any anti-aging therapy to humans.[221] Characterized inhibitors of mTOR pathway are already clinically approved, and others are under development. Johnson et al. recently pointed out that 'although adverse side effects currently preclude use in otherwise healthy individuals, drugs that target the mTOR pathway could one day become widely used to slow aging and reduce age-related pathologies in humans.' [228]

1.12.3.5 AMPK Pathway

The mTORC1 complex of mTOR is known to be regulated by cellular energy levels through the metabolic sensor, AMPK, which has emerged as another potentially important target in CR-based therapies. AMPK signaling pathway maintains the energy balance in the cell by modulation of ATP production. AMPK is a cellular energy sensor that monitors the AMP/ATP ratio inside the cell. The reduced ATP concentrations in the cell result in increase of AMP levels and to activation of AMPK.[195] Recent studies revealed that, apart from AMP, adenosine diphosphate (ADP) may also be crucially contributed to AMPK activation.[270] Activated AMPK coordinates an energy-conserving program by increase of cellular ATP production and reduction of ATP consumption by shutting down energy-consuming processes such as the mTOR-dependent protein translation.[271] Upon activation, AMPK switches on catabolic pathways that generate ATP, both in a short time frame, by promoting glycolysis and fatty acid oxidation, and in a long time frame, by increasing mitochondrial content and the use of mitochondrial substrates as an energy source, and also switches off the ATP-consuming processes such as biosynthesis as well as cell growth and proliferation.[272] Although these processes can occur to respond to metabolic stress at the cellular level, cytokines and hormones such as leptin, insulin, and adiponectin may interact with this system, and it likely can play a crucial role in maintaining energy balance at the whole body level. AMPK responds to energy stress by suppressing the cell growth and biosynthetic processes, partially via the inhibition of the mTORC1 pathway.[273,274] Moreover, AMPK activation leads to an increased glucose uptake in skeletal muscles, and to a decreased hepatic glucose production and enhanced fatty acid oxidation in various tissues.[275] Numerous data indicate that AMPK inhibits mTOR through the phosphorylation and activation of the tuberous sclerosis complex (TSC) as well as via the direct phosphorylation of the RAPTOR subunit of mTORC1.[276] Recent results suggest that activation of AMPK by the upstream kinase, the tumor suppressor LKB1, in response to nutrient lack occurs at the surface of the lysosome.[277] Thereby, AMPK is an important player in regulation of energy balance at both cellular and whole-body levels via the regulation of insulin sensitivity and mitochondrial biogenesis, as well as in processes of autophagy and stress resistance.[278]

The AMPK system may be partly responsible for the health benefits of exercise. It is a key player in the development of new treatments for obesity, type 2 diabetes and the metabolic syndrome. In addition, it is known as the key integrator and mediator of processes linking metabolism to longevity.[279,280] Because modulation of AMPK signaling is also known to contemporaneously modulate other biochemical pathways which are considered as key anti-aging pathways, including the PPAR gamma coactivator a (PGC-1a), SIRT1 and TOR,[22] AMPK pathway is assumed to be a promising drug target for healthspan and life span extension.

1.12.3.5.1 Metformin

A number of drugs have been developed demonstrating the AMPK-activating properties, including several FDA-approved drugs such as resveratrol, biguanides, salicylates, thiazolidinediones, and glucagon-like peptide-1 receptor agonists.[281] Among them, metformin (1,1-dimethylbiguanide hydrochloride), a biguanide antidiabetic medication derived from French lilac, is in the focus of research activity. Currently, it is considered to be one of the most effective medications for treating type 2 diabetes because it is known to be able to specifically inhibit the hepatic gluconeogenesis without increasing insulin secretion, inducing weight gain or posing a risk of hypoglycaemia.[282,283] It might also act as a CR mimetic since it has been shown to acutely decrease hepatic glucose production, mostly owing to mild and transient inhibition of the mitochondrial respiratory-chain complex 1.[284]

Several studies have shown that administration with metformin and other biguanides, such as phenformin and buformin, can extend the life span of experimental animals such as worms, fruit flies and rodents, although the results have been somewhat inconsistent (**Table 4**).

Increasing evidence for beneficial effects of metformin has been obtained in human studies as well. For example, in a very recent study by Luong et. al.,[298] metformin treatment resulted in significant improvement in body mass index, total cholesterol, low-density lipoprotein cholesterol, and non-high density lipoprotein cholesterol in children with metabolic syndrome. The

Table 4 Summary of the effects of biguanides on the life span and associated functional traits of model organisms

Model organism	*Biguanide*	*Effects observed*	*Reference*
Caenorhabditis elegans	Metformin	Extended median life span, slowed lipofuscin accumulation, prolonged youthful locomotory ability	Onken and Driscoll[285]
	Metformin Phenformin	Increase of mean life span by 18%, 36%, and 3% in worms treated with doses of 25, 50, and 100 mM, respectively; altered microbial folate and methionine metabolism; Increase of mean life span by 5%, 21%, and 26% in worms treated with doses of 1.5, 3, and 4.5 mM, respectively	Cabreiro et al.[286]
	Metformin	Significant life extension; 45% increase in respiration and 38% increase in metabolic heat production	De Haes et al.[287]
Drosophila melanogaster	Metformin	Males: no effect on life span of flies supplemented with 1 to 50 mM, decreased life span at 100 mM; Females: no effect on survival of flies supplemented with 1 to 10 mM, dose-dependent decrease in life span at doses above 10 mM; activation of AMPK and reduced lipid store	Slack et al.[288]
Mus musculus	Metformin	C57BL/6 strain: 5.83%, increase of mean life span in males treated with 0.1%; 14.4% decrease of mean life span in mice treated with 1%; B6C3F1 strain: 4.15% increase of mean life span in males treated with 0.1%	Martin-Montalvo et al.[289]
	Metformin	8% increase of mean life span in female transgenic HER-2/neu mice supplemented with 100 mg kg^{-1}; decreased food consumption; slowdown of the age-related rise in blood glucose and triglycerides level, as well as the age-related switch-off of estrous function	Anisimov et al.[290]
	Metformin	Increase of mean life span up to 37.8% and maximum life span up to 10.3% in female outbred SHR mice supplemented with 100 mg kg^{-1}; slowdown the age-related switch-off of estrous function	Anisimov et al.[291]
	Metformin	8% increase of mean life span in transgenic HER2/neu mice supplemented with 0.5 mg ml^{-1}; increased latency of mammary adenocarcinoma by 13.2%	Anisimov et al.[292]
	Metformin	13.4% decreased mean life span of inbred 129/Sv male mice treated with 100 mg kg^{-1}; no significant effect on female life span; 3.5 times decreased incidence of malignant neoplasms in female mice	Anisimov et al.[293]
	Metformin	Decreased body temperature and postponed age-related switch-off of estrous function in female outbred SHR mice; 14% increase of mean life span in mice treated started at the age of 3 months; no effects on longevity in mice treated starting from the ages of 9 or 15 months. Delayed detection of the first tumor by 22% and 25% in mice treated since the ages of 3 and 9 months, respectively.	Anisimov et al.[294]
	Phenformin	Increase of mean life span of female C3H/Sn mice by 21.1% and the maximum life span by 26%.	Anisimov et al.[295]
Rattus norvegicus	Buformin	9% increase of mean life span in LIO rats, 1.6-fold reduction in cumulative incidence of spontaneous tumors	Anisimov[296]
	Metformin	Reduced body weight, no effect on life span in Fischer-344 rats	Smith et al.[297]

anti-cancer effects of metformin among both diabetic and non-diabetic patients have been also observed.[299–301] In addition, treatment with metformin caused the 30 % reduction in the lifetime risk of cancer incidence in diabetic patients.[302] Remarkably, microarray analysis revealed a considerable similarity between the gene expression patterns generated by both metformin and CR.[303]

There is an increasing recognition that metformin can directly act on tumor cells, primarily affecting the mitochondrial respiratory chain, thereby resulting in the activation of AMPK. Recent research findings, however, indicate that AMPK-independent pathways may also explain both beneficial and unfavorable effects of metformin.[304] These pathways include suppression of glucagon signaling, alteration of intestinal microbiota, inhibition of mitochondrial shuttles, induction of mitochondrial stress, activation of autophagy, attenuation of inflammasome activation, induction of incretin receptors and reduction of terminal endoplasmic reticulum stress.[305] Thus, therapeutic and pro-healthspan effects of metformin have been well established. However, as it was recently stressed by Longo et al., 'to consider metformin for clinical trials testing its potential anti-aging effect, it will be important to closely examine the known effects of long-term use on a wide range of subjects and particularly those who are relatively healthy, but also those with specific conditions for whom chronic metformin use may have been shown to be detrimental.' [161]

Summarizing the research findings on the effects of CR mimetics, it should be noted that, despite the increasing interest in applying these substances in anti-aging medicine, any proven CR mimetics have been identified until now. Several candidate medications, such as resveratrol, rapamycin and metformin, however, appear highly promising. By arguing that both CR and CR mimetics induce their beneficial effects through numerous signaling pathways, Ingram and Roth (2015) have recently proposed to use the "cocktails" of CR mimetics to simultaneously affect multiple pathways. [144] For example, metformin might be expected to block the glucose dysmetabolism caused by rapamycin treatment via inhibiting the gluconeogenesis by downregulating expression of glucose-6-phosphatase and phosphoenolpyruvate carboxykinase.[306] Such combined strategy would likely be more secure and provide a more balanced therapeutic approach, especially in relatively healthy subjects.

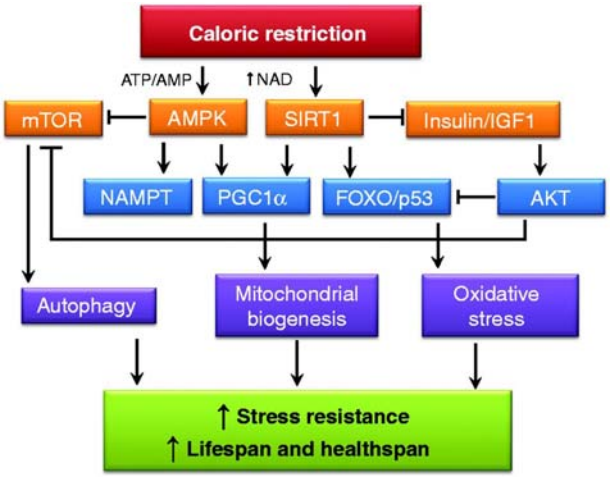

Fig. 7 The complex metabolic network of potential players in the mechanism of CR. A reduction in energy intake influences cellular energy levels, activating the AMPK and SIRT1 pathways. Antagonistic responses include the inhibition of the anabolic pathways mTOR and insulin/IGF1. Downstream effects result in increased stress resistance and improved life span and healthspan. The figure is reproduced with permission of the copyright holders from Solon-Biet, S.M.; McMahon, A.C.; Ballard, J.W.; Ruohonen, K.; Wu, L.E.; Cogger, V.C.; Warren, A.; Huang, X.; Pichaud, N.; Melvin, R.G.; Gokarn, R.; Khalil, M.; Turner, N.; Cooney, G.J.; Sinclair, D.A.; Raubenheimer, D.; Le Couteur, D.G.; Simpson, S.J., The ratio of macronutrients, not caloric intake, dictates cardiometabolic health, aging, and longevity in ad libitum-fed mice, Cell Metab 19 (3) (2014) 418–430.

The complex metabolic network of potential players in the mechanism of CR and CR-mimicking interventions is presented in Fig. 7.

1.12.4 Autophagy

Autophagy is a cytoplasmic catabolic process of protecting cells against stressful conditions. By this process, damaged or defective cellular components are engulfed into the lysosomes for degradation and recycling of their components; then they can be used for protein synthesis and cellular repair.[307] Depending on the mode of delivery of cellular material to lysosomes, autophagy is generally classified into three major categories: microautophagy, macroautophagy, and chaperone-mediated autophagy.[308] Among them, macroautophagy (usually referred to as 'autophagy'), a degradative pathway wherein cytoplasmatic components such as aggregated/misfolded proteins and organelles are engulfed within double-membrane vesicles (autophagosomes) and then delivered to lysosomes for degradation, is the most prominent and best-studied form of autophagy. This process is involved in degrading and recycling macromolecules and damaged organelles to maintain intracellular homeostasis in conditions of metabolic stress.

The autophagy pathway is evolutionarily conserved across diverse species ranging from yeast to mammals. For decades, this process has been regarded as a predominantly unspecific and destructive, contributing to 'autophagic cell death'. However, recent research has uncovered important cytoprotective functions of this pathway including fuel utilization, cellular differentiation and protection against cell death.[309] The cytoprotective effects of autophagy are generally attributed to the digestion of potentially harmful intracellular structures, including aggregates of misfolded proteins and damaged organelles.[310,311] Madeo et al.[312] speculated in their recent review that major mechanistic pathways contributing to cytoprotection by autophagy are: '(a) buffering of cellular stress in conditions of fluctuating nutrient availability by enhanced provision of substrates for bioenergetic metabolism and anabolic reactions, (b) removal of dysfunctional and harmful organelles, including uncoupled mitochondria, and (c) clearance of aggregate-prone, potentially toxic proteins.' On the whole-organism level, these pathways can be expanded by the immunoregulatory effects of autophagy, suppression of carcinogenesis as well as by hormetic responses.[312]

The autophagic cytoprotective response allows cell to mobilize the energy resources from recycled organelles in order to cope with stress, particularly in conditions of hypoxia, amino acid and/or glucose deprivation, genotoxic stress and viral infection.[313–315] As a consequence, autophagy induced by hypoxia or nutrient deprivation enhances cellular survival, and thereby improves cellular fitness, while inhibiting this pathway can precipitate bioenergetic failure and cell death.[316] The autophagy-induced enhanced stress resistance has been revealed at the organismal level as well. The induction of autophagy is believed to be contributed to the beneficial effects of fasting,[317] low-dose radiation (radiation hormesis)[318] and low doses of toxins and other stressors.[311] It can also play an important role in aging process because they counteract the age-associated accumulation of damaged organelles and proteins. Since the capacity of the cell for autophagic degradation is known to decline with age, it is not surprising that autophagy has an important impact on pathological processes common to the elderly. A deficient autophagy is suggested to

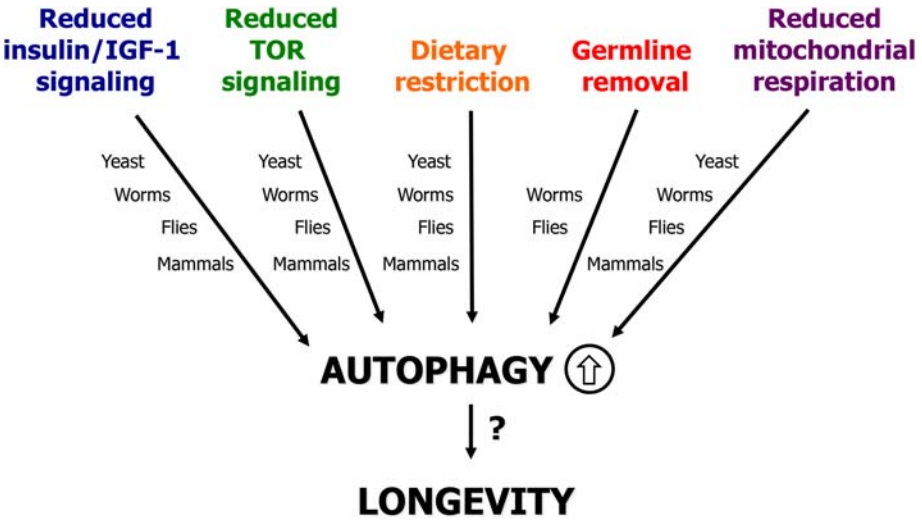

Fig. 8 Conserved longevity pathways and processes, which modulate aging via autophagy. Additional interventions not listed here, e.g., the polyamine spermidine may also engage autophagy as a possible effector mechanism to extend life span. For simplicity, the interactions between the pathways are not shown, whereas the degree of conservation is indicated. While the mechanisms by which autophagy affects aging through these longevity paradigms are not yet fully elucidated, several positive regulators of autophagy have been identified, including the forkhead transcription factor FOXO, the histone deacetylase SIRT1, the energy sensor AMPK, and the forkhead transcription factor PHA-4/FOXA. The figure is reproduced with permission of the copyright holders from Gelino, S.; Hansen, M., Autophagy – an emerging anti-aging mechanism?, J Clin Exp Pathol (4) (2012) pii:006, with correction.

contribute to a variety of age-related pathological conditions such as excessive lipid accumulation, glucose intolerance, reduction of muscle mass (sarcopenia), neurodegeneration and cardiac malfunction.[309]

Autophagy-related genes (ATGs) have been shown to be significantly implicated in the life extending effects observed in fruit flies, nematodes and mice.[319] In experimental models, autophagy has been demonstrated to be induced by the same genetic manipulations that are known to extend longevity, such as mutations in crucial signaling pathways like the TOR, SIRT1 and insulin/IGF-1 pathways.[307,320] Moreover, life extending effects have been repeatedly obtained by the pharmacologic induction of autophagy in experimental studies.[312] The schematic presentation of autophagy-mediated pathways potentially influencing longevity is presented in Fig. 8.

Biological mechanisms underlying the role of autophagy in health and disease are not properly understood to date, however there are several plausible explanations for this. Enhanced autophagy can improve the resistance of the cell to stress by increasing its metabolic buffering capacity or, alternatively, it can enhance the organelles' turnover, thereby preventing the accumulation of old or damaged organelles.[321–323] Moreover, the reduced autophagy can contribute to the progression of cancer, whereas the increased level of autophagy is characteristic to cancerous cells where the availability of nutrients and oxygen is restricted and represents a mechanism of cell survival aimed to overcome the cellular stress and cytotoxicity induced by drugs.[324]

1.12.4.1 Pharmacological Induction of Autophagy

Depending on the pathophysiological context, pharmacological suppression or induction of autophagy can cause therapeutic effects through promoting either survival or death of particular cell groups which may be critically important when attempting to treat chronic human disorders, including cancer.[325] Currently, it is commonly believed that modulating the autophagy activity via targeting specific components of its molecular machinery can affect the development and progression of the chronic pathological processes, thereby representing a promising pharmacological target for therapeutic application in treatment of age-associated diseases. Many recent data indicate that autophagy can mediate CR-dependent life span extension, and also that induction of autophagy may contribute to the pharmacologically-induced life extension in various experimental models.[326]

Involvement of autophagy in life-extending effects of rapamycin has been demonstrated in yeast, worms and fruit flies. In yeast, rapamycin was not able to extend the chronological life span of mutants lacking the essential autophagic genes, *ATG1* and *ATG7*.[327,328] Autophagy was also found to be required for life span extension by rapamycin in *C. elegans*: no positive effect on longevity was observed when the essential autophagy genes, *VPS34* and *BEC-1*, were knocked down.[329] Role of autophagy in rapamycin-induced life extension has been also found for *Drosophila melanogaster*.[241]

Resveratrol is another commonly used drug whose health-promoting effects are believed to be mediated by autophagy. In many organisms, including humans, resveratrol was found to substantially increase the level of SIRT1, which is a key regulator of both autophagy and longevity, but failed to extend life span under the lack of SIRT1. For example, resveratrol treatment caused life extension in the autophagy-proficient nematodes in conditions of CR. These beneficial effects, however, were abolished by the

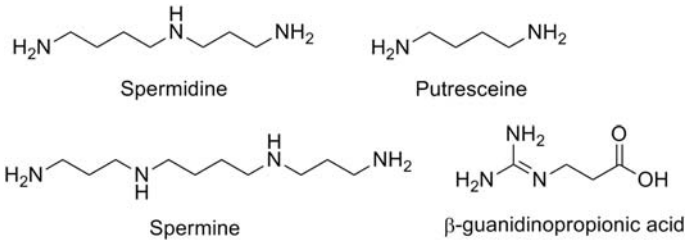

Fig. 9 Autophagy-inducing agents.

knockdown of the essential autophagic modulator Beclin-1.[330] These findings indicate that life-extending effects of resveratrol are consistent with SIRT1-dependent induction of autophagy.

Similarly to the resveratrol, which is the histone deacetylase activator, the histone acetylase inhibitor, spermidine, can induce autophagy by upregulation of ATG genes and extend life span in a range of model organisms from yeast to mice.[326,331–333] This ubiquitous molecule is a naturally occurring polyamine interacting, along with other polycations, with negatively charged molecules, including RNA, DNA and lipids, thereby substantially influencing basic cellular functions such as DNA stability, as well as cell growth, proliferation and death. The intracellular concentrations of spermidine have been shown to decline through the aging process.[334] Recently, spermidine has been emerged as promising anti-aging substance.[334–336] The supplementation with this agent was shown to increase the resistance to stress and life span in yeast, nematode worms and fruit flies, as well as to decrease the loss of age-related locomotor activity and the incidence of age-related pathological changes.[334,336,337] Supplementation with spermidine and other physiologically relevant polyamines, putrescine and spermine (**Fig. 9**), also increased both healthspan and life span in mice,[332,333] although implication of autophagy has not been examined in this research.

Since spermidine can affect the acetylation profile of many proteins (mostly belonging to the autophagy protein network), autophagy is currently believed to be the main mechanism mediating the anti-aging effects of this substance. Involvement of autophagy in the life-extending effects of spermidine is evident from the fact that these effects were abolished in yeast, worms and fruit flies if autophagy was blocked by knockout or knockdown of the essential autophagy genes, *ATG7* or *BECN1*.[326] Remarkably, the deletion of SIRT1 did not abolish the life-extending capability of spermidine, indicating that spermidine can promote longevity by pathways other than SIRT1.[326] Other candidate pathways, mTOR and AMPK, are also unlikely to play a crucial role, because of spermidine does not alter the phosphorylation status of mTOR, AMPK and their substrates.[338] In addition, recent research has demonstrated that spermidine may act through mechanisms such as control of inflammation and lipid metabolism, as well as regulation of cell growth, proliferation and death.[337] It is currently believed that another important signalling pathway mediating the effects of spermidine is the MAPK pathway, which is known to interact with polyamines. This pathway was shown to be involved in the control of cellular functions such as cell proliferation, inflammation, and programmed cell death, and also in autophagy modulation.[339,340] It should be, however, noted that since the health benefits and life-extending effects of spermidine are generally mediated by inhibition of histone acetylase activity, whereas similar beneficial effects of resveratrol are due to the activation of the histone deacetylase, SIRT1, it may be indicative of the important role of histone acetylation in both the autophagy and longevity pathways. Supplementation with spermidine can cause histone deacetylation, thereby inducing changes in gene expression.[334]

In recent years, other potent autophagy-inducing agents have emerged as exhibiting life-extending properties. For example, it has been demonstrated that β-guanidinopropionic acid (a creatine analog that causes ATP depletion) (**Fig. 9**) can extend the life span of *Drosophila melanogaster* via an AMP-activated protein kinase-dependent increase in autophagy.[341] Administration of ethanolamine (a precursor of phosphatidylethanolamine which is an essential component of most biological membranes) was also shown to positively regulate the autophagy and longevity in yeast.[342] Experimental findings on the life span-modulating effects of autophagy-inducing agents are summarized in **Table 5**.

1.12.5 Melatonin

Melatonin (**Fig. 3**) is a natural hormone produced predominantly by pineal gland in the brain and released into circulation in a pulsatile fashion with the sharpest peaks in the early morning hours.[343] It is a highly pleiotropic agent acting not only as an orchestrating chronobiotic required for some high-amplitude rhythms, but also a potent antioxidant that prevents excessive free radical formation thus supporting the redox balance, a modulator and protectant of mitochondrial electron flux, a coregulator of metabolic sensing and antagonist of insulin resistance, as well as an immune modulator.[344] In addition, its effects appear to be mediated by autophagy and regulation of some signaling pathways that influence energy metabolism, including insulin/IGF1, Akt and phosphoinositide 3 kinase (PI3K), as well as mTOR signaling pathway.[345]

The role of melatonin in aging process is evident from the observation that both aging and age-associated disorders are linked to loss in melatonin secretion and decline of circadian amplitude of the melatonin rhythm. Recently, it has also been suggested that life span-modulating effects of melatonin may be attributed to SIRT1 activation.[346] On this background and since melatonin is shown to be a safe and well tolerated substance, it attracts great interest for the application in anti-aging medicine. Its potent aging-

Table 5 Summary of the effects of autophagy-inducing agents on the life span and associated functional traits of model organisms

Model organism	*Substance/dose*	*Effects observed*	*Reference*
Saccharomyces cerevisiae	Rapamycin (0.1–40 nM)	Extension of chronological life span accompanied by induction of autophagy in wild-type strain; no effects on life span in autophagy-deficient mutant strains, ATG1 and ATG7	Alvers et al.[327,328]
	Spermidine (1 mM)	Extension of chronological life span in an autophagy-dependent fashion	Eisenberg et al.[334]
	Ethanolamine (10 mM)	Extension of chronological life span in an autophagy-dependent fashion	Rockenfeller et al.[342]
Caenorhabditis elegans	Spermidine (0.2 mM)	Extension of life span in an autophagy-dependent fashion	Eisenberg et al.[334]
Drosophila melanogaster	Spermidine (1 mM)	Extension of life span in an autophagy-dependent fashion	Eisenberg et al.[334]
	Spermidine (0.1 and 1 mM)	Increased median life spans, enhances starvation resistance, improved survival on paraquat, reduced female fecundity; abolished life extension by downregulation of autophagy through the reduction in expression of ATG5 gene by RNA interference	Bjedov et al.[241]
	β-guanidinopropionic acid (>900 mM)	Life extension via an AMP-activated protein kinase-dependent increase in autophagy; abolished life extension by downregulation of autophagy through the reduction in expression of ATG5 gene by RNA interference	Yang et al.[341]
Mus musculus	Mixture of spermine, spermidine and putrescine (374 to 1540 nmol g^{-1})	Increased survival, lower incidence of glomerulosclerosis in kidney	Soda et al.[332]
	Mixture of spermine, spermidine and putrescine (374 to 1540 nmol g^{-1})	Reduced mortality in advanced age; decreased age-associated pathological changes, suppressed age-associated increase in pro-inflammatory status, inhibited age-associated global alteration in DNA methylation status and 1,2-dimethylhydrazine-induced tumorigenesis	Soda et al.[333]

modulating properties were investigated in a range of model systems.[347] Life-extending capabilities of melatonin have been repeatedly demonstrated in *Drosophila melanogaster* and in mice.[348] Findings from these studies are summarized in the **Table 6**.

1.12.6 Perspective and conclusion

This chapter is devoted to review literature related to the development of theoretical concepts, as well as advances and perspectives in the field of anti-aging pharmacology. Based on analysis of research findings reviewed in the chapter, the conclusion can be made that this research field has evolved from the reductionistic to more systemic holistic thinking and approaches. It seems increasingly clear that a single cause cannot properly explain the anti-aging and longevity-promoting effects of various pharmacological classes. In the middle of the past century it was generally believed that cellular damages induced by free radicals are the main cause of aging and that supplementation with exogenous antioxidants can protect against such damages, thereby slowing the aging process and preventing the age-related chronic pathologies. Presently, however, it is becoming increasingly obvious that pro-longevity effects of most potential anti-aging drugs are complex and may be attributable to multiple interacting signaling pathways. For example,

Table 6 Summary of the effects of melatonin on the life span and associated functional traits of model organisms

Model organism	*Effects observed*	*Reference*
Drosophila melanogaster	Increase of life span up to 19% in males and up to 12% in females	Izmaylov and Obukhova [72]
	13.5% increase in median life span; 33.2% increase in maximum life span; increased resistance to paraquat and to heightened temperature (36°C)	Bonilla et al.[349]
	27.8% decrease in mean life span, 25.4% increase in maximum life span; increased eclosion rate and the locomotor activity; decreased concentration of malondialdehyde	Terán et al.[350]
Mus musculus	5.4% increase in mean life span of female CBA mice; decreased locomotor activity and body temperature; delay of the age-related switching-off of estrous function; 20% increase in malignant tumor incidence	Anisimov et al.[351]
	10% increase in maximum life span of female SHR mice; delay of the age-related switching-off of estrous function	Anisimov et al.[352]
	17.4% increase in maximum life span of SAMP8 mice; normalized redox and bioenergetic status of the mitochondria and increased ATP levels	Rodríguez et al.[96]

resveratrol, in addition to being the well-known sirtuin-activating substance, also showed other beneficial properties, such as antioxidant activity. Moreover, both resveratrol and other promising anti-aging drug, spermidine, can induce autophagy by differing pathways, the first one by SIRT1 activation and the second one through protein hypoacetylation. In addition, hormesis (beneficial effects from low doses of potentially toxic substances) may also be involved in pro-longevity effects of various compounds.[105,353,354] Such substances can cause the mild stress-induced activation of several stress response pathways and stimulation of repair mechanisms, thereby reducing the age-related accumulation of molecular damage.[355] Thereby, it can be assumed that, taking into account the complexity of the aging process, application of hormesis-based systemic approach addressed primarily to mechanisms of central regulation of the aging process could be a novel promising strategy to slow down aging and to extend the healthspan and life span.[99]

Taking into account the extraordinary complexity of mechanistic pathways underlying aging process, the recognition of these pathways and development of anti-aging interventions seems a challenging task. Significant progress, however, has been achieved in this research field during the past years. A number of pharmacological agents with the potential to target particular pathways associated with aging and to produce protective responses against age-related pathologies are currently under investigation. Nowadays, there is an active search for new classes of pharmacological agents capable of modulating the rate of aging. Apart from the substances with potential clinical value in the treatment of aging-related conditions, which are described in detail in this review, other agents also may be classified as potent anti-aging therapeutic compounds. All these compounds are multi-functional and targeted at multiple signaling pathways affecting aging. Among them, there are phytochemicals such as curcumin, a natural extract from the turmeric spice which is a powerful antioxidant and efficient inhibitor of mTOR and NF-kappaB,[356] as well as epigallocatechin gallate (EGCG), a flavonoid extracted from green tea shown to prevent age-related inflammation and oxidative stress via the inhibition of NF-kappaB signaling by activation of the pro-longevity factors including forkhead box transcription factor FoxO3a and SIRT1 (Fig. 6).[98] A lot of hope is also being pinned on pharmacological agents targeted to epigenetic regulators of gene activity, such as inhibitors of DNA methyltransferases and histone deacetylases (HDACs). Life-extending properties of HDACs including sodium buthyrate, trichostatin A (TSA), sodium 4-phenylbutyrate (PBA) and suberoylanilide hydroxamic acid (SAHA) (Fig. 10) have been reported repeatedly in *Drosophila* studies.[357–359] The evidence remains however limited regarding the overall health benefits of these substances, including epidemiological studies exploring the impacts of various intake levels on human health.

In summarizing it can be concluded that targeting aging per se can be more effective approach to postpone or prevent age-associated disorders than treatments targeted to specific pathological conditions. Because of the aging population, such therapeutic strategy is undoubtedly an area of enhancing relevance for pharmaceutical industry and public health organizations. Longo et al. concluded in their recent review that 'the time has come not only to consider several therapeutic options for the treatment of age-related comorbidities, but to initiate clinical trials with the ultimate goal of increasing the healthspan (and perhaps longevity) of human populations, while respecting the guiding principle of physicians primum non nocere.[161] Currently, this is the consensus among physicians and health professionals that the optimization of physiological and mental functioning throughout the life span should be a major emphasis of any contemporaneous biomedical policy addressing global aging. The healthy lifestyle comprising proper diet and physical activity represents the first-line function-preserving strategy. Pharmacological compounds, both existing and potential, can serve as prospective complementary approach.[11]

In a modern pharmacy, anti-aging is likely one of the most promising markets because the target group can potentially include each person. Current marketing research indicates that most people are willing to pay for long-term pharmacological therapy to prevent or delay the aging-related decline in physical and mental functions.[153] Optimistic predictions of the feasibility of health- and life-extending interventions, however, should certainly be critically discussed in the light of their ethical, economic and social implications. Only after in-depth examination and following comprehensive debates, the implementation of such approaches in clinical practice will be possible. To meet the requirements created by the rapid aging of the population in both developed and developing countries, a new emphasis in physiological geroscience is needed that will demand the joint efforts of interdisciplinary researchers working throughout the continuum of translational research from basic science to health care.

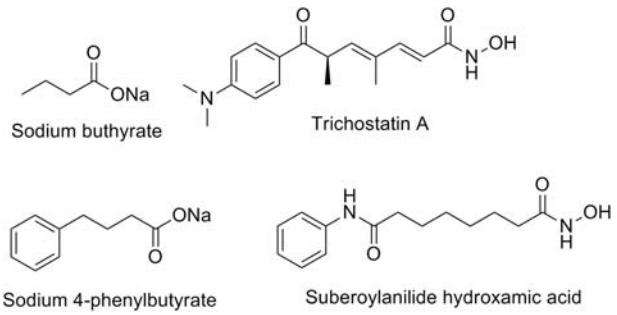

Fig. 10 Inhibitors of histone deacetylases.

Acknowledgments

The author thanks Oksana Zabuga for the assistance in preparing the manuscript.

References

1. de Magalhães, J. P. The scientific quest for lasting youth: prospects for curing aging. *Rejuvenation Res* **2014,** *17* (5), 458–467.
2. Vijg, J.; de Grey, A. D. Innovating aging: promises and pitfalls on the road to life extension. *Gerontology* **2014,** *60* (4), 373–380.
3. Kennedy, B. K.; Pennypacker, J. K. Drugs that modulate aging: the promising yet difficult path ahead. *Transl Res* **2014,** *163* (5), 456–465.
4. Hung, W. W.; Ross, J. S.; Boockvar, K. S.; Siu, A. L. Recent trends in chronic disease, impairment and disability among older adults in the United States. *BMC Geriatr* **2011,** *11,* 47.
5. Petsko, G. A. A seat at the table. *Genome Biol* **2008,** *9* (12), 113.
6. Beard, J. R.; Bloom, D. E. Towards a comprehensive public health response to population ageing. *Lancet* **2015,** *385* (9968), 658–661.
7. Harper, S. Economic and social implications of aging societies. *Science* **2014,** *346,* 587–591.
8. Le Bourg, E. Obsolete ideas and logical confusions can be obstacles for biogerontology research. *Biogerontology* **2013,** *14* (2), 221–227.
9. Fontana, L.; Partridge, L.; Longo, V. D. Extending healthy life span – from yeast to humans. *Science.* **2010,** *328,* 321–326.
10. Willcox, B. J.; Willcox, D. C.; Ferrucci, L. Secrets of healthy aging and longevity from exceptional survivors around the globe: Lessons fom octogenarians to supercentenarians. *J Gerontol A Biol Sci Med Sci.* **2008,** *63,* 1181–1185.
11. Seals, D.R.; Justice, J.N.; LaRocca, T.J., Physiological geroscience: targeting function to increase healthspan and achieve optimal longevity, J Physiol (2015) (In press). http://dx.doi.org/10.1113/jphysiol.2014.282665.
12. Kennedy, B. K.; Berger, S. L.; Brunet, A.; Campisi, J.; Cuervo, A. M.; Epel, E. S.; Franceschi, C.; Lithgow, G. J.; Morimoto, R. I.; Pessin, J. E.; Rando, T. A.; Richardson, A.; Schadt, E. E.; Wyss-Coray, T.; Sierra, F. Geroscience: Linking aging to chronic disease. *Cell* **2014,** *159,* 709–713.
13. Kirkland, J. L. Translating advances from the basic biology of aging into clinical application. *Exp Gerontol* **2013,** *48,* 1–5.
14. Fontana, L.; Kennedy, B. K.; Longo, V. D.; Seals, D.; Melov, S. Medical research: Treat ageing. *Nature* **2014,** *511,* 405–407.
15. Epel, E. S.; Lithgow, G. J. Stress biology and aging mechanisms: Toward understanding the deep connection between adaptation to stress and longevity. *J Gerontol A Biol Sci Med Sci* **2014,** *69* (l), S10–S16.
16. Barazzetti, G.; Reichlin, M. Life-extension: A biomedical goal? Scientific prospects, ethical concerns. *Swiss Med Wkly* **2011,** *141,* w13181.
17. Klatz, R. New horizons for the clinical speciality of anti-aging medicine. The future with biomedical technologies. *Ann NY Acad Sci* **2005,** *1057,* 536–544.
18. Tosato, M.; Zamboni, V.; Ferrini, A.; Cesari, M. The aging process and potential interventions to extend life expectancy. *Clin Interv Aging* **2007,** *2* (3), 401–412.
19. Anton, B.; Vitetta, L.; Cortizo, F.; Sali, A. Can we delay aging? The biology and science of aging. *Ann NY Acad Sci* **2005,** *1057,* 525–535.
20. Caplan, A. L. An unnatural process: Why it is not inherently wrong to seek a cure for aging. In *The Fountain of Youth. Cultural, Scientific, and Ethical Perspectives on a Biomedical Goal;* Post, S. G., Binstock, R. H., Eds.; Oxford University Press: Oxford, 2004; pp 271–285.
21. Lemaître, J. F.; Berger, V.; Bonenfant, C.; Douhard, M.; Gamelon, M.; Plard, F.; Gaillard, J. M. Early-late life trade-offs and the evolution of ageing in the wild. *Proc Biol Sci* **2015,** *282* (1806), 20150209.
22. Verdaguer, E.; Junyent, F.; Folch, J.; Beas-Zarate, C.; Auladell, C.; Pallàs, M.; Camins, A. Aging biology: a new frontier for drug discovery. *Expert Opin Drug Discov* **2012,** *7* (3), 217–229.
23. Zhou, Y.; Huang, N. Binding site druggability assessment in fragment-based drug design. *Methods Mol Biol* **2015,** *1289,* 13–21.
24. Paul, S. M.; Mytelka, D. S.; Dunwiddie, C. T.; Persinger, C. C.; Munos, B. H.; Lindborg, S. R.; Schacht, A. L. How to improve R&D productivity: the pharmaceutical industry's grand challenge. *Nat Rev Drug Discov* **2010,** *9,* 203–214.
25. Moskalev, A. A.; Aliper, A. M.; Smit-McBride, Z.; Buzdin, A.; Zhavoronkov, A. Genetics and epigenetics of aging and longevity. *Cell Cycle* **2014,** *13* (7), 1063–1077.
26. Lindborg, C. M.; Property, K. J.; Pignolo, R. J. Conservation of pro-longevity genes among mammals. *Mech Ageing Dev* **2015,** *146–148,* 23–27.
27. Shadyab, A. H.; LaCroix, A. Z. Genetic factors associated with longevity: A review of recent findings. *Ageing Res Rev* **2015,** *19,* 1–7.
28. Seals, D. R.; Kaplon, R. E.; Gioscia-Ryan, R. A.; LaRocca, T. J. You're only as old as your arteries: translational strategies for preserving vascular endothelial function with aging. *Physiology (Bethesda)* **2014,** *29,* 250–264.
29. Huber, W. R.; Sierra, F. The longevity dividend: Why invest in basic aging reserach? *Can J Aging* **2009,** *28* (4), 391–394.
30. Olshansky, S. J. Articulating the case for the longevity dividend. *Public Policy & Aging Report* **2013,** *23* (4), 3–6.
31. Seals, D. R.; Melov, S. Translational Geroscience: Emphasizing function to achieve optimal longevity. *Aging (Albany)* **2014,** *6,* 718–730.
32. Goldman, D. P.; Cutler, D.; Rowe, J. W.; Michaud, P. C.; Sullivan, J.; Peneva, D.; Olshansky, S. J. Substantial health and economic returns from delayed aging may warrant a new focus for medical research. *Health Aff.* **2013,** *32,* 1698–1705.
33. Le Couteur, D. G.; Sinclair, D. A. A blueprint for developing therapeutic approaches that increase healthspan and delay death. *J Gerontol A Biol Sci Med Sci* **2010,** *65,* 693–694.
34. Harman, D. Aging: a theory based on free radical and radiation chemistry. *J Gerontol* **1956,** *11,* 298–300.
35. Pandey, K. B.; Rizvi, S. I. Markers of oxidative stress in erythrocytes and plasma during aging in humans. *Oxid Med Cell Longev* **2010,** *3* (1), 2–12.
36. Bouayed, J.; Bohn, T. Exogenous antioxidants – Double-edged swords in cellular redox state: Health beneficial effects at physiologic doses versus deleterious effects at high doses. *Oxid Med Cell Longev* **2010,** *3* (4), 228–237.
37. Liu, Y.; Long, J.; Liu, J. Mitochondrial free radical theory of aging: Who moved my premise? *Geriatr Gerontol Int* **2014,** *14* (4), 740–749.
38. Pinto, M.; Moraes, C. T. Mechanisms linking mtDNA damage and aging. *Free Radic Biol Med* **2015,** *85,* 250–258.
39. Si, H.; Liu, D. Dietary antiaging phytochemicals and mechanisms associated with prolonged survival. *J Nutr Biochem* **2014,** *25* (6), 581–591.
40. Sadowska-Bartosz, I.; Bartosz, G. Effect of antioxidants supplementation on aging and longevity. *Biomed Res Int* **2014,** *2014,* 404680.
41. Niki, E.; Noguchi, N.; Tsuchihashi, H.; Gotoh, N. Interaction among vitamin C, vitamin E, and beta-carotene. *Am J Clin Nutr* **1995,** *62* (6), 1322S–1326S.
42. Meydani, M. Vitamin E and atherosclerosis: beyond prevention of LDL oxidation. *J Nutr* **2001,** *131* (2), 366S–368S.
43. Ganie, S. A.; Dar, T.; Bhat, A.; Dar, K.; Anees, S.; Masood, A.; Zargar, M.A., Melatonin: A potential antioxidant therapeutic agent for mitochondrial dysfunctions and related disorders, Rejuvenation Res (2015) (In press).
44. Hargreaves, I. P. Coenzyme Q10 as a therapy for mitochondrial disease. *Int J Biochem Cell Biol* **2014,** *49,* 105–111.
45. Bast, A.; Haenen, G. R. Lipoic acid: A multifunctional antioxidant. *Biofactors* **2003,** *17* (1–4), 207–213.
46. Gruber, J.; Fong, S.; Chen, C. B.; Yoong, S.; Pastorin, G.; Schaffer, S.; Cheah, I.; Halliwell, B. Mitochondria-targeted antioxidants and metabolic modulators as pharmacological interventions to slow ageing. *Biotechnol Adv* **2013,** *31* (5), 563–592.
47. Skulachev, V. P. Cationic antioxidants as a powerful tool against mitochondrial oxidative stress. *Biochem Biophys Res Commun* **2013,** *441* (2), 275–279.
48. Quick, K. L.; Ali, S. S.; Arch, R.; Xiong, C.; Wozniak, D.; Dugan, L. L. A carboxyfullerene SOD mimetic improves cognition and extends the lifespan of mice. *Neurobiol Aging* **2008,** *29* (1), 117–128.

49. Inoue, S.; Koya-Miyata, S.; Ushio, S.; Iwaki, K.; Ikeda, M.; Kurimoto, M. Royal Jelly prolongs the life span of C3H/HeJ mice: Correlation with reduced DNA damage. *Exp Gerontol* **2003,** *38* (9), 965–969.
50. Farr, S. A.; Price, T. O.; Banks, W. A.; Ercal, N.; Morley, J. E. Effect of alpha-lipoic acid on memory, oxidation, and lifespan in SAMP8 mice. *J Alzheimers Dis* **2012,** *32* (2), 447–455.
51. Rodríguez, M. I.; Escames, G.; López, L. C.; López, A.; García, J. A.; Ortiz, F.; Sánchez, V.; Romeu, M.; Acuña-Castroviejo, D. Improved mitochondrial function and increased life span after chronic melatonin treatment in senescent prone mice. *Exp Gerontol* **2008,** *43* (8), 749–756.
52. Niu, Y.; Na, L.; Feng, R.; Gong, L.; Zhao, Y.; Li, Q.; Li, Y.; Sun, C. The phytochemical, EGCG, extends lifespan by reducing liver and kidney function damage and improving age-associated inflammation and oxidative stress in healthy rats. *Aging Cell* **2013,** *12* (6), 1041–1049.
53. Suckow, B. K.; Suckow, M. A. Lifespan extension by the antioxidant curcumin in Drosophila melanogaster. *Int J Biomed Sci* **2006,** *2* (4), 402–405.
54. Shen, L. R.; Xiao, F.; Yuan, P.; Chen, Y.; Gao, Q. K.; Parnell, L. D.; Meydani, M.; Ordovas, J. M.; Li, D.; Lai, C. Q. Curcumin-supplemented diets increase superoxide dismutase activity and mean lifespan in Drosophila. *Age (Dordr)* **2013,** *35* (4), 1133–1142.
55. Chandrashekara, K. T.; Shakarad, M. N. Aloe vera or resveratrol supplementation in larval diet delays adult aging in the fruit fly Drosophila melanogaster. *J Gerontol A Biol Sci Med Sci* **2011,** *66* (9), 965–971.
56. Saul, N.; Pietsch, K.; Menzel, R.; Stürzenbaum, S. R.; Steinberg, C. E. Catechin induced longevity in C. elegans: from key regulator genes to disposable soma. *Mech Ageing Dev* **2009,** *130* (8), 477–486.
57. Abbas, S.; Wink, M. Epigallocatechin gallate from green tea (Camellia sinensis) increases lifespan and stress resistance in Caenorhabditis elegans. *Planta Med* **2009,** *75* (3), 216–221.
58. Zhang, L.; Jie, G.; Zhang, J.; Zhao, B. Significant longevity-extending effects of EGCG on Caenorhabditis elegans under stress. *Free Radic Biol Med* **2009,** *46* (3), 414–421.
59. Sayed, A. A. Ferulsinaic acid attenuation of advanced glycation end products extends the lifespan of Caenorhabditis elegans. *J Pharm Pharmacol* **2011,** *63* (3), 423–428.
60. Moriwaki, T.; Kato, S.; Kato, Y.; Hosoki, A.; Zhang-Akiyama, Q. M. Extension of lifespan and protection against oxidative stress by an antioxidant herb mixture complex (KPG-7) in Caenorhabditis elegans. *J Clin Biochem Nutr* **2013,** *53* (2), 81–88.
61. Wu, Z.; Smith, J. V.; Paramasivam, V.; Butko, P.; Khan, I.; Cypser, J. R.; Luo, Y. Ginkgo biloba extract EGb 761 increases stress resistance and extends life span of Caenorhabditis elegans. *Cell Mol Biol (Noisy-le-grand)* **2002,** *48* (6), 725–731.
62. Oh, S. I.; Park, J. K.; Park, S. K. Lifespan extension and increased resistance to environmental stressors by N-Acetyl-L-Cysteine in Caenorhabditis elegans. *Clinics (Sao Paulo)* **2015,** *70* (5), 380–386.
63. Park, J. K.; Kim, C. K.; Gong, S. K.; Yu, A. R.; Lee, M. Y.; Park, S. K. Acanthopanax sessiliflorus stem confers increased resistance to environmental stresses and lifespan extension in Caenorhabditis elegans. *Nutr Res Pract* **2014,** *8* (5), 526–532.
64. Surco-Laos, F.; Cabello, J.; Gómez-Orte, E.; González-Manzano, S.; González-Paramás, A. M.; Santos-Buelga, C.; Dueñas, M. Effects of O-methylated metabolites of quercetin on oxidative stress, thermotolerance, lifespan and bioavailability on Caenorhabditis elegans. *Food Funct* **2011,** *2* (8), 445–456.
65. Wang, C.; Yolitz, J.; Alberico, T.; Laslo, M.; Sun, Y.; Wheeler, C. T.; Sun, X.; Zou, S. Cranberry interacts with dietary macronutrients to promote healthy aging in Drosophila. *J Gerontol A Biol Sci Med Sci* **2014,** *69* (8), 945–954.
66. Lee, K. S.; Lee, B. S.; Semnani, S.; Avanesian, A.; Um, C. Y.; Jeon, H. J.; Seong, K. M.; Yu, K.; Min, K. J.; Jafari, M. Curcumin extends life span, improves health span, and modulates the expression of age-associated aging genes in Drosophila melanogaster. *Rejuvenation Res* **2010,** *13* (5), 561–570.
67. Zuo, Y.; Peng, C.; Liang, Y.; Ma, K. Y.; Yu, H.; Edwin Chan, H. Y.; Chen, Z. Y. Black rice extract extends the lifespan of fruit flies. *Food Funct.* **2012,** *3* (12), 1271–1279.
68. Peng, C.; Zuo, Y.; Kwan, K. M.; Liang, Y.; Ma, K. Y.; Chan, H. Y.; Huang, Y.; Yu, H.; Chen, Z. Y. Blueberry extract prolongs lifespan of Drosophila melanogaster. *Exp Gerontol* **2012,** *47* (2), 170–178.
69. Wang, L.; Li, Y. M.; Lei, L.; Liu, Y.; Wang, X.; Ma, K. Y.; Chen, Z. Y. Cranberry anthocyanin extract prolongs lifespan of fruit flies. *Exp Gerontol* **2015,** *69,* 189–195.
70. Zuo, Y.; Peng, C.; Liang, Y.; Ma, K. Y.; Chan, H. Y.; Huang, Y.; Chen, Z. Y. Sesamin extends the mean lifespan of fruit flies. *Biogerontology* **2013,** *14* (2), 107–119.
71. Dueñas, M.; Surco-Laos, F.; González-Manzano, S.; González-Paramás, A. M.; Gómez-Orte, E.; Cabello, J.; Santos-Buelga, C. Deglycosylation is a key step in biotransformation and lifespan effects of quercetin-3-O-glucoside in Caenorhabditis elegans. *Pharmacol Res* **2013,** *76,* 41–48.
72. Keaney, M.; Gems, D. No increase in lifespan in Caenorhabditis elegans upon treatment with the superoxide dismutase mimetic EUK-8. *Free Radic Biol Med* **2003,** *34* (2), 277–282.
73. Bayne, A. C.; Sohal, R. S. Effects of superoxide dismutase/catalase mimetics on lifespan and oxidative stress resistance in the housefly Musca domestica. *Free Radical Biol Med.* **2002,** *32,* 1229–1234.
74. Banks, R.; Speakman, J. R.; Selman, C. Vitamin E supplementation and mammalian lifespan. *Mol Nutr Food Res* **2010,** *54* (5), 719–725.
75. Spindler, S. R.; Mote, P. L.; Flegal, J. M. Lifespan effects of simple and complex nutraceutical combinations fed isocalorically to mice. *Age (Dordr)* **2014,** *36* (2), 705–718.
76. Magwere, T.; West, M.; Riyahi, K.; Murphy, M. P.; Smith, R. A.; Partridge, L. The effects of exogenous antioxidants on lifespan and oxidative stress resistance in Drosophila melanogaster. *Mech Ageing Dev* **2006,** *127* (4), 356–370.
77. Blackett, A. D.; Hall, D. A. Vitamin E – its significance in mouse ageing. *Age Ageing* **1981,** *10* (3), 191–195.
78. Vaiserman, A. M. Aging-modulating treatments: from reductionism to a system-oriented perspective. *Front Genet.* **2014,** *5,* 446.
79. Le Bourg, E. Oxidative stress, aging and longevity in Drosophila melanogaster. *FEBS Lett* **2001,** *498* (2–3), 183–186.
80. Frankel, E. N. Antioxidants in lipid foods and their impact on food quality. *Food Chem.* **1996,** *57,* 51–55.
81. Carocho, M.; Ferreira, I. C. A review on antioxidants, prooxidants and related controversy: natural and synthetic compounds, screening and analysis methodologies and future perspectives. *Food Chem Toxicol.* **2013,** *51,* 15–25.
82. Mao, L.; Franke, J. Hormesis in aging and neurodegeneration-a prodigy awaiting dissection. *Int J Mol Sci* **2013,** *14* (7), 13109–13128.
83. Juránek, I.; Nikitovic, D.; Kouretas, D.; Hayes, A. W.; Tsatsakis, A. M. Biological importance of reactive oxygen species in relation to difficulties of treating pathologies involving oxidative stress by exogenous antioxidants. *Food Chem Toxicol.* **2013,** *61,* 240–247.
84. Rattan, S. I. Molecular gerontology: from homeodynamics to hormesis. *Curr Pharm Des* **2014,** *20* (18), 3036–3039.
85. Ristow, M.; Schmeisser, K. Mitohormesis: promoting health and lifespan by increased levels of reactive oxygen species (ROS). *Dose Response* **2014,** *12* (2), 288–341.
86. Padurariu, M.; Ciobica, A.; Lefter, R.; Serban, I. L.; Stefanescu, C.; Chirita, R. The oxidative stress hypothesis in Alzheimer's disease. *Psychiatr Danub* **2013,** *25* (4), 401–409.
87. Blesa, J.; Trigo-Damas, I.; Quiroga-Varela, A.; Jackson-Lewis, V. R. Oxidative stress and Parkinson's disease. *Front Neuroanat.* **2015,** *9,* 91.
88. Stadler, K. Oxidative stress in diabetes. *Adv Exp Med Biol.* **2012,** *771,* 272–287.
89. Polimeni, L.; Del Ben, M.; Baratta, F.; Perri, L.; Albanese, F.; Pastori, D.; Violi, F.; Angelico, F. Oxidative stress: New insights on the association of non-alcoholic fatty liver disease and atherosclerosis. *World J Hepatol* **2015,** *7* (10), 1325–1336.
90. Jain, A. K.; Mehra, N. K.; Swarnakar, N. K. Role of antioxidants for the treatment of cardiovascular diseases: Challenges and opportunities. *Curr Pharm Des* **2015,** *21* (30), 4441–4455.
91. Sinha, N.; Dabla, P. K. Oxidative stress and antioxidants in hypertension - a current review. *Curr Hypertens Rev* **2015,** *11* (2), 132–142.
92. Cerullo, F.; Gambassi, G.; Cesari, M. Rationale for antioxidant supplementation in sarcopenia. *J Aging Res* **2012,** *2012,* 316943.
93. Callaway, D. A.; Jiang, J. X. Reactive oxygen species and oxidative stress in osteoclastogenesis, skeletal aging and bone diseases. *J Bone Miner Metab* **2015,** *33* (4), 359–370.
94. Jung, C.; Rong, Y.; Doctrow, S.; Baudry, M.; Malfroy, B.; Xu, Z. Synthetic superoxide dismutase/catalase mimetics reduce oxidative stress and prolong survival in a mouse amyotrophic lateral sclerosis model. *Neurosci Lett* **2001,** *304,* 157–160.

95. Peng, J.; Stevenson, F. F.; Doctrow, S. R.; Andersen, J. K. Superoxide dismutase/catalase mimetics are neuroprotective against selective paraquat-mediated dopaminergic neuron death in the substantial nigra: Implications for Parkinson disease. *J Biol Chem* **2005,** *280* (32), 29194–29198.
96. Redout, E. M.; van der Toorn, A.; Zuidwijk, M. J.; van de Kolk, C. W.; van Echteld, C. J.; Musters, R. J.; van Hardeveld, C.; Paulus, W. J.; Simonides, W. S. Antioxidant treatment attenuates pulmonary arterial hypertension-induced heart failure. *Am J Physiol Heart Circ Physiol* **2010,** *298* (3), H1038–H1047.
97. van Empel, V. P.; Bertrand, A. T.; van Oort, R. J.; van der Nagel, R.; Engelen, M.; van Rijen, H. V.; Doevendans, P. A.; Crijns, H. J.; Ackerman, S. L.; Sluiter, W.; De Windt, L. J. EUK-8, a superoxide dismutase and catalase mimetic, reduces cardiac oxidative stress and ameliorates pressure overload-induced heart failure in the harlequin mouse mutant. *J Am Coll Cardiol* **2006,** *48* (4), 824–832.
98. Kawakami, S.; Matsuda, A.; Sunagawa, T.; Noda, Y.; Kaneko, T.; Tahara, S.; Hiraumi, Y.; Adachi, S.; Matsui, H.; Ando, K.; Fujita, T.; Maruyama, N.; Shirasawa, T.; Shimizu, T. Antioxidant, EUK-8, prevents murine dilated cardiomyopathy. *Circ J* **2009,** *73* (11), 2125–2134.
99. Makino, N.; Maeda, T.; Oyama, J.; Sasaki, M.; Higuchi, Y.; Mimori, K.; Shimizu, T. Antioxidant therapy attenuates myocardial telomerase activity reduction in superoxide dismutase-deficient mice. *J Mol Cell Cardiol* **2011,** *50* (4), 670–677.
100. Kris-Etherton, P. M.; Lichtenstein, A. H.; Howard, B. V.; Steinberg, D.; Witztum, J. L. Nutrition Committee of the American Heart Association Council on Nutrition, Physical Activity, and Metabolism. Antioxidant vitamin supplements and cardiovascular disease. *Circulation* **2004,** *110* (5), 637–641.
101. Sahebkar, A.; Serban, C.; Ursoniu, S.; Wong, N. D.; Muntner, P.; Graham, I. M.; Mikhailidis, D. P.; Rizzo, M.; Rysz, J.; Sperling, L. S.; Lip, G. Y.; Banach, M. Lipid and Blood Pressure Meta-analysis Collaboration Group. Lack of efficacy of resveratrol on C-reactive protein and selected cardiovascular risk factors – Results from a systematic review and meta-analysis of randomized controlled trials. *Int J Cardiol* **2015,** *189,* 47–55.
102. Schürks, M.; Glynn, R. J.; Rist, P. M.; Tzourio, C.; Kurth, T. Effects of vitamin E on stroke subtypes: Meta-analysis of randomised controlled trials. *BMJ* **2010,** *341,* c5702.
103. Sheikh-Ali, M.; Chehade, J. M.; Mooradian, A. D. The antioxidant paradox in diabetes mellitus. *Am J Ther* **2011,** *18* (3), 266–278.
104. Suksomboon, N.; Poolsup, N.; Juanak, N. Effects of coenzyme Q10 supplementation on metabolic profile in diabetes: a systematic review and meta-analysis. *J Clin Pharm Ther* **2015,** *40* (4), 413–418.
105. Doss, M. Shifting the paradigm in radiation safety. *Dose Response* **2012,** *10* (4), 562–583.
106. Halliwell, B. Free radicals and antioxidants – quo vadis? *Trends Pharmacol Sci* **2011,** *32,* 125–130.
107. Lawson, K. A.; Wright, M. E.; Subar, A.; Mouw, T.; Hollenbeck, A.; Schatzkin, A.; Leitzmann, M. F. Multivitamin use and risk of prostate cancer in the National Institutes of Health-AARP Diet and Health Study. *J Natl Cancer Inst* **2007,** *99,* 754–764.
108. Ristow, M.; Zarse, K.; Oberbach, A.; Kloting, N.; Birringer, M.; Kiehntopf, M.; Stumvoll, M.; Kahn, C. R.; Bluher, M. Antioxidants prevent health-promoting effects of physical exercise in humans. *Proc Natl Acad Sci U S A* **2009,** *106,* 8665–8670.
109. Albanes, D.; Heinonen, O. P.; Taylor, P. R.; Virtamo, J.; Edwards, B. K.; Rautalahti, M.; Hartman, A. M.; Palmgren, J.; Freedman, L. S.; Haapakoski, J.; Barrett, M. J.; Pietinen, P.; Malila, N.; Tala, E.; Liippo, K.; Salomaa, E. R.; Tangrea, J. A.; Teppo, L.; Askin, F. B.; Taskinen, E.; Erozan, Y.; Greenwald, P.; Huttunen, J. K. Alpha-tocopherol and beta-carotene supplements and lung cancer incidence in the alpha-tocopherol, beta-carotene cancer prevention study: effects of base-line characteristics and study compliance. *J Natl Cancer Inst.* **1996,** *88,* 1560–1570.
110. Omenn, G. S.; Goodman, G. E.; Thornquist, M. D.; Balmes, J.; Cullen, M. R.; Glass, A.; Keogh, J. P.; Meyskens, F. L.; Valanis, B.; Williams, J. H.; Barnhart, S.; Hammar, S. Effects of a combination of beta-carotene and vitamin A on lung cancer and cardiovascular disease. *N Engl J Med* **1996,** *334* (18), 1150–1155.
111. Dolara, P.; Bigagli, E.; Collins, A. Antioxidant vitamins and mineral supplementation, lifespan expansion and cancer incidence: a critical commentary. *Eur J Nutr* **2012,** *51,* 769–781.
112. Goyal, A.; Terry, M. B.; Siegel, A. B. Serum antioxidant nutrients, vitamin A, and mortality in U.S. Adults. *Cancer Epidemiol Biomarkers Prev* **2013,** *22,* 2202–2211.
113. Bjelakovic, G.; Nikolova, D.; Gluud, C. Antioxidant supplements and mortality. *Curr Opin Clin Nutr Metab Care* **2014,** *17,* 40–44.
114. Curtis, A. J.; Bullen, M.; Piccenna, L.; McNeil, J. J. Vitamin E supplementation and mortality in healthy people: a meta-analysis of randomised controlled trials. *Cardiovasc Drugs Ther* **2014,** *28* (6), 563–573.
115. Liu, Z. Q. Antioxidants may not always be beneficial to health. *Nutrition* **2014,** *30* (2), 131–133.
116. Halliwell, B. The antioxidant paradox: less paradoxical now? *Br J Clin Pharmacol* **2013,** *75* (3), 637–644.
117. Bast, A.; Haenen, G. R. Ten misconceptions about antioxidants. *Trends Pharmacol Sci* **2013,** *34* (8), 430–436.
118. Masoro, E. J. Overview of caloric restriction and ageing. *Mech Ageing Dev* **2005,** *126,* 913–922.
119. Fontana, L.; Partridge, L. Promoting health and longevity through diet: from model organisms to humans. *Cell* **2015,** *161* (1), 106–118.
120. McCay, C. M.; Crowell, M. F.; Maynard, L. A. The effect of retarded growth upon the length of life span and upon the ultimate body size. 1935. *Nutrition* **1989,** *5* (3), 155–171.
121. Selman, C. Dietary restriction and the pursuit of effective mimetics. *Proc Nutr Soc* **2014,** *73* (2), 260–270.
122. Testa, G.; Biasi, F.; Poli, G.; Chiarpotto, E. Calorie restriction and dietary restriction mimetics: a strategy for improving healthy aging and longevity. *Curr Pharm Des* **2014,** *20* (18), 2950–2977.
123. Ingram, D. K.; Roth, G. S. Calorie restriction mimetics: can you have your cake and eat it, too? *Ageing Res Rev* **2015,** *20,* 46–62.
124. Colman, R. J.; Anderson, R. M.; Johnson, S. C.; Kastman, E. K.; Kosmatka, K. J.; Beasley, T. M.; Allison, D. B.; Cruzen, C.; Simmons, H. A.; Kemnitz, J. W.; Weindruch, R. Caloric restriction delays disease onset and mortality in rhesus monkeys. *Science* **2009,** *325* (5937), 201–204.
125. Mattison, J. A.; Roth, G. S.; Beasley, T. M.; Tilmont, E. M.; Handy, A. M.; Herbert, R. L.; Longo, D. L.; Allison, D. B.; Young, J. E.; Bryant, M.; Barnard, D.; Ward, W. F.; Qi, W.; Ingram, D. K.; de Cabo, R. Impact of caloric restriction on health and survival in rhesus monkeys from the NIA study. *Nature* **2012,** *489* (7415), 318–321.
126. Kemnitz, J. W. Calorie restriction and aging in nonhuman primates. *ILAR J* **2011,** *52* (1), 66–77.
127. Colman, R. J.; Beasley, T. M.; Kemnitz, J. W.; Johnson, S. C.; Weindruch, R.; Anderson, R. M. Caloric restriction reduces age-related and all-cause mortality in rhesus monkeys. *Nat Commun* **2014,** *5,* 3557.
128. Holloszy, J. O.; Fontana, L. Caloric restriction in humans. *Exp Gerontol* **2007,** *42* (8), 709–712.
129. Cava, E.; Fontana, L. Will calorie restriction work in humans? *Aging (Albany NY)* **2013,** *5* (7), 507–514.
130. Rizza, W.; Veronese, N.; Fontana, L. What are the roles of calorie restriction and diet quality in promoting healthy longevity? *Ageing Res Rev* **2014,** *13* (3), 8–45.
131. Ingram, D. K.; Zhu, M.; Mamczarz, J.; Zou, S.; Lane, M. A.; Roth, G. S.; deCabo, R. Calorie restriction mimetics: an emerging research field. *Aging Cell.* **2006,** *5* (2), 97–108.
132. Le Couteur, D. G.; McLachlan, A. J.; Quinn, R. J.; Simpson, S. J.; de Cabo, R. Aging biology and novel targets for drug discovery. *J Gerontol A Biol Sci Med Sci* **2012,** *67* (2), 168–174.
133. Mouchiroud, L.; Molin, L.; Dallière, N.; Solari, F. Life span extension by resveratrol, rapamycin, and metformin: The promise of dietary restriction mimetics for an healthy aging. *Biofactors* **2010,** *36* (5), 377–382.
134. Anisimov, V. N. Metformin: do we finally have an anti-aging drug? *Cell Cycle* **2013,** *12* (22), 3483–3489.
135. Bonomini, F.; Rodella, L. F.; Rezzani, R. Metabolic syndrome, aging and involvement of oxidative stress. *Aging Dis* **2015,** *6* (2), 109–120.
136. Sato, Y.; Kondo, T.; Ohshima, T. Estimation of age of human cadavers by immunohistochemical assessment of advanced glycation end products in the hippocampus. *Histopathology* **2001,** *38* (3), 217–220.
137. Rajaobelina, K.; Cougnard-Gregoire, A.; Delcourt, C.; Gin, H.; Barberger-Gateau, P.; Rigalleau, V. Autofluorescence of skin advanced glycation end products: marker of metabolic memory in elderly population. *J Gerontol A Biol Sci Med Sci* **2015,** *70* (7), 841–846.
138. Gristina, V.; Cupri, M. G.; Torchio, M.; Mezzogori, C.; Cacciabue, L.; Danova, M. Diabetes and cancer: A critical appraisal of the pathogenetic and therapeutic links. *Biomed Rep* **2015,** *3* (2), 131–136.
139. Anisimov, V. N. Insulin/IGF-1 signaling pathway driving aging and cancer as a target for pharmacological intervention. *Exp Gerontol* **2003,** *38,* 1041–1049.

140. Longo, V. D.; Antebi, A.; Bartke, A.; Barzilai, N.; Brown-Borg, H. M.; Caruso, C.; Curiel, T. J.; de Cabo, R.; Franceschi, C.; Gems, D.; Ingram, D. K.; Johnson, T. E.; Kennedy, B. K.; Kenyon, C.; Klein, S.; Kopchick, J. J.; Lepperdinger, G.; Madeo, F.; Mirisola, M. G.; Mitchell, J. R.; Passarino, G.; Rudolph, K. L.; Sedivy, J. M.; Shadel, G. S.; Sinclair, D. A.; Spindler, S. R.; Suh, Y.; Vijg, J.; Vinciguerra, M.; Fontana, L. Interventions to slow aging in humans: are we ready? *Aging Cell.* **2015,** *14* (4), 497–510.
141. Minor, R. K.; Smith, D. L., Jr.; Sossong, A. M.; Kaushik, S.; Poosala, S.; Spangler, E. L.; Roth, G. S.; Lane, M.; Allison, D. B.; de Cabo, R.; Ingram, D. K.; Mattison, J. A. Chronic ingestion of 2-deoxy-D-glucose induces cardiac vacuolization and increases mortality in rats. *Toxicol Appl Pharmacol* **2009,** *243,* 332–339.
142. Xi, H.; Kurtoglu, M.; Lampidis, T. J. The wonders of 2-deoxy-D-glucose. *IUBMB Life* **2014,** *66* (2), 110–121.
143. Ingram, D. K.; Roth, G. S. Glycolytic inhibition as a strategy for developing calorie restriction mimetics. *Exp Gerontol* **2010,** *46,* 148–154.
144. Ganapathy-Kanniappan, S.; Geschwind, J. F. Tumor glycolysis as a target for cancer therapy: progress and prospects. *Mol Cancer* **2013,** *12,* 152.
145. Taormina, G.; Mirisola, M. G. Longevity: epigenetic and biomolecular aspects. *Biomol Concepts* **2015,** *6* (2), 105–117.
146. Pawlikowska, L.; Hu, D.; Huntsman, S.; Sung, A.; Chu, C.; Chen, J.; Joyner, A. H.; Schork, N. J.; Hsueh, W. C.; Reiner, A. P.; Psaty, B. M.; Atzmon, G.; Barzilai, N.; Cummings, S. R.; Browner, W. S.; Kwok, P. Y.; Ziv, E. Study of Osteoporotic Fractures. Association of common genetic variation in the insulin/IGF1 signaling pathway with human longevity. *Aging Cell* **2009,** *8* (4), 460–472.
147. Tazearslan, C.; Huang, J.; Barzilai, N.; Suh, Y. Impaired IGF1R signaling in cells expressing longevity-associated human IGF1R alleles. *Aging Cell* **2011,** *10* (3), 551–554.
148. Suh, Y.; Atzmon, G.; Cho, M. O.; Hwang, D.; Liu, B.; Leahy, D. J.; Barzilai, N.; Cohen, P. Functionally significant insulin-like growth factor I receptor mutations in centenarians. *Proc Natl Acad Sci USA* **2008,** *105,* 3438–3442.
149. Milman, S.; Atzmon, G.; Huffman, D. M.; Wan, J.; Crandall, J. P.; Cohen, P.; Barzilai, N. Low insulin-like growth factor-1 level predicts survival in humans with exceptional longevity. *Aging Cell* **2014,** *13,* 769–771.
150. Vitale, G.; Brugts, M. P.; Ogliari, G.; Castaldi, D.; Fatti, L. M.; Varewijck, A. J.; Lamberts, S. W.; Monti, D.; Bucci, L.; Cevenini, E.; Cavagnini, F.; Franceschi, C.; Hofland, L. J.; Mari, D.; Janssen, J. Low circulating IGF-I bioactivity is associated with human longevity: findings in centenarians' offspring. *Aging (Albany NY)* **2012,** *4* (9), 580–589.
151. Zhou, Y.; Xu, B. C.; Maheshwari, H. G.; He, L.; Reed, M.; Lozykowski, M.; Okada, S.; Cataldo, L.; Coschigamo, K.; Wagner, T. E.; Baumann, G.; Kopchick, J. J. A mammalian model for Laron syndrome produced by targeted disruption of the mouse growth hormone receptor/binding protein gene (the Laron mouse). *Proc Natl Acad Sci USA* **1997,** *94,* 13215–13220.
152. Ikeno, Y.; Hubbard, G. B.; Lee, S.; Cortez, L. A.; Lew, C. M.; Webb, C. R.; Berryman, D. E.; List, E. O.; Kopchick, J. J.; Bartke, A. Reduced incidence and delayed occurrence of fatal neoplastic diseases in growth hormone receptor/binding protein knockout mice. *J. Gerontol A Biol Sci Med Sci* **2009,** *64,* 522–529.
153. Guevara-Aguirre, J.; Balasubramanian, P.; Guevara-Aguirre, M.; Wei, M.; Madia, F.; Cheng, C. W.; Hwang, D.; Martin-Montalvo, A.; Saavedra, J.; Ingles, S.; de Cabo, R.; Cohen, P.; Longo, V. D. Growth hormone receptor deficiency is associated with a major reduction in pro-aging signaling, cancer, and diabetes in humans. *Sci Transl Med.* **2011,** *3* (70), 70ra13.
154. Steuerman, R.; Shevah, O.; Laron, Z. Congenital IGF1 deficiency tends to confer protection against post-natal development of malignancies. *Eur J Endocrinol* **2011,** *164,* 485–489.
155. Giustina, A.; Chanson, P.; Kleinberg, D.; Bronstein, M. D.; Clemmons, D. R.; Klibanski, A.; van der Lely, A. J.; Strasburger, C. J.; Lamberts, S. W.; Ho, K. K.; Casanueva, F. F.; Melmed, S. Expert consensus document: a consensus on the medical treatment of acromegaly. *Nat Rev Endocrinol* **2014,** *10,* 243–248.
156. Kopchick, J. J.; Parkinson, C.; Stevens, E. C.; Trainer, P. J. Growth hormone receptor antagonists: discovery, development, and use in patients with acromegaly. *Endocr Rev* **2002,** *23,* 623–646.
157. Kopchick, J.J., Lessons learned from studies with the growth hormone receptor, Growth Horm IGF Res (2015) (In press) doi: 10.1016/j.ghir.2015.06.003.
158. van der Lely, A. J.; Kopchick, J. J. Growth hormone receptor antagonists. *Neuroendocrinology* **2006,** *83* (3–4), 264–268.
159. van der Lely, A. J.; Biller, B. M.; Brue, T.; Buchfelder, M.; Ghigo, E.; Gomez, R.; Hey-Hadavi, J.; Lundgren, F.; Rajicic, N.; Strasburger, C. J.; Webb, S. M.; Koltowska-Haggstrom, M. Long-term safety of pegvisomant in patients with acromegaly: comprehensive review of 1288 subjects in ACROSTUDY. *J. Clin. Endocrinol. Metab.* **2012,** *97,* 1589–1597.
160. Conover, C. A. PAPP-A: a new anti-aging target? *Aging Cell* **2010,** *9* (6), 942–946.
161. Conover, C. A. Role of PAPP-A in aging and age-related disease. *Exp Gerontol* **2013,** *48,* 612–613.
162. Imai, S.; Armstrong, C. M.; Kaeberlein, M.; Guarente, L. Transcriptional silencing and longevity protein Sir2 is an NAD-dependent histone deacetylase. *Nature* **2000,** *403* (6771), 795–800.
163. Boily, G.; Seifert, E. L.; Bevilacqua, L.; He, X. H.; Sabourin, G.; Estey, C.; Moffat, C.; Crawford, S.; Saliba, S.; Jardine, K.; Xuan, J.; Evans, M.; Harper, M. E.; McBurney, M. W. SirT1 regulates energy metabolism and response to caloric restriction in mice. *PLoS One* **2008,** *3.* e1759.
164. Liu, T. F.; McCall, C. E. Deacetylation by SIRT1 reprograms inflammation and cancer. *Genes Cancer* **2013,** *4* (3–4), 135–147.
165. Giblin, W.; Skinner, M. E.; Lombard, D. B. Sirtuins: guardians of mammalian healthspan. *Trends Genet* **2014,** *30* (7), 271–286.
166. Bordone, L.; Cohen, D.; Robinson, A.; Motta, M. C.; van Veen, E.; Czopik, A.; Steele, A. D.; Crowe, H.; Marmor, S.; Luo, J.; Gu, W.; Guarente, L. SIRT1 transgenic mice show phenotypes resembling calorie restriction. *Aging Cell* **2007,** *6,* 759–767.
167. Civitarese, A. E.; Carling, S.; Heilbronn, L. K.; Hulver, M. H.; Ukropcova, B.; Deutsch, W. A.; Smith, S. R.; Ravussin, E. CALERIE Pennington Team, Calorie restriction increases muscle mitochondrial biogenesis in healthy humans. *PLoS Med* **2007,** *4,* e76.
168. Kaeberlein, M.; Kirkland, K. T.; Fields, S.; Kennedy, B. K. Sir2-independent life span extension by calorie restriction in yeast. *PLoS Biol* **2004,** *2,* E296.
169. Smith, D. L., Jr.; McClure, J. M.; Matecic, M.; Smith, J. S. Calorie restriction extends the chronological lifespan of Saccharomyces cerevisiae independently of the sirtuins. *Aging Cell* **2007,** *6,* 649–662.
170. Burnett, C.; Valentini, S.; Cabreiro, F.; Goss, M.; Somogyvári, M.; Piper, M. D.; Hoddinott, M.; Sutphin, G. L.; Leko, V.; McElwee, J. J.; Vazquez-Manrique, R. P.; Orfila, A. M.; Ackerman, D.; Au, C.; Vinti, G.; Riesen, M.; Howard, K.; Neri, C.; Bedalov, A.; Kaeberlein, M.; Soti, C.; Partridge, L.; Gems, D. Absence of effects of Sir2 overexpression on lifespan in C. elegans and Drosophila. *Nature* **2011,** *477,* 482–485.
171. Baur, J. A.; Ungvari, Z.; Minor, R. K.; Le Couteur, D. G.; de Cabo, R. Are sirtuins viable targets for improving healthspan and lifespan? *Nat Rev Drug Discov* **2012,** *11,* 443–461.
172. Shackelford, D. B.; Shaw, R. J. The LKB1-AMPK pathway: metabolism and growth control in tumour suppression. *Nat Rev Cancer* **2009,** *9* (8), 563–575.
173. Cantó, C.; Gerhart-Hines, Z.; Feige, J. N.; Lagouge, M.; Noriega, L.; Milne, J. C.; Elliott, P. J.; Puigserver, P.; Auwerx, J. AMPK regulates energy expenditure by modulating NAD+ metabolism and SIRT1 activity. *Nature* **2009,** *458,* 1056–1060.
174. Hardie, D. G. AMPK: positive and negative regulation, and its role in whole-body energy homeostasis. *Curr Opin Cell Biol* **2015,** *33,* 1–7.
175. Kitada, M.; Koya, D. Renal protective effects of resveratrol. *Oxid Med Cell Longev* **2013,** *2013,* 568093.
176. de Ligt, M.; Timmers, S.; Schrauwen, P. Resveratrol and obesity: Can resveratrol relieve metabolic disturbances? *Biochim Biophys Acta* **2015,** *1852* (6), 1137–1144.
177. Catalgol, B.; Batirel, S.; Taga, Y.; Ozer, N. K. Resveratrol: French paradox revisited. *Front Pharmacol* **2012,** *3,* 141.
178. Howitz, K. T.; Bitterman, K. J.; Cohen, H. Y.; Lamming, D. W.; Lavu, S.; Wood, J. G.; Zipkin, R. E.; Chung, P.; Kisielewski, A.; Zhang, L. L.; Scherer, B.; Sinclair, D. A. Small molecule activators of sirtuins extend Saccharomyces cerevisiae lifespan. *Nature* **2003,** *425,* 191–196.
179. Viswanathan, M.; Kim, S. K.; Berdichevsky, A.; Guarente, L. A role for SIR-2.1 regulation of ER stress response genes in determining C. elegans life span. *Dev Cell* **2005,** *9* (5), 605–615.
180. Wood, J. G.; Rogina, B.; Lavu, S.; Howitz, K.; Helfand, S. L.; Tatar, M.; Sinclair, D. Sirtuin activators mimic caloric restriction and delay ageing in metazoans. *Nature* **2004,** *430,* 686–689.
181. Bauer, J. H.; Goupil, S.; Garber, G. B.; Helfand, S. L. An accelerated assay for the identification of lifespan-extending interventions in Drosophila melanogaster. *Proc Natl Acad Sci U S A* **2004,** *101* (35), 12980–12985.

182. Wang, C.; Wheeler, C. T.; Alberico, T.; Sun, X.; Seeberger, J.; Laslo, M.; Spangler, E.; Kern, B.; de Cabo, R.; Zou, S. The effect of resveratrol on lifespan depends on both gender and dietary nutrient composition in Drosophila melanogaster. *Age (Dordr)* **2013,** *35* (1), 69–81.
183. Rascón, B.; Hubbard, B. P.; Sinclair, D. A.; Amdam, G. V. The lifespan extension effects of resveratrol are conserved in the honey bee and may be driven by a mechanism related to caloric restriction. *Aging (Albany NY)* **2012,** *4* (7), 499–508.
184. Valenzano, D. R.; Terzibasi, E.; Genade, T.; Cattaneo, A.; Domenici, L.; Cellerino, A. Resveratrol prolongs lifespan and retards the onset of age-related markers in a short-lived vertebrate. *Curr Biol* **2006,** *16,* 296–300.
185. Yu, X.; Li, G. Effects of resveratrol on longevity, cognitive ability and aging-related histological markers in the annual fish Nothobranchius guentheri. *Exp Gerontol* **2012,** *47* (12), 940–949.
186. Baur, J. A.; Pearson, K. J.; Price, N. L.; Jamieson, H. A.; Lerin, C.; Kalra, A.; Prabhu, V. V.; Allard, J. S.; Lopez-Lluch, G.; Lewis, K.; Pistell, P. J.; Poosala, S.; Becker, K. G.; Boss, O.; Gwinn, D.; Wang, M.; Ramaswamy, S.; Fishbein, K. W.; Spencer, R. G.; Lakatta, E. G.; Le Couteur, D.; Shaw, R. J.; Navas, P.; Puigserver, P.; Ingram, D. K.; de Cabo, R.; Sinclair, D. A. Resveratrol improves health and survival of mice on a high-calorie diet. *Nature.* **2006,** *444,* 337–342.
187. Pearson, K. J.; Baur, J. A.; Lewis, K. N.; Peshkin, L.; Price, N. L.; Labinskyy, N.; Swindell, W. R.; Kamara, D.; Minor, R. K.; Perez, E.; Jamieson, H. A.; Zhang, Y.; Dunn, S. R.; Sharma, K.; Pleshko, N.; Woollett, L. A.; Csiszar, A.; Ikeno, Y.; Le Couteur, D.; Elliott, P. J.; Becker, K. G.; Navas, P.; Ingram, D. K.; Wolf, N. S.; Ungvari, Z.; Sinclair, D. A.; de Cabo, R. Resveratrol delays age-related deterioration and mimics transcriptional aspects of dietary restriction without extending life span. *Cell Metab.* **2008,** *8* (2), 157–168.
188. Bhullar, K. S.; Hubbard, B. P. Lifespan and healthspan extension by resveratrol. *Biochim Biophys Acta* **2015,** *1852* (6), 1209–1218.
189. Timmers, S.; Konings, E.; Bilet, L.; Houtkooper, R. H.; van de Weijer, T.; Goossens, G. H.; Hoeks, J.; van der Krieken, S.; Ryu, D.; Kersten, S.; Moonen-Kornips, E.; Hesselink, M. K.; Kunz, I.; Schrauwen-Hinderling, V. B.; Blaak, E. E.; Auwerx, J.; Schrauwen, P. Calorie restriction-like effects of 30 days of resveratrol supplementation on energy metabolism and metabolic profile in obese humans. *Cell Metab* **2011,** *14,* 612–622.
190. Konings, E.; Timmers, S.; Boekschoten, M. V.; Goossens, G. H.; Jocken, J. W.; Afman, L. A.; Müller, M.; Schrauwen, P.; Mariman, E. C.; Blaak, E. E. The effects of 30 days resveratrol supplementation on adipose tissue morphology and gene expression patterns in obese men. *Int J Obes (Lond)* **2014,** *38* (3), 470–473.
191. Hubbard, B. P.; Sinclair, D. A. Small molecule SIRT1 activators for the treatment of aging and age-related diseases. *Trends Pharmacol Sci* **2014,** *35* (3), 146–154.
192. Vang, O. Resveratrol: challenges in analyzing its biological effects. *Ann N Y Acad Sci* **2015,** *1348* (1), 161–170.
193. Minor, R. K.; Baur, J. A.; Gomes, A. P.; Ward, T. M.; Csiszar, A.; Mercken, E. M.; Abdelmohsen, K.; Shin, Y. K.; Canto, C.; Scheibye-Knudsen, M.; Krawczyk, M.; Irusta, P. M.; Martín-Montalvo, A.; Hubbard, B. P.; Zhang, Y.; Lehrmann, E.; White, A. A.; Price, N. L.; Swindell, W. R.; Pearson, K. J.; Becker, K. G.; Bohr, V. A.; Gorospe, M.; Egan, J. M.; Talan, M. I.; Auwerx, J.; Westphal, C. H.; Ellis, J. L.; Ungvari, Z.; Vlasuk, G. P.; Elliott, P. J.; Sinclair, D. A.; de Cabo, R. SRT1720 improves survival and healthspan of obese mice. *Sci Rep.* **2011,** *1,* 70.
194. Mitchell, S. J.; Martin-Montalvo, A.; Mercken, E. M.; Palacios, H. H.; Ward, T. M.; Abulwerdi, G.; Minor, R. K.; Vlasuk, G. P.; Ellis, J. L.; Sinclair, D. A.; Dawson, J.; Allison, D. B.; Zhang, Y.; Becker, K. G.; Bernier, M.; de Cabo, R. The SIRT1 activator SRT1720 extends lifespan and improves health of mice fed a standard diet. *Cell Rep* **2014,** *6* (5), 836–843.
195. Gano, L. B.; Donato, A. J.; Pasha, H. M.; Hearon, C. M., Jr.; Sindler, A. L.; Seals, D. R. The SIRT1 activator SRT1720 reverses vascular endothelial dysfunction, excessive superoxide production, and inflammation with aging in mice. *Am J Physiol Heart Circ Physiol* **2014,** *307* (12), H1754–H1763.
196. Mercken, E. M.; Mitchell, S. J.; Martin-Montalvo, A.; Minor, R. K.; Almeida, M.; Gomes, A. P.; Scheibye-Knudsen, M.; Palacios, H. H.; Licata, J. J.; Zhang, Y.; Becker, K. G.; Khraiwesh, H.; González-Reyes, J. A.; Villalba, J. M.; Baur, J. A.; Elliott, P.; Westphal, C.; Vlasuk, G. P.; Ellis, J. L.; Sinclair, D. A.; Bernier, M.; de Cabo, R. SRT2104 extends survival of male mice on a standard diet and preserves bone and muscle mass. *Aging Cell* **2014,** *13* (5), 787–796.
197. Ehninger, D.; Neff, F.; Xie, K. Longevity, aging and rapamycin. *Cell Mol Life Sci* **2014,** *71* (22), 4325–4346.
198. Johnson, S. C.; Sangesland, M.; Kaeberlein, M.; Rabinovitch, P. S. Modulating mTOR in aging and health. *Interdiscip Top Gerontol* **2015,** *40,* 107–127.
199. Lee, K. P. Dietary protein: carbohydrate balance is a critical modulator of lifespan and reproduction in Drosophila melanogaster: a test using a chemically defined diet. *J Insect Physiol* **2015,** *75,* 12–19.
200. Solon-Biet, S. M.; McMahon, A. C.; Ballard, J. W.; Ruohonen, K.; Wu, L. E.; Cogger, V. C.; Warren, A.; Huang, X.; Pichaud, N.; Melvin, R. G.; Gokarn, R.; Khalil, M.; Turner, N.; Cooney, G. J.; Sinclair, D. A.; Raubenheimer, D.; Le Couteur, D. G.; Simpson, S. J. The ratio of macronutrients, not caloric intake, dictates cardiometabolic health, aging, and longevity in ad libitum-fed mice. *Cell Metab* **2014,** *19* (3), 418–430.
201. Laplante, M.; Sabatini, D. M. mTOR signaling in growth control and disease. *Cell* **2012,** *149,* 274–293.
202. Solon-Biet, S. M.; Mitchell, S. J.; de Cabo, R.; Raubenheimer, D.; Le Couteur, D. G.; Simpson, S. J. Macronutrients and caloric intake in health and longevity. *J Endocrinol* **2015,** *226* (1), R17–R28.
203. Albert, V.; Hall, M. N. mTOR signaling in cellular and organismal energetic. *Curr Opin Cell Biol* **2015,** *33,* 55–66.
204. Inoki, K.; Kim, J.; Guan, K. L. AMPK and mTOR in cellular energy homeostasis and drug targets. *Annu Rev Pharmacol Toxicol* **2012,** *52,* 381–400.
205. Kaeberlein, M. Rapamycin and ageing: when, for how long, and how much? *J Genet Genomics* **2014,** *41* (9), 459–463.
206. Kapahi, P.; Chen, D.; Rogers, A. N.; Katewa, S. D.; Li, P. W.; Thomas, E. L.; Kockel, L.; With, T. O. R. less is more: a key role for the conserved nutrient-sensing TOR pathway in aging. *Cell Metab* **2010,** *11,* 453–465.
207. Finch, C. E. *Longevity, Senescence, and the Genome;* University of Chicago Press: Chicago, 1990.
208. Johnson, S. C.; Rabinovitch, P. S.; Kaeberlein, M. mTOR is a key modulator of ageing and age-related disease. *Nature* **2013,** *493* (7432), 338–345.
209. Vellai, T.; Takacs-Vellai, K.; Zhang, Y.; Kovacs, A. L.; Orosz, L.; Müller, F.; et al. Genetics: influence of TOR kinase on lifespan in C. elegans. *Nature.* **2003,** *426* (6967), 620.
210. Jia, K.; Chen, D.; Riddle, D. L. The TOR pathway interacts with the insulin signaling pathway to regulate C. elegans larval development, metabolism and life span. *Development.* **2004,** *131,* 3897–3906.
211. Kapahi, P.; Zid, B. M.; Harper, T.; Koslover, D.; Sapin, V.; Benzer, S. Regulation of lifespan in Drosophila by modulation of genes in the TOR signaling pathway. *Curr Biol* **2004,** *14,* 885–890.
212. Lamming, D. W.; Ye, L.; Katajisto, P.; Goncalves, M. D.; Saitoh, M.; Stevens, D. M.; Davis, J. G.; Salmon, A. B.; Richardson, A.; Ahima, R. S.; Guertin, D. A.; Sabatini, D. M.; Baur, J. A. Rapamycin-induced insulin resistance is mediated by mTORC2 loss and uncoupled from longevity. *Science* **2012,** *335* (6076), 1638–1643.
213. Passtoors, W. M.; Beekman, M.; Deelen, J.; van der Breggen, R.; Maier, A. B.; Guigas, B.; Derhovanessian, E.; van Heemst, D.; de Craen, A. J.; Gunn, D. A.; Pawelec, G.; Slagboom, P. E. Gene expression analysis of mTOR pathway: association with human longevity. *Aging Cell* **2013,** *12* (1), 24–31.
214. Lamming, D. W.; Ye, L.; Sabatini, D. M.; Baur, J. A. Rapalogs and mTOR inhibitors as anti-aging therapeutics. *J Clin Invest* **2013,** *123* (3), 980–989.
215. Ingle, G. R.; Sievers, T. M.; Holt, C. D. Sirolimus: continuing the evolution of transplant immunosuppression. *Ann Pharmacother* **2000,** *34* (9), 1044–1055.
216. Blagosklonny, M. V. An anti-aging drug today: From senescence-promoting genes to anti-aging pill. *Drug Discov Today* **2007,** *12,* 218–224.
217. Powers, R. W., 3rd; Kaeberlein, M.; Caldwell, S. D.; Kennedy, B. K.; Fields, S. Extension of chronological life span in yeast by decreased TOR pathway signaling. *Genes Dev* **2006,** *20* (2), 174–184.
218. Medvedik, O.; Lamming, D. W.; Kim, K. D.; Sinclair, D. A. MSN2 and MSN4 link calorie restriction and TOR to sirtuin-mediated lifespan extension in Saccharomyces cerevisiae. *PLoS Biol* **2007,** *5,* e261.
219. Ha, C. W.; Huh, W. K. Rapamycin increases rDNA stability by enhancing association of Sir2 with rDNA in Saccharomyces cerevisiae. *Nucleic Acids Res* **2011,** *39* (4), 1336–1350.
220. Robida-Stubbs, S.; Glover-Cutter, K.; Lamming, D. W.; Mizunuma, M.; Narasimhan, S. D.; Neumann-Haefelin, E.; Sabatini, D. M.; Blackwell, T. K. TOR signaling and rapamycin influence longevity by regulating SKN-1/Nrf and DAF-16/FoxO. *Cell Metab* **2012,** *15* (5), 713–724.
221. Bjedov, I.; Toivonen, J. M.; Kerr, F.; Slack, C.; Jacobson, J.; Foley, A.; Partridge, L. Mechanisms of life span extension by rapamycin in the fruit fly Drosophila melanogaster. *Cell Metab* **2010,** *11* (1), 35–46.

222. Sun, X.; Komatsu, T.; Lim, J.; Laslo, M.; Yolitz, J.; Wang, C.; Poirier, L.; Alberico, T.; Zou, S. Nutrient-dependent requirement for SOD1 in lifespan extension by protein restriction in Drosophila melanogaster. *Aging Cell* **2012,** *11* (5), 783–793.
223. Harrison, D. E.; Strong, R.; Sharp, Z. D.; Nelson, J. F.; Astle, C. M.; Flurkey, K.; Nadon, N. L.; Wilkinson, J. E.; Frenkel, K.; Carter, C. S.; Pahor, M.; Javors, M. A.; Fernandez, E.; Miller, R. A. Rapamycin fed late in life extends lifespan in genetically heterogeneous mice. *Nature* **2009,** *460* (7253), 392–395.
224. Miller, R. A.; Harrison, D. E.; Astle, C. M.; Baur, J. A.; Boyd, A. R.; de Cabo, R.; Fernandez, E.; Flurkey, K.; Javors, M. A.; Nelson, J. F.; Orihuela, C. J.; Pletcher, S.; Sharp, Z. D.; Sinclair, D.; Starnes, J. W.; Wilkinson, J. E.; Nadon, N. L.; Strong, R. Rapamycin, but not resveratrol or simvastatin, extends life span of genetically heterogeneous mice. *J Gerontol A Biol Sci Med Sci* **2011,** *66* (2), 191–201.
225. Miller, R. A.; Harrison, D. E.; Astle, C. M.; Fernandez, E.; Flurkey, K.; Han, M.; Javors, M. A.; Li, X.; Nadon, N. L.; Nelson, J. F.; Pletcher, S.; Salmon, A. B.; Sharp, Z. D.; Van Roekel, S.; Winkleman, L.; Strong, R. Rapamycin-mediated lifespan increase in mice is dose and sex dependent and metabolically distinct from dietary restriction. *Aging Cell* **2014,** *13* (3), 468–477.
226. Anisimov, V. N.; Zabezhinski, M. A.; Popovich, I. G.; Piskunova, T. S.; Semenchenko, A. V.; Tyndyk, M. L.; Yurova, M. N.; Antoch, M. P.; Blagosklonny, M. V. Rapamycin extends maximal lifespan in cancer-prone mice. *Am J Pathol* **2010,** *176* (5), 2092–2097.
227. Anisimov, V. N.; Zabezhinski, M. A.; Popovich, I. G.; Piskunova, T. S.; Semenchenko, A. V.; Tyndyk, M. L.; Yurova, M. N.; Rosenfeld, S. V.; Blagosklonny, M. V. Rapamycin increases lifespan and inhibits spontaneous tumorigenesis in inbred female mice. *Cell Cycle* **2011,** *10* (24), 4230–4236.
228. Zhang, Y.; Bokov, A.; Gelfond, J.; Soto, V.; Ikeno, Y.; Hubbard, G.; Diaz, V.; Sloane, L.; Maslin, K.; Treaster, S.; Réndon, S.; van Remmen, H.; Ward, W.; Javors, M.; Richardson, A.; Austad, S. N.; Fischer, K. Rapamycin extends life and health in C57BL/6 mice. *J Gerontol A Biol Sci Med Sci* **2014,** *69* (2), 119–130.
229. Neff, F.; Flores-Dominguez, D.; Ryan, D. P.; Horsch, M.; Schröder, S.; Adler, T.; Afonso, L. C.; Aguilar-Pimentel, J. A.; Becker, L.; Garrett, L.; Hans, W.; Hettich, M. M.; Holtmeier, R.; Hölter, S. M.; Moreth, K.; Prehn, C.; Puk, O.; Rácz, I.; Rathkolb, B.; Rozman, J.; Naton, B.; Ordemann, R.; Adamski, J.; Beckers, J.; Bekeredjian, R.; Busch, D. H.; Ehninger, G.; Graw, J.; Höfler, H.; Klingenspor, M.; Klopstock, T.; Ollert, M.; Stypmann, J.; Wolf, E.; Wurst, W.; Zimmer, A.; Fuchs, H.; Gailus-Durner, V.; Hrabe de Angelis, M.; Ehninger, D. Rapamycin extends murine lifespan but has limited effects on aging. *J Clin Invest.* **2013,** *123* (8), 3272–3291.
230. Wilkinson, J. E.; Burmeister, L.; Brooks, S. V.; Chan, C. C.; Friedline, S.; Harrison, D. E.; Hejtmancik, J. F.; Nadon, N.; Strong, R.; Wood, L. K.; Woodward, M. A.; Miller, R. A. Rapamycin slows aging in mice. *Aging Cell* **2012,** *11* (4), 675–682.
231. Kolosova, N. G.; Muraleva, N. A.; Zhdankina, A. A.; Stefanova, N. A.; Fursova, A. Z.; Blagosklonny, M. V. Prevention of age-related macular degeneration-like retinopathy by rapamycin in rats. *Am J Pathol* **2012,** *181* (2), 472–477.
232. Shioi, T.; McMullen, J. R.; Tarnavski, O.; Converso, K.; Sherwood, M. C.; Manning, W. J.; Izumo, S. Rapamycin attenuates load-induced cardiac hypertrophy in mice. *Circulation* **2003,** *107* (12), 1664–1670.
233. Spilman, P.; Podlutskaya, N.; Hart, M. J.; Debnath, J.; Gorostiza, O.; Bredesen, D.; Richardson, A.; Strong, R.; Galvan, V. Inhibition of mTOR by rapamycin abolishes cognitive deficits and reduces amyloid-beta levels in a mouse model of Alzheimer's disease. *PLoS One* **2010,** *5* (4), e9979.
234. Halloran, J.; Hussong, S. A.; Burbank, R.; Podlutskaya, N.; Fischer, K. E.; Sloane, L. B.; Austad, S. N.; Strong, R.; Richardson, A.; Hart, M. J.; Galvan, V. Chronic inhibition of mammalian target of rapamycin by rapamycin modulates cognitive and non-cognitive components of behavior throughout lifespan in mice. *Neuroscience* **2012,** *223,* 102–113.
235. Chen, C.; Liu, Y.; Zheng, P. mTOR regulation and therapeutic rejuvenation of aging hematopoietic stem cells. *Sci Signal.* **2009,** *2* (98), ra75.
236. Blagosklonny, M. V. Rapalogs in cancer prevention: anti-aging or anticancer? *Cancer Biol Ther* **2012,** *13* (14), 1349–1354.
237. Saran, U.; Foti, M.; Dufour, J. F. Cellular and molecular effects of the mTOR inhibitor everolimus. *Clin Sci (Lond)* **2015,** *129* (10), 895–914.
238. Perluigi, M.; Di Domenico, F.; Butterfield, D.A., mTOR signaling in aging and neurodegeneration: At the crossroad between metabolism dysfunction and impairment of autophagy, Neurobiol Dis (2015) (In press). http://dx.doi.org/10.1016/j.nbd.2015.03.014.
239. Maiese, K. Stem cell guidance through the mechanistic target of rapamycin. *World J Stem Cells* **2015,** *7* (7), 999–1009.
240. Araki, K.; Ellebedy, A. H.; Ahmed, R. TOR in the immune system. *Curr Opin Cell Biol* **2011,** *23* (6), 707–715.
241. Hipkiss, A. R. On why decreasing protein synthesis can increase lifespan. *Mech Ageing Dev* **2007,** *128* (5–6), 412–414.
242. Cetrullo, S.; D'Adamo, S.; Tantini, B.; Borzi, R. M.; Flamigni, F. mTOR, AMPK, and Sirt1: Key players in metabolic stress management. *Crit Rev Eukaryot Gene Expr* **2015,** *25* (1), 59–75.
243. Houde, V. P.; Brûlé, S.; Festuccia, W. T.; Blanchard, P. G.; Bellmann, K.; Deshaies, Y.; Marette, A. Chronic rapamycin treatment causes glucose intolerance and hyperlipidemia by upregulating hepatic gluconeogenesis and impairing lipid deposition in adipose tissue. *Diabetes* **2010,** *59* (6), 1338–1348.
244. Deblon, N.; Bourgoin, L.; Veyrat-Durebex, C.; Peyrou, M.; Vinciguerra, M.; Caillon, A.; Maeder, C.; Fournier, M.; Montet, X.; Rohner-Jeanrenaud, F.; Foti, M. Chronic mTOR inhibition by rapamycin induces muscle insulin resistance despite weight loss in rats. *Br J Pharmacol* **2012,** *165* (7), 2325–2340.
245. Richardson, A. Rapamycin, anti-aging, and avoiding the fate of Tithonus. *J Clin Invest* **2013,** *123* (8), 3204–3206.
246. Zafar, I.; Belibi, F. A.; He, Z.; Edelstein, C. L. Long-term rapamycin therapy in the Han: SPRD rat model of polycystic kidney disease (PKD). *Nephrol Dial Transplant* **2009,** *24* (8), 2349–2353.
247. Salmon, A. B. About-face on the metabolic side effects of rapamycin. *Oncotarget* **2015,** *6* (5), 2585–2586.
248. Liu, Y.; Diaz, V.; Fernandez, E.; Strong, R.; Ye, L.; Baur, J. A.; Lamming, D. W.; Richardson, A.; Salmon, A. B. Rapamycin-induced metabolic defects are reversible in both lean and obese mice. *Aging (Albany NY)* **2014,** *6* (9), 742–754.
249. Flynn, J. M.; O'Leary, M. N.; Zambataro, C. A.; Academia, E. C.; Presley, M. P.; Garrett, B. J.; Zykovich, A.; Mooney, S. D.; Strong, R.; Rosen, C. J.; Kapahi, P.; Nelson, M. D.; Kennedy, B. K.; Melov, S. Late-life rapamycin treatment reverses age-related heart dysfunction. *Aging Cell* **2013,** *12* (5), 851–862.
250. Gowans, G. J.; Hardie, D. G. AMPK: A cellular energy sensor primarily regulated by AMP. *Biochem Soc Trans* **2014,** *42* (1), 71–75.
251. Towler, M. C.; Hardie, D. G. AMP-activated protein kinase in metabolic control and insulin signaling. *Circ Res* **2007,** *100* (3), 328–341.
252. Canto, C.; Auwerx, J. AMP-activated protein kinase and its downstream transcriptional pathways. *Cell Mol Life Sci* **2010,** *67,* 3407–3423.
253. Gwinn, D. M.; Shackelford, D. B.; Egan, D. F.; Mihaylova, M. M.; Mery, A.; Vasquez, D. S.; Turk, B. E.; Shaw, R. J. AMPK phosphorylation of raptor mediates a metabolic checkpoint. *Mol Cell* **2008,** *30* (2), 214–226.
254. Hindupur, S. K.; González, A.; Hall, M. N. The opposing actions of target of rapamycin and AMP-activated protein kinase in cell growth control. *Cold Spring Harb Perspect Med* **2015,** *5* (7), a019141.
255. Ruderman, N. B.; Carling, D.; Prentki, M.; Cacicedo, J. M. AMPK, insulin resistance, and the metabolic syndrome. *J Clin Investig* **2013,** *123,* 2764–2772.
256. Potter, W. B.; O'Riordan, K. J.; Barnett, D.; Osting, S. M.; Wagoner, M.; Burger, C.; Roopra, A. Metabolic regulation of neuronal plasticity by the energy sensor AMPK. *PLoS One* **2010,** *5* (2), e8996.
257. Hardie, D. G.; Ross, F. A.; Hawley, S. A. AMPK: a nutrient and energy sensor that maintains energy homeostasis. *Nat Rev Mol Cell Biol* **2012,** *13* (4), 251–262.
258. Ha, J.; Guan, K.L.; Kim, J., AMPK and autophagy in glucose/glycogen metabolism, Mol Aspects Med (2015) (In press) doi: 10.1016/j.mam.2015.08.002.
259. Salminen, A.; Kaarniranta, K. AMP-activated protein kinase (AMPK) controls the aging process via an integrated signaling network. *Ageing Res Rev* **2012,** *11* (2), 230–241.
260. Burkewitz, K.; Zhang, Y.; Mair, W. B. AMPK at the nexus of energetics and aging. *Cell Metab* **2014,** *20* (1), 10–25.
261. Coughlan, K. A.; Valentine, R. J.; Ruderman, N. B.; Saha, A. K. AMPK activation: a therapeutic target for type 2 diabetes? *Diabetes Metab Syndr Obes* **2014,** *7,* 241–253.
262. Madiraju, A. K.; Erion, D. M.; Rahimi, Y.; Zhang, X. M.; Braddock, D. T.; Albright, R. A.; Prigaro, B. J.; Wood, J. L.; Bhanot, S.; MacDonald, M. J.; Jurczak, M. J.; Camporez, J. P.; Lee, H. Y.; Cline, G. W.; Samuel, V. T.; Kibbey, R. G.; Shulman, G. I. Metformin suppresses gluconeogenesis by inhibiting mitochondrial glycerophosphate dehydrogenase. *Nature* **2014,** *510,* 542–546.
263. Moreira, P. I. Metformin in the diabetic brain: friend or foe? *Ann Transl Med* **2014,** *2* (6), 54.

264. Viollet, B.; Guigas, B.; Sanz Garcia, N.; Leclerc, J.; Foretz, M.; Andreelli, F. Cellular and molecular mechanisms of metformin: an overview. *Clin Sci (Lond)* **2012,** *122* (6), 253–270.
265. Onken, B.; Driscoll, M. Metformin induces a dietary restriction-like state and the oxidative stress response to extend C. elegans healthspan via AMPK, LKB1, and SKN-1. *PLoS One* **2010,** *5*, e8758.
266. Cabreiro, F.; Au, C.; Leung, K. Y.; Vergara-Irigaray, N.; Cochemé, H. M.; Noori, T.; Weinkove, D.; Schuster, E.; Greene, N. D.; Gems, D. Metformin retards aging in C. elegans by altering microbial folate and methionine metabolism. *Cell* **2013,** *153* (1), 228–239.
267. De Haes, W.; Frooninckx, L.; Van Assche, R.; Smolders, A.; Depuydt, G.; Billen, J.; Braeckman, B. P.; Schoofs, L.; Temmerman, L. Metformin promotes lifespan through mitohormesis via the peroxiredoxin PRDX-2. *Proc Natl Acad Sci U S A* **2014,** *111* (24), E2501–E2509.
268. Slack, C.; Foley, A.; Partridge, L. Activation of AMPK by the putative dietary restriction mimetic metformin is insufficient to extend lifespan in Drosophila. *PLoS One* **2012,** *7* (10), e47699.
269. Martin-Montalvo, A.; Mercken, E. M.; Mitchell, S. J.; Palacios, H. H.; Mote, P. L.; Scheibye-Knudsen, M.; Gomes, A. P.; Ward, T. M.; Minor, R. K.; Blouin, M. J.; Schwab, M.; Pollak, M.; Zhang, Y.; Yu, Y.; Becker, K. G.; Bohr, V. A.; Ingram, D. K.; Sinclair, D. A.; Wolf, N. S.; Spindler, S. R.; Bernier, M.; de Cabo, R. Metformin improves healthspan and lifespan in mice. *Nat Commun* **2013,** *4,* 2192.
270. Anisimov, V. N.; Berstein, L. M.; Egormin, P. A.; Piskunova, T. S.; Popovich, I. G.; Zabezhinski, M. A.; Kovalenko, I. G.; Poroshina, T. E.; Semenchenko, A. V.; Provinciali, M.; Re, F.; Franceschi, C. Effect of metformin on life span and on the development of spontaneous mammary tumors in HER-2/neu transgenic mice. *Exp Gerontol* **2005,** *40* (8–9), 685–693.
271. Anisimov, V. N.; Berstein, L. M.; Egormin, P. A.; Piskunova, T. S.; Popovich, I. G.; Zabezhinski, M. A.; Tyndyk, M. L.; Yurova, M. V.; Kovalenko, I. G.; Poroshina, T. E.; Semenchenko, A. V. Metformin slows down aging and extends life span of female SHR mice. *Cell Cycle* **2008,** *7* (17), 2769–2773.
272. Anisimov, V. N.; Egormin, P. A.; Piskunova, T. S.; Popovich, I. G.; Tyndyk, M. L.; Yurova, M. N.; Zabezhinski, M. A.; Anikin, I. V.; Karkach, A. S.; Romanyukha, A. A. Metformin extends life span of HER-2/neu transgenic mice and in combination with melatonin inhibits growth of transplantable tumors in vivo. *Cell Cycle* **2010,** *9* (1), 188–197.
273. Anisimov, V. N.; Piskunova, T. S.; Popovich, I. G.; Zabezhinski, M. A.; Tyndyk, M. L.; Egormin, P. A.; Yurova, M. V.; Rosenfeld, S. V.; Semenchenko, A. V.; Kovalenko, I. G.; Poroshina, T. E.; Berstein, L. M. Gender differences in metformin effect on aging, life span and spontaneous tumorigenesis in 129/Sv mice. *Aging (Albany NY)* **2010,** *2* (12), 945–958.
274. Anisimov, V. N.; Berstein, L. M.; Popovich, I. G.; Zabezhinski, M. A.; Egormin, P. A.; Piskunova, T. S.; Semenchenko, A. V.; Tyndyk, M. L.; Yurova, M. N.; Kovalenko, I. G.; Poroshina, T. E. If started early in life, metformin treatment increases life span and postpones tumors in female SHR mice. *Aging (Albany NY)* **2011,** *3* (2), 148–157.
275. Anisimov, V. N.; Semenchenko, A. V.; Yashin, A. I. Insulin and longevity: antidiabetic biguanides as geroprotectors. *Biogerontology* **2003,** *4,* 297–307.
276. Anisimov, V. N. Life span extension and cancer risk: myths and reality. *Exp Gerontol* **2001,** *36* (7), 1101–1136.
277. Smith, D. L., Jr.; Elam, C. F., Jr.; Mattison, J. A.; Lane, M. A.; Roth, G. S.; Ingram, D. K.; Allison, D. B. Metformin supplementation and life span in Fischer-344 rats. *J Gerontol A Biol Sci Med Sci* **2010,** *65* (5), 468–474.
278. Luong, D. Q.; Oster, R.; Ashraf, A. P. Metformin treatment improves weight and dyslipidemia in children with metabolic syndrome. *J Pediatr Endocrinol Metab* **2015,** *28* (5–6), 649–655.
279. He, H.; Ke, R.; Lin, H.; Ying, Y.; Liu, D.; Luo, Z. Metformin, an old drug, brings a new era to cancer therapy. *Cancer J* **2015,** *21* (2), 70–74.
280. Coperchini, F.; Leporati, P.; Rotondi, M.; Chiovato, L. Expanding the therapeutic spectrum of metformin: from diabetes to cancer. *J Endocrinol Invest* **2015,** *38* (10), 1047–1055.
281. Provinciali, N.; Lazzeroni, M.; Cazzaniga, M.; Gorlero, F.; Dunn, B. K.; DeCensi, A. Metformin: risk-benefit profile with a focus on cancer. *Expert Opin Drug Saf* **2015,** *14* (10), 1573–1585.
282. Leone, A.; Di Gennaro, E.; Bruzzese, F.; Avallone, A.; Budillon, A. New perspective for an old antidiabetic drug: Metformin as anticancer agent. *Cancer Treat Res* **2014,** *159,* 355–376.
283. Dhahbi, J. M.; Mote, P. L.; Fahy, G. M.; Spindler, S. R. Identification of potential caloric restriction mimetics by microarray profiling. *Physiol Genomics* **2005,** *23,* 343–350.
284. Zheng, J.; Woo, S. L.; Hu, X.; Botchlett, R.; Chen, L.; Huo, Y.; Wu, C. Metformin and metabolic diseases: a focus on hepatic aspects. *Front Med* **2015,** *9* (2), 173–186.
285. Hur, K.Y.; Lee, M-Sh., New mechanisms of metformin action: Focusing on mitochondria and the gut, J Diab Invest (2015) (In press).
286. Mendelsohn, A. R.; Larrick, J. W. Dissecting mammalian target of rapamycin to promote longevity. *Rejuvenation Res* **2012,** *15* (3), 334–337.
287. Gelino, S.; Hansen, M. Autophagy – an emerging anti-aging mechanism?". *J. Clin Exp Pathol* **2012,** *4,* pii:006.
288. Jia, G.; Sowers, J. R. Autophagy: A housekeeper in cardiorenal metabolic health and disease. *Biochim Biophys Acta* **2015,** *1852* (2), 219–224.
289. Martinez-Lopez, N.; Athonvarangkul, D.; Singh, R. Autophagy and aging. *Adv Exp Med Biol* **2015,** *847,* 73–87.
290. Morselli, E.; Galluzzi, L.; Kepp, O.; Criollo, A.; Maiuri, M. C.; Tavernarakis, N.; Madeo, F.; Kroemer, G. Autophagy mediates pharmacological lifespan extension by spermidine and resveratrol. *Aging (Albany NY)* **2009,** *1* (12), 961–970.
291. Martins, I.; Galluzzi, L.; Kroemer, G. Hormesis, cell death and aging. *Aging (Albany NY)* **2011,** *3* (9), 821–828.
292. Madeo, F.; Zimmermann, A.; Maiuri, M. C.; Kroemer, G. Essential role for autophagy in life span extension. *J Clin Invest* **2015,** *125* (1), 85–93.
293. He, C.; Klionsky, D. J. Regulation mechanisms and signaling pathways of autophagy. *Annu Rev Genet* **2009,** *43,* 67–93.
294. Feng, Y.; Yao, Z.; Klionsky, D. J. How to control self-digestion: transcriptional, post-transcriptional, and post-translational regulation of autophagy. *Trends Cell Biol* **2015,** *25* (6), 354–363.
295. Filomeni, G.; De Zio, D.; Cecconi, F. Oxidative stress and autophagy: the clash between damage and metabolic needs. *Cell Death Differ* **2015,** *22* (3), 377–388.
296. Tasdemir, E.; Maiuri, M. C.; Galluzzi, L.; Vitale, I.; Djavaheri-Mergny, M.; D'Amelio, M.; Criollo, A.; Morselli, E.; Zhu, C.; Harper, F.; Nannmark, U.; Samara, C.; Pinton, P.; Vicencio, J. M.; Carnuccio, R.; Moll, U. M.; Madeo, F.; Paterlini-Brechot, P.; Rizzuto, R.; Szabadkai, G.; Pierron, G.; Blomgren, K.; Tavernarakis, N.; Codogno, P.; Cecconi, F.; Kroemer, G. Regulation of autophagy by cytoplasmic p53. *Nat Cell Biol* **2008,** *10* (6), 676–687.
297. Moore, M. N.; Shaw, J. P.; Ferrar Adams, D. R.; Viarengo, A. Anti-oxidative cellular protection effect of fasting-induced autophagy as a mechanism for hormesis. *Mar Environ Res* **2015,** *107,* 35–44.
298. Szumiel, I. Radiation hormesis: Autophagy and other cellular mechanisms. *Int J Radiat Biol* **2012,** *88* (9), 619–628.
299. Yamaguchi, O.; Otsu, K. Role of autophagy in aging. *J Cardiovasc Pharmacol* **2012,** *60* (3), 242–247.
300. Morselli, E.; Maiuri, M. C.; Markaki, M.; Megalou, E.; Pasparaki, A.; Palikaras, K.; Criollo, A.; Galluzzi, L.; Malik, S. A.; Vitale, I.; Michaud, M.; Madeo, F.; Tavernarakis, N.; Kroemer, G. The life span-prolonging effect of sirtuin-1 is mediated by autophagy. *Autophagy* **2010,** *6* (1), 186–188.
301. Levine, B.; Kroemer, G. Autophagy in aging, disease and death: the true identity of a cell death impostor. *Cell Death Differ* **2009,** *16,* 1–2.
302. Eisenberg-Lerner, A.; Bialik, S.; Simon, H. U.; Kimchi, A. Life and death partners: apoptosis, autophagy and the cross-talk between them. *Cell Death Differ* **2009,** *16,* 966–975.
303. Shimizu, S.; Yoshida, T.; Tsujioka, M.; Arakawa, S. Autophagic cell death and cancer. *Int J Mol Sci* **2014,** *15* (2), 3145–3153.
304. Tucci, P. Caloric restriction: is mammalian life extension linked to p53? *Aging (Albany NY)* **2012,** *4* (8), 525–534.
305. Cheng, Y.; Ren, X.; Hait, W. N.; Yang, J. M. Therapeutic targeting of autophagy in disease: biology and pharmacology. *Pharmacol Rev* **2013,** *65* (4), 1162–1197.
306. He, L. Q.; Lu, J. H.; Yue, Z. Y. Autophagy in ageing and ageing-associated diseases. *Acta Pharmacol Sin* **2013,** *34* (5), 605–611.
307. Alvers, A. L.; Fishwick, L. K.; Wood, M. S.; Hu, D.; Chung, H. S.; Dunn, W. A., Jr.; Aris, J. P. Autophagy and amino acid homeostasis are required for chronological longevity in Saccharomyces cerevisiae. *Aging Cell* **2009,** *8* (4), 353–369.
308. Alvers, A. L.; Wood, M. S.; Hu, D.; Kaywell, A. C.; Dunn, W. A., Jr.; Aris, J. P. Autophagy is required for extension of yeast chronological life span by rapamycin. *Autophagy* **2009,** *5* (6), 847–849.

309. Hansen, M.; Chandra, A.; Mitic, L. L.; Onken, B.; Driscoll, M.; Kenyon, C.; Hansen, M.; Chandra, A.; Mitic, L. L.; Onken, B.; Driscoll, M.; Kenyon, C. A role for autophagy in the extension of lifespan by dietary restriction in C. elegans. *Plos Genet* **2008,** *4* (2), e24.
310. Morselli, E.; Maiuri, M. C.; Markaki, M.; Megalou, E.; Pasparaki, A.; Palikaras, K.; Criollo, A.; Galluzzi, L.; Malik, S. A.; Vitale, I.; Michaud, M.; Madeo, F.; Tavernarakis, N.; Kroemer, G. Caloric restriction and resveratrol promote longevity through the Sirtuin-1-dependent induction of autophagy. *Cell Death Dis* **2010,** *1,* e10.
311. Mariño, G.; Morselli, E.; Bennetzen, M. V.; Eisenberg, T.; Megalou, E.; Schroeder, S.; Cabrera, S.; Bénit, P.; Rustin, P.; Criollo, A.; Kepp, O.; Galluzzi, L.; Shen, S.; Malik, S. A.; Maiuri, M. C.; Horio, Y.; López-Otín, C.; Andersen, J. S.; Tavernarakis, N.; Madeo, F.; Kroemer, G. Longevity-relevant regulation of autophagy at the level of the acetylproteome. *Autophagy* **2011,** *7* (6), 647–649.
312. Soda, K.; Dobashi, Y.; Kano, Y.; Tsujinaka, S.; Konishi, F. Polyamine-rich food decreases age-associated pathology and mortality in aged mice. *Exp Gerontol* **2009,** *44,* 727–732.
313. Soda, K.; Kano, Y.; Chiba, F.; Koizumi, K.; Miyaki, Y. Increased polyamine intake inhibits age-associated alteration in global DNA methylation and 1,2-dimethylhydrazine-induced tumorigenesis. *PLoS One* **2013,** *8* (5), e64357.
314. Eisenberg, T.; Knauer, H.; Schauer, A.; Büttner, S.; Ruckenstuhl, C.; Carmona-Gutierrez, D.; Ring, J.; Schroeder, S.; Magnes, C.; Antonacci, L.; Fussi, H.; Deszcz, L.; Hartl, R.; Schraml, E.; Criollo, A.; Megalou, E.; Weiskopf, D.; Laun, P.; Heeren, G.; Breitenbach, M.; Grubeck-Loebenstein, B.; Herker, E.; Fahrenkrog, B.; Fröhlich, K. U.; Sinner, F.; Tavernarakis, N.; Minois, N.; Kroemer, G.; Madeo, F. Induction of autophagy by spermidine promotes longevity. *Nat Cell Biol.* **2009,** *11* (11), 1305–1314.
315. Madeo, F.; Eisenberg, T.; Büttner, S.; Ruckenstuhl, C.; Kroemer, G. Spermidine: a novel autophagy inducer and longevity elixir. *Autophagy* **2010,** *6* (1), 160–162.
316. Minois, N. Molecular basis of the 'anti-aging' effect of spermidine and other natural polyamines – a mini-review. *Gerontology* **2014,** *60* (4), 319–326.
317. Minois, N.; Rockenfeller, P.; Smith, T. K.; Carmona-Gutierrez, D. Spermidine feeding decreases age-related locomotor activity loss and induces changes in lipid composition. *PLoS One* **2014,** *9* (7), e102435.
318. Morselli, E.; Marino, G.; Bennetzen, M. V.; Eisenberg, T.; Megalou, E.; Schroeder, S.; Cabrera, S.; Benit, P.; Rustin, P.; Criollo, A.; Kepp, O.; Galluzzi, L.; Shen, S.; Malik, S. A.; Maiuri, M. C.; Horio, Y.; Lopez-Otin, C.; Andersen, J. S.; Tavernarakis, N.; Madeo, F.; Kroemer, G. Spermidine and resveratrol induce autophagy by distinct pathways converging on the acetylproteome. *J Cell Biol* **2011,** *192,* 615–629.
319. Yang, S. H.; Sharrocks, A. D.; Whitmarsh, A. J. MAP kinase signalling cascades and transcriptional regulation. *Gene* **2013,** *513* (1), 1–13.
320. Vellai, T.; Takacs-Vellai, K.; Sass, M.; Klionsky, D. J. The regulation of aging: does autophagy underlie longevity? *Trends Cell Biol* **2009,** *19,* 487–494.
321. Yang, S.; Long, L.H.; Li, D.; Zhang, J.K.; Jin, S.; Wang, F.; Chen, J.G., β-Guanidinopropionic acid extends the lifespan of Drosophila melanogaster via an AMP-activated protein kinase-dependent increase in autophagy, Aging Cell (2015) (In press). http://dx.doi.org/10.1111/acel.12371.
322. Rockenfeller, P.; Koska, M.; Pietrocola, F.; Minois, N.; Knittelfelder, O.; Sica, V.; Franz, J.; Carmona-Gutierrez, D.; Kroemer, G.; Madeo, F. Phosphatidylethanolamine positively regulates autophagy and longevity. *Cell Death Differ* **2015,** *22* (3), 499–508.
323. Claustrat, B.; Leston, J. Melatonin: Physiological effects in humans. *Neurochirurgie* **2015,** *61* (2–3), 77–84.
324. Hardeland, R. Melatonin and circadian oscillators in aging – a dynamic approach to the multiply connected players. *Interdiscip Top Gerontol* **2015,** *40,* 128–140.
325. Jenwitheesuk, A.; Nopparat, C.; Mukda, S.; Wongchitrat, P.; Govitrapong, P. Melatonin regulates aging and neurodegeneration through energy metabolism, epigenetics, autophagy and circadian rhythm pathways. *Int J Mol Sci* **2014,** *15* (9), 16848–16884.
326. Ramis, M. R.; Esteban, S.; Miralles, A.; Tan, D. X.; Reiter, R. J. Caloric restriction, resveratrol and melatonin: Role of SIRT1 and implications for aging and related-diseases. *Mech Ageing Dev* **2015,** *146–148,* 28–41.
327. Hardeland, R. Melatonin and the theories of aging: A critical appraisal of melatonin's role in antiaging mechanisms. *J Pineal Res* **2013,** *55* (4), 325–356.
328. Anisimov, V. N.; Popovich, I. G.; Zabezhinski, M. A.; Anisimov, S. V.; Vesnushkin, G. M.; Vinogradova, I. A. Melatonin as antioxidant, geroprotector and anticarcinogen. *Biochim Biophys Acta* **2006,** *1757* (5–6), 573–589.
329. Izmaylov, D. M.; Obukhova, L. K. Geroprotector effectiveness of melatonin: investigation of lifespan of Drosophila melanogaster. *Mech Ageing Dev* **1999,** *106* (3), 233–240.
330. Bonilla, E.; Medina-Leendertz, S.; Díaz, S. Extension of life span and stress resistance of Drosophila melanogaster by long-term supplementation with melatonin. *Exp Gerontol* **2002,** *37* (5), 629–638.
331. Terán, R.; Bonilla, E.; Medina-Leendertz, S.; Mora, M.; Villalobos, V.; Paz, M.; Arcaya, J. L. The life span of Drosophila melanogaster is affected by melatonin and thioctic acid. *Invest Clin* **2012,** *53* (3), 250–261.
332. Anisimov, V. N.; Zavarzina, N. Y.; Zabezhinski, M. A.; Popovich, I. G.; Zimina, O. A.; Shtylick, A. V.; Arutjunyan, A. V.; Oparina, T. I.; Prokopenko, V. M.; Mikhalski, A. I.; Yashin, A. I. Melatonin increases both life span and tumor incidence in female CBA mice. *J Gerontol A Biol Sci Med Sci* **2001,** *56* (7), B311–B323.
333. Anisimov, V. N.; Alimova, I. N.; Baturin, D. A.; Popovich, I. G.; Zabezhinski, M. A.; Rosenfeld, S. V.; Manton, K. G.; Semenchenko, A. V.; Yashin, A. I. Dose-dependent effect of melatonin on life span and spontaneous tumor incidence in female SHR mice. *Exp Gerontol* **2003,** *38* (4), 449–461.
334. Vaiserman, A. M. Life extension by anti-aging drugs: hormetic explanation? *Am J Pharmacol Toxicol* **2008,** *2,* 14–18.
335. Rattan, S. I. S., Le Bourg, E., Eds. *Hormesis in Health and Disease;* Boca Raton: CRC Press, FL, 2014.
336. Rattan, S. I.; Kryzch, V.; Schnebert, S.; Perrier, E.; Nizard, C. Hormesis-based anti-aging products: A case study of a novel cosmetic. *Dose Response* **2013,** *11* (1), 99–108.
337. Sikora, E.; Bielak-Zmijewska, A.; Mosieniak, G.; Piwocka, K. The promise of slow down ageing may come from curcumin. *Curr Pharm Des* **2010,** *16* (7), 884–892.
338. Vaiserman, A. M.; Pasyukova, E. G. Epigenetic drugs: a novel anti-aging strategy? *Front Genet* **2012,** *3,* 224.
339. Kang, H.-L.; Benzer, S.; Min, K.-T. Life extension in *Drosophila* by feeding a drug. *Proc Natl Acad Sci USA* **2002,** *99,* 838–843.
340. Arking, R. Independent chemical regulation of health and senescent spans in Drosophila. *Invertebr Reprod Dev* **2015,** *59* (1), 28–32.
341. Sawada, M.; Enesco, H. E. Vitamin E extends lifespan in the short-lived rotifer Asplanchna brightwelli. *Exp Gerontol* **1984,** *19* (3), 179–183.
342. Poeggeler, B.; Sambamurti, K.; Siedlak, S. L.; Perry, G.; Smith, M. A.; Pappolla, M. A. A novel endogenous indole protects rodent mitochondria and extends rotifer lifespan. *PLoS One* **2010,** *5* (4), e10206.
343. Ishii, N.; Senoo-Matsuda, N.; Miyake, K.; Yasuda, K.; Ishii, T.; Hartman, P. S.; Furukawa, S. Coenzyme Q10 can prolong C. elegans lifespan by lowering oxidative stress. *Mech Ageing Dev* **2004,** *125* (1), 41–46.
344. Harrington, L. A.; Harley, C. B. Effect of vitamin E on lifespan and reproduction in Caenorhabditis elegans. *Mech Ageing Dev* **1988,** *43* (1), 71–78.
345. Wen, H.; Gao, X.; Qin, J. Probing the anti-aging role of polydatin in Caenorhabditis elegans on a chip. *Integr Biol (Camb)* **2014,** *6* (1), 35–43.
346. Liao, V. H.; Yu, C. W.; Chu, Y. J.; Li, W. H.; Hsieh, Y. C.; Wang, T. T. Curcumin-mediated lifespan extension in Caenorhabditis elegans. *Mech Ageing Dev* **2011,** *132* (10), 480–487.
347. Grünz, G.; Haas, K.; Soukup, S.; Klingenspor, M.; Kulling, S. E.; Daniel, H.; Spanier, B. Structural features and bioavailability of four flavonoids and their implications for lifespan-extending and antioxidant actions in C. elegans. *Mech Ageing Dev* **2012,** *133* (1), 1–10.
348. Pietsch, K.; Saul, N.; Chakrabarti, S.; Stürzenbaum, S. R.; Menzel, R.; Steinberg, C. E. Hormetins, antioxidants and prooxidants: defining quercetin-, caffeic acid- and rosmarinic acid-mediated life extension in C. elegans. *Biogerontology* **2011,** *12* (4), 329–347.
349. Melov, S.; Ravenscroft, J.; Malik, S.; Gill, M. S.; Walker, D. W.; Clayton, P. E.; Wallace, D. C.; Malfroy, B.; Doctrow, S. R.; Lithgow, G. J. Extension of life-span with superoxide dismutase/catalase mimetics. *Science* **2000,** *289,* 1567–1569.
350. Cañuelo, A.; Gilbert-López, B.; Pacheco-Liñán, P.; Martínez-Lara, E.; Siles, E.; Miranda-Vizuete, A. Tyrosol, a main phenol present in extra virgin olive oil, increases lifespan and stress resistance in Caenorhabditis elegans. *Mech Ageing Dev* **2012,** *133* (8), 563–574.
351. Honda, Y.; Fujita, Y.; Maruyama, H.; Araki, Y.; Ichihara, K.; Sato, A.; Kojima, T.; Tanaka, M.; Nozawa, Y.; Ito, M.; Honda, S. Lifespan-extending effects of royal jelly and its related substances on the nematode Caenorhabditis elegans. *PLoS One* **2011,** *6* (8), e23527.
352. Kim, J.; Takahashi, M.; Shimizu, T.; Shirasawa, T.; Kajita, M.; Kanayama, A.; Miyamoto, Y. Effects of a potent antioxidant, platinum nanoparticle, on the lifespan of Caenorhabditis elegans. *Mech Ageing Dev* **2008,** *129* (6), 322–331.

353. Krementsova, A. V.; Roshina, N. V.; Tsybul'ko, E. A.; Rybina, O. Y.; Symonenko, A. V.; Pasyukova, E. G. Reproducible effects of the mitochondria-targeted plastoquinone derivative SkQ1 on Drosophila melanogaster lifespan under different experimental scenarios. *Biogerontology* **2012,** *13* (6), 595–607.
354. Khavinson, V. K.; Izmaylov, D. M.; Obukhova, L. K.; Malinin, V. V. Effect of epitalon on the lifespan increase in Drosophila melanogaster. *Mech Ageing Dev* **2000,** *120* (1–3), 141–149.
355. Stvolinsky, S.; Antipin, M.; Meguro, K.; Sato, T.; Abe, H.; Boldyrev, A. Effect of carnosine and its Trolox-modified derivatives on life span of Drosophila melanogaster. *Rejuvenation Res* **2010,** *13* (4), 453–457.
356. Bahadorani, S.; Hilliker, A. J. Cocoa confers life span extension in Drosophila melanogaster. *Nutr Res* **2008,** *28* (6), 377–382.
357. Morley, A. A.; Trainor, K. J. Lack of an effect of vitamin E on lifespan of mice. *Biogerontology* **2001,** *2* (2), 109–112.
358. Kitani, K.; Osawa, T.; Yokozawa, T. The effects of tetrahydrocurcumin and green tea polyphenol on the survival of male C57BL/6 mice. *Biogerontology* **2007,** *8* (5), 567–573.
359. Anisimov, V. N.; Egorov, M. V.; Krasilshchikova, M. S.; Lyamzaev, K. G.; Manskikh, V. N.; Moshkin, M. P.; Novikov, E. A.; Popovich, I. G.; Rogovin, K. A.; Shabalina, I. G.; Shekarova, O. N.; Skulachev, M. V.; Titova, T. V.; Vygodin, V. A.; Vyssokikh, M. Y.; Yurova, M. N.; Zabezhinsky, M. A.; Skulachev, V. P. Effects of the mitochondria-targeted antioxidant SkQ1 on lifespan of rodents. *Aging (Albany NY)* **2011,** *3* (11), 1110–1119.

Relevant websites

360. http://www.anti-agingfirewalls.com/–AGINGSCIENCES™ – Anti-Aging Firewalls™. A weblog on the sciences and practices of living healthily very long – perhaps hundreds of years.
361. www.AntiAging.com.http://www.antiaging.com/.Rejuvenation and anti-aging medicine from one of the premiere experts in the United States.
362. http://www.aging-no-more.com/–Aging No More.This website will equip you with practical information and effective strategies to help you slow down and/or reverse the aging process!.
363. http://www.onewithwellness.com/–One With Wellness.Anti-aging, vitamins, supplements, wellness, beauty, cosmetics.
364. http://expert-anti-aging-advice.com/–Expert Anti Aging Advice: Vitality, Beauty & Health From the Inside Out.Educational advice on how to apply the scientific principles of anti aging medicine in order to improve your level of health, vitality and well-being.
365. Anti-Aging Medicine.Living a long and healthy life is easy with the right nutritional support. Protecting the body's cellular integrity is important for an anti-aging approach. Live better longer with advanced technology in nutritional medicine.
366. http://best-antiagingproducts.com/–Best Anti-Aging Products.At Best Anti-Aging Products we analyze many of the products on the market that are designed to reverse the effects of aging. We also collect reviews and feedback from customers using the product.

1.13 Regenerative Medicine

SG Davies, PD Kennewell, AJ Russell, L Silpa, R Westwood, and GM Wynne, University of Oxford, Oxford, United Kingdom

© 2017 Elsevier Ltd. All rights reserved.

1.13.1	**Introduction**	379
1.13.1.1	Definitions	380
1.13.1.2	Literature Trends in This Research Area	384
1.13.2	**Studies on Specific Organs**	385
1.13.2.1	Blood and Bone	385
1.13.2.1.1	Hematopoietic stem cells	385
1.13.2.1.2	Mesenchymal multipotent stromal cells	386
1.13.2.1.3	Bone marrow stem cell niche and signaling pathways	386
1.13.2.1.4	Diseases involving these cells	387
1.13.2.1.5	Current therapies	387
1.13.2.1.6	Chemical manipulation of HSCs	388
1.13.2.1.7	Eltrombopag: a case study in drug discovery of small molecule stem cell modulation	389
1.13.2.1.8	Bone	391
1.13.2.2	Cardiac Regeneration	393
1.13.2.2.1	In vitro chemically guided cardiac differentiation	393
1.13.2.2.2	In vivo	400
1.13.2.3	Neuronal System	402
1.13.2.3.1	Neuronal regeneration: neuronal stem cells and drug discovery	402
1.13.2.3.2	Neural stem cell culture	403
1.13.2.3.3	Directed differentiation of NSCs and NPCs in vitro	403
1.13.2.3.4	Directed differentiation of other cell types	404
1.13.2.3.5	Cell-based therapies for neurological disorders	409
1.13.2.3.6	Disease screening and drug discovery	413
1.13.2.4	Muscle Regeneration Using Small Molecules	414
1.13.2.4.1	Muscle-based applications of small molecule stem cell modulators	414
1.13.2.5	The Pancreas	416
1.13.2.5.1	Chemical manipulation of pancreatic regeneration	416
1.13.2.5.2	Ex vivo generation of replacement β-cells	416
1.13.2.5.3	Different sources of β-cells	419
1.13.2.5.4	In vivo expansion of β-cells	420
1.13.2.5.5	In vivo studies in zebrafish	421
1.13.2.6	Ocular Disease	422
1.13.2.6.1	Ocular applications of small molecule stem cell modulators	422
1.13.2.6.2	Corneal disease	422
1.13.2.6.3	Retinal disease	422
1.13.2.6.4	Retinal therapies using stem cells	423
1.13.2.6.5	Small molecule modulation of hES and iPS cells to retinal cells	425
1.13.2.6.6	New assays and assay technologies	426
1.13.3	**Conclusion**	427
References		428

1.13.1 Introduction

Stemistry[1] is the term given to describe the search for, and use of, small molecules able to affect the behavior of endogenous stem, stemlike, or progenitor cells. "Affecting the behavior" includes the stimulation of the proliferation of these cells, their directed differentiation to specific cells, their migration, and the dedifferentiation/transdifferentiation of differentiated cells. Such molecules could be used in regenerative medicine to repair tissue in two general ways. The ex vivo approach would remove cells from the patient and expand and differentiate them in vitro before transplanting into the patient. A particular medical advantage of this approach is that the cells to be transplanted could be subjected to rigorous quality control and inspection to ensure that only the desired cells were present and that teratoma formation would be highly unlikely. In the clinical situation, however, the resources needed for this are, except in a research environment, likely to be high and possibly difficult to justify at a time when all health systems are under significant financial pressures. There have been reports of successful applications of this procedure although definitive treatments

have yet to be confirmed. The alternative approach that would be much simpler for both the health professional and the patient is the in vivo one in which the transforming drug(s) were dosed directly to the patient.

Current research reviewed by us[1] and others[2,3] has shown considerable progress in identifying small molecules able to affect cell behavior in the desired manner. Whereas the major emphasis in this article are studies toward finding in vivo active small molecules, and several pioneering examples have been described in recent years, a significant body of work published to date has come from in vitro studies. In many instances these latter studies have found utility in cell-based transplantation therapies. While a full discussion of cell transplantation therapies is beyond the scope of this review, these systems also represent useful models and selected examples are discussed in this context. Before reviewing some of these findings it will be helpful to define the terminology used in this research.

1.13.1.1 Definitions

The terms and their definitions that are used in this article are as follows (Fig. 1).

Self-renewal is the process whereby a stem cell divides to produce at least one copy of itself.

Proliferation is the production of multiple exact copies of any cell.

Differentiation is the process whereby a cell is transformed into a new cell type. In the context of this article it refers to the change of a stem or progenitor cell into a particular cell type.

Dedifferentiation or transdifferentiation is either the reversion of a cell type to a progenitor cell or directly to a different, differentiated cell type.

Stem cells possess two critical properties, namely, the ability to repeatedly self-replicate through cell division while maintaining an undifferentiated state and the capacity to differentiate into specialized cell types. They are conveniently divided into a number of types depending on their location and ability to produce differentiated cells. In decreasing ability to produce different cell types, these are:

Totipotent stem cells are only found in the fertilized egg and the first few cell divisions. They are able to produce all the 200+ cell types of the adult human as well as the placenta and extra-embryonic tissue.

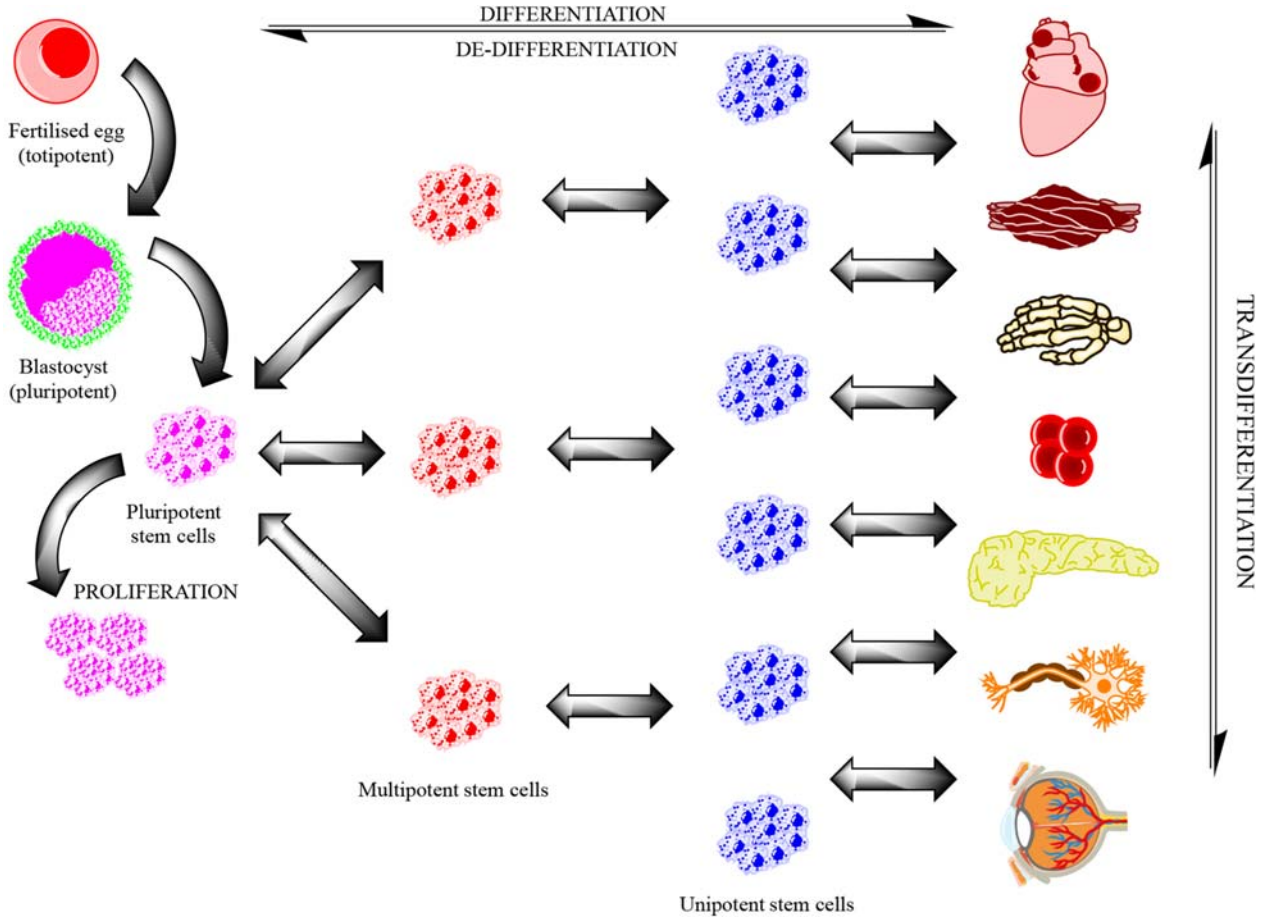

Fig. 1 Stem cell ontogeny and manipulation.

Pluripotent stem cells are derived from the epiblast tissue of the inner cell mass of the very early stage, that is, less than 5 days old, embryo and are capable of producing all the cells of the embryo and the adult except for the placenta and the extra-embryonic tissue. Historically, these cells could not be isolated without bringing about the death of the embryo and this has made the use of human embryonic stem cells (hESCs) problematic or unacceptable to a number of cultures and religions.

A major breakthrough occurred with the finding that adult terminally differentiated cells could be reprogrammed to produce pluripotent stem cells. These so-called induced pluripotent stem cells were initially derived from skin fibroblasts and later from those of the stomach, liver, skin, and blood. They were reprogrammed using the transcription factors (TFs) Oct 3/4, Sox2, c-Myc, and K1f4, but this procedure is complicated, inefficient, and carries the risk of tumor formation.[4] It is of particular relevance to this article that recently Deng and coworkers have been able to replace the TF Oct 4 by one of three candidate molecules (**Fig. 2**; forskolin (1), 2-methyl-5-hydroxytryptamine (2), D4476 (3)) and, in a separate study, the TFs Sox2, c-Myc, and K1f4 by a combination of four small molecules (valproic acid (4), CHIR99021 (5), 616452 (6), and tranylcypromine (7)). They went on to optimize this small molecule cocktail to develop a chemically induced reprogramming protocol, albeit with only 0.2% frequency.[5]

Multipotent/unipotent stem cells can only produce one or more differentiated cell types usually associated with specific tissues or organs. Examples include hematopoietic stem cells found in the bone marrow that give rise to red and white blood cells and platelets. Mesenchymal stem cells (MSCs) are also found in the bone marrow and give rise to stromal cells, fat cells, and bone cells. Epithelial stem cells give various types of skin cells while satellite cells contribute to differentiated muscle cells.

Progenitor cells have a tendency to differentiate into a specific target type of cell, although unlike the case with stem cells this cannot occur indefinitely and is restricted to a limited number of stages.

Adult or somatic stem cells are found in both children and adults and occur throughout the body and their role in natural repair processes is a subject of ongoing research. They can self-renew and generate the cell types comprising the organs where they reside including the hematopoietic system, bone marrow, central nervous system, liver, skin, cornea, gut, skeletal muscle, and adipose tissue. While compared with hESC and hiPSC they do have limited proliferation and differentiation capacity in vitro they confer a low risk of tumor formation after being transplanted to patients. In fact, a number of clinical trials are currently in place to investigate the use of adult stem cells to restore normal functioning in neurodegeneration, spinal cord injury, graft-*versus*-host disease (GVDH), and diabetes.[3]

To reiterate, the medicinal chemistry approach to regenerative medicine is to identify small molecules able to selectively influence stem cells in vivo in a therapeutically valuable way to produce new, healthy tissues, a process that has been termed "molecular organ repair."[6] The obvious question that a critic could pose is "is there any evidence that such an approach is at all feasible?" Poss[7] has discussed known in vivo tissue repair such as that seen in the liver while pointing out that mammalian tissues such as cardiac muscle and the spinal cord appear to have little regenerative capacity. He did also note that stem cells are not necessarily involved even in well-established instances of tissue regeneration. In particular, in the salamander, which is usually taken as the example *par excellence* of regeneration, the process seems to be one of dedifferentiation of tissue-specific cells rather than stem cell differentiation. These studies indicate that test systems designed to detect activity arising from a range of cell types can be established and could be used for the detection of small molecules that influence their behavior.

The hESCs contain the potential to produce exact daughter cells and to differentiate into all other adult cell types, which have only limited ability to change further. Thus the stem cell under the influence of the correct signaling factors is able to produce gene products that cause the cell to proliferate or to begin the differentiation process leading to the new cell lineages. A key feature in

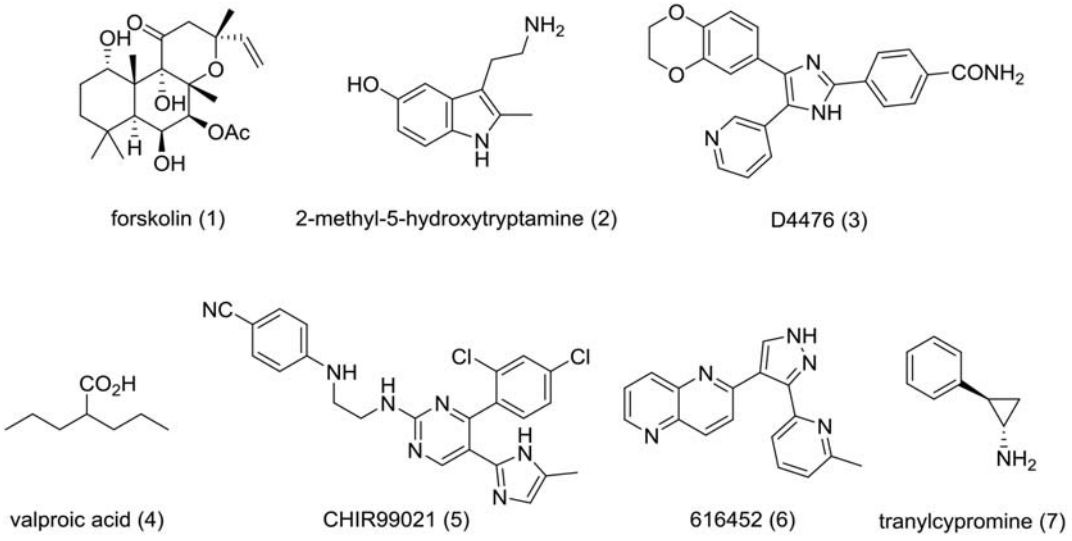

Fig. 2 Small molecules which used in combination are able to reprogram differentiated cells to pluripotent stem cells.

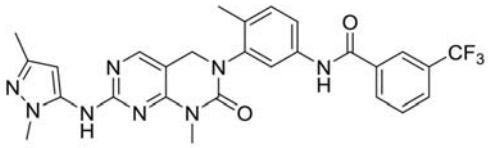

(8)

Fig. 3 Chemical structure of Pluripotin SC1 (8).

development is that conversion of a pluripotent stem cell to, say, a kidney cell, takes place through a number of steps all of which require the sequential production of signaling factors. Each of these processes produces only the targeted cell in a specific location so that, for example, a kidney cell ends up in the kidney and not the heart. Since in vitro studies demonstrate that the stem cell cannot itself "decide" to make a particular cell, this must mean that at a certain point in the development of the embryo signaling from other cells in the vicinity must play a role in the differentiation process. This microenvironment in which a stem cell resides has been designated the "niche" and it seems highly likely that growth factors either released into the niche or present in the extracellular matrix or on the surface of adjacent cells are responsible for the differentiation of the stem cell. In the later section of this article dealing with the pancreas, work will be described in which a prepared extracellular matrix is able to direct the differentiation of a stem cell to a pancreatic β-cell during in vitro culture.

Thus differentiated cells are produced as a result of growth factor interactions, that is, by protein–protein and ligand–receptor interactions and modulation of enzyme activity; medicinal chemistry has a substantial history at being able to find agents capable of interrupting such interactions to great therapeutic benefit. But how might such compounds be discovered? Initially with little information on the biochemistry/cell biology of the stem cell being known the way forward was via high-throughput screening of libraries of compounds using stem cell proliferation or differentiation readouts. Our previous perspective[1] discusses a number of such studies so one example will suffice here to show the principle involved. Schultz et al. used a reporter murine embryonic stem cell line from transgenic OG2 mice, which had been transfected with the regulatory region of the Oct-4 gene (a widely used pluripotency marker) fused with that for green fluorescent protein (GFP).[8] Under incubation conditions such cells lose both GFP expression and their compact colony morphology completely in 4–6 days in the absence of feeder cells and leukemia inhibitory factor so the maintenance of GFP expression in the presence of test compounds is a good indication of maintaining pluripotency of the stem cells. One active compound found in a library of 50,000 compounds was SC1 (pluripotin) ((8), Fig. 3), which on further biochemical investigation showed to be a dual function inhibitor of both extracellular signal-related kinases (ERK) and Ras GTPase activating protein (Ras GAP). Thus pluripotin allows the propagation of murine ESCs in an undifferentiated pluripotent state under chemically defined conditions and also gives ideas about some of the biochemical pathways involved in this process, which might be further exploited in the search for new agents.

Lu and Atala[3] give lists of compounds that cause self-renewal of stem cells, of others that affect differentiation of stem cells or generation of iPSCs from other cell lines and dedifferentiation of cells along with possible modes of action. Most of these have been discovered using variations of the original work described earlier. Once active molecules have been identified the next stage is to try to determine its mode of action but of course the fact that a compound is an inhibitor of, say, a kinase does not necessarily mean that the inhibition of that kinase actually causes the cellular changes. Questions relating to both the potency and specificity of the compounds naturally arise in the mind of the medicinal chemist, thus investigations into the action of other inhibitors of the kinase on stem cells should at least take place. In many instances such studies have not yet been undertaken or reported.

A word of caution regarding the use of murine stem cells as model for the human is necessary. Significant differences in behavior between the two species have been discovered including responsiveness to different signaling pathways and the vulnerability of human cells toward apoptosis following single cell dissociation. As this represents a significant hurdle to the use of hESCs a search was made to discover molecules able to enhance cell survival after dissociation and to maintain pluripotency.[9] From a library of 50,000 compounds, thiazovivin (9) and pyrintegrin (10) had the desired activities (Fig. 4) and it was suggested that the mechanism

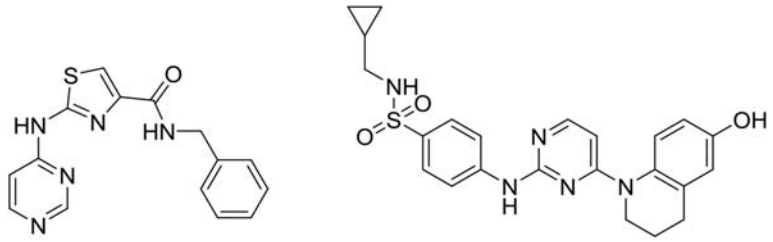

thiazovivin (9) pyrintegrin (10)

Fig. 4 Compounds reported to enhance hESC survival and maintain pluripotency.

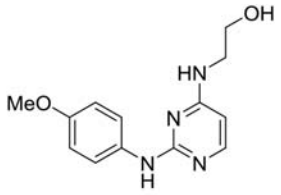

(11)

Fig. 5 Chemical structure of Cardiogenol C (11).

of activity is the enhancement of ECM-cell adhesion-mediated integrin activity. Thiazovivin was subsequently shown to inhibit Rho-associated kinase and to stabilize E-cadherin, thus promoting E-cadherin mediated cell–cell adhesion. Again the importance of interactions with elements of the niche is emphasized.

The discovery of agents able to control differentiation of stem cells is illustrated by the use of the mouse embryonic carcinoma cell line, P19, transfected by the promoter region of the rat atrial natriuretic factor, a polypeptide hormone synthesized primarily in cardiac myocytes[10] fused with a luciferase gene. As the natriuretic factor is considered as a specific cardiomyocyte (CM) marker, an increase in luciferase activity was taken as indicative of differentiation to cardiac cells. From a library of 100,000 compounds the most active was cardiogenol C ((11), Fig. 5) and cardiac activity was supported both by the detection of sarcomeric myosin heavy chain, one of the motor proteins essential for cardiac muscle contractibility and also the production of GATA-4, a TF expressed in the developing heart.

Small molecule-mediated or -enhanced dedifferentiation has been investigated mainly as an alternative route to iPSCs particularly from fibroblasts or keratinocytes, examples being the TGF-β inhibitor SB431542 (12) and MEK inhibitor PD0325901 (13).[11–13] Myoseverin (14), which binds tubulin, thus causing degradation of the microtubule cytoskeleton, was reported to convert muscle cells to a myoblast-like phenotype and, later, reversine (15) was shown to induce myogenic lineage-committed cells to become multipotent progenitor cells (Fig. 6).[14] Further examples of all of the earlier processes are discussed in the following sections.

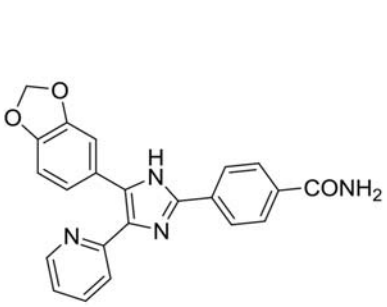

SB431542 (12)

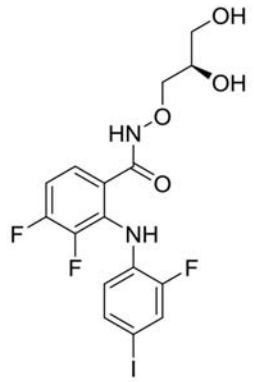

PD0325901 (13)

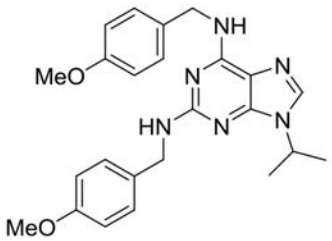

myoseverin (14)

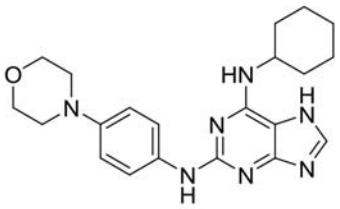

reversine (15)

Fig. 6 Compounds used in the dedifferentiation of cells to iPSCs.

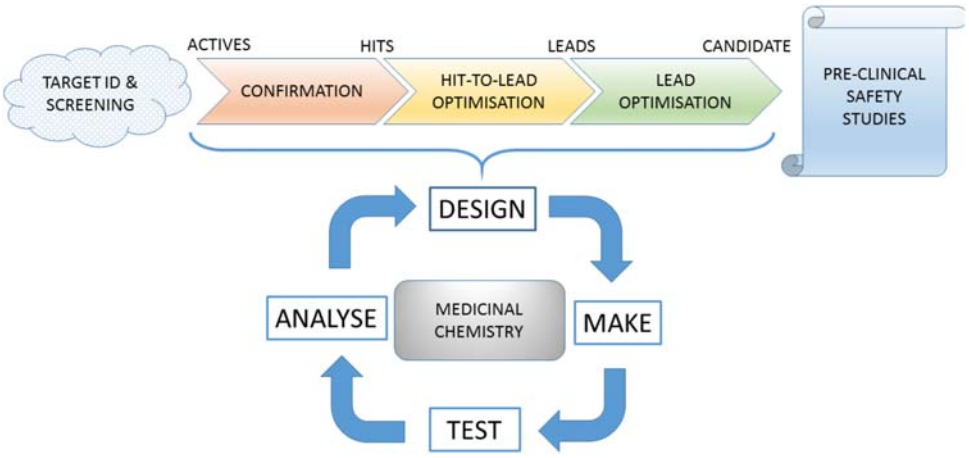

Fig. 7 The DMTA (Design-make-test-analyse) optimization cycle for drug discovery.

In vivo test systems are of course essential in the route from in vitro findings to animal studies to clinical trials and a number of results are described further. In particular, the zebrafish and its embryo have been used as a test system due to its innate ability to repair many types of tissue damage. Examples of specific in vivo investigations are also discussed in the later sections of this article.

1.13.1.2 Literature Trends in This Research Area

Recent years have seen a significant rise in publications relating to stem cells and their application in regenerative medicine. While many of these refer to cell-based therapies, and are therefore outside the scope of this article, the utilization of small molecules to modulate stem cell function and fate is on the rise. As already described, this enables the medicinal chemist to contemplate a rather more conventional Design-Make-Test-Analyse (DMTA) drug discovery project paradigm akin to the well-established workflow illustrated in Fig. 7.

It can be seen that the term "stem cells," while first described in the literature around 1900, has only really started to come to prominence during the late 1990s (Fig. 8, searches conducted using SciFinder™). Interestingly, a similar trend applies to the patent literature, though as one might expect, the rise in publications relative to the primary peer reviewed literature lags by a few years.

When a more applied stem cell paradigm is considered, in this case colocation of the terms "stem cells" and "small molecule" one can see that this only really emerges in the 1990s, and starts to increase in the mid 2000–10 decade (Fig. 9).[1] Again, as shown in a recent review, the patent literature lags somewhat behind the primary literature,[15] and while filings in this area are on the rise, one could expect this to be the growth area of the next decade, as true industrial application and drug discovery opportunities begin to be fully realized.

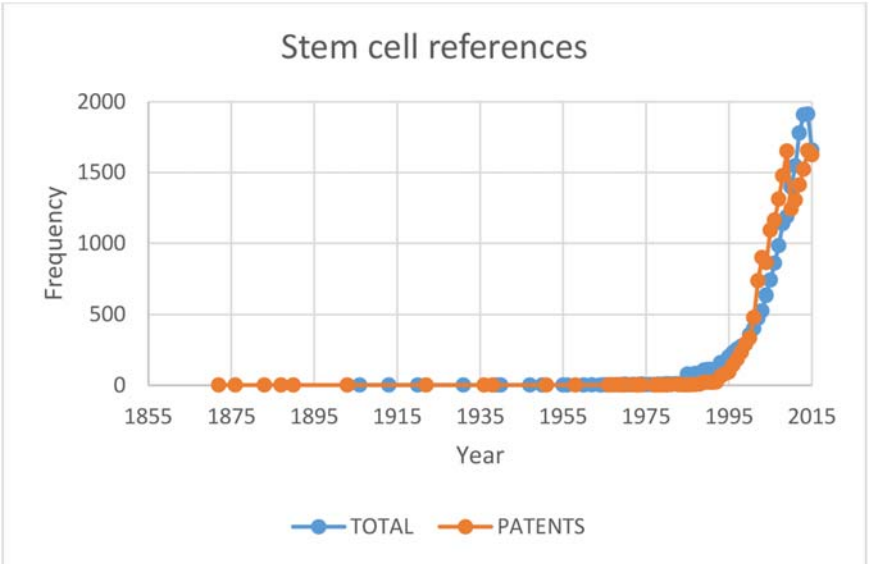

Fig. 8 Stem cell citation analysis.

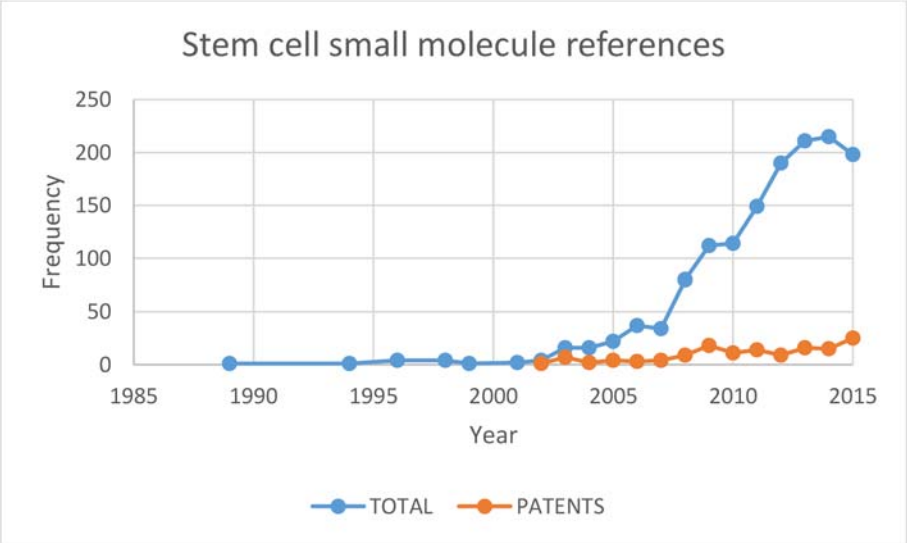

Fig. 9 Stem cell and small molecule citation analysis.

1.13.2 Studies on Specific Organs

1.13.2.1 Blood and Bone

1.13.2.1.1 Hematopoietic stem cells

The blood system is one of the organs of the body with the greatest capacity for regeneration and is maintained by a small pool of multipotent hematopoietic stem cells (HSCs), which is sufficient for replenishing all human blood cell lineages at a rate of millions of cells per second throughout life. Within the HSCs there are two large and distinct subsets responsible for the production of myeloid cells including monocytes, macrophages, neutrophils, basophils, eosinophils, erythrocytes, and dendritic cells and lymphoid cells producing T and B cells and natural killer cells. Recently it has been shown that there exists in the mouse a distinct HSC subset primed for platelet-specific gene expression with enhanced propensity for short- and long-term reconstitution of platelets.[16] As platelets are crucial for preventing bleeding, the discovery of specific targets with the potential to be targeted by drugs could be essential to medicinal chemistry programs aimed at enhancing their production following bone marrow transplantation or chemotherapy. Since the platelet-biased HSCs also frequently have a long-term myeloid-lineage bias and can give rise to lymphoid-biased HSCs, it was suggested that these cells could lie at the apex of HSC subtypes.

The self-renewing HSCs occupy the top of a hierarchical population of multipotent and progenitor cells, which differentiate along defined pathways via increasingly lineage-restricted cell types in response to various signaling events, thus giving rise to all the specialized functional cells of the bloodstream. Studies in mice have indicated the presence of both long-term (LT) and short-term (ST) HSCs.[17] Engraftment of human HSCs into immune-deficient mouse strains such as the nonobese diabetic/severe combined immunodeficiency (NOD/SCID) mouse has allowed the characterization of human HSCs.[18] Combinations of cell surface markers have been used to identify both human and mouse HSCs but, unfortunately, these are not conserved between species.[19] A number of endogenously synthesized growth factors including erythropoietin (EPO), thrombopoietin (TPO), granulocyte-macrophage colony stimulating factor (G-CSF), macrophage colony stimulating factor (GM-CSF), stem cell factor (SCF), and various interleukins (IL) have been shown to influence the proliferation, survival, and differentiation of HSCs.[20] A full review of the activity of TPO as the primary regulator of megakaryocyte progenitor expansion and differentiation, its activity, structure, mechanisms of action, and therapeutic use to increase platelet production has been produced.[21] The expectation that it should be possible to find small organic molecules able to influence the behavior of HSCs is perhaps given credence by the report that compounds P18IN003 (16) and P18IN011 (17), which block the activity of the G1 phase regulator protein, P18, are able to enhance ex vivo expansion of HSCs (Fig. 10).[22]

The details of endogenous hematopoiesis mechanisms in animals, particularly mice, have only recently been addressed. Earlier studies had involved following cells after transplantation and it is proposed that the stresses involved in such studies may give results different from the normal situation. In fact, Camargo et al. have shown that a large number of long-lived progenitors rather than classically defined HSCs are the main drivers of steady-state hematopoiesis during most of adulthood.[23] An even more recent report[24] agrees with the idea that the transplantation model is unlikely to give results showing the situation in the normal animal but believes that adult hematopoiesis is largely sustained by short-term stem cells downstream of HSCs, which nearly fully self-renew and receive rare but polyclonal HSC input. The authors postulate that the reservoir property of the ST-HSCs might explain the differences between their results and those of Camargo.[23] In any event, it is clearly very difficult to gain a full picture of the complex events taking place inside the bone marrow.

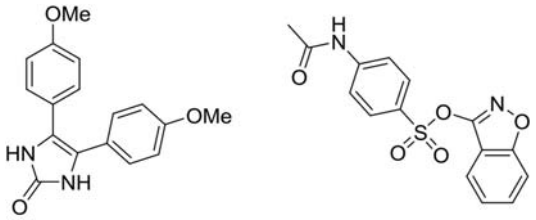

Fig. 10 Compounds reported to enhance ex vivo expansion of HSCs.

While HSCs self-renew indefinitely, their functional activity declines over time, which results in degraded blood production. Evidence has recently been reported to support this decline being due to replication stress and that the minichromosomal maintenance DNA helicase could be a potential molecular target for agents designed to alleviate this process.[25] In mice, HSCs divide significantly more frequently in female than in male mice. Further, estrogen levels increase in pregnancy and increase HSC division, frequency, cellularity, and erythropoiesis in the spleen via the estrogen receptor-α.[26]

1.13.2.1.2 Mesenchymal multipotent stromal cells

This is an overarching term used to describe multipotent cells able to produce other differentiated cells of which MSCs may be a subset.[27] These cells are also found in the bone marrow and are responsible for sustaining the integrity of the adult skeleton by the maintenance of the bone-forming osteoblasts and bone resorbing osteoclasts. Additional cell lineages produced by MSCs are chondrocytes and adipocytes for the maintenance of cartilage and lipid, respectively. In vitro populations of mesenchymal multipotent stromal cells, which self-renew and differentiate, can be derived from multipotent mesenchymal stem or progenitor cells. However, MSCs are significantly less well characterized than HSCs and as yet, appear to have no universally accepted unique surface markers. They may in fact be a heterogeneous population.[28] Bara et al.[29] have recently produced a detailed review of MSCs in their native environment focusing on the distinct phenotypic differences between them and MSCs cultured in vitro. The implications of these changes on potential clinical use are discussed.[29] Their possible interaction with HSCs is discussed in the next section.

1.13.2.1.3 Bone marrow stem cell niche and signaling pathways

The concept of a niche is that there is a defined area in which a particular cell exists and interacts with the cells and structures within the local microenvironment, this interaction controlling the behavior of the cell. The idea of the HSC niche was first introduced by Schofield in 1978[30] as a microenvironment in which stem cell populations reside and are maintained through a variety of cues. Of all adult stem cell niches, bone marrow HSC niches have been the most extensively studied, although many aspects remain poorly understood.[31,32] The main problem seems to lie in the difficulty with trying to get a clear picture of the nature of the cells and their precise status deep inside the bone marrow and in deciding which interactions are likely to be important under which circumstances. Morrison et al. have used GFP linked to the gene for α-catulin allied to deep confocal imaging to indicate that HSCs were more common in central marrow than near bone surfaces and that most HSCs, both dividing and nondividing, were located near sinusoidal blood vessels and distant from arterioles, transition zone vesicles, and bone surfaces. It was concluded that these cells reside mainly in perisinusoidal niches.[33] A very detailed review of the niche has been presented by Morrison and Scadden,[34] who suggest that HSCs reside in a specialized niche that is distinct from those that nurture other hematopoietic progenitors. Each niche may be created by multiple cell types that contribute to the niches in unique as well as redundant ways. Overall, the niche is perivascular and is created partly by mesenchymal stromal cells and endothelial cells. How these niches react in response to factors such as stress from infection, myeloablation, or neoplasia could shed light on disease progression or suggest ways of treating the condition. Mendez-Ferrer et al. have discussed the difficulties in precisely identifying the role of MSCs in the niche, difficulties caused by partial characterization of cell lines, redundancy and compensatory effects of the cells, and technical difficulties in the experimental procedures.[35] The role of interactions with the extracellular matrix components and adhesion molecules released from surrounding cells has been discussed by Klamer and Voemans.[36] They point out that normally the majority of HSCs are present in a quiescent state with, in mice, division only taking place on average once per 32 days while a subpopulation only divides five times during the lifespan of the mouse. However, these cells are reversibly activated upon massive hematopoietic cell loss. Presumably, this takes place following input from surrounding cells and tissue. Among the signaling molecules identified as playing a role in HSC stimulation are VLA4, VCAM1, CD44/hyaluronic acid, CXCR4/SDF1, SCF, ANG1, TIE2, TPO, MPL, Notch, and hedgehog signaling.[37] As well as these biochemical modulators, the physical environment imposed by the extracellular matrix within the niche such as shear stress and rigidity have also been reported to play a role in the regulation and maintenance of HSCs.[38] Furthermore, the changing role of the HSC niche through ontogeny to adulthood has been discussed by Fraser et al.[39]

1.13.2.1.4 Diseases involving these cells

HSCs and mesenchymal stem/progenitor cells are essential for maintenance of blood and bone and thus it is to be expected that faults in the functioning of either could lead to human diseases. These include myeloproliferative neoplasms such as leukemia, cell-based anemia, for example, thrombocytopenia (platelet deficiency) or osteoporosis in which osteoclast destruction is not matched by osteoblast mediated bone formation.[40,41]

1.13.2.1.5 Current therapies

HSCs form the basis of one of the oldest and most widely employed stem cell-based therapies, namely, their transplantation into patients suffering from bone marrow failure or myeloablative chemo/radiotherapy for leukemia. These transplantations may be autologous, where the bone marrow is sourced from the patient before myeloablation or allogenic, where the HSCs are sourced from a human leukocyte antigen (HLA) matched donor. Autologous donations hold the promise of a successful engraftment without the appearance of dangerous GVDH, while allogenic donations are preferred in cases of acute myeloid leukemia where the reintroduction of the patient's own cells is likely to lead to the reappearance of the cancer.[42] Aspiration of bone marrow, peripheral blood, and umbilical cord blood (UCB) are the three main sources of HSCs for transplantation. As harvesting bone marrow is an invasive procedure that requires the use of general anesthetic, its use has largely been replaced by the use of peripheral blood. This seems surprising as the number of HSCs circulating in peripheral blood is generally very low but it has been found that administration of G-CSF prior to harvesting promotes migration of HSCs out of the bone marrow.[43] This would seem to be an attractive case for small molecule intervention and indeed AMD3100 (plerixafor; marketed as Mozobil, (18), Fig. 11), a CXCR4 agonist, has been shown to promote mobilization of HSCs either alone or in combination with granulocyte-colony stimulating factor (G-CSF).[44] AMD3100 was approved by the FDA for the mobilization of HSCs to peripheral blood for autologous transplants in non-Hodgkin lymphoma and multiple myeloma patients.[45]

UCB has the advantage of availability from a variety of donors of different genetic background, who are otherwise underrepresented among donors and has been found to be more tolerant of HLA mismatches between donor and recipient. However, the small quantities of UCB available from each donor have historically limited transplants to children or very small adults. Even in these cases the low number of HSCs leads to a delay in hematopoietic reconstitution leaving recipients with reduced immune cell and platelet numbers with the associated risk of infection and bleeding. Cells from more than one source could be used but this increases the risk of GVHD. Thus strategies to expand the HSC populations from these sources are being investigated.[46,47] Recently O'Brien et al. have taken earlier findings that UCB derived hematopoietic progenitor cells (HPC) are depleted of Wnt signaling and proposed that inhibition of GSK-3β could reactivate this. They showed that culture of ex vivo expanded HPC in the presence of BIO ((19), Fig. 12), a GSK-3β inhibitor (albeit a relatively nonspecific one), increased engrafting of human cells into the NOD–SCID mouse and suggested that this could be a way of increasing the clinical usefulness of UCB.[48]

MSCs have also shown promise for cell-based therapy. Their therapeutic effects are increasingly being recognized as arising as a result of paracrine signaling in situ. For instance, the immunomodulatory activity of MSCs has led to them being used in clinical

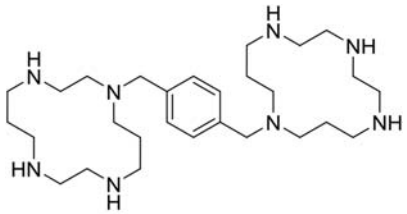

(18)

Fig. 11 Chemical structure of AMD3100, perixator, Mozobil (18).

(19)

Fig. 12 Chemical structure of BIO (19).

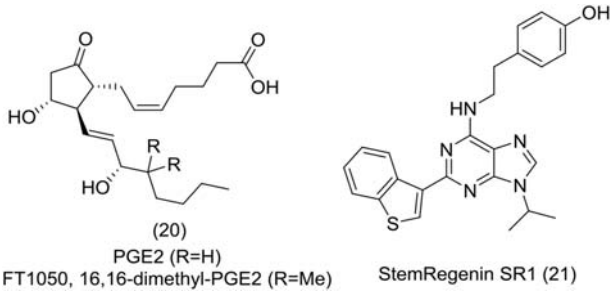

Fig. 13 Compounds reported to promote HSC expansion in vivo and ex vivo.

trials against various inflammatory diseases including GVHD and Crohn's disease. MSCs have also been shown to exhibit a paracrine effect to promote healing in other organs including the heart following myocardial infarction. Cell-based therapies in which MSCs/progenitor cells or chondroprogenitors are used to improve fracture healing or cartilage regeneration in osteoarthritic joints are also under investigation (see below).

1.13.2.1.6 Chemical manipulation of HSCs

While growth factors such as EPO and TPO stimulate HSCs and their progeny, small molecules would have the advantage of easier production and dosage and the search for such agents has been pursued with vigor. Prostaglandin E2 (PGE2) ((20), R=H, **Fig. 13**) and its more stable chemical analog 16,16-dimethylPGE2 ((20), R=Me, dmPGE2, FT1050) were found in a high-throughput screen using zebrafish embryos to enhance HSC expansion during embryogenesis.[49] This molecule, dmPGE2, was subsequently found to promote recovery of kidney marrow in sublethally irradiated zebrafish, which suggests a role also for this agent in adult HSC homeostasis. Human HSCs are also expanded by dmPGE2,[50] and the ex vivo dmPGE2-treated CB (ProHema®-modulated CB), very recently completed a Phase 2 clinical trial to evaluate its effects in a double CB transplant in patients with hematological malignancies (Clinical Trials.gov ID: NCT01627314). Further in 2011 the FDA granted this compound orphan drug status for the ex vivo treatment of human allogenic HSCs to enhance stem cell engraftment by treating neutropenia, thrombocytopenia, lymphopenia, and anemia.

In an approach similar to a number of others described in this article, Schultz and coworkers identified StemRegenin (SR1, (21)) from 100,000 heterocycles in a cell-based assay assessing ex vivo expansion of primary human CD34+ cells derived from HSC-mobilized peripheral blood.[51,52] SR1 acts as an agonist of the aryl hydrocarbon receptor (AhR), thus identifying another target for the design of molecules able to promote the ex vivo expansion of HSCs. It should be noted that SR1 did not promote the ex vivo expansion of mouse HSCs due to a lack of activity on the murine AhR, thus underlining another difference between human and murine cells.

Inhibition of p53 activity has been shown to enable the expansion of HSCs and it was found that pifithrin β ((22), **Fig. 14**), an inhibitor of p53, acts in mice to increase numbers of HSCs in vivo and promotes their mobilization into peripheral blood.[53,54] Given the widely studied role of p53 as a tumor suppressor, the strategy of inhibiting p53 activity for expansion of stem cell populations could, in principle, give rise to safety concerns. However, Gudkov et al.[53] found that administration of a single dose of pifithrin β to p53+/− heterozygous tumor susceptible mice prior to a dose of total body radiation did not lead to increased tumor incidence compared to control. Their conclusion was that short-term inhibition of p53 may not lead to increased incidence of tumors and it therefore could represent a viable strategy for HSC expansion.

From a 50,000 member library, MK1 ((23), **Fig. 15**) was identified as enhancing differentiation of primary human mobilized peripheral blood-derived CD34+ HSCs into CD41+ megakaryocytes.[55] MK1 was found to inhibit platelet-derived growth factor receptor (PDGFR), which leads to the production of megakaryocyte/erythrocyte progenitors (MEP). In a separate study, the natural product, euphohelioscopin A (24), was found to promote differentiation of CD34+ cells to the granulocyte/monocyte lineage at least in part via activation of protein kinase C.[56]

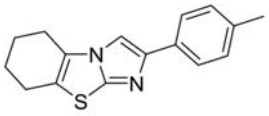

(22)

Fig. 14 Chemical structure of Pifithrin β (22).

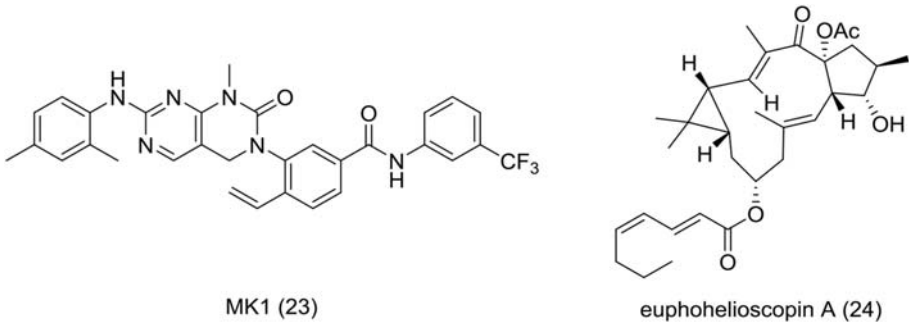

Fig. 15 Compounds reported to be able to differentiate megakaryocyte/erythrocyte progenitors.

1.13.2.1.7 Eltrombopag: a case study in drug discovery of small molecule stem cell modulation

The existence of TPO as a growth factor released from the liver and kidneys and involved in the production of platelets was first hypothesized over 50 years ago but this was only experimentally confirmed in 1994.[57] It is a 332-amino acid protein that has ca. 23% homology in its N-terminal region to EPO. However, its C-terminal region has homology to no known proteins and is thought to provide in vivo stability against proteolytic breakdown. Binding of TPO to its receptor, c-mpl, initiates multiple signaling pathways that lead ultimately to the production of megakaryocytes and thus to increased production of platelets (Fig. 16).

Following the isolation of TPO, a first generation of recombinant human TPO (rhTPO) and pegylated recombinant human megakaryocyte growth and development factor (PEG-rhMGDF) entered clinical trials and increased platelet counts in humans undergoing nonmyeloablative chemotherapy, but not in those undergoing stem cell transplantation. However, several healthy volunteers were found to develop neutralizing antibodies against PEG-rhMGDF, paradoxically leading to a drop in platelet levels and development of these proteins was halted. Another large molecule, romiplostim (AMG531) a conjugate of a peptide, which binds to the TPO receptor and an antibody Fc domain, which increases its half-life in the bloodstream, has been approved by the FDA and NICE for long-term treatment of chronic idiopathic (immune) thrombocytopenic purpura (ITP). Clinical use does require monitoring for thrombocytosis, the overproduction of platelets, which can lead to potentially hazardous blood clots.[58]

In view of the positive clinical activity of these macromolecules, the discovery of a safe, effective, and orally available, nonpeptidic TPO mimetic would seem to be highly desirable. Researchers at SmithKline Beecham in collaboration with Ligand Pharmaceuticals used high-throughput phenotypic screening of their in-house libraries to identify a number of classes of compounds, which upregulated TPO-responsive signaling pathways using a luciferase reporter assay.[59] From initial hit structure ((25), Fig. 17) extensive lead optimization led to the identification of eltrombopag (26), which was shown to be a potent TPO receptor agonist.[60,61]

Eltrombopag stimulates megakaryocyte proliferation and differentiation and increases platelet counts without activating them. Interestingly eltrombopag binds to the TPO receptor at a different site from that bound by TPO itself and the two agents act additively.[62] A histidine residue within the transmembrane region of the TPO receptor was found to be critical for binding of eltrombopag; only the human and chimpanzee TPO receptors have this residue and this may provide a rationale for why

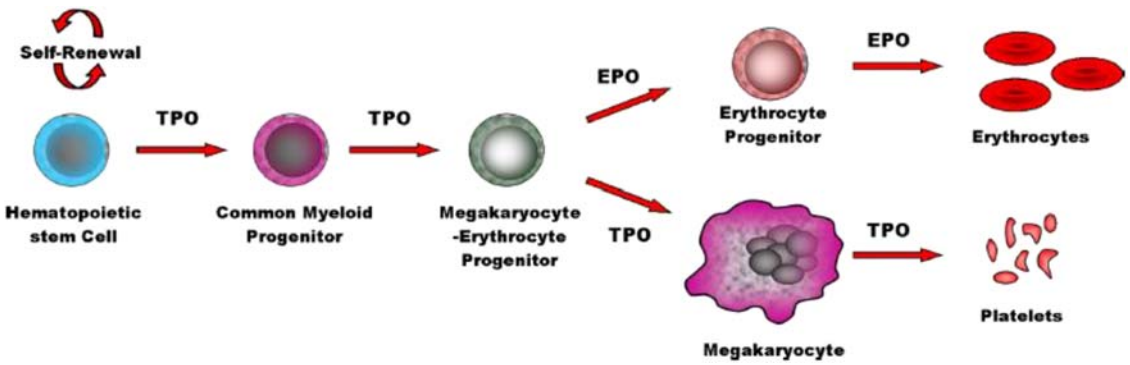

Fig. 16 The role of TPO in megakaryocyte and platelet production in vivo. Reprinted with permission from Davies, S. G.; Kennewell, P. D.; Russell, A. J.; Seden, P. T.; Westwood, R.; Wynne, G. M., Stemistry: The Control of Stem Cells *In Situ* Using Chemistry. *J. Med. Chem.* **2015**, *58* (7), 2863–2894.

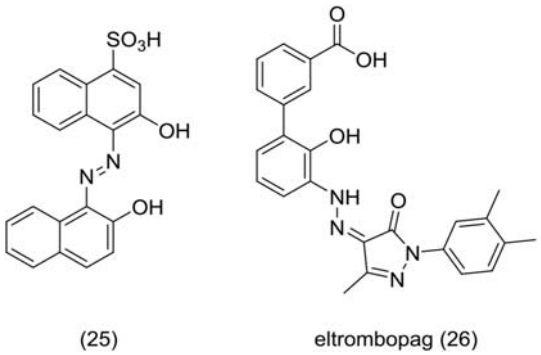

Fig. 17 Lead structure and final TPO receptor agonist.

eltrombopag only shows efficacy in these species. Binding to the receptor leads to activation of the Janus kinase (JAK) and signal transducer and activator of transcription (STAT) pathways but in a response distinct from that produced by TPO or romiplostim (Fig. 18).

Eltrombopag was granted orphan drug status and was approved by the FDA in 2008 for the treatment of thrombocytopenia (platelet deficiency) and in 2014 for the treatment of aplastic anemia. Numerous clinical trials have established that it is effective, and safe, for the treatment of both adult and childhood thrombocytopenia and in severe aplastic anemia.[57] In addition, it has been

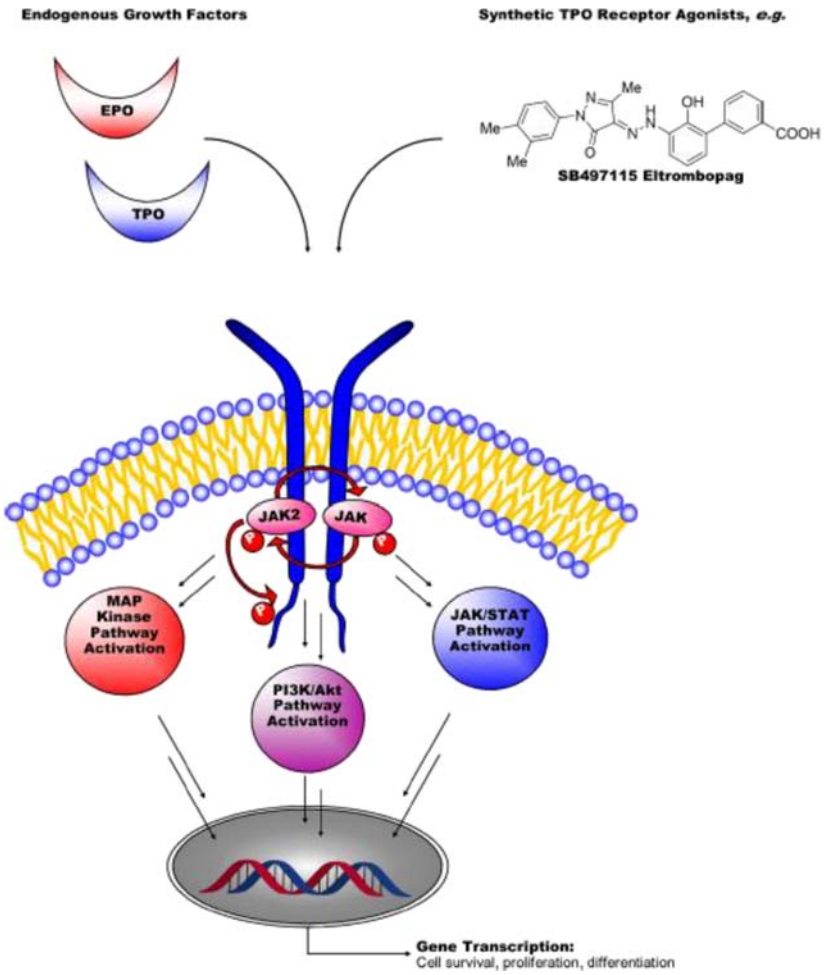

Fig. 18 Proposed mode of action for eltrombobag. Reprinted with permission From Davies, S. G.; Kennewell, P. D.; Russell, A. J.; Seden, P. T.; Westwood, R.; Wynne, G. M., Stemistry: The Control of Stem Cells *In Situ* Using Chemistry. *J. Med. Chem.* **2015**, *58* (7), 2863–2894. Copyright 2015 American Chemical Society.

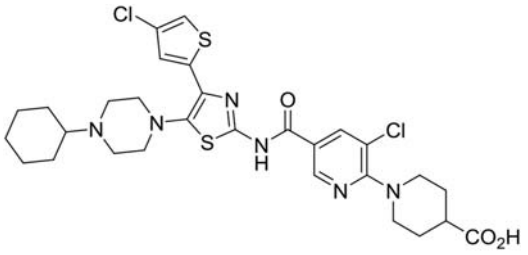

(27)

Fig. 19 Chemical structure of Avaltrombopag (27).

found to be of use in the treatment of thrombocytopenia in patients with chronic hepatitis C.[63] A very interesting finding was that of Desmond et al. who found that eltrombopag treatment was successful in patients with severe aplastic anemia, but remarkably the hematological responses were maintained even after discontinuation of drug treatment.[64] It was hypothesized that the drug was acting by the stimulation of residual HSCs, which would represent a new approach to the treatment of aplastic anemia.[65] It would also represent a further successful application of medicinal chemistry to the modulation of stem cell behavior to the benefit of the patient.

Other TPO mimetics have been progressed to clinical trials. Eisai have developed avatrombopag ((27), **Fig. 19**), which is claimed to have greater pharmacological activity than eltrombopag as a TPO agonist.[66] It is reported to be in Phase III trials in patients with thrombocytopenia associated with liver disease. Positive results have also been reported in patients with chronic immune thrombocytopenia[67] and in increasing platelet counts in patients with cirrhosis undergoing invasive procedures.[68] Another compound is LGD-4665 from Ligand that, despite being in development, has not yet had its structure disclosed.

1.13.2.1.8 Bone

Mesenchymal multipotent stromal cells and their role in sustaining bone and cartilage structure were introduced earlier. Here their potential role in correcting diseases of bone and cartilage is examined. The main disease of bone is osteoporosis, where the balance of bone resorption and reformation is disturbed, resulting in loss of bone mass and eventually severely weakened bone structure. In the case of cartilage, the main disease is osteoarthritis where damage results in pain and inflammation of the joint. Both of these conditions are widespread, cause significant levels of distress to the patient, and are largely treated by palliative interventions or significant invasive surgery. Thus drug treatments capable of giving bone and/or cartilage regeneration would be of significant benefit. A very recent review of orthopedic tissue regeneration using cells, scaffolds, and small molecules has appeared.[69]

As stated earlier, MSCs are adult stem cells capable of giving rise to tissues of mesodermal origin including bone, dentine, and ligament and so have been the most widely studied stem cell in this area. The ex vivo osteogenic differentiation of MSCs was discussed in our previous review.[1] One proosteogenic compound, purmorphamine ((28), **Fig. 20**), identified by high-throughput screening of a 50,000-member library, was shown to act by activation of the Hedgehog (Hh) signaling pathway as an agonist of the transmembrane receptor Smoothened (Smo). This compound acts synergistically with bone morphogenetic protein 4 (BMP-4) in osteogenic activity. The bone morphogenetic proteins are a group of 20 growth hormones initially identified by their ability to induce the formation of bone and cartilage. Recombinant BMP-2 and BMP-7 are approved by the FDA to stimulate the production of bone in orthopedics and dentistry. Other small molecules identified included H-8 (29), an ATP competitive inhibitor of protein kinase A, C, G and myosin light chain kinase, N6-benzoyladenosine-3′5′-cyclic monophosphate (30), a PKA-selective cAMP analog, CW008 (31), an inducer of cAMP production and SKL2001 (32), a specific activator of Wnt/β-catenin signaling. More recently, Ito et al. identified by means of a phenotypic screen the flavonoid natural product kaempferol (33) as being effective in the induction of osteogenesis in MSCs and as possessing in vivo activity in an ovariectomised mouse model, although the mechanism is as yet unclear.[70] As part of an excellent survey of the use of stem cells in the treatment of osteoporosis, Gazit et al. commented that Phase I trials investigating the ability of the anabolic agent, parathyroid hormone (PTH), with alendronic acid (34) to recruit MSCs to the sites of bone fractures were underway.[71] Finally, Cashman and coworkers reported that two small Wnt signaling modulators, THQ-1a (35) and PP-9 (36), increased the differentiation of C2C12 cells synergistically in the presence of an osteoinductive TCP ceramic.[72] C2C12 is a myoblast cell line that has been used for in vitro studies of osteoporosis and these results may even suggest an approach to directing cell lineage commitment for bone regeneration in vivo using a mixture of these sorts of small molecules along with osteoinductive ceramics.

The direct use of MSCs in dentistry has been recently reviewed; however, clinical trials conducted to date in this area have not yet allowed conclusions as to their utility to be drawn.[73]

It has been shown that cartilaginous grafts could be assembled from fat pad-derived stem cells by incorporating them onto fiber membranes, thus opening up the possibility that similarly engineered tissue derived from the cells of patients with osteoarthritis could be used in the treatment of damaged joints.[74] In the field of cartilage repair, Denaro et al. have cautioned that the limitations in animal models of osteoarthritis are rarely predictive of the equivalent disease in humans and that this is hindering the use of stem cells and gene therapy for the management of cartilage lesions.[75] The stepwise, controlled large-scale and effective differentiation of

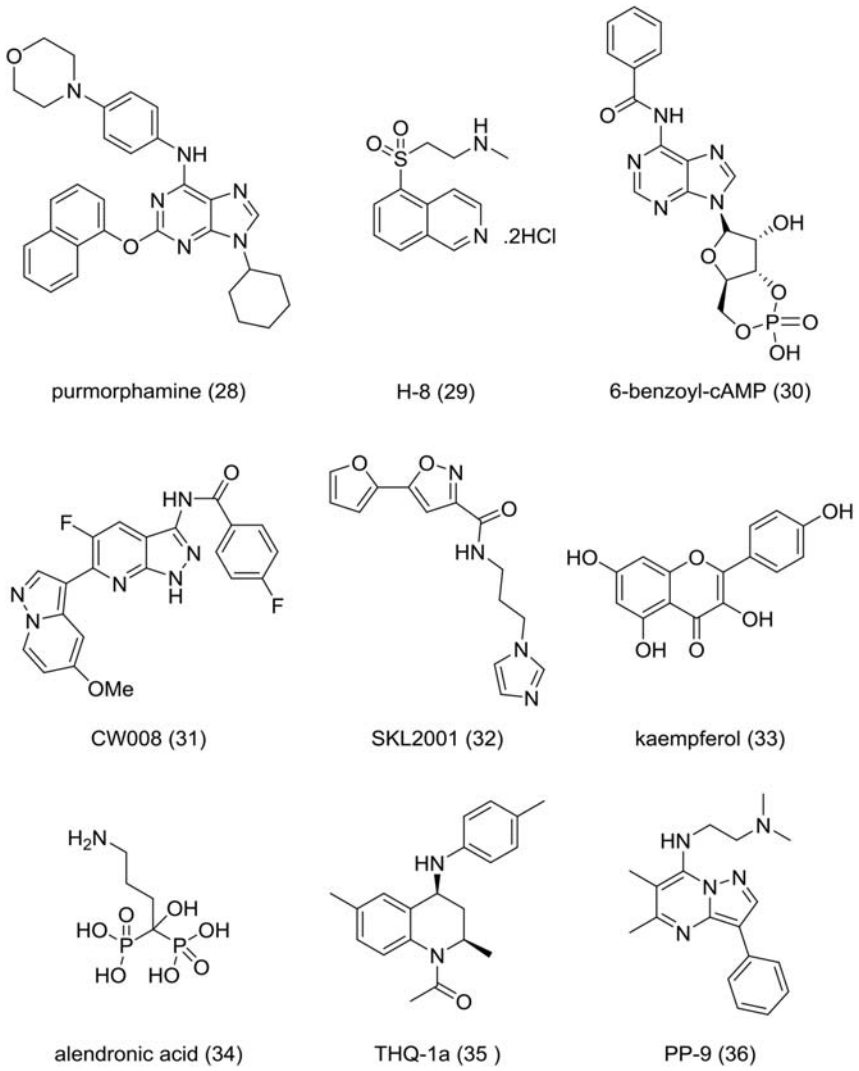

Fig. 20 Compounds with osteogenic properties.

mouse embryonic stem cells (mESC) and mouse- and human-induced pluripotent stem cells (hiPSCs) into osteoblasts has been described.[76] The four compounds (**Fig. 21**) used in the sequential steps for this process were CHIR99021 (5), cyclopamine (37), a smoothened/Hh antagonist, TH (38), and SAG (39), a smoothened/Hh agonist. While the molecular target for TH is unknown, this potentially offers a tool for mechanistic studies of osteoblast development and cell-based therapies for bone defects.

As might be expected, the BMP family of proteins has attracted considerable interest in their use in bone repair or as targets for the design of small molecule mimetics. A recent review[77] has discussed the complications involved in using both growth factors themselves in the clinic and small molecule mimetics. Difficulties with the proteins themselves include manufacture, specificity, and immunogenic potential while small molecules do have tremendous possibilities; of the BMP mimetics described to date several questions relating to their mode of action, specificity, and delivery remain. BMP acts on MSCs to stimulate differentiation into osteoblasts and as osteoporotic patients show reduced capacity for bone healing; it was surmised that impaired signal transduction and reduced osteogenic differentiation capacity in response to BMP-2 could be the cause of this.[78] In fact, while changes in BMP-2 signaling were observed, nonetheless osteogenic differentiation was retained in response to BMP-2 suggesting that this cytokine could be of use in the treatment of this disease.

The quinoline KM 11073 ((40), **Fig. 22**) was found to enhance the induction of BMP-2 stimulated effects in vitro and demonstrated in vivo osteogenic activity in zebrafish and mouse models suggesting its use in the stimulation of bone formation either alone or in combination with BMP-2.[79]

Lee et al. showed that a combination of BMP-2 and phenamil (41) promotes the osteogenic differentiation of adipose-derived stem cells in vitro and confirmed in a mouse calvarial repair model the usefulness of this combination in vivo. It was suggested that this combination using slow-release technology could represent a cost-effective, efficient approach to clinical bone repair.[80] An excellent overview of the state of research on regenerative medicine in osteoarthritis has been presented by Osch.[81]

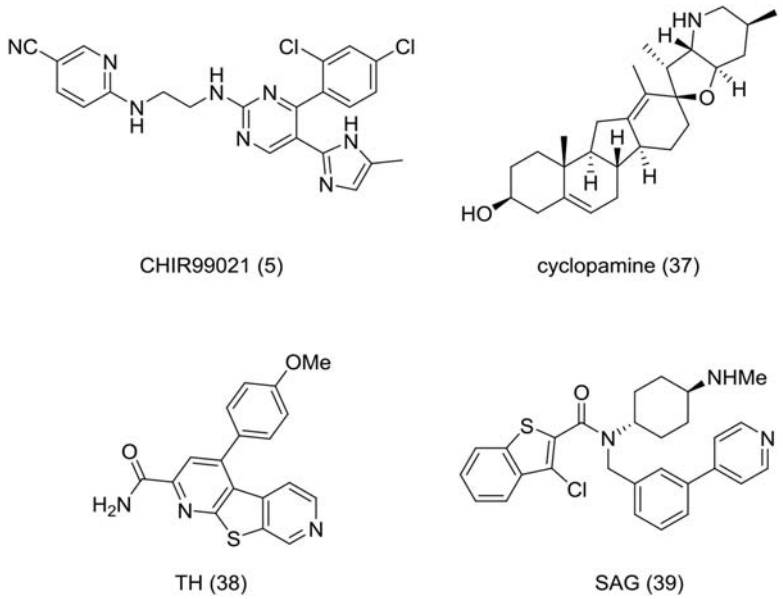

Fig. 21 Compounds reported to differentiate iPSCs into osteoblasts.

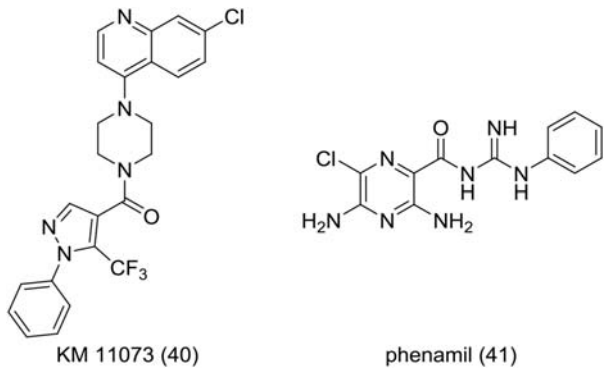

Fig. 22 Osteogenic agents.

1.13.2.2 Cardiac Regeneration

Progression to heart failure is usually coupled with a severe loss of CMs, the contracting muscle cells of heart tissue.[82] After injury, the heart undergoes a series of steps in wound healing. As adult mammalian CMs have little regenerative capacity, the result of the wound healing in the heart is the formation of a scar at the injury site that is mainly comprised of fibroblasts. These fibroblasts help maintain the structural integrity of the heart after an injury but have no contractile ability.[83] As a consequence the surviving CMs work more to compensate and support cardiac output. Over time, the CMs become hypertrophic, which eventually leads to heart failure.

Although today's medical and device therapies aim to optimize the cardiovascular hemodynamic, they do not account for the loss of the functional CMs, which are the cause of the failing myocardium. In general, embryonic cardiac development can be simplified into four key steps involving mesoderm induction, mesoderm structuring, cardiac mesoderm formation (cardiac progenitor cells) followed by CM induction and maturation. The prospect of being able to regenerate human heart tissue either in vivo by controlling the differentiation of stemlike/progenitor cells in situ, or ex vivo by subsequent implantation of the generated CMs is of great interest. The ability to achieve this goal by screening small molecules represents an important challenge and opportunity for medicinal chemists. Many cardiopoietic factors involved in CM generation are known and multiple publications have reported the effect of small molecules on this process.

1.13.2.2.1 In vitro chemically guided cardiac differentiation

1.13.2.2.1.1 Unspecific mode of action

Until relatively recently, few small molecules affecting cardiac differentiation from pluripotent stem cells had been reported and many of these had unspecific modes of action.[84] Among one of the first examples was ascorbic acid (AA).[85] More recently, in 2015, two research groups have reported the use of AA ((42), Fig. 23) to enhance differentiation of stem cells into CMs.

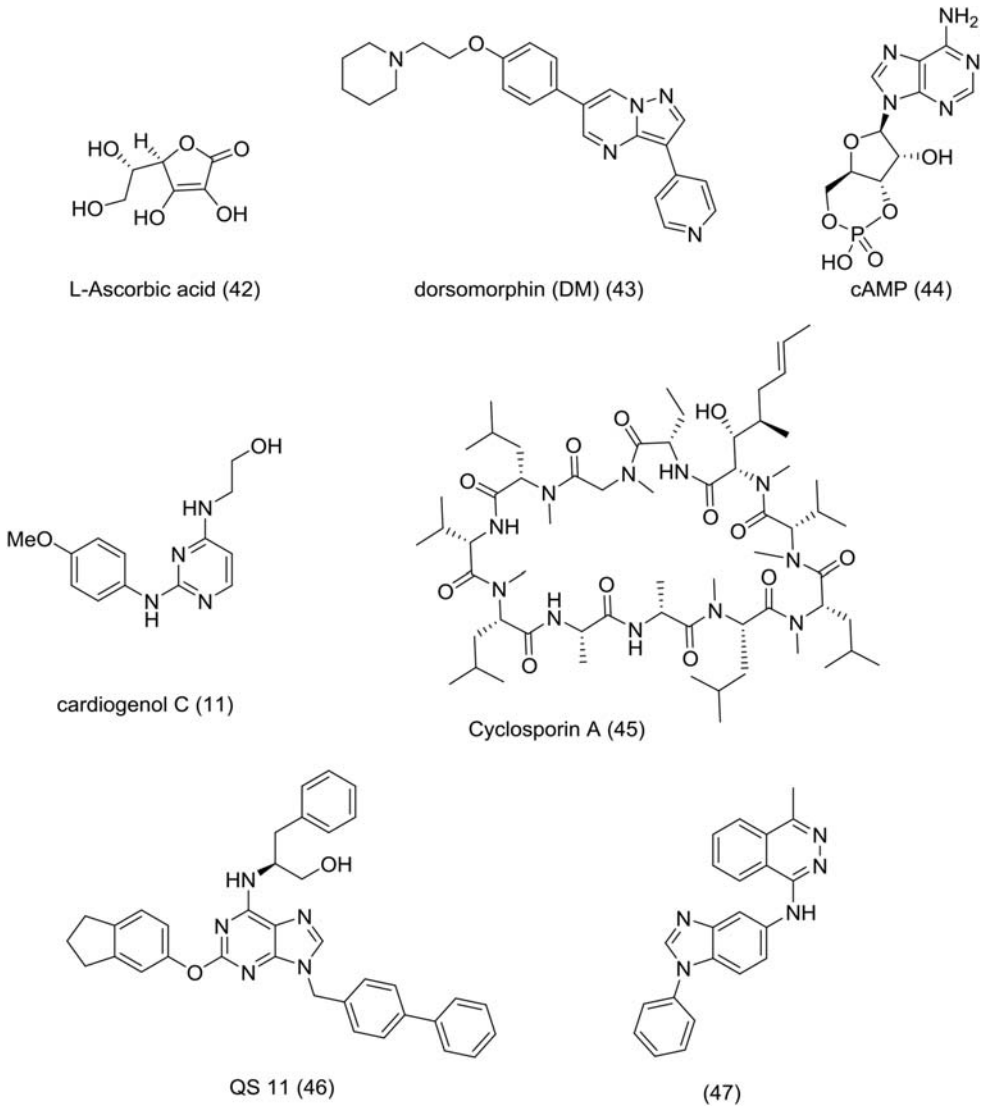

Fig. 23 Compounds reported to be able to differentiate iPSCs into cardiomyocytes.

In the paper published by Talkhabi et al., retrovirally transduced fibroblasts with reprogramming genes encoding all four TFs *Oct4*, *Sox2*, *Klf4*, and *c-Myc* and used these to screen small molecules that could augment the direct conversion of mouse fibroblasts into beating CMs.[86] Daily observation of the cells allowed the identification of AA as an efficient inducer. Moreover it was noticed that pretreatment of cells with AA at days 6–9 followed by cotreatment with both AA and recombinant BMP4 enhanced the conversion. Flow cytometry analysis showed that the cotreatment also increased the number of cardiac lineage cells (Flk1+, GATA4+, and MHC+) when compared to the control, leading to approximatively 20–30% of Flk1+ cardiac progenitors at day 14. The resulting directly converted beating CMs exhibit mature cardiac electrophysiological activity.

Ivanyuk et al. have evaluated the cardiac enhancing properties of small reported molecules such as AA, dorsomorphin (43), cyclic adenosine 3′,5,-monophosphate (cAMP, 44), cardiogenol C (11), and cyclosporin A (45) on ESC and iPSC lines.[87] Of concern was the observation that cardiogenesis induced by previously reported compounds was not reproducible from one pluripotent stem cell line to another, serving to underscore the significant differences between these lines. Among these five compounds, the most reproducible cardiogenic effect was only observed in the CGR8 ESC line when treated with AA alone. Further experiments have shown that AA treatment during the first 2 days of differentiation was sufficient to efficiently enhance differentiation of ESCs into CMs. When identifying functional categories enriched by AA-induced gene expression, cardiac-specific transcripts (Mef2, Myl7) along with early mesodermal marker T-brachyury were upregulated in day 5 embryonic bodies (EBs). TFs involved in angiogenesis, hematopoiesis, and vasculature development were also induced. In addition, what appeared to be an additive effect was observed when treating cells with both AA and QS11 (46), a small molecule synergist of the Wnt/β-catenin signaling pathway, significantly increasing the expression of TnnT2, cardiac α-actinin (Actn2), α-myosin heavy

chain (αMHC), and Nkx2.5 transcripts. No significant differences were found between control CMs and AA/QS11 CMs in electrophysiological analyses, suggesting that these chemically induced CMs were functionally intact.

To identify small molecules that stimulated stem cell differentiation, Okolotowicz et al. have screened chemically diverse compounds in a high-content cell-based assay using mESC.[88] The hit followed up from the small molecule screen was 1-phenyl-5(4′-methylphthalazin-1′-yl)aminobenzimidazole, (47), a robust and reproducible inducer of cardiomyogenesis: mESCs were differentiated into CMs upon chemical treatment from days 2 to 6. In addition to αMHC activation observed in mesoderm-derived cardiac muscle from day 10-differentiated mESC cultures, this new benzimidazole hit enhanced other biological markers such as Cer1 and Sox17 for the endoderm linage and Cdx2 and MesP1 for the mesoderm linage. Structure activity relationship studies and medicinal chemistry optimization afforded more potent and drug-like derivatives that stimulated differentiation of CMs upon a more restricted time window from days 2 to 4.

1.13.2.2.1.2 Targeting cardiopoietic signaling pathways

1.13.2.2.1.2.1 TGFβ pathway

The TGFβ superfamily is known to influence several cellular functions such as proliferation, apoptosis, and differentiation. Ifkovits et al. have reported that inhibiting the TGFβ pathway increased the direct conversion of both mouse embryonic fibroblasts (MEFs) and adult cardiac fibroblasts to induced cardiomyocytes (iCMs).[89] It was shown that treatment with SB431542 ((12), **Fig. 24**) in conjunction with ectopic expression of the TFs *Hand2*, *Nkx2.5*, *Gata4*, *Mefc2*, and *Tbx5* (HNGMT) increased the conversion of MEFs to iCMs in a dose-dependent manner. SB431542 (12) is a small molecule known to inhibit the Activin/Nodal/TGFβ signaling pathways, showing specificity for the Alk4, Alk5, and Alk7 components of the TGFβ signaling pathway. The authors reported that adding (12) prior to inducing HNGMT expression (day 1) resulted in a 3.5-fold increase of iCMs with Troponin T-GCaMP activity at day 14 post-HNGMT induction. Inhibition of this signaling pathway by (12) in the cardiac fibroblasts led to converted iCMs displaying several CM markers such as Troponin-T, α-actinin, αMHC, MHC-2, and beating of the iCMs was evident as early as day 16 postinduction. Interestingly, generation of iCMs was also observed when adding LY364947 (48), a known inhibitor of TGFβ but not Activin or Nodal components, on day 1.[90] Taken together these findings strongly suggest that the increase in iCM yield associated with (12) or (48) treatment is due to inhibition of TGFβ signaling as opposed to inhibition of Activin or Nodal family members.

Embryonic Nkx2.5+ cells are potent for both CMs and smooth muscle differentiation. In contrast neonatal Nkx2.5+ cells, which lack the capacity to differentiate into CMs nonetheless retain a limited ability to generate smooth muscle cells.[91] Using transgenic Nkx2.5 cardiac enhancer eGFP mice (Nkx2.5-eGFP) to label Nkx2.5+ cardiomyoblasts with eGFP, Chen et al. have demonstrated that A83-01 (49), a pharmacological inhibitor of type 1 TGFβ receptor (TGFβR1), could induce proliferation of

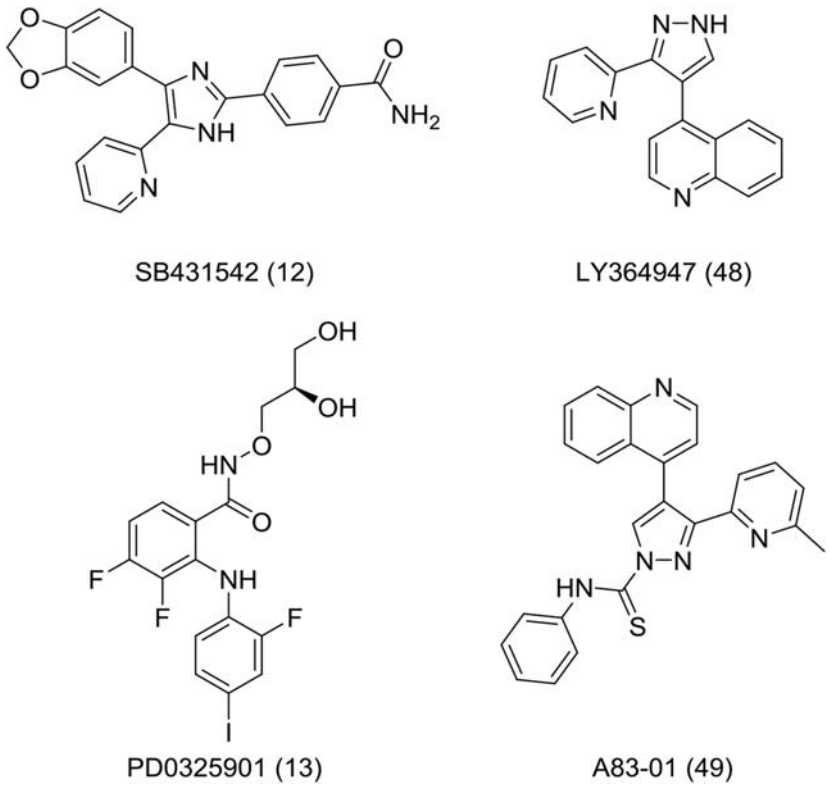

Fig. 24 Compounds affecting the TGFβ pathway in cardiac fibroblasts.

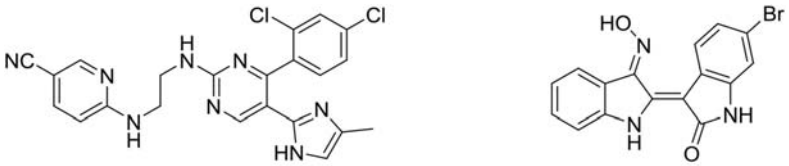

Fig. 25 Compounds affecting the Wnt signaling pathway in cardiogenesis.

postnatal Nkx2.5+ cardiomyoblasts in vitro and improve their cardiomyogenic differentiation.[92] After 7 days of culturing, A83-01 was shown to increase the percentage of eGFP+ cells up to 49% in a dose-dependent manner. The authors also demonstrated that A83-01 inhibited smooth muscle cell differentiation of Nkx2.5+ cardiomyoblasts but stimulated their differentiation into CMs. In addition, it was suggested that a direct cross-talk between TGFβ and FGF signaling pathways are necessary to retain the Nkx2.5+ cardiomyoblast phenotype as cotreatment with PD0325901 (13) an inhibitor of the mitogen-activated protein kinase kinase (MEK), a component of the FGF signaling, abolished the effect.

1.13.2.2.1.2.2 Wnt pathway

The Wnt signaling pathway is known as one of the key regulators of cardiogenesis in vitro and in vivo. A mechanism of activation of canonical Wnt signaling is via inhibition of the glycogen synthase kinase 3β (GSK3β), which leads to β-catenin nuclear accumulation and specific gene transcription activation. Canonical Wnt ligands induce cell proliferation and determine cell fate during embryonic development. Lian et al. have reported the use of CHIR99021, a GSK3β inhibitor ((5), **Fig. 25**), to modulate regulatory elements of the Wnt/β-catenin signaling pathway.[93] Populations of up to 98% of cTnT+ CMs were generated by chemically manipulating Wnt signaling activity during hPSCs differentiation under growth factor-free conditions. In this same article knockdown studies have shown the importance of β-catenin in hPSC differentiation to mesoderm and cardiac progenitors induced by GSK3β inhibitors. Various chemotypes of GSK3β inhibitors have been explored and in addition to CHIR99021, BIO (19) was also found to induce cardiac differentiation.[94]

In contrast to Wnt pathway stimulation, Wnt inhibition is also feasible for cardiac induction. Indeed, Willems et al. have reported the use of *endo*-IWR-1 ((50), **Fig. 26**) to induce beating foci from monolayer cultures of MESP1+ and KDR+ cardiac

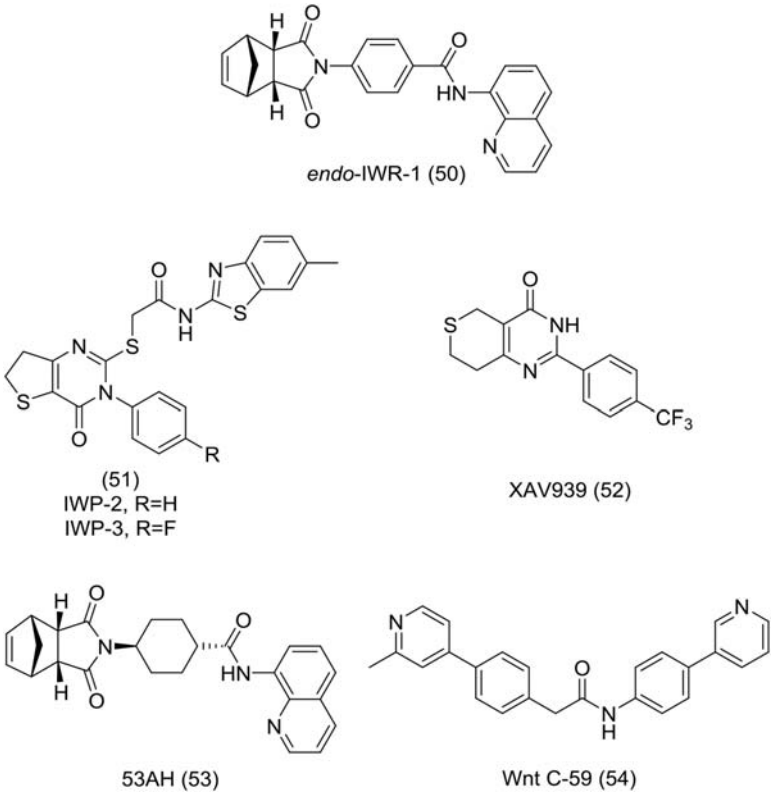

Fig. 26 Compounds affecting the Wnt signaling pathway in cardiogenesis.

mesoderm cells derived from hESCs.[95] *endo*-IWR-1s maximal cardiac induction was observed when added from days 4 to 5. Up to 30% CMs were generated, which was a 200-fold increase in yield over control cultures. Further analysis demonstrated that cardiac TFs (Mef2c and Nkx2.5) as well as CM structural genes (Myh6, Actn2, and Tnnt2) were increased upon treatment with *endo*-IWR-1. Other inhibitors of the Wnt pathway able to induce cardiogenesis were also used as examples. The porcupine inhibitors ((51); IWP-2, R=H and IWP-3, R=F), which prevent Wnt ligand palmitoylation[96]; the tankyrase inhibitor XAV939 (XAV, 52), which is cardiogenic in mESCs; and the most potent *endo*-IWR-1 analog 53AH (53) were tested and all three classes were found to promote cardiogenesis. Together these data strongly support a role for Wnt inhibition in cardiac induction using this system.

In an attempt to optimize a chemically defined medium, Burridge et al. have analyzed the importance of the timing of activation or inhibition of the Wnt signaling pathway, which may go some way to account for the apparent discrepancies in the examples described earlier.[94] Interestingly, treatment with Wnt activator CHIR99021 (5) for 2 days followed by its inhibition with Wnt-C59 (54) in CDM3 medium resulted in the production of TNNT2+ CMs.

1.13.2.2.1.2.3 Bone morphogenetic protein (BMP)

In 1997, the role of BMP in cardiac myogenesis was demonstrated by Schultheiss et al.[97] A fine balance between BMP, Nodal/Activin, and Wnt is desired for optimal mesoderm induction requiring BMP stimulation using recombinant BMP4 and Activin A. Interestingly, Hao et al. have reported that timely application of dorsomorphin (DM, (43), **Fig. 27**) in the early stages of mESCs induced cardiac differentiation, which they initially attributed to BMP inhibition.[98] However, in a series of studies prior to and following this report, (43) was shown to be nonspecific for Smad-dependent BMP signaling and also affected non-BMP signaling (AMP-kinase, receptor tyrosine kinases for PDGF and VEGF signaling) accounting for the delayed induction of early cardiac progenitor cells. The highly potent and selective analog (dorsomorphin homologue 1, DMH-1, (55)) was synthesized and characterized in a detailed in vitro study, and was reported to be a more selective inhibitor for the BMP Type 1 receptors compared to DM and LDN-193189 (56) inhibitors.[99] More recently, Ao et al. have compared the use of (55) with (43) to increase CM progenitors and promote cardiac differentiation in mESCs.[100] The authors reported that both (43) and (55) significantly increased beating EBs formation and reached a peak at about 70–75% efficiency on days 9 to 10 after induction; both compounds showed a fivefold induction increase. However, when (55) was compared with (43), it was observed that (55) induced beating EBs began to beat a day earlier than those induced by (43). As shown by rt-PCR the main difference between the two compounds appeared to be in their ability to modulate cardiac progenitor markers. Whereas (55)-treated cells expressed premesoderm (Bry-T) and mesoderm lineage (Mesp1) markers on days 3 and 4 in an upregulated manner, the expression of these factors was delayed or limited in (43) treated samples. Expression of CM-specific Nkx2.5 markers was also significantly increased in (55)-induced cells but showed less robust expression in samples treated with compound (43). It was suggested that (55)-induced cardiomyogenesis involves a canonical pathway requiring known premesoderm and mesoderm-specific TFs. Moreover, due to these differences in expression profiles, Ao et al. speculated that DM-induced CMs require a noncanonical pathway that remains unknown.

1.13.2.2.1.2.4 Small molecule cocktails

To circumvent the carcinogenicity and genetic insertion of the iPSCs obtained by viral-based methods, Hou et al. generated chemical-induced pluripotent stem cells (CiPSCs) from MEFs with a small molecule combination CRFVPTZ (C, CHIR99021 (5); R, RepSox (6); F, forskolin (1); V, valproic acid (4); P, parnate (7); T, TTNPB (57); Z, DZnep (58), **Fig. 28**).[5] A few years later,

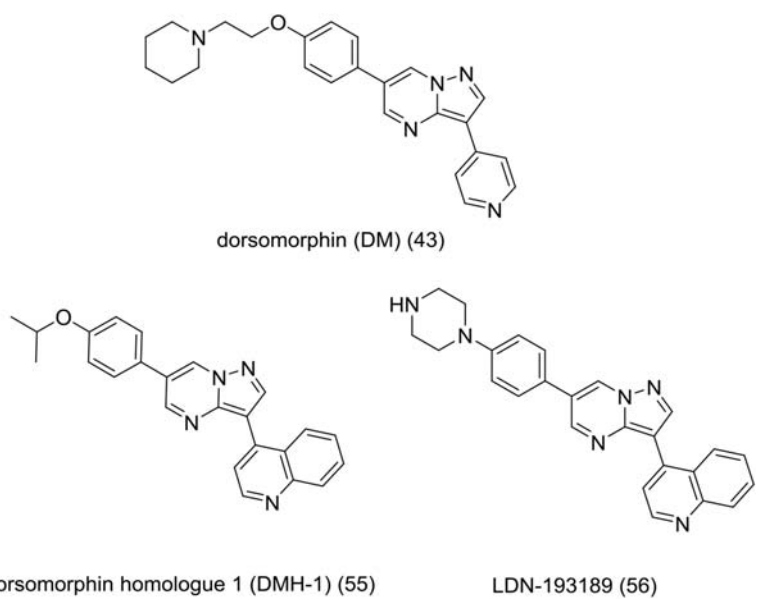

Fig. 27 BMP Type 1 receptor inhibitors.

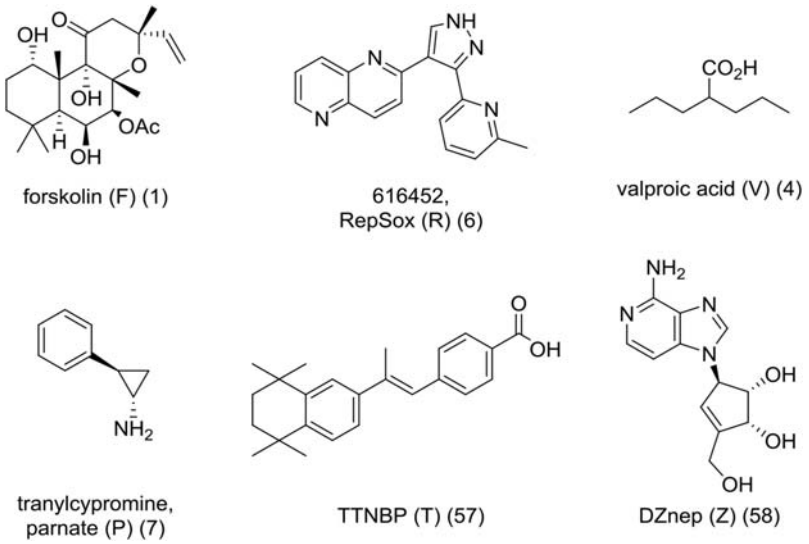

Fig. 28 Compounds inducing production of chemically induced cardiomyocyte-like cells.

Fu et al. also reported the use of a chemical cocktail to directly reprogram MEFs and neonatal mouse tail-tip fibroblasts (TTFs) into contracting cells named chemically induced cardiomyocyte-like cells (CiCMs).[101] However, their results suggested that the use of the CRFV cocktail was sufficient to generate CiCMs from MEFs after optimization of media.

Having identified conditions to produce CiCMs from MEFs, several additional compounds were trialed to enhance the transdifferentiation process including modulators of pathways that affect cardiac development or somatic cell reprogramming (Fig. 29). Both icariin (59) and PD169316 (60) were found to be effective. Phosphodiesterase (PDE) 4 inhibitors such as rolipram (61) and cilomilast (62) were also highly effective. Other PDE 1, 2, and 3 inhibitors were less efficient, while PDE 5 inhibitors were similarly found to be ineffective.

When using TTFs, the cells had to be treated with the CRFVPT cocktail. However, the reprogramming efficiency from TTFs to CiCMs was lower than from MEFs. With the aim to enhance the efficiency of CiCM generation from TTFs, numerous growth factors and chemicals were trialed. Addition of NRG1 and/or G-CSF and rolipram significantly enhanced the number of beating cells.

Further characterization of the CiCMs has shown that they express CM-specific markers. Important TFs for both cardiac development and function, including Mef2c, Gata4, and Nkx2.5 were expressed in the MEF-CiCMs whereas the TTF-CiCMs

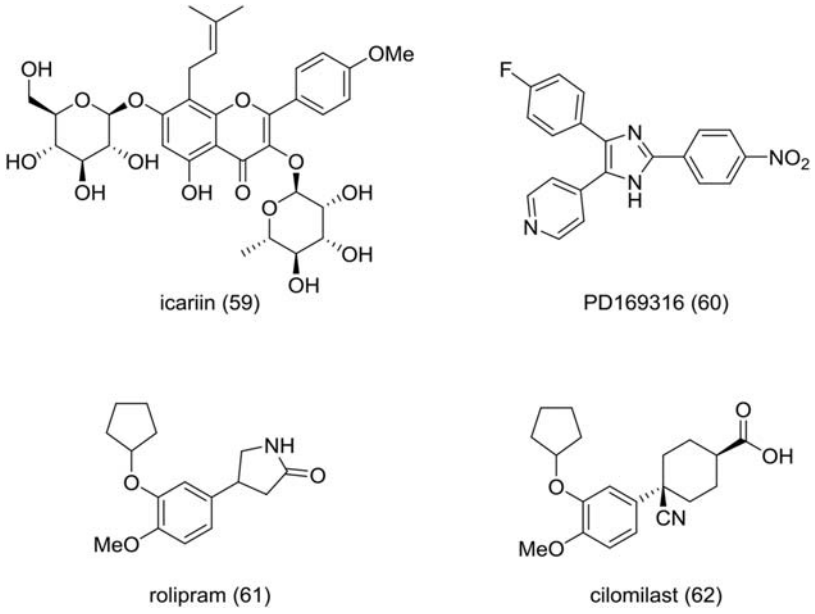

Fig. 29 Compounds reported to transdifferentiate cells to chemically induced cardiomyocyte-like cells.

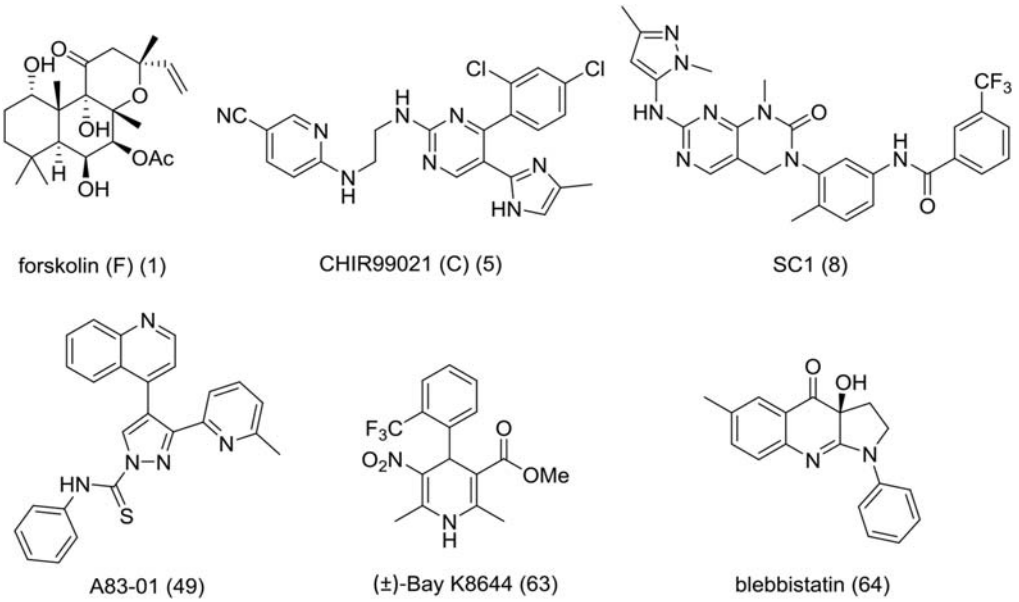

Fig. 30 Compounds reported to transform mouse embryonic fibroblasts to cardiomyocytes.

expressed Mef2c, Gata4, cardiac troponin-T, α-MHC, and α-actinin. Furthermore, these cells exhibit sarcomeric organization and possess typical cardiac calcium flux and electrochemical features.

It is noteworthy that both atrial-like and ventricular-like cells were found in the culture. These results suggest that specific cell types could be generated with further manipulation and optimization of both the chemical cocktail and culture conditions.

Park et al. have reported the conversion of MEFs into spontaneously contracting, cardiac troponin T-positive (cTnT+) cells using a combination of small molecules.[102] After treating MEFs for more than 2 weeks with the small molecule cocktail, features of CMs such as contraction and cTnT expression were observed. Flow cytometry analysis showed that the treatment of MEFs with five small molecules, termed FASCB (forskolin, F (1), A83-01, A (49), SC1, S (8), CHIR99021, C (5), (±)-Bay K8644, B (63), **Fig. 30**) significantly increased the percentage of cTnT+ cells. The authors were also able to report the importance of culture medium supplements; fibroblast growth factor 2 (FGF2), AA, and insulin transferrin-selenite (ITS) were indispensable to induce the differentiation of MEFs into cTnT+ cells. Further analysis using alternative chemotypes targeting common pathways to the FASCB components was consistent with cTnT+ cell induction by FASCB being mediated by the modulation glycogen synthase kinase 3 (GSK-3), activating receptor-like kinase 5 (ALK-5), and cyclic AMP (cAMP), although it suggested other pathways were also involved. The treatment with this small molecule cocktail also enabled the induction of both mesodermal (Flk-1, c-kit) and cardiac progenitor (Mesp1, Isl1, Nkx2.5) markers in MEFs. Further to these results, the role of each molecule in the FASCB cocktail was investigated. While the expression of most cardiac genes was induced by CHIR99021 (5) and A83-01 (49), forskolin (1) on the other hand suppressed the expression of mesoderm/cardiac progenitor markers but promoted the expression of CM markers. Based on these results, ASCB small molecules were used in the initiation stage to induce cardiac progenitors whereas medium supplement with FASCB would preferably enable cardiac differentiation. This suggests that treatment of fibroblasts with the appropriate small molecule cocktail allows the formation of small molecule-induced cardiomyocyte-like cells (smiCLCs).

In work from Karakikes et al., the authors have put in place a combination of small molecules and growth factors to develop a direct differentiation system to induce ventricular-like-cardiomyocytes (VCMs) from hESCs.[103] The chemically defined protocol was divided into two steps. In stage 1 (days 0–4.5), EB formation was initially induced by blebbistatin ((64), **Fig. 31**), a small molecule inhibitor of programmed cell death. As a result, apoptosis was inhibited and EBs formation was increased. A combinatorial activation of the BMP and Nodal/Activin signaling pathways by BMP4 and Activin A generated a multipotent cardiovascular

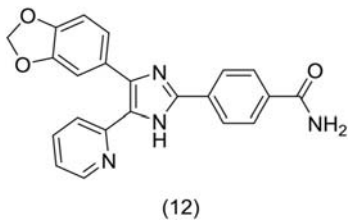

Fig. 31 Chemical structure of SB431542 (SB) (12).

progenitor population. In stage 2 (days 4.5–8), inhibition of the Wnt signaling pathway was realized by a small molecule IWR-1 (50) and yielded up to 90% terminally differentiated ventricular-like CMs as indicated by the expression of cardiac-specific (TNNT2) and ventricular CM (MLCV2) markers and the ventricle-specific TF (IRX4).

Wang et al. have screened for small molecule conditions that replaced TFs and enabled cardiac reprogramming of mouse fibroblasts with only one TF, Oct4.[104] A small molecule cocktail consisting of SB431542 ((12), Fig. 31, Alk4/5/7 inhibitor), CHIR99021 ((5), Fig. 30, GSK-3 inhibitor), parnate ((7), Fig. 28, LSD1/KDM1 inhibitor), and forskolin ((1), Fig. 30, adenylyl cyclase activator) was discovered. The fibroblasts were converted to spontaneously beating CMs that exhibit a ventricular phenotype. Immunocytochemistry analysis of the cells was consistent with the expression of cardiac troponin-T and α-actinin while qRT-PCR revealed the expression of cardiac-specific genes such as Myh6, Tnnt2, Gata4, and Nkx2.5. In addition, these chemically induced CMs also exhibited typical electrophysiological properties.

1.13.2.2.1.2.5 microRNAs

An alternative strategy for reprogramming is the use of microRNAs, as over the past several years, mounting evidence has indicated that virtually all aspects of cardiac function and adaptation are under the control of the microRNA (miRNA) network.[105,106] Four muscle-specific miRNAs—*miR-1*, *miR-133*, *miR-208*, and *miR-499*—are abundantly expressed in CMs, regulating many aspects of cardiac biology. In their study to redirect cardiac cell fate, Jayawardena et al. have developed a strategy to identify specific miRNAs capable of reprogramming cardiac fibroblasts directly to the cardiac lineage. miRNAs were selected based on their roles in cardiac muscle development and differentiation.[107–109] Synthetic and chemically modified mimics of miRNAs 1, 133a, 208a, and miRNA-499 were introduced into the mouse cardiac fibroblast via a single transient transfection. Using αMHC-CFP (cyan fluorescent protein, CFP) transgenic mice as cardiac reporters, they found that the in vitro transfection induced 5% of αMHC-CFP+ cells; this percentage was higher than the expression obtained in the control. Furthermore, RT-PCR revealed a shift in fibroblastic cells (Ddr2 and Vim) to early CMs (Isl1, Nkx2.5, Gata4, Hand2, and Mef2c) and late cardiac myocytes (Tnni3, Cx43). The starting cells were able to be converted to a CM-like lineage in vitro albeit with low efficiency. However, a 10-fold enhancement of miRNA-mediated reprogramming was realized upon treatment with Janus tyrosine kinase (JAK) inhibitor I ((65), Fig. 32). CM-like cells can be induced from noncardiac cells by ectopic expression of TFs and microRNAs. While these findings represent a promising avenue for future research, at the current time these methods have significant drawbacks that limit their application in therapies.

1.13.2.2.2 In vivo

1.13.2.2.2.1 Murine model

Chen et al. have described the effect of A83-01 (49) treatment on in vivo cardiomyogenesis using inducible Nkx2.5+ enhancer Cre transgenic mice to label postnatal Nkx2.5+ cardiomyoblasts and their differentiated progenies after myocardial injury.[110] Indeed, a recent study has demonstrated that Nkx2.5+ cardiomyoblasts may participate in the ability of neonatal heart to regenerate after induced injury. Treatment of Nkx2.5-GFP mice with A83-01 expanded postnatal Nkx2.5+ cardiomyoblasts contributing to the maintenance of ventricular wall thickness and cardiac function in post MI-mice.

Graichen et al. have generated CMs with promising efficiency when treating human ESCs with SB203580 ((66), Fig. 33), a p38 MAP kinase inhibitor, in the presence of factors released from endoderm-like (END-2) cells.[111] In addition, a synergistic effect was

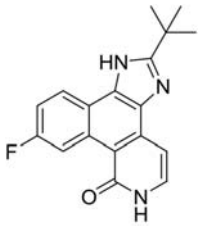

(65)

Fig. 32 Chemical structure of JAK Inhibitor 1 (65).

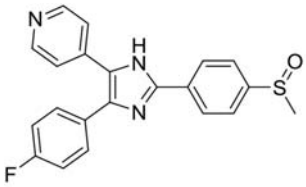

SB203580 (66)

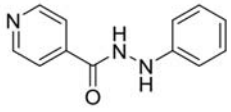

PluriSIn-1 (67)

Fig. 33 Compounds involved in cardiomyocyte differentiation in vitro and in vivo.

observed when using the same p38 MAP kinase inhibitor in combination with FGF1. While in vitro studies showed that mitosis was induced in cultured CMs, in vivo experiments showed reduced scarring and improved cardiac function in rats after acute myocardial infarction. In a separate study, Low et al. designed and prepared a series of imidazole analogs and tested them for their ability to both inhibit MAP kinase and to induce CM differentiation.[112] Although they demonstrated that analogs of SB203580 could induce CM differentiation from ESCs, the correlation between this and MAP kinase inhibition could not be established. Further work in this area is needed.

While the earlier examples illustrate the successful translation of in vitro active modulators of CM production to in vivo models, in general of the numerous examples of small molecules acting in vitro there have been very few reports of translation to achieve efficacy in vivo. This may be due to the inherent limitations of in vitro screening systems, but may also be due to controversies as to which cell populations within the adult heart are most relevant or susceptible to target to promote cardiac regeneration in vivo. In the past few years, several studies have demonstrated that epicardial-derived cells (EPDCs) can contribute either directly or indirectly to cardiac regeneration in vivo in animal models post injury, and that this effect can be augmented by treatment with exogenous agents. For instance, it has been shown that in response to injury resident adult EPDCs treated with the peptide thymosin β4 undergo migration and differentiation in vivo into what appear to be structurally and functionally coupled CMs.[113] Thymosin β4 has multiple potential applications in regenerative therapies, and RegeneRx are currently conducting a Phase 3 clinical trial on this agent for neurotrophic keratopathy (RGN-259, Clinicaltrials.gov ID NCT02600429).

Another significant challenge in regenerative therapies is that in adult mammals the wound healing response also involves inflammation and scarring. This response allows the maintenance of the structural integrity of the heart after an injury but, as the scar tissue has no contractile ability, significantly impacts on heart function. To regenerate cardiac tissue to restore functional capacity it will likely be necessary, to some extent, to intervene in the inflammation process to either reduce or reverse scar formation. A very recent study has revealed insights into how this may be achieved.[114] The cardiac lymphatic system is a crucial component of the immune system, and in 2015 it was shown that myocardial infarction in adult mice stimulated a significant lymphangiogenic response. Importantly, this response was shown to be enhanced by treatment with vascular endothelial growth factor C (VEGF-C) and led to an unprecedented 40% increase in functional recovery.

One crucial hurdle for therapeutic application of iPSCs or iPSC derivatives (iPSCD) can be the risk of teratoma formation after transplantation if residual undifferentiated iPSCs are not fully eliminated by cell differentiation or purification protocols.[115] As inhibition of stearoyl CoA desaturase (SCD) was recently reported to eliminate undifferentiated hESCs, Zhang et al. have tested the effect of PluriSIn 1 (67), a small molecule inhibitor of SCD, on iPSC-derived CMs.[116] Moreover, Nanog-positive cells have also been correlated to tumorigenicity. As a result, the authors asked whether (67) would eliminate Nanog-positive iPSCD, thus preventing tumorigenicity of transplanted cells in mouse model of myocardial infarction. CMs were differentiated from ESCs and inhibition of SCD with (67) resulted in a decrease of nearly all cultured iPSCD spheroids after 4 days of treatment. As shown by immunoblots and qRT-PCR, Nanog level was downregulated 16-fold by (67) treatment in comparison to DMSO. Moreover, treatment with (67) prevented in vivo tumorigenicity of iPSCD in a mouse myocardial infarction model. Indeed, 2 weeks after cell transplantation, tumor formation was observed in hearts injected with DMSO-treated iPSCD, while no tumor formation was detected following injection of (67)-treated iPSCD, thus enhancing the safety of iPSCs transplantation in mouse ischemic myocardium.

1.13.2.2.2.2 Zebrafish model

Zebrafish represent an interesting model to identify manipulation of, blocking of, or enhancement of CM proliferation, since the animal husbandry is straightforward and embryos are transparent. Indeed, in contrast to adult mammalian cells, zebrafish CMs have the capacity to proliferate in response to injury. Ni et al. have developed an in vivo small molecule screen that modulates heart size and CM generation.[117] To test these compounds, the authors have carried out a screen using transgenic zebrafish embryos (cmlc2:EGFP). Three related compounds, cardionogen-1 ((68), **Fig. 34**), cardionogen-2 (69), and cardionogen-3 (70), induced cardiomyogenesis and were subsequently shown to act by inhibiting Wnt/β-catenin-dependent transcription in both zebrafish embryos and murine ESCs. Further it was shown that the cardionogens increased the expression of Nkx2.5, cmlc2, and vhmc at only 17 h post fertilization leading to expansion of cardiac progenitor cells. Similarly, the authors have observed that in IWR-1 (50)-treated embryos, expression of the cardiac progenitor cell marker Nkx2.5 was increased. However, in contrast to the cardionogens, IWR-1 caused anterior–posterior axis development defects.

In another example of the use of phenotypic assay in zebrafish embryos, Choi et al. have adapted transgenic zebrafish lines that utilize the fluorescent ubiquitylation-based cell cycle indicator (FUCCI) system.[118] The cmlc2:FUCCI line was developed to monitor CM proliferation allowing the discovery of chemical modifiers of heart regeneration. When 3 days postfertilization embryos were exposed to a variety of compounds targeting developmental signaling pathways, only drugs targeting the Hedgehog (Hh), Insulin-like growth factor (IGF), and TGFβ signaling pathways seemed to modify CM proliferation. Indeed, similar results were obtained when modulating these signaling pathways. Modulation of the Hh pathway in CM production has demonstrated that a Smoothened agonist (SAG) (39) enhanced the proliferation of CMs up to 60% whereas cyclopamine (37), a Smoothened antagonist decreased this production to 27%. Treatment with IGF signaling agonist NBI-31772 (71), a potent inhibitor of IGF-binding proteins, increased the number of CMs by 41% while cardiomyocyte production was reduced to 31% in the presence of the IGF receptor antagonist NVP-AEW541 (72). It was also found that SB431542 (12), a TGFβ inhibitor, reduced the number of proliferating cells by 30%. Consistent with these findings, these pathways were also found to be activated in adult zebrafish following partial ventricular

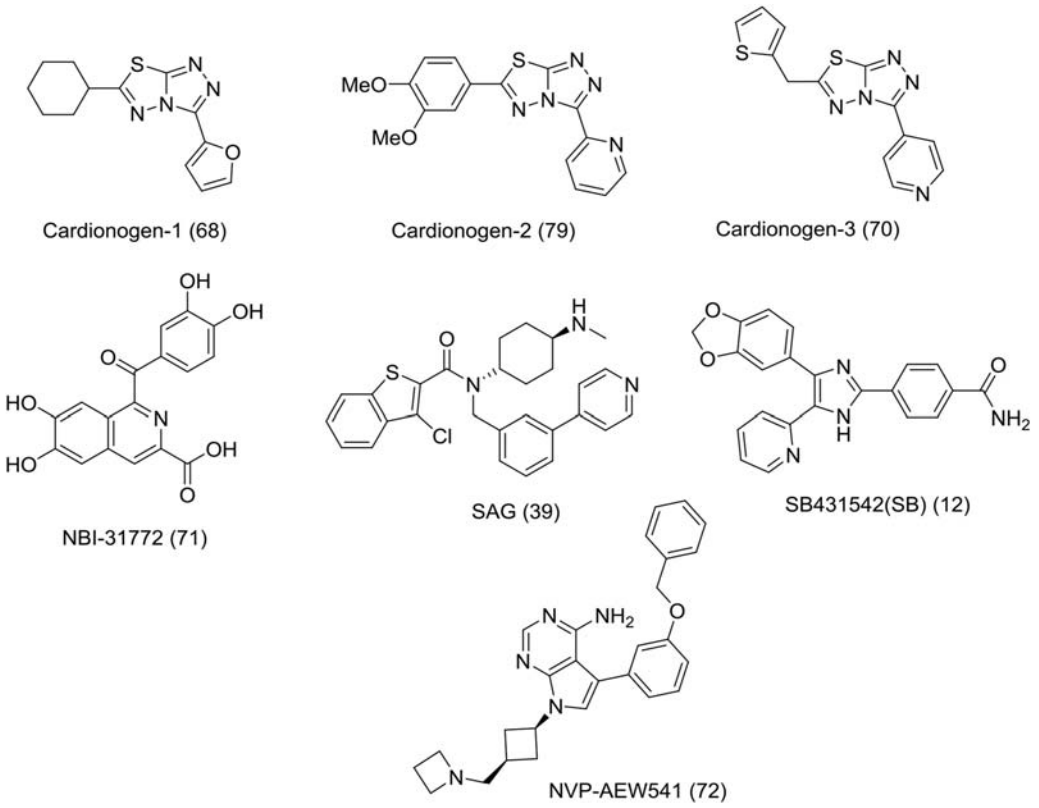

Fig. 34 Compounds involved in in vivo cardiomyocyte formation.

resection and genetic ablation of cardiac muscle and their effects on cardiomyocyte proliferation could be augmented by Hh and IGF agonist treatment. Interestingly, no response was observed in uninjured adult zebrafish.

1.13.2.3 Neuronal System

1.13.2.3.1 Neuronal regeneration: neuronal stem cells and drug discovery

Neurogenesis is the process whereby neurons are generated from precursor cells, namely neural stem cells (NSCs), and progenitor cells (NPCs). In addition, differentiated cells, in particular fibroblasts, have been transdifferentiated into neurons and this is discussed later in this section. While the process of neurogenesis is most active during prenatal development where it is responsible for populating the growing brain with neurons, there is now convincing evidence that the process continues in defined brain areas into adulthood. The precise details of neurogenesis, particularly in the adult human brain, are still being discovered and understood but what is clear is that cell signaling using factors from the stem cell niche, from other cells including neurons and from the bloodstream are involved in controlling the behavior of NSCs. As further details are revealed, the scope and potential of drug intervention in the process should also become clearer.

It is well-known that damage to the central and peripheral nervous systems affects large numbers of individuals with estimates of perhaps 1 billion sufferers throughout the world. In view of the fact that the average lifespan in many countries is increasing, it is predicted that these numbers can only increase in future. These disorders include the widely prevalent Parkinson and Alzheimer's diseases and less common conditions such as motor neurone disease, multiple sclerosis, and rare diseases such as spinal muscular atrophy. Also there are numerous psychiatric conditions for which a neurodegenerative component is being increasingly recognized. As many of the physical and psychiatric conditions are often imperfectly helped by current drug treatments, there is a pressing need for novel therapies to alleviate the suffering. The deliberate stimulation of neuronal stem cells/progenitor cells to produce new neurons or to repair existing, but damaged, ones could offer a route to such novel treatments.

The growth of understanding of adult mammalian NSCs and neurogenesis over the past 50 years has recently been authoritatively reviewed by Bond, Ming, and Song.[119] They titled their review on the fact that it was in the 1960s that Altman first suggested that neurogenesis takes place in the adult brain[120] with NSCs and NPCs being detected in 1989 and widely accepted during the 1990s.[121,122] NSCs are self-renewing multipotent cells that can generate neurons, astrocytes, and oligodendrocytes.[123] Endogenous NSCs have been shown to reside in three neurogenic niches in the adult mammalian brain. Of these the two most widely studied are the subventricular zones (SVZs) lining the lateral ventricles and the subgranular zone (SGZ) within the dentate gyrus of the

hippocampus, but there is also recent evidence to support a neurogenic niche within the hypothalamus. From their position in the SVZ NSCs are able to access both the cerebrospinal fluid and blood vessels from which presumably they receive growth factors and other stimuli essential to their development. NPCs differ in that while they are multipotent they do not self-renew indefinitely and appear to exist between NSCs and differentiated cells. It is also becoming clear that the population of NSCs at any time is very heterogeneous with, in particular, cells from different locations giving markedly different differentiated cells. This must be dependent on different signaling molecules in the niches as NSCs from both niches generate all three cell lineages when propagated in vitro in the presence of high concentrations of growth factors. Thus, in vivo SVZ NSCs generate olfactory bulb interneurons and corpus callosum oligodendrocytes while SGZ NSCs generate dentate granule neurons and astrocytes.

Elsewhere in this article the importance of the niche in which the particular stem cell exists has been stressed and this is true also for NSCs. NSCs in the SVZ are in close contact with cerebrospinal fluid (CSF) and the ependymal cell layer which excretes, inter alia, noggin, an inhibitor of bone morphogenetic protein signaling, whose presence allows the activation of the stem cell. NSCs are also exposed to signaling factors such as VEGF from endothelial cells, which promote self-renewal; and neurotrophin-3 (NT-3), which further promote quiescence and long-term maintenance. These signaling processes are not one-way streets and NSCs release signaling factors, which affect the structures that make up the niche. Also, and very remarkably, NSCs are regulated by neurotransmitters released by mature neurons and they express receptors, which respond to a variety of neurotransmitters including γ-aminobutyric acid (GABA), which also promotes quiescence. Many factors have been identified as affecting NSC behavior and no doubt many more remain to be detected but this surely shows the potential for discovering molecules able to affect the interactions involved in these signaling pathways.

Quiescence is an important state for the NSC, but it is not a dormant or passive state as there appear to be active expression of various receptors for niche signals and downstream signals. After activation most, if not all, of these are downregulated. Once the cell is activated a whole range of signaling processes, many of them acting in combinations, generate progression through NPCs to the final neuron or glial cell. Thus, for example, NSCs from the SVZ give rise first to transient amplifying progenitors, which divide a number of times to form neuroblasts. These neuroblasts then migrate to the olfactory bulb where they migrate radially and differentiate into different subtypes of interneurons. In a very interesting study, which perhaps sheds some light on normal ongoing processes in the central nervous system, Song et al.[124] have shown that in the adult mouse nestin (an intermediate filament protein expressed mainly in nerve cells where they are implicated in the radial growth of the axon)-expressing radial glia-like quiescent NSCs respond to GABA via the γ_2-subunit-containing $GABA_A$ receptor. Depletion of this subunit causes the cells to leave quiescence and undergo self-renewal. As stated earlier, decreasing GABA leads to quiescent NSC activation. The GABA responses are potentiated by diazepam, which specifically enhances γ_2-containing $GABA_A$ receptor responses to GABA.

It was the initial theory that the role of NSCs was to produce new neurons, which could repair or replace those damaged by disease or injury. It now appears that neurogenesis rather confers a unique mode of plasticity to the adult mammalian brain. However, this does not mean that with the right reagents the role of repair could not be achieved and that NSCs and NPCs could be stimulated to replace damaged neurons with functioning normal ones and that this approach could also be applied to conditions resulting from trauma injury to the CNS. As with other organs, at least three potential approaches are being actively investigated:

(1) The manipulation of NSCs and NPCs in vitro to generate tissue types for disease modeling and drug efficacy and toxicity testing
(2) Stem and progenitor cell therapy approaches involving ex vivo stimulation and differentiation followed by transplantation back into the patient and
(3) In situ stem cell modulation

However, obtaining neuronal stem cells from the patient would not be straightforward and it is likely that approach [3] will be more clinically acceptable. Alternatively, redifferentiation or transdifferentiation of more readily available adult cells into neuronal cells, or using cells from donors, would seem to be an attractive approach.

1.13.2.3.2 Neural stem cell culture

NSCs have proved difficult to culture in vitro as single cells and most work has involved the use of 3D aggregations of free-floating clusters of cells, which only contain a small percent of NSCs known as neurospheres. These are formed by suspending putative NSCs in a medium lacking adherent substrates but containing necessary growth factors such as epidermal growth factor (EGF) and fibroblast growth factor (FGF). A detailed protocol for producing neurospheres from mouse brain has been published by Pacey et al.[125] While neurospheres have proved to be highly useful in studying NSCs, there are problems that have to be taken into account. For instance, the culture formation is highly sensitive to the procedure so that different neurospheres can contain differences in composition of cell types and properties thus making interpretation of results obtained by their use difficult to interpret. It is known that neurospheres contain cells at multiple stages of differentiation, including stem cells, NPCs, neurons, and various glial cells. Nonetheless animal studies on the use of neurospheres or NSCs obtained from them are under investigation. Recently, Liebl et al. have published a detailed procedure for the preparation of cultures of adherent monolayer cells, which may act more consistently.[126] Also, the signaling pathways involved in NSC self-renewal and differentiation are becoming clearer with EGF, Hedgehog, vascular endothelial growth factor (VEGF), BMP, Notch, LIF-JAK-STAT identified to date.

1.13.2.3.3 Directed differentiation of NSCs and NPCs in vitro

As with any stem cell differentiation, the initial challenge is to prevent self-renewal and to initiate the differentiation pathway; in effect to inhibit one set of signaling pathways and/or stimulate the appropriate one. Rolfs et al. showed that inhibitors of glycogen

SB216763 (73) kenpaullone (74)

Fig. 35 Compounds involved in neurogenesis in human neural progenitor cells.

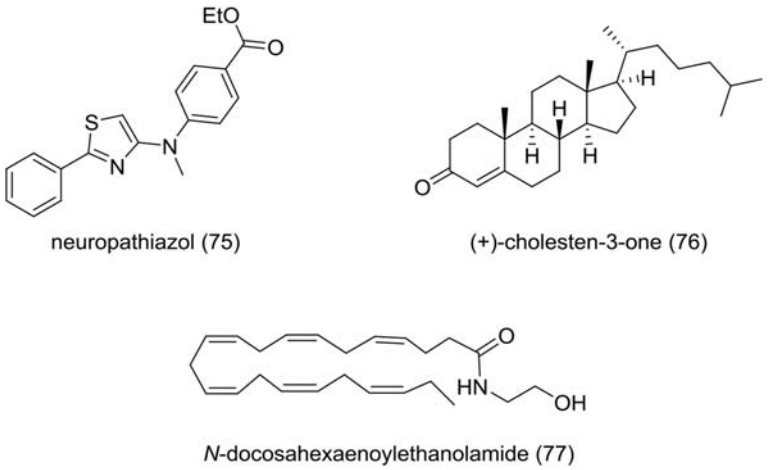

neuropathiazol (75) (+)-cholesten-3-one (76)

N-docosahexaenoylethanolamide (77)

Fig. 36 Compounds causing neuronal differentiation.

synthase kinase-3 (GSK-3), in particular SB216763 ((73), Fig. 35) and kenpaullone (74), enhance neurogenesis in human NPCs.[127] GSK-3 is a multifunctional enzyme, which is involved in glucose metabolism, Wnt/β-catenin, Sonic Hedgehog, Notch, and FGF signaling. It was proposed that these two compounds stimulate the Wnt/β-catenin pathway and that stimulation of this pathway is one route to differentiation.

Earlier, Schultz et al. had found that neuropathiazol ((75), Fig. 36) was able to enhance neurogenesis while suppressing astrogliogenesis in rat NPCs albeit via an unknown mechanism.[128] (+)-Cholesten-3-one (76) has been shown to induce the differentiation of NSCs from embryonic rat forebrain into dopaminergic neurons.[129] (+)-Cholesten-3-one (76) was shown to increase BMP receptor expression leading the authors to conclude that its effect is mediated through indirect stimulation of BMP signaling. Finally, N-docosahexaenoylethanolamine (77) promotes neuronal differentiation of NSCs both in vivo and in vitro.[130]

1.13.2.3.4 Directed differentiation of other cell types

1.13.2.3.4.1 Embryonic stem cells

A recent report describes the use of a cellular model involving hESCs first cultured toward a dopaminergic lineage, which are then treated with candidate molecules to detect those able to complete the differentiation to dopaminergic neurons.[131] From a range of tea catechins and ginsenosides, compound Rb1 ((78), Fig. 37) was found to be the most effective at generating dopaminergic neurons. It would appear that this approach could also be used to screen a wider range of structures. A different approach grew hESCs on monolayers in the presence of human leukemia inhibiting factor (LIF) and two small molecules, CHIR99021 (5), an inhibitor of GSK-3, and SB431542 (12), a TGF-β inhibitor. This produced primitive NSCs that can self-renew and respond to neural patterning cues toward midbrain and hindbrain neuronal subtypes. The authors subsequently showed that these cells could be transplanted into the lateral ventricle of neonatal mice and, satisfyingly, were then found to be distributed in many brain areas including the corpus callosum, the subcallosal zone, and the caudate-putamen.[132] A compound that had previously been reported to possess antiaging activity, icaritin (79), has been found to increase the differentiation of mESCs into cholinergic neurons in vitro[133] while isobavachin (80) also induced the differentiation of mESCs into neuronal cells.[134] Mechanistic studies were consistent with isobavachin acting via modulating protein prenylation.

Noggin is a protein that inhibits signal transduction within the TGFβ superfamily, and when present in the growth medium for hESCs the cells produce neuroectoderm. Further it was shown that treatment with FGF2/EGF gives neurospheres, which in the presence of Y-27632 ((81), Fig. 38), a Rho kinase inhibitor, produces increased levels of migrating neural cell-like cells, which were able to colonize explants of embryonic mouse gut and there to differentiate into enteric neurons.[135]

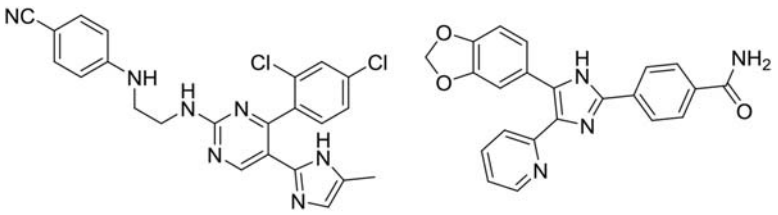

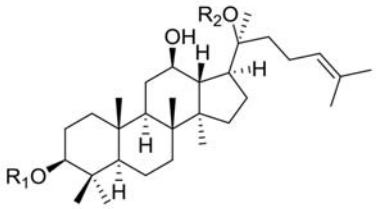

Rb1 R_1= glc-β(1-2)glc; R_2= glc-β(1-6)glc (78)

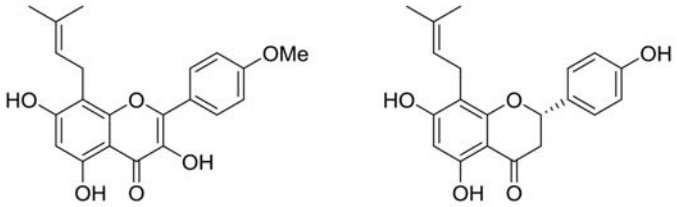

Fig. 37 Compounds causing the differentiation of mouse embryonic stem cells into neuronal cells.

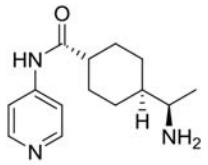

Fig. 38 Chemical structure of Y-27632 (81).

Inhibition of a different signaling pathway, namely Notch, by the γ-secretase inhibitor DAPT in hESC-derived NSCs markedly accelerates neuronal differentiation of the cells.[136] Further, hNSCs pretreated with DAPT ((82), Fig. 39) before transplantation into the mid-striatum of 9–12-week-old SCID-beige mice showed increased doublecortin staining, indicating that DAPT treatment also enhances neuronal differentiation in this context.

Two clinically useful drugs have also been found to have distinct effects on the differentiation of hESCs. The urinary analgesic drug phenazopyridine (83) was found using a high-throughput screen to increase total neurite outgrowth from hESCs and to produce a neuronal precursor cell population. After 1 week of incubation glutamatergic, GABAergic, and tyrosine hydroxylase-positive neurons were seen while after 4 weeks additionally nestin, β3-tubulin, SOX1, and vimentin-positive neurons were detected along with mature neurons and astrocyte and oligodendrocyte progenitors.[137] Zeng et al. showed that the antiarrhythmic drug, amiodarone ((84), Fig. 39), is selectively toxic to NSCs but not to dopaminergic neurons derived from hESCs, thus providing a way of producing a purer enriched population of desired neurons from these precursors.[138]

Of course, the generation of neurons from stem cells will only be of use if the resultant neurons can recapitulate the properties of native cells. A review has detailed the evidence that spinal motor neurons and cortical pyramidal neurons derived from stem cells show a remarkable degree of fidelity with those produced in normal embryonic development.[139] Further, it has also been shown that spinal motor neurons generated from hESCs show expected morphological and electrophysiological development along with neurite outgrowth and increased soma area.[140,141]

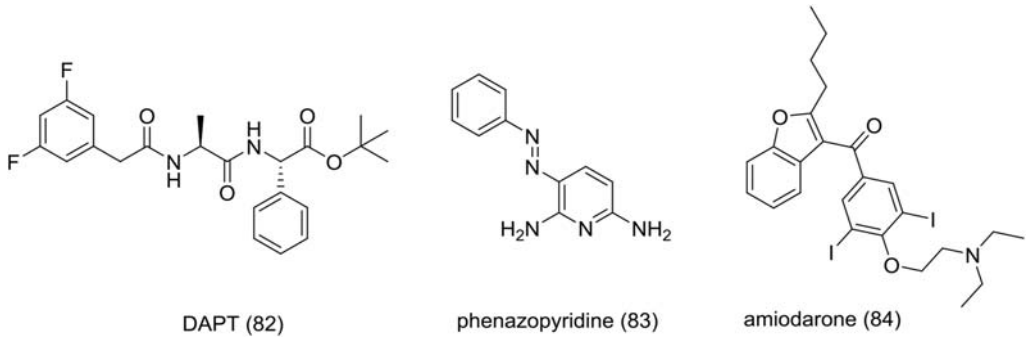

Fig. 39 Compounds causing the differentiation of hESCs into neurons.

Recently, Shin et al. took a mouse embryonic carcinoma cell line, P19, which, on treatment with appropriate growth factors and small molecules, could be differentiated into a range of cells including neurons, glia, cardiac, and skeletal muscle cells, and using a high-throughput screen found that two imidazoles, neurodazine ((85), **Fig. 40**) and neurodazole (86), promote the production of functional neurons.[142] Interestingly, these compounds do not also promote formation of astrocytes and this distinguishes them from other endogenous and synthetic mediators such as retinoic acid.

1.13.2.3.4.2 Induced pluripotent stem cells

In view of the ethical, sociological, and political difficulties arising from the use of hESCs it is not surprising that much work has been concentrated on the use of human iPSCs as potential sources of neurons for pharmacological studies and, hopefully, clinical use. A detailed review of the potential role of iPSC technology in understanding in vivo neurogenesis, neurological disorders, and in the discovery of potential new treatments for these disorders has been produced by Compagnucci et al.[143] In particular, they highlight how advances in carefully controlled culturing and differentiation of iPSCs in vitro feed into advances in the understanding of neurogenesis in vivo and vice versa. The differences between mouse and human cells are noted along with words of caution on extrapolating from one to the other.

Among other studies, Eggan et al. showed that 16 iPSC samples isolated from 7 individuals gave functional motor neurons with a range of efficiencies similar to that given by hESCs.[144] A detailed description of the rapid conversion of both hESCs and hiPSCs into motor neurons with defined subtypes of activities potentially useful for the study of neurodegenerative diseases has been published.[145,146] These studies used the small molecules Y-27632 (81), SB435142 (12), and LDN193189 ((56), **Fig. 41**) along with growth factors in the culturing media. Compound (12) was also used in combination with dorsomorphin (43) to enhance the neural induction of hESCs and hiPSCs.[147,148] A more specific BMP inhibitor than dorsomorphin, DMH1 (55), has been used with (12) and, separately, with SB218078 (87) in inducing neuronal differentiation of hiPSCs.[149,150] Gonzalez[150] used hiPSCs grown on Matrigel in N2B27 medium supplemented with primitive neuroepithelium to produce a highly enriched population of NSCs with concomitant downregulation of markers for pluripotency. These cells were found to be particularly suitable for the formation of dopaminergic cells.

The problem of producing sufficient specific neurons for clinical use has also been addressed by Iwata et al.[151] These authors used aggregates of dopamine neuron precursor cells in alginate-Ca^{+} microbeads followed by 25 days culturing to ensure cell maturation. The long maturation process has been shown to avoid teratoma formation following implantation into test rodents. This process gave dopamine-releasing neurons and the aggregates could be transplanted into rat brains where they were found to

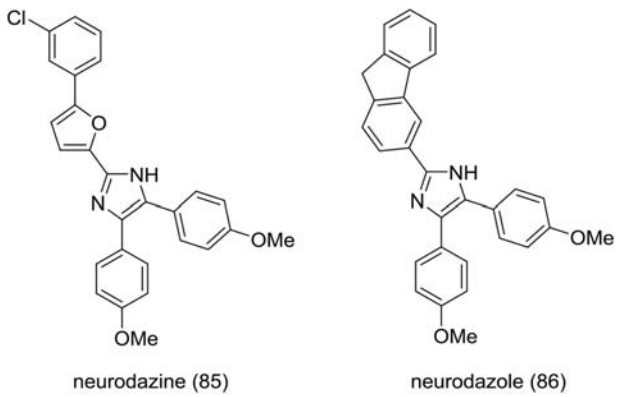

Fig. 40 Compounds involved in the production of functional neurons.

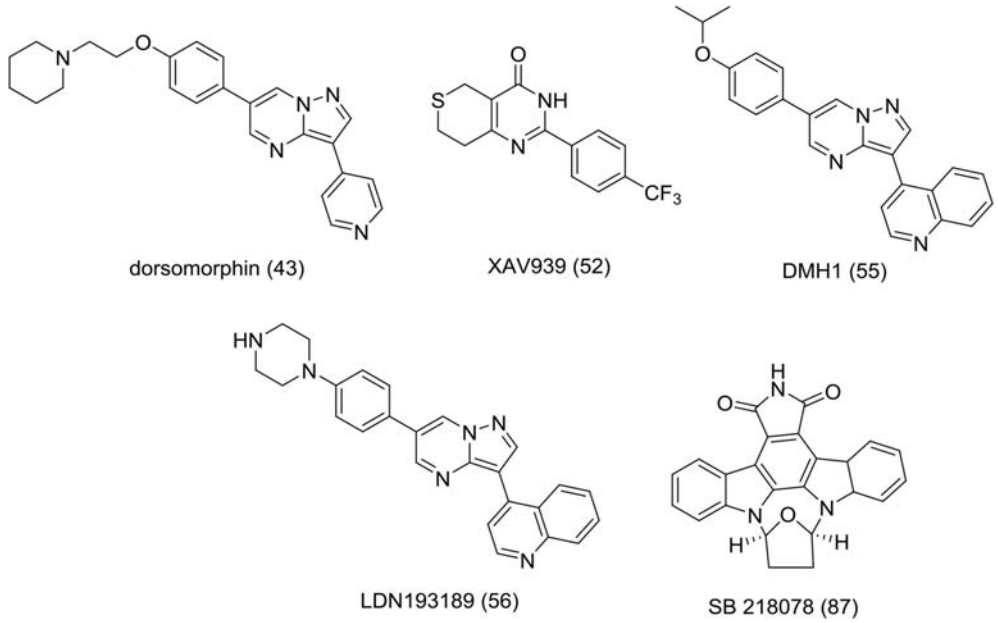

Fig. 41 Compounds differentiating hIPSCs to neurons.

produce neurites extending into the host tissue. Further studies are underway to investigate their functionality following transplantation.

Neurons in the hypothalamus are known to secrete a significant number of neuropeptides, which play roles in human health and disease. Among these are melanin-concentrating hormone, oxytocin, arginine vasopressin, corticotropin-releasing hormone, thyrotropin-releasing hormone, pro-opiolemelanocortin, agouti-related peptide, hypocretin/orexin, and melanin-concentrating hormone. Thus these neurons are under investigation as the basis of cellular models of the functioning of the hypothalamus, as potential screens in the discovery of new drugs to treat a number of human diseases or as cell-based therapies. Eggan et al. have described the generation of significant quantities of these neurons from hiPSCs by both a self-patterning strategy and, better, by a directed differentiation technique in cell culture. In the latter approach the hiPSCs were cultured on the growth medium in the presence of SB431542 (12), LDN193189 (56), and XAV939 (52) followed by purmorphamine (28) and SAG (39) and the resultant neurons were found to possess the characteristic morphological properties and gene expression patterns with in vivo neurons and were able to integrate into the mouse brain upon transplantation.[152] A similar approach to the study of hippocampal neurons was reported by Gage et al.[153] who produced dentate gyrus granule neurons from hiPSCs by culturing in the presence of, inter alia, Dkk1, SB431542 (12), Noggin, cyclopamine ((37), Fig. 42), and a number of growth factors. The final neurons that were shown to express characteristic expression factors were able to integrate into the dentate gyrus of the mouse and, very interestingly, the use of iPSCs derived from patients with schizophrenia showed lower levels of neuronal marker expression, reduced neuronal activity, and transmitter release by comparison with those from their healthy volunteer counterparts.

One feature of the development of a particular cell type from both ESCs and iPSCs is that different signaling pathways are operating at different times in the culture medium. A recent report[154] has generated transcriptomic data sets containing the expression levels from three ESC lines and two iPSC lines at four stages of differentiation. These were undifferentiated stem cells, NSCs, dopaminergic precursor cells, and dopaminergic neurons and showed clear differences in gene expression between the four stages. Thus they were able to systematically analyze the gene/pathways, networks, and cellular/molecular processes

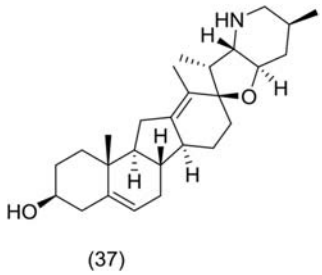

Fig. 42 Chemical structure of Cyclopamine (37).

controlling cell fates and the resultant information should provide great insights into how these processes could be improved by use of chemical mediators.

1.13.2.3.4.3 Bone marrow-mesenchymal stem cells

Mesenchymal multipotent stromal cells, of which MSCs are thought to be a constituent subtype, can be isolated from bone marrow and other tissues such as fat muscle and umbilical cord.[155] In fact the use of Wharton's jelly, the umbilical cord matrix, as the source of MSCs is regarded as a highly suitable source thanks to the primitive nature of the cells and their easy isolation without particular ethical concerns. The direct use of MSCs in animals and the clinic is discussed further, but they have also been used to produce neurons and other cells including osteocytes, adipocytes, chondriocytes, CMs, and endothelial cells. While a number of combinations of small and large molecules have been identified as directing cultures of MSCs to neurons, a recent paper claims that the presence of FGF2 alone is sufficient to generate dopaminergic neurons.[156] Previously a small molecule inhibitor of PI3K (phosphatidylinositol 3-kinase)/AKT signal pathways, LY294002 ((88), **Fig. 43**), was also shown to inhibit MSC proliferation and direct the neuronal differentiation of MSCs.[157]

Petri et al. [158] used human cord-blood-derived induced pluripotent stem cells, which hold the promise of lower genetic mutation burden or epigenetic alterations than iPSCs, to generate motor neurons by culturing in the presence of SB431542 (12), dorsomorphin (43), CHIR99021 ((5), **Fig. 44**), and purmorphamine (28). The resultant neurons showed characteristic functional neuronal properties such as sodium-inward currents and the ability to fire action potentials.

1.13.2.3.4.4 Transdifferentiation of other cell types

As has been mentioned elsewhere in this article, a potential problem arising from the use of transplanted ESC and iPSC-derived neuronal, and other, cells in the clinic is the potential for uncontrolled growth and teratoma production, which has been ascribed in part to the proliferative capacity of contaminating undifferentiated precursor cells. One means of circumventing this problem is to derive the target cells directly from a nonpluripotent, less/nonproliferative cell type, in particular from fibroblasts. Initial studies used the growth factors Asc11, Brn2, and Myt11 on mouse fibroblasts,[159] while Eggan et al. converted fibroblasts from both the mouse and human to motor neurons by using a limited number of TFs, namely, Asc11, Brn2, Myt11, Lhx3, Hb9, Isl1, and Ngn2 for the mouse and with one more, NEURODI for the human.[160] Interestingly, this conversion does not appear to involve a neural progenitor stage but the resultant neurons behave normally. Subsequently, a member of the forkhead box class O (FoxO) TFs, FoxO3a has been shown to be a critical regulator in the reprogramming of MEFs to iPSCs and thence to NSCs.[161] More recently, two groups have used only small molecules to achieve this transformation (**Fig. 45**). Cheng et al.[162] first used a combination of valproic acid ((4), histone deacetylase inhibitor), CHIR99021 ((5), a GSK-3 inhibitor), and RepSox ((6), an inhibitor of TGF-β pathways) under hypoxic conditions to produce neural progenitor cells. They then added a number of small molecules, forskolin (1), SP600125 (89), Go6983 (90), and Y-27632 (81) known to promote neural differentiation of NPCs[163]

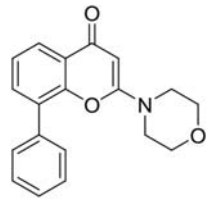

(88)

Fig. 43 Chemical structure of LY294002 (88).

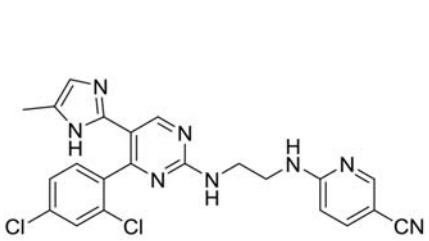

CHIR99021 (5)

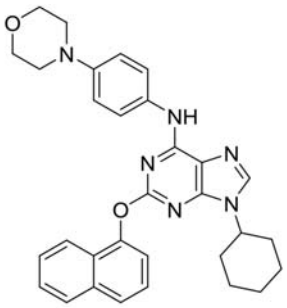

purmorphamine (28)

Fig. 44 Compounds reported to generate neurons from human cord-blood-derived pluripotent stem cells.

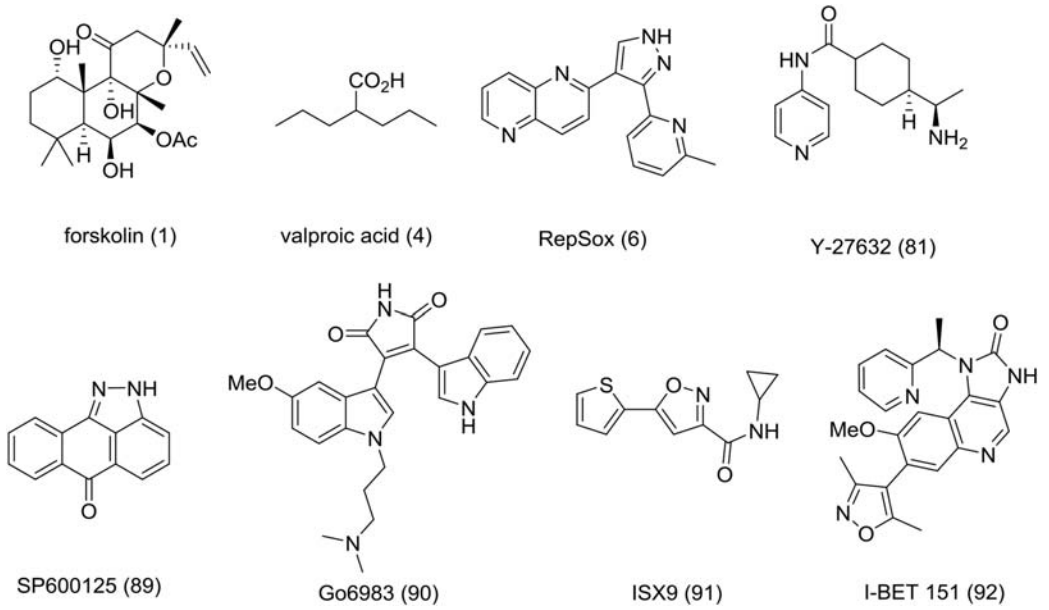

Fig. 45 Compounds reported to differentiate fibroblasts to neurons.

and produced mainly glutamatergic neurons from human fibroblasts. Fibroblasts from patients with familial Alzheimer's disease could also be differentiated and produced neurons with the expected elevated extracellular Aβ42 levels and Aβ42/Aβ40 ratio. A second Chinese group[164] has found that a combination of forskolin (1), ISX9 (91), CHIR99021 (5), and 1-BET151 (92) was able to generate with a very high-efficiency functional neurons from mouse fibroblasts. As was found earlier, these processes do not seem to involve the neural progenitor stage. Dopaminergic neurons were produced from mouse fibroblasts by use of a combination of transcription and neurotropic factors.[165]

It has been recently shown that adult neuroprogenitor cells can be isolated from subcortical white matter very much more conveniently than from the hippocampus and that they are able to produce neurons, astrocytes, and olidodendrocytes in amounts comparable to fetal NSCs.[166] Human dental pulp stem cells have been isolated and cultured to give first neurospheres and then cells with neuronal characteristics.[167] These may prove more readily accessible sources of human precursor cells in the future.

1.13.2.3.5 Cell-based therapies for neurological disorders

Since many neurological disorders and traumas involve irreversible damage to some brain tissue and as most current therapies provide only limited symptomatic treatments, the idea of replacing or regenerating the damaged tissue is a highly attractive one. The use of neuronal cells from a variety of sources has been reviewed by Das et al. [168] and, very recently by Steinbeck and Studer[169] who discussed in detail the history of cell-based treatments for neurological disorders, in particular Parkinson's disease (PD), and the switch to cells generated in vitro and the difficulties of establishing that the transplanted cells in both animal models and humans are functioning as anticipated. Initial studies in PD used fetal cell transplants and gave some indications of positive results. A recent paper has described the situation of two patients who, 15 and 18 years posttransplantation, show positive clinical improvements in their condition along with abandonment of any pharmacological dopaminergic therapy.[170] Two cases are hardly sufficient to draw definitive conclusions; nonetheless, this is a dramatic result for these two individuals. More recently the ethical and practical difficulties of this approach caused a shift to the use of neurons or neuron precursor cells derived from stem cells. These have their own difficulties such as ensuring proper quality control of cultivated cells and again establishing that any transplanted cells are behaving as required in the brain of both animal models and humans. For example, human adipose tissue-derived stromal cells (hASCs) were cultured and grafted into severed sciatic nerves of athymic nude female rats and found to significantly improve functional recovery in the damaged limb.[171] However, it was found that the hASCs did not differentiate into neurons and it was suggested that improvement was due to the production and local secretion of neurotrophins such as neural growth factor. Due to these difficulties, the number of clinical trials currently underway is very small but Asterias Biotherapeutics are running Phase 1/2 trials of a preparation of cells containing oligodendrocyte progenitor cells for patients with severe spinal cord injury. A detailed discussion of the potential and challenges of using NSCs in the treatment of neurological disorders along with a listing of clinical trials in the area has been given by Conti et al.[172] These authors stress that improving knowledge of the CNS microenvironment following injury will affect future treatment protocols and emphasize that the potential of NSCs to regenerate the brain also relies on the competence of other cells to be involved in the process. Lo et al. have discussed biomaterials, which might help the dosing and integration of transplanted cells.[173]

In other work, the direct transplantation of bone marrow MSCs to lineage stroke–prone spontaneously hypertensive rat resulted in levels of superoxide, apoptotic cells, and the by-products of lipid peroxidation fell to control levels and there was evidence of repair of morphological damage at the hippocampal region.[174]

A crucial feature of any cell-based treatment is that the transplanted cells should integrate into the recipient nervous system. Evidence that this is possible was provided by Ding et al. [175] who took human primitive NSCs transfected with GFP under the control of the elongation factor-1α promoter to show that following injection into the site of injury of athymic nude rats with lesioned spinal cords, the cells survived and largely differentiated into neurons. Further they grew away from the injury site and were also found to be predominantly serotonergic neurons. A different class of neurons, the inhibitory interneurons, has been discussed by Alvarez-Buylla et al.[176] These neurons are of particular interest because in their development they migrate through the brain to form inhibitory neural circuits and transplanted embryonic interneurons are found to do likewise. They therefore may be of interest in their own right as treatments for neurological disorders but also for what they can reveal about the formation of neurological circuits.

1.13.2.2.5.1 In situ stem cell modulation

It is an intriguing thought that existing drugs may exert some or all of their effects by promoting effects, including neurogenesis, on brain cells and the potential relationship between antidepressants and neurogenesis has been reviewed.[177,178] Antidepressants from multiple pharmacological classes have been shown to increase neurogenesis in human and animal models, although the link between neurogenesis and antidepressant activity remains controversial. Sertraline ((93), **Fig. 46**), an antidepressant, has been shown to increase adult human hippocampal neurogenesis via a mechanism that appears, at least in part, to involve activation of glucocorticoid receptors, which requires PKA signaling, glucocorticoid receptor phosphorylation, and gene activation.[179,180] Interestingly and importantly, the effect of such agents appears to be restricted to one NSC nest within the brain rather than exerting pleiotropic effects on other resident stem cell populations, an observation for which a possible explanation could be the reported synergy between sertraline and endogenous glucocorticoids,[179,180] thus raising the prospect of being able to find selective agents. Chronic fluoxetine (94) treatment of middle-aged rats increases the volume of the hippocampus and increases the expression of molecules related to structural plasticity and inhibitory neurotransmission with lesser effects in the amygdala.[181]

Allopregnanolone (95), a metabolite of progesterone, significantly increases neurogenesis in the SGZ of the dentate gyrus and the SVZ of a mouse model of Alzheimer's disease (3xTgAD mouse) and thus is currently the only small molecule with the ability to promote neurogenesis, to reduce cognitive defects, and to reduce the AD pathology burden.[182] A different class of active molecules, the histone deacetylase inhibitors, is effective neuroprotective agents following acute traumatic brain injury (TBI) in rodent models. LB-205 (96) treatment was reported to increase expression of CNS survival factors such as nerve growth factor (NGF) and activate the neurotrophic tyrosine kinase receptor type 1 (TrkA), repress astrocyte production, and augment the proliferation of nestin-expressing stemlike cells.[183]

Also active in models of TBI is LM11A-31 ((97), **Fig. 47**), a ligand for the p75 neurotrophic receptor, which is a major contributor to pathological processes in the CNS, and which decreases impairment of learning induced by injury, promotes neural progenitor cell survival, improves the outcome of TBI, and enhances the production of mature neurons from adult hippocampal neural progenitors in vitro.[184] The antiepileptic drug ethosuximide (98) has been shown to increase GABAergic neurons in rat forebrain cortex stem cells in vitro, but whether this could be the basis of its clinical effects has not been established.[185]

1.13.2.2.5.2 Augmenting neurogenesis in vivo

An attractive strategy to tackle neurodegenerative disease would be to promote differentiation of neural stem/progenitor cells especially as promotion of terminal differentiation rather than self-renewal of disregulated cancer stem/progenitor cells could

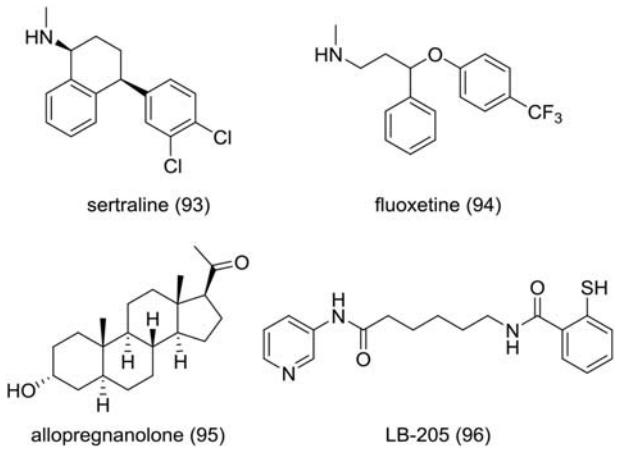

Fig. 46 CNS active agents able to induce neurogenesis.

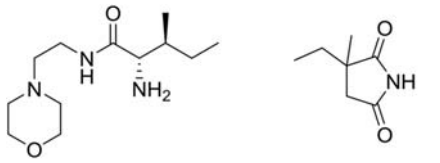

Fig. 47 Compounds active against traumatic brain injury and epilepsy.

play a key role in halting the progression of various neurological malignancies. However, it is apparent that the use of such agents discovered using in vitro methods in an in vivo pharmacological/clinical situation is likely to be particularly complicated due to the usual pharmacokinetic constraints, including the need to penetrate the blood–brain barrier. Notwithstanding these caveats, in vivo active compounds have been discovered. A group of molecules including P7C3 ((99), Fig. 48) and its derivative P7C3A20 (100) were discovered in an in vivo study monitoring hippocampal neurogenesis in neonatal mice. The authors went on to demonstrate that these molecules act through inhibition of apoptosis of new-born neurons in the subgranular zone of dentate gyrus, an effect mediated through activation of NAMPT, a key mediator in the NAD salvage pathway.[186] In addition, the compounds were able to protect adult mice against the effect of the neurotoxin 1-methyl-4-phenyl-1,2,3,6-tetrahydropyridine (MPTP, (101)), especially on dopaminergic neurons.[187] Further, P7C3A420 (100) was particularly active in the G93A-SOD1 mutant model of amyotropic lateral sclerosis (ALS) in protecting ventral horn spinal cord motor neurons,[188] indicating that this class of compounds do possess an exciting range of neuroprotective activities, although their broader specificity has yet to be reported.

1.13.2.2.5.3 NSC differentiation in vivo

To illustrate that this differentiation is possible, it should be noted that perfluorooctane sulfonate at environmentally relevant levels decreases proliferation and increases neuronal differentiation in NSCs in vitro via PPAR-γ (peroxisome proliferator response element) and in utero in the developing mouse brain.[189] The effect of hypoxia on neural development has been reviewed[190] and Fuller et al. showed that the NPCs isolated from SVZ tissue from 4 day old C57BL/6 mice, which had been exposed to intermittent hypoxia had greater capacity for expansion, increased cellular metabolic activity, and an increase in hypoxia-inducible factor 1-α signaling.[191] Novel medicinal chemistry discoveries may be facilitated by discovering the details of the biochemical processes involved in a particular target organ or tissue. Among such targets are the Notch/RBPJk (recombining bonding protein suppressor of hairless)-signaling pathway, which is highly active in NSCs and its inactivation leads first to increased neuronal differentiation and later, suppression of hippocampal neurogenesis,[192] which is accompanied by loss of expression of Sox2 (sex determining region-Y-box 2). A crucial role for cGMP in the in vivo differentiation of NSCs to neurons in rat prefrontal cortex and hippocampus has been shown and treatment of pregnant rats with L-NAME ((102), Fig. 49), a nitric oxide synthase inhibitor, which significantly reduces levels of cGMP in the fetus brain results in reduced neuron production and increased production of nonneuronal cells.[193] The effect was reversed on concomitant treatment with sildenafil (103), a cGMP-specific phosphodiesterase-5 inhibitor.

Schultz et al.[194] developed KHS101 ((104), Fig. 50) from a group of thiazoles identified in a phenotypic screen for compounds able to promote the neuronal differentiation of rat hippocampal NPCs. Further studies using chemical proteomics identified transforming acidic coiled-coil-containing protein 3 (TACC3) as a protein target bound by KHS101 leading to increased nuclear localization of the TF ARNT2. KHS101 also suppressed NPC proliferation and BMP4 induced astrogenesis in vitro and on subcutaneous injection into rats crossed the blood–brain barrier and promoted neurogenesis of NPCs in the subgranular layer of the dentate gyrus at the expense of proliferation.

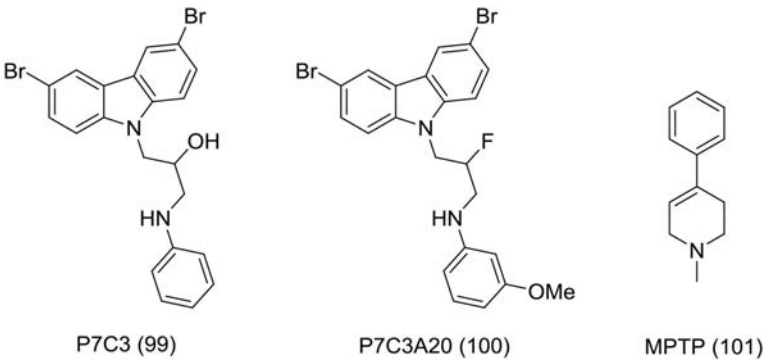

Fig. 48 Neuroprotective agents.

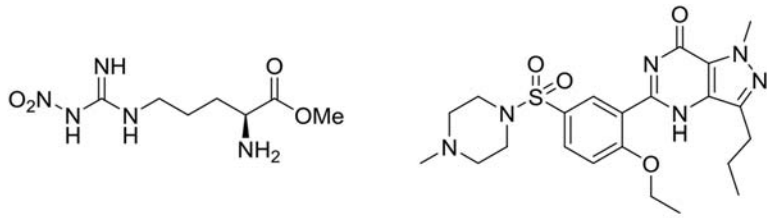

Fig. 49 Compounds involved in in vivo differentiation to neurons.

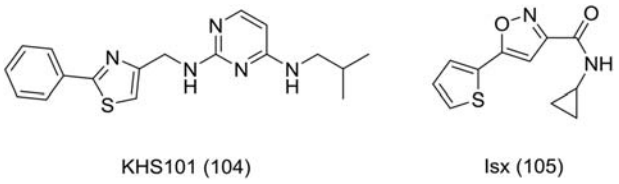

Fig. 50 Neuroactive isoxazoles.

A series of isoxazoles, exemplified by Isx (isoxazole stem cell modulator of small molecules) (105), which promote neurogenesis in NSCs in vivo were linked through a chemical proteomics study to the activity of a protein GPR68, a proton sensing G protein-coupled receptor with no previously reported function in the brain.[195] Isx and GPR68 were both found to increase levels of neuronal target genes such as Bex 1 (brain-enriched X-linked protein-1) in hippocampal progenitor cells. Furthermore, after TBI cerebral cortical astrocytes express GPR68 indicating a crucial role for the effect of brain pH and the authors speculate that lactic acidosis could explain the beneficial effect of exercise on Alzheimer's disease. Microarray gene expression analysis showed that Isx promoted upregulation of genes associated with neurogenesis and cell cycle progression in primary mouse dentate gyrus cells in vitro, which would be consistent with the conversion of quiescent NSCs converting to proliferative transit amplifying progenitors prior to terminally differentiated neurons. Isx is able to penetrate the blood–brain barrier and can promote enhanced hippocampal neurogenesis following intraperitoneal injection in young mice with an associated decrease in NSC populations. However, while Isx-treated mice increased neurogenesis as assessed by dentate gyrus volume combined with nestin-GFP + cell count and cell lineage tracing, they did not display any learning or memory enhancement over controls in behavioral tests likely due to the young age of the mice tested. It would be interesting to see the effects on cognitive behavior of these compounds in aged animals. Taken together these studies suggest a link between pH, which is often linked to hypoxia, and regulation of neurogenesis and that this may play part of the coordination of the body's response to injury. These findings may also pave the way for other opportunities for small molecule therapeutic intervention.

1.13.2.2.5.4 Neural cell migration in vivo

Neurogenesis in both embryonic and adult zebrafish has been the subject of a recent review[196] and methods of imaging the neural migration, axonal, and dendrite formation have also been described.[197] Clearly, being able to understand the mechanisms of these processes could lead to the discovery of agents able to constructively affect them and to influence the migration of neurons into functioning brain structures. N-Cadherin is known to regulate β-catenin and Wnt signaling, and has recently been shown to maintain β-catenin signaling via AKT (protein kinase B) in mouse cortical development.[198] Further, inhibition of AKT signaling in neural precursors in vivo leads to reduced β-catenin-dependent transcriptional activation, increased migration from the ventricular zone, premature neuronal differentiation, and increased apoptotic death. The growth factor, insulin-like growth factor-1 (IGF-1), has been found to act on SVZ-derived adult neuronal precursor cells in mice to induce migration along the rostral migratory stream (RMS) through both chemokinesis and chemotaxis.[199] Although less migration has been observed for human SVZ-derived neurons compared to mouse, this nonetheless suggests a possible target for further exploration to increase precursor cell recruitment into areas of cellular damage resulting from brain injury or illness.

Interestingly and in contradiction of previous claims, it has been shown that AMP-activated protein kinase activity (AMPK) is not required for proper cortical neurogenesis, radial migration, cortical layer formation, and axon-dendrite formation both in vivo and in vitro.[200] Hyperactivation of this enzyme complex does however have profound consequences on early neural development with inhibition of axon specification via the mTOR-dependent pathway (mammalian target of rapamycin complex-1).

1.13.2.2.5.5 Reprogramming in vivo

Evidence of the natural processes involved in neuronal development was provided by Lie et al.[201] who showed that in the adult mouse hippocampus expression of the SoxC TFs Sox4 and Sox11 is initiated at the time of neuronal commitment to adult

NSCs and is maintained in immature neurons. Further, both of these factors work with Ngn2 to reprogram astrocytes into neurons and understanding these processes is likely to lead to fresh targets for drug intervention.

1.13.2.3.6 Disease screening and drug discovery

The ability to produce the neurons and glial cells that are possibly involved in neuropathies and then use them in high-throughput screening could represent a highly significant approach to the discovery of new therapeutic agents. Thus for example the groups of Eggan and Wichterle have shown that hiPSCs generated from patients with amyotrophic lateral sclerosis (ALS) could be differentiated into motor neurons, thereby giving a route to the understanding of the molecular details of this disease.[202] The problems of such approaches to "in vitro disease modeling" have been discussed in thoughtful and comprehensive reviews by Eggan.[203–205] In particular, these reviews show how detailed studies of the cell type-specific gene expression of the damaged neurons could lead to an understanding of the true molecular nature of the disease and consequently the discovery of agents able to correct or alleviate this. Further, the potential problems arising from the use of hiPSCs from individuals, the variable behavior of such cells in culture, and epigenetic variations are discussed. It is possible that recent advances in reprogramming techniques and more stringent quality criteria will allow the production of large cohorts of disease and control subject pluripotent cell lines and that this should reduce the possibility of the results being distorted by the presence of aberrant cell lines.[206]

The most recent studies in this area include the use of polysialic acid-neural cell adhesion molecule (PSA-NCAM)-positive neural precursor cells derived from hESCs in a rat stroke model,[207] hiPSCs in modeling and therapy development in epilepsy.[208] The use of GABAergic interneuron transplants, which migrate tangentially from the subcortical forebrain into the cerebral cortex and become synaptically connected with host circuitry, have also been recently reported in the study of disease mechanisms and toward the development of cell-based therapies,[209] as has the transplantation of cholinergic neuron-like cells into APP/PS1 transgenic mice, a model for Alzheimer's disease.[210] Earlier studies included those on neuropathic Gaucher's disease using patient-derived iPSCs,[211] on neurodegeneration using stem cell-derived motor neurons and astrocytes with activated microglia,[212] on PD using iPSC-derived dopaminergic neurons,[213] and on neuroactivity/neurotoxicity with stem cells under the control of neural cell-specific tetralin-α promoter.[214] It has also been shown that cortical neurons can be generated from iPSCs of patients harboring mutations of a key protein involved in PD, namely α-synuclein. The protein NAB2 that affects the E3 ubiquitin ligase Nedd4 was identified as being able to reverse the pathological phenotypes in these neurons.[215]

Chandross et al.[216] have recently reported a high-content phenotypic screening strategy to identify molecules able to elicit the differentiation of oligodendrocyte precursor cells, which could be of use in the treatment of multiple sclerosis. The screen was capable of testing a library of 73,000 compounds from which 22 nontoxic compounds were identified that were capable of selectively stimulating primary rat oligodendrocyte precursor cells but not muscle myoblast cells. A different approach to the production of oligodendrocytes has been reported by Hickman et al.[217] who have described a three-dimensional environment in which human multipotent progenitor cells from umbilical cord were differentiated in the presence of noradrenaline to give committed oligodendrocytes that expressed myelin basic protein.

Previous mention has been made of the rapidly progressing neurodegenerative disease ALS, which is characterized by the death of motor neurons and for which there is currently no effective treatment. However, Rubin has described a high-throughput screen using motor neurons from wild-type and mutant SCPD1 mouse ESCs, which has shown that kenpaullone ((74), **Fig. 51**), a dual inhibitor of GSK-3 and HGK (an STE 20 serine/threonine kinase family member also known as MAP4K4), is able to prolong the survival of both types of motor neurons and, most interestingly, improved the survival of human motor neurons derived from ALS patient-derived iPSCs.[218]

A key necessity for studies of this kind is the reproducible expression of the necessary cell lines and a technique for the differentiation of hESCs and hiPSCs using small molecules including dorsomorphin (43), SB431542 (12), CHIR99021(5), and purmorphamine (28) to early neural progenitors has been described. These NSCs are robust, exhibit immortal expansion, and have the potential to clonally and efficiently differentiate into neural tube lineages, including motor neurons and midbrain dopaminergic neurons as well as neural crest lineages such as peripheral neurons and mesenchymal cells.[219]

Finally and of particular interest to medicinal chemists is the review by Kundu[220] on the range of small molecule inhibitors of epigenetic enzymes which also have been shown to be involved in the regulation of adult neurogenesis.

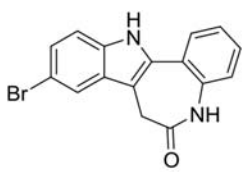

(74)

Fig. 51 Chemical structure of Kenpaullone (74).

1.13.2.4 Muscle Regeneration Using Small Molecules

There is a vast array of diseases associated with the loss of muscle tone, or degeneration of muscle fibers including ischemic heart disease and cachexia (muscle wasting often found in cancer patients and suffers of COPD, AIDS, and other diseases) through to less common genetic diseases such as Duchenne and Becker Muscular Dystrophies (DMD, BMD). The reversal of muscle loss via the use of stem cells as described in other sections of this article would appear to be an attractive therapeutic option. A comprehensive review describing a wide range of compounds that repair or replace defective muscle tissue has recently been published.[221] However, there are currently no small molecule drugs targeting muscle stem cells, which have been approved for that specific purpose and, more importantly there are, as yet, no muscle-focused cell-based therapeutic agents on the market, though a monoclonal antibody, bimagrumab is making progress in clinical trials of sporadic inclusion body myositis.[222] There is, though, an active body of research into agents that can affect muscle repair and a considerable number of examples of these have been described in the literature.

1.13.2.4.1 Muscle-based applications of small molecule stem cell modulators

During embryonic development, myoblasts, that is, progenitor cells that differentiate to produce muscle cells, fuse to form multinucleated fibers called myotubes en route to muscle fibers. Myoblasts can either undergo an asymmetric cell division or directly differentiate into myotubes, but it is not clear what controls this choice in vivo. In emerging stem cell-based therapeutic approaches to muscle disorders, initial publications have focused very much on the relatively small, but growing, number of well characterized promiscuous small molecules, which have been described as being able to modulate stem cell fate in other target tissues. For example, a number of small molecules including the GSK3β inhibitor BIO ((19), Fig. 52), a p38 MAPK inhibitor (SB203580, (66)), a broad spectrum GPCR activator (lysophosphatidic acid, (106)), and the adenylyl cyclase inhibitor SQ22536 (107) have been described as inducing dedifferentiation to multipotent cells from myoblast-like cells.[223,224] Furthermore, the small molecules dorsomorphin (43) and its derivative LDN193189 (56), both BMP/Activin receptor inhibitors have been described by Knaus and coworkers as inhibiting myostatin (GDF8, growth differentiation factor 8) signaling, with the result of promoting differentiation of myoblasts and their ensuing contractile activity.[225]

In related work, intriguing data has been published very recently by Wagers et al.,[226] in which the administration of a related protein growth differentiation factor 11 (GDF11) was reported to induce functional recovery in the skeletal muscle of aged mice and restore genomic integrity in muscle satellite cells. Indeed, the authors speculate that increased levels of GDF11 in aged mice may act on muscle satellite (stem) cells to restore regenerative function and induce a more promyogenic niche. No small molecules having a corresponding effect have yet been described, although this potentially represents an attractive medicinal chemistry strategy for muscle regeneration.

In a separate study, Ryan et al. have demonstrated that multiday treatment of hESCs with the pleiotropic stem cell modulator retinoic acid ((108), Fig. 53) leads to an increase in expression of the myogenic regulatory factor, which they correlated with an enhanced progenitor population and increased skeletal myogenesis.[227]

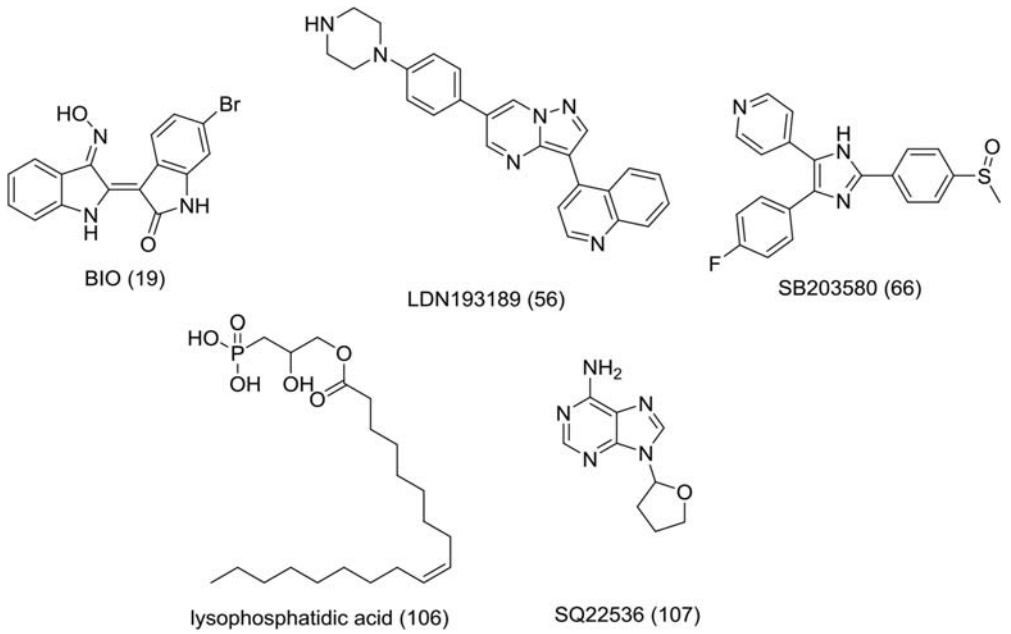

Fig. 52 Compounds reported to promote the differentiation of myoblasts.

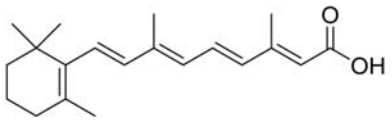

(108)

Fig. 53 Chemical structure of retinoic acid (108).

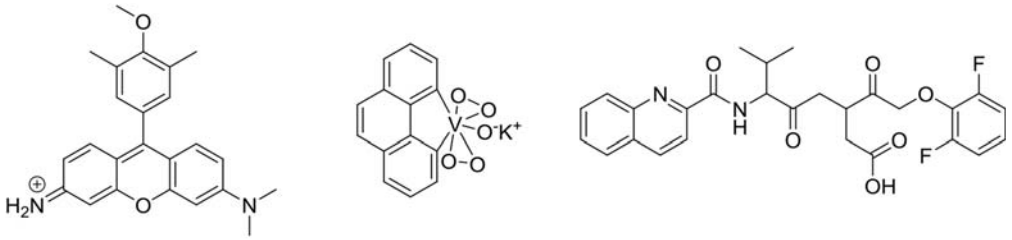

B25 (109) Bpv(phen) (110) Q-VD-OPh (111)

Fig. 54 Compounds reported to dedifferentiate myotubes to progenitor myogenic cells.

A mitochondria-targeted fluorophore has also been reported as being able to block muscle myoblast differentiation.[228] Interestingly, the authors had intended to undertake a screen to identify biosensor molecules, which were capable of distinguishing between stages of muscle differentiation through reporting on differential mitochondrial activity. However, the screen resulted in the identification of the rosamine derivative B25 ((109), **Fig. 54**), which acts to reverse myotubes to a dedifferentiated myoblast-like mononuclear phenotype. Unlike the previously described myoseverin (14), compound (109) did not appear to act via disruption of microtubule stability or modulation of the cell cycle, but rather through a mechanism involving activation of NF-kB signaling. Phosphatase and apoptosis inhibitors BpV(phen) (110) and Q-VD-OPh(111) used in combination have recently been documented as also being able to dedifferentiate myotubes to progenitor myogenic cells with high efficiency (12%).[229] Moreover, the resulting progenitor muscle cells were shown to be functionally competent, and capable of self-renewal and redifferentiation. The latter was demonstrated both in vitro, and, most interestingly, in vivo using SCID mice. Other researchers have shown that the same inorganic chemical, BpV(phen) (110), can also dedifferentiate myoblast cells to a multipotent circulating phenotype as evidenced through phenotypic and gene expression analyses of their progeny.[230]

The Type 1 TGFβ inhibitor (616452, also known as RepSox, (6), **Fig. 55**) has been shown to restore regenerative function to stem cells in muscle in vivo in aged mice. Inhibition of TGFβ following administration of (6) was supported by the observed reduction in the level of, for example, pSmad-3. This study provides additional evidence to support the role of TGFβ modulation in manipulating regenerative potential for muscle.[231] In a separate study of the biological activity of natural product extracts from *Geum japonicum*, a pure fraction was found to stimulate activation and differentiation of quiescent myoblast precursor cells to myocytes in vitro. Subsequent in vivo administration of the active principal "Trit" in a rat model of muscle injury led to reported improvements in myofiber regeneration and more efficient muscle repair, although no comparative quantitative data was presented.[232] Structural elucidation of the active principal was found to correspond to a previously described triterpenoid natural product, although it was unclear whether the corresponding carboxylic acid or its glycone conjugate was isolated, and many of the sterochemical features remain undefined (112).[233]

A recent publication has examined the effect of treating muscle-derived stem cells using in vitro assays with a range of nutritional supplements.[234] Of the 16 supplements tested, a significant number was found to enhance either proliferation

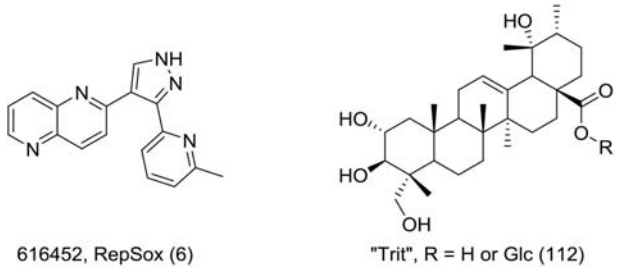

616452, RepSox (6) "Trit", R = H or Glc (112)

Fig. 55 In vivo muscle repair agents.

(ten) or differentiation (four). This is an intriguing finding, but further studies on the precise modes of action associated with these observations would appear to be warranted.

1.13.2.5 The Pancreas

1.13.2.5.1 Chemical manipulation of pancreatic regeneration

Diabetes mellitus, an endocrine disorder in which the natural control of blood glucose levels is compromised, is separated into two types. Type I is the result of an, as yet unexplained, autoimmune attack on the β-cells of the pancreas, which are responsible for the production of the hormone, insulin, and requires life-long daily subcutaneous injections or infusions of insulin for survival. The much more common Type II diabetes is a metabolic disorder in which insulin production is compromised along with the target cells becoming resistant to insulin signaling and probably arises from genetic disposition, obesity, lifestyle, and food choices. It can often be controlled by diet and/or hypoglycaemic drugs but does sometimes require insulin injection. In the pancreas of nondiabetic healthy adults, there are 1–2 g of β-cells dispersed among a vastly greater number of cells that release digestive enzymes into the gastrointestinal tract. A regenerative medicine approach to treatment would replace damaged cells with healthy, functioning ones. It is therefore an archetypical example of the regenerative medicine approach; a clear cause and a clear need for tissue/cell replacement. Of course, to achieve this requires a detailed knowledge of the cell biology, and ideally the biochemistry, of the β-cell.

While Type I diabetes has been treated successfully by transplantation of all or part of the pancreas by tissue recovered from cadavers, this lies outside the scope of this article that concentrates on the use of new β-cells generated either ex vivo or in vivo.

1.13.2.5.2 Ex vivo generation of replacement β-cells

1.13.2.5.2.1 In vitro β-cell expansion

In a series of three detailed papers, Stewart et al.[235–237] have summarized the current understanding of intracellular signaling pathways coupled to proliferation in pancreatic β-cells in both man and rodents. The knowledge of the human situation is, unfortunately, much less complete than that of the rodent but in both species a cell surface receptor specific solely to the β-cell has yet to be identified. While this means that any proliferating agent could, in principle, have similar effects on other cell types in the pancreas, it will be recalled that medicinal chemistry has a good history of finding selective agents in other therapeutic areas. It is also becoming clear that there are very significant differences between rodent and human β-cells; differences that, inter alia, include rats having two insulin genes and humans only one, different glucose transporters, different TFs and different pancreatic architecture. In the human cell, the cell cycling molecules are not found largely in the nucleus but in the cytoplasm for reasons that are not as yet clear. Finally mitogenic signaling pathways are difficult to activate in human cells and mediate only weak effects. Thus the extrapolation of information derived from the study of rodent cells to human ones may not be straightforward. While continually growing transformed rodent insulinoma cell lines are available for study, it is only recently that equivalent human lines have been developed. Thus the creation of a conditionally immortalized human β-cell line, EndoC-βH2, has been reported and should provide more direct information on the cell biology of this cell line.[238]

This is not to say that studies on rodent cell lines have not been useful. In one of the earliest studies Schultz et al. studied the effect of a library of ~800,000 compounds on the growth of a reversibly immortalized mouse β-cell line R7T1 using a luminescent assay to measure intracellular ATP content as a measure of viable cell number.[239] Approximately 80 of the compounds showed significant activity and these included phorbol esters, which probably act by activation of protein kinase C isoenzymes, and small molecules identified as Wnt activators (eg, (113), Fig. 56) or L-type calcium channel agonists (eg, (114)). Further work identified WS6 (115) as being able to induce proliferation of primary rodent and human islets in vitro and, importantly, to increase β-cell numbers in vivo and to correct hyperglycemia in a mouse model of β-cell ablation.[240] Affinity chromatography using a biotin-conjugated analog of WS6 revealed Erb-binding protein and IkB kinase as binding partners, the latter of which plays a role in regulating the NFkB pathway proinflammatory stress response.

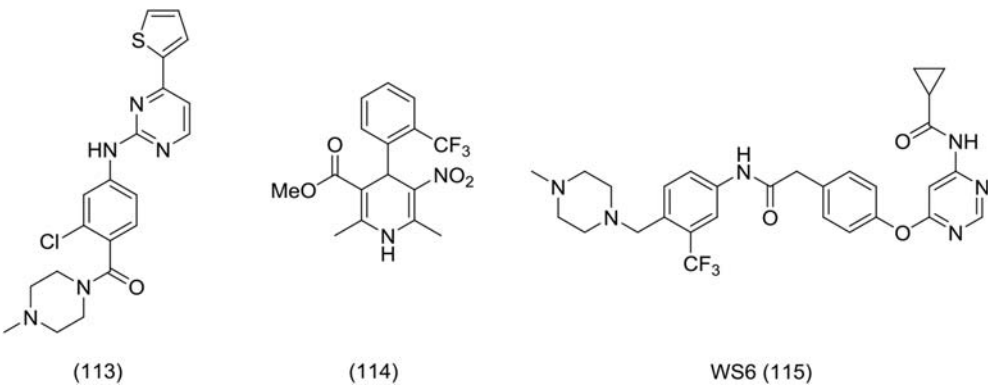

Fig. 56 Compounds reported to affect the growth of an immortalized mouse β-cell line.

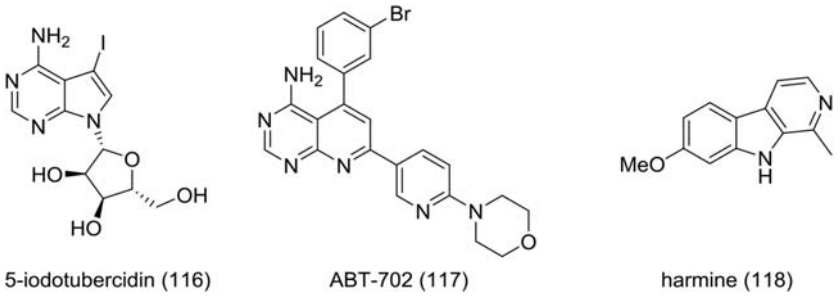

Fig. 57 Compounds reported to enhance the proliferation of β-cells.

Another group has shown that inhibitors of the adenosine kinase pathway, especially 5-iodotubercidin ((116), Fig. 57) and ABT-720 (117) enhance proliferation of β-cells from the islets of rat, mouse, and pig.[241] More recently, Sarvetnic et al.[242] have shown that WS6 stimulates both α- and β-cell proliferation in human islets in vitro while maintaining the differentiated β-cell phenotype. The use of a human hepatocyte cell line HepG2 that expresses a luciferase reporter under control of the human *MYC* gene (a regulator gene which codes for TFs) in a high-throughput in vitro screen enabled the identification of harmine (118) and its analogs as human β-cell mitogenic compounds. Subsequent analyses were consistent with harmine acting, at least in part, to inhibit the dual specificity kinase DYRK1A. Using three different in vivo models based on either murine or human islets, the authors went on to show that harmine can induce β-cell proliferation, increase islet mass, and improve glycaemic control.[243] There are therefore multiple independent lines of evidence that small molecules can be found, which promote proliferation of these cells at least in vitro and in vivo.

1.13.2.5.2.2 β-Cell derivation from stem cells

It is difficult to see how a supply of β-cells for ex vivo expansion could be obtained from the patient, so the challenge of this approach can be expressed very simply, that is, to devise the technology to reliably and economically produce sufficient β-cells from an alternative, more readily accessible source of a patient's or donor's precursor cells. There has been much work done on this but, at the time of writing, very limited clinical work using such cells has been reported.[244] The obvious alternative stem cells are hESCs, the less ethically contentious hiPSCs, or human MSCs derived from the bone marrow.

The pancreas develops from the mesoderm of the blastocyst and the differentiation process whereby the initial stem cell eventually develops into a functioning β-cell has been investigated in considerable detail and this provides the basis for attempts to replicate the process.[245–253] Melton et al.[253] have recently described a six-stage process over 27–34 days to convert hPSCs to generate glucose-responsive "stem cell-derived β-cells (SC-β)" capable of being scaled-up to generate hundreds of millions of cells. Furthermore, these cells behave very similarly to adult β-cells in that they express the same markers, exhibit characteristic Ca^{2+} flux in response to glucose, package insulin into secretory granules, and secrete comparable quantities of insulin in response to multiple sequential glucose challenges in vitro. Most encouragingly, these cells secrete human insulin into the serum of mice shortly after transplantation and ameliorate hyperglycemia in diabetic mice. Different combinations of large molecule growth factors and small molecules are required for each stage (Fig. 58). These include Activin A, keratinocyte growth factor, heparin, betacellulin, CHIR99021 (5), retinoic acid (108), SANT1 (119), LDN193189 (56), phorbol 12,13-dibutyrate (120), triiodothyronine (121), γ-secretase inhibitor XXI (122), and Alk5i ((6), also known as RepSox). The authors point out that the SC-β cells are not exactly the same as adult β-cells in that they produce slightly larger islets and the gene expression patterns are not identical. However, they do produce human insulin in diabetic mouse models and do this very quickly after transplantation. Also they point out that their procedure could make sufficient cells for human transplantation in two 500 mL flasks. Further, a single 500 mL flask could produce sufficient cells to enable 30,000 compounds to be screened in a 384-well plate seeded with 10,000 cells/well in a search for novel compounds able to influence the behavior of this cell type. Ongoing work has apparently generated equivalent cell lines from hiPSCs from diabetics which should provide a resource for fundamental studies on the disease. Incorporation of these cells into tissue-like structures for transplantation is envisaged.

The generation of β-cells from hESCs and hiPSCs by five different protocols has also been discussed by Suresh Kumar et al.[251] Gene expression profiles at the different stages were described, along with a discussion of the various signaling pathways induced or inhibited by the stimulating molecules used in the different stages. The authors also considered starting from MSCs and these can produce functional β-cells but, at the moment, expansion to large scale for clinical use does not seem practical. A detailed account of the likely role of the growth factors, Activin A, FGF, retinoic acid (108), cyclopamine ((37), Fig. 59), wortmannin (123), sodium butyrate (124), betacellulin, noggin, EGF, HGF, KGF, and IGF was also provided (Fig. 59).

A different approach has been taken by Viacyte Inc., who has conducted similar detailed research into the stepwise differentiation of hESCs to functional pancreatic progenitors on a manufacturing scale. These cells are a mixed population comprised of pancreatic endoderm (PE) and polyhormonal endocrine cells. Implantation of PE cells gives rise to functioning islet-like structures through a mechanism that appears to primarily involve the de novo commitment of pancreatic progenitors to the endocrine lineages followed by further maturation to glucose-responsive β-cells. Their protocol goes through four stages, ESC, mesendoderm, definitive

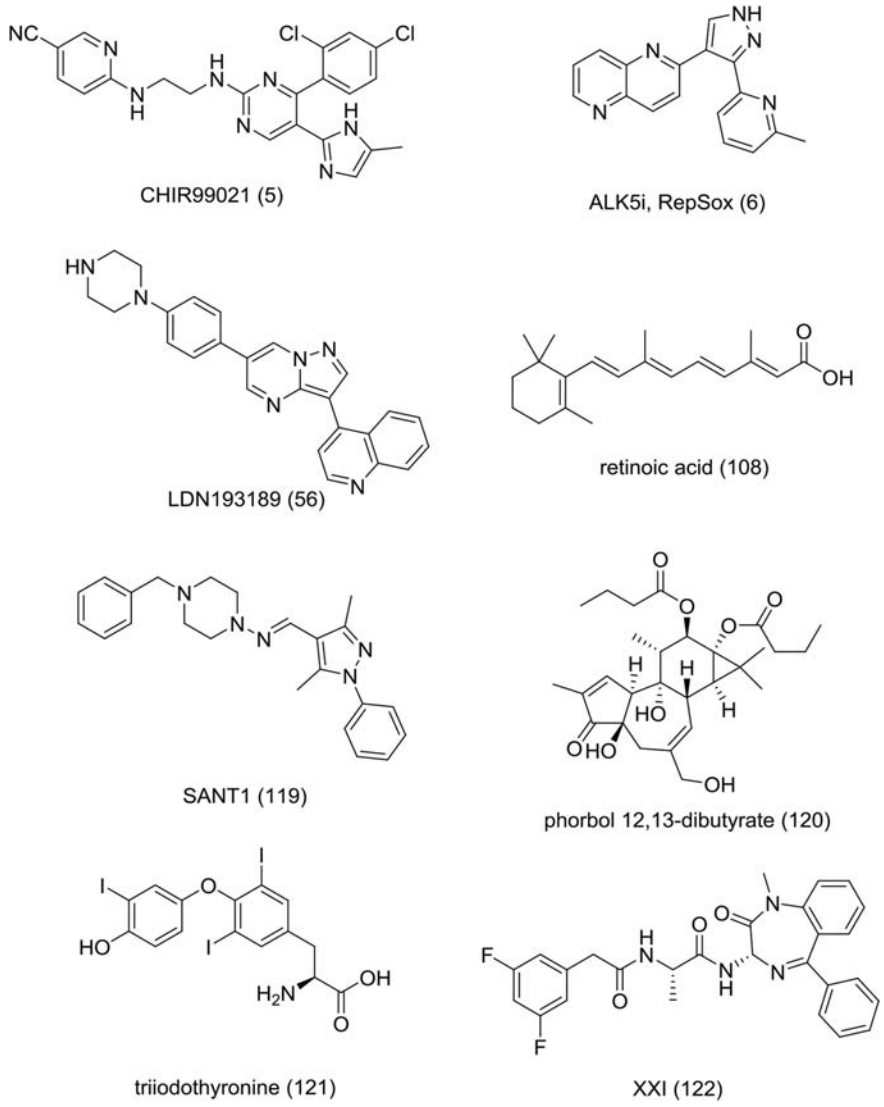

Fig. 58 Compounds reported to form "stem cell-derived β-cells."

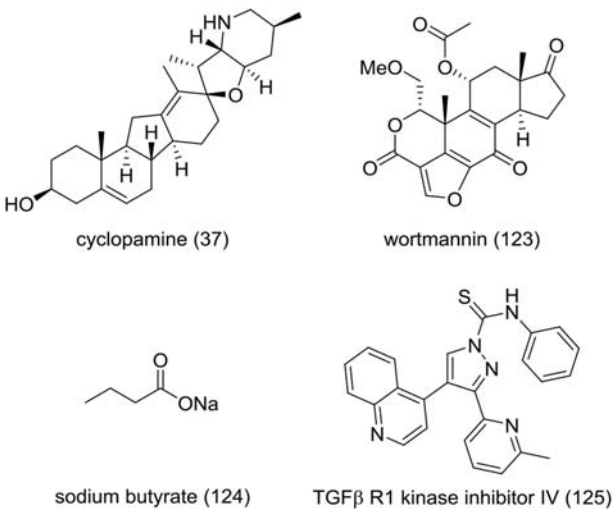

Fig. 59 β-Cell generating compounds.

endoderm, primitive gut tube, and posterior foregut to give the final cell mixture and takes around 13 days of incubation. The growth and differentiation factors involved are TGF-β R1 kinase inhibitor IV (125), insulin–transferrin–selenium, heregulin 1β, cyclopamine (37), and noggin. It is envisaged that the final cells could be transplanted into the patient or the company has developed an implantable delivery system (VC-01™) in which the cells are contained within a semipermeable capsule protected from the immune system but open to the bloodstream so that insulin can be released.[254] The company has stated that permission has been granted for a Phase 1/2a clinical trial of this device. This approach clearly uses the natural mechanisms to finish the differentiation process to the β-cell and shows that interaction of a cell within its native microenvironment it is part of the normal maturation process. Another approach using cell interactions is due to Narayanan,[255] who first grew β-cells on a tissue culture plate which was then decellularized. The derived extracellular matrix and conditioned media were then used for the culture of ESCs. This technique produced up to 38% of insulin-positive cells and gene expression studies indicated the presence of β-cell-specific markers. Subcutaneous implantation of these cells in a diabetic mouse model restored normoglycaemia in a long-term study. However, teratomas developed and this potentially indicates that residual pluripotent cells are still present and that methodologies to isolate the desired β-cells are required.

1.13.2.5.3 Different sources of β-cells

1.13.2.5.3.1 Other pancreatic cells

The transformation of other pancreatic cells to β-cells and the signaling molecules involved has been reviewed by Warnock et al., [249] Koblas et al., [256] and Melton et al.[257] In a seminal study using mice, Melton showed that in vivo adenovirus-mediated delivery of the genes for three TFs, Ngn3, Pdx1, and Mafa resulted in fully differentiated pancreatic exocrine cells being differentiated into cells that closely resemble β-cells and do secrete insulin. Koblas showed that the differentiation of adult human pancreatic nonendocrine cells into insulin-producing cells increased on treatment with the growth factors IGF-1, EGF, and Extendin-4. As all of these are known to act via the PI3K pathways and the effect is reversed on addition of a PI3K pathway inhibitor wortmannin (123), it was concluded that stimulation of this signaling pathway might be used to stimulate the differentiation of the nonendocrine cells into insulin-secreting cells.

It is known that the ventral pancreas and liver arise from the same cell population within the embryonic endoderm and thus efforts have been made to use progenitor cells from the liver as starting material to produce β-cells. While this might be useful for in vitro /ex vivo and transplantation work it is difficult at this time to see how the approach could work directly in vivo. Nevertheless, small cells were isolated from neonatal pig liver and these showed positive staining for immature liver and pancreatic endocrine markers. They could also be cultured to produce pancreatic-like β-cells but no in vivo results were reported.[258] More recently, Han has shown that rat liver epithelial stemlike WB-F344 cells can be transformed in a stepwise manner to functional insulin-secreting cells by use of a combination of large and small molecules.[259]

1.13.2.5.3.2 Mesenchymal stem cells

The ready availability of MSCs cells from bone marrow makes them a potentially attractive source of cells for differentiation to β-cells. Zuo and Yu[260] screened a 2500-compound library and identified XW4.4 ((126), **Fig. 60**), an aminopyrrole derivative, as being able to stimulate differentiation of rat MSCs into cells with the characteristics of insulin-producing cells including islet-like clusters displaying spherical, grape-like morphology, insulin secretion, glucose stimulation, and expression of pancreatic endocrine cell marker genes. Further investigation suggests that hepatocyte nuclear factor 3β may be involved in the pancreatic differentiation process.

Perhaps more remarkably, Wujun-Xue et al.[261] treated mice rendered diabetic by the injection of streptozotocin (127), with an infusion of MSCs and an injection of nicotinamide (128) resulting in raised insulin and decreased glucose levels and higher levels of expression of β-cell-related gene expression than in controls. The mechanism through which nicotinamide operates was unclear, but the authors hypothesized that it both promotes the homing of MSCs to the damaged pancreatic tissue and facilitates their differentiation to functional insulin-producing cells.

1.13.2.5.3.3 Fibroblasts

In a recent report Li[262] and coworkers described a scheme that converts engineered MEFs firstly into definitive endoderm-like cells (DELCs). These were isolated and expanded before being directed into pancreatic progenitor-like cells (PPLCs) by a combination of

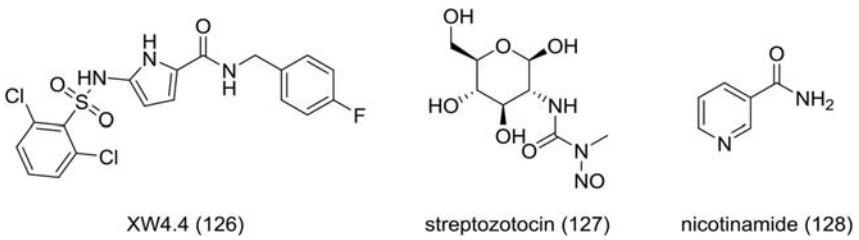

Fig. 60 Compounds reported to differentiate mesenchymal stem cells to β-cells.

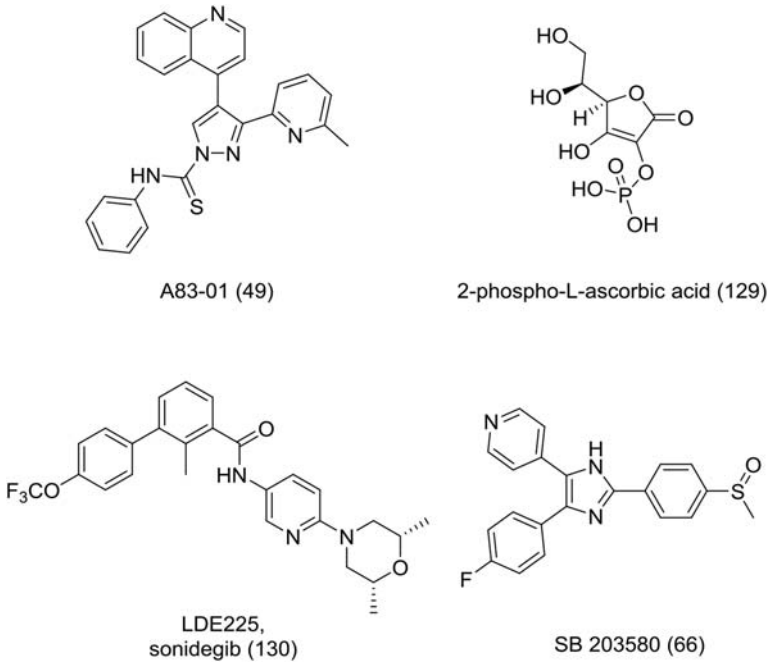

Fig. 61 Compounds reported to affect the formation of pancreatic progenitor-like cells.

signaling molecules and small molecules identified from screening libraries. The three-stage process uses Activin A and lithium chloride to generate DELCs, retinoic acid (108), A83-01 (49), a TGF-β receptor inhibitor, 2-phospho-L-ascorbic acid (pVc) (129) and LDE 225 (130), a hedgehog pathway inhibitor to generate PPLCs and finally SB203580 (66) (Fig. 61) and pVc to increase the yield of active cells. The resultant PPLCs were transplanted under the kidney capsule of immune-deficient mice rendered hyperglycaemic by streptozotocin and found, over time, to reduce glucose levels to normal. Analysis of the kidneys showed the presence of glucagon-producing pancreatic α-like cells, insulin-producing pancreatic β-like cells, amylase-producing pancreatic acinar-like cells, and Pdx1+/Ck19+ pancreatic duct-like cells. Although the authors did not conduct a rigorous lineage tracing analysis in this study, it appears that these cells may be capable of differentiating into cells of all three pancreatic lineages in vivo upon transplantation. Importantly, this procedure did not involve the MEFs passing through the iPSC stage and so it may be safer and reduce the risk of teratoma formation compared to earlier protocols.

1.13.2.5.4 In vivo expansion of β-cells

While the control of type I diabetes may be achieved by the transplantation of new β-cells, a better and less costly approach might be to trigger the renewal process in vivo by dosing with compounds able to provoke the expansion of the remaining β-cells. In addition, of course, as with any proliferation-inducing agent there is the possibility of activating oncogenic pathways. Thus there would need to be devised dosing protocols able to minimize this risk if ever a molecule acting in this way was introduced into clinical practice. One very interesting finding has been that patients who have survived more than 50 years of type I diabetes can still show residual β-cell functionality. Thus even under prolonged autoimmune and metabolic stress, pancreatic β-cells do seem to be able to be replenished but in this study the source of the β-cells was unclear, that is, are the β-cells themselves regenerating or are they being formed from other pancreatic cells?[263] All of this suggests that therapeutic intervention to replenish β-cells may not be a fanciful idea. The human pancreas contains ~1–2 g of β-cells but even in healthy individuals the range of values is from 0.1 to 2.0 g. Further, the rate of proliferation is highest, but still relatively low, in the first 2 years of life and then declines to a very low level by the age of 50. This leads to two considerations; the first being that a proliferation of ~2% such as is found in 1-year-olds might be all that is needed for therapy but on a more negative note the very people likely to need such therapy are the ones most resistant to it.[264]

This may seem discouraging for finding therapeutic agents, but it has also been pointed out that in pregnancy there is an increase in β-cell mass.[265] Although recent analysis of pancreatic sections from pregnant human donors did not find that proliferation contributed significantly to this increase, additional studies to understand the process might lead to the identification of new therapeutic targets. An alternative approach is to inhibit cell apoptosis in β-cells and inhibition of histone deacetylases by compounds such as vorinostat (131) and givinostat (132) (Fig. 62) had protective effects on the development of diabetes in a mouse model.[266]

Panadian et al.[252] have reviewed similar approaches to discovering clinically active agents. Also Wagner et al. have reported that a compound BRD0476 ((133), Fig. 63) suppresses cell death in β-cells and enhances cancer cell death.[267] This molecule acts to

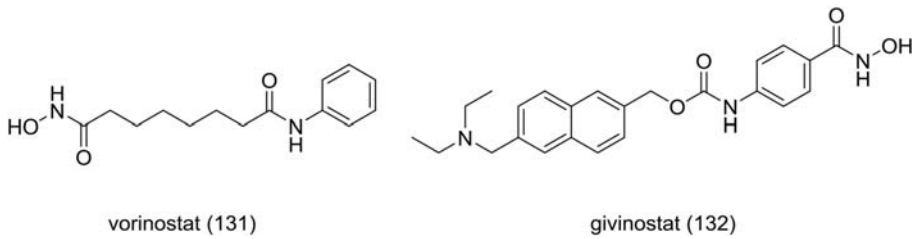

Fig. 62 Compounds with protective effects on the development of diabetes in a mouse model.

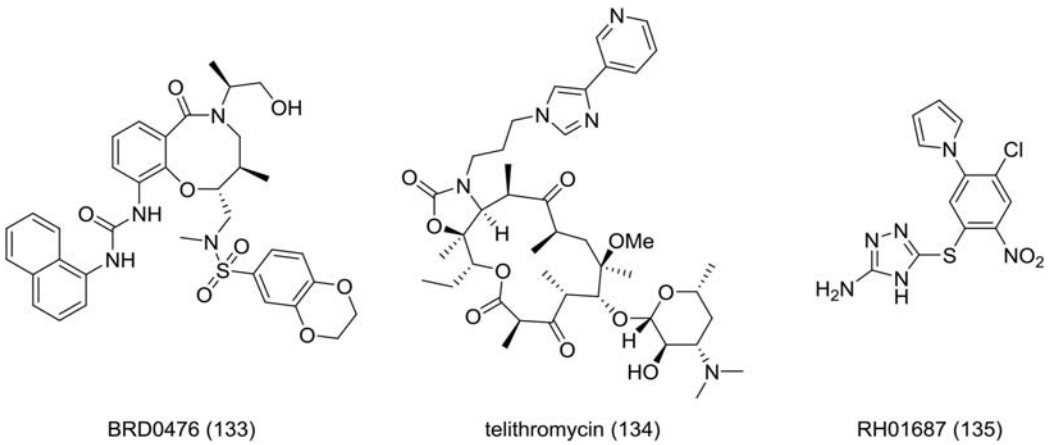

Fig. 63 Compounds suppressing β-cell death.

repress interferon gamma-induced Janus kinase 2 and signal inducer and activation of transcription 1(STAT1) signaling to promote β-cell survival. Interestingly, unlike other reported JAK-STAT inhibitors the mode of action was not through the inhibition of JAK kinase activity, but a proteomics analysis suggested the target to be the deubiquitinase ubiquitin-specific peptidase 9X (USP9X). This finding was supported by subsequent USP9X knockdown studies and comparison with another known USP9X inhibitor. Unfortunately, metabolic instability prevents the in vivo activity of this compound being assessed. A different approach to countering pancreatic β-cell death found that telithromycin (134) and RH01687 (135) are able to protect these cells from cell death induced by endoplasmic reticulum stress. The authors went on to show that a number of genes associated with cell survival and the unfolded protein response were upregulated, although the precise molecular mechanism of action of these compounds is not yet understood.[268]

As has been alluded to in other sections, increased levels of β-cells in vivo could be achieved from stem cell differentiation and transdifferentiation of other pancreatic cell types, especially α-cells. Initial work using genetic modification to introduce three TFs, *Ngn3*, *Pdx1*, and *Mafa* differentiated pancreatic exocrine cells in adult mice into cells that closely resemble β-cells.[257] Subsequently, it was shown that the growth factors IGF-1, EGF, and Extendin-4 that are known activators of the PI3K pathway differentiate human pancreatic nonendocrine cells into insulin-producing cells.[256] In addition, the Viacyte work and the finding that the endoderm cellular matrix can direct the differentiation of pancreatic progenitor cells gives some indication that this may be possible. Obviously, further efforts to understand the behavior of cells in the pancreas and, especially, of the interactions between them needs to be done so that the true biochemistry/cell biology of the human cells in the pancreas is properly understood and druggable targets begin to emerge.

1.13.2.5.5 In vivo studies in zebrafish

A number of groups have been studying the zebrafish and have shown significant similarities between its pancreatic development and that of mammals and shown that it is possible to do high-throughput screening to identify molecules able to affect differentiation to β-cells.[269] A transgenic zebrafish embryos were generated engineered to express a fusion protein of CFP and nitroreductase under the regulation of the insulin promotor. Nitroreductase expression allowed the local production toxic metabolites from metronidazole to damage the pancreas with temporary controlled β-cell ablation.[270] A high-throughput screen then identified four compounds capable of regenerating β-cells, all of which modulated the adenosine signaling pathway. Of these the most active was NECA, 5-*N*-ethylcarboxamido-adenosine ((136), Fig. 64). Significantly, the effects of NECA were shown to be specific to β-cells. NECA was also shown to promote β-cell proliferation both ex vivo in isolated murine islets and in vivo in a murine model of

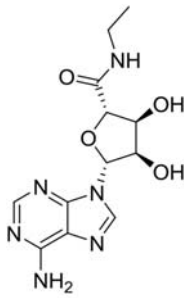

(136)

Fig. 64 Chemical structure of NECA (136).

diabetes. It was later demonstrated that adenosine receptor A2a signaling was the target pathway through which NECA exerted its effects, a discovery that suggests possible molecular targets for the development of future therapies.

A very significant amount of information on the cell biology of the β-cell and other pancreatic cell types has been, and continues to be developed and this knowledge, along with the molecules that have been identified through high-throughput screening gives hope that radical new treatments for both forms of diabetes can be found.

1.13.2.6 Ocular Disease

1.13.2.6.1 Ocular applications of small molecule stem cell modulators

Various diseases of the eye can result in blindness or visual degeneration and impairment, with notable examples including disorders affecting the retina (such as age-related macular degeneration, AMD),[271] and the corneal epithelium (for example, limbal stem cell deficiency, LSCD).[272] Stem and progenitor cell-modulating small molecule therapeutics offer considerable potential for treatment of these conditions, and a selection of examples follows. Therapeutic options and approaches to prolific and debilitating ocular fibrotic diseases such as glaucoma have been recently reviewed,[273] and evidence is also emerging that phenotypic reversion approaches may hold promise in this area.[274] Thus visual impairments involving regions of the eye such as the limbal epithelium are also potentially amenable to intervention with therapies that modulate stem cell function.[275]

As well as new approaches using small molecules to directly manipulate various cell populations for therapeutic benefit, development of new assay technologies to facilitate study and drug discovery efforts is an important area of exploration.

1.13.2.6.2 Corneal disease

The cornea, located in front of the iris and pupil, is the transparent outer layer of the eye, which provides protection against exogenous factors such as bacteria and solid particles. As well as disorders affecting the retina, corneal disease causes blindness and affects vision in a significant number of people worldwide. Of these, around 70% of cases of blindness are caused by LSCD.[276] The underlying cause of this disease is conjunctivalization of the corneal surface due to aberrant maintenance of the corneal epithelium. Cell-based therapies are being investigated clinically for LSCD, but to date no small molecule approaches have reached a similar stage.[277]

In recent years there have been emerging signs of interest in small molecule approaches for modulation of stem cells for potential treatment of corneal disorders. Skottman and coworkers have described the development and use of a new protocol for differentiating hiPSC into corneal epithelial cells using small molecules.[278] As well as offering the first uses of small molecules for applications toward corneal blindness such as LSCD, this work potentially allows for the discovery and development of new assay systems to study eye diseases. In other studies Chen and coworkers have described work that investigated the reprogramming of adipose-derived stem cells (ADSC) into corneal epithelial cells using various factors including small molecules.[279] ADSCs have advantages over use of cells from other lineages in that it is both quicker and easier to obtain significant quantities of these cells from the donor.

1.13.2.6.3 Retinal disease

The inner layer of the eye containing the light-sensitive cells is called the retina, and the structure and function of these cells and tissue is thus essential for effective vision. The degeneration of one or more cell types within the retina is responsible for a number of debilitating conditions, which ultimately results in visual impairment. The various cell types that comprise the retina are derived from multipotent retinal progenitor cells through modulation of a range of signaling pathways including hedgehog and notch, and various biomolecules, including FGF although the details are, at this time, incompletely understood.[280]

Retinal diseases such as AMD (AMD —accumulation of cellular debris between the choroid and the retina), diabetic retinopathy, (DR —degradation of retinal blood vessels), and retinitis pigmentosa (RP —loss of photoreceptors) are prevalent throughout the developed and developing world, AMD for example affects almost 15 million people worldwide.[281] It is often underappreciated

that these diseases do not just affect the more elderly segment of the population but are common across all age groups. This is a group of diseases where significant unmet medical need exists; from both a healthcare and economic perspective the area is lacking in current therapies and is urgently in need of new therapeutic agents and novel approaches.

Current drug treatments for all of the aforementioned diseases are sparse. The mainstay of therapies for AMD are drugs such as Lucentis, Macugen, and Avastin, all of which are anti-VEGF biomolecules. These also enjoy some use in treatment of DR. Currently there are no small molecule drugs that are used to treat the underlying cause of any of these diseases; however, it is not a significant leap to imagine that the multitude of small molecule inhibitors of VEGFr-mediated signaling could be explored in this context. Since current AMD therapeutics are currently delivered by intraocular injection, alternative therapeutic approaches using either orally delivered drugs or drugs delivered topically to the eye such as the aforementioned VEGFr-inhibitors or small molecule stem cell modulators would be an attractive option. A key consideration would of course be the appropriate pharmacokinetic profile of any such agent and its biodistribution in tissues so as to avoid or minimize any undesirable side effects in other tissues.

A number of potential assay systems that have utility in assessing modulation of retinal progenitor cells by small molecules and other agents have been described, and thus could represent a rich resource for drug discovery projects targeting new therapies for ocular disorders.[282]

1.13.2.6.4 Retinal therapies using stem cells

One of the first therapeutic areas to benefit from the discovery and evolution of stem cell therapeutics has been retinal disease, where a number of companies and organizations have initiated clinical trials in recent years.[283,284] This rapid advance is likely due not just to the significant unmet medical need but in no small part to the relatively self-contained nature of the inner eye, and the relative ease with which cell-based therapies can be introduced directly to the disease site by intraocular injection. Furthermore, in the case of cell-based therapeutic agents the immune privilege of the eye might be expected to result in fewer rejection events when using allogenic approaches.

Two therapeutic paradigms are envisaged with current stem cell treatments —regenerative and trophic. Regenerative stem cell-based therapies rely on the introduction of differentiated cell types, such as RPE (retinal pigment epithelial) cells, directly into the eye, the RPE cells having been produced previously from precursor cells such as hESCs or iPSCs. Trophic therapies on the other hand are predicated on the direct introduction of stem cells such as MSCs into the eye, with the expectation that the transplanted SCs rather than differentiating themselves, act to repair the underlying defects through the secretion of trophic factors, which act on resident cell populations through altering the local microenvironment. This latter phenomenon exploiting the paracrine influence of stem cell types in therapy is gaining increasing acceptance.[285]

In the former category, regenerative trials of note include those from advanced cell technology, using hESC-derived RPE cells.[286] The resulting RPE cultures were established as being 99% pure and free of any pathogens. In these studies, patients suffering from advanced vision loss due to either Stargardt's macular dystrophy ($n=1$) or AMD ($n=1$) were treated with subretinal implanations (injections) of between 50,000 and 200,000 RPE cells directly to the diseased area of the eye. The treatment was established as being safe, with no adverse events noted in either arm of the trial after cell transplantation, and also, critically, no rejection or tumorigenic response, the latter of which is a concern that has been associated with pluripotent stem cell-based therapies for some time. Four months after transplantation, improvement in visual acuity was evident in both patients, with assessment of the Stargardt's macular dystrophy patient demonstrating increased levels of pigmentation as assessed by optical coherence tomography. However, it was noted that in the corresponding AMD patient, there was actually no anatomical evidence of engraftment, perhaps due to the fact that the patient had not complied with the immunotherapy regime following transplantation. While the results are encouraging, given the relatively ST nature of the trial, as well as the very small patient numbers, further studies are needed in order to establish in more detail the nature and extent of any derived therapeutic benefit and anatomical consequences of these hESC-derived RPE cell-based therapies for retinal disorders.[287] Appropriate treatment paradigms will also need establishing, particularly the optimal cell numbers and timing of dosing for treatment.

As discussed elsewhere, the use of iPSCs avoids a number of issues associated with hESCs, and accordingly are an attractive alternative. Until recently there had been no reports of clinical studies using iPSCs as treatment for retinal disorders. However, very recently the first human clinical trial of iPSC-derived cells has been announced in Japan.[288] In this small pilot study that has recently been approved and will be conducted by the Kobe Center for Developmental Biology,[289] six patients over the age of 50 years suffering from macular degeneration will be treated with retinal epithelial cell grafts, which are intended to slow the progress of their eye disease.

Direct in vivo modulation of endogenous progenitor and stem cells is the emerging and alternative approach. While there have been relatively few reports to date of small molecule modulation of retinal stem cells, either in vitro or in vivo, with the emphasis being instead primarily focused on cell-based therapies, there is increasing evidence of a shift toward the use of small molecules, with examples now being published of studies using some of the better characterized, more promiscuous stem cell modulator compounds (discussed below). Furthermore, as more detailed investigations are carried out regarding the key signaling pathways involved in directing retinal stem, or progenitor cell fate, the discovery and study of small molecules that modulate these pathways can be expected to follow. For example, disruption of TGFβ signaling in retinal/eye disorders was described in the literature during 2005, although no small molecules were studied in this case.[290] Development of ocular cells of various lineages from the neural crest is reportedly influenced by TGFβ signaling, since disruption of this pathway led to ocular defects and was found to result in downregulation of two TFs known to be important for development of the eye (Pitx2 and Foxc1). Given numerous disclosures in the primary and patent literature since that date of the effect and therapeutic potential of TGFβ inhibitors in other therapeutic

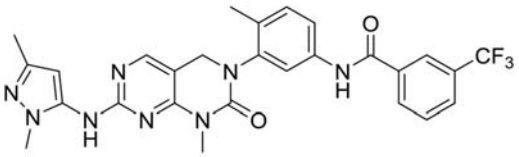

(8)

Fig. 65 Chemical structure of Pluripotin (8).

areas,[291] and also of TGFβ mimetics,[292] it is reasonable to suppose that reports will be forthcoming in the area describing the application of such molecules and whether they recapitulate these findings, or can rescue ocular defects. This also gives confidence that the approach to discovering active small molecules described elsewhere in this article could be applied to the eye.

Details of experiments describing the potential retinal applications of a number of stem cell-modulating compounds from studies on other organs have been published. For example, pluripotin ((8), Fig. 65) has been reported to promoting the production of rabbit limbal epithelial cells in vitro, putatively through a mechanism involving the enhanced proliferation of limbal stem cells.[293] Application of 200 nM of pluripotin enhanced RLEC numbers significantly and also doubled the colony forming efficiency of RLECs (26% vs. 13% in controls). However, concentrations higher than 200 nM were found to show toxicity, raising a concern over a very narrow therapeutic index.

Schultz et al. have recently described the effects of the drug-like small molecule WS3 ((137), Fig. 66) on the proliferation of primary RPE cells ex vivo.[294] Interestingly this compound, and derivatives (eg, WS6, (115)) were originally described by the same workers as being able to stimulate the proliferation of β-cells. RPE cells cultured ex vivo in the absence of compound were found to have significantly reduced doubling rates by the sixth passage. In contrast those cells treated with 25 nM of WS3 were observed to maintain doubling rates even up to passage 15. Analysis of the genomic integrity of the expanded cells showed no genetic alterations, nor were any tumorigenic events observed. These observations were important since the intended clinical application of this methodology is the provision of cells for transplantation therapy, assessment of the safety of the product cells is of critical importance.

The cells were demonstrated to be functionally competent after multiple passages: following removal of WS3 the cells differentiated in vitro to a monolayer with characteristic pigmented and cobblestone-type morphology. These morphological analyses were supported by RT-PCR analyses, which demonstrated the presence of markers characteristic of mature RPE cells, including RPE65, RAX, MITF, and others. Furthermore, implantation of WS3-expanded RPE cells in vivo in using the Royal College of Surgeons (RCS) rat model[295] resulted in retinas with more photoreceptors and lower luminescent thresholds compared with untreated animals, supporting an increase in functional photoreceptor numbers. In accordance with the group's previous target identification studies using WS6 in β-cells, a common target protein, Ebp1, was revealed.[240] In contrast to the studies on β-cells, IKKε was not detected as a target of WS3 in RPE cells.

Retinoic acid ((108), Fig. 67) has been shown to promote photoreceptor differentiation in various vertebrate retinal studies, including zebrafish and human, although the precise mechanism by which it does so has yet to be elucidated.[296]

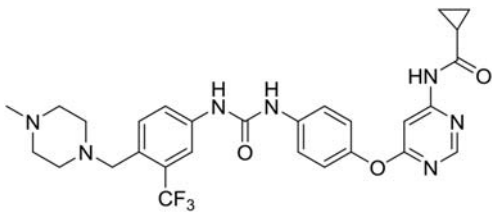

(137)

Fig. 66 Chemical structure of WS3 (137).

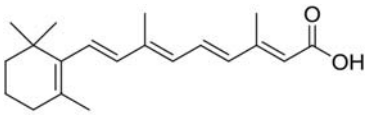

(108)

Fig. 67 Chemical structure of retinoic acid (108).

1.13.2.6.5 Small molecule modulation of hES and iPS cells to retinal cells

Nicotinamide ((128), Fig. 68) has been reported to stimulate the differentiation of human ESCs to RPE cells, via neural precursor cells.[297] Gene expression analysis at various stages of the differentiation protocol was undertaken in an effort to understand in greater detail the underlying mechanisms in the differentiation process. After 4 weeks of treatment with nicotinamide expression, analysis revealed that a number of genes were upregulated relating to differentiation to neural and retinal lineages as well as those relating to hematopoesis and melanogenesis. After 8 weeks of nicotinamide treatment, 70% of cell clusters were found to exhibit pigmented areas and 5% of cells being both pigmented and expressing a marker, MiTF, characteristic of RPE cells. The authors went on to show that these hESC-derived RPE cells were viable and led to functional and structural rescue of the retina 6 weeks after implantation in vivo in the RCS rate model.

The use of a combination of casein kinase inhibitor CKI-7 ((138), Fig. 69), TGFβ inhibitor SB-431542 (12), and Rho kinase inhibitor Y-27632 (81) has been reported to produce retinal precursor cells from hESCs.[298] The authors demonstrated that the resulting hES-derived retinal progenitor cells were capable of differentiating into RPE and photoreceptor cells by induction with retinoic acid and taurine. Finally, it was demonstrated that the same set of protocols was also applicable to human iPSCs, and their differentiation into retinal cells in vitro was illustrated. Other methods have also been reported describing the differentiation of RPE cells from murine or human iPSCs, for instance using delivery of TFs such as Oct4, Sox2, Nanog, and Lin28.[299,300]

The reprogramming of human primary neonatal epidermal keratinocytes to hiPSCs and their subsequent differentiation into RPE cells has recently been described using a cocktail of small molecules and growth factors (Fig. 70). This method used the dual TF "2F" conditions, consisting of either OCT4/KLF4 and CHIR99021 (5)/tranylcypromine (7) or OCT4/KLF4 and CHIR99021 (5)/SB-431542 (12)/tranylcypromine (7)/PD0325901 (13). The single TF "1F" protocol was also applied, which consisted of OCT4 along with sodium butyrate (124)/PS48 (139)/A83-01 (49)/PD0325901 (13).[301] The authors went on to show that the resulting cells expressed the markers bestrophin, CRALBP, and RPE65, consistent with terminal RPE cells. Comparison of the 1F- and 2F-derived RPE cells with human fetal RPE cells through metabolomic and proteomic analyses showed a high degree of similarity. Remarkably, bolus intraocular injection of 1F-derived RPE cells in vivo in the RCS rat model showed that the cells appeared to implant as a correctly polarized and extended monolayer. Preliminary studies of electrical responses of the engrafted retinas to light stimulation suggested that they were also functionally competent. This therapeutic strategy does therefore appear to significant promise for the treatment of retinal diseases.

The field of regenerative medicine as applied to ocular indications continues to move at a fast pace. During 2015 there have been a number of other important disclosures describing methods to differentiate stem cells to RPE cells. A nonsmall molecule approach using new chemically defined media conditions to convert human PSCs to retinal progenitor cells has been described by Zhou and coworkers. A detailed step-by-step analysis of the differentiation process was provided, which elegantly demonstrated how this in vitro approach recapitulates human embryogenesis, and ultrastructures were detected in the hPSC-derived RPE and neural retina that have not been reported in previous conditions.[302] The method appears promising; however, the authors have not yet reported any study on the transplantation of these cells in vivo and so the both the feasibility and safety questions remain to be resolved before any translation to the clinic could be envisaged. Other recent work outlining the use of additional small molecules that promote RPE differentiation has been published. For example, Maruotti et al. have described a high-throughput, quantitative PCR-based screening approach using the "StemSelect" compound library to identify compounds that promote RPE differentiation from human PSCs.[303] Critically, the hit molecules identified in this first assay were tested using an orthogonal assay, using hiPSCs engineered to express GFP under the regulation of an RPE-specific tyrosinase enhancer to confirm activity. Chetomin ((140), Fig. 71) was found to significantly increase the amount of RPE differentiation in a number of human PSC lines, an effect which

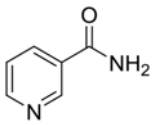

(128)

Fig. 68 Chemical structure of nicotinamide (128).

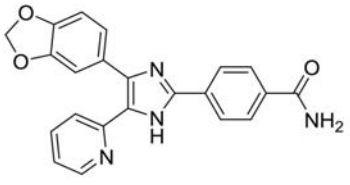

SB431542(SB) (12)

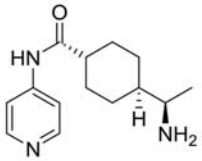

Y-27632 (81)

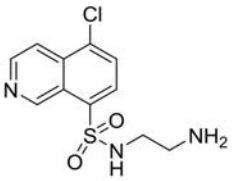

CKI-7 (138)

Fig. 69 Compounds reported to produce retinal precursor cells from hESCs.

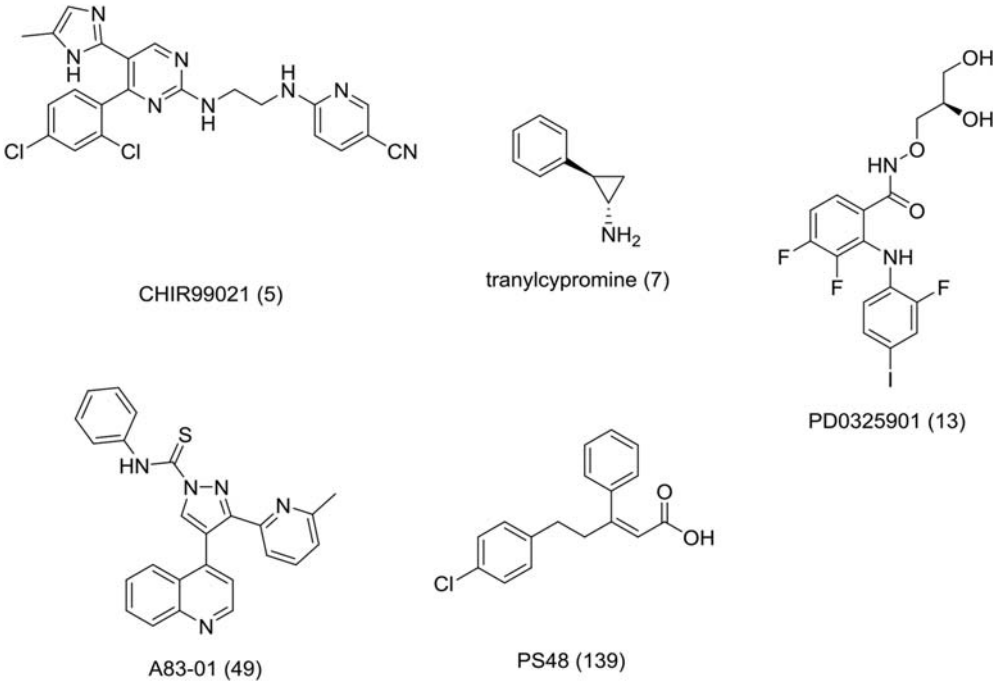

Fig. 70 Compounds reported to reprogram human primary neonatal epidermal keratinocytes to retinal pigment epithelial cells.

was potentiated by nicotinamide. Further studies were consistent with chetomin acting via a previous ascribed mechanism of inhibition of p300-mediated transcriptional activity, but other, as yet undefined pathways were also implicated.

In other work, Westenskow et al. have published a simplified protocol for directed differentiation of retinal pigment epithelium cells using PSCs.[304] The use of nicotinamide along with Activin A, or the small molecule IDE-1 ((141), Fig. 72) was found to significantly enhance the yield of RPE cells.

An important recent study was published by Parvani et al.[305] In this work, using a stepwise process, treatment of hESCs with a combination of small molecules resulted in increased expression levels of eye-field-specific genes, and intriguingly, also resulted in a subset of cells acquiring the features of advancing retinal differentiation, albeit transiently. Three previously described small molecules stem cell modulators dorsomorphin ((43), Fig. 73), the Wnt modulator XAV939 (52), and ALK inhibitor A83-01 (49) were used in the multistep differentiation process.

1.13.2.6.6 New assays and assay technologies

The effectiveness of a medicinal program is critically dependent not only on the chemical matter synthesized by project scientists but also on the testing methodologies employed. An effective and disease relevant assay system is a prerequisite for all drug discovery projects, and the application of stem cells to ocular disease is no exception.

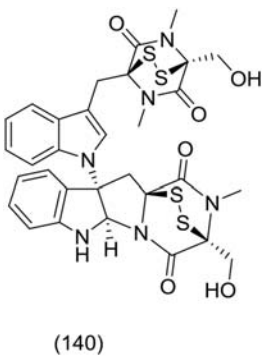

Fig. 71 Chemical structure of chetomin (140).

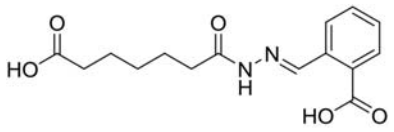

(141)

Fig. 72 Chemical structure of IDE 1 (141).

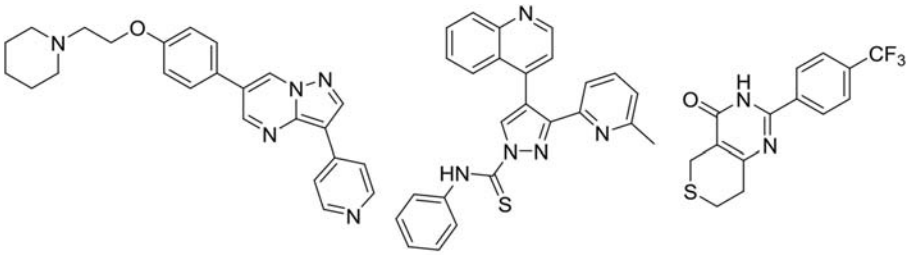

dorsomorphin (DM) (43) A83-01 (49) XAV939 (52)

Fig. 73 Compounds affecting the formation of eye-field specific genes from hESCs.

To this end, a number of interesting new assays systems have been described in recent years, and can reasonably be expected to have a significant impact on both the pace and predictability of compound progression toward proof-of-principle experiments for small molecule stem cell modulators for retinal, corneal, and other eye diseases.

Fuller et al. have described an elegant high-throughput assay that monitors for photoreceptor number and survival using primary murine retinal cells.[306] This assay may prove useful in both the identification of compounds with clinical utility for retinal disease, and for probing the underlying mechanisms of differentiation and survival. In related studies, Ferrer et al. have published work outlining a miniaturized 96 or 384 microtiter plate assay for application in screening small molecules, which influence retinal pigment epithelium pathology and physiology in vitro, and thereby potentially have therapeutic benefit.[307]

Improving the reliability, throughput, and physiological relevance of assay systems is also a critical consideration in all aspects of drug discovery. To this end, Lane et al. have evaluated the primary variable in the hESC-RPE differentiation process.[308] The authors document and quantify how factors such as cell density, passage number, and cell line used affect RPE yield. Finally, Jasty et al. have described a new 3D culture system that can in theory be used for modeling small molecule-based approaches to modulating retinal stem cell function.[309]

1.13.3 Conclusion

The purpose of this article has been to draw the attention of medicinal chemists to the challenges and benefits of discovering small molecules able to selectively stimulate stem cells, stemlike, and progenitor cells to produce new tissue to correct diseased and damaged organs in a number of serious disease states. Studies described herein show that progress is being made in this field although significant challenges remain. However, these challenges are familiar to medicinal chemists even if they differ significantly from the usual enzyme modulation/receptor interaction drug paradigm. The search for "hit" molecules in areas where mechanistic pathways are less than fully established will be aided by the use of more efficient phenotypic screening techniques described elsewhere in this series. Of course, as more active small molecules emerge and as more information is gained on the precise signaling mechanisms used by these cells, then the opportunities to use established structure-based drug design techniques will grow.

The discovery of a "hit" compound is of course only the first stage of the development of a clinical candidate and further optimization and downstream development will require the successful resolution and tuning of all the compounds properties such as ADMET, off-target idiosyncratic activity, in vivo animal model activity, synthetic route development, stability, formulation, etc., familiar to all practicing medicinal chemists.

Where this new paradigm diverges from existing approaches can be illustrated by consideration of the systems under study. It is obvious that a high degree of selectivity will be needed so that only stem cells in target organs are stimulated and that the degree of stimulation is controlled so that undesired side effects in other tissues and other outcomes, such as oncogenesis, fibrosis, or even depletion of the endogenous stem cell pool are avoided. However, as achieving selectivity and the appropriate levels of potency have long been the criteria to which medicinal chemists operate, it is reasonable to expect that these challenges will not be insurmountable. Advances in iPSC technology and our understanding of the stem cell niche will surely lead to the introduction of more robust and reliable in vitro screening tools that better recapitulate the in vivo situation, which should facilitate the achievement of these goals.

It will be a major challenge to discover small molecules with all the desired activities and none of the undesired ones but the rewards in terms of patient care will be considerable. Many of the long-term illnesses that cause so much suffering to patients such as diabetes, neuronal degeneration, and cardiac failure and so much damage to the economics of healthcare systems throughout the world could be addressed by this approach. It is to be hoped that medicinal chemists will rise to this challenge.

References

1. Davies, S. G.; Kennewell, P. D.; Russell, A. J.; Seden, P. T.; Westwood, R.; Wynne, G. M. Stemistry: The Control of Stem Cells in Situ Using Chemistry. *J. Med. Chem.* **2015,** *58* (7), 2863–2894.
2. Dimmeler, S.; Ding, S.; Rando, T. A.; Trounson, A. Translational Strategies and Challenges in Regenerative Medicine. *Nat. Med.* **2014,** *20* (8), 814–821.
3. Lu, B.; Atala, A. Small Molecules and Small Molecule Drugs in Regenerative Medicine. *Drug Discov. Today* **2014,** *19* (6), 801–808.
4. Takahashi, K.; Yamanaka, S. Induction of Pluripotent Stem Cells From Mouse Embryonic and Adult Fibroblast Cultures by Defined Factors. *Cell* **2006,** *126,* 663–676.
5. Hou, P.; Li, Y.; Zhang, X.; Liu, C.; Guan, J.; Li, H.; Zhao, T.; Ye, J.; Yang, W.; Liu, K.; Ge, J.; Xu, J.; Zhang, Q.; Deng, H. Pluripotent Stem Cells Induced From Mouse Somatic Cells by Small-Molecule Compounds. *Science* **2013,** *341,* 651–654.
6. Hoffman, T.; Metternich, R. The Future of Medicinal Chemistry. *Angew. Chem. Int. Ed.* **2012,** *51,* 8760–8761.
7. Poss, K. D. Advances in Understanding Tissue Regenerative Capacity and Mechanisms in Animals. *Nat. Rev. Genet.* **2010,** *11,* 710–722.
8. Chen, S.; Do, J. T.; Zhang, Q.; Yao, S.; Yan, F.; Peters, E. C.; Scholer, H. R.; Schultz, P. G.; Ding, S. Self-Renewal of Embryonic Stem Cells by a Small Molecule. *Proc. Natl. Acad. Sci. U. S. A.* **2006,** *103,* 17266–17271.
9. Xu, Y.; Zhu, X.; Hahm, H. S.; Wei, W.; Hao, E.; Hayek, A.; Ding, S. Revealing a Core Signalling Regulatory Mechanism for Pluripotent Stem Cell Survival and Self-Renewal by Small Molecules. *Proc. Natl. Acad. Sci. U. S. A.* **2010,** *107,* 8129–8134.
10. Wu, X.; Ding, S.; Ding, Q.; Gray, N. S.; Schultz, P. G. Small Molecules that Induce Cardiomyogenesis in Embryonic Stem Cells. *J. Am. Chem. Soc.* **2004,** *126* (6), 1590–1591.
11. Efe, J. A.; Ding, S. The Evolving Biology of Small Molecules: Controlling Cell Fate and Identity. *Philos. Trans. R. Soc. Lond. B Biol. Sci.* **2011,** *366,* 2208–2221.
12. Li, W.; Jiang, K.; Ding, S. Concise Review: A Chemical Approach to Control Cell Fate and Function. *Stem Cells* **2012,** *30,* 61–68.
13. Zhu, S.; Wei, W.; Ding, S. Chemical Strategies for Stem Cell Biology and Regenerative Medicine. *Annu. Rev. Biomed. Eng.* **2011,** *13,* 73–90.
14. Chen, S.; Zhang, Q.; Wu, X.; Schultz, P. G.; Ding, S. Dedifferentiation of Lineage-Committed Cells by a Small Molecule. *J. Am. Chem. Soc.* **2004,** *126* (2), 410–411.
15. Anwar, M. A.; Kim, S.; Choi, S. The Triumph of Chemically Enhanced Cellular Reprogramming: A Patent Review. *Expert Opin. Ther. Pat.* **2016,** *26* (2), 265–280.
16. Sanjuan-Pla, A.; Macaulay, I. C.; Jensen, C. T.; Woll, P. S.; Luis, T. C.; Mead, A.; Moore, S.; Carella, C.; Matsuoka, S.; Jones, T. B.; Chowdhury, O.; Stenson, L.; Lutteropp, M.; Green, J. C.; Facchini, R.; Boukarabila, H.; Grover, A.; Gambardella, A.; Thongjuea, S.; Carrelha, J.; Tarrant, P.; Atkinson, D.; Clark, S. A.; Nerlov, C.; Jacobsen, S. E. Platelet-Biased Stem Cells Reside at the Apex of the Haematopoietic Stem-Cell Hierarchy. *Nature* **2013,** *502,* 232–236.
17. Morrison, S. J.; Weissman, I. L. The Long-Term Repopulating Subset of Hematopoietic Stem Cells Is Deterministic and Isolable by Phenotype. *Immunity* **1994,** *1* (8), 661–673.
18. Shultz, L. D.; Lyons, B. L.; Burzenski, L. M.; Gott, B.; Chen, X. H.; Chaleff, S.; Kotb, M.; Gillies, S. D.; King, M.; Mangada, J.; Greiner, D. L.; Handgretinger, R. Human Lymphoid and Myeloid Cell Development in NOD/LtSz-Scid IL2R Gamma(Null) Mice Engrafted With Mobilised Human Haemopoietic Stem Cells. *J. Immunol.* **2005,** *174* (10), 6477–6489.
19. Doulatov, S.; Notta, F.; Laurenti, E.; Dick, J. E. Haematopoiesis: A Human Perspective. *Cell Stem Cell* **2012,** *10* (2), 120–136.
20. Kaushansky, K. Mechanisms of Disease: Lineage-Specific Haematopoietic Growth Factors. *N. Engl. J. Med.* **2006,** *354* (19), 2034–2045.
21. Hitchcock, I. S.; Kaushansky, K. Thrombopoietin From Beginning to End. *Br. J. Haematol.* **2014,** *165* (2), 259–268.
22. Gao, Y.; Yang, P.; Shen, H.; Yu, H.; Song, X.; Zhang, L.; Zhang, P.; Cheng, H.; Xie, Z.; Hao, S.; Donmg, F.; Ma, S.; Ji, Q.; Bartlow, P.; Ding, Y.; Wang, L.; Liu, H.; Cheng, H.; Miao, W.; Yuan, W.; Yuan, Y.; Cheng, T.; Xie, X.-Q. Small Molecule Inhibitors Targeting INK4 Protein p18INK4C Enhance ex vivo Expansion of Haematopoietic Stem Cells. *Nat. Commun.* **2015,** *6,* 6328.
23. Sun, J.; Ramos, A.; Chapman, B.; Johnnidis, J. B.; Le, L.; Ho, Y.-J.; Klein, A.; Hofmann, O.; Camargo, F. D. Clonal Dynamics of Native Haematopoiesis. *Nature* **2014,** *514,* 322–327.
24. Busch, K.; Klapproth, K.; Barile, M.; Flossdorf, M.; Holland-Letz, T.; Schlenner, S. M.; Hofer, M. T.; Rodewald, H.-R. Fundamental Properties of Unperturbed Haematopoiesis From Stem Cells *In Vivo*. *Nature* **2015,** *518,* 524–526.
25. Flach, J.; Bakker, S. T.; Mohrin, M.; Conroy, P. C.; Pietras, E. M.; Reynauld, D.; Alvarez, S.; Diolati, M. E.; Ugarte, F.; Forsberg, E. C.; Le Beau, M. M.; Stohr, B. A.; Mendez, J.; Morrison, C. G.; Passegue, E. Replication Stress Is a Potent Driver of Functional Decline in Ageing Haematopoietic Stem Cells. *Nature* **2014,** *512,* 198–202.
26. Nakada, D.; Oguro, H.; Levi, B. P.; Ryan, N.; Kitano, A.; Saltoh, Y.; Takeichi, M.; Wendt, G. R.; Morrison, S. J. Oestrogen Increases Haematopoietic Stem-Cell Self-Renewal in Females and During Pregnancy. *Nature* **2014,** *505,* 555–558.
27. Keating, A. Mesenchymal Stromal Cells. *Curr. Opin. Hematol.* **2006,** *13* (6), 419–425.
28. Nombela-Arrieta, C.; Ritz, J.; Silberstein, L. E. The Elusive Nature and Function of Mesenchymal Stem Cells. *Nat. Rev. Mol. Cell Biol.* **2011,** *12* (2), 126–131.
29. Bara, J. J.; Richards, R. G.; Alini, M.; Stoddart, M. J. Concise Review: Bone Marrow-Derived Mesenchymal Stem Cells Change Phenotype Following *In Vitro* Culture: Implications for Basic Research and the Clinic. *Stem Cells* **2014,** *32* (7), 1713–1723.
30. Schofield, R. Relationship Between Spleen-Colony Forming Cell and Hematopoietic Stem-Cell-Hypothesis. *Blood Cells* **1978,** *4* (1-2), 7–25.
31. Lo Celso, C.; Scadden, D. T. The Haematopoietic Stem Cell Niche at a Glance. *J. Cell Sci.* **2011,** *124* (21), 3529–3535.
32. Wang, H.; Zhang, P.; Liu, L.; Zuo, L. Hierarchical Organisation and Regulation of the Hematopoietic Stem Cell Osteoblastic Niche. *Crit. Rev. Oncol. Hematol.* **2013,** *85* (1), 1–8.
33. Acar, M.; Kocherlakota, K. S.; Murphy, M. M.; Peyer, J. G.; Oguro, H.; Inra, C. N.; Jalyeola, C.; Zhao, Z.; Luby-Phelps, K.; Morrison, S. J. Deep Imaging of Bone Marrow Shows Non-Dividing Stem Cells Are Mainly Perisinusoidal. *Nature* **2015,** *526,* 126–130.
34. Morrison, S. J.; Scadden, D. T. The Bone Marrow Niche for Haematopoietic Stem Cells. *Nature* **2014,** *505,* 327–334.
35. Mendez-Ferrer, S.; Scadden, D. T.; Sanchez-Aguilera, A. Bone Marrow Stem Cells: Current and Emerging Concepts. *Ann. N. Y. Acad. Sci.* **2015,** *1335,* 32–44.
36. Klamer, S.; Voemans, C. The Role of Novel and Known Extracellular Matrix and Adhesion Molecules in the Homeostatic and Regenerative Bone Marrow Microenvironment. *Cell Adhes. Migr.* **2014,** *8* (6), 563–577.
37. Takubo, K.; Goda, N.; Yamada, W.; Iriuchishima, H.; Ikeda, E.; Kubota, Y.; Shima, H.; Johnson, R. S.; Hirao, A.; Suematsu, M.; Suda, T. Regulation of the HIF1 Alpha Level Is Essential for Haematopoietic Stem Cells. *Cell Stem Cell* **2010,** *7* (3), 391–402.
38. Choi, J. S.; Harley, B. A. C. The Combined Influence of Substrate Elasticity and Ligand Density on the Viability and Biophysical Properties of Haematopoietic Stem and Progenitor Cells. *Biomaterials* **2012,** *33* (18), 4460–4468.
39. Al-Drees, M. A.; Yeo, J. H.; Boumelhem, B. B.; Antas, V. I.; Brigden, K. W.; Colonne, C. K.; Fraser, S. T. Making Blood: The Haematopoietic Niche Throughout Ontogeny. *Stem Cells Int.* **2015,** *2015,* 571893.
40. Long, F. Building Strong Bones: Molecular Regulation of the Osteoblast Lineage. *Nat. Rev. Mol. Cell Biol.* **2012,** *13* (1), 27–38.
41. Shi, C. Recent Progress Toward Understanding the Physiological Function of Bone Marrow Mesenchymal Stem Cells. *Immunology* **2012,** *136* (2), 133–138.

42. Bruno, B.; Rotta, M.; Patriaca, F.; Mordini, N.; Allione, B.; Carnevale-Schianca, F.; Giaccone, L.; Sorasio, R.; Omede, P.; Baldi, I.; Bringhen, S.; Massaia, M.; Aglietta, M.; Levis, A.; Gallamini, A.; Fanin, R.; Palumbo, A.; Storb, R.; Ciccone, G.; Boccadoro, M. A Comparison of Allografting With Autografting for Newly Diagnosed Myeloma. *N. Engl. J. Med.* **2007,** *356* (11), 1110–1120.
43. Matsunaga, T.; Sakamaki, S.; Kohgo, Y.; Ohi, S.; Hirayama, Y.; Niitsu, Y. Recombinant Human Granulocyte Colony-Stimulating Factor Can Mobilize Sufficient Amounts of Peripheral-Blood Stem-Cells in Healthy Volunteers for Allogenic Transplantation. *Bone Marrow Transplant.* **1993,** *11* (2), 103–108.
44. Flomenberg, N.; Devine, S. M.; DiPersio, J. F.; Liesveld, J. L.; McCarty, J. M.; Rowley, S. D.; Vesole, D. H.; Badel, K.; Calandra, G. The Use of AMD3100 Plus G-CSF for Autologous Haematopoietic Progenitor Cell Mobilization Is Superior to G-CSF Alone. *Blood* **2005,** *106* (5), 1867–1874.
45. Brave, M.; Farrell, A.; Lin, S. C.; Ocheltree, T.; Miksinski, S. P.; Lee, S.-L.; Saber, H.; Fourie, J.; Tornoe, C.; Booth, B.; Yuan, W.; He, K.; Justice, R.; Pazdur, R. FDA Review Summary: Mozobil in Combination With Granulocyte Colony-Stimulating Factor to Mobilize Haematopoietic Stem Cells to the Peripheral Blood for Collection and Subsequent Autologous Transplantation. *Oncology* **2010,** *78* (3-4), 282–288.
46. Nishino, T.; Osawa, M.; Iwama, A. New Approaches to Expand Hematopoietic Stem and Progenitor Cells. *Expert Opin. Biol. Ther.* **2012,** *12* (6), 743–756.
47. Le Blanc, K.; Mougiakakos, D. Multipotent Mesenchymal Stromal Cells and the Innate Immune System. *Nat. Rev. Immunol.* **2012,** *12* (5), 383-U17.
48. Dolnikov, A.; Xu, N.; Shen, S.; Song, E.; Holmes, T.; Klamer, G.; O'Brien, T. A. GSK-3beta Inhibition Promotes Early Engraftment of Ex-Vivo-Expandes Haematopoietic Stem Cells. *Cell Prolif.* **2014,** *47* (2), 113–123.
49. North, T. E.; Goessling, W.; Walkley, C. R.; Lengerke, C.; Kopane, K. R.; Lord, A. M.; Weber, G. J.; Bowman, T. V.; Jang, I.-H.; Grosser, T.; Fitzgerald, G. A.; Daley, G. Q.; Orkin, S. H.; Zon, L. I. Prostaglandin E2 Regulates Vertebrate Haematopoietic Stem Cell Homeostasis. *Nature* **2007,** *447,* 1007–1011.
50. Hoggatt, J.; Singh, P.; Sampath, J.; Pelus, L. M. Prostaglandin E-2 Enhances Haematopoietic Stem Cell Homing, Survival and Proliferation. *Blood* **2009,** *113* (22), 5444–5455.
51. Boitano, A. E.; Wang, J.; Romeo, R.; Bouchez, L. C.; Parker, A. E.; Sutton, S. E.; Walker, J. R.; Flaveny, C. A.; Perdew, G. H.; Denison, M. S.; Schultz, P. G.; Cooke, M. P. Aryl Hydrocarbon Receptor Antagonists Promote the Expansion of Human Haematopoietic Stem Cells. *Science* **2010,** *329* (5997), 1345–1348.
52. Bouchez, L. C.; Boitano, L. C.; de Lichtervelde, L.; Romero, R.; Cooke, M. P.; Schultz, P. G. Small-Molecule Regulators of Human Stem Cell Self-Renewal. *Chembiochem* **2011,** *16* (6), 854–857.
53. Leonova, K. I.; Shneyder, J.; Antoch, M. P.; Toshkov, I. A.; Novototskaya, L. R.; Komarov, P. G.; Komorova, E. A.; Gudkov, A. V. A Small Molecule Inhibitor of p53 Stimulates Amplification of Haematopoietic Stem Cells but Does Not Promote Tumour Development in Mice. *Cell Cycle* **2010,** *9* (7), 1434–1443.
54. Liu, Y.; Elf, S. E.; Miyata, Y.; Sashida, G.; Liu, Y.; Huang, G.; Di Giandomenico, S.; Lee, J. M.; Deblasio, A.; Menendez, S.; Antipin, J.; Reva, B.; Koff, A.; Nimer, S. D. p53 Regulates Haematopoietic Stem Cell Quiescence. *Cell Stem Cell* **2009,** *4* (1), 37–48.
55. Boitano, A. E.; de Lichtervelde, L.; Snead, J. L.; Cooke, M. P.; Schultz, P. G. An Image-Based Screen Identifies a Small Molecule Regulator of Megakaryopoiesis. *Proc. Natl. Acad. Sci. U. S. A.* **2012,** *109* (35), 14019–14023.
56. de Lichtervelde, L.; Antal, C. E.; Boitano, A. E.; Wang, Y.; Krastel, P.; Peterson, F.; Newton, A. C.; Cooke, M. P.; Schultz, P. G. Euphohelioscopin A Is a PKC Activator Capable of Inducing Macrophage Differentiation. *Chem. Biol.* **2012,** *19* (8), 994–1000.
57. Kuter, D. J. Milestones in Understanding Platelet Production: A Historical Overview. *Br. J. Haematol.* **2014,** *165,* 248–258.
58. Frampton, J. E.; Lyseng-Williamson, K. A. Romiplostim. *Drugs* **2009,** *69* (3), 307–317.
59. Duffy, K. J.; Darcy, M. G.; Delorme, E.; Dillon, S. B.; Eppley, D. F.; Erickson-Miller, C.; Giampa, L.; Hopson, C. B.; Huang, Y.; Keenan, R. M.; Lamb, P.; Leong, L.; Liu, N.; Miller, S. G.; Price, A. T.; Rosen, J.; Shah, R.; Shaw, T. N.; Smith, H.; Stark, K. C.; Tian, S. S.; Tyree, C.; Wiggall, K. J.; Zhang, L.; Luengo, J. I. Hydrazinonaphthalene and Azonaphthalene Thrombopoietin Mimics Are Nonpeptidyl Promoters of Megakaryocytopoiesis. *J. Med. Chem.* **2001,** *44* (22), 3730–3745.
60. Kuter, D. J. New Thrombopoietic Growth Factors. *Blood* **2007,** *109* (11), 4607–4616.
61. Erickson-Miller, C. L.; Delorme, E.; Tian, S.-S.; Hopson, C. B.; Landis, A. J.; Valoret, E. I.; Sellers, T. S.; Rosen, J.; Miller, S. G.; Luengo, J. I.; Duffy, K. J.; Jenkins, J. M. Preclinical Activity of Eltrombopag (SB-497115), an Oral Nonpeptide Thrombopoietin Receptor Agonist. *Stem Cells* **2009,** *27,* 424–430.
62. Kuter, D. J. What Is the Potential for Thrombopoietic Agents in Acute Leukemia? *Best Pract. Res. Clin. Haematol.* **2011,** *24,* 553–558.
63. Burness, C. B. Eltrombopag: A Review of Its Use in the Treatment of Thrombocytopenia in Patients With Chronic Hepatitis C. *Drugs* **2014,** *74* (16), 1961–1971.
64. Desmond, R.; Ankur, R.; Townsley, D. M.; Dumitriu, B.; Olines, M. J.; Scheinberg, P.; Bevans, M.; Parikh, A. R.; Broder, K.; Calvo, K. R.; Wu, C. O.; Young, N. S.; Dunbar, C. E. Eltrombopag Restores Trilineage Haematopoiesis in Refracting Severe Aplastic Anaemia that Can be Sustained on Discontinuation of Drug. *Blood* **2014,** *123* (12), 1818–1825.
65. Marsh, J. C. W.; Mufti, C. J. Eltrombopag: A Stem Cell Cookie? *Blood* **2014,** *123* (12), 1774–1775.
66. Abe, M.; Suzuki, K.; Sakata, C.; Sugasawa, K.; Hirayama, F.; Koga, Y.; Kawasaki, T.; Naganuma, S.; Itoh, H. Pharmacological Profile of AS1670542, a Novel Orally-Active Human Thrombopoietin Receptor Agonist. *Eur. J. Pharmacol.* **2011,** *650* (1), 58–63.
67. Stasi, R. Avatrombopag Maleate: Thrombopoietin Receptor Agonist Treatment of Thrombocytopenia. *Drugs Future* **2012,** *37* (5), 309–314.
68. Terrault, N. A.; Hassanein, T.; Howell, C. D.; Joshi, S.; Lake, J.; Sher, L.; Vargas, H.; McIntosh, J.; Tang, S.; Jenkins, T. M. Phase II Studies of Avatrombopag in Thrombocytopenic Patients With Cirrhosis Undergoing an Elective Procedure. *J. Hepatol.* **2014,** *61* (6), 1253–1259.
69. Jeon, O. H.; Elisseeff, J. Orthopedic Tissue Regeneration: Cells, Scaffolds and Small Molecules. *Drug Deliv. Transl. Res.* **2016,** *6* (2), 105–120.
70. Mazaki, T.; Kitajima, T.; Shiozaki, Y.; Sato, M.; Mino, M.; Yoshida, A.; Nakamura, M.; Yoshida, Y.; Tanaka, M.; Ozaki, T.; Matsukawa, A.; Ito, Y. In Vitro and in vivo Enhanced Osteogenesis by Kaemferol Found by a High-Throughput Assay Using Human Mesenchymal Stromal Cells. *J. Funct. Foods* **2014,** *6,* 241–247.
71. Antebi, B.; Pelled, G.; Gazit, D. Stem Cell Therapy for Osteoporosis. *Curr. Osteoporosis Res.* **2014,** *12,* 41–47.
72. Chen, S.; Ryan, D. A.; Dwyer, M. A.; Cashman, J. R. Synergistic Effect of Wnt Modulatory Small Molecules and an Osteoinductive Ceramic on C2C12 Cell Osteogenic Differentiation. *Bone* **2014,** *67,* 109–121.
73. Vina, J.-A.; El-Alami, M.; Gambini, J.; Borras, C.; Vina, J.; Penarrocha, M.-A. Application of Mesenchymal Stem Cells in Bone Regenerative Procedures in Oral Implantology. A Literature Review. *J. Clin. Exp. Dent.* **2014,** *6* (1), e60–e65.
74. Liu, Y.; Buckley, C. T.; Almeida, H. V.; Mulhall, K. J.; Kelly, D. J. Infrapatellar Fat Pad-Derived Stem Cells Maintain Their Chondrogenic Capacity in Disease and Can Be Used to Engineer Cartilaginous Grafts of Clinically Relevant Dimensions. *Tissue Eng. Part A* **2014,** *20* (21–22), 3050–3062.
75. Longo, U. G.; Petrillo, S.; Franceschetti, E.; Berton, A.; Maffulli, N.; Denaro, V. Stem Cells and Gene Therapy for Cartilage Repair. *Stem Cells Int.* **2012,** *2012,* 9. http://dx.doi.org/10.1155/2012/168385. Article ID 168385.
76. Kanke, K.; Masaka, H.; Saito, T.; Komiyama, Y.; Hojo, H.; Nakauchi, H.; Lichter, A. C.; Takato, T.; Chung, U.; Ohba, S. Stepwise Differentiation of Pluripotent Stem Cells Into Osteoblasts Using Four Small Molecules Under Serum-Free and Feeder-Free Conditions. *Stem Cell Rep.* **2014,** *2* (6), 751–760.
77. Laurencin, C. T.; Ashe, K. M.; Henry, N.; Kan, H. M.; Lo, K. W.-H. Delivery of Small Molecules for Bone Regenerative Engineering: Preclinical Studies and Potential Applications. *Drug Discov. Today* **2014,** *19* (6), 794–800.
78. Prall, W. C.; Haasters, F.; Heggebo, J.; Polzer, H.; Schwarz, C.; Gassner, C.; Grote, S.; Anz, D.; Jager, M.; Mutschler, W.; Schieker, M. Mesenchymal Stem Cells From Osteoarthritic Patients Feature Impaired Signal Transduction but Sustained Osteoinduction in Response to BMP-2 Stimulation. *Biochem. Biophys. Res. Commun.* **2013,** *440,* 617–622.
79. Baek, S. H.; Choi, S. W.; Park, S. J.; Lee, S. H.; Chun, H. S.; Kim, S. H. Quinoline Compound KM11073 Enhances BMP-2-Dependent Osteogenic Differentiation of C2C12 Cells via Activation of p38 Signaling and Exhibits in vivo Bone Forming Activity. *PLoS One* **2015,** *10* (3), e0120150.
80. Fan, J.; I'm, C. S.; Cui, Z.-K.; Guo, M.; Bezouglaia, O.; Fartash, A.; Lee, J.-Y.; Nguyen, J.; Wu, B. M.; Aghaloo, T.; Lee, M. Delivery of Phenamil Enhances BMP-2-Induced Osteogenic Differentiation of Adipose-Derived Stem Cells and Bone Formation in Calvarial Defects. *Tissue Eng. Part A* **2015,** *21* (13–14), 2053–2065.

81. van Osch, G. J. V. M. Osteoarathritis Year in Review 2014: Highlighting Innovations in Basic Research and Clinical Applications in Regenerative Medicine. *Osteoarthritis Cartilage* **2014,** *22,* 2013–2016.
82. Harvey, P. A.; Leinward, L. A. Cellular Mechanisms of Cardiomyopathy. *J. Cell Biol.* **2011,** *194,* 355–365.
83. Camelliti, P.; Borg, T. K.; Kohl, P. Structural and Functional Characterisation of Cardiac Fibroblasts. *Cardiovasc. Res.* **2005,** *65,* 40–51.
84. Willems, E.; Bushway, P. J.; Mercola, M. Natural and Synthetic Regulators of Embryonic Stem Cell Cardiogenesis. *Pediatr. Cardiol.* **2009,** *30* (5), 635–642.
85. Takahashi, T.; Lord, B.; Schulze, P. C.; Fryer, R. M.; Sarang, S. S.; Gullans, S. R.; Lee, R. T. Ascorbic Acid Enhances Differentiation of Embryonic Stem Cells Into Cardiac Myocytes. *Circulation* **2003,** *107* (14), 1912–1916.
86. Talkhabi, M.; Pahlavan, S.; Aghdami, N.; Baharvand, H. Ascorbic Acid Promotes the Direct Conversion of Mouse Fibroblasts Into Beating Cardiomyocytes. *Biochem. Biophys. Res. Commun.* **2015,** *463* (4), 699–705.
87. Ivanyuk, D.; Budash, G.; Zheng, Y.; Gaspar, J. A.; Chaudhari, U.; Fatima, A.; Bahmanpour, S.; Grin, V. K.; Popandopulo, A. G.; Sachinidis, A.; Hescheler, J.; Šarić, T. Ascorbic Acid-Induced Cardiac Differentiation of Murine Pluripotent Stem Cells: Transcriptional Profiling and Effect of a Small Molecule Synergist of Wnt/β-Catenin Signaling Pathway. *Cell. Physiol. Biochem.* **2015,** *36* (2), 810–830.
88. Okolotowicz, K. J.; Bushway, P.; Lanier, M.; Gilley, C.; Mercola, M.; Cashman, J. R. 1,5-Disubstituted Benzimidazoles That Direct Cardiomyocyte Differentiation From Mouse Embryonic Stem Cells. *Bioorg. Med. Chem.* **2015,** *23* (17), 5282–5292.
89. Ifkovits, J. L.; Addis, R. C.; Epstein, J. A.; Gearhart, J. D. Inhibition of TGFβ Signaling Increases Direct Conversion of Fibroblasts to Induced Cardiomyocytes. *PLoS One* **2014,** *9* (2), e89678.
90. Sawyer, J. S.; Anderson, B. D.; Beight, D. W.; Campbell, R. M.; Jones, M. L.; Herron, D. K.; Lampe, J. W.; McCowan, J. R.; McMillen, W. T.; Mort, N.; Parsons, S.; Smith, E. C.; Vieth, M.; Weir, L. C.; Yan, L.; Zhang, F.; Yingling, J. M. Synthesis and Activity of New Aryl- and Heteroaryl-Substituted Pyrazole Inhibitors of the Transforming Growth Factor-Beta Type I Receptor Kinase Domain. *J. Med. Chem.* **2003,** *46* (19), 3953–3956.
91. Wu, S. M.; Fujiwara, Y.; Cibulsky, S. M.; Clapham, D. E.; Lien, C. L.; Schultheiss, T. M.; Orkin, S. H. Developmental Origin of a Bipotential Myocardial and Smooth Muscle Cell Precursor in the Mammalian Heart. *Cell* **2006,** *127* (6), 1137–1150.
92. Chen, W. P.; Wu, S. M. Small Molecule Regulators of Postnatal Nkx2.5 Cardiomyoblast Proliferation and Differentiation. *J. Cell. Mol. Med.* **2012,** *16* (5), 961–965.
93. Lian, X.; Hsiao, C.; Wilson, G.; Zhu, K.; Hazeltine, L. B.; Azarin, S. M.; Raval, K. K.; Zhang, J.; Kamp, T. J.; Palecek, S. P. Robust Cardiomyocyte Differentiation From Human Pluripotent Stem Cells via Temporal Modulation of Canonical Wnt Signaling. *Proc. Natl. Acad. Sci. U. S. A.* **2012,** *109* (27), E1848–E1857.
94. Burridge, P. W.; Matsa, E.; Shukla, P.; Lin, Z. C.; Churko, J. M.; Ebert, A. D.; Lan, F.; Diecke, S.; Huber, B.; Mordwinkin, N. M.; Plews, J. R.; Abilez, O. J.; Cui, B.; Gold, J. D.; Wu, J. C. Chemically Defined Generation of Human Cardiomyocytes. *Nat. Methods* **2014,** *11* (8), 855–860.
95. Willems, E.; Spiering, S.; Davidovics, H.; Lanier, M.; Xia, Z.; Dawson, M.; Cashman, J.; Mercola, M. Small-Molecule Inhibitors of the Wnt Pathway Potently Promote Cardiomyocytes From Human Embryonic Stem Cell-Derived Mesoderm. *Circ. Res.* **2011,** *109* (4), 360–364.
96. Chen, B.; Dodge, M. E.; Tang, W.; Lu, J.; Ma, Z.; Fan, C. W.; Wei, S.; Hao, W.; Kilgore, J.; Williams, N. S.; Roth, M. G.; Amatruda, J. F.; Chen, C.; Lum, L. Small Molecule-Mediated Disruption of Wnt-Dependent Signaling in Tissue Regeneration and Cancer. *Nat. Chem. Biol.* **2009,** *5* (2), 100–107.
97. Schultheiss, T. M.; Burch, J. B.; Lassar, A. B.. A Role for Bone Morphogenetic Proteins in the Induction of Cardiac Myogenesis. *Genes Dev.* **1997,** *11* (4), 451–462.
98. Hao, J.; Daleo, M. A.; Murphy, C. K.; Yu, P. B.; Ho, J. N.; Hu, J.; Peterson, R. T.; Hatzopoulos, A. K.; Hong, C. C. Dorsomorphin, a Selective Small Molecule Inhibitor of BMP Signaling, Promotes Cardiomyogenesis in Embryonic Stem Cells. *PLoS One* **2008,** *3* (8), e2904.
99. Cross, E. E.; Thomason, R. T.; Martinez, M.; Hopkins, C. R.; Hong, C. C.; Bader, D. M. Application of Small Organic Molecules Reveals Cooperative TGFβ and BMP Regulation of Mesothelial Cell Behaviors. *ACS Chem. Biol.* **2011,** *6* (9), 952–961.
100. Ao, A.; Hao, J.; Hopkins, C. R.; Hong, C. C. DMH1, a Novel BMP Small Molecule Inhibitor, Increases Cardiomyocyte Progenitors and Promotes Cardiac Differentiation in Mouse Embryonic Stem Cells. *PLoS One* **2012,** *7* (7), e41627.
101. Fu, Y.; Huang, C.; Xu, X.; Gu, H.; Ye, Y.; Jiang, C.; Qiu, Z.; Xie, X. Direct Reprogramming of Mouse Fibroblasts Into Cardiomyocytes With Chemical Cocktails. *Cell Res.* **2015,** *25* (9), 1013–1024.
102. Park, G.; Yoon, B. S.; Kim, Y. S.; Choi, S. C.; Moon, J. H.; Kwon, S.; Hwang, J.; Yun, W.; Kim, J. H.; Park, C. Y.; Lim, D. S.; Kim, Y. I.; Oh, C. H.; You, S. Conversion of Mouse Fibroblasts into Cardiomyocyte-Like Cells Using Small Molecule Treatments. *Biomaterials* **2015,** *54,* 201–212.
103. Karakikes, I.; Senyei, G. D.; Hansen, J.; Kong, C. W.; Azeloglu, E. U.; Stillitano, F.; Lieu, D. K.; Wang, J.; Ren, L.; Hulot, J. S.; Iyengar, R.; Li, R. A.; Hajjar, R. J. Small Molecule-Mediated Directed Differentiation of Human Embryonic Stem Cells Toward Ventricular Cardiomyocytes. *Stem Cells Transl. Med.* **2014,** *3* (1), 18–31.
104. Wang, H.; Cao, N.; Spencer, C. L.; Nie, B.; Ma, T.; Xu, T.; Zhang, Y.; Wang, X. Small Molecules Enable Cardiac Reprogramming of Mouse Fibroblasts With a Single Factor Oct 4. *Cell Rep.* **2014,** *6,* 951–960.
105. Liu, N.; Olson, E. N. MicroRNA Regulatory Networks in Cardiovascular Development. *Dev. Cell* **2010,** *18* (4), 510–525.
106. Porrello, E. R. microRNAs in Cardiac Development and Regeneration. *Clin. Sci. (Lond.)* **2013,** *125* (4), 151–166.
107. Morton, S. U.; Scherz, P. J.; Cordes, K. R.; Ivey, K. N.; Stainier, D. Y.; Srivastava, D. microRNA-138 Modulates Cardiac Patterning During Embryonic Development. *Proc. Natl. Acad. Sci. U. S. A.* **2008,** *105* (46), 17830–17835.
108. Townley-Tilson, W. H.; Callis, T. E.; Wang, D. MicroRNAs 1, 133, and 206: Critical Factors of Skeletal and Cardiac Muscle Development, Function, and Disease. *Int. J. Biochem. Cell Biol.* **2010,** *42* (8), 1252–1255.
109. Callis, T. E.; Pandya, K.; Seok, H. Y.; Tang, R. H.; Tatsuguchi, M.; Huang, Z. P.; Chen, J. F.; Deng, Z.; Gunn, B.; Shumate, J.; Willis, M. S.; Selzman, C. H.; Wang, D. Z. MicroRNA-208a Is a Regulator of Cardiac Hypertrophy and Conduction in Mice. *J. Clin. Invest.* **2009,** *119* (9), 2772–2786.
110. Chen, W.-P.; Liu, Y.-H.; Ho, Y.-J.; Wu, S. M. Pharmacological Inhibition of TGF-Beta Receptor Improves Nkx 2.5 Cardiomyoblast-Mediated Regeneration. *Cardiovasc. Res.* **2015,** *105* (1), 44–54.
111. Graichen, R.; Xu, X.; Braam, S. R.; Balakrishnan, T.; Norfiza, S.; Sieh, S.; Soo, S. Y.; Tham, S. C.; Mummery, C.; Colman, A.; Zweigerdt, R.; Davidson, B. P. Enhanced Cardiomyogenesis of Human Embryonic Stem Cells by a Small Molecular Inhibitor of p38 MAPK. *Differentiation* **2008,** *76* (4), 357–370.
112. Low, J. L.; Jürjens, G.; Seayad, J.; Seow, J.; Ting, S.; Laco, F.; Reuveny, S.; Oh, S.; Chai, C. L. Tri-Substituted Imidazole Analogues of SB203580 as Inducers for Cardiomyogenesis of Human Embryonic Stem Cells. *Bioorg. Med. Chem. Lett.* **2013,** *23* (11), 3300–3303.
113. Smart, N.; Bollini, S.; Dubé, K. N.; Vieira, J. M.; Zhou, B.; Davidson, S.; Yellon, D.; Riegler, J.; Price, A. N.; Lythgoe, M. F.; Pu, W. T.; Riley, P. R. De Novo Cardiomyocytes From Within the Activated Adult Heart After Injury. *Nature* **2011,** *474* (7353), 640–644.
114. Klotz, L.; Norman, S.; Vieira, J. M.; Masters, M.; Rohling, M.; Dubé, K. N.; Bollini, S.; Matsuzaki, F.; Carr, C. A.; Riley, P. R. Cardiac Lymphatics Are Heterogeneous in Origin and Respond to Injury. *Nature* **2015,** *522* (7554), 62–67.
115. Lee, A. S.; Tang, C.; Rao, M. S.; Weissman, I. L.; Wu, J. C. Tumorigenicity as a Clinical Hurdle for Pluripotent Stem Cell Therapies. *Nat. Med.* **2013,** *19* (8), 998–1004.
116. Zhang, L.; Pan, Y.; Qin, G.; Chen, L.; Chatterjee, T.; Weintraub, N.; Tang, Y. Inhibition of Stearoyl-CoA Desaturase Selectively Eliminates Tumorigenic Nanog-Positive Cells Improving the Safety of iPS Cell Transplantation to Myocardium. *Cell Cycle* **2014,** *13,* 762–771.
117. Ni, T. T.; Rellinger, E. J.; Mukherjee, A.; Xie, S.; Stephens, L.; Thorne, C. A.; Kim, K.; Hu, J.; Lee, E.; Marnett, L.; Hatzopoulos, A. K.; Zhong, T. P. Discovering Small Molecules That Promote Cardiomyocyte Generation by Modulating Wnt Signaling. *Chem. Biol.* **2011,** *18* (12), 1658–1668.
118. Choi, W.-Y.; Gemberling, J. W.; Holdway, J. E.; Shen, M.-C.; Karlstrom, R. O.; Poss, K. D. In Vivo Monitoring of Cardiomyocyte Proliferation to Identify Chemical Modifiers of Heart Regeneration. *Development* **2013,** *140,* 660–666.
119. Bond, A. M.; Guo-li, M.; Song, H. Adult Mammalian Neural Stem Cells and Neurogenesis: Five Decades Later. *Cell Stem Cell* **2015,** *17,* 385–395.
120. Altman, J.; Das, D. G. Autoradiographic and Histological Evidence of Postnatal Hippocampal Neurogenesis in Rats. *J. Comp. Neurol.* **1965,** *124,* 319–335.
121. Temple, S. Division and Differentiation of Isolated CNS Blast Cells in Microculture. *Nature* **1989,** *340* (6233), 471–473.

122. Reynolds, B. A.; Weiss, S. Generation of Neurons and Astrocytes From Isolated Cells of the Adult Mammalian Central Nervous System. *Science* **1992,** *255* (5052), 1707–1710.
123. Lairson, L. L.; Lyssiotis, C. A.; Zhu, S.; Schultz, P. G. Small Molecule-Based Approaches to Adult Stem Cell Therapies. *Annu. Rev. Pharmacol. Toxicol.* **2013,** *53,* 107–125.
124. Song, J.; Zhong, C.; Bonaguidi, M. A.; Sun, G. J.; Hsu, D.; Gu, Y.; Meletis, K.; Huang, J. Z.; Ge, S.; Enikolopov, G.; Deisseroth, K.; Luscher, B.; Christian, K. M.; Ming, G.-l.; Song, H. Neuronal Circuitry Mechanism Regulating Adult Quiescent Neural Stem-Cell Fate Decision. *Nature* **2012,** *489,* 150–155.
125. Pacey, L.; Stead, S.; Gleave, J.; Tomczyk, K.; Doering, L. Neural Stem Cell Culture: Neurosphere Generation, Microscopic Analysis and Cryopreservation. *Protocol Exchange* **2006;** http://dx.doi.org/10.1038/nprot.2006.215.
126. Theus, M. H.; Ricard, J.; Liebl, D. J. Reproducible Expansion and Characterization of Mouse Neural Stem/Progenitor Cells in Adherent Cultures Derived From the Adult Subventricular Zone. *Current Protocols in Stem Cell Biology* **2012**, 20:D:2D.8:2D.8.1–2D.8.10.
127. Lange, C.; Mix, E.; Frahm, J.; Glass, A.; Müller, J.; Schmitt, O.; Schmöle, A. C.; Klemm, K.; Ortinau, S.; Hübner, R.; Frech, M. J.; Wree, A.; Rolfs, A. Small Molecule GSK-3 Inhibitors Increase Neurogenesis of Human Neural Progenitor Cells. *Neurosci. Lett.* **2011,** *488* (1), 36–40.
128. Warashina, M.; Min, K. H.; Kuwabara, T.; Huynh, A.; Gage, F. H.; Schultz, P. G.; Ding, S. A Synthetic Small Molecule That Induces Neuronal Differentiation of Adult Hippocampal Neural Progenitor Cells. *Angew. Chem. Int. Ed. Engl.* **2006,** *45* (4), 591–593.
129. Chen, D. F.; Meng, L. J.; Du, S. H.; Zhang, H. L.; Li, H.; Zhou, J. H.; Li, Y. W.; Zeng, H. P.; Hua, Z. C. (+)-Cholesten-3-one Induces Differentiation of Neural Stem Cells Into Dopaminergic Neurons Through BMP Signaling. *Neurosci. Res.* **2010,** *68* (3), 176–184.
130. Rashid, M. A.; Katakura, M.; Kharebava, G.; Kevala, K.; Kim, H. Y. N-Docosahexaenoylethanolamine Is a Potent Neurogenic Factor for Neural Stem Cell Differentiation. *J. Neurochem.* **2013,** *125* (6), 869–884.
131. Hsieh, W.-T.; Chiang, B.-H. A Well Refined in vitro Model Derived From Human Embryonic Stem Cell for Screening Phytochemicals With Potential With Midbrain Dopaminergic Differentiation Boosting Potential for Improving Parkinson's Disease. *J. Agric. Food Chem.* **2014,** *62* (27), 6326–6336.
132. Li, W.; Sun, W.; Zhang, Y.; Wei, W.; Ambasudhan, R.; Xia, P.; Talantova, M.; Lin, T.; Kim, J.; Wang, X.; Kim, W. R.; Lipton, S. A.; Zhang, K.; Ding, S. Rapid Induction and Long-Term Self-Renewal of Primitive Neural Precursors From Human Embryonic Stem Cells by Small Molecule Inhibitors. *Proc. Natl. Acad. Sci. U. S. A.* **2011,** *108* (20), 8299–8304.
133. Wang, Z.; Wang, H.; Wu, J.; Zhu, D.; Zhang, X.; Ou, L.; Yu, Y.; Lou, Y. Enhanced Co-Expression of Beta-Tubulin III and Choline Acetyltransferase in Neurons From Mouse Embryonic Stem Cells Promoted by Icaritin in an Estrogen Receptor-Independent Manner. *Chem. Biol. Interact.* **2009,** *179* (2-3), 375–385.
134. Wang, D. Y.; Hu, Y. Z.; Kong, S. S.; Yu, Y. P.; Zhu, D. Y.; Lou, Y. J. Promoting Effects of Isobavachin on Neurogenesis of Mouse Embryonic Stem Cells Were Associated With Protein Prenylation. *Acta Pharmacol. Sin.* **2011,** *32* (4), 425–432.
135. Hotta, R.; Pepdjonovic, L.; Anderson, R. B.; Zhang, D.; Bergner, A. J.; Leung, J.; Pébay, A.; Young, H. M.; Newgreen, D. F.; Dottori, M. Small-Molecule Induction of Neural Crest-Like Cells Derived From Human Neural Progenitors. *Stem Cells* **2009,** *27* (12), 2896–2905.
136. Borghese, L.; Dolezalova, D.; Opitz, T.; Haupt, S.; Leinhaas, A.; Steinfarz, B.; Koch, P.; Edenhofer, F.; Hampl, A.; Brüstle, O. Inhibition of Notch Signaling in Human Embryonic Stem Cell-Derived Neural Stem Cells Delays G1/S Phase Transition and Accelerates Neuronal Differentiation in vitro and In Vivo. *Stem Cells* **2010,** *28* (5), 955–964.
137. Suter, D. M.; Preynat-Seauve, O.; Tirefort, D.; Feki, A.; Krause, K. H. Phenazopyridine Induces and Synchronizes Neuronal Differentiation of Embryonic Stem Cells. *J. Cell. Mol. Med.* **2009,** *13* (9B), 3517–3527.
138. Han, Y.; Miller, A.; Mangada, J.; Liu, Y.; Swistowski, A.; Zhan, M.; Rao, M. S.; Zeng, X. Identification by Automated Screening of a Small Molecule that Selectively Eliminates Neural Stem Cells Derived From hESCs but not Dopamine Neurons. *PLoS One* **2009,** *4* (9), e7155.
139. Peljto, M.; Wichterle, H. Programming Embryonic Stem Cells to Neuronal Subtypes. *Curr. Opin. Neurobiol.* **2011,** *21* (1), 43–51.
140. Takazawa, T.; Croft, G. F.; Amoroso, M. W.; Studer, L.; Wichterle, H.; Macdermott, A. B.. Maturation of Spinal Motor Neurons Derived From Human Embryonic Stem Cells. *PLoS One* **2012,** *7* (7), e40154.
141. Peljto, M.; Dasen, J. S.; Mazzoni, E. O.; Jessell, T. M.; Wichterle, H. Functional Diversity of ESC-Derived Motor Neuron Subtypes Revealed Through Intraspinal Transplantation. *Cell Stem Cell* **2010,** *7* (3), 355–366.
142. Kim, G.-H.; Halder, D.; Park, J.; Namkung, W.; Shin, I. Imidazole-Based Small Molecules that Promote Neurogenesis in Pluriopotent Cells. *Angew. Chem. Int. Ed.* **2014,** *53,* 9271–9274.
143. Compagnucci, C.; Nizzardo, M.; Corti, S.; Zanni, G.; Bertini, E. In Vitro Neurogenesis: Development and Functional Implications of iPSC Technology. *Cell. Mol. Life Sci.* **2014,** *71,* 1623–1639.
144. Boulting, G. L.; Kiskinis, E.; Croft, G. F.; Amoroso, M. W.; Oakley, D. H.; Wainger, B. J.; Williams, D. J.; Kahler, D. J.; Yamaki, M.; Davidow, L.; Rodolfa, C. T.; Dimos, J. T.; Mikkilineni, S.; MacDermott, A. B..; Woolf, C. J.; Henderson, C. E.; Wichterle, H.; Eggan, K. A Functionally Characterized Test Set of Human Induced Pluripotent Stem Cells. *Nat. Biotechnol.* **2011,** *29* (3), 279–286.
145. Amoroso, M. W.; Croft, G. F.; Williams, D. J.; O'Keeffe, S.; Carrasco, M. A.; Davis, A. R.; Roybon, L.; Oakley, D. H.; Maniatis, T.; Henderson, C. E.; Wichterle, H. Accelerated High-Yield Generation of Limb-Innervating Motor Neurons From Human Stem Cells. *J. Neurosci.* **2013,** *33* (2), 574–586.
146. Wichterle, H.; Przedborski, S. What can Pluripotent Stem Cells Teach Us About Neurodegenerative Diseases? *Nat. Neurosci.* **2010,** *13* (7), 800–804.
147. Kim, D. S.; Lee, J. S.; Leem, J. W.; Huh, Y. J.; Kim, J. Y.; Kim, H. S.; Park, I. H.; Daley, G. Q.; Hwang, D. Y.; Kim, D. W. Robust Enhancement of Neural Differentiation From Human ES and iPS Cells Regardless of Their Innate Difference in Differentiation Propensity. *Stem Cell Rev.* **2010,** *6* (2), 270–281.
148. Morizane, A.; Doi, D.; Kikuchi, T.; Nishimura, K.; Takahashi, J. Small-Molecule Inhibitors of Bone Morphogenic Protein and Activin/Nodal Signals Promote Highly Efficient Neural Induction From Human Pluripotent Stem Cells. *J. Neurosci. Res.* **2011,** *89* (2), 117–126.
149. Neely, M. D.; Litt, M. J.; Tidball, A. M.; Li, G. G.; Aboud, A. A.; Hopkins, C. R.; Chamberlin, R.; Hong, C. C.; Ess, K. C.; Bowman, A. B.. DMH1, a Highly Selective Small Molecule BMP Inhibitor Promotes Neurogenesis of hiPSCs: Comparison of PAX6 and SOX1 Expression During Neural Induction. *ACS Chem. Neurosci.* **2012,** *3* (6), 482–491.
150. Gonzalez, R.; Garitaonandia, I.; Abramihina, T.; Wambua, G. K.; Ostrowska, A.; Brock, M.; Noskov, A.; Boscolo, F. S.; Craw, J. S.; Laurent, L. C.; Snyder, E. Y.; Semechkin, R. A. Deriving Dopaminergic Neurons for Clinical Use. A Practical Approach. *Sci. Rep.* **2013,** *3,* 1463.
151. Komatsu, M.; Konagaya, S.; Edgar, E. Y.; Iwata, H. Maturation of Human iPSC Cell-Derived Dopamine Precursors in Alginate-Ca+ Hydrogel. *Biochim. Biophys. Acta* **2015,** *1850,* 1669–1675.
152. Merkle, F. G.; Maroof, A.; Wataya, T.; Sasai, Y.; Studer, L.; Eggan, K.; Schier, A. Generation of Neuropeptidergic Hypothalamic Neurons From Human Pluripotent Stem Cells. *Development* **2015,** *142,* 633–643.
153. Yu, D. X.; Di Giorgio, F. P.; Yao, J.; Marchetto, M. C.; Brennand, K.; Wright, R.; Mei, A.; Mchenry, L.; Lisuk, D.; Grasmick, J. M.; Silberman, P.; Silberman, G.; Jappelli, R.; Gage, F. H. Modeling Hippocampal Neurogenesis Using Human Pluripotent Stem Cells. *Stem Cell Rep.* **2014,** *2,* 295–310.
154. Momcilovic, O.; Liu, Q.; Swistowski, A.; Russo-Tait, T.; Zhao, Y.; Rao, M. S.; Zeng, X. Genome Wide Profiling of Dopaminergic Neurons Derived From Human Embryonic and Induced Pluripotent Stem Cells. *Stem Cells Dev.* **2014,** *23* (4), 406–420.
155. Frausin, S.; Viventi, S.; Falzacappa, L. V.; Quattromani, M. J.; Leanza, G.; Tommasini, A.; Valencic, E. Wharton's Jelly Derived Mesenchymal Stromal Cells: Biological Properties, Induction of Neuronal Phenotype and Current Applications in Neurodegeneration Research. *Acta Histochem.* **2015,** *117,* 329–338.
156. Nandy, S. B.; Mohanty, S.; Singh, M.; Behari, M.; Airan, B. Fibroblast Growth Factor-2 Alone as an Efficient Inducer for Differentiation of Human Bone Marrow Mesenchymal Stem Cells Into Dopaminergic Neurons. *J. Biomed. Sci.* **2014,** *21,* 83/1–83/10.
157. Wang, Y.; He, W.; Bian, H.; Liu, C.; Li, S. Small Molecule Induction of Neural-Like Cells From Bone Marrow-Mesenchymal Stem Cells. *J. Cell. Biochem.* **2012,** *113* (5), 1527–1536.
158. Naujock, M.; Stanslowsky, N.; Reinhardt, P.; Sterneckert, J.; Haase, A.; Martin, U.; Kim, K.-S.; Dengler, R.; Wegner, F.; Petri, S. Molecular and Functional Analyses of Motor Neurons Generated From Human Cord-Blood-Derived Induced Pluripotent Stem Cells. *Stem Cells Dev.* **2014,** *24,* 3011–3020.

159. Vierbuchen, T.; Ostermeier, A.; Pang, Z. P.; Kokubu, Y.; Sudhof, T. C.; Wernig, M. Direct Conversion of Fibroblasts to Functional Neurons by Defined Factors. *Nature* **2010,** *463,* 1035–1041.
160. Son, E. Y.; Ichida, J. K.; Wainger, B. J.; Toma, J. S.; Rafuse, V. F.; Woolf, C. J.; Eggan, K. Conversion of Mouse and Human Fibroblasts Into Functional Spinal Motor Neurons. *Cell Stem Cell* **2011,** *9* (3), 205–218.
161. Wang, Y.; Tian, C.; Zheng, J. C. FoxO3a Contributes to the Reprogramming Process and the Differentiation of Induced Pluripotent Stem Cells. *Stem Cells Dev.* **2013,** *22* (22), 2954–2963.
162. Cheng, L.; Hu, W.; Qiu, B.; Zhao, J.; Yu, Y.; Guan, W.; Wang, M.; Yang, W.; Pei, G. Generation of Neural Progenitor Cells by Chemical Cocktails and Hypoxia. *Cell Res.* **2014,** *24,* 665–679.
163. Hu, W.; Qiu, B.; Guan, W.; Wang, Q.; Wang, M.; Li, W.; Gao, L.; Shen, L.; Huang, Y.; Xie, G.; Zhao, H.; Jin, Y.; Tang, B.; Yu, Y.; Zhao, J.; Pei, G. Direct Conversion of Normal and Alzheimer's Disease Human Fibroblasts Into Neuronal Cells by Small Molecules. *Cell Stem Cell* **2015,** *17,* 204–212.
164. Li, X.; Zuo, X.; Jing, J.; Ma, Y.; Wang, J.; Liu, D.; Zhu, J.; Du, X.; Xiong, L.; Du, Y.; Xu, J.; Xiao, X.; Wang, J.; Chai, Z.; Zhao, Y.; Deng, H. Small-Molecule Driven Direct Reprogramming of Mouse Fibroblasts Into Functional Neurons. *Cell Stem Cell* **2015,** *17,* 195–203.
165. Oh, S.-i.; Park, H.-s.; Hwang, I.; Park, H.-k.; Choi, K.-A.; Jeong, H.; Kim, S. W.; Hong, S. Efficient Programming of Mouse Fibroblasts to Neuronal Cells Including Dopaminergic Neurons. *Sci. World J.* **2014,** *2014,* 8. http://dx.doi.org/10.1155/2014/957548. Article ID 957548.
166. Lojewski, X.; Hermann, A.; Wegner, F.; Arauzo-Bravo, M. J.; Hallmeyer-Elgner, S.; Kirsch, M.; Schwartz, J.; Sholer, H. R.; Alexander, S. Human Adult White Matter Progenitor Cells Are Multipotent Neuroprogenitors Similar to Adult Hippocampal Progenitors. *Stem Cells Transl. Med.* **2014,** *3,* 458–469.
167. Gervois, P.; Struys, T.; Hilkens, P.; Bronckaers, A.; Ratajczak, J.; Politis, C.; Brone, B.; Lambrichts, I.; Martens, W. Neurogenic Maturation of Human Dental Pulp Stem Cells Following Neurosphere Generation Induces Morphological and Electrophysiological Characteristics of Functional Neurons. *Stem Cells Dev.* **2015,** *24* (3), 296–311.
168. Dutta, S.; Singh, G.; Sreejith, S.; Mamidi, M. K.; Husin, J. M.; Datta, I.; Pal, R.; Das, A. K. Cell Therapy: The Final Frontier for Treatment of Neurological Diseases. *CNS Neurosci. Ther.* **2013,** *19* (1), 5–11.
169. Steinbeck, J. A.; Studer, L. Moving Stem Cells to the Clinic: Potential and Limitations for Brain Repair. *Neuron* **2015,** *86,* 187–206.
170. Kefalopoulou, Z.; Politis, M.; Piccini, P.; Mencacci, N.; Bhatia, K.; Jahanshahi, M.; Widner, H.; Rehncrona, S.; Brundin, P.; Bjorklund, A.; Lindvall, O.; Limousin, P.; Quinn, N.; Foltynie, T. Long-Term Clinical Outcome of Fetal Cell Transplantation for Parkinson's Disease. *JAMA Neurol.* **2014,** *71* (1), 83–87.
171. Scholz, T.; Sumarto, A.; Krichevsky, A.; Evans, G. R. Neuronal Differentiation of Human Adipose Tissue-Derived Stem Cells for Peripheral Nerve Regeneration In Vivo. *Arch. Surg.* **2011,** *146* (6), 666–674.
172. Casarosa, S.; Bozzi, Y.; Conti, L. Neural Stem Cells: Ready for Therapeutic Applications? *Mol. Cell Ther.* **2014,** *2,* 31.
173. Wong, F. S. Y.; Chan, B. P.; Lo, A. C. Y. Carriers in Cell-Based Therapies for Neurological Disorders. *Int. J. Mol. Sci.* **2014,** *15,* 10669–10723.
174. Calio, M. L.; Marinho, D. S.; Ko, G. M.; Ribeiro, R. R.; Carbonel, A. F.; Oyama, L. M.; Ormanji, M.; Guirao, T. P.; Calio, P. L.; Reis, L. A.; Simoes, M. D. J.; Lisboa-Nascimento, T.; Ferreira, A. T.; Beertoncini, C. R. A. Transplantation of Bone Marrow Mesenchymal Stem Cells Decreases Oxidative Stress, Apoptosis and Hippocampal Damage in Brain of a Spontaneous Stroke Model. *Free Radic. Biol. Med.* **2014,** *70,* 141–154.
175. Zhao, J.; Sun, W.; Cho, H. M.; Ouyang, H.; Li, W.; Lin, Y.; Do, J.; Zhang, L.; Ding, S.; Liu, Y.; Lu, P.; Zhang, K. Integration and Long Distance Axonal Regeneration in the Central Nervous System From Transplanted Primitive Neural Stem Cells. *J. Biol. Chem.* **2013,** *288* (1), 164–168.
176. Southwell, D. G.; Nicholas, C. R.; Basbaum, A. I.; Stryker, M. P.; Kriegstein, A. R.; Rubenstein, J. L.; Alvarez-Buylla, A. Interneurons From Embryonic Development to Cell-Based Therapy. *Science* **2014,** *344,* 1240622.
177. Taupin, P. Neurogenesis and the Effect of Antidepressants. *Drug Target Insights* **2006,** *1,* 13–17.
178. Duman, R. S. Role of Neurotrophic Factors in the Etiology and Treatment of Mood Disorders. *Neuromol. Med.* **2004,** *5* (1), 11–25.
179. Anacker, C.; Zunszain, P. A.; Cattaneo, A.; Carvalho, L. A.; Garabedian, M. J.; Thuret, S.; Price, J.; Pariante, C. M. Antidepressants Increase Human Hippocampal Neurogenesis by Activating the Glucocorticoid Receptor. *Mol. Psychiatry* **2011,** *16* (7), 738–750.
180. Malberg, J. E.; Eisch, A. J.; Nestler, E. J.; Duman, R. S. Chronic Antidepressant Treatment Increases Neurogenesis in Adult Rat Hippocampus. *J. Neurosci.* **2000,** *20* (24), 9104–9110.
181. Guirado, R.; Sanchez-Matarredona, D.; Varea, E.; Crespo, C.; Blasco-Ibáñez, J. M.; Nacher, J. Chronic Fluoxetine Treatment in Middle-Aged Rats Induces Changes in the Expression of Plasticity-Related Molecules and in Neurogenesis. *BMC Neurosci.* **2012,** *13,* 5.
182. Irwin, R. W.; Wang, J. M.; Chen, S.; Brinton, R. D. Neuroregenerative Mechanisms of Allopregnanolone in Alzheimer's Disease. *Front. Endocrinol. (Laussane)* **2011,** *2,* 117.
183. Lu, J.; Frerich, J. M.; Turtzo, L. C.; Li, S.; Chiang, J.; Yang, C.; Wang, X.; Zhang, C.; Wu, C.; Sun, Z.; Niu, G.; Zhuang, Z.; Brady, R. O.; Chen, X. Histone Deacetylase Inhibitors Are Neuroprotective and Preserve NGF-Mediated Cell Survival Following Traumatic Brain Injury. *Proc. Natl. Acad. Sci. U. S. A.* **2013,** *110* (26), 10747–10752.
184. Shi, J.; Longo, F. M.; Massa, S. M. A Small Molecule p75(NTR) Ligand Protects Neurogenesis After Traumatic Brain Injury. *Stem Cells* **2013,** *31* (11), 2561–2574.
185. Sondossi, K.; Majdzadeh, M.; Ghaeli, P.; Ghahremani, M. H.; Shafaroodi, H.; Babek, P.; Ostad, S. N. Analysis of the Antiepileptic, Ethosuximide Impacts on Neurogenesis of Rat Forebrain Stem Cells. *Fundam. Clin. Pharmacol.* **2014,** *28,* 512–518.
186. MacMillan, K. S.; Naidoo, J.; Liang, J.; Melito, L.; Williams, N. S.; Morlock, L.; Huntington, P. J.; Estill, S. J.; Longgood, J.; Becker, G. L.; McKnight, S. L.; Pieper, A. A.; De Brabander, J. K.; Ready, J. M. Development of Proneurogenic, Neuroprotective Small Molecules. *J. Am. Chem. Soc.* **2011,** *133* (5), 1428–1437.
187. De Jesús-Cortés, H.; Xu, P.; Drawbridge, J.; Estill, S. J.; Huntington, P.; Tran, S.; Britt, J.; Tesla, R.; Morlock, L.; Naidoo, J.; Melito, L. M.; Wang, G.; Williams, N. S.; Ready, J. M.; McKnight, S. L.; Pieper, A. A. Neuroprotective Efficacy of Aminopropyl Carbazoles in a Mouse Model of Parkinson Disease. *Proc. Natl. Acad. Sci. U. S. A.* **2012,** *109* (42), 17010–17015.
188. Tesla, R.; Wolf, H. P.; Xu, P.; Drawbridge, J.; Estill, S. J.; Huntington, P.; McDaniel, L.; Knobbe, W.; Burket, A.; Tran, S.; Starwalt, R.; Morlock, L.; Naidoo, J.; Williams, N. S.; Ready, J. M.; McKnight, S. L.; Pieper, A. A. Neuroprotective Efficacy of Aminopropyl Carbazoles in a Mouse Model of Amyotrophic Lateral Sclerosis. *Proc. Natl. Acad. Sci. U. S. A.* **2012,** *109* (42), 17016–17021.
189. Wan Ibrahim, W. N.; Tofighi, R.; Onishchenko, N.; Rebellato, P.; Bose, R.; Uhlén, P.; Ceccatelli, S. Perfluorooctane Sulfonate Induces Neuronal and Oligodendrocytic Differentiation in Neural Stem Cells and Alters the Expression of PPARγ in vitro and In Vivo. *Toxicol. Appl. Pharmacol.* **2013,** *269* (1), 51–60.
190. Vieira, H. L.; Alves, P. M.; Vercelli, A. Modulation of Neuronal Stem Cell Differentiation by Hypoxia and Reactive Oxygen Species. *Prog. Neurobiol.* **2011,** *93* (3), 444–455.
191. Ross, H. H.; Sandhu, M. S.; Cheung, T. F.; Fitzpatrick, G. M.; Sher, W. J.; Tiemeier, A. J.; Laywell, E. D.; Fuller, D. D. In Vivo Intermittent Hypoxia Elicits Enhanced Expansion and Neuronal Differentiation in Cultured Neural Progenitors. *Exp. Neurol.* **2012,** *235* (1), 238–245.
192. Ehm, O.; Göritz, C.; Covic, M.; Schäffner, I.; Schwarz, T. J.; Karaca, E.; Kempkes, B.; Kremmer, E.; Pfrieger, F. W.; Espinosa, L.; Bigas, A.; Giachino, C.; Taylor, V.; Frisén, J.; Lie, D. C. RBPJkappa-Dependent Signaling Is Essential for Long-Term Maintenance of Neural Stem Cells in the Adult Hippocampus. *J. Neurosci.* **2010,** *30* (41), 13794–13807.
193. Gómez-Pinedo, U.; Rodrigo, R.; Cauli, O.; Herraiz, S.; Garcia-Verdugo, J. M.; Pellicer, B.; Pellicer, A.; Felipo, V. cGMP Modulates Stem Cells Differentiation to Neurons in Brain In Vivo. *Neuroscience* **2010,** *165* (4), 1275–1283.
194. Wurdak, H.; Zhu, S.; Min, K. H.; Aimone, L.; Lairson, L. L.; Watson, J.; Chopiuk, G.; Demas, J.; Charette, B.; Halder, R.; Weerapana, E.; Cravatt, B. F.; Cline, H. T.; Peters, E. C.; Zhang, J.; Walker, J. R.; Wu, C.; Chang, J.; Tuntland, T.; Cho, C. Y.; Schultz, P. G. A Small Molecule Accelerates Neuronal Differentiation in the Adult Rat. *Proc. Natl. Acad. Sci. U. S. A.* **2010,** *107* (38), 16542–16547.
195. Schneider, J. W.; Goetsch, S. C.; Leng, X.; Ludwig, S. M.; Russell, J. L.; Yang, C. P.; Zhang, Q. J. Coupling Hippocampal Neurogenesis to Brain pH Through Proneurogenic Small Molecules That Regulate Proton Sensing G Protein-Coupled Receptors. *ACS Chem. Neurosci.* **2012,** *3* (7), 557–568.
196. Schmidt, R.; Strähle, U.; Scholpp, S. Neurogenesis in Zebrafish—From Embryo to Adult. *Neural Dev.* **2013,** *8,* 3.
197. Hocking, J. C.; Distel, M.; Köster, R. W. Studying Cellular and Subcellular Dynamics in the Developing Zebrafish Nervous System. *Exp. Neurol.* **2013,** *242,* 1–10.

198. Zhang, J.; Shemezis, J. R.; McQuinn, E. R.; Wang, J.; Sverdlov, M.; Chenn, A. AKT Activation by N-Cadherin Regulates Beta-Catenin Signaling and Neuronal Differentiation During Cortical Development. *Neural Dev.* **2013,** *8,* 7.
199. Maucksch, C.; McGregor, A. L.; Yang, M.; Gordon, R. J.; Connor, B. IGF-I Redirects Doublecortin-Positive Cell Migration in the Normal Adult Rat Brain. *Neuroscience* **2013,** *241,* 106–115.
200. Williams, T.; Courchet, J.; Viollet, B.; Brenman, J. E.; Polleux, F. AMP-Activated Protein Kinase (AMPK) Activity Is not Required for Neuronal Development but Regulates Axogenesis During Metabolic Stress. *Proc. Natl. Acad. Sci. U. S. A.* **2011,** *108* (14), 5849–5854.
201. Mu, L.; Berti, L.; Masserdotti, G.; Covic, M.; Michaelidis, T. M.; Doberauer, K.; Merz, K.; Rehfeld, F.; Haslinger, A.; Wegner, M.; Sock, E.; Lefebvre, V.; Couillard-Despres, S.; Aigner, L.; Berninger, B.; Lie, D. C. SoxC Transcription Factors Are Required for Neuronal Differentiation in Adult Hippocampal Neurogenesis. *J. Neurosci.* **2012,** *32* (9), 3067–3080.
202. Dimos, J. T.; Rodolfa, K. T.; Niakan, K. K.; Weisenthal, L. M.; Mitsumoto, H.; Chung, W.; Croft, G. F.; Saphier, G.; Leibel, R.; Goland, R.; Wichterle, H.; Henderson, C. E.; Eggan, K. Induced Pluripotent Stem Cells Generated From Patients With ALS Can be Differentiated Into Motor Neurons. *Science* **2008,** *321* (5893), 1218–1221.
203. Sandoe, J.; Eggan, K. Opportunities and Challenges of Pluripotent Stem Cell Neurodegenerative Disease Models. *Nat. Neurosci.* **2013,** *16* (7), 780–789.
204. Merkle, F. T.; Eggan, K. Modeling Human Disease With Pluripotent Stem Cells: From Genome Association to Function. *Cell Stem Cell* **2013,** *12* (6), 656–668.
205. Han, S. S.; Williams, L. A.; Eggan, K. C. Constructing and Deconstructing Stem Cell Models of Neurological Disease. *Neuron* **2011,** *70* (4), 626–644.
206. Yung, J. S.; Tam, P. K.; Ngan, E. S. Pluripotent Stem Cell for Modeling Neurological Diseases. *Exp. Cell Res.* **2013,** *319* (2), 177–184.
207. Kim, H.-S.; Choi, S.-M.; Yang, W.; Kim, D.-S.; Lee, D. R.; Cho, S.-R.; Kim, D.-W. PSA-NCAM+ Neural Precursor Cells From Human Embryonic Stem Cells Promote Neural Tissue Integrity and Behavioural Performance in a Rat Stroke Model. *Stem Cell Rep.* **2014,** *10,* 761–771.
208. Du, X.; Parent, J. M. Using Patient-Derived Induced Pluripotent Stem Cells to Model and Treat Epilepsies. *Curr. Neurol. Neurosci. Rep.* **2015,** *15,* 71.
209. Tyson, J. A.; Anderson, S. A. GABAergic Interneuron Transplants to Study Development and Treat Disease. *Trends Neurosci.* **2014,** *37* (3), 169–177.
210. Gu, G.; Zhang, W.; Li, M.; Ni, J.; Wang, P. Transplantation of NSC-Derived Cholinergic Neuron-Like Cells Improves Cognitive Function in APP/PS1 Transgenic Mice. *Neuroscience* **2015,** *291,* 81–92.
211. Tiscornia, G.; Vivas, E. L.; Matalonga, L.; Berniakovich, I.; Barragán Monasterio, M.; Eguizábal, C.; Gort, L.; González, F.; Ortiz Mellet, C.; García Fernández, J. M.; Ribes, A.; Veiga, A.; Izpisua Belmonte, J. C. Neuronopathic Gaucher's Disease: Induced Pluripotent Stem Cells for Disease Modelling and Testing Chaperone Activity of Small Compounds. *Hum. Mol. Genet.* **2013,** *22* (4), 633–645.
212. Höing, S.; Rudhard, Y.; Reinhardt, P.; Glatza, M.; Stehling, M.; Wu, G.; Peiker, C.; Böcker, A.; Parga, J. A.; Bunk, E.; Schwamborn, J. C.; Slack, M.; Sterneckert, J.; Schöler, H. R. Discovery of Inhibitors of Microglial Neurotoxicity Acting Through Multiple Mechanisms Using a Stem-Cell-Based Phenotypic Assay. *Cell Stem Cell* **2012,** *11* (5), 620–632.
213. Peng, J.; Liu, Q.; Rao, M. S.; Zeng, X. Using Human Pluripotent Stem Cell-Derived Dopaminergic Neurons to Evaluate Candidate Parkinson's Disease Therapeutic Agents in MPP+ and Rotenone Models. *J. Biomol. Screen.* **2013,** *18* (5), 522–533.
214. Kern, I.; Xu, R.; Julien, S.; Suter, D. M.; Preynat-Seauve, O.; Baquié, M.; Poncet, A.; Combescure, C.; Stoppini, L.; Thriel, C. V.; Krause, K. H. Embryonic Stem Cell-Based Screen for Small Molecules: Cluster Analysis Reveals Four Response Patterns in Developing Neural Cells. *Curr. Med. Chem.* **2013,** *20* (5), 710–723.
215. Chung, C. Y.; Khurana, V.; Auluck, P. K.; Tardiff, D. F.; Mazzulli, J. R.; Soldner, F.; Baru, V.; Lou, Y.; Freyzon, Y.; Cho, S.; Mungenast, A. E.; Muffat, J.; Mitalipova, M.; Pluth, M. D.; Jui, N. T.; Schüle, B.; Lippard, S. J.; Tsai, L. H.; Krainc, D.; Buchwald, S. L.; Jaenisch, R.; Lindquist, S. Identification and Rescue of α-Synuclein Toxicity in Parkinson Patient-Derived Neurons. *Science* **2013,** *342* (6161), 983–987.
216. Peppard, J. V.; Rugg, C. A.; Smicker, M. A.; Powers, E.; Harnish, E.; Prisco, J.; Cirovic, D.; Wright, P. S.; August, P. R.; Chandross, K. J. High-Content Phenotypic Screening and Triaging Strategy to Identify Small Molecules Driving Oligodendrocyte Progenitor Cell Differentiation. *J. Biomol. Screen.* **2015,** *20* (3), 382–390.
217. Davis, H.; Guo, X.; Lambert, S.; Stanescu, M.; Hickman, J. J. Small Molecule Induction of Human Umbilical Stem Cells Into Myelin Basic Protein Positive Oligodendrocytes in a Defined Three-Dimensional Environment. *ACS Chem. Neurosci.* **2012,** *3* (1), 31–39.
218. Yang, Y. M.; Gupta, S. K.; Kim, K. J.; Powers, B. E.; Cerqueira, A.; Wainger, B. J.; Ngo, H. D.; Rosowski, K. A.; Schein, P. A.; Ackeifi, C. A.; Arvanites, A. C.; Davidow, L. S.; Woolf, C. J.; Rubin, L. L. A Small Molecule Screen in Stem-Cell-Derived Motor Neurons Identifies a Kinase Inhibitor as a Candidate Therapeutic for ALS. *Cell Stem Cell* **2013,** *12* (6), 713–726.
219. Reinhardt, P.; Glatza, M.; Hemmer, K.; Tsytsyura, Y.; Thiel, C. S.; Höing, S.; Moritz, S.; Parga, J. A.; Wagner, L.; Bruder, J. M.; Wu, G.; Schmid, B.; Röpke, A.; Klingauf, J.; Schwamborn, J. C.; Gasser, T.; Schöler, H. R.; Sterneckert, J. Derivation and Expansion Using Only Small Molecules of Human Neural Progenitors for Neurodegenerative Disease Modeling. *PLoS One* **2013,** *8* (3), e59252.
220. Swaminathan, A.; Kumar, M.; Sinha, S. H.; Schneider-Anthony, A.; Boutillier, A.-L.; Kundu, T. K. Modulation of Neurogenesis by Targeting Epigenetic Enzymes Using Small Molecules: An Overview. *ACS Chem. Neurosci.* **2014,** *5,* 1164–1177.
221. Jung, D. W.; Williams, D. R. Reawakening Atlas: Chemical Approaches to Repair or Replace Dysfunctional Musculature. *ACS Chem. Biol.* **2012,** *7* (11), 1773–1790.
222. Amato, A. A.; Sivakumar, K.; Goyal, N.; David, W. S.; Salajegheh, M.; Praestgaard, J.; Lach-Trifilieff, E.; Trendelenburg, A. U.; Laurent, D.; Glass, D. J.; Roubenoff, R.; Tseng, B. S.; Greenberg, S. A. Treatment of Sporadic Inclusion Body Myositis With Bimagrumab. *Neurology* **2014,** *83* (24), 2239–2246.
223. Trokovic, R.; Weltner, J.; Manninen, T.; Mikkola, M.; Lundin, K.; Hämäläinen, R.; Suomalainen, A.; Otonkoski, T. Small Molecule Inhibitors Promote Efficient Generation of Induced Pluripotent Stem Cells From Human Skeletal Myoblasts. *Stem Cells Dev.* **2013,** *22* (1), 114–123.
224. Kim, W. H.; Jung, D. W.; Kim, J.; Im, S. H.; Hwang, S. Y.; Williams, D. R. Small Molecules That Recapitulate the Early Steps of Urodele Amphibian Limb Regeneration and Confer Multipotency. *ACS Chem. Biol.* **2012,** *7* (4), 732–743.
225. Horbelt, D.; Boergermann, J. H.; Chaikuad, A.; Alfano, I.; Williams, E.; Lukonin, I.; Timmel, T.; Bullock, A. N.; Knaus, P. Small Molecules Dorsomorphin and LDN-193189 Inhibit Myostatin/GDF8 Signaling and Promote Functional Myoblast Differentiation. *J. Biol. Chem.* **2015,** *290* (6), 3390–3404.
226. Sinha, M.; Jang, Y. C.; Oh, J.; Khong, D.; Wu, E. Y.; Manohar, R.; Miller, C.; Regalado, S. G.; Loffredo, F. S.; Pancoast, J. R.; Hirshman, M. F.; Lebowitz, J.; Shadrach, J. L.; Cerletti, M.; Kim, M. J.; Serwold, T.; Goodyear, L. J.; Rosner, B.; Lee, R. T.; Wagers, A. J. Restoring Systemic GDF11 Levels Reverses Age-Related Dysfunction in Mouse Skeletal Muscle. *Science* **2014,** *344* (6184), 649–652.
227. Ryan, T.; Liu, J.; Chu, A.; Wang, L.; Blais, A.; Skerjanc, I. S. Retinoic Acid Enhances Skeletal Myogenesis in Human Embryonic Stem Cells by Expanding the Premyogenic Progenitor Population. *Stem Cell Rev.* **2012,** *8* (2), 482–493.
228. Kim, Y. K.; Ha, H. H.; Lee, J. S.; Bi, X.; Ahn, Y. H.; Hajar, S.; Lee, J. J.; Chang, Y. T. Control of Muscle Differentiation by a Mitochondria-Targeted Fluorophore. *J. Am. Chem. Soc.* **2010,** *132* (2), 576–579.
229. Paliwal, P.; Conboy, I. M. Inhibitors of Tyrosine Phosphatases and Apoptosis Reprogram Lineage-Marked Differentiated Muscle to Myogenic Progenitor Cells. *Chem. Biol.* **2011,** *18* (9), 1153–1166.
230. Castaldi, L.; Serra, C.; Moretti, F.; Messina, G.; Paoletti, R.; Sampaolesi, M.; Torgovnick, A.; Baiocchi, M.; Padula, F.; Pisaniello, A.; Molinaro, M.; Cossu, G.; Levrero, M.; Bouché, M. Bisperoxovanadium, a Phospho-Tyrosine Phosphatase Inhibitor, Reprograms Myogenic Cells to Acquire a Pluripotent, Circulating Phenotype. *FASEB J.* **2007,** *21* (13), 3573–3583.
231. Carlson, M. E.; Conboy, M. J.; Hsu, M.; Barchas, L.; Jeong, J.; Agrawal, A.; Mikels, A. J.; Agrawal, S.; Schaffer, D. V.; Conboy, I. M. Relative Roles of TGF-beta1 and Wnt in the Systemic Regulation and Aging of Satellite Cell Responses. *Aging Cell* **2009,** *8* (6), 676–689.
232. Cheng, L.; Gu, X.; Sanderson, J. E.; Wang, X.; Lee, K.; Yao, X.; Liu, H.; Cheung, W. L.; Li, M. A New Function of a Previously Isolated Compound That Stimulates Activation and Differentiation of Myogenic Precursor Cells Leading to Efficient Myofiber Regeneration and Muscle Repair. *Int. J. Biochem. Cell Biol.* **2006,** *38* (7), 1123–1133.
233. Choi, J.; Lee, K.; Ha, J.; Yun, S.; Ko, C.; Jung, H.; Park, H. Antinociceptive and Antiinflammatory Effects of Niga-Ichigoside F-1 and 23-Hydroxytormentic Acid Obtained From Rubus Coreanus. *Biol. Pharm. Bull.* **2003,** *26* (10), 1436–1441.

234. Fernyhough, M. E.; Bucci, L. R.; Feliciano, J.; Dodson, M. V. The Effect of Nutritional Supplements on Muscle-Derived Stem Cells In Vitro. *Int. J. Stem Cells* **2010,** *3* (1), 63–67.
235. Kulkami, R. N.; Mizrachi, E. B.; Ocana, A. G.; Stewart, A. F. Human Beta-Cell Proliferation and Intracellular Signalling: Driving in the Dark Without a Road Map. *Diabetes* **2012,** *61,* 2205–2213.
236. Bernal-Mizrachi, E.; Kulkami, R. N.; Scott, D. K.; Mauvais-Jarvis, F.; Stewart, A. F. Human Beta-Cell Proliferation and Intracellular Signalling: Still Driving in the Dark Without a Road Map. *Diabetes* **2014,** *63,* 819–831.
237. Stewart, A. F.; Hussain, M. A.; Garcia-Ocana, A.; Vasavada, R. C.; Bhushan, A.; Bernal-Mizrachi, E.; Kulkarni, R. N. Human Beta-Cell Proliferation and Intracellular Signalling: Part 3. *Diabetes* **2015,** *64,* 1872–1884.
238. Scharfmann, R.; Pechberty, S.; Hazhouz, Y.; von Bulow, M.; Bricout-Neveu, E.; Grenier-Godard, M.; Guez, F.; Rachdi, L.; Lohmann, M.; Czernichow, P.; Ravassard, P. Development of a Conditionally Immortalizsed Human Pancreatic Beta-Cell Line. *J. Clin. Invest.* **2014,** *124* (5), 2087–2098.
239. Wang, W.; Walker, J. R.; Wang, X.; Tremblay, M. S.; Lee, J. W.; Wu, X.; Schultz, P. G. Identification of Small-Molecule Inducers of Pancreatic Beta-Cell Expansion. *Proc. Natl. Acad. Sci. U. S. A.* **2009,** *106* (5), 1427–1432.
240. Shen, W.; Tremblay, M. S.; Deshmukh, V. A.; Wang, W.; Filippi, C. M.; Harb, G.; Zhang, Y. Q.; Kamireddy, A.; Baaten, J. E.; Jin, Q.; Wu, T.; Swoboda, J. G.; Cho, C. Y.; Li, J.; Laffitte, B. A.; McNamara, P.; Glynne, R.; Wu, X.; Herman, A. E.; Schultz, P. G. Small-Molecule Inducer of β Cell Proliferation Identified by High-Throughput Screening. *J. Am. Chem. Soc.* **2013,** *135* (5), 1669–1672.
241. Annes, J. P.; Ryu, J. H.; Lam, K.; Carolan, P. J.; Utz, K.; Hollister-Lock, J.; Arvanites, A. C.; Rubin, L. L.; Weir, G.; Melton, D. A. Adenosine Kinase Inhibition Selectively Promotes Rodent and Porcine Islet β-Cell Replication. *Proc. Natl. Acad. Sci. U. S. A.* **2012,** *109* (10), 3915–3920.
242. Boerner, B. P.; George, N. M.; Mir, S. U. R.; Sarvetnick, N. E. WS6 Induces Both Alpha and Beta Cell Proliferation Without Cell Stem Cellffecting Differentiation or Viability. *Endocr. J.* **2015,** *62* (4), 379–396.
243. Wang, P.; Alvarez-Perez, J.-C.; Felsenfield, D. P.; Liu, H.; Sivendran, S.; Bender, A.; Kumar, A.; Sanchez, R.; Scott, D. K.; Garcia-Ocana, A.; Stewart, A. F. A High-Throughput Chemical Screen Reveals That Harmine-Mediated Inhibition of DYRK1A Increases Human Pancreatic Beta Cell Replication. *Nat. Med.* **2015,** *21* (4), 383–388.
244. O'Sullivan, E.; Vegas, A.; Anderson, D. G.; Weir, G. C. Islets Transplanted in Immunoisolation Devices: A Review of the Progress and the Challenges That Remain. *Endocr. Rev.* **2011,** *32* (6), 827–844.
245. Borowiak, M. The New Generation of Beta-Cells: Replication, Stem Cell Differentiation, and the Role of Small Molecules. *Rev. Diabet. Stud.* **2010,** *7* (2), 93–104.
246. Baetge, E. E. Production of Beta-Cells From Human Embryonic Stem Cells. *Diabetes Obes. Metab.* **2008,** *10* (Suppl. 4), 186–194.
247. Zhang, D.; Jiang, W.; Liu, M.; Sui, X.; Yin, X.; Chen, S.; Shi, Y.; Deng, H. Highly Efficient Differentiation of Human ES Cells and iPS Cells Into Mature Pancreatic Insulin-Producing Cells. *Cell Res.* **2009,** *19* (4), 429–438.
248. Champeris Tsaniras, S.; Jones, P. M. Generating Pancreatic Beta-Cells From Embryonic Stem Cells by Manipulating Signaling Pathways. *J. Endocrinol.* **2010,** *206* (1), 13–26.
249. Wang, X.; Metzger, D. L.; Meloche, M.; Hao, J.; Ao, Z.; Warnock, G. L. Generation of Transplantable Beta Cells for Patient-Specific Cell Therapy. *Int. J. Endocrinol.* **2012,** *2012,* 414812.
250. Fryer, B. H.; Rezania, A.; Zimmerman, M. C. Generating Beta-Cells In Vitro: Progress Towards a Holy Grail. *Curr. Opin. Endocrinol. Diabetes Obes.* **2013,** *20* (2), 112–117.
251. Kumar, S. S.; Alarfaj, A. A.; Munusamy, M. A.; Singh, R. A. J. A.; Peng, I.-C.; Priya, S. P.; Hamat, R. A.; Higuchi, A. Recent Developments in Beta-Cell Differentiation of Pluripotent Stem Cells Induced by Small and Large Molecules. *Int. J. Mol. Sci.* **2014,** *15,* 23418–23447.
252. Pandian, G. N.; Taniguchi, J.; Sugiyama, H. Cellular Reprogramming for Pancreatic Beta-Cell Regeneration: Clinical Potential of Small Molecule Control. *Clin. Trans. Med.* **2014,** *3* (6), 1–12.
253. Pagliuca, F. W.; Millman, J. R.; Gurtler, M.; Segel, M.; van Dervort, A.; Ryu, J. H.; Peterson, Q. P.; Greiner, D.; Melton, D. A. Generation of Functional Human Pancreatic Beta-Cells In Vitro. *Cell* **2014,** *159,* 428–439.
254. Schultz, T. C.; Young, H. Y.; Agulnick, A. D.; Babin, J. M.; Baetge, E. E.; Bang, A. G.; et al. A Scalable System for Production of Functional Pancreatic Progenitors From hum. *PLoS One* **2012,** *7* (5), e37004.
255. Narayanan, K.; Lim, V. Y.; Shen, J.; Tan, Z. W.; Rajendran, D.; Luo, S.-C.; Gao, S.; Wan, A. C. A.; Ying, J. Y. Extracellular Matrix-Mediated Differentiation of Human Embryonic Stem Cells: Differentiation to Insulin-Secreting Beta Cells. *Tissue Eng. Part A* **2014,** *20* (1/2), 424–434.
256. Koblas, T.; Zacharovova, K.; Berkova, Z.; Girman, P.; Saudek, F. An Acidic pH and Activation of Phosphoinositide 3-Kinase Stimulate Differentiation of Pancreatic Progenitors Into Insulin-Producing Cells. *Transplant. Proc.* **2010,** *42,* 2075–2080.
257. Zhou, Q.; Brown, J.; Kanarek, A.; Rajagopal, J.; Melton, D. A. *In Vivo* Reprogramming of Adult Pancreatic Exocrine Cells to Beta-Cells. *Nature* **2008,** *455,* 627–632.
258. Racanicchi, L.; Basta, G.; Montanucci, P.; Guido, L.; Pensato, A.; Conti, V.; Calafiore, R. Neonatal Pig Liver-Derived Progenitors for Insulin-Producing Cells: An in vitro Study. *Tissue Eng.* **2007,** *13* (12), 2923–2931.
259. Liu, J.; Liu, Y.; Wang, H.; Hao, H.; Han, Q.; Shen, J.; Shi, J.; Li, C.; Mu, Y.; Han, W. Direct Differentiation of Hepatic Stem-Like WB Cells Into Insulin-Producing Cells Using Small Molecules. *Sci. Rep.* **2013,** *3,* 1185.
260. Ouyang, J.; Huang, W.; Yu, W.; Xiong, W.; Mula, R. V.; Zou, H.; Yu, Y. Generation of Insulin-Producing Cells From Rat Mesenchymal Stem Cells Using an Aminopyrrole Derivative XW4.4. *Chem. Biol. Interact.* **2014,** *208,* 1–7.
261. Yang, S.-F.; Xue, W.-J.; Duan, Y.-F.; Xie, L.-Y.; Lu, W.-H.; Zheng, J.; Yin, A.-P. Nicotinamide Facilitates Mesenchymal Stem Cell Differentiation Into Insulin-Producing Cells and Homing to Pancreas in Diabetic Mice. *Transplant. Proc.* **2015,** *47,* 2041–2049.
262. Li, K.; Zhu, S.; Russ, H. A.; Xu, S.; Xu, T.; Zhang, Y.; Ma, T.; Hebrok, M.; Ding, S. Small Molecules Facilitate the Reprogramming of Mouse Fibroblasts Into Pancreatic Lineages. *Cell Stem Cell* **2014,** *14,* 228–236.
263. Keenan, H. A.; Sun, J. K.; Levine, J.; Doria, A.; Aiello, L. P.; Eisenbarth, G.; Bonner-Weir, S.; King, G. L. Residual Insulin Production and Pancreatic Beta-Cell Turnover After 50 Years of Diabetes: Joslin Medalist Study. *Diabetes* **2010,** *59,* 2846–2853.
264. Wang, P.; Fiaschi-Taesch, N. M.; Vasavada, R. C.; Scott, D. K.; Garcia-Ocana, A.; Stewart, A. F. Diabetes Mellitus- Advances and Challenges in Human Beta-Cell Proliferation. *Nat. Rev. Endocrinol.* **2015,** *11,* 201–211.
265. Vetere, A.; Choudhary, A.; Burns, S. M.; Wagner, B. K. Targeting the Pancreatic Beta-Cell to Treat Diabetes. *Nat. Rev. Drug Discov.* **2014,** *13,* 277–289.
266. Christensen, D. P.; Gysemans, C.; Lundh, M.; Dahllöf, M. S.; Noesgaard, D.; Schmidt, S. F.; Mandrup, S.; Birkbak, N.; Workman, C. T.; Piemonti, L.; Blaabjerg, L.; Monzani, V.; Fossati, G.; Mascagni, P.; Paraskevas, S.; Aikin, R. A.; Billestrup, N.; Grunnet, L. G.; Dinarello, C. A.; Mathieu, C.; Mandrup-Poulsen, T. Lysine Deacetylase Inhibition Prevents Diabetes by Chromatin-Independent Immunoregulation and β-Cell Protection. *Proc. Natl. Acad. Sci. U. S. A.* **2014,** *111* (3), 1055–1059.
267. Chou, D. H.-C.; Schreiber, S. L.; Wagner, B. K.; et al. Kinase-Independent Small Molecule Inhibition of JAK-STAT Signaling. *J. Am. Chem. Soc.* **2015,** *137,* 7929–7934.
268. Tran, K.; Li, Y.; Duan, H.; Arora, D.; Lim, H.-Y.; Wang, W. Identification of Small Molecules that Protect Pancreatic Beta Cells Against Endoplasmic Reticulum Stress-Induced Cell Death. *ACS Chem. Biol.* **2014,** *9,* 2796–2806.
269. Tiso, N.; Moro, E.; Argenton, F. Zebrafish Pancreas Development. *Mol. Cell. Endocrinol.* **2009,** *312* (1-2), 24–30.
270. Andersson, O.; Adams, B. A.; Yoo, D.; Ellis, G. C.; Gut, P.; Anderson, R. M.; German, M. S.; Stanier, D. Y. R. Adenosine Signaling Promotes Regeneration of Pancreatic Beta-Cells In Vivo. *Cell Metab.* **2012,** *15,* 885–894.
271. Banerjee, S. A Review of Developments in the Management of Retinal Diseases. *J. R. Soc. Med.* **2006,** *99* (3), 125–127.
272. Sejpal, K.; Bakhtiari, P.; Deng, S. X. Presentation, Diagnosis and Management of Limbal Stem Cell Deficiency. *Middle East Afr. J. Ophthalmol.* **2013,** *20* (1), 5–10.
273. Yu-Wai-Man, C.; Khaw, P. T. Developing Novel Anti-Fibrotic Therapeutics to Modulate Post-Surgical Wound Healing in Glaucoma: Big Potential for Small Molecules. *Expert Rev. Ophthalmol.* **2015,** *10* (1), 65–76.

274. Xu, S. W.; Liu, S.; Eastwood, M.; Sonnylal, S.; Denton, C. P.; Abraham, D. J.; Leask, A. Rac Inhibition Reverses the Phenotype of Fibrotic Fibroblasts. *PLoS One* **2009,** *4* (10), e7438.
275. Li, D. Q.; Wang, Z.; Yoon, K. C.; Bian, F. Characterization, Isolation, Expansion and Clinical Therapy of Human Corneal Epithelial Stem/Progenitor Cells. *J. Stem Cells* **2014,** *9* (2), 79–91.
276. Ahmad, S. Concise Review: Limbal Stem Cell Deficiency, Dysfunction, and Distress. *Stem Cells Transl. Med.* **2012,** *1* (2), 110–115.
277. Osei-Bempong, C.; Figueiredo, F. C.; Lako, M. The Limbal Epithelium of the Eye—A Review of Limbal Stem Cell Biology, Disease and Treatment. *Bioessays* **2013,** *35* (3), 211–219.
278. Mikhailova, A.; Ilmarinen, T.; Uusitalo, H.; Skottman, H. Small-Molecule Induction Promotes Corneal Epithelial Cell Differentiation From Human Induced Pluripotent Stem Cells. *Stem Cell Rep.* **2014,** *2* (2), 219–231.
279. Dai, Y.; Guo, Y.; Wang, C.; Liu, Q.; Yang, Y.; Li, S.; Guo, X.; Lian, R.; Yu, R.; Liu, H.; Chen, J. Non-Genetic Direct Reprogramming and Biomimetic Platforms in a Preliminary Study for Adipose-Derived Stem Cells Into Corneal Endothelia-Like Cells. *PLoS One* **2014,** *9* (10), e109856.
280. Klassen, H.; Sakaguchi, D. S.; Young, M. J. Stem Cells and Retinal Repair. *Prog. Retin. Eye Res.* **2004,** *23* (2), 149–181.
281. Huang, Y.; Enzmann, V.; Ildstad, S. T. Stem Cell-Based Therapeutic Applications in Retinal Degenerative Diseases. *Stem Cell Rev.* **2011,** *7* (2), 434–445.
282. Meyer, J. S.; Shearer, R. L.; Capowski, E. E.; Wright, L. S.; Wallace, K. A.; McMillan, E. L.; Zhang, S. C.; Gamm, D. M. Modeling Early Retinal Development With Human Embryonic and Induced Pluripotent Stem Cells. *Proc. Natl. Acad. Sci. U. S. A.* **2009,** *106* (39), 16698–16703.
283. Wong, I. Y.; Poon, M. W.; Pang, R. T.; Lian, Q.; Wong, D. Promises of Stem Cell Therapy for Retinal Degenerative Diseases. *Graefes Arch. Clin. Exp. Ophthalmol.* **2011,** *249* (10), 1439–1448.
284. Tibbetts, M. D.; Samuel, M. A.; Chang, T. S.; Ho, A. C. Stem Cell Therapy for Retinal Disease. *Curr. Opin. Ophthalmol.* **2012,** *23* (3), 226–234.
285. Culme-Seymour, E. J.; Davie, N. L.; Brindley, D. A.; Edwards-Parton, S.; Mason, C. A Decade of Cell Therapy Clinical Trials (2000–2010). *Regen. Med.* **2012,** *7* (4), 455–462.
286. Schwartz, S. D.; Hubschman, J. P.; Heilwell, G.; Franco-Cardenas, V.; Pan, C. K.; Ostrick, R. M.; Mickunas, E.; Gay, R.; Klimanskaya, I.; Lanza, R. Embryonic Stem Cell Trials for Macular Degeneration: A Preliminary Report. *Lancet* **2012,** *379* (9817), 713–720.
287. Gonzalez-Cordero, A.; West, E. L.; Pearson, R. A.; Duran, Y.; Carvalho, L. S.; Chu, C. J.; Naeem, A.; Blackford, S. J.; Georgiadis, A.; Lakowski, J.; Hubank, M.; Smith, A. J.; Bainbridge, J. W.; Sowden, J. C.; Ali, R. R. Photoreceptor Precursors Derived From Three-Dimensional Embryonic Stem Cell Cultures Integrate and Mature Within Adult Degenerate Retina. *Nat. Biotechnol.* **2013,** *31* (8), 741–747.
288. Cyranoski, D. Stem Cells Cruise to Clinic. *Nature* **2013,** *494* (7438), 413.
289. Castelvecchi, D. *Japan to Start Stem-Cell Study on Humans.* http://blogs.nature.com/news/2013/07/japan-to-start-stem-cell-study-on-humans.html (accessed February 06, 2016).
290. Ittner, L. M.; Wurdak, H.; Schwerdtfeger, K.; Kunz, T.; Ille, F.; Leveen, P.; Hjalt, T. A.; Suter, U.; Karlsson, S.; Hafezi, F.; Born, W.; Sommer, L. Compound Developmental Eye Disorders Following Inactivation of TGFbeta Signaling in Neural-Crest Stem Cells. *J. Biol.* **2005,** *4* (3), 11.
291. Bonafoux, D.; Lee, W. C. Strategies for TGF-Beta Modulation: A Review of Recent Patents. *Expert Opin. Ther. Pat.* **2009,** *19* (12), 1759–1769.
292. Glaser, K. B.; Li, J.; Aakre, M. E.; Morgan, D. W.; Sheppard, G.; Stewart, K. D.; Pollock, J.; Lee, P.; O'Connor, C. Z.; Anderson, S. N.; Mussatto, D. J.; Wegner, C. W.; Moses, H. L. Transforming Growth Factor Beta Mimetics: Discovery of 7-[4-(4-Cyanophenyl)Phenoxy]-Heptanohydroxamic Acid, a Biaryl Hydroxamate Inhibitor of Histone Deacetylase. *Mol. Cancer Ther.* **2002,** *1* (10), 759–768.
293. Duan, H.; Wang, Y.; Yang, L.; Qu, M.; Wang, Q.; Shi, W.; Zhou, Q. Pluripotin Enhances the Expansion of Rabbit Limbal Epithelial Stem/Progenitor Cells In Vitro. *Exp. Eye Res.* **2012,** *100,* 52–58.
294. Swoboda, J. G.; Elliott, J.; Deshmukh, V.; de Lichtervelde, L.; Shen, W.; Tremblay, M. S.; Peters, E. C.; Cho, C. Y.; Lu, B.; Girman, S.; Wang, S.; Schultz, P. G. Small Molecule Mediated Proliferation of Primary Retinal Pigment Epithelial Cells. *ACS Chem. Biol.* **2013,** *8* (7), 1407–1411.
295. Bourne, M. C.; Gruneberg, H. Degeneration of the Retina and Cataract, a New Recessive Gene in the Rat. *J. Hered.* **1939,** *6,* 131.
296. Hyatt, G. A.; Dowling, J. E. Retinoic Acid. A key Molecule for Eye and Photoreceptor Development. *Invest. Ophthalmol. Vis. Sci.* **1997,** *38* (8), 1471–1475.
297. Idelson, M.; Alper, R.; Obolensky, A.; Ben-Shushan, E.; Hemo, I.; Yachimovich-Cohen, N.; Khaner, H.; Smith, Y.; Wiser, O.; Gropp, M.; Cohen, M. A.; Even-Ram, S.; Berman-Zaken, Y.; Matzrafi, L.; Rechavi, G.; Banin, E.; Reubinoff, B. Directed Differentiation of Human Embryonic stem Cells Into Functional Retinal Pigment Epithelium Cells. *Cell Stem Cell* **2009,** *5* (4), 396–408.
298. Osakada, F.; Jin, Z. B.; Hirami, Y.; Ikeda, H.; Danjyo, T.; Watanabe, K.; Sasai, Y.; Takahashi, M. In Vitro Differentiation of Retinal Cells From Human Pluripotent Stem Cells by Small-Molecule Induction. *J. Cell Sci.* **2009,** *122* (Pt 17), 3169–3179.
299. Buchholz, D. E.; Hikita, S. T.; Rowland, T. J.; Friedrich, A. M.; Hinman, C. R.; Johnson, L. V.; Clegg, D. O. Derivation of Functional Retinal Pigmented Epithelium From Induced Pluripotent Stem Cells. *Stem Cells* **2009,** *27* (10), 2427–2434.
300. Hirami, Y.; Osakada, F.; Takahashi, K.; Okita, K.; Yamanaka, S.; Ikeda, H.; Yoshimura, N.; Takahashi, M. Generation of Retinal Cells From Mouse and Human Induced Pluripotent Stem Cells. *Neurosci. Lett.* **2009,** *458* (3), 126–131.
301. Krohne, T.; Westenskow, P.; Kurihara, T.; Friedlander, D.; Lehmann, M.; Dorsey, A.; Li, W.; Zhu, S.; Schultz, A.; Wang, J.; Siuzdak, G.; Ding, S.; Friedlander, M. Generation of Retinal Pigment Epithelial Cells From Small Molecules and OCT4 Reprogrammed Human Induced Pluripotent Stem Cells. *Stem Cells Transl. Med.* **2012,** *1* (2), 96–109.
302. Wang, X.; Xiong, K.; Lin, C.; Lv, L.; Chen, J.; Xu, C.; Wang, S.; Gu, D.; Zheng, H.; Yu, H.; Li, Y.; Xiao, H.; Zhou, G. New Medium Used in the Differentiation of Human Pluripotent Stem Cells to Retinal Cells Is Comparable to Fetal Human Eye Tissue. *Biomaterials* **2015,** *53,* 40–49.
303. Maruotti, J.; Sripathi, S. R.; Bharti, K.; Fuller, J.; Wahlin, K. J.; Ranganathan, V.; Sluch, V. M.; Berlinicke, C. A.; Davis, J.; Kim, C.; Zhao, L.; Wan, J.; Qian, J.; Corneo, B.; Temple, S.; Dubey, R.; Olenyuk, B. Z.; Bhutto, I.; Lutty, G. A.; Zack, D. J. Small-Molecule-Directed, Efficient Generation of Retinal Pigment Epithelium From Human Pluripotent Stem Cells. *Proc. Natl. Acad. Sci. U. S. A.* **2015,** *112* (35), 10950–10955.
304. Westenskow, P.; Sedillo, Z.; Barnett, A.; Friedlander, M. Efficient Derivation of Retinal Pigment Epithelium Cells From Stem Cells. *J. Vis. Exp.* **2015,** *97,* e52214.
305. Parvini, M.; Parivar, K.; Safari, F.; Tondar, M. Generation of Eye Field/Optic Vesicle-Like Structures From Human Embryonic Stem Cells Under Two-Dimensional and Chemically Defined Conditions. *In Vitro Cell. Dev. Biol. Anim.* **2015,** *51* (3), 310–318.
306. Fuller, J. A.; Shaw, G. C.; Bonnet-Wersinger, D.; Hansen, B. S.; Berlinicke, C. A.; Inglese, J.; Zack, D. J. A high Content Screening Approach to Identify Molecules Neuroprotective for Photoreceptor Cells. *Adv. Exp. Med. Biol.* **2014,** *801,* 773–781.
307. Ferrer, M.; Corneo, B.; Davis, J.; Wan, Q.; Miyagishima, K. J.; King, R.; Maminishkis, A.; Marugan, J.; Sharma, R.; Shure, M.; Temple, S.; Miller, S.; Bharti, K. A Multiplex High-Throughput Gene Expression Assay to Simultaneously Detect Disease and Functional Markers in Induced Pluripotent Stem Cell-Derived Retinal Pigment Epithelium. *Stem Cells Transl. Med.* **2014,** *3* (8), 911–922.
308. Lane, A.; Philip, L. R.; Ruban, L.; Fynes, K.; Smart, M.; Carr, A.; Mason, C.; Coffey, P. Engineering Efficient Retinal Pigment Epithelium Differentiation From Human Pluripotent Stem Cells. *Stem Cells Transl. Med.* **2014,** *3* (11), 1295–1304.
309. Jasty, S.; Suriyanarayanan, S.; Krishnakumar, S. Influence of Self-Assembling Peptide Nanofibre Scaffolds on Retinal Differentiation Potential of Stem/Progenitor Cells Derived From Ciliary Pigment Epithelial Cells. *J. Tissue Eng. Regen. Med.* **2014;** http://dx.doi.org/10.1002/term.1947.

1.14 Data Integration and Sharing Supporting Drug R&D

F Sanz, Universitat Pompeu Fabra, Barcelona, Spain

© 2017 Elsevier Ltd. All rights reserved.

1.14.1	Introduction	436
1.14.2	Seeking Relevant Knowledge for a Drug Discovery Project	437
1.14.3	Information Supporting Target Identification	437
1.14.4	Information Supporting Hit Identification and Drug Design and Development	438
1.14.5	Information Sharing and Integrative Approaches in Predictive Toxicology	438
1.14.6	Using and Reusing Clinical Data for Biomedical Research	441
1.14.7	Integrating Clinical Data and Biomedical Evidence in Pharmacovigilance	441
1.14.8	Final Considerations	442
References		443

1.14.1 Introduction

Drug discovery and development is a knowledge-intensive process that implies the generation, management, and analysis of huge amounts of data (see Fig. 1). The first step of the process is the identification and analysis of all the preexisting knowledge that is relevant for the intended project. Regarding the new data to be generated during the project, they start with the results of the wide scope of biological experiments that are required for the discovery and validation of novel biological targets. Currently, the research on new targets uses to include "omics" experiments (genomics, transcriptomics, proteomics, metabolomics, etc.), which generate a huge amount of data. Once a new therapeutic target has been identified and validated, the following step usually is the execution of virtual and experimental screening campaigns, which assign affinities for the studied targets to series of thousands to millions of drug-like compounds and identify hits as compounds with promising biological profiles. The hits are subsequently transformed into leads through modification of their structures in order to improve the biological properties, using information on structure–activity relationships. The lead compounds are then submitted for preclinical assessment, which generates data informing about key aspects such as pharmacokinetics and toxicology. Once a drug candidate enters into clinical trials, another vast collection of data from the enrolled patients is accumulated. Last but not least, the drugs that are finally authorized for being marketed continue generating useful data about the therapeutic and adverse effects of their use in clinical practice. In summary, the whole pharmaceutical research pipeline uses and produces a massive and diverse assortment of data.

A point to be particularly stressed is the high degree of compartmentalization of the information management and analysis between the different stages of the drug discovery and development process. There are silos of information and expertise that hamper the efficiency of biomedical and pharmaceutical research.[1] This is an adverse scenario that requires to be overcome, since the integration of heterogeneous biomedical information (of different types and from different sources) constitutes an opportunity for gaining a more complete and powerful view on diseases and their therapeutics (Fig. 2). In order to maximize the effectiveness of efforts for integrating data in pharmaceutical R&D, it is crucial to identify and adopt relevant standards, or to develop them if they are unavailable. It is also vital for the annotation of the data in terms of their provenance and quality in order to make possible a critical assessment of their suitability for reuse. Another challenge that has to be addressed is the fact that most of the knowledge that is generated in the biomedical research is only disseminated by means of free-text scientific publications. Taking into account

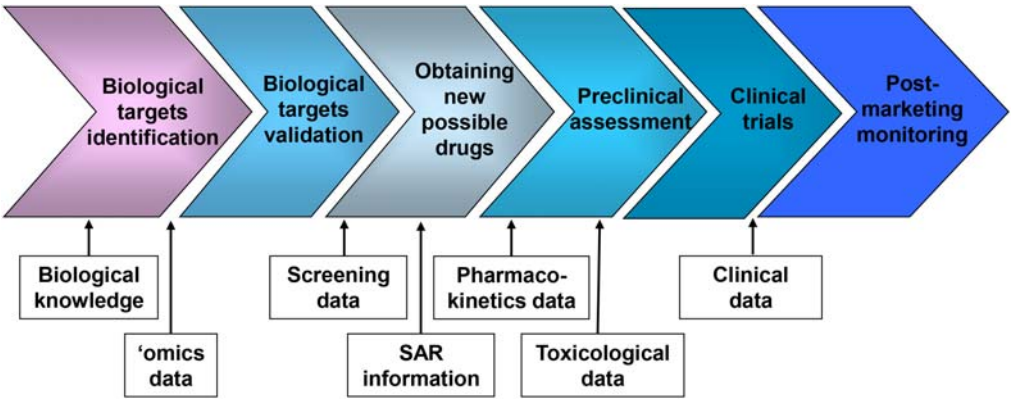

Fig. 1 Data and knowledge generation and use along the drug discovery and development pipeline.

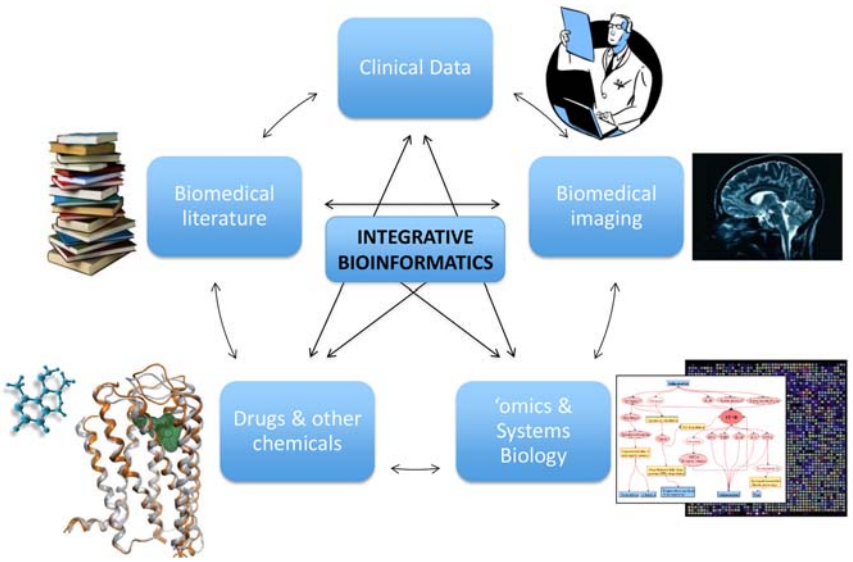

Fig. 2 Integration of heterogeneous biomedical information for gaining a more complete and powerful view on diseases and therapeutics.

the huge amount of biomedical publications that are generated and the fact that all of them are currently published electronically (eg, PubMed is an electronic repository that contains more than twenty million abstracts of scientific publications and to which about 700,000 more are added every year), we need to put in place computational methods for automatically extract information from free-text digital documents. This necessity also applies to the enormous amounts of clinical documents that record relevant evidences and that have free-text format. Finally, it has to be pointed out that the sustainability of data collections should be considered a key policy and the promotion of data sharing should be understood as a responsibility, especially when data are derived from public funding.[2]

The present article reviews different strategies and initiatives in integrative data approaches that facilitate the pharmaceutical R&D. They are presented following the sequence of the different stages of the drug discovery and development pipeline as depicted in Fig. 1.

1.14.2 Seeking Relevant Knowledge for a Drug Discovery Project

As it was previously stated, the first stage of such a pipeline is the identification of existing knowledge that constitutes the background for a particular project. In this respect, we need tools that facilitate the extraction and integration of data and information from different resources. A recent and successful initiative on the matter has been the Open PHACTS project, carried out in the framework of the Innovative Medicines Initiative (IMI), which is jointly funded by the European Commission and the EFPIA.[3] Open PHACTS Discovery Platform uses semantic web technology approaches to enable scientists to easily access and process data from multiple sources to solve real-world drug discovery problems.[4] Open PHACTS was built to address drug discovery questions that are of high priority to the pharmaceutical industry. Most of these frequently asked questions (FAQs) revolve around the combination of data concerning compounds, targets, pathways, and diseases. An example of them may be: *For disease X, which targets have ligands in different stages of the development process with publications and/or patents describing these compounds*? Computational drug discovery using workflow tools and the integrated resources of Open PHACTS can deliver answers to most of these questions.[5]

Another useful resource for reviewing information about marketed and experimental drugs is DrugBank.[6,7] It combines detailed drug data (ie, chemical, pharmacological, and pharmaceutical) with comprehensive drug target (ie, sequence, structure, and pathway) information. DrugBank v4.3 contains 8312 drug entries including 2036 FDA-approved small molecule drugs, 233 FDA-approved biotech (protein/peptide) drugs, 93 nutraceuticals, and over 6000 experimental drugs. Additionally, 4317 nonredundant protein (ie, drug target/enzyme/transporter/carrier) sequences are linked to these drug entries. Each drug entry contains more than 200 data fields with half of the information being devoted to drug/chemical data and the other half devoted to drug target or protein data.[6]

1.14.3 Information Supporting Target Identification

One of the information resources developed in the framework of Open PHACTS is DisGeNET,[8,9] a database that summarizes information on gene–disease associations. This kind of information is crucial in the process of studying the molecular basis of diseases

and to identify putative drug targets for its pharmacological treatment. It has to be pointed out that there is a large volume of biomedical information that connects genomic elements to disease phenotypes, but such information is fragmented across different repositories and hidden in the biomedical literature. Consequently, there was a need for computational resources which *gather*, *integrate*, and *analyze* medically relevant information on the genetic causes of diseases, and that was the motivation of the DisGeNET development.

DisGeNET is a comprehensive resource on gene–disease associations (about half a million of them), which integrates information from publicly available databases and directly from the biomedical literature by text-mining (more than 80% of gene–disease associations). Text-mining is a computational process that first identifies relevant entities in free text (eg, proteins, diseases, drugs). This identification implies the use of adequate vocabularies and tricks for managing the variability of texts associated with a specific entity (eg, *melanocortin-4 receptor*, *MC4R*, and *MC4-R* are different texts referring to the same protein, or *obese* and *obesity* indicate the same disease). Once the entities have been identified, a natural language processing (NLP) algorithm is used to detect relationships between entities within sentences (eg, *MC4R is associated with obesity*). DisGeNET includes a user-friendly interface that facilitates the interrogation of the system (see **Fig. 3**). It has to be stressed that DisGeNET ranks the lists of gene–disease associations by means of a score based in the reliability of the source (greater for resources curated by experts and lower for associations obtained only by text-mining), as well as in the number of evidences that support the association.

Another type of information that is key for the study of the disease mechanisms and their potential pharmacological targets regards systems biology, that is, information about the biological processes and mechanisms. The Reactome knowledgebase[10,11] provides molecular details of signal transduction, transport, DNA replication, metabolism, and other cellular processes as an ordered network of molecular transformations (an extended version of a classic metabolic map) in a single consistent data model.[11] There are also databases that contain information on protein–protein interactions (PPIs), such as STRING[12,13] or the human Interactome database,[14,15] or resources that facilitate the access to this type of information, such as HIPPIE[16,17] or Biana.[18,19]

1.14.4 Information Supporting Hit Identification and Drug Design and Development

The identification of hits for the selected targets and the process that goes from targets to drug candidates benefit from the availability of comprehensive repositories of information about the physicochemical and biological properties of drug-like compounds. A paradigmatic example of this type of resources is ChEMBL,[20,21] which is an open large-scale bioactivity database containing information largely manually extracted from the medicinal chemistry literature. Information regarding the compounds tested (including their structures), the biological or physicochemical assays performed on these, and the targets of these assays are recorded in a structured form.[21] In Jan. 2016, ChEMBL_20 reported data corresponding to activities of 1,463,270 distinct compounds versus 10,774 targets, totalizing 13,520,737 activity data. Obviously, the biological behavior of each compound is only tested in front of minority of the possible targets and most of the compound–target combinations remain undetermined,[22] even been required for an appropriate appraisal of the therapeutic and safety profiles of the drugs. For this reason, there are different methods and software that provide estimates for the missing values based on similarity strategies (see Ref.[23] as an example). It deserves to be pointed out that ChEMBL is complemented by the SureChEMBL database,[24] which is a publicly available large-scale resource containing compounds extracted from the full text, images, and attachments of patent documents. SureChEMBL provides access to a timely set of annotated compound-patent associations. Currently, the database contains 17 million compounds extracted from 14 million patent documents.[25]

1.14.5 Information Sharing and Integrative Approaches in Predictive Toxicology

The toxicological assessment of the potential drug candidates is a key aspect in the preclinical drug development. They imply sequences of long and expensive in vivo studies using different animal species. In the framework of three 3Rs policy (Replacement, Reduction, and Refinement in the use of animals in scientific research), the reuse of the experience accumulated in previous analogous projects for generating reliable predictions on new compounds under investigation is a must. The best historical data for such a purpose remains generally buried in the archives of the pharmaceutical companies. Some years ago, a large group of pharmaceutical companies, in collaboration with academic experts and small- and medium-sized enterprises, decided to launch the eTOX project[26] in the framework of the IMI. This project has the aim of building and exploiting a database that contains legacy in vivo toxicological studies donated by the pharmaceutical companies. The data of the resulting database is shared among all the project partners, and will be made accessible to external parties after the project finalization. In May 2016, the eTOX database contained more than 7000 repeated-dose toxicological studies corresponding to more than 2000 compounds. The studies correspond to different animal species (mainly rat, but also dog, monkey and mouse, among others) and report different kinds of toxicological findings (histopathology, organ weights, clinical chemistry, clinical signs, hematology, etc.), observed in different organs (liver, spleen, thymus, kidney, lung, etc.).[27] The database incorporates the chemical structures of the compounds and, in most of the cases, information about their pharmacological mode of action. The eTOX project also collects and links complementary information from other sources, such the ChEMBL database. All this data is used for developing a wide scope of predictive models, which use different methodological approaches, including multilevel and multiscale strategies.[28] The structure of the eTOX project is

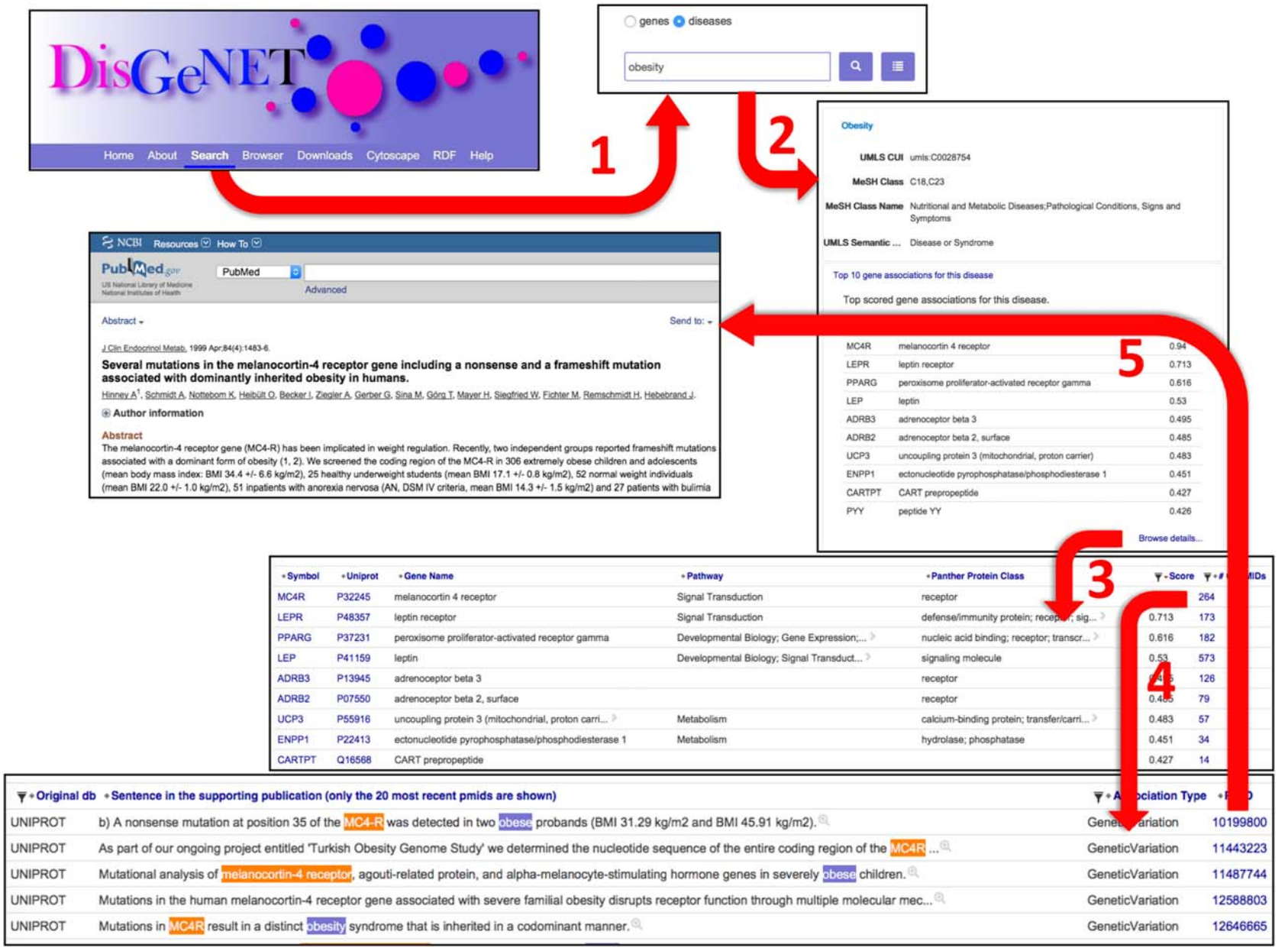

Fig. 3 Screenshots of DisGeNET showing a typical information query.

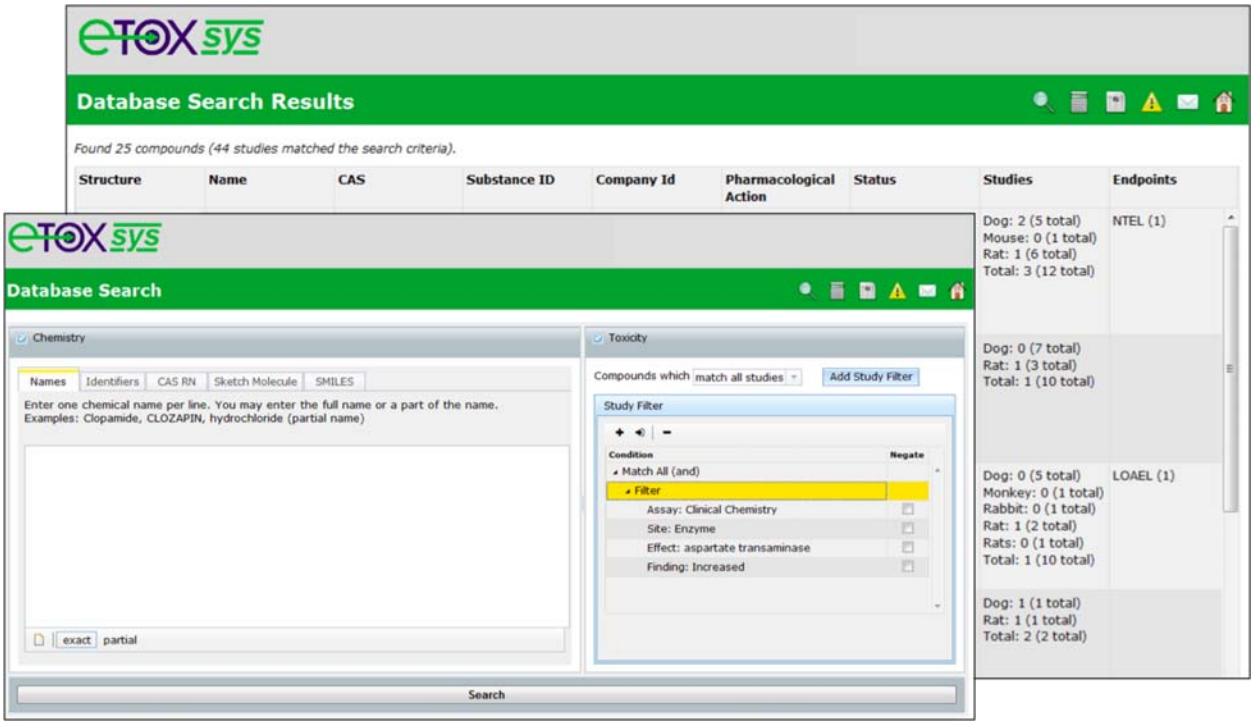

Fig. 4 Scheme showing the data integration and exploitation in the eTOX project.

summarized in the scheme shown in Fig. 4. The interrogation of the database, the selection of the predictive models, and the display of the results are done through an integrated graphical interface named eTOXsys (Fig. 5).

Other resources that contain useful public high-throughput chemical-toxicological data are ToxCast and Tox21, which are promoted by the US Environmental Protection Agency (EPA). ToxCast has data on over 1800 chemicals from a broad range of sources including industrial and consumer products, food additives, and potentially "green" chemicals that could be safer alternatives to

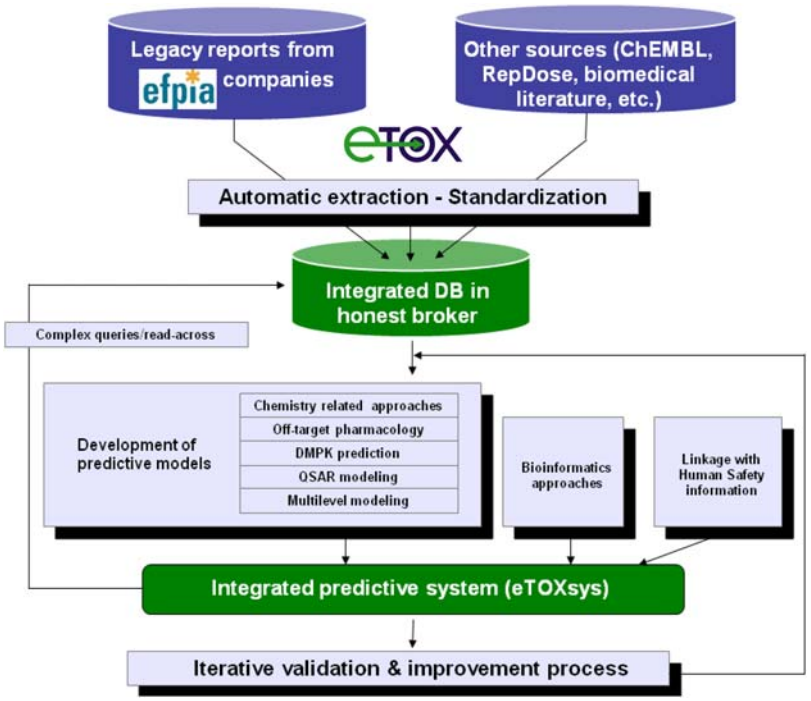

Fig. 5 Screenshots of eTOXsys showing a typical query of the database and the output obtained.

existing chemicals. ToxCast screens chemicals in over 700 high-throughput assays that cover a range of high-level cell responses and approximately 300 signaling pathways.[29] Regarding Tox21, it aims to extend the toxicological screening to 10,000 chemicals.[30] The Distributed Structure-Searchable Toxicity (DSSTox) Database provides a public chemistry resource for supporting improved predictive toxicology, including the ToxCast and Tox21 high-throughput toxicology efforts.[31] Though, it has to be pointed out that ToxCast and Tox21 are not specifically focused to drug-like compounds, but to chemicals at large. Lastly, it has to be pointed out that there is an interesting European-centric initiative (diXa) for depositing and accessing to toxicogenomics data.[32] There is public data warehouse supporting the diXa data operations.[33]

1.14.6 Using and Reusing Clinical Data for Biomedical Research

Nowadays, clinical research and healthcare practice generate huge amounts of data, which in all the cases are stored in electronic format. Regarding the clinical trials, there is a trend toward transparency supported by health authorities and the pharmaceutical industry, which is leading to the creation of useful databases where an increasing amount of public information about clinical trials can be found. This is the case of ClinicalTrials.gov in United States[34] and EudraPharm[35] and EudraCT[36] in the EU.

On the other hand, the electronic healthcare records (EHR) constitute a priceless source of evidence for biomedical research. There are recent international initiatives such the EU-ADR[37] and the IMI EMIF[38] EU-funded projects that reuse millions of EHRs from several European countries for answering to research questions that would not be easily afforded by alternative means. A point that deserves particular attention, and even some societal controversy, is the protection of the privacy of personal data in such type of projects. The most extended position among the scientific community is that such a protection can be reasonability attained if the data is carefully anonymized. There are additional precautions that use to be adopted, such as the approval and follow-up of the projects by health authorities or scientific bodies, or the only dissemination of aggregated data. An additional precaution consisting in the requirement of previous individual patient consent for carrying out observational retrospective studies (opt-in) remains almost impossible to be implemented for databases containing millions of EHRs. In this respect, the only procedure that looks feasible is the implementation of a public and easy procedure for removing patients that wish to be excluded (opt-out).

1.14.7 Integrating Clinical Data and Biomedical Evidence in Pharmacovigilance

In the last section of the present article, we describe with some detail the EU-ADR project that constitutes a relevant example of how the integration of data and knowledge from diverse sources and different types can support pharmaceutical research, post-marketing pharmacovigilance in this particular case.[37] The EU-ADR project was conceived for implementing and testing an alternative approach for detecting adverse drug reactions (ADR) generated by the use of medicines, in a way that goes beyond the traditional spontaneous reporting system.[39] It consisted of several stages depicted in Fig. 6. The first stage of the project was to put in place appropriate data management procedures for making possible the joint pharmacoepidemiological analysis of several (seven) population-based healthcare databases from different countries (Denmark, Italy, and the Netherlands) using anonymized demographic, clinical, and prescription/dispensing data. The studied databases represented 21,171,291 individuals with 154,474,063 person-years of follow-up in the period 1996–2010. The project implied the use of text-mining techniques for extracting the references to drugs and adverse clinical events, the implementation of adequate terminology mapping to address the fact that each database used different terminologies and even different languages, as well as the local implementation of an ad hoc software for extracting aggregated figures from each database in way that they can be integrated with those from other databases. The resulting infrastructure was tested for investigating the potential increased risk of suffering from myocardial infarction after the use of the drugs.[37] An innovative aspect of the workflow implemented in the EU-ADR project was the incorporation of a sophistical computational pipeline for discovering potential biological explanations for the drug-ADR signals detected by epidemiological methods.[40] The biological substantiation process (see Fig. 7) incorporated:

- automatic detection of similar compounds for the drug under study and its metabolites,
- in silico pharmacological profiling (exhaustive computational screening of interacted proteins) for any molecule (drug, metabolite or similar compound),
- determination of the common proteins between the ones that interact with the compounds and those described elsewhere as potentially related to the ADR (using DisGeNET[9]),
- consideration of the potential relationship between the proteins interacted by the drug and those related with the ADR through biological pathways, and
- contemplation of the potential effect of interindividual genetic variants in the drug metabolism or in the involved proteins.

Consequently, the integrated reuse of clinical data and biological knowledge contained in databases and in the biomedical literature offers a powerful way of discovering and biologically substantiating the rare but important ADRs produced by drugs that are used in therapeutics.

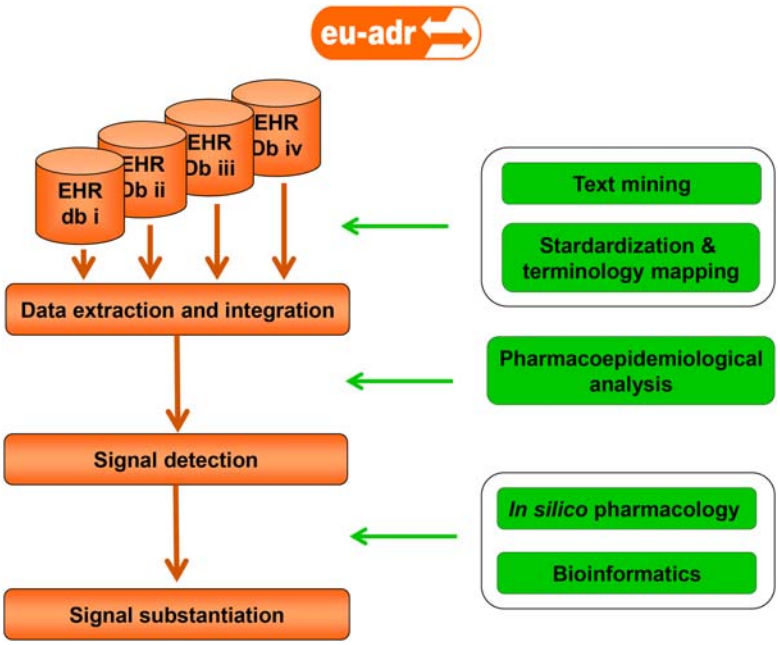

Fig. 6 Scheme of the EU-ADR project workflow.

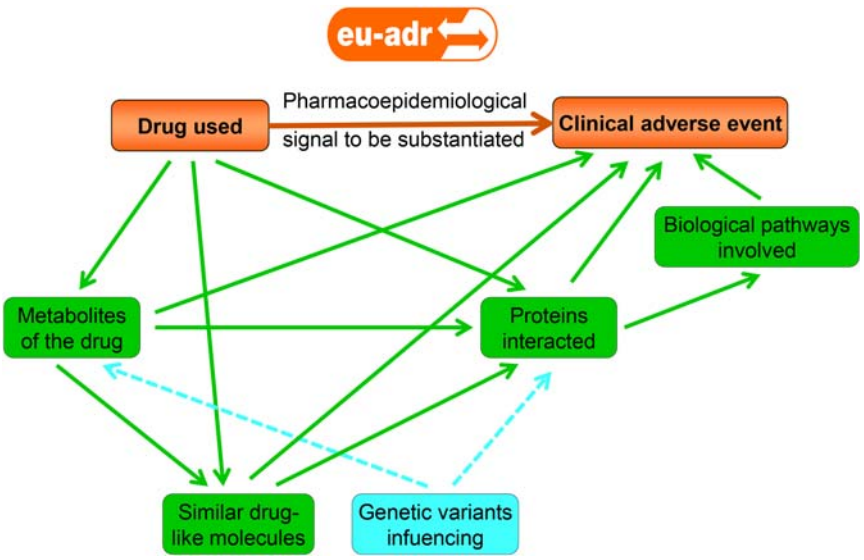

Fig. 7 Signal substantiation in the EU-ADR project by means of integrative knowledge management.

1.14.8 Final Considerations

In conclusion, we have to be aware that there is a plethora of strategies and computational tools that are available for facilitating and empowering the tasks to be done along the drug discovery and development pipeline. Most of such computational tools are publicly available and can be easily used or downloaded through Internet.

The integrative analysis of information from several types and several sources (the biomedical Big Data) offers great opportunities for gaining a more complete and powerful view on the biology, the diseases, and their pharmacological treatment.

References

1. Cases, M.; Furlong, L. I.; Albanell, J.; Altman, R. B.; Bellazzi, R.; Boyer, S.; Brand, A.; Brookes, A. J.; Brunak, S.; Clark, T. W.; Gea, J.; Ghazal, P.; Graf, N.; Guigó, R.; Klein, T. E.; López-Bigas, N.; Maojo, V.; Mons, B.; Musen, M.; Oliveira, J. L.; Rowe, A.; Ruch, P.; Shabo, A.; Shortliffe, E. H.; Valencia, A.; van der Lei, J.; Mayer, M. A.; Sanz, F. Improving Data and Knowledge Management to Better Integrate Health Care and Research. *J. Intern. Med.* **2013,** *274* (4), 321–328.
2. Marti-Solano, M.; Birney, E.; Bril, A.; Della Pasqua, O.; Kitano, H.; Mons, B.; Xenarios, I.; Sanz, F. Integrative Knowledge Management to Enhance Pharmaceutical R&D. *Nat. Rev. Drug Discov.* **2014,** *13* (4), 239–240.
3. https://www.openphacts.org/.
4. Ratnam, J.; Zdrazil, B.; Digles, D.; Cuadrado-Rodriguez, E.; Neefs, J. M.; Tipney, H.; Siebes, R.; Waagmeester, A.; Bradley, G.; Chau, C. H.; Richter, L.; Brea, J.; Evelo, C. T.; Jacoby, E.; Senger, S.; Loza, M. I.; Ecker, G. F.; Chichester, C. The Application of the Open Pharmacological Concepts Triple Store (open PHACTS) to Support Drug Discovery Research. *PLoS One* **2014,** *9* (12), e115460.
5. Chichester, C.; Digles, D.; Siebes, R.; Loizou, A.; Groth, P.; Harland, L. Drug Discovery FAQs: Workflows for Answering Multidomain Drug Discovery Questions. *Drug Discov. Today* **2015,** *20* (4), 399–405.
6. http://www.drugbank.ca/.
7. Wishart, D. S.; Knox, C.; Guo, A. C.; Shrivastava, S.; Hassanali, M.; Stothard, P.; Chang, Z.; Woolsey, J. DrugBank: A Comprehensive Resource for In Silico Drug Discovery and Exploration. *Nucleic Acids Res.* **2006,** *34* (Database issue), D668–D672.
8. http://www.disgenet.org/web/DisGeNET/.
9. Piñero, J.; Queralt-Rosinach, N.; Bravo, À.; Deu-Pons, J.; Bauer-Mehren, A.; Baron, M.; Sanz, F.; Furlong, L. I. DisGeNET: A Discovery Platform for the Dynamical Exploration of Human Diseases and Their Genes. *Database (Oxford)* **2015**. :bv028.
10. http://www.reactome.org/.
11. Fabregat, A.; Sidiropoulos, K.; Garapati, P.; Gillespie, M.; Hausmann, K.; Haw, R.; Jassal, B.; Jupe, S.; Korninger, F.; McKay, S.; Matthews, L.; May, B.; Milacic, M.; Rothfels, K.; Shamovsky, V.; Webber, M.; Weiser, J.; Williams, M.; Wu, G.; Stein, L.; Hermjakob, H.; D'Eustachio, P. The Reactome Pathway Knowledgebase. *Nucleic Acids Res.* **2016,** *44* (D1), D481–D487.
12. http://string-db.org/.
13. Szklarczyk, D.; Franceschini, A.; Wyder, S.; Forslund, K.; Heller, D.; Huerta-Cepas, J.; Simonovic, M.; Roth, A.; Santos, A.; Tsafou, K. P.; Kuhn, M.; Bork, P.; Jensen, L. J.; von Mering, C. STRING v10: Protein–Protein Interaction Networks, Integrated Over the Tree of Life. *Nucleic Acids Res.* **2015,** *43* (Database issue), D447–D452.
14. http://interactome.dfci.harvard.edu/H_sapiens/index.php?page=download.
15. Rolland, T.; Taşan, M.; Charloteaux, B.; Pevzner, S. J.; Zhong, Q.; Sahni, N.; Yi, S.; Lemmens, I.; Fontanillo, C.; Mosca, R.; Kamburov, A.; Ghiassian, S. D.; Yang, X.; Ghamsari, L.; Balcha, D.; Begg, B. E.; Braun, P.; Brehme, M.; Broly, M. P.; Carvunis, A. R.; Convery-Zupan, D.; Corominas, R.; Coulombe-Huntington, J.; Dann, E.; Dreze, M.; Dricot, A.; Fan, C.; Franzosa, E.; Gebreab, F.; Gutierrez, B. J.; Hardy, M. F.; Jin, M.; Kang, S.; Kiros, R.; Lin, G. N.; Luck, K.; MacWilliams, A.; Menche, J.; Murray, R. R.; Palagi, A.; Poulin, M. M.; Rambout, X.; Rasla, J.; Reichert, P.; Romero, V.; Ruyssinck, E.; Sahalie, J. M.; Scholz, A.; Shah, A. A.; Sharma, A.; Shen, Y.; Spirohn, K.; Tam, S.; Tejeda, A. O.; Trigg, S. A.; Twizere, J. C.; Vega, K.; Walsh, J.; Cusick, M. E.; Xia, Y.; Barabási, A. L.; Iakoucheva, L. M.; Aloy, P.; De Las, Rivas J.; Tavernier, J.; Calderwood, M. A.; Hill, D. E.; Hao, T.; Roth, F. P.; Vidal, M. A Proteome-Scale Map of the Human Interactome Network. *Cell* **2014,** *159* (5), 1212–1226.
16. http://cbdm-01.zdv.uni-mainz.de/~mschaefer/hippie/.
17. Schaefer, M. H.; Fontaine, J. F.; Vinayagam, A.; Porras, P.; Wanker, E. E.; Andrade-Navarro, M. A. HIPPIE: Integrating Protein Interaction Networks With Experiment Based Quality Scores. *PLoS One* **2012,** *7* (2), e31826.
18. http://sbi.imim.es/web/index.php/research/servers/biana.
19. Garcia-Garcia, J.; Guney, E.; Aragues, R.; Planas-Iglesias, J.; Oliva, B. Biana: A Software Framework for Compiling Biological Interactions and Analyzing Networks. *BMC Bioinformat.* **2010,** *11,* 56.
20. https://www.ebi.ac.uk/chembl/.
21. Bento, A. P.; Gaulton, A.; Hersey, A.; Bellis, L. J.; Chambers, J.; Davies, M.; Krüger, F. A.; Light, Y.; Mak, L.; McGlinchey, S.; Nowotka, M.; Papadatos, G.; Santos, R.; Overington, J. P. The ChEMBL Bioactivity Database: An Update. *Nucleic Acids Res.* **2014,** *42* (Database issue), D1083–D1090.
22. Mestres, J.; Gregori-Puigjané, E.; Valverde, S.; Solé, R. V. Data Completeness—The Achilles Heel of Drug-Target Networks. *Nat. Biotechnol.* **2008,** *26* (9), 983–984.
23. Mestres, J.; Martín-Couce, L.; Gregori-Puigjané, E.; Cases, M.; Boyer, S. Ligand-Based Approach to In Silico Pharmacology: Nuclear Receptor Profiling. *J. Chem. Inf. Model.* **2006,** *46* (6), 2725–2736.
24. https://www.surechembl.org/search/.
25. Papadatos, G.; Davies, M.; Dedman, N.; Chambers, J.; Gaulton, A.; Siddle, J.; Koks, R.; Irvine, S. A.; Pettersson, J.; Goncharoff, N.; Hersey, A.; Overington, J. P. SureChEMBL: A Large-Scale, Chemically Annotated Patent Document Database. *Nucleic Acids Res.* **2016,** *44* (D1), D1220–D1228.
26. Cases, M.; Briggs, K.; Steger-Hartmann, T.; Pognan, F.; Marc, P.; Kleinöder, T.; Schwab, C. H.; Pastor, M.; Wichard, J.; Sanz, F. The eTOX Data-Sharing Project to Advance In Silico Drug-Induced Toxicity Prediction. *Int. J. Mol. Sci.* **2014,** *15,* 21136–21154.
27. Briggs, K.; Barber, C.; Cases, M.; Marc, P.; Steger-Hartmann, T. Value of Shared Preclinical Safety Studies—The eTOX Database. *Tox. Rep.* **2015,** *2,* 210–221.
28. Sanz, F.; Carrió, P.; López, O.; Capoferri, L.; Kooi, D. P.; Vermeulen, N. P. E.; Geerke, D. P.; Montanari, F.; Ecker, G. F.; Schwab, C. H.; Kleinöder, T.; Magdziarz, T.; Pastor, M. Integrative Modeling Strategies for Predicting Drug Toxicities at the eTOX Project. *Mol. Inf.* **2015,** *34,* 477–484.
29. http://www.epa.gov/chemical-research/toxicity-forecasting.
30. http://ntp.niehs.nih.gov/results/hts/index.html.
31. http://www.epa.gov/chemical-research/distributed-structure-searchable-toxicity-dsstox-database.
32. Hendrickx, D. M.; Aerts, H. J.; Caiment, F.; Clark, D.; Ebbels, T. M.; Evelo, C. T.; Gmuender, H.; Hebels, D. G.; Herwig, R.; Hescheler, J.; Jennen, D. G.; Jetten, M. J.; Kanterakis, S.; Keun, H. C.; Matser, V.; Overington, J. P.; Pilicheva, E.; Sarkans, U.; Segura-Lepe, M. P.; Sotiriadou, I.; Wittenberger, T.; Wittwehr, C.; Zanzi, A.; Kleinjans, J. C. DiXa: A Data Infrastructure for Chemical Safety Assessment. *Bioinformatics* **2015,** *31* (9), 1505–1507.
33. http://wwwdev.ebi.ac.uk/fg/dixa/index.html.
34. https://clinicaltrials.gov/ct2/help/how-find/find-study-results#Overview.
35. http://www.eudrapharm.eu/eudrapharm/selectLanguage.do?NOCOOKIE=NOCOOKIE&NEW_SESSION=true.
36. https://eudract.ema.europa.eu/index.html.
37. Coloma, P. M.; Schuemie, M. J.; Trifirò, G.; Furlong, L.; van Mulligen, E.; Bauer-Mehren, A.; Avillach, P.; Kors, J.; Sanz, F.; Mestres, J.; Oliveira, J. L.; Boyer, S.; Helgee, E. A.; Molokhia, M.; Matthews, J.; Prieto-Merino, D.; Gini, R.; Herings, R.; Mazzaglia, G.; Picelli, G.; Scotti, L.; Pedersen, L.; van der Lei, J.; Sturkenboom, M.; EU-ADR consortium. Drug-Induced Acute Myocardial Infarction: Identifying 'prime suspects' From Electronic Healthcare Records-Based Surveillance System. *PLoS One* **2013,** *8* (8), e72148.
38. http://www.emif.eu/.
39. Rawlins, M. D. Spontaneous Reporting of Adverse Drug Reactions. I: The Data. *Br. J. Clin. Pharmacol.* **1988,** *26* (1), 1–5.
40. Bauer-Mehren, A.; van Mullingen, E. M.; Avillach, P.; Carrascosa Mdel, C.; Garcia-Serna, R.; Piñero, J.; Singh, B.; Lopes, P.; Oliveira, J. L.; Diallo, G.; Ahlberg Helgee, E.; Boyer, S.; Mestres, J.; Sanz, F.; Kors, J. A.; Furlong, L. I. Automatic Filtering and Substantiation of Drug Safety Signals. *PLoS Comput. Biol.* **2012,** *8* (4), e1002457.

1.15 Structural Chemogenomics Databases to Navigate Protein–Ligand Interaction Space

GK Kanev, AJ Kooistra, IJP de Esch, and C de Graaf, Vrije Universiteit Amsterdam, Amsterdam, The Netherlands

© 2017 Elsevier Ltd. All rights reserved.

1.15.1	**Introduction**	444
1.15.1.1	Chemogenomics: Interrogating Protein Targets With (Bioactive) Compounds	444
1.15.1.2	Publicly Available Sequence, Structural, and Activity Data	446
1.15.1.3	Structural Chemogenomics Ontology for the Integration of Curated Chemical and Biological Data	447
1.15.1.4	Protein Sequence and Structure for Structural Chemogenomics Analyses	449
1.15.2	**Systematic Analysis and Classification of Structural Chemogenomics Databases**	450
1.15.2.1	Database Classification Criteria	450
1.15.2.1.1	Data browse and search functionalities	451
1.15.2.1.2	Ligand data types	451
1.15.2.1.3	Protein data types	452
1.15.2.1.4	Protein–ligand interaction data types	453
1.15.2.1.5	Database update frequency	454
1.15.3	**Protein Structure-Annotated Biological Activity Databases**	454
1.15.3.1	Proteome-Wide Biological Activity Databases	454
1.15.3.1.1	Protein family-customized biological activity databases	456
1.15.3.1.2	Mechanism-specific biological activity databases	457
1.15.4	**Structural Protein–Ligand Interaction Databases**	457
1.15.4.1	General Structural Protein–Ligand Interaction Databases	457
1.15.4.2	Mechanism-Based Structural Protein–Ligand Interaction Databases	459
1.15.4.3	Protein Family-Customized Structural Chemogenomics Databases	460
1.15.5	**Examples of Applications of Structural Chemogenomics Databases in Drug Discovery**	461
1.15.5.1	Combined Bioactivity Data Mining and Chemical Similarity Search for Ligand-Based Target Prediction	461
1.15.5.2	Protein Binding Site Similarity Assessments for Ligand Repurposing and Off-Target Prediction	462
1.15.5.3	Integrated Structure-Based Medicinal Chemistry Toolbox for Drug Discovery and Design	463
1.15.5.4	Combined Navigation of Protein–Ligand Interaction and Ligand Chemistry Space	463
1.15.6	**Conclusions and Outlook**	466
References		467
Relevant Websites		471

1.15.1 Introduction

In the post genomic era, data generation in the pharmaceutical sciences has massively accelerated meaning that new analytic (eScience) approaches are needed to adequately exploit this new chemical and biological information.[1] Many new protein targets have been discovered recently, and it has been shown that clinical efficacy is often the result of polypharmacological action of drug molecules (i.e., the interaction with more than one protein target).[2] In addition, for a drug to be safe, certain off-target activities on other proteins should be avoided. For targets and off-targets, a plethora of different ligand-based and protein-based data are being generated and collected in databanks. For example, the Protein Data Bank (PDB)[3] currently holds 117,240 three-dimensional (3-D) protein structures, while the ChEMBL[4,5] database contains data relating to 13,967,816 biological activities of 1,928,903 compounds and 11,019 protein targets (**Fig. 1**). All these rapidly accumulating data hold great promise for more efficient structure-based discovery and design of ligands with desirable protein selectivity and polypharmacological profiles. Efficient exploitation is, however, hampered because a good approach to efficiently integrate large volumes of heterogeneous data from different disciplines is still missing. The data heterogeneity, volume, and noise levels preclude simple integration of data from multiple sources in, for example, a relational database. The data need to be properly processed and subsequently integrated in order to extract useful information that is manageable and applicable in various life science disciplines.

1.15.1.1 Chemogenomics: Interrogating Protein Targets With (Bioactive) Compounds

The completion of the Human Genome Project (HGP) in 2003 provided scientists with a near-complete reference of the human genome and the opportunity to study diseases at molecular level and accelerate drug development.[6] For example, while the discovery of the gene causing cystic fibrosis took 9 years in the 1980s, the gene responsible for Parkinson's disease was identified

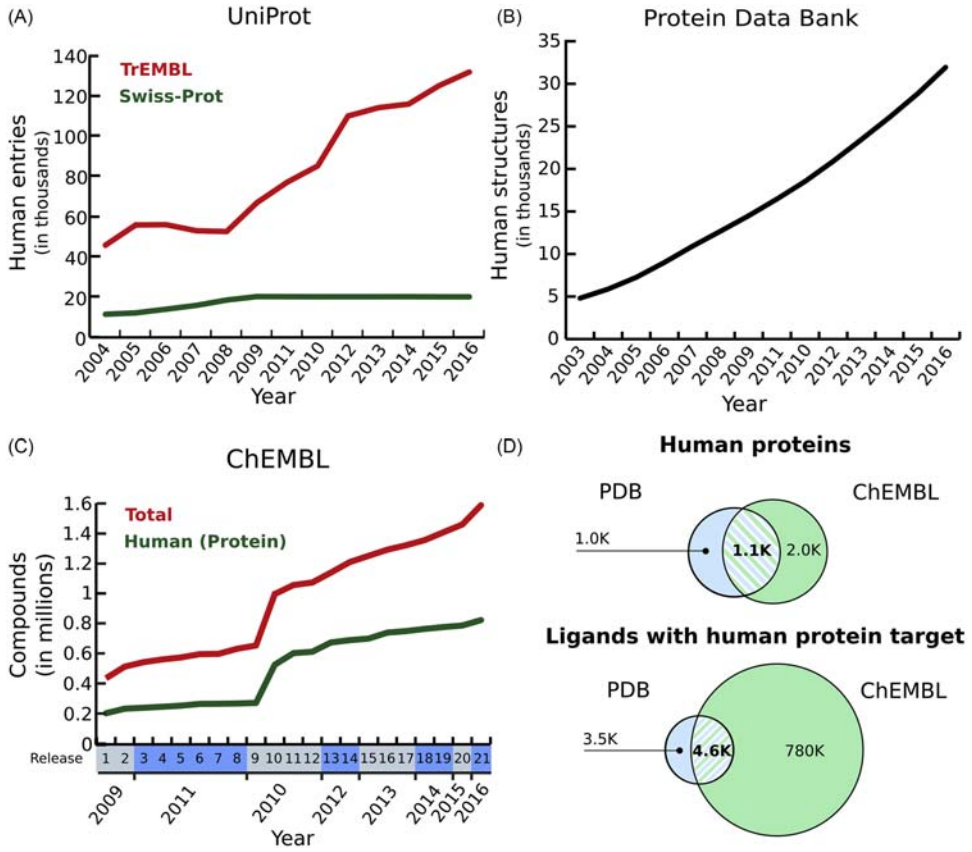

Fig. 1 An overview of the increase of structural chemogenomics data. The amount of (A) protein sequences in TrEMBL and Swiss-Prot (curated TrEMBL entries) integrated in UniProt, (B) structures in the Protein Data Bank (*PDB*), (C) Number of molecules for which biological activity data is available at human protein targets and all protein targets of ligands in ChEMBL, and (D) the overlap of the human protein targets and ligands with human protein targets covered by PDB and ChEMBL. The gene overlap was calculated based on accession IDs extracted from ChEMBL and PDB, while the ligand overlap was calculated based on extracted InChi keys from both databases.

within 9 days in 1998.[7] In addition to that, the human genome provided the potential to uncover new drug targets[8] by assessing the number of human genes, the druggable targets, and their druggability, which is the ability of small molecules to modulate protein targets.[9] The overwhelming majority of approved drugs bind to (specific) protein targets,[10] and these proteins could be used as templates to extend the number of protein targets as "similar ligands bind to similar targets."[11] Hopkins and Groom were among the first to estimate the number of drug targets.[12] By analyzing the overlap of all members of protein families with a precedent for binding drug-like molecules (~3000) and genes related to disease (~3000), they estimated the number of human drug targets to be between ~600 and 1500.[12] This estimation was adjusted to between 2000 and 3000 in 2005.[13] Overington et al. were able to assign 324 drug targets to the 1357 approved drugs up to that time.[14] This showed that all approved drugs up to 2006 targeted only 10–15% of the estimated number of druggable targets. Since the completion of the HGP, the pharmaceutical industry is continuously in pursuit of ways to reduce this gap by introducing new drugs that aim at previously untargeted proteins. For example, in 2014 and 2015, the FDA-approved drugs that had a novel mechanism of action and aimed at novel drug targets constituted of 17 (of 41 approved drugs) and 16 (of 45 approved drugs), respectively.[15] The advances made by the HGP simultaneously provided a new challenge to the pharmaceutical industry—selection and validation of drug targets.[16]

Chemogenomics, defined as the study of the effects of small molecules on target gene families, aims to convert the acquired wealth of genomic data combined with structural, phenotypic, and bioactivity data into drugs.[17,18] This new and highly interdisciplinary field combined medicinal chemistry, bioinformatics, and cheminformatics with the aim to develop novel strategies to tackle the significant challenges that the pharmaceutical industry was facing at the time. In particular, the increasing research costs and low approval rate of drugs aiming at new targets was a major concern.[19–21] In the decade before the completion of the HGP, for example, the approved drugs by the FDA had only three new targets each year on average.[12] In contrast to conventional methods, chemogenomics uses large and diverse compound libraries for screenings and applies interdisciplinary approaches to systematically link the readouts to drug targets.[17] To assist the process of identifying new drug candidates, experimental and computational approaches are commonly used within the field.[17] In the former approach, the workflow typically involves testing of compound libraries in representative biological systems, performing assays to generate readouts, and then analyzing those readouts to identify active compounds. In the case of computational (or predictive) chemogenomics, the workflow involves collecting, generating, and

integrating, (whenever available) genomic, structural, and activity data; and applying machine learning algorithms to predict phenotypic responses and effects of (novel) compounds on targets.[17,22] Given that experimental data are often incomplete because of time and resource savings applied on screening methods,[23,24] the computational approaches provide the means to predict the missing data, discover new protein targets, and lead the field closer to its ultimate aim to identify all drugs for all targets.[25,26]

In the post genomic era, along with the rise of chemogenomics, the industry started to shift away from the rational drug design paradigm—that is "one drug, one target"—toward drug polypharmacology as it became apparent that drugs typically act on more than one target.[2,27–29] Drug polypharmacology builds on these multiple drug–target observations and attempts to utilize this in order to improve major drug development obstacles like efficacy and toxicity by trying to optimize on- and off-target activity profiles, lower the drug resistance, and modulate beneficial pathways.[27,30] Analyses of ChEMBL and PubChem suggest that 30–50% of biologically active compounds and most drugs interact with multiple protein targets and therefore may exhibit polypharmacological profiles.[31–34] The already-established large and continuously increasing sources of publicly available data[35–37] provide input to computational chemogenomics approaches to predict the selectivity and polypharmacological action of drugs.[38–42] The large number of diverse compounds and their annotated targets could indeed serve as a starting point for such an endeavor.

1.15.1.2 Publicly Available Sequence, Structural, and Activity Data

Access to high-quality sequence, structural and activity data provide more than just the ability to study the direct relationships between ligands, targets, and their affinities. It also allows to predict previously unexplored ligand–target interactions and to correlate the predicted interactions to clinical efficacy. This is crucial for drug discovery as drugs typically act on multiple targets and are therefore likely to influence multiple pathways. The GenBank along with its European and Japanese counterparts were used to store the huge amount of sequence data produced by the HGP that started in 1990 and finished in 2003.[43,44] In order to make use of the genome reference to study and diagnose diseases, new human sequences had to be mapped to the reference human genome. The amount of bases in the GenBank increased fourfold in the last 10 years, from 50 trillion bases in 2005 (collected over 10 years) to over 200 trillion in 2015. In 2004, PIR-PSD,[45] Swiss-Prot,[46] and TrEMBL[47] united to form a central resource of protein sequence data: the Universal Protein Knowledgebase (UniProt).[48] Swiss-Prot and TrEMBL are separate sections of the UniProt database: Swiss-Prot consists of manually annotated protein sequence records, while TrEMBL consists of computationally analyzed sequence records that after curation are transferred to Swiss-Prot (**Fig. 1A**). In UniProtKB/TrEMBL, fragments, isoforms, and variants of full-length protein sequences (encoded by the same gene and from the same species) are represented in separate entries. In UniProtKB/Swiss-Prot, all protein products encoded by one gene in a given species, including alternative splicing isoforms, fragments, and polymorphisms, are all reported in a single entry. The manual curation procedure of UniProtKB/Swiss-Prot includes (i) sequence curation (identification of, e.g., alternative splicing, natural variations, frameshifts, incorrect initiation sites, and incorrect exon boundaries), (ii) sequence analysis (predicted annotation of, e.g., posttranslational modifications, subcellular location, transmembrane domains, protein topology, domain identification, and protein family classification), (iii) literature curation (check predicted annotations complemented by additional information summarized in section "**Protein sequence and structure for structural chemogenomics analyses**," and assignment of relevant gene ontology (GO) terms based on experimental data from the literature), (iv) family-based curation (data standardization across homologous proteins), (v) evidence attribution (links to the original information source), and (vi) quality assurance, integration, and update. In 2015, redundant proteomes were removed from UniProtKB/TrEMBL (decreasing the number of entries from 92 million to 46 million entries), and currently, UniProtKB/TrEMBL contains 63,686,057 entries. From 2004 to 2009, the number of curated protein sequence entries in UniProtKB/Swiss-Prot rapidly increased by 3.5-fold to more than 514,292 entries in 2009 (with an increase of 108,200 entries in 2009). In the past 5 years, the number of entries has grown at a slower rate than in 2004–09 and now contains 550,960 entries (with an increase of 3031 entries in 2015).

The PDB, established in 1971,[49] contains a standardized collection of macromolecular structure data derived primarily from X-ray diffraction (89.3%) and solution NMR (9.6%).[50] The PDB format[51] was introduced in 1977 to standardize the crystallographic data. During the years, it became mandatory for researchers to deposit their crystal structures in the databank,[52] which along with the continuously improving technology enormously increased the collection of 3-D structures in the databank—from only 7 initially to 10,000 in 1999[53] and more than 117,000 as of Mar. 2016 (**Fig. 1B**). The PDB is now the single repository of experimentally determined macromolecular structures[3] and among the most widely used structural databases.[52] The rapidly growing amount of protein structures in the 1990s (from 500 in 1990 to over 13,500 in the year 2000) and compound libraries allowed medicinal chemist to use computational approaches to enrich compound libraries and limit the costs and time needed to perform screenings.[54,55] ChEMBL, a database of bioactive drug-like small molecules and annotated bioactivities, was launched in 2009 with 440,055 bioactive compounds, 3622 protein targets, 329,250 assays, and 1,936,969 activities.[5] A year and half after its initial release ChEMBL reached over million compounds for the first time (tenth release, the lower red dot in 1C) and just recently, on its twenty-first release, 1.5 million compounds (the higher red dot in 1C). The total amount of bioactivities annotated in ChEMBL has increased more than sevenfold to 13,968,617 on the 1st of Feb. 2016, covering 1,592,191 compounds (>3-fold increase), 11,019 targets (including 6262 proteins, >3-fold increase), and 1,212,831 assays (>3-fold increase). **Fig. 1D** shows that for 1083 of the 3057 human protein targets (genes) for which bioactivity data is available in ChEMBL, there is also structural information available in the PDB. ChEMBL contains bioactivity data for 4575 of the 8048 ligands for which a protein bound structure is available in the PDB. This analysis suggests that for a large part of the protein targets for which bioactivity data is available, structure-based ligand discovery and optimization approaches may be used to optimize existing biologically active molecules or identify new

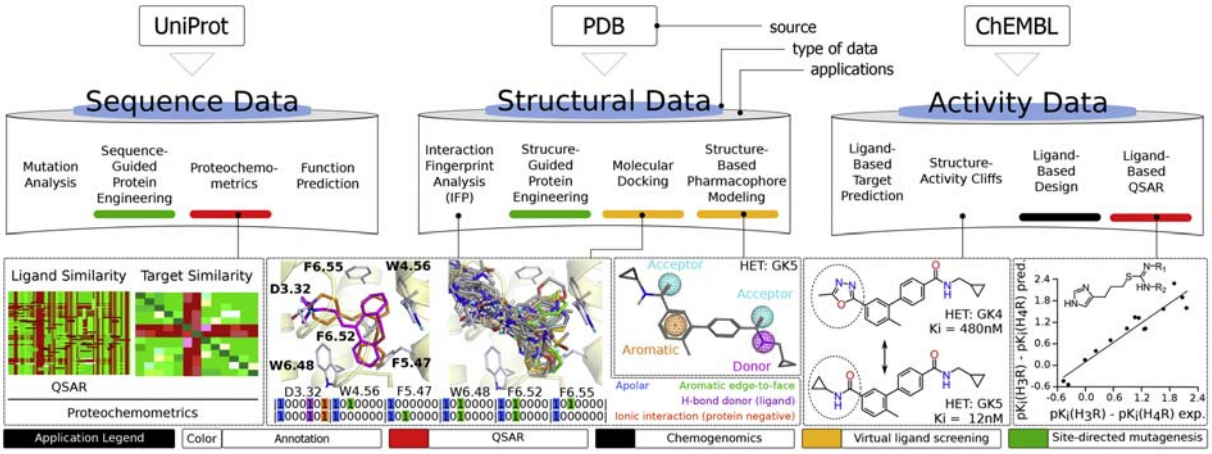

Fig. 2 Application of structural chemogenomics data. Schematic depiction of bioinformatics and chemoinformatics approaches and applications that can be used to transform information in protein sequence (e.g., UniProt[58]), (ligand-bound) protein structure (e.g., PDB[3]), and target-annotated ligand bioactivity (e.g., ChEMBL[5]) databases into models to predict structural protein–ligand interactions. Bio/chemoinformatics modeling applications based on protein amino acid sequence information (e.g., mutational analysis,[59] sequence-guided protein engineering,[60] proteochemometrics,[61,62] and function prediction[63]), protein–ligand structure data (e.g., structural protein–ligand interaction fingerprint (IFP) analysis,[64,65] structure-guided protein engineering,[60] molecular docking,[56] protein-based pharmacophore modeling[66]), and bioactivity data (e.g., ligand-based QSAR,[67] structure–activity cliffs,[68] ligand-based target prediction,[69] and ligand-based design[70]) can be used to, for example, guide site-directed mutagenesis studies, virtual screening to discover new ligands for specific protein targets and identify the protein target(s) of specific small molecules, and the construction and application of QSAR models to guide the design and optimization of ligands with desired protein affinity, activity, and selectivity profiles.

ligands. For a large part of the protein targets for which structural information is available, bioactivity data is still lacking to efficiently elucidate the molecular determinants of protein–ligand binding. Molecular docking of a small set of known biologically active molecules (e.g., drugs) against libraries of binding sites of protein for which few ligands are available (inverse docking) can, for example, be an efficient structure-based approach for ligand repurposing.[56] Only a very small number of the known biologically active molecules have been cocrystallized as a protein–ligand complex (<0.001%), emphasizing the need of computational methods to predict structures of protein–ligand complexes for which no structural information is available. Shan et al. were the first to accurately predict the binding mode of a ligand to a target without prior knowledge of the binding site using molecular dynamics (MD) simulations.[57] Fig. 2 shows examples of different bioinformatics and chemoinformatics methods that can be used to transform information in protein sequence (e.g., UniProt[58]), (ligand-bound) protein structure (e.g., PDB[3]), and target-annotated ligand bioactivity (e.g., ChEMBL[5]) databases into models to predict structural protein–ligand interactions. It should be noted, however, that the predictive power and information content of models (primarily) based on specific data sources can be significantly improved by the *combination* of sequence, structure, and bioactivity data: for example, the use of bioactivity data for optimization and training of pharmacophore models and docking studies,[71] the use of protein structures and bioactivity data in 3D-QSAR approaches,[72] and the integration of sequence information, bioactivity data, and sometimes also protein structures in proteochemometric models for the bioactivity prediction of protein–ligand pairs.[61,73] The current article focuses on the analysis of structural chemogenomics databases that allow integration of bioactivity and structural information for structure-based prediction of protein selectivity and ligand polypharmacology.

1.15.1.3 Structural Chemogenomics Ontology for the Integration of Curated Chemical and Biological Data

Structural chemogenomics data is highly heterogeneous—from experimental bioactivity data in large public databases such as ChEMBL[5] to molecular fingerprints and pharmacophores of ligands (generated using algorithms like ChemAxon,[74] EDprints[75]), protein–ligand interaction descriptors (IFP[64] and KRIPO[76]), and protein–ligand structure databases (PDB,[3,77] KLIFS,[64] PDESTrIAn,[65] and GPCRdb[78,79]). However, most databases use a relatively small set of IDs to link their data and analyses to comprehensive structural, sequence resources such as the PDB and UniProt. To facilitate systematic comparison between the biological and chemical databases reviewed in this article, we prepared a controlled dictionary in the form of a glossary (Table 1). This glossary comprises identifiers that are both relevant to the subject of this article and can, for example, be used to link to resources like PDB and UniProt. All entries in the glossary consist of an identifier, its definition, whether the PDB and/or UniProt have mapped their data to the identifier, a link to the original source (database) for the identifier (if applicable), and an example. In addition to the ontology and data mapping efforts unified in the PDB and UniProt databases, several other integrated databases have contributed to the definition of common ontologies that facilitate integrated structural chemogenomics analysis, ranging from broad platforms to integrated chemical identifiers (UniChem), pharmacological data resources (open PHACTS[93]), pharmacological targets

Table 1 Glossary used to define a structural chemogenomics ontology that facilitates systematic curation, mapping, integration, and comparison protein, ligand, and protein–ligand interaction data provided by the different databases described in Sections **Protein structure-annotated biological activity databases, Structural protein–ligand interaction databases**, and **Examples of applications of structural chemogenomics databases in drug discovery**

ID	*Definition*	*Mapped*	*Link*	*Example*
UniProt ID	ID linked to protein sequence and functional information in the UniProt database[80]	PDB	www.uniprot.org/	P00519
PDB ID	PDB code: four-character ID linked to DNA/protein structural information in the Protein Data Bank[81]	UniProt	www.rcsb.org/pdb	1HW9
HET code	PDB ligand ID: three-character ID linked to ligand information in the Protein Data Bank		www.rcsb.org/pdb	2P5
GI number	The GenInfo identifier is linked to a sequence record processed by NCBI[82]		www.ncbi.nlm.nih.gov/genbank/	62362414
RefSeq ID	The Reference Sequence ID is linked to comprehensive reference sequence information in the NCBI RefSeq database[83]	UniProt	www.ncbi.nlm.nih.gov/refseq/	NP_005148.2
UniGene code	Links to computationally derived transcripts from the same locus and expression data in the UniGene database[84]	UniProt	www.ncbi.nlm.nih.gov/unigene	Hs.431048
ChEMBL ID	ID linked to compound, target, assay bioactivity information in the ChEMBL database	UniProt	www.ebi.ac.uk/chembl/	CHEMBL1862
IUPHAR/BPS ID	ID linked to information on approved or experimental drug or target in the Guide To Pharmacology[85]	UniProt	www.guidetopharmacology.org	5687
PubChem ID	ID linked to compound, target, assay, activity, or patent information in the PubMed database		pubchem.ncbi.nlm.nih.gov/	PubChem CID 5291
SMILES	Simplified molecular input line-entry system describes molecular species in a string form			C1=NC2=C(N1)C(=NC=N2)N
CAS	Links to unique numerical identifier of compound described in the scientific literature			152459-95-5
InChi	IUPAC International Chemical identifier is a character identifier for chemical species			InChI=1S/C5H5N5/c6-4-3-5 (9-1-7-3)10-2-8-4/h1-2H,(H3,6,7,8,9,10)
InChi key	Fixed-length character representation of the InChi			GFFGJBXGBJISGV-UHFFFAOYSA-N
CATH ID	ID linked to information on classification of a protein structure in the CATH database[86]	PDB	www.cathdb.info/	3cs9A01
SCOP ID	ID linked to information on classification of a protein structure in the SCOP database[87]	PDB, UniProt	scop.berkeley.edu/	173427
PubMed ID	ID linked to scientific publication in the PubMed database	PDB, UniProt	www.ncbi.nlm.nih.gov/pubmed	26496949
OMIM ID	ID linked to thesaurus of human genomic information in the OMIM database	UniProt	www.omim.org/	608232
MeSH	ID linked to entry in the controlled vocabulary thesaurus of the US national library of medicine	PDB	www.ncbi.nlm.nih.gov/mesh	D015464
Ensembl ID	ID linked to genetic information in the Ensembl database[88]	UniProt	www.ensembl.org/	ENSG00000097007
KEGG ID	ID linked to genomic and biological pathway information in the KEGG database[89]	UniProt	www.genome.jp/kegg/	hsa:25
TaxID	ID linked to the taxonomy of the target as identified in NCBI Taxonomy[90]	PDB, UniProt	www.ncbi.nlm.nih.gov/taxonomy	9606
EC number	Number linked to information on the nomenclature of enzyme as defined by International Union of Biochemistry and Molecular Biology (IUBMB)[91]	PDB	http://www.iubmb.org/	EC 3.5.1.n3
GO terms	Links to controlled vocabularies used to describe biological, molecular, or cellular component or function[92]	PDB, UniProt	geneontology.org/	GO:0005524

Each entry consists of an identifier, definition including the original database that uses the identifier, whether the PDB and UniProt have linked their data to the original database of the identifier, link to the original database, and an example of the identifier.

(IUPHAR[94]), and target-specific data (e.g., G protein-coupled receptor data in the GPCRdb[79]). These resources are frequently used to combine and integrate data from multiple databases. Partially due to this integration, the amount of readily available data keeps increasing, and data quality, data comparability, and data curation remain important but challenging endeavors. This issue is due to several factors, including reproducibility,[95] errors while processing the experimental data, errors while writing a publication, incomplete method descriptions, quality of data collection, integration, and annotation in databases, assay conditions (e.g., the use of different protein constructs), compound properties (e.g., impure compounds, racemic mixtures, and PAINS[96]), or ligand topology errors.[97–99] As computational drug development approaches rely heavily on the published data,[100] chemogenomics databases are implementing methods to address the challenges regarding data quality and curation.[89] ChEMBL, for example, has implemented structural alerts for compounds containing scaffolds/moieties that could be problematic (e.g., PAINS) and provides a confidence score for each bioactivity entry. PDBBind-CN reduces the amount of annotation mistakes by performing the annotation of each datapoint twice, independently by two persons. Additionally, more and more frequently (computational) curation workflows are applied before using the data for the development of chemogenomics models, which significantly increase the data quality.[101]

For structural approaches, there is the concern of issues in the elucidation of a protein structure. Several factors can impact the experimental determination of protein structure, for example, crystallographic artifacts (e.g., crystal packing), conformational changes due to the creation of crystallographic constructs (e.g., fusion proteins and thermostabilizing mutations), and errors while modeling the structure. Two examples of databases that address the latter issue are ValidatorDB[102] and PDB_REDO.[103] ValidatorDB provides summaries of precomputed validation results describing correctness and errors in the structures of the PDB. The validation protocol analyzes all ligands and nonstandard residues in the PDB and the topology and geometry of the data including atom substitutions, atom naming, foreign atoms, bad root mean square deviation, and conformations as well as overall completeness and chirality. PDB_REDO[103] uses a fully automated pipeline that optimizes the PDB structures by performing iterative refinement and subsequent validation of the crystal structures using R-values and validation scores. The PDB itself is also continuously updating its requirements and policies in order to ensure the quality of the structures that are deposited into the database.[3]

1.15.1.4 Protein Sequence and Structure for Structural Chemogenomics Analyses

The UniProt Knowledgebase (UniProtKB, www.uniprot.org/uniprot/)[80] is a central database that incorporates large collections of functional information on proteins, including the annotation and reference information of the protein name(s) and taxonomy, function, subcellular location and structural topology, pathology, posttranslational modifications, expression, interactions with proteins and/or small-molecule ligands, protein family and domains, amino acid sequence, and structural information. In particular, the UniProt protein name, Enzyme Commission (EC), and gene names provide identifiers (**Table 1**) that are frequently used in structural chemogenomics databases described in sections **Protein structure-annotated biological activity databases** and **Structural protein–ligand interaction databases**. The organism name and NCBI taxonomy identifier are used throughout all databases in which organism-specific information is presented, high-profile examples of which are ChEMBL and PDB. GO (geneontology.org)[92] codes are used to annotate the cellular components where the protein is active. The published or predicted structural topology (e.g., protein crystal structure publication or sequence similarity to an experimentally determined structure), including (transmembrane) helical regions, and beta-strands are mapped on the amino acid sequence of the protein. Also, the predicted or reported posttranslational amino acid modifications, including glycosylation, phosphorylation, and disulfide bonds, reported in, for example, Phosphosite (www.phosphosite.org) and iPTMnet (research.bioinformatics.udel.edu/iptmnet), are mapped on the protein sequence. Protein–ligand and protein–protein interactions are extracted from different databases, including ChEMBL, DrugBank (www.drugbank.ca),[104] GuideToPharmacology (www.guidetopharmacology.org),[85] DIP (dip.doe-mbi.ucla.edu/dip), and IntAct (www.ebi.ac.uk/intact). Protein polymorphism and mutations are extracted from among others BioMuta (hive.biochemistry.gwu.edu) and DMDM (bioinf.umbc.edu/dmdm) databases, while several databases including Bgee (bgee.unil.ch/bgee)[105] and Expression Atlas (www.ebi.ac.uk/gxa/genes)[106] contain information on protein expression levels in, for example, different cell types and tissues. Links to experimental structures are provided via RCSB Protein Data Bank (PDB), Protein Data Bank in Europe (PDBe, www.ebi.ac.uk/pdbe/),[107] and Protein Data Bank Japan (PDBj, pdbj.org),[108] while predicted structural models of the protein entry can be automatically generated via links to ProteinModelPort (www.proteinmodelportal.org),[109] including models extracted from, for example, SWISS-MODEL (swissmodel.expasy.org),[110] ModBase (modbase.compbio.ucsf.edu),[111] and GPCRdB (GPCRdb.org).[79] Links to family and domain databases including InterPro (www.ebi.ac.uk/interpro/),[112] Pfam (pfam.xfam.org),[113] PRINTS (www.bioinf.manchester.ac.uk/dbbrowser/PRINTS/), PROSITE (prosite.expasy.org), and ProtoNet (www.protonet.cs.huji.ac.il) provide protein and protein family classification. All literature resources that are used for the annotation of each entry in UniProt are reported including the specification of which annotation is based on that specific publication. All annotations can be downloaded in multiple formats (plain text, XML, RDF, and GFF), and the protein sequence can be downloaded in FASTA format. Furthermore, from a UniProt entry, one can directly link and submit requests to BLAST, ProtParam, ProtScale, PeptideMass, and PeptideCutter and calculate the molecular weight and isoeletric point of the protein.

The Protein Data Bank United States (RCSB PDB, www.rcsb.org/pdb),[3] Biological Magnetic Resonance Data Bank (BRMB, www.bmrb.wisc.edu),[114] Protein Data Bank Japan (PDBj, pdbj.org),[108] and PDBe (www.ebi.ac.uk/pdbe)[107] are united in Worldwide PDB (wwPDB organization, www.wwpdb.org)[115] and maintain a centralized PDB archive of macromolecular structures. The organization of the corresponding website and search features are however different. In the current description, we will focus on the RCSB PDB website and shortly indicate unique features of the websites of BRMB, PDBj, and PDBe. The RCSB PDB can be browsed by enzyme nomenclature (EC number, enzyme.expasy.org), protein structure class (SCOP, scop.mrc-lmb.cam.ac.uk/scop/),[87] protein domain structure (CATH class, www.cathdb.info),[86] membrane protein class (mpstruc, blanco.biomol.uci.edu/mpstruc/), transporter class (TC, www.tcdb.org), genome location (NCBI gene name, www.ncbi.nlm.nih.gov/gene), biological process, cell

component, and molecular function (GO ID, geneontology.org), source organism (NCBI Taxonomy class, www.ncbi.nlm.nih.gov/taxonomy),[90] anatomical therapeutic chemical class (ATC, www.whocc.no/atc/structure_and_principles), and publication keywords (Medical Subject Headings (MeSH), www.nlm.nih.gov/mesh). The RCSB PDB can be searched based on the structure annotation mentioned earlier (see RCSB PDB browse options), (other) IDs and keywords, deposition information, structure features, sequence features, chemical components (ligands, protein, drugs, and drug–target combinations), biology, experimental methods used to determine the macromolecular structure, and the publication corresponding to the PDB coordinate file. IDs include PDB ID, PubMed ID, UniProtKB AC, Pfam AC, and UniProt Gene name. In addition, drugs and drug targets in the PDB have been mapped to DrugBank. Structure feature search options include protein stoichiometry and symmetry, molecular weight, and secondary structure content and length, while sequence features include amino acid sequence BLAST search, sequence of the wild-type protein (e.g., excluding mutations to facilitate crystallization), and sequence motifs. Chemical component search options include chemical name, chemical formula, SMILES string, InChI or InChIKey, chemical formula or molecular weight, or chemical substructure or similarity (interactive chemical sketcher Marvin JS). Biology search options include expression organism of the protein, in addition to the many browse options described earlier. Methods search options include experimental method (including X-ray crystallography, solution NMR, solid-state NMR, electron microscopy, and electron crystallography), X-ray resolution, X-ray average B-factor, and refinement R factors. PDB entries contain the results of most of the search and browse options. Along more common features like annotations of the structure, classification, reference publication, 3-D view of the structure and ligand, ligand representations, interactions, 2-D structures, and links to bioactivity data, the database provides in-depth overview of the sequence data, sequence and structure similarities, the experimental data and validation, and citations in the literature. 2-D representations of interactions between ligands and proteins are drawn with PoseView.[116] The in-depth analysis of sequence data consists of sequence viewer and the optional third party annotations DSSP,[117] STRIDE,[118] MSDsite,[119] InterPro,[120] protein domain decomposition,[121] calculated alignments,[122] and domain parser,[123] which upon selection will map their predictions on the sequence. The in-depth analysis of sequence similarity consists of prepared with BLAST[124] sequence similarity clusters using 30–100% sequence similarity cutoffs. The in-depth analysis of structural similarity consists of detailed comparison of structural similarities computed with either Blast2seq, the Smith–Waterman algorithm, the Needleman–Wunsch algorithm, and jCE or the external servers TM-align, FATCAT,[125] TopMatch server, and Dali. PDB provides several tools to analyze the structural data, including tools to perform sequence and structure alignment, assess structure quality (backbone Ramachandran plot, clash score, or residue sidechains), and map genomic position to protein sequence and 3-D structure and many links to external tools. The database provides many links to external databases, including general biological and chemical databases (see browse options: Entrez NCBI, ExPaSy, GenBank, mpstruc, Pfam, and UniProtKB), biological activity databases (BindingDB, PDBbind-CN, and Binding MOAD), a database of commercially available compounds (ZINC), other databases that contain molecular structures (CCDC containing small-molecule crystal structures, www.ccdc.cam.ac.uk), EMDataBank containing CryoEM structures (www.emdatabank.org), ModBase (modbase.compbio.ucsf.edu/modbase-cgi/index.cgi) and SWISS-MODEL Repository (swissmodel.expasy.org/repository/) containing comparative protein structure homology models), and protein–ligand interaction analyses (ReliBase, www.ccdc.cam.ac.uk/solutions/csd-discovery/components/relibase/).

1.15.2 Systematic Analysis and Classification of Structural Chemogenomics Databases

1.15.2.1 Database Classification Criteria

While UniProt and PDB represent the largest protein sequence and structure depositories, respectively, ChEMBL is currently the largest curated and publically available database of target-annotated biologically active molecules (**Fig. 1**). We have analyzed additional target-annotated biologically activity databases, including general bioactivity databases BindingDB,[126] Intact,[127] STITCH,[128] SuperTarget,[129] PubChem Bioassay,[130] DrugBank,[104] PDSP K_i[131] (kidbdev.med.unc.edu/databases/pdsp.php), PDBbind-CN,[132] Binding MOAD,[133] the target family-specific bioactivity databases focusing on G protein-coupled receptors (GLASS[134]) and kinases (K-Map[135]), and two mechanism-specific bioactivity databases Platinum (site-directed mutagenesis effects)[136] and TIMBAL (protein–protein interaction modulators).[137] We have furthermore selected representative structural chemogenomics databases containing and combining protein, structure, and biological activity data of protein–ligand complexes that have been based on the following criteria: The database (i) includes structural protein–ligand interaction information, (ii) is up to date (created or updated within the past 3 years), (iii) should be publically available, and (iv) have a web interface to browse and/or search the data. While the bioactivity databases contain information on the pharmacological parameters defining, for example, the affinity, potency, and efficacy of ligands for specific protein targets, structural chemogenomics databases offer (additional) information on the structural features of protein–ligand interactions. It should be noted that there are several extensive commercial biological activity databases, including MDDR,[138] WOMBAT,[139] and Reaxys Bioactivity (www.reaxys.com). Furthermore, several biological activity databases (SuperTarget (insilico.charite.de/supertarget),[129] GPCR SARfari (www.ebi.ac.uk/chembl/sarfari/gpcrsarfari), GLIDA (pharminfo.pharm.kyoto-u.ac.jp/services/glida)[140] and structural protein–ligand interaction databases (KidFAMmap (gemdock.life.nctu.edu.tw/KIDFamMap)[141] and Kinase SARfari (www.ebi.ac.uk/chembl/sarfari/kinasesarfari)) have been set up, but unfortunately, these databases have not been created or updated in the past 3 years and are therefore not included within this systematic analysis and comparison (Apr. 2016). The selected structural chemogenomics databases are classified according to their focus and coverage of protein targets, including general structural protein–ligand interaction databases PoSSuM, IBIS, BioLip, CREDO, PLIC, ProBis, sc-PDB, Bival-Bind, Pocketome, iPfam, and PSCDB; protein target class-specific structural protein–ligand interaction databases focusing on kinases (KLIFS[99]), GPCRs (GPCRdb),[79] and phosphodiesterases (PDEStrIAn)[65]; and mechanism-specific structural protein–ligand interaction databases 2P2Idb (protein–protein interactions and protein–protein modulators)[142] and ASD (allosteric modulation).[143] Databases are analyzed according to the type of data they contain with respect

Table 2 Classification of biological activity and structural chemogenomics databases

Database					Features														Latest Updates
Name	Targets	Compounds	Complexes		Ligand										Complex				
			Structures	Activity	PROP	2D	3D	ID	SEQ	PROP	SITE	2D-SP	WATER	SIM	ACT	IFP	2D	3D	
General biological activity databases																			
ChEMBL	11019	1592191		13967816														PDB	Feb 2016
BindingDB	6191	519724	2291	1186317														PDB	Mar 2016
IntAct				586731					UniPr									PDB	Apr 2016
STITCH	9600000	430000			NCB													PDB	Oct 2015
PubChem	9961	88933741		109390														PDB	Mar 2016
DrugBank	4333	8206																	Feb 2016
PDSP Ki	352	5335		59239	NCB	NCB			NCB										Apr 2016
PDBbind-CN	2849	12843	14620	14620														PDB	Dec 2015
Binding MOAD	7599	12440	25771	9142														PDB	2014
SuperTarget	6219	195770					PubC		UniPr										2012
Target class-specific biological activity databases																			
GLASS	3056	276324		441667			NCB								EMBL			PDB	Dec 2015
Kmap	724	241		98312															
Mechanism-specific biological activity databases																			
Platinum	742*	185	1008	1008		PDB		PDB	PDB									PDB	Oct 2014
TIMBAL	50	8889	1695	18940					UniPr									PDB	Jun 2015
General structural protein-ligand interaction databases																			
PoSSuM			88290					UniPr	PDB					3D					Oct 2014
IBIS			105712											1D					Feb 2016
BioLiP	19564	18442	337865*	23492					UniPr										Mar 2016
CREDO			95151																2013
PLIC	30956	11042	84846*						UniPr					3D					Mar 2013
ProBis			42270						UniPr										Jul 2015
sc-PDB	3678	5608	9283						UniPr					1D					Feb 2014
Bival-Bind			9153			PDB		PDBs	PDBs						MOAD				2014
Pocketome	2744		2744			PDB			UniPr					3D					Dec 2015
iPfam	15540																		Jun 2013
Target class-specific structural protein-ligand interaction databases																			
KLIFS	247*	1899	6398*											1D			scPDB		Mar 2016
GPCRDB	18788*	305	134	13213										1D					Sep 2015
PDEStrIan	16	173	240											1D			scPDB		Mar 2016
Mechanism-specific structural protein-ligand interaction databases																			
ASD	1473	71538	1930	75462					UniPr										2015
2P2idb	27	242	301						UniPr										2015

to (ligand, protein target, and protein–ligand complex information) (Table 2, Fig. 3), the way the data can be searched and/or browsed, and the frequency that the databases are updated.

1.15.2.1.1 Data browse and search functionalities

In addition to the analysis of the way that data types can be accessed and analyzed, we have evaluated whether the data can be browsed and/or searched. Most databases allow browsing, sometimes facilitated by predefined classifications of proteins and/or ligands. Search options are in some databases relatively limited and based only on protein or ligand names, PDB, UniProt, or ChEMBL IDs. Most biological activity and structural chemogenomics databases however, include search options based on 2-D chemical structure (SMILES and/or interactive chemical drawer), while several general structural chemogenomics databases (e.g., sc-PDB) and target-customized structural chemogenomics database (e.g., KLIFS, PDEStrIAn, or GPCRdb) include additional search options based on properties of the protein target binding site and/or protein–ligand interactions. More examples of different browse and search functionalities are described in more detail in sections Ligand data types, Protein data types, Protein–ligand interaction data types, and Protein structure-annotated biological activity databases.

1.15.2.1.2 Ligand data types

The following ligand data types are considered in the analysis of the target-annotated bioactivity and structural chemogenomics databases:

- *Physical–chemical properties*, including number of H-bond donors, H-bond acceptors, rotatable bonds, and hydrophobicity/log *P*. Many databases have this feature, including sc-PDB, KLIFS, and SuperTarget, which allow the extraction of entries that contain ligands with specific ranges of physical–chemical properties.
- *2-D chemical structure of the ligands* is included in most databases as 2-D depictions of the molecular structure and/or chemical structures that can be extracted from the database in, for example, SMILES or SDF format. Most biological activity databases include

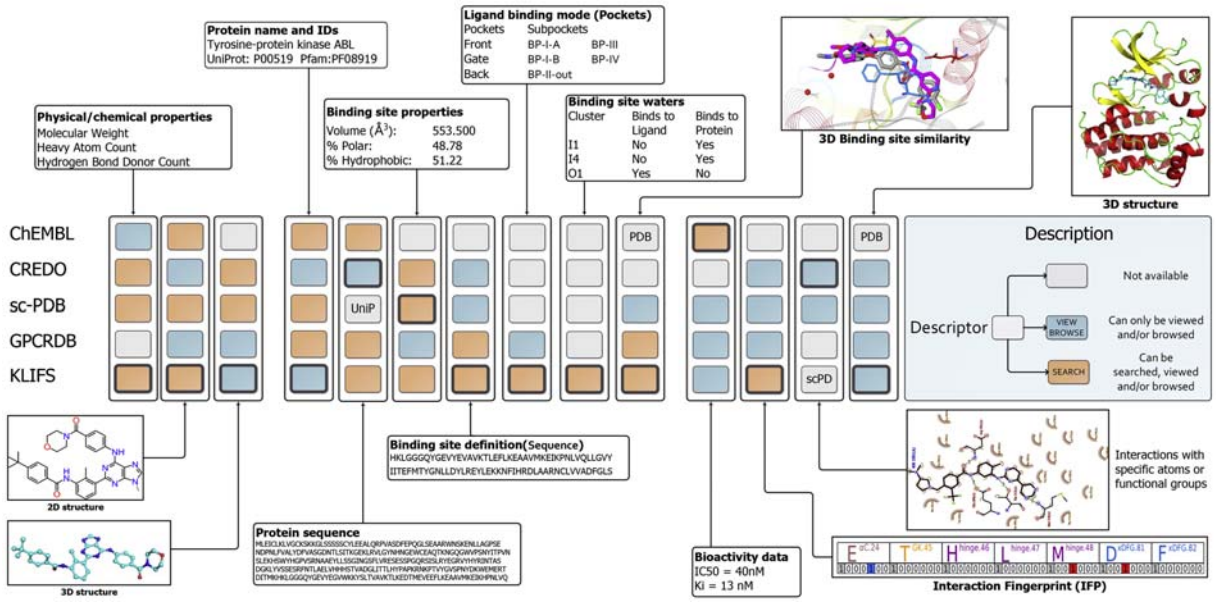

Fig. 3 Systematic structural chemogenomics comparison example. The comparison of representative proteome-wide biological activity (ChEMBL[4]), proteome-wide structural protein–ligand interaction (CREDO[144] and sc-PDB[145]), and protein family-focused structural protein–ligand interaction (GPCRdb[79] and KLIFS[99]) databases enables user to search (*orange*) and/or view/browse (*blue*) different features in the databases. For example, the ligand binding mode comparison shows that searching and viewing ligand binding mode information are possible only in KLIFS. GPCRDB allows to view/browse this type of information but not search, while sc-PDB, CREDO, and ChEMBL do not provide the option to search, view, or browse for ligand binding mode information at all. In addition to that, in some cases, the databases do not provide information directly on their website but instead provide links to external databases that contain that information, for example, UniProt (abbreviated as UniP), PDB, and sc-PDB (*scPD*). In the case of sc-PDB, the database does not show protein sequences in its result pages but provides links to UniProt where users can view it. The analysis of protein structure-annotated biological activity databases (described in Section **Protein structure-annotated biological activity databases**) and structural protein–ligand interaction databases (section **Structural protein–ligand interaction databases**) is presented in **Table 2**.

extensive search options including an interactive chemical sketch application to define queries and select entries that contain ligands with specific substructures, superstructures, scaffolds, and/or chemically similar molecules. In contrast, only three of the structural chemogenomics databases contain 2-D chemical structure search options: sc-PDB, KLIFS, and PDEStrIAn. Bival-Bind and Pocketome provide such information via the PDB. Applications relying on 2-D information include bioactivity data mining and chemical similarity search for ligand-based target prediction (Section "**Combined bioactivity data mining and chemical similarity search for ligand-based target prediction**") and integrated structure-based medicinal chemistry toolbox for drug discovery and design as described in Section "**Integrated structure-based medicinal chemistry toolbox for drug discovery and design**".

- *3-D chemical structure of the ligands* is included in all structural chemogenomics databases and most biological activity databases as coordinate files (e.g., PDB, MOL2, SDF) and/or links to PDB coordinates of cocrystallized ligands bound to protein structures. Only few databases include search options based on 3-D structural information of ligands. CREDO enables shape-based ligand similarity search, while sc-PDB and Bival-Bind provide search options based on indirect 3-D structural ligand information regarding ligand buried surface area (sc-PDB) and distance between two ligands targeting different binding site (Bival-Bind).

1.15.2.1.3 Protein data types

The following protein data types were considered in the analysis of the target-annotated bioactivity and structural chemogenomics databases:

- *Protein identifiers* can be used to search most databases and connect databases with each other allowing efficient data mapping. Frequently used IDs are shown in **Table 1**.
- *Amino acid sequence data*, along with structural data, form the essence when studying binding complexes, and as such, it is almost always either annotated in the databases or linked to databases that provide access to it (e.g., UniProt).
- *Physical–chemical properties* of protein binding sites can be searched in only a few databases to identify, for example, druggable binding sites (e.g., sc-PDB and CREDO).
- *Ligand binding sites* based on, for example, amino acid sequence or ligand distance cutoffs are defined in all structural chemogenomics databases while completely missing in the bioactivity databases. Examples of structural databases that enable users to view this information interactively include KLIFS, PDEStrIAn, PLIC, and BioLip.

- *Subpocket annotations* are reported in protein family-customized structural chemogenomics databases, as these databases allow the systematic annotation of (sub)pockets that are targeted by specific ligands. Complementary information on the chemical scaffolds that target-specific (sub)pockets could be extracted from a structure-based medicinal chemistry toolbox as described for KLIFS and PDEStrIAn in Section "**Integrated structure-based medicinal chemistry toolbox for drug discovery and design**."
- *Binding site water molecule annotations* based on superposed structures in protein family-focused structural chemogenomics databases allow the identification of areas in the binding sites in which a significant number of water molecules have been found within certain proximity. Consistent annotation of water clusters is included in KLIFS and PDEStrIAn databases and can be used to identify water molecules that can be displaced or targeted in structure-based ligand design.
- *Binding site similarity* assessments to other protein targets are provided by structural chemogenomics databases to facilitate the identification of sequentially, structurally, and/or chemically similar binding sites. Several databases allow binding site similarity assessments based on sequence similarity (IBIS, KLIFS, and PDEStrIAn), structure-based similarity (sc-PDB, PLIC, ProBis, and BioLip), or protein–ligand interaction pattern similarity (KLIFS, PDEStrIAn, and Pocketome). Applications of protein binding site similarity assessments for ligand repurposing and off-target prediction are described in Section "**Protein binding site similarity assessments for ligand repurposing and off-target prediction**."

1.15.2.1.4 Protein–ligand interaction data types

The following protein–ligand complex data types are considered in the analysis of the target-annotated bioactivity and structural chemogenomics databases (**Fig. 4**):

- *Bioactivity data* can be searched based on quantitative bioactivity data ranges and/or source data (e.g., PubMed ID and author names) in most biological activity databases. Only parts of the structural chemogenomics databases provide direct information on bioactivity data, including BioLip, sc-PDB, KLIFS, PDEStrIAn, GPCRdb, 2P2Idb, and ASD. Platinum contains experimentally

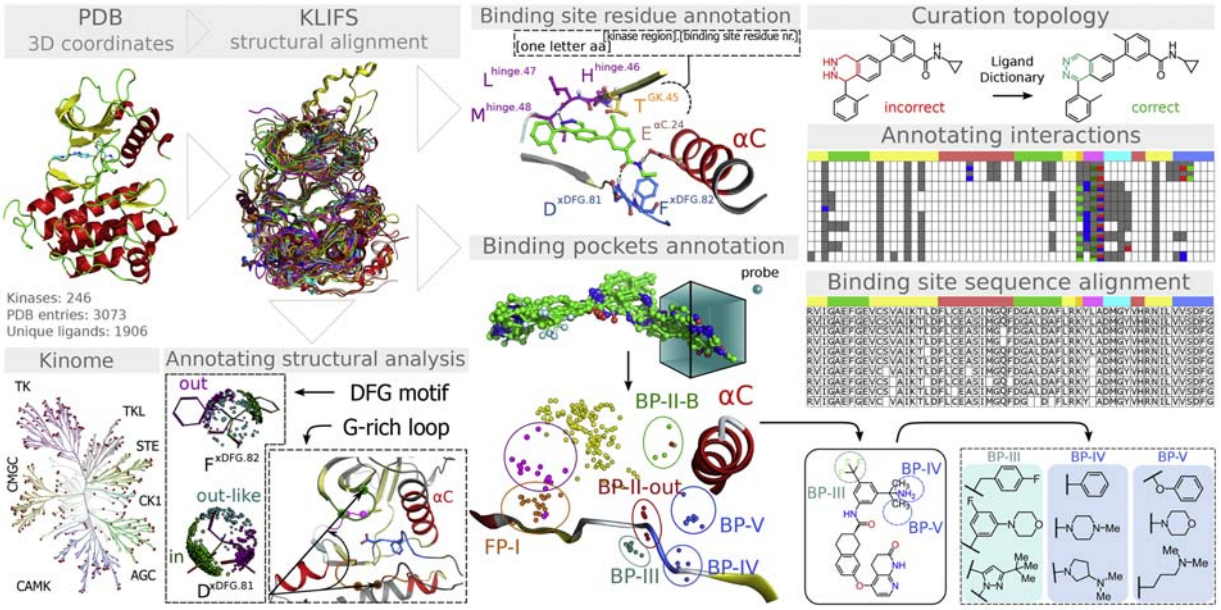

Fig. 4 Example of an integrated structural chemogenomics database to analyze structural protein–ligand interactions. The tools and analysis shown in this figure are extracted from the KLIFS database. New protein kinase structures (*top left corner*) are aligned to manually corrected structural and sequence alignments that allow automatic annotation of binding residues (shown under "Binding site residue annotation"), binding pockets (shown under "Binding pocket annotation") and interactions (shown under "Annotating interactions"). The positions and the residue coding of the aligned binding residues are annotated using the scheme (one letter amino acid)$^{(\text{kinase region}).(\text{binding site residue number})}$ as described by Kooistra et al. 2016.[99] This annotation allows for easy comparisons between different structures—for example, one could effortlessly compare the aspartic acid of the DFG motif in different structures as this residue is annotated consistently in the structures, that is, $D^{xDFG.81}$. The binding pocket annotation method uses probes and sets of aligned ligands to identify sets of probes that describe the binding pockets. Each set of probes (colored with a color) describes a binding pocket by using probes that are found within 1 Å of ligands that bind to that pocket; thus, each set of probes forms a sphere in the 3-D space that is unique to ligands that bind to a particular pocket. The identified probes can then be used to assign binding pockets to new ligands. On the *bottom right corner*, the back pockets(BP) III, IV, and V are annotated for the ligand with PDB ID 0NF. Interactions between ligands and protein kinases can be annotated using interaction fingerprint methods. These methods typically check if any of the atoms of a bound ligand fulfills any of the interaction rules, and if it does, it is annotated along with the type of interaction. Typical interaction rules are distances and angles. The interaction fingerprints allow easy comparison of the interactions that ligands make. The table under "Annotating interaction" shows interactions (represented with unique color) bound ligands make with protein kinase targets (each row represent unique protein kinase target).

measured effects of mutants of a set of protein–ligand complexes for which experimental data is available, while GPCRdb contains a large number of mutation data on G-protein-coupled receptors.

- *Residue-based interaction fingerprint*: Interaction fingerprints are binary representations (yes/no) that encode different types of interactions that a ligand makes with residues of their bound target. This descriptor indicates if such representations are available in the considered databases. It should be noted that the PDB format does not sufficiently annotated chemical topology of non-protein molecules to allow accurate annotation and analysis of protein–ligand interactions. A more appropriate format is, for example, the atom- and bond-type annotated Tripos MOL2 format, which is, for example, used to analyze protein–ligand interaction fingerprints deposited in, for example, sc-PDB, KLIFS, and PDEStrIan. Transformation of PDB into MOL2 format, however, requires careful curation of the chemical topology and protonation of ligands and proteins to allow for proper protonation of the molecules and accurate analysis of protein–ligand interactions, including H-bond interaction networks. In KLIFS and PDEStrIAn, for example, the data in the chemical component dictionary are used to identify and correct errors in atom and bond types complemented by manual curation steps (Fig. 3).
- *Atom-based 2-D interaction information* indicates whether protein–ligand interaction information is available in a 2-D representation. In contrast to residue-based interaction fingerprint that represents the interactions in a simple binary form, atom-based 2-D interaction information shows at least the interacting residues in 2-D and the interaction they make with the ligand, which is also represented in a 2-D. The 2-D representation should make it possible to determine the interacting atoms of both the protein and ligand. Most general structural protein–ligand interaction databases provide this feature. A well-known program that is frequently used to visualize protein–ligand interactions in 2-D diagram is LigPlot.[146]
- *3-D structural information*: All general, target class-specific, and mechanism-specific, structural protein–ligand interaction databases contain 3-D coordinates of the protein–ligand complex. All general and target class-specific structural protein–ligand interaction databases provide processed structural data files in which binding sites are annotated, residues are protonated, and/or the molecular topology is curated, which allow consistent analysis of structural protein–ligand interactions. Most of these databases annotate the interactions with interaction fingerprint and/or 2-D interaction information. Almost all general biological activity databases provide links to the coordinates PDB.

1.15.2.1.5 Database update frequency

To anticipate the continuous growth in sequence information deposited in the UniProt (>5.7 billion sequences over the period between Apr. 2015 and Apr. 2016), structural information in the PDB (9334 structures in 2015), and bioactivity information in the ChEMBL database (>440,000 bioactivity data points over the period between Feb. 2015 and Feb. 2016), it is important to know what the frequency is with which databases are updated and what the latest update was. For the analysis presented in Table 2, we have reported the latest updated on Apr. 2016. The update frequencies of the databases were categorized into weekly, montly, between 1 and 3 months, between half year and one year, not updated in the last 2 years, and never updated. The most regularly updated databases are BioLip, KLIFS, and PDEStrIAN, which are updated weekly to keep in sync the PDB to keep up with the continuous growth in published catalytic kinase domain structures (>337 new structures in 2015) and PDE structures (>18 new structures in 2015). DrugBank, PDSP Ki, and IntAct are updated monthly, while BindingDB and K-Map are updated every 1–3 months. Although ChEMBL used to have very frequent updates (up to six times a year, Fig. 1C), the two most recent versions of the database have been on a yearly basis. GPCRDB, PDBbind-CN, 2P2idb, Pocketome, and TIMBAL are updated every half a year to a year. ProBis used to be updated twice a year, but in the recent years, its update frequency decreased to only once a year or 2 years. GLASS is updated irregularly, but the time intervals between the updates span typically within a year. On the other hand, Binding MOAD, CREDO, PLIC, and sc-PDB have not been updated in the past 2 years (Apr. 2016). iPfam, Bival-Bind, and Platinum have never been updated since their initial release. PubChem is the only database that updates its content daily basis.

1.15.3 Protein Structure-Annotated Biological Activity Databases

1.15.3.1 Proteome-Wide Biological Activity Databases

PubChem[130,147] (pubchem.ncbi.nlm.nih.gov) contains 9960 protein, 19,260 gene targets, and 88,837,058 compounds, of which 2,101,179 tested in 1,154,436 bioassays, resulting in 230,042,050 bioactivity data (Apr. 2016, updated daily). PubChem can be searched by compound, patent, target, bioactivity, or bioassay. Compound searches can be performed based on name/keywords, PubChem CID, SMILES, InChI, molecular formula, and 2-D chemical (sub)structure and chemical similarity. Patent queries can be performed using keyword, inventor, applicant, structure, and molecular formula. Bioassays and bioactivities can be queried by only names, and in the case of bioactivity, the names can be genes or chemical names. The database can be browsed by bioassays and in particular activity types/potency, assay types, cell lines/types, data sources, detection methods, HTS projects, publications, targets, and taxonomy. The results of compound queries contain 2-D and 3-D structures of the compound and information on names and identifiers, chemical and physical properties, related records, chemical vendors, drug and medication information, pharmacology and biochemistry, toxicity, literature, patents, biomolecular interactions and pathways, biological test results, classification, and information sources. The chemical and physical properties consist of computed and experimental properties including MS–MS spectra. Related records provide links to similar compounds, conformers, components, and substances or records with similar connectivity and similar or exact patent. This part also offers links to journals, government organizations, and other

R&D databases to name just a few. The remaining parts provide information about involved disease, pharmacology, protein targets (including action, function, and references), ADME, mechanism of action, toxicity and protein binding, links to PubMed publications, patents, involved pathways, results of bioassays, and links to many external sources. The assay queries contain a description of the assay, tested substances and their outcome and activity, information from ChEMBL and other sources, assays from the same publication, and related bioassays. Target and bioactivity queries return the relevant compounds, their best activity value, and provide links to view the compound information, while patent queries give links to external source of the patent.

ChEMBL[5] (www.ebi.ac.uk/chembl) contains 13,967,816 biological activities for 1,592,191 distinct compounds and 11,019 targets, collected from 65,501 publications (Apr. 2016, v21, latest update Feb. 2016). ChEMBL can be browsed by protein target, drug, drug targets, and drug indications. The molecular structures of compounds in ChEMBL are curated and standardized and provided as SMILES string. Protein targets are classified in 15 main protein classes (7089 in total), 6 main taxonomy classes (10,657 in total), and 3 main gene ontologies (15,642 in total) and can be browsed by name, UniProt ID, and organism, among others. Drugs can be browsed based on 27 parameters, including patent number, applicants, clinical phase, indication class, and administration (oral, parenteral, or topical), and whether the drug is first in class, a prodrug, and whether the targets/mechanisms of action are (un)known (black box). Drug targets can be browsed based on 19 parameters, including drug molecule, drug target name, mechanism of action/action type (activator, inhibitor, agonist, and antagonist, including reference), and binding site. Drug indications can be browsed based on 11 parameters, including MeSH (ID and heading) and EFO (ID and term) information and indication reference. ChEMBL can be searched based on protein target (name/keyword, BLAST search), compound (ChEMBL ID, name/keyword, SMILES string, chemical (sub)structure, chemical similarity, and biological BLAST search), assays (keyword), documents (keyword), and cells (keyword). Protein target entries contain information on the target name and classification (including UniProt ID) and overviews of approved drugs and clinical candidates targeting the protein, associated bioactivities and assays, and analyses of target ligand efficiencies, target compound properties, and cross-references to external sources regarding target gene (including Ensembl, GO, Wikipedia), protein (including UniProt and Guide to Pharmacology[85]), and domain (including Pfam) information. Ligand entries contain information on compound name and classification (ChEMBL ID and synonyms), molecular representations (SMILES string, mol file, InChi, and InChi key), calculated physical–chemical properties, associated bioactivities and assays, protein target predictions, available clinical data, and compound (ChemSpider, Wikipedia) and UniChem (including BindingDB, eMolecules, LINCS, and PubChem ID) cross-references. Bioactivities can be filtered based on activity parameter and value and are described by 54 parameters, including parent compound ChEMBL ID (to allow mapping of similar compounds), compound key (name or code mentioned in the source), SMILES string, bioactivity parameter (value, relationship, and unit), pChEMBL value (to allow comparison of different bioactivity parameters), assay ChEMBL ID, protein target UniProt ID, assay type (binding or functional), cell type, and reference information (PubMed ID, ChEMBL document ID, and citation). The ChEMBL Virtual Machine (MyChEMBL) integrates ChEMBL, PostgreSQL, and the chemoinformatics tools in RDKit in order to provide a user-friendly environment for performing chemogenomics studies.[148]

STITCH[128] (stitch.embl.de, v4.0) contains experimentally determined and predicted protein–ligand interactions between 300,000 small molecules and 2.6 million proteins from 1133 organisms, including more than 2.2 million interactions between human proteins and small molecules (Apr. 2016, updated Oct. 2015). STITCH can be searched by protein information (name, UniProt, Swiss-Prot, sequence, and organism) and ligand information (name, InChi keys, ChEMBL, PubChem, and chemical structure (SMILES, upload)). The resulting STITCH protein–ligand interaction network can be interactively viewed. The individual connections (i.e., edges in the network) contain supporting experimental data and the associated databases (including ChEMBL, PubChem, PDSP-K_iDB, DrugBank, and KEGG), as well as predicted interactions, while the nodes contain information regarding the proteins (Ensemble, UniProt, Genecards, PfAm, and NextProt) and ligands (description, 2-D chemical structure and ChEMBL, PubChem, DrugBank, KEGG, ChemSpider, and Google links) involved in the network.

BindingDB[126] (www.bindingdb.org) contains 1,161,912 binding data of 6929 protein targets and 505,999 small molecules, collected from literature not covered by other public databases (Apr. 2016, latest update Mar. 2016, updated every 1–3 months). BindingDB includes affinity data for protein–ligand complexes of 2291 identical (100% protein sequence identity) and 5816 similar (85% protein sequence identity) proteins for which crystal structures are deposited in the PDB. BindingDB can be searched (and browsed) based on binding data (K_d, K_i, IC_{50}, k_{on}, k_{off}, ΔG^0, ΔH^0, and $-T\Delta S^0$), experimental details (pH enzymatic assays and pH ITC), protein target (name, UniProt ID, amino acid sequence, and PDB code), ligand (name, molecular weight, and SMILES string), 2-D chemical structure (substructure, similarity search), and reference (PubMed and PubChem). BindingDB can be browsed (but not searched) based on source organism, pathway, and reference (author, journal/citation, institution, and US Patent). BindingDB furthermore provides lists of the number of compounds per target, ligands per target (csv), PDB codes per ligand (sdf), and approved and experimental drugs. BindingDB (curated literature) data downloads can be complemented by binding data from ChEMBL, PubChem, PDSP K_i, CSAR, and US Patents.

IntAct[149] (www.ebi.ac.uk/intact, v4.0) contains 586,731 experimentally determined interactions between ligands and 83,536 proteins (Apr. 2016, updated monthly). IntAct can be searched by protein information (protein, RNA, gene name, UniProtKB, RNA, and IMex ID), ligand information (name and ChEBI), and reference (PubMed). Intact entries contain an overview of the interacting protein(s) (name, type, UniProtKB and CHEBI ID/AC links, and organism), the interacting ligand(s) (name, chemical structure, and CHEBI ID), and description of their experimentally determined interactions (interaction detection method, literature reference, and CHEBI interaction AC). Search links are provided based on the individual interacting molecules.

PDSP K_i database[131] (kidbdev.med.unc.edu/databases/pdsp.php) contains 59,239 K_i binding data, of 352 proteins and 5335 ligands, extracted from literature (Apr. 2016, latest update Mar. 2016, updated montly). The PDSP K_i database can be browsed

(but not searched) based on protein UniGene code and PubMed ID, PubChem ID, and ChEMBL ID source reference data. The PDSP K_i database can be searched (and browsed) based on K_i binding data range, protein target (name, organism, source, and anatomic profile), ligand (test ligand name, SMILES string, CAS, NSC code, and hot radioligand name), and reference source (author/date). The database furthermore offers different search options to investigate and visualize protein–ligand selectivity. Querying the database reveals the K_i information for protein–ligand complexes. In addition, PDSP K_i provides links to PubChem, ChEMBL, and PubMed.

PDBbind-CN[132] (www.pdbbind-cn.org/) provides highly curated experimentally determined binding data for biomolecular complexes available in the PDB, including binding data for 14,620 complexes, most of which are protein–ligand complexes (11,987), followed by protein–protein (1807), protein–nucleic acid (717), and nucleic acid–ligand (109) complexes (Apr. 2016, v2015, latest update Dec. 2015, updated every half year to one year). The database is updated on an annual basis and uses a combination of scripts and automation tools followed by double manual curation for the annotation of experimentally measured binding data (K_d, K_i, and IC_{50}) from literature (>27,000 unique references). It furthermore provides a set of high-quality "core" structures containing 195 protein–ligand complexes comprising 65 protein families. This set can, for example, be used for retrospective docking and scoring evaluation purposes. All data is available for download as a set of processed structures and all annotated binding data in plain text and PDF format. The web interface of PDBbind-CN provides four ways of traversing through the data. The first option is *Browse*, which allows the user to browse through the database starting from the first entry. The second option is *Data* and provides several search options: PDB code, ligand name, release year, structure resolution, binding affinity, EC number, and protein name. The third option is *Structure* and allows a user to specify (SMILES or PDB code) or draw a molecule for a chemical (sub)structure or similarity search. The fourth option is *Sequence*, which allows the user to perform blast queries using a PDB entry or a specific fasta sequence. All search results can be downloaded in PDF and Excel format and also provides the option to download the selected structures (ligand, protein, ligand and protein, or pocket and ligand). The detail page of each structure shows a summary of the entry, a 3-D viewer of the structure, a list of database entries with a high sequence similarity, and links to PDB, PDBsum, and PubChem.

Binding MOAD[133] (www.bindingmoad.org, v2014) contains well-resolved crystal structures (resolution ≤2.5 Å) of 25,771 biomolecular complexes of 7599 proteins and 12,440 different biologically relevant ligands (peptide ≤10 amino acids, oligonucleotide ≤4 nucleotides, and small organic molecules) collected from the PDB, annotated with 9142 experimentally determined binding data (K_d, K_i, IC_{50}) reported in the primary reference of each PDB file (Apr. 2016, latest update 2014). Crystallographic additives, salts, buffers, metals, metallic catalytic centers, or solvents are *not* considered as ligands. Database entries can be browsed and filtered based on protein target class (7 enzyme families organized by EC number and 11 nonenzyme groups), the availability and value ranges of binding affinity data, crystal structure resolution, and ligand molecular weight. Entries can be searched based on PDB code, EC number, protein source, ligand HET group and the molecular structure (substructure, superstructure, similarity, fragment, or duplicate), keywords, and author surname.

DrugBank[104] (www.drugbank.ca) focuses on FDA-approved, experimental, nutraceutical, and other types of drugs. The database currently contains 8198 drugs and 4331 protein sequences and many forms of related information (Apr. 2016, v4.3, latest update Feb. 2016, updated every 1–3 months). For each drug, there is an extensive list of annotations and datapoints available, which are categorized into identification, taxonomy, pharmacology, ADMET, pharmacoeconomics, properties, spectra, references, interactions, targets, enzymes, and transporters. Identification provides information on the name, structure, synonyms, approval status, (generic) prescription/over-the-counter products, brands, categories, and chemical descriptors and molecular identifiers. Taxonomy describes the classification of the drug in detail. Pharmacology reports detailed information regarding the indications for the use of this drug, the pharmacodynamics, the mechanism of action, experimental ADMET properties, and the affected pathways. "ADMET" provides a list of predicted ADMET properties (from admetSAR) and the probability of each property. "Pharmacoeconomics" list manufacturers, packagers, dosage forms, prices, and patents of a given compound. "Properties" list both experimental and predicted chemical properties of the drug (e.g., melting point, pK_a, and PSA). "Spectra" provide links to available MS and NMR spectra. "References" links to key patents, scientific articles, ATC codes, and many external resources (e.g., ChEMBL, KEGG, ChemSpider, and IUPHAR). "Interactions" list available drug–drug and drug–food interactions. The final three categories targets, enzymes, and transporters, offer detailed information regarding the interactions between the selected drug and proteins divided in these three categories. For each interaction entry, the type of interaction and the pharmacological classification as well as references to articles listing the interaction including a link to the UniProt identifiers of the interacting protein are given. Besides a browse option, the DrugBank also provides many search options including searching using structure, drug name, pathway name, target name, molecular weight, interaction, sequence, and (MS/GC)MS and (1-D/2-D) NMR spectra. All data are also available as download in XML/CSV/Fasta/SDF format depending on the type of data that is downloaded.

1.15.3.1.1 Protein family-customized biological activity databases

GLASS[134] (zhanglab.ccmb.med.umich.edu/GLASS/) contains 441,667 experimentally validated GPCR–ligand interactions extracted from 811,966 experimental data entries, covering 687 GPCRs (GLASS contains 3056 different GPCR entries, including 825 human GPCRs) and 276,324 ligands (including 192,251 Lipinski's drug-like entries) (Apr. 2016, latest update Dec. 2015). GLASS contains GPCR–ligand interaction data systematically extracted from biological activity databases (ChEMBL, BindingDB, IUPHAR, DrugBank, and PDSP), GPCR diseases association database TTD, GPCR experimental structural data (PDB and BioLiP), and predicted models of GPCRs (GPCRRD), and the respective IDs of these databases can be used to search GLASS. GLASS GPCR–ligand interaction entries are complemented with ligand (PubChem and InChI) and protein (UniProt) data and contain overviews of experimental data for a ligand with all known targets and for a target with all known ligands.

K-Map[135] (tanlab.ucdenver.edu/kMap/kMapv1.0/) contains bioactivity data for 98,312 kinase–ligand complexes, covering 742 protein kinases (including mutated kinases) and 241 compounds (Apr. 2016, updated every 1–3 months). K-Map provides a rank-ordered list of compounds for the queried kinases based on their normalized connectivity scores and *p*-values. The database can be searched by kinase name and browsed by kinase name, family, GO terms, and drug name in combination with IC_{50}, K_d, or both. Additional information about compounds and targets can be found via the following links to external sources: PubMed, PubChem, ChEMBL, ChemSpider, KEGG, GDSC, and clinical trials.

1.15.3.1.2 Mechanism-specific biological activity databases

TIMBAL[137] (mordred.bioc.cam.ac.uk/timbal) contains 18,940 bioactivity data of 8889 small-molecule ligands that modulate protein–protein interactions collected from ChEMBL based on UniProt codes of 50 known PPI targets and their orthologs (1137 entries in total, Apr. 2016, v2015, latest updated Jun. 2015, updated every half year to one year). Data have been selected from binding assays that are directly assigned to either a single protein or its homolog or a protein complex or its homologs.

1.15.4 Structural Protein–Ligand Interaction Databases

1.15.4.1 General Structural Protein–Ligand Interaction Databases

IBIS[150] (www.ncbi.nlm.nih.gov/Structure/ibis/ibis.cgi) contains 381,223 annotated protein–ligand interactions including 5981 protein–DNA interactions, 18,838 protein–RNA interactions, 199,819 protein–protein interactions, 6737 protein–peptide interactions, 53,927 protein–ion interactions, and 95,921 protein–chemical interactions (Apr. 2016, latest update Feb. 2016). IBIS can be searched based on PDB, UniProt, or Gene ID. Each IBIS entry (PDB link) provides an overview of the type and number of interaction sites and the interaction partner (protein, chemical, DNA/RNA, and ion), which can serve as a query to identify similar protein structures. The query result consists of a comparative binding site alignment of the residues interacting with different ligands targeting of the protein target and homologous proteins.

BioLip[151] (zhanglab.ccmb.med.umich.edu/BioLiP) contains 344,248 annotated protein–ligand interactions including 41,038 protein–DNA/RNA interactions, 16,169 peptide–protein interactions, 97,430 metal–protein interactions, and 189,611 regular protein–ligand interactions derived from 74,069 PDB entries (Apr. 2016, updated weekly). In total, 23,492 entries are annotated with experimentally determined binding data (K_d, K_i, and IC_{50}) derived from Binding MOAD (10,971), PDBbind-CN (16,980), BindingDB (7331), and 64 manually collected from original literature. BioLip contains a hierarchical procedure for assessing the biological relevance of ligands present in the PDB structures. BioLiP can be browsed and searched based on PDB ID, PDB ligand ID, ligand name, UniProt ID, EC numbers, and GO terms. BioLiP can be browsed (but not searched) based on ligand binding residues, catalytic sites (derived from Catalytic Site Atlas), and PubMed entry. To facilitate the use of BioLiP for function annotation of uncharacterized proteins, a consensus-based algorithm COACH is used to predict ligand binding sites from protein sequence or using 3-D structure. Each BioLip entry provides a definition of the ligand binding site and global view of protein–ligand interactions.

ProBIS[152] (probis.cmm.ki.si) allows structure-based comparison of specific ligand binding sites with the binding sites in 42,270 protein–ligand crystal structures collected from the PDB (Apr. 2016, latest update Jul. 2015, updated every 1 to 2 years). To search ProBIS, the query binding site can be defined interactively (JSmol) based on distance from specific HET codes observed in the query PDB file. ProBIS entries contain an overview of annotated binding sites, predicted ligands (small molecule, protein, nucleic acid, and ion), and a *z*-score ranked list of similar proteins in the PDB that can be browsed (including links to corresponding PDB entries).

PoSSuM[153] (possum.cbrc.jp/PoSSuM) contains 300,122 known and 5,213,569 putative binding sites collected from 98,458 PDB entries, covering 12,220 unique protein structures and 5312 unique ligands, excluding buffers, water molecules, DNA/RNA, and peptide (Apr. 2016, latest update Oct. 2014, updated every 1 to 2 years). Binding sites extracted from crystal structures ($\leq$4.0 Å resolution) and NMR structures (only model 1) consist of six residues or more that are within 5.0 Å from an interaction probe cluster (consisting of 200 probes or more) generated with Ghecom.[154] PoSSuM can be searched based on protein (PDB code) and ligand (HET code, HET chain ID, and HET residue number) information and customizable search settings considering the ligand binding site (known and/or putative), sequence redundancy, similarity cutoff, and aligned sequence length cutoff to identify 530,989 target binding sites that are similar to 2595 query binding pockets targeted by 194 known small-molecule drugs (covering 1289 PDB entries and 452 UniProt IDs). PoSSuM entries have been annotated with various protein and gene data (UniProt, CATH, SCOP, EC, and GO), and structural alignments of similar binding sites can be viewed in an interactive manner (with JSmol). The annotated drugs in PoSSuM can be browsed based on name/ID (preferred name, HET code, and ChEMBL ID), therapeutic application (WHO ATC classification), chemical properties (heavy atom, rotatable bonds, log*P*), chemical structure (2-D image, SMILES, and InChi key), and the number of query and target binding sites (and number of associated proteins, PDB entries, EC numbers, and CATH codes).

CREDO[144] (marid.bioc.cam.ac.uk/credo/) contains protein–ligand interactions in 95,515 crystal structures collected from the PDB (Apr. 2016, latest update 2013). CREDO entries contain the structural interaction fingerprint (SiFT[155]) analyses of interactions between the atoms of surface-exposed residues of all molecules inside macromolecular structures from the PDB (including proteins, nucleic acids, carbohydrates, and small-molecule ligands) and the annotation of protein structure variations (EnsEMBL Variation). CREDO can be searched based on ligand information, including physicochemical properties, 2-D similarity (substructure/

superstructure, RDKit, OpenEye fingerprints, and TriGRAM) and 3-D (ultrafast shape recognition) chemical similarity search, and nine filters (including amino acid, drug-like and lead-like). CREDO can be browsed based on protein information (PDB, protein type, protein domains (Pfam, CATH), and secondary structure fragment), ligand information (name, type, chemical components, and fragments), protein–ligand interactions (drug-/substrate-/product-/kinase-binding sites, interfaces, grooves, ligand–ligand interactions, ligand–nucleic acid interactions, halogen bonds, and metal complexes), genetic variations, and (disease) phenotypes. The protein, ligand, and protein–ligand information in CREDO entries can be used as reference for subsequent ligand 3-D similarity (USR) searches. In addition to the extensive structural protein–ligand interaction analyses (residue-based and atom-based contact analyses, 13 SiFT interaction types), CREDO provides overviews of structure quality criteria parameters (including identification of disordered regions, diffraction-component precision index (DPI), incomplete residues, and clashes).

sc-PDB[145] (cheminfo.u-strasbg.fr/scPDB/) contains annotated protein–ligand interactions in 9283 PDB entries, covering 3678 proteins and 5608 ligands collected from the PDB and their bioactivity data collected from ChEMBL (v.2013, latest update Feb. 2014). Sc-PDB can be searched based on (i) ligand properties (PDB HET code, ranges of molecular weight, aLogP, logS, rotatable bonds, rings, Lipinski rule of five violations, number of H-bond acceptors, H-bond donors, negatively ionizable atoms, and positively ionizable atoms) and 2-D chemical structure (exact, substructure, superstructure, and fragment), (ii) protein classification (EC number, UniProt (AC, name), organism, TaxID, and kingdom) and experimental structure information (PDB ID, experimental method, and resolution), (iii) binding site properties (presence cofactor, ion, number of water molecules and nonstandard amino acids, number of chains, range in size and cavity volume, and average B-factor), and (iv) binding mode (number of hydrophobic contacts, aromatic contacts, H-bond acceptor (protein) to H-bond donor (ligand) and H-bond donor (protein) to H-bond acceptor (ligand) interactions, cation (protein) to anion (ligand) and anion (protein) to cation (ligand) interactions, and ligand buried surface area). sc-PDB entries contain in addition to the search parameters the following information: (i) ChEMBL ID and activity data; (ii) 2-D structure of the ligand; (iii) comparison of protein and ligand properties to average values in the sc-PDB; (iv) atom- and residue-based report and 2-D (Poseview) and 3-D (AstexViewer) views of protein–ligand interaction distances, angles, and interaction types[156]; (v) assessment of binding site similarity (based on Shaper cavity fingerprint descriptor); (vi) and protein–ligand binding mode similarity (based on Grim[157] interaction fingerprint descriptor) and 3-D structural alignment with respect to other sc-PDB entries. sc-PDB-Frag[158] (cheminfo.u-strasbg.fr/scPDBFrag/, v.2013, latest update 2014) builds on the sc-PDB, contains fragments of protein-bound ligands, and allows users to search for bioisosteric replacements of ligands.

Bival-Bind[159] (agknapp.chemie.fu-berlin.de/bivalbind) contains 9153 crystal structures of bi- and multivalent protein–ligand complexes (containing at least two ligands of the same type) collected from PDB, BindingDB, and Binding MOAD (Apr. 2016, created 2014, not updated since). Bival-Bind can be searched based on PDB and ligand HET codes, distance between two ligands targeting different binding sites, sequence identities between the structures containing the binding sites, and several geometric parameters of the binding sites, including convexity, barrier, depth, and vectors alpha and beta defining the length and orientation of the two binding pockets. Bival-Bind entries furthermore contain the surface height profiles of the different ligands (PDB).

PLIC[160] (proline.biochem.iisc.ernet.in/PLIC) contains 84,846 protein–ligand binding sites in 30,956 proteins and 11,042 ligands collected from the PDB (Apr. 2016, latest update Mar. 2013). PLIC can be searched based on protein (UniProtID, EC number, CATH ID, and name) and ligand (PDB HET code and name) information and text search. PLIC entries (annotated ligand binding sites) contain overviews of similar binding sites, 2-D (LigPlot) and 3-D (Jmol) visualization, the analysis and structural 3-D alignments of binding site clusters (based on PocketMatch and PocketAlign), and detailed analyses of binding sites (based on fPocket shape descriptors) and protein–ligand interactions (atom-based and residue-based protein–ligand contact analyses, and water contacts, and interaction energies (using AutoDock)).

Pocketome[161] (pocketome.org, v15.12) contains conformational ensembles of protein–ligand binding sites of 2744 different proteins (Apr. 2016, latest update Dec. 2015, updated every half year to one year). The Pocketome database includes proteins that have an Swiss-Prot entry and, have been cocrystallized in complex with at least one drug-like small molecule, and are represented by at least two PDB entries. Pocketome can be searched based on protein (protein name, family, domains, UniProt name, and PDB code) and ligand (HET code and ligand name) information. In addition, similar Pocketome binding sites can be searched based on ICM binding site selection. Pocketome entries contain protein (PDB codes associated with the entry, protein, family, domain, and UniProt names of the master chain and second chain, organism), ligand information (HET code), and binding site annotation, atomic coordinates of superimposed structures, contact matrices, and the results of pairwise structure comparison within the pocket ensemble. Pocketome entries provide interactive structure visualization (ActiveICM) and can be downloaded in a variety of file formats including ICB (ICM binary format) and extensible markup language (XML).

Platinum[136] (bleoberis.bioc.cam.ac.uk/platinum) contains experimentally measured effects of 600 (single or double) mutants of 142 unique proteins and 185 ligands, representing 1008 protein–ligand combinations in total (Apr. 2016, created Oct. 2014, not updated since). Platinum can be browsed based on protein name, mutation, ligand ID, and UniProt ID. Platinum can be searched based on ligand type (amino acid, bound, nucleotide, and saccharide), organism category, mutation effect (decrease or increase), 12 protein classes, experimental method (kinetic, ITC, FRET, optical binding, radioligands, SPR, and others), protein structure resolution range, mutation type (all or single-point), and affinity constant ($K_D/K_i/K_m$). Platinum entries contain information on the protein (PDB ID and UniProt ID), ligand (name, PDB HET code, PDBe link, and SMILES string), definition of the mutant and its affinity compared with wild-type protein (affinity constant, unit), the experimental method used to determine the affinity, experimental parameters of the determined protein structure (including experimental method and resolution, R_{free}), and reference source (doi and PubMed ID).

1.15.4.2 Mechanism-Based Structural Protein–Ligand Interaction Databases

2P2Idb[142] (2p2idb.cnrs-mrs.fr) contains structural analyses of 27 protein–protein interaction interfaces and physical–chemical descriptors of 224 small-molecule PPI inhibitors collected from the PDB[3] (v2.0, latest update 2015). PPIs are classified in three classes, and each 2P2Idb PPI entry contains overviews of the structures of the protein–protein complex, free protein target, free protein partner, and protein–inhibitor complex that can be browsed and downloaded. Global PPI parameters (including gap volume, number of contacts, H-bonds, interface secondary structure, and planarity) and atom- and residue-based annotation of structural interactions (contacts, H-bonds, and salt bridges) are reported and visualized with JSmol[162] for each PPI interface. PPI inhibitors can be searched based on chemical descriptors (10 MOE (Chemical Computing Group Inc.) and 13 DRAGON[163] descriptors). Links to external databases provide (additional) information on the protein target and partner (UniProt, PDB, and PDBsum), dissociation constants (K_d) of protein–protein and protein–inhibitor complexes (PDBbind-CN), and small-molecule PPI inhibitor properties (ChemSpider, LigandRCSB, Ligand CREDO, LigandExpo, and HicUp). The information returned by the search or browse options is divided into four categories: protein–protein, free protein (target), free protein (partner), and protein inhibitor. The protein–protein contains 3-D representation of the proteins and provides the possibility to view the contacts and hydrogen bonds per residue (also in 3-D). The free protein sections contain the 3-D structure of the protein (in viewer) and information from Structural Biology Knowledgebase[164] and report additional links to literature. The protein inhibitor contains, in addition to 3-D representation, descriptors of the ligand generated by MOE and DRAGON and 2-D representation of the ligand. This section contains also additional links to CREDO, ChemSpider (www.chemspider.com), LigandExpo (ligand-expo.rcsb.org), and HIC-Up.[165] The combined information of the chemical and structural properties of PPIs and their inhibitors provided by the 2P2Idb database can be exploited by complementary chemoinformatics tools to analyze PPI interfaces (2P2I Inspector), predict the druggability of PPIs (2P2I score), and design focused chemical libraries to target PPIs (2P2I hunter).[166]

ASD (Allosteric Database)[143] (mdl.shsmu.edu.cn/ASD, v3.0) contains 1473 allosteric protein target entries, 71,538 allosteric modulator entries, 75,462 allosteric interactions, 1930 defined allosteric binding sites, 57 structural allosteric modulation pathways, 261 allosteric modulation networks, and 3350 diseases related to allosteric modulation of protein function, collected from scientific literature and web resources, including PubMed, Drugbank, IUPARM, PDB, and US and European patents (Apr. 2016, latest update 2015). Allosteric binding sites can be searched by name and are classified according to family, including 5 E-proteins, 21 phosphatases (30 orthologues), 19 nuclear hormone receptors (26), 42 transcription factors (55), 53 peptidases (59), 98 GPCRs (118), 100 channels (134), 141 kinases (207), and 616 other human proteins (838 orthologues). The allosteric modulation mechanism of each of the 1473 protein targets is annotated according to 87 different mechanisms. Allosteric target entries contain gene information, tissue and cell localization, keywords and summaries of biological function and processes of the target, and whether structural information is available (link to PDB or theoretical model), summary of the secondary structure topology of the target, the ASD ID and 2-D structure of allosteric modulators, and literature references describing the allosteric mechanism and include links to UniProt, EMBL, and KEGG databases. Allosteric modulators can be browsed (but cannot be searched) and are classified by three modulator classes (52 ions, 70983 organic compounds, and 503 polypeptides), three modulator types (33 activators, 26 inhibitors, and 29 regulators), and whether they are endogenous and/or drug-like modulators. Allosteric (and corresponding orthosteric) binding sites are defined in 1930 annotated in PDB files that can be downloaded. For 57 allosteric interactions, the structural allosteric modulation pathway is defined and can be browsed based on target, the amino acid residues involved, and the supporting publication and experimental method used to elucidate the pathway. ASD contains 261 allosteric modulation networks that are classified according to six different network types (cellular processes, environmental information processing, genetic information processing, human diseases, metabolism, and organismal systems) that can be interactively visualized with Cytoscape (including links to KEGG). Comprehensive maps of the allosterome of kinases and GPCRs are provided, including the annotation of allosteric crystal structure complexes. The combined information of the allosteric targets, modulators, structural pathways, and biological networks can be exploited by complementary tools to estimate whether a molecule is likely to be an allosteric modulator (Allo-Like),[167] predict (potential) allosteric sites in proteins (AlloSite),[168] predict the binding affinity of allosteric protein–ligand interactions (AlloScore),[169] analyze and visualize the structural features of allosteric binding sites (Asbench),[170] identify potential novel allosteric targets based on sequence similarity search (P-search), and identify potential novel allosteric modulators based on chemical similarity and/or substructure search (M-search).

iPfam[171] (ipfam.org, v1.0) provides detailed domain–domain and domain–ligand interactions data (DDI and DLI, respectively) on 9516 unique domain pairings, 15,540 ligands, and 50,886 unique domain–ligand pairings (Apr. 2016, created Jun. 2013, not updated since). iPfam can be search by keyword, accession ID, PDB ID, protein sequence, iPfam ligand, and family entries and browsed by family and ligand entry names. The iPfam query results contain a summary from Wikipedia (for both ligand and family) accompanied with references to PubMed articles, the corresponding family and ligand interactions, and 3-D structures. The formula, molecular weight, InChI, SMILES, and the 2-D structure of ligands are also included in the results. The family interactions consist of the interacting families and the number of intrachain and interchain interactions. Furthermore, the database gives a graphical representation of the sequences of the interacting pairs. In this representation, the domains of the sequences are annotated along with their type of interaction; in the case of domain–ligand pair, the domains are annotated along with the ligand interactions. iPfam distinguishes five types of interactions: Van der Waal, hydrogen bond (with backbone and chain), electrostatic, and covalent bonds. As part of its analysis, iPfam also provides a 3-D viewer in the query results in which the users can view dynamically the different domains.

1.15.4.3 Protein Family-Customized Structural Chemogenomics Databases

GPCRdb[79] (www.gpcrdb.org) contains sequence, structure, and protein–ligand interaction information on 18,788 G protein-coupled receptors (including 398 human nonolfactory GPCRs) of 3096 different species collected from UniProt, 134 experimentally determined GPCR structures collected from the PDB, and 12,150 GPCR mutant–ligand combinations and 1063 GPCR–ligand interactions collected from literature (Apr. 2016, latest update Sep. 2015, updated every half year to one year). GPCRdb can be filtered by species (human, all) and source (UniProt, all), searched by name, and browsed by 6 classes, 19 families, and 76 subfamilies. GPCR entries contain information on the name and classification (including UniProt ID, Guide to Pharmacology, and ChEMBL links), structure-annotated amino acid sequence (secondary structure assignment and structure-based residue numbering), and helical wheel diagrams and snake plots that can be mapped with the effects of mutation data collected from literature and protein–ligand interaction information derived from crystal structures deposited in the PDB. GPCRdb contains several tools to analyze the sequence, structure, mutation data, and ligand binding sites of GPCRs. GPCRdb sequence data analyses include structure-based sequence alignments and tools to perform sequence similarity searches (GPCRdb and BLAST) and to construct phylogenetic trees and sequence similarity matrices of specific combinations of GPCRs. GPCRdb structure data analyses include GPCR crystal structure browser and statistics and tools to superposition structures, annotate generic GPCR residue numbers to PDB files, and assess global and local sequence similarities to GPCRs for which experimental structures are available. GPCRdb mutation data, the comparison of the affinity/activity of a ligand at point mutant with wild-type receptor, can be analyzed for specific combinations of GPCRs and mapped on helical wheel and snake plots in an interactive manner. GPCR–ligand interaction data include reports of residue-based protein–ligand interactions (generic residue number, segment, and interaction types), interactive 3-D viewer of the ligand binding site and a 2-D interaction plot (Poseviewer), and tools to identify the GPCR–ligand binding site (manual, derived from PDB) and generate pharmacophore models from ligand substructures. Developers can incorporate the database in local workflows by either using the provided python API or downloading the source code and data that is freely available on GitHub. Recently, GPCRdb KNIME nodes have been developed to allow automated GPCR data extraction and incorporation in integrated structural bioinformatics and chemoinformatics modeling workflows.[172]

KLIFS[99] (klifs.vu-compmedchem.nl, v2.0) contains sequence, structure, and protein–ligand interaction information on 247 protein kinases (human and mouse) covering 3103 PDB structures and 1931 unique ligands (Apr. 2016, v2.0, updated weekly). The database can be searched by PDB code, kinase name, family and group, SMILES, 2-D structure, state of DFG conformation and αC-helix conformation, any combination of interaction pattern, any combination of sequence composition, ligand properties (e.g., number of heavy atoms, log *P*, number of hydrogen donors/acceptors, and number of rotatable bonds), structural properties (X-ray resolution, quality score, G-rich loop angle, G-rich loop rotation, and G-rich loop distance), any combination of 15 annotated ligand binding modes, and any combination of conserved pocket water presence including if they make a hydrogen bond with either the protein or ligand. Furthermore, the database can be browsed independent of a search query. KLIFS contains information on kinase classification (name, family, group, and species); 2-D representations of the ligands (if present); comprehensive structural and binding mode information that include annotations of the conformations of the DFG motif, the αC helix, the G-rich loop (angle and rotation), structure resolution, missing atoms, and residues in the binding site; a quality score that represents the completeness and conformity of the structure and the ability of KLIFS to accurately process the structure; and the pockets and subpockets that the ligands address and cluster water molecules within the pocket. Mutations and gaps in the sequences of the structures are annotated based on a comparison of the crystal structure sequence with the UniProt sequence. If a structure contains a ligand and is present in the ChEMBL database also, all kinase affinity data, including species, kinase name, the type of affinity, the median and average values of the affinities, and the total amount of records, is presented. Moreover, if bioactivity data for the specific ligand–kinase combination is available, it is highlighted in red. Key within KLIFS is the annotation of the kinase–ligand interaction pattern. This interaction pattern encodes seven types of interactions for each binding pocket residue, which again can be used to search for other kinase structures in which a similar interaction profile is observed based on a user-defined cutoff. Additionally, the database allows further exploration of its structure and ligand entries by providing an interactive 3-D viewer, iview.[173] This 3-D viewer also provides users with the opportunity to perform a 3-D comparison of ligand binding modes with different structures. Moreover, all PDB entries are linked to external databases—the PDB, sc-PDB, KIDFamMap, PubMed, and Guide to Pharmacology/IUPHARdb.

PDEStrIAn[65] (pdestrian.vu-compmedchem.nl, v1.0) contains sequence, structure, and protein–ligand interaction information from 18 phosphodiesterase (PDE) subtypes (human, rat, and parasite) covering 245 PDB structures and 185 unique ligands (Apr. 2016, updated weekly). The database can be searched by PDE type, species, ligand (sub)structures and similarity (using SMILES or by drawing the 2-D structure), sequence composition, ligand properties (e.g., number of heavy atoms, logP, number of hydrogen donors/acceptors, and number of rotatable bonds), structural properties (X-ray resolution and quality score), and protein–ligand information (e.g., interaction patterns, targeted subpockets, the presence of conserved waters including their interaction patterns). Furthermore, the database can also be browsed. The browse and search results of PDEStrIAn contain information on classifications (type and species), 2-D representations of the bound ligands (if available), and the option to download the processed complex. The detail pages offer comprehensive binding information, structure resolution, missing atoms and residues, quality scores (that represent both the quality of a structure and the ability of PDEStrIAn to accurately process this structure; the higher the score, the better), the subpockets the ligands address, and the observed water molecules in predefined conserved clusters. In addition to that, the database allows further exploration of its structure and ligand entries by providing an interactive 3-D viewer, iview,[173] and linking its entries to four external databases—the ChEMBL, PDB, sc-PDB, and PubMed. Along its many display and manipulation options, the 3-D viewer also provides the opportunity to compare the binding mode of ligands with different

structures. Furthermore, POVME calculations have been integrated that allow the user to visualize the pocket volume within the 3-D viewer. Mutations and gaps in the sequences of the structures are annotated by comparing the crystal structure sequence with the sequence deposited in the UniProt database. In addition to the 2-D representation and annotation of the binding modes, the structure–ligand interaction pattern is shown. This interaction pattern encodes seven types of interactions for each binding pocket residue, which again can be used to search for other PDE structures in which a similar protein–ligand binding mode is observed based on a user-defined cutoff. Furthermore, data from the ChEMBL database is integrated (and linked) showing all available affinities for PDEs from the ligand that is bound in a structure and provides a full overview of these entries listing the median, minimum, and maximum of the available bioactivities per species, PDE type, and measure type (e.g., K_i/IC_{50}).

1.15.5 Examples of Applications of Structural Chemogenomics Databases in Drug Discovery

In this section, applications of (off-)target prediction, detection of target similarity, ligand design and all-against-all analysis of ligand structures and interaction fingerprints, and using structural chemogenomics databases are described thoroughly. The section contains three examples of using the similarity ensemble approach (SEA) to predict unknown targets for known compounds (the targets were also experimentally validated), two examples of the key representation of interaction in POckets (KRIPO) method to identify off-targets for known inhibitors, an example of detecting target similarity using the SiteAlign[174] method and the sc-PDB database, an example of ligand design using an integrated structure-based medicinal chemistry toolbox and the PDEStrIAn database, and three examples of all-against-all analysis of ligand structures and interaction fingerprints using KLIFS, PDEStrIAn, and an in-house GPCR dataset.

1.15.5.1 Combined Bioactivity Data Mining and Chemical Similarity Search for Ligand-Based Target Prediction

Biological activity databases can be used to construct ligand-based target prediction models that correlate chemical structural features of small molecules to the probability to interact with a specific protein target.[162] ChEMBL compound entries contain ligand-based target predictions, and several webservers like SwissTargetPrediction[175] (www.swisstargetprediction.ch) and SEA[69] (sea.bkslab.org) can be used to perform ligand-based target for individual molecules. The SwissTargetPrediction webserver uses a combination of 2-D and 3-D chemical similarity methods to assess the similarity of the query molecule to 280,000 compounds active on more than 2000 targets of five different organisms. The SEA relates proteins based on the setwise 2-D chemical similarity among their ligands,[69] and the SEA webserver can perform queries against previous versions of ChEMBL, MDDR,[138] WOMBAT,[139] and KEGG.[89] The SEA method has been successfully applied to identify main and off-targets for several bioactive compounds, illustrating the potential of prospective ligand-based target prediction based on target-annotated biological activity databases.[39,176,177] SEA models have been built to predict off-target binding of 3655 FDA-approved drugs for 246 protein targets extracted from three databases (MDDR, WOMBAT, and StARlite), using ECFP4 molecular fingerprints to assess ligand similarity. The resulting SEA models identified 23 new experimentally validated drug–target combinations (of the 30 combinations that were tested),[39] including antagonistic effect of Prozac (fluoxetine) at the β_1 adrenergic receptor, inhibition of the serotonin transporter by Vadilex (ifenprodil), and antagonistic effect of Rescriptor (delavirdine) at the histamine H_4 receptor.[22] In another study, the SEA method was used to assess the safety of 656 marketed drugs against 73 promiscuous proteins that are associated with side effects based on bioactivity data from the ChEMBL database and the ECFP4 and 2048-bit Daylight molecular fingerprints to characterize the ligands of 73 protein targets. The SEA models identified 151 novel predicted drug–target combinations with micromolar potencies (out of the 694 that were tested), including inhibition of cyclooxygenase 1 (COX-1) by the estrogen receptor (ER) ligand chlorotrianisene.[176] The SEA method has furthermore been used to identify the protein targets of compounds that induce a photomotor response (PMR) in zebrafish.[177] A SEA search of the 681 phenotypic hits against 167,000 compounds in ChEMBL biologically annotated toward 2000 targets using ECFP4 and other molecular fingerprints yielded the prediction of 1328 compound–target interactions, of which 12 were confirmed by literature search and 54 novel combinations that were experimentally tested (covering 20 compounds and 31 targets).[177] The activity of 11 of the 20 compounds against 22 of the 31 predicted targets was confirmed in experimental assays. Nine of the 11 compounds targeted G protein-coupled receptors, and 2 compounds targeted protein kinases.

Other examples of prospectively validated ligand-based protein target prediction methods based on publically available biological activity data are the target-dependent composite workflow method PROFILER[178] and a ligand similarity-based Bayesian probabilistic activity modeling method (**Fig. 5B**).[179] Meslamani and Rognan et al.[178] constructed workflows that combine four ligand-based (SVM classification, SVR affinity prediction, nearest-neighbor interpolation, and shape similarity)[178] and two structure-based approaches (docking and protein–ligand pharmacophore match). Protein target-customized workflows were trained and evaluated based on target-specific bioactivity data extracted from on ChEMBL, PubChem BioAssay, and Guide to Pharmacology databases, correctly identifying 136 of the main target of 189 clinical candidates and successfully predicting 2 novel off-targets (out of 10 predicted protein–ligand combinations). The adenosine A_1 receptor antagonist Rolofylline was experimentally confirmed to inhibit phosphodiesterase 5, while the phosphodiesterase 10A inhibitor (PF-2545920) binds cysteinyl leukotriene type 1 G protein-coupled receptor.[178] Besnard et al. trained ligand-based Bayesian probabilistic activity models for 784 protein targets based on 215,967 bioactivity data points extracted from the ChEMBL database and used circular ECFP-6 fingerprints to compare ligand similarity.[179] Optimal Bayesian probability cutoff scores were determined by retrospective evaluation of Matthews correlation coefficients (MCC), reflecting the ability of the models to distinguish active from inactive compounds. The validated target-

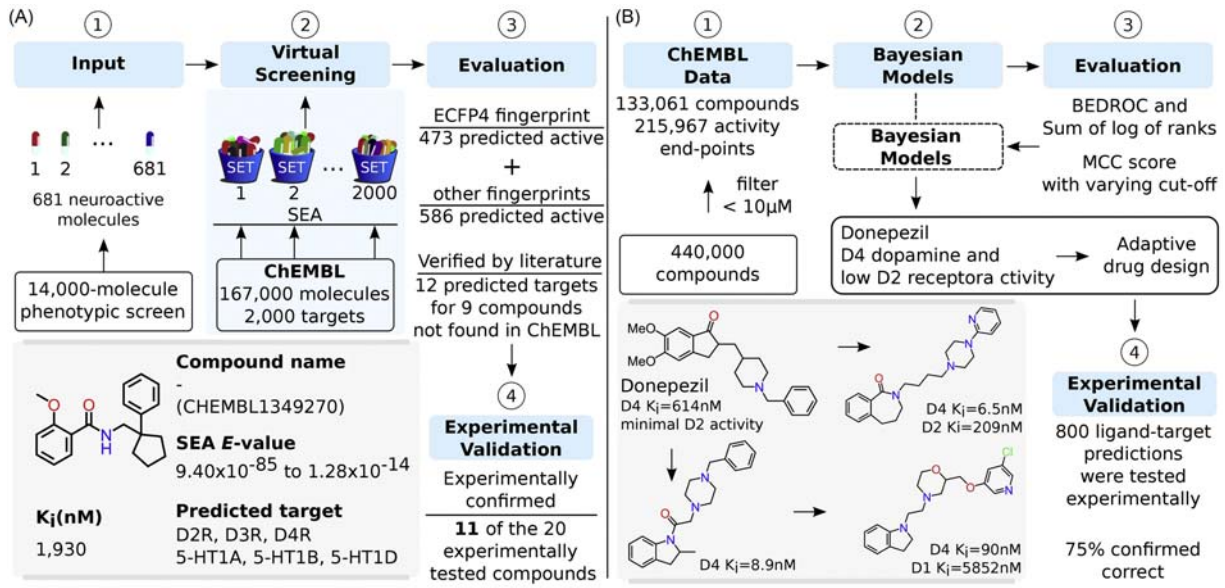

Fig. 5 Examples of ligand-based target prediction by bioactivity data mining. (1A) 681 neuroactive molecules were screened against 167,000 molecules from ChEMBL using the similarity ensemble approach (*SEA*) with ECFP4 and other fingerprints. In order to apply SEA, the molecules from ChEMBL were clustered according to their 2000 targets. Eleven of the 20 tested experimentally compounds were confirmed active. (1B) Bayesian models were trained on filtered ChEMBL bioactivity and compound data using circular ECFP6 fingerprints and applied to assist adaptive drug design. Using donepezil as a starting point (1B, *top left* compound), the authors predicted and experimentally tested the polypharmacological profile for 28 further evolved compounds on 20 G-protein-coupled receptors (GPCR) targets. Examples of highly selective dopamine D_4 compounds and an exquisite selective dopamine D_4 and dopamine D_1 compound are shown in (1B). Overall, 75% of the 800 ligand–target predictions were experimentally confirmed.

customized Bayesian models were incorporated as scoring functions in a multiobjective evolutionary optimization algorithm to design new ligands with polypharmacological activity at 5-HT_{1A} serotonin receptor and D_2, D_3, and D_4 dopamine receptors with selectivity over α1-adrenoreceptors antitargets α_{1A}, α_{1B}, and α_{1D} while maintaining CNS penetration. The resulting ligands were subsequently optimized for D_4 potency and brain penetrability and then for D_4 selectivity (Fig. 5B). Overall, 800 ligand–target predictions of 39 prospectively designed ligands were tested experimentally against 20 aminergic GPCRs, of which 75% were experimentally confirmed.[179]

1.15.5.2 Protein Binding Site Similarity Assessments for Ligand Repurposing and Off-Target Prediction

Diverse methods have been developed that allow for the comparison of protein binding sites based on their shape, pharmacophore features, and/or bound ligands.[180,181] These methods enable the identification of similar binding sites for, for example, ligand repurposing efforts and off-target prediction, as exemplified in this section by the successful prospective applications of the KRIPO[76] and SiteAlign[174] methods to screen large numbers of binding sites extracted from structures in the PDB (Fig. 6). KRIPO[76] is a fingerprinting method that enables the quantitative comparison of binding site (sub)pockets. This method defines a fingerprint for protein–ligand binding sites (and fragments of the ligand) based on the pharmacophore features of the surrounding amino acids and enables the comparison of such a fingerprint to that of all available structures in the PDB. KRIPO has been used to predict the Q_0 binding site of mitochondrial complex III (CIII) as off-target for simvastatin lactone (Fig. 6A).[183] KRIPO pharmacophore models of HMG-CoA reductase binding site were compared to the entries in the PDB revealing the Q_0 and Q_1 binding sites of CIII as possible off-target. Docking studies suggested that simvastatin lactone can adopt a binding mode in the Q_0 binding site of CIII that was consistent with the KRIPO binding site similarity assessment, while simvastatin acid cannot be accommodated due to possible repulsive interaction of the Glu-272 residue. The authors also experimentally validated their findings by reducing the CIII activity in statin-induced myopathies patients by 18%. In another study, KRIPO[76] has been used to identify potential off-targets of the cannabinoid receptor 1 (CB_1R) ibipinabant given the mitochondrial toxicity that was observed in preclinical trials.[184] A homology model of ibipinabant-bound CB_1R served as input for the KRIPO comparison with all available structures in the PDB. From the resulting list of most similar targets, according to KRIPO, only those targets that play a role in mitochondrial ADP/ATP exchange were selected. Two remaining targets were further investigated using docking, which indicated that ibipinabant could potentially bind to mitochondrial adenine nucleotide translocator 1 (ANT1). Subsequent experimental validation confirmed this hypothesized off-target effect as the mode of action for the observed mitochondrial toxicity of ibipinabant. The 3-D binding site comparison method SiteAlign[174] is a fingerprinting method encoding eight topological and physicochemical properties for the amino acids lining the binding site. SiteAlign has been used to prospectively predict the cross-reactivity of protein kinase

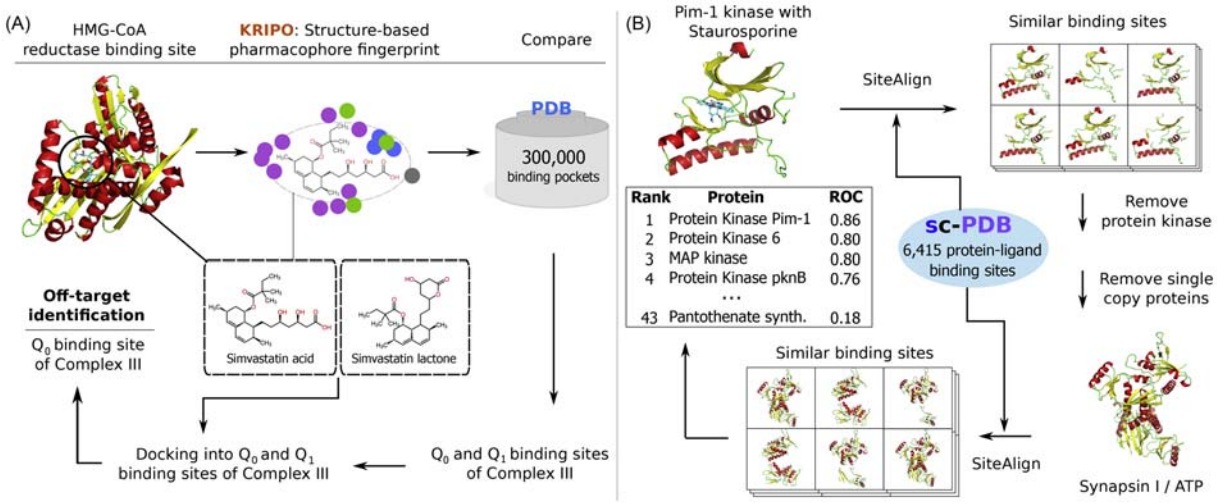

Fig. 6 Examples of protein–ligand binding site similarity search against the PDB. (A) In silico off-target prediction by protein–ligand binding site comparison with KRIPO. The binding site of HMG-CoA reductase was used as input for KRIPO to generate structure-based pharmacophore fingerprint, and then, those were evaluated against 300,000 binding pockets in the PDB in order to find new off-targets. After the screening, docking studies were performed to explore different binding modes of simvastatin acid and simvastatin lactone. The authors identified the Q_0 binding site of mitochondrial complex III (CIII) as off-target of the simvastatin lactone. (B) In silico ligand repurposing by protein–ligand binding site comparison with SiteAlign. The binding site of Pim-1 kinase is compared using SiteAlign against the sc-PDB database. After the removal of kinase structures from the same family and single copy proteins, the only remaining structure, synapsin I, was once again compared with SiteAlign to 978 binding sites in sc-PDB. From the comparison, De Franchi et al. concluded that some of the protein kinases are similar to synapsin I.[182] Part B adapted from Defranchi, E.; Schalon, C.; Messa, M.; Onofri, F.; Benfenati, F.; Rognan, D., Binding of Protein Kinase Inhibitors to Synapsin I Inferred From Pair-Wise Binding Site Similarity Measurements. *PLoS One*, **2010**, *5*, e12214.

inhibitors (Fig. 6B).[182] A pairwise comparison of the staurosporine binding site of the Pim-1 proto-oncogene serine/threonine kinase with over 6000 binding sites in the sc-PDB was made.[145] After removal of all protein kinase hits (given that staurosporine is a known promiscuous kinase inhibitor) and all proteins with only one structure, the only hit that remained was synapsin I. Subsequent in vitro competition assays validated that staurosporine indeed also has an inhibitory effect on synapsin I ($IC_{50} = 0.3\ \mu M$). This study furthermore validated the interaction of other kinase inhibitors with synapsin I.

1.15.5.3 Integrated Structure-Based Medicinal Chemistry Toolbox for Drug Discovery and Design

Protein-family oriented structural databases like KLIFS[99] and PDEStrIAn[65] can enrich a medicinal chemistry program by supporting ligand design with new ideas linked to a structure-based rationale. One way in which this can be obtained is by generating a medicinal chemistry toolbox containing scaffolds and substituents based on available crystal structures and known ligand libraries. The deconstruction of crystallized ligands into core scaffolds and their substituents while annotating their binding regions can yield such a structurally-aware toolbox. This knowledge-based toolbox can be further expanded by, for example, also deconstructing ligands without a crystal structure (e.g., from ChEMBL) that contain one of the core scaffolds of the cocrystallized ligands. The resulting resource can be exploited by medicinal chemists by providing substitution ideas and scaffold replacement options or even be used for ligand merging and novel ligand design efforts. Fig. 7 presents an example from the PDEStrIAn resource in which a selection of the deconstruction of 203 PDE inhibitors into 77 core scaffolds and 244 substituents is presented. Since for each scaffold and substituent the binding region is known, one can efficiently start interchanging substituents to optimally target a (sub)pocket to improve, for example, selectivity, potency, or physicochemical or ADMET properties. One step further, the so-called Markush enumeration of the fragmented ligands (the creation of a combinatorial library by combining the scaffolds with all possible substituents) can be performed in order to obtain (large) datasets with protein family-specific virtual compound sets that again can be explored for ligand discovery, design, and optimization. Such datasets can furthermore be utilized in virtual screening studies and other computer-aided drug design and drug optimization efforts to identify optimal ways to probe specific (combinations) of subpockets in order to obtain the desired polypharmacological or selectivity profile.

1.15.5.4 Combined Navigation of Protein–Ligand Interaction and Ligand Chemistry Space

Structural chemogenomics databases such as KLIFS[99] and PDEStrIAn[65] allow for the direct comparison and integration of ligand, protein, and ligand–protein interaction information. With these data, new insights can be obtained and used in drug discovery and design programs. As a proof of concept, we collected all preprocessed ligand-bound kinase (2662 unique PDBs), phosphodiesterase

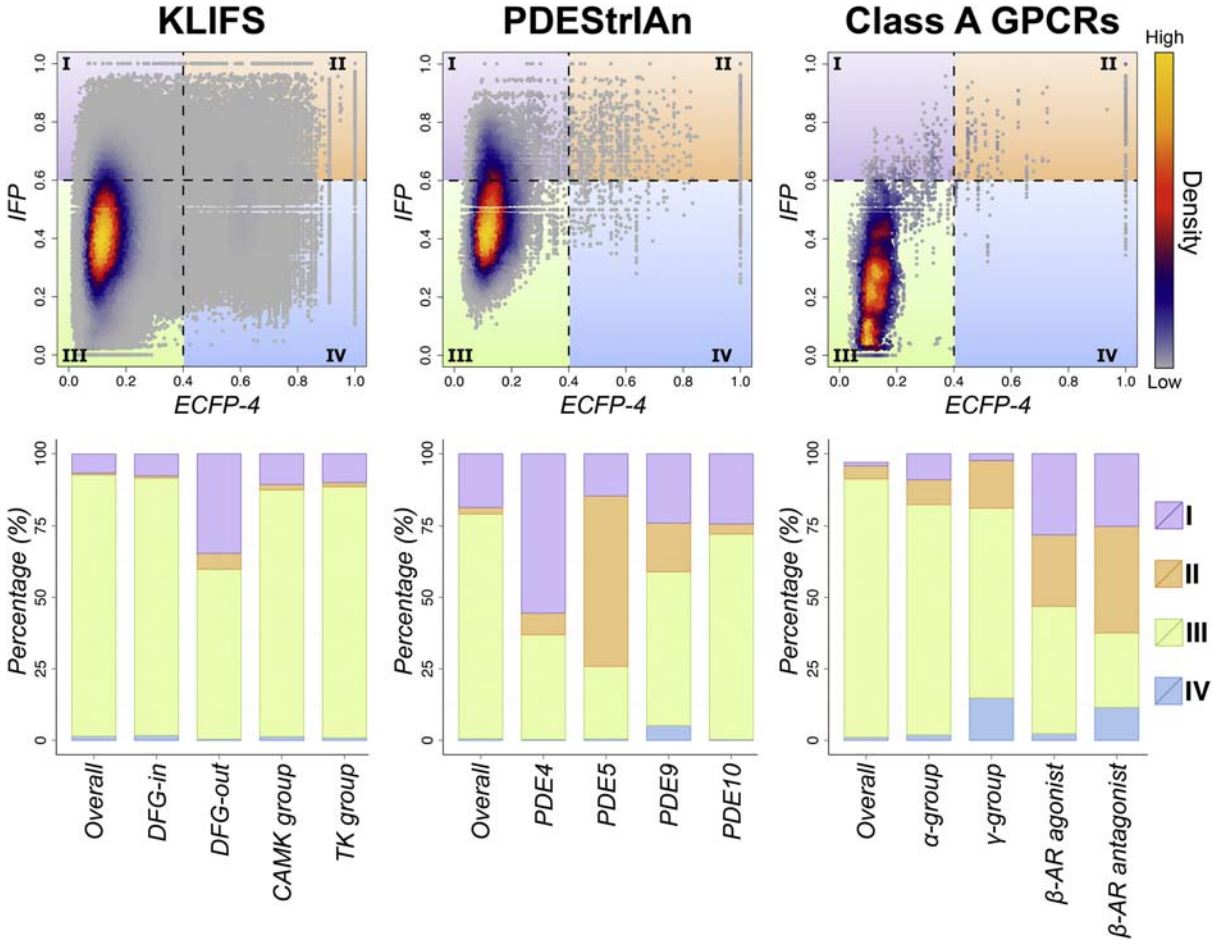

Fig. 7 The PDEStrIAn resource as a structure-based medicinal chemistry toolbox. The binding site of the catalytic PDE domain is colored according to the division into 10 regions: the hydrophobic clamp regions (HC, HC1, and HC2), the metal binding region (MB, MB1, and MB2), the region around the invariant glutamine (Q, Q1, and Q2), and the solvent region (S). Two hundred and three ligands of 220 PDE structures were deconstructed into core scaffolds binding in the HC and Q region, and all remaining substituents were assigned to their respective binding subpockets. This allows for the creation of a knowledge-based and structure-guided combinatorial PDE ligand library by combining all core scaffolds with all substituents from all respective regions providing novel ideas to further explore the chemical space of PDE inhibitors.

(236 unique PDBs), and class A GPCR (105 unique PDBs) structures from KLIFS, PDEStrIAn, and an in-house dataset of processed class A GPCR structures (excluding retinal-bound structures to prevent a bias) and used the interaction fingerprint data and ligand structures to perform an all-against-all analysis (Fig. 8). Subsequently, for each pair of ligands, the ligand similarity was assessed by generating the frequently applied molecular fingerprint ECFP-4 in combination with the Tanimoto coefficient.[187] Since each of these databases uses a consistent pocket definition with the same number of pocket residues (corrected for gaps), all interaction fingerprints of a database could directly be compared with each other, and their similarity was also quantified using the Tanimoto coefficient. The resulting scatterplots are shown in Fig. 8. An ECFP-4 cutoff of 0.4[185] was used to distinguish between high and low molecular similarity, and an IFP cutoff of 0.6[186] was used to distinguish between high and low binding mode similarity. These cutoffs were used to subdivide all data into four categories: (I) high binding mode similarity and low chemical similarity, (II) high binding mode similarity and high chemical similarity, (III) low binding mode similarity and low chemical similarity, and (IV) low binding mode similarity and high chemical similarity (Fig. 8). The highest density for all datasets was observed in category III, implying that most molecule pairs with a high chemical diversity also show a diverse binding mode. Interestingly, for the kinases and phosphodiesterases, category I was the second-most dense category, indicating that despite the difference in molecular structure, a similar binding mode was conserved for these ligand pairs. The pairs in this category have a high scaffold hopping potential as they provide information on chemical moieties that can be interchanged while maintaining the same binding mode (similar to the bioisosteric replacement theory behind sc-PDB-frag[158]). Such resources can be used to design new ligands, to resolve undesired physicochemical properties, and to escape patents.[188] When using IFP as a post-processing and filtering tool in a prospective virtual screening, this is also the category that is aimed for. In such studies, the goal is to discover ligands with diverse chemical compositions while maintaining a binding mode similar to a specific reference ligand (as performed in, e.g., a virtual screening study against the histamine H_1 structure[71] and the *Trypanosoma brucei* PDEB1 structure[189]). Category II is the category that adheres to

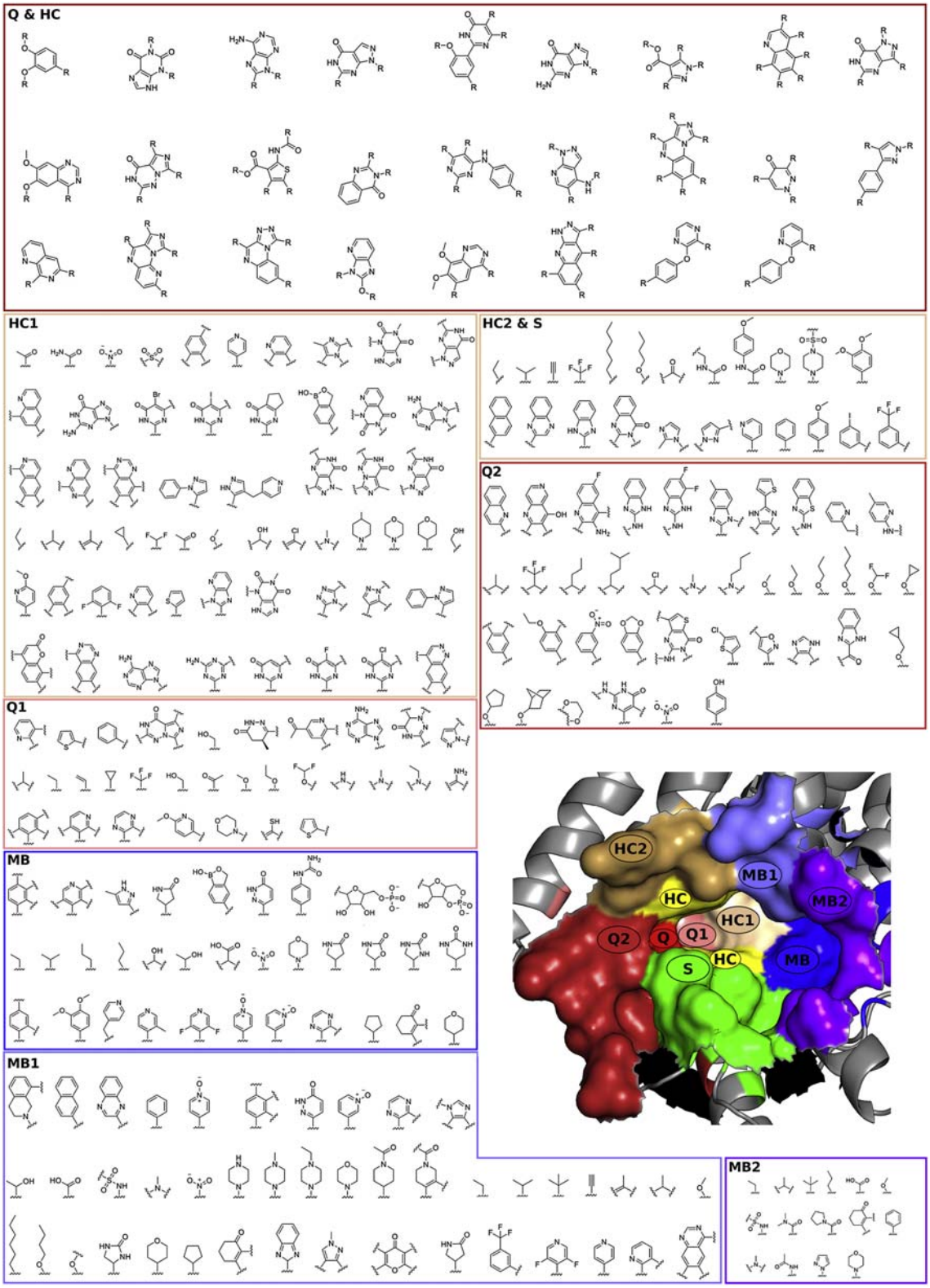

Fig. 8 All-against-all comparison of protein–ligand interaction patterns (*IFP*) versus molecular similarity (*ECFP-4*) for kinases, phosphodiesterases, and class A GPCRs. The scatterplots highlight the molecular similarity versus the interaction pattern similarity of all ligand pairs in KLIFS (2662 unique PDBs), PDEStrIAn (236 unique PDBs), and an in-house GPCR dataset (105 unique PDBs) based on the PDB. The scatterplots have been divided into four categories based on a low/high molecular similarity cutoff (ECFP-4 $\geq$ 0.4[185]) and a low/high binding mode similarity cutoff (IFP $\geq$ 0.6[186]). The stacked bar plots represent the density in each category for each of the datasets and smaller (more specific) subsets.

the chemogenomics principles that similar ligands have similar binding modes (and thus targets). The final category with the lowest occupancy is category IV, which is reserved for ligands with a similar structure but a different binding mode. It can also be seen that in all datasets even identical ligands (with and ECFP-4 of 1) can adopt different binding modes (IFP < 0.6). An example of such a ligand is the PDE-inhibitor IBMX, which can adopt multiple binding modes in phosphodiesterases (e.g., PDE5 PDB code 1RKP versus PDE4D PDB code 1ZKN[65]).

The dataset for kinases is by far the most extensive set with over 2662 ligand-bound complexes and shows a large chemical and binding mode diversity even within specific kinase groups (CAMK and TK) and also within the set of kinase structures in the DFG-in conformation. Some kinase inhibitors inhibit the kinase in a DFG-out conformation and can therefore address a more specific back pocket of the kinase (e.g., BPIII, BPIV, and BPV; see **Fig. 4**).[64] Almost 35% of the ligand pairs in this subset have a conserved binding mode despite the chemical diversity compared with less than 8% of the ligand pairs from structures in the DFG-in conformation. This also reflects the open nature of the front pocket that allows DFG-in inhibitors to address this pocket with a diverse range of binding modes. For PDEs, we see a much larger subtype dependency of the binding mode diversity. For PDE4, more than 55% of the ligand pairs adopt a similar binding mode despite their chemical diversity. On the other hand, there is a low chemical diversity for the ligands in complex PDE5 and therefore, as expected, also adopt similar binding modes. The ligands in complex with class A GPCRs show similar overall trends as the kinases and PDEs. However, only when looking at specific receptors (e.g., β-adrenoceptors 22.8% and 16.8% in categories I and II, respectively) and even ligand function specific subsets (e.g., β-adrenoceptor agonists and antagonists/inverse agonists), a high conservation of the binding mode is observed. IFPs can therefore also be used to predict the function of ligands based on their (predicted) binding modes as was shown in a retrospective all-against-all virtual screening using IFPs of 31 β-adrenoceptor crystal structures.[190] It should be noted that due to the limited number of available structures for GPCRs and PDEs, these statistics can be biased, such as the limited chemical diversity for PDE5.

1.15.6 Conclusions and Outlook

Structural chemogenomics databases allow the integration and exploration of heterogeneous genomic, structural, chemical, and pharmacological data in order to extract useful information that is applicable for the discovery of new protein targets and biologically active molecules. The use of common ontologies allows efficient protein and ligand data curation and mapping that enable the integration of bioactivity data mining, ligand and protein similarity assessment, and structural protein–ligand interaction analyses for the identification of new protein–drug combinations. The UniProt, PDB, and ChEMBL represent the largest databases comprising protein sequences, protein–ligand structures, and target-annotated biologically active molecules, respectively. Complementary integrated structural chemogenomics databases provide proteome-wide, target family-specific, or mechanism-specific information depending on the way that different types of protein–ligand interaction data can be explored. The general proteome-wide target-annotated biological activity databases, like BindingDB, Intact, STITCH, PubChem Bioassay, DrugBank, PDSP K_i, PDBbind-CN, and Binding MOAD, contain 10^4–10^7 bioactivity data points covering 10^2–10^6 protein targets and compounds 10^4–10^6, provide extensive information on ligands, and also contain (links to) general information on the associated protein targets (including IDs, sequence, and links to PDB structures). Target-annotated biological activity databases do not cover detailed structural information on binding sites or protein–ligand interactions, although protein target family-specific biological activity databases like GLASS (GPCRs) and K-Map (kinases) provide integrated and curated protein family-specific information regarding 10^4–10^5 protein–ligand complexes (including consistently annotated links to other databases). Unfortunately, such target family-specific databases are often created and not maintained or frequently updated afterward. Automated data mining protocols provide an alternative to facilitate efficient extraction and post-processing of customized data sets from, for example, ChEMBLdb or other databases in a consistent and automated manner.[148] Careful and consistent annotation of the chemical structure of ligands allows efficient combination of bioactivity data mining with chemical similarity assessment for ligand-based target prediction and the identification of new protein–ligand combinations. Mechanism-specific biological activity databases are generally relatively small, containing 10^3–10^4 data points and covering up to 10^3 protein targets and 10^2–10^4 compounds, but do contain complementary information like pairwise mutation data (Platinum) and protein–protein interaction modulators (Timbal).

Proteome-wide structural protein–ligand interaction databases like PoSSuM, IBIS, BioLip, CREDO, PLIC, ProBis, sc-PDB, BivalBind, Pocketome, iPfam, and PSCDB contain structural information on 10^4–10^5 protein–ligand binding sites of 10^3–10^4 compounds in 10^3–10^4 distinct proteins and provide additional consistent systematic analyses and search options of different properties of the binding sites (including physical–chemical properties) and characteristics of the protein–ligand interactions (using, for example, interaction fingerprint methods). Many proteome-wide structural protein–ligand interaction databases, including sc-PDB, PoSSum, CREDO, PLIC, and Pocketome, furthermore provide precalculated or on the fly binding site comparison and search options that enable structure-based ligand repurposing, target identification, and off-target prediction. Protein target class-specific structural protein–ligand interaction databases like KLIFS (kinases), GPCRdb (GPCRs), and PDEStrIAn (phosphodiesterases) facilitate search options to investigate and compare the protein–ligand binding sites and interactions in more detail, providing systematic analyses of the properties and molecular interactions of amino acid residues, subpockets, and water molecules, consistently annotated based on their position in the aligned binding sites of structures of a specific protein family. The protein family-customized setup in KLIFS, GPCRdb, and PDEStrIAn allows for consistent extraction, curation, analysis, visualization, and integration of structural chemogenomics data for efficient exploitation such as structure-based identification and prediction of the structural determinants of protein–ligand selectivity. The careful curation of ligand topology (e.g., definition of atom and chemical

bond types in customized databases such as the chemical component dictionary) and the consistent construction of binding site alignments are essential for the accurate and systematic analysis, comparison, and visualization of protein–ligand interactions (e.g., the comparison and assignment of interaction fingerprints to specific residues, subpockets, water molecules, or chemical groups in the ligand). KLIFS and PDEStrIAn demonstrate how the definition of a curated ontology of protein family-specific structural chemogenomics data allows for the construction of an automated data extraction that keeps in sync with, for example, weekly (PDB), monthly (UniProt), and (bi)annual (ChEMBL) updates of large sequence, structure, and bioactivity databases. Mechanism-specific structural protein–ligand interaction databases such as 2P2Idb (PPIs) and ASD (allosteric modulation) provide orthogonal information that can provide insights into general mechanisms and structural derminants of specific molecular processes that are relevant for drug discovery. The definition of general ontologies of biological, chemical, and structural information enables the construction of standardized chemoinformatics and bioinformatics workflows to integrate and exploit these data for structure prediction of, for example, protein selectivity and drug polypharmacology.[191] Moreover, the customized integration of structural chemogenomics information with other data sources such as phenotypic, (epi)genetics, and clinical data may ultimately enable the extension and translation of structural chemogenomics analyses, multidimensional analysis, and prediction of patient population-specific drug action.

See also: 3.06. Using 3-D Structural Information in Computational Design.

References

1. Lusher, S. J.; McGuire, R.; van Schaik, R. C.; Nicholson, C. D.; de Vlieg, J. Data-Driven Medicinal Chemistry in the Era of Big Data. *Drug Discov. Today* **2014,** *19,* 859–868.
2. Peters, J. U. Polypharmacology—Foe or Friend? *J. Med. Chem.* **2013,** *56,* 8955–8971.
3. Rose, P. W.; Prlic, A.; Bi, C.; Bluhm, W. F.; Christie, C. H.; Dutta, S.; Green, R. K.; Goodsell, D. S.; Westbrook, J. D.; Woo, J.; Young, J.; Zardecki, C.; Berman, H. M.; Bourne, P. E.; Burley, S. K. The RCSB Protein Data Bank: Views of Structural Biology for Basic and Applied Research and Education. *Nucleic Acids Res.* **2015,** *43,* 345–356.
4. Bento, A. P.; Gaulton, A.; Hersey, A.; Bellis, L. J.; Chambers, J.; Davies, M.; Kruger, F. A.; Light, Y.; Mak, L.; McGlinchey, S.; Nowotka, M.; Papadatos, G.; Santos, R.; Overington, J. P. The ChEMBL Bioactivity Database: An Update. *Nucleic Acids Res.* **2013,** *42,* 1083–1090.
5. Gaulton, A.; Bellis, L. J.; Bento, A. P.; Chambers, J.; Davies, M.; Hersey, A.; Light, Y.; McGlinchey, S.; Michalovich, D.; Al-Lazikani, B.; Overington, J. P. ChEMBL: A Large-Scale Bioactivity Database for Drug Discovery. *Nucleic Acids Res.* **2012,** *40,* 1100–1107.
6. Human Genome Sequencing Consortium. Finishing the Euchromatic Sequence of the Human Genome. *Nature* **2004,** *431,* 931–945.
7. Venkatesh, T. V.; Bowen, B.; Lim, H. A. Bioinformatics, Pharma and Farmers. *Trends Biotechnol.* **1999,** *17,* 85–88.
8. Human Genome Sequencing Consortium. Initial Sequencing and Analysis of the Human Genome. *Nature* **2001,** *409,* 860–921.
9. Owens, J. Determining Druggability. *Nat. Rev. Drug Discov.* **2007,** *6,* 187.
10. Rask-Andersen, M.; Almén, M. S.; Schiöth, H. B. Trends in the Exploitation of Novel Drug Targets. *Nat. Rev. Drug Discov.* **2011,** *10,* 579–590.
11. Klabunde, T. Chemogenomic Approaches to Drug Discovery: Similar Receptors Bind Similar Ligands. *Br. J. Pharmacol.* **2007,** *152,* 5–7.
12. Hopkins, A. L.; Groom, C. R. The Druggable Genome. *Nat. Rev. Drug Discov.* **2002,** *1,* 727–730.
13. Russ, A. P.; Lampel, S. The Druggable Genome: An Update. *Drug Discov. Today* **1607–1610,** *10,* 2005.
14. Overington, J. P.; Al-Lazikani, B.; Hopkins, A. L. How Many Drug Targets Are There? *Nat. Rev. Drug Discov.* **2006,** *5,* 993–996.
15. Jarvis, L. M. The Year in New Drugs. *Chem. Eng. News* **2015,** *93,* 11–16.
16. Ohlstein, E. H.; Ruffolo, R. R., Jr.; Elliott, J. D. Drug Discovery in the Next Millennium. *Annu. Rev. Pharmacol. Toxicol.* **2000,** *40,* 177–191.
17. Bredel, M.; Jacoby, E. Chemogenomics: An Emerging Strategy for Rapid Target and Drug Discovery. *Nat. Rev. Genet.* **2004,** *5,* 262–275.
18. Caron, P. R.; Mullican, M. D.; Mashal, R. D.; Wilson, K. P.; Su, M. S.; Murcko, M. A. Chemogenomic Approaches to Drug Discovery. *Curr. Opin. Chem. Biol.* **2001,** *5,* 464–470.
19. Kubinyi, H. Drug Research: Myths, Hype and Reality. *Nat. Rev. Drug Discov.* **2003,** *2,* 665–668.
20. Drews, J. Strategic Trends in the Drug Industry. *Drug Discov. Today* **2003,** *8,* 411–420.
21. Scannell, J. W.; Blanckley, A.; Boldon, H.; Warrington, B. Diagnosing the Decline in Pharmaceutical R&D Efficiency. *Nat. Rev. Drug Discov.* **2012,** *11,* 191–200.
22. Koutsoukas, A.; Simms, B.; Kirchmair, J.; Bond, P. J.; Whitmore, A. V.; Zimmer, S.; Young, M. P.; Jenkins, J. L.; Glick, M.; Glen, R. C.; Bender, A. From in Silico Target Prediction to Multi-Target Drug Design: Current Databases, Methods and Applications. *J. Proteomics* **2011,** *74,* 2554–2574.
23. Mestres, J.; Gregori-Puigjane, E.; Valverde, S.; Sole, R. V. Data Completeness—The Achilles Heel of Drug–Target Networks. *Nat. Biotechnol.* **2008,** *26,* 983–984.
24. Jalencas, X.; Mestres, J. On the Origins of Drug Polypharmacology. *Med. Chem. Commun.* **2013,** *4,* 80–87.
25. Jacoby, E. Computational Chemogenomics. *Wiley Interdiscip. Rev.: Comput. Mol. Sci.* **2011,** *1,* 57–67.
26. Bajorath, J. A Perspective on Computational Chemogenomics. *Mol. Inf.* **2013,** *32,* 1025–1028.
27. Hopkins, A. L. Network Pharmacology: The Next Paradigm in Drug Discovery. *Nat. Chem. Biol.* **2008,** *4,* 682–690.
28. Vogt, I.; Mestres, J. Drug–Target Networks. *Mol. Inform.* **2010,** *29,* 10–14.
29. Geppert, T.; Koeppen, H. Biological Networks and Drug Discovery—Where Do We Stand? *Drug Dev. Res.* **2014,** *75,* 271–282.
30. Anighoro, A.; Bajorath, J.; Rastelli, G. Polypharmacology: Challenges and Opportunities in Drug Discovery. *J. Med. Chem.* **2014,** *57,* 7874–7887.
31. Hu, Y.; Bajorath, J. How Promiscuous Are Pharmaceutically Relevant Compounds? A Data-Driven Assessment. *AAPS J.* **2013,** *15,* 104–111.
32. Hu, Y.; Bajorath, J. What Is the Likelihood of an Active Compound to be Promiscuous? Systematic Assessment of Compound Promiscuity on the Basis of PubChem Confirmatory Bioassay Data. *AAPS J.* **2013,** *15,* 808–815.
33. Karaman, M. W.; Herrgard, S.; Treiber, D. K.; Gallant, P.; Atteridge, C. E.; Campbell, B. T.; Chan, K. W.; Ciceri, P.; Davis, M. I.; Edeen, P. T.; Faraoni, R.; Floyd, M.; Hunt, J. P.; Lockhart, D. J.; Milanov, Z. V.; Morrison, M. J.; Pallares, G.; Patel, H. K.; Pritchard, S.; Wodicka, L. M.; Zarrinkar, P. P. A Quantitative Analysis of Kinase Inhibitor Selectivity. *Nat. Biotechnol.* **2008,** *26,* 127–132.
34. Knight, Z. A.; Lin, H.; Shokat, K. M. Targeting the Cancer Kinome Through Polypharmacology. *Nat. Rev. Cancer* **2010,** *10,* 130–137.
35. Bader, G. D.; Cary, M. P.; Sander, C. Pathguide: A Pathway Resource List. *Nucleic Acids Res.* **2006,** *34,* D504–D506.
36. Villoutreix, B. O.; Lagorce, D.; Labbé, C. M.; Sperandio, O.; Miteva, M. A. One Hundred Thousand Mouse Clicks Down the Road: Selected Online Resources Supporting Drug Discovery Collected Over a Decade. *Drug Discov. Today* **2013,** *18,* 1081–1089.
37. Ekins, S.; Clark, A. M.; Swamidass, S. J.; Litterman, N.; Williams, A. J. Bigger Data, Collaborative Tools and the Future of Predictive Drug Discovery. *J. Comput.-Aided Mol. Des.* **2014,** *28,* 997–1008.

38. Bajorath, J. Computational Analysis of Ligand Relationships Within Target Families. *Curr. Opin. Chem. Biol.* **2008,** *12,* 352–358.
39. Keiser, M. J.; Setola, V.; Irwin, J. J.; Laggner, C.; Abbas, A. I.; Hufeisen, S. J.; Jensen, N. H.; Kuijer, M. B.; Matos, R. C.; Tran, T. B.; Whaley, R.; Glennon, R. A.; Hert, J.; Thomas, K. L.; Edwards, D. D.; Shoichet, B. K.; Roth, B. L. Predicting New Molecular Targets for Known Drugs. *Nature* **2009,** *462,* 175–181.
40. Besnard, J.; Ruda, G. F.; Setola, V.; Abecassis, K.; Rodriguiz, R. M.; Huang, X. P.; Norval, S.; Sassano, M. F.; Shin, A. I.; Webster, L. A.; Simeons, F. R.; Stojanovski, L.; Prat, A.; Seidah, N. G.; Constam, D. B.; Bickerton, G. R.; Read, K. D.; Wetsel, W. C.; Gilbert, I. H.; Roth, B. L.; Hopkins, A. L. Automated Design of Ligands to Polypharmacological Profiles. *Nature* **2012,** *492,* 215–220.
41. Oprea, T. I.; Tropsha, A.; Faulon, J.-L.; Rintoul, M. D. Systems Chemical Biology. *Nat. Chem. Biol.* **2007,** *3,* 447–450.
42. Schenone, M.; Dancik, V.; Wagner, B. K.; Clemons, P. A. Target Identification and Mechanism of Action in Chemical Biology and Drug Discovery. *Nat. Chem. Biol.* **2013,** *9,* 232–240.
43. Sanger, F.; Air, G. M.; Barrell, B. G.; Brown, N. L.; Coulson, A. R.; Fiddes, J. C.; Hutchison, C. A.; Slocombe, P. M.; Smith, M. Nucleotide Sequence of Bacteriophage phi X174 DNA. *Nature* **1977,** *265,* 687–695.
44. Venter, J. C.; Adams, M. D.; Myers, E. W.; Li, P. W.; Mural, R. J.; Sutton, G. G.; Smith, H. O.; Yandell, M.; Evans, C. A.; Holt, R. A.; Gocayne, J. D.; Amanatides, P.; Ballew, R. M.; Huson, D. H.; Wortman, J. R.; Zhang, Q.; Kodira, C. D.; Zheng, X. H.; Chen, L.; Skupski, M.; Subramanian, G.; Thomas, P. D.; Zhang, J.; Gabor Miklos, G. L.; Nelson, C.; Broder, S.; Clark, A. G.; Nadeau, J.; McKusick, V. A.; Zinder, N.; Levine, A. J.; Roberts, R. J.; Simon, M.; Slayman, C.; Hunkapiller, M.; Bolanos, R.; Delcher, A.; Dew, I.; Fasulo, D.; Flanigan, M.; Florea, L.; Halpern, A.; Hannenhalli, S.; Kravitz, S.; Levy, S.; Mobarry, C.; Reinert, K.; Remington, K.; Abu-Threideh, J.; Beasley, E.; Biddick, K.; Bonazzi, V.; Brandon, R.; Cargill, M.; Chandramouliswaran, I.; Charlab, R.; Chaturvedi, K.; Deng, Z.; Francesco, V. D.; Dunn, P.; Eilbeck, K.; Evangelista, C.; Gabrielian, A. E.; Gan, W.; Ge, W.; Gong, F.; Gu, Z.; Guan, P.; Heiman, T. J.; Higgins, M. E.; Ji, R.-R.; Ke, Z.; Ketchum, K. A.; Lai, Z.; Lei, Y.; Li, Z.; Li, J.; Liang, Y.; Lin, X.; Lu, F.; Merkulov, G. V.; Milshina, N.; Moore, H. M.; Naik, A. K.; Narayan, V. A.; Neelam, B.; Nusskern, D.; Rusch, D. B.; Salzberg, S.; Shao, W.; Shue, B.; Sun, J.; Wang, Z. Y.; Wang, A.; Wang, X.; Wang, J.; Wei, M.-H.; Wides, R.; Xiao, C.; Yan, C.; Yao, A.; Ye, J.; Zhan, M.; Zhang, W.; Zhang, H.; Zhao, Q.; Zheng, L.; Zhong, F.; Zhong, W.; Zhu, S. C.; Zhao, S.; Gilbert, D.; Baumhueter, S.; Spier, G.; Carter, C.; Cravchik, A.; Woodage, T.; Ali, F.; An, H.; Awe, A.; Baldwin, D.; Baden, H.; Barnstead, M.; Barrow, I.; Beeson, K.; Busam, D.; Carver, A.; Center, A.; Cheng, M. L.; Curry, L.; Danaher, S.; Davenport, L.; Desilets, R.; Dietz, S.; Dodson, K.; Doup, L.; Ferriera, S.; Garg, N.; Gluecksmann, A.; Hart, B.; Haynes, J.; Haynes, C.; Heiner, C.; Hladun, S.; Hostin, D.; Houck, J.; Howland, T.; Ibegwam, C.; Johnson, J.; Kalush, F.; Kline, L.; Koduru, S.; Love, A.; Mann, F.; May, D.; McCawley, S.; McIntosh, T.; McMullen, I.; Moy, M.; Moy, L.; Murphy, B.; Nelson, K.; Pfannkoch, C.; Pratts, E.; Puri, V.; Qureshi, H.; Reardon, M.; Rodriguez, R.; Rogers, Y.-H.; Romblad, D.; Ruhfel, B.; Scott, R.; Sitter, C.; Smallwood, M.; Stewart, E.; Strong, R.; Suh, E.; Thomas, R.; Tint, N. N.; Tse, S.; Vech, C.; Wang, G.; Wetter, J.; Williams, S.; Williams, M.; Windsor, S.; Winn-Deen, E.; Wolfe, K.; Zaveri, J.; Zaveri, K.; Abril, J. F.; Guigó, R.; Campbell, M. J.; Sjolander, K. V.; Karlak, B.; Kejariwal, A.; Mi, H.; Lazareva, B.; Hatton, T.; Narechania, A.; Diemer, K.; Muruganujan, A.; Guo, N.; Sato, S.; Bafna, V.; Istrail, S.; Lippert, R.; Schwartz, R.; Walenz, B.; Yooseph, S.; Allen, D.; Basu, A.; Baxendale, J.; Blick, L.; Caminha, M.; Carnes-Stine, J.; Caulk, P.; Chiang, Y.-H.; Coyne, M.; Dahlke, C.; Mays, A. D.; Dombroski, M.; Donnelly, M.; Ely, D.; Esparham, S.; Fosler, C.; Gire, H.; Glanowski, S.; Glasser, K.; Glodek, A.; Gorokhov, M.; Graham, K.; Gropman, B.; Harris, M.; Heil, J.; Henderson, S.; Hoover, J.; Jennings, D.; Jordan, C.; Jordan, J.; Kasha, J.; Kagan, L.; Kraft, C.; Levitsky, A.; Lewis, M.; Liu, X.; Lopez, J.; Ma, D.; Majoros, W.; McDaniel, J.; Murphy, S.; Newman, M.; Nguyen, T.; Nguyen, N.; Nodell, M.; Pan, S.; Peck, J.; Peterson, M.; Rowe, W.; Sanders, R.; Scott, J.; Simpson, M.; Smith, T.; Sprague, A.; Stockwell, T.; Turner, R.; Venter, E.; Wang, M.; Wen, M.; Wu, D.; Wu, M.; Xia, A.; Zandieh, A.; Zhu, X. The Sequence of the Human Genome. *Science* **2001,** *291,* 1304–1351.
45. Barker, W. C.; Garavelli, J. S.; McGarvey, P. B.; Marzec, C. R.; Orcutt, B. C.; Srinivasarao, G. Y.; Yeh, L.-S. L.; Ledley, R. S.; Mewes, H.-W.; Pfeiffer, F.; Tsugita, A.; Wu, C. The PIR-International Protein Sequence Database. *Nucleic Acids Res.* **1999,** *27,* 39–43.
46. Boeckmann, B. The SWISS-PROT Protein Knowledgebase and Its Supplement TrEMBL in 2003. *Nucleic Acids Res.* **2003,** *31,* 365–370.
47. Bairoch, A.; Apweiler, R. The SWISS-PROT Protein Sequence Data Bank and Its New Supplement TREMBL. *Nucleic Acids Res.* **1996,** *24,* 21–25.
48. Apweiler, R.; Bairoch, A.; Wu, C. H.; Barker, W. C.; Boeckmann, B.; Ferro, S.; Gasteiger, E.; Huang, H.; Lopez, R.; Magrane, M.; Martin, M. J.; Natale, D. A.; O'Donovan, C.; Redaschi, N.; Yeh, L. S. L. UniProt: The Universal Protein Knowledgebase. *Nucleic Acids Res.* **2004,** *32,* D115–D119.
49. Bank, P. D. Protein Data Bank. *Nat. New Biol.* **1971,** *233,* 223.
50. Berman, H. M. The Protein Data Bank: A Historical Perspective. *Acta Crystallogr. A* **2007,** *64,* 88–95.
51. Bernstein, F. C.; Koetzle, T. F.; Williams, G. J. B; Meyer, E. F., Jr.; Brice, M. D.; Rodgers, J. R.; Kennard, O.; Shimanouchi, T.; Tasumi, M. The Protein Data Bank: A Computer-Based Archival File for Macromolecular Structures. *J. Mol. Biol.* **1977,** *112,* 535–542.
52. Berman, H. M.; Kleywegt, G. J.; Nakamura, H.; Markley, J. L. The Protein Data Bank Archive as an Open Data Resource. *J. Comput. Aided Mol. Des.* **2014,** *28,* 1009–1014.
53. Berman, Helen M.; Kleywegt, Gerard J.; Nakamura, H.; Markley, John L. The Protein Data Bank at 40: Reflecting on the Past to Prepare for the Future. *Structure* **2012,** *20,* 391–396.
54. Walters, W. P.; Stahl, M. T.; Murcko, M. A. Virtual Screening—An Overview. *Drug Discov. Today* **1998,** *3,* 160–178.
55. Jorgensen, W. L. The Many Roles of Computation in Drug Discovery. *Science* **1813–1818,** *303,* 2004.
56. Rognan, D. Proteome-Scale Docking: Myth and Reality. *Drug Discov. Today Technol.* **2013,** *10,* 403–409.
57. Shan, Y.; Kim, E. T.; Eastwood, M. P.; Dror, R. O.; Seeliger, M. A.; Shaw, D. E. How Does a Drug Molecule Find Its Target Binding Site? *J. Am. Chem. Soc.* **2011,** *133,* 9181–9183.
58. UniProt, C. Activities at the Universal Protein Resource (UniProt). *Nucleic Acids Res.* **2014,** *42,* D191–D198.
59. Kooistra, A. J.; Kuhne, S.; de Esch, I. J. P; Leurs, R.; de Graaf, C. A Structural Chemogenomics Analysis of Aminergic GPCRs: Lessons for Histamine Receptor Ligand Design. *Br. J. Pharmacol.* **2013,** *170,* 101–126.
60. Woolfson, D. N.; Bartlett, G. J.; Burton, A. J.; Heal, J. W.; Niitsu, A.; Thomson, A. R.; Wood, C. W. De Novo Protein Design: How Do We Expand Into the Universe of Possible Protein Structures? *Curr. Opin. Struct. Biol.* **2015,** *33,* 16–26.
61. van Westen, G. J. P; Wegner, J. K.; Ijzerman, A. P.; van Vlijmen, H. W. T; Bender, A. Proteochemometric Modeling as a Tool to Design Selective Compounds and for Extrapolating to Novel Targets. *Med. Chem. Commun.* **2011,** *2,* 16–30.
62. Cortés-Ciriano, I.; Ain, Q. U.; Subramanian, V.; Lenselink, E. B.; Méndez-Lucio, O.; Ijzerman, A. P.; Wohlfahrt, G.; Prusis, P.; Malliavin, T. E.; van Westen, G. J. P; Bender, A. Polypharmacology Modelling Using Proteochemometrics (PCM): Recent Methodological Developments, Applications to Target Families, and Future Prospects. *Med. Chem. Commun.* **2015,** *6,* 24–50.
63. Clark, W. T.; Radivojac, P. Analysis of Protein Function and Its Prediction From Amino Acid Sequence. *Proteins* **2011,** *79,* 2086–2096.
64. van Linden, O. P.; Kooistra, A. J.; Leurs, R.; de Esch, I. J.; de Graaf, C. KLIFS: A Knowledge-Based Structural Database to Navigate Kinase–Ligand Interaction Space. *J. Med. Chem.* **2014,** *57,* 249–277.
65. Jansen, C.; Kooistra, A. J.; Kanev, G. K.; Leurs, R.; de Esch, I. J.; de Graaf, C. PDEStrIAn: A Phosphodiesterase Structure and Ligand Interaction Annotated Database as a Tool for Structure-Based Drug Design. *J. Med. Chem.* **2016,** *59,* 7029–7065.
66. Sanders, M. P. A; McGuire, R.; Roumen, L.; de Esch, I. J. P; de Vlieg, J.; Klomp, J. P. G; de Graaf, C. From the protein's Perspective: The Benefits and Challenges of Protein Structure-Based Pharmacophore Modeling. *Med. Chem. Commun.* **2012,** *3,* 28–38.
67. Cherkasov, A.; Muratov, E. N.; Fourches, D.; Varnek, A.; Baskin, I. I.; Cronin, M.; Dearden, J.; Gramatica, P.; Martin, Y. C.; Todeschini, R.; Consonni, V.; Kuz'min, V. E.; Cramer, R.; Benigni, R.; Yang, C.; Rathman, J.; Terfloth, L.; Gasteiger, J.; Richard, A.; Tropsha, A. QSAR Modeling: Where Have you Been? Where Are You Going to? *J. Med. Chem.* **2014,** *57,* 4977–5010.
68. Stumpfe, D.; Hu, Y.; Dimova, D.; Bajorath, J. Recent Progress in Understanding Activity Cliffs and Their Utility in Medicinal Chemistry. *J. Med. Chem.* **2014,** *57,* 18–28.
69. Keiser, M. J.; Roth, B. L.; Armbruster, B. N.; Ernsberger, P.; Irwin, J. J.; Shoichet, B. K. Relating Protein Pharmacology by Ligand Chemistry. *Nat. Biotechnol.* **2007,** *25,* 197–206.
70. Schneider, G. De Novo Design—Hop(p)ing Against Hope. *Drug Discov. Today Technol.* **2013,** *10,* 453–460.

71. de Graaf, C.; Kooistra, A. J.; Vischer, H. F.; Katritch, V.; Kuijer, M.; Shiroishi, M.; Iwata, S.; Shimamura, T.; Stevens, R. C.; de Esch, I. J.; Leurs, R. Crystal Structure-Based Virtual Screening for Fragment-Like Ligands of the Human Histamine H(1) Receptor. *J. Med. Chem.* **2011,** *54,* 8195–8206.
72. Istyastono, E. P.; Nijmeijer, S.; Lim, H. D.; van de Stolpe, A.; Roumen, L.; Kooistra, A. J.; Vischer, H. F.; de Esch, I. J.; Leurs, R.; de Graaf, C. Molecular Determinants of Ligand Binding Modes in the Histamine H(4) Receptor: Linking Ligand-Based Three-Dimensional Quantitative Structure–Activity Relationship (3D-QSAR) Models to In Silico Guided Receptor Mutagenesis Studies. *J. Med. Chem.* **2011,** *54,* 8136–8147.
73. Ain, Q. U.; Mendez-Lucio, O.; Ciriano, I. C.; Malliavin, T.; van Westen, G. J.; Bender, A. Modelling Ligand Selectivity of Serine Proteases Using Integrative Proteochemometric Approaches Improves Model Performance and Allows the Multi-Target Dependent Interpretation of Features. *Integr. Biol. (Camb)* **2014,** *6,* 1023–1033.
74. ChemAxon. http://www.chemaxon.com/.
75. Kooistra, A. J.; Binsl, T. W.; van Beek, J. H. G. M.; de Graaf, C.; Heringa, J. Electron Density Fingerprints (EDprints): Virtual Screening Using Assembled Information of Electron Density. *J. Chem. Inf. Model.* **2010,** *50,* 1772–1780.
76. Wood, D. J.; de Vlieg, J.; Wagener, M.; Ritschel, T. Pharmacophore Fingerprint-Based Approach to Binding Site Subpocket Similarity and Its Application to Bioisostere Replacement. *J. Chem. Inf. Model.* **2012,** *52,* 2031–2043.
77. Protein Data Bank. Protein Data Bank. *Nature New Biol.* **1971**, *233*, 223.
78. Munk, C.; Isberg, V.; Mordalski, S.; Harpsøe, K.; Rataj, K.; Hauser, A. S.; Kolb, P.; Bojarski, A. J.; Vriend, G.; Gloriam, D. E. GPCRdb: the G protein-coupled receptor database–an introduction. *Br. J. Pharmacol.* **2016,** *173,* 2195–2207.
79. Isberg, V.; Vroling, B.; van der Kant, R.; Li, K.; Vriend, G.; Gloriam, D. GPCRDB: An Information System for G Protein-Coupled Receptors. *Nucleic Acids Res.* **2014,** *42,* D422–D425.
80. UniProt, C. UniProt: A Hub for Protein Information. *Nucleic Acids Res.* **2015,** *43,* D204–D212.
81. Berman, H. M.; Westbrook, J.; Feng, Z.; Gilliland, G.; Bhat, T. N.; Weissig, H.; Shindyalov, I. N.; Bourne, P. E. The Protein Data Bank. *Nucleic Acids Res.* **2000,** *28,* 235–242.
82. Benson, D. A.; Cavanaugh, M.; Clark, K.; Karsch-Mizrachi, I.; Lipman, D. J.; Ostell, J.; Sayers, E. W. GenBank. *Nucleic Acids Res.* **2013,** *41,* D36–D42.
83. Pruitt, K. D.; Tatusova, T.; Brown, G. R.; Maglott, D. R. NCBI Reference Sequences (RefSeq): Current Status, New Features and Genome Annotation Policy. *Nucleic Acids Res.* **2012,** *40,* D130–D135.
84. Schuler, G. D. Pieces of the Puzzle: Expressed Sequence Tags and the Catalog of Human Genes. *J. Mol. Med.* **1997,** *75,* 694–698.
85. Southan, C.; Sharman, J. L.; Benson, H. E.; Faccenda, E.; Pawson, A. J.; Alexander, S. P.; Buneman, O. P.; Davenport, A. P.; McGrath, J. C.; Peters, J. A.; Spedding, M.; Catterall, W. A.; Fabbro, D.; Davies, J. A.; Nc, I. The IUPHAR/BPS Guide to PHARMACOLOGY in 2016: Towards Curated Quantitative Interactions Between 1300 Protein Targets and 6000 Ligands. *Nucleic Acids Res.* **2016,** *44,* D1054–D1068.
86. Sillitoe, I.; Lewis, T. E.; Cuff, A.; Das, S.; Ashford, P.; Dawson, N. L.; Furnham, N.; Laskowski, R. A.; Lee, D.; Lees, J. G.; Lehtinen, S.; Studer, R. A.; Thornton, J.; Orengo, C. A. CATH: Comprehensive Structural and Functional Annotations for Genome Sequences. *Nucleic Acids Res.* **2015,** *43,* D376–D381.
87. Fox, N. K.; Brenner, S. E.; Chandonia, J. M. SCOPe: Structural Classification of Proteins—Extended, Integrating SCOP and ASTRAL Data and Classification of New Structures. *Nucleic Acids Res.* **2014,** *42,* D304–D309.
88. Yates, A.; Akanni, W.; Amode, M. R.; Barrell, D.; Billis, K.; Carvalho-Silva, D.; Cummins, C.; Clapham, P.; Fitzgerald, S.; Gil, L. Ensembl 2016. *Nucleic Acids Res.* **2016,** *44,* D710–D716.
89. Kanehisa, M.; Sato, Y.; Kawashima, M.; Furumichi, M.; Tanabe, M. KEGG as a Reference Resource for Gene and Protein Annotation. *Nucleic Acids Res.* **2016,** *44,* D457–D462.
90. Federhen, S. The NCBI Taxonomy Database. *Nucleic Acids Res.* **2012,** *40,* D136–D143.
91. International Union of Biochemistry and Molecular Biology (IUBMB). Biochemical Nomenclature, and Enzyme Nomenclature. *Eur. J. Biochem.*, **1993,** *213*, 1-1.
92. Ashburner, M.; Ball, C. A.; Blake, J. A.; Botstein, D.; Butler, H.; Cherry, J. M.; Davis, A. P.; Dolinski, K.; Dwight, S. S.; Eppig, J. T.; Harris, M. A.; Hill, D. P.; Issel-Tarver, L.; Kasarskis, A.; Lewis, S.; Matese, J. C.; Richardson, J. E.; Ringwald, M.; Rubin, G. M.; Sherlock, G. Gene Ontology: Tool for the Unification of Biology. *Nat. Genet.* **2000,** *25,* 25–29.
93. Williams, A. J.; Harland, L.; Groth, P.; Pettifer, S.; Chichester, C.; Willighagen, E. L.; Evelo, C. T.; Blomberg, N.; Ecker, G.; Goble, C. Open PHACTS: Semantic Interoperability for Drug Discovery. *Drug Discov. Today* **2012,** *17,* 1188–1198.
94. Menikarachchi, L. C.; Hill, D. W.; Hamdalla, M. A.; Mandoiu, I. I.; Grant, D. F. In Silico Enzymatic Synthesis of a 400,000 Compound Biochemical Database for Nontargeted Metabolomics. *J. Chem. Inf. Model.* **2013,** *53,* 2483–2492.
95. Prinz, F.; Schlange, T.; Asadullah, K. Believe It or not: How Much Can We Rely on Published Data on Potential Drug Targets? *Nat. Rev. Drug Discov.* **2011,** *10,* 712.
96. Baell, J. B.; Holloway, G. A. New Substructure Filters for Removal of Pan Assay Interference Compounds (PAINS) From Screening Libraries and for Their Exclusion in Bioassays. *J. Med. Chem.* **2010,** *53,* 2719–2740.
97. Baell, J.; Walters, M. A. Chemical Con Artists Foil Drug Discovery. *Nature* **2014,** *513,* 481–483.
98. Kalliokoski, T.; Kramer, C.; Vulpetti, A. Quality Issues With Public Domain Chemogenomics Data. *Mol. Inform.* **2013,** *32,* 898–905.
99. Kooistra, A. J.; Kanev, G. K.; van Linden, O. P.; Leurs, R.; de Esch, I. J.; de Graaf, C. KLIFS: A Structural Kinase–Ligand Interaction Database. *Nucleic Acids Res.* **2015,** *44* (D1), D365–D371.
100. Begley, C. G.; Ellis, L. M. Drug Development: Raise Standards for Preclinical Cancer Research. *Nature* **2012,** *483,* 531–533.
101. Fourches, D.; Muratov, E.; Tropsha, A. Curation of Chemogenomics Data. *Nat. Chem. Biol.* **2015,** *11,* 535.
102. Sehnal, D.; Svobodova Varekova, R.; Pravda, L.; Ionescu, C. M.; Geidl, S.; Horsky, V.; Jaiswal, D.; Wimmerova, M.; Koca, J. ValidatorDB: Database of Up-to-Date Validation Results for Ligands and non-Standard Residues From the Protein Data Bank. *Nucleic Acids Res.* **2015,** *43,* D369–D375.
103. Joosten, R. P.; Long, F.; Murshudov, G. N.; Perrakis, A. The PDB_REDO Server for Macromolecular Structure Model Optimization. *IUCrJ* **2014,** *1,* 213–220.
104. Law, V.; Knox, C.; Djoumbou, Y.; Jewison, T.; Guo, A. C.; Liu, Y.; Maciejewski, A.; Arndt, D.; Wilson, M.; Neveu, V.; Tang, A.; Gabriel, G.; Ly, C.; Adamjee, S.; Dame, Z. T.; Han, B.; Zhou, Y.; Wishart, D. S. DrugBank 4.0: Shedding New Light on Drug Metabolism. *Nucleic Acids Res.* **2014,** *42,* D1091–D1097.
105. Bastian, F.; Parmentier, G.; Roux, J.; Moretti, S.; Laudet, V.; Robinson-Rechavi, M. Bgee: Integrating and Comparing Heterogeneous Transcriptome Data Among Species. In *Data Integration in the Life Sciences: 5th International Workshop, DILS 2008, Evry, France, June 25-27, 2008. Proceedings;* Bairoch, A., Cohen-Boulakia, S., Froidevaux, C., Eds.; Springer: Berlin, Heidelberg, 2008; pp 124–131.
106. Petryszak, R.; Keays, M.; Tang, Y. A.; Fonseca, N. A.; Barrera, E.; Burdett, T.; Füllgrabe, A.; Fuentes, A. M.-P.; Jupp, S.; Koskinen, S.; Mannion, O.; Huerta, L.; Megy, K.; Snow, C.; Williams, E.; Barzine, M.; Hastings, E.; Weisser, H.; Wright, J.; Jaiswal, P.; Huber, W.; Choudhary, J.; Parkinson, H. E.; Brazma, A. Expression Atlas Update—An Integrated Database of Gene and Protein Expression in Humans, Animals and Plants. *Nucleic Acids Res.* **2016,** *44,* D746–D752.
107. Velankar, S.; van Ginkel, G.; Alhroub, Y.; Battle, G. M.; Berrisford, J. M.; Conroy, M. J.; Dana, J. M.; Gore, S. P.; Gutmanas, A.; Haslam, P. PDBe: Improved Accessibility of Macromolecular Structure Data From PDB and EMDB. *Nucleic Acids Res.* **2015,** *44* (D1), D385–D395. gkv1047.
108. Kinjo, A. R.; Suzuki, H.; Yamashita, R.; Ikegawa, Y.; Kudou, T.; Igarashi, R.; Kengaku, Y.; Cho, H.; Standley, D. M.; Nakagawa, A.; Nakamura, H. Protein Data Bank Japan (PDBj): Maintaining a Structural Data Archive and Resource Description Framework Format. *Nucleic Acids Res.* **2012,** *40,* D453–D460.
109. Haas, J.; Roth, S.; Arnold, K.; Kiefer, F.; Schmidt, T.; Bordoli, L.; Schwede, T. The Protein Model Portal—A Comprehensive Resource for Protein Structure and Model Information. *Database* **2013**. bat031.
110. Biasini, M.; Bienert, S.; Waterhouse, A.; Arnold, K.; Studer, G.; Schmidt, T.; Kiefer, F.; Cassarino, T. G.; Bertoni, M.; Bordoli, L.; Schwede, T. SWISS-MODEL: Modelling Protein Tertiary and Quaternary Structure Using Evolutionary Information. *Nucleic Acids Res.* **2014,** *42,* W252–W258.
111. Pieper, U.; Webb, B. M.; Dong, G. Q.; Schneidman-Duhovny, D.; Fan, H.; Kim, S. J.; Khuri, N.; Spill, Y. G.; Weinkam, P.; Hammel, M.; Tainer, J. A.; Nilges, M.; Sali, A. ModBase, a Database of Annotated Comparative Protein Structure Models and Associated Resources. *Nucleic Acids Res.* **2014,** *42,* D336–D346.
112. Mitchell, A.; Chang, H.-Y.; Daugherty, L.; Fraser, M.; Hunter, S.; Lopez, R.; McAnulla, C.; McMenamin, C.; Nuka, G.; Pesseat, S.; Sangrador-Vegas, A.; Scheremetjew, M.; Rato, C.; Yong, S.-Y.; Bateman, A.; Punta, M.; Attwood, T. K.; Sigrist, C. J. A.; Redaschi, N.; Rivoire, C.; Xenarios, I.; Kahn, D.; Guyot, D.; Bork, P.; Letunic, I.; Gough, J.; Oates, M.; Haft, D.; Huang, H.; Natale, D. A.; Wu, C. H.; Orengo, C.; Sillitoe, I.; Mi, H.; Thomas, P. D.; Finn, R. D. The InterPro Protein Families Database: The Classification Resource After 15 Years. *Nucleic Acids Res.* **2015,** *43,* D213–D221.

113. Finn, R. D.; Coggill, P.; Eberhardt, R. Y.; Eddy, S. R.; Mistry, J.; Mitchell, A. L.; Potter, S. C.; Punta, M.; Qureshi, M.; Sangrador-Vegas, A.; Salazar, G. A.; Tate, J.; Bateman, A. The Pfam Protein Families Database: Towards a More Sustainable Future. *Nucleic Acids Res.* **2016,** *44,* D279–D285.
114. Ulrich, E. L.; Akutsu, H.; Doreleijers, J. F.; Harano, Y.; Ioannidis, Y. E.; Lin, J.; Livny, M.; Mading, S.; Maziuk, D.; Miller, Z.; Nakatani, E.; Schulte, C. F.; Tolmie, D. E.; Kent Wenger, R.; Yao, H.; Markley, J. L. BioMagResBank. *Nucleic Acids Res.* **2008,** *36,* D402–D408.
115. Berman, H.; Henrick, K.; Nakamura, H. Announcing the Worldwide Protein Data Bank. *Nat. Struct. Mol. Biol.* **2003,** *10,* 980.
116. Stierand, K.; Rarey, M. Drawing the PDB: Protein–Ligand Complexes in Two Dimensions. *ACS Med. Chem. Lett.* **2010,** *1,* 540–545.
117. Kabsch, W.; Sander, C. Dictionary of Protein Secondary Structure: Pattern Recognition of Hydrogen-Bonded and Geometrical Features. *Biopolymers* **1983,** *22,* 2577–2637.
118. Frishman, D.; Argos, P. Knowledge-Based Protein Secondary Structure Assignment. *Proteins* **1995,** *23,* 566–579.
119. Golovin, A.; Dimitropoulos, D.; Oldfield, T.; Rachedi, A.; Henrick, K. MSDsite: A Database Search and Retrieval System for the Analysis and Viewing of Bound Ligands and Active Sites. *Proteins* **2005,** *58,* 190–199.
120. Mulder, N. J.; Apweiler, R.; Attwood, T. K.; Bairoch, A.; Bateman, A.; Binns, D.; Bork, P.; Buillard, V.; Cerutti, L.; Copley, R.; Courcelle, E.; Das, U.; Daugherty, L.; Dibley, M.; Finn, R.; Fleischmann, W.; Gough, J.; Haft, D.; Hulo, N.; Hunter, S.; Kahn, D.; Kanapin, A.; Kejariwal, A.; Labarga, A.; Langendijk-Genevaux, P. S.; Lonsdale, D.; Lopez, R.; Letunic, I.; Madera, M.; Maslen, J.; McAnulla, C.; McDowall, J.; Mistry, J.; Mitchell, A.; Nikolskaya, A. N.; Orchard, S.; Orengo, C.; Petryszak, R.; Selengut, J. D.; Sigrist, C. J.; Thomas, P. D.; Valentin, F.; Wilson, D.; Wu, C. H.; Yeats, C. New Developments in the InterPro Database. *Nucleic Acids Res.* **2007,** *35,* D224–D228.
121. Xu, Y.; Xu, D.; Gabow, H. N. Protein Domain Decomposition Using a Graph-Theoretic Approach. *Bioinformatics* **2000,** *16,* 1091–1104.
122. Prlic, A.; Bliven, S.; Rose, P. W.; Bluhm, W. F.; Bizon, C.; Godzik, A.; Bourne, P. E. Pre-Calculated Protein Structure Alignments at the RCSB PDB Website. *Bioinformatics* **2010,** *26,* 2983–2985.
123. Alexandrov, N.; Shindyalov, I. PDP: Protein Domain Parser. *Bioinformatics* **2003,** *19,* 429–430.
124. Altschul, S. F.; Gish, W.; Miller, W.; Myers, E. W.; Lipman, D. J. Basic Local Alignment Search Tool. *J. Mol. Biol.* **1990,** *215,* 403–410.
125. Ye, Y.; Godzik, A. Flexible Structure Alignment by Chaining Aligned Fragment Pairs Allowing Twists. *Bioinformatics* **2003,** *19,* ii246–ii255.
126. Gilson, M. K.; Liu, T.; Baitaluk, M.; Nicola, G.; Hwang, L.; Chong, J. BindingDB in 2015: A Public Database for Medicinal Chemistry, Computational Chemistry and Systems Pharmacology. *Nucleic Acids Res.* **2016,** *44,* D1045–D1053.
127. Orchard, S.; Ammari, M.; Aranda, B.; Breuza, L.; Briganti, L.; Broackes-Carter, F.; Campbell, N. H.; Chavali, G.; Chen, C.; del-Toro, N.; Duesbury, M.; Dumousseau, M.; Galeota, E.; Hinz, U.; Iannuccelli, M.; Jagannathan, S.; Jimenez, R.; Khadake, J.; Lagreid, A.; Licata, L.; Lovering, R. C.; Meldal, B.; Melidoni, A. N.; Milagros, M.; Peluso, D.; Perfetto, L.; Porras, P.; Raghunath, A.; Ricard-Blum, S.; Roechert, B.; Stutz, A.; Tognolli, M.; van Roey, K.; Cesareni, G.; Hermjakob, H. The MIntAct Project—IntAct as a Common Curation Platform for 11 Molecular Interaction Databases. *Nucleic Acids Res.* **2014,** *42,* D358–D363.
128. Szklarczyk, D.; Santos, A.; von Mering, C.; Jensen, L. J.; Bork, P.; Kuhn, M. STITCH 5: Augmenting Protein–Chemical Interaction Networks With Tissue and Affinity Data. *Nucleic Acids Res.* **2016,** *44,* D380–D384.
129. Hecker, N.; Ahmed, J.; von Eichborn, J.; Dunkel, M.; Macha, K.; Eckert, A.; Gilson, M. K.; Bourne, P. E.; Preissner, R. SuperTarget Goes Quantitative: Update on Drug–Target Interactions. *Nucleic Acids Res.* **2012,** *40,* D1113–D1117.
130. Wang, Y.; Suzek, T.; Zhang, J.; Wang, J.; He, S.; Cheng, T.; Shoemaker, B. A.; Gindulyte, A.; Bryant, S. H. PubChem BioAssay: 2014 Update. *Nucleic Acids Res.* **2014,** *42,* D1075–D1082.
131. Roth, B. L.; Lopez, E.; Patel, S.; Kroeze, W. K. The Multiplicity of Serotonin Receptors: Uselessly Diverse Molecules or an Embarrassment of Riches? *Neuroscientist* **2000,** *6,* 252–262.
132. Liu, Z.; Li, Y.; Han, L.; Li, J.; Liu, J.; Zhao, Z.; Nie, W.; Liu, Y.; Wang, R. PDB-Wide Collection of Binding Data: Current Status of the PDBbind Database. *Bioinformatics* **2015,** *31,* 405–412.
133. Ahmed, A.; Smith, R. D.; Clark, J. J.; Dunbar, J. B., Jr.; Carlson, H. A. Recent Improvements to Binding MOAD: A Resource for Protein–Ligand Binding Affinities and Structures. *Nucleic Acids Res.* **2015,** *43,* D465–D469.
134. Chan, W. K.; Zhang, H.; Yang, J.; Brender, J. R.; Hur, J.; Ozgur, A.; Zhang, Y. GLASS: A Comprehensive Database for Experimentally Validated GPCR–Ligand Associations. *Bioinformatics* **2015,** *31,* 3035–3042.
135. Kim, J.; Yoo, M.; Kang, J.; Tan, A. K-Map: Connecting Kinases With Therapeutics for Drug Repurposing and Development. *Hum. Genomics* **2013,** *7,* 20.
136. Pires, D. E.; Blundell, T. L.; Ascher, D. B. Platinum: A Database of Experimentally Measured Effects of Mutations on Structurally Defined Protein–Ligand Complexes. *Nucleic Acids Res.* **2015,** *43,* D387–D391.
137. Higueruelo, A. P.; Jubb, H.; Blundell, T. L. TIMBAL v2: Update of a Database Holding Small Molecules Modulating Protein–Protein Interactions. *Database* **2013**. bat039.
138. Schuffenhauer, A.; Zimmermann, J.; Stoop, R.; van der Vyver, J.-J.; Lecchini, S.; Jacoby, E. An Ontology for Pharmaceutical Ligands and Its Application for In Silico Screening and Library Design. *J. Chem. Inf. Comput. Sci.* **2002,** *42,* 947–955.
139. Olah, M.; Mracec, M.; Ostopovici, L.; Rad, R.; Bora, A.; Hadaruga, N.; Olah, I.; Banda, M.; Simon, Z.; Mracec, M. WOMBAT: World of Molecular Bioactivity. In *Chemoinformatics in Drug Discovery;* Oprea, T. I., Ed.; Wiley-VCH: Weinheim, 2004; pp 223–239.
140. Okuno, Y.; Tamon, A.; Yabuuchi, H.; Niijima, S.; Minowa, Y.; Tonomura, K.; Kunimoto, R.; Feng, C. GLIDA: GPCR—Ligand Database for Chemical Genomics Drug Discovery—Database and Tools Update. *Nucleic Acids Res.* **2008,** *36,* D907–D912.
141. Chiu, Y. Y.; Lin, C. T.; Huang, J. W.; Hsu, K. C.; Tseng, J. H.; You, S. R.; Yang, J. M. KIDFamMap: A Database of Kinase-Inhibitor-Disease Family Maps for Kinase Inhibitor Selectivity and Binding Mechanisms. *Nucleic Acids Res.* **2013,** *41,* D430–D440.
142. Basse, M. J.; Betzi, S.; Morelli, X.; Roche, P. 2P2Idb v2: Update of a Structural Database Dedicated to Orthosteric Modulation of Protein–Protein Interactions. *Database* **2016**. baw007.
143. Huang, Z.; Mou, L.; Shen, Q.; Lu, S.; Li, C.; Liu, X.; Wang, G.; Li, S.; Geng, L.; Liu, Y.; Wu, J.; Chen, G.; Zhang, J. ASD v2.0: Updated Content and Novel Features Focusing on Allosteric Regulation. *Nucleic Acids Res.* **2014,** *42,* D510–D516.
144. Schreyer, A. M.; Blundell, T. L. CREDO: A Structural Interactomics Database for Drug Discovery. *Database* **2013**. bat049.
145. Desaphy, J.; Bret, G.; Rognan, D.; Kellenberger, E. sc-PDB: A 3D-Database of Ligandable Binding Sites—10 Years on. *Nucleic Acids Res.* **2015,** *43,* D399–D404.
146. Laskowski, R. A.; Swindells, M. B. LigPlot+: Multiple Ligand–Protein Interaction Diagrams for Drug Discovery. *J. Chem. Inf. Model.* **2011,** *51,* 2778–2786.
147. Kim, S.; Thiessen, P. A.; Bolton, E. E.; Chen, J.; Fu, G.; Gindulyte, A.; Han, L.; He, J.; He, S.; Shoemaker, B. A.; Wang, J.; Yu, B.; Zhang, J.; Bryant, S. H. PubChem Substance and Compound databases. *Nucleic Acids Res.* **2016,** *44,* D1202–D1213.
148. Davies, M.; Nowotka, M.; Papadatos, G.; Atkinson, F.; van Westen, G.; Dedman, N.; Ochoa, R.; Overington, J. MyChEMBL: A Virtual Platform for Distributing Cheminformatics Tools and Open Data. *Challenges* **2014,** *5,* 334–337.
149. Kerrien, S.; Aranda, B.; Breuza, L.; Bridge, A.; Broackes-Carter, F.; Chen, C.; Duesbury, M.; Dumousseau, M.; Feuermann, M.; Hinz, U.; Jandrasits, C.; Jimenez, R. C.; Khadake, J.; Mahadevan, U.; Masson, P.; Pedruzzi, I.; Pfeiffenberger, E.; Porras, P.; Raghunath, A.; Roechert, B.; Orchard, S.; Hermjakob, H. The IntAct Molecular Interaction Database in 2012. *Nucleic Acids Res.* **2012,** *40,* D841–D846.
150. Shoemaker, B. A.; Zhang, D.; Tyagi, M.; Thangudu, R. R.; Fong, J. H.; Marchler-Bauer, A.; Bryant, S. H.; Madej, T.; Panchenko, A. R. IBIS (Inferred Biomolecular Interaction Server) Reports, Predicts and Integrates Multiple Types of Conserved Interactions for Proteins. *Nucleic Acids Res.* **2012,** *40,* D834–D840.
151. Yang, J.; Roy, A.; Zhang, Y. BioLiP: A Semi-Manually Curated Database for Biologically Relevant Ligand–Protein Interactions. *Nucleic Acids Res.* **2013,** *41,* D1096–D1103.
152. Konc, J.; Miller, B. T.; Stular, T.; Lesnik, S.; Woodcock, H. L.; Brooks, B. R.; Janezic, D. ProBiS-CHARMMing: Web Interface for Prediction and Optimization of Ligands in Protein Binding Sites. *J. Chem. Inf. Model.* **2015,** *55,* 2308–2314.
153. Ito, J.; Ikeda, K.; Yamada, K.; Mizuguchi, K.; Tomii, K. PoSSuM v. 2.0: Data Update and a New Function for Investigating Ligand Analogs and Target Proteins of Small-Molecule Drugs. *Nucleic Acids Res.* **2015,** *43,* D392–D398.
154. Kawabata, T.; Go, N. Detection of Pockets on Protein Surfaces Using Small and Large Probe Spheres to Find Putative Ligand Binding Sites. *Proteins* **2007,** *68,* 516–529.

155. Velankar, S.; Dana, J. M.; Jacobsen, J.; van Ginkel, G.; Gane, P. J.; Luo, J.; Oldfield, T. J.; O'Donovan, C.; Martin, M. J.; Kleywegt, G. J. SIFTS: Structure Integration With Function. Taxonomy and Sequences Resource. *Nucleic Acids Res.* **2013,** *41,* D483–D489.
156. Li, Z.; Lazaridis, T. Water at Biomolecular Binding Interfaces. *Phys. Chem. Chem. Phys.* **2007,** *9,* 573–581.
157. Desaphy, J.; Raimbaud, E.; Ducrot, P.; Rognan, D. Encoding Protein–Ligand Interaction Patterns in Fingerprints and Graphs. *J. Chem. Inf. Model.* **2013,** *53,* 623–637.
158. Desaphy, J.; Rognan, D. sc-PDB-Frag: A Database of Protein–Ligand Interaction Patterns for Bioisosteric Replacements. *J. Chem. Inf. Model.* **2014,** *54,* 1908–1918.
159. Meyer, T.; Knapp, E.-W. Database of Protein Complexes With Multivalent Binding Ability: Bival-Bind. *Proteins* **2014,** *82,* 744–751.
160. Anand, P.; Nagarajan, D.; Mukherjee, S.; Chandra, N. PLIC: Protein–Ligand Interaction Clusters. *Database* **2014**. bau029.
161. Volkamer, A.; Eid, S.; Turk, S.; Jaeger, S.; Rippmann, F.; Fulle, S. Pocketome of Human Kinases: Prioritizing the ATP Binding Sites of (yet) Untapped Protein Kinases for Drug Discovery. *J. Chem. Inf. Model.* **2015,** *55,* 538–549.
162. Hanson, R. M.; Prilusky, J.; Renjian, Z.; Nakane, T.; Sussman, J. L. JSmol and the Next-Generation Web-Based Representation of 3D Molecular Structure as Applied to Proteopedia. *Isr. J. Chem.* **2013,** *53,* 207–216.
163. Mauri, A.; Consonni, V.; Pavan, M.; Todeschini, R., Dragon Software: An Easy Approach to Molecular Descriptor Calculations. *Commun. Math. Comput. Chem.* **2006**, *56*, 237–248.
164. Gabanyi, M. J.; Adams, P. D.; Arnold, K.; Bordoli, L.; Carter, L. G.; Flippen-Andersen, J.; Gifford, L.; Haas, J.; Kouranov, A.; McLaughlin, W. A.; Micallef, D. I.; Minor, W.; Shah, R.; Schwede, T.; Tao, Y. P.; Westbrook, J. D.; Zimmerman, M.; Berman, H. M. The Structural Biology Knowledgebase: A Portal to Protein Structures, Sequences, Functions, and Methods. *J. Struct. Funct. Genomics* **2011,** *12,* 45–54.
165. Kleywegt, G. J. Crystallographic Refinement of Ligand Complexes. *Acta Crystallogr. D Biol. Crystallogr.* **2007,** *63,* 94–100.
166. Hamon, V.; Bourgeas, R.; Ducrot, P.; Theret, I.; Xuereb, L.; Basse, M. J.; Brunel, J. M.; Combes, S.; Morelli, X.; Roche, P. 2P2I HUNTER: A Tool for Filtering Orthosteric Protein–Protein Interaction Modulators via a Dedicated Support Vector Machine. *J. R. Soc. Interface* **2014,** *11,* 20130860.
167. Wang, Q.; Zheng, M.; Huang, Z.; Liu, X.; Zhou, H.; Chen, Y.; Shi, T.; Zhang, J. Toward Understanding the Molecular Basis for Chemical Allosteric Modulator Design. *J. Mol. Graph. Model.* **2012,** *38,* 324–333.
168. Huang, W.; Lu, S.; Huang, Z.; Liu, X.; Mou, L.; Luo, Y.; Zhao, Y.; Liu, Y.; Chen, Z.; Hou, T.; Zhang, J. Allosite: A Method for Predicting Allosteric Sites. *Bioinformatics* **2013,** *29,* 2357–2359.
169. Li, S.; Shen, Q.; Su, M.; Liu, X.; Lu, S.; Chen, Z.; Wang, R.; Zhang, J. Alloscore: A Tool for Predicting Allosteric Ligand–Protein Interactions. *Bioinformatics* **2016,** *32* (10), 1574–1576.
170. Huang, W.; Wang, G.; Shen, Q.; Liu, X.; Lu, S.; Geng, L.; Huang, Z.; Zhang, J. ASBench: Benchmarking Sets for Allosteric Discovery. *Bioinformatics* **2015,** *31,* 2598–2600.
171. Finn, R. D.; Miller, B. L.; Clements, J.; Bateman, A. iPfam: A Database of Protein Family and Domain Interactions Found in the Protein Data Bank. *Nucleic Acids Res.* **2014,** *42,* D364–D373.
172. Verhoeven, S.; Vass, M.; McGuire, R.; Ritschel, T.; Graaf, C. D., 3D-e-Chem GPCRdb KNIME Nodes: v1.0.8. **2016**. http://dx.doi.org/10.5281/zenodo.50042.
173. Li, H.; Leung, K.-S.; Nakane, T.; Wong, M.-H. Iview: An Interactive WebGL Visualizer for Protein–Ligand Complex. *BMC Bioinf.* **2014,** *15,* 1–6.
174. Schalon, C.; Surgand, J. S.; Kellenberger, E.; Rognan, D. A Simple and Fuzzy Method to Align and Compare Druggable Ligand-Binding Sites. *Proteins* **2008,** *71,* 1755–1778.
175. Gfeller, D.; Grosdidier, A.; Wirth, M.; Daina, A.; Michielin, O.; Zoete, V. SwissTargetPrediction: A Web Server for Target Prediction of Bioactive Small Molecules. *Nucleic Acids Res.* **2014,** *42,* W32–W38.
176. Lounkine, E.; Keiser, M. J.; Whitebread, S.; Mikhailov, D.; Hamon, J.; Jenkins, J. L.; Lavan, P.; Weber, E.; Doak, A. K.; Cote, S.; Shoichet, B. K.; Urban, L. Large-Scale Prediction and Testing of Drug Activity on Side-Effect Targets. *Nature* **2012,** *486,* 361–367.
177. Laggner, C.; Kokel, D.; Setola, V.; Tolia, A.; Lin, H.; Irwin, J. J.; Keiser, M. J.; Cheung, C. Y.; Minor, D. L., Jr.; Roth, B. L.; Peterson, R. T.; Shoichet, B. K. Chemical Informatics and Target Identification in a Zebrafish Phenotypic Screen. *Nat. Chem. Biol.* **2012,** *8,* 144–146.
178. Meslamani, J.; Bhajun, R.; Martz, F.; Rognan, D. Computational Profiling of Bioactive Compounds Using a Target-Dependent Composite Workflow. *J. Chem. Inf. Model.* **2013,** *53,* 2322–2333.
179. Paolini, G. V.; Shapland, R. H.; van Hoorn, W. P.; Mason, J. S.; Hopkins, A. L. Global Mapping of Pharmacological Space. *Nat. Biotechnol.* **2006,** *24,* 805–815.
180. Vulpetti, A.; Kalliokoski, T.; Milletti, F. Chemogenomics in Drug Discovery: Computational Methods Based on the Comparison of Binding Sites. *Future Med. Chem.* **2012,** *4,* 1971–1979.
181. Ehrt, C.; Brinkjost, T.; Koch, O. The Impact of Binding Site Comparisons on Medicinal Chemistry and Rational Molecular Design. *J. Med. Chem.* **2016,** *59* (9), 4121–4151.
182. Defranchi, E.; Schalon, C.; Messa, M.; Onofri, F.; Benfenati, F.; Rognan, D. Binding of Protein Kinase Inhibitors to Synapsin I Inferred From Pair-Wise Binding Site Similarity Measurements. *PLoS One* **2010,** *5,* e12214.
183. Schirris, T. J.; Renkema, G. H.; Ritschel, T.; Voermans, N. C.; Bilos, A.; van Engelen, B. G.; Brandt, U.; Koopman, W. J.; Beyrath, J. D.; Rodenburg, R. J.; Willems, P. H.; Smeitink, J. A.; Russel, F. G. Statin-Induced Myopathy Is Associated With Mitochondrial Complex III Inhibition. *Cell Metab.* **2015,** *22,* 399–407.
184. Schirris, T. J.; Ritschel, T.; Herma Renkema, G.; Willems, P. H.; Smeitink, J. A.; Russel, F. G. Mitochondrial ADP/ATP Exchange Inhibition: A Novel Off-Target Mechanism Underlying Ibipinabant-Induced Myotoxicity. *Sci. Rep.* **2015,** *5,* 14533.
185. Wawer, M.; Bajorath, J. Similarity–Potency Trees: A Method to Search for SAR Information in Compound Data Sets and Derive SAR Rules. *J. Chem. Inf. Model.* **2010,** *50,* 1395–1409.
186. Marcou, G.; Rognan, D. Optimizing Fragment and Scaffold Docking by Use of Molecular Interaction Fingerprints. *J. Chem. Inf. Model.* **2007,** *47,* 195–207.
187. Rogers, D.; Hahn, M. Extended-Connectivity Fingerprints. *J. Chem. Inf. Model.* **2010,** *50,* 742–754.
188. Langdon, S. R.; Ertl, P.; Brown, N. Bioisosteric Replacement and Scaffold Hopping in Lead Generation and Optimization. *Mol. Inform.* **2010,** *29,* 366–385.
189. Jansen, C.; Wang, H.; Kooistra, A. J.; de Graaf, C.; Orrling, K. M.; Tenor, H.; Seebeck, T.; Bailey, D.; de Esch, I. J.; Ke, H.; Leurs, R. Discovery of Novel Trypanosoma Brucei Phosphodiesterase B1 Inhibitors by Virtual Screening Against the Unliganded TbrPDEB1 Crystal Structure. *J. Med. Chem.* **2013,** *56,* 2087–2096.
190. Kooistra, A. J.; Leurs, R.; de Esch, I. J.; de Graaf, C. Structure-Based Prediction of G-Protein-Coupled Receptor Ligand Function: A Beta-Adrenoceptor Case Study. *J. Chem. Inf. Model.* **2015,** *55,* 1045–1061.
191. 3D-eChem VM. http://3d-e-chem.github.io.

Relevant Websites

http://www.uniprot.org/uniprot—UniProt Knowledgebase (UniProtKB), a database that incorporates large collection of functional information on proteins.
http://www.rcsb.org/pdb—Protein Databank (PDB), a repository of macromolecular structure data.
http://www.ebi.ac.uk/chembl—ChEMBL, a database of bioactive molecules and target annotated bioactivities.
http://cheminfo.u-strasbg.fr/scPDB—sc-PDB revolves around the druggable binding sites from the Protein Data Bank.
http://www.gpcrdb.org—GPCRdb contains data, diagrams and web tools for G protein-coupled receptors (GPCRs).
http://klifs.vu-compmedchem.nl—Kinase–Ligand Interaction Fingerprints and Structures database (KLIFS) a database containing sequence, structure, and protein–ligand interaction information on Protein Kinases.
http://pdestrian.vu-compmedchem.nl—PhosphoDiEsterase Structure and ligand Interaction Annotated (PDEStrIAn) database revolves around the protein structure of catalytic PDE domains and the way PDE inhibitors can interact with them.
http://pocketome.org—Pocketome, a database of conformational ensembles of protein–ligand binding sites.

1.16 Nontest Methods for REACH Legislation

A Gissi, European Chemicals Agency (ECHA), Helsinki, Finland
GF Mangiatordi, Università degli Studi di Bari Aldo Moro, Bari, Italy
T Sobański and T Netzeva, European Chemicals Agency (ECHA), Helsinki, Finland
O Nicolotti, Università degli Studi di Bari Aldo Moro, Bari, Italy

© 2017 Elsevier Ltd. All rights reserved.
The views expressed in this article are solely those of the authors, and the content of the article does not represent an official position of the European Chemicals Agency.

1.16.1 Introduction 472
1.16.1.1 Understanding REACH 472
1.16.1.1.1 The legal framework 472
1.16.1.1.2 The promotion of alternative methods 473
1.16.1.2 Obligations for Pharmaceutical Companies under REACH 474
1.16.1.3 REACH Annex XI Requirements for (Q)SAR and Read-Across 474
1.16.1.3.1 (Q)SAR 474
1.16.1.3.2 Grouping of substances and read-across approach 474
1.16.1.4 Dissemination of REACH Data 475
1.16.2 Nontest Methods 475
1.16.2.1 OECD Principles for the Validation of (Q)SAR 475
1.16.2.1.1 About principle 1: a defined endpoint 475
1.16.2.1.2 About principle 2: an unambiguous algorithm 476
1.16.2.1.3 About principle 3: a defined domain of applicability 476
1.16.2.1.4 About principle 4: appropriate measures of goodness of fit, robustness, and predictivity 479
1.16.2.1.5 About principle 5: a mechanistic interpretation, if possible 483
1.16.2.2 Grouping and Read-Across 483
1.16.2.3 (Q)SAR Toolbox 485
1.16.2.3.1 (Q)SAR Toolbox main functionalities 485
1.16.3 Practical Example on the Use of (Q)SAR under REACH: Mutagenicity 487
1.16.4 Conclusions 488
References 488

1.16.1 Introduction

1.16.1.1 Understanding REACH

1.16.1.1.1 The legal framework

In 2006, the European Union adopted the regulation (EC) No. 1907/2006 concerning the Registration, Evaluation, Authorization, and Restriction of Chemicals (REACH).

> Quoting REACH Article 1, "the purpose of this Regulation is to ensure a high level of protection of human health and the environment, including the promotion of alternative methods for assessment of hazards of substances, as well as the free circulation of substances on the internal market while enhancing competitiveness and innovation […]."

REACH brought a revolution in the chemical regulatory world, shifting for the first time the burden of proof for the safe use of chemicals from public authorities to the companies, which are manufacturing or importing chemical substances. With the entry into force of REACH, companies have to register their substances to the European Chemicals Agency (ECHA) according to the "no data, no market" principle, if the manufacture or import of the chemical exceeds 1 ton year^{-1}. The registration includes the preparation of a dossier for each substance, where industry has to show that the chemical hazard and risk are properly understood, adequately controlled, and communicated through the supply chain. The objective of REACH is to reduce and replace the most dangerous substances (known as substances of very high concern (SVHC)) with safer alternatives. This goal is achieved by collecting data (registration, done by industry), assessing these data (dossier compliance check, done by ECHA), and identifying SVHC (substance evaluation and SVHC identification, done by member state competent authorities and coordinated by ECHA). When an SVHC is identified, its use is limited with specific processes like authorization and/or restriction.

A cornerstone of the registration process is the preparation of the dossier containing, among others, hazard information. The minimum set of information to be provided is called standard information requirement (SIR). SIR includes physicochemical, toxicological (also termed as human health), ecotoxicological, and environmental fate endpoints. The amount of endpoints to take into account is proportional to the tonnages of a substance (i.e., the produced or imported volume of a chemical per year). The higher the tonnage, the higher the SIR. This tiered approach guarantees that the toxicity of chemicals produced or imported in larger amounts is studied more thoroughly. Based on such proportionality principle, the endpoints are listed in REACH Annexes VII, VIII, IX, and X for the substances produced or imported in quantities equal or above 1, 10, 100, and 1000 tons year^{-1}, respectively. These annexes are given in the form of tables with two columns. The first column reports the list of the demanded endpoints (SIR), while the second column contains the list of specific adaptation rules, describing the conditions under which the test can be adapted or waived. As an example of column two adaptations, a substance does not need to be tested for skin sensitization if it is already classified as corrosive. More details on the SIRs for toxicological (human health) endpoints are reported in **Table 1**.

1.16.1.1.2 The promotion of alternative methods

The promotion of alternative methods and animal welfare considerations has a central place in REACH. ECHA has the legal obligation to report to the European Commission the status of implementation and use of nonanimal methods for meeting the SIR. So far, ECHA has published two reports on this matter in 2011[1] and 2014.[2]

In order to minimize unnecessary animal testing, REACH offers to registrants several possibilities: using existing data, joining other registrant of the same substance (one substance, one registration principle) in order to avoid double testing, and using the so-called adaptation and alternative methods. If none of these elements is sufficient to meet the requirements, the registrant may perform the standard animal test. However, before performing a test on Annex IX and X endpoints, the registrant shall prepare a testing proposal (TP) that is evaluated by ECHA before the study is conducted.

The general rules for adaptation of the standard testing regime are explained in Annex XI as follows:

- *Testing does not appear scientifically necessary*.

  This is the case when it is possible to use existing data, weight of evidence (WoE), (quantitative) structure–activity relationships ((Q)SARs), *in vitro* methods, grouping of substances, and/or read-across. Please note that the definition of the WoE according to Annex XI is "sufficient weight of evidence from several independent sources of information leading to the assumption/conclusion that a substance has or has not a particular dangerous property, while the information from each single source alone is regarded insufficient to support this notion."
- *Testing is technically not possible*.

  This may happen due to particular physicochemical properties of a substance (e.g., very volatile, very reactive, or unstable substances) making the conduction of the study unfeasible.
- *Substance-tailored exposure-driven testing*.

Table 1 Overview of the toxicological standard information requirements (SIRs) as defined in REACH

REACH Annex	*Toxicological standard information requirements (SIRs)*
Annex VII	Skin irritation or skin corrosion (*in vitro*)
	Eye irritation (*in vitro*)
	Skin sensitization (*in vivo*)
	Mutagenicity (gene mutation in bacteria)
	Acute toxicity (by oral route)
Annex VIII	Skin irritation (*in vivo*)
	Eye irritation (*in vivo*)
	Cytogenicity in mammalian cells (*in vitro*)
	Gene mutation in mammalian cells (*in vitro*)
	Acute toxicity (by inhalation)
	Acute toxicity (by dermal route)
	Short-term repeated dose toxicity test (28 days). Screening for reproductive/developmental toxicity toxicokinetics
Annex IX	Short-term repeated dose toxicity test (28 days). Subchronic toxicity (90 days)
	Prenatal developmental toxicity
	Two-generation reproductive toxicity
Annex X	Long-term repeated dose toxicity ($\geq$12 months). Developmental toxicity
	Two-generation reproductive toxicity
	Carcinogenicity

The reader is reminded that the requirements of annexes are cumulative, that is, for registering a substance falling under Annex IX, the registrant needs to include the information in Annexes VII, VIII, and IX.
Adapted from ECHA, Guidance on registration, version 2.0, **2012**, http://echa.europa.eu/documents/10162/13632/registration_en.pdf (last accessed date, 19 February 2016).

Certain tests may be omitted if the manufacturers/importers document and demonstrate the absence of exposure or unlikely no relevant or no significant exposure.

It is also worth mentioning that in Mar. 2013, the use of animals for testing the toxicity of cosmetic products was banned,[3] making even more relevant for regulatory toxicology the need to find alternative methods and to use optimally existing data.

In this article, we will mainly focus on the "nontest" adaptations foreseen by REACH and particularly on (Q)SAR, grouping of substances, and read-across approach. It is noted that read-across often relies on existing information; however, in some cases, testing of the source chemical may be needed. *In chemico* and *in vitro* studies, which are also alternative methods (to the use of animals) but require testing of the substances, are not discussed here. WoE is also not discussed further in this article.

1.16.1.2 Obligations for Pharmaceutical Companies under REACH

At first sight, pharmaceutical products may look outside the scope of REACH. Indeed, Article 2 of REACH ("Application") exempts "medicinal products for human or veterinary use" from the registration process. The rationale beyond this exemption is that medicinal products are dealt under different EU regulations. Nevertheless, pharmaceutical companies have a number of obligations under REACH. In fact, this regulation still applies to medicinal products if they are produced for any other use. In this case, the information requirements depend on the volume of production (see **Table 1**). Isolated pharmaceutical intermediates, as any other transported or on-site isolated chemical intermediate, have to be registered too. The information requirements for intermediates are less demanding than those needed for substances with nonintermediate use and are listed in REACH Articles 17 and 18. They include, among others, information on substance identity, classification, any (eco)toxicological data available, and risk management measures applied. Furthermore, all the raw materials or any substance used during manufacture is subject to REACH. In practice, this means that, if the pharmaceutical company is producing or importing any raw material in a quantity more than 1 ton $year^{-1}$, a registration is needed. On the other hand, if the company is buying the raw material from a supplier, it should investigate whether the supplier plans to or have already registered it. On the positive side, REACH has improved and will continue to improve the quality of the hazard information available in safety data sheets for substances used also by pharmaceutical industry, with a positive impact on workers and environmental protections.

1.16.1.3 REACH Annex XI Requirements for (Q)SAR and Read-Across

1.16.1.3.1 (Q)SAR

The results of (Q)SAR models have to meet some mandatory regulatory requirements, described by Annex XI—paragraph 1.3 of REACH regulation:

1. Results are derived from a (Q)SAR model whose scientific validity has been established.
2. The substance falls within the applicability domain (AD) of the (Q)SAR model.
3. Results are adequate for the purpose of classification and labeling and/or risk assessment.
4. Adequate and reliable documentation of the applied method is provided.

In this respect, the evaluation of a (Q)SAR result requires the assessment of both the model (as set in condition 1) and its prediction (as set in conditions 2 and 3). In addition, appropriate documentation has to be provided (condition 4). The scientific validity of a (Q)SAR model is assessed in light of the Organization for Economic Cooperation and Development (OECD) principles for the validation of (Q)SARs.[4] These principles were specifically introduced for regulatory purposes and comprise five elements, which are deemed essential for the assessment of the validity of the model.

Once the model has been considered valid, predictions should be individually evaluated through a case-by-case exercise. It might happen that an unreliable or inadequate prediction is derived from otherwise valid (Q)SAR model. To elaborate further this issue, ECHA has made available guidance (Chapter R.6)[5] and practical guides,[6] has produced webinars,[7] and has developed illustrative examples[8,9] explaining how to obtain reliable and adequate (Q)SAR predictions.

1.16.1.3.2 Grouping of substances and read-across approach

The rationale behind the read-across approach[10] is that similar substances are expected to have similar properties. As a result, a property of a chemical that has not been tested yet (named as target) can be predicted by using available data from one or more similar compounds (named as source chemicals).

According to Annex XI, the similarity may be based (a) on common functional groups; (b) on common precursors and/or on the likelihood of common breakdown products via physical and biological processes, which result in structurally similar chemicals; and (c) on constant patterns in the changing of the potency of the properties across the category. In any case, results should

- be adequate for the purpose of classification and labeling and/or risk assessment;
- have adequate and reliable coverage of the key parameters addressed in the corresponding test method;
- cover an exposure duration comparable to, or longer than, the corresponding test method if exposure duration is a relevant parameter;
- be provided with adequate and reliable documentation of the applied method.

Also in this case, ECHA has prepared guidance, practical guides,[11] webinars, and illustrative examples[12,13] of read-across predictions.

In this respect, a recent milestone achieved by ECHA is the publication of the read-across assessment framework (RAAF),[14] whose aim is to provide a structured approach to the scientific evaluation of read-across justifications prepared by registrants in their dossiers.[15] The first publication covers read-across of human health endpoints for monoconstituent substances.

1.16.1.4 Dissemination of REACH Data

It may be of interest for the readers to be aware that ECHA makes available all the nonconfidential information for the substances registered under REACH and information from other regulations (e.g., from classification and labeling inventory).[16] This large database full of physicochemical and (eco)toxicological information on chemicals is available online free of charge.[16] The dissemination website has been revamped at the beginning of 2016 to make the information more clearly available to both general public and stakeholders.

1.16.2 Nontest Methods

(Q)SAR predictions are a cost-effective and efficient option for screening and prioritization of chemicals.[17] They also represent an opportunity for replacement of experimental tests for some endpoints and some chemicals. The need of a harmonized regulatory application of (Q)SAR among the OECD countries has been addressed in 2004 by the publication of internationally agreed principles, known as "OECD principles for the validation, for regulatory purposes, of (Q)SAR models."[4] These principles constitute a solid yardstick for regulators, providing a scientific framework for making informed decisions on the acceptability of (Q)SAR predictions and, in the same time, a chance for enhancement of the transparency of the (Q)SAR models and for improving the consistency of (Q)SAR reporting. The OECD principles provide a useful guidance on how not only regulatory agencies but also (Q)SAR practitioners and (Q)SAR end-users can (a) evaluate specific (Q)SAR models, (b) better understand the usefulness and the uncertainty of (Q)SAR estimates, (c) make regulatory decisions, and (d) support stakeholders with transparent models and documentations. It has to be highlighted that the acceptance of (Q)SAR as a nontest alternative source of data is highly context-dependent (i.e., a case-by-case assessment of the specific prediction from a specific (Q)SAR model for a specific purpose is needed). In this respect, both reliability and transparency represent key elements to evaluate (Q)SAR performances beyond a merely statistical evaluation.

1.16.2.1 OECD Principles for the Validation of (Q)SAR

At the 37th Joint Meeting of Chemicals Committee and Working Party on Chemicals, Pesticides and Biotechnology (Paris, 2004), the OECD member countries agreed to issue the following five principles for establishing the validity of (Q)SAR models for regulatory purposes:

1. A defined endpoint
2. An unambiguous algorithm
3. A defined AD
4. Appropriate measures of goodness of fit, robustness, and predictivity
5. A mechanistic interpretation, if possible

Each OECD principle is not sufficient as a standalone but needs to be considered with respect to all the others. Indeed, there is an interplay among the nature of the endpoints defined in OECD test guidelines for the testing of chemicals and the mechanistic interpretation, domain of applicability, algorithm used, and purpose of the (Q)SAR prediction. Taken all together, the OECD principles are expected to enhance both transparency and validity of (Q)SAR and, thus, to promote an international harmonization in the use of (Q)SAR for regulatory purposes.[18]

1.16.2.1.1 About principle 1: a defined endpoint

The term endpoint refers to any physicochemical, biological, or environmental effect, which can be measured under specific conditions. It can be defined at different levels. An endpoint can be (a) *a specific biological effect* (e.g., binding to a specific receptor); (b) a *test protocol endpoint* (i.e., skin irritation/corrosion as yes/no result or acute oral toxicity in rats in terms of LD_{50}), useful for regulatory purposes and adopting standardized and harmonized toxicological test protocols (i.e., those established in the OECD test guidelines); and (c) a *regulatory endpoint* concerned with a much more complex organizational level of regulatory work, which could require the adoption of different protocols (or similar protocols in different species/organisms) for the purpose of classification and labeling. In principle, the higher is the level of organization of living material tested, the wider could be the variability of the results. In addition, often, there is no established link between a measured molecular event (e.g., EC_{50} of receptor binding) and a quantitative measure of an apical endpoint (e.g., liver or kidney toxicity in repeated dose study). Approximately in the last decade, the theory of the adverse outcome pathway (AOP) approach has been developed by academia with support of OECD and regulatory bodies with the aim to relate one or more key events (including potential molecular initiating events) with potential adverse outcome by understanding the toxicity path between these two.[19]

Some well-established regulatory endpoints can be predicted with a higher level of confidence by (Q)SAR models. For instance, a (Q)SAR model built from a training set (TS) of *Salmonella* mutagenicity data, obtained following the OECD test guideline 471,[20] is expected to return highly reliable predictions for the endpoint *Salmonella* mutagenicity. The reason for this expectation is that the mechanisms of *Salmonella* mutagenicity are relatively simple and well understood. Nevertheless, strain-specific consideration would need to be taken into account for an acceptable prediction (i.e., TG 471 foresees the use of five strains to cover different mutagenicity mechanisms and the (Q)SAR prediction has to take this into account[20]). Conversely, global prediction of a repeated dose lowest-observed-adverse-effect level (LOAEL) from a TS of LOAEL data, which are concerned with a number of different mechanisms and effects, compiled by mixing results from different species using different test protocols, will hardly be reliable.[21]

In REACH legal text, endpoints are gathered in four main groups.[22] The first is related to physicochemical properties (i.e., melting/freezing point, boiling point, relative density, vapor pressure, surface tension, water solubility, partition coefficient, flash point, dissociation constants, and viscosity). The second is the toxicological group (i.e., skin irritation or corrosion, eye irritation, skin sensitization, mutagenicity, acute toxicity, repeated dose toxicity, reproductive toxicity, toxicokinetics, and carcinogenicity). The third is known as the ecotoxicological group (i.e., aquatic toxicity and effects on terrestrial organism). The fourth comprises the environmental fate properties (i.e., degradation and fate and behavior in the environment).

Some basic, although nonexhaustive, recommendations are needed for (Q)SAR developers and users about the endpoints to model: (a) endpoints should be defined along with detailed information about factors affecting variability, knowledge of uncertainties, and possible deviations from standardized test guidelines; (b) differences in the experimental protocols for measuring a given endpoint should not imply significant differences in the results that cannot be explained; and (c) the chemical and response domains of the (Q)SAR and of the test protocol should overlap.

1.16.2.1.2 About principle 2: an unambiguous algorithm

OECD second principle highlights the importance of developing unambiguous algorithms for building (Q)SAR models. In particular, typical algorithms can be mathematical functions or rule-based approaches. Mathematical algorithms for model derivation can be distinguished as (a) linear, that is, the activity is predicted as a linear function of molecular descriptors, or (b) nonlinear, that is, structure–activity relationships (SARs) are obtained by using nonlinear functions. The former are more straightforward and easier to interpret, enough accurate for small data sets of similar compounds. The latter are normally preferred for larger and more diverse data sets, but they could be often difficult to interpret and eventually lead to data overfitting. Rule-based approaches are generally based on an expert knowledge. This knowledge could have been extracted also with the help of computerized methods. One example of expert knowledge system is the Benigni–Bossa rule[23] making use of structural alerts for predicting mutagenicity of chemicals. Providing examples for the alerts is helpful to the user to understand the rules. The higher is the number of examples confirming the rule, the higher is the confidence in it. Another aspect to consider is the confidence in the expert system as a whole, including, for example, the TS used (for some historical models, this information is lost) or the chemical space intended to be covered with the predictions. As a result, unambiguous algorithms should ensure the full comprehension of how a predicted value is obtained, making models reproducible and acceptable from a regulatory perspective. To assess the goodness of an algorithm, it is wise to carefully consider (a) the data set of chemicals, endpoint, and descriptor values; (b) the nature and source of descriptors; (c) the composition of the validation set (VS) and TS with regard to the occurrence of outliers (and a clear justification); (c) the form of the mathematical models employed to sample the descriptor and endpoint relationship; and (d) statistical parameters defining the model performance.

1.16.2.1.3 About principle 3: a defined domain of applicability

The third OECD principle claims the need to report, along with a (Q)SAR model, its AD, or, in other terms, the projection space where the model is expected to produce meaningful predictions. Notably, a (Q)SAR model cannot reliably predict any possible chemical but only those within its AD. Compounds within AD are supposed to have physicochemical, structural, and biological features similar to those of TS compounds. In this respect, TS compounds define the boundaries of the chemical space where predictions could be considered the result of data interpolation. On the other hand, predictions made outside of such space are the result of data extrapolation and, thus, associated with higher uncertainty. Keeping this in mind, the definition of AD can be considered an essential step for both scientific and regulatory purposes being useful to increase the confidence in predictions and to allow the practical use of (Q)SAR models.[24] A definition of AD was given in 2003 at the Setubal workshop.[25] The AD was defined as "the physico-chemical, structural, or biological space, knowledge, or information on which the training set of the model has been developed, and for which it is applicable to make predictions for new compounds […]. Ideally, the (Q)SAR should only be used to make predictions within that domain by interpolation not extrapolation." A more concise definition was proposed in the report of the 52nd European Centre for the Validation of Alternative Methods workshop [26]: "the applicability domain of a (Q)SAR model is the response and chemical structure space in which the model makes predictions with a given reliability." Since then, several approaches have been developed to quantify AD.[24,25,27–30] They are inspired by the three main domains of the (Q)SAR space, explicitly cited in both the earlier reported definitions: (a) the physicochemical, (b) the structural, and (c) the biological (or response) domain.

The physicochemical domain is based on the coordinates of molecular descriptors enabling the allocation of TS compounds into a multidimensional space from which deriving, through interpolation, a space exploitable as AD. In this respect, the use of physicochemical descriptors has led to develop four major approaches[27,29,31] that are (a) range-based, (b) distance-based, (c) geometric-based, and (d) probability density distribution-based methods.

Range-based methods consider the interval of values of each descriptor included in the (Q)SAR model. A test compound exceeding the range defined by the maximum and minimum value for compounds of the TS for even one of the model descriptors would be considered out of the AD. This approach is limited by the fact that it does not account for the occurrence of empty spaces (i.e., interpolation regions where the relationship is not proved) nor intercorrelation among the descriptors.[26,27,29,31] Principal component analysis (PCA) could address, albeit partially, such issues, each principal component (PC) being a linear combination of the original descriptors and being derived to cover the largest possible variance.

Convex hull strategy is instead a geometric-based method, which estimates the model AD by computing the smallest convex area within the *n*-dimensional descriptor space that contains TS compounds (**Fig. 1**). Similarly to range-based methods, such strategy is also applicable on the dimensionally reduced space obtained by PCA. There are efficient algorithms for convex hull calculation, although their complexity increases at the increase of dimensions.[32] However, convex hull is unable, like the range-based methods, to take into account the density of TS data and the presence of potential internal empty regions.[26,27,29,31] To overcome this limitation, it is possible to restrict the convex hull to include a smaller percentage (e.g., the top 98%) of TS compounds on the basis of their closeness to the centroid of data distribution and, thus, to reduce the likelihood of inclusion of underrepresented areas.[33]

Distance-based methods calculate the chemical distance of a test compound from TS chemicals. In this respect, the Euclidean, Mahalanobis, and city block distances are the most employed in (Q)SAR.[26,28,31] The basic rationale is that a test chemical exceeding a user-defined distance threshold is considered chemically different from TS compounds and, thus, outside of the AD. A valuable option is the measure of the leverage (h), which quantifies the distance of a compound from the center of TS compounds. As a result, the value of the leverage evaluates the degree of influence that a particular TS chemical has on the model. Test compounds with $h > h^*$ (being h^* a threshold value equal to $3p/n$, where p is the number of model descriptors plus one and n is the number of chemicals included in the TS) are chemically distant from TS compounds and outside of the AD.[34] The Williams plot allows the graphic detection of compounds that are both response outliers (i.e., compounds with cross validated standardized residuals greater than three standard deviation units) and structurally different chemicals outside of the AD ($h > h^*$) (**Fig. 2**).

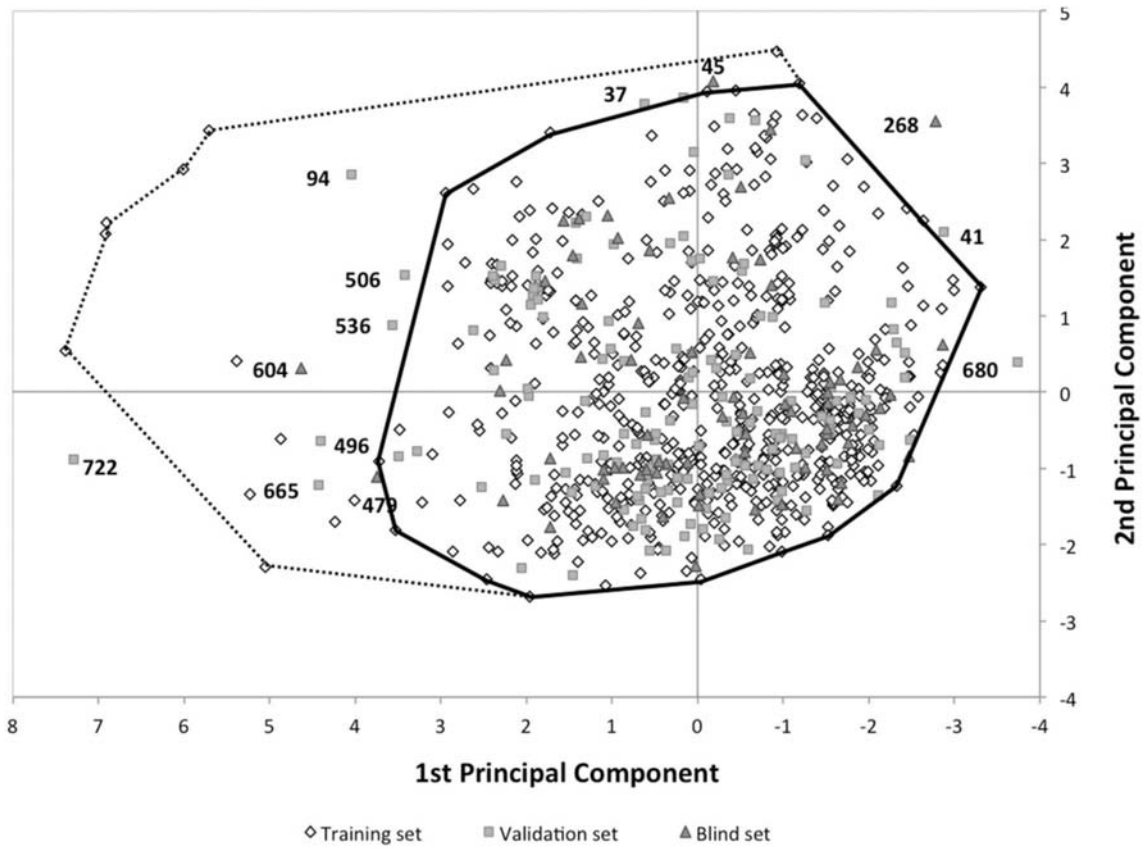

Fig. 1 Example of geometric-based AD. The convex hull is defined on the first two PC derived from the value of the nine descriptors for TS compounds. The outer polygon (*dashed line*) takes into account all the chemicals in the TS (*white diamonds*), while the inner polygon (*solid line*) retains the 98% of them, based on a user-dependent inclusive threshold. Chemicals included into two different validation sets (*gray squares* and *triangles*) outside the inner 98% polygon are flagged as outside AD. Adapted from Gissi, A.; Gadaleta, D.; Floris, M.; Olla, S.; Carotti, A.; Novellino, E.; Benfenati, E.; Nicolotti, O. An Alternative QSAR-Based Approach for Predicting the Bioconcentration Factor for Regulatory Purposes. *ALTEX* **2014**, *31*(1), 23–36.

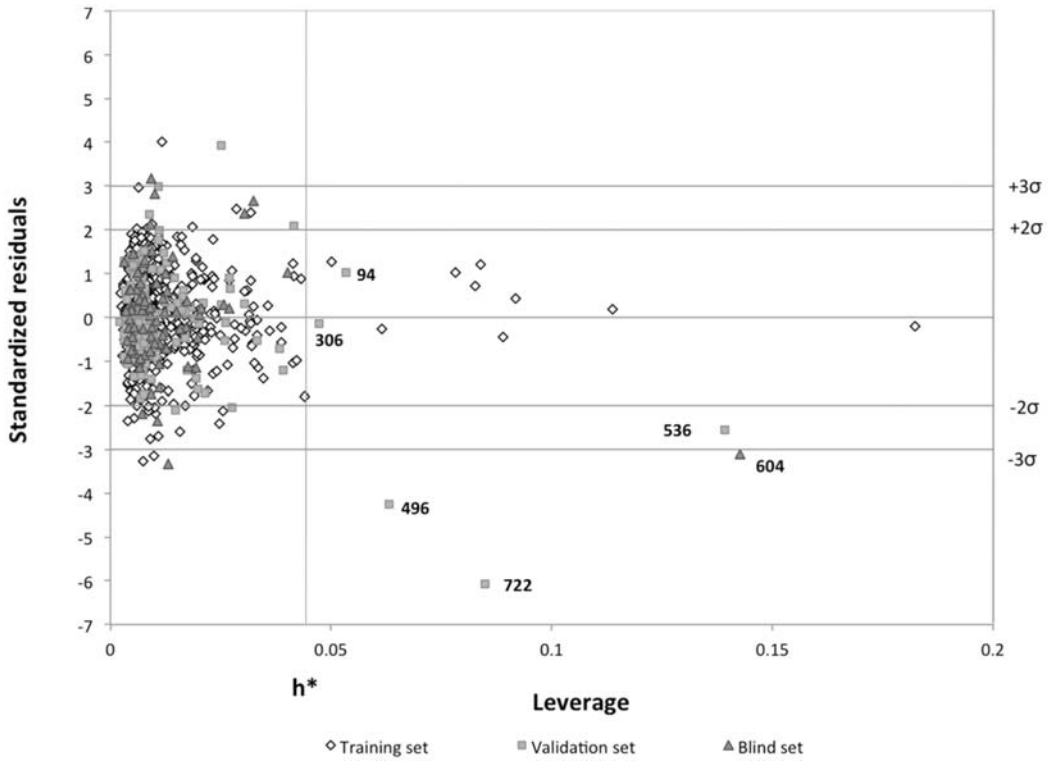

Fig. 2 Example of leverage-based AD. Leverage values computed from model descriptors for TS compounds (*white circles*) are plotted toward the corresponding standardized residuals. Chemicals included into the VS (*gray circles*) and violating the h^* threshold are flagged as outside AD. Adapted from Gissi, A.; Gadaleta, D.; Floris, M.; Olla, S.; Carotti, A.; Novellino, E.; Benfenati, E.; Nicolotti, O. An Alternative QSAR-Based Approach for Predicting the Bioconcentration Factor for Regulatory Purposes. *ALTEX* **2014**, *31*(1), 23–36.

Probability density function-based methods are classified as parametric and nonparametric methods. The former assumes standard distributions of TS data, such as Gaussian or Poisson distributions, while the latter does not make any a priori assumption and, thus, estimates the probability density from the original TS distribution. Unlike previous approaches, these methods allow to capture the real density distribution of data by the creation of concave regions reflecting the occurrence of empty spaces near to the limits of the convex hull.[26,28,31] Most of nonparametric methods focus on low-dimensional densities due to computation complexity. Kernel density estimation methods allow to handle *n*-dimensional densities such as multidimensional descriptor spaces.[35,36]

The evaluation of structural domain relies on the old, but yet valid, concept that a (Q)SAR model cannot be expected to return reliable predictions for compounds whose chemical types are not encountered in the TS.

Similarity-based methods employ the molecular similarity among the compounds in the TS and the target chemical to estimate the uncertainty of predictions.[37] Among the different methods proposed to measure molecular similarity, those based on fingerprints are perhaps the most largely used.[38,39] Fingerprints are fixed-length strings of bits, obtained by detecting all linear patterns encoding bonds and atoms of a structure, including branching points at the end of each linear pattern and cycles. Fingerprints allow to store the molecular structural complexity into simple numerical strings, which can be used to assess the similarity between molecules using, for instance, the popular Tanimoto index.[40]

Approaches based on the k-nearest neighbors (k-NN), the simplest algorithm among those used in machine learning, have been successfully used for assessing AD of (Q)SAR models.[28,37,41] In doing that, the average distance of a test compound from its k closest TS samples (i.e., neighbors) is compared with a predefined similarity threshold to determine its inclusion within the AD. Recently, it was proposed a novel method for the AD definition,[42] which integrates the classical k-NN approach with the ability of kernel probability density estimation methodologies to handle inhomogeneous data distribution. The advantage of this method is that there is not a fixed threshold such as in classical k-NN, since it is able to fit the neighborhood density of each compound, being particularly useful in case of data sets with sparse data regions.

Moreover, the structural domain can be evaluated employing structural fragment-based approaches. The assumption is that the structural closeness of test compounds to those of TS can be straight assessed[26,43] on the basis of the occurrence of known/unknown fragments. A test chemical containing fragments not observed in the TS fragment pool is, thus, considered outside of the AD and could not be reliably predicted. Fragment-based strategies are very effective since they can indirectly capture mechanistic aspects of (Q)SAR. Recurring fragments in TS could represent some reactive functional groups that may undergo a chemical reaction

responsible for a toxic effect.[44] For each test compound, the fragments of TS are, thus, searched to identify matched and unmatched fragments. Normally, only molecules with at least the 75% of matched fragments are considered within the AD, whereas those with 25% or less matched fragments are outside of the AD. Compounds with 25–75% matched fragments are considered questionable, accounting for the "fuzzy" nature of AD boundaries.[26] In addition, the frequency of unmatched fragments could be considered as an indicator of the likelihood that a compound is inside/outside of the AD. Atom-centred fragments (ACFs) are obtained by using other fragmenting strategy for decomposing molecules.[44–46]

The evaluation of response domain is strictly related to the range and mechanism of the response covered by TS compounds. There is no assurance whether a model, which has proved to be reliable in a defined range of activity, is also suitable for the prediction of compounds not comprised in that interval or mechanistic domain. As a result, the range of biological activity and, possibly, the mechanism of toxic action should be also taken into account to define whether a test compound is inside/outside of the AD. However, some concerns in this respect are due to the presence of empty regions in the activity space and the occurrence of sudden activity cliffs (i.e., compounds with high structural similarity and similar properties but unexpectedly high activity difference).[47] Such cliffs can have different explanations. One of these is metabolism, when products with different reactivities than the parent compounds are generated.

The earlier described strategies, which are based on the physicochemical, structural, and biological (or response) domain, should not to be considered mutually exclusive. Instead, an even better definition of the model AD could be obtained by integrating multiple different approaches,[26] thus, ideally intercepting different domain faces. An integrated-based strategy is expected to further increase the level of confidence associated with (Q)SAR predictions.[44] For instance, a stepwise approach[48] was proposed, which consists of four sequential stages. Moreover, there are combined computerized approaches resulting in the so-called applicability domain index (ADI) (implemented in the VEGA software[49,50]), a value ranging from zero to one to quantify whether a test compound is outside/inside of the AD. The ADI is calculated by weighting several other indices, most of them based on the calculation of the most similar compounds[51] found in the TS of the model. Each of the indices provides a particular measure relevant for defining AD, which are (a) the presence of similar molecules within the TS, (b) the accuracy of prediction for similar molecules, (c) the concordance with similar molecules (i.e., the difference between the predicted value and the experimental values of the most similar compounds), (d) the maximum error in prediction among similar molecules, (e) ACFs check, and (f) model descriptor range check.

1.16.2.1.4 About principle 4: appropriate measures of goodness of fit, robustness, and predictivity

Data-driven and *knowledge-driven* strategies can be adopted for model development. The former are particularly useful when large TS are available. Data-driven approaches rely mostly on algorithms for statistical optimization. Knowledge-driven approaches exploit on expert knowledge of chemistry and toxicology and put emphasis on mechanistic considerations rather than focusing on statistical results.

Within a highly context-dependent process, the evaluation of model statistics is important to provide valuable scientific information about (a) *goodness of fit*, (b) *robustness*, and (c) *predictivity*.

The goodness of fit is a measure of how well a model accounts for the variance of the response in the TS. The robustness of a model is related to its internal stability, assessed after data perturbation (i.e., deletion of one or more chemicals from the TS); the robustness could be quantified by the so-called internal validation. A stable model is not significantly affected by perturbations, and thus, stable perturbed models should recalculate values that are similar to those of the base model built by using the whole data set. The predictivity of the model is quantified by the accuracy in predicting test set chemicals during the so-called external validation.

Data-driven strategies make largely use of the regression and classification statistics techniques. The most popular regression technique is the multiple linear regression (MLR). The regression coefficients are estimated by using the least square method, which minimizes the sum of the squared residuals. The relative importance of descriptors is assessed by autoscaling, a process that standardizes variables to have a mean value equal to zero and a standard deviation equal to one.[52] Partial least squares (PLS)[53,54] is an MLR method to derive relationships between an X-block of p predictors and a single y response (PLS1) or a Y-block of r responses (PLS2). It is particularly useful for handling situations where the number of descriptors is much larger than the number of TS chemicals. PLS can tolerate up to 10–20% of missing data and found large application in 3-D (Q)SAR.[55,56]

The coefficient of multiple determination (r^2) and the root-mean-square error (RMSE) are used to assess goodness of fit and are computed following Eqs. (1) and (2), respectively:

$$r^2 = \frac{\mathrm{MSS}}{\mathrm{TSS}} = 1 - \frac{\mathrm{RSS}}{\mathrm{TSS}} = 1 - \frac{\sum_{i=1}^{n} (y_i - \hat{y}_i)^2}{\sum_{i=1}^{n} (y_i - y_{\mathrm{avg}})^2} \tag{1}$$

$$\mathrm{RMSE} = \sqrt{\frac{\sum_{i=1}^{N} (y_i - \hat{y}_i)^2}{n}} \tag{2}$$

where y_i is the observed dependent variable (the experimental response), $\hat{y}_i$ is the calculated response, and y_{avg} is the mean value of the observed dependent variable, for n elements of the modeled data set. The residual sum of squares (RSS) accounts for the gap between experimental and calculated values; the model sum of squares (MSS) quantifies the fluctuation of calculated values around the average of experimental responses; the total sum of squares (TSS) measures the variance associated to experimental data.

Basically, r^2 ranges from zero to one to estimate the proportion of the variation of the endpoint that is explained by the regression,[57] while RMSE is the standard error of estimate and measures the extent of deviations of the observed values from the regression line. High values of r^2 and low values of RMSE, preferably in line with the experimental variability of the endpoint, are associated with statistically good models. It is assumed that r^2 value >0.5 means that the explained variance by the model is higher than the unexplained one. Moreover, it is acknowledged that $r^2 \geq 0.81$ for *in vitro* data and $r^2 \geq 0.64$ for *in vivo* data can be regarded as good.[58]

In this respect, r^2 should be considered cautiously given that its value increases by adding additional variables to the model, even when these variables do not reduce the unexplained variance of the dependent variable, thus returning overfitted models. This means that the model identifies apparent and misleading relationships that fit well TS data points but has poor degree of generalization on external compounds. Such relationships are clearly meaningless and are not suitable for real-life applications. Such models could tend to comprise a large number of intercorrelated variables,[59] thus increasing the model complexity (i.e., the explained variance in fitting) irrespective of the predictive power (i.e., the explained variance in prediction). Similarly, RMSE values smaller than the experimental errors contained into the biological data would likely be indication of an overfitted model[53] since a (Q)SAR model could not generate predictions whose accuracy is higher than that of the experimental data.[60] As a result, good fitting models (i.e., small RMSE and large r^2) need further validation to assess their reliability in predicting new data.

Data used for model derivation are taken from the TS. However, a real predictive power can be claimed only if a model shows good performance in forecasting the activity/toxicity of compounds, which are not comprised in the TS. There is, thus, the need to challenge models through validation. In this respect, a number of statistical validation techniques are largely employed aiming at (a) finding a fair trade-off between the two extremes of overfitted (noisy) and underfitted (too simple) models[61,62] and (b) discarding spurious models resulting from chance correlations occurring when there is an apparent but meaningless and not predictive relationship between the predictor and response variables.[63–65]

A simple way to preassess the model validity makes use of the so-called Topliss ratio, that is, the proportion between the number of chemicals and of selected variables. As a rule of thumb, a Topliss ratio of at least five is recommended.[66]

Internal and external model validation techniques exist. Among internal validation techniques,[67,68] the most popular ones are (a) cross validation, (b) bootstrapping, (c) Y-scrambling, and (d) training/test set splitting.

Cross validation is the most applied validation technique to challenge model robustness. It implies the generation of cancellation groups obtained by deleting one or more compounds, once and only once. Each reduced data set is used to predict the compounds left out and, thus, to measure the predictive residual sum of squares (PRESS), from which the values of q^2 (or cross validated r^2_{CV}) and RMSE in prediction are calculated.[69] The leave-one-out (LOO) is the simplest cross validation technique, which implies the removal of one compound at a time. Straight comparisons of different models can be made, being the deletion scheme univocal.

The cross validated coefficient of determination q^2 is returned by comparing experimental and estimated values for each compound, as described by Eq. (3):

$$q^2 = 1 - \frac{\text{PRESS}}{\text{TSS}} = 1 - \frac{\sum_{i=1}^{n} \left(y_i - \hat{y}_{i,i}\right)^2}{\sum_{i=1}^{n} \left(y_i - y_{\text{avg}}\right)^2} \tag{3}$$

where y_i is the observed dependent variable (the experimental response), $\hat{y}_{i,i}$ is the response estimated during LOO, y_{avg} is the mean value of the observed dependent variable, and PRESS quantifies the accuracy of the internal prediction for n elements of the modeled data set.[70]

The value of q^2 increases until the optimal number of components is achieved, for instance, in a PLS analysis, defining the model structural complexity. In this respect, a difference between r^2 and q^2 larger than 0.3 is a warning of overfitted model, indicating the presence of irrelevant descriptor values or outliers in the data (**Fig. 3**).[59]

However, overoptimistic predictions (i.e., high apparent q^2) can be obtained especially when large data sets are investigated, because data perturbation is too small when only one compound is omitted. To avoid this inconvenience, the leave-many-out (LMO) cross validation procedures can be carried out. On the basis of rules set by the user, the data set is divided into a number of cancellation groups so that a group of compounds are left out for prediction under the condition that each compound should be excluded only once.

Bootstrap resampling is another technique largely exploited to perform internal validation.[71] In a typical bootstrap validation, the initial size n of the data set is kept unchanged by randomly selecting with repetition n compounds. In doing that, some compounds can be included in the same random sample several times at the expense of others that remain excluded. The theoretical number of resampling for sample containing, at least, two diverse compounds is given by Eq. (4):

$$k = \frac{(2n-1)!}{n!(n-1)!} \tag{4}$$

The squared differences between experimental and predicted responses of the excluded compounds are counted in the PRESS statistics. Likewise other LMO techniques, a high average of q^2 in bootstrap validation is indicative of model robustness and is, thus, a measure of internal predictivity.

Y-scrambling is a widely used technique to avoid models based on chance correlation. The basic premise for valid models is that endpoint values (i.e., independent variables) are not randomly distributed. If the original model has no chance correlation, a significant difference in terms of quality (i.e., r^2 and q^2) is, thus, expected by comparing it to random models. The procedure is repeated thousands of times to ensure that such difference is kept considering any originated random model.

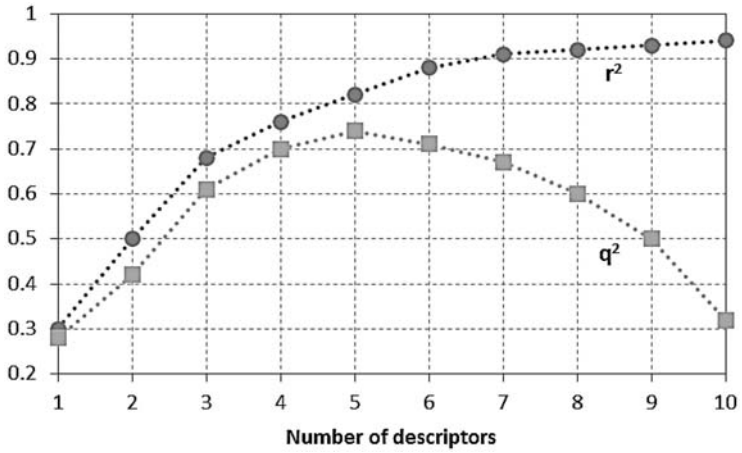

Fig. 3 Comparison of the explained variance in fitting with the explained variance in prediction. In this case, the optimum number of descriptors intercepting the maximum value of q^2 is equal to five. Adapted from Worth, A. P.; Bassan, A.; Gallegos, A.; Netzeva, T. I.; Patlewicz, G.; Pavan, M.; Tsakovska, I.; Vracko, M. The Characterisation of (Quantitative) Structure-Activity Relationships: Preliminary Guidance. ECB Report EUR 21866 EN, 95 pp. European Commission, Joint Research Centre; **2005**, Ispra, Italy.

Training/validation set splitting is perhaps the validation technique more frequently used.

The quality of internal validation depends upon the goodness of fit and robustness. However, internal validation gives almost no information about predictivity, an issue of vital importance when handling large amounts of correlated information and a large number of noisy variables.

No relationship between internal and external predictions has been described so far, and very often, high internal predictivity may result in low external predictivity and vice versa. This dilemma, also known as Kubinyi paradox,[72] represents the ultimate and perhaps unsolvable challenge for (Q)SAR practitioners.

In this respect, a more challenging approach in prediction is known as external validation. Unlike TS, the VS is used to evaluate the model external predictivity. In doing that, the user should ensure that (a) the TS and VS should cover the descriptor space of the entire data set, and (b) the structural types in the two sets are not too dissimilar.[73–76] In addition, the response space should be properly sampled[77] to ensure that TS and VS compounds span the entire range of the experimental responses and are numerically representative of the whole data set. Activity sampling[27,73,78] is a widely used example of rational selection methods and consists in dividing the whole range of activities into bins, randomly (or in some regular way) selecting compounds belonging to each bin that will be assigned to TS or VS.

In addition, external validation can be further challenged by using a blind set (BS). It must consist of compounds with known activities that are not included in either TS or VS. Unlike VS, the BS is selected through a mere random selection from the entire initial data set. The size of the BS should be about 15–20% of the entire data set. The remaining part of the data set is called modeling set, which can be divided into TS (about 80% of modeling set) and VS (about 20% of modeling set).[79] External validation, which should be regarded as a supplementary procedure to internal validation (rather than as an alternative), can be difficult to apply when the number of data of sufficient quality is scarce.

The calculation of external r^2_{ext} and RMSE in external prediction gives an indication of the real model predictivity. Additionally, a series of conditions[73] that a model must meet to be considered predictive have been also established. They are outlined in Eqs. (5)–(8):

$$r^2_{ext} > 0.5 \tag{5}$$

$$q^2 > 0.6 \tag{6}$$

$$\frac{r^2 - r_0^2}{r^2} < 0.1 \quad \text{or} \quad \frac{r^2 - r'^2_0}{r^2} < 0.1 \tag{7}$$

$$0.85 \leq k \leq 1.15 \quad \text{or} \quad 0.85 \leq k' \leq 1.15 \tag{8}$$

where r_0^2 and r'^2_0 are the coefficients of determination of the linear regression with the line of regression forced to pass through the origin of axes. In particular, the former is associated to observed versus predicted values, and the latter is related to predicted versus observed values; k and k' are the slopes of the same regression lines forced through zero, referring to observed versus predicted and predicted versus observed values, respectively.

When the variability of certain endpoints is too large to enable reasonable quantitative predictions or when the endpoints are of qualitative nature, it is wise to derive *classification models* (CMs) (e.g., toxic/nontoxic and mutagenic/nonmutagenic). For instance,

binary classification systems are commonly used to provide a convenient mean of labeling chemicals in regulatory toxicology. Several statistical techniques have been extensively reported in the literature[80] for deriving linear CMs, such as multivariate discriminant analysis, logistic regression, and decision or classification trees. Nonetheless, rule-based models, coded through "if…then" decision rules, can be implemented. Nonlinear CMs exploit other techniques such as embedded cluster modeling,[81] neural networks, and k-NN.

The goodness of fit of a CM can be assessed by using Cooper statistics, introduced in late 1970s to describe the validity of carcinogen screening tests.[82]

In this regard, predictions given by CMs are defined as (a) true positives (TPs), that is, positive compounds correctly classified; (b) true negatives (TNs), that is, negative compounds correctly classified; (c) false negatives (FNs), that is, positive compounds misclassified; and (d) false positives (FPs), that is, negative compounds misclassified.

The results of a CM can be arranged in the so-called confusion matrix,[83,84] where the main diagonal represents the cases where the true class matches the assigned class, that is, the number of objects correctly classified in each class, while off-diagonal elements quantify the types of error in the classification (**Table 2**).

The performance of a CM is quantified through the value of *accuracy* (Eq. 9), *sensitivity* (Eq. 10), and *specificity* (Eq. 11).

Accuracy, also defined concordance, is equal to the ratio between correctly predicted molecules (TP and TN) and total number of compounds:

$$\text{Accuracy} = \frac{\text{TP} + \text{TN}}{\text{TP} + \text{TN} + \text{FN} + \text{FP}} \tag{9}$$

Sensitivity measures the proportion of chemicals tested as positives that are correctly identified as positives. The parameter takes into account the number of FNs and is defined as the ratio between TPs and the total of the compounds experimentally positive:

$$\text{Sensitivity} = \frac{\text{TP}}{\text{TP} + \text{FN}} \tag{10}$$

Specificity quantifies the proportion of chemicals tested as negatives that are correctly identified as negative. It takes into account the number of FPs and is equal to the ratio of TNs and the total of the compounds experimentally negative.

$$\text{Specificity} = \frac{\text{TN}}{\text{TN} + \text{FP}} \tag{11}$$

As a result, a high value of sensitivity is associated with a high TP rate, while a high value of specificity is associated with a high TN rate. On the other hand, the FP and FN rates can be calculated from the complement of specificity and sensitivity, respectively. High values of sensitivity are welcomed to consider models adequate for the regulatory context: minimizing the number of FNs is in fact a major concern according to a precautionary approach aimed at the protection of environment and human health. In other words, a high sensitivity value for a model is necessary to consider it adequate to the regulatory context with the aim of avoiding the occurrence of FNs, which are toxic compounds wrongly predicted as not hazardous. There are also purposes for which a high specificity is preferred, for example, in screening activities aimed at finding potentially active (or toxic) substances for further actions. In these cases, it is important for an efficient use of resources that the substances selected for additional studies are TPs.

Cooper statistics are often not suitable in assessing the goodness of classification when the populations of the two classes are unevenly distributed. In this case, a useful parameter is the Matthews correlation coefficient (MCC).[85] The MCC accounts for the uneven distribution of compounds between actives and inactives and ranges between -1 and $+1$ (Eq. 12). A coefficient of $+1$ represents a perfect prediction and 0 no better than random prediction, and -1 indicates total disagreement between prediction and observation.

$$\text{MCC} = \frac{(\text{TP} \times \text{TN}) - (\text{FP} \times \text{FN})}{\sqrt{(\text{TP} + \text{FP})(\text{TP} + \text{FN})(\text{TN} + \text{FP})(\text{TN} + \text{FN})}} \tag{12}$$

The receiver operating characteristic (*ROC*) curve is used to compare the performance of CMs (**Fig. 4**). In the ROC graph, the *x*-axis reports 1-specificity (which accounts for the FP rate) and the *y*-axis the sensitivity (which accounts for the TP rate). A CM with no discriminating power would give a straight line at an angle of 45 degrees, which means equal rates of TPs and FPs [86,87]; beyond/below that straight line, the discriminating power increases/decreases accordingly. The area under the curve (AUC) quantifies the goodness of the CM: the higher the AUC, the better the CM.

Table 2 Confusion matrix for binary classification

	Predicted		
Observed	*Negatives*	*Positives*	*Total*
Negatives	TN	FP	$N_{\text{Negatives}} = \text{TN} + \text{FP}$
Positives	FN	TP	$N_{\text{Positives}} = \text{FN} + \text{TP}$
Total	TN + FN	FP + TP	$N_{\text{Total}} = N_{\text{Negatives}} + N_{\text{Positives}}$

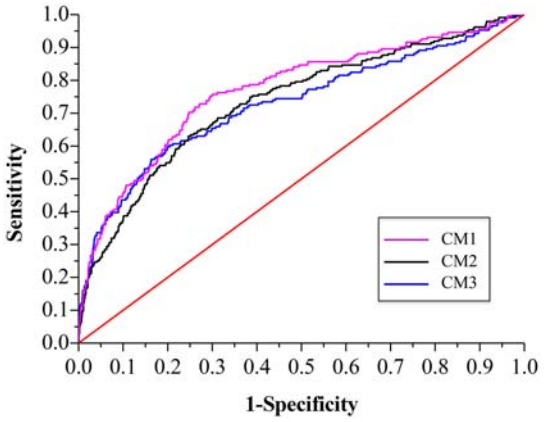

Fig. 4 Example of ROC curves derived from three different CMs. Based on the AUC values, CM1 (AUC = 0.72) is the best performing model with respect to CM2 (AUC = 0.70) and CM3 (AUC = 0.69). Adapted from Trisciuzzi, D.; Alberga, D.; Mansouri, K.; Judson, R.; Cellamare, S.; Catto, M.; Carotti, A.; Benfenati, E.; Novellino, E.; Mangiatordi, G. F.; Nicolotti, O. Docking-Based Classification Models for Exploratory Toxicology Studies on High-Quality Estrogenic Experimental Data. *Future Med. Chem.* **2015**, *7*(14), 1921–1936.

Knowledge-driven models (also known as *expert systems*[88]) are defined as formalized systems making use of specific rational rules for the prediction of the toxicity of chemicals. The rules are conceived to implement valuable information concerned with mechanism-based knowledge and available experimental data. In this respect, the rules can be derived on the basis of mathematical induction by using (Q)SAR models or on the basis of expert judgment about reactive chemistry.[89]

1.16.2.1.5 About principle 5: a mechanistic interpretation, if possible

It is important to provide a comprehensive mechanistic interpretation of a given (Q)SAR model for improving the acceptance of its results. This interpretation[90] relies on the in-depth understanding of the causal relationships relating desirable molecular descriptors to a specific endpoint. In this respect, the mechanistic rationale of a (Q)SAR can be established a priori, by choosing descriptors on a knowledge base before modeling, or a posteriori, by selecting descriptors on the basis of statistical performance, with their mechanistic rationale explained after modeling. A compromise can be found by developing models by trading-off these two approaches. The choice of molecular descriptors is particularly important for the formulation of a solid mechanistic interpretation. The descriptors are defined as "the final result of a logic and mathematical procedure which transforms chemical information encoded within a symbolic representation of a molecule into a useful number or the result of some standardized experiment."[91] Indeed, when a (Q)SAR model provides a wealth of information coherent with well-documented knowledge of mechanisms and existing hypotheses, a higher level of confidence is achieved. In this respect, the clause "if possible," mentioned in the original text from OECD, encourages the attempts of finding mechanistic interpretations, which will add a valuable plus to the model beyond its mere statistical validity. On the basis of this principle, the development of a (Q)SAR model is intended as a continuous process aimed at achieving a rational mechanistic explanation through some basic iterative steps, which are (a) the statistical exploration of data, (b) the hypothesis generation, and (c) the hypothesis testing.

The milestone work of Hansch on a set of esters binding to the enzyme papain[92] represents perhaps the first example of how a (Q)SAR could provide valuable mechanistic information:

$$\log\frac{1}{K_m} = 1.03\pi_3 + 0.57\sigma + 0.61\,MR_4 + 3.8$$
$$n = 25,\ r = 0.907,\ s = 0.208 \tag{13}$$

As reported in Eq. (13), electron-withdrawing substituents (i.e., $\sigma > 0$) favor the formation of the enzyme substrate complex. Such information is coherent with the well-documented evidence that an electron-rich thiol group of a cysteine residue is determinant for binding. The positive molar refractivity (i.e., MR > 0) suggests that bulkier substituents at the position 4 still favor binding. The same biological effect is obtained by the positive hydrophobic substituent (i.e., $\pi > 0$) at position 3.[93] Interestingly, Hansch's approach for interpreting mechanisms represents an early example of ligand-based methods for the indirect sampling of the hydrophobic, electronic, and steric properties of the protein active sites.[94] However, the mechanistic strength of Hansch's approach is obtained at the expense of its breadth of application, being AD made of few and structurally close compounds.

1.16.2.2 Grouping and Read-Across

As the understanding about SARs was growing, more confidence had started to be put into "reading" toxicological data from one substance to another. This process began in the 1980s in the United States, where US Environmental Protection Agency (US EPA) started to assess hazards and risk of chemicals based on grouping of substances. Such an approach was found cheaper, faster, and

applicable to many types of chemicals than traditional testing. In addition, finding the same effect in several similar chemicals increased the confidence of the regulator in the correctness of a prediction. The categorization approach to chemicals for regulatory purposes was taken also by OECD that, for many years, run a successful project for screening and assessment of chemicals and employing chemical categories and read-across (Screening Information Assessment Meeting (SIAM), lately known as Cooperative Chemicals Assessment Meeting), under their hazard assessment program.[95]

In 2007, the OECD Chemicals Program published the OECD guidance on grouping of chemicals[96] (No. 80 in the Series on Testing and Assessment, published by Interorganization Program for the Sound Management of Chemicals, IOMC[97]). It was based on the OECD SIAM experience with building and evaluating categories, and it also provided a basis for the REACH guidance on grouping and read-across. The OECD guidance was updated and published in 2014.[98]

In REACH, a chemical category is defined as a group of chemicals whose physicochemical and human health and/or ecotoxicological properties and/or environmental fate properties are likely to be similar or follow a regular pattern, usually as a result of structural similarity. The read-across methodology as such is based on the premise that similar chemical structures are expected to have similar biological/toxicological actions (Fig. 5).

There are different principles for grouping of substances and building categories for predictive purposed under different regulatory frameworks. Most often, the substances were grouped on a basis of common functional group (e.g., long-chain aliphatic alcohols and primary amines). Grouping and read-across were also applied to a range of substances including substances of unknown or variable composition, complex reaction products, or biological materials, where testing of every substance for every endpoint was not feasible and even not possible. In particular, the OECD program was seeking for a group description and data analysis in order to assess the hazard related to the group as a whole and the need for further testing, if any. It was clearly hypothesized that in a data matrix, where few data points are missing, one can predict them by interpolation or, in certain cases extrapolation, from other members of the group.

For the first time in the European regulation of chemicals, REACH included grouping and read-across as one of the five adaptations to the SIRs in the legal text, that is, in Annex XI, which says that "substances, whose physicochemical, toxicological and ecotoxicological properties are likely to be similar or follow a regular pattern as a result of the structural similarity may be considered as a group, or "category" of substances." In the same context, the interpolation in the prediction (read-across) approach was emphasized.

As a result of two ECHA analyses of registration data,[1,2] it was found that the registrants made a significant use of alternatives and particularly of read-across. It was found that for around 75% of the substances, a read-across adaptation is made, at least, once. It is noted that the analysis was not limited to only endpoints requiring vertebrate animal testing. Read-across was used mostly for complex health endpoints, such as repeated dose toxicity, toxicity to reproduction, and developmental toxicity. Read-across was also used for prediction of acute toxicity (all routes) and skin sensitization. Concerning environmental endpoints, read-across was used mostly for prediction of bioaccumulation potential of chemicals and short-term and long-term toxicity to fish. Noteworthy, it was observed that, in general, read-across was used much more frequently than (Q)SAR, especially in relation to the complex endpoints, which need specific mechanistic considerations. Endpoints such as physicochemical properties and environmental fate are often predicted with (Q)SARs, but this statistics is largely not available from the reports on animal testing for REACH.

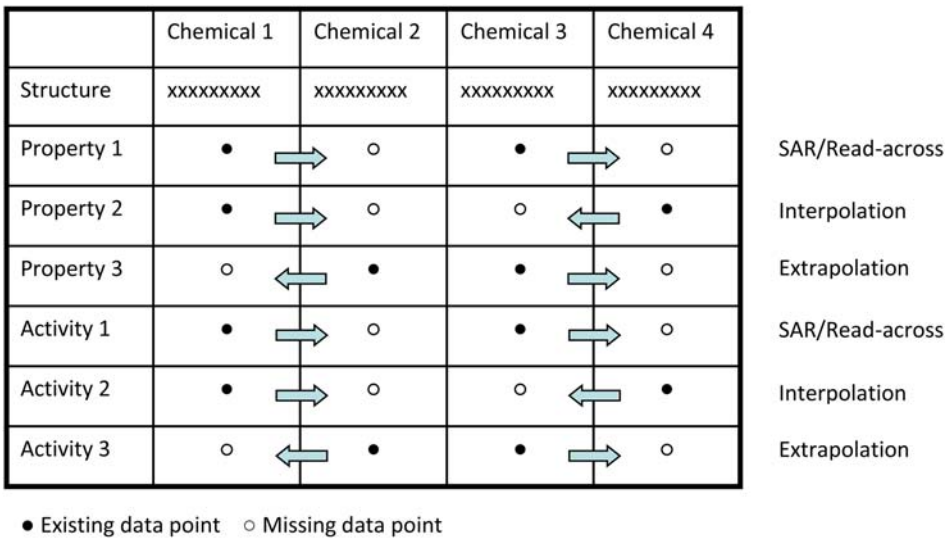

Fig. 5 Graphic illustration of a chemical category. Taken from OECD, Grouping of Chemicals: Chemical Categories and Read-Across, http://www.oecd.org/chemicalsafety/risk-assessment/groupingofchemicalschemicalcategoriesandread-across.htm (last accessed date, 19 February 2016).

The extensive use of read-across by the REACH registrants prompted ECHA to develop a systematic assessment approach in order to increase the transparency and consistency of read-across evaluation. To this end, ECHA developed and published on its website the RAAF.[10] It is important to highlight that RAAF is not a guidance and does not replace the guidance as such. The main REACH guidance dealing with read-across is Chapter R.6[5] of the Guidance on Information Requirements, which is dealing with (Q)SAR and grouping. The RAAF explains the approach that ECHA evaluators would undertake in assessing a case. It highlights the important pieces of information for assessing the read-across depending on which "scenario" the registrant may have. A scenario includes a series of assessment elements, and their integration leads to a conclusion concerning the overall assessment of the read-across adaptation, that is, either acceptance or rejection of the read-across case.

ECHA is making an enormous effort to help registrants in improving the quality of their registration dossiers in general and the quality of adaptations in particular. REACH framework increased the requirements in term of quality of the scientific justification. First, the justification needs to accommodate the definition of substance and to account for the main (or all) constituent(s) and impurities included in the substance. Second, the description of the logical read-across rationale should include the structural similarity as a basic requirement for grouping. Any difference in chemical structure between the source substance(s) and the target needs to be explained, for example, why it is expected under given hypothesis that a structural difference will bring or not bring to additional effect(s) or it will lead to a systematic (predictable) change of effect relevant for the endpoint to be predicted. Third, it should be clear what are the key aspects to be considered given the chemistry of the substances and the set of available data. Only then, the read-across can be built and the prediction model explained.

It is expected that the read-across will continue in the near future. The main aspects that need to be improved include the hypothesis and the justification, including also any nonstandard data that can support the explanation. The evidence may derive from mechanistic studies, AOP, high-throughput data (e.g., ToxCast data), or high-content data such as various omics. Very valuable information to support the read-across justification is toxicokinetics, which could be estimated through measurements or predictions. Expanding experimental methods to include additional toxicokinetics measurements can potentially increase their utility by facilitating their reuse in supporting read-across. Building ab initio predictions without a test result with phenotypic expression of adversity (or the lack of it) for comparison is currently considered uncertain with respect to the complex and expensive human health endpoints.[99] The combination of data in a strategic manner (e.g., IATA, which stands for integrated assessment and testing approaches, an approach supported by OECD) will become more important with the time.

1.16.2.3 (Q)SAR Toolbox

In read-across or category approach, data gap filling on intrinsic properties from source chemical(s) is used to predict property of another (target) chemical(s) belonging to the same category. Two types of uncertainties can be defined for the predicted property of the target chemical(s): the uncertainty related to data quality generated for source chemical(s) and the uncertainty related to grouping principles (how accurate our assumption that both source and target chemicals have same intrinsic property is). The quality of data can be assessed based on many criteria (widely recognized guidelines, good laboratory practice (GLP), and data consistency); the second uncertainty strongly depends on the knowledge about the main factors driving the toxicity effect within the property and experience of the hazard assessor dealing with the case.

In order to standardize the category formation approach, OECD decided to develop a tool, which supports the category building approach: the (Q)SAR Toolbox.[100] Under (Q)SAR Toolbox platform, six main steps in categorization process have been implemented:

1. Substance identification—input
2. Determination of the structural and mechanistic features of the substance—profiling
3. Grouping of substances sharing the same features (many iterations might be needed)—categorization
4. Data gathering for the substances in the category
5. Identification of data gaps and application of various interpolation techniques to fill identified data gaps
6. Reporting the data gap-filling outcome

(Q)SAR Toolbox platform provides a wide collection of tools to fully support the substance categorization process (from substance identification to reporting). The toolbox is therefore not a classic (Q)SAR or a library of (Q)SARs; it is rather a platform for applying category approaches and for deriving and applying customized (Q)SAR models. Such approach gives a unique opportunity to build local prediction, based on transparent empiric/mechanistic features, which normally better address specificity of the target substance compared with general models and, as a consequence, has higher probability for regulatory acceptance. However, the user needs of a certain amount of expertise and knowledge for an informed use.

1.16.2.3.1 (Q)SAR Toolbox main functionalities

As mentioned before, hazard assessment of the substance can be described in six major steps. As a result, the toolbox functionalities have also been structured accordingly.

This section is a brief explanation of these functionalities. Interested users can find more technical details on the (Q)SAR Toolbox website[100] and literature.[101]

1.16.2.3.1.1 Input

The input module allows defining the structure (and composition) of the target substance; the input structure can be defined by

- registry number (e.g., Chemical Abstracts Service – CAS and European Inventory of Existing Commercial Chemical Substances – EINECS),
- name (e.g., common, International Union of Pure and Applied Chemistry – IUPAC, commercial names are supported),
- 2-D structural representation (e.g., Simplified Molecular Input Line Entry System – SMILES, IUPAC-NIST Chemical Identifier – InChi, Structure Data Format – SDF, MOL, and XYZ)
- drawing,
- list of chemicals, inventory, or database.

In addition to the chemical names, regulatory agencies are also using international (or their own) registry numbers. Very often, the explicit structural information is missing from regulatory inventories. Likewise category approach, precise structural information is crucial, and thus, a dedicated substance identity (SID) module has been implemented in the (Q)SAR Toolbox. This module applies a search for all possible relations between CAS, structure, and name(s) in all toolbox inventories and databases. The outcomes of the search are all the chemical structures associated with name or inventory number, with five levels of confidence in the reliability of the retrieved structure (high, moderate, low, conflict, and N/A). Conflicts in relations between CAS/name and structure are resolved based on predefined hierarchy of inventories (which is related to reliability of SID information). Therefore, nonresolved conflicts are very rare and occur where for the same CAS number different structures are found in the sources with equivalent quality.

1.16.2.3.1.2 Profiling

The profiling module provides information about structural and mechanistic features of the target substance—that is, information about reactivity, potential to damage macromolecules, possible interaction mechanisms with receptors, etc. The implemented profilers are not only used to provide brief information about the toxicological profile of the substances. They are used later in the workflow to drive the categorization and data gap-filling processes (because the profiling outcome might indicate some hazardous potential and is used as a basis for grouping similar substances). Profilers in the toolbox are arranged according to the type of information they are providing:

- Affiliation profilers determine the substance affiliation with databases and inventories.
- Generic profilers determine predominantly (bio)chemical properties of the substance that could trigger a variety of adverse effects.
- Endpoint-specific profilers determine substance properties that are related to specific adverse effects such as acute oral toxicity, bioaccumulation, or mutagenicity.
- Empirical profilers provide basic chemical information such as chemical elements or organic functional groups constituting the substance.
- Custom profilers are user-defined.

Important additions to the profilers are the simulators (i.e., S9 metabolism, rat liver, skin autoxidation, microbial degradation, and hydrolysis). In general, profilers are covering the toxicodynamic part, while the simulators are covering the toxicokinetics part of the substance profile. As a first tier, the user can apply the profilers to parent chemicals and later to specific metabolites, if relevant.

1.16.2.3.1.3 Endpoint

The endpoint module allows users to retrieve (eco)toxicological and environmental data from a number of databases. The user has the option to specify which part of data should be retrieved (all properties or only specific ones). (Q)SAR Toolbox contains a wide collection of data on chemicals donated to OECD by regulatory institutions, research organizations, and companies. For user convenience, databases are thematically grouped in the following categories:

- Physicochemical properties, 42,000 substances and 157,000 experimental values [100]
- Environmental fate and transport, 8000 substances and 86,000 endpoint values [100]
- Ecotoxicological information, 12,000 substances and 608,000 endpoint values [100]
- Human health hazard, 19,000 substances and 688,000 endpoint values[100]

In order to normalize the data from different sources, the endpoint module dynamically processes the data and represents it in unified manner (e.g., all units are converted into default one defined by the user). Regardless of the data normalization process, the original information from the source (and about the source) is easily accessible. In addition, statistical information and visualization of the data aiming at improving the user's knowledge and effectiveness of decision-making are also available.

1.16.2.3.1.4 Category definition

This module provides the user with tools for grouping chemicals into a meaningful category based on their similarity with the target substance. Here, similarity is restricted not only to structural similarity but also to physicochemical properties, mechanism of interaction (e.g., same protein-binding mechanism), reactive potency, or toxicological effects. In the regulatory context for category definition, it is necessary to define the specific context of the similarity. As an example, chemicals that are similar with respect to skin

sensitization (which is driven by protein reactivity) can be dissimilar with respect to endocrine disruption (which is often driven by noncovalent receptor-mediated interactions).

Categorization can be performed with and without accounting for transformations of the analogs (metabolic, abiotic, autoxidation, and hydrolysis). In addition, a complete categorization process is normally required for several subcategorization steps. The order of subcategorization steps should start from wide categories and narrow them down later on during the subcategorization. Nonendpoint-specific profilers (e.g., based on organic functional groups, US EPA new chemicals categories, OECD HPV chemicals categories, or nonconservative structural similarity) are suitable for a first broad grouping, while for the endpoint-specific subcategorization, those profilers based on the specific mechanisms could be more appropriate (e.g., biodegradation fragments of BioWIN, classification by Mode of action (MOA) by OASIS,[108] Ecological Structure Activity Relationships – ECOSAR categorization, and carcinogenicity alerts).

1.16.2.3.1.5 Data gap filling

Data gap filling is the process of estimating the property of a nontested member of a category using the test results available for other members of the category. The toolbox offers three approaches to predict such property: read-across, trend analysis, and (Q)SAR model (the latter only if available for the given endpoint).

In normal situations, the toxic property is a multivariable function of many contributing features. Contribution of each feature can be covered in the individual (sub)categorization steps so that the final data gap step can be performed by relating the property (endpoint) data extracted from the category members to the variable that is related to bioavailability (e.g., water solubility, lipophilicity, and Henry's law constant). However, other data can be also used (i.e., endpoint–endpoint correlation, structural similarity between the target chemical, and category members) for more complex endpoints.

Data analysis focuses on the identification of the relevant data pattern. The (Q)SAR Toolbox provides a variety of formal, statistical, and logical approaches to systematically analyze the data patterns. Among them, there are data transformation (e.g., unit conversion) and data filtering by test conditions, marking substances with properties outside of a specified interval. Statistical techniques include correlation and regression analysis, confidence intervals and central data tendency calculation, leave-one-out validation, and residuals distribution.

1.16.2.3.1.6 Reporting

Three types of reports according to fixed formats approved by OECD and ECHA are produced by the toolbox:

- Chemical Category Reporting Format (CCRF)
- Toolbox Prediction Reporting Format (TPRF)
- Toolbox Model Reporting Format (TMRF)

The reports are accommodating the information, which is produced by the Toolbox. They can be used as background documentation for external purposes (such as regulatory submissions). Many fields in the reports can be automatically filled by the toolbox; other fields can only be filled by the users. Each of the three reports fulfills specific goals. The CCRF is based on OECD's guidance on grouping of chemicals.[96] The format is used to summarize information about the formed category.

The TPRF is based on the (Q)SAR Prediction Reporting Format (QPRF) version 1.1 created by the European Chemicals Bureau[102] and was modified to accommodate the functionalities of the Toolbox.

The TMRF is based on the (Q)SAR Model Reporting Format (QMRF) version 1.2 created by the European Chemicals Bureau[103] and was modified to accommodate the functionalities of the OECD Toolbox.

1.16.2.3.1.7 Summary

The popularity and usage of the toolbox are constantly growing since the launch of the first prototype of the system. The total number of registered users by Feb. 2016 exceeds 8600. It seems that the concept of building single prediction platform, which is combining extensive collection of databases, computational tools, theoretical knowledge, and transformation simulators, has a big practical value for regulatory hazard assessment.

1.16.3 Practical Example on the Use of (Q)SAR under REACH: Mutagenicity

The testing requirements for mutagenicity under REACH are designed in a tiered fashion. Positive outcomes from simpler tests (e.g., *in vitro*) trigger more complex tests (i.e., *in vivo*). The standard requirement for registered chemicals at 1 ton or more is the *in vitro* bacterial mutagenicity test (i.e., Ames test). This test is ideal for computational modeling thanks to the availability of large compilation of data, standardized experimental test protocols with high statistical reliability and low variability, and the well-studied mode of action involving DNA binding. Furthermore, already before the entry into force of REACH, the need of pharmaceutical companies of the early identification of potential mutagen substances has led to the development and validation of many reliable models. Most of these models identify structural alerts known to trigger specific toxicological pathways leading to mutagenicity (there are probably around 100 or more known groups). One example is represented by the arenediazonium salts, whose genotoxicity is caused by the interaction with purine bases. Evidence shows that the mechanism of genotoxicity of arenediazonium salts is governed by the arenediazonium salt itself or by the aryl radicals generated, which can react directly with DNA macromolecules or

can be converted by reduction or decomposition to other reactive and genotoxic species. For example, arenediazonium ions can also undergo one-electron reduction to diazenyl radicals, which, by losing nitrogen, can give rise to aryl radicals. Aryl and diazenyl radicals form adducts with DNA at the C8 carbon atom of adenine or guanine.[104,105] The presence of such structural alert would lead a positive prediction implying further testing for the definitive assessment of its mutagenicity. On the other hand, proving the absence of effect using SAR is always challenging, because it is difficult to link the absence of alerts with the absence of toxicity. To support a negative prediction, it is important to prove that the fragments present in the target chemical are also represented in the TS chemicals with negative experimental outcome. Otherwise, the lack of an alert could be just due to the presence of fragments unknown to the model, and the absence of toxicity would not be supported by experimental evidence. It is also important to consider as many models as possible to cover the chemical and toxicological space to the maximum extent. Finally, it is crucial to document all the predictions and expert judgment to allow an independent assessment of the predictions by regulators.

1.16.4 Conclusions

SARs are well known in the pharmaceutical arena, where they have been exploited for decades in the attempt to reduce costs required to design new potentially bioactive substances having high potency and minimal side effects. The onset of their use can be linked to the first documented examples in the literature[106] reporting as the increase in the potency of general anesthetics was related to the increase in the octanol–water partition coefficient (log *P*) of the chemical agents. This evidence laid the foundation to (Q)SAR, the most used nontest method in drug discovery whose history has been retraced in a recent paper.[107] Today, REACH provides an invaluable opportunity for medicinal chemists willing to tailor their purposes toward predictive toxicology, that is, playing a key role in the regulatory context. However, a full awareness of the more restrictive conditions to which nontest methods are subjected in the regulatory world is required to face this challenge. While pharmaceutical applications are more prone to trial and error principle, regulatory ones require high standards of quality and validity of the statements, as thoroughly stated by the OECD validation principles. In particular, the accurate assessment of AD in the regulatory practice is crucial for both (Q)SAR practitioners and downstream users encouraging a greater consciousness in predicting new data and decision-making. The model fit, robustness, and predictivity returned even by highly sophisticated statistical methods are meaningless for chemicals outside of the AD, while even predictions within AD are not necessarily reliable. This happens when the chemical of interest acts by a different mechanism of action, not captured by the model, or metabolism is causing a "cliff" in activity. Importantly, a thorough knowledge of the restrictive conditions of the regulatory field allows medicinal chemists to play a leading role in the multidisciplinary approach required to achieve the ultimate goal of the REACH program: the protection of human health and environment.

See also: 2.04. Predictive Toxicology: Latest Scientific Developments and Their Application in Safety Assessment. 2.09. Computational Models to Predict Toxicological Endpoints in Drug Discovery and Strategies for Data Integration. 4.16. Toxicity Prediction-Regulatory Perspective.

References

1. ECHA, The Use of Alternatives to Testing on Animals for the REACH Regulation, **2011**, http://echa.europa.eu/documents/10162/13639/alternatives_test_animals_2011_en.pdf (last accessed: 19 February 2016).
2. ECHA, The Use of Alternatives to Testing on Animals for the REACH Regulation, **2014**, http://echa.europa.eu/documents/10162/13639/alternatives_test_animals_2014_en.pdf (last accessed: 19 February 2016).
3. Pauwels, M.; Rogiers, V. *Toxicol. Appl. Pharmacol.* **2010,** *243* (2), 260–274.
4. European Commission, joint research centre, European Union Reference Laboratory for Alternatives to Animal Testing, OECD Principles for the Validation of (Q)SARs, https://eurl-ecvam.jrc.ec.europa.eu/laboratories-research/predictive_toxicology/background/oecd-principles (last accessed: 19 February 2016).
5. ECHA, Guidance on information requirements and chemical safety assessment, chapter R.6: QSARs and grouping of chemicals, https://echa.europa.eu/documents/10162/13632/information_requirements_r6_en.pdf (last accessed date: 19 February 2016).
6. ECHA, Practical Guide 5, How to report (Q)SARs, http://echa.europa.eu/documents/10162/13655/pg_report_qsars_en.pdf (last accessed date: 19 February 2016).
7. ECHA Webinar, Introduction to OECD QSAR toolbox, http://echa.europa.eu/documents/10162/21893819/qsar_toolbox_webinar_agenda_en.pdf (last accessed date: 19 February 2016).
8. ECHA, Illustrative example with the OECD QSAR Toolbox workflow, Part 1: Introductory note, https://echa.europa.eu/documents/10162/21655633/illustrative_example_qsar_part1_en.pdf (last accessed date: 19 February 2016).
9. ECHA, Illustrative example with the OECD QSAR Toolbox workflow, Part 2: Case studies, https://echa.europa.eu/documents/10162/21655633/illustrative_example_qsar_part2_en.pdf (last accessed date: 19 February 2016).
10. ECHA, Grouping of substances and read-across, http://echa.europa.eu/support/grouping-of-substances-and-read-across (last accessed date: 19 February 2016).
11. ECHA, Pratical Guide 6. How to report read-across and categories, http://echa.europa.eu/documents/10162/13655/pg_report_readacross_en.pdf (last accessed date: 19 February 2016).
12. ECHA, Grouping of substances and read-across approach. Part 1: Introductory note, http://echa.europa.eu/documents/10162/13628/read_across_introductory_note_en.pdf (last accessed date: 19 February 2016).
13. ECHA, Read-across illustrative example. Part 2. Example 1—Analogue approach: similarity based on breakdown, http://echa.europa.eu/documents/10162/13628/read_across_example_1_en.pdf (last accessed date: 19 February 2016).
14. ECHA, Read-Across Assessment Framework (RAAF), http://echa.europa.eu/documents/10162/13628/raaf_en.pdf (last accessed date: 19 February 2016).

15. ECHA, Assessing read-across-how ECHA does it, http://echa.europa.eu/view-article/-/journal_content/title/assessing-read-across-how-echa-does-it (last accessed date: 19 February 2016).
16. ECHA, Information on Chemicals, http://echa.europa.eu/information-on-chemicals (last accessed date: 19 February 2016).
17. Mansouri, K.; Abdelaziz, A.; Rybacka, A.; Roncaglioni, A.; Tropsha, A.; Varnek, A.; Zakharov, A.; Worth, A.; Richard, A. M.; Grulke, C. M.; Trisciuzzi, D.; Fourches, D.; Horvath, D.; Benfenati, E.; Muratov, E.; Wedebye, E. B.; Grisoni, F.; Mangiatordi, G. F.; Incisivo, G. M.; Hong, H.; Ng, H. W.; Tetko, I. V.; Balabin, I.; Kancherla, J.; Shen, J.; Burton, J.; Nicklaus, M.; Cassotti, M.; Nikolov, N. G.; Nicolotti, O.; Andersson, P. L.; Zang, Q.; Politi, R.; Beger, R. D.; Todeschini, R.; Huang, R.; Farag, S.; Rosenberg, S. A.; Slavov, S.; Hu, X.; Judson, R. S. Environ. *Health Perspect.* **2016**, in press.
18. Guidance Document on the Validation of (Quantitative) Structure-Activity Relationship [(Q)SAR] Models, OECD Series on Testing and Assessment, No. 69, *OECD Publishing*, DOI: http://dx.doi.org/10.1787/9789264085442-en.
19. OECD, Adverse Outcome Pathways, Molecular Screening and Toxicogenomics, http://www.oecd.org/chemicalsafety/testing/adverse-outcome-pathways-molecular-screening-and-toxicogenomics.htm, (last accessed date: 19 February 2016).
20. Test No. 471: Bacterial Reverse Mutation Test, OECD Guidelines for the Testing of Chemicals, Section 4, *OECD Publishing*, DOI: http://dx.doi.org/10.1787/9789264071247-en.
21. Gadaleta, D.; Pizzo, F.; Lombardo, A.; Carotti, A.; Escher, S. E.; Nicolotti, O.; Benfenati, E. *ALTEX* **2014,** *31* (4), 423–432.
22. Nicolotti, O.; Benfenati, E.; Carotti, A.; Gadaleta, D.; Gissi, A.; Mangiatordi, G. F.; Novellino, E. *Drug Discov. Today* **2014,** *19* (11), 1757–1768.
23. Benigni, R.; Bossa, C.; Jeliazkova, N.; Netzeva, T.; Worth, A. *JRC Sci. Tech. Rep.* **2008,** 1–78.
24. Weaver, S.; Gleeson, M. P. *J. Mol. Graph. Model.* **2008,** *26* (8), 1315–1326.
25. Jaworska, J. S.; Comber, M.; Auer, C.; Van Leeuwen, C. J. *Environ. Health Perspect.* **2003,** *111* (10), 1358–1360.
26. Netzeva, T. I.; Worth, A.; Aldenberg, T.; Benigni, R.; Cronin, M. T. D.; Gramatica, P.; Jaworska, J. S.; Kahn, S.; Klopman, G.; Marchant, C. A.; Myatt, G.; Nikolova-Jeliazkova, N.; Patlewicz, G. Y.; Perkins, R.; Roberts, D.; Schultz, T.; Stanton, D. W.; van de Sandt, J. J. M.; Tong, W.; Veith, G.; Yang, C. *Altern. Lab. Anim.* **2005,** *33* (2), 155–173.
27. Worth, A. P.; Bassan, A.; Gallegos, A.; Netzeva, T. I.; Patlewicz, G.; Pavan, M.; Tsakovska, I.; Vracko, M. The Characterisation of (Quantitative) Structure-Activity Relationships: Preliminary Guidance. ECB Report EUR 21866 EN, 95 pp. European Commission, Joint Research Centre; **2005**, Ispra, Italy.
28. Sahigara, F.; Mansouri, K.; Ballabio, D.; Mauri, A.; Consonni, V.; Todeschini, R. *Molecules* **2012,** *17* (5), 4791–4810.
29. Kunal, R. *Quantitative Structure-Activity Relationships in Drug Design, Predictive Toxicology, and Risk Assessment;* IGI Global: Hershey, Pennsylvania, 2015.
30. Gadaleta, D.; Mangiatordi, G. F.; Catto, M.; Carotti, A.; Nicolotti, O. *Int. J. Quant. Struct. Prop. Relat.* **2016,** *1* (1), 44–61.
31. Jaworska, J.; Nikolova-Jeliazkova, N.; Aldenberg, T. *Altern. Lab. Anim.* **2005,** *33* (5), 445–459.
32. Cormen, T. H.; Leiserson, C. E.; Rivest, R. L.; Stein, C. *Introduction to Algorithms,* 2nd ed.; MIT Press and McGraw-Hill: Cambridge, Massachusetts, 2001. Section 33.3: Finding the convex hull. 947–957.
33. Gissi, A.; Gadaleta, D.; Floris, M.; Olla, S.; Carotti, A.; Novellino, E.; Benfenati, E.; Nicolotti, O. *ALTEX* **2014,** *31* (1), 23–36.
34. Gramatica, P. In *Recent Advances in QSAR Studies;* Puzyn, T., Leszczynski, J., Cronin, M. T., Eds.; *Challenges and Advances in Computational Chemistry and Physics;* Springer: Netherlands, 2010; pp 327–366.
35. Gray, A. G.; Moore, A. W. SIAM International Conference on Data Mining (SDM), 2003, pp. 203–211.
36. Gray, A. G.; Moore, A. W.; Nichol, R. C.; Connolly, A. J.; Genovese, C.; Wasserman, L. Astronomical Data Analysis Software and Systems (ADASS) XIII, Proceedings of the Conference Held 12–15 October, 2003 in Strasbourg, France. ASP Conference Proceedingsvol. 314; Astronomical Society of the Pacific: San Francisco, 2004; p 249.
37. Sheridan, R. P.; Feuston, B. P.; Maiorov, V. N.; Kearsley, S. K. *J. Chem. Inf. Comput. Sci.* **2004,** *44* (6), 1912–1928.
38. Willett, P. *Drug Discov. Today* **2006,** *11* (23–24), 1046–1053.
39. Willett, P. *Methods Mol. Biol.* **2011,** *672,* 133–158.
40. Haranczyk, M.; Holliday, J. *J. Chem. Inf. Model.* **2008,** *48* (3), 498–508.
41. Tetko, I. V.; Sushko, I.; Pandey, A. K.; Zhu, H.; Tropsha, A.; Papa, E.; Oberg, T.; Todeschini, R.; Fourches, D.; Varnek, A. *J. Chem. Inf. Model.* **2008,** *48* (9), 1733–1746.
42. Sahigara, F.; Ballabio, D.; Todeschini, R.; Consonni, V. *J. Cheminform.* **2013,** *5,* 27.
43. Ellison, C. M.; Enoch, S. J.; Cronin, M. T.; Madden, J. C.; Judson, P. *Altern. Lab. Anim.* **2009,** *37* (5), 533–545.
44. Kühne, R.; Ebert, R.-U.; Schüürmann, G. *J. Chem. Inf. Model.* **2009,** *49* (12), 2660–2669.
45. Dimitrov, S. D.; Low, L. K.; Patlewicz, G. Y.; Kern, P. S.; Dimitrova, G. D.; Comber, M. H. I.; Phillips, R. D.; Niemela, J.; Bailey, P. T.; Mekenyan, O. G. *Int. J. Toxicol.* **2005,** *24* (4), 189–204.
46. Patlewicz, G.; Dimitrov, S. D.; Low, L. K.; Kern, P. S.; Dimitrova, G. D.; Comber, M. I. H.; Aptula, A. O.; Phillips, R. D.; Niemela, J.; Madsen, C. B.; Wedebye, E. B.; Roberts, D. W.; Bailey, P. T.; Mekenyan, O. G. *Regul. Toxicol. Pharmacol.* **2007,** *48* (2), 225–239.
47. Cruz-Monteagudo, M.; Medina-Franco, J. L.; Pérez-Castillo, Y.; Nicolotti, O.; Cordeiro, M. N. D. S.; Borges, F. *Drug Discov. Today* **2014,** *19* (8), 1069–1080.
48. Dimitrov, S.; Dimitrova, G.; Pavlov, T.; Dimitrova, N.; Patlewicz, G.; Niemela, J.; Mekenyan, O. *J. Chem. Inf. Model.* **2005,** *45* (4), 839–849.
49. http://www.vega-qsar.eu (last accessed date: 19 February 2016).
50. Gissi, A.; Nicolotti, O.; Carotti, A.; Gadaleta, D.; Lombardo, A.; Benfenati, E. *Sci. Total Environ.* **2013,** *456–457,* 325–332.
51. Floris, M.; Manganaro, A.; Nicolotti, O.; Medda, R.; Mangiatordi, G. F.; Benfenati, E. *J. Cheminform.* **2014,** *6* (1), 39.
52. Nicolotti, O.; Carotti, A. *J. Chem. Inf. Model.* **2006,** *46* (1), 264–276.
53. Wold, S.; Ruhe, A.; Wold, H.; Dunn, W. J., III *SIAM J. Sci. Stat. Comput.* **1984,** *5* (3), 735–743.
54. Wold, S.; Johansson, E.; Cocchi, M. In *3D-QSAR in Drug Design: Theory, Methods and Applications;* Kubinyi, H., Ed.; ESCOM Science: Leiden, The Netherlands, 1993; pp 523–550.
55. Verma, J.; Khedkar, V. M.; Coutinho, E. C. *Curr. Top. Med. Chem.* **2010,** *10* (1), 95–115.
56. Nicolotti, O.; Giangreco, I.; Miscioscia, T. F.; Carotti, A. *J. Chem. Inf. Model.* **2009,** *49* (10), 2290–2302.
57. Massart, D. L.; Vandeginste, B. G. M.; Buydens, L. M. C.; De Jong, S.; Lewi, P. J.; Smeyers-Verbeke, J. In *Handbook of Chemometrics and Qualimetrics*; vol. 20A; Elsevier: New York, NY, 1997, .
58. Kubinyi, H. *QSAR: Hansch Analysis and Related Approaches;* Wiley: Weinheim, 1993.
59. Eriksson, L.; Jaworska, J.; Worth, A. P.; Cronin, M. T. D.; McDowell, R. M.; Gramatica, P. *Environ. Health Perspect.* **2003,** *111* (10), 1361–1375.
60. Lombardo, A.; Roncaglioni, A.; Boriani, E.; Milan, C.; Benfenati, E. *Chem. Cent. J.* **2010,** *4* (Suppl 1), S1.
61. Jouan-Rimbaud, D.; Massart, D. L.; de Noord, O. E. *Chemom. Intell. Lab. Syst.* **1996,** *35* (2), 213–220.
62. Hawkins, D. M. *J. Chem. Inf. Comput. Sci.* **2004,** *44* (1), 1–12.
63. Topliss, J. G.; Edwards, R. P. *J. Med. Chem.* **1979,** *22* (10), 1238–1244.
64. Wold, S.; Dunn, W. J. *J. Chem. Inf. Comput. Sci.* **1983,** *23* (1), 6–13.
65. Clark, M.; Cramer, R. D. *Quant. Struct. Act. Relat.* **1993,** *12* (2), 137–145.
66. Topliss, J. G.; Costello, R. J. *J. Med. Chem.* **1972,** *15* (10), 1066–1068.
67. Diaconis, P.; Efron, B. *Sci. Am.* **1983,** *248,* 96–108.
68. Cramer, R. D.; Bunce, J. D.; Patterson, D. E.; Frank, I. E. *Quant. Struct. Act. Relat.* **1988,** *7* (1), 18–25.
69. Cruciani, G.; Baroni, M.; Clementi, S.; Costantino, G.; Riganelli, D.; Skagerberg, B. *J. Chemom.* **1992,** *6* (6), 335–346.
70. Tropsha, A.; Gramatica, P.; Gombar, V. K. *QSAR Comb. Sci.* **2003,** *22* (1), 69–77.

71. Wehrens, R.; Putter, H.; Buydens, L. M. C. *Chemom. Intell. Lab. Syst.* **2000,** *54* (1), 35–52.
72. Van Drie, J. H. *Curr. Pharm. Des.* **2003,** *9* (20), 1649–1664.
73. Golbraikh, A.; Tropsha, A. *J. Comput. Aided Mol. Des.* **2002,** *16* (5–6), 357–369.
74. Gramatica, P.; Pilutti, P.; Papa, E. *J. Chem. Inf. Comput. Sci.* **2004,** *44* (5), 1794–1802.
75. Gramatica, P.; Papa, E. *QSAR Comb. Sci.* **2005,** *24* (8), 953–960.
76. Papa, E.; Villa, F.; Gramatica, P. *J. Chem. Inf. Model.* **2005,** *45* (5), 1256–1266.
77. Kauffman, G. W.; Jurs, P. C. *J. Chem. Inf. Comput. Sci.* **2001,** *41* (6), 1553–1560.
78. Golbraikh, A.; Shen, M.; Xiao, Z.; Xiao, Y.-D.; Lee, K.-H.; Tropsha, A. *J. Comput. Aided Mol. Des.* **2003,** *17* (2–4), 241–253.
79. Tropsha, A. *Mol. Inform.* **2010,** *29* (6–7), 476–488.
80. Worth, A. P.; Cronin, M. T. D. *J. Mol. Struct. Theochem.* **2003,** *622* (1–2), 97–111.
81. Worth, A. P.; Cronin, M. T. D. In *Progress in the Reduction, Refinement and Replacement of Animal Experimentation;* Balls, M., van Zeller, A. M., Halder, M. E., Eds.; Elsevier Science: Amsterdam, The Netherlands, 2000; pp 479–491.
82. Cooper, J. A.; Saracci, R.; Cole, P. *Br. J. Cancer* **1979,** *39* (1), 87–89.
83. Kohavi, R.; Provost, F. *Mach. Learn.* **1998,** *30* (2–3), 271–274.
84. Kumar, S.; Kumar, M.; Thurow, K.; Stoll, R.; Kragl, U. *Environ. Model. Softw.* **2009,** *24* (1), 44–53.
85. Matthews, B. W. *Biochim. Biophys. Acta* **1975,** *405* (2), 442–451.
86. Hanley, J. A. *Crit. Rev. Diagn. Imaging* **1989,** *29* (3), 307–335.
87. Provost, F.; Fawcett, T. *Mach. Learn.* **2001,** *42* (3), 203–231.
88. Merlot, C. *Drug Discov. Today* **2010,** *15* (1–2), 16–22.
89. Dearden, J. C.; Barratt, M. D.; Benigni, R.; Bristol, D.; Combes, R. D.; Cronin, M.; Judson, P.; Payne, M.; Richard, A.; Tichy, M.; Worth, A.; Yourick, J. *Altern. Lab. Anim.* **1998,** *25,* 223–252.
90. Nicolotti, O.; Gillet, V. J.; Fleming, P. J.; Green, D. V. S. *J. Med. Chem.* **2002,** *45* (23), 5069–5080.
91. Todeschini, R.; Consonni, V. *Handbook of Molecular Descriptors*; vol. 11; John Wiley & Sons: New York, 2008.
92. Hansch, C.; Smith, R. N.; Rockoff, A.; Calef, D. F.; Jow, P. Y.; Fukunaga, J. Y. *Arch. Biochem. Biophys.* **1977,** *183* (2), 383–392.
93. Livingstone, D. L. *Data Analysis for Chemists: Applications to QSAR and Chemical Product Design;* Oxford Science Publications: Oxford, 1995.
94. Nicolotti, O.; Miscioscia, T. F.; Carotti, A.; Leonetti, F.; Carotti, A. *J. Chem. Inf. Model.* **2008,** *48* (6), 1211–1226.
95. OECD, Hazard Assessment, http://www.oecd.org/env/ehs/risk-assessment/hazardassessment.htm (last accessed date: 19 February 2016).
96. OECD. *Guidance on Grouping of Chemicals, ENV/JM/MONO(2007) 28;* Organisation for Economic Cooperation and Development: Paris, 2007.
97. IOMC—Inter-organisation Programme for the Sound Management of Chemicals, http://www.who.int/iomc/en/ (last accessed date: 19 February 2016).
98. OECD, Guidance on grouping of chemicals, second edition; series on testing & assessment, http://www.oecd.org/officialdocuments/publicdisplaydocumentpdf/?cote=env/jm/mono(2014)4&doclanguage=en (last accessed date: 19 February 2016).
99. Berggren, E. In *Towards the Replacement of in vivo Repeated Dose Toxicity Testing;* Gocht, T., Shcwarz, M., Eds.; vol. 5; Imrimerie Mouzet: France, 2015; pp 89–90.
100. QSAR Toolbox v3.3.5, http://www.qsartoolbox.org (last accessed date: 19 February 2016).
101. Dimitrov, S. D.; Diderich, R.; Sobanski, T.; Pavlov, T. S.; Chankov, G. V.; Chapkanov, A. S.; Karakolev, Y. H.; Temelkov, S. G.; Vasilev, R. A.; Gerova, K. D.; Kuseva, C. D.; Todorova, N. D.; Mehmed, A. M.; Rasenberg, M.; Mekenyan, O. G. *SAR QSAR Environ. Res.* **2016,** *19,* 1–17.
102. International Uniform Chemical Information Database, available at https://iuclid6.echa.europa.eu/ (last accessed date: 19 February 2016).
103. Joint Research Centre, available at https://eurl-ecvam.jrc.ec.europa.eu/laboratories-research/predictive_toxicology/qsar_tools/qrf/ (last accessed date: 19 February 2016).
104. Lawson, T.; Gannett, P. M.; Yau, W. M.; Dalal, N. S.; Toth, B. *J. Agric. Food Chem.* **1995,** *43,* 2627–2635.
105. Malaveille, C.; Brun, G.; Kolar, G.; Bartsch, H. *Cancer Res.* **1982,** *42,* 1446–1453.
106. Meyer, H. *Arch. Exp. Pathol. Pharmacol.* **1899,** *42,* 109–118.
107. Dearden, J. C. *Int. J. Quant. Struct. Prop. Relat.* **2016,** *1* (1), 1–44.
108. Laboratory of Mathematical Chemistry, University "Prof. D-R Asen Zlatarov", Bulgaria, http://oasis-lmc.org/about.aspx (last accessed date: 29 August 2016).

1.17 New Models of Drug Discovery and Development for Neglected Disease Populations

TNC Wells, R Hooft van Huijsduijnen, and JN Burrows, Medicines for Malaria Venture (MMV), Geneva, Switzerland

© 2017 Elsevier Ltd. All rights reserved.

1.17.1	Parasitic Infections: Neglected Disease and Neglected Populations	491
1.17.2	Drug Discovery in the World of Negative Net Present Value	492
1.17.3	Creating a Pipeline of New Candidates	493
1.17.4	New Collaborative Models for Partnerships and for Building Teams	497
1.17.5	The Circle of Life: Back to New Targets	498
1.17.6	Data Sharing—Dealing With Fragmentation	500
1.17.7	Bringing the Compounds to the Biology or the Biology to the Compounds	500
1.17.8	Intellectual Property and Drug Discovery in Neglected Disease	501
1.17.9	Conclusions	502
Acknowledgments		502
References		502
Relevant Websites		504

Over the last decade there has been a renaissance in the discovery and development of new medicines targeting infectious parasitic diseases, and this has led to new medicines being registered, but also to a range of new compounds entering clinical development against malaria,[1] tuberculosis,[2] other protozoans, parasites[3] and worms.[4] This has been driven by the availability of new high-content assay systems, which have allowed high-throughput screening of compound collections directly against the parasites, rather than against isolated molecular targets.[5,6] This approach has yielded two dividends in many areas: first of all, molecules that can be optimized and moved into clinical development. Second, the technologies for target identification have improved sufficiently that it has often been possible to rapidly identify the targets of these phenotypic screening hits.[7,8] These pharmacologically validated targets have the advantage that they are known to be important, but also demonstrated to be tractable. For malaria, rapid proof of concept in human experimental infection models[9–12] has also allowed us to quickly validate these new targets clinically, further increasing the confidence in this approach.

To achieve these goals, new models of collaboration have been developed, bringing together the strengths of academia and industry, close integration of science and medicine, but most importantly a move to increased sharing of data and transparency. In this review, using malaria as an example, the evolution of pipeline of molecules and targets is discussed. New modalities of collaborations and interdisciplinary teams have been necessary, as well as a continual review of data sharing and openness. These lessons can be translated at least in part to other therapeutic areas, and the next decade should see new models of collaboration permeating other disease areas, which were traditionally seen as profitable, but increasingly are becoming neglected due to a lack in progress using established *modi operandi*.

1.17.1 Parasitic Infections: Neglected Disease and Neglected Populations

Infectious tropical diseases, such as malaria, schistosomiasis, sleeping sickness, and leishmaniasis, are responsible for a significant proportion of the world's mortality.[13,14] More importantly, they have a disproportionate impact on children, which means their impact on global morbidity tends to be even larger than the headline figures on mortality would suggest; in 2013, almost 3.3 million children died before the age of five from infectious disease.[15] The effect is therefore a loss of so much potential for the future. For those who survive, disease causes children to miss significant amounts of schooling, and so the overall education levels are also suppressed. Many of these diseases are chronic with significant comorbidities, especially anemia. Even diseases, such as malaria, which has a relatively acute course of infection, effectively become chronic because in hyper-endemic regions a child may be infected as many as eight times in a year, transforming a short-term illness of a couple of weeks' duration into a long-term underlying health challenge.

These disease areas have often been called neglected diseases, because of the lack of funding in terms of drug development. To be fair, there has always been significant investment in the basic sciences on parasitic diseases, such as malaria, with contributions from national funding bodies, and also from organizations, such as the Wellcome Trust. In the past, this has been boosted by research expenditure in the military, since many of the conflicts from the Second World War through to the end of the Vietnam War involved large numbers of soldiers entering malaria-endemic zones. The difficulty has been twofold. First, that over the last two or three decades, many companies have stopped working on infectious diseases, especially protozoan pathogens, and fungal infections. The pressure within industry has been on finding new drugs with large commercial potential (the "blockbuster"

pharmacoeconomic model[16]). Failure to achieve this in an economically viable manner has now led to an increased focus on disease areas that have fewer and fewer patients,[17] with the double advantage that clinical trials tend to be much smaller and therefore much cheaper, but also that the final product can be sold at a super-premium price. Neglected diseases are in the exact opposite quadrant of this commercial space: millions of patients, with many significant underlying issues, and an inability to pay a significant price. The military today has less of a problem with parasitic infections and is more focused on battlefield injuries and post-traumatic stress. The second problem is that of fragmentation: beyond the big three of HIV, tuberculosis, and malaria, there are officially 17 diseases in the World Health Organization (WHO) list of neglected tropical diseases. Even this hides another level of complexity, as these 17 diseases break out into many more pathogens, and the pathogens themselves have subspecies and strains that may or may not respond equally well to each new drug. The effect is almost fractal: the more one looks into the number of potential diseases, the more of them there are. Clearly, any approach to neglected disease has to have an element of synergy. The lessons we learn from working against one parasite must be translated to other, similar parasites: ideas, targets, and compounds need to be freely shared.

These two issues can be addressed by new models of drug discovery and development. The first requires a reanalysis of the financing of neglected tropical disease. The second needs a more open framework for sharing of information and compounds. Fortunately, these challenges are related.

1.17.2 Drug Discovery in the World of Negative Net Present Value

The first issue can be boiled down to a simple observation. It is often stated that there is no money to be made from developing new molecules for neglected tropical diseases,[18] but this is clearly an oversimplification, and a more in-depth analysis is required. Typically, a project is viewed in terms of its risk-adjusted net present value.[19] This is a composite number. On the positive side, we can take the projected sales, adjusted for attrition (risk of failure). Here the one key advantage that infectious disease has is that the translation between an idea of killing a parasite *in vitro* or in a mouse, and curing the infection in humans is much more precise than the similar translation in, say, neurodegenerative diseases. Second, the molecular target(s) are nonhuman, a clear benefit toward safety. For instance, medicinal chemistry efforts have succeeded in finding molecules that selectively inhibit *Plasmodium* DHODH (dihydroorotate dehydrogenase) rather than its human ortholog.[20] But the opportunities go well beyond orthologous differences: the malaria parasite has a vestigial but essential plastid organelle (the apicoplast[21]), it must export hundreds of proteins into red blood cells that hosts it,[22] and it must also detoxify the heme it produces from degrading hemoglobin[23]; structures and processes that are all eminently druggable and nonexistent in healthy humans. For these reasons, the overall probability of success is much higher for drug discovery in malaria[24] and systemic antiinfectives in general[25] than for other therapeutic areas. On the negative side, there is still the cost of doing the research and development, which again has to be adjusted for the probability of success. The complexity here is working out how much a drug development project actually costs, and striving to reduce these costs. Analyses of the clinical costs of development for a classical antiinfective in industry tend to produce a number over $300 million.[26] In the malaria space, we can show that the cost of clinical development of a new molecule is a fraction of this,[24] which some have used as evidence that neglected disease researchers are somehow more efficient than researchers in other areas. However, this conclusion is premature: many of our projects involve pharmaceutical companies who provide in-kind support. Some, for example AbbVie, do not actually partner in the traditional sense of retaining intellectual property, but help out providing advice, and other services which have significant material value, and thus provide significant cost savings.

On the positive side, there are three areas of value creation that can be discussed. The first is of course sales of the final drug in commercial markets. Typically there are three markets in neglected disease. Firstly, the prices paid by United Nations Agencies, and government tenders for the public health services in developing countries, where volumes are in the hundreds of millions of doses with prices around $1–2 for an adult treatment.[27] The profit margins on these products are negligible, and under constant pressure. Secondly, there is the premium private market with patients buying directly from the pharmacist, where the volumes will be single-digit millions but the price will be around $10 per treatment, with a 90% gross margin. Finally, there are the Western prices; an Artemisinin-based Combination Therapy (ACT) in the United States can cost $100, with a 99% gross margin, but US annual sales are extremely small for antimalarials. (This of course is completely different for products that can be used to protect against infection, where most travellers take some chemoprevention, and for which there is a global commercial market.) From a commercial perspective, therefore, medicines that are used to treat parasitic diseases will never repay their development costs. Companies nevertheless manifest an interest in being involved, to a large extent in the context of Corporate Social Responsibility, but also as part of their overall strategy of having a greater Global Footprint. This means that having new drugs for malaria, for example, is a sign of commitment to the emerging markets, which may support the overall commercial goals in these regions (for other indications and their disease populations). Both of these factors combined mean that a project has a net present value at registration which is positive, an observation that is confirmed by the presence of generic manufacturers in the market place. The question is how to pay for and assume the risks in the upstream research and development process.

The challenge in any drug development initiative is therefore to close the funding gap, and move the projects closer to the break-even point from where expected NPV (or eNPV, expected Net Present Value) becomes positive. Over the last decade, donor money has helped kick-start this process. Molecules that move through development toward the clinic are bound to increase in value, provided they hit their efficacy and safety targets. The challenge is therefore to provide sufficient funding to reach this zero point, but no more. This negotiation is at the heart of the work of Product Development Partnerships, such as Medicines for Malaria

Venture (MMV), Drugs for Neglected Diseases *Initiative* (DND*i*), and the Global Alliance against Tuberculosis (GATB). A second component that drives positive eNPVs is the availability of rewards. In the diagnostics space, rewards such as a £10M "Longitude Prize"[28] for a new Fever diagnostic provide some way of closing this gap. Such rewards have not been made available as cash incentives for new medicines against parasitic disease, and one could argue that these would have to be quite substantial if they were to incentivize end-to-end drug discovery and development, certainly in excess of the $300M figure quoted above. However, one innovative approach that has been put in place is the US Priority Review Voucher.[29] This innovative new scheme allows any group which registers a drug for any one of a long list of neglected infectious diseases to receive a transferable voucher entitling its owner to a Priority Review for a second project, one in a commercial area. The first of these vouchers was awarded to Novartis for their work on artemether–lumefantrine (Coartem), and the voucher was used to accelerate review for Ilaris/canakinumab, an anti-IL1 antibody (an application that was rejected).[30] More recently, the power of these vouchers was illustrated by the purchase of one by Sanofi–Regeneron, who are in a neck-and-neck race with Amgen to launch an antibody against the cardiovascular target PSCK9. Given reasonably similar profiles for the two products, then the 6-month acceleration given by priority review has tremendous commercial potential for a potential blockbuster drug, and Sanofi paid $62M for their voucher.[31] Since then, other vouchers have been sold at ever increasing prices,[32] for $125M to Gilead in 2014, for $245M to Sanofi, and most recently for $350M to AbbVie.[33,34] Clearly, we are now at the stage where the value of the voucher is perceived by some to be higher than the cost of the complete clinical development of a new medicine against neglected disease. This means that with the addition of the voucher, projects already yield a positive eNPV once they enter clinical development. This has had a significant impact in our (MMV's) ability to find pharmaceutical partners for projects in the early stages of clinical development. **Fig. 1** shows that the time to reach eNPV break-even (arrows) is shorter for malaria (A) than for example, Alzheimer's disease (AD; B) with the sum invested "at risk" much lower. Of course the stakes (potential benefits) and risks are much higher for an AD drug. Note also that without a Priority Voucher, malaria projects do not reach positive eNPVs (C, D).

1.17.3 Creating a Pipeline of New Candidates

In many disease areas, investments in R&D over the last decade have significantly strengthened the pipelines of new molecules. There is still a long way to go before we can claim to have reached a critical mass, and there are many gaps, but the overall trend is in the right direction (see **Fig. 2** for the antimalarial portfolio). One exciting observation is that the vast majority of the molecules in "patient exploratory" studies or earlier in the pipeline have been discovered in the last decade. Another encouraging factor is the richness of the portfolio, with an unprecedented number of new scaffolds under development. In many cases, novel targets or underappreciated targets have been brought forward.

These molecules have come from three areas: improvements on existing known scaffolds, molecules rationally designed against molecular targets, and most importantly, from phenotypic screening. For malaria, these have been summarized in a recent review,[1] therefore only the key points are referred to below.

(a) Improving on the current generation of therapies

The gold standard for treating malaria is a fixed-dose combination of an artemisinin derivative, plus an aminoquinoline or aminoalcohol partner drug. The artemisinin activity has been shown to be due to the endoperoxide moiety, prompting the question whether a better endoperoxide could be developed. A collaboration between four academic groups, managed by MMV, was able to optimize synthetic endoperoxides and produce OZ277 (see **Fig. 3**), now sold as arterolane, part of the combination Synriam™, by Ranbaxy.[36,37]

OZ277/Rbx11160 shows potential replacing artesunate in a 3-day treatment and has the significant advantage that it is fully synthetic, and so will not suffer from any of the price fluctuations seen in the artesunate market over the last decade.[38,39] Further refinement of this molecule has produced a next-generation endoperoxide, OZ439, currently in phase II clinical trials. This compound was optimized to reduce the metabolic liabilities, but also to make it stable in the presence of free ferrous iron. The resulting compound has a much longer half-life and has potential to shorten treatment from 3 days down to one day, as well as showing superior safety against granulocytes and leukocytic populations in culture, and embryofetal safety.[40–42] There have also been improvements in the partner drugs: recently, a new version of a 4-aminoquinoline, ferroquine, showed good activity in clinical trials,[43,44] and an historical hybrid of quinacrine and amodiaquine, pyronaridine (see **Fig. 4**) was approved for use in adults and children by the European Medicines Agency (EMA).[45] In all cases where a new version of an old scaffold is produced, it is important to verify that the compounds are active against all clinically identified resistant isolates, and this was indeed the case here.

(b) Better by design

Structure-based design has also had an impact on the delivery of new clinical candidates. The best case so far in malaria is the development of DSM265, an inhibitor of the plasmodial enzyme DHODH. This target had been proposed from genetic validation, and a high-throughput screen was performed in which the original triazolopyrimidine screening hit was identified. This was subsequently optimized to increase potency and to remove both metabolic and genotoxic liabilities (the β-naphthylamine in the original structure; **Fig. 5**).

This compound has now been optimized[47,48] and entered phase I studies in 2013. It was one of the first molecules to take advantage of a human experimentally induced malaria infection model, run at the Queensland Institute of Medical Research in

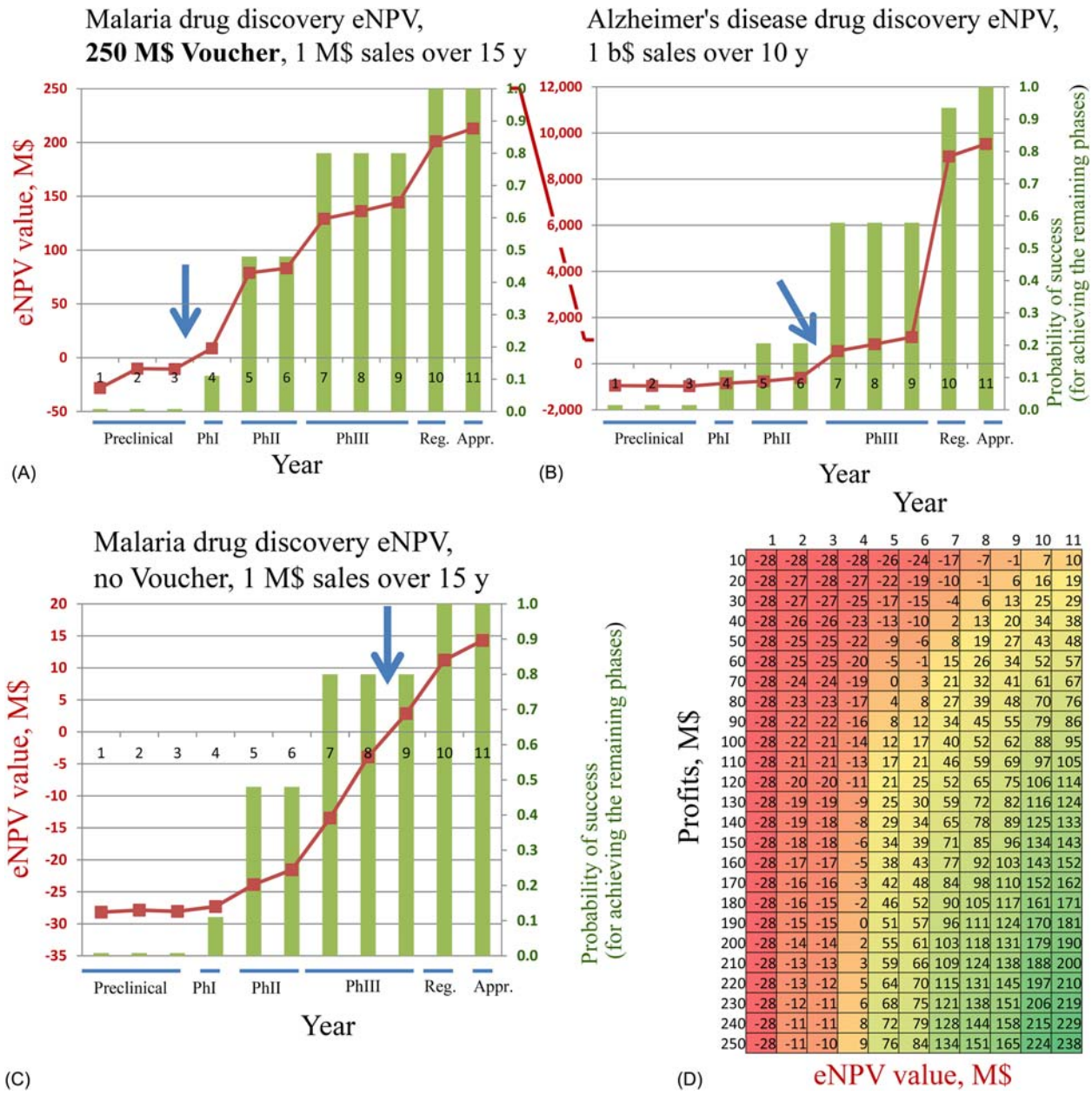

Profits, M$	1	2	3	4	5	6	7	8	9	10	11
10	-28	-28	-28	-28	-26	-24	-17	-7	-1	7	10
20	-28	-27	-28	-27	-22	-19	-10	-1	6	16	19
30	-28	-27	-27	-25	-17	-15	-4	6	13	25	29
40	-28	-26	-26	-23	-13	-10	2	13	20	34	38
50	-28	-25	-25	-22	-9	-6	8	19	27	43	48
60	-28	-25	-25	-20	-5	-1	15	26	34	52	57
70	-28	-24	-24	-19	0	3	21	32	41	61	67
80	-28	-23	-23	-17	4	8	27	39	48	70	76
90	-28	-22	-22	-16	8	12	34	45	55	79	86
100	-28	-22	-21	-14	12	17	40	52	62	88	95
110	-28	-21	-21	-13	17	21	46	59	69	97	105
120	-28	-20	-20	-11	21	25	52	65	75	106	114
130	-28	-19	-19	-9	25	30	59	72	82	116	124
140	-28	-19	-18	-8	29	34	65	78	89	125	133
150	-28	-18	-18	-6	34	39	71	85	96	134	143
160	-28	-17	-17	-5	38	43	77	92	103	143	152
170	-28	-16	-16	-3	42	48	84	98	110	152	162
180	-28	-16	-15	-2	46	52	90	105	117	161	171
190	-28	-15	-15	0	51	57	96	111	124	170	181
200	-28	-14	-14	2	55	61	103	118	131	179	190
210	-28	-13	-13	3	59	66	109	124	138	188	200
220	-28	-13	-12	5	64	70	115	131	145	197	210
230	-28	-12	-11	6	68	75	121	138	151	206	219
240	-28	-11	-11	8	72	79	128	144	158	215	229
250	-28	-11	-10	9	76	84	134	151	165	224	238

Fig. 1 Illustrative risk-corrected eNPV for drug discovery projects in malaria (A, C) and Alzheimer's disease (B). The costs and duration in years per phase for antimalarial development, and their probability of success were taken from a MMV portfolio analysis and reference [24] For the graph in A, final revenue was set at $15M drug sales profits, plus an FDA Priority Review Voucher valued at $250M. Panel (C) represents the scenario without the Voucher. For Alzheimer's disease (B), average "out of pocket costs" ($1.4b) was taken from the 2014 Tufts Center analysis (csdd.tufts.edu) and distributed over time as in the antimalarial example. The probabilities of success for the phase transitions were taken from reference [35] and cumulative revenue was conservatively set at $10 billion over the lifetime of the product. The *arrows* in (A) and (B) indicate the time (year) where the eNPV reaches break-even. The *red line* between the graphs (B) and (C) illustrates the difference in scale for their left *Y*-axes. NPVs were calculated using Microsoft Excel's NPV function, set as a discount of 3%, and corrected for revenues by the probability of (final) success. Panel (D) represents the result of an Excel "*What if*" analysis for malaria drug discovery with different profit scenarios (*Y*-axis), showing the eNPVs for each, by year. Under the assumptions of this model, profits of at least $50M are required to produce positive eNPVs. *Reg.*: regulatory submission; *Appr.*: Market approval. The key message is that in malaria, projects do not have a positive eNPV until they reach the clinic and are supported by a Priority Review Voucher, in the absence of additional pull or push mechanisms.

Australia.[49] During the phase I, a dose of 150 mg was tested in human volunteers who had been infected with a very low dose of parasitized erythrocytes, and where the infection was allowed to progress to a state where it can be measured by PCR, while remaining subclinical. The results were positive and were used to model the dose needed in phase II, where the studies were started at 400 mg dose in Peru in early 2015. This type of human volunteer data is useful for de-risking projects, but also helped

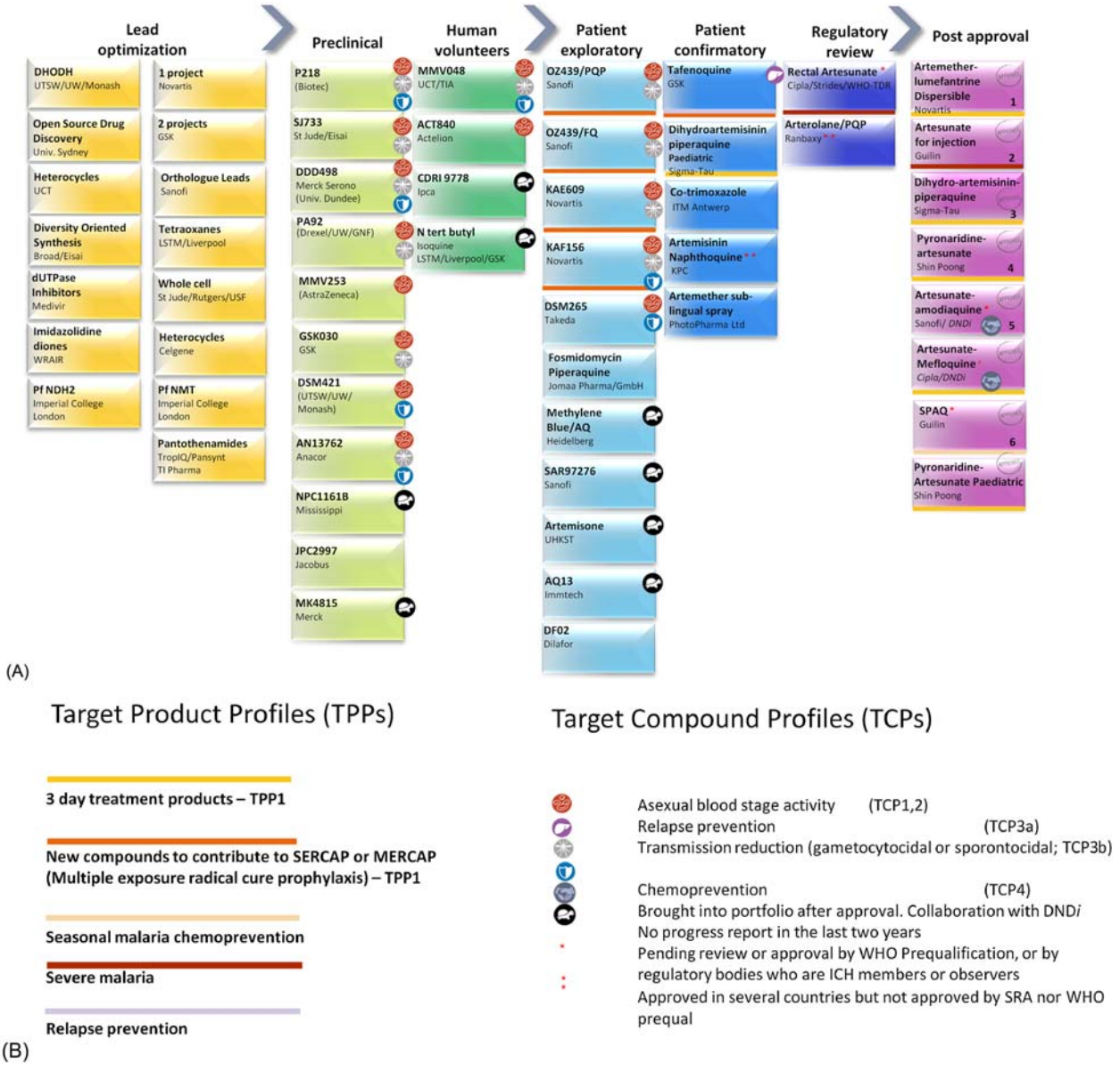

Fig. 2 (*Top*) The global portfolio of antimalarial drugs as of January 2016. The full details of the portfolio and an up-to-date version of this table can be downloaded from the MMV website at www.mmv.org. (*Bottom*) The malaria community has defined two target product profiles (*TPPs*) for medicines to make eradication achievable: *TPP1*: a treatment combination that is ideally a single exposure radical cure and prophylaxis (SERCaP) and *TPP2*: single exposure chemoprotection (*SEC*). To develop the individual compounds for combination into the TPPs, MMV has defined five target candidate profiles (*TCPs*). Footnotes: Brand names are 1: Coartem® Dispersible; 2: Artesun®; 3: Eurartesim®; 4: Pyramax®; 5: Coarsucam™ ASAQ/ Winthrop®; 6: SPAQ-CO™. The black tortoise marks projects which have not reported progress in the last 2 years. One of the consequences of limited funding is that often projects have to wait at each decision point for funding of the next stage to be clarified. This is especially true in clinical development where it is an ethical requirement to have secured complete funding of the trial before recruiting patients.

define critical pharmacodynamic parameters guiding the clinical dose early on. Other human volunteer challenge models are available; one uses sporozoites (the stage which is normally injected by the mosquito during the blood meal) and this is a good way to see the activity of compounds against the initial dividing stages of the parasite in the liver.[50,51] DSM265 is currently also being tested here—activity against the liver stages would be a useful asset for a molecule which could be used to protect against malaria infection.

(c) A renaissance in phenotypic screening: new models for interacting with Industry

The main contribution to the portfolio of new molecules in discovery over the last decade has come from phenotypic screening. It is important that these assays accurately reflect disease relevance—one harvests what is screened for. A compound that kills replicating *Trypanosomes* may leave nonreplicating forms, such as trypomastigotes, capable of reinitiating infection

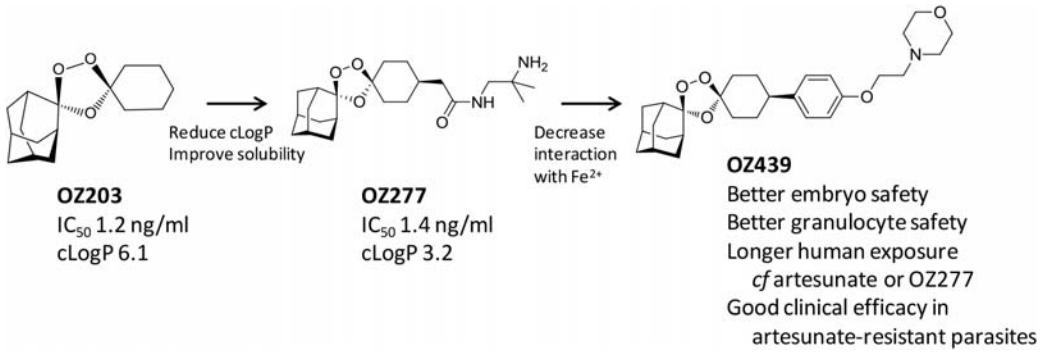

Fig. 3 Summary of discovery of OZ277 and OZ439 from OZ03 starting point.

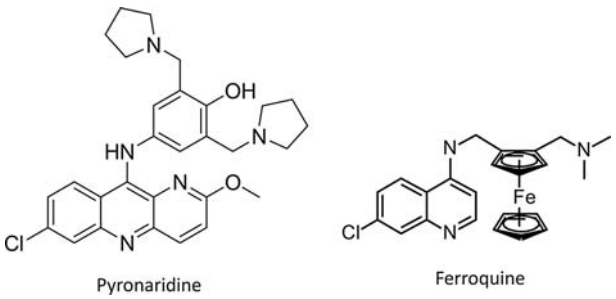

Fig. 4 Structures of pyronaridine and ferroquine.

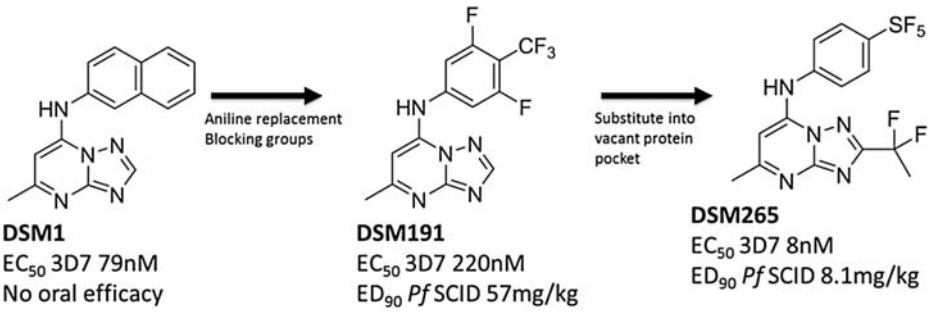

Fig. 5 Progression from the DSM1 "hit" to the DS191 "lead" and finally to DSM265, the preclinical candidate. "3D7" refers to *P. falciparum* strain 3D7. "*Pf*SCID" refers to the humanized mouse (NOD–SCID IL2R$^{-/-}$) malaria model described earlier,[46] with ED_{90} as the dose with 90% efficacy. The EC_{50} refers to the half maximal effective concentration.

long after the end of the treatment.[52] Ivermectin is a wonderful drug that kills microfilaria (*Onchocerca volvulus*), the cause of river blindness, yet does not kill the adult worms that produce these.[53] Compounds that kill *Leishmania* parasites *in vitro* may not reach the amastigotes, which reside inside acidic phago-lysosomes within macrophages. Similarly, *Trypanosoma cruzi*, the parasite that causes Chagas disease infects many cells types, with variable drug exposure. The key challenge for *Mycobacterium tuberculosis* bacteria is that few compounds affect the latent, nonreplicating stage[54]; moreover, bacteria may reside in poorly vascularized lung tissue with challenging drug irrigation. For these reasons, tuberculosis treatments take months to complete in regimens that are eminently designed to generate drug-resistant strains. Considerable efforts have been made to develop assays that address these other aspects so that compounds can be tested against rapidly replicating bacteria[54] but also when metabolically inert in low-oxygen conditions[55] and when residing in macrophages.[56,57] In the symptomatic phase of malaria, *Plasmodium* replicates in a single cell type (erythrocytes), and drugs that kill this stage have the capacity to completely clear patients from the disease (although they often do a poor job in preventing transmission back to mosquitoes, see below). Changes in the technologies for imaging in high-throughput assays, and improved biomass production[58] meant that parasites could be imaged in 384 and 1536 well plates. This meant that antiparasitic assays could be performed outside of the major screening centers of the pharmaceutical industry. This was a critical success factor—the malaria infection assay is relatively straightforward, but still requires live parasites and human erythrocytes—a setting which would not be allowed on the main

screening platforms of many pharmaceutical companies. The other advantage was that the price of screening dropped by almost 100-fold over a relatively short period of time. Three initial projects led by Novartis,[59] GlaxoSmithKline (GSK[60]), and St Jude Children's Research Hospital, Memphis, TN[61] screened large decks of up to 2 million compounds in-house. The technology was also taken up at the Eskitis Institute in Queensland Australia,[62] and over the following 3 to 4 years, over 7 million compounds from multiple libraries were screened, and a large collection of actives were identified. The advantage of the relatively low cost of the assay meant that a new model of interaction with the pharmaceutical industry was possible. The compounds were screened first and positives were identified, before any agreement was made over disclosing the structures. In most cases where positives have been identified, there was a desire by the partner company to carry on the collaboration into the Hits-to-Leads phase. Occasionally, strategic changes within the company meant that the project could not be continued, but in those cases the scaffolds were handed over to MMV for further work.

1.17.4 New Collaborative Models for Partnerships and for Building Teams

Even in cases where companies were interested in progressing compounds, not every company should, or indeed could have all of the assays in house. The role of MMV as a research catalyst was to make sure that standardized assays for all of the different stages of the parasite lifecycle were in place.[63] Thus, a system could be set up, whereby interesting compounds from a variety of different projects could be tested in the same assay—one for blood stages, one for the liver stages, and one for transmission blocking. This also included two standardized mouse models: one using the malaria parasite species *P. berghei*, which can infect mice, and the other using "human" *Plasmodium falciparum*, which infects NOD/SCID/IL2R$\gamma^{-/-}$ (NSG) mice engrafted with human erythrocytes.[46] We also set up a clear set of target candidate and target product profiles[24] which are updated every 2 or 3 years. These are the fruit of an extensive discussion with our advisory boards, which include experts in clinical malaria, but also experts in drug discovery from malaria and other therapeutic areas. The other critical success factor is the definition of standardized stage gates. Working with our pharmaceutical partners, and also with the other product development partnerships (PDPs), we have been able to define the characteristics of a molecule which is at the lead (activity *in vivo*) or the optimized lead stage (active *in vivo*, and with a need for early safety testing prior to becoming a clinical candidate).[64] In addition, we have produced a standardized list of parameters for compounds which can be considered preclinical development candidates. The creation of a standardized vocabulary and criteria between the different projects is critical, as most companies have very similar processes, but often use very different language that describes the phase transitions. This standardization of stage gates using data from standardized assay in the MMV network also means that it is easier for us to track the times taken between different stage gates for different projects, as well as the costs associated.

About half of the molecules in the portfolio come from industrial collaborations, and the other half from partnerships with academia. In all cases, we made sure that the projects had an industrial mentor. One of the advantages of working in neglected infectious disease is that we have been able to draw on the skills of a wide variety of senior experts, often recently retired from the pharmaceutical industry. Therefore even groups with relatively little experience of the early stages of drug discovery were properly advised and able to quickly identify the key issues, and design strategies to solve them. Each project is reviewed at least once per year by our External Scientific Advisory Committee (ESAC), and this review, plus the continual presence of ESAC members as mentors of the projects, ensures that the best practice is shared between projects. One message that comes out of this is that in neglected disease, we have a chance to observe first-hand how peer review across companies works. The increase in transparency and the discussions between companies mean that we can avoid unnecessary duplication, but also that common standards can be applied across all the projects.

The DSM265 project, mentioned above, has an interesting background. The fact that it is accepted that early-stage malaria drug research is in negative NPV territory, and therefore not seen as a commercially viable activity, means that we were able to take the transparency to a new level. Several groups were working on the same target, and we were able to organize a meeting between the University of Texas, Southwestern, Harvard University, GSK, and Genzyme, where the different groups talked about their approaches, and where everyone agreed that any ideas contributed to the existing projects remained with the existing teams. This resulted in unique partnerships in which, for example, GSK chose to support the University of Texas Southwestern in exchange for crystallography efforts. In this configuration, the collaboration fostered intellectual sharing between the teams that contributed to the ultimate success and the first batch of DSM265, that was synthesized by GSK and handed back to the University of Texas team for further characterization. It was not simply the openness of data sharing that was important here, but also the openness of critique. This raises the question about how much more efficient industrial drug discovery would be if all projects had some sort of external peer review: duplication of projects in industry is only wasteful if the individual insights cannot be shared. Clearly, this sharing cannot easily take place in disease areas which are seen to be highly profitable, but the success of this business model does suggest that more work to create open sharing in profitable diseases could significantly enhance success rates (and decrease attrition). It is also important to have a clear view about which diseases are not profitable: there is still quite a split in the tuberculosis community, where some believe there is a small profit to be made, and therefore operate as commercial companies. Others would take a more extreme view and consider many areas of medicine, such as psychiatric disease, to be unlikely to be profitable, and these are areas where more open collaboration models should be considered in the future.

1.17.5 The Circle of Life: Back to New Targets

Initially, it was difficult to convince many medicinal chemists of the possibility of optimizing compounds coming from phenotypic screens, without knowing the mechanism of action nor having a primary biochemical assay. One frequent comment was that it would never be possible to register a drug without having some understanding of the mechanism of action (which overlooks the fact that there are still many safe and effective drugs where the precise mechanism is a matter of debate; indeed, the question of mechanism was not even raised at the FDA review of Coartem®). However, the identification of the target has come naturally as part of the optimization. Two compounds can be used to illustrate this. The first is KAE609, a spiroindolone, under development by Novartis in collaboration with MMV and the Wellcome Trust, which was originally discovered as part of a collaboration between Novartis, the Swiss Tropical and Public Health Institute, and the Dutch Biomedical Primate Research Centre.[65–67] The optimization of this compound included a certain amount of effort to increase its potency, but mainly the removal of metabolic liabilities, knowing that the target candidate profile for this type of molecule ideally requires a long pharmacological duration of cover (Fig. 6).

Once the initial hit was confirmed and some structure–activity relationship data were available, a subproject was launched to identify the target. Early on in any project there is an assessment of the risk of development of resistance.[68] This initially focuses on two factors: the number of parasites that have to be cultured before a resistant parasite can be detected in the presence of a specific drug concentration, and the degree to which the IC_{50} shifts in the cloned resistant parasites. In most cases (with the exception of the endoperoxides and one or two other scaffolds), it has been possible to raise resistant mutants, and then sequence their genomes. Formally speaking, it is actually more important to know the mechanism of resistance than it is to know the mechanism of action—two compounds that hit the same target are clearly still going to add value provided they do not fall to identical patterns of resistance generation. In the case of KAE609, the target identified was the membrane channel *Pf*ATP4,[69] a sodium channel which had been identified and annotated over a decade earlier, but had not been the subject of intense research.[70] Clearly, the technical difficulties of screening against a membrane channel had kept most groups away from it in the absence of compelling pharmacological data. Now that KAE609 has successfully shown activity at an extremely low, oral dose (30 mg) in patients in Thailand[67] there is a renewed interest in what can be done directly on the target. There are a couple of other compounds in development, which are inhibitors of the same target, the second most advanced being SJ733 (SJ557733[61,71]), which is planned to start in phase I human volunteer studies in 2016. Once again this compound came from phenotypic screening. We are not yet at the stage where new scaffolds have been designed jumping between the various active pharmacophores using insights from structural biology(Fig. 7).

The other leading example of new target identification comes from a project led by the University of Cape Town, South Africa. Preliminary screening of an industrial library at the Eskitis Institute in Queensland led to the identification of four members of the same aminopyridine family. Medicinal chemistry optimization of the compound led to the development candidate MMV 390048 ("compound 15" in[727]), which is now completing human challenge studies, and should be ready for phase II studies in 2016 (Fig. 8).

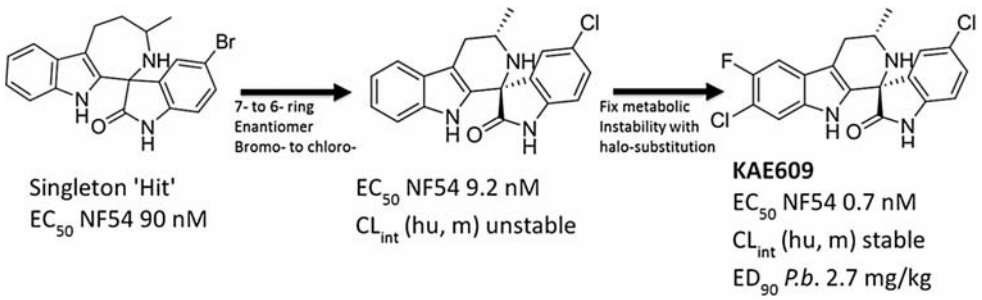

Fig. 6 Efficient optimization of a singleton "hit" from a "natural product-like" library through to KAE609. "NF54" refers to *P. falciparum* strain NF54.

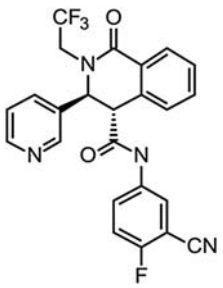

Fig. 7 Structure of SJ733 (SJ557733).

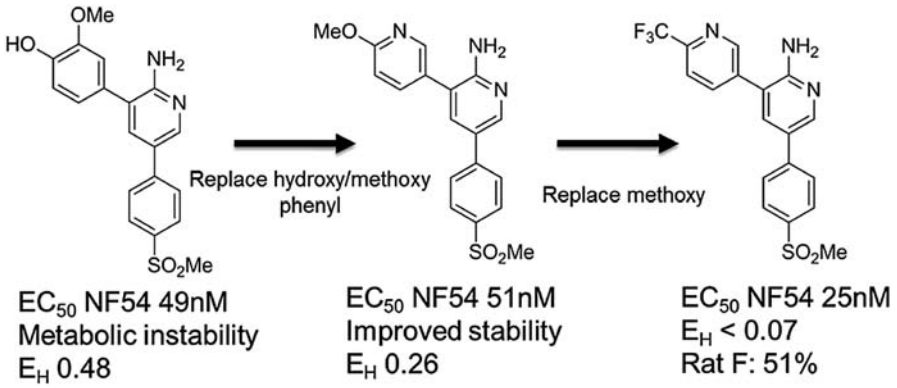

Fig. 8 Optimization of the Softfocus kinase "hit" into the lead and, finally, candidate MMV390048. E_H stands for Hepatic Extraction ratio—*eg* if the E_H is 0.3, it means that the *in vitro* data would predict that *in vivo* 30% of the compound would be removed by a first pass in the liver.

The target for these compounds was identified as a lipid kinase, phosphoinositol (PI) 4-kinase (*Pf*PI4K), by two different methods. First, a different project team independently identified the enzyme target as being the mechanism of resistance for their compound. Second, pull-down experiments using members of this chemical series have identified the enzyme by mass spectrometry.[7]

Chemical biology approaches to identify the targets are clearly going to be very important in the future. As the ideal target is one where it is difficult to raise resistant strains, then any target identification strategy which relies purely on this approach is going to be somewhat limited.

What is fascinating about both of these targets, which emerged from phenotypic screening, is their poor overlap with targets which were prioritized over the previous decade from genetic target validation approaches. In 2010, we could identify over 100 targets, which had been proposed to MMV as part of target-based drug discovery, and these did not include *Pf*ATP4. The list did include a large number of kinases, as would be expected, but the one that was conspicuously missing was *Pf*PI4K. One of the keys to future success is to make sure that the list of targets where there is a pharmacological validation is continuously updated and in the public domain. Naturally, one of the difficulties is to balance the academic needs of the original teams to achieve high-quality publications with the need for this transparency. Currently, the delays involved in preparing a high-quality manuscript submission and having it accepted greatly determine the time required for a new target to enter the public domain. This is something which needs some attention.

There are now quite a few new targets which have been described (the current state of the art is summarized in **Table 1**).

These now offer the chance to go back to primary screening collections and identify new scaffolds. Some of these targets are now validated in human patients, and many more will be validated over the next 3 or 4 years. It is important to keep reminding the community that the entrance of one molecule in the pipeline does not guarantee getting a drug out at the other end. Candidate profiles for inhibitors of each molecular target can be improved with each lesson learned by the front runners. Even when a molecule is in phase II, it still has less than a 50% chance of making it to Phase III.[24]

Table 1 New targets to fight against *Plasmodium falciparum*

Target	*Target name*	*Key molecules*	*Clinically validated*	*Key references*
*Pf*ATP4	Na^+-ATPase 4	KAE609, SJ557733, 21A092	Y	8,71
*Pf*PI4K	Phosphatidylinositol-4 kinase	MMV390048, KAF156	Y	7
*Pf*DHFR	Dihydrofolate reductase	P218	Y	73
*Pf*DXR	DXP reductoisomerase	Fosmidomycin	Y	74
*Pf*DHODH	Dihydroorotate dehydrogenase	DSM265	Y	75
*Pf*CYT bc1	Cytochrome bc1	Atovaquone	Y	76
*Pf*FP2-3	Falcipain cysteine proteases 2/3	Falcitidin	N	77,78
*Pf*HDAC1	Histone deacetylase	SB939, trichostatin A	N	79–81
*Pf*CARL	Cyclic amine resistance locus	KAF156—though uncertainty whether Carl is mechanism of resistance or action	Y	59
*Pf*EF2	Elongation factor 2	DDD107498	N	82
*Pf*PRS	Prolyl-tRNA synthetase	Halofuginone, Febrifugine	Y	83
*Pf*ThRS	Threonyl-tRNA synthetase	Borrelidin	N	84

1.17.6 Data Sharing—Dealing With Fragmentation

Access to data is a key catalyst to drug discovery. The first action which opened up the data for the malaria community was the publication of the primary datasets from the phenotypic screens.[61] The surprise was that the number of hits (roughly defined as a compound that causes significant inhibition of parasite growth at 1 μM) was around 0.7% in many of the screens, and so there are currently some 22,000 compounds where the structures have been placed into the public domain. Beyond this, in 2012, MMV and the European Bioinformatics Institute (EBI) started a collaboration to establish a one-stop shop for malaria drug data, consolidating publicly available malaria drug research into one easy-to-search database as part of the online ChEMBL database, hosted by the European Molecular Biology Laboratory-EBI (EMBL-EBI). One of the difficulties in interpreting these data is the absence of all the negative data, which helps to define pharmacophores. In theory, this could be achieved if all of the original compounds screened were made available. In practice, provided the key molecular descriptors of the inactive molecules are known, then that should suffice to start building models, which could enrich compound diversity proposals for molecules that will show activity. We are currently exploring this as a next step.

The push now is to obtain data on as much of the malaria lifecycle as possible for these compounds: as mentioned earlier, compounds with activities against the dividing liver stages, or hepatic schizonts, have potential use in chemoprotection. Compounds that kill the sexual stages (the ones which are transmitted back to the mosquito in the blood meal) could play a role in blocking the cycle of transmission—only few of today's malaria drugs achieve this. Such transmission blockade is a critical weapon in any campaign to eliminate or eradicate malaria; stopping humans infecting mosquitoes is arguably easier than stopping the mosquitoes infecting humans and certainly easier than specifically trying to cure mosquitoes once infected!

The ultimate goal of malaria research is the eradication of the disease. One of the key tools here is to simplify the treatment of disease down from the current 3-day regimen to a single encounter, as either a one-dose treatment, or as two doses taken with a short interval between them. Bearing in mind that the current artemisinin combination therapies often contain more than 3 g of active pharmaceutical ingredients, plus the excipients, it becomes clear that having more potent molecules will be a challenge that must be met. A second challenge required by the clinical community is to have molecules with improved safety. This translates into weeding out as early as possible molecules with no chance of being safe so that resources can be focused on the compounds which have the highest probability of success. In phase III trials for treatment, then any grade III adverse event is a concern, among the 1,000-2,000 (using the same style as below for 13,000, and 22,000 above) patients on the experimental medicine, and although it is clearly not possible to evaluate this without doing a large clinical study, any hints of adverse activity have to be closely followed up. One significant issue in malaria is that we need to know that the medicines are safe in children, because 85% of the patients are under the age of 5 years, and half of them are under 2, moreover this represents a very vulnerable population with high malaria mortality. In addition, the pregnancy status of many of the female patients may be difficult to assess in the field, so it is important to take into consideration any early flags in embryofetal safety studies. Although the mantra "kill [molecules] early, kill cheap" is beloved by portfolio managers, it is important not to prune the portfolio so thoroughly that nothing remains. It is also important to remember that some adverse event signals have become less significant as more and more patients, and also different types of patients, are added to the clinical trial databases.

1.17.7 Bringing the Compounds to the Biology or the Biology to the Compounds

The TCAMS (Tres Cantos Anti-Malarial Set): One of the major problems in drug discovery against protozoa is to bring together the excellent biology that exists in the academic centers with medicinal chemistry expertise, which still largely resides in industry, and in those who have recently left industry. Having identified over 13,000 screen-positive compounds, GSK has produced the TCAMS, which is available for screening, and groups interested in identifying compounds which hit their target or influence their pathway can collaborate to access the compounds.[85,86] Currently, though, the easiest way to test against such a large number of compounds is to take the biology to the compounds.

Malaria Box: We took an alternative approach and tried to identify a key set of compounds that could be shipped around the world. The first experiment, called Malaria Box[87] started by clustering the available hits into groups, and then purchasing one or more compounds from each group. The resultant compounds were then retested for quality control purposes, as it would be frustrating for biologists to test compounds, which are not known to be active against the parasite. Some 400 compounds were selected, and these were made available to anyone who requested them through a web server at www.mmv.org. There were no restrictions placed on the requestors in terms of intellectual property; if new intellectual property was identified, then the requestors were left free to proceed as they saw fit. (This is the paradox of open source, in that by being open, one cannot compel others to be open.) The Malaria Box has been shipped to over 260 different groups (Van Voorhis et al., submitted) in 30 different countries and in the first 2 years after release has already resulted in over 30 publications and 33 papers being prepared for submission. These assays have shown how producing decks of compounds and making them freely available is one way of overcoming the fragmentation of the community that works on neglected diseases. The sets have now been tested against multiple protozoan parasites as well as helminths and bacteria, with some important insights into the overall hit rates against the various parasites. By making the metabolic and pharmacokinetic data available for the compounds (currently on demand, but the goal is to publish this all as soon as possible), then any group finding a compound with potency *in vitro* can rapidly assess whether the compound has a chance of being active in an *in vivo* assay. Several groups have shown compounds to have significant *in vitro* and even *in vivo* activity.

The compounds do have potential for activity against host targets. Although a preliminary screening against human cell lines (THP-1 and MRC-5) showed no significant activity at 10 μM, subsequent testing against the National Cancer Institute panel of 60 tumor cell lines[88] showed several compounds with activity in the low micromolar range against one or more of these lines. Some of these compounds are being worked up for further analysis and *in vivo* testing. The low micromolar cut-off is also justified by the results seen in the mouse pharmacokinetics. All 400 compounds were subjected to a mouse snapshot pharmacokinetic experiment, and around one-third were capable of maintaining a close to micromolar plasma concentration over the first 24 h, from a single oral dose. This presumably reflects the fact that to kill the parasite, the compounds have to cross a number of membranes, and so the *Plasmodium* assay is already screening for highly drug-like molecules.

Pathogen Box. A second compound collection, known as the Pathogen Box, became available for delivery at the end of 2015. The key differences here were that because of a specific grant from the Bill & Melinda Gates Foundation, we obtained resources to synthesize key compounds, and so were not limited to commercially available compounds. In addition, the source for the original compounds came from a variety of different phenotypic screens including mycobacteria, other protozoan pathogens, a small number of infectious helminths, and some from emerging viruses. Again, the critical metabolism and pharmacokinetic data will be made available for all of these compounds. The selection of the compounds was done by a group of medicinal chemistry experts from the Product Development Partnerships (groups like MMW, DND*i*, TB Drug Accelerator, *etc.*) and our advisors, and so this represents the fruit of many years of screening, but also the insights from a wide variety of medicinal chemists with many different backgrounds.

Further directions for new compound collections. The broad distribution of the Malaria Box exposed the widespread hunger for interesting collections of new compounds to test in biology. In other words: for protozoan infections, most of the biology research groups are far in advance of medicinal chemistry support when compared with other neglected diseases. However, it was quite obvious that the number of groups asking for the compounds coming from disease-endemic countries was relatively small, and so in late 2014, we were able to run a call for proposals for pilot grants of $100,000 to enable researchers from Africa, Asia, and South America to test these compound decks. The hope is that there will be some common success factors here, but also that we can transfer some of the lessons on scientific and medicinal chemistry leadership to these groups. Other compound collections could be considered in a similar vein. There are over 1,500 compounds available in sets of FDA-approved medicines, but searches of the Cortellis Life Sciences information database (Thomson Reuters) show that there are almost 8,000 compounds which have been taken into clinical development for infectious diseases and so far have not been launched (most of these are discarded projects). Many of these will be able to achieve significant plasma exposure, and although some will have been stopped for safety reasons, many will have been stopped because of an insufficient pharmacodynamics effect for the specific indication(s) they were developed for, portfolio decisions and other specific reasons. Ensuring wider access to such compounds would be of great interest to the biological and medical community. The outbreak of Ebola in 2014–15 underlined the need to be prepared and to better understand the activity of known compound sets against potentially pandemic viruses. Ebola itself was not new, but very few compounds had actually been tested against it. There is clearly a need for a compound set similar to the Malaria Box, but made up of scaffolds which have been shown to have activity against a wide variety of pathogenic viruses. The prescreening of such a compound collection against existing strains of viruses, as well as the elucidation of pharmacokinetics and metabolism data would enable the community to have a head start when a new pandemic fever virus emerges. As always, the easiest way to move quickly is actually to start early.

1.17.8 Intellectual Property and Drug Discovery in Neglected Disease

One of the most widely discussed aspects of working in infectious diseases of neglected populations is the role of intellectual property. At its most basic, one of the arguments is that protection of intellectual property leads to a lack of transparency, which then slows down the discovery and development of new medicines. Although in many discussions, patents are seen as a part of the process of secrecy and control, it should not be forgotten that the patent is a contract exchanging rights to some commercial exclusivity in exchange for being transparent. Several factors therefore need to be considered in this discussion. As discussed above, one key impediment to transparency would appear to be the specific need for high-profile publications from the academic community, as discussed earlier in the target identification section. These delays may become quite lengthy, especially when papers are sent to three or four journals before being finally accepted. This sets a natural delay on data arriving in the public domain. One interesting problem we have seen with the Malaria Box is that much of the information is contained in the assays that show no activity for a particular compound, or marginal activity. These data are of course notoriously hard to publish: even with the combined data set of over 200 assays, many journals reject papers which report purely a collection of data. A second consideration about patents and intellectual property, something which has been at the heart of all of our projects at MMV, has been to see intellectual property as more of a responsibility than a right in this area. The traditional thinking that intellectual property is linked to a right to commercial exploitation cannot easily be translated into a world where there is hardly any commercial margin. In this case, the better descriptor would be *stewardship* of intellectual property rather than *ownership*. The goal would be to facilitate as wide an access as possible, with an affordable price. By gaining control of intellectual property, market access and pricing clauses can be put in at a very early stage, and the correct expectations set. Partnership with pharmaceutical companies depends on having a clear vision on the intellectual property and clarity on the freedom to operate.

1.17.9 Conclusions

Over the last decade, there has been a significant improvement in the number of new molecules and new scaffolds entering preclinical development in malaria, and in other diseases of neglected populations. In addition, the results of early screening have also led to new scaffolds in hits to leads, meaning that there should be a steady flow of new clinical candidates over the next few years, provided that funding can be sustained. In the longer term then these new molecules have led to the identification of new mechanisms of action, and the reprioritization of previously overlooked or undervalued mechanisms of action. This means that in the future we should be well-placed to identify backup compounds, for when our current frontrunner compounds fail. The project teams necessary to achieve this success consisted of a mix of academia and industry: bringing the best of both worlds together. One of the other unforeseen boosters has been the community of drug hunters outside of the mainstream pharmaceutical companies, the large numbers of advisors and mentors who have brought their many years of experience to guide and train the next generation.

There remain many gaps. Although the portfolio is numerically quite strong, the attrition rates that we are seeing are no different from the industry benchmarks for infectious disease in general. This means that there will always be a need for new chemical series, and different ways of looking at the old series. The push toward eradication means that more potent medicines will be needed in the future, but also safer medicines as they are to be used in increasingly larger number of patients and (as chemoprevention) in healthy individuals. It will be important to be able to develop a clear view on whether it is possible to realistically achieve both goals, and if not then which one is the higher priority. In any case, one of the lessons from drug discovery against parasitic diseases is that it is possible to achieve a new level of transparency of data and transparency of review, with this transparency resulting in clear scientific peer review. With the combined power of all of our teams, mentors, and advisors, we can be optimistic in the way we approach these very difficult questions. This is very important given the number of lives that depend on our future success.

Acknowledgments

The authors thank Matthew Todd (University of Sydney), Robert Don (DND*i*), and Alejandra Palermo (Royal Society of Chemistry, UK), and their MMV colleagues for helpful discussions.

References

1. Wells, T. N. C.; Hooft van Huijsduijnen, R.; Van Voorhis, W. C. Malaria Medicines: A Glass Half Full? *Nat. Rev. Drug Discov.* **2015,** *14,* 424–442.
2. Mdluli, K.; Kaneko, T.; Upton, A. The Tuberculosis Drug Discovery and Development Pipeline and Emerging Drug Targets. *Cold Spring Harb. Perspect. Med.* **2015,** *5* (6), 1–24. http://tinyurl.com/hd9jfo2.
3. Phillips, M. A. Stoking the Drug Target Pipeline for Human African Trypanosomiasis. *Mol. Microbiol.* **2012,** *86* (1), 10–14.
4. Tripathi, R. P.; Katiyar, D.; et al. Recent Developments in Search of Antifilarial Agents. *Curr. Med. Chem.* **2006,** *13* (27), 3319–3334.
5. Buckingham, S. D.; Partridge, F. A.; Sattelle, D. B. Automated, High-Throughput, Motility Analysis in Caenorhabditis Elegans and Parasitic Nematodes: Applications in the Search for New Anthelmintics. *Int. J. Parasitol. Drugs Drug Resist.* **2014,** *4* (3), 226–232.
6. Pena, I.; Pilar Manzano, M.; et al. New Compound Sets Identified From High Throughput Phenotypic Screening Against Three Kinetoplastid Parasites: An Open Resource. *Sci. Rep.* **2015,** *5,* 8771.
7. Ghidelli-Disse, S.; Lafuente-Monasterio, M. J.; et al. Identification of *Plasmodium* PI4 Kinase as Target of MMV390048 by Chemoproteomics. *Malar. J.* **2014,** *13* (Suppl. 1), 38. S21.
8. McNamara, C. W.; Lee, M. C.; et al. Targeting *Plasmodium* PI(4)K to Eliminate Malaria. *Nature* **2013,** *504* (7479), 248–253.
9. Engwerda, C. R.; Minigo, G.; Amante, F. H.; McCarthy, J. S. Experimentally Induced Blood Stage Malaria Infection as a Tool for Clinical Research. *Trends Parasitol.* **2012,** *28* (11), 515–521.
10. McCarthy, J. S.; Griffin, P. M.; et al. Experimentally Induced Blood-Stage *Plasmodium vivax* Infection in Healthy Volunteers. *J. Infect. Dis.* **2013,** *208* (10), 1688–1694.
11. McCarthy, J. S.; Sekuloski, S.; et al. A Pilot Randomised Trial of Induced Blood-Stage *Plasmodium falciparum* Infections in Healthy Volunteers for Testing Efficacy of New Antimalarial Drugs. *PLoS One* **2011,** *6* (8), e21914.
12. Stanisic, D. I.; Liu, X. Q.; et al. Development of Cultured *Plasmodium falciparum* Blood-Stage Malaria Cell Banks for Early Phase *in vivo* Clinical Trial Assessment of Anti-Malaria Drugs and Vaccines. *Malar. J.* **2015,** *14* (1), 143.
13. Bhutta, Z. A.; Sommerfeld, J.; et al. Global Burden, Distribution, and Interventions for Infectious Diseases of Poverty. *Infect. Dis. Poverty* **2014,** *3,* 21.
14. Global Burden of Disease Study, Collaborators. Global, Regional, and National Incidence, Prevalence, and Years Lived With Disability for 301 Acute and Chronic Diseases and Injuries in 188 Countries, 1990–2013: A Systematic Analysis for the Global Burden of Disease Study 2013. *Lancet* **2015,** *386* (9995), 743–800.
15. Liu, L.; Oza, S.; et al. Global, Regional, and National Causes of Child Mortality in 2000–13, With Projections to Inform Post-2015 Priorities: An Updated Systematic Analysis. *Lancet* **2015,** *385* (9966), 430–440.
16. Augen, J. Industrialized Molecular Biology, Information Biotechnology, and the Blockbuster Drug Model—Alive and Well at Age 50. *Drug Discov. Today* **2002,** *7* (20 Suppl), S157–159.
17. Kumar Kakkar, A.; Dahiya, N. The Evolving Drug Development Landscape: From Blockbusters to Niche Busters in the Orphan Drug Space. *Drug Dev. Res.* **2014,** *75* (4), 231–234.
18. Trouiller, P.; Olliaro, P.; et al. Drug Development for Neglected Diseases: A Deficient Market and a Public-Health Policy Failure. *Lancet* **2002,** *359* (9324), 2188–2194.
19. Svennebring, A. M.; Wikberg, J. E. Net Present Value Approaches for Drug Discovery. *Springerplus* **2013,** *2* (1), 140.
20. Deng, X.; Gujjar, R.; et al. Structural Plasticity of Malaria Dihydroorotate Dehydrogenase Allows Selective Binding of Diverse Chemical Scaffolds. *J. Biol. Chem.* **2009,** *284* (39), 26999–27009.
21. Kalanon, M.; McFadden, G. I. Malaria, *Plasmodium falciparum* and Its Apicoplast. *Biochem. Soc. Trans.* **2010,** *38* (3), 775–782.
22. Goldberg, D. E.; Cowman, A. F. Moving in and Renovating: Exporting Proteins From *Plasmodium* Into Host Erythrocytes. *Nat. Rev. Microbiol.* **2010,** *8* (9), 617–621.

23. Nakatani, K.; Ishikawa, H.; Aono, S.; Mizutani, Y. Heme-Binding Properties of Heme Detoxification Protein From *Plasmodium falciparum*. *Biochem. Biophys. Res. Commun.* **2013,** *439* (4), 477–480.
24. Burrows, J. N.; Hooft van Huijsduijnen, R.; et al. Designing the Next Generation of Medicines for Malaria Control and Eradication. *Malar. J.* **2013,** *12,* 187.
25. DiMasi, J. A.; Feldman, L.; Seckler, A.; Wilson, A. Trends in Risks Associated With New Drug Development: Success Rates for Investigational Drugs. *Clin. Pharmacol. Ther.* **2010,** *87* (3), 272–277.
26. Frantz, S. Therapeutic Area Influences Drug Development Costs. *Nat. Rev. Drug Discov.* **2004,** *3* (6), 466–467.
27. Watsierah, C. A.; Ouma, C. Access to Artemisinin-Based Combination Therapy (ACT) and Quinine in Malaria Holoendemic Regions of Western Kenya. *Malar. J.* **2014,** *13,* 290.
28. Rees, M. A Longitude Prize for the Twenty-First Century. *Nature* **2014,** *509* (7501), 401.
29. Noor, W. Placing Value on FDA's Priority Review Vouchers. *Vivo* **2009,** *27* (8), 1–8.
30. Robertson, A. S.; Stefanakis, R.; Joseph, D.; Moree, M. The Impact of the US Priority Review Voucher on Private-Sector Investment in Global Health Research and Development. *PLoS Negl. Trop. Dis.* **2012,** *6* (8), e1750.
31. Simpson, I.; Blakemore, J. Industry Update. *Ther. Deliv.* **2015,** *6* (4), 411–417.
32. Kesselheim, A. S.; Maggs, L. R.; Sarpatwari, A. Experience With the Priority Review Voucher Program for Drug Development. *JAMA* **2015,** *314* (16), 1687–1688.
33. Morrison, C. AbbVie Buys Last Available Priority Voucher for $350 Million. *Nat. Biotechnol.* **2015,** *33* (11), 1120.
34. Mullard, A. Priority Review Voucher Pitfalls. *Nat. Rev. Drug Discov.* **2015,** *14* (12), 811.
35. Calcoen, D.; Elias, L.; Yu, X. What Does It Take to Produce a Breakthrough Drug? *Nat. Rev. Drug Discov.* **2015,** *14* (3), 161–162.
36. Mossallam, S. F.; Amer, E. I.; El-Faham, M. H. Efficacy of Synriam, a New Antimalarial Combination of OZ277 and Piperaquine, Against Different Developmental Stages of Schistosoma Mansoni. *Acta Trop.* **2015,** *143,* 36–46.
37. Toure, O. A.; Valecha, N.; et al. A Phase 3, Double-Blind, Randomized Study of Arterolane Maleate-Piperaquine Phosphate vs Artemether-Lumefantrine for Falciparum Malaria in Adolescent and Adult Patients in Asia and Africa. *Clin. Infect. Dis.* **2016,** *62* (8), 964–971.
38. Kindermans, J. M.; Pilloy, J.; Olliaro, P.; Gomes, M. Ensuring Sustained ACT Production and Reliable Artemisinin Supply. *Malar. J.* **2007,** *6,* 125.
39. Peplow, M. Synthetic Biology's First Malaria Drug Meets Market Resistance. *Nature* **2016,** *530* (7591), 389–390.
40. Moehrle, J. J.; Duparc, S.; et al. First-in-Man Safety and Pharmacokinetics of Synthetic Ozonide OZ439 Demonstrates an Improved Exposure Profile Relative to Other Peroxide Antimalarials. *Br. J. Clin. Pharmacol.* **2013,** *75* (2), 524–537.
41. Phyo, A. P.; Jittamala, P.; et al. Antimalarial Activity of Artefenomel (OZ439), a Novel Synthetic Antimalarial Endoperoxide, in Patients with *Plasmodium falciparum* and *Plasmodium vivax* Malaria: An Open-Label Phase 2 Trial. *Lancet Infect. Dis.* **2015,** *16,* 61–69.
42. Wang, X.; Dong, Y.; et al. Comparative Antimalarial Activities and ADME Profiles of Ozonides (1,2,4-Trioxolanes) OZ277, OZ439, and Their 1,2-Dioxolane, 1,2,4-Trioxane, and 1,2,4,5-Tetraoxane Isosteres. *J. Med. Chem.* **2013,** *56,* 2547–2555.
43. Held, J.; Supan, C.; et al. Ferroquine and Artesunate in African Adults and Children With *Plasmodium falciparum* Malaria: A Phase 2, Multicentre, Randomised, Double-Blind, Dose-Ranging, Non-Inferiority Study. *Lancet Infect. Dis.* **2015**.
44. Wells, T. N. C.; Hooft van Huijsduijnen, R. Ferroquine: Welcome to the Next Generation of Antimalarials (Commentary). *Lancet Infect. Dis.* **2015,** *15* (12), 1365–1366. http://dx.doi.org/10.1016/S1473-3099(15)00148-6.
45. Kurth, F.; Belard, S.; Basra, A.; Ramharter, M. Pyronaridine: A New 'Old' Drug on the Verge of Entering the Antimalarial Armamentarium. *Expert Rev. Anti Infect. Ther.* **2011,** *9* (4), 393–396.
46. Jiménez-Díaz, M. B.; Mulet, T.; et al. Improved Murine Model of Malaria Using *Plasmodium falciparum* Competent Strains and Non-Myelodepleted NOD–SCID IL2Rγ−Null Mice Engrafted With Human Erythrocytes. *Antimicrob. Agents Chemother.* **2009,** *53* (10), 4533–4536.
47. Coteron, J. M.; Marco, M.; et al. Structure-Guided Lead Optimization of Triazolopyrimidine-Ring Substituents Identifies Potent *Plasmodium falciparum* Dihydroorotate Dehydrogenase Inhibitors With Clinical Candidate Potential. *J. Med. Chem.* **2011,** *54* (15), 5540–5561.
48. Phillips, M. A.; Lotharius, J.; et al. A Long-Duration Dihydroorotate Dehydrogenase Inhibitor (DSM265) for Prevention and Treatment of Malaria. *Sci. Transl. Med.* **2015,** *7* (296), 296ra111.
49. McCarthy, J. S.; Lotharius, J.; et al. A Phase I/Ib Study to Investigate the Safety, Tolerability and Pharmacokinetic Profile of DSM265 in Healthy Subjects and Then Its Antimalarial Activity in Induced Blood Stage *Plasmodium falciparum* Infection. ASTMH Annual Meeting, Abstract 675**;** 2014; pp 204–205.
50. Gomez-Perez, G. P.; Legarda, A.; et al. Controlled Human Malaria Infection by Intramuscular and Direct Venous Inoculation of Cryopreserved *Plasmodium falciparum* Sporozoites in Malaria-Naive Volunteers: Effect of Injection Volume and Dose on Infectivity Rates. *Malar. J.* **2015,** *14,* 306.
51. Shekalaghe, S.; Rutaihwa, M.; et al. Controlled Human Malaria Infection of Tanzanians by Intradermal Injection of Aseptic, Purified, Cryopreserved *Plasmodium falciparum* Sporozoites. *Am. J. Trop. Med. Hyg.* **2014,** *91* (3), 471–480.
52. Chatelain, E. Chagas Disease Drug Discovery: Toward a New Era. *J. Biomol. Screen.* **2015,** *20* (1), 22–35.
53. Van Voorhis, W. C.; Hooft van Huijsduijnen, R.; Wells, T. N. C. Profile of William C. Campbell, Satoshi Ōmura, and Youyou Tu, 2015 Nobel Laureates in Physiology or Medicine: Where New Drugs Come From: A Nobel Tale of Ancient Chinese Texts and a Japanese Golf Course. *Proc. Natl. Acad. Sci. U. S. A.* **2015,** *112,* 52. http://dx.doi.org/10.1073/pnas.1520952112.
54. Payne, D. J.; Gwynn, M. N.; Holmes, D. J.; Pompliano, D. L. Drugs for Bad Bugs: Confronting the Challenges of Antibacterial Discovery. *Nat. Rev. Drug Discov.* **2007,** *6* (1), 29–40.
55. Cho, S. H.; Warit, S.; et al. Low-Oxygen-Recovery Assay for High-Throughput Screening of Compounds Against Nonreplicating *Mycobacterium tuberculosis*. *Antimicrob. Agents Chemother.* **2007,** *51* (4), 1380–1385.
56. Pethe, K.; Bifani, P.; et al. Discovery of Q203, a Potent Clinical Candidate for the Treatment of Tuberculosis. *Nat. Med.* **2013,** *19* (9), 1157–1160.
57. Silva-Miranda, M.; Ekaza, E.; et al. High-Content Screening Technology Combined With a Human Granuloma Model as a New Approach to Evaluate the Activities of Drugs Against *Mycobacterium tuberculosis*. *Antimicrob. Agents Chemother.* **2015,** *59* (1), 693–697.
58. Schuster, F. L. Cultivation of *Plasmodium* spp. *Clin. Microbiol. Rev.* **2002,** *15* (3), 355–364.
59. Meister, S.; Plouffe, D. M.; et al. Imaging of *Plasmodium* Liver Stages to Drive Next-Generation Antimalarial Drug Discovery. *Science* **2011,** *334* (6061), 1372–1377.
60. Gamo, F. J.; Sanz, L. M.; et al. Thousands of Chemical Starting Points for Antimalarial Lead Identification. *Nature* **2010,** *465* (7296), 305–310.
61. Guiguemde, W. A.; Shelat, A. A.; et al. Chemical Genetics of *Plasmodium falciparum*. *Nature* **2010,** *465* (7296), 311–315.
62. Avery, V. M.; Bashyam, S.; et al. Screening and Hit Evaluation of a Chemical Library Against Blood-Stage *Plasmodium falciparum*. *Malar. J.* **2014,** *13* (1), 190.
63. Leroy, D.; Campo, B.; et al. Defining the Biology Component of the Drug Discovery Strategy for Malaria Eradication. *Trends Parasitol.* **2014,** *30* (10), 478–490.
64. Katsuno, K.; Burrows, J. N.; et al. Hit and Lead Criteria in Drug Discovery for Infectious Diseases of the Developing World. *Nat. Rev. Drug Discov.* **2015,** *14,* 751–758.
65. Leong, F. J.; Li, R.; et al. A First-in-Human Randomized, Double-Blind, Placebo-Controlled, Single- and Multiple-Ascending Oral Dose Study of Novel Antimalarial Spiroindolone KAE609 (Cipargamin), to Assess the Safety, Tolerability and Pharmacokinetics in Healthy Adult Volunteers. *Antimicrob. Agents Chemother.* **2014,** *58* (10), 6209–6214.
66. Stein, D. S.; Jain, J. P.; et al. Open-Label, Single-Dose, Parallel-Group Study in Healthy Volunteers To Determine the Drug–Drug Interaction Potential Between KAE609 (Cipargamin) and Piperaquine. *Antimicrob. Agents Chemother.* **2015,** *59* (6), 3493–3500.
67. White, N. J.; Pukrittayakamee, S.; et al. Spiroindolone KAE609 for Falciparum and Vivax Malaria. *N. Engl. J. Med.* **2014,** *371* (5), 403–410.
68. Chugh, M.; Scheurer, C.; et al. Identification and Deconvolution of Antimalarial Compounds Cross-Resistance Signals Using Multidrug-Resistant *Plasmodium falciparum* Strains. *Antimicrob. Agents Chemother.* **2014,** *59* (2), 1110–1118.
69. Spillman, N. J.; Allen, R. J.; et al. Na(+) Regulation in the Malaria Parasite *Plasmodium falciparum* Involves the Cation ATPase PfATP4 and Is a Target of the Spiroindolone Antimalarials. *Cell Host Microbe* **2013,** *13* (2), 227–237.

70. Krishna, S.; Woodrow, C.; et al. Expression and Functional Characterization of a *Plasmodium falciparum* Ca2 + − ATPase (PfATP4) Belonging to a Subclass Unique to Apicomplexan Organisms. *J. Biol. Chem.* **2001,** *276* (14), 10782–10787.
71. Jimenez-Diaz, M. B.; Ebert, D.; et al. (+)-SJ733, a Clinical Candidate for Malaria that Acts Through ATP4 to Induce Rapid Host-Mediated Clearance of *Plasmodium*. *Proc. Natl. Acad. Sci. U. S. A.* **2014,** *111* (50), E5455–E5462.
72. Younis, Y.; Douelle, F.; et al. 3,5-Diaryl-2-Aminopyridines as a Novel Class of Orally Active Antimalarials Demonstrating Single Dose Cure in Mice and Clinical Candidate Potential. *J. Med. Chem.* **2012,** *55* (7), 3479–3487.
73. Yuthavong, Y.; Tarnchompoo, B.; et al. Malarial Dihydrofolate Reductase as a Paradigm for Drug Development Against a Resistance-Compromised Target. *Proc. Natl. Acad. Sci. U. S. A.* **2012,** *109* (42), 16823–16828.
74. Jomaa, H.; Wiesner, J.; et al. Inhibitors of the Nonmevalonate Pathway of Isoprenoid Biosynthesis as Antimalarial Drugs. *Science* **1999,** *285* (5433), 1573–1576.
75. Deng, X.; Kokkonda, S.; et al. Fluorine Modulates Species Selectivity in the Triazolopyrimidine Class of *Plasmodium falciparum* Dihydroorotate Dehydrogenase Inhibitors. *J. Med. Chem.* **2014,** *57* (12), 5381–5394.
76. Looareesuwan, S.; Viravan, C.; et al. Clinical Studies of Atovaquone, Alone or in Combination With Other Antimalarial Drugs, for Treatment of Acute Uncomplicated Malaria in Thailand. *Am. J. Trop. Med. Hyg.* **1996,** *54* (1), 62–66.
77. Salas-Sarduy, E.; Cabrera-Munoz, A.; et al. Antiparasitic Effect of a Fraction Enriched in Tight-Binding Protease Inhibitors Isolated From the Caribbean Coral Plexaura Homomalla. *Exp. Parasitol.* **2013,** *135* (3), 611–622.
78. Wang, J.; Kaiser, M.; Copp, B. R. Investigation of Indolglyoxamide and Indolacetamide Analogues of Polyamines as Antimalarial and Antitrypanosomal Agents. *Mar. Drugs* **2014,** *12* (6), 3138–3160.
79. Hansen, F. K.; Sumanadasa, S. D.; et al. Discovery of HDAC Inhibitors With Potent Activity Against Multiple Malaria Parasite Life Cycle Stages. *Eur. J. Med. Chem.* **2014,** *82C,* 204–213.
80. Sumanadasa, S. D.; Goodman, C. D.; et al. Antimalarial Activity of the Anticancer Histone Deacetylase Inhibitor SB939. *Antimicrob. Agents Chemother.* **2012,** *56* (7), 3849–3856.
81. Trenholme, K.; Marek, L.; et al. Lysine Acetylation in Sexual Stage Malaria Parasites Is a Target for Antimalarial Small Molecules. *Antimicrob. Agents Chemother.* **2014,** *58* (7), 3666–3678.
82. Baragaña, B.; Hallyburton, I.; et al. A Novel Multiple-Stage Antimalarial Agent that Inhibits Protein Synthesis. *Nature* **2015,** *522* (7556), 315–320.
83. Herman, J. D.; Pepper, L. R.; et al. The Cytoplasmic Prolyl-tRNA Synthetase of the Malaria Parasite Is a Dual-Stage Target of Febrifugine and Its Analogs. *Sci. Transl. Med.* **2015,** *7* (288), 288ra277.
84. Aczárate, I. G.; Marin-Garcia, P.; et al. Insights Into the Preclinical Treatment of Blood-Stage Malaria by the Antibiotic Borrelidin. *Br. J. Pharmacol.* **2013,** *169* (3), 645–658.
85. Rueda, L.; Castellote, I.; et al. Cyclopropyl Carboxamides: A New Oral Antimalarial Series Derived from the Tres Cantos Anti-Malarial Set (TCAMS). *ACS Med. Chem. Lett.* **2011,** *2* (11), 840–844.
86. Weidner, T.; Nasereddin, A.; et al. Novel 2-Phenoxyanilide Congeners Derived From a Hit Structure of the TCAMS: Synthesis and Evaluation of Their *in vitro* Activity Against *Plasmodium falciparum*. *Molecules* **2016,** *21* (2).
87. Spangenberg, T.; Burrows, J. N.; et al. The Open Access Malaria Box: A Drug Discovery Catalyst for Neglected Diseases. *PLoS One* **2013,** *8* (6), e62906.
88. Shoemaker, R. H. The NCI60 Human Tumour Cell Line Anticancer Drug Screen. *Nat. Rev. Cancer* **2006,** *6* (10), 813–823.

Relevant Websites

www.mmv.org—Medicines for Malaria Venture (MMV).
www.ebi.ac.uk/chembl/malaria—Molecular Biology Laboratory-European Bioinformatics Institute (EMBL-EBI).

1.18 European Lead Factory

F Giordanetto, Taros Chemicals GmbH & Co. KG, Dortmund, Germany
P Jones, University of Dundee, Dundee, Scotland, United Kingdom
A Nelson, University of Leeds, Leeds, United Kingdom
J Benningshof and G Müller, Mercachem, Nijmegen, The Netherlands
A Pannifer, University of Dundee, Dundee, Scotland, United Kingdom
S van Boeckel, Pivot Park Screening Center, Oss, The Netherlands
D Tzalis, Taros Chemicals GmbH & Co. KG, Dortmund, Germany

© 2017 Elsevier Ltd. All rights reserved.

1.18.1 Introduction 505
1.18.2 The Joint European Compound Library 505
1.18.2.1 EFPIA-Contributed Collection 505
1.18.2.2 Public Compound Collection 506
1.18.3 European Screening Center and Hit List Generation 512
1.18.3.1 HTS Assay Requirements and Assay Development 513
1.18.3.2 Screening Cascade, Triaging to a Qualified Hit List (QHL), and Development to an Improved Hit List (IHL) 513
1.18.3.3 The Intricate Triaging Process, What Is the Context of a Program? 514
1.18.3.4 Development to IHL; Hit Characterization 515
1.18.4 The Honest Data Broker 515
1.18.4.1 Triage Tools 515
1.18.4.2 Intellectual Property Protection and Enforcement of ELF Rules 517
1.18.4.3 Project Organization 517
1.18.5 Summary and Outlook 517
Acknowledgments 518
References 518
Relevant Websites 519

1.18.1 Introduction

Despite the significant investments and advances that have been made into basic and applied pharmaceutical research in recent decades, the overall success rate in drug discovery remains low.[1,2] As a result, the unmet medical need in virtually all therapeutic areas is still considerable and poses a serious threat to the well-being of society.[3] In response to this, the drug research landscape is constantly modifying itself in search of a more sustainable business model and precompetitive, open innovation approaches are evaluated.[4] In this regard, the focus is on sharing the investment risks and improving the attrition rates of drug discovery by accessing the best ideas and solutions to problems and pooling together complementary talents and resources. With this in mind, the Innovative Medicine Initiative's European Lead Factory (ELF) project was launched with the aim to create a collaborative lead generation platform to seed and execute the early stages of drug discovery.[5] By combining an industrial quality high-throughput screening (HTS) infrastructure (European Screening Center) and the state-of-the-art Joint European Compound Collection (JECL), the ELF is granting any European private company or public entity access to resources that were once the pride and prerogative of only the largest pharmaceutical companies. In the following, we describe the ELF assets in detail and how these are intimately interlinked and successfully exploited in the ELF hit identification, evaluation, and exploration workflow.

1.18.2 The Joint European Compound Library

Identifying drug-like, well-validated, hit-and-lead compounds active against novel biological targets is the central aim of the ELF. Building a competitive HTS library to identify the initial hit matter underpins the efforts of the ELF consortium to achieve this goal. The following describes the dual approach taken by the ELF to assemble and maintain a high-quality compound collection for target-based biological screening.

1.18.2.1 EFPIA-Contributed Collection

The ELF's HTS library (the Joint European Compound Library—JECL) was initially established through the contribution of a total of 327,000 compounds from seven company members of the European Federation of Pharmaceutical Industries and Associations

(EFPIA). Combining these seven subsets into a coherent single library was the first goal and ensuring that the collection consisted of diverse, physicochemically attractive compounds, without duplicates, was crucial.[6] The main challenge in deduplication and assessing compound similarity was the requirement for compound structure confidentiality. The structures could not be exported beyond each company's firewall making direct comparison between subsets problematic. This difficulty was overcome by distributing a Pipeline Pilot protocol[7] to each of the EFPIA members, which calculated a range of physicochemical properties (eg, molecular weight, logP, topological polar surface area (TPSA)) together with the extended connectivity fingerprints (ECFP6) of all the molecules in the subset they were proposing to contribute. This protocol was run internally within each company. The results were returned to a central location at the University of Dundee for analysis and compounds with identical ECFP6 fingerprints were identified and deduplicated. Replacement compounds were requested and after a small number of iterations, a unique set was achieved. Prior to selecting compounds as candidate molecules for the ELF, property-based filtering was carried out within the EFPIA companies to ensure drug/lead-likeness of the library. An example of the filtering done included SMARTS filtering to remove compounds with undesirable features, purity check, physicochemical property filtering, removal of compounds having associated intellectual property, and, crucially, removal of compounds present in commercial databases. As a result, the physicochemical properties of the subsets were already attractive when contributed to the JECL, as shown in **Fig. 1**. Diversity analysis within and between the seven subsets showed that each subset largely sampled different areas of chemical space while within each subset, many compounds had analogs within a Tanimoto distance of 0.5. These analogs are likely to provide structure activity relationships (SAR) and support clustering and activity model-building in the HTS triage process. Consequently, the JECL has a high diversity content, as displayed in **Fig. 1**. This was a highly attractive combination and these compounds form the foundation of the JECL. In compiling the JECL, there was very little overlap of identical compounds prior to deduplication, which is in accordance with analyses done by AstraZeneca/Bayer and Johnson & Johnson/3DP,[9–11] who compared large HTS sets and further highlights that compound swaps are a simple and efficient way to rapidly increase library diversity and fully exploit assets.

1.18.2.2 Public Compound Collection

This initial set is now being complemented with up to an additional 200,000 compounds (here termed the Public Compound Collection (PCC)) in a collaborative effort involving a unique blend of chemistry expertise from 10 academic groups and 6 small & medium enterprises (SMEs), which form the ELF Chemistry Consortium.[12] The PCC will have drug-relevant properties, but also aims to capture novel and biologically relevant motifs that are poorly represented in current compound collections. The PCC is based on proposals for small molecule libraries that are submitted to the ELF via a web-based chemoinformatic tool.[12] Library proposals may be defined by specifying the structure of a scaffold, including the positions of variable substituents (as R1, R2, R3, etc.); alternative possible substituents can then be selected from predefined lists. Before submission to the ELF, the submitter is presented with information on the novelty and molecular properties of the compounds proposed. Once satisfied, that the assessment criteria have been addressed, the submitter may submit the proposal for consideration. Library proposals are considered by the ELF's Library Selection Committee that comprises eight scientists with complementary backgrounds (academic and industrial; synthetic and medicinal chemistry). The proposals are assessed against six criteria (**Table 1**) using a simple scoring system: from 0 (criterion not met) to 3 (excellent fit with the criterion). The committee reaches a consensus by scoring against each of the criteria and decides on an outcome for the proposal. Crucially, subsequent to processing of the proposal, the scores, feedback, and outcome are communicated to the submitter.

The accepted library proposals are then validated experimentally by academic and SME ELF consortium partners. The overall goal of this validation phase is to maximize the probability of progress of a library idea to the final production phase, where the actual library is synthesized in its entirety and added to the JECL. Key success factors, such as chemical feasibility, scalability, and final diversity of the envisioned scaffold, and the derivable library are thus being probed. The chances of success are highest when the chemistry involved is well validated rather than speculative in nature. This includes, for example, the scalability of key synthetic steps and the tolerability of diversity steps to the planned reagent space. Conversely, when only slight relatedness to chemical steps for which an ambiguous precedent is available in the literature is proposed, an increased amount of resources and time need to be invested during validation. Clearly, the majority of ELF library proposals having very high novelty content typically fall into this latter category. For entirely virtual proposals, different routes toward the scaffold are being devised and reduced to practice, commonly on a multigram scale. Routes are being optimized with respect to the required number of synthetic manipulations, upscaling potential, orthogonality of decoration chemistry, and availability of required starting materials and reagents. Once difficulties with the originally proposed and selected scaffold occur (eg, nonscalable chemistry route, limited decoration chemistry), the ELF Validation Chemistry Management Team is tasked with deciding on either further examination involving additional chemistry resources, modification of the original scaffold into a more feasible scaffold, or rejection of the scaffold.

In the following, three distinct examples will highlight (i) a validation attempt that failed, (ii) a scaffold validation project that succeeded within the very short time frame of only 1 month, and (iii) a validation project in which a specific approach was required to handle dangerous intermediates at large scale. **Scheme 1** depicts the envisioned synthetic route toward the final decorated library scaffold **5** clearly highlighting the synthetic step that failed, that is, the amide formation converting acid **3** to amide **4**. The key intermediate **3** was prepared in three steps.[18] During the envisioned amide coupling, the exocyclic double bond isomerized leading to a loss of the stereogenic center, as in by-product **6** (**Scheme 1**).

Library proposal yielding **14** (**Scheme 2**) progressed through the validation process in only 1 month, due to the fact that key steps in the planned route were based on solid literature precedence.[19] Key step in the preparation of **14** is the enantioselective

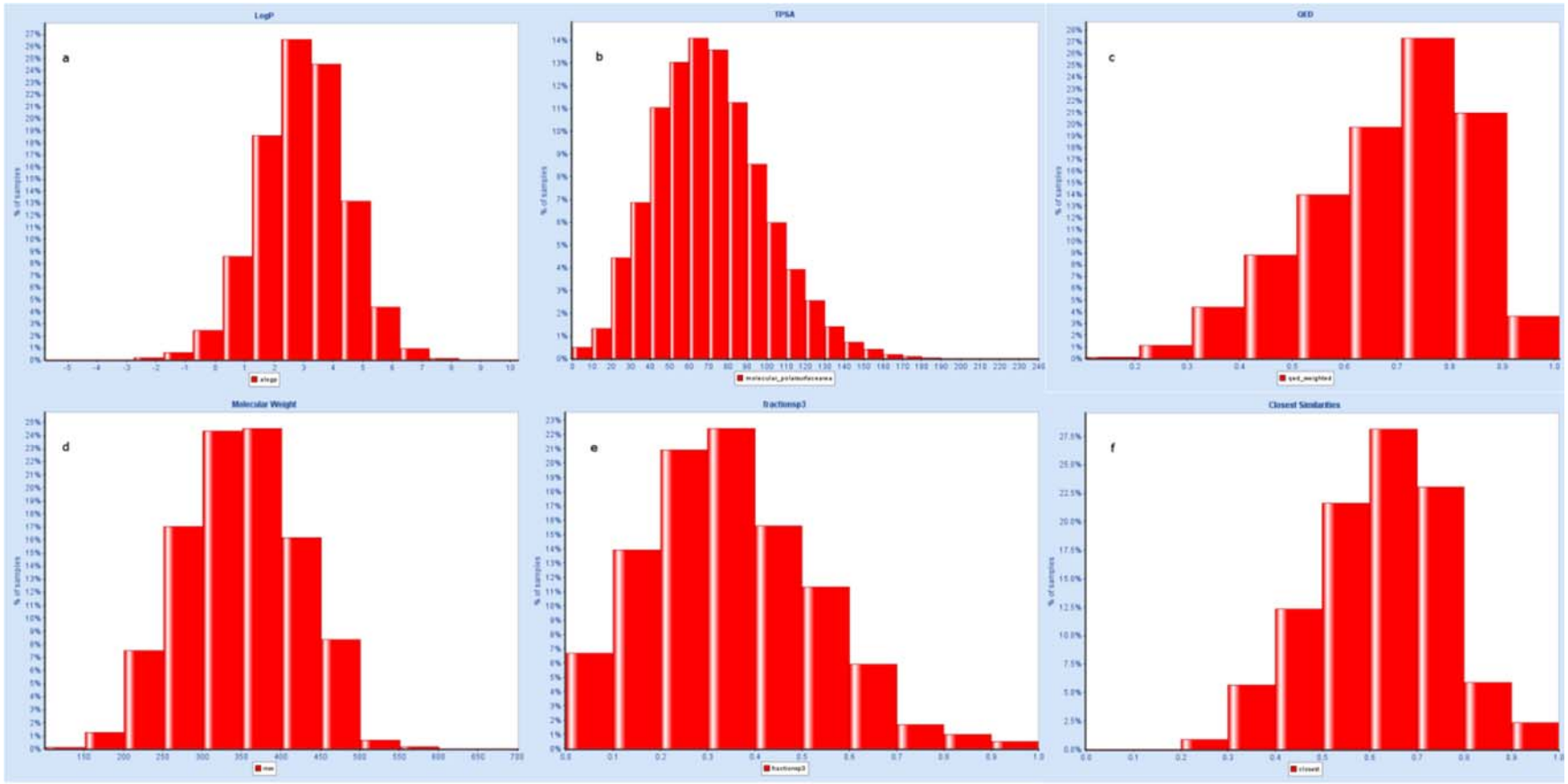

Fig. 1 Physicochemical and diversity profile of the JECL. Frequency analysis of (A) calculated logP, (B) topological polar surface area (*TPSA*), (D) molecular weight (*MW*), (E) fraction of sp^3 carbon atoms, and (C) quantitative estimate of drug-likeness (*QED*) score,[8] (F) nearest neighbor Tanimoto similarity based on extended connectivity fingerprints (ECFP6).

Table 1 Criteria for the review and selection of library proposals for inclusion in the public compound collection (*PCC*) set of the ELF's JECL

Criterion	*Notes*
Molecular properties	Assessment for drug-relevant molecular properties [13–15]
Structural features	Assessment of structural features that may constitute a liability in screening compounds, as defined by a collection of substructure filters contributed by the pharmaceutical companies participating in the ELF,[6] for example, alkylating agents, or potential intercalating compounds
Novelty	Assessment of novelty with respect to commercially available compounds[16]; patented compounds[17]; existing JECL compounds and compounds based on previous submissions to the consortium. Please note that novelty with respect to the scientific literature is not assessed during the selection of library proposals
Diversity potential	Assessment of the ability to deliver a library of diverse compounds. It is usually preferable for variable groups to be introduced late in the synthetic sequence. Most libraries require at least two diversity points
Synthetic tractability	Assessment of the likely synthetic accessibility of the library based on the precedent provided and consideration of issues of selectivity
Innovative library design	Assessment of the rationale that has been used for library design. Many different approaches might be considered to be innovative; for example, natural product-inspired libraries, or libraries designed to address a particular class of protein targets

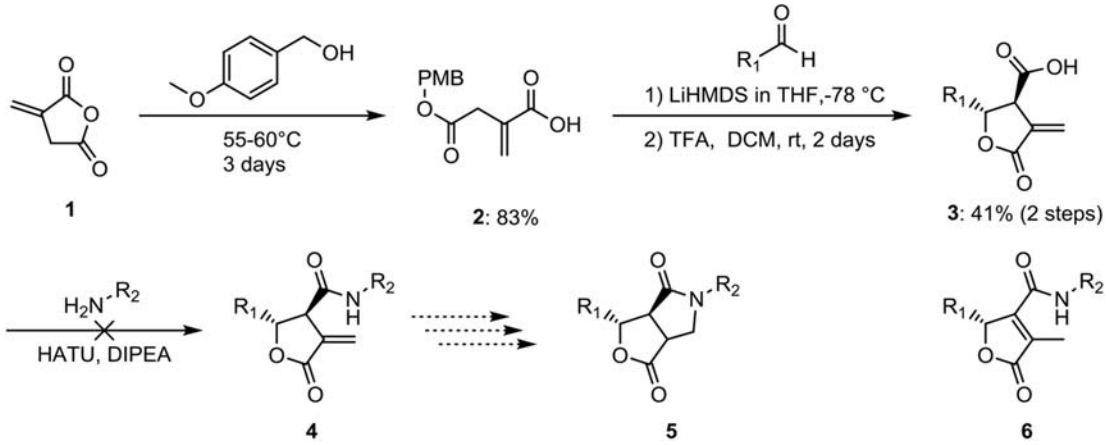

Scheme 1 A failed library validation project.

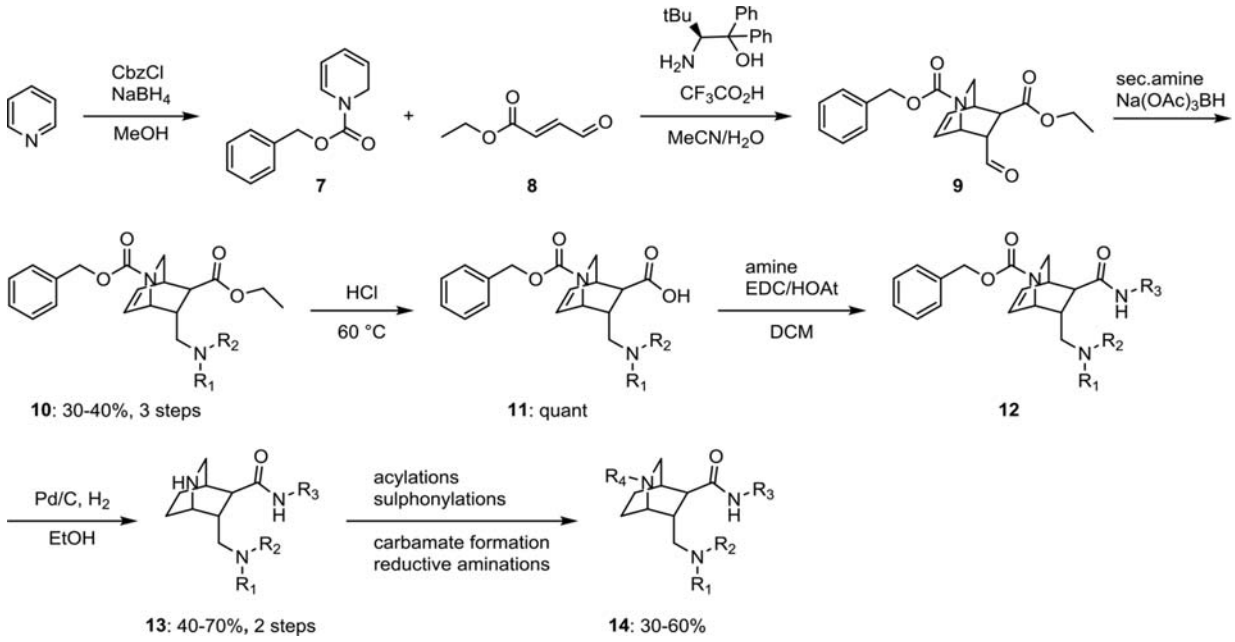

Scheme 2 A successful library validation project completed within a 1-month time frame.

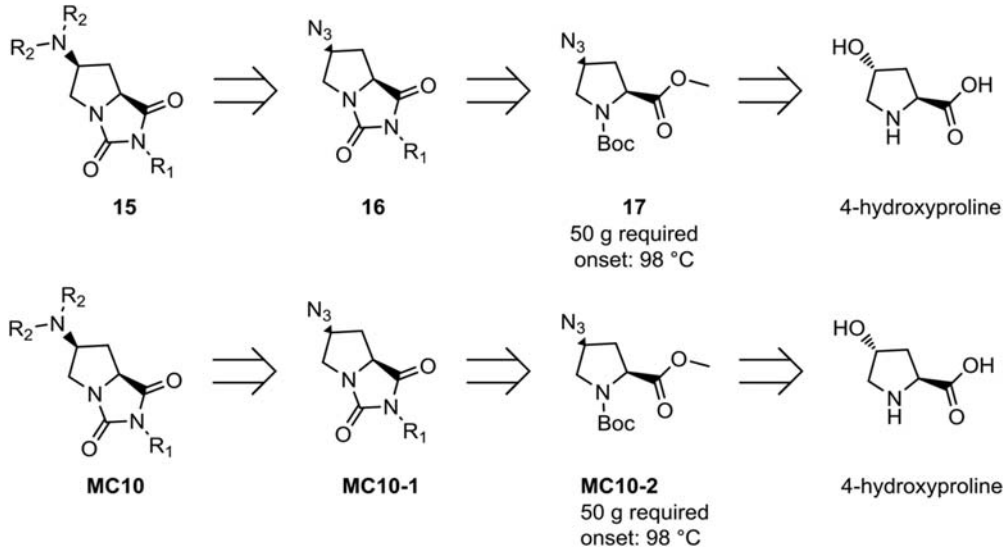

Scheme 3 Retrosynthetic analysis of library scaffold **15**.

Diels-Alder reaction of 1,2-dihydropyridine **7** and aldehyde **8** using an β-amino alcohol organo-catalyst. The isolated isoquinuclidine **9** was not stable and hence was used crude in the subsequent reductive amination affording compound **10**. Further synthetic manipulations proceeded without any issues.

Finally, the chemical validation toward the 6-aminotetrahydro-1*H*-pyrrolo[1,2-c]imidazole-1,3(2*H*)-dione-based library (**15**, Scheme 3) features a chemically interesting detail in that a flow chemistry-based process had to be established to ensure scalability of the scaffold. The retrosynthetic analysis leads to hydroxyproline via azide intermediate **17** that is finally required in a multigram scale.

During chemical validation, the synthesis of azide **17** from mesylated hydroxyproline **19** (Scheme 4) was possible, but only at elevated temperatures. It turned out that the azide is thermally unstable and has a low onset temperature of 98°C, rendering any

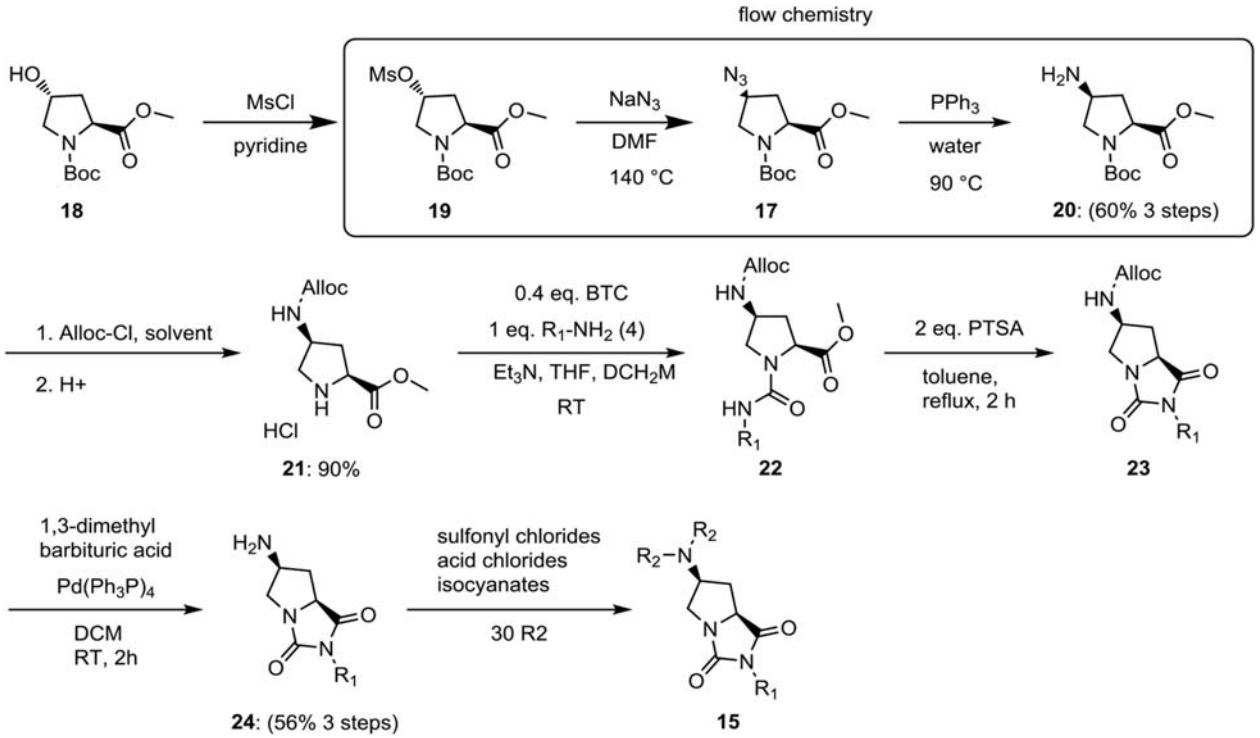

Scheme 4 Library validation project in which a flow chemistry approach was required to handle dangerous intermediates at large scale.

production scale synthesis prohibitive. For the synthesis of ELF library **15**, 50 g of the azide was required and safety regulations would not permit the preparation of the material on this scale. To mitigate these safety concerns, a flow process was designed, as depicted in Fig. 2. The preparation of azide **17** as well as its direct reduction was carried out in flow. After isolation of amine **20**, the material was protected as a carbamate. For the introduction of the first peripheral R group, an isocyanate intermediate was prepared, which was reacted for validation purposes with four different amines. Urea intermediate **22** was cyclized under acidic conditions. Removal of the Alloc group using an amine-free scavenger gave building blocks **24**, which were used to probe the library chemistry with acyl chlorides, sulfonyl chlorides, and isocyanates, respectively.

As of the end of Q3/2015, of approximately 450 accepted scaffold proposals, validation campaigns have been completed for 230 proposals. Here, around 170 succeeded in the chemical validation process, thus being progressed to library production. In total, 60 approved scaffold ideas were stopped due to failure during the chemical validation. The longest route that was established for a final library compound comprised 16 distinct synthetic steps, whereas the shortest routes toward final compounds usually employ multicomponent reactions in which a final compound is produced in a single synthetic step. On average, a scaffold is produced over a synthetic procedure of five to six steps, often followed by protective group manipulations prior to introduction of the final decorating R groups. After more than 2 years and 6 months of experience in scaffold and library validation work, best practice routines to aid the ELF library validation process have been defined, as shown in Table 2.

After the chemical validation step has succeeded, for each scaffold approximately 800–900 distinct Public Compounds with an individually optimized decoration pattern are nominated for synthesis considering optimal coverage of the feasible chemical space (also allowing for initial SAR of screening hits) and providing compliance with predefined physicochemical properties of the individual Public Compounds.[19] This target number of Public Compounds allows for attrition due to chemical reactivity, instability, or purification issues in the library production run. Selection of the distinct reagents that will constitute the final set of decorating groups will be furthermore directed by a set of medicinal chemistry-based guidelines to avoid, for example, toxic functionalities and groups with frequent hitter and pan-assay interference potential.[19]

The validated synthetic protocol is then executed during the production phase, and final compounds meeting the JECL quality criteria for purity (LC–MS purity >85%) and quantity (>5 μmol) are then added to the JECL and plated for the ELF high-throughput screens. Data sharing across the various ELF chemistry consortium partners, from the original library enumeration to experimental validation procedures, to the shipment of the final compounds to the screening centers is facilitated by TarosGate 2, a chemistry management solution especially designed for the ELF project. By providing a transparent, centralized repository

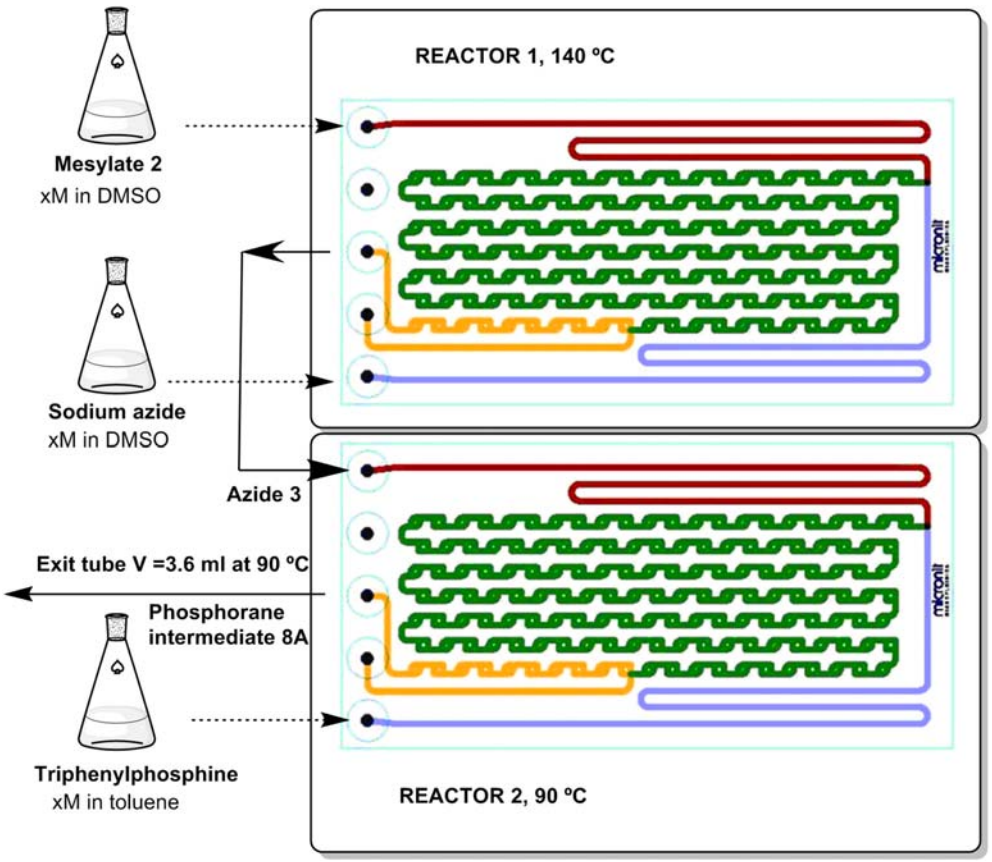

Fig. 2 Flow process to synthesize building block **20**.

Table 2 Key considerations during library validation activities as part of the ELF workflow

Criterion	*Notes*
Synthetic route	● Consider route length as from number of steps including starting materials and building blocks ● Fast track to the rate-determining "high risk" steps ● Definition of a target date to complete validation ● Ensure scalability of synthetic steps ● Demonstrate the synthetic route is robust, safe, and cost effective ○ Validate the exact route that will be used on scale up ○ Assess practical limitations of scale: temperature, equipment, and purification
Library generation	● Use truly representative reagent set to validate diversity step ● Favor well-known, robust, and generalized organic reactions ● Late diversification preferred with 2–3 points of variation ● Evaluate access to suitable building blocks and diversity reagent
Compounds properties	● Test chemical stability and solubility of intermediates and final compounds
Chemical costs	● Assess cost of library when projecting to final library production

of actionable chemical data across the ELF consortium, TarosGate 2 enables the ELF partners to monitor their productivity and efficiency with respect to the final goal of delivering c. 200,000 innovative compounds by the end of 2017. The software combines three important aspects of the collaborative chemistry workflow: (i) work documentation, (ii) management of the project, and (iii) communication. It creates a stable, secure platform for data collection of a daily work in synthetic chemical laboratories and provides the coordinator and project partners with an overview on the current progress of the ongoing library projects, facilitating efficient decisions in real time. Accordingly, it enables the planning of the resources required for project delivery; the monitoring of the status of projects during different project phases; the tracking of the use of resources versus plans and to the compound logistics. TarosGate 2 is filling an important niche among electronic lab-journals in supporting parallel synthesis by having an out-of-the-box plate module implemented representing the process flow in reality (Fig. 3).

As of Q4/2015, more than 100,000 final compounds were successfully delivered to the ELF compound management facilities. This batch of compounds is unique and diverse when compared with commercial sources and typical chemical compound repositories.[12] Furthermore, the delivered compounds share a similar profile in molecular properties space with typical Lipinski rule-of-five[13] characteristics for size and lipophilicity. The main differences between the libraries emerge when the number of chiral centers, fraction of sp^3 hybridized carbon atoms (Fsp^3), and molecular shape are considered. Here, the PCC compounds are markedly more complex in their structure and shape (Fig. 4).

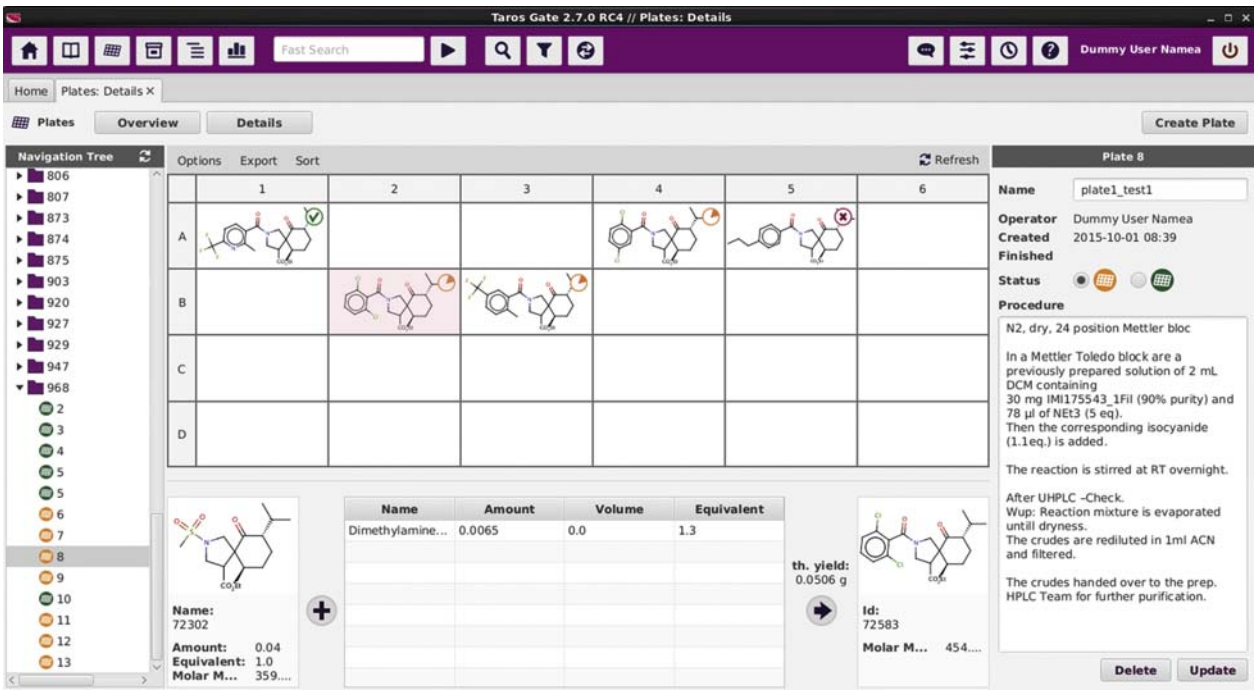

Fig. 3 The plate module that facilitates the parallel chemistry within an e-lab journal functionality of TarosGate 2.

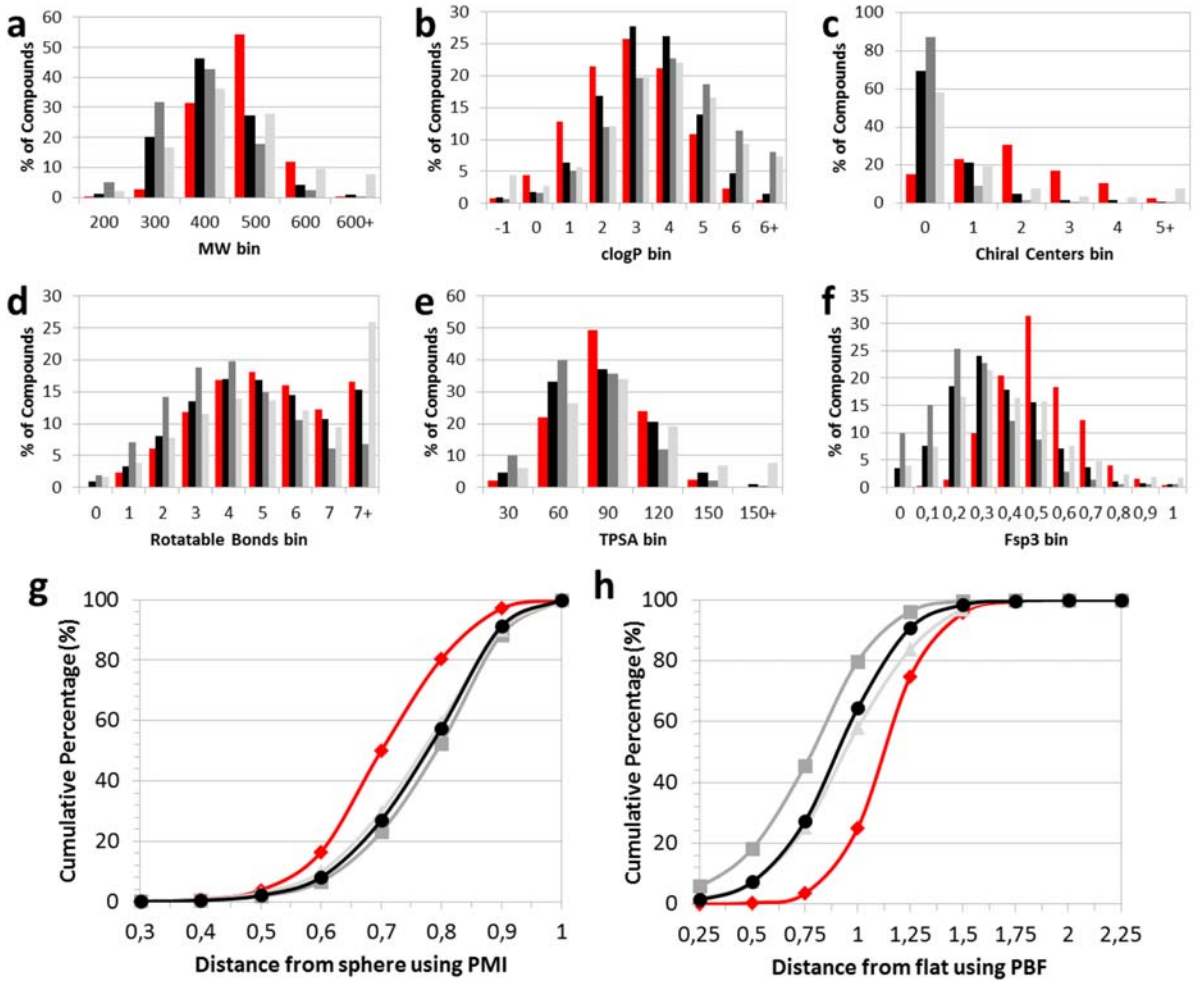

Fig. 4 (A) Molecular weight, (B) calculated logP (clogP), (C) number of chiral centers, (D) number of rotatable bonds, (E) topological polar surface area (*TPSA*), and (F) fraction of sp^3-hybridized carbon atoms profiles for PCC (*red bars*), MLP (*black bars*), Maybridge (*dark gray bars*), and ChEMBL (*light gray bars*) compounds. Cumulative distributions of distances from canonical sphere (G) and flat (H) shapes using principal moments of inertia (*PMI*) and plane of best-fit (*PBF*) descriptors, respectively, for PCC (*red diamonds*), MLP (*black circles*), Maybridge (*dark gray squares*), and ChEMBL (*light gray triangles*) compounds.

An important attribute of the delivered PCC compounds is their high degree of structural novelty. A large proportion (56%) of the Bemis–Murcko frameworks[20] exemplified by the PCC compounds are absent in medicinal chemistry-oriented compound collections.[12] For instance, a significant share of unprecedented spiro, bridged, and fused polycycles with different saturation, conjugation, and substitution patterns have been synthesized as part of the ELF activities.[21–38] This represents a fertile and practical avenue for the design and sampling of novel compound libraries, as the majority of theoretical ring systems remains largely unexplored, [39] and bodes well with the ELF remit of populating areas of chemical space which are not directly accessible from commercial sources or the scientific literature, thus offering a significant opportunity for the generation of intellectual property and innovation.

1.18.3 European Screening Center and Hit List Generation

The JECL comprising the EFPIA-contributed and ELF-synthesized compounds is stored at the state-of-the-art compound logistic facilities of BioAscent Discovery, Ltd. in Newhouse, Scotland. The Automated Compound Store (ACS) houses the JECL samples in DMSO solutions in barcoded tubes. Samples of the JECL collection are distributed among EFPIA members, the Pivot Park Screening Center (PPSC) in Oss (Fig. 5), the Netherlands, and cherry-picked sets to the University of Dundee group at Newhouse. Both the complete collection and selected subsets of the JECL are delivered with minimum turnaround time, ensuring expedient delivery during the hit finding and evaluation process for a given ELF program.

ELF program submissions by Program Owners (PO) include proposals for hit finding on biological targets for all disease areas. Novel molecular target screening programs of high scientific quality are required, for which HTS compatible assays are available. In this context, novel means: new target, new assay approach, or new chemistry required for existing targets. After a technical feasibility assessment of the screening assay by the PPSC, the submitted programs are reviewed and selected by the ELF Screening Selection Committee, consisting of assay developers, biologists, and medicinal chemists working for pharmaceutical companies and SMEs adhering to the ELF, or as independent consultants, all bound by strict confidentiality and nondisclosure agreements.

1.18.3.1 HTS Assay Requirements and Assay Development

Submitted programs should describe assays in 384-well format meeting specified requirements and which preferably are scalable to 1536-well format, the most suitable format for ultra-high-throughput screening (uHTS). Optimizing assays for uHTS is performed by PPSC and requires, among other things, the generation of stable reagents and the logical timing of incubation periods, while taking into consideration the total assay time and maximizing the total number of compounds to be tested. Homogenous assays are required and readout technologies should be compatible with mix and measure formats including Absorbance, Luminescence, Fluorescence intensity, Fluorescence polarization, Fluorescence resonance energy transfer (FRET), Time-Resolved Fluorescence (TRF/HTREF/TR-FRET), and alternatives that give highly specific readouts (eg, AlphaScreen technology, fluorescence lifetime, fragment complementation, or FLIPR for calcium readout). Furthermore, Signal/Background (S/B) in 384-well plate format should be preferentially higher than 3 and Z prime (Z') [40] higher than 0.6, taking into account a maximum assay end volume of 30 μL and a compound screening concentration of 10^{-5} M. If the PO's assay does not fully meet the technical feasibility assessment, scientists at PPSC can provide advice and support on developing the assay further to meet the specified criteria. ELF lab automation and assay specialists develop the majority of assays to run in 1536-well format to run on the uHTS facilities (Fig. 5). Cell culturing is performed at the PPSC, and protein production capability is provided by the University of Oxford.

1.18.3.2 Screening Cascade, Triaging to a Qualified Hit List (QHL), and Development to an Improved Hit List (IHL)

It is well recognized that successful drug discovery depends on high-quality hits, leads, and clinical candidates. Thus, the better the hit identified during screening, the faster the lead optimization process and the sooner the start of clinical trials. It is often not difficult to set the criteria for a hit from a primary screen and most screening campaigns deliver confirmed actives, although many will have suboptimal properties based on the program specifications. Consequently, the follow-up screening cascade involves various steps aimed at triaging the list of hits to identify those with the balance of properties, which provide the highest likelihood of long-term success.

In the ELF project, there are two distinct phases to generating high-quality hits. The first is a multistep triage process, which aims to select the best compounds from the uHTS. This phase will result in a qualified hit list (QHL) comprising up to 50 compounds. The second phase is a development phase, which aims to confirm the results from the original selection and then characterize the nature of the interaction between the hits and the target. The most promising hits can then be used as the basis for the preparation of analogs by carrying out design–synthesis–testing cycles to develop the compounds further and yield an improved hit list (IHL). During both phases, communication between the ELF and the PO is essential. However, due to the constraints applied to protect the associated intellectual property, chemical structures are not shared with the PO until the QHL is generated. Where programs progress beyond the QHL and toward the IHL within the ELF, a full collaboration can be established with the sharing of data, assets, and expertise between the ELF and the PO, thus greatly simplifying project progression.

Fig. 5 Ultra-HTS facilities of Pivot Park Screening Center.

During 2015, a typical ELF uHTS campaign takes place at PPSC and consists of a screen of the entire library of approximately 370,000 compounds using a target-based primary assay. Typically 1000–3000 actives are then cherry-picked and retested to identify a set of confirmed actives. These confirmed actives are further progressed in the screening cascade and triaged to deliver quality hits. This process is conducted both by scientists at the PPSC and at the European Screening Center (ESC) in Newhouse, the University of Dundee. The triaging process of confirmed actives can include both negative selection (eg, use of deselection assays) and positive selection (eg, active confirmation in an orthogonal assay). In addition, dose response curves are generated and Bayesian models are utilized to further increase the information content and confidence level around actives and inactives. Promising candidate hits are further tested to confirm target engagement using technologies, such as surface plasmon resonance (SPR) or microscale thermophoresis (MST). Up to this point in the process all of the decision-making has been driven by experimental and computational data and facilitates the selection of a preliminary hit list (PHL) of approximately 300–500 compounds. The chemical structures of compounds in the PHL are then revealed to the Program Clearance Team (PCT), consisting of expert medicinal chemists at ESC, all bound by confidentiality. The PCT carefully scrutinizes the molecules on the PHL and performs a liability check. Undesired molecular properties (eg, high molecular weight, high LogP, amphiphilicity, strong basicity, presence of electrophilic sites, active ester, or large flat aromatic systems) are highlighted and data/knowledge-based issues (eg, promiscuous motifs, frequent hitters, aggregators, Pan-Assay Interference Compounds (PAINS) [41]) are taken into account. Finally, the most promising PHL hits are analyzed by LC–MS to provide evidence of purity and structural identity. Subsequently, the QHL is generated and a report provided to the PO. This report includes a full description of the steps carried out in reaching the QHL including all protocols and metadata. Vitally, it also includes the structures and biological data of all the QHL compounds together with calculated physicochemical properties, the LC–MS results, an assessment of the novelty of the compounds, and potential suggestions for further hit evaluation work. In order to protect the potential intellectual property of the PO, all the compounds that appear on a QHL are automatically removed from the ELF compound library and will therefore not be available for screening in subsequent ELF campaigns. Following delivery of the QHL, a considerable amount of further work is still required to validate the hits. For example, up to this stage, all work has been carried out on the original screening solution and recapitulation of activity with freshly synthesized compounds is a vital early progression step.

The whole process of generating the QHL is supported by the Honest Data Broker (HDB), a bespoke IT system, which ensures the contractual business rules are enforced, facilitates the protection of intellectual property, and assists the scientific selection of compounds by providing an array of visualization tools, calculated data (eg, clogP, PSA), access to computational models, and cross-program information. The HDB will be described in more detail below.

1.18.3.3 The Intricate Triaging Process, What Is the Context of a Program?

The selection procedure from confirmed active to QHL during a screening campaign is far from a generic process and the investigators need to know the context of the program and its therapeutic target in detail. Here, it should be emphasized that for each target (class), a tailor-made screening/deselection cascade has to be designed. This should originate from considerations about the nature and location of the target in its physiological context as it can influence the desired property set of a molecule. As an example, for a centrally acting target, medicinal chemists could seek leads with low MW and moderate lipophilicity, whereas for a target in the liver high MW and high lipophilicity could be desirable. Additionally, off-target selectivity issues could be more stringent for cardiovascular or diabetes indications than for a cancer target. The desired mode of action (eg, agonist, antagonist, allosteric or orthosteric, enhancing or disrupting a protein–protein interaction) or the target class is also important determinants in the definition of an appropriate screening cascade. For instance, some target classes are especially sensitive to undesirable mechanisms of inhibition. Here, thiol (cysteine)-dependent proteins may be oxidized or react with electrophiles and, therefore, require special deselection assays. Metallo-enzymes may also be susceptible to redox reactions which can be catalyzed by compounds that will appear as positives in the screen but the nonspecific mechanism of action is unsuitable for further development of the compound.[42] In addition, promiscuous metal chelators showing inhibitory activity on many classes of metallo-enzymes may occur.

Screens, which involve enzymes and protein–protein interactions, are susceptible to particular false positive artifacts, such as lipophilic and amphiphilic molecules, causing aggregation or protein precipitation.[43] Primary assays should be established with appropriate concentrations of detergent (eg, Tween) to disrupt the formation of compound aggregates, and deselection strategies can involve changing the detergent concentration to look for changes in hit compound activity, which may indicate aggregation issues. Alternatively, for enzymatic assays, decreases in compound efficacy upon increasing the protein concentration are another recognized technique for identifying aggregators.[44] The identified aggregator compounds can subsequently be removed from the hit list, if appropriate. For targets, such as kinases, many potent inhibitors may appear in the PHL and finding the right selectivity against a panel of related targets could be of interest. This is just one of the areas where cross-program information can play an important role. As data from more screens is stored in the HDB, it can be used to identify compounds, which hit multiple targets either reflecting "frequent hitting" characteristics or because of genuine lack of selectivity at the target. Accordingly, this information can be incorporated into the compound selection for a given ELF campaign.

Apart from target-oriented screening design, more generic issues should also be taken into account, such as "compound interference," which encompasses mode of actions caused by undesired chemical and physical properties of compounds interfering with a wide variety of biochemical and cellular assays. Here, colored or fluorescent compounds and aggregators are well-known examples.[45,46]

1.18.3.4 Development to IHL; Hit Characterization

The overall goal of the IHL is to provide evidence of the quality of the hit series by providing data and physical samples of the compounds. This will hopefully facilitate the PO in securing further investment or funding to develop the compounds to leads and hopefully beyond to clinical candidates and ultimately new medicines. The ELF defines high-quality hits as having: (a) proven chemical structure, (b) on-target activity and selectivity, (c) emerging SAR, and (d) properties favorable for further optimization. The majority of the work toward an IHL is carried out at Newhouse although key capabilities are available at Dundee (SPR, in vitro distribution, metabolism, and pharmacokinetics (DMPK) assays) and Oxford (X-ray crystallography). In most cases, the dose–response assay used to generate the QHL will be transferred from PPSC to Newhouse creating an important opportunity for interlaboratory verification of the results. Samples of the QHL compounds, if still available in the store, are sent to the PO for use in their own assays. Following confirmation of activity at Newhouse and in the PO's lab, a sharing of data and conversation with the PO allows selection of a prioritized list of hits for resynthesis. Confirmation of structure by LC–MS and NMR provides unambiguous proof of structure and purity and recapitulation of the assay results with these new samples significantly reduces the possibility that decomposition by-products or sample impurities were the source of activity in the original screening sample. Further characterization of the compounds is then carried out with mechanism of action studies (ie. reversibility and competitivity) and selectivity measurements across a panel of assays available at Newhouse or with the PO. Cell-based toxicity is routinely assessed at Newhouse and again compounds are provided for testing in cellular disease models run by the PO.

Depending on the results and available resources, an analog program can be initiated to address identified issues with the QHL compounds. Typically, this will aim to explore potency determinants, ideally demonstrating progressive SAR. However, if the final goal of the ELF campaign is to identify a starting point for a drug discovery program, the wider properties of the compounds (eg, physicochemical properties) will also be important to consider. Medicinal chemists at the ELF work in close collaboration with the PO to create and execute a plan of design–synthesis–testing cycles to achieve these goals. Additionally, computational chemists from the ELF are involved in the design process using ligand-based and structure-based modeling techniques together with an array of cheminformatic tools. The importance of biostructural information is recognized and, where possible, data is generated by the ELF to support the medicinal chemistry and to provide further evidence of target engagement. The University of Oxford provides this expertise and aims to generate relevant protein–ligand structures to aid the design process. These experts are engaged from the initiation of the project so that the probability of success is maximized. Finally, as optimized compounds become available, the best examples can be profiled in in vitro drug DMPK and physicochemical assays to assess properties, such as hepatocyte/microsomal stability, plasma protein binding, solubility, and pK_a to further characterize risks and opportunities to further project progression. The final IHL package consists of all data, a report describing the studies, conclusion, and recommendations for further work and the remaining physical samples synthesized during the program. The goal for the ELF Screening Center is to execute a total of 90 screening campaigns from external investigators and 120 from the EFPIA companies adhering to the consortium. As of the end of Q3/2015, a total of 95 target proposals from investigators external to the ELF have been received; 52 of these have been approved and processed, 18 QHLs and 5 IHLs have been delivered to the original POs.

1.18.4 The Honest Data Broker

Reducing the output of the ELF's high-throughput screens to a list of high-quality compounds that could form the basis of a drug discovery or chemical biology project is a key step in the ELF workflow. The HDB is a cloud-based application hosting all of the ELF's chemical and biological data and provides the computational tools necessary to perform this triage while enforcing the intellectual property protection rules of the project. The ELF's HTS triage workflow is unique due to these rules and the workflow is depicted in Fig. 6 and briefly summarized here.

1.18.4.1 Triage Tools

The structure-blinded initial stages of the triage place particular demands on the computational tools to enable accurate selection of the best compounds. Identification of similar compounds to establish plausible SAR has been one of the most frequently used features, and a variety of approaches to achieve this are available. These include clustering by conventional FCFP4/Tanimoto methods, scaffold-based clustering by Bemis–Murcko frameworks [20] and clustering by an implementation of the ScaffoldTree algorithm.[47] These enable the PT members to get multiple perspectives on compound similarity. Compounds can also be used as query molecules for similarity searches within the HDB, again allowing users to understand the chemical neighborhood around their hits. SMARTS filters uploaded by each partner organization are available in the HDB and can be used to identify general undesirable functionality. For more program-specific searches, PT and PCT members can upload substructures of up to 10 heavy atoms to search their lists of hits. This allows the removal of, for example, quinolines in a kinase project if the program owner already feels they have enough examples of this chemotype. Conversely, it could be used to positively identify compounds for retention and further analysis. "Cross-program" information allows a user to see how many times a compound has been active in all the screens deposited in the ELF's HDB. This information can be used to identify frequent hitter or nonspecific compounds. Classical hard cut-off filtering is implemented and an array of calculated physicochemical properties (including molecular weight, logP, TPSA, H-bond donors/

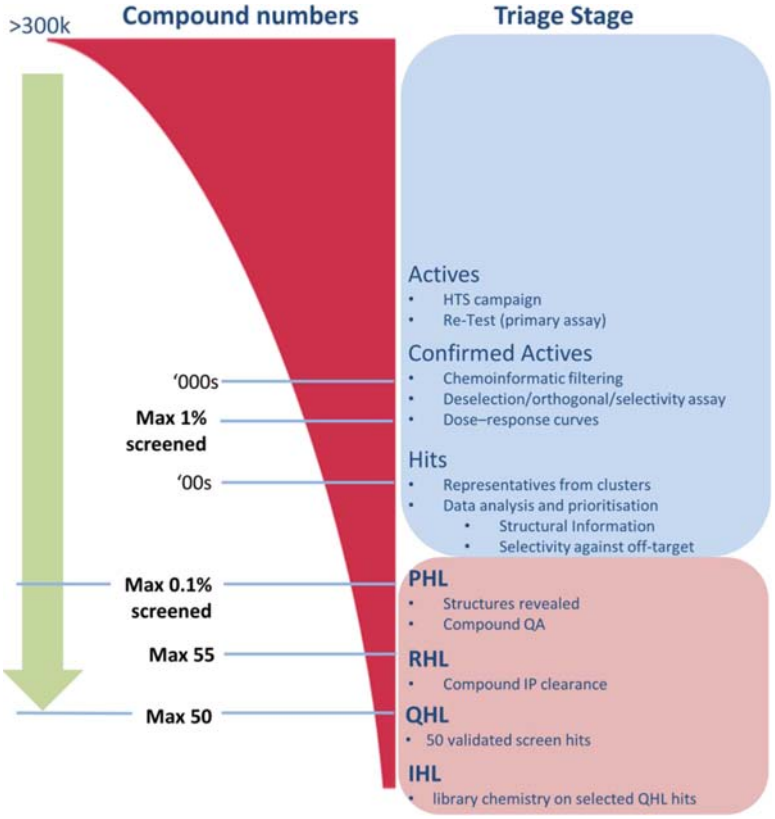

Fig. 6 ELF's HTS triage workflow. *PHL*, preliminary hitlist; *RHL*, refined hitlist; *QHL*, qualified hitlist; *IHL*, improved hitlist.

acceptors) is available in addition to biological data and all these features can be used for filtering. In some cases, desirability scoring rather than hard cut-off filtering can be more successful and Pareto and Derringer desirability methods are also available. List logic to combine compound lists through AND/OR/NOT/XOR operators is also a frequently used tool. A table summarizing the key triage tools is shown in Table 3. Visualization of data is essential in understanding the data for compound selection and this is enabled through the Pipette application.[48] Data can be seamlessly transferred to and from Pipette for visualization and interactive selection.

Table 3 Key triage tools in the HDB

Triage tool	*Function*
Property calculators (logP, Mwt, TPSA…)	Generation of key drug-likeness properties
Scaffold clustering	Group molecules by core structure
On-the-fly clustering	FCFP6/Tanimoto clustering of arbitrary compound lists
Filtering	Filter by Range, Top N, Outlier filtering
Activity model calculation	False negative rescue/unusual hit identification
Precomputed ChEMBL activity models	Off-target biological activity identification
Ligand Efficiency, LLE	Size and logP normalized activity estimation
List Logic	AND/NOT/OR/XOR joining of compound lists
Limited substructure filtering	(De)select compounds with structural feature
Binned similarity search	Identify compounds similar to query molecule
Pareto/Derringer Desirability scoring	"Soft" selection of compounds without hard filter limits
Basic Math & Statistics	
Cross-program Information	Shows activity of compounds to against enzyme/receptor classes to facilitate selectivity estimation
CNS filter	Desirability model to identify likely CNS-penetrant compounds
SMARTS filtering	Substructures encoding structural alerts to identify potentially undesirable features

Emphasis is placed on understanding the similarity relationships between compounds when structures are not visible in the early stages of the triage. Deriving knowledge from data deposited in the HDB to inform triage is also made possible and is an area under active development.

1.18.4.2 Intellectual Property Protection and Enforcement of ELF Rules

The rules of the ELF place a number of limits on the visibility of compound structures and on the use of physical compound samples in the compound store. These preserve the intellectual property associated with a compound and also prevent unnecessary depletion of physical sample. Structure visibility rules have been described[49] but additional rules govern the number of compounds that can be ordered for dose response or LC–MS structure validation, while other rules limit how many compounds can be passed from the SRL to the PHL and on to the QHL. All these rules are enforced by the HDB and prevent users from accessing or ordering too many compounds. A final step in the selection of a compound is an intellectual property check with the company that contributed the compound. This ensures that a compound that has intellectual property entanglement or has become part of an active project internal to that company is not released to the PO. Near the end of the triage process, each compound owner is alerted within the HDB to the compounds that have been selected and has the option to block their release. The compound owner has no knowledge of the PO or biological target and the grounds for blocking release are tightly defined. [49]

1.18.4.3 Project Organization

The ELF is carrying out a large number of HTSs with up to 20 per year being executed in the ESC alone. A core team of PT and PCT members carries out the triage for all of these public programs and these must be dealt with confidentially, to a high scientific standard and on a reasonable timescale. The HDB maintains strict separation of programs and provides a number of tools to organize and facilitate each program. Temporary work-lists can be saved, date-stamped, and shared within the HDB to facilitate HTS triage by scientists based at multiple sites. This eliminates the need for spreadsheets to be circulated and ensures complete control of access to information. The HDB also includes a compound ordering feature allowing PT and PCT members to request compounds from the liquid store for dispatch to user-selected locations in user-selected plate format, again obviating the need for creation and circulation of ad hoc text files. Auditing of the whole ELF process is an important part of the consortium and the ability of project management to track what has happened to compounds and who has access to information associated with a compound is recorded. This is available to project management to view through a suite of reporting tools.

1.18.5 Summary and Outlook

The ELF was established to offer researchers from academia, SMEs, and patient organizations, the opportunity to access a world-class infrastructure dedicated to the early phase of preclinical research. European investigators engaging the ELF can now exploit an innovative compound collection and industrial quality uHTS platform with the aim of discovering novel small molecule hits, suitable for subsequent optimization either to drug candidates or to high-quality pharmacological tools for the experimental validation of targets. In the open innovation model established by the ELF, seven pharmaceutical companies have contributed a total of 327,000 compounds from their proprietary and complementary collections, [6] thus maximizing their intrinsic values through compound collection sharing.[9–11] A crowd-sourcing, collaborative effort involving intersectoral chemistry research groups from the ELF consortium aims to deliver an additional 200,000 compounds to build the final JECL library to a size in excess of 527,000 compounds. Here, following a rigorous compound library design and synthesis workflow focused on chemistry innovation and compound attractiveness, the ELF chemistry consortium has already delivered more than 100,000 novel compounds to the JECL. Importantly, these compounds significantly differ from currently available commercial collections and medicinal chemistry databases in that they are chiral molecules with nonaromatic, nonplanar moieties, and a strong propensity for a globular three-dimensional shape. Their systematic evaluation against biological targets within the ELF will thus provide a very useful test of the general relevance of such compound characteristics to specific target classes, assay types, and ultimately programs' outcome and success.

While the availability of a novel, high-quality screening collection is a clear determinant of successful drug discovery,[50] an appropriate and stringent triage workflow is also a necessity. The ELF has assembled a multidisciplinary infrastructure consisting of state-of-the-art compound management facilities, assay development expertise, target-based uHTS technologies, medicinal chemistry know-how, chemoinformatics and modeling tools, secondary biological assays, X-ray crystallography, and in vitro DMPK readouts. These capabilities are aptly exploited by the ELF to craft and execute individual, project-centric HTS triage programs in order to deliver the best possible set of hits for a given ELF target proposal. This has already resulted in the completion of 52 screening campaigns, out of the planned 90 from external investigators, with 18 QHLs and 5 IHLs delivered to the respective POs. It is interesting to note that, by gathering and managing such critical hit evaluation talent and expertise, and routinely deploying it to a large portfolio of campaigns, the ELF plays an important role in establishing a de facto best practice in hit finding, evaluation, and hit-to-lead activities, critically contributing to training and formation of scientists in such phases, and eventually serving as a center of excellence in lead generation. Because of the collaborative, multidisciplinary nature of the ELF, the intellectual property sensitivity of lead generation activities, and associated competitive advantages, the need to establish a complete, functional, and safeguarded environment is paramount. The ELF has therefore invested significant efforts in establishing an "honest data broker" system allowing seamless execution of hit triaging campaigns in perfect compliance with the scientific and legal requirements of modern-day drug discovery. It is noteworthy that the ELF's HDB set-up provides a potential model for an IT system able to support a large, public–private, precompetitive consortium by enabling diverse organizations to collaborate and by providing a highly effective array of scientific tools for HTS triage.

In response to productivity pressures from multiple stakeholders, the pharmaceutical industry is attempting to explore alternative business models and precompetitive, open-source options have attracted significant attention.[4] The ELF has made significant progress in establishing an integrated lead generation platform that builds on intersectoral, complementary strengths and expertise within the consortium. Successful exploitation of the ELF model and infrastructure by adhering pharmaceutical companies and investigators external to the ELF across Europe will provide sound information on the overall sustainability and effectiveness of such approach.

Acknowledgments

We thank Stuart McElroy, Angus Morrison, and Silvia Stotani for useful comments and discussions on the article. The research leading to these results has received support from the Innovative Medicines Initiative Joint Undertaking under grant agreement no. 115489, resources of which are composed of financial contribution from the European Union's Seventh Framework Program (FP7/2007-2013) and EFPIA companies' in-kind contribution.

References

1. Hay, M.; Thomas, D. W.; Craighead, J. L.; Economides, C.; Rosenthal, J. Clinical Development Success Rates for Investigational Drugs. *Nat. Biotechnol.* **2014,** *32,* 40–51.
2. Khanna, I. Drug Discovery in Pharmaceutical Industry: Productivity Challenges and Trends. *Drug Discov. Today* **2012,** *17,* 1088–1102.
3. Schmid, E. F.; Smith, D. A. Pharmaceutical R&D in the Spotlight: Why Is There Still Unmet Medical Need? *Drug Discov. Today* **2007,** *12,* 998–1006.
4. Munos, B. Can Open-Source Drug R&D Repower Pharmaceutical Innovation? *Clin. Pharmacol. Ther.* **2010,** *87,* 534–536.
5. Mullard, A. European Lead Factory Opens for Business. *Nat. Rev. Drug Discov.* **2013,** *12,* 173–175.
6. Besnard, J.; Jones, P. S.; Hopkins, A. L.; Pannifer, A. D. The Joint European Compound Library: Boosting Precompetitive Research. *Drug Discov. Today* **2015,** *20,* 181–186.
7. BIOVIA Pipeline Pilot | Scientific Workflow Authoring Application for Data Analysis. At http://accelrys.com/products/collaborative-science/biovia-pipeline-pilot/.
8. Bickerton, G. R.; Paolini, G. V.; Besnard, J.; Muresan, S.; Hopkins, A. L. Quantifying the Chemical Beauty of Drugs. *Nat. Chem.* **2012,** *4,* 90–98.
9. Schamberger, J.; Grimm, M.; Steinmeyer, A.; Hillisch, A. Rendezvous in Chemical Space? Comparing the Small Molecule Compound Libraries of Bayer and Schering. *Drug Discov. Today* **2011,** *16,* 636–641.
10. Engels, M. F. M.; et al. A Cluster-Based Strategy for Assessing the Overlap Between Large Chemical Libraries and Its Application to a Recent Acquisition. *J. Chem. Inf. Model.* **2006,** *46,* 2651–2660.
11. Kogej, T.; et al. Big Pharma Screening Collections: More of the Same or Unique Libraries? The AstraZeneca-Bayer Pharma AG Case. *Drug Discov. Today* **2013,** *18,* 1014–1024.
12. Karawajczyk, A.; et al. Expansion of Chemical Space for Collaborative Lead Generation and Drug Discovery: The European Lead Factory Perspective. *Drug Discov. Today* **2015,** *20* (11), 1310–1316. http://dx.doi.org/10.1016/j.drudis.2015.09.009.
13. Lipinski, C. A. Lead- and Drug-Like Compounds: The Rule-of-Five Revolution. *Drug Discov. Today Technol.* **2004,** *1,* 337–341.
14. Teague, S. J.; Davis, A. M.; Leeson, P. D.; Oprea, T. The Design of Leadlike Combinatorial Libraries. *Angew. Chem. Int. Ed Engl.* **1999,** *38,* 3743–3748.
15. Walters, W. P.; Green, J.; Weiss, J. R.; Murcko, M. A. What Do Medicinal Chemists Actually Make? A 50-Year Retrospective. *J. Med. Chem.* **2011,** *54,* 6405–6416.
16. Chemical Structure Drawing Search—eMolecules. At http://emolecules.com/.
17. Overington, J. *The ChEMBL-og: SureChEMBL—Chemical Structure Information in Patents*. At. http://chembl.blogspot.de/2013/12/surechembl-chemical-structure.html.
18. Biel, M.; Kretsovali, A.; Karatzali, E.; Papamatheakis, J.; Giannis, A. Design, Synthesis, and Biological Evaluation of a Small-Molecule Inhibitor of the Histone Acetyltransferase Gcn5. *Angew. Chem. Int. Ed.* **2004,** *43,* 3974–3976.
19. Kohari, Y.; et al. Enantioselective Diels–Alder Reaction of 1,2-Dihydropyridines with Aldehydes Using β-Amino Alcohol Organocatalyst. *J. Org. Chem.* **2014,** *79,* 9500–9511.
20. Bemis, G. W.; Murcko, M. A. The Properties of Known Drugs. 1. Molecular Frameworks. *J. Med. Chem.* **1996,** *39,* 2887–2893.
21. Craven, P.; et al. Design, Synthesis and Decoration of Molecular Scaffolds for Exploitation in the Production of Alkaloid-Like Libraries. *Bioorg. Med. Chem.* **2015,** *23* (11), 2629–2635. http://dx.doi.org/10.1016/j.bmc.2014.12.048.
22. Murali, A.; Medda, F.; Winkler, M.; Giordanetto, F.; Kumar, K. Branching Cascades Provide Access to Two Amino-Oxazoline Compound Libraries. *Bioorg. Med. Chem.* **2015,** *23* (11), 2656–2665. http://dx.doi.org/10.1016/j.bmc.2015.01.009.
23. Sankar, M. G.; et al. Stereoselective Synthesis of a Natural Product Inspired Tetrahydroindolo[2,3-a]-Quinolizine Compound Library. *Bioorg. Med. Chem.* **2015,** *23* (11), 2614–2620. http://dx.doi.org/10.1016/j.bmc.2015.01.019.
24. Petersen, R.; et al. Synthesis of Hexahydropyrrolo[2,1-a]Isoquinoline Compound Libraries Through a Pictet-Spengler Cyclization/Metal-Catalyzed Cross Coupling/Amidation Sequence. *Bioorg. Med. Chem.* **2015,** *23* (11), 2646–2649. http://dx.doi.org/10.1016/j.bmc.2015.01.039.
25. Padwal, J.; et al. Cyclopentitol as a Scaffold for a Natural Product-Like Compound Library for Drug Discovery. *Bioorg. Med. Chem.* **2015,** *23* (11), 2650–2655. http://dx.doi.org/10.1016/j.bmc.2015.01.040.
26. van der Pijl, F.; van Delft, F. L.; Rutjes, F. P. J. T. Synthesis and Functionalization of Bicyclic N, O-Acetal Scaffolds From Furfural. *Bioorg. Med. Chem.* **2015,** *23* (11), 2721–2729. http://dx.doi.org/10.1016/j.bmc.2014.12.045.
27. Storr, T. E.; et al. Combining Two-Directional Synthesis and Tandem Reactions. Part 21: Exploitation of a Dimeric Macrocycle for Chain Terminus Differentiation and Synthesis of an sp3-Rich Library. *Bioorg. Med. Chem.* **2015,** *23* (11), 2621–2628. http://dx.doi.org/10.1016/j.bmc.2014.12.050.
28. Nortcliffe, A.; Moody, C. J. Seven-Membered Ring Scaffolds for Drug Discovery: ACCESS to Functionalised Azepanes and Oxepanes Through Diazocarbonyl Chemistry. *Bioorg. Med. Chem.* **2015,** *23* (11), 2730–2735. http://dx.doi.org/10.1016/j.bmc.2015.01.010.
29. Petersen, M.Å.; et al. Synthesis of 1,4,5 Trisubstituted γ-Lactams via a 3-Component Cascade Reaction. *Bioorg. Med. Chem.* **2015,** *23,* 2695–2698.
30. Nickel, S.; et al. Synthesis of a Hexahydropyrrolo Indole (HPI) Compound Library. *Bioorg. Med. Chem.* **2015,** *23,* 2636–2645.
31. Patil, P.; Khoury, K.; Herdtweck, E.; Dömling, A. MCR Synthesis of a Tetracyclic Tetrazole Scaffold. *Bioorg. Med. Chem.* **2015,** *23,* 2699–2715.
32. Ortega, R.; et al. Design and Synthesis of 1,1-Disubstituted-1-Silacycloalkane-Based Compound Libraries. *Bioorg. Med. Chem.* **2015,** *23* (11), 2716–2720. http://dx.doi.org/10.1016/j.bmc.2015.01.046.
33. Neochoritis, C. G.; et al. Leuckart-Wallach Route Toward Isocyanides and Some Applications. *ACS Comb. Sci.* **2015,** *17* (9), 493–499. http://dx.doi.org/10.1021/acscombsci.5b00066.
34. Neochoritis, C. G.; Stotani, S.; Mishra, B.; Dömling, A. Efficient Isocyanide-Less Isocyanide-Based Multicomponent Reactions. *Org. Lett.* **2015,** *17,* 2002–2005.
35. Foley, D. J.; Doveston, R. G.; Churcher, I.; Nelson, A.; Marsden, S. P. A Systematic Approach to Diverse, Lead-Like Scaffolds from α, α-Disubstituted Amino Acids. *Chem. Commun. Camb. Engl.* **2015,** *51,* 11174–11177.
36. Doveston, R. G.; et al. A Unified Lead-Oriented Synthesis of Over Fifty Molecular scaffolds. *Org. Biomol. Chem.* **2015,** *13,* 859–865.

37. Colomer, I.; et al. Aminomethylhydroxylation of Alkenes: Exploitation in the Synthesis of Scaffolds for Small Molecule Libraries. *Bioorg. Med. Chem.* **2015,** *23,* 2736–2740.
38. Firth, J.; et al. Exploitation of the Ugi–Joullié Reaction in the Synthesis of Libraries of Drug-Like Bicyclic Hydantoins. *Synthesis* **2015,** *47,* 2391–2406.
39. Lipkus, A. H.; et al. Structural Diversity of Organic Chemistry. A Scaffold Analysis of the CAS Registry. *J. Org. Chem.* **2008,** *73,* 4443–4451.
40. Zhang, J.-H.; Chung, T. D. Y.; Oldenburg, K. R. A Simple Statistical Parameter for Use in Evaluation and Validation of High Throughput Screening Assays. *J. Biomol. Screen.* **1999,** *4,* 67–73.
41. Baell, J. B.; Holloway, G. A. New Substructure Filters for Removal of Pan Assay Interference Compounds (PAINS) From Screening Libraries and for Their Exclusion in Bioassays. *J. Med. Chem.* **2010,** *53,* 2719–2740.
42. Jadhav, A.; et al. Quantitative Analyses of Aggregation, Autofluorescence, and Reactivity Artifacts in a Screen for Inhibitors of a Thiol Protease. *J. Med. Chem.* **2010,** *53,* 37–51.
43. Sassano, M. F.; Doak, A. K.; Roth, B. L.; Shoichet, B. K. Colloidal Aggregation Causes Inhibition of G Protein-Coupled Receptors. *J. Med. Chem.* **2013,** *56,* 2406–2414.
44. Habig, M.; et al. Efficient Elimination of Nonstoichiometric Enzyme Inhibitors From HTS Hit Lists. *J. Biomol. Screen.* **2009,** *14,* 679–689.
45. Thorne, N.; Auld, D. S.; Inglese, J. Apparent Activity in High-Throughput Screening: Origins of Compound-Dependent Assay Interference. *Curr. Opin. Chem. Biol.* **2010,** *14,* 315–324.
46. Acker, M. G.; Auld, D. S. Considerations for the Design and Reporting of Enzyme Assays in High-Throughput Screening Applications. *Perspect. Sci.* **2014,** *1,* 56–73.
47. Ertl, P.; Schuffenhauer, A.; Renner, S. The Scaffold Tree: An Efficient Navigation in the Scaffold Universe. *Methods Mol. Biol. Clifton NJ* **2011,** *672,* 245–260.
48. BLOG Pipette Analysis | ScienceCloud. At https://www.sciencecloud.com/blog-pipette-analysis/index.html.
49. Rights & Obligations. At https://www.europeanleadfactory.eu/how-to-submit/drug-target-assays/rights-obligations/#c34812.
50. Wigglesworth, M. J.; Murray, D. C.; Blackett, C. J.; Kossenjans, M.; Nissink, J. W. M. Increasing the Delivery of Next Generation Therapeutics From High Throughput Screening Libraries. *Curr. Opin. Chem. Biol.* **2015,** *26,* 104–110.

Relevant Websites

www.europeanleadfactory.eu—Official Website of the European Lead Factory.
www.bayer.com—Coordinator of the European Lead Factory.
www.lygature.com—Coordinator for the European Screening Center.
www.taros.de—Coordinator for the Chemistry and Library Production.

1.19 Closing Distances Between Academia and Market

F Cesaroni, D Baglieri, and A Crupi, University of Messina, Messina, Italy

© 2017 Elsevier Ltd. All rights reserved.

1.19.1	**Introduction**	520
1.19.2	**Development and Commercialization of Biotechnology-Based New Drugs**	521
1.19.2.1	The Upsurge of Biotechnology	521
1.19.2.2	The Traditional Contribution of DBFs in Drug Development and Commercialization	521
1.19.2.3	The Recent Evolution of the Biotechnology Industry	522
1.19.3	**The Recent Evolution of DBFs: An Empirical Assessment**	523
1.19.3.1	Upstream Vertical Relationships Between DBFs and Academic Institutions	523
1.19.3.2	Downstream Vertical Relationships Among DBFs, Pharmaceutical Companies, and Other Organizations	524
1.19.4	**Conclusions**	527
1.19.5	**Limitations and Further Research**	528
References		528

1.19.1 Introduction

The three decades since the first breakthrough in biotechnology have seen a huge rise in the industry–university collaboration in the development of biotech-based novel medicines, diagnostics, and new discovery techniques. The first biotechnology product (insulin) was approved in 1982 and, although the scientific revolution involving biotechnology has been slower than expected, there are more than 200 biotechnology products commercially available, and more than 900 biotechnology products in clinical trials.[1] At the beginning, the pharma industry engaged with biotechnology companies only to a small extent with their in-licensing of a few recombinant molecules, led by Roche, Eli Lilly, and Johnson and Johnson. Subsequently, over the last 25 years, biotechnology has become a cornerstone in new product development in all pharmaceutical companies. Currently, they are substantially engaged in both the clinical development of these products and their commercialization. To achieve this result, pharma companies have shifted their focus from blockbuster medicines, which are progressively declining due also to the patent expiration, to the progressive application of biotechnology, which includes, among others, the increasing trend of personalized medicines.

The global pharmaceutical industry is facing several challenges stemming from a variety of sources. One of the major issues is the high and risky investment in research and development (R&D) to create profitable blockbusters. In addition, the huge expansion of generics implies that big pharma are devoting more attention to two distinct strategic paths that are respectively: (1) improving clinical margins, and (2) increasing biotech opportunities. The former refers to companies that are investing in acquisitions of generic companies to counterbalance patent cliff and to gain access to emerging markets. Some examples include Novartis owning an in-house generics arm in Sandoz, and Sanofi-Aventis making takeover bids for the generics company Zentiva. The latter refers to pharmaceutical companies that are seeking to diversify their product portfolios to foster a more flexible and broad-ranging business model. These include Novartis, no longer exists-now is part of Pfizer, Abbvie, BMS and Roche, but also other big pharmaceutical companies more generally. Overall, the pharmaceutical industry is paying attention to the novel healthcare trends that are personalized medicine based on patient genomes, combined with the application of biotechnology.

Therefore, it is not surprising to learn that biotechnology firms are growing far more rapidly than the pharmaceutical firms, with US biotechnology recording a unique year in 2014, setting a new all-time record in total capital raised (US$45.1 billion) as well as funds raised through IPOs (US$4.9 billion) and debt (US$23.3 billion).[2] Also the European biotechnology firms have achieved these exceptional financial outcomes, although not quite as robust as that of its US counterpart. **Table 1** briefly highlights the key numbers of the biotechnology industry, comparing the latest 2 years (2013–14).

The pharmaceutical industry is, therefore, looking to close this gap by investing more in biotechnology, including acquisitions, in order to address revenue shortfalls that have arisen due to pricing pressures, slower growth in emerging markets, and R&D challenges. Accordingly, the marriage of biotechnology and the pharmaceutical industry is based both on industry dynamics and an evolution in technology and product innovation.

Against this background, this article provides an overview of the key evolutionary dynamics occurring in the biotechnology industry since its inception. This technological breakthrough has required new forms of division of labor and collaboration from both the pharmaceutical industry and basic researchers in academia to bridge the translation into new biotechnology-based medicines. This article describes upstream and downstream strategic partnerships and the different modalities of cross-fertilization between university and the dedicated biotech firms (DBFs) within the pharmaceutical industry. Two key factors in this important translational bridge can be identified: new governance of both partnering organizations to open up for new and, sometimes, disruptive ideas, and creation of trust-based relationships between different institutional partners (private–public

Table 1 Main facts and figures about the recent biotechnology industry

	2014	*2013*	*% change*
Public company data			
Revenues	123.1	99.0	24%
R&D expense	35.4	29.4	20%
Net income	14.9	4.5	231%
Market capitalization	1063.4	794.8	34%
Number of employees	183,610.0	168,010.0	9%
Number of companies			
Public companies	714	619	15%

Source: Ernst & Young. *Biotechnology Annual Industry Reports*; Ernst & Young: Palo Alto, CA, various years.

partnerships) enabling long-term scientific collaborations, while acknowledging that value creation and value appropriation are essential factors for successful collaboration.

The article is structured as follows. Section "**Development and Commercialization of Biotechnology-Based New Drugs**" briefly describes the evolution of biotechnology and the key role played by DBFs in closing the gap between academia and market. Section "**The Recent Evolution of DBFs: An Empirical Assessment**" highlights descriptive findings from our sample of 146 DBFs and their upstream and downstream collaboration during the period 1993–2013. Section "**Conclusions**" focuses on the implications stemming from empirical findings. "**Limitations and Further Research**" conclude the article.

1.19.2 Development and Commercialization of Biotechnology-Based New Drugs

1.19.2.1 The Upsurge of Biotechnology

During the 1980s, the pharmaceutical industry witnessed an upsurge of a technological discontinuity (biotechnology) that dramatically and persistently changed the way in which new drugs were conceived and developed, and dramatically affected the organization of the industry that had existed since its origins in the second half of the 19th century. While until that moment the knowledge base of pharmaceuticals was mainly based on organic chemistry, biotechnologies were based on a completely new paradigm drawn upon molecular biology rather than organic chemistry. For this reason, the technological breakthrough introduced by biotechnological research challenged severely the core competences of pharmaceutical firms.[3,4]

Historically, the origin of biotechnology has to be dated back to 1953, when Watson and Crick discovered the double helix structure of DNA. However, it was only 20 years later, in 1973 that a modern biotechnology industry could emerge, thanks to the breakthrough finding made by Cohen and Boyers of the recombinant DNA methodology. Following that invention, the first biotechnology firm, Genentech, was founded in San Francisco in 1976 and the US Food and Drugs Administration (FDA) approved the first biotechnological outcome, recombinantly produced human insulin, in 1982. The discovery of recombinant DNA represented a radical process innovation, capable of manipulating microorganisms, thanks to the convergence of multiple technologies such as molecular biology, genetics, combinatorial chemistry, immunology, and more recently, bioinformatics.[5] In this sense, biotechnology embodied a radically new combination of existing technologies, whose outcomes cover a wide range of disciplines and scientific and technological fields, ranging from health (both diagnostic and therapeutic phases), to agro industry, environmental protection, and so forth.

Both the technological bases composing biotechnology and the various application domains were not, however, part of traditional technological portfolios of incumbent pharmaceutical companies. As a consequence, following the development of this new technological paradigm, (large) pharmaceutical companies were forced to find the most efficient way to interact with (small) dedicated biotechnology firms (DBFs), which were specialized in developing biotechnologies and were in possession of the competences to master the new knowledge base.

Traditionally, large pharmaceutical companies have thus reacted to the upsurge of biotechnology by seeking alliances with new entrant DBFs that possessed R&D competences and capabilities they were lacking. To these new firms, large pharmaceutical companies were offering downstream complementary assets (such as clinical trials, manufacturing and marketing capabilities, access to market) that allowed innovative technological solutions to be converted into new drugs to be introduced into the market. As a matter of facts, seven of the top-ten biotechnology drugs that have been marketed during the late 1990s have been introduced by pharmaceutical companies, even though all of them have been originally developed by small biotechnology firms.[3]

1.19.2.2 The Traditional Contribution of DBFs in Drug Development and Commercialization

Since their original appearance, dedicated biotechnology start-ups have traditionally represented the organizational bridge between the upstream phase of biotechnology-based new drug development and the downstream phase of new drugs' market introduction. In performing their role, DBFs have thus engaged in two different types of vertical collaborative agreements: on the one hand, they have collaborated with universities and other public research organizations to enlarge their knowledge base, acquire new research

skills and expertise, and refine their technological capabilities; on the other hand, they have collaborated with incumbent large pharmaceutical firms for the commercialization of biotechnology products. For example, firms like Millennium Pharmaceuticals have built their business models by focusing on the early portions of drug development and then seeking the collaboration with large firms (such as Pfizer and Merck) to pursue the later stages of drug development and commercialization (from clinical trials to market introduction). DBFs that have been the original and largest founders of the US biotechnology industry during the 1980s (e.g., Amgen, Quintiles Transnational Corporation, Genentech, Genzyme Corporation, Allergan, Dow Agro Science, Chiron) have followed similar patterns.

In performing their bridging role, DBFs have organized R&D activities by following an open innovation model. According to the Open Innovation paradigm,[6] the innovation process can be subdivided into five stages: (1) seeking opportunities, (2) evaluating innovativeness and market value; (3) recruiting partners for the development stage; (4) valuating invention's commercialization opportunities; (5) extending the innovation offering. In the case of the pharmaceutical sector, stages 1–3 characterize the macrophase of "drug discovery," while stages 4–5 compose the macrophase of "drug development and market introduction."[7] In each one of these stages, scientific and technological knowledge in-flows and out-flows from an organization to others and the final outcome of a new product (drug) introduction is, indeed, the result of the complementary effort of a set of diverse actors possessing specialized knowledge, skills, resources, and capabilities. Within this network of relationships DBFs have often acted as focal point, by coordinating various partnerships with academic institutions and research organizations, upstream, and with pharmaceutical companies, downstream.

The vertical (downstream) relationships between DBFs and pharmaceutical companies were beneficial to both types of firms. From the point of view of a DBF, pursuing an alliance with a well-known pharmaceutical company was seen not only as a possibility to get access to the final market (i.e., to get access to downstream complementary assets), but also as the means to build credibility and, eventually, improve the firm's reputation.[8,9] From the point of view of a large pharmaceutical company, pursuing a set of alliances with promising DBFs was seen as a means to acquire expertise and know-how on the emerging biotechnological solutions (i.e., to acquire the needed absorptive capacity to explore the biotechnology sector[10]), integrate external knowledge with internal R&D capabilities, maximize the returns from investments done in manufacturing and marketing capabilities, and eventually support over time the firm's competitive position.[11–13]

This model of division of labor at the industry level has allowed the growth of the biotechnology industry and the commercialization of a growing share of biotechnology-based new drugs. To secure a consistent share of biotechnology drugs within their product portfolios, in some cases large pharmaceutical companies have moved a step forward, by integrating backward in the value chain, and by replacing vertical alliances with DBFs with the acquisition of the same biotechnology firms.[14–17] It is worth noticing that, while these cases of vertical merger and acquisitions have been clearly beneficial to large pharmaceutical companies aiming at acquiring new capabilities, knowledge, and technologies protected by intellectual property rights (e.g., patents), they have received acceptance also by most DBFs, incapable of facing the complexity and costs of regulation concerning new drug introduction. For DBFs, merging with large pharmaceutical company thus represented the possibility to exploit the strengths of big pharmaceutical companies, pertaining to their regulatory and marketing expertise.[18]

Even though this model of division of labor has worked well for almost two decades, during the last years a new model of industry organization is emerging, with DBFs evolving from their traditional "bridging" position between science and market, to assume a more active role in the development and commercialization of biotechnology products, in direct competition with large pharmaceutical companies.

1.19.2.3 The Recent Evolution of the Biotechnology Industry

The main problem with the traditional pattern of industry organization was that DBFs were often exposed at an excessive bargaining power by large pharmaceutical companies, with the consequent risk of losing control over property rights on new technologies or, at least, the impossibility to secure a consistent share of revenues arising from the commercialization of drugs based on the new technology. For this reason, DBFs have started to engage more and more in alliances with other DBFs (bio-to-bio alliances), with the aim of expanding their knowledge base and exploiting stronger economies of scale. In doing so, some DBFs have started to build those capabilities in downstream activities (such as clinical trials, FDA's market approval, manufacturing, commercialization, and marketing) they were originally lacking. They have started to become relevant competitors to traditional large pharmaceutical companies, having acquired in some cases the capability to reach the final market autonomously. Furthermore, contrary to bio-to-pharma alliances, bio-to-bio alliances reduce the risk of knowledge leakages for DBFs and the possibility to get involved in legal disputes and litigations over the control of property rights. By contrast, allied DBFs have the possibility of integrating their resources, knowledge, skills, and capabilities to create value and compete successfully. Such firms have transformed themselves from specialized high-tech developers to specialty biopharma companies,[19] competing with incumbent large pharmaceutical companies in an increasingly competitive and fragmented market,[20] in which a specialized biotech niche is emerging.

As for incumbent pharmaceutical companies operating in this changing environment, their traditional competitive advantage may slowly disappear due to the fact that the largest biotechnology firms have started to develop the needed complementary capabilities to operate in the final drug market.[21,22] As a matter of facts, several new firms have entered the pharmaceutical market in the last few years, and the number of bio-to-bio alliances has strongly increased in the same period of time. While traditional DBFs were focused on shaping the knowledge building blocks of a nascent technological trajectory, by collaborating with and expanding the knowledge base of universities and public research organizations, the new model of biotechnology firms seeks to pursue

a commercial exploitation of the technological solutions they have contributed to develop. Such firms both compete and cooperate with large pharmaceutical incumbents, and simultaneously take part in a larger network of collaborations and alliances with a diversified plethora of actors located at different levels of the value chain. Vertical partnerships have been complemented with (but not replaced by) horizontal partnership and the consequences for the processes of drug discovery and commercialization have to be fully understood, yet.

1.19.3 The Recent Evolution of DBFs: An Empirical Assessment

To better understand how DBFs contribute to closing the gap between academia and market, and to assess how their role has been evolving during the last years, we performed a descriptive statistical analysis focused on the behavior of a sample of biotechnology firms. Specifically, we included in the sample all biotechnology firms having closed at least one biotechnology-related deal during the period 1993–2013 (data were drawn from the Thomson Reuters' Recap IQ database, which reports in-depth information on most recent deals in pharmaceuticals, ranging from licensing agreements, merger and acquisitions, marketing deals and manufacturing agreements). Overall, 146 national and international DBFs were included in the sample. As **Table 2** shows, most firms have headquarters located in the United States (94 out of 146) and have been created at the end of 1990s. Even though most firms are small in size (a half of them have obtained revenues of no more than $120 millions), some of them (among which Amgen, Applera, Arcion Therapeutics, and Cambridge Antibody Technology) are characterized by a much larger size, having obtained revenues of billions of dollars during the last year.

On these firms, we addressed two complementary issues. On the one hand, we explored how DBFs cooperate with universities and public research organizations to develop new biotechnological solutions suitable to be patented. On the other hand, we explored how DBFs seek the exploitation of possessed technologies by engaging in partnerships of different types with external firms.

1.19.3.1 Upstream Vertical Relationships Between DBFs and Academic Institutions

In order to pursue the first goal, we analyzed the patent portfolios of sampled firms. Data on patents has been drawn from the Orbit-QPat database (ORBIT-QPAT is a service powered by Questel IP Business Intelligence providing information on patent documentation. It collects more than 100 databases for specialists in patents and designs. It covers more than 95 national patent offices, and reports patent information grouped by invention-based families and enriched with full-text data). For each patent possessed by samples firms, we explored whether it was coowned with other organizations, and, specifically, with universities and public research organizations. It is worth noticing that patent coownership reveals the existence of a cooperative agreement between the different coowners. Indeed, when two or more organizations perform joint research and decide to seek patent protection for the innovative technological solutions they jointly develop, they might decide either to allocate full property rights of the invention to only one of the partners, or to share ownership of property rights (coownership). In this sense, coowned patents can be considered an underestimated measure of cooperative agreements among coowners, and information on coowned patents can be used to assess whether and with whom a focal firm engages in research collaborations.

We performed a similar analysis on the total number of family patents possessed by our sample firms (**Table 3**). Among all these patents, we searched for those patents that sample firms coown with academic partners (universities, colleges, and other research organizations). As **Fig. 1** shows, the share of patents that DBFs coown with academic partners has remained almost stable over the last decade, thus revealing how the recent changes (as outlined earlier) that have characterized the organization of the biotechnological and pharmaceutical industry have not affected the importance that academic research and knowledge generated by universities has for the development of biotechnologies.

Nevertheless, if the number of academic institutions that sampled DBFs partner with is taken into account, then it is possible to observe a gradual evolution of collaborative agreements among the two organizations. As **Fig. 2** shows, over time, the share of academic patent coowners has constantly increased, by shifting from an average of $<4\%$ academic coowners at the beginning of 2000s (with respect to the total number of patent coowners), to more than 10% at the beginning of 2010s. Jointly with **Fig. 1**, this figure thus highlights a singular trend in the relationship between DBFs and the academia. It emerges that while the "quantity" of research produced (in terms of numbers of patents registered) in collaboration with academic actors has remained almost

Table 2 Sample firms' characteristics

	Value	*Mean*	*Median*	*Standard deviation*
Foundation year		1996	1999	11.89
Last year revenues ($ mln)		3441.16	120.00	7942.09
Location: United States	94			
Location: Europe	25			
Location: Other countries	27			

Table 3 Patent families owned by sample firms

Year	*# Patent families*
2003	2226
2004	2126
2005	2127
2006	2234
2007	2199
2008	2025
2009	1764
2010	1771
2011	1643
2012	1838
2013	1816
Total	*21,769*

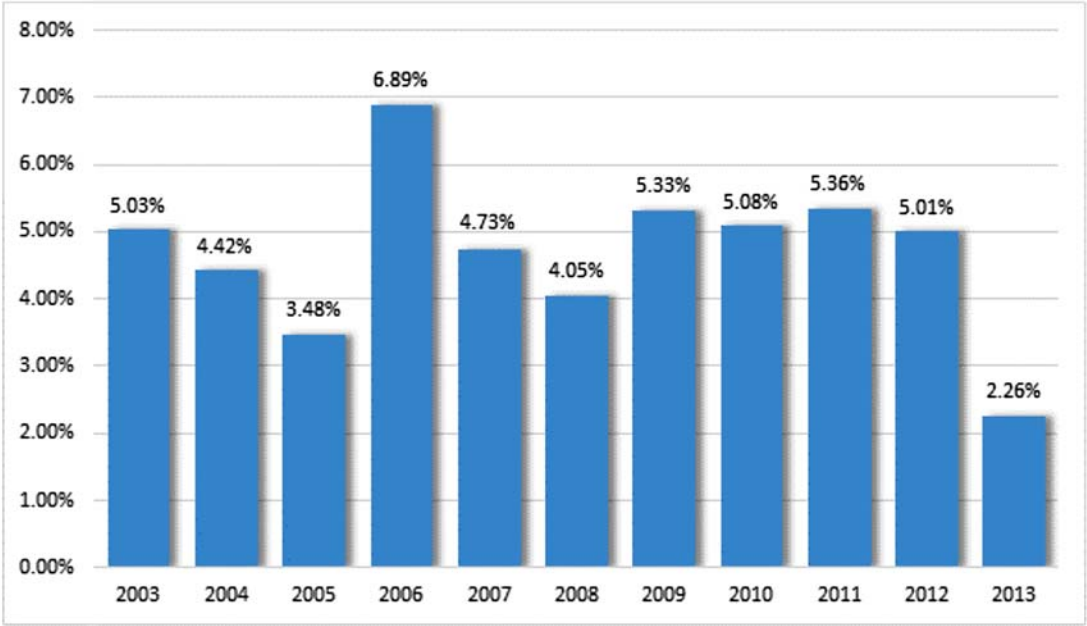

Fig. 1 Share of coowned patents with academic partners.

constant over time, the number of academic actors involved in patenting with DBFs has been constantly growing over the last years. This trend reveals an increasing need by DBFs to diversify and increase the number of knowledge sources, thus suggesting that the development of new biotechnology solutions currently requires the integration of a knowledge base which is larger than what it was a decade ago. Put differently, the fast pace of technological change in the biotechnology industry and the market demands require continuous innovation, which derives from multidisciplinary research through a transformation process that converts science-oriented knowledge into marketable products. Findings reveal that some certain transition mechanisms from monodisciplinary collaboration to multidisciplinary university–industry alliances are emerging. These relationships are a useful channel to accelerate the knowledge transfer from the university to industry aiming at the effective transition of science into products.

Alternatively, these figures may reveal that DBFs tend to reduce the risk of remaining locked-in in strict relationships with a reduced number of academic institutions by enlarging the portfolio of research alliances. More in details, in order to contrast patent expirations on blockbuster drugs and declining innovation in the industry, DBFs are restructuring their (R&D) operations and are pursuing an aggressive strategy of licensing deals and research collaborations in an attempt to fill the gaps in their product pipelines.

1.19.3.2 Downstream Vertical Relationships Among DBFs, Pharmaceutical Companies, and Other Organizations

In order to pursue the second goal of our analysis, we explored the different partnership agreements that DBFs belonging to our sample signed during the last decade. Data has been obtained from the Thomson Reuters' Recap IQ database, which includes all

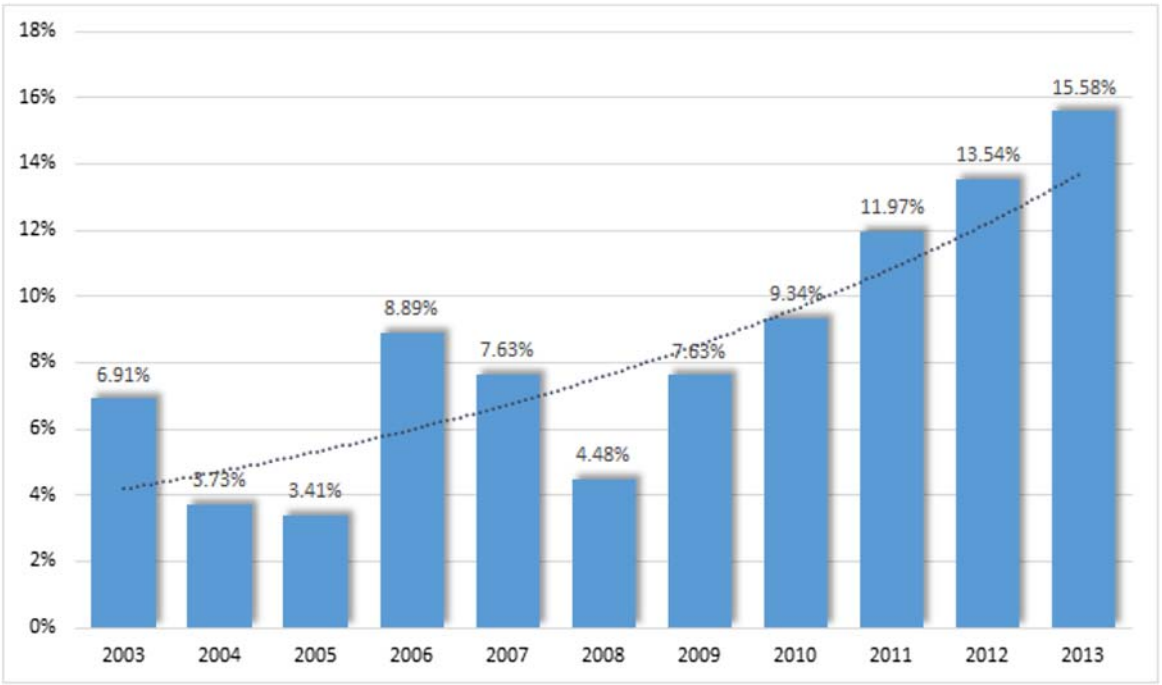

Fig. 2 Share of academic patent coowners (with respect to total patent coowners).

market deals closed in the pharmaceutical industry during the 2003–13 period. Within this period of time, DBFs have undertaken partnerships with various organizations (other DBFs, pharmaceutical companies, biopharma companies, and firms from other industries), both as promoters (i.e., acquirers or investor companies with an active role in promoting the partnership agreement) and as targets (i.e., recipient companies being "object" of the deal). Partnerships may take different forms, ranging from "research and discovery" agreements aimed at performing collaborative research activity on a specific molecule, methodology, or technological component, to "comarketing" agreements aimed at pursuing a collaborative marketing strategy in order to introduce into the market or to sustain the sales of a given drug or biotechnology product. In most cases, transactions take a complex form and include several single agreements joint together. For example, it is very likely that a technology license contract also includes an agreement on the acquisition of property rights (or an option to acquire property rights) on the licensed technology. Similarly, often a manufacturing contract also includes an agreement to subsequently commercialize the manufactured biotechnology product. Furthermore, all the possible types of agreements can also be classified into two main categories, namely "Drug Research and Development" and "Drug Exploitation and Commercialization." These two categories of deals correspond to the two stages of "drug discovery" and "drug development and market introduction" that compose the Open Innovation model described in the previous section, which characterize the activity of DBFs. As for the case of disaggregated agreements, also in this case it is possible that a deal between two companies takes a complex form, by including both elements of Drug Research and Development, and elements of Drug Exploitation and Commercialization.

Overall, our analyses confirm most of the tendencies suggested by prior research. As far as agreements in which a DBF appears as the target company are concerned, results show (Table 4) that most deals (290 out of 409 in total, equal to 70.90% of total deals) refer to Drug Exploitation and Commercialization agreements, while the remaining cases concern to Drug Research and Development agreements (199 deals, equal to 29.10% of total deals). This result confirms that DBFs act primarily as integrators of knowledge, skills, and resources related to biotechnology. DBFs thus aim at developing new biotechnology outcomes, which then they transfer to other organizations that are in charge of developing the technology further, create new products out of it (mainly, drugs), and introduce the new products into the final market. In some cases, however, agreements with external organizations are also aimed at performing research for the development of new biotechnologies, much before the exploitation and commercialization stage. Such deals complement those collaborative research agreements that DBFs sign with academic institutions and public research laboratories, and which we analyzed in the previous section by making use of patent statistics.

Table 4 also provides information on the type of organization that has promoted the agreements involving DBFs. It emerges that most of the deals in both drug development and drug exploitation stages are promoted by pharmaceutical companies. As suggested by prior research, these companies often lack updated know-how and competences to develop biotechnological-based new drugs and thus need to cooperate with specialized DBFs in possession of complementary capabilities. Furthermore, for the pharmaceutical companies such agreements also present the advantage of avoiding to remain locked-in with existing resources and competences. Since biotechnology research evolves very rapidly and entails a growing number of scientific disciplines (see, e.g., the case of

Table 4 Deals involving a DBF as target (period: 2003–13)

	Acquirer/partner/investor company				
Deal type	*DBF (%)*	*Pharmaceutical company (%)*	*Biopharma company (%)*	*Other (%)*	*Total (%)*
Drug research and development					
Research and discovery	0.73	3.18	1.22	0.00	5.13
Development	2.20	9.78	4.16	1.47	17.60
Collaboration	0.24	1.96	0.98	0.00	3.18
Codevelopment	0.49	1.22	1.47	0.00	3.18
Cross-license	0.00	0.00	0.00	0.00	0.00
Joint venture	0.00	0.00	0.00	0.00	0.00
Total drug R&D	*3.67*	*16.14*	*7.82*	*1.47*	*29.10*
Drug exploitation and commercialization					
Acquisition of rights	4.65	9.54	5.13	1.47	20.78
Licensing agreement	5.13	10.27	4.65	2.20	22.25
Sublicense	0.24	0.00	0.00	0.24	0.49
Option announced	0.00	0.24	0.00	0.24	0.49
Option exercised	0.49	0.00	0.24	0.24	0.98
Manufacturing	0.00	1.47	0.73	0.00	2.20
Distribution	0.24	0.73	0.49	0.00	1.47
Commercialization	1.96	7.58	4.16	1.22	14.91
Sales	0.73	1.71	0.98	0.24	3.67
Supply	0.00	0.00	0.24	0.00	0.24
Copromotion	0.00	0.24	0.00	0.00	0.24
Marketing	0.00	2.20	0.73	0.24	3.18
Comarketing	0.00	0.00	0.00	0.00	0.00
Total drug exploitation and commercialization	*13.45*	*33.99*	*17.36*	*6.11*	*70.90*
Total	*17.11*	*50.12*	*25.18*	*7.58*	*100.00*

bioinformatics), outsourcing biotechnology research from external providers (DBFs) allows large pharmaceutical companies to modify the setting of controlled competences without incurring the high costs of re-training internal staff. Furthermore, compared to pharmaceutical companies, DBFs can exploit their smaller size to move quickly towards new promising technological trajectories, investing in the exploration of new research possibilities, without facing the heavy fixed costs of larger companies.

However, Table 4 also shows that other DBFs also act as promoters of deals with their peers. As suggested by recent managerial literature, albeit always existed, these types of agreements have become more and more common in the last years (i.e., those covered by our data), revealing the tendency of some DBFs to acquire enough size to compete in the final market for drugs and other biotechnology products. As a matter of facts, most of bio-to-bio agreements do not concern the stages of Drug Research and Development, but those of exploitation and commercialization. This evidence thus confirms that the main aim of DBFs promoting agreements with other DBFs is that of acquiring and/or developing those downstream complementary assets in manufacturing, commercialization, and marketing that are needed to address final consumers. In this, their goal is to start competing with incumbent pharmaceutical companies in specialized niches of the market for biotechnology products.

To better explore this issue, we further analyzed in greater details the agreements that DBFs have signed during the period 2003–13 by taking the role of promoter (either, acquirer, partner or investor company). As Table 5 shows, gross results clearly mimic those obtained by Table 4—most of the agreements (148 out of 202, equal to 73.27% of total agreements) concern the Drug Exploitation and Commercialization stage, while only a minority (54 out 202, equal to 26.73%) refer to the stage of Drug Research and Development.

Nevertheless, results reported in Table 5 also provide insightful suggestions on how DBFs are attempting to move downward the value chain to reach the final market. First, it emerges that the largest share of downstream agreements are signed with other DBFs, and take primarily the form of technology licensing agreements. This result confirms what has been already expressed earlier, of an attempt made by DBFs to consolidate their market position by partnering with organizations having similar bargaining power, thus avoiding (or, at least, limiting) the risk of knowledge leakage and loss of control over property rights on possessed technologies.

Second, it emerges that not only DBFs are the target of agreements promoted by pharmaceutical companies, but also that in many cases the same DBFs do promote agreements with pharmaceutical companies for the exploitation of owned technologies. As a matter of facts, while licensing agreements do remain the preferred form of agreement as in the case of DBFs, manufacturing, commercialization, copromotion, and marketing deals are promoted almost exclusively with pharmaceutical companies. With these organizations, DBFs thus seek to get access to those downstream complementary assets they lack.

Finally, Table 5 also reveals that an important target of deals promoted by DBFs is biopharma companies. Such firms are usually identified as companies making a large fraction of drug revenues (usually, at least 50%) from selling biologics and vaccines. As such, these firms are those that have a research profile very close to that of biotechnology firms and that may benefit the most from

Table 5 Deals involving a DBF as promoter (period: 2003–13)

	Target/source/recipient company				
Deal type	*DBF (%)*	*Pharmaceutical company (%)*	*Biopharma company (%)*	*Other (%)*	*Total (%)*
Drug research and development					
Research and discovery	1.49	0.99	1.49	0.99	4.95
Development	4.46	5.45	4.95	1.49	16.34
Collaboration	0.50	0.00	2.48	0.00	2.97
Codevelopment	0.99	0.00	0.99	0.00	1.98
Cross-license	0.00	0.50	0.00	0.00	0.50
Joint venture	0.00	0.00	0.00	0.00	0.00
Total drug R&D	*7.43*	*6.93*	*9.90*	*2.48*	*26.73*
Drug exploitation and commercialization					
Acquisition of rights	9.41	5.45	4.46	1.49	20.79
Licensing agreement	10.40	6.44	4.95	1.98	23.76
Sublicense	0.50	0.00	0.99	0.00	1.49
Option announced	0.00	0.00	0.00	0.00	0.00
Option exercised	0.99	0.00	0.00	0.00	0.99
Manufacturing	0.00	0.99	0.99	0.50	2.48
Distribution	0.50	0.50	0.00	0.00	0.99
Commercialization	3.96	5.45	4.46	0.50	14.36
Sales	1.49	0.99	2.48	0.00	4.95
Supply	0.00	0.50	0.00	0.00	0.50
Copromotion	0.00	0.50	0.00	0.00	0.50
Marketing	0.00	1.49	0.50	0.50	2.48
Comarketing	0.00	0.00	0.00	0.00	0.00
Total drug exploitation and commercialization	*27.23*	*22.28*	*18.81*	*4.95*	*73.27*
Total	*34.65*	*29.21*	*28.71*	*7.43*	*100.00*

partnering with DBFs. In some cases, these firms are, indeed, prior DBFs that have integrated downward in the value chain to reach the final market. Results of our analysis seem to suggest that sample DBFs consider biopharma companies in a similar vein as large pharmaceutical companies, since with them too they seek various types of agreements, from technology licensing to manufacturing, commercialization, and marketing. Also in this case, the attempt is that of getting access to downstream complementary assets.

1.19.4 Conclusions

Over the last decades, the scientific revolution of biotechnology has drawn an increasing attention both from academia and industry and is producing truly novel therapeutics for unmet patient needs. Our findings from the analysis of both university–industry and industry–industry collaborations during the period 1993–2013 reveal that new interinstitutional and cross-domain relationships are emerging due to the novel technological trends and the new industry landscape. The pharmaceutical industry is facing significant barriers in the continued patent expirations that are eroding firms' profit margins, challenging market dynamics, and existing forms of pricing and reimbursement.

A number of biopharmaceutical patents are due to expire in the next few years, or have already expired. The subsequent production of follow-on products, or "biosimilars" has aroused interest within the pharmaceutical industry as biosimilar manufacturers strive to obtain part of an already large and rapidly-growing market. This represents a new challenge that pharmaceutical firms have to face.

Another challenge for the pharmaceutical industry stems from developing countries. To successfully develop a local biotechnology industry in these countries, it is critical to understand and improve the system of health innovation, as well as the role of each innovative sector and the linkages existing among sectors. Accordingly, academia and public research centers have to improve their capabilities to create nonlinear linkages and strong interrelations among players throughout the entire innovation process. These relationships generate and transfer knowledge related to commercialization of the innovative health products. The private sector is one of the main actors in healthcare innovation, contributing significantly to the development of biotechnology via knowledge, expertise, resources, and relationships that translate basic R&D into new commercial products and innovative processes. Thanks to these relationships, several developing countries that have been actively involved in health biotechnology are becoming the main players in this industry (e.g., South Korea, India, Brazil).

Our findings reveal that DBFs are adopting a flexible concept of collaboration in R&D and technology exploitation. This concept represents one new approach chosen by the DBFs to tackle current challenges posed by declining internal R&D success rates and emerging novel technological trends. For this reason, DBFs have gradually modified their partnering strategy, now seeking to larger

extent than it was in the past collaborations with actors in possession of downstream complementary assets they lack. In doing so, their aim is to get closer to the diversified final application markets (among which, the health sector), thus granting themselves a greater ability to control property rights and to secure higher and more stable flow of revenues.

Indeed, the identification and development of novel breakthrough medicines have recently undergone significant changes, in part because of the extraordinary complexity that is associated with tackling diseases of high unmet need, and also because of the increasingly demanding requirements that have been placed on the pharmaceutical industry by investors and regulatory authorities. Taken together, these trends have led DBFs to increase the diversification of actors they partner with in drug discovery and development. This trend has in turn led to increasing partnering interactions between the specialized biotechnology sector and the more diversified sector of big pharma. In addition, as our analyses revealed, the biotechnology sector has itself become further engaged in partnering with other biotechnology companies to accelerate the knowledge transfer and create a translational bridge able to increase the probability of success associated with identifying novel medicines to treat unmet medical needs.

1.19.5 Limitations and Further Research

The analyses presented in this article clearly suffer some limitations that require further research to be addressed and fixed. First, our patent analysis aimed at exploring the linkages that DBFs establish with academic institutions by observing the frequency of coownership. This event, however, only represent one among several other mechanisms of university–industry interaction. Not only, patent coownership does represent an explicit and formal interaction means, which only marginally captures the complexity of forms of interaction between the two institutions that often prefer to operate at an informal level. In turn, further research should address the problem at hand by complementing patent coownership data with information drawn from other sources.

Second, in analyzing the partnership strategies of DBFs, we only focused on the last 11 years (from 1993 to 2013). Even though such period of time has been characterized by dramatic changes in the biotechnology and pharmaceutical industries (for reasons that have been highlighted in the previous sections), a longer period of observation is needed to obtain a more complete picture of the dynamics of the two industries. Thus, further research should take a longer perspective and make a clearer distinction between long-term trends and short-term fluctuations.

Finally, our analysis has been mainly descriptive and quantitative. While we spent effort to infer from our results possible implications for company strategies and industry dynamics, more sophisticated econometric quantitative estimations would be needed to discover the exact causal relationships that may explain observed phenomena. Similarly, qualitative analyses (e.g., in-depth case studies) would help disentangling the picture of what motivates firms' moves, what obstacles impede their strategies to be fully implemented, and what directions firms should take to shape the boundaries of the future pharmaceutical industry.

References

1. Evens, R. P.; Kaitin, K. I. The Biotechnology Innovation Machine: A Source of Intelligent Biopharmaceuticals for the Pharma Industry—Mapping Biotechnology's Success. *Clin. Pharmacol. Ther.* **2014,** *95* (5). http://dx.doi.org/10.1038/clpt.2014.14.
2. Ernst & Young. *Biotechnology Annual Industry Reports*; Ernst & Young: Palo Alto, CA, various years.
3. Powell, W.; Koput, K.; Smith-Doerr, L. Inter-Organizational Collaboration and the Locus of Innovation: Networks of Learning in Biotechnology. *Adm. Sci. Q.* **1996,** *41,* 116–145.
4. Stuart, T. E.; Hoang, H.; Hybels, R. C. Inter-Organizational Endorsements and the Performance of Entrepreneurial Ventures. *Adm. Sci. Q.* **1999,** *44,* 315–349.
5. Young & Ernst. *Integration: Eighth Annual European Life Sciences Report 2001: Meeting the Needs of the Life Science Industry;* Ernst & Young's: Palo Alto, CA, 2001.
6. Chesbrough, H. W. *Open Innovation: The New Imperative for Creating and Profiting from Technology;* Harvard Business School Press: Boston, MA, 2003.
7. Bianchi, M.; Cavaliere, A.; Ciaroni, D.; Frattini, F.; Chiesa, V. Organisational Modes for Open Innovation in the Bio-Pharmaceutical Industry: An Explanatory Analysis. *Technovation* **2011,** *31,* 22–33.
8. Dollinger, M. J.; Golden, P. A.; Saxton, T. The Effect of Reputation on the Decision to Joint Venture. *Strateg. Manag. J.* **1997,** *18* (2), 127–140.
9. Hagedoorn, J.; Roijakkers, N. Small Entrepreneurial Firms and Large Companies in Inter-Firm R&D Networks: The International Biotechnology Industry. In *Strategic Entrepreneurship: Creating a New Mindset;* Hitt, M., Irleland, R., Camp, S., Sexton, D., Eds.; Blackwell: Oxford, 2002.
10. Cohen, W.; Levinthal, D. Absorptive Capacity: A new Perspective on Learning and Innovation. *Adm. Sci. Q.* **1990,** *35,* 128–152.
11. Oliver, A. L. On the Duality of Competition and Collaboration: Network-Based Knowledge Relations in the Biotechnology Industry. *Scand. J. Manag.* **2004,** *20,* 151–171.
12. Oliver, A. L. Strategic Alliances and the Learning Life-Cycle of Biotechnology Firms. *Organ. Stud.* **2001,** *22* (3), 467–489.
13. Kale, P.; Dyer, J. H.; Singh, H. Alliance Capability, Stock Market Response, and Long-Term Alliance Success: The Role of Alliance Function. *Strateg. Manag. J.* **2002,** *23,* 747–767.
14. Danzon, P.; Epstein, A.; Nicholson, S. Mergers and Acquisitions in the Pharmaceutical and Biotech Industries. *Manag. Decis. Econ.* **2007,** *28,* 307–328.
15. Rafferty, M. A. Managing Change in Biotech: Mergers and Acquisitions. *Nat. Biotechnol.* **2007,** *25,* 689.
16. Malik, N. N. Mergers and Acquisitions in the Pharmaceutical and Biotech Industries. *Drug Discov. Today* **2009,** *14* (17–18), 818–821.
17. Hora, M.; Dutta, D. Partnering With Goliath: Impact of Alliance Depth and Product Development Orientation on Entrepreneurial Success. In Academy of Management Annual Meeting Proceedings; 2010; pp 1–6.
18. Schweizer, L. Organizational Integration of Acquired Biotechnology Companies into Pharmaceutical Companies: The Need for a Hybrid Approach. *Acad. Manag. J.* **2005,** *48* (6), 1051–1074.
19. Hernández-Cuevas, C. Collaborative Innovation: The Future of Biopharma. *J. Technol. Manag. Innov.* **2007,** *2* (3), 1–3.
20. Bingham, A.; Ekins, S. Competitive Collaboration in the Pharmaceutical and Biotechnology Industry. *Drug Discov. Today* **2009,** *14* (23), 1079–1081.
21. Rothaermel, F. T. Incumbent's Advantage Through Exploiting Complementary Assets Via Interfirm Cooperation. *Strateg. Manag. J.* **2001,** *22,* 687–699.
22. Rothaermel, F. T.; Hill, W. Technological Discontinuities and Complementary Assets: A Longitudinal Study of Industry and Firm Performance. *Organ. Sci.* **2005,** *16* (1), 52–70.

1.20 Present and Future Challenges and Opportunities for Intellectual Property in an Open Landscape: Open Labs and the Internet

H Céster Schlaak, Integral BioConsulting, Las Rozas, Spain

© 2017 Elsevier Ltd. All rights reserved.

1.20.1	**Introduction**	529
1.20.2	**Open Laboratories**	529
1.20.2.1	Maintenance of Confidentiality in Open Lab Spaces	529
1.20.2.2	Inventorship in Open Lab Spaces	530
1.20.2.2.1	Some definitions	530
1.20.2.2.2	Inventorship: concerns in open lab spaces	531
1.20.3	**Lack of Control Over Information in the New Technological Era**	532
1.20.3.1	Smartphones and Computers	532
1.20.3.2	Multiple Devices	532
1.20.3.3	E-Mail	532
1.20.3.4	Publications in Scientific Congresses, Now and Before	532
1.20.4	**Patents in the Internet: Is "Do It Yourself" a Reasonable Option?**	533
1.20.4.1	Some Useful Information Resources in the Internet	533
1.20.4.1.1	World Intellectual Property Organization (WIPO)	533
1.20.4.1.2	United States Patent and Trademark Office (USPTO)	535
1.20.4.1.3	European Patent Office (EPO)	537
1.20.4.1.4	Japanese Patent Office (JPO)	537
1.20.4.2	How to Make Reasonable Use of the Available Resources	538
1.20.4.2.1	Searching	539
1.20.4.2.2	Drafting and Prosecution	539
1.20.4.2.3	Legal status of patents and patent applications	539
1.20.5	**Conclusion and Perspective**	539
Further Reading		539

1.20.1 Introduction

In this article, a reflection on the possible threats to intellectual property caused by the design of laboratories as open spaces and the extended use of new technology devices is presented. Further, a review of information on intellectual property, mainly patents, available on the Internet for free, is performed, including recommendations on how to use it reasonably.

1.20.2 Open Laboratories

Both public and private research institutions are increasingly designing their research facilities as "open" laboratories. The aim behind this kind of design is mainly to support team-based work and inter-team work, rather than isolated individual work: researchers do not only share the research space itself but also all the equipment, tools, their bench space, meeting spaces, and their support staff, often not only with colleagues from their own team, but also with colleagues from other teams. Modern science is expected to be an intensely social activity, the individual scientists being aware of the work and style of their colleagues, as the communication and exchange of information between the scientists is intended to be strongly increased.

Nevertheless, besides the main complaint expressed by scientists who are working in an open lab environment (ie, typically, the lack of sufficient capacity for concentration), there are also some relevant problems of various nature that should not at all be underestimated. In the following sections, some of the possible complications are explained. The effect of these complications on intellectual property is also highlighted.

1.20.2.1 Maintenance of Confidentiality in Open Lab Spaces

Maintaining the integrity and confidentiality of scientific information and results is absolutely crucial. Scientific research leads to the generation of immense amounts of information, which encompasses the accomplishments of the scientific staff and represents the real assets of any research institution, and as such due care has to be taken. The confidentiality of scientific information is especially relevant if at some point of the research a patent application is intended to be filed; but also if a publication in a peer review journal is envisaged; or sensitive information from third parties is handled with; or the information is intended to be withheld from the public as a trade secret; among other scenarios. Maintaining confidentiality of all the information is essential, as any disclosure can have adverse effects for any of the abovementioned actions or activities.

Nevertheless, in open lab spaces, especially those that are occupied by different organizations, such information, know-how, and results may be exposed to high risks, due precisely to the laboratory's design.

Regarding the request for patent protection, the risk may be especially high. It is well known that in order to obtain such protection, three main requirements have to be fulfilled: the invention has to be novel, involve an inventive step, and have some defined utility ("industrial applicability"). The latter requirement is not sensitive to prior disclosures, and as such will not be considered here. Nevertheless, the first two requirements will be adversely affected by any disclosure related to the object of the invention. As a reference, for example, according to the *Guidelines for Examination* published by the European Patent Office (EPO), paragraph G-VI-1, an "invention is considered to be new if it does not form part of the state of the art." On the other hand, the state of the art is defined within the same guidelines as, "everything made available to the public by means of a written or oral description, by use, or in any other way, before the date of filing of the European patent application." It will be noted that such a definition is wide, without any restrictions regarding the geographical location, the language or manner in which the information was made available to the public. That is, a disclosure of even only part of an invention could mean that the invention is not considered novel, and as such is not patentable. Although a resource from the EPO has been used herein to better explain this concept, the novelty requirement exists worldwide and is interpreted very similarly from country to country.

With respect to the inventive step (according to the *Guidelines for Examination* by the EPO, paragraph G-VII-4), "an invention is considered as involving an inventive step if, having regard to the state of the art, it is not obvious to a person skilled in the Art." Once more, the inventive step is evaluated with regard to the state of the art as was already defined above with regard to the novelty requirement. Further, the person skilled in the art "should be presumed to be a skilled practitioner in the relevant field of technology, who is possessed of average knowledge and ability and is aware of what was common general knowledge in the art at the relevant date […]. He should also be presumed to have had access to everything in the 'state of the Art'." That is, again a disclosure of even only part of an invention could mean that the invention is not considered patentable, in this case due to lack of inventive step. The requirement of inventive step also exists worldwide, although different terms may be used therefore, for example, non-obviousness in the case of the United States Patent and Trademark Office. Although the interpretation of the terms also varies slightly from country to country, in any case a prior disclosure would most probably be hazardous for the compliance of this requirement.

In view of the above, it will become clear that it is immensely important that public and private institutions working in an open lab environment take the necessary measurements and actions to protect and assure the confidentiality of the information held and generated by their staff. This includes corresponding confidentiality agreements, both with the staff and with anyone that has access at some point to the open lab and also an intense raising of awareness among their staff, by corresponding training and education, and serious repercussions in cases of breach of confidentiality.

The same confidentiality policy should also apply, if not even more, to information acquired by collaborations or agreements with external institutions. Such institutions expect that the information provided to third parties is treated with maximum confidentiality, and in such a case any minimal leak of information is absolutely unacceptable. Some institutions may even be thrown back when considering collaborating with an institution having an open lab, once they are aware of this circumstance, unless an impeccable reputation precedes the lab, and strong confidentiality agreements are signed before exchanging any information. Any minimal leak of information may irreparably harm the reputation of a lab and may lead to negative effects of other institutions avoiding collaborations with the lab.

Summing up, the socialization happening in open labs seems to be a great spawning ground for the generation of potentially patentable scientific advances. Nevertheless, precisely such socialization means also a hazard to the same inventions, as the confidentiality of the information underlying such inventions is at risk. Delicate information may be disclosed, displayed, or discussed in the presence of other laboratory staff not related to the project itself. Therefore, it is immensely important to make sure that all the staff with access to the laboratory (including not only scientific staff, but also maintenance or cleaning staff) signs corresponding confidentiality agreements. Also any temporary staff has to be made sure to sign such agreements regarding any information they may have access to in the open lab environment. But this arrangement should not end with one's signature on a confidentiality agreement, which may easily be broken without having the certainty of who is liable. It is increasingly important to raise the awareness of the staff regarding the importance of confidential information and the responsibility they share for understanding and respecting the importance of such information and maintaining such confidentiality with regard to their own and their colleagues' work.

1.20.2.2 Inventorship in Open Lab Spaces

The socialization intended by the open laboratories design leads to a further issue that is never simple, but may become even more problematic in open lab spaces: the determination of inventorship, the monitoring thereof, and the registering thereof.

At this point it seems important to define inventorship versus authorship: the terms "inventor" (the term used for patents and utility models) and "author" (the term used for scientific publications) are not synonymous.

1.20.2.2.1 Some definitions

The phrase "Authorship on a publication is determined by custom; Inventorship on a Patent is determined by law" (source: www.unemed.com) very well reflects the difference between the two terms.

Authorship is generally determined by custom: for a scientific publication, a large variety of people may be legitimately considered as authors, including those persons involved in the experimental design, who actually performed the experiments, who wrote or edited the manuscripts leading to the actual publication, or even those persons who contributed their general expertise. Authorship is sometimes also granted for the recognition of hard work or for financial support, or simply professional courtesy to collaborators and mentors.

In contrast, inventors of subject matter in patents have to be determined by law and on the basis of judicial decisions, and may differ from country to country. Any violation of the law regarding inventorship may have severe impacts on a resulting patent, and "corteous" giving of inventorship may have serious negative consequences in some countries (including, eg, the United States). Such a violation includes both an erroneously designated "inventor," who did not actually contribute to the conception of an invention, or an omitted inventor. In the extreme, such mistakes can result in the patent being invalidated. Inventorship is therefore a crucial issue in patent law.

1.20.2.2.1.1 United States

The legal meaning of the term "invention" is composed of two aspects:

(i) Conception of the invention, that is, the formation of a definite idea of the complete and operative invention in the mind of the inventor and
(ii) Reduction to practice of the invention, that is, the process of showing on the basis of experimental data that the claimed invention in fact works for its purpose.

Thus, an inventor is a person who made some inventive contribution to the invention as defined by the claims of the patent application, particularly the inventive contribution must go to the conception of the claimed invention. Therefore, in a first step it has to be determined when complete conception of the invention occurred. When the original conception is complete enough to enable another person, that is, the practitioner, to reduce the invention to practice, without contributing anything further than mere routine skill, the contributor to the conception of the claimed invention is an inventor; the practitioner reducing the invention to practice, without a contribution to the conception of the invention, will not be entitled to be designated as an inventor.

It is important to keep in mind that the claims are the part of a patent (application) that define the invention, and the contribution to the invention has to be determined based on the claims. During prosecution, particularly during examination of the patent application, claims are frequently amended or even deleted, and inventorship should necessarily be reviewed after each amendment, as it may be that a person listed as inventor in the originally filed patent application, is not anymore entitled to inventorship in the patent having amended claims.

1.20.2.2.1.2 European Patent Convention (EPC)

In the European Patent Convention (EPC) and its case law, no explicit, accurate definition of who exactly is an inventor is provided. The definition may slightly vary from one European country to another. Inventorship is generally not considered to be a patentability criterion under European patent law.

1.20.2.2.2 Inventorship: concerns in open lab spaces

As outlined before, the intention of open labs is to promote and encourage not only team-based work but also inter-team work, that is, the interaction between different teams to incite the generation of new and creative ideas. So far, the laboratory work was normally discussed, organized, and designed mainly in formal or informal team meetings. Especially for formal meetings, ideally some kinds of minutes were written as a record of the meeting. Also each of the scientists should be daily completing a laboratory notebook, or introducing the corresponding information into their computer with particular software, to record all the work and ideas he or she has generated during the work day. But what about those informal meetings that are intended to be promoted by the open lab design? Those aisle conversations encouraged by the open lab design? How may the information generated in such meetings and conversations be recorded?

As noted before, an inventor is a person who made some inventive contribution to the invention to the conception of the claimed invention, and not a person who reduced the invention to practice by performing experimental work in the laboratory; the latter could be easily followed, and it would be easy to determine who carried out the extensive experimental work; nevertheless, the former, that is the conception of the invention, is a much more subtle, ephemeral concept. And such a conception may in any case happen in such an informal meeting, which contents are difficult to be recorded or with hindsight be determined what was discussed during such meetings.

The only "legal" way of recording the content of such meetings (as I do not believe any worker would accept permanent voice recording, nor will any law on protection of personal data allow it, nor would it be humanly possible to review hours and hours of recording!) seems to be making references to such improvised meetings, if they seemed to refer to some information that could become relevant for generating an invention, in the individual notebooks or notes in the corresponding software.

Nevertheless, the issue of inventorship is always a complicated item (firms in countries where the inventors have a right to a retribution on the basis of their percentage of participation in the conception of an invention have particular departments in their structure, committed to determine such percentages as a basis of calculating the retribution), but it will become increasingly complicated within the open lab environment.

1.20.3 Lack of Control Over Information in the New Technological Era

An additional risk, which in some cases seems to be highly underestimated, in my view and experience, both in the personal and the professional environment, are also the risks arousing from the use of e-mail, social media, modern smartphones, and online storage ("the cloud").

1.20.3.1 Smartphones and Computers

Things have been changing rapidly during the last decade or more. Nowadays everyone owns a smartphone having high resolution camera, ready to take pictures and videos at any time, as well as a sound recorder, right there in their pocket. Prohibition signs regarding their use are not always respected, see for example the behavior of people at hospitals or at the cinema; there will always be someone that unfortunately does not follow the rules. And at work, everyone will have their mobile phone (mainly smartphones) ready to answer any calls, and as ready also to take any pictures. A similar landscape will apply to computers or laptops, equipped with webcams and microphones. Additionally, both smartphones and computers are constantly connected to the Internet. Any information recorded by any of such devices may immediately be shared with others by e-mail, shared folders, messaging programs, etc., or immediately a safety copy is stored in some part of "the cloud": many people's devices are configured to automatically make a safety copy of all the generated information or files, either intentionally, due to panic about losing any of their valuable information, or unintentionally, as their devices are automatically configured that way, once connected to, for example, Google or Apple iCloud. Many of us have been surprised about how much of your personal information, pictures, contacts, files, etc. are back-copied automatically, without asking for confirmation. Also our social behavior has been changing: things that were normally shared over a cup of coffee or tea, or over a telephone call, are now shared over social media, e-mail, messaging, etc., that is, in written form, and even if deleted, traces will for sure be maintained somewhere.

1.20.3.2 Multiple Devices

It is also common than people do not only work on one technological device, many having two or more devices out of a PC, a laptop, a tablet, and a smartphone, for example, or do not only work from one localization, but from more than one branch office or from the office and from home, or during travels; this fact, in combination with the wish of immediacy, that is the made-up necessity of immediately being able to access all the files from any device and from any location at any time, increasingly is leading to the use of online storage, which is accessible from anywhere whenever an Internet connection is available. Many providers offer such an online storage service, many of them even for free (subject to publicity). Nevertheless, with the exception of some providers, who against a fee, offer an encoded storage, that is, an encoding of the information stored that should make the information, even if accessed by third persons, illegible and useless, the security of such online storage is not guaranteed. This should be a concern with regard to personal information, such as family pictures or lists of addresses, but even the more with sensible information generated during work, for which confidentiality may be absolutely crucial. Therefore, in order to avoid any unwanted confidentiality breaks caused by online storage of information, the service offered by the corresponding provider should be thoroughly checked before use. The use of such storage should also be checked and confirmed with the employer, as internal policies may exist that such storage is not allowed, or a particular storage only is allowed.

1.20.3.3 E-Mail

Something similar occurs with e-mail communications: lots of information is shared through corporate or personal e-mails, repeatedly, both with individuals and groups of contacts. Generally, the communications should be secure, but it seems that someone with superior computing skills could be able to hack most of the e-mail communications if an interest therein exists. Therefore, for especially sensitive information, it should be considered to use some encoding software: such software encodes the information shared through the e-mail before sending, and may be decoded, by the use of shared passwords, by the receiver.

1.20.3.4 Publications in Scientific Congresses, Now and Before

As a particular example, only a decade ago, the only information that most probably would have been considered to have entered the state of the art in a poster session of a scientific congress is the poster itself; attendees would have made some manual notes from the corresponding oral exposure, but it would have been difficult that the integral exposure itself would have been considered to form part of the state of the art. Nowadays, it is highly probable that at least one attendee will be taking pictures of the PowerPoint slides for later referral, or even record the exposure, with or without the additional recording of images. That is, the information may get out of control. You will never become certain regarding the treatment the attendee will make of such information. Will (s)he be sharing it with friends or colleagues? Send it by e-mail? Publish it in social media? Or on a website? In any of such cases, the information would most probably be considered to have become part of the state of the art. Thus, it becomes increasingly important to thoroughly consider the content of any poster or exposition, even more than some years before.

In view of all of the above, the determination of the state of the art, in order to decide on the compliance of an invention with the requirements of novelty and inventive step has never been a simple issue, but increasingly there will be new challenges in said determination, and interesting situations may arise in this sense, both during prosecution and corresponding lawsuits later on.

1.20.4 Patents in the Internet: Is "Do It Yourself" a Reasonable Option?

Internet, with its many uses, is widely used as a source of information. The Internet has become the best source of information, as there seems to be nothing on which you cannot find information by browsing the Internet, whether about technology, science, engineering, mathematics, medicine, intellectual property, patents, geography, jobs, hobbies, history, sports, arts, games, music, gardening, wood working, sewing, etc. Online encyclopedias, video browsers, journals, newspapers, and innumerable sites on various subjects make the task of gathering information about a topic, even if it is the first contact with said topic, an easy task, for any field of study, research, or interest.

Nevertheless, one has to be careful when making contact with a topic for the first time. On the one hand, one must be careful to choose the appropriate correct information, as any individual can upload information on the Internet, and no one can be sure of the accuracy and correctness of the information, unless you are already knowledgeable about the topic; also may the information not be updated. On the other hand, the immense amounts of information available on the Internet, often very detailed or in the form of tutorials, may give the impression to have all the information necessary for a new task right there at your fingertips, without the hiring of an expert anymore; this may be a risky action.

1.20.4.1 Some Useful Information Resources in the Internet

In the following, a review of some of the most valuable information sources available on the Internet, related to patents, will be made. Later on, a consideration of what a layman, that is, someone without an expertise in patents, should make use of and for what (s)he should be asking for help to an expert.

Most of the websites pertaining to national patent or intellectual property offices, to regional patent offices, or to the WIPO (World Intellectual Property Organization, in charge of the PCT applications (Patent Cooperation Treaty)), provide useful, interesting, and free general information about patent applications.

1.20.4.1.1 World Intellectual Property Organization (WIPO)

On the WIPO website (www.wipo.int), various information is offered, which may become useful at some point for anyone having an interest in patents, either due to the intention of filing an application themselves, or due to the need of knowing about third parties' patents. For example, information about how to file, manage, or search applications is provided (http://www.wipo.int/pct/en/):

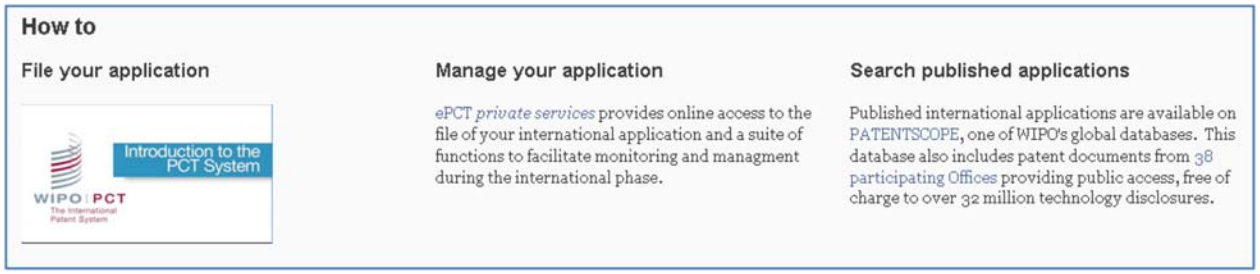

Also several guidelines are available, such as a PCT Applicant's Guide, which provides detailed information about the intricate PCT system and peculiarities of the national offices adhered thereto, as well as links to the laws that are relevant to PCT applications.

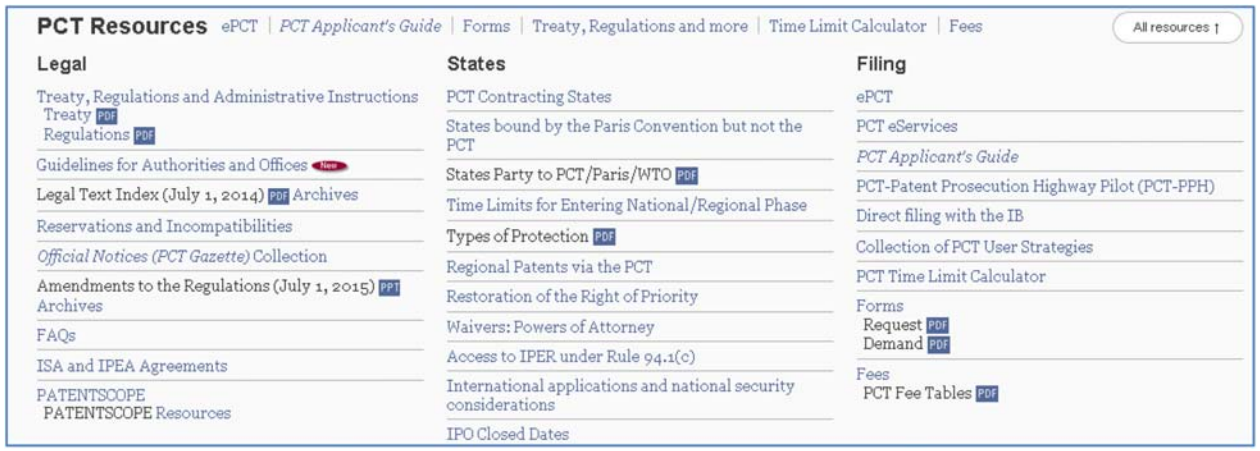

Even a detailed guideline regarding patent drafting is made available: the 138 pages long *WIPO Patent Drafting Manual* may be downloaded (http://www.wipo.int/edocs/pubdocs/en/patents/867/wipo_pub_867.pdf):

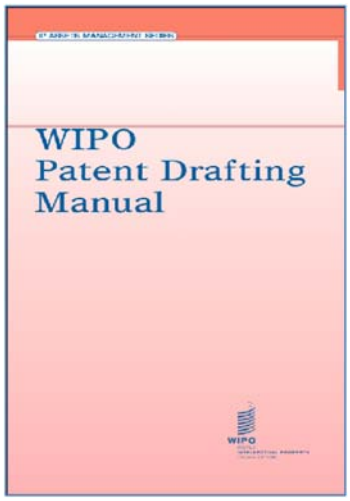

Therein a lot of information regarding what is a patent or patent application, what may be the subject/object of a patent, the legal requirements for patentability, recommendations about how to search prior art and which are the parts of a patent application, is provided.

A further, very useful utility offered by the WIPO website is the search interface Patentscope, which provides the possibility of searching for international patent applications by the use of various search fields, such as publication or application number, terms in the title or abstract, inventor names, applicant name, or international class code (https://patentscope.wipo.int/search/en/structuredSearch.jsf). The relevant documents, including publication document, search report, etc., may be downloaded for the corresponding patent application.

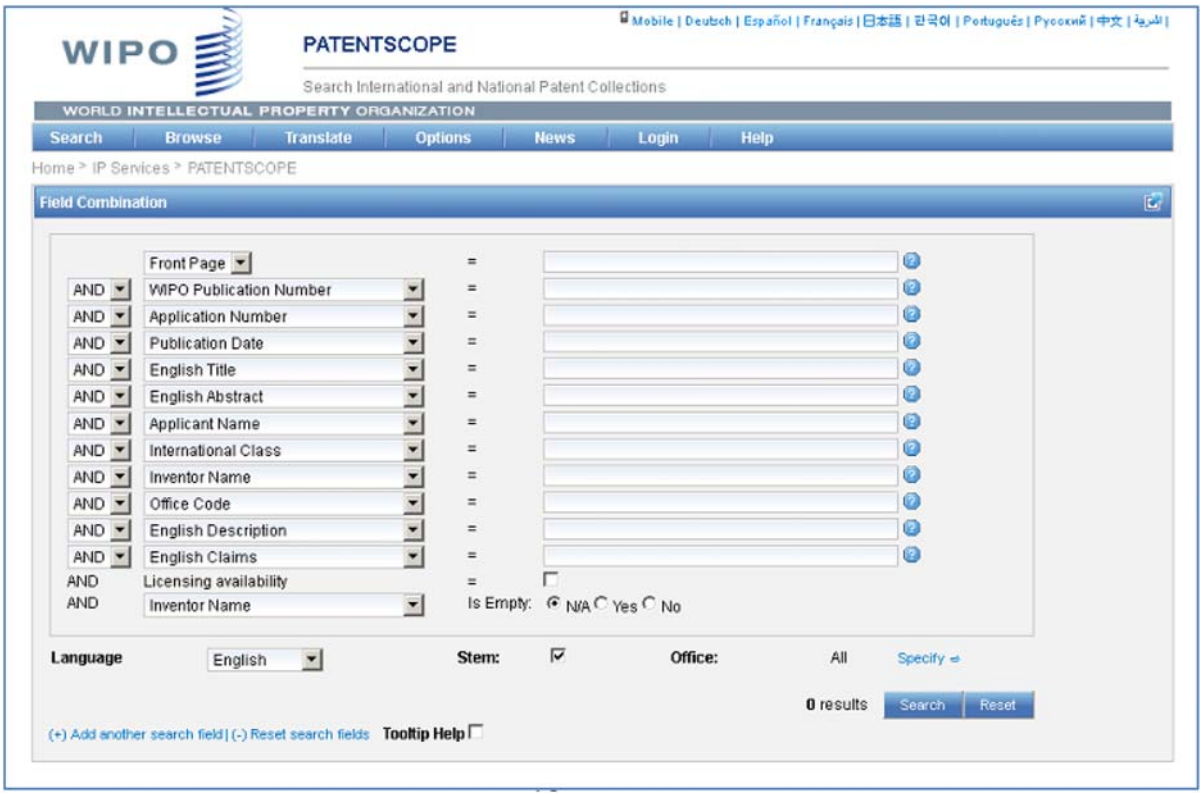

1.20.4.1.2 United States Patent and Trademark Office (USPTO)

The USPTO website (www.uspto.gov) provides general information concerning patents (http://www.uspto.gov/patents-getting-started/general-information-concerning-patents, http://www.uspto.gov/patents-application-process/search-patents), including basic information, such as what is a patent, what can be patented, and which are the parts of a specification, or more advanced information regarding the conditions for obtaining a patent, fees that have to be paid, or information about the examination procedure and other proceedings before the USPTO.

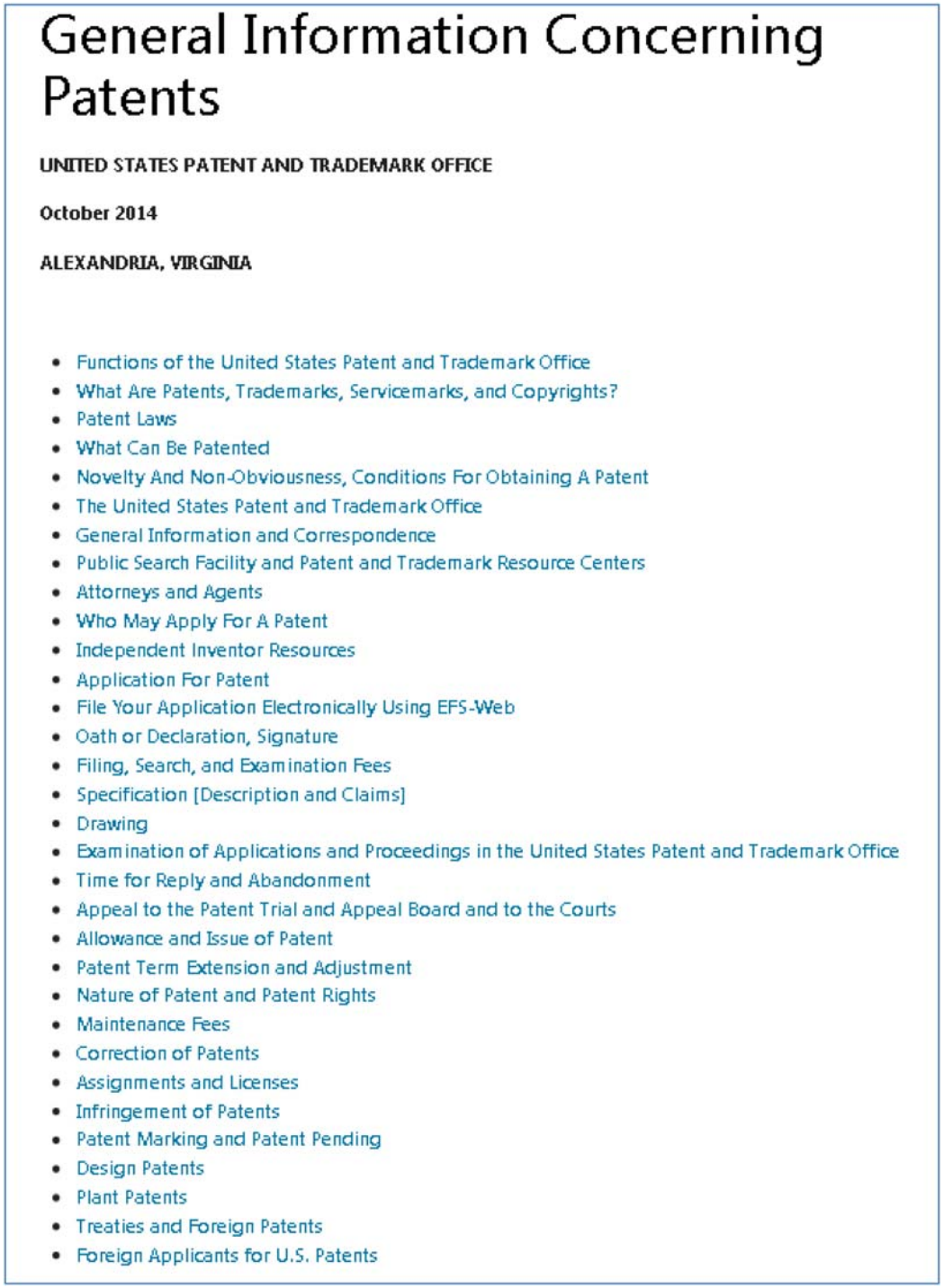

General Information Concerning Patents

UNITED STATES PATENT AND TRADEMARK OFFICE

October 2014

ALEXANDRIA, VIRGINIA

- Functions of the United States Patent and Trademark Office
- What Are Patents, Trademarks, Servicemarks, and Copyrights?
- Patent Laws
- What Can Be Patented
- Novelty And Non-Obviousness, Conditions For Obtaining A Patent
- The United States Patent and Trademark Office
- General Information and Correspondence
- Public Search Facility and Patent and Trademark Resource Centers
- Attorneys and Agents
- Who May Apply For A Patent
- Independent Inventor Resources
- Application For Patent
- File Your Application Electronically Using EFS-Web
- Oath or Declaration, Signature
- Filing, Search, and Examination Fees
- Specification [Description and Claims]
- Drawing
- Examination of Applications and Proceedings in the United States Patent and Trademark Office
- Time for Reply and Abandonment
- Appeal to the Patent Trial and Appeal Board and to the Courts
- Allowance and Issue of Patent
- Patent Term Extension and Adjustment
- Nature of Patent and Patent Rights
- Maintenance Fees
- Correction of Patents
- Assignments and Licenses
- Infringement of Patents
- Patent Marking and Patent Pending
- Design Patents
- Plant Patents
- Treaties and Foreign Patents
- Foreign Applicants for U.S. Patents

Regarding searching for patents, the USPTO offers to the user a range of different searches, in dependence of the particular needs (http://portal.uspto.gov/pair/PublicPair).

One utility that may become useful to the layman are the searches by terms, contained in any of the fields related to the application, including words in the title or the abstract.

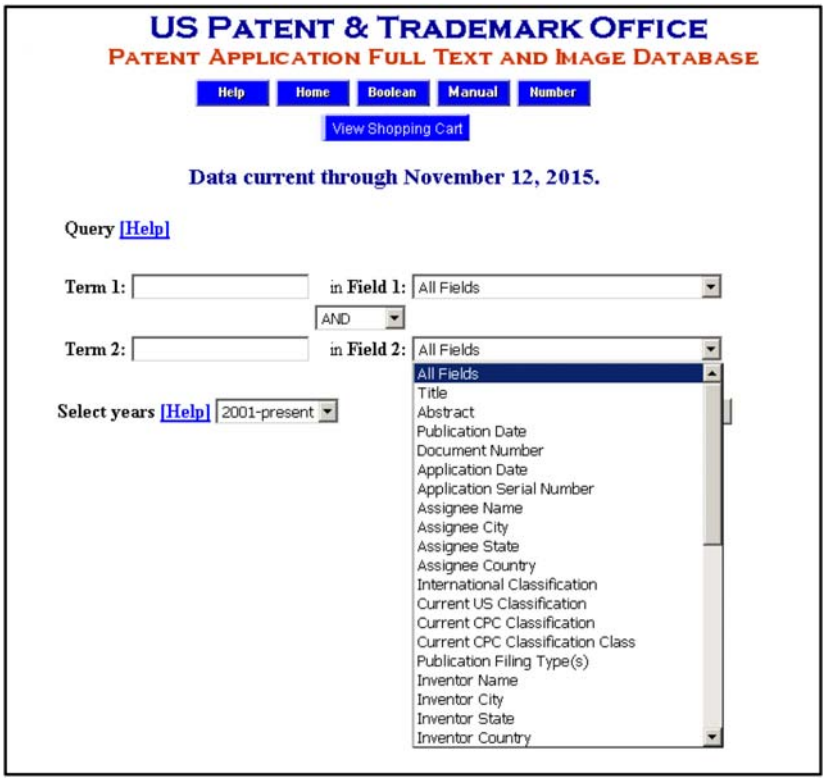

This allows easily retrieving and downloading publications of patent applications related to a technical field of interest.

Another useful search is the PAIR (Patent Application Information Retrieval; http://portal.uspto.gov/pair/PublicPair), which allows to retrieve and download information regarding the application status of particular applications, also including most of the documents from the file wrapper. The search is performed by any of the file numbers related to the application, that is, application number, patent number, or corresponding PCT application number.

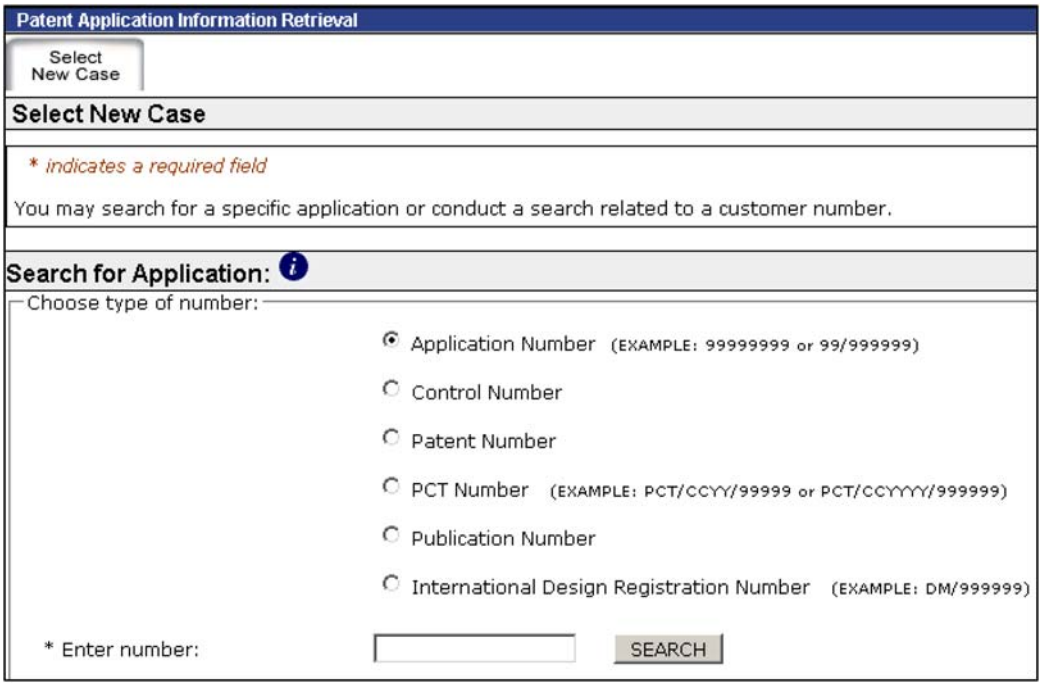

1.20.4.1.3 European Patent Office (EPO)

The EPO is in charge of prosecuting and granting European Patents, which are a regional patent that enables the applicant to seek patent protection in up to 40 European countries. The EPO is supervised by the Administrative Council; the Office is the executive arm of the European Patent Organisation.

On the EPO website (www.epo.org) again numerous, free resources are offered online, from which only a few will be referred to herein.

The EPO offers a complete "Guide for applicants" (https://www.epo.org/applying/european/Guide-for-applicants.html, which provides basic information around the European Patent Convention, general recommendations for the best route of protection to choose (ie, national applications, European Patent application, PCT application, etc.), an explanation of the patentability requirements, how to prepare and file a patent application, information about the European patent grant, opposition and appeals procedures, among many other information. The guide is available online, as a downloadable PDF, or may be ordered in printed form.

A more detailed guideline regarding examination at the EPO is also available online (https://www.epo.org/law-practice/legal-texts/guidelines.html). That is the case of the *Guidelines for Examination*, a document which has already been referred to in the present article (please refer back to http://www.wipo.int/pct/en/).

The EPO also offers access to a search facility known as Espacenet (http://worldwide.espacenet.com/?locale=en_EP), which allows searching and retrieving worldwide patent applications and patents. This database is very easy to use, as it offers a "Smart search" interface, which makes searching extremely simple to the layman.

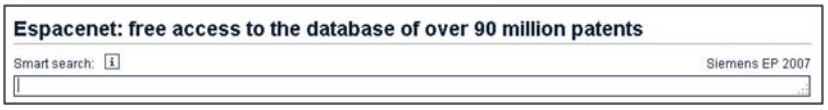

Nevertheless, also an advanced search interface is offered, which makes searching, in particular fields, simple.

1.20.4.1.4 Japanese Patent Office (JPO)

Searching at the Japanese Patent Office (JPO) (www.jpo.go.jp) may also provide some useful information, by use of a tool that is quite unknown for laymen.

If an interest in a Japanese patent document arises, either due to a prior search performed in one of the before mentioned search facilities, due to the results provided by a professional search, or as a reference made in another document, it may be interesting to check out the contents of said document. The JPO offers a search interface (https://www.j-platpat.inpit.go.jp/web/all/top/BTmTopEnglishPage, https://www4.j-platpat.inpit.go.jp/eng/tokujitsu/tkbs_en/TKBS_EN_GM101_Top.action) where any Japanese patent document, either an application or a granted patent, may be retrieved by number:

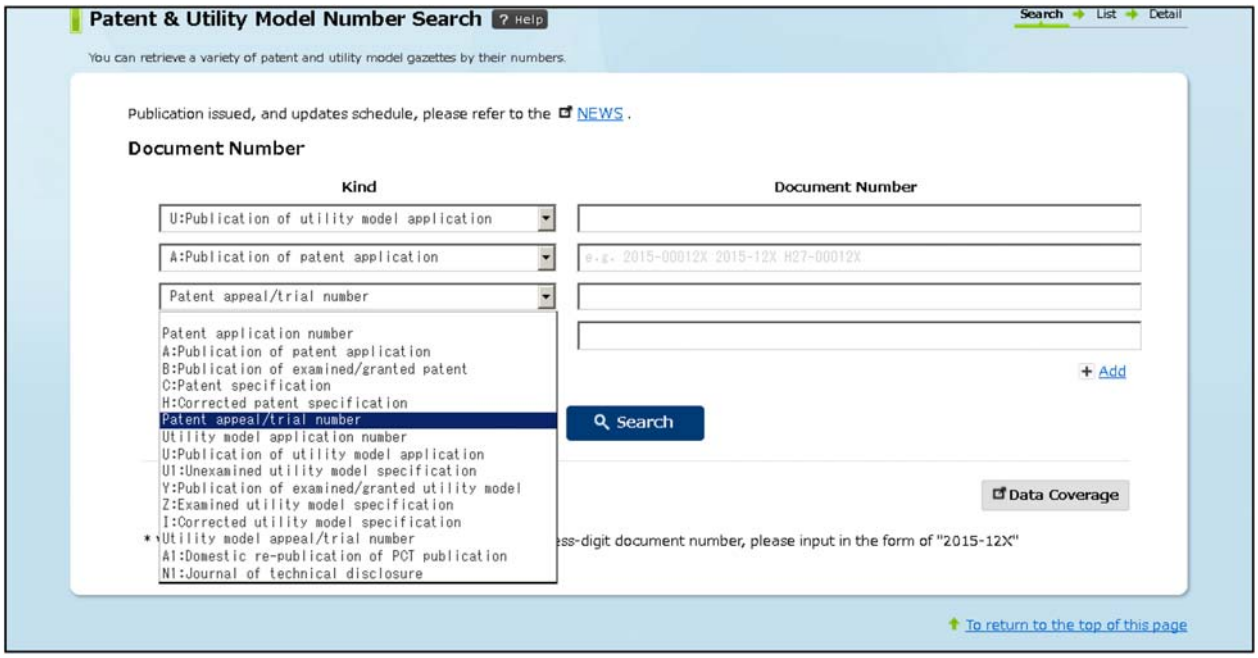

Nevertheless, as Japanese may not be within our language skills, and a translation into Japanese is a cost-intensive matter, at a first glance this information may not have any utility. However, the JPO also offers a free service of computer-assisted, automatic translation of the complete patent document. Once the document is retrieved through the search interface, at the top of the website three tabs will appear; when clicked on the "Detail" tab, automatically a translation into English language will be offered, separated by the parts of the application (ie, prior art, examples, claims, etc.).

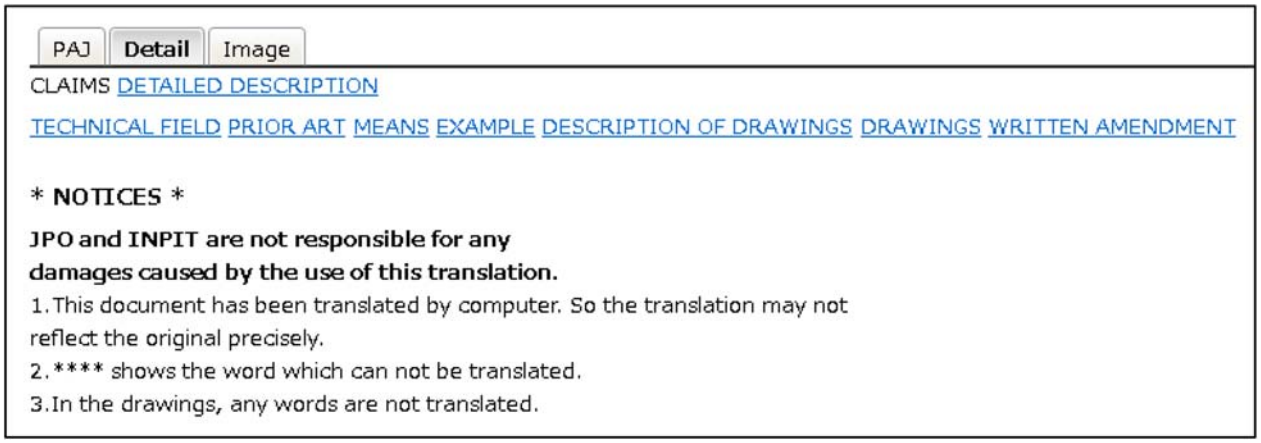

Of course the obtained translation will under no circumstances be a perfect translation, but it will provide the reader with a good idea of the actual contents of the document, beyond the abstract of the patent document. In some cases the computer-assisted translation may be enough for our needs, in other cases it will provide us with the information necessary to decide which parts of the document we would need to have fully translated by a specialized translator.

1.20.4.2 How to Make Reasonable Use of the Available Resources

The abovementioned information resources are only a small sample of the information that may be retrieved from the Internet, and a specific search in one of the known search engines will provide the link to much more information.

Nevertheless, one should not lose sight of the importance intellectual property and patents may have. Therefore, in the following a short explanation of what should be done and what should not be done with the information available is provided.

1.20.4.2.1 Searching

Patent and patent application publications (in the following, the term "patent publications" will be used in short, but is meant to include both patents and patent applications) usually provide lots of useful information regarding the technical field in which they are encompassed, in many cases very updated information, with cross-references to other documents with further useful information. As such, when starting to work at a new project or research, or when a new aspect is entered into a project, it would be a good habit to search for patent publications related to the matter in one or more of the available patent databases, and read through them to obtain useful scientific information, but also information regarding whether someone may have followed the same path earlier, and thus it may save a lot of work, or it may become clear that it makes no sense to work in that direction. This may become especially relevant if it was intended to apply for a patent at the end of the project, as subject matter which is already part of state of the art may not be patented.

Nevertheless, if a search is needed, either to evaluate the patentability of an invention or to evaluate the potential risk of infringing third parties' rights by bringing a project's result to the market ("freedom to operate"), it is highly recommended to ask for help to a patent attorney or a person with similar knowledge. This may avoid that unnecessary risks taken while taking a decision, and in the long term it will save a lot of money: the initial investment will for sure mean significant cost savings in the future.

1.20.4.2.2 Drafting and Prosecution

Regarding the drafting, filing, and prosecution of a patent application, it would for sure make sense to get used to some of the most relevant patent terms, especially to improve and speed up the communication with the corresponding patent attorney (reducing the time invested and consequently reducing the associated costs), who should at the end be in charge of the drafting, filing, and prosecuting of the application. Drafting a patent application, by use of the available information and examples in the Internet, may seem a trivial matter at a first glance. Nevertheless, the drafting of a patent application is a skill acquired during years of education, experience, and intensive dedication, and errors in the initial drafting and later during prosecution, may have fatal consequences, which may reach up to the loss of a patent, or at least mean high expenses to try to solve problems that may arise. Therefore, the drafting and prosecution of a patent application should be entrusted to a specialist, that is, a patent attorney.

1.20.4.2.3 Legal status of patents and patent applications

Most national patent offices, but also regional patent offices such as the EPO, offer online information regarding the legal status of applications of patent applications. Making such online consultations may save money, by avoiding the costs of a corresponding patent attorney. Nevertheless, this should only be made in cases where the correctness of the result obtained is not crucial to a decision (eg, check the legal status of a patent, which may be infringed by a product we are launching); in any other case, the legal status check should be performed once again by a specialist, that is, a patent attorney, as it may become tricky and more than one status resource should normally be checked.

1.20.5 Conclusion and Perspective

In the coming years, the tendency of designing laboratories as open spaces is expected to continue; also the use of electronic devices and the Internet is most certainly going to extend even more. Simultaneously to the beneficial consequences, an awareness of the new existing risks has to be awaken at all personnel levels of the corresponding institution, public or private, in order to take any possible preventive measures, to avoid any kind of information leak or unwanted publication of information. "*Scientia potentia est*" (knowledge is power) since time immemorial, and will increasingly be in the future; therefore, it is essential to take due care of knowledge and information.

Further Reading

1. Durham, A. L. *Patent Law Essentials: A Concise Guide*, 4th ed.; ABC CLIO-Greenwood: Santa Barbara, 2013. ISBN: 978–1440828782.
2. Mueller, J. M. *Patent Law*, 4th ed.; Wolters Kluwer Business & Law: New York, 2013. ISBN: 978–1454822448.
3. How to get a European Patent: Guide for applicants, 16th ed.; European Patent Office, Munich, 2016.

1.21 Ethics in Drug Discovery

M Snape, AMO Pharma Ltd, Surrey, United Kingdom

© 2017 Elsevier Ltd. All rights reserved.

1.21.1	**Introduction**	540
1.21.2	**Ethical Reasons to Perform Drug Discovery**	540
1.21.2.1	Medical Need in Orphan Populations	540
1.21.2.2	Medical Need in Older Age	541
1.21.2.3	Medical Need in Developing World Populations	541
1.21.3	**Ethics in Animal Research**	542
1.21.4	**Ethics in Clinical Studies**	542
1.21.4.1	Benefits to Participation in Clinical Studies of Potential Medicines	542
1.21.4.2	Ethical Consideration in Study Design Including Consent and Assent	543
1.21.4.2.1	Study design	543
1.21.4.2.2	Consent and assent	545
1.21.4.2.3	Role of the independent review board	546
1.21.4.3	Reporting of Clinical Study Results	546
1.21.5	**Ethics in Sales and Marketing**	546
1.21.5.1	Accurate Representation	546
1.21.5.2	Pricing	547
1.21.5.3	Role of Regulators	547
1.21.5.4	Conclusion	547
References		547

1.21.1 Introduction

The discovery of new drugs has changed the history of human healthcare. From the advent of analgesics to treat pain, anticonvulsants to treat seizures, control of hypertension, and antibiotics to treat infection, novel medicines have altered the probability of survival of humans radically, also impacting quality of life according to multiple dimensions. Nonetheless, there remains substantial unmet medical need, and therefore, further drug discovery efforts are in demand. This means that the ethical considerations inherent to the drug discovery process continue to be required as much as ever.

All stages of the drug discovery process generate a need to consider ethics. The selection of the areas of medical need before the process even starts raises ethical concerns. Historically, certain categories of healthcare have been underserved. Included among these are rare diseases, conditions that having increasing impact as the world population ages, and neglected infectious disease in the developing world.

The discovery of new drugs relies heavily on the use of nonhuman animals. In many regions, drug discovery mandates safety and toxicology testing that is a legal or regulatory requirement. Consideration of the ethics of animal experimentation has led to legislation and guidelines seeking to ensure animal welfare and appropriate experimentation.

Investigational medicines selected after safety and toxicology testing are advanced into clinical studies to investigate potential benefit and determine a safety and tolerability profile. Inherent to clinical studies is the ethical need to balance the risks of drug discovery against the benefit that may be obtained for affected patients. There is, therefore, an ethical need to ensure that clinical studies are optimally designed and able to fulfill the purpose of defining the profile of an investigational medicine, as well as ethical need to protect the welfare of study participants.

Once clinical study has led to a drug being approved for marketing as a medicine, the promotion of that medicine in the market and the price charged are not presently governed by formal ethical guidelines.

1.21.2 Ethical Reasons to Perform Drug Discovery

Drug discovery is the process of inventing new medicines to treat conditions that negatively impact human health. There is an obligation on scientists and humanity generally to implement this process since the personal, societal, and economic cost of human disorders and diseases has such an impact. We can illustrate this need by considering a number of categories of human ill-health as exemplars.

1.21.2.1 Medical Need in Orphan Populations

Orphan diseases are rare disorders that occur with a prevalence that is low. The definition of low varies between, for example, 4 in 10,000 of the population in Japan, and 7.5 in 10,000 of the population in the United States. These definitions of rarity are enshrined

in relevant national legislation and regulations in such territories as the United States, EU, Australia, Japan, and Singapore. This legislation was first put in place to stimulate drug discovery in disorders, which were under served and neglected due to the small size of the patient population affected and, therefore, the perceived commercial return. A series of incentives offered under this legislation are intended to increase the commercial viability of efforts in this area. Further, the regulators in relevant territories offer protocol assistance during discussion of the design of clinical studies required to be conducted in order to allow authorization for marketing of novel medicines for orphan disorders. This is of relevance since the rarity of the disorders in question means that design of studies with numbers of patients conventionally used is unlikely to be feasible.

There are at least 7000 orphan drug disorders, which are invariably serious in terms of their presentation. Most such disorders are genetically determined and first manifest in infancy. Only 5% of rare diseases do have any form of approved treatment.[1] The mortality and morbidity associated with these disorders is high. For example, 30% of children with rare disease will not live to see their fifth birthday and rare diseases are responsible for 35% of deaths in the first year of life.[1] In disorders with an onset early in childhood, where affected individuals survive, morbidity is high. For example, consider the condition congenital myotonic dystrophy. Congenital myotonic dystrophy is a life-threatening disorder, with a mortality rate of 25% by age 1.5 years and 50% by age 30 years.[2] This study also reports 50% of subjects unable to walk unaided with 4% of subjects requiring wheel chairs. Less than a quarter of congenital myotonic dystrophy patients were able to attend mainstream schooling due to intellectual disability, 15% were still fecally incontinent at 5 years of age, and in patients who lived to 20 years of age 79% were unemployed. Complementary data were reported by Ekström et al.,[3] who reported learning disability in 95 and 89% of congenital and juvenile myotonic dystrophy patients, respectively. Ekström et al.[4] also report that 68% and 50%, respectively, of individuals with congenital and juvenile congenital myotonic dystrophy type 1 (or Steinhert's disease) have an autism spectrum disorder. This is just one example if a disorder where there is a clear imperative to develop novels treatments via drug discovery.

The process of drug discovery in orphan drug disorders can make a difference. Following the introduction of orphan drug legislation in the United States, in the period 1999–2006, orphan drugs were estimated to reduce premature mortality in rare diseases by 3.3% (against a predicted increase of 0.9%).[5] The fact that rare disorders are clearly treatable when drug discovery is directed toward them makes the ethical case for further effort to prevent mortality and suffering in this field.

1.21.2.2 Medical Need in Older Age

Health conditions of older age represent a large and presently incompletely unaddressed problem. The developed world is aging. Life expectancy has increased dramatically over the past century, for example, in the United States increasing from 45 years in 1902 to 76 years in 2004. However, the health and capability of aged persons has not necessarily kept pace. As the proportion of the population that is older increases, so the relative impact of age-specific health concerns will increase.

For example, the UK Alzheimer Disease Society Dementia Report Update[6] estimates at the current estimated rate of prevalence, there will be 850,000 people with dementia in the United Kingdom in 2015. The number of people with dementia in the United Kingdom is forecast to increase to over 1 million by 2025 and over 2 million by 2051.[6] The current cost to the United Kingdom of dementia is £26.3 billion a year. Similarly, in the United States, it is predicted that the size of the population with Alzheimer's disease will increase from 5.3 million to 10 million by the middle of the century, with total payments for healthcare for Alzheimer patients expected to be $226 billion in 2015.[7]

Other health concerns related to older age also have a significant economic burden and impact on quality of life. Osteoarthritis affects over a third of individuals over the age of 65 years[8] and the cost of hospital treatment of osteoarthritis was already $42 billion in 2009.[9] The national economic burden of Parkinson's disease for the United States was estimated as exceeding $14 billion in 2010, with the prevalence of Parkinson's disease is expected to be double from 2010 levels by 2040.[10] Approximately one-third of individuals over the age of 65 have hearing loss, with the numbers of older individuals affected predicted to increase by between 18.4% and 49.7% according to geographic region between 2010 and 2010 according to the World Health Organization. Cardiovascular disease is the leading cause of death in people over 65 years of age. In the age range 60–79 years, over 42 million US citizens have cardiovascular disease.[11] The global cost of cardiovascular disease is forecast to rise from $863 billion in 2010 to $1044 in 2030.[12]

From these data it is apparent that the human and societal cost of an increasing proportion of presently untreated age-related disorders represents an enormous need requiring further drug discovery effort.

1.21.2.3 Medical Need in Developing World Populations

According to the World Health Organization, in low-income countries, nearly 4 in every 10 deaths are among children under 15 years, and only 2 in every 10 deaths are among people aged 70 years and older.[13] People predominantly die of infectious diseases: lower respiratory infections, HIV/AIDS, diarrheal diseases, malaria, and tuberculosis collectively account for almost one-third of all deaths in these countries. Accordingly, the World Health Organization lists 17 neglected tropical diseases to be treated as a priority.[14] According to the World Health Organization, these infectious conditions "are a diverse group of communicable diseases that prevail in tropical and subtropical conditions in 149 countries and affect more than one billion people, costing developing economies billions of dollars every year."[14]

Traditionally such conditions have not been a priority for drug discovery efforts progressed by institutions based in the developed world. There is a compelling ethical case for further work in this field. As of 2014, the 20 largest pharmaceutical companies are

active in this area, with 18 of the largest 20 companies implementing equitable pricing strategies and 11 having drug approvals relevant to this need.[15]

1.21.3 Ethics in Animal Research

Drug development typically progresses through a number of stages that can be grouped into categories. After chemical design and synthesis, potential novel medicines are assessed to determine their efficacy using in vitro or test tube methods. Following this, testing will be conducted to establish proof of the concept that benefits could be achieved by the medicine using animal models of disease. Then the potential for harm in humans is assessed using tests of pharmacokinetics, safety, and toxicology in nonhuman species. Assuming the profile of the molecule is acceptable, then clinical studies in human beings will be initiated. Clinical studies will be progressed through a number of stages (Phase I, Phase II, and Phase III) and the accumulated data presented to the regulatory authorities to determine whether a marketing authorization for the medicine can be granted.

The advent of transgenic animals has led to the ability to investigate a large range of disorders including rare orphan disorders. For example, transgenic mouse models of disorders, such as Fragile X Syndrome and Rett Syndrome, have stimulated clinical studies of novel therapeutics in these disorders.[16]

The nonhuman pharmacokinetic, safety, and toxicology testing is intended to establish predictions of the likely profile in humans. These tests are required by law in all territories where drug discovery takes place. Pharmacokinetic testing is intended to determine how much of the potential medicine is exposed to the tissues of the body. For example, although a given amount of medication might be administered via a tablet, not all of the medicine will be absorbed into the body and gain access to the blood stream. Therefore, it is important to know the actual exposure rather than make safety calculations based on the amount given. The level of exposure to the potential medicine achieved after administration of different doses of the medication can then be correlated to any side effects seen. These data overall can be used to generate a predicted maximum safe dose to be administered in clinical studies.

The use of nonhuman species in drug discovery is the subject of ethical review and regulation in many territories. For example, in the United Kingdom, use of animals is controlled by the Animals (Scientific Procedures) Act 1986. Enshrined within this legislation is a commitment to the "3Rs," meaning reduction, replacement, and refinement. This translates to a requirement to reduce the use of animals in testing, replacement of animal studies with alternatives wherever possible, and refinement of techniques so as to minimize pain suffering and distress. There is also a requirement that institutions authorized to conduct animal research establish an Animal Welfare and Ethical Review Body to provide local independent oversight. The number of procedures conducted on genetically normal animals has fallen by about half since 1990 under this legislation.[17]

Similar legislation and regulation is present in the United States (the Animal Welfare Act of 1966), the European Union (Directive 2010/63/EU), Japan (Law for the Humane Treatment and Management of Animals, 2005 and The Standards Relating to the Care and Management, and Alleviation of Pain and Distress of Experimental Animals, 2006) with regulations also being in place in, for example, Canada, Australia, and New Zealand.

Ethical considerations around the use of nonhuman species in drug discovery are, therefore, highly relevant.

1.21.4 Ethics in Clinical Studies

Once the process of drug discovery has identified novel potential therapeutics that have successfully completed preclinical development, human studies can begin and the novel therapeutic becomes an investigational medicine. A variety of ethical issues arise as a consequence of progression into studies in the clinic. These ethical issues relate to the exposure of human subjects, who have vulnerabilities, to a new potential medicine with associated risks. The potential for detection of benefit in these studies needs to be balanced against the risks to the participants concerned. This means putting in place specific protections and also ensuring that the studies conducted deliver the optimum output.

1.21.4.1 Benefits to Participation in Clinical Studies of Potential Medicines

The enrollment of human subjects into clinical studies of investigational medicines requires consideration of multiple ethical issues. These involve processing of the potential benefits of involvement in such studies, the risks inherent in participation, and the ability of the potential enrollee to understand these considerations and agree to participate.

There are three ways a human subject may benefit by participation in the clinical study of an investigational medicine. In Phase I studies, healthy volunteer subjects undergo administration of a novel potential medicine during the first exposures of human subjects to the substance in question. Commonly, participation in studies of this kind is subject to a financial inducement. The ethics of financial inducements to participants in Phase I studies have been the subject of review.[18] For example, The National Research Ethics Advisors Panel (an independent panel hosted by the National Health Service Health Resource Authority in the United Kingdom) has issued guidance on incentives and payments in this area.[18] This guidance discusses the distinctions between coercion and undue inducements (the former involving threat, the latter excessively attractive offers), the issue of whether payments should be related to risk in Phase I studies, and whether patients should be rewarded for participation above and beyond

reimbursement of costs. The same guidance endorses the premise that children and incapacitated adults should never be offered financial inducements above and beyond reimbursement of expenses. In general, the guidance is that ethical review should consider payments that are proportional to burden, rather than risk, burden meaning inconvenience and effort. Otherwise, the ethical review should consider the study justification in terms of weighing other potential benefits against the risks of participation.

A second way human subjects may benefit is by virtue of any efficacy inherent to the novel potential medicine. The importance of this benefit may be great, particularly for rare and life-threatening disorders. For example, initial clinical study of the drug Rilutek™ (riluzole) in amyotrophic lateral sclerosis used survival as an endpoint—a benefit to participating subjects was, therefore, an extension of their life.[19] Multiple rare genetic diseases can be life threatening, examples including congenital myotonic dystrophy, in which less than half of affected individuals survive to adulthood.[1] Another example is spinal muscular atrophy, the type 1 form (Werdnig–Hoffmann's disease) having a 50% mortality rate at 2 years of age.[20] As well as receiving potential benefit during placebo-controlled phases of clinical studies, many studies of investigational medicines include open-label extension phases. These extension studies allow patients optional access to more extended treatment with the investigational medicine. An extended follow up of a clinical study of the experimental medicine idebenone revealed persistent benefit in patients suffering from Leber's hereditary optic neuropathy, a condition causing blindness.[21] Lastly, as it has previously been proposed that participation in clinical studies may benefit even subjects receiving placebo treatment, as study protocols specify care and attention at a high level, and the placebo effect itself can reduce reported severity of symptoms.[22]

Aside from treatment effects related to the investigational medicine, patients and their caregivers may benefit from participating in development of research into therapeutics for the condition affected them. In orphan drug disorders, it may be the case that few or no clinical studies have been conducted in the disorder previously. In such cases, progression of initial clinical studies provides the opportunity to establish outcome measures and agreement with regulators as to requirements for approvals of potential marketing authorizations, as well as encouraging drug discovery efforts by other sponsors. Therefore, the general contribution of information is an advance in the specific field concerned, as well as providing a test of the scientific hypothesis driving the rationale behind study of the investigational medicine.

1.21.4.2 Ethical Consideration in Study Design Including Consent and Assent

Participation in clinical studies of investigational medicines is associated with risks. All medicines have the potential for induction of adverse events and during the early stages of drug discovery the safety and tolerability profile is still being developed. Therefore, the risks of participation need to be acceptable and balanced against the potential benefit. Further, this assessment needs to be made independently and needs to be understood by the participants. Beyond an individual risk-benefit consideration, the study itself needs to be considered, since if it is not capable of providing useful information then the risks involved cannot be justified. These elements can be considered separately.

1.21.4.2.1 Study design

Clinical studies of investigational medicines need to be optimized to have the best chance of success. An inadequate study will not only fail to provide a test of the underlying scientific rational for the study, and therefore fail to benefit the community via provision of new information, but will also fail to justify the potential risk or risks assumed by the individual participants. The study design needs to weigh multiple factors that might impact on risk versus benefit. The following sections describe these factors in greater detail.

1.21.4.2.1.1 Use of placebo

As mentioned earlier, participation in a study in and of itself may induce a placebo effect. In the absence of a placebo control group, delineation of a true effect of treatment might not be achievable and, therefore, the lack of such a control might complicate detection or interpretation of treatment effects. However, the use a placebo group may not be ethical. Where a condition is life threatening, historical data on the course of the condition might serve as an adequate reference against which to gauge treatment effects in a design that seeks avoid denying potential benefit to critically ill patients. Likewise, the use of a placebo treatment condition may be ethically challenging where an existing approved treatment is available for a serious disorder. Guidance for these issues is enshrined in the Declaration of Helsinki, a set of ethical principles for human experimentation developed by the World Medical Association.[23] Interpretation of the Declaration of Helsinki in relation to the ethics of use of a placebo group has been discussed in a variety of publications.[25]

1.21.4.2.1.2 Assessment of safety

For a study to have an acceptable risk-benefit profile, the risks of administration of the investigational medicine need to be monitored and recorded. This involves a variety of safety assessments. Monitoring is conducted by an independent review board to determine the presence and severity of adverse events. An adverse event is any untoward medical occurrence associated with the use of a drug in humans, whether or not considered drug related. Adverse events can be recorded as nonserious, serious, or severe, and related or unrelated to administration of the investigational medicine. A serious adverse event not predicted by the adverse event profile known for the investigational medicine is classified as a suspected unexpected serious adverse reaction or SUSAR. Adverse events detected will commonly be coded according to systems such as the Medical Dictionary for Regulatory Activities or World Health Organization Drug Dictionary Enhanced, for example.[38] This coding process will categorize the nature of adverse events

in order to aid analysis of the profile of safety and tolerability of the investigational medicine and to facilitate comparison of, for example, frequency or incidence of adverse events compared to placebo treatment.

1.21.4.2.1.3 Assessment of efficacy

Determination of the potential benefit of an investigational medicine produced via the process of drug discovery is made by the use of quantitative and/or qualitative outcome measures that are predefined by the sponsor. The art of developing an outcome measure to reliably and reproducibly translate the benefit produced into a number amenable to statistical analysis. Outcomes may be a biochemical or physiological marker that substitutes for a clinical endpoint, or an actual clinical measure that relates to the benefit in the context of the indication being treated. A clinical endpoint in a study in oncology might be shrinkage of the size of a tumor, or survival over the duration assessed. In many indications, the endpoint study can be objective, such as automated determination of blood pressure. In other indications, the outcome might be more subjective, such as patient reported experience of severity of pain. Selection of outcome measures is vital for success in detecting benefit. Conventionally, a primary outcome is prioritized and selected. Metrics relating to the primary outcome will be used for power analysis (see section "Study Size") and a criterion set for defining a study as positive on the basis of change on the primary outcome.

1.21.4.2.1.4 Study size

The size of a clinical study, in terms of the number of subjects recruited, may be planned by statistical modeling. By making an assumption about the likely magnitude of the effect of the investigational medicine, and inputting the known variability of inherent to the outcome measures selected, statistical power can be calculated.[26] Statistical power represents the ability to detect a statistically significant effect assuming there is genuine benefit, usually expressed as a percentage. A proposed study size associated with low statistical power may not be justified as subjects will be exposed to risk without real potential for successful detection of benefit.

There is a need for ethical consideration of the size of a study, in terms of the number of subjects that will be enrolled. Exposing large numbers of subjects to early-stage clinical investigations where there is limited available information on safety and potential benefit may not be warranted. Conversely, very small studies will have limited ability to distinguish true increases in adverse events and therefore very small studies are potentially futile and, therefore, not justified. The ethical determination of appropriate study size is not the same analysis as determination of the optimal study size for statistical purposes. The determination of the optimal study size purely in terms of ability to detect an effect is determined by statistical means in derivation of acceptable power to detect an effect (frequently desired to be 80% or 90%). The ethical determination of appropriate study size has been proposed as a function of the summed burden incurred by individual patients contrasted with projected study value. This measure shows that lower conventional statistical power does not make a study less ethical.[26] In general in drug development, Phase I studies are fairly small, as these studies are initial "first-in-man" study. Phase II studies for conventional investigational drugs are larger in size as Phase I studies have derisked somewhat with respect to safety and, therefore, greater numbers of subjects can be recruited in order to give a better opportunity to detect signals of efficacy and inform on choice of dose. Phase III studies are typically largest of all since at this point there is a need to have a safety database of sufficient size to detect rarer safety signals, and to show the robustness of reported benefits in broader patient populations and increased numbers of study sites. These rules are not hard and fast and may be significantly changed in orphan drug disorders where scarcity of patients to be enrolled for study needs to be taken account of in study design.

1.21.4.2.1.5 Study population

Selection of subjects eligible to participate in has an ethical dimension. Clinical study of investigational medicines conventionally uses study and treatment-specific criteria to determine which subjects can be included for enrollment into a study and which subjects will be excluded. Typically such criteria will be intended to attempt mitigation of safety considerations and to increase the probability of the study providing useful information. Subjects might be excluded from initial studies if they have health concerns above and beyond the indication intended to be investigated, as a protection for such individuals. Other inclusion/exclusion criteria might seek to make the study population more homogenous in order to reduce variability in the data obtained or to ensure the presentation of symptoms under study is sufficient to detect a treatment effect.

One consideration is that these criteria should not be discriminatory in entitlement in respect of eligibility to benefit from study participation. Therefore, restriction according to, for example, gender or ethnicity would need to be justified ethically. There may be valid reasons for such a consideration relating to the scientific rational for the treatment, the nature of the medical condition, or, for example, gender or ethnically specific pharmacokinetics and metabolism. For example, tacrimolus, a medicine used in prevention of rejection of transplants, achieves greater plasma levels in white and Latin-American subjects than in African–American subjects.[27] Similarly, the commonly prescribed anticoagulant warfarin achieves higher plasma levels in Asian subjects than whites, whites achieving greater levels than African-Americans.[27]

Other groups who may be under researched or inappropriately excluded have reduced entitlement to participation include children and the elderly. Concerns over the participation of children in clinical studies have related to age-specific safety vulnerabilities and the ability of younger subjects to report and inform on beneficial treatment effects. However, a lack of investigation in these populations may result in off-label use in children where formal investigation has not validated this use. Pharmacokinetic parameters in children may not always be accurately estimated by adjusting adult data for weight—children are not always "small adults." Concern that there is a potential gap in the available data guiding prescription has lead the European Medicines Agency, for example, to develop a priority list for studies on off-patent pediatric medicinal products.[28] Relative under study of elderly subjects,

who may also have altered drug absorption and metabolism and differing background comorbid medical conditions, represents a similar concern.

The participation of subjects with intellectual handicap in clinical studies of investigational medicines represents a further ethical consideration. Exploitation and abuse of such subjects during medical investigations during the mid-20th century has stimulated a need for clear ethical protection of vulnerable individuals.[29] Conversely, recent neurobiological advances have led to the development of novel therapeutics with potential to ameliorate cognitive deficits in such conditions as Fragile X Syndrome.[30] Therefore, the importance of protection may need to be balanced against the potential for benefit. Beyond this, there is a need to determine the relevance of benefit. Empirically, it is known that the presence of intellectual disability reduces the probability of the individual affected gaining employment, living independently, or forming adult relationships.[31] However, while such outcomes are concerning for caregivers and societally, such outcomes might or might not represent an issue for the individual themselves.[32]

1.21.4.2.2 Consent and assent

An ethical concern impacting drug discovery is the consent of subjects to participate in the study of investigational medicines. There is a requirement that study subjects fully understood the implications of their participation in research and agree to take part. The need for informed consent raises special considerations in children and those with intellectual disability, including analysis of capacity to consent and consent on another person's behalf.

Consent is a central tenet of the Declaration of Helsinki and has two key features—that the subject understands the purpose, method, risks if any, uses, and potential benefits of the study, and that the subject agrees to participate of their own volition and without coercion. Consent therefore is a process, not a single decision. The methodology used to establish consent conventionally will be the subject of independent review by a specific convened panel who will have the ability to refuse endorsement of commencement of the study in question. The independent ethical review will examine the information and materials provided to ensure the subject is properly informed, and the process for obtaining consent. The materials used during the process should clearly define what the study will involve, potential known and unknown safety risks, and procedures that will be implemented. The materials and explanations given must be appropriate and understandable. For example, regulatory guidance issued by the US Food and Drug Administration (FDA) alerts researchers preparing consent that one-third of US adults, being 77 million people, have basic or below basic health literacy.[33] Explanation of the detail of the study needs to include information on, for example, the use of placebo treatment, the nature of the investigational medicine under test, how often the participant will need to undergo assessment, and the duration of the study. Reasonably foreseeable risks should be outlined without being understated, covering the nature of the risk, its magnitude, and duration. Risks to others and in relation to pregnancy should also be covered, as should discomforts associated with study procedures. Currently unforeseeable risks should also be discussed by mentioning such risks exist. Benefits in terms of intended relief of signs and symptoms should be stated as well as benefits more broadly and in the future as a result of generation of knowledge. Payments to patients should not be identified as a benefit. The consent should also point out alternatives to participation in the study. If an alternative is participation in another study, the consent needs to highlight any exclusion criteria restricting participation in other studies. Procedures for patient confidentiality must be explained, as does compensation and handling of medical treatment required as a consequence of study participation. The participant also needs to be given contact information relevant to the study, such as the telephone number of the investigating clinician who can be contacted in the event of medical concerns and their care, as well details regarding voluntary or involuntary withdrawal from the study. The subject should also be told the size of the study to inform their thinking on the significance of the data to be obtained.

Consideration of consent may differ in some populations such as children, those with intellectual disability, or those affected by a medical emergency. In some regions, it may not be legal for a minor to consent to study participation, and the ability of young children to fully understand the information required to be understood for truly informed consent can be questioned. Generally, it is the parent or legal guardian of the child who gives consent for study participation on behalf of the child. However, it is generally the case that a child should be required to give assent to participation. Assent is given via a form that covers similar concepts to the consent form, but in language appropriate for a child. While assent may not be legally binding, the assent process gives the opportunity for the child to determine their willingness to participate.

Consent by subjects with intellectual disability requires ethical consideration. As discussed previously, subjects with intellectual disability may be under-involved in participation in clinical studies as an intended consequence of measures designed to protect against their vulnerability.[34,35] A key question for ethical debate is the ability of a subject with intellectual disability to understand the information provided in the consent process and, therefore, the risks and benefits of participation. However, the assumption that intellectual disability is a barrier to informed consent may not be correct.[36] Therefore, streamlined methods for assessing capacity to consent should be developed.[37] Some authorities and institutions require consent by a surrogate with accompanying assent by the subject with intellectual disability.

Another situation with requirement for specific ethical consideration is enrollment in study of investigational medicines intended to treat traumatic brain injury. Traumatic brain injury is a medical emergency that can render a subject incapable of conventional informed consent. Recent scientific advances have generated plausible hypotheses of potential benefit with novel potential medicines. Therefore, there is potential benefit for subjects with this condition being enrolled into clinical study without the ability to consent. Frameworks have been developed to address the situation of exempting from consent requirements in a life-threatening situation. For example, in the United States, FDA and the Department of Health and Human Services have developed such regulations[24] (cited in Ref.[37]). This process involved allows subjects to be enrolled in an emergency setting if the legally

authorized representative of the subject cannot be contacted within a specified time window and prior consultations over the study have been undertaken.

1.21.4.2.3 Role of the independent review board

Consent and assent takes place in the context of an independent review, conducted by a specific institutional body. The role of the Independent Review Board or Ethics Committee is to protect the welfare of human subjects participating in clinical studies. The Board may be local to the institution carrying out the study, or a central specialized facility undertaking the review process on behalf of one or more participating institutions. The Board will usually consider some form of risk-benefit analysis and the justification and rationale for the study, materials describing the investigational medicine, as well as approving the materials used to recruit participants into the study and obtain their consent. The Ethics Committee will also consider the suitability of the investigator(s) and the institution.

The review board should be constituted appropriately and regulatory authorities make recommendations on their constitution. For example, the Clinical Trials Directive of the EU (Directive 2001/20/EC) defines the role of the Ethics Committee under Good Clinical Practice in European states, and in the United States FDA regulation 21 CFR 56.107 sets out the role of the Institutional Review Board. In both cases, the constitution will require a minimum number of members for a quorum (often more than five), that members are independent of the investigator, and that there is scientific and lay representation. The membership should also have the ability to evaluate medical aspects of the proposed study.

The review board should evaluate all of the materials used to recruit subjects and guard against undue influence or coercion. The board should also examine financial interests relating to the study. As well as reviewing the materials involved and their suitability allow informed consent, the board needs to evaluate the process for obtaining and maintaining the consent, and the board may have the ability to observe the consent process and will need to review changes to the material and consent as a consequence of any changes that occur or new information that is generated during the conduct of the study. As the investigator running the study is responsible for implementing the consent process, the investigator will need to disclose their sources of funding in conducting the study, and any financial interests in the study. As well as the independent review board, some regulatory authorities such as the FDA will require to review materials such as the informed consent form. The review board will also have to make provision for situations in which subjects might be recruited who do not speak the language used for the consent process and materials. The review board will also consider matters pertaining to assent by, for example, children. Actions pertaining to suspension or termination of a study will also require involvement of the board.

1.21.4.3 Reporting of Clinical Study Results

Consideration should be given to ethical issues in the reporting of clinical study results. A clinical study may be successful in detecting benefit associated with an investigational medicine that has an acceptable safety and tolerability profile. An accumulation of such data will be considered during assessment by regulators ahead of a potential approval for marketing and grant of marketing authorization. However, not all clinical studies are positive in the sense of detecting benefit. A failure to detect benefit in a negative study might be the consequence of more than one cause. It is possible that the study conducted was designed in such a way that genuine benefit was not detected. In this case, a failed study has occurred. Alternatively, an appropriately designed study may show that no genuine benefit can be attributed to the investigational medicine. In the latter scenario, the drug has failed to meet study goals. It is reasonable to determine a novel medicine is useful, even when some of the studies conducted with the investigational medicine have been negative, if these failed studies lead to corrected designs leading to positive data. However, the rationale for concluding negative studies do not reflect failure of the drug and can, therefore, be discounted in determining safety and efficacy needs to be presented and reported appropriately. Failure to report negative studies has been an issue historically, and the World Health Organization has drawn up proposals for prompt reporting and public disclosure of study results.[39] Relevant examples include data on the antidepressants seroxat[40] and reboxetine.[41]

1.21.5 Ethics in Sales and Marketing

Approval of a new medicine at the end of the drug discovery process is an approval to market the medicine. Marketing is conducted in relation to the label of the medicine, which is a list of approved claims approved by the regulator that can be justified on the basis of the data submitted to the regulator as part of the application for approval. The label determines what can be proposed in promotion of the new medicine, and also impacts the price that can be charged. A medicine linked to a broader and more significant label can be promoted to more patients and as more attractive than alternative medicines for the same indications.

1.21.5.1 Accurate Representation

During advertising and promotion, the language used to describe a medicine must be accurate. Analysis of direct to consumer advertising for medicines on television, for prescription, and nonprescription medicines proposes that misleading claims can occur.[42] The marketing of medicines is a complex and extensive activity. Expenditure on marketing by pharmaceutical companies on drug promotion was estimated as $70.7 billion globally in 2014.[43]

1.21.5.2 Pricing

The price charged for supply of a medicine is determined by multiple factors, including the claims that can be made about the effectiveness and safety described on the label, the number of patients that may be prescribed the medicine, the impact of the condition being treated, the cost of producing the active ingredients of the medicine, and competition from similar medicines. Expenditure on medicines is increasing—the US total prescription sales in 2014 were $360.7 billion, 12.2% higher than the preceding 12 months.[44] Average prices for medicines increased by more than 10% in 2015.[45] The cost of modern medicines for cancer and rare diseases has been the subject of reporting. The most expensive medicines available include treatments for rare diseases, such as Soliris® and Glybera®, which treat the rare diseases paroxysmal nocturnal hemoglobinuria and familial lipoprotein lipase deficiency, respectively. The pricing of medicines for rare diseases integrates recouping the cost of the research and development spend on drug discovery by the companies that produce the medicines, the need to make a profit from a small number of patients, and the affordability of the medicine for individuals and national healthcare systems. Reconciling these factors is an important issue in the context of future provision of new medicines in rare conditions.[46] Pricing for medication is not generally governed by formal ethical review, but is the subject of debate from an ethical perspective.[47]

1.21.5.3 Role of Regulators

The regulation of advertising of medicines is conducted by organizations such as FDA in the United States and EMA in Europe. Regulators are able to level fines in the event of inappropriate marketing practices. Kessel details fines of $100 million and over in the years from 2009 to 2014[48] with violations resulting from promotions for unlicensed uses such as prescriptions to the elderly, promotion of unapproved doses, and filing false price reports.

1.21.5.4 Conclusion

The process of drug discovery is vital for healthcare, particularly in relation to developing new treatments for underserved areas that include rare diseases, disorders relating to the increasing age of the populations, and neglected diseases in the developing world. Every stage of the discovery process, from selecting indications to address through to marketing of medicines once approved carries the need for consideration of ethical issues.

References

1. RARE Diseases: Facts and Statistics Global Genes website: https://globalgenes.org/rare-diseases-facts-statistics/.
2. Reardon, W.; Newcombe, R.; Fenton, I.; Sibert, J.; Harper, P. S. The Natural History of Congenital Myotonic Dystrophy: Mortality and Long Term Clinical Aspects. *Arch. Dis. Child.* **1993,** *68,* 177–181.
3. Ekström, A. B.; Hakenäs-Plate, L.; Samuelsson, L.; Tulinius, M.; Wentz, E. Autism Spectrum Conditions in Myotonic Dystrophy Type 1: A Study on 57 Individuals With Congenital and Childhood Forms. *Am. J. Med. Genet. B Neuropsychiatr. Genet.* **2008,** *147B,* 918–926.
4. Ekström, A. B.; Hakenäs-Plate, L.; Tulinius, M.; Wentz, E. Cognition and Adaptive Skills in Myotonic Dystrophy Type 1: A Study of 55 Individuals With Congenital and Childhood Forms. *Dev. Med. Child Neurol.* **2009,** *51,* 982–990.
5. Lichtenberg, F. R. The Impact of New (Orphan) Drug Approvals on Premature Mortality From Rare Diseases in the United States and France, 1999–2007. *Eur. J. Health Econ.* **2013,** *14* (1), 41–56.
6. Prince, M.; Knapp, M.; Guerchet, M.; McCrone, P.; Prina, M.; Comas-Herrera, A.; Wittenberg, R.; Adelaja, B.; Hu, B.; King, D.; Rehill, A.; Salimkumar, D. *Dementia UK: Update;* Alzheimer's Society, 2014.
7. Alzheimer's Association. 2015 Alzheimer's Disease Facts and Figures. *Alzheimers Dement.* **2015,** *11* (3), 332–384.
8. Lawrence, R. C.; Felson, D. T.; Helmick, C. G.; et al. Estimates of the Prevalence of Arthritis and Other Rheumatic Conditions in the United States. Part II. *Arthritis Rheum.* **2008,** *58* (1), 26–35.
9. Murphy, L.; Helmick, C. G. The Impact of Osteoarthritis in the United States: A Population-Health Perspective. *Am. J. Nurs.* **2012,** *112* (3 Suppl 1), S13–S19.
10. Kowal, S. L1.; Dall, T. M.; Chakrabarti, R.; Storm, M. V.; Jain, A. The Current and Projected Economic Burden of Parkinson's Disease in the United States. *Mov. Disord.* **2013,** *28* (3), 311–318.
11. National Heart, Lung, and Blood Institute. *Incidence and Prevalence: 2006 Chart Book on Cardiovascular and Lung Diseases;* National Heart, Lung, and Blood Institute: Bethesda, MD, 2006.
12. http://www.championadvocates.org/en/champion-advocates-programme/the-costs-of-cvd (accessed February 2016).
13. http://www.who.int/mediacentre/factsheets/fs310/en/index2.html (accessed February 2016).
14. http://www.who.int/neglected_diseases/diseases/en/ (accessed January 2016).
15. Connelly, D. Drug Development: Targeting Disease in the Developing World. *Pharm. J.* **2014,** *293,* 629.
16. ClinicalTrials.gov study Identifiers NCT01894958 and NCT01703533.
17. UK Government Statistics: http://www.understandinganimalresearch.org.uk/animals/numbers-animals/ (accessed January 2016).
18. HRA Guidance: Payments and Incentives in Research 2014: http://www.hra.nhs.uk/documents/2014/05/hra-guidance-payments-incentives-research-v1-0-final-2014-05-21.pdf (accessed February 2016).
19. Bensimon, G.; Lacomblez, L.; Meininger, V. A Controlled Trial of Riluzole in Amyotrophic Lateral Sclerosis. ALS/Riluzole Study Group. *N. Engl. J. Med.* **1994,** *330,* 585–591.
20. Park, H. B.; Lee, S. M.; Lee, J. S.; Park, M. S.; Park, K. I.; Namgung, R.; Lee, C. Survival Analysis of Spinal Muscular Atrophy Type I. *Korean J. Pediatr.* **2010,** *53,* 965–970.
21. Klopstock, T.; Metz, G.; Yu-Wai-Man, P.; et al. Persistence of the Treatment Effect of Idebenone in Leber's Hereditary Optic Neuropathy. *Brain* **2013,** *136* (Pt 2), e230.
22. Finniss, D. G.; Kaptchuk, T. J.; Miller, F.; Benedetti, F. Placebo Effects: Biological, Clinical and Ethical Advances. *Lancet* **2010,** *375* (9715), 686–695.
23. Human, D.; Fluss, S. *The World Medical Association's Declaration of Helsinki: Historical and Contemporary Perspectives*, 5th draft.; WMA: France, 2001
24. Yamal, J. M1.; Robertson, C. S.; Rubin, M. L.; Benoit, J. S.; Hannay, H. J.; Tilley, B. C. Enrollment of Racially/Ethnically Diverse Participants in Traumatic Brain Injury Trials: Effect of Availability of Exception From Informed Consent. *Clin. Trials* **2014,** *11* (2), 187–194.

25. Simon, R. Are Placebo-Controlled Clinical Trials Ethical or Needed When Alternative Treatment Exists? *Ann. Intern. Med.* **2000,** *133,* 474–475.
26. Bacchetti, P1.; Wolf, L. E.; Segal, M. R.; McCulloch, C. E. Ethics and Sample Size. *Am. J. Epidemiol.* **2005,** *161,* 105–110.
27. Yasuda, S. U.; Zhang, L.; Huang, S.-M. The Role of Ethnicity in Variability in Response to Drugs: Focus on Clinical Pharmacology Studies. *Clin. Pharmacol. Ther.* **2008,** *84,* 417.
28. EMA, 2013. Human Medicines Development and Evaluation Revised priority list for studies on off-patent paediatric medicinal products EMA/PDCO/98717/2012 Rev. 2013/14 http://www.ema.europa.eu/docs/en_GB/document_library/Other/2009/10/WC500004017.pdf (accessed January 2016).
29. Carlson, L. Research Ethics and Intellectual Disability: Broadening the Debates Yale. *J. Biol. Med.* **2013,** *86,* 303–314.
30. Deacon, R. M.; Glass, L.; Snape, M.; Hurley, M. J.; Altimiras, F. J.; Biekofsky, R. R.; Cogram, P. NNZ-2566, a Novel Analog of (1–3) IGF-1, as a Potential Therapeutic Agent for Fragile X Syndrome. *Neuromol. Med.* **2015,** *17,* 71–82.
31. Hartley, S. L.; Seltzer, M. M.; Raspa, M.; Olmstead, M.; Bishop, E.; Bailey, D. B. Exploring the Adult Life of Men and Women With Fragile X Syndrome: Results From a National Survey. *Am. J. Intellect. Dev. Disabil.* **2011,** *116,* 16–35.
32. Armstrong, T. The Myth of the Normal Brain: Embracing Neurodiversity. *AMA J. Ethics* **2015,** *17* (4), 348–352.
33. Kutner, M.; Greenberg, E.; Jin, Y.; Paulsen, C. *The Health Literacy of America's Adults: Results From the 2003 National Assessment of Adult Literacy (NCES 2006–483);* U.S. Department of Education, National Center for Education Statistics: Washington, DC, 2006.
34. Lennox, N.; Taylor, M.; Rey-Conde, T.; Bain, C.; Purdie, D. M.; Boyle, F. Beating the Barriers: Recruitment of People With Intellectual Disability to Participate in Research. *J. Intellect. Disabil. Res.* **2005,** *49,* 296–305.
35. Horner-Johnson, W.; Bailey, D. Assessing Understanding and Obtaining Consent From Adults With Intellectual Disabilities for a Health Promotion Study. *J. Policy Pract. Intellect. Disabil.* **2013,** *10* (3). http://dx.doi.org/10.1111/jppi.12048.
36. McDonald, K. E.; Kidney, C. A. What is Right? Ethics in Intellectual Disabilities Research. *J. Policy Pract. Intellect. Disabil.* **2012,** *9,* 27–39.
37. Offices of the Secretary, DHHS, FDA. Protection of Human Subjects: Informed Consent and Waiver of Informed Consent Requirements in Certain Emergency Research: Final Rules. *Fed Regist.* **1996,** *61,* 51497–51531.
38. Babre, D. Medical Coding in Clinical Trials. *Perspect. Clin. Res.* **2010,** *1,* 29–32.
39. Moorthy, V. S.; Karam, G.; Vannice, K. S.; Kieny, M. P. Rationale for WHO's New Position Calling for Prompt Reporting and Public Disclosure of Interventional Clinical Trial Results. *PLoS Med.* **2015,** *12* (4), e1001819.
40. McGoey, L.; Jackson, E. Seroxat and the Suppression of Clinical Trial Data: Regulatory Failure and the Uses of Legal Ambiguity. *J. Med. Ethics* **2009,** *35,* 107–112.
41. Eyding, D1.; Lelgemann, M.; Grouven, U.; Härter, M.; Kromp, M.; Kaiser, T.; Kerekes, M. F.; Gerken, M.; Wieseler, B. Reboxetine for Acute Treatment of Major Depression: Systematic Review and Meta-Analysis of Published and Unpublished Placebo and Selective Serotonin Reuptake Inhibitor Controlled Trials. *BMJ* **2010,** *341,* c4737.
42. Faerber, A. E.; David, H.; Kreling, D. H. Content Analysis of False and Misleading Claims in Television Advertising for Prescription and Nonprescription Drugs. *J. Gen. Intern. Med.* **2014,** *29* (1), 110–118.
43. http://www.imshealth.com:90/files/web/Global/Market%20Insights/IMSH%20GPMCR_2015_GlobalExtract.pdf (accessed February 2016).
44. Schumock, G. T.; Li, E. C.; Suda, K. J.; Wiest, M. D.; Stubbings, J.; Matusiak, L. M.; Hunkler, R. J.; Vermeulen, L. C. National Trends in Prescription Drug Expenditures and Projections for 2015. *Am. J. Health Syst. Pharm.* **2015,** *72* (9), 717–736.
45. https://www.washingtonpost.com/news/to-your-health/wp/2016/01/11/prescription-drug-prices-jumped-more-than-10-percent-in-2015/ (accessed February 2016).
46. Hyry, H. I.; Cox, T. M.; Roos, J. C. Saving the Orphan Drug Legislations: Misconceptions and Clarifications. *Expert Rev. Pharmacoecon. Outcomes Res.* **2016,** *16* (1), 111–117.
47. Reinhardt, U. Probing Our Moral Values in Health Care: The Pricing of Specialty Drugs. *JAMA* **2015,** *314* (10), 981–982.
48. Mark Kessel, M. Restoring the Pharmaceutical Industry's Reputation. *Nat. Biotechnol.* **2014,** *32,* 983–990.

1.22 The Rise of Rare Disease Foundations: How Patient Associations Can Drive the Drug Discovery Process

MR Tranfaglia, FRAXA Research Foundation, Newburyport, MA, United States

© 2017 Elsevier Ltd. All rights reserved.

1.22.1	**Introduction**	549
1.22.2	**The Early Days: How Treatments Used to be Discovered**	549
1.22.3	**Major Diseases, Large Foundations: Attempts to Shift the Paradigm**	550
1.22.4	**The Human Genome Project Spawns a Vast New Generation**	551
1.22.5	**Social and Economic Inputs Driving These Trends**	551
1.22.6	**Stages of Therapeutic Development**	551
1.22.7	**How RDFs Can Help**	552
1.22.7.1	Basic Research	552
1.22.7.2	Translational Research	554
1.22.7.3	Genetic Rescue Versus Rational Approach	554
1.22.7.4	Preclinical Research	555
1.22.7.5	Clinical Trials	556
1.22.7.6	Limitations of This Approach — and Possible Solutions	557
1.22.7.6.1	Biomedical research is expensive	557
1.22.7.6.2	University-based research can be inefficient	557
1.22.7.6.3	The drug discovery process is very risky	557
1.22.7.6.4	Impatient patients — everything takes too long	557
1.22.8	**Conclusions**	558
References		558

1.22.1 Introduction

Many factors have contributed to explosive growth in the number of patient-advocacy organizations around the world in recent years. Typically started and run by people affected by a specific disorder, these organizations seek to improve current and future quality of life in a number of ways. While there is certainly a role for patient and family support, increasingly patient-run medical foundations aim to change actual disease outcomes. By improving public awareness and rates of diagnosis, these groups can increase the chances that disease sufferers get the best available treatments. By lobbying governments, they can increase public funding dedicated to their disease. By raising private funds and directly supporting biomedical research, they may speed the development of new disease-modifying therapeutics. By collaborating with industry (biotech and pharmaceutical companies) they can facilitate clinical trials of new treatments.

This article will focus on the ways that rare disease foundations (RDFs) can directly facilitate and expedite the drug discovery process, based on the author's direct experience in this field. Many of these basic principles apply to more common diseases, or to those with nongenetic origins. For the purposes of this discussion, we will focus on the case of the rare genetic disease as an example of how patients, their friends, and families can make a difference in the drug discovery process and accelerate the development of new therapeutics.

1.22.2 The Early Days: How Treatments Used to be Discovered

Astute clinical observation and pure serendipity were the most common sources of medical advances throughout the history. Indeed, most of the common therapeutics in use today were derived from such ancient discovery mechanisms. The classical medical education emphasized the study of anatomy and physiology, as well as physical examination and a decidedly low-tech approach to the diagnosis of disease. This approach may have lacked the sophistication of modern medical diagnostics, but it cast a wider net, allowing for novel observations. The causes of major diseases were generally not known, their genetics were often poorly understood, and basic mechanisms of disease were purely a matter for speculation.

Ironically, in today's diagnostics-driven medical environment, serendipitous observations of novel drug effects may be more difficult to make. As understanding of disease mechanisms has increased, clinicians have fundamentally changed their approach to patients over the past century, with a much greater focus on "evidence-based medical practice," which generally assumes that it will always be possible to develop treatments for diseases via basic research.

As James Le Fanu notes in "The Rise and Fall of Modern Medicine":

> These, and a multitude of other developments, have been of immeasurable benefit, freeing people from the fear of illness and untimely death, and significantly ameliorating the chronic disabilities of ageing.
>
> This post-war medical achievement is well recognized, but much less appreciated is the means by which it was brought about. For the previous 2000 years doctors had sought in vain for the "magic bullets" that would alleviate their patients' suffering and then, quite suddenly and without warning, they came cascading out of the research laboratories just as if medicinal chemists had hit the jackpot (as they had). Or again, in 1945, desirable objectives such as transplanting organs or curing cancer were rightly perceived as being unattainable, as there was simply no way of overcoming the biological problems of the rejection of foreign tissue or the selective destruction of cancer cells. But these and many other obstacles were surmounted. The past fifty years have been a unique period of prodigious intellectual ferment that, quite naturally, invite investigation.
>
> …yet their significance has for the most part been concealed from view by the common perception, profoundly influenced by medicine's historic achievements, of it being on a continuous and upward curve of knowledge. Here the unknown is merely waiting to be known with, in principle, no limits to its further beneficent advance.[1]

1.22.3 Major Diseases, Large Foundations: Attempts to Shift the Paradigm

Disease-focused charities are a relatively new concept. Although charitable organizations often played a role in the care of the sick, only recently did they attempt to tackle the diseases themselves. This is not surprising, given that doctors traditionally rarely attempted to cure disease outright, but rather tried to provide supportive and palliative care to allow time for natural healing. With a growing understanding of infectious diseases (the major cause of mortality at the time) in the 18th and 19th centuries, physicians had the opportunity to utilize public health measures and vaccination to decrease disease burden. At the same time, advances in surgical techniques and aseptic methods allowed for the possibility of surgical cures in some cases. Thus, during the course of the 19th century a major change in thinking occurred: disease was no longer simply the illness of an individual, it was increasingly seen as a foreign entity which could be fought.

Naturally, the most common and most deadly diseases were the first to be joined in this battle (for there is little point in tackling rare diseases (RDs) when many more common threats to health and life abound!). Examples of advocacy organizations founded to address major health concerns of the time include the American Lung Association (ALA),[2] founded in 1904 as a response to the toll exacted by tuberculosis (TB). Public health efforts promoted by the ALA were so successful that TB declined in prevalence long before antitubercular drugs were widely used. With the virtual disappearance of TB as a major cause of morbidity and mortality in the United States, the AMA changed its focus to prevention of lung cancer by advocating smoking cessation. This is an early example of a now common transformation among larger patient-advocacy groups: successful organizations may accomplish their primary mission, but that rarely results in organizational retirement. More often, larger organizations have simply taken on new missions.

The American Cancer Society[3] was founded in 1913 in response to rising rates of cancer, with a primary strategy of destigmatizing the illness and promoting early diagnosis. It seems almost inconceivable today, with regular, well-attended fundraising events for virtually all types of cancer, that there could be a stigma associated with this disease, but this is an intriguing window into changing cultural perceptions of disease. While research funding would come later, early detection and treatment were seen as the best option for helping the most people with the technology of the time. As efforts to destigmatize cancer were met with success, to the point that "cancer survivor" is now considered a badge of honor, the organization shifted its goal to funding of clinical research to improve cancer treatment and basic biomedical studies of mechanisms of disease. It is worth noting that massive funding of cancer research, totaling hundreds of billions of (US) dollars, has yet to produce the kind of "silver bullet" cure that many have hoped for. Indeed, while some improved therapeutics have emerged from research on cancer disease mechanisms, these improvements have been surprisingly slow and incremental. This supports the notion that it may be more difficult than first thought to promote a specific scientific advance, such as a cure for cancer, regardless of the investment of resources. If science and medical technologies advance by capitalizing on serendipitous discoveries, then we will continue to see progress, but we may not be able to determine its course as precisely as we might hope.

In similar fashion, the American Heart Association (AHA)[4] began in 1924 with the goal of enhancing clinical management of heart disease, but quickly moved to improve public health by making dietary recommendations that might reduce the occurrence of heart disease. Again, prevention was seen as far more efficient and more likely than a cure. The AHA became an early proponent of diet and lifestyle modifications which were seen as the best way to prevent heart disease, only later funding research on actual disease mechanisms.

When poliomyelitis became the scourge of western societies in the pre-World War II era, the March of Dimes[5] was founded in 1938 by President Franklin Roosevelt, a polio patient himself, to combat the disease. Much of its early funding was devoted to treatment of polio patients rather than research into any disease-modifying strategy. Once again, public health measures began to reduce the impact of the polio virus even before a vaccine, but the steady push from patient advocates (and the governments they lobbied) certainly sped the development of the polio vaccine, which rendered this condition a rarity in the modern era. Since polio is no longer a major public health concern, the March of Dimes has shifted its mission and its methods entirely to focus on prevention of birth defects, and has moved to more direct funding of biomedical research.

1.22.4 The Human Genome Project Spawns a Vast New Generation

Genetically based RDFs have blossomed as the Human Genome Project (HGP) has revealed the genetic underpinnings of many conditions.[6] In many cases, these conditions were long recognized as heritable diseases, but the precise mutations responsible for them were unknown. While medical genetics could offer counseling to prevent the occurrence of some of the classically Mendelian autosomal recessive conditions, along with occasional screening for some of the better-recognized diseases (eg, Tay-Sachs), medicine rarely had much to offer to those diagnosed with RDs. This changed rather abruptly with the advent of modern genetic technologies.

In the modern era, the idea that virtually any problem can be solved via technology is widely held by the general public.[7] Science has advanced and we are surrounded by technological wonders; this is easy to see as inexorable progress which will continue ad infinitum. So it is with medical science: we have come a long way in recent years, and it only seems reasonable to expect more great things. As the HGP uncovered the genetic basis for many long-recognized but poorly understood conditions, RDFs have formed rapidly (sometimes 2 or 3 per disease) to exploit this new information. It is now estimated that there are over 7000 distinct, recognized RDs,[8] the vast majority with no specific treatment available.

1.22.5 Social and Economic Inputs Driving These Trends

The explosion of RDFs in recent years cannot be attributed entirely to the HGP, nor to general advances in medicine and technology. While the hope offered by the HGP undoubtedly motivated the formation of many patient organizations, private charitable funding of biomedical research requires a considerable amount of financing. The social and economic context is thus critical to understanding the rise of RDFs.

Economic expansion following World War II, and accelerating after the end of the Cold War, led to widespread prosperity in the developed world. Unprecedented credit expansion and increasing affluence have led to greater charitable giving, especially in the United States and Western Europe. Charitable giving can be roughly divided into two basic categories: major and minor philanthropy — "high net worth" donors giving very large (often one-time) donations versus much larger numbers of less affluent donors making (often repeat) smaller donations. Economic expansion and globalization simultaneously increased the general affluence of western populations, increasing minor philanthropy, while also increasing the proportion and absolute numbers of very affluent major philanthropists. As traditional religious organizations have decreased in their relative influence, a larger proportion of charitable giving has flowed to health-related charities. This confluence of factors has fueled a dramatic expansion of disease-specific charities in general, and RDFs in particular. Of course, patterns of charitable giving vary dramatically by country, and are profoundly affected by tax laws and overall levels of affluence. Nonetheless, these economic factors have permitted RDFs to flourish, and have fueled a movement which allows even those of modest means to finance a rather expensive undertaking.[9]

One of the biggest obstacles facing RD groups is that there are, by definition, few motivated people in any one place. One goal of RDFs is to bring people together to work for a common cause; that task is considerably more difficult when very few people share that cause. Even the simplest support group becomes logistically complex when the target audience is spread out over a large area. The Internet and modern communications have made that problem tractable. It is now possible for RD patients and families to connect entirely via the Internet, with no need for physical meetings at all.[10] While businessmen may still feel the need for personal contact, people with severe disabilities do not always consider this essential, and much can be done in the virtual arena.

Thus, a convergence of advancing medical and genetic technology with worldwide economic expansion and a radical transformation in communications has enabled a boom in the formation of patient-driven organizations attempting to address unmet medical needs.

1.22.6 Stages of Therapeutic Development

Most RDFs follow a plan of rational drug discovery with emphasis on different stages of the process, depending largely on the maturity of their field. RDFs involved in relatively newly discovered genetic conditions, for example, may focus largely on understanding basic disease mechanisms, whereas organizations working with well-known conditions (ie, muscular dystrophy, cystic fibrosis) will typically focus on more preclinical and clinical research. Note that while the basic plan of attack parallels the drug discovery process in the pharmaceutical, it is not the same. RDFs will rarely take a direct interest in activities such as toxicology or lead optimization. Rather, most foundations prefer an "open source" approach beginning in university-based labs. That approach can be summarized in Fig. 1.

The emphasis on the particular stage in the product development cycle of any given RDF will depend on the overall maturity of the research field, but the key for any RDF is to leverage each step of this process to the maximum extent possible, and to take advantage of partnerships and collaborations to do something significant with funding which will always be inadequate to the task. These "force multipliers" and opportunities for leverage will be described at each step.

Fig. 1 Stages of research for rare disease foundations attempting to develop new therapeutics for rare and neglected diseases.

1.22.7 How RDFs Can Help

Summarized in Table 1.

1.22.7.1 Basic Research

The most obvious way that RDFs can assist in the development of new therapeutics for rare and neglected disorders is to fund basic biomedical research investigating mechanisms of disease. This is typically the way most RDFs start, and this type of work can be especially valuable in otherwise neglected disorders.[11] In most cases, this process begins when a relative handful of established authorities in the field are funded to extend their studies. As funding increases in a small field, more scientists are drawn into the field, with a concomitant infusion of new ideas. With any luck, pilot projects funded by an RDF lead to more substantial funding by more traditional sources (government, larger medical research foundations, etc.). Leveraging the RDF's funding by increasing financial support from these other sources is crucial, since few nonprofits have the finances to go it alone. Fortunately, most governmental agencies are responsive to the needs of neglected and rare disorders, and pilot funding can often attract much larger grants.[12]

Table 1 Methods used by rare disease foundations to further their goals

Stage of research	*Major goals*	*Methods*	*RDF contributions*
Basic	● Understand basic mechanisms of disease ● Develop disease models for future studies	Basic biology (primarily university-based)	● Direct funding ● Organize scientific meetings ● Distribute critical reagents ● Distribute animal models ● Facilitate collection and distribution of human tissues
Translational	● Identify and validate targets for therapeutic intervention	Rational drug discovery versus high-throughput screens versus genetic "fix"	● Direct funding ● Focused meetings ● Distribute advanced transgenic animal models (conditional, inducible, double knockout, knock-in, reporter constructs, etc.)
Preclinical	● Validate specific therapeutic agents in model systems ● Enable clinical trials	In vitro rescue experiments In vivo rescue experiments Biomarker studies	● Direct funding ● Facilitate MTAs with pharma ● Contract studies (CRO or university-based) ● Collaborative studies with pharma partners
Clinical	● Test promising therapeutics in disease patient population ● Enable marketing of new drugs ● Establish efficacy of available drugs	Pilot studies (small/inexpensive) Open trials (medium/moderately expensive) Randomized controlled trials (large/very expensive)	● Direct funding ● Patient/family organizing ○ Specialty clinics ○ Registries ○ Recruiting for trials ● Pharma industry liaison

However, it is critical for RDFs to understand that this leveraging is the goal, and to direct pilot grants toward the projects and the scientists who are most likely to secure these other sources of funding.

It seems entirely logical that greater understanding of the disease process would lead to enhanced therapeutics for any given condition. However, as noted previously, the history of medicine does not contain many examples of success for this method. Major advances in medicine have more often occurred serendipitously, with rational drug discovery methods more often providing rather gradual improvements over existing treatments.[13] However, there is a method which can be seen as a way of inducing or accelerating serendipity: high-throughput screening (HTS), where hundreds, thousands, or even hundreds of thousands of compounds are tested (often robotically) for therapeutic effects in a disease model system. This is an attractive proposition for an RDF, and it is a standard approach in the pharmaceutical industry. Part of its attraction lies in the brute force approach of simply trying every known drug in the disease model of interest to find beneficial effects which could not be anticipated otherwise. This bypasses entirely the need for detailed understanding of the disease process, and it would seem like potentially valuable shortcut. Unfortunately, HTS results are often disappointing. As many pharma companies have come to appreciate, the choice of model system is critical — the wrong choice of model system "readout" for the disease can lead to identification of many false-positive results, which will all require extensive validation. Conversely, false negatives are also a distinct possibility if researchers do not have an adequate understanding of the range of desirable outcomes. For example, a drug screen may be established to look for compounds which could increase transcription of a silenced gene; however, this approach would likely miss entirely other compounds which could generate compensatory downstream effects. Either way, a poorly chosen HTS readout can lead to much lost time and money. How can optimal readouts be devised? One of the best ways is basic research on disease mechanisms, but of course this brings us full circle, minimizing the advantage of the shortcut.

With these caveats in mind, what can a modest-size RDF expect to accomplish in the basic research realm? Certainly, one of the most useful strategies for promoting biomedical research in any given area, and one within reach of even relatively small organizations, is the development and dissemination of disease-specific research tools, such as antibodies, animal models, or human tissues.

Many of the recently formed RDFs focus on genetically based disorders, in which transgenic animal models play a key role in basic mechanisms of disease research. These animal models are also critical for translational elaboration of any findings made during the course of basic research, and they are essential for preclinical validation of potential therapeutic strategies. Transgenic mice are one of the most common model systems for the study of disease, offering an entry level mammalian model. The technology for creating knockout, knock-in, and other forms of transgenics is well established and cost-effective, though it should be noted that creating a transgenic mouse model for a given disease is often the easiest step in the process. Characterizing the resulting model systems is often more difficult, but at least as important, since animal phenotypes rarely match human phenotypes precisely.[14]

Phenotypic characterization of transgenic animal models can be especially challenging when a major transition in specialization is required. For example, fragile X was known as a developmental disorder with X-linked inheritance; when the FMR1 gene was discovered, the field was dominated by geneticists and molecular biologists. When the knockout mouse model of fragile X was created by some of the same scientists who first discovered the gene, these research groups had little experience with in vivo mouse research or even general neuroscience. Formation of collaborations and recruitment of neuroscientists took many years to bring about adequate characterization of reliable phenotypes in this model system.

Some degree of interdisciplinary transition must necessarily occur in virtually any field. The acknowledged experts in a particular RD (assuming it is genetically based) prior to the discovery of its genetic basis will typically be geneticists and clinical specialists involved in routine treatment of the condition. While molecular biologists may make quick work of developing a knockout mouse for a single gene, loss of function mutation, using this model system to understand the underlying pathophysiology of the disease will require a very different set of experts, scientists with experience studying the organ systems affected by the mutation (the full extent of which may take many years to appreciate). Thus, RDFs will often convene meetings to introduce new scientists to the field, and disseminate information as quickly as possible.

Recent advances have made many species viable as animal models for genetically based disease. Transgenic rats are now in common use, and offer the advantage of greater intelligence, more "human-like" physiology, and more complex social interaction, though at a greater cost than mice for acquisition and housing.[15] Drosophila mutants can be excellent models for the study of human disease, offering low cost, ease of genetic manipulation, and short generation times.[16] However, their genome is greatly simplified compared to humans, and their nonmammalian brains and metabolism can vary significantly from those of humans. Increasingly, patient-derived induced pluripotent stem cells are seen as important model systems for future research. Here RDFs can make an enormous contribution by organizing tissue donation and banking; in a similar fashion, surgical and postmortem tissue samples from patients with RDs are difficult for most scientists to obtain unless RDFs take the lead in making these tissues available for the study.

Biomedical research is a complex undertaking, but even the most complex systems usually have bottlenecks or rate-limiting steps. The crucial task of an effective RDF is to identify these bottlenecks and relieve them as quickly and efficiently as possible. If no mouse model exists, or if specific antibodies are unavailable, RDFs can fund academic labs to make these, or pay a Contract Research Organization (CRO) to make them.[14] While it is perhaps more traditional for nonprofit RDFs to fund research at nonprofit universities, while for-profit pharma companies are more likely to outsource research to for-profit CROs, cost inflation in the university system has made CROs competitive with academic labs at many levels. This alternative pathway may be especially productive when providing research resources to a burgeoning field. CROs can make antibodies, transgenic animals, or novel reagents quickly

and without intellectual property claims which might hinder their later use in the field. Likewise, the RDF may then distribute these without encumbrance to all interested parties (including, ultimately, industry partners). In comparison, an academic lab may be able to produce an antibody or generate a knockout mouse rather quickly, but standard academic etiquette would allow the lab (absent specific prior contracts) to retain exclusive use of these until their work is published, a process which can delay dissemination for several years.

Leverage Potential: Direct funding by RDFs can serve as seed money to obtain much larger grants from governmental agencies or larger, endowed private funding sources. Basic disease mechanisms for a number of conditions may also intersect, revealing common research interests and other sources of funding. For example, fragile X and other monogenic causes of autism cause impairments in signaling pathways regulating synaptically driven protein translation; thus fragile X researchers have had success in obtaining grants from autism foundations. Many smaller RDFs limit the duration of funding to avoid long-term dependence of academic labs on their relatively meager resources, and to encourage applications to other funding organizations. This can be seen as an attempt to maximize leverage.

1.22.7.2 Translational Research

While this category often defies precise definition (indeed, the term "translational research" is sometimes used more generally to refer to the entire development process), translational research can be seen as the attempt to use the information gained from basic science discoveries to develop new treatment targets.[17] This is a relatively new concept and one with broad appeal. In the context of RD research, translational research is a critical step in the development of new therapies. While true translational research may be hard to come by, this is one area in which RDFs can have a major impact and can hope to drive the drug discovery process.

Typically, translational research begins when basic scientists make a significant finding concerning disease mechanisms. For example, research on a genetic disease may reveal that a mutant protein product results in abnormal intracellular signaling in a specific pathway. The question for the research field is then, how much of the disease is caused by this one abnormality? Is this a valid treatment target, or only one small facet of a much larger disorder? With the emergence of powerful animal transgenic technologies, one straightforward way to answer this question is to attempt genetic rescue of the identified pathway. Expression of individual elements of involved pathways can be increased or decreased, and this can now be done with a reasonable degree of spatial and temporal specificity using inducible systems (eg, Cre-Lox).[18] This allows scientists to isolate the effects of specific alterations in protein expression and to validate potential therapeutic targets (other than the affected gene/gene product, of course).

Generally speaking, small molecule therapies are more effective in inhibiting biological processes than in replacing them, but most genetic diseases result in loss of function (loss or mutation of a protein). This is the essential quandary faced by anyone attempting to develop treatments for genetic disorders from the ground up. It is very difficult to replace the function of a complex biological molecule (a protein) with a simple small molecule (a drug), but it is relatively easy to find small molecules which inhibit the function(s) of virtually any protein. Occasional exceptions, such as channel openers or receptor agonists, are the rare exceptions which only reinforce this general principle. One challenge in translational research, therefore, is to find a useful "double negative" — a process which can be inhibited to compensate for the loss of function caused by the disease mutation. Clearly, significant understanding of basic pathophysiology is required to make this approach work, and often the studies required to enable translational research are quite specific. In this situation, RDFs can play an important role by plugging gaps in research — recruiting scientists to look at specific questions which are holding a particular field back, using "double knockout" rescue models of disease (and making them available), and generally studying aspects of the disease which may not be considered of general intellectual interest, but of great interest to patients suffering from that particular condition.

1.22.7.3 Genetic Rescue Versus Rational Approach

Another approach to RDs, especially genetic disorders whose disease mechanisms are not well understood, is to simply attempt "genetic rescue" of patients. Newer technologies offer the promise of gene therapy, gene repair, gene editing, gene knockdown, gene reactivation, and these possibilities have brought great excitement to the RDF world. This is a (conceptually) simple way of bypassing all the trouble and expense of understanding disease mechanisms by fixing the problem at its source — the defective gene. Unfortunately, this promise has been largely unfulfilled, and most of these techniques have been far more difficult to implement in humans than in animal models. It is encouraging that more and more biotechnology industry funding has flowed into these new technologies, and this may help speed the maturation of this field. However, for most RDs (and even for most common ones) the idea of genetic rescue remains more science fiction than near-term reality.[19,20]

For an understanding of the technical difficulties inherent in these approaches, one need only look to the surprisingly sluggish development of protein replacement therapies. There would seem to be few problems as simple as a single missing protein, and few solutions as simple as replacing that protein. Indeed, for some diseases, like diabetes or hemophilia, this simple and straightforward approach works quite well. Once the protein is produced and purified, replacement results in an excellent therapeutic effect. However, this represents a best case scenario. Most proteins are not secreted; many are involved in complex regulatory functions, where precise spatial and temporal control of concentration is required and dosage is critical. Simply dumping these proteins into the circulatory system in an uncontrolled fashion can be toxic in many cases.[21] Likewise, global reactivation of a silenced gene may result simultaneously in therapeutic effects in target organs and toxic effects in unanticipated locations. It seems likely that for each

new technology, some "low hanging fruit" will be picked — conditions which are especially amenable to this new intervention. However, the vast body of RDs will invariably encounter technical difficulties.

Leverage Potential: Simply by offering grant funding to identify and validate therapeutic targets for a given RD, an RDF can incentivize this type of treatment-oriented translational research. In many cases, especially for RDs, this kind of research might not otherwise take place. Many larger governmental and private funding organizations have expressed interest in funding translational research, but this type of work is often perceived as particularly risky. This makes pilot funding of early translational studies especially important, and a particularly good candidate for leveraging RDF funding.

1.22.7.4 Preclinical Research

RDFs can play an important role in preclinical research leading to new therapeutics; that role is characterized by two main strategies: *derisking* and *repurposing*.[22] If basic research in a specific disease area has revealed possible disease mechanisms, and translational follow-up has identified specific therapeutic targets, the field may be ready to move on to preclinical research.

The point of preclinical research is to learn as much as possible about any proposed treatment strategy from model systems before moving into the next (very expensive) stage of clinical trials. The value of models systems can vary quite a bit, depending on the model and the disease condition being studied; the high rate of failure in transitioning from preclinical research, through clinical trials and into marketing, has led many critics to question the value of preclinical validation in animal models.[23] Clearly, mice are not humans; indeed, even human cells are not humans. No model system can replicate the complexity of a live human being, so the predictive value of any preclinical research must be kept in perspective. Nevertheless, clinical trials are so expensive that any groundwork which can be done to enhance their chances of success is quite valuable.[24] Derisking is perhaps in the eye of the beholder, but if an RDF can show particularly good effects of a therapeutic strategy in relevant model systems, that strategy can be deemed "derisked." An accumulation of data can convince potential industry partners (not to mention governmental agencies and larger healthcare foundations) that investment in therapeutic development for this indication is less risky.

One of the greatest challenges faced by RDFs operating primarily in the academic arena (funding university labs) is that many academic scientists are reluctant to conduct experiments which are essentially following up another academic scientist's work. Such studies are not considered especially innovative, and may be considered a breach of etiquette in some cases. Funding may be difficult to obtain. Preclinical validation of potential therapeutics also usually involves a major transition in experimental methods compared to translational research. For example, basic research may have implicated a particular signaling pathway in the pathogenesis of a genetically based developmental disorder using electrophysiological methods in hippocampal slices from a transgenic mouse model. Translational research may have shown that a class of small molecules can rescue this disease-related phenotype by inhibiting one element of the pathway; this might be demonstrated by adding a research reagent to the bath surrounding the slice of brain tissue. Preclinical validation of this therapeutic strategy might require administration of an actual drug candidate (whether an available drug or one in development) to a live animal model; this requires a completely different skill set and equipment which may not be available to the same researchers. If they are unable to form collaborations (via meetings and research networks), progress on this treatment strategy could easily stall at this point.

A potential method that RDFs can employ to overcome this common obstacle is to develop contract lab facilities to conduct vital translational and preclinical studies as needed. Certainly, there are many commercial CROs which can conduct preclinical validation studies quickly and cost-effectively. While these facilities are not inexpensive, their rapid turnaround time compared to academic labs can be a distinct advantage; in addition, the sponsoring RDF will usually retain all intellectual property rights from these studies, simplifying further development. An alternative to the usual commercial CRO is a specialized academic lab functioning as a "nonprofit CRO." This could be an academic lab with experience in the field which is willing to do this kind of work on a contract basis, or a dedicated university-based facility.[19] Studies of this kind could be seen as a radical departure from typical academic research, in that the academic contractor is being asked to work at the behest of the RDF, rather than pursuing independent intellectual interests. However, university-based labs are increasingly willing and eager to take on this kind of project, especially at times when traditional funding is harder to find, making this an attractive option for RDFs with more advanced research programs facing a preclinical validation bottleneck. For example, when researchers discovered a promising new drug target (mGluR5) for rescuing synaptic plasticity in fragile X syndrome,[25] most lab groups in the field lacked the animal model resources to conduct preclinical validation studies of mGluR5 antagonists. FRAXA Research Foundation contracted with the Columbia University laboratory run by Robert Bauchwitz, a transgenic animal expert, to test this drug class in the fragile X knockout mouse model. This resulted in the first validation of the "mGluR Theory of Fragile X"[26] and supported development of this drug class for a fragile X indication. Subsequently, increasing demand for preclinical validation of promising therapeutic candidates has led FRAXA to establish a long-running Drug Validation Initiative at the University of Chile and Frauenhofer-Chile Research Institute,[27] which maintains animal models of fragile X and conducts validation studies utilizing standardized methods for any interested industry partner.

Repurposing strategies may also begin in earnest at this point. If the goal is to bring innovative new treatments into clinical use, and translational research has uncovered drugs in development which may be of use, then it is much quicker and less expensive to repurpose an existing drug than to attempt development from scratch. Obviously, available drugs which are on the market may be validated with no permission required, and this type of "off-the-shelf" treatment is everyone's first choice. However, this is not always possible, given the relatively limited repertoire of available drugs. Pharmaceutical companies have developed vast numbers of investigational new drugs (INDs) over the past 50 years, the great majority of which have never found an approvable use. This great age of drug discovery was, unfortunately, not accompanied by the requisite "disease discovery," so huge numbers of

compounds, characterized to varying degrees, languish in pharma vaults, waiting to be paired with the ideal indication. For any RDF, this is the great promise of repurposing.[28]

While it is possible to do some preclinical validation with class prototype drugs, it is still most desirable to validate the same compounds available for repurposing from pharma partners[29]; however, this requires establishment of relationships between scientists, RDFs, and pharmaceutical partners. This process faces several obstacles. Long-dormant drugs-in-development may be considered safe to restart for a new indication, but drugs in active development may not be viewed this way at all. The conventional wisdom is that development for an orphan/niche indication could jeopardize development for a mainstream indication, especially if previously unseen toxicity is encountered during preclinical or clinical studies. Thus, timing is critical, and often the ideal time for repurposing comes when the blockbuster indication begins to falter.

Another major problem in negotiating Material Transfer Agreements (MTAs) for compounds in development is that universities, especially in the United States, have become increasingly aggressive in asserting intellectual property rights. This poses a significant problem for any industry collaborator, in that MTAs can be very difficult and time-consuming to negotiate, and academic institutions may be unwilling to waive potential intellectual property (IP) claims. The prospect of competing IP interests can cause significant distrust between industry and academia, but an RDF can often be seen as an honest third party to facilitate these collaborations. An attractive option for RDFs at this stage can also be found in contracting with foreign labs, a form of nonprofit off-shoring. A great many high-quality academic labs in Asia and Latin America are available to perform contract studies in an environment which can be more pharma-friendly. Indeed, universities outside of the United States and Western Europe are significantly less aggressive in pursuing potential IP claims.

Leverage Potential: RDFs can use contract labs of various types (commercial CRO vs. academic contractor) in various locations (potentially offshore) to achieve quicker and more cost-effective preclinical validation. Derisking and repurposing can make a rare or neglected disease indication much more attractive to industry partners, and can attract funding for clinical trials which would otherwise be unavailable to most RDFs.

1.22.7.5 Clinical Trials

Traditionally, RDFs and other patient organizations have played a role in clinical trials by assisting with recruitment of subjects. Patient associations are in an ideal position to do this if they have a patient registry or even an extensive database.[22] As noted previously, modern web-based communications make the dissemination of clinical trial information easy, efficient, and inexpensive. However, RDFs are increasingly taking a more direct approach in funding and even organizing clinical trials.

Derisking strategies can encourage pharmaceutical companies to pursue an indication for a target disease. However, the market for any given RD therapeutic may not appear attractive enough. RDFs may, at this stage, opt to organize and/or fund studies via investigator-initiated IND studies.[30] RDF-funded clinical trials will necessarily be smaller than most industry-sponsored studies, even in the RD field, where all clinical trials are relatively small. This is not necessarily a problem, however, in that clinical trial methodology usually must be developed for each new indication, and most rare and neglected disorders do not have a well-worn path for drug development. Many of the elements of clinical trials methodology, such as outcome measures, must be tailored to the target disorder in an iterative validation process. For instance, in the case of outcome measures, specific rating scales may be designed to capture the prominent features of the RD; these outcome measures may be validated in disease populations to document interrater and test–retest reliability. However, until these disease-specific outcome measures can be shown to capture not just disease symptoms, but also treatment response, they cannot be considered fully validated. This iterative process may require several cycles.[13] Early, smaller, RDF-funded trials can help to pave the way for larger industry-sponsored clinical trials. This can be considered an important form of derisking, and illustrates the usefulness of early clinical trials of available agents to facilitate the development of proper trials methodology in a given field.

It is important to recognize that while the specifics will vary with each disease indication, some variant of this iterative process is always required to develop adequate clinical trial methods. Even the best preclinical validation simply cannot predict human therapeutic effects with precision, and even the best-designed outcome measures for a new indication will themselves require repeated validation in their own development cycle.

Leverage Potential: Ultimately, the most effective leveraging strategy for RDFs is to use the previous development stages to convince industry or governmental agencies to fund larger clinical trials. Larger trials are required for approval of new chemical entities, or even to establish efficacy of available drugs for a new RD indication. By organizing and funding smaller early-stage trials, improving clinical trial methodology through the necessary iterative process, RDFs can derisk this process substantially. Those fortunate RDFs with sufficient funding may even engage in full partnerships with pharmaceutical companies; perhaps the best-known and most successful example is the partnership between Vertex Pharmaceuticals (http://www.vrtx.com) and the Cystic Fibrosis Foundation (http://www.cff.org). The exceptionally well-funded CF Foundation invested more than $150 million in Vertex, beginning in the late 1990s, with the express goal of developing a new class of drugs to treat a subset of CF patients. This eventually led to the approval of Kalydeco (ivacaftor), which increases chloride transport via cystic fibrosis transmembrane conductance regulator, the protein impaired in cystic fibrosis.[31] Royalties to the CF Foundation from this deal are now estimated to exceed $3 billion, and will likely fund the Foundation's operations for many years. However, the ethics and incentives of this partnership have caused concern in many circles,[32] in part because of the astronomical cost of the drug. Clearly, this type of collaboration is reserved for the wealthiest of RDFs, but other groups, such as the SMA Foundation, have embraced this direct funding partnership model.[33]

1.22.7.6 Limitations of This Approach — and Possible Solutions

1.22.7.6.1 Biomedical research is expensive

Just as tuition at universities in the western world has increased at a rate far higher than the background rate of inflation, the cost of conducting research at these institutions has also skyrocketed. Average college tuition in the United States increased by 498.49% versus only 114.85% increase in the overall Consumer Price Index (the official figure for price inflation in the United States) between 1985 and 2011.[34] This university price inflation has made academic research much more expensive over the past 30 years. Likewise, rapidly increasing healthcare costs have driven inflation of pharmaceutical research costs, with players competing for limited research resources in an effort to exploit increasingly lucrative markets. Outsourcing some of this work to more cost-effective areas may be a solution for RDFs, especially in earlier phases of research, where regulatory requirements are not a major concern. For example, a custom synthesis firm in India may be able to produce an essential reagent for significantly less than a US firm. For example, during FRAXA's partnership with the UK-based startup Neuropharm to develop fenobam (an mGluR5 antagonist) for fragile X, it was necessary to synthesize large quantities of the compound. Bids for a (several kilogram) Good Manufacturing Practices (GMP) synthesis of fenobam were obtained from multiple US firms and a well-known Indian pharmaceutical manufacturer; the cost of the GMP fenobam from the Indian source was approximately one-fourth the cost of the lowest US firm. It is unlikely that the development project could have proceeded at the higher cost, given the limited resources of this small company.

1.22.7.6.2 University-based research can be inefficient

Academic labs do not always share the same culture of accountability as industry research facilities, and many RDFs are unaccustomed to enforcing strict accountability. They are, after all, charities, not businesses. Add to this different incentive structure the increasing pressure from ever larger numbers of RDFs seeking high-quality research, and we can see an emerging problem: competition within the conventional university-based research paradigm limits the ability of RDFs to demand accountability from academic labs, since successful research groups may have many options for funding. Nonetheless, many RDFs have adopted policies which can increase the efficiency and accountability of its grantees. For example, an RDF may limit funding of any given research group to a 2- or 3-year time span, to reduce dependence on RDF funding and encourage scientists to seek out other funding sources. Most importantly, the issue of accountability must be considered from the start of the grant-making process. Expectations must be specified and enumerated in grant contracts, and monitoring mechanisms should be accepted by all parties. Likewise, intellectual property issues must be decided in advance and specified in any grant contract. For example, if a disease foundation would like a transgenic mouse model produced for the benefit of the research community, and it has elected to pursue a nonprofit/academic route, it should issue a request for proposals (RFPs) for this model. It should have some guidelines for the funding available, and the timeline required. The foundation should also specify in its RFP any requirements for sharing of the mouse model, the mechanism for distribution, and the ownership of intellectual property. These issues will all be critical for future work, but they are very difficult to negotiate after the fact. Consideration of these issues in advance can make academic research more efficient, and move this model closer to the CRO model, while still allowing for the utilization of the often unique expertise of academic labs.

1.22.7.6.3 The drug discovery process is very risky

Pharmaceutical industry researchers are well aware of the risks of developing new drugs. However, the influence of RDFs and other nonprofit funding sources may actually introduce new perils into the process. Repurposing, in particular, has one potentially fatal flaw: drugs are typically developed for an initial indication, with a particular dose range in mind. In most cases, the drug's mechanism of action is not directly related to the disease mechanism. For example, most patients with hypertension do not have excess angiotensin converting enzyme activity, but angiotensin converting enzyme (ACE) inhibitors will still lower their blood pressure. The preclinical toxicology package for the drug's indication often reflects the anticipated use, and this may not align with the requirements of the RD indication. Consider a case where research into the mechanism of a RD has shown excessive enzyme activity, perhaps as a result of the disease's genetic mutation. If a drug class in development is known to inhibit this enzyme quite potently and specifically, it might appear to be a perfect candidate for repurposing. However, we might reasonably anticipate that the effective dose in the RD patient population could actually be much higher than the dose for the original indication in the general population, since the RD group is known to have higher baseline, constitutive activity of this enzyme. Indeed the RD patients may be able to tolerate higher doses without significant adverse effects. However, repurposing may be heavily constrained by the preclinical toxicology already done on this class of compounds, originally targeted at the general population. While preclinical toxicology could be repeated for the RD, with the higher dosage in mind, this greatly decreases the attraction of repurposing, increasing the time and expense involved in pursuing the rare/orphan indication.

1.22.7.6.4 Impatient patients — everything takes too long

Curing disease is no easy task. When one considers that most of the effective treatments we have in modern medicine today were essentially discovered serendipitously, the prospect of developing a specific treatment for a particular disease from the ground up seems even more daunting. Even when everything goes right in the drug discovery process, many years are still required to develop a new treatment. Clearly, those embarking on this kind of project must be prepared for a long and arduous journey. Not surprisingly, many patients and families are losing patience with the current RDF model and starting their own biotech and pharma companies:

Tracy and Benjamin Seckler in 2011 helped found a startup, now known as Akashi Therapeutics Inc., in Cambridge, Mass., after growing frustrated that some compounds their foundation supported for Duchenne muscular dystrophy weren't moving forward in development. Their son, Charley, 14, has the fatal condition.

Jill Wood of Brooklyn, N.Y., cofounded Phoenix Nest Inc. to seek treatments for Sanfilippo syndrome, a fatal genetic condition affecting her son Jonah, 6. She and her husband also have a nonprofit, but she says she realized "I can't nickel and dime my friends and family forever."

The for-profit approach is a harder slog than many anticipate, says Harvey Lodish, a Massachusetts Institute of Technology molecular biologist who advises parents wanting to start companies to develop drugs for their children. He was an original scientific adviser to Genzyme, now Sanofi unit, which has developed drugs for Gaucher disease, a rare disorder that can swell internal organs and weaken bones. He later discovered it affects his grandson Andrew, 12.[35]

Anyone entering the RDF world should be prepared for a long haul, yet the impatience of RD patients and families to find improved treatment can itself be a major driving force. RDFs have shown great potential for motivating drug discovery, and these patient-driven organizations have certainly helped to accelerate the pace of drug discovery in many ways.[13] Though actual progress in biomedical research is often frustratingly gradual, this trend shows no signs of abating, and RDFs will likely continue to play a growing role in the future of drug discovery.

1.22.8 Conclusions

As medical technology has progressed, our perceptions of medicine and disease have changed. As we have seen once incurable scourges of modern societies like TB and polio become preventable, treatable, and even eradicable, our expectations have changed significantly. Economic expansion and advances in telecommunications have allowed newly affluent people around the world to coalesce around the causes that are most important to them. Thus, small groups of people affected by even the rarest conditions now feel empowered to change the course of diseases. Vast numbers of RDFs have formed in recent years, and while their specific missions vary, most aim to promote biomedical research into the mechanisms of their diseases, with the goal of expediting the development of improved medical treatment. Some of these patient associations have successfully navigated the long and complex drug discovery process, and found ways to improve the long odds facing any new treatment strategy. A greater understanding of how nonprofits can participate in the drug discovery process benefits both patient-run, disease-focused groups and their potential partners in industry.

From the perspective of a patient association, drug discovery entails basic research to elucidate disease mechanisms, translational research to identify treatment targets, preclinical research to evaluate the effectiveness of potential treatments, and clinical trials to test new therapeutics in patients. RDFs and other patient-run groups can contribute at every stage of this process, though the means employed will necessarily be determined by the resources available. Most importantly, the personal commitment and added motivation of patient associations can be an important factor in overcoming the significant obstacles posed by drug development in the modern era and promoting medical advances for otherwise neglected conditions.

References

1. Le Fanu, J. The Rise and Fall of Modern Medicine, revised ed; Basic Books: New York, 2012; p. 1
2. http://www.lung.org.
3. http://www.cancer.org.
4. http://www.heart.org.
5. http://www.marchofdimes.org.
6. Joyce, C. Transforming Our Approach to Translational Neuroscience: The Role and Impact of Charitable Nonprofits in Research. *Neuron* **2014,** *84* (3), 526–532.
7. Porter, R. *The Greatest Benefit to Mankind: A Medical History of Humanity from Antiquity to the Present;* Harper Collins: London, 1997.
8. European Organisation for Rare Diseases (EURORDIS). *Rare Diseases: Understanding This Public Health Priority (PDF).* http://www.eurordis.org/IMG/pdf/princeps_document-EN.pdf.
9. Fumagalli, D. C.; Gouw, A. M. Crowdfunding for Personalized Medicine Research. *Yale J. Biol. Med.* **2015,** *88* (4), 413–414.
10. Sommer, J.; Wessel, L. One in a Million: A Common Goal for an Uncommon Cause Connects Patients Who Share a Rare Disease. *Mark. Health Serv.* **2012,** *32* (4), 3–5.
11. Ingelfinger, J. R.; Drazen, J. M. Patient Organizations and Research on Rare Diseases. *N. Engl. J. Med.* **2011,** *364* (17), 1670–1671.
12. Groft, S. C. Rare Diseases Research: Expanding Collaborative Translational Research Opportunities. *Chest* **2013,** *144* (1), 16–23.
13. Swinney, D. C.; Xia, S. The Discovery of Medicines for Rare Diseases. *Future Med. Chem.* **2014,** *6* (9), 987–1002.
14. Vandamme, T. F. Rodent Models for Human Diseases. *Eur. J. Pharmacol.* **2015,** *759,* 84–89.
15. Dwinell, M. R.; Lazar, J.; Geurts, A. M. The Emerging Role for Rat Models in Gene Discovery. *Mamm. Genome* **2011,** *22,* 466–475.
16. Simmons, D. The Use of Animal Models in Studying Genetic Disease: Transgenesis and Induced Mutation. *Nat. Educ.* **2008,** *1* (1), 70.
17. Rubio, D. M.; Schoenbaum, E. E.; Lee, L. S.; et al. Defining Translational Research: Implications for Training. *Acad. Med.* **2010,** *85* (3), 470–475.
18. NIH blueprint for neuroscience: Cre driver network. http://www.neurosciencebluprint.nih.gov/factSheet/CreDriver.htm.
19. Moos, W. H.; Kodukula, K. Nonprofit Pharma: Solutions to What Ails the Industry. *Curr. Med. Chem.* **2011,** *18* (22), 3437–3440.
20. Liang, P.; Xu, Y.; Zhang, X.; Ding, C.; Huang, R.; Zhang, Z.; Lv, J.; Xie, X.; Chen, Y.; Li, Y.; Sun, Y.; Bai, Y.; Songyang, Z.; Ma, W.; Zhou, C.; Huang, J. CRISPR/Cas9-Mediated Gene Editing in Human Tripronuclear Zygotes. *Protein Cell* **2015,** *6* (5), 363–372.
21. Reis, S. A.; Willemsen, R.; van Unen, L.; Hoogeveen, A. T.; Oostra, B. A. Prospects of TAT-Mediated Protein Therapy for Fragile X Syndrome. *J. Mol. Histol.* **2004,** *35* (4), 389–395.
22. Litterman, N. K.; Rhee, M.; Swinney, D. C.; Ekins, S. Collaboration for Rare Disease Drug Discovery Research. *F1000Res* **2014,** *3,* 261.

23. McGonigle, P.; Ruggeri, B. Animal Models of Human Disease: Challenges in Enabling Translation. *Biochem. Pharmacol.* **2014,** *87* (1), 162–171.
24. Wood, J.; Sames, L.; Moore, A.; et al. Multifaceted Roles of Ultra-Rare and Rare Disease Patients/Parents in Drug Discovery. *Drug Discov. Today* **2013,** *18* (21–22), 1043–1051.
25. Huber, K. M.; Gallagher, S. M.; Warren, S. T.; Bear, M. F. Altered Synaptic Plasticity in a Mouse Model of Fragile X Mental Retardation. *Proc. Natl. Acad. Sci. U. S. A.* **2002,** *99* (11), 7746–7750.
26. Yan, Q. J.; Rammal, M.; Tranfaglia, M.; Bauchwitz, R. P. Suppression of Two Major Fragile X Syndrome Mouse Model Phenotypes by the mGluR5 Antagonist MPEP. *Neuropharmacology* **2005,** *49* (7), 1053–1066.
27. http://www.fraxa.org/research/resources/.
28. Haugh, R. Pharmaceuticals. Disease Foundations Prime the Drug Pump. *Hosp. Health Netw.* **2010,** *84* (2), 19.
29. Bartek, R. J. Foundation-Industry Relationships — A New Business Model Joint-Venture Philanthropy in Therapy Development. *Curr. Top. Med. Chem.* **2014,** *14* (3), 313–318.
30. http://www.fda.gov/Drugs/DevelopmentApprovalProcess/HowDrugsareDevelopedandApproved/ApprovalApplications/InvestigationalNewDrugINDApplication/ucm343349.htm.
31. Eckford, P. D.; Li, C.; Ramjeesingh, M.; Bear, C. E. Cystic Fibrosis Transmembrane Conductance Regulator (CFTR) Potentiator VX-770 (ivacaftor) Opens the Defective Channel Gate of Mutant CFTR in a Phosphorylation-Dependent but ATP-Independent Manner. *J. Biol. Chem.* **2012,** *287* (44), 36639–36649.
32. http://www.nytimes.com/2014/11/19/business/for-cystic-fibrosis-foundation-venture-yields-windfall-in-hope-and-cash.html.
33. http://www.smafoundation.org/collaborators.
34. http://inflationdata.com/Inflation/Inflation_Articles/Education_Inflation.asp.
35. https://globalgenes.org/raredaily/wsj-reports-parents-start-companies-cure-children/.

1.23 Contemporary Considerations for Discovering a Successful Medicine

MM Hann and MK Bayliss, GSK Medicines Research Centre, Stevenage, SG1 2NY, Hertfordshire, United Kingdom
AR Leach, GSK Medicines Research Centre, Stevenage, SG1 2NY, Hertfordshire, United Kingdom; and The European Bioinformatics Institute (EMBL-EBI), Wellcome Genome Campus, CB10 1SD, United Kingdom

© 2017 Elsevier Ltd. All rights reserved.

1.23.1 Introduction 560
1.23.2 Molecular Properties, Drug-Like Chemical Space, and "Rules" 560
1.23.3 Drug at Target 564
1.23.4 Target and Off-Target Engagement 569
1.23.5 Pharmacokinetics and Pharmacodynamics 571
1.23.6 Target Choices 573
Acknowledgments 574
References 574

1.23.1 Introduction

While there are many successful medicines now in use, there is abundant evidence of the many financial, scientific, and societal challenges for today's drug discovery and pharma industry, including:

- Patients are still in need of more effective drugs for many diseases.
- Payers are increasingly only prepared to pay for innovative rather than derivative drugs.
- Investors often believe they can get a better return on investment elsewhere, especially when a short-term view is taken.
- Legislators demand that only the very safest possible drugs are licensed.
- Researchers are frustrated that despite all our accumulated knowledge and the continued introduction of new technologies, the challenge of successfully navigating the scientific, administrative, and regulatory hurdles to find novel, effective medicines seems to get harder rather than easier and with high rates of attrition.

One consequence of these and related considerations is that the average cost of developing a new drug once all the failures are accounted for is now $1.8 billion.[1]

Drug discovery is so challenging in part because of the multitude of factors that need to be delivered successfully, across many different scientific, clinical, and business areas as summarized in the "equation" shown in Fig. 1. A "miss" on any one of these factors can lead to overall failure.

In this article, we will focus primarily on the "molecule" component, with an emphasis on small molecule therapeutics. Prompted by the challenges outlined earlier, and in part as a response to the perceived failure of combinatorial chemistry and high-throughput screening in the 1990s, the drug discovery and medicinal chemistry communities subsequently tried to understand the drivers for success or failure. We will review some of the discoveries and learnings (and in some cases, rediscoveries and relearnings) from these studies and analyses. At the same time, we will endeavor to indicate future challenges and opportunities and so provide the reader with a practical and pragmatic toolbox to help with the challenging yet rewarding task of finding effective and safe new medicines.

1.23.2 Molecular Properties, Drug-Like Chemical Space, and "Rules"

The notion of drug-like chemical space has evolved over the last 20 years both as a concept and as a practical tool to improve the probability that molecules being designed and synthesized in pharmaceutical research have the potential to deliver useful medicines. Just as overall success in drug discovery is dependent on a multiplicative array of components (molecule, target, study, etc., see Fig. 1), so for the molecule itself it is necessary to achieve, in a single entity, a multitude of properties that together confer the efficacy, safety, absorption, distribution, metabolism, excretion, and toxicology (ADMET), physicochemical, physical form, synthetic accessibility,

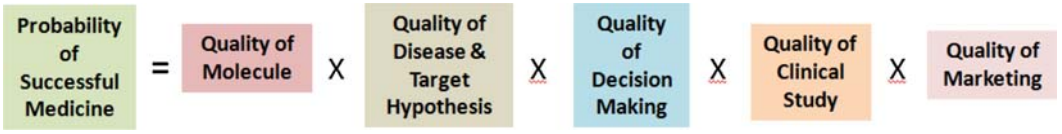

Fig. 1 The overall probability of success in making an impactful new medicine is dependent on many components.

and other properties that are required to enable the successful delivery of a medicine to patients. A perennial challenge in drug discovery, and one that will be a constant theme throughout this article, concerns the need for methods to assess and predict complex properties of molecules using simple in vitro measurements and in silico methods. Of course, it might be considered that trying to represent complex pharmacokinetic, pharmacodynamic, and toxicological phenomena using simple molecular properties is a fool's errand. Nevertheless, as we will endeavor to show, there have been some successes in moving toward this objective. It is very important however to recognize that in many cases, these properties and parameters are only indirectly related to the true molecular phenomena of interest. Another consideration, and one that has caused much debate, is that many of these studies have expressed these characteristics in the form of "rules." Some practitioners have chosen to interpret and apply these in a very rigid way. However, if the approach adopted is "rules are for the obedience of fools and the guidance of wise men," then there is a strong case to support their role in drug discovery, as we will try to show using our own drug discovery experiences.

The most frequently (and first) quoted "rule" of drug space was defined by Chris Lipinski, whose rule of fives (Ro5) refers to the probability that a compound will be orally bioavailable in humans.[2] The Ro5 states that if a compound has more than one violation of the following four criteria, then it is unlikely to be orally bioavailable: (1) greater than 5 hydrogen bond donors (defined as the total number of hydrogens directly bonded to O or N), (2) greater than 10 hydrogen bond acceptors (defined by all N or O atoms in the molecule), (3) a molecular weight greater than 500, and (4) a calculated octanol–water partition coefficient log *P* greater than 5. The Ro5 refers to only one aspect (i.e., oral absorption) of the overall ADMET profile of a compound, and it has frequently and erroneously been misquoted as "the" rule of drug-like space, no doubt helped by its simple formulation and it being the first major study of its type. This common conflation of Ro5 with drug space is probably due to the fact that most drug discovery projects do aspire to achieve oral bioavailability. However, while this may be desirable it is certainly not sufficient. To more fully define a drug-like space, we need guidance on parameters such as solubility, permeability, dose, toxicity, metabolism, etc. In part inspired by Lipinski, over the past 5–10 years, many analyses of data sets from the literature and from internal Pharma company projects have been published that aim in whole or in part to extend Lipinski's work. These studies typically involve comparisons between compounds that successfully progress through a particular test or milestone (e.g., candidate selection, animal safety testing, or a clinical phase) and compounds that do not, with the goal of finding a few simple properties that can account for the observed differences. The work of Wenlock and colleagues is a good example of this type of analysis; they concluded that the properties with the strongest influence on the successful passage of a candidate drug through the different stages of development are molecular weight and lipophilicity.[3] This and other analyses are summarized in **Table 1**.

It should be noted that lipophilicity is the most common parameter in **Table 1**. The importance of controlling lipophilicity is not new and was integral to the conclusions described in particular by Corwin Hansch et al. in the early days of quantitative structure activity relationships (QSAR) where the emphasis was more on properties such as absorption. In today's target-based approach to drug discovery, the role of lipophilicity as a key parameter in modulating target potency has also become an important consideration. The challenge here is to avoid an excess of lipophilicity driven interactions in a drive for improved potency. This phenomenon has been described by Hann as molecular obesity, in recognition of the similarities with medical obesity.[12] Some of the more common drivers for increased lipophilicity are summarized in **Table 2**.

The "rules" summarized in **Table 1** are all reported using hard cut-offs. While simple to articulate and incorporate into computational filters there are well-known dangers of expressing conclusions in this way. First, rules such as these do not reflect effectively the complete spectrum of molecules that are medicines. Second, they do not reflect the inherent uncertainties in the experimental measurements (or indeed, in computed properties). The third drawback comes from the potential for misuse, insofar as all compounds that "pass" a rule are deemed acceptable and all that "fail" are unacceptable. To take an extreme case, there is no real difference between two compounds, one of which may fail the Lipinski rule because of a calculated log *P* of 5.1 versus a closely

Table 1 Guidance "rules of thumb" for physchem property influence on ADMET outcomes[4]

Drug-like property considered	*Guidance*	*References*
Lipinski/Pfizer Ro5 for oral bioavailability	Violating two or more of MW < 500, log *P* < 5, HBD < 5, and HBA < 10 results in poor oral bioavailability	2
AZ receptor promiscuity	Maximize LLE = pIC50–log *P* to reduce promiscuity	5
Pfizer 3/75 rule for toxicity	Keep c log *P* < 3 and PSA > 75 to minimize toxicity	6
GSK 4/400 rule for general ADMET	Keep c log *P* < 4 and MW < 400 for generally favorable ADMET properties	7
AZ permeability model	Larger "small molecules" need more lipophilicity to penetrate membranes	8
GSK PFI model for general drug-like properties (including solubility)	Favored space from property forecast index (PFI) when PFI = mChromLogD7.4 + Number of aromatic rings < 6. But note that permeability max is PFI = 6–8	9
Pfizer dosage guidance for reducing toxicity	Keep predicted human efficacious dosage of < 250 nM (total drug) and < 40 nM (free drug)	10
GSK developability classification system DCS based on permeability, dose, and solubility	Compounds with DCS classification I, IIa, or III are much easier to develop	11

Table 2 Reasons for molecular obesity and mitigating strategies[4]

Reason for lipophilicity increase	*How to avoid or alleviate*	*References*
Potency is easily driven by nondirectional lipophilic interactions and which are therefore easier to make	Ensure maximum potency is initially achieved through polar (enthalpic) interactions	13,14
Permeability sweet spot is often found by indiscriminate use of lipophilicity—particularly for larger molecules	Use lipophilic ligand efficiency metric LLE to control lipophilicity driven membrane effects	5,15
Organic synthesis favors purification of lipophilic compounds	Design synthesis, work up, and purification schemas which can cope with more polar molecules	16

related compound from the same series with a corresponding value of 4.9. To counter this particular limitation, Bickerton et al. introduced the concept of desirability which they termed the quantitative estimate of drug likeness (QED) that can reflect more effectively the underlying distribution of molecular properties.[17]

Clearly there are effective oral drugs that lie outside drug space, as defined by Lipinski's Ro5 or indeed one or more of the other rules listed earlier. Equally, there are many compounds that meet the Ro5 but which for any of a whole variety of reasons will never be an effective medicine. What can we learn from drugs that fall outside the Ro5? In a recent study, Doak et al. identified 226 clinical or preclinical candidate drugs which have a MW greater than 500 Da. The set includes macrolides, peptides, rifamycins, HSV NS3/4A and NS5A inhibitors, HIV protease inhibitors, azole antifungals, cyclosporins, taxanes, cardiac glycosides, etc.[18] They use this set to define a "beyond rule of 5" (bRo5) space, although it should be pointed out that the criterion for inclusion in the set is a violation of one or more of the Lipinski criteria, whereas the original Lipinski publication required two violations to be excluded. Furthermore, as we noted earlier, Lipinski was focused on oral absorption rather than "drug likeness." The bRo5 set represents approximately 10% of the total number of oral clinical and preclinical agents. This may seem quite a significant percentage but it should be noted that many of the compounds in the bRo5 set are from a limited set of chemotypes based on natural products, and there is a preponderance of antiinfective therapies. These compounds have likely benefitted from significant evolutionary pressures, often against the infective agents or related pathogens for which they are primarily prescribed.

There is thus an apparent discrepancy between the numbers and structural diversity of oral drugs that conform broadly to the Lipinski guidelines and the smaller numbers in the bRo5 space that represent a much more limited set of chemotypes. Can we identify possible explanations for this? Has the medicinal chemistry community been too dismissive of bRo5 compounds because they do not conform to what a "typical" drug molecule "looks like"? One viewpoint is to consider this problem from the perspective of the distribution of drugs within chemical space. It is estimated that there are of the order of 10^{30} compounds with MW < 500 Da that could in principle exist. From this, there are ca. 2×10^3 drugs, giving a hit rate of $1{:}10^{27}$. There are $\sim 10^{78}$ possible compounds with 500 Da < MW < 1000 Da, which has so far yielded 0.1×10^3 drugs, equivalent to a hit rate of $1{:}10^{76}$. In other words, if drug-like molecules are equally distributed throughout chemical space (a big assumption, granted), then it will be much more difficult to find them in the bRo5 region than in the Lipinski space. This simple argument, albeit based on very approximate statistics, suggests that the probability of success is likely to be higher in the Ro5 space and so it is incumbent on teams to ensure that they have fully explored the options here before venturing into the more challenging arena of bRo5. This perspective is supported by Ritchie and Macdonald who used the QED drug likeness score on a set of 771 clinical drugs to compare the top scoring compounds with the worst scoring compounds and they clearly show that it is the absorption and bioavailability characteristics of the different subsets that are the most striking differences and these characteristics are much better understood and predictable in drug-like space.[19]

How can an organization or a team practically apply the myriad rules and guidelines now available in the literature? At GSK, our increased understanding of compound attributes that can influence successful candidate drug progression has resulted in documented guidance to project teams designed to improve the probability of success of oral candidates. Our compound quality criteria have been created by combining three measures which can variously be predicted or measured as the project progresses: property forecast index (PFI, a composite measure of lipophilicity and aromaticity), solubility, and dose. For each of these three properties benchmarked guidelines are provided, based on the distributions of marketed oral small molecule drugs.[20] It is important to highlight that these are intended as guidelines; teams are not prohibited from progressing or selecting molecules outside the defined regions. Compounds that are far outside the guideline regions are nevertheless considered to have a higher risk that may warrant performing certain preclinical studies earlier in the progression cascade. The guidelines are also intended to ensure that teams thoroughly explore drug-like space before moving far from it. Also of note is the inclusion in our criteria of solubility and dose which are tangible experimental quantities rather than the more abstract property counts used in the Lipinski-type guidance.

Just as important as the actual guidelines have been the communication, educational, and support mechanisms. These have focused on providing access to the underlying data together with practical and pragmatic insights into the rationale for selecting the particular properties and their guideline values. For example, the developability classification scheme (DCS) is a straightforward yet highly effective way to assess the solubility and permeability properties required in a potential drug to enable absorption in the gastrointestinal (GI) tract.[11] The *X*-axis in the DCS plot is the ratio of dose and solubility, which may appear at first sight a somewhat abstract concept but has physical meaning as the volume required to dissolve the intended dose. The logarithmic scale along the *X*-axis corresponds to values ranging from a tea-spoon to a small swimming pool. Volumes exceeding approximately 1 L (i.e., the

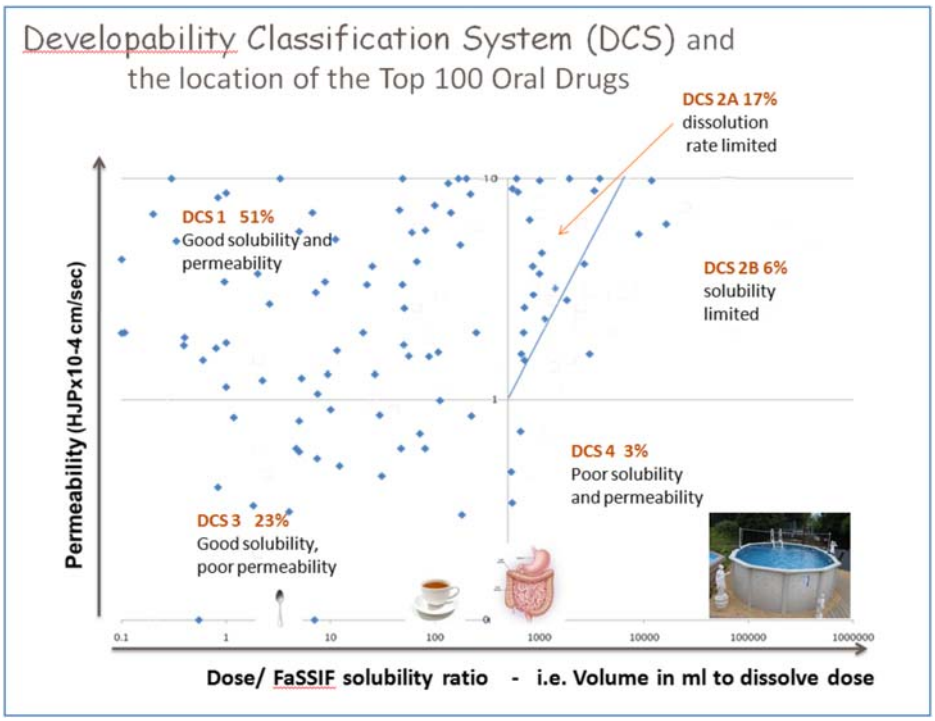

Fig. 2 Distribution of top 100 oral drugs[22] in developability classification system (DCS) space and visualization of volumes needed to dissolve intended dose. Drawn with the help of Anthony Taylor, GSK Stevenage.

approximate volume of the gut in its fed state) can be problematic as there is insufficient volume to dissolve the intended dose again emphasizing the influence physicochemical properties such as solubility on dissolution of drugs in the GI tract[21] (see Fig. 2).

The picture emerging thus far is one where appropriate monitoring of key physicochemical properties is important in the early phases of drug discovery, with well-understood risks of being in the wrong space (though as always there are successful medicines that lie outside the norms). Lipophilicity is a key molecular property where inadequate monitoring or control can have undesirable consequences. In some cases, there is a direct link and/or molecular rationale between too high or too low a lipophilicity value and the undesired property. In other cases such as off-target toxicity, the link may be less clear but there is ample circumstantial evidence in support. However, as a recent pan-Pharma analysis suggested,[23] simple physicochemical properties will not be sufficient to solve all of the challenges. We concur; at GSK we consider our physicochemical property-based guidelines as just the first phase of a series of tools and techniques designed to address attrition across the entire portfolio and through all phases. Clearly the discovery and development of molecules which have the greatest likelihood of success requires a combined evaluation of *all* the contributing factors during the lead optimization phase including lipophilicity, protein binding, solubility, in vitro and in vivo clearance, and exposure. Moreover, it is important to take a broad perspective. We therefore need to find a new language to capture some of the more complex processes involved in the later preclinical and clinical phases of drug discovery and development. The challenge then is to identify effective and cost-efficient ways to incorporate any learning's into our Discovery programs.

In a series of publications, scientists at Pfizer and Astra Zeneca sought to understand some of the more fundamental reasons why projects progress or fail. The first of these studies was from the Pfizer group who examined the underlying reasons for success or failure at the critical transition from Phase II to Phase III—Fig. 3A summarizes the findings from the retrospective analysis of information available at the time that the Phase II trial was initiated.[24] Key to successful progression were the following three critical requirements (termed the "three Pillars of survival"): (1) Does the molecule get to the site of action? (2) Does it engage the target effectively? (3) Does the target engagement elicit a pharmacological response? In a subsequent publication a fourth pillar was added: (4) Does this translate into therapeutic benefit)?[25] The importance of getting firm evidence for each pillar is emphasized in the temple diagram shown in Fig. 3B. We similarly believe that these concepts are critical for the delivery of a successful medicine and will expand on each of these concepts in the subsequent sections of this article. It should be noted that these do not obviate the need for a quality molecule and in particular for the therapeutic index to be sufficiently high to enable a clinically effective dose to be delivered.

Another useful set of considerations for successful drug discovery has come from a longitudinal review of AstraZeneca's small molecule drug projects from 2005 to 2010 which identified the most important technical determinants of project success and drug pipeline quality.[26] These criteria have been termed the 6Rs: the right target, the right patient, the right tissue, the right safety, the right culture, and the right commercial potential. They thus mirror to some extent the components in Fig. 1; the need is for effective integration of knowledge and data throughout the lifecycle of a project to ensure a thorough understanding of the

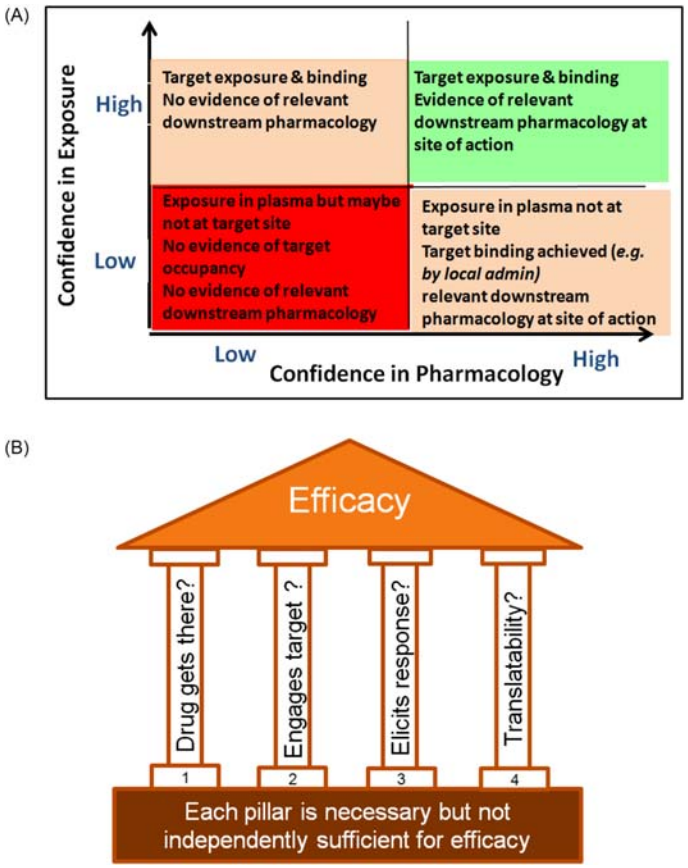

Fig. 3 (A) Causes of high/low confidence in exposure and pharmacology for Phase II Survival (adapted from Morgan, P.; Van Der Graaf, P. H.; Arrowsmith, J.; Feltner, D. E.; Drummond, K. S.; Wegner, C. D.; Street, S. D. A. *Drug Discov. Today* **2012**, *17*, 419–424); (B) iconic representation of the necessity of having each pillar in place to guarantee efficacy.

relationships between systemic exposure, target engagement, efficacy, and safety potential of any asset progressed to the clinic. Of these six criteria, the right culture is perhaps the hardest of all to measure as it is far more subjective than the other criteria but is critically important for enabling high-quality decision making based on the data relevant to the remaining 5Rs. Organizational aspects have also been the subject of analyses of medicinal chemistry strategies, for instance in how different companies appear to have embraced the challenge of dealing with excess lipophilicity.[27]

The Pfizer and Astra Zeneca reviews, together with other publications and in-house analysis at GSK, provide us with useful indicators for the challenges and issues that the next generation of attrition tools will need to address. In the following sections, we consider a number of these topics: understanding drug concentrations distribution and concentrations; monitoring the binding interactions between drug and target (and drug/off-targets); pharmacokinetic and pharmacodynamic analysis and modeling and how this relates to accurate human dose prediction.

1.23.3 Drug at Target

Clearly, a medicine cannot be effective if it does not get to the target location at a sufficient concentration to enable a molecular interaction. In those cases where there is clear and definitive evidence that the compound is demonstrating the required effects in vitro and in vivo, then it is highly likely that it is present at the target. However, as with many aspects of drug discovery, the lack of such an observation can be due to a number of factors of which only one is an insufficient amount of drug at the target over the required time period. Further, it is rarely possible to work backward from an observed phenotypic effect and/or target engagement study to understand precisely how much compound really is present and available to bind to the target. Even when such calculations can be done, it is useful to be able to measure directly compound disposition both total and free. This can also help understand the location of compound that is not contributing to the desired activity.

Important data come from tissue distribution studies using radiolabeled development compounds. An example of such a dataset is that from an analysis of ca. 200 quantitative whole body autoradiography (QWBA) studies conducted at GSK over a number of years.[28] The results show that in vivo distribution to compartments (Fig. 4) is strongly influenced by lipophilicity and ionization state

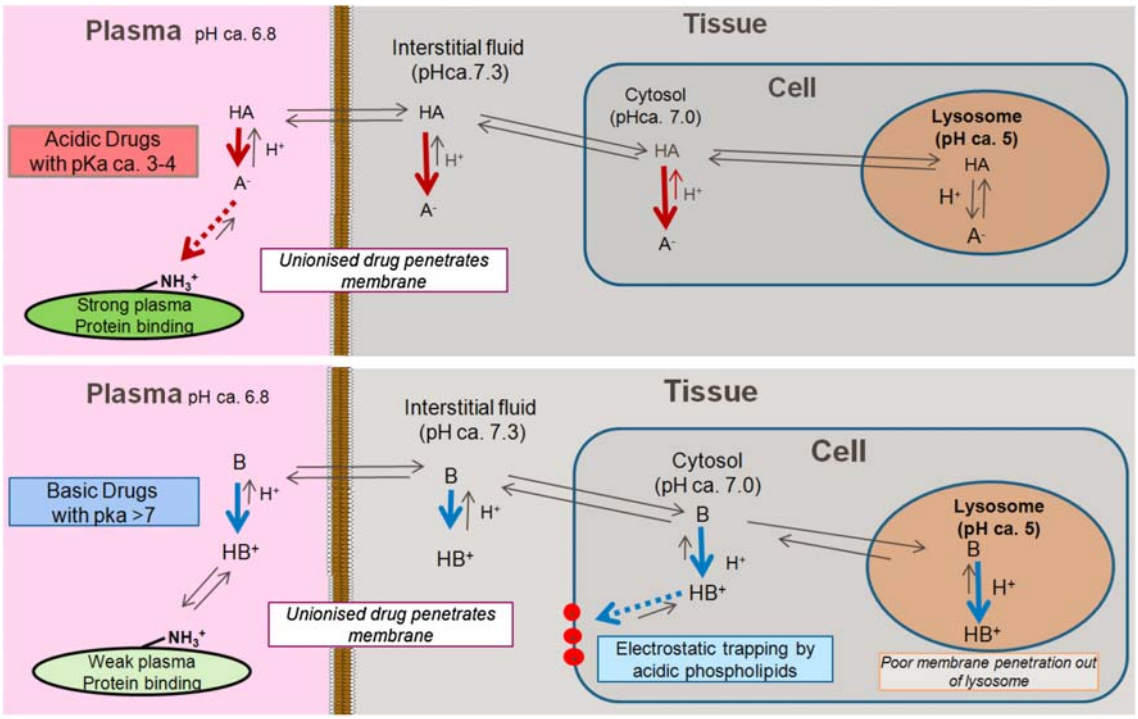

Fig. 4 The effect of pH and pK_a on the distribution of molecules between plasma, tissues, cells, and subcellular organelles. Drawn with help from Andy Harrell, GSK Ware.

as a consequence of their role in determining phospholipid and plasma protein binding. Basic and neutral molecules are more effectively distributed due to weaker plasma protein and stronger phospholipid binding. By contrast, the poor distribution of acidic drugs into tissues is due to high plasma protein and weak phospholipid binding. However, anionic uptake transporters in liver and kidney can favor the uptake of several anionic drugs into these organs. From these studies it is clear that for many molecules the role of drug binding to endogenous macromolecules heavily influences the distribution of total drug. Reducing lipophilicity decreases the effect of nonspecific binding on drug distribution in tissues, confirming again the critical role that this parameter has in drug disposition.

Studies in the discovery phase are traditionally limited to nonradiolabeled compounds due to the costs, complexities, and timescales associated with radiolabeling experiments. An alternative is to use mass spectrometric methods which are widely used to determine levels of total or free drug (and/or known metabolites) in plasma and other compartments such as Cerebrospinal fluid (CSF) or in tissue homogenates. The advent of spatially resolved mass spectrometric methods such as Matrix Assisted Laser Desorption/Ionization (MALDI) and secondary ion mass spectrometry (SIMS) offer exciting new opportunities to observe the distribution of compounds at resolutions below the subcellular, as we will discuss shortly. The more traditional approach is to perform in vivo (or in vitro) measurements in plasma and then apply the free drug hypothesis. This states that at equilibrium, the free drug concentration is the same on both sides of a biomembrane and that at the site of action, it is the free drug concentration that drives target engagement.[29] However, Smith et al. have argued that over reliance on the free drug hypothesis is dangerous due to the number of implicit assumptions.[29] This is particularly true for compounds of low passive permeability or when there is low blood flow to the tissue or cells, or when efflux or influx of the drug is mediated by active transporters. Other causes of the breakdown of the free drug hypothesis occur when there is irreversible inactivation of the target, or when in vitro assays are used for which the therapeutic target concentration of drug differs from that in the in vivo environment.

A situation commonly encountered occurs when the target of interest is intracellular, where the free intracellular concentration of drug is important for driving target engagement.[30] Use and application of the free drug hypothesis can be particularly problematic here. A typical example of such an issue is shown in **Fig. 5** where the potency of a series of compounds assayed for syk inhibition in a biochemical assay (full-length syk in HTRF format) is plotted against their cellular potency (as measured by Erk phosphorylation in a B-cell assay that identifies inhibitors of activation mediated by B-cell receptor signaling events including syk).[31]

This cellular assay is typical of those used prior to in vivo studies as part of a lead optimization screening cascade. It is clear that there is a degree of correlation between the two measurements, but also a pronounced deviation from the line of unity. The main explanation for this is presumed to be due to varying levels of free compound in the cells due to compound binding to cell membranes, lipid binding proteins, and other macromolecules. This variability was first studied by Corwin Hansch and colleagues in their QSAR studies.[32,33] Invariably it was found that lipophilicity (as measured by the octanol–water partition log P or calculated as the equivalent c log P) was a key parameter in relating cellular, tissue, or whole animal activity to target-based biochemical activity and this was well understood in the era where drug discovery usually started with a cellular or tissue assay.

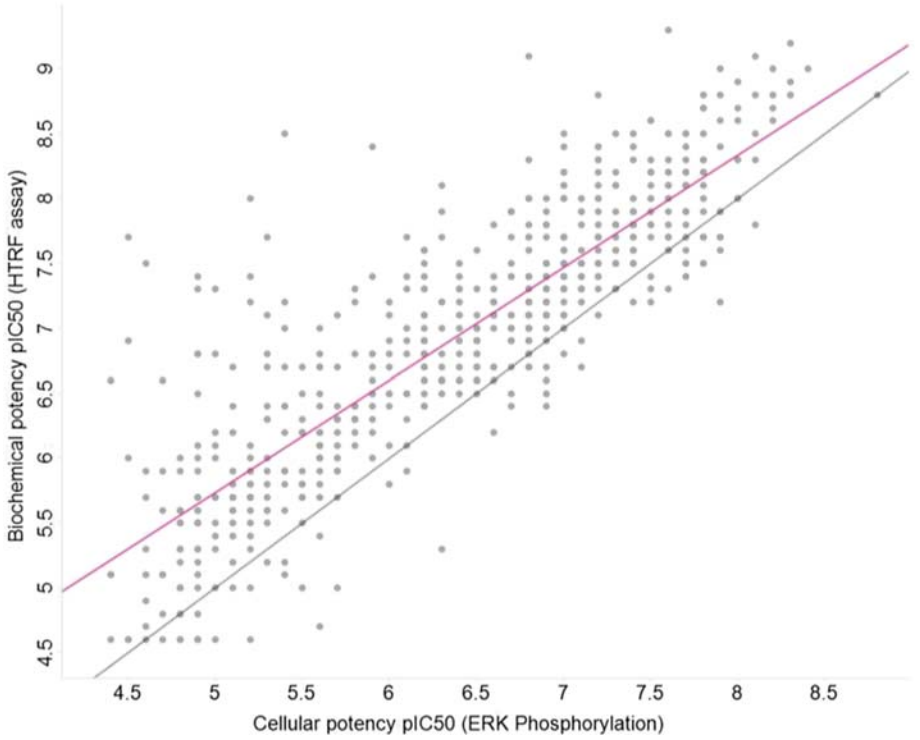

Fig. 5 Plot of biochemical potency (pIC50) versus cellular potency (pEC50) across multiple chemotypes studied as syk inhibitors at GSK. *Black line* represents 1:1 correspondence; *red line* represents correlation line of best fit ($r^2 = 0.7$).

With the advent of contemporary screening cascades where achieving potency in biochemical assays is often the starting norm, it is clear that understanding how much compound is actually available at the site of action in a subsequent cellular assay is a key consideration in lead optimization. Without this information it is difficult to determine how much of the total dose is available for effective target engagement rather than being lost through metabolism and excretion, or distribution to nonproductive compartments, potentially leading to unwanted interactions with off-targets, causing side effects.

This balance between potency and compound concentration at the site of action has always been a key consideration in medicinal chemistry. Recently, a simple mathematical formalism has been introduced that expresses this in a succinct manner. Drug efficiency (D_{eff}) is defined as the fraction of the dose (usually oral) that is available, that is, free, in the compartment of interest (traditionally the plasma). D_{eff} (sometimes also referred to as Kpu) is thus a useful measure of the free bioavailability of the drug.[34] Montanari et al. subsequently defined the drug efficiency index (DEI) as the sum of $\log D_{\text{eff}}$ and the measured potency of the drug at its target (expressed as pIC50 or pK_a). DEI can be considered as a potency corrected for the amount of drug at the site of action.[35] If the D_{eff} equals 1%, then $\log D_{\text{eff}}$ is zero and the DEI equals the intrinsic potency. If D_{eff} is greater than 1% (which is true only for some drugs), then DEI is greater than the intrinsic potency. Conversely, if D_{eff} is less than 1% (a situation not uncommon with known drugs), the intrinsic potency is less than the target potency, and becomes increasingly lower as D_{eff} gets smaller. As discussed in the article, DEI also relates to the likely receptor occupancy that can be achieved, another key parameter that needs to be understood in lead optimization studies. DEI thus provides a convenient way to monitor the balance between potency and compound availability. Further, this simple index was found to be a very good predictor of dose—compounds with a higher DEI (>7) show a corresponding reduction in the efficacious dose. An additional benefit of the DEI is that it helps to emphasize that low intrinsic potency is not as essential a requirement for a good drug as is often perceived. Indeed, it is worth pointing out that the average potency of drugs at their molecular site of action (when known) is only 50 nM (equivalent to pK 7.8).[36]

D_{eff} is an experimentally determined parameter that relies on in vivo experiments to determine the plasma free concentration. This typically requires animal studies and significant compound requirements. An in vitro alternative that may be more suitable for lead optimization where only a few milligrams may be available was developed by Valko et al. using biomimetic partition coefficient data for compounds of known D_{eff}, giving an expression for an in vitro $D_{\text{eff max}}$[37]:

$$D_{\text{eff max}} = 100/10(0.23 \times \log K \text{ HSA} + 0.43 \times \log K \text{ IAM} - 0.72)$$

HSA and IAM refer to human serum albumin (HSA) and immobilized artificial membrane (IAM), respectively. It should be noted that this model should be considered the best case scenario as it assumes that a compound's bioavailability is 100%, and no active transport and/or permeability barriers impact the free biophase concentration.

The equation shows that low drug efficiency is related to high protein binding (the HSA term) and high lipid binding (K_{IAM}). $D_{\text{eff max}}$ can also be understood in more classical terms through its link to the volume of distribution. A high volume is often

considered to give an extended drug half-life, but likely to give a low free drug concentration.[38] As in silico predictions of HSA and IAM binding can be made, it is also possible to make predictions of in vitro $D_{\text{eff max}}$ in advance of synthesis, thus enabling a much more predictive approach to drug design.

Mateus et al. have described a platform for the routine and comparative analysis of total and free drug in cells routinely used in drug discovery programs such as HeLa, HEK293, or even primary cells.[39] This is achieved by incubating cells with compound and then after a rapid wash, the cells are ruptured and the total concentration of cell-associated compound is measured by LC/MS. In a separate experiment, they use cell homogenates and equilibrium dialysis to estimate the free intracellular concentration of compound. At GSK, an assay similar to this has been automated with the aid of a Rapidfire LC/MS platform to provide routine and robust data sets for use in early lead optimization.[40] **Fig. 6** shows a plot of the total compound in the cells expressed as a concentration against the free concentration. The plot shows compounds color coded by their lipophilicity using PFI values and confirms the expectation that as the compounds become more lipophilic the free concentration is not greatly affected while the total concentration associated with the cell rises. Note that for the most lipophilic compounds (*red* and *yellow*), the total concentrations can be up to two orders of magnitude higher than the applied concentration of 20 μM, while the free concentration is typically below 20 μM, the maximum expected from the free drug hypothesis. This shows that as compounds become more lipophilic, they are increasingly bound to lipid and protein and that there is no parallel increase of free drug concentration. This is also fully consistent with the bell-shaped curves of biological response with log *P* that Corwin Hansch first pointed out ca. 50 years ago and is highlighted by Yvonne Martin in her review of his many contributions to QSAR.[33]

While increasing the free concentration of a drug at the site of action is generally considered a good strategy during lead optimization, it should also be born in mind that a high free concentration means that the compound is also free to interact with off-targets, which may in turn result in a lack of specificity and potential toxicity. Wenlock has suggested that a value of over 100 nM (free concentration in plasma) is likely to be associated with adverse effects.[41] This is only slightly higher than the value of $\leq$40 nM as free drug concentration (or $\leq$250 nM (total drug)) which was suggested in a study by Pfizer scientists as an acceptable concentration to avoid toxicity problems.[10] It is interesting to note that a concentration of 250 nM for a 500 Da molecule is equivalent to 10 mg dissolved in 80 L (i.e., the approximate size of an average adult); a daily dose of 10 mg has been proposed as the threshold below which idiosyncratic toxicity is less likely to occur.[42] We can thus see, through the key property of administered dose, some convergence of the desired values of these more complex properties, similar to the situation for lipophilicity.

Earlier, we discussed the insights gained from QWBA on tissue distribution for radiolabeled compounds. Unfortunately such studies are often limited to very few compounds and are rarely performed in lead optimization. More suitable for lead optimization studies are the mass spectrometry imaging (MSI) methods that have become available in the last 15 years due to improvements in MS sensitivity and ionization methods. The most widely used approach is the MALDI MSI approach in which a tissue slice from a drug treated animal is sprayed with MALDI matrix and then raster imaged using a laser beam to produce ions which are analyzed

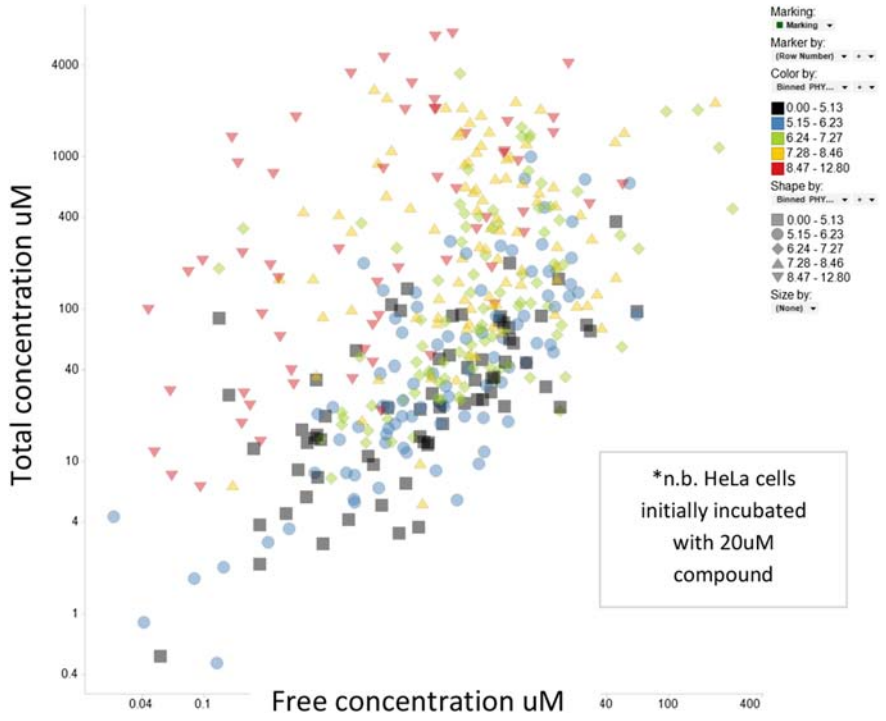

Fig. 6 Plot of total versus free concentration of compounds of multiple chemotypes in the GSK HeLa cell concentration assay.

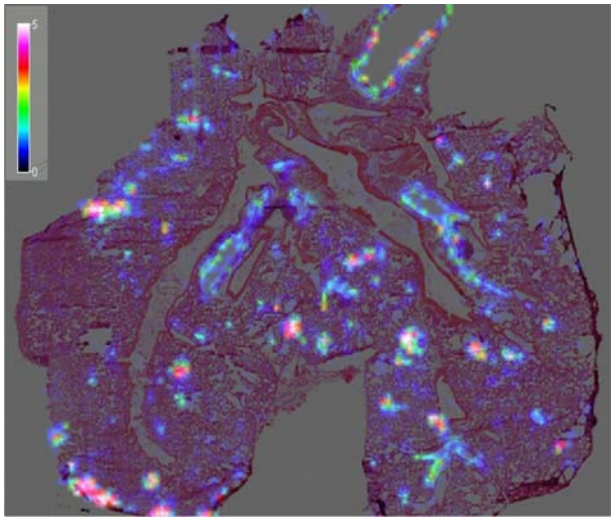

Fig. 7 MALDI MS imaging of drug distribution of an inhaled drug in rat coregistered with histology H&E image showing drug distributed predominantly in the airways. Image courtesy of Peter Marshall, GSK Stevenage.

in either TOF, TOF–TOF, or Fourier Transform Ion Cyclotron Resonance (FTICR) MS instruments.[43] This enables specific ion detection at increasingly high-mass resolution to provide spatial mapping of drugs, metabolites, and endogenous molecules (see **Fig. 7**).

While MS sensitivity continues to improve thus lowering the limits of detection, ion suppression by endogenous compounds (particularly lipids) remains a problem.[44] The alternative ionization method of desorption electrospray ionization is also being developed for MSI of tissue slices.[45] Relying on charged droplets for the ionization process, the spatial resolution is currently limited by droplet size production to around 50 μm. The spatial resolution of MALDI MSI is limited to around 5–10 μm by the size of the matrix crystals formed and lateral diffusion of compounds into them, thus limiting resolution to approximately cellular resolution. While this is at least as good as QWBA, neither method is able to achieve cellular or subcellular resolution. To address this limitation, SIMS imaging methods are being developed for application to biological samples (both tissue slices[46] and single cells[47]), allowing spatial resolution down to 100 nm. Moreover, 3D images can be generated by etching through the sample with ion beams. The next generation of SIMS instruments will undoubtedly reveal new insights into the spatial distribution of compounds within cells, hopefully down to suborganelle resolution.

A different approach to understanding compound disposition at high resolution has been the use of optical imaging methods. Intrinsically fluorescent compounds can be tracked by fluorescence microscopy at sub-micron resolution. However, most drug molecules are not fluorescent. For proteins the addition of a fluorescent tag can be considered to have minimal effect on its properties, enabling, for example, super resolution microscopy to track protein–protein interactions (PPIs) in real time.[48] However, the challenge of faithfully tracking small drug-like molecules is far greater because addition of even a small fluorescent ligand such as Bodipy adds a significant amount of chemical material to the drug, thus altering its likely distribution and other properties. An alternative approach, termed biorthogonal chemistry by Sletten and Bertozzi,[49] is to incorporate an even smaller moiety on the drug molecule which can subsequently be chemically linked within cells to a separately introduced fluorescent tag using, for example, the tetrazine and *trans*-cyclooctene Cu-free click reactions.[50] However, even this elegant approach cannot guarantee that the distribution of the unlabeled and labeled drug molecule is the same. Competition experiments with unlabeled drug can however be used to help in the correct interpretation of such experiments.[51] With some types of microscopy, the change in the fluorescence life time or correlation time on ligand binding to macromolecule can be deconvoluted and studies using unlabeled drug to compete with labeled ligand give a better indication of compound disposition and even target engagement.[52] Raman spectroscopy methods are capable of imaging unlabeled compounds provided there is a functional group in the drug which is Raman active at a frequency distinct from those found in endogenous compounds. Groups such as nitriles, alkynes, halo, or deutero are possible moieties of interest. One of the major challenges with Raman is an intrinsic lack of sensitivity, but multiphoton enhancement techniques such as coherent anti-Stokes Raman spectroscopy show promise for tracking species at high concentrations such as lipids. The related stimulated Raman spectroscopy method does have greater sensitivity but still fails to reach the micro- and submicro-molar concentration of drugs that will be required to be truly transformational as a technique.[53]

The discussion in this section has so far considered drug disposition from the perspective of the free drug hypothesis, which is generally considered to be reliant on passive diffusion, without reference to the contribution that transporters play in moving drugs across membranes in either direction. It has been understood for many years that drugs can be facilitated in their movements into and out of cells by channel and carrier proteins which can be important determinants governing ultimate drug absorption into target organs and their excretion. Alterations in these transporter functions, either due to genetic polymorphisms, drug–drug interactions (DDIs), or external factors (e.g., diet), can result in unexpected toxicity or lack of efficacy.[54] This may be due to the interplay between uptake and efflux transporters leading to pronounced in vivo variability in drug disposition of certain drugs between

individuals. Thus it is important to understand as early as possible in drug discovery if these problems exist; many drug discovery projects have had to be terminated or seriously delayed by issues related to lack of understanding or resolution of the role of transporters in a compound's ADMET profile. With the advent of technologies for creating transporter knockouts or by the use of inhibitors it has become easier to identify issues with compounds using for instance Caco-2 or Madin Darby canine kidney (MDCK) cell-based intestinal permeability assay. However the challenge of recognizing issues in lead optimization still suffers from a limited range of suitable tools and reagents for use in these early stages of discovery. There are also conflicting opinions about the importance of transporters in drug disposition which will require further rigorous experimentation on cell lines with specific transporter knockouts.[55,56] Drugs that rely on transporters for access to the site of action as opposed to passive diffusion are not only subject to the vagaries of genetic differences, DDIs, and dietary effects, but there is the added challenge that for antiinfectives (and likely oncology drugs) mutations may lead to resistance. A recent review of how antimalarial drugs reach their intracellular targets highlights the importance of this and how passive diffusion across a minimum of three membranes is actually achieved by most antimalarials.[57]

Barton and Riley have attempted to incorporate the effects of transporters into a decision tree to understand the compound risk.[58] They do so by introducing the effects of polar surface area into the widely-cited lipophilic ligand efficiency index of Leeson and Springthorpe.[5] As can be seen from the flowchart in Fig. 8, this results in another efficiency index termed the ADMET efficiency index (AEI) which is defined as $AEI = (pActivity - \log P) \times 100/PSA$ and is in effect LLE normalized by polar surface area which is introduced to characterize the effects of transporters. The flow chart in Fig. 8 enables potential issues with a compound (or series of compounds) to be flagged in early lead optimization so that any risks identified can be mitigated by appropriate follow-up experiments.

The challenges of dealing with both the upsides and downsides of transporters have led the International Transporter Consortium, a collective of academic, industrial, and regulatory scientists, which aims to provide guidance on current thinking on drug transporters with a particular focus on clinical relevance. This guidance is similarly based on decision trees which can be used to assess the potential risks of drug interactions. While generic decision trees such as these can help, it is clear that a customized strategy must be built for each clinical drug candidate to mitigate the risks. There is also a clear need for such understanding to be brought earlier into drug discovery where it is easier to change the molecule for an improved candidate.[59]

1.23.4 Target and Off-Target Engagement

Having obtained evidence that a candidate drug molecule is present at or in the vicinity of the target, the second pillar requires evidence of target engagement. It is also important to consider the potential for off-target engagement which may lead to toxicity. Evidence that

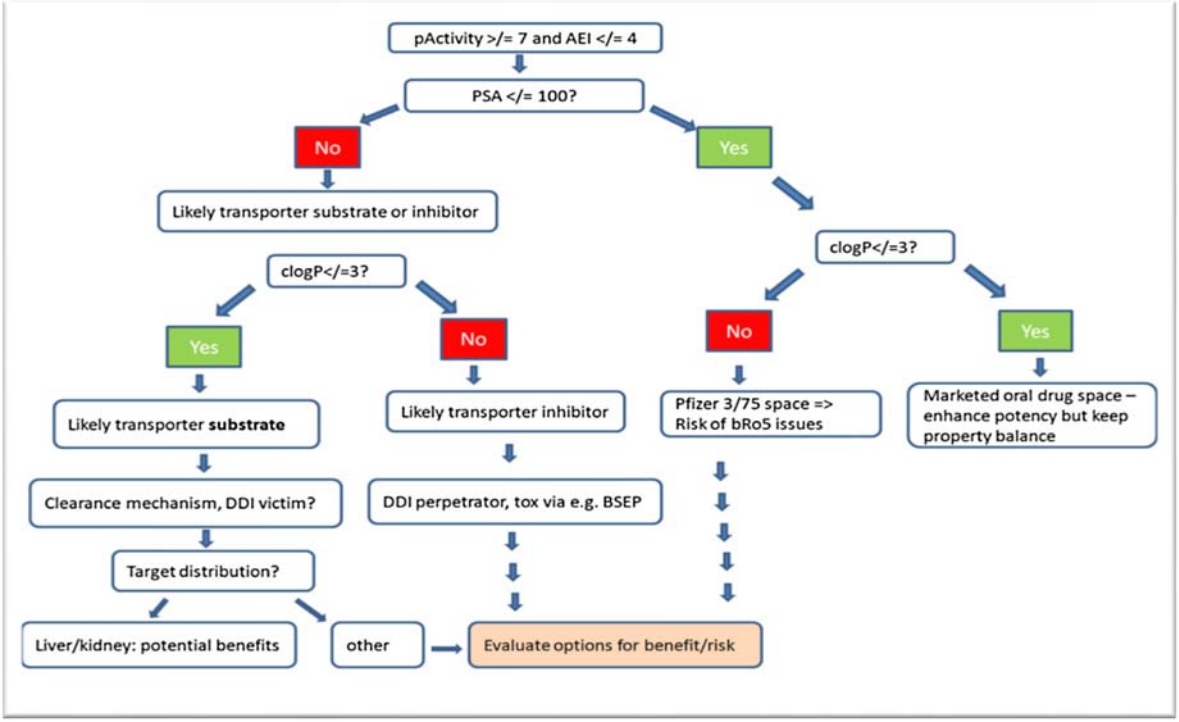

Fig. 8 Decision tree for use of ADMET efficiency index (AEI) in alerting to potential transporter issues. Based on Barton, P.; Riley, R. J. *Drug Discov. Today* **2016**, *21*, 72–81.

the compound binds to the required target in cell free, biochemical, or biophysical assays will most likely have been used as part of the initial compound or compound series selection and subsequent potency optimization. However, demonstrating that the compound effectively engages the target in cells and then in vivo, firstly in animals and then in clinical studies, can be difficult. This is especially an issue if there is an unexpected drop or total loss of activity. Provided the compound has been shown to be present at the target, then the most obvious explanation must be that the target protein is somehow different to that which was used for biochemical studies (e.g., due to posttranslational modification—PTM) or there are differences in the concentration of cofactors or reactants (e.g., ATP). Bunnage et al. have cataloged both target and compound related issues relevant to this pillar as summarized here.[60]

Target related issues

- Subcellular distribution of target may be different to that anticipated from transcriptomic or proteomic studies due to translocation or compartmentalization into organelles.
- Target exists as isoforms, splice variants, or PTMs which may also differ in different species or tissues.
- Endogenous ligand concentration or interaction in disease state may be different to that in healthy tissue.
- The target protein may be part of a larger complex in vivo which modulates its behavior in a different way to how the protein expressed for biochemical experiments behaves.
- The pharmacodynamic effect of a covalent or degradation promoting drug will be influenced by the resynthesis rate of the target and this rate may be variable in different situations.
- Target abundance data derived from transcriptomic and proteomic data can be very different.
- Closely related off-target proteins may be key determinants of selectivity.

Compound related issues

- What targets and off-targets does the compound bind to and what efficacy or toxicity consequence does each have?
- Understanding required target occupancy sets expectations about potency and likely efficacious drug concentration required.
- Characterization of binding kinetics can aid in understanding of pharmacodynamics.

Early signs of off-target engagement can be recognized by profiling compounds of interest in a panel of in vitro safety-related drug attrition assays. Such methods for in vitro pharmacological profiling have recently been reviewed using experiences from four major pharmaceutical companies (AstraZeneca, GlaxoSmithKline, Novartis, and Pfizer) with the conclusion that the use of a minimal core panel of <60 targets can reduce safety-related attrition of drug molecules during drug discovery.[61] Assays focussed on whole cell or organism phenotypic assays can also be used, but these will likely need target deconvolution to determine the specific off-targets. Traditionally, this has been a challenging task, but a number of significant new technologies have been recently introduced which can help to deconvolute the results from phenotypic assays and provide evidence of target engagement (for both "on" targets and "off" targets) through direct observation rather than relying on downstream intrinsic or engineered pharmacology readouts. Phenotypic screening has seen a resurgence of interest in recent years, prompted in part by the analysis of Swinney and Anthony which showed that first in class drugs have historically been discovered more often through phenotypic screening than through target-based approaches.[62] This conclusion has been challenged by more recent work from Eder et al. which takes into account the lag time in drug discovery whereby the impact of target-based approaches is only recently being seen.[63] With this current renewed interest in using phenotypic screening to source new points of effective intervention in pathways and molecules that can affect this, it is vital that appropriate cell-based assays are set up. Useful guidance on the value of getting the right stimulus, cell/tissue type, and readout to ensure the most faithful reproduction of the disease situation has been provided by Vincent et al.[64] Designing assays with an endogenous stimulus using relevant human disease cells/tissue without over engineering the readout so that the assay is still fit for purpose in high-throughput screening is considered the pinnacle of design.

Techniques that are now routinely used to deconvolute points of intervention on biological pathways include pull-down experiments where compounds of interest are immobilized on solid support (e.g., with kinobeads[65]) and used to identify proteins from lysates. Stable Isotope Labelleing with Amino acids in Culture (SILAC)[66] or isobaric Tags for Relative and Absolute Quantification. (iTRAQ)[67] enhanced mass spectrometry methods enable such studies to be performed at a proteome-wide scale. Such approaches are even more powerful when combined with whole genome sequencing[68] and functional genomics.[69] The ever-increasing sensitivity of modern mass spectrometry now enables unbiased open proteomics[70] and similar technical advances in genomic sequencing down to, for example, single molecule and single cell levels,[71] continue to enhance capabilities in these areas for target deconvolution. The complementary use of shRNA-based gene knock out, suppression, or overexpression techniques is also now being widely used to confirm the significance of the deconvoluted targets. The advent of gene editing methods such as Zinc fingers, Talens, and CRISPR-Cas9 continues to bring increasingly powerful and specific tools to the armory for target engagement and identification studies.[72]

For situations where the target is known and confirmation of effective target engagement is required, a number of recently introduced protocols may help. These rely on compound-induced stabilization of the target protein inside living cells. Such compound-induced stabilization protects the protein from aggregation; the stabilization is detected by having preengineered the protein to provide a readout of the amount of protein remaining in solution. Two such methods are fragment complementation using β-galactosidase (InCell Hunter technology) or time-resolved fluorescence resonance energy transfer using affinity-tagged proteins (NanoLuc technology) and they have both been effectively used to show target engagement in bromodomain studies.[73,74]

A more recent approach to the problem of demonstrating target engagement in cellular or in vivo systems is the cellular thermal shift assay (CETSA) pioneered by Nordlund's group[75] (see **Fig. 9**). Again, this relies on ligand-induced stabilization against thermal

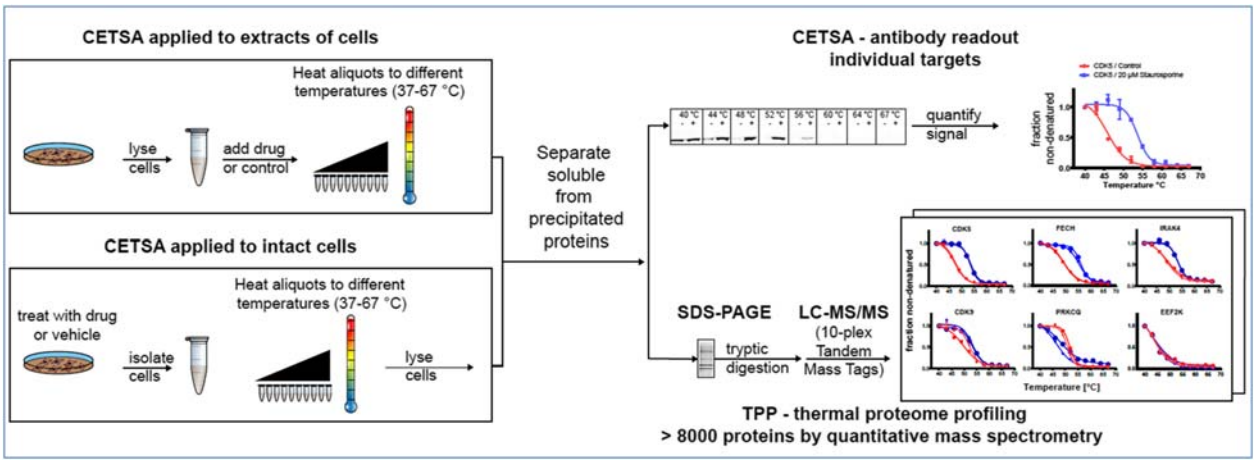

Fig. 9 Cellular thermal shift assay (CETSA) and thermal proteome profiling (TPP) modalities. Figure courtesy of Friedrich Reinhard, GSK Cellzome, Heidelberg.

denaturation but does not require protein engineering to introduce a label onto the target protein of interest. Instead the stabilized protein that remains in solution at different temperatures is monitored with a western blot readout, so all that is required is a high affinity and specific antibody for the protein of interest to enable a readout of the melting temperature (T_m) of the protein. Such assays can either be run at several temperatures and constant ligand concentration or at a selected elevated temperature with increasing ligand concentration so as to get a more classical dose response curve. However, as with all T_m-based assays, the experiment is performed on systems that are not at equilibrium and thus it is not easy to get a true binding affinity.

The use of the antibody readout for CETSA limits the experiment to a specific predefined protein, but this limitation can be addressed through the use of mass spectrometry-based proteomic studies and the thermal proteome profiling (TPP)[76] approach. In TPP, no cell engineering is required and thermal profiles for up to 7000 proteins in their native cellular environment can be performed to identify the direct targets of compounds in cells or homogenates, as well as downstream effectors. Huber et al. used the TPP method to profile targets of the drugs methotrexate and (*S*)-crizotinib and the metabolite 2′3′-cGAMP; in the latter case, they identified the 2′3′-cGAMP cognate transmembrane receptor STING which is involved in immune signaling.[77] The power of the method for identifying off-target engagement is illustrated in a study by Klaeger et al. which revealed ferrochelatase as a common off-target of kinase inhibitors.[78] The main limitation of the CETSA and TPP approaches is that not all interacting ligands cause stabilization (or destabilization, which can also be detected) so there will likely be false negatives in these unbiased/open proteomic studies. This may be ameliorated if downstream stabilization of a protein in a biological pathway occurs, so indicating that the compound engages somewhere in the pathway. A current limitation is that membrane-bound proteins, and possibly those in larger complexes, are often difficult to study as the method relies on aggregation of unstabilized protein followed by subsequent detection of that remaining. This may not occur in membrane systems, which serve to keep the protein folded in the first place. This limitation is likely to be overcome by further development of the protocols for handling membrane-bound targets.[79]

1.23.5 Pharmacokinetics and Pharmacodynamics

The third pillar focuses on the lack of efficacy which is all too often the cause of failure in Phase II trials. While historically, drug metabolism and pharmacokinetic properties have been cited as the reasons that oral compounds fail and have been the subject of several reviews,[80–82] more recent studies have shown that the survival of new molecular entities is now more significantly impacted by insufficient or lack of clinical efficacy in Phases II and III.[83] These authors also indicated that the attrition due to lack of efficacy in Phase II was higher in the 2011–12 analysis verses a previous analysis in 2008–10. A lack of biological efficacy continues to be a root cause of attrition in Phase II as highlighted in the publications by Hay et al.[84] as well as the studies from the Pfizer and AstraZeneca groups already summarized earlier.

Human dose prediction has been recognized as an important parameter in molecule selection.[85] The consequent recent emphasis on earlier effective dose prediction prior to selecting a candidate molecule has prompted an improved understanding of the balance of a molecule's intrinsic potency, pharmacokinetic, pharmacodynamic, and toxicological properties and how such properties can be predicted.

A great deal of effort has been focused on accurate methods for predicting human pharmacokinetic parameters including clearance and scaling from animal exposure data, with varying levels of accuracy.[86] These methods can be described as:

1. allometry-related methods and include simple allometric scaling in a single species such as rat, dog, and or monkey or in multiple species, scaling corrected by various factors such as life span, intrinsic clearance, and/or plasma protein binding;

2. methods that focus on in vitro hepatic clearance, for example, the well-stirred model; and
3. physiologically based pharmacokinetic (PBPK) prediction methods using both in vitro and in vivo data.

These methods have been the subject of review articles and regulatory guidance. The FDA guidance on first human dose does not explicitly mention pharmacokinetic prediction but recommends a human dose estimation method which is consistent with single species allometry and assumes the same bioavailability between human and the nonhuman species. Allometry, a method that has been used routinely for many years for human pharmacokinetic prediction, has been explored retrospectively using 50 compounds for which it was shown that using a single species approach was as accurate or more accurate than using multi-species allometry.[87] However, work from Goteti et al. evaluating 45 different compounds contradicted this finding, suggesting that two species scaling is useful for prediction purposes and that the prediction of clearance from three species was far more accurate than two species scaling.[88] Yet others have indicated that the prediction from allometry suffers from a lack of predictive power.[89] In practice, since monkey data are now not routinely generated for small molecule compounds, only two species are usually available for prediction, which makes the allometry approach challenging.

More mechanistic methods, such as PBPK, have been suggested to perform no better than allometry in accurately predicting human pharmacokinetics.[90] PBPK estimate the dose required at the target tissue by taking into account the rate of absorption into the body, the distribution and retention in tissues, the metabolism and excretion of the compound based on the relationship between physiological, physicochemical, and biochemical parameters and is required to provide insights to PK and pharmacokinetic and pharmacodynamics modeling (PKPD) when a target is located in a tissue. The application in drug discovery has been reviewed.[91] The use of PKPB in regulatory submissions to support dose selections has also been explored[92,93] and in addition the value of PBPK in designing clinical studies has been reviewed.[91] However, these pharmacokinetic-based methods do not take into account the pharmacology of the compound when determining the initial dose, which is an essential consideration when progressing to the clinic. More recently human dose prediction has been recognized as an important parameter in molecule selection in the early stages of drug discovery.[85] These authors validated a method to predict human dose and free C_{max} for a number of molecules using in vitro data and predicted parameters which were incorporated into a pharmacokinetic model. The authors further developed the work of McGinty et al. who were able to predict clinical doses taking into account all parameters contributing to human pharmacokinetics; clearance, volume of distribution, protein binding (fraction unbound), bioavailability, and dosing interval assuming that efficacy would be observed if unbound plasma concentrations exceed an in vitro measure of potency.[94] This work relies on the use of in vitro intrinsic clearance data produced in vitro using human tissue and has been supported by other workers.[87,95,96] However, the work of McGinty et al. includes the use of in vivo preclinical data. Page et al. enhanced and developed the dose prediction methodology of McGinty et al. without the use of in vivo data so that it could be reliably used in the early stages of drug discovery to select compounds for progression earlier.[85] These authors were able to produce a reliable human dose prediction across a wide range of chemistry with the use of in vitro data and QSAR-predicted parameters. One of the challenges of the approach of Page and colleagues is the use of human tissues. A recent survey highlighted a number of challenges to a wider uptake, including regulatory barriers, supply issues, practical, and scientific barriers.[97] However to aid in chemical design and influence early drug discovery, the use of in vitro approaches will be key. In addition these in vitro approaches have limits when exploring low clearance compounds which will require further work.[98] Nevertheless, the approaches defined by McGinty and Page represent significant progress. The science of human pharmacokinetic predictions has continued to develop but at times has been limited by the fact that we are unable to discriminate between closely related compounds, that additional preclinical data adds no further value to the prediction, and that the quest for potency associated with novel targets pushes the physicochemical properties to a challenging space where human pharmacokinetic properties are difficult to assess. These challenges make prediction of human parameters open to challenge and to address these challenges alternative strategies such as microdosing using subpharmacological doses can be considered.

The term microdosing refers to a pharmacokinetic study where the dose is administered at a subpharmacological level and where the focus is predominately on analysis of pharmacokinetic parameters.[99] This approach requires a dose of either 1/100th of the known active dose or < 100 μg total dose and therefore requires a reduced toxicology package comprising a single dose in the rodent via the clinical route of administration for progression. If the total dose is < 500 μg, then a 7-day rodent study is required administering the dose via the clinical route. The requirements for these exploratory clinical studies are detailed in the International Conference on Harmonisation (ICH) guidance documentation.[100] A key advantage of microdosing studies is that they enable early evaluation of candidate molecules when the preclinical data in animal species is conflicting, leading to wide variability in human pharmacokinetic predictions and therefore the best approach is to understand the outcome in human. Additional advantages include less animal use, less drug requirements, and less time to acquire human data. The endpoints following an intravenous dose are clearance, volume, and half-life and following an oral dose the absolute bioavailability can be determined when combined with intravenous dosing. However, when to use this approach has attracted some discussion as the key assumption of microdosing is that the pharmacokinetic parameters determined using the microdosing approach are predictive of the pharmacokinetics of the efficacious dose.[101] Work by Rowland indicates that the number of microdose studies has increased significantly between 2002 and 2011, the rationale for this being the lack of success of approaches such as allometry and PBPK to predict human pharmacokinetics from preclinical and in vitro data.[102] There has also been some debate on the additional cost and time required to complete the microdose studies before completing the full regulatory package for a first time in human study. Furthermore, data from Bosgra et al. showed that nonlinear kinetics between an efficacious dose and a microdose could be anticipated from preclinical data. These authors also presented a strategy that could be utilized in the decision to progress with a microdose study as part of the development

of a drug candidate.[101] The improvement in analytical technologies such as liquid chromatography coupled with tandem mass spectrometry (LC MS-MS) and accelerated mass spectrometry (AMS) may provide the tools which could enhance the use of microdosing although the AMS approach would require the use of trace amounts of a ^{14}C radio isotope-labeled compound.[103]

The need to improve our understanding of the drivers of efficacy has been highlighted as key to advancing drug discovery. PKPD and simulation is an important tool in understanding the efficacy of a molecule earlier within the drug discovery process.[104] PKPD analysis quantitatively interrelates drug behavior and its effects on the biological systems using mathematical functions. Mechanism-based PKPD modeling allows the quantitative analysis of identified species differences in factors such as pharmacokinetics or in vivo efficacy studies, enabling the relationship of concentration to a pharmacodynamic effect from often variable in vivo preclinical efficacy data. Recently, there have been several examples published outlining the use of PKPD analysis to translate findings in preclinical experiments to the human situation.[105–108] Ultimately the development of PKPD models enables integration of all available data to develop a prospective simulation. As described previously, the early assessment of pharmacokinetics has been shown to reduce attrition due to poor or in appropriate pharmacokinetics[80–82] an improved understanding of drug effect using preclinical PKPD analysis offers an important tool to potentially reduce attrition due to a lack of efficacy.[23,25] Schuck et al. completed a survey of the pharmaceutical industry members of the International Consortium for Quality and Innovation in Pharmaceutical development and showed that the majority of pharma companies in the group used preclinical PKPD in all therapy areas and an important goal was the selection and optimization of doses and dose regimens including the prediction of efficacious human doses.[104] These authors highlighted oncology as one therapeutic area where PKPD had a major impact; most companies had observed an impact of the preclinical PKPD analysis; and preclinical PKPD analysis was increasingly used in regulatory submissions. The authors also reported that there was an opportunity for PKPD modeling to impact future drug discovery and development. Furthermore, an opportunity exists to incorporate the consistent use of systems pharmacology and physiologically based PK models with PKPD modeling.

An additional strategy to the approaches to reduce late-stage efficacy failures outlined earlier is to consider the impact of biomarkers of both efficacy and safety. The strategy is to identify a biomarker or biomarkers that can be objectively measured and evaluated as an indicator of a change in a biological process in response to a drug intervention. A biomarker is defined as "a characteristic that is objectively measured and evaluated as an indicator of normal biologic processes, pathogenic processes, or pharmacologic responses to a therapeutic intervention."[109] Once validated, a biomarker can play a key role in disease diagnosis, the prediction of disease progression, and the monitoring of a response following drug intervention. The use of biomarkers is recommended by regulators in the development of a chemical entity and is also a key focus of the Strategic Research agenda for the European Union Innovative Medicine Initiative. The use of biomarkers has been the subject of an extensive review.[110] Further work to assess the next generation of biomarkers has been described by Caberlotto and Lauria.[111] These authors suggest that biomarkers and companion diagnostics will require technologies that are able to integrate the advances in high-throughput biology in the field of –omic technologies such as genomics, proteomics, metabolomics, and transcriptomics. This approach will help to further reduce failure and enhance access to personalized medicine for patients.

1.23.6 Target Choices

Target choice is fundamental to the likely outcome of a drug discovery program. The prospect of improved understanding of the translatability of a hypothesis into a drug is being driven by the deeper understanding of genetic linkage of diseases to targets and pathways, and this can be referred to as improved biological tractability of a target.[112] However this is not sufficient to guarantee success, because the ligandability of the target is equally important. Ligandability is the likelihood that a drug-like molecule can be found to effectively engage with the target to illicit the biological response needed. Both chemical and biological tractability of a target are therefore essential.

Historically, many drugs have been targeted at proteins that can be accessed extracellularly and when their 3D structures are examined it is often found that the binding sites are amenable to small, Lipinski-compliant Ro5 small molecules. As the history of drug discovery has shown, this region of chemical space is also compatible with the properties required for traditional once or twice a day oral delivery. Clearly there are many effective nonoral drugs, though a high proportion of these are for extracellular targets. However, there is increased interest in intracellular proteins as potential targets and in particular those involved in PPIs. Many PPIs are considered to have low chemical tractability because they are intractable to traditional Lipinski-compliant small molecules. Doak et al., using X-ray structural information, have analyzed the properties of complexes to understand more about the nature of binding sites for bRo5 molecules compared to Ro5 compliant molecules.[113] Not surprisingly, larger molecules (e.g., macrocycles) have lower local curvature and thus will have higher contact area which allows them to bind to flat sites. Analyses by the Morelli[114] and Blundell[115] groups have confirmed these types of findings from PPI inhibitor databases (e.g., 2P2I, TIMBAL) which include a wider range of nonclinical molecules. PPI-disrupting interacting small molecules (where they can be found) are generally larger, have more sp3 character, and are more lipophilic than non-PPI-interacting compounds.

The challenge of finding drug-like ligands for difficult targets raises the question of whether such targets should be considered ligandable and ultimately "druggable" in the first place. The genomic revolution is leading to a rapidly growing body of biological and disease knowledge, but some of the best biologically and genetically validated targets (e.g., PCSK9) are proving intractable to small molecule intervention. In the case of PCSK9, of course, whose binding to the Low Density Lipoprotein (LDL) receptor is an extracellular event, then intervention by injected antibodies is proving an effective strategy.[116] Understanding as early as possible the

likely tractability of an intracellular target to small molecule intervention can be used to help reduce attrition due to failure in hit generation. Methods for assessing the ligandability of a target by either experimental methods such as fragment screening[117] or in silico[118] analysis are important tools for carrying out such assessments.

With such a high level of attrition prevalent in drug discovery, it can often appear that there is a significant amount of luck associated with the small proportion of projects that are ultimately successful in bringing a new drug to patients. While serendipity often does play a role, it is also true that "chance favors the prepared mind." Put another way, improving the odds of success by exploring fully the most statistically likely approaches first is surely the most fruitful approach to adopt for improving return on investment in the pharmaceutical industry. However, the desire for novelty in new therapeutics and technologies, almost by definition, drives us to the unknown regions of science where low probability of success is unfortunately intrinsically too often the norm until sufficient experience is gained. However while new biology opportunities continue to unfold, it is essential that quality and rigorous methods of drug discovery are applied if low probabilities of success are going to deliver anything. We hope that this article has helped to ensure that the learnings of the recent years continue to be valued and applied as we enter into an era of renewed hope in turning the advances in basic biology and understanding into, efficacious and affordable new drugs.

Acknowledgments

We would like to thank the many GSK and other pharma and academic colleagues who have contributed to the ideas that we have set out to express in this article. In particular we thank Peter Marshall, Andy West, Andy Harrell, Friedrich Reinhard, Valeriu Damian, and Anthony Taylor for help with diagrams and thoughtful input.

References

1. Paul, S. M.; Mytelka, D. S.; Dunwiddie, C. T.; Persinger, C. C.; Munos, B. H.; Lindborg, S. R.; Schacht, A. L. *Nat. Rev. Drug Discov.* **2010,** *9* (3), 203–214.
2. Lipinski, C. A.; Lombardo, F.; Dominy, B. W.; Feeney, P. J. *Adv. Drug Deliv. Rev.* **1997,** *23,* 3–25.
3. Wenlock, M. C.; Austin, R. P.; Barton, P.; Davis, A. M.; Leeson, P. D. *J. Med. Chem.* **2003,** *46* (7), 1250–1256.
4. Hann, M. M. In *Introduction: Learnings From the Past—Characteristics of Successful Leads;* Holenz, J., Ed.; Wiley-VCH: Weinheim, 2016.
5. Leeson, P. D.; Springthorpe, B. *Nat. Rev. Drug Discov.* **2007,** *6* (11), 881–890.
6. Hughes, J. D.; Blagg, J.; Price, D. A.; Bailey, S.; DeCrescenzo, G. A.; Devraj, R. V.; Ellsworth, E.; Fobian, Y. M.; Gibbs, M. E.; Gilles, R. W.; Greene, N.; Huang, E.; Krieger-Burke, T.; Loesel, J.; Wager, T.; Whiteley, L.; Zhang, Y. *Bioorg. Med. Chem. Lett.* **2008,** *18* (17), 4872–4875.
7. Gleeson, M. P. *J. Med. Chem.* **2008,** *51* (4), 817–834.
8. Waring, M. J. *Bioorg. Med. Chem. Lett.* **2009,** *19* (10), 2844–2851.
9. Young, R. J.; Green, D. V. S.; Luscombe, C. N.; Hill, A. P. *Drug Discov. Today* **2015,** *16* (17–18), 822–830.
10. Wager, T. T.; Kormos, B. L.; Brady, J. T.; Will, Y.; Aleo, M. D.; Stedman, D. B.; Kuhn, M.; Chandrasekaran, R. Y. *J. Med. Chem.* **2013,** *56* (23), 9771–9779.
11. Butler, J. M.; Dressman, J. B. *J. Pharm. Sci.* **2010,** *99* (12), 4940–4954.
12. Hann, M. M. *Med. Chem. Commun.* **2011,** *2,* 349.
13. Olsson, T. S. G.; Williams, M. A.; Pitt, W. R.; Ladbury, J. E. *J. Mol. Biol.* **2008,** *384* (4), 1002–1017.
14. Hann, M. M.; Keserü, G. M. *Nat. Rev. Drug Discov.* **2012,** *11* (5), 355–365.
15. Waring, M. J. *Expert Opin. Drug Discov.* **2010,** *5* (3), 235–248.
16. Nadin, A.; Hattotuwagama, C.; Churcher, I. *Angew. Chem. Int. Ed.* **2012,** *51,* 1114–1122.
17. Bickerton, G. R.; Paolini, G. V.; Besnard, J.; Muresan, S.; Hopkins, A. L. *Nat. Chem.* **2012,** *4* (2), 90–98.
18. Doak, B. C.; Over, B.; Giordanetto, F.; Kihlberg, J. *Chem. Biol.* **2014,** *21* (9), 1115–1142.
19. Ritchie, T. J.; Macdonald, S. J. F. *Drug Discov. Today* **2014,** *19* (4), 489–495.
20. Bayliss, M. K.; Butler, J.; Feldman, P. L.; Green, D. V. S.; Leeson, P. D.; Palovich, M. R.; Taylor, A. J. *Drug Discov. Today* **2016**.
21. Horter, D.; Dressman, J. B. *Adv. Drug Deliv. Rev.* **1997,** *25* (1), 3–14.
22. Top 100 drugs—Internet Drug IndexIndex, Internet Drug https://www.drugs.com/stats/top100/2012/sales.
23. Waring, M. J.; Arrowsmith, J.; Leach, A. R.; Leeson, P. D.; Mandrell, S.; Owen, R. M.; Pairaudeau, G.; Pennie, W. D.; Pickett, S. D.; Wang, J.; Wallace, O.; Weir, A. *Nat. Rev. Drug Discov.* **2015,** *14* (7), 475–486.
24. Morgan, P.; Van Der Graaf, P. H.; Arrowsmith, J.; Feltner, D. E.; Drummond, K. S.; Wegner, C. D.; Street, S. D. A. *Drug Discov. Today* **2012,** *17,* 419–424.
25. Bunnage, M. E.; Chekler, E. L. P.; Jones, L. H. *Nat. Chem. Biol.* **2013,** *9* (4), 195–199.
26. Cook, D.; Brown, D.; Alexander, R.; March, R.; Morgan, P.; Satterthwaite, G.; Pangalos, M. N. *Nat. Rev. Drug Discov.* **2014,** *13* (6), 419–431.
27. Leeson, P. D.; St-Gallay, S. A. *Nat. Rev. Drug Discov.* **2011,** *10* (10), 749–765.
28. Harrell, A. W.; Sychterz, C.; Ho, M. Y.; Weber, A.; Valko, K.; Negash, K. *Pharmacol. Res. Perspect.* **2015,** *3* (5), 1–12.
29. Smith, D. A.; Di, L.; Kerns, E. H. *Nat. Rev. Drug Discov.* **2010,** *9,* 929–939.
30. Jack, D. *Drug Des. Deliv.* **1989,** *4* (3), 167–186.
31. Hann, M. M.; Simpson, G. L. *Methods* **2014,** *68* (2), 283–285.
32. Hansch, C. *Acc. Chem. Res.* **1969,** *2* (8), 232–239.
33. Martin, Y. C. *Wiley Interdiscip. Rev. Comput. Mol. Sci.* **2012,** *2* (3), 435–442.
34. Braggio, S.; Montanari, D.; Rossi, T.; Ratti, E. *Expert Opin. Drug Discov.* **2010,** *5* (March), 609–618.
35. Montanari, D.; Chiarparin, E.; Gleeson, M. P.; Braggio, S.; Longhi, R.; Valko, K.; Rossi, T. *Expert Opin. Drug Discov.* **2011,** *6* (9), 913–920.
36. Gleeson, M. P.; Hersey, A.; Montanari, D.; Overington, J. *Nat. Rev. Drug Discov.* **2011,** *10* (3), 197–208.
37. Valko, K.; Chiarparin, E.; Nunhuck, S.; Montanari, D. *J. Pharm. Sci.* **2012,** *101* (11), 4155–4169.
38. Valkó, K. L.; Nunhuck, S. B.; Hill, A. P. *J. Pharm. Sci.* **2011,** *100* (3), 849–862.
39. Mateus, A.; Matsson, P.; Artursson, P. *Mol. Pharm.* **2013,** *10,* 2467–2478.
40. Gordon, L. J.; Allen, M.; Artursson, P.; Hann, M. M.; Leavens, B. J.; Mateus, A.; Readshaw, S.; Valko, K.; Wayne, G. J.; West, A. *J. Biomol. Screen.* **2015,** *21,* 1–9.
41. Wenlock, M. C. *Med. Chem. Commun.* **2016,** *7,* 706–719.

42. Uetrecht, J. *Annu. Rev. Pharmacol. Toxicol.* **2007,** *47,* 513–539.
43. Castellino, S.; Groseclose, M. R.; Wagner, D. *Bioanalysis* **2011,** *3* (21), 2427–2441.
44. Tomlinson, L.; Fuchser, J.; Futterer, A.; Baumert, M.; Hassall, D. G.; West, A.; Marshall, P. S. *Rapid Commun. Mass Spectrom.* **2014,** *28* (9), 995–1003.
45. Swales, J. G.; Tucker, J. W.; Strittmatter, N.; Nilsson, A.; Cobice, D.; Clench, M. R.; Mackay, C. L.; Andren, P. E.; Takats, Z.; Webborn, P. J. H.; Goodwin, R. J. A. *Anal. Chem.* **2014,** *86* (16), 8473–8480.
46. Carado, A.; Kozole, J.; Passarelli, M.; Winograd, N.; Loboda, A.; Bunch, J.; Wingate, J.; Hankin, J.; Murphy, R. *Appl. Surf. Sci.* **2008,** *255* (4), 1572–1575.
47. Passarelli, M. K.; Newman, C. F.; Marshall, P. S.; West, A.; Gilmore, I. S.; Bunch, J.; Alexander, M. R.; Dollery, C. T. *Anal. Chem.* **2015,** *87* (13), 6696–6702.
48. Liu, Z.; Xing, D.; Su, Q. P.; Zhu, Y.; Zhang, J.; Kong, X.; Xue, B.; Wang, S.; Sun, H.; Tao, Y.; Sun, Y. *Nat. Commun.* **2016,** *21,* 72–81.
49. Sletten, E. M.; Bertozzi, C. R. *Angew. Chem. Int. Ed.* **2009,** *48,* 6974–6998.
50. Simon, G. M.; Niphakis, M. J.; Cravatt, B. F. *Nat. Chem. Biol.* **2013,** *9* (4), 200–205.
51. Rutkowska, A.; Thomson, D.; Vappiani, J.; Werner, T.; Mueller, K.; Dittus, L.; Krause, J.; Muelbaier, M.; Bergamini, G.; Bantscheff, M. *ACS Chem. Biol.* **2016.** http://dx.doi.org/10.1021/acschembio.6b00346.
52. Dubach, J. M.; Vinegoni, C.; Mazitschek, R.; Fumene Feruglio, P.; Cameron, L. A.; Weissleder, R. *Nat. Commun.* **2014,** *5* (May), 3946.
53. Saar, B. G.; Freudiger, C. W.; Reichman, J.; Stanley, C. M.; Holtom, G.; Xie, X. S. *Science* **2010,** *330* (6009), 1368–1370.
54. Zheng, X.; Diao, L.; Ekins, S.; Polli, J. E. *Biochem. Pharmacol.* **2010,** *80* (7), 1087–1092.
55. Sugano, K.; Kansy, M.; Artursson, P.; Avdeef, A.; Bendels, S.; Di, L.; Ecker, G. F.; Faller, B.; Fischer, H.; Gerebtzoff, G.; Lennernaes, H.; Senner, F. *Nat. Rev. Drug Discov.* **2010,** *9* (8), 597–614.
56. Kell, D. B.; Dobson, P. D.; Oliver, S. G. *Drug Discov. Today* **2011,** *16* (15–16), 704–714.
57. Basore, K.; Cheng, Y.; Kushwaha, A. K.; Nguyen, S. T.; Desai, S. A. *Front. Pharmacol.* **2015,** *6,* 91.
58. Barton, P.; Riley, R. J. *Drug Discov. Today* **2016,** *21,* 72–81.
59. Tweedie, D.; Polli, J. W.; Berglund, E. G.; Huang, S. M.; Zhang, L.; Poirier, A.; Chu, X.; Feng, B.; International Transporter Consortium. *Clin. Pharmacol. Ther.* **2013,** *94* (1), 113–125.
60. Bunnage, M. E.; Gilbert, A. M.; Jones, L. H.; Hett, E. C. *Nat. Chem. Biol.* **2015,** *11* (6), 368–372.
61. Bowes, J.; Brown, A. J.; Hamon, J.; Jarolimek, W.; Sridhar, A.; Waldron, G.; Whitebread, S. *Nat. Rev. Drug Discov.* **2012,** *11* (12), 909–922.
62. Swinney, D. C.; Anthony, J. *Nat. Rev. Drug Discov.* **2011,** *10* (7), 507–519.
63. Eder, J.; Sedrani, R.; Wiesmann, C. *Nat. Rev. Drug Discov.* **2014,** *13* (8), 577–587.
64. Vincent, F.; Loria, P.; Pregel, M.; Stanton, R.; Kitching, L.; Nocka, K.; Doyonnas, R.; Steppan, C.; Gilbert, A.; Schroeter, T.; Peakman, M. *Sci. Transl. Med.* **2015,** *7* (293), 293ps15.
65. Bantscheff, M.; Eberhard, D.; Abraham, Y.; Bastuck, S.; Boesche, M.; Hobson, S.; Mathieson, T.; Perrin, J.; Raida, M.; Rau, C.; Reader, V.; Sweetman, G.; Bauer, A.; Bouwmeester, T.; Hopf, C.; Kruse, U.; Neubauer, G.; Ramsden, N.; Rick, J.; Kuster, B.; Drewes, G. *Nat. Biotechnol.* **2007,** *25* (9), 1035–1044.
66. Ong, S.-E.; Schenone, M.; Margolin, A. A.; Li, X.; Do, K.; Doud, M. K.; Mani, D. R.; Kuai, L.; Wang, X.; Wood, J. L.; Tolliday, N. J.; Koehler, A. N.; Marcaurelle, L. A.; Golub, T. R.; Gould, R. J.; Schreiber, S. L.; Carr, S. A. *Proc. Natl. Acad. Sci. U. S. A.* **2009,** *106* (12), 4617–4622.
67. Ross, P. L.; Huang, Y. N.; Marchese, J. N.; Williamson, B.; Parker, K.; Hattan, S.; Khainovski, N.; Pillai, S.; Dey, S.; Daniels, S.; Purkayastha, S.; Juhasz, P.; Martin, S.; Bartlet-Jones, M.; He, F.; Jacobson, A.; Pappin, D. J. *Mol. Cell. Proteomics* **2004,** *3* (12), 1154–1169.
68. Roemer, T.; Davies, J.; Giaever, G.; Nislow, C. *Nat. Chem. Biol.* **2011,** *8* (1), 46–56.
69. Nijman, S. *Nat. Chem. Biol.* **2015,** *11* (12), 942–948.
70. Schirle, M.; Bantscheff, M.; Kuster, B. *Chem. Biol.* **2012,** *19* (1), 72–84.
71. Gawad, C.; Koh, W.; Quake, S. R. *Nat. Rev. Genet.* **2016,** *17* (3), 175–188.
72. Moore, J. D. *Drug Discov. Today* **2015,** *20* (4), 450–457.
73. Schulze, J.; Moosmayer, D.; Weiske, J.; Fernandez-Montalvan, A.; Herbst, C.; Jung, M.; Haendler, B.; Bader, B. *J. Biomol. Screen.* **2015,** *20* (2), 180–189.
74. Theodoulou, N. H.; Bamborough, P.; Bannister, A. J.; Becher, I.; Bit, R. A.; Che, K. H.; Chung, C.-W.; Dittmann, A.; Drewes, G.; Drewry, D. H.; Gordon, L.; Grandi, P.; Leveridge, M.; Lindon, M.; Michon, A.-M.; Molnar, J.; Robson, S. C.; Tomkinson, N. C. O.; Kouzarides, T.; Prinjha, R. K.; Humphreys, P. G. *J. Med. Chem.* **2015,** *15,* 1425–1439.
75. Molina, D. M.; Jafari, R.; Ignatushchenko, M.; Seki, T.; Larsson, E. A.; Dan, C.; Sreekumar, L.; Cao, Y.; Nordlund, P. *Science* **2013,** *341* (6141), 84–87.
76. Savitski, M. M.; Reinhard, F. B. M.; Franken, H.; Werner, T.; Savitski, M. F.; Eberhard, D.; Martinez Molina, D.; Jafari, R.; Dovega, R. B.; Klaeger, S.; Kuster, B.; Nordlund, P.; Bantscheff, M.; Drewes, G. *Science* **2014,** *346* (6205), 1255784.
77. Huber, K. V. M.; Olek, K. M.; Müller, A. C.; Tan, C. S. H.; Bennett, K. L.; Colinge, J.; Superti-Furga, G. *Nat. Methods* **2015,** *12* (11), 1055–1057.
78. Klaeger, S.; Gohlke, B.; Perrin, J.; Gupta, V.; Heinzlmeir, S.; Helm, D.; Qiao, H.; Bergamini, G.; Handa, H.; Savitski, M. M.; Bantscheff, M.; Médard, G.; Preissner, R.; Kuster, B. *ACS Chem. Biol.* **2016,** *11* (5), 1245–1254.
79. Reinhard, F. B. M.; Eberhard, D.; Werner, T.; Franken, H.; Childs, D.; Doce, C.; Savitski, M. F.; Huber, W.; Bantscheff, M.; Savitski, M. M.; Drewes, G. *Nat. Methods* **2015,** *12* (12), 1129–1131.
80. Prentis, R. A.; Lis, Y.; Walker, S. R. *Br. J. Clin. Pharmacol.* **1988,** *25* (3), 387–396.
81. Kola, I.; Landis, J. *Nat. Rev. Drug Discov.* **2004,** *3,* 711–715.
82. Summerfield, S.; Jeffrey, P. *Expert Opin. Drug Discov.* **2009,** *4* (3), 207–218.
83. Arrowsmith, J.; Miller, P. *Nat. Rev. Drug Discov.* **2013,** *12* (8), 569.
84. Hay, M.; Thomas, D. W.; Craighead, J. L.; Economides, C.; Rosenthal, J. *Nat. Biotechnol.* **2014,** *32* (1), 40–51.
85. Page, K. M. *Mol. Pharm.* **2016,** *13* (2), 609–620.
86. Beaumont, K.; Smith, D. A. *Curr. Opin. Drug Discov. Dev.* **2009,** *12* (1), 61–71.
87. Hosea, N. A.; Collard, W. T.; Cole, S.; Maurer, T. S.; Fang, R. X.; Jones, H.; Kakar, S. M.; Nakai, Y.; Smith, B. J.; Webster, R.; Beaumont, K. *J. Clin. Pharmacol.* **2009,** *49* (5), 513–533.
88. Goteti, K.; Edwin Garner, C.; Mahmood, I. *J. Pharm. Sci.* **2010,** *99* (3), 1601–1613.
89. Bonate, P. L.; Howard, D. *J. Clin. Pharmacol.* **2000,** *40,* 665–670. discussion 671–676.
90. Rowland, M.; Benet, L. Z. *J. Pharm. Sci.* **2011,** *100* (10), 4047–4049.
91. Rowland, M.; Peck, C.; Tucker, G. *Annu. Rev. Pharmacol. Toxicol.* **2011,** *51,* 45–73.
92. Shepard, T.; Scott, G.; Cole, S.; Nordmark, A.; Bouzom, F. *CPT Pharmacometrics Syst. Pharmacol.* **2015,** *4* (4), 221–225.
93. Wagner, C.; Zhao, P.; Pan, Y.; Hsu, V.; Grillo, J.; Huang, S. M.; Sinha, V. *Clin. Pharmacol. Ther.* **2015,** *4* (4), 226–230.
94. McGinnity, D. F.; Collington, J.; Austin, R. P.; Riley, R. J. *Curr. Drug Metab.* **2007,** *8* (5), 463–479.
95. Ito, K.; Houston, J. B. *Pharm. Res.* **2005,** *22* (1), 103–112.
96. Houston, J. B.; Galetin, A. *Curr. Drug Metab.* **2008,** *9* (9), 940–951.
97. Holmes, A.; Bonner, F.; Jones, D. *Nat. Rev. Drug Discov.* **2015,** *14,* 585–587.
98. Bonn, B.; Svanberg, P.; Janefeldt, A.; Hultman, I.; Grime, K. H. *Drug Metab. Dispos.* **2016,** *44,* 527–533.
99. Lappin, G.; Noveck, R.; Burt, T. *Expert Opin. Drug Metab. Toxicol.* **2013,** *9* (7), 817–834.
100. International Conference on Harmonisation. *Int. Conf. Harmon.* **2009**, *3* (June), 25.

101. Bosgra, S.; Vlaming, M. L. H.; Vaes, W. H. J. *Clin. Pharmacokinet.* **2016,** *55* (1), 1–15.
102. Rowland, M. *J. Pharm. Sci.* **2012,** *101* (11), 4067–4074.
103. Lappin, G. *J. Clin. Oncol.* **2015,** *56* (1), 11–23.
104. Schuck, E.; Bohnert, T.; Chakravarty, A.; Damian-Iordache, V.; Gibson, C.; Hsu, C.-P.; Heimbach, T.; Krishnatry, A. S.; Liederer, B. M.; Lin, J.; Maurer, T.; Mettetal, J. T.; Mudra, D. R.; Nijsen, M. J.; Raybon, J.; Schroeder, P.; Schuck, V.; Suryawanshi, S.; Su, Y.; Trapa, P.; Tsai, A.; Vakilynejad, M.; Wang, S.; Wong, H. *AAPS J.* **2015,** *17* (2), 462–473.
105. Liu, L.; Di Paolo, J.; Barbosa, J.; Rong, H.; Reif, K.; Wong, H. *J. Pharmacol. Exp. Ther.* **2011,** *338* (1), 154–163.
106. Maurer, T. S.; Ghosh, A.; Haddish-Berhane, N.; Sawant-Basak, A.; Boustany-Kari, C. M.; She, L.; Leininger, M. T.; Zhu, T.; Tugnait, M.; Yang, X.; Kimoto, E.; Mascitti, V.; Robinson, R. P. *AAPS J.* **2011,** *13* (4), 576–584.
107. Wong, H.; Choo, E. F.; Alicke, B.; Ding, X.; La, H.; McNamara, E.; Theil, F. P.; Tibbitts, J.; Friedman, L. S.; Hop, C. E. C. A.; Gould, S. E. *Clin. Cancer Res.* **2012,** *18* (14), 3846–3855.
108. Zager, M. G.; Kozminski, K.; Pascual, B.; Ogilvie, K. M.; Sun, S. *J. Pharmacokinet. Pharmacodyn.* **2014,** *41* (2), 127–139.
109. Atkinson, A. J., Jr.; Colburn, W. A.; DeGruttola, V. G.; DeMets, D. L.; Downing, G. J.; Hoth, D. F.; Oates, J. A.; Peck, C. C.; Schooley, R. T.; Spilker, B. A.; Woodcock, J.; Zeger, S. L. *Clin. Pharmacol. Ther.* **2001,** *69* (3), 89–95.
110. Halim, A. Drug Discovery and Development—Present and Future. In Kapetanović, I., Ed.; InTech: Croatia, 2011; pp 401–424.
111. Caberlotto, L.; Lauria, M. *Expert. Rev. Mol. Diagn.* **2015,** *15* (2), 255–265.
112. Sarntivijai, S.; Vasant, D.; Jupp, S.; Saunders, G.; Bento, A. P.; Gonzalez, D.; Betts, J.; Hasan, S.; Koscielny, G.; Dunham, I.; Parkinson, H.; Malone, J. *J. Biomed. Semantics* **2016,** *7* (1), 8.
113. Doak, B. C.; Zheng, J.; Dobritzsch, D.; Kihlberg, J. *J. Med. Chem.* **2016,** *59* (6), 2312–2327.
114. Bourgeas, R.; Basse, M. J.; Morelli, X.; Roche, P. *PLoS One* **2010,** *5* (3), e9598.
115. Higueruelo, A. P.; Jubb, H.; Blundell, T. L. *Database* **2013,** *2013,* 1–5.
116. Joseph, L.; Robinson, J. G. *Prog. Cardiovasc. Dis.* **2015,** *58* (1), 19–31.
117. Edfeldt, F. N. B.; Folmer, R. H. A.; Breeze, A. L. *Drug Discov. Today* **2011,** *16* (7–8), 284–287.
118. Nisius, B.; Sha, F.; Gohlke, H. *J. Biotechnol.* **2012,** *159* (3), 123–134.

1.24 Perspectives of Carbohydrates in Drug Discovery

J Rojo, A Sousa-Herves, and A Mascaraque, IIQ, CSIC—Universidad de Sevilla, Seville, Spain

© 2017 Elsevier Ltd. All rights reserved.

1.24.1	**Relevance of Carbohydrates**	577
1.24.2	**Current Uses of Carbohydrates in Drug Discovery**	578
1.24.2.1	Modulation of Enzymes	581
1.24.2.2	Lectin Inhibitors	583
1.24.2.2.1	Inhibition of selectins	583
1.24.2.2.2	Inhibition of galectins	585
1.24.2.2.3	Inhibition of bacterial lectins: adhesins and toxins	585
1.24.2.2.4	Targeting DC-SIGN lectin	589
1.24.2.3	Carbohydrates in Vaccine Development	591
1.24.2.3.1	Carbohydrates as immune modulators	593
1.24.2.3.2	Carbohydrate-based vaccines	596
1.24.3	**Carbohydrate-Mediated Drug and Gene Delivery**	598
1.24.4	**Carbohydrate-Based Diagnostics**	601
1.24.5	**Glycoengineering in Therapeutics**	602
1.24.6	**Conclusions and Perspectives**	603
References		604
Relevant Websites		610

1.24.1 Relevance of Carbohydrates

This article will describe how carbohydrates in their different forms (glycans, glycoconjugates, or glycomimetics) can be considered as very interesting tools in chemical biology and medicinal chemistry and the perspectives of their use in drug development with emphasis on those examples already approved for use or under clinical trials. This article does not intend to be an exhaustive collection of all potential carbohydrate drug candidates, but a compilation of significant and illustrative examples of those carbohydrate-based compounds that represent novel structures with promising activity to be considered as potential drug candidates in the future.

Carbohydrates are a very important class of biomolecules present at the surface of most of eukaryotic cells as glycoconjugates (glycolipids and glycoproteins) as well as in the extracellular space.[1] Among other important functions, they are responsible for cellular communication and protein folding. They have key roles in many biological processes such as inflammation, angiogenesis, pathogen infection, immune modulation, cell development, fertilization and embryogenesis, tumor progression, and metastasis.[1] In fact, some of these glycan structures have been selected as specific biomarkers for diseases such as congenital disorders and cancer and other pathological processes. For this reason, carbohydrates, involved in many human diseases and disorders (depicted in Fig. 1), can be considered as potential targets for drug development.[2]

The term glycome (similarly to proteome and genome) has been recently coined to describe the whole glycans within a biological system. Nowadays, a new "omics" comes on the scene, glycomics, which describes the structures and functions of glycans in a biological system (Fig. 1).[3] Glycans encode a large amount of molecular information that is decoded by lectins, proteins able to read out this information through their interaction with these glycans. The complexity of the glycan structures present in nature, their heterogeneity, and the difficulty to synthesize them in amounts enough to study the structure–activity relationships have delayed the boom of the glycoscience.[4] The direct consequence of this is a deficient development of carbohydrate-based therapeutics over the last years. Advances in both analytic techniques and the synthetic methods (in solution, enzymatic, or in solid phase, manual or automatic) have finally allowed access to pure complex carbohydrates that facilitated the understanding of carbohydrate function and their activity in nature. This has opened new avenues of remarkable interest in chemical biology and medicinal chemistry for the development of carbohydrate-based therapeutics and diagnostics.

Glycans are biomolecules with very interesting properties from the point of view of drug development such as low toxicity and poor immunogenicity; however, the chemical and physical properties of carbohydrates (specially, their polarity and their instability against degradation by glycosidases) have limited, in some cases, their use as drugs. Also, carbohydrates frequently interact with their receptors with weak affinities that are compensated in nature by multivalent interactions through the presence of multiple copies (multivalency) of both ligands (carbohydrates) and receptors (lectins). All these points lead to consider these molecules as poor candidates for drug development by the pharmaceutical industry. In fact, the percentage that represents carbohydrate-based drugs in the pharmaceutical market is still very small. In spite of all the drawbacks concerning the use of carbohydrates as drugs and the reticence that medicinal chemists have to work with these polar molecules, there are some remarkable examples in the market that demonstrate that this kind of molecules can be used effectively. As reviewed recently, more than 130 natural carbohydrate drugs are present in four pharmacopeias (the United States, China, Japan, and EU) as drugs or as excipients.[2] These

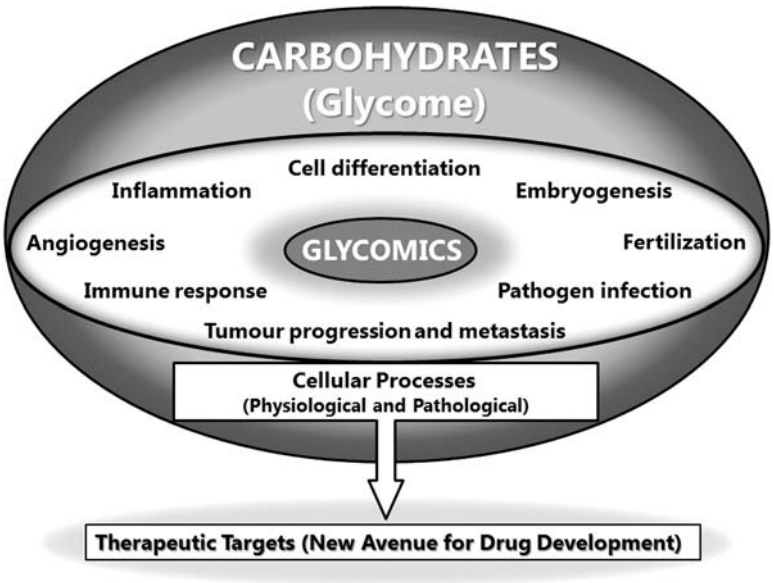

Fig. 1 The carbohydrate world as a source for the development of therapeutics.

drugs include natural compounds from simple monosaccharides as glucose to complex polysaccharides as heparin. In some cases, the biological target is not known, although the carbohydrate drug is active against a particular disease. Therefore, a deep understanding at molecular level of the carbohydrate role in biological processes and the mechanism of action of these natural ligands should lead to new synthetic promising compounds to increase, in following years, the arsenal of therapeutics against a large variety of diseases.

1.24.2 Current Uses of Carbohydrates in Drug Discovery

A large variety of carbohydrates and glycomimetics are available as drugs or are in clinical phases as promising candidates. This pool of carbohydrate-based candidates shows very different structures, from simple monosaccharide derivatives to complex polymers. The different structures of these compounds, the biological targets, and the diseases where they can be used are so complex and diverse that many different classifications are possible. In this section, the organization is based on biological targets of the carbohydrate drugs, with the exception of the glycosaminoglycan (GAG) derivatives, which represent a large family of drugs with different targets and in some cases without well-defined ones.

Heparin, one of the first glycans with medical applications, is a very popular drug. This oligosaccharide, a highly sulfated GAG clinically used since the 1930s to treat thrombosis in humans, is a classic natural carbohydrate-based drug that is still commonly used.[5] Heparin and derivatives are carbohydrate-based drugs that do not have, strictly speaking, a target enzyme, but modulate the activity of an enzyme through an interaction with one of its inhibitors. The mechanism of action of heparin is based on its binding to the enzyme inhibitor antithrombin III,[6] causing a conformational change that results in its activation. The activated antithrombin then inactivates thrombin and other enzymes that promote coagulation, most notably factor Xa.[7] This glycan is in fact a heterogeneous mixture of complex structures obtained from natural sources. The main source of heparin is porcine mucosa, although relevant advances have been performed in the last decade to prepare synthetic heparin[8] as well as low-molecular-weight heparin (LMWH) derivatives from simple precursors.[9] In 2008, contaminated batches of heparin and LMWH led to an international health crisis, emphasizing the need of a reliable method for generating well-defined (homogeneous) heparin therapeutics.[10] In this context, a series of low-molecular-weight carbohydrate-based drugs have been developed and clinically approved as alternative antithrombotic agents (Table 1 and Fig. 2). A relevant example is fondaparinux (Arixtra, **1**; Fig. 2),[11] the first synthetically well-defined small-molecule heparin derivative, on the market since 2002. Fondaparinux (**1**) is a pentasaccharide widely used for the treatment of deep vein thrombosis. Its chemical structure is almost identical to the antithrombin-binding pentasaccharide sequence found in natural heparin and heparan sulfate. It is noteworthy that some low-molecular-weight derivatives present additional advantages, such as quality control manufacturing, enhanced potency, and reduced risk of thrombocytopenia, which makes them more selective and reduces adverse events.

Apart from heparin, other common GAGs with applications in the pharmaceutical industry are hyaluronic acid (HA, also known as hyaluronan), chondroitin sulfate, dermatan sulfate, and keratan sulfate. In nature, GAGs are often covalently linked to a protein forming proteoglycans, which are located in the membranes of all animal tissues, on the surface of cells, or in the extracellular matrix, where they perform a variety of biological functions.[18]

Table 1 LMWH-based drugs with antithrombotic and anticoagulant activity currently on the market

Compound	*Trade name*	*Company*	*References*
Fondaparinux (**1**)	Arixtra	GlaxoSmithKline	11,12
Enoxaparin (**2**)	Lovenox	Sanofi Aventis	13
Nadroparin (**3**)	Fraxiparine	Aspen Pharmacare	14
Dalteparin (**4**)	Fragmin	Pfizer	15
Certoparin	Sandoparin	Novartis	16
Parnaparin	Fluxum	Alfa Wassermann	17

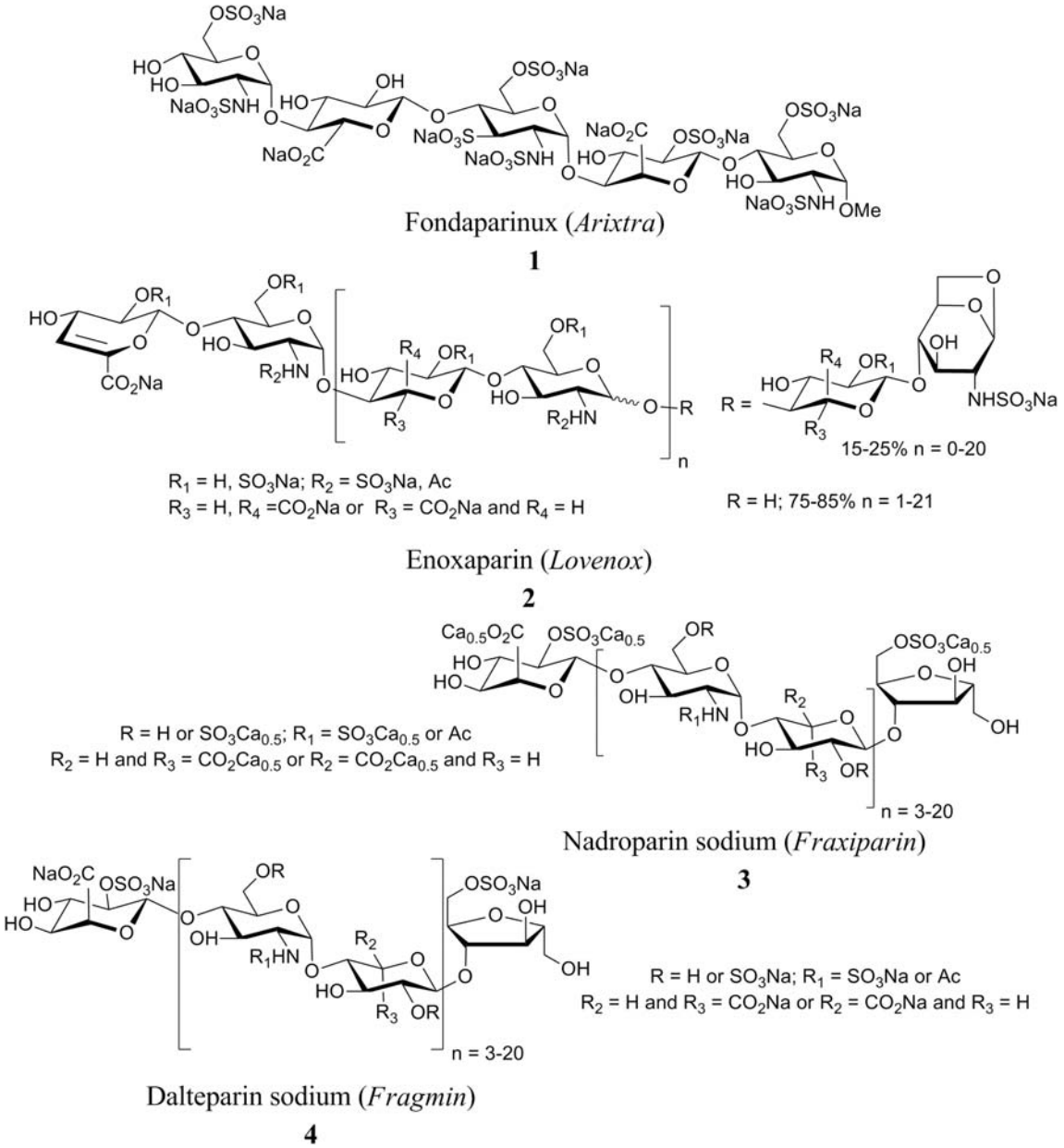

Fig. 2 Chemical structures of some clinically used LMWH.

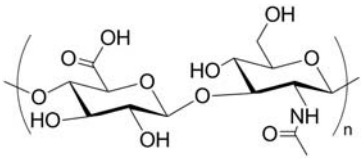

Hyaluronic acid repeating unit (**5**)

Fig. 3 Chemical structure of HA (**5**).

Some of the biological roles of GAGs have been exploited for the preparation of drugs with applications in tissue engineering and repair. For instance, HA has been used therapeutically for several years. HA is a nonsulfated, high-molecular-weight GAG made of repeating units of disaccharides composed of glucuronic acid and *N*-acetyl-glucosamine linked by a glucuronidic β(1 → 3) bond (**5**; Fig. 3).[19] It is naturally produced by hyaluronan synthases and is degraded by a category of enzymes called hyaluronidases. HA can be found both in the skin, where it plays a major role in tissue repair, and in cartilage and connective tissues, where it works as a lubricant and as a constituent of the extracellular matrix.

In this particular context, Anika Therapeutics has launched several drugs based on HA to the market (mainly in Europe), with many others in the pipeline (Table 2).[20] Anika Therapeutics uses naturally sourced HA, which is properly manufactured in order to obtain a purified, high-quality, and medical grade HA. The company offers therapeutic products in orthobiologics, dermatology, surgery, ophthalmology, and veterinary. One of the most successful products is Orthovisc, employed for the treatment of osteoarthritis. The mechanism of action is complex and most likely involves both the viscoelastic properties of the polymer and effects on synovial cells in the joint capsule. In addition, HA has been proved to suppress cartilage degeneration, act as a lubricant, and reduce pain perception.

Finally, it is important to remark the growing use of HA in popular beauty treatments such as soft tissue augmentation or as fillers for the "treatment" of the aging face.[21]

Table 2 Some examples of HA-based drugs developed by Anika Therapeutics[20]

Trade name	*Application*	*Description*	*Clinical status*
Orthovisc	Orthobiologics. Treatment of joint pain caused by osteoarthritis	High-molecular-weight injectable HA	Approved worldwide
Monovisc	Orthobiologics. Treatment of joint pain caused by osteoarthritis	HA single-injection treatment. Delivers the maximum dose of HA currently available in any single-injection treatment	Approved worldwide
Hyalofast	Orthobiologics. Treatment of lesions in the knee and ankle	HA-based implant for cartilage regeneration. It supports mesenchymal stem cell attachment, proliferation, and differentiation	CE-marked
Hyaloglide	Orthobiologics. Prevention or reduction of adhesions or fibrosis after surgical procedures	Auto-cross-linked HA gel that creates an antiadhesion barrier that keeps the adjacent tissues separated while repair occurs after surgery	CE-marked
Hyalomatrix/ Hyalomatrix PA	Dermal. Suited for a range of wounds that include pressure ulcers, diabetic foot ulcers, and deep second-degree burns	Pad composed of a wound contact layer made of a derivative of HA with an outer layer composed of a semipermeable silicone membrane. The wound contact layer acts as a 3-D scaffold for cellular invasion and capillary growth	Approved worldwide
Hyalofill-R	Dermal. Treatment of deep exuding wounds, sinuses, and fistulae	Absorbent and soft fibrous rope composed of an ester of HA. In contact with wound, it turns into a gel that keeps a wet environment, promotes wound healing, and allows a painless removal of the dressing	FDA-cleared and CE-marked
Elevess/Hydrelle	Dermal. Correction of facial lines and wrinkles	Injectable dermal filler made of cross-linked HA that contains the anesthetic lidocaine	Approved worldwide
Anikavisc	Ophthalmology	Viscoelastic for use in eye surgery	Approved worldwide
Hyaloss matrix	Dental surgery. Promotes bone graft application in the bone defect	Matrix constituted by bundles of fibers entirely made of a solid derivative of HA	CE-marked
Hyvisc	Veterinary. Treatment of noninfectious synovitis associated with equine osteoarthritis	HA-based viscous fluid	FDA-approved
Cingal	Orthobiologics. Treatment of pain caused by osteoarthritis of the knee	Palliative treatment	About to be launched

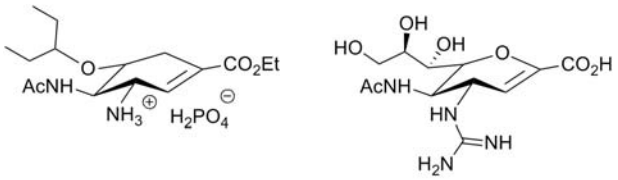

Oseltamivir (*Tamiflu*) **6** Zanamavir (*Relenza*) **7**

Fig. 4 Chemical structures of the neuraminidase inhibitors oseltamivir (**6**) and zanamivir (**7**).

1.24.2.1 Modulation of Enzymes

Glycoconjugates (glycolipids and glycoproteins) are posttranslational modifications of lipids and proteins, respectively, mediated by specific enzymes, the so-called glycosyltransferases. The improper operation of these enzymes leads to aberrant glycosylation patterns, one of the most significant marks of several pathologies such as cancer, congenital disorders, and autoimmune diseases. Glycomimetics able to interact and interfere with the activity of these enzymes have been developed as therapeutics to be applied in the treatment of these pathologies. Representative examples of drugs marketed or under clinical studies will be highlighted in the succeeding text.

One common approach toward the preparation of novel carbohydrate-based therapeutics is the rational design of low-molecular-weight compounds able to mimic (glycomimetics) the bioactive conformation of the native functional carbohydrate ligand in its target binding site.[2,22] Probably, the most well-known examples are the glycomimetic inhibitors of the influenza virus neuraminidase enzyme (NA).[23] The antiviral drugs oseltamivir phosphate (Tamiflu, Hoffman La Roche, **6**; Fig. 4)[24] and zanamivir (Relenza, GlaxoSmithKline, **7**; Fig. 4)[25] perfectly illustrate the rational design of potent and effective glycomimetic drugs. These drugs are indicated for the treatment of both influenza A and B (flu) in adults and children. Their mechanism of action is based on mimicking the high-affinity transition state of the sialic acid substrate before being cleaved by the influenza NA, rendering the influenza virus unable to escape its host cell and infect others.

Carbohydrate analogs that target α-glucosidases, intestinal enzymes that release glucose from larger polysaccharides, have also been developed for the treatment of diabetes. Examples of these drugs are miglitol (Glyset, Bayer, **8**; Fig. 5),[26] voglibose (Glustat, Takedo/Abbott, **9**; Fig. 5),[27] and acarbose (Glucobay, Bayer, **10**; Fig. 5).[28] Voglibose (**9**; Fig. 5) was first launched in 1994 and is an α-glucosidase inhibitor used for lowering postprandial blood glucose levels in people with diabetes mellitus. Acarbose (**10**; Fig. 5) is a modified tetrasaccharide of microbial origin that acts as a reversible α-glucosidase inhibitor, specifically of those enzymes in the brush border of the small intestine and pancreatic α-amylase.

Similarly, phosphomannopentaose sulfate (PI-88, Progen/Medigen Biotechnology Corporation, **11**; Fig. 6)[29] inhibits the enzyme endo-β-D-glucuronidase heparanase, thereby interfering with the heparanase-mediated degradation of heparan sulfate proteoglycans in extracellular matrices, an important step in the metastatic process. Heparanase expression has been directly correlated with the metastatic spread of various tumors.[30] PI-88 (**11**; Fig. 6) is a mixture of oligosaccharides mimicking heparan sulfate that exhibited antirecurrence and antimetastatic activity to hepatocellular carcinoma in preliminary clinical trials.[31] Phase I and II clinical studies have demonstrated good safety profiles and promising efficacy in the treatment of liver cancer,[32] while phase III clinical trials are currently being carried out.

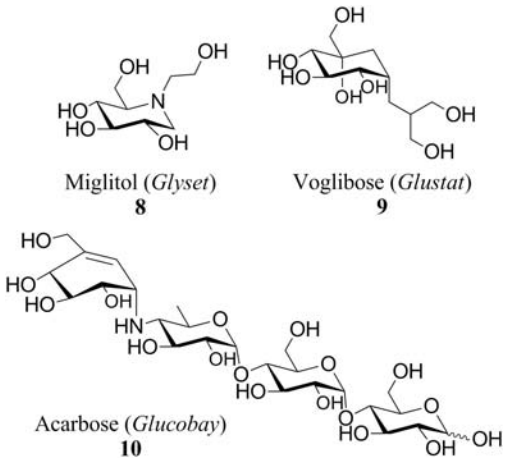

Miglitol (*Glyset*) **8** Voglibose (*Glustat*) **9**

Acarbose (*Glucobay*) **10**

Fig. 5 Chemical structures of α-glucosidase inhibitors employed in the treatment of diabetes.

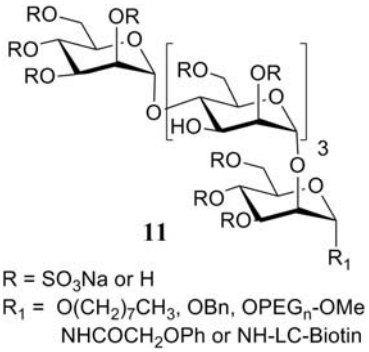

Fig. 6 Chemical structure of phosphomannopentaose sulfate (PI-88, **11**).

Another relevant glycomimetic that also inhibits carbohydrate biosynthesis is miglustat (Zavesca, Actelion Pharmaceuticals, **12**; Fig. 7), used to treat Gaucher disease and type C Niemann–Pick disease (NP-C). Zavesca was approved in Europe in 2002 and by the US Food and Drug Administration (FDA) in 2003 to treat adults with mild to moderate type I Gaucher disease for whom enzyme replacement therapy is unsuitable.[33] It is also approved for the treatment of NP-C disease in 45 countries, including the European Union since 2009. Miglustat reduces the biosynthesis of glucosylceramide from ceramide through the inhibition of the enzyme glucosylceramide synthase, thus reducing the production of glycosphingolipids in cells. This is expected to slow down or prevent the development of the symptoms of type 1 Gaucher disease and to reduce the symptoms of NP-C disease in adult and pediatric patients.[34]

Finally, another significant carbohydrate-based drug on the market is topiramate (Topamax, Johnson & Johnson, **13**; Fig. 7), employed as an antiepileptic medicine and to prevent migraine headaches.[35] The precise mechanism of action of topiramate is relatively complex and is not completely understood. However, preclinical studies have revealed some properties that may contribute to topiramate's efficacy: this drug blocks voltage-dependent Na^+ channels, increases activity of the neurotransmitter γ-aminobutyrate (GABA) at some subtypes of the GABA-A receptor, antagonizes the α-amino-3-hydroxy-5-methyl-4-isoxazolepropionic acid (AMPA)/kainate subtype of the glutamate receptor, and inhibits carbonic anhydrase.

Another vast family of enzyme-modulating carbohydrate-based drugs is composed of natural products that possess glycan components. This group includes chemotherapeutic drugs, antibiotics, and compounds to treat cardiovascular diseases (Fig. 8). Some of these drugs, described in the next paragraphs, are contained within the World Health Organization List of Essential Medicines, which compiles the most important medications needed in a basic health system.

Doxorubicin (**14**) and daunorubicin (**15**) are cytotoxic drugs in the anthracycline family (Fig. 8). These drugs are potent neoplastic agents that bind to nucleic acids, apparently by specific intercalation of the planar anthracycline nucleus with the DNA double helix. This intercalation inhibits nucleotide replication and action of DNA and RNA polymerases. Topoisomerase II-mediated DNA damage is followed by cell death.[36]

Streptomycin (**16**) and erythromycin (**17**) are examples of antibiotics of natural origin for which their sugar moiety is an essential component (Fig. 8).[37] Removal of this carbohydrate residue typically leads to elimination of the drug's therapeutic properties. Streptomycin inhibits both Gram-positive and Gram-negative bacteria and is therefore a useful broad-spectrum antibiotic. It is a bacterial protein synthesis inhibitor and was the first efficient treatment for tuberculosis.[38] In a similar way, erythromycin, an antibiotic of microbial origin used for several infections, hampers the production of functional proteins in bacteria. It induces peptidyl transferase activity and interferes with translocation of amino acids during translation and assembly of proteins. Several semisynthetic antibiotics derived from erythromycin—dirithromycin, clarithromycin (Biaxin, Abbott), and azithromycin (Zithromax, Pfizer)—are currently on the market.[39]

Digoxin (**18**; Fig. 8) is a glycoside used in the treatment of various heart disorders, namely, atrial fibrillation, atrial flutter, and sometimes heart failure that cannot be controlled by other medication.[40] Digoxin's mechanism of action involves inhibition of the Na^+/K^+ ATPase, mainly in the myocardium, which eventually leads to a decrease in heart rate and smooth muscle contraction and vasoconstriction.

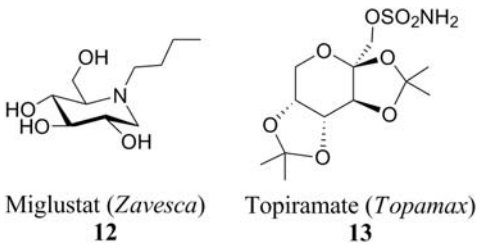

Fig. 7 Chemical structures of miglustat (**12**) and topiramate (**13**).

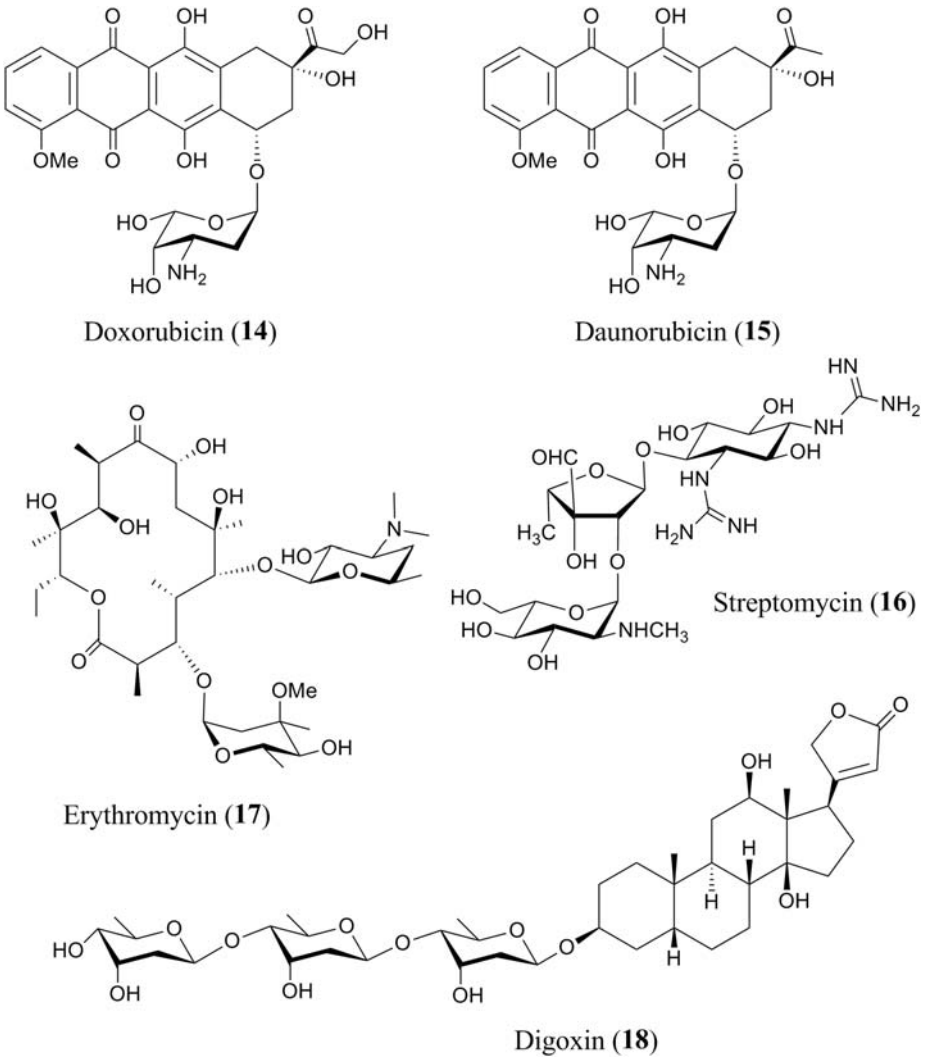

Fig. 8 Chemical structures of some chemotherapeutic, antibiotic, and cardiac drugs derived from carbohydrates.

1.24.2.2 Lectin Inhibitors

Lectins were first discovered at the end of the nineteenth century as plant proteins capable to agglutinate erythrocytes, a process that later was demonstrated to occur through the specific recognition of the carbohydrates present at the surface of these blood cells. Since then, many members of this family have been identified, isolated, and characterized in a broad range of different species (lectins occur ubiquitously in nature), and nowadays lectins are very useful tools in chemical biology.[41] These proteins received little attention until the discovery of animal lectins implicated in many relevant biological processes. Based on this fact, lectins are considered as very important therapeutic targets for the development of carbohydrate-based drugs. Some of these lectins, selectins, galectins, and C-type lectins, such as dendritic cell-specific intercellular adhesion molecule 3-grabbing nonintegrin (DC-SIGN) among others, have attracted the interest of scientists to develop new drugs. The progress in this field is summarized in the next sections.

1.24.2.2.1 Inhibition of selectins

Selectins mediate the initial attachment of leukocytes to endothelial cells at sites of inflammation.[42] Selectins were discovered in the late 1980s and probably are one of the best known carbohydrate-binding proteins. The selectin family is composed of three members: E-selectin (expressed on endothelial cells), P-selectin (expressed on activated platelets and stored in endothelial cells), and L-selectin (expressed by most leukocytes). L-selectin plays a major role in the trafficking of lymphocytes through the blood and lymphatic system. The L-selectins regulate the attraction of leukocytes to sites of inflammation through the binding of their carbohydrate domains to sialyl Lewis^x (SLe^x) and sialyl Lewis^a (SLe^a) oligosaccharides present on the cell surface.[43] Remarkably, these carbohydrate sequences were originally discovered as cancer-associated antigens and are prognostic indicators of metastatic

diseases.[44] Apart from cancer, selectins take part in many other inflammatory diseases such as rheumatoid arthritis, psoriasis, asthma, transplant rejection, inflammatory bowel disease, and multiple sclerosis (MS), among others.[45] Therefore, selectins are considered very appealing therapeutic targets in oncology and other medical fields.

Initially, strong efforts were made to synthesize small mimetics of SLe^x to inhibit the selectins (Fig. 9). The first selectin antagonist was cylexin (CY-1503, **19**; Fig. 9),[46] developed by the company Cytel, although clinical results were not satisfactory mainly due to a poor oral availability and lack of potency. Structural modifications have been made in order to prepare synthetically simpler structures,[47] like the fucosylated mimetics of SLe^x bimosiamose (TBC-1269, Revotar, **20**; Fig. 9) and rivipansel (GMI-1070, GlycoMimetics/Pfizer, **21**; Fig. 9). Bimosiamose showed promising results in the treatment of asthma, but was discontinued after phase II clinical trials.[48] Rivipansel is about to start a phase III clinical trial to assess its efficacy and safety for the treatment of vaso-occlusive crisis in patients with sickle cell disease.[49]

Interestingly, E-selectins have also been reported to play an important role in the dissemination of hematologic cancers and the homing of leukemic stem cells to the bone marrow. In this context, GlycoMimetics has also launched a small-molecule E-selectin antagonist (GMI-1271), which is currently being evaluated in phase I/II trials in combination with chemotherapy for the treatment of acute myeloid leukemia.

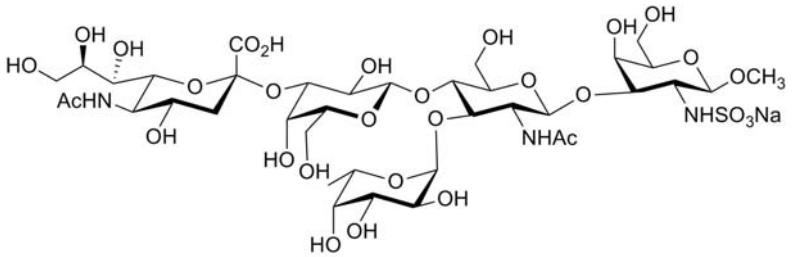

Cylexin (CY-1503)
19

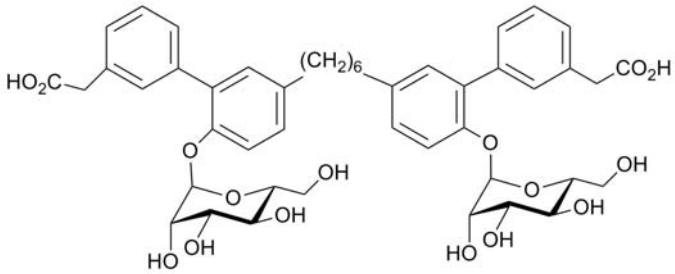

Bimosiamose (TBC-1269)
20

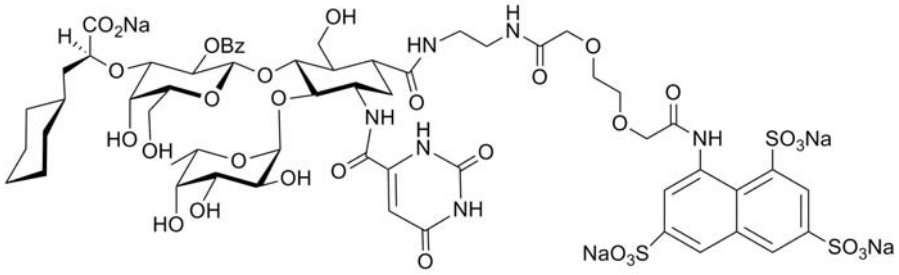

Rivipansel (GMI-1070)
21

Fig. 9 Chemical structures of relevant small-molecule mimetics of SLe^x.

1.24.2.2.2 Inhibition of galectins

Galectins are a family of lectins characterized by a galactose-specific carbohydrate-binding domain that interacts with galactose moieties located on glycoproteins.[50] These lectins are known to be involved in a plethora of biological processes, such as inflammation, immune response regulation, and tumor progression and metastasis.[51] They can be found in cellular compartments or in the extracellular space where they interact with cell surface and extracellular glycoproteins.

To date, 15 different galectins have been identified. Among them, galectin-1 and galectin-3 are the two galectins most frequently involved in pathological processes. In addition, these galectins are overexpressed in several diseases including inflammation and fibrosis and several types of cancer.[52] As a consequence, targeting and blocking galectins may have an efficacious therapeutic effect on some of these diseases. To this end, several strategies have been reported to obtain natural[53] or synthetic derivatives[54] that could behave as effective and safe pharmacological inhibitors.

One of the most successful examples is the potent galectin-3 inhibitor (TD139, **22**; **Fig. 10**) developed by Galecto Biotech,[55] which specifically blocks the binding of galectin-3 to carbohydrate structures inhibiting various biological actions like modulation of immune processes and profibrotic activity. TD139 is a small glycan derived from thiodigalactoside that has shown very promising results in clinical trials for the treatment of patients with idiopathic pulmonary fibrosis, an irreversible and fatal lung disease with no effective treatments. According to the studies, TD139 interferes with signaling from receptors for the cytokine *transforming growth factor* (TGFβ), a potent inducer of lung fibrosis, ultimately showing strong antifibrotic potential.[56] In 2015, the US FDA has approved an Investigational New Drug application for the treatment of patients with idiopathic pulmonary fibrosis, and TD130 has entered in phase Ib/IIa trials.

In a complementary approach, Galectin Therapeutics uses naturally occurring carbohydrate polymers to prepare well-defined, pharmaceutical grade polysaccharides that serve as galectin ligands and interfere with their function. This company has developed GM-CT-01 (also known as Davanat, **23**; **Fig. 10**) and GR-MD-02 (galactoarabino-rhamnogalacturonate) as promising galectin inhibitors for the treatment of liver fibrosis, fatty liver disease, diabetic kidney disease, and metastatic melanoma.[57] Davanat is the galactomannan isolated from seeds of *Cyamopsis tetragonoloba*, or guar gum, and subjected to a controlled partial chemical degradation. It was the first polymeric carbohydrate-based drug candidate proved to be an effective ligand for galectin-1.[58]

Due to the interest on targeting galectins and their implication in several diseases as mentioned in the preceding text, nowadays, there is a strong activity in the search of new therapeutics based on galactose derivatives looking for more efficient and selective drugs.

1.24.2.2.3 Inhibition of bacterial lectins: adhesins and toxins

Bacteria express on their surfaces many glycan-binding proteins or lectins (often called adhesins) that show strong and specific binding for carbohydrates expressed on human cells. Such interactions constitute an essential part of the infection pathway, as their primary function is to facilitate attachment or adherence of bacteria to host cells, a prerequisite for bacterial colonization and infection.

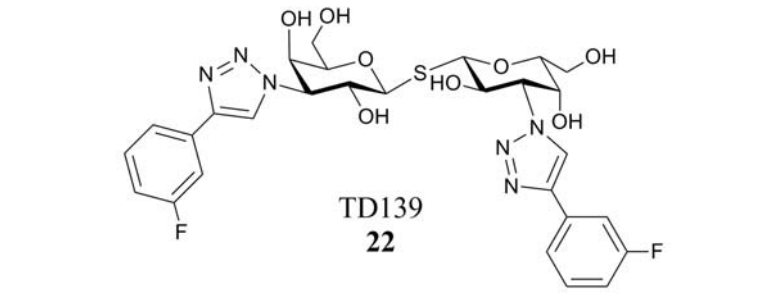

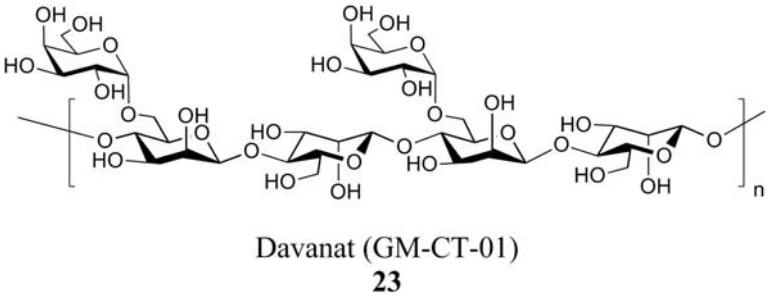

Fig. 10 Chemical structure of the galectin-3 inhibitors TD139 (**22**) and GM-CT-01 (Davanat, **23**).

Bacteria also produce toxins, whose actions often depend on carbohydrate-binding subunits that allow the toxin to combine with host membranes and deliver the active toxic subunit across the plasma. For instance, the family of the AB_5 toxins, important virulence factors for several major bacterial pathogens,[59] are so termed because they comprise a catalytic A subunit (or disease-causing component), which is responsible for disruption of essential host functions, and a pentameric B subunit that binds to specific glycan ligands on the target cell surface.[60] Toxins producing diseases such as cholera or hemolytic uremic syndrome (HUS) can be found within this family. Cholera, still a life-threatening disease in many parts of the world, is caused by the cholera toxin (CT) produced by *Vibrio cholerae*, while *Shigella dysenteriae* and *Shiga toxigenic Escherichia coli* generate shiga toxins (Stx), whose the associated symptoms include diarrhea and hemorrhagic colitis, but it could also result in life-threatening HUS.[61]

In addition to the cytotoxicity of bacterial lectins, it has been suggested that many of them contribute to the formation of bacterial microcolonies and biofilms,[62] thereby promoting colonization of host tissues and being one of the key factors responsible for the virulence and antibiotic resistance of pathogens.

To prevent or suppress infection, soluble forms of human cell surface oligosaccharides or glycomimetics are being investigated to block the initial attachment of microbes and toxins to the cell surfaces. Development of such potential antiadhesive drugs against bacterial infection[63] is emerging as a relevant strategy due to the increasing antibiotic resistance of several bacterium strains.[64] It has also been postulated that, since antiinfective agents rely on disrupting carbohydrate–lectin interactions, any mutation that provides the bacteria with resistance to the antiinfective carbohydrate agents should also render on bacteria unable to bind the host's carbohydrates.[2]

To this end, some monosaccharides have been tested to limit bacterial infection through competition, for example, with LecA (or PA-IL) and LecB (or PA-IIL), main lectins of *Pseudomonas aeruginosa*, an opportunistic pathogen involved not only in a large number of diseases[65] such as septicemia and urinary tract infections but also in lung infections in immunocompromised and cystic fibrosis patients.[66] It was demonstrated that solutions of galactose and fucose, LecA and LecB ligands, respectively, were active against the spread of infection of *P. aeruginosa* in mice models[67] and cystic fibrosis patients,[66] particularly in combination with antibiotics.[68] Adhesion of *P. aeruginosa* to human respiratory epithelial cells was also significantly prevented by human milk oligosaccharides.[69] In addition, other LecA and LecB ligands such as plant- and microbial-derived polysaccharides were identified as candidates with potential applications in gastrointestinal and external infections.[70]

However, difficulties with carbohydrate-based antiadhesion therapies still remain, not only making necessary the development of more potent inhibitors through rational design[71] but also overcoming the low affinity of free carbohydrates for microbial lectins, which may be afforded with optimized multivalent carrier carbohydrates conjugates.[63]

Although reaching submicromolar affinity with monovalent ligands has proved to be a rather complicated task, the use of rational drug design and several medicinal chemistry strategies can strongly improve the affinity of these saccharides in comparison with the natural ligands, providing efficient antiadhesive strategies against bacteria. In this context, hydrophobic aglycon modification is a commonly used approach because hydrophobic interactions are usually possible in the surroundings of the lectin's binding site.[72] For instance, some modified monovalent ligands of FimH lectin from uropathogenic *E. coli* were identified as improved ligands for the bacterial lectin in terms of affinity.[73] This rational design led to one of the best FimH inhibitors to date ($EC_{>90} = 10$ nM), which additionally inhibited the biofilm formation with an IC_{50} value of 43 nM (**24**; **Fig. 11**).[74] A monoamide derivative of the previous inhibitor was also synthesized (**25**; **Fig. 11**) and, although the inhibitory properties were slightly decreased ($IC_{50} = 62$ nM) in comparison with the 3,5-diamide (**24**; **Fig. 11**), such compound appears as a promising candidate after successful in vivo assays.[75]

Another strategy in rational design is introduction on the aglycon derivative of relevant protein's recognition motifs such as those of the serum amyloid P (SAP) protein, an endogenous protein that plays an important role in the clearance of several pathogens.[76] The conjugation of a CT ligand with a proline group (an SAP recognition motif) on the aglycon derivative provided a bifunctional construct that allowed the preorganization of such ligand with the CT B subunits (CTB) and the SAP protein in a ternary complex. This noncovalent and multivalent preorganization enhanced the potency against CTB from an IC_{50} in the high micromolar range, without preorganizing SAP, to submicromolar IC_{50} when noncovalently bound to SAP. It was demonstrated that this increase was promoted by the formation of the CTB/bifunctional ligand/SAP ternary complex in solution.[76] The latter approach was also employed in the optimization of the so-called STARFISH (**26**; **Fig. 12**) and DAISY (**27**; **Fig. 12**) glycodendrimers,[77] the landmark studies in the Stx inhibitor field.

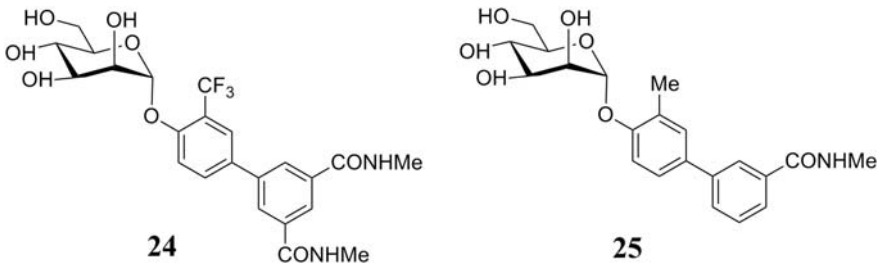

Fig. 11 Lead monovalent inhibitors of FimH.

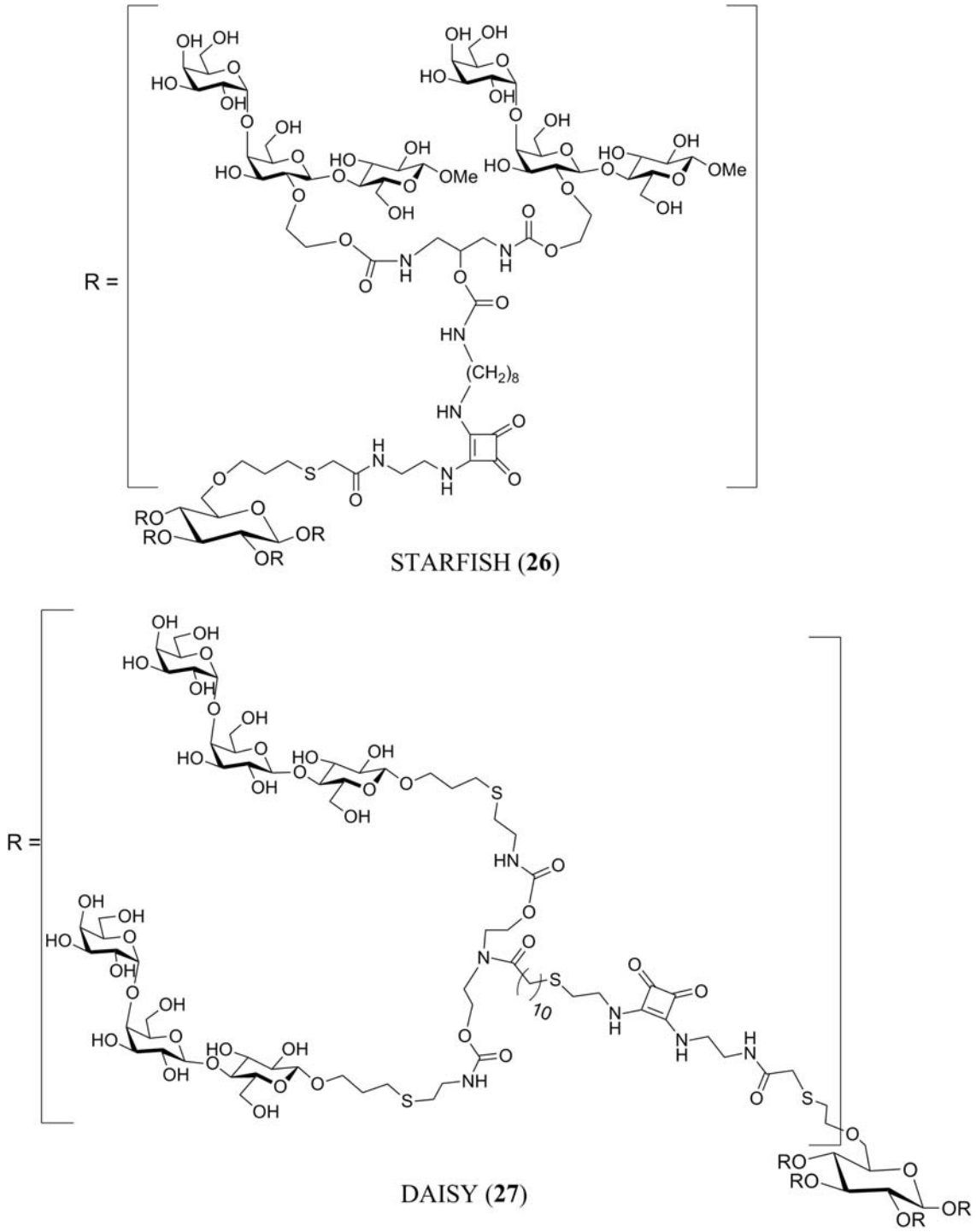

Fig. 12 STARFISH (**26**) and DAISY (**27**) inhibitors of Stx.

STARFISH dendrimer (**26**; Fig. 12) utilized a central pentavalent glucose core functionalized with 10 trisaccharide epitopes (Galα(1,4)Galβ(1,4)Glc or P^k glycan) and displayed IC_{50} values in the subnanomolar range against Stx1 (8.75×10^6-fold more potent when compared with the natural ligand). Unfortunately, this system did not show the biological activity expected in mice infection models.[78] DAISY (**27**; Fig. 12), a refined structure of STARFISH (where the trisaccharide was conjugated to the scaffold through the anomeric position of the glucose at the reducing end), was also tested in in vivo experiments demonstrating protection from both Stx1 and Stx2.[78]

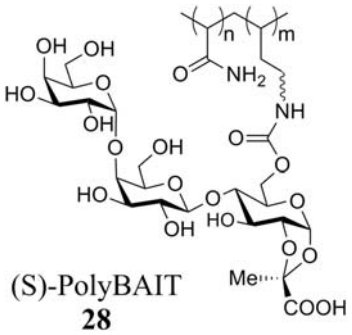

Fig. 13 Glycopolymer (S)-PolyBAIT (**28**).

The STARFISH inhibitor was improved by creating the glycopolymer (S)-PolyBAIT (**28**; **Fig. 13**), composed of a monomer containing the P^k glycan with a cyclic pyruvate ketal (CP),[79] a known binder of serum amyloid P (SAP) component.[79] An intravenous injection of this polymer protected 100% of mice that were subcutaneously inoculated with a lethal dose of Stx1. Interestingly, mice treated with a copolymer, in which P^k and CP were randomly distributed, developed severe signs of shigatoxemia. These results highlight the importance of the ligand placement on a polymeric scaffold in recruiting the necessary protein components for toxin clearance and drug efficacy.

Such important adhesin inhibitor rational design has also been conducted to the development of lead candidates in the antimicrobial drug field based on structure–activity relationship studies. Guided by the structural knowledge at the molecular level, divalent LecA ligands against *P. aeruginosa* infection were designed,[80] providing the best ligand to date (**29**; **Fig. 14**) with an $IC_{50} = 2.7$ nM (over 7500-fold stronger than the relevant reference compound) and a K_d value of 28 nM toward LecA (close to 800-fold more potent than the monovalent probe).[81] The study focused on the design of a rigid spacer based on the alternation of a different number of glucose moieties linked at 1 and 4 positions by a 1,2,3-triazole unit via "click chemistry." Docking studies revealed that the two terminal galactose units of the divalent ligand match in a "perfect" chelate-binding mode in the adjacent binding sites of a single LecA tetramer.[81]

Structure–activity relationship studies have also demonstrated the need for multivalency to achieve strong inhibitory activities, since ligand–lectin recognition processes usually go through multivalent interactions. A plethora of multivalent glycoconjugates have been investigated, displaying high affinities toward many bacterial lectins[73,82] with some of them applied in studying biofilm dispersion.[83] Scaffolds like proteins, peptides, fullerenes, calixarenes, and gold nanoparticles (GNPs), with different valencies (number of ligands), linkers, and spatial organization, have been used to multimerize carbohydrates and to enhance affinity of the monomers toward their respective targets.[73,82,84] Among these molecules, the 1,3-alternate conformer of calix[4]arene (**30**; **Fig. 15**) demonstrated the most efficient and dramatic increase in affinity to LecA from *P. aeruginosa*. A chelate-binding mode in which two galactose residues interact with two neighboring binding sites in a single LecA could be confirmed by atomic force microscopy.[85] The study of its inhibitory properties on *P. aeruginosa* aggregation, biofilm formation, adhesion on epithelial cells, and destruction of alveolar tissues was performed, and antiadhesive properties were evaluated through several in vitro bioassays. The use of this compound in in vivo mouse models of lung infection demonstrated an almost complete protection against *P. aeruginosa* infection. Such multivalent ligands now appear as promising drug candidates for the treatment of bacterial infections.[86]

Multivalent scaffolds have also been used to obtain inhibitors with nanomolar[87] to picomolar[88] activities against bacterial toxins. The combination of "click chemistry" with chemoenzymatic synthesis enabled the assembly of multivalent versions of the GM1os glycan (natural ligand of CT)[89] into glycodendrimers.[90] The octavalent version glycodendrimer (**31**; **Fig. 16**), with an $IC_{50} = 50$ pM, was 380,000-fold more potent compared with the GM1os natural ligand.[90,91]

GNPs have also reached very high affinities toward Stx.[92] P^k-functionalized GNPs, decorated with around 2000 copies of this ligand, showed binding constants in the picomolar range ($IC_{50} = 1.14$ pM and $K_i = 0.254$ pM), providing the highest relative

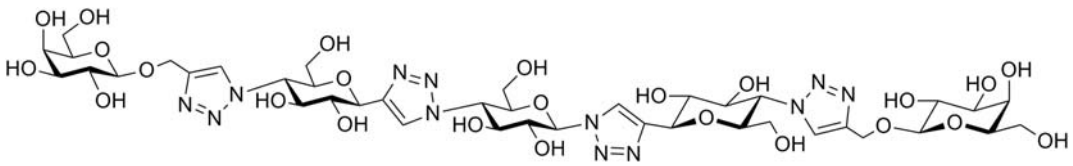

Fig. 14 Chemical structure of the best inhibitor for LecA lectin (**29**).

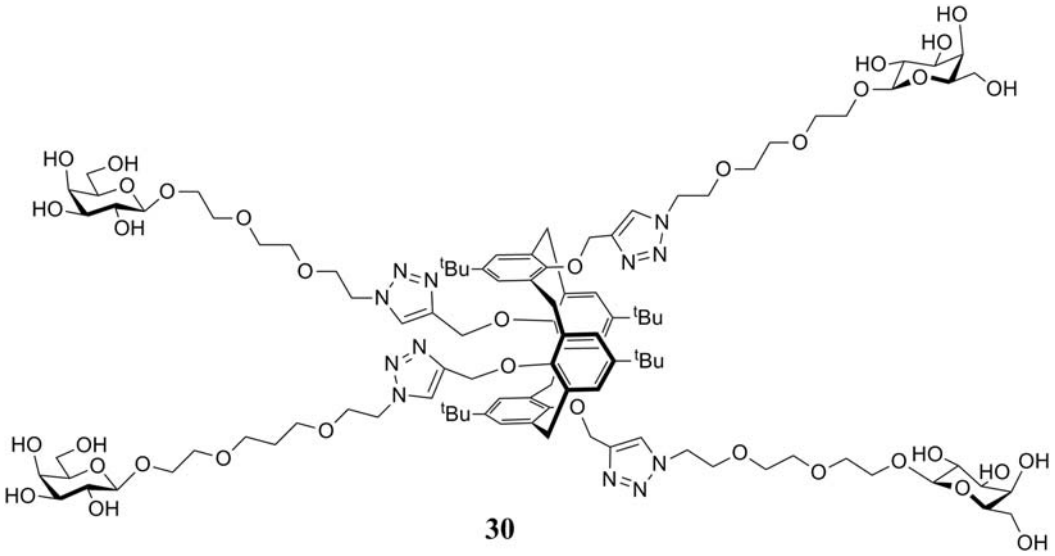

Fig. 15 Galactosyl calix[4]arene (**30**).

potency (β) to date when compared with the natural monovalent ligand Gb3.[93] Such hyperavidity has been applied to the purification of Stx from bacterial extracts.

Clinical trials up to phase III have been performed using multivalent systems of Gb3 or other epitopes.[94] The company Synsorb Biotech has developed two antiinfective agents that consisted of insoluble powders bearing carbohydrates that mimic the natural cell-bound carbohydrate targets of two bacterial toxins, namely, Synsorb Pk (**32**; **Fig. 17**) and Synsorb Cd. Synsorb Pk targets the Stx-producing *E. coli* enterohemorrhagic infections, and Synsorb Cd has demonstrated to be effective against *Clostridium difficile*-associated diarrhea. Both compounds underwent phase III clinical trials, but, unfortunately, these studies have now been discontinued as in vivo experimentation seems to be highly challenging in this field.[2]

Multivalent glycoconjugates have also proved higher affinities toward bacterial lectins with just one binding site. That is the case of fimbrial adhesin FimH, a protein located on the tip of type 1 pili (or fimbriae) from uropathogenic *E. coli*.[95] Since only one α-mannoside fits in the FimH binding site, the observed multivalency effects[96] cannot be explained on the basis of the structure of mannose-specific lectin FimH. Nevertheless, avidity effects have frequently been demonstrated with a variety of multivalent mannose-containing glycomimetics.[73] Interestingly, adhesion on multivalent glycomaterials can be utilized for aggregating *E. coli* and removing them from solution with the use of appropriate filters. For instance, glyconanodiamonds decorated with mannose (**33**; **Fig. 18**) have been shown to be able to clean bacteria-polluted water.[97]

1.24.2.2.4 Targeting DC-SIGN lectin

DC-SIGN is a C-type lectin mainly expressed at the surface of macrophages and immature dendritic cells (DCs). This lectin plays a critical role in the recognition of viruses (e.g., HIV, Ebola, dengue, and cytomegalovirus) and other pathogens (e.g., *Leishmania*, *Candida albicans*, *Mycobacterium tuberculosis*, *Streptococcus pneumoniae*, and *Aspergillus fumigatus*).[98] DC-SIGN is naturally expressed at the surface of DCs as a homotetramer presenting four carbohydrate recognition domains,[99] which binds glycoconjugates containing mannose or fucose in a multivalent and calcium-dependent manner.[100] The main natural ligands recognized by DC-SIGN are the high-mannose glycan, $(Man)_9(GlcNAc)_2$ or Man_9 (**34**; **Fig. 19**) and a group of fucosylated oligosaccharides bearing Lewis-type epitopes such as Lewis X (Le^x) or Lewis Y (Le^y) (**35**; **Fig. 19**).[101] This lectin is substantially involved in innate immunity internalizing highly glycosylated antigens into DCs to be processed and presented to T lymphocytes, activating and tailoring adaptive immune responses against different pathogens. Because of its crucial relevance in the immunological system, DC-SIGN has been extensively targeted with the aim of interfering with pathogenic processes through the development of not only new antiviral drugs but also immune modulators (see Section "**Carbohydrates as immune modulators**").[102] In this section, we will focus on the former application, highlighting the most relevant discoveries in the design and development of DC-SIGN inhibitors against viral infections, such as those of HIV or Ebola.

The design of DC-SIGN high-affinity ligands can be performed through glycomimetics of the high-mannose glycan (Man_9), which mimic the two or three terminal mannose residues (**34**; **Fig. 19**),[103] through structural analogs of the Le^x trisaccharide (Galβ(1,4)[Fucα(1,3)]GlcNAc) (**35a**; **Fig. 19**)[104] or through the construction of highly glycosylated polyvalent compounds.[73,82] Although most of the work concerns with mannose or mannose analogs,[105] fucose-based antagonists have been reported as well[106] providing moderately potent DC-SIGN ligands (similar to, or slightly better than, the natural ligand Le^x).

In 2008, a nonavalent mannose glycodendron that displayed nanomolar IC_{50} values toward DC-SIGN (10^6-fold more potent than mannose) was developed, inhibiting the binding of the HIV envelope glycoprotein gp120 to anti-HIV antibodies and

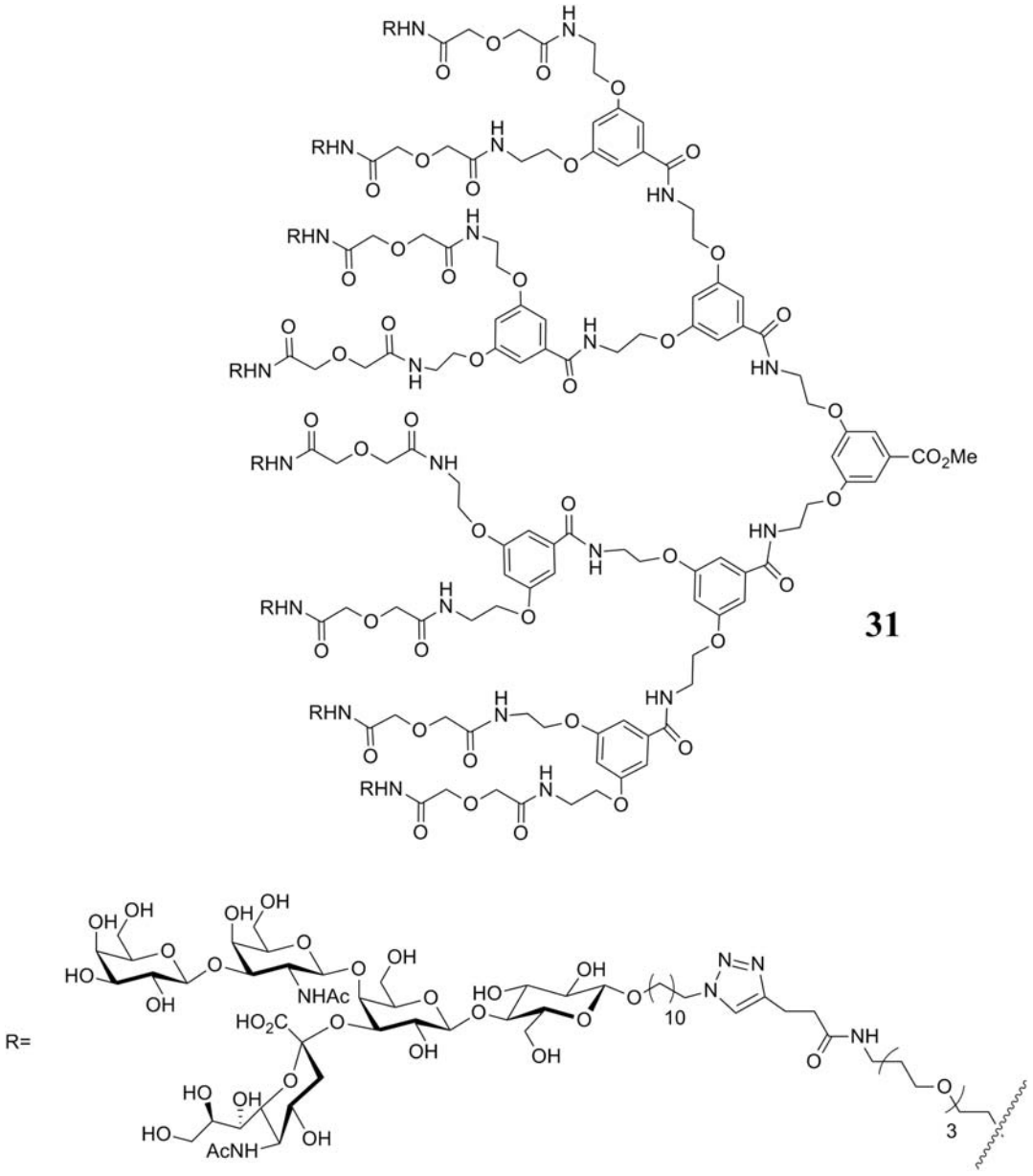

Fig. 16 Octavalent glycodendrimer conjugated with the GM1os ligand (**31**).

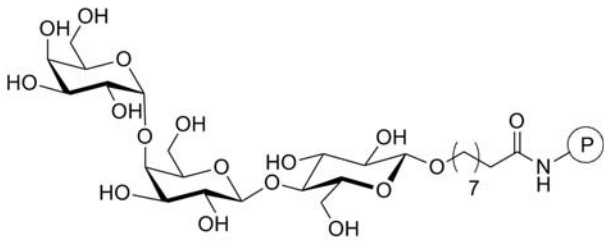

Synsorb Pk (**32**)

Fig. 17 Chemical structure of Synsorb Pk (**32**).

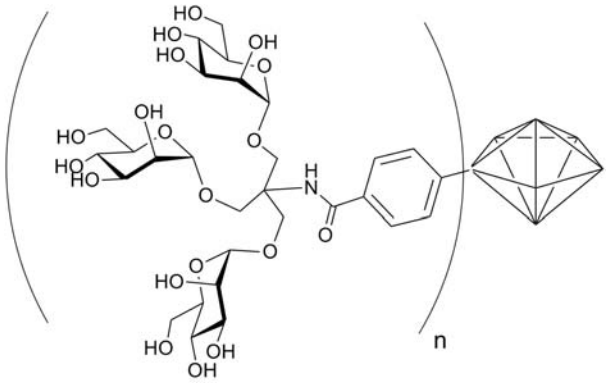

33

Fig. 18 Mannosylated nanodiamonds (**33**).

a recombinant dimeric DC-SIGN.[107] Since then, several examples have shown the importance of carbohydrate multivalency in the design and development of viral inhibitors (Fig. 20).[73,82] For instance, the conjugation of a trimannoside analog[105] to a tetravalent scaffold resulted in a glycocluster displaying improved binding properties and also better inhibition of DC-SIGN-mediated HIV infection.[108] The same linear trimannoside analog was conjugated to a Boltorn H30 dendrimer,[109] yielding a glycodendrimer functionalized with 30–32 copies of the synthetic epitope (**36**; Fig. 20).[110] While related mannosylated glycodendrimers were active against Ebola or HIV viral infections in the micromolar range,[111] this glycomimetic construct inhibited the Ebola virus infection in the nanomolar range.[110]

In order to mimic the cluster presentation of high mannose-type glycans on the HIV envelope, GNPs functionalized with gp120 oligomannosides (**37**; Fig. 20) have been prepared and tested as anti-HIV agents.[112] DC-SIGN/gp120 binding was inhibited by these manno-GNPs at nanomolar concentrations, a remarkable improved activity compared with those of monovalent oligomannosides (in the millimolar range).[112] Furthermore, it was demonstrated that manno-GNPs were uptaken by DCs,[113] thus explaining the inhibition observed for the DC-SIGN-mediated HIV transinfection of human activated peripheral blood mononuclear cells.[114]

In another attempt to prepare virus-like particles as potential inhibitors, fullerenes seemed to emerge as great scaffolds for a multivalent presentation of carbohydrates. In this regard, hexakis adducts of C60 fullerene are useful building blocks because they maintain a globular shape and, at the same time, allow the control over the size and multivalency. New glycodendritic compounds displaying a wide variety of valencies and spatial presentations of carbohydrate ligands have been prepared using a C60 fullerene as a central core.[115] Glycofullerenes decorated with 120 peripheral mannoses, the so-called superballs (**38**; Fig. 20), appeared as potent inhibitors of cell infection by using an artificial Ebola virus with IC_{50} in the subnanomolar range.[116]

Proteins have also been used as platforms in the development of multivalent antiviral inhibitors. A methodology in which glycodendrimers were attached to multiple sites of a protein producing highly valent glycodendriproteins was recently described.[117] This technology was employed in the conjugation of mannose dendrimers to the bacteriophage Qβ capsid. The resulting glycodendrinanoparticles (**39**; Fig. 20) are the highest multivalent glycodendrimeric constructs described to date, bearing up to 1620 glycan units, and were obtained as pure and well-defined entities with diameters of up to 32 nm. This kind of glycodendrinanoparticles are capable of mimicking pathogens both in size and in their highly glycosylated surfaces. Through this mimicry, they were able to inhibit the Ebola infection of DCs by blocking viral binding to DC-SIGN in the nanomolar to picomolar range.[118]

All these examples represent interesting multivalent strategies to afford the development of successful and potent carbohydrate-based antiviral drugs that inhibit the cell entry by an antiadhesive effect. Although the in vitro results are very promising, up to now, none of these carbohydrate multivalent systems have been tested in vivo. These studies will be necessary in the future to confirm the application of these systems as therapeutics.

1.24.2.3 Carbohydrates in Vaccine Development

The development of an effective and successful vaccine involves the induction of protective immune responses. These types of responses are best achieved by the generation of long-term protection through a precise integration between innate and adaptive (antigen-specific) immunities.

The innate immune cells, mainly antigen-presenting cells (APCs), detect pathogen-associated molecular patterns (PAMPs) through their surface pattern recognition receptors (PRRs), including the Toll-like receptor (TLR) family and the C-type lectins such as DC-SIGN. APCs, in particular DCs, provide an essential link between innate and adaptive immune systems. PRR stimulation leads to antigen uptake, full maturation of DCs, and intracellular processing of antigens. Antigen presentation to *naive* T cells at the lymph nodes triggers a specific adaptive response (mediated by T and/or B lymphocytes), depending on the antigen exposed on the DC surface. The long-term immunity requires the persistence of vaccine-induced antibodies (or immunoglobulins (Ig)) and/or the generation of immune memory cells. As T lymphocytes are essential to the induction of high-affinity antibodies and immune

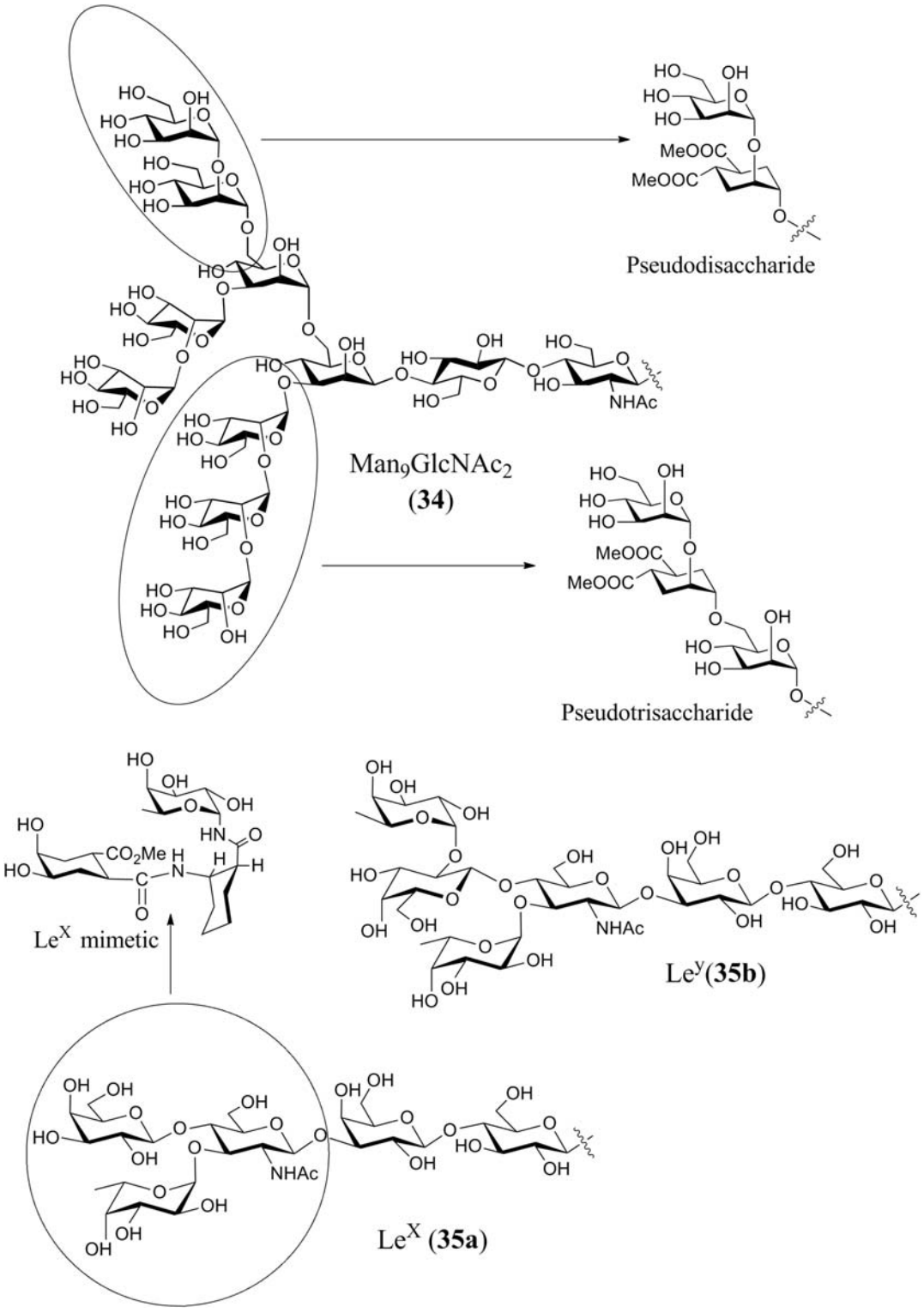

Fig. 19 Chemical structures of high mannose ($(Man)_9(GlcNAc)_2$) (**34**), Le^x (**35a**), and relevant fucose- and mannose-based glycomimetics designed to interact with DC-SIGN.

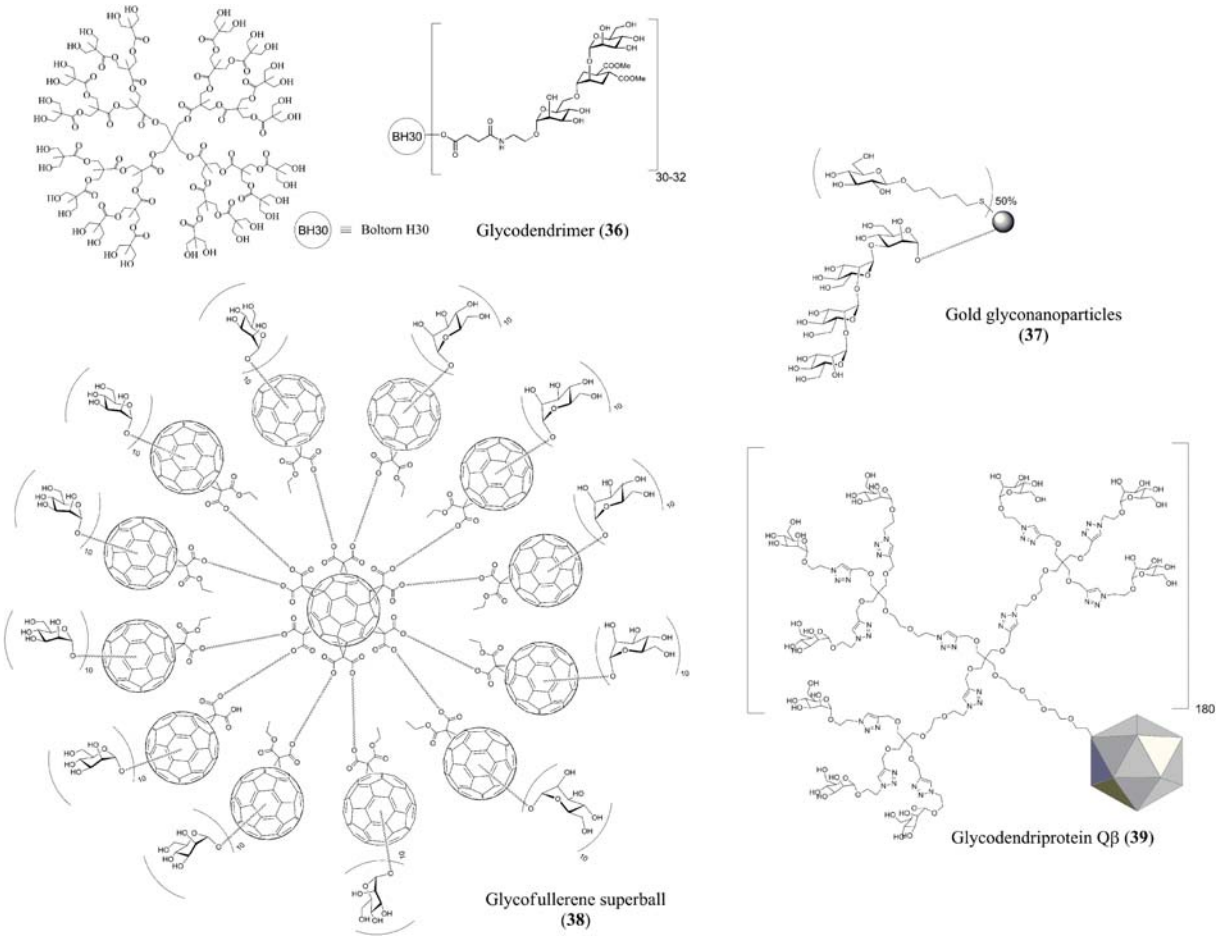

Fig. 20 Selected examples of carbohydrate multivalent systems that inhibit DC-SIGN.

memory, triggering T cell-dependent responses should be the foremost aim on the designing and development of novel vaccine candidates.

In this context, pathogen oligosaccharides, as one of the major PAMPs recognized by host immune cells, can be exploited as the basis for the design of carbohydrate vaccines.[119] As well as specific pathogenic carbohydrates, *tumor-associated carbohydrate antigens* (TACAs) can be recognized by the host immune system, thus employed as cancer vaccine epitopes. Most of the human cancers are characterized by aberrant glycosylation, expressing abnormal oligosaccharides (TACAs) that are not produced by normal tissues or at least in a quantitative or qualitative different form.[120] However, two main problems are related to the use of TACAs as epitopes: their poor immunogenicity and that they sometimes are regarded as "self-antigens." These TACAs have been generally classified into four main groups: *gangliosides* (such as GM2, GM3, GD2, GD3, and fucosyl-GM1, compounds **40–43**), overexpressed in melanoma, and colon, and prostate cancers; *blood group determinants* (SLe^x, SLe^a, Le^y, and KH-1 antigens, compounds **44–47**), implicated in tumor invasion and metastasis; *glycophorins* (including Tn, STn, and TF antigens, compounds **48–50**), typically associated with mucin proteins implicated in epithelial cancers such as breast, prostate, and ovarian; and the *globo series* (globo H and Gb3 oligosaccharides, compounds **51–52**) (Fig. 21).[121] It is important to notice that, whereas classical pathogen vaccines have generally a prophylactic preventing action against future infections, cancer vaccines are intended to induce an immune response against an already existing disease.[121]

Carbohydrates have been widely explored in the design and development of vaccines relying on two main approaches: (a) using antigenic carbohydrates as immunogens to trigger responses against the related pathogenic oligosaccharides (*carbohydrate-based vaccines*) and (b) employing the sugar moiety as an "adjuvant" or immune modulator to target several PPRs, thus improving the immune profiles for a more effective response against other antigens such as peptides (*carbohydrates as immune modulators*). In some cases, both roles are synergistically overlapped.

1.24.2.3.1 Carbohydrates as immune modulators

It has been postulated that, since peptide and protein mannosylations facilitate their uptake by APCs through interaction with some receptors at their surfaces (such as DC-SIGN or mannose receptor (MR)),[122] carbohydrate constructs can be used in the design and

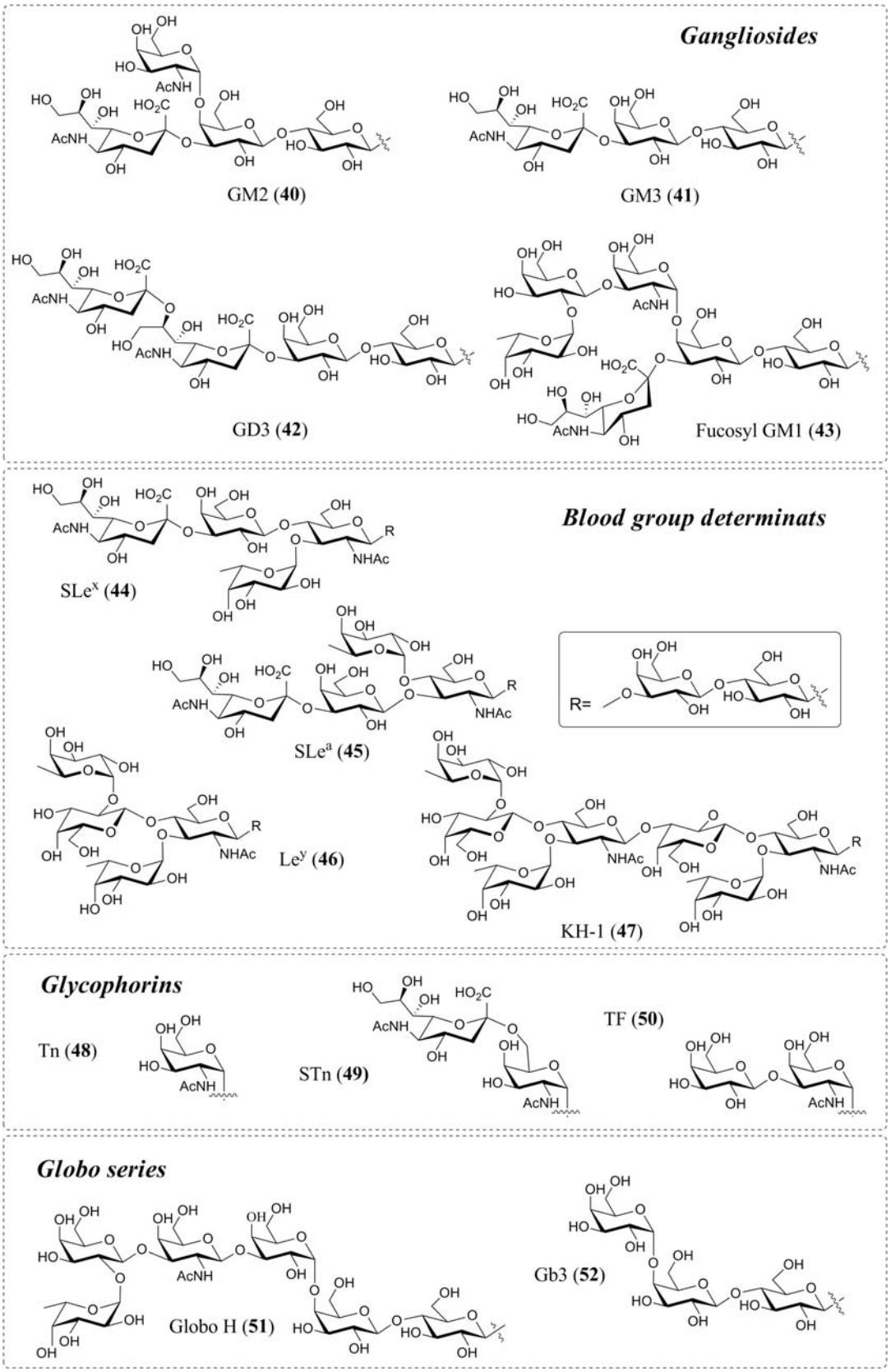

Fig. 21 Selected tumor-associated carbohydrate antigens (TACAs).

development of vaccines with the aim of improving the peptidic epitope delivery and/or initiating DC-mediated signaling, which should result in a better immune response against the mentioned epitopes. Based on this hypothesis, several groups have employed their multivalent glycoconstructs not only to inhibit lectin–carbohydrate-mediated infections but also to develop synthetic vaccine candidates.[123] For instance, ovalbumin (OVA) protein was modified with a DC-SIGN targeting multivalent glycan construct. This structure consisted on poly(amidoamine) dendrimers conjugated with the Le^b tetrasaccharide.[124] The glycan modification enhanced both CD4 + and CD8 + T-cell responses compared with the unmodified OVA, through DC-SIGN interaction in transgenic DCs. In a latter work, it was demonstrated that the use of an OVA peptide, instead of the full entire protein, produced stronger DC activation and subsequent T-cell stimulation.[125] In another attempt to develop a new synthetic vaccine against *influenza A virus*, hybrid constructs named glycodendropeptides (GDPs) and constituted by both peptide- and carbohydrate-functionalized dendrons were designed.[126] Recently, in vitro assays were carried out, demonstrating that these GDPs were recognized by the immunological system inducing DC maturation and CD8 T-lymphocyte proliferation.[127] All these works highlight the observation that APC targeting via PPR interaction might be an important strategy to improve vaccine design.

In the context of vaccine formulation, synthetic carbohydrates are also useful tools for the development of immunoadjuvants (Fig. 22).[2c,128] In this sense, TLR carbohydrate agonist, mainly palmitoylated TLR2 ligands (e.g., Pam_3CysSK_4, **53**; Fig. 22), can be

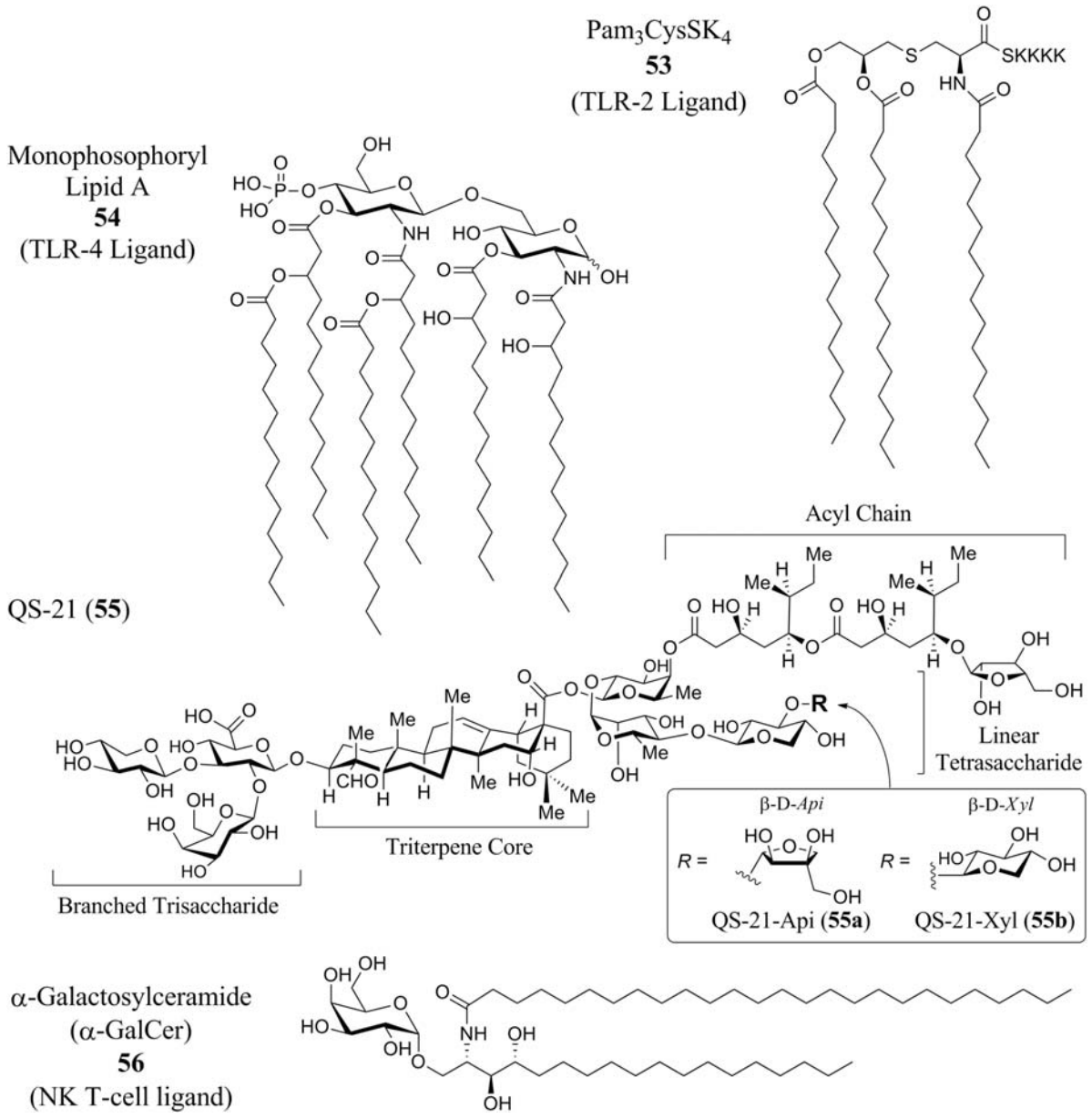

Fig. 22 Carbohydrate adjuvant molecules: Pam_3CysSK_4 (**53**), monophosphoryl lipid A (**54**), QS-21 (**55**), and α-GalCer (**56**).

included in synthetic molecules to improve their immunological responses. Lipopolysaccharides,[82] as TLR4 ligands, can be chemically modified to be conjugated to synthetic vaccines as adjuvant (e.g., the synthetic monophosphoryl lipid A,[129] **54**; Fig. 22). The oligosaccharide-containing natural product saponin QS-21 (**55**; Fig. 22), from the *Quillaja saponaria* tree, is one of the most investigated adjuvants. Two QS-21 active components, QS-21-Api (**55a**; Fig. 22) and QS-21-Xyl (**55b**; Fig. 22), were synthesized, and adjuvant activity was demonstrated by immunological assays.[130] Subsequently, structure–activity relationship studies led to several carbohydrate-truncated Q-21 versions with improved activity–toxicity profiles.[131] Synthetic phosphatidylinositol mannosides from *M. tuberculosis* also exhibit adjuvant activity.[132] Another carbohydrate-based immunoadjuvant is the α-galactosyl ceramide (α-GalCer, **56**; Fig. 22), a natural killer (NK) T-cell ligand. This lead compound, in particular their synthetic analogs, have demonstrated to highly stimulate NK cells in animal models in a range of diseases such as malaria and melanoma.[133] For instance, a capsular polysaccharide antigen covalently linked to α-GalCer induced protection in mice against *S. pneumoniae* by eliciting potent carbohydrate-specific humoral responses.[134] Zwitterionic polysaccharides (ZPSs) have also been employed as immune stimulators as they are able to elicit MHC-II-mediated T-cell responses in the absence of carrier proteins.[135] In an example, a ZPS extracted from *Bacteroides fragilis* was chemoselective conjugated to the GalNAc tumor Tn epitope, with the aim of developing an entirely carbohydrate-based cancer vaccine.[136] The in vivo assays in Tn-ZPS-conjugated immunized mice demonstrated that carbohydrate-specific IgG3 antibodies were produced. These immunoglobulins were able to both bind and recognize human tumor cells displaying the Tn hapten.[137]

1.24.2.3.2 Carbohydrate-based vaccines

The use of carbohydrate antigens as potential vaccines was firstly demonstrated in 1930, when a bacterial capsular polysaccharide could elicit antibody responses against *Streptococcus pneumoniae*.[138] The first polysaccharide-based vaccine, Pneumovax, was commercially launched by Merck in 1983. The current version of this vaccine is composed by an unconjugated capsular polysaccharide isolated from 23 out of around 90 known pneumonia serotypes.[139] Although this vaccine resulted in good protective immune responses in healthy adults, polysaccharide-based vaccines are generally poorly immunogenic with no induced protection in infants, elderly, and immunocompromised patients.[140] This is mainly due to the fact that usually carbohydrate-associated antigens just trigger B-cell responses by cross-linking the B-cell receptor, and they cannot be processed by APCs (an exception is represented by the previously mentioned zwitterionic polysaccharides A from *B. fragilis*). This results in T cell-independent immunity without any MHC-II CD4+ interaction, which is the major obstacle associated with the development of carbohydrate-based vaccines.[141] These T cell-independent responses are less robust and primarily consist of short-lived low-affinity IgM antibody-mediated reactions. *Conjugate vaccines*,[142] consisting of a carbohydrate antigen and an immunogenic T-cell epitope protein (protein carriers like keyhole limpet hemocyanin (KLH), OVA, holo-acyl (HA), and tetanus toxoid (TT)), have proved to overcome this problem, promoting an antibody class switching from IgM to carbohydrate-specific long-term antibodies (IgG) and memory responses. When polysaccharides are covalently linked to proteins, after binding to the carbohydrate B-cell receptor, the protein portion is digested by proteases in the B-cell endosomes. The released peptide epitopes are exposed on the surface of B cells in association with MHC-II and presented to CD4+ T cells. Peptide/MHC-II-activated T cells produce cytokines to stimulate B-cell maturation to memory cells and induce the mentioned immunoglobulin class switch from IgM to IgG.

Many currently commercialized vaccines are based on this glycoconjugated vaccine approach and have proved to be very efficient in preventing a range of human diseases. Among them, vaccines as Menactra (against *Neisseria meningitidis*), Typhim VI (*Salmonella typhi*), Prevnar (*S. pneumoniae*), and Hib Comvax (*Haemophilus influenzae* type b, Hib) can be selected as examples.[2f,143] However, polysaccharide antigens used in these constructs are derived from natural sources, a challenging task that is not always readily available.

In general, polysaccharides obtained from natural sources are heterogeneous mixtures that might imply hard isolation and purification processes, difficulty in the characterization, unavailability of enough amounts of material, loss of activity, and not always safety profiles. Consequently, strategies on the development of new carbohydrate-based vaccines are focusing on the use of more defined fully synthetic oligosaccharides as antigens. A breakthrough in this regard was the Cuban Hib vaccine developed in 2004, which consisted of a synthetic carbohydrate epitope covalently linked to the TT.[144] This first clinically approved fully synthetic carbohydrate vaccine is based on the structure of the capsular polysaccharide antigen from Hib (Fig. 23), and it can be produced in scales large enough to be incorporated into Cuba's current routine vaccination system. Other synthetic glycan epitopes from several pathogens have been attached to carrier proteins, many of them conferring protection against their respective pathologies in animal models.[121,145] Among them can be mentioned those against *Staphylococcus aureus*, *S. pneumoniae*, *Leishmania*,[146] *Plasmodium falciparum*-caused malaria,[147] and even surface spores of *Bacillus anthracis* (anthrax)[148] (Fig. 23). The carrier protein selection is of acute importance in the design of cancer vaccines due to the poor immunogenicity of TACAs. For instance, Theratope (Biomira), a promising candidate vaccine that consisted of an STn-KLH conjugate, failed in the phase III clinical trial because of its low efficiency against breast and metastatic colon cancers.[149]

Despite the conjugation to carrier proteins having demonstrated to be a good approach, preexisting immunity to the protein may suppress the immune response to the conjugated carbohydrate antigen.[150] This phenomenon, known as *carrier-induced epitope suppression*, is particularly problematic when "self-antigens" such as TACAs are employed for the vaccine construct.[151] Using peptidic epitopes instead of the full-length protein has been deeply studied to overcome this matter. This, in combination with the covalent link of immunoadjuvants, may improve the immune response against the pathogenic carbohydrate epitopes, especially for those poor immunogenics as TACAs.[152] Such adjuvants include TLR2 agonist (Pam_2CysSK_4 or Pam_3CysSK_4),[153] saponin QS-21, and α-GalCer.

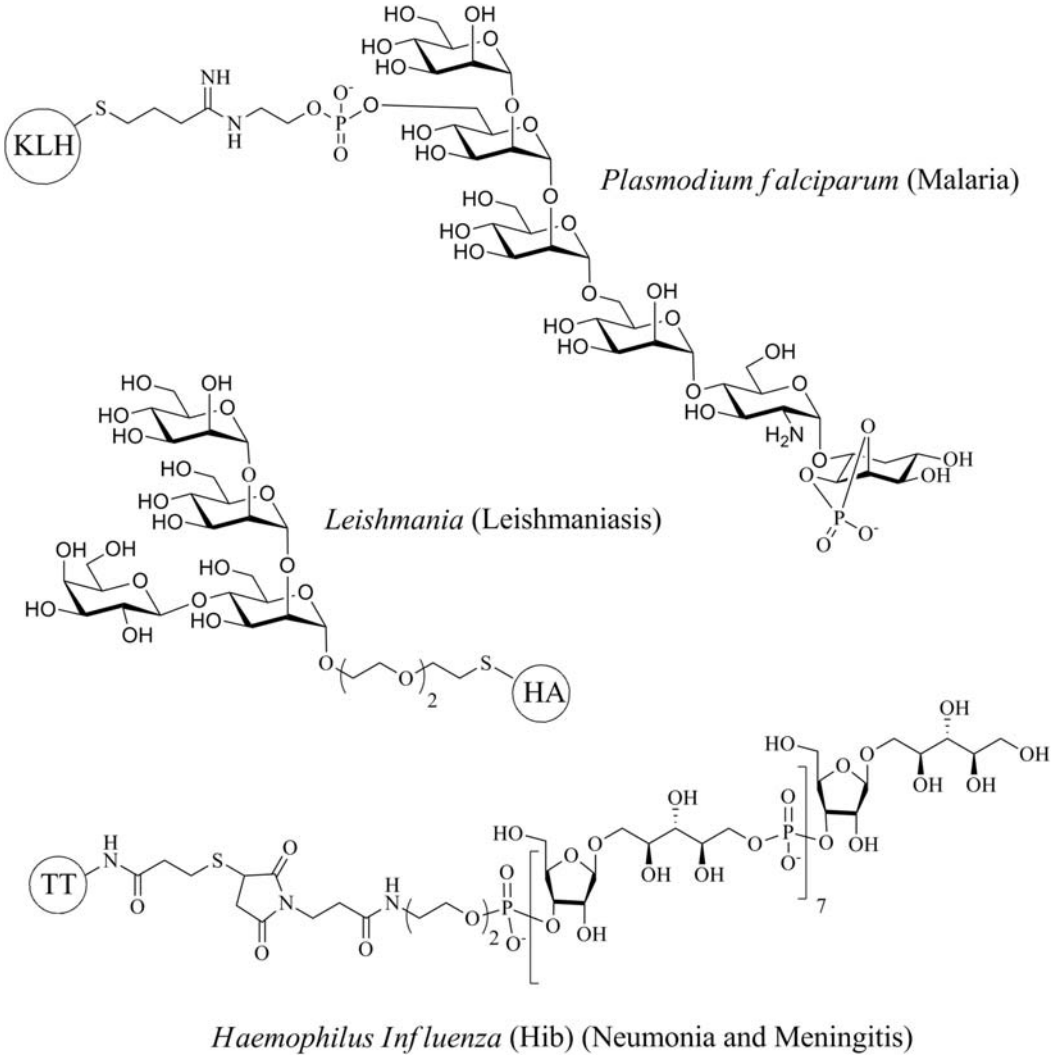

Fig. 23 Synthetic carbohydrate-based vaccines against several microbial pathogens: *H. influenzae type b* (Hib), *Leishmania*, and *P. falciparum*.

With the aim of overcoming the immune tolerance against TACAs, multicomponent self-adjuvanting approaches have been employed to develop totally synthetic vaccines that incorporate the carbohydrate antigen (B-cell epitope), a synthetic adjuvant and/or a selected T-cell peptide. A representative example of this strategy is the design of a tricomponent vaccine candidate composed of a tumor-associated glycopeptide (Tn-MUC1), a T-helper peptide epitope derived from poliovirus ($PV_{103–115}$), and a TLR2 ligand (Pam_2CysSK_4 or Pam_3CysSK_4) (Fig. 24). This all-in-one construct was able to induce high titers of anti-MUC1 IgG antibodies against the Tn antigen of human cancer cells.[154] More recently, those multicomponent self-adjuvant constructs proved to elicit both cellular and humoral immunity, leading to a therapeutic IgG production in a mouse model of breast cancer.[155]

Carbohydrate-based compounds also represent a promising strategy for the development of an effective HIV vaccine, in order to stimulate neutralizing antibodies that bind oligosaccharide high mannose (Man_9) and glycopeptide epitopes from the gp120 envelope protein. Among these antibodies, the most highly studied variant is the 2G12, which neutralizes HIV infection by slowing down the entry of the virus into cells and inhibiting replication after passive transfer into patients.[156] Accordingly, early efforts to elicit an immune response against the high-mannose epitope of gp120 focused on the design and synthesis of multivalent glycoconjugate vaccines on a variety of carrier proteins such as bovine serum albumin. Unfortunately, while these conjugates were able to elicit anticarbohydrate antibodies in animal models, the resulting antibodies were not capable to bind the native gp120 *N*-glycans or neutralize the virus.[157] In a further attempt to prompt protective immunity, synthetic analogs were used instead of mannose to create more immunogenic nonself epitopes. Conjugation of this carbohydrate mimic onto the viruslike particle Qβ resulted in a compound able to bind to the antibody 2G12 with high affinity and elicited a greater antibody response than vaccines constructed with only mannose. However, they failed to bind the native gp120 and did not exhibit HIV-neutralizing activity.[158] In a representative example, the synthesis of several glycopeptides containing the epitope for another HIV-neutralizing antibody (PG9) has been described.[159] The synthetic constructs containing the two closely spaced high-mannose glycans at the amino acids Asn160

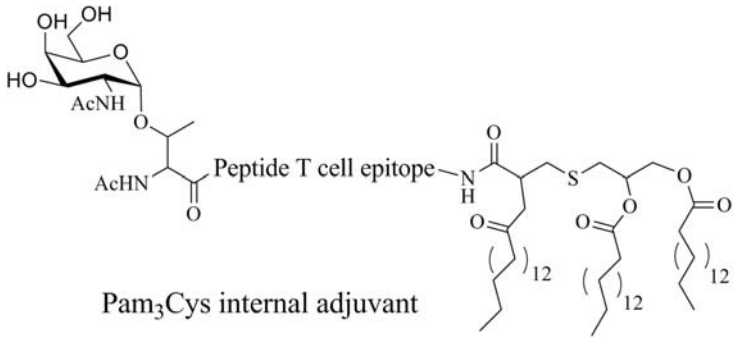

Fig. 24 Tricomponent synthetic vaccine construct composed of the Tn antigen, a T-helper peptide epitope, and a TLR2 ligand (Pam_3CysSK_4).

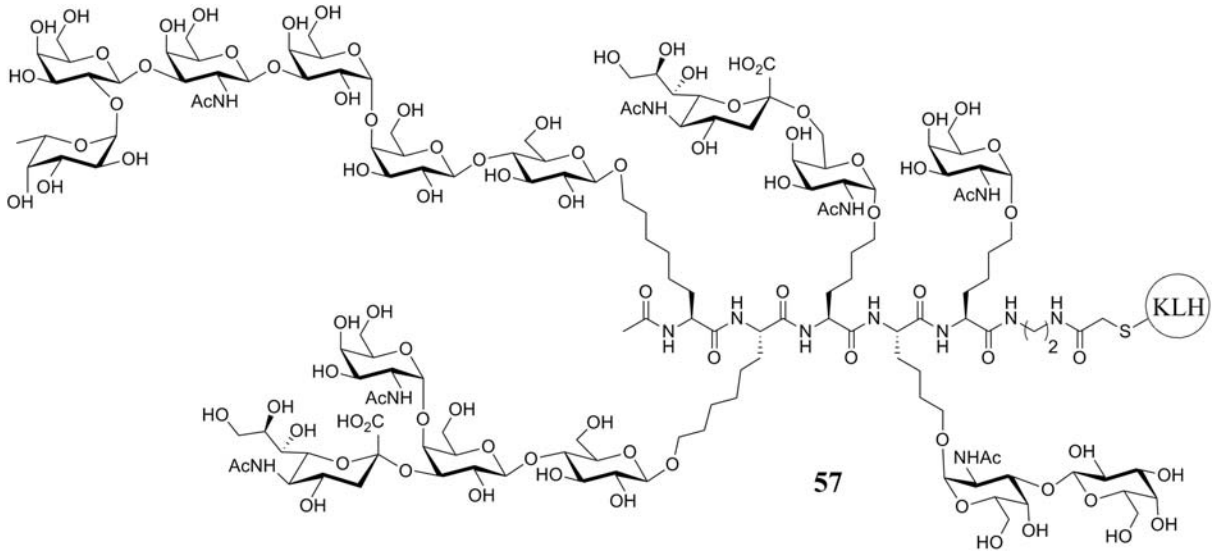

Fig. 25 A peptidic construct containing the antigens globo H, GM2, STn, TF, and Tn (**57**).

and Asn156 of gp120 could bind with high affinity to the PG9 antibody, while the glycans alone were not good ligands. Promising experiments are currently in progress to evaluate their immunogenicity and HIV protection in animal models.

The multivalent presentation of sugar antigens has also been exploited to enhance the immunogenicity of conjugate vaccines against cancer. With the goal of mimicking more closely the heterogeneity of tumor cell surface, trimeric clusters of one carbohydrate antigen[160] and, subsequently, a broader combination of several prostate and breast cancer-associated carbohydrate antigens were developed. This latter construct containing globo H, GM2, STn, TF, and Tn antigens on a single peptide backbone was conjugated to the KLH carrier protein (**57**; Fig. 25).[161] This extraordinary synthetic molecule, in combination with the QS-21 immunoadjuvant, elicited a successful antibody response in mice and is currently in clinical trials against ovarian cancer.

As a summary, the considerations generally applicable to the design of carbohydrate-based conjugate vaccines can be englobed in the good choice of the antigen source, the protein/peptidic carrier, the conjugation method, the adjuvant, and, sometimes, the required multivalency.

1.24.3 Carbohydrate-Mediated Drug and Gene Delivery

Many efforts of the biopharmaceutical industry have been focused on the development of targeted drug delivery in order to improve the efficacy and reduce the side effects of medicaments. A drug delivery system (DDS) is defined as a formulation or a device that enables a therapeutic substance to selectively reach its site of action without reaching the nontarget cells, organs, or tissues. The term therapeutic substance refers not only to a prodrug (a pharmacologically inert substance that undergoes to an active drug in vivo by either chemical or enzymatic reactions) but also to agents such as those for gene therapy. Besides other tools, receptor-mediated endocytosis has been commonly used to deliver drugs to specific types of cells or tissues, and it is particularly applicable to cytotoxic therapy for cancer and gene therapy.

A number of carrier systems and devices have been developed for targeted delivery, like monoclonal antibodies, resealed erythrocytes, and nanocarriers such as nanoparticles, polymers, micelles, carbon-based materials, liposomes, and gels. The early-stage nanocarriers were mostly built up from inorganic materials[162] or artificial polymers.[163] However, mainly due to hydrophobic interactions, most of these nanocarriers adsorb proteins on their surfaces in a process known as *opsonization*.[164] This opsonization can result in a fast nanocarrier clearance from the bloodstream through MPS (*mononuclear phagocyte system*) phagocytosis, turning any in vivo application into a challenge.[164] Enhanced blood circulation times have been usually achieved by the attachment of polyethylene glycol (PEG) moieties to the surface of the carriers, which increases the hydrophilicity and the steric repulsion to proteins,[165] thus resulting in a decreased protein adsorption.[162] Despite the PEG benefits, it is not biodegradable, and several drawbacks might be associated to its use.[158]

In this context, the development of safer and biocompatible nanocarriers, such as those functionalized or performed with mono-, oligo-, or polysaccharides, is currently discussed as alternatives for the traditional ones.[166] Moreover, specific recognition processes mediated by carbohydrate ligands and their respective cell receptors resulted in useful applications for targeting drug or gene delivery.[2f,167] Besides their biodegradation and their active biological function to interact with certain proteins/cell surfaces, their inherent hydrophilicity and their low unspecific protein adsorption make them attractive candidates in the design of DDS for biomedical applications.[165] It has been reported that the polysaccharide hydroxyethyl starch,[168] a synthetically modified starch derivative, dextrin[169], or other saccharides[170] can reduce or even suppress the unspecific uptake of nanocarriers, prolonging their circulation half-life times in the bloodstream.

With the aim of targeting several pathogenic processes such as cancer, infection, or metabolic diseases, many studies have been carried out in the drug delivery field, showing that carbohydrate-functionalized nanodevices (such as liposomes, microspheres, and nanoparticles) or saccharide constructs are excellent tools to target specific cells, tissues, or organs.[171] For example, lactosylated microspheres, micelles, liposomes, or polymers with high specificity for the asialoglycoprotein receptor found on mammalian hepatocytes have been created for liver-specific delivery of drugs and genes.[172] Furthermore, some of these studies have verified that the saccharide shells can be cleaved under a reductive environment that mimics the cell's interior.[173] Mannose-modified liposomes, selectively targeting their MRs, have also been developed as efficient alveolar macrophage selective drug carriers.[174]

Cyclodextrins (CDs), as they are composed of a hydrophilic outside surface and a hydrophobic internal cavity, have been successfully exploited to form inclusion complexes with various hydrophobic drugs to intensely improve their water solubility (**58**; **Fig. 26**).[177] Additionally, these cyclodextrin scaffold glycotransporters have also been widely studied for gene delivery (**59**; **Fig. 26**).[178]

Besides these examples, chitosan and HA have been deeply investigated as novel materials for drug delivery due to their unique biomedical properties.[179] Chitosan is a linear cationic polysaccharide composed of *N*-acetyl-D-glucosamine and glucosamine. The positive charge plays a very important role in mucoadhesion of chitosan DDSs. Also, due to these cationic charges, chitosan can be electrostatically anchored onto the surface of negatively charged polymers or particles. For instance, chitosan-coated particles showed significantly increased uptake by the breast cancer MCF-7 cell line compared with the unmodified nanoparticles. Furthermore, the proapoptotic effect of chitosan proved synergistic with the chemotherapy drug docetaxel.[171] Additionally, multilayered polysaccharide vesicles have been generated from starch as the core and HA as the shell, resulting in self-assembled nanoparticles with a hollow inner core. The enzymatic degradation of the HA shell by hyaluronidase enzyme contributed to accelerate the release of the payload.[180] Antibacterial nanodevices have also been developed by using HA nanocapsules containing the antimicrobial agent polyhexanide. They could be specifically cleaved in the presence of bacterial hyaluronidases, "spreading factors" of pathogens such as *Staphylococcus aureus* and *E. coli*.[181]

A novel strategy named *lectin-directed enzyme-activated prodrug therapy* (LEAPT) has been developed for a regioselective drug release into specific cells that display lectins (**Fig. 27**). LEAPT has been designed as a two-component delivery system that employs a nonmammalian glycosylated enzyme (e.g., α-L-rhamnosidase from *Penicillium decumbens*) and a sugar-bearing prodrug, which is itself the substrate for the enzyme.[182] Through specific carbohydrate–lectin interactions, both the enzyme and the prodrug are internalized into the target cell. Colocalization of both components allows the selective drug release at the target cell, as it only occurs within the vicinity of the enzyme. In this way, by modifying the carbohydrate attached to the glycosidase enzyme, different cell types can be targeted for the release of a given drug.

In the context of lectin-mediated therapies, a class of cell surface receptors expressed in hematopoietic cells and known as siglecs (from *sialic acid-binding immunoglobulin-like lectins*) have been considered attractive targets, not only for carbohydrate-directed therapy for leukemia, lymphomas, and immune cell-mediated diseases but also for carbohydrate recognition-based drug delivery.[183] A number of multivalent sialoside siglec ligands have been successfully applied to direct drug-loaded liposomal nanoparticles to lymphoma cells expressing these lectins.[184] These approaches provide new targets in gene delivery and anticancer therapies.[183] In a sophisticated study, doxorubicin-loaded liposomal nanoparticles were decorated with a high-affinity ligand of the CD22 siglec lectin. These devices were evaluated for targeting B-lymphoma cells, and it was demonstrated that these constructs were actively bound and endocytosed by B cells and able to kill primary malignant B cells from patients with hairy leukemia. Moreover, these CD22-targeted liposomes significantly extended survival in a xenograft model of disseminated Daudi human B-cell lymphoma.[184]

In summary, carbohydrate-based nanocarriers have shown several advantageous properties, such as biodegradability, specific targeting to different cell types, protection and decreased toxicity of the payload, controlled release of the drug by specific protein interaction, and prolonged in vivo plasma half-life times due to reduced protein adsorption. Such behavior makes these sugar constructs highly potential platforms for developing targeted drug devices against many pathogenic processes.

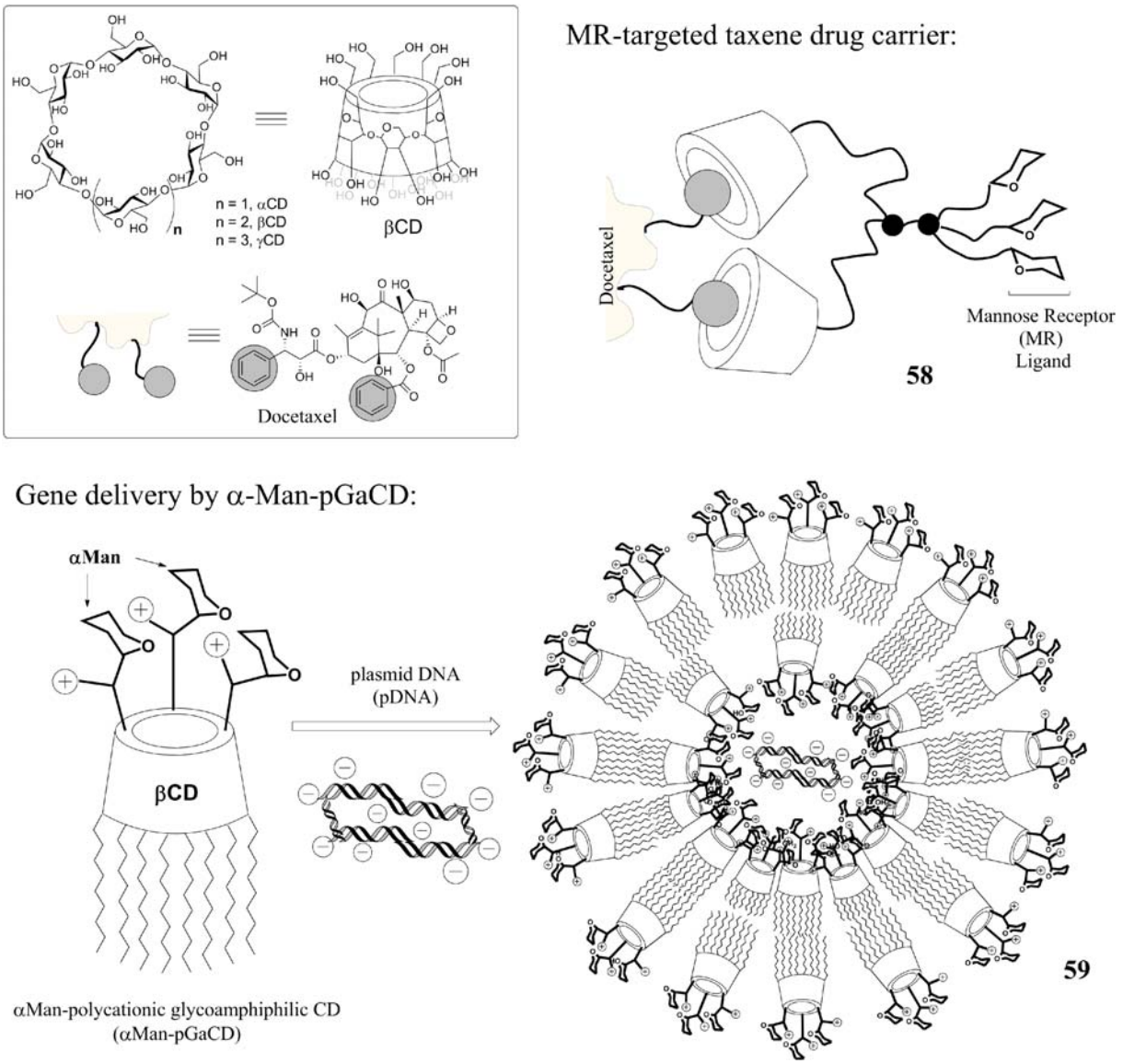

Fig. 26 Examples of cyclodextrins (CDs) employed in drug (**58**)[175] and gene (**59**)[176] delivery.

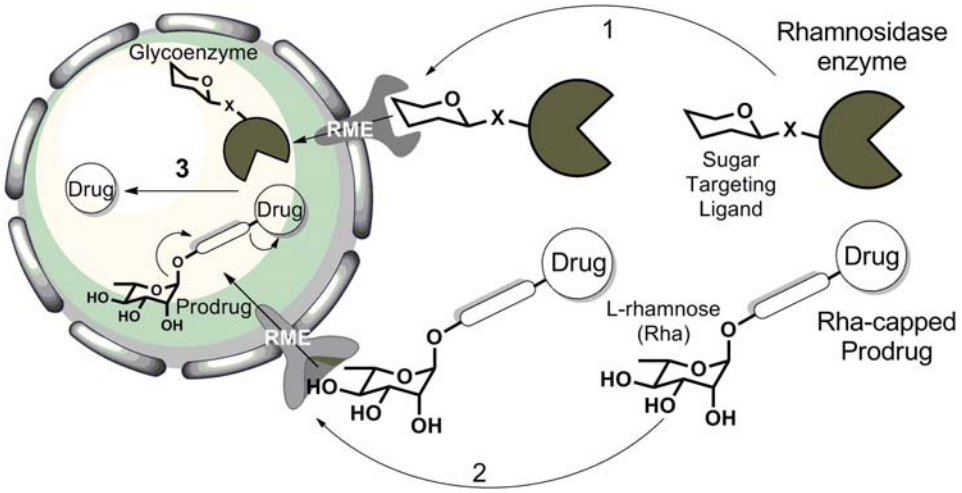

Fig. 27 LEAPT strategy.

1.24.4 Carbohydrate-Based Diagnostics

In the last decades, several methods have been established to study the interactions of carbohydrates with other relevant biomolecules. Among them, carbohydrate[185] and lectin microarrays[186] have emerged as new tools for glycan analysis and diagnosis purposes. Carbohydrate microarrays were independently developed by several groups in 2002 with the aim of obtaining fast and reliable information about the interactions between glycans and antibodies or other carbohydrate-recognizing proteins. Carbohydrate microarrays are composed of diverse glycans densely and orderly attached to a solid surface. One advantage of this microarray-based technology is that it permits the simultaneous evaluation of many glycan–protein interactions using small amounts of samples. More importantly, another relevant hallmark of microarrays is that the glycans anchored on the solid surface are presented in a multivalent fashion, allowing the formation of multivalent complexes with glycan-binding proteins. As a result, proteins that weakly interact with monovalent glycans in solution can strongly bind to carbohydrates on the microarrays (cluster effect).

Apart from the rapid detection of glycan–protein interactions, carbohydrate microarrays have also been employed to study binding properties of several viruses' strains, which has cleared up the differences in binding specificities of pandemic strains and seasonal ones. Similarly, the knowledge gained from the multiple microarray analyses of the interactions related to the HIV infection has been essential for the design of carbohydrate-based HIV vaccine candidates.[187] Other examples, like the screening of human sera to correlate the presence of specific antibodies with resistance to malaria[147] or to identify markers for Crohn's disease,[188] highlight the relevance of carbohydrate microarrays in the diagnostics field.

Overexpression of certain glycoproteins or the alteration in glycan expression can be a hallmark of severe pathologies, including cancer and autoimmune diseases. Accordingly, many efforts have been devoted to the identification of molecular targets that allow the early detection of diseases and the evaluation of the effects of therapy.

The discovery of 2-fluorodeoxy-D-glucose (^{18}FDG)[189] was a huge boost for the routine application of positron emission tomography as a screening tool in oncology, neurology, and cardiology.[190] The employment of FDG in this noninvasive imaging technology relies on its increased concentration in tumor cells or diseased tissues, as they are more glucose-demanding than other cell types.[191]

More recently, the so-called metabolic oligosaccharide engineering (MOE; Fig. 28) was developed to achieve molecular imaging of glycans in living organisms. In a pioneering approach, cell surface carbohydrates were modified with unnatural sugars that

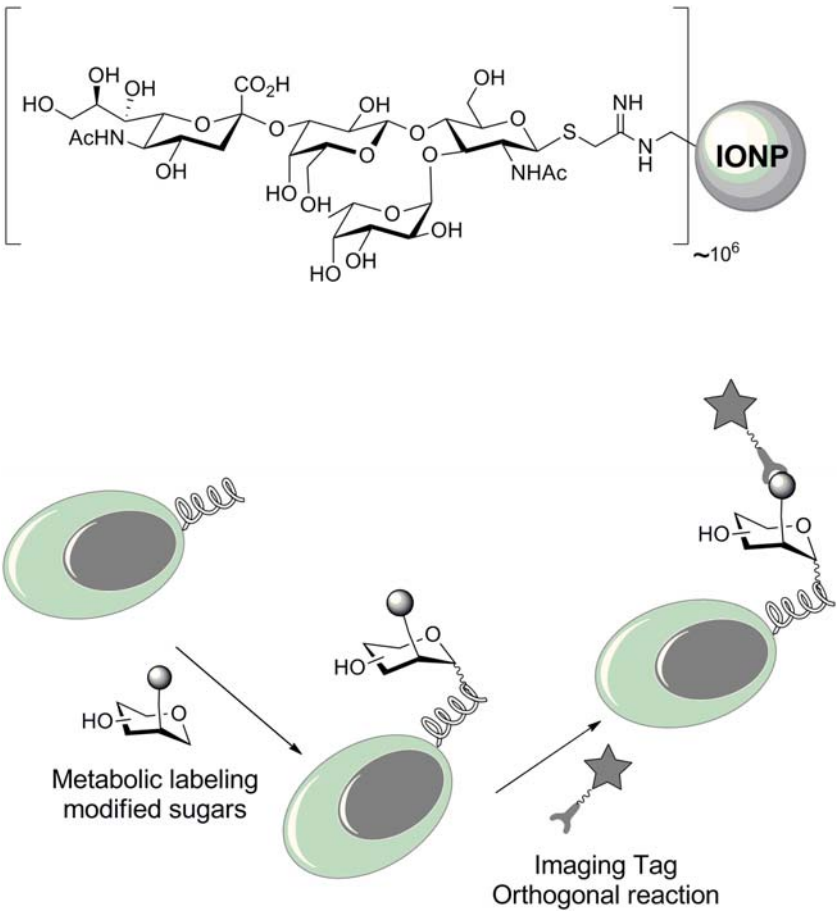

Fig. 28 Schematic representation of SLe^x glyconanoparticles (*above*) and MOE (*below*).

subsequently underwent bioorthogonal reaction with imaging probes. Considering that cancer cells are more metabolically active, this technique should allow discrimination of altered tissues from normal ones using noninvasive detection by magnetic resonance imaging of the preferentially tagged glycans. More broadly, this chemical imaging platform paves the road to the diagnosis of several pathologies related to changes in glycosylation.[192]

Iron oxide nanoparticles (Fig. 28) functionalized with an impressive number of SLe^x have been used to detect presymptomatic brain diseases. The strategy exploited the affinity of the multivalent SLe^x glyconanoparticles toward E- and P-selectins to selectively target and image cerebral inflammation in animal models of MS and stroke.

1.24.5 Glycoengineering in Therapeutics

Most protein-based drugs (antibodies, hormones, enzymes, etc.) are glycoproteins.[193] The glycan part of these molecules modulates the chemical and physical properties as well as the stability, immunogenicity, serum half-life, and clearance from serum. Therefore, control of glycans present in the glycoproteins is essential to maintain their therapeutic properties. An additional problem is the presence of several glycoforms, structural variations in the glycan moieties, frequently found in natural glycoproteins, that complicates the quality control of the therapeutics and the isolation of homogeneous samples.

The development of glycoscience has facilitated the understanding of the glycan role in glycoconjugates, the importance of glycan structures, the definition of their biological targets, and the identification of the glycosyltransferases involved in their biosynthesis. With all this information and the current tools of molecular biology, now it is possible to address the large-scale production of recombinant glycoprotein therapeutics in high quality and purity with a reasonable cost. Moreover, control of the protein glycosylation process in a tailor-made fashion can provide the way to obtain neoglycoproteins with improved therapeutic properties, an emerging field of remarkable interest in particular for the biotechnology industry. There are already some notable examples of glycoprotein therapeutics in the market (Table 3).

To address the preparation of these glycoprotein-based therapeutics, different strategies are described such as modification of the glycosyl pattern of native proteins (entries 1, 2, and 3; Table 3), proteins chemically modified (entry 4; Table 3), engineered fusion proteins (entries 5 and 11; Table 3), antibodies (entries 6, 7, and 8; Table 3), cytokines (entries 9 and 10; Table 3), and recombinant enzymes (entry 12; Table 3).

A very well-known example is erythropoietin, also known as EPO, a glycoprotein hormone that controls erythropoiesis, or red blood cell production, and therefore prescribed for the treatment of anemia. This drug is very popular due to its use by athletes to increase aerobic capacity by maximizing the uptake of O_2 in order to enhance its transport to the muscles. Erythropoietin is considered a performance-enhancing drug and a doping agent by various athletic governing bodies. EPO plays other important roles in the brain's response to neuronal injury and is also involved in the wound healing process. Exogenous erythropoietin is produced by recombinant DNA technology in cell culture. Several different pharmaceutical agents are available with a variety of glycosylation patterns and are collectively called erythropoiesis-stimulating agents such as epoetin alfa (Procrit, Johnson & Johnson, or Epogen, Amgen) and, a second generation based on a different glycosylation pattern with improved therapeutic properties, darbepoetin alfa (Aranesp, Amgen).[194] A different strategy to improve the therapeutic activity of EPO derivatives is the chemical modification of the glycoprotein introducing a polyethylene glycol (PEG). Methoxy PEG-epoetin beta (Mircera, Roche) is a continuous erythropoietin receptor activator. It is indicated for patients with anemia associated with chronic kidney disease. This molecule is based on erythropoietin where methoxy polyethylene glycol butanoic acid is conjugated to the N-terminal amino group or to the ε-amino group of any lysine present in the protein.[195]

Imiglucerase (Cerezyme and Genzyme) is an enzyme-based glycoprotein for the treatment of Gaucher disease. This disorder is characterized by the accumulation of glucosylceramide in cells of certain organs due to the lack of glucocerebrosidase enzyme activity. The treatment of patients by direct injection of the native glucocerebrosidase is not efficient due to the fast clearance of

Table 3 Glycoprotein-based drugs approved for their use

Entry	*Compound (trade name)*	*Indication*	*Company*
1	Epoetin alfa (*Procrit*, *Epogen*)	Anemia	Johnson & Johnson, Amgen
2	Darbepoetin alfa (*Aranesp*)	Anemia	Amgen
3	Imiglucerase (*Cerezyme*)	Gauche disease	Genzyme
4	Methoxy polyethylene glycol-epoetin beta (*Mircera*)	Anemia	Roche
5	Rilonacept (*Arcalyst*)	Cryopyrin-associated periodic syndromes (CAPS)	Regeneron Pharmaceuticals
6	Bevacizumab (*Avastin*)	Metastatic colorectal cancer	Genentech
7	Cetuximab (*Erbitux*)	Colorectal cancer	Eli Lilly, BMS
8	Trastuzumab (*Herceptin*)	Breast cancer	Roche
9	Interferon alpha (*Wellferon*)	Chronic hepatitis B	Wellcome
10	Interferon beta-1a (Avonex)	Multiple sclerosis	Biogen
11	Etanercept (Enbrel)	Rheumatoid arthritis	Pfizer, Amgen
12	Idursulfase (*Elaprase*)	Hunter syndrome (mucopolysaccharidosis II)	Shire Pharmaceuticals

the enzyme by the liver. Imiglucerase is based on modified glycans in which the native sialic acid residues have been removed, thereby allowing exposure of mannose sugar residues that notably reduces its clearance by the liver, enhancing its therapeutic effects.[196]

Rilonacept (Arcalyst, Regeneron) is an engineered dimeric fusion protein consisting of the ligand-binding domains of the extracellular portions of the human interleukin-1 receptor component and interleukin-1 (IL-1) receptor accessory protein linked to the Fc region of human immunoglobulin IgG1. This protein binds and neutralizes IL-1. The drug is used for the treatment of cryopyrin-associated periodic syndrome (CAPS).[197] Another example of the fusion protein strategy is etanercept (Enbrel, Amgen). This fusion protein is indicated for the treatment of active rheumatoid arthritis. The protein is produced by recombinant DNA and contains the tumor necrosis factor (TNF) receptor fused with the constant end of the IgG1. Its mechanism of action is based on the interaction with TNF inhibiting the pro-inflammatory effects caused by TNF.[198]

Probably, one of the more active research fields in the glycoengineering area is the production of antibodies due to their high selectivity and efficiency to interact with target molecules. Bevacizumab (Avastin, Genentech) is a recombinant humanized monoclonal antibody that interacts with the vascular endothelial growth factor A and inhibits angiogenesis. This molecule is indicated for colorectal cancer.[199] Cetuximab (Erbitux, Eli Lilly) is a monoclonal antibody that specifically blocks the epidermal growth factor receptor (EGFR) overexpressed in colorectal cancer cells. This receptor is related with the tumor progression. The inhibition of EGFR will induce the downregulation of this receptor and will modulate the cell division.[200] Another example is trastuzumab (Herceptin, Roche), a humanized monoclonal antibody that interferes with a receptor of the EGFR family, the HER2 receptor, overexpressed in breast cancer.[201]

Two examples of interferon cytokines are commercialized to treat different diseases. Interferon alpha-n1 (Wellferon, Wellcome) is a natural glycosylated human interferon alpha produced from a lymphoid cell line and consists of multiple subtypes. This interferon presents antiviral, immunomodulatory, and antiproliferative properties and is indicated for the treatment of chronic viral hepatitis B.[202] Interferon beta-1a (Avonex, Biogen) is another cytokine of the interferon family used to treat MS reducing neuron inflammation. The mechanism of action is complex and probably comprises several pathways.[203]

A final example comprises the use of an enzyme, idursulfase (Elaprase, Shire), a recombinant enzyme used in enzyme replacement therapy to treat mucopolysaccharidosis type II (Hunter syndrome). MPS is a lysosomal storage disease characterized by a deficiency of iduronate-2-sulfatase, an enzyme responsible for cleavage of O-linked sulfate from GAGs dermatan sulfate and heparan sulfate.[204]

1.24.6 Conclusions and Perspectives

The understanding of the role that carbohydrates play in many relevant biological processes and the progress of glycoscience have boosted the development of carbohydrate-based drugs. Modern analytic tools and the application of glycoarrays have facilitated the identification and characterization of glycan structures involved in defining physiological and pathological processes as well as the identification of new therapeutic targets. The development of efficient synthetic strategies has provided the tools to access to complex carbohydrate structures in the pure forms and quantities required for carbohydrate-based drug developments. The high selectivity of carbohydrate–protein interactions involved in these biological events and the huge possibilities that carbohydrate scaffolds offer to design new drugs based on them, improving their drug-like properties, their affinity, and even the selectivity, are important items to be taken into account. For this reason, the search for new carbohydrate-based drugs can be considered as a hot topic in medicinal chemistry.

Several examples described in the preceding text, where the typical heat to lead the medicinal chemistry process has been applied, show how this strategy can be successful for the development of new therapeutics based on carbohydrates. There is still plenty of room to improve the current available carbohydrate-based drug candidates and for the discovery of new ones. Up to now, some important contributions to the pharmaceutical arsenal came from the glycomimetics. Probably, one of the most recent remarkable and very popular examples is the well-known drug oseltamivir (Tamiflu), which was in high demand when the avian influenza (bird flu) pandemic by the strain H5N1 caused a world health crisis in 2005.

Today, new avenues are envisaged with the development of carbohydrate multivalent systems to be applied in many biological processes where carbohydrate participates through the interaction with lectins. A priori, these high-molecular-weight molecules do not seem adequate to be considered as drugs; however, these compounds have attracted the attention of medicinal chemists due to their potential therapeutic applications.

Glycoengineering and the development of tools in molecular biology pave the way to create de novo glycoproteins as therapeutics (biotherapeutics) with remarkable selectivities and efficiencies for their targets. The reduction of the production cost and the improvement of the bioengineering processes to generate large-scale glycoproteins are fundamental issues to the progress of this field. More recently, the application of carbohydrates in the development of synthetic vaccines represented a landmark in the area, although a large road waits until the role that carbohydrates play in immune modulation and immunogenicity can be fully understood.

A very promising future is ahead for the carbohydrate field in the area of medicinal chemistry. The development of new carbohydrate-based drugs and the progress in the glycoscience field should go hand in hand to face persistent, chronic, and new diseases, for which new medications are demanded, a challenge to be certainly achieved with the participation of glycoscientists.

References

1. Varki, A. *Essentials of Glycobiology;* Cold Spring Harbor Laboratory Press: Cold Spring Harbor, N.Y, 2009; (b) Stick, R. V. *Carbohydrates: The Sweet Molecules of Life;* Academic: San Diego, California; London, 2001; (c) Varki, A. Biological Roles of Oligosaccharides: All of the Theories Are Correct. *Glycobiology* **1993,** *3* (2), 97–130.
2. (a) Jimenez-Barbero, J.; Cañada, F. J.; Martin-Santamaria, S. *Carbohydrates in Drug Design and Discovery;* RSC Publishing: London, 2015; (b) Zhang, Y.; Wang, F. Carbohydrate Drugs: Current Status and Development Prospect. *Drug Discov. Ther.* **2015,** *9* (2), 79–87; (c) Fernández-Tejada, A.; Cañada, F. J.; Jiménez-Barbero, J. Recent Developments in Synthetic Carbohydrate-Based Diagnostics, Vaccines, and Therapeutics. *Chem. Eur. J.* **2015,** *21* (30), 10616–10628; (d) Klysov, A. A. *Glycobiology and Drug Design;* American Chemical Society: Washington DC, 2012; (e) Ernst, B.; Magnani, J. L. From Carbohydrate Leads to Glycomimetic Drugs. *Nat. Rev. Drug Discov.* **2009,** *8* (8), 661–677; (f) Osborn, H. M. I.; Evans, P. G.; Gemmell, N.; Osborne, S. D. Carbohydrate-Based Therapeutics. *J. Pharm. Pharmacol.* **2004,** *56* (6), 691–702; (g) Wong, C.-H. *Carbohydrate-Based Drug Discovery;* Wiley-VCH: Weinheim, 2003.
3. (a) Gupta, G.; Surolia, A. Glycomics: An Overview of the Complex Glycocode. *Adv. Exp. Med. Biol.* **2012,** *749,* 1–13; (b) Shriver, Z.; Raguram, S.; Sasisekharan, R. Glycomics: A Pathway to a Class of New and Improved Therapeutics. *Nat. Rev. Drug Discov.* **2004,** *3* (10), 863–873.
4. (a) Kamerling, J. P.; Boons, G.-J. *Comprehensive Glycoscience: From Chemistry to Systems Biology;* Elsevier: Amsterdam; Boston, 2007; (b) Fraser-Reid, B. O.; Tatsuta, K.; Thiem, J. *Glycoscience Chemistry and Chemical Biology;* Springer: Berlin; New York, 2008; (c) Taylor, M. E.; Drickamer, K. *Introduction to Glycobiology,* 3rd ed.; Oxford University Press: New York, 2011.
5. Linhardt, R. J. 2003 Claude S. Hudson Award Address in Carbohydrate Chemistry. Heparin: Structure and Activity. *J. Med. Chem.* **2003,** *46* (13), 2551–2564.
6. Lindahl, U.; Backstrom, G.; Hook, M.; Thunberg, L.; Fransson, L. A.; Linker, A. Structure of the Antithrombin-Binding Site in Heparin. *Proc. Natl. Acad. Sci. U. S. A.* **1979,** *76* (7), 3198–3202.
7. Hirsh, J.; Raschke, R.; Warkentin, T. E.; Dalen, J. E.; Deykin, D.; Poller, L. Heparin: Mechanism of Action, Pharmacokinetics, Dosing Considerations, Monitoring, Efficacy, and Safety. *Chest* **1995,** *108* (4 Suppl), 258S–275S.
8. Linhardt, R. J.; Liu, J. Synthetic Heparin. *Curr. Opin. Pharmacol.* **2012,** *12* (2), 217–219.
9. Xu, Y.; Masuko, S.; Takieddin, M.; Xu, H.; Liu, R.; Jing, J.; Mousa, S. A.; Linhardt, R. J.; Liu, J. Chemoenzymatic Synthesis of Homogeneous Ultralow Molecular Weight Heparins. *Science* **2011,** *334* (6055), 498–501.
10. Liu, H.; Zhang, Z.; Linhardt, R. J. Lessons Learned From the Contamination of Heparin. *Nat. Prod. Rep.* **2009,** *26* (3), 313–321.
11. Petitou, M.; van Boeckel, C. A. A. A Synthetic Antithrombin III Binding Pentasaccharide Is Now a Drug! What Comes Next? *Angew. Chem. Int. Ed.* **2004,** *43* (24), 3118–3133.
12. Reynolds, N. A.; Perry, C. M.; Scott, L. J. Fondaparinux Sodium: A Review of Its Use in the Prevention of Venous Thromboembolism Following Major Orthopaedic Surgery. *Drugs* **2004,** *64* (14), 1575–1596.
13. Noble, S.; Peters, D. H.; Goa, K. L. Enoxaparin. A Reappraisal of Its Pharmacology and Clinical Applications in the Prevention and Treatment of Thromboembolic Disease. *Drugs* **1995,** *49* (3), 388–410.
14. Barradell, L. B.; Buckley, M. M. Nadroparin Calcium. A Review of Its Pharmacology and Clinical Applications in the Prevention and Treatment of Thromboembolic Disorders. *Drugs* **1992,** *44* (5), 858–888.
15. Dunn, C. J.; Sorkin, E. M. Dalteparin Sodium. A Review of Its Pharmacology and Clinical Use in the Prevention and Treatment of Thromboembolic Disorders. *Drugs* **1996,** *52* (2), 276–305.
16. Krieter, D. H.; Fink, S.; Dorsch, O.; Harenberg, J.; Melzer, N.; Wanner, C.; Lemke, H. D. Pharmacokinetics of Certoparin During in vitro and in vivo Dialysis. *Artif. Organs* **2015,** *39* (11), 951–959.
17. McKeage, K.; Keating, G. M. Parnaparin: A Review of Its Use in the Management of Venous Thromboembolism, Chronic Venous Disease and Other Vascular Disorders. *Drugs* **2008,** *68* (1), 105–122.
18. (a) Islam, T.; Linhardt, R. J. Chemistry, Biochemistry, and Pharmaceutical Potentials of Glycosaminoglycans and Related Saccharides. In *Carbohydrate-Based Drug Discovery;* Wiley-VCH, Verlag GmbH & Co. KGaA: Weinheim (Germany), 2005; pp 407–439; (b) Esko, J. D.; Kimata, K.; Lindahl, U. Proteoglycans and Sulfated Glycosaminoglycans. In *Essentials of Glycobiology;* Varki, A., Cummings, R. D., Esko, J. D., Freeze, H. H., Stanley, P., Bertozzi, C. R., Hart, G. W., Etzler, M. E., Eds., 2nd ed.; Cold Spring Harbor Laboratory Press: Cold Spring Harbor (NY), 2009.
19. Hascall, V.; Esko, J. D. Hyaluronan. In *Essentials of Glycobiology;* Varki, A., Cummings, R. D., Esko, J. D., Freeze, H. H., Stanley, P., Bertozzi, C. R., Hart, G. W., Etzler, M. E., Eds., 2nd ed.; Cold Spring Harbor Laboratory Press: Cold Spring Harbor (NY), 2009.
20. www.anikatherapeutics.com.
21. Gold, M. H. Use of Hyaluronic Acid Fillers for the Treatment of the Aging Face. *Clin. Interv. Aging* **2007,** *2* (3), 369–376.
22. Magnani, J. L.; Ernst, B. Glycomimetic Drugs—A New Source of Therapeutic Opportunities. *Discov. Med.* **2009,** *8* (43), 247–252.
23. Cooper, N. J.; Sutton, A. J.; Abrams, K. R.; Wailoo, A.; Turner, D.; Nicholson, K. G. Effectiveness of Neuraminidase Inhibitors in Treatment and Prevention of Influenza A and B: Systematic Review and Meta-Analyses of Randomised Controlled Trials. *BMJ* **2003,** *326* (7401), 1235–1242.
24. Kim, C. U.; Lew, W.; Williams, M. A.; Liu, H.; Zhang, L.; Swaminathan, S.; Bischofberger, N.; Chen, M. S.; Mendel, D. B.; Tai, C. Y.; Laver, W. G.; Stevens, R. C. Influenza Neuraminidase Inhibitors Possessing a Novel Hydrophobic Interaction in the Enzyme Active Site: Design, Synthesis, and Structural Analysis of Carbocyclic Sialic Acid Analogues With Potent Anti-Influenza Activity. *J. Am. Chem. Soc.* **1997,** *119* (4), 681–690.
25. von Itzstein, M.; Wu, W.-Y.; Kok, G. B.; Pegg, M. S.; Dyason, J. C.; Jin, B.; Phan, T. V.; Smythe, M. L.; White, H. F.; Oliver, S. W.; Colman, P. M.; Varghese, J. N.; Ryan, D. M.; Woods, J. M.; Bethell, R. C.; Hotham, V. J.; Cameron, J. M.; Penn, C. R. Rational Design of Potent Sialidase-Based Inhibitors of Influenza Virus Replication. *Nature* **1993,** *363* (6428), 418–423.
26. Campbell, L. K.; Baker, D. E.; Campbell, R. K. Miglitol: Assessment of Its Role in the Treatment of Patients With Diabetes Mellitus. *Ann. Pharmacother.* **2000,** *34* (11), 1291–1301.
27. Dabhi, A. S.; Bhatt, N. R.; Shah, M. J. Voglibose: An Alpha Glucosidase Inhibitor. *J. Clin. Diagn. Res.* **2013,** *7* (12), 3023–3027.
28. Truscheit, E.; Frommer, W.; Junge, B.; Müller, L.; Schmidt, D. D.; Wingender, W. Chemistry and Biochemistry of Microbial α-Glucosidase Inhibitors. *Angew. Chem. Int. Ed.* **1981,** *20* (9), 744–761.
29. Karoli, T.; Liu, L.; Fairweather, J. K.; Hammond, E.; Li, C. P.; Cochran, S.; Bergefall, K.; Trybala, E.; Addison, R. S.; Ferro, V. Synthesis, Biological Activity, and Preliminary Pharmacokinetic Evaluation of Analogues of a Phosphosulfomannan Angiogenesis Inhibitor (PI-88). *J. Med. Chem.* **2005,** *48* (26), 8229–8236.
30. Hulett, M. D.; Freeman, C.; Hamdorf, B. J.; Baker, R. T.; Harris, M. J.; Parish, C. R. Cloning of Mammalian Heparanase, an Important Enzyme in Tumor Invasion and Metastasis. *Nat. Med.* **1999,** *5* (7), 803–809.
31. Liao, B. Y.; Wang, Z.; Hu, J.; Liu, W. F.; Shen, Z. Z.; Zhang, X.; Yu, L.; Fan, J.; Zhou, J. PI-88 Inhibits Postoperative Recurrence of Hepatocellular Carcinoma via Disrupting the Surge of Heparanase After Liver Resection. *Tumour Biol.* **2015,** *28,* 1–12.
32. Basche, M.; Gustafson, D. L.; Holden, S. N.; O'Bryant, C. L.; Gore, L.; Witta, S.; Schultz, M. K.; Morrow, M.; Levin, A.; Creese, B. R.; Kangas, M.; Roberts, K.; Nguyen, T.; Davis, K.; Addison, R. S.; Moore, J. C.; Eckhardt, S. G. A Phase I Biological and Pharmacologic Study of the Heparanase Inhibitor PI-88 in Patients With Advanced Solid Tumors. *Clin. Cancer Res.* **2006,** *12* (18), 5471–5480.
33. Cox, T.; Lachmann, R.; Hollak, C.; Aerts, J.; van Weely, S.; Hrebícek, M.; Platt, F.; Butters, T.; Dwek, R.; Moyses, C.; Gow, I.; Elstein, D.; Zimran, A. Novel Oral Treatment of Gaucher's Disease With *N*-Butyldeoxynojirimycin (OGT 918) to Decrease Substrate Biosynthesis. *Lancet* **2000,** *355* (9214), 1481–1485.
34. Lyseng-Williamson, K. A. Miglustat: A Review of Its Use in Niemann-Pick Disease Type C. *Drugs* **2014,** *74* (1), 61–74.

35. (a) Shank, R. P.; Gardocki, J. F.; Streeter, A. J.; Maryanoff, B. E. An Overview of the Preclinical Aspects of Topiramate: Pharmacology, Pharmacokinetics, and Mechanism of Action. *Epilepsia* **2000,** *41* (1), S3–S9; (b) Faught, E. Topiramate in the Treatment of Partial and Generalized Epilepsy. *Neuropsychiatr. Dis. Treat.* **2007,** *3* (6), 811–821; (c) Ruiz, L.; Ferrandi, D. Topiramate in Migraine Progression. *J. Headache Pain* **2009,** *10* (6), 419–422; (d) Diener, H. C.; Bussone, G.; Van Oene, J. C.; Lahaye, M.; Schwalen, S.; Goadsby, P. J. Topiramate Reduces Headache Days in Chronic Migraine: A Randomized, Double-Blind, Placebo-Controlled Study. *Cephalalgia* **2007,** *27* (7), 814–823.
36. Bodley, A.; Liu, L. F.; Israel, M.; Seshadri, R.; Koseki, Y.; Giuliani, F. C.; Kirschenbaum, S.; Silber, R.; Potmesil, M. DNA Topoisomerase II-Mediated Interaction of Doxorubicin and Daunorubicin Congeners With DNA. *Cancer Res.* **1989,** *49* (21), 5969–5978.
37. Igarashi, K.; Ishitsuka, H.; Kaji, A. Comparative Studies on the Mechanism of Action of Lincomycin, Streptomycin, and Erythromycin. *BBRC* **1969,** *37* (3), 499–504.
38. Wassersug, J. D. Pulmonary Tuberculosis. *N. Engl. J. Med.* **1946,** *235* (7), 220–229.
39. Kirst, H. A. Semi-Synthetic Derivatives of Erythromycin. *Prog. Med. Chem.* **1993,** *30,* 57–88.
40. The-Digitalis-Investigation-Group. The Effect of Digoxin on Mortality and Morbidity in Patients With Heart Failure. *N. Engl. J. Med.* **1997,** *336* (8), 525–533.
41. (a) Sharon, N. Lectins: Carbohydrate-Specific Reagents and Biological Recognition Molecules. *J. Biol. Chem.* **2007,** *282* (5), 2753–2764; (b) Kilpatrick, D. C. *Handbook of Animal Lectins. Properties and Biomedical Applications;* John Wiley and Sons Ltd: Chichester, UK, 2000.
42. Ley, K.; Laudanna, C.; Cybulsky, M. I.; Nourshargh, S. Getting to the Site of Inflammation: The Leukocyte Adhesion Cascade Updated. *Nat. Rev. Immunol.* **2007,** *7* (9), 678–689.
43. (a) Lasky, L. A. Selectin-Carbohydrate Interactions and the Initiation of the Inflammatory Response. *Annu. Rev. Biochem.* **1995,** *64,* 113–139; (b) Berg, E. L.; Robinson, M. K.; Mansson, O.; Butcher, E. C.; Magnani, J. L. A Carbohydrate Domain Common to Both Sialyl Le(a) and Sialyl Le(X) is Recognized by the Endothelial Cell Leukocyte Adhesion Molecule ELAM-1. *J. Biol. Chem.* **1991,** *266* (23), 14869–14872.
44. (a) Magnani, J. L. Letters to the Glyco-Forum: The Tumor Markers, Sialyl Lea and Sialyl Lex Bind ELAM-1. *Glycobiology* **1991,** *1* (4), 318–320; (b) Fukushima, K.; Hirota, M.; Terasaki, P. I.; Wakisaka, A.; Togashi, H.; Chia, D.; Suyama, N.; Fukushi, Y.; Nudelman, E.; Hakomori, S. Characterization of Sialosylated Lewisx as a New Tumor-Associated Antigen. *Cancer Res.* **1984,** *44* (11), 5279–5285.
45. (a) Bevilacqua, M. P.; Nelson, R. M.; Mannori, G.; Cecconi, O. Endothelial-Leukocyte Adhesion Molecules in Human Disease. *Annu. Rev. Med.* **1994,** *45* (1), 361–378; (b) Coussens, L. M.; Werb, Z. Inflammation and Cancer. *Nature* **2002,** *420* (6917), 860–867.
46. Kerr, K. M.; Auger, W. R.; Marsh, J. J.; Comito, R. M.; Fedullo, R. L.; Smits, G. J.; Kapelanski, D. P.; Fedullo, P. F.; Channick, R. N.; Jamieson, S. W.; Moser, K. M. The Use of Cylexin (CY-1503) in Prevention of Reperfusion Lung Injury in Patients Undergoing Pulmonary Thromboendarterectomy. *Am. J. Respir. Crit. Care Med.* **2000,** *162* (1), 14–20.
47. (a) Wong, C.-H.; Moris-Varas, F.; Hung, S.-C.; Marron, T. G.; Lin, C.-C.; Gong, K. W.; Weitz-Schmidt, G. Small Molecules as Structural and Functional Mimics of Sialyl Lewis X Tetrasaccharide in Selectin Inhibition: A Remarkable Enhancement of Inhibition by Additional Negative Charge and/or Hydrophobic Group. *J. Am. Chem. Soc.* **1997,** *119* (35), 8152–8158; (b) Kranich, R.; Busemann, A. S.; Bock, D.; Schroeter-Maas, S.; Beyer, D.; Heinemann, B.; Meyer, M.; Schierhorn, K.; Zahlten, R.; Wolff, G.; Aydt, E. M. Rational Design of Novel, Potent Small Molecule Pan-Selectin Antagonists. *J. Med. Chem.* **2007,** *50* (6), 1101–1115.
48. (a) Beeh, K. M.; Beier, J.; Meyer, M.; Buhl, R.; Zahlten, R.; Wolff, G. Bimosiamose, an Inhaled Small-Molecule Pan-Selectin Antagonist, Attenuates Late Asthmatic Reactions Following Allergen Challenge in Mild Asthmatics: A Randomized, Double-Blind, Placebo-Controlled Clinical Cross-Over-Trial. *Pulm. Pharmacol. Ther.* **2006,** *19* (4), 233–241; (b) Kogan, T. P.; Dupre, B.; Bui, H.; McAbee, K. L.; Kassir, J. M.; Scott, I. L.; Hu, X.; Vanderslice, P.; Beck, P. J.; Dixon, R. A. Novel Synthetic Inhibitors of Selectin-Mediated Cell Adhesion: Synthesis of 1,6-Bis[3-(3-carboxymethylphenyl)-4-(2-alpha-D-mannopyranosyloxy)phenyl]hexane (TBC1269). *J. Med. Chem.* **1998,** *41* (7), 1099–1111.
49. (a) Telen, M. J.; Wun, T.; McCavit, T. L.; De Castro, L. M.; Krishnamurti, L.; Lanzkron, S.; Hsu, L. L.; Smith, W. R.; Rhee, S.; Magnani, J. L.; Thackray, H. Randomized Phase 2 Study of GMI-1070 in SCD: Reduction in Time to Resolution of Vaso-Occlusive Events and Decreased Opioid Use. *Blood* **2015,** *125* (17), 2656–2664; (b) Wun, T.; Styles, L.; DeCastro, L.; Telen, M. J.; Kuypers, F.; Cheung, A.; Kramer, W.; Flanner, H.; Rhee, S.; Magnani, J. L.; Thackray, H. Phase 1 Study of the E-Selectin Inhibitor GMI 1070 in Patients With Sickle Cell Anemia. *PLoS One* **2014,** *9* (7), e111690; (c) Chang, J.; Patton, J. T.; Sarkar, A.; Ernst, B.; Magnani, J. L.; Frenette, P. S. GMI-1070, a Novel Pan-Selectin Antagonist, Reverses Acute Vascular Occlusions in Sickle Cell Mice. *Blood* **2010,** *116* (10), 1779–1786.
50. Di Lella, S.; Sundblad, V.; Cerliani, J. P.; Guardia, C. M.; Estrin, D. A.; Vasta, G. R.; Rabinovich, G. A. When Galectins Recognize Glycans: From Biochemistry to Physiology and Back Again. *Biochemistry* **2011,** *50* (37), 7842–7857.
51. Klyosov Anatole, A.; Traber Peter, G. *Galectins and Disease Implications for Targeted Therapeutics*; vol. 1115; American Chemical Society: Washington, DC, 2012.
52. Liu, F.-T.; Rabinovich, G. A. Galectins as Modulators of Tumour Progression. *Nat. Rev. Cancer* **2005,** *5* (1), 29–41.
53. Inohara, H.; Raz, A. Effects of Natural Complex Carbohydrate (Citrus Pectin) on Murine Melanoma Cell Properties Related to Galectin-3 Functions. *Glycoconj. J.* **1994,** *11* (6), 527–532.
54. Hakon, L.; Ulf, J. N. Low-Molecular Weight Inhibitors of Galectins. In *Galectins and Disease Implications for Targeted Therapeutics*; vol. 1115; American Chemical Society: Washington, DC, 2012, ; pp 47–59.
55. Garber, K. Galecto Biotech. *Nat. Biotechnol.* **2013,** *31* (6), 481.
56. (a) MacKinnon, A. C.; Gibbons, M. A.; Farnworth, S. L.; Leffler, H.; Nilsson, U. J.; Delaine, T.; Simpson, A. J.; Forbes, S. J.; Hirani, N.; Gauldie, J.; Sethi, T. Regulation of Transforming Growth Factor-β1-Driven Lung Fibrosis by Galectin-3. *Am. J. Respir. Crit. Care Med.* **2012,** *185* (5), 537–546; (b) Henderson, N. C.; Mackinnon, A. C.; Farnworth, S. L.; Poirier, F.; Russo, F. P.; Iredale, J. P.; Haslett, C.; Simpson, K. J.; Sethi, T. Galectin-3 Regulates Myofibroblast Activation and Hepatic Fibrosis. *Proc. Natl. Acad. Sci. U. S. A.* **2006,** *103* (13), 5060–5065.
57. (a) Traber, P. G.; Zomer, E. Therapy of Experimental NASH and Fibrosis With Galectin Inhibitors. *PLoS One* **2013,** *8* (12), e83481; (b) Traber, P. G.; Chou, H.; Zomer, E.; Hong, F.; Klyosov, A.; Fiel, M.-I.; Friedman, S. L. Regression of Fibrosis and Reversal of Cirrhosis in Rats by Galectin Inhibitors in Thioacetamide-Induced Liver Disease. *PLoS One* **2013,** *8* (10), e75361; (c) Anatole, K.; Eliezer, Z.; David, P. DAVANAT (GM-CT-01) and Colon Cancer: Preclinical and Clinical (Phase I and II) Studies. In *Glycobiology and Drug Design*; vol. 1102; American Chemical Society: Washington, DC, 2012, ; pp 89–130.
58. Miller, M. C.; Klyosov, A.; Mayo, K. H. The Alpha-Galactomannan Davanat Binds Galectin-1 at a Site Different From the Conventional Galectin Carbohydrate Binding Domain. *Glycobiology* **2009,** *19* (9), 1034–1045.
59. Beddoe, T.; Paton, A. W.; Le Nours, J.; Rossjohn, J.; Paton, J. C. Structure, Biological Functions and Applications of the AB5 Toxins. *Trends Biochem. Sci.* **2010,** *35* (7), 411–418.
60. Merritt, E. A.; Hol, W. G. J. AB5 Toxins. *Curr. Opin. Struct. Biol.* **1995,** *5* (2), 165–171.
61. Tarr, P. I.; Gordon, C. A.; Chandler, W. L. Shiga-Toxin-Producing *Escherichia coli* and Haemolytic Uraemic Syndrome. *Lancet* **2005,** *365* (9464), 1073–1086.
62. Diggle, S. P.; Stacey, R. E.; Dodd, C.; Cámara, M.; Williams, P.; Winzer, K. The Galactophilic Lectin, LecA, Contributes to Biofilm Development in *Pseudomonas aeruginosa*. *Environ. Microbiol.* **2006,** *8* (6), 1095–1104.
63. Sharon, N. Carbohydrates as Future Anti-Adhesion Drugs for Infectious Diseases. *Biochim. Biophys. Acta* **2006,** *1760* (4), 527–537.
64. (a) Blango, M. G.; Mulvey, M. A. Persistence of Uropathogenic *Escherichia coli* in the Face of Multiple Antibiotics. *Antimicrob. Agents Chemother.* **2010,** *54* (5), 1855–1863; (b) Cholley, P.; Thouverez, M.; Hocquet, D.; van der Mee-Marquet, N.; Talon, D.; Bertrand, X. Most Multidrug-Resistant *Pseudomonas aeruginosa* Isolates From Hospitals in Eastern France Belong to a Few Clonal Types. *J. Clin. Microbiol.* **2011,** *49* (7), 2578–2583; (c) Davies, D. Understanding Biofilm Resistance to Antibacterial Agents. *Nat. Rev. Drug Discov.* **2003,** *2* (2), 114–122; (d) Livermore, D. M. Multiple Mechanisms of Antimicrobial Resistance in *Pseudomonas aeruginosa*: Our Worst Nightmare? *Clin. Infect. Dis.* **2002,** *34* (5), 634–640.
65. de Bentzmann, S.; Plésiat, P. The *Pseudomonas aeruginosa* Opportunistic Pathogen and Human Infections. *Environ. Microbiol.* **2011,** *13* (7), 1655–1665.

66. (a) Callaghan, M.; McClean, S. Bacterial Host Interactions in Cystic Fibrosis. *Curr. Opin. Microbiol.* **2012,** *15* (1), 71–77; (b) Venkatakrishnan, V.; Packer, N. H.; Thaysen-Andersen, M. Host Mucin Glycosylation Plays a Role in Bacterial Adhesion in Lungs of Individuals With Cystic Fibrosis. *Expert Rev. Resp. Med.* **2013,** *7* (5), 553–576; (c) Hauber, H. P.; Schulz, M.; Pforte, A.; Mack, D.; Zabel, P.; Schumacher, U. Inhalation With Fucose and Galactose for Treatment of *Pseudomonas aeruginosa* in Cystic Fibrosis Patients. *Int. J. Med. Sci.* **2008,** *5* (6), 371–376.
67. Chemani, C.; Imberty, A.; de Bentzmann, S.; Pierre, M.; Wimmerová, M.; Guery, B. P.; Faure, K. Role of LecA and LecB Lectins in *Pseudomonas aeruginosa*-Induced Lung Injury and Effect of Carbohydrate Ligands. *Infect. Immun.* **2009,** *77* (5), 2065–2075.
68. Bucior, I.; Abbott, J.; Song, Y.; Matthay, M. A.; Engel, J. N. Sugar Administration Is an Effective Adjunctive Therapy in the Treatment of *Pseudomonas aeruginosa* Pneumonia. *Am. J. Physiol. Lung Cell. Mol. Physiol.* **2013,** *305* (5), L352–L363.
69. Weichert, S.; Jennewein, S.; Hufner, E.; Weiss, C.; Borkowski, J.; Putze, J.; Schroten, H. Bioengineered 2'-Fucosyllactose and 3-Fucosyllactose Inhibit the Adhesion of *Pseudomonas aeruginosa* and Enteric Pathogens to Human Intestinal and Respiratory Cell Lines. *Nutr. Res.* **2013,** *33* (10), 831–838.
70. Zinger-Yosovich, K. D.; Gilboa-Garber, N. Blocking of *Pseudomonas aeruginosa* and *Ralstonia solanacearum* Lectins by Plant and Microbial Branched Polysaccharides Used as Food Additives. *J. Agric. Food Chem.* **2009,** *57* (15), 6908–6913.
71. (a) Fan, E.; O'Neal, C. J.; Mitchell, D. D.; Robien, M. A.; Zhang, Z.; Pickens, J. C.; Tan, X.-J.; Korotkov, K.; Roach, C.; Krumm, B.; Verlinde, C. L. M. J.; Merritt, E. A.; Hol, W. G. J. Structural Biology and Structure-Based Inhibitor Design of Cholera Toxin and Heat-Labile Enterotoxin. *Int. J. Med. Microbiol.* **2004,** *294* (4), 217–223; (b) Liu, J.; Begley, D.; Mitchell, D. D.; Verlinde, C. L. M. J.; Varani, G.; Fan, E. Multivalent Drug Design and Inhibition of Cholera Toxin by Specific and Transient Protein–Ligand Interactions. *Chem. Biol. Drug Des.* **2008,** *71* (5), 408–419; (c) Ivarsson, M. E.; Leroux, J.-C.; Castagner, B. Targeting Bacterial Toxins. *Angew. Chem. Int. Ed.* **2012,** *51* (17), 4024–4045; (d) Fan, E.; Merritt, E. A.; Verlinde, C. L. M. J.; Hol, W. G. J. AB5 Toxins: Structures and Inhibitor Design. *Curr. Opin. Struct. Biol.* **2000,** *10* (6), 680–686.
72. (a) Minke, W. E.; Roach, C.; Hol, W. G. J.; Verlinde, C. L. M. J. Structure-Based Exploration of the Ganglioside GM1 Binding Sites of *Escherichia coli* Heat-Labile Enterotoxin and Cholera Toxin for the Discovery of Receptor Antagonists. *Biochemistry* **1999,** *38* (18), 5684–5692; (b) Merritt, E. A.; Sarfaty, S.; Feil, I. K.; Hol, W. G. Structural Foundation for the Design of Receptor Antagonists Targeting *Escherichia coli* Heat-Labile Enterotoxin. *Structure* **1997,** *5* (11), 1485–1499; (c) Pickens, J. C.; Merritt, E. A.; Ahn, M.; Verlinde, C. L. M. J.; Hol, W. G. J.; Fan, E. Anchor-Based Design of Improved Cholera Toxin and *E. coli* Heat-Labile Enterotoxin Receptor Binding Antagonists That Display Multiple Binding Modes. *Chem. Biol.* **2002,** *9* (2), 215–224; (d) Pickens, J. C.; Mitchell, D. D.; Liu, J.; Tan, X.; Zhang, Z.; Verlinde, C. L. M. J.; Hol, W. G. J.; Fan, E. Nonspanning Bivalent Ligands as Improved Surface Receptor Binding Inhibitors of the Cholera Toxin B Pentamer. *Chem. Biol.* **2004,** *11* (9), 1205–1215; (e) Mitchell, D. D.; Pickens, J. C.; Korotkov, K.; Fan, E.; Hol, W. G. J. 3,5-Substituted Phenyl Galactosides as Leads in Designing Effective Cholera Toxin Antagonists: Synthesis and Crystallographic Studies. *Bioorg. Med. Chem.* **2004,** *12* (5), 907–920.
73. Cecioni, S.; Imberty, A.; Vidal, S. Glycomimetics Versus Multivalent Glycoconjugates for the Design of High Affinity Lectin Ligands. *Chem. Rev.* **2015,** *115* (1), 525–561.
74. Han, Z.; Pinkner, J. S.; Ford, B.; Chorell, E.; Crowley, J. M.; Cusumano, C. K.; Campbell, S.; Henderson, J. P.; Hultgren, S. J.; Janetka, J. W. Lead Optimization Studies on FimH Antagonists: Discovery of Potent and Orally Bioavailable Ortho-Substituted Biphenyl Mannosides. *J. Med. Chem.* **2012,** *55* (8), 3945–3959.
75. Totsika, M.; Kostakioti, M.; Hannan, T. J.; Upton, M.; Beatson, S. A.; Janetka, J. W.; Hultgren, S. J.; Schembri, M. A. A FimH Inhibitor Prevents Acute Bladder Infection and Treats Chronic Cystitis Caused by Multidrug-Resistant Uropathogenic *Escherichia coli* ST131. *J. Infect. Dis.* **2013,** *208* (6), 921–928.
76. Liu, J.; Zhang, Z.; Tan, X.; Hol, W. G. J.; Verlinde, C. L. M. J.; Fan, E. Protein Heterodimerization Through Ligand-Bridged Multivalent Pre-Organization: Enhancing Ligand Binding Toward Both Protein Targets. *J. Am. Chem. Soc.* **2005,** *127* (7), 2044–2045.
77. Kitov, P. I.; Sadowska, J. M.; Mulvey, G.; Armstrong, G. D.; Ling, H.; Pannu, N. S.; Read, R. J.; Bundle, D. R. Shiga-Like Toxins Are Neutralized by Tailored Multivalent Carbohydrate Ligands. *Nature* **2000,** *403* (6770), 669–672.
78. Mulvey, G. L.; Marcato, P.; Kitov, P. I.; Sadowska, J.; Bundle, D. R.; Armstrong, G. D. Assessment in Mice of the Therapeutic Potential of Tailored, Multivalent Shiga Toxin Carbohydrate Ligands. *J. Infect. Dis.* **2003,** *187* (4), 640–649.
79. Kitov, P. I.; Mulvey, G. L.; Griener, T. P.; Lipinski, T.; Solomon, D.; Paszkiewicz, E.; Jacobson, J. M.; Sadowska, J. M.; Suzuki, M.; Yamamura, K.-i.; Armstrong, G. D.; Bundle, D. R. In Vivo Supramolecular Templating Enhances the Activity of Multivalent Ligands: A Potential Therapeutic Against the *Escherichia coli* O157 AB5 Toxins. *Proc. Natl. Acad. Sci. U. S. A.* **2008,** *105* (44), 16837–16842.
80. Pertici, F.; Pieters, R. J. Potent Divalent Inhibitors With Rigid Glucose Click Spacers for *Pseudomonas aeruginosa* Lectin LecA. *Chem. Commun.* **2012,** *48* (33), 4008–4010.
81. Pertici, F.; de Mol, N. J.; Kemmink, J.; Pieters, R. J. Optimizing Divalent Inhibitors of *Pseudomonas aeruginosa* Lectin LecA by Using a Rigid Spacer. *Chem. Eur. J.* **2013,** *19* (50), 16923–16927.
82. Bernardi, A.; Jimenez-Barbero, J.; Casnati, A.; De Castro, C.; Darbre, T.; Fieschi, F.; Finne, J.; Funken, H.; Jaeger, K.-E.; Lahmann, M.; Lindhorst, T. K.; Marradi, M.; Messner, P.; Molinaro, A.; Murphy, P. V.; Nativi, C.; Oscarson, S.; Penades, S.; Peri, F.; Pieters, R. J.; Renaudet, O.; Reymond, J.-L.; Richichi, B.; Rojo, J.; Sansone, F.; Schaffer, C.; Turnbull, W. B.; Velasco-Torrijos, T.; Vidal, S.; Vincent, S.; Wennekes, T.; Zuilhof, H.; Imberty, A. Multivalent Glycoconjugates as Anti-Pathogenic Agents. *Chem. Soc. Rev.* **2013,** *42* (11), 4709–4727.
83. (a) Johansson, E. M. V.; Crusz, S. A.; Kolomiets, E.; Buts, L.; Kadam, R. U.; Cacciarini, M.; Bartels, K.-M.; Diggle, S. P.; Cámara, M.; Williams, P.; Loris, R.; Nativi, C.; Rosenau, F.; Jaeger, K.-E.; Darbre, T.; Reymond, J.-L. Inhibition and Dispersion of *Pseudomonas aeruginosa* Biofilms by Glycopeptide Dendrimers Targeting the Fucose-Specific Lectin LecB. *Chem. Biol.* **2008,** *15* (12), 1249–1257; (b) Consoli, G. M. L.; Granata, G.; Cafiso, V.; Stefani, S.; Geraci, C. Multivalent Calixarene-Based C-Fucosyl Derivative: A New *Pseudomonas aeruginosa* Biofilm Inhibitor. *Tetrahedron Lett.* **2011,** *52* (44), 5831–5834.
84. Hudak, J. E.; Bertozzi, C. R. Glycotherapy: New Advances Inspire a Reemergence of Glycans in Medicine. *Chem. Biol.* **2014,** *21* (1), 16–37.
85. Sicard, D.; Cecioni, S.; Iazykov, M.; Chevolot, Y.; Matthews, S. E.; Praly, J.-P.; Souteyrand, E.; Imberty, A.; Vidal, S.; Phaner-Goutorbe, M. AFM Investigation of *Pseudomonas aeruginosa* Lectin LecA (PA-IL) Filaments Induced by Multivalent Glycoclusters. *Chem. Commun.* **2011,** *47* (33), 9483–9485.
86. Boukerb, A. M.; Rousset, A.; Galanos, N.; Méar, J.-B.; Thépaut, M.; Grandjean, T.; Gillon, E.; Cecioni, S.; Abderrahmen, C.; Faure, K.; Redelberger, D.; Kipnis, E.; Dessein, R.; Havet, S.; Darblade, B.; Matthews, S. E.; de Bentzmann, S.; Guéry, B.; Cournoyer, B.; Imberty, A.; Vidal, S. Antiadhesive Properties of Glycoclusters Against *Pseudomonas aeruginosa* Lung Infection. *J. Med. Chem.* **2014,** *57* (24), 10275–10289.
87. Mattarella, M.; Garcia-Hartjes, J.; Wennekes, T.; Zuilhof, H.; Siegel, J. S. Nanomolar Cholera Toxin Inhibitors Based on Symmetrical Pentavalent Ganglioside GM1os-sym-corannulenes. *Org. Biomol. Chem.* **2013,** *11* (26), 4333–4339.
88. Garcia-Hartjes, J.; Bernardi, S.; Weijers, C. A. G. M.; Wennekes, T.; Gilbert, M.; Sansone, F.; Casnati, A.; Zuilhof, H. Picomolar Inhibition of Cholera Toxin by a Pentavalent Ganglioside GM1os-calix[5]arene. *Org. Biomol. Chem.* **2013,** *11* (26), 4340–4349.
89. Pukin, A. V.; Weijers, C. A. G. M.; van Lagen, B.; Wechselberger, R.; Sun, B.; Gilbert, M.; Karwaski, M.-F.; Florack, D. E. A.; Jacobs, B. C.; Tio-Gillen, A. P.; van Belkum, A.; Endtz, H. P.; Visser, G. M.; Zuilhof, H. GM3, GM2 and GM1 Mimics Designed for Biosensing: Chemoenzymatic Synthesis, Target Affinities and 900 MHz NMR Analysis. *Carbohydr. Res.* **2008,** *343* (4), 636–650.
90. Pukin, A. V.; Branderhorst, H. M.; Sisu, C.; Weijers, C. A. G. M.; Gilbert, M.; Liskamp, R. M. J.; Visser, G. M.; Zuilhof, H.; Pieters, R. J. Strong Inhibition of Cholera Toxin by Multivalent GM1 Derivatives. *ChemBioChem* **2007,** *8* (13), 1500–1503.
91. Sisu, C.; Baron, A. J.; Branderhorst, H. M.; Connell, S. D.; Weijers, C. A. G. M.; de Vries, R.; Hayes, E. D.; Pukin, A. V.; Gilbert, M.; Pieters, R. J.; Zuilhof, H.; Visser, G. M.; Turnbull, W. B. The Influence of Ligand Valency on Aggregation Mechanisms for Inhibiting Bacterial Toxins. *ChemBioChem* **2009,** *10* (2), 329–337.
92. Kulkarni, A. A.; Fuller, C.; Korman, H.; Weiss, A. A.; Iyer, S. S. Glycan Encapsulated Gold Nanoparticles Selectively Inhibit Shiga Toxins 1 and 2. *Bioconjug. Chem.* **2010,** *21* (8), 1486–1493.
93. Chien, Y.-Y.; Jan, M.-D.; Adak, A. K.; Tzeng, H.-C.; Lin, Y.-P.; Chen, Y.-J.; Wang, K.-T.; Chen, C.-T.; Chen, C.-C.; Lin, C.-C. Globotriose-Functionalized Gold Nanoparticles as Multivalent Probes for Shiga-Like Toxin. *ChemBioChem* **2008,** *9* (7), 1100–1109.
94. Karmali, M. A. Prospects for Preventing Serious Systemic Toxemic Complications of Shiga Toxin-Producing *Escherichia coli* Infections Using Shiga Toxin Receptor Analogues. *J. Infect. Dis.* **2004,** *189* (3), 355–359.

95. Knight, S. D.; Bouckaert, J. Structure, Function, and Assembly of Type 1 Fimbriae. *Top. Curr. Chem.* **2009,** *288,* 67–107.
96. (a) Heidecke, C. D.; Lindhorst, T. K. Iterative Synthesis of Spacered Glycodendrons as Oligomannoside Mimetics and Evaluation of Their Antiadhesive Properties. *Chem. Eur. J.* **2007,** *13* (32), 9056–9067; (b) Almant, M.; Moreau, V.; Kovensky, J.; Bouckaert, J.; Gouin, S. G. Clustering of *Escherichia coli* Type-1 Fimbrial Adhesins by Using Multimeric Heptyl α-D-Mannoside Probes With a Carbohydrate Core. *Chem. Eur. J.* **2011,** *17* (36), 10029–10038; (c) Dubber, M.; Sperling, O.; Lindhorst, T. K. Oligomannoside Mimetics by Glycosylation of 'Octopus Glycosides' and Their Investigation as Inhibitors of Type 1 Fimbriae-Mediated Adhesion of *Escherichia coli*. *Org. Biomol. Chem.* **2006,** *4* (21), 3901–3912; (d) Durka, M.; Buffet, K.; Iehl, J.; Holler, M.; Nierengarten, J.-F.; Taganna, J.; Bouckaert, J.; Vincent, S. P. The Functional Valency of Dodecamannosylated Fullerenes With *Escherichia coli* FimH-Towards Novel Bacterial Antiadhesives. *Chem. Commun.* **2011,** *47* (4), 1321–1323; (e) Hartmann, M.; Lindhorst, T. K. The Bacterial Lectin FimH, a Target for Drug Discovery—Carbohydrate Inhibitors of Type 1 Fimbriae-Mediated Bacterial Adhesion. *Eur. J. Org. Chem.* **2011,** *2011* (20–21), 3583–3609; (f) Touaibia, M.; Wellens, A.; Shiao, T. C.; Wang, Q.; Sirois, S.; Bouckaert, J.; Roy, R. Mannosylated G(0) Dendrimers With Nanomolar Affinities to *Escherichia coli* FimH. *ChemMedChem* **2007,** *2* (8), 1190–1201.
97. Hartmann, M.; Betz, P.; Sun, Y.; Gorb, S. N.; Lindhorst, T. K.; Krueger, A. Saccharide-Modified Nanodiamond Conjugates for the Efficient Detection and Removal of Pathogenic Bacteria. *Chem. Eur. J.* **2012,** *18* (21), 6485–6492.
98. (a) van Kooyk, Y.; Geijtenbeek, T. B. DC-SIGN: Escape Mechanism for Pathogens. *Nat. Rev. Immunol.* **2003,** *3* (9), 697–709; (b) Geijtenbeek, T. B. H.; Torensma, R.; van Vliet, S. J.; van Duijnhoven, G. C. F.; Adema, G. J.; van Kooyk, Y.; Figdor, C. G. Identification of DC-SIGN, a Novel Dendritic Cell-Specific ICAM-3 Receptor That Supports Primary Immune Responses. *Cell* **2000,** *100* (5), 575–585.
99. Feinberg, H.; Guo, Y.; Mitchell, D. A.; Drickamer, K.; Weis, W. I. Extended Neck Regions Stabilize Tetramers of the Receptors DC-SIGN and DC-SIGNR. *J. Biol. Chem.* **2005,** *280* (2), 1327–1335.
100. Van Liempt, E.; Imberty, A.; Bank, C. M. C.; Van Vliet, S. J.; Van Kooyk, Y.; Geijtenbeek, T. B. H.; Van Die, I. Molecular Basis of the Differences in Binding Properties of the Highly Related C-type Lectins DC-SIGN and L-SIGN to Lewis X Trisaccharide and *Schistosoma mansoni* Egg Antigens. *J. Biol. Chem.* **2004,** *279* (32), 33161–33167.
101. Kwon, D. S.; Gregorio, G.; Bitton, N.; Hendrickson, W. A.; Littman, D. R. DC-SIGN-Mediated Internalization of HIV Is Required for Trans-Enhancement of T Cell Infection. *Immunity* **2002,** *16* (1), 135–144.
102. Sánchez-Navarro, M.; Rojo, J. Targeting DC-SIGN With Carbohydrate Multivalent Systems. *Drug News Perspect.* **2010,** *23* (9), 557–572.
103. Bernardi, A.; Cheshev, P. Interfering With the Sugar Code: Design and Synthesis of Oligosaccharide Mimics. *Chem. Eur. J.* **2008,** *14* (25), 7434–7441.
104. Guo, Y.; Feinberg, H.; Conroy, E.; Mitchell, D. A.; Alvarez, R.; Blixt, O.; Taylor, M. E.; Weis, W. I.; Drickamer, K. Structural Basis for Distinct Ligand-Binding and Targeting Properties of the Receptors DC-SIGN and DC-SIGNR. *Nat. Struct. Mol. Biol.* **2004,** *11* (7), 591–598.
105. (a) Reina, J. J.; Sattin, S.; Invernizzi, D.; Mari, S.; Martínez-Prats, L.; Tabarani, G.; Fieschi, F.; Delgado, R.; Nieto, P. M.; Rojo, J.; Bernardi, A. 1,2-Mannobioside Mimic: Synthesis, DC-SIGN Interaction by NMR and Docking, and Antiviral Activity. *ChemMedChem* **2007,** *2* (7), 1030–1036; (b) Sattin, S.; Daghetti, A.; Thépaut, M.; Berzi, A.; Sánchez-Navarro, M.; Tabarani, G.; Rojo, J.; Fieschi, F.; Clerici, M.; Bernardi, A. Inhibition of DC-SIGN-Mediated HIV Infection by a Linear Trimannoside Mimic in a Tetravalent Presentation. *ACS Chem. Biol.* **2010,** *5* (3), 301–312.
106. Timpano, G.; Tabarani, G.; Anderluh, M.; Invernizzi, D.; Vasile, F.; Potenza, D.; Nieto, P. M.; Rojo, J.; Fieschi, F.; Bernardi, A. Synthesis of Novel DC-SIGN Ligands With an α-Fucosylamide Anchor. *ChemBioChem* **2008,** *9* (12), 1921–1930.
107. Wang, S.-K.; Liang, P.-H.; Astronomo, R. D.; Hsu, T.-L.; Hsieh, S.-L.; Burton, D. R.; Wong, C.-H. Targeting the Carbohydrates on HIV-1: Interaction of Oligomannose Dendrons With Human Monoclonal Antibody 2G12 and DC-SIGN. *Proc. Natl. Acad. Sci. U. S. A.* **2008,** *105* (10), 3690–3695.
108. Berzi, A.; Reina, J. J.; Ottria, R.; Sutkeviciute, I.; Antonazzo, P.; Sanchez-Navarro, M.; Chabrol, E.; Biasin, M.; Trabattoni, D.; Cetin, I.; Rojo, J.; Fieschi, F.; Bernardi, A.; Clerici, M. A Glycomimetic Compound Inhibits DC-SIGN-Mediated HIV Infection in Cellular and Cervical Explant Models. *AIDS* **2012,** *26* (2), 127–137.
109. Rojo, J.; Delgado, R. Glycodendritic Structures: Promising New Antiviral Drugs. *J. Antimicrob. Chemother.* **2004,** *54* (3), 579–581.
110. Luczkowiak, J.; Sattin, S.; Sutkevičiūtė, I.; Reina, J. J.; Sánchez-Navarro, M.; Thépaut, M.; Martínez-Prats, L.; Daghetti, A.; Fieschi, F.; Delgado, R.; Bernardi, A.; Rojo, J. Pseudosaccharide Functionalized Dendrimers as Potent Inhibitors of DC-SIGN Dependent Ebola Pseudotyped Viral Infection. *Bioconjug. Chem.* **2011,** *22* (7), 1354–1365.
111. Lasala, F.; Arce, E.; Otero, J. R.; Rojo, J.; Delgado, R. Mannosyl Glycodendritic Structure Inhibits DC-SIGN-Mediated Ebola Virus Infection in Cis and in Trans. *Antimicrob. Agents Chemother.* **2003,** *47* (12), 3970–3972.
112. Martínez-Ávila, O.; Hijazi, K.; Marradi, M.; Clavel, C.; Campion, C.; Kelly, C.; Penadés, S. Gold Manno-Glyconanoparticles: Multivalent Systems to Block HIV-1 gp120 Binding to the Lectin DC-SIGN. *Chem. Eur. J.* **2009,** *15* (38), 9874–9888.
113. Arnáiz, B.; Martínez-Ávila, O.; Falcon-Perez, J. M.; Penadés, S. Cellular Uptake of Gold Nanoparticles Bearing HIV gp120 Oligomannosides. *Bioconjug. Chem.* **2012,** *23* (4), 814–825.
114. Martínez-Ávila, O.; Bedoya, L. M.; Marradi, M.; Clavel, C.; Alcamí, J.; Penadés, S. Multivalent Manno-Glyconanoparticles Inhibit DC-SIGN-Mediated HIV-1 Trans-Infection of Human T Cells. *ChemBioChem* **2009,** *10* (11), 1806–1809.
115. (a) Luczkowiak, J.; Muñoz, A.; Sánchez-Navarro, M.; Ribeiro-Viana, R.; Ginieis, A.; Illescas, B. M.; Martín, N.; Delgado, R.; Rojo, J. Glycofullerenes Inhibit Viral Infection. *Biomacromolecules* **2013,** *14* (2), 431–437; (b) Nierengarten, J.-F.; Iehl, J.; Oerthel, V.; Holler, M.; Illescas, B. M.; Munoz, A.; Martin, N.; Rojo, J.; Sanchez-Navarro, M.; Cecioni, S.; Vidal, S.; Buffet, K.; Durka, M.; Vincent, S. P. Fullerene Sugar Balls. *Chem. Commun.* **2010,** *46* (22), 3860–3862; (c) Sánchez-Navarro, M.; Muñoz, A.; Illescas, B. M.; Rojo, J.; Martín, N. [60]Fullerene as Multivalent Scaffold: Efficient Molecular Recognition of Globular Glycofullerenes by Concanavalin A. *Chem. Eur. J.* **2011,** *17* (3), 766–769.
116. Muñoz, A.; Sigwalt, D.; Illescas, B. M.; Luczkowiak, J.; Rodríguez-Pérez, L.; Nierengarten, I.; Holler, M.; Remy, J.-S.; Buffet, K.; Vincent, S. P.; Rojo, J.; Delgado, R.; Nierengarten, J.-F.; Martín, N. Synthesis of Giant Globular Multivalent Glycofullerenes as Potent Inhibitors in a Model of Ebola Virus Infection. *Nat. Chem.* **2016,** *8* (1), 50–57.
117. Rendle, P. M.; Seger, A.; Rodrigues, J.; Oldham, N. J.; Bott, R. R.; Jones, J. B.; Cowan, M. M.; Davis, B. G. Glycodendriproteins: A Synthetic Glycoprotein Mimic Enzyme With Branched Sugar-Display Potently Inhibits Bacterial Aggregation. *J. Am. Chem. Soc.* **2004,** *126* (15), 4750–4751.
118. Ribeiro-Viana, R.; Sánchez-Navarro, M.; Luczkowiak, J.; Koeppe, J. R.; Delgado, R.; Rojo, J.; Davis, B. G. Virus-Like Glycodendrinanoparticles Displaying Quasi-Equivalent Nested Polyvalency Upon Glycoprotein Platforms Potently Block Viral Infection. *Nat. Commun.* **2012,** *3,* 1303–1311.
119. (a) Vliegenthart, J. F. G. Carbohydrate Based Vaccines. *FEBS Lett.* **2006,** *580* (12), 2945–2950; (b) Oppenheimer, S. B.; Alvarez, M.; Nnoli, J. Carbohydrate-Based Experimental Therapeutics for Cancer, HIV/AIDS and Other Diseases. *Acta Histochem.* **2008,** *110* (1), 6–13; (c) Huang, Y. L.; Wu, C. Y. Carbohydrate-Based Vaccines: Challenges and Opportunities. *Expert Rev. Vaccines* **2010,** *9* (11), 1257–1274.
120. (a) Hakomori, S.-I. Aberrant Glycosylation in Tumors and Tumor-Associated Carbohydrate Antigens. *Adv. Cancer Res.* **1989,** *52,* 257–331; (b) Kim, Y. J.; Varki, A. Perspectives on the Significance of Altered Glycosylation of Glycoproteins in Cancer. *Glycoconj. J.* **1997,** *14* (5), 569–576.
121. Morelli, L.; Poletti, L.; Lay, L. Carbohydrates and Immunology: Synthetic Oligosaccharide Antigens for Vaccine Formulation. *Eur. J. Org. Chem.* **2011,** *2011* (29), 5723–5777.
122. (a) Engering, A. J.; Cella, M.; Fluitsma, D.; Brockhaus, M.; Hoefsmit, E. C. M.; Lanzavecchia, A.; Pieters, J. The Mannose Receptor Functions as a High Capacity and Broad Specificity Antigen Receptor in Human Dendritic Cells. *Eur. J. Immunol.* **1997,** *27* (9), 2417–2425; (b) Tan, M. C. A. A.; Mommaas, A. M.; Drijfhout, J. W.; Jordens, R.; Onderwater, J. J. M.; Verwoerd, D.; Mulder, A. A.; van der Heiden, A. N.; Scheidegger, D.; Oomen, L. C. J. M.; Ottenhoff, T. H. M.; Tulp, A.; Neefjes, J. J.; Koning, F. Mannose Receptor-Mediated Uptake of Antigens Strongly Enhances HLA Class II-Restricted Antigen Presentation by Cultured Dendritic Cells. *Eur. J. Immunol.* **1997,** *27* (9), 2426–2435.
123. Berzi, A.; Varga, N.; Sattin, S.; Antonazzo, P.; Biasin, M.; Cetin, I.; Trabattoni, D.; Bernardi, A.; Clerici, M. Pseudo-Mannosylated DC-SIGN Ligands as Potential Adjuvants for HIV Vaccines. *Viruses* **2014,** *6* (2), 391–403.
124. Singh, S. K.; Stephani, J.; Schaefer, M.; Kalay, H.; García-Vallejo, J. J.; den Haan, J.; Saeland, E.; Sparwasser, T.; van Kooyk, Y. Targeting Glycan Modified OVA to Murine DC-SIGN Transgenic Dendritic Cells Enhances MHC Class I and II Presentation. *Mol. Immunol.* **2009,** *47* (2–3), 164–174.

125. García-Vallejo, J. J.; Ambrosini, M.; Overbeek, A.; van Riel, W. E.; Bloem, K.; Unger, W. W. J.; Chiodo, F.; Bolscher, J. G.; Nazmi, K.; Kalay, H.; van Kooyk, Y. Multivalent Glycopeptide Dendrimers for the Targeted Delivery of Antigens to Dendritic Cells. *Mol. Immunol.* **2013,** *53* (4), 387–397.
126. Kowalczyk, W.; Mascaraque, A.; Sánchez-Navarro, M.; Rojo, J.; Andreu, D. Convergent Synthesis of Glycodendropeptides by Click Chemistry Approaches. *Eur. J. Org. Chem.* **2012,** *2012* (24), 4565–4573.
127. Mascaraque, A.; Kowalczyk, W.; Fernandez, T.; Palomares, F.; Mayorga, C.; Andreu, D.; Rojo, J. Glycodendropeptides Stimulate Dendritic Cell Maturation and T Cell Proliferation: A Potential Influenza A Virus Immunotherapy. *Med. Chem. Commun.* **2015,** *6* (10), 1755–1760.
128. Toussi, D.; Massari, P. Immune Adjuvant Effect of Molecularly-Defined Toll-Like Receptor Ligands. *Vaccines* **2014,** *2* (2), 323–353.
129. Cui, W.; Joshi, N. S.; Liu, Y.; Meng, H.; Kleinstein, S. H.; Kaech, S. M. TLR4 Ligands Lipopolysaccharide and Monophosphoryl Lipid a Differentially Regulate Effector and Memory CD8+ T Cell Differentiation. *J. Immunol.* **2014,** *192* (9), 4221–4232.
130. (a) Deng, K.; Adams, M. M.; Damani, P.; Livingston, P. O.; Ragupathi, G.; Gin, D. Y. Synthesis of QS-21-Xylose: Establishment of the Immunopotentiating Activity of Synthetic QS-21 Adjuvant With a Melanoma Vaccine. *Angew. Chem. Int. Ed.* **2008,** *47* (34), 6395–6398; (b) Deng, K.; Adams, M. M.; Gin, D. Y. Synthesis and Structure Verification of the Vaccine Adjuvant QS-7-Api. Synthetic Access to Homogeneous *Quillaja saponaria* Immunostimulants. *J. Am. Chem. Soc.* **2008,** *130* (18), 5860–5861.
131. (a) Fernández-Tejada, A.; Chea, E. K.; George, C.; Gardner, J. R.; Livingston, P. O.; Ragupathi, G.; Tan, D. S.; Gin, D. Y. Design, Synthesis, and Immunologic Evaluation of Vaccine Adjuvant Conjugates Based on QS-21 and Tucaresol. *Bioorg. Med. Chem.* **2014,** *22* (21), 5917–5923; (b) Chea, E. K.; Fernández-Tejada, A.; Damani, P.; Adams, M. M.; Gardner, J. R.; Livingston, P. O.; Ragupathi, G.; Gin, D. Y. Synthesis and Preclinical Evaluation of QS-21 Variants Leading to Simplified Vaccine Adjuvants and Mechanistic Probes. *J. Am. Chem. Soc.* **2012,** *134* (32), 13448–13457; (c) Fernández-Tejada, A.; Chea, E. K.; George, C.; Pillarsetty, N.; Gardner, J. R.; Livingston, P. O.; Ragupathi, G.; Lewis, J. S.; Tan, D. S.; Gin, D. Y. Development of a Minimal Saponin Vaccine Adjuvant Based on QS-21. *Nat. Chem.* **2014,** *6* (7), 635–643.
132. Boonyarattanakalin, S.; Liu, X.; Michieletti, M.; Lepenies, B.; Seeberger, P. H. Chemical Synthesis of all Phosphatidylinositol Mannoside (PIM) Glycans From *Mycobacterium tuberculosis*. *J. Am. Chem. Soc.* **2008,** *130* (49), 16791–16799.
133. (a) Li, X.; Chen, G.; Garcia-Navarro, R.; Franck, R. W.; Tsuji, M. Identification of C-Glycoside Analogues That Display a Potent Biological Activity Against Murine and Human Invariant Natural Killer T Cells. *Immunology* **2009,** *127* (2), 216–225; (b) Franck, R. W.; Tsuji, M. α-C-Galactosylceramides: Synthesis and Immunology. *Acc. Chem. Res.* **2006,** *39* (10), 692–701.
134. (a) Cavallari, M.; Stallforth, P.; Kalinichenko, A.; Rathwell, D. C. K.; Gronewold, T. M. A.; Adibekian, A.; Mori, L.; Landmann, R.; Seeberger, P. H. A Semisynthetic Carbohydrate-Lipid Vaccine That Protects Against *S. pneumoniae* in Mice. *Nat. Chem. Biol.* **2014,** *10* (11), 950–956; (b) Tzianabos, A.; Onderdonk, A.; Rosner, B.; Cisneros, R.; Kasper, D. Structural Features of Polysaccharides That Induce Intra-Abdominal Abscesses. *Science* **1993,** *262* (5132), 416–419.
135. Stephen, T. L.; Groneck, L.; Kalka-Moll, W. M. The Modulation of Adaptive Immune Responses by Bacterial Zwitterionic Polysaccharides. *Int. J. Microbiol.* **2010,** *2010,* 0–12.
136. De Silva, R. A.; Wang, Q.; Chidley, T.; Appulage, D. K.; Andreana, P. R. Immunological Response From an Entirely Carbohydrate Antigen: Design of Synthetic Vaccines Based on Tn−PS A1 Conjugates. *J. Am. Chem. Soc.* **2009,** *131* (28), 9622–9623.
137. De Silva, R. A.; Appulage, D. K.; Pietraszkiewicz, H.; Bobbitt, K. R.; Media, J.; Shaw, J.; Valeriote, F. A.; Andreana, P. R. The Entirely Carbohydrate Immunogen Tn-PS A1 Induces a Cancer Cell Selective Immune Response and Cytokine IL-17. *Cancer Immunol. Immunother.* **2012,** *61* (4), 581–585.
138. (a) Heidelberger, M.; Avery, O. T. The Soluble Specific Substance of *Pneumococcus*. *J. Exp. Med.* **1924,** *40* (3), 301–317; (b) Heidelberger, M.; Dilapi, M. M.; Siegel, M.; Walter, A. W. Persistence of Antibodies in Human Subjects Injected With Pneumococcal Polysaccharides. *J. Immunol.* **1950,** *65* (5), 535–541.
139. Robbins, J. B.; Austrian, R.; Lee, C.-J.; Rastogi, S. C.; Schiffman, G.; Henrichsen, J.; Makela, P. H.; Broome, C. V.; Facklam, R. R.; Tiesjema, R. H.; Parke, J. C. Considerations for Formulating the Second-Generation Pneumococcal Capsular Polysaccharide Vaccine With Emphasis on the Cross-Reactive Types Within Groups. *J. Infect. Dis.* **1983,** *148* (6), 1136–1159.
140. (a) Segal, S.; Pollard, A. J. Vaccines Against Bacterial Meningitis. *Br. Med. Bull.* **2004,** *72* (1), 65–81; (b) González-Fernández, Á.; Faro, J.; Fernández, C. Immune Responses to Polysaccharides: Lessons From Humans and Mice. *Vaccine* **2008,** *26* (3), 292–300.
141. Mond, J. J.; Lees, A.; Snapper, C. M. T Cell-Independent Antigens Type 2. *Annu. Rev. Immunol.* **1995,** *13* (1), 655–692.
142. Avery, O. T.; Goebel, W. F. Chemo-Immunological Studies on Conjugated Carbohydrate-Proteins V: The Immunological Specificity of an Antigen Prepared by Combining the Capsular Polysaccharide of Type III *Pneumococcus* With Foreign Protein. *J. Exp. Med.* **1931,** *54* (3), 437–447.
143. (a) Astronomo, R. D.; Burton, D. R. Carbohydrate Vaccines: Developing Sweet Solutions to Sticky Situations? *Nat. Rev. Drug Discov.* **2010,** *9* (4), 308–324; (b) Zhang, Y.; Wang, F. Carbohydrate Drugs: Current Status and Development Prospect. *Drug Discov. Ther.* **2015,** *9* (2), 79–87.
144. Verez-Bencomo, V.; Fernández-Santana, V.; Hardy, E.; Toledo, M. E.; Rodríguez, M. C.; Heynngnezz, L.; Rodriguez, A.; Baly, A.; Herrera, L.; Izquierdo, M.; Villar, A.; Valdés, Y.; Cosme, K.; Deler, M. L.; Montane, M.; Garcia, E.; Ramos, A.; Aguilar, A.; Medina, E.; Toraño, G.; Sosa, I.; Hernandez, I.; Martínez, R.; Muzachio, A.; Carmenates, A.; Costa, L.; Cardoso, F.; Campa, C.; Diaz, M.; Roy, R. A Synthetic Conjugate Polysaccharide Vaccine Against *Haemophilus influenzae* Type b. *Science* **2004,** *305* (5683), 522–525.
145. Phalipon, A.; Tanguy, M.; Grandjean, C.; Guerreiro, C.; Bélot, F.; Cohen, D.; Sansonetti, P. J.; Mulard, L. A. A Synthetic Carbohydrate-Protein Conjugate Vaccine Candidate Against *Shigella flexneri* 2a Infection. *J. Immunol.* **2009,** *182* (4), 2241–2247.
146. (a) Gening, M. L.; Maira-Litrán, T.; Kropec, A.; Skurnik, D.; Grout, M.; Tsvetkov, Y. E.; Nifantiev, N. E.; Pier, G. B. Synthetic β-(1→6)-Linked *N*-Acetylated and Nonacetylated Oligoglucosamines Used to Produce Conjugate Vaccines for Bacterial Pathogens. *Infect. Immun.* **2010,** *78* (2), 764–772; (b) Benaissa-Trouw, B.; Lefeber, D. J.; Kamerling, J. P.; Vliegenthart, J. F. G.; Kraaijeveld, K.; Snippe, H. Synthetic Polysaccharide Type 3-Related Di-, Tri-, and Tetrasaccharide–CRM197 Conjugates Induce Protection Against *Streptococcus pneumoniae* Type 3 in Mice. *Infect. Immun.* **2001,** *69* (7), 4698–4701; (c) Liu, X.; Siegrist, S.; Amacker, M.; Zurbriggen, R.; Pluschke, G.; Seeberger, P. H. Enhancement of the Immunogenicity of Synthetic Carbohydrates by Conjugation to Virosomes: A Leishmaniasis Vaccine Candidate. *ACS Chem. Biol.* **2006,** *1* (3), 161–164.
147. Schofield, L.; Hewitt, M. C.; Evans, K.; Siomos, M.-A.; Seeberger, P. H. Synthetic GPI as a Candidate Anti-Toxic Vaccine in a Model of Malaria. *Nature* **2002,** *418* (6899), 785–789.
148. (a) Tamborrini, M.; Werz, D. B.; Frey, J.; Pluschke, G.; Seeberger, P. H. Anti-Carbohydrate Antibodies for the Detection of Anthrax Spores. *Angew. Chem. Int. Ed.* **2006,** *45* (39), 6581–6582; (b) Werz, D. B.; Seeberger, P. H. Total Synthesis of Antigen *Bacillus anthracis* Tetrasaccharide—Creation of an Anthrax Vaccine Candidate. *Angew. Chem. Int. Ed.* **2005,** *44* (39), 6315–6318.
149. (a) Adis-International-Ltd. Cancer Vaccine THERATOPE-Biomira. *Drugs R D* **2003,** *4* (4), 236–240; (b) Gilewski, T. A.; Ragupathi, G.; Dickler, M.; Powell, S.; Bhuta, S.; Panageas, K.; Koganty, R. R.; Chin-Eng, J.; Hudis, C.; Norton, L.; Houghton, A. N.; Livingston, P. O. Immunization of High-Risk Breast Cancer Patients With Clustered sTn-KLH Conjugate Plus the Immunologic Adjuvant QS-21. *Clin. Cancer Res.* **2007,** *13* (10), 2977–2985; (c) Holmberg, L. A.; Sandmaier, B. M. Vaccination With Theratope® (STn-KLH) as Treatment for Breast Cancer. *Expert Rev. Vaccines* **2004,** *3* (6), 655–663; (d) Holmberg, L. A.; Sandmaier, B. M. Theratope® Vaccine (STn-KLH). *Expert Opin. Biol. Ther.* **2001,** *1* (5), 881–891.
150. (a) Jegerlehner, A.; Wiesel, M.; Dietmeier, K.; Zabel, F.; Gatto, D.; Saudan, P.; Bachmann, M. F. Carrier Induced Epitopic Suppression of Antibody Responses Induced by Virus-Like Particles Is a Dynamic Phenomenon Caused by Carrier-Specific Antibodies. *Vaccine* **2010,** *28* (33), 5503–5512; (b) Dagan, R.; Poolman, J.; Siegrist, C.-A. Glycoconjugate Vaccines and Immune Interference: A Review. *Vaccine* **2010,** *28* (34), 5513–5523.
151. (a) Buskas, T.; Thompson, P.; Boons, G.-J. Immunotherapy for Cancer: Synthetic Carbohydrate-Based Vaccines. *Chem. Commun.* **2009**, (36), 5335–5349; (b) Buskas, T.; Ingale, S.; Boons, G.-J. Towards a Fully Synthetic Carbohydrate-Based Anticancer Vaccine: Synthesis and Immunological Evaluation of a Lipidated Glycopeptide Containing the Tumor-Associated Tn Antigen. *Angew. Chem. Int. Ed.* **2005,** *44* (37), 5985–5988.
152. Rakoff-Nahoum, S.; Medzhitov, R. Toll-Like Receptors and Cancer. *Nat. Rev. Cancer* **2009,** *9* (1), 57–63.
153. Toyokuni, T.; Dean, B.; Cai, S.; Boivin, D.; Hakomori, S.; Singhal, A. K. Synthetic Vaccines: Synthesis of a Dimeric Tn Antigen-Lipopeptide Conjugate That Elicits Immune Responses Against Tn-Expressing Glycoproteins. *J. Am. Chem. Soc.* **1994,** *116* (1), 395–396.

154. Ingale, S.; Wolfert, M. A.; Gaekwad, J.; Buskas, T.; Boons, G.-J. Robust Immune Responses Elicited by a Fully Synthetic Three-Component Vaccine. *Nat. Chem. Biol.* **2007,** *3* (10), 663–667.
155. Lakshminarayanan, V.; Thompson, P.; Wolfert, M. A.; Buskas, T.; Bradley, J. M.; Pathangey, L. B.; Madsen, C. S.; Cohen, P. A.; Gendler, S. J.; Boons, G.-J. Immune Recognition of Tumor-Associated Mucin MUC1 is Achieved by a Fully Synthetic Aberrantly Glycosylated MUC1 Tripartite Vaccine. *Proc. Natl. Acad. Sci. U. S. A.* **2012,** *109* (1), 261–266.
156. Platt, E. J.; Gomes, M. M.; Kabat, D. Kinetic Mechanism for HIV-1 Neutralization by Antibody 2G12 Entails Reversible Glycan Binding That Slows Cell Entry. *Proc. Natl. Acad. Sci. U. S. A.* **2012,** *109* (20), 7829–7834.
157. (a) Astronomo, R. D.; Lee, H.-K.; Scanlan, C. N.; Pantophlet, R.; Huang, C.-Y.; Wilson, I. A.; Blixt, O.; Dwek, R. A.; Wong, C.-H.; Burton, D. R. A Glycoconjugate Antigen Based on the Recognition Motif of a Broadly Neutralizing Human Immunodeficiency Virus Antibody, 2G12, Is Immunogenic but Elicits Antibodies Unable to Bind to the Self Glycans of gp120. *J. Virol.* **2008,** *82* (13), 6359–6368; (b) Joyce, J. G.; Krauss, I. J.; Song, H. C.; Opalka, D. W.; Grimm, K. M.; Nahas, D. D.; Esser, M. T.; Hrin, R.; Feng, M.; Dudkin, V. Y.; Chastain, M.; Shiver, J. W.; Danishefsky, S. J. An Oligosaccharide-Based HIV-1 2G12 Mimotope Vaccine Induces Carbohydrate-Specific Antibodies That Fail to Neutralize HIV-1 Virions. *Proc. Natl. Acad. Sci. U. S. A.* **2008,** *105* (41), 15684–15689.
158. Doores, K. J.; Fulton, Z.; Hong, V.; Patel, M. K.; Scanlan, C. N.; Wormald, M. R.; Finn, M. G.; Burton, D. R.; Wilson, I. A.; Davis, B. G. A Nonself Sugar Mimic of the HIV Glycan Shield Shows Enhanced Antigenicity. *Proc. Natl. Acad. Sci. U. S. A.* **2010,** *107* (40), 17107–17112.
159. Aussedat, B.; Vohra, Y.; Park, P. K.; Fernández-Tejada, A.; Alam, S. M.; Dennison, S. M.; Jaeger, F. H.; Anasti, K.; Stewart, S.; Blinn, J. H.; Liao, H.-X.; Sodroski, J. G.; Haynes, B. F.; Danishefsky, S. J. Chemical Synthesis of Highly Congested gp120 V1V2 N-Glycopeptide Antigens for Potential HIV-1-Directed Vaccines. *J. Am. Chem. Soc.* **2013,** *135* (35), 13113–13120.
160. Slovin, S. F.; Ragupathi, G.; Musselli, C.; Fernandez, C.; Diani, M.; Verbel, D.; Danishefsky, S.; Livingston, P.; Scher, H. I. Thomsen-Friedenreich (TF) Antigen as a Target for Prostate Cancer Vaccine: Clinical Trial Results With TF Cluster (c)-KLH Plus QS21 Conjugate Vaccine in Patients With Biochemically Relapsed Prostate Cancer. *Cancer Immunol. Immunother.* **2005,** *54* (7), 694–702.
161. Zhu, J.; Wan, Q.; Lee, D.; Yang, G.; Spassova, M. K.; Ouerfelli, O.; Ragupathi, G.; Damani, P.; Livingston, P. O.; Danishefsky, S. J. From Synthesis to Biologics: Preclinical Data on a Chemistry Derived Anticancer Vaccine. *J. Am. Chem. Soc.* **2009,** *131* (26), 9298–9303.
162. (a) Cheng, J.; Teply, B. A.; Sherifi, I.; Sung, J.; Luther, G.; Gu, F. X.; Levy-Nissenbaum, E.; Radovic-Moreno, A. F.; Langer, R.; Farokhzad, O. C. Formulation of Functionalized PLGA-PEG Nanoparticles for in vivo Targeted Drug Delivery. *Biomaterials* **2007,** *28* (5), 869–876; (b) Qian, X.; Peng, X.-H.; Ansari, D. O.; Yin-Goen, Q.; Chen, G. Z.; Shin, D. M.; Yang, L.; Young, A. N.; Wang, M. D.; Nie, S. In Vivo Tumor Targeting and Spectroscopic Detection With Surface-Enhanced Raman Nanoparticle Tags. *Nat. Biotechnol.* **2008,** *26* (1), 83–90; (c) Gao, X.; Cui, Y.; Levenson, R. M.; Chung, L. W. K.; Nie, S. In Vivo Cancer Targeting and Imaging With Semiconductor Quantum Dots. *Nat. Biotechnol.* **2004,** *22* (8), 969–976; (d) Liong, M.; Lu, J.; Kovochich, M.; Xia, T.; Ruehm, S. G.; Nel, A. E.; Tamanoi, F.; Zink, J. I. Multifunctional Inorganic Nanoparticles for Imaging, Targeting, and Drug Delivery. *ACS Nano* **2008,** *2* (5), 889–896; (e) Tkachenko, A. G.; Xie, H.; Coleman, D.; Glomm, W.; Ryan, J.; Anderson, M. F.; Franzen, S.; Feldheim, D. L. Multifunctional Gold Nanoparticle−Peptide Complexes for Nuclear Targeting. *J. Am. Chem. Soc.* **2003,** *125* (16), 4700–4701.
163. (a) Liu, Z.; Cai, W.; He, L.; Nakayama, N.; Chen, K.; Sun, X.; Chen, X.; Dai, H. In Vivo Biodistribution and Highly Efficient Tumour Targeting of Carbon Nanotubes in Mice. *Nat. Nanotechnol.* **2007,** *2* (1), 47–52; (b) Wu, W.; Wieckowski, S.; Pastorin, G.; Benincasa, M.; Klumpp, C.; Briand, J.-P.; Gennaro, R.; Prato, M.; Bianco, A. Targeted Delivery of Amphotericin B to Cells by Using Functionalized Carbon Nanotubes. *Angew. Chem. Int. Ed.* **2005,** *44* (39), 6358–6362; (c) Nasongkla, N.; Bey, E.; Ren, J.; Ai, H.; Khemtong, C.; Guthi, J. S.; Chin, S.-F.; Sherry, A. D.; Boothman, D. A.; Gao, J. Multifunctional Polymeric Micelles as Cancer-Targeted, MRI-Ultrasensitive Drug Delivery Systems. *Nano Lett.* **2006,** *6* (11), 2427–2430.
164. (a) Salvati, A.; Pitek, A. S.; Monopoli, M. P.; Prapainop, K.; Bombelli, F. B.; Hristov, D. R.; Kelly, P. M.; Aberg, C.; Mahon, E.; Dawson, K. A. Transferrin-Functionalized Nanoparticles Lose Their Targeting Capabilities When a Biomolecule Corona Adsorbs on the Surface. *Nat. Nanotechnol.* **2013,** *8* (2), 137–143; (b) Pino, P. D.; Pelaz, B.; Zhang, Q.; Maffre, P.; Nienhaus, G. U.; Parak, W. J. Protein Corona Formation Around Nanoparticles—From the Past to the Future. *Mater. Horiz.* **2014,** *1* (3), 301–313.
165. Knop, K.; Hoogenboom, R.; Fischer, D.; Schubert, U. S. Poly(ethylene glycol) in Drug Delivery: Pros and Cons as Well as Potential Alternatives. *Angew. Chem. Int. Ed.* **2010,** *49* (36), 6288–6308.
166. Pelegri-O'Day, E. M.; Lin, E.-W.; Maynard, H. D. Therapeutic Protein–Polymer Conjugates: Advancing Beyond PEGylation. *J. Am. Chem. Soc.* **2014,** *136* (41), 14323–14332.
167. (a) Wirth, M.; Fuchs, A.; Wolf, M.; Ertl, B.; Gabor, F. Lectin-Mediated Drug Targeting: Preparation, Binding Characteristics, and Antiproliferative Activity of Wheat Germ Agglutinin Conjugated Doxorubicin on Caco-2 Cells. *Pharm. Res.* **1998,** *15* (7), 1031–1037; (b) Wangyang, Y.; Na, Z.; Changjun, L. Saccharide Modified Pharmaceutical Nanocarriers for Targeted Drug and Gene Delivery. *Curr. Pharm. Des.* **2009,** *15* (32), 3826–3836.
168. (a) Besheer, A.; Vogel, J.; Glanz, D.; Kressler, J.; Groth, T.; Mäder, K. Characterization of PLGA Nanospheres Stabilized With Amphiphilic Polymers: Hydrophobically Modified Hydroxyethyl Starch vs. Pluronics. *Mol. Pharm.* **2009,** *6* (2), 407–415; (b) Lemarchand, C.; Gref, R.; Couvreur, P. Polysaccharide-Decorated Nanoparticles. *Eur. J. Pharm. Biopharm.* **2004,** *58* (2), 327–341; (c) Noga, M.; Edinger, D.; Kläger, R.; Wegner, S. V.; Spatz, J. P.; Wagner, E.; Winter, G.; Besheer, A. The Effect of Molar Mass and Degree of Hydroxyethylation on the Controlled Shielding and Deshielding of Hydroxyethyl Starch-Coated Polyplexes. *Biomaterials* **2013,** *34* (10), 2530–2538; (d) Noga, M.; Edinger, D.; Rödl, W.; Wagner, E.; Winter, G.; Besheer, A. Controlled Shielding and Deshielding of Gene Delivery Polyplexes Using Hydroxyethyl Starch (HES) and Alpha-Amylase. *J. Control. Release* **2012,** *159* (1), 92–103.
169. (a) Ferguson, E. L.; Duncan, R. Dextrin−Phospholipase A2: Synthesis and Evaluation as a Bioresponsive Anticancer Conjugate. *Biomacromolecules* **2009,** *10* (6), 1358–1364; (b) Hardwicke, J.; Ferguson, E. L.; Moseley, R.; Stephens, P.; Thomas, D. W.; Duncan, R. Dextrin–rhEGF Conjugates as Bioresponsive Nanomedicines for Wound Repair. *J. Control. Release* **2008,** *130* (3), 275–283; (c) Duncan, R.; Gilbert, H. R. P.; Carbajo, R. J.; Vicent, M. J. Polymer Masked−Unmasked Protein Therapy. 1. Bioresponsive Dextrin−Trypsin and −Melanocyte Stimulating Hormone Conjugates Designed for α-Amylase Activation. *Biomacromolecules* **2008,** *9* (4), 1146–1154.
170. (a) Ohyanagi, T.; Nagahori, N.; Shimawaki, K.; Hinou, H.; Yamashita, T.; Sasaki, A.; Jin, T.; Iwanaga, T.; Kinjo, M.; Nishimura, S.-I. Importance of Sialic Acid Residues Illuminated by Live Animal Imaging Using Phosphorylcholine Self-Assembled Monolayer-Coated Quantum Dots. *J. Am. Chem. Soc.* **2011,** *133* (32), 12507–12517; (b) Österberg, E.; Bergström, K.; Holmberg, K.; Schuman, T. P.; Riggs, J. A.; Burns, N. L.; Van Alstine, J. M.; Harris, J. M. Protein-Rejecting Ability of Surface-Bound Dextran in End-On and Side-On Configurations: Comparison to PEG. *J. Biomed. Mater. Res.* **1995,** *29* (6), 741–747.
171. Kang, B.; Opatz, T.; Landfester, K.; Wurm, F. R. Carbohydrate Nanocarriers in Biomedical Applications: Functionalization and Construction. *Chem. Soc. Rev.* **2015,** *44* (22), 8301–8325.
172. (a) Davis, B. G.; Robinson, M. A. Drug Delivery Systems Based on Sugar-Macromolecule Conjugates. *Curr. Opin. Drug Discov. Devel.* **2002,** *5* (2), 279–288; (b) Vyas, S. P.; Singh, A.; Sihorkar, V. Ligand-Receptor-Mediated Drug Delivery: An Emerging Paradigm in Cellular Drug Targeting. *Crit. Rev. Ther. Drug Carrier Syst.* **2001,** *18* (1), 76.
173. Chen, W.; Zou, Y.; Meng, F.; Cheng, R.; Deng, C.; Feijen, J.; Zhong, Z. Glyco-Nanoparticles With Sheddable Saccharide Shells: A Unique and Potent Platform for Hepatoma-Targeting Delivery of Anticancer Drugs. *Biomacromolecules* **2014,** *15* (3), 900–907.
174. (a) Tiwari, S.; Chaturvedi, A. P.; Tripathi, Y. B.; Mishra, B. Macrophage-Specific Targeting of Isoniazid Through Mannosylated Gelatin Microspheres. *AAPS PharmSciTech* **2011,** *12* (3), 900–908; (b) Lu, Y.; Kawakami, S.; Yamashita, F.; Hashida, M. Development of an Antigen-Presenting Cell-Targeted DNA Vaccine Against Melanoma by Mannosylated Liposomes. *Biomaterials* **2007,** *28* (21), 3255–3262.
175. Benito, J. M.; Gómez-García, M.; Ortiz Mellet, C.; Baussanne, I.; Defaye, J.; García Fernández, J. M. Optimizing Saccharide-Directed Molecular Delivery to Biological Receptors: Design, Synthesis, and Biological Evaluation of Glycodendrimer−Cyclodextrin Conjugates. *J. Am. Chem. Soc.* **2004,** *126* (33), 10355–10363.
176. Diaz-Moscoso, A.; Guilloteau, N.; Bienvenu, C.; Mendez-Ardoy, A.; Blanco, J. L.; Benito, J. M.; Le Gourrierec, L.; Di Giorgio, C.; Vierling, P.; Defaye, J.; Mellet, C. O.; Fernandez, J. M. Mannosyl-Coated Nanocomplexes From Amphiphilic Cyclodextrins and pDNA for Site-Specific Gene Delivery. *Biomaterials* **2011,** *32* (29), 7263–7273.
177. Chen, J.; Lu, W.-L.; Gu, W.; Lu, S.-S.; Chen, Z.-P.; Cai, B.-C.; Yang, X.-X. Drug-in-Cyclodextrin-in-Liposomes: A Promising Delivery System for Hydrophobic Drugs. *Expert Opin. Drug Deliv.* **2014,** *11* (4), 565–577.

178. (a) Martinez, A.; Ortiz Mellet, C.; Garcia Fernandez, J. M. Cyclodextrin-Based Multivalent Glycodisplays: Covalent and Supramolecular Conjugates to Assess Carbohydrate-Protein Interactions. *Chem. Soc. Rev.* **2013,** *42* (11), 4746–4773; (b) Benito, J. M.; García Fernández, J. L.; Ortiz-Mellet, C. Cyclodextrin-Scaffolded Glycotransporters for Gene Delivery. *Pure Appl. Chem.* **2013,** *85* (9), 1825–1845.
179. Morris, G.; Kok, S.; Harding, S.; Adams, G. Polysaccharide Drug Delivery Systems Based on Pectin and Chitosan. *Biotechnol. Genet. Eng. Rev.* **2010,** *27,* 257–284.
180. Kwag, D. S.; Oh, K. T.; Lee, E. S. Facile Synthesis of Multilayered Polysaccharidic Vesicles. *J. Control. Release* **2014,** *187,* 83–90.
181. Baier, G.; Cavallaro, A.; Vasilev, K.; Mailänder, V.; Musyanovych, A.; Landfester, K. Enzyme Responsive Hyaluronic Acid Nanocapsules Containing Polyhexanide and Their Exposure to Bacteria to Prevent Infection. *Biomacromolecules* **2013,** *14* (4), 1103–1112.
182. Garnier, P.; Wang, X.-T.; Robinson, M. A.; van Kasteren, S.; Perkins, A. C.; Frier, M.; Fairbanks, A. J.; Davis, B. G. Lectin-Directed Enzyme Activated Prodrug Therapy (LEAPT): Synthesis and Evaluation of Rhamnose-Capped Prodrugs. *J. Drug Target.* **2010,** *18* (10), 794–802.
183. Jandus, C.; Simon, H.-U.; von Gunten, S. Targeting Siglecs—A Novel Pharmacological Strategy for Immuno- and Glycotherapy. *Biochem. Pharmacol.* **2011,** *82* (4), 323–332.
184. Chen, W. C.; Completo, G. C.; Sigal, D. S.; Crocker, P. R.; Saven, A.; Paulson, J. C. In Vivo Targeting of B-Cell Lymphoma With Glycan Ligands of CD22. *Blood* **2010,** *115* (23), 4778–4786.
185. Park, S.; Gildersleeve, J. C.; Blixt, O.; Shin, I. Carbohydrate Microarrays. *Chem. Soc. Rev.* **2013,** *42* (10), 4310–4326.
186. Hirabayashi, J.; Yamada, M.; Kuno, A.; Tateno, H. Lectin Microarrays: Concept, Principle and Applications. *Chem. Soc. Rev.* **2013,** *42* (10), 4443–4458.
187. Seeberger, P. H.; Werz, D. B. Synthesis and Medical Applications of Oligosaccharides. *Nature* **2007,** *446* (7139), 1046–1051.
188. Dotan, I.; Fishman, S.; Dgani, Y.; Schwartz, M.; Karban, A.; Lerner, A.; Weishauss, O.; Spector, L.; Shtevi, A.; Altstock, R. T.; Dotan, N.; Halpern, Z. Antibodies Against Laminaribioside and Chitobioside Are Novel Serologic Markers in Crohn's Disease. *Gastroenterology* **2006,** *131* (2), 366–378.
189. Ido, T.; Wan, C. N.; Casella, V.; Fowler, J. S.; Wolf, A. P.; Reivich, M.; Kuhl, D. E. Labeled 2-Deoxy-D-glucose Analogs. 18 F-Labeled 2-Deoxy-2-fluoro-D-glucose, 2-Deoxy-2-fluoro-D-mannose and 14C-2-Deoxy-2-fluoro-D-glucose. *J. Labelled Comp. Radiopharm.* **1978,** *14* (2), 175–183.
190. Hoh, C. K. Clinical Use of FDG PET. *Nucl. Med. Biol.* **2007,** *34* (7), 737–742.
191. Gambhir, S. S. Molecular Imaging of Cancer With Positron Emission Tomography. *Nat. Rev. Cancer* **2002,** *2* (9), 683–693.
192. Agard, N. J.; Bertozzi, C. R. Chemical Approaches to Perturb, Profile, and Perceive Glycans. *Acc. Chem. Res.* **2009,** *42* (6), 788–797.
193. Bork, K.; Horstkorte, R.; Weidemann, W. Increasing the Sialylation of Therapeutic Glycoproteins: The Potential of the Sialic Acid Biosynthetic Pathway. *J. Pharm. Sci.* **2009,** *98* (10), 3499–3508.
194. Steensma, D. P.; Loprinzi, C. L. Epoetin Alfa and Darbepoetin Alfa Go Head to Head. *J. Clin. Oncol.* **2006,** *24* (15), 2233–2236.
195. Curran, M. P.; McCormack, P. L. Methoxy Polyethylene Glycol-Epoetin Beta: A Review of Its Use in the Management of Anaemia Associated With Chronic Kidney Disease. *Drugs* **2008,** *68* (8), 1139–1156.
196. Deegan, P. B.; Cox, T. M. Imiglucerase in the Treatment of Gaucher Disease: A History and Perspective. *Drug Des. Devel. Ther.* **2012,** *6,* 81–106.
197. Hoffman, H. M. Rilonacept for the Treatment of Cryopyrin-Associated Periodic Syndromes (CAPS). *Expert. Opin. Biol. Ther.* **2009,** *9* (4), 519–531.
198. Alldred, A. Etanercept in Rheumatoid Arthritis. *Expert. Opin. Pharmacother.* **2001,** *2* (7), 1137–1148.
199. Ferrara, N. From the Discovery of Vascular Endothelial Growth Factor to the Introduction of Avastin in Clinical Trials—An Interview With Napoleone Ferrara by Domenico Ribatti. *Int. J. Dev. Biol.* **2011,** *55,* 383–388.
200. Reynolds, N. A.; Wagstaff, A. J. Cetuximab: In the Treatment of Metastatic Colorectal Cancer. *Drugs* **2004,** *64* (1), 109–118.
201. Albanell, J.; Baselga, J. Trastuzumab, a Humanized Anti-HER2 Monoclonal Antibody, for the Treatment of Breast Cancer. *Drugs Today* **1999,** *35* (12), 931–946.
202. Perry, C. M.; Wagstaff, A. J. Interferon-alpha-n1: A Review of Its Pharmacological Properties and Therapeutic Efficacy in the Management of Chronic Viral Hepatitis. *BioDrugs* **1998,** *9* (2), 125–154.
203. Clerico, M.; Contessa, G.; Durelli, L. Interferon-beta1a for the Treatment of Multiple Sclerosis. *Expert. Opin. Biol. Ther.* **2007,** *7* (4), 535–542.
204. (a) Burrow, T. A.; Leslie, N. D. Review of the Use of Idursulfase in the Treatment of Mucopolysaccharidosis II. *Biol. Targets Ther.* **2008,** *2* (2), 311–320; (b) Zareba, G. Idursulfase in Hunter Syndrome Treatment. *Drugs Today* **2007,** *43* (11), 759–767.

Relevant Websites

http://www.functionalglycomics.org/—This is the webpage of the Consortium for Functional Glycomics (CFG), a large international research initiative that provide a networking forum and glycomics resources to reveal functions of glycans and glycan-binding proteins (GBPs) that impact human health and disease.

http://canadianglycomics.ca/—The Network GlycoNet's research program focuses primarily on applications in human health and is based on five synergistic themes: antimicrobials, rare genetic diseases, diabetes and obesity, chronic diseases and therapeutic proteins and vaccines. In addition, GlycoNet will offer a set of four core service facilities for researchers: high-throughput screening, glycan screening, glycan structure analysis and chemical synthesis.

http://www.egsf.org/—ESF Euroglycoforum. This webpage is an online resource for all scientists interested in aspects of glycoscience and includes a forum for discussions. We provide links to databases, on-line tools, textbooks and other teaching materials.

http://www.glycoforum.gr.jp/index.html—This Web site in which FCCA (Forum: Carbohydrates Coming of Age) and other world glycoscientists introduce a series of topics on rapidly growing glycoscience.

http://www.glycopedia.eu/—This a webpage devoted to promote the field of carbohydrates with emphasis to provide material for education.

COMPREHENSIVE MEDICINAL CHEMISTRY III

This page intentionally left blank

COMPREHENSIVE MEDICINAL CHEMISTRY III

EDITORS-IN-CHIEF

Samuel Chackalamannil
Rutgers University, Piscataway, NJ, United States

David Rotella
Montclair State University, Montclair, NJ, United States

Simon E. Ward
University of Sussex, Brighton, United Kingdom

VOLUME 2

DRUG DISCOVERY TECHNOLOGIES

VOLUME EDITORS

Helmut Buschmann
Savira Pharmaceuticals GmbH, Vienna, Austria

Norbert Handler
Savira Pharmaceuticals GmbH, Vienna, Austria

Andrea Wolkerstorfer
Baxalta Innovations GmbH — Now part of Shire, Vienna, Austria

ELSEVIER

Elsevier
Radarweg 29, PO Box 211, 1000 AE Amsterdam, The Netherlands
The Boulevard, Langford Lane, Kidlington, Oxford OX5 1GB, United Kingdom
50 Hampshire Street, 5th Floor, Cambridge, MA 02139, United States

Copyright © 2017 Elsevier Ltd. All rights reserved

No part of this publication may be reproduced or transmitted in any form or by any means, electronic or mechanical, including photocopying, recording, or any information storage and retrieval system, without permission in writing from the publisher. Details on how to seek permission, further information about the Publisher's permissions policies and our arrangements with organizations such as the Copyright Clearance Center and the Copyright Licensing Agency, can be found at our website: www.elsevier.com/permissions.

This book and the individual contributions contained in it are protected under copyright by the Publisher (other than as may be noted herein).

Notices
Knowledge and best practice in this field are constantly changing. As new research and experience broaden our understanding, changes in research methods, professional practices, or medical treatment may become necessary.

Practitioners and researchers may always rely on their own experience and knowledge in evaluating and using any information, methods, compounds, or experiments described herein. In using such information or methods they should be mindful of their own safety and the safety of others, including parties for whom they have a professional responsibility.

To the fullest extent of the law, neither the Publisher nor the authors, contributors, or editors, assume any liability for any injury and/or damage to persons or property as a matter of products liability, negligence or otherwise, or from any use or operation of any methods, products, instructions, or ideas contained in the material herein.

Library of Congress Cataloging-in-Publication Data
A catalog record for this book is available from the Library of Congress

British Library Cataloguing-in-Publication Data
A catalogue record for this book is available from the British Library

ISBN 978-0-12-803200-8

For information on all publications visit our website at
http://store.elsevier.com

Working together
to grow libraries in
developing countries
www.elsevier.com • www.bookaid.org

Publisher: Oliver Walter
Acquisition Editor: Rachel Gerlis
Content Project Manager: Gemma Tomalin
Associate Content Project Manager: Marise Willis
Designer: Mark Rogers

Printed and bound in the United Kingdom

PREFACE

Previous editions of *Comprehensive Medicinal Chemistry*, published in 1990 and 2006, provided an integrated reference source that encompassed all major aspects of drug discovery research. The third edition follows this tradition and considerably expands its scope and content.

The trailblazing scientific discoveries of the 21st century have brought new opportunities for drug discovery research. The discipline of medicinal chemistry continues to evolve as it adapts to these new opportunities and strives to solve new challenges. Covered in the new edition are not only the breakthrough therapies of the past decade in cancer, hepatitis C, heart failure, dyslipidemia, cystic fibrosis, multiple sclerosis, HIV, etc., but also extensive discussion of new business models in drug discovery research, shifting industry demographics, emerging technologies, *in silico* drug discovery tools, experimental ADME and toxicology, and biologics medicine. The tone of this edition is prospective in which contributors identify outstanding issues and paths forward in their area of expertise. The aim is to provide drug discovery scientists in industry, government, academia, and research organizations with a contemporary global perspective on the field that includes a look ahead in selected areas.

The eight individual volumes fulfill these objectives and include extensive discussion of biomolecular therapeutics, drug targeting and delivery, development of chemical biology tools, data collection and analysis, *in silico* models as predictors for biological properties, identification/validation of new targets, approaches to quantify target engagement, new methods for synthesis of drug candidates such as green chemistry, development of novel scaffolds for drug discovery, and the role of regulatory agencies in drug discovery.

The individual volume editors have done an outstanding job to identify topics and contributors to meet these goals and we thank them for their hardwork and diligence. In volume 1, Ana Martinez and Carmen Gil recruited an international group of contributors who provide chapters on the emerging role of organizations other than traditional pharmaceutical companies in drug discovery, the evolving science of chemical biology, and new organic chemistry contributions to the discipline. In volume 2, Helmut Buschmann, Norbert Handler, and Andrea Wolkerstorfer have accomplished a seemingly impossible task and attracted world-leading experts across the wide field of drug discovery enabling technologies, covering contemporary thinking in a wide range of key disciplines that enable modern medicinal chemistry and drug discovery and development. The computational enabling technologies are the focus of volume 3, in which Andy Davis and Colin Edge have assembled chapters covering both ligand-based and protein structure–based advances as well as exciting new methodologies and case studies exploiting these. Alan Wilson identified experts in the fields of pharmacokinetics and toxicology who describe a wide range of contemporary advances in prediction and analysis of pharmaceutical properties and drug safety in volume 4. In volume 5, Ian Collins, Louis Lombardo, and Will Watkins have assembled leading experts to discuss high impact drug discovery accomplishments over the past decade in cancer chemotherapeutics, immunology and inflammation, and infectious diseases therapeutic areas. Ved Srivastava edited volume 6 on biologic medicines, a significant and rapidly evolving area where medicinal chemistry plays an important role. The chapters in this volume provide timely information on not only protein-based drugs, such as monoclonal antibodies and therapeutic proteins, but also peptides and nucleic acid–based therapeutics. Volume 7, edited by Adrian Hall, Santhosh Neelamkavil, and Rob Jones, presents a detailed account of the major advances in CNS, metabolic, and cardiovascular fields over the past decade and the promising new opportunities. Joerg Holenz edited volume 8 that presents case histories of successful drug discovery and strategic differentiation that have resulted in commercialized drugs and candidates in advanced clinical trials.

We are truly grateful to the publishing team at Elsevier that includes Gemma Tomalin, Rachel Gerlis, Marise Willis, and Sean Simms for their assistance and support throughout the process. With their expertise, this project became what we believe is a noteworthy and valuable resource for the discipline of medicinal chemistry. We look forward to the response and feedback of our colleagues who will use this information in their own work.

Samuel Chackalamannil, David P. Rotella, and Simon E. Ward

EDITORS-IN-CHIEF: BIOGRAPHIES

Dr. Samuel Chackalamannil

Dr. Chackalamannil obtained his PhD in chemistry from Yale University in 1984 and subsequently worked in drug discovery research at Schering-Plough Corporation and Merck Research Laboratories, where he was a distinguished fellow when he left in 2011. Since then, he has been teaching at Ernest Mario School of Pharmacy, Rutgers University, New Jersey.

Dr. Chackalamannil has significant accomplishments in the discovery of new medicines. He led the discovery of vorapaxar (Zontivity®), an FDA-approved antiplatelet drug for the prevention of heart attack and stroke. His group also discovered a PDE-5 inhibitor clinical candidate dasantafil and an adenosine A2a antagonist clinical candidate for the treatment of Parkinson's disease. Altogether, he was responsible for the discovery of nine development candidates in cardiovascular, central nervous system, and metabolic disease areas.

Dr. Chackalamannil is a coinventor of 62 allowed US patents and numerous patent applications worldwide. He has published 81 peer-reviewed articles and has coauthored a book. He has also given numerous lectures at international meetings and academic institutions.

Dr. Chackalamannil is a two-time recipient of the Thomas Alva Edison Award for Emerging Technology Patent and a two-time recipient of the Presidential Award for Discovery at Schering-Plough Research Institute. He has chaired several sessions at American Chemical Society national meetings and Gordon Research Conference on Medicinal Chemistry and was an organizer for Chemistry as a Life Science Symposium.

Dr. David Rotella

Dr. Rotella earned a PhD in medicinal chemistry from The Ohio State University and carried out postdoctoral research in organic chemistry at Penn State University. He joined the faculty at Montclair State University in July 2011 as the Margaret and Herman Sokol Professor of medicinal chemistry after a successful career in the pharmaceutical industry. He is an expert in the discovery and optimization of small molecule drug candidates for use in metabolic, cardiovascular, cancer, and central nervous system diseases. His current research is focused on discovering new lead compounds for use in parasitic and central nervous system diseases. He has coedited the seventh edition of *Burger's Medicinal Chemistry* and is a senior editor for the Royal Society of Chemistry's Drug Discovery book series. He has authored over 40 peer-reviewed articles, is an inventor on 8 issued US patents, and has contributed 10 book chapters.

Simon E. Ward

Simon Ward has an MA in natural sciences and PhD in synthetic organic chemistry from Cambridge University, UK. He has a wide-ranging experience of drug discovery in both large and small companies (GlaxoSmithKline, Knoll Pharmaceuticals, Vernalis, Chiroscience, BioCrea) and specialist experience of discovering and developing drugs for central nervous system indications. He has led multidisciplinary project teams and medicinal chemistry groups from target identification through to early clinical studies, delivering multiple clinical development candidates across indications. He is a fellow of the Royal Society of Chemistry. He is currently a professor of medicinal chemistry at the University of Sussex, UK, and the director of the Sussex Drug Discovery Centre, which he established within the University of Sussex in 2010.

This page intentionally left blank

CONTRIBUTORS TO VOLUME 2

D Armstrong
Novartis Institutes for Biomedical Research, Cambridge, MA, United States

A Bergner
Boehringer-Ingelheim RCV GmbH Co KG, Vienna, Austria

A Brigo
F. Hoffmann-La Roche, Ltd., Basel, Switzerland

R Chaudhari
MD Anderson Cancer Center, Houston, TX, United States

H Chen
Fuzhou University, Fuzhou, Fujian, China; and University of Texas Medical Branch, Galveston, Texas, United States

M E Cvijic
Bristol-Myers Squibb, Princeton, NJ, United States

L Detalle
Ablynx Technologiepark, Zwijnaarde, Belgium

P Ettmayer
Boehringer-Ingelheim RCV GmbH Co KG, Vienna, Austria

Y Fang
Corning Incorporated, Corning, NY, United States

D Fiegen
Boehringer Ingelheim Pharma GmbH & Co. KG, Biberach an der Riss, Germany

W Frieauff
Novartis Institutes for Biomedical Research, Cambridge, MA, United States

Y Gao
Fuzhou University, Fuzhou, Fujian, China

M P Gleeson
Kasetsart University, Bangkok, Thailand

I Gonzalez Suarez
Quai Jeanrenaud 5, Neuchatel, Switzerland

J Hoeng
Quai Jeanrenaud 5, Neuchatel, Switzerland

G A Holdgate
Cambridge Science Park, Cambridge, United Kingdom

S Hörer
Boehringer Ingelheim Pharma GmbH & Co. KG, Biberach an der Riss, Germany

N V Ivanov
Quai Jeanrenaud 5, Neuchatel, Switzerland

A M Jones
Manchester Metropolitan University, Manchester, United Kingdom

J T Jørgensen
Dx-Rx Institute, Fredensborg, Denmark

A Knorr
Quai Jeanrenaud 5, Neuchatel, Switzerland

D V LaBarbera
University of Colorado Anschutz Medical Campus, Aurora, CO, United States

L Li
University of Colorado Anschutz Medical Campus, Aurora, CO, United States

S Li
Novartis Institutes for Biomedical Research, Cambridge, MA, United States

Z Li
Bristol-Myers Squibb, Princeton, NJ, United States

Z Liu
University of Texas Medical Branch, Galveston, TX, United States

J Loscalzo
Harvard Medical School, Boston, MA, United States

S Lu
Shanghai Jiao Tong University, Shanghai, China

F Martin
Quai Jeanrenaud 5, Neuchatel, Switzerland

H-J Martus
Novartis Institutes for Biomedical Research, Cambridge, MA, United States

D Mikhailov
Novartis Institutes for Biomedical Research, Cambridge, MA, United States

D Montanari
H. Lundbeck A/S, Valby, Denmark

W Muster
F. Hoffmann-La Roche, Ltd., Basel, Switzerland

H Nar
Boehringer Ingelheim Pharma GmbH & Co. KG, Biberach an der Riß, Germany

K B Nielsen
Agilent Technologies Inc, Glostrup, Denmark

M C Noe
Pfizer Worldwide Research and Development, Groton, CT, United States

A Pautsch
Boehringer Ingelheim Pharma GmbH & Co. KG, Biberach an der Riss, Germany

M-C Peakman
Pfizer Worldwide Research and Development, Groton, CT, United States

M C Peitsch
Quai Jeanrenaud 5, Neuchatel, Switzerland

R Rajesh Singh
The University of Texas MD Anderson Cancer Center, Houston, TX, United States

J Reilly
Novartis Institutes for Biomedical Research, Cambridge, MA, United States

D Reinert
Boehringer Ingelheim Pharma GmbH & Co. KG, Biberach an der Riss, Germany

M L Sargentini-Maier
Ablynx Technologiepark, Zwijnaarde, Belgium

R Schnitzer
Boehringer-Ingelheim RCV GmbH Co KG, Vienna, Austria

A Sewer
Quai Jeanrenaud 5, Neuchatel, Switzerland

T Stöhr
A2M Pharma GmbH, Monheim, Germany

M Talikka
Quai Jeanrenaud 5, Neuchatel, Switzerland

Z Tan
MD Anderson Cancer Center, Houston, TX, United States

B Titz
Quai Jeanrenaud 5, Neuchatel, Switzerland

L Urban
Novartis Institutes for Biomedical Research, Cambridge, MA, United States

K Vanheusden
Ablynx Technologiepark, Zwijnaarde, Belgium

R-S Wang
Harvard Medical School, Boston, MA, United States

S Whitebread
Novartis Institutes for Biomedical Research, Cambridge, MA, United States

E A Wold
University of Texas Medical Branch, Galveston, TX, United States

P M Woster
Medical University of South Carolina, Charleston, SC, United States

J Zhang
Shanghai Jiao Tong University, Shanghai, China

L Zhang
Bristol-Myers Squibb, Princeton, NJ, United States

S Zhang
MD Anderson Cancer Center, Houston, TX, United States

J Zhou
University of Texas Medical Branch, Galveston, TX, United States

J Zhou
University of Texas Medical Branch, Galveston, Texas, United States

X Zhou
Fuzhou University, Fuzhou, Fujian, China

CONTENTS OF VOLUME 2

Preface *v*

Editors-in-Chief: Biographies *vii*

Contributors to Volume 2 *ix*

Editorial Board *xiii*

2.01 Drug Discovery Technologies: Current and Future Trends 1
M C Noe and M-C Peakman

2.02 Hit and Lead Generation Strategies 33
P Ettmayer, R Schnitzer, A Bergner, and H Nar

2.03 Multiobjective Optimization of Biological and Physical Properties in Drug Discovery 64
M P Gleeson and D Montanari

2.04 Predictive Toxicology: Latest Scientific Developments and Their Application in Safety Assessment 94
D Armstrong, S Li, W Frieauff, H-J Martus, J Reilly, D Mikhailov, S Whitebread, and L Urban

2.05 Privileged Structures and Motifs (Synthetic and Natural Scaffolds) 116
A M Jones

2.06 High-Throughput Crystallography and Its Applications in Drug Discovery 153
H Nar, D Fiegen, S Hörer, A Pautsch, and D Reinert

2.07 Kinetics, Thermodynamics, and Ligand Efficiency Metrics in Drug Discovery 180
G A Holdgate

2.08 Fragment-Based Drug Design: Strategic Advances and Lessons Learned 212
H Chen, X Zhou, Y Gao, H Chen, and J Zhou

2.09 Computational Models to Predict Toxicological Endpoints in Drug Discovery and Strategies for Data Integration 233
A Brigo and W Muster

2.10 Overview of Drug Polypharmacology and Multitargeted Molecular Design 259
R Chaudhari, Z Tan, and S Zhang

2.11 Allosteric Modulators 276
S Lu and J Zhang

2.12 Novel Therapeutics Targeting Epigenetics 297
P M Woster

2.13 Small-Molecule Inhibitors of Protein–Protein Interactions 329
Z Liu, H Chen, E A Wold, and J Zhou

2.14 Next Generation Sequencing Technologies 354
R Rajesh Singh

2.15 Cellular Imaging in Drug Discovery: Imaging and Informatics for Complex Cell Biology 362
Z Li, M E Cvijic, and L Zhang

2.16 3D High-Content Screening of Organoids for Drug Discovery 388
L Li and D V LaBarbera

2.17 Label-Free Screening Technologies 416
Y Fang

2.18 Systems Biology: Methods and Applications 434
B Titz, A Knorr, A Sewer, F Martin, N V Ivanov, M Talikka, I Gonzalez Suarez, M C Peitsch, and J Hoeng

2.19 Systems Chemical Biology: Integrating Medicinal Chemistry and Systems Biology for Drug Discovery 481
R-S Wang and J Loscalzo

2.20 Translational Aspects in Drug Discovery 495
L Detalle, K Vanheusden, M L Sargentini-Maier, and T Stöhr

2.21 Companion Diagnostics: From Biomarkers to Diagnostics 530
J T Jørgensen and K B Nielsen

EDITORIAL BOARD

EDITORS-IN-CHIEF

Samuel Chackalamannil
Rutgers University, Piscataway, NJ, United States

David Rotella
Montclair State University, Montclair, NJ, United States

Simon E. Ward
University of Sussex, Brighton, United Kingdom

VOLUME 1
GENERAL PERSPECTIVE - THE FUTURE OF DRUG DISCOVERY

VOLUME EDITORS

Ana Martinez
Centro de Investigaciones Biologicas-CSIC, Madrid, Spain

Carmen Gil
Centro de Investigaciones Biologicas-CSIC, Madrid, Spain

VOLUME 2
DRUG DISCOVERY TECHNOLOGIES

VOLUME EDITORS

Helmut Buschmann
Savira Pharmaceuticals GmbH, Vienna, Austria

Norbert Handler
Savira Pharmaceuticals GmbH, Vienna, Austria

Andrea Wolkerstorfer
Baxalta Innovations GmbH — Now part of Shire, Vienna, Austria

VOLUME 3
IN SILICO DRUG DISCOVERY TOOLS

VOLUME EDITORS

Andrew M. Davis
AstraZeneca R&D Gothenburg, Gothenburg, Sweden

Colin Edge
GlaxoSmithKline Medicines Research Centre, Stevenage, United Kingdom

VOLUME 4
EXPERIMENTAL ADME AND TOXICOLOGY

VOLUME EDITOR

Alan G. E. Wilson
Lexicon Pharmaceuticals, The Woodlands, TX, United States

VOLUME 5
CANCER, IMMUNOLOGY AND INFLAMMATION, AND INFECTIOUS DISEASE

VOLUME EDITORS

Ian Collins
The Institute of Cancer Research, London, United Kingdom

William Watkins
Gilead Sciences, Foster City, CA, United States

Louis J. Lombardo
Bristol-Myers Squibb Research and Development, Princeton, NJ, United States

VOLUME 6
BIOLOGICS MEDICINE

VOLUME EDITOR

Ved Srivastava
Intarcia Therapeutics, Durham, NC, United States

VOLUME 7
CNS, PAIN, METABOLIC SYNDROME, CARDIOVASCULAR, TISSUE FIBROSIS AND URINARY INCONTINENCE

VOLUME EDITORS

Adrian Hall
UCB BioPharma SPRL, Brussels, Belgium

Santhosh Neelamkavil
Merck Research Laboratories, Kenilworth, NJ, United States

Rob Jones
BlackThorn Therapeutics, San Francisco, CA, United States

VOLUME 8
CASE HISTORIES IN RECENT DRUG DISCOVERY

VOLUME EDITOR

Joerg Holenz
R&D Neurosciences TAU, GSK, PA, United States

PERMISSION ACKNOWLEDGMENTS

The following material is reproduced with kind permission of Taylor & Francis

Scheme 2 Cellular Imaging in Drug Discovery: Biomolecular Imaging and Informatics (HCS, HCA, HCI)
Figure 2 Past Present Future
Figure 5 Past Present Future
Figure 6 Past Present Future
www.taylorandfrancisgroup.com

The following material is reproduced with kind permission of Oxford University press

Table 1 Targeting G-quadruplex Nucleic Acids for Cancer Therapy
Table 2 Targeting G-quadruplex Nucleic Acids for Cancer Therapy
Figure 1 Protein Structure Prediction and Homology Modelling
www.oup.com

The following material is reproduced with kind permission of American Association for the Advancement of Science

Figure 3b,c Cellular Imaging in Drug Discovery: Biomolecular Imaging and Informatics (HCS, HCA, HCI)
www.aaas.org

The following material is reproduced with kind permission of Nature Publishing Group

Table 4 Use of Stem Cells in Toxicology
Table 6 Use of Stem Cells in Toxicology
Figure 17 Strategy and Tactics for Designing Analogs; Biochemical Characterization of the Large Molecules
Figure 30 Strategy and Tactics for Designing Analogs; Biochemical Characterization of the Large Molecules
Figure 2 Cellular Imaging in Drug Discovery: Biomolecular Imaging and Informatics (HCS, HCA, HCI)
Figure 3a Cellular Imaging in Drug Discovery: Biomolecular Imaging and Informatics (HCS, HCA, HCI)
Figure 4 Cellular Imaging in Drug Discovery: Biomolecular Imaging and Informatics (HCS, HCA, HCI)
Figure 5a Cellular Imaging in Drug Discovery: Biomolecular Imaging and Informatics (HCS, HCA, HCI)
Figure 9a Cellular Imaging in Drug Discovery: Biomolecular Imaging and Informatics (HCS, HCA, HCI)
Figure 20 Epigenetics: Novel Therapeutics Targeting Epigenetics
Figure 1 UCB5857
Figure 6 Empirical and Physics Based Calculations of Physical Properties
Figure 4 Progress and Challenges in the Development if PET Ligands to Aid CNS Drug Discovery
http://www.nature.com

2.01 Drug Discovery Technologies: Current and Future Trends

MC Noe and M-C Peakman, Pfizer Worldwide Research and Development, Groton, CT, United States

© 2017 Elsevier Ltd. All rights reserved.

2.01.1	**Introduction**	1
2.01.2	**New Modalities for Target Modulation and Validation**	2
2.01.2.1	Gene Editing and Gene therapy	2
2.01.2.2	Biased Receptor Signaling	4
2.01.2.3	Modulators of Protein Transcription, Translation, and Translocation	5
2.01.2.4	Modulating Proteostasis and Protein Degradation	8
2.01.3	**Hit Identification Methods**	10
2.01.3.1	Phenotypic Screening	10
2.01.3.2	New Technologies for Target-Based Screening	12
2.01.4	**Hit Characterization Using Computational Approaches and Biophysical Assays**	14
2.01.5	**Lead Optimization**	18
2.01.5.1	Expanding drug-like chemical space: Rational design of covalent inhibitors	21
2.01.5.2	Expanding drug-like chemical space: Designing permeable compounds beyond the Lipinski Rule of Five	22
2.01.5.3	Developing Design Principles for Asymmetric Tissue Distribution	23
2.01.5.4	Screening Technologies for ADME and Safety Optimization	24
2.01.6	**Perspective and Future Direction**	27
References		28

2.01.1 Introduction

Since the early days of human civilization, humankind has searched for medicinal remedies to treat disease. The earliest medicines were derived from plant or herbal extracts discovered through pure empiricism—either by experiencing their effects after human consumption or through observing their impact on animals that consumed them. These discoveries led to the compendium of folk medicines used in Ancient Rome, China, Egypt, and Greece.[1] The practice of medicine became considerably more refined during the Renaissance, which laid the foundation for applying the scientific method to understanding disease and to developing medical practices and treatments.[1] The development of synthetic organic chemistry was transformative in allowing structural analogues to be prepared and tested for superior properties and led to the emergence of the pharmaceutical industry in the early 20th Century. The introduction of molecular biology and decoding of the human genome led to a revolution in the pharmaceutical industry, wherein drug discovery could be translated from a purely phenotypic screening approach to a target-based strategy that begins with a molecular hypothesis impacting the disease state. Modern drug discovery captures elements from each of these periods: empirical observations leading to new indications for existing medicines, use of natural products as leads for drug discovery programs, application of phenotypic screening to identify novel targets for disease intervention, and target-based approaches leveraging genome-wide association studies that implicate a target in disease.

Despite these advances, drug discovery remains perhaps the most challenging applied science—largely due to the complexity of human biology, the vastness of chemical space, the discontinuous impact of functional group changes on molecular properties, and the inability to optimize a single variable (potency, selectivity, permeability, metabolic stability, solubility) without having simultaneous and sometimes detrimental effects on other critical parameters. For these reasons, a successful drug discovery campaign often emerges after investigating dozens of pharmacological targets, with each one requiring thousands of chemical hits to be triaged and hundreds of close-in synthetic analogues to be evaluated. A recent 2016 publication based on 106 new drugs from 10 pharmaceutical firms estimated that the overall investment in discovery and clinical development approaches $2.6 billion for each successful launch.[2] Prior studies, dated 2003–12, have given estimates ranging from $0.8 billion to $2.2 billion, and although the numbers are hotly debated, there is a clear trend for increasing costs in recent years.[2] Technologies that enable more effective selection of productive biomolecular targets, provide novel ways to engage targets, or appropriately guide design to the most effective regions of chemical space will lead to transformative improvements in drug discovery efficiency.

The complexity of human biology contributes most directly to the challenge of drug discovery, as a flawed biological hypothesis will lead to certain failure no matter how elegantly the screening and medicinal chemistry components of the process are devised. There are an estimated 25,000 protein encoding genes in the human genome.[3,4] These genes are regulated by processes that govern the transcription, splicing variation, translation and post-translational modification of the resulting proteins. Many of these proteins interact as part of larger intracellular signaling systems or multiprotein complexes with different functions. Chronic diseases such as cancer, diabetes, Alzheimer's disease, and rheumatoid arthritis likely have their origins in several dysregulated proteins or pathways, making it very difficult to identify single targets that will lead to efficacious and durable therapies in a broad patient population. Advances in genome-wide association studies to identify polymorphisms associated with disease, coupled with gene editing and

molecular biology tools to probe specific proteins and pathways, will lead to more informed drug target selection with greater confidence in translational pharmacology.

Another major challenge for drug discovery is the vastness of chemical space. It is estimated that there are $>10^{40}$ possible structures in the universe of drug-like small molecules—more than the total number of atoms in the universe.[5] Typical compound collections within the pharmaceutical industry range between 10^6 real compounds and 10^{20} virtual compounds and are limited by the practicality of chemical synthesis and screening of real compounds along with computing power needed for virtual screening. Regardless of the methodology used for hit identification, either figure is dwarfed by the breadth of drug-like chemical space. The fact that any drug discovery efforts are successful is believed to result from the finite number of protein folds and similarity of binding pockets across targets within a gene family that, over time, have focused pharmaceutical company collections on biological hotspots in chemical space. In order to further expand the diversity of corporate collections, companies have broadened their chemical equity to include products of Diversity-Oriented Synthesis (DOS),[6–8] DNA-encoded massively parallel libraries,[9,10] and fragments for fragment-based drug discovery (FBDD).[11–14] Additionally, companies are broadening their definition of drug-like chemical space to extend beyond the boundaries contemplated by applying the Lipinski Rule of Five—to include cyclic peptides and natural product derivatives.

In order for a drug to demonstrate efficacy, it must reach the target tissue and safely attain sustained concentrations to deliver the appropriate degree of pharmacological modulation over the course of the dosing interval.[15] While this statement sounds intrinsically simple, optimizing for biopharmaceutic, pharmacokinetic, and safety properties can be extraordinarily difficult while retaining potency, selectivity, and the desired mechanism of action (antagonism, agonism, or allosteric modulation) on the primary pharmacological target. All drugs must persist for a reasonable period of time after administration, which is a function of their absorption rate, distribution into tissues, metabolism, and excretion. Absorption and tissue distribution occurs as a function of passive permeability together with transporter-mediated uptake and efflux. In addition, distribution is also a function of plasma and tissue protein binding. Metabolism can occur through oxidative processes mediated by enzymes such as CYPs (Cytochrome p450 family enzymes, of which there are 57 isoforms[16]), amine oxygenases, and aldehyde oxidase. Alternatively, conjugative processes, such as glucuronidation and sulfation, modify polar functional groups such as acids and alcohols. Finally, excretion can occur through biliary transporters, active renal transport or passive renal excretion without reabsorption. While there are widely known medicinal chemistry principles for modulating many of these pharmacokinetic parameters, their application is often challenged by limited flexibility of the biomolecular target to allow appropriate modification of the pharmacophore.

Moreover, safety is a multiparametric property that depends on the intrinsic effects of modulating the primary pharmacological target, absence of detrimental off-target pharmacology, absence of intrinsically reactive functionality, and negligible propensity to form reactive metabolites that induce indiscriminate covalent protein modification. While most compounds possess one or more of these effects at some level, it is often a question of efficacious dose and whether the off-target effects can be minimized or tolerated at low enough doses where repair and clearance mechanisms can effectively handle insults. For example, the generation of reactive metabolites can sometimes be managed by glutathione trapping in the cytosol, provided doses are low enough to prevent persistence of electrophilic species that could covalently modify proteins.[17] Likewise, the heterogeneity of protein-binding pockets will lead to a narrowing of secondary targets that are modulated as exposure decreases, provided that the compound possesses some modicum of selectivity.

To address these challenges, medicinal chemists utilize a wide array of technologies to better understand how lead compounds interact with their targets, address off target pharmacology through understanding selectivity at a molecular level, develop design strategies to reduce metabolism or alter clearance pathways, and optimize distribution to specific tissue compartments. This chapter will provide a broad overview of established technologies and will emphasize advances in enabling technologies that have occurred in the last ten years. Our emphasis will be on technologies that enable quality drug design: identifying quality starting points for drug discovery, determining their molecular mode of action, and understanding their pharmacokinetic properties. The equally important areas of enabling technologies in chemical synthesis and formulations will not be covered owing to limitations of space.

2.01.2 New Modalities for Target Modulation and Validation

Classical drug discovery was largely driven by phenotypic assays due to a limited understanding of the biomolecular basis of disease, and many therapeutic agents were advanced to clinical practice with only a limited understanding of their molecular mode of action. Major advances in genetics and molecular biology, coupled with the decoding of the human genome, drove a target-centric approach to drug discovery and unleashed a broad array of tools to associate specific genetic targets to disease. Despite these advances, the pharmaceutical industry continues to struggle with clinical candidate attrition, which in many cases is due to insufficient efficacy or differentiation. This attrition has been ascribed in part to insufficient validation of drug targets, prompting investment in chemical biology and genetic methods to increase confidence in targets and the molecular basis for their modulation by drug candidates.[18,19]

2.01.2.1 Gene Editing and Gene therapy

Throughout the late 1990s, target validation studies were conducted in vivo using embryonic or conditional gene knockouts to understand the impact of target inhibition on the disease state. These transgenic organisms are created through the generation of engineered embryonic stem cells, using plasmids that encompass part of the gene target and exploiting homologous recombination

to introduce a nonfunctional sequence into the target gene. These methods provide valuable information on the physiological role of the protein target but are complicated by the potential for embryonic lethality of the genetic knockout in cases where the target gene is critical for organismal development, making phenotypic study of the knockout impossible. Additionally, developmental compensation through altered expression of other genes has the potential to ameliorate the impact of the target knockout. Finally, these studies are time-consuming and expensive. Over the past few years, a variety of molecular genetic tools have emerged that make these studies more efficient, enable temporal alterations in gene function, and can be conducted in fully developed cells or organisms. Moreover, gene-editing tools can in principle enable the study of target modulation through genetic manipulation as opposed to simple target inhibition through genetic knockout. With greater access to human patient-derived tissues, these gene-editing techniques are now routinely used to create isogenic cell lines in which specific disease-related mutations are induced or corrected to enable holistic interrogations of cellular alterations in normal vs disease state.[20]

Discovery of the CRISPR-Cas9 (Clustered Regularly Interspersed Palindromic Repeats—CRISPR-associated protein 9) system has revolutionized genetic manipulation in cells and whole organisms. In comparison to earlier gene-editing technologies such as ZFNs (zinc finger nucleases) and TALENs (Transcription activator-like effector nucleases), the CRIPSR system is much simplified leading to an increased ability to test for the most efficient design, increased speed of model creation, reduced cost of reagents, and a higher editing activity. While we focus primarily on the concept of the CRISPR system here due to its broad availability and widespread application, there may still be merit to using TALENs and ZFNs to give greater specificity when targeting genes with very homologous family members.[21,22] The native CRISPR-Cas system functions as a bacterial innate immune system, which protects against bacteriophage replication by cleaving phage DNA at specific points. The cleavage sites are defined by portions of bacteriophage DNA from prior infections that become incorporated into the bacterial genome and are contained between the palindromic repeats in a larger CRISPR array.[23] This CRISPR array begins with a leader sequence that promotes its transcription and subsequent processing into small CRISPR RNAs. These RNAs function as a prokaryotic analogue to shRNA in eukaryotic cells and guide the Cas endonuclease complex to cleave complementary sequence from the DNA of the new invading bacteriophage. This system was adapted to function in eukaryotic cells using the *S. pyogenes* Cas9 system, which requires two short RNAs for specificity—the CRISPR RNA and the noncoding transactivating crRNA (tracrRNA), which are combined into a single-chimeric guide RNA (sgRNA).[24] Endonuclease cleavage produces a specific double-stranded DNA break only when the targeted site is located immediately downstream from a PAM (protospacer adjacent motif) nucleotide triplet. The cleaved DNA is then repaired through nonhomologous end joining that introduces frameshift insertion/deletion (indel) mutations, rendering the targeted gene nonfunctional. By using two guide RNAs directed at multiple sites in the target gene, complete deletion of the intervening sequence can be achieved (see **Fig. 1**).

One liability of the early CRISPR-Cas9 technology was incomplete specificity resulting from cleavage at partially mismatched sites relative to the guide RNA. Mutant Cas9 proteins (Cas9 D10A) have been developed to effect only single-strand cleavage of the target DNA sequence, precluding the nonhomologous end joining repair mechanism.[25] Through delivering two such guide RNAs directed at proximal sequences on both strands of DNA within the target gene, two single-strand breaks will occur in close proximity, triggering nonhomologous end joining with increased specificity. The Cas9 D10A mutant also enables the introduction of new genetic sequences through homology-directed repair, wherein a coexpressed exon serves as a homology-directed repair donor and is inserted into the target sequence. This technique offers the possibility of genetic knock in using the CRISPR-Cas9 editing system.

In addition to its editing capabilities, the CRISPR-Cas9 system offers exciting potential for genetic and epigenetic regulation to further dissect gene function and linkage to disease. Mutation of the two nuclease domains of Cas9 to create a nuclease-deactivated Cas9 (dCas9) followed by subsequent fusion to a transcriptional activator (CRISPRa) or repressor (CRISPRi) converts this system into an easily programmable transcription factor when paired with its target specific sgRNA.[26] Additionally, fusion of dCas9 with a histone acetyltransferase was shown to create a platform capable of manipulating the epigenome.[27]

The extension of this technology to pooled genetic screening has enabled the interrogation of many genes at once, and all three versions of the CRISPR-Cas system described earlier have been used for mammalian cell screening.[28] In 2014, multiple reports were almost simultaneously published describing pooled screens that used the wild-type humanized Cas9 system.[29–32] Cells were transduced with lentiviral vectors containing the guide RNA libraries and then positively selected for resistance to toxin-mediated death. Most guide RNAs do not confer resistance and therefore "drop out" in the subsequent selection process, whereas those that do confer resistance become enriched.[29–32] CRIPSRa and CRIPSRi screens have also been described[33,34] and together with CRIPSR knockout screens provide complementary systems. Genes that are highly enriched with CRISPRa are likely to "drop out" of

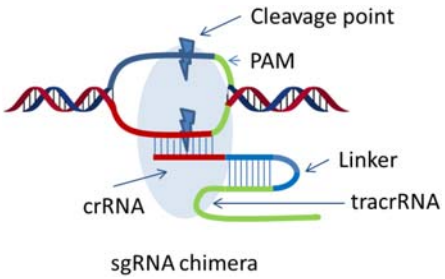

Fig. 1 Illustration of targeted DNA cleavage by CRISPR single-guide RNA.

a CRISPRi or knockout screen and vice versa. Since there is less sensitivity and more noise in the guide RNAs that drop out of a screen, upregulation and downregulation may offer complementary sensitivities.[26]

One of the most significant challenges associated with the CRISPR-Cas9 system is efficient delivery of the Cas9 nuclease DNA and guide RNA to the target cells. This delivery can be accomplished through liposomal-mediated transfection or electroporation.[35] However, these systems are not suitable for in vivo delivery of the CRISPR-Cas9 machinery, which would be necessary for in vivo target validation studies or adaptation of the CRISPR-Cas9 system for gene therapy. Adenoviral delivery of Cas9 and sgRNA is attractive in principle due to the low immunogenicity and oncogenic risk from incorporation into the host genome. However, adenoviral vectors are limited with respect to their genetic payload size (c.4.5 kb), which is insufficient to carry the commonly used *S. pyogenes* Cas9 DNA alongside its sgRNA in the same vector. A systematic screen of smaller Cas9 orthologues revealed that the *S. aureus* Cas9 protein possesses properties conducive to efficient, selective gene editing with a sequence small enough for adenoviral delivery (1053 amino acids vs. 1368 amino acids for *S. pyogenes* Cas9).[36] To demonstrate proof of concept, a U6-driven sgRNA encoding either the ApoB or PCSK9 gene and a cytomegalovirus-driven or thyroxine-binding globulin-driven *S. aureus* Cas9 expression vector were delivered in a single adenoviral vector to C57BL/6 mice.[36] Genetic and phenotypic evidence of selective target knockdown was demonstrated in each case. The ApoB-transfected animals demonstrated 5% indel incorporation and increased hepatic lipid levels, and the PCSK9-transfected animals showed 40% indel incorporation and lowered PCSK9 and LDL cholesterol levels as expected for this mechanism.

2.01.2.2 Biased Receptor Signaling

The concept of using sensors to measure physiological changes within cellular systems has been a mainstay of cell-based high-throughput screening since the 1980s. This strategy has ranged from the use of molecular indicators, such as the calcium-responsive dyes (Fura-2, Fluo-3, Fluo-4, etc.) to genetically encoded reporters such as luciferase. As scientific advances continue to reveal the increasing complexity of the cellular milieu, genetically encoded biosensors are being refined and applied to further dissect signaling cascades and understand the protein interactome. Fluorescence/bioluminescence resonance energy transfer techniques (FRET/BRET) have been applied to measure conformational changes within a single protein or to monitor protein–protein interactions and are well reviewed by Lohse et al.[37] Panels of FRET/BRET biosensors have been developed to interrogate all the nodes of the GPCR signaling cascade, and as the understanding that these pathways can be modulated independently has emerged, these biosensors have been leveraged to guide the design of biased ligands that preferentially signal through specific pathways in order to tease apart therapeutic benefits from unwanted adverse effects. This approach has formed the premise for the development of TRV130 (**1**, currently in Phase 2 clinical trials), a potent analgesic at the μ-opioid receptor that has reduced β-arrestin recruitment and receptor internalization and is reported to show less gastrointestinal dysfunction and respiratory suppression than morphine at equianalgesic doses.[38] The physiological importance of functional bias at GPCRs has also been demonstrated through the beneficial cardiac effects displayed by angiotensin-1 receptor (AT1R) ligands that selectively activate β-arrestin and not G-proteins [TRV027, **2**, Phase 2b].[39,40] Moreover, the G-protein-biased GPR109A agonist MK0354 (**3**) that does not activate β-arrestin and ERK reduces triglyceride levels without promoting the unwanted cutaneous flushing caused by nicotinic acid.[41]

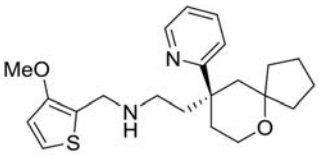

1

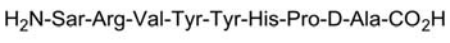

2

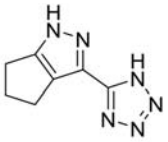

3

FRET technologies have also been exploited to investigate receptor heteromers which are defined as macromolecular complexes formed of at least two functional receptor units with biochemical properties different from their individual counterparts.[42] A screen for δ-opioid-μ-opioid heteromer ligands led to the identification of CYM51010 (**4**), which exhibited antinociceptive activity similar to morphine with lower levels of tolerance and provides an alternate potential path to analgesics with reduced side effects.[43] While there is still some controversy around the existence and physiological relevance of GPCR heteromers in native tissues, a number of examples including A2A-D2R, MT1-MT2, α_{1A}AR-CXCR4, and α_{1B}AR-CXCR4 have been described.[42] The biased ligand and GPCR heteromer approaches to modulating intracellular signaling cascades represent evolving tactics for the design of GPCR-directed therapeutics, which currently comprise almost 30% of marketed drugs.

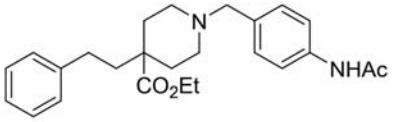

4

One caveat of the FRET/BRET biosensor systems is that they are frequently generated as stably transfected cell lines in which the receptor of interest is overexpressed. The drive to improve translation into the clinic calls for more physiologically relevant systems early in screening cascades, and thus emphasis is shifting to the expression of biosensors in primary[44] and stem cell[45] derived systems.

2.01.2.3 Modulators of Protein Transcription, Translation, and Translocation

The vast majority of small molecule and nonvaccine biological agents in the human pharmacopeia exert their pharmacology through direct modulation of their protein target—either through orthosteric or allosteric receptor modulation, or via competitive, noncompetitive or uncompetitive modulation of enzyme activity. As the proverbial "low hanging" fruit of therapeutic targets are successfully modulated with these specific ligands, we are observing an expansion of innovative therapeutic approaches. These approaches aim to fine tune efficacy and reduce adverse effects, to provide differentiation from available therapies or to overcome hurdles posed by difficult targets with strong links to disease. Some examples include: undruggable proteins (with large or shallow binding pockets or highly conserved active sites), complex protein–protein interactions, and mutant or misfolded proteins that may initiate cellular damage *per se* or may be unrecognizable to the cell's trafficking machinery and become misrouted to incorrect subcellular locations. Therapeutic modulators of gene expression, including read-through compounds, RNA splicing modulators, epigenetic regulators, pharmacological chaperones, and proteostasis regulators, have all received attention. This section will briefly touch on all these mechanisms of action, using some key disease and therapeutic examples to provide context.

Cystic fibrosis (CF), the most common fatal genetic disorder affecting 1 of 3000 live newborns in Caucasian populations, is caused by mutations in the gene encoding the cAMP-regulated CF transmembrane conductance regulator (CFTR) chloride channel. The loss of CFTR function/expression at the apical membrane in bronchial epithelia impairs ion homeostasis and mucociliary clearance, leading to obstruction, infection, and inflammation. More than 2000 CFTR mutations have been identified and categorized by their alteration of CFTR function and/or expression and phenotypic consequences.[46] Class I mutations cause nonsense, frameshift or mRNA splicing mutations, resulting in the absence of CFTR synthesis. In general, class II mutations lead to defective protein maturation and premature degradation. Class III and IV mutations are responsible for gating defects and lower conductance respectively, while class V mutations lead to reduced CFTR protein due to alternative splicing of CFTR mRNA. Class VI mutations cause a decreased stability of CFTR protein at plasma membranes.

In about 5–10% of CF patients, at least one allele is affected with a nonsense (class I) mutation that creates a PTC (premature termination codon) in the mRNA open reading frame. This mutation leads to truncation and almost total absence of full-length protein. In trying to identify compounds that enable read-through of these premature, nonsense stop signs, PTC Therapeutics has developed Translarna™ (ataluren, PTC124 (**5**)), a nonaminoglycoside compound for oral administration. Ataluren is believed to interact with the ribosome to enable production of a full-length functional CFTR protein. Unfortunately, outcome measures were insufficient to provide a clinical benefit in CF patients, and in the meantime, ataluren has been conditionally approved for the treatment of Duchenne muscular dystrophy which can be linked to a similar premature termination codon etiology.

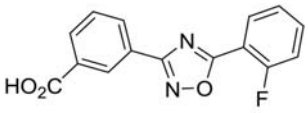

5

The process of pre-mRNA splicing, that is the precise ligation of exons and removal of introns, is essential for the correct expression and regulation of the majority of human genes. The splicing process is highly complex, requiring an array of *cis*-elements embedded in the mRNA and *trans*-factors that bind to them. Perhaps not surprisingly, this process is susceptible to derangement, and numerous diseases are attributable to mutations that alter splicing. Mutations in *cis* elements cause missplicing of genes, thereby altering gene function and contributing to disease pathology. Mutations of core spliceosomal factors are associated with hematolymphoid neoplasias, retinitis pigmentosa, and microcephalic osteodysplastic primordial dwarfism type 1 (MOPD1). Mutations in the *trans*-regulatory factors that control alternative splicing are associated with autism spectrum disorder, amyotrophic lateral sclerosis (ALS), and various cancers. A good review of the outcomes of these mutations together with references to a comprehensive list of splicing-associated diseases can be found in Singh and Cooper, 2012.[47] In addition to the use of antisense oligonucleotides (such as ISIS-SMNRx; ISIS Pharmaceuticals/Biogen), therapeutic advances have been made in the identification of small molecules to control splicing rearrangements. For example, various antitumor drugs have been reported to inhibit splicing: isoginkgetin (**6**), pladienolide B (**7**), herboxidiene (**8**,GEX1A), and spliceostatin A (**9**).[47,48] Three small molecule candidate therapeutics are currently in development for the correction of SMN2 splicing in spinal muscular atrophy (SMA). SMA is an inherited, automsomal recessive, motor neuron disease that affects 1 in 6,000 to 1 in 10,000 live births. It is characterized by loss of function of the survival of motorneuron 1, telomeric (SMN1) gene which leads to degeneration of motor neurons in the spinal cord and to muscle atrophy. The paralogous gene in humans, SMN2, contains a silent mutation in exon 7 that leads to exon skipping and a truncated, unstable SMN protein that does not compensate for the loss of SMN1. Paratek Pharmaceuticals identified PTK-SMA1 (**10**), a tetracycline derivative that promoted exon 7 inclusion.[49,50] A partnership between PTC Therapeutics, Roche, and the SMA Foundation has RG7800 currently

in phase 1b/2a clinical trials (see PTC website for status updates).[49] Independently, Novartis identified another orally active small molecule (**11**) that modulates splicing of SMN2 to increase levels of SMA protein.[49,51]

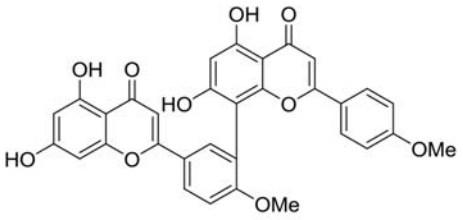

6

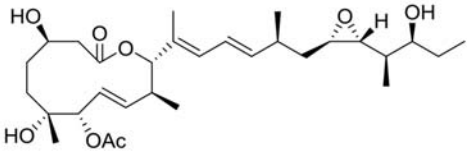

7

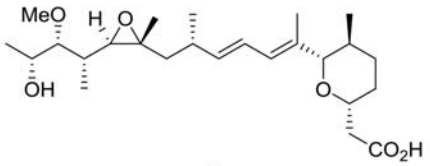

8

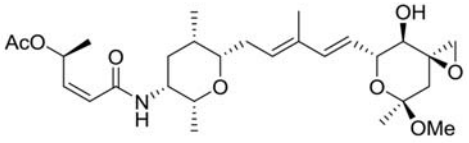

9

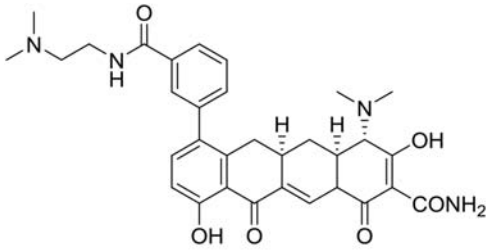

10

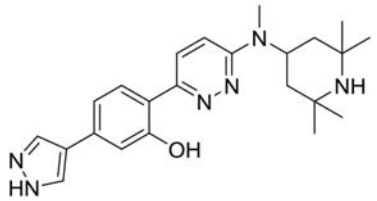

11

Regulating of gene expression through manipulating epigenetic factors has accrued some credence as a therapeutic approach as an increased understanding of the role of epigenetics in various diseases has emerged. Epigenetics relates genetics to a varied phenotypic outcome as a result of external or environmental factors that influence *how* genes are read as opposed to being caused by changes in the DNA sequence. At the molecular level this process refers to chemical modifications of chromatin through DNA modifications, histone modifications, histone variants, noncoding RNAs, and nucleosome remodeling.

DNA methylation is controlled by DNA methyltransferase enzymes and plays a crucial role in cell development and physiology. DNA methylation at CpG islands represses gene expression. For example, SMN2 is silenced by DNA methylation specifically at CpG islands within or in close proximity of the SMN2 promoter.[49] However, deregulation of methylation can lead to silencing of tumor-suppressor genes and the subsequent onset of cancer. Azacytidine (**12**) and its deoxy derivative, decitabine (**13**), are two nucleoside inhibitors, originally synthesized as potential chemotherapeutics that have FDA approval for the treatment of myelodysplasia. These compounds are believed to act in part through DNA methyltransferase inhibiton, causing hypomethylation of DNA, in addition to having a direct cytotoxic effect on abnormal hematopoietic cells. Despite their early promise as potential therapeutic targets in cancer, DNA methyltransferase inhibitors have not demonstrated single agent efficacy in other cancers, and reported compounds are generally low in potency and have poor metabolic or chemical stability.[52]

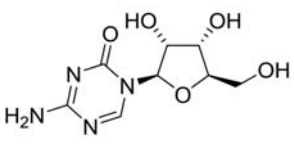

12

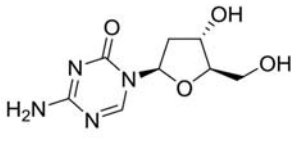

13

A causal role for epigenetic modifications of histone proteins in disease has also attracted the awareness of the research community to targets previously considered merely "packaging proteins." Multiple lysine residues can be acetylated in histone proteins, and numerous enzymes can write (histone acetyltransferases) or erase (histone deacetylases, HDACs) these modifications. HDACs

suppress transcriptionally active genes, and in 2001 the HDAC inhibitor sodium butyrate was shown to increase SMN levels in patient-derived cells and in mouse models of mild SMA.[53] Two HDAC inhibitors (vorinostat (**14**) and romidepsin (**15**)) have FDA approval for the treatment of refractory cutaneous T-cell lymphoma, although in a similar vein to the DNA methyltransferase inhibitors, there is some skepticism on the value of HDAC inhibitors for single agent therapy in general oncology. Histone methylation provides higher contextual environments than DNA methylation or histone acetylation. Histone proteins may be methylated on lysine residues (mono-, di-, or tri-), and on arginine residues (mono- or di-), and the position of methylation may vary. Each of these modifications may attract a different complex of reader proteins and have different cellular effects, for example: gene expression or gene repression.[54] Activating mutations in the histone methyltransferase, EZH2, which is responsible for trimethylating Lys27 of histone H3 (H3K27), have been reported to contribute to B-cell non-Hodgkin lymphomas. EZH2 inhibitors still retain promise as effective chemotherapeutic agents.[55] In addition to being methylated and acetylated, histone proteins can also be (de) phosphorylated, (de) ubiquitinated, and (de) SUMOylated leading to a complex intricacy of potential regulatory signals. Reader proteins recognize these chromatin modifications and activate the appropriate intracellular pathways, for example, BRD4, which contains a BET domain that binds to acetyl-lysine in histone proteins. There is hope that inhibitors of BRD4 will prove clinically useful in the treatment of midline carcinomas and acute myeloid leukemia.[54] While oncology remains the key area of focus for epigenetic therapies, interest is spreading to other areas such as autoimmune disorders and diabetes. Much work is needed, however, to deliver a second generation of epigenetic therapies that have greater efficacy and tolerability than seen in currently developed compounds.

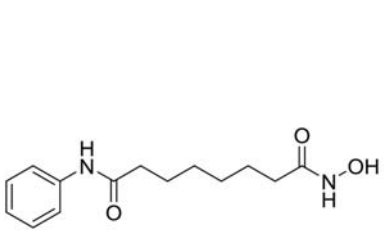

14

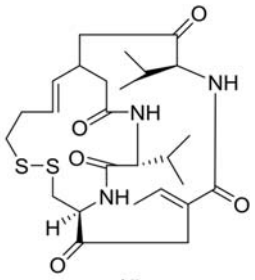

15

The potential to arrest protein translation by stalling a translating ribosome on its nascent peptide has recently emerged as a potential therapeutic opportunity to reduce the synthesis of mutant proteins that contribute to a disease phenotype. During protein translation the ribosome polymerizes amino acid building blocks into the elongating nascent polypeptide chain by forming a new peptide bond at the peptidlytransferase center. The rate of this nucleophilic attack varies with each amino acid, and specific amino acids or combinations of amino acids can slow or even stop translation in a *cis* fashion, stalling the self-synthesizing ribosome. In eukaryotes for example, stretches of positively charged amino acids (such as lysine or arginine) and motifs of three or more consecutive proline residues have all been shown to induce stalling.[56] Stalling during translation of the upstream open reading frames of arginine attenuator peptide (AAP), cytomegalovirus (CMV), and S-adenosyl-methionine decarboxylase (SAM-DC) prevents further ribosomal scanning and represses expression of the downstream genes.[56] Most of the sequences that pause translation, the so-called arrest peptides, are active only in the presence of specific environmental cues and modulate the cell's downstream response. For example, in bacteria, exposure to antibiotics causes ribosomal stalling to induce an upregulation of downstream antibiotic-resistance genes. High-resolution cryo-EM structures demonstrated that erythromycin, either through direct contact with an upstream open reading frame or through limiting its conformation, induces interactions between the peptide and the ribosome that render the peptidlytransferase center inactive and stall the ribosome on the uORF.[57,58] This stalled ribosome induces an alternative conformation that exposes a new ribosomal binding site and enables translation of the downstream rRNA methyltransferase, ErmC. This enzyme dimethylates ribosomes at the erythromycin binding site, conferring antibiotic resistance.[56,59] Regulation of translation in response to a small molecule has been demonstrated in additional systems. For example, stalling of the bacterial TnaC arrest peptide occurs in response to L-tryptophan,[56] however, only recently has it been conceived that this could be a potential therapeutic mechanism, and should this activity be translated into the clinical setting, this modality will open the doors for greater therapeutic impetus in this area.

Mutations in receptors, ion channels, and enzymes frequently interfere with the tertiary folded protein structure alerting the cellular quality control system and leading to protein retention in the endoplasmic reticulum (ER) or other misrouting. These outcomes result in loss of function at the normal site of biological activity. A pharmacological chaperone (or pharmacoperone, from "protein chaperone") is a small molecule that serves as molecular scaffolding to induce the correct folding and trafficking of mutant proteins within the cell, bypassing the quality control systems, and thereby ameliorating disease symptoms. Candidate diseases that may be susceptible to such treatments include neurodegenerative diseases, such as: Alzheimer's, Parkinson's, and Huntington's diseases, diabetes, inherited cataracts and cystic fibrosis.[60] In 2013 Michael Conn and coworkers demonstrated the ability of pharmacoperone, IN3, to rescue the plasma membrane localization of mutant gonadotropin-releasing hormone receptor (GnRHR) in a knock-in mouse model that mirrors the mutation causing human hypogonadotropic hypogonadism (failed puberty).[61] Restoration of plasma membrane localization was associated with renewed responsiveness to the endogenous ligand, gonadotropin-releasing hormone, and a mutant-specific agonist. Moreover, pharmacoperone treatment in the mice improved testis function (restored spermatogenesis and testosterone production) and restored fertility.

The prototype class II mutation in CF is a deletion of the phenylalanine in position 508 (F508del-CFTR). This mutation is found in 90% of CF alleles and impairs the protein folding leading to protein retention in the endoplasmic reticulum (ER) and degradation by the proteasomal pathway. VX-809 (Iumacaftor (**16**), Vertex Pharmaceuticals) was the most promising of the first generation of pharmacological chaperones or correctors for CFTR restoring about 15% of normal CFTR function in human epithelial airway cells. Unfortunately, in phase IIa clinical studies a number of patient outcome parameters were not improved, and therefore polypharmacology approaches combining additional mechanisms of action with these corrector compounds is expected to be necessary for effective protein repair. A potentiator compound (e.g., VX-770 (**17**)) increases the cAMP-regulated chloride channel gating of the CFTR channel and is most likely to have positive impact on Class III and IV mutations. Successful phase III trials were reported for patients with gating deficiency mutations, but monotherapy in F508del-CFTR patients failed due to limited CFTR expression at the plasma membrane. VX-809 and a second-generation chaperone, VX-661 (**18**), have both been combined with VX-770 for clinical testing.

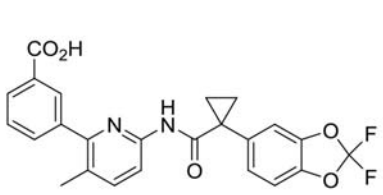

16

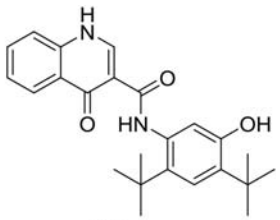

17

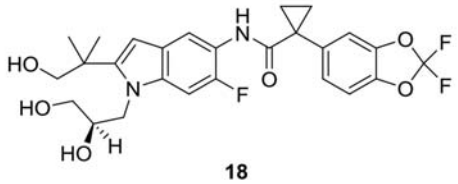

18

2.01.2.4 Modulating Proteostasis and Protein Degradation

An alternate approach to treating protein misfolding disorders is to address the proteostasis network, the cellular machinery that controls protein homeostasis.[62,63] Cystic fibrosis serves yet again as a good context for this approach, with multiple examples being reported that increase pathway capacity, modulate intracellular signaling, or affect protein degradation.[46] Silencing expression of the heat shock protein 90 co-chaperone, Aha1, partially restores folding, trafficking and chloride conductance of F508del-CFTR. Additionally, the decrease of ubiquitinated F508del-CFTR via overexpression of ubiquitin protease 10 leads to increased expression at plasma membranes in human epithelial airway cells. Transglutaminase 2 inhibitors have been tested in an attempt to correct defective autophagy. Nivalis Therapeutics is working to increase intracellular concentrations of GSNO (s-nitrosoglutathione) to prevent CFTR degradation, and Bayer is testing Riociguat (FDA approved for pulmonary arterial hypertension and chronic thromboembolic pulmonary hypertension) for stimulation of CFTR activity via elevation of intracellular cGMP levels. Accordingly, phosphodiesterase type 5 inhibitors (PDE5), which also enhance cGMP accumulation, have also been studied for potential therapeutic benefit in CF.

Targeted protein degradation strategies exploit the ubiquitin-proteasome system to achieve selective destruction of a target protein.[64] Ubiquitin is a small regulatory protein that is expressed in almost all human tissues. Its attachment to target proteins by ubiquitin ligases can result in several outcomes, one of which is altered subcellular localization and protein destruction by the 26S proteasome. The latter outcome is typically signaled by polyubiquitination of a target protein at lysine. Protein ubiquitination is reversible, the forward reaction being catalyzed by ubiquitin ligases, and the reverse reaction being effected by deubiquitinases. Ubiquitin ligases are modular proteins, comprised of an E3 substrate recognition domain, an E1 ubiquitin-activating enzyme, and an E2 ubiquitin-conjugating enzyme. Of these three modules, the E3 ubiquitin ligase is the most heterogeneous, and it is estimated that there are over 600 different E3 ligases in the human genome.[65] The targeted protein degradation strategy relies on reprogramming the E3 ligase to operate on a neomorphic substrate through the use of a chimeric ligand possessing a moiety that binds to the target protein and another subunit that binds to the E3 ligase being exploited for target destruction (see **Fig. 2**).

Four ligases have been exploited for targeted protein degradation: VHL, Cereblon, MDM2, and cIAP2.[64] In addition, a hydrophobic tagging strategy has been devised to exploit the general ubiquitination and destruction of proteins with exposed hydrophobic cores, a hallmark of misfolded proteins. Because these protein degraders must simultaneously bind to the E3 ligase and the target protein in order to be effective, their design typically involves two elaborated ligands for each protein (with affinities between 1 nM and 1 μM) and a flexible linker. The resulting physicochemical property space poses challenges for cellular permeability and oral absorption. However, unlike typical enzyme inhibition and receptor antagonism approaches which are stoichiometric in ligand, targeted protein degradation is catalytic and irreversible.[64] This unique mechanistic property should dramatically reduce the intracellular concentration of chimeric ligand needed to suppress target protein function relative to conventional approaches. Additionally, the protein degrader approach requires that one identify a ligand that binds to the desired target; it

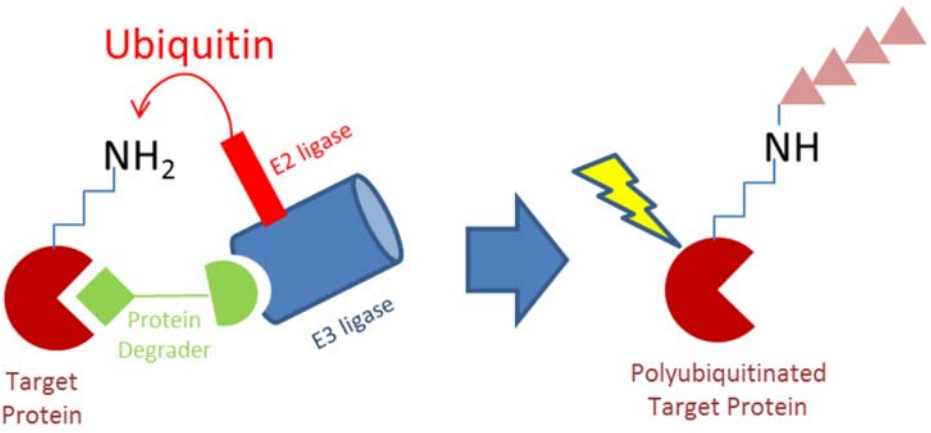

Fig. 2 Targeted protein degradation through the recruitment of ubiquitin ligases by a bispecific ligand.

does not need to possess intrinsic functional activity. Therefore, protein degrader strategies theoretically expand the number of useful binding sites on the target protein, enabling selection of the most drugable pocket for chimera design.

The first E3 ligase hijacked for protein degradation is cIAP1, which interacts with other protein targets through its BIR3 (Baculoviral IAP Repeat) domain.[66] Small-molecule ligands like methyl bestatin were shown to bind the BIR3 domain and induce autoubiquitination; therefore, methyl bestatin was selected as a target binder for further study. Early proof of concept was demonstrated with chimeric degraders (SNIPERS) of CRABP I and CRABP II (Cellular Retinoic Acid Binding Protein).[66] Bestatin-based protein degraders were found to induce autoubiquitination and degradation of the cIAP1 protein, which could lead to reduced efficacy over time due to depletion of the E3 ligase. While methyl bestatin (**19**) is known to induce this autodegradation, as are ester-based SNIPERs, the corresponding N-methyl amide of bestatin **20** does not despite its tight binding to the BIR3 domain. Therefore, the amide-based SNIPER **21** was designed.[67,68] This compound demonstrates nearly complete degradation of CRABP II after 6 h of treatment at 3 μM, whereas no degradation of cIAP1, cIAP2, or XIAP was observed over the entire concentration range (up to 30 μM) for 48 h. The earlier SNIPER **22** demonstrated nearly complete loss of cIAP from 6-24 h under these conditions. Other proteins that have been successfully degraded by cIAP1-based degraders include the retinoic acid receptor (RAR), the estrogen receptor (ER), and the androgen receptor (AR).[69]

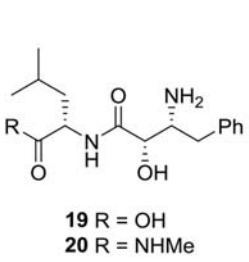

19 R = OH
20 R = NHMe

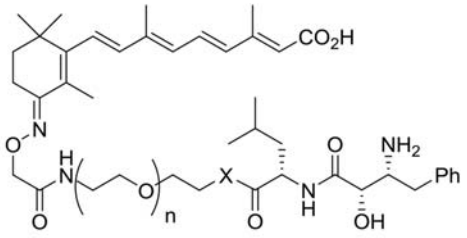

21 X = O, n = 2
22 X = NH, n = 2

The Von Hippel Lindau ligase (VHL) has been repeatedly exploited for targeted protein degradation in vitro and in vivo. The VHL protein is an E3 ligase that is responsible for degrading Hypoxia Inducible Factor (HIF), a protein that regulates erythropoiesis under hypoxic conditions. Under normoxic conditions, P402/564 is hydroxylated by HIF prolyl hydroxylase. The VHL ligase recognizes the hydroxylated proline residue, catalyzing ubiquitination of the protein as a negative feedback mechanism. The unique recognition of hydroxyproline was exploited in the design of VHL targeting ligands for protein degrader chimeras—for example, the ERRα degrader **23**. These chimeras typically possess a tripeptide-based VHL ligand featuring 4-hydroxyproline as the central residue. Targeted protein degradation has been accomplished for the Estrogen Receptor,[70,71] Androgen Receptor, FKBP,[70] TrkA,[72] ErbB2/ErbB3,[72] RIPK2,[71] BCR-ABL,[73] and BET[74] using VHL chimeras.

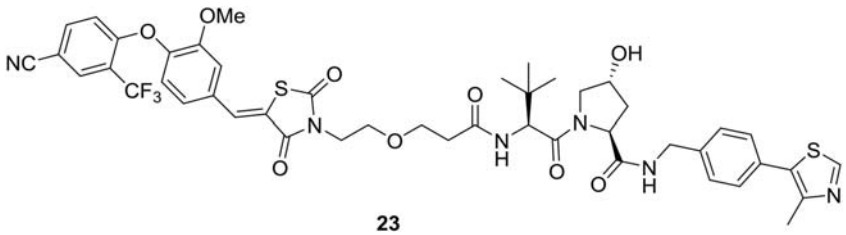

23

Cereblon is an E3 ligase that binds to damaged DNA-binding protein 1 (DDB1), cullin 4A, and regulator of cullins 1.[75] It is the biomolecular target of thalidomide, pomalidomide, and lenalidomide, which associate with its substrate binding site and alter substrate specificity for the protein, inducing ubiquitination of neomorphic substrates and preventing modification of its endogenous substrate.[76] It is this mechanism of action that is postulated to result in the teratogenic effects of these agents. Because these ligands are small, drug-like compounds, they have been exploited for targeted protein degradation through linkage to target-binding compounds through the phthalimide ring—for example, the BRD4 degrader **24**. Cereblon-containing protein degraders have successfully been designed for Androgen Receptor, Estrogen Receptor, BRD4,[77,78] FKBP,[77,78] and TBK1.

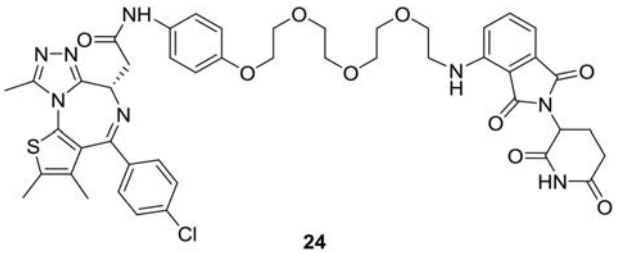

24

While targeted protein degradation is a promising new modality for target inhibition or antagonism, the technology has primarily been demonstrated in vitro, with few reports describing in vivo efficacy after subcutaneous administration.[71,78] Moreover, given the requirement for simultaneous binding of the protein target and the E3 ligase in a manner that allows positioning of a surface lysine residue near the E2 ubiquitin thioester bond, it can be challenging to design effective degraders for a given protein target. Design principles for effective protein degrader design have yet to be described but will need to consider: (1) the physicochemical properties required for effective cell penetration; (2) linker group properties such as length, polarity, and flexibility to allow formation of an effective ternary complex; and (3) optimum affinity for the target and ligase-binding moieties to generate that complex under physiologically relevant concentrations of the chimera. The lack of published design strategies is to be expected for a technology in its nascent stage, and further advances promise to yield effective target inhibition strategies for proteins that are otherwise challenging to pursue.

2.01.3 Hit Identification Methods

Advances in the molecular understanding of enzymes and receptors throughout the 20th century[79,80] together with the revelation of the human genomic sequence[81] and the concepts of drugability[3] heralded an era of molecular target-based drug discovery in the 1990s and the early 2000s. Modern drug discovery strategies now typically begin from the hypothesis that modulating a single biomolecular target or pathway is expected to deliver a beneficial effect on the disease state. Early confidence in rationale is established using genetic analysis, bioinformatics and pathway mining, molecular biology tools, and chemical probes. Upon determination that the target merits pursuing a drug discovery campaign, efforts begin toward the identification of lead matter to initiate medicinal chemistry optimization. Early screening strategies can encompass high-throughput, target-based, biochemical, functional assays; binding assays; or cell-based screens to identify chemical starting points. There is a wide array of well-established screening technologies for this purpose, and this section will focus on alternate philosophies and newer methods that have emerged or matured over the last 10 years.

2.01.3.1 Phenotypic Screening

Recent commentaries on the productivity crisis in the pharmaceutical industry have pointed to the highly reductionist approach applied in target selection and target-centric campaigns as contributing to poor clinical translation, and hence there has been a resurgence of interest in phenotypic screening as a mechanism to identify new drug targets and molecular mechanisms for treating disease.[82,83] Phenotypic screening potentially offers several advantages over target-based approaches.[84] Its inherent lack of target bias opens the possibility of targeting any biomolecular entity in its cellular context. In principle, this property enables discovering new targets for modulating cellular pathways and disease states. Because many drug targets reside within the cell, an attractive aspect of phenotypic screening is that it generally selects for compounds with favorable molecular properties for cellular penetration. It also selects for compounds that can attain intracellular concentrations sufficient to modulate their target in the presence of physiologically relevant concentrations of cofactors that might be competitive with compound binding. Finally, a phenotypic approach allows for discovering new molecular modes of action that might not be found in an isolated target-based assay with a defined molecular endpoint that could limit the number functional mechanisms that can be detected for modulating target activity. For example, a phenotypic screen using live bacteria led to Linezolid, a member of a novel antibiotic class that blocks the initiation of protein translation.[85] Similarly, the antiepileptic Lacosamide (**25**) was identified through testing in an in vivo rat model of epilepsy; following its FDA approval, it was documented to promote slow inactivation of voltage-gated sodium channels rather than blocking them directly.[86,87] The essence of the phenotypic movement proposes that the value of a phenotypic screen lies in

its ability to predict the successful translation of a compound or molecular mechanism of action to patients. As a result the greatest success is anticipated from an assay that uses a cellular system with a clear link to disease (e.g., patient-derived primary cells), a physiologically relevant stimulus (e.g., an intrinsic disease stimulus already provided in patient-derived cells), and a proximal and/or clinically relevant readout (e.g., a functional manifestation of disease).[88]

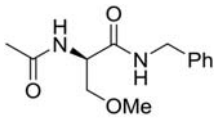

25

Technological advances have helped in the generation of more physiologically relevant systems in which to screen. Greater access to patient tissues and cells together with advances in the ability to induce pluripotency and to subsequently differentiate these iPS cells (IPSCs, induced pluripotent stem cells) in culture to a cell type of interest enables the development of a system using relevant cells that are compromised and demonstrate a disease phenotype in vivo. The genomic editing techniques described above are frequently applied to generate isogenic "normal or corrected" cells in diseases where a specific genetic mutation is being investigated. This practice allows for the comparison of normal and disease cell populations that can be tested for recapitulating a disease phenotype in vitro. If this phenotype can be established and quantitatively measured, then the identification of compounds that can correct/modify the phenotype comes with an increased confidence of clinical translation. Likewise, it is easy to understand the appeal of iPSC-derived hepatocytes to the drug metabolism and pharmacokinetics discipline that has traditionally been limited to working with labor intensive, high cost, and variable primary human hepatocytes for an understanding of clearance mechanisms. A key challenge with the use of iPSCs has been the inability to generate mature differentiated phenotypes that accurately mimic the expression profiles of the gold standard: primary human tissue. As a result, more complex coculture, three-dimensional (3D) culture, and microphysiological systems are emerging that are anticipated to provide the appropriate signals and growth factors for greater cell maturity and physiological relevance.

Spatial control is one of the fundamental premises of 3D cell culture, allowing for patterning of multiple cell types in a way that more faithfully represents the organization of tissues and organs. Four major platforms are typically used for the generation of 3D cultures: spheroids or cellular aggregates, synthetic scaffolds, naturally derived matrices, and hydrogels. Multiple reports have revealed significant changes in gene expression profiles of 3D vs. 2D cultured cells.[89] Many physiological processes take place under flow conditions, for example, blood flowing through vasculature and cancer cells circulating through the body. High-throughput microfluidic systems can be used to mimic these conditions, creating a physiologically relevant shear profile, and these systems have advantages in the design of assays to interrogate processes such as cell or platelet adhesion, rolling velocity, or transmigration.[90] Such cellular models may still be relatively simple from the context of one cell type flowing across a simple immortalized cell monolayer. In contrast, simple in vitro models of kidney function for efficacy, safety, and ADME testing have been challenging to develop for a variety of reasons.[91] The functional filtering unit of the kidney, the nephron, is composed of several cell types with multiple interactions and a specific architecture. There are apical and basal surfaces displaying unique protein expression profiles that drive transport of endogenous substrates and xenobiotics. Isolated primary kidney cells in the absence of 3D cues lose these properties when extracted from the body; moreover, these cells are limited in supply. Immortalized cells derived from the kidney similarly often retain only a subset of renal properties in two-dimensional (2D) cell cultures. The expression of relevant solute transporters has been documented to increase in proximal kidney tubule cells cultured under flow conditions, and a growing body of evidence suggests that extrinsic cues such as appropriate architecture and fluid flow are necessary to establish polarity and promote functional maturation of in vitro kidney cells.[92–94] Enter microphysiological systems, cellular and organ microsystems which have a multicellular architecture representing the characteristics and functions of the tissue of origin and demonstrate a reproducible and viable operation under physiological conditions over a long culture period. These systems, which are often referred to as organs-on-a-chip or tissues-on-a-chip, integrate advances in microfabrication and microfluidics to present highly controlled extracellular cues to cultured cells in a physiologically relevant context. Fluid flow and tissue deformation can be controlled, and the design enables the formation of independent channels with their own fluid access for co-culture systems in order to mimic typical barriers found in the human body. Microphysiological systems have been described for a variety of tissues including the liver, heart, lung, intestine, kidney, brain, vasculature, and bone. The competitive landscape is rapidly evolving although to date most testing has been low-throughput evaluations of efficacy or toxicity.[95]

One significant drawback of running phenotypic screens, even in physiologically relevant systems, is uncertainty of the molecular mechanism of compound action. Anticipation of this challenge and the desire of many chemists to ultimately deconvolute phenotypic hits to their specific protein target for lead optimization often engenders careful consideration of the chemical equity tested in the primary screen. The creation of well-annotated compound collections that are selected based on biological activity against key pathway targets is a typical approach with the hope being that specific cohorts of hits, known to demonstrate activity at the same target or at targets in the same pathway, might lead to a hypothesis for modulating the phenotypic outcome measured. The libraries are generally designed to cover broad areas of pharmacological space and frequently take into account primary target potency, selectivity, and cellular data, or at least physicochemical properties to ensure cell penetration. Compounds that have good lead-like properties and are cell permeable are favorable for phenotypic screens, and clearly compounds with clinical or patient data

can provide invaluable mechanistic hypotheses in addition to fast routes to in vivo testing if they show activity. Compounds that have demonstrated in vivo toxicity are also frequently well annotated within Pharma compound collections and can serve as learning tools within the context of a phenotypic project through indentifying key safety liabilities as well as providing substrate for tool compounds or SAR. Genetic screens such as the CRISPR-Cas9 described previously, or siRNA/shRNA screens provide a complementary approach to small molecule phenotypic screening. Using an arrayed format targeting one gene per well, a very similar approach to small-molecule screening can be taken, often with the very same assay format. These approaches rely on the identification or reversal of the endpoint in question after knockdown of a specific gene, and they are essentially target or pathway identification efforts that can subsequently be converted to target-centric projects. Combining hits from a small-molecule screening campaign with specific genes that impact the phenotype in question can provide a key to unlocking disease physiology.

Recent advances in genetic and proteomic analysis have enabled more rigorous and efficient determination of the target and molecular mode of action for phenotypic screening hits. Activity-based proteomic profiling (ABPP) enables the identification of specific enzyme targets for inhibitors using proteomic technology.[96] This technology relies on the development of mechanistic probes that covalently modify the catalytically active residue of enzymes within a specific gene family. These probes possess molecular features that enable their general activation and covalent labeling only of proteins within that gene family. Activity-based probes generally have fluorescent labels or cell capture tags (typically biotin) attached to them, enabling fluorescent analysis after gel electrophoresis or mass spectral identification after capture on streptavidin-coated beads.[97] The typical ABPP workflow involves incubating drug-treated cell lysates with the fluorescently labeled activity-based probe, quenching the reaction and separating the proteins by gel electrophoresis. Proteins for which compounds compete with the probe produce a reduced fluorescent signal in the compound-treated lysates relative to the untreated controls. The bands corresponding to these differentially labeled proteins can be excised from the gel, digested with trypsin and analyzed by mass spectrometry to identify the protein target from its tryptic peptides. Alternatively, SILAC (Stable Isotope Labeling by Amino Acids in Cell Culture) labeling can be used to produce differentially labeled cells that can be used for the compound treated and control lysates for subsequent treatment by a biotin-labeled activity-based probe.[98,99] Streptavidin capture of the labeled proteins, followed by digestion and mass spectral analysis, allows identification of target proteins by virtue of different quantities of tryptic peptides captured in the compound treated vs. control samples.

Activity-based probes exist for the ATP-site of protein kinases, serine hydrolases, and glucosidases.[100] ATP-based acylphosphonate probes (e.g., **26**) enable general labeling of the catalytic lysine in over 75% of all protein kinases, providing a general method for kinome selectivity profiling and identifying kinase targets for phenotypic screening hits. Probes for serine hydrolases are typically based on fluorophosphonates (e.g., **27**) owing to their broad reactivity with this enzyme family. The requirement for enzyme activity is elegantly demonstrated by the lack of reactivity with serine hydrolase zymogens.[97] Glucosidases contain a nucleophilic aspartate or glutamate residue that is covalently labeled by cyclophellitol. Activity-based probes containing an analogous epoxide or aziridine function (e.g., **28**) as activity-based probes against this enzyme family and can also modify nucleophilic acidic residues in related enzymes.[100] Additionally, general covalent probes for nucleophilic cysteines enable covalent tagging of the reactive cysteinome. These electrophilic compounds can be used to interrogate the differential reactivity of cysteines, which has important implications for understanding their function as potential nucleophiles or as sites for oxidation as a potential regulatory mechanism for protein function.[100–103] Compounds that bind proximally to a site of cysteine alkylation by these electrophiles produce a reduction in reactivity that can be detected by differential fluorimetric or mass spectrometric analysis.

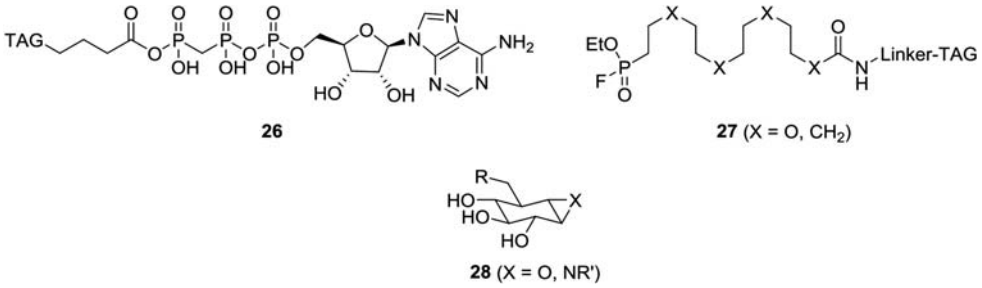

26 **27** (X = O, CH_2) **28** (X = O, NR')

2.01.3.2 New Technologies for Target-Based Screening

Affinity selection mass spectrometry (ASMS) is a high-throughput technology for the unbiased identification of target binders.[104,105] It enables massive parallel screening of compound libraries that can be compressed to >100 compounds per well, provided that each has a unique molecular weight for structural identification by mass spectrometry. In ASMS, the target protein is incubated with a set of potential binders and is then subjected to a separation step that discards unbound compounds (see **Fig. 3**). This separation step is critical for the success of the technique, and several methods have been employed including size exclusion chromatography and ultrafiltration.[106] Size exclusion methods are unique in that they are nonequilibrium methods owing to retention of the unbound compounds relative to rapid elution of the target protein. As a result, this separation method selects for compounds that have a low dissociation rate relative to the elution time of the protein. By contrast, centrifugal ultrafiltration techniques are more likely to select binders based on affinity due to the equilibrium that is established with each washing step. Once the target

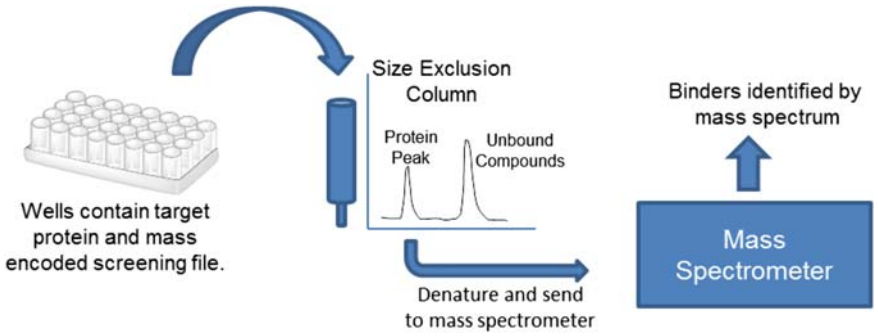

Fig. 3 Schematic representation of the process of affinity selection mass spectrometry used for identification of target binders.

protein is eluted, it is denatured or precipitated, and bound compounds are analyzed by mass spectrometry. Binders are identified by comparing the molecular weights of the bound compounds with a mass table that contains the structures and unique molecular weights of the compounds present in the incubation mixture.

Affinity selection mass spectrometry offers advantages of speed and a low false positive rate once the separation step is optimized. It is also relatively immune to artifacts, provided that the buffers used do not interfere with mass spectrometric analysis through ion suppression. One downside of the technique is that it can require large amounts of the target protein due to sensitivity limitations of the mass spectral readout. It is also impossible to infer the extent of target binding based on signal strength, as each compound has a different ionization efficiency that can vary by orders of magnitude. However, it is possible to determine affinity constants by conducting the ASMS experiment across a range of ligand concentrations and fitting the ASMS response as a function of ligand concentration to a saturation-binding curve.[107] Competition experiments with ligands of known affinity can also be used to estimate K_d for mixtures of compounds.[108] Because ASMS identifies target binders without regard for functional activity, subsequent validation steps are needed to characterize whether and how hits modulate the target. These validation steps typically consist of an orthogonal biophysical technique to validate binding and characterize the binding site, along with a functional assay to determine whether the hit compound inhibits, activates or has no effect on the target protein's activity. Through adding high concentrations of agents that are known to occupy one binding site on the target, it is possible to select for noncompetitive binders or to characterize whether hits identified in an unbiased screen bind at a particular site.[107]

DNA-encoded libraries take the compound compression that can be achieved through ASMS to another level, screening over 100 billion compounds in a single experiment.[109] Once again this is, at its foundation, an affinity-based approach; however, DNA-encoded libraries can dwarf conventional small-molecule libraries and offer a complementary approach for finding structures that bind to novel or challenging targets based on the diversity of chemical space covered just from sheer numbers. DNA-encoded libraries can be synthesized in several different ways, but the largest libraries (including GSK's which comprises 1×10^{12} compounds) tend to be built using a DNA-recording approach. A chemical building block is synthesized and tagged with a unique DNA barcode. A new building block is added to create a small molecule, and subsequently the DNA tag is lengthened to represent the new addition. Through a split and pool chemistry approach, the number of potential combinations is enormous. The protein target of interest is engineered with a purification tag, and then the library and target are combined and passed through a purification column. Binders are identified through sequencing the DNA tag, and an advantage over ASMS appears to be the revelation of a full structure–activity matrix including weaker binders. Clinical candidates are beginning to emerge from DNA-encoded library hits with the most advanced being the soluble epoxide hydrolase inhibitor, GSK2256294 (**29**), which is currently in phase 1.[110,111] This approach is not without its caveats. The DNA tag can sometimes interfere with target binding, and some library members can bind to the purification column causing false positives. The next wave of developments looks to move beyond soluble targets to membrane-bound proteins, and multiple large pharma are investing in collaborations or internal libraries for hit identification.[109]

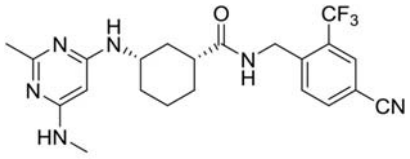

29

Fragment-based drug discovery (see Fig. 4) is a lead identification technique that has matured considerably over the last decade.[11–14] This strategy also relies on biophysical techniques to detect binders—typically using surface plasmon resonance, NMR-binding assays, or X-ray crystallography. Fragment screens are focused on identifying compounds with low molecular weight (<250) that incompletely occupy a binding site on the target protein.[112,113] Due to their limited binding surface, these compounds usually possess low affinity (sometimes approaching 1 mM), placing a higher hurdle on subsequent medicinal chemistry

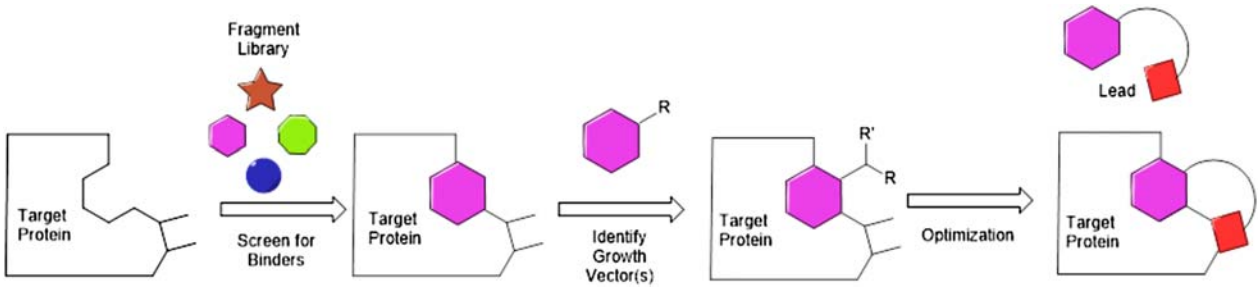

Fig. 4 Schematic representation of fragment-based drug discovery.

optimization for potency. Structure-guided optimization allows growth of the fragment to yield compounds with lead-like potency. Because the chemical starting points are small, chemical space is significantly more limited in the universe of fragments, making it possible upon fragment growth to penetrate regions of chemical space that are not covered in a corporate compound collection. Therefore, fragment screening offers the potential to identify or create diverse leads for protein targets that would not otherwise deliver compelling hits from a traditional functional high-throughput assay.

As with ASMS, the biophysical techniques that identify fragment hits will only select for target binders. It is not uncommon for functional activity to be undetectable due to the limited dynamic range of functional biological assays. Therefore, early optimization efforts are sometimes undertaken with the belief that increasing affinity will lead to measurable functional activity. Also, it is typical for hit optimization efforts to rely on crystallographic information that guides structure-based optimization of potency and selectivity.

Fragment screening approaches claimed early success with kinases, demonstrating regular propensity to identify compounds that bind at their ATP-binding site. However, corporate collections readily yield elaborated leads that are potent inhibitors binding to these sites. Some early examples of fragment-linking strategies, wherein fragments that bind adjacent sites are attached by a chemical linker to deliver a compound with dramatically improved potency, yielded high-molecular-weight compounds with poor drug-like properties. For these reasons, fragment-based drug discovery took a while before being broadly embraced across the pharmaceutical industry. The emergence of compelling leads from fragment approaches toward difficult targets like beta-secretase (BACE),[114] coupled with the recent approval of vemurafenib (**30**), a fragment-derived drug that targets the BRAF mutant kinase V600E,[115–117] have contributed to wider acceptance of fragment-based drug design as a viable approach for drug discovery.

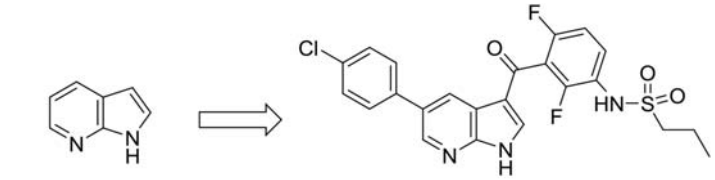

Original Fragment Hit **30**

2.01.4 Hit Characterization Using Computational Approaches and Biophysical Assays

In any screening campaign (target centric or phenotypic) the first round of hit identification approaches will ideally yield multiple series of compounds that reproducibly demonstrate activity in a dose-dependent manner in the identifying assay/technology. Subsequently, multiple techniques are employed to confirm the validity of these hits, to demonstrate target binding and pharmacological modulation following a target centric screen and, in the case of phenotypic screens, to further deconvolute the biological mechanism of activity.

Computational expertise can frequently be applied immediately to weed out likely false positives based on the wealth of data that already exists in a corporate database and literature examples.[118] For example, some hit compounds may be promiscuous binders, or the so-called frequent hitters. In a recent study, colleagues of ours surveyed 96 high-throughput screening campaigns (HTS) run within Pfizer (82 different targets, 66 gene families, ~300 million data points), and characterized the common features among frequent hitters.[119] The topology and physical attributes of these compounds were analyzed and compared with random sets of compounds generating a fingerprint-based Bayesian model to predict frequent hitters and potentially reduce the time and cost of HTS triage and chemistry follow-up during hit-to-lead optimization. Currently, this model is used as part of Pfizer's tool box for HTS triage and hit follow-up. Multiple groups have published on the nonspecific inhibition of enzymes by compounds that form organic small-molecule aggregates, and more recently, Brian Shoichet's lab have attempted to describe the mechanism of action of aggregate-based promiscuous inhibitors as a partial protein unfolding.[120] Historically, fluorescent compounds were often false

positives in fluorescence-based assays and were triaged out of hit lists or passed through nonfluorescence-based assays for confirmation. Newer generations of fluorescent probes and fluorescent technologies, together with improved compound file characteristics however, have reduced the impact of these compounds on screening campaigns.

Computational expertise is also highly valuable in determining a biological fingerprint of activities to enable the expansion of an initial hit list or build hypothesis around mode of action. Similarity searches based on chemocentric attributes have long been standard approaches for hit expansion and the defining of Structure–Activity Relationships (SAR) using the computational toolbox. Additionally, mining large biological datasets across multiple screens or cell lines enables the clustering of compounds based on their biological similarity. In 2005, Anton Fliri and Pfizer colleagues used percent activities of over 1500 compounds against 92 targets to demonstrate that comparing biological profiles of molecules provides an unbiased quantitative relationship between chemical structure and broad biological effects.[121–123] More recently Novartis identified bioactivity relationships using 195 biochemical- and cell-based assays, highlighting value for virtual screening, scaffold hopping, and designing new subsets.[124] The authors also found that their HTS-fingerprint clustering enriched the gene ontology categories in each cluster, illustrating that compounds in a cluster may not share the same chemical structure, nor target the same proteins, yet they participate in related cellular processes. Hence, biological fingerprint analysis (within a screen and across preexisting datasets) can be a valuable way to characterize hits from a phenotypic screen. Building on this concept, platforms of cell-based assays and informatics models are becoming available to profile compounds in a focused manner. Primary human cells cultured in systems representative of vascular, immune, and inflammatory biology and of sites of human exposure (skin and lung) have been used to classify novel agents according to mechanism of action and to provide insight into clinical phenomena.[125] Similarly a so-called cell painting assay in immortalized cell lines (U2OS) utilizes six stains to profile seven different cellular compartments (nucleus, nucleoli, golgi, plasma membrane, endoplasmic reticulum, mitochondria, and F-actin), and this assay has been shown to similarly cluster compounds with like actions.[126] What is needed now is a way to bring together physiological models and higher-throughput capacities at lower cost to enable disease relevant molecular profiling at scale in the earliest stages of lead identification and optimization. Hypotheses that are generated for the mechanism of action of hits at the conclusion of phenotypic campaigns, for example, from an annotated compound subset with known activities or from biological fingerprint clustering, can be validated through targeted siRNA/shRNA experiments designed to modulate the targets or pathways in question in an attempt to phenocopy the compound activity.

In addition to being biologically validated, hits identified from target-centric high-throughput screening need to have their target-binding properties characterized in order to have confidence in their suitability for lead optimization efforts. This process involves using an orthogonal technology, typically a biophysical or biochemical assay that is complimentary to that used in primary screening so that binding kinetics and thermodynamics can be characterized alongside functional activity. Well-designed studies provide information on molecular mode of action in addition to triaging compounds that emerge as false positives due to undesired mechanisms of target modulation.

Surface plasmon resonance is a general technique for characterizing binding affinity, association rate, and dissociation rate. This technique measures subtle refractive index fluctuations that occur when effective target mass changes upon ligand binding. Flow-based systems are commonly used for this purpose, as they enable direct measurement of binding kinetics. The target protein is immobilized—typically through biotinylation of surface lysine residues and capture on a streptavidin chip. The protein-treated chip is then exposed to a running buffer across a control and treatment channel. Upon addition of compound to the running buffer on the treated channel, a difference in refractive index is captured as a function of time, enabling association rate to be quantified. After equilibration, the treated channel is washed with running buffer, enabling the measurement of dissociation kinetics. Saturation binding can be measured by treating the chip with different concentrations of the test compound. As such, it is possible to measure binding kinetics and affinity in a single experiment. Because this technique requires immobilized protein, it is important to ensure that the immobilization process does not alter the structural properties of the target-binding site. The observation of similar control compound affinity as measured by SPR and solution techniques gives confidence in the structural relevance of the immobilized protein. It is also possible for the protein to bind test compounds so tightly that regeneration of the unbound protein is impossible or occurs very slowly upon treatment with the running buffer. In these cases, the utility of SPR is compromised by the expense and limited lifetime of the protein-treated chip.

Microscale thermophoresis (MST) is a related technique that allows direct measurement of binding affinity. It is an optical technique that requires a fluorescent tag to be attached to the protein; alternatively, label-free MST can be used, provided there is sufficient fluorescent signal from tryptophan residues in the protein.[127] This technique relies on compound-induced thermophoretic mobility shifts, which result from differences in solvation entropy, size, or charge of the bound vs. unbound protein.[128] In MST, the protein sample is introduced into a capillary on a thermally controlled stage. Local heating by an IR laser induces changes in the fluorophore's fluorescence due to conformational alterations in its local environment. These rapid changes are followed by a slower, diffusion-controlled depletion of protein concentration in the local field of heating due to thermophoresis. Upon termination of the IR-laser-induced heating, the fluorophore's environment changes again due to local cooling, resulting in a rapid reversion to the initial intrinsic fluorescence of the protein complex. This event is followed by diffusion-controlled re-equilibration of the concentration gradient through thermophoresis. The fluorescent signal changes produced from each of these properties can, in principle, be influenced by compound binding.

Microscale thermophoresis offers the advantages of studying proteins in solution, and with the use of a suitable fluorescent tag, proteins can be studied in mixtures or even cell lysates provided the target protein can be selectively observed. Furthermore, by titrating test compound in the presence of cofactors or other binding partners, it is possible to determine the molecular mode of action (competitive or noncompetitive) relative to the other agents.[127] As examples of its utility, MST was used to characterize

the binding affinity of several protein–protein interactions, such as the binding of TEM-1 β-lactamase to the β-lactamase inhibitory protein BLIP.[127] The binding affinity of the Grb2 homodimer was studied by titrating fluorescently tagged Grb2 with untagged protein.[127] Here, the technique demonstrates superiority to isothermal calorimetry due to the relative insensitivity of that technique, limiting its use in studying high-affinity protein dimerization events. The MST technique was also successfully used to characterize the interaction of caffeine, theophylline, and amiloride with the adenosine A2a receptor, where results concurred well with radiolabeled ligand affinity studies.[127]

Isothermal titration calorimetry is a technique by which binding free energy, enthalpy, and entropy can be determined.[129] It directly measures heat evolution from the incubation chamber, which is held at constant temperature while the test compound is introduced. Its sensitivity is directly dependent on the amount of enthalpy generated by binding of the analyte ligand to the protein target. Free energy of binding can be calculated from the K_d, which can be derived from titrating the test sample and looking for saturation of the binding enthalpy curve. Binding entropy is then calculated using the Gibbs free energy equation, given that the free energy and enthalpy of binding are directly determined from the experiment. While the technique is generally useful for determining binding thermodynamics, conventional ITC requires a relatively large amount of pure protein. Moreover, the energetics of binding can be significantly influenced by experimental conditions such as buffer composition. Recent reviews of drug discovery campaigns have suggested that binding thermodynamics are characteristic of lead quality, with enthalpically driven binding events being regarded as highly beneficial relative to entropically driven affinity.[130] During lead optimization, it is common to see entropy–enthalpy compensation, a process by which increasing enthalpic interactions drives a corresponding decrease in the favorability of the entropy term in the Gibbs free energy equation. This phenomenon can be understood chemically from the observation that increasing binding enthalpy through improving H-bonding, van der Waals, and pi-stacking interactions generally rigidifies the protein–ligand complex, resulting in lower entropy upon binding.

The ability to monitor target engagement directly within cells or tissue was provided by the development of the cellular thermal shift assay (CETSA).[131] In this procedure, cell lysates, intact cells, or live animals can be dosed with compound. For in vivo experiments, frozen organs are homogenized, lysed, and then cleared of lipids and cell debris. Small aliquots of lysates or intact cells are heated to different predetermined temperatures for short period of time (~3 min) and then cooled at room temperature (~3 min). Intact cells are lysed at this stage, and subsequently soluble protein is isolated (typically by filtration or centrifugation) and quantitated (by western, ELISA, antibody, mass spectrometry, etc).[132] In the first proof-of-principle study, all samples were centrifuged to separate soluble fractions from precipitates, and the supernatants were separated by SDS-PAGE and quantitated by Western blotting. Plotting amount of soluble protein against temperature yields the CETSA melting curve, and subsequent addition of a ligand results in a shift of this melting curve. For a range of drug concentrations measured at constant temperature, the isothermal dose–response curve generated is used as a fingerprint of target engagement along the drug concentration range. Absolute binding affinities cannot be derived, since the protein precipitation on unfolding is not reversible, and the system is clearly not in equilibrium. However, at high concentrations of compound the aggregation temperature approximates the melting temperature and can be used to relatively rank affinities. Although CETSA data are highly related to the data achieved with pure protein (such as in isothermal calorimetry), the melting curves in cells and lysates are more dispersed than in purified proteins, and this phenomenon has been suggested to reflect the presence of multiple forms of protein in the cell. Combining pulsed temperature denaturation with enzyme fragmentation complementation technology[133] is proposed to generate a facile HTS-compatible protocol with a sensitive and quantitative readout. In this refinement, the target of interest is tagged with a label that can be detected by its complimentary binding partner, thus creating the signal readout. A differential signal post-heating therefore identifies a stabilized target bound by compound. Using quantitative mass spectrometry as the CETSA detection method enables parallel binding experiments in proteome-wide studies, and the identification of downstream thermal shifts representing altered signaling changes provides an exciting opportunity for MS-CETSA to play a role in phenotypic deconvolution and discovering mechanistic biomarkers.[132]

Back-scattering interferometry provides another label-free, binding detection methodology which is performed in solution, is matrix-tolerant and has low sample requirements. Sample contained within a microfluidic channel on a chip is placed in the beam from a He-Ne laser. Combinations of reflection and refraction at the air-chip and fluid-chip interfaces create constructive and destructive interference fringe patterns, which can be detected in the direction of the back-scattered light. The fringe patterns are collected by a mirror and directed to a CCD array. When molecules combine, the refractive index in the detection zone changes, creating a phase shift pattern at the fringes. This phenomenon allows for quantitative equilibrium K_d measurements to be performed even in complex biological or chemical matrices. Both positive and negative changes in the refractive index can be detected by back-scattering interferometry relating, respectively, to an increase and a decrease in the molecular footprint (solvent addressable surface area and mean radius of gyration). A publication from AstraZeneca demonstrates the use of back-scattering interferometry in a recent effort to assess whether GPR39 agonists might enhance β-cell function in type 2 diabetes, leading to improved insulin release and glucose control.[134] Three compounds identified in a high-throughput screen were assessed for their ability to bind GPR39 in the presence of Zn^{2+}, which is known to modulate GPR39 function. Compound binding affinities were calculated using a one site model, and, interestingly, the technique also allowed the detection of Zn^{2+} binding to GPR39 at both high- and low-affinity sites.

Second-harmonic generation can also be used to detect structural and conformational changes of proteins. It is an optical technique in which two photons of equal energy are combined by a nonlinear molecule or material to generate one photon with twice the energy. The protein of interest is labeled with proprietary dyes conjugated to either amines or thiols and tethered to a lipid bilayer surface via a His-tag. Upon stimulation by a femtosecond laser, the dyes generate second harmonic light, and the intensity of the signal is highly sensitive to the average angular orientation of the dye. Even sub-Ångström shifts in orientation cause a detectable signal change that is not affected by mass or structure, and so is amenable to proteins of varying molecular weight and ligands

ranging from small fragments to protein complexes, including antibody-antigen interactions. Moree et al. recently used second-generation harmonics to identify hits from a fragment library that can modulate the confirmation of α-synuclein and reduce protein aggregation in cells.[135]

X-ray fluorescence is analogous to optical fluorescence but uses X-ray photons rather than optical or ultraviolet wavelengths for excitation. Each excited element emits X-rays at a unique frequency dependent on its atomic number, and analysis of a frequency spectrum can reveal the elements present in a sample. Since all elements with atomic number greater than 12 can be assessed, this approach could prove valuable as an orthogonal technique for transporter or ion channel assays to measure flux of monovalent and divalent cations, to track halogens, first-row transition metals, and small molecules.[136]

Nuclear Magnetic Resonance (NMR) provides a powerful set of methods for screening fragment collections to identify binders, characterizing protein–ligand interactions, studying the dynamics of protein motion, and determining functional inhibition of enzyme action. As such, it is a commonly used biophysical technique for both primary screening and hit characterization. NMR methods offer the advantage of good sensitivity, enabling the study of weak protein–ligand interactions that are typically found with fragments used as starting points for fragment-based drug discovery. Moreover, protein NMR spectroscopy offers the possibility of determining the precise binding site and molecular mode of action for hits, delivering mechanistic information that can be difficult to obtain using other techniques. With the evolution of 1.7 mm cryoprobes, protein requirements have diminished considerably due to the threefold sensitivity improvement and reduced material requirements relative to earlier 5 mm cryoprobes.

Saturation Transfer Difference NMR spectroscopy is commonly used as a screening technique for fragments and other weakly binding compounds. The basic principle of STD spectroscopy involves the transfer of energy from irradiated methyl groups on the protein to bound small molecules.[137] Upon dissociation of the small molecule from the protein, some of this transferred energy is retained and can be detected in the 1D NMR spectrum. Compounds that do not bind to the protein will receive no transferred energy and therefore will not present signals in an STD NMR experiment. A related method for detecting protein binders is Water-LOGSY.[138] Like STD spectroscopy, this technique relies on the transfer of energy across interacting molecules—in this case from water to the protein–ligand complex and then to the bound ligand. These techniques are more sensitive to weak binders and are preferred for screening fragments or for confirming the binding of compounds that are identified via other methods.

The protein requirements for NMR screening can be dramatically reduced by adapting these screening methods to a flow-based system, wherein the target protein is immobilized on a solid support. Target Immobilized NMR Screening (TINS) relies on the principle that transverse relaxation times increase for ligands that are bound to an immobilized protein, resulting in a loss of their resonances from a proton NMR spectrum due to line broadening.[139] By examining difference spectra between the initial mixture of test compounds in solution and in the presence of immobilized protein in a flow NMR probe, one can determine the identity of compounds that bind to the target protein. The TINS technique is quite sensitive, being able to detect compounds with affinities as low as 1 mM. Because the technique does not rely on magnetization transfer, it is more sensitive to compounds that bind tightly to the target protein. Targets are typically biotinylated and immobilized on a streptavidin-containing sepharose support.

Protein NMR spectroscopy can also be used to characterize the binding site for small-molecule ligands by observing ligand-induced changes in TROSY (transverse relaxation-optimized spectroscopy) spectra.[140] TROSY spectroscopy reduces the multiplicity of peaks in an HSQC spectrum by exploiting relaxation mechanisms that cancel out the different relaxation components of multiplet peaks, enabling the study of large molecule spectra. This technique is most powerful where spectral peak assignments have been made on the target protein, but it is still useful for comparing the likely molecular mode of action between different ligands even in the absence of peak assignments. Selective isotope labeling of one amino acid type with ^{15}N and ^{13}C atoms (Phe, for example), dramatically simplifies the HSQC spectrum by restricting observations to only that subset of residues. Single residue assignments can be made through site-directed mutagenesis and noting the absence of that particular residue in the TROSY spectrum of the labeled protein. Upon ligand binding, local changes in the environment of the ligand's binding pocket result in chemical shift changes for adjacent amino acid residues. These chemical shift changes feature prominently in the TROSY spectrum, allowing definitive placement of the ligand by assignment of the perturbed resonances.[140] While it is possible to see long-range chemical shift perturbations induced by compound-induced protein motions, the largest changes are typically observed for the ^{15}N-^{13}C correlations that correspond to backbone amide groups closest to the compound's binding site. This technique is quite reliable for determining the similarity or uniqueness of the molecular mode of action for a series of protein ligands. For example, TROSY spectroscopy was used to characterize the binding site of PDK inhibitors by observing the similarity of chemical shift perturbation fingerprints for test compounds relative to spectra collected for a known ATP-site binder (staurosporine) or a substrate analogue.[140] Thus, fragment screening hit **31** was determined to bind to the ATP site based on similar chemical shift perturbations relative to staurosporine, whereas fragment hit **32** was determined to bind at the allosteric PIF pocket by virtue of similar chemical shift perturbations to a short peptide PIF-site binder.[140]

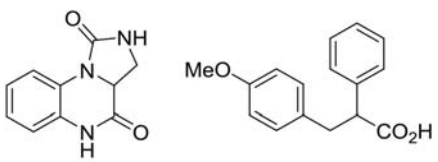

31 **32**

Spin labeling is another method, wherein compounds can be localized within a protein.[141,142] This technique relies on paramagnetic acceleration of relaxation rates for nuclei that are proximal to a spin label that has been introduced on a specific site of the protein. Compounds that are bound within 20 Ångström of the spin label experience accelerated relaxation rates, leading to further line broadening and signal reduction.

While NMR spectroscopy has demonstrated significant utility for directly assessing compound binding and determining molecular mode of action, it is also useful for studying functional modulation of enzyme action. Like mass spectrometry, NMR has been used to follow the course of enzymatic reactions and thereby characterize small molecule potency and function. In principle, NMR-based functional activity screening offers significant specificity advantages over optical methods for following the course of an enzymatic reaction. It is insensitive to optical artifacts induced by compound fluorescence or absorption in regions of the visible spectrum that are used to detect enzymatic reactions. Therefore, studies can be conducted at high concentrations of test compounds, enabling the characterization of weak binders such as fragments. The practicality of this method depends on the ability to detect substrate and product resonances without interference from compound signals. A strategy for reducing interference is to use fluorinated substrates and track the ^{19}F NMR signal, taking advantage of its broad chemical shift dispersion and high NMR sensitivity. Incorporation of a trifluoromethyl group was used to create functional peptide probes for the AKT1 Ser/Thr kinase and for trypsin as a model protease.[143] This technique was dubbed 3-FABS (Three Fluorine Atoms for Biochemical Screening). Because the 3-FABS technique is insensitive to interference from compounds lacking fluorine, it is possible to screen in the presence of human serum albumin to enable estimation of plasma protein binding.

One limitation of the 3-FABS approach is its requirement for a trifluoromethyl group, which in some cases may not be tolerated on the protein substrate or cofactor. Proton-decoupled NMR data collection enables use of a single fluorine atom, which is a more conservative substitution. This approach was successfully extended to the study of fluorinated ATP analogues as substrates for ATP-dependent enzymes, including kinases, hydrolases, and ligases.[144] A survey of two fluorinated ATP derivatives revealed that 2′-Fluoro ATP (**33**) is a substrate for some ATP-dependent enzymes, including the kinase PDK1 and the bacterial ligase MurC. However, it was not a functional substrate for the bacterial enzyme NadE. The related substrate 2-fluoro-ATP is a functional substrate for nine different enzymes, including NadE, PDK1, the bacterial thymidylate kinase TMK, adenylate kinase, hexokinase, pyruvate kinase, myosin ATPase, creatinine kinase, and RNA polymerase. This broad substrate compatibility suggests that 2-fluoro-ATP (**34**) could serve as a general tool for developing NMR-based functional assays across a wide array of ATP-dependent enzymes. The conversion of ATP to ADP and AMP can be monitored for either substrate by monitoring the ^{19}F NMR resonances near 24 ppm (2-fluoro ATP) or −127 ppm (2′-fluoro-ATP) using this technique. The broad chemical shift dispersion associated with fluorine led to very little interference from fluorine-containing test compounds.

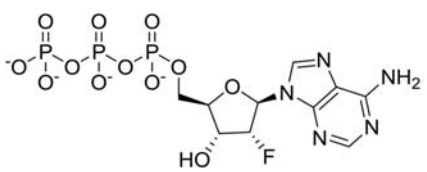

33

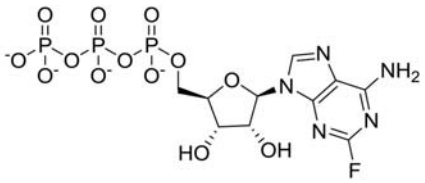

34

2.01.5 Lead Optimization

It is rare for a lead compound to possess all of the attributes required of a clinical candidate suitable for development. The lead optimization process requires careful medicinal chemistry design to optimize protein–ligand interactions, which have a direct bearing on potency and selectivity, while paying careful attention to physicochemical properties that are conducive to favorable pharmacokinetic, biopharmaceutic and safety properties, and avoiding functional groups that are associated with toxicity. The complexity of this process results from interplay of these variables, the number of parameters requiring optimization, and the frequent concomitant deterioration of some of these properties during attempts to optimize others. The flow of design ideas occurs more rapidly than the pace of synthetic chemistry, placing a premium on technologies that enable selection of those design hypotheses with the greatest probability of success. Despite the power of technologies that will be highlighted in this section, it is sometimes prudent to challenge models that are used to drive design by occasionally preparing and testing compounds that are orthogonal to the direction that they suggest. Doing so enables model refinement and builds confidence in the tools being used to drive drug design.

The optimization of binding affinity, selectivity, and functional activity is greatly enhanced through structure-based drug design using protein–ligand structures or homology models. The field of structural biology has undergone a renaissance in recent years with breakthrough advances in membrane protein crystallography, cryo-electron microscopy of multiprotein complexes, and new techniques for ultrafast crystallographic data collection that have broadly expanded the structural genome. These technology achievements have opened new frontiers in understanding the molecular basis of receptor and ion channel function, RNA splicing, ribosomal protein synthesis, epigenetic regulation of gene expression and transporter function, to name a few.

The G-Protein-Coupled Receptor family has been an extraordinarily productive hunting ground for drug targets, in part because of the pivotal role these receptors play in cellular signal transduction, but also because a number of them have very drug-like endogenous ligands. The human genome encodes for over 390 nonolfactory GPCRs, and approximately 150 drugs in the human pharmacopeia have at least one GPCR as their primary target. However, there remains a lot of opportunity for drug discovery within this gene family. Despite the number of drugs developed for GPCR proteins, roughly 80% of this gene family remains without a marketed drug agent. Recent advances in understanding GPCR pharmacology have also opened new opportunities for differentiated therapeutics directed at GPCRs that are already targeted by a marketed drug agent. GPCR's signal through two second messenger systems G-proteins and β-arrestin. It is possible to bias this signaling toward one of these two pathways through structural modification of orthosteric agonists or through allosteric modulation. As such, it is conceivable to dissociate some of the adverse effects or tachyphalaxis from therapeutic effects in certain diseases as described earlier.

Integral membrane proteins are significantly challenging targets for structural biology. Their membrane localization results in extensively exposed hydrophobic surface that often leads to poor expression and aggregation in aqueous buffers used for purification and crystallization. The seven transmembrane helical domain of GPCRs generally lacks polar surface residues that are important for forming crystal contacts. Finally, G-protein-coupled receptors and transporters tend to be very dynamic proteins, creating particularly high entropic barriers to crystallization in an ordered lattice. As such, stabilizing mutations, fusion proteins, antibodies, or tightly binding ligands must be used to stabilize these proteins for crystallization.[145] Finally, crystals from these protein targets can exhibit significant instability to radiation, requiring merging of datasets across several crystals or X-ray free-electron laser technology to collect a complete data set from one crystal.

Many of these challenges have been addressed through technology advances that enable more facile protein purification and crystallization. Issues of protein instability and the absence of adequate polar contacts for crystallization can be addressed through introducing stabilized mutations (STaR technology), designing fusion constructs with BRIL or T4-lysozyme proteins, or complexation with Fab antibody fragments. The StaR approach involves scanning mutagenesis of transmembrane residues to identify point mutations that increase thermal melting temperature of the protein, which is an indicator of its stability. Mutations conferring this property are analyzed for their effect on protein expression and ligand pharmacology to ensure the mutant receptor retains function and that protein can be produced in adequate quantities for structural studies. Fusion protein constructs aim to introduce polar crystal contacts and reduce protein aggregation through introduction of a highly crystalline protein fragment in one of the intracellular or extracellular loops. A similar, noncovalent strategy involves the use of antibody Fab fragments or nanobodies raised to conformational epitopes of the GPCR to stabilize the receptor and enable its crystallization. Crystallization of the protein is typically accomplished in lipidic cubic phases, which enable the protein to crystallize in an environment resembling its native membrane. The membrane protein is typically purified in an aqueous mixture with detergents and is then homogenized with monoacylglycerol, which forms a cubic phase in which the aqueous and bilayer components are continuous in all three dimensions. Addition of a precipitant then forces crystallization of the protein in an environment enriched in one of the lipidic cubic-phase components, which form lamellar sheets onto which the regular ordered array of protein molecules assembles.

The first nonrhodopsin GPCR to deliver a high-resolution crystal structure was the β2-adrenergic receptor, the structure of which was reported in 2007. Since then, structures from each major class of GPCRs have appeared in the literature.[146] Many of the first GPCR structures were delivered with antagonists bound to the orthosteric site. Subsequent structures with bound agonists and allosteric modulators have dramatically expanded our understanding of the molecular basis for GPCR pharmacology.[147] Specifically, agonist structures of the β2-adrenergic receptor with Gs-heterotrimer protein[148] or of rhodopsin complexed with β-arrestin[149] have given insights into interactions that are critical for binding these partner proteins and affecting signaling through their cognate pathways.[150]

The ion channels constitute an important family of signaling proteins and drug targets. These proteins regulate the passage of calcium, sodium, potassium, chloride, and other ions through the plasma membrane and are responsible for regulating a number of physiological processes, such as muscle contraction and synaptic transmission. There are over 200 ion channels encoded by the human genome, reflecting the diversity of signaling pathways which they regulate. Ion channels are able to respond to many extracellular stimuli, such as temperature, pH and membrane potential, and their activity can be regulated by a variety of small-molecule ligands that bind to the pore domain or to various allosteric sensor domains. Many drugs have been discovered which modulate ion channels, including (1) the benzodiazepines, which modulate GABA channels and are important anxiolytics; (2) topical anesthetics, which modulate voltage-gated ion channels; (3) calcium channel blockers, which function as antihypertensives; and (4) GABA analogs, such as gabapentin, which regulate voltage-gated calcium channels and are effective agents for treating neuropathic pain and epilepsy.[151] Despite the discovery of many therapeutic agents that target ion channels, there remains considerable untapped opportunity for discovering new agents given the number of family members with no known ligands, or for which only weakly active, nonselective ligands are known. Recent advances in ion channel structural biology have provided insights into the diverse mechanisms of their regulation and promise to enable more efficient optimization of potency and selectivity through structure-based drug design.

Ion channels are transmembrane proteins which function through gating of a central pore that passes ions across the membrane. This gating event typically involves stimulus-induced molecular movements in the pore domain which alter its size and can occur based on ligand binding or gradients of voltage, temperature, or pH.[152,153] Most ion channels are highly selective for the ions that they transport. This selectivity is driven by a region known as the selectivity filter, which adopts dimensions closely aligned with the ion that the channel transports. Ion conduction is facilitated by an array of backbone carbonyls or polar side chains that line the pore and enable transport of ions in either their hydrated or partially dehydrated form through a polar channel of defined size. Ion

channel antagonists function by blocking the pore at either its extracellular or intracellular face or through allosteric modulation of the protein.

For over 50 years, protein crystallography has been the preferred technique for studying protein structure at high resolution. Advances in crystallization techniques, the evolution of microfocused synchrotron beamlines, development of highly sensitive detectors, and the introduction of novel phasing methods have made protein crystallography almost a routine practice, enabling structure-based drug design for a wide range of protein targets. Furthermore, the range of biomolecules able to be studied by X-ray crystallography spans crambin at the lower end of molecular weight to the 70S ribosome. Despite this progress, the requirement for protein crystals makes X-ray crystallography a demanding technique for studying large biomolecules or multiprotein complexes. Cryo-electron microscopy (CryoEM) offers a complementary method for studying these systems based on its ability to image single particles in a 2-dimensional array and its greater effectiveness with larger proteins.[154,155] The Cryo-EM technique uses transmission electron microscopy to deliver a 2-dimensional projection-image of the protein. These 2-dimensional projections can be reconstructed into a 3-dimensional model, yielding structural information with near-atomic resolution.

Recent advances in technology have overcome some of the key hurdles impeding high-resolution cryoEM studies of protein assemblies.[154,155] One of the challenges with sample preparation for electron microscopy is dehydration of the protein sample in the vacuum environment required for EM studies. Through plunging the hydrated sample into a cryogen, the protein becomes trapped in a layer of vitrified ice, which obviates this issue. The lack of heavy atoms in biological specimens limits the extent of electron scattering. The radiation sensitivity of many protein specimens requires low electron doses to preserve sample integrity. This fact, coupled with the lack of heavy atoms in biological specimens which limits the extent of electron scattering, leads to low signal-to-noise ratio. The low signal-to-noise ratio for protein cryoEM can be managed through aligning and averaging across thousands of 2D projection images. This strategy requires the protein sample to be very pure so as to not complicate analysis with the presence of interfering contaminant particles. Likewise, the need to align across many projections requires easily identifiable features on the molecule being studied, which is more likely with larger samples or protein assemblies bearing symmetry. The introduction of direct electron detection (DED) cameras addresses one of the principal barriers to obtaining high-resolution structures: the movement of the protein molecule upon collision with the electron beam. This motion results in blurring of the 2D image, limiting resolution. The DED camera allows image collection in movie mode, which enables tracking beam-induced motion of the protein and its surroundings. Relatively few protein structures have been solved at high resolution by cryoEM, but several noteworthy recent examples include the gamma secretase complex[156,157] and the TRPV1[158,159] and TRPA1[160] ion channels. These examples illustrate the promise of cryoEM in enabling structural studies of targets that would be difficult address with protein crystallography and as an addition to the armamentarium of techniques supporting structure-based drug design.

Experimentally determined structural information forms the basis for computational modeling of protein–ligand interactions that lead to new hypotheses on how to design for increased potency and selectivity of lead compounds. The era of structure-based drug design was ushered in with the discovery of the angiotensin-converting enzyme (ACE) inhibitor captopril, which used homology modeling of the related zinc peptidase, carboxypeptidase A, to design succinyl amino acid-based ligands bearing a thiol-based zinc chelator.[161–163] Since that discovery, computational modeling of crystal structures has become a central feature of many successful drug discovery programs targeting kinases, proteases, and hydrolases.[164] Early techniques employed in structure-based drug design used manual assessment of ligand-based functional group replacements based on their compatibility with neighboring residues in the protein–ligand complex. The accurate prediction of binding energetics is critical to the success of modern structure-based drug design and relies on having a high-performance potential energy function and molecular dynamics simulations to estimate the conformational space of both the ligand- and the protein-binding pocket. Significant effort has been devoted to the development of force fields that estimate the energetics of protein–ligand binding interactions. Newer force fields, such as OPLS2.1 (Optimized Potentials for Liquid Simulations—Schrodinger, New York, 2014), which is trained on thousands of organic compounds that are representative of small molecule drug space, promise to deliver more accurate estimation of torsional energies and nonbonded interactions that are critical for computing binding free energy.[165] In order to reduce the number of protein residues that are required for sampling the conformational space of the ligand-binding pocket, REST (Replica Exchange with Solvent Tempering) is employed to determine the regions of the protein and ligand that are subjected to simulated annealing. While it is computationally challenging to conduct accurate absolute free energy prediction, the use of free energy perturbation (FEP) analysis to compare the impact of minor structural changes on binding energy is more feasible and useful in potency optimization. The combined FEP/REST approach involves the collection of a series of structurally related molecules that are sorted by similarity, and free energy perturbation cycles are then created between a limited number of related compounds.[165] Free energy perturbation calculations then generate a series of $\Delta\Delta G$ values between each structural member of a given free energy cycle, leading to potency predictions for every molecule in the set. A study of eight different protein targets comprising 330 free energy perturbations demonstrated that the FEP/REST method employing the OPLS2.1 force field delivered accuracy to within RMSE of 1 kcal/mol across the data set.[165] Furthermore, this method was accurate in predicting the direction and magnitude of affinity change resulting from ligand pairs emphasizing differences in electrostatic interactions, hydrophobic interactions, ionic interactions and ability to expel unfavorable water molecules from the ligand-binding pocket.[165]

An important component of binding free energy for a protein–ligand interaction is derived from displacement of water molecules upon binding a ligand with functional groups that complement residues in the ligand-binding pocket.[166] Displacing these water molecules is often entropically favorable due to the protein-inducing constraints on their motion relative to bulk solution. Moreover, water molecules enclosed within a largely hydrophobic protein pocket suffer from unfavorable enthalpy due to an incomplete complement of hydrogen bonds relative to their completely solvated state. It is now possible to estimate the binding

energy, entropy, and enthalpy of water molecules in the ligand-binding site using explicit solvent models such as Watermap®. In the Watermap® application, solvent sites are defined by conducting a short molecular dynamics simulation on an explicitly solvated binding pocket and defining bound waters through examination of solvent clusters (density peaks) relative to a uniform solvation model.[166,167] The chemical potential of the bound state of each water molecule is then computed. Inhomogeneous solvent theory is used to calculate the average system interaction energy of each water molecule in the bound state relative to bulk solvent, which delivers an estimate of the water molecule's binding enthalpy. The system interaction energy is defined as the average interaction energy of a given water molecule with the rest of the system (protein residues, backbone atoms, and other solvent molecules). Likewise, the excess entropy resulting from the bound state of the water molecule defines its binding entropy. This information delivers more accurate estimates of ligand-binding energy and potency prediction across a series of compounds but also provides useful physical insight that is applicable to drug design. Specifically, this information is helpful in estimating whether a design strategy should target displacement of a given structural water molecule or building in functional groups to form productive hydrogen-bonding interactions with it. Water molecules that are predicted to have favorable binding energies driven through strong enthalpic interactions become appropriate for targeting hydrogen-bonding interactions with the inhibitor, whereas those with unfavorable entropy that is not offset by highly favorable enthalpic interactions become targets for displacement strategies.

Applications of the WaterMap approach include improving the performance of docking and scoring calculations using implicit solvent models (MM-GB/SA) to orient the ligand in the protein, followed by replacing the GB/SA component with the explicit solvent model from WaterMap to calculate interaction energies. This combination was shown to be better than GLIDE XP, Watermap, or MM-GB/SA alone for predicting binding affinities within congeneric series for inhibitors of CDK2 and Factor Xa.[168] The use of WaterMap alone for predicting binding affinity needs to be treated with caution. While desolvation of a protein-binding pocket accounts for the majority of binding energy in most cases, WaterMap does not consider ligand strain energy, ligand desolvation, conformational entropy penalties, protein–ligand electrostatic interactions, or protein strain energies. As an example, WaterMap performance in predicting the binding energies of a series of SRC inhibitors was only qualitative; although it successfully clustered highly potent and less active compounds across a 4 kcal/mol energy range, it performed poorly in predicting potency trends for compounds with intermediate affinity.[169] WaterMap was used to analyze complexes of tofacitinib with JAK family members (JAK1, JAK2, JAK3, and Tyk2), ascribing a tentative role for tofacitinib's nitrile group in displacing a highly unfavorable water molecule near the glycine-rich loop of the kinase. The role of this nitrile group in imparting exquisite potency to tofacitinib is otherwise unapparent from protein crystal structures.[170] Watermap also successfully explained structure–activity relationships for a congeneric series of spiropiperidine BACE inhibitors based on the propensity of groups binding to the S1 and S1a pockets to displace energetically unfavorable water molecules.[171] Applying WaterMap to a series of matriptase inhibitors revealed unstable water molecules in the S1′ pocket that when displaced by compounds bearing larger groups projecting into the S1′ region led to a 100x improvement in binding affinity.[172] Solvent modeling using WaterMap combined with a related protocol SZMAP was able to rationalize differences in off rate of a series of adenosine 2a receptor binders.[173] While this combination afforded reasonable prediction of binding affinity when used in conjunction with MMSA, it did not perform as well as a combined GRID search using water and a CRY probe for lipophilicity in conjunction with MMSA. Finally, WaterMap analysis has been used to understand the relative binding thermodynamics of core fragments and auxiliary binding groups in fragment to lead optimization and to develop principles for protein druggability analysis based on the association of fragment hotspots with clusters of energetically unfavorable water molecules.[174]

2.01.5.1 Expanding drug-like chemical space: Rational design of covalent inhibitors

Medicinal chemistry strategies for improving potency and selectivity typically involve optimizing nonbonded interactions between the drug molecule and its target protein. This reversible, noncovalent target modulation strategy enables understanding PK/PD relationships in terms of equilibrium binding affinity relative to steady-state plasma concentrations and reduces the risk of idiosyncratic toxicity due to immunogenic reactions against modified proteins. However, there are instances where a covalent inhibition strategy might be preferred: for instance, when highly homologous binding sites exist between a desired target and close family members for which selectivity is desired. In cases where the target resynthesis rate is slow, covalent target modulation strategies also capitalize on prolonged pharmacodynamic effects long after dissipation of free drug concentrations in plasma. These advantages have led to a recent resurgence of interest in covalent target modulation strategies.[175,176] However, these advantages come with two principal risks: the generation of immunogenic responses to haptens created by irreversible covalent modulation of a drug target and the potential for reduced selectivity in cases where the functional group forming the covalent bond is too reactive. Recent advances in proteomic technology, coupled with a better understanding of the capacity of physiological mechanisms to manage low doses of reactive species, have led to a better appreciation of how to quantify and manage these risks.[17,177]

The question of covalent inhibitor selectivity can be elegantly addressed using recent advances in proteomic technology. In cases where the covalent inhibitor binds to the active site of a kinase or serine hydrolase target, the aforementioned competitive activity-based proteomic profiling (ABPP) technique can be used to interrogate selectivity within the target protein gene family.[97,178] In a basic implementation of this technique, a broadly reactive activity-based probe is used to interrogate the proteome with which it reacts. Competition experiments utilizing the test compound deliver a selectivity profile through comparing the treated and untreated cell lysates for differences in signal generated by the activity-based probe. This technique can use fluorescently tagged activity-based probes for in-gel analysis or biotinylated probes to allow capture of labeled proteins, followed by mass spectral analysis. One important limitation of this technique is that selectivity across the broader proteome must be inferred from the inhibition profile within the target gene family that was interrogated. A more thorough technique involves generating an activity-based probe

using the covalent inhibitor itself, wherein a clickable handle is introduced at a position that is tolerated for target binding.[177] After incubating either cells (or cell lysates) with the covalent probe, the resultant cell lysate is subjected to click chemistry with either a fluorescent tag or a biotinylated tag to allow direct visualization or capture of the labeled proteins. Because some level of indiscriminate labeling occurs, usually as a function of protein abundance, a competition experiment is needed to delineate the selectivity profile of the actual test compound. It is also important to conduct these experiments across a range of probe concentrations, as it was observed with EGFR- and BTK-based probes that indiscriminate labeling surmounting compound competition occurs at probe concentrations above 1 μM. Comparing the test compound treated and untreated samples yields the selectivity profile of the original inhibitor. This technique assumes that the activity-based probe binds to every target that the test compound binds; the presence of a small clickable handle (usually a tethered terminal alkyne, with which an azide-containing tag reacts to form a 1,2, 3-triazole under copper catalysis) offers minimal perturbation of binding interactions or physical properties related to cellular permeability.

The resurgence of covalent inhibitors has also been aided by an increased appreciation of the relationship between dose and toxicity for reactive compounds. Idiosyncratic toxicity is believed to occur when a reactive species (either the compound itself or a metabolite thereof which bears an electrophilic group) forms a covalently modified protein to which an immunogenic response is mounted. These toxicities are difficult to predict through preclinical toxicology studies and have resulted in several withdrawals of marketed drug compounds or late-stage clinical candidates. The extent of covalent labeling associated with a test compound can be assessed through the use of radiolabeled derivatives and quantitating the residual reactivity upon incubation with liver microsomes. It has been proposed that an in vivo covalent labeling threshold of 50 pmol/mg of protein should be used to reduce the probability of toxicity based on a safety margin of 20× relative to levels of covalent labeling typically associated with liver toxicity in animal studies of prototypic hepatotoxins.[179] It has also been observed that thresholds of total daily dose can be used to define the probability of drug-induced toxicity for compounds that form reactive species—either due to reduced cell stress or the induction of immune tolerance at low doses.[180] The combination of dose, propensity to covalently modify proteins and percentage of metabolism that results in reactive species has been proposed as a predictive measure for the propensity of reactive compounds to cause toxicity (as defined by the presence of a black box label or withdrawal from the market).[17,181] These guidelines are based on retrospective studies of the safety of clinical compounds that are known to form reactive species.

The design of targeted covalent inhibitors is assisted by methods to quantify and predict the reactivity of electrophilic functional groups. The intrinsic activity of a covalent inhibitor is best defined by k_{inact}/K_i, the second-order rate constant for reaction of the protein with the inhibitor. Maximizing selectivity, therefore, depends on optimizing this parameter for the target protein relative to secondary targets. The k_{inact} parameter is defined by the intrinsic reactivity of both the nucleophile and the electrophile, along with the unique arrangement of residues that can minimize the transition state energy for forming the covalent bond between the protein and the inhibitor. Compounds that possess a highly electrophilic group have the potential for eroded selectivity with nucleophilic residues on other proteins, coupled with a greater propensity for reaction with endogenous nucleophiles (such as glutathione), which result in high clearance. Therefore, a sensible design strategy is to minimize the intrinsic reactivity of the electrophilic species while maximizing nonbonding interactions that enhance inhibitor affinity. As such, several groups have compiled tables of pseudo first-order rate constants for the reaction of electrophilic groups with biologically relevant nucleophiles.[182–185] These tools, coupled with computational transition state modeling, allow medicinal chemists to incorporate these parameters into design of more selective covalent inhibitors.

2.01.5.2 Expanding drug-like chemical space: Designing permeable compounds beyond the Lipinski Rule of Five

There have been numerous attempts to codify design principles that maximize drug-likeness, often defined by the molecular properties that correlate with oral absorption. One of the most commonly used guidelines is the Lipinski Rule of Five, which defines property boundaries for molecular weight, number of hydrogen bond donors, number of N and O atoms, and *C*log *P*.[186] Intuitively, this heuristic set of guidelines is aimed at maximizing solubility without compromising permeability by a large number of polar groups that must be desolvated prior to passing through the lipid bilayer of the cell membrane. While small molecule drug discovery efforts are typically focused in chemical space that aligns with the Rule of Five, there are several examples of targets for which Rule of Five compliant chemical matter is unlikely to deliver the level of potency required for a successful drug candidate. Examples include proteases, peptide GPCRs, and direct modulation of protein–protein interactions, where it is often necessary to explore chemical space that pushes beyond the Rule of Five boundaries for molecular weight, polar functional group and lipophilicity. As such, there has been a resurgence of effort in the past several years to define molecular properties associated with reasonable permeability and metabolic stability for such compounds, particularly small peptides.

The cyclic peptide cyclosporine is an orally administered immunosuppressant that binds to cyclophilin. It has a remarkably high oral bioavailability of 29% given its structure. Cyclosporine is known to adopt multiple conformations in solution and is endowed with chameleon-like properties. It can display its polar backbone functionality to confer adequate solubility in an aqueous environment, while adopting an alternative conformation in apolar solvents where lipophilic groups project to the exterior of the molecule and polar groups are engaged in intramolecular hydrogen bonds on its interior. These structural preferences were observed in X-ray structural studies of cyclosporine crystallized from both water and chloroform (which mimics the interior environment of the apolar lipid bilayer), along with solution NMR studies in $CDCl_3$.[187] Another factor assisting the membrane permeability of cyclosporine is the extensive N-methylation of its peptide backbone, which removes several hydrogen bond donors that would exist in the native cyclic peptide. The importance of intramolecular hydrogen bonding in elevating passive permeability of cyclic peptides

was also shown in a study of synthetic cyclic peptides bearing no backbone nitrogen methylation.[188] A systematic evaluation of permeability as a function of stereochemistry at individual amino acid residues showed the importance of peptides being able to adopt conformations favoring intramolecular H-bonding for conferring good permeability. This same scaffold was subjected to electrophilic methylation conditions on solid support to probe the accessibility of exposed N-H groups, which should be reflective of lesser engagement in transannular intramolecular hydrogen bonding. Methylation of exposed peptide backbone NH groups led to a reduction in H-D exchange (reflecting extensive intramolecular hydrogen bonding of the remaining backbone amide NH groups) and improved permeability.[189] The extent of methylation could be varied based on the polarity of the reaction solvent, reflecting altered conformational dynamics in apolar vs. polar solvents. A more extensive assessment of permeability for 1152 cyclic hexapeptide stereoisomers and N-methylated variants prepared from this same scaffold found that sterically masking polar functionality by subtle effects of side-chain orientation, in addition to intramolecular hydrogen bonding, had profound effects on permeability.[190] Likewise, an evaluation of 39 cyclic peptide natural products illustrated the importance of backbone alkylation and intramolecular hydrogen bonding in improving the membrane permeability of these high-molecular-weight compounds.[191] It was noted that many natural products and synthetic peptides that exhibit good cellular permeability possess nonproteinogenic amino acids or functionality, which contributes to conformational flexibility and shielding of polar groups.[192]

A physics-based model was developed to guide design toward maximizing permeability for cyclic peptides.[189] The physics-based model offers advantages over statistical models in that it does not rely on a training set to bootstrap calculations. This model assesses multiple conformational states in aqueous solution, while presuming membrane permeability is conferred by a single low energy conformation in the apolar cell membrane. This low dielectric conformation is selected from the ensemble of states in aqueous solution, and membrane flux is modeled by calculating the free energy of transitioning the low dielectric conformation from water to the low dielectric environment. The observed free energies showed good correlation to PAMPA permeability ($\log P_e$). This model was improved by incorporating terms for the energy of neutralizing ionizable centers, diffusion across the membrane, and thickness of the membrane.[193,194] The physics-based model showed good correlation across six datasets with experimental PAMPA values and eight datasets with cell-based permeability values.[194]

The experimental assessment of hydrogen bonding has been assessed using a variety of methods for compounds outside Rule of Five chemical space. The most common techniques involve evaluation of the temperature dependence of NMR chemical shift changes for exchangeable protons, hydrogen-deuterium exchange rates, delta log *P* and chromatographic assays. Variable temperature NMR chemical shift changes were used to characterize intramolecular hydrogen-bonding patterns for cyclosporine and atazanavir.[187] Hydrogen–Deuterium exchange was used to characterize intramolecular hydrogen bonding in a series of cyclic peptide analogues.[189] The assessment of log *P* differences between octanol–water and toluene–water systems leads to some inference into intramolecular hydrogen-bonding propensity, as compounds with extensive intramolecular hydrogen bonding are expected to show smaller differences in log *P* across octanol (which has hydrogen-bonding capability) and toluene (which does not).[195] None of these methods provides a high-throughput experimental assessment of hydrogen-bonding capability. Chromatographic methods have been established to evaluate molecular polarity and intramolecular hydrogen bonding. Critical to their success is the use of nonpolar supercritical fluid eluents that maximize propensity for compounds to form intramolecular hydrogen bonds. The exposed polarity (termed EPSA) method utilizes supercritical CO_2 supplemented with methanol as a mobile phase with a Chirex 3014 stationary phase that possesses lipophilic and polar attributes and is able to separate compounds across a wide range of polarity differences.[196,197] In a set of cyclic peptides evaluated by the EPSA method, only compounds with EPSA values less than 80 were shown to have appreciable permeability in RRCK assays.[197] Moreover, small molecules with the capability of forming intramolecular H-bonds demonstrated significantly lower EPSA values than corresponding isomers lacking the ability to form an intramolecular hydrogen bond.[196]

2.01.5.3 Developing Design Principles for Asymmetric Tissue Distribution

In order for drugs to demonstrate efficacy, they must distribute to the tissue where the pharmacological target governing their activity resides. The efficacy of most permeable small molecule drugs is governed by the free drug hypothesis, which states that only the unbound concentration of a drug is available for binding to its pharmacological target. This unbound concentration generally reaches equilibrium across different tissues such that at steady state the unbound concentration in tissue equals the unbound concentration in plasma. Under these circumstances, total tissue levels can vary significantly relative to total plasma concentrations due to differences in affinity for plasma or tissue proteins. An important exception to this free drug equilibrium between plasma and tissues occurs where there are active transport systems that are involved in uptake or efflux of the drug. These processes have the potential to create very different free drug concentrations within certain tissues, which have important implications for efficacy and safety. Where active transport leads to higher concentrations in a target tissue of interest, lower plasma free drug concentrations will be required for efficacy. Likewise, efflux mechanisms that actively pump drug out of a tissue compartment will raise the plasma free drug levels required to achieve sufficient concentrations needed for efficacy in that tissue.

There are over 400 membrane transporters encoded in the human genome.[198] However, only a handful of these transporters have been implicated in the absorption, excretion, or asymmetric tissue distribution of most small-molecule drugs.[199200] Aside from cancerous tumors, the principal organs where asymmetric tissue distribution is most often noted include the liver, brain/CNS, and kidney. Common transporters affecting drug uptake in the intestinal lumen include members of the organic anion transporters (OATP2B1) and peptide transporters (PEPT1).[199] Efflux pumps limiting oral bioavailability include the multidrug resistance proteins MDR1 and BCRP along with P-glycoprotein P-gp.[199] The latter protein is often implicated in limiting brain and CNS

exposure of drugs as well as biliary excretion. Hepatic uptake transporters include members of the OAT family, such as OATP1B1, OATP1B3, and OATP2B1, along with the organic cation transporter OCT1.[199] Biliary elimination is facilitated by members of the MDR and MRP families of transporters (MDR1, MDR3, MRP2 and BCRP) as well as bile salt efflux pumps (BSEP). Several transporters are implicated in active renal excretion, which requires carrier-mediated transport at both the basolateral and apical sides of the tubule cell.[198] Basolateral transporters that accept drug substrates from the blood include OAT1, OAT3, OCT2 and OATP4C1.[198] Apical transporters include the multidrug resistance proteins MDR1, BCRP, MRP2 and MRP4, along with multidrug and toxin extrusion proteins MATE1 and MATE2/2 K.[198] There are several challenges associated with incorporating active transport approaches in drug discovery. Variations in cross-species transporter expression and tissue localization create potential translational pharmacology problems. Likewise, the potential to saturate the function of a transporter creates the potential for drug–drug interactions with other substrates of the same transporter or safety issues in the event that physiological transport processes are interrupted.[201]

The diversity of transporters implies that selective asymmetric tissue distribution strategies could be developed provided knowledge of structure–activity relationships for exploiting different transporters. In practice this is quite challenging due to conflicting recognition motifs for designed transporter uptake relative to activity against the desired pharmacological target. An additional limitation is the lack of structural information for many of these transporters owing to the difficulty associated with crystallizing membrane proteins. Finally, genetic polymorphisms that impact transporter expression and function have the potential to introduce variability in tissue exposure across diverse patient populations.[202,203] Despite these factors, transport strategies have been devised for achieving hepatoselective drug delivery for several metabolic disease targets.[204]

For many drug discovery programs, achieving high CNS concentrations is challenging due to the tight junctions present at the blood–brain barrier, coupled with high expression of several efflux transporters. These challenges have typically restricted CNS drug discovery programs to pursuing lipophilic amines, which traditionally have achieved high central concentrations. However, these physicochemical properties are commonly associated with toxicity and are not compatible with several protein families that are implicated in neurological disorders. Recent efforts to evaluate CNS penetration across large sets of small molecules revealed significantly expanded chemical space for CNS penetration. These studies have led to the development of a CNS MPO (multiparameter optimization) algorithm that incorporates *C* log *P*, *C* log *D*, MW, TPSA, HBD number and pK_a based on physicochemical properties of 119 CNS drugs and 108 clinical candidates.[205–207] These physicochemical properties were chosen based on their association with common ADME and safety endpoints, and for each a combination of linear functions was used to derive a desirability score of 0–1 based on their individual association with favorable ADME and safety properties.[206] A composite CNS MPO score is derived through combining the individual property scores. Statistical analysis showed that CNS drugs typically were associated with a higher CNS MPO score than CNS candidates (some of which experienced safety or ADME attrition), reflecting the need to shift molecular properties to more drug-like space. Since implementation of the CNS MPO algorithm at Pfizer, neuroscience drug candidates display higher *C* log *D*, lower median basic pKa, higher TPSA, and higher molecular weight compared to either the drug or candidate component of the original test set.[208] The higher *C* log *D* value was derived from significantly lower mean basicity (pK_a 4.1 vs. 8.0 in the drug or candidate test set). The higher TPSA value was intentionally designed to avoid safety issues associated with compounds having *C* log $P > 3$ and TPSA < 75. The fact that these post-MPO CNS candidates occupy very different property space from either the pre-MPO CNS candidate or drug test sets speaks to the effectiveness of the MPO algorithm in expanding property space for CNS penetrant compounds by considering multiple combinations of physicochemical properties that achieve high passive permeability and avoid efflux.[208]

Conversely, it is sometimes desirable to restrict CNS exposure in order to avoid safety issues associated with modulation of a target that is expressed both centrally and peripherally, but where modulation of central activity produces a harmful effect. One effective strategy to restrict compounds to peripheral tissues is to combine low-moderate passive permeability with structural features that impart efflux by pumps at the blood–brain barrier.[203] While some of these efflux transporters are also present in the GI lumen, they can be surmounted by high local concentrations of drug in the GI tract, provided sufficient aqueous solubility exists to effect saturation of the efflux transporter. In this way, central restriction can be achieved without adversely impacting oral bioavailability.

2.01.5.4 Screening Technologies for ADME and Safety Optimization

In the 1990s poor PK and biopharmaceutical properties caused a high percentage of clinical candidate attrition.[209–212] Safety has also been, and continues to be, a key attrition factor, though as mechanistic toxicity and adverse drug reactions (ADR's) become better understood, it is possible to proactively avoid some recognized issues.[213,214] Unfortunately, since we do not fully understand the mechanisms contributing to PK or safety profiles, it is unlikely that attrition due to these factors will ever be totally eliminated, particularly since, as described in this volume, experimental strategies to treat disease constantly evolve and diversify. However, in spite of this complexity, significant progress has been made to increase success in these areas over the last two decades. A key strategic approach has been to measure significant properties that define the PK profile and eliminate known safety liabilities early in discovery while the opportunity remains to influence candidate design and selection. This strategy has led to plate-based measurements of physical properties and to in vitro absorption, distribution, metabolism, and elimination (ADME) assays and safety assays run at a throughput that matches discovery chemistry output. As a result, profiling of multiple series and property optimization in large numbers of compounds can occur in parallel with efforts to improve potency. Moreover, as data from these assays have been accumulated, powerful in silico tools have been built that can help to avoid liabilities or to optimize desirable profiles at the concept

stage of the drug design process.[215–217] Optimizing ADME properties early in lead molecules has additional positive impact, over and above directly reducing attrition from poor PK, for example, by enabling lower compound doses, thus avoiding solubility challenges that may occur at higher levels.[211,218,219]

Realizing the ability to conduct ADME profiling on a high-throughput scale has required several unique scientific and technical advancements.[211] Perhaps one of the key scientific advancements was the establishment of a relationship between ADME properties and the PK profile. Indeed, much work has been done building relationship models correlating in vivo (whole organism), in situ (organ), in vitro (cell and tissue models), physical properties, and in silico predicted properties. Consequently, the in vivo to in vitro correlation (IVIVC) is now well understood for many properties and mechanisms with varying degrees of sophistication from binning to accurate prediction. Pharmaceutical research organizations have amassed well-annotated compound sets that can be used to establish quantitative or semiquantitative translation from experimental models to potential clinical outcomes. Keeping pace with parallel medicinal chemistry capabilities has required in vitro ADME models that can be tested rapidly on plate-based scales with minimal amounts of compound. The widespread establishment of cell culture models (e.g., Caco-2, MDCK) and readily available reagents (e.g., human liver microsomes and hepatocytes) has provided key tools for in vitro ADME assay development. These systems are amenable to miniaturization, and given their ease of use a high number of studies can be performed per design cycle. Complementary technological advances in workflow and sample analysis have also had significant impact on the early discovery cycle. Typically, the endpoint measured in ADME profiling is the compound of interest itself, rather than a downstream physiological consequence as is the case in pharmacology and safety assays. This change presented four major challenges to be overcome.[218] First, an ability to rapidly generate analytical methods was needed, given the thousands of compounds requiring analysis. The solution involved creating automated methods development, applicable on the microtiter plate scale together with informatics capabilities to manage compound details and the resulting analytical conditions specific to each test compound.[220–222] A second challenge was that miniaturized assays using small amounts of compound required highly sensitive instruments for sample analysis. In this case, the utilization of mass spectrometry (MS) technology played a powerful role by providing the necessary sensitivity to quantify samples in the nanomolar to micromolar ranges. The third major challenge was a requirement for high analytical throughput and capacity since multiple assays, each yielding many sets of samples, are commonly performed per given compound. One approach to overcoming this challenge was the creation of high-throughput autosamplers to take samples from plates and introduce them to the mass spectrometer. These autosamplers are capable of handling many samples per minute, and plates per hour.[221,222] Examples include the RapidFire® system from Agilent and the Apricot Designs Dual-Arm Autosampler. The former integrates a fast autosampler and automated micro-scale solid-phase extraction enabling a cycle time of 5–10 s/sample, and the latter achieves its speed (also under 10 s/sample in trap and elute mode) with two robotic arms each equipped with a needle and up to four injection ports. Tandem mass spectrometry (MS/MS) played a significant role in increasing sample throughput by creating a rapid and highly specific analytical method that can be utilized by multiple instruments and reducing the need to perform chromatographic separations for reliable analysis. A final challenge required the ability to manipulate large volumes of data in rapid fashion for reviewing each sample analysis and summarizing endpoints from multiple samples. Automated approaches to each problem have been created and typically involve laboratory information systems. The establishment of this high-throughput analytical platform represents a major step forward in enabling early ADME profiling both from the standpoint of meeting capacity and demand, along with being universally applicable as an approach to measure samples across a wide variety of ADME endpoints.

A compound's PK profile is a reflection of: (1) its bioavailability and distribution, or ability to reach the target site following an acceptable dosing route (typically oral); (2) residence time in the body required to yield efficacy (described by half-life and elimination, expressed as clearance); and (3) the potential for drug–drug interactions (DDI). In depth discussions of these areas will occur in subsequent chapters, so here we will highlight mechanistic elements of bioavailability, distribution, clearance and DDI, and provide some example systems that are used for profiling. Since most drugs are dosed orally, a prerequisite to attaining their site of action (unless they target the gut wall) is absorption from the gut lumen into blood. This factor is determined by a balance of solubility and permeability characteristics, which are attributable to physical properties such as lipophilicity, hydrogen-bonding abilities (to donate and to accept), polar surface area and molecular size as described by Lipinski's rule of 5.[223,224] These properties can be calculated or computationally derived values, but lipophilicity may also be experimentally measured, often using octanol–water shake-flask methods, immobilized artificial membrane, or chromatographic approaches.[225,226] Measures of solubility and permeability are typically assessed in an ADME suite of assays. For solubility determinations, UV detection, nephelometry, turbidity, or mass spectrometry are typically employed to kinetically assess the dissolved concentration of a compound as it equilibrates in an appropriate buffer system.[227,228] Intestinal permeability can be measured using artificial or tissue culture models, where the ability of a compound to partition into and to diffuse across a membrane is determined by using bicameral systems with donor and acceptor chambers. The parallel artificial membrane permeability assay (PAMPA) utilizes common lipids (such as dodecane and phosphatidylcholine) or extracts (such as soy lecithin) to form the membrane.[229,230] Advantages of this approach include the ease of reagent generation and optimization, whereas disadvantages include challenges of translation to true tissue permeability. Tissue culture models such as Caco-2 and MDCK, which spontaneously differentiate into polarized epithelium under normal culture conditions, have been widely utilized.[231–233] Both models allow for a multimechanistic study of transport processes across intestinal epithelium, though both require labor-intensive cell culture efforts.

Subsequent to absorption, permeability will also govern a compound's distribution within the body and its access to the required site of action. This is particularly relevant for brain-localized targets, where the blood–brain barrier (BBB) poses a significant hurdle. Unfortunately, models of the BBB have been challenging to develop, and consequently focus has shifted to understanding

that role that membrane transporters play in tissue distribution. Many of the ABC transporters, notably P-glycoprotein (P-gp), Breast Cancer Resistance Protein (BCRP), and Multidrug-Related Protein (MRP), can efflux a wide spectrum of drugs and exist in barrier tissues throughout the body. It is thought that these transporters serve a protective role to limit exposure of these pharmacological sanctuaries to foreign compounds. Assays to profile efflux potential have tended to utilize Caco-2 cells (P-gp and BCRP), or transfected MDCK cells (P-gp, BCRP, MRP) and to determine transport polarity via comparing absorptive transport (apical to basolateral) vs. secretory transport (basolateral to apical).[234,235] Another key factor involved in distribution is protein binding, notably plasma protein binding. While this parameter is routinely profiled for establishing the free drug concentration, which is necessary for PK predictions, it plays no role in drug action and should not be used in compound design optimization.[211] Commonly used methods to measure protein binding in high-throughput formats include ultrafiltration and equilibrium dialysis.[236–238]

Residence time in the body is an important factor in governing therapeutic efficacy, and that rate at which a compound is eliminated is commonly expressed as the flow parameter clearance, which is dependent on metabolic stability (metabolic clearance is typically observed for more lipophilic compounds), and biliary and renal excretion. The liver is the major drug metabolizing organ, and reagents used to gauge metabolic stability are typically derived from liver tissue, for example, human liver microsomes, and hepatocytes. Microsomes have been used successfully to profile Phase I, or oxidative, metabolism where polarity is imparted to the parent compound.[239] Hepatocytes provide an intact whole-cell system that can be used to assess both phase I and II metabolism. Phase II metabolism imparts hydrophilicity to the compound and includes synthesis and conjugation reactions such as glucuronidation and sulfation. Reports have shown that data generated using these assays can be used to inform PK predictions when metabolism is the rate-limiting event that determines clearance.[240] The amenability of these reagents to high-throughput approaches, translation to clinical outcomes and applicability to a large majority of drug-like chemical space has led to them being placed on the front lines of ADME profiling. The emerging importance of biliary and renal excretion as major pathways of clearance for metabolically stable compounds has led to greater focus on their characterization. These processes involve passive and/or active transport from blood into bile and urine, respectively, and when they have been important contributors to overall clearance, active transport mediated by transporters has often played a significant role. Whole-cell systems such as sandwich-cultured human hepatocytes have been used to determine biliary elimination,[241,242] and cell lines expressing a suite of key transporters such OATP, OAT and OCT isoforms are becoming more prevalent.[243,244]

A compound's PK profile can be significantly shifted through biochemical interactions with enzymes, transporters, other proteins and even other drugs. Hence, it is important to assess this interaction potential to reveal any variability that may be displayed in the patient population with particular focus on identifying any key safety liabilities. Numerous clinical reports have revealed CYP-mediated DDI,[245] and therefore routine high-throughput profiling of the major Cytochrome P450 enzymes, CYP1A2, CYP2C8/9/19, CYP2B6, CYP2D6 and CYP3A4 using either recombinant CYP enzymes or microsomes together with marker substrates is typically performed early in discovery. Some CYP isoforms are important to profile due to the large variety of substrates metabolized (e.g., CYP3A4), while others are important to profile due to the existence of polymorphisms within the population (e.g., CYP2D6). CYP-mediated DDI experiments evaluate competitive inhibition, time/mechanism-based inhibition, and induction. Induction experiments may study perpetrator propensity to bind and activate the nuclear receptors, PXR and CAR, or profile changes in CYP expression in whole-cell models such as primary hepatocytes.[246] These data are typically included in regulatory submissions; therefore, the degree of rigor of the assays typically increases as a candidate compound progresses from discovery into development. Once again, transporters are emerging as important factors in this space. Interactions between P-gp and digoxin have been seen clinically, and assays have been developed to profile these events.[247,248] It is likely that as more candidates, for which transporters play a major ADME role, reach the clinic, a greater need to profile transporter-mediated DDI will emerge.

The advances in parallel medicinal chemistry and high-throughput profiling of compounds in plate-based pharmacology and ADME studies, combined with the reduced amounts of compound being synthesized in these chemistry methodologies, required a consequential evolution of safety strategies that previously called for large amounts of compounds and significant resources in the planning and use of animals. These studies were typically conducted in the later stages of discovery when reoptimization of lead compounds becomes more challenging. Today, in vitro assays for safety profiling are taking their place alongside potency and ADME assays for use during lead identification and optimization. The strategic approach here often biases toward allowing false negatives rather than false positives to avoid the risk of deselecting potentially useful compounds and therefore relies on downstream techniques to ultimately identify unsafe compounds.[249] The Ames assay, which addresses a compound's potential to cause genotoxicity, is the most widely utilized assay and is a prerequisite to dosing in humans.[249] Scaled down versions of the Ames test and surrogates, including the in vitro micronucleus assay, have been developed for high-throughput profiling.[250,251] Recently, a high-throughput assay using transformed human liver epithelial (THLE) cells and monitoring ATP depletion was shown to successfully predict cytotoxicity,[252,253] and a glucose/galactose assay is frequently used in early discovery as a surrogate for mitochondrial toxicity.[254]

High-content screening attempts to assess numerous endpoints and to define an overall toxic profile for compounds. The human hepatocellular liver carcinoma (HepG2) cell line has been used in a high-content format to profile cell number, nuclear area, calcium content and mitochondrial membrane potential.[255] A commercially available assay with primary human hepatocytes is offered by CellCiphr that includes markers for oxidative stress, organelle function, stress pathway activation, cytoskeletal integrity, cell cycle, and DNA damage. Luxcel Biosciences has developed assays that can profile mitochondrial toxicity using soluble phosphorescence and fluorescence-based sensors for extracellular oxygen consumption. These assays can be adapted to the system of interest, for example, isolated mitochondria, organisms or tissues.[256–258] Genomic-based technologies have led to the creation of micorarrays that probe expression changes in specific pathways including oxidative stress, mitochondrial

dysfunction, differentiation, inflammation and apoptosis pathways allowing a targeted profiling of these outcomes.[249] These efforts require informatics support to map profiles against a database providing a greater understanding of translation to clinical outcomes and to guide decisions on next steps to eliminate safety risks. Furthermore, in order to become a more main stream early discovery profiling technology microarrays will require increases in capacity and reductions in cost.

In addition to profiling markers of general toxicity, some safety studies are directed toward specific pharmacological interactions. Profiling against the heterologously expressed, human voltage-gated potassium channel subfamily H member (hERG) is required for regulatory submission due to the association of compounds that block this channel with potentially fatal arrhythmia (Torsades de Pointe).[214] Typically, profiling includes a binding assay using astemizole or dofetilide, followed by patch-clamp assays.[259,260] The technologies utilized for in vitro safety pharmacology profiling are very much the same as those used in plate-based primary pharmacology, and include ligand-binding approaches and functional approaches performed in single-concentration and dose–response formats to obtain an effect profile. A recent publication from Bowes et al.[214] compares the collective safety experiences of four major pharmaceutical companies and suggests a strategic approach together with a baseline set of targets, including receptors, ion channels, enzymes and transporters against which to profile using in vitro models.[214]

2.01.6 Perspective and Future Direction

Advances in drug discovery technology over the last 15 years have created tremendous opportunity to accelerate the discovery and development of novel therapeutic agents to treat devastating human diseases. These advances have touched nearly every area of the drug discovery process and leave us poised on a threshold of innovation. We have the opportunity to assimilate big data sets from large patient cohorts and combine this information with genome-wide association studies to correlate genotype and phenotype. The decoding of the human genome, coupled with advances in our understanding of processes regulating transcription, translation, and the role of posttranslational modification have expanded the number of compelling drug targets, increased confidence in their association with disease and introduced new modalities for modulating their function. Rapid and precise genomic editing capabilities can be applied to build systems of greater physiological relevance and disease significance. Additionally we have greater access to the specific cell types impacted by disease using primary patient cells, stem cell-derived models, 3D organoids and tissue models. The expansion of accessible chemical space—through diversity oriented synthetic libraries, DNA-encoded library technology, fragment screening, newer high-throughput screening technologies and an increased appreciation for the merits of covalent drug discovery have enabled drug discovery targets once considered inaccessible for small molecule therapeutic development to be pursued with higher quality leads. Moreover, the landscape of chemical space believed to be privileged for oral absorption or access to restricted tissue compartments (such as the central nervous system) is changing with the introduction of multiparameter optimization techniques and design principles to access uptake transporters and avoid efflux. Phenotypic screening, the mainstay of classical drug discovery efforts briefly set aside in favor of hypothesis-driven, target-directed approaches, is undergoing a resurgence given the development of tools enabling scientists to confidently determine mechanism of action. These same technologies are also finding application for developing target engagement probes used to guide preclinical and clinical efficacy studies. Finally, our ability to predict pharmacokinetics and safety—even to the extent of once challenging areas such as transporter-mediated clearance, aldehyde oxidase-driven metabolism, and hepatic safety, are improving thanks to new screening technologies and an understanding of the capacity of physiological detoxification mechanisms.

Despite these advances, there are still gaps that impede swift progress from medical need to candidate molecule identification. The leap from genetic association data to a therapeutically relevant drug target is still a daunting one, requiring the demonstration of causality, determining directionality for target modulation, further target validation, and demonstrating drugability. Complex multifactorial diseases such as Alzheimer's and diabetes markedly demonstrate these challenges. While newer screening technologies such as ASMS and DNA-encoded libraries may require less assay development time and can be relatively quick to execute, these techniques are not routinely successful with membrane proteins and complex targets. Disease models, on the other hand, while more physiologically relevant are also more costly, labor intensive and time-consuming. Moreover, the heterogeneity and lower reproducibility in stem cell and 3D model systems present new challenges to the standard approaches of traditional biochemical or cellular screens. A phenotpypic screening campaign yielding small molecule hits is still just the beginning of a long haul to identify mechanisms of action for the hits, deconvolute them to targets and understand safety properties.

Improving drug discovery productivity in the next decade will require generating physiologically relevant disease models for major therapeutic areas, including robust and reproducible stem-cell differentiation protocols for a broad range of target tissues. It will be necessary to run high-throughput, small-molecule screens with a clinically relevant stimulus and endpoints to generate phenotypic hits and, in parallel, to probe these endpoints with genomic perturbagens such as siRNA, shRNA, CRISPRa and CRISPRi for new target identification. Currently, pooled genomic screens are best suited to oncology (using synthetic lethal or dropout approaches) or to cell surface markers that can be monitored at the single cell level by high-throughput flow cytometry. Innovative technologies such as microfluidics will be necessary to capture the advantage of pooled genomic screens and apply them more broadly across other therapeutic areas. We also need to see a step change in the efficiency of phenotypic deconvolution and target identification in order to rapidly assess multiple hit series and effectively triage the most valuable active compounds from a screen.

As drug discovery efforts venture into more complex modalities, such as interfering with protein–protein interactions, modulating peptidergic GPCRs and influencing complex intracellular multiprotein assemblies, medicinal chemists will be challenged to think beyond traditional small-molecule drug discovery paradigms. Emerging technologies such as targeted protein degraders

(PROTACs) bring challenges associated with poor cellular permeability that limits their effectiveness. Despite advances in understanding permeability of cyclic peptides and other macrocyclic compounds, it is still difficult to combine potency, permeability and metabolic stability into the same molecular entity for programs reliant on this type of chemical matter. Finally, newer modalities such as targeted inhibition of protein translation and RNA splicing modulators have yet to be proven as general strategies for addressing challenging drug targets. Progress in each of these areas will further expand options for drug discovery scientists in pursuing challenging targets of the future.

Medicinal chemistry was once considered to be a discipline integrating organic synthesis and bioorganic chemistry. That narrow focus is now changing with the breadth of these new technologies impacting the entire drug discovery process and the intimate involvement of chemistry as a central science in their development and implementation. The ever expanding landscape of new technology makes it more important than ever for medicinal chemists, analytical chemists, structural biologists, screening biologists, and computational scientists to integrate their efforts into fluid cross-disciplinary collaborations and to become more familiar with the challenges and new science occurring in these respective areas. Often it is the creative advances in the application of new science in a seemingly unrelated area that provokes transformative change in how drug discovery is practiced, ultimately enabling scientists to surmount challenges once presumed to be extremely difficult or impossible to overcome. This creativity requires scientists to expand their interests beyond the immediate problem at hand in a drug discovery program and ask how new science might be more broadly applied to address obstacles encountered in other programs. We have attempted to provide a high level overview of the most impactful advances in drug discovery technologies over the past decade. Subsequent chapters in this volume will treat these topics in greater detail and hopefully inspire new applications that will enable further advances in medicinal chemistry and drug discovery approaches.

See also: 4.01. Role of ADME/PK in Drug Discovery, Safety Assessment, and Clinical Development.

References

1. Ng, R. Drugs: From Discovery to Approval, 3rd edition, pub. John Wiley & Sons, 2015.
2. DiMasi, J. A.; Grabowski, H. G.; Hansen, R. W. *J. Health Econ.* **2016,** *47,* 20.
3. Hopkins, A. L.; Groom, C. R. *Nat. Rev. Drug Discov.* **2002,** *1,* 727.
4. Overington, J. P.; Al-Lazikani, B.; Hopkins, A. L. *Nat. Rev. Drug Discov.* **2006,** *5,* 993.
5. Gribbon, P.; Sewing, A. *Drug Discov. Today* **2005,** *10,* 17.
6. Schreiber, S. L. *Nature* **2009,** *457,* 153.
7. Dandapani, S.; Marcaurelle, L. A. *Curr. Opin. Chem. Biol.* **2010,** *14,* 362.
8. Morton, D.; Leach, S.; Cordier, C.; Warriner, S.; Nelson, A. *Angew. Chem. Int. Ed.* **2008,** *48,* 104.
9. Mannocci, L.; Leimbacher, M.; Wichert, M.; Scheuermann, J.; Neri, D. *Chem. Commun. (Cambridge, UK)* **2011,** *47,* 12747.
10. Franzini, R. M.; Randolph, C. J. *Med. Chem.* **2016**. *59*, 6629.
11. Coyne, A. G.; Scott, D. E.; Abell, C. *Curr. Opin. Chem. Biol.* **2010,** *14,* 299.
12. Scott, D. E.; Coyne, A. G.; Hudson, S. A.; Abell, C. *Biochemistry* **2012,** *51,* 4990.
13. Chessari, G.; Woodhead, A. *J. Drug Discov. Today* **2009,** *14,* 668.
14. Carr, R. A. E.; Congreve, M.; Murray, C. W.; Rees, D. C. *Drug Discov. Today* **2005,** *10,* 987.
15. Bunnage, M. E. *Nat. Chem. Biol.* **2011,** *7,* 335.
16. Ingelman-Sundberg, M. *Toxicol. Appl. Pharmacol.* **2005,** *207,* 52.
17. Nakayama, S.; Atsumi, R.; Takakusa, H.; Kobayashi, Y.; Kurihara, A.; Nagai, Y.; Nakai, D.; Okazaki, O. *Drug Metab. Dispos.* **2009,** *37,* 1970.
18. Bunnage, M. E.; Chekler, E. L. P.; Jones, L. H. *Nat. Chem. Biol.* **2013,** *9,* 195.
19. Bunnage, M. E.; Gilbert, A. M.; Jones, L. H.; Hett, E. C. *Nat. Chem. Biol.* **2015,** *11,* 368.
20. Cox, D. B. T.; Platt, R. J.; Zhang, F. *Nat. Med. (New York, NY)* **2015,** *21,* 121.
21. Gasiunas, G.; Barrangou, R.; Horvath, P.; Siksnys, V. *Proc. Natl. Acad. Sci. U. S. A.* **2012,** *109,* E2579.
22. Jinek, M.; Chylinski, K.; Fonfara, I.; Hauer, M.; Doudna, J. A.; Charpentier, E. *Science (Washington, DC)* **2012,** *337,* 816.
23. Marraffini, L. A. *Nature (London)* **2015,** *526,* 55.
24. Moore, J. D. *Drug Discov. Today* **2015,** *20,* 450.
25. Mali, P.; Yang, L.; Esvelt, K. M.; Aach, J.; Guell, M.; DiCarlo, J. E.; Norville, J. E.; Church, G. M. *Science (Washington, DC)* **2013,** *339,* 823.
26. La Russa, M. F.; Qi, L. S. *Mol. Cell. Biol.* **2015,** *35,* 3800.
27. Hilton, I. B.; D'Ippolito, A. M.; Vockley, C. M.; Thakore, P. I.; Crawford, G. E.; Reddy, T. E.; Gersbach, C. A. *Nat. Biotechnol.* **2015,** *33,* 510.
28. Taylor, J.; Woodcock, S. *J. Biomol. Screen.* **2015,** *20,* 1040.
29. Wang, T.; Wei, J. J.; Sabatini, D. M.; Lander, E. S. *Science (Washington, DC)* **2014,** *343,* 80.
30. Zhou, Y.; Zhu, S.; Cai, C.; Yuan, P.; Li, C.; Huang, Y.; Wei, W. *Nature (London)* **2014,** *509,* 487.
31. Koike-Yusa, H.; Li, Y.; Tan, E. P.; Velasco-Herrera, M. D. C.; Yusa, K. *Nat. Biotechnol.* **2014,** *32,* 267.
32. Shalem, O.; Sanjana, N. E.; Hartenian, E.; Shi, X.; Scott, D. A.; Mikkelsen, T. S.; Heckl, D.; Ebert, B. L.; Root, D. E.; Doench, J. G.; Zhang, F. *Science (Washington, DC)* **2014,** *343,* 84.
33. Gilbert, L. A.; Horlbeck, M. A.; Adamson, B.; Villalta, J. E.; Chen, Y.; Whitehead, E. H.; Guimaraes, C.; Panning, B.; Ploegh, H. L.; Bassik, M. C.; Qi, L. S.; Kampmann, M.; Weissman, J. S. *Cell (Cambridge, MA)* **2014,** *159,* 647.
34. Konermann, S.; Brigham, M. D.; Trevino, A. E.; Joung, J.; Abudayyeh, O. O.; Barcena, C.; Hsu, P. D.; Habib, N.; Gootenberg, J. S.; Nishimasu, H.; Nureki, O.; Zhang, F. *Nature (London)* **2015,** *517,* 583.
35. Schumann, K.; Lin, S.; Boyer, E.; Simeonov, D. R.; Subramaniam, M.; Gate, R. E.; Haliburton, G. E.; Ye, C. J.; Bluestone, J. A.; Doudna, J. A.; Marson, A. *Proc. Natl. Acad. Sci. U. S. A.* **2015,** *112,* 10437.
36. Ran, F. A.; Cong, L.; Yan, W. X.; Scott, D. A.; Gootenberg, J. S.; Kriz, A. J.; Zetsche, B.; Shalem, O.; Wu, X.; Makarova, K. S.; Koonin, E. V.; Sharp, P. A.; Zhang, F. *Nature (London)* **2015,** *520,* 186.

37. Lohse, M. J.; Nuber, S.; Hoffmann, C. *Pharmacol. Rev.* **2012,** *64,* 299.
38. DeWire, S. M.; Yamashita, D. S.; Rominger, D. H.; Liu, G.; Cowan, C. L.; Graczyk, T. M.; Chen, X.-T.; Pitis, P. M.; Gotchev, D.; Yuan, C.; Koblish, M.; Lark, M. W.; Violin, J. D. *J. Pharmacol. Exp. Ther.* **2013,** *344,* 708.
39. Rajagopal, K.; Whalen, E. J.; Violin, J. D.; Stiber, J. A.; Rosenberg, P. B.; Premont, R. T.; Coffman, T. M.; Rockman, H. A.; Lefkowitz, R. J. *Proc. Natl. Acad. Sci. U. S. A.* **2006,** *103,* 16284.
40. Violin, J. D.; DeWire, S. M.; Yamashita, D.; Rominger, D. H.; Nguyen, L.; Schiller, K.; Whalen, E. J.; Gowen, M.; Lark, M. W. *J. Pharmacol. Exp. Ther.* **2010,** *335,* 572.
41. Walters, R. W.; Shukla, A. K.; Kovacs, J. J.; Violin, J. D.; DeWire, S. M.; Lam, C. M.; Chen, J. R.; Muehlbauer, M. J.; Whalen, E. J.; Lefkowitz, R. J. *J. Clin. Invest.* **2009,** *119,* 1312.
42. Gomes, I.; Ayoub, M. A.; Fujita, W.; Jaeger, W. C.; Pfleger, K. D. G.; Devi, L. A. *Annu. Rev. Pharmacol. Toxicol.* **2016,** *56,* 403.
43. Gomes, I.; Fujita, W.; Gupta, A.; Saldanha, S. A.; Negri, A.; Pinello, C. E.; Eberhart, C.; Roberts, E.; Filizola, M.; Hodder, P.; Devi, L. A. *Proc. Natl. Acad. Sci. U. S. A.* **2013,** *110,* 12072.
44. Remus, T. P.; Zima, A. V.; Bossuyt, J.; Bare, D. J.; Martin, J. L.; Blatter, L. A.; Bers, D. M.; Mignery, G. A. *J. Biol. Chem.* **2006,** *281,* 608.
45. Kapoor, N.; Maxwell, J. T.; Mignery, G. A.; Will, D.; Blatter, L. A.; Banach, K. *PLoS One* **2014,** *9,* e83715/1.
46. Dhooghe, B.; Haaf, J. B.; Noel, S.; Leal, T. *Expert Opin. Invest. Drugs* **2016,** *25,* 423.
47. Singh, R. K.; Cooper, T. A. *Trends Mol. Med.* **2012,** *18,* 472.
48. Butler, M. S. *J. Med. Chem.* **2013,** *56,* 6573.
49. d'Ydewalle, C.; Sumner, C. J. *Neurotherapeutics* **2015,** *12,* 303.
50. Hastings, M. L.; Berniac, J.; Liu, Y. H.; Abato, P.; Jodelka, F. M.; Barthel, L.; Kumar, S.; Dudley, C.; Nelson, M.; Larson, K.; Edmonds, J.; Bowser, T.; Draper, M.; Higgins, P.; Krainer, A. R. *Sci. Transl. Med.* **2009,** *1,* 5ra12.
51. Palacino, J.; Swalley, S. E.; Song, C.; Cheung, A. K.; Shu, L.; Zhang, X.; Van Hoosear, M.; Shin, Y.; Chin, D. N.; Keller, C. G.; Beibel, M.; Renaud, N. A.; Smith, T. M.; Salcius, M.; Shi, X.; Hild, M.; Servais, R.; Jain, M.; Deng, L.; Bullock, C.; McLellan, M.; Schuierer, S.; Murphy, L.; Blommers, M. J. J.; Blaustein, C.; Berenshteyn, F.; Lacoste, A.; Thomas, J. R.; Roma, G.; Michaud, G. A.; Tseng, B. S.; Porter, J. A.; Myer, V. E.; Tallarico, J. A.; Hamann, L. G.; Curtis, D.; Fishman, M. C.; Dietrich, W. F.; Dales, N. A.; Sivasankaran, R. *Nat. Chem. Biol.* **2015,** *11,* 511.
52. Mai, A. *ChemMedChem* **2014,** *9,* 415.
53. Chang, J.-G.; Hsieh-Li, H.-M.; Jong, Y.-J.; Wang, N. M.; Tsai, C.-H.; Li, H. *Proc. Natl. Acad. Sci. U. S. A.* **2001,** *98,* 9808.
54. Carey, N. *Med. Chem. Commun.* **2012,** *3,* 162.
55. Morin, R. D.; Johnson, N. A.; Severson, T. M.; Mungall, A. J.; An, J.; Goya, R.; Paul, J. E.; Boyle, M.; Woolcock, B. W.; Kuchenbauer, F.; Yap, D.; Humphries, R. K.; Griffith, O. L.; Shah, S.; Zhu, H.; Kimbara, M.; Shashkin, P.; Charlot, J. F.; Tcherpakov, M.; Corbett, R.; Tam, A.; Varhol, R.; Smailus, D.; Moksa, M.; Zhao, Y.; Delaney, A.; Qian, H.; Birol, I.; Schein, J.; Moore, R.; Holt, R.; Horsman, D. E.; Connors, J. M.; Jones, S.; Aparicio, S.; Hirst, M.; Gascoyne, R. D.; Marra, M. A. *Nat. Genet.* **2010,** *42,* 181.
56. Wilson, D. N.; Arenz, S.; Beckmann, R. *Curr. Opin. Struct. Biol.* **2016,** *37,* 123.
57. Arenz, S.; Meydan, S.; Starosta, A. L.; Berninghausen, O.; Beckmann, R.; Vazquez-Laslop, N.; Wilson, D. N. *Mol. Cell* **2014,** *56,* 446.
58. Arenz, S.; Ramu, H.; Gupta, P.; Berninghausen, O.; Beckmann, R.; Vazquez-Laslop, N.; Mankin, A. S.; Wilson, D. N. *Nat. Commun.* **2014,** *5,* 4501/1.
59. Alonzo, D. A.; Schmeing, T. M. *Nat. Chem. Biol.* **2016,** *12,* 127.
60. Quick, D. Oregon Health And Science University http://newatlas.com/pharmacoperones-drug-protein-misfolding/30074/, **2013**.
61. Janovick, J. A.; Stewart, M. D.; Jacob, D.; Martin, L. D.; Deng, J. M.; Stewart, C. A.; Wang, Y.; Cornea, A.; Chavali, L.; Lopez, S.; Mitalipov, S.; Kang, E.; Lee, H.-S.; Manna, P. R.; Stocco, D. M.; Behringer, R. R.; Conn, P. M. *Proc. Natl. Acad. Sci. U. S. A.* **2013,** *110,* 21030.
62. Brehme, M.; Voisine, C.; Rolland, T.; Wachi, S.; Soper, J. H.; Zhu, Y.; Orton, K.; Villella, A.; Garza, D.; Vidal, M.; Ge, H.; Morimoto, R. I. *Cell Rep.* **2014,** *9,* 1135.
63. Bouchecareilh, M.; Balch, W. E. *Curr. Mol. Med.* **2012,** *12,* 815.
64. Toure, M.; Crews, C. M. *Angew. Chem. Int. Ed.* **2016,** *55,* 1966.
65. Li, W.; Bengtson, M. H.; Ulbrich, A.; Matsuda, A.; Reddy, V. A.; Orth, A.; Chanda, S. K.; Batalov, S.; Joazeiro, C. A. *PLoS One* **2008,** *3,* e1487.
66. Itoh, Y.; Ishikawa, M.; Naito, M.; Hashimoto, Y. *J. Am. Chem. Soc.* **2010,** *132,* 5820.
67. Itoh, Y.; Ishikawa, M.; Kitaguchi, R.; Sato, S.; Naito, M.; Hashimoto, Y. *Bioorg. Med. Chem.* **2011,** *19,* 3229.
68. Okuhira, K.; Ohoka, N.; Sai, K.; Nishimaki-Mogami, T.; Itoh, Y.; Ishikawa, M.; Hashimoto, Y.; Naito, M. *FEBS Lett.* **2011,** *585,* 1147.
69. Itoh, Y.; Kitaguchi, R.; Ishikawa, M.; Naito, M.; Hashimoto, Y. *Bioorg. Med. Chem.* **2011,** *19,* 6768.
70. Schneekloth, J. S., Jr.; Fonseca, F. N.; Koldobskiy, M.; Mandal, A.; Deshaies, R.; Sakamoto, K.; Crews, C. M. *J. Am. Chem. Soc.* **2004,** *126,* 3748.
71. Bondeson, D. P.; Mares, A.; Smith, I. E. D.; Ko, E.; Campos, S.; Miah, A. H.; Mulholland, K. E.; Routly, N.; Buckley, D. L.; Gustafson, J. L.; Zinn, N.; Grandi, P.; Shimamura, S.; Bergamini, G.; Faelth-Savitski, M.; Bantscheff, M.; Cox, C.; Gordon, D. A.; Willard, R. R.; Flanagan, J. J.; Casillas, L. N.; Votta, B. J.; den Besten, W.; Famm, K.; Kruidenier, L.; Carter, P. S.; Harling, J. D.; Churcher, I.; Crews, C. M. *Nat. Chem. Biol.* **2015,** *11,* 611.
72. Hines, J.; Gough, J. D.; Corson, T. W.; Crews, C. M. *Proc. Natl. Acad. Sci. U. S. A.* **2013,** *110,* 8942.
73. Lai, A. C.; Toure, M.; Hellerschmied, D.; Salami, J.; Jaime-Figueroa, S.; Ko, E.; Hines, J.; Crews, C. M. *Angew. Chem. Int. Ed.* **2016,** *55,* 807.
74. Zengerle, M.; Chan, K.-H.; Ciulli, A. *ACS Chem. Biol.* **2015,** *10,* 1770.
75. Ito, T.; Ando, H.; Suzuki, T.; Ogura, T.; Hotta, K.; Imamura, Y.; Yamaguchi, Y.; Handa, H. *Science (Washington, DC)* **2010,** *327,* 1345.
76. Chamberlain, P. P.; Lopez-Girona, A.; Miller, K.; Carmel, G.; Pagarigan, B.; Chie-Leon, B.; Rychak, E.; Corral, L. G.; Ren, Y. J.; Wang, M.; Riley, M.; Delker, S. L.; Ito, T.; Ando, H.; Mori, T.; Hirano, Y.; Handa, H.; Hakoshima, T.; Daniel, T. O.; Cathers, B. E. *Nat. Struct. Mol. Biol.* **2014,** *21,* 803.
77. Lu, J.; Qian, Y.; Altieri, M.; Dong, H.; Wang, J.; Raina, K.; Hines, J.; Winkler, J. D.; Crew, A. P.; Coleman, K.; Crews, C. M. *Chem. Biol. (Oxford, UK)* **2015,** *22,* 755.
78. Winter, G. E.; Buckley, D. L.; Paulk, J.; Roberts, J. M.; Souza, A.; Dhe-Paganon, S.; Bradner, J. E. *Science (Washington, DC)* **2015,** *348,* 1376.
79. Johnson, K. A. *FEBS Lett.* **2013,** *587,* 2753.
80. Winquist, R. J.; Mullane, K.; Williams, M. *Biochem. Pharmacol. (Amsterdam, Neth.)* **2014,** *87,* 4.
81. Venter, J. C.; Adams, M. D.; Myers, E. W.; Li, P. W.; Mural, R. J.; Sutton, G. G.; Smith, H. O.; Yandell, M.; Evans, C. A.; Holt, R. A.; Gocayne, J. D.; Amanatides, P.; Ballew, R. M.; Huson, D. H.; Wortman, J. R.; Zhang, Q.; Kodira, C. D.; Zheng, X. H.; Chen, L.; Skupski, M.; Subramanian, G.; Thomas, P. D.; Zhang, J.; Miklos, G. L. G.; Nelson, C.; Broder, S.; Clark, A. G.; Nadeau, J.; McKusick, V. A.; Zinder, N.; Levine, A. J.; Roberts, R. J.; Simon, M.; Slayman, C.; Hunkapiller, M.; Bolanos, R.; Delcher, A.; Dew, I.; Fasulo, D.; Flanigan, M.; Florea, L.; Halpern, A.; Hannenhalli, S.; Kravitz, S.; Levy, S.; Mobarry, C.; Reiner, K.; Remington, K.; Abu-Threide, J.; Beasle, E.; Biddick, K.; Bonazzi, V.; Brandon, R.; Cargill, M.; Chandramouliswaran, I.; Charlab, R.; Chaturved, K.; Deng, Z.; Di Francesco, V.; Dunn, P.; Eilbeck, K.; Evangelista, C.; Gabrielian, A. E.; Gan, W.; Ge, W.; Gon, F.; Gu, Z.; Guan, P.; Heiman, T. J.; Higgins, M. E.; Ji, R.-R.; Ke, Z.; Ketchum, K. A.; Lai, Z.; Lei, Y.; Li, Z.; Li, J.; Liang, Y.; Lin, X.; Lu, F.; Merkulov, G. V.; Milshina, N.; Moore, H. M.; Naik, A. K.; Narayan, V. A.; Neelam, B.; Nusskern, D.; Rusch, D. B.; Salzberg, S.; Shao, W.; Shue, B.; Sun, J.; Wang, Z. Y.; Wang, A.; Wang, X.; Wang, J.; Wei, M.-H.; Wides, R.; Xiao, C.; Yan, C. *Science (Washington, DC)* **2001,** *291,* 1304.
82. Swinney, D. C.; Anthony, J. *Nat. Rev. Drug Discov.* **2011,** *10,* 507.
83. Brown, D. *Drug Discov. Today* **2007,** *12,* 1007.
84. Eggert, U. S. *Nat. Chem. Biol.* **2013,** *9,* 206.
85. Wilson, D. N.; Schluenzen, F.; Harms, J. M.; Starosta, A. L.; Connell, S. R.; Fucini, P. *Proc. Natl. Acad. Sci. U. S. A.* **2008,** *105,* 13339.
86. Errington, A. C.; Stohr, T.; Heers, C.; Lees, G. *Mol. Pharmacol.* **2008,** *73,* 157.
87. Choi, D.; Stables, J. P.; Kohn, H. *J. Med. Chem.* **1996,** *39,* 1907.
88. Vincent, F.; Loria, P.; Pregel, M.; Stanton, R.; Kitching, L.; Nocka, K.; Doyonnas, R.; Steppan, C.; Gilbert, A.; Schroeter, T.; Peakman, M.-C. *Sci. Transl. Med.* **2015,** *7,* 1.

89. Ruedinger, F.; Lavrentieva, A.; Blume, C.; Pepelanova, I.; Scheper, T. *Appl. Microbiol. Biotechnol.* **2015,** *99,* 623.
90. Shi, X.; Yang, J.; Huang, J.; Long, Z.; Ruan, Z.; Xiao, B.; Xi, X. *Mol. Med. Rep.* **2016,** *13,* 2447.
91. DesRochers, T. M.; Suter, L.; Roth, A.; Kaplan, D. L. *PLoS One* **2013,** *8,* e59219.
92. Jang, K.-J.; Mehr, A. P.; Hamilton, G. A.; McPartlin, L. A.; Chung, S.; Suh, K.-Y.; Ingber, D. E. *Integr. Biol.* **2013,** *5,* 1119.
93. Sciancalepore, A. G.; Sallustio, F.; Girardo, S.; Passione, L. G.; Camposeo, A.; Mele, E.; Di Lorenzo, M.; Costantino, V.; Schena, F. P.; Pisignano, D. *PLoS One* **2014,** *9,* e87496/1.
94. Jang, K.-J.; Suh, K.-Y. *Lab Chip* **2010,** *10,* 36.
95. van Duinen, V.; Trietsch, S. J.; Joore, J.; Vulto, P.; Hankemeier, T. *Curr. Opin. Biotechnol.* **2015,** *35,* 118.
96. Jessani, N.; Cravatt, B. F. *Curr. Opin. Chem. Biol.* **2004,** *8,* 54.
97. Cravatt, B. F.; Wright, A. T.; Kozarich, J. W. *Annu. Rev. Biochem.* **2008,** *77,* 383.
98. Xu, H.; Majmudar, J. D.; Davda, D.; Ghanakota, P.; Kim, K. H.; Carlson, H. A.; Showalter, H. D.; Martin, B. R.; Amidon, G. L. *Mol. Pharm.* **2015,** *12,* 3399.
99. Adibekian, A.; Martin, B. R.; Wang, C.; Hsu, K.-L.; Bachovchin, D. A.; Niessen, S.; Hoover, H.; Cravatt, B. F. *Nat. Chem. Biol.* **2011,** *7,* 469.
100. Shannon, D. A.; Weerapana, E. *Curr. Opin. Chem. Biol.* **2015,** *24,* 18.
101. Weerapana, E.; Wang, C.; Simon, G. M.; Richter, F.; Khare, S.; Dillon, M. B. D.; Bachovchin, D. A.; Mowen, K.; Baker, D.; Cravatt, B. F. *Nature (London)* **2010,** *468,* 790.
102. Wang, C.; Weerapana, E.; Blewett, M. M.; Cravatt, B. F. *Nat. Methods* **2014,** *11,* 79.
103. Couvertier, S. M.; Zhou, Y.; Weerapana, E. *Biochim. Biophys. Acta, Proteins Proteomics* **2014,** *1844,* 2315.
104. Annis, A.; Chuang, C.-C.; Nazef, N. In *Mass Spectrometry in Medicinal Chemistry;* Wanner, K. T., Hofner, G., Eds.; Wiley-VCH: Weinheim, 2007; p 121.
105. Zehender, H.; Mayr, L. M. *Expert Opin. Drug Discov.* **2007,** *2,* 285.
106. Annis, D. A.; Nickbarg, E.; Yang, X.; Ziebell, M. R.; Whitehurst, C. E. *Curr. Opin. Chem. Biol.* **2007,** *11,* 518.
107. Annis, D. A.; Nazef, N.; Chuang, C.-C.; Scott, M. P.; Nash, H. M. *J. Am. Chem. Soc.* **2004,** *126,* 15495.
108. Annis, D. A.; Shipps, G. W., Jr.; Deng, Y.; Popovici-Mueller, J.; Siddiqui, M. A.; Curran, P. J.; Gowen, M.; Windsor, W. T. *Anal. Chem. (Washington, DC)* **2007,** *79,* 4538.
109. Mullard, A. *Nature (London)* **2016,** *530,* 367.
110. Thalji, R. K.; McAtee, J. J.; Belyanskaya, S.; Brandt, M.; Brown, G. D.; Costell, M. H.; Ding, Y.; Dodson, J. W.; Eisennagel, S. H.; Fries, R. E.; Gross, J. W.; Harpel, M. R.; Holt, D. A.; Israel, D. I.; Jolivette, L. J.; Krosky, D.; Li, H.; Lu, Q.; Mandichak, T.; Roethke, T.; Schnackenberg, C. G.; Schwartz, B.; Shewchuk, L. M.; Xie, W.; Behm, D. J.; Douglas, S. A.; Shaw, A. L.; Marino, J. P., Jr. *Bioorg. Med. Chem. Lett.* **2013,** *23,* 3584.
111. Ding, Y.; Belyanskaya, S. L.; DeLorey, J. L.; Israel, D.; Messer, J. A.; Morgan, B. A.; Skinner, S.; Clark, M. A.; Cuozzo, J. W. *Am. Chem. Soc.* **2015,** MEDI.
112. Lau, W. F.; Withka, J. M.; Hepworth, D.; Magee, T. V.; Du, Y. J.; Bakken, G. A.; Miller, M. D.; Hendsch, Z. S.; Thanabal, V.; Kolodziej, S. A.; Xing, L.; Hu, Q.; Narasimhan, L. S.; Love, R.; Charlton, M. E.; Hughes, S.; Hoorn, W. P. V.; Mills, J. E. *J. Comput. Aided Mol. Des.* **2011,** *25,* 621.
113. Boyd, S. M.; Kloe, G. E. D. *Drug Discov. Today Technol.* **2010,** *7,* e173.
114. Mergott, D. J.; May, P. C.; Dean, R. A.; Lowe, S. L.; Martenyi, F.; Sheehan, S. M.; Boggs, L. N.; Mathes, B. M.; Watson, B. M.; Stout, S. L.; Timm, D. E.; Smith LaBell, E.; Gonzales, C. R.; Nakano, M.; Jhee, S. S.; Yen, M.; Ereshefsky, L.; Lindstrom, T. D.; Calligaro, D. D.; Cocke, P. J.; Hall, D. G.; Friedrich, S.; Citron, M.; Audia, J. E. *Am. Chem. Soc.* **2011,** CERM.
115. Tsai, J.; Lee, J. T.; Wang, W.; Zhang, J.; Cho, H.; Mamo, S.; Bremer, R.; Gillette, S.; Kong, J.; Haass, N. K.; Sproesser, K.; Li, L.; Smalley, K. S. M.; Fong, D.; Zhu, Y.-L.; Marimuthu, A.; Nguyen, H.; Lam, B.; Liu, J.; Cheung, I.; Rice, J.; Suzuki, Y.; Luu, C.; Settachatgul, C.; Shellooe, R.; Cantwell, J.; Kim, S.-H.; Schlessinger, J.; Zhang, K. Y. J.; West, B. L.; Powell, B.; Habets, G.; Zhang, C.; Ibrahim, P. N.; Hirth, P.; Artis, D. R.; Herlyn, M.; Bollag, G. *Proc. Natl. Acad. Sci. U. S. A.* **2008,** *105,* 3041.
116. Bollag, G.; Tsai, J.; Zhang, J.; Zhang, C.; Ibrahim, P.; Nolop, K.; Hirth, P. *Nat. Rev. Drug Discov.* **2012,** *11,* 873.
117. Ibrahim, P. N.; Zhang, J.; Zhang, C.; Bollag, G. *Annu. Rep. Med. Chem.* **2013,** *48,* 435.
118. Baell, J.; Walters, M. A. *Nature (London)* **2014,** *513,* 481.
119. Song, K.; Wang, J.; Boehm, M.; Mathiowetz, A.; Klug-McLeod, J.; Bhattacharya, S.; Carpino, P. *Am. Chem. Soc.* **2011,** COMP.
120. Coan, K. E. D.; Maltby, D. A.; Burlingame, A. L.; Shoichet, B. K. *J. Med. Chem.* **2009,** *52,* 2067.
121. Fliri, A. F.; Loging, W. T.; Thadeio, P. F.; Volkmann, R. A. *J. Med. Chem.* **2005,** *48,* 6918.
122. Fliri, A. F.; Loging, W. T.; Thadeio, P. F.; Volkmann, R. A. *Proc. Natl. Acad. Sci. U. S. A.* **2005,** *102,* 261.
123. Fliri, A. F.; Loging, W. T.; Thadeio, P. F.; Volkmann, R. A. *Nat. Chem. Biol.* **2005,** *1,* 389.
124. Petrone, P. M.; Simms, B.; Nigsch, F.; Lounkine, E.; Kutchukian, P.; Cornett, A.; Deng, Z.; Davies, J. W.; Jenkins, J. L.; Glick, M. *ACS Chem. Biol.* **2012,** *7,* 1399.
125. Berg, E. L.; Yang, J.; Melrose, J.; Nguyen, D.; Privat, S.; Rosler, E.; Kunkel, E. J.; Ekins, S. *J. Pharmacol. Toxicol. Methods* **2010,** *61,* 3.
126. Gustafsdottir, S. M.; Ljosa, V.; Sokolnicki, K. L.; Wilson, J. A.; Walpita, D.; Kemp, M. M.; Seiler, K. P.; Carrel, H. A.; Golub, T. R.; Schreiber, S. L.; Clemons, P. A.; Carpenter, A. E.; Shamji, A. F. *PLoS One* **2013,** *8,* e80999/1.
127. Seidel, S. A. I.; Dijkman, P. M.; Lea, W. A.; van den Bogaart, G.; Jerabek-Willemsen, M.; Lazic, A.; Joseph, J. S.; Srinivasan, P.; Baaske, P.; Simeonov, A.; Katritch, I.; Melo, F. A.; Ladbury, J. E.; Schreiber, G.; Watts, A.; Braun, D.; Duhr, S. *Methods (Amsterdam, Neth.)* **2013,** *59,* 301.
128. Duhr, S.; Braun, D. *Proc. Natl. Acad. Sci. U. S. A.* **2006,** *103,* 19678.
129. Freire, E. *Drug Discov. Today Technol.* **2004,** *1,* 295.
130. Freire, E. *Drug Discov. Today* **2008,** *13,* 869.
131. Martinez, M. D.; Jafari, R.; Ignatushchenko, M.; Seki, T.; Larsson, E. A.; Dan, C.; Sreekumar, L.; Cao, Y.; Nordlund, P. *Science* **2013,** *341,* 84.
132. Martinez Molina, D.; Nordlund, P. *Annu. Rev. Pharmacol. Toxicol.* **2016,** *56,* 141.
133. Treiber, D. K.; Menichelli, E.; Discoverx Corporation, USA, **2016**, 61pp.
134. Fjellstrom, O.; Johansson, A.; Larsson, N.; Lundqvist, S.; Brengdahl, J.; Geschwindner, S.; Yasuda, S.-I.; Tsuchida, T.; Oguma, T.; Sasaki, K.; Marley, A.; Priest, C.; Wennberg-Huldt, C.; Benthem, L.; Hovdal, D.; Fukuda, H.; Yoneyama, Y.; Isaacs, R. J.; Brown, D.; Turnbull, A. *PLoS One* **2015,** *10,* e0145849.
135. Moree, B.; Yin, G.; Lazaro, D. F.; Munari, F.; Strohaker, T.; Giller, K.; Becker, S.; Outeiro, T. F.; Zweckstetter, M.; Salafsky, J. *J. Biol. Chem.* **2015,** *290,* 27582.
136. Peterson, L. J.; Mortillaro, C. A.; Warner, B. P.; Zahler, N. H.; Bharti, P.; Hsieh, C.-T.; Solomon, E. A.; US Patent Application US20120093286 A1, Caldera Pharmaceuticals, Inc., USA; Xrpro Sciences, Inc.
137. Pellecchia, M.; Bertini, I.; Cowburn, D.; Dalvit, C.; Giralt, E.; Jahnke, W.; James, T. L.; Homans, S. W.; Kessler, H.; Luchinat, C.; Meyer, B.; Oschkinat, H.; Peng, J.; Schwalbe, H.; Siegal, G. *Nat. Rev. Drug Discov.* **2008,** *7,* 738.
138. Dalvit, C.; Fogliatto, G.; Stewart, A.; Veronesi, M.; Stockman, B. *J. Biomol. NMR* **2001,** *21,* 349.
139. Vanwetswinkel, S.; Heetebrij, R. J.; van Duynhoven, J.; Hollander, J. G.; Filippov, D. V.; Hajduk, P. J.; Siegal, G. *Chem. Biol.* **2005,** *12,* 207.
140. Stockman, B. J.; Kothe, M.; Kohls, D.; Weibley, L.; Connolly, B. J.; Sheils, A. L.; Cao, Q.; Cheng, A. C.; Yang, L.; Kamath, A. V.; Ding, Y.-H.; Charlton, M. E. *Chem. Biol. Drug Des.* **2009,** *73,* 179.
141. Vazquez, J.; Tautz, L.; Ryan, J. J.; Vuori, K.; Mustelin, T.; Pellecchia, M. *J. Med. Chem.* **2007,** *50,* 2137.
142. Jahnke, W.; Floersheim, P.; Ostermeier, C.; Zhang, X.; Hemmig, R.; Hurth, K.; Uzunov, D. P. *Angew. Chem. Int. Ed.* **2002,** *41,* 3420.
143. Dalvit, C.; Ardini, E.; Flocco, M.; Fogliatto, G. P.; Mongelli, N.; Veronesi, M. *J. Am. Chem. Soc.* **2003,** *125,* 14620.
144. Stockman, B. J. *J. Am. Chem. Soc.* **2008,** *130,* 5870.
145. Granier, S.; Kobilka, B. *Nat. Chem. Biol.* **2012,** *8,* 670.
146. Lagerstrom, M. C.; Schioth, H. B. *Nat. Rev. Drug Discov.* **2008,** *7,* 339.
147. Bouvier, M. *Nat. Struct. Mol. Biol.* **2013,** *20,* 539.

148. Rasmussen, S. G. F.; DeVree, B. T.; Zou, Y.-Z.; Kruse, A. C.; Chung, K.-Y.; Kobilka, T.-S.; Thian, F.-S.; Chae, P.-S.; Pardon, E.; Calinski, D.; Mathiesen, J. M.; Shah, S. T. A.; Lyons, J. A.; Caffrey, M.; Gellman, S. H.; Steyaert, J.; Skiniotis, G.; Weis, W. I.; Sunahara, R. K.; Kobilka, B. K. *Nature (London)* **2011,** *477,* 549.
149. Kang, Y.; Zhou, X. E.; Gao, X.; He, Y.; Liu, W.; Ishchenko, A.; Barty, A.; White, T. A.; Yefanov, O.; Han, G. W.; Xu, Q.; de Waal, P. W.; Ke, J.; Tan, M. H. E.; Zhang, C.; Moeller, A.; West, G. M.; Pascal, B. D.; Van Eps, N.; Caro, L. N.; Vishnivetskiy, S. A.; Lee, R. J.; Suino-Powell, K. M.; Gu, X.; Pal, K.; Ma, J.; Zhi, X.; Boutet, S.; Williams, G. J.; Messerschmidt, M.; Gati, C.; Zatsepin, N. A.; Wang, D.; James, D.; Basu, S.; Roy-Chowdhury, S.; Conrad, C. E.; Coe, J.; Liu, H.; Lisova, S.; Kupitz, C.; Grotjohann, I.; Fromme, R.; Jiang, Y.; Tan, M.; Yang, H.; Li, J.; Wang, M.; Zheng, Z.; Li, D.; Howe, N.; Zhao, Y.; Standfuss, J.; Diederichs, K.; Dong, Y.; Potter, C. S.; Carragher, B.; Caffrey, M.; Jiang, H.; Chapman, H. N.; Spence, J. C. H.; Fromme, P.; Weierstall, U.; Ernst, O. P.; Katritch, V.; Gurevich, V. V.; Griffin, P. R.; Hubbell, W. L.; Stevens, R. C.; Cherezov, V.; Melcher, K.; Xu, H. E. In *Nature (London, U. K.)* **2015,** *523*; p 561.
150. Audet, M.; Bouvier, M. *Cell (Cambridge, MA)* **2012,** *151,* 14.
151. Bagal, S. K.; Brown, A. D.; Cox, P. J.; Omoto, K.; Owen, R. M.; Pryde, D. C.; Sidders, B.; Skerratt, S. E.; Stevens, E. B.; Storer, R. I.; Swain, N. A. *J. Med. Chem.* **2013,** *56,* 593.
152. Alam, A.; Jiang, Y. *J. Gen. Physiol.* **2011,** *137,* 397.
153. daCosta, C. J. B.; Baenziger, J. E. *Structure* **2013,** *21,* 1271.
154. Binshtein, E.; Ohi, M. D. *Biochemistry* **2015,** *54,* 3133.
155. Cheng, Y.; Grigorieff, N.; Penczek, P. A.; Walz, T. *Cell (Cambridge, MA)* **2015,** *161,* 438.
156. Lu, P.; Bai, X.-C.; Ma, D.; Xie, T.; Yan, C.; Sun, L.; Yang, G.; Zhao, Y.; Zhou, R.; Scheres, S. H. W.; Shi, Y. *Nature (London)* **2014,** *512,* 166.
157. Bai, X.-C.; Yan, C.; Yang, G.; Lu, P.; Ma, D.; Sun, L.; Zhou, R.; Scheres, S. H. W.; Shi, Y. *Nature (London)* **2015,** *525,* 212.
158. Cao, E.; Liao, M.; Cheng, Y.; Julius, D. *Nature (London)* **2013,** *504,* 113.
159. Liao, M.; Cao, E.; Julius, D.; Cheng, Y. *Nature (London)* **2013,** *504,* 107.
160. Paulsen, C. E.; Armache, J.-P.; Gao, Y.; Cheng, Y.; Julius, D. *Nature (London)* **2015,** *520,* 511.
161. Ondetti, M. A.; Rubin, B.; Cushman, D. W. *Science* **1977,** *196,* 441.
162. Cushman, D. W.; Cheung, H. S.; Sabo, E. F.; Ondetti, M. A. *Prog. Cardiovasc. Dis.* **1978,** *21,* 176.
163. Cushman, D. W.; Ondetti, M. A. *Nat. Med.* **1999,** *5,* 1110.
164. Noe, M. C.; Kurumbail, R. G. *Annu. Rev. Med. Chem.* **2015,** *50,* 299.
165. Wang, L.; Wu, Y.; Deng, Y.; Kim, B.; Pierce, L.; Krilov, G.; Lupyan, D.; Robinson, S.; Dahlgren, M. K.; Greenwood, J.; Romero, D. L.; Masse, C.; Knight, J. L.; Steinbrecher, T.; Beuming, T.; Damm, W.; Harder, E.; Sherman, W.; Brewer, M.; Wester, R.; Murcko, M.; Frye, L.; Farid, R.; Lin, T.; Mobley, D. L.; Jorgensen, W. L.; Berne, B. J.; Friesner, R. A.; Abel, R. *J. Am. Chem. Soc.* **2015,** *137,* 2695.
166. Abel, R.; Young, T.; Farid, R.; Berne, B. J.; Friesner, R. A. *J. Am. Chem. Soc.* **2008,** *130,* 2817.
167. Young, T.; Abel, R.; Kim, B.; Berne, B. J.; Friesner, R. A. *Proc. Natl. Acad. Sci. U. S. A.* **2007,** *104,* 808.
168. Guimaraes, C. R. W.; Mathiowetz, A. M. *J. Chem. Inf. Model.* **2010,** *50,* 547.
169. Kohlmann, A.; Zhu, X.; Dalgarno, D. *ACS Med. Chem. Lett.* **2012,** *3,* 94.
170. Chrencik, J. E.; Patny, A.; Leung, I. K.; Korniski, B.; Emmons, T. L.; Hall, T.; Weinberg, R. A.; Gormley, J. A.; Williams, J. M.; Day, J. E.; Hirsch, J. L.; Kiefer, J. R.; Leone, J. W.; Fischer, H. D.; Sommers, C. D.; Huang, H.-C.; Jacobsen, E. J.; Tenbrink, R. E.; Tomasselli, A. G.; Benson, T. E. *J. Mol. Biol.* **2010,** *400,* 413.
171. Brodney, M. A.; Barreiro, G.; Ogilvie, K.; Hajos-Korcsok, E.; Murray, J.; Vajdos, F.; Ambroise, C.; Christoffersen, C.; Fisher, K.; Lanyon, L.; Liu, J.; Nolan, C. E.; Withka, J. M.; Borzilleri, K. A.; Efremov, I.; Oborski, C. E.; Varghese, A.; O'Neill, B. T. *J. Med. Chem.* **2012,** *55,* 9224.
172. Goswami, R.; Mukherjee, S.; Wohlfahrt, G.; Ghadiyaram, C.; Nagaraj, J.; Chandra, B. R.; Sistla, R. K.; Satyam, L. K.; Samiulla, D. S.; Moilanen, A.; Subramanya, H. S.; Ramachandra, M. *ACS Med. Chem. Lett.* **2013,** *4,* 1152.
173. Bortolato, A.; Tehan, B. G.; Bodnarchuk, M. S.; Essex, J. W.; Mason, J. S. *J. Chem. Inf. Model.* **2013,** *53,* 1700.
174. Ichihara, O.; Shimada, Y.; Yoshidome, D. *ChemMedChem* **2014,** *9,* 2708.
175. Singh, J.; Petter, R. C.; Baillie, T. A.; Whitty, A. *Nat. Rev. Drug Discov.* **2011,** *10,* 307.
176. Noe, M. C.; Gilbert, A. M. *Annu. Rep. Med. Chem.* **2012,** *47,* 413.
177. Lanning, B. R.; Whitby, L. R.; Dix, M. M.; Douhan, J.; Gilbert, A. M.; Hett, E. C.; Johnson, T. O.; Joslyn, C.; Kath, J. C.; Niessen, S.; Roberts, L. R.; Schnute, M. E.; Wang, C.; Hulce, J. J.; Wei, B.; Whiteley, L. O.; Hayward, M. M.; Cravatt, B. F. *Nat. Chem. Biol.* **2014,** *10,* 760.
178. Long, J. Z.; Nomura, D. K.; Cravatt, B. F. *Chem. Biol.* **2009,** *16,* 744.
179. Evans, D. C.; Watt, A. P.; Nicoll-Griffith, D. A.; Baillie, T. A. *Chem. Res. Toxicol.* **2004,** *17,* 3.
180. Uetrecht, J. P. *Chem. Res. Toxicol.* **1999,** *12,* 387.
181. Obach, R. S.; Kalgutkar, A. S.; Soglia, J. R.; Zhao, S. X. *Chem. Res. Toxicol.* **2008,** *21,* 1814.
182. Flanagan, M. E.; Abramite, J. A.; Anderson, D. P.; Aulabaugh, A.; Dahal, U. P.; Gilbert, A. M.; Li, C.; Montgomery, J.; Oppenheimer, S. R.; Ryder, T.; Schuff, B. P.; Uccello, D. P.; Walker, G. S.; Wu, Y.; Brown, M. F.; Chen, J. M.; Hayward, M. M.; Noe, M. C.; Obach, R. S.; Philippe, L.; Shanmugasundaram, V.; Shapiro, M. J.; Starr, J.; Stroh, J.; Che, Y. *J. Med. Chem.* **2014,** *57,* 10072.
183. Schwobel, J. A.; Koleva, Y. K.; Enoch, S. J.; Bajot, F.; Hewitt, M.; Madden, J. C.; Roberts, D. W.; Schultz, T. W.; Cronin, M. T. *Chem. Rev.* **2011,** *111,* 2562.
184. Friedman, M.; Cavins, J. F.; Wall, J. S. *J. Am. Chem. Soc.* **1965,** *87,* 3672.
185. Toda, N.; Asano, S.; Barbas, C. F., III. *Angew. Chem. Int. Ed.* **2013,** *52,* 12592.
186. Lipinski, C. A.; Lombardo, F.; Dominy, B. W.; Feeney, P. *J. Adv. Drug Deliv. Rev.* **1997,** *23,* 3.
187. Alex, A.; Millan, D. S.; Perez, M.; Wakenhut, F.; Whitlock, G. A. *Med. Chem. Commun.* **2011,** *2,* 669.
188. Rezai, T.; Yu, B.; Millhauser, G. L.; Jacobson, M. P.; Lokey, R. S. *J. Am. Chem. Soc.* **2006,** *128,* 2510.
189. White, T. R.; Renzelman, C. M.; Rand, A. C.; Rezai, T.; McEwen, C. M.; Gelev, V. M.; Turner, R. A.; Linington, R. G.; Leung, S. S. F.; Kalgutkar, A. S.; Bauman, J. N.; Zhang, Y.; Liras, S.; Price, D. A.; Mathiowetz, A. M.; Jacobson, M. P.; Lokey, R. S. *Nat. Chem. Biol.* **2011,** *7,* 810.
190. Hewitt, W. M.; Leung, S. S. F.; Pye, C. R.; Ponkey, A. R.; Bednarek, M.; Jacobson, M. P.; Lokey, R. S. *J. Am. Chem. Soc.* **2015,** *137,* 715.
191. Ahlbach, C. L.; Lexa, K. W.; Bockus, A. T.; Chen, V.; Crews, P.; Jacobson, M. P.; Lokey, R. S. *Future Med. Chem.* **2015,** *7,* 2121.
192. Bockus, A. T.; Lexa, K. W.; Pye, C. R.; Kalgutkar, A. S.; Gardner, J. W.; Hund, K. C. R.; Hewitt, W. M.; Schwochert, J. A.; Glassey, E.; Price, D. A.; Mathiowetz, A. M.; Liras, S.; Jacobson, M. P.; Lokey, R. S. *J. Med. Chem.* **2015,** *58,* 4581.
193. Rand, A. C.; Leung, S. S. F.; Eng, H.; Rotter, C. J.; Sharma, R.; Kalgutkar, A. S.; Zhang, Y.; Varma, M. V.; Farley, K. A.; Khunte, B.; Limberakis, C.; Price, D. A.; Liras, S.; Mathiowetz, A. M.; Jacobson, M. P.; Lokey, R. S. *Med. Chem. Commun.* **2012,** *3,* 1282.
194. Leung, S. S. F.; Mijalkovic, J.; Borrelli, K.; Jacobson, M. P. *J. Chem. Inf. Model.* **2012,** *52,* 1621.
195. Shalaeva, M.; Caron, G.; Abramov, Y. A.; O'Connell, T. N.; Plummer, M. S.; Yalamanchi, G.; Farley, K. A.; Goetz, G. H.; Philippe, L.; Shapiro, M. J. *J. Med. Chem.* **2013,** *56,* 4870.
196. Goetz, G. H.; Farrell, W.; Shalaeva, M.; Sciabola, S.; Anderson, D.; Yan, J.; Philippe, L.; Shapiro, M. J. *J. Med. Chem.* **2014,** *57,* 2920.
197. Goetz, G. H.; Philippe, L.; Shapiro, M. J. *ACS Med. Chem. Lett.* **2014,** *5,* 1167.
198. Morrissey, K. M.; Stocker, S. L.; Wittwer, M. B.; Xu, L.; Giacomini, K. M. *Annu. Rev. Pharmacol. Toxicol.* **2013,** *53,* 503.
199. Kim, R. B. *Mol. Pharm.* **2006,** *3,* 26.
200. Dantzig, A. H.; Hillgren, K. M.; de Alwis, D. P. *Annu. Rep. Med. Chem.* **2004,** *39,* 279.
201. Cheng, Y.; El-Kattan, A.; Zhang, Y.; Ray, A. S.; Lai, Y. *Chem. Res. Toxicol.* **2016**. *29,* 545.

202. DeGorter, M. K.; Xia, C. Q.; Yang, J. J.; Kim, R. B. *Annu. Rev. Pharmacol. Toxicol.* **2012,** *52,* 249.
203. Bagal, S.; Bungay, P. *Drug Discov. Today Technol.* **2014,** *12*, e79.
204. Tu, M.; Mathiowetz, A. M.; Pfefferkorn, J. A.; Cameron, K. O.; Dow, R. L.; Litchfield, J.; Di, L.; Feng, B.; Liras, S. *Curr. Top. Med. Chem. (Sharjah, UAE)* **2013,** *13,* 857.
205. Wager, T. T.; Chandrasekaran, R. Y.; Hou, X.; Troutman, M. D.; Verhoest, P. R.; Villalobos, A.; Will, Y. *ACS Chem. Neurosci.* **2010,** *1,* 420.
206. Wager, T. T.; Hou, X.; Verhoest, P. R.; Villalobos, A. *ACS Chem. Neurosci.* **2010,** *1,* 435.
207. Wager, T. T.; Villalobos, A.; Verhoest, P. R.; Hou, X.; Shaffer, C. L. *Expert Opin. Drug Discovery* **2011,** *6,* 371.
208. Wager, T. T.; Hou, X.; Verhoest, P. R.; Villalobos, A. *ACS Chem. Neurosci.* **2016,** *7*, 767.
209. Baillie, T. A.; Pearson, P. G.; Humana Press, p. 481, 2000.
210. Kola, I.; Landis, J. *Nat. Rev. Drug Discov.* **2004,** *3,* 711.
211. Smith, D. A.; John Wiley & Sons, Inc., p. 231, 2010.
212. Smith, D. A.; Schmid, E. F. *Curr. Opin. Drug Discov. Dev.* **2006,** *9,* 38.
213. Kramer, J. A.; Sagartz, J. E.; Morris, D. L. *Nat. Rev. Drug Discov.* **2007,** *6,* 636.
214. Bowes, J.; Brown, A. J.; Hamon, J.; Jarolimek, W.; Sridhar, A.; Waldron, G.; Whitebread, S. *Nat. Rev. Drug Discov.* **2012,** *11,* 909.
215. Keefer, C. E.; Kauffman, G. W.; Gupta, R. R. *J. Chem. Inf. Model.* **2013,** *53,* 368.
216. Keefer, C. E.; Chang, G.; Kauffman, G. W. *Bioorg. Med. Chem.* **2011,** *19,* 3739.
217. Honorio, K. M.; Moda, T. L.; Andricopulo, A. D. *Med. Chem.* **2013,** *9,* 163.
218. Hop, C. E. C. A.; Cole, M. J.; Davidson, R. E.; Duignan, D. B.; Federico, J.; Janiszewski, J. S.; Jenkins, K.; Krueger, S.; Lebowitz, R.; Liston, T. E.; Mitchell, W.; Snyder, M.; Steyn, S. J.; Soglia, J. R.; Taylor, C.; Troutman, M. D.; Umland, J.; West, M.; Whalen, K. M.; Zelesky, V.; Zhao, S. X. *Curr. Drug Metab.* **2008,** *9,* 847.
219. Di, L.; Kerns, E. H.; John Wiley & Sons, Inc., p. 101, 2012.
220. Whalen, K.; Gobey, J.; Janiszewski, J. *Rapid Commun. Mass Spectrom.* **2006,** *20,* 1497.
221. Janiszewski, J. S.; Rogers, K. J.; Whalen, K. M.; Cole, M. J.; Liston, T. E.; Duchoslav, E.; Fouda, H. G. *Anal. Chem.* **2001,** *73,* 1495.
222. Whalen, K. M.; Rogers, K. J.; Cole, M. J.; Janiszewski, J. S. *Rapid Commun. Mass Spectrom.* **2000,** *14,* 2074.
223. Amidon, G. L.; Lennernaes, H.; Shah, V. P.; Crison, J. R. *Pharm. Res.* **1995,** *12,* 413.
224. Gleeson, M. P.; Hersey, A.; Montanari, D.; Overington, J. *Nat. Rev. Drug Discov.* **2011,** *10,* 197.
225. van de Waterbeemd, H.; Gifford, E. *Nat. Rev. Drug Discov.* **2003,** *2,* 192.
226. Lombardo, F.; Shalaeva, M. Y.; Tupper, K. A.; Gao, F. *J. Med. Chem.* **2001,** *44,* 2490.
227. Avdeef, A. *Curr. Top. Med. Chem. (Hilversum, Neth.)* **2001,** *1,* 277.
228. Bevan, C. D.; Lloyd, R. S. *Anal. Chem.* **2000,** *72,* 1781.
229. Kansy, M.; Senner, F.; Gubernator, K. *J. Med. Chem.* **1998,** *41,* 1007.
230. Avdeef, A. *Expert Opin. Drug Metab. Toxicol.* **2005,** *1,* 325.
231. Cho, M. J.; Thompson, D. P.; Cramer, C. T.; Vidmar, T. J.; Scieszka, J. F. *Pharm. Res.* **1989,** *6,* 71.
232. Di, L.; Whitney-Pickett, C.; Umland, J. P.; Zhang, H.; Zhang, X.; Gebhard, D. F.; Lai, Y.; Federico, J. J.; Davidson, R. E.; Smith, R.; Reyner, E. L.; Lee, C.; Feng, B.; Rotter, C.; Varma, M. V.; Kempshall, S.; Fenner, K.; El-kattan, A. F.; Liston, T. E.; Troutman, M. D. *J. Pharm. Sci.* **2011,** *100,* 4974.
233. Artursson, P.; Karlsson, J. *Biochem. Biophys. Res. Commun.* **1991,** *175,* 880.
234. Augustijns, P. F.; Bradshaw, T. P.; Gan, L. S.; Hendren, R. W.; Thakker, D. R. *Biochem. Biophys. Res. Commun.* **1993,** *197,* 360.
235. Troutman, M. D.; Thakker, D. R. *Pharm. Res.* **2003,** *20,* 1210.
236. Banker, M. J.; Clark, T. H.; Williams, J. A. *J. Pharm. Sci.* **2003,** *92,* 967.
237. van, L. S.; Morrison, D.; Sysmans, L.; Nelis, P.; Mortishire-Smith, R. *J. Lab. Autom.* **2011,** *16,* 56.
238. Pacifici, G. M.; Viani, A. *Clin. Pharmacokinet.* **1992,** *23,* 449.
239. Obach, R. S.; Baxter, J. G.; Liston, T. E.; Silber, B. M.; Jones, B. C.; Macintyre, F.; Rance, D. J.; Wastall, P. *J. Pharmacol. Exp. Ther.* **1997,** *283,* 46.
240. Hosea, N. A.; Collard, W. T.; Cole, S.; Maurer, T. S.; Fang, R. X.; Jones, H.; Kakar, S. M.; Nakai, Y.; Smith, B. J.; Webster, R.; Beaumont, K. *J. Clin. Pharmacol.* **2009,** *49,* 513.
241. Bi, Y.-A.; Kazolias, D.; Duignan, D. B. *Drug Metab. Dispos.* **2006,** *34,* 1658.
242. Hoffmaster, K. A.; Turncliff, R. Z.; LeCluyse, E. L.; Kim, R. B.; Meier, P. J.; Brouwer, K. L. R. *Pharm. Res.* **2004,** *21,* 1294.
243. Kusuhara, H.; Sugiyama, Y. *Drug Metab. Pharmacokinet.* **2009,** *24,* 37.
244. Feng, B.; Hurst, S.; Lu, Y.; Varma, M. V.; Rotter, C. J.; El-Kattan, A.; Lockwood, P.; Corrigan, B. *Mol. Pharm.* **2013,** *10,* 4207.
245. Obach, R. S.; Walsky, R. L.; Venkatakrishnan, K.; Gaman, E. A.; Houston, J. B.; Tremaine, L. M. *J. Pharmacol. Exp. Ther.* **2006,** *316,* 336.
246. Fahmi, O. A.; Ripp, S. L. *Expert Opin. Drug Metab. Toxicol.* **2010,** *6,* 1399.
247. Fenner, K. S.; Troutman, M. D.; Kempshall, S.; Cook, J. A.; Ware, J. A.; Smith, D. A.; Lee, C. A. *Clin. Pharmacol. Ther. (New York, NY)* **2009,** *85,* 173.
248. Cook, J. A.; Feng, B.; Fenner, K. S.; Kempshall, S.; Liu, R.; Rotter, C.; Smith, D. A.; Troutman, M. D.; Ullah, M.; Lee, C. A. *Mol. Pharm.* **2010,** *7,* 398.
249. Thomas, C. E.; Will, Y. *Expert Opin. Drug Discovery* **2012,** *7,* 109.
250. Bryce, S. M.; Avlasevich, S. L.; Bemis, J. C.; Phonethepswath, S.; Dertinger, S. D. *Mutat. Res. Genet. Toxicol. Environ. Mutagen.* **2010,** *703,* 191.
251. Mondal, M. S.; Gabriels, J.; McGinnis, C.; Magnifico, M.; Marsilje, T. H.; Urban, L.; Collis, A.; Bojanic, D.; Biller, S. A.; Frieauff, W.; Martus, H.-J.; Suter, W.; Bentley, P. *Toxicol. Sci.* **2010,** *118,* 71.
252. Greene, N.; Aleo, M. D.; Louise-May, S.; Price, D. A.; Will, Y. *Bioorg. Med. Chem. Lett.* **2010,** *20,* 5308.
253. Benbow, J. W.; Aubrecht, J.; Banker, M. J.; Nettleton, D.; Aleo, M. D. *Toxicol. Lett.* **2010,** *197,* 175.
254. Hynes, J.; Nadanaciva, S.; Swiss, R.; Carey, C.; Kirwan, S.; Will, Y. *Toxicol. In Vitro* **2013,** *27,* 560.
255. O'Brien, P. J.; Irwin, W.; Diaz, D.; Howard-Cofield, E.; Krejsa, C. M.; Slaughter, M. R.; Gao, B.; Kaludercic, N.; Angeline, A.; Bernardi, P.; Brain, P.; Hougham, C. *Arch. Toxicol.* **2006,** *80,* 580.
256. Will, Y.; Hynes, J.; Ogurtsov, V. I.; Papkovsky, D. B. *Nat. Protoc.* **2006,** *1,* 2563.
257. Papkovsky, D. B.; Hynes, J.; Will, Y. *Expert Opin. Drug Metab. Toxicol.* **2006,** *2,* 313.
258. Hynes, J.; Marroquin, L. D.; Ogurtsov, V. I.; Christiansen, K. N.; Stevens, G. J.; Papkovsky, D. B.; Will, Y. *Toxicol. Sci.* **2006,** *92,* 186.
259. Chadwick, C. C.; Ezrin, A. M.; O'Connor, B.; Volberg, W. A.; Smith, D. I.; Wedge, K. J.; Hill, R. J.; Briggs, M.; Pagani, E. D.; et al. *Circ. Res.* **1993,** *72,* 707.
260. Chiu, P. J. S.; Marcoe, K. F.; Bounds, S. E.; Lin, C.-H.; Feng, J.-J.; Lin, A.; Cheng, F.-C.; Crumb, W. J.; Mitchell, R. *J. Pharmacol. Sci. (Tokyo, Jpn.)* **2004,** *95,* 311.

2.02 Hit and Lead Generation Strategies

P Ettmayer, R Schnitzer, and A Bergner, Boehringer-Ingelheim RCV GmbH Co KG, Vienna, Austria
H Nar, Boehringer Ingelheim Pharma GmbH & Co. KG, Biberach an der Riß, Germany

© 2017 Elsevier Ltd. All rights reserved.

2.02.1	**Introduction**	33
2.02.2	**The Major Approaches for Hit and Lead Discovery**	33
2.02.2.1	Analog-Based Drug Discovery	33
2.02.2.2	"De-novo" Structure-Based Design	34
2.02.2.3	Screening	36
2.02.2.3.1	Screening and its impact in drug discovery	36
2.02.2.3.2	Chemical space considerations	37
2.02.2.3.3	Virtual screening	40
2.02.2.3.4	Assay technology advances for functional screens	43
2.02.2.3.5	Fragment-based drug discovery	44
2.02.2.3.6	Phenotypic screening	46
2.02.2.4	How to Best Identify Valid Hits?	50
2.02.3	**Hit-to-Lead Process**	51
2.02.3.1	Chemical Probes for Novel Therapeutic Concepts	52
2.02.4	**Origin of First-in-Class Drugs: Past and Future Outlook**	53
References		59
Relevant Websites		63

2.02.1 Introduction

How does one best identify a pharmacologically active compound? This important milestone in every low molecular weight (MW) drug discovery endeavor can be a starting point for further optimization (hit/lead) or already a drug from past preclinical and clinical development. The need for efficient hit and lead discovery has not changed over the past century—it is only the approach that has changed, and the technologies involved have progressed significantly. Analog- or chemocentric-based starting points still play an important role in medicinal chemistry, especially for systems-based target-agnostic approaches, but are of limited use for novel unprecedented targets. Hundreds of thousands of primary hits are now almost routinely identified using functional, biophysical, or even phenotypic high-throughput screens (HTS). Here the challenge has matured to the efficient identification of validated hits as starting points worth investing chemistry resources on. The characterization of confirmed and validated hits is discussed, as well as the paradigm shift from screening ever-increasingly large number of compounds to smaller targeted, and often well annotated, libraries. Among the approved new molecular entities, biologics (eg, antibodies) have an increasing role in addressing unmet medical needs. Since 2009, approximately 50% of the approved drugs are biologics. The recent advances in new biological entities (NBEs) and their success highlight the fact that the often proclaimed productivity and innovation drought in pharmaceutical industry are not due to a lack of new therapeutic concepts or druggable targets. Since biologics still have to face the cellular membrane barrier it is estimated that 10–20% of the target space will be addressable by antibodies, and the remaining 80–90% will be reserved for creative medicinal chemists and their teams.[1]

2.02.2 The Major Approaches for Hit and Lead Discovery

There are basically three major routes toward hit and lead discovery, the analog-based "chemocentric" approach, "de-novo" structure-based design, and the screening approach. The analog-based and screening approach can be pursued in a systems-based, target-agnostic, manner or in a target-based manner. Depending on the feasibility, technical availability, and priority setting these routes are often explored in parallel, thereby benefiting from the mutual synergies between the hit-finding approaches.

2.02.2.1 Analog-Based Drug Discovery

The analog-based approach considers lead structures that have well-defined medicinal properties, such as natural products, substrate or product derivatives, or other drugs. Camille Wermuth differentiates between three categories of analogs based on chemical and pharmacological similarity;[2] however, agreeing on what defines these similarities renders this classification difficult.[3] For simplicity, drugs, which did not require a screen or upfront structural research investment as a starting point for their drug discovery,

were labeled as originating from an analog-based approach. In 1988, Kurt Freter noted that all new drugs that had been approved by the Food and Drug Administration (FDA) in 1985 appeared to be the result of analog-based approaches.[4] The number of exploited lead structures was relatively small; in 1996, Walter Sneader categorized 244 drug prototypes, fewer than 140 of which would be considered drug-like as currently defined.[5] Until about 1980, information on drug targets at the molecular level was scarce, and drug discovery was mostly driven by data obtained from testing a limited number of compounds in animal models or microorganism cultures.[6–9] One of the most spectacular examples of such analog-based drug discovery approaches was the discovery of Warfarin. Warfarin, a coumarin derivative that acts as a vitamin K antagonist, was approved by the FDA in 1952 as a rat poison.[10] When a US soldier survived a suicide attempt with Warfarin unharmed, the idea for the pharmacological use of this approved rodenticide as an anticoagulant in humans was born.[10] In 1954, Warfarin's use as medication in humans was approved by the FDA, and other close coumarin analogs, such as acenocoumarol and phenprocoumon, followed in due course. The mode of action of these coumarins was only later discovered in 1978.[11]

Interestingly, even in the third millennium, more than half of the approved drugs (new chemical entities, NCEs) still originated from analog-based approaches (**Fig. 1**). There have been exciting and important discoveries highlighting the fact that analog-based approaches deliver first-in-class medicines (**Table 1**). Innovative analog-based drugs include, for example, the thalidomide analogs pomalidomide[12] and lenalidomide,[12] which were approved by the FDA for the treatment of mantel cell lymphoma in 2013, and apremilast,[13] which was approved in 2014 for the treatment of psoriatic arthritis. Thalidomide was first marketed in 1957 under the trade name Contergan. It was primarily prescribed as a sedative, but was also, unfortunately, prescribed to pregnant women to alleviate morning sickness. Due to its high teratogenicity, its use was discontinued in the early 1960s. Observations of the immunomodulatory and antiangiogenic effects of the withdrawn sedative thalidomide led to its investigation as a treatment for multiple myeloma. Phenotypic optimization of analogs in turn led to the discovery of lenalidomide. This drug was found to be 50,000-fold more potent in downregulating tumor necrosis factor production while having reduced sedative and neuropathic adverse effects compared to thalidomide.[12] The identification of a primary target of thalidomide teratogenicity lead to the identification of CRBN E3 ubiquitin ligase as the target of the "lidomides,"[14] and opened up a new approach for targeted therapies.[15] Another example for innovative analog-based drug discovery is afatinib, as a first-in-class irreversible dual specificity EGFR/HER2 inhibitor derived from anilinoquinazoline chemical series that was designed to covalently bind to Cys 797 of EGFR and Cys 805 of HER2.[16] Although the anilinoquinazoline chemical series was well known from gefitinib and erlotinib,[17] the addition of the functional Michael acceptor was an innovative step for increased efficacy in the treatment of EGFR-mutated lung cancers.[18]

2.02.2.2 "De-novo" Structure-Based Design

Advances in molecular biology provided access to many potential drug targets as pure or overexpressed proteins, and made them available for molecular or cellular assays as well as for structural biology.[7] These advances led to a paradigm shift in drug discovery from "phenotypic" to a target-based approach that relies on a profound understanding, on the molecular level, of the target under investigation. In the 1970s, structural biology started to have an ever-increasing role in drug discovery.[19] Detailed knowledge about protein–ligand interactions allowed a more rational design of new drugs, and X-ray structures of natural ligand–protein complexes offered new starting points for hit and lead identification. As the advances in technology are covered in another chapter in this article we concentrate on the key examples of marketed drugs that originated from "de-novo" structure-based drug design. Of course, structure-based design has a very important role beyond hit and lead selection in the lead optimization phase. Lead optimization

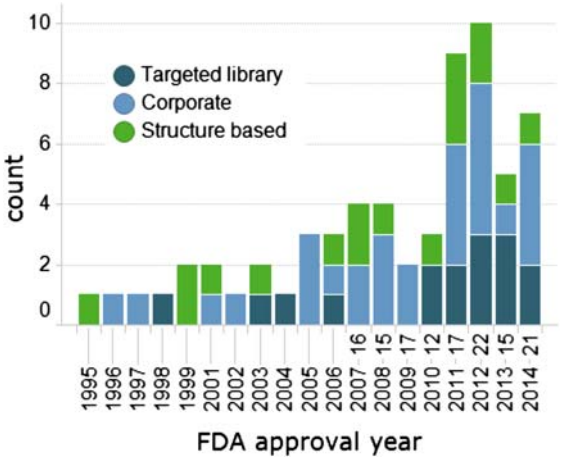

Fig. 1 Number of marketed drugs (*bars*) that emerged from screening (*blue*) or from structure-based design leads (*green*), summarized by their respective FDA approval date.[47] The number under the bars indicate the total number of novel NCEs approved between 2007 and 2014 including those originating from analog-based approaches.

Table 1 Representative examples for analog-based and "de-novo" structure-based design hit and lead discovery approaches

Drug	*Approach*	*Unmet medical need*	*Origin*
Warfarin[10] 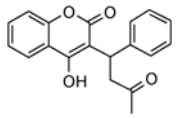	Analog	High: New use for pharmacological active compound	Warfarin used as rodenticide
Phenprocoumon[11] 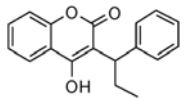	Analog	Low (me-too/me-better)	Warfarin
Pomalidomide[12] 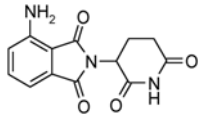	Analog	High: New use of old drug	Thalidomide[12] 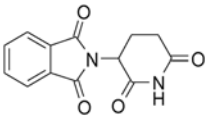
Afatinib[16,18] 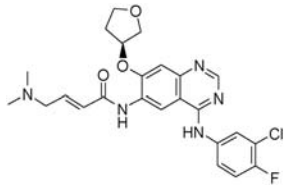	Analog	High: First-in-class irreversible dual specificity EGFR/HER2 inhibitor	Gefitinib[17]: First-in-class EGFR family inhibitor from screening 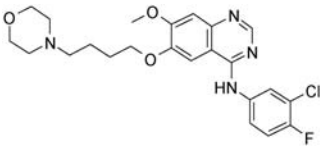
Erelotinib[17] 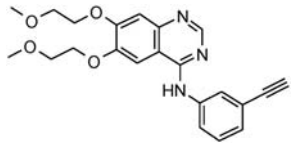	Analog	Low (me-too/me-better)	Gefitinb
Saquinavir[20] 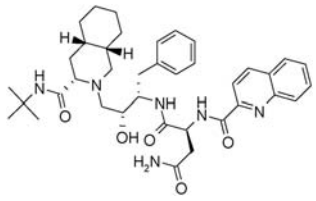	"De-novo" structure-based design	High: First-in-class HIV-protease inhibitor	Peptides containing reduced amide and hydroxyethylamine transition state mimetics
Oseltamivir[21] 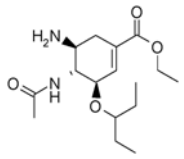	"De-novo" structure-based design	High: First-in-class oral neuraminidase inhibitor	2,3-Didehydro-2-deoxy-*N*-acetyl neuraminic acid 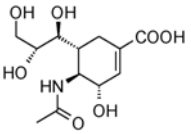

is significantly accelerated when X-ray structure determination is enabled for the hit and lead candidate. These success stories have been extensively reviewed[19] and are not covered here.

Table 2 lists the 17 marketed drugs that were approved by the FDA between 1996 and 2014, where a literature review suggests that they had been derived from structure-based "de-novo" design starting points. It is interesting to note that there are quite a number of protease inhibitors where a peptidomimetic starting point has been used. Some protease inhibitors were designed to mimic the transition state of the protease's actual substrates. For example, for aspartyl proteases an –NH–CO– peptide linkage is replaced by an hydroxyethylene group (–CH_2–CH(OH)–, the "statin" moiety), which cannot be cleaved by the protease.

Table 2 Drugs derived from "de-novo" structure-based design leads

Drug	*Target-based actions*	*FDA approved*
Saquinavir[20]	HIV-1 protease inhibitor	1995
Oseltamivir[21]	Neuraminidase inhibitor	1999
Zanamivir[22]	Neuraminidase inhibitor	1999
Imatinib[23]	Protein-tyrosine kinase	2001
Bortezomib[24]	Proteasome inhibitor	2003
Darunavir[25]	HIV-1 protease inhibitor	2006
Aliskiren[26]	Renin inhibitor	2007
Nilotinib[27]	Protein-tyrosine kinase	2007
Dabigatran[28]	Factor IIa antagonist	2010
Boceprevir[29]	Hepatitis C virus NS3 protease inhibitor	2011
Rilpivirine[30]	Nonnucleoside reverse transcriptase inhibitor	2011
Telaprevir[31]	Hepatitis C virus NS3 protease inhibitor	2011
Carfilzomib[32]	Proteasome inhibitor	2012
Ponatinib[33]	Protein-tyrosine kinase	2012
Alogliptin[34]	Dipeptidyl peptidase IV inhibitor	2013
Apremilast[13]	PDE 4 inhibitor	2014

Substrate competitive HIV-protease inhibitors were rationally designed utilizing knowledge of the aspartyl protease's mode of action. The most promising transition state mimic was hydroxyethylamine that led to the discovery of the first protease inhibitor; saquinavir.[20] Following this discovery, another HIV-protease inhibitor (darunavir) was designed using the same principle.[25]

2.02.2.3 Screening

Over the years, various screening strategies have been applied to the identification of drug and lead candidates. The screening of natural product extracts for bioactivity, followed by the isolation of the active principle or principles, has been a successful source of initial leads for drug discovery. The identification of cyclosporin A as an effective immunosuppressive drug is illustrative for this process.[35] Screening of a fungal extract for antimicrobial activity led to the isolation of a number of cyclosporins that were subsequently found to possess immunosuppressive properties. The molecular target mediating the pharmacological activity was only identified several years after market approval was obtained for the drug.[36] The microtubulin inhibitor eribulin mesylate[37] and fingolimod,[38] a novel immunosuppressive, are further examples of marketed drugs that originate from natural products. Natural products have been the most productive source of leads for new drugs in the past: 36 out of 114 first-in-class low molecular drugs approved between 1999 and 2013 originate from natural products (see **Table 6**). Interestingly, they are currently out of fashion with the pharmaceutical industry,[39] and many pharmaceutical companies stopped the screening of extracts and the labor-intensive isolation of the active principle. Given the past contributions of natural products to drug discovery, it seems surprising that natural product-based drug discovery is no longer routinely used by the pharmaceutical industry. Some of the reasons behind this shift relate to the difficulties in accessing natural products in ways that are compatible with target-based HTS. Natural products are often synthesized in small quantities or are present as mixtures in extracts, which require labor-intensive and time-consuming purification procedures. Obtaining further quantities for lead optimization or preclinical development requires large-scale reacquisition or fermentation, resulting in a substantial impact on the development timeline. Furthermore, the rediscovery of known compounds is a major problem when screening natural product libraries. The time-consuming processes of dereplication and purification are not compatible with the present regime of HTS campaigns. From a medicinal chemist point of view, natural products are often structurally complex and modification of complex natural products using synthetic organic chemistry is often challenging.[40] Finally, a mixture of natural compounds in a natural extract can be required for activity and this concerted activity of various compounds against several targets is an additional challenge for target-based drug discovery.

Screening of discrete synthetic compounds in vivo or in vitro for a targeted pharmacological or phenotypic effect constitutes the second approach. This approach was employed by Ehrlich in the early part of the last century to identify arsphenarnine, an important early antiinfective drug.[5] From the 1950s, the National Cancer Institute screened many thousands of samples per year in vivo and in vitro,[41] and identified anticancer agents such as hydroxyurea[42] and the lead structure for carmustine[43] using this approach. The access to many potential drug targets as pure or overexpressed proteins has made them more readily available for biochemical or cellular assays.[7] The feasibility of probing the mode of action at the target level has triggered further advancements in assay technologies, automation, and miniaturization—and the era of HTS was born.[44]

2.02.2.3.1 Screening and its impact in drug discovery

Testing against isolated targets in a high-throughput manner to identify novel lead structures was previously limited by the relatively small numbers of synthetic compounds available for screening. Improved automation and informatics have provided tools for the organization of screening libraries and the collection and interpretation of the large quantities of data generated by screening

campaigns. Finally, combinatorial chemistry and high-throughput synthesis methods have provided large collections of compounds to fuel the screening process. The combined application of these new technologies has enabled an HTS approach to lead identification, and large numbers of discrete small molecules can now be assessed for activity against a well-defined biological target within a relatively short period of time. The widespread adoption of HTS, and associated technologies for lead identification, has led to the expectation that an increased number of drug candidates would progress through the clinic. Indeed, in 2006, a study involving 58 HTS laboratories and 34 suppliers revealed a twofold increase in HTS-derived leads having progressed to clinical trials from 2000 to 2004.[45] As the success of any drug discovery technology has to be evaluated based on the final product, the marketed drug, the origin of the marketed small-molecule drugs approved by the FDA between 1996 and 2014 was investigated. John Proudfoot found that from 2005 onward a significant number of approved small-molecule drugs have emerged from screening leads.[46] Between 2007 and 2014, 98 NBEs and 270 NCEs have been approved by the FDA (see relevant websites). The 270 NCEs can be further split into: 97 (36%) new formulations/indications for approved drugs, 38 (14%) fixed combinations, and 135 (50%) active substances that have never before been approved for the market in any form in the United States. As shown in **Fig. 1** and **Table 3**, the positive trend for approved drugs emerging from screening derived leads has continued. "De-novo" structure-based design leads also contribute to new therapies, but to a lesser extent when compared to screening. Until 2004, only one new drug per year originated from any screening approach, while in 2012 seven such drugs were granted approval by the FDA. The average timeline of approximately 12 years from the new therapeutic concept discovery to the approved drug explains the time lag from the start of the HTS era mid-1990s to its positive impact. However, the time required to develop processes that effectively leverage the application of these new technologies to lead identification has contributed to this delay. The drop in the number of approvals in 2009 (**Fig. 1**), for instance, might reflect the learning phase in the early days of combinatorial chemistry. Chris Lipinski et al. noted in 1997 that HTS campaigns tended to produce relatively large, lipophilic lead molecules.[77,78] Since it is common during LO (lead optimization) to enhance potency through the addition of lipophilic substituents, many discovery campaigns based on screening leads provided large, poorly soluble, lipophilic drug-candidate molecules that were difficult to progress successfully through the clinic.[79]

Since the compound collections screened are not always disclosed by the respective authors and also come in many flavors, the available information was summarized as follows: When the corporate compound collection was screened in an HTS format, the screening library is designated "corporate." "Targeted library" summarizes all customized libraries (eg, lead-like, fragments, natural products, in silico preselected libraries) of a smaller size. Interestingly, among the drugs emerging from screening leads there is a general trend toward targeted libraries from 2010 onward. This trend likely relates to the observation made in 1997 that HTS campaigns tended to produce relatively large and lipophilic leads with a high failure rate in subsequent drug development.[77,78] PLX4720, the predecessor of the first-in-class B-Raf protein kinase inhibitor vemurafenib, was discovered by screening a targeted library of 20,000 compounds ranging in molecular mass from 150 to 350 Da at a concentration of 200 μM through three divergent but structurally characterized kinases.[58] A total of 238 hits were subjected to cocrystallographic analysis in at least one of these three kinases. The combination of screening a set of lead-like molecules at high concentration with large-scale X-ray structure analysis can be seen as the first successful example of fragment-based drug discovery (FBDD).

2.02.2.3.2 Chemical space considerations

The advances in HTS technologies in terms of quality, throughput, and efficiency have resulted in an ever-increasing importance of the nature (lead-likeness) of the compounds in the screening collection. Corporate screening collections often exceed one million compounds, combining the output from NCE projects, combinatorial chemistry efforts, and purchases from commercial vendors.[80] These libraries are often complemented by DNA-encoded libraries[81] and dynamic combinatorial libraries (DCLs)[82] that require customized screening processes. DNA-encoded chemical libraries represent a relatively new and inexpensive tool for the fast and efficient identification of ligands to target proteins of choice by affinity capture at subpicomolar concentrations. Such libraries consist of mixtures of millions of organic molecules, covalently linked to a unique DNA tag serving as an amplifiable identification bar code. The implementation of next-generation high-throughput sequencing has enabled the rapid identification of binding molecules. Dynamic combinatorial chemistry (also known as dynamic covalent chemistry) is a method for the generation of new molecules formed by the reversible reaction of simple building blocks under thermodynamic control. The library of these reversibly interconverting building blocks is called a DCL. When a DCL is exposed to an external influence (such as proteins or nucleic acids), the equilibrium shifts and those components that interact with the external influence are stabilized and amplified, allowing more of the active compound to be formed.

Compounds produced by early combinatorial chemistry methods were designed based on synthetic accessibility and diversity of structure, and tended to be high MW, lipophilic structures of questionable purity. The current emphasis on the quality of compounds produced by high-throughput synthesis, rather than on the sheer numbers, has led to libraries where drug-like properties[78] are considered before synthesis is initiated, and where the design is often focused on providing leads against particular targets or target classes.

As the building and maintenance of large libraries is expensive, there are constant debates as to the optimal size. Suggestions range from two to three million compounds being sufficient to deliver multiple starting points from any given screen[83] to an estimate that up to 24 million compounds would be needed to ensure potent hits for all targets.[84] Interestingly, in recent years some pharmaceutical companies started to open up their vaults to share their collections, in order to increase the chemical space and therefore the chance of finding suitable hit molecules.[80] The recent open sharing of compound collection property information also highlights the progress made with respect to the quality of the compound collections. The analysis of the European lead factory

Table 3 Drugs derived from screening leads

Drug	*Target-based actions*	*FDA approved*	*Screening library*
Nevirapine[46]	Nonnucleoside reverse transcriptase inhibitor	1996	Corporate
Delavirdine[46]	Nonnucleoside reverse transcriptase inhibitor	1997	Corporate
Tirofiban[46]	GP IIb IIIa antagonist	1998	Targeted library
Bosentan[46]	Endothelin antagonist	2001	Corporate
Efavirenz[46]	Nonnucleoside reverse transcriptase inhibitor	2002	Corporate
Gefitinib[46]	EGFR family tyrosine kinase receptor inhibitor	2003	Targeted library
Cinacalcet[46]	Parathyroid hormone ligand inhibitor	2004	Targeted library
Conivaptan[46]	Vasopressin antagonist	2005	Corporate
Sorafenib[46]	Tyrosine kinase inhibitor	2005	Corporate
Tipranavir[46]	HIV-1 protease inhibitor	2005	Corporate
Dasatinib[46]	Tyrosine kinase inhibitor	2006	Targeted library
Ditagliptin[46]	Dipeptidyl peptidase IV inhibitor	2006	Corporate
Ambrisentan[46]	Endothelin ET-A antagonist	2007	Corporate
Maraviroc[46]	CCR5 chemokine antagonist	2007	Corporate
Eltrombopag[48]	Thrombopoietin receptor agonist	2008	Corporate
Etravirine[49]	Nonnucleoside reverse transcriptase inhibitor	2008	Corporate
Plerixafor[50]	CXCR4 chemokine antagonist	2008	Corporate
Mozavaptan[51]	Vasopressin V2 antagonist	2009	Corporate
Tolvaptan[52]	Vasopressin V2 antagonist	2009	Corporate
Eribulin mesylate[37]	Microtubule inhibitor	2010	Targeted library
Fingolimod[38]	Sphingosine-1-phosphate receptor-1 modulator	2010	Targeted library
Crizotinib[53]	Protein kinase inhibitor	2011	Corporate
Linagliptin[54]	Dipeptidyl peptidase IV inhibitor	2011	Corporate
Rivaroxaban[55]	Factor Xa antagonist	2011	Corporate
Roflumilast[56]	PDE 4 inhibitor	2011	Targeted library
Sunitinib[57]	Tyrosine kinase inhibitor	2011	Corporate
Vemurafenib[58]	B-Raf protein kinase inhibitor	2011	Targeted library
Apixaban[59]	Factor Xa antagonist	2012	Targeted library
Bedaquiline[60]	ATP synthase inhibitor	2012	Corporate
Bosutinib[61]	Abl tyrosine kinase inhibitor	2012	Targeted library
Ivacaftor[62]	CFTR stimulator	2012	Targeted library
Lomitapide[63]	Microsomal triglyceride transfer protein inhibitor	2012	Corporate
Perampanel[64]	AMPA receptor antagonist	2012	Corporate
Tofacitinib[65]	JAK tyrosine kinase inhibitor	2012	Corporate
Vismodegib[66]	Smoothened receptor antagonist	2012	Corporate
Dabrafenib[67]	Raf B protein kinase inhibitor	2013	Targeted library
Ibrutinib[68]	Btk tyrosine kinase inhibitor	2013	Targeted library
Luliconazole[69]	Fungicide	2013	Targeted library
Trametinib[70]	MEK protein kinase inhibitor	2013	Corporate
Ceritinib[71]	Protein kinase inhibitor	2014	Targeted library
Eliglustat[72]	Glucosylceramide synthase inhibitor	2014	Corporate
Olaparib[73]	PARP inhibitor	2014	Corporate
Olodaterol[74]	Beta 2 adrenoceptor agonist	2014	Targeted library
Ombitasvir[75]	Hepatitis C virus NS5A inhibitor	2014	Corporate
Suvorexant[76]	Orexin receptor antagonist	2014	Corporate

The lead source "corporate" was shown when the corporate compound collection was screened in HTS format. "Targeted library" summarizes all customized libraries (eg, lead-like, fragments, natural products, virtual screening libraries) of a smaller size.

compound collection (seven pharmaceutical companies collaborated to generate a pooled resource) shows good quality with respect to lead-like properties with a MW centered around 350 Da, a log *P* of 2–3, and diversity based on Tanimoto similarity (the most popular similarity measure for comparing chemical structures). Two structures are usually considered similar if $T > 0.85$ (for daylight fingerprints, **Fig. 2**).[85] The progression of leads into drugs tends to increase the MW (Δ69 Da), lipophilicity [ΔLogD(pH 7.4) = 1], and complexity, therefore it seems obvious that lead structures should be relatively simple, of low MW and not too lipophilic.[86]

In addition to keeping the focus on heavy atom count (HAC), MW, Log *P*, and topological polar surface area (TPSA) in the lead-like and drug-like space to avoid false positives,[87] structural elements that frequently result in assay artifacts are now well recognized. Many of these molecules—pan-assay interference compounds, or PAINS—have defined structures and cover several structural classes (**Table 4**). Most PAINS act as reactive chemicals rather than discriminating drugs, and contain, for example, alkylating, acylating, and redox active groups, as well as aggregating and chelating moieties.[88] Although software tools can easily filter

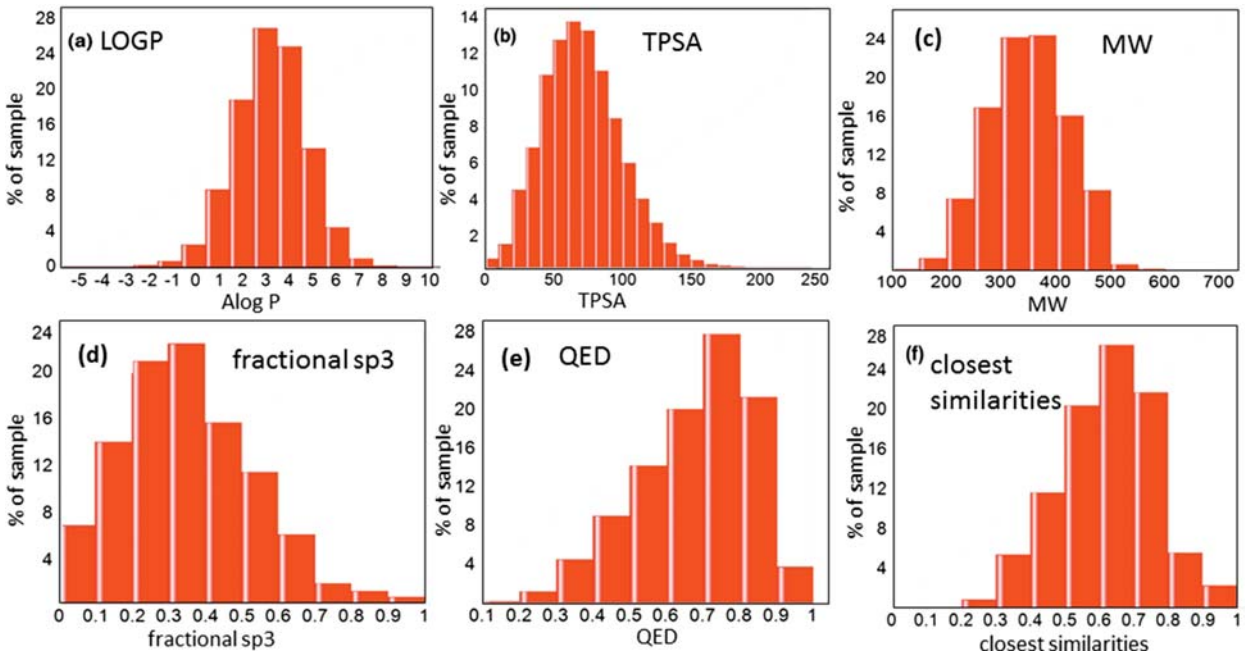

Fig. 2 Key physicochemical parameters and diversity of the Joint European Compound Library (JECL). The key physicochemical parameters of (A) log *P*, (B) topological polar surface area (TPSA), (C) molecular weight (MW), (D) fraction sp^3 carbon atoms, and (E) the quantitative estimate of drug-likeness (QED) desirability score, are typical of a lead-like library and centered on a MW of 350 Da and a log *P* of 2–3. The fraction of sp^3-hybridized carbon atoms indicates a broad spread of 3-dimensionality. (F) The nearest-neighbor diversity of the collection using Tanimoto similarity with extended connectivity fingerprint (ECFP6). Reproduced from Besnard, J.; Jones, P.S.; Hopkins, A.L.; Pannifer, A.D. The Joint European Compound Library: Boosting Precompetitive Research. Drug Discov. Today **2015**, *20*, 181–186.

PAINS from screening libraries, not all PAINS can be identified by structural features. False-positive hits may occur due to synthesis-related impurities that might not be noticed in liquid chromatography/mass spectrometry (LC/MS) or nuclear magnetic resonance (NMR) quality control checks. These include metal ions and long-term storage condition-dependent decomposition products.[89] It proved extremely valuable to check (database or literature search) if the hits interacted with unrelated proteins or had been implicated in nondrug-like mechanisms. The Boehringer-Ingelheim (BI) corporate and a collaborator library were recently screened against 10 protein–protein interaction (PPI) assays using the Alpha Screen® technology. Analysis of the 91,000 primary hits for the presence of PAINS structural elements, and unrelated targets where the compound was also found as a primary hit (frequent hitter (FH) score) revealed that there is merely a trend indicating that FHs contain a higher percentage of PAINS structural elements (Fig. 3). Interestingly, only the bin with an FH score of 1–2 and no PAIN structural alerts contained validated hits (see next section on the definition) against several PPIs. Significant resources and profiling time were saved by restricting further triaging of the primary hits to PAIN-free compounds (43,500, 48%). At BI, for future Alpha Screens® hits a FH score of ≤ 2 will be applied, that in a retrospective analysis would have disqualified a further 14,000 (32%) primary Alpha Screen hits from further profiling.

In addition, or as an alternative to screening increasingly large numbers of complex molecules, many pharmaceutical companies utilize much smaller but well-designed and characterized sets of low MW compounds for fragment-based screening (FBS). A fragment is commonly defined by the Astex Rule of 3 in which the MW is ≤ 300 and the number of hydrogen-bond acceptors, donors, and rotatable bonds is ≤ 3 in each case.[90] The HAC (already well-established for ligand efficiency (LE) calculation) was found to be a better descriptor for lead-likeness than MW since halogen atoms have a higher impact on the MW gain than on the volume of a molecule. Therefore at BI, a heavy atom (HA) range was defined from 10 to 22, as the preferred compound space for hit finding (Hit Zone). Hits from this zone should permit effective hit-to-lead optimization toward the Oral Drug Zone [HAC 14–34 and pIC50-cLogP (lipophilic ligand efficiency, LLE) >2.4].

Screening in the Hit Zone, however, comes at the price of lower binding affinity/potency, requiring higher screening concentrations, and a special focus on sufficiently high solubility. LE is defined as the free binding energy per ligand atom to its binding partner. Mathematically, LE is defined as $LE = (\Delta G)/N = -RT\ln K_i/N$ where N is the number of HAs in a ligand.[91] LE is not only an excellent tool for ranking hits coming from any screening campaign; it also helps to relate the molecular size of the screening compound to the expected potency or binding affinity (Fig. 4). While an HTS hit with $LE = 0.3$ can be found when screening at 10 μM, a fragment with the same LE can require millimolar screening concentrations. To enable screening concentrations in the mM range, aqueous solubility data were measured experimentally and only fragments that passed this threshold were included in the fragment library.

Table 4 Frequent pan-assay interference compounds (PAINS): These, and related compounds, should set off alarm bells if found as hits in functional screens

Toxoflavin	*Redox cycler: can produce hydrogen peroxide which can activate or inactivate different proteins*	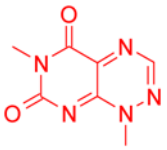
Isothiazolone	Covalent modifier: reacts chemically with proteins in nonspecific, nondrug-like ways	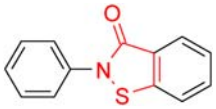
Curcumin	Covalent modifier, membrane disruptor: muddles response of membrane receptors	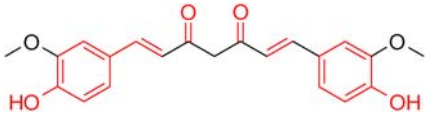
Hydroxyphenyl hydrazones	Covalent modifier, metal complexer: sequesters metal ions that inactivate proteins	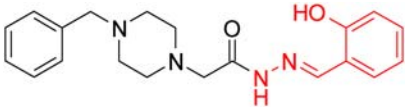
Ene-rhodanine	Covalent modifier, metal complexer	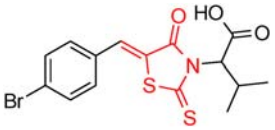
Phenol-sulphonamides	Redox cycler, covalent modifier, unstable compound: breaks down into molecules that give false signals	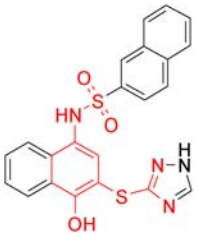
Enones	Covalent modifier	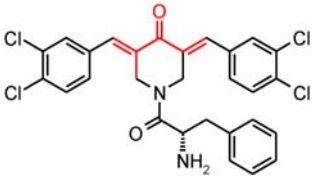
Quinones and catechols	Redox cycler, metal complexer, covalent modifier	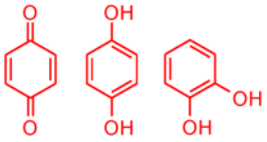

Reactive parts are colored *red* (reproduced from Baell, J.; Walters, M.A. Chemistry: Chemical Con Artists Foil Drug Discovery. Nature **2014**, *513*, 481–483).

Since some compound-related pan-assay interferences properties like aggregation, quenching of fluorescent readouts, or the impact of sample impurities are more critical at higher concentrations, it is not recommended that biochemical assays are used for screening at concentrations $\geq 200\ \mu M$, unless the tolerability of the assay principle at such high concentrations has been demonstrated. The optimal screening technology for a given concentration is shown in Fig. 4. Ligand-based NMR studies are most sensitive and can reliably pick binders with mM Kd values. Target-based NMR Heteronuclear Single-Quantum Coherence Spectroscopy (HSQC), isothermal calorimeter (ITC), microscale thermophoresis (MST), and surface plasmon resonance (SPR) all have the advantage of detecting the specific and saturable interaction of the ligand with its target protein, and thereby discriminate between true binders and aggregators.

2.02.2.3.3 Virtual screening

Hit-finding campaigns are increasingly supported or even driven by smart computational techniques,[92] and virtual screening (VS) has matured into an invaluable approach that can significantly save time and costs (eg, screening a smartly selected small subset of

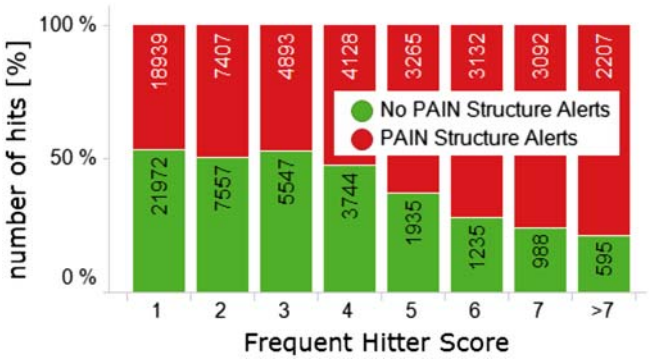

Fig. 3 Histogram representation of the number of hits without (*green*) or with (*red*) structural pain alerts versus the number of unrelated targets where the compound was found as a hit (frequent hitter score) in 10 PPI assays using the AlphaScreen® technology.

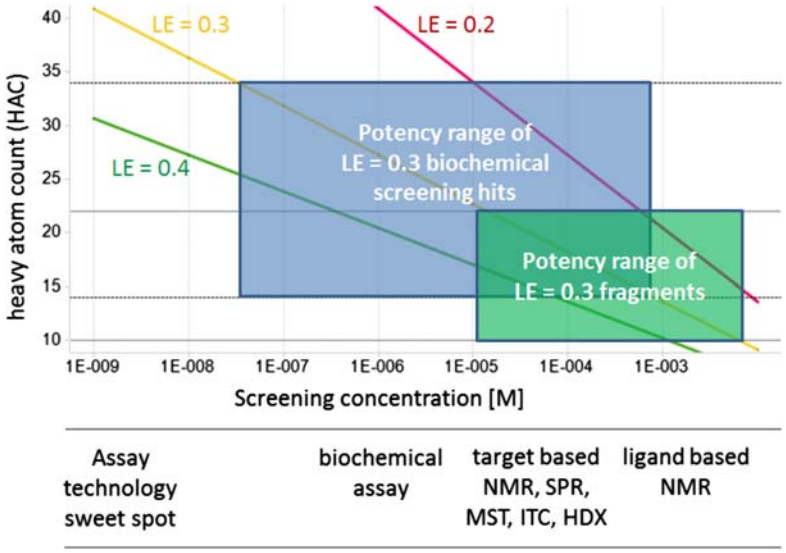

Fig. 4 Relationship between heavy atom count (size) and required screening concentration to find hits within an LE range of 0.2–0.4. The potency range for LE = 0.3 biochemical screening hits (HA = 24 ± 10) is shown in *green* and the potency range for LE = 0.3 fragments ($10 \leq HA \leq 22$) is shown in *blue*. The best-suited assay technology (sweet spot) for a screening concentration range is listed here.

a corporate library instead of running an HTS). It has also been clearly shown that VS has contributed to the discovery of compounds that ultimately reached the market.[93]

VS, or in silico screening,[94] is a general term for a broad range of computational methods for selecting compounds from a database that are likely to bind and exhibit activity against a target of interest. VS approaches are driven by various types of additional knowledge concerning the target or active compounds, which are available prior to executing a VS campaign. Depending upon the type of information that is utilized and embraced in the concept of a VS method, VS methods are designated as ligand-based VS (LBVS) methods and structure-based VS (SBVS).

2.02.2.3.3.1 Ligand-based VS (LBVS)

The starting point for LBVS is the chemical structures of known active compounds, without using any 3D-structural information of their target protein. In situations where abundant structural information of active and inactive compounds is available, machine learning tools such as, for example, Bayesian classifiers, supper vector machines, neural networks, decision trees, and random forests, can be applied for generating activity prediction models to be used in VS. Here, we focus on methods that can be applied if only one or few active compounds are known. For an overview and applications of machine learning in LBVS, we refer the reader to the recent review by Lavecchia.[95]

Most of the chemoinformatics-based LBVS[96] methods are based upon the similar property principle, that is, the fundamental hypothesis that similar compounds have similar properties,[97] as in a compound that is similar to an active molecule is also likely active. LBVS is the search for molecules in a database that are similar to known active compounds, referred to as template (also query or seed) structures. However, there is no absolute measure of similarity, and different similarity metrics result in different sets of

similar compounds. Since the advent of chemoinformatics, a huge multitude of similarity search methods has been established, each with its particular purpose representing a certain aspect of chemical similarity. Molecular fingerprints (FPs) have now been used for a long time in analogging and VS, and still remain amongst the most commonly applied LBVS methods.[98] A recent advancement of FP-based VS is turbo similarity searching,[99] an approach that uses the results of a similarity search as the query molecules in a subsequent second similarity search step. The idea of using successive similarity searches has been extended to using bioisosteric enumerations and combining different similarity methods in multistep searches.[100]

While FPs encode the composition of molecules in terms of certain features that are present or absent in a molecule, other methods work with abstractions of molecules, thereby aiming to represent certain physicochemical characteristics in a way that allows fast comparisons by computer algorithms. Feature trees and pharmacophore graphs condense atom groups that embody, for example, donors, acceptors, aromatic moieties, as the nodes of a tree. Such trees can be considered as generic 2D pharmacophores, and graph-theory based methods enable rapid comparison of template (query) structure trees with trees that are calculated from large compound databases.[101]

More physics-based descriptions of molecules accrue if the 3D-shape and electrostatic potential is used. Contrary to the 2D methods described above, which depend only upon the connectivity tables of the molecule, shape-based search methods depend upon reasonable 3D conformations of the query molecules. Knowledge or at least a sound hypothesis of the bioactive conformation of the query molecules is clearly advantageous. The use of such computationally more demanding 3D methods such as ShaEP(Molecular Overlay Based on Shape and Electrostatic Potential),[102] ROCS (Software from OpenEye),[103] or BLAZE (Software from Cresset)[104] against large databases is nowadays easily viable on multicore computers or clusters, and often leads to high-quality hits.

The development of methods that use more physics-based descriptions of molecules suggests, at a first glance, that such methods should be superior to simpler and less physics-aware methods, rendering many of the initially developed methods such as FPs obsolete for LBVS. However, evidence has been provided that it is difficult to gauge a priori which VS method is best suited to a particular project situation, and there is consensus that the success of VS is extremely hard to predict.[94]

On the other hand, it has been suspected for a long time that the parallel use of various VS approaches promises a higher rate of success.[105] This notion is strongly supported by a number of studies that systematically assess the assumption that multiple searches truly increase the likelihood of finding more active compounds, see for example the study by Holliday et al.[106] This is not surprising given that different molecular descriptors describe different aspects of molecular structure, and hence, different methods probe a compound's neighborhood in chemical space in different ways.[107] A key task when using multiple methods is the stringent aggregation of the individual results, the systematic approach to do so is referred to as data fusion. According to Willet, data fusion is the name given to a body of techniques that combine multiple sources of data into a single source, with the expectation that the resulting fused source will be more informative than the individual input sources.[108] A number of advanced data fusion approaches for aggregating multisearch results have been developed, including theoretically derived fusion rules[109] and a method based upon belief theory.[110]

2.02.2.3.3.2 Structure-based VS

SBVS relies on the 3D structure of a protein with a suitable binding site of interest that can accommodate compounds of interest. In essence, SBVS is the automated positioning (docking) of compounds in a database into such a binding site, whereupon generating different 3D conformations (poses) that should represent likely binding modes of the compound. This procedure is driven or complemented by a scoring scheme that aims to rank the compounds by their likelihood of binding.

The challenges, limitations, and successes of SBVS have been extensively discussed and reviewed. In this article, we only outline some of the key issues, in particular the treatment of the target protein and its binding site in the docking process, and the handling of the poses. For further details we refer the reader to the literature and recommend, for example, the following recent reviews by Spyrakis.[111]

Binding site: The specification of what can be considered a suitable binding site for docking is by no means a trivial task. In most cases, the relevant area on the protein surface is known, but cavity detection methods[112] can be applied if this is not the case. The preparation of the protein prior to docking, as in the correct protonation and specification of, for example, Asn/Gln side chain flip status, is of utmost importance. The latter aspect points to the much more general issue of protein flexibility. While some docking programs consider side chain flexibility, as an example for small structural change, in their pose generation method to a certain level, and are hence apt to adapting different ligands that can trigger side chain flips, the more general dynamic behavior of a binding site cannot be easily treated in this way. Rather, multiple conformations, for example, from different X-ray crystal structures with slightly different binding site arrangements can be used. Furthermore, snapshots from molecular dynamics simulations have also successfully been used. Such approaches are commonly termed ensemble docking. While their success in comparison to docking against one single structure is a priori not predictable, it is commonly accepted that ensemble docking normally outperforms docking into a single structure.[113] Various approaches for handling protein flexibility in docking have been reviewed recently,[114] and include docking to an ensemble of structures (ensemble docking). Recently, basic guidelines for selecting the best binding site for docking from an ensemble of X-ray structures have also been published.[115]

Another crucial aspect of protein–ligand binding is the involvement of water molecules. Water molecules can bind tightly to the protein surface and, as conserved water molecules that are localized across a number of X-ray crystal structures in the same position, considered to be part of the binding pocket. Other water molecules can mediate protein–ligand contact in some complex structures of a target, and not in others. Hence, the involvement of water molecules in protein–ligand binding is extremely heterogenous, and highly depends upon the targets and the ligand binding to it. Docking programs generally allow the specification of the water

molecules that are part of the pocket. In the FlexX docking program,[116] a particle placement concept has been pioneered that allows the placement of energetically favorable water molecules on-the-fly during the docking process, similar mechanisms have been implemented in other docking tools, such as GOLD (Genetic Optimisation for Ligand Docking) and Glide.[117] These few examples show that an in-depth analysis of the available structural information of a target, its dynamics and hydration behavior, and the selection and preparation of proteins with the most promising binding sites for docking, is of great importance for conducting successful SBVS campaigns.

In the absence of suitable 3D X-ray crystal structures, homology models can also be used as structures for docking. The usefulness of such models in SBVS has been a topic of controversial discussions, but their value has been demonstrated in a number of studies,[118] see also examples in a recent review on homology modeling in drug discovery.[119] Interestingly, the quality of hits identified using individual or ensembles of homology models can be even higher than for hits identified by docking into X-ray structures. This underpins that the success of SBVS campaigns is intimately linked to adequate treatment of binding site flexibility, and in particular the adaptation of the ligand binding cavity to bound ligands, which can have a more significant impact on docking success than the intrinsic methodical errors of homology modeling. Nevertheless, as for experimental structures, the selection of the most suitable model for docking from a pool of generated models remains a problem.

2.02.2.3.3.3 Scoring

The fundamental physical principles of protein–ligand binding are essentially formulated by the theory of statistical thermodynamics. However, it only recently became possible to approximate the free binding energy ΔG of a ligand binding to a protein with an accuracy that is even worthwhile discussing. Such approaches still have their limitations and are computationally extremely demanding, and will clearly not be applicable to SBVS with large compound sets for the foreseeable future. Since the advent of SBVS, major attempts have been made to develop different types of scoring functions that would, ideally, approximate ΔG with reasonable accuracy to enable the selection of poses that are most likely to represent true binders. At the same time, such functions need to be fast enough to allow calculations for very large data sets. Unfortunately, the correlation between ΔG and typical scoring functions is very low, which can most likely be attributed to the fact that ΔG cannot, principally, be decomposed into a sum of its components.[120] Nevertheless, scoring functions serve an important purpose as a rough first filter. As a result of these failures, various pose postprocessing methods have been established as a crucial step for successful SBVS campaigns showing a reasonable enrichment. A typical way of filtering poses is by applying constraints, for example, by enforcing the presence of certain hydrogen bonds or other protein-ligand interactions in the pose. The downside of such an approach is clearly that novel and unprecedented binding modes, and hence relevant new chemical matter, could be missed. A common postprocessing method is consensus scoring, that is, the rescoring of poses with different scoring functions. The principle of consensus scoring is the same as for data fusion, as outlined in the LBVS section, using the combination of information from different sources. In spite of all these efforts, careful visual inspection of the remaining top ranked poses by an experienced computational chemist is still often the best filtering method for distinguishing meaningful poses from artifacts.

2.02.2.3.3.4 Conclusion

The compilation of some key aspects of both LBVS and SBVS in this article demonstrates that devising a promising VS strategy for a target in a particular project situation requires detailed analysis of the available knowledge that operates the VS campaign. Obviously, for well-known pharmaceutical targets there is often a wealth of structural and ligand information available that allows precise SBVS and LBVS screening campaigns to be set up in parallel, including machine learning techniques. Knowledge of active chemical matter enables an a priori estimation of the success rates to be expected. The rescue or retrieval of known active compounds from a set of inactive compounds can be simulated and exploited for adjusting and optimizing the VS protocols before use in the actual campaign. Moreover, in such situations LBVS and SBVS can complement each other such that ligand-based methods can guide the specification of the SBVS protocol, thus exploiting the best of both worlds.[121] However, in projects on new targets, the knowledge base on protein structure and chemical matter is often small, and such estimations prior to the VS campaign can be difficult or impossible. Although a high level of automation in the VS search procedures is key to drug discovery projects, the composition of the most suitable VS approach still depends highly upon experience.

A common approach for fast follow-up of hits obtained by the first round of screening is hit expansion (HE). Validated hit structures and relevant structures obtained from data-mining procedures can be employed for defining small compound decks using in silico compound selection methods. The compound decks are then used in subsequent rounds of screening. HE can serve multiple purposes, depending on the outcome of the primary screen and the aim of a hit-finding project. It can consolidate and expand knowledge about active regions in chemical space by scaffold hopping and by finding derivatives of active scaffolds, hence establishing or broadening SAR information. Alternative naming conventions include structure activity relationship (SAR) expansion and hit-directed nearest-neighbor searching. HE is intended to strengthen the knowledge base for direct use in hit-to-lead campaigns.

2.02.2.3.4 Assay technology advances for functional screens

The increasing number of compounds available for testing and a growing number of molecular targets triggered parallel advances in assay technologies and automation, achieving adequate throughput. Suitable assay technologies had to be easily automated and robust. This led to the development of new homogeneous assay techniques without separation, washing, or transfer steps. Another driving factor for technology development was cost pressure, which brought forth the miniaturization of plates, to 384-well and

1536-well formats. While medicinal chemists rarely setup and run functional screens, it is of utmost importance that the medicinal chemist understands the scope and limitation of a given screening system.

One of the earliest homogeneous assay technologies was the scintillation proximity assay (SPA),[122] which consists of microspheres with embedded scintillant coated with acceptor molecules. The energy of β-particles from ^{3}H decay is absorbed in assay buffer and only stimulates light emission of the scintillant if it is in close proximity to the bead. The adaption of radioimmunoassays to SPA technology made them amenable to HTS. The great convenience of this format is that no tag is required, which could affect binding affinities. However, its downside is radioactivity and radioactive waste.

As a result, fluorescence and luminescence became established as the most widely applied assay principles. There are a whole range of fluorescent technologies available, the simplest being direct measurement of fluorescence intensity including fluorescence quenching. Fluorescence polarization (FP) exploits the size-dependent rotation rate of molecules, which is reflected by the extent of polarization of the fluorescently labeled molecule when excited by polarized light.[123,124] This allows binding of small molecules like DNA, RNA, or peptides to proteins to be monitored. Since the assay window is dependent on the difference of the fraction of tracer bound, a high saturation of tracer is needed. Depending on the Kd of the binding partners, this can require very high concentrations of protein and test compounds. Furthermore, a careful design of the fluorescent labeling is important to avoid a propeller effect and steric hindrance. FRET (Förster or fluorescence resonance energy transfer)[125] uses dipole coupling of donor–acceptor pairs (eg, 5-((2-Aminoethyl)amino)naphthalene-1-sulfonic acid (EDANS) and 4-(dimethylaminoazo)benzene-4-carboxylic acid (DABCYL))) to quantify binding events. The strong distance dependence of the energy transfer limits the detection range of binding events to 5–10 nm. All fluorescent assays are prone to artifacts due to debris and compound fluorescence, which can be reduced by using a red-shifted fluorescent label.[126] The possibility of a ratiometric measurement of FRET offers some improvement in this regard. A further improvement is obtained by time-resolved FRET, which uses long-lived lanthanide cryptate or chelate donor fluorophores with a large Stokes shift. A time delay between excitation and measurement of emission reduces background, debris, and compound fluorescence.[127] Unlike fluorescence, chemiluminescence is the result of an exothermic chemical reaction and not light absorption.[128] The light intensities of chemiluminescent assays are usually below those of fluorescent assays, but their great advantage is an extremely low background and a smaller fraction of interfering compounds in compound collections. Bioluminescence is the reaction of luciferase with its substrate luciferin resulting in a very efficient photon emission due to the enzymatic amplification.[129] It is used in cellular assay systems to quantify changes in Adenosine triphosphate (ATP) levels or modulation of gene transcription in cases where luciferase has been introduced into the cells as reporter gene. Aequorin, a calcium-sensitive photoprotein, allows intracellular calcium levels to be measured. Bioluminescent resonance energy transfer (BRET) is a bioluminescent assay format for measuring PPIs in cells. It is composed of luciferase or another bioluminescent donor fused to the protein of interest and a fluorescent receptor linked to the binding partner.[130] The quantification of ATP levels can also be used to quantify kinase activity in biochemical assays. The application of modified versions of enzyme or substrate extends the application of this assay principle to various other enzyme activities (eg, proteases, Monoamine oxidase (MOA), P450) in biochemical assays.[131] One source of interference in bioluminescent assays is the tested compounds, which affect the luciferase activity.[132] In biochemical assays, this effect can be minimized by using high luciferase concentrations. Another very important chemiluminescent assay technology is AlphaScreen[133] (amplified luminescent proximity homogeneous assay), which is based on a donor–acceptor bead pair. The partners interact directly or indirectly via tags, antibodies, or biotin-SA coupled to each of the two types of beads. Excitation at 680 nm of the photosensitizer in the donor bead converts triplet oxygen to singlet oxygen, which induces chemiluminescence and subsequent light emission at 520–620 nm at the acceptor bead if close to it. The short half-life of the singlet oxygen limits the detectable distance between the beads to 200 nm, which is significantly above the range which is covered by FRET and Time-Resolved Fluorescence Resonance Energy Transfer (TR-FRET), and thus enables monitoring of larger interacting molecules. This assay technology has a very low background and a very high sensitivity, which makes it amenable to miniaturization down to a 1536-well format. It can also be used in cellular assays to identify modification of target molecules for which antibodies are available (eg, Surefire). As with all homogeneous assay technologies, where the compounds remain in the assay, this one is also prone to interferences, in particular, singlet oxygen quenchers, such as NaN_3, divalent ions, and blue-colored compounds.

Compound-dependent assay interference leads to artifacts and these must be excluded to identify the true hits modulating the biological activity of interest. Chemoinformatic filters have been described to rule out assay technology-specific FHs.[134,135] Although these filters allow a proportion of these compounds to be eliminated the prediction is not very reliable. Tags can also be targets of compound interference. In addition to spectroscopic artifacts, chemical artifacts can occur as a result of aggregate formation.[136] Experience has shown that confirmation of biological activity should necessarily include testing in an orthogonal assay technology.[137] In 2003, FP and TR-FRET were ranked as the most suitable HTS assay technologies followed by AlphaScreen.[138] The analysis of a large set of historical data at AstraZeneca identified luminescence and FRET technologies as more successful than the average. Future directions might be the use of more complex and multiplexed assay systems. Two attractive assay principles are direct quantification via mass spectroscopy (MS) and quantification of gene expression using real-time quantitative reverse transcription polymerase chain reaction (RT-qPCR). In spite of significant technological advancement in terms of automated sampling and miniaturization, these technologies still suffer from limited throughput.[139]

2.02.2.3.5 Fragment-based drug discovery

FBDD is a complementary approach for finding new leads that during the past 15 years has increasingly been adopted by research groups in the pharmaceutical industry. The goal of FBDD is to identify small organic molecules (MW <300 Da), "fragments" of

lead-like molecular entities, that bind to a functional pocket of the target protein, and to further optimize them into potent leads using strategies that are similar to the traditional structure-based design approaches used for hits derived from HTS. Since the introduction of this concept in the mid-1990s through a seminal work by a group from Abbott,[140] the field has rapidly matured. A great variety of success stories have been published[141], which are good show cases for the efficiency and versatility of the approach. To date, there are numerous FBDD-derived clinical compounds and with vemurafenib (PLX4032)[58] the first representative has reached the market.

The great conceptual appeal of FBDD is based on considerations of sampling efficiency and of the optimal physicochemical or drug-like properties of lead compounds. Since the chemical space of organic molecules with drug-like properties is vast [estimations indicate that there are approximately 10^{50} molecules with [HAC of 15–35]; screening of corporate libraries of up to 10^{7} compounds with limited structural diversity will not get anywhere close to a representative sampling of the chemical space of potential lead structures. In contrast, screening a set of 10^{3}–10^{4} structurally diverse fragments with HAC between 10 and 22 will sample the corresponding chemical space of approximately 10^{20} molecules more efficiently.[142] In addition, due to the lower complexity of the screened compounds, hit rates are much higher.[143] Due to the small size and fewer options of forming interactions with the target receptor, fragment hits are weak binders. Therefore, in order to detect the binding event, fragments need to be screened at high compound concentrations, which in turn necessitate the selection of polar and highly water soluble specimens in the design of a fragment screening library. While this may seem a restriction at first glance, it in fact yields the advantage that such fragment hits have better physicochemical properties than typical HTS-derived hits and are thus usually better starting points for a chemical optimization effort.

The typical workflow of FBDD starts with a biophysics and structural biology dominated FBS process followed by a round of hit analogging and a fragment-hit-to-lead/drug (FHTL) phase in which synthetic medicinal chemistry activities need to be resourced.

FBS typically comprises a primary screening step in which various biophysical methods are employed to screen for the weak binding events between target and fragment. The most commonly utilized technologies are ligand- or protein-detecting NMR spectroscopy, SPR, differential scanning fluorimetry (DSF), and MST. Fluorescence displacement assays or mass spectrometry (MS) or calorimetry-based technologies are reported, but less frequently used. The selection of technologies is based on throughput and sensitivity. Throughput must be such that a library of a few thousand compounds can be screened in a (semi)-automated fashion in a timeframe of a few days or weeks. An ideal fragment screening technology should be sensitive enough to measure high micro- to millimolar interactions without any interference due to unspecific binding events. In reality, all existing technologies have liabilities that lead to false-negative and false-positive screening results. Therefore, strategies need to be devised to extract the most reliable hit set. This can be done for instance by using a triaging scheme that employs multiple screening technologies consecutively or in parallel.[144] In almost all published cases of FBDD, the identification of the primary FBS hit set is followed by a second process step in which X-ray crystallography is used to elucidate the binding site and the details of the protein–ligand interaction. Cocrystallography thereby not only provides another orthogonal proof of binding, but, more importantly, enables the structurally informed design of optimization strategies of selected fragment hits.

In the ensuing process step, selected fragment hits with suitable binding affinity and binding mode are further validated using analogging approaches in which hypotheses about determining factors for binding affinity are probed with close structural analogs of the hits. Ideally, initial fragment structure–activity relationships can be derived, the binding mode of the fragment and its analogs is found to be preserved, and promising growth vectors are identified in the process. Improving the affinity of fragments can be achieved through various avenues, most prominently fragment growing, merging, and linking.[145] In the first examples of industrial FBS, the SAR-by-NMR approach pioneered by Abbott,[140] fragment linking was used and emphasis was put on the profound effect on the resulting affinity when covalently linking two weakly binding fragments. In retrospect, fragment linking has been used relatively rarely compared to fragment growing strategies, which elaborate leads by stepwise and structure-guided growing of the starting fragment hit (Fig. 5).

There are numerous biotech companies that specialize in FBDD, and for these enterprises FBDD is typically the only accessible hit generation technology. Major pharmaceutical companies, in contrast, have built FBS units that operate in parallel to HTS units.

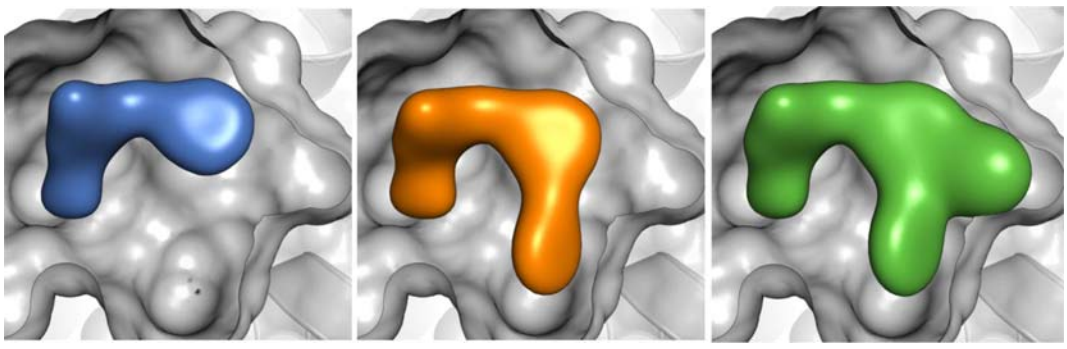

Fig. 5 Fragment-based drug discovery: Structure-guided fragment growing leads to high affinity lead candidates.

Thus, typical hit generation strategies in major pharmaceutical companies employ various approaches simultaneously. In such a scenario, FBS, HTS, and VS all produce hit sets that yield complementary information at the end of the hit-finding phase. A decision point is then reached at which the most suitable chemical starting points to be prosecuted are selected. At the start, and along the course of compound optimization, information derived from the original FBS campaign is of great use, even if the original fragment hits are not directly used as optimization starting points. In the literature, this opportunity is referred to as "fragment assisted" drug discovery.[142] For example, an HTS hit with some "functional" activity in a biochemical assay can be decorated with a substituent or merged/hybridized with a moiety that was identified in a parallel FBS. The particular way in which decoration or hybridization is done is informed by the available high resolution structural information. In literature, examples documenting merging or linking approaches spectacular improvements in potency were achieved in a single round of medicinal chemistry optimization.[146] This mix-and-match strategy can also be employed to modulate physicochemical properties of compounds, for example, by replacing a hydrophobic substituent in an HTS-derived lead by a more polar fragment, leading to an improved LLE of the resulting structural class.[147]

Synergy between the concepts of FBS and HTS can be further used to setup a separate biochemical screening scenario, in which the fragment subset of the corporate screening deck is screened in a high-concentration screening (HiCoS) regime and yields yet another functionally active fragment hit set that can be prosecuted in a similar fashion to biophysically derived hit sets (Fig. 6).

Notwithstanding the details of FBDD implementation it has become clear that this relatively new hit generation paradigm in pharmaceutical research represents a highly useful resource and time efficient approach that in a short period of time has become an integral part of drug discovery in the industry.

Future areas of development and expansion of FBDD will encompass (1) technology improvements leading to higher throughput and data quality and, in turn, to faster access to a higher quality fragment hit set, (2) enhancements in data-mining capabilities that will lead to improved fragment selection and optimization strategies, and, finally, (3) work on difficult target classes such as oligonucleotides, PPI targets, and integral membrane proteins such as G-Protein-Coupled Receptors (GPCRs).

2.02.2.3.6 Phenotypic screening

As the technology advance are covered in this paragraph concentrates on the past and future role of phenotypic screening in drug discovery. Among the factors contributing to the growing interest in phenotypic screening in drug discovery in general is the perception that, by avoiding oversimplified reductionist assumptions regarding molecular targets and instead focusing on functional effects, compounds that are discovered in phenotypic assays may be more likely to show clinical efficacy.

We would like to define "phenotypic screening" as the testing of a large number of—in most cases randomly selected—compounds in a systems-based assays. This should not be confused with systems-based chemocentric approaches. The latter typically includes an active ingredient from a plant or microbial extract with known pharmacological activity (eg, aspirin) or the derivation of a pharmacologically active natural substance (eg, prostaglandins, steroids, nucleosides, amino acids, and biogenic amines) or a synthetic compound, often based on serendipitous findings made decades before. In addition, optimization of such analogs using phenotypic assays does not classify them as phenotypic screening leads. The term "phenotypic screening" in particular appears to be used rather loosely and with different meanings. In a recent and frequently cited analysis,[148] focusing on first-in-class drugs,[149] phenotypic screening was considered to encompass all nontarget based approaches to drug discovery.

Indeed, there are highly encouraging recent examples of approved first-in-class drugs derived from phenotypic screening. However, between 1999 and 2014, only eight of the approved drugs were discovered through phenotypic screening. Fingolimod, sirolimus, and plerixafor are immunomodulatory drugs; daptomycin, artemether-lumefantrine, and bedaquiline are antibacterial/antiparasitic drugs;

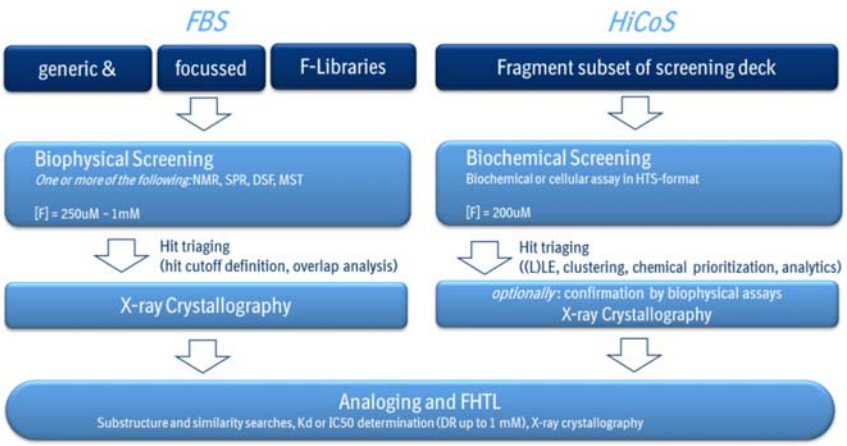

Fig. 6 Parallel prosecution of biophysical FBS and biochemical high-concentration screening (HiCoS) merging into the same downstream pipeline of FHTL activities.

and eribulin and trametinib are anticancer drugs[150] (Table 5). The fascinating case study of the discovery of fingolimod[38] illustrates nicely why developing a phenotypic screening hit can be a lengthy and twisted process (Fig. 7).

Myriocin (ISP-1), a natural product first characterized in 1972,[151] was rediscovered as an immunosuppressive metabolite in 1990[152] using MLR (mouse allogeneic mixed lymphocyte reaction). The phenotypic screening hit was subsequently assessed for prolongation of allograft survival in a rat skin allogeneic transplantation model and found to be efficacious but also toxic. Simplified derivatives were prepared with the objective of identifying ISP-1 derivatives with reduced toxicity. Out of the in-vivo characterized 2-alkyl-2-amino-propane-1,3-diols derivatives, ISP-I55 was found to be more efficacious than ISP-1 in the rat skin transplantation model but no longer inhibited MLR.[153] The different in-vitro profile compared to Cyclosporine A (CsA) and ISP-1 at that time was already pointing toward a mode of action switch. Based on ISP-I55 further conformationally constrained derivatives were prepared and the importance of correct position of the phenyl ring for the in-vivo efficacy noted. The first patent containing FTY-720 was filed in 1993 and the SAR published in 1995.[154] Only in 2002, it was disclosed that FTY-720 actually gets enantioselectively phosphorylated by sphingosine kinase and that (S)FT720-P is the active principle.[155] The obvious similarity of FTY-720P to sphingosine phosphate further stimulated research in this area and the binding of FTY-720P to the very recently discovered S1P receptor family was published.[156] At the same time, the utility of this prodrug for the treatment of multiple sclerosis was discovered and development of fingolimod was focused toward a first-in-class multiple sclerosis therapeutic with a novel mechanism of action (MoA).[157] In contrast to CsA, FTY-720 and its active principle FTY-720P do not inhibit Il-2 production and lymphocyte proliferation. Fingolimod sequesters circulating mature lymphocytes into peripheral and mesenteric lymph nodes and thereby reduces the number of lymphocytes in peripheral blood. There was a lot of speculation and uncertainty how FTY720P accomplishes this in the presence of exceeding amounts of the natural ligand of S1PR, sphingosine-1-phosphate, until Brinkmann et al. published in 2009 that FTY-720P causes long lasting internalization of the S1P receptors and thereby acts as a functional antagonist.[158]

One of the many challenges of phenotypic screening is the selection of a few interesting compounds from a list of typically thousands of hits. These hit lists are often heavily dominated by unselective or toxic compounds, substances with already known unwanted MoA or false positives. Usually, potency is the sole criterion by which such hit lists are sorted and compounds selected for further studies, but this criterion might be inappropriate for identifying the best chemotypes. Usually these hits are progressed to more physiological cellular assays, but it is important to understand that new methodologies and approaches are required to increase the success rate of phenotypic screens. Validation strategies like recently established for target-based screens are not easily translatable for phenotypic screens.

Another challenge is the definition of the correct phenotype to mimic the disease in the patient. For example, phenotypic screening for the induction of cell death in cancer cell lines has frequently yielded the same "low-hanging fruit" in terms of mode of actions (MoA)—such as targeting microtubule dynamics and DNA modifications—and has thus made relatively little contribution to the identification of drugs with novel MoAs.[150] Many diseases today are still difficult to faithfully mirror in test plates and model organisms, and the use of stem cell technology or whole-organism screens might enable the establishment of more physiological assay systems that better reflect the actual disease. Reporter gene assays are a specific category of phenotypic screens, although they are somewhat artificial and have limitations.[159,160] Many reporter gene assays have been run in pharmaceutical companies and academic institutions over the past 20 years, with a peak in the mid to late 1990s, apparently with little success in terms of delivering drug candidates. To our knowledge, there is not yet an example of a first-in-class drug originating from such a screen. Progress here will certainly increase the likelihood of finding disease-relevant pathways, but it may not enable a more effective selection of interesting compounds, and so more innovation is required.

A third challenge poses the target identification for a phenotypic lead or drug.[161] Traditionally, the follow-up work of target identification and elucidating the MoA of hits from phenotypic screens have been slow and at times fruitless. Knowledge of the efficacy target, the protein through which the drug elicits the phenotype of interest via direct binding and modulation is not necessarily an absolute requirement during initial development stages. However, the definition of the on- and off-target space remains a crucial step toward full development for a drug candidate; it facilitates the definition of a patient selection biomarker, the optimization of potency within a lead scaffold, and the translation from a simplified cellular model to in vivo models. Progress has been made with respect to the identification of intracellular binding partners of the hit by affinity-based approaches like small-molecule affinity proteomics and proteomic target stability profiling.[162] Chemoproteomics approaches interrogate proteins directly in cell lysates or live cells. Despite the ever-increasing sensitivity of detection methods, the differences in cellular abundance of putative interactors that are being interrogated in parallel still pose a challenge (protein levels span 10 orders of magnitude). In addition, most of these methods do not differentiate between direct and indirect binding. A popular version of chemoproteomics combines small-molecule affinity chromatography with MS-based proteomics.[163] For unbiased target deconvolution, the compound of interest is immobilized on solid support via a functionalized linker introduced at a permissive site so that the resulting affinity probe retains cellular activity. Like in every screening process, the challenge is in the follow-up work with the identified potential targets and their functional characterization. Alternatively, genetic suppression or potentiation of compound mechanism has been achieved in human cells by combining compound treatment with cDNA overexpression[164] as well as with Ribonucleic Acid Interference (RNAi), reviewed in Palchaudhuri et al.,[165] in genome-wide screens. Small Interfering RNA (siRNA) and pooled Small hairpin RNA (shRNA) screens are amenable to unbiased, genome-wide compound-sensitization experiments. As an example, successful target ID was achieved for STF118804, a compound that reduced viability of most B-ALL cell lines, using a genome-wide pooled shRNA screen, where the direct target, nicotinamide phosphoribosyltransferase, was the most statistically significant gene conferring drug sensitivity.[166] Finally, knowledge-based approaches for target ID are the fastest, making them the first approaches

Table 5 Low molecular weight first-in-class drugs approved between 1999 and 2014 originating from phenotypic screening

Sirolimus (transplantation, coronary stent coating)

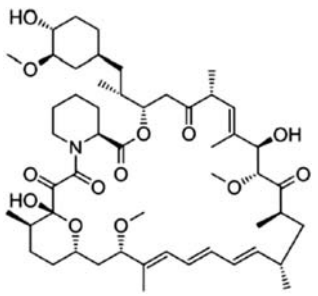

Natural product (derived) MoA: mTOR (in complex with FKBP12), kinase inhibitor

Sirolimus was isolated from a streptomycetes and found to have antifungal activity (1975). It was later found to be immunosuppressive (1978), and its utility for allograph rejection was published in 1989. Its mechanism of action was only later elucidated (1991). FDA approval was granted in 1999

Daptomycin (antibacterial)

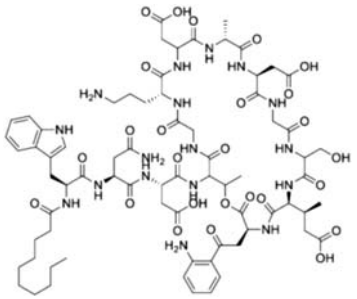

Natural product (derived) MoA: Antibacterial

The drug is a lipopeptide which binds to the bacterial cell membrane and causes rapid polarization

1980, the chemotype with indication was discovered in a cellular in vitro phenotypic screen. The final molecule was published in 1986, FDA approval was granted in 2003

Artemether-lumefantrine (malaria)

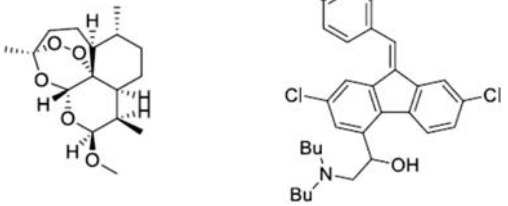

Combination of a natural product derivative (artemether) and a l.m.w. synthetic compound (lumefantrine) Target/MoA unknown

Discovered in 1972 by testing various traditional Chinese medicines in a rodent model of malaria (artemisinin). Little has been published about the discovery since this project was regarded secret by the Chinese military. Lumefantrine was also discovered in the same project

Fingolimod (multiple sclerosis)

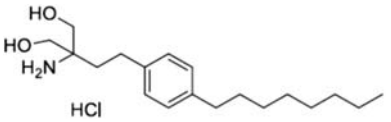

Natural product (derived) MoA: Sphingosine 1-phosphate receptor modulator

The chemotype was discovered through a phenotypic screen for novel immunosuppressive natural products using a cellular assay (mixed lymphocyte reaction). Subsequent chemical optimization using in vitro and in vivo models serendipitously changed the mechanism of action which later was established to be sphingosine 1-phosphate receptor modulation

Eribulin [cancer (breast cancer)]

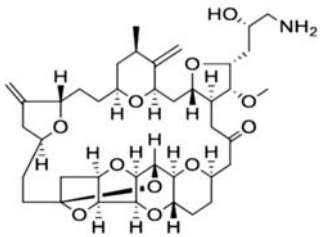

Natural product (derived) MoA: Microtubule inhibitor

Studying active substances of marine organisms, halichondrin B was isolated (1985) and shown to have antitumor activity in a cellular assay. The final molecule was synthesized as a structurally simplified, fully synthetic analog (2001). The mechanism of action was established subsequently in 2005

Bedaquiline (tuberculosis)

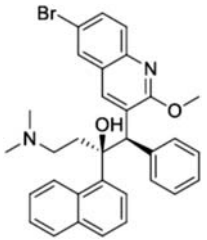

Synthetic molecule *MoA: Mycobacterium tuberculosis* ATP synthase, enzyme inhibitor

The final molecule was discovered at least 7 years prior to the first publication in 2007. The chemotype was found by high-throughput screening using *M. smegmatis* cultures. The target was subsequently identified through the characterization of resistant mutants

Trametinib (melanoma)

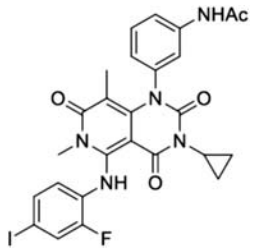

Synthetic molecule MoA: MEK1 and MEK2, allosteric kinase inhibitor

The chemotype was discovered using a cellular screen for inducers of p15INK4B and p27Kip1/CDKN1B (2007) and subsequently shown to be a specific, allosteric MEK1/MEK2 inhibitor (2011)

Plerixafor (immunostimulant)

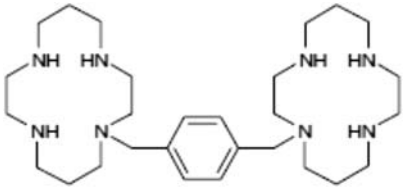

Synthetic molecule CXCR4 antagonist

The chemotype was discovered as a chemical impurity in a whole cell screen searching for compounds that prevent HIV infection (1995). In 1998, it was characterized as an inhibitor of HIV-1 entry via the CXCR4 co-receptor. Development as an anti-HIV agent was redirected toward stem cell-mobilizing agent in 2002

Adapted from Eder, J.; Sedrani, R.; Wiesmann, C. The Discovery of First-in-Class Drugs: Origins and Evolution. Nat. Rev. Drug Discov. **2014**, *13*, 577–586.

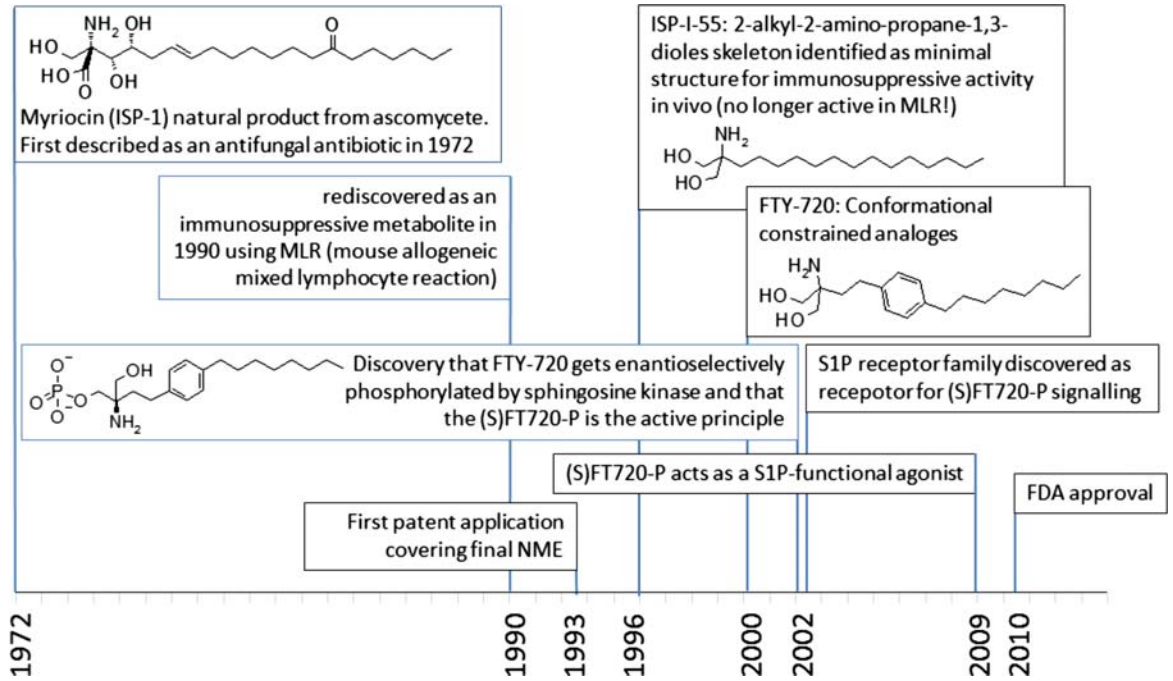

Fig. 7 The long and twisted journey of Fingolimod from the natural product phenotypic screening hit Myriocin to the first-in-class drug approved by the FDA.

implemented for deconvoluting phenotypic screening hits. However, like all approaches relying on correlation to reference compounds, they are limited in their breadth of targets that can be predicted, and ultimately depend on experimental validation of efficacy targets. Knowledge-based approaches, at their core, rely on exploitation of integrated compound–target associations gleaned from bioactivity data.

Consequently, in order for phenotypic screening to be successful, it will be important to recognize it as a new discipline that needs new technologies and methods, and for which lessons must be learnt to avoid frustration from unrealistic expectations and premature conclusions if the current investments do not yield quick returns. Now, with an increased chemical space, the time might be right to further broaden the target space and open up new avenues. This could well be achieved by investing in phenotypic screening using the compound libraries and the many tools that have been established in the context of target-based approaches, but it also requires further technological advancements. The choice should not be between phenotypic screening and target-based discovery, as both approaches can complement each other and are interconnected they should be run in parallel. Therefore, the goal will be to screen phenotypically in an efficient and effective manner and to combine phenotypic screening sensibly and productively with target-based drug discovery.

2.02.2.4 How to Best Identify Valid Hits?

In any target-based screening campaign involving a large number of samples, it is likely that a hundred to several thousand samples can be identified that display activity above a statistical significant threshold. While there is hardly a screen with any hits, a hit rate in the single digit percent range is more concerning than reassuring. A large number of primary hits always translate to big work packages to identify those hits that show specific, drug-like interaction between molecule and protein. Validated (true) hits inhibit or activate a protein by fitting into a binding site on the protein. Saturable interaction of the ligand with its target protein is best shown with biophysical assays[167] like resonant waveguide (RWG), Thermal Shift Assay (TSA) DSF, SPR, MST, or ITC. The specificity of binding is ideally deduced from the cocrystal structure, 2D (HSQC) NMR techniques, or HDX exchange studies. Covalent inhibitors can be validated by proving the specific covalent labeling of the target protein and ideally the target epitope by chemoproteomics. All these biophysical methods need to be carefully validated using validated binders, like natural substrates or validated hits from another screen, for example, an FBS campaign, before being applied in triaging schemes for inhibitors out of a functional assay. Not all methods are suitable for all targets, and not all have the same information content. As most of the biophysical methods are more resource intensive, and of slower throughput than the functional screening assay the primary hits must be smartly triaged down to a number that is compatible with the profiling assays.

This triaging process of the primary hits to validated hits is often underestimated or seen as part of the hit-to-lead process. The latter is especially unfortunate since synthetic chemistry on assay artifacts is probably the biggest waste of resources in preclinical drug discovery. Retrospective analysis of the timelines for the 10 PPI screens done with a collaborator revealed that the initial screen

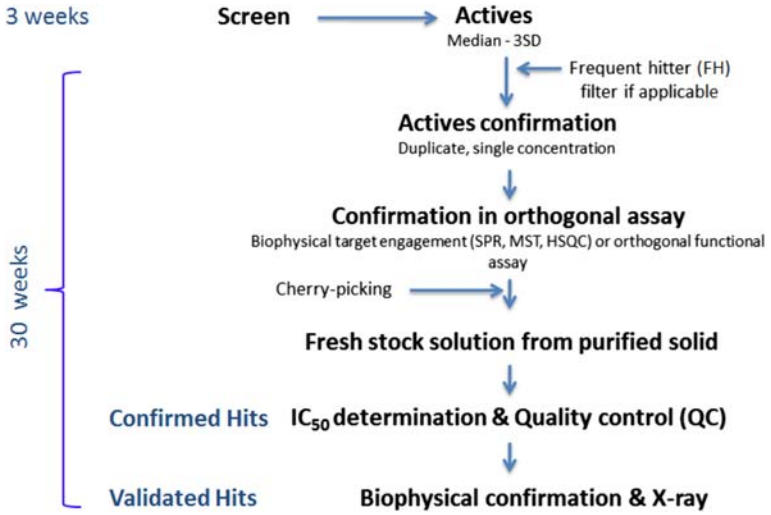

Fig. 8 Generic triaging process for functional screens.

of 1,700,000 samples took only 3 weeks, while the triaging process to validated hits needed on average 30 weeks. In terms of efficiency, much more is gained from designing a smarter triaging scheme than to further increase the throughput of the primary screen. The triaging scheme should also be geared toward the rapid identification of some validated hits with the anticipated risk of not finding all validated hits in the deck. As much time can be lost rescuing presumed "false negatives" as submitting "false positive" to the next profiling round.

Based on our experience we suggest a generic hit triaging process as outlined in Fig. 8. The primary actives from a large (>200,000) biochemical or cellular assay are submitted for confirmation in the identical assay. Those that display activity above a statistically significant threshold (confirmed actives) are ideally tested for binding to the target by a biophysical method with sufficient throughput like RWG, DSF, or SPR. At this stage, a single concentration thermal shift value or a SPR sensogram for the target protein as well as a control protein is likely to be more efficient than a full Kd determination. If a biophysical assay is not feasible, we recommend retesting the confirmed actives in an orthogonal assay utilizing a different technology than the primary screening assay. We and others[88] find this "active in both assays" flag much more efficient than the typical assay technology and compound property specific counter screens, where each potential liability needs to be addressed in a separate experiment. Those confirmed actives are then assessed for dose-responsive inhibition (or activation) and those that pass are cherry picked for retesting from a freshly prepared stock solution, ideally from purified solid. As not all confirmed hits will be readily available as solids, cherry picking based on cluster representatives at this stage will be required. Those that confirm in the primary screening assay (confirmed hits) are submitted to Kd determination using suitable biophysical assays. If saturable and sufficiently potent binding (LE $\geq$ 0.3) to the target protein can be obtained, then the sample is prioritized for elucidation of the binding site information by X-ray cocrystallography or HSQC.

2.02.3 Hit-to-Lead Process

The process usually referred to as "hit-to lead" is geared toward the identification of lead series around validated hits with satisfactory molecular potency, and a more detailed assessment of the liabilities and opportunities with respect to selectivity, patentability, and ADME properties (absorption, distribution, metabolism, and excretion). In the hit-to-lead phase, systematic and sometimes quite intensive SAR investigations are performed on several core structures in parallel. Experience shows that it is important to pursue several structurally diverse series in parallel to balance the risk of dead ends due to incompatible pharmacokinetics/pharmacodynamics (PK)/PD.

It is now common to demonstrate that an appropriate PK or pharmacological profile can be achieved for selected compounds.[168] Obstacles to a targeted PK profile, for example, poor permeability or rapid metabolism, can now be readily identified through well-established in vitro surrogates such as permeability in a Caco-2 assay or by in vitro metabolism as measured in microsomal or hepatocyte preparations. Off-target liabilities such as human ether-a-go-go-related gene (hERG) (life-threatening long QT syndrome (long interval between Q and T wave in the hearts electric cycle) due to block of the hERG channel) or Cytochrom P450 (CYP) inhibition[169,170] or phospho-lipidoses[171] should also be identified at this early stage—it is not necessary to fix all the issues that are identified, but the data should indicate that there is a path forward during LO (Fig. 9). These assays are now fairly high throughput and allow the characterization of a large number of hit derivatives. However, sometimes the throughput is achieved by making compromises on the predictability of the surrogate assay. High-throughput microsomal stability assays have less

Fig. 9 Medicinal Chemists face many challenges. Reproduced from Bleicher, K.H.; Böhm, H.-J.; Müller, K.; Alanine, A.I. A Guide to Drug Discovery: Hit and Lead Generation: Beyond High-Throughput Screening. Nat. Rev. Drug Discov. **2003**, *2*, 369–378.

predictability than more labor-intensive hepatocyte preparations.[172] Many companies also prefer the more labor-intensive functional patch-clamp assay to a radiometric or fluorescence-based hERG binding assay for an early risk assessment of hERG channel blockage.

2.02.3.1 Chemical Probes for Novel Therapeutic Concepts

The recent years witnessed an increased acceptance of the usefulness of high-quality chemical probes for improved understanding of human biology. Especially for novel, unprecedented targets the detailed understanding of their role in disease is potentially of greater importance than ADME properties in line with oral dosage. Classical hit-to-lead work and the development of chemical probes both require validated hits as starting points; however, the objectives of these processes can be significantly different. So what is a chemical probe and why should it be different from a lead for a drug discovery campaign targeting an unmet medical need? (Fig. 10). A chemical probe is simply a reagent—a selective small-molecule modulator of a protein's

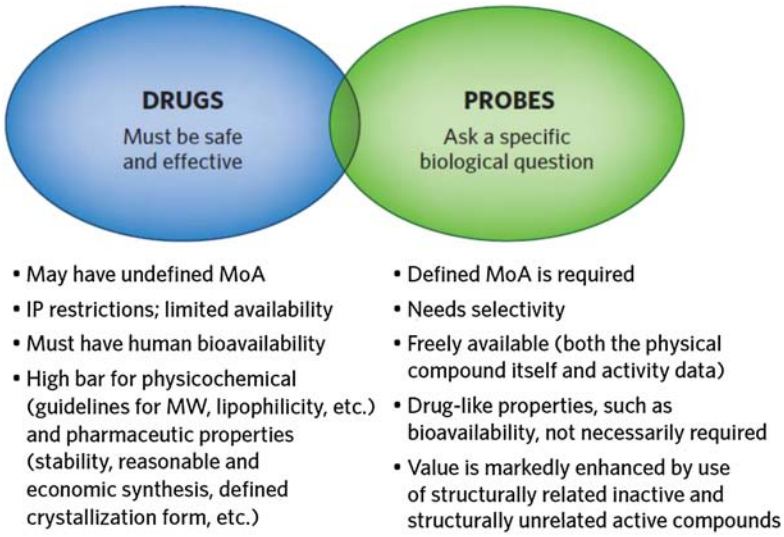

Fig. 10 Different purposes and requirements for chemical probes and drugs. Reproduced from Arrowsmith, C.H.; Audia, J. E.; Austin, C.; Baell, J.; Bennett, J.; Blagg, J.; Bountra, C., et.al. The Promise and Peril of Chemical Probes. Nat. Chem. Biol. **2015**, *8*, 536-541.

function that allows the user to ask mechanistic and phenotypic questions about its molecular target in biochemical, cell-based, or animal studies. Chemical probes do not need to meet the same requirements as a successful medicine, such as good PDs and oral bioavailability, but they must exhibit high potency, selectivity, and proven intracellular target engagement to be useful probes of biological questions. The prime objective of a chemical probe will always be to interrogate system biology. Making such a probe publicly available can significantly increase the learning curve and therefore enable an earlier understanding about the validity of a novel therapeutic concept. A lead compound is almost always kept secret until the patent application is filed and published.

Chemical probes have proven to be very impactful not only because they are complementary to genetic approaches, such as CRISPR (Clustered Regularly Interspaced Short Palindromic Repeat) and RNAi,[173] but also because they have unique advantages. They can rapidly and reversibly inhibit a protein or a protein domain in cells or animals, be used in almost any cell type and reveal temporal features of target inhibition. They allow the interrogation the catalytic versus scaffolding functions of an enzyme. A target family restricted polypharmacology can be an additional upside potential compared to RNAi studies. Finally, and importantly, the results obtained with chemical probes are more relevant for translational studies as they are more likely to mimic the pharmacology realized when a therapeutic small-molecule drug is used.

The difference in IP restriction between a lead for a drug (keep secret) and a chemical probe (share with the community to learn more about the biology) make such approaches attractive for private–public partnerships. About a decade ago, academia substantially increased its efforts in chemical biology and drug discovery. These efforts arose in part because of the availability of large numbers of uncharacterized potential drug targets emerging from genome sequencing efforts, from the development and commoditization of new screening technologies and from the possibility of inventing new medicines. In the context of public–private partnerships for chemical probes, the Structure Genomics Consortium (SGC; http://www.thesgc.org/) is the leading example for a large collaboration of academic and industry scientists.[174] SGC probes for epigenetic targets require minimally to have in vitro potency at the target protein of <100 nM (ideally by biophysical assays), possess >30-fold selectivity relative to other sequence-related proteins of the same target family, be profiled against an "industry standard" selection of pharmacologically relevant off-targets and against large protein families of relevance to drug discovery and, finally, have demonstrated target engagement in cells at <1 μM. In addition the consortium now also requires that the chemical probe be accompanied by an inactive close analog of the compound (eg, for chiral probes the distomer) to serve as a negative control.

By mid-2015, more than 30 chemical probes have been made publicly available by the SGC and over 6000 samples of SGC probes have been used in various experiments proving the validity of the open access approach.[174] Early successes of open access inhibitors have been driven by bromodomain and, in particular, Bromodomain and extraterminal domain family (BET) inhibitors, but as more probes become available, insights into other target areas and therapeutic potentials are emerging (**Fig. 11**). Importantly, in less than 5 years after the publication of the first BRD4 chemical probe, inhibitors of the BET family have entered clinical trials enabled, in part, through a solid new therapeutic concept validation by the scientific community.

2.02.4 Origin of First-in-Class Drugs: Past and Future Outlook

In 1997, Drews and Ryser[175] published their seminal analysis on escalating research and development (R&D) costs in the pharmaceutical industry. Many additional studies and perspectives have been published since then on the trends, metrics, and measures that drive R&D productivity and the potential causes for the productivity and innovation draught. Groundbreaking scientific discoveries and technological advances like the modern molecular biology method toolbox, fragment, and HTS advances, structure-based drug design, combinatorial and parallel chemistry, and the sequencing of the human genome have allowed a rational, target- and hypothesis-driven approach to drug discovery. They were implemented with the promise of greatly enhancing the productivity of R&D; however, so far there has been little apparent impact of these advances on the number of drug approvals by the US FDA. So was this paradigm shift from the "phenotypic" systems-based drug discovery approach to the target-based the wrong decision for drug discovery? Has the pharmaceutical industry invested trillions in the wrong technologies for almost three decades?

Eder et al.[150] address this worrisome question with the analysis of the origin of first-in-class drugs approved by the FDA between 1999 and 2013. Drugs were designated as first-in-class drugs based on their modulation of—until then— an unprecedented target or biological pathway. This was considered to be independent of the mechanism of modulation, so if for the same target several drugs with different mode of action (eg, reversible and irreversible or competitive and allosteric) exist, only the drug that was approved first was included in the analysis. Using these stringent criteria the drugs were categorized if they emerged from a systems-based approach (target-agnostic approach that is based on a phenotypic change in vitro or in vivo) or target-based approaches (aims to manipulate a biological system by pharmacologically modulating a specific component or target). According to this analysis, of the 114 first-in-class drugs, 34 (30%) were discovered through systems-based approaches and more than double (78, 70%) were discovered from target-based approaches (**Fig. 12A**). While there is no statistically significant trend over the 15-year period that would indicate a clear superiority of one approach over the other, there is a positive trend for an increasing number of newly approved target-based first-in-class drugs (**Fig. 12A** and **Table 6**).

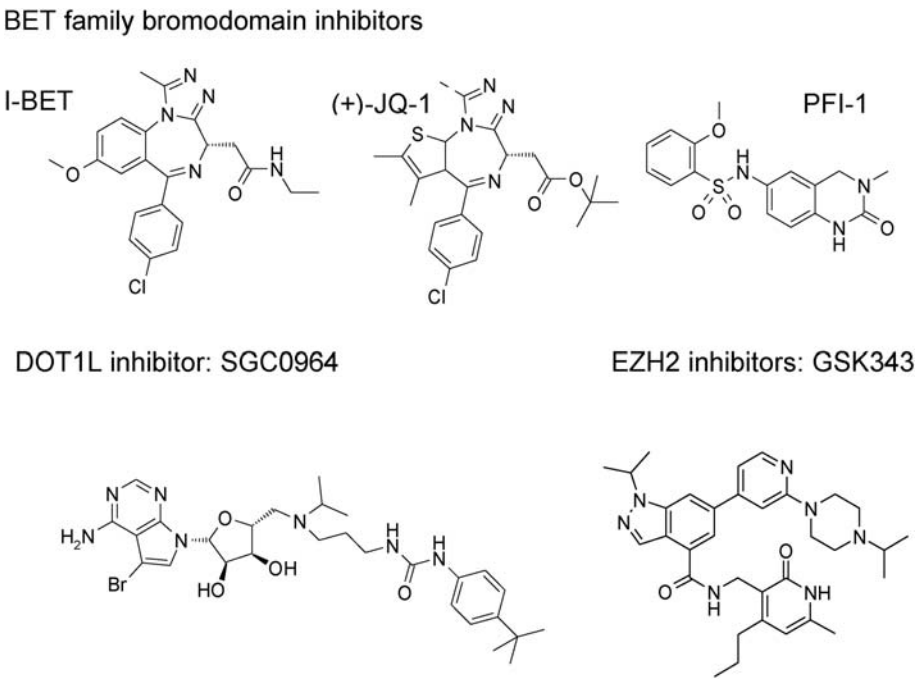

Fig. 11 SGC chemical probes that enabled new therapeutic concept validation and subsequent start of clinical trials (not necessarily with the same compound).

Confirming that the increased investment in target-based approaches translates into more first-in-class drugs, we wondered if the investment in high-throughput and FBS technologies as well as in structural research and improved compound collections in the last decades translates into increased number of first-in-class drugs. Out of the 114 drugs, 34 are biologics and were excluded from further analysis since the finding approaches for antibodies and biologics in general differ significantly from low MW drug discovery. From the remaining 80 first-in-class low molecular drugs, 49 are natural product derived or from existing drugs, 26 drugs originated from screening campaigns, and 5 drugs were derived by de-novo structure-based design (**Fig. 12B**). Although there is a trend for more first-in-class drugs originating from screening leads even in the second decade of the new millennium, the majority of first-in-class drugs did not require sophisticated screening technology or early structural research investments to be discovered. This puzzling finding needs closer examination. Upon additional inspection it becomes clear that approximately half of the first-in-class drugs (26) that originated from analogs were discovered using a systems-based approach. This is different to the screening and "de-novo" structure-based design derived lead-derived drugs where only eight originate from a phenotypic screen. So how have these starting points for analog-based drug discovery been discovered? Thirty-one (63%) of these 49 analogs are actually natural product derived and only 18 (37%) are from former synthetic leads or drugs (see **Table 7** for examples approved in 2013). Looking at patent filing dates for these drugs one has to note that interestingly, all but four, systems-based drugs have their beginnings before 1985. So, the finding that a considerable number of systems-based drugs have been approved over the past 10 years is likely to be due in part to the length of time these projects took. Low MW first-in-class drugs that originated from target-based screening or de-novo structure-based design (taking 8 years) took only half the time as the systems-based approaches (taking 16 years). The data also suggest that target-based drug discovery might have helped reduce the median time for drug discovery and development. However, this does not change the fact that technology driven target-based approaches failed to live up the high expectations put into them. Based on the previously described analysis, systems-based, target-agnostic, approaches seem to be a productive source for first-in-class drugs addressing unmet medical needs. There are principally two major shortcomings for systems-based low MW drug discovery: (1) The shortage of existing chemotypes. Natural products have been a successful source in this respect, but fall out of fashion with the move to target-based approaches. (2) The long time it needs to bring a systems-based drug to the market.

In this context, phenotypic screening could be an important contribution as it offers the potential to provide important new pharmacological tools to study new biology at a faster pace than classical chemocentric systems-based approaches. Phenotypic screening as a new discipline holds the promise to uncover new therapeutic principles and molecular pathways of currently untreatable diseases (see section on Cellular imaging in drug discovery: biomolecular imaging and informatics). In order for phenotypic screening to be successful, it will be important to recognize it as a new discipline that needs new technologies and

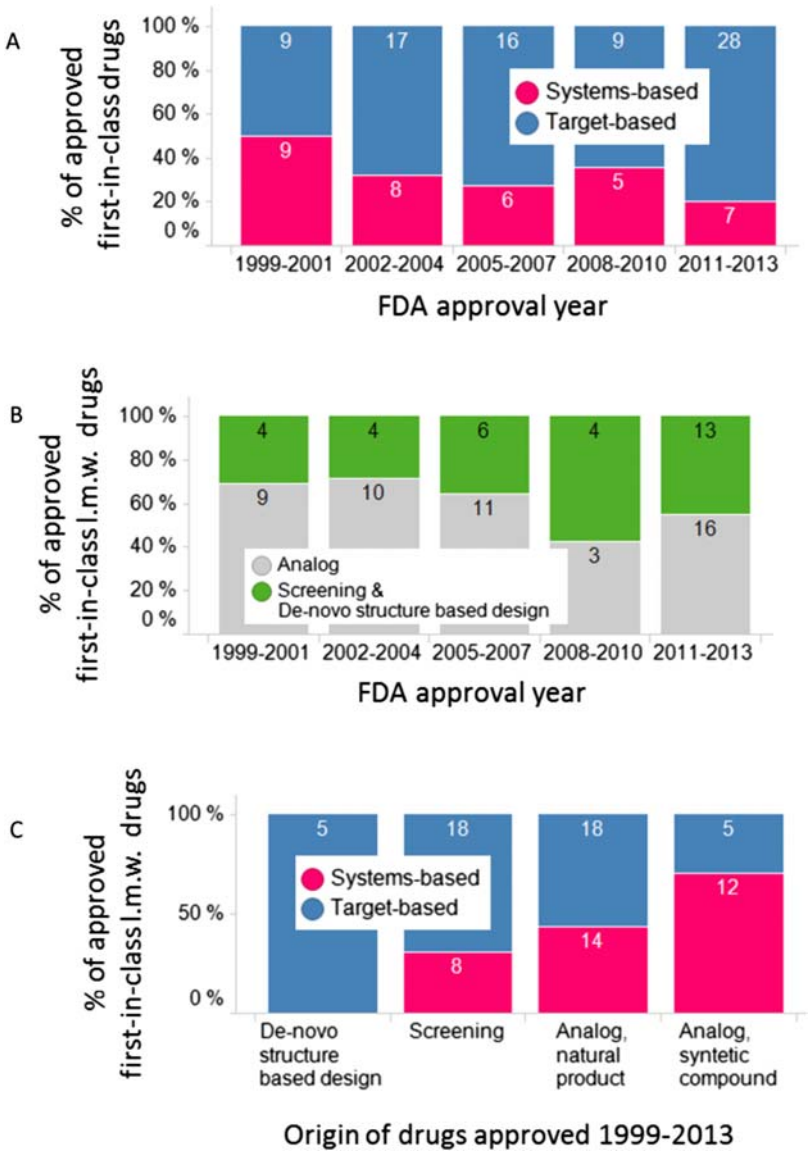

Fig. 12 (A) Percentage of 114 first-in-class drugs that were discovered through systems-based approaches (*red*) and target-based approaches (*blue*) by FDA approval date. Numbers in the bars reflect the discreet number of approved drugs in this category. (B) Percentage of first-in-class drugs that originated from a screening lead or "de-novo" structure-based design (*green*) and an analog-based approach (*gray*) by FDA approval date. Numbers in the bars reflect the discrete numbers of approved drugs in this category. (C) Origin of low molecular weight drugs approved by the FDA between 1999 and 2013.

methods, and for which lessons must be learnt to avoid frustration from unrealistic expectations and premature conclusions if the current investments do not yield quick returns. We therefore consider phenotypic screening not as a neoclassical approach that reverts to a supposedly more successful systems-based method of the past, but instead as a logical evolution of the current target-based activities in drug discovery. Moreover, phenotypic screening is not just dependent on the use of many tools that have been established for target-based approaches; it also requires further technological advancements. The choice should not be between phenotypic screening or target-based discovery, as both approaches can complement each other, are interconnected, and should be run in parallel. Although target or pathway discovery for chemotypes identified from phenotypic screens is not necessarily required for further drug development, it could be an advantage in order to discover additional pathway nodes for target-based therapeutic intervention or to enable the discovery of follow-on drugs. Therefore, the goal will be to screen phenotypically in an efficient and effective manner and to combine phenotypic screening sensibly and productively with target-based drug discovery.

Table 6 One hundred and fourteen first-in-class low molecular drugs approved between 1999 and 2013: Approach and origin of lead structure

Name	*Approach*	*Origin of lead*	*Indication*	*FDA approval*	*Years*[a]
Sofosbuvir	Target-based	Analog, natural product	Hepatitis C viral infection	2013	6
Ibrutinib	Target-based	Screening	Mantle cell lymphoma	2013	6
Riociguat	Target-based	Analog, synthetic compound	Pulmonary arterial hypertension and chronic thromboembolic pulmonary	2013	10
Trametinib	Systems-based	Screening	Melanoma	2013	8
Canagliflozin	Target-based	Analog, natural product	Type 2 diabetes	2013	8
Dimethyl fumarate	Systems-based	Analog, natural product	Multiple sclerosis	2013	16
Mipomersen sodium	Target-based	Analog, natural product	Homozygous familial hypercholesterolemia	2013	10
Crofelemer	Systems-based	Analog, natural product	Diarrhea	2012	6
Bedaquiline	Systems-based	Screening	Tuberculosis	2012	8
Lomitapide	Target-based	Screening	Familial hypercholesterolemia	2012	17
Teduglutide	Target-based	Analog, natural product	Short bowel syndrome	2012	16
Tofacitinib	Target-based	Screening	Rheumatoid arthritis	2012	10
Omacetaxine	Systems-based	Analog, natural product	Cancer (chronic myeloid leukemia)	2012	35
Perampanel	Target-based	Screening	Epilepsy	2012	11
Linaclotide	Target-based	Analog, natural product	Chronic idiopathic constipation, irritable bowel syndrome with constipation	2012	9
Mirabegron	Target-based	Analog, synthetic compound	Overactive bladder	2012	14
Lucinactant	Target-based	Analog, natural product	Respiratory distress syndrome	2012	15
Ivacaftor	Target-based	Screening	Cystic fibrosis	2012	7
Vismodegib	Target-based	Screening	Cancer (basal cell carcinoma)	2012	6
Ingenol mebutate	Systems-based	Analog, natural product	Cancer (actinic keratosis)	2012	11
Ruxolitinib	Target-based	Analog, synthetic compound	Cancer (intermediate or high-risk myelofibrosis)	2011	5
Crizotinib	Target-based	Screening	Cancer (ALK-positive nonsmall cell lung cancers)	2011	6
Icatibant	Target-based	Analog, natural product	Hereditary angioedema	2011	22
Vemurafenib	Target-based	Screening	Cancer (melanoma)	2011	5
Rivaroxaban	Target-based	Screening	Thrombosis	2011	9
Ezogabine	Systems-based	Analog, synthetic compound	Epilepsy	2011	19
Boceprevir	Target-based	De-novo structure-based design	Hepatitis C viral infection	2011	10
Abiraterone	Target-based	Analog, natural product	Cancer (prostate)	2011	18
Roflumilast	Target-based	Screening	Chronic obstructive pulmonary disease	2011	17
Eribulin	Systems-based	Screening	Cancer (breast cancer)	2010	11
Tesamorelin	Target-based	Analog, natural product	Lipodystrophy associated with HIV infection	2010	14
Fingolimod	Systems-based	Screening	Multiple sclerosis	2010	17
Carglumic acid	Target-based	Analog, natural product	Hyperammonemia	2010	44
Artemether-lumefantrine	Systems-based	Screening	Malaria	2009	22
Plerixafor	Systems-based	Screening	Immunostimulant	2008	18
Rufinamide	Systems-based	Analog, synthetic compound	Seizures, epilepsy, Lennox-Gastaut syndrome	2008	23
Tetrahydro-biopterin	Target-based	Analog, natural product	Phenylketonuria	2007	23
Raltegravir	Target-based	Analog, synthetic compound	HIV infection	2007	5
Maraviroc	Target-based	Screening	HIV infection	2007	6
Aliskiren	Target-based	De-novo structure-based design	Hypertension	2007	12
Sinecatechins	Systems-based	Analog, natural product	Genital and perianal warts (antiviral; topical)	2006	11
Sitagliptin	Target-based	Screening	Diabetes type-2	2006	4
Vorinostat	Systems-based	Analog, synthetic compound	Cutaneous T-cell lymphoma (hematologic and solid tumors)	2006	14
Varenicline	Systems-based	Analog, natural product	Smoking cessation	2006	5
Lubiprostone	Systems-based	Analog, natural product	Irritable bowel syndrome and chronic constipation	2006	15

Table 6 One hundred and fourteen first-in-class low molecular drugs approved between 1999 and 2013: Approach and origin of lead structure—cont'd

Name	*Approach*	*Origin of lead*	*Indication*	*FDA approval*	*Years*[a]
Ranolazine	Systems-based	Analog, synthetic compound	Chronic angina pectoris	2006	22
Sunitinib	Target-based	Screening	Cancer (renal cell carcinoma and gastrointestinal stromal tumor)	2006	5
Conivaptan	Target-based	Screening	Hyponatremia	2005	11
Sorafenib	Target-based	Screening	Cancer (renal, liver)	2005	6
Nelarabine	Systems-based	Analog, natural product	Cancer (T-cell acute lymphoblastic leukemia and T-cell lymphoblastic)	2005	17
Ramelteon	Target-based	Analog, natural product	Insomnia	2005	8
Exenatide	Target-based	Analog, natural product	Diabetes type 2	2005	8
Pramlintide	Target-based	Analog, natural product	Diabetes types 1 and 2	2005	12
Ziconotide	Systems-based	Analog, natural product	Severe chronic pain (intrathecal injection)	2004	14
Acamprosate	Target-based	Analog, natural product	Alcohol dependence	2004	7
Azacitidine	Systems-based	Analog, natural product	Myelodysplastic syndromes (cancer)	2004	43
Cinacalcet	Target-based	Screening	Secondary hyperparathyroidism and hypercalcemia in patients with parathyroid carcinoma	2004	8
Memantine	Systems-based	Analog, synthetic compound	Alzheimer's disease	2003	32
Daptomycin	Systems-based	Screening	Antibacterial	2003	18
Miglustat	Systems-based	Analog, natural product	Gaucher disease	2003	26
Bortezomib	Target-based	De-novo structure-based design	Cancer (multiple myeloma, mantle cell lymphoma)	2003	8
Gefitinib	Target-based	Screening	Cancer (breast, lung, others)	2003	7
Aprepitant	Target-based	Analog, synthetic compound	Chemotherapy induced nausea and vomiting	2003	8
Enfuvirtide	Target-based	Analog, natural product	HIV infection	2003	9
Nitazoxanide	Systems-based	Analog, synthetic compound	Antiparasitic (*Cryptosporidium* and *Giardia* infections)	2002	28
Ezetimibe	Systems-based	Analog, synthetic compound	Cardiovascular, LDL cholesterol lowering	2002	10
Nitisinone	Systems-based	Analog, natural product	Hereditary tyrosinemia type 1	2002	16
Bosentan	Target-based	Screening	Pulmonary arterial hypertension	2001	9
Imatinib	Target-based	De-novo structure-based design	Cancer (chronic myelogenous leukemia, gastrointestinal stromal tumors)	2001	8
Caspofungin	Systems-based	Analog, natural product	Fungal infections	2001	7
Mifepristone	Target-based	Analog, natural product	Termination of intrauterine pregnancies	2000	20
Docosanol	Systems-based	Analog, synthetic compound	Herpes simplex virus (topical treatment)	2000	9
Zonisamide	Systems-based	Analog, synthetic compound	Epilepsy	2000	23
Aminolevulinic acid	Systems-based	Analog, natural product	Actinic keratosis	1999	14
Levetiracetam	Systems-based	Analog, synthetic compound	Epilepsy	1999	15
Pemirolast	Systems-based	Analog, synthetic compound	Itch associated with allergic conjunctivitis	1999	22
Sirolimus	Systems-based	Screening	Transplantation, coronary stent coating	1999	26
Zanamivir	Target-based	De-novo structure-based design	Influenza viral infection	1999	8
Orlistat	Target-based	Analog, natural product	Obesity	1999	15
Cilostazol	Systems-based	Analog, synthetic compound	Intermittent claudication in peripheral vascular disease (inhibits platelet)	1999	20

[a]Timespan from first patent filing date to FDA approval.
Adapted from Eder, J.; Sedrani, R.; Wiesmann, C. The Discovery of First-in-Class Drugs: Origins and Evolution. Nat. Rev. Drug Discov. **2014**, *13*, 577–586.

Table 7 Examples of first-in-class drugs approved in 2013

Sofosbuvir (hepatitis C viral infection)

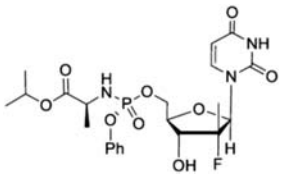

Approach: Target-based | Origin of lead: Analog, natural product | MoA: HCV NS5B polymerase, enzyme inhibitor

Rational design, the molecule is a cytidine analog (prodrug) optimized for selectivity and pharmacokinetic properties

Ibrutinib (mantle cell lymphoma)

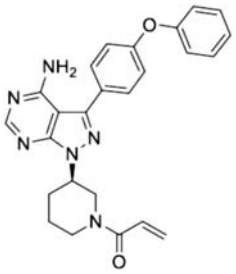

Approach: Target-based | Origin of lead: Screening | MoA: Bruton's tyrosine kinase inhibitor

The fundamental target biology was discovered in 1993. Pyrrolo[2,3-*d*]pyrimidines have been identified as tyrosine kinase inhibitors by screening various compound collections using biochemical kinase assays. The final molecule was rationally designed by introducing an electrophilic group capable of irreversibly inactivating the target. The lymphoma "melting" effect in patients was not predicted by preclinical models

Riociguat (pulmonary arterial hypertension)

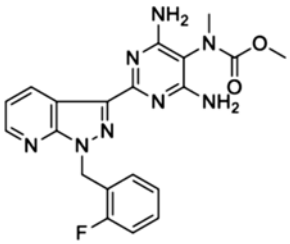

Approach: Target-based | Origin of lead: Analog, synthetic compound | MoA: Stimulator of soluble guanylate cyclase, enzyme

The target rationale was established in the late 1970s. The chemotype was discovered by a systems-based approach in 1994 and later used as a chemical starting point in a target-based drug discovery effort using the recombinant enzyme

Trametinib (melanoma)

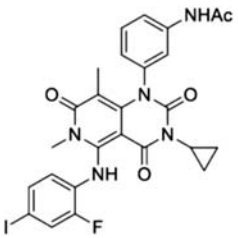

Approach: Systems-based | Origin of lead: Phenotypic screening | MoA: MEK1 and MEK2, allosteric kinase inhibitor

The chemotype was discovered using a cellular screen for inducers of p15INK4B and p27Kip1/CDKN1B and subsequently shown to be a specific, allosteric MEK1/MEK2 inhibitor

Canagliflozin (type 2 diabetes)

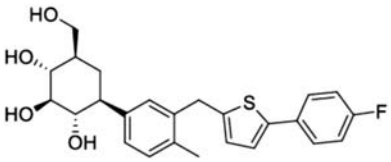

Approach: Target-based | Origin of lead: Analog, natural product | MoA: Sodium-glucose transport protein subtype 2 (SGLT2), enzyme inhibitor

The transporter was cloned in 1992 (Wells et al.). Cloning of a human kidney cDNA with similarity to the sodium-glucose cotransporter and characterized in 1994. The chemotype, inspired by the natural product phlorizin, was optimized to selectively inhibit SGLT2 using a cellular assay with an exogenously overexpressed transporter

Dimethyl fumarate (multiple sclerosis)

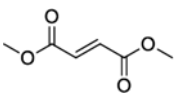

Approach: Systems-based | Origin of lead: Analog, natural product | MoA: Unclear

Serendipitous finding assuming that psoriasis might be caused by a metabolic disturbance involving the citrate cycle. Schweckendiek, who suffered from psoriasis, was working on C4 compounds of the citrate cycle and was taking fumaric acid in a self-experiment. The final molecule was approved for treatment of psoriasis in Germany in 1994 and it was found later that two psoriasis patients who also suffered from multiple sclerosis improved in both diseases. This triggered further clinical trials in multiple sclerosis

Adapted from Eder, J.; Sedrani, R.; Wiesmann, C. The Discovery of First-in-Class Drugs: Origins and Evolution. Nat. Rev. Drug Discov. **2014**, *13*, 577–586.

See also: 2.06. High-Throughput Crystallography and Its Applications in Drug Discovery. 2.08. Fragment-Based Drug Design: Strategic Advances and Lessons Learned. 2.17. Label-Free Screening Technologies. 3.06. Using 3D Structural Information in Computational Design. 3.09. 2/3D Pharmacophore Definitions and Their Application. 3.15. Quantitative Structure–Activity Relationships.

References

1. Verdine, G. L.; Hilinski, G. J. Chapter One—Stapled Peptides for Intracellular Drug Targets. In *Methods in Enzymology;* Dane Wittrup, K., Verdine, G. L., Eds.; vol. 503; Academic Press: Boston, 2012; pp 3–33.
2. Fischer, J.; Ganellin, C. R.; Rotella, D. P. *Analogue-Based Drug Discovery III;* John Wiley & Sons: Weinheim, 2012.
3. Wermuth, C. G. Strategies in the Search for New Lead Compounds or Original Working Hypotheses. In *The Practice of Medicinal Chemistry;* Wermuth, C. G., Ed.; Academic Press: London, 2008; pp 125–143.
4. Freter, K. R. Drug Discovery—Today and Tomorrow: The Role of Medicinal Chemistry. *Pharmaceut. Res.* **1988,** *5,* 397–400.
5. Sneader, W. S. *Drug Prototypes and Their Exploitation;* John Wiley & Sons: Chichester, 1996; p. 9.
6. Lombardino, J. G.; Lowe, J. A. The Role of Medicinal Chemistry in Drug Discovery—Then and Now. *Nat. Rev. Drug Discov.* **2004,** *3,* 853–862.
7. Drews, J. Drug Discovery: A Historical Perspective. *Science* **2000,** *287,* 1960–1963.
8. For example, during the first 4 years of the discovery campaign that led to cimetidine, some 200 compounds were synthesized and assessed Ganellin, C. R. Discovery of the Antiulcer Drug Tagamet. In *Drug Discovery and Development;* Chorghade, M. S., Ed.; vol. 1; John Wiley & Sons, Inc: Hoboken, New Jersey, 2006; p 300.
9. Smith, W. G. Pharmacological Screening Tests. *Progr. Med. Chem.* **1964,** *1,* 1–33.
10. Link, K. P. The Discovery of Dicumarol and its Sequels. *Circulation* **1959,** *19,* 97–107.
11. Whitlon, D. S.; Sadowski, J. A.; Suttie, J. W. Mechanism of Coumarin Action: Significance of Vitamin K Epoxide Reductase Inhibition. *Biochemistry* **1978,** *17* (8), 1371–1377.
12. Zhu, Y. X.; Kortuem, K. M.; Stewart, A. K. Molecular Mechanism of Action of Immune-Modulatory Drugs Thalidomide, Lenalidomide and Pomalidomide in Multiple Myeloma. *Leuk. Lymphoma* **2013,** *54,* 683–687.
13. Man, H.-W.; Schafer, P.; Wong, L. M.; Patterson, R. T.; Corral, L. G.; Raymon, H.; Blease, K.; Leisten, J.; Shirley, M. A.; Tang, Y.; et al. Discovery of (S)-N-{2-[1-(3-ethoxy-4-methoxyphenyl)-2-methanesulfonylethyl]-1,3-dioxo-2,3-dihydro-1H-isoindol-4-yl}acetamide (Apremilast), a Potent and Orally Active Phosphodiesterase 4 and Tumor Necrosis Factor-α Inhibitor. *J. Med. Chem.* **2009,** *52* (6), 1522–1524.
14. Ito, T.; Ando, H.; Suzuki, T.; et al. Identification of a Primary Target of Thalidomide Teratogenicity. *Science* **2010,** *327,* 1345–1350.
15. Carmony, K. C.; Kim, K.-B. PROTAC-Induced Proteolytic Targeting, Ubiquitin Family Modifiers and the Proteasome. *Methods Mol. Biol.* **2012,** *832,* 627–638.
16. Solca, F.; Dahl, G.; Zoephel, A.; Bader, G.; Sanderson, M.; Klein, C.; Kraemer, O.; Himmelsbach, F.; Haaksma, E.; Adolf, G. R. Target Binding Properties and Cellular Activity of Afatinib (BIBW 2992), an Irreversible ErbB Family Blocker. *JPET* **2012,** *343,* 342–350.
17. Dowell, D.; Minna, J. D.; Kirkpatrick, P. Fresh From the Pipeline: Erlotinib Hydrochloride. *Nat. Rev. Drug Discov.* **2005,** *4,* 13–14.
18. Nelson, V.; Ziehr, J.; Agulnik, M.; Johnson, M. Afatinib: Emerging Next-Generation Tyrosine Kinase Inhibitor for NSCLC. *Onco Targets Ther.* **2013,** *6,* 135–143.
19. Congreve, M.; Murray, C. W.; Blundell, T. L. Structural Biology and Drug Discovery. *Drug Discov. Today* **2005,** *10,* 895–907.
20. Roberts, N. A.; Martin, J. A.; Kinchington, D.; Broadhurst, A. V.; Craig, J. C.; Duncan, I. B.; Galpin, S. A.; Handa, B. K.; Kay, J.; et al. Rational Design of Peptide-Based HIV Proteinase Inhibitors. *Science* **1990,** *248* (4953), 358–361.
21. Kim, C. U.; Lew, W.; Williams, M. A.; Wu, H.; Zhang, L.; Chen, X.; Escarpe, P. A.; Mendel, D. B.; Laver, W. G.; Stevens, R. C. J. Structure-Activity Relationship Studies of Novel Carbocyclic Influenza Neuraminidase Inhibitors. *J. Med. Chem.* **1998,** *41* (14), 2451–2460.
22. von Itzstein, M.; Wu, W. Y.; Kok, G. B.; Pegg, M. S.; Dyason, J. C.; Jin, B.; Van Phan, T.; Smythe, M. L.; White, H. F.; et al. Rational Design of Potent Sialidase-Based Inhibitors of Influenza Virus Replication. *Nature* **1993,** *363,* 418–423.
23. Noble, M. E. M.; Endicott, J. A.; Johnson, L. N. Protein Kinase Inhibitors: Insights Into Drug Design From Structure. *Science* **2004,** *303,* 1800–1805.
24. Adams, J.; Palombella, V. J.; Sausville, E. A.; et al. Proteasome Inhibitors: A Novel Class of Potent and Effective Antitumor Agents. *Cancer Res.* **1999,** *59,* 2615–2622.
25. Surleraux, D. L. N. G.; Tahri, A.; Verschueren, W. G.; Pille, G. M. E.; de Kock, H. A.; Jonckers, T. H. M.; Peeters, A.; De Meyer, S.; Azijn, H.; Pauwels, R.; et al. Discovery and Selection of TMC114, a Next Generation HIV-1 Protease Inhibitor. *J. Med. Chem.* **2005,** *48* (6), 1813–1822.
26. Wood, J. M.; Maibaum, J.; Rahuel, J.; Grütter, M. G.; Cohen, N. C.; Rasetti, V.; Rüeger, H.; Göschke, R.; Stutz, S.; Fuhrer, W.; Schilling, W.; Rigollier, P.; Yamaguchi, Y.; Cumin, F.; Baum, H. P.; Schnell, C. R.; Herold, P.; Mah, R.; Jensen, C.; O'Brien, E.; Stanton, A.; Bedigian, M. P. Structure-Based Design of Aliskiren, a Novel Orally Effective Renin Inhibitor. *Biochem. Biophys. Res. Commun.* **2003,** *208,* 698–705.
27. Davies, S. L.; Bolos, J.; Serradell, N.; Bayes, M. Nilotinib. *Drugs Future* **2007,** *32* (1), 17–25.
28. Hauel, N. H.; Nar, H.; Priepke, H.; Ries, U.; Stassen, J.-M.; Wienen, W. Structure-Based Design of Novel Potent Nonpeptide Thrombin Inhibitors. *J. Med. Chem.* **2002,** *45* (9), 1757–1766.
29. Venkatraman, S.; Bogen, S. L.; Arasappan, A.; Bennett, F.; Chen, K.; Jao, E.; Liu, Y.-T.; Lovey, R.; Hendrata, S.; Huang, Y.; et al. Discovery of (1R,5S)-N-[3-Amino-1-(cyclobutylmethyl)-2,3-dioxopropyl]-3-[2(S)-[[[(1,1-dimethylethyl)amino]carbonyl]amino]-3,3-dimethyl-1-oxobutyl]-6,6-dimethyl-3-azabicyclo[3.1.0]hexan-2(S)-carboxamide (SCH 503034), a Selective, Potent, Orally Bioavailable Hepatitis C Virus NS3 Protease Inhibitor: A Potential Therapeutic Agent for the Treatment of Hepatitis C Infection. *J. Med. Chem.* **2006,** *49* (20), 6074–6086.
30. Janssen, P. A. J.; Lewi, P. J.; Arnold, E.; Daeyaert, F.; de Jonge, M.; Heeres, J.; Koymans, L.; Vinkers, M.; Guillemont, J.; Pasquier, E.; et al. In Search of a Novel Anti-HIV Drug: Multidisciplinary Coordination in the Discovery of 4-[[4-[[4-[(1E)-2-cyanoethenyl]-2,6-dimethylphenyl]amino]-2-pyrimidinyl]amino]benzonitrile (R278474, Rilpivirine). *J. Med. Chem.* **2005,** *48* (6), 1901–1909.
31. Lin, C.; Lin, K.; Luong, Y.-P.; Rao, B. G.; Wei, Y.-Y.; Brennan, D. L.; Fulghum, J. R.; Hsiao, H.-M.; Ma, S.; Maxwell, J. P.; et al. In Vitro Resistance Studies of Hepatitis C Virus Serine Protease Inhibitors, VX-950 and BILN 2061: Structural Analysis Indicates Different Resistance Mechanisms. *J. Bio. Chem.* **2004,** *279* (17), 17508–17514.
32. Zhou, H.-J.; Aujay, M. A.; Bennett, M. K.; Dajee, M.; Demo, S. D.; Fang, Y.; Ho, M. N.; Jiang, J.; Kirk, C. J.; Laidig, G. J.; et al. Design and Synthesis of an Orally Bioavailable and Selective Peptide Epoxyketone Proteasome Inhibitor (PR-047). *J. Med. Chem.* **2009,** *52* (9), 3028–3038.
33. Huang, W.-S.; Metcalf, C. A.; Sundaramoorthi, R.; Wang, Y.; Zou, D.; Thomas, R. M.; Zhu, X.; Cai, L.; Wen, D.; Liu, S.; et al. Discovery of 3-[2-(Imidazo[1,2-b]pyridazin-3-yl) ethynyl]-4-methyl-N-[4-((4-methylpiperazin-1-yl)methyl)-3-(trifluoromethyl)phenyl]benzamide (AP24534), a Potent, Orally Active Pan-Inhibitor of Breakpoint Cluster Region-Abelson (BCR-ABL) Kinase Including the T315I Gatekeeper Mutant. *J. Med. Chem.* **2010,** *53* (12), 4701–4719.
34. Feng, J.; Zhang, Z.; Wallace, M. B.; Stafford, J. A.; Kaldor, S. W.; Kassel, D. B.; Navre, M.; Shi, L.; Skene, R. J.; Asakawa, T.; et al. Discovery of Alogliptin: A Potent, Selective, Bioavailable, and Efficacious Inhibitor of Dipeptidyl Peptidase IV. *J. Med. Chem.* **2007,** *50* (10), 2297–2300.
35. Von Wartburg, A.; Traber, R. Cyclosporins, Fungal Metabolites With Immunosuppressive Activities. *Progr. Med. Chem.* **1988,** *25,* 1–33.
36. Takahashi, N.; Hayano, T.; Suzuki, M. Peptidyl-Prolyl Cis-Trans Isomerase Is the Cyclosporin A-Binding Protein Cyclophilin. *Nature* **1989,** *337,* 473–475.
37. Pettit, G. R.; Herald, C. L.; Boyd, M. R.; et al. Isolation and Structure of the Cell Growth Inhibitory Constituents From the Western Pacific Marine Sponge *Axinella* sp. *J. Med. Chem.* **1991,** *34,* 3339–3340.

38. Suzuki, S.; Enosawa, S.; Kakefuda, T.; Shinomiya, T.; Amari, M.; Naoe, S.; Hoshino, Y.; Chiba, K. A. Novel Immunosuppressant, FTY720, With a Unique Mechanism of Action, Induces Long-Term Graft Acceptance in Rat and Dog Allotransplantation. *Transplantation* **1996,** *61* (2), 200–205.
39. Harvey, A. L. Natural Products as a Screening Resource. *Curr. Opin. Chem. Biol.* **2007,** *11* (5), 480–484.
40. Lam, K. S. New Aspects of Natural Products in Drug Discovery. *Trends Microbiol.* **2007,** *15,* 279–289.
41. Shoemaker, R. H.; Scudiero, D. A.; Melillo, G.; Currens, M. J.; Monks, A. P.; Rabow, A. A.; Covell, D. G.; Sausville, E. A. Application of High-Throughput, Molecular-Targeted Screening to Anticancer Drug Discovery. *Curr. Top. Med. Chem.* **2002,** *2,* 229–246.
42. Stearns, B.; Losee, K. A.; Bernstein, J. Hydroxyurea, a New Type of Potential Antitumor Agent. *J. Med. Chem.* **1963,** *6,* 201.
43. Schabel, F. M.; Johnston, T. P.; McCaleb, G. S.; Montgomery, J. A.; Laster, W. R.; Skipper, H. E. Experimental Evaluation of Potential Anticancer Agents. VIII, Effects of Certain Nitrosoureas on Intracerebral L1210 Leukemia. *Cancer Res.* **1963,** *23,* 725–733.
44. Pereira, D. A.; Williams, J. A. Origin and Evolution of High Throughput Screening. *Br. J. Pharmacol.* **2007,** *152* (1), 53–61.
45. Fox, S.; Farr-Jones, S.; Sopchak, L.; et al. High-Throughput Screening: Update on Practices and Success. *J. Biomol. Screen.* **2006,** *11,* 864–869.
46. For drugs that emerged from screening leads between 1995 and 2007 see Proudfoot, J. R. High Throughput Screening and Drug Discovery. In *The Practice of Medicinal Chemistry;* Wermuth, C. G., Ed.; Academic Press: London, 2008; pp 125–143.
47. From 1995–2006 the numbers were taken from reference 48. From 2007–2014 the analysis was performed based on the FDA data (see relevant website) and primary literature review (referenced in Tables 3 and 4).
48. Revill, P.; Serradell, N.; Bolos, J. Eltrombopag. *Drugs Future* **2006,** *31* (9), 767–770.
49. Ludovici, D. W.; De Corte, B. L.; Kukla, M. J.; Ye, H.; Ho, C. Y.; Lichtenstein, M. A.; Kavash, R. W.; Andries, K.; de Bethune, M.-P.; Azijn, H.; et al. Evolution of Anti-HIV Drug Candidates. Part 3: Diarylpyrimidine (DAPY) Analogues. *Bioorg. Med. Chem. Lett.* **2001,** *11,* 2235–2239.
50. Bridger, G. J.; Skerlj, R. T.; Thornton, D.; Padmanabhan, S.; Martellucci, S. A.; Henson, G. W.; Abrams, M. J.; Yamamoto, N.; Vreese, K. D.; et al. Synthesis and Structure-Activity Relationships of Phenylenebis(methylene)-Linked Bis-Tetraazamacrocycles That Inhibit HIV Replication. Effects of Macrocyclic Ring Size and Substituents on the Aromatic Linker. *J. Med. Chem.* **1995,** *38,* 366–378.
51. Ogawa, H.; Yamashita, H.; Kondo, K.; Yamamura, Y.; Miyamoto, H.; Kan, K.; Kitano, K.; Tanaka, M.; Nakaya, K.; et al. Orally Active, Nonpeptide Vasopressin V2 Receptor Antagonists: A Novel Series of 1-[4-(Benzoylamino)benzoyl]-2,3,4,5-tetrahydro-1H-benzazepines and Related Compounds. *J. Med. Chem.* **1996,** *39* (18), 3547–3555.
52. Kondo, K.; Ogawa, H.; Yamashita, H.; Miyamoto, H.; Tanaka, M.; Nakaya, K.; Kitano, K.; Yamamura, Y.; Nakamura, S.; Onogawa, T.; et al. 7-Chloro-5-hydroxy-1-[2-methyl-4-(2-methylbenzoyl-Amino)benzoyl]-2,3,4,5-tetrahydro-1H-1-benzazepine (OPC-41061): A Potent, Orally Active Nonpeptide Arginine Vasopressin V2 Receptor Antagonist. *Bioorg. Med. Chem.* **1999,** *7* (8), 1743–1754.
53. Zou, H. Y.; Li, Q.; Lee, J. H.; Arango, M. E.; McDonnell, S. R.; Yamazaki, S.; Koudriakova, T. B.; Alton, G.; Cui, J. J.; Kung, P.-P.; et al. An Orally Available Small-Molecule Inhibitor of c-Met, PF-2341066, Exhibits Cytoreductive Antitumor Efficacy Through Antiproliferative and Antiangiogenic Mechanisms. *Cancer Res.* **2007,** *67* (9), 4408–4417.
54. Eckhardt, M.; Langkopf, E.; Mark, M.; Tadayyon, M.; Thomas, L.; Nar, H.; Pfrengle, W.; Guth, B.; Lotz, R.; Sieger, P.; et al. 8-(3-(R)-Aminopiperidin-1-yl)-7-but-2-ynyl-3-methyl-1-(4-methyl-quinazolin-2-ylmethyl)-3,7-dihydropurine-2,6-dione (BI 1356), a Highly Potent, Selective, Long-Acting, and Orally Bioavailable DPP-4 Inhibitor for the Treatment of Type 2 Diabetes. *J. Med. Chem.* **2007,** *50* (26), 6450–6453.
55. Roehrig, S.; Straub, A.; Pohlmann, J.; Lampe, T.; Pernerstorfer, J.; Schlemmer, K.-H.; Reinemer, P.; Perzborn, E. Discovery of the Novel Antithrombotic Agent 5-chloro-N-({(5S)-2-oxo-3-[4-(3-oxomorpholin-4-yl)phenyl]-1,3-oxazolidin-5-yl}methyl)thiophene-2-carboxamide (BAY 59–7939): An Oral, Direct Factor Xa Inhibitor. *J. Med. Chem.* **2005,** *48* (19), 5900–5908.
56. Sorbera, L. A.; Leeson, P. A.; Castaner, J. Roflumilast: Antiallergy/Antiasthmatic, Treatment of COPD, Phosphodiesterase 4 Inhibitor. *Drugs Future* **2000,** *25* (12), 1261–1264.
57. Li, R.; Stafford, J. A.; Sun, C. L.; Christensen, J. G.; McMahon, G. *Discovery and Development of Sunitinib (SU11248): A Multitarget Tyrosine Kinase Inhibitor of Tumor Growth, Survival, and Angiogenesis;* Wiley Online Library, 2009. Hoboken, NJ, USA, Chapter 1.
58. Tsai, J.; et al. Discovery of a Selective Inhibitor of Oncogenic B-Raf Kinase With Potent Antimelanoma Activity. *Proc. Natl. Acad. Sci.* **2008,** *105,* 3041–3046.
59. Pinto, D. J. P; Orwat, M. J.; Koch, S.; Rossi, K. A.; Alexander, R. S.; Smallwood, A.; Wong, P. C.; Rendina, A. R.; Luettgen, J. M.; Knabb, R. M.; He, K.; Xin, B.; Wexler, R. R.; Lam, P. Y. S. Discovery of 1-(4-Methoxyphenyl)-7-oxo-6-(4-(2-oxopiperidin-1-yl)phenyl)-4,5,6,7-tetrahydro-1H-pyrazolo[3,4-c]pyridine-3-carboxamide (Apixaban, BMS-562247), a Highly Potent, Selective, Efficacious, and Orally Bioavailable Inhibitor of Blood Coagulation Factor Xa. *J. Med. Chem.* **2007,** *50* (22), 5339–5356.
60. Andries, K.; Verhasselt, P.; Guillemont, J.; Göhlmann, H. W. H.; Neefs, J.-M.; Winkler, H.; Gestel, J. F.; Timmerman, P.; Zhu, M.; Lee, E.; Williams, P.; et al. A Diarylquinoline Drug Active on the ATP Synthase of *Mycobacterium tuberculosis*. *Science* **2005,** *307* (5707), 223–227.
61. Boschelli, D. H.; Wang, D. Y.; Ye, F.; Wu, B.; Zhang, N.; Dutia, M.; Powell, D. W.; Wissner, A.; Arndt, K.; Weber, J. M.; Boschelli, F. Synthesis and Src Kinase Inhibitory Activity of a Series of 4-Phenylamino-3-quinolinecarbonitriles. *J. Med. Chem.* **2001,** *44,* 822–833.
62. Van Goor, F.; Hadida, S.; Grootenhuis, P. D. J.; Burton, B.; Cao, D.; Neuberger, T.; Turnbull, A.; Singh, A.; Joubran, J.; Hazlewood, A.; et al. Rescue of CF Airway Epithelial Cell Function In Vitro by a CFTR Potentiator, VX-770. *PNAS* **2009,** *106* (44), 18825–18830.
63. Wetterau, J. R.; Gregg, R. E.; Harrity, T. W.; Arbeeny, C.; Cap, M.; Connolly, F.; Chu, C.-H.; George, R. J.; Gordon, D. A.; Jamil, H.; et al. An MTP Inhibitor That Normalizes Atherogenic Lipoprotein Levels in WHHL Rabbits. *Science* **1998,** *282* (5389), 751–754.
64. Hibi, S.; Ueno, K.; Nagato, S.; Kawano, K.; Ito, K.; Norimine, Y.; Takenaka, O.; Hanada, T.; Yonaga, M. Discovery of 2-(2-Oxo-1-phenyl-5-pyridin-2-yl-1,2-dihydropyridin-3-yl) benzonitrile (Perampanel): A Novel, Noncompetitive α-Amino-3-hydroxy-5-methyl-4-isoxazolepropanoic Acid (AMPA) Receptor Antagonist. *J. Med. Chem.* **2012,** *55* (23), 10584–10600.
65. Changelian, P. S.; Flanagan, M. E.; Ball, D. J.; Kent, C. R.; Magnuson, K. S.; Martin, W. H.; Rizzuti, B. J.; Sawyer, P. S.; Perry, B. D.; Brissette, W. H.; et al. Prevention of Organ Allograft Rejection by a Specific Janus Kinase 3 Inhibitor. *Science* **2003,** *302* (5646), 875–878.
66. Robarge, K. D.; Brunton, S. A.; Castanedo, G. M.; Cui, Y.; Dina, M. S.; Goldsmith, R.; Gould, S. E.; Guichert, O.; Gunzner, J. L.; Halladay, J.; Jia, W.; Khojasteh, C.; et al. GDC-0449—A Potent Inhibitor of the Hedgehog Pathway. *Bioorg. Med. Chem. Lett.* **2009,** *19,* 5576.
67. Rheault, T. R.; Stellwagen, J. C.; Adjabeng, G. M.; Hornberger, K. R.; Petrov, K. G.; Waterson, A. G.; Dickerson, S. H.; Mook, R. A.; Laquerre, S. G.; King, A. J.; et al. Discovery of Dabrafenib: A Selective Inhibitor of Raf Kinases With Antitumor Activity Against B-Raf-Driven Tumors. *Med. Chem. Lett.* **2013,** *4* (3), 358–362.
68. Pan, Z.; Scheerens, H.; Li, S.-J.; Schultz, B. E.; Sprengeler, P. A.; Burrill, L. C.; Mendonca, R. V.; Sweeney, M. D.; Scott, K. C. K.; Grothaus, P. G.; et al. Discovery of Selective Irreversible Inhibitors for Bruton's Tyrosine Kinase. *Chem. Med. Chem.* **2007,** *2* (1), 58–61.
69. Niwano, Y.; Ohmi, T.; Seo, A.; Kodama, H.; Koga, H.; Sakai, A. Lanoconazole and Its Related Optically Active Compound NND-502: Novel Antifungal Imidazoles With a Ketene Dithioacetal Structure. *Curr. Med. Chem.: Anti-Infect. Agents* **2003,** *2* (2), 147–160.
70. Abe, H.; Kikuchi, S.; Hayakawa, K.; Iida, T.; Nagahashi, N.; Maeda, K.; Sakamoto, J.; Matsumoto, N.; Miura, T.; Matsumura, K.; et al. Discovery of a Highly Potent and Selective MEK Inhibitor: GSK1120212 (JTP-74057 DMSO Solvate). *Med. Chem. Lett.* **2011,** *2* (4), 320–324.
71. Marsilje, T. H.; Pei, W.; Chen, B.; Lu, W.; Uno, T.; Jin, Y.; Jiang, T.; Kim, S.; Li, N.; Warmuth, M.; et al. Synthesis, Structure-Activity Relationships, and In Vivo Efficacy of the Novel Potent and Selective Anaplastic Lymphoma Kinase (ALK) Inhibitor 5-Chloro-N2-(2-isopropoxy-5-methyl-4-(piperidin-4-yl)phenyl)-N4-(2-(isopropylsulfonyl)phenyl) pyrimidine-2,4-diamine (LDK378) Currently in Phase 1 and Phase 2 Clinical Trials. *J. Med. Chem.* **2013,** *56* (14), 5675–5690.
72. Richards, S.; Larson, C. J.; Koltun, E. S.; Hanel, A.; Chan, V.; Nachtigall, J.; Harrison, A.; Aay, N.; Du, H.; Arcalas, A.; et al. Discovery and Characterization of an Inhibitor of Glucosylceramide Synthase. *J. Med. Chem.* **2012,** *55* (9), 4322–4335.
73. Menear, K. A.; Adcock, C.; Boulter, R.; Cockcroft, X.-l.; Copsey, L.; Cranston, A.; Dillon, K. J.; Drzewiecki, J.; Garman, S.; Gomez, S.; et al. 4-[3-(4-Cyclopropanecarbonylpiperazine-1-carbonyl)-4-fluorobenzyl]-2H-phthalazin-1-one: A Novel Bioavailable Inhibitor of Poly(ADP-ribose) Polymerase-1. *J. Med. Chem.* **2008,** *51* (20), 6581–6591.

74. Bouyssou, T.; Hoenke, C.; Rudolf, K.; Lustenberger, P.; Pestel, S.; Sieger, P.; Lotz, R.; Heine, C.; Buettner, F. H.; Schnapp, A.; et al. Discovery of Olodaterol, a Novel Inhaled β2-Adrenoceptor Agonist With a 24 h Bronchodilatory Efficacy. *Bioorg Med. Chem. Lett.* **2010,** *20* (4), 1410–1414.
75. DeGoey, D. A.; Randolph, J. T.; Liu, D.; Pratt, J.; Hutchins, C.; Donner, P.; Rueger, A. C.; Matulenko, M.; Patel, S.; Motter, C. E.; Nelson, L.; Keddy, R.; Tufano, M.; et al. Discovery of ABT-267, a Pan-Genotypic Inhibitor of HCV NS5A. *J. Med. Chem.* **2014,** *57,* 2047–2057.
76. Cox, C. D.; Breslin, M. J.; Whitman, D. B.; Schreier, J. D.; McGaughey, G. B.; Bogusky, M. J.; Roecker, A. J.; Mercer, S. P.; Bednar, R. A.; Lemaire, W.; et al. Discovery of the Dual Orexin Receptor Antagonist [(7R)-4-(5-Chloro-1,3-benzoxazol-2-yl)-7-methyl-1,4-diazepan-1-yl][5-methyl-2-(2H-1,2,3-triazol-2-yl)phenyl]methanone (MK-4305) for the Treatment of Insomnia. *J. Med. Chem.* **2010,** *53* (14), 5320–5332.
77. Lipinski, C. A.; Lombardo, F.; Dominy, B. W.; Feeney, P. J. Experimental and Computational Approaches to Estimate Solubility and Permeability in Drug Discovery and Development Settings. *Adv. Drug Dev. Rev.* **1997,** *23,* 3–25.
78. Lipinski, C. A. Drug-Like Properties and the Causes of Poor Solubility and Poor Permeability. *J. Pharmacol. Toxicol. Meth.* **2001,** *44,* 235–249.
79. Weolock, M. C.; Austin, R. P.; Barton, P.; Davis, A. M.; Leeson, P. D. A Comparison of Physiochemical Property Profiles of Development and Marketed Oral Drugs. *J. Med. Chem.* **2003,** *46,* 1250–1256.
80. Wigglesworth, M. J.; Murray, D. C.; Blackett, C. J.; Kossenjans, M.; Nissink, J. W. M. Increasing the Delivery of Next Generation Therapeutics From High Throughput Screening Libraries. *Curr. Opin. Chem. Biol.* **2015,** *26,* 104–110.
81. Mannocci, L.; Leimbacher, M.; Wichert, M.; Scheuermann, J.; Neri, D. 20 Years of DNA-Encoded Chemical Libraries. *Chem. Commun.* **2011,** *47,* 12747–12753.
82. Greaney, M. F.; Bhat, V. T. Protein-Directed Dynamic Combinatorial Chemistry. In *Dynamic Combinatorial Chemistry: In Drug Discovery, Bioinorganic Chemistry, and Materials Sciences;* Miller, B. L., Ed.; John Wiley & Sons: New Jersey, 2010; pp 43–82. Chapter 2.
83. Harper, G.; Pickeu, S. D.; Green, D. V. S. Design of a Compound Screening Selection for Use in High-Throughput Screening. *Comb. Chem. High Throughput Screen.* **2004,** *7,* 63–71.
84. Wintner, E. A.; Moallemi, C. C. Quantized Surface Complementarity Diversity (QSCD): A Model Based Small Molecule-Target Complementarity. *J. Med. Chem.* **2000,** *43,* 1993–2006.
85. Besnard, J.; Jones, P. S.; Hopkins, A. L.; Pannifer, A. D. The Joint European Compound Library: Boosting Precompetitive Research. *Drug Discov. Today* **2015,** *20,* 181–186.
86. Oprea, T. I.; Davis, A. M.; Teague, S. J.; Leeson, P. D. Is There a Bifference between Leads and Drugs? A Historical Perspective. *J. Chem. Inf. Comput. Sci.* **2001,** *41* (5), 1308–1315.
87. Leeson, P. D.; Springthorpe, B. The Influence of Drug-Like Concepts on Decision-Making in Medicinal Chemistry. *Nat. Rev. Drug Discov.* **2007,** *6,* 881–890.
88. Baell, J.; Walters, M. A. Chemistry: Chemical Con Artists Foil Drug Discovery. *Nature* **2014,** *513,* 481–483.
89. Lane, S.; Eggleston, D. S.; Brinded, K. A.; Hollerton, J. C.; Taytor, N. L.; Readshaw, S. A. Defining and Maintaining a High Quality Screening Collection: The GSK Experience. *Drug Discov. Today* **2006,** *11,* 267–272.
90. Gill, A.; Cleasby, A.; Jhoti, H. The Discovery of Novel Protein Kinase Inhibitors by Using Fragment-Based High Throughput X-ray Crystallography. *Chem. Bio. Chem.* **2005,** *6,* 506–512.
91. Hopkins, A. L.; Groom, C. R.; Alex, A. Ligand Efficiency: A Useful Metric for Lead Selection. *Drug Discov. Today* **2004,** *9,* 430–431.
92. Langer, T.; Hoffmann, R.; Bryant, S.; Lesur, B. Hit Finding: Towards 'Smarter' Approaches. *Curr. Opin. Pharmacol.* **2009,** *9,* 589–593.
93. Clark, D. E. What Has Virtual Screening Ever Done for Drug Discovery? *Exp. Opin. Drug Discov.* **2008,** *3,* 841–851.
94. Glick, M.; Jacoby, E. The Role of Computational Methods in the Identification of Bioactive Compounds. *Curr. Opin. Chem. Biol.* **2011,** *15,* 540–546.
95. Lavecchia, A. Machine-Learning Approaches in Drug Discovery: Methods and Applications. *Drug Discov. Today* **2015,** *20* (3), 318–331.
96. Ripphausen, P.; Nisius, B.; Bajorath, J. State-of-the-Art in Ligandbased Virtual Screening. *Drug Discov. Today* **2011,** *16,* 372–376.
97. Johnson, M. A., Maggiora, G. M., Eds. *Concepts and Applications of Molecular Similarity;* John Wiley & Sons: New York, 1990.
98. Eckert, H.; Bajorath, J. Molecular Similarity Analysis in Virtual Screening: Foundations, Limitations and Novel Approaches. *Drug Discov. Today* **2007,** *12,* 225–233.
99. Hert, J.; Willett, P.; Wilton, D. J.; Acklin, P.; Azzaoui, K.; Jacoby, E.; Schuffenhauer, A. Enhancing the Effectiveness of Similarity-Based Virtual Screening Using Nearest-Neighbor Information. *J. Med. Chem.* **2005,** *48,* 7049–7054; Willett, P. Similarity-Based Virtual Screening Using 2D Fingerprints. *Drug Discov. Today* **2006,** *11,* 1046–1053.
100. Bergner, A.; Parel, S. P. Hit Expansion Approaches Using Multiple Similarity Methods and Virtualized Query Structures. *J. Chem. Inf. Model.* **2013,** *53,* 1057–1066.
101. Rarey, M.; Dixon, J. S. Feature Trees: A New Molecular Similarity Measure Based on Tree Matching. *J. Comput.-Aided Mol. Des* **1998,** *12,* 471–490.
102. Vainio, M. J.; Puranen, J. S.; Johnson, M. S. ShaEP: Molecular Overlay Based on Shape and Electrostatic Potential. *J. Chem. Inf. Model.* **2009,** *49,* 492–502.
103. Nicholls, A.; McGaughey, G. B.; Sheridan, R. P.; Good, A. C.; Warren, G.; Mathieu, M.; Muchmore, S. W.; Brown, S. P.; Grant, J. A.; Haigh, J. A.; Nevins, N.; Jain, A. N.; Kelley, B. Molecular Shape and Medicinal Chemistry: A Perspective. *J. Med. Chem.* **2010,** *53,* 3862–3886.
104. Cheeseright, T.; Mackey, M.; Melville, J.; Vinter, J. G. FieldScreen: Virtual Screening Using Molecular Fields. Application to the DUD Data Set. *J. Chem. Inf. Model.* **2008,** *48,* 2108–2117.
105. Sheridan, R. P.; Kearsley, S. K. Why Do We Need So Many Chemical Similarity Search Methods? *Drug Discov. Today* **2002,** *7,* 903–911.
106. Holliday, J. D.; Kanoulas, E.; Malim, N.; Willett, P. Multiple Search Methods for Similarity-Based Virtual Screening: Analysis of Search Overlap and Precision. *J. Cheminform.* **2011,** *3,* 29.
107. Bender, A.; Jenkins, J. L.; Scheiber, J.; Sukuru, S. C.; Glick, M.; Davies, J. W. How Similar are Similarity Searching Methods? A Principal Component Analysis of Molecular Descriptor Space. *J. Chem. Inf. Model.* **2009,** *49,* 108–119.
108. Willett, P. Combination of Similarity Rankings Using Data Fusion. *J. Chem. Inf. Model.* **2013,** *53,* 1–10.
109. Whittle, M.; Gillet, V. J.; Willett, P.; Loesel, J. Analysis of Data Fusion Methods in Virtual Screening: Similarity and Group Fusion. *J. Chem. Inf. Model.* **2006,** *46,* 2206–2219.
110. Muchmore, S. W.; Debe, D. A.; Metz, J. T.; Brown, S. P.; Martin, Y. C.; Hajduk, P. J. Application of Belief Theory to Similarity Data Fusion for Use in Analog Searching and Lead Hopping. *J. Chem. Inf. Model.* **2008,** *48,* 941–948.
111. Spyrakis, F.; Cavasotto, C. N. Open Challenges in Structure-Based Virtual Screening: Receptor Modeling, Target Flexibility Consideration and Active Site Water Molecules Description. *Arch. Biochem. Biophys.* **2015,** *583,* 105–119.
112. Perot, S.; Sperandio, O.; Miteva, M. A.; Camproux, A. C.; Villoutreix, B. O. Druggable Pockets and Binding Site Centric Chemical Space: A Paradigm Shift in Drug Discovery. *Drug Discov. Today* **2010,** *15,* 656–667.
113. Yuriev, E.; Holien, J.; Ramsland, P. A. Improvements, Trends, and New Ideas in Molecular Docking: 2012–2013 in Review. *J. Mol. Recognit.* **2015,** *10,* 581–604.
114. Beier, C.; Zacharias, M. Tackling the Challenges Posed by Target Flexibility in Drug Design. *Expert Opin. Drug Discov.* **2010,** *5,* 347–359.
115. Ben Nasr, N.; Guillemain, H.; Lagarde, N.; Zagury, J. F.; Montes, M. Multiple Structures for Virtual Ligand Screening: Defining Binding Site Properties-Based Criteria to Optimize the Selection of the Query. *J. Chem. Inf. Model.* **2013,** *53* (2), 293–311.
116. Kämper, A.; Apostolakis, J.; Rarey, M.; Marian, C. M.; Lengauer, T. Fully Automated Flexible Docking of Ligands into Flexible Synthetic Receptors Using Forward and Inverse Docking Strategies. *J. Chem. Inf. Model.* **2006,** *46* (2), 903–911.
117. Verdonk, M. L.; Cole, J. C.; Hartshorn, M. J.; Murray, C. W.; Taylor, R. D. Improved Protein-Ligand Docking Using GOLD. *Proteins* **2003,** *52* (4), 609–623.
118. Kairys, V.; Fernandes, M. X.; Gilson, M. K. Screening Drug-Like Compounds by Docking to Homology Models: A Systematic Study. *J. Chem. Inf. Model.* **2006,** *46,* 365–379.
119. Schmidt, T.; Bergner, A.; Schwede, T. Modelling Three-Dimensional Protein Structures for Applications in Drug Design. *Drug Discov. Today* **2014,** *19* (7), 890–897.
120. Mark, A. E.; van Gunsteren, W. F. Decomposition of the Free Energy of a System in Terms of Specific Interactions. Implications for Theoretical and Experimental Studies. *J. Mol. Biol.* **1994,** *240* (2), 167–176.
121. Broccatelli, F.; Brown, N. Best of Both Worlds: On the Complementarity of Ligand-Based and Structure-Based Virtual Screening. *J. Chem. Inf. Model.* **2014,** *54* (6), 1634–1641.

122. Bosworth, N.; Towers, P. Scintillation Proximity Assay. *Nature* **1989,** *341,* 167–168.
123. Owicki, J. C. Fluorescence Polarization and Anisotropy in High Throughput Screening: Perspectives and Primer. *J. Biomol. Screen.* **2000,** *5,* 297–306.
124. Wendy, A. L.; Simeonov, A. Fluorescence Polarization Assays in Small Molecule Screening. *Expert Opin. Drug Discov.* **2011,** *6,* 17–32.
125. Clegg, R. M. Fluorescence Resonance Energy Transfer. In *Fluorescence Imaging Spectroscopy and Microscopy;* Wang, X. F., Herman, B., Eds.; John Wiley & Sons: New York, 1995; pp 179–252.
126. Simeonov, A.; Jadhav, A.; Thomas, C. J.; Wang, Y.; Huang, R.; Southall, N. T.; Shinn, P.; Smith, J.; Austin, C. P.; Auld, D. S.; Inglese, J. Fluorescence Spectroscopic Profiling of Compound Libraries. *J. Med. Chem.* **2008,** *51,* 2363–2371.
127. Kolb, J. M.; Yamanaka, G.; Manly, S. P. Use of a Novel Homogeneous Fluorescent Technology in High-Throughput Screening. *J. Biomol. Screen.* **1996,** *1,* 203–210.
128. Roda, A.; Guardigli, M.; Pasini, P.; Mirasoli, M. Bioluminescence and Chemiluminescence in Drug Screening. *Anal. Bioanal. Chem.* **2003,** *377,* 826–833.
129. de Wet, J. R.; Wood, K. V.; DeLuca, M.; Helsinki, D. R.; Subramani, S. Firefly Luciferase Gene: Structure and Expression in Mammalian Cells. *Mol. Cell. Biol.* **1987,** *7,* 725–737.
130. Bradley, W. D.; Arora, S.; Busby, J.; Balasubramanian, S.; Gehling, V. S.; Nasveschuk, C. G.; Vaswani, R. G.; et al. EZH2 Inhibitor Efficacy in Non-Hodgkin's Lymphoma Does Not Require Suppression of H3K27 Monomethylation. *Chem. Biol.* **2014,** *21,* 1463–1475.
131. Fan, F.; Wood, K. V. Biochemical Assays for High-Throughput Screening. *Assay Drug Dev. Technol.* **2007,** *5,* 127–136.
132. Bakhtiarova, A.; et al. Resveratrol Inhibits Firefly Luciferase. *Biochem. Biophys. Res. Commun.* **2006,** *351,* 481–484.
133. Ullman, E. F.; et al. Luminescent Oxygen Channeling Immunoassay: Measurement of Particle Binding Kinetics by Chemiluminescent. *Proc. Natl. Acad. Sci. U. S. A.* **1994,** *91,* 5426–5430.
134. Schorp, K.; Rothenaigner, I.; Salmina, E.; Reinshagen, J.; Low, T.; Brenke, J. K.; Gopalakrishnan, J.; Tetko, I. V.; Gul, S.; Hadian, K. Identification of Small-Molecule Frequent Hitters From AlphaScreen High-Throughput Screens. *J. Biomol. Screen.* **2014,** *19,* 715–726.
135. Baell, J. B.; Holloway, G. A. New Substructure Filters for Removal of Pan Assay Interference Compounds (PAINS) From Screening Libraries and for Their Exclusion in Bioassays. *J. Med. Chem.* **2010,** *53* (7), 2719–2740.
136. Shoichet, B. K. Screening in a Spirit Haunted World. *Drug Discov. Today* **2006,** *11,* 607–615.
137. Mayr, L. M.; Fürst, P. The Future of High-Throughput Screening. *J. Biomol. Screen.* **2008,** *13,* 443–448.
138. Thorne, N.; Auld, D. S.; Inglese, J. Apparent Activity in High-Throughput Screening: Origins of Compound-Dependent Assay Interference. *Curr. Opin. Chem. Biol.* **2010,** *14,* 315–324.
139. Clark, R.; Harper, P.; Wigglesworth, M. Technological and Sociological Advances in HTS: Evolution and Revolution? *Eur. Pharm. Rev.* **2013,** *18,* 55–60.
140. Shuker, S. B.; Hajduk, P. J.; Meadows, R. P.; Fesik, S. W. Discovering High-Affinity Ligands for Proteins: SAR by NMR. *Science* **1996,** *274* (5292), 1531–1534.
141. Baker, M. Fragment-Based Lead Discovery Grows Up. *Nat. Rev. Drug Discov.* **2013,** *12,* 5–7.
142. Fink, T.; Reymond, J. L. Virtual Exploration of the Chemical Universe up to 11 Atoms of C, N, O, F: Assembly of 26.4 Million Structures (110.9 Million Stereoisomers) and Analysis for New Ring Systems, Stereochemistry, Physicochemical Properties, Compound Classes, and Drug Discovery. *J. Chem. Inf. Model.* **2007,** *47,* 342–353.
143. Hann, M. M.; Leach, A. R.; Harper, G. Molecular Complexity and Its Impact on the Probability of Finding Leads for Drug Discovery. *J. Chem. Inf. Comput. Sci.* **2001,** *41,* 856.
144. Schiebel, J.; Radeva, N.; Köster, H.; Metz, A.; Krotzky, T.; Kuhnert, M.; Diederich, W. E.; Heine, A.; Neumann, L.; Atmanene, C.; Roecklin, D.; Vivat-Hannah, V.; Renaud, J.-P.; Meinecke, R.; Schlinck, N.; Sitte, A.; Popp, F.; Zeeb, M.; Klebe, G. One Question, Multiple Answers: Biochemical and Biophysical Screening Methods Retrieve Deviating Fragment Hit Lists. *ChemMedChem* **2015,** *10,* 1511–1521.
145. Velvadapu, V.; Farmer, B. T.; Reitz, A. B. Fragment-Based Drug Discovery. In *The Practice of Medicinal Chemistry;* Wermuth, C. G., Ed., 4th ed.; Academic Press: London, 2015; pp 161–180.
146. Joseph-McCarthy, D.; Campbell, A. J.; Kern, G.; Moustakas, D. Fragment-Based Lead Discovery and Design. *J. Chem. Inf. Model.* **2014,** *54* (3), 693–704.
147. Taylor, S. J.; Padyana, A. K.; Abeywardane, A.; Liang, S.; Hao, M. H.; De Lombaert, S. D.; Proudfoot, J.; Bennett, S.; Farmer, S.; Li, X.; Collin, B.; Martin, L.; Albaugh, D. R.; Hill-Drzewi, M.; Pullen, S. S.; Takahashi, H. Discovery of Potent, Selective Chymase Inhibitors via Fragment Linking Strategies. *J. Med. Chem.* **2013,** *56,* 4465.
148. Swinney, D. C.; Anthony, J. How Were New Medicines Discovered? *Nat. Rev. Drug Discov.* **2011,** *10,* 507–519.
149. Swinney, D. C. Phenotypic Versus Target-Based Drug Discovery for First-in-Class Medicines. *Clin. Pharmacol. Ther.* **2013,** *93,* 299–301.
150. Eder, J.; Sedrani, R.; Wiesmann, C. The Discovery of First-in-Class Drugs: Origins and Evolution. *Nat. Rev. Drug Discov.* **2014,** *13,* 577–586.
151. Kluepfel, D.; Bagli, J.; Baker, H.; Charest, M. P.; Kudelski, A.; Sehgal, S. N.; Vezina, C. Myriocin, a New Antifungal Antibiotic From *Myriococcum albomyces*. *J. Antibiot.* **1972,** *25* (2), 109–115.
152. Fujita, T.; et al. Fungal Metabolites. Part 11. A Potent Immunosuppressive Activity Found in Isaria Sinclairii Metabolite. *J. Antibiot.* **1994,** *47,* 208–215.
153. Fujita, T.; Yoneta, M.; Hirose, R.; Sasaki, S.; Inoue, K.; Kiuchi, M.; Hirase, S.; et al. Simple Compounds, 2-Alkyl-2-amino-1,3-propanediols Have Potent Immunosuppressive Activity. *Bioorg. Med. Chem. Lett.* **1995,** *5* (8), 847–852.
154. Adachi, K.; et al. Design, Synthesis, and Structure-Activity-Relationships of 2-Substituted-2-Amino-1,3-Propanediols—Discovery of a Novel Immunosuppressant, Fty720. *Bioorg. Med. Chem. Lett.* **1995,** *5,* 853–856.
155. Mandala, S.; et al. Alteration of Lymphocyte Trafficking by Sphingosine-1-phosphate Receptor Agonists. *Science* **2002,** *296,* 346–349.
156. Spiegel, S.; Milstien, S. Sphingosine-1-phosphate: An Enigmatic Signalling Lipid. *Nat. Rev. Mol. Cell Biol.* **2003,** *4,* 397–407.
157. Brinkmann, V.; et al. The Immune Modulator FTY720 Targets Sphingosine 1-Phosphate Receptors. *J. Biol. Chem.* **2002,** *277* (24), 21453–21457.
158. Brinkmann, V. FTY720 (Fingolimod) in Multiple Sclerosis: Therapeutic Effects in the Immune and the Central Nervous System. *Br. J. Pharmacol.* **2009,** *158,* 1173–1182.
159. Naylor, L. H. Reporter Gene Technology: The Future Looks Bright. *Biochem. Pharmacol.* **1999,** *58,* 749–757.
160. Chiba, T.; Tsuchiya, T.; Mori, R.; Shimokawa, I. Protein Reporter Bioassay Systems for the Phenotypic Screening of Candidate Drugs: A Mouse Platform for Anti-Aging Drug Screening. *Sensors* **2012,** *12,* 1648–1656.
161. Schirle, M.; Jenkins, J. L. Identifying Compound Efficacy Targets in Phenotypic Drug Discovery. *Drug Discov. Today* **2015,** *21,* 82–89.
162. Martinez, M. D.; Jafari, R.; Ignatushchenko, M.; Seki, T.; Larsson, E. A.; Dan, C.; Sreekumar, L.; Cao, Y.; Nordlund, P. Monitoring Drug Target Engagement in Cells and Tissues Using the Cellular Thermal Shift Assay. *Science* **2013,** *341* (6141), 84–87.
163. Rix, U.; Superti-Furga, G. Target Profiling of Small Molecules by Chemical Proteomics. *Nat. Chem. Biol.* **2009,** *5,* 616–624.
164. Arnoldo, A.; et al. A Genome Scale Overexpression Screen to Reveal Drug Activity in Human Cells. *Genome Med.* **2014,** *6,* 32.
165. Palchaudhuri, R.; Hergenrother, P. J. Transcript Profiling and RNA Interference as Tools to Identify Small Molecule Mechanisms and Therapeutic Potential. *ACS Chem. Biol.* **2011,** *6,* 21–33.
166. Matheny, C. J.; et al. Next-Generation NAMPT Inhibitors Identified by Sequential High-Throughput Phenotypic Chemical and Functional Genomic Screens. *Chem. Biol.* **2013,** *20,* 1352–1363.
167. Genick, C. C.; Barlier, D.; Monna, D.; Brunner, R.; Bé, C.; Scheufler, C.; Ottl, J. Applications of Biophysics in High-Throughput Screening Hit Validation. *J. Biomol. Screen.* **2014,** *19* (5), 707–714.
168. Steinmeyer, A. The Hit-to-Lead Process at Schering AG: Strategic Aspects. *ChemMedChem* **2006,** *1,* 31–36.
169. Wunberg, T.; Hendrix, M.; Hillisch, A.; Lobell, M.; Meier, H.; Schmeck, C.; Wild, H.; Hinzen, B. Improving the Hit-to-Lead Process: Data-Driven Assessment of Drug-Like and Lead-Like Screening Hits. *Drug Discov. Today* **2006,** *11,* 175–180.
170. Baxter, A.; Brough, S.; Cooper, A.; Floettmann, E.; Poster, S.; Harding, C.; Kettle, J.; McInally, T.; Martin, C.; Mobbs, M.; Needham, M.; Newham, P.; Paine, S.; St-Gallay, S.; Salter, S.; Unitt, J.; Xue, Y. Hit-to-Lead Studies: The Discovery of Potent, Orally Active, Thiophenecarboxamide IKK-2 Irthibitors. *Bioorg. Med. Chem.* **2004,** *14* (11), 2817–2822.

171. Reasor, J. R.; Hasting, K. L.; Ulrich, R. G. Drug-Induced Phospholipidosis: Issues and Future Directions. *Expert Opin. Drug Saf.* **2006,** *5* (4), 567–583.
172. Chiba, M.; Ishii, Y.; Sugiyama, Y. Prediction of Hepatic Clearance in Human From *In Vitro* Data for Successful Drug Development. *AAPS J.* **2009,** *11* (2), 262–276.
173. Weiss, W. A.; Taylor, S. S.; Shokat, K. M. *Recognizing and exploiting differences between RNAi and small-molecule inhibitors.* Nat. Chem. Biol. **2007,** *3,* 739–744.
174. Brown, P. J.; Müller, S. Open Access Chemical Probes for Epigenetic Targets. *Future Med. Chem.* **2015,** *7,* 1901–1917 [Epub ahead of print].
175. Drews, J.; Ryser, S. The Role of Innovation in Drug Development. *Nat. Biotechnol.* **1997,** *15,* 1318–1319.

Relevant Websites

https://www.centerwatch.com/drug-information/fda-approved-drugs. The above link is to a database containing a listing of drugs (NMEs) approved by the Food and Drug Administration (FDA) for sale in the United States. Drug information typically includes the drug name, approval status, indication of use, and clinical trial results. A New Molecular Entity (NME) is defined by the FDA as a medication containing an active substance that has never before been approved for marketing in any form in the United States. The database also includes some recombinant proteins and biologics that were approved by the FDA's Center for Drug Evaluation and Research (CDER).

2.03 Multiobjective Optimization of Biological and Physical Properties in Drug Discovery

MP Gleeson, Kasetsart University, Bangkok, Thailand
D Montanari, H. Lundbeck A/S, Valby, Denmark

© 2017 Elsevier Ltd. All rights reserved.

2.03.1	**Introduction**	64
2.03.1.1	Multiobjective Optimization in Drug Discovery	65
2.03.1.2	Defining the Project Target Requirements	66
2.03.1.2.1	Target potency and selectivity requirements	67
2.03.1.3	Physical Properties	69
2.03.2	**Multiobjective Optimization and the Role of Physical Properties**	70
2.03.2.1	Drug-Like Property Space	70
2.03.2.2	DMPK, Safety, and Physical Properties	70
2.03.2.3	Target Activity and Physical Properties	71
2.03.2.3.1	Ligand efficiency	75
2.03.3	**Multiobjective Optimization of PK/PD Parameters**	76
2.03.3.1	Assessment of PK/PD Properties of Development Compounds	76
2.03.3.2	Achieving a Balanced PK/PD Profile	78
2.03.3.3	Drug Efficiency and the Free Drug Hypothesis	79
2.03.3.3.1	Definition of DRUG efficiency	80
2.03.3.3.2	Drug efficiency index	81
2.03.4	**Effect of Systematic Biases in Drug Discovery**	87
2.03.4.1	The Effect of Personal and Organization Biases	87
2.03.4.2	Overcoming Systematic Biases	88
2.03.5	**Conclusions**	89
Acknowledgment		89
References		90
Relevant websites		93

2.03.1 Introduction

The pharmaceutical industry has undergone dramatic changes over recent decades, adapting to an ever evolving understanding of how to target human diseases. This has resulted in the incorporation of additional assays, technologies and management practices into the drug discovery process.[1] It has invariably led to the earlier assessment of preclinical compounds using in vitro and animal models for efficacy, safety, and pharmacokinetics. The increased number of new targets under investigation, and the increasing front loading in the preclinical phase have led to a dramatic increase in research and development (R&D) costs.[2,3] Nevertheless, it has been predicted that without a considerable increase in productivity, or the adoption of new approaches and practices, that drug discovery will become unsustainable in the future.[3–5]

Recent analyses of marketed drugs showed that the mean development cost per drug molecule was approximately 1.8 billion US dollars (USD), with 32% of the cost coming from the preclinical phase and 63% in the clinical phase.[5,6] However, analysis of the total cost throughout development, both on projects that resulted in drugs, and those that were prematurely terminated, has shown that the total costs in clinical and preclinical development were similar. The two most cost intensive phases identified were lead optimization and phase III.[5,6] Yet > 90% of all drug candidates identified in the preclinical phase fail in clinical development, with in vivo safety and efficacy being the primary scientific causes for termination.[5,7,8] This would suggest that the predictive value of the preclinical scientific process is in need of improvement.[9–11]

Mergers and the widespread downsizing observed in the pharmaceutical industry are an unsurprising reaction to the high costs and the low predictive performance of the preclinical phases. This has forced the industry to cut R&D by moving to lower cost regions[5] as well as reorganize internally into smaller units.[12,13] The benefit of the latter approach is that dogmatic practices that can develop within large organizations are less likely to take hold, including standardized progression paths and milestones, which have the potential to limit true scientific innovation.[10,14,15]

The typical medicinal chemist follows a reasonable well defined process starting with target selection, hit identification and the subsequent lead optimization.[16] Target selection is often based on clinically unvalidated disease or systems-biology data; hit selection using simple, robust biochemical or cellular assays; lead optimization aided by in vitro and in vivo data on animals.[17] The sophistication of the models employed in this process is without question, yet the integration of this data to identify the best

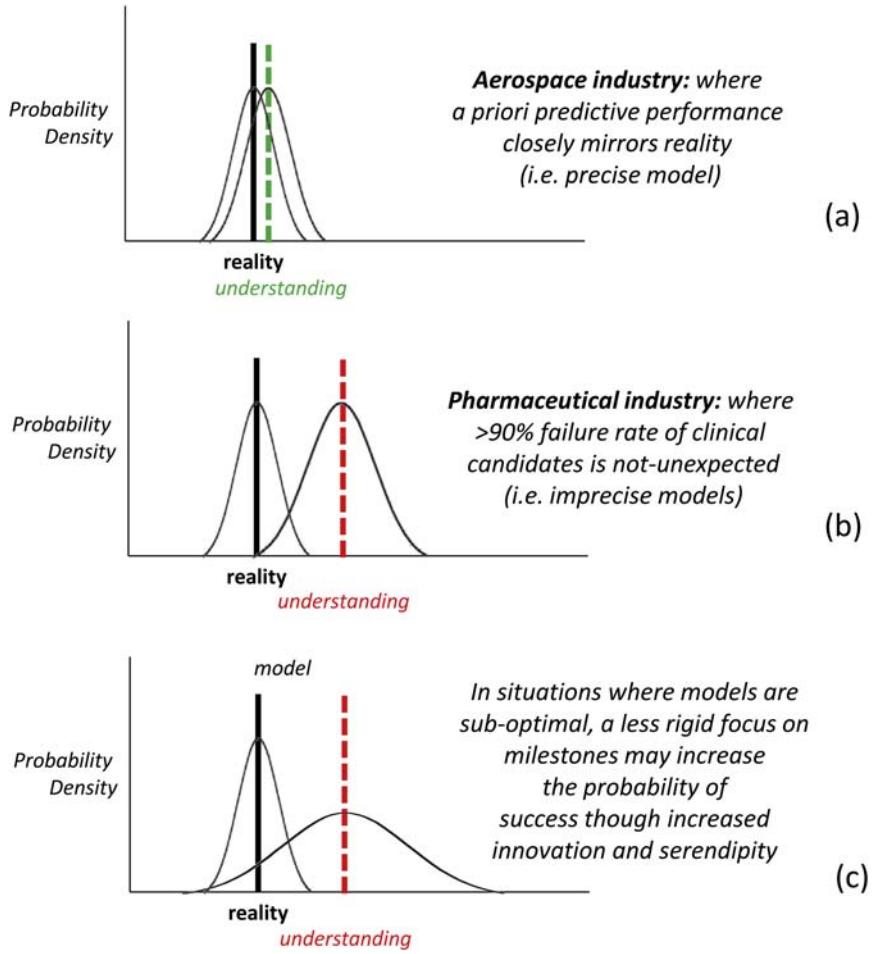

Fig. 1 Some models are of more utility than others: (A) the aerospace and (B) pharmaceutical industry. In the case of (C), models with more limited predictive capability can also be effectively used, however in such cases additional flexibility in the solutions should be considered to identify or include serendipitous and innovative discoveries.

possible compounds to test the disease-target hypothesis is perhaps not. The development statistics discussed above highlight that there is considerable potential to improve the discovery process: How and when we collect data and how it is integrated together in a multiobjective fashion.

In this chapter we consider whether the use of the term "process" in conjunction with drug discovery is perhaps optimistic, since it is difficult to define a rigid flow-chart process for something that is not fully understood or difficult to model.[18–22] Contrast the pharmaceutical and aerospace industries. The process of designing new aircraft, which also utilizes theoretical and physical models, is found to be considerable more predictive (Fig. 1). In the latter case, focusing development efforts on models that show good agreement with reality results in a design that translate well.[14] In contrast, when models show weaker agreement with reality, focusing rigidly to these will probably not result in translatable designs. In such a situation a more effective approach would be to incorporate information from these models, yet acknowledge the limitations of the methods, and in doing so, undertake parallel approaches to maximize the probability of success though true innovation and/or serendipity.[15,23]

We discuss issues regarding the drug-target hypothesizes, pharmacokinetics & dynamics (PK/PD), toxicity and physical properties, and whether they are fully accounted for in a systematic fashion during the translational process.

2.03.1.1 Multiobjective Optimization in Drug Discovery

The retrospective analysis of drug discovery data is a valuable means to gain insight into the phenomenally complex process that is drug discovery. Unfortunately, the available data generated on clinical candidates and drug molecules to date is insufficient, or not of sufficient quality or diversity, to fully understand or define with any accuracy, a universal concept of "drug-like" properties. Indeed, at present drug-likeness is more often framed in terms of the physical property space occupied by oral drugs rather than being a definition of a precise location in biological/pharmacological space. Nevertheless, analysis of the available data generated in drug discovery can still shed light on the challenges we face and how we can adapt to them.

Morgan et al.[8] reported an insightful retrospective analysis of phase II compounds from Pfizer. Forty four compounds for which progression decisions were made were analyzed in terms of the underlying causes of success and failure. They defined 3 criteria, the 3 pillars of survival, to assess the outcome of the phase II trials:

(1) exposure time profile at the target site of action,
(2) binding to the pharmacological target and receptor engagement,
(3) confidence in the validity of the target and the pharmacological outcome.

It was found that just 14 (33%) of the compounds that had successfully exited preclinical research, and progressed through phase I trials, achieved a positive proof of concept by meeting all 3 of the criteria.[8] Efficacy (ie, 1&2) was the principal cause of failures (27%), while exposure issues (2&3) led to a further 13%. The final 27% of compound failed to meet any of the criteria. The authors stated that a back to basic approach to better integrate pharmacology and PK is needed to improve the chances of success.

Scientists from AstraZeneca reported a retrospective analysis of 142 small molecule projects between 2005–10 to understand the causes of project failure and to identify the features associated with successful outcomes.[10] Phase II failures were identified as being the greatest issue, with safety and efficacy being the main causes of attrition. It was found that unacceptable safety was the most important reason for failure overall, accounting for more than half of all project closures. The majority of these failures occurred before clinical testing and in phase I. Safety related failures remained an important reason for project closure in later development with approximately 30% of projects failing due to safety issues in Phase II. The other highest cause of project closure overall was a lack of efficacy in the chosen disease indication. Overall, 65% of projects failed owing to efficacy issues in Phase II. Failures due to exposure were lower than that reported by Morgan et al. at Pfizer,[8] which is potentially due to the definitions used and the level of detail in which project failures were analyzed. The authors came up with recommendations to target the main causes of failure by suggesting a careful consideration of the most appropriate parameters needed from the outset:

(1) Right target
(2) Right tissue
(3) Right safety
(4) Right patients
(5) Right commercial potential
(6) Right culture

AstraZeneca, Eli Lilly, GlaxoSmithKline, and Pfizer joined together to analyze their development failures in terms of the role of physicochemical properties.[7] This collaboration was driven by the fact that no individual company has sufficient numbers of compounds, or the chemical diversity, to determine statistically reliable trends. The authors found that toxicology and safety issues were the principal causes of failures, with portfolio rationalization also being a major issue. In phase II, efficacy, followed by clinical safety were the dominant reasons for termination. Failures due to exposure were low. The authors also noted the importance of physicochemical properties in controlling absorption, distribution, metabolism, excretion, and toxicity (ADMET) but that beyond a certain point (ie, after preclinical optimization is complete), the effect of such factors become negligible.[7]

2.03.1.2 Defining the Project Target Requirements

Target selection and the definition of a desired pharmacokinetic profile are critical steps in a discovery project. This will fundamentally influence the nature of the compounds selected in hit identification and their subsequent optimization.[10,24] It has been demonstrated that the success of a project is predicated on the strength of the target validation available and the types of assays used to identify and optimize compounds.[5,7,10,25] Recent reports have highlighted the problems associated with target validation, with one study from Novartis noting that only 23% of 70 published claims in the literature could be verified.[18] Additionally, Amgen scientists were able to reproduce just 6 out of 53 landmark studies in the oncology area,[26] highlighting the need for increased rigor in target validation.[19,27]

Target based approaches have dominated the drug discovery process due to the benefits of selectively modulating a single target that is relevant to the disease pathway.[28] Network pharmacology studies have suggested that disease-target pathways are highly complex and having compounds which have polypharmacology, but are not promiscuous,[29] may in fact be desirable. The question is how we can identify the required pharmacological profile, from a target based or phenotypic based screening. Swinney et al.[30,31] reported that projects that have employed phenotypic assays either as the primary assay, or a secondary assay, were identified as having a greater probability of success than those that used target based approaches.[31,32] It is presumed that a further benefit of the phenotypic approach is that permeability and solubility are concomitantly optimized along with the pharmacologically relevant target interaction. However, Eder et al.[33] suggest the success of the phenotypic approach has been overstated and the full effect of target based approaches has yet to be observed. Furthermore, a limitation of the phenotypic approach is the difficulty in identifying the precise target,[34,35] and/or the precise mode of action.[36]

Castoreno and Eggert[37] stated that in vitro assays based on purified proteins, while extremely useful to identify potent and selective compounds, have limits including: (i) they primarily target very specific and measurable functions of a protein or complex of proteins, either particular enzymatic activities or particular functional interactions between defined proteins; (ii) potent and selective in vitro activity is not necessarily predictive of actual activity in cells, for example, due to poor cell permeability; and (iii) the

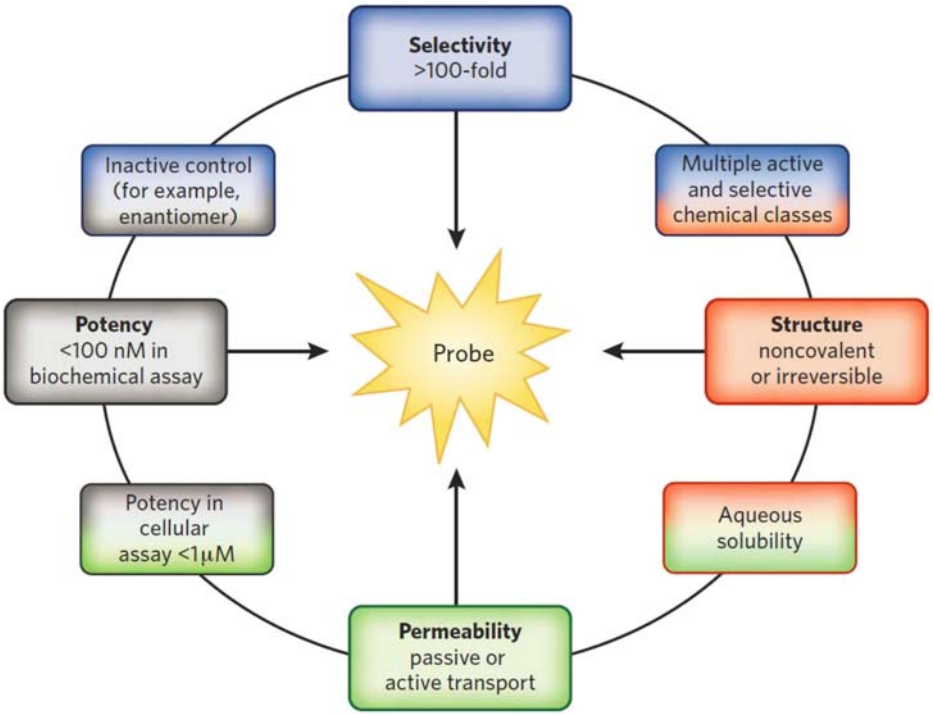

Fig. 2 Important criteria for designing and creating effective chemical probes. Selectivity against close-family-member biological targets, chemical structure and mode of inhibition, cell permeability, and biochemical activity are four essential considerations in designing successful chemical probes. Additional considerations may include aqueous solubility and potency in cellular assays, the value of building a chemical tool kit that includes probes from orthogonal active and selective chemical classes and the importance of having structurally related inactive controls. Figure reproduced with permission from reference Bunnage, M.E.; Chekler, E.L.P.; Jones, L.H., Target Validation Using Chemical Probes. *Nat. Chem. Biol.* **2013**, 9(4), 195–199.

scope of off-target cellular effects due to, for example, similarities between related proteins, eg, kinases, as well as toxicity is not readily discernible.

It has been suggested that project teams can sometimes place too much confidence in the early disease-target hypothesis and that without due-diligence to validate that link, the project risks wasting time and resource before failing in later development.[38] Indeed, this is consistent with the large failure rates due to efficacy in phase II trials and suggests greater effort should be made to produce selective chemical probes to validate the hypothesis prior to late stage development.[2,39] In practice, the requirements for a probe are not so far from those of a clinical candidate (Fig. 2). Both require good solubility and permeability, potency <100 nM and selectivity of >100-fold. Obtaining the required selectivity can be challenging as the screening panels used to assess compounds are not necessarily sufficient to meet this criteria completely, meaning a positive or negative response may still have a degree of uncertainty.[40,41] Validation in preclinical cellular or animal models using both active and inactive variants of a chemotype at the suggested target offers a means to confirm the role of the target in the disease.[2,39] In addition, detailed preclinical studies in models of diseased[17] and healthy tissue are not necessarily performed early in the life of a project. However their deployment towards the start of the project have been suggested to help confirm target engagement and the expected pharmacology.[42]

Covalent binding compounds are often avoided due to increased safety risk, however, given the large number of drugs that function via this mechanism, there are some who argue that this neglected mechanism offers great potential.[43,44] Indeed the blocker buster drug omeprazole, as well as penicillins, act in a covalent fashion, indicating their potential.[45] The known limitation with this approach is that the reactive functionality employed in such molecules have the potential to cause unintended off-target pharmacological effects.[22] The majority of these drugs were identified by serendipity, but more recently a number of compounds in clinical development have been specifically developed to target such a mechanism.[44]

2.03.1.2.1 Target potency and selectivity requirements

It is necessary to consider the expression levels of the target in question and how it is distributed, and what level of activity and exposure will be needed to modulate it. As is common with any multidimensional problem, focus at the early stage typically turns to those variables that are more easily controllable. Compounds are assessed for potency as measured in an in vitro assay system as the primary filter. Potency is typically expressed as $pXC_{50} = -\text{Log}XC_{50}$, where XC_{50} is the concentration of a substance that results in

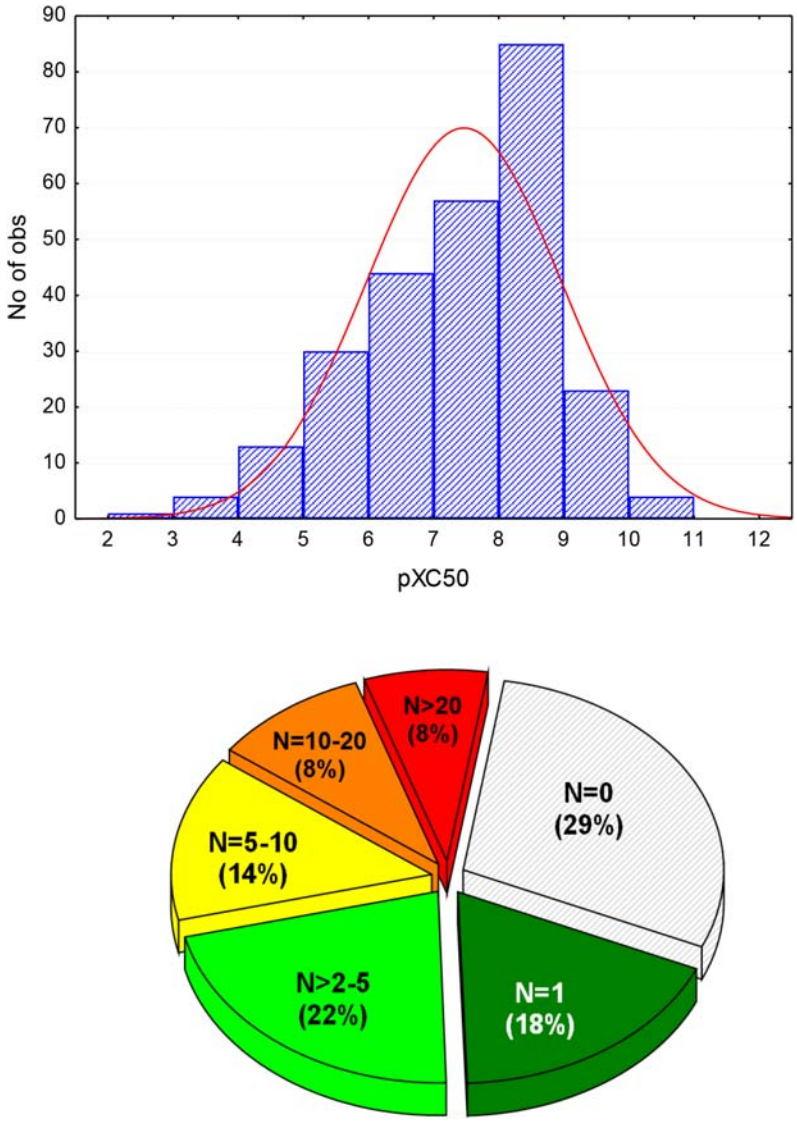

Fig. 3 The reported (A) therapeutically relevant pXC_{50}s values for 261 oral drugs has a mean value of 63 μM. (B) Promiscuity of oral drugs where *N* is the number of reported hits in target based assays in ChEMBL with an XC50 $\leq$ 1 μM. Adapted with permission from reference Gleeson, M.P.; Hersey, A.; Montanari, D.; Overington, J., Probing the Links Between in vitro Potency, ADMET and Physicochemical Parameters. *Nat. Rev. Drug Discov.* **2011**, 10, 197–208.

a 50% biological effect at the therapeutic target. It is common to aim for $<$ 100 nM, yet many projects extol the benefits of even greater potency ($\sim$1 nM) as can be appreciated from the perusal of articles in the medicinal chemistry literature.

Analysis of the biological activities of a set of drugs would appear to suggest these are somewhat arbitrary cut-offs. Overington et al.[46] extracted the reported on and off-target potencies of drug molecules and found that the median XC_{50} was approximately 16 nM. Later, Gleeson et al.[47] extracted and analyzed the mean target potencies of 261 oral drugs, finding a median value of approximately 50 nM. Irrespective of the precise median value, the XC_{50} distribution in Fig. 3A suggests that a large percentage of molecules have XC_{50} at or around 1 μM.[47]

The distribution presented Fig. 3A suggests that potency cut-offs should be taken as approximate given the need to balance a wide range of biological parameters in the eventual candidate molecule, as well as the uncertainty or relevance of the assay system being used. It could be argued that benefit should exist in probing lower potency compounds in certain circumstances. Moreover, setting an arbitrary cut-off of 0.1 μM for compounds to progress to a secondary screening assay may have the unintended consequence of excluding compounds with more optimal characteristics (ie, solubility & permeability) that might allow improved efficacy.

Drug selectivity can also be assessed from data reported in the literature (Fig. 3B). The data associated with 291 oral drugs shows that a large number of these compounds hit multiple targets at or below 1 μM and suggests they are not totally selective.[46]

This data can be considered in the context of the current discussions around designing in specific target selectivity to a molecule,[34,48–50] as well as the desire to avoid high promiscuity, particularly at known antitargets such as the potassium channel encoded by the human ether a go-go related gene (hERG) and cytochrome P450 enzymes (CYP).[40] Reports on anticancer compounds show that while avoiding particular pathways is desirable, the complexity of the disease means that poly pharmacology approaches are highly attractive.[51,52] This is consistent with a move away from the traditional "1 disease—1 target" hypothesis,[34,48–50] which has been accompanied by an increased interest in target nonspecific, phenotypic screening methods.[17,28,32,35,36,53]

2.03.1.3 Physical Properties

The physical properties of legacy oral drugs are found to cluster into a relatively tight area of chemical space. The earliest, and most notable observation was provided by Lipinski et al who noted that oral drugs and late stage development compounds were found to have no more than 1 parameter outside of the following: molecular weight (MWT) $\leq$ 500, lipophilicity (logP) $\leq$ 5, hydrogen bond donors (HBD) $\leq$ 10 and hydrogen bond acceptors (HBA) $\leq$ 5.[54] The so called "Lipinski rule of 5" was general considered to represent a property range in which good solubility and permeability, which are important for oral exposure, was more likely.

Teague et al. subsequently introduced the distinction between lead-like and drug-like molecules, noting that the low potency leads obtained from high throughput screening (HTS) were often optimized beyond drug-like space in an effort to obtain potency.[55] They defined medicinal chemistry "lead-like space," wherein lead-like structures are, on the average, less complex.[56] Libraries consisting of molecules with MWT between 100–350 and calculated logP (clogP) between 1 and 3 were therefore proposed to be superior to ones consisting of drug-like compounds.[55,57] Later Oprea et al. were to show that it was also possible to define a literature publication-like (pub-like, or data reported in the peer reviewed literature) chemical space which lay beyond lead or drug-like space.[58] They proposed that these highly optimized, typically potent compounds derived from failed drug discovery or academic projects, therefore had higher mean MWT and logP.[58] This effect can be seen from a comparison of ChEMBL compounds (pub-like) to oral drugs (Fig. 4). The ChEMBL dataset is made up of 112,586 unique compounds while the oral drug dataset consists of approximately 2000.[59] As can be seen from the density contours, the area occupied by pub-like compounds is dramatically larger, and shifted upwards in terms of the MWT and logP of oral drugs.

Wenlock et al.[60] considered how parameters such as MWT and logP affected the progression of compounds though the different phases of development. The properties showing the clearest influence on the successful passage of a candidate drug through the different stages of development are MWT and logP. Statistical analysis shows that the mean MWT of orally administered drugs in development decreases on passing through each of the different clinical phases and gradually converges toward the mean MWT of marketed oral drugs. A more recent analysis of attrition also noted a link between these two physicochemical properties and clinical failure due to safety issues, and that the parameters identified in the former analysis should be restrained, though only up to a point (ie, no absolute guarantee of success).[7]

Proudfoot analyzed the variation in physical properties of oral drugs over the period 1937–97 and found that the most notable change in molecular properties was a steady increase in MWT.[59] In contrast, the logP was found not to have changed. In addition, fewer than 5% of oral marketed drugs have more than 4 H-bond donors and a small number exceed both the MWT $\leq$ 500 and HBD $\leq$ 5 rules suggesting that Lipinski's rule is a relatively generous definition of legacy drug-like space (as it was designed to be). Nonetheless, drug molecules that violate the rule of 5 are not negligible ($\sim$12%) and there is some concern that restricting physical properties to those of legacy drugs might stifle our ability to target less druggable targets. While target classes do show differences in terms of the molecular properties of their ligands, these differences do not appear to justify searching beyond drug-like space.[24,61]

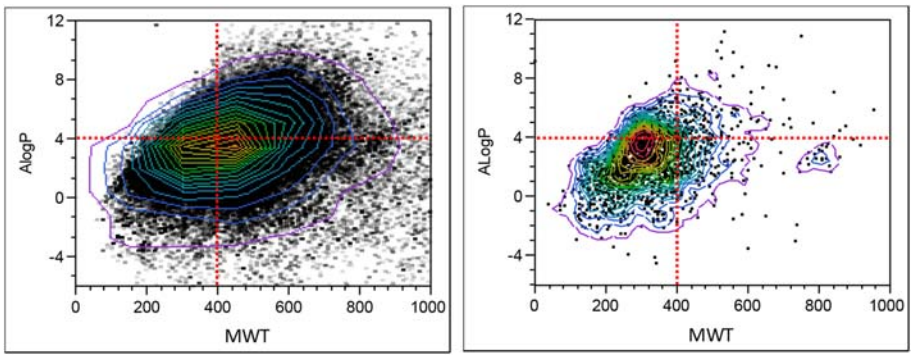

Fig. 4 Plot of MWT against calculated logP (ALogP) for ChEMBL database pub-like compounds (N=112,586) and oral drugs (N=1791). Red contours represent area of maximum density while blue represent lowest. Adapted with permission from reference Gleeson, M.P.; Hersey, A.; Montanari, D.; Overington, J., Probing the Links Between in vitro Potency, ADMET and Physicochemical Parameters. *Nat. Rev. Drug Discov.* **2011**, 10, 197–208.

2.03.2 Multiobjective Optimization and the Role of Physical Properties

The job of identifying a molecule that meets the project requirements (ie, can safely modulate a therapeutic target in human with minimal side effects) is a massively complex undertaking with many unknowns. The medicinal chemist lies at the center of this endeavor and is tasked with distilling the information from disparate disciplines in the discovery effort to synthesize and deliver a suitable candidate.[62–65] This process involves a degree of subjective decision making to select and iterative modify a lead series to achieve the desired criteria. The decisions made by an individual are based on a unique combination of their unique expertise, educational background, past project experiences and organizational culture.

The process of drug discovery involves trying to standardize the decision making such that we try to tackle known issues (ie, commonly experienced) in drug discovery. Yet it is clear that our current understanding represents the tip of the iceberg, with many "known-unknowns" and "unknown-unknowns." Thus, the definition of rigid progression path and milestones, may act to restrict the choices open to the medicinal chemist, thereby stifling the opportunity for progress achieved through trial and error, serendipity, and innovative thinking. The drug discovery scientist must be given sufficient leeway to think outside of the box, without fear of re-percussions should it fail. This requires a less rigid process with better and more flexible management oversight less driven by metrics.[10]

The challenge for the medicinal chemist, and indeed their partners in drug discovery, is to know when to think outside of the box and when to follow convention. This is a challenge in the serial drug discovery process as the decisions made early in the project will invariably lead the project team down a restrictive path that offers little room for maneuver. Yet, there is now an acknowledgment that a parallel process, where the aim is to assess many compounds rapidly, and fail them rapidly, may be a more effective way to perform drug discovery.[5,14]

2.03.2.1 Drug-Like Property Space

Despite Lipinski's et al.'s seminal paper[54] being close to 2 decades old, the restraining of physicochemical parameters to an area of drug-like space is still somewhat controversial.[66,67] Analyses have shown that moving outside drug-like space leads to poorer ADMET parameters and increased promiscuity, yet there are many who see these constraints potentially hamper the search for drugs for less druggable targets.[68] Focusing on the exceptions to the rule can be desirable for reasons of diversity, but only up to a point as the probability of success is expected to drop accordingly. The consensus opinion is that properties should be restrained within drug-like space unless there are clear reasons to move beyond them. [47,54,67,69–71]

Drug discovery must be pursued with a view to maximizing the chances of success and all data to date suggest that drug-like space is a confined area of parameter space where it is probabilistically more likely to obtain a molecule with a good balance of properties. Should a project team feel it was pertinent to spend a percentage of medicinal chemistry resource to explore this region, for the purpose of generating structure activity relationships (SAR), then that could certainly be justified so as to not restrict innovation or serendipity. [64,72] However, it would be prudent for organizations to look at their preclinical drug discovery efforts as a whole and ensure that the overall molecular properties of the compounds they are working on can be justified given the range of target classes and due to the apparent benefits of remaining within legacy drug-like space.

2.03.2.2 DMPK, Safety, and Physical Properties

Lipinski et al.[54] reported that marketed drugs and drugs in clinical development had distinctive molecular property distributions. Over approximately two decades since this analysis, numerous researchers have worked to improve our understanding of link between ADMET parameters and physicochemical properties.[47,72–78]

The role of some key physicochemical parameters (MWT, logP, and ionization state) were demonstrated quite clearly using 10,000 s of proprietary GSK data on commonly measured ADMET parameters (**Table 1**).[79]

Table 1 List of the ADMET assays evaluated in references[79,80]

Assay type	*Description*
Solubility	Phosphate buffer pH 7.4
Permeability	Permeability assay pH 7.4
Oral bioavailability	Rat—in vivo PK studies
Volume of distribution	Rat—in vivo PK studies
Plasma protein binding	Rat plasma—equilibrium dialysis
CNS penetration	Rat—in vivo PK studies
P-gp substrate efflux	MDCK assay with and without a P-gp inhibitor
Brain tissue binding	Rat brain homogenate—equilibrium dialysis
In vivo clearance	Rat—*in vivo* PK studies
hERG inhibition	[^{3}H] dofetilide assay
CYP inhibition	Fluorescence based assay

Analyses demonstrated the underlying intercorrelation between common physicochemical properties and a range of measured ADMET parameters (Table 2). This allowed for a direct comparison between the physicochemical parameters having a simultaneous impact on multiple ADMET endpoints. The effects observed using proprietary GSK compounds[79] can also be demonstrated using open access ChEMBL data.[47] This data consisted of diverse compounds from a range of assays including solubility, bioavailability, plasma protein binding and P450 3A4 inhibition (Fig. 5). It is apparent there is an overall detrimental effect of increasing logP and MWT on average within these diverse sets. Furthermore, the results are in agreement with SAR observations on smaller congeneric series.[79]

Due to the fact the datasets are highly diverse in nature, the trends observed are relatively weak compared to those often observed within a congeneric series. However, the results demonstrate that the probability of obtaining favorable ADMET across all assays is probabilistically less likely with increased logP and MWT. It also offers a quick method of assessing what ADMET properties might be modulated for a given series to give rise to the desired property change. For example, a basic compound with significant P450 2D6 inhibition would generally be expected to improve by reducing lipophilicity, as well as removing any basic center, assuming it was tolerated by the target pharmacophore. Alternatively, one could add an acidic center, yet this would also likely to lead to a drop in permeability (Table 3).

Safety represents an altogether more challenging endpoint to predict as the causes can be both target specific and nonspecific in nature. Unlike many ADME endpoints, relatively little bulk property SAR exists (excluding hERG and P450s) for the multitude of known toxicity pathways. The following represent the key causes of safety related issues:

(1) due to primary pharmacology of the molecule,
(2) secondary pharmacology of the molecule,
(3) due to a structural fragment or toxicophore in the molecule,
(4) the overall physicochemical properties of the molecule.

The progression of a molecule through development rarely occurs in the absence of some form of toxicity, thus it is necessary that this risk be mitigated using the predicted safety margins and the therapeutic exposure level required to modulate the target. Prediction of the therapeutic index is a nontrivial process that according to Muller and Milton requires more effective approaches to systematically and quantitatively compare the in vitro and in vivo data and to apply this knowledge more effectively.[82]

Some toxicity endpoints have been shown to correlate to some degree with physicochemical parameters. Unintended off-target activity is often a source of side effects and a number of studies have shown that making molecules larger (not necessarily more complex) and more lipophilic is likely to increase this effect.[47,74,75,83] Basicity has also been shown to be a factor that increases the probability of off-target effects.[83] It has been clearly demonstrated that strong hERG inhibition correlates with the presence of a basic center and higher lipophilicity.[79,84,85]

Nevertheless, molecular properties can get you only so far, as revealed by Leach et al.[86] The authors showed sizeable differences in certain ADMET parameters (ie, solubility, intrinsic clearance and volume of distribution) for different enantiomeric pairs. The large differences could not be explained by properties alone which is in line with reports from clinical attrition data that while important, molecular properties will get you only so far.[7]

2.03.2.3 Target Activity and Physical Properties

The identification of a therapeutic target allows for the instigation of assay development, and medicinal chemistry efforts can subsequently start. HTS is the primary source of hits at this early stage.[87,88] HTS has a reported success rate $>60\%$[88] for identifying tractable leads, however doubt regarding its effectiveness remain.[89] The origin of this doubt relates to the suitability of the compounds in terms of their molecular properties.

Over two decades ago a survey of the tightest binding compounds for a variety of protein targets showed that the free energy of binding increases with the number of nonhydrogen atoms. For ligands with more than 15 nonhydrogen atoms, the free energy of binding plateaus, increasing very little with additional MWT.[90] This and other analyses[91] inferred that potency can be built into compounds by increasing the number of Van der Waals interactions and overall hydrophobicity. These fundamental observations, rather than being an effective way to quickly increase the potency of a molecular series, could potentially be a distraction in the generation of molecules with balanced biological and physical properties. A more recent analysis by Hajduk et al. showed that an optimal 64 Da increase in MWT was needed per 1 log unit increase in activity.[92]

To demonstrate the correlation between MWT, logP and target activity, we have analyzed six target specific sets[93] containing a single chemotype and a diverse set of molecules with activities at a variety of receptors (Figs. 6 and 7).[47] Analysis of variance (ANOVA) was used to show the relationship between the molecular properties, which are binned, and the target activity. A diverse dataset of 205,582 unique target-compound activities (112,586 unique compounds) derived from the ChEMBL database shows a statistically significant relationship (Fig. 7). It can be seen that the higher MWT and logP compounds have higher potencies on average. It is also apparent that a 100 Da increase in MWT appears to have a stronger effect on the mean affinity than a 1 log unit increase in logP. Broken down by specific target-molecular series pairs also reveals similar relationships (Fig. 6). The effect of increasing MWT was found to be statistically significant for 4 out of 5 chemotypes, while the effect for logP was observed for 2 (logP and MWT show some degree of intercorrelation). This indicates these two properties do play a role in defining the level of potency of a series. As we will show, restraint needs to be exercised in the pursuit of potency so that project teams focus on specific enthalpic gains through new interactions rather than though nonspecific effects.

Table 2 An indication of how changes in key molecular properties will affect a range of ADMET parameters. Green indicates, better, orange neutral, and red poorer values of the ADMET parameter in question (relative to the mean of the distribution). MWT and logP (calculated logP) cut-offs of 400 and 4 respectively are used

Neutral Molecules	Mwt<400 & clogP<4	Mwt>400 &/or clogP>4
Solubility	Average	Lower
Permeability[a]	Higher	Average/Higher
Bioavailability	Average	Lower
Volume of Dist.[b]	Average	Average
Protein Binding	Average	Higher
CNS Penetration[c]	Higher/Average	Average/Lower
Brain Tissue Binding	Lower	Higher
P-gp Efflux	Average	Higher/Average
In-vivo Clearance	Average	Average
hERG Inhibition	Lower	Lower
P450 Inhibition[d]	Lower 2C9, 2C19, 2D6 & 3A4 inhibition	Higher 2C9, 2C19 & 3A4 inhibition
"	Higher 1A2 inhibition	Lower 1A2
"		Average 2D6 inhibition
Basic Molecules	**Mwt<400 & clogP<4**	**Mwt>400 &/or clogP>4**
Solubility	Average/Higher	Average/Lower
Permeability[a]	Higher/Average	Average
Bioavailability	Average	Lower
Volume of Dist.[b]	Average/Higher	Higher
Protein Binding	Lower	Average
CNS Penetration[c]	Higher/Average	Average/Lower
Brain Tissue Binding	Lower	Higher
P-gp Efflux	Average	Higher/Average
In-vivo Clearance	Average	Higher/Average
hERG Inhibition	Average/Higher	Higher
P450 Inhibition[d]	Lower 1A2, 2C9, & 2C19 inhibition	Lower 1A2 inhibition
"	Average 2D6 & 3A4 inhibition	Average 2C9, 2C19 inhibition
"		Higher 2D6 & 3A4 inhibition
Acidic Molecules	**Mwt<400 & clogP<4**	**Mwt>400 &/or clogP>4**
Solubility	Higher	Average/Higher
Permeability[a]	Lower	Lower/Average
Bioavailability	Low/Average	Average
Volume of Dist.[b]	Lower	Lower
Protein Binding	High/Average	Higher
CNS Penetration[c]	Lower	Lower
Brain Tissue Binding	Lower	Higher
P-gp Efflux	Lower	Lower
In-vivo Clearance	Lower/Average	Average
hERG Inhibition	Lower	Lower
P450 Inhibition[d]	Lower 1A2, 2C9, 2C19, 2D6 & 3A4 inhibition	Lower 1A2, 2C19, 2D6 & 3A4 inhibition
"		Higher 2C9 inhibition
Zwitterionic Molecules	**Mwt<400 & clogP<4**	**Mwt>400 &/or clogP>4**
Solubility	Higher	Average/Higher
Permeability[a]	Lower	Lower/Average
Bioavailability	Lower	Lower
Volume of Dist.[b]	Lower	Average/Lower
Protein Binding	Low/Average	Higher
CNS Penetration[c]	Average/Lower	Lower
Brain Tissue Binding	Lower	Higher
P-gp Efflux	Average	Average
In-vivo Clearance	Average	Average
hERG Inhibition	Lower	Average/Lower
P450 Inhibition[d]	Lower 1A2, 2C9, 2C19, 2D6 & 3A4 inhibition	Lower 1A2, 2C19 & 3A4 inhibition
"		Average 2C9, 2D6 inhibition

[a]Optimum clogP bin is 3–5 with respect to permeability.
[b]Average to high volumes rather than high, low or average generally considered optimum.
[c]Low CNS considered optimum, although for targets in the brain this will be reversed.
[d]Some isoforms show a nonlinear relationship with clogP and/or MWT.
Reproduced from reference Gleeson, M.P., Generation of a Set of Simple, Interpretable ADMET Rules of Thumb. *J. Med. Chem.* **2008**, 51,(4), 817–834 with the permission of the American Chemical Society.

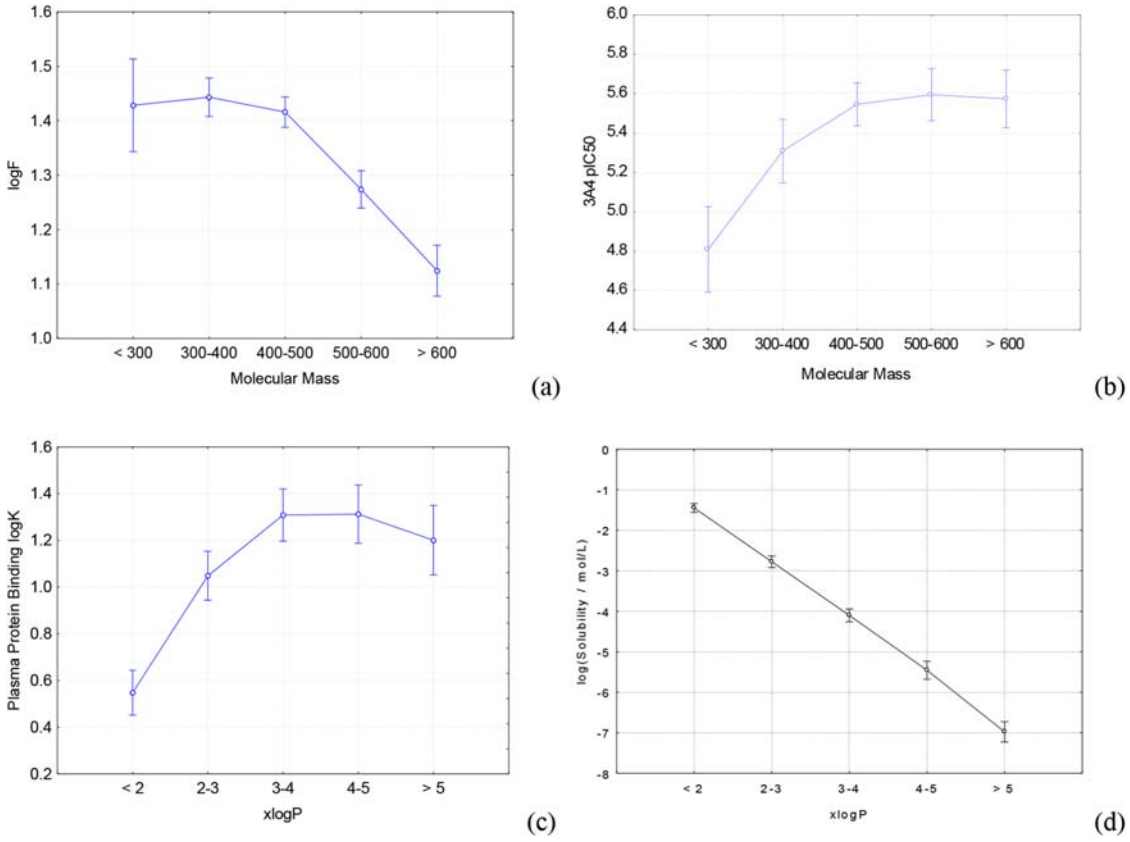

Fig. 5 The relationship between 4 different ADMET parameters and either molecular mass or logP. Bioavailability ($N=3644$), 3A4 inhibition ($N=742$) and plasma protein binding data ($N=1101$) was obtained from the ChEMBL database. Solubility data ($N=1144$) was taken from reference.[81] Adapted with permission from reference Gleeson, M.P.; Hersey, A.; Montanari, D.; Overington, J., Probing the Links Between in vitro Potency, ADMET and Physicochemical Parameters. *Nat. Rev. Drug Discov.* **2011**, 10, 197–208.

Table 3 Typical DMPK and exploratory toxicological assays during hit to lead (HtoL) and lead optimization (LO) phases

Phase	*DMPK*	*Exploratory toxicology*
HtoL & LO	In silico physicochemical profiling	In silico physicochemical profiling
HtoL & LO	In silico ADME profiling	In silico TOX profiling
HtoL & LO	Permeability and efflux ratio (ie, P-gp)	Target safety assessment
HtoL & LO	CYP450 inhibition (automated)	hERG (automated)
HtoL & LO	Metabolic stability (clint) in liver microsomes in rat and human	Hepatotoxicity: mitochondrial toxicity
HtoL & LO	Evidence of systemic exposure after oral or desired route of administration dosing in PD species	Hepatotoxicity: cytotoxicity
HtoL & LO	Plasma protein binding in relevant species	Hepatotoxicity: oxidative stress
HtoL & LO	Target tissues binding (ie, brain)	Hepatotoxicity: glutathione depletion
LO	Metabolic stability (clint) in hepatocytes in rat, human, and relevant species	Hepatotoxicity: transporter assays
LO	CYP450 induction	Genotoxicity: MiniAmes
LO	Metabolite id	Genotoxicity: In vitro micronucleus
LO	Low dose iv/po PK in rat	Genotoxicity: GreenScreen
LO	Low dose full PK in nonrodent species	CV Ion channels
LO	PK at different doses	In vivo cardiac electrophysiology and hemodynamic in relevant species
LO	DDI and bioactivation assessment (ie, Glutatione trapping and CYP450 Mechanism-based inhibition)	Exploratory in vivo toxicity studies

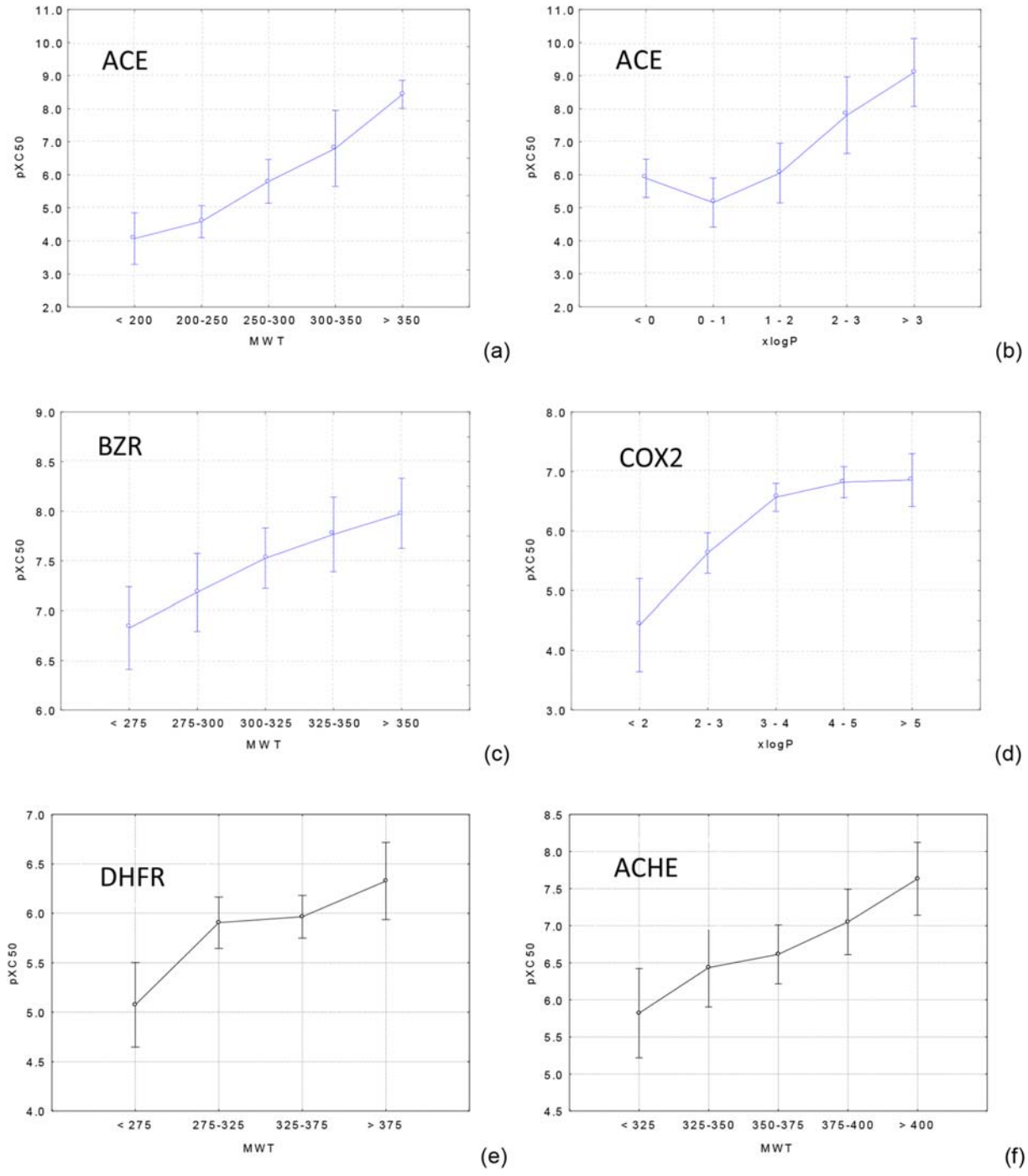

Fig. 6 The relationship between the in vitro potency, MWT and calculated logP for 5 different chemotypes (specific structural scaffold/class of compound), each acting at a single target.[94] Adapted with permission from reference Gleeson, M.P.; Hersey, A.; Montanari, D.; Overington, J., Probing the Links Between in vitro Potency, ADMET and Physicochemical Parameters. *Nat. Rev. Drug Discov.* **2011**, 10, 197–208.

Increasing logP and MWT will also affect compound selectivity. The theoretical analyses of Harper et al. demonstrated that as the complexity of a molecule increased the probability of inhibiting multiple different targets decreases.[95] While nominally larger molecules might be considered more complex, due to increased lipophilicity/bulk that may not be the case. The addition of substituents that can form van der Waals (VDW) interactions in essentially nonspecific binding pockets, i.e. the addition of "grease," which drives the entropic partitioning of the molecule from solution (hydrophobic effect). Thus, while an approach to increase potency though increases in size and logP may work in the short term, the probability of having off-target activity increases accordingly. Experimental evidence for this comes from the work of Leeson et al. analyzed a dataset of approximately 2000 compound screened

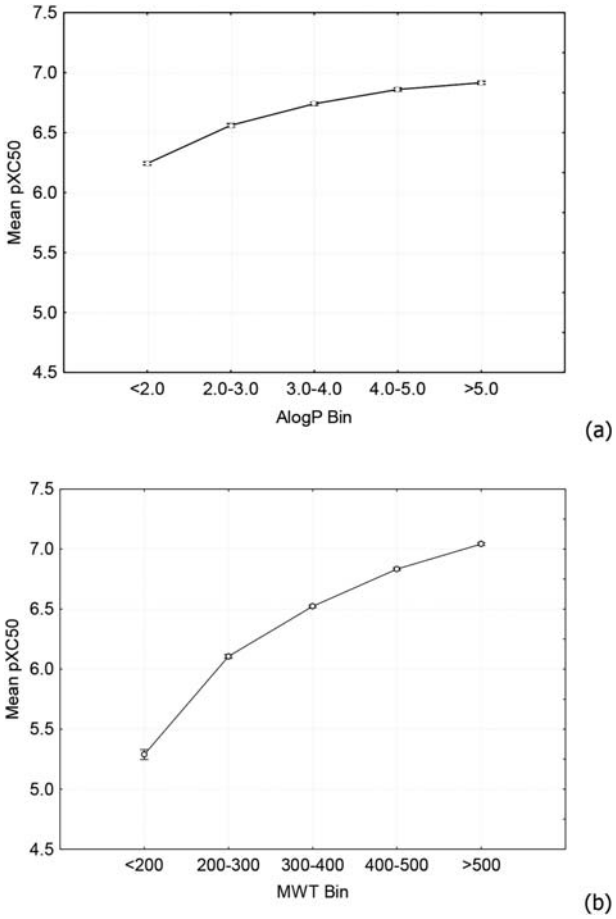

Fig. 7 The relationship between the mean reported in vitro potency (pXC_{50}), MWT and calculated logP for 201,355 compounds with reported activity measurements in the ChEMBL. Adapted with permission from reference Gleeson, M.P.; Hersey, A.; Montanari, D.; Overington, J., Probing the Links Between in vitro Potency, ADMET and Physicochemical Parameters. *Nat. Rev. Drug Discov.* **2011**, 10, 197–208.

in the Bioprint® database which had % inhibition data at approximately 140 targets. They noted a significant relationship between increasing promiscuity with increasing clogP and to a lesser extent MWT.[75] A subsequent analysis of pXC_{50} values of oral drugs derived from ChEMBL by Gleeson et al.[47] also demonstrated the negative effect of logP and also MWT on selectivity. Additionally, Peters et al. analyzed an updated Bioprint® dataset and identified lipophilicity and the basic pKa as key drivers for promiscuity.[83]

2.03.2.3.1 Ligand efficiency

It would appear that the availability of relatively cheap, high throughput purified protein and recombinant cellular assays at the inception of the project, and the relative ease with which SAR can be established, may represent a key strategic problem due to the effect this may have on physicochemical properties, and thus impact the overall balanced biological profile.[76]

Ligand efficiency represents a surprisingly simple and effective way of meeting one of the key challenges in drug discovery, namely restraining compounds within drug-like space (at least logP and MWT) by indirectly minimizing the focus on nonspecific potency gains.[96] This parameter may also have the unintended effect of helping to increase the probability that the ADMET parameters associated with the series in question will therefore be more acceptable (since logP and MWT are restrained).[97]

A range of different ligand efficiency metrics have been proposed in the literature, which has led to criticism by some.[98,99] The key feature of all of these metrics is to focus on potency gains per unit mass, atom or lipophilicity (Eqs. 1, 2).[69] The two principle parameters are obtained by dividing the pXC_{50} by the heavy atom count (or MWT):

$$\text{Ligand efficiency (LE)} = pXC_{50} \times 1.37/\text{Heavy atom count}^{96} \quad (1)$$

$$\text{Lipophilic ligand efficiency (LLE or LiPE)} = pXC_{50} - \text{LogP(or LogD)}^{75} \quad (2)$$

Ligand efficiency metrics are useful for placing the potency gains within a series into perspective. Issues include the nonlinearity of LE after approximately 25 heavy atoms (HA) and the use of predicted clogP values in the equation for LLE.[100]

A retrospective analysis of marketed oral drugs by Hopkins et al.[69] showed that they frequently have highly optimized ligand efficiency values for their target. They propose (a) replacing carbon atoms with oxygen or nitrogen atoms (especially converting phenyl rings to heteroaromatic rings), (b) adding polar substitutions/functional groups where possible, (c) removing or replacing lipophilic substituents and templates, and (d) controlling growth of heavy atom count. The authors conclude that optimizing on combined LE and LLE measures have the potential to reverse the molecular inflation that pervades current practice in medicinal chemistry, and to increase the developability of drug candidates. Perola et al. describe suggested guidelines for utilizing the different efficiency parameters to increase the overall potency of a lead by carefully controlling the changes in logP and MWT. They noted that 90% of leads have LE values over 12.4, whereas 90% of drugs have binding efficiencies over 14.7.[101]

2.03.3 Multiobjective Optimization of PK/PD Parameters

The integration challenge in drug discovery is how to achieve a dosing regimen and concentration time profile in the body which attains an appropriate balance between drug efficacy and potential adverse drug reactions (ADRs).[102] It has been reported that about 75% of ADRs are dose dependent and can be predicted by the exposure of a given tissue to the drug and on the basis of the pharmacological profile, primary and secondary effects, of the candidates compound.[103–105] Under an exposure centered approach, a thorough characterization of the lead compounds aimed at the identification of the inherent pharmacokinetic and safety liabilities includes, but it is not restricted to, an early generation of quantitative pharmacokinetic-pharmacodynamics (PK/PD) relationship, linking in vitro and in vivo pharmacology to target exposure and efficacy in animal studies, and therapeutic window, which is a quantitative relationship between the exposure level at the chosen safety end point and the exposure level at the chosen efficacy end point. As the extent of efficacy and safety data increases as a candidate drug progresses from in vitro to animal to human studies, the understanding of both PK/PD and therapeutic window increases.

It is important to emphasize that there is a continuum of information, which must be refined and have to be put into context during the process, and that there is no fixed tiered screening tree that can guarantee success. Project teams may decide to adopt a classical approach based on:

(1) potency and selectivity in biochemical and cellular assays,
(2) physicochemical properties (ie, drug-likeness parameters, solubility, and permeability) to eliminate unwanted compounds,
(3) ADME, drug–drug interaction (DDI) and safety in vitro profile (ie, intrinsic metabolic clearance, permeability, cytochrome P450 (CYP) inhibition and induction, panel of secondary pharmacological targets, hepatotoxicity and genotoxicity assays),
(4) in vivo pharmacokinetic (PK) profile in rodent and pharmacodymanic (PD) species,
(5) preliminary in vivo PD experiments,
(6) in vivo non rodent PK (ie, dog and monkey), and
(7) exploratory in vivo toxicity studies.

However, whatever the screening tree adopted, it is the relationship between PK, PD and safety that needs to be rigorously understood to define the drivers for robust in vivo efficacy, desired human PK and for the prediction of human therapeutic dose and safety margins. After more than a decade since drug metabolism and pharmacokinetic (DMPK) representatives have become part of discovery project teams, and helped in the reduction of the PK related attrition to ca. 10% today,[11,106–108] it is now time that discovery toxicologists also become part of discovery project teams to actively influence decision making.[109,110] Despite the availability of toxicology assays and models in early phases, safety related attrition is still high (~30% of all new drugs) and there is the need for an integrated in vitro, ex vivo and in vivo strategy to steer away safety hazards.[111–117]

It is worth noting that DMPK is increasingly being seen as a problem that is no longer a significant issue in drug discovery. At a simplistic level this appears to be true, yet is becoming increasingly clear that our understanding of the DMPK concept is evolving, and its role in failures due to efficacy.[8] It is also worth noting that 10 years ago it was common for discovery to optimize protein binding to maximize free fraction (not concentration) yet now it is accepted that the effect of the free fraction on the free concentration is generally negated by the simultaneous effects on increased clearance.[118] Furthermore, the desire for increased efficacy though increased receptor off-rates[119,120] have been brought into question due to the confounding effects of PK/PD. The receptor off rates can only have a significant effect on efficacy if the off rates are longer than the plasma elimination rate.[119] Data extracted by Dahl and Akerud[119] for several drugs and development compounds indicate that they have a slower elimination compared with dissociation. These observations greatly reduce the usability of drug-target residence times for estimating the duration of effect of a drug in vivo. It appears that consensus is still to be found in terms of what parameters should be optimized to achieve the required plasma concentration and target binding necessary for efficacy and once a day dosing.

2.03.3.1 Assessment of PK/PD Properties of Development Compounds

The identification of tractable chemical series that modulates the target means the hit to lead phase can start. Many properties of the hit series are assessed and the most promising are progressed for further characterization. The decision regarding which series to promote is based on a variety of data usually generated from both cheminformatics based searches, using scientific literature and/or available public databases, followed by high-content screening assays, such as lipophilicity, permeability, solubility, target affinity, potency in relevant cellular assay, metabolic stability, CYP450 inhibition, initial exposure data, cytotoxicity, hERG, and

genotoxicity (Table 3). Other information regarding the patentability, synthetic feasibility are also considered. The purpose of the characterization at this stage is not necessarily to prevent progression of a compound series but rather to flag potential issues that might indicate a significant liability in an individual chemical series. This would allow a project team to take an informed decision based on an assessment of risk.[121–123]

The aim of the project team during the lead optimization phase is to explore whether an appropriate balance of properties can be achieved in a single compound, and ideally a number of diverse backups. Many structural features and properties can change dramatically meaning extensive characterization of relevant physicochemical, pharmacological, DMPK, and exploratory toxicology in vitro and in vivo assays is needed to define, confirm and derive a working hypothesis and understand the SAR (Table 1).[118,124,125]

It is widely accepted that while the optimization of a single endpoint is often doable, achieving the desired balanced profile and the understanding of what makes that specific compound a disease-modifying drug is difficult, requiring a sound understanding of the relationship between the primary and off-target pharmacology, pharmacokinetic and toxicological properties. It is important to evaluate, with quantitative and reliable data, whether structural modifications, introduced to improve one property, do not lead to other liabilities negatively affecting the overall developability profile. Among the most important processes characterized during lead optimization are the classical processes: absorption, distribution, metabolism, and excretion, collectively referred to as ADME. These processes are described in vivo by the conventional pharmacokinetic parameters (ie, bioavailability, clearance, distribution volumes, half-life) as well as using in vitro data (ie, plasma and target tissue binding, transporters efflux ratios, and permeability). An incorrect assumption is that each individual ADME parameter is somehow independent and can be separately "optimized" one by one. This may drive scientists to adopt unsuitable practices by trying to establish SAR and optimize individual properties but neglecting other factors that will also change concomitantly (ie, PK/PD and therapeutic dose). The reality is that there is interdependency between different PK/PD phenomena, including acting in correlated or inversely correlated manner. The search for the best drug candidate is almost always a search for the molecule with the most balanced properties. The decision making strategy will therefore be heavily affected by the availability of data at a given time in the project which will have implications for product profile.[79,126,127]

Prior to the first-in-human (FIH) study, a number of preclinical in vivo and in vitro experiments are performed on a drug candidate to understand the PK/PD/safety and efficacy. Typically, the preclinical species are mouse, rat, and dog. The relationship between dose, kinetics of the unbound drug concentration, target engagement, functional response (MoA) and in vivo efficacy must be understood in the animal disease model. Then, translation of these parameters to predict PK/PD/safety outcomes in a human population is required. The process can be summarized as follow:

1. Human PK prediction
2. Human therapeutic exposure (dose) prediction
3. Estimation of therapeutic window

There are several approaches currently used to predict human PK.[128–130] These approaches could be broadly divided into three areas: allometry, in vitro–in vivo extrapolation (IVIVE), and physiologically based pharmacokinetics (PBPK).

Allometry, involving scaling to humans PK data in test animals (often rat and dog and nonhuman primate), relates in vivo derived parameters across species as a function of differences in body weight and is the mainstay approach by industry. Allometry tends to be successful in the prediction of volume of distribution and flow dependent pathways such as renal clearance, but has limited predictive capacity for hepatic clearance compounds (most often oral drugs), since it does not take into consideration species differences in metabolism.

IVIVE, which may be regarded as a subcomponent of PBPK, has been applied to predict hepatic metabolic clearance based on animal and human-derived tissues or expression systems. It aims to address particularly the known species differences in enzymatic and/or active processes.[131] A PBPK model consists of anatomically and physiologically meaningful compartments connected by flow rates that relate to circulating blood and the lymph system. It integrates physiological parameters and in vitro and in vivo DMPK data and represents a quantitative framework for mechanistic translation across species.

PBPK is highly mechanistic and can be employed upstream by linking processes to physicochemical and structure properties and hence guide in the design of more optimal compounds. In addition, it has the potential to explain the observed in vivo behavior of drugs, and can be used beyond dose selection in FIH studies, by helping to guide various aspects of clinical development, such as prediction of the impact of DDIs, age, and disease. However, PBPK is inherently mathematically complex and many underlying assumptions are difficult to verify. Animal data are not inherently required in PBPK prediction of human PK, although development and verification of the methodology are often undertaken in animals. It has been reported that although some prediction methods are definitely better than others, there is currently no universally outstanding method and that the prediction of human pharmacokinetic parameters following intravenous administration is much better than the prediction of events following oral administration due to the complex physiology of the gastrointestinal tract and the complex processes occurring during the absorption phase.[140] Despite its limitations, allometry is likely to remain a key approach by industry for prediction of human PK in lead optimization. However, as the refinement and commercialization of PBPK methodologies, together with the understanding of processes controlling both PK and PD, improves, the adoption of more mechanistic PBPK approach will become essential for drug discovery.[142]

The effective unbound concentration time profile for both plasma and the effect compartment, as determined in animal disease models, provides the corresponding target concentration time profile as required for efficacy in human. The estimation of the pharmacologically active therapeutic exposure should be based on a set of dedicated PK/PD studies with quantitative data analysis in

relevant PD and/or efficacy models, and with different doses and dosing schedules. For targets residing in the body's periphery, it is important to characterize and describe the blood—target site equilibrium according to the free drug hypothesis and evaluate if the unbound plasma concentration fully represents the unbound concentration at the target site.[132,133] For CNS drugs, the target site is located behind the blood–brain barrier (BBB) and additional data, such as interaction with efflux transporters P-glycoprotein (P-gp/MDR1/ABCB1), are needed to translate unbound plasma concentration into relevant brain concentration.[134]

The human therapeutic dose is estimated by considering the human PK prediction and the pharmacologically active therapeutic exposure. The prediction of the human therapeutic dose reflects all the uncertainties of the available data and therefore often results in a range of predictions originating from different assumptions and scenarios.[135] The amount of safety and efficacy data increases as the front running compound progresses along the discovery process, from in vitro to animal PK, PD, and toxicology studies. Off-target pharmacology interactions that are often the cause of ADRs in animal models or clinical studies, and the evaluation of the potential DDI risks are needed to carefully characterize compounds at the early stages of the process.[136,137]

In vitro pharmacological and DDI profiling involves the screening of compounds against a broad range of targets distinct for the primary therapeutic targets to identify specific molecular interactions that may cause safety hazards in human, and the characterization of the potential for CYP inhibition, CYP induction and transporter protein interactions, respectively. Good laboratory practice (GLP) safety pharmacology and toxicology studies are conducted according to regulatory guidelines, candidate drugs are evaluated in project and compound specific non-GLP pilot studies, such as 2-week toxicology studies in relevant preclinical species, usually rat and dog. The data generated from these studies constitute the basis for the initial estimate of the therapeutic window. Safety margins, which are ratios derived from concentration data (IC_{50}) from in vitro safety and efficacy studies, and therapeutic indices, ratios derived from concentration data from animal and human in vivo safety and in vivo efficacy studies, are calculated to put the target product profile into context.[82]

2.03.3.2 Achieving a Balanced PK/PD Profile

As stated above, for a drug to achieve a therapeutic effect it should have the ability to access the effective compartment at the "right" time and concentration. The selection of high quality drug candidates is a complex and multidimensional exercise where project teams must integrate data from various in vitro and in vivo assays in order to ensure a sound understanding of the PK/PD/safety relationships. Indeed, in **Fig. 8**, the relationship between the dose and in vitro potency at the therapeutic target is found to be relatively poor. Potency is a key driver of efficacy yet it is obvious from the poor correlation that other factors are at play.[47]

To that end a number of issues and misconceptions need to be considered:

- From a technical perspective, there are limitations to the validity of some in vitro pharmacological, toxicological, and DMPK assays. These assays are often validated in very static conditions (ie, time of incubation, reagent concentrations, protein content etc.) and therefore may not be totally representative of the in vivo situation.
- Measuring and understanding the pharmacokinetics of the unbound drug is critical, as it is the unbound drug that is able to interact with the target and elicit the effect. This can be problematic for some nonperipheral targets (ie, CNS). For these targets, understanding the mechanisms involved in uptake into and efflux from the effective and plasma compartments is essential to describe the drug effect.

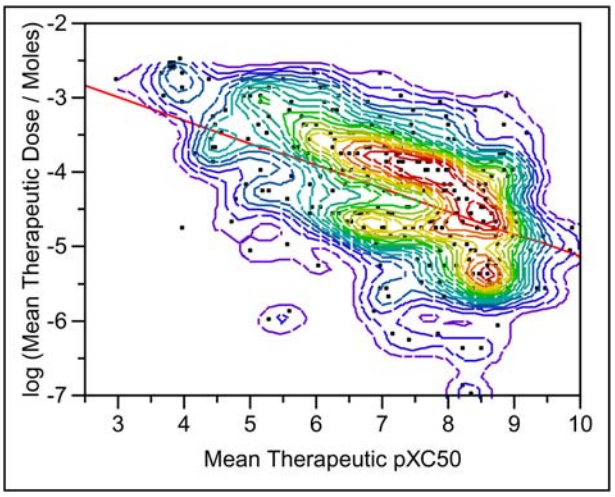

Fig. 8 The relationship between the reported mean therapeutic dose and the mean therapeutically relevant pXC_{50} reported for a set of 261 oral drugs. Adapted from reference Gleeson, M.P.; Hersey, A.; Montanari, D.; Overington, J., Probing the Links Between in vitro Potency, ADMET and Physicochemical Parameters. *Nat. Rev. Drug Discov.* **2011**, 10, 197–208.

- A reduction in plasma protein binding has occasionally been attempted to improve the systemic exposure of new compounds in a chemical series. However, it has now become clear that for compounds that are cleared predominantly by hepatic clearance, the protein binding has no impact on plasma levels.[118]
- It is necessary to consider drug-receptor theory for quantifying the efficacy of drugs and minimize the therapeutic dose. It is the optimal balance of properties (ie, physicochemical properties, target affinity and unbound concentration in the effect compartment, and not their absolute values that dictates the quality and potential of drug molecules.
- One challenging scientific problem is the need for better understanding of the biological mechanism and the underlying PK/PD relationships. The lack of appropriate disease models and the complexity and, sometimes, impossibility of testing pharmacological outcomes in preclinical species limit the confidence a project can have in the validity of the biological hypothesis. Project teams may not be able to ask the right questions if they do not have the right tools to test the hypothesis.
- Some biological and physiological systems operate in different ways under different conditions. Understanding the drug effect under a variety of circumstances important. Innovative experimental procedures are needed to uncover the factors that govern the PK/PD relationship. The dynamic regulation of context related mechanisms contribute to the variability in drug effect. Hence, heterogeneity in species, gender, genetic background, tissue, age, diet, disease condition etc., must be considered for the prediction of human response.[138]
- Sophisticated mathematical modeling techniques are needed to reveal complex PK/PD relationships and extrapolate pharmacokinetic parameters. These techniques (ie, PBPK modeling) are complex and many underlying assumptions are difficult to verify experimentally.

2.03.3.3 Drug Efficiency and the Free Drug Hypothesis

The free drug hypothesis is extensively applied in drug discovery and development to select and design new chemical entities, to support and establish the design and interpretation of PK/PD studies, to predict the therapeutic relevant dose and to monitor drug concentration in clinical studies. According to the free drug hypothesis, it is the time profile of the unbound drug concentration in the effect compartment which is responsible for receptor occupancy (RO%) and hence the in vivo efficacy. The assessment of a compound's exposure profile allows us to generate a hypothesis as to how best elicit the required pharmacological response. This facilitates the identification of compounds that are likely to maximize target exposure per unit of dose which should be a central strategy for any discovery project.

The establishment of solid PK/PD relationships is a fundamental as it allows the building of a rational basis for the prediction of human therapeutic dose and dose regimens, and for the estimation of the therapeutic window in human. This is to allow us to understand the in vivo target RO% (drug action), how it translates to the expected MOA, and the in vivo efficacy of the disease model.[139] To this end, theoretical models which use in vitro potency data and in vivo experimental determinations of the RO% are required. This requires an estimation of the therapeutic effect as early as possible in order to effectively guide the selection of optimal drug candidate. The level of RO% can be assessed using Eq. 3, with K_d being the in vitro potency and $C_{u,e}$ the unbound concentration in the effect compartment.

$$RO\% = C_{u,e} \times 100/(C_{u,e} + K_d) \tag{3}$$

Once the level of RO% needed for efficacy in vivo, and the relevance of C_u in the effect compartment has been established, the information must be related to the dose and peripheral PK using appropriate PK/PD models.

Targeting low therapeutic dose by maximizing efficacy in vivo is essential to reduce the risk of attrition. It has been estimated that ~75% of all ADRs are dose related and can be predicted from either the pharmacology (target and/or off-target) or the structure of the of the candidate compound.[104,140] Maximizing target RO% per unit of dose is therefore a valuable strategy to do this. There are two ways to improve a series: either by increasing target affinity and by improving the concentration unbound in the effective compartment. It is, therefore, the optimal balance of these properties, and not their absolute values that dictates the potential of a compound to achieve a low in vivo efficacious dose.

According to the free drug hypothesis, at steady state, drugs that have a high rate of membrane permeation must therefore have unbound drug concentration that are the same on both sides of the biomembrane (intracellular, extracellular, and cerebrospinal).[118] The free drug hypothesis can be represented by Eq. 4.

$$C_{u,p} = C_{u,e} \tag{4}$$

Here $C_{u,p}$ is the unbound plasma concentration and $C_{u,e}$ is the unbound effect compartment concentration. Exceptions to the free drug hypothesis mainly refer to when a drug has low passive permeability, when influx or efflux of the drug occurs from the tissue of the therapeutic target by active transporters and when the drug encounters tissues with low discontinuous blood flow. After oral dosing, the unbound plasma concentration of compounds that are cleared predominantly by hepatic clearance is affected by the dose, the fraction of a dose absorbed, intrinsic clearance and the dose interval according to the following Eq. 5 where $C_{u,av}$ is the average unbound plasma concentration, Fa is the fraction of a dose absorbed, Clint is intrinsic clearance and T is the dose interval.

$$C_{u,av} = (Fa \times dose) \div (Clint \times T) \tag{5}$$

The assumption that there is an absence of barriers between the different physiological compartments (unbound levels would be identical) holds true for most peripheral tissues, however, for other tissues, such as CNS, which is separated from the plasma by the BBB, the unbound concentration in plasma and tissue (effect compartment) will differ by a factor equivalent to $K_{p,uu,e}$ (the ratio of the unbound concentration in the effect compartment and the unbound plasma concentration) (Eq. 6) if either active transport is involved or if there is a significant gradient between the diffusion rate from blood to tissue.

$$K_{p,uu,e} = C_{u,e}/C_{u,p} \tag{6}$$

Eqs. 5, 6 can therefore be generalized as follows:

$$C_{u,e} = (Fa \times dose) \times K_{p,uu,e} \div (Clint \times T) \tag{7}$$

Strategies to increase the unbound concentration in the effect compartment ($C_{u,e}$) for oral drugs that are cleared predominantly by hepatic clearance, and which are consistent with Eq. 7, require the following:

1. Reducing intrinsic clearance (Clint) in liver microsomes and or hepatocytes.
2. Increasing the fraction of dose absorbed (Fa): which can be achieved by
   - increasing the solubility of the compound.
   - increasing intestinal permeability.
3. Minimizing interactions with active transporters (ie, P-glycoprotein).

2.03.3.3.1 Definition of DRUG efficiency

The drug efficiency (DRUGeff) measure relates the estimate of the compound potency to the free concentration of the administered dose.[141–144] DRUGeff is a straightforward parameter that takes into account the factors influencing the concentration of a given compound at the site of action and can be used, in combination with in vitro potency, in the selection of the compounds with optimized in vivo potency to be progressed for further characterization.

In contrast to in vitro testing, where almost all the dose is available to interact with the target, in the in vivo situation only a small portion of the dose effectively reaches the effective compartment, the biophase, and is available to interact with the desired biological target as a consequence of all ADME processes occurring after administration. DRUGeff is estimated through the Eq. 8:

$$DRUGeff(\%) = C_{u,e} \times 100/Dose \tag{8}$$

In Eq. 8, the $C_{u,e}$ is expressed in μg/mL and the dose is expressed in mg/kg, (with the assumption that 1 L is equivalent to 1 kg as done for tissues to blood calculations). Thus the DRUGeff can be considered as a percentage. For compounds that are cleared predominantly by hepatic clearance can be generalized as follows:

$$DRUGeff(\%) = Fa \times K_{p,uu,e} \times 100/(Clint \times T) \tag{9}$$

The assessment of the exposure profile, required to elicit the pharmacological response and the identification of compounds that are likely to maximize DRUGeff are essential for any discovery project working toward a low dose drug. One of the key benefits of the DRUGeff parameter is that it takes an integrated view on the pharmacokinetic profile and helps correct the ranking of compounds for further progression.

The impact of DRUGeff on discovery project strategy is shown in **Table 4**. A series of analogs targeting a peripheral receptor for which the biophase has been defined to be the plasma unbound concentration is considered. All candidates show an acceptable profile based on the classical PK parameters and therefore the selection of the compound for progression into further assessment would probably be driven mainly by the target affinity (Drug C). When DRUGeff values are calculated it becomes apparent that

Table 4 In vitro and In vivo pharmacokinetic parameters of a series of potential candidates. In vitro target affinity (pKi), in vitro permeability (Papp), in vitro plasma protein binding (F_u plasma), in vitro metabolic stability (clint), in vivo volume of distribution (Vd_{ss}), in vivo blood clearance (CLb), in vivo half-life ($t_{1/2}$), in vivo oral bioavailability (F), and drug efficiency (DRUGeff)

Parameter	*DRUG A*	*DRUG B*	*DRUG C*	*DRUG D*
pKi	6.9	7.0	7.5	7.4
Papp (nm/s)	85	90	122	143
F_u plasma (%)	5.4	2.4	1.5	2.4
Clint (ng/min/g)	0.5	0.6	0.5	0.7
Vd_{ss} (L/Kg)	0.4	0.4	2.3	2.1
CLb (mL/min/Kg)	3.0	2.0	18	42
$t_{1/2}$ (hr)	1.5	2.3	1.5	0.6
F (%)	60	80	67	50
DRUGeff (%)	1.8	2.7	0.25	0.12

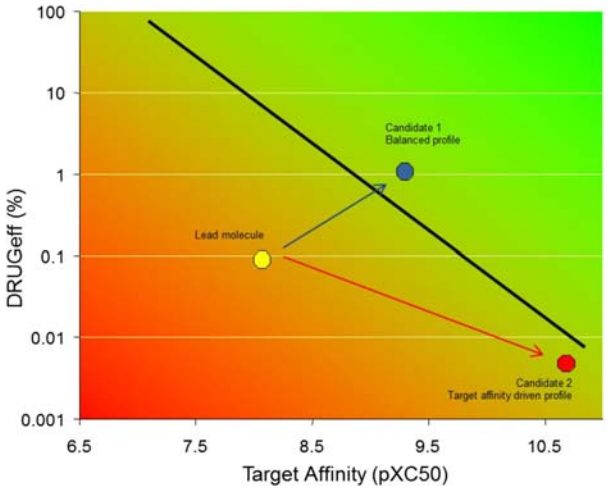

Fig. 9 DRUGeff versus target affinity (pXC_{50}) analysis. The solid black line represent the level of combined DRUGeff and affinity required to reach the PK/PD target of 90% of RO%, at the dose of 1 mg/kg. Figure adapted from reference Braggio, S.; Montanari, D.; Rossi, T.; Ratti, E., Drug Efficiency: A New Concept to Guide Lead Optimization Programs Towards the Selection of Better Clinical Candidates. *Expert Opin. Drug Discovery* **2010**, 5, (7), 609–618. www.tandfonline.com

Drugs A and B have a significantly higher efficiency with 15–20-fold higher biophase concentrations compared to Drugs C and D. Considering both DRUGeff and in vitro affinity, Drug B appears to be the one with the more balanced profile and higher potential for in vivo potency assessment (ie, lowest dose).

The prioritization of compounds using DRUGeff is summarized in Fig. 9, which shows a plot of DRUGeff versus target affinity. The solid black line represents the level of DRUGeff and affinity that is required to reach the PK/PD target of 90% RO% at the dose of 1 mg/kg. The same efficacious dose can be achieved with a compound having a high affinity and low DRUGeff or vice versa. Compounds with DRUGeff versus target affinity combinations in the upper right-hand region of the plot (*green*) will have lower efficacious doses. Compounds with DRUGeff versus target affinity combinations in the lower-left hand region (*red*) will have higher efficacious doses. The direction taken from the lead to the candidate illustrate the impact of using a "balanced" approach (*blue* arrow) rather than selecting on target affinity alone (*red arrow*).

The utility of the DRUGeff parameter can be further illustrated from a consideration of 215 oral drugs compiled from a variety of literature sources (see below). The therapeutically relevant potency, the daily dose, as well as plasma concentration and protein binding were collated and analyzed. The mean DRUGeff(%) for this set of oral drugs is 9.0. About 5% of the 215 oral drugs have DRUGeff(%) <0.1 and $\sim$30% have DRUGeff(%) <1 meaning that very few marketed drugs have poor DRUGeff.

Literature sources

- Drugdex
- Martindales
- Physcians desk reference
- Index nominum: (http://micromedex.com/)
- Pubmed (http://www.ncbi.nlm.nih.gov/sites/entrez)
- RXList: (http://www.rxlist.com/script/main/hp.asp)
- Pharmacology and Experimental Therapeutics: (http://jpet.aspetjournals.org)

If the target affinity (XC_{50}) is also considered (Fig. 10), $\sim$8% of the 215 oral drugs have a DRUGeff(%) <1 and a reported $XC_{50}>0.1$ uM, while $\sim$37% have a DRUGeff(%) >1 and a reported $XC_{50}<0.1$ uM. This suggests that the majority of the oral drugs ($\sim$55%) are either biased toward high DRUGeff or high target affinity, with a preference for the former. If the therapeutic dose is considered, there is a clear trend suggesting that achieving low therapeutic dose is often the result of a compromise between DRUGeff and target affinity. In fact about 82% of low therapeutic dose drugs lie to towards the top right of the plot.

2.03.3.3.2 Drug efficiency index

Fig. 10 clearly shows that DRUGeff can be used to enhance the chances of achieving a balance of affinity and ADMET properties and low therapeutic dose. This observation has been rationalized by considering classical receptor theory, which states that, at equilibrium, receptor-ligand interactions must obey the law of mass action that follows the basic laws of thermodynamics (Eq. 10). A theoretical estimation of the target RO% can be obtained as a function of the biophase concentration, the unbound concentration in the effect compartment $C_{u,\,e}$ (Eq. 11), where K_d (or K_i) is the in vitro estimation of the drug affinity (binding) to the specific receptor.

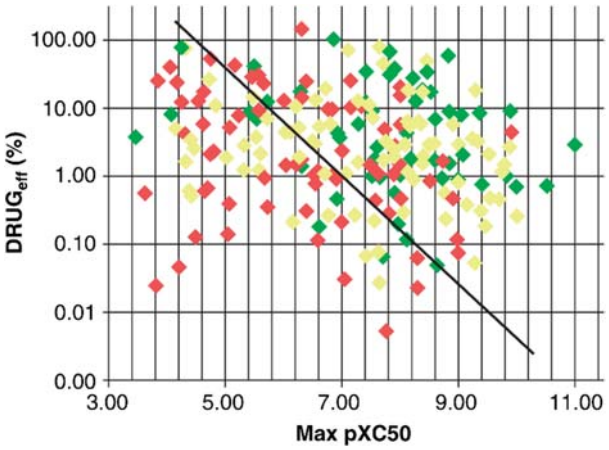

Fig. 10 The relations between the calculated DRUGeff and the reported in vitro pXC_{50} color-coded by therapeutic dose for oral drugs ($N=215$). Green spots represent therapeutic dose $<=$ 10 mg/day, orange spots represent therapeutic dose in the range 10–100 mg/day, *red spots* represent therapeutic dose $>=100$ mg/Day. Solid black line represents 50% RO% achieved at a therapeutic dose of 10 mg/day. Figure adapted from reference Braggio, S.; Montanari, D.; Rossi, T.; Ratti, E., Drug Efficiency: A New Concept to Guide Lead Optimization Programs Towards the Selection of Better Clinical Candidates. *Expert Opin. Drug Discovery* **2010**, 5, (7), 609–618. www.tandfonline.com

$$\text{Receptor} + \text{Ligand} \leftrightarrow \text{Receptor} - \text{Ligand} \tag{10}$$

$$\text{RO\%} = C_{u,e} \times 100/\left(K_d + C_{u,e}\right) \tag{11}$$

By inserting $C_{u,e}$ from Eq. 8 into Eq. 11, the result is that the sum of the DRUGeff and in vitro efficacy, defined as drug efficiency index (DEI) is directly proportional to the RO% and inversely proportional to the Dose.

$$\text{Log}[\text{DRUGeff}(\%)] + pK_d = \text{Log}[\text{RO\%}/(100 - \text{RO\%})] - \text{Log}(\text{Dose}) + 2 \tag{12}$$

The right-hand side of Eq. 12 is found to increase with increasing RO%. Thus the left-hand side term $\text{Log}(\text{DRUGeff}) + pK_d$ should be larger for drugs with larger RO%. Thus, the DEI can be defined by Eq. 13 with larger values leading to lower dose drugs. This can be achieved by either increasing the affinity of the compound to target receptor (smaller K_d), or through a larger value DRUGeff(%). DRUGeff positively adds to DEI if the DRUGeff $>1\%$. In this case lower in vitro potency results in the same RO%. Higher DEI values predict lower doses, thus lower risk of attrition.

$$\text{Log}[\text{DRUGeff}(\%)] + pK_d = \text{DEI} \tag{13}$$

The relation between DEI and therapeutic dose for the set of 215 oral drugs is shown in **Table 5**. DEI, which can be seen as a correction of the in vitro target affinity by the in vivo pharmacokinetic potential (DRUGeff), increases from 6.7 to 8.4 for high (>100 mg/day) dose to low (<10 mg/day) therapeutic dose regimens. It is worth noting that high DRUGeff appears to be the main driver in achieving low (<10 mg/day) therapeutic dose. A high therapeutic dose appears to be the result of profiles where a low target affinity is not sufficiently compensated by the DRUGeff.

In **Fig. 11** the pXC_{50} values for marketed oral drugs (**Table 6**) are plotted against the DEI parameter. The diagonal line corresponds to DRUGeff $=1\%$, ie, to $pXC_{50}=$DEI. Note that most of the marketed drugs lie below the diagonal line as they possess DRUGeff $>1\%$. For the highlighted drug, the in vitro pXC_{50} of 8 corresponds to a DEI above 9. This difference of 1 unit between the DEI and the target affinity reflects a 10-fold lower therapeutic dose required for a given receptor engagement.

The DEI is a simple descriptor which is directly connected to efficacy and therapeutic dose and has the potential to help us understand the balance between in vitro affinity and ADME properties. To illustrate how DEI can prove advantageous to select molecules we highlight the situation for three lead and candidate pairs for different CNS indications (**Table 7**) Drug pair 1 represents a balanced example of a lead optimization strategy: the increase in DEI values from lead to candidate is achieved by increasing both affinity and DRUGeff. An Eight-fold increase in affinity combined to a 220-fold increase in DRUGeff leads to a dramatic

Table 5 Therapeutic dose, in vitro pXC_{50}, DRUGeff, and DEI for oral drugs ($N=215$)

Therapeutic dose (mg/day)	*Mean pXC_{50} (SEM)*	*Mean DRUGeff% (SEM)*	*Mean DEI (SEM)*
≤ 10 ($n=53$)	7.8 (0.2)	13.0 (2.8)	8.4 (0.2)
10–100 ($n=89$)	7.3 (0.2)	7.8 (1.6)	7.6 (0.2)
>100 ($n=73$)	6.4 (0.2)	7.7 (1.3)	6.7 (0.2)

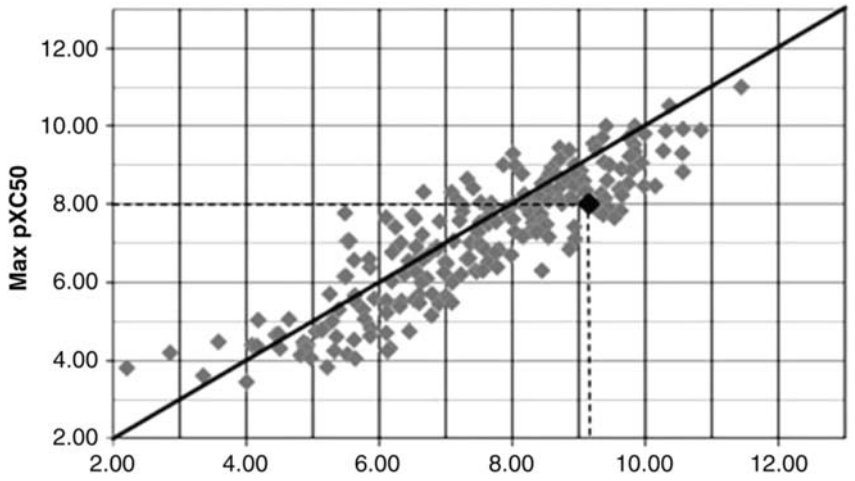

Fig. 11 The relation between the reported in vitro pXC_{50} and DEI for oral drugs ($N=215$). Dark spot is marketed drug with reported in vitro pXC_{50} of 8 and DEI above 9. Figure adapted from Braggio, S.; Montanari, D.; Rossi, T.; Ratti, E., Drug Efficiency: A New Concept to Guide Lead Optimization Programs Towards the Selection of Better Clinical Candidates. *Expert Opin. Drug Discovery* **2010**, 5, (7), 609–618. www.tandfonline.com

Table 6 List of drug molecules and associated values used to construct **Fig. 11**

Drug name	*Class*	*Disease*	*pXC_{50}*	*$DRUG_{eff}$%*	*DEI*	*Therapeutic dose (mg/day)*	*Reference*
Abacavir	Antiinfective	Infection, Hiv	7.15	39.20	8.74	300	DRUGDEX®
Acebutolol hydrochloride	Cardiovascular	Angina	6.76	9.58	7.74	400	DRUGDEX®
Acetylsalicylic acid	Neurology	Pain	5.45	28.00	6.90	1200	G&G
Acrivastine	Immunology	Allergic rhinitis	8.46	49.22	10.15	16	DRUGDEX®
Adefovir dipivoxil	Antiinfective	Infection, Hiv	5.7	12.36	6.79	10	DRUGDEX®
Albuterol sulfate	Respiratory	Asthma	7.4	11.81	8.47	4	G&G
Alfuzosin	Urogenital	Benign prostatic hyperplasia	7.64	0.95	7.62	10	DRUGDEX®
Almotriptan malate	Neurology	Migraine	8.14	18.02	9.40	12.5	DRUGDEX®
Alosetron hydrochloride	Gastroenterology	Irritable bowel syndrome	7.3	9.45	8.28	1	DRUGDEX®
Alprazolam	Neurology	Anxiety	7.05	0.03	5.53	1000	G&G
Amitriptyline hydrochloride	Neurology	Depression	6.15	0.22	5.49	100	G&G
Amlodipine besylate	Cardiovascular	Hypertension	8.72	0.79	8.62	10	DRUGDEX®
Amprenavir	Antiinfective	Infection, Hiv	7.92	4.47	8.57	1200	DRUGDEX®
Anastrozole	Oncology	Cancer	7.82	64.40	9.63	3	DRUGDEX®
Aprepitant	Gastroenterology	Emesis, chemotherapy induced	9.92	4.48	10.57	125	DRUGDEX®
Aripiprazole	Neurology	Bipolar disorder	9.7	1.06	9.73	20	DRUGDEX®
Atomoxetine hydrochloride	Neurology	Depression	8.65	1.20	8.73	90	DRUGDEX®
Atorvastatin calcium	Cardiovascular	Hyperlipidemia	7.4	0.07	6.25	40	DRUGDEX®
Atovaquone	Antiinfective	Pneumocystis carinii	6.57	0.11	5.61	750	DRUGDEX®
Bendroflumethiazide	Cardiovascular	Hypertension	3.44	3.61	4.00	10	DRUGDEX®
Bezafibrate	Cardiovascular	Hyperlipidemia	4.52	12.51	5.62	400	DRUGDEX®
Bicalutamide	Oncology	Cancer	6.1	4.73	6.77	50	DRUGDEX®
Bosentan	Cardiovascular	Hypertension	8.74	1.62	8.95	125	DRUGDEX®
Bromazepam	Neurology	Anxiety	7.82	29.58	9.29	6	DRUGDEX®
Buflomedil	Cardiovascular	Vascular disease	6.3	14.00	7.45	450	DRUGDEX®
Bupropion Hydrochloride	Neurology	Depression	6.26	1.09	6.30	150	DRUGDEX®
Buspirone Hydrochloride	Neurology	Anxiety	7.62	0.08	6.52	20	G&G
Busulfan	Oncology	Cancer	5.48	97.83	7.47	4	G&G
Caffeine	Neurology	Fatigue	4.74	51.20	6.45	700	DRUGDEX®
Candesartan cilexetil	Cardiovascular	Hypertension	10.52	0.70	10.37	8	DRUGDEX®
Captopril	Cardiovascular	Hypertension	7.72	44.59	9.37	100	DRUGDEX®
Carbamazepine	Neurology	Epilepsy	4.6	12.13	5.68	1288	G&G
Carvedilol	Cardiovascular	Hypertension	9.7	0.45	9.35	50	DRUGDEX®
Celecoxib	Musculoskeletal	Arthritis	8.52	0.84	8.44	200	DRUGDEX®
Cerivastatin sodium	Cardiovascular	Hyperlipidemia	9	0.88	8.94	0.2	DRUGDEX®

(Continued)

Table 6 List of drug molecules and associated values used to construct **Fig. 11**—cont'd

Drug name	*Class*	*Disease*	pXC_{50}	$DRUG_{eff}$%	*DEI*	*Therapeutic dose (mg/day)*	*Reference*
Cetirizine hydrochloride	Immunology	Allergic rhinitis	8.52	16.71	9.74	10	DRUGDEX®
Cevimeline hydrochloride	Endocrine	Stomatitis	5.52	3.73	6.09	90	DRUGDEX®
Chloroquine phosphate	Antiinfective	Malaria	7.32	0.80	7.22	300	G&G
Chlorpheniramine maleate	Immunology	Allergic reaction	9.05	21.07	10.37	4	G&G
Chlorpromazine hydrochloride	Neurology	Depression	9.29	0.06	8.07	100	G&G
Cilostazol	Cardiovascular	Vascular disease	6.7	1.09	6.74	100	DRUGDEX®
Citalopram hydrobromide	Neurology	Depression	8.34	1.75	8.58	40	G&G
Clemastine fumarate	Immunology	Allergic rhinitis	8.64	0.05	7.34	2.68	DRUGDEX®
Clomipramine hydrochloride	Neurology	Obsessive compulsive dsorder	7.86	2.57	8.27	49	DRUGDEX®
Clonidine hydrochloride	Cardiovascular	Hypertension	8.46	33.60	9.99	0.1	G&G
Cyclobenzaprine hydrochloride	Musculoskeletal	Muscle sprain	7.21	0.27	6.64	15	DRUGDEX®
Cyproterone	Endocrine	Male hypersexuality	4.3	1.60	4.50	50	DRUGDEX®
Dapsone	Dermatology	Acne	4.82	11.20	5.87	100	G&G
Delavirdine mesylate	Antiinfective	Infection, Hiv	6.59	1.16	6.65	300	DRUGDEX®
Desipramine hydrochloride	Neurology	Depression	6.77	0.26	6.18	100	DRUGDEX®
Desloratadine	Immunology	Allergy	9.4	0.73	9.26	5	DRUGDEX®
Dexfenfluramine	Metabolic	Obesity	5.52	3.88	6.11	30	DRUGDEX®
Diclofenac potassium	Musculoskeletal	Osteoarthritis	9.01	0.84	8.93	25	DRUGDEX®
Didanosine	Antiinfective	Infection, Hiv	8	15.46	9.19	400	G&G
Diflunisal	Neurology	Pain	4.24	12.04	5.32	500	DRUGDEX®
Digitoxin	Cardiovascular	Arrhythmia	4.06	7.98	4.96	0.25	DRUGDEX®
Diphenhydramine hydrochloride	Immunology	Allergic Rhinitis	8.12	1.18	8.19	100	DRUGDEX®
Dofetilide	Cardiovascular	Fibrillation	7.5	8.78	8.44	0.55	DRUGDEX®
Domperidone	Gastroenterology	Emesis	9.82	0.98	9.81	10	DRUGDEX®
Donepezil hydrochloride	Neurology	Alzheimers disease	8.17	1.72	8.41	5	G&G
Doxazosin mesylate	Cardiovascular	Benign prostatic hypertrophy	10	0.70	9.85	8	DRUGDEX®
Doxepin hydrochloride	Neurology	Anxiety	7	0.21	6.32	150	G&G
Duloxetine hydrochloride	Neurology	Depression	7.55	0.23	6.91	20	DRUGDEX®
Ebastine	Immunology	Allergic rhinitis	7.65	0.03	6.13	20	DRUGDEX®
Efavirenz	Antiinfective	Infection, Hiv	8.92	0.47	8.59	600	DRUGDEX®
Eletriptan hydrobromide	Neurology	Migraine	9.34	3.20	9.85	20	DRUGDEX®
Encainide (Withdrawn—1991)	Cardiovascular	Arrhythmia	5.68	8.21	6.59	75	DRUGDEX®
Entacapone	Neurology	Parkinsons disease	8	1.51	8.18	400	DRUGDEX®
Eplerenone	Cardiovascular	Hypertension	7.1	66.61	8.92	100	DRUGDEX®
Eprosartan mesylate	Cardiovascular	Heart failure	8.77	0.61	8.56	100	DRUGDEX®
Escitalopram oxalate	Neurology	Depression	6.53	2.90	6.99	20	DRUGDEX®
Estazolam	Neurology	Insomnia	8.22	26.95	9.65	1	DRUGDEX®
Fenofibrate	Cardiovascular	Hyperlipidemia	4.74	2.01	5.04	300	DRUGDEX®
Fexofenadine hydrochloride	Immunology	Allergy	7.27	4.59	7.93	60	DRUGDEX®
Finasteride	Urogenital	Benign prostatic hyperplasia	7.28	5.71	8.04	10	DRUGDEX®
Fluoxetine hydrochloride	Neurology	Depression	8.59	3.06	9.08	60	DRUGDEX®
Flurbiprofen	Musculoskeletal	Inflammation	6.2	10.64	7.23	100	DRUGDEX®
Fluvastatin sodium	Cardiovascular	Hyperlipidemia	8.42	1.24	8.51	40	DRUGDEX®
Fluvoxamine maleate	Neurology	Depression	8.3	0.06	7.08	150	DRUGDEX®
Fosinopril sodium	Cardiovascular	Hypertension	7.96	0.20	7.26	10	DRUGDEX®
Furosemide	Cardiovascular	Hypertension	5	1.93	5.29	20	DRUGDEX®
Gabapentin	Neurology	Epilepsy	6.85	11.32	7.90	2400	G&G
Ganciclovir	Antiinfective	Cytomegalovirus	6	12.49	7.10	1000	DRUGDEX®
Gemfibrozil	Cardiovascular	Hyperlipidemia	7	2.33	7.37	600	G&G
Gliclazide	Metabolic	Diabetes	4.13	4.81	4.81	80	DRUGDEX®
Glimepiride	Metabolic	Diabetes	5.38	6.16	6.17	4	DRUGDEX®
Glipizide	Metabolic	Diabetes	5.52	6.51	6.33	5	G&G
Granisetron hydrochloride	Gastroenterology	Emesis, chemotherapy induced	9.89	20.09	11.19	1	DRUGDEX®
Guanabenz acetate	Cardiovascular	Hypertension	8.24	0.88	8.18	16	DRUGDEX®
Guanfacine hydrochloride	Cardiovascular	Hypertension	7.6	2.58	8.01	2	DRUGDEX®
Haloperidol	Neurology	Anxiety	10	0.26	9.41	20	G&G
Hydrochlorothiazide	Cardiovascular	Hypertension	4.7	27.59	6.14	100	DRUGDEX®
Hydroxyurea	Oncology	Cancer	3.6	0.56	3.35	2000	G&G
Hydroxyzine pamoate	Neurology	Anxiety	8.4	0.10	7.40	49	DRUGDEX®
Ibuprofen potassium	Neurology	Pain	6.62	6.25	7.42	400	DRUGDEX®

Table 6 List of drug molecules and associated values used to construct **Fig. 11**—cont'd

Drug name	*Class*	*Disease*	*pXC_{50}*	*$DRUG_{eff}$%*	*DEI*	*Therapeutic dose (mg/day)*	*Reference*
Imatinib mesylate	Oncology	Cancer	4.77	2.01	5.07	400	DRUGDEX®
Imipramine hydrochloride	Neurology	Depression	6.55	0.77	6.44	200	G&G
Indapamide	Cardiovascular	Hypertension	4.24	76.44	6.12	5	DRUGDEX®
Indinavir sulfate	Antiinfective	Infection, Hiv	7.05	0.03	5.53	800	DRUGDEX®
Indometacin	Musculoskeletal	Inflammation	6.48	2.80	6.93	50	DRUGDEX®
Irbesartan	Cardiovascular	Hypertension	9.3	14.00	10.45	100	DRUGDEX®
Isradipine	Cardiovascular	Hypertension	6.6	0.18	5.86	2.5	DRUGDEX®
Itraconazole	Antiinfective	Infection, fungal	4.19	0.08	3.09	200	DRUGDEX®
Ketoconazole	Antiinfective	Infection, fungal	4.65	0.61	4.44	200	G&G
Ketoprofen	Musculoskeletal	Arthritis	7.63	1.09	7.67	200	DRUGDEX®
Lamotrigine	Neurology	Epilepsy	4.04	36.54	5.60	50	DRUGDEX®
Lansoprazole	Gastroenterology	Ulcer, peptic	7.05	2.20	7.39	15	DRUGDEX®
Letrozole	Oncology	Breast cancer	7.89	36.96	9.46	2.5	G&G
Lorazepam	Neurology	Epilepsy	8.85	8.82	9.80	2	G&G
Lovastatin	Cardiovascular	Hyperlipidemia	9.52	0.04	8.12	40	DRUGDEX®
Maprotiline hydrochloride	Neurology	Depression	4.39	0.49	4.08	50	DRUGDEX®
Meclofenamate sodium	Musculoskeletal	Arthritis	4.35	3.36	4.88	100	DRUGDEX®
Mefloquine hydrochloride	Antiinfective	Malaria	4.47	0.22	3.81	1170	DRUGDEX®
Memantine hydrochloride	Neurology	Alzheimers disease	6	15.86	7.20	20	DRUGDEX®
Mesalamine	Gastroenterology	Colitis	4.8	3.15	5.30	1000	DRUGDEX®
Metformin hydrochloride	Metabolic	Diabetes	5.65	1.74	5.89	850	DRUGDEX®
Methyltestosterone	Endocrine	Hormone replacement therapy	6.9	0.45	6.55	10	DRUGDEX®
Metoclopramide hydrochloride	Gastroenterology	Emesis	8.38	16.80	9.61	20	DRUGDEX®
Metoprolol tartrate	Cardiovascular	Hypertension	7.47	11.09	8.51	100	G&G
Mexiletine hydrochloride	Cardiovascular	Arrhythmia	4.29	4.04	4.90	400	DRUGDEX®
Mibefradil dihydrochloride	Cardiovascular	Hypertension	6.15	0.10	5.15	40	DRUGDEX®
Mifepristone	Endocrine	Pregnancy, abortion	8.02	0.46	7.68	600	DRUGDEX®
Minocycline hydrochloride	Antiinfective	Infection, Oral	5.15	42.84	6.78	200	DRUGDEX®
Mirtazapine	Neurology	Depression	9	2.93	9.47	15	G&G
Misoprostol	Gastroenterology	Ulcer, Peptic	7.9	0.56	7.65	0.4	DRUGDEX®
Moricizine hydrochloride	Cardiovascular	Arrhythmia	6.21	1.45	6.37	200	DRUGDEX®
Morphine sulfate	Neurology	Pain	6.96	2.25	7.31	100	DRUGDEX®
Nadolol	Cardiovascular	Hypertension	8.9	5.52	9.64	55	DRUGDEX®
Naltrexone hydrochloride	Neurology	Addiction, Opioid	9.87	2.77	10.31	50	DRUGDEX®
Naproxen	Musculoskeletal	Inflammation	5.22	11.06	6.26	500	DRUGDEX®
Nefazodone Hcl	Neurology	Depression	5.05	0.39	4.64	400	DRUGDEX®
Nevirapine	Antiinfective	Infection, Hiv	8	28.00	9.45	200	DRUGDEX®
Nicardipine hydrochloride	Cardiovascular	Hypertension	5.58	2.21	5.92	40	DRUGDEX®
Nilutamide	Oncology	Prostate cancer	6.39	24.08	7.77	300	DRUGDEX®
Nimesulide	Musculoskeletal	Inflammation	4.4	3.28	4.92	100	DRUGDEX®
Nimodipine	Cardiovascular	Vascular disease	9.55	0.47	9.22	60	DRUGDEX®
Nitazoxanide	Antiinfective	Parasitic infection	7.89	1.05	7.91	200	DRUGDEX®
Nitrendipine	Cardiovascular	Hypertension	7.64	78.75	9.54	20	DRUGDEX®
Nortriptyline hydrochloride	Neurology	Depression	8.98	0.12	8.06	125	G&G
Olanzapine	Neurology	Schizophrenia	7.52	0.98	7.51	10	G&G
Olmesartan medoxomil	Cardiovascular	Hypertension	8.11	6.30	8.91	20	DRUGDEX®
Omeprazole	Gastroenterology	Ulcer	6.6	8.13	7.51	20	DRUGDEX®
Oseltamivir phosphate	Antiinfective	Infection, influenza virus	9.22	9.42	10.19	150	DRUGDEX®
Oxazepam	Neurology	Anxiety	7.92	1.90	8.20	15	DRUGDEX®
Oxycodone	Neurology	Pain	8.36	5.57	9.11	15	DRUGDEX®
Paroxetine hydrochloride	Neurology	Depression	9.44	0.19	8.72	20	DRUGDEX®
Penbutolol sulfate	Cardiovascular	Hypertension	7.7	1.74	7.94	100	DRUGDEX®
Perindopril erbumine	Cardiovascular	Hypertension	8.82	56.00	10.57	8	DRUGDEX®
Phenytoin	Neurology	Epilepsy	4.15	23.33	5.52	300	G&G
Pimecrolimus	Dermatology	Eczema	7.27	0.82	7.18	60	DRUGDEX®
Pioglitazone hydrochloride	Metabolic	Diabetes	4.46	2.77	4.90	30	DRUGDEX®
Piroxicam	Musculoskeletal	Arthritis	6.7	19.25	7.98	20	DRUGDEX®
Polythiazide	Cardiovascular	Edema	6.92	4.20	7.54	1	DRUGDEX®
Pramipexole dihydrochloride	Neurology	Parkinsons disease	6.3	17.92	7.55	0.5	G&G
Pranlukast	Respiratory	Asthma	5.03	0.14	4.18	225	DRUGDEX®

(Continued)

Table 6 List of drug molecules and associated values used to construct **Fig. 11**—cont'd

Drug name	*Class*	*Disease*	pXC_{50}	$DRUG_{eff}$%	*DEI*	*Therapeutic dose (mg/day)*	*Reference*
Pravastatin sodium	Cardiovascular	Atherosclerosis	8.16	5.20	8.88	20	G&G
Praziquantel	Antiinfective	Parasitic infection	7.49	0.42	7.11	2800	DRUGDEX®
Prazosin hydrochloride	Cardiovascular	Hypertension	8.85	1.51	9.03	5	G&G
Probenecid	Musculoskeletal	Gout	3.82	24.71	5.21	500	DRUGDEX®
Propafenone hydrochloride	Cardiovascular	Fibrillation	5.7	0.36	5.26	300	DRUGDEX®
Propranolol Hcl	Cardiovascular	Hypertension	9.38	0.30	8.86	80	G&G
Quetiapine fumarate	Neurology	Schizophrenia	5.3	2.86	5.76	25	DRUGDEX®
Quinapril hydrochloride	Cardiovascular	Hypertension	6.3	1.37	6.44	10	DRUGDEX®
Quinidine gluconate	Cardiovascular	Arrhythmia	5.06	5.25	5.78	400	DRUGDEX®
Quinine sulfate	Antiinfective	Malaria	6.3	1.74	6.54	1000	DRUGDEX®
Rabeprazole sodium	Gastroenterology	Gastroesophageal Reflux	7.74	3.36	8.27	20	DRUGDEX®
Ramipril	Cardiovascular	Hypertension	9.36	8.18	10.27	10	DRUGDEX®
Ranitidine bismuth citrate	Gastroenterology	Ulcer, Duodenal	7.57	0.43	7.20	150	DRUGDEX®
Repaglinide	Metabolic	Diabetes	7.54	3.57	8.09	2	DRUGDEX®
Rifapentine	Antiinfective	Infection	7.16	9.93	8.16	600	DRUGDEX®
Riluzole	Musculoskeletal	Amyotrophic lateral sclerosis	4.37	0.75	4.25	50	DRUGDEX®
Rimantadine hydrochloride	Antiinfective	Infection, influenza A	6.03	1.43	6.19	200	DRUGDEX®
Ritonavir	Antiinfective	Infection, Hiv	5.66	0.93	5.63	400	DRUGDEX®
Rivastigmine tartrate	Neurology	Dementia	8.37	17.92	9.62	6	DRUGDEX®
Rizatriptan benzoate	Neurology	Migraine	8.26	13.70	9.40	40	DRUGDEX®
Ropinirole hydrochloride	Neurology	Parkinsons disease	6.27	4.37	6.91	3	DRUGDEX®
Rosiglitazone maleate	Endocrine	Diabetes	8	1.05	8.02	2	DRUGDEX®
Rosuvastatin calcium	Cardiovascular	Hyperlipidemia	9.8	0.78	9.69	40	DRUGDEX®
Roxithromycin	Antiinfective	Infection	6.83	9.33	7.80	300	DRUGDEX®
Saquinavir	Antiinfective	Infection, Hiv	8.3	0.02	6.60	600	DRUGDEX®
Selegiline hydrochloride	Neurology	Parkinsons disease	8.1	2.81	8.55	1	DRUGDEX®
Sertraline hydrochloride	Neurology	Depression	9	0.10	8.00	200	DRUGDEX®
Sildenafil citrate	Urogenital	Erectile dysfunction	8.46	2.92	8.93	100	DRUGDEX®
Spironolactone	Cardiovascular	Hypertension	4.67	0.65	4.48	200	G&G
Sumatriptan	Neurology	Migraine	8.07	2.99	8.55	100	G&G
Tadalafil	Urogenital	Erectile dysfunction	8.3	6.80	9.13	20	DRUGDEX®
Tamsulosin hydrochloride	Urogenital	Prostatic hyperplasia	11	2.80	11.45	0.4	G&G
Tegaserod maleate	Gastroenterology	Constipation	7.7	0.06	6.48	6	DRUGDEX®
Telmisartan	Cardiovascular	Hypertension	8.04	0.30	7.52	80	DRUGDEX®
Terazosin hydrochloride	Cardiovascular	Hypertension	8.6	6.72	9.43	1	G&G
Terbinafine hydrochloride	Antiinfective	Infection, dermatophyte	7.8	0.28	7.25	250	DRUGDEX®
Terfenadine	Immunology	Allergic rhinitis	7.76	0.01	5.76	180	DRUGDEX®
Tizanidine hydrochloride	Musculoskeletal	Spasticity	7.51	6.32	8.31	20	DRUGDEX®
Tocainide hydrochloride	Cardiovascular	Arrhythmia	3.8	24.84	5.20	400	DRUGDEX®
Topiramate	Neurology	Epilepsy	4.31	70.21	6.16	100	DRUGDEX®
Torasemide	Urogenital	Renal failure	6.52	12.95	7.63	20	DRUGDEX®
Toremifene citrate	Oncology	Breast cancer	5.52	1.28	5.63	60	G&G
Tramadol hydrochloride	Neurology	Pain	5.55	17.25	6.79	100	DRUGDEX®
Trandolapril	Cardiovascular	Heart failure	8.6	1.16	8.66	4	DRUGDEX®
Trazodone hydrochloride	Neurology	Depression	6.25	5.25	6.97	100	G&G
Triamterene	Cardiovascular	Edema	5.3	1.22	5.39	50	G&G
Triazolam	Neurology	Behavioral disorder	9.07	2.04	9.38	1.75	DRUGDEX®
Trimethoprim hydrochloride	Antiinfective	Infection	5.57	29.40	7.04	160	G&G
Troglitazone	Metabolic	Diabetes	6.38	0.28	5.83	400	DRUGDEX®
Valdecoxib	Musculoskeletal	Arthritis	8.4	1.99	8.70	20	DRUGDEX®
Vardenafil Hydrochloride	Urogenital	Erectile dysfunction	9.15	0.37	8.72	20	DRUGDEX®
Venlafaxine hydrochloride	Neurology	Depression	7.74	12.84	8.85	150	DRUGDEX®
Verapamil hydrochloride	Cardiovascular	Hypertension	6.9	0.92	6.86	120	DRUGDEX®
Vigabatrin	Neurology	Epilepsy	4.62	17.43	5.86	2129	DRUGDEX®
Zidovudine	Antiinfective	Infection, Hiv	8	14.73	9.17	140	DRUGDEX®
Zileuton	Respiratory	Asthma	6.52	1.02	6.53	2400	DRUGDEX®
Ziprasidone hydrochloride	Neurology	Schizophrenia	8.77	0.24	8.15	20	G&G
Zolmitriptan	Neurology	Migraine	8.1	4.20	8.72	10	DRUGDEX®
Zolpidem tartrate	Neurology	Insomnia	6.82	6.00	7.60	12.5	DRUGDEX®
Zopiclone	Neurology	Insomnia	7.41	33.37	8.93	7.5	DRUGDEX®

Data taken from Micromedex® DRUGDEX® and Goodman & Gilman's The Pharmacological Basis of Therapeutics, 10 Ed. (G&G).

Table 7 The relation between target affinity, DRUGeff, and DEI for 3 CNS lead-candidate pairs

	MWT (Da)	*clogP*	*pKi*	*DRUGeff (%)*	*DEI*
Pair 1					
Lead	415.5	3.3	7.1	0.025	4.6
Candidate	363.5	3.5	8.0	5.49	6.4
Pair 2					
Lead	545	6.4	9.4	0.001	6.4
Candidate	615	5.6	10	0.017	8.24
Pair 3					
Lead	363.5	2.9	6.4	0.1	5.4
Candidate	472	4.9	7.9	0.08	6.8

increase in DEI and the corresponding in vivo efficacy potential. Drug pair 2 represents an example of profile biased toward in vitro affinity as DRUGeff is very low. The optimized candidate shows slight improvements in both in vitro affinity and DRUGeff; however this molecule has very high MWT and logP leading to suboptimal ADMET properties. In drug pair 3, the increase in DEI value for the candidate with respect to the lead drug is achieved mainly by increasing the in vitro potency, as DRUGeff remains constant. In this case the directions taken by the project team involved chasing target affinity.

2.03.4 Effect of Systematic Biases in Drug Discovery

The systematic, multivariate optimization of disparate biological measurements obtained from in vitro and in vivo models of efficacy, safety and PK is a relatively new and evolving area of pharmaceutical research.[145] Our ability to identify and understand the reasons for compound attrition points to a renewed need to consider how we rank order preclinical compounds using the data generated in drug discovery. Ranking compounds using data from 10–100 s of different assay systems is complicated by the fact that each assay has a different relative importance to efficacy and safety, can have linear or nonlinear relationship with the probability of success. Each parameter will have an intrinsically different relevance/accuracy to the endpoint they are supposed to model.[28,37,146] The ability to effectively manage a large number of parameters, some of which can be orthogonal, correlated or inversely correlated, is absolutely critical in lead optimization, yet it remains one of the key challenges.[147,148]

Many of the highly complex decisions that must be made over the course of a discovery project will be heavily influenced by the personal backgrounds and experience of the individual(s) involved, or the organization where the research is undertaken. It is important to acknowledge that when decisions are made on complex problems a reductionist approach is required. A situation may arise where the solutions obtained by taking the reductionist step may involve a project team following the same path, rather than exploring diverse solutions. Indeed, concepts such as lean sigma are increasingly being proposed to improve the efficiency and streamline processes in R&D, and can be beneficial unless they somehow limit scientific innovation in the pursuit of standardization and data reproducibility.[149,150]

A concern is that the causes of undesirable, systematic biases in decision making may limit creativity and reduce the diversity of the solutions investigated to probe a given problem. This is important since the goal of the discovery process is to probe a problem with a set of diverse solutions that are probabilistically more likely to work, or at least answer a question that may help influence the future direction of the project, or indeed close it.

2.03.4.1 The Effect of Personal and Organization Biases

Management, metrics, and the culture of an organization contribute significantly to the decision making and thus output of a drug discovery project. A number of groups have noted how an industry-wide pressure existed for increased number of hits, leads and candidates, rather than a focus on quality science.[10,63] Furthermore, Leeson et al. have shown that the physicochemical properties from AstraZeneca, GlaxoSmithKline, Merck, and Pfizer showed marked intercompany differences even on the same target class, driven by different corporate cultures.[75] A subsequent more extensive patent based analysis on a wider set of companies demonstrated similar findings and suggested that differences in physical properties between the organization's compounds are not influenced very much by the targets or target classes pursued, but more by the different strategies and tactics followed.[10,61]

Personal biases will invariable affect lead optimization where a quantitative balance of a range of diverse parameters must be developed in the lead series. Unlike a binary classification of good or bad, the search for optimal pharmacokinetics, dynamics and safety involves considering an array of assay parameters that constitutes a multidimensional hypersurface that is not easily navigated using the human brain. A further complication is that not all parameters are as meaningful as others, yet selection bias may mean some parameters take greater precedence over others. Once an apparently desirable solution has been achieved there may also be a reticence on the part of the team to stray too far from this solution when searching for a backup molecule. This can sometimes mean that the backup series contains the same fundamental safety issues or mode of action issue as the molecule that preceded it.[151]

Lajiness et al.[152] demonstrated the bias displayed by individuals by asking different chemists to assess the suitability of 2000 compounds based on their "attractiveness" and/or synthetic feasibility as a basis for launching a drug discovery campaign. Intriguingly, they found that medicinal chemists were not even internally consistent when reviewing compounds as it was shown that the review of the same compounds a second time but in a different set, saw the rejection of the same compounds only about 50% of the time. It is therefore no surprise that the average agreement between a pair of chemists was approximately 28%. These findings were given additional support by an exercise to separate a set of approximately 4000 fragments into lead-like and non lead-like sets which was reported by Kutchukian et al.[153] It was found that the 19 chemists involved adopted a simplified selection strategy, taking into account no more than 2–3 parameters, with ring topology and functional groups being the key factors. In addition, the chemists involved were often unaware of the parameters they had instinctively used (such as size), and overestimated the number of overall parameters they employed.

The difficultly in identifying molecules with the required balance in properties might explain why project teams frequently synthesize more molecules than are needed.[151] This finding was echoed by Bennani[154] who found that between 20–30% of effort within a project was spent "over fitting" the molecular series to fit the disease model. The over synthesis of compounds must be viewed in the context of (a) the approximate nature of the biological profile at the start of a project, and (b) the approximate nature of the in vitro and in vivo models used to meet the profile.

Suggested Guidelines for Project Progression:

- Aim to meet the proposed biological profile set by the project team as best as possible with the series(s) under investigation.
  - However, avoid a box ticking exercise with parameters. Assess the relevance and meaning of the assumptions and try to validate.
- Acknowledge that the biological profile is an estimate and adjust
  - Remain conscious that it may not be necessary to meet the required profile defined at the outset given the limited understanding at that particular time.
- Acknowledge that the in vitro and in vivo assays used to prioritize compounds at each stage are reductionist. Values are approximate, and discordance with in vivo models can be sizeable.
  - Perfect agreement with the model(s) is not expected.
- Be aware that meeting one criterion typically leads to deterioration in others, often due to their conflicting physicochemical dependences.

2.03.4.2 Overcoming Systematic Biases

Cognitive biases can also affect the integration of data that is critical in defining a clinical candidate (Table 8). Types of biases that can arise include (a) overconfidence in the project rationale leading to a lack of due-diligence in the mode of action studies (MOA), (b) insufficient understanding of the reliability of individual parameters leading to poor decisions being made,[155] (c) over focusing on one's own experience and neglecting probabilistically important lessons, and (d) focus on parameters under ones control and neglecting more relevant parameters which are harder to understand or influence. Such biases could in theory lead to the progression of less lead-like molecules should potency considerations dominate decision making,[47,156] or allow the progression of compounds that should have failed in earlier development.

The use of arbitrary cut-offs or the overreliance on certain individual parameters out of the many generated increases the risk of biased solutions emerging from a drug discovery project. Consider a case where we have two equally important parameters (ie, the free concentration vs. the potency), a large number of equally acceptable solutions will exist in terms of the Pareto ranking[155,157] yet often it is the most potent molecules that are taken forward (ie, seldom above 0.1 uM) before even considering the free concentration in vivo. This essentially limits the coverage of parameter space and will bias the solutions in ways that might not be easily rationalized a priori (Fig. 12). This is despite the fact that the relevance of in vitro potency has been questioned in the past,[28,29,37,156] and that it is known that a focus on absolute potency values can lead to the inflation of MWT and logP.[47,96,156] This of course means that lower logP and MWT compounds, which traditionally have better overall ADMET parameters,[54,79,80] including (exposure, clearance, and protein binding) are more likely to be excluded earlier on in the process.

Table 8 Cognitive biases discussed in this paper, their potential implications for drug discovery decision-making[147]

	Bias	*Implications*
a	Overconfidence: reluctance and/or inability to "prove a negative" and instigate premature closure	Projects failed too late. Insufficiently wide search before choosing a lead series or candidate
b	Poor calibration of judgements on estimating and forecasting reliability	Inappropriate weight given to results from early screening methods, or rules of thumb, that might too often reject drugs that should have survived
c	"Availability" bias: over-attention to the vivid and recent, with neglect of prior information	Failure to apply and learn from the "big picture" of industry project successes and failures
d	Excess focus on certainty when considering whether to accept one or more sources of residual risk	Inefficient use of resources when screening across multiple risk factors or possible indications

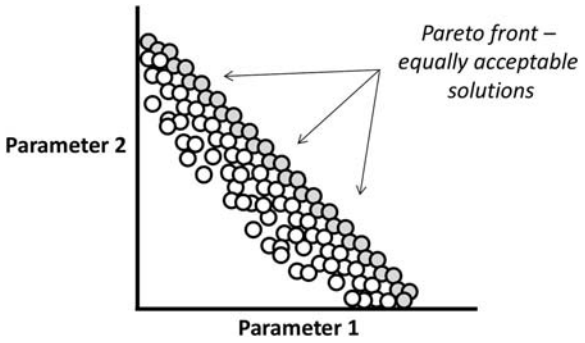

Fig. 12 An example of a Pareto front[155,157] obtained from two equally weighted variables. A large number of equally acceptable solutions are obtained (*gray circles*).

2.03.5 Conclusions

Achieving a molecule with balanced PK/PD and safety properties, that meets or exceeds the project goals, is a very difficult undertaking. This is especially true for projects associated with novel targets where little historical validation data is available. The current rates of attrition point to failures in utilizing the current battery of assays in preclinical and early clinical development to weed out problematic compounds. Moreover, it suggests further scientific effort is needed to rectify the situation, including the development and validation of more predictive toxicity assays to help reduce the large numbers of failures due to safety, as well as earlier proof of concept studies to tackle failures due to efficacy. A process that can identify and fail problematic compounds faster and more cheaply is a key goal.[5]

Despite Lipinski's seminal paper[54] being close to 2 decades old, the restraining of physicochemical parameters to an area of drug-like space is still somewhat controversial.[66,67] It could be argued that physical properties should be restrained within drug-like space unless there are justifiable reasons to move beyond them. We also question whether we take enough risks with lower potency compounds, given this is a major cause of property inflation. Justification for this is clear given that oral drugs display mean XC_{50} of ~0.1 μM (ie, 50% of compounds have XC_{50}s below this cut-off)[46,47]. Medicinal chemistry teams are highly effective at optimizing compounds against these high throughput assays, yet the relevance of them towards efficacy is often not always clear,[28] especially since efficacy is the single largest failure of compounds in clinical development.[158] A more effective strategy may be for the drug discovery project to work towards developing 2–3 distinctly novel chemical series to target the most optimal areas of physical property space, thereby maximizing the probability of obtaining an a balanced PK/PD and safety profile.

From a PK/PD perspective a more effective translational approach is to target low therapeutic doses by maximizing target affinity and the free drug concentration. This has the potential to reduce the risk of attrition related to drug burden and direct organ toxicity. This strategy sees the maximization of the target RO% per unit of dose which can be achieved in two ways: either by increasing the target affinity and/or by improving the unbound concentration in the relevant compartment. It is the optimal balance of these properties, and not their absolute values per se that dictates the potential to achieve a low in vivo efficacious dose. This forms the basis of the DEI, a method that allows the comparison of leads and candidates in terms of their RO% per unit of dose.

List of Recommendations:

- Take a probabilistic approach to drug discovery; there are clearly unknowns so following a standard strategy that results in a 96% failure rate is not practical.
- Focus initially on ideal area of property space—but don't be afraid to make undesirable compounds for reasons of diversity
- Aim for backup molecules with truly different structures and properties (PK/PD and physicochemical properties)
- There will be a need to compromise on certain parameters—avoid the desire to maintain potency over other parameters as this is typically a refined protein or recombinant assays which by their very nature have questionable disease/phenotype relevance.[28]
- Follow best practice in target activity/selectivity, PK/PD, and molecular properties, but do not be afraid to "break from the model" to test a hypothesis.

Acknowledgment

MPG would like to acknowledge funding from The Thailand Research Fund (RSA5780068) and the Kasetsart University Research and Development Institute (KURDI).

See also: 3.16. Empirical and Physics-Based Calculations of Physical–Chemical Properties. 4.01. Role of ADME/PK in Drug Discovery, Safety Assessment, and Clinical Development. 4.02. ADME Optimization in Drug Discovery. 4.08. A Comprehensive Overview of the Current Status and Application of Predictive ADMET: Introduction and Overview.

References

1. Scannell, J. W.; Blanckley, A.; Boldon, H.; Warrington, B. Diagnosing the Decline in Pharmaceutical R&D Efficiency. *Nat. Rev. Drug Discov.* **2012,** *11* (3), 191–200.
2. Bunnage, M. E.; Chekler, E. L. P.; Jones, L. H. Target Validation Using Chemical Probes. *Nat. Chem. Biol.* **2013,** *9* (4), 195–199.
3. Plenge, R. M.; Scolnick, E. M.; Altshuler, D. Validating Therapeutic Targets Through Human Genetics. *Nat. Rev. Drug Discov.* **2013,** *12* (8), 581–594.
4. Munos, B. How to Avert biopharma's R&D Crisis. *In Vivo* **2011,** *29*, 2011800050.
5. Paul, S. M.; Mytelka, D. S.; Dunwiddie, C. T.; Persinger, C. C.; Munos, B. H.; Lindborg, S. R.; Schacht, A. L. How to Improve R&D Productivity: The Pharmaceutical industry's Grand Challenge. *Nat. Rev. Drug Discov.* **2010,** *9* (3), 203–214.
6. Milne, G. M., Jr. Pharmaceutical Productivity—the Imperative for New Paradigms. In *Annual Reports in Medicinal Chemistry,* vol. 38; Academic Press, 2003; pp 383–396. Chapter 35.
7. Waring, M. J.; Arrowsmith, J.; Leach, A. R.; Leeson, P. D.; Mandrell, S.; Owen, R. M.; Pairaudeau, G.; Pennie, W. D.; Pickett, S. D.; Wang, J.; Wallace, O.; Weir, A. An Analysis of the Attrition of Drug Candidates from Four Major Pharmaceutical Companies. *Nat. Rev. Drug Discov.* **2015,** *14* (7), 475–486.
8. Morgan, P.; Van Der Graaf, P. H.; Arrowsmith, J.; Feltner, D. E.; Drummond, K. S.; Wegner, C. D.; Street, S. D. A. Can the Flow of Medicines be Improved? Fundamental Pharmacokinetic and Pharmacological Principles Toward Improving Phase II Survival. *Drug Discov. Today* **2012,** *17* (9–10), 419–424.
9. Ullman, F.; Boutellier, R. A Case Study of Lean Drug Discovery: From Project Driven Research to Innovation Studios and Process Factories. *Drug Discov. Today* **2008,** *13* (11–12), 543–550.
10. Cook, D.; Brown, D.; Alexander, R.; March, R.; Morgan, P.; Satterthwaite, G.; Pangalos, M. N. Lessons Learned From the Fate of AstraZeneca's Drug Pipeline: A Five-Dimensional Framework. *Nat. Rev. Drug Discov.* **2014,** *13* (6), 419–431.
11. Empfield, J. R.; Leeson, P. D. Lessons Learned From Candidate Drug Attrition. *IDrugs* **2010,** *13* (12), 869–873.
12. Owens, P. K.; Raddad, E.; Miller, J. W.; Stille, J. R.; Olovich, K. G.; Smith, N. V.; Jones, R. S.; Scherer, J. C. A Decade of Innovation in Pharmaceutical R&D: The Chorus Model. *Nat. Rev. Drug Discov.* **2015,** *14* (1), 17–28.
13. Munos, B. Lessons From 60 Years of Pharmaceutical Innovation. *Nat. Rev. Drug Discov.* **2009,** *8* (12), 959–968.
14. Laufer, S.; Holzgrabe, U.; Steinhilber, D. Drug Discovery: A Modern Decathlon. *Angew. Chem. Int. Ed.* **2013,** *52* (15), 4072–4076.
15. Pammolli, F.; Magazzini, L.; Riccaboni, M. The Productivity Crisis in Pharmaceutical R&D. *Nat. Rev. Drug Discov.* **2011,** *10,* 428–438.
16. Davis, A. M.; Keeling, D. J.; Steele, J.; Tomkinson, N. P.; Tinker, A. C. Components of Successful Lead Generation. *Curr. Top. Med. Chem.* **2005,** *5* (4), 421–439.
17. Edwards, A. M.; Arrowsmith, C. H.; Bountra, C.; Bunnage, M. E.; Feldmann, M.; Knight, J. C.; Patel, D. D.; Prinos, P.; Taylor, M. D.; Sundstrom, M.; Barker, P.; Barsyte, D.; Bengtson, M. H.; Bell, C.; Bowness, P.; Boycott, K. M.; Buser-Doepner, C.; Carpenter, C. L.; Carr, A. J.; Clark, K.; Das, A. M.; Dhanak, D.; Dirks, P.; Ellis, J.; Fantin, V. R.; Flores, C.; Fon, E. A.; Frail, D. E.; Gileadi, O.; O'Hagan, R. C.; Howe, T.; Isaac, J. T. R.; Jabado, N.; Jakobsson, P.-J.; Klareskog, L.; Knapp, S.; Lee, W. H.; Lima-Fernandes, E.; Lundberg, I. E.; Marshall, J.; Massirer, K. B.; MacKenzie, A. E.; Maruyama, T.; Mueller-Fahrnow, A.; Muthuswamy, S.; Nanchahal, J.; O'Brien, C.; Oppermann, U.; Ostermann, N.; Petrecca, K.; Pollock, B. G.; Poupon, V.; Prinjha, R. K.; Rosenberg, S. H.; Rouleau, G.; Skingle, M.; Slutsky, A. S.; Smith, G. A. M.; Verhelle, D.; Widmer, H.; Young, L. T. Preclinical Target Validation Using Patient-Derived Cells. *Nat Rev Drug Discov* **2015,** *14* (3), 149–150.
18. Dolgin, E. Drug Discoverers Chart Path to Tackling Data Irreproducibility. *Nat. Rev. Drug Discov.* **2014,** *13* (12), 875–876.
19. Peers, I. S.; Ceuppens, P. R.; Harbron, C. In Search of Preclinical Robustness. *Nat. Rev. Drug Discov.* **2012,** *11* (10), 733–734.
20. Chu, X.; Bleasby, K.; Evers, R. Species Differences in Drug Transporters and Implications for Translating Preclinical Findings to Humans. *Expert Opin. Drug Metab. Toxicol.* **2013,** *9* (3), 237–252.
21. Volpe, D. A. Variability in Caco-2 and MDCK Cell-Based Intestinal Permeability Assays. *J. Pharm. Sci.* **2008,** *97* (2), 712–725.
22. Park, B. K.; Boobis, A.; Clarke, S.; Goldring, C. E. P.; Jones, D.; Kenna, J. G.; Lambert, C.; Laverty, H. G.; Naisbitt, D. J.; Nelson, S.; et al. Managing the Challenge of Chemically Reactive Metabolites in Drug Development. *Nat. Rev. Drug Discov.* **2011,** *10* (4), 292–306.
23. Dahlin, J. L.; Inglese, J.; Walters, M. A. Mitigating Risk in Academic Preclinical Drug Discovery. *Nat. Rev. Drug Discov.* **2015,** *14* (4), 279–294.
24. Morphy, R. The Influence of Target Family and Functional Activity on the Physicochemical Properties of Pre-Clinical Compounds. *J. Med. Chem.* **2006,** *49* (10), 2969–2978.
25. Lindsay, M. A. Target Discovery. *Nat. Rev. Drug Discov.* **2003,** *2* (10), 831–838.
26. Begley, C. G.; Ellis, L. M. Drug Development: Raise Standards for Preclinical Cancer Research. *Nature* **2012,** *483* (7391), 531–533.
27. Steward, O.; Balice-Gordon, R. Rigor or Mortis: Best Practices for Preclinical Research in Neuroscience. *Neuron* **2014,** *84* (3), 572–581.
28. Eggert, U. S. The Why and how of Phenotypic Small-Molecule Screens. *Nat. Chem. Biol.* **2013,** *9* (4), 206–209.
29. Morphy, R.; Rankovic, Z. The Physicochemical Challenges of Designing Multiple Ligands. *J. Med. Chem.* **2006,** *49* (16), 4961–4970.
30. Swinney, D. C. Phenotypic Versus Target-Based Drug Discovery for First-in-Class Medicines. *Clin. Pharmacol. Ther.* **2013,** *93,* 299–301.
31. Swinney, D. C.; Anthony, J. How Were New Medicines Discovered? *Nat. Rev. Drug Discov.* **2011,** *10,* 507–519.
32. Vincent, F.; Loria, P.; Pregel, M.; Stanton, R.; Kitching, L.; Nocka, K.; Doyonnas, R.; Steppan, C.; Gilbert, A.; Schroeter, T.; Peakman, M.-C. Developing Predictive Assays: The Phenotypic Screening "Rule of 3". *Sci. Transl. Med.* **2015,** *7* (293), 293 ps15.
33. Eder, J.; Sedrani, R.; Wiesmann, C. The Discovery of First-in-Class Drugs: Origins and Evolution. *Nat. Rev. Drug Discov.* **2014,** *13* (8), 577–587.
34. Schenone, M.; Dancik, V.; Wagner, B. K.; Clemons, P. A. Target Identification and Mechanism of Action in Chemical Biology and Drug Discovery. *Nat. Chem. Biol.* **2013,** *9* (4), 232–240.
35. Harrison, C. Phenotypic Screening: A More Rapid Route to Target Deconvolution. *Nat. Rev. Drug Discov.* **2014,** *13* (2), 102–103.
36. Moffat, J. G.; Rudolph, J.; Bailey, D. Phenotypic Screening in Cancer Drug Discovery—Past, Present and Future. *Nat. Rev. Drug Discov.* **2014,** *13* (8), 588–602.
37. Castoreno, A. B.; Eggert, U. S. Small Molecule Probes of Cellular Pathways and Networks. *ACS Chem. Biol.* **2011,** *6* (1), 86–94.
38. Sweis, R. F. Target (In)Validation: A Critical, Sometimes Unheralded, Role of Modern Medicinal Chemistry. *ACS Med. Chem. Lett.* **2015,** *6* (6), 618–621.
39. Arrowsmith, C. H.; Audia, J. E.; Austin, C.; Baell, J.; Bennett, J.; Blagg, J.; Bountra, C.; Brennan, P. E.; Brown, P. J.; Bunnage, M. E.; Buser-Doepner, C.; Campbell, R. M.; Carter, A. J.; Cohen, P.; Copeland, R. A.; Cravatt, B.; Dahlin, J. L.; Dhanak, D.; Edwards, A. M.; Frye, S. V.; Gray, N.; Grimshaw, C. E.; Hepworth, D.; Howe, T.; Huber, K. V. M.; Jin, J.; Knapp, S.; Kotz, J. D.; Kruger, R. G.; Lowe, D.; Mader, M. M.; Marsden, B.; Mueller-Fahrnow, A.; Muller, S.; O'Hagan, R. C.; Overington, J. P.; Owen, D. R.; Rosenberg, S. H.; Roth, B.; Ross, R.; Schapira, M.; Schreiber, S. L.; Shoichet, B.; Sundstrom, M.; Superti-Furga, G.; Taunton, J.; Toledo-Sherman, L.; Walpole, C.; Walters, M. A.; Willson, T. M.; Workman, P.; Young, R. N.; Zuercher, W. J. The Promise and Peril of Chemical Probes. *Nat. Chem. Biol.* **2015,** *11* (8), 536–541.
40. Harrison, C. Kinase Inhibitors: Analysing Kinase Inhibitor Selectivity. *Nat. Rev. Drug Discov.* **2012,** *11* (1), 21.
41. Davis, M. I.; Hunt, J. P.; Herrgard, S.; Ciceri, P.; Wodicka, L. M.; Pallares, G.; Hocker, M.; Treiber, D. K.; Zarrinkar, P. P. Comprehensive Analysis of Kinase Inhibitor Selectivity. *Nat. Biotechnol.* **2011,** *29* (11), 1046–1051.
42. Bunnage, M. E. Getting Pharmaceutical R&D Back on Target. *Nat. Chem. Biol.* **2011,** *7* (6), 335–339.
43. Mah, R.; Thomas, J. R.; Shafer, C. M. Drug Discovery Considerations in the Development of Covalent Inhibitors. *Bioorg. Med. Chem. Lett.* **2014,** *24* (1), 33–39.
44. Singh, J.; Petter, R. C.; Baillie, T. A.; Whitty, A. The Resurgence of Covalent Drugs. *Nat. Rev. Drug Discov.* **2011,** *10* (4), 307–317.
45. Wilson, A. J.; Kerns, J. K.; Callahan, J. F.; Moody, C. J. Keap Calm, and Carry on Covalently. *J. Med. Chem.* **2013,** *56* (19), 7463–7476.
46. Overington, J. P.; Al-Lazikani, B.; Hopkins, A. L. How Many Drug Targets Are There? *Nat. Rev. Drug Discov.* **2006,** *5,* 993–996.
47. Gleeson, M. P.; Hersey, A.; Montanari, D.; Overington, J. Probing the Links Between in vitro Potency, ADMET and Physicochemical Parameters. *Nat. Rev. Drug Discov.* **2011,** *10,* 197–208.
48. Bain, J.; Plater, L.; Elliott, M.; Shpiro, N.; Hastie, C. J.; McLauchlan, H.; Klevernic, I.; Arthur, J.; Simon, C.; Alessi, D. R.; Cohen, P. The Selectivity of Protein Kinase Inhibitors: A Further Update. *Biochem. J.* **2007,** *408* (3), 297–315.

49. Morphy, R. Selectively Nonselective Kinase Inhibition: Striking the Right Balance. *J. Med. Chem.* **2010,** *53* (4), 1413–1437.
50. Morphy, R.; Rankovic, Z. Fragments, Network Biology and Designing Multiple Ligands. *Drug Discov. Today* **2007,** *12* (3–4), 156–160.
51. Dar, A. C.; Das, T. K.; Shokat, K. M.; Cagan, R. L. Chemical Genetic Discovery of Targets and Anti-Targets for Cancer Polypharmacology. *Nature* **2012,** *486* (7401), 80–84.
52. Flemming, A. Cancer: Of Targets and Anti-Targets. *Nat. Rev. Drug Discov.* **2012,** *11* (7), 515.
53. Guiguemde, W.; Shelat, A.; Garcia-Bustos, J.; Diagana, T.; Gamo, F.; Guy, R. Global Phenotypic Screening for Antimalarials. *Chem. Biol.* **2012,** *19,* 116–129.
54. Lipinski, C. A.; Lombardo, F.; Dominy, B. W.; Feeney, P. J. Experimental and Computational Approaches to Estimate Solubility and Permeability in Drug Discovery and Development Settings. *Adv. Drug Deliv. Rev.* **1997,** *23* (2–3), 3–25.
55. Teague, S. J.; Davis, A. M.; Leeson, P. D.; Oprea, T. The Design of Leadlike Combinatorial Libraries. *Angew. Chem. Int. Ed. Engl.* **1999,** *38* (24), 3743–3748.
56. Oprea, T. I.; Davis, A. M.; Teague, S. J.; Leeson, P. D. Is There a Difference Between Leads and Drugs? A Historical Perspective. *J. Chem. Inf. Comput. Sci.* **2001,** *41* (5), 1308–1315.
57. Hann, M. M.; Oprea, T. I. Pursuing the Leadlikeness Concept in Pharmaceutical Research. *Curr. Opin. Chem. Biol.* **2004,** *8* (3), 255–263.
58. Oprea, T. I.; Allu, T. K.; Fara, D. C.; Rad, R. F.; Ostopovici, L.; Bologa, C. G. Lead-Like, Drug-Like or "Pub-Like": How Different are They? *J. Comput. Aided Mol. Des.* **2007,** *21* (1–3), 113–119.
59. Proudfoot, J. R. The Evolution of Synthetic Oral Drug Properties. *Bioorg. Med. Chem. Lett.* **2005,** *15* (4), 1087–1090.
60. Wenlock, M. C.; Austin, R. P.; Barton, P.; Davis, A. M.; Leeson, P. D. A Comparison of Physiochemical Property Profiles of Development and Marketed Oral Drugs. *J. Med. Chem.* **2003,** *46* (7), 1250–1256.
61. Leeson, P. D.; St-Gallay, S. A. The Influence of the 'Organizational Factor' on Compound Quality in Drug Discovery. *Nat. Rev. Drug Discov.* **2011,** *10* (10), 749–765.
62. Johnstone, C. Medicinal Chemistry Matters—A Call for Discipline in Our Discipline. *Drug Discov. Today* **2012,** *17* (11–12), 538–543.
63. Nussbaumer, P. Medicinal Chemists of the 21st Century—Who Are We and Where to Go? *ChemMedChem* **2015,** *10* (7), 1133–1139.
64. Tsukamoto, T. Tough Times for Medicinal Chemists: Are We to Blame? *ACS Med. Chem. Lett.* **2013,** *4* (4), 369–370.
65. Lowe, D. B. Nowhere to Go But Up: The Return of Medicinal Chemistry. *ACS Med. Chem. Lett.* **2012,** *3* (1), 3–4.
66. Kenny, P.; Montanari, C. Inflation of Correlation in the Pursuit of Drug-Likeness. *J. Comput. Aided Mol. Des.* **2013,** *27* (1), 1–13.
67. Leeson, P. D.; Young, R. J. Molecular Property Design: Does Everyone Get It? *ACS Med. Chem. Lett.* **2015,** *6* (7), 722–725.
68. Hajduk, P. J.; Huth, J. R.; Tse, C. Predicting Protein Druggability. *Drug Discov. Today* **2005,** *10* (23–24), 1675–1682.
69. Hopkins, A. L.; Keserü, G. M.; Leeson, P. D.; Rees, D. C.; Reynolds, C. H. The Role of Ligand Efficiency Measures in Drug Discovery. *Nat. Rev. Drug Discov.* **2014**. *13*, 105–121.
70. Leeson, P. Drug Discovery: Chemical Beauty Contest. *Nature* **2012,** *481* (7382), 455–456.
71. Johnson, T. W.; Dress, K. R.; Edwards, M. Using the Golden Triangle to Optimize Clearance and Oral Absorption. *Bioorg. Med. Chem. Lett.* **2009,** *19* (19), 5560–5564.
72. Waring, M. J. Lipophilicity in Drug Discovery. *Expert Opin. Drug Discovery* **2010,** *5* (3), 235–248.
73. Meanwell, N. A. Improving Drug Candidates by Design: A Focus on Physicochemical Properties as a Means of Improving Compound Disposition and Safety. *Chem. Res. Toxicol.* **2011,** *24* (9), 1420–1456.
74. Tarcsay, Á.; Keserű, G. M. Contributions of Molecular Properties to Drug Promiscuity. *J. Med. Chem.* **2013,** *56,* 1789–1795.
75. Leeson, P. D.; Springthorpe, B. The Influence of Drug-Like Concepts on Decision-Making in Medicinal Chemistry. *Nat. Rev. Drug Discov.* **2007,** *6,* 881–890.
76. Hann, M. M.; Keserü, G. M. Finding the Sweet Spot: The Role of Nature and Nurture in Medicinal Chemistry. *Nat. Rev. Drug Discov.* **2012,** *11* (5), 355–365.
77. Gleeson, M. P.; Montanari, D. Strategies for the Generation, Validation and Application of In Silico ADMET Models in Lead Generation and Optimization. *Expert Opin. Drug Metab. Toxicol.* **2012,** *8* (11), 1435–1446.
78. Gleeson, M. P.; Hersey, A.; Hannongbua, S. In-Silico ADME Models: A General Assessment of Their Utility in Drug Discovery Applications. *Curr. Top. Med. Chem.* **2011,** *11* (4), 358–381.
79. Gleeson, M. P. Generation of a Set of Simple, Interpretable ADMET Rules of Thumb. *J. Med. Chem.* **2008,** *51* (4), 817–834.
80. Gleeson, P.; Bravi, G.; Modi, S.; Lowe, D. ADMET Rules of Thumb II: A Comparison of the Effects of Common Substituents on a Range of ADMET Parameters. *Bioorg. Med. Chem.* **2009,** *17* (16), 5906–5919.
81. Huuskonen, J. Estimation of Aqueous Solubility for a Diverse Set of Organic Compounds Based on Molecular Topology. *J. Chem. Inf. Comput. Sci.* **2000,** *40* (3), 773–777.
82. Muller, P. Y.; Milton, M. N. The Determination and Interpretation of the Therapeutic Index in Drug Development. *Nat. Rev. Drug Discov.* **2012,** *11* (10), 751–761.
83. Peters, J. U. Can We Discover Pharmacological Promiscuity Early in the Drug Discovery Process? *Drug Discov. Today* **2012,** *17,* 325–335.
84. Aptula, A. O.; Cronin, M. T. Prediction of hERG K+ Blocking Potency: Application of Structural Knowledge. *SAR QSAR Environ. Res.* **2004,** *15* (5–6), 399–411.
85. Vaz, R. J.; Li, Y.; Rampe, D. Human Ether-A-Go-Go Related Gene (HERG): A Chemist's Perspective. *Prog. Med. Chem.* **2005,** *43,* 1–18.
86. Leach, A. G.; Pilling, E. A.; Rabow, A. A.; Tomasi, S.; Asaad, N.; Buurma, N. J.; Ballard, A.; Narduolo, S. Enantiomeric Pairs Reveal That Key Medicinal Chemistry Parameters Vary More Than Simple Physical Property Based Models Can Explain. *Med. Chem. Commun.* **2012,** *3* (5), 528–540.
87. Dahlin, J. L.; Walters, M. A. The Essential Roles of Chemistry in High-Throughput Screening Triage. *Future Med. Chem.* **2014,** *6* (11), 1265–1290.
88. Macarron, R. Impact of High-Throughput Screening in Biomedical Research. *Nat. Rev. Drug Discov.* **2011,** *10,* 188–195.
89. Keseru, G. M.; Makara, G. M. The Influence of Lead Discovery Strategies on the Properties of Drug Candidates. *Nat. Rev. Drug Discov.* **2009,** *8* (3), 203–212.
90. Kuntz, I. D.; Chen, K.; Sharp, K. A.; Kollman, P. A. The Maximal Affinity of Ligands. *Proc. Natl. Acad. Sci. U. S. A.* **1999,** *96* (18), 9997–10002.
91. Andrews, P. R.; Craik, D. J.; Martin, J. L. Functional Group Contributions to Drug-Receptor Interactions. *J. Med. Chem.* **1984,** *27* (12), 1648–1657.
92. Hajduk, P. J.; Greer, J. A Decade of Fragment-Based Drug Design: Strategic Advances and Lessons Learned. *Nat. Rev. Drug Discov.* **2007,** *6* (3), 211–219.
93. Sutherland, J. J.; O'Brien, L. A.; Weaver, D. F. A Comparison of Methods for Modeling Quantitative Structure – Activity Relationships. *J. Med. Chem.* **2004,** *47* (22), 5541–5554.
94. Myint, K.-Z.; Wang, L.; Tong, Q.; Xie, X.-Q. Molecular Fingerprint-Based Artificial Neural Networks QSAR for Ligand Biological Activity Predictions. *Mol. Pharm.* **2012,** *9* (10), 2912–2923.
95. Hann, M. M.; Leach, A. R.; Harper, G. Molecular Complexity and Its Impact on the Probability of Finding Leads for Drug Discovery. *J. Chem. Inf. Comput. Sci.* **2001,** *41* (3), 856–864.
96. Hopkins, A. L.; Groom, C. R.; Alex, A. Ligand Efficiency: A Useful Metric for Lead Selection. *Drug Discov. Today* **2004,** *9* (10), 430–431.
97. Reynolds, C. H. Ligand Efficiency Metrics: Why All the Fuss? *Future Med. Chem.* **2015,** *7* (11), 1363–1365.
98. Shultz, M. D. The Thermodynamic Basis for the Use of Lipophilic Efficiency (LipE) in Enthalpic Optimizations. *Bioorg. Med. Chem. Lett.* **2013,** *23* (21), 5992–6000.
99. Kenny, P.; Leitão, A.; Montanari, C. Ligand Efficiency Metrics Considered Harmful. *J. Comput. Aided Mol. Des.* **2014,** *28* (7), 699–710.
100. Ferenczy, G. G.; Keseru, G. M. Enthalpic Efficiency of Ligand Binding. *J. Chem. Inf. Model.* **2010,** *50* (9), 1536–1541.
101. Perola, E. An Analysis of the Binding Efficiencies of Drugs and Their Leads in Successful Drug Discovery Programs. *J. Med. Chem.* **2010,** *53* (7), 2986–2997.
102. Stevens, J. L. Future of ToxicologyMechanisms of Toxicity and Drug Safety: Where Do We Go From Here? *Chem. Res. Toxicol.* **2006,** *19* (11), 1393–1401.
103. Redfern, W. S. Safety Pharmacology—A Progressive Approach. *Fundam. Clin. Pharmacol.* **2002,** *16,* 161–173.
104. Smith, D. A.; Schmid, E. F. Drug Withdrawals and the Lessons Within. *Curr. Opin. Drug Discov. Devel.* **2006,** *9,* 38–46.
105. Sanguinetti, M. C.; Jiang, C.; Curran, M. E.; Keating, M. T. A Mechanistic Link Between an Inherited and an Acquired Cardiac Arrhythmia: HERG Encodes the IKr potassiμM Channel. *Cell* **1995,** *81,* 299–307.
106. Kennedy, T. Managing the Drug Discovery/Development Interface. *Drug Discov. Today* **1997,** *2,* 436–444.
107. Frank, R.; Hargreaves, R. Clinical Biomarkers in Drug Discovery and Development. *Nat. Rev. Drug Discov.* **2003,** *2* (7), 566–580.

108. DiMasi, J. A.; Feldman, L.; Seckler, A.; Wilson, A. Trends in Risks Associated With New Drug Development: Success Rates for Investigational Drugs. *Clin. Pharmacol. Ther.* **2010,** *87,* 272–277.
109. Hornberg, J. J.; Laursen, M.; Brenden, N.; Persson, M.; Thougaard, A. V.; Toft, D. B.; Mow, T. Exploratory Toxicology as an Integrated Part of Drug Discovery. Part II: Screening Strategies. *Drug Discov. Today* **2014,** *19* (8), 1137–1144.
110. Hornberg, J. J.; Laursen, M.; Brenden, N.; Persson, M.; Thougaard, A. V.; Toft, D. B.; Mow, T. Exploratory Toxicology as an Integrated Part of Drug Discovery. Part I: Why and How. *Drug Discov. Today* **2014,** *19* (8), 1131–1136.
111. Budnitz, D. S.; Pollock, D. A.; Weidenbach, K. N.; Mendelsohn, A. B.; Schroeder, T. J.; Annest, J. L. National Surveillance of Emergency Department Visits for Outpatient Adverse Drug Events. *JAMA* **2006,** *296* (15), 1858–1866.
112. Lazarou, J.; Pomeranz, B. H.; Corey, P. N. Incidence of Adverse Drug Reactions in Hospitalized Patients: A Meta-Analysis of Prospective Studies. *JAMA* **1998,** *279* (15), 1200–1205.
113. Kramer, J. A.; Sagartz, J. E.; Morris, D. L. The Application of Discovery Toxicology and Pathology Towards the Design of Safer Pharmaceutical Lead Candidates. *Nat. Rev. Drug Discov.* **2007,** *6* (8), 636–649.
114. Sasseville, V. G.; Lane, J. H.; Kadambi, V. J.; Bouchard, P.; Lee, F. W.; Balani, S. K.; Miwa, G. T.; Smith, P. F.; Alden, C. L. Testing Paradigm for Prediction of Development-Limiting Barriers and Human Drug Toxicity. *Chem. Biol. Interact.* **2004,** *150* (1), 9–25.
115. Thomas, E. E.; Will, Y. The Impact of Assay Technology as Applied to Safety Assessment in Reducing Compound Attrition in Drug Discovery. *Expert Opin. Drug Discovery* **2012,** *7* (2), 109–122.
116. Arrowsmith, J. Trial Watch: Phase II Failures: 2008–2010. *Nat. Rev. Drug Discov.* **2011,** *10* (5), 328–329.
117. Arrowsmith, J. Trial Watch: Phase III and Submission Failures: 2007–2010. *Nat. Rev. Drug Discov.* **2011,** *10* (2), 87.
118. Smith, D. A.; Di, L.; Kerns, E. H. The Effect of Plasma Protein Binding on in vivo Efficacy: Misconceptions in Drug Discovery. *Nat. Rev. Drug Discov.* **2010,** *9* (12), 929–939.
119. Dahl, G.; Akerud, T. Pharmacokinetics and the Drug–Target Residence Time Concept. *Drug Discov. Today* **2013,** *18* (15–16), 697–707.
120. Copeland, R. A.; Pompliano, D. L.; Meek, T. D. Drug-Target Residence Time and Its Implications for Lead Optimization. *Nat. Rev. Drug Discov.* **2006,** *5* (9), 730–739.
121. Roberts, S. A. High-Throughput Screening Approaches for Investigating Drug Metabolism and Pharmacokinetics. *Xenobiotica* **2001,** *31* (8–9), 557–589.
122. Roberts, S. A. Drug Metabolism and Pharmacokinetics in Drug Discovery. *Curr. Opin. Drug Discov. Devel.* **2003,** *6* (1), 66–80.
123. Tsaioun, K.; Kates, S. A. *ADMET for Medicinal Chemists: A Practical Guide;* John Wiley & Sons: Hoboken, New Jersey, 2010.
124. Wang, J.; Urban, L. *Predictive ADMET: Integrated Approaches in Drug Discovery and Development;* John Wiley & Sons: Hoboken, New Jersey, 2014.
125. Smith, D. A., Allerton, C., Kubinyi, H., van de Walker, H., Walker, D. K., Eds.; 3rd ed.; *Pharmacokinetics and Metabolism in Drug Design*; Wiley-VCH Verlag & Co KGaA: Weinheim, Germany, 2012.
126. Ballard, P.; Brassil, P.; Bui, K. H.; Dolgos, H.; Petersson, C.; Tunek, A.; Webborn, P. J. H. The Right Compound in the Right Assay at the Right Time: An Integrated Discovery DMPK Strategy. *Drug Metab. Rev.* **2012,** *44* (3), 224–252.
127. Plowright, A. T.; Johnstone, C.; Kihlberg, J.; Pettersson, J.; Robb, G.; Thompson, R. A. Hypothesis Driven Drug Design: Improving Quality and Effectiveness of the Design-Make-Test-Analyse Cycle. *Drug Discov. Today* **2012,** *17* (1–2), 56–62.
128. Beaumont, K.; Smith, D. A. Does Human Pharmacokinetic Prediction Add Significant Value to Compound Selection in Drug Discovery Research? *Curr. Opin. Drug Discov. Devel.* **2009,** *12* (1), 61–71.
129. Van den Bergh, A.; Sinha, V.; Gilissen, R.; Straetemans, R.; Wuyts, K.; Morrison, D.; Bijnens, L.; Mackie, C. Prediction of Human Oral Plasma Concentration-Time Profiles Using Preclinical Data. *Clin. Pharmacokinet.* **2011,** *50* (8), 505–517.
130. Grime, K. H.; Barton, P.; McGinnity, D. F. Application of In Silico, in vitro and Preclinical Pharmacokinetic Data for the Effective and Efficient Prediction of Human Pharmacokinetics. *Mol. Pharm.* **2012,** *10* (4), 1191–1206.
131. McGinnity, D. F.; Collington, J.; Austin, R. P.; Riley, R. J. Evaluation of Human Pharmacokinetics, Therapeutic Dose and Exposure Predictions Using Marketed Oral Drugs. *Curr. Drug Metab.* **2007,** *8* (5), 463–479.
132. Kalgutkar, A. S.; Gardner, I.; Obach, R. S.; Shaffer, C. L.; Callegari, E.; Henne, K. R.; Mutlib, A. E.; Dalvie, D. K.; Lee, J. S.; Nakai, Y.; O'Donnell, J. P.; Boer, J.; Harriman, S. P. A Comprehensive Listing of Bioactivation Pathways of Organic Functional Groups. *Curr. Drug Metab.* **2005,** *6* (3), 161–225.
133. Valko, K.; Chiarparin, E.; Nunhuck, S.; Montanari, D. In Vitro Measurement of Drug Efficiency Index to Aid Early Lead Optimization. *J. Pharm. Sci.* **2012,** *101* (11), 4155–4169.
134. Gabrielsson, J.; Dolgos, H.; Gillberg, P.-G.; Bredberg, U.; Benthem, B.; Duker, G. Early Integration of Pharmacokinetic and Dynamic Reasoning is Essential for Optimal Development of Lead Compounds: Strategic Considerations. *Drug Discov. Today* **2009,** *14* (7–8), 358–372.
135. Gabrielsson, J.; Fjellstrom, O.; Ulander, J.; Rowley, M.; Van Der Graaf, P. H. Pharmacodynamic-Pharmacokinetic Integration as a Guide to Medicinal Chemistry. *Curr. Top. Med. Chem.* **2011,** *11* (4), 404–418.
136. Reichel, A. Addressing Central Nervous System (CNS) Penetration in Drug Discovery: Basics and Implications of the Evolving New Concept. *Chem. Biodivers.* **2009,** *6* (11), 2030–2049.
137. Lowe, P. J.; Hijazi, Y.; Luttringer, O.; Yin, H.; Sarangapani, R.; Howard, D. On the Anticipation of the Human Dose in First-in-man Trials From Preclinical and Prior Clinical Information in Early Drug Development. *Xenobiotica* **2007,** *37* (10–11), 1331–1354.
138. Bowes, J.; Brown, A. J.; Hamon, J.; Jarolimek, W.; Sridhar, A.; Waldron, G.; Whitebread, S. Reducing Safety-Related Drug Attrition: The Use of in vitro Pharmacological Profiling. *Nat. Rev. Drug Discov.* **2012,** *11* (12), 909–922.
139. Giacomini, K. M.; Huang, S. M.; Tweedie, D. J.; Benet, L. Z.; Brouwer, K. L.; Chu, X.; Dahlin, A.; Evers, R.; Fischer, V.; Hillgren, K. M.; Hoffmaster, K. A.; Ishikawa, T.; Keppler, D.; Kim, R. B.; Lee, C. A.; Niemi, M.; Polli, J. W.; Sugiyama, Y.; Swaan, P. W.; Ware, J. A.; Wright, S. H.; Yee, S. W.; Zamek-Gliszczynski, M. J.; Zhang, L. Membrane Transporters in Drug Development. *Nat. Rev. Drug Discov.* **2010,** *9* (3), 215–236.
140. de Lange, E. The Mastermind Approach to CNS Drug Therapy: Translational Prediction of Human Brain Distribution, Target Site Kinetics, and Therapeutic Effects. *Fluids Barriers CNS* **2013,** *10* (1), 12.
141. Shaffer, C. L. Defining Neuropharmacokinetic Parameters in CNS Drug Discovery to Determine Cross-Species Pharmacologic Exposure-Response Relationships. *Annu. Rep. Med. Chem.* **2010,** *45,* 55–70.
142. Benet, L. Z.; Hoener, B. A. Changes in Plasma Protein Binding Have Little Clinical Relevance. *Clin. Pharmacol. Ther.* **2002,** *71,* 115–121.
143. Montanari, D.; Chiarparin, E.; Gleeson, M. P.; Braggio, S.; Longhi, R.; Valko, K.; Rossi, T. Application of Drug Efficiency Index in Drug Discovery: A Strategy Towards Low Therapeutic Dose. *Expert Opin. Drug Discovery* **2011,** *6* (9), 913–920.
144. Braggio, S.; Montanari, D.; Rossi, T.; Ratti, E. Drug Efficiency: A New Concept to Guide Lead Optimization Programs Towards the Selection of Better Clinical Candidates. *Expert Opin. Drug Discovery* **2010,** *5* (7), 609–618.
145. van der Graaf, P.; Benson, N. Systems Pharmacology: Bridging Systems Biology and Pharmacokinetics-Pharmacodynamics (PKPD) in Drug Discovery and Development. *Pharm. Res.* **2011,** *28* (7), 1460–1464.
146. Paine, S. W.; Ménochet, K.; Denton, R.; McGinnity, D. F.; Riley, R. J. Prediction of Human Renal Clearance From Preclinical Species for a Diverse Set of Drugs That Exhibit Both Active Secretion and Net Reabsorption. *Drug Metab. Dispos.* **2011,** *39* (6), 1008–1013.
147. Chadwick, A. T.; Segall, M. D. Overcoming Psychological Barriers to Good Discovery Decisions. *Drug Discov. Today* **2010,** *15* (13–14), 561–569.
148. Segall, M. D. Multi-Parameter Optimization: Identifying High Quality Compounds With a Balance of Properties. *Curr. Pharm. Des.* **2012,** *19,* 1292–1310.
149. Johnstone, C.; Pairaudeau, G.; Pettersson, J. A. Creativity, Innovation and Lean Sigma: A Controversial Combination? *Drug Discov. Today* **2011,** *16* (1–2), 50–57.
150. Andersson, S.; Armstrong, A.; Björe, A.; Bowker, S.; Chapman, S.; Davies, R.; Donald, C.; Egner, B.; Elebring, T.; Holmqvist, S.; Inghardt, T.; Johannesson, P.; Johansson, M.; Johnstone, C.; Kemmitt, P.; Kihlberg, J.; Korsgren, P.; Lemurell, M.; Moore, J.; Pettersson, J. A.; Pointon, H.; Pontén, F.; Schofield, P.; Selmi, N.; Whittamore, P. Making Medicinal Chemistry More Effective—Application of Lean Sigma to Improve Processes, Speed and Quality. *Drug Discov. Today* **2009,** *14* (11–12), 598–604.

151. Cheshire, D. R. How Well do Medicinal Chemists Learn From Experience? *Drug Discov. Today* **2011,** *16* (17–18), 817–821.
152. Lajiness, M. S.; Maggiora, G. M.; Shanmugasundaram, V. Assessment of the Consistency of Medicinal Chemists in Reviewing Sets of Compounds. *J. Med. Chem.* **2004,** *47* (20), 4891–4896.
153. Kutchukian, P. S.; Vasilyeva, N. Y.; Xu, J.; Lindvall, M. K.; Dillon, M. P.; Glick, M.; Coley, J. D.; Brooijmans, N. Inside the Mind of a Medicinal Chemist: The Role of Human Bias in Compound Prioritization During Drug Discovery. *PLoS One* **2012,** *7* (11), e48476.
154. Bennani, Y. L. Drug Discovery in the Next Decade: Innovation Needed ASAP. *Drug Discov. Today* **2011,** *16* (17–18), 779–792.
155. Segall, M. D.; Beresford, A. P.; Gola, J. M. R.; Hawksley, D.; Tarbit, M. H. Focus on Success: Using a Probabilistic Approach to Achieve an Optimal Balance of Compound Properties in Drug Discovery. *Expert Opin. Drug Metab. Toxicol.* **2006,** *2* (2), 325–337.
156. Hann, M. M. Molecular Obesity, Potency and Other Addictions in Drug Discovery. *Med. Chem. Commun.* **2011,** *2* (5), 349–355.
157. Kell, D. B. Scientific Discovery as a Combinatorial Optimisation Problem: How Best to Navigate the Landscape of Possible Experiments? *Bioessays* **2012,** *34* (3), 236–244.
158. Macdonald, S. J. F.; Smith, P. W. Lead Optimization in 12 Months? True Confessions of a Chemistry Team. *Drug Discov. Today* **2001,** *6* (18), 947–953.

Relevant websites

https://www.ebi.ac.uk/chembl: A link to bioactivity data compiled by the European Bioinformatics Institute.
https://pubchem.ncbi.nlm.nih.gov: A link to screening data generated by the institute of national health.
http://www.drugbank.ca: A link to data pertaining to marketed drugs.
http://www.rxlist.com: A link to data pertaining to marketed drugs.
http://www.ncbi.nlm.nih.gov/pubmed: A link to target and compound pharmacology data.

2.04 Predictive Toxicology: Latest Scientific Developments and Their Application in Safety Assessment

D Armstrong, S Li, W Frieauff, H-J Martus, J Reilly, D Mikhailov, S Whitebread, and L Urban, Novartis Institutes for Biomedical Research, Cambridge, MA, United States

© 2017 Elsevier Ltd. All rights reserved.

2.04.1	**Introduction**	94
2.04.1.1	Why Drugs Fail	94
2.04.1.2	The Proportionality and Predictability of Adverse Drug Reactions	94
2.04.1.3	Regulatory Context	95
2.04.1.4	3Rs	95
2.04.1.5	What Are We Trying to Predict?	95
2.04.1.6	Assessment of Predictivity	96
2.04.2	**Model Systems for Toxicology**	97
2.04.2.1	Individual Target Screening	97
2.04.2.2	Simple Cellular Models	100
2.04.2.3	Complex Cellular Models	100
2.04.2.4	Organ Chips	101
2.04.2.5	Isolated Tissues and Organs	101
2.04.2.6	Animal Models: How Good Are They?	102
2.04.3	**OMICS Technologies**	102
2.04.3.1	Genomics	102
2.04.3.2	Proteomics	103
2.04.3.3	Metabolomics	104
2.04.4	**Predictive Genetic Toxicology**	105
2.04.4.1	The Standard Genotoxicity Testing Battery	105
2.04.4.2	The Two-Strain Ames Screen	106
2.04.4.3	The Micronucleus Test *In Vitro*	106
2.04.5	**Physicochemical Properties Link With Drug Promiscuity and *In Vivo* Toxicologic Outcomes**	106
2.04.5.1	Lipophilicity and Promiscuity	107
2.04.5.2	Basicity and Promiscuity	107
2.04.5.3	Phospholipid Affinity: Incorporating Both Lipophilic and Ionic Interactions	107
2.04.6	***In Silico* Approaches to Predictive Toxicology**	108
2.04.7	**Summary**	110
References		110

2.04.1 Introduction

2.04.1.1 Why Drugs Fail

The probability of successfully launching a new small-molecule drug is very small,[1,2] with the likelihood of progressing from phase I clinical trial to FDA approval being in the region of 10%.[3] An analysis of reasons for late-stage (phase II and phase III) failure identified lack of efficacy as the major contributor in >50% of cases between 2007 and 2012,[4] suggesting that investing in target validation might have the greatest impact on attrition. Arrowsmith and Miller[4] identified that the next largest cause of late-stage failure, accounting for 19–35%, is safety. It is notable that this is a rather different picture from that in 1991 when the pharmacokinetics and bioavailability of compounds were by far the largest challenge to success, accounting for around 40% of failures.[5] By 2000, the implementation of early *in vitro* absorption, distribution, metabolism, and excretion (ADME) assays early in the drug discovery process and utilizing *in vitro* intestinal permeability and hepatic metabolism assays alongside physiochemical understanding, had reduced this to ~10%, and this figure remains low. Here, we discuss key *in vitro* technologies that can make early predictions of drug safety, offering the opportunity for significant improvement on the probability of success in drug discovery and development.

2.04.1.2 The Proportionality and Predictability of Adverse Drug Reactions

Around 75% of adverse drug reactions (ADRs) in hospitalized patients (those admitted to the hospital due to an ADR or those experiencing an ADR while undergoing hospitalized treatment)[6] have been classified[7] as "type A" ADRs: those that are dose-dependent,

those that are related to a pharmacological action of the drug, and (perhaps most importantly) those that are predictable. This suggests that, with early characterization of the pharmacological properties of candidate molecules, there is an opportunity to eliminate a large proportion of the undesired effects of molecules selected to enter the development phase.

Given the immensely complex nature of normal physiology, the key question is where to focus in implementing early testing, detection, and elimination strategies. Redfern and colleagues[8] provide a meta-analysis identifying the proportional contribution of key organ systems to adverse events or causes of attrition broken down by phase. For example, genetic toxicity accounts for 5% of attrition in nonclinical phases of drug discovery.[8] Importantly, genetic toxicity does not feature as a cause of any attrition during clinical development or postmarketing: The decision-enabling data are generated in the nonclinical phase and appropriate decisions are made to avoid progression of genetically toxic molecules. In order to assess potential metabolites of the tested compounds that may be generated *in vivo*, genetic toxicity tests employ an *in vitro* metabolic activation system (normally the so-called S9 mix from rat liver). Interestingly, cardiovascular toxicology accounts for 27% of attrition in the nonclinical phase but only 9% of ADRs reported during phase I clinical trials. However, 45% of postmarketing drug withdrawals are due to cardiovascular ADRs. This suggests that nonclinical data enable selection of molecules that are relatively safe in populations of (often healthy) volunteers in phase I trials, whereas in larger patient populations, where the disease state may compromise the cardiovascular system and chronic treatment is not limited by the set period of clinical trials, ADRs occur, which were not predicted by nonclinical models, presumably because such models are based on the normal healthy physiological state.

2.04.1.3 Regulatory Context

In addition to the economic drivers demanding improvement in attrition, there are of course ethical requirements for safe medicines that are embodied in guidelines issued by the International Council for Harmonization of Technical Requirements for Pharmaceuticals for Human Use (ICH). The "S" series guidance contains descriptions of both recommended and required nonclinical tests for assessment of the safety of candidate molecules (http://www.ich.org/products/guidelines/safety/article/safety-guidelines.html). Three of the 10 guidelines explicitly encourage *in vitro* testing: S2 for genetic toxicology, S7A/B for safety and secondary pharmacology and specifically prolongation of the QT interval of the surface electrocardiogram, and S10 for photosafety. ICH guidance S2 is quite explicit in requiring assessment of genetic toxicologic potential in bacterial reverse gene mutation (Ames) tests in addition to *in vivo* tests. ICH guidance S10 recommends characterization of UV–visible absorption spectra as an initial experiment to determine whether further testing is required, and the initial toxicity testing involves a test in 3T3 fibroblasts *in vitro*. Although ICH S7A does not specify methodologies for secondary pharmacology, many in the industry have chosen to use *in vitro* biochemical and pharmacological assays as a means to assess off-target activity.[9,10] ICH S7B recommends *in vitro* electrophysiological assays for the activity of compounds at cardiac ion channels as part of an integrated risk assessment of cardiovascular safety. Thus, it is clear that a major aspect of the ICH S guidelines involves the results of *in vivo* tests for candidate drugs. This leaves a wide opportunity to develop rapid, cost-effective, and predictive medium- and high-throughput *in vitro* methodologies to enable selection of the best molecules to move forward into *in vivo* testing without the constraints of the regulatory environment.

2.04.1.4 3Rs

Notwithstanding a regulatory requirement for animal testing prior to first human testing of new chemical entities, there has been a strong movement to "refine, reduce, and replace" animal studies in toxicologic testing, based on the framework proposed by Russell and Burch.[11] In part, this reduction in some *in vivo* testing is driven by the understanding that models or tests should provide useful information on which to base decisions to design and select drug-like molecules and that some *in vitro* systems can be more predictive of human effects than some animal tests. For example, in 2001, the LD_{50} Draize test (a test that determines the acute oral dose at which 50% of animals tested are killed) was abolished by the Organization for Economic Co-operation and Development (OECD) with the realization that the test did not provide particularly useful information for specific understanding of toxicity. Such examples are simplistic and rare; much stronger, current drivers for the pharmaceutical industry to implement more *in vitro* and *in silico* toxicity and safety testing are the need to improve predictivity, throughput, and quality while minimizing sample requirement and cost.

One approach to reducing the need for testing is in the application of a "read-across" process. This is the concept that compounds with defined structures and toxicologic end points (source compounds) may be grouped into categories. The aim would be to use the known end points to predict the toxicologic effect of an untested compound (target compound).[12] While perhaps more commonly applied in areas such as environmental toxicology or cosmetics, read-across has been successfully applied in the pharmaceutical development, for example, in generating alerts for structures associated with the potential for causing hepatotoxicity,[13] offering the opportunity to evaluate *in silico* before synthesis or testing.

2.04.1.5 What Are We Trying to Predict?

The search for new medicines that are both efficacious and safe in humans requires the ability to make predictions based on data from nonclinical models to likely effects in humans. However, given a regulatory requirement for *in vivo* safety testing prior to first human testing, it may also be appropriate to generate *in silico* or *in vitro* models that are predictive of effects obtained from preclinical species. The use of drug combinations is becoming more common, particularly in the areas of oncology and infectious disease.

The ability to predict whether administration of drug combinations affects the toxicologic profile, through synergistic effects on off-target pathways, effects on bioavailability, or changes in metabolism, is becoming an important component of predictive toxicology and may be amenable to *in silico* system informatics approaches.[14]

The selection of appropriate end points is also of interest: some models may provide specific molecular detail and understanding related to a well-defined physiological end point. Perhaps the most common example of this is the electrophysiological assessment of block of the delayed rectifier potassium current IKr carried by the human ether-à-go-go (hERG) potassium channel. It is now well established that block of the hERG channel is linked to lengthening of the QT interval of the surface electrocardiogram, which in a small number of cases is associated with life-threatening cardiac arrhythmias including torsades de pointes (TdP).[15] While it is possible to build a chain of ever more integrative models in order to assess the risk of arrhythmia in humans, with models ranging from electrophysiological recordings of recombinant ion channels[16] or Purkinje fibers,[17] isolated cardiomyocyte action potential duration recording,[18] ventricular wedge preparations,[19] isolated heart,[20,21] to conscious telemetered dogs,[22] it may not be efficient or desirable to utilize all of the available models. At present, the most conservative approach is mandated by regulatory authorities, based on hERG channel inhibition measured in recombinant channels expressed in immortalized cells by manual patch clamp, followed by nonrodent telemetry. This approach is open to criticism, as arrhythmogenesis in the heart is the result of integrated effects of the modulation of ion channel kinetics and other pharmacological factors. Importantly, the mode of inhibition of the hERG channel might differentiate in the translation to arrhythmia.[15] The comprehensive *in vitro* proarrhythmia assay initiative (http://cipaproject.org/) is a coordinated effort between regulatory authorities, industry, and academia, to address these questions and provide suite of mechanistically based *in vitro* assays coupled to *in silico* reconstructions of cellular cardiac electrophysiological activity that could integrate the various components of chronotropy. A body of evidence can be generated to provide an integrated risk assessment of the likelihood of the occurrence of specific functional end points.

At the other end of the scale, some end points such as manifestation of phospholipidosis may be reasonably well defined,[23] and *in vitro* black-box assays are available to predict the effects;[24] however, the underlying molecular mechanisms driving the effect either *in vitro* or *in vivo* are less clear. In these cases, using an appropriately characterized set of compounds to evaluate the *in vitro* model allows calculation of sensitivity, specificity, and predictive value of an assay.[25]

It is also important to have an understanding of the predictive value of animal models themselves. Ultimately an integrated risk assessment involving the understanding of toxicologic findings and their underlying mechanisms is required to determine the safety profile relevant to human use. In a recent example, ticagrelor, a reversible $P2Y_{12}$ receptor antagonist for the treatment of acute coronary syndrome, was found to affect the incidence of uterine and mammary tumor in a 2-year rat carcinogenicity study,[26] which was performed to meet the requirement of ICH guidance S1. At face value, it may appear that ticagrelor would pose a carcinogenic risk for human patients. However, mechanistic investigations using *in vitro* biochemical and pharmacological assays to understand the off-target profile (secondary pharmacology) revealed that ticagrelor inhibits the function of the dopamine transporter, increasing dopaminergic signaling so modulating prolactin release from the anterior pituitary.[27] Understanding the fundamental differences in rat and human physiology, specifically that prolactin is eutrophic in rats but not in humans,[28] allows an integrated assessment, combining the *in vitro* off-target activity, *in vitro* genotoxicity, and *in vivo* data. Taken together, these findings do not indicate a patient safety risk, based on qualitative species differences between rat and human.[26] The learning from this example is that for a chain of different models from *in vitro* to *in vivo* to the clinic, it is essential to understand both the predictivity of each model to the next and the relevance of every model to the clinical setting.

2.04.1.6 Assessment of Predictivity

A key element in the assessment of predictivity is the availability of well-characterized reference compounds. While the dynamic range of a model may be explored with pharmacological tool compounds, the ability to correctly classify the activity or lack of activity of compounds whose effects have previously been characterized in humans is essential to gain an understanding of the predictive value of a safety or toxicologic model. Selection of drugs for model validation requires evidence of effect or lack of effect on the desired end point, an understanding of the prevalence of the end point in the human population, an understanding of the population in which the end point was studied (eg, healthy volunteers versus patient), characterization of the exposure (AUC and free C_{max}) at which the effect occurred/did not occur, and understanding whether there are active metabolites with a similar or diverse pharmacological profile to the parent relevant to the measured end point.

Cooper et al.[25] describe a contingency matrix (**Table 1**) that clearly defines terms to describe the characteristics of an assay. Of greatest interest are sensitivity—the finding of true-positive outcomes as a proportion of both true-positive and false-negative outcomes—and specificity—the finding of true-negative outcomes as a proportion of both true-negative and false-positive outcomes. The definition of a true outcome is in the hands of the assay developer, and the characterization of the test is dependent on this definition; thus, the selection of appropriate reference compounds, as discussed in the preceding text, is critical in assay development. The balance of sensitivity and specificity required of an early *in vitro* safety assay will depend on the severity of the adverse event that the assay is attempting to predict, the context of when the assay will be used in the discovery process, and the availability of additional confirmatory assays. It may be that for very early, higher throughput safety assays, specificity is the most important parameter in order to avoid discarding compounds too early in the discovery process. It is worth noting that in the selection of reference compounds for characterization of an assay, there should be a good balance of both positive and negative compounds; if the training set is heavily weighted to either positive or negative compounds, the assessment of sensitivity and specificity will be biased.

Table 1 Terms used to characterize *in vitro* assays[25]

		Reference compound annotation	
		Toxic	*Nontoxic*
In vitro assay outcome	Positive	True positive (TP)	False positive (FP)
	Negative	False negative (FN)	True negative (TN)

(from Cooper, J.A.; Saracci, R.; Cole, P. Describing the Validity of Carcinogen Screening Tests. *Br. J. Cancer* **1979**, *39*(1), 87–89). Reference compounds are grouped according to defined criteria as either toxic or nontoxic (eg, based on clinical finding), and the outcome of the assay under evaluation is shown as either positive or negative. Sensitivity = TP/(TP + FN). Specificity = TN/(TN + FP)

2.04.2 Model Systems for Toxicology

2.04.2.1 Individual Target Screening

In vitro pharmacological profiling, using simple biochemical, enzymological, and pharmacological assays to assess the interaction of test molecules with individual molecular targets from a broad range of target classes typically including G protein-coupled receptors (GPCRs), enzymes, kinases, nuclear hormone receptors, ion channels, and transporters, is now well established in the pharma industry as a preferred method of assessing secondary pharmacodynamics early in the discovery process.[9,10] These techniques offer rapid, cost-effective methods with low sample requirement to generate an understanding of off-target activity. Often, assays are grouped into panels ranging from a handful to hundreds of targets, and testing may be performed at single concentration or over a range of concentrations, with assays being readily available at several contract research organizations (CROs). Typically, a small number of targets with key links to safety end points are screened early, with broader coverage of targets employed for more advanced compounds. Since there is little regulatory guidance on the appropriate selection of targets for *in vitro* profiling,[29] a minimum panel of 44 targets has been proposed based on the shared experience of four large pharma companies.[9]

Selection of appropriate targets for *in vitro* pharmacology screening has to be considered at two levels: (1) identification of targets that are associated with a known hazard when affected by drugs or modulated by genetic modifications and (2) selection of targets from the collection identified at level 1 for screening and profiling *in vitro* and also *in silico*. The composition of the second level is largely dependent on the indication, therapeutic targets, preferred chemical structure, and availability of high-quality assays. It is important to maintain a broad focus in panel design: in a mapping on "pharmacological space," Paolini and colleagues[30] demonstrated that many compounds bind to more than one target and that the promiscuity is not limited to like-target classes; in other words, if the primary target is a kinase, it is not sufficient to screen only kinases as off-targets.

Some understanding of the physiological role of a target is usually obtained in a number of different sources, including extensive literature surveys, cataloging data from human genetics (OMIM http://www.ncbi.nlm.nih.gov/omim provides a useful resource), knockout animal studies (although of course the long-term absence of a target is not necessarily the same as pharmacological antagonism), clinical trial data (databases such as PharmaPendium provide helpful curation of compound, exposure, and ADR reports), and pharmacological studies using previously characterized and reference compounds.

It should be remembered that adverse events may be driven by primary drug targets, for example, skin rash caused by EGFR inhibitors,[31] or opiate analgesics associated with abdominal distension, pain, constipation, nausea, and vomiting,[32] and this can provide valuable evidence linking target to effect. However, the use of reference compounds can be challenging in that certainty of the mechanism of action (MOA) can be difficult to demonstrate. For example, CGP 71683A has been described as a selective neuropeptide NPY Y_5 antagonist that reduces food intake in rats. Indeed, Criscione and colleagues[33] showed >1000-fold selectivity of the compound for the NPY_5 subtype over Y_1, Y_2, Y_4 receptors in *in vitro* radioligand binding assays. However, this study did not examine the effects of CGP 71683A at targets outside the immediate receptor family, and Della Zuna[34] subsequently found high affinity for muscarinic receptors and serotonin reuptake sites (presumably the 5-HT transporter) within approximately threefold of the affinity for the NPY Y_5 receptor. A number of hypotheses can be generated to relate these off-target activities with modulation of food intake in addition to the action at NPY Y_5 receptors[34]; thus, the hypothesis that NPY Y_5 receptors affect food intake is not conclusively supported by data from studies using CGP 71683A as a reference compound.

Interpretation of the off-target profile on a target-by-target basis involves some assessment of the potency in the *in vitro* assay relative to free plasma concentrations (free C_{max}, for reasons reviewed in[35]): those likely to be achieved in humans for efficacy and those achieved in preclinical species as part of an integrated risk assessment. Typically, a 100-fold difference between free C_{max} and *in vitro* potency is taken as likely to be of little concern (**Fig. 1**). For the shortlist of targets where separation between *in vitro* potency and (likely) *in vivo* plasma exposure is <100-fold, it may be appropriate to assess safety margins on an individual target basis. For example, Smith[36] has shown that for a range of GPCR antagonists, there is a strong correlation between the clinical free C_{max} required for efficacy and 3x the *in vitro* affinity for the receptor (K_i); therefore, for the specific subgroup of GPCR antagonist hits, it may be that >3x separation between *in vitro* affinity and free C_{max} would be accepted as low risk. For other targets, individual assessments can be made by comparing the exposures for known drug/ADR pairs at a given target to determine a safety margin unique to the target.[37] A comprehensive review of the therapeutic index, the relationship of exposure data to a variety of assay and clinical data, is provided by Muller and Milton.[38]

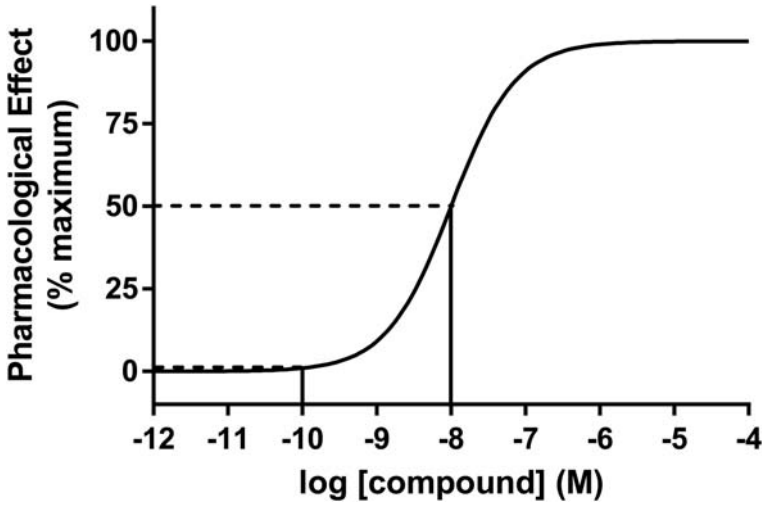

Fig. 1 A standardized pharmacological concentration–response curve using the Hill–Langmuir equation to relate increasing concentrations of the compound of interest to increasing effect. The curve is described by a lower asymptote of 0% and an upper asymptote of 100%, a slope of unity, and a midpoint of 10 nM. It can be seen that at a concentration of drug 100x lower (0.1 nM) than the midpoint of the curve, the pharmacological effect is approximately 1%.

Examining the profiles for known compounds can give confidence that *in vitro* profiling is able to detect target interactions that are relevant to drug discovery. For example, in Fig. 2, the *in vitro* target profile of three generations of antidepressants is shown grouped with the oldest generation at the top of the table. While most of the compounds have strong interactions with the 5-hydroxytryptamine (5-HT) transporter, it can be seen that the newer generations of compounds are less promiscuous, especially among muscarinic, histaminergic, and adrenergic receptors, which appears to correlate with fewer ADRs. A second example is shown in Fig. 3 where the *in vitro* activity at phosphodiesterase 3 (PDE3) was found to translate to both histopathologic and functional changes in rat heart for a number of tyrosine kinase inhibitors. The link between PDE3 and myocardial toxicity has been described for both milrinone, for which the primary target is assumed to be PDE3, and other kinase inhibitors for which PDE3 is a secondary target.[39]

The overall promiscuity of a drug in the context of likelihood of success may also be considered. An analysis of marketed and withdrawn drugs shows that a higher proportion of withdrawn drugs are promiscuous than those that remain on the market (see Fig. 2 in[9]). Typically, promiscuity is expressed as the proportion of targets at which a compound has a defined activity (eg, $IC_{50} < 10$ μM or shows >50% effect at a given test concentration); however, to our knowledge, there is no validated scaling factor that would encompass, in a single summary value, both the number of hits and the potency at each of the targets.

Generic name	5-HT1A	5-HT2A	5-HT2B	5-HT2C	5-HT Transporter	Adenosine A1	Adenosine A2A	Adenosine Transporter	Alpha1A adrenoceptor	Alpha2A adrenocetor	Alpha2B adrenoceptor	Alpha2C adrenoceptor	Beta1 adrenoceptor	Beta2 adrenoceptor	Noradrenaline Transporter	Dopamine D1	Dopamine D2L	Dopamine D3	Dopamine Transporter	hERG	Histamine H1	Delta Opioid	Kappa Opioid	Muscarinic M1	Muscarinic M2	Muscarinic M3
Amitriptyline	3.77	0.92	1.10	0.15	0.01	>30	>30	>30	0.03	9.10	0.28	0.29	22.70	22.74	0.52	0.45	0.55	0.44	14.20	6.73	0.01	>30	1.10	0.61	0.19	0.26
Clomipramine	>10	0.90	5.60	0.53	<0.01	>30	>30	>30	0.04	>10	1.70	4.50	5.90	19.00	0.60	>20	0.39	0.30	14.63	2.69	0.07	>30	4.11	0.70	>10	1.70
Desipramine	>30	19.00	27.00	3.20	0.12	>30	>30	>30	0.57	>30	2.20	5.10	>30		0.01	>30	8.40	1.70	13.00	1.90	0.14	>30	30.00	3.60	4.70	2.90
Imipramine	>10	10.00	5.00	0.13	0.02	>30	>30	>30	0.08	>10	0.32	2.10	>10	>10	0.08	3.20	1.30	0.41	>10	4.06	0.02	>10	2.61	0.49	0.45	0.78
Nortriptyline	8.00	0.51	0.73	0.18	0.17	>30	>30	>30	0.13	9.40	0.42	0.90	24.00	4.70	0.03	0.39	5.70	0.51	3.20	2.59	0.02	>30	0.69	0.51	0.63	0.58
Protriptyline	>10	1.80	3.80	3.50	>30	>10	>10	>30	0.46	>10	6.40	11.00	>10	>10	>30	>10	5.20	0.85	17.80	1.00	0.05	>30	2.12	0.57	0.65	0.24
Fluoxetine	>10	3.50	>10	0.15	0.02	>30	>30	>30	5.28	>10	3.90	>10	>10	>10	2.30	12.97	8.30	>10	>10	5.33	6.00	>10	2.34	15.00	11.55	4.10
Paroxetine	17.00	27.00	28.00	>30	0.00	>30	>30	>30	1.86	>10	>10	7.80	>10	9.50	0.07	>10	>10	>10	1.18	3.00	>10	0.83	1.45	1.50	1.15	0.45
Sertraline	12.00	9.80	9.45	5.40	0.00	>30	>30	>30	1.01	12.23	2.90	2.70	12.00	>30	6.30	>20	11.00	15.00	0.29	1.90	23.00	>30	0.24	9.80	24.00	11.00
Citalopram	>10	>30	2.00	4.10	0.01	>30	>30	>30	1.10	>10	>10	>10	>10	>10	5.80	7.30	>10	1.90	>10	2.81	1.90	>30	>10	13.00	>10	>10
Duloxetine	8.90	20.00	12.00	13.00	0.00	>30	>30	>30	1.05	>10	3.90	1.40	15.00		0.05	>10	6.60	4.60	1.15	2.38	8.80	>30	1.96	>10	>10	>30
Fluvoxamine	>10	>10	>10	>30	0.00	>10	>10	>30	2.55	>10	>10	>10	>10	>10	28.00	>10	>10	>30	>30	4.00	>10	>30	10.67	>10	>10	>30
Lofepramine	>30	6.60	>30	2.70	0.04	>30	>30	>30	4.40	>30	4.00	17.00	>30	20.00	0.02	>30	19.00	3.00	21.00	3.30	0.65	30.00	4.80	4.30	>30	4.70
Venlafaxine	>30	>30	>10	>30	0.03	>30	>30	>30	>30	>10	>10	>10	>10	>10	12.85	>20	>10	>30	26.32	>30	1.10	>30	>10	>10	>10	>30

Fig. 2 *In vitro* secondary target profile for selected antidepressants with the first-generation compounds at the top of the table. Values are *in vitro* A_{50} in μM. Color-coded red <1 μM; orange 1–10 μM; yellow 10–30 μM; white >30 μM. Data from Novartis in house screening.

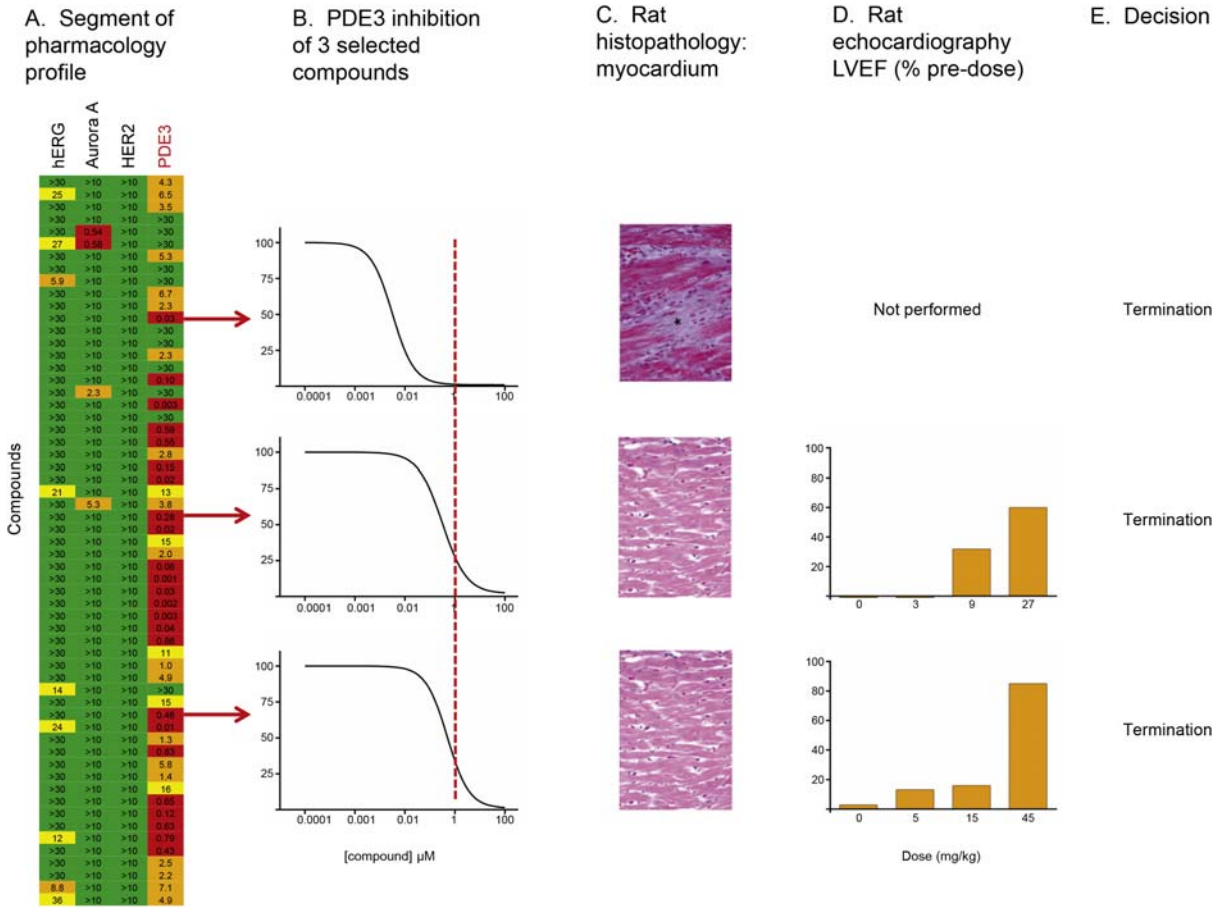

Fig. 3 Translation of PDE3 from *in vitro* to *in vivo* effects. (A) Excerpt of *in vitro* secondary pharmacology profile for a range of compounds from a tyrosine kinase inhibitor project. Each row represents a single compound, each column the result of an *in vitro* target assay; red high activity; yellow moderate activity; green low activity. (B) Concentration–response curves showing inhibition of PDE3 by 3 example compounds from panel A. Dashed red line indicates approximate free plasma concentration achieved in *in vivo* rat studies (panels C and D). (C) Histopathologic effects of 3 example compounds in rat myocardium from free plasma exposures around 1 μM. Compound 1 shows necrosis. (D) Evaluation of compounds 2 and 3 in rat using echocardiography, measured 1 h post dose. Percentage increase in left ventricular ejection fraction for control and 3 increasing doses. Maximum free plasma exposure at high dose for all 3 compounds was approximately 1 μM. (E) Integrating 4 preceding data sets to make a decision on compound progression.

One of the appeals of individual target screening is the ability to access specific molecular-level information about the activity of a compound; often, this is useful in reverse pharmacology: understanding the underlying mechanisms of *in vivo* or clinical observations. One of the most common examples of reverse pharmacology is the relationship between agonism of the 5-HT_{2B} receptor and cardiac valvulopathy, which has been found to be caused by norfenfluramine, pergolide, methysergide and cabergoline.[40] The original finding of valve disease caused by fenfluramine's metabolite, norfenfluramine, showed striking similarities to valvulopathies caused by serotonin-releasing tumors[41] that pointed toward the involvement of 5-HT receptors. Specific association between agonism of the 5-HT_{2B} receptor and valvulopathy was demonstrated by Rothman and colleagues[42] by screening both positive (compounds known or suspected of causing cardiac valvular damage) and negative controls for activity at 11 cloned 5-HT receptors in radioligand binding and functional assays in a classic example of *in vitro* secondary pharmacology. The underlying mechanism appears to relate to the role of 5-HT_{2B} receptors in valve fibroblasts, with overstimulation causing upregulation of mitogenesis and induction of differentiation into myofibroblasts that overproduce interstitial collagen affecting the function of the valve (extensively reviewed in[43–45]).

Scaling of individual target screening using traditional biochemical assays is dependent on the ability to source appropriate reagents, develop an appropriate assay, and synthesize an appropriate quantity of test compound. Catalogs of major CROs offer in the 100s to low 1000s of individual assays. However, this represents only a fraction of the ~19,000 proteins that are encoded by the human genome,[46] and an increasing number of different assays and reagents pose a logistic challenge to perform. Grouping targets into shared technology assays may be one way of addressing this challenge. For example, GPCRs may be "force-coupled" to the same G protein, thereby allowing a single functional platform, often a calcium-based technology[47,48]; circular dielectric spectroscopy may also be appropriate for GPCR functional measures.[49] Cell microarray technology may offer an alternate approach

to measurement of direct ligand–receptor interaction, although at the present time, this requires labeling of the test compound with, for example, radioactive isotope and luminescent or antigenic tags, and is limited to targets expressed on the cell surface. This technology, which uses ink jet printing technology to transfect discrete groups of cells within a monolayer cultured on glass slides, each with a vector encoding a unique protein, was successfully used to identify the human endothelial protein C receptor as a key target in *Plasmodium falciparum*-induced malaria from an array of 2505 cell surface proteins.[50]

2.04.2.2 Simple Cellular Models

Simple cellular models fall into two categories: First, those addressing individual molecular targets in a whole cell (eg, cell-based kinase assays, whole-cell GPCR functional assays, and reporter gene assays) may be grouped into the preceding category of *in vitro* pharmacological profiling by single-target screening. The second category of simple cellular models uses whole cells as models of functional or pathway end points where the action of a test compound may be mediated by a number of different mechanisms that may not be readily distinguished. In essence, a toxicologic end point is defined for which it is intended that the effects of test compounds in single cells will reflect the effect in whole tissue or organism. One of the common applications of simple cellular models is the prediction of hepatic toxicity since drug-induced liver injury manifests in a range of different phenotypes with a number of different potential underlying mechanisms.[51] Isolated primary hepatocytes have been used for many years as the gold standard *in vitro* test for hepatotoxicity.[52] Typically, some measure of cytotoxicity is used as an end point, for example, membrane permeability by DNA stain or depletion of metabolites such as ATP after exposure of test compound for 24–48 h. However, isolated primary hepatocytes cultured in monolayers experience changes in morphology and gene expression toward a more dedifferentiated phenotype, which change intracellular metabolism, cell–cell interactions, and cell integrity.[53] These changes may underlie some of the limitations in the ability of these assays to detect some hepatotoxins.[54] The challenges of obtaining and culturing primary cells, coupled with low sensitivity of cytotoxicity assays (even though specificity is generally very good, $>80\%$[54]), have encouraged exploration of immortalized cell lines. Human hepatocellular carcinoma-derived cell lines such as HepG2 and HepaRG are cheaper and easier to culture. However, their liver-like morphology and function are more removed from the whole organ than primary cells, and these cell lines also show very limited sensitivity: one study reported 6–13%,[55] although again specificity is generally good. Hepatotoxicity is a good example of a multifactorial end point for which very simple models are insufficient to provide reliable prediction of the *in vivo* toxicity.

For some cardiovascular risk assessments, single-cell analyses show promise. For example, human-induced pluripotent stem cell-derived cardiomyocytes (iPS-CM) provide a model for arrhythmia and QT interval prolongation. Guo and colleagues[56] defined sensitivity and specificity of $>80\%$ for both of these end points using cellular impedance to quantitate the effects of 88 reference compounds on beat rate and rhythm. Despite this success, it must be noted that iPS-CM are not perfect replicas of adult cardiomyocytes, with perhaps the most noticeable difference being spontaneous beating in iPS-CM not found in isolated adult cardiomyocytes.[57]

2.04.2.3 Complex Cellular Models

One of the key limitations of simple cellular models is the lack of physiologically relevant cell–cell interaction. Culturing one or more cell types together in 3-D, rather than as monolayers, offers opportunities to explore more complex biology. Perhaps the simplest of the 3-D models is the culture of cells together as spheroids in which cells aggregate into small (up to $\sim 600\ \mu M$) spherical clusters. These spheroids, which are long-established tumor models useful in drug discovery, provide a microenvironment of self-secreted extracellular matrix and generate inherent metabolic and proliferative gradients (see[58] for review). Ramaiahgari and colleagues[59] have successfully cultured HepG2 cells in spheroids that appear to differentiate to develop hepatic phenotypes including storage of glycogen, transport of bile salts, and the formation of structures resembling bile canaliculi and increased expression of albumin, urea, and xenobiotic transcription factors. This differentiated state can last for up to 28 days and has been shown to be sensitive to a small number of known hepatotoxins. Similarly, primary human hepatocytes in 3-D culture are more sensitive to acetaminophen than 2-D monolayers,[60] although a thorough evaluation of the sensitivity and specificity of these cultures as a model of hepatotoxicity is yet to be published.

Further physiological approximation of an *in vivo* functionality can be achieved for some systems by coculturing different cell types. For example, a liver model with microscale architecture and optimal stromal interactions (micropatterned cocultures [MPCCs]) has displayed phenotypic stability for several weeks *in vitro* as assessed by major liver-specific functions, and gene expression has been developed.[61,62] In MPCCs, primary hepatocytes are patterned onto extracellular matrix domains of optimized dimensions and then surrounded by 3T3-J2 murine embryonic fibroblasts. This model was found to be somewhat more sensitive than monoculture of primary hepatocytes in predicting hepatotoxicity with a sensitivity of around 50% at a specificity of 90%.[63]

A different take on complex cell systems has been described by Plavec and colleagues[64] who developed a test and data analysis system termed biologically multiplexed activity profiling (BioMAP). This system, originally described as a method for analyzing biological processes associated with endothelial cell responses to inflammatory stimuli, involves the culture of primary human endothelial cells under a number of different conditions with a select set of stimuli (cytokines such as TNF-α and IL-1β) and with select overexpression of genes in pathways of interest (eg, TNF receptors, MEK1 kinase, RAF, and PI3K). The response of the cell systems to stimulus and/or test compound is measured by ELISA, detecting changes in the expression level of specific proteins in the pathways of interest (eg, VCAM-1, E-selectin, and CXCL8). Using this system, relationships between pathways

and responses were built, for example, in endothelial cells expressing constitutively active *MEK1* or *MEK2*, the protein expression profiles were similar in cells treated with IL-1β and TNFα but different from those stimulated with INFγ or unstimulated cells. Berg and colleagues[65–67] have since expanded the range of cells and biological pathways that are able to be interrogated to include human primary cells from the endothelial system, bronchial cells, smooth muscle cells, fibroblasts, and others. Most recently, this system has been used to screen 776 diverse environmental and industrial chemicals as part of the US Environmental Protection Agency's ToxCast program.[68] Using a combination of 8 primary cell lines and 87 measurements per test compound concentration, a detailed fingerprint of the effects of test chemicals has been built in the BioMAP system with end points potentially relating to cardiovascular and respiratory diseases, inflammation, dermatitis, and oncology, among others. Initial success has been reported both in clustering compounds by fingerprint and known mechanism, such as mitochondrial toxins, and in identifying known and suspected activities such as the association between MAP kinase inhibitors and skin rash. The future value of such a data set is dependent on the quality of annotation that can be associated with each compound: clustering by bioassay fingerprint allows association of novel compound to already screened compounds; if these latter compounds share known toxicologic effects, then predictions may be made about the potential toxicity of the novel compound.

2.04.2.4 Organ Chips

The current cutting edge of cell-based models is in the generation of complex multicellular 3-D structures with integrated microscale structure and microfluidics, "organs-on-chips" (so called because the microengineering technology involved in the construction of the structures is analogous to that used in generating computer microchips). Models of bone, brain, breast, eye, gut, liver, lung, and kidney tissues have been generated (reviewed in[69]). These microengineered models generate the opportunity to explore multicell interactions in the context of organ-relevant spatial and structural constraints and in the presence of mechanical stresses. For example, in a "lung-on-a-chip" model,[70] human alveolar epithelial cells and human pulmonary microvascular endothelial cells were cultured on opposite sides of a porous, flexible membrane made of poly(dimethylsiloxane) (PDMS) contained in a microengineered structure able to be stretched to mimic inspiration and with microchannels able to deliver air or liquid to each face of the membrane. Beyond confirming basic functional interactions formed between the alveolar epithelial and endothelial cells, Huh and colleagues[70] showed that the "organ" was able to respond to the presence of a bacterial pathogen, *Escherichia coli*, introduced to the alveolar face, by recruitment of neutrophils circulating in the endothelial channel that migrated to the alveolar channel and engulfed the pathogen.

While the organ-on-a-chip technology is still in its early stages, many of the systems are being characterized to support toxicologic studies. One example of this is the generation of a biomimetic of the human kidney proximal tubule.[71] Jang and colleagues generated two microfluidic channels separated by a PDMS membrane on which human kidney proximal tubule epithelial cells were seeded. An apical channel allowed flow of culture medium to provide shear stress analogous to the lumen of the proximal tubule, while the opposing channel was filled with culture medium to mimic the interstitial space. The resulting organ model was sensitive to the known nephrotoxin cisplatin (reviewed in[72]) as measured by LDL release and by apoptosis, and this toxicity was antagonized by cimetidine, an inhibitor of the OCT-2 transporter by which cisplatin is taken up by proximal tubule cells.

Connection of multiple organs-on-chips has already been achieved, giving the opportunity to study ADME of drugs across different organ systems. Such linkage is also relevant to toxicology in detecting effects of metabolites or the active parts of prodrugs. In one example, Viravaidya and colleagues[73] connected liver and lung chips and administered naphthalene that was converted by the liver compartment to its reactive metabolites, 1,2-naphthalenediol and 1,2-naphthoquinone. These metabolites circulated to the lung compartment where it was possible to detect a reduction in glutathione levels as a measure of toxicity.

2.04.2.5 Isolated Tissues and Organs

Isolated perfused organs have long been used as pharmacological tools to investigate the MOA of drugs (see[74] for review), and many different organs have been successfully isolated and maintained in perfusate allowing measurements of function to be made. In toxicology, one of the more common isolates is the heart, isolated and maintained by a technique pioneered by Langendorff (reviewed in[75]). Many functional end points relevant to safety pharmacological evaluation of drug effects may be measured including left ventricular pressure, contractility, perfusion pressure, electrograms delivering the equivalent to standard surface ECG wave form (PR, QRS, and QT intervals), and monophasic action potential. One particularly successful application of the isolated rabbit heart by Hondeghem[21] was validated in two studies of clinically characterized drugs and correctly classified arrhythmogenic and nonarrhythmogenic compounds in 14 of 14[76] and 49 of 52[77] cases.

Working with isolated tissues is not a high-throughput screening methodology; the key advantage is the rich detail of conserved physiology available when testing compounds for effects on an organ or tissue. The closest to the "whole human" one may reasonably expect to achieve is by using isolated human tissues. This offers a species-relevant model, overcoming many concerns of differential sensitivity between species, but can present a challenge in trying to assure that the tissue donor is a reasonable representative of a desired population (eg, healthy versus diseased state), the tissue is in a representative condition, and there is no contamination of drugs. Sources are typically organs residual from surgery (diagnostic or cosmetic procedures), unused organs from transplant surgery, or tissues retrieved post-mortem. It should be noted that in many countries, acquisition, storage, and use of human tissues for research are very highly regulated (eg, Human Tissue Act 2004, the United Kingdom; Code of Federal Regulations Title 21 Part 1271, the United States).

2.04.2.6 Animal Models: How Good Are They?

The translatability of animal models to human outcome has been the subject of detailed scrutiny with particular focus on animal models of disease used to test the efficacy of candidate drugs and in the field of nuclear medicine.[78–81] Successful translation rates appear to vary from abject failure of 0% for prediction of vaccination development against acquired immunodeficiency syndrome by nonhuman primates,[80] to low 5% for oncology models to 20% for cardiovascular disease.[79] Martic-Kehl and colleagues[78,79] suggest that some of the reasons for low success rates of translation may be in the design, execution, and analysis of animal experiments, rather than inherent issues of species difference or inappropriate biology.

One of the key studies addressing the predictivity of animal models for human toxicology (as opposed to efficacy of candidate drugs) is presented by Olson and colleagues[82]: a summary of data shared by multinational pharmaceutical companies and the output of an International Life Sciences Institute (ILSI) meeting in 1999. This study concludes that for 150 compounds and 221 human toxicities, the true-positive concordance rate was 71% across rodent and nonrodent species, which at first may suggest that animal models are a reasonable predictor of human toxicity and have a success rate far in excess of animal models of disease. However, the study was unable to analyze a full matrix of true- and false-positive and negative data (refer to **Table 1** for definitions): only compounds that were found to be toxic in humans were considered and compared with preclinical animal data. No compounds were assessed that had been shown to be nontoxic for a given end point in humans; thus, the ability to detect false-negative and true-negative compounds was not assessed. This and other studies have been heavily criticized by Shanks et al. in a paper published in 2009,[83] questioning the statistical methods employed, inclusion criteria for data, and the retrospective approach. In the absence of a definitive analysis, it is very unlikely that regulatory authorities will abandon the requirement for *in vivo* preclinical testing of candidate drugs, especially for the assessment of general (whole-body) toxicologic effects. However, as more *in vitro* systems are validated against clinical data for specific end points, the predictive power of integrated preclinical risk assessments will increase.

2.04.3 OMICS Technologies

2.04.3.1 Genomics

The concept that changes in gene expression may be correlated with toxicologic events induced by xenobiotics was recognized in the 1990s,[84,85] and the profiling of gene transcription in toxicology is termed toxicogenomics.

The technology underpinning the advent of toxicogenomics is the DNA microarray: substrates typically of silica, plastic, or glass onto which thousands of DNA probes are anchored, representing either a set of genes of specific interest or a sample of genes across the whole genome. Total RNA is extracted from the sample and used in reverse transcription as a template to synthesize cDNA. Either the cDNA is labeled with fluorophore and hybridized to the microarray chip or the cDNA is used to synthesize cRNA including biotinylated nucleotides to label the cRNA that is subsequently hybridized to the chip. After hybridization, the chip is washed to remove unbound molecules and visualized in a scanner to detect the bound nucleotide. The intensity of the signal is related to the extent of gene expression. Detailed technical descriptions are beyond the scope of this article and the reader is referred to existing publications.[86,87] Expression of genes is determined either in relation to other genes in the same experiment (one-channel analysis) or relative to control or reference samples (two-channel analysis).[88,89]

The majority of toxicogenomics studies are conducted using the rat as the most common laboratory small species with complete genome annotation. Studies typically use homogeneous tissues (eg, heart and liver) as these are most consistent in their transcriptome and so give more robust and reliable detection of expression changes; more heterogeneous tissues (eg, brain) with different cell types and different transcriptomes depending on regional location give greater challenges in resolving changes in signal.[90] While cultured cell systems offer homogeneity and simplicity and have been successfully used as model systems in toxicogenomics (eg,[91,92]), the advantage is also the limitation: the lack of interaction with the whole tissue or whole organism provides a major challenge in detecting specific toxicogenomics effects.

In common with the preceding discussion of molecular and cell-based technologies, the application of toxicogenomics has typically been to either characterize organ-specific toxicities (hepatotoxins, cardiotoxins, and nephrotoxins) or identify molecular mechanisms or pathways underlying a specific toxicity. For example, Waring et al.[93] have shown that global gene expression analysis could distinguish groups of hepatotoxins in both rat and cultured rat hepatocytes based on their MOA. Interestingly, Hamadeh et al.[94] found that for methapyrilene, gene expression changes correlated with histopathologic changes and preceded the observation of overt toxicity suggesting the potential to use shorter term studies with the same or increased sensitivity compared with traditional toxicology.

Using a set of 64 known nephrotoxic and nonnephrotoxic drugs, an expression profile of 35 genes was identified by Fielden and colleagues[95] as a signature of renal tubular degeneration in rats. This signature was validated with 21 test compounds: 7 of 9 nephrotoxins were correctly identified (2 false negatives) and 9 of 12 nonnephrotoxins (3 false positives). What makes the toxicogenomics approach unique in this application is that the change in gene expression was detected in samples from only three rats in each treatment group on day 5 of a 28-day repeat-dose study at which point no significant histopathologic evidence of renal tubular degeneration was found; traditional toxicologic end points were informative only after the 4 weeks of dosing.

Similarly, Thukral and colleagues[96] used a set of 4 known nephrotoxins to evaluate renal gene expression profiles in rats after 1, 3, and 7 days of dosing. The gene expression profiles were clustered by both the severity and the type of tubular degeneration found

pathologically. The profiles were used to generate a predictive model that was tested against the expression profiles of 28 compounds and found 82% sensitivity. The study also identified individual genes for which the expression profile changed in a time- and dose-dependent manner aligned to the progression of proximal tubular toxicity. Perhaps unsurprisingly several of these genes are transporters (*Slc21a2*, *Slc15*, and *Slc34a2*) that can offer potential biomarkers for renal toxicology.

Key to the utilization of predictive toxicogenomics is the development of reference databases of gene expression profiles: often, it is the changes in expression profiles of a number of genes together that represent modulation of toxicologically relevant pathways, rather than the expression profile of a single gene. However, the vast array of patterns that may result from treatment with a xenobiotic must be placed in an appropriate context: it is necessary to separate the expression changes relevant to the toxicity from those that are adaptive, compensatory, or unrelated to the toxicity. For example, decreased food consumption is a common adverse reaction to xenobiotic treatment and may have wide-ranging effects on standard toxicologic end points,[97] yet it may be secondary to a specific end point of interest. Generation of such databases requires not only reference compound profiles but also sufficient annotation of technological and biological information to appropriately contextualize the data sets. Several public and commercial toxicogenomics databases exist, such as those of Gene Logic, the Toxicogenomics Project–Genomics Assisted Toxicity Evaluation (TG-GATE) system (http://toxico.nibiohn.go.jp/english/),[98] Drug Matrix (https://ntp.niehs.nih.gov/drugmatrix/index.html),[99] the EU PredTox 6 initiative outcome (http://www.ebi.ac.uk/bioinvindex/browse_studies.seam),[100] and the IMI eTOX initiative (http://www.e-tox.net/).[101]

In 2005, the FDA issued a Guidance for Industry: Pharmacogenomics Data Submissions that described in broad terms how and when pharmacogenomics data should be submitted including the concept of a Voluntary Genomic Data Submission system, which is intended to enhance the learning of both sponsors and regulators in the exploration of this new technology.[102] Importantly, the guidance provides reassurance to sponsors that early/exploratory toxicogenomics studies would not result in negative regulatory consequences, thus providing a motivation to apply this technology and drive the field forward. There are opportunities to improve the sensitivity of toxicologic studies and to refine some current studies, particularly long-term carcinogenicity studies.[103]

2.04.3.2 Proteomics

Proteomics, as originally described by Wilkins et al. in 1996,[104] is the study of the protein complement of the genome, and of course, toxicoproteomics is the term now used to describe the study of the response of the proteome to toxicants.

Although a detailed technical description is beyond the scope of this article, the key technologies underlying toxicoproteomics are electrophoresis, chromatography, and mass spectrometry (MS) (see[105,106] for reviews). In essence, to study the proteome, total protein must be isolated from a donor cell, tissue, biological fluid, or organism. The proteins of interest must be solubilized in standard chemicals including urea, guanidine hydrochloride, detergents such as Triton X-100, and sodium dodecyl sulfate (SDS). Certain groups of proteins have differential solubility and so lend themselves to studies of subgroups by type, for example, cytosolic, membrane, or glycoproteins. Some very abundant proteins may be selectively removed from the sample by immunodepletion, that is, using antibodies to remove very abundant proteins (such as albumin, IgG, and IgA present in plasma), which might otherwise mask signal from proteins of lower abundance. The sample of soluble proteins is separated by 2-D electrophoresis, first by isoelectric focus and then by polyacrylamide gel electrophoresis. This results in a 2-D separation of proteins into spots that may be stained and visualized with, for example, Coomassie, silver, or fluorescent dyes. Typically, a control sample is compared against a treatment sample to identify patterns of spots that change in intensity. Identification of the protein constituents of the spots of interest is performed using MS of fragments of the proteins that have been digested with endoproteases such as trypsin. Comparison of the fragmented sequences against protein sequence databases allows identification of the original protein. Alternatively, proteins may be digested to peptides and then separated by liquid chromatography (LC), rather than gel electrophoresis, directly coupled to a mass spectrometer. Major advances in the throughput of MS and in data handling have facilitated the development of proteomics.[107]

In essence, toxicoproteomics and toxicogenomics share principles and aims in either studying broad responses to challenge or identifying biomarkers of toxicity and are very complementary approaches. For example, it is suggested that around 50% of the measured changes in mRNA correspond to changes in expressed protein[108–110] such that proteomics may provide a level of filtration of findings from genomic studies. Toxicoproteomics also shares with toxicogenomics the requirement to filter out "background" or "nonspecific" responses. For example, Wang and colleagues[111] identified a list of 44 proteins for which a change in expression is generally detected regardless of species or experimental objective and a list of 28 protein families commonly detected in different studies. These appear to be generally related to stress response, protein stabilization, and homoeostatic control.

Specific application of toxicoproteomics has tended to focus on common organ-level toxicities such as liver, kidney, and heart in an effort to characterize the response of the proteome to a small number of specific toxins to identify markers of toxicities in these organs and understand underlying mechanisms. Success has been modest thus far; for example, Van Summeren and colleagues[112] identified 86 proteins differentially expressed in HepG2 cells in response to the known hepatotoxin cyclosporin A. However, the pattern of change was unable to distinguish two other hepatotoxins, amiodarone and acetaminophen, from the control sample, though it is unclear whether this is a limitation of the technique or the choice of HepG2 cells as a model.

Proteomic assessment of the whole liver from mice treated with acetaminophen identified 35 proteins changed by treatment with this hepatotoxicant[113] including proteins known to interact with the metabolite n-acetyl-p-benzoquinoneimine. Similarly, 33 protein targets of bromobenzene were identified as targets of this compound,[114] indicating that proteomics can identify changes in the proteome relevant to specific toxicities.

In one of the few proteomic studies to use a relatively large number of compounds, Yamanaka et al.[115] measured changes in the proteome of rat livers after 28 days of dosing with 63 carcinogenic and noncarcinogenic compounds, identifying a set of 30 changes that showed >70% concordance in classification of the reference compound set, offering the potential to create predictive analyses of carcinogenicity based on proteomic measurements. Similar proteomic studies of a large number of reference compounds of known effect/no effect in order to generate predictive tools are currently lacking.

2.04.3.3 Metabolomics

In a broad sense, metabolites are endogenous chemical entities other than DNA, RNA, proteins, and polymeric saccharides, and the measurement of such molecules has come to be termed metabolomics, although other terms including metabonomics and metabolic profiling have also been used.[116,117] Typical metabolites inspected by metabolomics are small molecules including nucleic acids, amino acids, small peptides, lipids, and sterols. The analytic tools in the metabolomics fields are naturally those that are effective in small-molecule analysis. Since metabolomics studies metabolite modulation in one or a few pathways, if not on the system level, an ideal analytic strategy should permit accurate identification and quantification of multiple interesting metabolites from biological matrices including cells, tissues, and blood.

Metabolomics studied by nuclear magnetic resonance (NMR)[118] is typically more stable and has smaller variability across samples and labs than MS. While NMR is a versatile and powerful tool, the sensitivity of NMR can be orders of magnitude lower than MS.[119] MS can be used by itself in some metabolomics applications, as in the direct infusion method for lipidomics[120]; but more often, MS is coupled online to separation methods, such as gas chromatography, LC, and capillary electrophoresis, thanks to the advance in interfacing technologies such as electrospray.[121] Separation delineates the mixture of metabolites along the time axis and reduces the complexity of the copresent metabolites at any time point. This reduces the possibility of ion suppression, which in many applications is essential to improve the sensitivity of detection and quality of quantification for MS quantification.[122] In addition, under the same chromatographic method, a metabolite of the same molecular structure is eluted at the same retention time (RT); thus, RT can be used as an orthogonal matrix for metabolite identification.[123] A so-called untargeted MS-based strategy scans and measures the entire range of molecular weight accurately.[124] Metabolites are identified by searching the measured molecular weight against metabolite database. Because the identification is solely based on molecular weight, isomeric metabolites or, in practice, those of similar molecular weights cannot be differentiated. To increase the reliability of metabolite identification, fragmentation patterns may be obtained by additional LC/MS experiment and compared with standard spectra generated previously. An alternative approach, the so-called targeted method,[125] does not look for a comprehensive coverage of metabolite space, but rather is focused on a subset of metabolites for which standards are available. Using metabolite standards, knowledge such as molecular fragmentation pattern and RT can be obtained experimentally. The sensitivity of detection and the reliability of identification of metabolites can be improved by incorporating this knowledge to build analytic methods. For these reasons, although limited to a subset of metabolites, targeted metabolomics has enjoyed great success in recent years.[126–129]

Small molecular metabolites can be indicators of disease progression, and discovery of disease-relevant biomarkers is always one of the top applications for metabolomics. As examples, the concentration of creatinine has been used to indicate renal dysfunction,[130] and a panel of metabolites in plasma is used for rare disease diagnostics for newborns.[131] Since metabolites are the end products of biochemical reactions, they reflect the working status of protein machinery. The functionality of protein machinery depends not only on the protein sequence, expression level, and posttranslational modification, traditional topics for proteomic studies, but also on factors such as the folding and binding partners, which can be extremely difficult to measure at the system level. Thus, the change in the metabolome may be most indicative of a phenotypic change, and metabolomics is well positioned to study the efficacy and side effects of drug treatment. In this regard, metabolomics in toxicology and the so-called pharmacometabolomics[132,133] have coincided,[134] with the latter focusing more on the efficacy but not excluding side effects.

While change in the metabolome is indicative of phenotypic change, the understanding of MOA often cannot be derived from metabolomics alone. The technical challenge is that no method can measure the entire metabolome accurately. In addition, intricate knowledge of how a metabolite interacts with the biological system is needed to link the change of metabolite level to MOA. A metabolite may stand at the intersection of several pathways, its production or transportation may be modulated by other proteins or other metabolites, it may inhibit or activate enzymes, and it may bind to translational factors to modulate several pathways at the same time. Databases such as KEGG (Kyoto Encyclopedia of Genes and Genomes)[135] capture knowledge of how metabolites interact with enzymes; however, our knowledge about metabolites and metabolism is far from complete, as has been demonstrated in many publications in the active field of cancer metabolism[136,137] and immunometabolism.[138,139]

Despite these challenges, metabolomics, in combination with other technologies, has been used successfully to elucidate MOA. In a metabolomics study of prostate cancer, sarcosine was found to be an important metabolic intermediary of prostate cancer progress.[140,141] Using metabolomics profiling, elevated adenosine was found in the blood of humans with sickle cell disease, inducing 2,3-diphosphoglycerate, an erythrocyte-specific metabolite that decreases the oxygen-binding affinity of hemoglobin.[142] In another study, the previously unidentified mechanism of GMX1778 antitumor activity was found to be due to inhibition of NAD+ biosynthesis.[143] In a recent study, metabolomics was used with transcriptomics to uncover significant alterations in the nucleotide metabolism networks of pink1 mutant flies, which leads to the conclusion that mitochondrial dysfunction and neurodegeneration of Parkinson's disease may be protected against by enhancing nucleotide metabolism.[144]

There are also a few examples where metabolomics has been applied to elucidate a toxicologic MOA. Ethylene glycol monomethyl ether was revealed to induce toxicity by inhibiting the flavoprotein dehydrogenase enzyme family.[145] The source of

drug-induced acute kidney injury was found via the interaction with the microbiota.[146] In another study, *in vitro* and *in vivo* models were used to evaluate epigenetic toxicity of trichloroethylene at the genetic, transcriptomic, metabolomics, and signaling levels.[147] Irinotecan (CPT-11), a first-line anti-colon cancer drug, was found to suppress IL-10 expression by causing metabolic changes in the composition of bile acids.[148]

As with other omics techniques, in order to generate predictive tools applicable to toxicology, the key to success is the generation of an annotated reference database relating known compounds, toxicologic end points, and metabolomics profiles. Two notable attempts have been made: the Consortium for Metabonomic Toxicology (COMET)[149] generated NMR profiles of the urine and blood serum of rats used in acute toxicity studies dosed with 147 compounds, with particular focus on liver and kidney toxicants of interest to pharmaceutical development. The database was annotated with histopathologic data as the reference for toxicity. Lindon reported that, using a subset of the compounds as a test set, the database identified the main organ of toxicity "in over 50% of cases" and that in 5% of cases, an incorrect prediction was made.[149] Subsequently Ebbels and colleagues[150] reported a model built on this database with sensitivities of 67% and 41% and specificities of 77% and 100% for hepatic and renal toxicity, respectively.

BASF have generated a database, MetaMapTox®, of the effects of over 500 reference compounds (chemicals, agrochemicals, and drugs) in 28-day rat toxicology studies including metabolomics profiles generated by MS and claim to be able to distinguish metabolomics profiles associated with different target organ toxicities.[151–153] Although no broad assessment of the predictivity of the database is provided, case studies are available in which the database correctly predicts the presence/absence of renal toxicity for 5 agents.[154]

Some nontoxicologic signatures can be found in metabolomics. For example, Saito and colleagues[155] describe that differential lipid profiles in rats discriminated by food intake and as described for both genomics and proteomics may relate to nontoxicologic effects.[60] Similarly, age, diet, diurnal, and estrus cycles all give measurable changes in metabolic profiles in urine.[156–158] A list of "usual suspects," that is, metabolites frequently found to change in response to toxicant administration, regardless of class, is given by Robertson,[116] analogous to the changes in 44 proteins found to occur frequently in proteomic analyses, described by Wang et al.[111] It is important to be able to distinguish and suspend where necessary these potentially distracting signatures in order to focus on the most predictive data sets, although it must be remembered there is no indication that these effects are artifactual.

2.04.4 Predictive Genetic Toxicology

Genotoxicity assessment provides mechanistic evidence for a major pathway of cancer induction, that is, by genomic alterations that lead to oncogene activation or tumor suppressor gene inactivation. Genotoxicity assessment is an interesting example of predictive toxicology where two tiers of assays are employed. While a thorough assessment of potential for genotoxicity is prescribed in regulatory guidance (ie, assays to predict effects in humans), low throughput and expense have driven the evolution of simpler, higher throughput assays employed earlier in the drug development process that are well correlated with the regulatory assays.

A scientific and regulatory framework for genotoxicity testing in the development of pharmaceutically active ingredients for human drugs is well established. ICH guidance S2[159] focuses on two fundamental areas of genotoxicity testing: the identification of a standard set of suitable and predictive assays to be performed to support clinical trials and drug registration and guidance for result interpretation (eg, extent of confirmatory experimentation). The purpose of the document is to recommend an optimized standard genetic toxicology battery for the prediction of a potential human risk and to provide guidance on the interpretation of results, with the ultimate goal of improving risk characterization for carcinogenic effects that have their basis in changes in the genetic material.

However, testing for genotoxicity extends to many other chemical areas (cosmetics and industrial or environmental chemicals), and a broader set of important guidelines include the OECD technical guidelines for the testing of chemicals, which describe the specific tests that are used routinely, such as OECD TG 471, Bacterial Reverse Mutation Test[160]; TG487, *In Vitro* Mammalian Cell Micronucleus Test[161]; TG474, Mammalian Erythrocyte Micronucleus Test[162]; and TG 489, *In Vivo* Mammalian Alkaline Comet Assay.[163]

Genotoxicity testing may comprise regulatory testing, exploratory testing, screening, and special strategies for batch/impurity/metabolite qualification. Here, we will focus on screening approaches to predict the regulatory assays as covered by ICH guidance S2.

2.04.4.1 The Standard Genotoxicity Testing Battery

According to ICH S2, the standard test battery of regulatory assays consists of the assessment of mutagenicity in a bacterial reverse gene mutation test (Ames test) and the evaluation of genotoxicity in mammalian cells *in vitro* and/or *in vivo* as covered by two options: a cytogenetics test for chromosomal damage (chromosome aberration test, micronucleus test, or a mouse lymphoma TK test) and an *in vivo* test for chromosomal damage in rodent hematopoietic cells (usually the micronucleus test in bone marrow or peripheral blood cells). Alternatively, leaving aside the mammalian *in vitro* option, an *in vivo* assessment of genotoxicity using two different assays can be conducted. Usually, this would include a micronucleus test in rodent hematopoietic cells and a second *in vivo* assay addressing DNA damage in a relevant organ: either the single-cell gel electrophoresis ("comet") assay or, more generally, an alkaline elution assay or the *in vivo* transgenic mouse mutation assay.

A common testing strategy for pharmaceutical products is the conduction of an Ames test and an *in vitro* micronucleus test, later to be complemented by an *in vivo* micronucleus test following option 1 of the ICH S2 guidance, with oncology compounds

addressed slightly differently (reduced genotoxicity testing for lifesaving indications, based on a risk–benefit approach). A requirement is that all tests conducted to support clinical testing or marketing authorization adhere to the principles of good laboratory practice (GLP).

The standard test battery may consist of an Ames test in 5 strains of *Salmonella typhimurium* (TA97a, TA98, TA100, TA102, and TA1535). The objective of the Ames assay is to evaluate the mutagenic potential of a test item by measuring its effect on the histidine-requiring bacterial strains to revert to histidine proficiency, which is a reliable method for characterizing compounds with regard to induction of mutagenic activity at the nucleotide level (such as point mutations, frameshifts, and small deletions). The micronucleus test in primary human lymphocytes or TK6 cells serves as an *in vitro* test for the assessment of chromosomal damage, which is an essential part in the characterization of the genotoxic potential of a test compound. For this purpose, the induction of micronuclei in cultured cells has shown to be a sensitive and reliable alternative to the time-consuming metaphase analysis.[164] Micronuclei are generated upon cell division, from parts of chromosomes or whole chromosomes that are lost from the nucleus during mitosis, and they can be specifically detected as extranuclear particles. As a measure for numerical and structural chromosome aberrations, the micronucleus test consists of determining the frequency of micronucleated cells in a representative fraction of cells, which is indicative for a clastogenic and/or aneugenic effect of the test item *in vitro* and *in vivo*. In order to cover potential metabolites of the tested compounds, in all *in vitro* tests, a modification using a metabolic activation system (normally the so-called S9 mix from rat liver) is included.

The micronucleus test in the bone marrow or in the peripheral blood of rats from a 4-week general toxicology study, analyzed by flow cytometry, provides the necessary information *in vivo*.[165]

Besides the well-established micronucleus test in rodent bone marrow that has been an integral part of industrial genotoxicity testing for many years,[166] the comet assay *in vivo* has emerged as the second *in vivo* test to further elucidate potentially clastogenic mechanisms by measuring DNA strand breaks in isolated cells (DNA migration in an electric field).[167] Before the revision of ICH S2(R1), the comet assay was mainly used as a mechanistic assay to follow up on *in vitro* and/or *in vivo* positives. Now, option 2 recommends the assay as a second *in vivo* genotoxicity test, for example, to follow up on *in vitro* positive genotoxicity results (option 1) or as a second *in vivo* test parallel to the *in vivo* micronucleus test (option 2).

The *in vivo* alkaline comet assay is especially suitable to assess genotoxic hazard in different organs because the assay can be conducted in any organ or cell type from which a single-cell suspension can be obtained. Usually, the liver as a metabolically active organ, areas of the gastrointestinal tract such as the jejunum and duodenum as site-of-contact tissues, and blood for systemic exposure are considered as standard organs. However, other target organs can be evaluated as well.

2.04.4.2 The Two-Strain Ames Screen

A genotoxicity testing strategy that integrates screening to predict the outcome of the regulatory assays (as outlined in the preceding text) can consist of an Ames screen and an *in vitro* micronucleus test, either in primary lymphocytes or in a cell line. For the Ames screen, designed to predict the 5-strain GLP version of the Ames test, often only the two strains TA98 and TA100 are used.[168] This strategy has also been adopted by Novartis where data show that all mutagenic compounds were identified by just using TA98 and TA100. We have found that a positive result in any of the other three strains only occurs for around 20% of synthesis intermediates showing structural alerts [unpublished Novartis internal data]. In order to further minimize test compound consumption, a miniaturized 6-well format was introduced, with which Novartis has accumulated a large database confirming the ability to detect genetically active compounds of most chemical classes with 100% sensitivity while minimizing the amount of test compound and increasing the throughput.

2.04.4.3 The Micronucleus Test *In Vitro*

Similar to the 2-strain Ames screen, the *in vitro* micronucleus test using adherent or suspension cells, designed to predict the GLP version in human lymphocytes, has evolved to include fully automated liquid handlers, flow cytometry, and image analysis.

Immortalized cell lines such as V79, CHO, and TK6 cells have been used routinely in many laboratories for conducting chromosomal aberration studies *in vitro* for many years. They have been found to be genetically stable and easy to handle and thus well suited for large-scale routine screening, with an excellent correlation between *in vitro* chromosomal aberration and *in vitro* micronucleus data in various cell lines.[169] Automated sample analysis[170] further helped to establish a simple and reliable screen for genotoxic effects, more than doubling the compound screening throughput. In order to reduce the number of positive results due to the oversensitivity of rodent cell lines such as V79, CHO, and mouse lymphoma L5178Y, when compared with the results of chromosome aberration tests in human lymphocytes, we have found that the use of the human p53-proficient TK6 cell line provides sensitivity and specificity for predicting chromosome aberration or micronucleus test in human lymphocytes of $>80\%$ [Novartis, unpublished data].

2.04.5 Physicochemical Properties Link With Drug Promiscuity and *In Vivo* Toxicologic Outcomes

Pharmaceutical companies require drug candidates to have a favorable balance of pharmacological, pharmacokinetic, and physicochemical properties. Undesirable physicochemical properties can lead to the drug having a "promiscuous" profile, which refers

to activity against multiple targets for a single molecule including nontherapeutic "off-targets."[171,172] Of course, it must be remembered that not all promiscuity is "bad"; many central nervous system (CNS) disorders such as depression, schizophrenia, and bipolar disorder present with complex pharmacology, and treatment is achieved through polypharmacological drugs such as clozapine, risperidone, and haloperidol (see[173] for a review). However, outside of the CNS, promiscuity is a major safety concern, and there is a drive within the pharmaceutical industry to detect an unfavorable profile as early as possible in the drug discovery process as it has been recognized that undesirable off-target activity profiles can prevent the development of drug compounds and even in some cases lead to market withdrawal when discovered after the drug has been approved.[9] Gaining a much better perspective and understanding of the potential safety profile at an earlier stage in the drug discovery process is essential. Physicochemical properties such as lipophilicity, size, and polarity are routinely examined in relation to drug disposition and ADME characteristics; these parameters should also be studied closely with a view on potential drug promiscuity and inherent toxicologic liabilities. Insight into property–promiscuity relationships can lead to an early recognition of potential toxic liabilities in a series and can be extremely useful in the optimization stage.

We will focus on the physicochemical parameters lipophilicity and ionization state and demonstrate how these factors combined aid in a better prediction of drug promiscuity. We will also introduce the concept of combining in one methodology the ability to rank order potential drug promiscuity by phospholipid affinity, which is a combination of both lipophilic and electrostatic interactions, and describe how this correlates with drug promiscuity.

2.04.5.1 Lipophilicity and Promiscuity

Lipophilicity is generally recognized as an important parameter of potential promiscuity, and many published property–promiscuity analyses report that drug promiscuity increases with lipophilicity. Both Hopkins et al. and Peters et al.[174,175] found that maximum promiscuity is observed for compounds when cLogP hits a threshold higher than 2.5–3. This trend can be a concern as increasing the lipophilicity of a molecule can often increase the potency of the molecule at the primary target; however, this may be offset with an increase in off-target promiscuity. Waring and Johnstone[176] concluded that the overall trend for increasing hERG potency is also driven by lipophilicity. Inhibition of the hERG potassium channel can cause delayed cardiac repolarization, which, in a very small percentage of people, is associated with a potentially fatal cardiac arrhythmia, TdP. This has resulted in a number of drugs being withdrawn from the market and represents a significant regulatory hurdle for new molecular entities in development.[177] A review of the physical properties of compounds interacting with this channel has shown that there is a low probability of lipophilic bases achieving an acceptable hERG potency.[176]

2.04.5.2 Basicity and Promiscuity

For a given lipophilicity, basic compounds tend to be more promiscuous.[178] An example of increasing basicity, while maintaining similar lipophilicity, can be found in the gentamicin series of aminoglycoside antibiotics. Increasing nephrotoxicity is seen with an increasing number of basic groups in the aminoglycoside molecule. This is due to increased binding of the drug to the anionic phospholipids on the brush border of the proximal tubular cells of the kidney and subsequent accumulation in secondary lysosomes. These cells become necrotic after repeated dosing as the time required for the tissue concentration to decrease after treatment termination is 5–6 days.[179] This is an example where increasing basicity while maintaining lipophilicity is associated with risk of compound accumulation in tissues.

When the analyses of a large data set of promiscuous molecules are further reviewed, it becomes clearer that the majority of promiscuous compounds are strong bases and bear a positive charge at pH7.[171] This research correlates well with an analysis by Peters et al.[175] and also a study by Lounkine et al. of promiscuity of 656 marketed drugs that concluded that promiscuous drugs are often both hydrophobic and cationic.[180] The link between increasing adverse *in vivo* outcomes and increasing lipophilicity and pKa for basic molecules was also recently published.[181] There is clear evidence that compounds with a cLogP > 3 and containing a basic center with a $pK_a > 8$ have physicochemical properties that can lead to phospholipidosis,[181] where intracellular accumulation of phospholipids and vacuole formation occur. A strategy to move drug design away from the physicochemical property space of these phospholipidosis potentiators is exemplified by disobutamide, a dibasic lipophilic molecule modified to reduce the risk of vacuole formation.[182]

2.04.5.3 Phospholipid Affinity: Incorporating Both Lipophilic and Ionic Interactions

Accumulation of drug in the cell membrane can be undesirable, not only reducing the ability of the drug to reach its intended target but also resulting in toxicologic consequences such as phospholipidosis or nonspecific modification of the function of membrane proteins. Cationic amphiphilic compounds are known to sequester into cell membranes, and some phospholipogenics cause liver toxicity in preclinical species such as rats[183–187] and dogs.[187] It has been documented previously that the phospholipogenic potential of drugs can be predicted by chromatographic methods including the phosphatidylcholine affinity retention factor.[188] The chance of a phospholipidotic response increases with increasing affinity for phospholipid. A statistical correlation has been found between the measured chromatographic retention factors of 36 drugs and their phospholipidosis-inducing potential.[187] It has also been demonstrated that the extent of nonspecific tissue binding of ligands used for positron emission tomography can be predicted by the retention factor in phospholipid affinity chromatographic methods,[188] which is additional information to suggest that higher

phospholipid affinity may correlate with increased risk of drug promiscuity. Finally, an in-house study at Novartis was compiled for a large data set (550) of marketed drugs and candidate drug molecules. Here, the HPLC phospholipid affinity was determined by an immobilized artificial membrane (IAM) assay, a method that incorporates not only lipophilic but also ionic contributions of test compounds.[189] In this study, there was much stronger correlation with promiscuity than lipophilicity alone as shown in Fig. 4. High values of chromatographic hydrophobicity index using IAM (CHI $IAM_{7.4}$) (>60) serve as a cautionary flag for compound promiscuity.

Physicochemical properties in small-molecule drug discovery programs are controllable by medicinal chemistry methods, and some measure of these properties can be calculated before chemical synthesis. In drug discovery, early lead generation approaches often start with small, more hydrophilic molecules but frequently expand to larger more hydrophobic and basic molecules to drive potency at the primary target. The suboptimal physicochemical properties that can arise during this stage need to be taken into account when balancing improvement in potency with promiscuity and potential toxic liabilities. Lipophilicity and ionization state of the molecule are important parameters that can be adjusted to reduce drug promiscuity and the associated safety risk. It has been demonstrated that a simple IAM HPLC phospholipid affinity measurement can incorporate the ionic and lipophilic interactions between drugs and tissue and is an efficient experimental method to rank order molecules in respect to nonspecific binding to tissue, drug phospholipidosis, and drug promiscuity potential.[188]

2.04.6 *In Silico* Approaches to Predictive Toxicology

Traditional predictive toxicology has used molecular structure information collected by experts to build knowledge-based rules or toxicophores to alert for possible toxicity end point. This approach is represented by systems like DEREK.[190] Here, we focused on computational algorithms that use 2-D or 3-D structural information along with biological activity data to generate statistical models for risk assessment, implemented with tools such as MultiCASE, MDL, BioEpisteme, and Leadscope.[191]

Consistent with the experimental tools for drug candidate risk assessment described in this article, available *in silico* predictive tools range from single- or multiple-target models to system biology approaches, from cell-based toxicity end points to whole system organ models.

For specific target models, it is appropriate to start with analyzing hERG, which is a well-recognized safety target linked to a cardiac arrhythmia called TdP. hERG blockade has been modeled using a variety of different techniques and continues to serve as a good example of how different modeling approaches can complement each other.

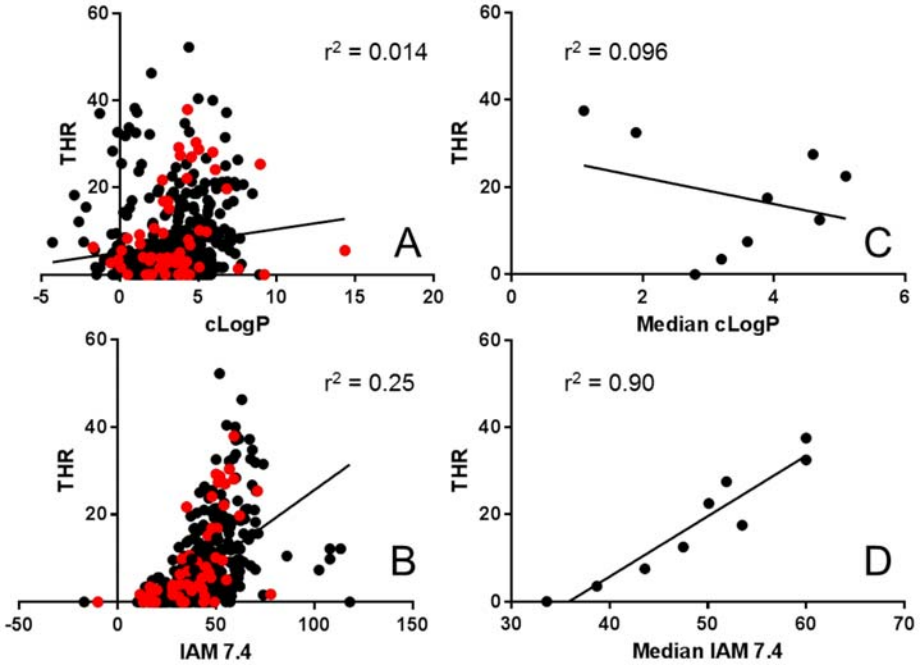

Fig. 4 Phosphatidylcholine affinity (IAM) is superior to lipophilicity alone (cLogP) to predict drug promiscuity. Promiscuity index (target hit rate (THR)) compared with cLogP (A) and chromatographic hydrophobicity index using immobilized artificial membrane (IAM) (B) for 57 marketed drugs (red) and 493 research compounds (black); the same data are shown in (C) and (D), but the THR has been binned into 9 groups, and the median cLogP (C) and median IAM (D) for each THR bin have been plotted. The THR is defined as the percentage of targets giving greater than 50% inhibition at 10 μM from a panel of at least 50 targets; higher values represent increased promiscuity.

Several pharmacophore models for hERG binding have been developed since the discovery of this ion channel linkage to LQT and TdP. The early pharmacophore model contained a tertiary or quaternary amine along with two or three aromatic rings.[192–194] Further examination of known hERG modulators shows that not all pharmacophore features are necessary and molecules with two (in case of clofilium) or three (in case of dofetilide) features can bind hERG with high affinity. The classical hERG pharmacophore model was later augmented by a possibility to have an aliphatic tail attached to a positively charged amine group to describe additional hERG blockers (C10-TEA).[195]

To provide additional insight into how hERG blockers interact with residues within the ion channel pore, Farid et al.[196] performed a number of induced-fit docking studies. The hERG homology model was built as a tetramer using MthK and KvAP structures, and six ligands known to be strong hERG binders were computationally docked into the hERG model. All six molecules demonstrate multiple ring stacking and hydrophobic interactions with the Tyr652 and Phe656 side chains of each subunit (**Fig. 5**), thus suggesting that the promiscuity of the channel is in part due to the possibilities for interactions of aromatic or hydrophobic side chains of a ligand with eight aromatic residues of the hERG tetramer.

While pharmacophore and docking modules provide chemists with visual and qualitative assessment of potential hERG binders, QSAR models can provide a quantitative assessment of the risk. The available hERG QSAR models range from those establishing a regression model between cLogP and hERG activity for a specific chemical series[176] to more complex multivariate type models using neural networks or support vector machines.[197,198] The application of QSAR models in ligand-based virtual screening is not limited to ion channels: Luo and colleagues[199] have shown the strength of such models in predicting binding affinity at a number of G protein-coupled receptors.

While blockade of the hERG ion channel remains the main focus for cardiosafety risk assessment during lead optimization, it becomes increasingly clear that modulation or perturbation of multiple cardiac ion channels can affect QT prolongation and result in life-threatening arrhythmias. This interplay of multiple targets was a subject of an integrated system-based computer model of the heart study.[200]

Recent years have seen increased attention to off-target polypharmacology, whether by design or adversely modulating many safety-related antitargets. Although chemistry optimization around several safety target liabilities is a daunting task, attempts have been made to build computational models to help with that. One example is the use of the *in vitro* secondary pharmacology profiling that involves screening lead candidates across a panel of binding and functional assays including a diverse set of GPCRs, nuclear hormone receptors, transporters, enzymes, and ion channels—all linked with documented clinical ADRs.[201] Promiscuous molecules that hit many targets in this secondary pharmacology profiling panel carry various ADR liabilities that need to be addressed earlier during lead optimization. As a result, a simple scoring model was built to classify promiscuity and selectivity.[202] As expected, the authors observed a strong correlation between a higher model score (low promiscuity) for marketed drugs than for compounds in early clinical development or compounds that failed in the clinic. This also demonstrates the relevance of a low promiscuity in the *in vitro* secondary pharmacology panel and therefore the benefit of using the promiscuity predictive model during early lead optimization.

The development of more extensive computational models came with the emergence of large public and internal databases amenable to computational modeling. These so-called chemogenomics data sets have computer-readable chemical structures, well-annotated biological targets (eg, Entrez gene ID), and activity values (eg, IC_{50}, EC_{50}, and K_d). Once these data are available, it can be used to predict potential targets based on a chemical structure. These predictions rely on chemical similarity search, using

Fig. 5 Positions of Y652 and F656 predicted from KvAP-based hERG homology model. Y652 and F656 side chains are shown in magenta. Molecular surfaces drawn amino acid side chains in contact with terfenadine (rendered in spheres). The view direction is from intracellular hERG domain to extracellular. Courtesy of R. Pearlstein.

a tool such as SciFinder. Alternatively, statistical Bayesian models were built using extended connectivity fingerprints for each target or target class in the chemogenomics database, thus resulting in predictions for activities of multiple targets based on chemical structure.[201]

The utility of these multitarget predictions becomes clear in cases of reverse pharmacology, when generating hypotheses for an observed *in vivo* toxicity can help in designing experiments to determine the mechanism of that toxicity.[180] Combining multiple data sources (eg, biochemical activities, chemical proteomics, chemical genetics, and toxicogenomics) with known biological pathway data can further enhance predictive power for possible mechanisms of toxicities[203] and help reduce liabilities in backup compounds.

So far, the main focus of this section has been on chemical modulation of safety pharmacology targets. Apart from that, there has been significant effort on predicting direct safety end points, without focusing on specific pharmacological mechanisms. Examples include the use of chemical structural alerts[190] and QSAR models for drug-induced phototoxicity,[204] to name a few.

In summary, predictive computational models can be used either prospectively during chemical lead optimization or retrospectively when toxicity is already observed in animals or clinical trial. These powerful predictive tools can help design better compounds with reduced safety liabilities or help understand mechanisms of toxicities for clinical candidates and estimate safety margins necessary to enable risk-based decision for further clinical development.

2.04.7 Summary

It is an exciting time for early predictive toxicology. A wide range of methods are available to support filtration of drug candidates to those most likely to succeed in the clinic. It seems unlikely that established tools such as *in vitro* pharmacological profiling will be entirely replaced in the near future; focus will be more on ensuring that the selected set of targets tested[9] is an appropriate subset of the whole[46] or drug-able[174,205] genome and will consider nontraditional modes of action such as disruption of protein–protein interactions.[206] Integrated *in vitro* toxicologic models will offer the opportunity to explore organ-level toxicology in a specific manner[69] and perhaps explore species-specific effects in greater detail than ever before. The opportunity exists to blur the boundary between phenotypic screening and targeted mechanistic toxicology,[66] and the curation of toxicologic reference databases will enable the development of powerful *in silico* predictive tools.

One of the key hurdles in developing new platforms, particularly those with low throughput, is to screen a sufficient number of reference compounds to enable a broad characterization of the system. The omics technologies, for example, may at this time be best suited to identifying novel biomarkers of toxic effects for which simpler, higher throughput assays could be developed, rather than being screening technologies in themselves. Underlying all *in vitro* toxicology assay development is the need for well-annotated reference compounds—those whose characteristics are well understood, with safety and toxicologic end points clearly related not only to dose but also to exposure in humans. Of necessity, this set is limited in size and the challenge is frequently to be able to find and access robust data.

Selection of techniques depends on the phase of drug discovery and development: medium- and high-throughput methods are required in early phases to triage a large number of compounds; sensitive and highly predictive methods to characterize in detail the safety profiles of candidate molecules are employed later in development. The challenge is always to be able to perform these studies quickly, accurately, and with as little cost as possible while at the same time understanding the translational value.

In an age of increasing regulatory risk awareness, there is also an enthusiasm to explore new technologies to improve our predictive ability.

See also: 4.08. A Comprehensive Overview of the Current Status and Application of Predictive ADMET. 4.16. Toxicity Prediction—Regulatory Perspective.

References

1. Waring, M. J.; Arrowsmith, J.; Leach, A. R.; Leeson, P. D.; Mandrell, S.; Owen, R. M.; Pairaudeau, G.; Pennie, W. D.; Pickett, S. D.; Wang, J.; Wallace, O.; Weir, A. An Analysis of the Attrition of Drug Candidates From Four Major Pharmaceutical Companies. *Nat. Rev. Drug Discov.* **2015,** *14* (7), 475–486.
2. Bunnage, M. E. Getting Pharmaceutical R&D Back on Target. *Nat. Chem. Biol.* **2011,** *7* (6), 335–339.
3. Hay, M.; Thomas, D. W.; Craighead, J. L.; Economides, C.; Rosenthal, J. Clinical Development Success Rates for Investigational Drugs. *Nat. Biotechnol.* **2014,** *32* (1), 40–51.
4. Arrowsmith, J.; Miller, P. Trial Watch: Phase II and Phase III Attrition Rates 2011–2012. *Nat. Rev. Drug Discov.* **2013,** *12* (8), 569.
5. Koala, I.; Landis, J. Can the Pharmaceutical Industry Reduce Attrition Rates? *Nat. Rev. Drug Discov.* **2004,** *3,* 711.
6. Lazarou, J.; Pomeranz, B. H.; Corey, P. N. Incidence of Adverse Drug Reactions in Hospitalized Patients: A Meta-Analysis of Prospective Studies. *JAMA* **1998,** *279* (15), 1200–1205.
7. Edwards, I. R.; Aronson, J. K. Adverse Drug Reactions: Definitions, Diagnosis, and Management. *Lancet* **2000,** *356* (9237), 1255–1259.
8. Redfern, W.; Ewart, L. C.; Hammond, T. G.; Bialecki, R.; Kinter, L.; Lindgren, S.; Pollard, C. E.; Roberts, R.; Rolf, M. G.; Valentin, J. P. Impact and Frequency of Different Toxicities Throughout the Pharmaceutical Life Cycle. *Toxicologist: Suppl. Toxicol. Sci.* **2010,** *114* (1), 231.
9. Bowes, J.; Brown, A. J.; Hamon, J.; Jarolimek, W.; Sridhar, A.; Waldron, G.; Whitebread, S. Reducing Safety-Related Drug Attrition: The Use of in vitro Pharmacological Profiling. *Nat. Rev. Drug Discov.* **2012,** *11* (12), 909–922.
10. Whitebread, S.; Hamon, J.; Bojanic, D.; Urban, L. Keynote Review: in vitro Safety Pharmacology Profiling: An Essential Tool for Successful Drug Development. *Drug Discov. Today* **2005,** *10* (21), 1421–1433.

11. Russell, W. M. S.; Burch, R. L. *The Principles of Humane Experimental Technique;* Methuen: London, 1959.
12. Schultz, T. W.; Amcoff, P.; Berggren, E.; Gautier, F.; Klaric, M.; Knight, D. J.; Mahony, C.; Schwarz, M.; White, A.; Cronin, M. T. A Strategy for Structuring and Reporting a Read-Across Prediction of Toxicity. *Regul. Toxicol. Pharmacol.* **2015,** *72* (3), 586–601.
13. Hewitt, M.; Enoch, S. J.; Madden, J. C.; Przybylak, K. R.; Cronin, M. T. Hepatotoxicity: A Scheme for Generating Chemical Categories for Read-Across, Structural Alerts and Insights Into Mechanism(S) of Action. *Crit. Rev. Toxicol.* **2013,** *43* (7), 537–558.
14. Bulusu, K. C.; Guha, R.; Mason, D. J.; Lewis, R. P.; Muratov, E.; Kalantar Motamedi, Y.; Cokol, M.; Bender, A. Modelling of Compound Combination Effects and Applications to Efficacy and Toxicity: State-of-the-Art, Challenges and Perspectives. *Drug Discov. Today* **2016,** *21* (2), 225–238.
15. Pearlstein, R. A.; MacCannell, K. A.; Erdemli, G.; Yeola, S.; Helmlinger, G.; Hu, Q.-Y.; Farid, R.; Egan, W.; Whitebread, S.; Springer, C.; Beck, J.; Wang, H.-R.; Maciejewski, M.; Urban, L.; Duca, J. S. Implications of Dynamic Occupancy, Binding Kinetics, and Channel Gating Kinetics for hERG Blocker Safety Assessment and Mitigation. Current Topics in Medicinal Chemistry **2016,** *16,* 1792–1818.
16. Dunlop, J.; Bowlby, M.; Peri, R.; Vasilyev, D.; Arias, R. High-Throughput Electrophysiology: An Emerging Paradigm for Ion-Channel Screening and Physiology. *Nat. Rev. Drug Discov.* **2008,** *7* (4), 358–368.
17. Ideker, R. E.; Kong, W.; Pogwizd, S. Purkinje Fibers and Arrhythmias. *Pacing Clin. Electrophysiol.* **2009,** *32* (3), 283–285.
18. Abi-Gerges, N.; Valentin, J.-P.; Pollard, C. E. Comparison of Dog Myocytes and Purkinje Fibres for Assessment of Drug-Induced Changes in Action Potential Duration. *J. Pharmacol. Toxicol. Methods* **2008,** *58* (2), 164.
19. Yan, G.-X.; Antzelevitch, C. Cellular Basis for the Normal T Wave and the Electrocardiographic Manifestations of the Long-QT Syndrome. *Circulation* **1998,** *98* (18), 1928–1936.
20. Zabel, M.; Hohnloser, S. H.; Behrens, S.; Yi-Gang, L.; Woosley, R. L.; Franz, M. R. Electrophysiologic Features of Torsades de Pointes: Insights From a New Isolated Rabbit Heart Model. *J. Cardiovasc. Electrophysiol.* **1997,** *8* (10), 1148–1158.
21. Hondeghem, L. M.; Carlsson, L.; Duker, G. Instability and Triangulation of the Action Potential Predict Serious Proarrhythmia, but Action Potential Duration Prolongation Is Antiarrhythmic. *Circulation* **2001,** *103* (15), 2004–2013.
22. Hanson, L. A.; Bass, A. S.; Gintant, G.; Mittelstadt, S.; Rampe, D.; Thomas, K. ILSI-HESI Cardiovascular Safety Subcommittee Initiative: Evaluation of Three Non-Clinical Models of QT Prolongation. *J. Pharmacol. Toxicol. Methods* **2006,** *54* (2), 116–129.
23. Anderson, N.; Borlak, J. Drug-Induced Phospholipidosis. *FEBS Lett.* **2006,** *580* (23), 5533–5540.
24. Donato, M. T.; Gomez-Lechon, M. J. Drug-Induced Liver Steatosis and Phospholipidosis: Cell-Based Assays for Early Screening of Drug Candidates. *Curr. Drug Metab.* **2012,** *13* (8), 1160–1173.
25. Cooper, J. A.; Saracci, R.; Cole, P. Describing the Validity of Carcinogen Screening Tests. *Br. J. Cancer* **1979,** *39* (1), 87–89.
26. Brott, D. A.; Andersson, H. A. S.; Stewart, J.; Ewart, L.; Christoph, G.; Harleman, J.; Armstrong, D.; Kinter, L. B. A Peripherally Restricted P2Y12 Receptor Antagonist Altered Rat Tumor Incidences With No Human Relevance: Mode of Action Consistent With Dopamine Agonism. *Toxic. Rep.* **2014,** *1,* 1202–1212.
27. Brott, D.; Werkheiser, J.; Campbell, P.; Bentley, P.; Andersson, H.; Stewart, J.; Huby, R.; Altekar, M.; Kinter, L. Inhibition of Oestradiol-Induced Prolactin Release in a Dual-Cannulated Ovariectomized Rat Model by Carmoxirole, a Peripherally Restricted Dopamine Agonist. *Basic Clin. Pharmacol. Toxicol.* **2012,** *111,* 411–416.
28. Neumann, F. Early Indicators for Carcinogenesis in Sex-Hormone-Sensitive Organs. *Mutat. Res. Fundam. Mol. Mech. Mutagen.* **1991,** *248* (2), 341–356.
29. Papoian, T.; Chiu, H. J.; Elayan, I.; Jagadeesh, G.; Khan, I.; Laniyonu, A. A.; Li, C. X.; Saulnier, M.; Simpson, N.; Yang, B. Secondary Pharmacology Data to Assess Potential Off-Target Activity of New Drugs: a Regulatory Perspective. *Nat. Rev. Drug Discov.* **2015,** *14* (4), 294.
30. Paolini, G. V.; Shapland, R. H.; van Hoorn, W. P.; Mason, J. S.; Hopkins, A. L. Global Mapping of Pharmacological Space. *Nat. Biotechnol.* **2006,** *24* (7), 805–815.
31. Wu, P. A.; Balagula, Y.; Lacouture, M. E.; Anadkat, M. J. Prophylaxis and Treatment of Dermatologic Adverse Events From Epidermal Growth Factor Receptor Inhibitors. *Curr. Opin. Oncol.* **2011,** *23* (4), 343–351.
32. Kurz, A.; Sessler, D. Opioid-Induced Bowel Dysfunction: Pathophysiology and Potential New Therapies. *Drugs* **2003,** *63* (7), 649–671.
33. Criscione, L.; Rigollier, P.; Batzl-Hartmann, C.; Rueger, H.; Stricker-Krongrad, A.; Wyss, P.; Brunner, L.; Whitebread, S.; Yamaguchi, Y.; Gerald, C.; Heurich, R. O.; Walker, M. W.; Chiesi, M.; Schilling, W.; Hofbauer, K. G.; Levens, N. Food Intake in Free-Feeding and Energy-Deprived Lean Rats Is Mediated by the Neuropeptide Y5 Receptor. *J. Clin. Invest.* **1998,** *102* (12), 2136–2145.
34. Zuana, D. O.; Sadlo, M.; Germain, M.; Félétou, M.; Chamorro, S.; Tisserand, F.; de Montrion, C.; Boivin, J. F.; Duhault, J.; Boutin, J. A.; Levens, N. Reduced Food Intake in Response to CGP 71683A May Be Due to Mechanisms Other Than NPY Y5 Receptor Blockade. *Int. J. Obes. (Lond)* **2001,** *25* (1), 84–94.
35. Smith, D. A.; Di, L.; Kerns, E. H. The Effect of Plasma Protein Binding on in vivo Efficacy: Misconceptions in Drug Discovery. *Nat. Rev. Drug Discov.* **2010,** *9* (12), 929–939.
36. Smith, D. Pharmacokinetics. In *Pharmacokinetics and Metabolism in Drug Design;* Smith, D., van deWaterbeemd, H., Walker, D., Eds.; WILEY-VCH Verlag GmbH & Co. KGaA: Weinheim, 2006; pp 19–37.
37. Rosenbrier Ribeiro, L.; Morton, M. J.; Wirght, L.; Kavanagh, S. L.; Rolf, M. G.; Armstrong, D.; Bowes, J.; Valentin, J.-P. Acetylcholinesterase: Is There a Recommended Level of Off Target Activity That Can Be Tolerated and Predicted Safe? *J. Pharmacol. Toxicol. Methods* **2014,** *70* (3), 327.
38. Muller, P. Y.; Milton, M. N. The Determination and Interpretation of the Therapeutic Index in Drug Development. *Nat. Rev. Drug Discov.* **2012,** *11* (10), 751–761.
39. Aguirre, S. A.; Heyen, J. R.; Collette, W., 3rd; Bobrowski, W.; Blasi, E. R. Cardiovascular Effects in Rats Following Exposure to a Receptor Tyrosine Kinase Inhibitor. *Toxicol. Pathol.* **2010,** *38* (3), 416–428.
40. Roth, B. L. Drugs and Valvular Heart Disease. *N. Engl. J. Med.* **2007,** *356* (1), 6–9.
41. Connolly, H. M.; Crary, J. L.; McGoon, M. D.; Hensrud, D. D.; Edwards, B. S.; Edwards, W. D.; Schaff, H. V. Valvular Heart Disease Associated With Fenfluramine–Phentermine. *N. Engl. J. Med.* **1997,** *337* (9), 581–588.
42. Rothman, R. B.; Baumann, M. H.; Savage, J. E.; Rauser, L.; McBride, A.; Hufeisen, S. J.; Roth, B. L. Evidence for Possible Involvement of 5-HT2B Receptors in the Cardiac Valvulopathy Associated With Fenfluramine and Other Serotonergic Medications. *Circulation* **2000,** *102* (23), 2836–2841.
43. Cavero, I.; Guillon, J. M. Safety Pharmacology Assessment of Drugs With Biased 5-HT(2B) Receptor Agonism Mediating Cardiac Valvulopathy. *J. Pharmacol. Toxicol. Methods* **2014,** *69* (2), 150–161.
44. Elangbam, C. S. Drug-Induced Valvulopathy: An Update. *Toxicol. Pathol.* **2010,** *38* (6), 837–848.
45. Hutcheson, J. D.; Setola, V.; Roth, B. L.; Merryman, W. D. Serotonin Receptors and Heart Valve Disease—It Was Meant 2B. *Pharmacol. Ther.* **2011,** *132* (2), 146–157.
46. Ezkurdia, I.; Juan, D.; Rodriguez, J. M.; Frankish, A.; Diekhans, M.; Harrow, J.; Vazquez, J.; Valencia, A.; Tress, M. L. Multiple Evidence Strands Suggest That There May Be as Few as 19,000 Human Protein-Coding Genes. *Hum. Mol. Genet.* **2014,** *23* (22), 5866–5878.
47. Conklin, B. R.; Farfel, Z.; Lustig, K. D.; Julius, D.; Bourne, H. R. Substitution of Three Amino Acids Switches Receptor Specificity of Gq[Alpha] to That of Gi[Alpha]. *Nature* **1993,** *363* (6426), 274–276.
48. Charlton, S. J.; Vauquelin, G. Elusive Equilibrium: The Challenge of Interpreting Receptor Pharmacology Using Calcium Assays. *Br. J. Pharmacol.* **2010,** *161* (6), 1250–1265.
49. Ciambrone, G. J.; Liu, V. F.; Lin, D. C.; McGuinness, R. P.; Leung, G. K.; Pitchford, S. Cellular Dielectric Spectroscopy: A Powerful New Approach to Label-Free Cellular Analysis. *J. Biomol. Screen.* **2004,** *9* (6), 467–480.
50. Turner, L.; Lavstsen, T.; Berger, S. S.; Wang, C. W.; Petersen, J. E.; Avril, M.; Brazier, A. J.; Freeth, J.; Jespersen, J. S.; Nielsen, M. A.; Magistrado, P.; Lusingu, J.; Smith, J. D.; Higgins, M. K.; Theander, T. G. Severe Malaria Is Associated With Parasite Binding to Endothelial Protein C Receptor. *Nature* **2013,** *498* (7455), 502–505.
51. Fontana, R. J. Pathogenesis of Idiosyncratic Drug-Induced Liver Injury and Clinical Perspectives. *Gastroenterology* **2014,** *146* (4), 914–928.
52. Jover, R.; Ponsoda, X.; Castell, J. V.; Gómez-Lechón, M. J. Evaluation of the Cytotoxicity of Ten Chemicals on Human Cultured Hepatocytes: Predictability of Human Toxicity and Comparison With Rodent Cell Culture Systems. *Toxicol. in Vitro* **1992,** *6* (1), 47–52.
53. Elaut, G.; Henkens, T.; Papeleu, P.; Snykers, S.; Vinken, M.; Vanhaecke, T.; Rogiers, V. Molecular Mechanisms Underlying the Dedifferentiation Process of Isolated Hepatocytes and Their Cultures. *Curr. Drug Metab.* **2006,** *7,* 629–660.

54. Xu, J. J.; Diaz, D.; O'Brien, P. J. Applications of Cytotoxicity Assays and Pre-Lethal Mechanistic Assays for Assessment of Human Hepatotoxicity Potential. *Chem. Biol. Interact.* **2004,** *150* (1), 115–128.
55. Gerets, H. H.; Tilmant, K.; Gerin, B.; Chanteux, H.; Depelchin, B. O.; Dhalluin, S.; Atienzar, F. A. Characterization of Primary Human Hepatocytes, HepG2 Cells, and HepaRG Cells at the mRNA Level and CYP Activity in Response to Inducers and Their Predictivity for the Detection of Human Hepatotoxins. *Cell Biol. Toxicol.* **2012,** *28* (2), 69–87.
56. Guo, L.; Coyle, L.; Abrams, R. M.; Kemper, R.; Chiao, E. T.; Kolaja, K. L. Refining the Human iPSC-Cardiomyocyte Arrhythmic Risk Assessment Model. *Toxicol. Sci.* **2013,** *136* (2), 581–594.
57. Knollmann, B. C. Induced Pluripotent Stem Cell-Derived Cardiomyocytes: Boutique Science or Valuable Arrhythmia Model? *Circ. Res.* **2013,** *112* (6), 969–976. discussion 976.
58. Weiswald, L. B.; Bellet, D.; Dangles-Marie, V. Spherical Cancer Models in Tumor Biology. *Neoplasia* **2015,** *17* (1), 1–15.
59. Ramaiahgari, S. C.; den Braver, M. W.; Herpers, B.; Terpstra, V.; Commandeur, J. N.; van de Water, B.; Price, L. S. A 3D in vitro Model of Differentiated HepG2 Cell Spheroids With Improved Liver-Like Properties for Repeated Dose High-Throughput Toxicity Studies. *Arch. Toxicol.* **2014,** *88* (5), 1083–1095.
60. Schyschka, L.; Sánchez, J. J.; Wang, Z.; Burkhardt, B.; Müller-Vieira, U.; Zeilinger, K.; Bachmann, A.; Nadalin, S.; Damm, G.; Nussler, A. K. Hepatic 3D Cultures but not 2D Cultures Preserve Specific Transporter Activity for Acetaminophen-Induced Hepatotoxicity. *Arch. Toxicol.* **2013,** *87* (8), 1581–1593.
61. Bhatia, S. N.; Balis, U. J.; Yarmush, M. L.; Toner, M. Effect of Cell–Cell Interactions in Preservation of Cellular Phenotype: Cocultivation of Hepatocytes and Nonparenchymal Cells. *FASEB J.* **1999,** *13* (14), 1883–1900.
62. Khetani, S. R.; Bhatia, S. N. Microscale Culture of Human Liver Cells for Drug Development. *Nat. Biotechnol.* **2008,** *26,* 120–126.
63. Khetani, S. R.; Kanchagar, C.; Ukairo, O.; Krzyzewski, S.; Moore, A.; Shi, J.; Aoyama, S.; Aleo, M.; Will, Y. Use of Micropatterned Cocultures to Detect Compounds That Cause Drug-Induced Liver Injury in Humans. *Toxicol. Sci.* **2013,** *132* (1), 107–117.
64. Plavec, I.; Sirenko, O.; Privat, S.; Wang, Y.; Dajee, M.; Melrose, J.; Nakao, B.; Hytopoulos, E.; Berg, E. L.; Butcher, E. C. Method for Analyzing Signaling Networks in Complex Cellular Systems. *Proc. Natl. Acad. Sci. U. S. A.* **2004,** *101* (5), 1223–1228.
65. Berg, E. L.; Kunkel, E. J.; Hytopoulos, E.; Plavec, I. Characterization of Compound Mechanisms and Secondary Activities by BioMAP Analysis. *J. Pharmacol. Toxicol. Methods* **2006,** *53* (1), 67–74.
66. Berg, E. L.; Yang, J.; Melrose, J.; Nguyen, D.; Privat, S.; Rosler, E.; Kunkel, E. J.; Ekins, S. Chemical Target and Pathway Toxicity Mechanisms Defined in Primary Human Cell Systems. *J. Pharmacol. Toxicol. Methods* **2010,** *61* (1), 3–15.
67. Berg, E. L.; Yang, J.; Polokoff, M. A. Building Predictive Models for Mechanism-of-Action Classification From Phenotypic Assay Data Sets. *J. Biomol. Screen.* **2013,** *18* (10), 1260–1269.
68. Kleinstreuer, N. C.; Yang, J.; Berg, E. L.; Knudsen, T. B.; Richard, A. M.; Martin, M. T.; Reif, D. M.; Judson, R. S.; Polokoff, M.; Dix, D. J.; Kavlock, R. J.; Houck, K. A. Phenotypic Screening of the ToxCast Chemical Library to Classify Toxic and Therapeutic Mechanisms. *Nat. Biotechnol.* **2014,** *32* (6), 583–591.
69. Huh, D.; Hamilton, G. A.; Ingber, D. E. From 3D Cell Culture to Organs-on-Chips. *Trends Cell Biol.* **2011,** *21* (12), 745–754.
70. Huh, D.; Matthews, B.; Mammoto, A.; Montoya-Zavala, M.; Hsin, H.; Ingber, D. Reconstituting Organ-Level Lung Functions on a Chip. *Science* **2010,** *328* (5986), 1662–1668.
71. Jang, K. J.; Mehr, A. P.; Hamilton, G. A.; McPartlin, L. A.; Chung, S.; Suh, K. Y.; Ingber, D. E. Human Kidney Proximal Tubule-on-a-Chip for Drug Transport and Nephrotoxicity Assessment. *Integr. Biol. (Camb)* **2013,** *5* (9), 1119–1129.
72. Pabla, N.; Dong, Z. Cisplatin Nephrotoxicity: Mechanisms and Renoprotective Strategies. *Kidney Int.* **2008,** *73* (9), 994–1007.
73. Viravaidya, K.; Sin, A.; Shuler, M. L. Development of a Microscale Cell Culture Analog to Probe Naphthalene Toxicity. *Biotechnol. Prog.* **2004,** *20* (1), 316–323.
74. van Bronswijk, P.; Cohen, A. F. The First Recordings of Pharmacological Effects. *Br. J. Clin. Pharmacol.* **2008,** *66* (5), 588–593.
75. Skrzypiec-Spring, M.; Grotthus, B.; Szelag, A.; Schulz, R. Isolated Heart Perfusion According to Langendorff—Still Viable in the New Millennium. *J. Pharmacol. Toxicol. Methods* **2007,** *55* (2), 113–126.
76. Hondeghem, L. M.; Hoffmann, P. Blinded Test in Isolated Female Rabbit Heart Reliably Identifies Action Potential Duration Prolongation and Proarrhythmic Drugs: Importance of Triangulation, Reverse Use Dependence, and Instability. *J. Cardiovasc. Pharmacol.* **2003,** *41,* 14–24.
77. Lawrence, C. L.; Bridgland-Taylor, M. H.; Pollard, C. E.; Hammond, T. G.; Valentin, J. P. A Rabbit Langendorff Heart Proarrhythmia Model: Predictive Value for Clinical Identification of Torsades de Pointes. *Br. J. Pharmacol.* **2006,** *149* (7), 845–860.
78. Martić-Kehl, M.; Schibli, R.; Schubiger, P. Can Animal Data Predict Human Outcome? Problems and Pitfalls of Translational Animal Research. *Eur. J. Nucl. Med. Mol. Imaging* **2012,** *39,* 1492–1496.
79. Martic-Kehl, M. I.; Wernery, J.; Folkers, G.; Schubiger, P. A. Quality of Animal Experiments in Anti-Angiogenic Cancer Drug Development—A Systematic Review. *PLoS One* **2015,** *10* (9), e0137235.
80. Langley, G. The Validity of Animal Experiments in Medical Research. *RSDA* **2009,** *1,* 161–168.
81. Matthews, R. A. Medical Progress Depends on Animal Models—Doesn't It? *J. R. Soc. Med.* **2008,** *101* (2), 95–98.
82. Olson, H.; Betton, G.; Robinson, D.; Thomas, K.; Monro, A.; Kolaja, G.; Lilly, P.; Sanders, J.; Sipes, G.; Bracken, W.; Dorato, M.; Van Deun, K.; Smith, P.; Berger, B.; Heller, A. Concordance of the Toxicity of Pharmaceuticals in Humans and in Animals. *Regul. Toxicol. Pharmacol.* **2000,** *32* (1), 56–67.
83. Shanks, N.; Greek, R.; Greek, J. Are Animal Models Predictive for Humans? *Philos. Ethics Humanit. Med.* **2009,** *4,* 2.
84. Farr, S.; Dunn, R. T., II Concise Review: Gene Expression Applied to Toxicology. *Toxicol. Sci.* **1999,** *50,* 1–9.
85. Macgregor, J. T.; Farr, S.; Tucker, J. D.; Heddle, J. A.; Tice, R. R.; Turteltaub, K. W. New Molecular Endpoints and Methods for Routine Toxicity Testing. *Fundam. Appl. Toxicol.* **1995,** *26* (2), 156–173.
86. Shi, L.; Tong, W.; Fang, H.; Scherf, U.; Han, J.; Puri, R. K.; Frueh, F. W.; Goodsaid, F. M.; Guo, L.; Su, Z.; Han, T.; Fuscoe, J. C.; Xu, Z. A.; Patterson, T. A.; Hong, H.; Xie, Q.; Perkins, R. G.; Chen, J. J.; Casciano, D. A. Cross-Platform Comparability of Microarray Technology: Intra-Platform Consistency and Appropriate Data Analysis Procedures Are Essential. *BMC Bioinf.* **2005,** *6* (Suppl 2), S12.
87. Churchill, G. A. Fundamentals of Experimental Design for cDNA Microarrays. *Nat. Genet.* **2002,** *32* (Suppl), 490–495.
88. Hayes, K. R.; Bradfield, C. A. Advances in Toxicogenomics. *Chem. Res. Toxicol.* **2005,** *18* (3), 403–414.
89. Vinciotti, V.; Khanin, R.; D'Alimonte, D.; Liu, X.; Cattini, N.; Hotchkiss, G.; Bucca, G.; de Jesus, O.; Rasaiyaah, J.; Smith, C. P.; Kellam, P.; Wit, E. An Experimental Evaluation of a Loop Versus a Reference Design for Two-Channel Microarrays. *Bioinformatics* **2005,** *21* (4), 492–501.
90. Mirnics, K.; Pevsner, J. Progress in the Use of Microarray Technology to Study the Neurobiology of Disease. *Nat. Neurosci.* **2004,** *7* (5), 434–439.
91. Waring, J. F.; Ciurlionis, R.; Jolly, R. A.; Heindel, M.; Ulrich, R. G. Microarray Analysis of Hepatotoxins in vitro Reveals a Correlation Between Gene Expression Profiles and Mechanisms of Toxicity. *Toxicol. Lett.* **2001,** *120,* 359–368.
92. Burczynski, M. E.; McMillian, M.; Ciervo, J.; Li, L.; Parker, J. B.; Dunn, R. T., II; Hicken, S.; Farr, S.; Johnson, M. D. Toxicogenomics-Based Discrimination of Toxic Mechanism in HepG2 Human Hepatoma Cells. *Toxicol. Sci.* **2000,** *58,* 399–415.
93. Waring, J. F.; Jolly, R. A.; Ciurlionis, R.; Lum, P. Y.; Praestgaard, J. T.; Morfitt, D. C.; Buratto, B.; Roberts, C.; Schadt, E.; Ulrich, R. G. Clustering of Hepatotoxins Based on Mechanism of Toxicity Using Gene Expression Profiles. *Toxicol. Appl. Pharmacol.* **2001,** *175* (1), 28–42.
94. Hamadeh, H. K.; Knight, B. L.; Haugen, A. C.; Sieber, S.; Amin, R. P.; Bushel, P. R.; Stoll, R.; Blanchard, K.; Jayadev, S.; Tennant, R. W.; Cunningham, M. L.; Afshari, C. A.; Paules, R. S. Methapyrilene Toxicity: Anchorage of Pathologic Observations to Gene Expression Alterations. *Toxicol. Pathol.* **2002,** *30* (4), 470–482.
95. Fielden, M. R.; Eynon, B. P.; Natsoulis, G.; Jarnagin, K.; Banas, D.; Kolaja, K. L. A Gene Expression Signature That Predicts the Future Onset of Drug-Induced Renal Tubular Toxicity. *Toxicol. Pathol.* **2005,** *33* (6), 675–683.

96. Thukral, S. K.; Nordone, P. J.; Hu, R.; Sullivan, L.; Galambos, E.; Fitzpatrick, V. D.; Healy, L.; Bass, M. B.; Cosenza, M. E.; Afshari, C. A. Prediction of Nephrotoxicant Action and Identification of Candidate Toxicity-Related Biomarkers. *Toxicol. Pathol.* **2005,** *33* (3), 343–355.
97. Levin, S.; Semler, D.; Ruben, Z. Effects of Two Weeks of Feed Restriction on Some Common Toxicologic Parameters in Sprague-Dawley Rats. *Toxicol. Pathol.* **1993,** *21* (1), 1–14.
98. Uehara, T.; Ono, A.; Maruyama, T.; Kato, I.; Yamada, H.; Ohno, Y.; Urushidani, T. The Japanese Toxicogenomics Project: Application of Toxicogenomics. *Mol. Nutr. Food Res.* **2010,** *54* (2), 218–227.
99. Ganter, B.; Tugendreich, S.; Pearson, C. I.; Ayanoglu, E.; Baumhueter, S.; Bostian, K. A.; Brady, L.; Browne, L. J.; Calvin, J. T.; Day, G. J.; Breckenridge, N.; Dunlea, S.; Eynon, B. P.; Furness, L. M.; Ferng, J.; Fielden, M. R.; Fujimoto, S. Y.; Gong, L.; Hu, C.; Idury, R.; Judo, M. S.; Kolaja, K. L.; Lee, M. D.; McSorley, C.; Minor, J. M.; Nair, R. V.; Natsoulis, G.; Nguyen, P.; Nicholson, S. M.; Pham, H.; Roter, A. H.; Sun, D.; Tan, S.; Thode, S.; Tolley, A. M.; Vladimirova, A.; Yang, J.; Zhou, Z.; Jarnagin, K. Development of a Large-Scale Chemogenomics Database to Improve Drug Candidate Selection and to Understand Mechanisms of Chemical Toxicity and Action. *J. Biotechnol.* **2005,** *119* (3), 219–244.
100. Suter, L.; Schroeder, S.; Meyer, K.; Gautier, J. C.; Amberg, A.; Wendt, M.; Gmuender, H.; Mally, A.; Boitier, E.; Ellinger-Ziegelbauer, H.; Matheis, K.; Pfannkuch, F. EU Framework 6 Project: Predictive Toxicology (PredTox)—Overview and Outcome. *Toxicol. Appl. Pharmacol.* **2011,** *252* (2), 73–84.
101. Cases, M.; Briggs, K.; Steger-Hartmann, T.; Pognan, F.; Marc, P.; Kleinoder, T.; Schwab, C. H.; Pastor, M.; Wichard, J.; Sanz, F. The eTOX Data-Sharing Project to Advance In Silico Drug-Induced Toxicity Prediction. *Int. J. Mol. Sci.* **2014,** *15* (11), 21136–21154.
102. Goodsaid, F.; Frueh, F. W. Implementing the U.S. FDA Guidance on Pharmacogenomic Data Submissions. *Environ. Mol. Mutagen.* **2007,** *48* (5), 354–358.
103. Ellinger-Ziegelbauer, H.; Gmuender, H.; Bandenburg, A.; Ahr, H. J. Prediction of a Carcinogenic Potential of Rat Hepatocarcinogens Using Toxicogenomics Analysis of Short-Term in vivo Studies. *Mutat. Res.* **2008,** *637* (1–2), 23–39.
104. Wilkins, M. R.; Sanchez, J.-C.; Gooley, A. A.; Appel, R. D.; Humphery-Smith, I.; Hochstrasser, D. F.; Williams, K. L. Progress With Proteome Projects: Why All Proteins Expressed by a Genome Should Be Identified and How to Do It. *Biotechnol. Genet. Eng. Rev.* **1996,** *13,* 19–50.
105. Barrier, M.; Mirkes, P. E. Proteomics in Developmental Toxicology. *Reprod. Toxicol.* **2005,** *19* (3), 291–304.
106. Messana, I.; Cabras, T.; Iavarone, F.; Vincenzoni, F.; Urbani, A.; Castagnola, M. Unraveling the Different Proteomic Platforms. *J. Sep. Sci.* **2013,** *36* (1), 128–139.
107. Nilsson, T.; Mann, M.; Aebersold, R.; Yates, J. R., 3rd; Bairoch, A.; Bergeron, J. J. Mass Spectrometry in High-Throughput Proteomics: Ready for the Big Time. *Nat. Methods* **2010,** *7* (9), 681–685.
108. Varambally, S.; Yu, J.; Laxman, B.; Rhodes, D. R.; Mehra, R.; Tomlins, S. A.; Shah, R. B.; Chandran, U.; Monzon, F. A.; Becich, M. J.; Wei, J. T.; Pienta, K. J.; Ghosh, D.; Rubin, M. A.; Chinnaiyan, A. M. Integrative Genomic and Proteomic Analysis of Prostate Cancer Reveals Signatures of Metastatic Progression. *Cancer Cell* **2005,** *8* (5), 393–406.
109. Griffin, T. J.; Gygi, S. P.; Ideker, T.; Rist, B.; Eng, J.; Hood, L.; Aebersold, R. Complementary Profiling of Gene Expression at the Transcriptome and Proteome Levels in Saccharomyces Cerevisiae. *Mol. Cell. Proteomics* **2002,** *1* (4), 323–333.
110. Baliga, N. S.; Pan, M.; Goo, Y. A.; Yi, E. C.; Goodlett, D. R.; Dimitrov, K.; Shannon, P.; Aebersold, R.; Ng, W. V.; Hood, L. Coordinate Regulation of Energy Transduction Modules in Halobacterium sp. Analyzed by a Global Systems Approach. *Proc. Natl. Acad. Sci. U. S. A.* **2002,** *99* (23), 14913–14918.
111. Wang, P.; Bouwman, F. G.; Mariman, E. C. Generally Detected Proteins in Comparative Proteomics—A Matter of Cellular Stress Response? *Proteomics* **2009,** *9* (11), 2955–2966.
112. Van Summeren, A.; Renes, J.; Bouwman, F. G.; Noben, J. P.; van Delft, J. H.; Kleinjans, J. C.; Mariman, E. C. Proteomics Investigations of Drug-Induced Hepatotoxicity in HepG2 Cells. *Toxicol. Sci.* **2011,** *120* (1), 109–122.
113. Fountoulakis, M.; Juranville, J.-F.; Berndt, P.; Langen, H.; Suter, L. Two-Dimensional Database of Mouse Liver Proteins. An Update. *Electrophor.* **2001,** *22* (9), 1747–1763.
114. Koen, Y. M.; Gogichaeva, N. V.; Alterman, M. A.; Hanzlik, R. P. A Proteomic Analysis of Bromobenzene Reactive Metabolite Targets in Rat Liver Cytosol In Vivo. *Chem. Res. Toxicol.* **2007,** *20* (3), 511–519.
115. Yamanaka, H.; Yakabe, Y.; Saito, K.; Sekijima, M.; Shirai, T. Quantitative Proteomic Analysis of Rat Liver for Carcinogenicity Prediction in a 28-day Repeated Dose Study. *Proteomics* **2007,** *7* (5), 781–795.
116. Robertson, D. G. Metabonomics in Toxicology: A Review. *Toxicol. Sci.* **2005,** *85* (2), 809–822.
117. Robertson, D. G.; Watkins, P. B.; Reily, M. D. Metabolomics in Toxicology: Preclinical and Clinical Applications. *Toxicol. Sci.* **2011,** *120* (Suppl 1), S146–S170.
118. Larive, C. K.; Barding, G. A.; Dinges, M. M. NMR Spectroscopy for Metabolomics and Metabolic Profiling. *Anal. Chem.* **2015,** *87* (1), 133–146.
119. Veenstra, T. D. Metabolomics: The Final Frontier? *Genome Med.* **2012,** *4* (4), 40.
120. Shiva, S.; Vu, H. S.; Roth, M. R.; Zhou, Z.; Marepally, S. R.; Nune, D. S.; Lushington, G. H.; Visvanathan, M.; Welti, R. Lipidomic Analysis of Plant Membrane Lipids by Direct Infusion Tandem Mass Spectrometry. *Methods Mol. Biol.* **2013,** *1009,* 79–91.
121. Dunn, W. B.; Broadhurst, D. I.; Atherton, H. J.; Goodacre, R.; Griffin, J. L. Systems Level Studies of Mammalian Metabolomes: The Roles of Mass Spectrometry and Nuclear Magnetic Resonance Spectroscopy. *Chem. Soc. Rev.* **2011,** *40* (1), 387–426.
122. Jessome, L. L.; Volmer, D. A. Ion Suppression: A Major Concern in Mass Spectrometry. *LCGC N. Am.* **2006,** *83–89.*
123. Kuehnbaum, N. L.; Britz-McKibbin, P. New Advances in Separation Science for Metabolomics: Resolving Chemical Diversity in a Post-Genomic Era. *Chem. Rev.* **2013,** *113* (4), 2437–2468.
124. Zhu, Z. J.; Schultz, A. W.; Wang, J. H.; Johnson, C. H.; Yannone, S. M.; Patti, G. J.; Siuzdak, G. Liquid Chromatography Quadrupole Time-of-Flight Mass Spectrometry Characterization of Metabolites Guided by the METLIN Database. *Nat. Protoc.* **2013,** *8* (3), 451–460.
125. Yuan, M.; Breitkopf, S. B.; Yang, X. M.; Asara, J. M. A Positive/Negative Ion-Switching, Targeted Mass Spectrometry-Based Metabolomics Platform for Bodily Fluids, Cells, and Fresh and Fixed Tissue. *Nat. Protoc.* **2012,** *7* (5), 872–881.
126. Shin, S. Y.; Fauman, E. B.; Petersen, A. K.; Krumsiek, J.; Santos, R.; Huang, J.; Arnold, M.; Erte, I.; Forgetta, V.; Yang, T. P.; Walter, K.; Menni, C.; Chen, L.; Vasquez, L.; Valdes, A. M.; Hyde, C. L.; Wang, V.; Ziemek, D.; Roberts, P.; Xi, L.; Grundberg, E.; Waldenberger, M.; Richards, J. B.; Mohney, R. P.; Milburn, M. V.; John, S. L.; Trimmer, J.; Theis, F. J.; Overington, J. P.; Suhre, K.; Brosnan, M. J.; Gieger, C.; Kastenmuller, G.; Spector, T. D.; Soranzo, N. An Atlas of Genetic Influences on Human Blood Metabolites. *Nat. Genet.* **2014,** *46* (6), 543–550.
127. Suhre, K.; Shin, S. Y.; Petersen, A. K.; Mohney, R. P.; Meredith, D.; Wagele, B.; Altmaier, E.; Deloukas, P.; Erdmann, J.; Grundberg, E.; Hammond, C. J.; de Angelis, M. H.; Kastenmuller, G.; Kottgen, A.; Kronenberg, F.; Mangino, M.; Meisinger, C.; Meitinger, T.; Mewes, H. W.; Milburn, M. V.; Prehn, C.; Raffler, J.; Ried, J. S.; Romisch-Margl, W.; Samani, N. J.; Small, K. S.; Wichmann, H. E.; Zhai, G. J.; Illig, T.; Spector, T. D.; Adamski, J.; Soranzo, N.; Gieger, C. Human Metabolic Individuality in Biomedical and Pharmaceutical Research. *Nature* **2011,** *477* (7362), 54–60.
128. Ferrannini, E.; Natali, A.; Camastra, S.; Nannipieri, M.; Mari, A.; Adam, K. P.; Milburn, M. V.; Kastemmuller, G.; Adamski, J.; Tuomi, T.; Lyssenko, V.; Groop, L.; Gall, W. E. Early Metabolic Markers of the Development of Dysglycemia and Type 2 Diabetes and Their Physiological Significance. *Diabetes* **2013,** *62* (5), 1730–1737.
129. Hsiao, E. Y.; McBride, S. W.; Hsien, S.; Sharon, G.; Hyde, E. R.; Mccue, T.; Codelli, J. A.; Chow, J.; Reisman, S. E.; Petrosino, J. F.; Patterson, P. H.; Mazmanian, S. K. Microbiota Modulate Behavioral and Physiological Abnormalities Associated With Neurodevelopmental Disorders. *Cell* **2013,** *155* (7), 1451–1463.
130. Gowda, S.; Desai, P. B.; Kulkarni, S. S.; Hull, V. V.; Math, A. A.; Vernekar, S. N. Markers of Renal Function Tests. *N. Am. J. Med. Sci.* **2010,** *2* (4), 170–173.
131. Shlomi, T.; Cabili, M. N.; Ruppin, E. Predicting Metabolic Biomarkers of Human Inborn Errors of Metabolism. *Mol. Syst. Biol.* **2009,** *5,* 263.
132. Kaddurah-Daouk, R.; Weinshilboum, R. M. Pharmacometabolomics: Implications for Clinical Pharmacology and Systems Pharmacology. *Clin. Pharmacol. Ther.* **2014,** *95* (2), 154–167.
133. Kaddurah-Daouk, R. Pharmacometabolomics: Global Biochemical Approach for Mapping Drug Effects. Abstracts from the 10th International ISSX Meeting. *Drug Metab. Rev.* **2014,** *45* (1), 1–286. http://dx.doi.org/10.3109/03602532.2013.868114.

134. Kaddurah-Daouk, R.; Kristal, B. S.; Weinshilboum, R. M. Metabolomics: A Global Biochemical Approach to Drug Response and Disease. *Annu. Rev. Pharmacol. Toxicol.* **2008,** *48,* 653–683.
135. Kanehisa, M.; Goto, S. KEGG: Kyoto Encyclopedia of Genes and Genomes. *Nucleic Acids Res.* **2000,** *28* (1), 27–30.
136. Eales, K. L.; Hollinshead, K. E.; Tennant, D. A. Hypoxia and Metabolic Adaptation of Cancer Cells. *Oncogenesis* **2016,** *5,* e190.
137. Beloribi-Djefaflia, S.; Vasseur, S.; Guillaumond, F. Lipid Metabolic Reprogramming in Cancer Cells. *Oncogenesis* **2016,** *5,* e189.
138. O'Neill, L. A. J.; Hardie, D. G. Metabolism of Inflammation Limited by AMPK and Pseudo-Starvation. *Nature* **2013,** *493* (7432), 346--355.
139. Pearce, E. L.; Poffenberger, M. C.; Chang, C. H.; Jones, R. G. Fueling Immunity: Insights Into Metabolism and Lymphocyte Function. *Science* **2013,** *342* (6155), 1242454.
140. Sreekumar, A.; Poisson, L. M.; Rajendiran, T. M.; Khan, A. P.; Cao, Q.; Yu, J.; Laxman, B.; Mehra, R.; Lonigro, R. J.; Li, Y.; Nyati, M. K.; Ahsan, A.; Kalyana-Sundaram, S.; Han, B.; Cao, X.; Byun, J.; Omenn, G. S.; Ghosh, D.; Pennathur, S.; Alexander, D. C.; Berger, A.; Shuster, J. R.; Wei, J. T.; Varambally, S.; Beecher, C.; Chinnaiyan, A. M. Metabolomic Profiles Delineate Potential Role for Sarcosine in Prostate Cancer Progression. *Nature* **2009,** *457* (7231), 910–914.
141. Abate-Shen, C.; Shen, M. M. Diagnostics: The Prostate-Cancer Metabolome. *Nature* **2009,** *457* (7231), 799–800.
142. Zhang, Y. J.; Dai, Y. B.; Wen, J. M.; Zhang, W. R.; Grenz, A.; Sun, H.; Tao, L. J.; Lu, G. X.; Alexander, D. C.; Milburn, M. V.; Carter-Dawson, L.; Lewis, D. E.; Zhang, W. Z.; Eltzschig, H. K.; Kellems, R. E.; Blackburn, M. R.; Juneja, H. S.; Xia, Y. Detrimental Effects of Adenosine Signaling in Sickle Cell Disease. *Nat. Med.* **2011,** *17* (1), 79–86.
143. Watson, M.; Roulston, A.; Belec, L.; Billot, X.; Marcellus, R.; Bedard, D.; Bernier, C.; Branchaud, S.; Chan, H.; Dairi, K.; Gilbert, K.; Goulet, D.; Gratton, M. O.; Isakau, H.; Jang, A.; Khadir, A.; Koch, E.; Lavoie, M.; Lawless, M.; Nguyen, M.; Paquette, D.; Turcotte, E.; Berger, A.; Mitchell, M.; Shore, G. C.; Beauparlant, P. The Small Molecule GMX1778 Is a Potent Inhibitor of NAD(+) Biosynthesis: Strategy for Enhanced Therapy in Nicotinic Acid Phosphoribosyltransferase 1-Deficient Tumors. *Mol. Cell. Biol.* **2009,** *29* (21), 5872–5888.
144. Tufi, R.; Gandhi, S.; de Castro, I. P.; Lehmann, S.; Angelova, P. R.; Dinsdale, D.; Deas, E.; Plun-Favreau, H.; Nicotera, P.; Abramov, A. Y.; Willis, A. E.; Mallucci, G. R.; Loh, S. H. Y.; Martins, L. M. Enhancing Nucleotide Metabolism Protects Against Mitochondrial Dysfunction and Neurodegeneration in a PINK1 Model of Parkinson's Disease. *Nat. Cell Biol.* **2014,** *16* (2), 157–166.
145. Takei, M.; Ando, Y.; Saitoh, W.; Tanimoto, T.; Kiyosawa, N.; Manabe, S.; Sanbuissho, A.; Okazaki, O.; Iwabuchi, H.; Yamoto, T.; Adam, K. P.; Weiel, J. E.; Ryals, J. A.; Milburn, M. V.; Guo, L. N. Ethylene Glycol Monomethyl Ether-Induced Toxicity Is Mediated Through the Inhibition of Flavoprotein Dehydrogenase Enzyme Family. *Toxicol. Sci.* **2010,** *118* (2), 643–652.
146. Zgoda-Pols, J. R.; Chowdhury, S.; Wirth, M.; Milburn, M. V.; Alexander, D. C.; Alton, K. B. Metabolomics Analysis Reveals Elevation of 3-Indoxyl Sulfate in Plasma and Brain During Chemically-Induced Acute Kidney Injury in Mice: Investigation of Nicotinic Acid Receptor Agonists. *Toxicol. Appl. Pharmacol.* **2011,** *255* (1), 48–56.
147. Ren, W.; Zhou, Z. W.; Irudayaraj, J. M. K. Trichloroethylene Sensing in Water Based on SERS With Multifunctional Au/TiO_2 Core-Shell Nanocomposites. *Analyst* **2015,** *140* (19), 6625–6630.
148. Fang, Z. Z.; Zhang, D.; Cao, Y. F.; Xie, C.; Lu, D.; Sun, D. X.; Tanaka, N.; Jiang, C.; Chen, Q.; Chen, Y.; Wang, H.; Gonzalez, F. J. Irinotecan (CPT-11)-Induced Elevation of Bile Acids Potentiates Suppression of IL-10 Expression. *Toxicol. Appl. Pharmacol.* **2016,** *291,* 21–27.
149. Lindon, J.; Keun, H.; Ebbels, T.; Pearce, J.; Holmes, E.; Nicholson, J. The Consortium for Metabonomic Toxicology (COMET): Aims, Activities and Achievements. *Pharmacogenomics* **2005,** *6* (7), 691–699.
150. Ebbels, T. M. D.; Keun, H. C.; Beckonert, O. P.; Bollard, M. E.; Lindon, J. C.; Holmes, E.; Nicholson, J. K. Prediction and Classification of Drug Toxicity Using Probabilistic Modeling of Temporal Metabolic Data: The Consortium on Metabonomic Toxicology Screening Approach. *J. Proteome Res.* **2007,** *6* (11), 4407–4422.
151. van Ravenzwaay, B.; Cunha, G. C.; Leibold, E.; Looser, R.; Mellert, W.; Prokoudine, A.; Walk, T.; Wiemer, J. The Use of Metabolomics for the Discovery of New Biomarkers of Effect. *Toxicol. Lett.* **2007,** *172* (1–2), 21–28.
152. van Ravenzwaay, B.; Herold, M.; Kamp, H.; Kapp, M. D.; Fabian, E.; Looser, R.; Krennrich, G.; Mellert, W.; Prokoudine, A.; Strauss, V.; Walk, T.; Wiemer, J. Metabolomics: A Tool for Early Detection of Toxicological Effects and an Opportunity for Biology Based Grouping of Chemicals-From QSAR to QBAR. *Mutat. Res.* **2012,** *746* (2), 144–150.
153. Kamp, H.; Fabian, E.; Groeters, S.; Krennrich, G.; Mattes, W. B.; Prokoudine, A.; Mellert, W.; Ruiz-Noppinger, P.; Strauss, V.; Walk, T.; Wiemer, J.; van Ravenzwaay, B. Application of in vivo Metabolomics to Preclinical/Toxicological Studies: Case Study on Phenytoin-Induced Systemic Toxicity. *Bioanalysis* **2012,** *4* (18), 2291–2301.
154. Mattes, W. B.; Kamp, H. G.; Fabian, E.; Herold, M.; Looser, G.; Mellert, W.; Prokoudine, A.; Strauss, V.; van Ravenzwaay, B.; Walk, T.; Naraoka, H.; Omura, K.; Schuppe–Koistinen, I.; Nadanaciva, S.; Bush, E. D.; Moeller, N.; Ruiz–Noppinger, P.; Piccoli, S. P. Prediction of Clinically Relevant Safety Signals of Nephrotoxicity Through Plasma Metabolite Profiling. *BioMed Res. Int.* **2013,** *2013.* http://dx.doi.org/10.1155/2013/202497. Article ID 202497.
155. Saito, K.; Ishikawa, M.; Murayama, M.; Urata, M.; Senoo, Y.; Toyoshima, K.; Kumagai, Y.; Maekawa, K.; Saito, Y. Effects of Sex, Age, and Fasting Conditions on Plasma Lipidomic Profiles of Fasted Sprague-Dawley Rats. *PLoS One* **2014,** *9* (11), e112266. http://dx.doi.org/10.1371/journal.pone.0112266.
156. Robertson, D. G.; Reily, M. D.; Sigler, R. E.; Wells, D. F.; Paterson, D. A.; Braden, T. K. Metabonomics: Evaluation of Nuclear Magnetic Resonance (NMR) and Pattern Recognition Technology for Rapid in vivo Screening of Liver and Kidney Toxicants. *Toxicol. Sci.* **2000,** *57* (2), 326–337.
157. Bollard, M. E.; Holmes, E.; Lindon, J. C.; Mitchell, S. C.; Branstetter, D.; Zhang, W.; Nicholson, J. K. Investigations Into Biochemical Changes Due to Diurnal Variation and Estrus Cycle in Female Rats Using High-Resolution (1)H NMR Spectroscopy of Urine and Pattern Recognition. *Anal. Biochem.* **2001,** *295* (2), 194–202.
158. Holmes, E.; Loo, R. L.; Stamler, J.; Bictash, M.; Yap, I. K.; Chan, Q.; Ebbels, T.; De Iorio, M.; Brown, I. J.; Veselkov, K. A.; Daviglus, M. L.; Kesteloot, H.; Ueshima, H.; Zhao, L.; Nicholson, J. K.; Elliott, P. Human Metabolic Phenotype Diversity and Its Association With Diet and Blood Pressure. *Nature* **2008,** *453* (7193), 396–400.
159. Guideline, I. H. T. *Guidance on Genotoxicity Testing and Data Interpretation for Pharmaceuticals Intended for Human Use: S2 (R1),* 2011; pp 1–25.
160. OECD. Test No. 471: Bacterial Reverse Mutation Test. In *OECD Guidelines for the Testing of Chemicals;* OECD Publishing: Paris, 1997.
161. OECD. Test No. 487: in vitro Mammalian Cell Micronucleus Test. In *OECD Guidelines for the Testing of Chemicals,* Vol.; OECD Publishing: Paris, 2010.
162. OECD. Test No. 474: Mammalian Erythrocyte Micronucleus Test. In *OECD Guidelines for the Testing of Chemicals,* Vol.; OECD Publishing: Paris, 2014.
163. OECD. Test No. 489: in vivo Mammalian Alkaline Comet Assay. In *OECD Guidelines for the Testing of Chemicals,* Vol.; OECD Publishing: Paris, 2014.
164. Schmid, W. The Micronucleus Test. *Mutat. Res., Environ. Mutagen. Relat. Subj.* **1975,** *31* (1), 9–15.
165. Rothfuss, A.; Honma, M.; Czich, A.; Aardema, M. J.; Burlinson, B.; Galloway, S.; Hamada, S.; Kirkland, D.; Heflich, R. H.; Howe, J.; Nakajima, M.; O'Donovan, M.; Plappert-Helbig, U.; Priestley, C.; Recio, L.; Schuler, M.; Uno, Y.; Martus, H. J. Improvement of in vivo Genotoxicity Assessment: Combination of Acute Tests and Integration into Standard Toxicity Testing. *Mutat. Res.* **2011,** *723* (2), 108–120.
166. Romagna, F.; Staniforth, C. D. The Automated Bone Marrow Micronucleus Test. *Mutat. Res. Fundam. Mol. Mech. Mutagen.* **1989,** *213* (1), 91–104.
167. Speit, G.; Kojima, H.; Burlinson, B.; Collins, A. R.; Kasper, P.; Plappert-Helbig, U.; Uno, Y.; Vasquez, M.; Beevers, C.; De Boeck, M.; Escobar, P. A.; Kitamoto, S.; Pant, K.; Pfuhler, S.; Tanaka, J.; Levy, D. D. Critical Issues With the in vivo Comet Assay: A Report of the Comet Assay Working Group in the 6th International Workshop on Genotoxicity Testing (IWGT). *Mutat. Res. Genet. Toxicol. Environ. Mutagen.* **2015,** *783,* 6–12.
168. Zeiger, E.; Risko, K. J.; Margolin, B. H. Strategies to Reduce the Cost of Mutagenicity Screening With the Salmonella Assay. *Environ. Mutagen.* **1985,** *7* (6), 901–911.
169. Miller, B.; Albertini, S.; Locher, F.; Lorge, E. Comparative Evaluation of the in vitro Micronucleus Test and the in vitro Chromosome Aberration Test: Industrial Experience. *Mutat. Res.* **1997,** *392,* 45–59.
170. Frieauff, W.; Potter-Locher, F.; Cordier, A.; Suter, W. Automatic Analysis of the in vitro Micronucleus Test on V79 Cells. *Mutat. Res.* **1988,** *413,* 57–68.
171. Peters, J. U.; Hert, J.; Bissantz, C.; Hillebrecht, A.; Gerebtzoff, G.; Bendels, S.; Tillier, F.; Migeon, J.; Fischer, H.; Guba, W.; Kansy, M. Can We Discover Pharmacological Promiscuity Early in the Drug Discovery Process? *Drug Discov. Today* **2012,** *17* (7–8), 325–335.
172. Schuster, D.; Laggner, C.; Langer, T. Why Drugs Fail—A Study on Side Effects in New Chemical Entities. In *Antitargets;* Wiley-VCH Verlag GmbH & Co. KGaA: Weinheim, 2008; pp 1–22.

173. Roth, B. L.; Sheffler, D. J.; Kroeze, W. K. Magic Shotguns Versus Magic Bullets: Selectively Non-Selective Drugs for Mood Disorders and Schizophrenia. *Nat. Rev. Drug Discov.* **2004,** *3,* 353.
174. Hopkins, A. L.; Mason, J. S.; Overington, J. P. Can We Rationally Design Promiscuous Drugs? *Curr. Opin. Struct. Biol.* **2006,** *16* (1), 127–136.
175. Peters, J. U.; Schnider, P.; Mattei, P.; Kansy, M. Pharmacological Promiscuity: Dependence on Compound Properties and Target Specificity in a Set of Recent Roche Compounds. *ChemMedChem* **2009,** *4* (4), 680–686.
176. Waring, M. J.; Johnstone, C. A Quantitative Assessment of hERG Liability as a Function of Lipophilicity. *Bioorg. Med. Chem. Lett.* **2007,** *17* (6), 1759–1764.
177. Shah, R. R. Drugs, QT Interval Prolongation and ICH E14. *Drug Saf.* **2005,** *28* (2), 115–125.
178. Leeson, P. D.; Springthorpe, B. The Influence of Drug-Like Concepts on Decision-Making in Medicinal Chemistry. *Nat. Rev. Drug Discov.* **2007,** *6* (11), 881–890.
179. Timbrell, J. Principles of Biochemical Toxicology. In 3rd ed.; Taylor & Francis: London, 2000, 11 New Fetter Lane, London EC4P 4EE.
180. Lounkine, E.; Keiser, M. J.; Whitebread, S.; Mikhailov, D.; Hamon, J.; Jenkins, J. L.; Lavan, P.; Weber, E.; Doak, A. K.; Cote, S.; Shoichet, B. K.; Urban, L. Large-Scale Prediction and Testing of Drug Activity on Side-Effect Targets. *Nature* **2012,** *486,* 361–367.
181. Price, D. A.; Blagg, J.; Jones, L.; Greene, N.; Wager, T. Physicochemical Drug Properties Associated With in vivo Toxicological Outcomes: A Review. *Expert Opin. Drug Metab. Toxicol.* **2009,** *5* (8), 921–931.
182. Rorig, K. J.; Ruben, Z.; Anderson, S. N. Structural Determinants of Cationic Amphiphilic Amines Which Induce Clear Cytoplasmic Vacuoles in Cultured Cells. *Exp. Biol. Med.* **1987,** *184* (2), 165–171.
183. Reasor, M. J.; Hastings, K. L.; Ulrich, R. G. Drug-Induced Phospholipidosis: Issues and Future Directions. *Expert Opin. Drug Saf.* **2006,** *5* (4), 567–583.
184. Willard, J. FDA Phospholipidosis Working Group Preliminary Results and Developing Opinions. Society of Toxicologic Pathology (STP) 27th Annual Symposium, San Francisco.
185. Bernstein, P. R.; Ciaccio, P.; Morelli, J. Drug-Induced Phospholipidosis. *Annu. Rep. Med. Chem.* **2011,** *46,* 419–430.
186. Barone, L. R.; Boyer, S.; Damewood, J. R.; Fikes, J.; Ciaccio, P. J. Phospholipogenic Pharmaceuticals Are Associated With a Higher Incidence of Histological Findings Than Nonphospholipogenic Pharmaceuticals in Preclinical Toxicology Studies. *J. Toxicol.* **2012,** *2012,* 7.
187. Jiang, Z.; Reilly, J. Chromatography Approaches for Early Screening of the Phospholipidosis-Inducing Potential of Pharmaceuticals. *J. Pharm. Biomed. Anal.* **2012,** *61,* 184–190.
188. Jiang, Z.; Reilly, J.; Everatt, B.; Briard, E. A Rapid Vesicle Electrokinetic Chromatography Method for the in vitro Prediction of Non-Specific Binding for Potential PET Ligands. *J. Pharm. Biomed. Anal.* **2011,** *54* (4), 722–729.
189. Valko, K.; Du, C. M.; Bevan, C. D.; Reynolds, D. P.; Abraham, M. H. Rapid-Gradient HPLC Method for Measuring Drug Interactions With Immobilized Artificial Membrane: Comparison With Other Lipophilicity Measures. *J. Pharm. Sci.* **2000,** *89* (8), 1085–1096.
190. Dearden, J. C. In Silico Prediction of Drug Toxicity. *J. Comput. Aided Mol. Des.* **2003,** *17* (2–4), 119–127.
191. Matthews, E. J.; Kruhlak, N. L.; Benz, R. D.; Contrera, J. F.; Marchant, C. A.; Yang, C. Combined Use of MC4PC, MDL-QSAR, BioEpisteme, Leadscope PDM, and Derek for Windows Software to Achieve High-Performance, High-Confidence, Mode of Action-Based Predictions of Chemical Carcinogenesis in Rodents. *Toxicol. Mech. Methods* **2008,** *18* (2–3), 189–206.
192. Morgan, T. K., Jr.; Sullivan, M. E. An Overview of Class III Electrophysiological Agents: A new Generation of Antiarrhythmic Therapy. *Prog. Med. Chem.* **1992,** *29,* 65–108.
193. Cavalli, A.; Poluzzi, E.; De Ponti, F.; Recanatini, M. Toward a Pharmacophore for Drugs Inducing the Long QT Syndrome: Insights From a CoMFA Study of HERG K+ Channel Blockers. *J. Med. Chem.* **2002,** *45* (18), 3844–3853.
194. Aronov, A. M. Common Pharmacophores for Uncharged Human Ether-a-Go-Go-Related Gene (hERG) Blockers. *J. Med. Chem.* **2006,** *49* (23), 6917–6921.
195. Ficker, E.; Obejero-Paz, C. A.; Zhao, S.; Brown, A. M. The Binding Site for Channel Blockers That Rescue Misprocessed Human Long QT Syndrome Type 2 Ether-a-Gogo-Related Gene (HERG) Mutations. *J. Biol. Chem.* **2002,** *277* (7), 4989–4998.
196. Farid, R.; Day, T.; Friesner, R. A.; Pearlstein, R. A. New Insights About HERG Blockade Obtained From Protein Modeling, Potential Energy Mapping, and Docking Studies. *Bioorg. Med. Chem.* **2006,** *14* (9), 3160–3173.
197. Seierstad, M.; Agrafiotis, D. K. A QSAR Model of HERG Binding Using a Large, Diverse, and Internally Consistent Training Set. *Chem. Biol. Drug Des.* **2006,** *67* (4), 284–296.
198. Jia, L.; Sun, H. Support Vector Machines Classification of hERG Liabilities Based on Atom Types. *Bioorg. Med. Chem.* **2008,** *16* (11), 6252–6260.
199. Luo, M.; Wang, X. S.; Tropsha, A. Comparative Analysis of QSAR-Based vs. Chemical Similarity Based Predictors of GPCRs Binding Affinity. *Mol. Inf.* **2016,** *35* (1), 36–41.
200. Bottino, D.; Penland, R. C.; Stamps, A.; Traebert, M.; Dumotier, B.; Georgiva, A.; Helmlinger, G.; Lett, G. S. Preclinical Cardiac Safety Assessment of Pharmaceutical Compounds Using an Integrated Systems-Based Computer Model of the Heart. *Prog. Biophys. Mol. Biol.* **2006,** *90* (1–3), 414–443.
201. Bender, A.; Scheiber, J.; Glick, M.; Davies, J. W.; Azzaoui, K.; Hamon, J.; Urban, L.; Whitebread, S.; Jenkins, J. L. Analysis of Pharmacology Data and the Prediction of Adverse Drug Reactions and Off-Target Effects From Chemical Structure. *ChemMedChem* **2007,** *2* (6), 861–873.
202. Azzaoui, K.; Hamon, J.; Faller, B.; Whitebread, S.; Jacoby, E.; Bender, A.; Jenkins, J. L.; Urban, L. Modeling Promiscuity Based on in vitro Safety Pharmacology Profiling Data. *ChemMedChem* **2007,** *2* (6), 874–880.
203. Scheiber, J.; Chen, B.; Milik, M.; Sukuru, S. C. K.; Bender, A.; Mikhailov, D.; Whitebread, S.; Hamon, J.; Azzaoui, K.; Urban, L.; Glick, M.; Davies, J. W.; Jenkins, J. L. Gaining Insight Into Off-Target Mediated Effects of Drug Candidates With a Comprehensive Systems Chemical Biology Analysis. *J. Chem. Inf. Model.* **2009,** *49* (2), 308–317.
204. Peukert, S.; Nunez, J.; He, F.; Dai, M.; Yusuff, N.; DiPesa, A.; Miller-Moslin, K.; Karki, R.; Lagu, B.; Harwell, C.; Zhang, Y.; Bauer, D.; Kelleher, J. F.; Egan, W. A Method for Estimating the Risk of Drug-Induced Phototoxicity and Its Application to Smoothened Inhibitors. *Med. Chem. Commun.* **2011,** *2* (10), 973.
205. Overington, J. P.; Al-Lazikani, B.; Hopkins, A. L. How Many Drug Targets Are There? *Nat. Rev. Drug Discov.* **2006,** *5,* 993–996.
206. Villoutreix, B. O.; Kuenemann, M. A.; Poyet, J. L.; Bruzzoni-Giovanelli, H.; Labbe, C.; Lagorce, D.; Sperandio, O.; Miteva, M. A. Drug-Like Protein-Protein Interaction Modulators: Challenges and Opportunities for Drug Discovery and Chemical Biology. *Mol. Inf.* **2014,** *33* (6–7), 414–437.

2.05 Privileged Structures and Motifs (Synthetic and Natural Scaffolds)

AM Jones, Manchester Metropolitan University, Manchester, United Kingdom

© 2017 Elsevier Ltd. All rights reserved.

2.05.1	**Introduction**	116
2.05.1.1	The Concept of a Privileged Structure	116
2.05.2	**Privileged Scaffolds for Library Design and Drug Discovery**	120
2.05.2.1	Classes of Privileged Structure	120
2.05.2.1.1	Privileged 6,6 heterocyclic ring systems	120
2.05.2.1.2	Privileged 6,5 heterocyclic ring systems	123
2.05.2.1.3	Privileged 5,5 heterocyclic ring systems	124
2.05.2.1.4	Coumarin-/chromone-/pyran-derived privileged structures	125
2.05.2.1.5	Miscellanea	126
2.05.2.1.6	Arylated piperidine/piperazine ring systems	128
2.05.2.1.7	Benzodiazepine and related seven-membered ring systems	130
2.05.2.1.8	Single-cycle ring systems	132
2.05.2.1.9	Rhodanines (and related) as a special class of potentially privileged scaffolds	133
2.05.2.1.10	Spirocyclic structures	134
2.05.3	**Privileged Scaffolds to Identify Biologically Active Compounds Through Building Chemical Libraries**	135
2.05.3.1	Natural Product-Inspired Chemical Synthesis	135
2.05.3.1.1	Benzimidazolinopiperazinones	135
2.05.3.1.2	β-Lactams	136
2.05.4	**Natural Products as Lead Structures**	137
2.05.4.1	Lead-Like Natural Products?	137
2.05.5	**Chemical Transformations to Create Lead-Like Libraries**	139
2.05.5.1	Lead-Like Library Synthesis Approaches	139
2.05.6	**Conclusions and Outlook**	146
2.05.6.1	Future Directions for Privileged Structure Development	146
References		147
Relevant Websites		152

2.05.1 Introduction

2.05.1.1 The Concept of a Privileged Structure

When is a chemical structure a privileged structure? The definition adopted in this article is that of Evans[1] who stated that: "privileged structures are capable of providing useful ligands for more than one receptor." The privileged structures discussed in this article (Fig. 1) with two exceptions (prostanoic acid and morphine) generally have a molecular weight (MW) between 75 and 250 Da (with a median of 160 Da) and a cLog*P* (calculated partition solubility) −3 to +3 (with a median of +1.8). The topological polar surface area (tPSA) ranges from 0 to 110.4 Å with a median of 27 Å. This falls well within certain aspects of the rule of three (Ro3),[2] and therefore, privileged structures can be viewed as preferred fragments.[3,4] Biological targets are unconcerned with the minutia of chemical structures, but the overall size and charge are important factors. Privileged scaffolds, as we will discuss, are structures with favorable starting properties for drug discovery (such as obeying characteristics of Ro3) but importantly allow for the addition of multiple vectors to interact with the generic biological target via the addition of suitable functional groups. Importantly, this suggests most low MW (and as we will find almost exclusively nitrogen-containing) scaffolds have the potential to become privileged if sufficient biological data against a range of targets are obtained for multiple compounds containing that particular scaffold. We will also discuss examples that push the limits of the privileged argument that interact with nearly every biological target they are screened against (chelators, rhodanines, and reactive species, e.g., Michael acceptors). There is a panoply of privileged structures currently available, which have had significant impacts on medicinal chemistry, being a good starting point on discovery programs (the caveat to this is intellectual property (IP) considerations). We discuss outstanding examples of this and in Section "**Natural Products as Lead Structures**" look to the future in terms of the as yet not privileged but potentially so lead-like scaffold synthesis and what this may hold for medicinal chemists in the ever-changing world of drug discovery.

The conundrum that we have to contend with here is does ease of synthesis of certain scaffolds influence what we consider privileged scaffolds; for example, there is a panoply of low-cost methods to synthesis the indole skeleton, while there are more limited and expensive methods to prepare more elaborate heterocycles. Although the pharmaceutical industry has moved away from the preparation of large numbers (the quantity approach, e.g., 100–100,000 s) of new compounds (with potentially less structural diversity), the combinatorial chemistry approach to preparing "quality" compounds (with potentially more structural diversity

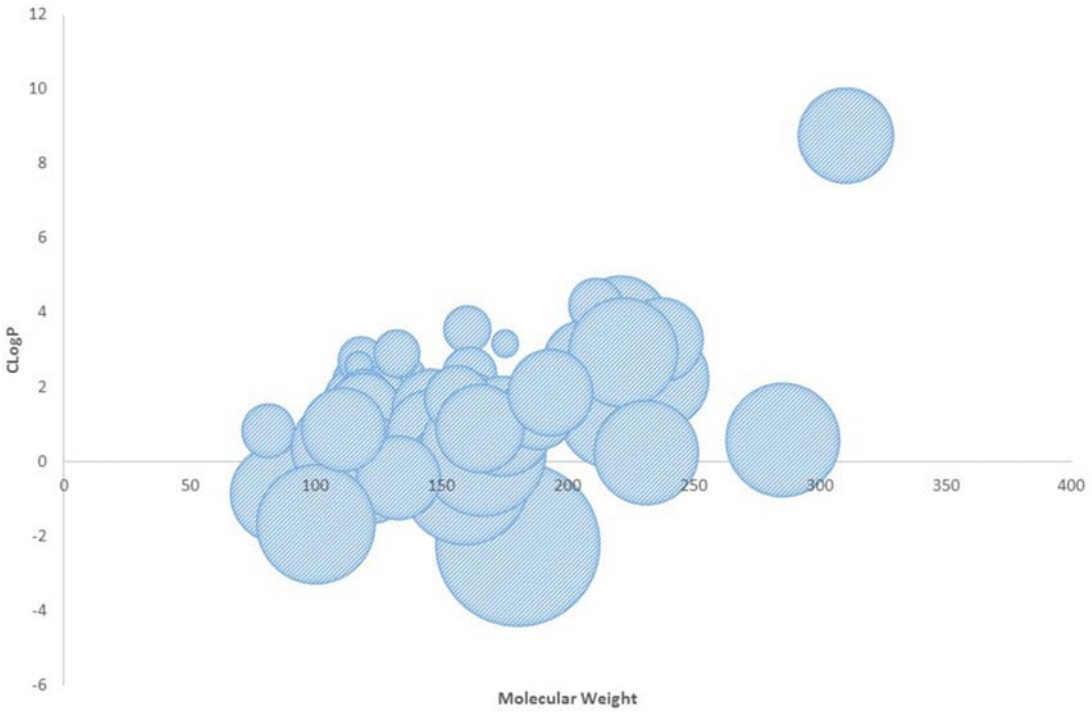

Fig. 1 Evaluation of the broad properties of the privileged structures discussed in this article (Size of the circle relates to tPSA).

but in smaller numbers) that interrogate less explored areas of chemical/biological space has more recently taken precedence. The literature explored in this article 2007–16 will undoubtedly have remnants of the quantity over quality structural approach. However, it is not the purpose of this article to question the validity of these alternate approaches, but to make the reader aware of the trends in chemical synthesis that when performed on an industrial scale whether in companies, research institutes or hybrid academic research models can artificially bias the compounds available to explore the privileged scaffold concept. Hot topics, trends, and even the general popularity of certain research areas within universities, companies, and the academe influence the pots of money and the resulting compounds prepared. High-risk fundamental synthetic work can go unnoticed (and unfunded) and research that builds on a narrow window of previous knowledge may be considered less risky and more fundable, perpetuating the cycle of looking narrowly for new biological activity. Certain research funders now appear to be bucking this trend with their pioneer awards. Of pertinence to this is a recent paper by Grzybowski's group[5] that has shone light onto the myriad of chemical networks and synthetic strategies employed by chemists during synthetic campaigns. Although we may believe that chemical synthesis by the multitude of research groups over the world is inherently random and free-spirited based on intuition and imagination, statistical analysis has shown this not to be the case, it is evolution of popular motifs through chemical decoration that wins out. With the assumption that there may be many other "privileged structures" languishing in research labs or yet to be isolated natural products or as the American politician, Donald Rumsfeld, aptly put it in his infamous quote "unknown unknowns," let us concentrate on the "known knowns" privileged structures that, can and often do, yield bioactive compounds.

With this caveat, we, the synthetic chemistry/medicinal chemistry community, have not systematically explored chemical space, iteratively building out from known scaffolds to new and as yet unprepared scaffolds examining the minutiae of functional group interconversions and testing the resulting materials for all possible bioactivity. Firstly, the costs would be prohibitive, and the number of small organic molecules (even at <500 Da) that can be possibly prepared, estimated at 166 billion structures (consisting of up to 17 atoms of C, N, O, S, and halogens),[6] is more than all the organic chemical matter available in the universe. Clearly this is impossible and coupled with an unsystematic exploration of chemical space and the presumption that analogs that are more tractable have been prepared in abundance (including the privileged scaffolds), we can still reach the following conclusion: there are privileged scaffolds. Certain scaffolds do tend to show biological activity to multiple different targets (discussed in Section "**Privileged Scaffolds for Library Design and Drug Discovery**"), possibly due to evolutionary recognition. Yet, these multitarget privileged scaffolds can branch over into the area of "frequent hitters/promiscuous inhibitors,"[7–10] and we will discuss the pros and cons of the privileged scaffold approach through a discussion of the famous class of rhodanine-like privileged scaffolds. These are examples of a chemotype that is prevalent in company and academic screening collections, which satisfies the maximal vector exploration needed in a privileged scaffold but has received a mixed response from the medicinal chemistry community. A caveat to identifying promiscuous compounds is that they are almost always well-established chemotypes identified from historical screening data where there is an abundance of cross target screening data. Understandably, analog design and synthesis of "promiscuous" chemotypes would only occur after detection of a protein–ligand response; this in turn would validate whether a chemotype is promiscuous.

As medicinal chemists, we cannot ignore this information at least as a starting point for developing new compounds. Herein lies a second consideration encountered with privileged scaffolds, the space to operate, for patent considerations, which may ultimately limit this approach with certain targets. Some privileged structures will also possess undesired off-target activity that needs to be dialed out early on in a campaign.

So with all these issues with the concept of "privileged structures," why do we still pursue it? Based on the current evidence, the strategy does appear to work and work well to deliver new clinical candidates, chemical tools, and drugs for patient benefit. Herein, the purpose of all our research to advance the field and contribute to scientific understanding can be more readily achieved using synthetically tractable routes to privileged scaffolds to design, develop, and optimize new inhibitors for patient benefit. Even if the privileged structure approach is proved wrong at a later point in the years to come, the privileged structure approach has led to the successful development of multiple small molecules described in the following sections. Having a rationale and increasing the often dire success rate of drug development can only be a good thing both for patients and companies and for the morale of the scientists in the lab. It should also be noted that the term "privileged structure" finds use in a number of disciplines, which complicates matters, but even within synthetic and medicinal chemistry, the term is often applied without much forethought to the spirit of the original definition.

Bringing the privileged structure approach up-to-date with modern advancements *in silico* developments, the approach of scaffold hopping[11] may be a particularly helpful addition to the drug discovery process when combined with privileged leads. Brown[11] has eloquently stated the drug discovery challenge as a "multiobjective optimization process" that ultimately satisfies the objectives of safety and efficacy. The process is reliant on (i) identifying a molecular scaffold and (ii) optimizing that scaffold through decoration or scaffold hopping improving efficacy, safety, and IP considerations. The privileged structure may therefore find intense use in the discovery and lead-optimization stages. In particular, the privileged scaffold, and it is often the case, acts as a *functional scaffold* interacting with the target and to a lesser extent as a *structural scaffold*, providing a framework for decoration that ultimately interacts with the target. Importantly, the privileged scaffold decoration pattern allows it to have significantly different functional engagements with targets. Langdon, Brown, and Blagg[12] have also analyzed the scaffold diversity of seven reported commercial compound libraries, demonstrating that the majority of compounds contain only a small number of well-represented scaffolds and the need to diversify these screening collections. Coupled with these limitations, the privileged scaffold has found extensive use in lead generation since the inception of the concept in 1988 and has become integrated into a variety of drug development platforms not purely as a standalone strategy. Zhao and Dietrich[13] have highlighted the strategic value of employing the privileged scaffold concept in both the mass production of compounds for high-throughput screening (HTS) and in the design of highly selective warhead-based ligands. The use of *privileged structures* has changed since its original inception and has allowed for the accelerated discovery of bioactive ligands for most currently investigated targets, with high levels of selectivity for the desired target or target space.

Kim and coworkers have coined the term *efficient chemical* "navigators" *of biological space* to get to new areas of bioactive chemical space[14] to explain the use of privileged structures as *activity beacons*. When coupled to diversity-oriented synthesis (DOS), the use of privileged substructure-based DOS results in compounds that can be used toward discovering bioactivity in traditionally "undruggable" targets. Collins and Jones[15] have recently reviewed the diversity-oriented landscape to preparing and discovering new molecular scaffolds, often incorporating privileged scaffold elements, to anticancer compounds. The privileged structure approach is compatible with the original tenets of chemical diversity-driven DOS.[16] At the extreme of the spectrum of limitations on skeletal diversity that may be considered, this approach becomes analogous to the privileged structure strategy familiar to medicinal chemists,[17] which typically involves substituent decoration of single scaffolds selected for their propensity to show particular bioactivities. In this context, it is interesting to note that minimal changes to the privileged scaffold may result in quite profound changes in biological activity despite high apparent similarity in the structural framework.

The reader is directed to these reviews (Nelson and coworkers[18] have reviewed natural product-inspired DOS. Waldmann and coworkers[19] have reviewed natural products as inspiration for the design of bioactive compounds. DeSimone and coworkers[20] have reviewed the many applications of privileged structures in drug discovery) and chapters and sections in the accompanying volumes in this compendium for further in-depth discussion of these concepts as they arise.

The most comprehensive definition of the types of scaffold that meet the criteria of a *privileged structure* since Evans (1988) first definition was by Stockwell and coworkers in 2010.[21] In this review, for the first time, a strategy for grouping and sorting privileged structures was offered and has served as inspiration for this article. The reader is directed to this article for its comprehensive coverage of the privileged structure landscape as of 2010.

The privileged structure approach also fits well with newer approaches to drug discovery, such as fragment-based drug discovery.[22] Chen and coworkers[23] have critically reviewed the evolution of fragment-based drug design and the deconstruction–reconstruction strategy of using privileged fragments from previously reported ligands. If we look at O'Donnell and colleagues comprehensive synthetic approaches, reviews to the new drugs of each year 2009–13[16-20,24-28] demonstrate the prevalence of the privileged structure in drugs launched each year. For instance, in 2009,[24] pazopanib hydrochloride, a multitargeted receptor tyrosine kinase of VEGFR-1, VEGFR-2, VEGFR-3, PDGFR-α/β, and c-Kit, contains the diaminopyrimidine privileged scaffold. In 2010,[25] bazedoxifene acetate, an estrogen receptor (ER) modulator for the treatment of osteoporosis in postmenopausal women, contains a central indole core. In 2011,[26] bilastine, a selective histamine H_2 antagonist for the treatment of rhinoconjunctivitis and urticarial, contains a benzimidazole privileged motif. In 2012,[27] bosutinib hydrate, a dual Src/Abl kinase inhibitor for the treatment of chronic myeloid leukemia, contains a central anilinoquinoline privileged hinge-binding motif. In 2013,[28] afatinib dimaleate containing the privileged quinazoline 6,6-ring system was approved for the treatment of nonsmall-cell lung cancer (NSCLC), highlighting some of the successes with incorporating the privileged scaffold approach.

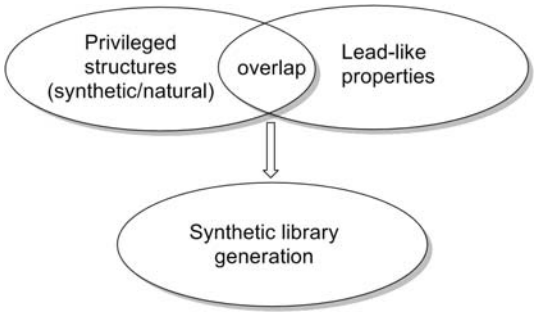

Fig. 2 Overlap between the main concepts described in this Chapter.

The structure of this article (Fig. 2) will first introduce and focus on (i) the most commonly encountered classes of privileged structures, directing the reader to seminal articles and comprehensive reviews within the field and (ii) the incorporation of privileged scaffolds into library design displaying examples of discovering bioactivity different to the scaffold source (or its known bioactivity). Next, we look at a potential source for discovering privileged scaffolds, natural products, and how they can be incorporated into library design. In the penultimate section, we look at the current trend of "lead-like" compounds by focusing on exemplar library synthesis and application to bioactive molecule discovery. Finally, we consider the outlook for privileged scaffold-based drug discovery and, in the changeable world of drug discovery, for instance, public-private partnerships (PPP) initiatives such as the European Lead Factory from IMI that also has and will identify new privileged structure scaffolds.[29]

Drugs on the market and a natural product that contains some of the privileged structures: Indomethacin **1** is a nonsteroidal antiinflammatory drug; tamoxifen **2** is an antiestrogen therapy for hormone receptor-positive breast cancer; camptothecin **3** is a cytotoxic quinoline containing alkaloid that inhibits topoisomerase I; gefitinib (Iressa) **4** is an epidermal growth factor receptor inhibitor used to treat, among others; NSCLC are shown in Fig. 3.

Chan and colleagues[30] have mined the protein data bank for chemical fragments that bind to the four most common side-chain residues: Asp, Glu, Arg, and His. Analysis of 8000 protein–ligand interactions revealed 2038 unique ligands containing a recurring 462 fragments. This work shows that certain fragments (or privileged structures) have a higher propensity for interaction with these key residues, and further global mapping of pharmacological space[31] may reveal other networks of privileged structure interactions. Related to this, Stahl and coworkers[32] have written an excellent perspective piece on molecular interactions between the ligand (which may be privileged) and the biological target from a medicinal chemist's viewpoint.

To give a flavor of this article, four articles have been selected to highlight examples of different privileged approaches. For instance, Kim and coworkers[33] have described the discovery and structure–activity relationships (SARs) of privileged pyrazolodiazepine scaffolds as the first reported agonists of the *Drosophila sex* peptide receptor (also known as *D. melanogaster* (DrmSPR)). DrmSPR is an important G-protein-coupled receptor (GPCR) involved in postmating responses such as egg laying, and the receptor is modulated by a natural peptide agonist (the sex peptide). A library of pyrazolodiazepines was screened against this target, and a weak agonistic effect was observed. A SAR was determined leading to the synthesis of variously substituted pyrazolodiazepines. Two examples bearing a pendant 6-benzyl moiety exhibited EC_{50} values of 3–4 μM, and they were also the first small molecules to achieve this effect.

Sun and coworkers[34] have developed an expedient synthesis of oxa-, thio-, and selenohydantoin-fused tetrahydrozaepino[4,5-*b*]indoles. These privileged scaffolds were inspired from the seven-membered azepino[4,5-*b*]indole ring found in the *iboga* class of naturally occurring alkaloids.

Che and Marshall have reviewed privileged scaffolds that target reverse-turn and helix recognition.[35] Disrupting protein–protein interactions through small-molecule inhibition is one of the key challenges of drug discovery at the time of writing, and the

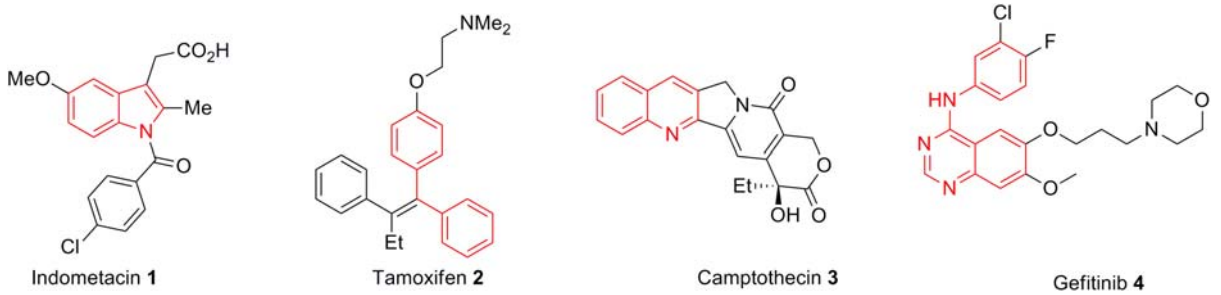

Fig. 3 Examples of drugs and natural products that contain privileged structures (indomethacin **1**, indole; tamoxifen **2**, diphenylmethane; camptothecin **3**, quinoline; and gefitinib **4**, anilinoquinazoline).

application of privileged scaffolds is advocated and finding new uses. For example, privileged structures that target reverse turns include the benzodiazepine scaffold, and α-helical recognition include trispyridylamides. Arkin, Tang, and Wells have written an excellent review of progress toward small-molecule inhibitors of protein–protein interaction.[36] The reader is directed to this article for further information on this rapidly evolving area. However, for the purpose of this article, it is of note that several research inhibitors contain privileged elements. For example, TL-32711 (birinapant) contains a bisindole motif, (+)-JQ1 contains the thienodiazepine scaffold as a BRD4 inhibitor, and BCL family inhibitors contain the aryl and benzylpiperazine scaffolds, for instance, in ABT-263 (navitoclax). These and others will be used to exemplify the privileged structure, development of privileged syntheses, and ultimately the use of privileged scaffolds in medicinal chemistry.

2.05.2 Privileged Scaffolds for Library Design and Drug Discovery

2.05.2.1 Classes of Privileged Structure

We have grouped Chapter 2 around general and repeating functional scaffolds that show bioactivity in more than one target depending on the substitution pattern. The potential for privileged scaffolds to become *promiscuous* is also highlighted. Han and coworkers[37] have studied the drug-likeness of bicyclic privileged structures (such as 6,5-, 6,6-, and 6,7-ring systems represented by purine, chromone, and benzodiazepine in the following sections) with the purpose of designing new bicyclic privileged structure combinatorial libraries. In particular, they focused on the physicochemical properties (such as MW, Log *P*, and tPSA) and noted a significant difference between the drug-likeness range of privileged bicyclic scaffolds compared with nonprivileged scaffolds. A 76% prediction accuracy for designing improved drug-like privileged scaffolds was obtained.

2.05.2.1.1 Privileged 6,6 heterocyclic ring systems

Examples of the privileged unsaturated 6,6 heterocyclic ring system are provided in Fig. 4.

There is a wealth of examples (Fig. 4) and reviews in this area. Bolognesi and coworkers have reported the privileged structure-guided synthesis of quinazolines as trypanothione reductase inhibitors[38] and quinolones as a privileged structure in antimicrobial drugs[39]; the 8-hydroxyquinoline scaffold (as a strong metal ion chelator) acts as an anticancer agent, anti-HIV properties, antifungal, chelator of metalloproteins, inhibitor of 2OG-dependent enzymes, antileishmanial, antischistosomal, *Mycobacterium tuberculosis* inhibitor, and botulinum neurotoxin inhibitor, among others.[40] Solomon and Lee have reviewed the application of the 6,6-ring system and quinoline in drug discovery.[41] Shiro and coworkers[42] have reviewed the privileged quinolinone-containing heterocyclic scaffold from both a synthetic and biological viewpoint. Quinolones are shown to act as antiinflammatory, antitumor, antidiabetic, and antipsychotic agents.

Ross and coworkers[43] have prepared ciprofloxacin dimers to explore atypical chemical space with bacterial permeability properties. Fluoroquinolones, such as ciprofloxacin, are well-known antibiotics; the dimer prepared showed enhanced inhibition of the intracellular target (DNA gyrase) and general antibacterial activity in whole cells, which in turn is governed by its cellular permeation and physicochemical properties. Principal component analysis showed that the privileged dimers occupied a unique region of chemical space most similar to macrolides.

Nakamura and coworkers[44] have evaluated 46 in-house synthesized 2,3-substituted quinoxalines as antileishmanial and antitrypanosomal drugs with inhibition levels of *T. cruzi* promastigotes and epimastigotes between $IC_{50} = 100–800$ nM for the most potent analogs.

Similarly, a collection of 2,3-substituted quinoxalin-6-amine analogs was evaluated by Natarajan and coworkers[45] for cancer cell line activity. A urea-containing analog showed cancer cell line growth inhibition at 20 μM with concomitant caspase-3/7 activation, PARP cleavage, and Mcl-1-dependent apoptosis.

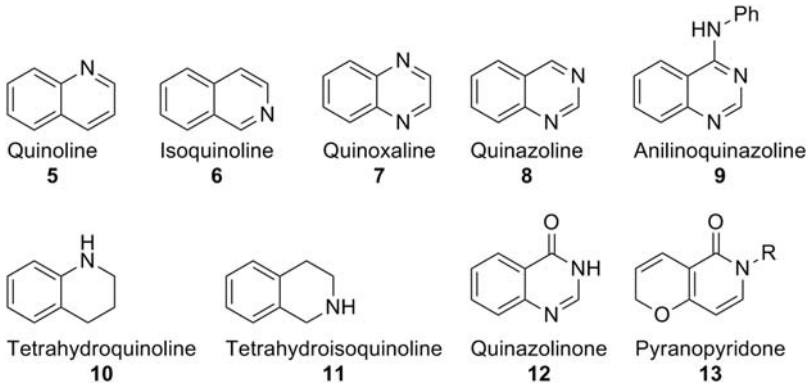

Fig. 4 Examples of privileged 6,6 heterocyclic ring systems **5–13** (saturated/unsaturated).

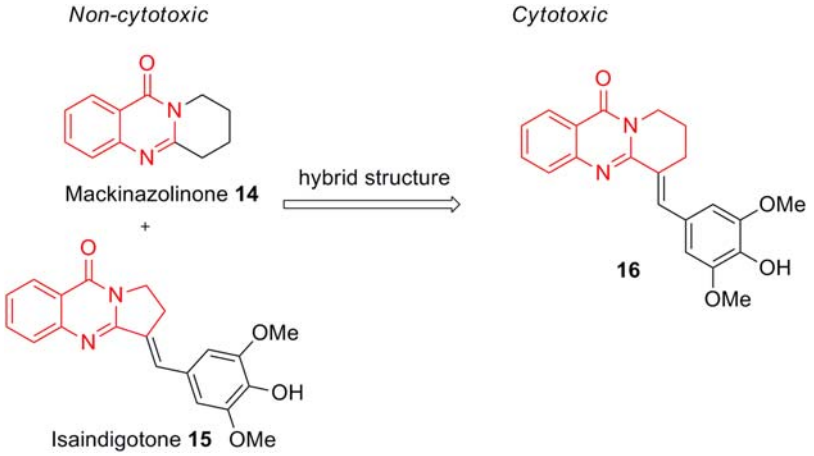

Fig. 5 Natural product hybridization strategy to privileged cytotoxic scaffolds.

The group of Liu and coworkers has reported[46] a focused library containing a privileged quinazolinone natural product motif (Fig. 5). Using a strategy of hybridizing the structures of two known natural products, mackinazolinone **14** and isaindigotone **15**, a library of natural product-related compounds was rapidly prepared. Prior to the synthesis campaign, a virtual library of 900 analogs was assembled using the ArQule software from a 30×30 collection of anthranilic acids and benzaldehydes. Using the diversity paradigm, 67 analogs were synthesized. Importantly, it should also be noted that neither parent natural product mackinazolinone **14** nor isaindigotone **15** is reported to exhibit cytotoxic activity. Screening of the 67-member library using an (3-(4,5-dimethylthiazol-2-yl)-5-(3-carboxymethoxyphenyl)-2-(4-sulfophenyl)-2H-tetrazolium) (MTS) cell proliferation assay (five cancer cell lines, NCI-H460, A549, DU-145, MDA-MB-231, and SF-268 and one primary cell culture Human Mammary Epithelial Cells (HMEC)) identified compounds such as the cytotoxic hybrid **16** (shown in Fig. 5) as a cytotoxic, an unexpected feature based on the structures the molecule was hybridized from. Particularly active analogs of the hybrid were further evaluated in a phosphohistone H3 (pH3) assay to demonstrate whether their inhibition of cell proliferation resulted from mitotic arrest. A dose-dependent response with pH3 EC_{50}'s from 0.3 to 11 μM gave support to this argument. The antimitotic agents were further evaluated in a tubulin polymerization assay; the inhibition observed suggests these compounds act through destabilization of tubulin polymerization. Taken together, the authors suggest that the cytotoxic hybrid may also be a new privileged structure for further development.

Liu and coworkers[47] applied a biased privileged structure-enriched library approach to the screening and identification of new hepatitis C virus (HCV) inhibitors. A quinoxalin-2(*1H*)-one derivative **17** (Fig. 6) showed potent HCV inhibition *in vitro* from the screening library; further synthesis identified key SARs leading to five advanced compounds with increased antiviral potency, EC_{50} range of 1–2 μM, while concomitantly reducing cytotoxic effects inherent to the hit compound, although the underlying mechanism of action was unclear at this stage.

The synthesis of derivatives of the hit compound was accomplished as follows: treatment of a difluoro dinitro benzene with methyl glycine afforded the first of two S_NAr products; the second fluoro group was displaced by a secondary amine, in this case, *N*-methyl cyclohexane. The quinoxalin-2(1*H*)-one ring system was formed via hydrogenation of both remaining nitro groups using hydrogen over palladium on carbon. A spontaneous cyclization of the ortho-amine to the glycine carbonyl atom effected this transformation. Finally, the remaining amino group was reacted with a benzoyl isothiocyanate to install the carbamothioylbenzamide functionality.

Manfroni and coworkers[48] have reevaluated their previously reported antibacterial- and antiviral-privileged 6-aminoquinolone scaffold as potent inhibitors of NS5B polymerase, a target for the development of HCV inhibitors. In particular, the 6-amino-7-[4-(2-pyridinyl)-1-piperazinyl]quinolone derivative possessed an IC_{50} value of 69 nM against NS5B polymerase and selective antiviral effect ($EC_{50} = 3.03$ μM) with no detectable cytostatic effects in the high micromolar range measured by MTS in Huh 9–13 cells; demonstrating the repurposability of privileged scaffolds to interact with other biological targets. We discuss this later in a secondary context in Section "**Arylated piperidine/piperazine ring systems**."

Kandi and coworkers[49] have noted the prevalence of the privileged scaffolds, curcumin, and 4-aminoquinolines that are often found in ligands that can modulate diseases such as cancer and malaria. Hybridization of these two privileged scaffolds with a triazole linker was postulated to give a dual privileged scaffold ligand with potentially improved anticancer activity. Evaluation of these new ligands in a diverse set of 60 human cancer cell lines revealed examples that showed nanomolar growth inhibition. Mechanistically, this was due to the privileged-linked compounds acting in an apoptotic-inducing manner.

D'hooghe and Vandekerckhove have reviewed[50] quinoline-derived antimalarial hybrid compounds. Joseph and coworkers[51] have reported a ketene-initiated domino reaction to the privileged quinolizidine class of molecules with multiple stereogenic centers and high diastereoselectivities. These quinolizidines are constrained mimetics of the privileged H-bonded conformation of (−)-Lobeline.

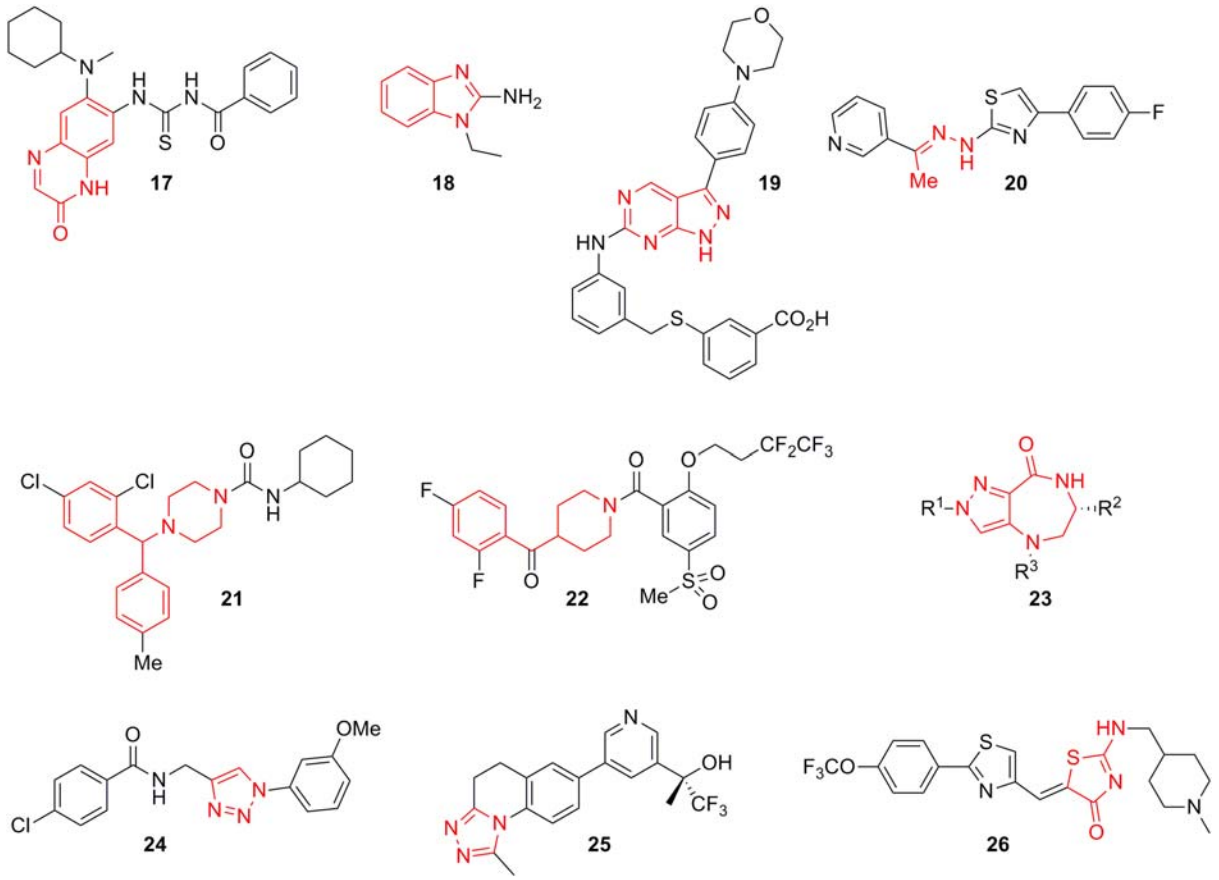

Fig. 6 Examples of singleton-privileged hit scaffolds discussed in this article **17–26**.

2.05.2.1.1.1 A special subset: kinase inhibitors

Gray and coworkers[52] have made a compelling argument for the extension of the privileged structure approach to the development of type II binding mode kinase inhibitors. In kinases, the Adenosine triphosphate (ATP) active site is conformationally flexible on its account of its ability to accept a range of small-molecule inhibitors. In turn, the conformation of the kinase, the activation segment, controls access to the substrate-binding pocket. This large conformational change leads to a DFG-in (active state) and a DFG-out (inactive state) (where DFG means D = aspartic acid, F = phenylalanine, and G = glycine). Type II kinase inhibitors typically bind to the DFG-out conformation of the kinase (while type I inhibitors bind to the DFG-in conformation). Gray and colleagues have reviewed the large number of reported type II kinase inhibitors and undertaken a crystallographic analysis of their previously determined binding modes. Using a small collection of type II inhibitors, over 200 kinases can be inhibited, suggesting they are not only less selective than type I inhibitors but also privileged to be able to modulate a range of kinases. Zhang and coworkers[53] have investigated the privileged pharmacophore elements of type II kinase inhibitors that target the v-RAF murine sarcoma viral oncogene homologue B1 (BRAF). BRAF is a protein kinase that is frequently mutated in cancer to BRAF V600E. In turn, this activates the RAS/RAF/MEK/ERK pathway (RAS = p21/RAS protein, RAF = RAF proto-oncogene serine/threonine-protein kinase, MEK = Mitogen-activated protein kinase kinase, ERK = extracellular signal–regulated kinase) and is therefore a validated target. Using two privileged pharmacophores in kinase inhibitor design, anilinopyrimidine and an unsymmetrical diaryl-substituted urea, a series of hybridized structures were prepared. The lead compound from the series is a selective inhibitor of BRAF and its oncogenic BRAF V600E and was demonstrated to possess antitumor efficacy in an A549 human NSCLC xenograft model through a once-daily po dosing regime. Furthermore, molecular docking studies showed that these privileged structure motifs might act in a type II kinase inhibition mode with the DFG-out conformation of BRAF.

Hoelder and coworkers[54] have updated the literature on the privileged-fused pyrimidine core, ubiquitous in kinase inhibitor scaffolds. In particular, they have developed a route to the underrepresented 2-amino-pyrido[3,4-*d*]-pyrimidine scaffold, a potential privileged scaffold of the future. As all privileged scaffolds are dependent on tractable syntheses, this work makes this scaffold more likely to be developed and explored in future medicinal chemistry campaigns. Furthermore, their effects in a checkpoint kinase 2 (CHK2) assay were evaluated and showed nanomolar inhibition. This work demonstrates that privileged scaffolds can be used as potential predictors of future privileged scaffolds that may be currently untractable but with effort and imagination can be overcome.

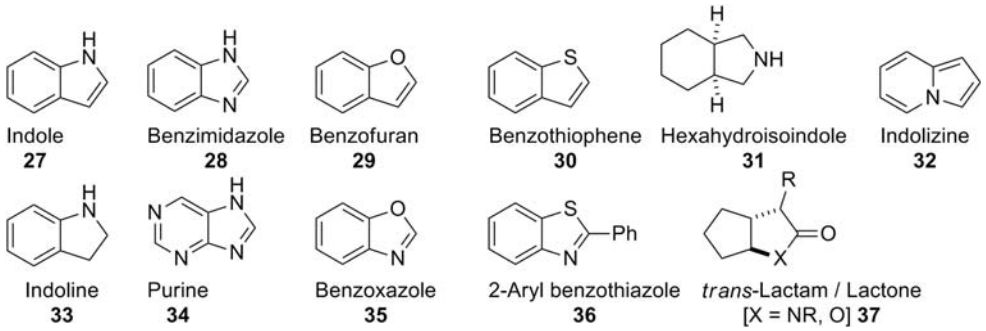

Fig. 7 Privileged 6,5 heterocyclic ring systems (saturated/unsaturated) **27–37**.

Zhan and coworkers[55] have reported anticancer dual c-Met and VEGFR-2 inhibitors derived from the privileged anilinopyrimidine scaffold. Two novel synthetic routes allowed for rapid library preparation and SAR interrogation of the privileged scaffold. At the enzyme level, nanomolar potency was detected. In a cellular environment, low micromolar antiproliferative effects against c-Met-dependent cell lines were found. The binding mode of the privileged anilinopyrimidine scaffold with c-Met was conclusively determined with a cocrystal determination.

Zhao and coworkers[56] have analyzed the chemical space coverage of reported kinase inhibitors. Deconstruction of 26,668 kinase inhibitors into their constituent fragments revealed that half of the 10,302 fragments are not commercially available and 5861 ring-containing fragments were capable of hinge-binding. This is only 1% of all the known ring systems (~75,000) capable of forming a bidentate hinge-binding interaction, leading to the conclusion "current kinase inhibitors cover a tiny fraction of fragment space."

2.05.2.1.2 Privileged 6,5 heterocyclic ring systems

The privileged 6,5 heterocyclic ring systems can be viewed as a subset of the privileged 6,6 heterocyclic ring systems in Section "**Privileged 6,6 heterocyclic ring systems**" but due to the panoply of examples reported is individually discussed here.

There is a wealth of examples (**Fig. 7**) and reviews in this area: Xiang and coworkers have extensively reviewed the synthetic routes to the indoline privileged scaffold,[57] and Fang and coworkers have reviewed the development of indole-containing antiviral agents.[58] Fraga and coworkers[59] have reviewed the indole as a privileged drug discovery motif, again from a natural product inspiration perspective. Zhang and coworkers[58] have reviewed recent strides in the development of the privileged indole-containing antiviral compounds from compounds on the market, clinical trials, and research in development. Likewise, Sonsona[60] has highlighted some of the methods to the synthesis and diversification of privileged indole-containing natural products and bioactive molecules. Keri and coworkers[61] have extensively reviewed the benzimidazole privileged structure, highlighting examples of antibacterial, antifungal, antiinflammatory, antioxidant, anticonvulsant, and antitubercular activities, among others. Lim and coworkers[62] have reviewed 1,3,5-triazine-derived analogs of purines not only as isosteres of the privileged purine class but also as privileged structures in their own right. Purines are one of the most prevalent heterocycles in biology, and through isosteric replacement with other *N*-containing heterocycles, seven purine isosteres can be determined. This range of privileged isosteres and their associated bioactivities such as inhibitors of kinases, phosphodiesterases, xanthine oxidases, and thymidine phosphorylases is reviewed. Zhang and coworkers[16] have reported a library of privileged heterocycles, including indoles, from an Ugi four-component reaction, which may also be considered a privileged reaction. Paul and colleagues[63] have reviewed the synthetic approaches and derivatization methods of the privileged imidazo[1,2-*a*]pyrimidine scaffold. Xiao and coworkers[64] have reviewed synthetic methods to and biological activities of privileged pyrroloquinazolines.

Bunders and colleagues[65] have investigated desformylflustrabromine (dFBr) analogs (**Fig. 8**) as an indole-derived privileged template for the discovery of novel inhibitors of the indole-signaling network in *Escherichia coli* and *Staphylococcus aureus*. The indole-signaling network is an important pathway in the bacterial kingdom. Using this privileged starting point for derivatives of dFBr, 10–1000-fold more potent analogs than indole were discovered demonstrating the value of the flustramine natural product family as a starting point for the design of bioactive small molecules. Analog, **38**, was a nonmicrobiocidal inhibitor of biofilm formation; mechanistic studies in wild-type (wt) and knockout *E. coli* strains showed a temperature-dependent mode of action. It was further suggested based on the indole template from flustramine that **38** may achieve its potency via modulation of indole-based signaling pathways. Furthermore, due to the activity of **38** against indole-positive and indole-negative bacteria and the putative role of indole-signaling in nature, the privileged structure-containing molecule, **38** and **39** will also be employed as chemical probes.

Pedersen and coworkers[66] have used the privileged 2-phenylindole scaffold to develop for the first time selective allosteric antagonists of the G-protein-coupled receptor (GPRC6A). GPCRs are an important biological target for drug development, and class C GPCRs are new drug targets. Using a fluorescence resonance energy transfer (FRET) FRET-based inositol monophosphate assay, three privileged 2-phenylindoles were identified as antagonists at the GPRC6A receptor in the low micromolar range, and two of these compounds displayed a greater than ninefold selectivity for the GPRC6A receptor over related GPCRs. This makes this privileged scaffold the most potent and selective inhibitor of GPRC6A reported to date.

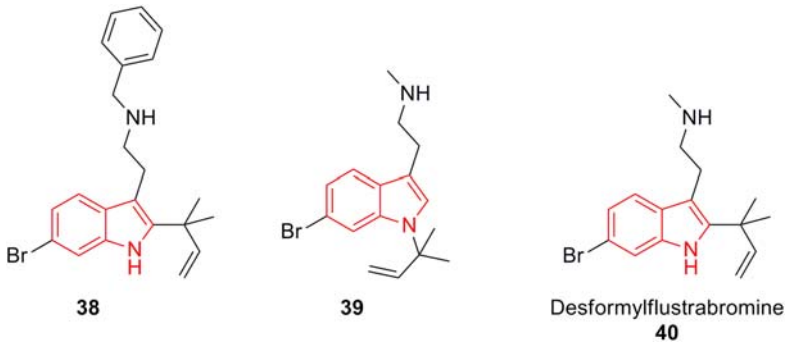

Fig. 8 Privileged bioactive desformylflustrabromine analogs **38** and **39**.

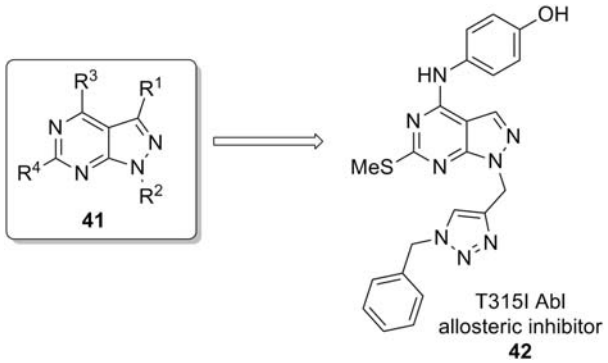

Fig. 9 Evolution of a hit privileged scaffold into a T315I Abl allosteric inhibitor **42**.

Vignaroli and coworkers[67] used a privileged pyrazolo[3,4-*d*]pyrimidine scaffold **41** (isosteric to purine) coupled with a diversification strategy to generate a library, using synthetic sequences to functionalize the C3, C4, C6, and N1 positions (Fig. 9). Screening the library prepared against enzymatic targets revealed several inhibitors of the Src and Abl kinases (including wt and T315I-mutated forms) with comparable levels of activities to known inhibitors. This area of kinase inhibitor discovery is often explored successfully using a target-oriented approach; therefore, a diversity-oriented approval is a novel update in this field. Of interest, a member of the library was demonstrated to be an allosteric inhibitor of the T315I form of Abl (**42**), opening up a new avenue of noncompetitive inhibition.

Using a fragment-based Nuclear Magnetic Resonance (NMR) spectroscopy screening platform, Miller and coworkers[68] discovered a series of privileged structures, such as benzothiazoles and benzoimidazoles, as in **18** (Fig. 6) that bind to the plant homeodomain (PHD)–the BCL9 HD1 domain interface, blocking protein–protein interactions. The chromatin reading Pygo–BCL9 complex is a novel and emerging target in oncology that anchors the histone H3 tail methylated at lysine 4 (H3K4me).

X-ray crystallography of the newly discovered privileged fragments revealed that, despite their small size, they bind to a cleft on the PHD–HD1 interface, displacing the native H3K4me peptide from the PHD finger. This demonstrated that the Pygo–BCL9 complex can be inhibited using a privileged fragment approach.

De La Cruz, Kapoor, and coworkers[69] utilized a purine privileged structure template in their discovery program of small-molecule probes (such as **19**, Fig. 6) of nonclass II myosins. Myosins are motor proteins that translate across the actin cytoskeleton, important for muscle contraction among other biological motions. There are now 18 classes of myosins, with small-molecule probes for class II myosins only. Intriguingly, purine derivatives are more commonly encountered as kinase inhibitors; therefore, this may be viewed as a scaffold hop to a kinase-like inhibitor that now targets a GTPase-fold protein. Iterative SAR afforded a selective myosin V inhibitor that does not interfere directly with nucleotide binding.

Wang and coworkers[70] have investigated novel thieno[2,3-*b*]pyridine analogs and their resulting SAR as HCV inhibitors. From an initial hit compound (from a larger privileged small-molecule library) containing a thienopyridine core, in cell-based screening, several noncytotoxic analogs with low micromolar EC_{50} were uncovered. Although a mechanism of action was not elucidated, this privileged scaffold showed potential as an anti-HCV agent.

2.05.2.1.3 Privileged 5,5 heterocyclic ring systems

A subset of the 6,5-ring systems are the ring-contracted 5,5-ring systems. Romagnoli and coworkers[71] have designed heterobivalent antiproliferative hybrids based on the privileged imidazo[2,1-*b*][1,3,4]thiadiazole and imidazo[2,1-*b*][1,3]thiazole structures. Using

a strategy of selecting two different pharmacophores that bind to different biological targets or indeed separate sites on the same molecular target, the two privileged scaffolds were selected for investigation. The scaffolds were fused at their respective C6 positions by a *meta*-(bromoacryloylamido)phenyl motif. Most of the prepared biprivileged hybrids showed antiproliferative activity against a wide panel of cancer cell lines with up to submicromolar IC_{50}. Selected promising candidates induced apoptosis via the release of cytochrome c and cleavage of a variety of caspases. Despite overexpression of Bcl-2 in the tested cell lines, this did not appear to confer protection from cell death from the biprivileged hybrids tested.

Sztanke and coworkers[72] have explored a novel class of thiophene bioisosteres based on the privileged 7,8-dihydroimidazo[2,1-*c*][1,2,4]triazin-4(6*H*)-one moiety for antiproliferative effects in cancer cell lines. Using the reaction of 1-aryl-2-hydrazonoimidazolidine hydroiodides with ethyl 2-oxo-2-(2-thienyl)acetate, a range of analogs were prepared in good overall yield. Upon testing in vitro in human tumor cell lines (A549, HeLa, T47D, and TOV112D), the compounds showed good levels of antiproliferation and were found to be in most cell lines more cytotoxic than pemetrexed. In normal cell lines, this cytotoxic effect was limited, demonstrating a potential window for further development. A bioassay using double fluorochrome staining provided some insight into how these privileged scaffolds gave rise to an anticancer effect in the tumor cell lines described.

2.05.2.1.4 Coumarin-/chromone-/pyran-derived privileged structures

Although the coumarin/chromone class is another example of the 6,6-ring system, particular bioactivity exclusively associated with this class merits its own section.

There is a wealth of examples (Fig. 10) in this area: Grover and Jachak have reviewed the coumarin privileged scaffold as a starting point in antiinflammatory drug discovery [73]; Keri and colleagues have extensively reviewed the chromone scaffold as a general privileged class,[74] which possesses a range of biological activity (e.g., anticancer, anti-HIV, wound healing, and antiinflammatory). Gaspar and colleagues[75] have extensively reviewed the properties of the chromone scaffold detailing the many and varied biological effects of this simple privileged structure.

Park and coworkers have developed a branching DOS library inspired by natural products containing the privileged benzopyran ring system.[76,77] The DOS strategy involved balancing two seeming opposites: biased incorporation of privileged structures and unbiased diversity. In total, 22 unique core structures were prepared with limited appendage diversity; this enabled the side-by-side evaluation of core structural diversity. From a 3- or 4-(pseudo)halo-substituted benzopyran, three key reactions were performed to generate the diastereo-enriched library: Diels–Alder cycloaddition, click chemistry, and palladium-catalyzed cross coupling. In particular, Stille cross coupling followed by endo-favored Diels–Alder cycloaddition generated steroid-like tetracycles (Fig. 11). Three-dimensional structures were generated by hydrogenation, while dichlorodicyanoquinone (DDQ)-mediated oxidation gave flat aromatic systems. Comparison of examples **52** and **53** highlighted the power of three-dimensional architectures to provide differential biological activity: a viability assay in A549 lung carcinoma cells demonstrated the cytotoxicity of **52** (1.0 μM) versus **53**(63.9 μM). Using a cell-based reporter assay in LNCaP human prostate adenocarcinoma cells, screening of a 2000-member benzopyran DOS library followed by focused screening of 19 second-round derivatives identified P01F01 (**54**) as an antagonist of the androgen receptor.[77,78] The compound was also shown to inhibit transcription mediated by androgen receptor mutants that are resistant to inhibition with conventional antagonists such as bicalutamide.

Gaspar and coworkers[79] have employed the chromone privileged scaffold to develop two new series of monoamine oxidase (MAO) inhibitors. SAR studies showed preference for MAO-B inhibition that could be enhanced via 3-position substitution, while identical 2-position substitution ablated activity. The optimal compound showed an MAO-B IC_{50} of 63 nM with a 1000-fold selectivity window over MAO-A inhibition, thus validating the chromone privileged scaffold as a MAO inhibition template. Massari and coworkers[80] have investigated both the irreversible and reversible small-molecule inhibition of monoamine B (MAO-B) using a range of biophysical techniques. MAO-B is an important target (involved in the metabolism of dopamine) for diseases and disorders associated with a decrease in dopaminergic neurotransmission, such as Parkinson's disease. Isothermal titration calorimetry and thermal shift approaches were used to identify interesting scaffolds to further investigate from a binding mode direction (reversible or irreversible) and also thermodynamically privileged chemical scaffolds for MAO-B inhibition. Due to the mechanism-based difference in the thermal shift assay from the MAO-B inhibitors, reversible and irreversible inhibitors were easily identified. Coupled with screening of privileged scaffolds, these biophysical approaches may help shed light on the next generation of MAO-B inhibitors. Ortuso and coworkers[81] have also probed the development of monoamine oxidase-B (MAO-B) inhibitors based on a known privileged 3-acetyl-2-dichlorophenyl-5-aryl-2,3-dihydro-1,3,4-oxadiazole scaffold for this target. Applying molecular interaction field analysis, several compounds were developed that displayed potent in vitro activity (IC_{50} medium to low nanomolar range).

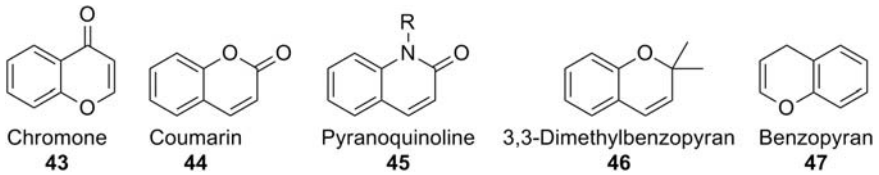

Fig. 10 Privileged coumarin/chromones/pyrans **43–44**.

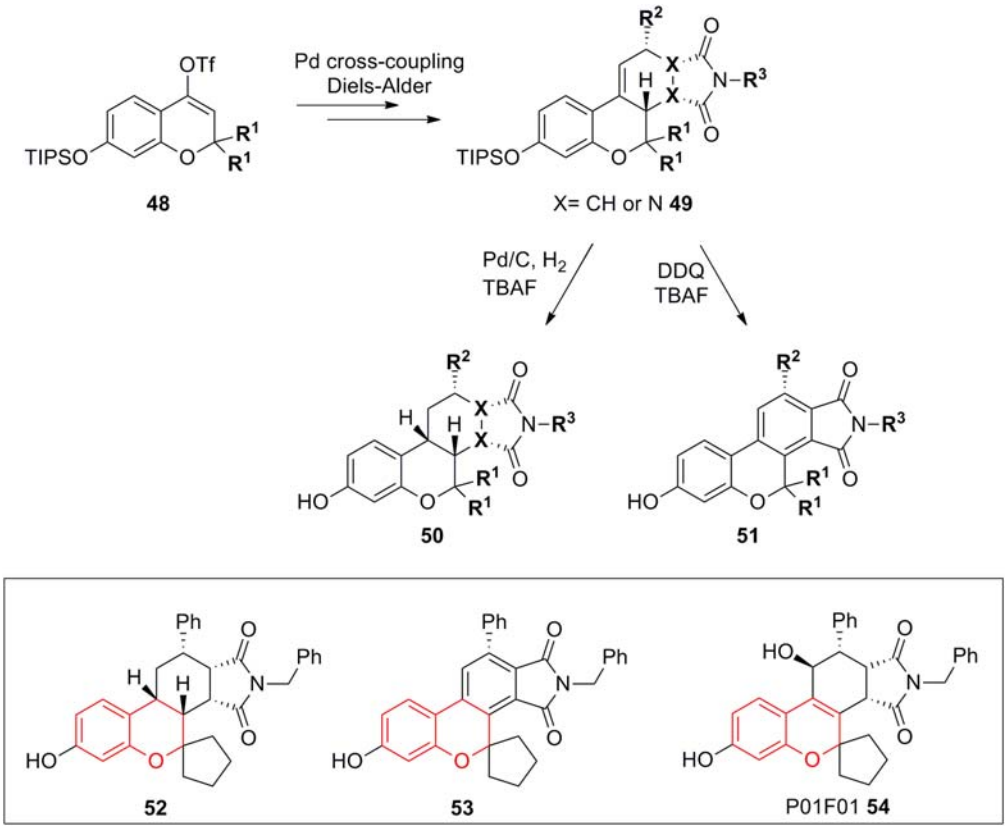

Fig. 11 DOS of privileged benzopyran-containing polycycles and identification of an androgen receptor antagonist **54**.

The enantiomers of the most promising compounds were separated, and the (*R*) enantiomer was found to be more active. Khan and coworkers[82] have also investigated triazolothiadiazole and triazolothiadiazine scaffolds as cholinesterase and MAO inhibitors.

2.05.2.1.5 Miscellanea

Unfortunately, not all scaffolds fall into a clustering system, due to either limited examples reported or the lack of investigations. Thus, in this section, examples from small scaffolds to steroids are represented.

There is a wealth of examples (Fig. 12) in this area that are mainly singletons rather than clusters of hit scaffolds, as in the previous sections.

2.05.2.1.5.1 N-Acylhydrazones and related diazo structures

Fraga and coworkers have reviewed the patent literature on the acylhydrazone privileged functional group.[83] For instance, the drug dantrolene contains this privileged motif and is used to treat malignant hyperthermia. The acylhydrazone core is used in research studies for pain, inflammation, cancer, and cardiovascular targets. Fraga and coworkers[84] have combined a rational design approach using molecular modeling studies with the acylhydrazone privileged template to generate a novel IKK-β inhibitor (*E*)-*N*-(4-nitrobenzylidene)-2-naphthohydrazide. Incorporation of two lipophilic motifs around the central privileged template led to a scaffold with increased selectivity over IKK-α and CHK2. Furthermore, the privileged compound was shown to suppress arachidonic acid-induced edema formation in vivo, demonstrating an antiinflammatory mode of action.

Barreiro and coworkers[85] have designed a new class of cyclohexyl-*N*-acylhydrazones using the prototype compound, LASSBio-294 with the aim of preparing analogs with analgesic and antiinflammatory properties. The *N*-acylhydrazone motif is considered a privileged scaffold with pluripotent biological activities. Most analogs demonstrated some antiinflammatory and/or analgesic activity, and one example showed remarkable activity in a chronic neuropathic pain model.

Secci and coworkers[86] synthesized a library of (4-substituted-thiazol-2-yl)hydrazines (such as **20**, Fig. 6) as potential reversible and selective in vitro inhibitors of human monoamine oxidase B (*h*MAO-B) with nanomolar potency and up to 58,820-fold selectivity over *h*MAO-A. These compounds show marked similarity to the privileged *N*-acyl hydrazine class and may be viewed as pseudoprivileged motifs, mimicking portions of a more understood pharmacophore. SAR revealed that substitution on the α-carbon to the N1 nitrogen atom had marked effects on potency and *h*MAO-B selectivity. Substitution of the 4-position of the thiazole with aryl ring systems, such as in **20**, has demonstrated further interactions with the well-documented aromatic cage in *h*MAOs. Prior to this work, arylalkylhydrazines were irreversible, nonselective *h*MAO inhibitors and show that privileged structures are not a panacea in

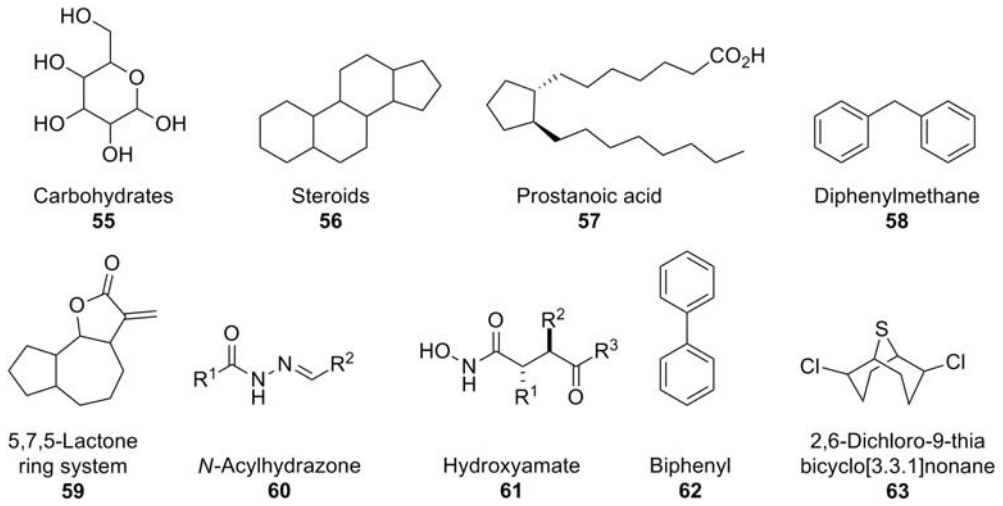

Fig. 12 Miscellaneous privileged structures **55–63**.

themselves but through SAR work, therapeutically relevant inhibitors can be derived. Abou-Gharbia and colleagues have also investigated the 2-aminothiazole scaffold[87] as methicillin-resistant Staphylococcus aureus (MRSA) antimicrobials.

2.05.2.1.5.2 Bispidines, tetralones, diphenyls, and related scaffolds

Haridas and coworkers[88] searched for new compounds to inhibit Japanese encephalitis virus (JEV) and the related West Nile virus (Fig. 13). Using the backbone of the natural product, sparteine, as a privileged scaffold template that mimics protein secondary structure, they identified and synthesized a collection of 3,7-diazabicyclo[3.3.1]nonanes based on the naturally occurring lupin alkaloid, sparteine, or more commonly known as bispidine analogs **65** that showed antiviral effects. These bispidine derivatives are rigid structures with a hydrophobic surface area that orients the R groups in defined geometries, ideal for mimicking protein–protein interactions. In particular, the decoration of the core structure with hydrophobic amino acids, such as tryptophan, showed a 100-fold improvement in inhibition of JEV infection in neuroblastoma cells at a concentration of 5 mM. The location of viral inhibition was postulated to be at the RNA replication stage, post-entry, and prior to protein translation. The same privileged scaffold demonstrated inhibition of similar viruses, West Nile virus and Chandipura virus, in the same concentration range.

Carro and coworkers[89] synthesized and evaluated a series of aminoalkyl-tetralones and tetralols as dual dopamine/serotonin ligands. The privileged molecules were evaluated to obtain their binding affinities for the 5-HT_{2A} and D_2 receptors (D_2Rs), with the goal of determining how the substitution pattern of the aromatic ring affects selectivity and affinity for these important targets for antischizophrenia drug development. Competitive antagonists with $pK_i > 8.3$ were obtained for 5-HT_{2A} and D_2 and may serve as a promising approach to developing dual inhibitors using a privileged structure approach.

Endo and coworkers[90] have developed SAR around the privileged diphenylamine scaffold as ER antagonists. The diphenylamine skeleton was selected as an improvement over the previously used diphenylmethane scaffold (another privileged moiety). Furthermore, incorporating basic alkylamino side chains on one of the phenyl groups was used to probe the ER antagonist effect. Cyclic alkylamine-containing derivatives were more potent ER antagonists in the MCF-7 cell proliferation assay. Indeed, the most potent antiestrogenic activity ($IC_{50} = 130$ nM) is more potent than tamoxifen.

Zhang and coworkers[91] have reported the synthesis of privileged pyrazole-based structures using a divergent cascade method. These enantio-enriched pyrazoles were in turn derived from easily accessible chiral pyrazole tetrahydropyran acetals. From these pluripotent acetals, a variety of reactions can be performed including Michael–aldol, reduction, lactonization, α-hydroxylation–acetalization–oxidation, Wittig–aldol, and Wittig–oxa-Michael synthetic cascades. From six simple starting materials, five molecular scaffolds could be accessed. Representative examples were screened and revealed potent anticancer activities.

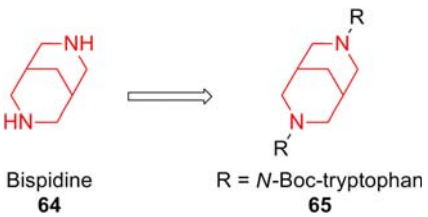

Fig. 13 Bispidine **64**-inspired privileged Japanese encephalitis virus inhibitor **65**.

2.05.2.1.5.3 Peptide and peptidomimetics

Assimon and coworkers[92] were inspired by the promising antibiotic properties of the natural product spergualin that is a privileged scaffold (amino acid-based). However, it is difficult to synthesize, and this had limited analog synthesis in an attempt to find compounds with broad-spectrum antibiotic activity. Using the recurring Ugi multicomponent reaction (MCR) (a privileged reaction), spergualin-inspired analogs were rapidly assembled. Testing the 43 novel compounds prepared in four Gram-negative and two Gram-positive strains revealed the most potent analog to have a MIC of 4–32 μg mL^{-1} against the six strains, which is comparable to spergualin (Minimum inhibitory concentration (MIC) 6.25–50 μg mL^{-1}).

Neubauer and coworkers[93] have investigated the selective targeting of the αvβ3 integrin subtype without targeting the structurally similar receptor α5β1 using a peptidomimetic approach. Peptidomimetic approaches may incorporate privileged heterocycles, but peptides themselves may also be viewed as privileged units. They report Arg-Gly-Asp (RGD) peptidomimetics for αvβ3 integrin with selectivity against α5β1. The incorporation of a privileged methoxypyridine unit into the peptidomimetic scaffold led to subnanomolar αvβ3-antagonistic activity. Docking studies helped elucidate the binding mode, and this privileged approach coupled with remarkable affinity and selectivity may help in the identification of personalized integrin-based medicines. Diederich and coworkers[94] have used the privileged structure C_2-symmetrical 3,4-disubstituted pyrrolidines as nonpeptidic human T-cell leukemia virus 1 protease (HTLV-1 PR) inhibitors, which may be a new avenue to explore HTLV-1. The scaffold selected had previously been designed and evaluated to inhibit the related HIV-1 protease, and therefore, it was logical to explore the related protease. This privileged scaffold exhibited nanomolar affinity and may be one of the most potent nonpeptidic inhibitors of HTLV-1 PR reported. X-ray data gave further insight into this small-molecule mode of interaction. Vilaivan[95] has reviewed using pyrrolidinyl peptide nucleic acid (PNA) with an α/β-dipeptide backbone, among others, as a possible new privileged avenue for the design of oligonucleotide mimics.

2.05.2.1.5.4 Steroidal scaffolds

Blanco-Ania and coworkers[96] have reported an unusual pressure-facilitated extension of the privileged steroid scaffold. Mohamed and coworkers[97] have utilized a Cu(I)-catalyzed alkyne–azide 1,3-dipolar cycloaddition reaction to synthesize privileged 17a-[1-(substituted phenyl)-1,2,3-triazol-4-yl]-19-nortestosterone-17b-yl acetates. These steroidal analogs were investigated for progestational and antiproliferative activities. Synthetic steroidal agonist can be optimized for progestational potency by placing large chemical moieties at the 17a-position of the steroid scaffold. Several analogs showed low nanomolar modification to the rat uterus using histopathologic endpoints. At up to 40 mg kg^{-1} dosage, the tested compounds were nontoxic. From an anticancer perspective, the privileged steroidal analogs showed 46–57% growth inhibition in the central nervous system (CNS) cancer SNB-75, renal cancer A498, and prostate cancer PC-3 cell lines mediated by cell cycle arrest.

2.05.2.1.5.5 Epoxy compounds

Tan and coworkers[98] have investigated the antibacterial activity of a range of epoxypyrrolidinones prepared by epoxidation of carboxamide-activated bicyclic lactams against *S. aureus* and *E. coli*. These scaffolds may be viewed as mimics of the natural products pramanicin and epolactaene. Lin and Tan have written an excellent review on the cross kingdom action of phytohormones,[99] naturally occurring molecules (such as the gibberellins, salicylic, and jasmonic acids) that act as a functional privileged scaffold. These molecules show a variety of bioactivities such as antitumour, antiviral, and immunomodulatory activity that justify their title as privileged scaffolds. Although phytohormones are outside the scope of this work, there may be many more complex, natural, privileged structures yet to be discovered and investigated.

2.05.2.1.6 Arylated piperidine/piperazine ring systems

We next consider the single unsaturated six-membered nitrogen-containing heterocycles joined to an aromatic ring system (**Fig. 14**).

Rutjes and coworkers have extensively reviewed the synthetic approaches to the 3-hydroxypiperidine privileged scaffold[100] that is prevalent in bioactive natural products. Kim and coworkers[101] have developed an efficient synthesis of 140 diversity-driven tetrasubstituted Δ^5-2-oxopiperazine privileged structures that mimics the β-turn structural motif of proteins without the loss of stereochemical purity using a fluorous tag approach. The claim that these privileged scaffolds mimicked β-turns was demonstrated via an in silico study that involved conformational overlapping with β-turns and distance measurements.

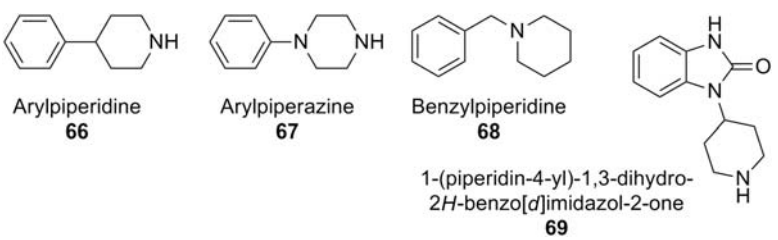

Fig. 14 Piperidine/piperazine ring systems linked to an aryl core **66**–**69**.

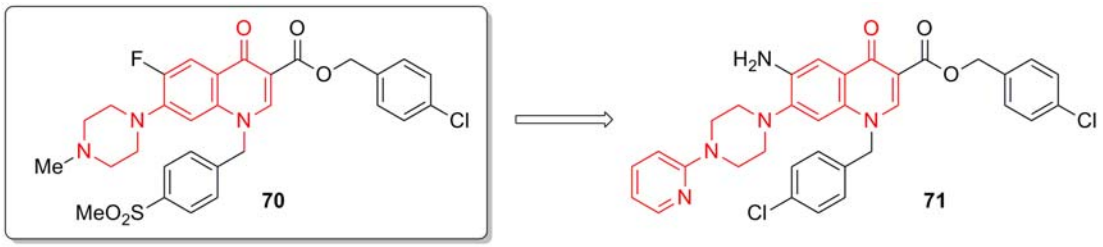

Fig. 15 The 6-aminoquinolone scaffold **70–71**.

Manfroni and coworkers[48] used their previously reported 6-aminoquinolone privileged scaffold **70** to prepare new antibacterial and antiviral agents (Fig. 15). In particular, they demonstrated inhibition of NS5B polymerase as a potential new therapeutic intervention for HCV. The most potent compound **71** prepared demonstrated inhibition of NS5B polymerase ($IC_{50} = 6.9$ nM), a selective antiviral effect ($EC_{50} = 3.03$ μM), and no cytostatic effect up to $CC_{50} > 163$ μM in Huh 9–13 cells by MTS assay. Key to the success was the early introduction of a further privileged motif at the C7 position, an arylpiperazine motif. The synthesis began with an acrylate that was reacted with 4-chlorobenzylamine, followed by base-mediated thermal S_NAr to form the core 6-aminoquinolone scaffold. Acid-mediated hydrolysis of the ethyl ester under microwave irradiation afforded the carboxylic acid to install the 4-chlorobenzyl ester. Finally, an S_NAr reaction with pyridyl piperazine followed by reduction revealed the amino functionality in the active compound.

Meng and coworkers[102] developed novel CB_1 receptor modulatory agents, using a privileged structure-based approach derived from the benzhydryl piperazine scaffold, as a strategy to investigate the control obesity. Structural modification to the original four hit compounds led to a lead series by iterative fragment A, B, C, and D SAR studies. In particular, compound **21** (shown in Fig. 6) had a >2000-fold selectivity profile for hCB_1 ($K_i = 0.15$ nM (hCB_1) versus 329 nM (hCB_2)). In diet-induced obese Sprague–Dawley rats, **5** was shown to reduce body weight for the first time for this scaffold.

Capuano and coworkers[103] investigated a privileged structure approach to dopamine D_2R ligands as an approach to the potentially therapeutically valuable biased agonism of GPCRs as antipsychotics (Fig. 16). By using three distinct privileged structures and varying changes to the linker and heterocycle cores, the relative activity and selectivity as a D_2R ligand were probed. Privileged structure-containing compounds prepared were profiled for biased agonism at the D_2R in Cyclic adenosine monophosphate (cAMP) and pERK1/2 signaling assays. It was found that substitution of the phenylpiperazine privileged structures affected agonism bias when the thienopyridine was removed. However, addition of the thienopyridine overruled the effect of phenylpiperazine substitution. This was rationalized by the proposed extended-binding mode present for this compound with the second heterocycle (thienopyridine) interacting with a secondary binding pocket. This is an unusual case where one privileged structure can overrule another privileged structure. **72** is the first example of a selection rule for an inhibitor containing multiple privileged structures.

The linker between the privileged structures (phenylpiperazine and thienopyridine) was another determinant of affinity. In particular, linker length (3–5 carbon atoms) gave rise to partial agonism at the D_2R. It was proposed that compounds containing one heterocycle plus the linker bind to the D_2R in a different orientation to the larger multipocket binding structure. It was found that simple substitution around the privileged heterocycle terminal groups led to similar affinity of D_2R ligands, as in aripiprazole, but has dramatically different bias profiles.

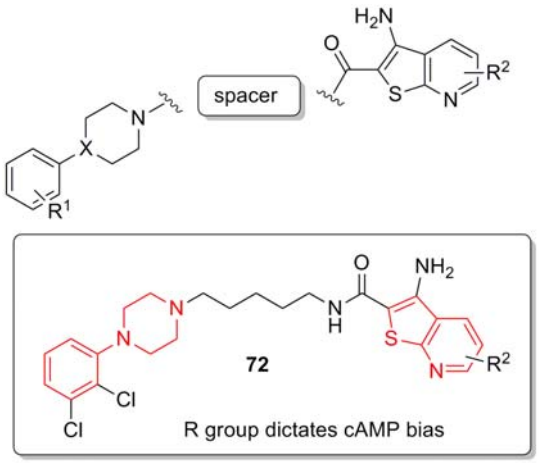

Fig. 16 A privileged approach to D_2R ligands.

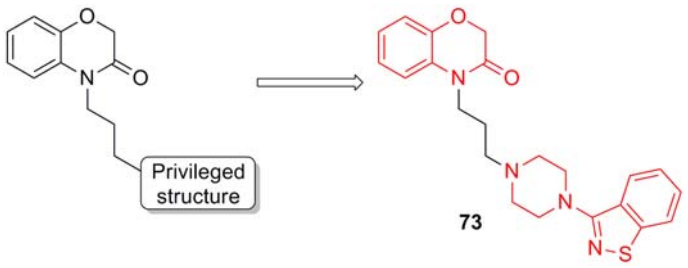

Fig. 17 A privileged structure approach to new antipsychotics.

Capuano and coworkers[104] have also recently shown that SB269652 interacts with one protomer of the dopamine D_2R and, via a dual mode of action, allosterically inhibits the binding of dopamine at the other protomer. To probe the structural cause of this allosteric action, various head groups were exchanged. For instance, the tetrahydroisoquinoline head group could be replaced with other D^2R "privileged structures" to generate orthosteric antagonists. Another privileged element, the indole NH, acting as a hydrogen-bond donor, was found to be crucial to maintaining the allosteric interaction. However, other related privileged structures such as the azaindole conferred a 30-fold increase in affinity while maintaining negative cooperativity. These privileged structure replacements were found to provide new SAR data on a class of bitopic ligands that are negative allosteric modulators of the D_2R.

Szabo and coworkers[105] used privileged structures found in clinically prescribed antipsychotics to develop new ligands (Fig. 17). Interaction with multiple targets is a useful drug design approach to treat the variety of symptoms of schizophrenia. For instance, the M_1AChR is a useful target for cognitive issues prevalent in many CNS disorders, and D_2 and 5-HT_{2A} receptors are useful targets to engage antipsychotic activity. A hybridization strategy of an M_1 scaffold (benzoxazinone) and a D_2 scaffold (substituted piperazine) was employed. Using this approach of hybridizing two known but separately engaging privileged structures, **73** was prepared that not only retained activity against M_1AChR and D_2R but also engaged 5-$HT_{2A}R$. This approach of "designing in" multiple pharmacologies is a new and enabling approach that is reliant on the privileged structures and their inherent effects against the multiple targets selected.

Liu and coworkers[106] developed a new series of 4-benzoylpiperidine derivatives as regulators of glycine transporter 1 (GlyT1) activity, a potential strategy in the management of schizophrenia. Bioisosteric replacement of the pyridine ring in RG1678 and modification of the piperazine ring based on incorporating extra heteroatoms and the need to compensate for the loss of binding energy resulted in potent ($\sim IC_{50} = 30$ nM) examples. Furthermore, based on the privileged structure template coupled with rigidification of the terminal acyl phenol to a benzo[*d*]isoxazole resulted in blood–brain barrier penetrant examples, such as **22** (Fig. 6), with good selectivity for GlyT1 over GlyT2, $D_{1/2/3}$, and 5-$HT_{1A/2A}$ receptors. Crucially, the most potent examples were effective on the Phencyclidine (PCP) treated schizophrenia-like behavioral model at 40 mg kg^{-1}. A rationale for the relatively high dose is explained by the poor pharmacokinetics of the compound.

Spadoni and coworkers[107] have developed 5-HT_7 ligands by combining the privileged serotonin-like and arylpiperazine scaffolds. Although these molecules are supposed to bind to the same pocket on the receptor, Spadoni has postulated that these two molecules can bind to the same target but in different binding pockets. Using 5-hydroxyindol-3-ylethyl (or a bioisostere such as 3-hydroxyanilinoalkyl) and a 1-arylpiperazine moieties connected by a short linker, the prepared compounds were tested for their effects on the human 5-HT_7 serotonin receptor. Examples of potent antagonist ligands of the 5-HT_7 receptor were uncovered but with limited selectivity. Molecular modeling studies showed that the 5-HT_7 receptor can accept both privileged scaffolds in the hybridized (or fragment-linked) mode. The serotonin-like scaffold exists in the orthosteric site, and the arylpiperazine exists in an accessory pocket. This work demonstrates that it may be possible to develop new 5-HT_7 ligands by merging multiple privileged structures into a larger hybrid molecule.

Liu and coworkers[108] adopted the strategy of privileged fragment hybridization to prepare a novel collection of 4-aminopiperidinyl-linked 3,5-disubstituted-1,2-6-thiadiazine-1,1-dione analogs. These compounds were evaluated in vitro for anti-HIV activity in MT-4 cells, and although only weak inhibition was observed against wild-type HIV1, a mode of action was determined using the HIV-1 RT inhibitory assay with micromolar activity.

2.05.2.1.7 Benzodiazepine and related seven-membered ring systems

A commonly encountered privileged scaffold is the seven-membered ring system, usually fused to cyclic ring systems, represented by the benzodiazepine class.

For a recent review of the biological significance of the 1,4-benzodiazepine scaffold, see[109] Fig. 18. Benzothiazepines[110] are another class of privileged structure that have reported bioactivities as antimicrobials, antifungals, Ca^{2+} antagonists, and CNS depressant, among others. The reader is directed to this review for a comprehensive evaluation of synthetic routes to this core scaffold. Lee and coworkers[111] were inspired by the first examples of "privileged structures," namely, 1,4-benzodiazepin-2-ones, which show a wide range of binding affinities to multiple drug targets. Analysis of the benzodiazepine core shows they conformationally mimic beta turns. Using the same strategy of attempting to mimic beta turns, the pyrazolodiazepine scaffold is advocated as a new

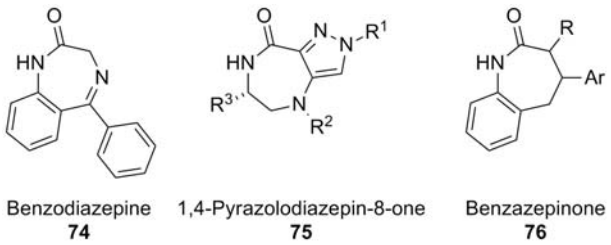

Fig. 18 Examples of the seven-membered privileged scaffolds **74–76**.

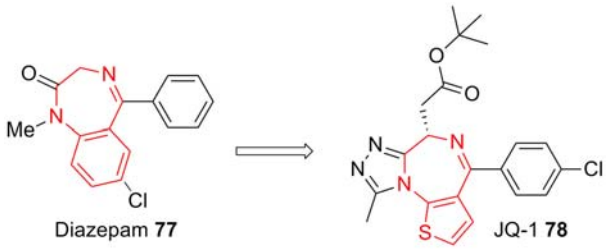

Fig. 19 Bromodomain inhibitors inspired by the privileged diazepam core.

privileged structure. One hundred and forty six examples of tetrahydro-1,4-pyrazolodiazepin-8(2*H*)-ones, such as **23** (Fig. 6), were prepared with three decoration points. Assessment of their bioactivity was through $P2X_7R$, BACE-1, and MC4R targets. It was found that examples from the collection showed activity against these targets based on the functional group decoration. Therefore, based on the conformation displayed, a variety of new and differing bioactivities were discovered derived from a privileged template.

Smith, Sanchez, and Zhou[112] have recently reviewed new applications of the privileged diazepine structure as bromodomain inhibitors. JQ-1 (**78**), for instance, (Fig. 19) based on a pseudodiazepam core is a potent inhibitor of acetyllysine binding activity and an important target for the gene transcriptional activity in inflammation and cancer, demonstrating new uses in the epigenetic age for the privileged structure methodology. In particular, an excellent commentary on the unique topological features of diazepine, which make it a versatile scaffold in drug discovery and chemical biology, is detailed, and the reader is directed to this article for further information outside the scope of this article. Medina-Franco and coworkers[113] have updated the chemoinformatics world with a take on the chemical space that is relevant to epigenetics, in particular, DNA methyltransferase (DNMTs) inhibition. DNA methylation is regulated on the epigenetics level by proteins, termed DNMTs. In turn, the covalent modification of DNA by the addition of a methyl group, if misregulated, is common in cancer and other diseases. Medina-Franco et al. have curated the blossoming collection of known inhibitors and revealed the structural diversity and chemical space coverage of this emerging field, showing the presence of privileged scaffolds within this new branch of chemical biology and drug discovery.

Galli and coworkers[114] have also exploited the privileged features of the 1,4-benzodiazepin-2-one core to prepare a novel class of *cis*-locked combretastatins (Fig. 20) that show similar cytotoxic and antitubulin activity in neuroblastoma cells compared with the natural product it is derived from, combretastatin A-4 (CA-4), together with an improved pharmacokinetic profile. CA-4 was in clinical trials; however, concerns relating to isomerism, half-life, and metabolism prompted the current research into conformationally

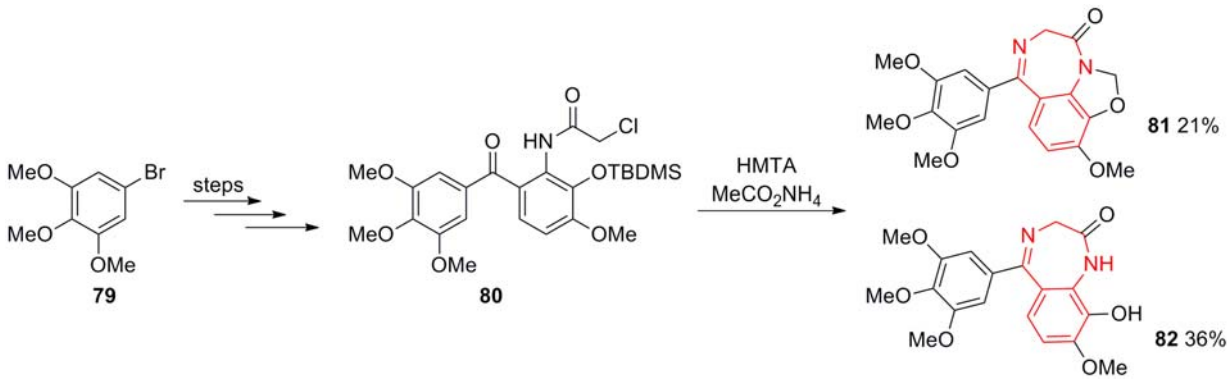

Fig. 20 A synthetic route to privileged *cis*-locked benzophenones **81–82** inspired by the combretastatin class.

locked analogs, which also contain a new privileged element. Compound **82** had a longer half-life than CA-4 in human liver microsomes (HLMs). It was found that the introduction of the 1,4-benzodiazepin-2-one not only retained activity but also prevented double-bond isomerization, O-demethylation, and aromatic hydroxylation metabolic pathways. Taken together, this privileged motif via the prevention of these pathways also mitigated the formation of glutathione conjugates, a previous disadvantage of CA-4.

The combretabenzodiazepine scaffold was prepared in five synthetic steps from the reaction of a 2-nitrobenzaldehyde (with *tert*-butyl dimethylsilane (TBDMS) protection of the phenolic oxygen) with an in situ prepared trimethoxyphenyl Grignard reagent in a 61% yield. Pyridinium dichromate (PDC) mediated oxidation of the newly formed racemic secondary alcohol afforded the diphenylketone scaffold (84%). Reduction of the ortho-nitro group with hydrogen over palladium on carbon smoothly afforded the ortho-amine functionality (78%). Treatment of the newly formed amine with 2-chloroacylchloride afforded the amide in 76% yield. Finally, treatment with ammonium acetate and hexamethylenetetramine (HMTA) mediated the formation of the imine and completed the ring closure with concomitant TBDMS group deprotection in a 36% yield. Intriguingly, it was also found that 6,7,5-ring system **81** was formed in a 21% yield, presumably from thermal decomposition of HMTA to yield formaldehyde to react with the OH and NH functionality. Viviano and colleagues[115] have developed a continuous flow process for synthesizing the privileged scaffold 1,4-benzodiazepin-5-one.

2.05.2.1.8 Single-cycle ring systems

Monocyclic scaffold can also possess privileged biological activity, often in combination with an extended network of ring decorations.

Palasz and Ciez[116] have reviewed the privileged scaffold uracil and related fused uracils from both a synthetic and biological activity viewpoint. Uracils (Fig. 21) are privileged motifs, with a panoply of bioactivities including antiviral and antitumor, herbicidal, insecticidal, and bactericidal properties. Ruvo and colleagues[117] note that 1,2,3 triazoles are privileged pharmacophores for inhibition of specific serine proteases, in particular the Acylamino-acid-releasing enzyme (APEH) enzyme inhibitor, opening a new therapeutic avenue.

Bai and coworkers[118] have used a privileged phenyltriazole core scaffold to prepare new inhibitors (such as **24**, shown in Fig. 6) of firefly luciferase. Firefly luciferase is one of the most widely applied and studied bioluminescent systems for the development of small-molecule probes through to imaging techniques. These compounds showed comparable activity to the widely studied inhibitor resveratrol but intriguingly were found to exhibit a novel inhibition mechanism based on kinetic studies. Kinetic studies showed a mixed noncompetitive response for the substrate amino-luciferin and were ATP-noncompetitive.

Hoyt and coworkers[119] discovered during a hit-to-lead campaign, a privileged structure-containing molecule, **25** (see Fig. 6) as a potent CYP11B2 inhibitor possessing selectivity over related cytochrome P450s (CYPs). Inhibition of CYP11B2, also known as aldosterone synthase, is validated in the clinic to lower blood pressure for treating hypertension. Coupled with good pharmacokinetics in rat and rhesus monkeys and lead-like properties, the privileged structure triazole-containing **25** has been considered for further drug development.

Cantley and coworkers[120] screened 9517 compounds (Fig. 22), pre-selected for their lead-like properties from a larger subset of 3,372,615 compounds against a dexamethasone-resistant T-cell acute lymphoblastic leukemia (T-ALL). One of the more potent examples found was the privileged structure-containing **90**; further SARs were determined leading to **91** and **92**. These compounds restored sensitivity to the current treatment, glucocorticoids, through upregulation of the self-named receptor. Further mechanistic experiments demonstrated the dependence on the expression of glucocorticoid receptor.

Terracciano and coworkers[121] have used structure-based techniques from the crystal structure of prostaglandin E_2 synthase 1 (mPGES-1) in complex with a known ligand to optimize the dihydropyrimidin-2-one, a privileged structure-containing scaffold.

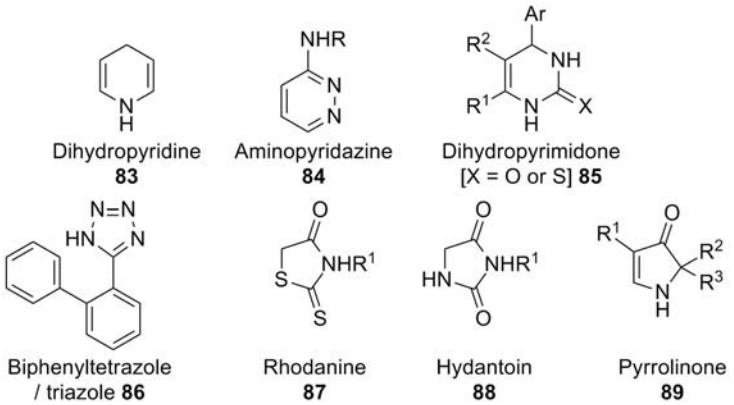

Fig. 21 Examples of the monocyclic scaffolds considered in this section **83–89**.

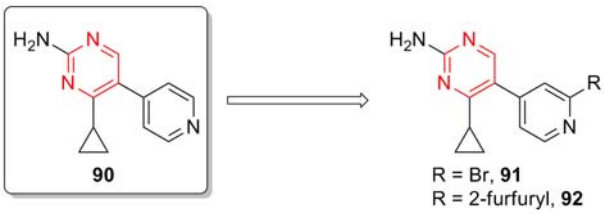

Fig. 22 Privileged hit and potent analogs for T-cell acute lymphoblastic leukemia.

A 10-fold improvement in mPGES-1 IC_{50} was obtained. Computational modeling suggested further dihydropyrimidine privileged scaffolds that may interact with mPGES-1.

Wermuth has recommended the pyridazine[122] scaffold as a possible new contender for a privileged structure due to their affinity to a variety of receptor proteins. From a physicochemical perspective, changing a phenyl ring to a pyridazine ring results in a two-logarithmic unit decrease in lipophilicity and concomitant increase in aqueous solubility, among other, changes in overall absorption, distribution, metabolism, and excretion (ADME) and toxicity improvements.

Gerona-Navarro and coworkers[123] have investigated a solid-phase synthesis of a library of amphipathic hydantoins. Hydantoins are another class of five-membered heterocycles that can be considered privileged due to the panoply of bioactivities associated with them, for example, antituberculosis and antiproliferative effects, among others. The library design consisted of attaching a privileged hydantoin molecule to a biologically diverse functional group, in this case guanidine-containing molecules. The library was prepared using parallel solid-phase synthesis upon an orthogonally protected Lys–Lys skeleton attached to the resin. The key synthetic step upon the Lys–Lys skeleton was the construction of the central hydantoin ring, which was accomplished via reaction of the terminal amino group with *N,N*-disuccinimidyl carbonate, and then, under basic conditions, the cyclization was completed. Removal of the alloc protecting group allowed the attachment of the guanidine-containing functional group to the C-terminal Lys side chain. In total, 112 amphipathic hydantoins were prepared from eight diverse guanidine functional groups and 14 different acyl terminal groups for the amino hydantoin alkyl linker. Screening of this library resulted in the discovery of novel TRPV1 ion channel blockers, in particular through blockage of capsaicin-induced Ca^{2+} influx. Particularly active hydantoins contained highly lipophilic fatty-type acyl substituents and substituted guanidines on the C-terminal chain. The thio-analogs of hydantoin, rhodanine, and related scaffolds pose a unique question of the privileged structure approach, which is worthy of further discussion in Section "**Single-cycle ring systems**."

2.05.2.1.9 Rhodanines (and related) as a special class of potentially privileged scaffolds

Mendgen and coworkers[124] have posed the following question regarding the rhodanine (and related) scaffold: *privileged structure or promiscuous binders?* Rhodanines are historically regarded as promiscuous binders by medicinal chemists. To probe whether the intuition of medicinal chemists toward this chemotype was indeed valid, a total of 163 rhodanines, hydantoins, thiohydantoins, and thiazolidinediones were tested against multiple biological targets in a focused and controlled campaign. Their behavior, including electrophilic reactivity and aggregation ability, was probed. A further comparison with binding mode behavior from published crystallography studies of these rhodanine-like structures was evaluated. Although promiscuous behavior can be identified at "screening concentration" levels, it is not sufficiently serious as to merit exclusion as a general criteria. It was found that the exocyclic double-bonded sulfur atom in some rhodanine-like structures is a critically important, high-density, binding site for both polar interactions and hydrogen bonding to the biological target. Intriguingly, the Michael acceptor capacity of the exocyclic alkene was found to be insignificant, and only 2 out of 163 examples demonstrated potential aggregation problems through particle size measurement (dynamic light scattering). The α-carbon attachment decoration proved key to selectivity of the rhodanine-like structures and limiting promiscuous effects.

As with any concept, there are limitations and rule breakers, for instance, examples of promiscuous inhibitors.[125–132] The rhodanine class, which meets some requirements of being privileged (showing activity in multiple assays) yet as often as they are shown to be a true hit, if proper precautions are not followed, turns out to aggregate and cause inhibition through less clear mechanisms. This warrants caution when interpreting biological results, leading to the policy of many academic and industrial labs to treat rhodanines as "guilty, until proved innocent" with regard to their promiscuous behavior.

Ge and coworkers[125] have reported the use of a catechol–rhodanine privileged scaffold for target and antitarget fishing experiments for NAD(P)(H) dehydrogenase-binding proteins. Using this chemical proteomics-based drug design strategy, they have reversed the common lead drug design strategy and identified NAD(P)(H)-binding proteins using privileged scaffolds to discover potential targets in *M. tuberculosis* and/or antitargets in the human liver.

Similarly, the thiazolidinedione-based drugs, rosiglitazone and pioglitazone, have been investigated by Hoffmann and coworkers[126] using a chemical proteomics approach to assess potential cardiotoxicity issues. Both drugs contain a common glitazone privileged core scaffold and, via a suitable linker, are attached to a resin. Although peroxisome proliferator-activated receptor γ (PPARγ) inhibition is well known with these drugs, they were further investigated to determine off-target binding events in the rat heart to rationalize reported cardiovascular risk factors associated with the drug molecules. Their results suggest that the glitazone

privileged scaffold has affinity for dehydrogenases, ion channels (such as voltage-dependent L-type calcium channels), and modulators.

Martinez and coworkers[127] have explored the SAR and 3-D-QSAR of a collection of thiadiazolidinone derivatives, with a view to identifying the structural features necessary for glycogen synthase kinase 3 (GSK-3) inhibition. In particular, the 2,4-substituted thiadiazolidinones were found to be the first ATP-noncompetitive GSK-3 inhibitors. Through a study of individual changes in the thiadiazolidinone heterocyclic ring, a molecular interaction network was identified with the approximate contribution of each heteroatom in the densely functionalized five-membered privileged ring system. Comparison with other five-membered heterocycles such as hydantoins, dithiazolidindiones, rhodanines, maleimides, and triazoles suggested the thiadiazolidinone core to be privileged for GSK-3 inhibition. Mapping studies have shown that the thiadiazolidinone core has two different binding modes with GSK-3, suggesting possible mechanistic differences in the GSK-3 inhibitory activity, for follow-up studies.

Raghubir and coworkers[128] have reinvestigated the thiazolidin-4-one privileged scaffold as a replacement for the alternative privileged thiazolidine-2,4-dione scaffold found in PPARγ agonists such as pioglitazone and rosiglitazone for neuroprotective effects in cerebral ischemia/reperfusion injury. Three of the 20 novel thiazolidin-4-one analogs of the generic glitazone scaffold were found to have significantly improved neuroprotection compared with rosiglitazone at the same dose, enhancing GLT-1 glutamate uptake and showing a 6 h postdose curative effect.

Zhou and coworkers[132] have designed and synthesized privileged 2-thioxo-4-thiazolidinone derivatives as PPAR-gamma-binding modulators. Two compounds were found to potently interact with peroxisome proliferator-activated receptor g (PPARg) with K_i values of between 12.15 and 14.46 nmol L^{-1}. SARs obtained with these privileged scaffolds were molecularly mapped on to the approved drug rosiglitazone (a PPARγ ligand-binding domain) to design new analogs and demonstrate the privileged scaffold approach.

If we look to the patent literature, we can find further examples of the employment of a privileged structure approach. Using a privileged structure as the starting hit, in a hit-to-lead campaign, a class of rhodanine-containing compounds (including **26**) was prepared by the Russell group at the University of Oxford.[133] These compounds displayed therapeutically relevant inhibition of proviral integration site for the Moloney murine leukemia virus kinase.

Zhao and coworkers[134] used a fragment-based drug discovery approach to the identification and optimization of a novel class of privileged 2-thiazolidinones as BET bromodomain, BRD4, inhibitors (**Fig. 23**). Several bromodomain inhibitors are potent anticancer agents, and some have reached clinical trials. Bromodomains act as a recognition site for signal transduction of acetylated lysines on the histone tail. The fragment-based approach adopted by the group was informed by crystal structure analysis, in particular the reversing of the direction of a sulfonamide group, which in turn led to the identification of a new binding mode. The most potent BRD4 inhibitors prepared had an $IC_{50} = 50–100$ nM measured via a fluorescence polarization assay and a $GI_{50} = 100–300$ nM in a cellular environment. Interrogation of the downstream c-Myc protein of BRD4 with the scaffold, alongside stability assays, reaffirmed the lead-like properties of this privileged fragment-derived series.

2.05.2.1.10 Spirocyclic structures

The reader is directed to this article for further background in this area (**Fig. 24**). The spirocyclic scaffold is an example of a 3-D-enriched scaffold, which can often exhibit privileged biological activity.

The privileged spirooxindole ring system was used as inspiration for a DOS library by the research groups of Zhang and Shi.[135] The 1,3-dipolar cycloaddition reaction between a range of electron-deficient alkynes and isatin-derived azomethine ylides afforded 36 spirooxindole-based 2,5-dihydropyrrole compounds in good to excellent yield (**Fig. 25**). Several compounds exhibited modest cytotoxic effects in vitro in MCF-7 cells (up to 28% inhibition at 100 μg mL^{-1}). The possible mechanism of the cytotoxicity of this compound was investigated using Hoechst 33 324 staining to determine whether the cytotoxic effects were related to cell apoptosis. A dose-dependent response was found by flow cytometry studies indicating that the observed cytotoxicity was due to cell apoptosis. To elucidate the mechanism of apoptosis, the levels of the signaling kinases ERK1/2, p38, and JNK and their respective phosphorylation states were measured. Levels of p38 and pJNK increased after 30 min, followed by pERK1/2 after 1 h, and remained high for 8 h post-treatment. Separate pretreatment of MCF-7 cells with a MEK1, an ERK1/2, or a c-Jun *N*-terminal kinase (JNK) inhibitor, respectively, did not affect the apoptotic response, and it was concluded that compound **101** acted on MCF-7 cells through the Mitogen-activated protein kinase (MAPK) pathway.

Mercurio and coworkers[136] have developed potent histone deacetylase (HDAC) inhibitors as anticancer probes using privileged spirochromanes as the key scaffold. In particular, using molecular modeling and biological evaluation feedback loops, their

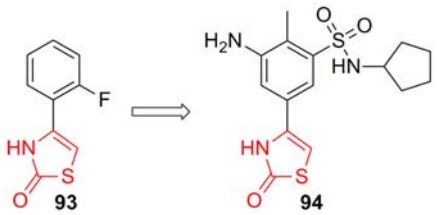

Fig. 23 Novel bromodomain inhibitors incorporating a privileged fragment.

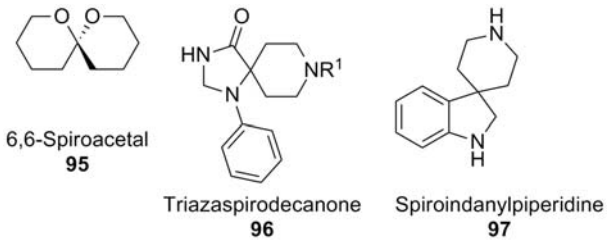

Fig. 24 Examples of spirocyclic structures considered in this section **95–97**.

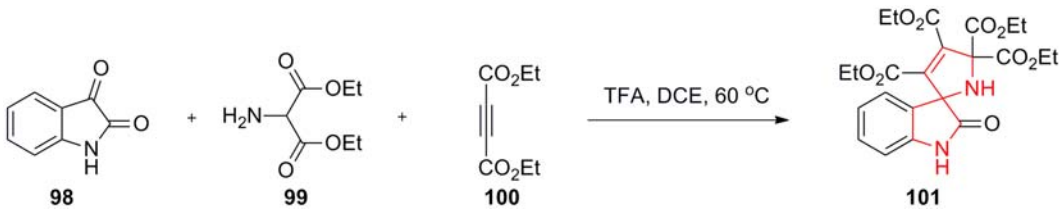

Fig. 25 A three-component reaction to a 2,5-dihydropyrrole spirooxindole-based library.

previously reported spiro[chromane-2,4′-piperidine]hydroxamic acid analogs were optimized via replacement of the piperidine ring with a range of cycloamines. These changes were made in the attempt to retain the potency of the privileged scaffold while improving the ADME profile.

He and coworkers[137] have reported SAR around a class of spiroindane *N*-methyl-1,2,4-triazole privileged structures as melanocortin transmembrane G-protein-coupled receptor subtype 4 (MC4R) agonists for the treatment of obesity. This privileged class of compounds showed subnanomolar *h*MC45 IC_{50} and in early experiments showed antiobesity efficacy in a mouse model; however, this was not reported to be solely due to the MC4R pathway. Further SAR studies revealed that it was possible to design a privileged scaffold that is both effective for in vitro inhibition of MC4R and obtain an MC4R-dependent mode of antiobesity efficacy in a mouse model. Lavieri and coworkers[138] have also reported the use of the 1,3-triazaspiro[4,5]decan-4-one privileged scaffold for isoform-2-selective phospholipase D inhibition.

2.05.3 Privileged Scaffolds to Identify Biologically Active Compounds Through Building Chemical Libraries

2.05.3.1 Natural Product-Inspired Chemical Synthesis

Natural products, often containing evolutionarily conserved privileged elements, can serve as inspiration for new chemical synthesis.

2.05.3.1.1 Benzimidazolinopiperazinones

Ventosa-Andrés and coworkers[139] used a solid-phase-supported route to highly decorated 2,3,10,10a-tetrahydrobenzo[4,5]imidazo[1,2-*a*]pyrazin-4(1*H*)-ones (Fig. 26), possessing a privileged structure element, namely, a benzimidazolinopiperazinone. These elements were incorporated to act as a peptide backbone conformational restraint. Critical to the success of their route was the modularity of their approach, in particular the tandem *N*-acyl-*N*-aryliminium ion cyclization–nucleophilic addition reaction, which proceeded with complete stereointegrity and control of the newly formed stereocentre.

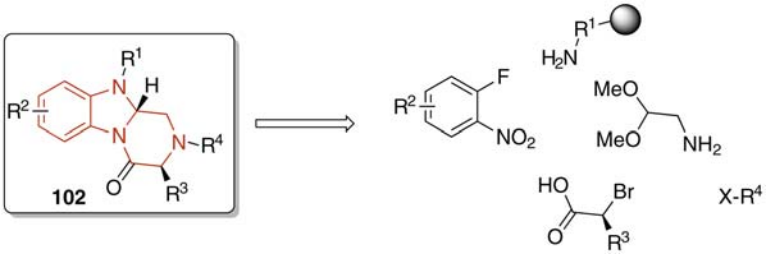

Fig. 26 Deconstruction of a highly decorated privileged structure.

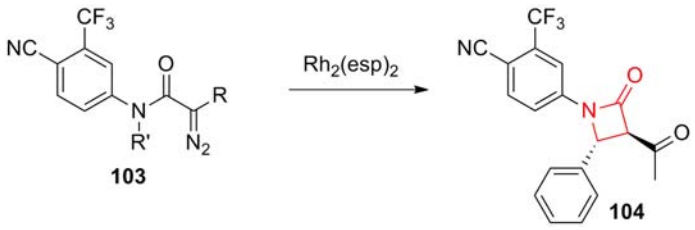

Fig. 27 Example of activity-directed synthesis.

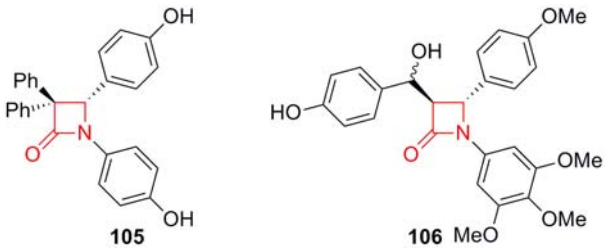

Fig. 28 The privileged β-lactam scaffold as an ER antagonist and tubulin-targeting compound.

2.05.3.1.2 β-Lactams

Karageorgis and coworkers[140] have reported an "activity-directed synthesis" discovery approach to the development of new biologically active small molecules (Fig. 27), in an analogous manner to evolutionary inspired biosynthetic pathways to natural products. As synthetic chemistry reactions have become more robust, medicinal chemistry has followed suit, utilizing these well-known reactions to prepare compounds that possibly are a smaller subset of the many molecular scaffolds that could be prepared. Methods such as DOS[15] and biology-inspired organic synthesis (BIOS) have expanded the collection of molecular scaffolds that have been tested for bioactivity, but there is still space for improvement. In the *activity-directed synthesis* approach advocated, bioactivity of the small-molecule product dictates the evolution of a synthetic strategy. In particular, substrates that could give rise to a wealth of alternative molecular scaffolds via modest changes to the catalyst and reaction conditions were used. After each round of array synthesis, the products formed were tested for androgen receptor agonism and showed dose dependency. Results obtained with round one of the array informed array two and so on, finally revealing after scale-up and purification biologically active ligands. In the current study, nanomolar ligands based on two templates with no previously reported activity androgen receptor were uncovered.

O'Boyle and coworkers[141] have reported a compound derived from the privileged β-lactam scaffold that is the first dual-targeting ER antagonist and tubulin depolymerization (Fig. 28). The majority of breast cancers express ER and treatment with a well-known ER antagonist; tamoxifen has contributed to a dramatic reduction in the lethality of this disease. Twelve analogs were prepared that decorated the core privileged scaffold derived from a Staudinger [2 + 2] cycloaddition to form the key β-lactam motif. In particular, compounds **105** and **106** showed the strongest binding affinity for the ERα form of ER ($IC_{50} = 40$ and 8 nM, respectively) and the ERβ form ($IC_{50} = 19$ and 15 nM, respectively). Compound **105** had the most potent antiproliferative effect in MCF-7 breast cancer cell assay. Of note, **105** led to the accumulation of cells in the G_2/M phase, which indicated mitotic blockade and depolymerization of tubulin in the MCF-7 cells. Compound **106** also induced apoptosis and downregulation of the expression of Bcl-2 and Mcl-1, prosurvival proteins. Despite other β-lactams being ER ligands, the unexpected and beneficial depolymerization of tubulin in MCF-7 cells can be attributed to a privileged starting point.

Waldmann and coworkers[142] have reviewed a powerful method for the construction of the privileged pyrrolidine scaffold, the 1,3-dipolar cycloaddition using azomethine ylides as the dipole. Due to the impressive regio- and stereocontrol, it has found uses in natural product synthesis and BIOS.

Collins and coworkers[143] used the natural product kinase inhibitor indirubin as their inspiration for the development of a lead-like kinase inhibitor screening library (Fig. 29). Using a parallel synthesis strategy, robust routes were developed to the 195 analogs prepared; these new compounds were designed to be consistent with guidelines for lead-like properties (many were also consistent with fragment-like guidelines). Members of their synthetic library consisted of 3-aminopyrazolopyridinones that mimicked the hydrogen-bond donor–acceptor motifs and the substitution vectors of indirubin. Indirubin itself contains the 6,5-ring system privileged scaffold, and the 3-aminopyrazolopyridinones synthesized possess an alternate heteroatom-rich 6,5-ring system with aryl substitution vectors; advantageously, this scaffold is >1000-fold more soluble than indirubin. The library was evaluated against a kinase screening collection, in particular diaryl-substituted compounds possessed submicromolar inhibition of tyrosine kinases with good levels of ligand efficiency. This result translated into the cellular environment and was confirmed via an antiproliferative assay in the MCF-7 breast cancer cell line ($GI_{50} = 40$–60 μM). *In silico* modeling was used to rationalize a probable binding mode to

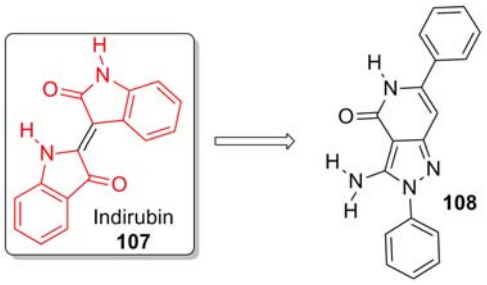

Fig. 29 Natural product-inspired privileged structure construction.

the kinase ATP active site. This research adds to the body of evidence that with careful consideration, natural product (privileged structure-containing)-inspired synthesis generates lead-like molecules with improved physicochemical properties and in this case, good levels of tyrosine kinase inhibition.

2.05.4 Natural Products as Lead Structures

2.05.4.1 Lead-Like Natural Products?

Pascolutti and Quinn have reviewed the concept of using natural products as lead structures.[144] In particular, they focus on controlling MW and the partition coefficient (log *P*) to generate natural product-like libraries that remain lead-like. Quinn and colleagues[145] have eloquently advanced the field of using natural products as drug-like screening candidates. From a survey of 126,140 unique natural products, 60% do not violate Lipinski's rule of five (Ro5), and through further data mining, a collection of 814 chemically diverse natural products with both drug-like and lead-like properties were determined. Similarly, Newman[146] has advocated the use of natural products or natural product-derived/inspired molecules as a source for the next generation of therapeutics. Kombarov and coworkers[147] have discovered an alternate systematic method to locate and describe the many variant of the privileged scaffolds through "BioCores." BioCores was developed through a detailed analysis of known drugs and natural products leading to the identification of privileged saturated and aromatic heterocyclic ring pairs. Medina-Franco and colleagues[148] have investigated a computer-aided discovery approach to natural products as DNMT inhibitors. Tao and coworkers[149] have defined natural product leads of drugs and, via molecular fingerprinting, clustered into discrete drug-productive groups. As a case example, Wezeman and colleagues[150] have reviewed the range of xanthone dimer-containing natural products that are both widespread in nature and, due to the range of reported bioactivities, privileged.

Balsera and coworkers[151] screened a library of natural products for in vitro activity against acetylcholine nicotine receptors (nAChRs) as possible starting points for the development of treatments for cognition disorders, schizophrenia, pain, and inflammation. In particular, their search for positive allosteric modulators of this target revealed privileged chalcone structure-containing molecules. The initial hit compound was isoliquiritigenin; a trihydroxy-substituted chalcone showed moderate positive allosteric modulation of nAChRs. Alteration of the hydroxylation pattern around the hit compound revealed SAR insights, leading to the synthesis of potent compound **110** (Fig. 30). Compound **110** demonstrated an $EC_{50} = 3.3$ mM. Coupled with no discernible cytotoxicity on human embryonic kidney (HEK) cells, primary hippocampal neurons, and no systemic effects on isolated rat organs, the privileged structure-containing **110** may be a viewed as a useful starting point for drug discovery approaches.

Foster and coworkers[152] took inspiration from the natural product canthaimide **111** (Fig. 31) to prepare a general synthesis of cantharimides. Using a [4 + 2] cycloaddition strategy of 3-alkoxyfurans with N-substituted maleimides provided an enabling *endo*-selective approach. The cantharimides prepared show promising lead-like properties for incorporation into medicinal chemistry approaches.

Rosini and coworkers[153] took inspiration from the natural product lipoic acid **115** (a privileged structure-containing natural antioxidant, Fig. 32) and a multiligand compound memoquin **116** and, via a hybridization strategy, prepared compound **117** as a multimodal compound to investigate Alzheimer's disease. Early work ruled out the need to develop a chiral synthesis of lipoic acid, and instead, racemic lipoic acid was coupled with known anticholinesterase agents, such as rivastigmine and memoquin.

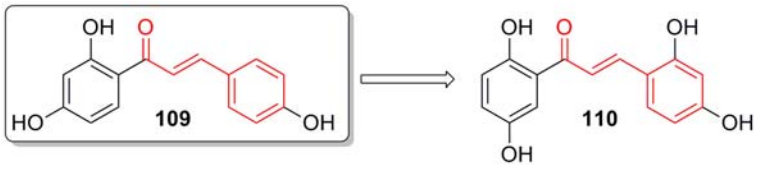

Fig. 30 Privileged natural product optimization.

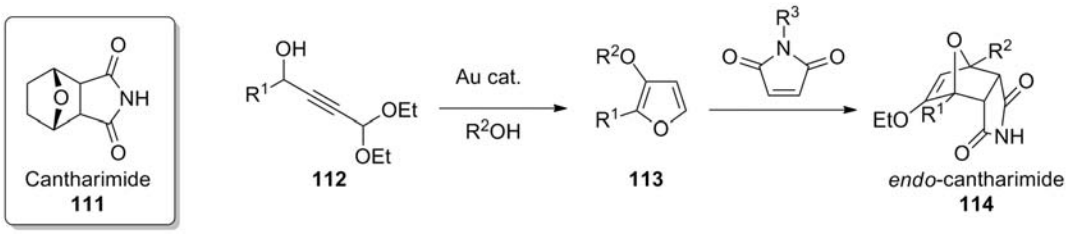

Fig. 31 Development of a lead-like synthesis of cantharimide derivatives.

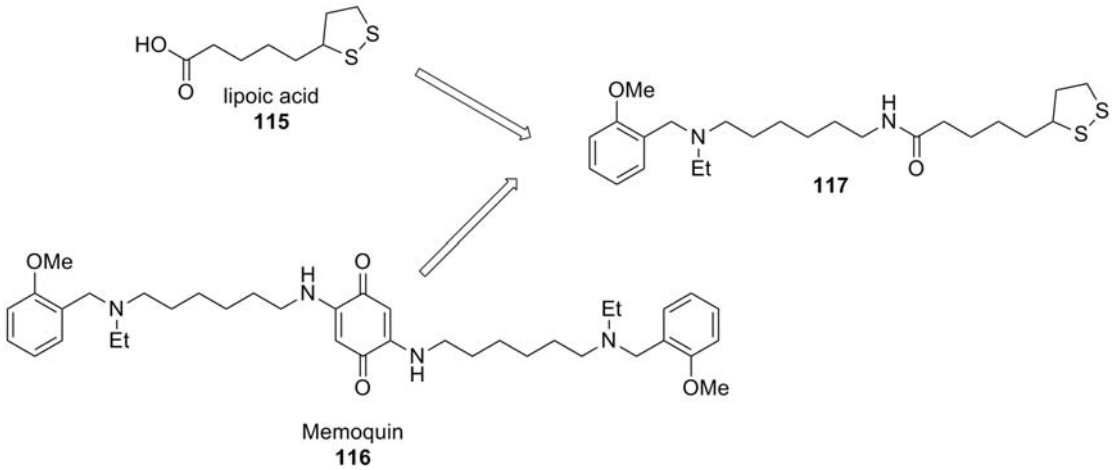

Fig. 32 Privileged multitarget-direct ligand from a hybridization strategy.

Compound **117** is an example of a multitarget-directed ligand (MTDL) that has balanced anticholinesterase and antioxidant capacities, coupled with limited cytotoxicity in neuronal-like cells (SH-SY5Y) at up to 50 mM concentration. This work has demonstrated the importance of using privileged structures to guide MTDL investigations.

Novaes and coworkers[154] investigated a natural product (−)-tarchonanthuslactone **118** (Fig. 33) that contains the privileged α,β-unsaturated lactone motif, but the bioactivity of which is unreported. Molecular simplification led to the synthesis of a collection of dihydropyran-2-ones derived from the natural product, using a strategy of Keck asymmetrical allylation as the key step. Evaluation of the compounds prepared in eight human tumor cell lines in vitro revealed the simplified compound (**119**) as the most cytotoxic and selective compound in six of the eight cancer cell lines analyzed. On one of the cancer cell lines, pancreatic cancer, apoptotic cell death occurs mediated by increased levels of reactive oxygen species. However, care needs to be taken due to the presence of both catechol and two Michael acceptor systems.

Porco and colleagues[155] have designed privileged β-lactone-containing compounds modeled on a natural product. These exhibited in vitro inhibition of the serine hydrolases ABHD10 and ACOT1/2 and the serine peptidases CTSA and SCPEP1, in PC3 cells. Camara and coworkers[156] have developed new privileged β-lactone-containing diverse scaffolds that target serine hydrolases combining aspects of activity-based protein profiling and the cross metathesis method. The β-lactone motif is a well-known scaffold in enzyme inhibitors and chemical probes.

Ononye and coworkers[157] took inspiration from a structurally modest family of natural products, thujaplicins (Fig. 34). In particular, beta-thujaplicin **120** contains a lead-like tropolone motif that is of low MW and has a multitude of diversification sites and of relevance to the intended metalloenzyme target, metal-binding functionality. The well-known anticancer drug target HDAC

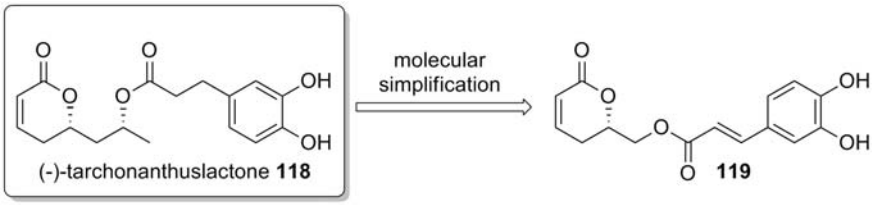

Fig. 33 Simplification as a route to privileged bioactive scaffolds.

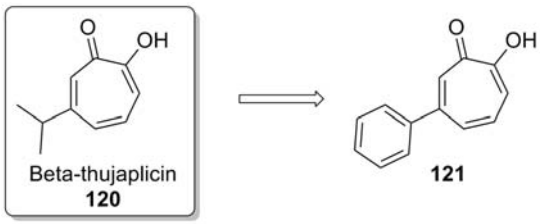

Fig. 34 Natural product-inspired development of thujaplicin analogs **121**.

was selected for biological interrogation. Of note, several tropolone derivatives including **121** displayed HDAC2 selectivity coupled with potent inhibition of T-cell lymphocyte cell lines and may be an underexploited scaffold for drug development.

Sen and coworkers[158] have described a natural product-inspired DOS library development of structurally discrete hybrid systems. Using a privileged pyrroloisoquinoline scaffold prepared via a tandem Pictet–Spengler lactamization reaction, further privileged scaffolds are attached to the core pyrroloisoquinoline unit. The natural product-inspired DOS library was screened for antiplasmodial activity against chloroquine-sensitive 3D7 cells with limited success (20–50 mM).

2.05.5 Chemical Transformations to Create Lead-Like Libraries

2.05.5.1 Lead-Like Library Synthesis Approaches

Bonnet has considered whether synthetic tractability can be computationally predicted for drug-like and lead-like molecules.[159] Intriguingly, the synthetic accessibility was compared via a scoring system between a computer prediction and 11 lab-based medicinal chemists who had to select the compounds. A good correlation (0.7) was obtained and suggests that to avoid missing some useful compounds, collective decisions should be reached on which compounds to synthesize. Oprea and coworkers have considered whether there are substantial differences between lead-like, drug-like, and "pub-like" in the chemical literature.[160] Examination of over 36,000 compounds in the literature (either high- or low-activity scaffolds) is based on MW, molecularly complexity, the number of hydrogen-bond acceptors and hydrogen-bond donors, cLog*P*, intrinsic water solubility (Log *Sw*), and the number of Ro5 violations. From this study, there were no significant differences between leads of known drugs and generally biologically active molecules. Intriguingly, compounds that displayed biological activity were generally less complex, less flexible, and more soluble than drugs and significantly smaller, less complex, and less hydrophobic than high-activity examples. Rishton has written an insightful review on the concept of lead-likeness in biochemical screening[161] with a particular emphasis on moving away from med chem dogma, avoiding the promiscuous inhibitor, frequent hitter, or warhead compounds to obtain meaningful results in biochemical assays. For this section, we will adopt Rishton's summary for the following "lead-likeness": MW = 200–350 Da, cLog*P* < 1.0–3.0, single charge present, and exclusion of chemically reactive functionality. This ordinarily differs from "drug-likeness": MW < 500 Da, cLog*P* < 5, H-bond donors < 5, H-bond acceptors < 10, polar surface area ≤ 140 A^2, and number of rotatable bonds ≤ 10. As the two concepts are interrelated from a lead compound, you would likely add 100–200 Da in weight with concomitant increases in cLog*P*, for instance, during drug development. Doveston and colleagues have described the problem of finding and synthesizing sufficiently large collections of compounds that are within the parameters of being lead-like molecules, using a strategy of lead-oriented synthesis.[162] Conversely, Leeson and colleagues have described the medicinal chemist as "recycling privileged structures"[163] in order to satisfy the concepts of "drug-like" and "lead-like" molecules. However, this biases the chemical profiles of screening collections to known scaffolds (e.g., compounds that we term as being privileged and/or tractable). Leeson proposes that we, although risky, travel the path less worn to new scaffolds. Lipinski[164] has looked back on his Ro5 guide and how it impacts on the next generation of drug-like and tool-like compounds. Jhoti and coworkers[165] have revisited the Ro3 philosophy and its relationship with the advances in fragment-based screening.

Soural and coworkers[166] have reviewed the synthesis of diverse privileged scaffolds using polymer-supported benzene sulfonamides as a general route to bioactive structures.

Tosatti and colleagues have reported a synthetic development in asymmetrical allylic amination[167] using an air-stable iridium catalyst and by employing dimethylsulfoxide (DMSO) as solvent allowed the incorporation of highly polar functionalized amines. The chiral products obtained are sp^3-rich in character and, with suitable physicochemical properties to be considered, valuable lead-like building blocks (**Fig. 35**).

Wang and coworkers[168] have investigated increasing ligand efficiency for the FK506-binding protein 51 through the development of conformational control (**Fig. 36**). Bischoff and coworkers have published the synthesis earlier.[169] In particular, two new classes of bicyclic sulfonamides were developed (a [4.3.1] and a [3.3.1] scaffold) to probe the contribution of conformational energy to ligand efficiency and simultaneously develop lead-like ligands for the protein target. It was found that the [4.3.1] scaffold had higher affinity compared with the [3.3.1] and monocyclic scaffolds, which was attributed to the conformational preorganization of the two key recognition sites. It was also shown that the [4.3.1] scaffold bound to FK506-binding protein 51 (FKBP51) was enthalpically driven and entropically disfavored in comparison with more flexible analogs. Furthermore, a cocrystal structure

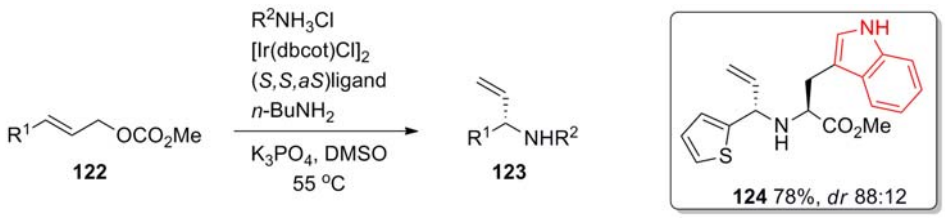

Fig. 35 Asymmetrical allylic amination to lead-like building blocks.

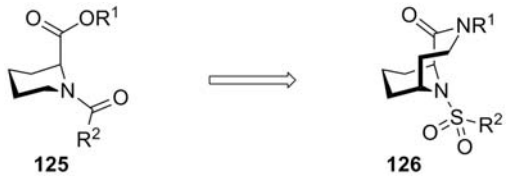

Fig. 36 Chemical transformation to increase conformational control and ligand efficiency in synthesis.

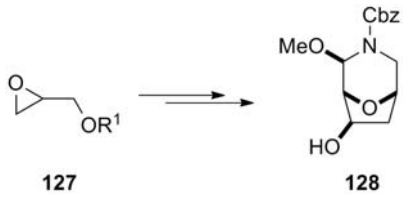

Fig. 37 Development of conformationally locked bicyclic morpholines **128**.

showed that the sulfonamide nitrogen in the bicyclic analogs accepts a hydrogen bond from W113 that mimics the FKBP transition state, giving rise to the first functionally active ligand for FKBP51. Taken together, these findings suggest that lead-like ligand rigidification can enhance affinity; however, it was not due to the expected entropic advantage but instead an enhanced geometric contact mimicking the highly conserved hydrogen bond–dipole contact in FKBP ligands.

Bogacki and coworkers[170] have developed a route to conformationally locked bicyclic morpholines **128** (Fig. 37), reminiscent of the bispidine scaffold (see Fig. 13) from commercially available building blocks. The flexible strategy employed allows for late-stage diversification of these lead-like motifs.

Doveston and coworkers[171] have addressed a challenging aspect of enumerating collections of lead-like compounds for primary screening that could target new lead-like chemical space (Fig. 38). In total, the synthesis of 52 lead-like scaffolds from only 13 chemical precursors was accomplished. Crucial to the success of the strategy was the use of robust, functional group tolerant reactions that were convergent in nature, such as in the preparation of **131**.

Rawling and coworkers[172] have contributed to preparing 3-D space-enriched libraries by developing a six-step method to a sp^3-rich chemical scaffold **134** (Fig. 39). Using a highly regio- and diastereoselective tandem nitrone synthesis followed by intramolecular nitrone–alkene [3 + 2] cycloaddition, 543 lead-like compounds were prepared, inspired by the core skeleton.

Craven and coworkers[173] have designed and developed modular syntheses of six small-molecule libraries inspired by alkaloid natural products (one example is shown in Fig. 40), using strategies such as palladium-catalyzed aminoarylation and/or dipolar cycloadditions. For example, inspired by the structures of nicotine **135** and anisomycin **136**, an elegant Pd-catalyzed

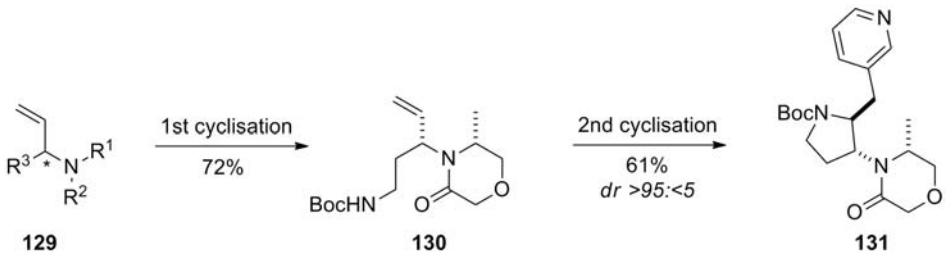

Fig. 38 Two-step route to over 50 diverse lead-like chemical scaffolds.

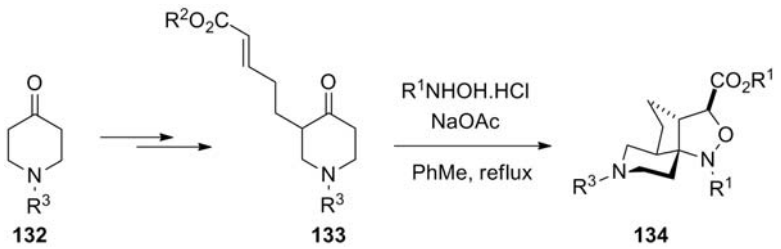

Fig. 39 Synthetic route to sp^3-enriched chemical scaffolds.

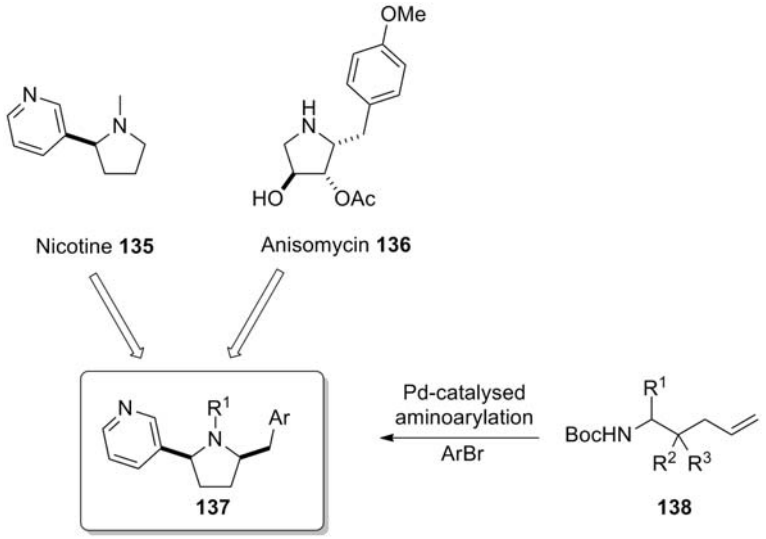

Fig. 40 An example of one of six modular syntheses of natural product-inspired libraries.

aminoarylation with an aryl bromide and a protected aminobutene **138**, a composite structure containing a lead-like privileged element was prepared, **137**. Five of the six libraries were subsequently validated through both scope and limitation studies and predicted molecular properties, leading to the production of over 2500 novel alkaloid-like small molecules for screening. A successful compound synthesis rate of between 58% and 84% was achieved during the library campaign.

Lüthy and coworkers[174] have developed lead-oriented synthetic routes to six 3-D enriched molecular scaffolds containing the privileged piperazine, pyrrolidine, and piperidine cores (representative examples **139–142** are shown in Fig. 41). Using a strategy of N-Boc α-lithiation followed by trapping. On the basis of this chemistry, a virtual library of 190 compounds was assembled, incorporating features from all six scaffolds, and 92 molecules met the lead-like criteria of Log *P*, number of heavy atoms, and tPSA. Furthermore, the 3-D shapes of the enumerated scaffolds were analyzed using normalized principal moments of inertia, giving 46 scaffolds that met both criteria.

Stocks and coworkers[175] have developed a pragmatic method to align the often separated concepts of compound diversity and lead-likeness to enable the scientist to pick with confidence compounds to investigate further from large virtual libraries (Fig. 42). As part of this paradigm shift, Stocks discloses (i) a method for decreasing synthetic attrition through grouping reagents by reaction type, (ii) a predictive method to minimize synthetic effort on compounds that have the potential to exhibit toxicity or less than desirable physicochemical properties, and (iii) a compound selection process that meets the earlier criteria yet also maintains diversity coverage. Taken together, this approach employed at AstraZeneca generated premium quality compounds with increased lead-likeness and novelty. As a case example, a virtual library of 100,299 potential compounds was filtered based on the outlined parameters to yield 12,837 or 12.8% of the compounds that passed these hard cutoffs. A further round of diversity analysis gave a final target size of 518 compounds that covered the complete chemical space of the previous selection. The synthesis of a bisazetidine spirocyclic library (represented by **145**) is one possible outcome.

Nelson and coworkers[176] have identified a paucity of approaches to both fused and C-substituted piperazines scaffolds, and through the development of a modular synthetic approach of the reaction of a cyclic sulfamidate (or hydroxyl sulfonamide) followed by cyclization, the synthesis of substituted piperazine and homologated 1,4-diazepine and 1,5-diazocane scaffolds was prepared (an example of the method to a 1,4-diazepine **148** is shown in the Fig. 43). Using this approach, a large collection of analogs with variations to ring size and substitution pattern of this underrepresented scaffold was achieved. These lead-like molecules were complementary to commercial compound screening collections. Furthermore, a virtual library was assembled using this

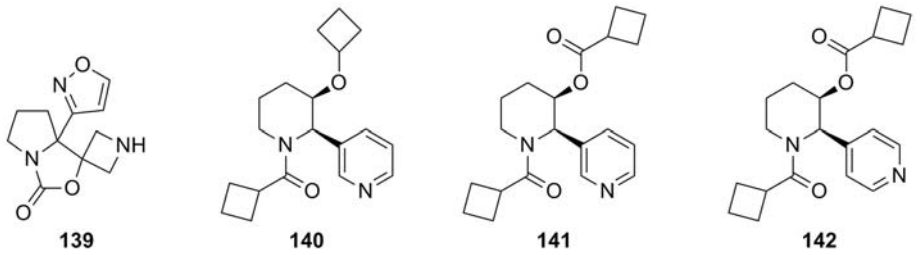

Fig. 41 A lead-oriented synthesis to 3-D-enriched scaffolds **139**–**142**.

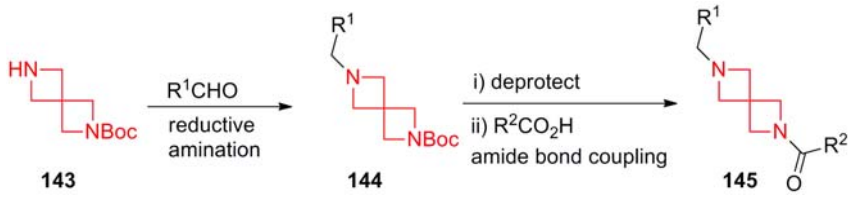

Fig. 42 An approach to align compound diversity and lead-likeness.

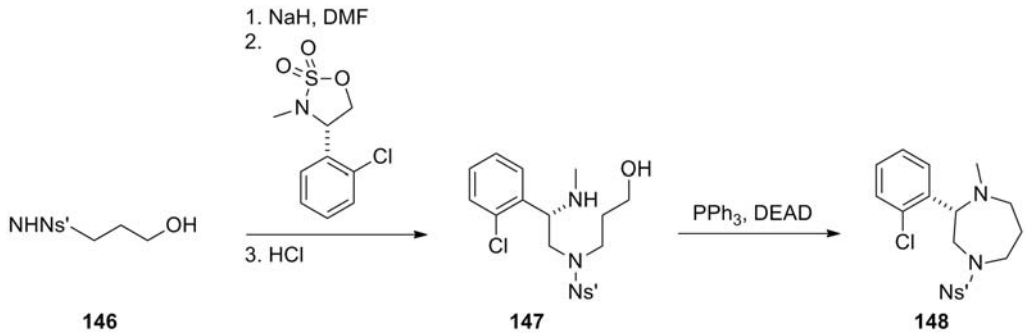

Fig. 43 An approach to C-substituted cyclodiazines, **148**.

synthetic route and followed by deprotection, and approximately one-third of the collection possessed lead-like molecular properties and 3-D shape complementarity properties.

The Wnt proteins are another group of extracellular proteins that initiate signaling cascades that can lead to transcriptional activation and are important in carcinogenesis and cell differentiation. A BIOS-derived library of 91-substituted oxepanes and oxepane-containing frameworks was designed, based on recognition of the oxepane ring as a privileged scaffold embedded in diverse natural products with varying biological activity.[177] Diels–Alder cycloadditions to intermediate 6-vinyl-2,3,4,7-tetrahydrooxepines were used to diversify the core scaffold. The compounds were screened in a cell reporter assay sensitized to detect stimulation of Wnt3a-dependent transcription. Pathway activators that acted synergistically with the presence of the Wnt3a isoform were detected, and subsequent SAR studies identified the activator wntepane 1 (**153**; Fig. 44; ED_{50} 1.8 μM). An affinity probe based on **153** linked to biotin was used to capture potential targets, and reversible binding to the Wnt membrane receptor Vangl1 was demonstrated, the first time a tool molecule targeting this protein was reported.

Also taking a privileged scaffold approach based on indoline alkaloids, Arya and coworkers designed a skeletally diverse DOS screening library that provided inhibitors of focal adhesion kinase (FAK), a protein involved in tumorigenesis and metastasis.[178] N-Alloc-protected 2-formylindolines or homologues were functionalized by addition of allylic or homoallylic Grignard reagents under Felkin–Anh control (Fig. 45). After alcohol protection, the resulting proximal vinyl groups were reacted using ring-closing metathesis (RCM) to afford 6-, 7- and 8-membered rings fused to the indoline scaffold. Compound **157** inhibited FAK activity (30% inhibition at 30 μM), but its mode of action (ATP-competitive or allosteric) was not determined, although docking studies suggested an ATP-site inhibitor. In a cell proliferation assay, **157** had a cytotoxicity of 39 μM and reduced expression of FAK autophosphorylation on pY397. The inhibitor also reduced MDA231-M cell invasion and motility, which may at least in part be due to FAK inhibition.

MacLellan and coworkers[179] have sought to shine a light and bring some redress to the historical unsystematic exploration of chemical space by outlining a new conceptual framework. The proposed framework seeks to "capture, analyze, and plan synthetic

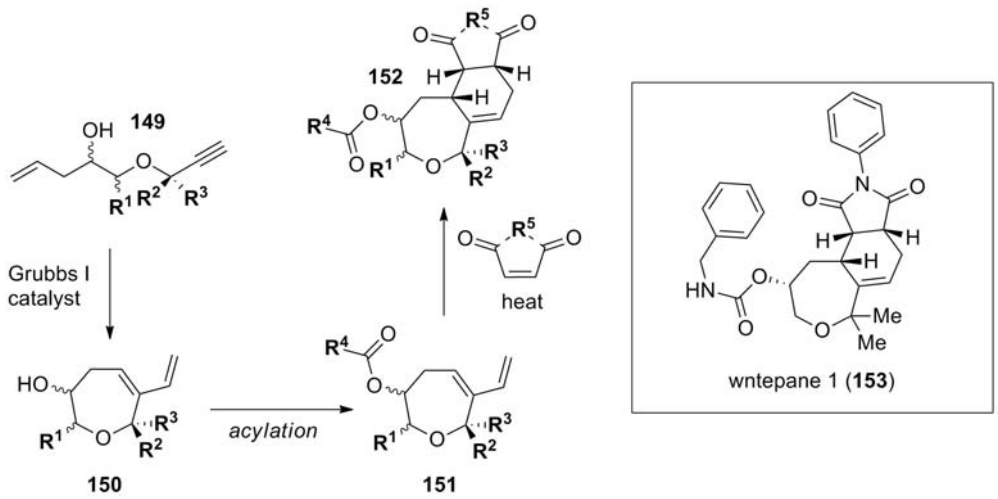

Fig. 44 BIOS and structure of an activator of Wnt signaling.

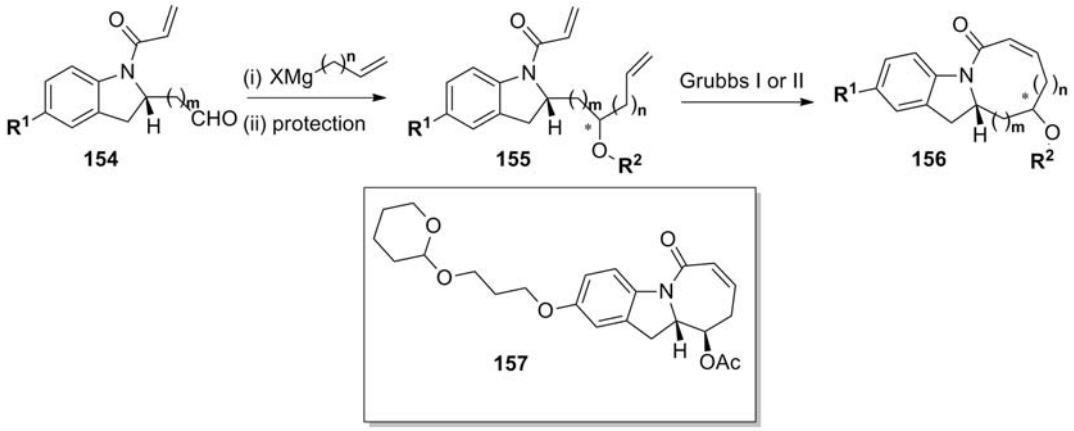

Fig. 45 DOS route to tricyclic indolines.

approaches" to help address this anomaly. An example of a synthetic approach to **160–162**, that is, modular in design to allow for combinatorial variants, is shown in Fig. 46 yet still able to target new expanses of lead-like chemical space. A key distinction to this framework is its ability to prioritize the relative synthetic power of often dissimilar approaches, with complexity generaton the guiding principle. In particular, this was achieved by exploitation of approaches that combine building blocks with greater possible connectivity or enumeration of the building blocks entered into a reaction.

Shaw and coworkers[180] have developed a one-pot, four-component reaction to a structurally diverse, lead-like library of 116 γ-lactams, such as **166** (Fig. 47). The key MCR to access the core scaffold occurred between ammonium acetate, *para*methoxythiophenol, *para*methyoxybenzaldehyde, and maleic anhydride. Through iterative chemical manipulation of the core γ-lactam, for example, amide-bond coupling, thioaryl cleavage, *N*-functionalization, and heterocycle-forming reactions, the complete library was assembled. Post-assembly, computational analysis of the library revealed that the molecular properties and 3-D shape diversity as being suitable for both drug lead discovery and chemical biology probe discovery.

James and coworkers[181] have developed a lead-like synthesis of tetrahydropyrazines (Fig. 48). Using a strategy of propargylic sulfonamide-mediated ring-opening of cyclic sulfamidates afforded intermediates suitable for Au-catalyzed cyclization to the tetrahydropyrazine core scaffold (**170**). Further reaction of the scaffold through chemical manipulation afforded a variety of carbon-substituted tetrahydropyrazine analogs with favorable lead-like properties.

A synthetic route to a new class of privileged tri- and tetracyclic quinazolines containing a medium-sized ring was reported by Hensbergen et al. (Fig. 49).[182] A synthetic route involving nucleophilic aromatic substitution and sequential Niementowski and (benzotriazol-1-yloxy)tris(dimethylamino)phosphonium hexafluorophosphate (BOP)-mediated ring closures afforded a collection of quinazoline-containing analogs (**174**) via the quinazolinone intermediate (**175**, another privileged structure). This application of a tandem cyclization strategy is a new and enabling route to rigidify kinase inhibitor-like quinazolines and has wide-ranging potential in the field of medicinal chemistry.

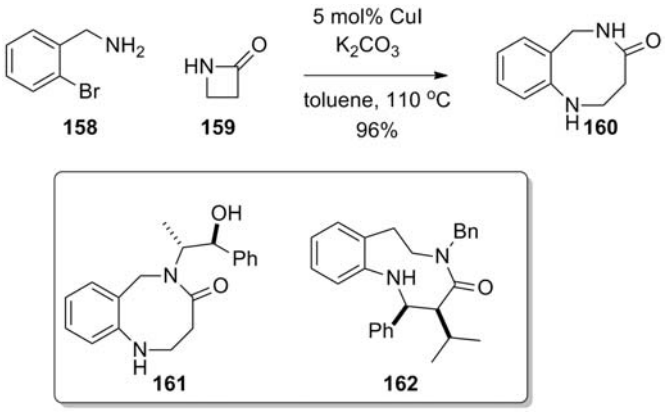

Fig. 46 A new conceptual approach to populating chemical space.

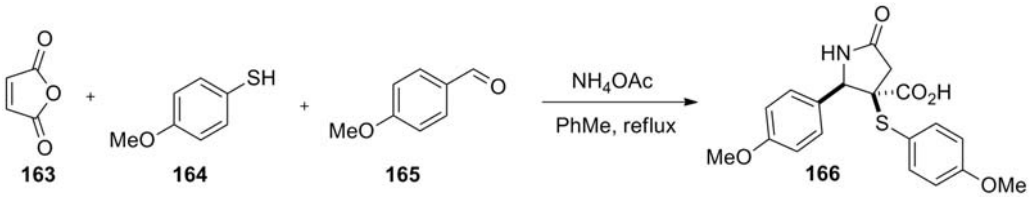

Fig. 47 A one-pot MCR to structurally diverse lead-like scaffolds.

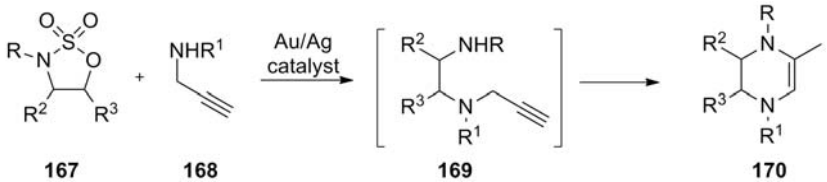

Fig. 48 Lead-like synthesis of tetrahydropyrazines.

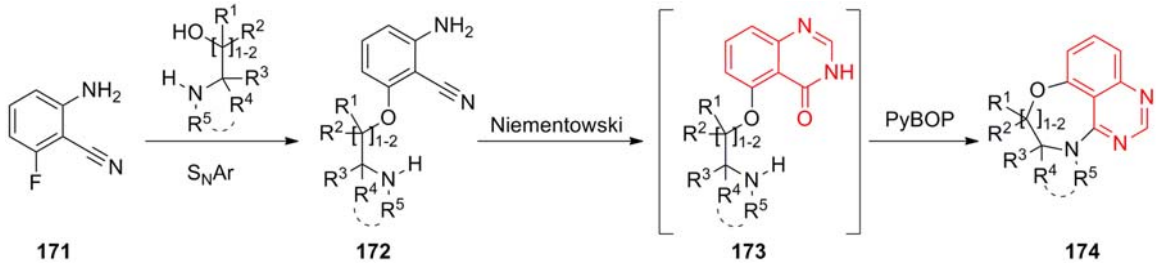

Fig. 49 An expedient synthesis of privileged tri(and tetra)-cyclic quinazolines.

Bull and coworkers[183] have developed an operationally straightforward, high-yielding, copper-catalyzed N-arylation of 2-imidazoles such as **177** (Fig. 50). The reaction is tolerant of a range of electron-rich and electron-poor (hetero)aromatic coupling partners and useful functional groups for late-stage diversification. The imidazole-containing products derived possess lead-like characteristics and are fragment-sized.

Lowe and coworkers[184] have developed a comprehensive synthesis of densely functionalized azetidine ring systems, including fused, bridged, and spirocyclic ring systems **178–184** (Fig. 51). These phenyl azetidine compounds are reminiscent of the phenylethylamine privileged structure (see **185**) prevalent in a variety of synthetic and natural drugs that affect the CNS. Using the solid-supported SynPhase lanterns, a 1976-member library of spirocyclic azetidines was also achieved. Representative examples of all the diverse azetidine families have had their physicochemical and pharmacokinetic properties evaluated in vitro to prioritize the classes

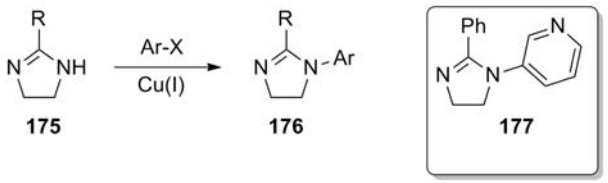

Fig. 50 Fragment- and lead-like synthesis of *N*-aryl imidazoles.

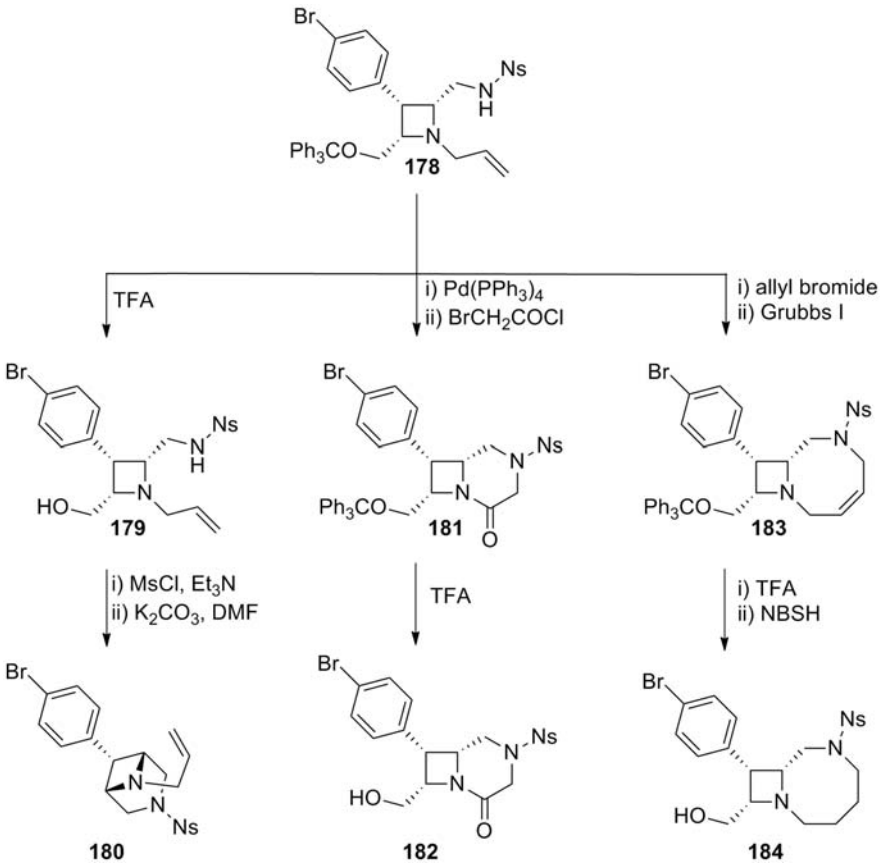

Fig. 51 DOS of densely functionalized azetidines.

to be taken forward for CNS studies. In particular, the *in silico* analysis of the library members showed a good balance of physicochemical properties for CNS application. Optimal compounds showed good ADME profiles in vitro.

The phenylethylamine scaffold has emerged as a versatile privileged motif prevalent in synthetic and natural drug molecules (Fig. 52), such as 3,4-methylenedioxymethamphetamine (MDMA). The area of natural product-inspired drug discovery has been extensively reviewed,[185,186] for instance, alkaloid-inspired libraries[185] and natural and physiologically ligands,[186] which are

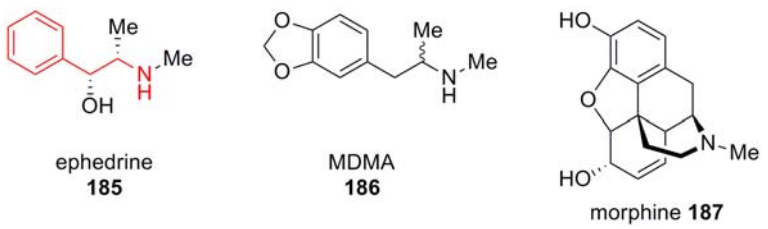

Fig. 52 Phenylethylamine, a privileged structure found in ephedrine **185**, MDMA **186**, morphine **187** (CNS BBB penetrant), and inter alia dopamine.

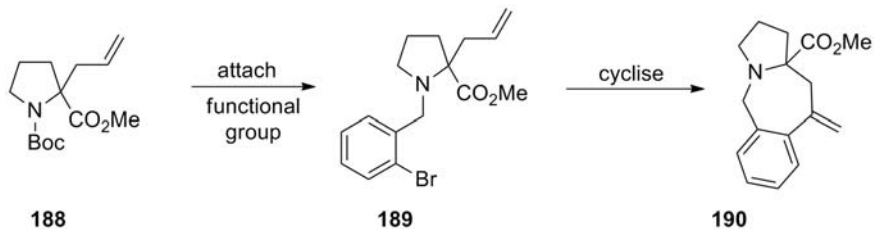

Fig. 53 Lead-oriented synthesis of over 20 new scaffolds.

also highly relevant starting points. Iterative deconstruction of natural product scaffolds can lead to privileged elements such as the indole and phenylethylamine scaffolds we see that are prevalent in the privileged structures discussed in Section "Privileged Scaffolds for Library Design and Drug Discovery."

Foley and coworkers[187] have developed a versatile strategy for lead-oriented synthesis of new scaffolds. As an example of the reaction products prepared, **190** is shown in Fig. 53; in total, 22 novel scaffolds, with the ability to interact with lead-like chemical space, were synthesized from only four alpha-amino acid-based building blocks and six linkage reactions. One aspect of developing new, diverse lead-like libraries is the fraction sp^3 (Fsp^3) challenge. Fsp^3 was first defined by Lovering[188] as a simple measure of the complexity of potential drug molecules. It is a twofold guideline: (1) carbon-bond saturation as defined by Fsp^3 where $Fsp^3 = (\text{number of } sp^3\text{-hybridized carbons/total carbon count})$ and (2) whether a chiral carbon exists in the molecule. The Fsp^3 has been shown to correlate with relative success of a drug candidate. It has been shown that attrition rate of small molecules in screening collections toward becoming drug candidates is correlated with the degree or lack of Fsp^3 present. Inspection of the virtual library showed that Foley's route prepared compounds with Fsp^3 ($m = 0.57$) versus commercial screening collections Fsp^3 ($m = 0.33$).

Ryabukhin and coworkers[189] developed a high-yielding and diastereoselective combinatorial approach to 1,2-disubstituted 5-oxopyrrolidines and 6-oxopiperidine-3-carboxylic acids (such as **193**) using a variant of the Castagnoli condensation of cyclic anhydrides, amines, and aldehydes (Fig. 54). Members of the collection of the compounds prepared meet the strictest criteria of lead-likeness based on their associated physicochemical properties.

Schmitt and coworkers[190] have utilized a lead-like design approach to a library of 2,4-bisheterocyclic-substituted thiophenes. These in turn represent a novel class of nanomolar Dyrk inhibitors with balanced pharmacokinetic properties and high ligand efficiency scores. This lead-like core translated into limited off-target activity against other kinases, namely, a dual Clk/Dyrk inhibition profile.

2.05.6 Conclusions and Outlook

2.05.6.1 Future Directions for Privileged Structure Development

The ubiquitous privileged structure will be with us for many years to come owing to the panoply of interactions with a range of biologically relevant targets and in many cases their ease of synthesis. With an eye on the future, an intriguing feature of some of the privileged structures detailed here is their potential ability to undergo hyperpolarization to enhance selectivity and detection in the NMR or magnetic resonance imaging (MRI) environment. For example, the tuberculosis drugs containing a privileged scaffold such as pyrazinamide and isoniazid have been probed in this manner.[191] For the same target, Ballell and collaborators[192] have described an approach to open-source tuberculosis drug discovery using 177 small-molecule leads. Intriguingly, the eight most promising families from the high-throughput screening (HTS) campaign all contain privileged elements. This demonstrates the potential of collaborative open-source screening, of which the privileged structure will remain a key element. Goldberg and colleagues[193] have made the case for designing novel building blocks as a key strategy to improve compound quality, and this

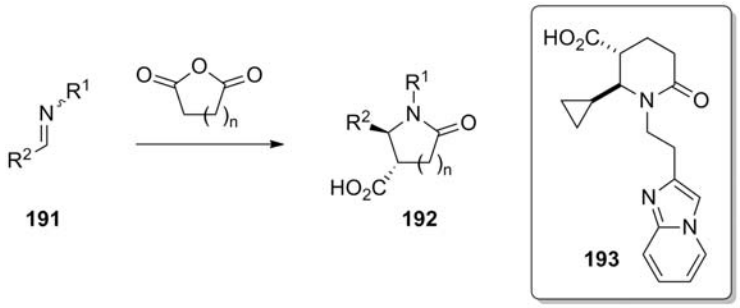

Fig. 54 A diastereoselective combinatorial approach to lead-like scaffolds.

may mean a shift away from the privileged scaffold in time. Open-source, collaborative research, informed with predictive in silico models, and new biophysical techniques will mean the privileged structure will be around until then and beyond.

See also: 1.06. Continuous Flow Processing as a Tool for Medicinal Chemical Synthesis. 1.08. Spirocyclic Scaffolds in Drug Discovery. 1.10. Click Chemistry in Medicinal Chemistry for Comprehensive Medicinal Chemistry III. 1.18. European Lead Factory. 2.02. Hit and Lead Generation Strategies. 2.12. Novel Therapeutics Targeting Epigenetics. 2.13. Small-molecule Inhibitors of Protein–Protein Interactions. 5.01. Cancer Biology and the Principles of Targeted Cancer Drug Discovery. 5.02. Selective Kinase Inhibitors in Cancer. 5.06. Protein–Protein Interaction Inhibitors in Cancer. 5.18. Direct-Acting Antiviral Agents for the Treatment of Hepatitis C Virus Infection.

References

1. Evans, B. E.; Rittle, K. E.; Bock, M. G.; DiPardo, R. M.; Freidinger, R. M.; Whitter, W. L.; Lundell, G. F.; Veber, D. F.; Anderson, P. S.; Chang, R. S. L.; Lotti, V. J.; Cerino, D. J.; Chen, T. B.; Kling, P. J.; Kunkel, K. A.; Springer, J. P.; Hirshfield, J. Methods for Drug Discovery: Development of Potent, Selective, Orally Effective Cholecystokinin Antagonists. *J. Med. Chem.* **1988,** *31,* 2235–2246.
2. Congreve, M.; Carr, R.; Murray, C.; Jhoti, H. A. Rule of Three' for Fragment-Based Lead Discovery? *Drug Discov. Today* **2003,** *8* (19), 876–877.
3. Erlanson, D. A.; McDowell, R. S.; O'Brien, T. Fragment-Based Drug Discovery. *J. Med. Chem.* **2004,** *47* (14), 3463–3482.
4. Congreve, M.; Chessari, G.; Tisi, D.; Woodhead, A. J. Recent Developments in Fragment-Based Drug Discovery. *J. Med. Chem.* **2008,** *51* (13), 3661–3680.
5. Grzybowski, B. A.; Bishop, K. J. M.; Kowalczyk, B.; Wilmer, C. E. The 'Wired' Universe of Organic Chemistry. *Nat. Chem.* **2009,** *1,* 31–36.
6. Ruddigkeit, L.; van Deursen, R.; Blum, L. C.; Reymond, J. L. Enumeration of 166 Billion Organic Small Molecules in the Chemical Universe Database GDB-17. *J. Chem. Inf. Model.* **2012,** *52,* 2864–2875.
7. Crisman, T. J.; Parker, C. N.; Jenkins, J. L.; Scheiber, J.; Thoma, M.; Kang, Z. B.; Kim, R.; Bender, A.; Nettles, J. H.; Davies, J. W.; Glick, M. Understanding False Positives in Reporter Gene Assays: In Silico Chemogenomics. Approaches to Prioritize Cell-Based HTS Data. *J. Chem. Inf. Model.* **2007,** *47,* 1319–1327.
8. Huth, J. R.; Mendoza, R.; Olejniczak, E. T.; Johnson, R. W.; Cothron, D. A.; Liu, Y.; Lerner, C. G.; Chen, J.; Hajduk, P. J. ALARM NMR: A Rapid and Robust Experimental Method to Detect Reactive False Positives in Biochemical Screens. *J. Am. Chem. Soc.* **2005,** *127,* 217–224.
9. Beck, B. BioProfile—Extract Knowledge From Corporate Databases to Assess Cross-Reactivities of Compounds. *Bioorg. Med. Chem.* **2012,** *20,* 5428–5435.
10. Schorpp, K.; Rothenaigner, I.; Salmina, E.; Reinshagen, J.; Low, T.; Brenke, J. K.; Gopalakrishnan, J.; Tetko, I. V.; Gul, S.; Hadian, K. Identification of Small-Molecule Frequent Hitters From AlphaScreen High-Throughput, Screens. *J. Biomol. Screen.* **2014,** *19* (5), 715–726.
11. Brown, N. *Scaffold Hopping in Medicinal Chemistry,* 1st ed.; Wiley-VCH: Weinheim, 2014. *58.*
12. Langdon, S. R.; Brown, N.; Blagg, J. Scaffold Diversity of Exemplified Medicinal Chemistry Space. *J. Chem. Inf. Model.* **2011,** *51,* 2174–2185.
13. Zhao, H.; Dietrich, J. Privileged Scaffolds in Lead Generation. *Expert Opin. Drug Discov.* **2015,** *10* (7), 781–790.
14. Kim, J.; Kim, H.; Park, S. B. Privileged Structures: Efficient Chemical "Navigators" Toward Unexplored Biologically Relevant Chemical Spaces. *J. Am. Chem. Soc.* **2014,** *136,* 14629–14638.
15. Collins, I.; Jones, A. M. Diversity-Oriented Synthetic Strategies Applied to Cancer Chemical Biology and Drug Discovery. *Molecules* **2014,** *19* (11), 17221–17225.
16. Zhang, L.; Zheng, M.; Zhao, F.; Zhai, Y.; Liu, H. Rapid Generation of Privileged Substructure-Based Compound Libraries With Structural Diversity and Drug-Likeness. *ACS Comb. Sci.* **2014,** *16,* 184–191.
17. Costantino, L.; Barlocco, D. Privileged Structures as Leads in Medicinal Chemistry. *Front. Med. Chem.* **2010,** *5,* 381–422.
18. Cordier, C.; Morton, D.; Murrison, S.; Nelson, A.; O'Leary-Steel, C. Natural Products as an Inspiration in the Diversity-Oriented Synthesis of Bioactive Compound Libraries. *Nat. Prod. Rep.* **2008,** *25,* 719–737.
19. Breinbauer, R.; Vetter, I. R.; Waldmann, H. From Protein Domains to Drug Candidates—Natural Products as Guiding Principles in the Design and Synthesis of Compound Libraries. *Angew. Chem. Int. Ed.* **2002,** *41,* 2878–2890.
20. DeSimone, R. W.; Currie, K. S.; Mitchell, S. A.; Darrow, J. W.; Pippin, D. A. Privileged Structures: Applications in Drug Discovery. *Comb. Chem. High Throughput Screen.* **2004,** *7,* 473–493.
21. Welsch, M. E.; Snyder, S. A.; Stockwell, B. R. Privileged Scaffolds for Library Design and Drug Discovery. *Curr. Opin. Chem. Biol.* **2010,** *14,* 347–361.
22. Rees, D. C.; Congreve, M.; Murray, C. W.; Carr, R. Fragment-Based Lead Discovery. *Nat. Rev. Drug Discov.* **2004,** *3* (8), 660–672.
23. Chen, H.; Zhou, X.; Wang, A.; Zheng, Y.; Gao, Y.; Zhou, J. Evolutions in Fragment-Based Drug Design: The Deconstruction–Reconstruction Approach. *Drug Discov. Today* **2015,** *20* (1), 105–113.
24. Liu, K. K.-C.; Sakya, S. M.; O'Donnell, C. J.; Flick, A. C. Synthetic Approaches to the 2009 New Drugs. *Bioorg. Med. Chem.* **2011,** *19,* 1136–1154.
25. Liu, K. K.-C.; Sakya, S. M.; O'Donnell, C. J.; Flick, A. C.; Ding, H. X. Synthetic Approaches to the 2010 New Drugs. *Bioorg. Med. Chem.* **2012,** *20,* 1155–1174.
26. Ding, H. X.; Liu, K. K.-C.; Sakya, S. M.; Flick, A. C.; O'Donnell, C. J. Synthetic Approaches to the 2011 New Drugs. *Bioorg. Med. Chem.* **2013,** *21,* 2795–2825.
27. Ding, H. X.; Leverett, C. A.; Kynr, R. E., Jr.; Liu, K. K.-C.; Sakya, S. M.; Flick, A. C.; O'Donnell, C. J. Synthetic Approaches to the 2012 New Drugs. *Bioorg. Med. Chem.* **2014,** *22,* 2005–2032.
28. Ding, H. X.; Leverett, C. A.; Kyne, R. E., Jr.; Liu, K. K.-C.; Fink, S. J.; Flick, A. C.; O'Donnell, C. J. Synthetic Approaches to the 2013 New Drugs. *Bioorg. Med. Chem.* **2015,** *23,* 1895–1922.
29. Karawajczyk, A.; Giordanetto, F.; Benningshof, J.; Hamza, D.; Kalliokoski, T.; Pouwer, K.; Morgentin, R.; Nelson, A.; Müller, G.; Piechot, A.; Tzalis, D. Expansion of Chemical Space for Collaborative Lead Generation and Drug Discovery: The European Lead Factory Perspective. *Drug Discov. Today* **2015,** *20* (11), 1310–1316.
30. Chan, A. W. E.; Laskowski, R. A.; Selwood, D. L. Chemical Fragments That Hydrogen Bond to Asp, Glu, Arg, and His Side Chains in Protein Binding Sites. *J. Med. Chem.* **2010,** *53* (8), 3086–3094.
31. Paolini, G. V.; Shapland, R. H.; van Hoorn, W. P.; Mason, J. S.; Hopkins, A. L. Global Mapping of Pharmacological Space. *Nat. Biotechnol.* **2006,** *24,* 805–815.
32. Bissantz, C.; Kuhn, B.; Stahl, M. A Medicinal Chemist's Guide to Molecular Interactions. *J. Med. Chem.* **2010,** *53,* 5061–5084.
33. Kim, J.-H.; Jeong, P.-H.; Lee, J.-Y.; Lee, J.-H.; Kim, Y.-J.; Kim, Y.-C. Discovery and Structure–Activity Relationships of Pyrazolodiazepine Derivatives as the First Small Molecule Agonists of the *Drosophila* Sex Peptide Receptor. *Bioorg. Med. Chem.* **2015,** *23,* 1808–1816.
34. Barve, I. J.; Dalvi, P. B.; Thikekar, T. U.; Chanda, K.; Liu, Y.-L.; Fang, C.-P.; Liu, C.-C.; Sun, C.-M. Design, Synthesis and Diversification of Natural Product-Inspired Hydantoin-Fused Tetrahydroazepino Indoles. *RSC Adv.* **2015,** *5,* 73169–73179.
35. Che, Y.; Marshall, G. R. Privileged Scaffolds Targeting Reverse-Turn and Helix Recognition. *Expert Opin. Ther. Targets* **2008,** *12* (1), 101–114.
36. Arkin, M. R.; Tang, Y.; Wells, J. A. Small-Molecule Inhibitors of Protein-Protein Interactions: Progressing Toward the Reality. *Chem. Biol.* **2014,** *21* (9), 1102–1114.
37. Han, C.; Zhang, J.; Zheng, M.; Xiao, Y.; Li, Y.; Liu, G. An Integrated Drug-Likeness Study for Bicyclic Privileged Structures: From Physicochemical Properties to in vitro ADME Properties. *Mol. Divers.* **2011,** *15,* 857–876.

38. Cavalli, A.; Lizzi, F.; Bongarzone, S.; Brun, R.; Krauth-Siegel, R. L.; Bolgnesi, M. L. Privileged Structure-Guided Synthesis of Quinazoline Derivatives as Inhibitors of Trypanothione Reductase. *Bioorg. Med. Chem. Lett.* **2009,** *19,* 3031–3035.
39. Musiol, R.; Magdziarz, T.; Kurczyk, A. Quinoline Scaffold as a Privileged Substructure in Antimicrobial Drugs. In *Science Against Microbial Pathogens: Communicating Current Research and Technological Advances Microbial Book Series Number 3 (Formatex, Spain);* Méndez-Vilas, A., Ed.; 2011; pp 72–83.
40. Song, Y.; Xu, H.; Chen, W.; Zhan, P.; Liu, X. 8-Hydroxyquinoline: A Privileged Structure With a Broad-Ranging Pharmacological Potential. *Med. Chem. Commun.* **2015,** *6,* 61–74.
41. Solomon, V. R.; Lee, H. Quinoline as a Privileged Scaffold in Cancer Drug Discovery. *Curr. Med. Chem.* **2011,** *18* (10), 1488–1508.
42. Shiro, T.; Fukaya, T.; Tobe, M. The Chemistry and Biological Activity of Heterocycle-Fused Quinolinone Derivatives: A Review. *Eur. J. Med. Chem.* **2015,** *97,* 397–408.
43. Ross, A. G.; Benton, B. M.; Chin, D.; De Pascale, G.; Fuller, J.; Leeds, J. A.; Reck, F.; Richie, D. L.; Vo, J.; LaMarche, M. J. Synthesis of Ciprofloxacin Dimers for Evaluation of Bacterial Permeability in Atypical Chemical Space. *Bioorg. Med. Chem. Lett.* **2015,** *25,* 3468–3475.
44. Cogo, J.; Kaplum, V.; Sangi, D. P.; Ueda-Nakamura, T.; Corréa, A. G.; Nakamura, C. V. Synthesis and Biological Evaluation of Novel 2,3-Disubstituted Quinoxaline Derivatives as Antileishmanial and Antitrypanosomal Agents. *Eur. J. Med. Chem.* **2014,** *90,* 107–123.
45. Chen, Q.; Bryant, V. C.; Lopez, H.; Kelly, D. L.; Luo, X.; Natarajan, A. 2,3-Substituted Quinoxalin-6-Amine Analogs as Antiproliferatives: A Structure–Activity Relationship Study. *Bioorg. Med. Chem. Lett.* **2011,** *21,* 1929–1932.
46. Liu, J.-F.; Wilson, C. J.; Ye, P.; Sprague, K.; Sargent, K.; Si, Y.; Beletsky, G.; Yohannes, D.; Ng, S.-C. Privileged Structure-Based Quinazolinone Natural Product-Templated Libraries: Identification of Novel Tubulin Polymerization Inhibitors. *Bioorg. Med. Chem. Lett.* **2006,** *16,* 686–690.
47. Liu, R.; Huang, Z.; Murray, M. G.; Guo, X.; Liu, G. Quinoxalin-2(1*H*)-One Derivatives as Inhibitors Against Hepatitis C Virus. *J. Med. Chem.* **2011,** *54,* 5747–5768.
48. Manfroni, G.; Cannalire, R.; Barreca, M. L.; Kaushik-Basu, N.; Leyssen, P.; Winquist, J.; Iraci, N.; Manvar, D.; Paeshuyse, J.; Guhamazumder, R.; Basu, A.; Sabatini, S.; Tabarrini, O.; Danielson, U. H.; Neyts, J.; Cecchetti, V. The Versatile Nature of the 6-Aminoquinolone Scaffold: Identification of Submicromolar Hepatitis C Virus NS5B Inhibitors. *J. Med. Chem.* **2014,** *57,* 1952–1963.
49. Kandi, S. K.; Manohar, S.; Gerena, C. E. V.; Zayas, B.; Malhotra, S. V.; Rawat, D. S. C5-Curcuminoid-4-Aminoquinoline Based Molecular Hybrids: Design, Synthesis and Mechanistic Investigation of Anticancer Activity. *New J. Chem.* **2015,** *39,* 224–234.
50. Vandekerckhove, S.; D'hooghe, M. Quinoline-Based Antimalarial Hybrid Compounds. *Bioorg. Med. Chem.* **2015,** *23,* 5098–5119.
51. Drège, E.; Venot, P. E.; Le Bideau, F.; Retailleau, P.; Joseph, D. Two-Component Domino Reactions Initiated From Ketenes: Serendipitous Synthesis of Quinolizidinones Analogous to Chelated Lobeline's Conformation. *J. Org. Chem.* **2015,** *80,* 10119–10126.
52. Zhao, Z.; Wu, H.; Wang, L.; Liu, Y.; Knapp, S.; Liu, Q.; Gray, N. S. Exploration of Type II Binding Mode: A Privileged Approach for Kinase Inhibitor Focused Drug Discovery? *ACS Chem. Biol.* **2014,** *9,* 1230–1241.
53. Zhang, Q.; Wang, J.; Wang, F.; Chen, X.; He, Y.; You, Q.; Zhou, H. Identification of Type II Inhibitors Targeting BRAF Using Privileged Pharmacophores. *Chem. Biol. Drug Des.* **2014,** *83,* 27–36.
54. Innocenti, P.; Woodward, H.; O'Fee, L.; Hoelder, S. Expanding the Scope of Fused Pyrimidines as Kinase Inhibitor Scaffolds: Synthesis and Modification of Pyrido[3,4-*d*]pyrimidines. *Org. Biomol. Chem.* **2015,** *13,* 893–904.
55. Zhan, Z.; Ai, J.; Liu, Q.; Ji, Y.; Chen, T.; Xu, Y.; Geng, M.; Duan, W. Discovery of Anilinopyrimidines as Dual Inhibitors of c-Met and VEGFR-2: Synthesis, SAR, and Cellular Activity. *ACS Med. Chem. Lett.* **2014,** *5,* 673–678.
56. Zhao, H.; Caflisch, A. Current Kinase Inhibitors Cover a Tiny Fraction of Fragment Space. *Bioorg. Med. Chem. Lett.* **2015,** *25,* 2372–2376.
57. Liu, D.; Zhao, G.; Xiang, L. Diverse Strategies for the Synthesis of the Indoline Scaffold. *Eur. J. Org. Chem.* **2010,** *2010* (21), 3975–3984.
58. Zhang, M.-Z.; Chen, Q.; Yang, G.-F. A Review on Recent Developments of Indole-Containing Antiviral Agents. *Eur. J. Med. Chem.* **2015,** *89,* 421–441.
59. Fraga, C. A. M.; Barreiro, E. J.; de Sa Alves, F. R. From Nature to Drug Discovery: The Indole Scaffold as a 'Privileged Structure'. *Mini Rev. Med. Chem.* **2009,** *9,* 782–793.
60. Sonsona, I. G. Indole, a Privileged Structural Core Motif. *Synlett* **2015,** *26,* 2325–2326.
61. Keri, R. S.; Hiremathad, A.; Budagumpi, S.; Nagaraja, B. M. Comprehensive Review in Current Developments of Benzimidazole-Based Medicinal Chemistry. *Chem. Biol. Drug Des.* **2015,** *86,* 19–65.
62. Lim, F. P. L.; Dolzhenko, A. V. 1,3,5-Triazine-Based Analogues of Purine: From Isosteres to Privileged Scaffolds in Medicinal Chemistry. *Eur. J. Med. Chem.* **2014,** *85,* 371–390.
63. Goel, R.; Luxami, V.; Paul, K. Synthetic Approaches and Functionalizations of Imidazo[1,2-a]pyrimidines: An Overview of the Decade. *RSC Adv.* **2015,** *5,* 81608–81637.
64. Chao, B.; Li, B. X.; Xiao, X. The Chemistry and Pharmacology of Privileged Pyrroloquinazolines. *Med. Chem. Commun.* **2015,** *6,* 510–520.
65. Bunders, C. A.; Minvielle, M. J.; Worthington, R. J.; Ortiz, M.; Cavanagh, J.; Melander, C. Intercepting Bacterial Indole Signaling With Flustramine Derivatives. *J. Am. Chem. Soc.* **2011,** *133,* 20160–20163.
66. Johansson, H.; Boesgaard, M. W.; Nørskov-Lauritsen, L.; Larsen, I.; Kuhne, S.; Gloriam, D. E.; Bräuner-Osborne, H.; Pedersen, D. S. Selective Allosteric Antagonists for the G Protein-Coupled Receptor GPRC6A Based on the 2-Phenylindole Privileged Structure Scaffold. *J. Med. Chem.* **2015,** *58,* 8938–8951.
67. Vignaroli, G.; Mencarelli, M.; Sementa, D.; Crespan, E.; Kissova, M.; Maga, G.; Schenone, S.; Radi, M.; Botta, M. Exploring the Chemical Space Around the Privileged Pyrazolo[3,4-*d*]pyrimidine Scaffold: Toward Novel Allosteric Inhibitors of T315I-Mutated Abl. *ACS Comb. Sci.* **2014,** *16,* 168–175.
68. Miller, T. C. R.; Rutherford, T. J.; Birchall, K.; Chugh, J.; Fiedler, M.; Bienz, M. Competitive Binding of a Benzimidazole to the Histone-Binding Pocket of the Pygo PHD Finger. *ACS Chem. Biol.* **2014,** *9,* 2864–2874.
69. Islam, K.; Chin, H. F.; Olivares, A. O.; Saunders, L. P.; De La Cruz, E. M.; Kapoor, T. A Myosin V Inhibitor Based on Privileged Chemical Scaffolds. *Angew. Chem. Int. Ed.* **2010,** *49,* 8484–8488.
70. Wang, N.-Y.; Zuo, W.-Q.; Xu, Y.; Gao, C.; Zeng, X.-X.; Zhang, L.-D.; You, X.-Y.; Peng, C.-T.; Shen, Y.; Yang, S. Y.; Wei, Y.-Q.; Yu, L.-T. Discovery and Structure–Activity Relationships Study of Novel Thieno[2,3-b]pyridine Analogues as Hepatitis C Virus Inhibitors. *Bioorg. Med. Chem. Lett.* **2014,** *24,* 1581–1588.
71. Romagnoli, R.; Baraldi, P. G.; Prencipe, F.; Balzarini, J.; Liekens, S.; Estevez, F. Design, Synthesis and Antiproliferative Activity of Novel Heterobivalent Hybrids Based on Imidazo[2,1-b][1,3,4]thiadiazole and Imidazo[2,1-b] [1,3]thiazole Scaffolds. *Eur. J. Med. Chem.* **2015,** *101,* 205–217.
72. Sztanke, M.; Rzymowska, J.; Sztanke, K. Synthesis, Structure Elucidation and Identification of Antiproliferative Activities of a Novel Class of Thiophene Bioisosteres Bearing the Privileged 7,8-Dihydroimidazo[2,1-c][1,2,4]triazin-4(6H)-one Scaffold. *Bioorg. Med. Chem.* **2015,** *23,* 3448–3456.
73. Grover, J.; Jachak, S. M. Coumarins as Privileged Scaffold for Anti-Inflammatory Drug Development. *RSC Adv.* **2015,** *5,* 38892–38905.
74. Keri, R. S.; Budagumpi, S.; Pai, R. K.; Balakrishna, R. G. Chromones as a Privileged Scaffold in Drug Discovery: A Review. *Eur. J. Med. Chem.* **2014,** *78,* 340–374.
75. Gaspar, A.; Matos, M. J.; Garrido, J.; Uriarte, E.; Borges, F. Chromone: A Valid Scaffold in Medicinal Chemistry. *Chem. Rev.* **2014,** *114,* 4960–4992.
76. Ko, S. K.; Jang, H. J.; Kim, E.; Park, S. M. Concise and Diversity-Oriented Synthesis of Novel Scaffolds Embedded With Privileged Benzopyran Motif. *Chem. Commun.* **2006,** *42,* 2962–2964.
77. Oh, S.; Park, S. M. A Design Strategy for Drug-Like Polyheterocycles With Privileged Substructures for Discovery of Specific Small-Molecule Modulators. *Chem. Commun.* **2011,** *47,* 12754–12761.
78. Oh, S.; Nam, H. J.; Park, J.; Beak, S. H.; Park, S. B. Development of a Benzopyran-Containing Androgen Receptor Antagonist to Treat Antiandrogen-Resistant Prostate Cancer. *ChemMedChem* **2010,** *5,* 529–533.
79. Gaspar, A.; Silva, T.; Yáñez, M.; Vina, D.; Orallo, F.; Ortuso, F.; Uriarte, E.; Alcaro, S.; Borges, F. Chromone, a Privileged Scaffold for the Development of Monoamine Oxidase Inhibitors. *J. Med. Chem.* **2011,** *54,* 5165–5173.
80. Rojas, R. J.; Edmondson, D. E.; Almos, T.; Scott, R.; Massari, M. E. Reversible and Irreversible Small Molecule Inhibitors of Monoamine Oxidase B (MAO-B) Investigated by Biophysical Techniques. *Bioorg. Med. Chem.* **2015,** *23,* 770–778.

81. Distinto, S.; Meleddu, R.; Yanez, M.; Cirilli, R.; Bianco, G.; Sanna, M. L.; Arridu, A.; Cossu, P.; Cottiglia, F.; Faggi, C.; Ortuso, F.; Alcaro, S.; Maccioni, E. Drug Design, Synthesis, in vitro and In Silico Evaluation of Selective Monoaminoxidase B Inhibitors Based on 3-Acetyl-2-dichlorophenyl-5-aryl-2,3-dihydro-1,3,4-oxadiazole Chemical Scaffold. *Eur. J. Med. Chem.* **2016,** *108,* 542–552.
82. Khan, I.; Bakht, S. M.; Ibrar, A.; Abbas, S.; Hameed, S.; White, J. M.; Rana, U. A.; Zaib, S.; Shahide, M.; Iqbal, J. Exploration of a Library of Triazolothiadiazole and Triazolothiadiazine Compounds as a Highly Potent and Selective Family of Cholinesterase and Monoamine Oxidase Inhibitors: Design, Synthesis, X-ray Diffraction Analysis and Molecular Docking Studies. *RSC Adv.* **2015,** *5,* 21249–21267.
83. Mala Rdo, C.; Tesch, R.; Fraga, C. A. M. Acylhydrazone Derivatives: A Patent Review. *Expert Opin. Ther. Pat.* **2014,** *24* (11), 1161–1170.
84. Avila, C. M.; Lopes, A. B..; Gonçalves, A. S.; da Silva, L. L.; Romerio, N. C.; Miranda, A. L. P.; Sant'Anna, C. M. R.; Barreiro, E. J.; Fraga, C. A. M. Structure-Based Design and Biological Profile of (*E*)-*N*-(4-Nitrobenzylidene)-2-naphthohydrazide, a Novel Small Molecule Inhibitor of IB Kinase-β. *Eur. J. Med. Chem.* **2011,** *46,* 1245–1253.
85. da Silva, T. F.; Júnior, W. B.; Alexandre-Moreira, M. S.; Costa, F. N.; da Silva Monteiro, C. E.; Ferreira, F. F.; Barroso, R. C. R.; Noël, F.; Sudo, R. T.; Zapata-Sudo, G.; Lima, L. M.; Barreiro, E. J. Novel Orally Active Analgesic and Anti-Inflammatory Cyclohexyl-*N*-Acylhydrazone Derivatives. *Molecules* **2015,** *20,* 3067–3088.
86. Secci, D.; Bolasco, A.; Carradori, S.; D'Ascenzio, M.; Nescatelli, R.; Yáñez, M. Recent Advances in the Development of Selective Human MAO-B Inhibitors: (Hetero)arylidene-(4-substituted-thiazol-2-yl)hydrazines. *Eur. J. Med. Chem.* **2012,** *58,* 405–417.
87. Annadurai, S.; Martinez, R.; Canney, D. J.; Eidem, T.; Dunman, P. M.; Abou-Gharbia, M. Design and Synthesis of 2-Aminothiazole Based Antimicrobials Targeting MRSA. *Eur. J. Med. Chem.* **2012,** *22,* 7719–7725.
88. Harida, V.; Rajgokul, K. S.; Sadanandan, S.; Agrawal, T.; Sharvani, V.; Gopalakrishna, M. V. S.; Bijesh, M. B.; Kumawat, K. L.; Basu, A.; Medigeshi, G. R. Bispidine-Amino Acid Conjugates Act as a Novel Scaffold for the Design of Antivirals That Block Japanese Encephalitis Virus Replication. *PLoS Negl. Trop. Dis.* **2013,** *7* (1), 1–11.
89. Carro, L.; Torrado, M.; Raviña, E.; Masaguer, C. F.; Lage, S.; Brea, J.; Loza, M. I. Synthesis and Biological Evaluation of a Series of Aminoalkyl-Tetralones and Tetralols as Dual Dopamine/Serotonin Ligands. *Eur. J. Med. Chem.* **2014,** *71,* 237–249.
90. Ohta, K.; Chiba, Y.; Kaise, A.; Endo, Y. Structure–Activity Relationship Study of Diphenylamine-Based Estrogen Receptor (ER) Antagonists. *Bioorg. Med. Chem.* **2015,** *23,* 861–867.
91. Zhang, Y.; Wu, S.; Wang, S.; Fang, K.; Dong, G.; Liu, Na.; Miao, Z.; Yao, J.; Li, J.; Zhang, W.; Sheng, C.; Wang, W. Divergent Cascade Construction of Skeletally Diverse "Privileged" Pyrazole-Derived Molecular Architectures. *Eur. J. Org. Chem.* **2015,** *9,* 2030–2037.
92. Assimon, V. A.; Shao, H.; Garneau-Tsodikov, S.; Gestwicki, J. E. Concise Synthesis of Spergualin-Inspired Molecules With Broad-Spectrum Antibiotic Activity. *Med. Chem. Commun.* **2015,** *6,* 912–918.
93. Neubauer, S.; Rechenmacher, F.; Brimioulle, R.; Di Leva, F. S.; Bochen, A.; Sobahi, T. R.; Schottelius, M.; Novellino, E.; Mas-Moruno, C.; Marinelli, L.; Kessler, H. Pharmacophoric Modifications Lead to Superpotent αvβ3 Integrin Ligands With Suppressed α5β1 Activity. *J. Med. Chem.* **2014,** *57* (8), 3410–3417.
94. Kuhnert, M.; Blum, A.; Steuber, H.; Diederich, W. E. Privileged Structures Meet Human T-Cell Leukemia Virus-1 (HTLV-1): C2-Symmetric 3,4-Disubstituted Pyrrolidines as Nonpeptidic HTLV-1 Protease Inhibitors. *J. Med. Chem.* **2015,** *58,* 4845–4850.
95. Vilaivan, T. Pyrrolidinyl PNA With α/β-Dipeptide Backbone: From Development to Applications. *Acc. Chem. Res.* **2015,** *48,* 1645–1656.
96. Blanco-Ania, D.; Aben, R. W. M.; van Berkom, L. W. A.; Scheeren, H. W.; Rutjes, F. P. J. T. High-Pressure-Mediated Extension of the Privileged Steroid Scaffold. *Eur. J. Org. Chem.* **2014,** *2014,* 1438–1444.
97. Mohamed, Z. H.; El-Koussi, N. A.; Mahfouz, N. M.; Youssef, A. F.; Abdel Jaleel, G. A.; Shouman, S. A. Cu (I) Catalyzed Alkyne-Azide 1,3-Dipolar Cycloaddition (CuAAC): Synthesis of 17a-[1-(Substituted phenyl)-1,2,3-triazol-4-yl]-19-nortestosterone-17b-yl Acetates Targeting Progestational and Antiproliferative Activities. *Eur. J. Med. Chem.* **2015,** *97,* 75–82.
98. Tan, S. W. B.; Chai, C. L. L.; Moloney, M. G.; Thompson, A. L. Synthesis of Mimics of Pramanicin From Pyroglutamic Acid and Their Antibacterial Activity. *J. Org. Chem.* **2015,** *80* (5), 2661–2675.
99. Lin, L.; Tan, R. X. Cross-Kingdom Actions of Phytohormones: A Functional Scaffold Exploration. *Chem. Rev.* **2011,** *111,* 2734–2760.
100. Wijdeven, M. A.; Willemsen, J.; Rutjes, F. P. J. T. The 3-Hydroxypiperidine Skeleton: Key Element in Natural Product Synthesis. *Eur. J. Org. Chem.* **2010,** *2010,* 2831–2844.
101. Kim, J.; Lee, W. S.; Koo, J.; Lee, J.; Park, S. B. Synthesis and Library Construction of Privileged Tetra-Substituted Δ5-2-Oxopiperazine as β-Turn Structure Mimetics. *ACS Comb. Sci.* **2014,** *16,* 24–32.
102. Meng, T.; Wang, J.; Peng, H.; Fang, G.; Li, M.; Xiong, B.; Xie, X.; Zhang, Y.; Wang, X.; Shen, J. Discovery of Benzhydrylpiperazine Derivatives as CB_1 Receptor Inverse Agonists via Privileged Structure-Based Approach. *Eur. J. Med. Chem.* **2010,** *45,* 1133–1139.
103. Szabo, M.; Herenbrink, C. K.; Christopoulos, A.; Lane, R. J.; Capuano, B. Structure–Activity Relationships of Privileged Structures Lead to the Discovery of Novel Biased Ligands at the Dopamine D_2 Receptor. *J. Med. Chem.* **2014,** *57,* 4924–4939.
104. Shonberg, J.; Draper-Joyce, C.; Mistry, S. N.; Christopoulos, A.; Scammells, P. J.; Lane, J. R.; Capuano, B. Structure−Activity Study of *N*-((trans)-4-(2-(7-Cyano-3,4-dihydroisoquinolin-2(1H)-yl)ethyl)cyclohexyl)-1H-indole-2-carboxamide (SB269652), a Bitopic Ligand That Acts as a Negative Allosteric Modulator of the Dopamine D2 Receptor. *J. Med. Chem.* **2015,** *58,* 5287–5307.
105. Szabo, M.; Lim, H. D.; Herenbrink, C. K.; Christopoulos, A.; Lane, J. R.; Capuano, B. Proof of Concept Study for Designed Multiple Ligands Targeting the Dopamine D_2, Serotonin 5-HT_{2A}, and Muscarinic M_1 Acetylcholine Receptors. *J. Med. Chem.* **2015,** *58,* 1550–1555.
106. Liu, Y.; Guo, L.; Duan, H.; Zhang, L.; Jiang, N.; Zhen, X.; Shen, J. Discovery of 4-Benzoylpiperidine and 3-(piperidin-4-yl)benzo[*d*]isoxazole Derivatives as Potential and Selective GlyT1 Inhibitors. *RSC Adv.* **2015,** *5,* 40964–40977.
107. Spadoni, G.; Bedini, A.; Bartolucci, S.; Pala, D.; Mor, M.; Riccioni, T.; Borsini, F.; Cabri, W.; Celona, D.; Marzi, M.; Tarzia, G.; Rivara, S.; Minetti, P. Towards the Development of 5-HT7 Ligands Combining Serotonin-Like and Arylpiperazine Moieties. *Eur. J. Med. Chem.* **2014,** *80,* 8–35.
108. Liu, T.; Huang, B.; Tian, Y.; Liang, X.; Liu, H.; Liu, H.; Zhan, P.; De Clercq, E.; Pannecouque, C.; Liu, X. Design, Synthesis, and Biological Evaluation of Novel 4-Aminopiperidinyl-linked 3,5-Disubstituted-1,2,6-thiadiazine-1,1-dione Derivatives as HIV-1 NNRTIs. *Chem. Biol. Drug Des.* **2015,** *86,* 107–113.
109. Kaur, N. An Insight Into Medicinal and Biological Significance of Privileged Scaffold: 1,4-Benzodiazepine. *Int J Pharm. Bio. Sci* **2013,** *4* (2), 318–337.
110. Saha, D.; Jain, G.; Sharma, A. Benzothiazepines: Chemistry of a Privileged Scaffold. *RSC Adv.* **2015,** *5,* 70619–70639.
111. Lee, J.-Y.; Kim, Y.-C. Combinatorial Library Synthesis and Biological Evaluation of Pyrazolo[4,3-*e*][1,4]diazepine as a Potential Privileged Structure. *Chem. Med. Chem.* **2009,** *4,* 733–737.
112. Smith, S. G.; Sanchez, R.; Zhou, M.-M. Privileged Diazepine Compounds and Their Emergence as Bromodomain Inhibitors. *Chem. Biol.* **2014,** *21,* 573–583.
113. Fernández de Gortari, E.; Medina-Franco, J. L. Epigenetic Relevant Chemical Space: A Chemoinformatic Characterization of Inhibitors of DNA Methyltransferases. *RSC Adv.* **2015,** *5,* 87465–87476.
114. Galli, U.; Travelli, C.; Aprile, S.; Arrigoni, E.; Torretta, S.; Grosa, G.; Massarotti, A.; Sorba, G.; Canonico, P. L.; Genazzani, A. A. Design, Synthesis, and Biological Evaluation of Combretabenzodiazepines: A Novel Class of Anti-Tubulin Agents. *J. Med. Chem.* **2015,** *58,* 1345–1357.
115. Viviano, M.; Milite, C.; Rescigno, D.; Castellano, S.; Sbardella, G. A Continuous-Flow Synthesis of 1,4-Benzodiazepin-5-ones, Privileged Scaffolds for Drug Discovery. *RSC Adv.* **2015,** *5,* 1268–1273.
116. Pałasz, A.; Ciez, D. In Search of Uracil Derivatives as Bioactive Agents. Uracils and Fused Uracils: Synthesis, Biological Activity and Applications. *Eur. J. Med. Chem.* **2015,** *97,* 582–611.
117. Sandomenico, A.; Celentano, V.; D'Andrea, L. D.; Palmieric, G.; Ruvo, M. Screening of b-Hairpin Peptide-Engrafted 1,2,3-Triazoles to Identify APEH Enzyme Inhibitors. *RSC Adv.* **2015,** *5,* 9965–9972.

118. Bai, H.; Zhu, P.; Wu, W.; Li, J.; Ma, Z.; Zhang, W.; Cheng, Y.; Du, L.; Li, M. Synthesis and Biological Evaluation of a Series of Aryl Triazoles as Firefly Luciferase Inhibitors. *Med. Chem. Commun.* **2015,** *6,* 418–424.
119. Hoyt, S. B.; Petrilli, W.; London, C.; Liang, G.-B.; Tata, J.; Hu, Q.; Yin, L.; van Koppen, C. J.; Hartmann, R. W.; Struthers, M.; Wisniewski, T.; Ren, N.; Bopp, C.; Sok, A.; Cai, T.-Q.; Stribling, S.; Pai, L.-Y.; Ma, X.; Metzger, J.; Verras, A.; McMasters, D.; Chen, Q.; Tung, E.; Tang, W.; Salituro, G.; Buist, N.; Clemas, J.; Zhou, G.; Gibson, J.; Maxwell, C. A.; Lassman, M.; McLaughlin, T.; Castro-Perez, J.; Szeto, D.; Forrest, G.; Hajdu, R.; Rosenbach, M.; Xiong, Y. Discovery of Triazole CYP11B2 Inhibitors With in vivo Activity in Rhesus Monkeys. *ACS Med. Chem. Lett.* **2015,** *6* (8), 861–865.
120. Cantley, A. M.; Welsch, M.; Ambesi-Impiombato, A.; Sanchez-Martin, M.; Kim, M.-Y.; Bauer, A.; Ferrando, A.; Stockwell, B. R. Small Molecule That Reverses Dexamethasone Resistance in T-Cell Acute Lymphoblastic Leukemia (T-ALL). *ACS Med. Chem. Lett.* **2014,** *5* (7), 754–759.
121. Terracciano, S.; Lauro, G.; Strocchia, M.; Fischer, K.; Werz, O.; Riccio, R.; Bruno, I.; Bifulco, G. Structural Insights for the Optimization of Dihydropyrimidin-2(1H)-one Based mPGES-1 Inhibitors. *ACS Med. Chem. Lett.* **2015,** *6,* 187–191.
122. Wermuth, C. G. Are Pyridazines Privileged Structures? *Med. Chem. Commun.* **2011,** *2,* 935–941.
123. Gerona-Navarro, G.; González-Muñiz, R.; Fernández-Carvajal, A.; González-Ros, J. M.; Ferrer-Montiel, A.; Carreño, C.; Alberico, F.; Royo, M. Solid-Phase Synthesis of a Library of Amphipathic Hydantoins. Discovery of New Hits for TRPV1 Blockade. *ACS Comb. Sci.* **2011,** *13,* 458–465.
124. Mendgen, T.; Steuer, C.; Klein, C. D. Privileged Scaffolds or Promiscuous Binders: A Comparative Study on Rhodanines and Related Heterocycles in Medicinal Chemistry. *J. Med. Chem.* **2012,** *55,* 743–753.
125. Ge, X.; Wakim, B.; Sem, D. S. Chemical Proteomics-Based Drug Design: Target and Antitarget Fishing With a Catechol-Rhodanine Privileged Scaffold for NAD(P)(H) Binding Proteins. *J. Med. Chem.* **2008,** *51,* 4571–4580.
126. Hoffmann, B. R.; El-Mansy, M. F.; Sem, D. S.; Greene, A. S. Chemical Proteomics-Based Analysis of Off-Target Binding Profiles for Rosiglitazone and Pioglitazone: Clues for Assessing Potential for Cardiotoxicity. *J. Med. Chem.* **2012,** *55,* 8260–8271.
127. Martinez, A.; Alonso, M.; Castro, A.; Dorronsoro, I.; Gelpí, J. L.; Luque, J.; Pérez, C.; Moreno, F. J. SAR and 3D-QSAR Studies on Thiadiazolidinone Derivatives: Exploration of Structural Requirements for Glycogen Synthase Kinase 3 Inhibitors. *J. Med. Chem.* **2005,** *48,* 7103–7112.
128. Raghubir, R.; Verma, R.; Samuel, S. S.; Raza, S.; Haq, W.; Katti, S. B. Anti-Stroke Profile of Thiazolidin-4-one Derivatives in Focal Cerebral Ischemia Model in Rat. *Chem. Biol. Drug Des.* **2011,** *78,* 445–453.
129. Baell, J. B.; Holloway, G. A. New Substructure Filters for Removal of Pan Assay Interference Compounds (PAINS) From Screening Libraries and for Their Exclusion in Bioassays. *J. Med. Chem.* **2010,** *53* (7), 2719–2740.
130. Baell, J. B.; Walters, M. A. Chemical Con Artists Foil Drug Discovery. *Nature* **2014,** *513,* 481–483.
131. Dahlin, J. L.; Nissink, J. W. M.; Strasser, J. M.; Francis, S.; Higgins, L.; Zhou, H.; Zhang, Z.; Walters, M. A. PAINS in the Assay: Chemical Mechanisms of Assay Interference and Promiscuous Enzymatic Inhibition Observed During a Sulfhydryl-Scavenging HTS. *J. Med. Chem.* **2015,** *58,* 2091–2113.
132. Zhou, L.; Zhong, Y.; Xue, M.-Z.; Kuang, D.; Cao, X.-W.; Zhao, Z.-J.; Li, H.-L.; Xu, Y.-F.; Wang, R. Design, Synthesis and Evaluation of PPAR Gamma Binding Activity of 2-Thioxo-4-thiazolidinone Derivatives. *Chin. Chem. Lett.* **2015,** *26,* 63–68.
133. Byrne, S.; Durbin, M.; Jones, A.M.; Montgomery, C.; Quevedo, C.; Liu, G.; Seden, P.; Bataille, C.; Guillermo, A.; Davies, S.; Westwood, R.; Russell, A.; Wynne, G.; Naylor, A. PIM Kinase Inhibitors. 2013. Patent Appl. No. GB1222826.8.
134. Zhao, L.; Wang, Y.; Cao, D.; Chen, T.; Wang, Q.; Li, Y.; Xu, Y.; Zhang, N.; Wang, X.; Chen, D.; Chen, L.; Chen, Y. L.; Xia, G.; Shi, Z.; Liu, Y. C.; Lin, Y.; Miao, Z.; Shen, J.; Xiong, B. Fragment-Based Drug Discovery of 2-Thiazolidinones as BRD4 Inhibitors: Structure-Based Optimization. *J. Med. Chem.* **2015,** *58* (3), 1281–1297.
135. Tan, W.; Zhu, X.-T.; Zhang, S.; Xing, G.-J.; Zhu, R.-Y.; Shi, F. Diversity-Oriented Synthesis of Spiro-Oxindole-Based 2,5-Dihydropyrroles via Three-Component Cycloadditions and Evaluation on Their Cytotoxicity. *RSC Adv.* **2013,** *3,* 10875–10886.
136. Thaler, F.; Moretti, L.; Amici, R.; Abate, A.; Colombo, A.; Carenzi, G.; Fulco, M. C.; Boggio, R.; Dondi, G.; Gagliardi, S.; Minucci, S.; Sartori, L.; Varasi, M.; Mercurio, C. Synthesis, Biological Characterization and Molecular Modeling Insights of Spirochromanes as Potent HDAC Inhibitors. *Eur. J. Med. Chem.* **2016,** *108,* 53–67.
137. He, S.; Ye, Z.; Dobbelaar, P. H.; Bakshi, R. K.; Hong, Q.; Dellureficio, J. P.; Sebhat, I. K.; Guo, L.; Liu, J.; Jian, T.; Lai, Y.; Franklin, C. L.; Reibarkh, M.; Holmes, M. A.; Weinberg, D. H.; MacNeil, T.; Tang, R.; Tamvakopoulos, C.; Peng, Q.; Miller, R. R.; Stearns, R. A.; Chen, H. Y.; Chen, A. S.; Strack, A. M.; Fong, T. M.; Wyvratt, M. J., Jr.; Nargund, R. P. Discovery of Highly Potent and Efficacious MC4R Agonists With Spiroindane *N*-Me-1,2,4-triazole Privileged Structures for the Treatment of Obesity. *Bioorg. Med. Chem. Lett.* **2010,** *20,* 6524–6532.
138. Lavieri, R.; Scott, S. A.; Lewis, J. A.; Selvy, P. E.; Armstrong, M. D.; Brown, H. A.; Lindsley, C. W. Design and Synthesis of Isoform-Selective Phospholipase D (PLD) Inhibitors. Part II. Identification of the 1,3,8-Triazaspiro[4,5]decan-4-one Privileged Structure That Engenders PLD2 Selectivity. *Bioorg. Med. Chem. Lett.* **2009,** *19,* 2240–2243.
139. Ventosa-Andrés, P.; Hradilová, L.; Krchňak, V. Privileged Structures as Peptide Backbone Constraints: Polymer-Supported Stereoselective Synthesis of Benzimidazolinopiperazinone Peptides. *ACS Comb. Sci.* **2014,** *16,* 359–366.
140. Karageorgis, G.; Warriner, S.; Nelson, A. Efficient Discovery of Bioactive Scaffolds by Activity-Directed Synthesis. *Nat. Chem.* **2014,** *6,* 872–876.
141. O'Boyle, N. M.; Pollock, J. K.; Carr, M.; Knox, A. J. S.; Nathwani, S. M.; Wang, S.; Caboni, L.; Zisterer, D. M.; Meegan, M. J. β-Lactam Estrogen Receptor Antagonists and a Dual-Targeting Estrogen Receptor/Tubulin Ligand. *J. Med. Chem.* **2014,** *57,* 9370–9382.
142. Narayan, R.; Potowski, M.; Jia, Z.-J.; Antonchick, A. P.; Waldmann, H. Catalytic Enantioselective 1,3-Dipolar Cycloadditions of Azomethine Ylides for Biology-Oriented Synthesis. *Acc. Chem. Res.* **2014,** *47,* 1296–1310.
143. Smyth, L. A.; Matthews, T. P.; Collins, I. Design and Evaluation of 3-Aminopyrazolopyridinone Kinase Inhibitors Inspired by the Natural Product Indirubin. *Bioorg. Med. Chem.* **2011,** *19* (11), 3569–3578.
144. Pascolutti, M.; Quinn, R. J. Natural Products as Lead Structures: Chemical Transformations to Create Lead-Like Libraries. *Drug Discov. Today* **2014,** *19* (3), 215–221.
145. Quinn, R. J.; Carroll, A. R.; Pham, N. B.; Baron, P.; Palframan, M. E.; Suraweera, L.; Pierens, G. K.; Muresan, S. Developing a Drug-Like Natural Product Library. *J. Nat. Prod.* **2008,** *71* (3), 464–468.
146. Newman, D. J. Natural Products as Leads to Potential Drugs: An Old Process or the New Hope for Drug Discovery? *J. Med. Chem.* **2008,** *51,* 2589–2599.
147. Kombarov, R.; Altieri, A.; Genis, D.; Kirpichenok, M.; Kochubey, V.; Rakitina, N.; Titarenko, Z. BioCores: Identification of a Drug/Natural Product-Based Privileged Structural Motif for Small-Molecule Lead Discovery. *Mol. Divers.* **2010,** *14* (1), 193–200.
148. Medina-Franco, J. L.; Lopez-Vallejo, F.; Kuck, D.; Lyko, F. Natural Products as DNA Methyltransferase Inhibitors: A Computer-Aided Discovery Approach. *Mol. Divers.* **2011,** *15* (2), 293–304.
149. Tao, L.; Zhu, F.; Qin, C.; Zhang, C.; Chen, S.; Zhang, P.; Zhang, C.; Tan, C.; Gao, C.; Chen, Z.; Jiang, Y.; Chen, Y. Z. Clustered Distribution of Natural Product Leads of Drugs in the Chemical Space as Influenced by the Privileged Target-Sites. *Sci. Rep.* **2015,** *5* (9325), 1–10.
150. Wezeman, T.; Brase, S.; Masters, K.-S. Xanthone Dimers: A Compound Family Which Is Both Common and Privileged. *Nat. Prod. Rep.* **2015,** *32,* 6–28.
151. Balsera, B.; Mulet, J.; Fernández-Carvajal, A.; de la Torre-Martínez, R.; Ferrer-Montiel, A.; Hernández-Jiménez, J. G.; Estévez-Herrera, J.; Borges, R.; Feritas, A. E.; López, M. G.; García-López, M. T.; González-Muñiz, R.; de Vega, M. J. P.; Valor, L. M.; Svobodová, L.; Sala, S.; Sala, F.; Criado, M. Chalcones as Positive Allosteric Modulators of α7 Nicotinic Acetylcholine Receptors: A New Target for a Privileged Structure. *Eur. J. Med. Chem.* **2014,** *86,* 724–739.
152. Foster, R. W.; Benhamou, L.; Porter, M. J.; Bucar, D.-K.; Hailes, H. C.; Tame, C. J.; Sheppard, T. D. Irreversible Endo-Selective Diels-Alder Reactions of Substituted Alkoxyfurans: A General Synthesis of Endo-Cantharimides. *Chem. Eur. J.* **2015,** *21* (16), 6107–6114.
153. Rosini, M.; Simoni, E.; Bartolini, M.; Tarozzi, A.; Matera, R.; Milelli, A.; Hrelia, P.; Andrisano, V.; Bolognesi, M. L.; Melchiorre, C. Exploiting the Lipoic Acid Structure in the Search for Novel Multitarget Ligands Against Alzheimer's Disease. *Eur. J. Med. Chem.* **2011,** *46,* 5435–5442.
154. Novaes, L. F. T.; Avila, C. M.; Pelizzaro-Rocha, K. J.; Vendramini-Costa, D. B.; Dias, M. P.; Trivella, D. B. B.; de Carvahlo, J. E.; Ferreira-Halder, C. V.; Pilli, R. A. (−)-Tarchonanthuslactone: Design of New Analogues, Evaluation of Their Antiproliferative Activity on Cancer Cell Lines, and Preliminary Mechanistic Studies. *Chem. Med. Chem.* **2015,** *10* (10), 1687–1699.

155. Lajkiewicz, N. J.; Cognetta, A. B..; Niphakis, M. J.; Cravatt, B. F.; Porco, J. A., Jr. Remodeling Natural Products: Chemistry and Serine Hydrolase Activity of a Rocaglate-Derived β-Lactone. *J. Am. Chem. Soc.* **2014,** *136,* 2659–2664.
156. Camara, K.; Kamat, S. S.; Lasota, C. C.; Cravatt, B. F.; Howell, A. R. Combining Cross-Metathesis and Activity-Based Protein Profiling: New B-Lactone Motifs for Targeting Serine Hydrolases. *Bioorg. Med. Chem. Lett.* **2015,** *25,* 317–321.
157. Ononye, S. N.; VanHeyst, M. D.; Oblak, E. Z.; Zhou, W.; Ammar, M.; Anderson, A. C.; Wright, D. L. Tropolones as Lead-Like Natural Products: The Development of Potent and Selective Histone Deacetylase Inhibitors. *ACS Med. Chem. Lett.* **2013,** *4,* 757–761.
158. Prabhu, G.; Agarwal, S.; Sharma, V.; Madurkar, S. M.; Munshi, P.; Singh, S.; Sen, S. A Natural Product Based DOS Library of Hybrid Systems. *Eur. J. Med. Chem.* **2015,** *95,* 41–48.
159. Bonnet, P. Is Chemical Synthetic Accessibility Computationally Predictable for Drug and Lead-Like Molecules? A Comparative Assessment Between Medicinal and Computational Chemists. *Eur. J. Med. Chem.* **2012,** *54,* 679–689.
160. Oprea, T. I.; Allu, T. K.; Fara, D. C.; Rad, R. F.; Ostopovici, L.; Bologa, C. G. Lead-Like, Drug-Like or "Pub-Like": How Different Are They? *J. Comp. Aid. Mol. Des.* **2007,** *21* (1–3), 113–119.
161. Rishton, G. M. Nonleadlikeness and Leadlikeness in Biochemical Screening. *Drug Discov. Today* **2002,** *8* (2), 86–96.
162. Doveston, R.; Marsden, S.; Nelson, A. Towards the Realisation of Lead-Oriented Synthesis. *Drug Discov. Today* **2014,** *19* (7), 813–819.
163. Leeson, P. D.; Davis, A. M.; Steele, J. Drug-Like Properties: Guiding Principles for Design—Or Chemical Prejudice? *Drug Discov. Today Technol.* **2004,** *1* (3), 189–195.
164. Lipinski, C. A. Lead—and Drug-Like Compounds: The Rule-of-Five Revolution. *Drug Discov. Today Technol.* **2004,** *1* (4), 337–341.
165. Jhoti, H.; Williams, G.; Rees, D. C.; Murray, C. W. The 'Rule of Three' for Fragment-Based Drug Discovery: Where Are We Now? *Nat. Rev. Drug Discov.* **2013,** *12,* 644–645 http://dx.doi.org/10.1038/nrd3926-c1.
166. Fulöpövá, V.; Soural, V. F. M. Mining the Chemical Space: Application of 2/4-Nitrobenzenesulfonamides in Solid-Phase Synthesis. *ACS Comb. Sci.* **2015,** *17,* 570–591.
167. Tosatti, P.; Horn, J.; Campbell, A. J.; House, D.; Nelson, A.; Marsden, S. P. Iridium-Catalyzed Asymmetric Allylic Amination With Polar Amines: Access to Building Blocks With Lead-Like Molecular Properties. *Adv. Synth. Cat.* **2010,** *352* (18), 3153–3157.
168. Wang, Y.; Kirschner, A.; Fabian, A.-K.; Gopalakrishnan, R.; Kress, C.; Hoogeland, B.; Koch, U.; Kozany, C.; Bracher, A.; Hausch, F. Increasing the Efficiency of Ligands for FK506-Binding Protein 51 by Conformational Control. *J. Med. Chem.* **2013,** *56* (10), 3922–3935.
169. Bischoff, M.; Sippel, C.; Bracher, A.; Hausch, F. Stereoselective Construction of the 5'Hydroxy diazabicyclo[4.3.1]decane-2-one Scaffold, a Privileged Motif for FK506-Binding Proteins. *Org. Lett.* **2014,** *16,* 5254–5257.
170. Bogacki, R.; Gill, D. M.; Kerr, W. J.; Lamont, S.; Parkinson, J. A.; Paterson, L. C. Flexible Access to Conformationally-Locked Bicyclic Morpholines. *Chem. Commun.* **2013,** *49* (79), 8931–8933.
171. Doveston, R. G.; Tosatti, P.; Dow, M.; Foley, D. J.; Li, H. Y.; Campbell, A. J.; House, D.; Churcher, I.; Marsden, S. P.; Nelson, A. A Unified Lead-Oriented Synthesis of Over Fifty Molecular Scaffolds. *Org. Biomol. Chem.* **2015,** *13* (3), 859–865.
172. Rawling, M. J.; Storr, T. E.; Bawazir, W. A.; Cully, S. J.; Lewis, W.; Makki, M. S. I. T.; Strutt, I. R.; Jones, G.; Hamza, D.; Stockman, R. A. Facile Access to a Heterocyclic, sp3-Rich Chemical Scaffold via a Tandem Condensation/Intramolecular Nitrone-Alkene [3+2] Cycloaddition Strategy. *Chem. Commun.* **2015,** *51* (64), 12867–12870.
173. Craven, P.; Aimon, A.; Dow, M.; Fleury-Bregeot, N.; Guilleux, R.; Morgentin, R.; Roche, D.; Kalliokoski, T.; Foster, R.; Marsden, S. P.; Nelson, A. Design, Synthesis and Decoration of Molecular Scaffolds for Exploitation in the Production of Alkaloid-Like Libraries. *Bioorg. Med. Chem.* **2015,** *23,* 2629–2635.
174. Luthy, M.; Wheldon, M. C.; Haji-Cheteh, C.; Atobe, M.; Bond, P. S.; O'Brien, P.; Hubbard, R. E.; Fairlamb, I. J. S. Lead-Oriented Synthesis: Investigation of Organolithium-Mediated Routes to 3-D Scaffolds and 3-D Shape Analysis of a Virtual Lead-Like Library. *Bioorg. Med. Chem.* **2015,** *23* (11), 2680–2694.
175. Stocks, M. J.; Wilden, G. R. H.; Pairaudeau, G.; Perry, M. W. D.; Steele, J.; Stonehouse, J. P. A Practical Method for Targeted Library Design Balancing Lead-Like Properties With Diversity. *Chem. Med. Chem.* **2009,** *4* (5), 800–808.
176. James, T.; Maclellan, P.; Burslem, G. M.; Simpson, I.; Grant, J. A.; Warriner, S.; Sridharan, V.; Nelson, A. A Modular Lead-Oriented Synthesis of Diverse Piperazine, 1,4-Diazepane and 1,5-Diazocane Scaffolds. *Org. Biomol. Chem.* **2014,** *12* (16), 2584–2591.
177. Basu, S.; Ellinger, B.; Rizzo, S.; Deraeve, C.; Schurmann, M.; Preut, H.; Arndt, H.; Waldmann, H. Biology-Oriented Synthesis of a Natural-Product Inspired Oxepane Collection Yields a Small-Molecule Activator of the Wnt-Pathway. *Proc. Natl. Acad. Sci. U. S. A.* **2011,** *108,* 6805–6810.
178. Prakesch, M.; Bijian, K.; Campagna-Slater, V.; Quevillon, S.; Jospeh, R.; Wei, C.-Q.; Sesmilo, E.; Reayi, A.; Poondra, R. R.; Barnes, M. L.; Leek, D. M.; Xu, B.; Lougheed, C.; Schapira, M.; Alaouli-Jamali, M.; Arya, P. Building Skeletally Diverse Architectures on the Indoline Scaffold: The Discovery of a Chemical Probe of Focal Adhesion Kinase Signalling Networks. *Bioorg. Med. Chem.* **2008,** *16,* 9596–9602.
179. MacLellan, P.; Nelson, A. A Conceptual Framework for Analyzing and Planning Synthetic Approaches to Diverse Lead-Like Scaffolds. *Chem. Commun.* **2013,** *49* (24), 2383–2393.
180. Martin, K. S.; Di Maso, M. J.; Fettinger, J. C.; Shaw, J. T. Synthesis of a Library of Lead-Like γ-Lactams by a One Pot, Four-Component Reaction. *ACS Comb. Sci.* **2013,** *15* (7), 356–362.
181. James, T.; Simpson, I.; Grant, J. A.; Sridharan, V.; Nelson, A. Modular, Gold-Catalyzed Approach to the Synthesis of Lead-Like Piperazine Scaffolds. *Org. Lett.* **2013,** *15* (23), 6094–6097.
182. Hensbergen, A. W.; Mills, V. R.; Collins, I.; Jones, A. M. An Expedient Synthesis of Oxazepino and Oxazocino Quinazolines. *Tetrahedron Lett.* **2015,** *56* (46), 6478–6483.
183. Davis, O. A.; Hughes, M.; Bull, J. A. Copper-Catalyzed N-Arylation of 2-Imidazolines With Aryl Iodides. *J. Org. Chem.* **2013,** *78* (7), 3470–3475.
184. Lowe, T.; Lee, M. D., IV; Akella, L. B.; Davoine, E.; Donckele, E. J.; Durak, L.; Duvall, J. R.; Gerard, B.; Holson, E. B.; Joliton, A.; Kesavan, S.; Lemercier, B. C.; Liu, H.; Marié, J.-C.; Mulrooney, C. A.; Muncipinto, G.; Welzel-O'Shea, M.; Panko, L. M.; Rowley, A.; Suh, B.-C.; Thomas, M.; Wagner, F. F.; Wei, J.; Foley, M. A.; Marcaurelle, L. A. Synthesis and Profiling of a Diverse Collection of Azetidine-Based Scaffolds for the Development of CNS-Focused Lead-Like Libraries. *J. Org. Chem.* **2012,** *77,* 7187–7211.
185. McLeod, M. C.; Singh, G.; Plampin, J. N.; Rane, D.; Wang, J. L.; Day, V. W.; Aubé, J. Probing Chemical Space With Alkaloid-Inspired Libraries. *Nat. Chem.* **2014,** *6* (2), 133–140.
186. Koehn, F. E.; Carter, G. T. The Evolving Role of Natural Products in Drug Discovery. *Nat. Rev. Drug Discov.* **2005,** *4,* 206–220.
187. Foley, D. J.; Doveston, R. G.; Churcher, I.; Nelson, A.; Marsden, S. P. A Systematic Approach to Diverse, Lead-Like Scaffolds From α, α-Disubstituted Amino Acids. *Chem. Commun.* **2015,** *51* (56), 11174–11177.
188. Lovering, F.; Bikker, J.; Humblet, C. Escape From Flatland: Increasing Saturation as an Approach to Improving Clinical Success. *J. Med. Chem.* **2009,** *52,* 6752–6756.
189. Ryabukhin, S. V.; Panov, D. M.; Granat, D. S.; Ostapchuk, E. N.; Kryvoruchko, D. V.; Grygorenko, O. O. Toward Lead-Oriented Synthesis: One-Pot Version of Castagnoli Condensation With Nonactivated Alicyclic Anhydrides. *ACS Comb. Sci.* **2014,** *16* (3), 146–153.
190. Schmitt, C.; Kail, D.; Mariano, M.; Empting, M.; Weber, N.; Paul, T.; Hartmann, R. W.; Engel, M. Design and Synthesis of a Library of Lead-Like 2,4-Bisheterocyclic Substituted Thiophenes as Selective Dyrk/Clk Inhibitors. *PLoS One* **2014,** *9* (3). e87851/1–e87851/20.
191. Zeng, H.; Xu, J.; Gillen, J.; McMahon, M. T.; Artemov, D.; Tyburn, J.-M.; Lohman, J. A. B.; Mewis, R. E.; Atkinson, K. D.; Green, G. G. R.; Duckett, S. B.; van Zijl, P. C. M. Optimization of SABRE for Polarization of the Tuberculosis Drugs Pyrazinamide and Isoniazid. *J. Magn. Reson.* **2013,** *237,* 73–78.
192. Ballell, L.; Bates, R. H.; Young, R. J.; Alvarez-Gomez, D.; Alvarez-Ruiz, E.; Barroso, V.; Blanco, D.; Crespo, B.; Escribano, J.; Gonzalez, R.; Losano, S.; Huss, S.; Santos-Villarejo, A.; Martin-Plaza, J. J.; Mendoza, A.; Rebollo-Lopez, M. J.; Remuiñan-Blanco, M.I.; Lavandera, J. L.; Pérez-Herran, E.; Gamo-Benito, F. J.; García-Bustos, J. F.; Barros, D.; Castro, J. P.; Cammack, N. Fueling Open-Source Drug Discovery: 177 Small-Molecule Leads Against Tuberculosis. *Chem. Med. Chem.* **2013,** *8* (2), 313–321.
193. Goldberg, F. W.; Kettle, J. G.; Kogej, T.; Perry, M. W. D.; Tomkinson, N. P. Designing Novel Building Blocks Is an Overlooked Strategy to Improve Compound Quality. *Drug Discov. Today* **2015,** *20* (1), 11–17.

Relevant Websites

https://llama.leeds.ac.uk/—Lead-Likeness and Molecular Analysis (LLAMA). LLAMA allows the lead-likeness of chemical scaffolds to be evaluated in silico.
https://www.europeanleadfactory.eu/—European Lead Factory creates new chemistry based on crowd-sourced ideas to boost drug discovery.
http://www.sigmaaldrich.com/chemistry/chemical-synthesis/learning-center/chemfiles.html—A range of articles including commercially available privileged scaffolds and related chemistry.
http://www.scripps.edu/baran/heterocycles/—The Scripps Research Institute comprehensive resources related to privileged heterocyclic chemistry.
https://clinicaltrials.gov/—Repository of results of recent clinical trials.

2.06 High-Throughput Crystallography and Its Applications in Drug Discovery

H Nar, D Fiegen, S Hörer, A Pautsch, and D Reinert, Boehringer Ingelheim Pharma GmbH & Co. KG, Biberach an der Riss, Germany

© 2017 Elsevier Ltd. All rights reserved.

2.06.1	**Introduction**	154
2.06.2	**Historical Development**	155
2.06.3	**Methods**	158
2.06.3.1	Generation of the Complex—Cocrystallisation and Soaking	158
2.06.3.1.1	Cocrystallization	158
2.06.3.1.2	Soaking	159
2.06.3.2	Crystal Harvesting, Flash-cooling, Storage, and Mounting	159
2.06.3.3	Diffraction Experiment, Structure Determination, Ligand Placement, and Refinement	160
2.06.3.4	The Challenge of Automation	161
2.06.3.5	Validation of the Final Structure	162
2.06.3.6	Communication of Results	163
2.06.4	**Applications**	163
2.06.4.1	Structure-based Target Assessment	163
2.06.4.1.1	Protein–Protein Interactions	164
2.06.4.2	Hit Validation	165
2.06.4.2.1	Characterization of the cocrystal structures of a chemically diverse set of CDK1 inhibitors	166
2.06.4.3	Fragment-Based Screening	168
2.06.4.3.1	Implementation of an X-ray crystallography-based FBS	168
2.06.4.4	Structure-Based Molecular Design	169
2.06.4.4.1	Isoform selective PI3Kγ inhibitors	169
2.06.4.4.2	Lead hopping in fXa	171
2.06.4.5	Biologics Discovery	172
2.06.5	**Outlook—Industrial structural biology of the future**	172
2.06.5.1	X-ray free electron lasers and cryo-electron microscopy	172
2.06.5.2	Structural biology of integral membrane proteins (IMP)	174
2.06.6	**Summary**	175
References		175

Abbreviations

ADP Atomic displacement parameter
COPD Chronic obstructive pulmonary disease
DMSO Dimethylsulfoxide
DMTA "design-make-test-analyse" cycle
DSF Differential scanning fluorimetry
FBDD Fragment-based drug discovery
FBS Fragment-based screening
GPCR G-protein coupled receptors
HAC Heavy atom count
HTL Hit-to-lead
HTS High-throughput screening
HTX High-throughput crystallography
IMP Integral membrane protein
ITC Isothermal titration calorimetry
LO Lead optimization
MR Molecular replacement
MST Microscale thermophoresis
MW Molecular weight
NBE New biological entity
NMR Nuclear magnetic resonance
NOAC Novel oral anticoagulant
PDB Protein data bank
PPI Protein–protein interactions
SAR Structure–activity relationships
SBDD Structure-based drug design
SFX Serial femtosecond crystallography
SILCS Site Identification by Ligand Competitive Saturation
SPR Surface plasmon resonance
SR Structural research
XFEL X-ray free electron laser

Software programs and their major applications

AFFIT Program for generating geometrical restraints for small molecules and automatic ligand fitting into electron density
AIMLESS Program for scaling and merging multiple observations of reflections into an average intensity
ARP/wARP Programs for automatic model building and ligand fitting into electron density

autoBUSTER Tools and programs for refining structures against X-ray data
autoPROC Tools and programs to automate the whole range of steps involved in X-ray data processing
BALBES Automatic pipeline for molecular replacement
BLAST or PSI-BLAST Program for finding homologous sequences by (iterative) sequence alignment
eLBOW Program for generating geometrical restraints for small molecules
FoldX Program for quantitatively estimating contributions to protein stability and complex formation
Grade Program for generating geometrical restraints for small molecules
GESAMT Program for structural alignment of macromolecular structures
HHBlits program for finding homologous sequences by iterative comparison of profile hidden Markov models
HKL-2000 Program for processing single crystal X-ray data, scaling and merging of intensities as well as visualization of diffraction images
LABELIT Tools for pre-processing diffraction images, mainly used for indexing single crystal X-ray data
LigandFit Program for automatic ligand fitting into electron density
MOE Integrated drug discovery package
MolProbity Program for validating macromolecular structures
MOLREP Versatile molecular replacement program
MOSFLM Program for processing single crystal X-ray data and visualization of diffraction images
MRage Automatic pipeline for molecular replacement
MrBUMP Automatic pipeline for molecular replacement
PHASER Tools and programs for phasing macromolecular crystal structures, mainly used for molecular replacement and SAD phasing
phenix.ligand_pipeline Automatic pipeline for molecular replacement, refinement and ligand fitting
phenix.refine Program for refining structures against X-ray data
Pipedream Automatic pipeline for processing, molecular replacement, refinement and ligand fitting
Polyphony Tools and methods for the statistical analysis of protein structure ensembles
Protein Ligand interaction Fingerprints application within MOE Application to analyse, categorize and summarize protein–ligand interactions across an ensemble of structures via a fingerprint scheme
PyMOL Program for molecular visualization
REFMAC5 Program for refining structures against X-ray or cryo-EM data
RhoFit Program for automatic ligand fitting into electron density
Robetta Program for building models of protein domains (ab initio or comparative)
Site Finder application within MOE Application for identifying and evaluating binding sites in macromolecular structures
SiteMap Program for identifying and evaluating binding sites in macromolecular structures
TRUNCATE Program for converting intensities into amplitudes and scaling to an approximate absolute scale
WONKA Application to analyse, categorize and summarize protein–ligand interactions, protein conformation and water conservation across an ensemble of structures via a fingerprint scheme
XDS Program for processing single crystal X-ray data
xia2 Tools and programs to automate the whole range of steps involved in X-ray data processing

2.06.1 Introduction

Information on the molecular architecture of important drug targets, the elucidation of their structure–function relationships, and understanding the details of target–ligand interactions have a strong impact on the paths and fates of today's drug discovery projects.

Protein crystallography is the dominant technology that delivers this information. While, in principle, there are also other methods that are able to generate structural information, most notably nuclear magnetic resonance (NMR) spectroscopy which looks at isotopically labeled proteins in solution, structure determination by single crystal X-ray structure determination has turned out to be the most successful, most timely delivering, most broadly applicable, and highest throughput method and has matured to be the "gold standard" technology for structural biology in pharmaceutical research. It is particularly well suited for drug discovery for a number of reasons. It can provide the experimental evidence that a small molecule ligand binds to its target protein and to which functional site it binds. The resolution obtained by X-ray diffraction is high enough to allow for the elucidation of the atomic details of ligand–receptor interactions and the protein conformational changes upon ligand binding. It has no limitations to the size of the studied objects which can be as large as entire ribosomes. It provides a platform for intuitive visualization of drug action and facilitates the understanding of molecular mechanisms of action. And it inspires new hypotheses and experiments to probe the feasibility of small molecule agents to serve as suitable initial scaffolds for lead compounds and to inform the optimization of these initial leads into drug candidate chemical matter.

During the last two decades we have witnessed an explosion both in the number of macromolecular structures as well as of protein complexes with small organic ligands.

This explosion is due to a number of technological developments. Firstly, significant progress has been achieved in methods for recombinant protein production and purification. Secondly, on the level of protein crystallization, the miniaturization and automation, both for initial crystallization screening and crystal hit optimization, lowered the hurdles for entering this process stage and enhanced the probability to obtain high quality crystals diffracting to atomic resolution. For refractive proteins, novel approaches for the optimization of sample preparation such as in situ proteolysis, reductive methylation, or surface entropy reduction have been developed and again improved the probability of crystallization. The mining of the growing body of crystallization data has led to creation of more efficient crystallization cocktail screens. Thirdly, fluorescence-based thermal shift assays and dynamic light scattering are now routinely used for choosing not only the most suitable protein constructs, but also protein buffers or stabilizing ligands prior to crystallization. Further, developments in X-ray data collection protocols, the availability of low noise detectors and sample handling robotics, third-generation synchrotron beamlines, structure phasing approaches using anomalous signal and cryo-crystallography, supported by the concomitant development of associated software have greatly reduced the efforts to collect data and solve, refine, and validate the crystal structures. These technological advances have been spurred for the most part by the initiatives that followed the genome sequencing projects and focused on protein structure and function ("structural proteomics").

As a consequence of these developments, nowadays protein crystallography in drug discovery is operating in a high-throughput mode (high-throughput crystallography—HTX). Enablement of project support is done on time scales aligned with other project time scales, which often means that the three-dimensional structure of the target and a crystal form allowing for fast ligand costructure determinations are available at early stages in the drug discovery process. Therefore, areas of application span the entire project lifetime, starting with structure-based analysis of the "ligandability" of a drug target, supporting the hit validation stage after a biochemical or cellular high-throughput screening (HTS), entertaining fragment-based screening (FBS) activities as well as informing hit selection, and the crucial early stages of the hit-to-lead (HTL) phase. Finally, even for the ever growing area of biologics discovery, protein crystallography has an impact for instance in the definition of the antigen epitope. In the following sections we will discuss first the historical development of industrial protein crystallography and methods applied to achieve high throughput, before focusing on applications in the aforementioned drug discovery project phases.

Despite the tremendous progress made during the last 20 years, there still remain significant challenges and limitations to the technology. These comprise, for example, difficulties in protein crystallization due to protein conformational diversity, limitations in the understanding or preparation of protein chemical heterogeneity such as posttranslational modifications, dealing with intrinsically disordered but functional sections of protein primary structure, as well as limited experience in the work on integral membrane proteins (IMP), an endeavor which still is not routinely used in today's pharmaceutical protein crystallography. All these factors contribute to the failure of our technology in supporting a significant subset of projects. Finally, there remains a significant challenge to exploit the vast body of structural information obtained throughout a project lifetime. Suitable and efficient tools for structural data mining and aggregation of the information of a multitude of ligand costructures are still largely missing and often main conclusions are drawn for inspecting superpositions of just a few individual structures.

Toward the end of this review, we are describing our view on the future development of the field by describing the recent advances in the field of IMP structural biology and the developments in the areas of X-ray free electron lasers (XFELs) as well as cryo-electron microscopy (Cryo-EM) and their expected impact on our field of expertise within drug discovery.

2.06.2 Historical Development

The determination of the three-dimensional structures of myoglobin and hemoglobin around 1960[1,2] heralded the advent of protein structural biology. It showed that protein structures could be determined at atomic resolution and that molecular structures could potentially be useful to unravel the molecular nature of disease processes.

However, it took another 15 years until protein structures were used to guide synthesis of ligands for hemoglobin,[3] to our knowledge the first report to describe the process of design of "compounds … to fit a site of known [protein] structure". In a *Nature* review in 1976, Max Perutz predicted that "knowledge of the three-dimensional structure of these enzymes may open the way to the synthesis of tailor-made inhibitors for the treatment of such diseases" using examples from the serine protease field and their role in blood coagulation and lung disorders.[4]

In the 1960s and 1970s, a number of crystal structures of pharmaceutically relevant protein class representatives were determined, among them members of the trypsin family of serine proteinases, of the aspartyl protease family and influenza virus neuraminidase.[5–9] The structural information was used to understand the molecular details of the function of the proteins, to derive models for the actual drug targets (eg, of the blood clotting enzymes from structures of the homologous chymotrypsin/trypsin) and to describe the topology of the binding sites and their interaction with physiological ligands.

Based on the great potential seen in the application of the technology in pharmaceutical research, in the 1980s the first industrial protein crystallography laboratories were established, often as an experimental section within existing groups of computational chemists.

The pioneers in the pharmaceutical industry had to face a multitude of difficulties: few crystallographic software tools were available, computing power was small, diffraction data collection was done on the first expensive, semiautomated X-ray detectors

mounted on low intensity in-house X-ray generators. All the steps of structure determination had to be done "manually" and throughput was low.

By the mid-1990s all major pharmaceutical companies had invested into protein crystallography units and with the foundation of Agouron and Vertex Pharmaceuticals the first biotech companies had emerged whose business concept relied on the use of structure-based design to develop superior drugs.

At that time, with the boost in computing power and development of improved software tools, the availability of synchrotron beamlines for efficient data collection and advanced structure validation tools, industrial protein crystallography aiming at resolving the structures of pharmacologically important drug targets and their ligand complexes had become much more a routine endeavor and "high-throughput" crystallography—in this context the concept of generating a multitude of protein–ligand costructures in a short period of time—had come within reach. Importantly, in this phase the advances of molecular biology and protein expression and purification technologies had made many drug targets accessible for the crystallography labs.

The sequencing of the human genome[10,11] led to the conception of "structural genomics" in the early 2000s. Many publicly and privately funded consortia across the world started to determine the structures of proteins from a certain species or involved in certain diseases.[12] Industry benefited tremendously from these initiatives because many new structures were determined and new methods were developed along the way. This enabled a further increase in throughput and new concepts like X-ray crystallography-based fragment screening were established.[13,14]

Finally, more recently, structural biology of membrane proteins, invoked in the late 1980s, but for a long time refractive to application in pharma research, has become amenable. This is particularly apparent in the field of G-protein coupled receptors (GPCRs), among the largest families of drug targets, for which an increasing number of representatives are being structurally characterized[15,16] (for an overview on the described timelines see **Fig. 1**).

But how did this technological development impact the output of drug discovery?

The first drug derived from structure-based approaches that came to the market was Captopril in 1981.[17,18] This antihypertensive drug is directed against angiotensin-converting enzyme (ACE). While the structure of ACE was determined in 2003,[19] the design of captopril was based on the then available crystal structure of bovine carboxypeptidase A and information on the mode of substrate binding to this surrogate structural model. In the following years, major contributions to the discovery of new drugs have been made especially for antiviral drugs, for example, nelfinavir,[20] amprenavir,[21] lopinavir,[22] zanamivir,[23] and oseltamivir[24] (**Table 1**). The two latter compounds were developed based on structural information on influenza virus neuraminidase.[8] The key observation leading to zanamivir was the binding mode of sialic acid, the product of the enzymatic reaction.[25,26]

By 2003, >40 compounds discovered by structure-guided approaches entered clinical trials[27] and 7 had become approved and marketed drugs.[17] As of today, this list has to be expanded with numerous kinase, proteinase, phosphodiesterase inhibitors which were discovered and optimized using structural information.[28] Given the lag time of approximately 10–12 years between the discovery of a drug and market approval, the success stories known today have their origin in the 2000–05 time frame. Prospects are such that the majority of drugs approved in the future will have been discovered with the help of knowledge of the structure of the target protein.

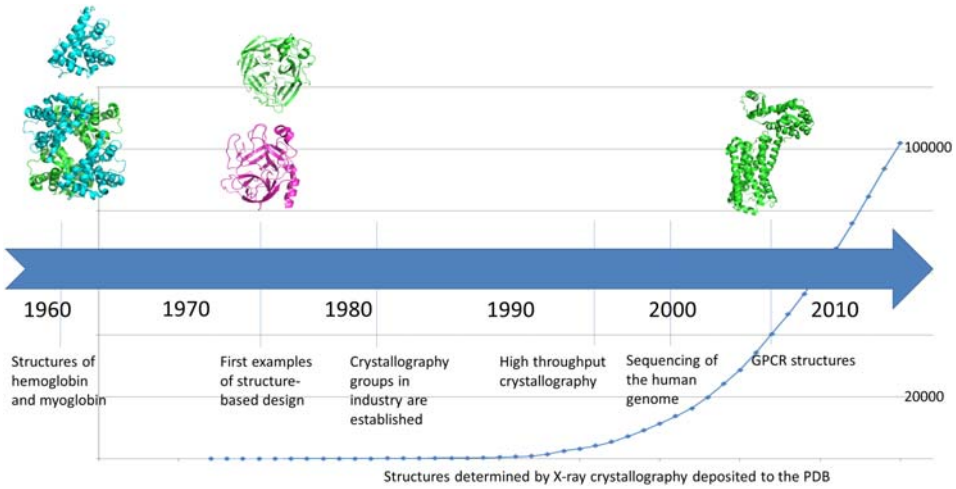

Fig. 1 Key dates and milestone achievements of protein crystallography in drug design. The structures shown are of hemoglobin, myoglobin, trypsin, neuraminidase, and β2-adrenergic receptor. The chart in the background shows the exponential growth in structural information contained in the PDB. Concerning the absolute numbers of structures deposited in the PDB, it is to be noted that the vast majority of protein–ligand complex structures determined in pharmaceutical industry in high-throughput manner is not deposited in the PDB due to both the confidentiality involved and the additional effort to do so.

Table 1 Antiviral drugs discovered with contributions from structure-based design

Trade name	*Generic name*	*Structure*	*Mechanism*
Viracept®	Nelfinavir	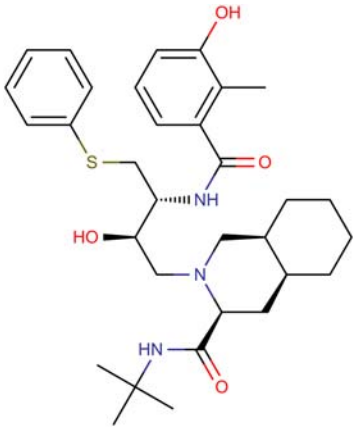	HIV protease inhibitor
Agenerase®	Amprenavir	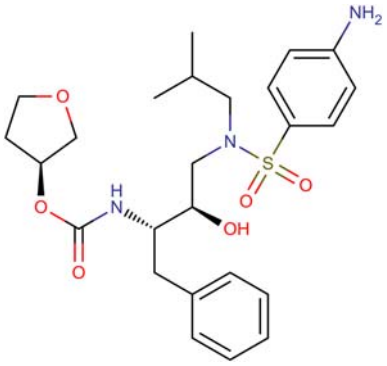	HIV protease inhibitor
Aluviran®	Lopinavir	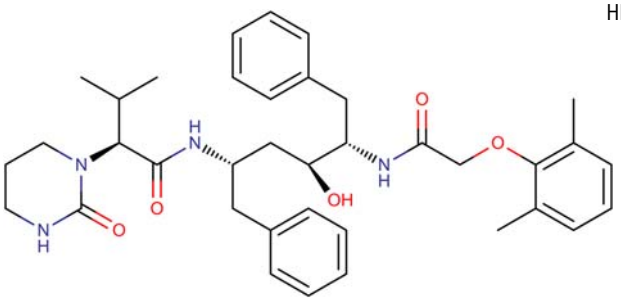	HIV protease inhibitor
Relenza®	Zanamivir	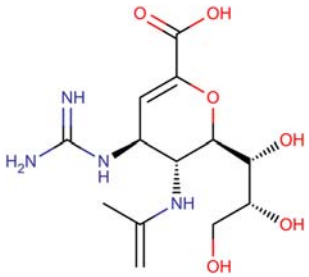	Neuraminidase inhibitor
Tamilfu®	Oseltamivir	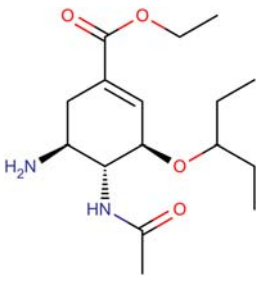	Neuraminidase inhibitor

2.06.3 Methods

Establishing high-throughput processes in structural biology involves the implementation of highly efficient workflows in the entire value chain from protein to 3D structure: protein cloning, expression and purification, protein quality control, crystallization, generation of protein–ligand cocrystals, crystal harvesting, storage and mounting, data collection and evaluation, and structure determination and validation (Fig. 2). We will not cover the issues of generating a relatively high amount of high quality, crystallization grade protein as well as the initial protein crystals in this review. Instead, in the following paragraphs, all steps from the generation of a cocrystal to structure validation are discussed with an emphasis on the establishment of robust high-throughput procedures.

2.06.3.1 Generation of the Complex—Cocrystallisation and Soaking

After obtaining the first crystals of the respective target protein, an essential step is to develop a robust protocol for the reproducible generation of a large number of high quality crystals. A typical goal would be to establish a crystallization protocol delivering tens to hundreds of crystals of constant quality diffracting to 2.5 Å or better from a setup of a few 24- or 96-well crystallization plates. Time invested at that early stage in the optimization of such a crystal system is well spent, since it makes all later process steps much easier. For this purpose screening of crystallization conditions using variations of buffer components and pH as well as other additives turn out to be very helpful.[29–32] For an increase in resolution after crystals have been obtained under optimized conditions crystal dehydration can be applied.[31,33–35]

There are two general methodologies of obtaining complexes between a target protein and a small molecule ligand: cocrystallization and compound soaking. There are pros and cons for each of the methods and the most suitable needs to be selected in a protein and crystal target dependent manner.

2.06.3.1.1 Cocrystallization

In the cocrystallization setting, protein and ligand are mixed prior to the crystallization experiment such that the protein crystals grow in the presence of the ligand. To get a good occupancy of the ligand at the protein binding site as a rule of thumb, the compound concentration should be around 10 times higher than the protein concentration. If the ligand solubility is very low, it is possible to mix protein and ligand at low protein concentration and concentrate the complex to the desired protein concentration prior to crystallization. Introducing the ligand at this stage can have a big positive or negative influence on the outcome

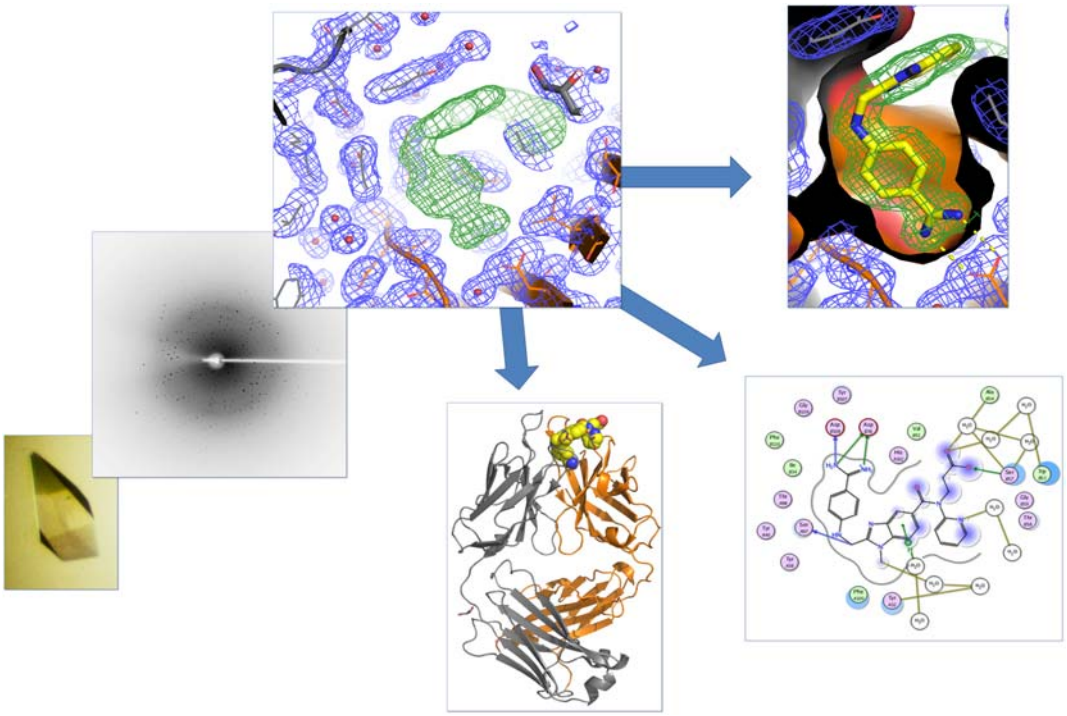

Fig. 2 Workflow in protein structure determination by X-ray crystallography. Depicted are a microscopic image of a protein crystal, an X-ray diffraction pattern, and a representation of the electron density and the protein model. The difference density (in green) clearly indicates the presence of a ligand. Different representations of the structural data are shown on the right. A surface representation of the binding pocket with bound ligand and polar interactions (yellow dashed lines), a ribbon representation of the complete protein:ligand complex, and a 2D representation of the interactions of the ligand (generated with PyMOL and MOE).

of the crystallization experiment. It is quite often observed that the addition of a ligand leads to a stabilization of the protein and thereby facilitates crystallization and improves crystal quality. On the other hand, ligand binding might induce conformational changes in the protein that do not fit the crystal packing arrangement of the unliganded protein. In such a case, for each new ligand a separate crystallization experiment, often even a small crystallization screen needs to be performed, so that the throughput for this method is limited.

2.06.3.1.2 Soaking

Protein crystals have a relatively loose crystal packing and a correspondingly high solvent content. Typical protein crystals have a protein volume content of $<50\%$. Solvent channels have diameters of 5–50 Å. A ligand can therefore quickly diffuse through the channels to the binding site of the target protein provided the respective binding site is freely accessible for the ligand, for instance by facing a solvent channel. The process of generating a protein–ligand complex in situ by letting the ligand diffuse into a preformed crystal of unliganded protein is called "soaking". This is done by addition of ligand to the *mother liquor* (the aqueous buffer within which the crystal has grown) or the *stabilizing solution* (a buffer that will prevent dissolution of the crystals, warrant a long-term stability of the crystals and maintains their diffraction quality) in which the preformed crystals reside. The ligand can be supplied either by dilution of a compound stock solution (eg, in dimethylsulfoxide (DMSO) or aqueous buffers) into the mother liquor or by addition of solid material which subsequently dissolves in the liquor surrounding the crystals. In any case, the concentration of the soaked ligand should exceed the expected dissociation constant of the ligand about 10 to 100 times. For low affinity binders such as fragments, it is often useful to approach the maximally possible concentration by generating a saturated solution of the ligand in the soaking buffer. Once the ligand is supplied to the medium, the ligand concentration gradient between the surrounding mother liquor and the solvent channels inside the crystal induces the onset of diffusion. Diffusion processes in the crystalline environment are relatively fast so that the interior crystal environment equilibrates within a few minutes. Depending on ligand binding kinetics, mass transport limitations and additional factors such as kinetic barriers to complex formation productive incubation times can vary from as short as a few minutes to hours or even a few days.

From the perspective of throughput optimization and process efficiency, crystal soaking is the ideal method to generate protein–ligand cocrystals. In contrast to cocrystallization, many crystals of the empty target protein can be generated using a given crystallization protocol and multiple ligands can be soaked in a highly parallelizable way to generate a multitude of different cocrystals within a few hours.

In the described ways, it is often straightforward to obtain protein–ligand complexes. However, there are cases in which soaking is problematic or even impossible. For instance, sometimes a ligand-free protein cannot be crystallized. If crystallization of a complex of this target protein with a relatively weakly binding tool compound can be achieved, these crystals can be used for soaking if it is possible to generate the ligand-free form of the crystals by diluting out the tool compound or if the added ligand is able to displace the cocrystallized tool compound in situ, a process called "counter-soaking." Other underlying reasons for the failure to establish a successful soaking protocol can be low aqueous ligand solubility or limited solubility in the soaking solution, a soaking buffer pH that is incompatible with the binding event or the partial or full occlusion of the binding site by neighboring protein molecules in the crystal lattice. To overcome the solubility problems solubilizing agents, pH, or temperature changes, exchange of buffers, salts, or precipitants can be explored. Another way to overcome solubility issues is to increase the solubility by added increasing amounts of solubilizing solvents to the aqueous soaking buffer. After suitable stabilization of the crystals, sometimes using crosslinking (see below), the crystals can be transferred into, for example, water/DMSO mixtures with high DMSO content ($>50\%$) in which ligands can be dissolved at much higher concentrations. A similar mechanism is used by Proteros using their "picodropper"-system which titrates DMSO solutions of the ligand onto crystals stabilized in a "free-mounting" system[35] and generates a new crystal saturated with ligand and DMSO.

With regard to occluded binding sites, it is often possible to screen for new crystallization conditions generating crystals with a different crystal packing.[36,37] If the crystals are sensitive to compound addition and significantly lose diffraction quality or even crack or dissolve once ligand is added, chemical stabilization of the crystal by crosslinking reagents, for example, glutaraldehyde can be a method of choice.[38]

At times it is claimed that soaking will not be able to produce an unbiased cocrystal structure, because binding within the solid state and the resulting limitations of protein dynamics will influence the binding mode. However, crystal packing energies for protein crystals are relatively small and proteins are highly dynamic even when fixed in a crystalline environment. Consequently, relatively large protein conformational rearrangement can be tolerated by the crystal lattice. Therefore, in many cases the structures obtained by ligand soaking and ligand cocrystallization are very similar and the numbers of examples in which an artifactual ligand pose was generated by soaking are rare.

2.06.3.2 Crystal Harvesting, Flash-cooling, Storage, and Mounting

After successful crystallization of a protein, the next step is to prepare the crystal for X-ray data collection. The crystal needs to be retrieved from the drop of stabilizing buffer. Nowadays, this is done by seizing the crystal with a small nylon loop mounted on a steel pin.

The crystals need to be flash-cooled in liquid nitrogen for long-term storage, transport, and data collection at a synchrotron light source. The crystallization conditions of proteins are often not suitable for flash-cooling and hence there is a need for finding a suitable cryoprotectant that hinders ordered ice formation. Identification of a good cryoprotectant is a trial and error process for which

a few screens are available.[30,39] Addition of the cryoprotectant to the stabilizing solution generates the *cryo buffer*. In the ideal case the stabilizing solution is already cryogenic. Flash-cooling the crystal is achieved by plunging the crystal into liquid nitrogen.

With this procedure, numerous crystals can be flash-cooled in a short period of time and stored in vials in liquid nitrogen containers. In this flash-cooled state, crystals have an essentially unlimited lifetime. The cryogenic storage provides a convenient way to send samples to a synchrotron light source for data collection. It is of utmost importance that the crystals do not undergo thaw-freeze cycles at any time when transferring the vials between storage and shipment dewars or from storage to the diffractometer. To ensure this, special cryo-tools are available to protect crystals during the transfer (dry mounting). The diffractometer has to be equipped with a cooling device which immerses the crystal in a stream of cool nitrogen gas (usually at 100 K) during data collection. It is also possible to transfer the crystal-pin together with the cap filled with liquid nitrogen in which it was stored to the instrument and quickly remove the cap (wet mounting). This procedure has the advantage to be faster than the dry mounting procedure but can cause turbulence around the crystal which can lead to a warm up of the sample.

Procedures for flash-cooling protein crystals were established in the 1990s and quickly popularized because of the ease of handling and because of the fact that in a flash-cooled state the crystals turned out to be much less sensitive to radiation damage especially when using synchrotron radiation. It should be noted that with the availability of new single pixel counting detectors which enable data collections speeds in the order of hundreds of images per second data collection might become faster than the progress of radiation damage that ultimately destroys the crystal's ability to diffract. This will lead to a renaissance of room temperature data collection for samples for which it is difficult to establish a cryo procedure.

2.06.3.3 Diffraction Experiment, Structure Determination, Ligand Placement, and Refinement

The steps to produce an X-ray crystal structure for a crystallized protein–ligand complex of a protein with a known structure usually are the following:

(i) X-ray data collection resulting in a set of diffraction images (Fig. 3)
(ii) Data processing resulting in a space group, a unit cell and structure factor amplitudes
(iii) Molecular replacement (MR)
(iv) Initial crystallographic refinement of the model
(v) Generating a model of the ligand and a restraints dictionary
(vi) Ligand fitting
(vii) Refinement of the protein–ligand complex
(viii) Model validation, inspection

X-ray data sets are either collected at a synchrotron beamline or using an in-house diffractometer. It includes mounting of a (cooled) crystal onto the goniometer, centring the crystal in the X-ray beam, and collecting a data set using an appropriate strategy. The data collection strategy depends upon the instrumentation and crystal properties such as space group, unit cell dimensions, mosaicity, and sensitivity to radiation damage but also highly on what is to be done with the data. The goal of a suitable data collection strategy for ligand binding studies is to achieve a high resolution and completeness as well as a moderate redundancy of the diffraction data while at the same time achieving a high turnover.[40] Special care has to be taken to avoid radiation damage. Bound ligands might be highly sensitive to radiation damage. Documented cases are cleavage of aromatic carbon–halogen bonds with release of the halogen atom and of sulfonamides.[41] Data processing includes the indexing and the integration of diffraction spots resulting in reflection intensities, the determination of the Laue group and Bravais lattice type, scaling and merging of symmetry equivalent reflections, as well as converting intensities into structure factor amplitudes. Programs widely used in the community

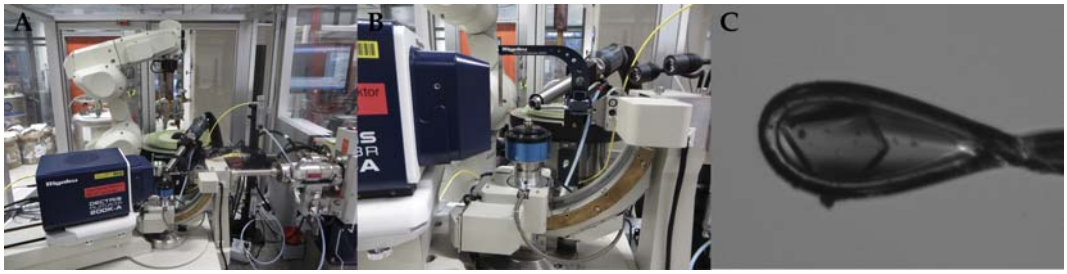

Fig. 3 Setup of an in-house, automated X-ray station. (A) Overall view upon the system. The rotating anode and X-ray optics are on the right. The beam traverses the collimator and hits the crystal, before reflected X-ray beams hit the Dectris Pilatus detector shown on the left (blue box). In the background, an ACTOR robot with its dewar are there to facilitate automated crystal mounting from storage positions inside the dewar. (B) Zoom on the crystal position. Using a mounting onto an automated "microglide" mount instead of a regular goniometer head, the crystal can be automatically centered in the X-ray beam. The crystal is positioned such that it resides in a nitrogen stream of nitrogen gas at 100 K. The nitrogen gas nozzle from an Oxford Cryosystems Cobra instrument protrudes from the upper right corner. (C) A flash-cooled crystal in a nylon loop during an ongoing X-ray diffraction experiment.

are XDS,[42] HKL-2000,[43] MOSFLM,[44] AIMLESS,[45] and TRUNCATE.[46] With autoPROC [47] and xia2,[48] powerful automated expert systems are available. Statistical (precision) indicators to assess quality and to deduce the high-resolution cut-off of the merged data set are Rmeas, CC1/2, Rpim, and mean(I/sig)mrgd. A detailed discussion can be found in Karplus and Diederichs.[49]

The MR step is optional, depending on the actual extent of nonisomorphism of the known structure used as initial model and the structure to be solved. It is run to correct coarse differences in orientation and placement of the initial model or components of the model and to account for a change of the number of molecules within the asymmetric unit. The programs MOLREP[50] and PHASER[51] are widely used for MR. MrBUMP,[52] MRage,[53] or BALBES[54] are all very robust automated MR pipelines allowing the input of a custom set of pdb files as search models. If there are only minor changes the MR step can be replaced by a thorough rigid-body refinement with a sufficient convergence radius.[55]

Refinement is run to improve the parameters of the current working model until a best fit to the experimental data is achieved. A sensible parameterization of the model is highly important since an over-parameterized model will cause overfitting of the data. Usually, only positional coordinates of atoms and B factors are refined. B factors or atomic displacement parameter (ADP), sometimes referred to as the "temperature factor," in theory should reflect the amplitude of atomic movement around an equilibrium position. In reality, B is a capacious parameter, capable of absorbing many other effects, such as static disorder or even experimental errors.[67] During refinement, typically, bond lengths, bond angles (and torsion angles), planar groups, repulsion between nonbonded atoms as well as B factor differences between bonded atoms are restrained to their ideal values. Since isotropic B factors are an oversimplification but anisotropic B factors can only be refined at atomic resolution (due to the sixfold increase in ADPs), the TLS parameterization has been introduced to model the anisotropic movement of sets of atoms (TLS groups[56]). For each TLS group, a pseudo-rigid body, parameters for translation, libration, and screw-rotation displacement are introduced and refined. Occupancies should only be included in the refinement when needed or justified by the quality of the data. To enlarge the convergence radius during early stages of initial refinement it is common to parameterize the model as rigid bodies of molecules or domains. The parameterization as torsion angles during refinement rounds of simulated annealing is also very powerful in terms of escaping local minima. Recently, real-space rotamer correction of amino acid side chains also became available as a routine during refinement further automating the correction of local misfits to the density.[57] If available, noncrystallographic symmetry should be exploited and (local) noncrystallographic symmetry restraints applied.[57–59] If needed, external restraints to a reference structure solved at high resolution can be used to stabilize low resolution refinement.[57–59] Water molecules are handled in different ways. The most common procedure is to either delete all waters or to only keep well defined, conserved water molecules of the starting model. Updating water molecules automatically during refinement is a common practise for high to medium resolution structures. Common programs for these tasks are autoBUSTER (Global Phasing Ltd.), REFMAC5,[58] and phenix.refine.[60]

The preferred starting point for generating a model and a dictionary of refinement restraints (idealized geometric parameters) for the ligand is a format describing connectivity, atom types, and stereochemistry. If there is no information on the latter, all possible stereocentres have to be enumerated. The tautomeric state of the molecule should also be considered as it can have a strong influence on the geometry of its 3D structure. Programs widely used include Grade (Global Phasing Ltd.), eLBOW,[61] and AFFIT.[62] eLBOW and Grade make use of geometry optimization using a quantum chemical method alone or in combination with data mining in small molecule databases. AFFIT uses a molecular mechanics force field to derive model restraints.

Ligand fitting starts with the assessment whether (difference) electron density blobs after refinement justify attempting ligand placement. After blobs of suitable size have been identified, the ligand or set of ligands (stereoisomers, tautomers) can be fit either automatically or manually. There are various programs available that produce excellent results in automatic fitting. Coot (either built-in routine or standalone executable findligand[63]), LigandFit,[64] RhoFit (Global Phasing Ltd.), AFFIT,[62] and ARP/wARP[65] are widely used. Usually, the fit to the density and the binding site are automatically assessed.

After ligand fitting, the protein–ligand complex is refined typically using a similar but less thorough protocol as during initial refinement. The final model needs to be validated and inspected manually. In the past, there have been cases in which a proper validation was not done.[66] In consequence, any published structural information has to be analysed with care prior to use.

2.06.3.4 The Challenge of Automation

To approach or achieve high-throughput hardware and software automation is essential for a structural research (SR) lab in industry. This is true for cloning, protein expression, and purification (not covered here), but even more important for crystallization, data collection, and processing as well as refinement and ligand fitting.

The availability of liquid handling systems and commercial crystallization kits has largely led to a standardization of protein crystallization.[67] Usually, a dedicated crystallization robot for setting up nano-liter sitting drops is used to screen sparse matrix and/or incomplete factorial screens.[68] Automating liquid handling has the benefit of increasing speed and decreasing sample volume. At the same time, it also increases the robustness of the whole process. Once initial crystallization conditions have been found, it may be beneficial to set up optimization trials using larger volumes by hand. Reservoir solutions for this step can conveniently be prepared using general or dedicated liquid handling systems such as the Formulator (Formulatrix, Inc.) or the dragonfly® (TTP Labtech Ltd).

Automated crystal harvesting is needed to bridge the gap between automated crystallization and data collection units and to improve the reliability and reproducibility of the whole process. Several (semi-) automatic procedures are available that demonstrate the feasibility by different methods (eg, microtools, microelectromechanical systems, or laser ablation) but are not yet commonly used.[69,70]

Data collection, either at the home source or at a synchrotron beamline, can be fully automated nowadays. Sample mounts and storage systems are to a great extent standardized. Sample changers are available from commercial suppliers and most synchrotron beamlines and many industrial home lab systems are equipped with automated sample mounting systems which can transfer crystals without user intervention. Software for automatic loop centring is also available.[71–73] If the sample is about the size of the loop and fairly homogeneous, results from this simple approach can be of sufficient quality. For challenging samples diffraction based centring has to be used to define the best diffracting volume of the sample.[74]

The quality of the data and the subsequent crystal structure are strongly affected by an adequate data collection strategy. Therefore a highly reliable, automatic determination of crystal symmetry, unit cell parameters, mosaicity, and radiation sensitivity is a pivotal step to successfully collect good quality data.[75] EDNA MX[76] has been developed for this purpose. The ESRF beamline MASSIF-1[74] is currently the only beamline where sample characterization and data collection is fully automated.

Solving the *n*th crystal structure in a project is unsatisfactory if done manually and a serious waste of time. Most pharmaceutical companies have developed proprietary pipelines to accomplish this task automatically (eg, see Refs.[78,79]). Companies focusing on FBS have published details of their automation process, for example, the Astex "Pyramid" Process[80] or the "FAST" approach at SGX.[81]

At synchrotrons, usually a data processing pipeline is available.[82,83] Recently, a pipeline encompassing all stages starting from integrated and scaled intensities has been implemented in Phenix (phenix.ligand_pipeline[84]). A pipeline named Pipedream that also includes data processing is available from Global Phasing Ltd.

An automation pipeline in industry is best organized on a project and sample orientated level. Information on space groups and unit cell dimensions, initial pdb files, or reference mtz files for a new sample can conveniently be defined by the project setup. Information on the ligand needs to be stored separately for each sample. Maintaining and retrieving this information in/from a laboratory information management system can be highly beneficial. The steps carried out by the pipelines usually are data processing (optional), molecular replacement (optional), initial refinement of the model without the ligand of interest, generating a ligand restraint dictionary, ligand fitting, refinement and validation of the complex.

A custom pipeline can be designed, making use of powerful existing standalone programs (described in **Diffraction Experiment, Structure Determination, Ligand Placement, and Refinement** section). The indexing routine to deduce the crystal lattice needs to be very robust to automatically deal with difficult diffraction patterns. LABELIT[77] is a very good choice for this task. Especially in projects where one has to rely on cocrystallization to generate crystals of the protein–ligand complex, support for multiple crystal systems is important. A robust algorithm needs to be in place to reliably identify the correct crystal system or to trigger processing without using a known crystal system as reference. For data processing, powerful expert systems such as autoPROC[46] or xia2[47] can conveniently be integrated. During refinement robust defaults for the parameterization have to be in place to properly refine structures from different projects and at different resolution. The advantage of a custom pipeline is the possibility to plug in several ligand fitting routines to maximize the success rate.

After refinement of the complex, a thorough validation is important to enable rapid elimination of problems during manual refinement rounds. Results should be accessible via an interface to ease browsing.

2.06.3.5 Validation of the Final Structure

The quality of protein–ligand structures is of high importance for structure-based design since the information is used to guide synthetic strategies aimed at improving protein–ligand interactions.

For all successive steps of the structure-based drug design (SBDD) workflow, therefore, a thorough validation of ligand costructures is essential to ensure that the structural models are correct. Two aspects need to be checked: Does the model fit the electron density (the primary evidence) and is it consistent with basic physics, chemistry, and biology (prior knowledge).[85]

The most important global validation measures indicative of the overall quality of the model are the R-factor and R-free.[86] Both measure the difference between observed and calculated diffraction data. R-free is being used for cross-validation during refinement to avoid overfitting. It is important to note that the resolution only places a limit on the precision of the model. It does not provide any information about its quality.[87] Local measures such as the real-space correlation coefficient, the real-space R,[88] or the recently proposed metrics for local model accuracy and precision, the real-space difference density Z-score, and the real-space observed density Z-score,[89] can be used to judge the local quality of the model in terms of fit to the electron density. (Of course, local measures can also be averaged into global measures.)

Consistency with basic knowledge can, to a great extent, be checked by locating implausible features in stereochemistry, in the chemical environment, or in coordination geometry, often combined with improbable refinement results such as absurdly high or low B factors.[90]

The root mean squared deviation of bond lengths, angles, and planes from their target value are used to assess the stereochemical quality of the model. Deviations from experimental target values are usually expressed in multiples of the standard deviation using statistics such as Z-score.[85] For the parameterization of the protein geometry, a standard set of means and standard deviations is used which was derived from atomic resolution structures of amino acids and peptides.[91] For ligands, Mogul can be used to derive target values and uncertainties from the Cambridge Structural Database and to validate geometry.[92]

Combinations of the main-chain φ and ψ torsion angles as well as side-chain χ torsion angles are a valuable source for validation as they are (still) rarely restrained.[93] Today, the program MolProbity[94] is commonly used to calculate validation statistics for these as

well as for all-atom contacts (physically impossible overlaps). Since hydrogens are usually not modeled explicitly in refinement the latter is a powerful validation tool as well.

2.06.3.6 Communication of Results

The delivery of results to customers, typically project teams consisting of medicinal chemists and computational chemists, is the final step of structure determination of protein–ligand complexes in industry. Since all colleagues that are not well-trained structural biologists will need assistance when looking at and using data from X-ray crystallography, a carefully implemented process to communicate results is essential.

Of course, the basis is a careful evaluation of the structure quality and the analysis of the resulting structure in terms of details of the protein–ligand interactions, the evaluation of the bound conformation of the ligand, and the changes in the protein structure and dynamics upon ligand binding. The resulting information package contains structure validation data and the interpretation of the structural data by the X-ray crystallographer. It is typically provided as a document or slide deck. For validation statistics spider diagrams (as used by POLYGON[95]) or slider representations (as used in the wwPDB validation report[96]) are generally more useful than tables.

Further, the final structure needs to be deposited in a structure repository or file archive. Easy access to structures can be supplied for instance either via PSILO® (Chemical Computing Group Inc.) or Proasis3 (Desert Scientific Software Pty Ltd).

Finally, it is also essential to provide project session files using molecular visualization systems like PyMOL (Schrödinger LLC.). These session files typically contain all structures of relevance for a given project, supplied as superimposed structures, and are used for interactive 3D sessions with the project team or for individual use. The structures can suitably be grouped by ligand classification based on chemistry and by the source of the data (public or in house). Access to electron density maps or at least to scoring via per-atom real-space quality indicators is very important to guide structure-based design. The visualization system has to be flexible enough to include (per-residue) comments and results from other sources such as computational chemistry or screening.

Despite the fact that in many projects a large number of costructures are determined today, only few systems have been developed to provide an aggregated view on information contained in the entire data set. The Protein Ligand Interaction Fingerprints application within MOE (Chemical Computing Group Inc.) can be used to analyse, categorize and summarize protein–ligand interactions across an ensemble of structures via a fingerprint scheme. WONKA[97] extends this kind of analysis to protein conformation and water conservation. Another option that is only infrequently seen in the literature is the analysis of ensembles of crystal structures by principle component analysis,[98–101] Polyphony[102] being a recent and powerful application to accomplish this task. However, despite the availability of these tools, common practice still is to visualize structures alone or as pairwise superpositions and conclusions are drawn from there.

In our experience, it is of paramount importance to entertain face-to-face discussion with project team members as the best form of communication as only in this way it is ensured that no information is lost and a detailed discussion of the implications of the structural data is possible.

2.06.4 Applications

The drug discovery process can be subdivided in a series of project phases that build upon each other, starting with the first idea for a new project and ideally culminating in the handover of a drug candidate molecule to preclinical development (**Fig. 4**).

We will outline in this article why structural biology support in general is a great asset in this process and how knowledge of the three-dimensional structures of protein targets and their ligands—be they endogenous or synthetic—can accelerate and guide drug discovery greatly. We will discuss the various steps using case examples from "real-life" projects conducted at BI.

Historically the focus of SR activities has been in the lead optimization (LO) phase, probably due to the difficulties of obtaining target crystal structures early and the low throughput for protein–ligand costructure determination. It is now commonly accepted that SR enabling should start as early as possible—ideally synchronized with project initiation in other functions—in order to have high-throughput systems for structure determination and biophysics in place once a project enters the lead identification phase.

We will see in the following paragraphs that in this way highest possible project impact is given both through timely validation and quantification of ligand binding, the latter via biophysics, and provision of binding modes of the various possible starting points via X-ray crystallography. Over the lifetime of a typical project nowadays up to 100–300 costructures are generated.

X-ray crystallography is the most widely used technique for protein structure determination in industry, which will be reflected in our choice of examples. Other biophysical technologies can be nicely complementary. In paragraphs "**Hit Validation**" and "**Structure-based Molecular Design**" we will show how these methods are integrated. In the last paragraph ("**Biologics discovery**") of this article we will discuss how X-ray crystallography can leverage the discovery of biological drug molecules (new biological entities, NBEs).

2.06.4.1 Structure-based Target Assessment

The huge amount of structural data that is available in the public domain enables the structural biologist to support the assessment of new target ideas. Typical questions raised in this context concern the nature of known binding pockets of the molecule, the

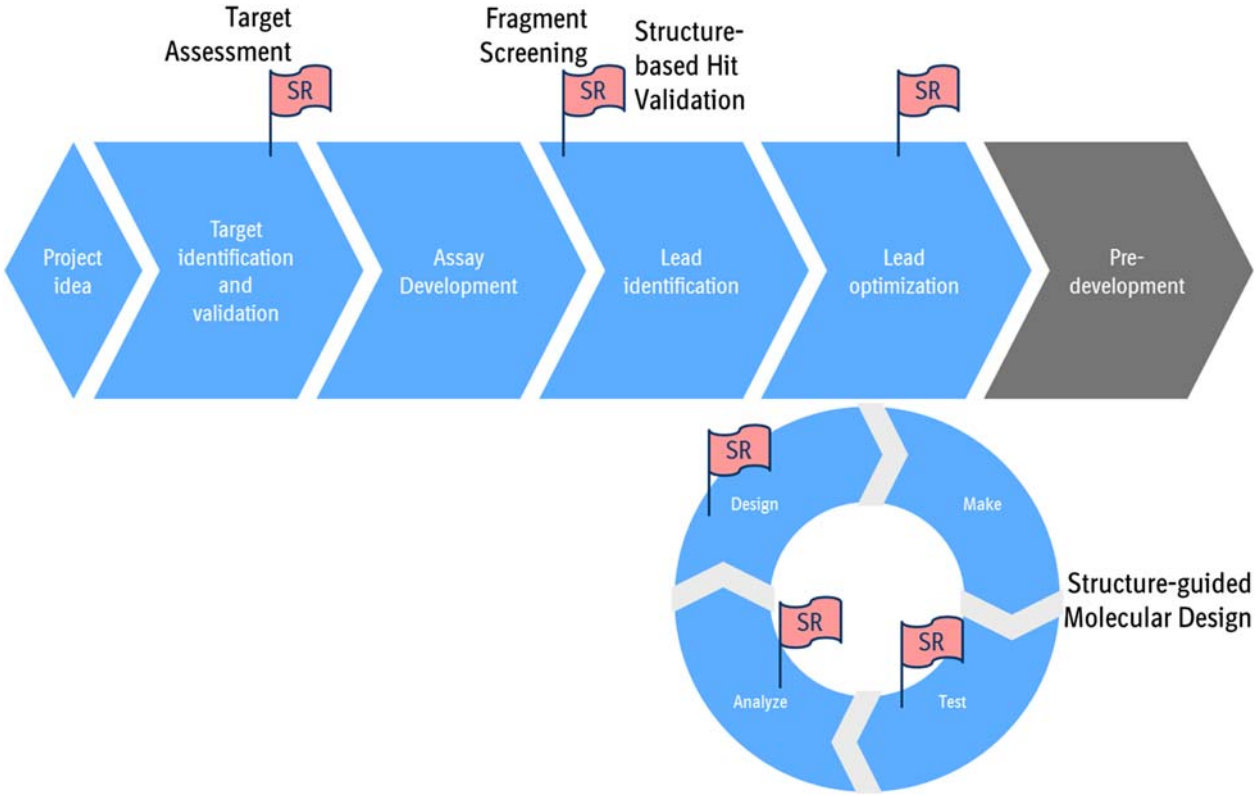

Fig. 4 Applications of structural biology and biophysics technologies in drug discovery. The various phases in the drug discovery process comprise the target identification, development of appropriate assays to test the target function and to screen for chemical starting points, identification of suitable starting points (leads) for medicinal chemistry, and the optimization of these leads toward a desired compound property set. Structural research (SR) can contribute to various phases: a structure-based target assessment, structure-based hit validation after a HTS-based finding activity or fragment-based screening, and supporting structure-based molecular design activities.

possible mechanism of action, or the chance to obtain selectivity against antitargets (see paragraph "**Fragment-based Screening**"). A common workflow usually starts with a query of a sequence database of the protein data bank (PDB) by using BLAST or PSI-BLAST,[103] HHBlits,[104] or a similar sequence search tool. Depending on the chosen cut-off value, one obtains a list of PDB entries of the target protein and proteins similar in sequence. If structural information for the target or a close sequence homolog is available it is possible to search for structurally similar proteins or domains by using the program GESAMT.[105] The structures of interest that are retrieved in these ways need to be superimposed and analysed. If there is prior knowledge about interesting binding sites available (eg, the active site or an effector binding site), these can be analysed with respect to their properties, that is, shape, size, and distribution of charged, polar, or hydrophobic surface patches or metal-ion binding. Taken together, these parameters define the propensity of the respective pocket to bind drug-like molecules, the "ligandability" or "drugability" of the putative functional site. Structures with bound ligands can be used to derive pharmacophore models, to generate a focussed library for screening, for example, and in turn to search the PDB for similar binding sites (eg, from within PSILO®, Chemical Computing Group Inc.). For proteins without known binding sites, pocket detection methods can be applied. These use either geometric algorithms, probe, and/or energy based methods.[106] Some also perform a quantitative drugability prediction of pockets (eg, SiteMap[107] or Site Finder within MOE, Chemical Computing Group Inc.). A limitation of all these methods is that they do not account for pocket flexibility. Using SILCS (Site Identification by Ligand Competitive Saturation) FragMaps[108] to derive information on putative pockets and their properties is a promising recent development to overcome this problem, since it relies on an algorithm employing molecular dynamics simulations that model protein conformational changes and the appearance of transient pockets.

2.06.4.1.1 Protein–Protein Interactions

Assessing protein–protein interactions (PPI) targets remains a challenge. Ideally, structural information is available to deduce the determinants of binding. In general, it is more promising to target an interface that features a pronounced pocket or several clustered smaller pockets (often these are filled by residues of the binding partner) instead of a relatively flat or even convex surface. Clustered hot spots, residues that account for most of the binding energy, are typically targeted when trying to interfere with protein–protein binding. These need to be identified either by experimental alanine-scanning or by in-silico methods. FoldX[109] and Robetta[110] are widely used for the latter.[111] When searching for putative binding pockets, protein flexibility has to be taken into account. This is

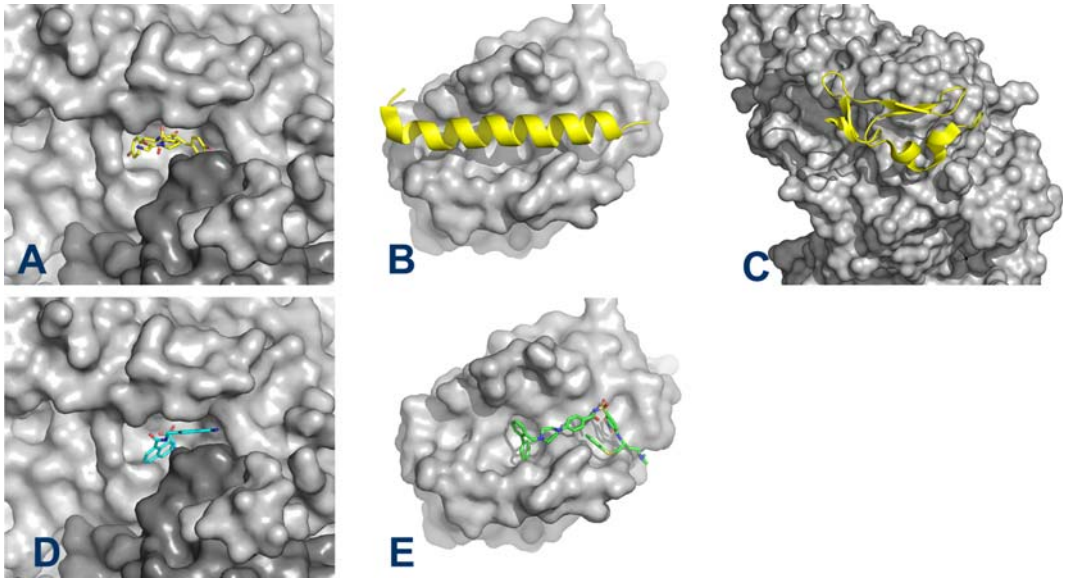

Fig. 5 Protein–protein interactions. The good, the bad, and the ugly PPI. (A and D) Linear epitope, short contiguous peptide sequence binds into relatively deep pocket, main interactions formed by one or few residues (HLGP-GL). The pocket is adressed by fragment or lead-like chemical matter (blue carbon atoms in (D)). (B and E) Linear epitope, contiguous peptide sequence located on a-helix or β-strand/turn, binds into relatively shallow groove, main interactions by few noncontiguous residues (Bcl-Xl-BAK). This binding site is adressed by a large ligand that needs to extend along the groove to pick up multiple interactions for nanomolar affinity (green carbon atom in (E)). (C) 3D epitope, longer noncontiguous peptide sequence binds on flat and convex surface region, main interactions formed by numerous residues (PCSK9–LDLR EGF domain). No small molecule ligand has been identified for this binding site.

especially true if only the structure of the unbound form of a target protein is known. Protein–protein interfaces might be inherently "wobbly,"[112] that is, pockets are transient in nature.

There are a number of possibilities to classify PPIs in groups of targets with low, medium, or high difficulty with respect to the identification of suitable interfering small molecules. For example, Smith and Gestwicki[113] differentiate PPIs according to two parameters: the binding affinity of the two proteins (tight–loose) and the extent of the interaction interface as measured by the surface area occluded from solvent in the complex (narrow–wide). A loose and wide PPI is much harder to target than a narrow and tight PPI. This is conceptually fairly easy to comprehend, since a loose and wide PPI is most probably characterized by a flat interaction surface exhibiting little topological or chemical features to be tackled by a small molecule drug. Here, we would like to introduce a relatively simplistic model to differentiate classes of PPIs (**Fig. 5**). Based on literature known examples of drug discovery projects in which PPIs were successfully or unsuccessfully targeted, we suggest that a PPI is a "good" target, if it consists for at least one of the binding proteins of a sequentially linear epitope, a short contiguous peptide sequence that binds into a relatively deep pocket with main interactions formed by one or just a few residues. Examples for this kind of PPI are the mdm2-p53, IAP BIR3 domain-caspase-9, bromodomain-histone, and HLGP-GL interactions.[112,114,115] For some of these well-known interactions, successful drug discovery efforts have been described that resulted in high affinity and highly ligand efficient drug candidates.

A "bad" PPI would be again a linear epitope on one of the binding proteins with a contiguous peptide sequence located on a secondary structural element, a α-helix or β-strand/turn, which binds into relatively shallow groove with main interactions formed by few noncontiguous residues. Examples for this type of interaction are Bcl-Xl–BAK, gastro-intestinal peptide–GIP receptor, and Nrf2–Keap1.[116,117] This type of PPI is more difficult to address with small molecules. A particularly striking example of a successful drug discovery program is the Abbott program on BCL-Xl which led to the discovery of ABT-199, a promising cancer drug.[118] The compound exhibits an extraordinarily high molecular weight (MW), only moderate ligand efficiency, and it took above-average time and capacity to identify it.

Finally, PPIs that exhibit 3D epitopes made up by longer, noncontiguous peptide sequences on one protein that bind on flat and convex surface regions on the other protein with main interactions formed by numerous residues on both sides would qualify as "ugly" PPIs that are extremely difficult to target. Documented examples are IL4–IL4 receptor and PCSK9–LDLR EGF domain for which no competitively binding small molecule drug has yet been identified.[119,120]

2.06.4.2 Hit Validation

The HTL phase in drug discovery commences after hits have been identified in a finding process that typically measures the ability of compounds to modulate a biochemical or cellular activity in the context of a HTS. The first step in this HTL phase is the "validation"

of the hits. The aim of the validation is to come up with a prioritized set of functionally active compounds that represent the best starting points for follow-on chemistry activities.

A range of criteria are applied to qualify compounds.[121] The screening assay is used to demonstrate reproducibility and concentration responsiveness of the activity. In a second step, employing technology counter screens, assay artifacts relating to an interference of the hits with the assay readout can be assessed and used to remove false positive hits. To test whether the activity is based on a specific mode-of-action on the target or on an undesired unspecific effect due to unwanted compound properties (such as compound aggregation-induced inactivation of the target protein,[122,123] unspecific modulation of an entire target family, or nonspecific cellular toxicity), a number of distinct and target-specific secondary assays are performed. Finally, after computational clustering of hit sets into chemically related hit series, all available project-related and historic assay data are compiled for the hit set and critically scrutinized to search for frequent hitters and initial structure–activity relationships (SAR) within a compound cluster.

At this stage of the process, a confirmation of the hits in orthogonal assays, which are devoid of agents like substrate or readout chemicals but rather measures binding in a binary assay format containing only compound and target, is highly valuable. During the last 15 years, biophysical methods have been increasingly employed to do this job. These methods can be used to either simply prove binding or demonstrate concentration dependence yielding affinity information that can be compared to the effective concentration derived from an activity assay. The biophysical methods are typically chosen and positioned in a screening cascade based on throughput, sensitivity, robustness, cost, and information content. Most prominent technologies in the industry are differential scanning fluorimetry (DSF), microscale thermophoresis (MST), surface plasmon resonance (SPR), NMR, and isothermal titration calorimetry (ITC). SPR and ITC can be used to determine affinities but at the same time characterize the binding kinetics and the thermodynamic profiles of the hits, data that contain valuable information toward the mode-of-action and may be used in prioritization of one hit series over another.[124,125]

Now, if for a given target a medium-high-throughput crystal system is available, the biophysical hit validation can be expanded by a structural component. An X-ray costructure of a ligand–target complex is the gold standard of hit validation, because it not only provides a clear proof of (specific) binding, but at the same time delivers a multitude of additional information. Most importantly at this stage, the binding site of the ligand is unequivocally defined giving immediate access to the mode-of-action of the compounds (eg, orthosteric–allosteric, reversible/noncovalent–irreversible). Further, changes in the target structure become apparent and can be evaluated (eg, larger scale changes such as domain movements, opening of a subpocket in the binding site, changes in protein dynamics upon binding). The details of the ligand–target interaction are revealed and form the basis for the interpretation of the observed SAR in the given hit cluster as well as the structure-guided design of optimization strategies if the particular hit is selected.

Since the crystallographic elucidation of the binding mode will define the main molecular interactions, at this stage the computational or manual classifications into hit clusters can be critically scrutinized at this stage. It may in fact turn out that compounds originally put into the same cluster actually entertain distinct binding modes and should be put into different baskets. Conversely, if compounds with distinct chemical structures initially put into different clusters turn out to form similar interactions, they should be placed in the same bin. Medicinal chemists tend to group and name hit compounds based on the molecular core structure or scaffold, oftentimes an aliphatic or aromatic heterocyclic ring system. This aids both in terms of communication as well as in the early stages of synthetic planning when modifications to the hits are designed. Structural information, however, may show that the scaffold has no direct contact to the target protein merely serving as a spacer that positions the interacting substituents into the right directions. In such a case, the scaffold may be switched without changing the key interactions and may give access to a new core structure that is more easily chemically explored.

While the above might seem trivial at a first glance, the results of this exercise will be extremely helpful during both hit prioritization and the first stages of chemical exploration of a hit cluster.

Since typically not just one hit class representative, but a representative set of hits from all hit clusters are crystallographically characterized, many possible ways to interact with the target protein within its functional sites are discovered, the binding sites are "mapped" by the distinct chemistries of the ligands so that a protein pharmacophore can be elucidated, and information can be extracted how certain moieties/substructures of one ligand class may be transferred to another.

The value and timing of this information cannot be underestimated. If a chemistry program is informed in such a comprehensive way by biophysics and structure at this early stage, even prior to any initiation of synthesis activity, an optimal basis for an informed selection of the ideal starting point as well as for a streamlined optimization process is granted. Therefore early enablement of biophysics and structural biology for all amenable targets is warranted even if this means a heavy capacity frontloading.

2.06.4.2.1 Characterization of the cocrystal structures of a chemically diverse set of CDK1 inhibitors

A historic example from our laboratory that nicely illustrates the above is the case of a CDK1 inhibitor project. At the time, the crystal structure of the target was not available. In order to support the program, we decided to use a previously enabled structural and sequential homolog to CDK1, CDK2, for ligand cocrystallography. An HTS delivered a relatively large hit set. After clustering of hits in groups with identical scaffold, a list of representative compounds was assembled for which the costructures were determined using a soakable high-throughput and high-resolution crystal system of CDK2. The compounds all turned out to be ATP-competitive binders, today classified as Type-I kinase inhibitors (Fig. 6). Superpositioning the entirety of costructures (Fig. 6C) illustrates emerging canonical interaction patterns formed by Type-I kinase inhibitors. The ligands and their distinct substitution patterns result in a broad occupation of the ATP pocket. The binding mode of two hits which exhibit a pyrazolo substructure (Fig. 6D) demonstrate that a distinct tautomer is involved in binding to the kinase, respectively. Finally, a pair of

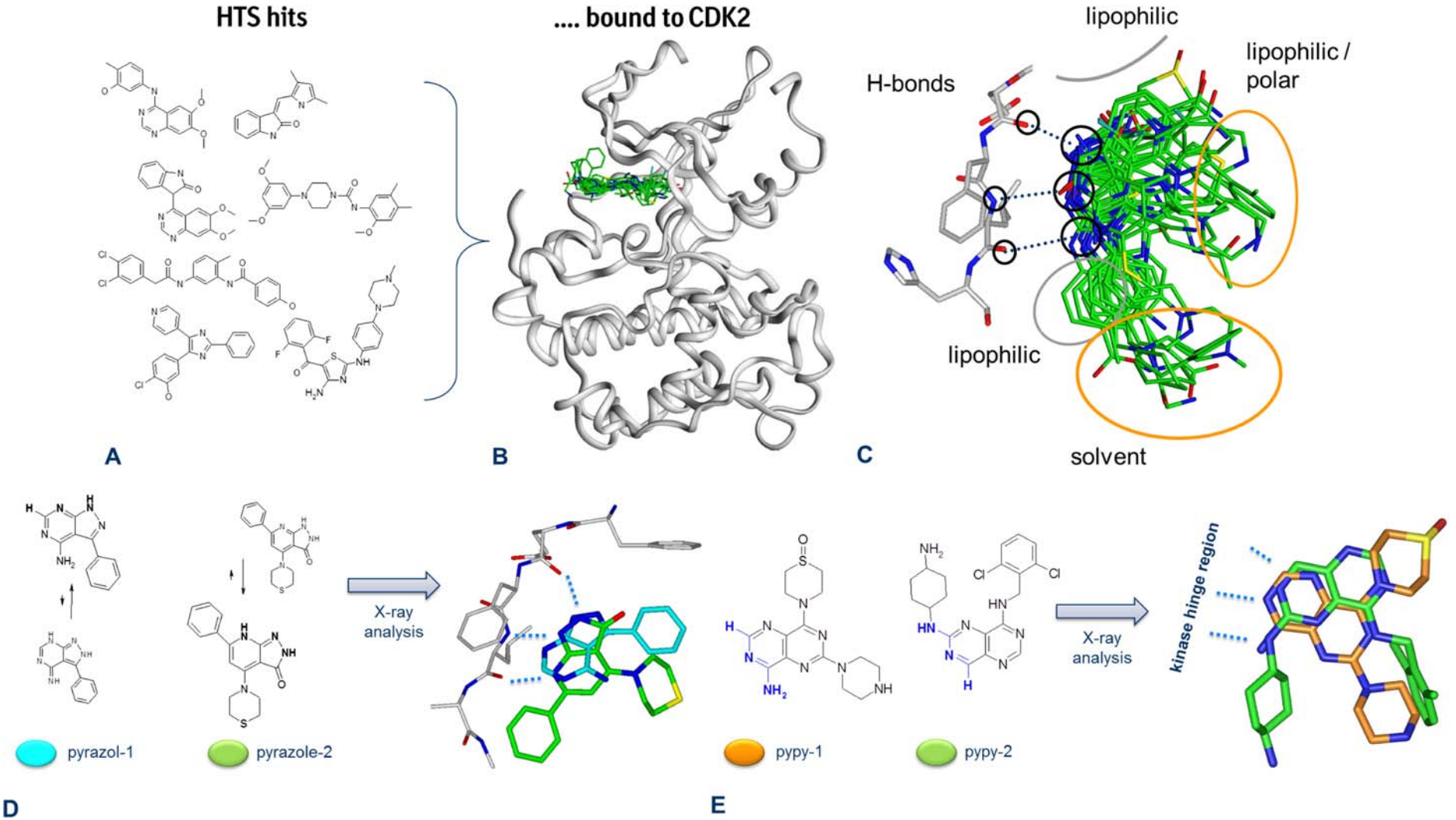

Fig. 6 Structure-based hit validation in the CDK1 project. (A) The chemical structures of a subset of the CDK1 HTS hits are shown. (B) Superposition of the costructures of the hits shown in (A) as bound to the surrogate target CDK2. (C) Interaction details derived from the superposition of a large number of cocrystal structures with chemically diverse hits. Interaction patterns emerge such as the well-known hydrogen bonding interactions with the kinase hinge region, exploration of the hydrophobic parts of the binding site below the glycine rich loop (not shown for clarity). (D) Identification of bound tautomer. The pyrazoles 1 and 2 can exist as different tautomers, with the bound tautomer and hinge-bonding atoms highlighted. A superposition of X-ray structures in complex with CDK2 is shown on the right-hand side. (E) Same scaffold—different binding modes: Variations in the substitution pattern of two pyrimidopyrimidines (left-hand side, with H-bonding atoms highlighted in blue) leads to a swap in binding mode (right-hand side).

pyrimidopyrimidine inhibitors binds in a distinct way to the target due to their different substitution patterns and are to be treated as independent hits despite their identical chemical scaffold (Fig. 6E).

2.06.4.3 Fragment-Based Screening

Fragment-based drug discovery (FBDD) is a complementary approach for finding new leads that during the last 15 years has increasingly been adopted by research groups in the pharmaceutical industry. The goal of FBDD is to identify small organic molecules (MW < 300 Da), "fragments" of lead-like molecular entities, that bind to a functional pocket of the target protein, and to further optimize them into potent leads using strategies that are similar to the traditional structure-based design approaches used for hits derived from HTS. The great conceptual appeal of FBDD is based on considerations of sampling efficiency and of the optimal physicochemical or drug-like properties of lead compounds. Since the chemical space of organic molecules with drug-like properties is vast (estimations indicate that there are approximately 10^{50} molecules with heavy atom count (HAC) of 15 to 35); screening of corporate libraries of up to 10^7 compounds with limited structural diversity will not get anywhere close to a representative sampling of the chemical space of potential lead structures. In contrast, screening a set of 10^3 to 10^4 structurally diverse fragments with HAC between 10 and 22 will sample the corresponding chemical space of approximately 10^{20} molecules more efficiently.[126] In addition, due to the lower complexity of the screened compounds hit rates are much higher.

In a typical FBS campaign, a screening library of a few thousand low MW compound (MW < 280 or HAC < 22) is screened by biophysical screening technologies like ligand- or protein detecting NMR spectroscopy, SPR, DSF, or MST being applied either in parallel or consecutively. The resulting primary FBS hit set (50–150 compounds) is then analyzed by X-ray crystallography.

In addition to validating the binding, the structural information is valuable for the subsequent analoging and optimization process. However, depending on the target it is often observed that only a subset of the hits that have been found in the biophysical prescreening will yield costructures.

This is because the low affinity of the fragments leads to an increase in false positive hit rates in the primary FBS due to the sensitivity of the screening technologies which may fail to differentiate between specific and unspecific binding.

The biophysical prescreen is the standard case in fragment-based lead discovery when larger (2000–15,000 compounds) fragment libraries are used. With smaller libraries, it is also possible to use X-ray analysis as primary screening technology. In the early days of FBS, X-ray crystallography in fact was used as a primary screening technology.[13,14] Recent developments revive the idea of using X-ray crystallography as a primary screening technology. Most prominently, at synchrotron beamlines, services are being set up which focus on the establishment of an efficient process to cocrystallize, perform data collection and structure determination of a fragment library of hundreds of compounds. Secondly, evidence is accumulating that if applied in parallel to biophysical screens, crystallographic screening delivers its own hit set and identifies fragment hits that were missed entirely by other methods.[67]

2.06.4.3.1 Implementation of an X-ray crystallography-based FBS

Both cocrystallization and soaking are used for fragment crystallography. During cocrystallization the small molecule is already present during the crystallization step of the protein and the growing crystals incorporate protein–ligand complexes. The drawback of cocrystallization in this context is that due to the low affinity of the fragments, high concentrations of the ligand are necessary which might hamper crystallization of the protein. The presence of a ligand during crystallization might even lead to a change of the original crystallization requiring new crystallization screens. In general a cocrystallization setting lowers the throughput and is not ideal for fragment-based approaches. The most efficient method in getting crystals that contain protein–ligand complexes is the soaking approach, in which crystals of the target protein that have an empty active site or contain a low affinity ligand are produced in large numbers. These crystals are then incubated in a stabilizing or ideally cryogenic solution with a high (eg, 100 mM) concentration of the fragment. The highest possible concentration of the fragments should be used and corresponds to a saturated solution with remaining solid material of compound in the droplet.

In order to reach high compound concentrations, special requirements in compound logistics are required. DMSO is often the solvent of choice for preparing fragment stock solutions. The concentration of the stocks should be high (100–500 mM), so that a later dilution into the stabilizing solution leads to a high concentration of fragment and a low DMSO content. High concentrations of DMSO can be problematic, for example, in cases where it destroys the crystal lattice or competes with the fragment for a binding site. If it is necessary to use premade DMSO stock solutions of lower concentration it can be an option to evaporate the DMSO. The dried fragment is then resolubilized to a higher concentration in the crystallization or stabilization buffer.[127] It should be noted that fragments can have a low vapor pressure and the fragment might coevaporate with the DMSO.

Depending on the expected hit rate of the target, fragments are pooled into cocktails of 3 to 10. Soaking of mixtures leads to a more efficient process and often reduces the number of datasets that need to be collected but also requires a deconvolution step. Once a cocktail has been found by X-ray analysis to produce significant difference electron density in a binding site, it is often possible to identify the binding fragment based on the shape and form of the electron density. In subsequent experiments the other elements of the cocktail need to be examined to find out whether another component of the mixture is able to bind in the absence of the first hit. Setting up the cocktails using a maximum of structural diversity can help in this deconvolution process.[14] Next to these advantages there are also pitfalls when using cocktails. The compound concentration in cocktail soaks is lower compared to single soaks and this can be critical with low affinity binding fragments. Further, some of the selected compounds might be reactive and lead to unexpected products. The probability of such unwanted reactions is likely to increase with the number of compounds per cocktail[128] (see also Zartler 2014, http://practicalfragments.blogspot.de/).

A nice example that shows that the throughput limitation of protein crystallography in the context of FBS can be overcome are the efforts at the Diamond I04-1 beamline where up to 500 crystals can be soaked and prepared in a day. The subsequent data collection takes about 24 hours (http://www.diamond.ac.uk/Beamlines/Mx/Fragment-Screening.html).

If one drives the fragment idea into extreme one enters the regime of very small fragment screening. Very small fragments (MW < 150 Da) are expected to bind with extremely low affinity (1–50 mM). A costructure with such compounds will only be obtained when the aqueous solubility is very high. In published procedures, soaking of crystals in organic solvents has been performed to address this issue. This technology called multiple solvent crystal structures has been used for locating and characterizing binding sites.[129] While being methodologically very interesting a direct impact on medicinal chemistry programs has not yet been shown.

2.06.4.4 Structure-Based Molecular Design

Objectives in the LO phase are to improve a variety of critical parameters relating to drug properties: functional activity, selectivity against antitargets, cellular activity, physicochemical properties, in vitro and in vivo pharmacokinetic properties, in vivo efficacy, safety and tolerability, and drug substance properties such as chemical stability and crystallizability. Only affinity and selectivity optimization can be directly impacted by structural biology. However, knowledge about the binding mode of a lead series will have a strong impact on the optimization of the other properties, mainly by clarifying to the medicinal chemist which changes to the molecular structure, planned to optimize these other properties, will be neutral or even beneficial to affinity. For instance, the costructure will instruct the chemist how to tackle problems of solubility by indicating positions on the molecule to which solubilizing groups can be attached without interfering with target interaction.

The multiparameter LO is an iterative process (the "design-make-test-analyse" DMTA cycle). Even if the structural changes to the lead structure are small in each cycle, it is strongly recommended to check by costructure determination if the binding mode is preserved. Especially, when SAR cannot be readily explained by existing structural information, it may turn out that the binding mode has changed.

If it turns out that a lead class has intrinsic issues with any of the optimization parameters that cannot be overcome applying structural information can be extremely powerful, for example, by suggesting modifications to the core chemical structure of a lead that changes the basic compound properties but leaves the binding mode unaltered.

The following paragraphs will illustrate the interplay of crystallography, medicinal chemistry, and biological testing with two case stories. Our fist example will focus on the design of potency and selectivity, while the second example will illustrate *lead hopping* to generate novel chemical matter.

2.06.4.4.1 Isoform selective PI3Kγ inhibitors

Signaling via phosphoinositide 3-kinases (PI3K) has been shown to be a key pathway in the regulation of the immune response[130] and is in the focus of many research programs in inflammatory diseases and cancer.[131] In an internal project, we attempted to generate isoform selective PI3Kγ inhibitors to block the underlying inflammation in chronic obstructive pulmonary disease (COPD).[132] PI3Kγ is one member of the class I PI3Ks, which phosphorylate PI(4,5)P2 to produce the critical second messenger PI(3,4,5)P3. The project was initiated under the hypothesis that PI3Kγ was the predominant isoform responsible for leucocyte migration (which is unwanted in COPD) and thus should be inhibited. Other PI3K isoforms should not be targeted in a chronic indication as COPD, to avoid potential toxicity issues. Due to its ubiquitous expression and central role in insulin signaling, the PI3Kα isoform in particular was closely monitored. Following a HTS campaign we identified lead structure BI-1 with an attractive MW and good initial potency. An early crystal structure of BI-1 bound to PI3Kγ was helpful to guide initial synthesis (Fig. 7). On the one hand, growth vectors for chemical exploration were identified; on the other hand, two hydrogen bonds were revealed to be critical for establishing the binding mode. These were not modified to maintain molecular recognition.

While BI-1 was already in the desired potency range (IC_{50}(PI3Kγ) < 50 nM) it showed no selectivity to PI3Kα and other isoforms (target values were IC_{50}(PI3Kα) > 200 nM absolute and > 100 × relative selectivity). In the absence of other PI3K isoform structures, similarity was assessed by mapping a PI3K family sequence alignment on the structure (Fig. 8A). It was immediately evident that, due to its small size, BI-1 was exclusively in contact to residues conserved throughout the family. We therefore designed a small series of modifications that were directed toward less conserved regions to engage residues unique to PI3Kγ (Fig. 8B) and thus held promise to improve selectivity. Compound BI-2 was identified with a tendency toward the right direction (ratio $\alpha/\gamma = 28$), but was still far from having the ideal selectivity range. A crystal structure of BI-2 confirmed our design hypothesis and revealed that the compound engages its basic pyrrolidine moiety in a salt bridge to nonconserved aspartic acid D950, which is a serine in PI3Kα. In a parallel exercise, we had discovered that modifications of the tri-cyclic core structure also resulted in a slight improvement in selectivity (ratio $\alpha/\gamma = 15$) for BI-3. We were initially puzzled by this observation, since BI-3 is not appreciably larger than BI-1 and was not predicted to contact nonconserved regions. A costructure of BI-3 (Fig. 8C) revealed that the exit vector of BI-3's phenyl ring had a slightly modified direction and could only be accommodated through a concomitant conformational change of the active site lid-region. Interestingly, this conformational adaptation propagated to a second shell of residues that is not conserved between isoforms. Although the ligand-induced conformational change came along with a slight loss in PI3Kγ-potency, we assumed based on the observed selectivity data that other isoforms were even less tolerant to these conformational changes. To combine both observations, we attached the previously identified c-hexyl-pyrrolidine fragment on BI-3 to obtain BI-4 (Fig. 8D). As expected, the new compound featured largely improved potency and selectivity (IC_{50}(PI3Kγ) = 6.5 nM; ratio $\alpha/\gamma = 55$) and made the desired interaction with PI3Kγ D950 (Fig. 8E). In a final step we "recycled" our initial exploration of *linker-selectivity probe*

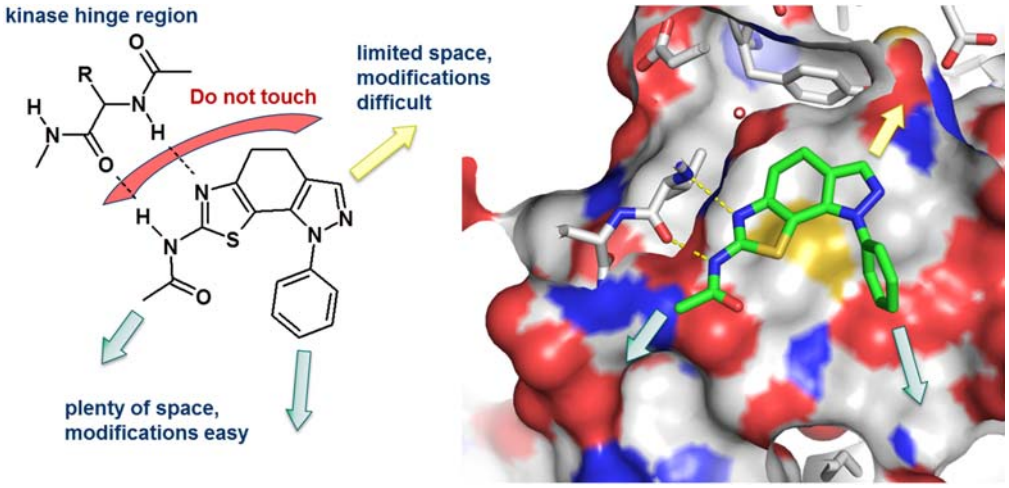

Fig. 7 Structure of lead BI-1 and potential growth vectors.

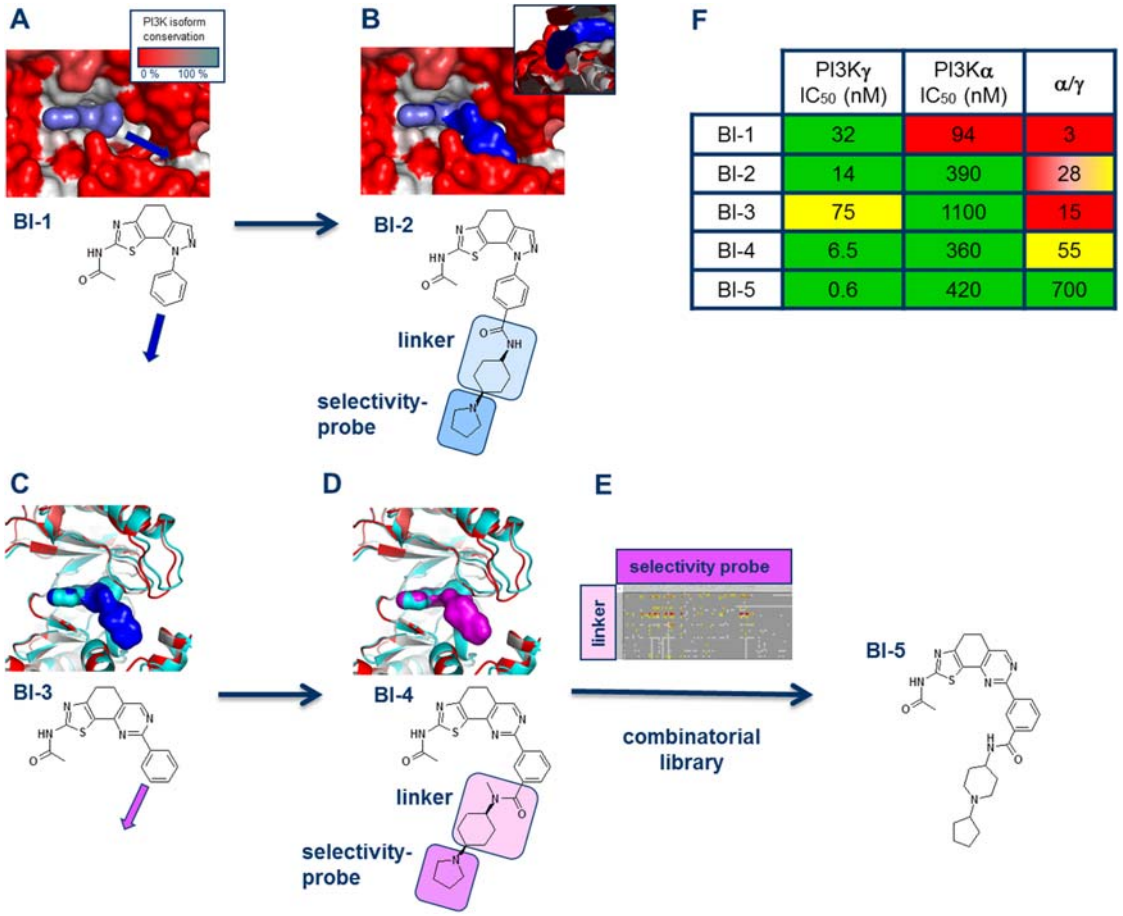

	PI3Kγ IC_{50} (nM)	PI3Kα IC_{50} (nM)	α/γ
BI-1	32	94	3
BI-2	14	390	28
BI-3	75	1100	15
BI-4	6.5	360	55
BI-5	0.6	420	700

Fig. 8 Iterative optimization of potency and selectivity. (A) Active site of PI3Kγ color coded according to sequence conservation between isoforms (α, β, γ, δ) with compound BI-1 (purple). (B) As in (A) and with superimposed compound BI-2 (blue). The insert shows the nonconserved selectivity-pocket. (C) Complex between BI-3 (cyan) and PI3Kγ (cyan ribbon) superimposed on the PI3Kγ BI-2 complex (color coded as in (B)). (D) As in (C) and with superimposed compound BI-4 (blue). (E) Schematic of the combinatorial library and final molecule BI-5. (F) Activity data and selectivity ratios.

combinations in a biased combinatorial library. The best compound, BI-5, bound to PI3Kγ in the predicted manner (Fig. 8F) and with ~10-fold improved potency and selectivity.

The presented case is a good example for the iterative nature of structure-based design: It usually takes multiple cycles of chemical synthesis, biological testing, structure analysis, and hypothesis generation to arrive at a molecule with the desired properties. More often than not, there is a need of an element of serendipity (in our case deliberately introduced through combinatorial chemistry) to succeed. We should be poised not to miss it!

2.06.4.4.2 Lead hopping in fXa

Focus of this endeavor was on direct inhibitors of factor Xa (fXa), a highly validated protease target to treat thromboembolic disorders such as stroke.[133,134] From the early days of research on thrombin (fIIa) and fXa inhibitors, conventional thinking was that a strong interaction of basic P1 groups with Asp-189 in the S1 specificity pockets of these trypsin-like serine proteases (Fig. 9A) was indispensable for potent inhibitors. However, by the late 1990s focus was shifting from strongly basic to less basic and, eventually to neutral compounds (Fig. 9B) that would provide a better chance of oral bioavailability without the need to resort to prodrug approaches.[135,136]

Characteristic for benzamidine containing compounds, such as the direct fIIa inhibitor dabigatran, the first novel oral anticoagulant (NOAC) to be brought to the market in 50 years,[137] is a bidentate salt bridge interaction with Asp-189 at the bottom of the pocket. A conserved, structural water molecule in a hydrophobic subpocket is hydrogen bonded between the amidine moiety and the Phe-227 carbonyl oxygen. Fig. 9B illustrates the binding of neutral compounds into the S1 pocket. Rivaroxaban, a fXa inhibitor and the second marketed NOAC, as an example of a compound with a nonbasic character binds with its chlorothiophene carboxamide into the fXa S1 pocket. It does not bind to Asp-189 but instead utilizes aryl halogen interaction with Tyr-228 and a hydrogen bond to Gly-219. Water displacement and an energetically favorable (Ar)C–Cl π interaction compensate for the loss of interaction with Asp-189.

At Boehringer Ingelheim, information on this distinct type of interaction in the S1 pocket was used early on to convert highly active benzamidine leads into equally potent nonbasic chloro-benzimidazoles.[138] Superposition of the crystal structures of a benzamidine lead class representative with a neutral chloropyridyl-diaminophenol (Fig. 9D) suggested a way to replace the m-substituted benzamidine by a chloro-substituted bicyclic ring system with the aim of generating an alternative neutral equipotent

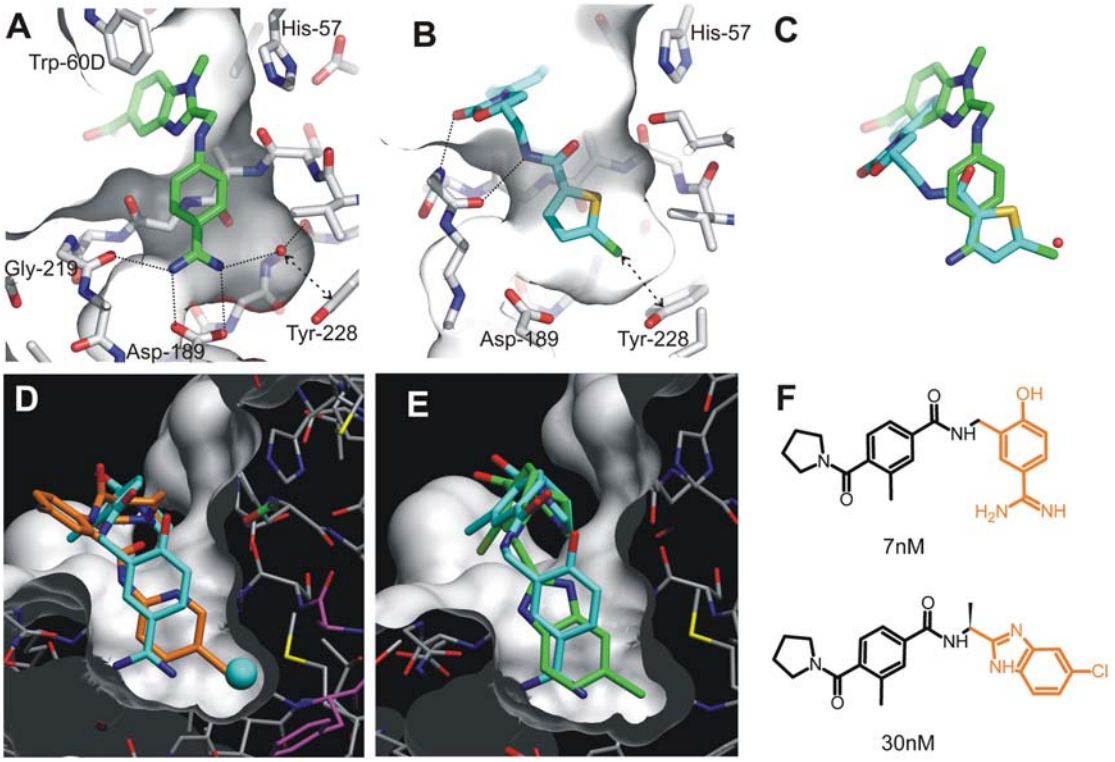

Fig. 9 Blood coagulation serine proteinase S1 pocket interaction principles and structure-based lead hopping. (A) The S1 pocket of fIIa in the dabigatran complex. (B) The S1 pocket of fXa in the rivaroxaban complex (PDB code 2w26). (C) Superposition of the two compounds as bound to the structurally aligned proteins. (D–F) Hybridization of an aryl halogen motif onto the benzamidine lead class. Benzamidine lead compound: blue carbon atoms in (D) and top molecule in (F). Chloropyridyl-diaminophenol competitor compound: orange carbon atoms in (D). New chlorobenzimidazole lead: green carbon atoms in E and bottom molecule in (F). Figure reproduced with permission from Trends in Pharmacological Sciences.

lead. A chlorobenzimidazole (Fig. 9E) was made that retains the left-hand side of the benzamidine compound with only a marginal loss of affinity (Fig. 9F).

The presented case is a good example for the need to look beyond one's own nose. It is always advisable to investigate binding modes of competitor molecules (or any other available chemical matter) to obtain new design inspirations, hybrid ideas, etc. Many of our ideas may fail, but the one that survives might be the next lead structure!

2.06.4.5 Biologics Discovery

Biopharmaceuticals made up around one-fourth of the 200 top selling drugs in 2013. Many different types of biological drugs (or NBEs) are on the market, the most prominent are antibodies, hormones, and vaccines. Among the 20 top selling drugs in 2013, 9 were proteins.[139] The antibody adalimumab (Humira®) was number one on the list and had worldwide sales of more than 10 billion dollars. This illustrates the growing role of biopharmaceuticals in drug discovery.

As for new chemical entity discovery, the knowledge about the 3D structures (of target molecules and the NBE itself) can be of great help for research and development. For many protein classes, representative structures can be found in the PDB. Especially for antibodies, SBDD can be applied readily because their structures are well understood. As of Nov. 2015, more than 2200 structures of Fab-parts have been deposited to the PDB.[140] Around 460 structures have been determined in complex with a (poly)peptidic antigen. This huge amount of information enables modeling of newly discovered antibody sequences and can help on the way of optimizing different properties of these drug candidates. 3D structures can, for example, be used to aid the humanization of antibodies from animal sources like rodents or camelids[141–147] or guide the optimization of affinity and efficacy.[148] Framework engineering, the optimization of the constant parts of an antibody, is a means to tailor a molecule for its purpose. This region is responsible for binding to effector molecules like Fcγ-receptors,[149,150] complement factor C1q,[151] or neonatal Fc-receptor FcRn.[152,153] Modifications in this region can alter antibody-dependent cell-mediated cytotoxicity, complement activation, and cell-dependent cytotoxicity. The half-life of an antibody can be modulated by altering its affinity to the FcRn-receptor.

Despite the already known structures of antibody fragments and their interaction with effector molecules, there is added value in the crystallization of an individual NBE-candidate alone and in complex with its antigen. Modeling of Fabs has its limitations, especially for the highly variable CDR-H3 loop. The detailed knowledge of the paratope region and structure is the starting point for the above-mentioned strategies for humanization and affinity maturation. Another advantage of antibody:antigen structures is the fact that apart from the paratope, one also gains insight into the nature of the epitope. This can be useful for patenting reasons or for a rational design to overcome species selectivity. The structure of a complete antibody or antibody fragments has also been shown to be of help in overcoming solubility issues for a certain antibody.[154,155] In these studies, the crystal structure of the Fab alone revealed a tetrameric arrangement of the molecules. The contacts between the molecule also involve parts of the paratope. The structure was used to guide the design of mutants that have 10 times higher solubility while retaining the activity of the antibody (Fig. 10).

The molecular properties of the antigen have a strong influence on the probability of a successful Fab:antigen crystallization. Therefore it is of high importance that SR is involved in NBE discovery from the very start of a new project. The knowledge of the structure of the antigen can be of help in the design of the optimal protein for immunization. This has been demonstrated in the design of several vaccines, where a structure-based design of the antigen leads to a higher immune response or a broader immunization against several isotypes of the pathogen.

2.06.5 Outlook—Industrial structural biology of the future

The generation of 3D structural information for use in drug discovery for the past 4 decades has been dominated by X-ray crystallography. While some target structures with limited MW (<50 kDa) have been determined by NMR methodology, the vast majority of structures were derived with crystallographic methods. Moreover, in contrast to NMR-based methods, the determination of multiple structures of target–ligand complexes is easily facilitated by either cocrystallization or soaking protocols and thus enables the essential domain of HTX in drug research. Recently, with the rising number of elucidated IMP structures, most notably GPCRs, this large group of pharmacologically relevant targets have finally become accessible to SBDD.

2.06.5.1 X-ray free electron lasers and cryo-electron microscopy

There are two relatively new developments in structural biology that promise to have a major impact to the field.

During the last ~3–4 years, the technology of XFELs has become accessible at several synchrotron facilities around the world. These generate ultrashort pulses of coherent and extremely intense X-radiation that exceed the brilliance of third-generation synchrotron sources by ~11 orders of magnitude.[156,157] The enormous energy input through femtosecond X-radiation pulses allows for rapid collection of diffraction information, but the samples are irreversibly destroyed ("diffraction before destruction"). Therefore, for collection of complete diffraction data sets, a large number of diffraction patterns have to be collected from either series of small crystals traversing the X-ray beam in a liquid carrier matrix supplied by injection devices or by irradiating multiple spots on crystals traditionally mounted on goniometers. With XFELs it is now possible to obtain structural information for notoriously difficult targets for which either only very small crystals can be obtained (which are not suitable for diffraction experiments

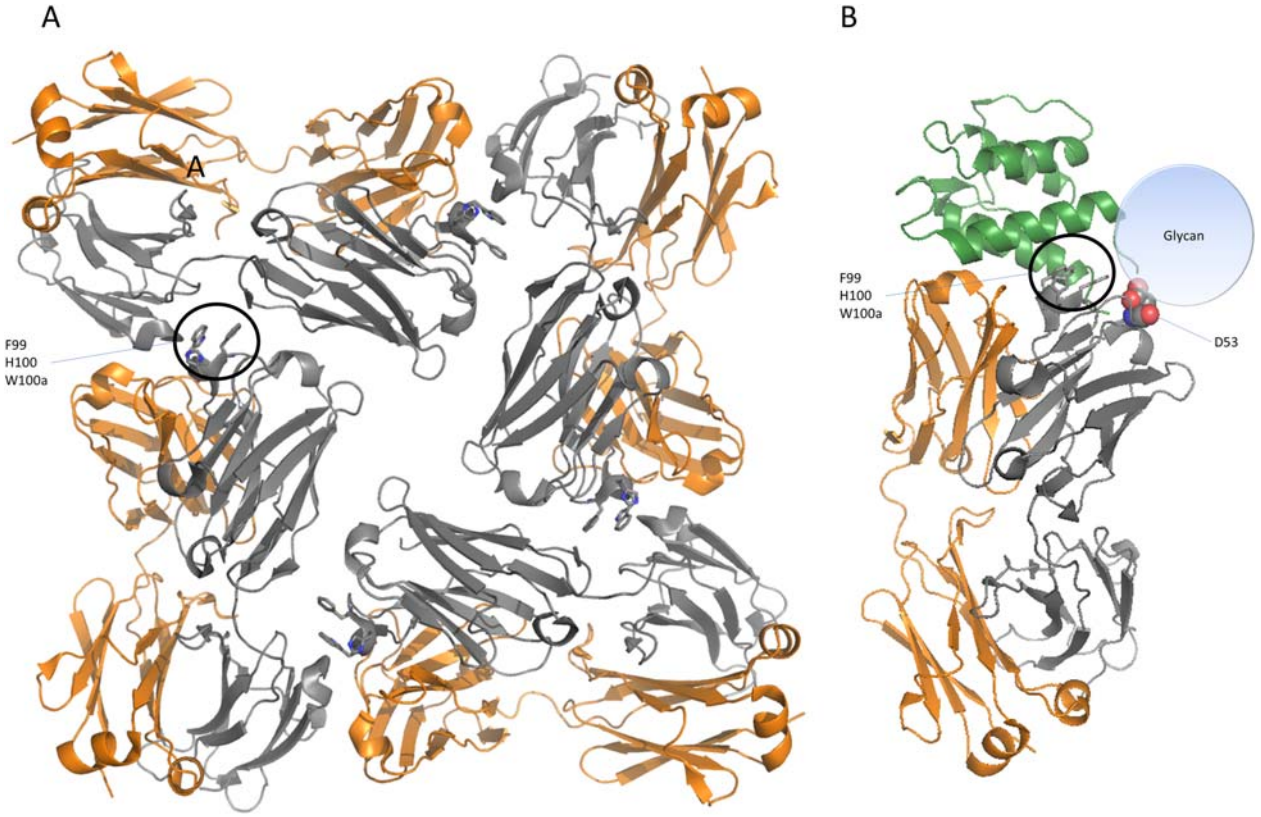

Fig. 10 Design of soluble versions of an anti IL13 antibody. (A) Tetrameric arrangement in the structure of the Fab, residues responsible for the packing (F99, H100, W100a) are shown as sticks. (B) Structure of the Fab in complex with the antigen IL13 (green), same orientation as in (A). The mutation D53N introduces a glycosylation site that prevents the formation of the tetramers but retains the antigen binding capacity of the antibody. Residue number annotations were determined according to Chothia's structure-based numbering scheme.[195]

on regular synchrotron beamlines) or radiation damage is a serious problem (eg, for metalloproteins[158]). Examples include the structure determination of GPCRs which were crystallized in lipidic cubic phase[159] and of recombinantly expressed proteins which, under conditions of overexpression, form nanocrystals within the expression host cells.[160] Further, XFELs offer opportunities that exceed those of traditional X-ray crystallography. For instance, it is now conceivable to derive details of molecular dynamics given the picosecond temporal resolution of XFELs.[161] In the context of drug discovery, the enhanced access to novel structures in particular of tough targets is of great value. Whether the XFEL technology will significantly impact the "productive" cocrystallography stage has to be seen. Currently, the very high effort involved to determine a structure by serial femtosecond crystallography (SFX) and, compared to traditional crystallography, the poorer data quality and resolution limit applications to nonroutine, low throughput, and high value projects.

Secondly, on the basis of revolutionary developments in the field of direct electron detectors and image processing algorithms,[162] with single-particle Cryo-EM 3D structures of biomolecules can now be determined at near-atomic resolution.[163] Study objects currently are mainly large macromolecular complexes (~500–4000 kDa size) some of which reside in membrane, can adopt multiple conformational states, and/or have been refractive to crystallization.[164] Recent examples of pharmacological targets studied by cryo-EM include TRPV1[165] and γ-secretase.[166] For β-galactosidase, a 2.2 Å resolution structure was obtained allowing for the resolution of atomic details of a ligand interaction site.[167] No crystals and only little amounts of sample are needed and sample heterogeneity can be dealt with at the image processing stage of a structure determination. Conformational heterogeneity, often detrimental to crystallization efforts, can even be used to ones favor in cryo-EM, because it can be analyzed after data collection and yields most valuable information pertaining to the mode-of-action of proteins for which structural dynamics is required for function.[168] All these circumstances define the great attractiveness and potential of the technology and explain why many people believe that cryo-EM will be the dominating technology in the structural biology of the future. Concerning applications in the field of pharmaceutical research it appears that currently, in favorable cases, cryo-EM is able to achieve the resolution needed to elucidate details of protein–ligand interactions thus enabling structure-based design. However, current applications are restricted to biomolecules with a minimal molecular size of about 100 kDa[169,170] so that for the time being a large set of relevant drug targets appears too small to be amenable to cryo-EM studies. Possibly, this limitation can be overcome by future methodological developments or circumvented by studying molecular targets in the context of larger, functional protein complexes.

2.06.5.2 Structural biology of integral membrane proteins (IMP)

Membrane proteins constitute a highly important target class. Most prominently, GPCR targeting molecules account for many of best-selling drugs and 30–40% of all prescribed pharmaceuticals.[92] Compounds modulating the function of channels and transporters—two other larger membrane protein classes—account for another ~10% of the pharmaceutical market.

X-ray crystallography of IMPs has been lagging behind that of soluble proteins[171] due to the large technical difficulties associated with overexpression, purification, stabilization, and crystallization. Illustrating that point, only 2.3% of the 114,080 entries in the PDB (as of Dec. 7, 2015) were annotated as IMPs. Consequently—despite its huge relevance—drug discovery for this target space was until recently only sparsely supported by experimental structures. A comprehensive discussion of SR and SBDD for membrane proteins is beyond the scope of this paragraph and instead we briefly touch on the three most important target classes: GPCRs, ion channels, and transporters.

The last decade has brought a game change to the field which has probably been most remarkable in the area of GPCR structural biology.[172,173] First crystal structures of beta-adrenergic receptors (bAR) bound to inverse agonists were reported in 2007[174] and 2008.[175] Already in 2011 the complex of activated bAR2 with G protein[176] contributed to another landmark in the field leading to the 2012 Nobel Prize in Chemistry. Meanwhile the PDB lists ~30 different GPCRs, many of them crystallized in various signaling states and with multiple ligands (**Fig. 11**). Many of the available structures are in complex with established drugs or drug candidates and are invaluable to better explain their molecular mechanism of action.[177] The remarkable progress in GPCR structure determination has come about by the combination of a number of techniques and a better understanding of factors influencing membrane protein stability (**Table 2**). Naturally, the main focus of this first wave of structures has been on obtaining structures "at all," allowing for a retrospective understanding of binding modes. As the field is maturing we are now starting to see examples where GPCR structures were determined in pharma companies to drive ongoing programs.[178–180] Moreover, the first companies are now pioneering FBS on GPCRs.[181–183] Despite the significant advances made, GPCR crystallography is still far from being routine and both timelines as well as throughput of ligand costructure delivery might be prohibitive for many internal drug discovery programs.

Similar to GPCRs, ion channel structural biology benefits from a rich and well explored pharmacology that provides tools to stabilize the protein of interest.[184–186] Several families, as for example the NMDA synaptic receptors, carry large extracellular domains for ligand or modulator binding, which can be separately expressed to facilitate structural studies.[187–189]

Membrane transporters are a large and heterogeneous superfamily,[190] but are still to large extents unexplored as a target space.[191] While initial progress in crystallography was made on simpler model systems from bacteria or thermophiles,[192] we now increasingly see structures from higher species being solved[193,194] making it likely that the field will soon experience first success stories of SBDD.

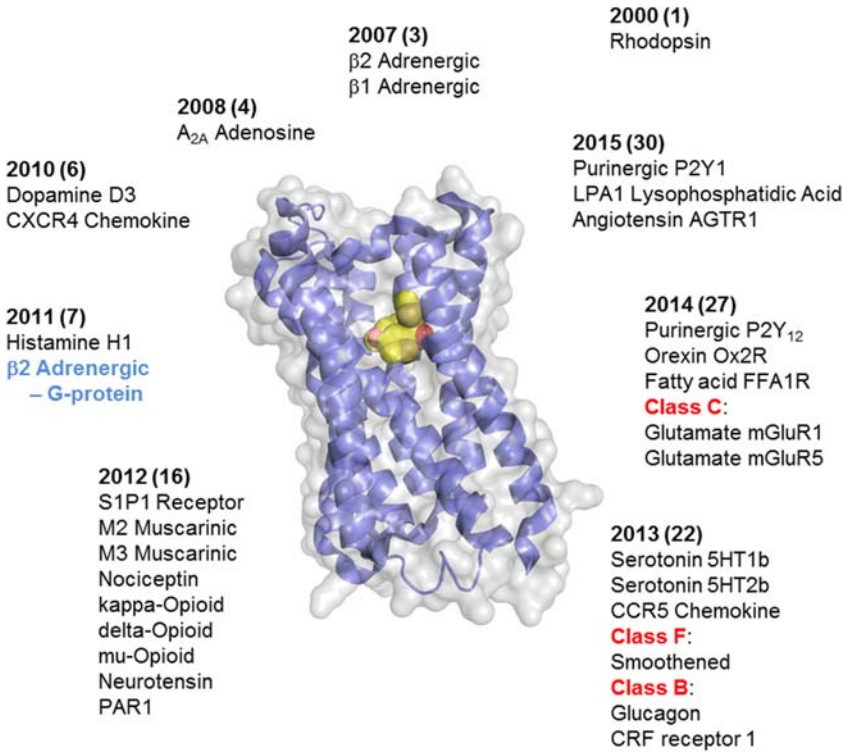

Fig. 11 Advances in GPCR structural biology. Only unique new GPCR structures are listed with the exception of the β2 adrenergic receptor–G-protein complex (blue). Orthologues and other ligand or effector complexes are not listed. The total number of GPCR structures in the PDB was ~150 by the end of 2015.

Table 2 Strategies and technological advances for membrane protein expression

Technology/strategy	*Explanation*	*Reference*
Thermophilic/bacterial protein	Use "easier" more stable surrogate targets to model human system. Not suitable for GPCRs	Indiveri (2013)[192] Baker (2010)[196]
Novel detergents	Milder detergents to solubilize and purify protein in functional state	Kang (2013)[172]
Thermostabilization mutants	Screen for mutations that stabilize protein, but do not affect function/ligand binding	Tate (2012)[197]
Fusion proteins	Replace flexible loops by fusion partner to reduce conformational heterogeneity and expand extracellular surface for crystal contacts	Chun (2012)[198]
Ligands	Ligands to stabilize desired conformation, preferably highly potent	Alexandrov (2008)[199] Andrews (2014)[183]
Crystallization chaperones	Fab fragments, nanobodies, or other binding partners to stabilize conformation and expand extracellular surface	Rasmussen (2011)[200] Lawson (2012)[201]
In meso crystallization	Specialized crystallization system in lipidic cubic phase	Caffrey (2015)[202]
SFX	Serial femto second crystallography	Liu (2014)[159]

2.06.6 Summary

HTX was established in the 1995–2005 decade and has found a precious application in structure-based drug discovery. The initial promises that using structural information combined with computational approaches would lead to superior quality drugs has not fully materialized. However, in our view the major contributions are that it leads to an increase of the probability to find new leads and to accelerate their optimization into drugs. Thereby, it has greatly contributed to major successes in drug discovery during the last decade and contributed to a large enhancement in process efficiency of industrial medicinal chemistry activities. Since computational approaches are suffering from still poor quality of protein structure and ligand pose predictions, for the foreseeable future the science of protein crystallography will continue to be a key success factor in drug discovery.

See also: 2.02. Hit and Lead Generation Strategies.

References

1. Kendrew, J. C.; et al. A Three-Dimensional Model of the Myoglobin Molecule Obtained by X-Ray Analysis. *Nature* **1958,** *181,* 662–666.
2. Perutz, M. F.; et al. Structure of Haemoglobin: A Three-Dimensional Fourier Synthesis at 5.5-A. Resolution, Obtained by X-Ray Analysis. *Nature* **1960,** *185,* 416–422.
3. Beddell, C. R.; Goodford, P. J.; Norrington, F. E.; Wilkinson, S.; Wootton, R. Compounds Designed to Fit a Site of Known Structure in Human Haemoglobin. *Br. J. Pharmacol.* **1976,** *57,* 201–209.
4. Perutz, M. F. Fundamental Research in Molecular Biology: Relevance to Medicine. *Nature* **1976,** *262,* 449–453.
5. Sweet, R. M.; Wright, H. T.; Janin, J.; Chothia, C. H.; Blow, D. M. Crystal Structure of the Complex of Porcine Trypsin With Soybean Trypsin Inhibitor (Kunitz) at 2.6-Å Resolution. *Biochemistry* **1974,** *13,* 4212–4228.
6. Stroud, R. M.; Kay, L. M.; Dickerson, R. E. The Structure of Bovine Trypsin: Electron Density Maps of the Inhibited Enzyme at 5 Å and at 2.7 Å Resolution. *J. Mol. Biol.* **1974,** *83,* 185–192. IN11–IN14,193–208.
7. Bode, W.; Fehlhammer, H.; Huber, R. Crystal Structure of Bovine Trypsinogen at 1.8 Å Resolution. I. Data Collection, Application of Patterson Search Techniques and Preliminary Structural Interpretation. *J. Mol. Biol.* **1976,** *106,* 325–335.
8. Varghese, J. N.; Laver, W. G.; Colman, P. M. Structure of the Influenza Virus Glycoprotein Antigen Neuraminidase at 2.9 Å Resolution. *Nature* **1983,** *303,* 35–40.
9. Hsu, I. N.; Delbaere, L. T.; James, M. N.; Hofmann, T. Penicillopepsin: 2.8 A Structure, Active Site Conformation and Mechanistic Implications. *Adv. Exp. Med. Biol.* **1977,** *95,* 61–81.
10. Lander, E. S.; et al. Initial Sequencing and Analysis of the Human Genome. *Nature* **2001,** *409,* 860–921.
11. Venter, J. C.; et al. The Sequence of the Human Genome. *Science* **2001,** *291,* 1304–1351.
12. Sharff, A.; Jhoti, H. High-Throughput Crystallography to Enhance Drug Discovery. *Curr. Opin. Chem. Biol.* **2003,** *7,* 340–345.
13. Nienaber, V. L.; et al. Discovering Novel Ligands for Macromolecules Using X-ray Crystallographic Screening. *Nat. Biotechnol.* **2000,** *18,* 1105–1108.
14. Hartshorn, M. J.; et al. Fragment-Based Lead Discovery Using X-ray Crystallography. *J. Med. Chem.* **2005,** *48,* 403–413.
15. Ghosh, E.; Kumari, P.; Jaiman, D.; Shukla, A. K. Methodological Advances: The Unsung Heroes of the GPCR Structural Revolution. *Nat. Rev. Mol. Cell Biol.* **2015,** *16,* 69–81.
16. Hollenstein, K.; et al. Insights Into the Structure of Class B GPCRs. *Trends Pharmacol. Sci.* **2014,** *35,* 12–22.
17. Congreve, M.; Murray, C. W.; Blundell, T. L. Structural Biology and Drug Discovery. *Drug Discov. Today* **2005,** *10,* 895–907.
18. Cushman, D. W.; Cheung, H. S.; Sabo, E. F.; Ondetti, M. A. Design of Potent Competitive Inhibitors of Angiotensin-Converting Enzyme. Carboxyalkanoyl and Mercaptoalkanoyl Amino Acids. *Biochemistry* **1977,** *16,* 5484–5491.
19. Natesh, R.; Schwager, S. L. U.; Sturrock, E. D.; Acharya, K. R. Crystal Structure of the Human Angiotensin-Converting Enzyme-Lisinopril Complex. *Nature* **2003,** *421,* 551–554.
20. Kaldor, S. W.; et al. Viracept (Nelfinavir Mesylate, AG1343): A Potent, Orally Bioavailable Inhibitor of HIV-1 Protease. *J. Med. Chem.* **1997,** *40,* 3979–3985.
21. Kim, E. E.; et al. Crystal Structure of HIV-1 Protease in Complex With VX-478, a Potent and Orally Bioavailable Inhibitor of the Enzyme. *J. Am. Chem. Soc.* **1995,** *117,* 1181–1182.
22. Sham, H. L.; et al. ABT-378, a Highly Potent Inhibitor of the Human Immunodeficiency Virus Protease. *Antimicrob. Agents Chemother.* **1998,** *42,* 3218–3224.
23. von Itzstein, M.; et al. Rational Design of Potent Sialidase-Based Inhibitors of Influenza Virus Replication. *Nature* **1993,** *363,* 418–423.
24. Kim, C. U.; et al. Structure-Activity Relationship Studies of Novel Carbocyclic Influenza Neuraminidase Inhibitors. *J. Med. Chem.* **1998,** *41,* 2451–2460.

25. Colman, P. M.; Varghese, J. N.; Laver, W. G. Structure of the Catalytic and Antigenic Site in Influenza Virus Neuraminidase. *Nature* **1983,** *303,* 41–44.
26. Varghese, J. N.; McKimm-Breschkin, J. L.; Caldwell, J. B.; Kortt, A. A.; Colman, P. M. The Structure of the Complex Between Influenza Virus Neuraminidase and Sialic Acid, the Viral Receptor. *Proteins Struct. Funct. Genet.* **1992,** *14,* 327–332.
27. Hardy, L. W.; Malikayil, A. The Impact of Structure-Guided Drug Design on Clinical Agents. *Curr. Drug Discov. Technol.* **2003,** *3,* 15–19.
28. Eder, J.; Sedrani, R.; Wiesmann, C. The Discovery of First-in-Class Drugs: Origins and Evolution. *Nat. Rev. Drug Discov.* **2014,** *13,* 577–587.
29. Hassell, A. M.; et al. Crystallization of Protein–Ligand Complexes. *Acta Crystallogr. D Biol. Crystallogr.* **2007,** *63,* 72–79.
30. Leulliot, N.; et al. High-Throughput Crystal-Optimization Strategies in the South Paris Yeast Structural Genomics Project: One Size Fits All? *Acta Crystallogr. D Biol. Crystallogr.* **2005,** *61,* 664–670.
31. Heras, B.; Martin, J. L. Post-Crystallization Treatments for Improving Diffraction Quality of Protein Crystals. *Acta Crystallogr. D Biol. Crystallogr.* **2005,** *61,* 1173–1180.
32. Newman, J. A Review of Techniques for Maximizing Diffraction From a Protein Crystal in Stilla. *Acta Crystallogr. D Biol. Crystallogr.* **2006,** *62,* 27–31.
33. Boettcher, J.; et al. Key Factors for Successful Generation of Proteinfragment Structures: Requirement on Protein, Crystals, and Technology. *Methods Enzymol.* **2011,** *493,* 61–89.
34. Kiefersauer, R.; Grandl, B.; Krapp, S.; Huber, R. IR Laser-Induced Protein Crystal Transformation. *Acta Crystallogr. D Biol. Crystallogr.* **2014,** *70,* 1224–1232.
35. Kiefersauer, R.; et al. A Novel Free-Mounting System for Protein Crystals: Transformation and Improvement of Diffraction Power by Accurately Controlled Humidity Changes. *J. Appl. Crystallogr.* **2000,** *33,* 1223–1230.
36. Skarzynski, T.; Thorpe, J. Industrial Perspective on X-Ray Data Collection and Analysis. *Acta Crystallogr. D Biol. Crystallogr.* **2006,** *62,* 102–107.
37. Danley, D. E. Crystallization to Obtain Protein–Ligand Complexes for Structure-Aided Drug Design. *Acta Crystallogr. D Biol. Crystallogr.* **2006,** *62,* 569–575.
38. Lusty, C. J. A Gentle Vapor-Diffusion Technique for Cross-Linking of Protein Crystals for Cryocrystallography. *J. Appl. Crystallogr.* **1999,** *32,* 106–112.
39. JBScreen Cryo Pro. Jena Bioscience, Jena (Germany). http://www.jenabioscience.com/images/PDF/CC-102.pdf
40. Rajashankar, K.; Dauter, Z. Data Collection for Crystallographic Structure Determination. *Methods Mol. Biol.* **2014,** *1140,* 211–237.
41. Färnegårdh, M.; et al. The Three-Dimensional Structure of the Liver X Receptor β Reveals a Flexible Ligand-Binding Pocket That Can Accommodate Fundamentally Different Ligands. *J. Biol. Chem.* **2003,** *278,* 38821–38828.
42. Kabsch, W. XDS. *Acta Crystallogr. Sect. D* **2010,** *66,* 125–132.
43. Otwinowski, Z.; Minor, W. Processing of X-ray Diffraction Data Collected in Oscillation Mode. *Methods Enzymol.* **1997,** *276,* 307–326.
44. Leslie, A. W.; Powell, H. Processing Diffraction Data With Mosflm. In *Evolving Methods for Macromolecular Crystallography,* vol. 245, Read, R., Sussman, J., Eds.; Springer: Netherlands, 2007; pp 41–51.
45. Evans, P. R.; Murshudov, G. N. How Good Are My Data and What Is the Resolution? *Acta Crystallogr. D Biol. Crystallogr.* **2013,** *69,* 1204–1214.
46. French, S.; Wilson, K. On the Treatment of Negative Intensity Observations. *Acta Crystallogr. A* **1978,** *34,* 517–525.
47. Vonrhein, C.; et al. Data Processing and Analysis With the autoPROC Toolbox. *Acta Crystallogr. D Biol. Crystallogr.* **2011,** *67,* 293–302.
48. Winter, G. xia2: An Expert System for Macromolecular Crystallography Data Reduction. *J. Appl. Crystallogr.* **2009,** *43,* 186–190.
49. Karplus, P. A.; Diederichs, K. Assessing and Maximizing Data Quality in Macromolecular Crystallography. *Curr. Opin. Struct. Biol.* **2015,** *34,* 60–68.
50. Vagin, A.; Teplyakov, A. MOLREP: An Automated Program for Molecular Replacement. *J. Appl. Crystallogr.* **1997,** *30,* 1022–1025.
51. McCoy, A. J.; et al. Phaser Crystallographic Software. *J. Appl. Crystallogr.* **2007,** *40,* 658–674.
52. Keegan, R. M.; Winn, M. D. MrBUMP: An Automated Pipeline for Molecular Replacement. *Acta Crystallogr. D Biol. Crystallogr.* **2008,** *64,* 119–124.
53. Adams, P. D.; et al. PHENIX: A Comprehensive Python-Based System for Macromolecular Structure Solution. *Acta Crystallogr. D Biol. Crystallogr.* **2010,** *66,* 213–221.
54. Long, F.; Vagin, A. A.; Young, P.; Murshudov, G. N. BALBES: A Molecular-Replacement Pipeline. *Acta Crystallogr. D Biol. Crystallogr.* **2008,** *64,* 125–132.
55. Afonine, P. V.; Grosse-Kunstleve, R. W.; Urzhumtsev, A.; Adams, P. D. Automatic Multiple-Zone Rigid-Body Refinement With a Large Convergence Radius. *J. Appl. Crystallogr.* **2009,** *42,* 607–615.
56. Winn, M. D.; Isupov, M. N.; Murshudov, G. N. Use of TLS Parameters to Model Anisotropic Displacements in Macromolecular Refinement. *Acta Crystallogr. D Biol. Crystallogr.* **2001,** *57,* 122–133.
57. Headd, J. J.; et al. Flexible Torsion-Angle Noncrystallographic Symmetry Restraints for Improved Macromolecular Structure Refinement. *Acta Crystallogr. D Biol. Crystallogr.* **2014,** *70,* 1346–1356.
58. Murshudov, G. N.; et al. REFMAC5 for the Refinement of Macromolecular Crystal Structures. *Acta Crystallogr. D Biol. Crystallogr.* **2011,** *67,* 355–367.
59. Smart, O. S.; et al. Exploiting Structure Similarity in Refinement: Automated NCS and Target-Structure Restraints in BUSTER. *Acta Crystallogr. D Biol. Crystallogr.* **2012,** *68,* 368–380.
60. Afonine, P. V.; et al. Towards Automated Crystallographic Structure Refinement With Phenix.Refine. *Acta Crystallogr. D Biol. Crystallogr.* **2012,** *68,* 352–367.
61. Moriarty, N. W.; Grosse-Kunstleve, R. W.; Adams, P. D. Electronic Ligand Builder and Optimization Workbench (eLBOW): A Tool for Ligand Coordinate and Restraint Generation. *Acta Crystallogr. D Biol. Crystallogr.* **2009,** *65,* 1074–1080.
62. Wlodek, S.; Skillman, A. G.; Nicholls, A. Automated Ligand Placement and Refinement With a Combined Force Field and Shape Potential. *Acta Crystallogr. D Biol. Crystallogr.* **2006,** *62,* 741–749.
63. Emsley, P.; Lohkamp, B.; Scott, W. G.; Cowtan, K. Features and Development of Coot. *Acta Crystallogr. D Biol. Crystallogr.* **2010,** *66,* 486–501.
64. Terwilliger, T. C.; Adams, P. D.; Moriarty, N. W.; Cohn, J. D. Ligand Identification Using Electron-Density Map Correlations. *Acta Crystallogr. D Biol. Crystallogr.* **2007,** *63,* 101–107.
65. Carolan, C. G.; Lamzin, V. S. Automated Identification of Crystallographic Ligands Using Sparse-Density Representations. *Acta Crystallogr. D Biol. Crystallogr.* **2014,** *70,* 1844–1853.
66. Davis, A. M.; St-Gallay, S. A.; Kleywegt, G. J. Limitations and Lessons in the Use of X-ray Structural Information in Drug Design. *Drug Discov. Today* **2008,** *13,* 831–841.
67. Wlodawer, A.; Minor, W.; Dauter, Z.; Jaskolski, M. Protein Crystallography for Aspiring Crystallographers or How to Avoid Pitfalls and Traps in Macromolecular Structure Determination. *FEBS J.* **2013,** *280,* 5705–5736.
68. Ferrer, J. L.; Larive, N. A.; Bowler, M. W.; Nurizzo, D. Recent Progress in Robot-Based Systems for Crystallography and Their Contribution to Drug Discovery. *Expert Opin. Drug Discovery* **2013,** *8,* 835–847.
69. Deller, M. C.; Rupp, B. Approaches to Automated Protein Crystal Harvesting. *Acta Crystallogr. F Struct. Biol. Commun.* **2014,** *70,* 133–155.
70. Marquez, J. A.; Cipriani, F. CrystalDirect: A Novel Approach for Automated Crystal Harvesting Based on Photoablation of Thin Films. *Methods Mol. Biol.* **2014,** *1091,* 197–203.
71. Juanhuix, J.; et al. Developments in Optics and Performance at BL13-XALOC, the Macromolecular Crystallography Beamline at the ALBA Synchrotron. *J. Synchrotron Radiat.* **2014,** *21,* 679–689.
72. Smith, C. A.; Cohen, A. E. The Stanford Automated Mounter: Enabling High-Throughput Protein Crystal Screening at SSRL. *JALA Charlottesv Va* **2008,** *13,* 335–343.
73. Muchmore, S. W.; et al. Automated Crystal Mounting and Data Collection for Protein Crystallography. *Structure* **2000,** *8,* R243–R246.
74. Svensson, O.; Malbet-Monaco, S.; Popov, A.; Nurizzo, D.; Bowler, M. W. Fully Automatic Characterization and Data Collection From Crystals of Biological Macromolecules. *Acta Crystallogr. D Biol. Crystallogr.* **2015,** *71,* 1757–1767.
75. Cymborowski, M.; et al. To Automate or Not to Automate: This Is the Question. *J. Struct. Funct. Genomics* **2010,** *11,* 211–221.
76. Incardona, M. F.; et al. EDNA: A Framework for Plugin-Based Applications Applied to X-Ray Experiment Online Data Analysis. *J. Synchrotron Radiat.* **2009,** *16,* 872–879.
77. Sauter, N. K.; Grosse-Kunstleve, R. W.; Adams, P. D. Robust Indexing for Automatic Data Collection. *J. Appl. Crystallogr.* **2004,** *37,* 399–409.

78. Kroemer, M.; Dreyer, M. K.; Wendt, K. U. APRV—A Program for Automated Data Processing, Refinement and Visualization. *Acta Crystallogr. D Biol. Crystallogr.* **2004,** *60,* 1679–1682.
79. Mooij, W. T.; et al. Automated Protein–Ligand Crystallography for Structure-Based Drug Design. *ChemMedChem* **2006,** *1,* 827–838.
80. Davies, T. G.; van Montfort, R. L. M.; Williams, G.; Jhoti, H. Pyramid: An Integrated Platform for Fragment-Based Drug Discovery. *Methods Princ. Med. Chem.* **2006,** *34,* 193–214.
81. Blaney, J.; Nienaber, V.; Burley, S. K. Fragment-Based Lead Discovery and Optimization Using X-Ray Crystallography, Computational Chemistry, and High-Throughput Organic Synthesis. *Methods Princ. Med. Chem.* **2006,** *34,* 215–248.
82. Monaco, S.; et al. Automatic Processing of Macromolecular Crystallography X-Ray Diffraction Data at the ESRF. *J. Appl. Crystallogr.* **2013,** *46,* 804–810.
83. Winter, G.; McAuley, K. E. Automated Data Collection for Macromolecular Crystallography. *Methods* **2011,** *55,* 81–93.
84. Echols, N.; et al. Automating Crystallographic Structure Solution and Refinement of Protein–Ligand Complexes. *Acta Crystallogr. D Biol. Crystallogr.* **2014,** *70,* 144–154.
85. Deller, M. C.; Rupp, B. Models of Protein–Ligand Crystal Structures: Trust, but Verify. *J. Comput. Aided Mol. Des.* **2015,** *29,* 817–836.
86. Brunger, A. T. Free R Value: A Novel Statistical Quantity for Assessing the Accuracy of Crystal Strucutres. *Nature* **1992,** *355,* 472–475.
87. Warren, G. L.; Do, T. D.; Kelley, B. P.; Nicholls, A.; Warren, S. D. Essential Considerations for Using Protein–Ligand Structures in Drug Discovery. *Drug Discov. Today* **2012,** *17,* 1270–1281.
88. Brändén, C.-I.; Jones, A. T. Between Objectivity and Subjectivity. *Nature* **1990,** *343,* 687–689.
89. Tickle, I. J. Statistical Quality Indicators for Electron-Density Maps. *Acta Crystallogr. D Biol. Crystallogr.* **2012,** *68,* 454–467.
90. Dauter, Z.; Wlodawer, A.; Minor, W.; Jaskolski, M.; Rupp, B. Avoidable Errors in Deposited Macromolecular Structures: An Impediment to Efficient Data Mining. *IUCrJ* **2014,** *1,* 179–193.
91. Engh, R. A.; Huber, R. Structure Quality and Target Parameters. In Arnold, E., Himmel, D. M., Rossmann, M. G., Eds.; pp 474–484. Vol. F, ch. 18.3.
92. Groom, C. R.; Allen, F. H.; Henderson, S. The Cambridge Structural Database (CSD), 2013.
93. Kleywegt, G. J.; Jones, T. A. Phi/Psi-Chology: Ramachandran Revisited. *Structure* **1996,** *4,* 1395–1400.
94. Chen, V. B.; et al. MolProbity: All-Atom Structure Validation for Macromolecular Crystallography. *Acta Crystallogr. D Biol. Crystallogr.* **2010,** *66,* 12–21.
95. Urzhumtseva, L.; Afonine, P. V.; Adams, P. D.; Urzhumtsev, A. Crystallographic Model Quality at a Glance. *Acta Crystallogr. D Biol. Crystallogr.* **2009,** *65,* 297–300.
96. Read, R. J.; et al. A New Generation of Crystallographic Validation Tools for the Protein Data Bank. *Structure* **2011,** *19,* 1395–1412.
97. Bradley, A. R.; et al. WONKA: Objective Novel Complex Analysis for Ensembles of Protein–Ligand Structures. *J. Comput. Aided Mol. Des.* **2015,** *29,* 963–973.
98. Jin, X.; et al. PDB-Explorer: A Web-Based Interactive Map of the Protein Data Bank in Shape Space. *BMC Bioinformat.* **2015,** *16,* 339.
99. Wallnoefer, H. G.; Handschuh, S.; Liedl, K. R.; Fox, T. Stabilizing of a Globular Protein by a Highly Complex Water Network: A Molecular Dynamics Simulation Study on Factor Xa. *J. Phys. Chem. B* **2010,** *114,* 7405–7412.
100. Kastenholz, M. A.; Pastor, M.; Cruciani, G.; Haaksma, E. E. J.; Fox, T. GRID/CPCA: A New Computational Tool to Design Selective Ligands. *J. Med. Chem.* **2000,** *43,* 3033–3044.
101. Howe, P. W. A. Principal Components Analysis of Protein Structure Ensembles Calculated Using NMR Data. *J. Biomol. NMR* **2001,** *20,* 61–70.
102. Pitt, W. R.; Montalvão, R. W.; Blundell, T. L. Polyphony: Superposition Independent Methods for Ensemble-Based Drug Discovery. *BMC Bioinformat.* **2014,** *15,* 339.
103. Altschul, S. F.; et al. Gapped BLAST and PSI-BLAST: A New Generation of Protein Database Search Programs. *Nucleic Acids Res.* **1997,** *25,* 3389–3402.
104. Remmert, M.; Biegert, A.; Hauser, A.; Soding, J. HHblits: Lightning-Fast Iterative Protein Sequence Searching by HMM-HMM Alignment. *Nat. Methods* **2012,** *9,* 173–175.
105. Krissinel, E. Enhanced Fold Recognition Using Efficient Short Fragment Clustering. *J. Mol. Biochem.* **2012,** *1,* 76–85.
106. Perot, S.; Sperandio, O.; Miteva, M. A.; Camproux, A. C.; Villoutreix, B. O. Druggable Pockets and Binding Site Centric Chemical Space: A Paradigm Shift in Drug Discovery. *Drug Discov. Today* **2010,** *15,* 656–667.
107. Halgren, T. New Method for Fast and Accurate Binding-Site Identification and Analysis. *Chem. Biol. Drug Des.* **2007,** *69,* 146–148.
108. Guvench, O.; MacKerell, A. D., Jr. Computational Fragment-Based Binding Site Identification by Ligand Competitive Saturation. *PLoS Comput. Biol.* **2009,** *5,* e1000435.
109. Schymkowitz, J.; et al. The FoldX Web Server: An Online Force Field. *Nucleic Acids Res.* **2005,** *33,* W382–W388.
110. Kortemme, T.; Kim, D. E.; Baker, D. Computational Alanine Scanning of Protein–Protein Interfaces. *Sci. STKE* **2004,** *2004* (219), e266.
111. Metz, A.; Ciglia, E.; Gohlke, H. Modulating Protein–Protein Interactions: From Structural Determinants of Binding to Druggability Prediction to Application. *Curr. Pharm. Des.* **2012,** *18,* 4630–4647.
112. Wells, J. A.; McClendon, C. L. Reaching for High-Hanging Fruit in Drug Discovery at Protein–Protein Interfaces. *Nature* **2007,** *450,* 1001–1009.
113. Smith, M. C.; Gestwicki, J. E. Features of Protein–Protein Interactions That Translate Into Potent Inhibitors: Topology, Surface Area and Affinity. *Expert Rev. Mol. Med.* **2012,** *14,* e16.
114. Berg, T. Small-Molecule Inhibitors of Protein–Protein Interactions. *Curr. Opin. Drug Discov. Devel.* **2008,** *11,* 666–674.
115. Pautsch, A.; et al. Molecular Recognition of the Protein Phosphatase 1 Glycogen Targeting Subunit by Glycogen Phosphorylase. *J. Biol. Chem.* **2008,** *283,* 8913–8918.
116. Parthier, C.; et al. Crystal Structure of the Incretin-Bound Extracellular Domain of a G Protein-Coupled Receptor. *Proc. Natl. Acad. Sci. U. S. A.* **2007,** *104,* 13942–13947.
117. Li, X.; Zhang, D.; Hannink, M.; Beamer, L. J. Crystal Structure of the Kelch Domain of Human Keap1. *J. Biol. Chem.* **2004,** *279,* 54750–54758.
118. Tse, C.; et al. ABT-263: A Potent and Orally Bioavailable Bcl-2 Family Inhibitor. *Cancer Res.* **2008,** *68,* 3421–3428.
119. Liu, M. H. Antihyperlipidemic Therapies Targeting PCSK9: Novel Therapeutic Agents for Lowering Low-Density Lipoprotein Cholesterol. *Int. J. Cardiol.* **2015,** *195,* 212–214.
120. Zhang, Y.; et al. Identification of a Small Peptide That Inhibits PCSK9 Protein Binding to the Low Density Lipoprotein Receptor. *J. Biol. Chem.* **2014,** *289,* 942–955.
121. Arkin, M.; Neitz, J. Hit Validation and Optimisation in Earlystage Drug Discovery. *Eur. Pharm. Rev.* **2014,** *19,* 48–52.
122. Feng, B. Y.; Shelat, A.; Doman, T. N.; Guy, R. K.; Shoichet, B. K. High-Throughput Assays for Promiscuous Inhibitors. *Nat. Chem. Biol.* **2005,** *1,* 146–148.
123. Feng, B. Y.; et al. A High-Throughput Screen for Aggregation-Based Inhibition in a Large Compound Library. *J. Med. Chem.* **2007,** *50,* 2385–2390.
124. Genick, C. C.; et al. Applications of Biophysics in High-Throughput Screening Hit Validation. *J. Biomol. Screen.* **2014,** *19,* 707–714.
125. Silvestre, H. L.; Blundell, T. L.; Abell, C.; Ciulli, A. Integrated Biophysical Approach to Fragment Screening and Validation for Fragment-Based Lead Discovery. *Proc. Natl. Acad. Sci. U. S. A.* **2013,** *110,* 12984–12989.
126. Fink, T.; Raymond, J. L. Virtual Exploration of the Chemical Universe up to 11 Atoms of C, N, O, F: Assembly of 26.4 Million Structures (110.9 Million Stereoisomers) and Analysis for new Ring Systems, Stereochemistry, Physicochemical Properties, Compound Classes, and Drug Discovery. *J. Chem. Inf. Model.* **2007,** *47,* 342–353.
127. Gelin, M.; et al. Combining 'Dry' Co-Crystallization and In Situ Diffraction to Facilitate Ligand Screening by X-ray Crystallography. *Acta Crystallogr. D Biol. Crystallogr.* **2015,** *71,* 1777–1787.
128. Hann, M.; et al. Strategic Pooling of Compounds for High-Throughput Screening. *J. Chem. Inf. Comput. Sci.* **1999,** *39,* 897–902.
129. Dechene, M.; Wink, G.; Smith, M.; Swartz, P.; Mattos, C. Multiple Solvent Crystal Structures of Ribonuclease A: An Assessment of the Method. *Proteins* **2009,** *76,* 861–881.
130. Stark, A.-K.; Sriskantharajah, S.; Hessel, E. M.; Okkenhaug, K. PI3K Inhibitors in Inflammation, Autoimmunity and Cancer. *Curr. Opin. Pharmacol.* **2015,** *23,* 82–91.
131. Fruman, D. A.; Rommel, C. PI3K and Cancer: Lessons, Challenges and Opportunities. *Nat. Rev. Drug Discov.* **2014,** *13,* 140–156.
132. Medina-Tato, D. A.; Ward, S. G.; Watson, M. L. Phosphoinositide 3-Kinase Signalling in Lung Disease: Leucocytes and Beyond. *Immunology* **2007,** *121,* 448–461.
133. Gustafsson, D.; et al. A New Oral Anticoagulant: The 50-Year Challenge. *Nat. Rev. Drug Discov.* **2004,** *3,* 649–659.
134. Pinto, D. J.; Smallheer, J. M.; Cheney, D. L.; Knabb, R. M.; Wexler, R. R. Factor Xa Inhibitors: Next-Generation Antithrombotic Agents. *J. Med. Chem.* **2010,** *53,* 6243–6274.
135. Lumma, W. C., Jr.; et al. Design of Novel, Potent, Noncovalent Inhibitors of Thrombin With Nonbasic P-1 Substructures: Rapid Structure-Activity Studies by Solid-Phase Synthesis. *J. Med. Chem.* **1998,** *41,* 1011–1013.

136. Tucker, T. J.; et al. Design and Synthesis of a Series of Potent and Orally Bioavailable Noncovalent Thrombin Inhibitors That Utilize Nonbasic Groups in the P1 Position. *J. Med. Chem.* **1998,** *41,* 3210–3219.
137. van Ryn, J.; et al. The Discovery of Dabigatran Etexilate. *Front. Pharmacol.* **2013,** *4,* 12. FEB.
138. Nar, H. The Role of Structural Information in the Discovery of Direct Thrombin and Factor Xa Inhibitors. *Trends Pharmacol. Sci.* **2012,** *33,* 279–288.
139. Weber, F.; Sedelmaier, G. Top 200 Pharmawirkstoffe. *Nachr. Chem.* **2014,** *62,* 1.
140. Dunbar, J.; et al. SAbDab: The Structural Antibody Database. *Nucleic Acids Res.* **2014,** *42,* D1140–D1146.
141. De Groot, A. S.; Goldberg, M.; Moise, L.; Martin, W. Evolutionary Deimmunization: An Ancillary Mechanism for Self-Tolerance? *Cell. Immunol.* **2006,** *244,* 148–153.
142. Tamura, M.; et al. Structural Correlates of an Anticarcinoma Antibody: Identification of Specificity-Determining Residues (SDRs) and Development of a Minimally Immunogenic Antibody Variant by Retention of SDRs Only. *J. Immunol.* **2000,** *164,* 1432–1441.
143. Kim, K. S.; Kim, H. J.; Han, B. W.; Myung, P. K.; Hong, H. J. Construction of a Humanized Antibody to Hepatitis B Surface Antigen by Specificity-Determining Residues (SDR)-Grafting and de-Immunization. *Biochem. Biophys. Res. Commun.* **2010,** *396,* 231–237.
144. Tan, P.; et al. "Superhumanized" Antibodies: Reduction of Immunogenic Potential by Complementarity-Determining Region Grafting With Human Germline Sequences: Application to an Anti-CD28. *J. Immunol.* **2002,** *169,* 1119–1125.
145. Lazar, G. A.; Desjarlais, J. R.; Jacinto, J.; Karki, S.; Hammond, P. W. A Molecular Immunology Approach to Antibody Humanization and Functional Optimization. *Mol. Immunol.* **2007,** *44,* 1986–1998.
146. Pelat, T.; et al. Germline Humanization of a Non-Human Primate Antibody That Neutralizes the Anthrax Toxin, by in vitro and In Silico Engineering. *J. Mol. Biol.* **2008,** *384,* 1400–1407.
147. Robert, R.; et al. Germline Humanization of a Murine Abeta Antibody and Crystal Structure of the Humanized Recombinant Fab Fragment. *Protein Sci.* **2010,** *19,* 299–308.
148. Fransson, J.; et al. Human Framework Adaptation of a Mouse Anti-Human IL-13 Antibody. *J. Mol. Biol.* **2010,** *398,* 214–231.
149. Radaev, S.; Motyka, S.; Fridman, W. H.; Sautes-Fridman, C.; Sun, P. D. The Structure of a Human Type III Fcgamma Receptor in Complex With Fc. *J. Biol. Chem.* **2001,** *276,* 16469–16477.
150. Sondermann, P.; Huber, R.; Oosthuizen, V.; Jacob, U. The 3.2-A Crystal Structure of the Human IgG1 Fc Fragment–Fc gammaRIII Complex. *Nature* **2000,** *406,* 267–273.
151. Idusogie, E. E.; et al. Mapping of the C1q Binding Site on Rituxan, a Chimeric Antibody With a Human IgG1 Fc. *J. Immunol.* **2000,** *164,* 4178–4184.
152. Oganesyan, V.; et al. Structural Characterization of a Human Fc Fragment Engineered for Extended Serum Half-Life. *Mol. Immunol.* **2009,** *46,* 1750–1755.
153. Oganesyan, V.; et al. Structural Insights Into Neonatal Fc Receptor-Based Recycling Mechanisms. *J. Biol. Chem.* **2014,** *289,* 7812–7824.
154. Wu, S. J.; et al. Structure-Based Engineering of a Monoclonal Antibody for Improved Solubility. *Protein Eng. Des. Sel.* **2010,** *23,* 643–651.
155. Bethea, D.; et al. Mechanisms of Self-Association of a Human Monoclonal Antibody CNTO607. *Protein Eng. Des. Sel.* **2012,** *25,* 531–537.
156. Marx, V. Structural Biology: 'Seeing' Crystals the XFEL Way. *Nat. Methods* **2014,** *11,* 903–908.
157. Schlichting, I. Serial Femtosecond Crystallography: The First Five Years. *IUCrJ* **2015,** *2,* 246–255.
158. Kern, J.; Yachandra, V. K.; Yano, J. Metalloprotein Structures at Ambient Conditions and in Real-Time: Biological Crystallography and Spectroscopy Using X-ray Free Electron Lasers. *Curr. Opin. Struct. Biol.* **2015,** *34,* 87–98.
159. Liu, W.; Wacker, D.; Wang, C.; Abola, E.; Cherezov, V. Femtosecond Crystallography of Membrane Proteins in the Lipidic Cubic Phase. *Philos. Trans. R. Soc. Lond. B Biol. Sci.* **2014,** *369,* 20130314.
160. Sawaya, M. R.; et al. Protein Crystal Structure Obtained at 2.9 Å Resolution From Injecting Bacterial Cells Into an X-ray Free-Electron Laser Beam. *Proc. Natl. Acad. Sci. U. S. A.* **2014,** *111,* 12769–12774.
161. Arnlund, D.; et al. Visualizing a Protein Quake With Time-Resolved X-ray Scattering at a Free-Electron Laser. *Nat. Methods* **2014,** *11,* 923–926.
162. Kuhlbrandt, W. Biochemistry. The Resolution Revolution. *Science* **2014,** *343,* 1443–1444.
163. Cheng, Y. Single-Particle Cryo-EM at Crystallographic Resolution. *Cell* **2015,** *161,* 450–457.
164. Bai, X. C.; McMullan, G.; Scheres, S. H. How Cryo-EM Is Revolutionizing Structural Biology. *Trends Biochem. Sci.* **2015,** *40,* 49–57.
165. Liao, M.; Cao, E.; Julius, D.; Cheng, Y. Structure of the TRPV1 Ion Channel Determined by Electron Cryo-Microscopy. *Nature* **2013,** *504,* 107–112.
166. Sun, L.; et al. Structural Basis of Human Gamma-Secretase Assembly. *Proc. Natl. Acad. Sci. U. S. A.* **2015,** *112,* 6003–6008.
167. Bartesaghi, A.; et al. 2.2 A Resolution Cryo-EM Structure of Beta-Galactosidase in Complex With a Cell-Permeant Inhibitor. *Science* **2015,** *348,* 1147–1151.
168. Zhao, J.; Benlekbir, S.; Rubinstein, J. L. Electron Cryomicroscopy Observation of Rotational States in a Eukaryotic V-ATPase. *Nature* **2015,** *521,* 241–245.
169. Cheng, Y.; Grigorieff, N.; Penczek, P. A.; Walz, T. A Primer to Single-Particle Cryo-Electron Microscopy. *Cell* **2015,** *161,* 438–449.
170. Henderson, R. The Potential and Limitations of Neutrons, Electrons and X-Rays for Atomic Resolution Microscopy of Unstained Biological Molecules. *Q. Rev. Biophys.* **1995,** *28,* 171–193.
171. White, S. H. The Progress of Membrane Protein Structure Determination. *Protein Sci.* **2004,** *13,* 1948–1949.
172. Kang, H. J.; Lee, C.; Drew, D. Breaking the Barriers in Membrane Protein Crystallography. *Int. J. Biochem. Cell Biol.* **2013,** *45,* 636–644.
173. Moraes, I.; Evans, G.; Sanchez-Weatherby, J.; Newstead, S.; Stewart, P. D. S. Membrane Protein Structure Determination—The Next Generation. *Biochim. Biophys. Acta Biomembr.* **2014,** *1838,* 78–87.
174. Cherezov, V.; et al. High-Resolution Crystal Structure of an Engineered Human Beta2-Adrenergic G Protein-Coupled Receptor. *Science* **2007,** *318,* 1258–1265.
175. Warne, T.; et al. Structure of a Beta1-Adrenergic G-Protein-Coupled Receptor. *Nature* **2008,** *454,* 486–491.
176. Rasmussen, S. G. F.; et al. Crystal Structure of the [bgr]2 Adrenergic Receptor–Gs Protein Complex. *Nature* **2011,** *477,* 549–555.
177. Lebon, G.; Warne, T.; Tate, C. G. Agonist-Bound Structures of G Protein-Coupled Receptors. *Curr. Opin. Struct. Biol.* **2012,** *22,* 482–490.
178. Srivastava, A.; et al. High-Resolution Structure of the Human GPR40 Receptor Bound to Allosteric Agonist TAK-875. *Nature* **2014,** *513,* 124–127.
179. Congreve, M.; et al. Discovery of 1,2,4-Triazine Derivatives as Adenosine A2A Antagonists Using Structure Based Drug Design. *J. Med. Chem.* **2012,** *55,* 1898–1903.
180. Congreve, M.; Langmead, C. J.; Mason, J. S.; Marshall, F. H. Progress in Structure Based Drug Design for G Protein-Coupled Receptors. *J. Med. Chem.* **2011,** *54,* 4283–4311.
181. Zhukov, A.; et al. Biophysical Mapping of the Adenosine A(2A) Receptor. *J. Med. Chem.* **2011,** *54,* 4312–4323.
182. Christopher, J. A.; et al. Fragment and Structure-Based Drug Discovery for a Class C GPCR: Discovery of the mGlu5 Negative Allosteric Modulator HTL14242 (3-Chloro-5-[6-(5-Fluoropyridin-2-yl)pyrimidin-4-yl]benzonitrile). *J. Med. Chem.* **2015,** *58,* 6653–6664.
183. Andrews, S. P.; Brown, G. A.; Christopher, J. A. Structure-Based and Fragment-Based GPCR Drug Discovery. *ChemMedChem* **2014,** *9,* 256–275.
184. Smart, T. G.; Paoletti, P. Synaptic Neurotransmitter-Gated Receptors. *Cold Spring Harb. Perspect. Biol.* **2012,** *4,* a009662.
185. Lemoine, D.; et al. Ligand-Gated Ion Channels: New Insights Into Neurological Disorders and Ligand Recognition. *Chem. Rev.* **2012,** *112,* 6285–6318.
186. daCosta Corrie, J. B.; Baenziger, John E. Gating of Pentameric Ligand-Gated Ion Channels: Structural Insights and Ambiguities. *Structure* **2013,** *21,* 1271–1283.
187. Jespersen, A.; Tajima, N.; Fernandez-Cuervo, G.; Garnier-Amblard, E. C.; Furukawa, H. Structural Insights Into Competitive Antagonism in NMDA Receptors. *Neuron* **2014,** *81,* 366–378.
188. Karakas, E.; Simorowski, N.; Furukawa, H. Subunit Arrangement and Phenylethanolamine Binding in GluN1/GluN2B NMDA Receptors. *Nature* **2011,** *475,* 249–253.
189. Kvist, T.; et al. Crystal Structure and Pharmacological Characterization of a Novel n-Methyl-d-Aspartate (NMDA) Receptor Antagonist at the glun1 Glycine Binding Site. *J. Biol. Chem.* **2013,** *288,* 33124–33135.
190. Yan, N. Structural Biology of the Major Facilitator Superfamily Transporters. *Annu. Rev. Biophys.* **2015,** *44,* 257–283.
191. César-Razquin, A.; et al. A Call for Systematic Research on Solute Carriers. *Cell* **2015,** *162,* 478–487.

192. Indiveri, C.; Galluccio, M.; Scalise, M.; Pochini, L. Strategies of Bacterial Over Expression of Membrane Transporters Relevant in Human Health: The Successful Case of the Three Members of OCTN Subfamily. *Mol. Biotechnol.* **2013,** *54,* 724–736.
193. Deng, D.; et al. Crystal Structure of the Human Glucose Transporter GLUT1. *Nature* **2014,** *510,* 121–125.
194. Nomura, N.; et al. Structure and Mechanism of the Mammalian Fructose Transporter GLUT5. *Nature* **2015,** *526,* 397–401.
195. Chothia, C.; Gelfand, I.; Kister, A. Structural Determinants in the Sequences of Immunoglobulin Variable Domain. *J. Mol. Biol.* **1998,** *278,* 457–479.
196. Baker, M. Making Membrane Proteins for Structures: A Trillion Tiny Tweaks. *Nat. Methods* **2010,** *7,* 429–434.
197. Tate, C. G. A Crystal Clear Solution for Determining G-Protein-Coupled Receptor Structures. *Trends Biochem. Sci.* **2012,** *37,* 343–352.
198. Chun, E.; et al. Fusion Partner Toolchest for the Stabilization and Crystallization of G Protein-Coupled Receptors. *Structure* **2012,** *20,* 967–976.
199. Alexandrov, A. I.; Mileni, M.; Chien, E. Y.; Hanson, M. A.; Stevens, R. C. Microscale Fluorescent Thermal Stability Assay for Membrane Proteins. *Structure* **2008,** *16,* 351–359.
200. Rasmussen, S. G.; et al. Structure of a Nanobody-Stabilized Active State of the Beta(2) Adrenoceptor. *Nature* **2011,** *469,* 175–180.
201. Lawson, A. D. Antibody-Enabled Small-Molecule Drug Discovery. *Nat. Rev. Drug Discov.* **2012,** *11,* 519–525.
202. Caffrey, M. A Comprehensive Review of the Lipid Cubic Phase or in Meso Method for Crystallizing Membrane and Soluble Proteins and Complexes. *Acta Crystallogr. F Struct. Biol. Commun.* **2015,** *71,* 3–18.

2.07 Kinetics, Thermodynamics, and Ligand Efficiency Metrics in Drug Discovery

GA Holdgate, Cambridge Science Park, Cambridge, United Kingdom

© 2017 Elsevier Ltd. All rights reserved.

2.07.1	**Introduction**	181
2.07.2	**Kinetics in Drug Discovery**	181
2.07.2.1	Biophysical Methods for Measuring Binding Kinetics	181
2.07.2.2	Principle of SPR	181
2.07.2.3	Experimental Considerations	182
2.07.2.4	Ligand Immobilization	182
2.07.2.5	Ligand Size/Molecular Weight Considerations	182
2.07.2.6	Choice of Coupling Methods	182
2.07.2.7	Ligand Quality Control Considerations	183
2.07.2.8	Consideration of Buffers	183
2.07.2.9	Association Phase	183
2.07.2.10	Steady-State Phase	184
2.07.2.11	Dissociation Phase	184
2.07.2.12	Regeneration Procedures	184
2.07.2.13	Biolayer Interferometry	185
2.07.2.14	Optical Waveguide Grating	186
2.07.2.15	Biochemical Methods to Determine Binding Kinetics	186
2.07.2.15.1	Radioligand binding	186
2.07.2.15.2	Measurement of dissociation rate constant: Direct dissociation of radiolabeled compound	186
2.07.2.15.3	Measurement of association rate constant	186
2.07.2.15.4	Fluorescence approaches	187
2.07.2.15.5	Competition methods	188
2.07.2.16	Enzyme Kinetics	188
2.07.2.17	Residence Times	188
2.07.2.18	Effect of Binding Kinetics on Fractional Occupancy and IC_{50}	189
2.07.2.19	Mechanistic Aspects to Binding Kinetics	190
2.07.2.20	Kinetic Selectivity	192
2.07.2.21	Role of Kinetics in Selectivity and Efficacy	192
2.07.2.22	Irreversible Inhibitors	194
2.07.2.23	Optimizing Residence Time	194
2.07.2.24	Binding Kinetics and PK/PD	196
2.07.2.25	Future Trends for Kinetic Characterization	197
2.07.3	**Thermodynamics in Drug Discovery**	197
2.07.3.1	Methods for Measuring Binding Thermodynamics	197
2.07.3.2	Direct Calorimetric Methods	198
2.07.3.2.1	Principle of ITC	198
2.07.3.2.2	Van't Hoff analysis	199
2.07.3.2.3	The thermodynamics of T_m shifting assays	200
2.07.3.3	Mechanistic Aspects to Binding Thermodynamics	201
2.07.3.3.1	Enthalpy–entropy compensation	201
2.07.3.3.2	Enthalpy–entropy transduction	202
2.07.3.3.3	The complex role of water	202
2.07.3.4	Role of Binding Thermodynamics in Selectivity and Efficacy	203
2.07.3.4.1	HIV-1 protease	203
2.07.3.4.2	Matrix metalloproteinase 12	203
2.07.3.4.3	Thrombin	203
2.07.3.4.4	HMGCoA reductase	204
2.07.3.4.5	Aldose reductase	204
2.07.3.5	Optimizing Enthalpy	204
2.07.3.6	Role of Binding Thermodynamics in Fragment-Based Drug Design	205
2.07.3.6.1	Experimental considerations for fragment ITC	206
2.07.3.7	Future Trends for Thermodynamic Characterization	206
2.07.4	**Use and Misuse of Efficiency Measures in Drug Discovery**	206

2.07.4.1 Common LEM 207
2.07.4.1.1 Ligand efficiency 207
2.07.4.1.2 Other size-based metrics 207
2.07.4.1.3 Ligand lipophilicity efficiency 207
2.07.4.1.4 Enthalpic efficiency 208
2.07.4.1.5 Kinetic efficiency 208
2.07.4.2 Future Trends for Application of LEM 209
2.07.5 Summary 209
References 210
Further Reading 211
Relevant Websites 211

2.07.1 Introduction

Drug discovery is a long and complex process, requiring multiparametric optimization. Detecting, characterizing, and optimizing molecular interactions lie at the heart of successful drug discovery, and these processes may be facilitated by understanding the kinetics and thermodynamics of ligand binding. Formation of a protein–ligand complex is driven by the change in free energy of binding, which itself is composed of enthalpic and entropic components, and so, the free energy change upon binding may be increased by improving the contributions from either or both components, providing different options for optimizing binding interactions. Of course, equilibrium considerations alone are not sufficient to fully describe a binding response, as the binding affinity is also composed of association and dissociation kinetic contributions. In fact, these contributions may be more important in the drug discovery setting, where the introduction of a drug to the body is more realistically represented by nonequilibrium considerations representative of an open system, where responses are not directly related to concentration. Hence, a greater understanding of the kinetic contribution to binding may offer further opportunity to optimize molecular interactions for greater efficacy under these nonequilibrium conditions.

The challenge for medicinal chemists is to understand both the thermodynamic and kinetic contributions and to exploit opportunities for modifying these contributions in order to make more effective and safer medicines. As a tool to help guide this process, various different measures of the efficiency of compound binding, termed ligand efficiency metrics (LEM), have been proposed that help to relate different binding parameters to various physicochemical properties of the compounds studied (such as molecular weight or hydrophobicity).

By employing rigorous experimental procedures to determine the thermodynamic and kinetic contributions to binding interactions and by applying simple tools and guidelines that help to identify compounds that outperform the trend in terms of the desired biological response, medicinal chemists will be able to use these principles to further optimize compounds toward improved clinical properties. Ultimately, this will decrease clinical attrition and help to make drug discovery more successful.

2.07.2 Kinetics in Drug Discovery

2.07.2.1 Biophysical Methods for Measuring Binding Kinetics

There are several different methods that allow binding kinetics to be measured and individual rate constants for association and dissociation derived. These include both biochemical and biophysical assays, which have different requirements for instrumentation and assay design. Of course, binding kinetics can be determined by any technique that is capable of measuring a change in bound or free analyte concentration with time. Ultimately, the choice of method will depend upon the desired information, the reagents available, and the access to specific instrumentation. Over the last few years, however, surface plasmon resonance (SPR) experiments have become particularly popular for determining both affinities and kinetics.

2.07.2.2 Principle of SPR

Optical biosensors measure changes in a particular characteristic of light, coupled to changes linked to binding at the sensor surface by making use of the electromagnetic evanescent wave formed at the gold interface of the sensor chip surface. Biosensors employing SPR are the most well-known optical biosensors, utilizing this phenomenon to enable detection of protein–ligand interactions in real time.

When total internal reflection occurs, the electromagnetic field component of the incident light (the evanescent wave) penetrates into the gold film on the sensor surface and interacts with free electrons, termed plasmons. Photons of the incident light are absorbed, the evanescent field strength is increased, and the light is no longer reflected. This decrease in the reflected light intensity occurs at an angle that is dependent upon the refractive index of the material in the flow cell and is called the SPR angle. The

refractive index of the flow cell changes with increased mass on the surface and thus allows detection of ligand binding. In a typical direct binding SPR experiment, the gold surface is coated with a carboxymethylated dextran matrix to which the target of interest can be immobilized. Test compounds or other binding partners are then flowed across the sensor chip surface, where binding during the association phase results in an increase in mass, a change in refractive index, and a measurable signal. Ligand dissociation can then be observed by simply flowing buffer, instead of ligand, across the protein surface.

Thus, these instruments potentially allow the kinetic rate constants and the equilibrium dissociation constant for an interaction to be measured, depending upon the experimental setup, the most common of which will be described in the succeeding text.

2.07.2.3 Experimental Considerations

The process employed in SPR experiments can be described by several key steps, which are required to generate useful data. Firstly, one binding partner must be immobilized; the association kinetics can then be monitored by injecting the other partner over this ligand surface; during the steady-state period, a kinetically independent affinity may be determined; subsequently, the dissociation of the analyte may be monitored, and finally, regeneration of the ligand surface must be achieved before the next analyte can be studied. These different stages of the SPR experiment will be briefly described in the succeeding text.

2.07.2.4 Ligand Immobilization

A requirement of SPR experiments is that one binding partner, termed the ligand, is attached to the biosensor surface. There are several options by which this capture may be achieved, including either covalent or noncovalent methods. Typically, it is the protein that is attached to the hydrogel matrix, and this must be achieved in a manner that retains authentic binding activity and capacity. Many factors contribute to the decision on which partner to immobilize, including the potential immobilization density required to produce a reasonable signal upon complexation, the routes for immobilization, and the type of assay required.

The successful immobilization of proteins requires consideration of the size/molecular weight of the protein, the amino acid composition, isoelectric point (pI), pH stability, and potential tagging sites for directional, homogeneous coupling. When possible, methods that minimize the possibility of heterogeneous coupling through different parts of the molecule should be prioritized. As with other biophysical methods, the quality of the protein is also important, and information about the quality and behavior of the protein can help to reduce problems with immobilization and subsequent affinity and kinetic measurements.

2.07.2.5 Ligand Size/Molecular Weight Considerations

Binding signals in SPR rely upon changes in refractive index caused by changes in mass on the sensor surface, with larger molecules producing correspondingly larger signal changes upon binding than smaller analytes. Sometimes, it can be advantageous to immobilize the smaller binding partner, as this will lead to larger responses during the experiment. Immobilization densities will need to be considered so that mass transfer does not limit the measurement of binding kinetics. This may be especially important if high densities of low-molecular-weight ligands are captured.

2.07.2.6 Choice of Coupling Methods

There are two general types of capture methods: covalent attachment and affinity capture. However, in order to capture the ligand onto the biosensor surface using either method, there must be a location at which either a chemical attachment (usually allowing complementary reaction with a surface bound group) or a capture tag can be placed without affecting binding functionality. Covalent attachment is often accomplished using amine, thiol, or aldehyde groups on the ligand, with complementary chemistry on the sensor surface allowing the formation of the covalent bond. These three coupling methods have been used extensively and are well understood and established. The immobilization density is relatively easily controlled, and reagent consumption is low. Disadvantages with this approach lie with the number or position of the reactive groups on the ligand: orientation of ligands containing more than one reactive group may be heterogeneous; coupling through a reactive group close to the analyte binding site may obscure the binding site resulting in reduced or abolished binding affinity.

Affinity capture of the ligand can often be achieved by initially introducing a high-affinity binding partner onto a site on the ligand, for a complementary partner that can be covalently attached to the sensor surface. Immobilization is then achieved via the high-affinity recognition between the two partners. Often, affinity capture approaches make use of the high-affinity interactions between antibodies and antigens or between biotin and streptavidin, for example, by capturing a biotinylated analog of the ligand onto a streptavidin-coated surface. High-affinity interactions such as these, although not irreversible, often provide stable enough surfaces that allow kinetic measurements to be made.

In the antibody capture approach, usually, the antibody can be covalently immobilized using amine capture, as described earlier, as often coupling occurs via the Fc region leaving the Fab region free to bind the antigen, which may be attached to the ligand, or the ligand itself (providing the antibody recognition site is distal to the analyte binding site).

It is also possible to combine both affinity capture and covalent approaches; for example, the weak affinity Ni-NTA–6His tag interaction may be used to directionally orient the ligand to the surface, allowing subsequent chemical interaction with groups in proximity to the surface.

The process involves activating the Ni-NTA chip with NHS/EDC in the standard manner for amine coupling (as the chip retains a significant proportion of nonderivatized carboxyl groups), followed by the introduction of the His-tagged ligand. The ligand is weakly but directionally noncovalently captured to the surface via the His–Ni-NTA interaction, but once it is close enough to the reactive esters on the chip, proximal free amines on the ligand can react to yield covalent coupling. The advantage of this method is twofold: It avoids the need for the low pH usually required for amine capture; it results in a more functional and robust immobilization, based upon the directionality of the capture. The chosen immobilization procedure often depends upon the type of ligand (protein, carbohydrate, nucleic acid, small molecule, etc.), the partner analyte to be used (small or large molecule), and the data required.

2.07.2.7 Ligand Quality Control Considerations

Purity of test compounds is seen as a key factor in screening and follow-up characterization, yet often, the purity and other quality control factors associated with the target protein have a lower profile. In fact, this should be a prioritized consideration, as the target protein is the key reagent used to identify and characterize all potential hits and leads. Before beginning immobilization procedures, it is good practice to verify the identity, purity, concentration, functionality, and stability of the target protein, using a combination of biochemical and biophysical methods. This can help to avoid problems associated with heterogeneous immobilization, which could result from impurities being coupled to the surface; it also helps to identify buffer conditions that are compatible for maintaining folded and active protein during both capture and subsequent kinetic binding experiments. Another factor not directly related to ligand quality is the availability of the ligand, as the requirements for this are often lower, in an individual experiment, than the analyte, which has to be injected at several different concentrations. However, the amount of ligand required to thoroughly analyze many different analytes may be considerable.

2.07.2.8 Consideration of Buffers

The choice of immobilization buffer, controlling the pH relative to the pI, and the ionic strength and the presence of other additives required for stability can make a considerable difference to both the attraction of the ligand to the surface and the final immobilization density. Buffers should be chosen carefully to achieve a reasonable preconcentration at the carboxymethyldextran sensor surface, as an initial high local ligand concentration promotes efficient coupling. Electrostatic preconcentration is accomplished by introducing a positive charge on the ligand while maintaining a negative charge on the hydrogel matrix by using a pH lower than the pI of the ligand and by having a low ionic strength. The pK_a of the typical carboxymethyldextran surface is around 3.5, and so, ligand preconcentration is not successful at pH values below this. Usually, the buffer with the highest pH, giving a reasonable preconcentration response, is used for the immobilization process.

A key consideration, especially when running kinetics experiments, is the ligand immobilization density. Kinetic measurements are best achieved with the lowest ligand immobilization density that gives a measurable response. This is because secondary effects including mass transfer and steric hindrance are reduced at lower immobilization densities.

The theoretical maximal binding capacity for the analyte is given by the Eq. (1):

$$R_{max} = \frac{MW_{\text{analyte}}}{MW_{\text{ligand}}} \text{x} R_{\text{ligand}} \text{x}\, n \tag{1}$$

where R_{max} is the maximum analyte binding capacity in RU, MW is the molecular weight of the indicated species, R_{ligand} is the amount of immobilized ligand in RU, and n is the stoichiometry of analyte binding to ligand.

This formula assumes that all the immobilized ligand molecules are accessible and fully functional, which may not always be the case. In order to characterize the surface before undertaking binding kinetics studies on test compounds, it is useful to employ a control or tool analyte that may be used to probe the ligand functionality and to test the sensor surface for stability over time and cycles of regeneration.

It is also beneficial for a reference ligand, which lacks the ability to bind analytes, to be immobilized to the same density as the target ligand. This surface provides a suitable reference allowing for changes in refractive index occurring from analyte injections or other injection artifacts to be corrected.

2.07.2.9 Association Phase

Once a suitable ligand surface has been prepared, the next step is the injection of the analyte over the ligand in order to monitor binding. Binding occurs when the injected analyte collides with the immobilized ligand, following the diffusion of the analyte from bulk flow to the sensor surface. Recognition occurs and a binding signal detected if the analyte has the correct direction of approach and sufficient energy. The binding response at any time, t, during the association phase is given by Eq. (2):

$$R = \frac{k_a.C.R_{\text{max}}}{k_a.C + k_d}\left(1 - e^{-(k_a.C+k_d).t}\right) + R_i \tag{2}$$

where R is the signal in RU, C is the concentration of injected analyte, R_{max} is the maximum signal, k_a is the association rate constant, k_d is the dissociation rate constant, and R_i is a curve-fitting parameter that allows for a nonzero signal at the start of the injection (often reflecting bulk refractive index changes).

As the association rate constant becomes larger, it becomes more difficult to reliably measure. Two factors contribute to this: the effect of mass transfer becomes more important and the assumption that the concentration of analyte in the flow remains constant at its injected value. Thus, the upper limit to reliable values lies in the range 10^7 $M^{-1}s^{-1}$.

As Eq. (2) shows, the association phase contains information about not only the association rate constant but also the dissociation rate constant, as dissociation events will also occur during analyte injection.

2.07.2.10 Steady-State Phase

As dissociation events occur during the injection of analyte, if the injection of analyte continues for long enough, then the net binding rate observed will fall to zero (shown when the binding response becomes parallel to the baseline), as the rate of dissociation becomes equal to the rate of association. This situation is called steady state (not equilibrium since there is continuous addition and removal of the analyte) and reflects the fact that the concentration of ligand–analyte complex is not changing. The responses at steady state, obtained for different concentrations of analyte, may then be used to calculate the steady-state affinity or equilibrium dissociation constant, K_D, as shown in Eq. (3):

$$K_D = \frac{[L][A]}{[LA]} = \frac{[A](R_{max} - R_{ss})}{R_{ss}} = \frac{k_d}{k_a} \tag{3}$$

where [L] is the free concentration of ligand, [A] is the free concentration of analyte, [LA] is the concentration of the ligand–analyte complex, and R_{ss} is the response at steady state for the injected analyte concentration. Often in SPR experiments, the ligand is the immobilized protein, and the analyte is the injected small-molecule ligand, so care should be used with the nomenclature.

Plotting the steady-state response, R_{ss}, versus the injected analyte concentration yields a rectangular hyperbola described by the Langmuir binding isotherm, and the K_D value is determined as the concentration of analyte producing a half maximal response (rearrangement of Eq. (3) in the preceding text). Since steady-state measurements of K_D are not affected by mass transport limitations or potential analyte rebinding, often affecting rate constants, this offers an internally consistent approach to check the validity of the kinetic rate constants by comparing the steady-state K_D with that calculated from k_d/k_a.

2.07.2.11 Dissociation Phase

After binding has taken place, the ligand and analyte remain bound in the complex until dissociation takes place. Dissociation is the process by which the analyte is released from the complex and is removed from the sensor surface of the SPR instrument by buffer flow. As stated previously, dissociation events occur during the association and steady-state phases of the sensorgram, but during these phases, any dissociated ligand is replaced by new analyte from the injection. However, when the flow of analyte is stopped and replaced with buffer, the concentration of the free analyte falls to zero, and the dissociation events are easily detected as a decrease in signal (in the absence of rebinding further along the flow cell, there are no further binding events to obscure the measurement).

The response at any time, t, during the dissociation phase is given by Eq. (4) in the succeeding text:

$$R = R_0.e^{-k_d t} + R_{(t \to \infty)} \tag{4}$$

where R_0 is the initial signal at the start of the dissociation phase (at the time the analyte injection is stopped and buffer flow started), k_d is the dissociation rate constant, and $R_{(t \to \infty)}$ is the response after infinite time (essentially a background term).

Dissociation rates that are very fast ($k_d > 1$ s^{-1}) or very slow ($k_d < 10^{-4}$ s^{-1}) are difficult to measure reliably. In the rapid case, the data sampling rate (even at 10 Hz) does not allow the collection of sufficient data for accurate data fitting (90% of the signal is lost in 2.3 s for a k_d of 1 s^{-1}). Conversely for the slow rate situation, data collection takes too long for enough dissociation phase to be collected to be reliable (10% reduction in starting signal for a $k_d = 10^{-4}$ s^{-1} takes 17.6 min). In the slow dissociation example, it is important that control experiments are carried out to account for any baseline drift during the long data collection times.

A typical example of multicycle kinetic data is shown in Fig. 1, top panel.

2.07.2.12 Regeneration Procedures

In SPR instruments with a single channel or flow cell for target immobilization or for higher throughput in multichannel instruments, when the aim is to characterize large numbers of interactions, it is important to remove any remaining analyte from the ligand following the monitored dissociation phase, without affecting the ligand functionality. This process is known as regeneration, as the aim is to regenerate the starting condition of free ligand so that a further cycle of analyte testing can take place. Conditions leading to regeneration have to be evaluated empirically since the physical forces driving the binding interaction usually are not known. Hence, a series of different regeneration conditions must be sampled for their ability to disturb the binding interaction without negatively affecting the binding competence of the ligand. Sometimes, regeneration occurs by partially unfolding the

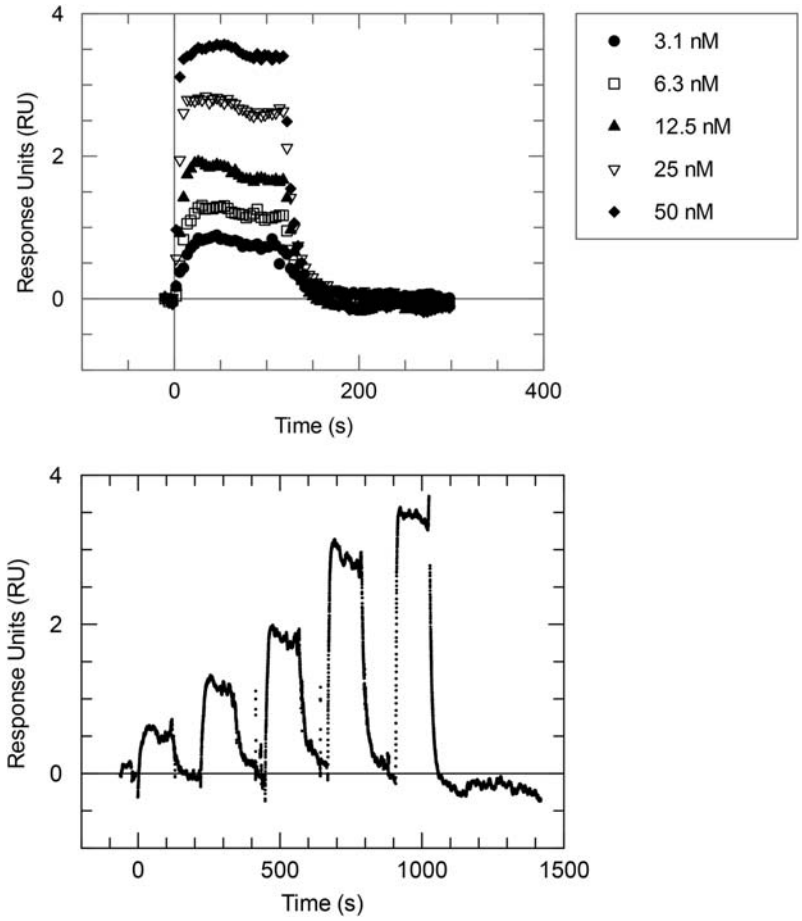

Fig. 1 Typical sensorgrams from a Biacore instrument, showing multicycle kinetics (top panel) and single-cycle kinetics (bottom panel).

protein ligand or by using pH, ionic strength, or chemicals to remove the analyte. Guidelines for regeneration suggest that the chosen conditions should be the mildest solution that completely disrupts the complex, producing free ligand.

Sometimes, it is possible to avoid the need for regeneration by employing single-cycle kinetics measurements. As the name suggests, this involves a series of injections of analyte at increasing concentrations in a single cycle, with no regeneration in between, Fig. 1, bottom panel. This effectively allows the monitoring of the increasing concentration of complex formation and can potentially be advantageous when working with slowly dissociating compounds.

Direct binding assays are dependent upon the MW and K_D of the test compound in order to produce a large enough signal, which potentially represents a challenge when working with fragments, where both the compound size and affinity are low.

However, problems in sensitivity due to ligand molecular size may be overcome by the use of alternative assay formats such as the surface competition assay (SCA) or inhibition in solution assay (ISA). In the SCA format, an analyte competes with a higher-molecular-weight analog for binding to a common partner immobilized on the sensor surface; for example, a peptide and protein could compete for binding to a second immobilized protein partner.

The ISA overcomes the size issue by measuring the binding of the macromolecule, whereby increasing test compound concentration results in a decrease in the observed signal due to competition.

The ISA format requires immobilization of a tool compound or so-called target definition compound (TDC) to the sensor surface, which then serves as a probe for the binding site. The binding interaction between the TDC and the target protein results in a control signal, which is reduced in the presence of competing test compounds. Only those test compounds demonstrating kinetic competition with the immobilized TDC will reduce the amount of free protein available at equilibrium to bind to the TDC. This approach allows affinity information for test compounds to be derived, although kinetic information is not easily obtained.

2.07.2.13 Biolayer Interferometry

Biolayer interferometry (BLI) is another optical technique that may also be used to measure binding kinetics. The BLI method is based on the interference wave pattern created from the reflection of white light as a function of the thickness of the biosensor

tip surface. Ligand (here used in its more traditional sense, compared with the SPR section in the preceding text), binding to the immobilized protein attached to the sensor surface, causes a change in the optical layer thickness. This results in a change in the interference pattern between this and the reference reflection that can be measured in overtime. This change is brought about because some of the wavelengths of light are subject to a change in path length during reflection, as a result of alteration in the surface thickness. Thus, the interference patterns for all wavelengths are changed, due to differences in the constructive and destructive interference patterns. The resulting interferometric profile is wavelength-shifted, by an amount that is proportional to the change in thickness, compared with the original sensor surface. Only molecules associating with or dissociating from the biosensor surface result in a change in thickness, generating a change in signal. This method is insensitive to changes in the refractive index of the surrounding solution and so may be used with complex mixtures without adverse effect.

2.07.2.14 Optical Waveguide Grating

Biosensor instruments employing optical waveguides may also allow direct measurements of binding interactions and are suitable for high-throughput measurements.

Similar to SPR, the instruments exploit evanescent waves generated when light traveling through a boundary of different refractive indices undergoes total internal reflection. Waveguides situated adjacent to each other allow coupling and propagation of the wave from one element to the next. Broadband light is used to illuminate the surface, which then reflects a specific wavelength dependent upon the refractive index close to the sensor surface. Ligand binding causes a change in refractive index, leading to a wavelength change in the reflected light. This measurement correlates with the change in mass on the sensor surface.

The largest difference between both BLI and optical waveguide grating (OWG) instruments and SPR-based instruments is the absence of a flow system. This means that BLI and OWG systems measure an approach to a new equilibrium during dissociation experiments, rather than a true dissociation rate constant. However, in practice, the large dilution of dissociating analyte means that the errors are often insignificant.

2.07.2.15 Biochemical Methods to Determine Binding Kinetics

2.07.2.15.1 Radioligand binding

Radioligand binding is an approach that makes use of a radioactively labeled compound, which binds at the target binding site. These long-established assays are potentially suitable for purified protein, tissue homogenates, cell lysates, and also even whole cells. The radioligand tool compound should have a specific activity high enough to allow detection of the protein–ligand complex (usually by a scintillation counting method) in the binding assay and should demonstrate a high degree of selectivity and being pure and stable. The kinetics of the binding interaction are measured by detecting the incorporation of the radioactivity into the protein over time. Most radioligand binding assays need a separation step (typically filtration or washout) to separate bound from free radioligand before the measurement of the incorporated radioactivity is undertaken.

An alternative radiolabeled approach is using scintillation proximity assays (SPA), where the protein of interest is captured onto a scintillant-containing solid support (usually beads or microtiter plates). SPA typically involves isotopes whose decay particles have only a short path length in aqueous solution (e.g., β-particle emitters such as tritium). This means that only a radioligand bound to the immobilized protein is close enough to excite the scintillant, which results in signal generation.

Competition experiments between the tool ligand and test compounds may be employed, as long as the tool compound is known to interact at the same binding site as the test compounds. This method allows determination of test compound binding kinetics without the need to label each individual compound.

Radioligand binding experiments may be used to determine both association and dissociation rate constants, depending upon the experimental design, discussed in the succeeding text. As with other methods, the direct binding experiment analysis assumes that binding follows the law of mass action so that at any time, the rate at which the protein–ligand complex is formed is proportional to the radioligand concentration and the number of binding sites unoccupied. In the dissociation experiment, the rate of dissociation is proportional to the concentration of protein–ligand complexes.

2.07.2.15.2 Measurement of dissociation rate constant: Direct dissociation of radiolabeled compound

Dissociation experiments, following dissociation of the radiolabeled molecule itself, directly measure the dissociation rate constant for radioligand dissociating from the protein. The setup involves allowing the ligand and receptor to bind, usually until equilibrium is reached, at which point, further binding of radioligand to the protein is prevented, for example, by adding unlabeled compound or by large dilution. The addition of a saturating level of a competitor compound in order to prevent rebinding of the dissociated ligand, especially in the case of fast association kinetics, may also be considered. The rate of dissociation can be described by a single exponential decay with a rate constant equal to the k_d for the ligand.

2.07.2.15.3 Measurement of association rate constant

Measurement of the association rate constant is achieved by adding radioligand to protein and measuring the specific binding component at various times. The binding signal increases with time until a plateau is reached. As described in the SPR section in the preceding text, this plateau is not the maximum binding signal, as the value of the plateau in this experiment depends upon the concentration of radioligand used, and so represents the steady state under the conditions used. The maximum binding

signal is given by extrapolation to an infinite concentration of radioligand or in practical terms a concentration that is much greater than K_D.

As shown in Eq. (2) for SPR in the preceding text, the rate with which the binding signal increases is controlled by three factors: the association rate constant itself, k_a, which needs to be determined in the experiment; the concentration of radioligand used (higher concentrations of radioligand result in faster equilibration times); and the dissociation rate constant, k_d. At first, it may be unexpected that the measured rate of association depends partially on the dissociation rate constant. However, consideration of the binding process reveals that during the association experiment, radioligand both binds to and may also dissociate from the protein. The system reaches steady state when the rates of the association and dissociation events are equal. Thus, the observed rate of association indicates the time to reach steady state, and it is not possible to fit a simple equation to association data to determine the association rate constant, unless the value of the dissociation rate constant is already known. It is possible to resolve the values if two or more concentrations of radioligand are used.

2.07.2.15.4 Fluorescence approaches

Fluorescence-based methodologies, such as fluorescence polarization (FP), Förster resonance energy transfer (FRET) or fluorescence intensity (FLINT), see Fig. 2, offer an alternative approach to radioactivity-based assays, along with potentially higher throughput.

In FP assays, the ligand, containing the fluorophore, is excited by linearly polarized light. The degree of polarization of the fluorescence emission is proportional to the rate of tumbling in solution of the fluorophore. The rate of tumbling is proportional to the size of the species to which the fluorophore is attached, with higher-molecular-weight species tumbling at lower frequencies. Hence protein-bound ligands retain more of the polarization of the excitation light. FP assays are applicable to both isolated protein assays but have also found application in cell-based methods, enabling the detection and kinetic characterization of ligand–cell surface receptor interactions.

The FRET method involves the nonradiative transfer of energy between a donor (usually a fluorescently labeled ligand) and an acceptor (often a fluorescently labeled protein). The FRET signal is dependent upon ligand since the FRET phenomenon is distance-dependent, with the maximal donor/acceptor distance being around 5–10 nm. Only when bound to the protein will the donor fluorophore be positioned close enough to be able to excite the acceptor fluorophore attached to the protein.

FLINT experiments rely upon the change in fluorescence signal brought about by a change in polarity of the environment experienced by the fluorophore. This may be the relocation from solvent to the protein-bound state for the (labeled) fluorescent ligand or due to conformational changes induce within the protein by ligand binding that alter the intrinsic protein fluorescence or that of a protein-bound fluorophore.

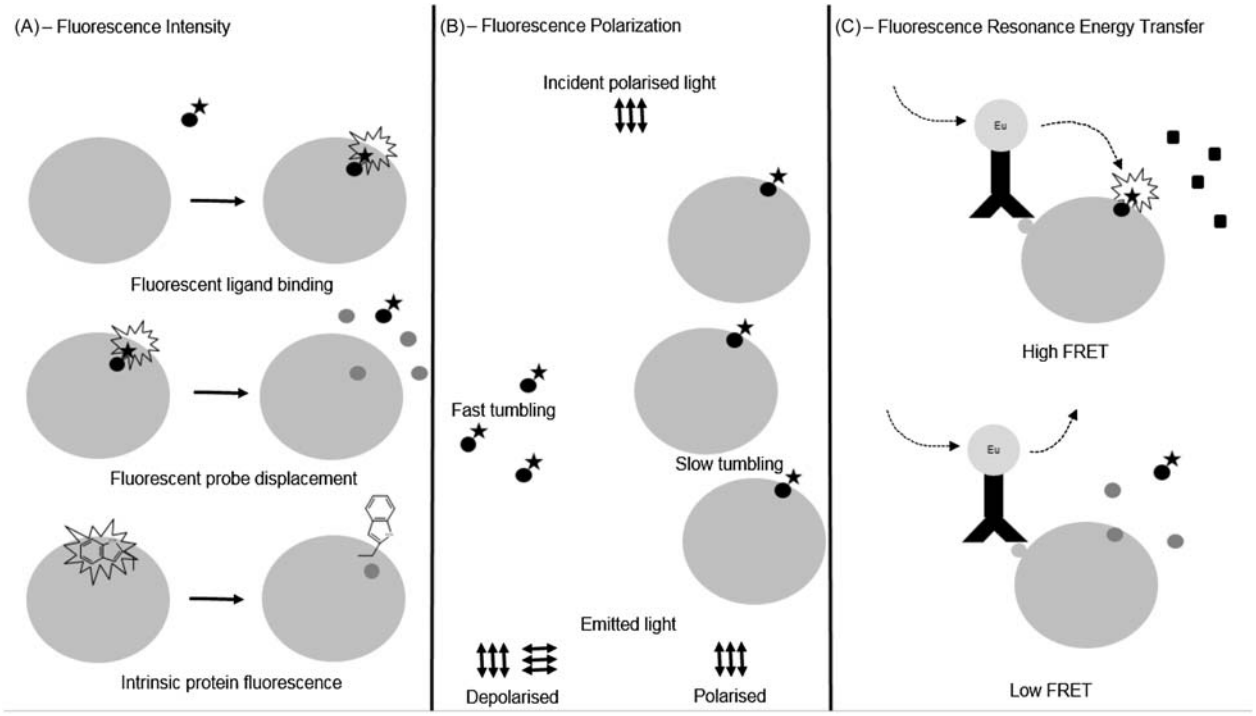

Fig. 2 Principles of fluorescence-based methodologies—(A) fluorescence intensity; (B) fluorescence polarization; and (C) fluorescence resonance energy transfer.

2.07.2.15.5 Competition methods

As mentioned earlier for radiolabeled methods, competition experiments are also useful in fluorescent approaches, as they preclude the need to label every compound. Such indirect, competition methodologies are suitable for use with both radioligand and fluorescence-based assays, making use of the kinetic competition between the test compound and the (radio)labeled tool ligand. In this type of experiment, the binding kinetics of the test compound are derived by the affect upon the kinetics of a labeled reporter molecule. Usually, it is desired for the labeled molecule to have rapid association/dissociation kinetics, such that these kinetics do not affect the kinetics of the test compound. Complications arise when the labeled ligand has its own, resolvable binding kinetics. In these cases, knowledge of the mechanism of inhibition/binding and knowledge of the binding kinetics of the labeled ligand are required in order to resolve the kinetics of the test compound. For the simple 1:1 binding situation, following the law of mass action, the method of Motulsky and Mahan, which has seen an increase in use again recently, can be employed.[1] Extending this, a model including an isomerization step upon compound binding, for example, as described for muscarinic receptors, has also been described.[2]

It should be noted that a potential problem when employing some label-based approaches (especially where the labels are large molecular entities, as can be the case for fluorescent labels) is the possibility that the incorporation of the label into the ligand may potentially affect its binding kinetics and affinity. Of course, label-free methods offer the opportunity to avoid this issue, and the use of biosensors to measure binding kinetics has increased dramatically over the last decade. While strictly not truly label-free (as the protein has to be coupled to the sensor surface), the use of these technologies does not require the use of small-molecule labels.

2.07.2.16 Enzyme Kinetics

Enzyme assays, which often can be followed using biophysical readouts, for example, quantification of the amount of a fluorescent product, can also be used to measure binding kinetics. However, knowledge of the inhibitor mechanism of action (MoA) is required in order to access the relevant parameters. An example is the derivation of the kinetic parameters for inhibitors of the enoyl-acyl carrier protein reductase, FabI, from forward reaction progress curves (enzyme assay time courses) through a detailed understanding of the MoA of the inhibitors coupled with computational methods.[3]

Jump dilution methods offer a more direct way to estimate inhibitor dissociation rate constants. In a similar way to the large dilution experiments described earlier, the enzyme is incubated with a saturating concentration of test compound, and this mixture is rapidly diluted into a large excess of substrate. Product accumulation is then again measured as a function of time, and the observed rate of enzyme activity recovery fits to a single exponential in order to derive the inhibitor dissociation rate constant. Two important factors in conducting this type of experiment are that the inhibitor concentration falls well below its apparent inhibition constant, K_i', upon dilution and that the final enzyme concentration, following the dilution, is sufficient to generate enough product for reliable detection.

2.07.2.17 Residence Times

The exploration of the use of residence times has gained popularity recently, with several authors proposing advantages over equilibrium-based affinity measurements[4–7] and describing applications of medium to high throughput in drug discovery.[8] Residence time, τ, is proportional to the half-life for dissociation and describes the time the protein is occupied by the ligand, and methods such as those described earlier have allowed more routine application of the measurement of the kinetics of biomolecular association and dissociation within drug discovery projects. Biophysical methods especially tend to play a larger role in the characterization of hits and leads, allowing kinetic data to be considered during the optimization of lead molecules.

In order for residence times to be compared and utilized, it is important to consider the mechanism of the binding interaction. Three simple mechanisms of single compound binding to target proteins have been described, with and without protein isomerization steps. An overview of these different mechanisms, along with the parameters describing them, are shown in **Table 1**.

Table 1 Parameters and their relationships to individual rate constants associated with the three common models of ligand binding

Parameter	*Model*		
	Single step	Induced fit	Conformational selection
	$R + L \underset{k_2}{\overset{k_1}{\rightleftharpoons}} RL$	$R + L \underset{k_2}{\overset{k_1}{\rightleftharpoons}} RL \underset{k_4}{\overset{k_3}{\rightleftharpoons}} R^*L$	$R + L \underset{k_4}{\overset{k_3}{\rightleftharpoons}} R^* + L \underset{k_2}{\overset{k_1}{\rightleftharpoons}} R^*L$
k_{obs}	$k_1[L] + k_2$	$k_4 + \left(k_3/\left(1 + K_D'/[L]\right)\right)$	$k_3 + \left(k_4/\left(1 + [L]/K_D''\right)\right)$
τ	$1/k_2$	$(k_2 + k_3 + k_4)/k_2k_4$	$1/k_2$
K_D	k_2/k_1	k_2/k_1	–
$K_D{}^*$	–	$k_2k_4/(k_1(k_3 + k_4))$	k_2/k_1

Note that for the one-step binding mechanism, k_1 is k_a, and k_2 is k_d.

k_{obs} is the observed rate constant for association. K_D and K_D^* are the equilibrium dissociation constants for the relevant bimolecular complexes (RL and R*L, respectively), and K_D' and $K_D^{*\prime}$ are their apparent values. These may be related to the true values, by the usual Cheng–Prusoff relationships, according to the mode of inhibition.

For a simple one-step reversible interaction, the residence time, τ, is the reciprocal of the dissociation rate constant and is correlated to the amount of time the protein is occupied by the ligand. The value of comparison of residence times really comes from the discrimination between hits and leads in terms of the dissection of the affinity into the component association and dissociation rate constants. Compounds with similar binding affinities may have very different kinetic contributions. The increased application of biophysical and biochemical methods to dissect the kinetics of ligand binding from affinity values will potentially lead to the development of more refined structure–kinetic relationships. The ultimate goal is a set of guidelines that may help to steer medicinal chemistry efforts in the modification of the kinetic behavior of compounds in order to achieve the desired kinetic profile required for the specific intervention at the protein target in the disease state.

2.07.2.18 Effect of Binding Kinetics on Fractional Occupancy and IC_{50}

The association and dissociation rate constants are important factors in determining the fractional occupancy and the correct inhibitor potency, as these may change according to time at which the fractional occupancy or IC_{50} is measured, dependent upon the value of the individual rate constants. This is because, where slow kinetics are involved and/or the time of the assay is short relative to the required equilibration times, then a lower fractional occupancy will be observed according to Eq. (5) in the succeeding text:

$$\text{Fractional occupancy} = \left(\frac{[\text{L}].k_a}{[\text{L}].k_a + k_d}\right).\left(1 - e^{-([\text{L}].+k_d).t}\right) \tag{5}$$

Usually, this is not a problem during the initial screening activities, as the potencies of initial hits are usually relatively low, test compound concentrations are usually high, and often assays are long enough, or contain preincubation periods that ensure that equilibration occurs, so that even very slowly, equilibrating compounds are still identified with the correct potency. For example, for 1 μM potency with an incubation time of 30 min, the true potency is observed for compounds with association rate constants ranging from 1×10^3 to 1×10^8 M^{-1} s^{-1}, and all the fractional occupancy versus concentration curves overlay, see **Fig. 3**.

However, for more potent compounds and lower assay times, then, differences between true and observed potencies become more problematic for compounds displaying slower kinetics, and now, the difference in the fractional occupancy versus concentration plots is easily observable for the slower association rate constants, **Fig. 4**.

It can be seen that as the association rate constant (and correspondingly the dissociation rate constant) decreases, for this time point (here 15 min), then, the concentration of compound required for 50% fractional occupancy increases significantly. Although for very rapid rate constants ($k_a = 1 \times 10^8$ M^{-1} s^{-1} and $k_d = 0.1$ s^{-1}), the observed affinity is similar to the true affinity; for the slowest rate constants depicted here ($k_a = 1 \times 10^3$ M^{-1} s^{-1} and $k_d = 1 \times 10^{-6}$ s^{-1}), the observed affinity is almost three orders of magnitude lower than the true affinity at this time point (top panel). It can also be seen that the slope of the curves increases as the rate constants become slower, with slope factors increasing from 1 to around 1.4 from the fastest to the slowest values of rate constants (bottom panel). This highlights the need to understand the potential for binding kinetics to vary during the hit to lead process in order to ensure that assays are conducted suitably so that compound ranking may be correctly assessed in terms of equilibrium affinity values and also to allow follow-up on interesting kinetic profiles.

Of course, binding kinetics and residence times will not be the only decisive factor considered during lead selection and the consequent optimization process. But together with approaches suggested by Lipinksi and Leeson[9,10] and the potential application

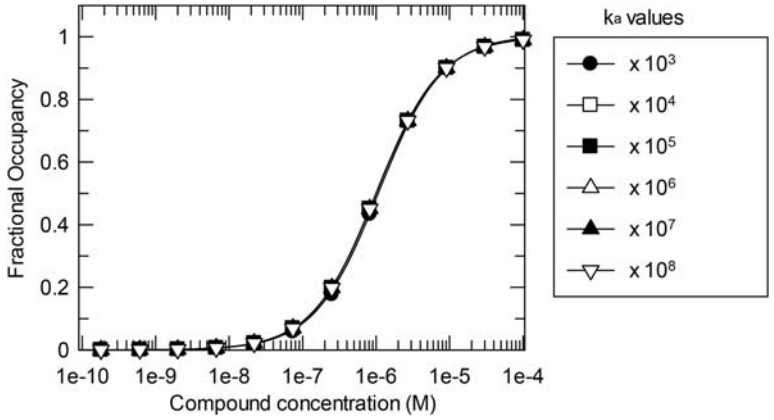

Fig. 3 Effect of various combinations of rate constants on the fractional occupancy for compounds of 1 μM potency, tested at a range of concentrations in an assay lasting 30 min. Even for a wide range of rate constants, varying by over five orders of magnitude, there is little difference in the plot of fractional occupancy versus concentration.

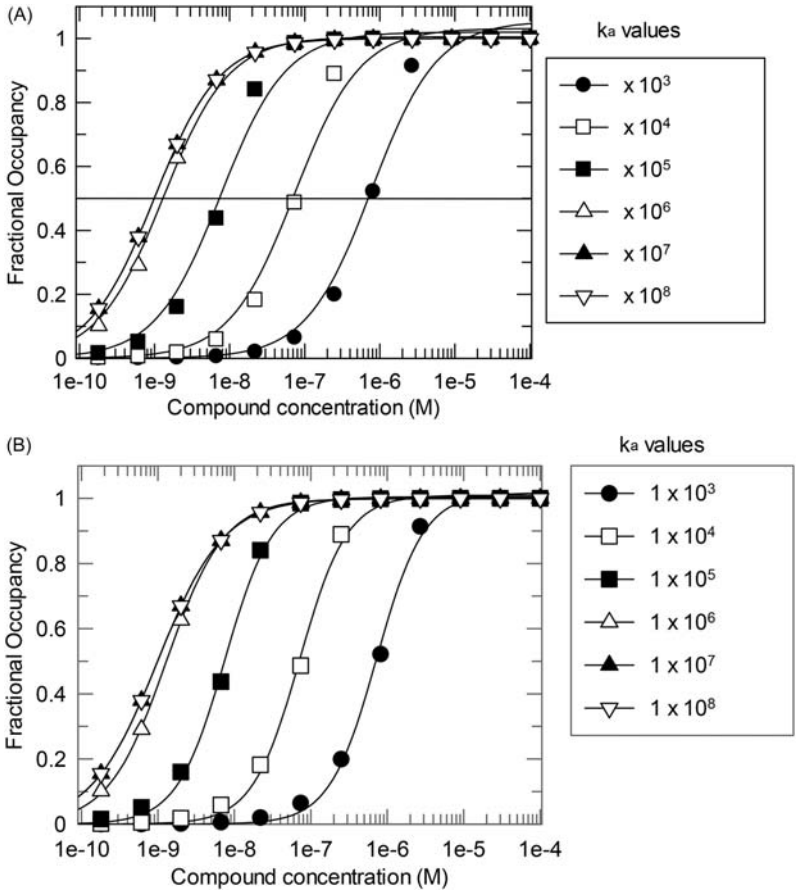

Fig. 4 Effect of various combinations of rate constants on the fractional occupancy for compounds of 1 nM potency, tested at a range of concentrations in an assay lasting 15 min. In this case, there may be a marked difference in the fractional occupancy achieved at each concentration, depending upon the kinetics of the interaction. Fits are shown to a simple 1:1 binding model (top panel) and to a binding model including a slope factor (bottom panel), representative of models that may be fitted to the data during the lead optimization phase of drug discovery.

of some recent LEM, for example, those suggested by Hopkins and Ladbury,[11,12] they form part of a collection of features that are accessible for the medicinal chemist to examine in order to construct a comprehensive and efficient strategy for optimization. This allows the optimization process to be based on the inclusion of a thorough overview of a range of different compound properties.

2.07.2.19 Mechanistic Aspects to Binding Kinetics

Ligand binding can be viewed most simply as the molecular collision between two molecules, described by the **Scheme 1**.

This simplistic view of ligand binding overlooks potential conformational effects and assumes that the complex results from ligand collisions with the binding site. The association rate constant is proportional to the frequency of productive encounters, and the dissociation rate constant, which is a measure of stability of the resulting complex, is inversely proportional to the residence time of the inhibitor.

The dissociation rate constant is directly accessible experimentally, as described earlier, and can be measured by dilution of the preformed complex. The association rate constant is measured only indirectly, because it is difficult to separate the formation of new complexes from the dissociation of complexes previously formed. Consequently, upon addition of ligand to the target protein, the concentration of the complex accumulates with rate constant k_{obs}, where the magnitude of k_{obs} is governed by both the production of the receptor–ligand complex and its simultaneous breakdown by dissociation back to the free partners, Eq. (6):

$$k_{obs} = k_a.[L] + k_d \tag{6}$$

$$R + L \underset{k_{diss}}{\overset{k_{ass}}{\rightleftharpoons}} RL$$

Scheme 1

The equilibrium dissociation constant, K_D, is given by

$$K_D = \frac{k_d}{k_a} \tag{7}$$

From Eq. (6) and **Scheme 1** in the preceding text, it can be seen that for a single-step mechanism, a simple plot of k_{obs} versus ligand concentration is linear with slope and intercept equal to k_a and k_d, respectively.

Sometimes, this simple model is insufficient to describe the interaction process, as often the free partners must undergo adjustments in shape in order to bind successfully, and the structures of the unbound and bound states differ significantly. Two different theories have been established that describe the potential mechanisms of these necessary conformational rearrangements. These are termed the induced fit and conformational selection models.

While these types of conformational rearrangements are often discussed from the perspective of the protein target, it should be remembered that ligands may also undergo rearrangement, and so, binding may occur via conformational selection or induced fit-type processes, which reflect ligand shape and the changes required to form high-affinity interactions.

The induced fit theory (**Scheme 2** and **Fig. 4**) describes the formation of a weak initial complex, which proceeds via intermediates that gradually rearrange to establish further interactions, until the final high-affinity state is reached.

The conformational selection model (**Scheme 3** and **Fig. 4**) suggests that the bound conformation of the protein preexists in the absence of ligand as a small population of different substructures available in conformational space. When ligand is added, complexes are only formed with that subset of protein molecules in the correct conformation to support binding.

The observed binding kinetics reflect the molecular processes that occur during the binding event, and so, the dependence of k_{obs} on [L] can be used to select the most appropriate model from the conformational selection and induced fit models. The induced fit model (**Scheme 2**) produces a hyperbolic plot of k_{obs} versus [L], which reflects the situation at high ligand concentrations, where initial complexes are formed rapidly, driven by the high ligand concentration, with the second step being rate-limiting. Addition of further ligand does not increase the rate of final complex formation, see Eq. (8):

$$k_{obs} = k_3 . \frac{[L]}{K_d + [L]} + k_4 \tag{8}$$

where K_d is given by

$$K_D = \frac{k_2}{k_1} \tag{9}$$

and $K_D{}^*$ is given by

$$K_D^* = \frac{k_2 . k_4}{k_1 (k_3 + k_4)} \tag{10}$$

A modified induced fit model may be applied to describe the binding of specific irreversible covalent inhibitors, where the second reversible step in **Scheme 2** is replaced by the irreversible covalent reaction process.

Conversely, for the conformational selection model (**Scheme 3**), the plot of k_{obs} versus [L] shows a hyperbolic decrease with increasing ligand concentration, Eq. (11). This can be understood since the concentration of binding competent protein decreases as these molecules become bound with ligand. Thus, at high ligand concentrations, all of the binding competent protein is rapidly complexed, and the formation of new binding competent conformations becomes rate-limiting:

$$k_{obs} = k_3 + k_4 . \frac{K_D^*}{K_D^* + [L]} \tag{11}$$

where $K_D{}^*$ is now given by

$$K_D^* = \frac{k_2}{k_1} \tag{12}$$

Of course, these two models rely on a number of assumptions, and often, the binding process may be more complicated, with both mechanisms potentially occurring at the same time. It is possible for both pathways to be followed simultaneously where the concentration of R* and R*L will determine which mechanism tends to dominate the observed kinetics. It is also possible for both

$$R + L \underset{k_2}{\overset{k_1}{\rightleftharpoons}} RL \underset{k_{-1}}{\overset{k_3}{\rightleftharpoons}} R^*L$$

Scheme 2

$$R + L \underset{k_4}{\overset{k_3}{\rightleftharpoons}} R^* + L \underset{k_2}{\overset{k_1}{\rightleftharpoons}} R^*L$$

Scheme 3

pathways to occur sequentially; for instance, binding may occur following a conformational selection step, with subsequent optimization of side chain and/or backbone interactions occurring via an induced fit.[13]

Clearly, medicinal chemistry applied during the lead optimization process can only impact the initial conformation of the ligand and not the target protein. This process often results in a decrease in conformational entropy as a result of ligand rigidification, aimed at minimizing entropic penalties upon binding.[14]

This approach, whether deliberate or serendipitous, may be considered as the advantageous exploitation of conformational selection.

There are examples in the literature describing systems that appear to conform to these models. The induced fit model has been proposed to occur for the binding of compounds such as imatinib to protein tyrosine kinases. Binding has been shown to occur in two different binding modes: a low-affinity, ATP-competitive form known as Type I, (where the aspartate–phenylalanine–glutamate motif (DFG motif) is in the DFG-in conformation)[15] and the high-affinity form, Type II form where the kinase adopts an inactive conformation (DFG-out).[16]

The conformational change between these two modes requires substantial rearrangement of the protein, where the DFG motif at the beginning of the activation loop moves to reposition the catalytic machinery into an inactive conformation.

Almost 40% of the imatinib–Abl kinase binding free energy appears to come from the DFG-in to DFG-out transition. Interestingly for imatinib binding to Src kinase, the DFG-out conformation contributes much lower free energy, which results in a high selectivity for binding to Abl compared with Src.[17,18] The DFG conformational change has been targeted in the development of other Type II Abl inhibitors such as nilotinib and ponatinib[19,20] and for inhibitors of other kinases.

The conformational selection model is exemplified by the mechanism of ligand recognition by ubiquitin. Lange et al.[21] used both NMR studies and computational approaches to identify the ensemble of conformations populated by free ubiquitin in solution. The group of conformations was demonstrated to contain all of the crystallographically observed structural changes in ubiquitin bound to different ligands, leading to the conformational selection mechanism being established as the preferred model to describe binding in this system.

2.07.2.20 Kinetic Selectivity

The kinetics of ligand binding are dictated by the energy barriers for the association and dissociation processes, which are themselves governed by the nature of the forces controlling the interactions between a ligand and its target. In a simplistic manner, we can consider these interactions to be dependent upon four primary aspects: binding site accessibility, the electrostatic nature of the interaction, the nature of hydrophobic interactions, and conformational dynamics.

The accessibility to and from the binding site plays a key role in controlling the observed binding kinetics of a ligand. Intuitively, the entry and exit of a ligand to and from a narrow binding cleft would be expected to produce slower kinetics than that of a ligand binding to a shallow, flat area of the protein. In a study of prostaglandin H2 synthase, slow-binding kinetics are observed due to restricted access to the binding site.[22] Although both slow tight-binding and rapidly reversible inhibitors bind in identical binding modes, the kinetic divergence of prostaglandin H2 synthase inhibitors is explained by the rate and effectiveness with which the compounds open the narrow channel and gain entrance to the binding site, and it is proposed that the kinetic differences may reflect differences in the efficiency with which the inhibitors perturb the hydrogen-bonding network in the vicinity of Arg-120 and Tyr-355.

Electrostatic interactions between charged ligands and charged binding site will influence both association and dissociation rates. This may be demonstrated by varying the solution ionic strength, which will greatly affect association rates (increasing ionic strength decreases the on-rate) but hardly affects off-rates. These effects are due to ions screening the electrostatic interactions between the associating partners during the association process, but the dissociation shows less dependence due to similar geometries in the bound and transition states, leading to relatively little difference in the electrostatic interaction energy between the transition state and the bound state.

Ligand binding to the charged binding site of acetylcholinesterase demonstrates the influence of electrostatics on binding kinetics.[23] Neutralization of the net positive charge of the m-trimethylammonium trifluoroacetophenone ligands leads to around 30-fold decrease in the association rate constant and greater than 10-fold increase in dissociation rate constant.

The hydrophobic effect and the role of water in stabilizing protein–ligand complexes have been well studied from a thermodynamic perspective, but the influence on ligand binding kinetics is less clear. However, it is thought that the kinetic consequences may be related to the distance from the binding location. Schmidtke et al.[24] investigated the role of hydrophobicity in determining binding kinetics by employing both experimental and computation methods in the model Hsp90 system. This study suggested that protein–ligand interactions that contain hydrogen bonds that are shielded from bulk water by hydrophobic residues may result in a kinetically more stable complex than when hydrogen-bonded waters are solvent exposed.

The role of conformational dynamics and the mechanisms of the induced fit and conformational selection models have been illustrated earlier.

2.07.2.21 Role of Kinetics in Selectivity and Efficacy

The principle of kinetic selectivity is relatively simple—potentially, the binding kinetics rather than the binding affinity may allow discrimination between the temporal occupancy of target versus secondary, off-target binding sites. It has been understood for many years that the relative difference between the activity of a drug at its primary and secondary (off-) targets is important in determining

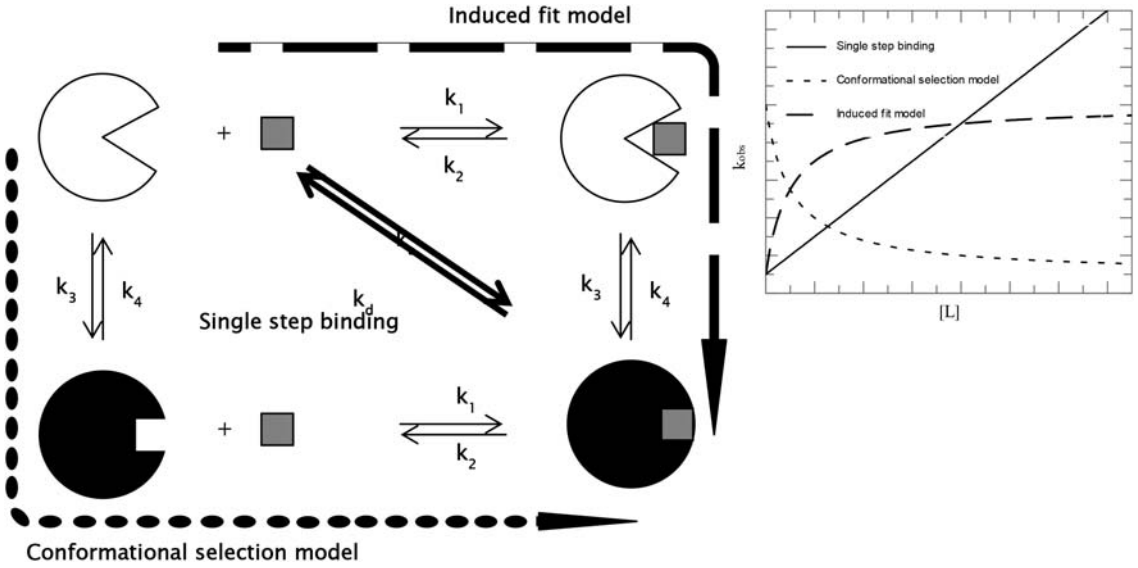

Fig. 5 Scheme showing the processes for single-step, induced fit, and conformational selection binding models. Rate constants relate to the parameters given in **Table 1**. Inset shows the variation of the observed rate constant, k_{obs}, with varying ligand concentration.

the therapeutic window of drug action (which is the difference in concentrations required for efficacy at the primary target and that leading to adverse effects in vivo). Most often, selectivity is characterized from thermodynamic values, such IC_{50} or K_d, measured in enzyme assays or ligand binding assays at equilibrium. However, since the affinity of a ligand for its protein target is also determined by the ratio of the dissociation and association rates (and the free ligand concentration at equilibrium), it is possible, at least theoretically, to obtain differences in kinetic selectivity via differences in association rate or residence time (**Fig. 5**). This figure shows that the binding kinetics may allow a higher fractional occupancy over time even at a target for which the compound binds 100-fold less tightly (according to the equilibrium K_D value). The fractional occupancy for the slower kinetic profile remains at 88% after 3 h, whereas the fractional occupancy for the faster kinetic profile has dropped to around 0.01%.

The concept of kinetic or temporal selectivity was promoted by Copeland et al.,[4] and it was suggested that a prolonged residence time for the primary target could provide beneficial selectivity against secondary, off-targets in vivo.

For a hypothetical drug binding to the primary target by a two-step mechanism that includes a second-step isomerization to form a tight-binding complex (see **Scheme 2**), the fractional occupancy for a primary target, with a 25-fold increased residence time compared with a 30-fold weaker secondary target, is shown in **Fig. 6**. The fractional occupancy remains above 95% after 10 h,

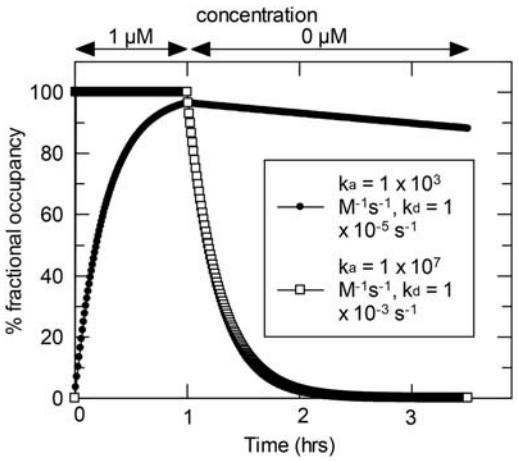

Fig. 6 Effects of kinetics on the fractional occupancy for compounds with different potencies. Prolonged occupancy is demonstrated even for a 100-fold weaker binding compound ($K_D = 10$ nM (filled circles) versus $K_D = 100$ pM (open squares)), following removal of free compound, due to its lower dissociation rate constant. This demonstrates that fractional occupancy at a particular time may be dictated by the binding kinetics of the interaction and is not just a consideration of the binding affinity.

even after the plasma concentration has dropped to almost zero, due to drug elimination. For the secondary target, the fractional occupancy falls to 40% for the 30-fold weaker affinity target.

In another well-known example, drugs binding to the angiotensin II type 1 receptor and displaying extended residence times, for example, candesartan, are more efficacious than compounds with faster off-rates, such as losartan. The two compounds bind in the same pocket, although with very different binding kinetics (residence times 174 and 4 min, respectively). This difference in residence time is assumed to account for the clinical differentiation between the compounds, allowing PD to outlast pharmacokinetics (PK) and to provide improved efficacy for candesartan.[25] However, the prolonged blood pressure lowering effect of candesartan is attributed not only to its long residence time but also to the rebinding of the drug to the receptor.[26]

Slow-binding inhibition of the acyl carrier protein enoyl reductase (FabI) in *Mycobacterium tuberculosis and Francisella tularensis* has been exemplified for drugs such as triclosan and isoniazid. An examination of the *F. tularensis* compounds demonstrated that there was poor correlation connecting affinity (K_i) or minimum inhibitory concentration values and in vivo efficacy. However, a much stronger linear correlation was revealed between residence time and efficacy (percent survival).[27]

The use of kinetic selectivity is exemplified by the development of subtype-selective muscarinic receptor antagonists. Tiotropium bromide, glycopyrronium bromide, and aclidinium bromide are inhaled long-acting muscarinic antagonist drugs for treatment of COPD.[28,29] It appears that the dissociation rate constant may be important for providing kinetic selectivity and may partly explain their therapeutic indices.[30] Glycopyrronium is slightly selective for the M3 receptor over the M2 receptor, whereas aclidinium and tiotropium show no selectivity in terms of binding affinity between the two receptors. All three drugs, however, dissociate more rapidly from the M2 receptor than the M3 receptor, giving them kinetic selectivity for the M3 receptor and so reducing side effects associated with M2 binding. The largest kinetic selectivity ratio of the three drugs is shown by glycopyrronium, which has a greater cardiovascular therapeutic index for hypotension and bradycardia compared with tiotropium in preclinical models.[31,32]

2.07.2.22 Irreversible Inhibitors

Understanding kinetic SAR should enable inhibitors with the desired kinetic profiles to be developed more effectively. Optimizing compound structures to give very slow dissociation rate constants has led to what has been termed ultimate physiological efficacy,[33] which indicates that inhibition is persistent until replacement of the inhibited target is accomplished by fresh protein synthesis. It would seem sensible for the most effective way to develop an ultimate physiological inhibitor being to optimize the binding kinetics (ideally increasing the association rate to enhance rebinding and decreasing the dissociation rate to prolong residence time). However, focusing on residence time optimization, without deliberately trying to optimize association kinetics (as this would seem a more difficult task), with the systematic application of SAR-driven medicinal chemistry effort seems the most practical way forward. The insights gained from taking the time to understand structure–kinetic relationships can be very valuable, and deriving empirical relationships can lead to improved PD effects.[34]

Clearly, the ultimate endpoint for the development of inhibitors with progressively longer residence times is the development of irreversible covalent inhibitors. Covalent compound development can be a successful strategy for targets where a suitable residue allowing covalent attachment is present in the binding site, where on-target toxicity is not a risk and target protein turnover is slow. The molecular recognition by and covalent reaction to related proteins must be scrutinized during the optimization process, particularly for proteins that share the residue for covalent attachment. Having a rapid clearance rate is also ideal for irreversible compounds, because this will tend to restrict off-target side effects.

Targeting kinases with irreversible compounds has been reviewed[35] and reveals an additional benefit—overcoming competition by high concentrations of natural substrates—demonstrating reduced ATP competition, which may be a problem for reversible competitive inhibitors, given that the cellular concentration of ATP is usually much higher than the K_m for ATP. This is due to the fact that covalent inhibition for kinases follows a modified induced fit model, where only the first step is competitive with respect to ATP.

The application of covalent inhibition is not restricted to kinases.

2.07.2.23 Optimizing Residence Time

To design new ligands with longer residence times, it would be useful to understand which molecular interactions contribute to increases in residence times so that this could be applied to any particular target. Cusack et al.[17] summarized the rationale for long residence time for a large number of ligand–target interactions. In these examples, prolonged residence time was attributed to a variety of different features including an increase in the kinetic barrier to dissociation, hydrophobic interactions, stabilization of the drug–target complex from multiple contacts, and the induction of conformational changes. Given that the contributions to increased residence time may be quite diverse and vary from target to target, it appears difficult to develop a generic approach for increasing residence times and to prospectively design slow dissociation kinetics into a given ligand.

Conversely, the principles underpinning the rational improvement of binding affinity during the lead optimization phase are relatively well understood. However, as described in the preceding text, the rational modulation of binding kinetics is not nearly as well characterized or understood. Whereas the magnitude of the equilibrium binding constant is directly associated with the structures and energies of the free and bound states, the kinetics of moving between these states is determined by the structure and corresponding energy of the transition state. Since the transition state is a low-abundance and highly unstable state, which often is difficult to characterize, understanding the kinetic constants associated with passing through this state is also difficult.

Although there are structural methods that facilitate the study of low-abundance conformations (e.g., Carr-Purcell-Meiboom-Gill pulse train sequences used for dynamic NMR measurements) and room-temperature and time-resolved Laue crystallography approaches,[36,37] the predetermined manipulation of compound binding kinetics remains intractable, and it is often only retrospectively that structure–kinetics relationships are revealed.

As a result, there is a current lack of detailed guidelines for kinetic-based ligand optimization, and the structural rationalization for differences in binding kinetics can really only be attempted for situations involving highly similar chemotypes or targets.

If kinetic modulation is to be undertaken, it is clear that in general, increasing residence time is more a realistic goal than modulation of the association rate constant. This can be realized by inspection of the simple free energy diagram describing a single-step binding mechanism following **Scheme 1**. The residence time (k_d^{-1}) can be increased by raising the energy barrier for dissociation, which can be accomplished either by increasing the energy of the transition state, by decreasing the energy of the complex, or by a combination of both effects, **Fig. 7**. Optimization of the binding energy is usually one of the main approaches taken during drug discovery, and the residence times of compounds may often increase in parallel with increases in affinity during lead optimization. An example of such a correlation was shown by Chang et al.[3] for inhibitors of enoyl-ACP reductase from *Staphylococcus aureus* (Fabl). The structure–affinity–kinetics relationships demonstrated that within the same chemical series, there was a strong relationship between K_i and k_d, whereas the corresponding k_a values remained similar for all of inhibitors within the chemical series.

By inspection of **Fig. 7**, it can be seen that increasing the energy of the transition state is another approach for kinetic modulation, as this will slow both the association and dissociation rates. As a general approach, restricting the accessibility to the binding site by increasing the molecular size of the compound often results in increasing the energy barrier, leading to slower rates.[38] Increasing the rigidity of compounds during lead optimization, as a means of reducing conformational entropy losses upon binding, also often leads to longer residence times, as a result of the concomitant increase in transition state energy.

Where the induced fit model best describes the binding process, it may be advantageous to retain a degree of flexibility in lead compounds in order to allow conformational rearrangements within the initial complex, which permit access to conformations that ultimately are more stable, and demonstrate higher affinity and slower dissociation.

It should be noted, however, that at least for some proteins, restricting the flexibility of the test compound may also have a corresponding effect on the association rate. An illustration of this point is provided by Fleck et al.[39] where it was shown that for a series of corticotropin-releasing factor type 1 receptor antagonists, constraining the active ligand conformation by ring substitution resulted in an increase in the association rate of around 33-fold. No effect on the dissociation rate was observed, suggesting a conformational selection mechanism.

Clearly, the logical extension of long residence time compounds is to move to irreversible complexes via covalent bond formation between the test compound and the protein target, as discussed earlier. There is renewed interest in covalent compounds, and as long as safety concerns stemming from the lack of specificity can be addressed, then approaches targeting nucleophilic cysteines with reactive warheads may be a useful approach. This strategy has been employed to target proteins such as EGFR[40] and the Ras G12C mutant.[41]

Covalent binding can often be described by a mechanism similar to the induced fit model, which involves initial molecular recognition, driven by noncovalent interactions, followed by the slower covalent chemical reaction. Gradually, an understanding of how to combine the fine-tuning of warhead reactivity, together with factors that modulate initial recognition, is developing,

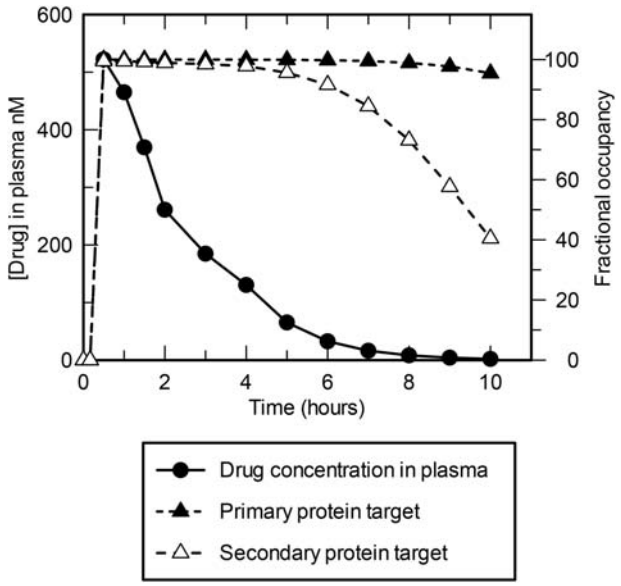

Fig. 7 Effect of kinetics and affinity on fractional occupancy for a primary target and a secondary target following a single-step binding mechanism.

which will eventually allow covalent inhibitors to be designed with the desired kinetic profiles. The utility of the covalent approach has been exemplified nicely by Bradshaw et al.[42] where the use of inverted cyanoacrylamides targeted to noncatalytic cysteines in kinases demonstrated the possibility of increasing residence times by chemical design.

2.07.2.24 Binding Kinetics and PK/PD

The interaction between a drug and the target protein, controlled by the relevant kinetic rate constants for association and dissociation, establishes the link between PK and PD effects. Clearly, a drug can only generate a biological response when it is bound to its target protein, and so, understanding the individual contributions that control the duration of target occupation is critical when trying to optimize these interactions for the particular target in the disease setting. The simplest model describing the relationship between binding kinetics and PK is shown in Fig. 8, although more complex models, for example, including the extra rate constants required to describe the induced fit and conformational selection models may be envisaged.

The free concentration of the drug in the location around the target protein governs the formation of the drug–protein complex. As can be seen from Fig. 8, this is controlled by the target protein concentration and a combination of rate constants, including the rate constants for distribution and clearance, which control the delivery and removal of drug to the target location, and the rate constants for association and dissociation, which control the formation of complex between the two partners, while the drug is in the vicinity of the target.

As long as binding reaction occurs more rapidly than the clearance of drug from the target location, then the drug will accumulate in the target vicinity and target occupation will be driven by mass action.

For different drugs with fixed affinity, since $K_D = k_d/k_a$, slower dissociation is coupled with slower association, and so, equilibrium may not be reached before significant clearance occurs. In these cases, frequent and multiple dosing may be required for slow associating drugs to reach equilibrium.

In the case of slow dissociating compounds, the limit to the value of increasing residence time even further is reached when the dissociation half-lives extend beyond that of protein turnover. In this case and also for the case of irreversible inhibitors, the rate of fresh protein synthesis dictates the ultimate limitation for the duration of effect, when the entire free compound pool has been eliminated.

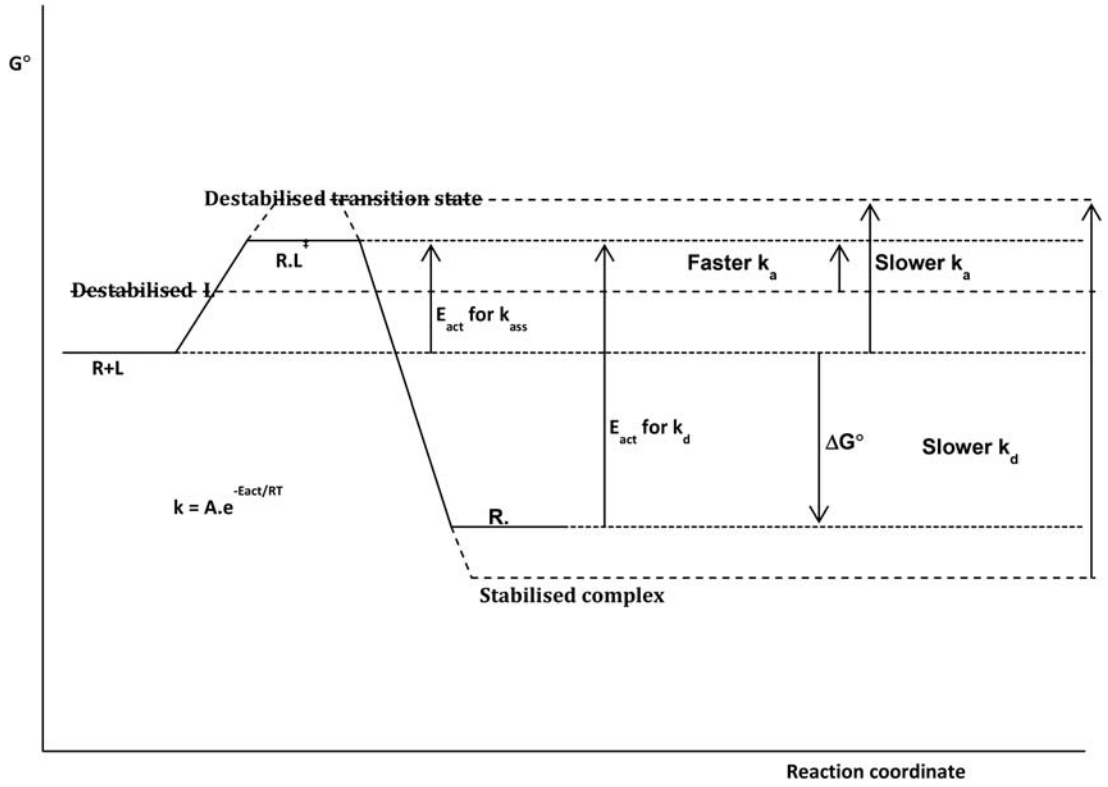

Fig. 8 Free energy diagram showing the effect of destabilizing the ligand or the transition state or stabilizing the protein–ligand complex on the observed rate constants. R.L‡ indicates the transition state between the free partners and the complex. E_{act} represents the activation energy barrier between the ground state and the transition state, controlling the magnitude of the rate constant for the binding or dissociation process as indicated—the larger the activation energy barrier, the slower the kinetics. ΔG° represents the change in free energy G° between the free partners and the bound complex. Slower dissociation rates may be achieved if the bound complex can be stabilized and/or the transition state destabilized. Faster association would require stabilization of the transition state (which opposes slow dissociation) or destabilization of the ligand.

When this situation occurs, a sustained pharmacological effect can only be achieved via PK exposure, when additional free compound is available to bind to newly produced protein. Thus, increasing residence time, by decreasing the dissociation rate constant, has a benefit only up to this limit, when PK effects are not considered. Fig. 8 demonstrates that there will be certain combinations of PK and BK rate constant profiles that will allow optimization of coverage but that conversely there will be some combinations that will not produce enough of a benefit to merit attempts to increase residence time further. In the induced fit case, exemplified in Scheme 2, if clearance is rapid, a decrease in the rate constant k_4 of over three orders of magnitude will be required in order to extend the time for which the fractional occupancy remains above 0.5 by only a factor of 10 (where the other parameters are $k_1 = 1 \times 10^6\ M^{-1}\ s^{-1}$, $k_2 = 1\ s^1$, $k_3 = 1 \times 10^{-3}\ s^{-1}$, clearance $t_{½} = 1$ h, $C_{max} = 500$ nM, and t_R varies from 2.8 to 2780 days with $k_4 = 1 \times 10^{-4}\ s^{-1}$ and $1 \times 10^{-7}\ s^{-1}$, respectively).

On the other hand, if clearance is slow, then there may be not a considerable advantage to efforts aimed at increasing the residence time. As an example, if we consider the same two-step binding mechanism where the clearance $t_{½}$ is now increased 24-fold to 24 h, a fractional occupancy of over 0.5 is maintained for 2.5 days when k_4 is left unchanged at $1 \times 10^{-4}\ s^{-1}$ ($t_R = 2.8$ days). Decreasing k_4 will extend this, but it is clear that once-daily dosing is sufficient to maintain the pharmacological effect with no requirement for any further chemical optimization.

Dahl and Akerud[43] have investigated the range of suitable kinetic values that permit high-target occupancy for a period of time after elimination. Their calculations suggest that k_a for a drug-like molecule should be in the range 2×10^3–$1 \times 10^8\ M^{-1}\ s^{-1}$, with a potency greater than a lower level of about 30 nM. Assuming there is a single-step binding process, this gives a range of equivalent k_d values of between $6\ s^{-1}$ and $6 \times 10^{-5}\ s^{-1}$. However, inspection reveals that not all of these combinations of rate constants allow the required occupancy, and so, optimization of k_d toward a maximum value of around $1 \times 10^{-4}\ s^{-1}$ is desirable if the fast k_a can be preserved. However, if as a result of chemistry efforts to decrease k_d, k_a is also reduced toward the lower values given earlier; then, k_d may need to be decreased further, by even another two orders of magnitude. This highlights the difficulties faced in kinetically optimizing test compounds, starting from initial hits, which may have affinities of the order of 1 μM, and assuming a reasonable value of k_a of $5 \times 10^5\ M^{-1}\ s^{-1}$, where the corresponding k_d would be of the order of $0.5\ s^{-1}$. This signifies that around a 5000-fold decrease in residence time is necessary to reach the suggested upper limit, with even additional improvement required to give the desired BK profile. Assuming there is no change in the corresponding association rate constant, the end result of the chemistry design efforts would be with a compound with 10 pM affinity.

2.07.2.25 Future Trends for Kinetic Characterization

Currently, designing a particular binding kinetics profile into a compound remains challenging but clearly remains a strategic goal for the medicinal chemist, as kinetics provides an opportunity to optimize compounds to gain a therapeutic advantage. Modifying binding kinetics can lead to improved therapeutic index and improve coverage via changes in PK/PD relationships.

Modifying binding kinetics will ultimately require changes to the energy levels of either the transition state or the protein–ligand complex, and understanding how to achieve these will be key. The increased measurement of binding kinetics, together with both structural information and computational approaches such as molecular modeling and molecular dynamics simulations, will help to provide a better understanding of both protein dynamics and the factors influencing binding kinetics.

Currently, we often think about lead optimization from an equilibrium perspective, since the interactions that are introduced relate to the two ends of an equilibrium, and we understand little of what happens in between. We may consider the modification of a compound structure and the result on residence times in two simplistic ways: Firstly, the structural change leads to a conformational change in the protein, leading to altered binding kinetics; secondly, the structural change changes the balance of interactions to favor the slowly dissociating ones. In this simplistic view, it would appear that the former would be very target-specific and understanding the effect on protein conformation might be challenging to accomplish in order to have impact in medicinal chemistry projects in a timescale that would be useful. The second approach seems more tractable, and we would hope that there may be some simple guidelines that could be established to promote rational design.

And even if this cannot be done directly, the strategy for optimizing long residence times can focus on optimizing affinity or by exploring additional binding interactions that are associated with larger kinetic barriers.

As our understanding of the implication of binding kinetics grows, the opportunity to impact projects will improve as we begin to implement kinetic optimization in order to decrease the number of iterations to move from lead to candidate drug or from first-in-class to best-in-class molecule.

Several recent articles have reviewed the current status of the use of binding kinetics in drug discovery for improved drug effects,[44] focusing on optimizing on rates,[45] and for GPCR kinetic optimization.[46]

2.07.3 Thermodynamics in Drug Discovery

2.07.3.1 Methods for Measuring Binding Thermodynamics

Thermodynamic data may be generated in two main ways, either directly employing ITC or indirectly utilizing the Van't Hoff approach and any method that can determine K_D as a function of temperature, for example, SPR or fluorescence.

2.07.3.2 Direct Calorimetric Methods

2.07.3.2.1 Principle of ITC

Isothermal titration calorimeters quantify the heat change that results when two molecules interact. Heat is almost always generated or absorbed as a result of the redistribution of noncovalent bonds when the interacting partners proceed from the initial free to the final bound state. Commercially available power compensation-based calorimeters detect these heat changes by monitoring the differential power required to preserve a zero temperature difference between the reference and sample cells as the binding partners are mixed and the binding reaction takes place.

The reference cell typically contains only the matched experimental buffer used for the individual interactants, while the sample cell contains one of the binding partners (often the macromolecule), and the injection syringe holds the other binding partner (often the ligand). In a typical injection protocol, aliquots of between 0.5 and 2 μL are injected, separated by enough time to allow equilibration between injections, until the final total ligand concentration attained is around two- to threefold greater than the total protein concentration. Each injection of ligand generates a heat pulse, and the power that is applied to maintain the temperature difference between the sample and reference cells close to zero is monitored. The power versus time plot shows a peak (for exothermic reactions, the peak represents a drop in applied power) that returns to the baseline level during the restoration of the thermal equilibrium. Each peak in the power versus time plot is subsequently integrated with respect to time and may be normalized versus concentration to produce a titration curve or binding isotherm, where enthalpy (kcal/mol) is plotted versus molar ratio (ligand/sample). In typical experiments, most of the injected ligand becomes bound in the early injections, since there is a large excess of free protein, and the differential ligand concentration is greatest. These initial injections therefore produce the largest heat changes, allowing estimation of the binding enthalpy. During subsequent injections, the heat changes are reduced as the titration proceeds. This is because the concentration of free protein decreases, due to complex formation, and some of the total added ligand remains free in solution.

During a typical experiment, the measured heat change is composed of at least three contributions: the heat of complex formation (which is the desired parameter), the heat of dilution of both binding partners, and the heat of mixing. In order to determine the heat of complex formation, a number of control experiments are required, in order to dissect this contribution from the total measured signal.[47] The heat of dilution of the protein can be measured by injecting buffer into fresh protein solution or may be estimated from the injection peaks near the end of the titration, after saturation is reached, as this dilution is often relatively modest. The dilution heat for the ligand can be measured by identical titration of ligand into buffer in the absence of protein. The heat of mixing is usually small and may sometimes be neglected, or it can be measured by titrating buffer into buffer. Identically matched buffers should be used throughout these experiments to contain components in the sample cell and the titration syringe, because differences in buffer composition may lead to additional heat signals during the titration, which will introduce additional complexity to the measurement of the heat of binding. In order to avoid this, the protein usually is dialyzed or buffer exchanged into the experimental buffer and the test compound dissolved in the stock buffer or that recovered from the dialysis.

A relevant binding model may then be fitted by nonlinear regression analysis to the data to obtain the affinity (K_D), stoichiometry (N), and enthalpy of interaction (ΔH) potentially from a single experiment. The binding enthalpy is estimated from the heat change per mole of added ligand during the early injections. The K_D is measured as the free ligand concentration at the midpoint of the cumulative heat change during the titration. The stoichiometry is calculated from the depletion of total ligand, giving a lower free ligand concentration, in a similar manner to tight-binding inhibition in concentration–response analysis of enzyme kinetic data. Further thermodynamic parameters including the Gibb's free energy change upon binding (ΔG) and the change in the entropy (ΔS) can be calculated from the equation in the succeeding text:

$$\Delta G = RT \ln K_d = \Delta H - T\Delta S \tag{13}$$

where R is the universal gas constant and T is the experimental temperature in Kelvin.

A typical thermogram, showing the raw power data, collected over time (top panel) and the integrated heat signals from each injection (bottom panel) are shown in Fig. 9. Using additional experiments, it is also possible to determine the change in heat capacity for the binding interaction (ΔC_p) by measuring the change in enthalpy at several different temperatures (T) and utilizing the relationship shown in the succeeding text:

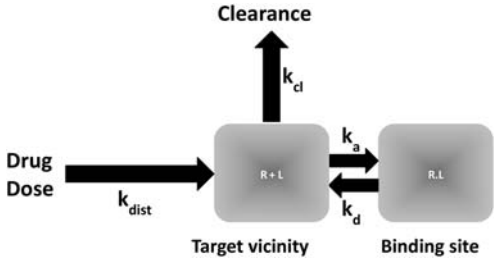

Fig. 9 Simplest scheme relating binding kinetics and PK.

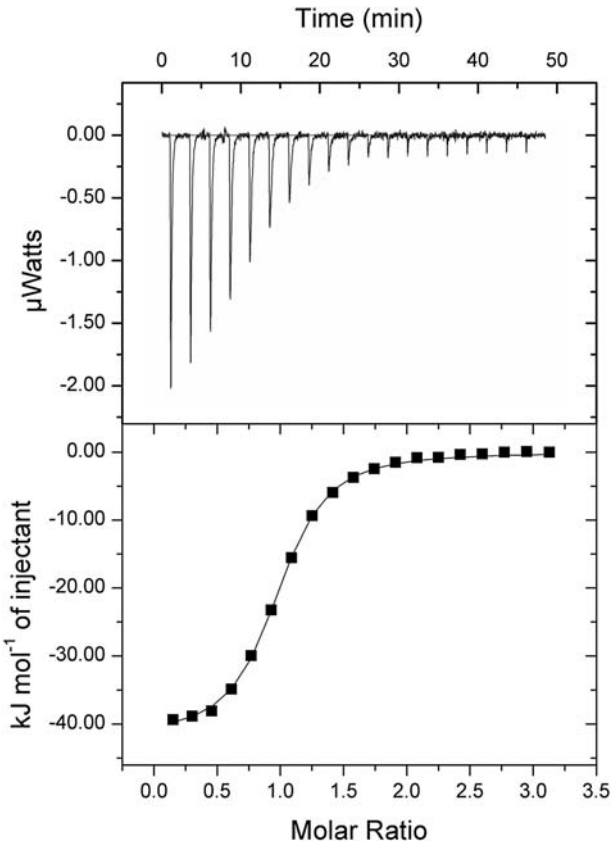

Fig. 10 A typical thermogram from an ITC instrument, showing raw data (top panel) and the integrated heats fitted to a simple 1:1 binding model (bottom panel).

$$\Delta C_p = \delta \Delta H / \delta T \tag{14}$$

The range of binding parameters that can be measured depends upon the concentration of protein required to give a measurable heat signal and the binding affinity of the ligand (Fig. 10). The nature of the thermogram is governed by the unitless parameter, c, whose value is given by the concentration of protein binding sites divided by the dissociation constant.[48] For high-affinity interactions ($c \rightarrow \infty$), all of the injected ligand becomes bound to the target protein until saturation is reached, and the resulting binding isotherm resembles a step shape and so only allows estimation of ΔH° and the binding stoichiometry. Conversely, for low-affinity interactions ($c \leq 0.1$), the thermogram resembles a horizontal trace. In both of these situations, little information is accessible on the value of K_d. In order to obtain reliable estimates of K_d, values of c in the range 1–1000 are suitable to allow nonlinear regression analysis to approximate the magnitude of K_d. In order to adjust the c-value, the protein concentration should be adjusted in order to produce an appropriate value of c. The injection protocol (injection number, injection volume, ligand concentration, and injection timing) often may be created to allow the estimation of ΔH°, K_d, and the heats of dilution in a single experiment.

2.07.3.2.2 Van't Hoff analysis

In the absence of calorimetric data, it is still possible to assess the enthalpic and entropic contributions to the binding affinity. These thermodynamic values may be elucidated using indirect methods, which involve the determination of the temperature dependence of the binding affinity, by analysis using the Van't Hoff equation. This approach allows estimates of entropy and enthalpy to be determined using any method that permits the determination of the binding affinity over a range of experimental temperatures. Eq. (15) shows an integrated version of the Van't Hoff equation, which demonstrates that the enthalpy can be calculated from temperature-dependent changes in the binding affinity, so as long as the constant pressure heat capacity change associated with the binding event (ΔC_p) is known or can be fitted by nonlinear regression. The entropic contribution can then be determined from the Gibbs–Helmholtz equation in the standard manner. In this way, a number of standard laboratory methods to measure K_d, including SPR, microscale thermophoresis, fluorescence, and radioligand binding assays, can be employed to measure the effects of temperature on K_d to determine Van't Hoff enthalpies. For Van't Hoff analysis, the experimental protocol should be designed so that individual binding affinities are measured over a broad enough temperature range (ensuring that the protein does not become unfolded), so that the enthalpy change associated with the binding interaction can subsequently be calculated from the Van't Hoff relationship shown in Eq. (15):

$$ln\, K_1/K_2 = \left(\Delta H_1 - T_1 \cdot \Delta C_p\right)/R \cdot (1/T_1 - - 1/T_2) + \Delta C_p/R \ln T_2/T_1 \tag{15}$$

where K_1 and K_2 are the dissociation constants at different temperatures, T_1 and T_2. R is the universal gas constant and ΔC_p the constant pressure heat capacity change for the binding interaction.

Although the use of the Van't Hoff approach can provide thermodynamic information without the need for a calorimeter, it is not without potential problems. Since the enthalpy is temperature-dependent, the inclusion of the ΔC_p term is required, necessitating the use of the more complex form of the Van't Hoff equation. Obtaining ΔC_p without calorimetric data is difficult since the estimation of ΔC_p from Eq. (14) requires the significant curvature in the Van't Hoff plot to be discernible from apparent curvature resulting from errors in the K_d values. Consequently, this indirect method requires both accurate and precise K_d measurements. Additionally, the temperature-dependent variation of ΔG often is comparatively small, making the derivation of two correlated parameters from the data rather difficult. Often, this results in a relatively large uncertainty in the fitted enthalpy in comparison with the direct, calorimetric approach.

2.07.3.2.3 The thermodynamics of T_m shifting assays

Thermal stability assays have become widespread for both screening and hit characterization over the last few years. In a manner similar to the Van't Hoff approach in the preceding text, it is possible to access affinity measurements from these assays, using the stabilization observed due to ligand binding during protein unfolding. When a ligand binds to the folded state of a target protein, this leads to a stabilization of the folded state. The degree of stabilization may be measured as an increase in the midpoint of the thermal melting transition, T_m. From the observed increase in the measured T_m values obtained in the presence of ligand, compared with control, it is possible to derive an equilibrium dissociation constant for the ligand binding event. The unfolding experiments may be carried out using differential scanning calorimetry or other noncalorimetric methods, where the degree of unfolding may, for example, be measured by fluorescence, circular dichroism, or some other biophysical method.

The equilibrium describing a simple, two-state, reversible unfolding reaction is described by Scheme 4.

Where the equilibrium constant for unfolding, in the absence of ligand, K_0, at any temperature can be described as the relative concentrations of unfolded and folded protein, Eq. (16):

$$K_0 = [U]/[N] \tag{16}$$

The Gibbs free energy of unfolding, ΔG_{unf}, is related to the equilibrium constant for unfolding, K_0, by modification to Eq. (13). It can also be written as difference in free energy between the unfolded and folded state, shown by Eq. (17):

$$\Delta G_{unf} = G_U - G_N \tag{17}$$

Similarly, the equilibrium association constant for ligand binding, K_A, is given by Eq. (18):

$$K_A = [NL]/[N][L] \tag{18}$$

Eqs. (16) and (18) can be combined to yield an equation for K_A at the melting temperature, $K_{A(Tm)}$; see Eq. (19) in the succeeding text:

$$K_{A(Tm)} = \left[K_{0(Tm)} - 1\right]/[L]_{(Tm)} \tag{19}$$

However, Eq.(19) must be modified to account for the transposition of K_A from T_m (the affinity at the melting temperature) to a more relevant temperature for ligand binding, T_{rel}, and hence to calculate binding affinity at a more relevant temperature, such as 25°C or 37°C. This produces Eq. (20):

$$K_{A(Trel)} = K_{A(Tm)} \exp\left[\left(-\Delta H_{L(Trel)}/R\right)(1/T_{rel} - 1/T_m) + \left(\Delta C_{pL}/R\right)(\ln(T_{rel}/T_m) + 1 - (T_{rel}/T_m))\right] \tag{20}$$

where $K_{A(Trel)}$ is the equilibrium association constant at a relevant temperature and $\Delta H_{L(Trel)}$ and ΔC_{PL} represent the ligand binding enthalpy at a relevant temperature and the heat capacity change on ligand binding, respectively.

It is also possible to determine K_D for ligand binding directly from fluorescence-based thermal shift assays using a two-stage process. Firstly, the fluorescence thermal shift data are analyzed to produce the T_m for each ligand concentration. Secondly, the T_m value at each ligand concentration is related to the expected effect for a given K_D, using Eqs. (21) and (22) in the succeeding text:

$$y(T) = y_{F,T_m} + m_F(T - T_m) + \frac{\left(y_{U,T_m} - y_{F,T_m}\right) + (m_U - m_F)(T - T_m)}{1 + e^{\frac{\Delta_U H_{T_m} + \Delta_U C_p (T - T_m) - T\left(\Delta_U S_{T_m} + \Delta_U C_p \ln\left(\frac{T}{T_m}\right)\right)}{RT}}} \tag{21}$$

where y is fluorescence, dependent upon temperature T; $y_{F,Tm}$ is the fluorescence of the probe bound to native protein; $y_{U,Tm}$ is the fluorescence bound to the unfolded protein; m_F is the slope of fluorescence when the probe is bound to the folded protein; m_U is the

$$N \Leftrightarrow U$$

Scheme 4

slope of fluorescence when the probe is bound to the unfolded protein; $\Delta_U H_{Tm}$ is the enthalpy of unfolding; $\Delta_U S_{Tm}$ is the entropy of unfolding; and $\Delta_U C_p$ is the change in heat capacity on unfolding.

$$L_t = \left(e^{\frac{-(\Delta_U H_{T_r} + \Delta_U C_p (T_m - T_r) - T_m \left(\Delta_U S_{T_r} + \Delta_U C_p \ln\left(\frac{T_m}{T_r}\right)\right)}{RT_m}} - 1 \right) \times \left[\frac{P_t}{2} \cdot \frac{1}{e^{\frac{-(\Delta_U H_{T_r} + \Delta_U C_p (T_m - T_r) - T_m \left(\Delta_U S_{T_r} + \Delta_U C_p \ln\left(\frac{T_m}{T_r}\right)\right)}{RT_m}}} + \frac{1}{e^{\frac{-(\Delta_b H_{T_0} + \Delta_b C_p (T_m - T_0) - T_m \left(\Delta_b S_{T_0} + \Delta_b C_p \ln\left(\frac{T_m}{T_0}\right)\right)}{RT_m}}} \right] \quad (22)$$

where P_t is the total protein concentration and T_0 is a reference temperature.

2.07.3.3 Mechanistic Aspects to Binding Thermodynamics

2.07.3.3.1 Enthalpy–entropy compensation

Enthalpy–entropy compensation (EEC) is a widely observed phenomenon that often has been examined in the thermodynamic literature over several years. It appears that EEC is a real and observable effect that has been experienced in many systems and by many groups, but its origin may be due to multiple effects occurring across and within experimental measurements.[49] The fundamental principle is reasonably simple. The binding event between a ligand and a target protein is the result of the disruption of interactions that each free partner has with the solvent and the concomitant formation of new interactions with each other in the complex. In the lead optimization process, the structure of the ligand is changed with the aim of increasing optimal bonding interactions with the target binding site. Generally, this often makes ΔH° more negative. By introducing further or more optimal points of interaction, this will tend to introduce increased order into the complex as a consequence of the alteration, which will generally lead to a more negative component to ΔS°. Frequently, the two opposing contributions to ΔG° have a tendency to be of similar size, in many instances in a number of biological systems. As a result, the conventional medicinal chemistry process of building new chemical functionality into a lead compound to optimize the interactions within the binding site (leading to favorable enthalpy) tends to establish restrictions to movement of the compound and also even the protein (leading to unfavorable entropy). Given that these two contributions to the free energy oppose each other, the overall change in ΔG° of binding often is fairly small, potentially thwarting the intention to increase affinity. Conceivably, this cause of EEC is not unexpected, given that both ΔH° and ΔS° themselves are dependent upon the change in heat capacity, ΔC_p. On the other hand, there are other reasons that may lead to the observation of real or apparent compensation. For instance, errors in the measurement of the enthalpy value can give rise to similar and opposite errors in the calculated entropy. This source of error may initiate from errors in the ligand concentration, which has a larger effect on the estimated ΔH° than on ΔG° or also from the error in the estimated parameter values due to the uncertainty in the nonlinear regression fit. Additionally, there is a moderately narrow window, both in terms of the quantifiable binding affinities that can be determined by ITC and also in terms of the affinity values that are actually physiologically relevant. This narrow window restricts the measurable range of ΔG°, but not ΔH° or ΔS°, and so leads to apparent compensation in plots of ΔH° versus $T\Delta S^\circ$.

The phenomenon of EEC, real or apparent, means that modifying the structure of a test compound often has a larger effect on ΔH° than on ΔG° (usually measured from K_D or IC_{50} values). This has significant repercussions for medicinal chemistry, as there may be variation in ΔH°, but not ΔG°, for structurally related compounds that may form diverse interactions with the protein. In the extreme case, a difference in binding mode, resulting from modifications to the compound leading to different thermodynamic profiles, but with modest change in affinity may be observed using ITC measurements. This is vital so that SAR may be understood correctly in the context of the changed interactions within a common binding mode, rather than being masked by the complicating effects of trying to understand changes across a completely different set of interactions in a switched binding mode.

The role of EEC and how to overcome or exploit it remain a key challenge for the medicinal chemist, when the objective is to make alterations to lead compounds in order to increase the binding affinity for the target protein.

It has been recommended that exploiting both enthalpic and entropic optimization options should be employed to direct lead optimization,[50] and clearly, this seems to be the most efficient approach to improve affinity. Clearly, in order to achieve this, the individual enthalpic and entropic components must first be dissected. Different thermodynamic profiles have often been attributed to different types of molecular interactions, and some simple guidelines have been proposed that chemists may apply; for instance, hydrogen bonds associated with favorable enthalpy, hydrophobic interactions tend to be entropically driven, release of water trapped in the binding sites is entropically favored, and increasing ligand rigidity reduces the entropy loss upon binding. However, even if these simple guidelines always held, there is also no constraint for these different types of interaction to contribute to the binding free energy in a simple and additive manner. This means that it is often complex for the chemist to interpret and utilize these signatures in straightforward prospective design setting.

Moreover, the general rule of thumb illustrated earlier often does not hold up to detailed scrutiny themselves, which adds to the difficulty in attempting to make alterations to lead series by employing enthalpic and entropic signatures, as numerous different contributions may give rise to the observed values.

So, if we expect that EEC, at least to some extent, may occur throughout lead optimization, how can the medicinal chemist make the best use of this accessible information?

The most powerful approach would still be to use a combination of thermodynamic data coupled with high-resolution crystal structures in attempting to decide upon a strategy to attempt to overcome this propensity toward compensation. Some of these strategies have been highlighted previously, for example, directing hydrogen bonds to previously structured regions of the protein or by introducing multiple hydrogen bonds from a single group so that the entropic penalty for constraining the test compound has already been paid.[51]

The existence of EEC suggests that even when specific interactions with likely enthalpic signatures are introduced, it will not be certain that these modifications will result in an increase in binding affinity. This highlights the advantage of having an excellent understanding of the structural features of the binding site and an appreciation of the flexibility and dynamics of the protein both within the binding site vicinity and beyond. Undoubtedly, in the absence of this detailed understanding, designing for improvements in affinity directly utilizing traditional SAR approaches may be more successful.

EEC thus represents a global phenomenon, as it reveals properties of the entire molecules associating or perturbed during the binding event. This includes the water molecules that may be relocated or reorganized during the interaction.

Of course, local increases in entropy upon binding are still possible. Zidek et al.[52] exemplified this via NMR studies on the binding interaction between mouse major urinary binding protein I and the ligand 2-sec-butyl-4,5-dihydrothiazole.

Recognition of the compensatory effects of the contribution of delicate changes in the network of water molecules surrounding a ligand and the resulting thermodynamic fingerprints have been highlighted recently.[53] These are not the water molecules displaced by the ligand upon binding (which also have been previously discussed in detail) but those on the protein surface that encounter the ligand on the exterior.

2.07.3.3.2 Enthalpy–entropy transduction

As described earlier, the measured values of binding enthalpy and entropy often can be complicated to interpret, especially in terms of the fundamental physical forces controlling the binding interaction. Alongside the problem of entropy–enthalpy compensation, another potential reason this can be complex includes understanding the correct binding equilibrium, as there may be other unknown linked equilibria that may confuse the interpretation of the observed thermodynamic data. Of course, errors in the experimentally determined values should also be handled cautiously, in order to avoid overinterpretation.

Another perplexing relationship between enthalpy and entropy that may hinder the use of these values in chemical design has been proposed recently, termed enthalpy–entropy transduction. A statistical thermodynamic examination of the primary conformations of the 1 ms MD simulation for the small trypsin inhibitor, BPTI, showed that three conformation clusters were carefully balanced in free energy. This delicate balance between conformations meant that even fairly small perturbations in the system could alter their probabilities.[54] In this situation, small adjustments to a test compound could, theoretically at least, lead to significant changes in enthalpy and entropy values for the binding interactions but only minor differences in free energy.

Selection for one of these three major conformational clusters may consequently influence the magnitude of the global enthalpy and entropy terms. So the thermodynamic nature of the local driving forces controlling the binding event need not be the same as the global thermodynamic results of complex formation. Hence, there may be a transduction of the local driving force into a different global thermodynamic profile, which leads to the term entropy–enthalpy transduction (EET). This expression basically arises because the protein may be able to switch conformational states upon binding allowing the conversion or transduction of binding enthalpy into entropy or vice versa.

Given that this phenomenon may occur for a small, comparatively rigid protein, such as BPTI, the trend may be even more common in larger, more flexible proteins often encountered in drug discovery. As a result, ligand binding events, even within a chemical series with relatively small modifications, such as generally experienced during lead optimization, may sometimes be expected to display large changes in entropy and enthalpy of binding if alternative conformational states are populated, particularly if the free energy difference between these states is small.

Since EET may be responsible for changes in entropy and enthalpy arising from global effects that may not be predicted from local considerations alone, it may be prudent to explore relevant possible conformational changes by undertaking structural- and dynamics-based studies, in an integrative structural biology approach that may be crucial in really interpreting experimental calorimetric data.

EET also may add to the difficulties in interpreting the measured thermodynamic signatures in the presence of substantial solvent reorganization and also even in systems where prominent EEC occurs.

In the case of solvent reorganization, it is believed that conformational rearrangement from one state to another of comparable free energy results in water release at sites away from the binding site, which may be overlooked when predicting or analyzing the experimental thermodynamic contributions.

In the example of combination with EEC, a series of related compounds binding to the same target protein could access a number of alternative protein conformations of similar free energy but with different enthalpic and entropic contributions. This would then produce the linear compensation plots typically observed during the lead optimization process.

2.07.3.3.3 The complex role of water

The hydrophobic effect may partly explain the binding of test compounds to protein target binding sites, as burial of hydrophobic surfaces on both partners occurs. Medicinal chemists increase the hydrophobicity of compounds as a common approach to improve binding affinity, since this leads to an increase in the total amount of hydrophobic surface area burial. The hydrophobic effect occurs via displacement of water molecules from around the hydrophobic surfaces of both the protein target and the test compound. The

ligand binding interaction can therefore be described by two steps—desolvation and association. Water is present in all biological systems, often at high concentration, but is often not considered in ligand binding experiments, although protein structures often reveal that water molecules are regularly present in binding sites and the role of water in modulating interactions is often discussed in the literature. Understanding the nature of the solvation state of the target protein, especially at the binding interface, is advantageous during lead optimization.[55] Water molecules occupying hydrophilic pockets tend to have the strongest binding affinities as they make optimal hydrogen-bonding interactions with charged amino acids. Hydrophobic cavities tend to contain more weakly bound water molecules. Often, binding interactions dislodge water from the binding surface, with a small gain in free energy (around 2 kcal mol^{-1}) resulting from the favorable entropy associated with this water release.[56] Numerous waters within protein pockets are disordered and exchange rapidly with bulk solvent, and so, these waters may be readily expelled from the pocket. However, some tightly bound water molecules may be more difficult to displace. Displacing these tightly bound waters incurs an enthalpic penalty, which often offsets any entropic gain. These tightly associated water molecules often can be identified from numerous X-ray structures of the same target protein as their positions are preserved and they usually have lower crystallographic temperature factors (*B* factors—which reflect the displacement of atomic positions from a mean value, identifying flexible regions as those with larger displacement from the mean and greater *B* factors) than the mean temperature factor for all waters in the structure. Temperature factors are related to the relative vibrational motion of atoms within the X-ray structure and so may be applied to help identify the reduced movement of these tightly bound waters. Identification of tightly associated water molecules allows them to be dealt with differently to weakly bound waters, during compound design. Tightly bound waters can in effect be considered as part of the protein structure, and often, these water molecules are even called "structural" waters. Design strategies would then not aim to displace these waters, but potentially even look for compounds to form interactions with them. Although the hydrophobic effect has been studied for many years, the full extent and the true role of water in binding interactions are still not fully understood. Several studies have established that hydrophobic interactions can be dominated by either enthalpy or entropy, signifying that simple explanations are not sufficient to fully explain the underlying driving forces.[57,58] Various computational approaches[59] including specialized software such as WaterMap[60] or protocols using freely available software[61] have been used to try to incorporate the effects of the water network into drug design. Additionally, studies using D_2O and osmolytes at a range of concentrations have been used to try to explain binding behavior in cell, where the effects of water are also complicated by molecular crowding effects.[62]

2.07.3.4 Role of Binding Thermodynamics in Selectivity and Efficacy

Several examples have been used to exemplify the role of thermodynamics in selectivity and efficacy, and some of these case studies will be briefly described in the succeeding text.

2.07.3.4.1 HIV-1 protease

Kawasaki and Freire studied the thermodynamic profile for two similar compounds binding to HIV-1 protease and two antitargets, cathepsin D and pepsin.[63] Even a relatively subtle change like the introduction of two methyl groups into a phenyl moiety produced a gain of around 11 kJ/mol in binding free energy, resulting from the favorable enthalpy component for the methylated derivative. This arises due to the optimal filling of the small cavity around the aryl moiety allowing the methyl groups to form advantageous contacts. Alongside the improvement in affinity, the selectivity over pepsin and cathepsin D increased by 13- and 34-fold, respectively. In a second example, the thioether group was substituted by a sulfonylmethyl moiety resulting in a decrease in binding free energy of about 1 kJ mol^{-1}. Although the binding free energy was less favorable, the binding enthalpy increased by approximately 16 kJ mol^{-1}, alongside an almost completely compensating decrease in entropy. X-ray structures show that the added sulfonyl group forms a strong hydrogen bond with Asp30 of the protease, which reflects the increase in enthalpy. The selectivity over pepsin and cathepsin D increased by seven- and ninefold, respectively. It was suggested that maximal selectivity could be achieved by establishing few but strong hydrogen bonds in the interaction with the target protein.

It was reasoned that suboptimal H-bonds formed with antitarget proteins are penalized resulting in a larger decrease in the binding free energy for the off-target proteins. This example suggests that as the enthalpic contribution to binding free energy is increased, the compounds are more specific for the primary target. Supporting this view is the fact that of the four compounds, it is the one with the most favorable binding enthalpy that is the most selective.

2.07.3.4.2 Matrix metalloproteinase 12

Another example demonstrating matrix metalloproteinase 12 (MMP12) inhibitor optimization, with a focus on selectivity over MMP13, shows a similar effect.[64] Highest selectivity was observed for the compound with the largest enthalpic component (around -40 kJ mol^{-1}) although this was not the highest affinity compound for the MMP12 target. Although these observations were on a limited congeneric compound set, the results further reinforce the hypothesis that the binding enthalpy has higher contribution to off-target selectivity.

2.07.3.4.3 Thrombin

Optimization of sulphonamide inhibitors of thrombin containing triazole and tetrazole moieties, with selectivity over trypsin, may also fit with the hypothesis of binding enthalpy being important for selectivity.[65] The lead compound showed over 800-fold selectivity versus trypsin, and selectivity over tryptase and chymase was also favorable. The lead compound was found to bind to

thrombin with binding enthalpy of around $-38\ \mathrm{kJ\ mol^{-1}}$ and a slightly unfavorable entropy. In this study, only the lead compound was characterized in terms of the thermodynamic components, but the high-selectivity and enthalpy-driven nature of binding to the target fits with the proposed relationship between these properties.

2.07.3.4.4 HMGCoA reductase

A retrospective analysis of the binding thermodynamic profiles of marketed statins inhibiting 3-hydroxy-3-methylglutaryl coenzyme A (HMGCoA) reductase suggested there may be advantages to enthalpically driven binding.[63] The study showed a correlation between market entry time and the enthalpic contribution of the binding affinity for the statins, a trend that has also been observed for HIV protease inhibitors[63] and inhibitors of farnesyl pyrophosphate synthase.[66] First-in-class drugs were entropically driven, with unfavorable or very low enthalpic components in each of these systems.

New drugs acting on the same target for the same biological effect must show advantages over existing therapies. In these cases, new drugs showed successively increased binding enthalpy. Of course, binding enthalpy alone may not explain the success of the later compounds, as other factors shown by the more enthalpic compounds may contribute to improved physicochemical properties, such as lipophilicity and solubility. These later drugs were all optimized without a focus on binding thermodynamics, and a large number of other parameters may have influenced the success, but the increased enthalpy contribution during drug evolution for each of these systems is still significant and certainly merits further investigation.

The contribution of enthalpy to selectivity may also be prevalent in the statin example, as hepatoselectivity is desired for statin drugs to avoid myalgia, which has been suggested to be linked to myocyte HMGCoA inhibition. Consistent with this, the most enthalpic binder, rosuvastatin has the highest hydrophilicity and hepatoselectivity, with almost 1000-fold selectivity over the myocyte. The hepatoselectivity of the less enthalpic binding compounds (e.g., pravastatin, atorvastatin, and cerivastatin) is lower than that of rosuvastatin, showing around 400-, 100-, and fourfold hepatoselectivity, respectively.

2.07.3.4.5 Aldose reductase

A further example suggesting a link between binding enthalpy and selectivity may be from work on aldose reductase (ALR2) and selectivity of inhibitors over aldehyde reductase (ALR1).[65] X-ray crystallography grouped the six studied compounds into those protruding into the specificity pocket and others leaving the pocket closed. The X-ray structures suggested that the favorable enthalpy displayed by IDD393 might result from specific polar contacts between the nitro moiety of the compound and Ser302 in the protein. Sorbinil was shown to form a strong H-bond with the backbone NH of Leu300. In both of these examples, the increased selectivity over ALR1 is suggested to come from the specific enthalpic engagement with the primary target that may be suboptimal for binding to ALR1.

Although the correlations between selectivity and binding enthalpy are not completely consistent across the entire dataset, this may arise from the differences in physicochemical profiles for the two types of ligand classes. Those compounds penetrating into the selectivity pocket are carboxylic acids, sharing similar pharmacophoric features, while those binding outside the pocket are small, weak NH acids, showing less pharmacophoric elements compared with compounds in the first cluster.

The correlation between enthalpy and selectivity may not always be clear, and obtaining thermodynamic profiles may not always enable the development of selective compounds. Undoubtedly, there will be a variety of factors that contribute toward selectivity and efficacy, and optimizing enthalpy alone will not be sufficient. However, the hypothesis first presented by Freire[67] provides a framework for attempting to increase ligand selectivity by improving protein–ligand complementarity. Precisely oriented interactions, accomplished from enthalpic binding, tend to result in a higher bias toward the primary target, leading to potentially less promiscuous compounds. It seems that there is already some evidence across a number of diverse ligands for several different validated drug targets (including HIV protease and HMGCoA reductase) showing selectivity profiles that support this concept. Only by exploiting this observation in compound optimization will the strength of this hypothesis be truly tested.

2.07.3.5 Optimizing Enthalpy

Observations by Freire[67] that for two important drug classes, the statins and the HIV protease inhibitors suggested that the best-in-class drugs tended to have the most favorable binding enthalpy. Although there are a large number of other factors that lead to a best-in-class molecule, this focus on thermodynamics initiated a drive by many pharmaceutical companies to begin to include thermodynamic data in some early-phase drug discovery decision-making.

Potentially, thermodynamic signatures could be used to identify compounds optimized in a number of different ways, including flexibility, helping to minimize drug resistance due to mutation occurring at the compound binding site[68]; specificity, reducing off-target effects caused by nonspecific binding interactions;[69] and water solubility, maximizing the ligand efficiency of polar interactions.[70]

These thermodynamic signatures have been used to produce guidelines that have been suggested may help to exploit thermodynamic data for advancing lead optimization.[67,69] Simplistically, hydrogen bonds tend to produce favorable enthalpy changes, hydrophobic interactions yield favorable entropic contributions, and conformational changes are often entropically unfavorable.

Although simplistic, these signatures and guidelines can be used during lead optimization to formulate strategies for new chemical design and to monitor the success of these strategies. For instance, the successful introduction of hydrogen-bonding interactions should lead to increases in potency potentially driven by favorable enthalpy gains, whereas ligand rigidification should reduce

entropic losses. Thus, the expected thermodynamic changes suggest that the strategy was successful, and differences from the profile expected suggest that structural information on the complex may be informative in understanding unexpected SAR.

Although the combination of ITC and X-ray structure with medicinal chemistry design is clearly a powerful tool, examples have emerged recently that suggest that thermodynamic-guided lead optimization is difficult to implement in prospective compound design.[71] Complicating factors such as EEC and transduction and the role of water have been highlighted in the preceding text, and it is important that these aspects should be considered carefully when trying to optimize binding enthalpy.

2.07.3.6 Role of Binding Thermodynamics in Fragment-Based Drug Design

Since fragment-based lead generation has become a successful paradigm for drug discovery, biophysical methods have established an even wider influence, since they are frequently used as the basis for primary fragment screens, due to their sensitivity in detecting small, weak compound binding. The foundation of fragment-based drug discovery (FBDD) is that small fragments sample chemical space more effectively than large molecules and therefore provide more effective and potentially more diverse start points for lead generation. However, since fragments often lack the substituents required for high affinity, the link with biophysical detection methods is ideal, as these methods are often preferred over biochemical assays to discover and quantify the weak binding that these fragments often demonstrate.

Some studies suggest that fragments bind to a target binding site with an average of two hydrogen bonds, which display close to optimal geometry.[72] Sites within a protein that permit optimal hydrogen-bonding interactions in a hydrophobic environment are frequently described as hot spots. From estimation of the free energy increase of hydrogen bond formation (around 1–2 kcal per mol per H-bond), as opposed to apolar desolvation, which is usually smaller (usually less than 0.25 kcal per mol per heavy atom), comes the suggestion that fragments require optimal hydrogen bonds in order to attain measurable binding affinities. This may be the basis of a benefit frequently asserted in fragment-based drug discovery—that fragment binding is inherently enthalpically driven—arising from the formation of these few but optimized polar interactions within the hot spot of the protein binding site.

Understandably, the effects of ligand size on the underlying thermodynamic contributions to the binding free energy change have been studied, and it has been demonstrated that these contributions show different effects when considered in the context of compound size, molecular weight, or heavy atom count. The entropic component becomes progressively more dominant with increased size of compounds, whereas enthalpy seems to lack a correlation with compound molecular weight. So what are the reasons for this behavior? There may be several explanations that may help explain these observations. As compound molecular weight rises, the probability for a corresponding group of H-bond donors and acceptors declines, thus lowering the likelihood for forming polar interactions. Another possible cause for the number of hydrogen bonds to remain essentially unchanged with compound size may be the constrained motion of the protein and compound with increasing numbers of polar interactions. The contribution from the unfavorable entropic penalty thus limits any enthalpic advantage of added polar interactions.

Additionally, larger compounds are likely to have increased amounts of apolar surface area, which means that the involvement of apolar desolvation in the contributing to the binding affinity becomes more significant.

These observed effects and the potential reasons behind them help to formulate a possible strategy for the use of thermodynamic data in fragment optimization. For example, suppose the most enthalpically driven, small polar fragments that often bind to protein hot spots could be identified, from the considerations in the preceding text, these compounds might be preferred start points for further optimization than fragments that may be entropy-driven. Starting from these interaction-rich fragments should theoretically be an advantage because affinity may be gained straightforwardly via typical structure-based expansion of these fragment cores, where the increase in affinity is brought about by an entropically favorable component, which is usually easier to incorporate. Analysis of 39 fragment to lead campaigns undertaken by the fragment-focussed company Astex showed that the positions of atoms in a starting fragment core are frequently well preserved in the final, larger, and optimized leads. This highlights that the original polar interactions, responsible for the enthalpy-driven nature of the fragment binding, are conserved during lead optimization.[72]

There are additional benefits to examining fragment thermodynamic profiles during the optimization process; for example, the ability to detect conformational changes that might occur as fragments is grown and also in assisting in identifying the most appropriate strategy for extracting a contribution to the binding free energy from water molecules in the binding site. Fragment growing might result in ligand-induced protein conformational changes as additional substituents are added that may contact the protein and constrain it to adopt alternative conformations. Should these differences in conformation or binding mode occur, then the thermodynamic signatures related to these different binding modes may be detected using ITC. This is an advantage of ITC over other affinity only techniques, since these methods for measuring binding affinity may, in the absence of structures, lead to misleading SAR, as changes in binding mode may be missed if there is no concomitant change in binding free energy change.[73]

The presence of high-energy water molecules located within a protein hot spot signifies that large desolvation energy may potentially be available if displacement of these waters can be achieved. Since it may be rather complicated to achieve displacement of these water molecules, which have large entropic terms, by standard fragment optimization design strategies, prioritizing fragments that previously displace these waters would seem an attractive approach. However, it can be difficult to categorize these water molecules and to identify those fragments that displace them, but the use of structural B factors and the simple enthalpy–entropy compensation plot can give some insight into which fragments achieve this displacement and should be prioritized for optimization.[74]

2.07.3.6.1 Experimental considerations for fragment ITC

Due to the weak affinity of fragment binding and potentially low solubility relative to achievable aqueous concentrations and sometimes even low-enthalpy values, characterizing the thermodynamic contributions to fragment binding can often be challenging. As a result, direct titrations with fragments often lead to low *c*-value (where *c* is the unitless parameter that governs the shape of the binding isotherm, whose value equals the stoichiometry of the interaction × the macromolecule concentration in the cell divided by the K_D value) situations, because the binding affinity is frequently only in the low mM to high μM range and often the achievable protein concentration only around tens of μM. This results in *c*-values potentially around 1 or lower (whereas values between 5 and 100 are ideal), which means that in order to resolve reliable binding parameter values, necessitates final test fragment concentrations that are significantly in excess of the K_D value. The ability to reach these concentrations so that a significant degree of saturation is reached depends upon the aqueous solubility of the fragment being used. In the low *c*-value regime, the ITC method resembles other traditional binding techniques, which do not permit differential measurements. Another disadvantage of experiments conducted under low *c*-value conditions is that the stoichiometry value must be arbitrarily fixed, and so, information about the number of binding sites from other sources should be used if possible.[75]

Thus, low *c*-value experiments with fragments may be challenging, but there are some modifications that can be made to standard ITC experimental methods that can be used to access some of the individual binding parameters, either directly or indirectly, to allow full characterization of the binding interaction.

Competition or displacement experiments may be carried out, if a suitable tool compound is accessible, which is known to compete for the binding site, and for which the binding affinity is measurable and is in the range of around 10–100 nM. This reference ligand is first characterized in a traditional direct titration in order to obtain its thermodynamic parameters. Next, the tool ligand titration is repeated but this time in the presence of a known, fixed concentration of the test fragment. This methodology allows the measurement of the degree of competition caused by the presence of the fixed concentration of fragment, and so consequently, the fragment binding parameters may be indirectly determined. Thorough descriptions and applications of the technique and the associated data analysis procedures are available.[76,77]

As mentioned earlier, there are certain requirements that the reference compound must satisfy in order to get reliable, accurate, and precise results. Obviously, the reference ligand has to compete with the binding of the fragment, and ideally, the enthalpy of the binding interaction should be significantly different to that of the fragment. Consideration should also be given to the fact that errors in the binding parameter values of the tool compound will be compounded during the calculation of the parameter values for fragment binding. Despite these issues, however, when carried out cautiously, both the low *c*-value methods and displacement experiments can provide comparable results, indicating the robustness of both methods.[78]

Finally, an adaptation to the typical displacement method has been described, termed single-injection thermal extinction (SITE), whereby it is feasible to determine relative enthalpies for fragments, compared with a reference ligand using only a single injection. Even though this does not give exact enthalpy values and the binding affinity must be measured separately, it offers a rapid method for identifying those fragments with a favorable enthalpic binding profile.[79]

2.07.3.7 Future Trends for Thermodynamic Characterization

Theoretically at least, it would appear that thermodynamic signatures are valuable in guiding compound selection and lead optimization. However, due to the many different contributing factors to both the enthalpic and entropic components, it has proved difficult to use these fingerprints effectively in prospective drug design. Rather, the combination of thermodynamic data with structural information has been used to postrationalize the optimization process. So the role of thermodynamics may be more subtle than previously believed. Certainly, ITC still has a major role to play in early lead identification and optimization. It is still regarded as one of the most powerful methods for characterizing both target proteins and tool ligands in terms of functionality, concentration, and affinity. It can also highlight important changes in the binding interactions that other affinity only methods may miss. The additional measure of the binding enthalpy is therefore useful in identifying unexpected changes in enthalpy that may indicate potential changes in binding mode that could lead to comparisons across different structure–activity relationships, which will ultimately confound optimization. So, ITC will remain useful during the early stages of drug discovery. But what of the future for thermodynamic-guided lead optimization? By combining thermodynamic data, especially for systems that show unexpected or unusual profiles, with structural information and computational methods that may enable the underlying intermolecular interactions to be better understood, we may begin to implement approaches where manipulation of enthalpic or entropic contributions to produce more favorable molecules may be successful.

2.07.4 Use and Misuse of Efficiency Measures in Drug Discovery

LEMs are used in drug discovery to normalize affinity or activity with respect to various physicochemical properties, and there has been debate in the literature recently over the value of using such metrics. In the succeeding text, we will provide an overview of the different metrics and will comment on the application in prioritizing and optimizing lead compounds.

The principle for employing LEMs is based around a potentially more relevant comparison of compounds than by considering affinity alone. This is because affinity is often linked to molecular size and so introduces a bias for the selection of larger compounds during lead optimization. Of course, affinity is not the only factor that has to be considered during lead optimization, and the

physicochemical properties of leads are also important. For example, it is usually considered that excess molecular weight or lipophilicity is associated with poor PK and toxicity, associated with off-target binding, and so should be constrained during ligand optimization. However, affinity for the primary target also increases with these factors, and so, modifying these variables should be carried out in the most efficient manner.

The role of different physicochemical properties for leads and drug-like compounds was highlighted some time ago by Lipinski,[80] and since this seminal paper, the "rule of five" has been a valuable guide for establishing the physicochemical boundaries associated with reduced attrition at the later drug discovery stages. A recent article by Gleeson emphasized the importance of selecting the most appropriate hits and for tracking increases in molecular weight and lipophilicity alongside affinity during lead optimization, as almost all ADMET parameters were shown to worsen with increasing compound size and lipophilicity.[81]

However, the use of LEMs should be employed in the knowledge that it is free concentration and affinity that determines the extent of target engagement, not the ligand efficiency value itself.

2.07.4.1 Common LEM

2.07.4.1.1 Ligand efficiency

Ligand efficiency (LE), the concept for which was first described in 1999,[82] is one of the most commonly used LEMs and is defined as the affinity of the ligand divided by the number of heavy (nonhydrogen) atoms,[83] given by the expression

$$\mathrm{LE} = -\Delta G/n_{\mathrm{HA}} \approx 1.4^{*}\mathrm{pIC}_{50}/N_{\mathrm{HA}} \tag{23}$$

where N_{HA} is the number of heavy (non-H) atoms and pIC_{50} is the negative logarithm of IC_{50}.

Its use and popularity was linked to the growth of fragment-based drug discovery and the desire to bring forward compounds into the optimization process that are smaller and with lower lipophilicity.

2.07.4.1.2 Other size-based metrics

Table 2 shows a number of other LEM that are dependent upon heavy atom count

As is evident from Table 2, efficiency metrics are mathematical functions that attempt to describe how efficiently potency is achieved relative to some other variable. Also evident from the table, which does not list all LEMs, is that there are many composite metrics that have been proposed to help medicinal chemists improve success rates by moving away from simple potency optimization. The premise of LEMs is that they encourage multiparametric optimization as they include other parameters that may be important to consider during compound optimization.

2.07.4.1.3 Ligand lipophilicity efficiency

Another frequently used LEM is ligand lipophilicity efficiency (or lipophilic ligand efficiency) (LLE) or lipophilic efficiency (LipE):

$$\mathrm{LLE} = (\mathrm{pIC}_{50} \text{ or } pK_i) - (\log \Delta \text{ or } C\log P) \tag{24}$$

$$\mathrm{LipE} = (\mathrm{pIC}_{50} \text{or } pK_i) - C\log P \tag{25}$$

where $C\log P$ is the calculated octanol–water partition coefficient and $\log D$ is the measured distribution coefficient.

These LEMs attempt to account for the lipophilicity of the compound rather than the molecular size and may be considered more useful than size-based metrics when trying to achieve optimal ADMET properties. Compounds with high LLE therefore are suggested to gain affinity through direct specific interactions, minimizing the probability for nonspecific interactions. In order to combine the effects of molecular size and lipophilicity into a single efficiency metric, lipophilicity measurements have been combined with potency and molecular size in two further LEMs: the Astex ligand lipophilic efficiency ($\mathrm{LLE}_{\mathrm{AT}}$) and the lipophilicity-dependent ligand efficiency (LELP):

$$\mathrm{LLE}_{\mathrm{AT}} = 0.11 - \left[\ln(10).RT(\log P - \mathrm{pIC}_{50})/N_{\mathrm{HA}}\right] \tag{26}$$

$$\mathrm{LELP} = C\log P/LE \tag{27}$$

Table 2 Selected commonly used LEM, with their abbreviations and definitions. HAC is heavy atom count (=N_{HA}), MW is molecular weight, and Δ represents a change in the associated parameter

Name	*Abbreviation*	*Definition*
Maximal ligand efficiency	%LE	(LE/max LE) × 100
Size-independent ligand efficiency	SILE	$1.4 \times \mathrm{pIC}_{50}/\mathrm{HAC}^{0.3}$
Scaled ligand efficiency	LE_scale	$0.0715 + 7.5328/\mathrm{HAC} + 25.7079/\mathrm{HAC}^2 + 361.4722/\mathrm{HAC}^3$
Fit quality	FQ	LE/LE_scale
Binding efficiency index	BEI	pIC_{50}/MW
Group efficiency	GE	$-\Delta\mathrm{pIC}_{50}/\Delta HAC$

The uptake of LEMs into the considerations of the medicinal chemist was driven by both the established use of the rule of five guidelines and the increasing application of fragment-based lead generation and its equivalent rule of three.[84] Ligand efficiency became a convenient way to track and prevent property inflation during optimization programs, as it offered a simple calculation to avoid making compounds unacceptably large.

2.07.4.1.4 Enthalpic efficiency

As described earlier, the measurement of ΔH potentially offers a direct estimate of the heat change associated changes in noncovalent bonding upon formation of the protein–ligand complex. Therefore, taken in its most simplistic form, a favorable enthalpy for ligand binding suggests that stronger or an increased number of bonds are formed when moving from the free to the bound state. As we have seen, it is very difficult to design compounds that are able to form new noncovalent bonds in the complex. If we take the example of hydrogen bonds, then there are relatively few examples where new bonds have been introduced in a rational and expected way in order to increase affinity. This is due to the precise orientation and distance constraints on both donor and acceptor moieties, which dictate the geometry of optimal hydrogen-bonding interactions introduced in the binding site. Since modification of small molecules to maintain existing interactions while introducing new ones is difficult to achieve from a rational design perspective, often, new hydrogen bonds arise by chance, as the medicinal chemist often is focussed upon increasing the entropic contribution to the binding free energy change. This may, however, suggest that the greatest value from ITC is in the measurement of the ΔH term, as this allows the monitoring of increasing bonding interactions.

Clearly, the exploitation of the binding enthalpy is most important when comparing and contrasting molecules of similar structure binding to the same target binding site, and so, it is the difference in enthalpy values, $\Delta\Delta H$, which is most informative. This is due to the fact that the effects of solvent removal from the surfaces buried during the formation of the complex will mostly cancel for compounds that are closely related structurally. Hence, a potential criterion for guiding subsequent optimization would be to prioritize those compounds with the most favorable comparative enthalpic contribution.

In fact, the use of the enthalpic component has been expressed as comparable to the use of other LEM to prioritize ligands for further optimization, and enthalpic efficiency, EE (defined in Eq. (28)), was introduced in order to compare compounds according to their net bond forming capability:[85]

$$\mathrm{EE} = \Delta H/N_{\mathrm{HA}} \tag{28}$$

So, it may be advantageous to calculate the enthalpic efficiency or break this down further to provide a measure of the specific enthalpic efficiency of polar groups, $\Delta H/N_{\mathrm{polar}}$, since it is the favorable interactions from the polar groups with the target protein that contribute to affinity, not the mere presence of a polar group in the ligand. Similar to many of the described LEMs, enthalpic efficiency can be corrected for molecular size to produce a size-independent enthalpic efficiency, SIHE, $(\mathrm{p}K_{\mathrm{H}}/40)\cdot {H_{\mathrm{A}}}^{0.3}$, where $\mathrm{p}K_{\mathrm{H}}$ is $-\Delta H/2.303 \bullet RT$.[86]

The maximum potential binding enthalpy has been suggested to decrease with molecular size, leading to the hypothesis that enthalpy-driven binding may be applicable only to smaller compounds. From this analysis, it seems that enthalpic optimization may represent a suitable strategy only while the molecular size of the compounds requiring optimization remains below around 30 heavy atoms.[87] After this size, it appears that affinity improvement may only be possible by predominantly increasing entropy, until solubility limits, protein binding and clearance limits, and other physicochemical property issues prevent further entropic gains from being achievable.

Clearly, EE has not replaced other more established LEMs, and it would not be appropriate to switch from one metric to another without understanding the thermodynamic basis of the metrics and the information they provide, but EE was proposed to add to the toolbox for facilitating the decision-making process.

2.07.4.1.5 Kinetic efficiency

In 2011, we proposed[88] that the kinetic parameters for the binding interaction per atom or kinetic efficiency (KE) could be used to complement ligand and enthalpic efficiencies:

$$\mathrm{KE} = \tau/N_{\mathrm{HA}} = \tau_{½}/(0.693N_{\mathrm{HA}}) \tag{29}$$

The application of kinetic data and the KE metric may be best applied later during lead optimization as rapid kinetics are often exhibited by low-molecular-weight compounds, which demonstrate low-affinity compounds, and so, there is often little discrimination in residence times. Once differences in residence time become apparent, for compounds from different chemical series where differences in molecular weight may still be significant, KE may be used to rank them in order of potential later-stage optimization and developability. Use in this way may be compared with the similar use of enthalpic efficiency, as it is often difficult to determine the binding enthalpy for small, weak binding hits.

In terms of binding kinetics, it may also be possible to dissect the ligand efficiency into an association efficiency and an alternative expression for a dissociation rate-based efficiency metric, for example, from Eq. (23) in the preceding text:

$$\mathrm{LE} = -\Delta G/nHA = RT\ln(k_{\mathrm{d}}/k_{\mathrm{a}})/nHA = RT\ln k_{\mathrm{d}}/nHA - RT\ln k_{\mathrm{a}}/nHA \tag{30}$$

However, we believe there is more value in utilizing dissociation rate measures as medicinal chemistry efforts can only modify the ligand in an effort to alter association kinetics, and usually, there is a more limited range of accessible values (typically spanning

three to four orders of magnitude), whereas it may be easier to modify the interactions formed by the ligand in the complex (and the accessible rate constant values often cover a wider dynamic range (often over six orders of magnitude)).

LEMs have been used increasingly to guide the hit to lead and lead optimization processes as they relate changes in certain measured parameters to changes in compound molecular weight and so may offer an advantage over the absolute parameters. The use of these metrics has been supported by retrospective analysis suggesting that many recently approved drugs have high ligand efficiency values for their targets, often due to the fact that the metrics have been used to restrict the previous tendency for uncontrolled property inflation.

However, there have been a number of publications that have questioned the use and even the validity of certain LEM.[89,90]

Some of the concerns may well be at least partially justified; for example, some drugs have low ligand efficiencies, LEMs have no power to resolve between different atom types or functional groups, and the increase in the number of different metrics may have introduced more complexity than the metrics themselves may be able to reduce.

Of course, these metrics should be applied cautiously and should not be employed as fixed rules, but as simple guidelines that may help to frame the optimization process in terms of kinetic or thermodynamic parameters, with a view to restricting the inflation of molecular weight and lipophilicity. They should be viewed as pragmatic tools that can offer insights into the evaluation of hits and leads, beyond affinity alone. What should be avoided is an excessive reliance on metrics, without also undertaking a thorough analysis of the available data.

In defense of LEM, they have been compared with fuel economy (miles/gallon), which allows comparison of the efficiency of motor vehicles. Of course, fuel efficiency is not the only criterion used when choosing a car, but it is one factor that helps the decision-making process when there are a large number of different factors to consider. LEM should be viewed in the same manner and the limitations and the application of the different metrics understood. For example, size-independent metrics should be preferred when comparing compounds of contrasting sizes, and consideration of the target binding site should also be kept in mind when thinking about LEMs, as lead compounds binding to large binding sites will naturally tend to have lower ligand efficiency than lead compounds binding to smaller binding sites. The short article by Reynolds[91] and the references contained within are recommended for a thorough appreciation of the role of LEM.

2.07.4.2 Future Trends for Application of LEM

LEMs will continue to be used as a tool for optimizing fragments and small molecules and applied by medicinal chemists during the optimization process. It is hoped that the recent debate in the literature around the validity and usefulness of these metrics will help to further the understanding of the physical basis of the various LEM calculations and the scaling or offsetting applied to the measured activity. Ultimately, the role of LEMs is to help to identify compounds that outperform the observed trend in the data, with respect to a chosen risk factor, so that these compounds can be prioritized for further optimization. It may be that there will be a move toward a least square-based approach for identifying these compounds as our understanding of the limitations of LEMs is increased, as suggested by Kenny et al.[89] But regardless of how lead compounds are actually identified, the general guiding principle that drugs should be as hydrophilic as possible while maintaining efficacy remains a key strategic objective in drug design.[92]

2.07.5 Summary

Ligand binding thermodynamics describes the differences in free energy between the two ends of an equilibrium, while binding kinetics are dependent upon the free energy barriers between those two states. Clearly, an appreciation of both is important to fully understand binding interactions and to maximize the opportunities for modifying compounds for improved activity and desired thermodynamic and kinetic profiles.

We are beginning to appreciate how these properties might be connected to both binding affinity, efficacy, and selectivity, and studies have been presented where attempts have been made to explain postrationally or utilize prospectively the kinetic and thermodynamic components to improved compound properties. Optimizing compounds via improved kinetics and/or thermodynamics remains a difficult task, and tools and guidelines for helping to do this are attractive and increasingly used. Some of the most widely used LEM have been discussed and some potential pitfalls with their application.

By increasing our understanding of protein–ligand interactions from a kinetic and thermodynamic perspective and by applying this learning throughout the optimization process, with a view to control undesired properties such as increasing hydrophobicity and molecular weight, we will become more successful in designing safe and effective medicines.

See also: 3.03. Recent Progress in Free Energy Methods. 3.04. Molecular Dynamics, Quantum Mechanics and Combined Quantum Mechanics/Molecular Mechanics Methods for Drug Discovery and Development. 3.05. Progress in the Understanding of Traditional and Nontraditional Molecular Interactions.

References

1. Motulsky, H.; Mahan, L. The Kinetics of Competitive Radioligand Binding Predicted by the Law of Mass Action. *Mol. Pharmacol.* **1983,** *25,* 1–9.
2. Schreiber, G. Analysis of Ligand Binding to Receptors by Competition Kinetics. *J. Biol. Chem.* **1985,** *206,* 8789–8794.
3. Chang, A.; et al. Rational Optimization of Drug-Target Residence Time: Insights from Inhibitor Binding to the *Staphylococcus aureus* FabI Enzyme-Product Complex. *Biochemistry* **2013,** *52,* 4217–4228.
4. Copeland, R.; et al. Drug-Target Residence Time and its Implications for Lead Optimization. *Nat. Rev. Drug Discov.* **2006,** *5,* 730–739.
5. Tummino, P.; Copeland, R. Residence Time of Receptor-Ligand Complexes and its Effect on Biological Function. *Biochemistry* **2008,** *47,* 5481–5492.
6. Zhang, R.; Monsma, F. Binding Kinetics and Mechanism of Action: Toward the Discovery and Development of Better and Best in Class Drugs. *Expert Opin. Drug Discovery* **2010,** *5,* 1023–1029.
7. Copeland, R. The Drug–Target Residence Time Model: A 10-Year Retrospective. *Nat. Rev. Drug Discov.* **2016,** *15,* 87–95.
8. Zhang, R.; et al. Moderate to High Throughput in vitro Binding Kinetics for Drug Discovery. *Front. Biosci. (Schol. Ed.)* **2016,** *8,* 278–297.
9. Lipinski, C. Drug Like Properties and the Causes of Poor Solubility and Poor Permeability. *J. Pharmacol. Toxicol. Methods* **2000,** *44,* 235–249.
10. Leeson, P.; Springthorpe, B. The Influence of Drug-Like Concepts on Decision-Making in Medicinal Chemistry. *Nat. Rev. Drug Discov.* **2007,** *6,* 881–890.
11. Hopkins, A.; et al. Ligand Efficiency: A Useful Metric for Lead Selection. *Drug Discov. Today* **2004,** *9,* 430–433.
12. Ladbury, J. Enthalpic Efficiency and the Role of Thermodynamic Data in Drug Development: Possibility or a Pipeline Dream!. *Eur. Pharm. Rev.* **2007,** *12,* 59–62.
13. Csermely, P.; et al. Induced Fit, Conformational Selection and Independent Dynamic Segments: An Extended View of Binding Events. *Trends Biochem. Sci.* **2010,** *35,* 539–546.
14. Klebe, G. Applying Thermodynamic Profiling in Lead Finding and Optimization. *Nat. Rev. Drug Discov.* **2015,** *14,* 95–110.
15. Atwell, S.; et al. A Novel Mode of Gleevec Binding is Revealed by the Structure of Spleen Tyrosine Kinase. *J. Biol. Chem.* **2004,** *279,* 55827–55832.
16. Nagar, B.; et al. Crystal Structures of the Kinase Domain of c-Abl in Complex With the Small Molecule Inhibitors PD173955 and Imatinib (STI-571). *Cancer Res.* **2002,** *62,* 4236–4243.
17. Cusack, K.; et al. Design Strategies to Address Kinetics of Drug Binding and Residence Time. *Bioorg. Med. Chem. Lett.* **2015,** *25,* 2019–2027.
18. Agafonov, R.; et al. Energetic Dissection of Gleevec's Selectivity Toward Human Tyrosine Kinases. *Nat. Struct. Mol. Biol.* **2014,** *21,* 848–853.
19. Wilson, C.; et al. Using Ancient Protein Kinases to Unravel a Modern Cancer drug's Mechanism. *Science* **2015,** *347,* 882–886.
20. Tse, A.; Verkhivker, G. Molecular Determinants Underlying Binding Specificities of the ABL Kinase Inhibitors: Combining Alanine Scanning of Binding hot Spots With Network Analysis of Residue Interactions and Coevolution. *PLoS One* **2015,** *10,* e0130203.
21. Lange, O.; et al. Recognition Dynamics up to Microseconds Revealed from an RDC-Derived Ubiquitin Ensemble in Solution. *Science* **2008,** *320,* 1471–1475.
22. Selinsky, B. Structural Analysis of NSAID Binding by Prostaglandin H_2 Synthase: Time-Dependent and Time Independent Inhibitors Elicit Identical Enzyme Conformations. *Biochemistry* **2001,** *40,* 5172–5180.
23. Radić, Z.; et al. Electrostatic Influence on the Kinetics of Ligand Binding to Acetylcholinesterase. Distinctions Between Active Center Ligands and Fasciculin. *J. Biol. Chem.* **1987,** *272,* 23265–23277.
24. Schmidtke, P.; et al. Shielded Hydrogen Bonds as Structural Determinants of Binding Kinetics: Application in Drug Design. *J. Am. Chem. Soc.* **2011,** *133,* 18903–18910.
25. Laciurciere, Y.; Asma, R. A Comparison of the Efficacy and Duration of Action of Candesartan Cilexetil and Losartan as Assessed by Clinic and Ambulatory Blood Pressure After a Missed Dose in Truly Hypertensive Patients. *Am. J. Hypertens.* **1999,** *12,* 1181–1187.
26. Vanderheyden, P.; et al. Angiotension II Type 1 Receptor Antagonists: Why Do Some of Them Produce Insurmountable Inhibition? *Biochem. Pharmacol.* **2000,** *60,* 1557–1563.
27. Lu, H.; Tonge, P. Drug-Target Residence Time: Critical Information for Lead Optimization. *Curr. Opin. Chem. Biol.* **2010,** *14,* 467–474.
28. Moulton, B.; Fryer, A. Muscarinic Receptor Antagonists, from Folklore to Pharmacology; Finding Drugs That Actually Work in Asthma and COPD. *Br. J. Pharmacol.* **2011,** *163,* 44–52.
29. Jones, P. Long-Acting Muscarinic Antagonists for the Prevention of Exacerbations of Chronic Obstructive Pulmonary Disease. *Ther. Adv. Respir. Dis.* **2015,** *9,* 84–96.
30. Gavalda, A.; et al. The *in vitro* and *in vivo* Profile of Aclidinium Bromide in Comparison With Glycopyrronium Bromide. *Pulm. Pharmacol. Ther.* **2014,** *28,* 114–121.
31. Sykes, D.; et al. The Influence of Receptor Kinetics on the Onset and Duration of Action and the Therapeutic Index of NVA237 and Tiotropium. *J. Pharmacol. Exp. Ther.* **2012,** *343,* 520–528.
32. Trifilieff, A.; et al. Comparing the Cardiovascular Therapeutic Indices of Glycopyrronium and Tiotropium in an Integrated Rat Pharmacokinetic, Pharmacodynamic and Safety Model. *Toxicol. Appl. Pharmacol.* **2015,** *287,* 9–16.
33. Lewandowicz, A.; et al. Achieving the Ultimate Physiological Goal in Transition State Analogue Inhibitors for Purine Nucleoside Phosphorylase. *J. Biol. Chem.* **2003,** *278,* 31465–31468.
34. Cumming, J.; et al. Potential Strategies for Increasing Drug-Discovery Productivity. *Future Med. Chem.* **2014,** *6,* 515–527.
35. Barf, T.; Kaptein, A. Irreversible Protein Kinase Inhibitors: Balancing the Benefits and Risks. *J. Med. Chem.* **2012,** *55,* 6243–6262.
36. Schotte, F.; et al. Picosecond Time-Resolved X-ray Crystallography: Probing Protein Function in Real Time. *J. Struct. Biol.* **2004,** *147,* 235–246.
37. Vallurupalli, P.; et al. Structures of Invisible, Excited Protein States by Relaxation Dispersion NMR Spectroscopy. *Proc. Natl. Acad. Sci. U. S. A.* **2008,** *105,* 11766–11771.
38. Pan, A.; et al. Molecular Determinants of Drug-Receptor Binding Kinetics. *Drug Discov. Today* **2013,** *18,* 667–673.
39. Fleck, B.; et al. Binding Kinetics Redefine the Antagonist Pharmacology of the Corticotropin-Releasing Factor Type 1 Receptor. *J. Pharmacol. Exp. Ther.* **2012,** *34,* 518–531.
40. Finlay, M.; et al. Discovery of a Potent and Selective EGFR Inhibitor (AZD9291) of Both Sensitizing and T790M Resistance Mutations That Spares the Wild Type Form of the Receptor. *J. Med. Chem.* **2014,** *57,* 8249–8267.
41. Ostrem, J.; et al. K-Ras(G12C) Inhibitors Allosterically Control GTP Affinity and Effector Interactions. *Nature* **2013,** *503,* 548–551.
42. Bradshaw, J.; et al. Prolonged and Tunable Residence Time Using Reversible Covalent Kinase Inhibitors. *Nat. Chem. Biol.* **2015,** *11,* 525–531.
43. Dahl, G.; Akerud, T. Pharmacokinetics and the Drug-Target Residence Time Concept. *Drug Discov. Today* **2013,** *18,* 697–707.
44. de Witte, W.; et al. Mechanistic Models Enable the Rational use of In Vitro Drug-Target Binding Kinetics for Better Drug Effects in Patients. *Expert Opin. Drug Discov.* **2015,** *11.*
45. Schoop, A.; Dey, F. On-Rate Based Optimization of Structure–Kinetic Relationship – Surfing the Kinetic Map. *Drug Discov. Today Technol.* **2015,** *17,* 9–15.
46. Swinney, D.; et al. The Role of Binding Kinetics in GPCR Drug Discovery. *Curr. Top. Med. Chem.* **2015,** *15,* 2504–2522.
47. Holdgate, G.; et al. The Application of Isothermal Titration Calorimetry to Drug Discovery. In *Biocalorimetry 2: Applications of Calorimetry in the Biological Sciences;* Ladbury, J., Doyle, M., Eds.; Wiley, 2004.
48. Wiseman, T.; et al. Rapid Measurement of Binding Constants and Heats of Binding Using a New Titration Calorimeter. *Anal. Biochem.* **1989,** *179,* 131–137.
49. Chodera, J.; Mobley, D. Entropy-Enthalpy Compensation: Role and Ramifications in Biomolecular Ligand Recognition and Design. *Annu. Rev. Biophys.* **2013,** *42,* 121–142.
50. Lafont, V.; et al. Compensating Enthalpic and Entropic Changes Hinder Binding Affinity Optimization. *Chem. Biol. Drug Des.* **2007,** *69,* 413–422.
51. Ward, W.; Holdgate, G. Isothermal Titration Calorimetry in Drug Discovery. *Prog. Med. Chem.* **2001,** *38,* 309–376.
52. Zidek, L.; et al. Increased Protein Backbone Conformational Entropy Upon Hydrophobic Ligand Binding. *Nat. Struct. Biol.* **1999,** *6* (12), 1118–1121.
53. Breiten, B.; et al. Water Networks Contribute to Enthalpy/Entropy Compensation in Protein-Ligand Binding. *J. Am. Chem. Soc.* **2013,** *135* (41), 15579–15584.
54. Fenley, A.; et al. Entropy –Enthalpy Transduction Caused by Conformational Shifts can Obscure the Forces Driving Protein-Ligand Binding. *PNAS* **2012,** *109* (49), 20006–20011.
55. Bronowska, A. Thermodynamics of Ligand-Protein Interactions: Implications for Molecular Design. In *Thermodynamics - Interaction Studies - Solids, Liquids and Gases;* Carlos Moreno Pirajáan, J., Ed.; 2011; ISBN 978-953-307-563-1; 2011.

56. Huggins, D. Quantifying the Entropy of Binding for Water Molecules in Protein Cavities by Computing Correlations. *Biophys. J.* **2015,** *108,* 928–936.
57. Snyder, P.; et al. Mechanism of the Hydrophobic Effect in the Biomolecular Recognition of Arylsulfonamides by Carbonic Anhydrase. *Proc. Natl. Acad. Sci. U. S. A.* **2011,** *108,* 17889–17894.
58. Biela, A.; et al. Dissecting the Hydrophobic Effect on the Molecular Level: The Role of Water, Enthalpy, and Entropy in Ligand Binding to Thermolysin. *Angew. Chem. Int. Ed.* **2013,** *52,* 1822–1828.
59. Young, T.; et al. Motifs for Molecular Recognition Exploiting Hydrophobic Enclosure in Protein–Ligand Binding. *Proc. Natl. Acad. Sci. U. S. A.* **2007,** *104,* 808–813.
60. Perlstein, R.; et al. New Hypotheses About the Structure–Function of Proprotein Convertase Subtilisin/Kexin Type 9: Analysis of the Epidermal Growth Factor-Like Repeat A Docking Site Using WaterMap. *Proteins* **2010,** *78,* 2571–2586.
61. Ross, G.; et al. Rapid and Accurate Prediction and Scoring of Water Molecules in Protein Binding Sites. *PLoS One* **2012,** *7* (3), e32036.
62. Duff, M.; Howell, E. Thermodynamics and Solvent Linkage of Macromolecule-Ligand Interactions. *Methods* **2015,** *76,* 51–60.
63. Kawasaki, Y.; Freire, E. Finding a Better Path to Drug Selectivity. *Drug Discov. Today* **2011,** *16,* 985–990.
64. Bertini, I.; et al. Exploring the Subtleties of Drug-Receptor Interactions: The Case of Matrix Metalloproteinases. *J. Am. Chem. Soc.* **2007,** *129,* 2466–2475.
65. Siles, R.; et al. Synthesis and Biochemical Evaluation of Triazole/Tetrazole-Containing Sulfonamides Against Thrombin and Related Serine Proteases. *Bioorg. Med. Chem. Lett.* **2011,** *21,* 5305–5309.
66. Kawasaki, Y.; et al. Thermodynamic Evaluation of the Binding of Bisphosphonates to Human Farnesyl Pyrophosphate Synthase. *Chem. Pharm. Bull. (Tokyo)* **2014,** *62,* 77–83.
67. Freire, E. Do Enthalpy and Entropy Distinguish First in Class From Best in Class? *Drug Discov. Today* **2008,** *13,* 869–874.
68. Ohtaka, H.; Freire, E. Adaptive Inhibitors of the HIV-1 Protease. *Prog. Biophys. Mol. Biol.* **2005,** *88,* 193–208.
69. Ferenczy, G.; Keseru, G. Thermodynamic Guided Lead Discovery and Optimization. *Drug Discov. Today* **2010,** *15,* 919–932.
70. Olsson, T.; et al. The Thermodynamics of Protein-Ligand Interaction and Solvation: Insights for Ligand Design. *J. Mol. Biol.* **2008,** *384,* 1002–1017.
71. Geschwinder, S.; et al. Ligand Binding Thermodynamics in Drug Discovery: Still a Hot Tip? *J. Med. Chem.* **2015,** *58,* 6321–6335.
72. Ferenczy, G.; Keseru, G. Thermodynamics of Fragment Binding. *J. Chem. Inf. Model.* **2012,** *52* (4), 1039–1045.
73. Edink, E.; et al. Fragment Growing Induces Conformational Changes in Acetylcholine-Binding Protein: A Structural and Thermodynamic Analysis. *J. Am. Chem. Soc.* **2011,** *133,* 5363–5371.
74. Ichihara, O.; et al. The Importance of Hydration Thermodynamics in Fragment-to-Lead Optimisation. *ChemMedChem* **2014,** *9,* 2708–2717.
75. Turnbull, W.; Daranas, A. On the Value of c: Can Low Affinity Systems be Studied by Isothermal Titration Calorimetry. *J. Am. Chem. Soc.* **2003,** *125,* 14859–14866.
76. Khalifah, R.; et al. Thermodynamics of Binding of the CO2-Competitive Inhibitor Imidazole and Related Compounds to Human Carbonic Anhydrase I: An Isothermal Titration Calorimetry Approach to Studying Weak Binding by Displacement With Strong Inhibitors. *Biochemistry* **1993,** *32,* 3058–3066.
77. Sigurskjold, B.; et al. Thermodynamics of Ligand Binding to the Starch-Binding Domain of Glucoamylase from Aspergillus Niger. *Eur. J. Biochem.* **1994,** *225,* 133–141.
78. Ruhmann, E.; et al. Thermodynamic Signatures of Fragment Binding: Validation of Direct Versus Displacement ITC Titrations. *Biochim. Biophys. Acta* **2015,** *1850,* 647–656.
79. Kobe, A.; et al. Incorporation of Rapid Thermodynamic Data in Fragment-Based Drug Discovery. *J. Med. Chem.* **2013,** *56,* 2155–2159.
80. Lipinksi, C. Experimental and Computational Approaches to Estimate Solubility and Permeability in Drug Discovery and Development Settings. *Adv. Drug. Deliv. Rev.* **1997,** *23,* 3–25.
81. Gleeson, M. Generation of a Set of Simple, Interpretable ADMET Rules of Thumb. *J. Med. Chem.* **2008,** *51,* 817–834.
82. Kuntz, I.; et al. The Maximal Affinity of Ligands. *Proc. Natl. Acad. Sci.* **1999,** *96,* 9997–10002.
83. Hopkins, A.; et al. Ligand Efficiency: A Useful Metric for Lead Selection. *Drug Discov. Today* **2004,** *9,* 430–431.
84. Congreve, M.; et al. A 'Rule of Three' for Fragment-Based Lead Discovery? *Drug Discov. Today* **2003,** *8,* 876–877.
85. Ladbury, J. Enthalpic Efficiency and the Role of Thermodynamic Data in Drug Development: Possibility or a Pipeline Dream!. *Eur. Pharm. Rev.* **2007,** *12,* 59–62.
86. Ferenczy, G.; Keseru, G. Enthalpic Efficiency of Ligand Binding. *J. Chem. Inf. Model.* **2010,** *50,* 1536–1541.
87. Hann, M.; Keseru, G. Finding the Sweet Spot: The Role of Nature and Nurture in Medicinal Chemistry. *Nat. Rev. Drug Discov.* **2012,** *11* (5), 355–365.
88. Holdgate, G.; Gill, A. Kinetic Efficiency: The Missing Metric for Enhancing Compound Quality? *Drug Discov. Today* **2011,** *16,* 910–913.
89. Kenny, P.; et al. Ligand Efficiency Metrics Considered Harmful. *J. Comput. Aided Mol. Des.* **2014,** *28,* 699–710.
90. Shultz, M. Improving the Plausibility of Success With Inefficient Metrics. *ACS Med. Chem. Lett.* **2013,** *5,* 2–5.
91. Reynolds, C. Ligand Efficiency Metrics: Why All the Fuss? *Future Med. Chem.* **2015,** *7* (11), 1363–1365.
92. Hopkins, A.; et al. The Role of Ligand Efficiency Metrics in Drug Discovery. *Nat. Rev.* **2015,** *13,* 105–121.

Further Reading

Rich, R. Higher-Throughput, Label-Free, Real-Time Molecular Interaction Analysis. *Anal. Biochem.* **2007,** *361,* 1–6.

Bocquet, N.; et al. Real-Time Monitoring of Binding Events on a Thermostabilized Human A2A Receptor Embedded in a Lipid Bilayer by Surface Plasmon Resonance. *Biochim. Biophys. Acta* **2015,** *1848,* 1224–1233.

Concepcion, J.; et al. Label-Free Detection of Biomolecular Interactions Using BioLayer Interferometry for Kinetic Characterization. *Comb. Chem. High Throughput Screen.* **2009,** *12,* 791–800.

Knezevic, J.; et al. Quantitation of Affinity, Avidity and Binding Kinetics of Protein Analytes With a Dynamically Switchable Biosurface. *J. Am. Chem. Soc.* **2012,** *134,* 15225–15228.

Fang, Y.; et al. Resonant Waveguide Grating Biosensor for Whole-Cell GPCR Assays. *Methods Mol. Biol.* **2009,** *552,* 239–252.

Zepperitz, C.; et al. MS-Binding Assays: Kinetic, Saturation, and Competitive Experiments Based on Quantitation of Bound Marker as Exemplified by the GABA Transporter mGAT1. *ChemMedChem* **2006,** *1,* 208–217.

Steuber, H.; et al. Merging the Binding Sites of Aldose and Aldehyde Reductase for Detection of Inhibitor Selectivity-Determining Features. *J. Mol. Biol.* **2008,** *379,* 991–1016.

Relevant Websites

http://www.k4dd.eu/—Kinetics for Drug Discovery.
http://www.sprpages.nl/—SPRpages.
https://www.bindingdb.org/bind/index.jsp—The Binding Database.

2.08 Fragment-Based Drug Design: Strategic Advances and Lessons Learned

H Chen, Fuzhou University, Fuzhou, Fujian, China; and University of Texas Medical Branch, Galveston, Texas, United States
X Zhou and Y Gao, Fuzhou University, Fuzhou, Fujian, China
H Chen and J Zhou, University of Texas Medical Branch, Galveston, Texas, United States

© 2017 Elsevier Ltd. All rights reserved.

2.08.1	**Introduction**	213
2.08.2	**Fragment-Based Screening (FBS)**	213
2.08.2.1	Nuclear Magnetic Resonance	213
2.08.2.2	X-ray Crystallography	213
2.08.2.3	Surface Plasmon Resonance	214
2.08.2.4	Mass Spectrometry	214
2.08.2.5	Thermal Shift Assay (TSA)	214
2.08.2.6	Isothermal Titration Calorimetry	214
2.08.2.7	High Concentration Screening	214
2.08.2.8	Virtual Screening	215
2.08.2.9	Combination Approaches	215
2.08.3	**From Fragments to Clinical Drug Candidates**	215
2.08.3.1	Ligand Efficiency	215
2.08.3.2	Fragment Elaboration	215
2.08.3.3	Medicinal & Synthetic Chemistry Rules	217
2.08.4	**Success Stories in FBDD**	217
2.08.4.1	Case 1: Vemurafenib (**PLX-4032**), FDA Approved Drug	217
2.08.4.2	Case 2: **ABT-199** (Venetoclax), Phase III	217
2.08.4.3	Case 3: **AT13387**, Phase II	220
2.08.4.4	Case 4: **AT9283**, Phase II	221
2.08.4.5	Case 5: **AT7519**, Phase II	221
2.08.4.6	Case 6: **NVP-AUY922**, Phase II	222
2.08.4.7	Case 7: Bruton's Tyrosine Kinase Inhibitor	223
2.08.4.8	Case 8: RSK2 Inhibitor RMM-46	225
2.08.4.9	Case 9: HCV NS3 Protein Modulator	225
2.08.4.10	Case 10: Dual pan-RET/VEGFR2 Kinase Inhibitors	226
2.08.5	**Lessons Learned From Success Stories in FBDD**	227
2.08.5.1	Fragment Identification	228
2.08.5.2	Fragment Elaboration	228
2.08.5.3	Drug Candidate Selection	228
2.08.6	**Conclusion and Outlook**	228
Acknowledgments		229
References		229

Abbreviations

ADMET Absorption, distribution, metabolism, excretion, and toxicity
Asp-Phe-Gly Aspartic acid, phenyl alanine, glycine
Btk Bruton's tyrosine kinase
DFG Region of conserved amino acids
FBDD Fragment-based drug discovery
FBS Fragment-based screening
FDA Food and drug administration
HCS High concentration screening
Hsp90 Heat-shock protein 90
HTS High-throughput screening
ITC Isothermal titration calorimetry
K_d Dissociation constant
K_i Inhibition constant
LE Ligand efficiency
LLE Lipophilic LE
MS Mass spectrometry
NMR Nuclear magnetic resonance
PK Pharmacokinetic
PPB Plasma protein binding
PPI Protein–protein interaction
RET Rearranged during transfection
RO3 Rule of three
RSK2 Ribosomal S6 kinase
SPR Surface plasmon resonance
TSA Thermal shift assay

VEGFR2 Vascular endothelial growth factor receptor 2
VS Virtual screening
XRC X-ray crystallography

2.08.1 Introduction

The identification of new chemical leads is a key step for the innovation and success in small-molecule drug design in drug discovery programs.[1] Over the past two decades, the pharmaceutical industry has committed to high-throughput screening (HTS) approaches through screening large libraries of compounds (up to 10^6) for lead discovery.[2–4] However, most HTS libraries tend to have a limited coverage of chemical space and structural diversity, leading to the difficulty in discovering ideal hit leads for drug development in this "finding a needle in a haystack" game.[5,6] Moreover, unfavorable ADMET (absorption, distribution, metabolism, excretion, and toxicity) drug properties and potential ambiguity about how best to increase potency are also obstacles for subsequent hit-to-lead development.[7] Obviously, the inherent limitations of HTS result in high attrition rates in drug discovery. Hence, there is an urgent need for new lead generation strategies to address such issues.[8]

With the scientific and technological advances in screening fragments, fragment-based drug discovery (FBDD) has emerged as an alternative to HTS in hit identification and hit-to-lead discovery.[9,10] Taking advantages of both random screening and structure-based drug design, FBDD constructs novel lead structures from weak-affinity fragments. Fragments are typically "rule of three" (RO3) compliant: MW $\leq$ 300 Da, LogP $\leq$ 3, and hydrogen bond acceptors/donors $\leq$ 3.[11] These properties allow a wider exploration of chemical space compared with larger lead-like compounds and this FBDD strategy has demonstrated a higher binding efficiency, higher hit rate, and more effective optimization capability relative to HTS. Notably, this approach has already yielded one marketed drug (ie, vemurafenib) within 6 years from concept to FDA approval, and a dozen of preclinical and clinical drug candidates in development to date.[12]

2.08.2 Fragment-Based Screening (FBS)

To date, an increasing number of commercial companies, such as ChemBridge, ChemDiv, Emerald Bio, and Enamine, provide a variety of well-defined fragment libraries for screening of new hits. Since the identification of fragments is the starting point for FBDD, selection of a suitable fragment-based screening assay is particularly critical.[13] However, fragments inherently have relatively weak binding affinities (medium μM to low mM range), thereby requiring highly sensitive techniques. The past decade has witnessed a huge development of FBS techniques, providing us with a wide range of screening methods for hit and hit-to-lead identification.[14] Therefore, the ability to choose the most suitable FBS techniques for a specific drug discovery program is especially important. To this end, it is imperative to understand the characteristics of each FBS approach, including its advantages and disadvantages.[15] Herein, the biophysical techniques, including nuclear magnetic resonance (NMR), X-ray crystallography (XRC), surface plasmon resonance (SPR), mass spectrometry (MS), thermal shift assay (TSA), and isothermal titration calorimetry (ITC), as well as other screening methods such as high concentration screening (HCS) and virtual screening (VS), are enumerated further; While their advantages and disadvantages are also discussed.

2.08.2.1 Nuclear Magnetic Resonance

NMR is one of the widely used approaches for FBS, which is able to detect very weak interactions (mM range) between a target and a fragment with unmatched sensitivity.[16–18] The various NMR techniques currently available for FBDD can be divided into two major groups: target-based and ligand-based approaches.[19] Target-based NMR monitors signal changes (mainly chemical shift) in isotopically (^{15}N or ^{13}C) labeled target protein upon ligand binding.[20] Other than the high-affinity fragments identified, the binding site can also be precisely localized and partially characterized with this method.[21] However, it is only applicable for proteins with high purity, suitable solubility, and modest molecular weight (typically smaller than 30–40 kDa).[22,23] In addition, it also requires large amounts of protein and a relatively long acquisition time.[24] Ligand-based NMR detects NMR parameters' changes in ligand upon binding to a target using relatively little protein. Moreover, ligand-based NMR allows rapid fragment identification, with target protein not isotopically labeled and its molecular mass practically unlimited.[25] However, ligand-based NMR is not able to provide the detailed information about the actual binding pocket. Foremost, once the fragment binds tightly with the target protein, there exist false negatives.[26]

2.08.2.2 X-ray Crystallography

As a primary screening method in construction of fragment library, XRC can provide detailed information regarding protein–ligand interactions like NMR spectroscopy.[27–29] This approach includes the following steps: The soaking of crystals in a solution containing fragments; X-ray data collection and processing; ligand identification by analyzing electron density maps. While XRC possesses a lot

of advantages compared to other FBS approaches, such as avoiding false positives, applicability to large proteins, and more importantly, providing detailed binding information with high resolution, there are also some disadvantages. Firstly, false negatives may occur because of crystal packing that would hamper fragments from entering into the protein crystal. Secondly, the throughput is low, mainly owning to the requirement for a crystallized protein. Thirdly, it is not feasible to quantitatively assess the binding affinity, due to the lack of inhibition data. Fourthly, despite recent several techniques and tools are available to improve crystallizability, crystallization of difficult targets remains a challenge, making screening by XRC sometimes impractical. Fifthly, due to poor crystallizability, resolution may be a significant problem in structural determination. In addition to the aforementioned shortcomings, low affinity requires high fragment concentrations, thereby leading to potential solubility issues.

2.08.2.3 Surface Plasmon Resonance

SPR, once known as a powerful and versatile tool investigating biomolecular interactions, is now emerging as a popular method for primary screening in FBDD.[30–32] In general, fragments are allowed to flow past a biosensor (usually a thin gold film) onto which a target protein is immobilized. Then the changes in the refractive index of the biosensor are observed upon ligand binding. Intrinsic advantages and recent technical advances, such as multiple biosensor channels, have made SPR a rapid, efficient, high-throughput, and cost-effective methodology for FBS. Compared to other biophysical and biochemical FBS methods, SPR has the following merits: Consuming less protein (as little as 25–50 μg) while keeping a high sensitivity to fragments with molecular weight as low as 100 Da; capable of providing kinetic and thermodynamic information of ligand binding, which is useful for later hit-to-lead optimization.[33] Despite these advantages, more attention should be paid to implementing all necessary steps, including assay design, data analysis, and interpretation to avoid false negatives.

2.08.2.4 Mass Spectrometry

More recently, MS has extended its application in fragment identification as a highly sensitive and accurate screening tool.[34–36] The fragments are detected with MS mainly in two approaches: Electrospray ionization MS and tethering, which detects noncovalent and covalent (disulfide bond) binding between fragments and target protein, respectively.[37,38] Based on the mass-to-charge ratio and abundance of a protein–ligand complex, it is possible to directly determine the fragment as well as its binding affinity and stoichiometry. In addition, MS requires small amounts of protein and fragments with significantly reduced constraints on purity, and there is no need to label them. Meanwhile, MS approach is rapid and automatable, indicating a very high screening capacity. These combined features provide significant advantages over other fragment screening methods.[39] However, it is worth noting that MS is unable to provide information concerning ligand-binding mode, which constitutes a major disadvantage of MS.

2.08.2.5 Thermal Shift Assay (TSA)

TSA is a thermal-denaturation assay to measure the thermal stability of proteins. It is a relatively high-throughput, inexpensive, and rapid method for fragment identification.[40] As binding to protein can enhance the stability of the protein, the unfolding temperature (also called melting temperature, T_m) of ligand-binding protein is higher than the nonligand binding, which may cause a temperature shift (ΔT_m) between them. Moreover, only those ligands with $\Delta T_m \geq 0.5°C$ are considered to be hits.[41] Based on this simple principle, TSA is able to distinguish hits from fragments requiring significantly reduced degree of technical expertise compared to previously described FS approaches. Meanwhile, TSA consumes small quantities of proteins, there is no need to know the function of the target protein, and it does not involve any target modification and separation step.[42] However, there also exist limitations and drawbacks with this method. Firstly, problems regarding fragment solubility and aggregation may be caused due to the high concentrations of fragments required for screening. In addition, it is difficult to detect very weakly binding fragments by TSA.[43] Moreover, the screening results may be false negatives or positives. Multiple binding events may occur and thereby generate either false increases or false decreases in T_m, indicating that the screening results determined by ΔT_m might be incorrect.

2.08.2.6 Isothermal Titration Calorimetry

ITC has been applied for FBS by directly measuring the heat change when a ligand binds to a target protein.[44] From these precise measurements, the binding affinity (K_a), stoichiometry (n), as well as the enthalpy ($\triangle H$) and entropy ($\triangle S$) changes of the intermolecular interaction can be calculated or determined. The parameters acquired can provide information about both binding events and structural features, which is quite useful for fragment identification and lead optimization.[45] Nonetheless, there exist some severe limitations with ITC, such as low throughput and resolution, high protein and ligand consumption. ITC is thus more suitable for secondary screening instead of primary screening, particularly for screening of large compound libraries.

2.08.2.7 High Concentration Screening

As a simple and rapid method, HCS with biochemical assays has been used for identifying fragments by measuring changes in the activity of a target upon fragment binding.[46] In addition to high-throughput, there are several major advantages with HCS: Various

available techniques for detection, small amounts of protein requirement, and upfront knowledge of biochemical activity. However, drawbacks still exist mainly due to the high concentration of fragment (250–1000 vs. 10–30 μM in HTS) and subsequent large quantities of organic solvents required. These drawbacks include false positives (compound aggregation induced), false negatives (caused by poor solubility of fragments), cell toxicity (induced by large amounts of organic solvents), and target denaturation (ditto). Hence, in order to minimize these potential artifacts, it is necessary to carefully design the screening cascade and preferably apply more sensitive biophysical and biochemical methods especially as initial screenings. The frequently conducted initial biochemical assays include needle screening, MULBITS (Multiple BITS), substrate activity screening, the cell-based functional assay, and combinatorial target-guided ligand assembly. Meanwhile, initial bioassay screens in combination with virtual fragment screening followed by fragment validation using other sensitive biological and biophysical screenings may be an effective approach to the identification of novel starting points for further fragment elaboration.

2.08.2.8 Virtual Screening

VS is a computational technique which uses computer programs to search potential hits from virtual fragment libraries.[47,48] There are two widely used approaches for VS: Structure-based methods (docking) and ligand-based methods.[49] In contrast to experimental methods, VS, on the one hand, is fast and cost-effective, but on the other hand, has relatively low accuracy of predictions and rapid accumulation of errors.[50,51] Notably, ZINC as one of the big free databases offers various fragment-like libraries including target-orientated libraries for VS.

2.08.2.9 Combination Approaches

Nothing is perfect, and FBS approach is no exception. Each FBS approach has its limitations, such as low throughput, high protein consumption, long time-consuming, and so on. Therefore, the combination of two or more screening methods might compensate the limitations of each method and fulfill a win–win situation.[52–54] Generally, the combination of FBS by biophysical screening approaches together with XRC offers more benefits. Several successful drug discovery campaigns, which are discussed here, provide the detailed examples for such combinations. VS may also assist other approaches to yield the potential fragments for further biophysical screening, and the predicted binding modes have attracted more and more interests, especially for the targets which are very difficult to crystallize. In short, experimental or computational predicted structural information about fragments binding to the target enables a more efficient chemical space exploration for further fragment elaboration to establish structure–activity relationships and explore potential drug candidates.

2.08.3 From Fragments to Clinical Drug Candidates

Once the potential fragment hits have been identified and validated, the next step is to improve potency through transforming these fragments into a drug-like lead compound without losing their original binding modes. A broad range of metrics, strategies, and methodologies have been developed to guide the fragment-based hit-to-lead generation.

2.08.3.1 Ligand Efficiency

Ligand efficiency (LE) as a widely applied metric was first proposed for selecting favorable fragments through comparing the values of average binding energy per atom.[55–57] It is simply the free binding energy divided by the number of heavy atoms, $LE = -\Delta G/N = -RT\ln(K_d)/N \approx -RT\ln(IC_{50})/N$. Fragments with higher LE values indicate more potential improvement in binding affinity through structural information guided drug design. Another extending metric based on LE is lipophilic LE, also known as LLE or LiPE ($LLE = pIC_{50}$ – CLogP).[58] Note that utilization of these metrics including the derivation of LE metrics during the overall drug design process to control the balance of molecular size and potency will significantly improve success rates.[59] The derivation of LE metrics is also discussed in more detail by Leeson.[60]

2.08.3.2 Fragment Elaboration

Despite recent numerous biophysical techniques that have benefited FBS and resulted in higher hit rates and more available chemical space, the subsequent chemical optimization of identified fragments toward high-affinity lead compounds remains a crucial aspect for the FBDD approach.[61] In general, as depicted in **Fig. 1**, there are four main strategies for converting low-affinity fragments into a fledged lead structure: (1) Fragment growing (a.k.a. fragment evolution), (2) fragment optimization, (3) fragment linking or merging, and (4) fragment self-assembly.[62,63] The increasing number of candidates progressing into clinical trials has demonstrated that available target structure is beneficial for elaboration of the fragments through utilizing the X-ray crystallographic and/or NMR spectral data.[64] Structural information about the binding mode of the initial fragment is very useful to know how to build up more complex compounds possessing additional interactions with the target. This "evolution" results in development of some tighter binding molecules, which can be used as the second starting points for further chemical optimization.[65]

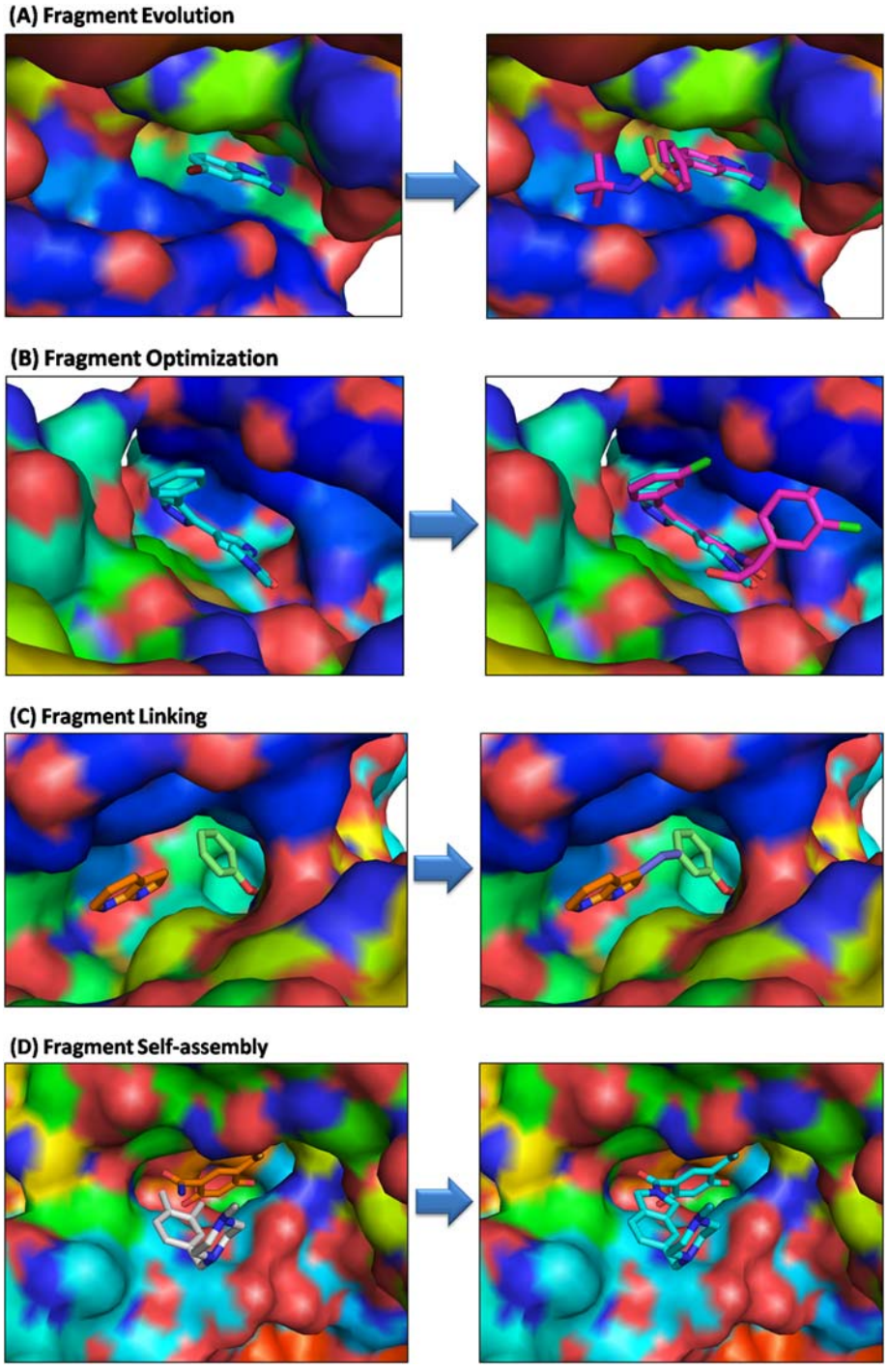

Fig. 1 Four different approaches for converting low-affinity fragments into a fledged lead structure: (A) Fragment evolution; (B) fragment optimization; (C) fragment linking or fragment merging; and (D) fragment self-assembly.

Iterative fragment growing (Fig. 1A) closely resembles traditional medicinal chemistry, and it is thus the most straightforward and preferred strategy in fragment optimization. Generally, functional features are added to adjacent regions of the initial fragment core for access to additional pockets at each chemical modification step during iterative cycles, eventually leading to a desired compound with enhanced potency and favorable pharmacological properties. As mentioned earlier, structural biology is crucial to guide the chemical optimization of initial fragment toward clinical candidate drugs. Fragment optimization (Fig. 1B) is similar to the traditional HTS campaign to maintain the initial scaffold without big chemical modification. Fragment linking (Fig. 1C) involves two identified privileged fragments binding to separate and adjacent pockets are chemically connected via an appropriate

linker in an ideal fashion, resulting in development of a hybrid molecule with significantly improved binding affinity and pharmacokinetic (PK) properties.[66] However, this strategy consumes more experimental time and effort to explore the right linker.[67] Fragment self-assembly (Fig. 1D) is the complementary functional groups of advancing fragments "automatically" assembled in the right places.[68] It should be noted that fragment self-assembly appears not to be the widely applied approach.[69]

2.08.3.3 Medicinal & Synthetic Chemistry Rules

The aforementioned four different approaches for converting identified fragments into potential drug candidates appear to be straightforward. Nevertheless, how to find the correct positions and select reasonable chemical reactions for further successive generations of structural modifications becomes an extremely challenging task. To address this issue, several computer-assisted drug design software programs have been developed to improve drug discovery process. Drug Guru™ as the first web-based software program was established to apply a set of medicinal chemical transformation rules for drug design.[70] AutoGrow, another computational method, combined the strengths of fragment growing and docking algorithms to explore new chemical space more efficiently.[71,72] MedChem Transformations (MCT) is a new algorithm for automatically generating new compounds guided by the set of 206 transformations including functional group addition, linker modification, atom removal, ring addition/modification/removal, and terminal group exchange.[73] Notably, Roughley et al. summarized the most commonly applied reaction types in the pursuit of drug candidates and classified them into 10 major categories.[74] No matter which software programs and reaction types are chosen, medicinal chemistry knowledge on the balance between pharmacological and pharmaceutical properties together with synthetic chemistry knowledge on the large diversity of reactions and functionalities will be beneficial for increasing drug design efficiency and clinical approval success rate.

2.08.4 Success Stories in FBDD

Recently, accumulating evidence indicates that FBDD approaches are widespread in both academia and industry settings, and the aforementioned four predominant strategies have been successfully utilized to generate the optimized drug candidates with enhanced potency as well as improved physicochemical or ADMET properties. A number of successful examples are provided below with more detailed information as to how the starting fragments have been advanced to the optimized drug candidates for human clinical trials or even reaching the market.

2.08.4.1 Case 1: Vemurafenib (PLX-4032), FDA Approved Drug

Vemurafenib (**PLX4032**, Zelboraf) was the first approved fragment-derived drug for the treatment of BRAF-mutant melanoma in Aug. 2011 in the United States.[75,76] Vemurafenib was discovered by Plexxikon Company through utilizing a combination of scaffold- and structure-based drug discovery.[77] Firstly, a library of 20,000 "scaffolds" with molecular mass of 150–350 Daltons was selected and screened at 200 μM against various kinases. Numerous weak and nonselective fragments were identified despite the fact that these small fragments would have been overlooked in a traditional HTS. In order to avoid potential false positives which were apt to occur in early drug screening at high concentrations, cocrystallographic screening was performed as secondary validation at next step. The cocrystals confirmed the binding between initial identified fragments and provided atomic-level details of the binding interactions. Combined with the structural information and criteria for scaffold selection, a nonselective 7-azaindole (initial fragment **1**, Fig. 2A) was selected for further chemical optimization. To address its multiple binding mode within the ATP-binding site and thus weak affinity ($IC_{50} > 200$ μM for Pim-1), additional hydrogen bonding interactions were introduced as shown in Fig. 2B, resulting in an enhanced potency with a single binding mode. Subsequently, a group of 7-azaindole derivatives were synthesized and screened against 17 kinases, such as wild-type and mutated B-RAF, which are present in most of melanomas. Derivatives bearing a difluorophenylsulfonamide motif displayed excellent potency and high selectivity toward mutated B-RAF. Their selectivity was confirmed in a panel assay of 70 kinases, while the anti-B-RAF activity was validated in different melanoma cell lines, including several drug-resistant cell lines. Structure-guided optimization led to the development of **PLX4720**, which exhibits good selectivity in both of enzyme- and cell-based assays ($IC_{50} = 13$ nM for B-RAF V600E, $IC_{50} = 160$ nM for wild-type B-RAF, $IC_{50} > 1$ mM for several other kinases).[77] Addition of a phenyl group afforded **PLX4032** (MW 490; clogP = 4.2), which was chosen over **PLX4720** due to its superior PK properties.[78] Clinical trials confirmed the excellent efficacy of **PLX4032** in patients with metastatic melanoma harboring the V600 B-RAF mutation, consistent with the notion of **PLX4032** as a personalized medicine.[78] The PK properties of vemurafenib prompted its progression into clinical studies that culminated in its approval in 2011.

2.08.4.2 Case 2: ABT-199 (Venetoclax), Phase III

The inhibition of a protein–protein interaction (PPI) is an extremely difficult challenge for medicinal chemists due to general large and flat PPI interfaces.[79] Given the fact that few molecules in existing compound libraries were designed for other PPIs, in contrast to enzyme inhibitors/receptor ligands, etc., traditional HTS fails to offer validated hits for further chemical discovery process.[80] To circumvent this challenge, FBS by the NMR method provides a particularly successful strategy to afford various small-size ligands for further chemical optimization.[81] Abbott Laboratories applied their pioneering developed technology of SAR by NMR[18] to

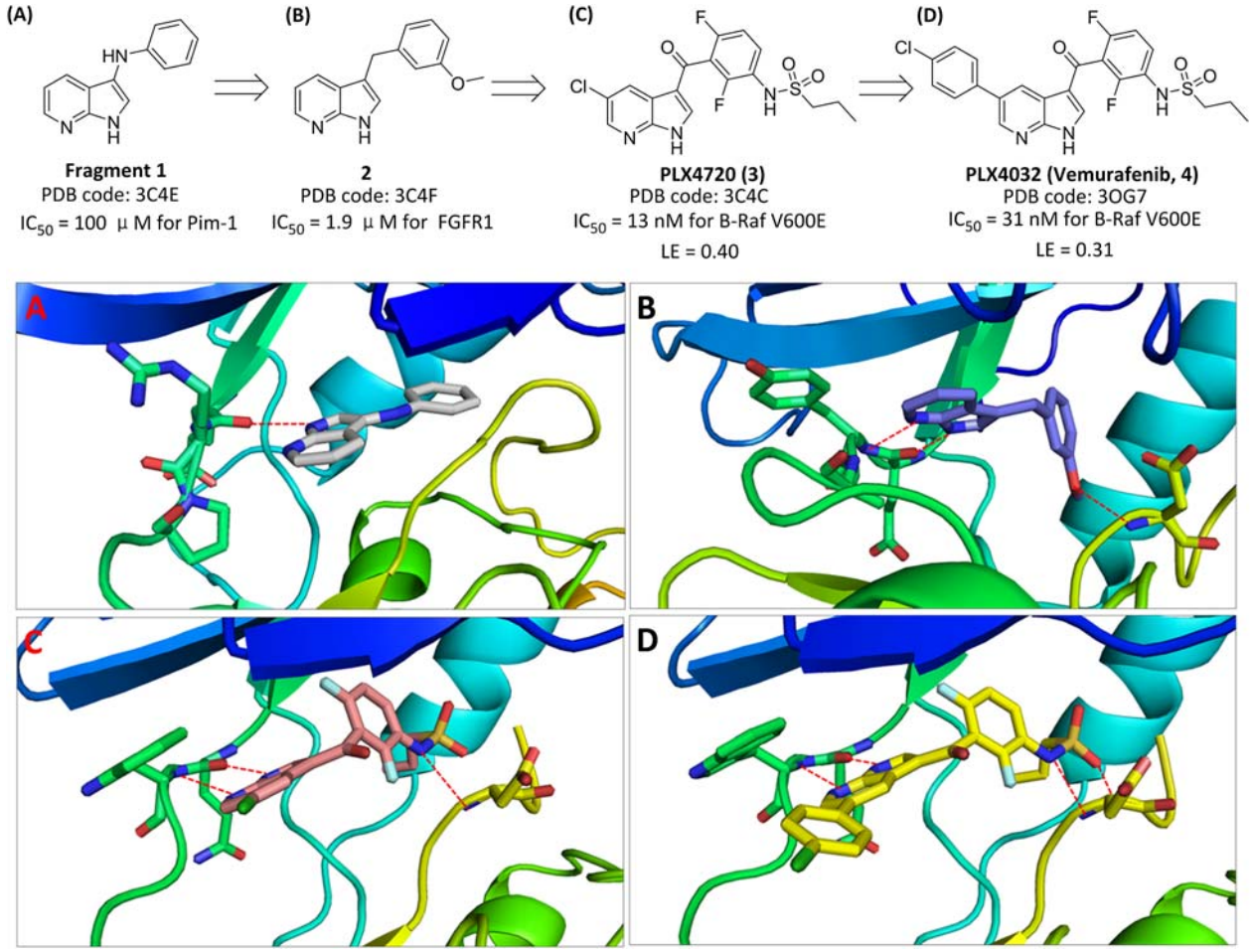

Fig. 2 Progression from initial fragment **1** to the approved drug **PLX-4032** (Vemurafenib). (A) The chemical structure of 3-aminophenyl-7-azaindole (fragment **1**) and its X-ray costructure with Pim-1 kinase. (B) The chemical structure of 3-(3-methoxybenzyl)-7-azaindole (compound **2**) and its X-ray costructure with the kinase domain of FGFR1. (C) The chemical structure of **PLX4720** and its X-ray costructure with B-RAF kinase. (D) The chemical structure of **PLX4032** and its X-ray costructure with B-RAF kinase.

discover potent and selective inhibitors targeting the intracellular Bcl-2 family PPI for the treatment of Bcl-2-dependent hematological cancers. Fig. 3 illustrates the long-lasting drug discovery effort of **ABT-199** as a new orally bioavailable therapeutic agent that is currently being evaluated in clinical trials for the treatment of chronic lymphocytic leukemia patients. Fragment **5**, with a dissociation constant (K_d) of about 300 μM, was identified from a screen of 10,000-compound small fragment library (average MW = 210 Da).[82] NMR-based structural investigation revealed that fragment **5** occupies the center of the hydrophobic pocket of Bcl-x_L, which is the same position as the BAK-binding site. In order to search for molecules binding into the proximal groove, the second screening was performed in the presence of excess fragment **5**. From this second-site ligand screen, fragment **6** with a K_d value of 6000 μM was identified by using a 3500-compound library (average MW = 125 Da).[82] The detailed structural interaction of fragment **5** and fragment **6** with the ternary complex of Bcl-x_L for FBDD was calculated using NMR data for structure-guided design and synthesis. Fragment linking strategy was utilized to merge these two fragments, and parallel chemistry ultimately resulted in development of compound **7** containing a trans-olefin moiety as an appropriate linker.[82] Despite this compound displayed a significant enhancement in potency with an inhibition constant (K_i) of 1.4 μM, further structural characterization from the NMR-based model revealed that the trans-olefin is not the ideal linker for the biaryl fragment and cannot fit effectively into the hydrophobic groove. To overcome this shortcoming, replacement of the carboxylic acid with an acylsulfonamide demonstrated that the sulfonamide represented as a suitable linker to bridge two initial fragments in an optimal fashion. This strategy eventually led to lead compound **8** with 8300-fold improvement in potency ($K_i = 36$ nM).[82] Due to its relatively low solubility and high binding to human serum albumin, further medicinal chemistry resulted in discovery of **ABT-737**, which binds to Bcl-2, Bcl-x_L, and Bcl-w with subnanomolar affinity ($K_i = 0.8$ nM) and exhibits impressive single-agent activity in several murine cancer xenograft models.[83] However, due to low aqueous solubility, it is not orally bioavailable. In order to improve flexible application in the clinical setting, Abbott eventually discovered an orally bioavailable Bcl-2/Bcl-x_L/Bcl-W inhibitor **ABT-263** (navitoclax) with improved pharmacodynamics, which finally entered Phase II clinical trials in patients with lung cancer and hematological

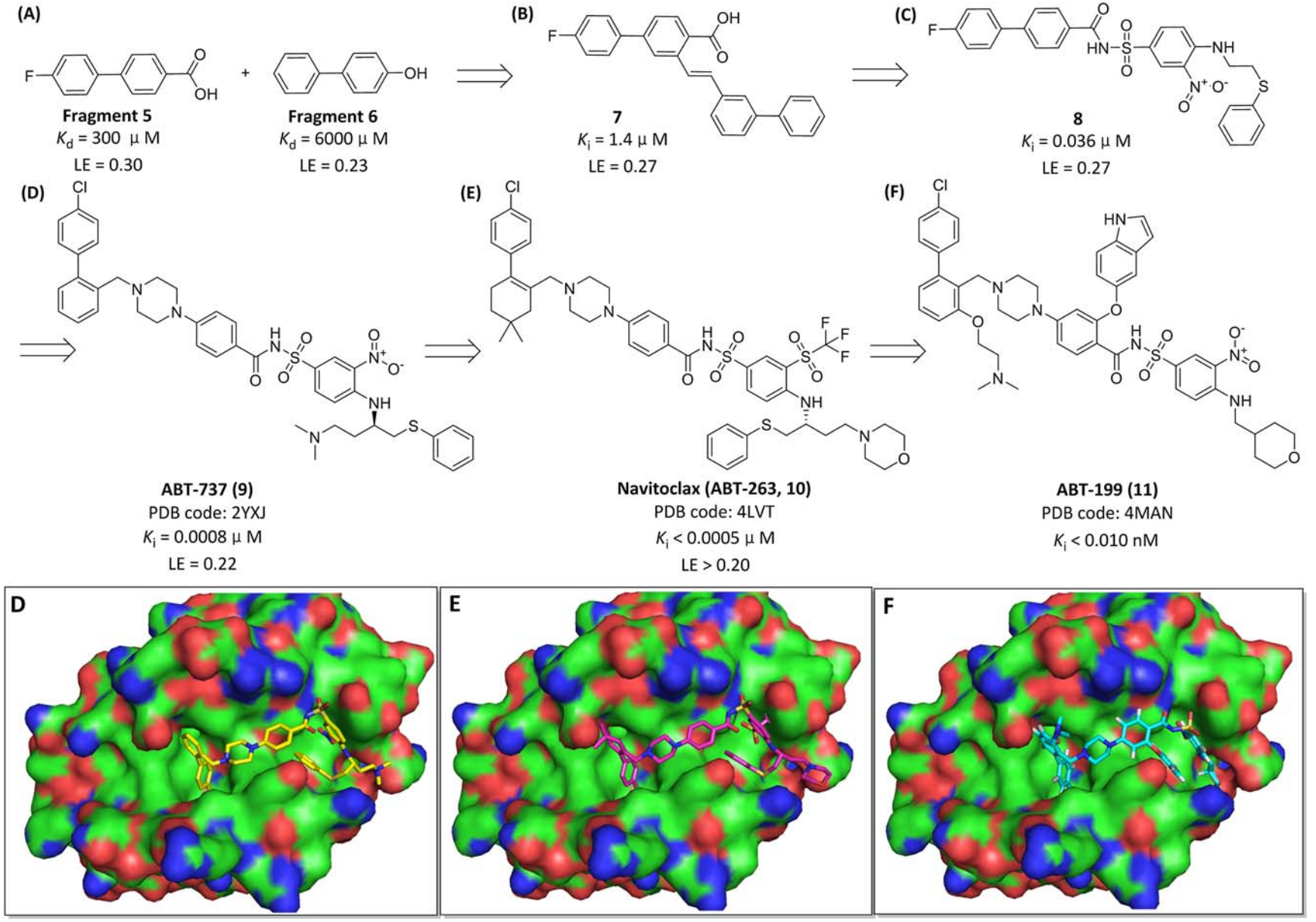

Fig. 3 Progression from initial fragment **5** and fragment **6** to the clinical candidate **ABT-199**. (A) The chemical structures of initial fragment **5** and fragment **6**. (B) The chemical structure of compound **7**. (C) The chemical structure of compound **8**. (D) The chemical structure of **ABT-737** and its X-ray costructure with Bcl-2. (E) The chemical structure of **ABT-263** and its X-ray costructure with Bcl-2. (F) The chemical structure of **ABT-199** and its X-ray costructure with Bcl-2.

malignancies.[84] During clinical investigation, the efficacy of **ABT-263** is limited by thrombocytopenia (platelet loss) caused by inhibition of Bcl-x_L.[85] In order to design a Bcl-2-selective inhibitor to avoid thrombocytopenia, **ABT-263** was cocrystalized with Bcl-2. The binding mode revealed that a tryptophan residue from a neighboring Bcl-2 sat very nearby to **ABT-263**. Addition of an indole near this position led to the discovery of **ABT-199** (venetoclax), which binds Bcl-2 about 10-fold more tightly than **ABT-263** and displays 5000-fold selectivity for Bcl-2 compared to Bcl-x_L.[85]**ABT-199** accesses the BAK-binding pockets without possessing the peptide backbone structure. It is noteworthy that **ABT-199** is more ligand efficient than **ABT-737** and **ABT-263**. Excitingly, **ABT-199** has been advanced into Phase III clinical trials, and very recently, granted breakthrough therapy designation by FDA as an investigational Bcl-2 inhibitor for the treatment of 17p deletion relapsed-refractory CCL (http://www.roche.com).

2.08.4.3 Case 3: AT13387, Phase II

The heat-shock protein 90 (Hsp90) as a popular oncology target is involved in cancer progression and has quickly captured the attention of medicinal chemists. Accumulating clinical advancement of Hsp90 inhibitors also demonstrated the potential therapeutic opportunities for human cancers and neurodegenerative disorders.[86] One of the most impressive drug candidates is **AT13387**, which was discovered by Astex Pharmaceuticals through a successful application of the FBDD approach. The whole drug discovery campaign is very useful for us to learn how to use different techniques and biological data to achieve the final structure with improved pharmaceutical properties. Approximately 1600 selected fragments spanning various chemotypes were firstly screened via water LOGSY (Water-**L**igand **O**bserved via **G**radient **S**pectroscop**Y**) as a primary method for NMR screening.[87] Fragments displaying obvious LOGSY signal were further characterized through competition experiments and high-throughput XRC assay. From this process, 26 cocrystal structures of fragments with Hsp90 were solved and the binding affinities (K_d) were determined by ITC. Among them, fragment **12** with the K_d value of 790 μM and LE of 0.26 was chosen as the starting point for further fragment optimization campaign (Fig. 4). The binding mode revealed that the carbonyl moiety forms an H-bond with the side chain of Thr184 and the methoxy group does not properly fill the proximal lipophilic groove around Met98, Leu107, Phe138,

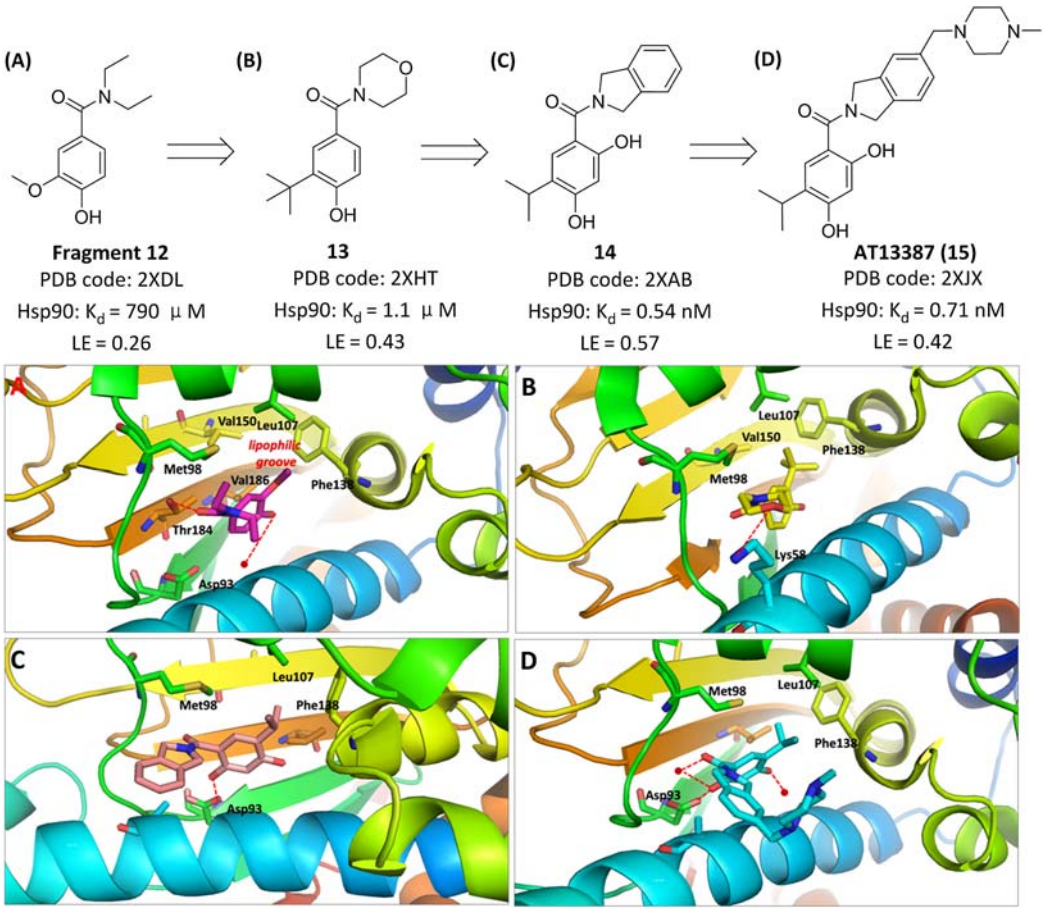

Fig. 4 Progression from initial fragment **12** to the clinical candidate **AT13387**. (A) The chemical structure of fragment **12** and its X-ray costructure with Hsp90. (B) The chemical structure of compound **13** and its X-ray costructure with Hsp90. (C) The chemical structure of compound **14** and its X-ray costructure with Hsp90. (D) The chemical structure of **AT13387** and its X-ray costructure with Hsp90.

Val150, and Val186, indicating that replacement with other substituents might be beneficial for rapid improvement in potency. Replacement of the methoxy group with a more lipophilic moiety provided compound **13** with significantly enhanced potency and improvement in LE. The crystal structure of compound **13**/Hsp90 confirmed that the *tert*-butyl moiety effectively fits into the lipophilic pocket and the H-bond forms between the morpholine oxygen and the side chain Lys58. However, Lys58 might also form the lipophilic interactions with the surrounding side chains including Ala55 and Ile96, indicating that morpholine moiety should be a potential position for further structural modification. Overlay analysis of cocrystal structures (the natural product radicicol/Hsp90, PDB code: 1BGQ) and fragment **12** revealed that the group of 2-OH in radicicol forms the direct H-bond with Asp93, suggesting that the additional hydroxyl moiety might bring additional benefit for affinity improvement.[88] Further synthetic manipulation resulted in isoindoline resorcinol **14** with subnanomolar affinity as well as excellent LE. The additional hydroxyl moiety as a polar positively charged group significantly improved potency and the distribution properties. The binding mode of compound **14** in Hsp90 also confirmed that the additional hydroxyl moiety forms H-bonds with Asp93. Further optimization of compound **14** was focused on the 2,4-dihydroxybenzamide moiety and the bicyclic isoindoline ring. In an attempt to block potential sites of oxidative metabolism and increase the p*K*a of the basic center, as well as reduce lipophilicity, **AT13387** was prepared containing the *N*-methylpiperazine group, exhibited favorable physicochemical and PK properties, and was selected as the drug candidate for further clinical investigation.[89] It is worth mentioning that LE was used as one of the criteria to guide the whole optimization campaign for controlling the molecular size. The superimposition with fragment **12** demonstrated that the binding mode was maintained during the process of fragment elaboration. As the advanced drug candidate, **AT13387** possesses the excellent balance of properties including potency, in vivo PK, acceptable risk profiles, as well as suboptimal physicochemical properties (p*K*a, $\log D_{7.4}$, and aqueous solubility).

2.08.4.4 Case 4: AT9283, Phase II

AT9283 is a novel multitargeted kinase inhibitor with potent Aurora kinase activity, which was also identified and developed by Astex Therapeutics.[90]**AT9283** displays potent antiproliferative and apoptotic properties in vitro, and the in vivo anticancer activity has been demonstrated in several human tumor xenograft models. Recently, clinical trials are ongoing to verify the effects of this fragment-derived compound. Unlike the previous fragments, fragment **16** was firstly identified as a starting point to explore CDK inhibitors (Fig. 5). Subsequently, FBDD resulted in identification of benzamide analogue **17** as a potent CDK2 inhibitor with an affinity of 0.052 μM. During the fragment optimization campaign, Astex researchers found that fragment **16** also exhibited superior inhibition for Aurora A with an IC_{50} value of 0.91 μM (LE = 0.59). Further characterization of fragment **16** and compound **17** through XRC revealed that fragment **16** fits deeply in the active site of Aurora A. The ligand H-bonds to backbone carbonyl of Glu211 and to the carbonyl and backbone NH of Ala213 of hinge region, the benzimidazole motif binds in the cleft around Ala213, Pro214, Leu215, and Gly216. This cleft has significant differences compared to the comparable region in CDK2. The binding mode of compound **17** also revealed the same three H-bonds to the hinge region. An intramolecular H-bond exists between the benzimidazole and the amide NH, holding the molecule in a planar conformation. The region of the ATP pocket occupied by the benzamide motif also displays significant differences between Aurora A and CDK2. With the aim to identify compounds with improvement on cellular potency via inhibition of Aurora kinases A and B, Astex researchers decided to add a basic motif on 5- or 6-position of the benzimidazole without causing any clashes. Weakly basic morpholine moiety ($pK_a \approx 7$) was selected with the aim to minimize the increase in effective H-bond donors since compound **17** has already possessed three H-bond donors. During this hit-to-lead phase, *p*-fluorophenyl analogue **18** displayed enhanced cellular potency and encouraging PK properties in mouse, while the plasma protein binding was found to be high (PPB = 99.5%). The X-ray cocrystal structure of compound **18**/Aurora A revealed that the motif of pyrazole–benzimidazole fills the narrow region of the ATP pocket, while the *p*-fluorophenyl fragment partially fills the surrounding region, indicating that the chemical space in this region needs further modification. The synthetic effects resulted in providing **AT9283** as a highly potent Aurora A inhibitor ($IC_{50} \approx 3$ nM, LE ≈ 0.42). The crystal structure of **AT9283**/Aurora A revealed that the urea linker allows a folded conformation, while the key H-bonds between initial fragment **16** and Aurora A are retained during the process of fragment elaboration. The high LE of the pyrazole–benzimidazole motif resulted in development of **AT9283** as the clinical drug candidate with low nanomolar potency and favorable pharmacological properties.

2.08.4.5 Case 5: AT7519, Phase II

AT7519 as a novel multi-CDK inhibitor is another example that was developed by Astex Therapeutics through utilization of fragment-based X-ray crystallographic screening and structure-based drug design (Fig. 6).[91] They began their drug discovery campaign by soaking crystals of CDK2 with a library of focused fragments. Approximately 30 low-affinity and small-size fragments binding to the active site of CDK2 were solved and identified with high LE and limited functionality. Despite indazole **20** displayed relative low binding affinity (>100 μM), the detailed binding mode revealed that this fragment with comparative higher LE (LE = 0.57) forms two classical H-bonds with CDK2 and it does not access the surrounding pocket, indicating that fragment indazole is suitable for potential substitution to occupy deep pocket of ATP-binding site. Structural analysis also suggested that addition of an aryl amide to the 3-position of indazole might form another hydrogen bonding interaction to Leu83. An alternative design strategy was pursued to decrease molecular weight through simplification by removal of the fused benzene ring without the significant loss in LE. The above-mentioned effects afforded the pyrazole **21** with the IC_{50} value of 97 μM and LE of 0.39. CDK2 cocrystal structure of compound **21** confirmed the additional hydrogen bonding interaction with Phe82. It is noteworthy to mention that the

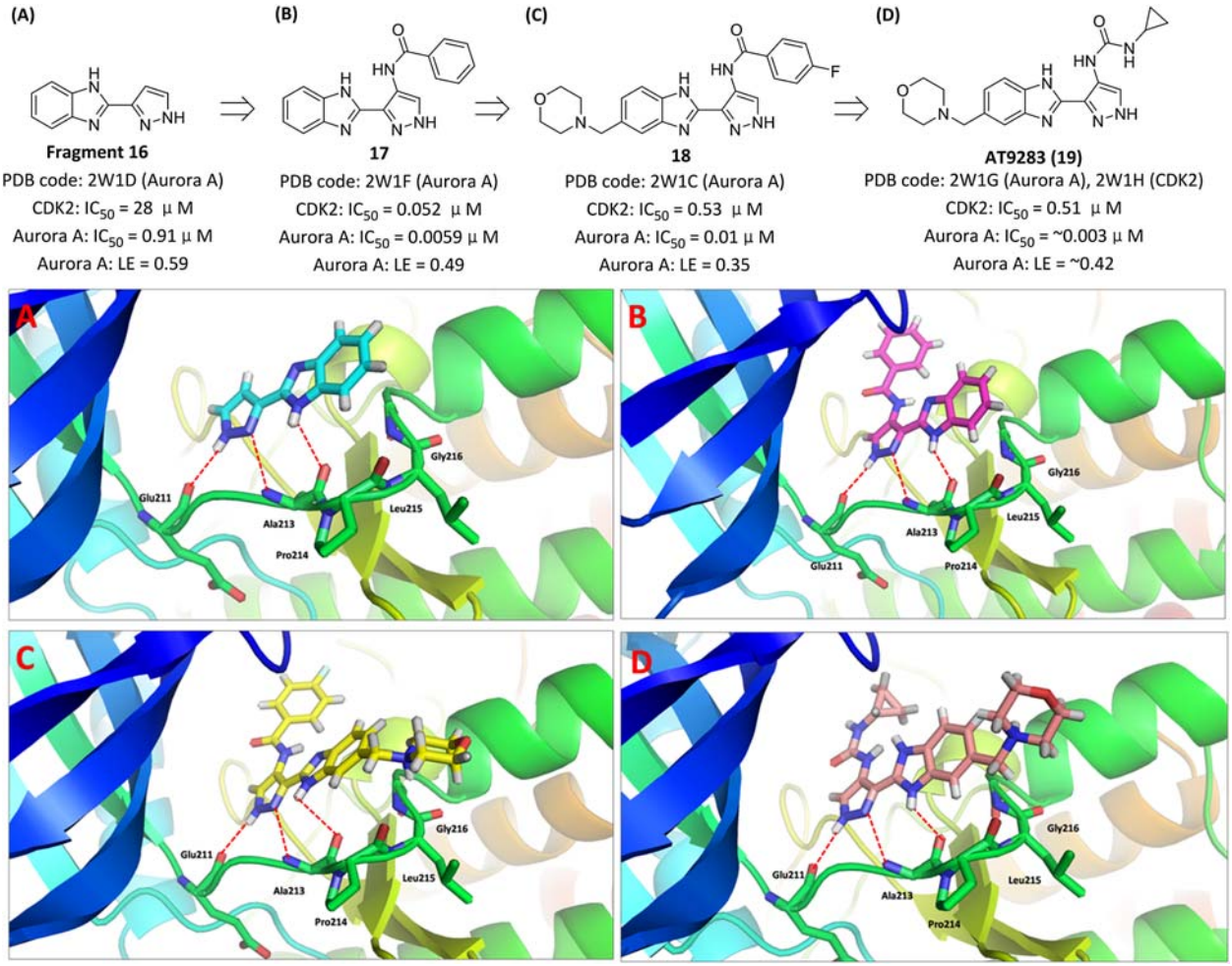

Fig. 5 Progression from initial fragment **16** to the clinical candidate **AT9283**. (A) The chemical structure of fragment **16** and its X-ray costructure with Aurora A. (B) The chemical structure of compound **17** and its X-ray costructure with Aurora A. (C) The chemical structure of compound **18** and its X-ray costructure with Aurora A. (D) The chemical structure of **AT9283** and its X-ray costructure with Aurora A and CDK2.

binding mode of pyrazole **21** remained identical to that of the starting fragment **20**, further indicating that the strategy applied herein is suitable for fragment optimization. The X-ray crystal structure also revealed that functionalizing the pyrazole moiety at the 4-position provided an opportunity to accommodate more space. Introduction of a 4-amino moiety gave compound **22**, resulting in a significant improvement in potency and enhanced LE ($IC_{50} = 0.003$ μM; LE = 0.45). The X-ray structure of **22**/CDK2 revealed that water-mediated H-bond from the amide carbonyl oxygen to the backbone NH of Asp145 benefits for improvement in affinity, while diortho substitution of the phenyl ring might be beneficial for stabilization of the twist. Although compound **22** exhibited potent kinase activity, due to its low cell permeability, this compound displayed moderate antiproliferative cell activity. Further optimization by replacement of the lipophilic 4-fluorophenyl moiety and modifications of the 2,6-difluorophenyl group ultimately led to the 2,6-dichlorophenyl derivative **AT7519**, which exhibited promising in vitro kinase, antiproliferative cell activity as well as low PPB and reasonable tumor distribution. The crystal structure of **AT7519** complexed with CDK2 reveals that the two chlorine atoms fill the lipophilic pocket more effectively than fluorine. **AT7519** demonstrated significant in vivo efficacy and is currently under evaluation in Phase II clinical development for multiple myeloma.

2.08.4.6 Case 6: NVP-AUY922, Phase II

NVP-AUY922 is one of small molecules targeting Hsp90 currently under Phase II clinical trials. Previous screening resulted in identification of small-molecular size 4,5-diarylpyrazoles including **CCT018159** as a new class of Hsp90 inhibitors (Fig. 7).[92] X-ray determination of **CCT018159**/Hsp90 cocrystal structure indicated that chemical modification on pyrazole ring especially methyl group might be beneficial for improvement in potency, and the resorcinol moiety seems to be important for two phenolic hydroxyls form two critical H-bonds with Hsp90. The structure-based drug design for the optimization of **CCT018159** led to the discovery of the amide-substituted pyrazole **VER-49009** that exhibited significant potency ($IC_{50} = 25$ nM). However, **VER-49009** did not show

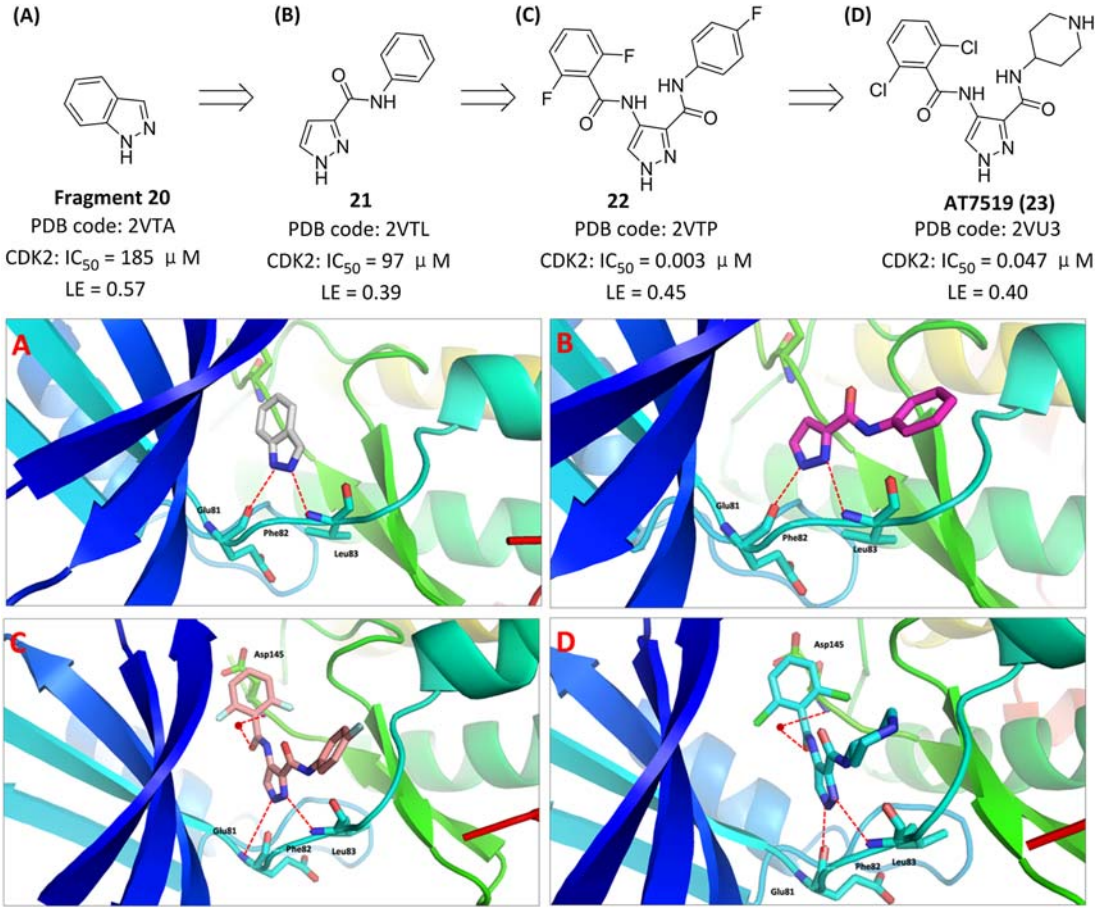

Fig. 6 Progression from initial fragment **20** to the clinical candidate **AT7519**. (A) The chemical structure of fragment **20** and its X-ray costructure with CDK2. (B) The chemical structure of compound **21** and its X-ray costructure with CDK2. (C) The chemical structure of compound **22** and its X-ray costructure with CDK2. (D) The chemical structure of **AT7519** and its X-ray costructure with CDK2.

ideal antiproliferative effects (HCT116 colon cancer cell line: $GI_{50} = 0.26$ μM). Subsequent structural analysis of Hsp90/**VER-49009** revealed that there is limited space for chemical modification around resorcinol group and pyrazole ring, while various substituents can be placed on the 5′-position of the resorcinol ring and incorporation of one solubilizing moiety on the 4-arylpyrazole substituents is recommended.[93] Additionally, modification of the pyrazole heterocycle provides another option to maintain the binding mode without changing the key scaffold core. Replacement of the pyrazole core with the isoxazole scaffold and the solubilizing group incorporation on the para position of the 4-aryl ring provided the isoxazole analogue **VER-50589** which showed significantly improved inhibition of cell proliferation against HCT116 cells with a GI_{50} value of 0.083 μM. Further replacement of the chlorine by an isopropyl group afforded **NVP-AUY922** as the desired drug candidate which exhibited excellent potency ($IC_{50} = 21$ nM) and inhibited proliferation in a wide range of human cancer cell lines with an average GI_{50} of 9 nM. X-ray crystal structure of Hsp90/**NVP-AUY922** confirmed an additional hydrophobic interaction with Leu107 in the flexible lipophilic pocket. **NVP-AUY922** exhibited excellent efficacy in a range of human tumor xenograft models covering major cancer types and diverse oncogenic profiles.

2.08.4.7 Case 7: Bruton's Tyrosine Kinase Inhibitor

Smith et al. sought to identify novel inhibitors of Bruton's tyrosine kinase (Btk) for the treatment of rheumatoid arthritis.[94] They began their drug discovery campaign by using a Caliper mobility shift assay to screen a library of 11,098 fragments. Small potential fragments were selected for XRC based on the novelty of fragment structure, LE, and the confirmation of binding data derived by NMR. Fragment **28** was selected for further structural optimization due to its high LE value (LE = 0.53) and the synthetic tractability (Fig. 8).[94] The binding mode of fragment **28** revealed that several potential accessible vectors can be modified for fragment evolution toward the floor pocket, P-loop, and the gatekeeper around the side chain residue Thr474. Of all possible vectors for fragment growth, 8-position of the cinnoline ring was selected to modify in order to enhance potency, selectivity, and ADME properties for this vector pointed to the center of ATP-binding site and might provide a great opportunity to grow the fragment toward the floor pocket and P-loop. The synthesis efforts resulted in the discovery of compound **29** with improved Btk potency. Further X-ray

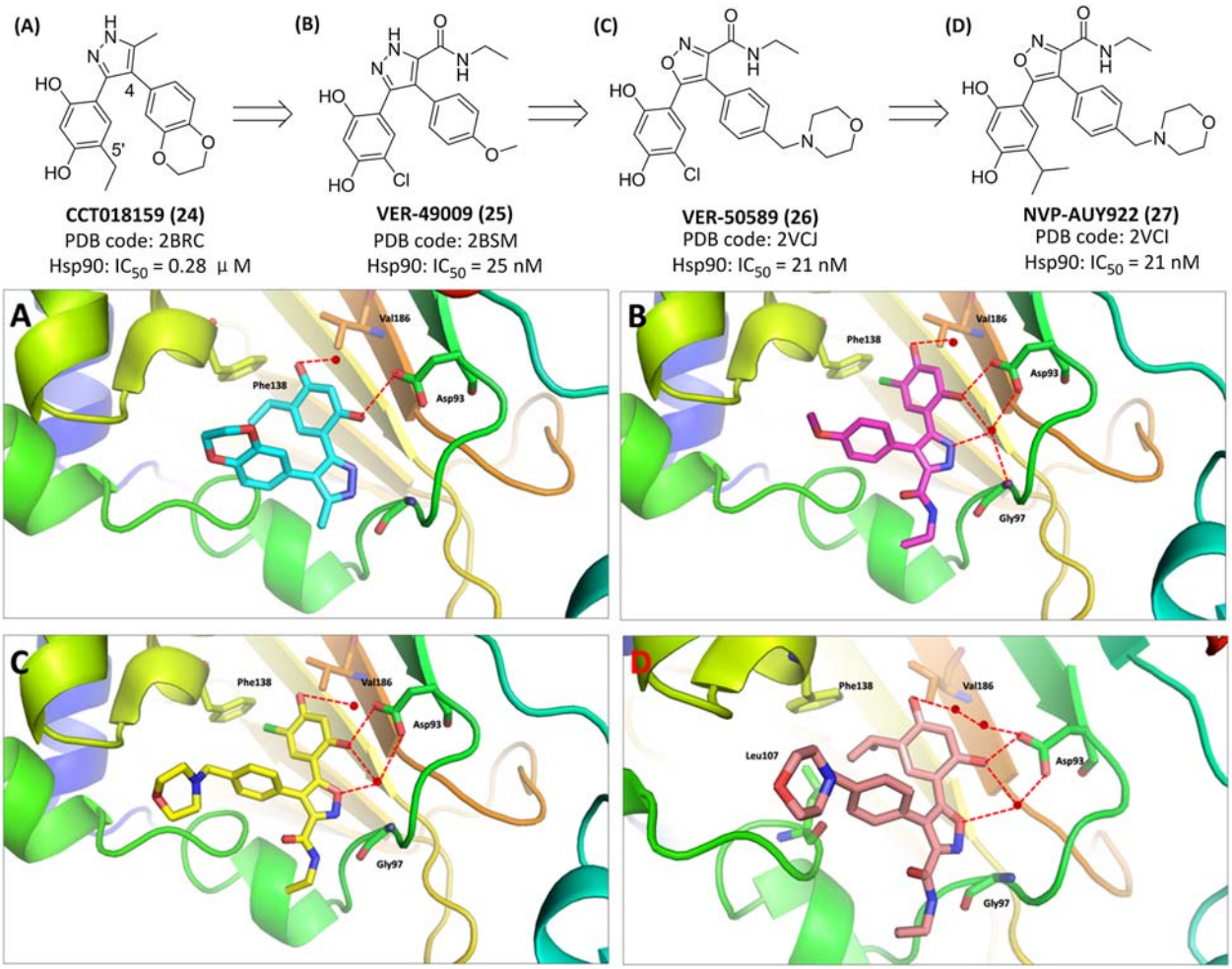

Fig. 7 Progression from initial fragment **24** to the clinical candidate **NVP-AUY922**. (A) The chemical structure of fragment **24** and its X-ray costructure with Hsp90. (B) The chemical structure of compound **25** and its X-ray costructure with Hsp90. (C) The chemical structure of compound **26** and its X-ray costructure with Hsp90. (D) The chemical structure of **NVP-AUY922** and its X-ray costructure with Hsp90.

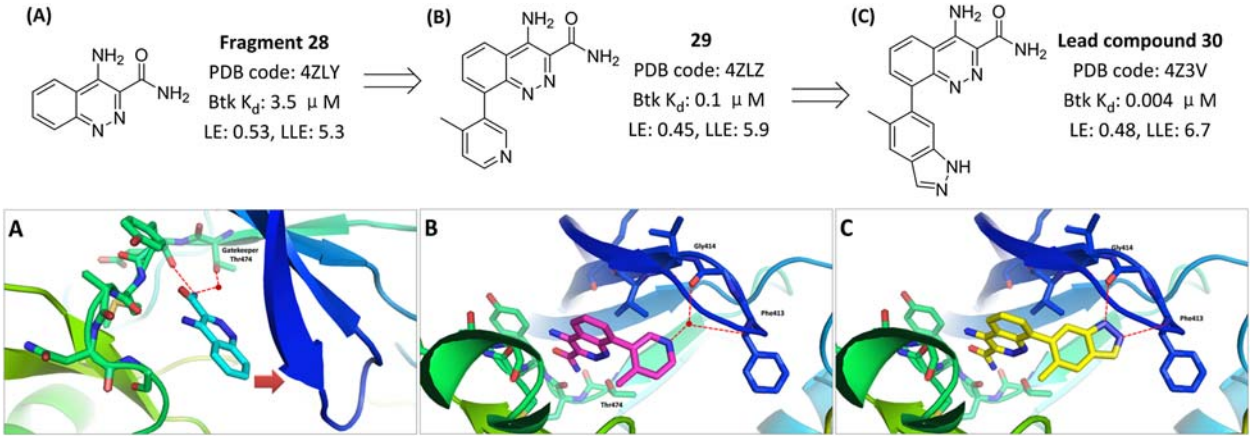

Fig. 8 Progression from initial fragment **28** to the lead compound **30**. (A) The chemical structure of fragment **28** and its X-ray costructure with Btk. (B) The chemical structure of compound **29** and its X-ray costructure with Btk. (C) The chemical structure of lead compound **30** and its X-ray costructure with Btk.

cocrystal structure revealed that the pyridine moiety of compound **29** makes a bifurcated water-mediated H-bond with P-loop. Therefore, with the goal to displace this water, a series of bicyclic heterocycles were designed and synthesized. 5-Methyl-indazol-6-yl analogue **30** was found to be a good lead compound with significant improved affinity, higher selectivity over Lck, and favorable cellular potency. The X-ray cocrystal structure revealed that the indazole moiety of the lead compound **30** forms two H-bonds with two strands of the P-loop and stabilizes the P-loop conformation, while the 4-amino and 3-carboxamide motifs make three H-bond interactions with the hinge, conserving the binding mode of the initial fragment **28**.

2.08.4.8 Case 8: RSK2 Inhibitor RMM-46

Recently, Taunton et al. used a fragment-based approach to develop the first reported inhibitor targeting RSK2 (ribosomal S6 kinase) C-terminal kinase domain.[95] They screened several heteroaryl-susbstituted cyanoacrylamides against three human kinases (RSK2, NEK2, and PLK1). Fragment indazole **31** and fragment azaindole **32** (Fig. 9) were found to inhibit RSK2 with submicromolar IC_{50} values and suitable ligand efficiencies (LE = 0.54 and 0.39, respectively). In order to gain detailed structural insight into the extraordinary LE, the cocrystals of these fragments with RSK2 were determined. The results revealed that the moiety of indazole forms two H-bonds with the side chains of Leu495 and Met496. However, this group does not properly fit into the ATP pocket around Ile428, Met496, and Leu546, indicating the potential position for further chemical optimization. The cocrystal structure of azaindole **32** revealed that the group of ketone formed an H-bond with the hinge residue Met496 and the azaindole moiety filled the entrance of the ATP pocket. Overlaying these two cocrystals revealed that aromatic substituents appended to the 3-position of indazole **31** might fill the hydrophobic cleft occupied by the azaindole moiety of **32**. Therefore, a series of analogues with 3-substituents on indazole and substituents on the primary amide were designed and synthesized. This provided the optimized inhibitor PMM-46 with significant improvement in potency toward RSK2 and higher selectivity over NEK2 and PLK1. The overlay of the cocrystals of PMM-46 and **31** revealed that the indazole cores of both compounds were aligned perfectly. Similar to compound **32**, trimethoxyphenyl moiety of PMM-46 was nestled around Ile428, Met496, and Leu546, while the fragment of 1,1-dimethyl-2-hydroxyethyl amide extended beneath the glycine-rich loop.

2.08.4.9 Case 9: HCV NS3 Protein Modulator

Astex Pharmaceuticals identified a series of fragments by high sensitive fragment screening using crystals of the HCV NS3-NS4a protein.[96] Some crystal structures revealed a new allosteric binding pocket at the interface between the protease and helicase domains. Fragment **34** bound to this relatively hydrophobic pocket with a fairly low potency and a high LE ($IC_{50} = \sim 500$ μM, LE = 0.3; Fig. 10). Examination of the crystal structures suggested that modification on the ring A and the side chain might lead

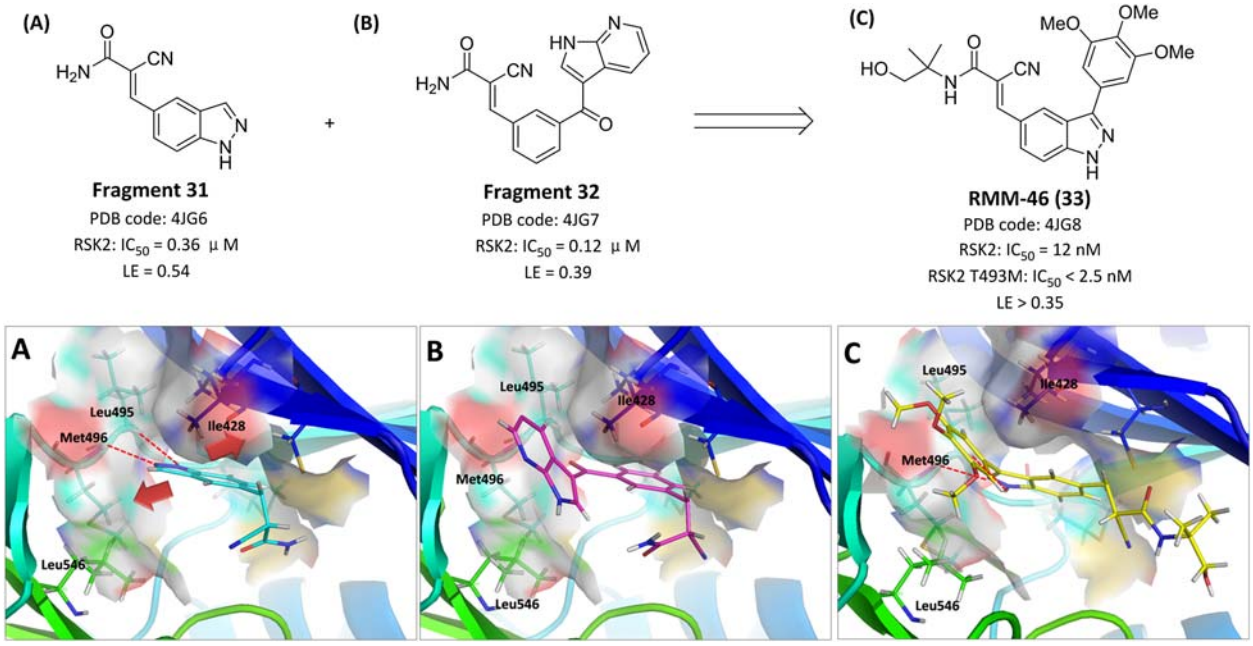

Fig. 9 Progression from initial fragment **31** to the lead compound **RMM-46** (**33**). (A) The chemical structure of fragment **31** and its X-ray costructure with RSK2. (B) The chemical structure of fragment **32** and its X-ray costructure with RSK2. (C) The chemical structure of lead compound **RMM-46** and its X-ray costructure with RSK2.

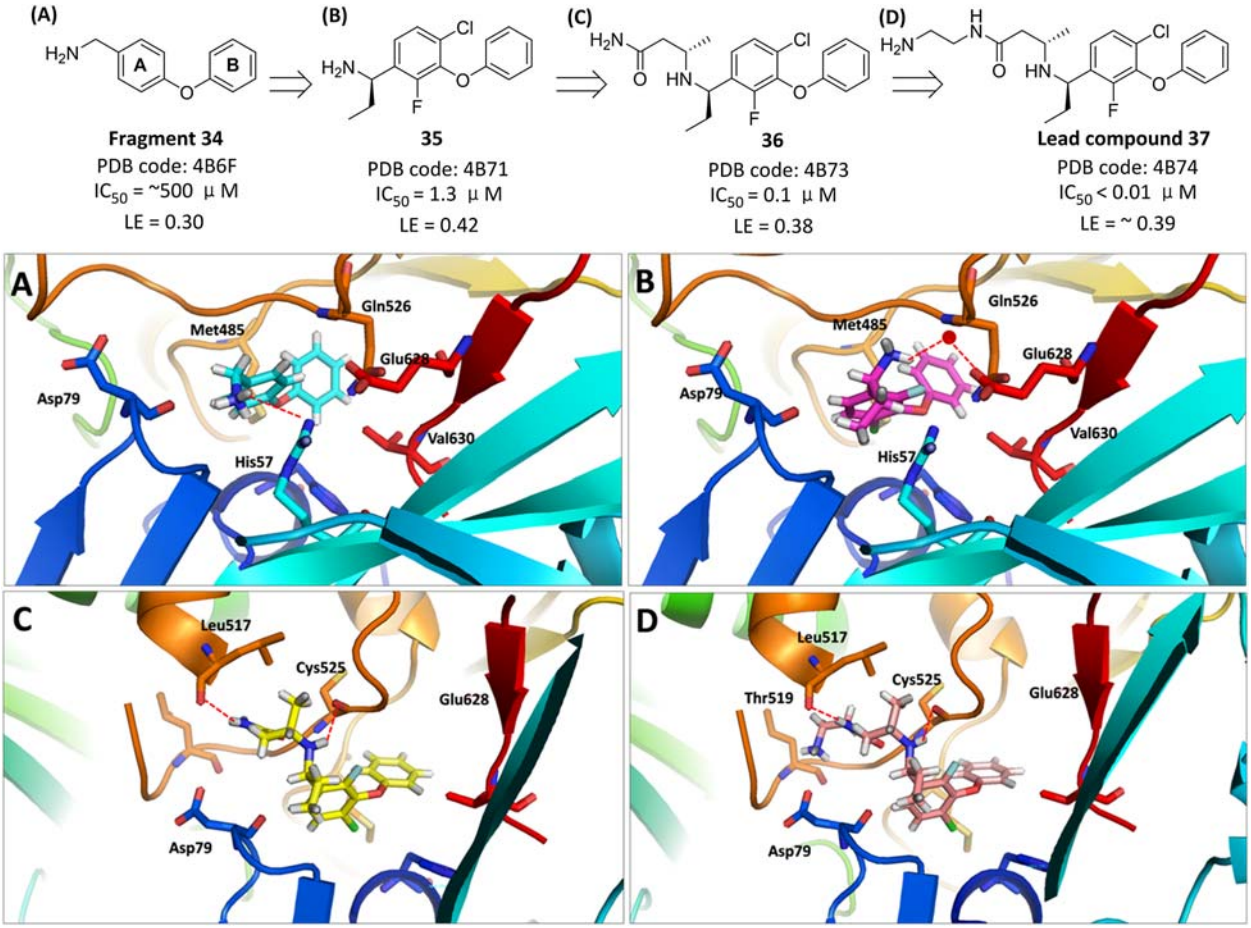

Fig. 10 Progression from initial fragment **34** to the lead compound **37**. (A) The chemical structure of fragment **34** and its X-ray costructure with HCV NS3 protein. (B) The chemical structure of compound **35** and its X-ray costructure with HCV NS3 protein. (C) The chemical structure of compound **36** and its X-ray costructure with HCV NS3 protein. (D) The chemical structure of the lead compound **37** and its X-ray costructure with HCV NS3 protein.

to afford more potent lead compound to efficiently fill the hydrophobic binding site, maximize van der Waals interactions, and stabilize the bound conformation. Initial effects resulted in a conformationally constrained compound **35** with a significant increase in binding affinity and a considerable improvement in LE ($IC_{50} = 1.3$ μM, LE = 0.42). Introduction of an ethyl group at the benzylic position restricted the rotation of the side chain. Modification on the side chain provided an excellent vector to identify more additional specific hydrogen bonding interactions. This effect led to the discovery of compound **36** which forms two key interactions with residues from both the protease and helicase domains. Addition of an ethylamino side chain led to the identification of the lead compound **37** with great improvement in potency ($IC_{50} < 0.01$ μM, LE ~0.39). Cocrystal structure revealed that the lead compound **37** forms further interactions with the pocket around the residues of Asp79, Thr519, and Leu522.

2.08.4.10 Case 10: Dual pan-RET/VEGFR2 Kinase Inhibitors

Li et al. recently identified a dual pan-RET/VEGFR2 kinase inhibitor **Pz-1** through successful application of the computational modeling-guided fragment-based approach (Fig. 11).[97] From a library of kinase-directed fragments, one benzimidazole scaffold **38** was identified as a promising starting point for a tyrosine kinase inhibitor targeting RET. This fragment was found to inhibit RET effectively at 20.0 μM. Molecular modeling of **38** in the RET kinase "DFG-in" (native active fold, the active DFG-in conformation) indicated that the chemical space around the position of bromine is solvent-exposed and the substitution at this region might be tolerated. The resulted compound **39** exhibited slightly enhanced potency against the RET kinase with an IC_{50} value of 18.2 μM. Further computational modeling revealed that the DFG pocket of RET could be accessed with the addition of a hydrophobic moiety connecting to the allosteric pocket. The optimized compound **40** displayed improved RET potency with an IC_{50} value of 2.1 μM. The combination of SAR information from both compounds **39** and **40** indicated that further optimization at the position of bromine and the allosteric region might lead to some promising compounds. The chemical synthesis and biological evaluation efforts resulted in identification of a significant potent lead compound **Pz-1** (**41**) containing a pyrazole at the solvent region

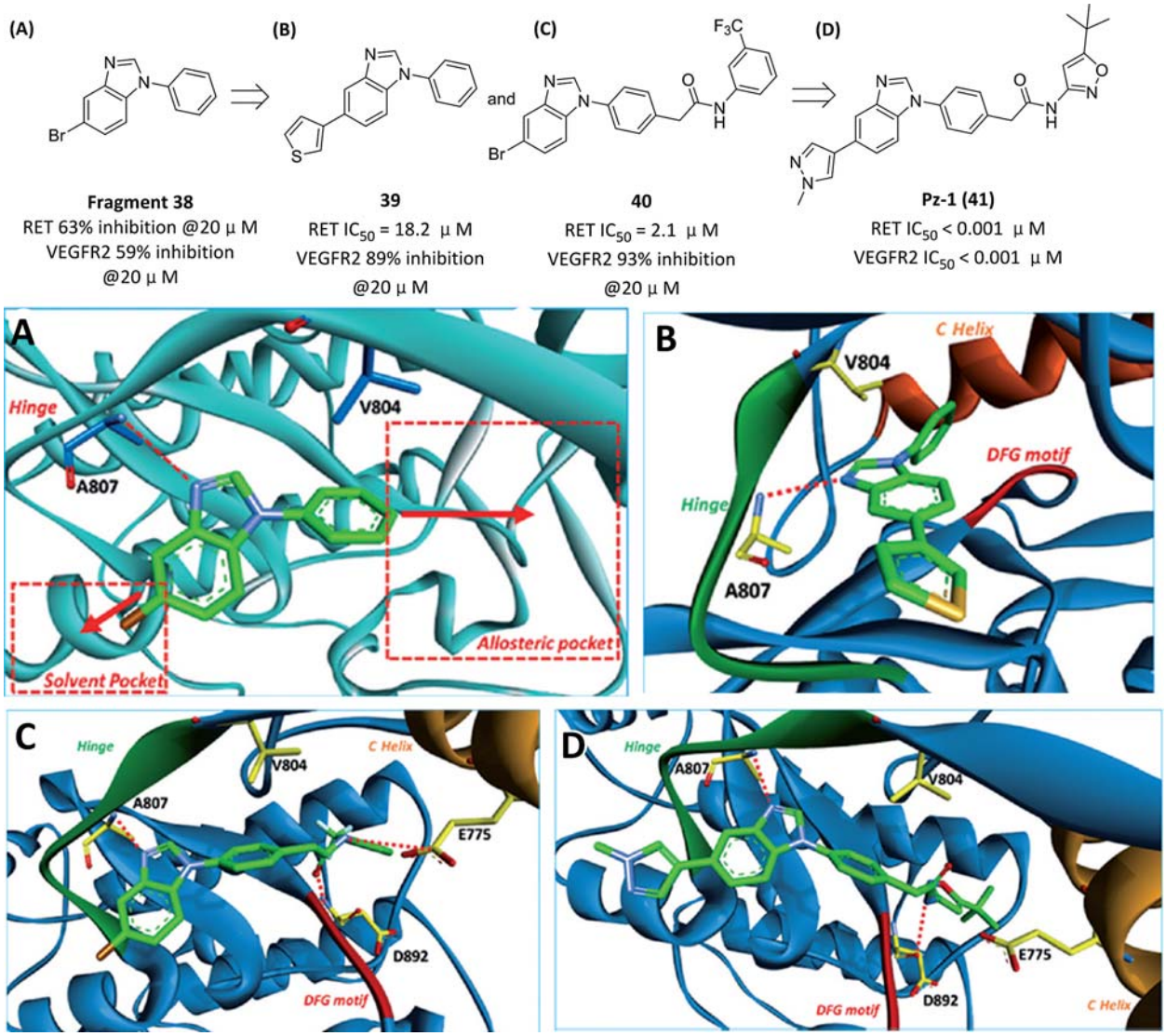

Fig. 11 Progression from initial fragment **38** to the clinical candidate **Pz-1** (**41**). (A) The chemical structure of fragment **38** and its computational modeling in the RET DFG-in crystal structure. (B) The chemical structure of compound **39** and its computational modeling in the RET DFG-out homology model. (C) The chemical structure of compound **40** and its computational modeling in the RET DFG-in crystal structure. (D) The chemical structure of **Pz-1** (**41**) and its computational modeling in the RET DFG-out homology model. Reproduced with permission from Frett, B.; Carlomagno, F.; Moccia, M. L.; Brescia, A.; Federico, G.; De Falco, V.; Admire, B.; Chen, Z.; Qi, W.; Santoro, M.; Li, H.Y. Fragment-based discovery of a dual pan-RET/VEGFR2 kinase inhibitor optimized for single-agent polypharmacology. *Angew. Chem. Int. Ed. Engl.***2015,** 54, 8717–8721.

and an isoxazole in the allosteric pocket. This clinical candidate **Pz-1** was found to be active against RET, RET mutants, and VEGFR2 with IC_{50} values at the subnanomolar level. Pz-1 can strongly block VEGFR2-mediated nutrient accumulation and inhibited RET/RET-mutant cell proliferation. Computational modeling of **Pz-1** within the RET kinase indicated that binding occurred >3.5 Å away from the side chain V804 of the gatekeeper region. Due to the large binding distance from the gatekeeper, **Pz-1** exhibits an improved binding affinity for the gatekeeper mutant RETV804M. It is worth noting that the clinical development of **Pz-1** represents a successful application of a computational modeling-guided FBDD.

2.08.5 Lessons Learned From Success Stories in FBDD

As we discussed, FBDD became a widespread applied approach throughout both the academia and industry settings over the past two decades. There are several key lessons that we can learn from the successful cases. Several areas with more attention should be considered so that future drug discovery opportunities may increase the impact and success of FBDD approaches even further.

2.08.5.1 Fragment Identification

As aforementioned, various techniques have been developed for FBS.[98] Therefore, more options are available to select one suitable assay for the first-round fragment screening to identify valuable fragments for further chemical modification.[99–101] As we mentioned earlier, combination of different methods to confirm the right fragments is critically important for the entire drug discovery campaign.[27] Utilization of XRC is the first choice to confirm the right fragments through achieving the detailed structural information about the binding mode with high resolution.[102–104] However, it requires high-purity protein, the automated infrastructures, and professional knowledge.[105] NMR spectroscopy also consumes large quantities of purified proteins and the expensive equipment, while target-based NMR needs ^{15}N-labeled protein to identify binding sites.[23] Other assays including several biochemical and functional assays that are rapid and cost-effective, while the detailed information about the localization of fragment binding is missing. Different from the FBS assays mentioned earlier, the appropriate deconstruction of reported ligands may also provide potential privileged fragments for further reconstruction of novel scaffolds with favorable drug-likeness.[106–108] Despite a number of methods are capable of identifying interesting fragments for further fragment elaboration, the quality of fragments with real potential is one crucial factor that should be taken into account to validate the effective fragment identification.[109] Ideally, these fragments are metabolically stable, pure, and unreactive with fewer off-target effects. Special attention should be paid to recognize the pan-assay interference compounds issues with many hits identified from HTS and FBS that are artifacts and promiscuous binders to a variety of biological targets.[110] Such hits should be eliminated early from the FBDD approaches to avoid a "garbage in, garbage out" process.

2.08.5.2 Fragment Elaboration

During fragment elaboration cycle, utilization of LE is very important to control the balance of molecular size and potency.[111,112] Structural information about the binding mode is useful to guide drug design. Such information may provide the potential structural sites that are tolerable for modification to increase the binding affinity, and identify which chemical sites are available for incorporating additional fragments to improve selectivity and PK properties. Several assays may be conducted to figure out the detailed structural information including XRC, target-based NMR, and molecular docking.[113] Even though molecular docking only predicts the potential binding mode, the suitable algorithms are widely applied to guide drug design, and several successful examples demonstrated their potential applications in rational drug design.[97,114,115] It is worth mentioning that retaining the binding mode of the initial fragments is critical in the course of fragment elaboration and structural optimization.[116] While there are relatively few approaches emerging as reliable and efficient methods for rapidly exploring chemical space for lead compound development, the aforementioned successful cases may provide some useful insights for utilizing the FBDD strategy.

2.08.5.3 Drug Candidate Selection

The initial fragments must be structurally optimized to yield favorable PK properties.[117] Therefore, how to select potential drug candidates for further clinical evaluation is challenging, especially when couple of ideal compounds are available with favorable drug ADMET properties and suitable aqueous solubility.[118] Oral bioavailability and the pharmacological efficacy have the top priority for drug candidate selection. The ease of chemical synthesis and the source of the starting materials are also important factors to be considered. In addition, some useful programs such as pkCSM for predicting small-molecule PK properties using graph-based signatures may facilitate a more effective drug-candidate selection in FBDD for further development.[119]

2.08.6 Conclusion and Outlook

With an increasing number of FBDD-derived drugs progressing into clinical trials, more and more attention from both industry and academia have been and will continue to be paid to FBDD.[120–122] As an alternative strategy to HTS in drug discovery, FBDD increases the hit rates via screening low MW fragments covering a relatively broader chemical space. However, initial fragment tends to display a weak binding affinity, thereby requiring highly sensitive screening methods to identify such weak interactions between fragments and the target protein. Fragment screening requires appropriate selection and integration of various techniques based on the available technology for identification and validation of right fragments. Each fragment screening technique has its advantages: XRC provides detailed structural information, NMR offers binding affinity and binding site, while other bioassays afford functionally relevant activity data for larger collections of fragments.[123] However, these experimental screening approaches require large quantities of purified proteins. The strength of biochemical screening is that the throughput allows large fragment collections to be screened in a short time period. This ensures that the most ligand efficient diverse starting points are available for medicinal chemists to select for subsequent optimization. The most effective way to perform fragment screening is not to rely on a single method but to use orthogonal methods in concert.

Regardless of the screening method, developing low-affinity fragment hits into a lead by fragment evolution, fragment optimization, fragment linking, or fragment self-assembly is challenging.[124] Of all cases described earlier, structural information played a profound role in both discovering fragments and advancing them into the clinic.[125] Both NMR and XRC are capable of providing detailed structural information, but recently tremendous progress in computational structure-based drug design leads to

development of novel therapeutic agents with promising pharmacological efficacy. This further demonstrates that the combination of different sophisticated and reproducible molecular modeling tools may also advance fragments to drug candidates, especially in case some membrane proteins are challenging to characterize using experimental structural methods.[126–129] With the experimental or predicted structural information in hand, how to effectively select the potential chemical sites for further structural optimization becomes crucial to improve potency and selectivity. Recently, several tools and software programs such as Drug Guru™, AutoGrow, and MCT are available to explore chemical space more efficiently as we discussed earlier. The optimal balance of properties including molecular weight, potency, selectivity, amphiphilicity, and druggability is quite sensitive in the fragment elaboration campaign. Notably, the adoption of early stage PK and PD studies has also contributed greatly to a significantly reduced late-stage attrition rate of clinical candidates.[130,131] Taken together, it is our hope that the strategic advances and lessons learned will continue to enable and expand the efficient applications of FBDD in the discovery and development of new drugs in the years to come.

Acknowledgments

Conflict of Interest
The authors declare no competing financial interest.
This work was supported by grants P30 DA028821 and R01 DA038446 from the National Institutes of Health, Cancer Prevention Research Institute of Texas (CPRIT) award, R. A. Welch Foundation Chemistry and Biology Collaborative Grant from the Gulf Coast Consortia (GCC), John Sealy Memorial Endowment Fund, Institute for Translational Sciences (ITS), Sealy Center for Molecular Medicine, and the Center for Addiction Research (CAR) at UTMB, the National Natural Science Foundation of China (Nos. 81402781 and 81571802), the Scientific Research Foundation for the Returned Overseas Chinese Scholars, and Technology Development Foundation of Fuzhou University.

See also: 2.13. Small-Molecule Inhibitors of Protein–Protein Interactions. 2.17. Label-Free Screening Technologies. 5.02. Selective Kinase Inhibitors In Cancer. 8.13. Fragment-Based Discovery of AZD2716: A Novel, Potent Secreted Phospholipase A_2 ($sPLA_2$) Inhibitor for the Treatment of Coronary Artery Disease.

References

1. Murray, C. W.; Rees, D. C. The Rise of Fragment-Based Drug Discovery. *Nat. Chem.* **2009,** *1,* 187–192.
2. Zhang, J. H.; Chung, T. D.; Oldenburg, K. R. A Simple Statistical Parameter for Use in Evaluation and Validation of High Throughput Screening Assays. *J. Biomol. Screen.* **1999,** *4,* 67–73.
3. Pammolli, F.; Magazzini, L.; Riccaboni, M. The Productivity Crisis in Pharmaceutical R&D. *Nat. Rev. Drug Discov.* **2011,** *10,* 428–438.
4. Pereira, D. A.; Williams, J. A. Origin and Evolution of High Throughput Screening. *Br. J. Pharmacol.* **2007,** *152,* 53–61.
5. Bohacek, R. S.; McMartin, C.; Guida, W. C. The Art and Practice of Structure-Based Drug Design: A Molecular Modeling Perspective. *Med. Res. Rev.* **1996,** *16,* 3–50.
6. Erlanson, D. A.; McDowell, R. S.; O'Brien, T. Fragment-Based Drug Discovery. *J. Med. Chem.* **2004,** *47,* 3463–3482.
7. Kola, I.; Landis, J. Can the Pharmaceutical Industry Reduce Attrition Rates? *Nat. Rev. Drug Discov.* **2004,** *3,* 711–715.
8. Hajduk, P. J.; Greer, J. A Decade of Fragment-Based Drug Design: Strategic Advances and Lessons Learned. *Nat. Rev. Drug Discov.* **2007,** *6,* 211–219.
9. Fattori, D. Molecular Recognition: The Fragment Approach in Lead Generation. *Drug Discov. Today* **2004,** *9,* 229–238.
10. Congreve, M.; Chessari, G.; Tisi, D.; Woodhead, A. J. Recent Developments in Fragment-Based Drug Discovery. *J. Med. Chem.* **2008,** *51,* 3661–3680.
11. Congreve, M.; Carr, R.; Murray, C.; Jhoti, H. A 'Rule of Three' for Fragment-Based Lead Discovery? *Drug Discov. Today* **2003,** *8,* 876–877.
12. Baker, M. Fragment-Based Lead Discovery Grows Up. *Nat. Rev. Drug Discov.* **2013,** *12,* 5–7.
13. Fattori, D.; Squarcia, A.; Bartoli, S. Fragment-Based Approach to Drug Lead Discovery: Overview and Advances in Various Techniques. *Drugs R. D.* **2008,** *9,* 217–227.
14. Leach, A. R.; Hann, M. M.; Burrows, J. N.; Griffen, E. J. Fragment Screening: An Introduction. *Mol. Biosyst.* **2006,** *2,* 430–446.
15. Ciulli, A.; Abell, C. Fragment-Based Approaches to Enzyme Inhibition. *Curr. Opin. Biotechnol.* **2007,** *18,* 489–496.
16. Campos-Olivas, R. NMR Screening and Hit Validation in Fragment Based Drug Discovery. *Curr. Top. Med. Chem.* **2011,** *11,* 43–67.
17. Hajduk, P. J.; Huth, J. R.; Fesik, S. W. Druggability Indices for Protein Targets Derived from NMR-Based Screening Data. *J. Med. Chem.* **2005,** *48,* 2518–2525.
18. Shuker, S. B.; Hajduk, P. J.; Meadows, R. P.; Fesik, S. W. Discovering High-Affinity Ligands for Proteins: SAR by NMR. *Science* **1996,** *274,* 1531–1534.
19. Klages, J.; Coles, M.; Kessler, H. NMR-Based Screening: A Powerful Tool in Fragment-Based Drug Discovery. *Analyst* **2007,** *132,* 693–705.
20. Jordan, J. B.; Poppe, L.; Xia, X.; Cheng, A. C.; Sun, Y.; Michelsen, K.; Eastwood, H.; Schnier, P. D.; Nixey, T.; Zhong, W. Fragment Based Drug Discovery: Practical Implementation Based on (1)(9)F NMR Spectroscopy. *J. Med. Chem.* **2012,** *55,* 678–687.
21. Jahnke, W. Perspectives of Biomolecular NMR in Drug Discovery: The Blessing and Curse of Versatility. *J. Biomol. NMR* **2007,** *39,* 87–90.
22. Ross, A.; Schlotterbeck, G.; Klaus, W.; Senn, H. Automation of NMR Measurements and Data Evaluation for Systematically Screening Interactions of Small Molecules With Target Proteins. *J. Biomol. NMR* **2000,** *16,* 139–146.
23. Pellecchia, M.; Bertini, I.; Cowburn, D.; Dalvit, C.; Giralt, E.; Jahnke, W.; James, T. L.; Homans, S. W.; Kessler, H.; Luchinat, C.; Meyer, B.; Oschkinat, H.; Peng, J.; Schwalbe, H.; Siegal, G. Perspectives on NMR in Drug Discovery: A Technique Comes of Age. *Nat. Rev. Drug Discov.* **2008,** *7,* 738–745.
24. Zartler, E. R.; Mo, H. Practical Aspects of NMR-Based Fragment Discovery. *Curr. Top. Med. Chem.* **2007,** *7,* 1592–1599.
25. Skinner, A. L.; Laurence, J. S. High-Field Solution NMR Spectroscopy as a Tool for Assessing Protein Interactions With Small Molecule Ligands. *J. Pharm. Sci.* **2008,** *97,* 4670–4695.
26. Dalvit, C. NMR Methods in Fragment Screening: Theory and a Comparison With Other Biophysical Techniques. *Drug Discov. Today* **2009,** *14,* 1051–1057.
27. Hennig, M.; Ruf, A.; Huber, W. Combining Biophysical Screening and X-ray Crystallography for Fragment-Based Drug Discovery. *Top. Curr. Chem.* **2012,** *317,* 115–143.
28. Jhoti, H.; Cleasby, A.; Verdonk, M.; Williams, G. Fragment-Based Screening Using X-ray Crystallography and NMR Spectroscopy. *Curr. Opin. Chem. Biol.* **2007,** *11,* 485–493.
29. Davies, T. G.; Tickle, I. J. Fragment Screening Using X-ray Crystallography. *Top. Curr. Chem.* **2012,** *317,* 33–59.
30. Neumann, T.; Junker, H. D.; Schmidt, K.; Sekul, R. SPR-Based Fragment Screening: Advantages and Applications. *Curr. Opin. Chem. Biol.* **2007,** *7,* 1630–1642.
31. Navratilova, I.; Hopkins, A. L. Emerging Role of Surface Plasmon Resonance in Fragment-Based Drug Discovery. *Future Med. Chem.* **2011,** *3,* 1809–1820.

32. Perspicace, S.; Banner, D.; Benz, J.; Muller, F.; Schlatter, D.; Huber, W. Fragment-Based Screening Using Surface Plasmon Resonance Technology. *J. Biomol. Screen.* **2009,** *14,* 337–349.
33. Navratilova, I.; Hopkins, A. L. Fragment Screening by Surface Plasmon Resonance. *ACS Med. Chem. Lett.* **2010,** *1,* 44–48.
34. Hofstadler, S. A.; Sannes-Lowery, K. A. Applications of ESI-MS in Drug Discovery: Interrogation of Noncovalent Complexes. *Nat. Rev. Drug Discov.* **2006,** *5,* 585–595.
35. Deng, G.; Sanyal, G. Applications of Mass Spectrometry in Early Stages of Target Based Drug Discovery. *J. Pharm. Biomed. Anal.* **2006,** *40,* 528–538.
36. Vivat Hannah, V.; Atmanene, C.; Zeyer, D.; Van Dorsselaer, A.; Sanglier-Cianferani, S. Native MS: An 'ESI' Way to Support Structure- and Fragment-Based Drug Discovery. *Future Med. Chem.* **2010,** *2,* 35–50.
37. Jefferson, E. A.; Seth, P. P.; Robinson, D. E.; Winter, D. K.; Miyaji, A.; Risen, L. M.; Osgood, S. A.; Bertrand, M.; Swayze, E. E. Optimizing the Antibacterial Activity of a Lead Structure Discovered by "SAR by MS" Technology. *Bioorg. Med. Chem. Lett.* **2004,** *14,* 5257–5261.
38. Swayze, E. E.; Jefferson, E. A.; Sannes-Lowery, K. A.; Blyn, L. B.; Risen, L. M.; Arakawa, S.; Osgood, S. A.; Hofstadler, S. A.; Griffey, R. H. SAR by MS: A Ligand Based Technique for Drug Lead Discovery Against Structured RNA Targets. *J. Med. Chem.* **2002,** *45,* 3816–3819.
39. Annis, D. A.; Nickbarg, E.; Yang, X.; Ziebell, M. R.; Whitehurst, C. E. Affinity Selection-Mass Spectrometry Screening Techniques for Small Molecule Drug Discovery. *Curr. Opin. Chem. Biol.* **2007,** *11,* 518–526.
40. Lo, M. C.; Aulabaugh, A.; Jin, G.; Cowling, R.; Bard, J.; Malamas, M.; Ellestad, G. Evaluation of Fluorescence-Based Thermal Shift Assays for Hit Identification in Drug Discovery. *Anal. Biochem.* **2004,** *332,* 153–159.
41. Kranz, J. K.; Schalk-Hihi, C. Protein Thermal Shifts to Identify Low Molecular Weight Fragments. *Methods Enzymol.* **2011,** *493,* 277–298.
42. Pantoliano, M. W.; Petrella, E. C.; Kwasnoski, J. D.; Lobanov, V. S.; Myslik, J.; Graf, E.; Carver, T.; Asel, E.; Springer, B. A.; Lane, P.; Salemme, F. R. High-Density Miniaturized Thermal Shift Assays as a General Strategy for Drug Discovery. *J. Biomol. Screen.* **2001,** *6,* 429–440.
43. Cimmperman, P.; Baranauskiene, L.; Jachimoviciute, S.; Jachno, J.; Torresan, J.; Michailoviene, V.; Matuliene, J.; Sereikaite, J.; Bumelis, V.; Matulis, D. A Quantitative Model of Thermal Stabilization and Destabilization of Proteins by Ligands. *Biophys. J.* **2008,** *95,* 3222–3231.
44. Leavitt, S.; Freire, E. Direct Measurement of Protein Binding Energetics by Isothermal Titration Calorimetry. *Curr. Opin. Struct. Biol.* **2001,** *11,* 560–566.
45. Ladbury, J. E.; Klebe, G.; Freire, E. Adding Calorimetric Data to Decision Making in Lead Discovery: A Hot Tip. *Nat. Rev. Drug Discov.* **2010,** *9,* 23–27.
46. Barker, J.; Courtney, S.; Hesterkamp, T.; Ullmann, D.; Whittaker, M. Fragment Screening by Biochemical Assay. *Expert Opin. Drug Discov.* **2006,** *1,* 225–236.
47. Mclnnes, C. Virtual Screening Strategies in Drug Discovery. *Curr. Opin. Chem. Biol.* **2007,** *11,* 494–502.
48. Zoete, V.; Grosdidier, A.; Michielin, O. Docking, Virtual High Throughput Screening and In Silico Fragment-Based Drug Design. *J. Cell. Mol. Med.* **2009,** *13,* 238–248.
49. Sheng, C.; Zhang, W. Fragment Informatics and Computational Fragment-Based Drug Design: An Overview and Update. *Med. Res. Rev.* **2013,** *33,* 554–598.
50. Rabal, O.; Urbano-Cuadrado, M.; Oyarzabal, J. Computational Medicinal Chemistry in Fragment-Based Drug Discovery: What, How and When. *Future Med. Chem.* **2011,** *3,* 95–134.
51. Wang, T.; Wu, M. B.; Chen, Z. J.; Chen, H.; Lin, J. P.; Yang, L. R. Fragment-Based Drug Discovery and Molecular Docking in Drug Design. *Curr. Pharm. Biotechnol.* **2015,** *16,* 11–25.
52. Orita, M.; Warizaya, M.; Amano, Y.; Ohno, K.; Niimi, T. Advances in Fragment-Based Drug Discovery Platforms. *Expert Opin. Drug Discov.* **2009,** *4,* 1125–1144.
53. Gozalbes, R.; Carbajo, R. J.; Pineda-Lucena, A. Contributions of Computational Chemistry and Biophysical Techniques to Fragment-Based Drug Discovery. *Curr. Med. Chem.* **2010,** *17,* 1769–1794.
54. Slack, M.; Winkler, D.; Kramer, J.; Hesterkamp, T. A Multiplexed Approach to Hit Finding. *Curr. Opin. Drug Discov. Devel.* **2009,** *12,* 351–357.
55. Kuntz, I. D.; Chen, K.; Sharp, K. A.; Kollman, P. A. The Maximal Affinity of Ligands. *Proc. Natl. Acad. Sci. U. S. A.* **1999,** *96,* 9997–10002.
56. Hopkins, A. L.; Groom, C. R.; Alex, A. Ligand Efficiency: A Useful Metric for Lead Selection. *Drug Discov. Today* **2004,** *9,* 430–431.
57. Abad-Zapatero, C.; Metz, J. T. Ligand Efficiency Indices as Guideposts for Drug Discovery. *Drug Discov. Today* **2005,** *10,* 464–469.
58. Perola, E. An Analysis of the Binding Efficiencies of Drugs and Their Leads in Successful Drug Discovery Programs. *J. Med. Chem.* **2010,** *53,* 2986–2997.
59. Murray, C. W.; Erlanson, D. A.; Hopkins, A. L.; Keseru, G. M.; Leeson, P. D.; Rees, D. C.; Reynolds, C. H.; Richmond, N. J. Validity of Ligand Efficiency Metrics. *ACS Med. Chem. Lett.* **2014,** *5,* 616–618.
60. Hopkins, A. L.; Keseru, G. M.; Leeson, P. D.; Rees, D. C.; Reynolds, C. H. The Role of Ligand Efficiency Metrics in Drug Discovery. *Nat. Rev. Drug Discov.* **2014,** *13,* 105–121.
61. Eitner, K.; Koch, U. From Fragment Screening to Potent Binders: Strategies for Fragment-to-Lead Evolution. *Mini Rev. Med. Chem.* **2009,** *9,* 956–961.
62. Rees, D. C.; Congreve, M.; Murray, C. W.; Carr, R. Fragment-Based Lead Discovery. *Nat. Rev. Drug Discov.* **2004,** *3,* 660–672.
63. Abad, M. C.; Gibbs, A. C.; Zhang, X. Electron Density Guided Fragment-Based Drug Design—A Lead Generation Example. *Methods Enzymol.* **2011,** *493,* 487–508.
64. Orita, M.; Ohno, K.; Niimi, T. Two 'Golden Ratio' Indices in Fragment-Based Drug Discovery. *Drug Discov. Today* **2009,** *14,* 321–328.
65. de Kloe, G. E.; Bailey, D.; Leurs, R.; de Esch, I. J. Transforming Fragments into Candidates: Small Becomes Big in Medicinal Chemistry. *Drug Discov. Today* **2009,** *14,* 630–646.
66. Chung, S.; Parker, J. B.; Bianchet, M.; Amzel, L. M.; Stivers, J. T. Impact of Linker Strain and Flexibility in the Design of a Fragment-Based Inhibitor. *Nat. Chem. Biol.* **2009,** *5,* 407–413.
67. Crisman, T. J.; Bender, A.; Milik, M.; Jenkins, J. L.; Scheiber, J.; Sukuru, S. C.; Fejzo, J.; Hommel, U.; Davies, J. W.; Glick, M. "Virtual Fragment Linking": An Approach to Identify Potent Binders From Low Affinity Fragment Hits. *J. Med. Chem.* **2008,** *51,* 2481–2491.
68. Erlanson, D. A.; Wells, J. A.; Braisted, A. C. Tethering: Fragment-Based Drug Discovery. *Annu. Rev. Biophys. Biomol. Struct.* **2004,** *33,* 199–223.
69. Erlanson, D. A.; Lam, J. W.; Wiesmann, C.; Luong, T. N.; Simmons, R. L.; DeLano, W. L.; Choong, I. C.; Burdett, M. T.; Flanagan, W. M.; Lee, D.; Gordon, E. M.; O'Brien, T. In Situ Assembly of Enzyme Inhibitors Using Extended Tethering. *Nat. Biotechnol.* **2003,** *21,* 308–314.
70. Stewart, K. D.; Shiroda, M.; James, C. A. Drug Guru: A Computer Software Program for Drug Design Using Medicinal Chemistry Rules. *Bioorg. Med. Chem.* **2006,** *14,* 7011–7022.
71. Durrant, J. D.; Amaro, R. E.; McCammon, J. A. AutoGrow: A Novel Algorithm for Protein Inhibitor Design. *Chem. Biol. Drug Des.* **2009,** *73,* 168–178.
72. Durrant, J. D.; Lindert, S.; McCammon, J. A. AutoGrow 3.0: An Improved Algorithm for Chemically Tractable, Semi-Automated Protein Inhibitor Design. *J. Mol. Graph. Model.* **2013,** *44,* 104–112.
73. Segall, M.; Champness, E.; Leeding, C.; Lilien, R.; Mettu, R.; Stevens, B. Applying Medicinal Chemistry Transformations and Multiparameter Optimization to Guide the Search for High-Quality Leads and Candidates. *J. Chem. Inf. Model.* **2011,** *51,* 2967–2976.
74. Roughley, S. D.; Jordan, A. M. The Medicinal Chemist's Toolbox: An Analysis of Reactions Used in the Pursuit of Drug Candidates. *J. Med. Chem.* **2011,** *54,* 3451–3479.
75. Bollag, G.; Tsai, J.; Zhang, J.; Zhang, C.; Ibrahim, P.; Nolop, K.; Hirth, P. Vemurafenib: The First Drug Approved for BRAF-Mutant Cancer. *Nat. Rev. Drug Discov.* **2012,** *11,* 873–886.
76. Das Thakur, M.; Salangsang, F.; Landman, A. S.; Sellers, W. R.; Pryer, N. K.; Levesque, M. P.; Dummer, R.; McMahon, M.; Stuart, D. D. Modelling Vemurafenib Resistance in Melanoma Reveals a Strategy to Forestall Drug Resistance. *Nature* **2013,** *494,* 251–255.
77. Tsai, J.; Lee, J. T.; Wang, W.; Zhang, J.; Cho, H.; Mamo, S.; Bremer, R.; Gillette, S.; Kong, J.; Haass, N. K.; Sproesser, K.; Li, L.; Smalley, K. S.; Fong, D.; Zhu, Y. L.; Marimuthu, A.; Nguyen, H.; Lam, B.; Liu, J.; Cheung, I.; Rice, J.; Suzuki, Y.; Luu, C.; Settachatgul, C.; Shellooe, R.; Cantwell, J.; Kim, S. H.; Schlessinger, J.; Zhang, K. Y.; West, B. L.; Powell, B.; Habets, G.; Zhang, C.; Ibrahim, P. N.; Hirth, P.; Artis, D. R.; Herlyn, M.; Bollag, G. Discovery of a Selective Inhibitor of Oncogenic B-Raf Kinase With Potent Antimelanoma Activity. *Proc. Natl. Acad. Sci. U. S. A.* **2008,** *105,* 3041–3046.

78. Bollag, G.; Hirth, P.; Tsai, J.; Zhang, J.; Ibrahim, P. N.; Cho, H.; Spevak, W.; Zhang, C.; Zhang, Y.; Habets, G.; Burton, E. A.; Wong, B.; Tsang, G.; West, B. L.; Powell, B.; Shellooe, R.; Marimuthu, A.; Nguyen, H.; Zhang, K. Y.; Artis, D. R.; Schlessinger, J.; Su, F.; Higgins, B.; Iyer, R.; D'Andrea, K.; Koehler, A.; Stumm, M.; Lin, P. S.; Lee, R. J.; Grippo, J.; Puzanov, I.; Kim, K. B.; Ribas, A.; McArthur, G. A.; Sosman, J. A.; Chapman, P. B.; Flaherty, K. T.; Xu, X.; Nathanson, K. L.; Nolop, K. Clinical Efficacy of a RAF Inhibitor Needs Broad Target Blockade in BRAF-Mutant Melanoma. *Nature* **2010,** *467,* 596–599.
79. Arkin, M. R.; Wells, J. A. Small-Molecule Inhibitors of Protein–Protein Interactions: Progressing Towards the Dream. *Nat. Rev. Drug Discov.* **2004,** *3,* 301–317.
80. Wells, J. A.; McClendon, C. L. Reaching for High-Hanging Fruit in Drug Discovery at Protein–Protein Interfaces. *Nature* **2007,** *450,* 1001–1009.
81. Coyne, A. G.; Scott, D. E.; Abell, C. Drugging Challenging Targets Using Fragment-Based Approaches. *Curr. Opin. Chem. Biol.* **2010,** *14,* 299–307.
82. Petros, A. M.; Dinges, J.; Augeri, D. J.; Baumeister, S. A.; Betebenner, D. A.; Bures, M. G.; Elmore, S. W.; Hajduk, P. J.; Joseph, M. K.; Landis, S. K.; Nettesheim, D. G.; Rosenberg, S. H.; Shen, W.; Thomas, S.; Wang, X.; Zanze, I.; Zhang, H.; Fesik, S. W. Discovery of a Potent Inhibitor of the Antiapoptotic Protein Bcl-xL From NMR and Parallel Synthesis. *J. Med. Chem.* **2006,** *49,* 656–663.
83. Oltersdorf, T.; Elmore, S. W.; Shoemaker, A. R.; Armstrong, R. C.; Augeri, D. J.; Belli, B. A.; Bruncko, M.; Deckwerth, T. L.; Dinges, J.; Hajduk, P. J.; Joseph, M. K.; Kitada, S.; Korsmeyer, S. J.; Kunzer, A. R.; Letai, A.; Li, C.; Mitten, M. J.; Nettesheim, D. G.; Ng, S.; Nimmer, P. M.; O'Connor, J. M.; Oleksijew, A.; Petros, A. M.; Reed, J. C.; Shen, W.; Tahir, S. K.; Thompson, C. B.; Tomaselli, K. J.; Wang, B.; Wendt, M. D.; Zhang, H.; Fesik, S. W.; Rosenberg, S. H. An Inhibitor of Bcl-2 Family Proteins Induces Regression of Solid Tumours. *Nature* **2005,** *435,* 677–681.
84. Park, C. M.; Bruncko, M.; Adickes, J.; Bauch, J.; Ding, H.; Kunzer, A.; Marsh, K. C.; Nimmer, P.; Shoemaker, A. R.; Song, X.; Tahir, S. K.; Tse, C.; Wang, X.; Wendt, M. D.; Yang, X.; Zhang, H.; Fesik, S. W.; Rosenberg, S. H.; Elmore, S. W. Discovery of an Orally Bioavailable Small Molecule Inhibitor of Prosurvival B-cell Lymphoma 2 Proteins. *J. Med. Chem.* **2008,** *51,* 6902–6915.
85. Souers, A. J.; Leverson, J. D.; Boghaert, E. R.; Ackler, S. L.; Catron, N. D.; Chen, J.; Dayton, B. D.; Ding, H.; Enschede, S. H.; Fairbrother, W. J.; Huang, D. C.; Hymowitz, S. G.; Jin, S.; Khaw, S. L.; Kovar, P. J.; Lam, L. T.; Lee, J.; Maecker, H. L.; Marsh, K. C.; Mason, K. D.; Mitten, M. J.; Nimmer, P. M.; Oleksijew, A.; Park, C. H.; Park, C. M.; Phillips, D. C.; Roberts, A. W.; Sampath, D.; Seymour, J. F.; Smith, M. L.; Sullivan, G. M.; Tahir, S. K.; Tse, C.; Wendt, M. D.; Xiao, Y.; Xue, J. C.; Zhang, H.; Humerickhouse, R. A.; Rosenberg, S. H.; Elmore, S. W. ABT-199, a Potent and Selective BCL-2 Inhibitor, Achieves Antitumor Activity While Sparing Platelets. *Nat. Med.* **2013,** *19,* 202–208.
86. Bhat, R.; Tummalapalli, S. R.; Rotella, D. P. Progress in the Discovery and Development of Heat Shock Protein 90 (Hsp90) Inhibitors. *J. Med. Chem.* **2014,** *57,* 8718–8728.
87. Murray, C. W.; Carr, M. G.; Callaghan, O.; Chessari, G.; Congreve, M.; Cowan, S.; Coyle, J. E.; Downham, R.; Figueroa, E.; Frederickson, M.; Graham, B.; McMenamin, R.; O'Brien, M. A.; Patel, S.; Phillips, T. R.; Williams, G.; Woodhead, A. J.; Woolford, A. J. Fragment-Based Drug Discovery Applied to Hsp90. Discovery of Two Lead Series With High Ligand Efficiency. *J. Med. Chem.* **2010,** *53,* 5942–5955.
88. Roe, S. M.; Prodromou, C.; O'Brien, R.; Ladbury, J. E.; Piper, P. W.; Pearl, L. H. Structural Basis for Inhibition of the Hsp90 Molecular Chaperone by the Antitumor Antibiotics Radicicol and Geldanamycin. *J. Med. Chem.* **1999,** *42,* 260–266.
89. Woodhead, A. J.; Angove, H.; Carr, M. G.; Chessari, G.; Congreve, M.; Coyle, J. E.; Cosme, J.; Graham, B.; Day, P. J.; Downham, R.; Fazal, L.; Feltell, R.; Figueroa, E.; Frederickson, M.; Lewis, J.; McMenamin, R.; Murray, C. W.; O'Brien, M. A.; Parra, L.; Patel, S.; Phillips, T.; Rees, D. C.; Rich, S.; Smith, D. M.; Trewartha, G.; Vinkovic, M.; Williams, B.; Woolford, A. J. Discovery of (2,4-Dihydroxy-5-isopropylphenyl)-[5-(4-methylpiperazin-1-ylmethyl)-1,3-dihydrois oindol-2-yl]methanone (AT13387), a Novel Inhibitor of the Molecular Chaperone Hsp90 by Fragment Based Drug Design. *J. Med. Chem.* **2010,** *53,* 5956–5969.
90. Howard, S.; Berdini, V.; Boulstridge, J. A.; Carr, M. G.; Cross, D. M.; Curry, J.; Devine, L. A.; Early, T. R.; Fazal, L.; Gill, A. L.; Heathcote, M.; Maman, S.; Matthews, J. E.; McMenamin, R. L.; Navarro, E. F.; O'Brien, M. A.; O'Reilly, M.; Rees, D. C.; Reule, M.; Tisi, D.; Williams, G.; Vinkovic, M.; Wyatt, P. G. Fragment-Based Discovery of the Pyrazol-4-yl urea (AT9283), a Multitargeted Kinase Inhibitor With Potent Aurora Kinase Activity. *J. Med. Chem.* **2009,** *52,* 379–388.
91. Wyatt, P. G.; Woodhead, A. J.; Berdini, V.; Boulstridge, J. A.; Carr, M. G.; Cross, D. M.; Davis, D. J.; Devine, L. A.; Early, T. R.; Feltell, R. E.; Lewis, E. J.; McMenamin, R. L.; Navarro, E. F.; O'Brien, M. A.; O'Reilly, M.; Reule, M.; Saxty, G.; Seavers, L. C.; Smith, D. M.; Squires, M. S.; Trewartha, G.; Walker, M. T.; Woolford, A. J. Identification of N-(4-Piperidinyl)-4-(2,6-dichlorobenzoylamino)-1H-pyrazole-3-carboxamide (AT7519), a Novel Cyclin Dependent Kinase Inhibitor Using Fragment-Based X-ray Crystallography and Structure Based Drug Design. *J. Med. Chem.* **2008,** *51,* 4986–4999.
92. Cheung, K. M.; Matthews, T. P.; James, K.; Rowlands, M. G.; Boxall, K. J.; Sharp, S. Y.; Maloney, A.; Roe, S. M.; Prodromou, C.; Pearl, L. H.; Aherne, G. W.; McDonald, E.; Workman, P. The Identification, Synthesis, Protein Crystal Structure and in vitro Biochemical Evaluation of a New 3,4-diarylpyrazole Class of Hsp90 Inhibitors. *Bioorg. Med. Chem. Lett.* **2005,** *15,* 3338–3343.
93. Brough, P. A.; Aherne, W.; Barril, X.; Borgognoni, J.; Boxall, K.; Cansfield, J. E.; Cheung, K. M.; Collins, I.; Davies, N. G.; Drysdale, M. J.; Dymock, B.; Eccles, S. A.; Finch, H.; Fink, A.; Hayes, A.; Howes, R.; Hubbard, R. E.; James, K.; Jordan, A. M.; Lockie, A.; Martins, V.; Massey, A.; Matthews, T. P.; McDonald, E.; Northfield, C. J.; Pearl, L. H.; Prodromou, C.; Ray, S.; Raynaud, F. I.; Roughley, S. D.; Sharp, S. Y.; Surgenor, A.; Walmsley, D. L.; Webb, P.; Wood, M.; Workman, P.; Wright, L. 4,5-Diarylisoxazole Hsp90 Chaperone Inhibitors: Potential Therapeutic Agents for the Treatment of Cancer. *J. Med. Chem.* **2008,** *51,* 196–218.
94. Smith, C. R.; Dougan, D. R.; Komandla, M.; Kanouni, T.; Knight, B.; Lawson, J. D.; Sabat, M.; Taylor, E. R.; Vu, P.; Wyrick, C. Fragment-Based Discovery of a Small Molecule Inhibitor of Bruton's Tyrosine Kinase. *J. Med. Chem.* **2015,** *58,* 5437–5444.
95. Miller, R. M.; Paavilainen, V. O.; Krishnan, S.; Serafimova, I. M.; Taunton, J. Electrophilic Fragment-Based Design of Reversible Covalent Kinase Inhibitors. *J. Am. Chem. Soc.* **2013,** *135,* 5298–5301.
96. Saalau-Bethell, S. M.; Woodhead, A. J.; Chessari, G.; Carr, M. G.; Coyle, J.; Graham, B.; Hiscock, S. D.; Murray, C. W.; Pathuri, P.; Rich, S. J.; Richardson, C. J.; Williams, P. A.; Jhoti, H. Discovery of an Allosteric Mechanism for the Regulation of HCV NS3 Protein Function. *Nat. Chem. Biol.* **2012,** *8,* 920–925.
97. Frett, B.; Carlomagno, F.; Moccia, M. L.; Brescia, A.; Federico, G.; De Falco, V.; Admire, B.; Chen, Z.; Qi, W.; Santoro, M.; Li, H. Y. Fragment-Based Discovery of a Dual Pan-RET/VEGFR2 Kinase Inhibitor Optimized for Single-Agent Polypharmacology. *Angew. Chem. Int. Ed. Engl.* **2015,** *54,* 8717–8721.
98. Ciulli, A.; Williams, G.; Smith, A. G.; Blundell, T. L.; Abell, C. Probing Hot Spots at Protein-Ligand Binding Sites: a Fragment-Based Approach Using Biophysical Methods. *J. Med. Chem.* **2006,** *49,* 4992–5000.
99. Reynolds, C. H.; Bembenek, S. D.; Tounge, B. A. The Role of Molecular Size in Ligand Efficiency. *Bioorg. Med. Chem. Lett.* **2007,** *17,* 4258–4261.
100. Murray, C. W.; Verdonk, M. L.; Rees, D. C. Experiences in Fragment-Based Drug Discovery. *Trends Pharmacol. Sci.* **2012,** *33,* 224–232.
101. Schulz, M. N.; Hubbard, R. E. Recent Progress in Fragment-Based Lead Discovery. *Curr. Opin. Pharmacol.* **2009,** *9,* 615–621.
102. Davis, A. M.; St-Gallay, S. A.; Kleywegt, G. J. Limitations and Lessons in the Use of X-ray Structural Information in Drug Design. *Drug Discov. Today* **2008,** *13,* 831–841.
103. Hartshorn, M. J.; Murray, C. W.; Cleasby, A.; Frederickson, M.; Tickle, I. J.; Jhoti, H. Fragment-Based Lead Discovery Using X-ray Crystallography. *J. Med. Chem.* **2005,** *48,* 403–413.
104. Carr, R.; Jhoti, H. Structure-Based Screening of Low-Affinity Compounds. *Drug Discov. Today* **2002,** *7,* 522–527.
105. Blundell, T. L.; Jhoti, H.; Abell, C. High-Throughput Crystallography for Lead Discovery in Drug Design. *Nat. Rev. Drug Discov.* **2002,** *1,* 45–54.
106. Babaoglu, K.; Shoichet, B. K. Deconstructing Fragment-Based Inhibitor Discovery. *Nat. Chem. Biol.* **2006,** *2,* 720–723.
107. Chen, H.; Zhou, X.; Wang, A.; Zheng, Y.; Gao, Y.; Zhou, J. Evolutions in Fragment-Based Drug Design: The Deconstruction–Reconstruction Approach. *Drug Discov. Today* **2015,** *20,* 105–113.
108. Chen, H.; Yang, Z.; Ding, C.; Chu, L.; Zhang, Y.; Terry, K.; Liu, H.; Shen, Q.; Zhou, J. Fragment-Based Drug Design and Identification of HJC0123, a Novel Orally Bioavailable STAT3 Inhibitor for Cancer Therapy. *Eur. J. Med. Chem.* **2013,** *62,* 498–507.
109. Davis, B. J.; Erlanson, D. A. Learning From Our Mistakes: The 'Unknown Knowns' in Fragment Screening. *Bioorg. Med. Chem. Lett.* **2013,** *23,* 2844–2852.
110. Baell, J.; Walters, M. A. Chemistry: Chemical Con Artists Foil Drug Discovery. *Nature* **2014,** *513,* 481–483.
111. Reynolds, C. H.; Tounge, B. A.; Bembenek, S. D. Ligand Binding Efficiency: Trends, Physical Basis, and Implications. *J. Med. Chem.* **2008,** *51,* 2432–2438.
112. Bembenek, S. D.; Tounge, B. A.; Reynolds, C. H. Ligand Efficiency and Fragment-Based Drug Discovery. *Drug Discov. Today* **2009,** *14,* 278–283.

113. Pellecchia, M.; Becattini, B.; Crowell, K. J.; Fattorusso, R.; Forino, M.; Fragai, M.; Jung, D.; Mustelin, T.; Tautz, L. NMR-Based Techniques in the Hit Identification and Optimisation Processes. *Expert Opin. Ther. Targets* **2004,** *8,* 597–611.
114. Chen, H.; Wang, C. Z.; Ding, C.; Wild, C.; Copits, B.; Swanson, G. T.; Johnson, K. M.; Zhou, J. A Combined Bioinformatics and Chemoinformatics Approach for Developing Asymmetric Bivalent AMPA Receptor Positive Allosteric Modulators as Neuroprotective Agents. *ChemMedChem* **2013,** *8,* 226–230.
115. Talele, T. T.; Khedkar, S. A.; Rigby, A. C. Successful Applications of Computer Aided Drug Discovery: Moving Drugs From Concept to the Clinic. *Curr. Top. Med. Chem.* **2010,** *10,* 127–141.
116. Hajduk, P. J. Fragment-Based Drug Design: How Big is Too Big? *J. Med. Chem.* **2006,** *49,* 6972–6976.
117. Albert, J. S.; Blomberg, N.; Breeze, A. L.; Brown, A. J.; Burrows, J. N.; Edwards, P. D.; Folmer, R. H.; Geschwindner, S.; Griffen, E. J.; Kenny, P. W.; Nowak, T.; Olsson, L. L.; Sanganee, H.; Shapiro, A. B. An Integrated Approach to Fragment-Based Lead Generation: Philosophy, Strategy and Case Studies From AstraZeneca's Drug Discovery Programmes. *Curr. Top. Med. Chem.* **2007,** *7,* 1600–1629.
118. Chessari, G.; Woodhead, A. J. From Fragment to Clinical Candidate-A Historical Perspective. *Drug Discov. Today* **2009,** *14,* 668–675.
119. Pires, D. E.; Blundell, T. L.; Ascher, D. B. pkCSM: Predicting Small-Molecule Pharmacokinetic and Toxicity Properties Using Graph-Based Signatures. *J. Med. Chem.* **2015,** *58,* 4066–4072.
120. Alex, A. A.; Flocco, M. M. Fragment-Based Drug Discovery: What Has It Achieved So Far? *Curr. Top. Med. Chem.* **2007,** *7,* 1544–1567.
121. Sancineto, L.; Massari, S.; Iraci, N.; Tabarrini, O. From Small to Powerful: The Fragments Universe and Its "Chem-Appeal". *Curr. Med. Chem.* **2013,** *20,* 1355–1381.
122. Warr, W. A. Fragment-Based Drug Discovery. *J. Comput. Aided Mol. Des.* **2009,** *23,* 453–458.
123. Zartler, E. R.; Shapiro, M. J. Protein NMR-Based Screening in Drug Discovery. *Curr. Pharm. Des.* **2006,** *12,* 3963–3972.
124. Erlanson, D. A. Fragment-Based Lead Discovery: A Chemical Update. *Curr. Opin. Biotechnol.* **2006,** *17,* 643–652.
125. Murray, C. W.; Blundell, T. L. Structural Biology in Fragment-Based Drug Design. *Curr. Opin. Struct. Biol.* **2010,** *20,* 497–507.
126. Law, R.; Barker, O.; Barker, J. J.; Hesterkamp, T.; Godemann, R.; Andersen, O.; Fryatt, T.; Courtney, S.; Hallett, D.; Whittaker, M. The Multiple Roles of Computational Chemistry in Fragment-Based Drug Design. *J. Comput. Aided Mol. Des.* **2009,** *23,* 459–473.
127. Kumar, A.; Voet, A.; Zhang, K. Y. Fragment Based Drug Design: From Experimental to Computational Approaches. *Curr. Med. Chem.* **2012,** *19,* 5128–5147.
128. Hubbard, R. E.; Davis, B.; Chen, I.; Drysdale, M. J. The SeeDs Approach: Integrating Fragments Into Drug Discovery. *Curr. Top. Med. Chem.* **2007,** *7,* 1568–1581.
129. Sondergaard, C. R.; Garrett, A. E.; Carstensen, T.; Pollastri, G.; Nielsen, J. E. Structural Artifacts in Protein-Ligand X-ray Structures: Implications for the Development of Docking Scoring Functions. *J. Med. Chem.* **2009,** *52,* 5673–5684.
130. Leeson, P. D.; Springthorpe, B. The Influence of Drug-Like Concepts on Decision-Making in Medicinal Chemistry. *Nat. Rev. Drug Discov.* **2007,** *6,* 881–890.
131. Keseru, G. M.; Makara, G. M. The Influence of Lead Discovery Strategies on the Properties of Drug Candidates. *Nat. Rev. Drug Discov.* **2009,** *8,* 203–212.

2.09 Computational Models to Predict Toxicological Endpoints in Drug Discovery and Strategies for Data Integration

A Brigo and W Muster, F. Hoffmann-La Roche, Ltd., Basel, Switzerland

© 2017 Elsevier Ltd. All rights reserved.

2.09.1	**Introduction**	233
2.09.2	**Methods for the Prediction of Toxicity**	234
2.09.2.1	Rule-Based Systems	234
2.09.2.1.1	Derek Nexus	234
2.09.2.1.2	ToxTree	235
2.09.2.1.3	CASE Ultra expert rules	235
2.09.2.1.4	Leadscope expert alert system	235
2.09.2.2	Statistical-Based Systems	235
2.09.2.2.1	Sarah Nexus	236
2.09.2.2.2	CASE Ultra	236
2.09.2.2.3	Leadscope model applier	236
2.09.2.2.4	OECD toolbox	237
2.09.2.2.5	Bioclipse	237
2.09.2.2.6	admetSAR	237
2.09.2.2.7	Symmetry	237
2.09.3	**Assessment of Genotoxic Impurities**	237
2.09.3.1	Regulatory Requirements	237
2.09.3.2	The ICH M7 Guideline	238
2.09.3.3	Prediction of Mutagenicity With Commercial In Silico Systems	238
2.09.4	**In Silico Models for the Prediction of Toxicity in Drug Discovery**	246
2.09.4.1	Target Identification (TI), Target Assessment, and Exploratory Work	246
2.09.4.2	Lead Identification Phase: Target Selected (TS) to Lead Series Identified (LSI)	249
2.09.4.3	Lead Optimization (LO) Phase: LSI to Clinical Candidate Selected (CLS)	249
2.09.4.4	Phase 0: After CLS to Entry Into Humans (EIH)	250
2.09.5	**Prediction of Complex Toxicity Endpoints**	250
2.09.5.1	Outcome of In Vivo Safety Studies: A Challenging Prediction	250
2.09.5.2	Drug-Induced Liver Injury	251
2.09.5.3	Data Integration of In Vivo Toxicity Studies	253
2.09.5.4	Development of Prediction Models	253
2.09.6	**Data Sharing Initiatives and Data Exchange for Regulatory Purposes**	254
2.09.6.1	IMI eTox and NextGets Initiatives: Data Sharing and Modeling Approaches	254
2.09.6.2	SEND Data Model and Electronic Submission to FDA	255
References		256

2.09.1 Introduction

Over the past few years, computational models have positioned themselves quite significantly within the pharmaceutical industry, particularly in the earlier phases of drug discovery, not only for the prediction of efficacy or affinity to specific pharmacological targets, but also for the optimization of safety and pharmacokinetics profile. The transition from a promising compound to a successful drug that can ultimately benefit patients is the result of a fine balance of a daunting number of favorable properties, including target potency, selectivity, ADME (absorption, distribution, metabolism, excretion), and (pre)-clinical safety profiles.[1,2]

As a clinical candidate needs to undergo rigorous preclinical optimization in various domains, multidimensional optimization (MDO) is a term often used to describe the intensive investigations during the first 3 to 4 years of drug development from the identification and validation of the target to the selection of the molecule most suitable for clinical development. The current MDO process comprises the use of in silico, in vitro, as well as in vivo models. In general, in silico tools have the intrinsic advantages to be fast and not to need the physical presence of the test compounds and can therefore be applied very early in drug development. Theoretically, in silico models can be developed for all endpoints and organisms, but the availability of large enough, balanced, and high-quality datasets are the main drawbacks for reliable predictions. An excellent correlation with the in vitro/in vivo data, that is, high sensitivity, as well as high specificity, an easy to use and easy to interpret in silico model are key requirements for its usefulness. In the past few years, computational toxicology prediction systems tremendously increased their predictive power for endpoints like

genotoxicity, carcinogenicity, phototoxicity, phospholipidosis, GSH adduct formation, hERG inhibition, CYP inductions, and DILI (drug-induced liver injury), but still have not achieved the major breakthrough due to lack of sufficiently large datasets covering more complex and broader toxicological endpoints (e.g., liver-, kidney-, cardio-toxicity). These are the critical toxicity endpoints, which needs to be further investigated in the next years to weed out potential safety issues in the clinics. Recent initiatives and consortia (e.g., IMI/eTOX, ToxCast, and ToxBank) dealing with data sharing of preclinical in vivo toxicology studies and development of computational approaches have the potential of significantly improving these endpoint predictions and filling the most data gaps.[3]

This article will outline general considerations on the mainly applied expert systems—rule-based and statistical-based models—in toxicology and ADME for pharmaceuticals and their application in the early drug discovery and optimization process as well as their regulatory impact on the assessment of potential impurities arising in the manufacturing process. Recent improvements and future perspectives on the main challenges of predicting complex in vivo endpoints will be summarized and discussed.

2.09.2 Methods for the Prediction of Toxicity

The thorough assessment of the safety profile of drug candidates is of great importance to ensure that no harm is posed to healthy volunteers and patients during and after clinical development throughout the entire lifecycle of the drug product. Drug toxicity can manifest itself in a number of ways and may interest one or more target organs or biological processes.

In particular, carcinogenicity, liver, renal, cardiovascular, reproductive, and genetic toxicities are among the most significant safety issues that can prevent drug candidates from progressing through clinical development or can cause the withdrawal of already marketed products. Overall, between 20% and 30% of failures can be attributed to safety reasons.[4–6]

In recent years, predictive computational approaches have gained more importance within industry, helping discovery teams to rank compound classes according to specified criteria and prioritize follow-up experiments, either in vitro or in vivo, with the most promising molecules. Few factors have been instrumental in the increased popularity of in silico approaches in drug discovery, among them:

(a) Broader availability of high quality datasets either via the public domain route or through focused data sharing initiatives;[7,8]
(b) More robust computational models that can provide more reliable predictions;[9]
(c) General pressure to reduce animal testing (e.g., ban on animal testing in the EU for the cosmetic sector);[10]
(d) Increased unmet medical needs calling for bringing innovative drugs to patients faster;
(e) Legislation on the assessment of potential genotoxic impurities;[11]
(f) Software and technology progress, both at a commercial and open source levels.

The most widely used platform-based computational methods specifically designed and developed for the prediction of toxicity endpoints can be roughly divided into two main categories, rule-based and statistical-based systems, depending on what type of methods they use to make their classifications.[3]

2.09.2.1 Rule-Based Systems

Computational tools included in this category store and manipulate knowledge to interpret information. They are often referred to as expert systems, which make use of a set of explicit rules (i.e., not implicitly embedded in a code) to make deductions and classifications. Such systems have the advantage that rules can be easily represented and developed by experts in the field of toxicology (or of any discipline the systems are applied to), rather than by information technology (IT) specialists. In addition, solid expert rules can be derived from limited amounts of data, as long as they are sufficiently representative of specific chemical and biological spaces. Both commercial and open source systems are available within the rule-based methodologies and they include, among others, Derek Nexus,[12–15] ToxTree,[16] CASE Ultra Expert Rules,[17] and Leadscope Expert Alert system.[18]

2.09.2.1.1 Derek Nexus

It is an expert, knowledge-based system which contains structural alerts (SAs) and expert knowledge rules (derived from both public and proprietary data by scientists at Lhasa Ltd.) for a wide range of toxicological endpoints and applies these to make in silico predictions about the toxicity of chemical entities. The knowledge-based expert rules represent knowledge from the literature, academic, industrial, and Lhasa Ltd. scientific experts and are regularly updated according to the newly available experimental data and publications. In making predictions, the expert rules, which take into account not only the presence or absence of a structural alert but also the species and a few calculated physicochemical parameters (where applicable) in a process akin to the human-based logic of argumentation. Proprietary data donated, by Lhasa Ltd. members, has been used in the development of approximately 25% of the bacterial in vitro (the Ames test) mutagenicity alerts in Derek Nexus and proprietary data sets are used to validate the performance of alerts for this, and other endpoints, to provide an indication of predictive performance within the chemical space of highest interest to users. In addition, proprietary and customized alerts can be defined by users and implemented through the Derek Knowledge Editor.

The most recent version of Derek Nexus contains expert-derived functionality to provide negative predictions for bacterial in vitro mutagenicity in order to give more confidence on nonpositive predictions. If a query compound does not match a structural

alert for mutagenicity, then it is compared to a Lhasa reference set of Ames test data and a negative prediction is provided based on the features within the query compound.[19] In case of absence of alerts for endpoints other than mutagenicity, negative calls should be made with caution as alerts that are not part of the rule base, hence unknown to the system, can still be relevant in the induction of certain toxicities.

Since Derek is an expert system, it has no training set in a strict sense as in QSAR-based systems, but there are example compounds for the alerts stored in its knowledge base.

2.09.2.1.2 ToxTree

It is a Java-based, freely available, open-source application for toxicity prediction. It was developed by Ideaconsult Ltd. (Sofia, Bulgaria) under the terms of a contract with the European Commission Joint Research Centre. The program is mainly based on structural alerts but also provides QSAR models for distinct chemical classes to refine the predictions. For mutagenicity, ToxTree implements the Benigni–Bossa rulebase[20] for carcinogenicity and mutagenicity. The alerts are only differentiated into genotoxic and a small number of nongenotoxic ones, without distinction between carcinogenicity and mutagenicity. Additionally, this module offers QSAR models for aromatic amines and α,β-unsaturated aldehydes, which should improve the predictivity for these specific chemical classes. However, the mutagenicity QSARs refer to Salmonella typhimurium TA100 only. With regards to structures that do not trigger any alert, the same considerations on negative predictions made for nonmutagenic endpoints for Derek Nexus apply.

2.09.2.1.3 CASE Ultra expert rules

As of version 1.5.2.0 of CASE Ultra, an *expert rule system* is built using rules from expert knowledge or scientific literature for the prediction of bacterial mutagenicity.[17] A detailed description of the software is given in the related section describing the statistically based systems.

2.09.2.1.4 Leadscope expert alert system

Leadscope Inc. produces several software modules applicable in the context of toxicological forecasting, particularly in the field of QSAR models. Recently, Leadscope developed a rule-based expert system for the prediction of mutagenicity, using an extensive high quality genetic toxicity database containing the results of the bacterial mutagenesis assay along with chemical structures.[21] Firstly, the chemical structures were merged using a chemical registration system to assign a unique identifier to each chemical and merging entries on the basis of this identifier. Next, the graded endpoints for *Salmonella* and *E. coli* were combined from the different sources, resulting in a database of over 7000 chemicals each with a positive/negative overall bacterial mutation call. The reference set also covers a diverse collection of compounds since they have been derived from many different sources, including pharmaceuticals, pesticides, industrial chemicals, and food additives. Clustering led to 1220 clusters with two or more examples, and 1049 singletons (clusters with one example). Once substructures are identified for alert definitions, the selected alerts are consolidated and organized hierarchically (i.e., parent/child). This helps in establishing a mechanistic explanation particularly where any child alert is lacking or has limited mechanistic information, as it may be inherited from the parent alert. When the expert alerts are used to make prediction, a score is calculated reflecting the precision of the alert.[21] In addition to the primary alert, it is also important to define any factors that would deactivate the alerts as a result of electronic or steric effects or by blocking an important metabolic step. In this context, the Leadscope software identified and quantitatively assessed deactivating factors using the 27,000 predefined structural features in Leadscope and generated new chemical scaffolds associated with negative bacterial mutagenicity. Any deactivating fragments identified were quantitatively evaluated using the reference set.

2.09.2.2 Statistical-Based Systems

Quantitative structure–activity relationship (QSAR) models are regression or classification models used in the chemical and biological sciences and other disciplines. Like other regression models, QSAR regression models relate a set of "predictor" variables (X) to the potency of the response variable (Y), while classification QSAR models correlate the predictor variables to a category value of the response variable.

The QSAR approach can be generally described as an application of data analysis methods and statistics to models development that could accurately predict biological activities or properties of compounds based on their structures. Any QSAR method can be generally defined as an application of mathematical and statistical methods to the problem of finding empirical relationships (QSAR models) in the form $P_i = k'(D1, D2,\ldots,Dn)$, where P_i are biological activities (or other properties) of molecules; $D1$, $D2,\ldots,Dn$ are calculated (or, sometimes, experimentally measured) structural properties (or molecular descriptors) of compounds; k' is some empirically established mathematical transformation that should be applied to descriptors to calculate the property values for all molecules. The goal of QSAR modeling is to establish a trend in the descriptor values, which parallels the trend in biological activity.[22]

Both commercial and open source systems are available within the QSAR-based methodologies and they include, among others, Sarah Nexus,[23] CASE Ultra,[17] Leadscope Model Applier,[24] OECD Toolbox,[25] Bioclipse,[26] admetSAR, and Prous Institute Symmetry.[27]

2.09.2.2.1 Sarah Nexus

It is a statistical system which utilizes a self-organising hypothesis network (SOHN) model to generate predictions for mutagenicity.[28] This hierarchical model not only retrieves matching fragments, it also further refines these results by considering the structure's similarity to the query structure. The methodology retains those fragments that are perceived to be of greater value; fragments may be of various sizes and can even overlap, ensuring greater accuracy in predictions. Fragments are generated from the provided training set of molecules and not selected from lists of predetermined fragments. Both global (broad coverage, not adequately sensitive to local variations) and local (more accurate for fragments that fall inside their chemical space, narrower in scope) models are available in Sarah Nexus. If the query structure is not an exact match to a compound within the training set (for which a prediction of 100% confidence is generated), the structure is fragmented and the software will select the most appropriate model for each fragment.

The structural explanation for the prediction provided by Sarah Nexus is conveyed by highlighting those fragment(s) that the model considers meaningful. Sarah Nexus provides a confidence score and a structural explanation for each prediction alongside direct access to supporting data to aid expert analysis.[29] The results of the validation of the system using 14 different in vitro mutagenicity data sets provided by nine pharmaceutical companies have been recently published by Barber et al.[30]

2.09.2.2.2 CASE Ultra

CASE Ultra's algorithm is mainly influenced by the original MCASE methodology,[31,32] a traditional QSAR system, which can automatically generate a predictive model from a training set of noncongeneric compounds with associated biological or toxicity data. The training set ideally should contain examples of both active and inactive chemicals in a nonoverly skewed ratio.

CASE Ultra can identify alerts that are not limited to linear paths of limited size or limited branching pattern and the training sets could be larger than 8000 molecules.[33] To build a model, CASE Ultra picks up one active chemical at a time from the training set and systematically generates a list of fragments for that chemical. Each fragment's relevance for activity is then determined using a two-objective criteria comprised of Shannon's entropy[34] as a fitness measure and the number of the active training set molecules containing this fragment (fragments that are optimal based on the two objectives, i.e., the ones that cannot be replaced by any other fragment without degrading one or both objectives, are selected and then sorted in descending order of the number of their active chemicals). A top few fragments (based on the aforementioned two-objective criteria, e.g., fragments that have low entropy as well as supported by higher number of active training chemicals) are selected. These fragments are considered as potential positive alerts. The fragment generation procedure produces simple linear chains of varying lengths and branched fragments as well as complex substructures generated by combining simple fragments. When the algorithm has finished scanning all the active chemicals, a search is made in the accumulated list of the potential positive alerts to find the alert that covers the highest number of active chemicals, and it is added to the final list of positive alerts. This step is repeated until enough positive alerts were identified to cover all the active chemicals in the training set. Once a final set of positive alerts is identified, CASE Ultra attempts to build separate local QSARs for each positive alert in order to explain the variation in activity within the training set chemicals covered by that alert. In addition, deactivating alerts are found using a very similar process but by scanning inactive chemicals and finding fragments that occur mainly in inactive chemicals. This collection of positive and deactivating alerts constitutes a model for a particular endpoint and can be used for predicting activity in test chemicals. During prediction, a test chemical is scanned against the list of the model's positive and deactivating alerts, and if no positive alerts could be identified in it, the chemical is considered inactive. In general, if the test chemical contains one or more positive alerts, it is predicted as "active." However, this active prediction call can be changed if the local QSAR of the positive alert modifies the prediction. The presence of a deactivating alert alongside a positive alert renders the prediction call as "inactive." If more than one positive alert is present, then the one with the highest number of active chemicals is used, and in the case of more than one deactivating alert, the one with the highest number of inactive chemicals is used. If a test chemical contains a positive alert that has been seen in just one or two active training set chemicals, the prediction result is considered "inconclusive" because of the alert low statistical confidence. CASE Ultra recognizes unusual features/fragments in test chemicals that do not match training data (unknown structural fragments). The presence of more than three unknown structural fragments in the test chemical results in an "out of domain" call.

2.09.2.2.3 Leadscope model applier

The Leadscope software employs a fragment-based QSAR paradigm; however, the fragments are not paths of distinct lengths but are predefined in a hierarchically organized dictionary that is closely related to common organic/medicinal chemistry building blocks. For binary classification problems, such as the Ames test results, the algorithm identifies toxicity modulating fragments using a χ^2-test. Furthermore, the software is able to build superstructures from smaller fragments if they improve predictivity. Together with eight global molecular properties, the set of fragments is then used as a descriptor set in a partial least squares (PLS) logistic regression model of the activity class. Therefore, the predictions from this algorithm are continuous probabilities of class membership rather than binary outputs. The program also assesses the applicability domain by measuring the distance to training set molecules. Typically, probabilities greater than 0.5 as can be used to give an "active" prediction and probabilities smaller than 0.5 an "inactive" prediction, which is the standard procedure used by the Model Applier for pretrained models. The system can also annotate compounds as "out of domain" or with "missing descriptors" when a conclusive prediction cannot be made.[24]

2.09.2.2.4 OECD toolbox

The OECD Toolbox (http://www.oecd.org/chemicalsafety/risk-assessment/theoecdqsartoolbox.htm)[25,35] represents a free source of various models. The Toolbox is a software application intended to the use of governments, chemical industry, and other stakeholders in filling gaps in (eco)toxicity data needed for assessing the hazards of chemicals. The Toolbox incorporates information and tools from various sources into a logical workflow. Crucial to this workflow is grouping chemicals into chemical categories. The seminal features of the Toolbox are: (i) identification of relevant structural characteristics and potential mechanism or mode of action of a target chemical; (ii) identification of other chemicals that have the same structural characteristics and/or mechanism or mode of action; (iii) use of existing experimental data to fill the data gap(s). The Toolbox includes a number of models predicting several toxicological endpoints, such as skin sensitization, Ames mutagenicity, acute and repeat-dose toxicity, aquatic toxicity, and others.[36]

2.09.2.2.5 Bioclipse

Bioclipse[26] is an open source cheminformatics toolkit with a wide array of toxicity models integrated, such as carcinogenicity, mutagenicity (Ames), hERG, aquatic tox (daphnia), and a wide array of models from OpenTox.[37] The Ames mutagenicity model in Bioclipse is built using the dataset published by Kazius et al. in 2005[38] containing 4337 chemical structures of which 2401 were classified as mutagen and 1936 nonmutagen. The datasets can be downloaded and the software can be used to generate many molecule descriptors (using the CDK)[39,40] and then QSAR models (through integration with the R-statistical software). The software is considered not as user friendly as some other commercial tools.[41]

2.09.2.2.6 admetSAR

admetSAR[42] is a free website (http://lmmd.ecust.edu.cn:8000/)[43] that enables a single input SMILES structure to be used to rapidly predict scores against a wide range of ADME/Tox models (at the time of writing, 26 qualitative classification and 5 quantitative regression models). These datasets can also be downloaded as most are based on other publications. Each model has some statistics describing the model as well as a probability to provide more confidence in the result. The software is simple to use and drawbacks appear to be the lack of batch processing operation, the "black box" nature of the models, and the lack of capability to build or update the models on the website.[41]

2.09.2.2.7 Symmetry

Symmetry[27] is a platform that applies advanced machine-learning techniques to a variety of structural features and physicochemical properties of small molecules to provide predictions about biological effects. Available Symmetry algorithms include binary classification for active/inactive data sets, meta-classifiers to achieve consensus predictions for sets of binary models, and multilabel learning that yields ranking and probabilistic estimates of the possible outcomes. Symmetry offers a wide range of predictive models (http://symmetry.prousresearch.com/symmetry-models/), including mechanism of action and phenotypic models, toxicity,[44] and human adverse effects.

2.09.3 Assessment of Genotoxic Impurities

2.09.3.1 Regulatory Requirements

The European Medicines Agency Committee for Medicinal Products for Human Use (CHMP) released in 2006[45] a "Guideline on the Limits of Genotoxic Impurities," which describes an approach for assessing genotoxic impurities of unknown carcinogenic potential based on the Threshold of Toxicological Concern (TTC) concept.

The TTC bases its rationale on the fact that it is possible to identify "safe levels of exposure" for chemicals with known toxicological profiles. TTC is a pragmatic risk assessment approach that aims at establishing a human exposure threshold value below which there is a very low probability of an appreciable risk to human health.[46]

Genotoxicity is a broad term that typically describes a deleterious action on cellular genetic material. Chemicals may induce DNA damage by directly interacting with it (e.g., alkylating agents) or by acting on non-DNA targets (e.g., mitotic spindle poisons, inhibitors of topoisomerase). For DNA-reactive genotoxins, the mechanism by which they induce genetic damage is assumed to follow a linear no-threshold model; on the other hand, for molecules not interacting directly with DNA, the existence of a threshold concentration required to induce the damage is accepted.[46] Impurities that belong to the second category of substances can be regulated according to the ICH Quality Guideline Q3C[47] which includes Class 2 Solvents. The thresholds or permissible daily exposures are calculated from the no-observed-effect Level (NOEL) obtained in the most relevant animal studies with the use of conservative conversion factors used to extrapolate the animal data to humans.

In terms of regulatory guidelines on this specific aspect of risk assessment, the European Medicines Agency Committee for Medicinal Products for Human Use (CHMP) released in 2006[45] a "Guideline on the Limits of Genotoxic Impurities," which describes an approach for assessing genotoxic impurities of unknown carcinogenic potential based on the TTC concept. The CHMP guideline suggests that the TTC concept should be applied to those genotoxic impurities that do not have sufficient evidence of a threshold-related mechanism of action. The reference values are taken from Kroes et al.,[48] where a TTC of 0.15 μg/day is proposed for impurities presenting a structural alert for genotoxicity, corresponding to a 10^{-6} lifetime risk of cancer. In the case of pharmaceuticals, the guideline suggests a 1 in 100,000 risk be applied, resulting in a TTC of 1.5 μg/day.[3,46]

Also in 2006, a task force established under the umbrella of the US Pharmaceutical Research and Manufacturing Association (PhRMA) for the first time proposed the ″staged TTC″ concept to be applied to pharmaceuticals.[49] The task force was established as a response to various clinical holds imposed by the FDA on investigational drugs in clinical trial phases based on suspicions to contain genotoxic impurities at levels potentially associated with a risk for the volunteers or patients involved in these trials.[50] The staged approach allows levels of daily intake of mutagenic impurities higher than 1.5 μg as defined by the lifetime TTC, namely 10 μg (for a 6-to-12-month duration), 20 μg (3–6 months), 40 μg (1–3 months), and 120 μg for not more than 1 month. The EMA adopted the staged TTC approach for limits of genotoxic impurities in clinical trials in the 2007 Q&A document (EMA 2010,[51]), but to be more conservative it reduced the staged TTC limits proposed in the PhRMA paper by a factor of 2.

In 2008, the FDA issued a draft "guidance for Industry on Genotoxic and Carcinogenic Impurities in Drug Substances and Products: Recommended Approaches" (FDA 2008) which was largely similar to the EU guidance. However, this document has not been finalized because in 2009 the topic "genotoxic impurities" was adopted by ICH for development of a new internationally harmonized guideline. Since the topic was considered to include both safety and quality aspects the projected guideline was assigned to the M (multidisciplinary) series of the ICH process and designated as ICH M7 with the title "Assessment and Control of DNA-Reactive (Mutagenic) Impurities in Pharmaceuticals to Limit Potential Carcinogenic Risk."[52] The document was adopted as a step 4 ICH Harmonised Tripartite Guideline in June 2014 (ICH 2014) and is currently on step 5, adopted by CHMP on 25 Sep. 2014 and issued as EMA/CHMP/ICH/83812/2013.

2.09.3.2 The ICH M7 Guideline

The ICH M7 guideline combines many of the principles set by the EU- and the draft FDA Guidelines on genotoxic impurities. Some aspects, though, have been updated and clear recommendations can be identified. A thorough description of all key aspects of the ICH M7 guideline, is beyond the scope of the present contribution.[50] It is nonetheless worthwhile mentioning few of the critical aspects that the ICH M7 guideline does enforce:

1. Structure-based assessment of potentially mutagenic impurities has to be carried out using two in silico systems that complement each other: one should be a rule-based and one a statistics-based method;
2. The impurities classification system proposed by the ICH M7 guideline has been derived from the scheme proposed by Müller et al. in 2006,[49] with five classes of impurities assigned according to data availability for the characterization of their mutagenicity and carcinogenicity potential;
3. ICH M7 replaced the term "genotoxic impurities" as applied by the EU Guideline on the Limits of Genotoxic Impurities with the term "DNA-reactive impurities" in order to specify that DNA reactive compounds (i.e., that typically covalently bind to DNA generating adducts, which, if unrepaired, can lead to point mutations and/or strand-breakage) are those that fall within the scope of the Guideline. There is also the assumption that DNA-reactive (Ames-positive) compounds are likely carcinogens with no threshold mechanism;
4. For DNA-reactive (Ames-positive) compounds lacking rodent carcinogenicity data, a generic TTC value would be applied as an acceptable intake level that poses a negligible risk of carcinogenicity;
5. If rodent carcinogenicity data is available for a (potentially) mutagenic impurity, the application of the TTC concept is not warranted and a compound-specific calculation of acceptable levels of impurity intake is recommended;[52]
6. Compound-specific calculations for acceptable intakes can be applied case-by-case for impurities which are chemically similar to a known carcinogen compound class (class-specific acceptable intakes) provided that a rationale for chemical similarity and supporting data can be demonstrated (Note 5);[46,52]
7. The acceptable intakes derived from compound-specific risk assessments can be adjusted for shorter duration of exposure. The TTC-based acceptable intake of 1.5 μg/day is considered to be protective for a lifetime of daily exposure (**Table 1**,[11]). To address Less Than Lifetime (LTL) exposures to mutagenic impurities in pharmaceuticals, a formula is applied in which the acceptable cumulative lifetime dose (1.5 μg/day × 25,550 days = 38.3 mg) is uniformly distributed over the total number of exposure days during LTL exposure. This allows higher daily intakes of mutagenic impurities than would be the case for lifetime exposure and still maintain comparable risk levels for daily and nondaily treatment regimens;
8. As far as multiple impurities are concerned, when there are more than two mutagenic (i.e., Ames positive) or alerting impurities, total mutagenic impurities should be limited as described in **Table 2** for clinical development and marketed products.

2.09.3.3 Prediction of Mutagenicity With Commercial In Silico Systems

In silico methods for the prediction of mutagenic activity have been available for many years and they have undergone continuous updates and improvements driven by advancements in technology and greater availability of high quality data.

Table 1 Acceptable Intakes for an Individual Impurity

Duration of treatment	*≤ 1 month*	*> 1–12 months*	*> 1–10 years*	*> 10 years*
Daily intake (μg/day)	120	20	10	1.5

Table 2 Acceptable intakes for an individual impurity

Duration of treatment	*≤ 1 month*	*> 1–12 months*	*> 1–10 years*	*> 10 years*
Daily intake (μg/day)	120	60	30	5

The specific use of such in silico tools in the pharmaceutical industry, in the context of the evaluation of genotoxic impurities, has been summarized and reviewed by Sutter et al.[53] The authors, representing a total of 14 pharmaceutical companies, compared the predictive value of the different methodologies analyzed in two surveys conveyed in the US and European pharmaceutical industry: most pharmaceutical companies used a rule-based expert system as their primary methodology, yielding negative predictivity values of ⩾78% in all participating companies. A further increase (>90%) was often achieved by an additional expert review and/or a second statistics-based methodology. Also in the latter case, an expert review was encouraged, especially when conflicting results were obtained. The conclusion was that a rule-based expert system complemented by either expert knowledge or a second (Q)SAR model is appropriate.

More recently, still using ICH M7 as binding guidance, Amberg and coworkers went deeper in elucidating scenarios where additional expert knowledge may be beneficial (on top of the in silico classification), what such an expert review may contain, and how the results and accompanying considerations may be documented.[54]

In order to comply with the ICH M7 guideline specifications, mandating the use two different methodologies, one expert-rule based and one statistical based, additional commercial in silico tools and novel models have been made available to the scientific community. Brigo and Muster[55] evaluated three expert-rule systems (*Derek Nexus v.4.0.5*,[12] *ToxTree v.2.6.6*,[16] *Leadscope Expert Alert v.3.2.4-1*[18]) and three statistical systems (*Sarah v.1.2.0*,[23] *Leadscope Model Applier v.3.2.4-1*,[24] *three models of CASE Ultra v.1.5.1.8*[17]—*GT1_7B; SALM2013; SALM2013PHARMA*) in an individual and combined fashion. All the examined programs (see **Table 3**) have been applied as commercially available, without internal customization or any follow-up expert knowledge driving the final classifications.

The evaluation was carried out using a large validation set of Ames mutagenicity data comprising over 10,000 compounds, 30% of which are Roche proprietary data (**Table 4**). The Roche datasets include the vast majority of compounds (not only impurities) tested in the Ames standard[57] and Microsuspension[58] protocols over the past 30 years.

The application of individual systems showed, as expected, adequate performance statistics with public domain datasets (concordance: 74–95%; sensitivity: 58–99%; specificity: 51–96%; **Fig. 1**), however there was a significant drop in sensitivity with the Roche data sets, down, in one case, to single digit (concordance: 66–88%; sensitivity: 8–54%; specificity: 69–95%; **Fig. 2**). The assessment of the overlap between training and validation data sets showed high values (up to 91% for Sarah) for the "public validation sets," which obviously contributed to good performance of the systems with these specific sets.[3,55]

Expert-rule based tools showed lower specificity with public domain datasets versus the statistical-based programs. Statistical tools showed a much higher number of compounds (up to 39% in one case) outside of their applicability domains and, hence, not predicted (**Fig. 2**).

Table 3 Software tools assessed in the validation experiments and main features

Software tool	*Methodology*	*Availability*	*Vendor*
Derek Nexus v.4.0.5	Rule-based	Commercial	Lhasa Limited
ToxTree v.2.6.6	Rule-based	Free Download	EU ECVAM JRC
Leadscope Expert Alert v.3.2.4-1	Rule-based	Commercial	Leadscope, Inc.
Sarah Nexus v.1.2.0	Statistical-based	Commercial	Lhasa Limited
Leadscope Model Applier v.3.2.4-1	Statistical-based	Commercial	Leadscope, Inc.
CASE Ultra v.1.5.1.8—*Model GT1_7B*	Statistical-based	Commercial	MultiCASE, Inc.
CASE Ultra v.1.5.1.8—*Model SALM2013*	Statistical-based	Commercial	MultiCASE, Inc.
CASE Ultra v.1.5.1.8—*Model SALM2013PHARMA*	Statistical-based	Commercial	MultiCASE, Inc.

Table 4 Summary of external validation sets

Data set	*Number of compounds*	*Positive*	*Negative*
Roche Ames Standard	1335	254	1081
Roche Ames Microsuspension	1785	190	1595
LSDB (public domain)	4699	2068	2631
Hansen (public domain)[56]	2647	1773	874
Total	*10,466*	*4285*	*6181*

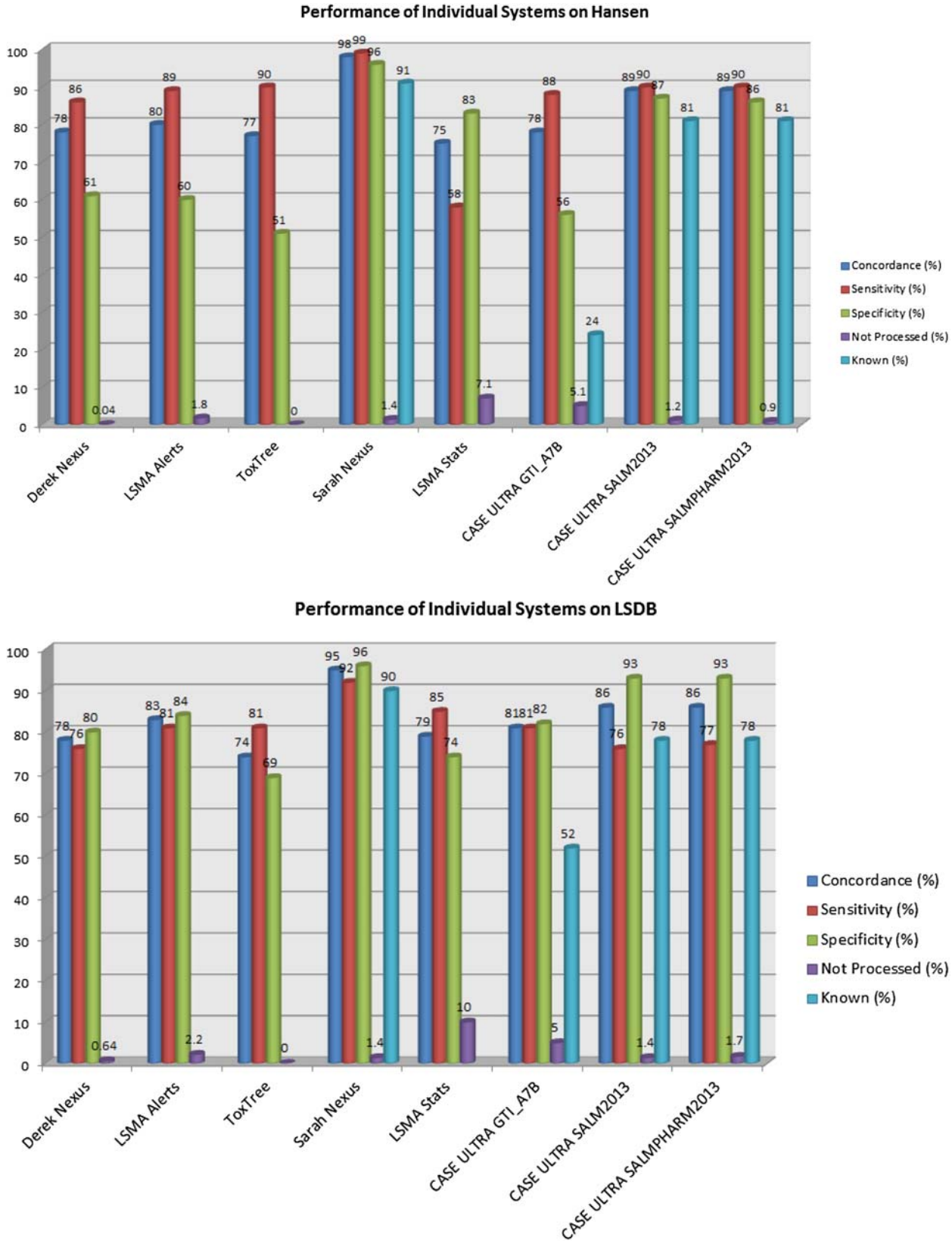

Fig. 1 Performance of individual systems on public datasets Hansen and LSDB.

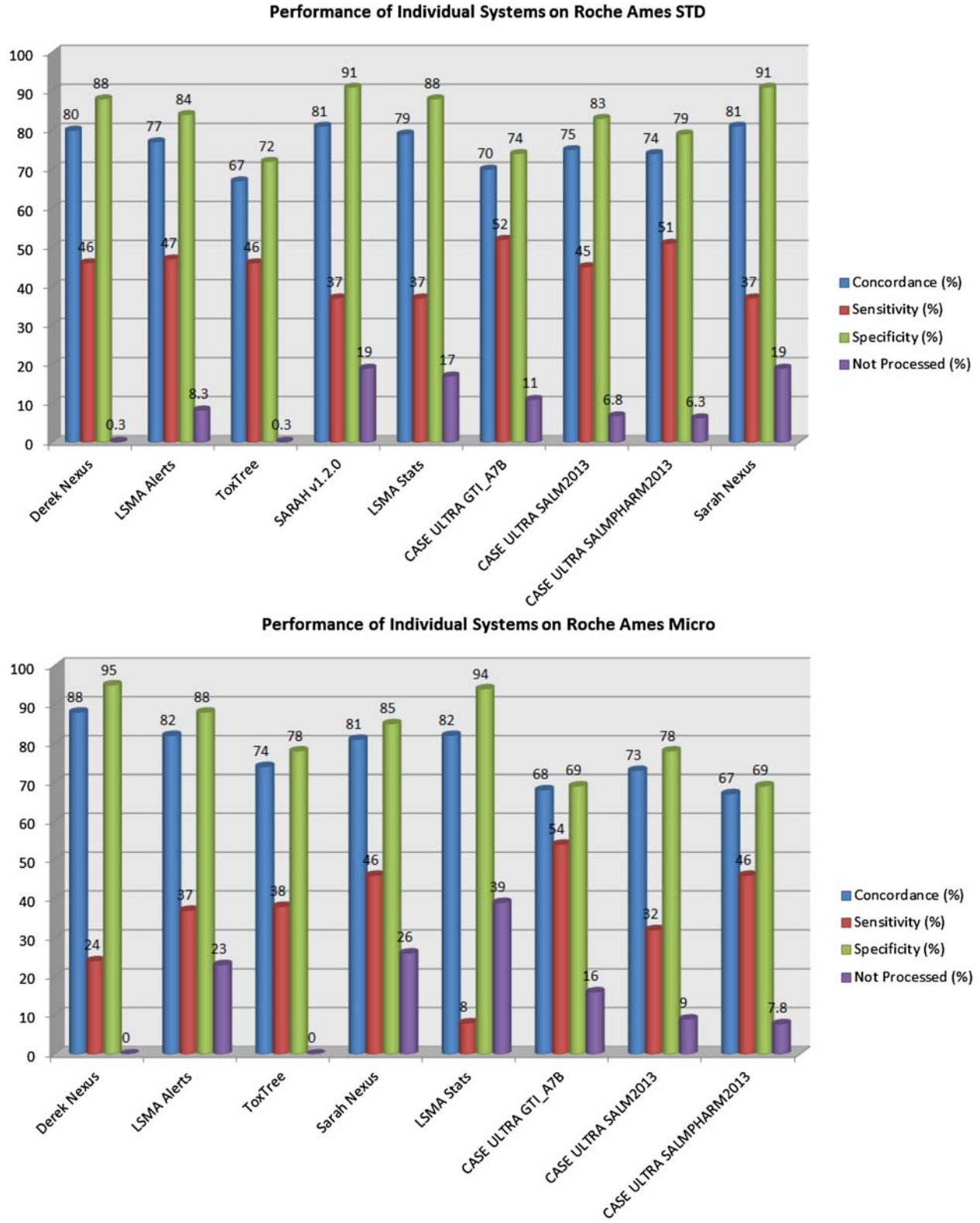

Fig. 2 Performance of individual systems on proprietary Roche datasets.

As previously mentioned, the ICH M7 requires the use of a single combination of one rule-based and one statistical-based tool for the assessment of potential genotoxic impurities. In order to evaluate how such a combined approach changes the overall prediction performance in comparison to the use of individual systems, the Roche validation data sets were submitted to all possible systems permutations (Figs. 3 and 4).

The combinations of all systems, compared to their individual performance with both Roche validation sets, improves the sensitivity to consistently above 50%, up to 71% for the combination "LSMA Alerts + SALM2013." As expected from a consistent increase in sensitivity, specificity is generally lower than with individual systems, but its reduction is limited for the majority of combinations with deltas lower than 20%.

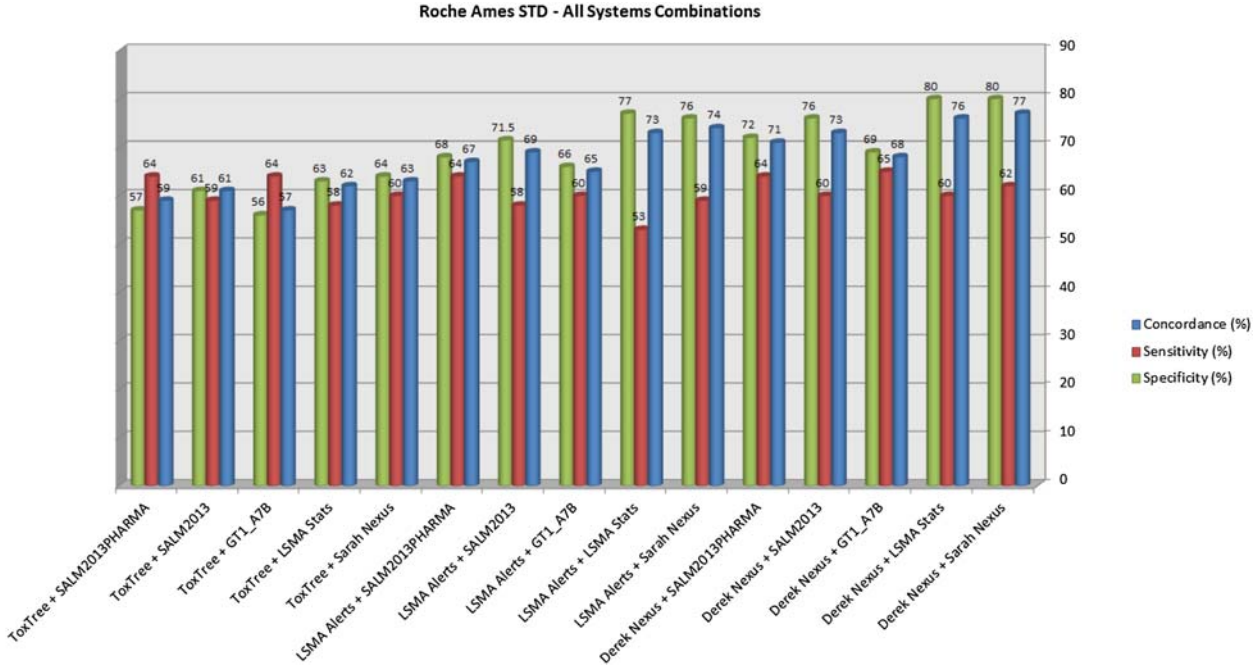

Fig. 3 Performance of individually combined systems on the Roche Ames Standard dataset.

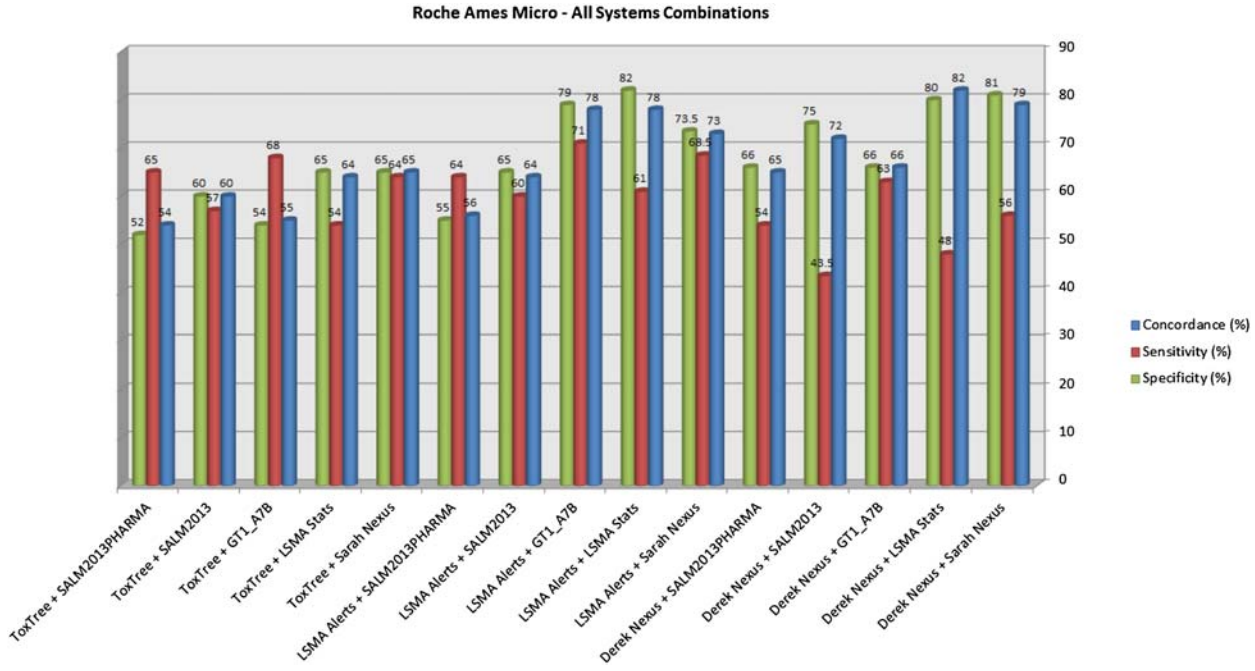

Fig. 4 Performance of individually combined systems on the Roche Ames Microsuspension dataset.

The Roche datasets used in this validation exercise include a rather broad proprietary chemical space not restricted to the usual potential genotoxic impurities domain. A rather quick way to focus the analysis specifically to impurities was the generation from both Roche validation sets of four subsets with molecular weights (MW) ≤ 400, ≤ 350, ≤ 300, and ≤ 250, respectively. Such subsets cover the chemical space of the large majority of the potential genotoxic impurities tested in Roche over the past 10 years.

All in silico programs have been tested against these subsets individually (Figs. 5 and 6) and in all possible permutations (Figs. 7 and 8).[3,55]

With individual systems, sensitivity shows a clear trend to increase proportionally to the decrease of MW. For example, in the Roche Ames Microsuspension set, sensitivity improves as follows: Derek from 27% to 64%; Sarah from 51% to 76%; ToxTree from 42% to 85%; CASE Ultra SALMPHARM2013 from 45% to 71%; LSMA Alerts and LSMA Stats show an increase in sensitivity to 60% up to MW ≤ 300, but there is a flection down to $\sim 55\%$ for both programs for MW ≤ 250. In general, sensitivity increases significantly with low-MW subsets with almost all programs and models (Figs. 5 and 6). The only exception is the CASE Ultra SALM2013 model, which keeps the same sensitivity values throughout all subsets (between 29% and 33%).[3,55] Changes in MW from ≤ 300 to ≤ 250 show overall a rather stable trend in sensitivity with rather small variations. In general, the specificity is affected but to a lesser than expected extent by the decrease in MW, with strong dependency on the system. Looking at the two MW extremes in the Ames Microsuspension subsets (i.e., MW ≤ 400 and MW ≤ 250), Derek Nexus sees a decrease in specificity from 94% to 87%, LSMA alerts from 83% to 61%, ToxTree from 76% to 54%, Sarah from 74% to 53%, and LSMA Stats from 91% to 72%.

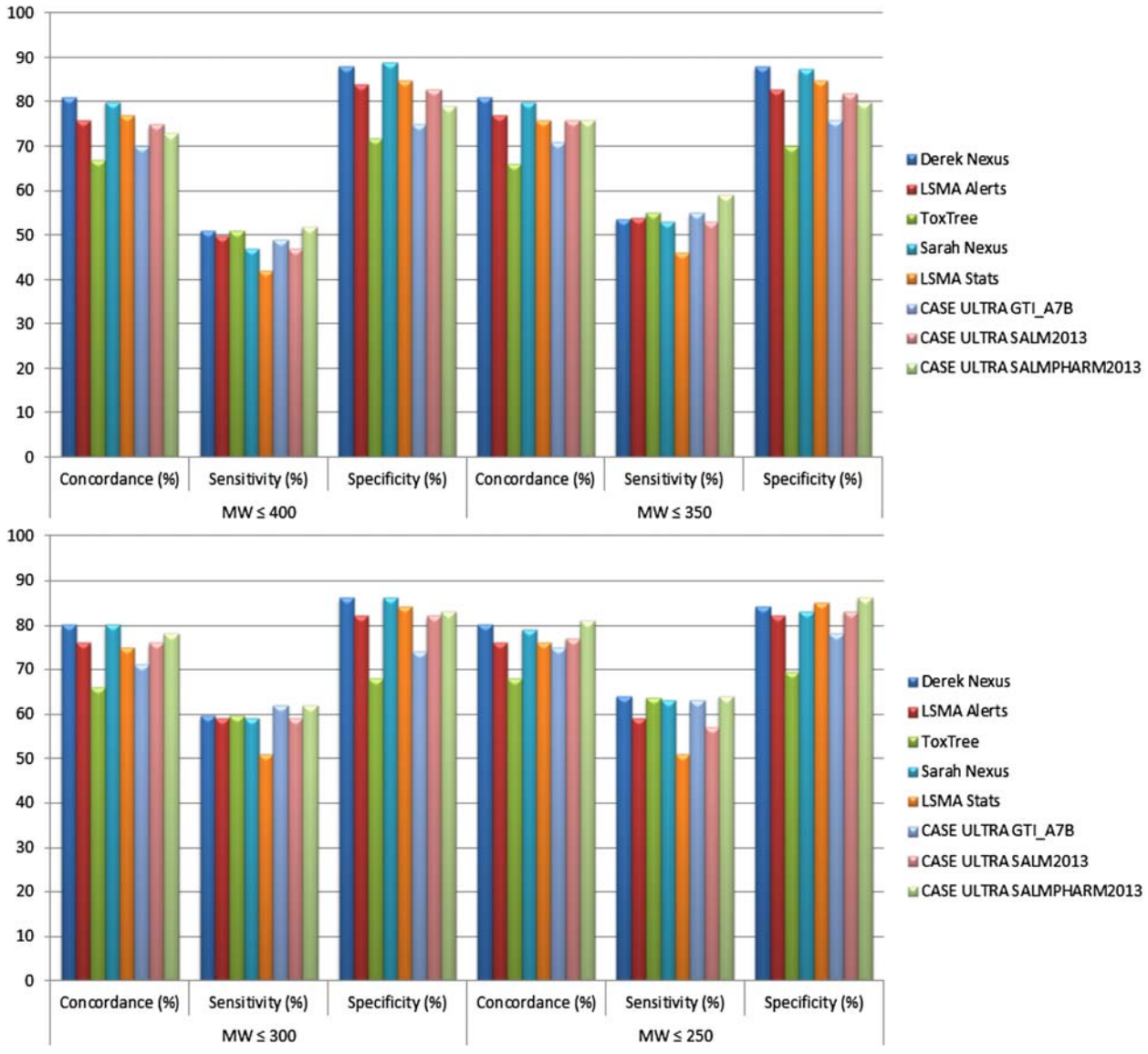

Fig. 5 Performance of individual systems on the Roche Ames Standard dataset filtered by MW.

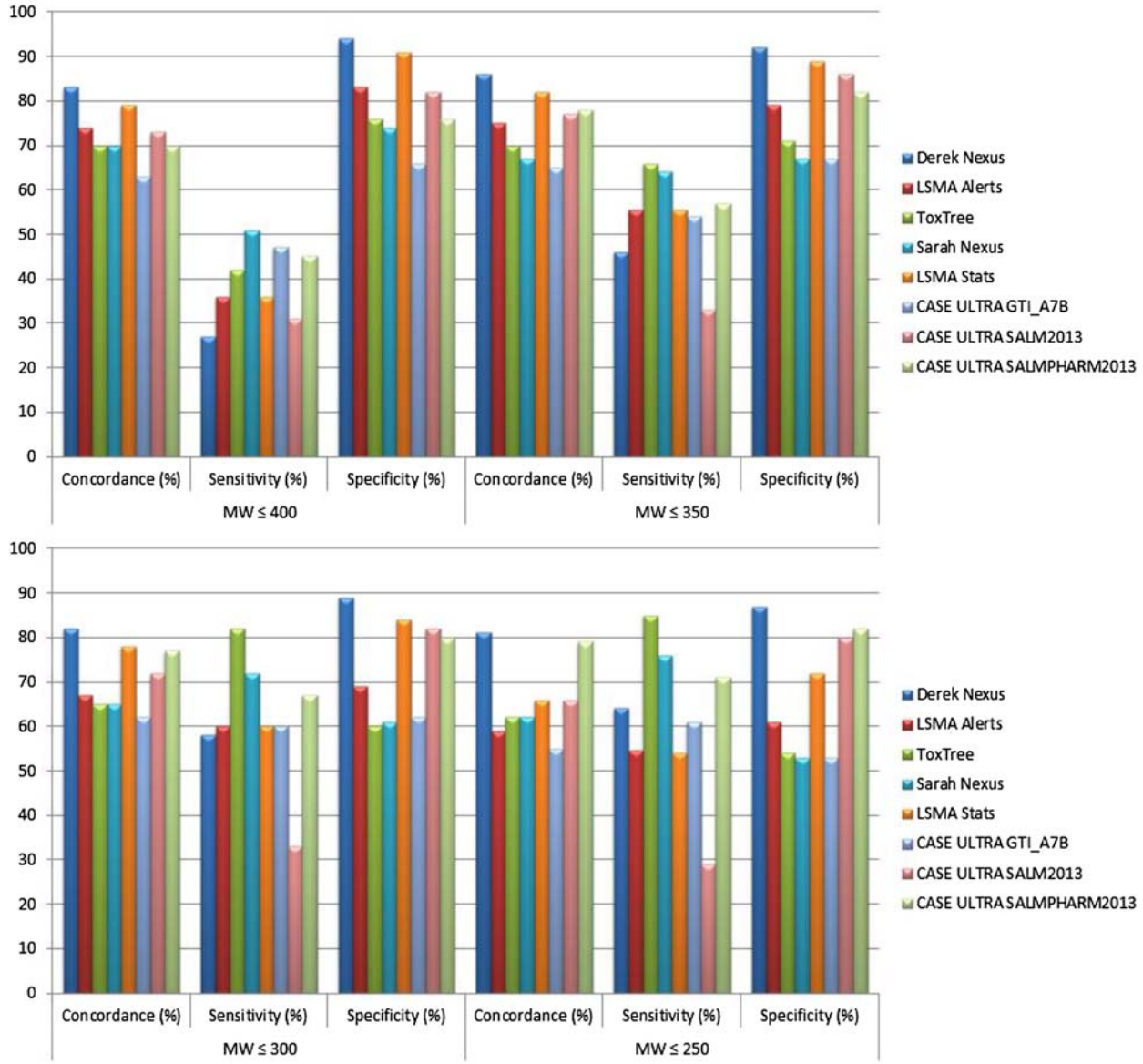

Fig. 6 Performance of individual systems on the Roche Microsuspension dataset filtered by MW.

The evaluation of combined systems with lower MW Roche subsets shows a significant increase in sensitivity, up to over 90% for sets with MW $\leq$300 and $\leq$250 with several combinations (Figs. 7 and 8). The increase in sensitivity is proportional to the decrease in MW; at the same time, there is a considerable decrease in specificity ($\sim$30% in some cases). Such deltas are generally more pronounced in the Ames Micro dataset (Fig. 8) compared to the Roche Ames Standard dataset (Fig. 7). Such effect on the specificity is in general more pronounced compared to single systems. In the Ames Standard subsets, specificity and sensitivity values are consistently comprised between 70% and 80% in nearly all Derek Nexus and LSMA Alerts combinations. In the latter combinations, values are a bit lower than 70% at higher MW. ToxTree combinations show lower sensitivity and specificity values at higher molecular weights and greater gaps between sensitivity and specificity within the subsets MW $\leq$300 and MW $\leq$250.[3,55]

As far as the Roche Ames Micro set is concerned, the sensitivity is in the range of 90% in the subset with MW $\leq$250 with several combinations, such as Derek Nexus + Sarah and Derek Nexus + GT1_A7B; LSMA Alerts + Sarah; LSMA Alerts + CASE Ultra models. Nearly all combinations with ToxTree gave sensitivity in the range of 90%. Nearly all combinations of LSMA Alerts showed high sensitivity also in the subset with MW $\leq$300.

Looking at the plots in Fig. 8, it is evident that more balanced results are obtained with all Derek Nexus combinations: in other words, the sensitivity increases proportionally to the decrease of the MW at a moderate expense of specificity. Compared to this, LSMA Alerts combinations have overall lower specificity than Derek combinations.

At the same time, ToxTree combinations, despite showing good sensitivity, have a greater corresponding decrease in specificity, down to approximately 50% and lower.

The aim of the earlier described in silico systems analysis is not to identify the best performing in silico tools, or combinations thereof, but rather to identify trends and assess their behavior specific to the test sets used. The performance metrics used in the present contribution (namely, sensitivity, specificity, and concordance) is known to be strictly dependent to the test sets used. Some software tools may perform rather poorly with one test set or very well with a different one. This observation is confirmed by the present analysis as well, since most tools performed very satisfactorily with the public domain datasets but their performance got worse with the Roche proprietary datasets.

Our study showed that the use of two systems does indeed improve the overall sensitivity values, meaning that they gain a higher ability to identify mutagenic compounds at a relatively minor increase of the rate of false positive calls.

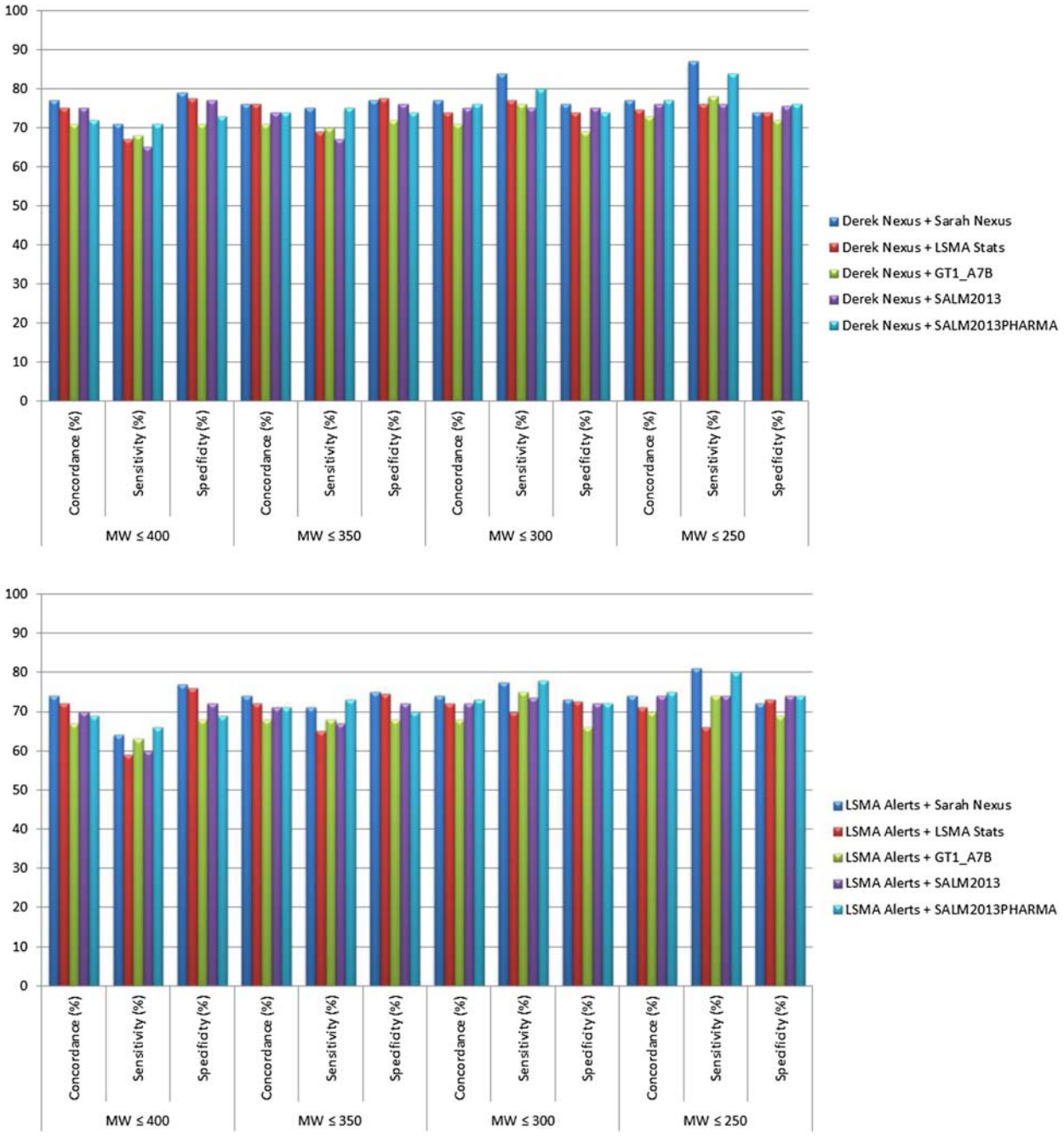

Fig. 7 Performance of individually combined systems on the Roche Ames Standard dataset filtered by MW.

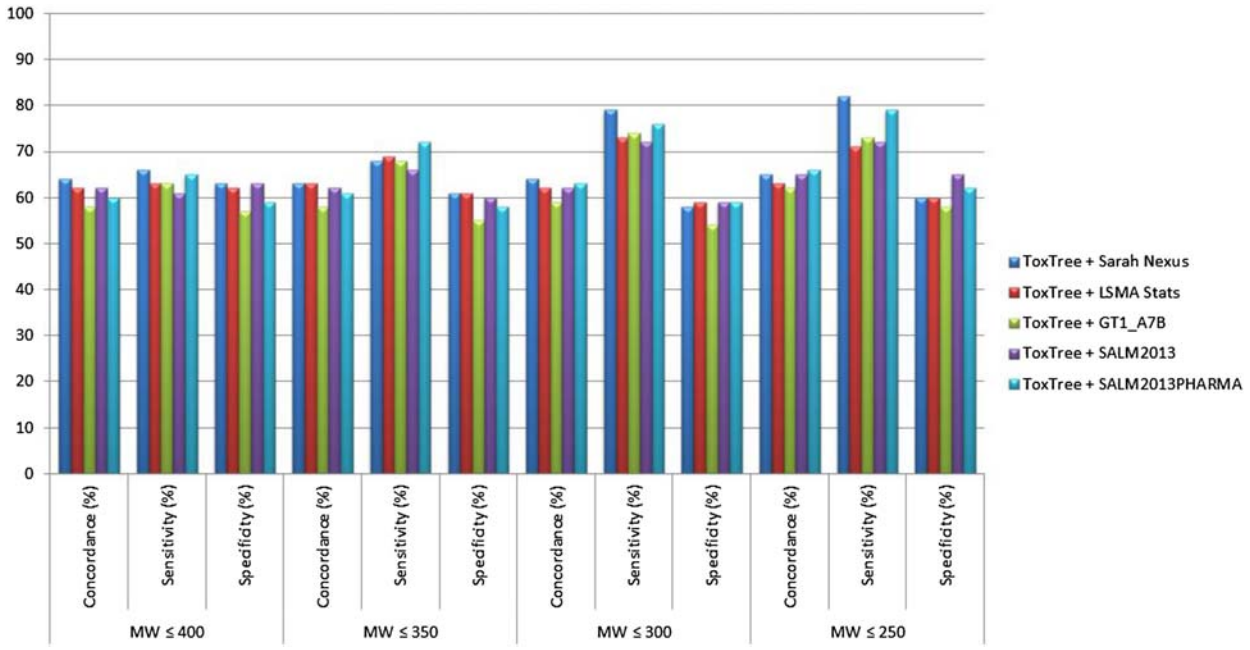

Fig. 7 (*continued*).

In general terms, the most obvious room for improvement lies within the expansion of the chemical space known by the in silico systems via the addition of new data, particularly within the proprietary domain. This goal can be achieved via cross-industry data sharing initiatives (some of them are already active) aiming at filling the gaps of specific chemical classes providing that there are no competitive conflicts.

Another area where some efforts should be directed to is the investigation and establishment of significant correlations between specific chemical properties (e.g., log *P*, PSA, MW), metabolic pathways, and the final biological (or toxic) effects. This would allow complementing the classic fragment-based or substructure-based approach with other parameters that in some cases are critical for the explanation of specific biological activities.

2.09.4 In Silico Models for the Prediction of Toxicity in Drug Discovery

In silico approaches to predict potential toxicities and drug metabolism on the basis of the chemical structure are of particular interest to the pharmaceutical industry as having the potential to impact the early drug discovery process as well as in the candidate selection phase. Prediction models for the identification of metabolic soft spots and potentially toxic substructures can be easily applied to a large number of chemical structures and are therefore integrated already during HTS (high-throughput screening) or even earlier as an automatically attributed alert for all new chemical entities. At this early stage, only a basic in silico profiling can be done, as only the most well validated endpoints can be reliably applied automatically and generated on-the-fly without an expert intervention. Later in the development, at the latest before the final candidate is selected, a more detailed in silico profiling also considering the whole profile of the compound is thoroughly conducted. According to the development scheme provided in Fig. 9, the further in silico tools and in vitro downstream activities are conducted.

2.09.4.1 Target Identification (TI), Target Assessment, and Exploratory Work

The first step after the target has been identified as potential development opportunity is a target assessment (TA) conducted by nonclinical safety experts, using appropriate databases and public sources. A proper target/functionality assessment in healthy and diseased status contains pathway mapping, information from knock-out and transgenic models, a target expression profile in relevant species, as well as a critical evaluation of potential off-target safety alerts (selectivity). Various software systems are available to assist the experts in these assessments (e.g., MetaCore,[59] Symmetry[27]).

Modern in silico prediction software is able to calculate thousands of chemical structures on-the-fly and can be therefore applied very early in the drug development process. Immediately after the chemical structure is known, meaning chemical libraries are added to the company's chemical database, a basic in silico prediction panel is applied using reliably validated toxicological endpoints like genotoxicity and carcinogenicity. As always, a large, homogeneous, and high-quality database is the prerequisite

for reliable predictions. Therefore, in vitro screens which have been used within pharmaceutical companies for years containing data generated often in one single lab are the best sources for the development of highly predictive models. For example, an in silico model predicting the potential of drug-induced phospholipidosis (a reversible storage disorder characterized by accumulation of phospholipids within cells) has been developed. Based on more than 600 in vitro assay, an accuracy of 86% led to a replacement of the in vitro by the in silico method. The model is calculating the free energy of amphiphilicity ($\Delta\Delta G_{AM}$) and log P value[60] of cationic amphiphilic drugs and can be applied in a high-throughput mode. Further endpoints that can be used for on-the-fly predictions are teratogenicity, GSH adduct formation, irritation, and skin sensitization.

At this early stage of development, the potential safety hazards identified by the application of an expert system in combination with a set of statistical models contribute to the overall compound profile (in silico default), but are not used as a decision pathway (see Fig. 10).

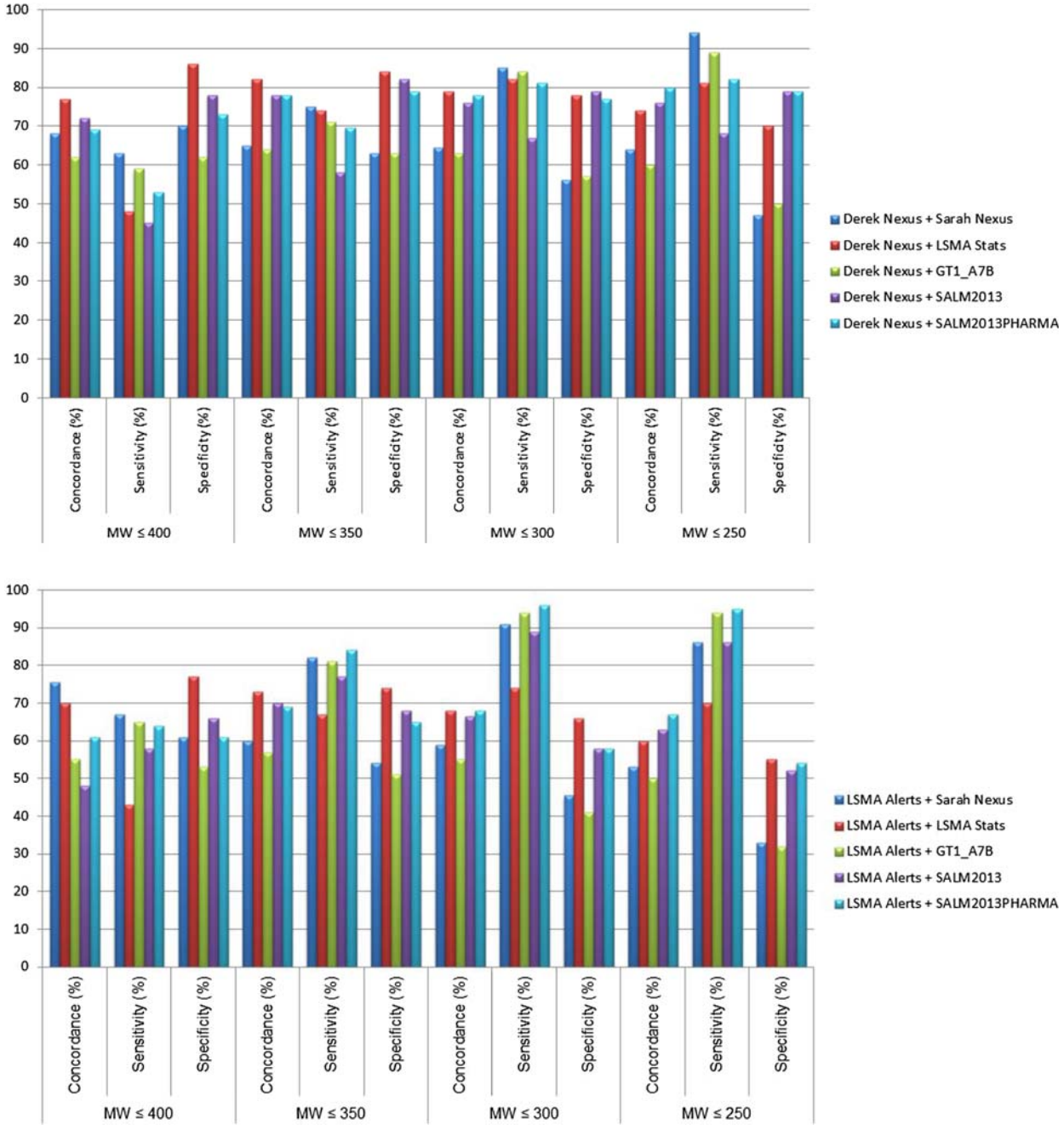

Fig. 8 Performance of individually combined systems on the Roche Ames Microsuspension dataset filtered by MW.

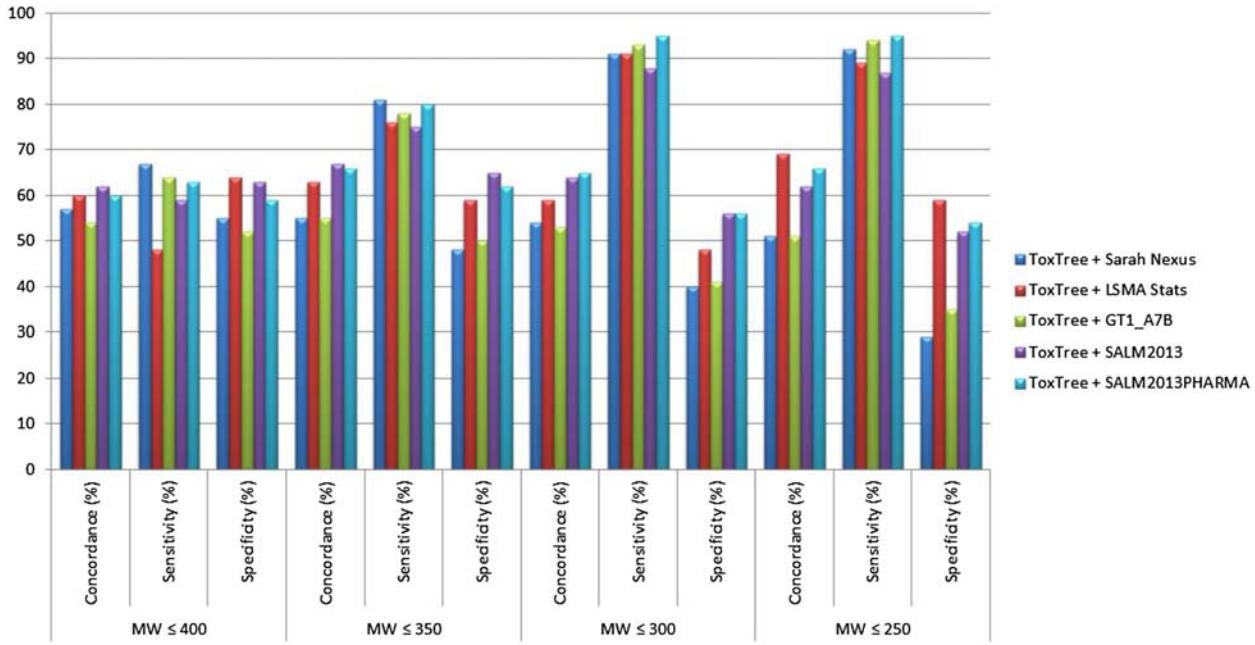

Fig. 8 (*continued*).

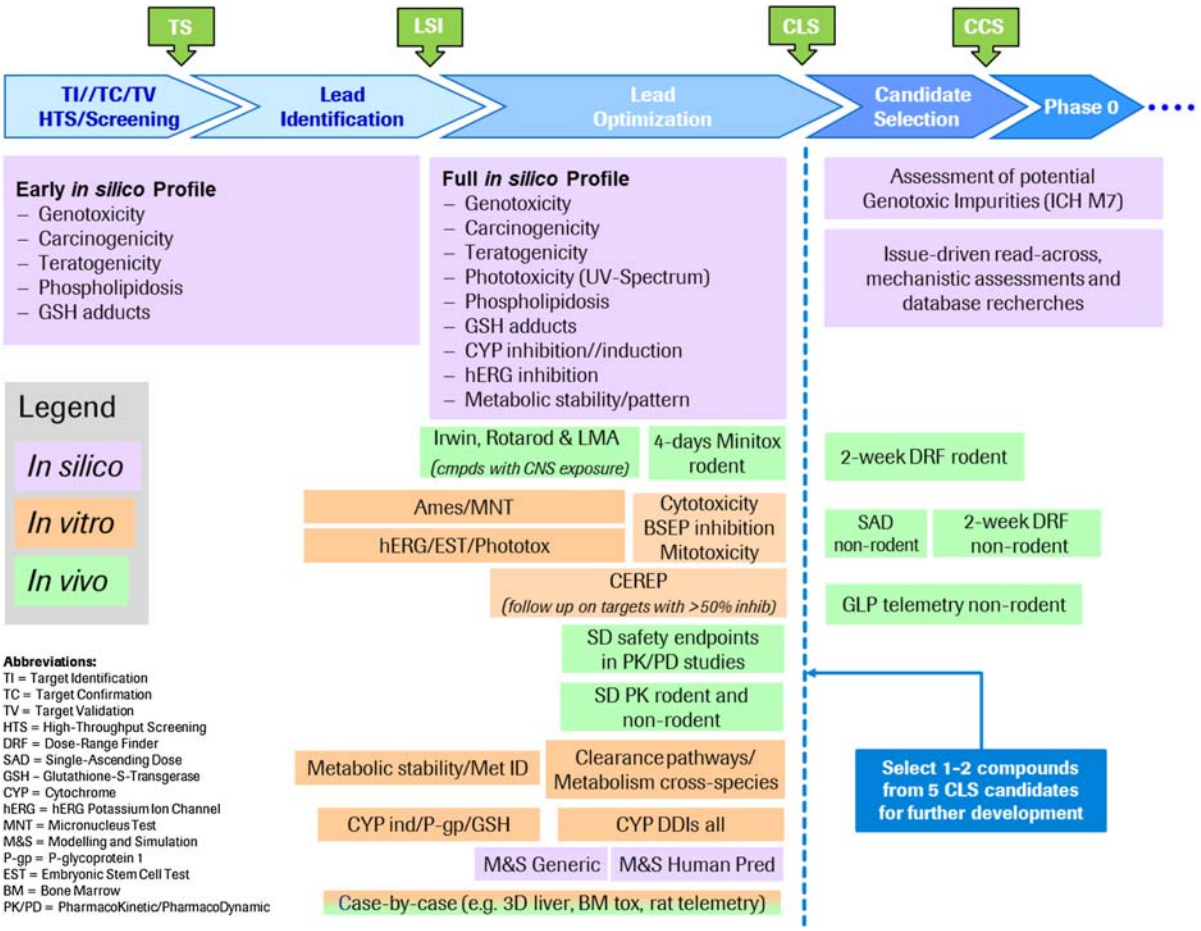

Fig. 9 Use of in silico tools and safety screening during the early drug development process.

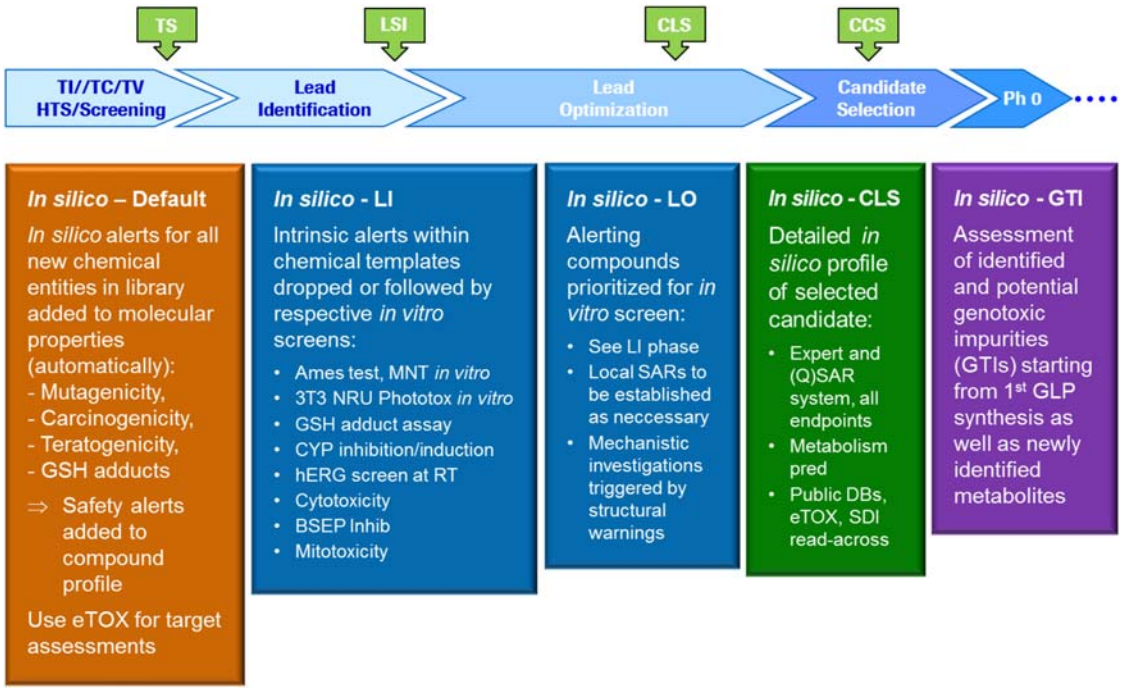

Fig. 10 Downstream activities following in silico alerts in the drug development process.

2.09.4.2 Lead Identification Phase: Target Selected (TS) to Lead Series Identified (LSI)

The main goal during lead identification (LI) is to identify valid chemical templates for further optimizing the efficacy and selectivity on the target, ideally multiple discrete series. Besides computational chemistry tools to calculate physicochemical properties, virtual screening, structure-based design, QSAR analysis of both the desired target but also off-target activities, chemical structures are analyzed continuously in silico for possible structure-related safety concerns to identify major issues with the templates (in silico LI). Insights into the toxicological potential of a scaffold or series of structures early in the drug discovery process could help medicinal chemists to prioritize particular scaffolds. Components of early avoidance of chemical structure safety liabilities include predictions for genotoxicity, carcinogenicity, hERG channel blockade, reactive metabolite formation, phospholipidosis, structural similarity to problematic molecules, CYP inductions, GSH adduct formation, and DMPK properties (cell penetration, microsomal stability, CYP3A inhibition). The in silico tools offer good guidance on what additional tests may be necessary or whether further characterization is warranted; however, they also have limitations.[61]

Drug, metabolism, and pharmacokinetics (DMPK) properties play a major role during lead identification. Numerous commercially available tools for the prediction of metabolites exist, such as METEOR,[13,19] MetabolExpert,[62] and MetaSite.[63] Most software packages correctly predict metabolites that are detected experimentally. However, a relatively high incidence of false predictions of metabolites is common to most unspecified computerized systems. In the hand of drug metabolism experts, these software packages have a certain value for hypothesis generation and guiding to experimental approaches for the identification of drug metabolites. However, the generation of additional new local rules, intended to predict the activity of a single enzyme (and often only within a chemical series), can significantly improve the prediction accuracy.

Experimental follow up of potential issues is conducted to build/refine safety plans moving forward. Even if in vitro assays clearly disprove identified in silico alerts further spot-checking of the distinctive endpoint will be conducted to avoid creeping in of a structural liability. The in vitro results always overrule the in silico warnings provided that the corresponding assays could have been conducted under reliable conditions (e.g., solubility, stability). Chemical templates with identified and confirmed intrinsic metabolic and/or safety concerns will be eliminated (see **Fig. 10**).

2.09.4.3 Lead Optimization (LO) Phase: LSI to Clinical Candidate Selected (CLS)

The task of the LO phase is to take a lead and convert it into a candidate for preclinical evaluation. This phase is intensively accompanied by early safety in vitro screening in various areas: genotoxicity, hERG and other ion channels, cytotoxicity, hepatic toxicity, bone marrow toxicity, transporters, metabolites identification, metabolic stability, CYP induction/inhibition, reactive metabolites, off-target pharmacology/secondary pharmacology, and cross-species comparisons, where applicable. Further screens might be applied based on the target liabilities or already identified potential safety issues. If adverse in vitro activities appear, specified

structure-activity relationships (SARs), the so-called local SARs, will be established to support the discovery projects in optimizing the clinical candidates toward safety/DMPK in parallel to efficacy (in silico LO).

At this stage, first, fit for purpose in vivo studies are conducted to address early target or chemistry-related safety concerns. The first general toxicology studies are maximal tolerated dose (MTD) and dose-range finding (DRF) studies generally performed in rodents and nonrodents. The value of performing exploratory drug safety studies before candidate nomination is to identify unwanted toxicities evident in a study of up to 14 days duration, as well as any potential toxicities anticipated based on a known cause for concern. In the absence of findings or the presence of findings that are judged manageable, these studies provide a greater comfort in the selection of a molecule for advancement into development with higher likelihood of success. Additional benefits of these studies are the identification of target organs to monitor in development and the selection of doses for the GLP toxicology studies. In addition, identification of the toxicity profile of a lead compound can be useful for the backup program where the goal is often an improved safety margin. In silico safety concerns might be included as part of pharmacokinetic/pharmacodynamics (PK/PD) characterization in vivo (disease) models to extract safety-relevant information and to build confidence in safety before expanding into larger regulatory animal studies (in silico CLS).

During LO, every in silico alert is immediately followed up by the corresponding in vitro screen, in case, even in vivo studies might be frontloaded. To avoid late failures of optimized candidates, spot-checking of the potential development candidates without alerts is conducted if the resources and throughput of the assay allow. In case of screening alerts, creation of local SARs can result in significant acceleration of project by optimizing the chemical improvement rounds. Specific and tailor-made local models normally have a significantly higher accuracy, if continuously updated with new incoming screening results. Learnings and newly identified alerting substructures should be implemented in general rules and models (customized systems) to continuously improve the performance of the computational tools used for drug optimization (see **Fig. 10**).

2.09.4.4 Phase 0: After CLS to Entry Into Humans (EIH)

The main usage of in silico tools after the final candidate has been selected encompasses the assessment of potentially genotoxic impurities according to the ICH M7 guideline as well as cross-reading and pathway analysis following an unexpected event in preclinical studies (in silico GTI). Furthermore, a backup or fast-follower program will trigger dedicated in silico profiling and screening of the new molecules, based on experiences and identified issues of the frontrunner compound.

Apart from the use of in silico tools to assess genotoxic impurities, there are no computational assessments which are mandatory requirements from regulatory agencies, but in case in silico models have been applied during drug development and influenced the testing strategy or triggered addition investigations, the information should be included in regulatory documents and adequately described.

2.09.5 Prediction of Complex Toxicity Endpoints

2.09.5.1 Outcome of In Vivo Safety Studies: A Challenging Prediction

Certain assays like the Ames assay,[57] present their outcome in what can be considered a binary way, in which the answer is a "yes" or "no" type. In such cases, in silico models have a higher chance to give a better predictive performance if compared to more complex assays and studies, where multiple parameters need to be brought together and analysed in relation to doses, time, and other factors to reach a final result or classification.

The mechanism of action of a molecule leading to a specific readout plays a critical role in the predictive performance of in silico models as it is one of the biggest challenges of, for instance, QSAR models. "Do the descriptors have any physicochemical interpretation that is consistent with a known biological mechanism?"[64] is often a very difficult question to answer. In vitro chromosome damage (an assay used to establish the clastogenicity potential of test compounds) can also be considered binary (i.e., the test item is "clastogenic" or "not clastogenic"). However, the mechanisms of action that may lead to clastogenicity are manifold and may involve the interaction of the compound with a number of proteins or enzymes, the disruption of one or more biological pathways that ultimately lead to a clastogenicity outcome. Such scenarios are quite difficult to be consistently accounted for within an in silico prediction system or model since the actual targets leading to the final assay outcome are mostly unknown. Even when using large proprietary datasets to improve the performance of existing models, the risk is to obtain better prediction metrics specific to the training set and not much broader than that since minor structural changes within a chemical class can have a large impact on the mechanism of action (e.g., the interaction with one or more proteins may be hampered, hence changing the final outcome of the assay).[3]

Even greater challenges are offered to the prediction of the outcome of single dose and repeat-dose toxicity in vivo studies. In the pharmaceutical industry, such studies are typically used to identify a Maximum Tolerated dose (MTD) and the NOAEL (Non-Observed Adverse Effect Level) for a test compound, in addition to the identification of a general toxicity profile and significant target organs that may show toxicity upon exposure to the compound tested.

Since animal models are very complex and the number of readouts collected in such studies is extremely wide, the development of in silico models that can reliably predict such outcomes is extremely challenging. If we reason in terms of dimensionality, if an Ames assay can be considered 2D, in vivo studies are multidimensional, making their accurate representation in a comprehensive model rather difficult. For example, a typical repeat-dose study requires the use of a control group plus 3 dose groups: each animal is

then carefully examined for clinical observations throughout the in-life part, including body weight and food consumption measurements as well as some behavioural evaluations; clinical pathology values are collected at different time points; urine analysis is performed; macroscopic and microscopic examinations are carried out on selected organs; toxicokinetics values are then calculated using the test item concentrations measured in blood from the samples collected throughout the study, which could be of different durations, from 5 days till 39 weeks (up to 2 years for the rodent bioassays for the evaluation of carcinogenicity) and in different species.

The variations, permanent or transient, of the parameters and values briefly described earlier may depend on the pharmacological target, on the chemical structure of the test item and related physico-chemical properties, on background incidences due to adaptations or other factors, such as major differences in plasma exposures. Because of this variability, building an in silico model capable of predicting all these different "degrees of freedom" is extremely challenging, in particular due to the fact that the identification of unequivocal mechanisms of action for whatever findings has been identified is not trivial. In addition, the development of robust SARs using the outcome of such studies is made more difficult by the very limited amount of publicly available data and, even within large pharmaceutical companies, the number of chemically similar compounds tested in such long and expensive studies for each investigated pharmacological target is often small (less than 5). This, of course, hampers the possibility to even develop local models since the number of similar compounds, designed for the same target, undergoing the same type of complex and expensive studies is rather limited.

Sophisticated in silico models may indeed become available for the prediction of the potential findings identified in, for example, repeat-dose studies, however all the limitations described earlier and the difficulties to conduct a proper validation with external data sets would make debatable, within the pharmaceutical industry, whether or not to accept them for decision making on compounds prioritization or as guidance for chemical optimization.

2.09.5.2 Drug-Induced Liver Injury

Drug-induced liver injury (DILI) is a major clinical and pharmaceutical concern and has remained one of the top two causes of drug attrition in the last decades.[65] DILI is responsible for about 30–50% of acute liver failure cases in the developed world and accounts for the withdrawal of a significant number of approved drugs from the market.[66–68] Hence, the early and reliable detection of hepatotoxicity during the drug discovery process is a must and would go a long way in reducing the drug development costs by decreasing the attrition rate. Nonetheless, DILI is complex and encompasses a wide range of effects, like liver enzymes elevation in serum, acute liver failure, and chronic liver dysfunction. In addition, patient-related factors play a significant role in liver injuries,[68,69] among them, age, race, co-medication, genetic polymorphism, and diet/nutritional state. Given the complexity of DILI and often the lack of understanding of its etiology, its prediction, using in vitro, in vivo, and in silico tools, has been very challenging with sporadic success. In the present contribution, we will give on overview of some of the in silico models that have been proposed and used for the prediction of DILI[70]; other in vitro and in vivo methods will not be illustrated.[65]

A variety of computational models have been developed with the aim to predict global hepatotoxicity, from nonspecific to idiosyncratic using several training set combinations.[70] Two models used in vitro data only,[71,72] one model used a combination of in vitro and in vivo data,[73] while the remaining one used only in vivo data, being human[74–79] or animal data.[80,81] The ideal situation for the prediction of hepatotoxicity is to have models with high sensitivity, that is, capable of identifying with high confidence compounds with high likelihood of being hepatotoxic. The reason is that excluding hepatotoxicants early from further development will have a much higher impact on patients' health and costs for pharmaceutical companies than excluding a false positive molecule (e.g., as a result of a low specificity of the model).

Clark and coworkers[71] applied Idiotropic Field Orientation for Comparative Molecular Field Analysis (IFO-CoMFA) as structural descriptors and Soft Independent Modeling of Class Analogy (SIMCA) to make a classification of hepatotoxicity from 654 drugs. Measurement of hepatotoxicity was done using four different in vitro assays assessing cell proliferation, lactate dehydrogenase (LDH), intracellular ATP, and levels of caspases 3 and 7. Greatest accuracy of 52% was achieved for a hierarchical ranking model combining all four assays. The global IFO-SIMCA approach showed poor predictivity for a large dataset of biologically active compounds, but significant improvements were achieved when the model was built for nonsteroidal antiinflammatory drugs (NSAIDs) as a single pharmacological class of chemicals. Such models, built on specific cytotoxicity indicators, may have the limitation to be performant only on individual chemical classes, which may share a similar mechanism of action. This aspect is deemed to limit the applicability domain of the model.

Fourches and coworkers[81] developed a QSAR model from mining published literature data for hepatotoxicity descriptors derived from in vitro and in vivo (animal and human) data. The model used hierarchical cluster analysis and QSAR with Support Vector Machines (SVM) using different types of descriptors to predict whether a compound would be hepatotoxic in humans. The predictivity of the models was assessed via internal and external fivefold cross-validation, which returned accuracies ranging from 61.9% to 67.5% and 55.7% and 72.6% for internal and external validations, respectively. The models were also applied to external test sets of 18 and 246 chemicals, respectively; the prediction accuracy for 78% for the former set and 67.5% for the latter set. Overall, the described approach showed reasonably good predictivity considering that the training sets were coming from an automated text mining technique with limited manual intervention.

In general terms, the availability of in vivo liver toxicity data is higher than in vitro data. In vivo liver toxicity can be divided into intrinsic, often linked to the presence of specific structural moieties within the molecules, and idiosyncratic, which is rare and dose-independent.

Cheng and Dixon[74] compiled a data set of liver toxicity data for drug and drug-like compounds from the literature collecting 149 toxicants and 233 nontoxicants. Recursive partitioning (RP)[82,83] with an ensemble approach was used to generate the models, from training set subsets, that will be then averaged into one single model. RP uses a number of decision trees to split the training set into mainly toxic and nontoxic compounds based on 1D and 2D descriptors selected by a Monte Carlo linear regression. A total of 151 trees were created and used to predict each compound as toxic or nontoxic and then averaged to make a final prediction. Leave-one-out (LOO) validation and leave-10%-out methods were used for internal validation with sensitivity of 78% and 76% and specificity of 90% and 75%, respectively. Overall concordance was 85% and 76%, respectively. External validation conducted on 54 compounds showed that the model could correctly predict 81% of the test set. The overall good accuracy suggests that this model could be applied to diverse classes of chemicals for the prediction of hepatotoxicity risk.

The prediction of idiosyncratic hepatotoxicity presents even more challenges as it is the product of the probability of each individual contributing factor, such as chemical properties of the drug, genetic polymorphism, and environmental aspects (i.e., tobacco, alcohol, age, gender, health status, and use of additional drugs).[70]

A model for the prediction of idiosyncratic hepatotoxicity implementing linear discriminant analysis (LDA), ANN, and machine learning algorithms (OneR) have been described in 2008.[79] Literature data was used to collect a set of 74 drugs, 33 with idiosyncratic hepatotoxicity and 41 without it. The models constructed with 3D radial distribution descriptors showed an accuracy of 84%, sensitivity of 78%, and specificity of 90% for the training set. The LDA model correctly predicted 86% of the compounds. Two external sets were also used for models validation. A first set consisted of six chemicals, which were similar in pharmacology and chemical structures, but with opposite toxicity profiles: LDA and OneR showed the same predictive accuracy of 83%. The second external test set consisted of 13 hepatotoxic drugs, 9 of which were correctly classified by the LDA model. These results may suggest that these computational approaches may find some applications in the lead selection or lead optimization stages to filter out some compounds with the potential to induce idiosyncratic hepatotoxicity.

On the regulatory side, the US FDA conducted a broad investigation aimed at setting up a health effect database and develop QSAR models to predict hepatobiliary adverse effects of drugs.[71,78,84] The effort resulted in a set of about 1660 chemical structures[85] with five hepatobiliary endpoints considered: liver enzyme disorders, cytotoxic injury, cholestasis and jaundice, bile duct, and gall bladder disorders. Four QSAR programs (MC4PC,[17] MDL-QSAR, Bioepisteme,[27] and Leadscope Predictive Data Miner (LPDM)[24]) were selected to build predictive models using the same training set. Leave-many-out validation methods showed an average sensitivity of 39% and a specificity of 86% for all four programs. A pairwise consensus approach was also tested giving an average sensitivity of 56% and specificity of 78%. An external validation set consisting of 18 compounds withdrawn from the market because of unacceptable hepatotoxicity was tested and almost 90% of the drugs were predicted to be hepatotoxic by at least one of the four programs. When applying a consensus scheme, 67%, 44%, and 11% of the external set were correctly predicted by two, three, and four programs, respectively. This analysis showed that carefully built QSAR models using robust data can provide valuable support in the early profiling of candidate leads.

Ekins et al.[76] used a 295-compound training set (including 158 DILI-positive molecules) to build a liver toxicity prediction model using a Bayesian classification approach. A test set of 237 compounds (114 DILI drugs) was also used for the model evaluation. 2D descriptors were used to differentiate the activities and highlight chemical substructures known to be critical for DILI. The Bayesian model correctly classified 56% of active chemicals and 67% of the inactive. Despite the performance metrics can be considered disappointing, the fact that a broad and diverse training set was used for the model development suggests that the approach may be applied early on in the drug discovery process.

Rodgers and coworkers[77] applied the *k*-nearest neighbor (*k*-NN) method to build a model for binary classification of drugs, inducing liver toxicity based on the chemical structure. A 200-compound subset of the HLEAD database (containing five different serum enzyme markers for liver toxicity: ALP, ALT, AST, LDH, and GGT) was used to construct the model using two types of descriptors. Models were built for the five endpoints and for a composite liver endpoint showing sensitivity greater than 73% and specificity greater than 94% in external validation settings. The applicability domain of the models was tested using the WDI, PCL, and the Biowisdom Liver Intelligence Module chemical databases. The exercise showed a rather poor coverage of the composite model, with 80% of the WDI database being out of domain. This study pointed out the general challenges of in silico methods to achieve an acceptable applicability domain as well as their inner limitations in identifying the correct mechanisms of action or biological pathways leading to liver toxicity.

Zhu et al.[86] constructed in silico models for human hepatotoxicity using both the chemical structure and in vitro assay data. The in vitro data were from human hepatocyte imaging assay technology (HIAT) that measured the intensity of biochemical indicators (e.g., lipids and glutathione) after the exposure of human hepatocytes to a single test compound. Models combining chemical descriptors and in vitro assay data were compared alongside the conventional QSAR, as well as models based on pure in vitro assay data. A dataset of 156 DILI positive and 136 DILI negative compounds were selected for model development. First, models based on chemical descriptors (CDK, Dragon, and MOE) and in vitro cell-imaging endpoints (HIAT) descriptors were built using random forest (RF) and fivefold cross-validation procedure. Then, three hybrid models were built using HIAT and a single type of chemical descriptors. Generally, the models based only on chemical descriptors were poor, with a correct classification rate (CCR) around 0.60 when threshold value of 0.50 was used. The hybrid models afforded a CCR of 0.73 with a specificity of 0.74 and a better true positive rate (sensitivity of 0.71). Stricter classification thresholds showed higher benefits of the hybrid models.

Egan and coworkers reported the development of structural alerts for hepatotoxicity as implemented in VERDI.[75] A series of 244 molecules was compiled, including 54 drugs that were withdrawn from the market due to liver toxicity. Based the dataset the authors developed 74 alerts, most of them related to functional groups converted to reactive metabolites. Predictive performance

of the alerts pool was not provided as according to the authors, liver toxicity prediction is not possible due to the wide variety of factors and mechanisms involved in such endpoint.

Greene et al.[87] described a four-stage approach for the development of structural alerts. In step 1, 1266 chemical structures were selected from the literature. Step 2 looked into the relationship between compounds and reported toxicity in order to derive specific structural classes. Subsequently, structure–activity relationships (SARs) were built for 38 classes and finally implemented in Derek Nexus[12] and the predictive performance was evaluated using an external validation set consisting of 626 compounds developed by Pfizer. Each validation compound was assigned to one of the four identified activity classes: (i) no evidence for hepatotoxicity; (ii) weak evidence for hepatotoxicity; (iii) animal hepatotoxicity; (iv) human hepatotoxicity. The four activity classes, for the purpose of validation, were combined into two classes (first two into one negative set and the last two into one positive set). Derek Nexus showed a sensitivity of 46%, a specificity of 73% with an overall concordance of 56%. Poor sensitivity was attributed to the limited mechanistic evidence for some classes of compounds and to the lack of good predictions for the pool of compounds hepatotoxic in preclinical studies and not tested in clinical trials.

2.09.5.3 Data Integration of In Vivo Toxicity Studies

Despite the obvious challenges described earlier and the disappointments given by some of the models attempting to predict DILI, a lot of efforts have been recently directed toward leveraging the information coming from complex in vivo models. Promises have been shown by some in silico methods that can be considered as a valuable support for the early selection of compounds with the potential of inducing hepatotoxicity. An obvious strategy aiming at the further improvement of prediction models is to keep adding new, high quality data, to existing (or totally new) models to (re)train them and expand their applicability domain. Another key aspect is to get the data classification right for the generation of more robust correlations with the most significant molecular properties or substructures.

Within the industry, it has been recognized that the consolidation of the results of in vivo toxicity within appropriate tools making use of the right technology would allow the full exploitation of the knowledge that such data can provide.

Large Pharma organizations can typically count on many years of drug discovery and research conducted across several sites on a significant number of therapeutic areas, pharmacological targets, and molecules. This consists of a large amount of complex datasets, stored in different repositories or Laboratory Information Management Systems (LIMS) each designed specifically to accommodate the data type of interest (e.g., Histopathology, Clinical Observation, Clinical Pathology, PK, Urinalysis). The organization of such wealth of information to generate specific knowledge from the integration of all of these data types has been considered several times in the past by many pharmaceutical companies. However, due to limited resources or inadequate technology, the outcome of such initiatives has often been disappointing or only partially successful.

In more recent years, there has been a tremendous focus across industries, not only pharma, to extract knowledge and identify patterns or trends from large amounts of data, being either omics, market research, customer purchase preferences in retail stores, people's favourite digital movies rental,[88] airplane estimated times of arrivals, and others. A lot of these initiatives often fall under the term "Big Data," generally underlying the intention of many organizations to look deeper into their databases and assess whether an improvement in the way such data are organized, stored, made accessible, and mined may provide any advantage for the business in terms of saving resources or increasing efficiency via surfacing hidden value. Another angle is to collect more data in a targeted way in order to ensure that critical information is promptly made available by analysing such data to identify or anticipate specific trends or make better, more informed decisions.

Along this line, Roche has been working on a number of "Big Data" projects across several areas of research and IT. One of them had the goal to integrate all in vivo nonclinical safety data generated by the company over the past 30 years across three research sites, two in the United States and one in Switzerland. The goal was to ensure that all different data types that are part of in vivo studies (i.e., histopathology, clinical observations, PK, clinical pathology, etc.) were brought together electronically in such a way that they could all be searched and made available at the same time to the users community. The scope for such a platform, internally called SDI (i.e., Safety Data Integration), is to allow scientists to identify specific patterns of findings across species and their historical relevance, correlations between molecular structures and toxicological effects, and, eventually, use the data to generate more reliable prediction algorithms. The application of a semantic data integration approach[89] for the harmonization of terms, formats, units, and taxonomy, allowed the implementation of a Non-Clinical study warehouse including more than 5000 studies of different types which can be interrogated with very complex queries such as: "Which compounds showed Spleen Hyperplasia AND Liver Necrosis AND Lung Leukocytosis AND an AST increase $>50\%$?" returning an answer in a matter of seconds. The identification of studies and compound matching the query above, in the absence of properly designed data integration efforts, would have been extremely labour intensive and time consuming, if possible at all.[3] Further integration efforts have seen the SDI platform being interfaced with other internal databases, such as the chemical structures and the in vitro biology data repositories to further expand the data integration beyond toxicology allowing the users to assess the compound profile in almost its entirety.

2.09.5.4 Development of Prediction Models

As far as models development is concerned, one of the advantages of the platform described earlier is the high data granularity available, down to the single animal level.

One of the challenges in the development of predictive models for complex endpoints, such as, for example, hepatotoxicity, is that the modeller is forced to make a generic binary classification (hepatotoxic vs. nonhepatotoxic), often neglecting safety margins (vs. pharmacological activity), doses at which specific toxicity is seen and ignoring the specific findings and whether it is transient or not. This is because, more often than not, all these elements are not easily available. All these factors make such classification relatively inaccurate: for example, paracetamol (or acetaminophen) an over-the-counter mild analgesic, commonly used to relieve headaches and reduce fever, is commonly classified as hepatotoxic (as its overdose can cause fatal liver damage[90]). However, at doses as high as up to 4 grams per day in adults, paracetamol is regarded as totally safe and can comfortably be used (at lower doses, of course) even in infants. This example explains how critical and challenging a correct classification is: it is correct to classify paracetamol as hepatotoxic, since an overdose would likely cause a fatal liver failure, however, in drug development settings, what type of decision can be made on a compound predicted to be hepatotoxic by a model based on the information gathered, among others, from paracetamol? Should this molecule be discontinued and any further investigation stopped before knowing what safety margins might there be with regards to its intended therapeutic indication? Disregarding this molecule immediately after a positive prediction bears the risk of losing a potentially valuable compound. Continuing the investigations to further profile the molecule for future clinical development may be the best option to get to a more solid data-driven decision on its potential to become a drug. The bottom line is that, in this context, the prediction model will have a negligible impact on the decision. The same can be said in relation to other potential liabilities beyond hepatotoxicity, such as cardiotoxicity.

In order to strengthen the reliability of in silico models for the prediction of complex endpoints, all information generated by in vivo single- and repeat-dose studies should be made available in a clear and searchable way at the highest possible level of details. This is the most critical starting point for experts to generate very specific models based on the correct compounds classifications for very specific findings engaging into a careful data analysis. For example, it will be possible to have models for AST and ALT increases above 50% versus control groups, or for the prediction of bilirubinemia, moving away from a nonspecific, for example, "hepatotoxicity" classification. Even better, it would allow correlating certain parameters changes in the blood with very specific organ microscopic findings. This approach would, in principle, also make the identification of sound mechanisms of action for the specific observed toxicities a bit easier to address.

2.09.6 Data Sharing Initiatives and Data Exchange for Regulatory Purposes

2.09.6.1 IMI eTox and NextGets Initiatives: Data Sharing and Modeling Approaches

Analysis of reasons for previous failures and exploitation of them should help in improving the efficiency of clinical development of new drugs and their safety profiles. So far, preclinical study reports have been rarely stored in a format that supports data mining or statistical analysis. Some pharmaceutical companies have realized these hidden treasures in their archives and started internal work to improve retrievability of their report data. It would clearly be of benefit to the whole industry to analyze these data across multiple companies in order to expand the chemical and biological space. However, extracting these data from the reports and building such a database requires considerable investment. Recent advances achieved in international initiatives, including IMI's eTOX project, have shown that sharing of preclinical data, both private and public, is achievable through the combination of legal (IP), IT, and honest broker concepts[91,92] (see **Fig. 11**).

The eTOX project aims to collect, extract, and organize preclinical safety data from pharmaceutical industry legacy study reports and publically available toxicology data into a searchable database to facilitate data mining and the development of innovative in silico models and software tools to predict potential safety liabilities of small molecules. The eTOX-consortium consists of 13 pharmaceutical companies, 11 academic institutions, and 6 SMEs working together under the sponsorship of the Innovative Medicines Initiative (IMI) since 2010. The participating partners embrace expert knowledge in computational modelling, toxicology, pathology, and database design, liaising within the project in an integrative working environment.

After establishing an effective data sharing intellectual property (IP) protection within an "honest broker" approach (see **Fig. 11**), the project was able to compile a unique, well-curated dataset of currently more than 7000 study reports, corresponding to c.2000 test compounds. The concept to divide the results from the legacy reports of the pharmaceutical companies in different "confidentiality classes" was fundamental to facilitate data sharing and overcome IP and legal hurdles. Public data (class 1) are accessible to the public on request, nonconfidential data (class 2) are open for eTOX consortium members, confidential data (class 3) are only accessible within the consortium with an additional secrecy agreement, and private date (class 4) are only for EFPIA data owners, but can be shared for model generation on request.

Treatment-related findings have been classified within the database, reflecting the interpreted study outcome of every report. A suite of ontologies, built through OntoBrowser now released by eTOX to the public domain, enables the user to directly compare observed effects or toxicities of chemically similar structures (read-across).

A new in silico tool—eTOXsys—has been developed with a single user interface, which manages search queries on the high-quality preclinical database and organizes requests to a steadily growing collection of independent prediction models. Aspects of IP rights for data sharing, definition of ontologies, design of database structure, development of in silico models, data analysis, validation, and sustainability are key aspects of the eTOX project.

The recent advances achieved in several international initiatives, including the beforehand described IMI eTOX project, have shown that sharing of preclinical data, both private and public, is achievable, ontology development has been fostered in the area, and systems to handle, mine, and exploit these data across studies, compounds, pharmacology, side effects, and other criteria

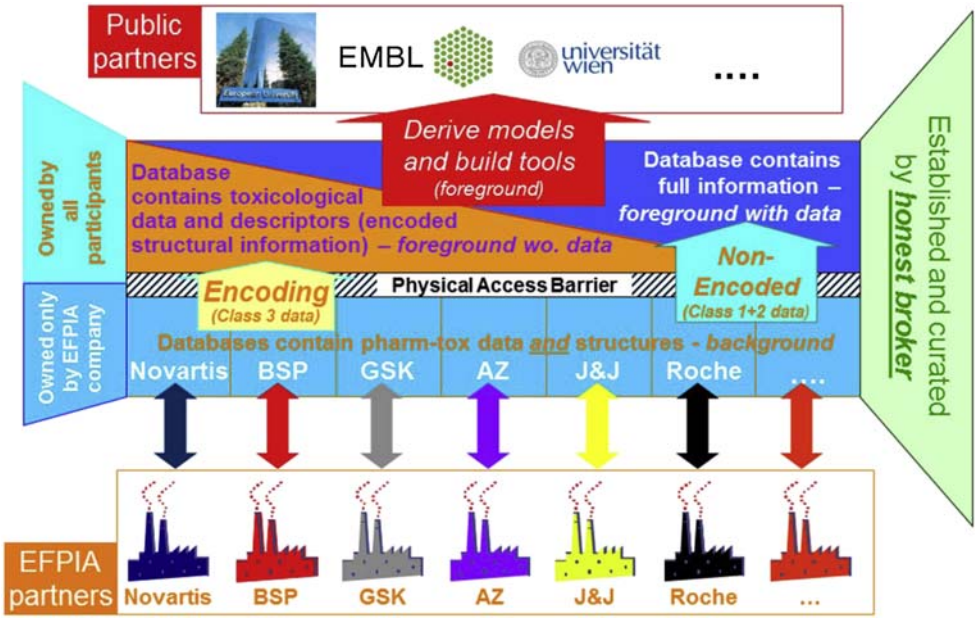

Fig. 11 The overall setup of the eTOX Project.

have been created and partly implemented within industry. In parallel, the electronic CDISC-SEND format has been chosen for file submission in IND/NDA/ANDA/BLA to FDA. This offers an opportunity for automatic collection of data, and sharing those into a common platform for reasons of data transparency, but also to obtain more powerful predictive data analyses. Existing initiatives in the field offer a relevant basis for an expanded IMI-based effort that leverages database and the data sharing. The so-called NexGETS initiative (*Nex*t Generation of *E*lectronic *T*ranslational *S*afety) is intended to provide a cost-efficient ideal environment for incorporating these data, optimizing tools, and providing linkage to human safety information to support the described regulatory-compliant, holistic perspective. In addition, tools for multivariate and multilevel data analysis and modelling, comparative data display across studies and compounds shall be developed within this proposed IMI2 project to enable meaningful exploitation of the accrued data.[93]

Beyond data sharing and mining, prediction of potential toxicity events both in preclinical species and in humans is key. The in-depth assessment of the preclinical species predictivity to human can only be achieved by analyzing as large an amount of organized data as possible. The linking of preclinical databases to chemical and biological knowledge, and to human clinical data probably represents the most powerful approach to achieve this endeavor and offers a unique opportunity. Such a translational approach will greatly advance the assessment of the relevance of animal findings for humans. In addition, it will contribute to the public discussion regarding the necessity of animal studies during drug development.

2.09.6.2 SEND Data Model and Electronic Submission to FDA

On Dec. 18th 2014 FDA issued the binding guidance titled "Providing Regulatory Submissions In Electronic Format—Standardized Study Data"[94] that requires Investigational New Drug (IND), New Drug Application (NDA), Abbreviated New Drug Application (ANDA), and Biologics License Application (BLA) submissions to be made in a standardized electronic format. The Clinical Data Interchange Standards Consortium (CDISC) Standard for Exchange of Nonclinical Data (SEND) is intended to guide the structure and format of standard nonclinical datasets for interchange between sponsors and Contract Research Organizations (CROs) and for submission to the US FDA.

SEND, or the *S*tandard for *E*xchange of *N*onclinical *D*ata, is an implementation of the CDISC Standard Data Tabulation Model (SDTM) which specifies a way to present nonclinical data in a consistent format.[95]

The current production version of the SEND Implementation Guide (SENDIG v.3.0) is designed to support single-dose general toxicology, repeat-dose general toxicology, and carcinogenicity studies.

The guidance requires submission of nonclinical safety studies in SEND format for the study types currently supported. In the near future, the standard will be expanded to include additional study types, such as Safety Pharmacology (cardiovascular and respiratory) and Developmental and Reproductive toxicology, which will also be required.

The guidance further stipulates that published FDA Specific SEND Validation Rules will be enforced for all submitted data sets. The Agency may refuse to file (for NDAs and BLAs) or refuse to receive (for ANDAs) an electronic submission that does not have study data in conformance to the required standards.

Under the guidance, supported studies (included in NDA, ANDA, and certain BLA submissions) starting after Dec. 18th, 2016 must be submitted in SEND.

For IND submissions supported studies starting after Dec. 18th, 2017 must be submitted in SEND.

Currently nonclinical safety data is provided as tabulated data within PDF Study Reports, Original electronic data, generated in-house, is normally stored on the originating LIMS systems until it is archived. In the case of CRO studies, original electronic data is typically not made available unless explicitly requested by the sponsor. The FDA now requires that, in addition to the PDF reports, the original electronic data also be submitted in SEND format. This is a new requirement that is currently unsupported at Roche.

While it is possible to build a SEND data set manually, the process is labor intensive, error prone, and very difficult to validate. Given the fact that data comprising a study may come from multiple data sources the challenge becomes unworkable.

An automated or semi-automated computerized system that can accurately and consistently transform original non-SEND data from multiple sources to the SEND standard and validate SEND data following published rules is required. Oversight, tools and processes for ensuring that source data sets are collected, curated, transformed to SEND, and made available for submission in an effective manner are also required. A number of vendors offer SEND solutions, among them: Instem;[96] Integrated Nonclinical Development Solutions, Inc.;[97] PDS;[98] PointCross LifeSciences;[89] Xybion;[99] Zifo RnD Solutions.[100] The vendors offer a number of features in their solutions to make it easy to handle the numerous aspects of data management and production, including the ability to define and maintain mappings from company-specific lexicons to SEND controlled terminologies.

Currently, FDA pharm/tox reviewers analyze the submitted study reports by manually extracting the tabulated data contained in the appendices of the PDF documents and loading them into any number of tools they see fit for visualizing and reviewing it. This first step is labor intensive and time consuming.

With the recently issued guidance for e-submissions, FDA reviewers have the opportunity to receive the study data directly in the appropriate format into one single platform called Non Clinical Information Management System (NIMS). FDA will use NIMS also to visualize the data, run their analyses, and draw their conclusions on the studies under review.

This approach will allow FDA reviewers to save time on data curation and formatting aspects and free resources for more in-depth scientific analyses, also leveraging the large amount of information and knowledge that NIMS will be capturing over the coming years.

Since clinical data is also electronically exchanged via standardized models (www.cdisc.org), it can be expected that one day, clinical and nonclinical data will be integrated under one single platform intra- and intercompany, which would represent a significant milestone in Translational Medicine arena.

See also: 4.08. A Comprehensive Overview of the Current Status and Application of Predictive ADMET: Introduction and Overview. 4.16. Toxicity Prediction—Regulatory Perspective.

References

1. Muller, L.; Breidenbach, A.; Funk, C.; Muster, W.; Paehler, A. Strategies for Using Computational Toxicology Methods in Pharmaceutical R&D. In *Computational Toxicology: Risk Assessment for Pharmaceutical and Environmental Chemicals;* Ekins, S., Ed.; Wiley: Hoboken, NY, 2008; pp 545–579.
2. Muster, W.; et al. Computational Toxicology in Drug Development. *Drug Discovery Today* **2008,** *13* (7–8), 303–310.
3. Brigo, A.; Muster, W. The Use of In Silico Models Within a Large Pharmaceutical Company. In *In Silico Methods for Predicting Drug Toxicity;* Benfenati, E., Ed.; Springer: New York, 2016; p 534.
4. Arrowsmith, J. Trial Watch: Phase III and Submission Failures: 2007–2010. *Nature Reviews Drug Discovery* **2011,** *10,* 87.
5. Arrowsmith, J. Trial Watch: Phase II Failures: 2008–2010. *Nature Reviews Drug Discovery* **2011,** *10,* 328–329.
6. Arrowsmith, J.; Miller, P. Trial Watch: Phase II and Phase III Attrition Rates 2011–2012. *Nature Reviews Drug Discovery* **2013,** *12,* 569.
7. Elder, D. P.; White, A.; Harvey, J.; Teasdale, A.; Williams, R.; Covey-Crump, E. Mutagenic Impurities: Precompetitive/Competitive Collaborative and Data Sharing Initiatives. *Organic Process Research & Development* **2015,** *19* (11), 1486–1494.
8. Briggs, K. A. Is Preclinical Data Sharing the New Norm? *Drug Discovery Today* **2016**, in press.
9. Hillebrecht, A.; et al. Comparative Evaluation of in Silico Systems for Ames Test Mutagenicity Prediction: Scope and Limitations. *Chemical Research in Toxicology* **2011,** *24,* 843–854.
10. EU, Ban on animal testing, 2013. Available from: http://ec.europa.eu/growth/sectors/cosmetics/animal-testing/index_en.htm.
11. ICH, M., ICH M7: Assessment and Control of DNA Reactive (Mutagenic) Impurities in Pharmaceuticals to Limit Potential Carcinogenicity Risk, 2014.
12. Lhasa, L. Derek Nexus. 2015; Available from: http://www.lhasalimited.org/products/derek-nexus.htm.
13. Greene, N.; Judson, P. N.; Langowski, J. J.; Marchant, C. A. Knowledge-Based Expert Systems for Toxicity and Metabolism Prediction: DEREK, StAR and METEOR. *SAR QSAR Environ. Res.* **1999,** *10,* 299–314.
14. Judson, P. N. Using Computer Reasoning about Qualitative and Quantitative Information to Predict Metabolism and Toxicity. In *Pharmacokinetic Profiling in Drug Research: Biological, Physicochemical, and Computational Strategies;* Testa, B., Kramer, S. D., Wunderli-Allespach, H., Volkers, G., Eds.; Wiley: New York, 2006; pp 183–215.
15. Sanderson, D. M.; Earnshaw, C. G. Computer Prediction of Possible Toxic Action From Chemical Structure; the DEREK System. *Hum. Exp. Toxicol.* **1991,** *10,* 261–273.
16. ToxTree version 2.6.6. 2015; Available from: https://eurl-ecvam.jrc.ec.europa.eu/laboratories-research/predictive_toxicology/qsar_tools/toxtree.
17. CASE Ultra version 1.5.2.0. 2015; Available from: http://www.multicase.com/case-ultra.
18. Leadscope Expert Alerts version 3.2.4-1. 2015; Available from: http://www.leadscope.com/expert_alerts/.
19. Lhasa. Derek Nexus: Negative Predictions for Bacterial Mutagenicity. 2015; Available from: http://www.lhasalimited.org/products/negative-predictions-for-bacterial-mutagenicity.htm.
20. Benigni, R.; Bossa, C. Structure Alerts for Carcinogenicity, and the Salmonella Assay System: A Novel Insight Through the Chemical Relational Databases Technology. *Mutation Research* **2008,** *659,* 248–261.

21. Leadscope® Genetox Expert Alerts White paper. 2014; Available from: http://www.leadscope.com/white_papers/Leadscope_alerts_white_paper.pdf.
22. Tropsha, A. Best Practices for QSAR Model Development, Validation, and Exploitation. *Molecular Informatics* **2010,** *29,* 476–488.
23. Sarah Nexus, 2015. Available from: http://www.lhasalimited.org/products/sarah-nexus.htm.
24. Leadscope Model Applier, 2015. Available from: http://www.leadscope.com/model_appliers/.
25. van Leeuwen, K.; Schultz, T. W.; Henry, T.; Diderich, B.; Veith, G. D. Using Chemical Categories to Fill Data Gaps in Hazard Assessment. *SAR and QSAR in Environmental Research* **2009,** *20,* 207–220.
26. Bioclipse, 2015. Available from: http://www.bioclipse.net/.
27. Prous Institute Symmetry, 2015. Available from: http://symmetry.prousresearch.com/about-symmetry/.
28. Hanser, T.; Barber, C.; Rosser, E.; Vessey, J. D.; Webb, S. J.; Werner, S. Self Organising Hypothesis Networks: A New Approach for Representing and Structuring SAR Knowledge. *Journal of Cheminformatics* **2014,** *6,* 21.
29. Sarah Nexus Methodology, 2015. Available from: http://www.lhasalimited.org/products/methodology-confidence-and-interpretation-of-predictions.htm.
30. Barber, C.; Cayley, A.; Hanser, T.; Harding, A.; Heghes, C.; Vessey, J. D.; Werner, S.; Weiner, S. K.; Wichard, J.; Giddings, A.; Glowienke, S.; Parenty, A.; Brigo, A.; Spirkl, H. P.; Amberg, A.; Kemper, R.; Greene, N. Evaluation of a Statistics-Based Ames Mutagenicity QSAR Model and Interpretation of the Results Obtained. *Reg. Tox. Pharm.* **2016,** *76,* 7–20.
31. Klopman, G. A Hierarchical Computer Automated Structure Evaluation Program. *Quant. Struct.–Act. Relat.* **1992,** *11,* 176–184.
32. Klopman, G. Artificial Intelligence Approach to Structure–Activity Studies. Computer automated structure evaluation of biological activity of organic molecules. *Journal of the American Chemical Society* **1984,** *106,* 7315–7321.
33. Chakravarti, S. K.; Saiakhov, R. D.; Klopman, G. Optimizing Predictive Performance of CASE Ultra Expert System Models Using the Applicability Domains of Individual Toxicity Alerts. *Journal of Chemical Information and Modeling* **2012,** *52,* 2609–2618.
34. Shannon, C. E. A Mathematical Theory of Communication. *Bell Syst. Tech. J.* **1948,** *27* (379–423), 379.
35. The OECD QSAR Toolbox, 2015. Available from: http://www.oecd.org/chemicalsafety/risk-assessment/theoecdqsartoolbox.htm.
36. OECD Toolbox guidance document, 2015.
37. OpenTox, 2015. Available from: http://www.opentox.org/.
38. Kazius, J.; McGuire, R.; Bursi, R. Derivation and Validation of Toxicophores for Mutagenicity Prediction. *J. Med. Chem.* **2005,** *48,* 312–320.
39. Kuhn, T.; Willighangen, E. L.; Zielesny, A.; Steinbeck, C. CDK-Taverna: An Open Workflow Environment for Cheminformatics. *BMC Bioinform.* **2010,** *11,* 159.
40. Steinbeck, C.; Hoppe, C.; Kuhn, S.; Floris, M.; Guha, R.; Willighagen, E. L. Recent Developments of the Chemistry Development Kit (CDK)—An Open-Source Java Library for Chemo- and Bioinformatics. *Curr. Pharmaceut. Des.* **2006,** *12,* 2111–2120.
41. Ekins, S. Progress in Computational Toxicology. *J. Pharmacol. Toxicol. Methods* **2014,** *69,* 115–140.
42. Cheng, A.; Li, W.; Zhou, Y.; Shen, J.; Wu, Z.; Liu, G.; et al. admetSAR: A Comprehensive Source and Free Tool for Assessment of Chemical ADMET Properties. *J. Chem. Inform. Modeling* **2012,** *52,* 3099–3105.
43. admetSAR, 2015. Available from: http://lmmd.ecust.edu.cn:8000/.
44. Valencia, A.; Prous, J.; Mora, Q.; Sadrieh, N.; Valerio, L. G., Jr. A Novel QSAR Model of Salmonella Mutagenicity and Its Application in the Safety Assessment of Drug Impurities. *Toxicol. Appl. Pharmacol.* **2013,** *273* (3), 427–434.
45. EMEA, G. Guideline on the limits of genotoxic impurities, 2006. Available from: http://www.emea.europa.eu/pdfs/human/swp/519902en.pdf.
46. Brigo, A.; Müller, L. Development of the Threshold of Toxicological Concern Concept and its Relationship to Duration of Exposure. In *Genotoxic Impurities;* Teasdale, A., Ed.; Wiley: Hoboken, NJ, USA, 2011; pp 27–63.
47. ICH, International Conference on Harmonisation of Technical Requirements for Registration of Pharmaceuticals for Human Use (ICH). Topic Q3C. Impurities: Residual Solvents, 1997.
48. Kroes, R.; Renwick, A. G.; Cheesemann, M.; Kleiner, J.; Mangelsdorf, I.; Piersma, A.; Schilter, B.; Schlatter, J.; van Schothorst, F.; Vos, J. G.; Wurtzen, G. Structure-based Thresholds of Toxicological Concern (TTC): Guidance for Application to Substances Present at Low Levels in the Diet. *Food Chem. Toxicol.* **2004,** *42,* 65–83.
49. Müller, L.; Mauthe, R. J.; Riley, C. M.; Andino, M. M.; Antonis, D. D.; Beels, C.; DeGeorge, J.; De Knaep, A. G.; Ellison, D.; Fagerland, J. A.; Frank, R.; Fritschel, B.; Galloway, S.; Harpur, E.; Humfrey, C. D.; Jacks, A. S.; Jagota, N.; Mackinnon, J.; Mohan, G.; Ness, D. K.; O'Donovan, M. R.; Smith, M. D.; Vudathala, G.; Yotti, L. A rationale for Determining, Testing, and Controlling Specific Impurities in Pharmaceuticals that Possess Potential for Genotoxicity. *Reg. Tox. Pharm.* **2006,** *44,* 198–211.
50. Kasper, P.; Müller, L. Genotoxic Impurities in Pharmaceuticals. In *Genotoxicity and Carcinogenicity Testing of Pharmaceuticals;* Jacobson-Kram, M. G.a. D., Ed.; Springer: New York, 2015.
51. EMA. Questions and answers on the 'Guideline on the limits of genotoxic impurities', 2010. Available from: http://www.ema.europa.eu/docs/en_GB/document_library/Scientific_guideline/2009/09/WC500002907.pdf.
52. M7, I., Assessment and Control of DNA Reactive (Mutagenic) Impurities in Pharmaceuticals to Limit Potential Carcinogenicity Risk, 2014.
53. Sutter, A.; Amberg, A.; Boyer, S.; Brigo, A.; Contrera, J. F.; Custer, L. L.; Dobo, K. L.; Gervais, V.; Glowienke, S.; van Gompel, J.; Greene, N.; Muster, W.; Nicolette, J.; Reddy, M. V.; Thybaud, V.; Vock, E.; White, A. T.; Müller, L. Use of in Silico Systems and Expert Knowledge for Structure-Based Assessment of Potentially Mutagenic Impurities. *Regul. Toxicol. Pharmacol.* **2013,** *67* (1), 39–52.
54. Amberg, A.; et al. Principles and Procedures for Implementation of ICH M7 Recommended (Q)SAR Analyses. *Reg. Tox. Pharm.* **2016,** *77,* 13–24.
55. Brigo, A., Muster, W. Comparative Assessment of Several In Silico Systems and Models to Predict the Outcome of the Ames Mutagenicity Assay. In Society of Toxicology Annual Meeting 2015, S.o. Toxicology, Editor 2015: San Diego, California, USA.
56. Hansen, K.; Mika, S.; Schroeter, T.; Sutter, A.; ter Laak, A.; Steger-Hartmann, T.; Heinrich, N.; Müller, K. R. Benchmark Data Set for In Silico Prediction of Ames Mutagenicity. *J. Chem. Inform. Modeling* **2009,** *49,* 2077–2081.
57. Ames, B. N.; Durston, W. E.; Yamasaki, E.; Lee, F. D. Carcinogens are Mutagens: A Simple Test System Combining Liver Homogenate for Activation and Bacteria for Detection. *Proc. Natl. Acad. Sci. U.S.A.* **1973,** *70,* 2281–2285.
58. Escobar, P. A.; Kemper, R. A.; Tarca, J.; Nicolette, J.; Kenyon, M.; Glowienke, S.; Sawant, S. G.; Christensen, J.; Johnson, T. E.; McKnight, C.; Ward, G.; Galloway, S. M.; Custer, L.; Gocke, E.; O'Donovan, M. R.; Braun, K.; Snyder, R. D.; Mahadevan, B. Bacterial Mutagenicity Screening in the Pharmaceutical Industry. *Mutat. Res.* **2013,** *752,* 99–118.
59. Reuters, T. Metacore—Data-mining and pathway analysis, 2015. Available from: http://thomsonreuters.com/en/products-services/pharma-life-sciences/pharmaceutical-research/metacore.html.
60. Fischer, H., et al., Prediction of In Vitro Phospholipidosis of Drugs by Means of Their Amphiphilic Properties. Rational Approaches to Drug Design, 2001; pp. 286–289.
61. Kruhlak, N. L.; et al. Progress in QSAR Toxicity Screening of Pharmaceutical Impurities and Other FDA Regulated Products. *Adv. Drug Delivery Rev.* **2007,** *59* (1), 43–55.
62. CompuDrug. MetabolExpert, 2015. Available from: http://www.compudrug.com/metabolexpert.
63. Molecular, D. MetaSite, 2015. Available from: http://www.moldiscovery.com/software/metasite/.
64. Cherkasov, A.; Muratov, E. N.; Fourches, D.; Varnek, A.; Baskin, I. I.; Cronin, M.; Dearden, J.; Gramatica, P.; Martin, Y. C.; Todeschini, R.; Consonni, V.; Kuz'min, V. E.; Cramer, R.; Benigni, R.; Yang, C.; Rathman, J.; Terfloth, L.; Gasteiger, J.; Richard, A.; Tropsha, A. QSAR Modeling: Where Have You Been? Where Are You Going To? *J. Med. Chem.* **2014,** *57,* 4977–5010.
65. Dambach, D. Drug-Induced Hepatotoxicity Advances in Preclinical Predictive Strategies and Tools. In *Predictive ADMET: Integrative Approaches in Drug Discovery and Development;* Wang, J., Urban, L., Eds.; Wiley-VCH: Weinheim, 2014.
66. Lee, W. M.; et al. Acute Liver Failure in the United States. *Semin Liver Dis* **2003,** *23,* 217–226.

67. Holt, M. P.; et al. Mechanism of Drug-Induced Liver Injury. *AAPS J.* **2006,** *8,* E48–E54.
68. Kaplowitz, N. Idiosyncratic Drug Hepatotoxicity. *Nature Rev. Drug Discov.* **2005,** *4* (489–499), 489.
69. Russmann, S. Current Concepts of Mechanisms of Drug-Induced Hepatotoxicity. *Curr. Med. Chem.* **2009,** *16,* 3041–3053.
70. Przybylak, K. R.; Cronin, M. T. D. In Silico Models for Drug-Induced Liver Injury—Current Status. *Expert Opin. Drug Metab. Toxicol.* **2012,** *8* (2), 201–217.
71. Clark, K.; et al. Modelling In Vitro Hepatotoxicity Using Molecular Interaction Fields and SIMCA. *J. Mol. Graph Model.* **2004,** *22,* 487–497.
72. Chan, K.; et al. Structure–Activity Relationships for Halobenzene Induced Cytotoxicity in Rat and Human Hepatocytes. *Chem. Biol. Interact.* **2007,** *165,* 165–174.
73. Sakuratani, Y.; et al. Category Analysis of the Substituted Anilines Studies in a 28-Day Repeat-Dose Toxicity Test Conducted on Rats: Correlation Between Toxicity and Chemical Structure. *SAR and QSAR in Environ. Res.* **2008,** *19,* 681–696.
74. Cheng, A.; Dixon, S. L. In Silico Models for the Prediction of Dose-Dependent Human Hepatotoxicity. *J. Comp. Aided Mol. Des.* **2003,** *17,* 811–823.
75. Egan, W. J.; et al. In Silico Prediction of Drug Safety: Despite Progress There is Abundant Room for Improvement. *Drug Discovery Today* **2004,** *1,* 381–387.
76. Ekins, S.; et al. A Predictive Ligand-Based Bayesian Model for Human Drug-Induced Liver Injury. *Drug Metab. Dispos.* **2010,** *38,* 2302–2308.
77. Rodgers, A. D.; et al. Modeling Liver-Related Adverse Effects of Drugs Using k-Nearest Neighbor Quantitative Structure–Activity Relationship Method. *Chem. Res. Toxicol.* **2010,** *23,* 724–732.
78. Matthews, E. J.; et al. Identification of Structure–Activity Relationships for Adverse Effects of Pharmaceuticals in Humans: Part B. Use of (Q)SAR Systems for Early Detection of Drug Induced Hepatobiliary and Urinary Tract Toxicities. *Reg. Tox. Pharm.* **2009,** *54,* 23–42.
79. Cruz-Monteagudo, M.; et al. Computational Chemistry Approach for the Early Detection of Drug-Induced Idiosyncratic Liver Toxicity. *J. Comp. Chem.* **2008,** *29,* 533–549.
80. Low, Y.; et al. Predicting Drug-Induced Hepatotoxicity Using Qsar and Toxicogenomics Approaches. *Chem. Res. Toxicol.* **2011,** *24,* 1251–1262.
81. Fourches, D.; et al. Chemoinformatics Analysis of Assertions Mined from Literature that Describe Drug-Induced Liver Injury in Different Species. *Chem. Res. Toxicol.* **2010,** *23,* 171–183.
82. Breiman, L.; et al. *Classification and Regression trees;* Wadsworth International Group: Belmont, CA, 1984.
83. Hawkins, D. M.; Kass, G. V. In *Topics in Applied Multivariate Analysis;* Hawkins, D. M., Ed.; Cambridge University Press: Cambridge, 1982; pp 269–302.
84. Matthews, E. J.; et al. Identification of Structure–Activity Relationships for Adverse Effects of Pharmaceuticals in Humans: Part C. Use of QSAR and An Expert System for the Estimation of the Mechanism of Action of Drug-Induced Hepatobiliary and Urinary Tract Toxicities. *Reg. Tox. Pharm.* **2009,** *54,* 43–65.
85. Ursem, C. J.; et al. Identification of Structure Activity Relationships for Adverse Effects of Pharmaceuticals in Humans. Part A: Use of FDA Post-Market Reports to Create a Database of Hepatobiliary and Urinary Tract Toxicities. *Reg. Tox. Pharm.* **2009,** *54,* 1–22.
86. Zhu, X.-W.; et al. Hybrid In Silico Models for Drug-Induced Liver Injury Using Chemical Descriptors and In Vitro Cell-Imaging Information. *J. Appl. Toxicol.* **2013,** *34,* 281–288.
87. Greene, N.; et al. Developing Structure–Activity Relationships for the Prediction of Hepatotoxicity. *Chem. Res. Toxicol.* **2010,** *23,* 1215–1222.
88. Piatetsky-Shapiro, G. Big Data Hype (and Reality), 2012. Available from: https://hbr.org/2012/10/big-data-hype-and-reality.
89. PointCross-Life-Sciences, 2016. Available from: http://pointcrosslifesciences.com/index.html.
90. James, L. P.; Mayeuy, P. R.; Hinson, J. A. Acetaminophen-Induced Hepatotoxicity. *Drug Metab. Dispos.* **2003,** *31* (12), 1499–1506.
91. Cases, M.; et al. The eTOX Data-Sharing Project to Advance in Silico Drug-Induced Toxicity Prediction. *Int. J. Mol. Sci.* **2014,** *15* (11), 21136–21154.
92. Briggs, K.; Cases, M.; Heard, D. J.; Pastor, M.; Pognan, F.; Sanz, F.; Schwab, C. H.; Steger-Hartmann, T.; Sutter, A.; Watson, D. K.; Wichard, J. D. Inroads to Predict In Vivo Toxicology-An Introduction to the eTOX Project. *Int. J. Mol. Sci.* **2012,** *13* (3), 3820–3846.
93. Proposal, I. Topic: Next Generation of Electronic Translational Safety—NexGETS, 2016. Available from: http://ec.europa.eu/research/participants/portal/desktop/en/opportunities/h2020/topics/19053-imi2-2016-09-04.html.
94. FDA, 2014. Available from: http://www.fda.gov/downloads/Drugs/Guidances/UCM292334.pdf.
95. PhUSE. SEND Implementation Wiki, 2016. Available from: http://www.phusewiki.org/wiki/index.php?title=SEND_Implementation_Wiki.
96. Instem, 2016. Available from: http://www.instem.com/.
97. INDS, 2016. Available from: http://inds-inc.com/.
98. PDS, 2016. Available from: http://www.pdslifesciences.com/.
99. Xybion, 2016. Available from: http://www.xybion.com/.
100. Zifo-RnD, 2016. Available from: http://www.zifornd.com/.

2.10 Overview of Drug Polypharmacology and Multitargeted Molecular Design

R Chaudhari, Z Tan, and S Zhang, MD Anderson Cancer Center, Houston, TX, United States

© 2017 Elsevier Ltd. All rights reserved.

2.10.1	**Introduction**	259
2.10.1.1	The Concept of Polypharmacology	259
2.10.1.2	Overview of the Current Status of Polypharmacology	260
2.10.1.3	Comparison of Polypharmacology With Monotherapy and Combination Therapy	261
2.10.2	**Methods to Study Polypharmacology**	262
2.10.2.1	Ligand-Based Methods	263
2.10.2.2	Structure-Based Methods	266
2.10.2.3	Network-Based Methods	267
2.10.2.4	Bioinformatics Methods	268
2.10.3	**Advantages of Polypharmacological Drugs**	268
2.10.4	**Challenges in Polypharmacology Design**	269
2.10.4.1	Avoiding the Off-Target Activity	269
2.10.4.2	Optimizing the Potency of Multitargeted Agents	269
2.10.4.3	Achieving Multitargeting Without Becoming Nonselective	270
2.10.4.4	Selecting the Best Multitargeted Strategies	270
2.10.5	**Applications of Polypharmacology**	270
2.10.5.1	Targeting Complex Diseases	270
2.10.5.1.1	Polypharmacology in cancer	270
2.10.5.1.2	Polypharmacology in CNS disorders	271
2.10.5.2	Targeting Drug Resistance	271
2.10.5.3	Drug Repositioning/Repurposing	271
2.10.6	**Conclusions**	272
References		272

2.10.1 Introduction

2.10.1.1 The Concept of Polypharmacology

In the past decades, the predominant paradigm of drug discovery and development has been the rational design of maximally selective drugs for a certain target.[1,2] Great success has been achieved in pharmaceutical industry using this method, especially regarding diseases with well-defined mechanisms.[3,4] Nevertheless, the pathology of many diseases is much more complex and it would be very unlikely to cure these diseases through hitting only one target.[5,6] Increasing evidence acquired from genomics studies have shown that many biological systems are insensitive to a single attacker.[7,8] Interestingly, it is also found that over 40% of these targets are involved in more than one disease through molecular network analysis.[9] Indeed, single gene-knockout studies have shown little effect on phenotype in many cases. Of all the "druggable" genes and targets in mice,[10] the number of models with knockdown of one gene that are valuable in target validation can be as little as 10%.[7,11,12]

The substantial and robust nature of these observations can be understood by considering redundancy inherent in the vital system such as the alternative, complementary, or compensatory signaling pathways. These biological networks are characterized by their high resilience to mutations of a random node, but high instability when the highly connected (or significant) hubs are deleted.[13,14] The studies suggest that organisms tend to develop compensatory signaling pathways in order to counteract the acquired mutation/deletion of a single node.[15] Such findings encourage new thinking of drug discovery: in order to modify a phenotype, modulation of several targets is often required.[13] The burgeoning molecular networks predict that deletion of a single node will not affect many disease states; modulation of multiple proteins in the network is required to alter functions and restore the normal phenotypes.[13,16] Even if perfectly selective drugs were developed toward specific targets, those targets are also likely to be involved in multiple pathways, and thus target specificity does not guarantee a real "functional" specificity.

To bring a new drug onto the market, the cost was proximately $800 million in 2003. However, current estimates place the value ranging from $900 million to $1.7 billion (USD).[17–19] The average success rate from first-in-man to registration has been reported by big pharmaceutical companies from 1991 to 2000 at around 11%, with oncology and central nervous system (CNS) disorder treatments showing ~5% and ~8% success, respectively.[20] However, the attrition rate increases in the later stages of clinical development (Phases IIb and III) with the highest cumulative investment to that point. Even more worrisome is that compounds with novel mechanisms of action (MOA) experience higher attrition than those with well-defined mechanisms (defined as hitting a known target or showing proof of concept in clinical trials).[20,21] For instance, during 2011–15 Food and Drug Administration (FDA) approved 19 kinase inhibitors,[22] and in 2015 only ~36% of the approved drugs are targeting novel mechanisms[23]

One may argue that the bleak outlook for the pharmaceutical industry is due to the social climate or the corporate structure; regulatory authorities now are stricter with drug safety than ever before, and the standard of health care is higher than ever. The true reason for the depressing outlook, however, could be more fundamental than those mentioned; the most critical manner in which drug development is executed might be flawed. It is difficult to ignore the growing rate of failures and attrition in drug development over the last two decades based on the "one drug for one target for one disease" model. This philosophy was in harmonious combination with genetic reductionism and classification of one disease-causing gene.[24] The goal of drug discovery at that time was to produce "clean" drugs that minimized toxic side effects by making ligands as selective as possible for their respective targets. However, the current efficiency of drug development cannot achieve this goal and a new paradigm is required to boost the progress of drug development. Polypharmacology, defined as "the specific binding of single or multiple ligands to two or more molecular targets,"[25] then was a property that was considered undesirable in rational drug design, now, becomes a new paradigm to develop more effective and less toxic agents. It is worthy of note that polypharmacology design is still a very challenging task in its infancy. Many of the drugs were found to be active against multiple targets only after introduced to the market. For example Gleevec was introduced as one of the most selective kinase inhibitors and later was found to be targeting multiple receptors.[26,27]

2.10.1.2 Overview of the Current Status of Polypharmacology

As a new concept, the goal of polypharmacology is to design compounds specifically binding to more than one molecular target.[6,25] On the one side, interaction with multiple targets is one of the major reasons that cause drug side effects and toxicities. For instance, terfenadine, an H1 receptor antagonist that entered the market in 1982, was later withdrawn due to its side effects including life-threatening ventricular tachyarrhythmia, torsades de pointes. Such toxicity is caused by the blockade of the human ether-à-go-go-related gene, which is a common reason of failure in early drug safety assessment.[28] Another example is propoxyphene, which is a *mu* opioid receptor agonist and noncompetitive $\alpha 3\beta 4$ neuronal nicotinic acetylcholine receptor antagonist used as analgesic. After 55 years, the drug was withdrawn from the market due to its fatal side effects.

However, on the other side, drug polypharmacology could be beneficial. It has been recurrently used to identify novel indications of existing drugs, also known as drug repurposing. Sildenafil (Viagra), for instance, is an inhibitor of the cyclic guanosine monophosphate (cGMP)-specific phosphodiesterase type 5 (PDE5), initially developed to treat ischemic heart disease and hypertension by Pfizer in 1980s. Its side effect of stimulating penile erections was reported during Phase I clinical trials. Soon after Phase II clinical trials failure for treating angina, sildenafil was repurposed for the treatment of erectile dysfunctions[29] and successfully approved by FDA in 1998. After that, sildenafil quickly became a blockbuster. Recently, the promiscuous nature of a variety of FDA approved drugs has led to redirection of their use in different diseases, and this helps pharmaceutical companies to cut down their drug development cost, since the toxicity and side effect data is available from previous clinical trial studies.

In recent years, polypharmacology has gained significant interest in drug discovery.[30] Using "polypharmacology" as the keyword to search in Google Scholar generated 3840 results as of Mar. 16, 2016. Out of these literatures, more than half reports (about 2810) were published within the last 5 years. In particular, kinase inhibitors are well-known examples for their polypharmacology profiles. For instance, imatinib is a tyrosine kinase inhibitor approved by FDA for treatment of multiple cancers. Initially, it was designed to selectively inhibit the breakpoint cluster region protein–ABL complex (BCR–ABL) for the treatment of chronic myelogenous leukemia (CML).[27] Later it was found also to inhibit CD117 and platelet-derived growth factor receptor (PDGFR) and improve conditions of the patients with gastrointestinal stromal tumors.[31] Currently it is known that imatinib inhibits many other targets to exert its pharmacological effects, and its polypharmacology profile is illustrated in **Fig. 1**. One of the advantages of such multitargeted drugs is that they are compatible with a larger population of patients and would show better overall efficacies in treatment.[32]

Although most of the current multitargeting drugs are serendipitous discoveries, understanding of molecular polypharmacology may also contribute to rational design of new compounds with better efficacy and less side effects.[33] For instance, Knapp and colleagues designed several compounds with dual inhibition of kinases and bromodomains.[34] Bromodomains play an important role in multiple diseases where kinase inhibitors are used as therapeutic drugs.[35–37] In order to rationally obtain dual kinase-bromodomain inhibitors, the team tested 628 kinase inhibitors against the first bromodomain of bromodomain-containing protein 4 (BRD4).[34] They identified PLK1 inhibitor BI2536 as the potent inhibitor of BRD1 receptor. To further understand the mechanism, analysis of crystal structures of Polo like kinase 1 (PLK1) and BRD4 was carried out for rational design and further optimization of novel multitargeting drugs.

In 2005, Murphy et al. published a comprehensive review article focused on rational design of multitargeted ligands.[38] In this article they described the main strategies and applications in this field reported from 1990 to 2004. Over the past years, more methods have been developed. For instance, Apsel et al. identified compounds that inhibit both tyrosine kinases and phosphatidylinositol-3-OH kinases (PI3K).[39] These kinase subfamilies are characterized by low overall sequence identity but share a similar fold (two-lobed structure) with conserved residue motifs in the ATP site. Using iterative chemical synthesis, X-ray crystallography and biochemical profiling, the authors discovered some compounds with promising dual target activity. Structural features were also examined to rationalize the selectivity toward their targets. More recently, Besnard and team members devised an automated approach to design ligands with desirable polypharmacological profiles.[40] Bayesian models were built to prioritize the compounds, and 800 ligand–target predictions were tested experimentally, of which 75% were confirmed as true. In particular, starting with the drug donepezil, an acetylcholine esterase inhibitor initially for Alzheimer's disease (AD) therapy, they predicted and confirmed weak polypharmacological activity on dopamine receptors D4 and D2. A recent review study by Katselau et al. focused on successful

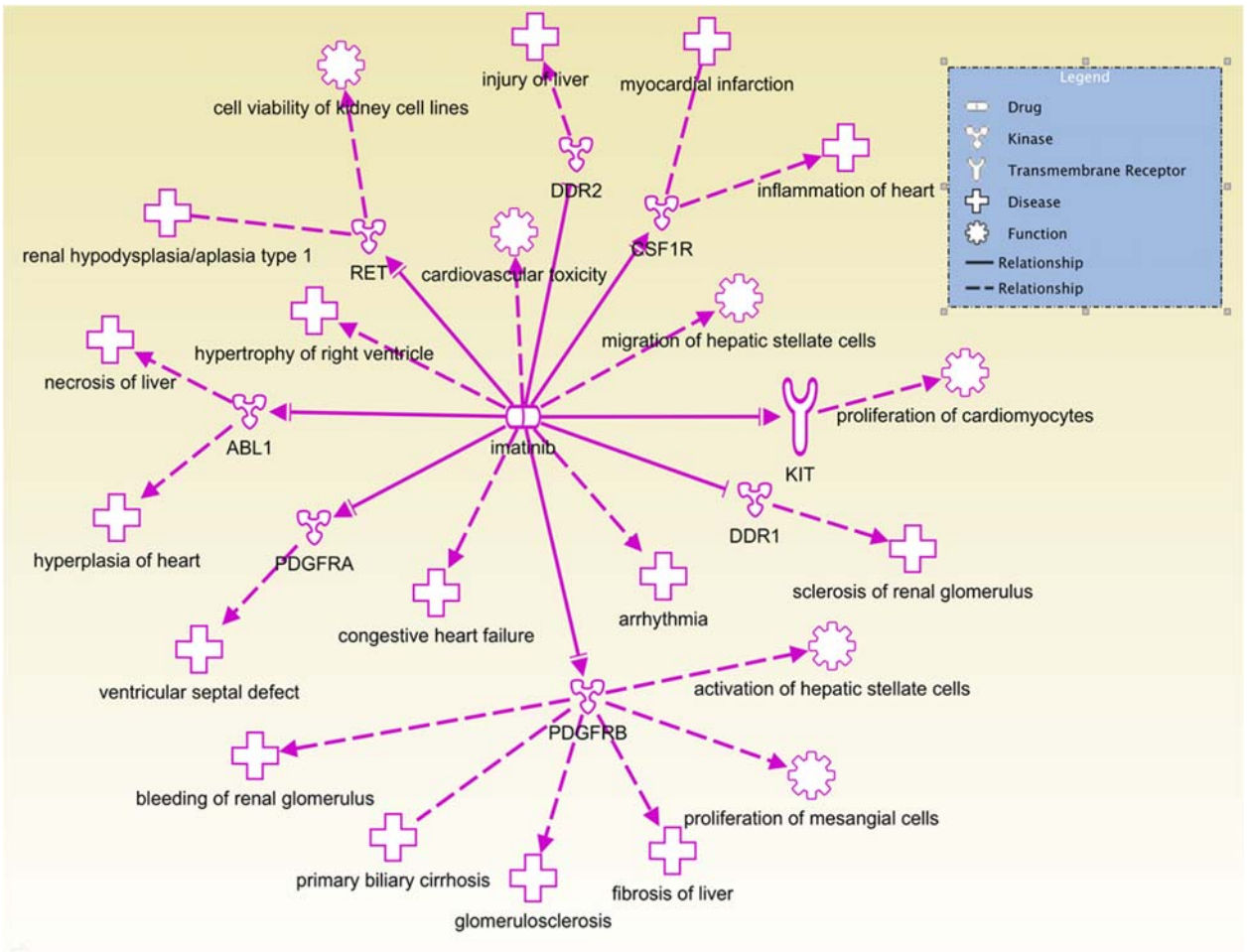

Fig. 1 Polypharmacology profile of imatinib. Generated using the QIAGEN's Ingenuity Pathway Analysis (IPA, QIAGEN Redwood City).

applications of multitargeted strategies for the treatment of chronic diseases like AD, Parkinson's disease, and cardiovascular and inflammatory diseases.[41]

2.10.1.3 Comparison of Polypharmacology With Monotherapy and Combination Therapy

In the last few decades, considerable research efforts have been made in the discovery and development of therapeutics that modulate individual disease-modifying targets. Based on different MOAs, there are many drugs in the market to treat disease conditions ranging from the simplest one to the most complicated one. These drugs can be classified as: (1) Drug acting on single targets, (2) Combinations of drugs acting on single or multiple targets, and (3) Single drug acting on multiple targets. The comparison of these therapies and some respective examples are shown in Fig. 2. These drugs have their own pros and cons and the limitation varies with the complexity of diseases.

Monotherapy is the preferred choice of medicine for most of the conditions. In most cases it is able to get the desired response and it also reduces potential drug adverse effects due to drug–drug interactions. The major disadvantage of this class of drugs is that the drug off-target activities are poorly known and lead to the consequences of reduced drug efficacy, increased drug resistance, and poor quality of life of the patients. Complex diseases such as cancer or those that affect multiple tissues such as diabetes and immune-inflammatory disorders are caused by multiple pathogenic mechanisms. Drugs designed to act against individual molecular targets usually are insufficient to combat multigenic diseases.[42] Attempts to develop more effective treatments by discovering highly selective single drugs have been largely unsuccessful in case of such complex diseases.

In comparison to single-target drugs, combinations of specific drugs that impact multiple targets simultaneously are found to be more effective at controlling complex diseases.[34,43,44] They are designed either in a way that one of the drugs facilitates the action of others, that is providing synergistic effect, or in the way that they exhibit a combined additive effect. A good combination of drugs is the one in which the drugs are individually active, are able to elicit a synergistic effect, have different MOA, have nonoverlapping mechanisms of resistance, and demonstrate distinct toxicities. In some cases, the risks of drug–drug interactions associated with combination therapies could be mitigated, resulting in a simplified therapeutic regimen. Many drug combination therapies have

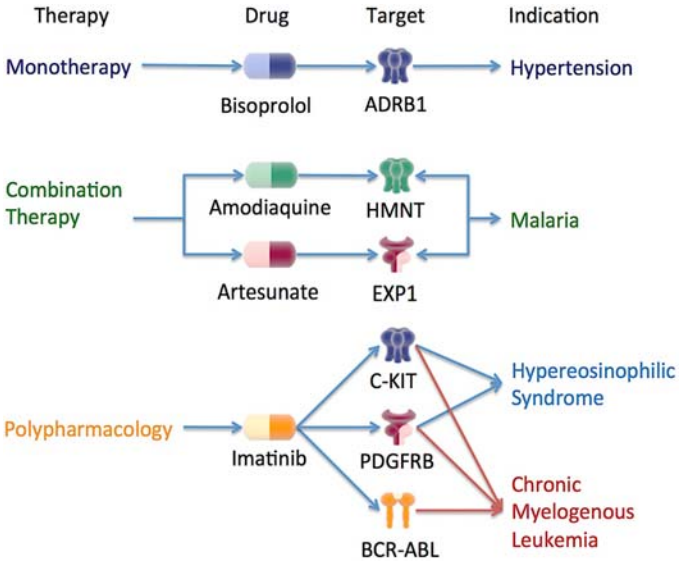

Fig. 2 Comparison of monotherapy, combination therapy, and polypharmacological agents.

been investigated in different disease conditions. For example, the implementation of artemisinin-based combination therapy was carried out to treat chloroquine-resistant and sulfadoxine–pyrimethamine-resistant malaria,[45] although it is not used as the preferred first-line antimalarial drug. Combination therapy is also explored in multiple sclerosis, a complex CNS inflammatory disease process that comprises multiple potential therapeutic targets. For example, one drug can be used to reduce the inflammation while another is able to augment neuroprotection or reduce side effects.

Though combination therapies have proved to be highly significant and therapeutically relevant, they have some disadvantages. Adverse effects of individual drugs can be additive or even synergistic, and drugs might interfere with each other, thereby reducing efficacy and exacerbating potential drug–drug interactions. If the combinatorial drugs are not highly selective, they could lead to a higher chance of acute or delayed toxicities. The use of drug cocktails often complicates dosing schedules and negatively impacts patient adherence to the treatment. Moreover, developing combination drugs is a time-consuming and arduous process, as it requires demonstration of the activity and safety of combination to regulatory agencies. In addition, problems may also arise if different pharmaceutical companies are developing two drugs selected for the combination therapy. In this case regulatory and intellectual property issues may delay clinical trials of these investigational drug combinations. To resolve this, the FDA recently expanded their patent portfolio. It is now possible to patent combination drugs in cocrystal format which could minimize some of the above combination therapy issues in the future.

On the other side, single drug acting on multiple targets have many advantages over drug acting on single targets or combination of drugs. They can act on multiple targets simultaneously; hence they show excellent efficacy compared to a compound with high specificity for a single target. They often show superior efficacy against advanced stage diseases. A single molecule with dual activity may have a more predictable pharmacokinetic (PK) profile compared to multiple molecules administered in combination. Therefore, it may display a superior PK and safety profile. This is particularly true if the adverse effects are molecule-based because a single molecule would be administered instead of combination. On the other hand, no clear advantage is obtained if the adverse effects are target-based. In this case two adverse effects will be independent of each other. The chance of developing target-based resistance to multitarget drugs is statistically lower than that of single-target drugs. Administering a single drug modulating multitarget guarantees the simultaneous presence of the molecule in tissues where the active principle is required to work such that the compound interacts with its multiple targets. Although it is arguable, developing a single agent binding to multiple targets might be easier compared to developing combination drugs. More detailed comparisons have been described by Anighoro et al.[30]

2.10.2 Methods to Study Polypharmacology

In polypharmacology, the ideal goal is to identify/develop compounds that act on multiple key targets involved in a given disease with increased efficacy and decreased side effects. Systematic method integration and data visualization is required to facilitate such studies. Significant efforts have been put forth to develop polypharmacology databases and computational methods. Some of the representative databases include STITCH,[46] Polypharma,[47] SuperTarget,[48] IBIS,[49] and SIDER.[50] Tools such as PyMine bring relevant data from databases and facilitate hypothesis generation for polypharmacology studies.[51] Various computational methods have been developed to predict on/off target activities for small molecules. One can use these methods to predict novel targets of known drugs and repurpose them to treat new indications. For example, Keiser et al. applied the similarity ensemble approach

(SEA) method and predicted new targets for methadone, emetine, and loperamide.[52] They found that these drugs might act as antagonist of muscarinic M3, α2 adrenergic, and neurokinin NK2 receptors, respectively. Experimental studies validated their prediction results. Recently, Kumar and Jasrai published a study in which they identified seven targets of kinetin using idTarget, a structure-based target prediction web server. Four of the seven predicted targets were experimentally validated in the subsequent literature search.[53] Although there have been a few successes, more accurate and robust approaches are still needed. Current methods can be divided into four categories: ligand-based, structure-based, network-based, and bioinformatics methods. In the rest of the article, we will review these methods (**Table 1**) and expect that a better understanding of their algorithms will greatly help to improve and develop novel technologies for polypharmacology studies. It is worth mentioning that since it is not realistic to cover all reported methods, herein we arbitrarily select and discuss some of them as examples in each category. We also provide an overview of the polypharmacological agents that have been discussed in this Chapter, including their 2D structures, mode of action, and indications to use (**Table 2**).

2.10.2.1 Ligand-Based Methods

A general assumption behind target identification using ligand-based methods is that similar compounds share similar targets. Many similarity-based methods and machine learning algorithms have been developed to predict targets of small molecule

Table 1 Methods and algorithms for polypharmacology studies

Methods	*Algorithms used*	*Web links*
Ligand-based methods		
SEA[52]	Daylight fingerprints, Kruskal's algorithm	http://sea.bkslab.org
TarPred[54]	Extended-connectivity fingerprint 4 (ECFP4), Tanimoto coefficient	http://www.dddc.ac.cn/tarpred
TargetHunter[55]	TAMOSIC algorithm	http://cbligand.org/TargetHunter
SuperPred[56]	Extended-connectivity fingerprint 4 (ECFP4), Tanimoto coefficient	http://prediction.charite.de
SwissTarget[57]	Chemical and structure similarity approach	http://www.swisstargetprediction.ch
Structure-based methods: inverse docking		
INVDOCK[58]	Geometric algorithm	http://bidd.nus.edu.sg/group/softwares/invdock.htm
idTarget[59]	Modified Dock algorithm	http://idtarget.rcas.sinica.edu.tw
DRAR-CPI[60]	Connectivity maps with Dock 6 algorithm	http://cpi.bio-x.cn/drar/
TarFisDock[61]	Modified Dock algorithm	http://www.dddc.ac.cn/tarfisdock/
Glide[62]	Stochastic search algorithm	http://www.schrodinger.com/Glide
Structure-based methods: binding site similarity search		
CavBase[63]	Clique detection algorithm	http://www.ccdc.cam.ac.uk/
SiteEngines[64]	Geometric hashing method	http://bioinfo3d.cs.tau.ac.il/SiteEngine/
SuMo[65]	Geometric matching of triplets	http://sumo-pbil.ibcp.fr/cgi-bin/sumo-welcome
ProBis[66]	Solvent accessible surface algorithm	http://probis.cmm.ki.si
IsoMIF[67] Finder	FLAP algorithm, Tanimoto coefficient	http://bcb.med.usherbrooke.ca/imfi.php
PocketMatch[68]	Greedy alignment algorithm, PM scoring method	http://proline.physics.iisc.ernet.in/pocketmatch/
PARIS[69]	Convolution kernel-based method	http://cbio.ensmp.fr/paris/paris.html
APoc[70]	Pocket similarity score	http://cssb.biology.gatech.edu/APoc
Structure-based methods: inverse pharmacophore search		
PharmMapper[71]	Kabsch algorithm	http://59.78.96.61/pharmmapper/
Network-based Methods		
Cmap[72]	Pattern matching algorithms	https://www.broadinstitute.org/cmap/
Bioinformatics-based methods		
Gene Expression Atlas[73,74]	Gene expression patterns under different conditions	https://www.ebi.ac.uk/gxa/home
Genecards[75]	Gene-centric databases integrated data from more than 100 web sources	http://www.genecards.org/
Gene Expression Omnibus[76,77]	Public database include microarray, NGS, and other high throughput functional genomics data	http://www.ncbi.nlm.nih.gov/geo/
KEGG[78]	Integrated database containing both genomic and molecular levels	http://www.kegg.jp/kegg/
Cancer Genome Anatomy Project (CGAP)[79]	Determination of gene expression levels of normal and cancer cells	http://cgap.nci.nih.gov/
The Cancer Genome Atlas (TCGA) Data Portal[80]	Large genome sequencing data of multiple cancer types	http://cancergenome.nih.gov/
1000 Human Genome[81]	Sequencing the genomes of a large number of people	http://www.1000genomes.org/
cBIOPortal[82]	Visualization, analysis, and download of large-scale cancer genomics data sets	http://www.cbioportal.org/

Table 2 Drug formulas, mode of action, and indications to use

Structure	*Name*	*Targets/mode of action*	*Indications*
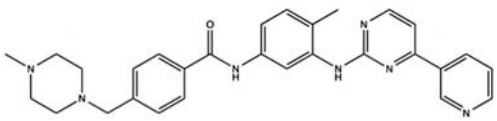	Imatinib	Tyrosine kinase inhibitor	Multiple cancers
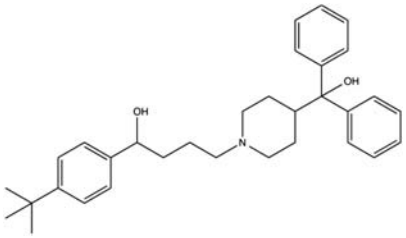	Terfenadine	H1 receptor antagonist	Withdrawn
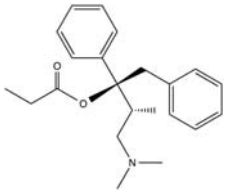	Propoxyphene	*Mu* receptor agonist and noncompetitive nAChR antagonist	Withdrawn
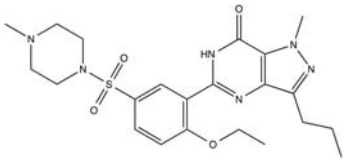	Sildenafil	cGMP–PDE5 inhibitor	Hypertension and erectile dysfunction
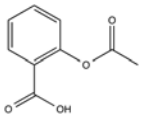	Aspirin	Suppression of prostaglandins and thromboxane, COX1 and COX2 inhibitors	Pain, cancer, and arthritis
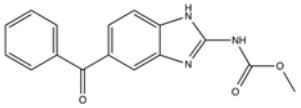	Mebendazole	Microtubule synthesis inhibitor	Nematode infestation, advanced colon cancer
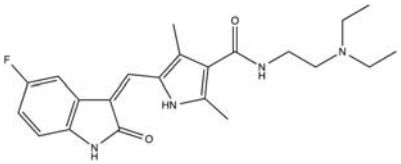	Sunitinib	VEGFR, PDGFR, KIT, FLT3 modulator	Renal cell carcinoma, GIST tumors
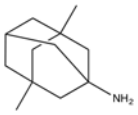	Memantine	Uncompetitive glutamatergic NMDA receptor antagonist	Alzheimer's disease
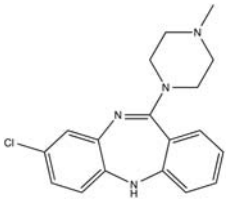	Clozapine	5HT1A partial agonist	Schizophrenia
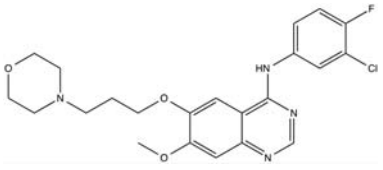	Gefitinib	EGFR inhibitor	Breast, lung, and other types of cancer

Table 2 Drug formulas, mode of action, and indications to use—cont'd

Structure	*Name*	*Targets/mode of action*	*Indications*
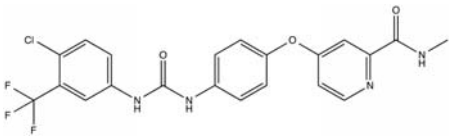	Sorafenib	Multiple kinase inhibitor including VEGFR, PDGFR and Raf family proteins	Kidney cancer and thyroid carcinoma
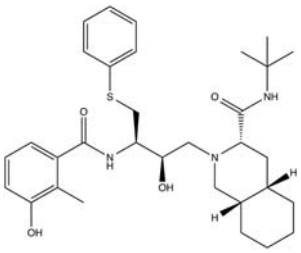	Nelfinavir	Inhibits angiogenesis, HSP90, HER2, and AKT signaling pathway	HIV and cancer

compounds (**Table 1**). SEA is one of the earliest similarity-based methods that generates similarity maps for targets based on their ligand topological similarities.[52] The statistical method of SEA is similar to the one used in basic local alignment search tool.[83] The dataset consists of 246 sets of targets acquired from MDL Drug Data Report with a unique set of ligands. In the first step, the 2D topological Daylight fingerprints are calculated for each ligand, and a pair-wise similarity metric is generated for each element of the two sets by calculating the Tanimoto coefficient (T_c).

$$T_c = \frac{A \cap B}{A \cup B}$$

Then the linear least square optimizer is used to predict raw scores of the two sets. These raw scores are then converted into z scores using the following formula:

$$z\text{score} = \frac{\text{raw score} - \text{random raw score at that set sizes}\,(\mu)}{\text{random standard deviation}\,(\sigma)}$$

The z scores are then converted to the E-value as a probability of score being achieved by random chance, as follows:

$$E(z) = P(z)N_{\text{db}}$$

where N_{db} is the number of set comparisons made in the database and $P(z)$ or $P(Z>z)$ is the probability of obtaining the same z score or better z score by random. In this case it was found that the background z scores have an extreme value distribution. Therefore, $P(Z>z)$ is calculated as follows:

$$P(Z > z) = 1 - exp(-e^x)$$

where $x = -\frac{z\pi}{\sqrt{6}} - \Gamma'(1)$ and $\Gamma'(1)$ is the Euler Mascheroni constant (≈ 0.577215665).

For numerical precision, when z score > 28, $P(Z>z)$ is approximated as:

$$P(Z > z) = -(x + (x2)/2 + (x3)/6)$$

A matrix of SEA E-values is then constructed for all pair of sets in the database. Using the Kruskal's algorithm, a minimum spanning tree is built as similarity map. Although the similarity map is calculated based on ligand similarities, it generates clusters of targets that are biologically related.

Another example is Shape Signature developed by Zauhar et al. It is a novel fragment-based ligand similarity search method that uses smooth molecular surface triangulator algorithm to generate surface of the ligand.[84] Along with the ligand similarity, it can also compare the shape of the ligand with the shape of the binding sites. This shape-based similarity function can be further explored for polypharmacology applications.

The structure–activity relationship (SAR) data has also enabled application of various machine-learning algorithms to derive relationship between small molecules and targets. Most of the similarity-based polypharmacology methods use Tanimoto coefficients whereas machine-learning algorithms include support vector machine (SVM), artificial neural networks, and Bayesian classifiers. In machine learning-based target prediction methods, similarity matrices between drug–drug and target–target are generated. A variety of machine learning methods such as Gaussian interaction profile,[85] pairwise kernel method (PKM),[86] Laplacian regularized least squares,[87] kernel regression,[88] bipartite local method,[89] and kernelized Bayesian matrix factorization with twin kernels (KBMF2K)[90] have been developed. For instance, Ding et al. carried out comparison studies on these methods and concluded that PKM and KBMF2K performed better than any other methods.[91] The PKM method was adopted by Jacob et al.,[86] and it is an

SVM-based method that precomputes drug–drug and target–target similarities and uses drug–target interaction as instances. The similarity of drug–target pairs from the drug similarity score and the target similarity score is computed by the following formula:

$$S((d,t),(d',t')) = S_{\mathrm{d}}(d,d')\cdot S_{\mathrm{t}}(t,t')$$

The generated similarity matrix (kernel) of drug–target pairs is then used to train SVM classifier for prediction of drug–target interactions. The authors tested this algorithm on three classes of receptors (enzymes, GPCRs, and ion channels) and reported that the methods did exceptionally well compared to traditional ligand-based methods, especially when target receptors did not have a set of known ligands.

2.10.2.2 Structure-Based Methods

Traditionally, structure-based methods such as molecular docking are used to screen small molecule libraries against targets of interest. In recent years, the significant increase of the number of unique 3D protein structures in Protein Data Bank (PDB) has paved the way for development of inverse docking methods. The primary goal of inverse docking is to dock the small ligand into active sites of multiple targets and rank those targets. Though available docking algorithms are capable of carrying out inverse docking, major challenge is to handle large amount of structural data and ranking of targets instead of small molecules. Multiple studies have suggested that energy scores used in traditional docking algorithms are not sufficient for ranking targets.[92–94] For example, Wang et al. reported limitations of Glide score in ranking targets.[92] They found that Glide score performed better when a correction term related to binding site description was added. Kellenberger et al. published a study on ranking of targets using Gold fitness score and topological molecular interaction fingerprint (IFP) and concluded that traditional single scoring function is not enough to rank targets accurately.[94] Their combination of gold fitness score with topological molecular IFPs performed better than any single scoring function. From these studies, it is clear that target-specific scoring functions are required to rank targets accurately for polypharmacology studies.

In recent years, various inverse docking methods such as INVDOCK,[58] TarFisDock,[61] and idTarget[59] were developed by using traditional docking algorithms with slightly modified parameters. For example, in 2001 Chen et al. developed the first automated inverse docking method INVDOCK.[58] It scores the protein targets based on ligand–protein interaction energy function (ΔE_{LP}) through calculation of two threshold values $\Delta E_{\mathrm{Threshold}}$ and $\Delta E_{\mathrm{competitor}}$ to screen potential targets. The first one is calculated from the analysis of PDB receptor–ligand complex analysis:

$$\Delta E_{\mathrm{Threshold}} = -\alpha N$$

where α is calculated by fitting above linear equation to the calculated ΔE_{LP} values of all receptor–ligand complexes in PDB database and N is the number of atoms in ligand. Based on the observed relation, targets are considered as binders if calculated $\Delta E_{\mathrm{LP}} < \Delta E_{\mathrm{Threshold}}$ kcal/mol.

The second threshold value $\Delta E_{\mathrm{competitor}}$ is applied to detect if the given small molecule is better competitor as compared to the ligand present in PDB structure of that receptor target. The threshold value is calculated from original receptor–ligand complex found in PDB database.

$$\Delta E_{\mathrm{competitor}} = \beta \Delta E_{(\mathrm{pdbcomplex})}$$

From computed energies of multiple compounds, it was suggested to use a value of 0.8 for β to produce statistically significant results. Targets are considered as binders if $\Delta E_{\mathrm{LP}} < \Delta E_{\mathrm{competitor}}$. Multiple studies have applied INVDOCK method for multitarget identification of small molecules.[95–98] For example, Zhao et al. identified multiple targets for Astragaloside IV.[98] Out of 32 predicted targets they experimentally validated three targets, namely calcineurin, angiotensin-converting enzyme, and c-Jun N-terminal kinase.

Later, Wang et al. developed idTarget, a web server for target fishing.[59] It employs a target scoring function based on binding pocket affinity profile modeled by a Gaussian function. A range of predicted binding affinities of multiple ligands for a given receptor determines the width of the Gaussian function. From this profile, a z score can be calculated where target prediction is considered significant if large negative Z value is observed. For ligand j to a given binding pocket i, the Z value can be calculated using the following equations:

$$Z_{ij} = \frac{E_{ij} - E_i}{sd_i}$$

$$E_i = \sum_{k=1}^{N_{\mathrm{c}}} E_k^{\mathrm{c}} / N_{\mathrm{c}}$$

$$sd_i = \sqrt{\frac{\left(E_k^{\mathrm{c}} - E_i\right)^2}{N_{\mathrm{c}} - 1}}$$

where E_{ij} is the dock energy of ligand j and binding pocket i; E^{c} is the dock energy from crystal pose; E_i is the center of the affinity profile for pocket I; and sd_i is the width of the affinity profile for pocket i.

Another widely used approach for target prediction is binding site similarity search. Based on the "lock & key model" postulated by Emil Fisher in 1894, it could be assumed that structurally similar proteins have similar molecular functions and therefore may

bind to structurally similar compounds. However it is worth to mention that many proteins do not share overall sequence similarity or structural similarity but they still have local similarities in form of binding sites and thus bind similar ligands. This is also an active area of research and a number of tools have been developed to identify similar binding sites (Table 1). Most of these methods use some variation of geometric pattern comparison, in which the 3D coordinates of the proteins are converted into simplified patterns such as pharmacophoric features or geometric triplets. Such patterns are then aligned using various search algorithms. Most commonly used strategies include geometric matching of triplets, where triplets are aligned based on measurements of distances between two points of the triplets.

Recently, the Fingerprints for Ligands And Proteins (FLAP) algorithm were developed by combining the GRID molecular interaction fields (GRID-MIFs) and pharmacophoric features.[99] First, MIFs are generated using various chemical probes covering all types of chemical interactions. The weighted energy-based and space-coverage function is then used to convert these MIFs into pharmacophoric features. All possible combinations of pharmacophoric features are used to generate four-point pharmacophore fingerprints, and they are used to find ligand–ligand, ligand–receptor, and receptor–receptor similarities. BioGPS is an automated method that calculates binding site similarities using FLAP algorithm.[100] It uses Fixpdb algorithm for automatic protein structure preparation and employs FLAPsite algorithm for binding site detection using 16 different GRID probes. Then with the FLAP protocol, MIFs are generated for the binding sites, and they are then superposed against all binding site MIFs in the database. For each solution, the algorithm calculates a set of Tanimoto coefficients.

Also, inverse pharmacophore methods have been implemented to map small molecule pharmacophoric features on structure-based pharmacophore models of the targets.[71,99] Traditionally, pharmacophore modeling is used as ligand-based virtual screening to identify compounds that match similar pharmacophoric features of known ligand. Liu et al. developed PharmMapper, a web server that can predict targets for a given small molecule by reverse mapping of pharmacophore to the receptor structure. The PharmMapper algorithm generates a triangle-hashing table from triplets of feature points, which resembles to the widely used geometric hashing method in pharmacophore modeling. These triangles from ligands are matched with precomputed library of triangles from receptor. The Kabsch algorithm is then used to optimize the alignment of these triangles. An evaluation of the alignment is carried out using distance-dependent scores.

$$\text{PointScore} = \sum_{i=1}^{n} w_i F(p)_i = \begin{cases} 1 - \left[\dfrac{d(p)_i}{T(p)_i}\right]^2, & d(p)_i \le T(p)_i \\ 0, & d(p)_i \le T(p)_i \end{cases}$$

$$\text{VectorScore} = \sum_{i=1}^{n} w_i F(v)_i \times cos\theta$$

where $d(p)_i$ is the distance between ligand point feature p and corresponding one in pharmacophore; $T(p)_i$ is the matching tolerance value; and θ is the angle between the two vectors from the matching pair of vector features in the ligand and pharmacophore. The final fit score is calculated using the following equation:

$$\text{FinalFitScore} = \text{PointScore} + \text{VectorScore} - \text{PenaltyScore}$$

where PenaltyScore is the PointScore calculated between ligand heavy atoms and pharmacophore excluded volumes. PharmMapper method was used to predict targets for a series of acenaphtho[1,2]pyrrole derivatives,[101] tyrosine kinases were identified as putative targets and then validated experimentally.

2.10.2.3 Network-Based Methods

High-throughput techniques in genomics, proteomics, and metabolomics are generating enormous amounts of data, which increases our understanding of complex diseases. Large efforts are being made to annotate and integrate such data to understand system-wide effects of small molecules. The Connectivity Map Project is the largest collection of gene-expression profiles for diseases, genetic mutations, and drug activities. One way to represent such data is by creating networks of various biological entities, and the graph algorithms can be used to deduce relation between biological entities, in this case the off-targets of small molecules. Recently, Vitali et al. developed a network-based method that builds a protein–protein interaction network in order to increase the number of possible associations retrieved, that is, the physical interaction between proteins and their binding type. It was then used to rank targets for polypharmacology studies.[102]

STITCH is an example that utilizes network-based methods and curated databases to predict protein–inhibitor interactions.[103,104] The authors extracted the interactions from literature using natural language processing text-mining techniques, and then used this data to predict interactions of query compounds. In the latest version, the authors added a new function to predict the protein–ligand interaction based on compound structures. They curated ligands with more than 100 binding proteins in ChEMBL database and utilized random forest to predict the binding proteins for query compounds. During the past several years, our group has embarked the development of using molecular networks that allows users to visually and efficiently navigate publicly available information on drug properties (biological targets, pharmacology, etc.) and can show relationships among drugs and their receptors based on their function annotation (biological targets, toxicity, side effects, metabolism, etc.) or chemical similarity.[105] Currently, this platform has been expanded to the analysis of more than 5000 drugs and 10 million virtual library compounds, along with 56,000 biological

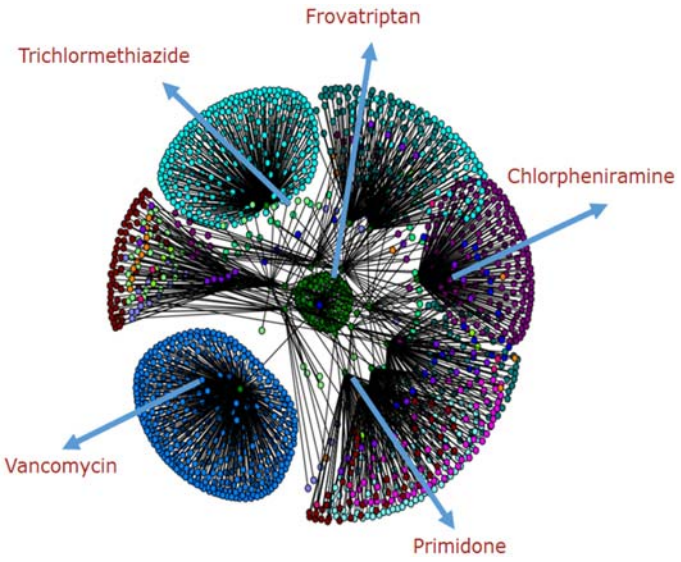

Fig. 3 *Drug network for butalbital*, generated based on shared targets with other approved drugs. Targets have been hidden in order to reduce the complexity, and drugs related to butalbital are shown in three levels with different colors. Butalbital is placed in the center of the graph; Frovatriptan is an example of innermost cluster *(dark green)*; Vancomycin, Trichlormethiazide, Chlorpheniramine, and Primidone are situated in blue, cyan, purple, and magenta clusters, respectively.

macromolecules with available high-resolution 3D structures. To fully explore the huge and complex molecular networks among ligand–ligand, ligand–receptor, and receptor–receptor molecules, integration of a diverse set of tools including chemical similarity searches, text mining, cheminformatics mapping, and high-throughput docking approaches are being implemented for in silico polypharmacology prediction and design. Fig. 3 demonstrates the drug network for Butalbital using our tools. Along this line, *Polypharma* is another database of multitargeted small molecules developed by our group recently.[47] In this database, we curated all drug-like ligands (953) that bind to more than two distinct proteins in PDB. Further analysis has shown that compared to single target-specific ligands, the multitargeted ligands have different chemical characteristics such as molecular weight and hydrophobicity. As a consequence, Polypharma provides a collection of confirmed multitargeted compounds that are very useful in the polypharmacology research such as novel target predictions and identification of new multitargeted compounds. The analyses of these multitargeted compounds provide insights of difference between multitargeted and single-targeted compounds.

2.10.2.4 Bioinformatics Methods

High-throughput methods, such as RNA-Seq, next generation sequencing, and reverse protein phase array, have generated large amount of gene expression data. With the help of genome-wide expression data from treated and untreated samples, one can study the overall functional effects of a small molecule and generate gene expression signatures that could be used for training data sets for polypharmacology studies. Sirota et al. developed a drug repositioning method that can predict novel therapeutic effect of the drugs based on gene expression pattern of 100 diseases and 164 drug treatments collected from public databases.[106] They demonstrated the capability of their method by recovering known drug–disease relationships. They also experimentally validated probable use of Cimetidine, an antiulcer drug in lung adenocarcinoma.

Currently, the NIH Library of Integrated Network-based Cellular Signatures Program (LINCS) (http://www.lincsproject.org) aims to collect and disseminate data and analytical tools needed to understand how human cells respond to perturbation by drugs, environment, and mutation. The database contains more than 1 million drug-induced gene expression profiles that can be explored to study drug polypharmacology. Another well-known tool for such studies is Ingenuity Pathway Analysis (IPA). It is developed by Qiagen with a significant amount of curated and annotated data of genes, chemicals, diseases, pathways, and toxicity studies. It helps in analyzing and visualizing gene expression data by mapping onto various canonical and novel pathways. Of note, bioinformatics-based polypharmacology applications can also be developed with Cytoscape, which is an open source molecular interaction network visualizer.[107] Other bioinformatics approaches that can be used for polypharmacology studies are summarized in Table 1.

2.10.3 Advantages of Polypharmacological Drugs

As already mentioned above, polypharmacological drugs have a number of advantages over single target drugs or combination. Generally, the therapeutic efficiency of the multitargeted drugs is increased as the result of their ability to target multiple cellular

pathways at the same time. More obviously, it is much easier to alter the physical and chemical properties of a single agent than combinations for better bioavailability. In addition, due to their promiscuous nature, multitargeted drugs may have multiple routes of elimination, thus less accumulation in the body and making them safer. Another advantage of multitargeted drugs is that they may be suitable for a larger population of patients and produce much better overall effects by targeting multiple signaling pathways as compared to selective drugs. This also creates incentives for pharmaceutical industry to invest more financial and research efforts in term of profitability. For instance due to its multitargeting activity, imatinib is effective in a more broad population while gefitinib as a selective EGFR inhibitor is shown to be effective only in patients with EGFR mutations.[32]

The multitargeted behavior of these drugs has proved to be a great asset in drug development. One of the most renowned examples is aspirin. This drug has not only been employed for pain relief, but frequently used for decreasing platelet aggregation, prevention of cancer and preeclampsia, and treating arthritis.[108–110] Its actions on several pain-related pathways have been well studied in depth and more MOA have been elucidated. Drugs like sorafenib and sunitinib have also shown favorable results with their multitargeted behavior. Especially sorafenib, which impedes the activity of several of kinase receptors such as platelet-derived growth factor (PDGF), vascular endothelial growth factor (VEGF), also triggers the RAF/MEF/ERK signaling pathway (inhibition of cell proliferation) and the VEGFR-2/PDGFR-β signaling cascade (curbing tumor angiogenesis).[111–113] On the other hand, sunitinib, a small molecule with inhibition of tyrosine kinase activities, acts on VEGF, PDGF, and FLT3 receptor tyrosine kinases.[114,115] They both are used as frontline drugs for treatment of a variety of cancers.

In many cases it is observed that the polypharmacological agents present relatively low binding affinity to their targets, as compared to the single targeted, selective drugs. However, such feature does not diminish their therapeutic effects. For example, memantine (a drug used to treat AD) and other multitargeted, noncompetitive NMDA receptor antagonists display minimal side effects and prevalence.[116] More encouraging, the low affinity binding molecules have been employed to inhibit unconventional targets such as unstructured proteins, where the weak binding properties prove to be very useful in modulating the signaling and regulation.[117] The low affinity binding also involves fleeting interactions with the targets, which may manifest in greater off-rate as compared to on-rate actions. Interestingly, the low affinity binding does not necessarily reduce the efficiency. It is observed that most of the signaling pathways and transcriptional networks involve weak linkage protein interactions, which are transient in nature,[118] and these reactions have low flux energy consumption. The polypharmacological drugs usually have transitory interactions with their targets in cells and such binding is adequate to modulate the required modifications needed to trigger the next step in the pathway.

The multitarget effects of these drugs not only aid in developing new strategies for rational drug design but also help understand the promiscuous binding, even in processes such as drug delivery and excretion. This has presented a new challenge for drug development across the disciplines, where further research will be needed for designing the next generation of therapeutics.

2.10.4 Challenges in Polypharmacology Design

Though multitargeted drug design is suitable for complex diseases, there are many challenging tasks that need to be overcome.

2.10.4.1 Avoiding the Off-Target Activity

By understanding the mechanisms behind off-target activities, we can devise strategies to avoid unintended effects, which may cause side effects or toxicities. For example, when the RNA-induced silencing complex processes siRNAs, it also downregulates unintended targets that result in measurable false-positive phenotypes.[119] This problem can be mitigated by understanding the basic mechanism, selecting appropriate relevant targets, and including phenotypic screening experiments. Additionally we can also optimize the chemical structure and carry out siRNA pooling to decrease potential side effects.[120,121] Again with the multikinase inhibitor sorafenib as the example, it was found to be also active against 5-HT receptors in the range of nanomolar concentrations.[122] Such issues could be addressed by developing more accurate computational methods to predict the promiscuous nature of drugs and their targets in the earlier stage of drug discovery.

2.10.4.2 Optimizing the Potency of Multitargeted Agents

With the help of combinatorial chemistry and SAR studies, it is feasible to optimize the compound potency for a particular target. For combination therapy targeting multiple receptors, it can be achieved by simply optimizing the ratio of the individual drug doses. It is rather difficult to optimize potencies at multiple receptors while optimizing the single chemical structure. However, multitargeted single drugs avoid drug–drug interactions and simplify the process of clinical trial development for new drug approval. To outweigh the advantages of monotherapy and combination therapy, computational methods can be used to optimize drug potencies against multiple targets. Recently, Besnard and Hopkins developed an automated and adaptive design method to develop drugs targeting multiple specific receptors also with potency optimization strategies.[40] Using the algorithm, the team was able to develop highly potent donepezil derivatives against the D4 dopamine receptor ($K_i = 8.9$ nM) as compared to donepezil ($K_i = 614$ nM).[40] Wermuth et al. in a recent publication described a novel approach termed as selective optimization of side effect (SOSA) which was used for optimization to increase affinity to the new target for a known drug, while reducing affinity to the primary target.[123] In the first step, screening is carried out to identify hits from carefully selected, structurally diverse compounds with known toxicity and bioavailability data. In the second step, the selected hits are optimized for their potency against the new target using traditional approaches such as

parallel or combinatorial chemistry. These studies have demonstrated that the potency of the multitarget agents can be optimized through rational design.

2.10.4.3 Achieving Multitargeting Without Becoming Nonselective

Again sunitinib was one of the first multikinase inhibitors used to selectively block VEGFR2 signaling to achieve antitumor efficacy that is by regulating both tumor proliferation and angiogenesis.[115] But one study found that the off-target effects of the RTK inhibitor might disturb the homeostatic barrier function of the host vasculature, leading to metastasis promotion.[124] Later, sunitinib was also found to be a nonselective drug that promotes some cancer towards the aggressive stage in animal models. The proposed mechanism behind this action is that the Akt/β-catenin pathway gets activated in response to drug-induced hypoxia and then it stimulates the growth of the distinct aggressive tumor cells.[125] To overcome this problem, combination therapy of this drug with agents that can block the Akt/β-catenin pathway was suggested.[126] This demonstrates that complete understanding of pathways and protein networks is required to treat complex diseases, and it is crucial to derive multitargeted, but still selective agents.

2.10.4.4 Selecting the Best Multitargeted Strategies

Information obtained from in vitro assays in developing multikinase inhibitors cannot be solely relied on, but rather additional cell-based studies are required to assess system-wide effects including membrane permeability, intracellular ATP concentrations, and the relative concentrations of the kinase targets and their substrates. In some cases such as relapsed or refractory lymphomas or Hodgkin disease after DHAP induction, clinicians need to prescribe a series of drugs with maximum tolerable doses to achieve sequenced action as the molecular target. Such highly potent and multiple targeted therapies are very difficult with multitargeted single drug therapy. Thus, combination therapies have to be used as complementary approaches to the multitargeted drug therapy in these cases.

2.10.5 Applications of Polypharmacology

2.10.5.1 Targeting Complex Diseases

The "one drug–one target" approach is beneficial when the underlying etiology of a disease is well studied and it produces the maximum efficacy by targeting a single receptor or enzyme. Unfortunately this does not hold true for complex diseases. Diseases such as cancer and AD arise from multiple factors including biological and environmental. In most of the cases the underlying mechanisms of these diseases are poorly known. Despite the large amount of money invested and recent success in target identification, the single drug approach and the combination therapy have failed to show expected results. On the other hand, multitargeted drugs indeed have been shown with significant advantages in treating cancer and AD. Next we briefly discuss some application of polypharmacology to the therapy of these diseases.

2.10.5.1.1 Polypharmacology in cancer

Utilization of molecular networks has been pivotal to have next big breakthroughs for treatment of this seemingly unstoppable disease. Cancer is poised to surpass heart disease to become the most common cause of death in the United States.[127] It is no surprise that, when compared to other diseases afflicting the current population, cancer is described as a malady "at best, minimally controlled by modern medicine."[128] While the mortality rates of cardiac, cerebrovascular, and infectious diseases have been brought down about two-thirds in the last 50 years, the mortality rates from cancer have remained largely the same.[127] The global market for cancer drugs has hit $100 billion in annual sales, and could reach $147 billion by 2018, even with numerous recent discoveries in many diverse fields of cancer studies.[129] Also, the active cancer patient population demands the latest aggressive chemotherapy regimens that can easily command high prices due to unmet need. Patients whose survival is limited are desperate for treatments in order to extend their livelihood. These factors allow drug prices to reach record high, and the demand for the next cancer breakthroughs has reached an unprecedented level.

Multitargeted kinase inhibitors are a specific subset of drugs that hold the promise of overcoming the woes of the current attrition rate, and rational design approaches can bring the pipe dream of cancer cure closer to reality. It should come as no surprise that because tyrosine kinases are involved in cell growth, survival, and proliferation, many model systems show that a perturbation of tyrosine kinase signaling results in malignant transformation and oncogenic mutations in tumors.[130–132] Tyrosine kinase inhibitors with impressive clinical efficacy have been attributed to a selectivity profile that incorporates multiple targets.[132,133] Examples include imatinib (Gleevec), used for CML and gastrointestinal stromal tumors (GIST), sunitinib (Sutent) for treatment of imatinib-resistant GIST and renal cell carcinoma (RCC), sorafenib (Nexavar) for RCC and hepatocellular carcinoma. Analysis of 974 anticancer agents from 1995 to 2007 in the area of oncology demonstrates an attrition rate from Phase I to registration of 82% as a whole, but in the subset of multitargeted kinase inhibitors, the observed attrition rate drops to 53%.[134]

Along with tyrosine kinases, the PI3K class of kinases are commonly mutated and activated in human cancers. While the two types of kinases lack a primary sequence homology, they share a kinase domain structure and a crucial function of tyrosine kinases is to activate the lipid kinases of the PI3K family.[135] PI3Ks are validated targets for drug development, and the isoform p110α is the most frequently mutated kinase in human cancer.[136,137] In an effort to generate molecules that preferentially inhibit both PI3Ks and tyrosine kinases, Apsel et al.[39] used kinome-wide biochemical profiling of compounds sharing a pyrazolopyrimidine (PP) core,

combined with X-ray crystallography and iterative chemical synthesis, to discover the small molecule PP121. The compound forms the same hydrogen bonds to kinases as the adenine of ATP, exploiting the conserved region in both tyrosine kinases and PI3Ks. The authors then showed that the selectivity of PP121 toward the PI3K/tyrosine kinases relative to serine/threonine kinases is due to a "gatekeeper residue" that is bulkier in serine/threonine. Given that PP121 can inhibit both tyrosine kinases and PI3Ks at nanomolar efficacy, they next examined its use in imatinib-resistant CML. PP121 was able to block proliferation by inducing G_0/G_1 cell cycle arrest, and the authors attribute this effect to PI3K pathway inhibition. The results show that consideration of potential inherent polypharmacological effects against two signaling pathways provides promising new anticancer agents with advantages over other treatments.

2.10.5.1.2 Polypharmacology in CNS disorders

Another area that has seen the first-hand benefits of polypharmacological drugs are the antipsychotic and anti-dementia medications. Profitability and demand from this new market have exploded, with over 45 million annual prescriptions as of 2007, and worldwide sales are over $17 billion.[138,139] While the profitability is large, the success rate of CNS drugs, as stated above, is significantly low from first-in-man trials to registrations. It has been well established that many mental illnesses are polygenic in origin and the embodiment of complexity, with substantial environmental and possibly even epigenetic components.[140,141] Although neurological disorders display deregulation of multiple signaling pathways, drug mechanistic studies of these diseases have only focused on specific targets, such as dopamine transmission for psychosis and acetylcholine and glutamate transmission for Alzheimer's dementia.[142]

Atypical antipsychotics, also known as the second-generation antipsychotics, differentiate themselves from typical antipsychotics by their ability to bind to both serotonin and dopamine receptors and their decreased extrapyramidal side effects. The first atypical antipsychotic is Clozapine, which remains the "gold standard" of atypical antipsychotic treatments. Interestingly, it was discovered through phenotypic screening/optimization and not originally designed to hit any one individual protein target. However, the pharmacological profile of Clozapine shows binding (with affinity values $K_i < 100$ nM) to at least 26 receptors.[139] Even more interesting, almost all attempts to target a single "magic receptor" thought to be involved in schizophrenia have resulted in much lower efficacy than multitarget drugs like Clozapine.[139] The pleiotypic nature of Clozapine is most likely accountable for its efficacy in treating schizophrenia and related disorders.[143,144] Examination of functional electrophysiology data demonstrated that antipsychotic and anti-dementia medications directly modulated multiple ligand- and voltage- gated ion channels.[142] A logical expansion of this fact is that enhanced understanding of the polypharmacological effects of these drugs can coincide with progress in disease subtyping, leading to personalized drugs toward patients with unique polymorphisms of ion channels.

Antidepressants are also trending toward polypharmacological effects. Genetic studies have shown that depression displays a complexity that spans many diverse genes.[145] Results show that dual-action antidepressants (serotonin and noradrenaline reuptake inhibitors, or SNRIs), which inhibit both 5-HT and dopamine and/or noradrenaline reuptake, are more effective than single-action antidepressants (selective serotonin reuptake inhibitors, SSRIs).[146,147] Clearly, the most clinically effective treatments for depression, schizophrenia, and possibly other mood disorders display multiple MOA, working as nonspecific "magic shotguns" rather than "magic bullets" on the CNS.[139]

2.10.5.2 Targeting Drug Resistance

Polypharmacology can also be applied to overcome drug resistance problem. As known with a long history, one of the common methods to deal with bacterial drug resistance is to use broad spectrum antibiotics. In cancer, a general drawback of target-specific monotherapy therefore derives from the fact that a single genetic alteration conferring target resistance to an individual tumor cell can eventually lead to relapse, as exemplified by the clonal selection for drug-resistant *BCR–ABL* alleles during imatinib therapy. Therefore, the ability of kinases to mutate in response to the selective pressure created by drug treatment provides a strong rationale for hitting more than one essential target at the same time in the tumor cells.[148] Alternatively, simultaneous targeted inhibition of multiple essential protein components in the cancer cells aims not only at increased therapeutic potency but also at reduction in the risk of molecular resistance formation by reducing the tumor cell population.[149]

The success of such efforts can be illustrated by a series of indolinone inhibitors. The first is SU5416 originally developed as a monospecific inhibitor of VEGFR involved in angiogenesis.[150] The follow-up compound SU6668 improved both pharmacological properties and potency due to its simultaneous inhibition of three RTKs (VEGFR2, PDGFRβ, and FGFR174). However, FGFR signaling was hardly affected by SU6668 and VEGFR2 seemed to be only partially blocked.[151,152] SU11248, later marketed as sunitinib, shows comparable potency against multiple RTKs including PDGFRα, PDGFRβ, VEGFR2, Kit, and FLT3.[153–155] Its balanced activity profile was well translated into simultaneous inhibition of disease-relevant RTKs in vivo and has resulted in therapeutic efficacy in neoplasias such as renal cell carcinoma.[149] In addition, sunitinib showed promising results in GIST tumors with acquired resistance to imatinib. In addition to Kit in tumor cells, sunitinib targets both VEGFR and PDGFR tyrosine kinases in endothelial and perivascular cells and interferes with tumor vascularization.[156] This explains why efficacious multitargeted kinase inhibitors such as sunitinib could potently thwart resistance formation.

2.10.5.3 Drug Repositioning/Repurposing

As already discussed, another beneficial aspect of polypharmacology is drug repositioning/repurposing (i.e., identifying new medical use for approved, discontinued, shelved, and experimental drugs). It has gained enormous attention during the last

10 years,[157] and there have been numerous examples of success in drug repurposing, including the aforementioned sildenafil repurposed from treating angina to erectile dysfunctions therapy,[29] imatinib from the initial CML treatment expanded to treat GIST,[31] aspirin for pain relief and then for treating cancer and cardiovascular diseases,[108–110] etc. Most of these successful efforts of drug repositioning have been serendipitous to date or through exploitation of the original drug mechanism of action for new indications. Currently, systematic approaches are being carried out to find novel use of marketed drugs. For instance, Liu et al. reviewed recent advances in drug repositioning for the discovery of new anticancer drugs.[158] They discussed many currently marketed drugs that are in clinical trials for their novel anticancer activity including Nelfinavir. Nelfinavir inhibits angiogenesis and this led to systematic studies of its anticancer activities. In addition further studies showed that the drug also inhibits HSP90, HER2, and AKT signaling pathways.[159–161]

The complexity of the problem clearly needs novel multimodal approaches for better solutions. To this end, our group developed an integrative computational framework based on classical structure-based drug design, chemical-genomic similarity, and molecular graph theories.[162] Briefly, we used pharmacophore modeling to guide docking pose selection resulting from our high-throughput virtual screening. Using a novel chemo-genomic similarity approach, we evaluated if any hits missed by docking can be obtained. We also developed drug–target bipartite graph to assess similarity of different inhibitors based on their connections to other compounds and targets. The approaches were applied to the repurposing of existing drugs against ACK1 through screening of 1447 marketed drugs. We identified 10 hits and 4 drugs were experimentally confirmed as potent ACK1 inhibitors. In particular dasatinib could inhibit ACK1 with $IC_{50} = 1$ nM. Currently we have also expanded our novel, integrative strategy to the screening of other biological targets with a more comprehensive coverage of known bio-chemical space for repurposing studies. Recently, Corbett and colleagues identified some drugs that are effective toward distinct pathological conditions such as hypertension, type 2 diabetes mellitus, and retinoid therapy, and these agents can be used to treat AD.[163] In a phenotypic screening study, Nygren et al. found novel use of mebendazole, an anthelmintic drug, in advanced colon cancer treatment,[164] and this has been confirmed by our own recent studies elucidating the novel mechanism of action through inhibiting the Wnt signaling pathway. All of these studies suggest that multitargeted agents are natural candidates for more innovative drug repositioning and advancement in computational modeling will significantly facilitate such efforts.

2.10.6 Conclusions

During the past decades, pharmaceutical companies have successfully carried out their drug discovery programs using reductionist approach. The increase of drug development cost has demanded for alternative strategies, and recent successes in discovering novel use of well-studied FDA approved drugs provide a great impetus for such efforts. The assumption that similar compounds share similar targets remains the basic principle behind most of the ligand-based and structured-based methods developed for polypharmacology studies. Although some computational methods can be used to calculate similarity, a major challenge is to develop scoring functions that can accurately and robustly rank targets instead of small molecules. In addition, novel approaches such as rational design of multitargeting small molecules are being explored. Apart from chemogenomics-based methods, interests in network-based and bioinformatics-based methods have been increased. These methods are not only able to predict new targets for small molecules but also help understand the complex dynamics of the diseases and molecular interaction pathways. Recently NIH and FDA initiated programs to identify new indications of existing drugs. These programs have been enhanced through collaborations with major pharmaceutical companies. Such efforts will boost the interests of general public as well as improve collaborations among government, industry, and academia for drug repurposing. In the near future we expect that, taking the advantages of the current big data studies and more advanced deep learning technologies, we will be able to develop robust computational approaches for modeling multitargeted drugs with optimal efficacies but minimum side effects. Of course significant challenges still lie ahead.

See also: 2.11. Allosteric Modulators. 7.10. Inhibiting Kinases in the CNS.

References

1. Morphy, R.; Kay, C.; Rankovic, Z. From Magic Bullets to Designed Multiple Ligands. *Drug Discov. Today* **2004,** *9* (15), 641–651.
2. Rastelli, G.; Pinzi, L. Computational Polypharmacology Comes of Age. *Front. Pharmacol.* **2015,** *6*, 157.
3. Bottegoni, G.; et al. The Role of Fragment-Based and Computational Methods in Polypharmacology. *Drug Discov. Today* **2012,** *17* (1-2), 23–34.
4. Tan, Z.; et al. Trans Fatty Acids Influence the Oxidation of LDL in ECV304 Cells. *Eur. J. Lipid Sci. Technol.* **2012,** *114* (8), 880–888.
5. Tan, Z.; Zhang, S. Past, Present, and Future of Targeting Ras for Cancer Therapies. *Mini-Rev. Med. Chem.* **2016,** *16* (5), 345–357.
6. Tan, Z.; Chaudhai, R.; Zhang, S. Polypharmacology in Drug Development: A Minireview of Current Technologies. *ChemMedChem* **2016,** *11* (12), 1211–1218.
7. Zambrowicz, B. P.; Sands, A. T. Knockouts Model the 100 Best-Selling Drugs—Will They Model the Next 100? *Nat. Rev. Drug Discov.* **2003,** *2* (1), 38–51.
8. Wagner, A. Robustness Against Mutations in Genetic Networks of Yeast. *Nat. Genet.* **2000,** *24* (4), 355–361.
9. Yildirim, M. A.; et al. Drug-Target Network. *Nat. Biotechnol.* **2007,** *25* (10), 1119–1126.
10. Hopkins, A. L.; Groom, C. R. The Druggable Genome. *Nat. Rev. Drug Discov.* **2002,** *1* (9), 727–730.
11. Austin, C. P.; et al. The Knockout Mouse Project. *Nat. Genet.* **2004,** *36* (9), 921–924.
12. Zambrowicz, B. P.; Turner, C. A.; Sands, A. T. Predicting Drug Efficacy: Knockouts Model Pipeline Drugs of the Pharmaceutical Industry. *Curr. Opin. Pharmacol.* **2003,** *3* (5), 563–570.

13. Barabasi, A. L.; Oltvai, Z. N. Network Biology: Understanding the Cell's Functional Organization. *Nat. Rev. Genet.* **2004,** *5* (2), 101–113.
14. Kitano, H. Towards a Theory of Biological Robustness. *Mol. Syst. Biol.* **2007,** *3,* 137.
15. Hartman, J. L.t.; Garvik, B.; Hartwell, L. Principles for the Buffering of Genetic Variation. *Science* **2001,** *291* (5506), 1001–1004.
16. Csermely, P.; Agoston, V.; Pongor, S. The Efficiency of Multi-Target Drugs: The Network Approach Might Help Drug Design. *Trends Pharmacol. Sci.* **2005,** *26* (4), 178–182.
17. DiMasi, J. A. The Value of Improving the Productivity of the Drug Development Process: Faster Times and Better Decisions. *PharmacoEconomics* **2002,** *20* (Suppl 3), 1–10.
18. Janga, S. C.; Tzakos, A. Structure and Organization of Drug-Target Networks: Insights From Genomic Approaches for Drug Discovery. *Mol. BioSyst.* **2009,** *5,* 1536–1548.
19. Collier, R. Drug Development Cost Estimates Hard to Swallow. *CMAJ* **2009,** *180* (3), 279–280.
20. Kola, I.; Landis, J. Can the Pharmaceutical Industry Reduce Attrition Rates? *Nat. Rev. Drug Discov.* **2004,** *3* (8), 711–715.
21. Ma, P.; Zemmel, R. Value of Novelty? *Nat. Rev. Drug Discov.* **2002,** *1* (8), 571–572.
22. Wu, P.; Nielsen, T. E.; Clausen, M. H. Small-Molecule Kinase Inhibitors: An Analysis of FDA-Approved Drugs. *Drug Discov. Today* **2016,** *21* (1), 5–10.
23. Mullard, A. 2015 FDA Drug Approvals. *Nat. Rev. Drug Discov.* **2016,** *15* (2), 73–76.
24. Sams-Dodd, F. Target-Based Drug Discovery: Is Something Wrong? *Drug Discov. Today* **2005,** *10* (2), 139–147.
25. Hopkins, A. L. Network Pharmacology: The Next Paradigm in Drug Discovery. *Nat. Chem. Biol.* **2008,** *4* (11), 682–690.
26. Ross, D. M.; Hughes, T. P. Cancer Treatment With Kinase Inhibitors: What Have we Learnt from Imatinib? *Br. J. Cancer* **2004,** *90,* 12–19.
27. Capdeville, R.; et al. Glivec (STI571, Imatinib), a Rationally Developed, Targeted Anticancer Drug. *Nat. Rev. Drug Discov.* **2002,** *1,* 493–502.
28. Du-Cuny, L.; Chen, L.; Zhang, S. A Critical Assessment of Combined Ligand- and Structure-Based Approaches to HERG Channel Blocker Modeling. *J. Chem. Inf. Model.* **2011,** *51* (11), 2948–2960.
29. DeBusk, R. F.; et al. Efficacy and Safety of Sildenafil Citrate in men With Erectile Dysfunction and Stable Coronary Artery Disease. *Am. J. Cardiol.* **2004,** *93* (2), 147–153.
30. Anighoro, A.; Bajorath, J.; Rastelli, G. Polypharmacology: Challenges and Opportunities in Drug Discovery. *J. Med. Chem.* **2014,** *57* (19), 7874–7887.
31. Joensuu, H.; et al. Effect of the Tyrosine Kinase Inhibitor STI571 in a Patient With a Metastatic Gastrointestinal Stromal Tumor. *N. Engl. J. Med.* **2001,** *344* (14), 1052–1056.
32. Chou, W. C.; et al. Different Responses to Gefitinib in Lung Adenocarcinoma Coexpressing Mutant- and Wild-Type Epidermal Growth Factor Receptor Genes. *Jpn. J. Clin. Oncol.* **2006,** *36* (8), 523–526.
33. Xie, L.; et al. Novel Computational Approaches to Polypharmacology as a Means to Define Responses to Individual Drugs. *Annu. Rev. Pharmacol. Toxicol.* **2012,** *52,* 361–379.
34. Ciceri, P.; et al. Dual Kinase-Bromodomain Inhibitors for Rationally Designed Polypharmacology. *Nat. Chem. Biol.* **2014,** *10* (4), 305–312.
35. Wyce, A.; et al. Inhibition of BET Bromodomain Proteins as a Therapeutic Approach in Prostate Cancer. *Oncotarget* **2013,** *4* (12), 2419–2429.
36. Mertz, J. A.; et al. Targeting MYC Dependence in Cancer by Inhibiting BET Bromodomains. *Proc. Natl. Acad. Sci. U. S. A.* **2011,** *108* (40), 16669–16674.
37. Shimamura, T.; et al. Efficacy of BET Bromodomain Inhibition in Kras-Mutant non-Small Cell Lung Cancer. *Clin. Cancer Res.* **2013,** *19* (22), 6183–6192.
38. Morphy, R.; Rankovic, Z. Designed Multiple Ligands. An Emerging Drug Discovery Paradigm. *J. Med. Chem.* **2005,** *48* (21), 6523–6543.
39. Apsel, B.; et al. Targeted Polypharmacology: Discovery of Dual Inhibitors of Tyrosine and Phosphoinositide Kinases. *Nat. Chem. Biol.* **2008,** *4* (11), 691–699.
40. Besnard, J.; et al. Automated Design of Ligands to Polypharmacological Profiles. *Nature* **2012,** *492* (7428), 215–220.
41. Katselou, M. G.; Matralis, A. N.; Kourounakis, A. P. Multi-Target Drug Design Approaches for Multifactorial Diseases: From Neurodegenerative to Cardiovascular Applications. *Curr. Med. Chem.* **2014,** *21* (24), 2743–2787.
42. Altieri, D. C. Mitochondrial Hsp90 Chaperones as Novel Molecular Targets in Prostate Cancer. *Future Oncol.* **2010,** *6* (4), 487–489.
43. Lehar, J.; et al. Synergistic Drug Combinations Tend to Improve Therapeutically Relevant Selectivity. *Nat. Biotechnol.* **2009,** *27* (7), 659–666.
44. Ryall, K. A.; Tan, A. C. Systems Biology Approaches for Advancing the Discovery of Effective Drug Combinations. *J. Cheminf.* **2015,** *7,* 7.
45. Eastman, R. T.; Fidock, D. A. Artemisinin-Based Combination Therapies: A Vital Tool in Efforts to Eliminate Malaria. *Nat. Rev. Microbiol.* **2009,** *7* (12), 864–874.
46. Kuhn, M.; et al. STITCH: Interaction Networks of Chemicals and Proteins. *Nucleic Acids Res.* **2008,** *36* (Database issue), D684–D688.
47. Reddy, A. S.; Tan, Z.; Zhang, S. Curation and Analysis of Multitargeting Agents for Polypharmacological Modeling. *J. Chem. Inf. Model.* **2014,** *54* (9), 2536–2543.
48. Gunther, S.; et al. SuperTarget and Matador: Resources for Exploring Drug-Target Relationships. *Nucleic Acids Res.* **2008,** *36* (Database issue), D919–D922.
49. Shoemaker, B.a.; et al. IBIS (Inferred Biomolecular Interaction Server) Reports, Predicts and Integrates Multiple Types of Conserved Interactions for Proteins. *Nucleic Acids Res.* **2012,** *40,* D834–D840.
50. Kuhn, M.; et al. The SIDER Database of Drugs and Side Effects. *Nucleic Acids Res.* **2016,** *44* (D1), D1075–D1079.
51. Chaudhari, R.; Li, Z. PyMine: A PyMOL Plugin to Integrate and Visualize Data for Drug Discovery. *BMC. Res. Notes* **2015,** *8,* 517.
52. Keiser, M. J.; et al. Relating Protein Pharmacology by Ligand Chemistry. *Nat. Biotechnol.* **2007,** *25* (2), 197–206.
53. Kumar, S. P.; et al. Prediction of Protein Targets of Kinetin Using in Silico and in vitro Methods: A Case Study on Spinach Seed Germination Mechanism. *J. Chem. Biol.* **2015,** *8* (3), 95–105.
54. Liu, X.; et al. TarPred: A web Application for Predicting Therapeutic and Side Effect Targets of Chemical Compounds. *Bioinformatics* **2015,** *31* (12), 2049–2051.
55. Wang, L.; et al. TargetHunter: An in Silico Target Identification Tool for Predicting Therapeutic Potential of Small Organic Molecules Based on Chemogenomic Database. *AAPS J.* **2013,** *15* (2), 395–406.
56. Nickel, J.; et al. SuperPred: Update on Drug Classification and Target Prediction. *Nucleic Acids Res.* **2014,** *42* (Web Server issue), W26–W31.
57. Gfeller, D.; et al. SwissTargetPrediction: A Web Server for Target Prediction of Bioactive Small Molecules. *Nucleic Acids Res.* **2014,** *42* (Web Server issue), W32–W38.
58. Chen, Y. Z.; Ung, C. Y. Computer Automated Prediction of Potential Therapeutic and Toxicity Protein Targets of Bioactive Compounds From Chinese Medicinal Plants. *Am. J. Chin. Med.* **2002,** *30* (1), 139–154.
59. Wang, J. C.; et al. idTarget: a Web Server for Identifying Protein Targets of Small Chemical Molecules With Robust Scoring Functions and a Divide-and-Conquer Docking Approach. *Nucleic Acids Res.* **2012,** *40* (Web Server issue), W393–W399.
60. Luo, H.; et al. DRAR-CPI: A Server for Identifying Drug Repositioning Potential and Adverse Drug Reactions via the Chemical-Protein Interactome. *Nucleic Acids Res.* **2011,** *39* (Web Server issue), p. W492–p. W498.
61. Li, H.; et al. TarFisDock: A Web Server for Identifying Drug Targets With Docking Approach. *Nucleic Acids Res.* **2006,** *34* (Web Server issue), W219–W224.
62. Friesner, R.a.; et al. Glide: A New Approach for Rapid, Accurate Docking and Scoring. 1. Method and Assessment of Docking Accuracy. *J. Med. Chem.* **2004,** *47,* 1739–1749.
63. Krotzky, T.; et al. Extended Graph-Based Models for Enhanced Similarity Search in Cavbase. *IEEE/ACM Trans. Comput. Biol. Bioinform.* **2014,** *11* (5), 878–890.
64. Shulman-Peleg, A.; Nussinov, R.; Wolfson, H. J. SiteEngines: Recognition and Comparison of Binding Sites and Protein-Protein Interfaces. *Nucleic Acids Res.* **2005,** *33* (Web Server issue), W337–W341.
65. Jambon, M.; et al. A new Bioinformatic Approach to Detect Common 3D Sites in Protein Structures. *Proteins* **2003,** *52* (2), 137–145.
66. Konc, J.; et al. ProBiS-Database: Precalculated Binding Site Similarities and Local Pairwise Alignments of PDB Structures. *J. Chem. Inf. Model.* **2012,** *52,* 604–612.
67. Chartier, M.; Adriansen, E.; Najmanovich, R. IsoMIF Finder: Online Detection of Binding Site Molecular Interaction Field Similarities. *Bioinformatics* **2016,** *32* (4), 621–623.
68. Yeturu, K.; Chandra, N. PocketMatch: A new Algorithm to Compare Binding Sites in Protein Structures. *BMC Bioinf.* **2008,** *9,* 543.
69. Hoffmann, B.; et al. A new Protein Binding Pocket Similarity Measure Based on Comparison of Clouds of Atoms in 3D: Application to Ligand Prediction. *BMC Bioinf.* **2010,** *11,* 99.
70. Gao, M.; Skolnick, J. APoc: Large-Scale Identification of Similar Protein Pockets. *Bioinformatics* **2013,** *29* (5), 597–604.
71. Liu, X.; et al. PharmMapper Server: A Web Server for Potential Drug Target Identification Using Pharmacophore Mapping Approach. *Nucleic Acids Res.* **2010,** *38* (Web Server issue), W609–W614.
72. Lamb, J.; et al. The Connectivity Map: Using Gene-Expression Signatures to Connect Small Molecules, Genes, and Disease. *Science* **2006,** *313* (5795), 1929–1935.

73. Petryszak, R.; et al. Expression Atlas Update—A Database of Gene and Transcript Expression from Microarray- and Sequencing-Based Functional Genomics Experiments. *Nucleic Acids Res.* **2014,** *42* (Database issue), D926–D932.
74. Petryszak, R.; et al. Expression Atlas Update—An Integrated Database of Gene and Protein Expression in Humans, Animals and Plants. *Nucleic Acids Res.* **2016,** *44* (D1), D746–D752.
75. Rebhan, M.; et al. GeneCards: Integrating Information About Genes, Proteins and Diseases. *Trends Genet.* **1997,** *13* (4), 163.
76. Clough, E.; Barrett, T. The Gene Expression Omnibus Database. *Methods Mol. Biol.* **2016,** *1418,* 93–110.
77. Edgar, R.; Domrachev, M.; Lash, A. E. Gene Expression Omnibus: NCBI Gene Expression and Hybridization Array Data Repository. *Nucleic Acids Res.* **2002,** *30* (1), 207–210.
78. Kanehisa, M.; Goto, S. KEGG: Kyoto Encyclopedia of Genes and Genomes. *Nucleic Acids Res.* **2000,** *28* (1), 27–30.
79. Krizman, D. B.; et al. The Cancer Genome Anatomy Project: EST Sequencing and the Genetics of Cancer Progression. *Neoplasia* **1999,** *1* (2), 101–106.
80. Tomczak, K.; Czerwinska, P.; Wiznerowicz, M. The Cancer Genome Atlas (TCGA): an Immeasurable Source of Knowledge. *Contemp. Oncol. (Pozn)* **2015,** *19* (1A), A68–A77.
81. Genomes Project, C.; et al. A Global Reference for Human Genetic Variation. *Nature* **2015,** *526* (7571), 68–74.
82. Gao, J.; et al. Integrative Analysis of Complex Cancer Genomics and Clinical Profiles Using the cBioPortal. *Sci. Signal.* **2013,** *6,* pl1.
83. Altschul, S. F.; et al. Basic Local Alignment Search Tool. *J. Mol. Biol.* **1990,** *215,* 403–410.
84. Zauhar, R. J.; Gianti, E.; Welsh, W. J. Fragment-Based Shape Signatures: A new Tool for Virtual Screening and Drug Discovery. *J. Comput. Aided Mol. Des.* **2013,** *27* (12), 1009–1036.
85. van Laarhoven, T.; Nabuurs, S. B.; Marchiori, E. Gaussian Interaction Profile Kernels for Predicting Drug-Target Interaction. *Bioinformatics* **2011,** *27* (21), 3036–3043.
86. Jacob, L.; Vert, J. P. Protein-Ligand Interaction Prediction: An Improved Chemogenomics Approach. *Bioinformatics* **2008,** *24* (19), 2149–2156.
87. Xia, Z.; et al. Semi-Supervised Drug-Protein Interaction Prediction From Heterogeneous Biological Spaces. *BMC Syst. Biol.* **2010,** *4* (Suppl 2), S6.
88. Yamanishi, Y.; et al. Prediction of Drug-Target Interaction Networks From the Integration of Chemical and Genomic Spaces. *Bioinformatics* **2008,** *24* (13), i232–i240.
89. Bleakley, K.; Yamanishi, Y. Supervised Prediction of Drug-Target Interactions Using Bipartite Local Models. *Bioinformatics* **2009,** *25* (18), 2397–2403.
90. Gonen, M. Predicting Drug-Target Interactions From Chemical and Genomic Kernels Using Bayesian Matrix Factorization. *Bioinformatics* **2012,** *28* (18), 2304–2310.
91. Ding, H.; et al. Similarity-Based Machine Learning Methods for Predicting Drug-Target Interactions: A Brief Review. *Brief. Bioinform.* **2014,** *15* (5), 734–747.
92. Wang, W.; et al. The Interprotein Scoring Noises in Glide Docking Scores. *Proteins* **2012,** *80* (1), 169–183.
93. Schomburg, K. T.; et al. Facing the Challenges of Structure-Based Target Prediction by Inverse Virtual Screening. *J. Chem. Inf. Model.* **2014,** *54* (6), 1676–1686.
94. Kellenberger, E.; et al. Comparative Evaluation of Eight Docking Tools for Docking and Virtual Screening Accuracy. *Proteins Struct. Funct. Genet.* **2004,** *57,* 225–242.
95. Yang, L.; et al. Exploring Off-Targets and Off-Systems for Adverse Drug Reactions via Chemical-Protein Interactome—Clozapine-Induced Agranulocytosis as a Case Study. *PLoS Comput. Biol.* **2011,** *7* (3), e1002016.
96. Yadav, D. K.; et al. Molecular Docking and ADME Studies of Natural Compounds of Agarwood Oil for Topical Anti-Inflammatory Activity. *Curr. Comput. Aided Drug Des.* **2013,** *9* (3), 360–370.
97. Zhao, S.; Iyengar, R. Systems Pharmacology: Network Analysis to Identify Multiscale Mechanisms of Drug Action. *Annu. Rev. Pharmacol. Toxicol.* **2012,** *52,* 505–521.
98. Qiu, X.; et al. Therapeutic Effect of Astragaloside-IV on Bradycardia is Involved in Up-Regulating Klotho Expression. *Life Sci.* **2016,** *144,* 94–102.
99. Cross, S.; et al. FLAP: GRID Molecular Interaction Fields in Virtual Screening. Validation Using the DUD Data Set. *J. Chem. Inf. Model.* **2010,** *50* (8), 1442–1450.
100. Siragusa, L.; et al. BioGPS: Navigating Biological Space to Predict Polypharmacology, Off-Targeting, and Selectivity. *Proteins* **2015,** *83* (3), 517–532.
101. Chen, Z.; et al. Acenaphtho[1,2-b]pyrrole-Based Selective Fibroblast Growth Factor Receptors 1 (FGFR1) Inhibitors: Design, Synthesis, and Biological Activity. *J. Med. Chem.* **2011,** *54* (11), 3732–3745.
102. Vitali, F.; et al. Network-Based Target Ranking for Polypharmacological Therapies. *J. Biomed. Inform.* **2013,** *46* (5), 876–881.
103. Kuhn, M.; et al. STITCH 2: An Interaction Network Database for Small Molecules and Proteins. *Nucleic Acids Res.* **2010,** *38* (Database issue), D552–D556.
104. Szklarczyk, D.; et al. STITCH 5: Augmenting Protein-Chemical Interaction Networks With Tissue and Affinity Data. *Nucleic Acids Res.* **2016,** *44* (D1), D380–D384.
105. Tian, L.; Zhang, S. Mapping Drug-Target Interaction Networks. *Conf. Proc. IEEE Eng. Med. Biol. Soc.* **2009,** *2009,* 2336–2339.
106. Sirota, M.; et al. Discovery and Preclinical Validation of Drug Indications Using Compendia of Public Gene Expression Data. *Sci. Transl. Med.* **2011,** *3* (96), 96ra77.
107. Shannon, P.; et al. Cytoscape: A Software Environment for Integrated Models of Biomolecular Interaction Networks. *Genome Res.* **2003,** *13,* 2498–2504.
108. Chan, A. T.; et al. Aspirin in the Chemoprevention of Colorectal Neoplasia: An Overview. *Cancer Prev. Res. (Phila.)* **2012,** *5* (2), 164–178.
109. Cuzick, J.; et al. Estimates of Benefits and Harms of Prophylactic use of Aspirin in the General Population. *Ann. Oncol.* **2015,** *26* (1), 47–57.
110. Lewis, H. D., Jr.; et al. Protective Effects of Aspirin Against Acute Myocardial Infarction and Death in Men With Unstable Angina. Results of a Veterans Administration Cooperative Study. *N. Engl. J. Med.* **1983,** *309* (7), 396–403.
111. Adnane, L.; et al. Sorafenib (BAY 43-9006, Nexavar), a Dual-Action Inhibitor That Targets RAF/MEK/ERK Pathway in Tumor Cells and Tyrosine Kinases VEGFR/PDGFR in Tumor Vasculature. *Methods Enzymol.* **2006,** *407,* 597–612.
112. Hwang, S. H.; et al. Synthesis and Biological Evaluation of Sorafenib- and Regorafenib-Like sEH Inhibitors. *Bioorg. Med. Chem. Lett.* **2013,** *23* (13), 3732–3737.
113. Wilhelm, S. M.; et al. Preclinical Overview of Sorafenib, a Multikinase Inhibitor That Targets Both Raf and VEGF and PDGF Receptor Tyrosine Kinase Signaling. *Mol. Cancer Ther.* **2008,** *7* (10), 3129–3140.
114. Patyna, S.; et al. Nonclinical Safety Evaluation of Sunitinib: A Potent Inhibitor of VEGF, PDGF, KIT, FLT3, and RET Receptors. *Toxicol. Pathol.* **2008,** *36* (7), 905–916.
115. Roskoski, R., Jr. Sunitinib: A VEGF and PDGF Receptor Protein Kinase and Angiogenesis Inhibitor. *Biochem. Biophys. Res. Commun.* **2007,** *356* (2), 323–328.
116. Rogawski, M. A. Low Affinity Channel Blocking (Uncompetitive) NMDA Receptor Antagonists as Therapeutic Agents—Toward an Understanding of Their Favorable Tolerability. *Amino Acids* **2000,** *19* (1), 133–149.
117. Cheng, Y.; et al. Rational Drug Design via Intrinsically Disordered Protein. *Trends Biotechnol.* **2006,** *24* (10), 435–442.
118. Csermely, P. Strong Links are Important, but Weak Links Stabilize Them. *Trends Biochem. Sci.* **2004,** *29* (7), 331–334.
119. Fedorov, Y.; et al. Off-Target Effects by siRNA Can Induce Toxic Phenotype. *RNA* **2006,** *12* (7), 1188–1196.
120. Jackson, A. L.; Linsley, P. S. Recognizing and Avoiding siRNA Off-Target Effects for Target Identification and Therapeutic Application. *Nat. Rev. Drug Discov.* **2010,** *9* (1), 57–67.
121. Hannus, M.; et al. siPools: Highly Complex but Accurately Defined siRNA Pools Eliminate Off-Target Effects. *Nucleic Acids Res.* **2014,** *42* (12), 8049–8061.
122. Lin, X.; et al. Life Beyond Kinases: Structure-Based Discovery of Sorafenib as Nanomolar Antagonist of 5-HT Receptors. *J. Med. Chem.* **2012,** *55* (12), 5749–5759.
123. Wermuth, C. G. Selective Optimization of Side Activities: The SOSA Approach. *Drug Discov. Today* **2006,** *11* (3-4), 160–164.
124. Chung, A. S.; et al. Differential Drug Class-Specific Metastatic Effects Following Treatment With a Panel of Angiogenesis Inhibitors. *J. Pathol.* **2012,** *227* (4), 404–416.
125. Ebos, J. M.; et al. Accelerated Metastasis After Short-Term Treatment With a Potent Inhibitor of Tumor Angiogenesis. *Cancer Cell* **2009,** *15* (3), 232–239.
126. Casanovas, O. Cancer: Limitations of Therapies Exposed. *Nature* **2012,** *484* (7392), 44–46.
127. Heron, M.; et al. Deaths: Final Data for 2006. *Natl. Vital Stat. Rep.* **2009,** *57* (14), 1–134.
128. Varmus, H. The New Era in Cancer Research. *Science* **2006,** *312* (5777), 1162–1165.
129. Booth, B.; Glassman, R.; Ma, P. Oncology's Trials. *Nat. Rev. Drug Discov.* **2003,** *2* (8), 609–610.
130. Blume-Jensen, P.; Hunter, T. Oncogenic Kinase Signalling. *Nature* **2001,** *411* (6835), 355–365.
131. Krause, D. S.; Van Etten, R. A. Tyrosine Kinases as Targets for Cancer Therapy. *N. Engl. J. Med.* **2005,** *353* (2), 172–187.
132. Sebolt-Leopold, J. S.; English, J. M. Mechanisms of Drug Inhibition of Signalling Molecules. *Nature* **2006,** *441* (7092), 457–462.
133. Petrelli, A.; Giordano, S. From Single- to Multi-Target Drugs in Cancer Therapy: When Aspecificity Becomes an Advantage. *Curr. Med. Chem.* **2008,** *15* (5), 422–432.
134. Walker, I.; Newell, H. Do Molecularly Targeted Agents in Oncology Have Reduced Attrition Rates? *Nat. Rev. Drug Discov.* **2009,** *8* (1), 15–16.

135. Shaw, R. J.; Cantley, L. C. Ras, PI(3)K and mTOR Signalling Controls Tumour Cell Growth. *Nature* **2006,** *441* (7092), 424–430.
136. Samuels, Y.; et al. High Frequency of Mutations of the PIK3CA Gene in Human Cancers. *Science* **2004,** *304* (5670), 554.
137. Samuels, Y.; Velculescu, V. E. Oncogenic Mutations of PIK3CA in Human Cancers. *Cell Cycle* **2004,** *3* (10), 1221–1224.
138. Snyder, E. M.; Murphy, M. R. Schizophrenia Therapy: Beyond Atypical Antipsychotics. *Nat. Rev. Drug Discov.* **2008,** *7* (6), 471–472.
139. Roth, B. L.; Sheffler, D. J.; Kroeze, W. K. Magic Shotguns Versus Magic Bullets: Selectively Non-Selective Drugs for Mood Disorders and Schizophrenia. *Nat. Rev. Drug Discov.* **2004,** *3* (4), 353–359.
140. Harrison, P. J.; Owen, M. J. Genes for Schizophrenia? Recent Findings and Their Pathophysiological Implications. *Lancet* **2003,** *361* (9355), 417–419.
141. Lewis, C. M.; et al. Genome Scan Meta-Analysis of Schizophrenia and Bipolar Disorder, Part II: Schizophrenia. *Am. J. Hum. Genet.* **2003,** *73* (1), 34–48.
142. Bianchi, M. T. Promiscuous Modulation of Ion Channels by Anti-Psychotic and Anti-Dementia Medications. *Med. Hypotheses* **2009,** *74,* 297–300.
143. Kane, J.; et al. Clozapine for the Treatment-Resistant Schizophrenic. A Double-Blind Comparison With Chlorpromazine. *Arch. Gen. Psychiatry* **1988,** *45* (9), 789–796.
144. Meltzer, H. Y.; et al. Clozapine Treatment for Suicidality in Schizophrenia: International Suicide Prevention Trial (InterSePT). *Arch. Gen. Psychiatry* **2003,** *60* (1), 82–91.
145. Zubenko, G. S.; et al. Genome-Wide Linkage Survey for Genetic Loci That Influence the Development of Depressive Disorders in Families With Recurrent, Early-Onset, Major Depression. *Am. J. Med. Genet. B Neuropsychiatr. Genet.* **2003,** *123B* (1), 1–18.
146. Anderson, I. M. Meta-Analytical Studies on New Antidepressants. *Br. Med. Bull.* **2001,** *57,* 161–178.
147. Thase, M. E.; Entsuah, A. R.; Rudolph, R. L. Remission Rates During Treatment With Venlafaxine or Selective Serotonin Reuptake Inhibitors. *Br. J. Psychiatry* **2001,** *178,* 234–241.
148. Druker, B. J. Overcoming Resistance to Imatinib by Combining Targeted Agents. *Mol. Cancer Ther.* **2003,** *2,* 225–226.
149. Hampton, T. 'Promiscuous' Anticancer Drugs That Hit Multiple Targets May Thwart Resistance. *JAMA* **2004,** *292,* 419–422.
150. Fong, T. A. SU5416 is a Potent and Selective Inhibitor of the Vascular Endothelial Growth Factor Receptor (Flk-1/KDR) That Inhibits Tyrosine Kinase Catalysis, Tumor Vascularization, and Growth of Multiple Tumor Types. *Cancer Res.* **1999,** *59,* 99–106.
151. Laird, A. D. SU6668 is a Potent Antiangiogenic and Antitumor Agent That Induces Regression of Established Tumors. *Cancer Res.* **2000,** *60,* 4152–4162.
152. Bergers, G.; et al. Benefits of Targeting Both Pericytes and Endothelial Cells in the Tumor Vasculature With Kinase Inhibitors. *J. Clin. Invest.* **2003,** *111,* 1287–1295.
153. Abrams, T. J.; et al. SU11248 Inhibits KIT and Platelet-Derived Growth Factor Receptor Beta in Preclinical Models of Human Small Cell Lung Cancer. *Mol. Cancer Ther.* **2003,** *2,* 471–478.
154. Mendel, D. B. In Vivo Antitumor Activity of SU11248, A Novel Tyrosine Kinase Inhibitor Targeting Vascular Endothelial Growth Factor and Platelet-Derived Growth Factor Receptors: Determination of a Pharmacokinetic/Pharmacodynamic Relationship. *Clin. Cancer Res.* **2003,** *9,* 327–337.
155. O'Farrell, A. M. SU11248 is a Novel FLT3 Tyrosine Kinase Inhibitor With Potent Activity in vitro and In Vivo. *Blood* **2003,** *101,* 3597–3605.
156. Schueneman, A. J. SU11248 Maintenance Therapy Prevents Tumor Regrowth After Fractionated Irradiation of Murine Tumor Models. *Cancer Res.* **2003,** *63,* 4009–4016.
157. Ashburn, T. T.; Thor, K. B. Drug Repositioning: Identifying and Developing New Uses for Existing Drugs. *Nat. Rev. Drug Discov.* **2004,** *3* (8), 673–683.
158. Shim, J. S.; Liu, J. O. Recent Advances in Drug Repositioning for the Discovery of New Anticancer Drugs. *Int. J. Biol. Sci.* **2014,** *10* (7), 654–663.
159. Jiang, W.; et al. HIV Protease Inhibitor Nelfinavir Inhibits Growth of Human Melanoma Cells by Induction of Cell Cycle Arrest. *Cancer Res.* **2007,** *67* (3), 1221–1227.
160. Srirangam, A.; et al. Effects of HIV Protease Inhibitor Ritonavir on Akt-Regulated Cell Proliferation in Breast Cancer. *Clin. Cancer Res.* **2006,** *12* (6), 1883–1896.
161. Pore, N.; et al. HIV Protease Inhibitors Decrease VEGF/HIF-1alpha Expression and Angiogenesis in Glioblastoma Cells. *Neoplasia* **2006,** *8* (11), 889–895.
162. Phatak, S. S.; Zhang S. A Novel Multi-Modal Drug Repurposing Approach for Identification of Potent ACK1 Inhibitors. Pac. Symp. Biocomput. **2013**, 29–40. http://dx.doi.org/10.1142/9789814447973_0004.
163. Corbett, A.; Williams, G.; Ballard, C. Drug Repositioning: An Opportunity to Develop Novel Treatments for Alzheimer's Disease. *Pharmaceuticals (Basel)* **2013,** *6* (10), 1304–1321.
164. Nygren, P.; et al. Repositioning of the Anthelmintic Drug Mebendazole for the Treatment for Colon Cancer. *J. Cancer Res. Clin. Oncol.* **2013,** *139* (12), 2133–2140.

2.11 Allosteric Modulators

S Lu and J Zhang, Shanghai Jiao Tong University, Shanghai, China

© 2017 Elsevier Ltd. All rights reserved.

2.11.1	**Introduction**	276
2.11.2	**Advantages and Disadvantages of Allosteric Protein Regulation**	276
2.11.3	**Allosteric Proteins**	279
2.11.3.1	Target Distribution	279
2.11.3.2	Target Properties	280
2.11.3.3	Allosteric Site Properties	280
2.11.4	**Allosteric Modulators**	282
2.11.4.1	Chemical Structure and Physicochemical Properties	283
2.11.4.2	"Allo-Modulator Like"	284
2.11.4.3	Privileged Scaffolds	284
2.11.5	**Allosteric Protein–Ligand Interactions**	285
2.11.5.1	Noncovalent Allosteric Modulators	285
2.11.5.2	Covalent Allosteric Modulators	285
2.11.5.3	Bitopic Ligands	288
2.11.5.4	Allo-Network Modulators	289
2.11.5.5	Allosteric and Orthosteric Collaboration	290
2.11.6	**Mechanisms of Allosteric Drug Action**	290
2.11.7	**Conclusions**	293
Acknowledgments		293
References		293

2.11.1 Introduction

Drugs on the market can be divided into orthosteric or allosteric drugs according to their molecular mechanism of action. Orthosteric drugs compete with the endogenous substrates or ligands to occupy the active site. By contrast, allosteric drugs bind to sites distinct from the active site, also referred to as allosteric sites. As such, allosteric drugs are resistant to orthosteric competition. Rather, they typically exert their effects in concert with the endogenous substrates or ligands in the active site. Allostery takes place when proteins propagate the perturbation signal from an allosteric site to an orthosteric site, giving rising to regulation of a protein's functional activity.[1–4] Allosteric regulation allows for exquisite control of numerous normal processes of cells, including signal transduction, metabolism, enzymatic catalysis, and gene regulation.[5–11]

Since the concept of allostery was introduced by Monod and Jacob in the 1960s,[12] the repertoire of allostery has undergone profound development.[13] In the theoretical aspect, many, if not all, allosteric models, such as Monod–Wyman–Changeux,[14] Koshland–Nemethy–Filmer,[15] population shift model,[16] morpheein model,[17–19] and dynamics-driven models,[20–23] have been formulated to elucidate the underpinnings of allosteric regulation (**Fig. 1** and **Table 1**). Several allosteric network methods, such as SPACER[24] and MCPath,[25] have been developed to predict likely allosteric pathways (communication) between orthosteric and allosteric sites. In addition, a gamut of computational approaches, encompassing AlloSite,[26] ASbench,[27] molecular dynamics (MD) simulations,[10,28–31] two-state Gō model,[32–34] normal mode analysis (NMA),[35–37] binding leverage,[38,39] graph theory,[40] and statistical coupling analysis (SCA),[41–45] have been developed to predict as-yet-unknown allosteric sites in proteins. Experimental methods to identify potential allosteric sites have also made great improvements currently. These methods include disulfide trapping,[46–48] high-throughput screening,[49,50] fragment-based screening,[51–53] alanine-scanning mutagenesis,[54,55] and photoaffinity labeling.[56–58] Significantly, the improvement of biophysical technologies such as X-ray crystallography and NMR,[59–66] together with several other novel methods including fluorescent labeling,[67] electrophysiology,[68] and patch clamp,[69] provides valuable avenues to detect allosteric protein binding sites and to design and develop novel efficient therapeutics aiming at allosteric sites. Therefore, the repertoire of allostery has been experiencing an upsurge, evidenced by an explosive growth in the number of allosteric proteins and allosteric modulators in recent years.[70–72] These lay the foundation for allosteric discoveries and applications.

2.11.2 Advantages and Disadvantages of Allosteric Protein Regulation

There are several features of allosteric regulation that offer considerable advantages for allosteric modulators as preferred therapeutic agents compared to classic orthosteric ligands. First, unlike the highly conserved orthosteric binding sites, allosteric binding sites are less well conserved. In theory, any evident cavities on protein surfaces distinct from the active site can potentially serve as

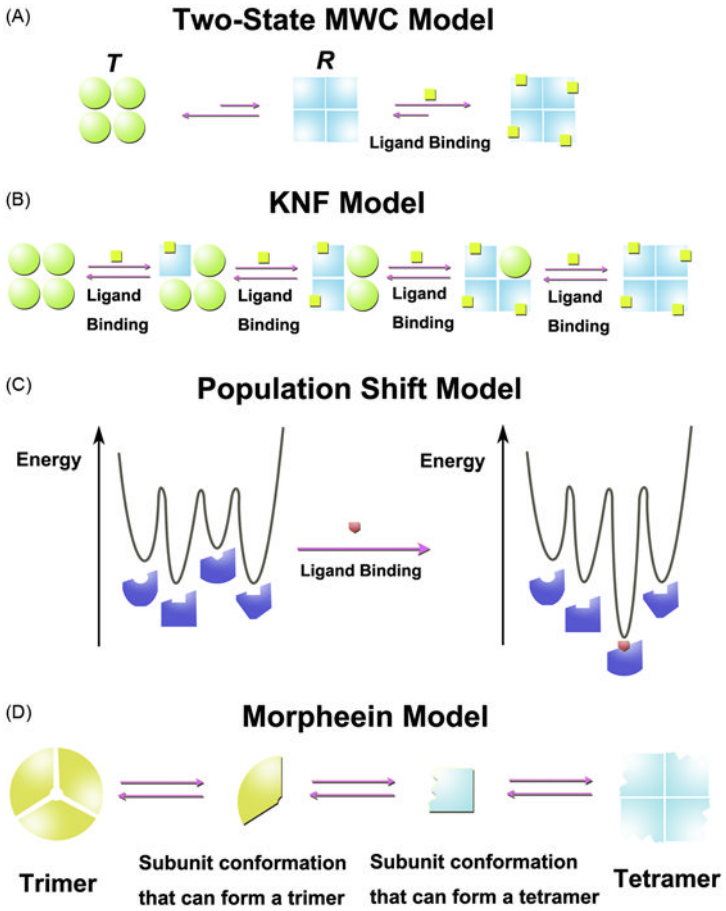

Fig. 1 Models of allostery. (A) The two-state concerted model of Monod–Wyman–Changeux (MWC). (B) The sequential model of Koshland–Nemethy–Filmer (KNF). (C) The population shift model of allostery. (D) The morpheein model of allostery.

Table 1 Models of allostery and their characteristics

Two-state concerted model of Monod–Wyman–Changeux (MWC)	(1) Regulatory proteins are symmetrical homooligomers (2) Conformation of the subunits (tertiary structure) of multimeric proteins changes in a concerted manner (3) Ligand-free oligomers spontaneously exist under two discrete and symmetrical conformations. Upon ligand binding, the equilibrium of the preexisting oligomer between two states (quaternary structure) is merely shifted
Sequential model of Koshland–Nemethy–Filmer (KNF)	The KNF model assumes that a ligand binding to one subunit of a multimeric protein can induce the conformational change of that subunit, thereby remodeling the conformation of the binding site to completely accommodate the ligand
Population shift model	In the unligand forms, proteins exist in an ensemble of conformations. When an allosteric effector is accessed to a specific protein, the conformer (substate) of the dynamically fluctuating protein whose binding site is most complementary to the effector conformation will be selected for binding. Following binding, the ensemble of dynamic conformations undergoes a population shift, redistributing the conformational states toward the conformation favored by the effector
Morpheein model	Two or more homooligomers (morpheein forms) with distinct functionality comprise a protein and is pertinent to homooligomeric proteins. The interchange of morpheein forms requires the obligatory dissociation of higher-order multimers into a lower-order multimer, and a conformational change occurs in the lower-order state prior to assembly into the alternate higher-order multimer
Dynamic-driven model	Allosteric effects are elicited by changes in protein dynamics, without changes in the shape of protein structure

allosteric sites that can be targeted by allosteric modulators. In this context, allosteric modulators can exploit a structurally diverse feature of an allosteric site that may distinguish the target protein from other homologous proteins, in particular in protein kinases and G-protein coupled receptors (GPCRs; also known as seven-transmembrane receptors).[73–77] In fact, a vast majority of small-molecule kinase inhibitors bound to the conserved ATP-binding sites interact with multiple members of the protein kinase family.[78] Davis et al. performed a comprehensive analysis of kinase inhibitor selectivity based on 72 kinase inhibitors and 442 protein kinases;[79] the latter covers >80% of the human catalytic protein kinome. The results showed that, in general, the selectivity of an orthosteric inhibitor to its primary target is fairly poor, with 10–40% of the tested inhibitors at a concentration of 3 μM interacting with >60% of kinases. Polypharmacology is referred to a single drug molecule able to simultaneously and specifically interact with multiple targets.[80–82] For instance, because of the highly conserved ATP-binding sites in the kinome, a designed inhibitor is able to modulate the activity of additional targets beyond the primary target. In contrast, a designed allosteric modulator bound to the less conserved allosteric site can reduce the possibility of polypharmacology, which facilitates the design of more specific drugs. In addition, the low evolutionary conservation of allosteric sites guarantees the high specificity of a designed allosteric modulator to the primary target, which has promise for application to personalized medicine.[83,84] For example, an orthosteric drug, zolmitriptan, was developed to treat migraine targeting serotonin receptors 5-HT-1B and 5-HT-1D.[85] The side effects such as increased pain sensitivity (hyperesthesia) occurred in response to the treatment of zolmitriptan. This effect is owing to the binding of zolmitriptan to the off-target (antitarget) 5-HT-7 (26% sequence identity between 5-HT-7 and 5-HT-1B, 5-HT-1D). However, the low evolutionary conservation of allosteric sites has the potential to cause significant *species differences*.[86,87] For instance, the allosteric effects of allosteric modulators are effective in recombinant human receptors in vitro. However, drug screening using rodent receptors or the investigation of drug effects in vivo using rodent models may disqualify them as effective allosteric modulators.

Second, allosteric modulators have the potential to achieve fewer side effects and lower toxicity compared to orthosteric ligands. Here, we define the allosteric modulators as that ligands bind to an allosteric site and modulate the binding and/or signaling efficacy of orthosteric ligands, while we define the allosteric agonists/antagonists as that ligands binds to an allosteric site and activate/inactivate proteins in the absence of "traditional" orthosteric ligands. The specific function of a protein depends on the extent that a macromolecule populates its active conformation.[20,88] The outcome of binding of an orthosteric ligand to the orthosteric site constrains the ensemble of the protein conformation to one predominant active or inactive conformation. As such, orthosteric ligands can immoderately shut off or turn on native protein function. In contrast, binding of an allosteric modulator to the allosteric site alters the population of the conformation at the orthosteric site, coupled with the occupation of orthosteric site by an orthosteric ligand simultaneously. As a result, allosteric regulation merely modulates the protein's function. In this context, an allosteric modulator can selectively tune cellular responses in tissues, while the endogenous orthosteric ligand exerts its normal physiological effects, thereby maintaining both the temporal and spatial aspects of endogenous physiological signaling.

Third, some proteins are amenable to allosteric regulation by allosteric modulators, whereas they are resistant to orthosteric activation or inhibition by orthosteric ligands. As in the case of class B GPCRs, a small family of peptide-binding receptors, although they are able to be orthosterically interacted with peptides, this cannot be achieved with small-molecule CNS drug space. This is due to the natural polypeptide ligands with varying lengths (ranging from 30 to 40 residues) outside classic oral drug-like space.[89] The fact that orthosteric sites in the class B GPCRs are relatively flat and narrow renders design of orthosteric ligands bound to these sites refractory. However, allosteric modulators can hit class B GPCRs through binding to their allosteric sites. In addition, allosteric GPCR modulators have good pharmacokinetic properties. In the case of metabotropic glutamate (mGlu) receptors, the endogenous ligand, glutamate, bound to the orthosteric site of mGlu receptors underscores the necessity of designing agonists or antagonists with amino acid-like structures for binding. Such polar, charged molecules are closely related to poor bioavailability and blood–brain barrier permeability. In contrast, allosteric sites of mGlu receptors are located in the seven-transmembrane (7TM) domain where they commonly are neutral and lipophilic, which allows for the design of hydrophobic allosteric modulators with favorable pharmacokinetic properties such as good brain permeability. However, allosteric GPCR modulators usually have micromolar affinities to receptors and frequently encounter "*flat*," *nontractable structure–activity relationships* (SAR).[86,87] This deficiency leads to the difficulty in improving allosteric GPCR modulators into bona fide lead compounds. Moreover, allosteric modulation in many cases of mGlu receptors has not achieved for clinical signals, suggesting that allosteric modulation of mGlu receptors may be less effective than orthosteric modulation.

Fourth, allosteric modulators, in combination with orthosteric ligands, can overcome drug-resistant mutations. Combination of both allosteric modulators and orthosteric ligands in the treatment of diseases has a potential advantage because of targeting allosteric sites alone where resistance escapes for nonfunctional site would be easier. For instance, the gatekeeper T315I mutation in the breakpoint cluster region/Abelson (Bcr/Abl) tyrosine kinase fusion protein is resistant to ATP-competitive drugs imatinib (STI-571/Gleevec) and nilotinib (AMN-107/Tasigna). The advent of drug resistance is resulting from the stabilization of active Abl conformation induced by the mutation.[90,91] GNF-5 is a selective allosteric inhibitor targeting the myristoyl-binding pocket of Abl in the C-terminal lobe.[92] The combination of imatinib with the allosteric inhibitor GNF-5 can repress the emergence of resistance mutations by shifting conformational equilibrium of Abl to the closed, inactive state.[93] In addition, combining allosteric modulators and orthosteric ligands can synergistically help to surmounting the diseases, which cannot be achieved by either agent alone. As in the case of mGlu4, a selective, brain-penetrant mGlu4-positive allosteric modulator, (1*S*, 2*R*)-N^1-(3,4-dichlorophenyl)-cyclohexane-1,2-dicarboxamide (Lu AF21934) (**Fig. 2**), in tandem with the dopamine precursor L-3,4-dihydroxyphenylalanine (L-DOPA), allows reducing the effective dose of L-DOPA and preventing the development of L-DOPA-induced dyskinesia.[94]

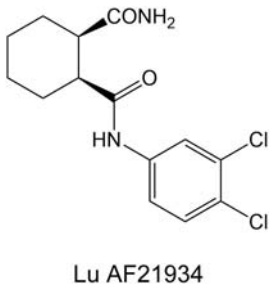

Fig. 2 Chemical structure of Lu AF21934.

Despite the existence of challenging in the design of allosteric modulators, however, owing to unparalleled advantages shared by allosteric modulators as mentioned earlier, current drug discovery efforts in pharmaceutical regimes have increasingly invested in the development of allosteric drugs.

2.11.3 Allosteric Proteins

2.11.3.1 Target Distribution

We have constructed a large dataset of known allosteric proteins and allosteric modulators deposited into the allosteric database (ASD),[70–72] which provides a comprehensive allosteric resource depicting the specific structure, function, and mechanism of allosteric proteins and allosteric modulators. The most direct evidence to determine whether a protein is an allosteric protein is to solve the cocrystal structures between the target protein and its allosteric modulators. In this case, the definite allosteric proteins in complex with their allosteric modulators were annotated. Otherwise, if cocrystal structures are currently unavailable, the indirect biochemical evidences must be satisfied with one of the three following cases, such as inactive mutation of allosteric residues, cooperativity of kinetic effect from two ligands, and uncompetitive binding assay with chromatography. These cases of proteins would also be identified as allosteric proteins. The first version of ASD was released in Aug. 2010, which contains only 316 allosteric proteins. The current ASD (Aug. 2015) is the third version, which contains 1930 allosteric proteins. Thus, in the past five years, the number of allosteric proteins was significantly increased owing to that a great deal of effort that has been focused on the detection of allosteric proteins.

As shown in Fig. 3A, systematic investigation of known allosteric proteins in the ASD exhibits that allosteric phenomena can be widely observed in the vast majority of proteins, such as GPCRs, protein kinases, ion channels, peptidases, phosphatases, transcription factors, nuclear receptors, and E-proteins. This observation reflects that in principle, in addition to orthosteric modulation, any protein has the ability to take advantage of additional allosteric modulation. As of yet, the number of allosteric proteins is mainly observed in the three categories, that is, GPCRs, kinases, and ion channels, which are three largest human drug targets. This phenomenon is ascribed to the fact that these therapeutic targets are amenable to allosteric (and orthosteric) regulation and have therefore gained more attention by academia and the pharmaceutical industry in modern drug discovery. Because of the remarkable structural conservation of orthosteric sites in the kinome and homologous GPCRs, it has been a long-standing conundrum in the discovery of highly specific kinase and GPCR orthosteric inhibitors or activators. Thus, targeting the structural diversity of allosteric sites in

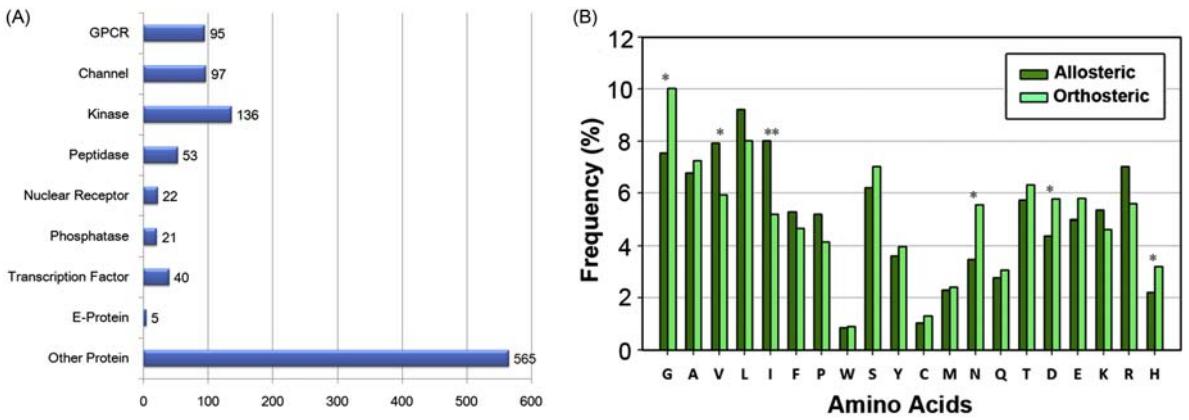

Fig. 3 (A) The distribution of allosteric drug targets. (B) Amino acid compositions of orthosteric and allosteric sites. The fraction of each amino acid of orthosteric and allosteric is shown.

protein kinases and GPCRs provides a promising new paradigm for the design of potent modulators with improved protein subtype selectivity, adverse effects, and pathway-biased signaling.[95] For instance, in class C GPCRs, allosteric modulators are capable of selectively activating these targets. Conversely, the discovery of selective orthosteric ligands against this subtype of GPCRs remains a daunting task because of a paucity of feasible modification positions in these small ligands.[96] In the case of protein kinases, allosteric modulators by targeting the less conserved allosteric sites outside the highly conserved ATP-binding site can achieve greater selectivity for a target kinase against others. For example, allosteric activators, 2-(3-Oxo-1,3-diphenylpropyl)malonic acids, highly selectively activate 3-phosphoinositide-dependent kinase-1 (PDK1) via binding to the interacting fragment (PIF) pocket compared to a panel of AGC kinases, including PKA, PKB/Akt, PKC, p70 S6 kinase (S6K), serum- and glucocorticoid-induced protein kinase (SGK), p90 ribosomal S6 kinase (RSK), and protein kinase C-related kinase 2 (PRK2), which all share a homologous PIF pocket with PDK1.[97] However, allosteric modulators may be easier to acquire resistance compared to orthosteric ligands because allosteric sites are not be conserved in wider population.

2.11.3.2 Target Properties

Traditionally, multimeric proteins are considered to be the prototypes of allosteric proteins, such as hemoglobin, SAM domain- and HD domain-containing protein 1 (SAMHD1), and *N*-methyl-D-aspartate receptor.[98,99] In the multimeric allosteric proteins, cooperativity can be achieved by conformational changes caused by ligand binding to one of the equivalent sites that propagate to the other clefts and facilitate or impair binding of other ligand molecules. Now, the observation of the allosteric phenomenon has expanded from multimeric proteins to monomeric proteins by means of crystallography and electron microscopy studies of signaling molecules, including regulatory enzymes, membrane receptors, and nuclear receptors.[3,100] For example, in the Bcr/Abl kinase, binding of allosteric inhibitor GNF-2 to the C-terminal myristate pocket of Abl resulted in changes in the structural dynamics of the ATP-binding site, facilitating the stabilization of an inactive conformation of Abl.[92] In the human δ-opioid GPCR, Fenalti et al. revealed the presence and fundamental role of a sodium ion in mediating allosteric control of receptor functional selectivity and constitutive activity.[101,102]

Recent experimental observations have suggested that intrinsically disordered proteins (IDPs) can also be allosterically regulated.[103,104] An IDP is a protein that lacks a fixed or ordered three-dimensional (3-D) structure, but in some cases, it has the ability to adopt a fixed 3-D structure after binding to other ligands or macromolecules.[105,106] As in the case of the intrinsically disordered segment of protein tyrosine phosphatase 1B (PTP1B), Krishman et al. demonstrated that binding of small-molecule inhibitor MSI-1436 to the intrinsically disordered segment close to the catalytic domain, with cooperative effects between the two sites, locked PTP1B in an inactive state.[107]

2.11.3.3 Allosteric Site Properties

Over the past few years, the rapid growth in the number of allosteric proteins determined by X-ray crystallography and NMR spectroscopy provides unparalleled insight into the structural properties of allosteric proteins.[70–72] A comprehensive analysis of sequence differences between allosteric sites in the allosteric proteins and orthosteric sites in the nonallosteric proteins using the relatively small allosteric protein set from ASD v1.0[70] was performed. Li et al.[108] and Yang et al.[109] revealed that allosteric sites bear more hydrophobic residues than orthosteric sites, with the emergence of a high frequency of hydrophobic residues in allosteric sites, such as isoleucine, proline, tryptophan, leucine, valine, phenylalanine, methionine, and tyrosine. Similarly, based on the analysis of intramolecular interactions between the allosteric protein set and the randomly generated protein set, Namboodiri et al.[110] demonstrated that hydrophobicity patterning assessed by recurrence quantification analysis descriptors, representative of allosteric hotspots signatures, plays a pivotal role in determining the allostery of proteins. On the basis of relatively large allosteric protein set from ASD v3.0,[72] we also investigated the physicochemical properties of allosteric sites and their corresponding orthosteric sites by comparing their amino acid compositions. As shown in **Fig. 3B**, the hydrophobic residues such as valine and isoleucine are highly enriched in allosteric sites, where polar residues glutamine, aspartic acid, histidine, and glycine are highly enriched in orthosteric sites. These differences in amino acid composition for the allosteric and orthosteric sites are attributed to the different functional roles of the sites. Yang et al.[109] explained that in orthosteric (catalytic) sites, ligands are subject to the heterolytic breakage and formation of covalent bonds, yet such bond breakage and formation do not occur in allosteric sites. In contrast, hydrophobic residues are enriched in allosteric sites to provide a binding pocket for a specific ligand, with only a small fraction of charged residues that are present to facilitate specific interactions during ligand binding.

Yang et al.[109] investigated sequence conservation of allosteric and orthosteric sites in 56 enzyme structures and found that residues of allosteric sites are significantly less conserved than residues of orthosteric sites. Consistently, previous comparative analysis of sequence conservation of ATP-binding sites between allosteric and substrate ATP-binding sites uncovered that residues in the allosteric ATP-binding sites, with the average conservation score of 0.63, were less conserved compared with residues in the substrate ATP-binding sites, with the average conservation score of 0.83 ($P = 1.2 \times 10^{-3}$).[111] As shown in **Fig. 4A**, residues of substrate ATP-binding sites that anchor and orient ATP are extremely conserved, including important motifs such as GXGXXG, DXXXXN, DFG, APE, and DXXXXG, with X indicating any amino acid and the conserved K/E ion pair; this finding is in good agreement with the previously aligned sequences available in the kinase sequence database.[112] By sharp contrast, residues of allosteric ATP-binding sites are markedly variable (**Fig. 4B**). **Fig. 4C** shows the projection of residues of allosteric ATP-binding sites onto residues of substrate ATP-binding sites in order to further unravel the differences in evolutionary conservation of allosteric and substrate

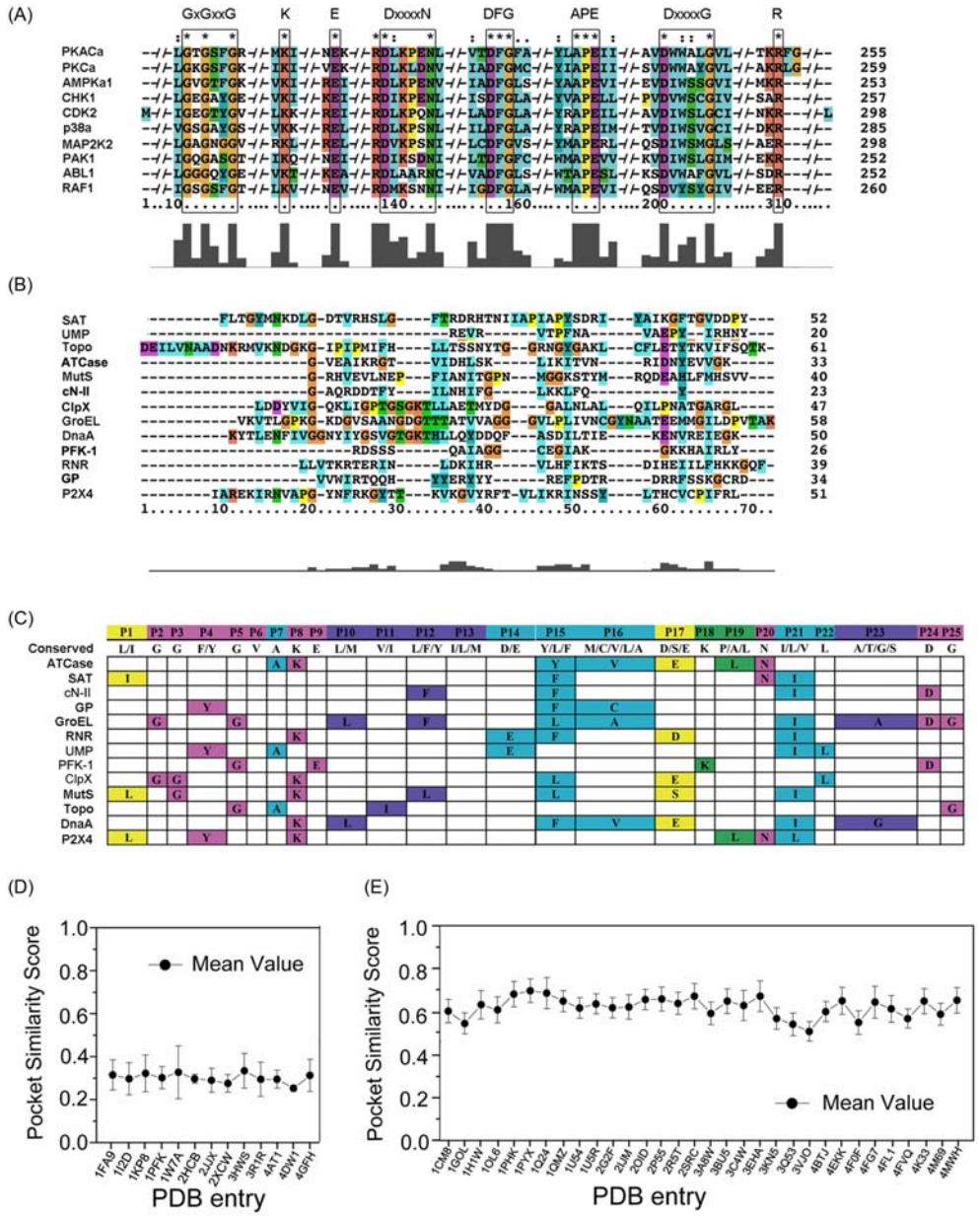

Fig. 4 Comparison of evolutionary conservation of allosteric and substrate ATP-binding sites. (A) A sequence alignment of residues of substrate ATP-binding sites exhibiting important motifs. Abbreviations: *PKACα*, protein kinase A catalytic subunit α; *PKCα*, protein kinase C α; *AMPKα1*, AMP-activated protein kinase catalytic subunit α1; *CHK1*, checkpoint kinase 1; *CDK2*, cyclin-dependent kinase 2; *MAP2K2*, mitogen-activated protein kinase kinase 2; *PAK1*, p21-activated kinase 1. (B) A sequence alignment of residues of allosteric ATP-binding sites. Abbreviations: *SAT*, ATP sulfurylase; *UMP*, uridine monophosphate kinase; *Topo*, DNA topoisomerase II; *ATCase*, aspartate carbamoyltransferase; *cN-II*, cytosolic 5′-nucleotidase II; *PFK-1*, phosphofructokinase 1; *RNR*, ribonucleotide reductase; *GP*, glycogen phosphorylase. (C) Mapping the residues of allosteric ATP-binding sites on residues of substrate ATP-binding sites. The 25 conserved residues derived from a multiple sequence alignment of all known human protein kinases are selected as a reference. (D) The global structural similarity of allosteric ATP-binding sites measured by a PS-score. The PS-score is between 0 and 1. (E) The global structural similarity of substrate ATP-binding sites measured by a PS-score.

ATP-binding sites. Twenty-five conserved residues (P1–P25, starting at the N terminus) that comprise the substrate ATP-binding sites were selected as a reference. These residues were identified by performing a multiple sequence alignment of all known human protein kinases.[113,114] The occurrences of residues in each position of the allosteric ATP-binding sites are significantly different compared with those in the substrate ATP-binding sites. Aside from the sequence difference between allosteric and substrate ATP-binding sites, the pocket similarity measured by the pocket similarity score (PS-score) between the two binding sites is also distinct. The PS-score was calculated based on backbone geometry, side-chain orientation, and chemical similarity of the aligned pocket-lining residues.[115] As shown in Fig. 4D, the global structural similarity of the allosteric ATP-binding sites is low, with

a mean PS-score of 0.3, compared with the high structural similarity of substrate ATP-binding sites, with a mean PS-score of 0.6 (Fig. 4E). Taken together, these data indicate that allosteric ATP-binding sites have evolved along different evolutionary pathways compared with the highly conserved substrate ATP-binding sites, which confers subtype selectivity on allosteric modulators as compared to orthosteric ligands.

2.11.4 Allosteric Modulators

Identification of allosteric sites in proteins is a prerequisite for the screening and optimization of allosteric modulators. Currently, it is challenging to find and characterize new allosteric sites by experimental approaches. Indeed, the vast majority of known allosteric sites were serendipitously discovered while measuring the binding affinities or kinetics between proteins and ligands. However, computational approaches for identifying allosteric sites provide useful empirical knowledge that complements existing experimental techniques. While impressive progress has currently been achieved, the predictive methods developed thus far still fall short of fully predicting experimental observations. The shape and pharmacophoric properties of allosteric sites are not necessarily similar to those of highly conserved orthosteric sites; that is, allosteric sites have evolved along different evolutionary pathways compared with orthosteric sites. In many cases, allosteric sites cannot be easily predicted from the unbound protein structures, thus emphasizing that most of the allosteric sites are remarkably adaptable. In addition, some of allosteric sites exist exclusively in intermediate states pertaining to activation or deactivation processes of proteins.

Thus far, ~71500 allosteric modulators in the library of ASD v3.0 bound to more than 1300 allosteric proteins have been reported, including GPCRs, protein kinases, ligand-gated ion channels, peptidases, phosphatases, transcription factors, and nuclear receptors. Fig. 5 shows time-dependent discovery of allosteric modulators. Overall, a small fraction of allosteric modulators was reported before the year 2000. After that, the interest in the discovery of allosteric modulators was fueled by technical breakthroughs in studying protein allostery, which was evidenced by the increasing number of allosteric modulators during the period of 2000–15. Remarkably, in the past 5 years, the number of allosteric modulators underwent an explosive growth. In particular, the number of allosteric modulators targeting the two largest families of drug targets, GPCRs and kinases, has been pronouncedly enriched.

Allosteric modulators can be divided into three classes, positive allosteric modulators (PAMs), negative allosteric modulators (NAMs), and neutral allosteric modulators or silent allosteric modulators (SAMs), based on their pharmacological effects on the affinity and efficacy of orthosteric ligands bound to the same target.[116] PAMs enhance the affinity of the orthosteric ligand, while NAMs decrease the affinity of the orthosteric ligand. Allosteric modulators function by exerting either positive or negative modulation in cooperation with orthosteric ligands to achieve a potential "ceiling effect" (i.e., maximal receptor occupancy may not translate into a maximal amplitude of receptor activation), which avoids side effects and receptor desensitization and downregulation that are elicited by chronic treatment with an orthosteric agonist.[117–120] In addition, SAMs refer to substances that occupy allosteric binding sites without affecting receptor function. The prominent differences in the magnitude of the allosteric effects induced by different allosteric modulators or the allosteric effects of a modulator that depend on the type of orthosteric ligand used as a probe for receptor activity are referred to as probe dependence.[116]

Interestingly, in the case of GPCRs, distinct chemical structures of allosteric modulators bound to the same receptor are capable of differentially activating specific subsets of downstream signaling pathways; this phenomenon is defined as functional selectivity (also known as stimulus bias, biased signaling, ligand-dependent stimulus trafficking, or biased agonism).[121–125] The origin of functional selectivity can be explained by the dynamic fluctuations in the conformation of receptors, and a specific agonist selects the conformation that is compatible with its binding, thereby stabilizing this receptor conformation at the exclusion of others. In

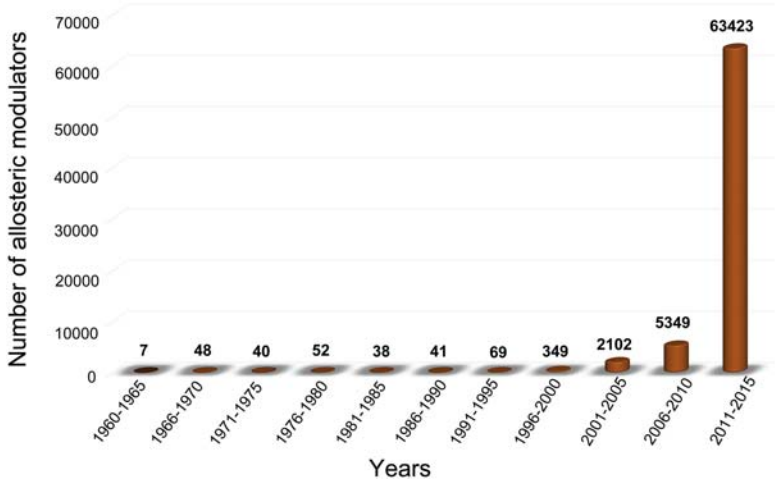

Fig. 5 Time period dependence of discovering allosteric modulators.

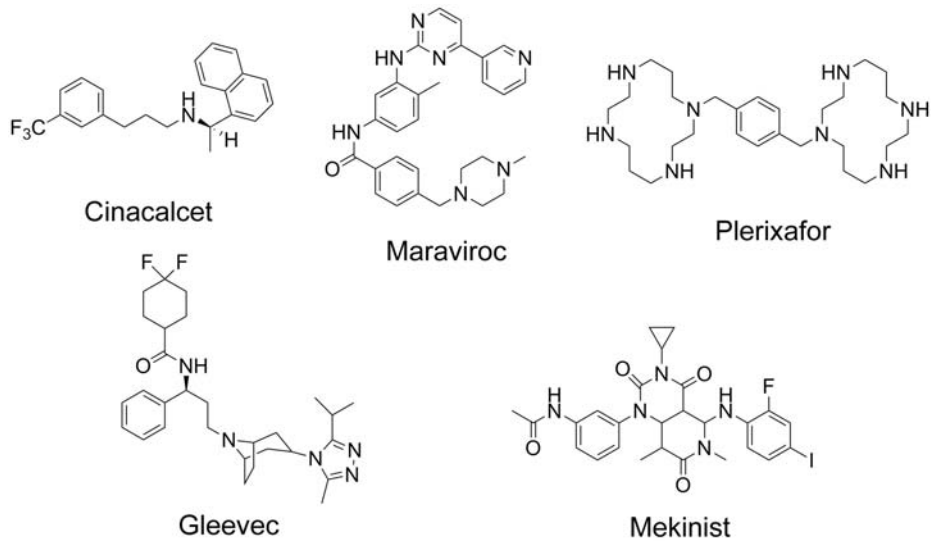

Fig. 6 Chemical structures of allosteric modulators already approved and marketed as drugs.

this scenario, a unique allosteric modulator can activate a specific pathway because each conformational state imparts a specific repertoire of signaling behaviors. As a result, allosteric modulators can induce specific changes in receptor conformation, which may exclusively activate a specific signaling pathway, thereby providing a basis for functional selectivity.[126–133]

Totally, five allosteric drugs have earned approval from the US Food and Drug Administration (FDA), including three GPCRs and two kinase allosteric drugs (Fig. 6). For example, Amgen's cinacalcet acts as a PAM of calcium-sensing receptor to treat chronic renal failure. Pfizer's maraviroc acts as a NAM to inhibit the CC chemokine receptor type 5 (CCR5) for the treatment of HIV infection. Genzyme's plerixafor, as a NAM of the chemokine receptor CXCR4, was used to mobilize hematopoietic stem cell in cancer patients. Novartis's Gleevec was used to treat chronic myelogenous leukemia and gastrointestinal stromal tumors in the Bcr–Abl tyrosine kinase. GlaxoSmithKline's Mekinist, in combination with dabrafenib, was approved for the treatment of patients with B-Raf V600E/K-mutated metastatic melanoma.

2.11.4.1 Chemical Structure and Physicochemical Properties

Currently, numerous allosteric modulators are under study in clinical trials to treat diseases ranging from chronic kidney failure to cancers, HIV, pain, diabetes, Alzheimer's disease, Parkinson's disease, and others.[86] Overall, the discovered allosteric modulators are helpful to the understanding of the structural and physicochemical properties of these substances, which may provide the principles and rationale for allosteric drug discovery.

By systematic investigation of the differences between allosteric modulators and nonallosteric compounds, van Westen et al.[134] showed that the molecular weight of allosteric modulators falls within a much narrower range compared with that of nonallosteric compounds. For example, in the class B GPCR ligands, statistical analysis shows that the molecule weight for the allosteric modulators is in a range from 305 to 569 Da for 95% of the allosteric modulators tested, whereas it is in a range from 334 to 3591 Da for 95% of the nonallosteric ligands tested. Moreover, allosteric modulators are predicted to be slightly better to Lipinski's rule of five (75% vs. 66%) than nonallosteric compounds. These observations suggest that allosteric modulators are more susceptible to development into orally available drugs than nonallosteric compounds. In addition, comparison of binding affinities between allosteric modulators and nonallosteric ligands shows that the absolute potency for allosteric modulators is lower than that of nonallosteric ligands (5.96 log units vs. 6.66 log units, $p < 0.01$).[134]

Regarding physicochemical properties, a comparative analysis between allosteric modulators in the ASD and nonallosteric ligands in other well-known databases, including MDL Drug Data Report (MDDR) (Accelrys, Inc., San Diego, the United States, 2009), Chinese Natural Product Database (CNPD) (NeoTrident Technol. Ltd., Beijing, China, 2005), Comprehensive Medicinal Chemistry (CMC) (Accelrys, Inc., San Diego, the United States, 2009), and DrugBank,[135] was performed. It should be noted that allosteric modulators tend to be more hydrophobic than nonallosteric ligands, supporting the notion that the predicted average hydrophobicity index (3.98) of allosteric modulators, quantified by a measure called SlogP, is generally greater than that of nonallosteric ligands (3.54 for MDDR, 2.77 for CNPD, 2.32 for CMC, and 0.91 for DrugBank) (Fig. 7). This result is reminiscent of the hydrophobic nature of allosteric sites, which, in turn, is suitable for recruiting hydrophobic allosteric modulators. Another remarkable difference is that the average number of rotatable bonds is calculated to be 7.47 for allosteric modulators in ASD, significantly smaller than that of nonallosteric ligands in other databases (11.0 for MDDR, 10.7 for CNPD, 9.33 for CMC, and 9.63 for DrugBank) (Fig. 7). Indeed, sp^2-hybridized carbon bonds and aromatic bonds are highly enriched in allosteric modulators,[134] indicating that allosteric modulators are more rigid than nonallosteric compounds. This finding is consistent with the mode of action of

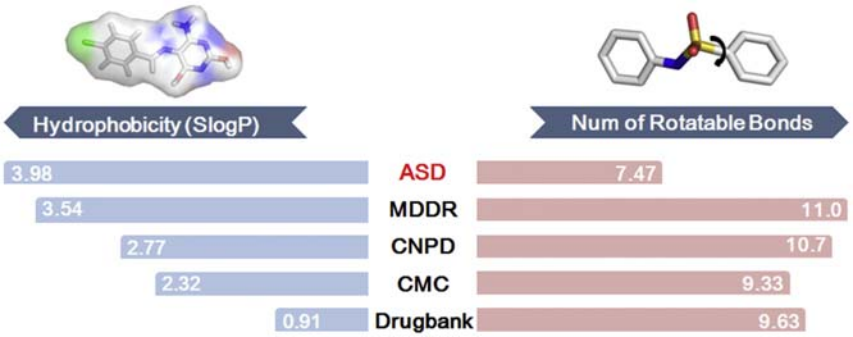

Fig. 7 The predicted average hydrophobicity and number of rotatable bonds for allosteric modulators in ASD and nonallosteric compounds in MDDR, CNPD, CMC, and DrugBank.

allosteric modulators via binding in distinct structural locations of proteins instead of orthosteric sites and the ability of the rigid structures of allosteric modulators to potentiate the specific ligand–host allosteric interactions that stabilize the active or inactive conformations of proteins.

2.11.4.2 "Allo-Modulator Like"

Based on the differences of chemical structure and physicochemical properties between allosteric modulators and nonallosteric ligands, Wang et al.[136] developed a classification model to distinguish allosteric modulators from nonallosteric ligands. They performed systematic analyses of eighteen molecular descriptors, including molecular weight (MW), average MW (MW per atom), number of atoms, number of bonds, number of rotatable bonds (RBN), rotatable bond fraction, unsaturation index, number of rings (nR), number of circuits, number of ring systems, number of rings in the largest ring system (nRIS), complexity of ring systems, number of hydrogen-bond acceptors, number of hydrogen-bond donors, hydrogen-bond acceptor fraction, hydrogen-bond donor fraction, SlogP, and topological polar surface area. They summarized several structural requirements that are shared by allosteric modulators. These features are referred to as "Allo-Modulator Like" and presented as follows: (i) $MW \leq 600$, (ii) $RBN \leq 6$, (iii) $2 \leq nR \leq 5$, (iv) $nRIS = 1$ or 2, and (v) $3 \leq SlogP \leq 7$. This empirical rule can positively filter more than 80% of the known allosteric modulators deposited in ASD and provides a guideline for the rational design and optimization of allosteric modulators. The "Allo-Modulator Like" rule was developed into a web server that can be accessed at http://mdl.shsmu.edu.cn/ASD/.[71]

2.11.4.3 Privileged Scaffolds

The concept of privileged scaffolds, first proposed by Evans and coworkers in 1988, is defined as the ability of multiple molecules of the same scaffold bearing bioactivity to cover a broad spectrum of target proteins.[137] In general, privileged scaffolds exhibit favorable drug-like properties and are amenable to the synthesis of combinatorial compound libraries with extensive pharmaceutical applications.[138] Over the past two decades, a host of privileged scaffold-based libraries have proved capable of effectively capturing potent and selective ligands for a wide variety of targets to improve R&D productivity.[139,140] Inspired by these advantages, the privileged scaffolds for allosteric modulators are explored, aiming to offer a viable starting point for the rapid discovery and optimization of novel allosteric modulators.

Table 2 lists the high frequencies of privileged scaffolds in allosteric modulators, with each privileged scaffold covering more than 15 types of allosteric targets. The 12 privileged scaffolds include indole, biphenyl, naphthalene, diphenylmethane, benzo[*d*][1,3]dioxole, *N*-phenylbenzamide, quinoline, oxydibenzene, 1*H*-benzo[*d*]imidazole, 1-benzylpiperazine, 2,3-dihydrobenzo[*b*][1,4]dioxine, and 1-phenylpiperazine, as enumerated in Table 2, among which indole appears to be the most frequently used as a privileged scaffold for allosteric modulators, with 44 protein targets associating with the indole-containing scaffold. Indole-containing derivatives have the advantage to mimic the structure of peptides, which represent a very important class of molecules to develop novel drugs with different modes of action.[141] More than 30 marketed drugs contain indole scaffold. Among them, seven drugs are in the top-200 best selling drugs by US retail sales in 2012.[142] Notwithstanding, there are no allosteric drugs containing indole scaffold in the market. Considering the availability of cocrystal structures of ligand–target complexes, nine types of targets in complex with their allosteric modulators harboring indole privileged scaffold have been determined by X-ray crystallography. In all of the aforementioned cases, indole-containing derivatives serve as allosteric inhibitors for modulating the functions of targets by either direct or indirect interactions (Fig. 8), such as tryptophan for anthranilate synthase (PDB ID: 1I1Q), chorismate mutase (PDB ID: 1CSM), and tryptamin 2,3-dioxygenase (PDB ID: 2NW8); 5-fluoro-1*H*-indole-2-carboxylic acid-(2-mercapto-ethyl)-amide for caspase 7 (PDB ID: 1SHL); 3-(2-carboxy-ethyl)-4,6-dichloro-1*H*-indole-2-carboxylic acid for fructose-1,6-bisphosphatase 1 (PDB ID: 1LEV); 3-(carboxymethyl)-5,7-dichloro-1*H*-indole-2-carboxylic acid for farnesyl pyrophosphate synthase

Table 2 The high frequency of privileged scaffolds found in allosteric modulators

Privileged scaffolds	*Num of targets*	*Privileged scaffolds*	*Num of targets*
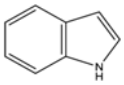	44	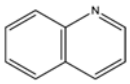	17
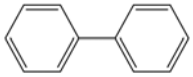	27	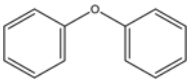	16
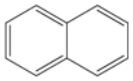	26	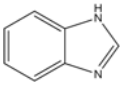	16
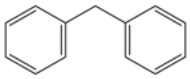	23	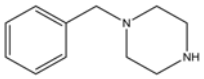	15
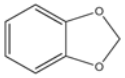	21	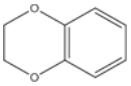	15
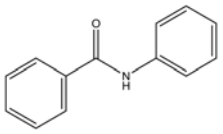	19	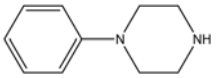	15

(PDB ID: 3N5J); *N*-[1*H*-indole-3-yl-acetyl]glycine for tryptophan synthase (PDB ID: 1K7E); 3-cyclohexyl-1-(2-morpholin-4-yl-2-oxoethyl)-2-phenyl-1*H*-indole-6-carboxylic acid for NS5B RNA-dependent RNA polymerase (PDB ID: 2BRK); and bis[5-chloro-1*H*-indole-2-yl-carbonyl-aminoethyl]-ethylene glycol for glycogen phosphorylase (PDB ID: 1EM6).

2.11.5 Allosteric Protein–Ligand Interactions

2.11.5.1 Noncovalent Allosteric Modulators

The vast majority of the currently reported allosteric modulators are noncovalent. For example, PDK1, a master kinase that belongs to the Ser/Thr AGC protein kinase family, plays a key role in the regulation of physiological processes, such as cell proliferation, differentiation, and survival.[143] PDK1 possesses a hydrophobic pocket positioned in the N-lobe of the kinase, referred to as the PIF pocket, which has been demonstrated to interact with the C-terminal hydrophobic motifs (HMs) of its substrates.[144,145] The catalytic activity of PDK1 can be allosterically enhanced by the binding of phosphorylated HMs to the PIF pocket;[146,147] this pocket is distant from the ATP-binding site. Based on the PIF pocket of PDK1, Rettenmaier et al.[148] recently developed a fluorescence polarization (FP) competitive binding assay to screen for small-molecule compounds that compete with PIFtides (an activating peptide motif on downstream substrate kinases) to bind to the PIF pocket. Using the FP assay, they screened ~154,000 compounds and identified 1280 hits for dose response. Among these initial hits, one of the small molecules, diaryl sulfonamide RS-HTS (**Fig. 9**), is the most potent, which had a K_d value of 15 μM measured by the FP assay and an IC_{50} value of 20 μM by the surface plasmon resonance (SPR) assay. Subsequent structural modifications of RS-HTS identified two regioisomers RS1 and RS2 (**Fig. 9**); the two small molecules bind to the PIF pocket of PDK1 with K_d values of 1.5 and 9 μM, respectively. The determination of the cocrystal complexes between PDK1 and RS1 (PDB ID: 4RQK) (**Fig. 10A**) and RS2 (PDB ID: 4RQV) (**Fig. 10B**), together with ATP, clearly exhibits that both RS compounds bind to the N-terminal PIF pocket, distal from the ATP-binding site. In the PIF pocket, the sulfonyl group of both RS compounds engages in a salt bridge with Arg131 in the helix αC, and both aromatic substituents of RS1 and RS2 form hydrophobic interactions with Leu155 in the β5 sheet.

2.11.5.2 Covalent Allosteric Modulators

A major challenge in drug discovery is how to reduce drug dosage and increase specificity of compound candidates, because high dosage is frequently associated with toxicity. Compared with noncovalent drugs, covalent drugs have potential pharmacological advantages because they may be administrated in lower doses due to the maintenance of longer lifetime of the drug–target complex.[149] Covalent drugs are compounds bearing a bond-forming functional group of low reactivity, following binding to the target protein and then reacting with a specific nucleophilic residue (usually cysteine) at the target site.[150,151] The irreversible binding of covalent drugs to proteins allows for the prolonged duration of drug action on the target, which has the potential to contribute the selectivity and reduce the toxicity that is often caused by high dosage. However, covalent allosteric drugs not only

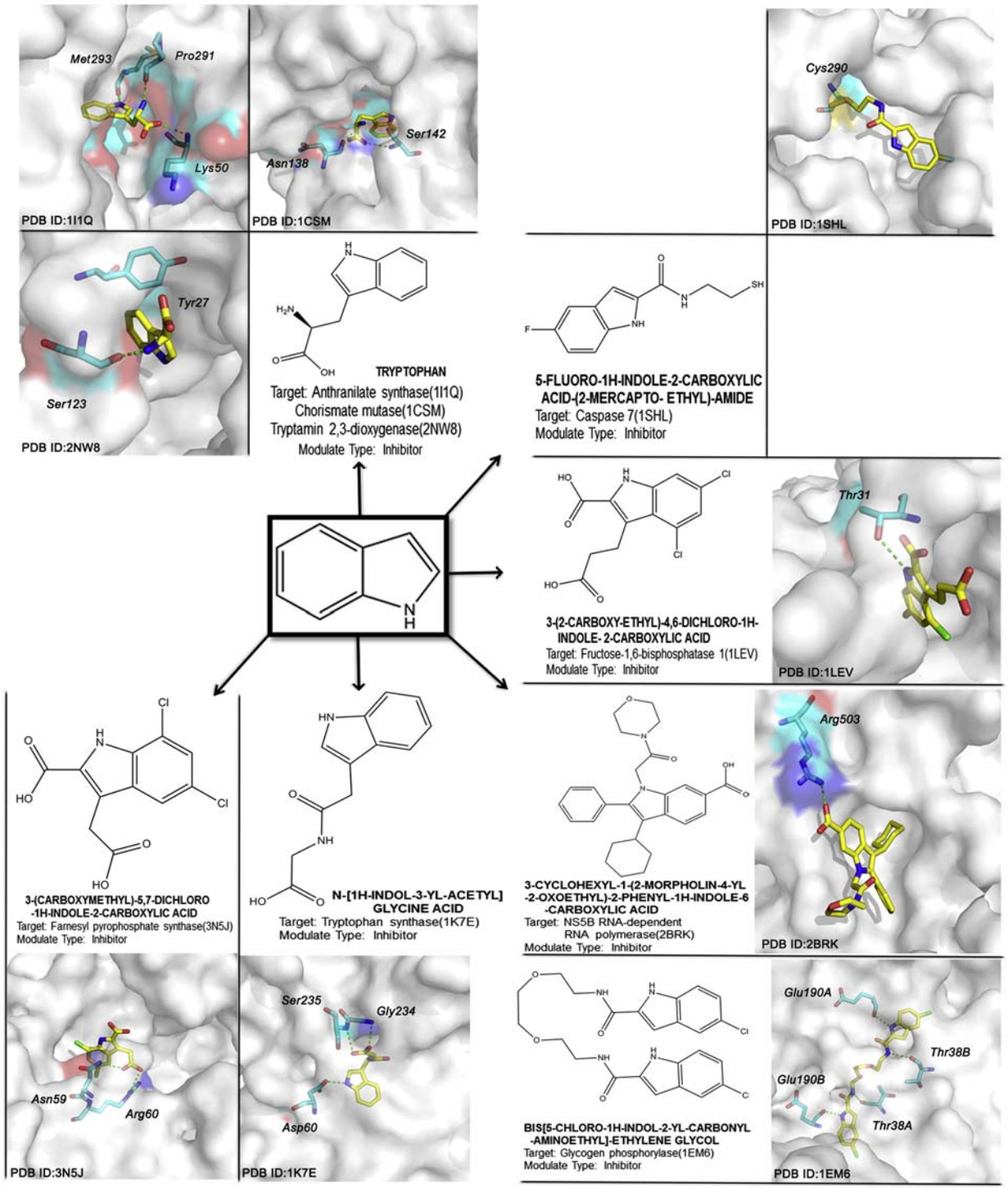

Fig. 8 Cocrystal structures of allosteric targets in complex with their allosteric modulators harboring indole scaffolds. Hydrogen-bonding interactions between allosteric targets and allosteric modulators are depicted by *green dotted lines*.

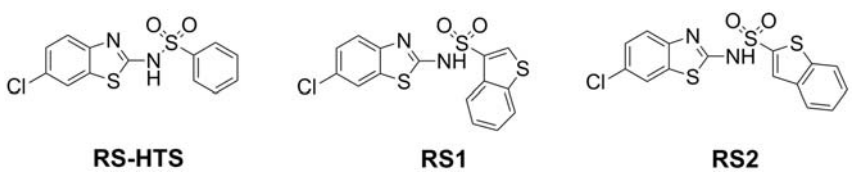

Fig. 9 Chemical structures of the diaryl sulfonamides RS-HTS, RS1, and RS2.

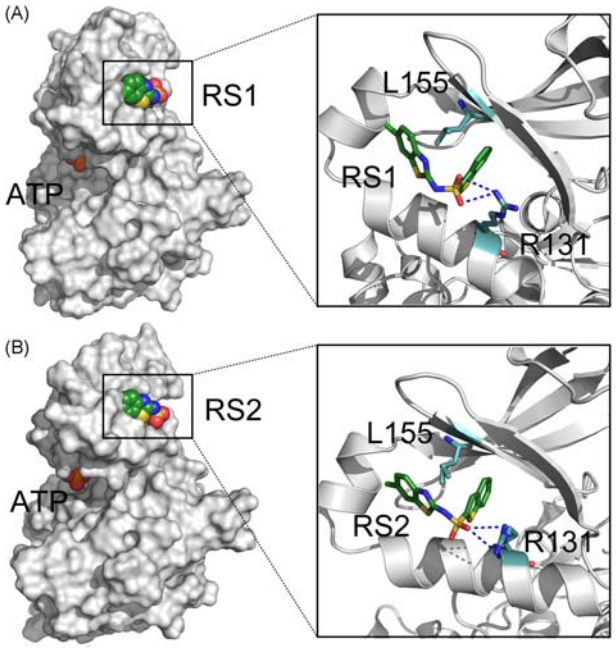

Fig. 10 The binding modes of RS1 (A) and RS2 (B) with PDK1. Salt bridges are depicted by *blue dotted lines*.

possess the pharmacological merits of covalent drugs but also have additional benefit of the higher specificity of allosteric drugs. Thus, covalent allosteric drugs present a novel direction in therapeutic drug development.[152,153]

In the oncogenic Ras protein, somatic mutations such as Gly12, Gly13, and Gln61 mutations are the most common activating lesions found in human cancers, including pancreatic, colorectal, and lung cancers.[154–156] In the case of G12C mutation, this mutation creates a nucleophilic cysteine that can be used to design covalent allosteric modulators. Ostrem et al.[157] harnessed a disulfide-fragment-based screening approach to screen a library of 480 disulfide-containing small-molecule compounds against K-Ras4B^{G12C}-GDP. Structure–activity optimizations of the initial hits identified the compound **6** (Fig. 11A), which showed a higher potency compared to initial hits. To uncover the structural details of the binding between compound **6** and G12C K-Ras4B, the X-ray

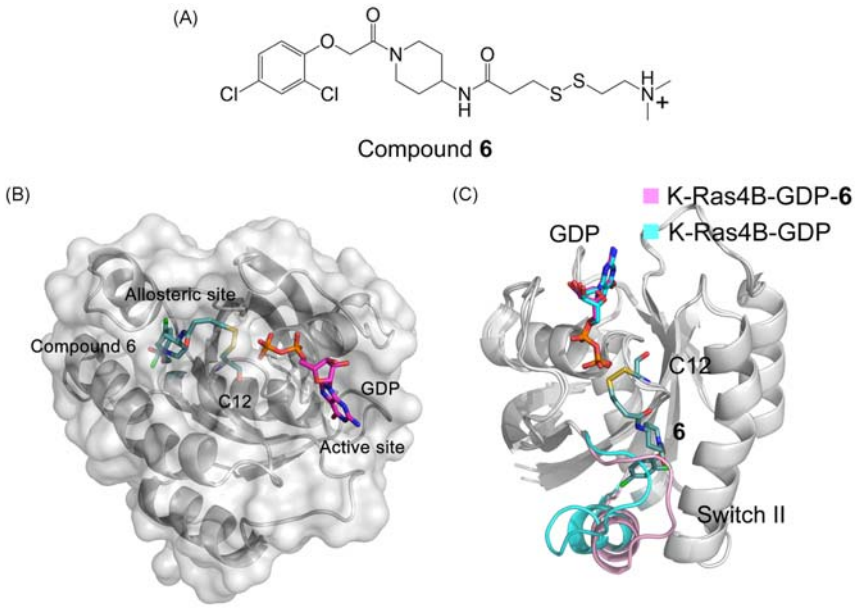

Fig. 11 (A) Chemical structure of compound **6**. (B) Surface representation of K-Ras4B^{G12C}-GDP-**6** (PDB ID: 4LUC) showing the compound **6** bound to the switch II pocket, S-IIP. (C) Backbone superimposition of the crystal structure of K-Ras4B^{G12C}-GDP-**6** onto that of K-Ras4B^{WT}-GDP (PDB ID: 4Q21). The switch II region in the structures of K-Ras4B^{G12C}-GDP-**6** and K-Ras4B^{WT}-GDP is colored in *pink* and *cyan*, respectively.

structure of G12C K-Ras4B-GDP in complex with compound **6** was determined (PDB ID: 4LUC). The structure revealed that compound **6** forms a disulfide bond with Cys12 (Fig. 11B), and because of this binding, a new allosteric pocket is generated beneath the effector binding switch II region, termed S-IIP (Fig. 11C). The covalent binding of compound **6** to K-Ras4B^{G12C} prevents the downstream effectors, such as Raf and PI3K, from binding to K-Ras4B^{G12C}, thereby inhibiting the downstream signaling mediated by Ras.

2.11.5.3 Bitopic Ligands

The bitopic ligand, also named dualsteric ligand, is a kind of allosteric modulators, which are referred to a single chemical entity consisted of an orthosteric pharmacophore covalently linked to an allosteric pharmacophore.[158] In this regard, a bitopic ligand can bind simultaneously to both the orthosteric and allosteric binding sites of proteins. In principle, the orthosteric portion is responsible for binding affinity, and the allosteric portion is accountable for the selectivity of the protein subtype of interest.[159] As a consequence, the ability of the bitopic ligands to achieve improved protein affinity and selectivity is gaining increasing recognition as a tactics in allosteric drug design.

The advantages of bitopic ligands include receptor-expression-dependent pharmacology and ligand-biased signaling.[86,160,161] As in the case of the muscarinic M_2 acetylcholine (ACh) receptor (mAChR), a prototype of class A GPCRs, the ACh orthosteric binding site of the M_2 mAChR is located in a narrow cavity formed by the seven-transmembrane (TM) domains of the receptor, and the allosteric binding site is located on the extracellular entrance of the receptor. The close proximity of these two binding sites suggests the possibilities of sculpting bitopic ligands to bridge orthosteric and allosteric binding sites. Founded on this hypothesis, Steinfeld et al.[162] designed a bitopic antagonist—THRX160209—that links the orthosteric and allosteric binding sites of the M_2 mAChR. THRX160209 contains an orthosteric pharmacophore, a benzhydryl (3-BHP) moiety, and an allosteric pharmacophore, a 4-aminopiperidine moiety (4-ABP); the two pharmacophores are connected by a C7 polymethylene chain (Fig. 12A). In the M_2 mAChR inhibition radioligand binding assay, the observed affinity for THRX160209 (apparent $pK_i = 9.51 \pm 0.22$) was several orders of magnitude greater than its two parent components (apparent pK_i values < 6.0). Moreover, THRX160209 exhibited markedly higher specificity for the M_2 receptor, in a range of one to two orders of magnitude greater compared with the other four highly conserved receptor subtypes (M_1, M_3, M_4, and M_5) of mAChR.

The dopamine receptors contain five subtypes (D_{1-5}Rs) that are expressed mainly in the vertebrate central nervous system (CNS). The physiological functions of DRs are mediated by the binding of the catecholamine neurotransmitter, dopamine, to the highly conserved orthosteric site of DRs. Aberrant DR functions in the CNS have been associated with numerous neuropsychiatric disorders, including schizophrenia, attention-deficit hyperactivity disorder, and social phobia.[163–165] Recently, Lane et al.[166] characterized the first drug-like allosteric modulator, SB269652, of the D_2R. The ligand, SB269652, harbors a structural hallmark of orthosteric D_2R antagonists, the tetrahydroisoquinoline (THIQ) moiety, and a lipophilic appendage, the indole-2-carboxamide moiety (Fig. 12B); the two pharmacophores are connected by a cyclohexane linker. Via the ERK1/2 phosphorylation assay, it was shown that the binding affinity of SB269652 is much greater than that of the THIQ moiety by 17-fold. Molecular modeling and site-directed mutagenesis experiments revealed that the THIQ moiety of SB269652 occupies the orthosteric site of D_2R, whereas the indole-2-carboxamide moiety protrudes into the allosteric site lined by the extracellular interface between TM2

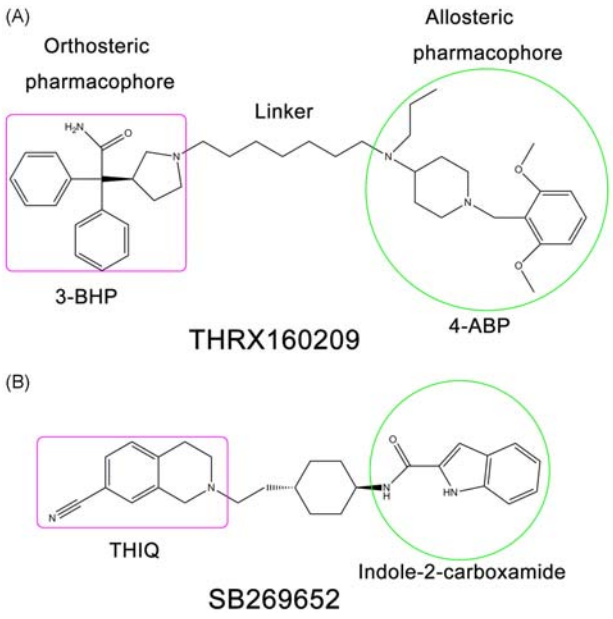

Fig. 12 Chemical structures of bitopic ligands for the THRX160209 (A) and SB269652 (B).

and TM7; the engagement of the latter is of fundamental importance to exert the allosteric pharmacology of SB269652. Furthermore, based on the functional complementation assay and [^{35}S] GTPγS binding assay, the allosteric underpinning of action of SB269652 is proposed as the binding of the bitopic ligand to one D_2R homodimer to allosterically modulate the binding of a ligand to the orthosteric site of another D_2R homodimer. This novel mechanism expands the repertoire of allosteric regulation than can be engendered by bitopic GPCR ligands.

2.11.5.4 Allo-Network Modulators

In living cells, a protein is not an isolated node. Rather, it has the potential to contact with its partners to form protein–protein interactions (PPI) in a specific circumstance.[167–169] For example, in the phosphatidylinositol 3-kinase (PI3K)/Akt signaling pathway, the master kinase PDK1 interacts with its downstream substrate, Akt, and subsequently phosphorylates the threonine in the activation loop of Akt. The active phosphorylated Akt has the ability to interact with its downstream substrate glycogen synthase kinase 3 (GSK3) and then phosphorylates the serine in the activation loop of GSK3.[170] As a result, a signal from one protein can be propagated over a long distance to the specific destination. This individual signal transduction process is called as cellular pathway. In fact, a certain protein may also be involved in more than one signaling pathway, thereby resulting in the signaling pathways in cells to be interconnected. This phenomenon is also referred to as cellular network, which, coupled with its environment, guides cell and organism behavior and is of prime importance to understanding the function and misfunction of proteins.[171,172]

The binding of a molecule may trigger conformational or dynamic changes in its target, which, in turn, propagates the perturbation signal to affect the conformations of its adjacent proteins. As such, the adjacent proteins can also transmit the conformational signal to their partners via the complex PPI interactome. Recently, Nussinov et al.[173–175] proposed a novel paradigm of drug action, "allo-network drugs," to parse out this kind of behavior. Unlike a conventional drug that directly targets an individual malfunctioning protein, an allo-network drug enables to initiate a perturbation signal in a distant protein in the cellular network to reach the target protein. Thus, the "allo-network drug" concept greatly broadens the scope of target proteins that can be exploited as drug discovery targets. Taking into account that allo-network drugs orchestrate a specific signaling pathway to shift its pathophysiological network status to normal, they are capable of achieving fewer side effects and lower toxicity.[174]

Despite the importance of allo-network drugs in the development of allosteric drugs, the exquisite characterization of PPI complex in the cellular network is a daunting task by experiments. The recent advances in the network analysis methodology, in-depth understanding of pathways and information flow in the cellular networks at atomic level, and the remarkable progress in the analysis of cellular system-level responses by means of cell-based assays will be beneficial to accelerate allo-network drugs discovery.[175,176] Thus far, several paradigms have witnessed the utilization of allo-network drugs to modulate the PPI network in the specific pathway. One quintessential example that takes advantage of allo-network drugs to interfere with a disease-specific pathway has been reported in the serine/threonine mammalian target of rapamycin (mTOR). mTOR, belonging to the PI3K-related kinase protein family, regulates cell growth, proliferation, survival, and protein synthesis. Dysregulation of the mTOR signaling pathway has implicated in human diseases, such as cancers, diabetes, and obesity.[177,178] mTOR exists in the two structurally different complexes: mTOR complex 1 (mTORC1) and mTOR complex 2 (mTORC2). The two complexes contain the same catalytic subunit, mTOR, but are engaged in significantly distinct signaling pathways. The allosteric inhibitor rapamycin/FKBP12 can selectively inhibit the mTORC1 signaling (Fig. 13), but not the mTORC2 signaling. Rapamycin/FKBP12 binds to the FKBP12-rapamycin-binding domain of mTOR, leading to allosterically disrupt the interactions between the mTOR C-terminus and the protein raptor in the mTORC1. Under this circumstance, the conformation of the protein raptor undergoes changes, preventing

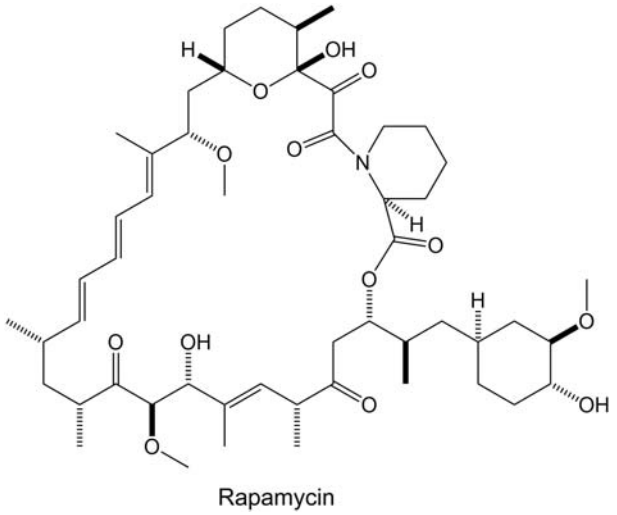

Fig. 13 Chemical structure of rapamycin.

it from the interaction with the eukaryotic translation initiation factor 4E (eIF4E) binding protein (4E-BP) substrates. This effect inhibits the downstream signaling of mTORC1.

2.11.5.5 Allosteric and Orthosteric Collaboration

In the c-Abl, modulation of c-Abl activity is achieved by an autoinhibition involving the N-terminal SH2 and SH3 domains of the protein. In the oncogenic fusion protein Bcr-Abl, the autoinhibition conformation of Abl is disrupted, resulting in CML or acute lymphoblastic leukemia.[179] The "gatekeeper" T334I mutation renders the ATP-binding site inhibitors imatinib (STI-571/Gleevec), nilotinib (AMN-107/Tasigna), and dasatinib (Sprycel) ineffective and causes clinical relapse in advanced-phase patients. Addition of GNF-5 to occupy the C-terminal Abl myristoyl allosteric pocket, coupled with the occupation of ATP-binding site by imatinib, allosterically locks c-Abl in the closed, inactivated state.[93] The cooperative actions of imatinib and GNF-5 can be used to overcome drug resistance. The determination of the cocrystal structure between c-Abl and an analog of imatinib, PD166326 (**Fig. 14A**) and myristic acid (PDB ID: 2FO0)[180] displayed that the myristic acid occupies a deep pocket in the C-lobe of the kinase domain, whereas the PD166326 is bound to the ATP-binding site (**Fig. 14B**).

The most encouraging case is the combination of the MEK inhibitor trametinib and the B-Raf inhibitor dabrafenib for the treatment of mutant B-Raf$^{V600E/K}$ metastatic melanoma.[75] This combinational strategy was approved by the FDA in the early 2014 and has been utilized to overcome the drug resistance within about 6 months in response to the treatment of B-Raf inhibitors.[181,182] The determination of the cocrystal structure between MEK1 and an analog of trametinib, TAK-733 (**Fig. 15A**), displayed that the TAK-733 is located in an allosteric pocket proximal to the ATP-binding site (PDB ID: 3PP1),[183] a typical type III binding mode (**Fig. 15B**).

2.11.6 Mechanisms of Allosteric Drug Action

The recent unified view of allostery introduced by Nussinov and Tsai suggests the existence of structural coupling between the orthosteric and allosteric sites.[184] The allosteric signals propagate from allosteric sites to orthosteric sites by virtue of multiple,

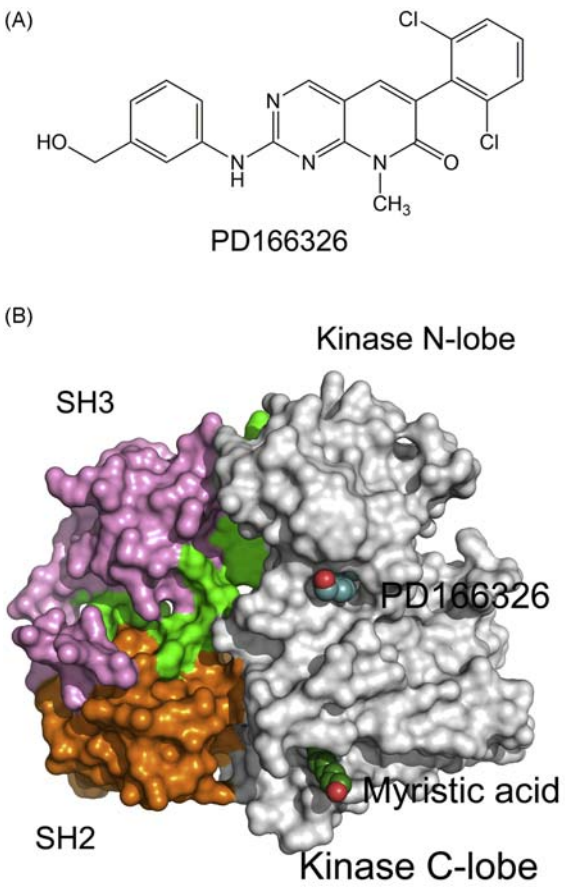

Fig. 14 (A) Chemical structure of PD166326. (B) Crystal structure of c-Abl in complex with an allosteric modulator, myristic acid located in the C-lobe of the kinase domain, and an orthosteric inhibitor, PD166326 (PDB ID: 2FO0). SH3 domain, SH2 domain, interdomain linkers, and kinase domain are colored in *pink*, *orange*, *green*, and *gray*.

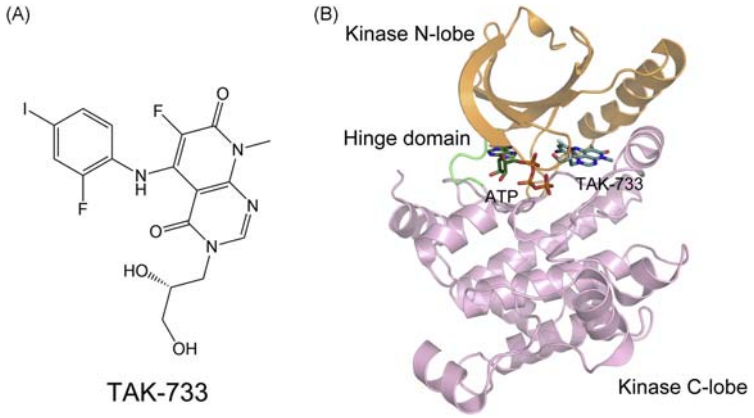

Fig. 15 (A) Chemical structure of TAK-733. (B) Crystal structure of MEK1 in complex with an allosteric modulator TAK-733 (PDB ID: 3PP1). ATP and TAK-733 are depicted by stick models. N-lobe, hinge domain; C-lobe are colored in *orange*, *green*, and *pink*.

preexisting pathways in all proteins, but which pathways are dominated, associated with protein topologies, specific binding events (small molecules, proteins, and DNA/RNA), covalent modifications, and cellular conditions.[185,186] Allosteric drugs bound to allosteric sites merely shift the preexisting ensemble of pathways to one specific pathway, resulting in the variation of the relative populations of the different substrates. Consequently, different chemical types of allosteric drugs can produce distinctly functional and dynamical allosteric effects of proteins. The specific allosteric ligand–protein interactions determine the extent of relative increase of the active state population of proteins in solution as a result of stabilizing the active conformation and/or destabilizing the inactive conformation.[184] This principle plays a pivotal role in specifying the allosteric drug action.

Recently, Nussinov and Tsai emphasized that allosteric drugs consist of anchor and driver atoms.[187,188] The anchor atoms, by definition, occupy the allosteric site and are engaged in favorable interactions with a highly populated conformation in the inactive and active states. These interactions between the anchor atoms of allosteric drugs and proteins do not undergo change during the protein switch from the inactive to active states and vice versa. In contrast, the driver atoms interact with proteins, and these interactions profoundly differ between the inactive and active states. The driver atoms can be further divided into attractive "pulling" or repulsive "pushing" atoms, depending on the specific interactions between the driver atoms and their corresponding residues in the allosteric sites. Guided by this concept, a formation of a stabilizing attractive interaction between drive atoms and proteins has the potential to pull the inactive conformation into the active conformation. Conversely, formation of a repulsive interaction between driver atoms and proteins can push the active conformation into the inactive conformation. Furthermore, the characteristic properties of driver atoms can be exploited to decipher allosteric ligand–protein interactions where minor or subtle modifications in allosteric drugs can lead to opposite allosteric effects, such as from agonism to antagonism. Identification of driver atoms in allosteric drugs can contribute to allosteric drug discovery.

For example, Ras proteins, small GTPases, are signal switch molecules that regulate cell fates by coupling receptor activation to downstream effector pathway that control diverse cellular responses including proliferation, differentiation and survival.[154] Ras proteins are activated by the exchange of Ras-bound guanosine diphosphate (GDP) (Ras-GDP, inactive state) with guanosine triphosphate (GTP) (Ras-GTP, active state). This exchange results in large conformational changes in the switch I and switch II regions of the Ras catalytic domains, rendering the Ras proteins in the active state that can bind to various effector proteins to stimulate signaling pathways. According to the anchor and driver identification protocol[187] that is applied on the catalytic domain of Ras in the GNP-bound (PDB ID: 3GFT) and GDP-bound (PDB ID: 4LPK) structures, two oxygen atoms from the γ-phosphate group of GNP are identified as driver atoms, which form hydrogen-bonding interactions with the residue Thr35 from the switch I region and Gly60 from the switch II region (**Fig. 16**). The two hydrogen bonds are absent in the GDP-bound structure. The driver's pulling action from the two oxygen atoms from the γ-phosphate group of GNP may pull the inactive to active Ras conformation and stabilize the Ras-GNP-bound conformation. In addition, the anchor atoms are derived from the adenine, ribose, and α-/β-phosphate groups in the both of two structures. These atoms interact with the inactive/active Ras through hydrogen-bonding interactions; these interactions do not change between the inactive and active states. For example, in the both structures, residues that interact with the anchor atoms include Gly13, Gly15, Lys16, Ser17, Ala18, Val29, Asp30, Asp119, and Ala146.

In the case of the regulatory subunit of protein kinase A (R_A), R_A functions to modulate the activity of protein kinase A in a cAMP-dependent manner and exists in two distinct and structurally dissimilar, active cAMP-bound "B" and inactive C-subunit "H" conformations.[189] The replacement of the equatorial oxygen of the cyclic phosphate of cAMP to a sulfur atom yields the R_p-cAMP. R_p-cAMP functions as an antagonist that binds to the *cyclic* nucleotide-binding (CNB) domain of R_A, thereby locking the R_A in its inactive "H" conformation. As shown in **Fig. 17**, superimposition of the crystal structures of the active cAMP bound (PDB ID: 3PNA) and inactive R_p-cAMP bound (PDB ID: 3PLQ) reveals that the dramatic conformational changes between the two structures are observed in the α subdomain distant from the CNB domain, with only small differences in the β subdomain.

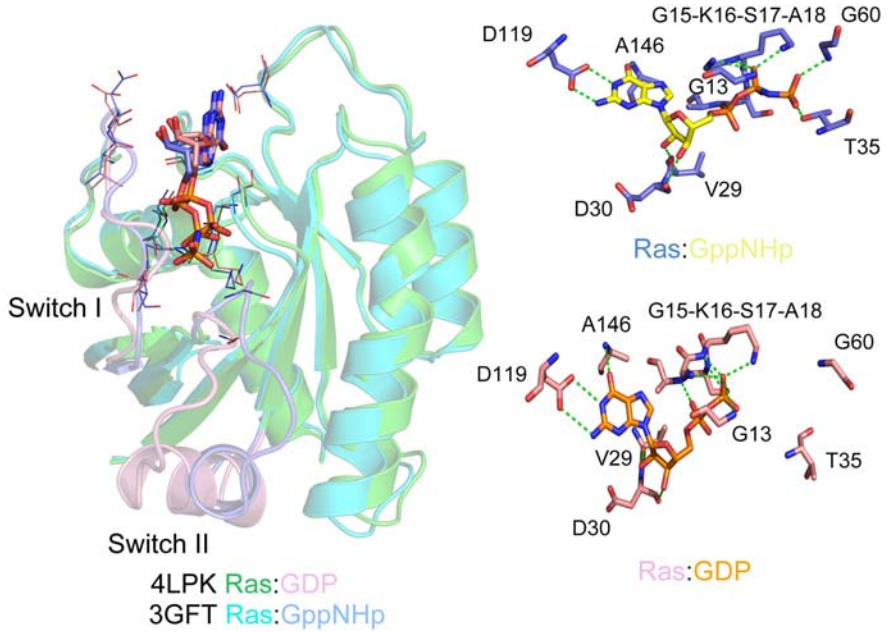

Fig. 16 Structural presentation of identified driver and anchor atoms for Ras.

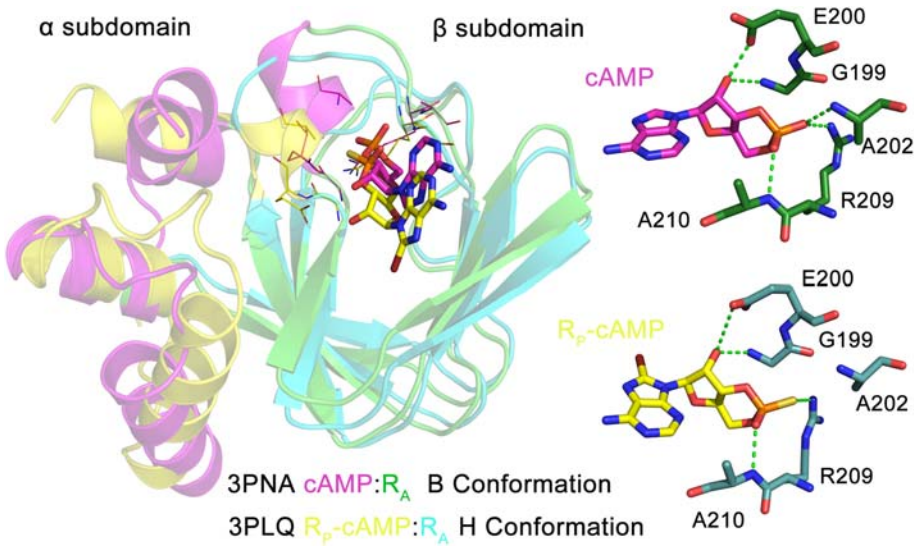

Fig. 17 Structural presentation of identified driver and anchor atoms for PKA.

The crystallographic information indicates that the activation mechanism of cAMP action is through allosteric regulation. Based on the anchor and driver identification protocol, the equatorial oxygen atom in the cAMP that is substituted with a sulfur atom R_p-cAMP is identified as a driver atom, which forms a hydrogen bond with the residue Ala202. This hydrogen bond is absent in the R_p-cAMP-bound structure. The driver's pulling action from the equatorial oxygen atom from the cyclic phosphate of cAMP may pull the inactive to active R_A conformation and stabilize the R_A-cAMP-bound conformation. In addition, the anchor atoms are derived from the hydroxyl group of ribose, one oxygen atom from the cyclic phosphate of cAMP in the both of two structures. These atoms interact with the inactive/active R_A through hydrogen-bonding interactions; these interactions do not change between the inactive and active states. For example, in the both structures, residues that interact with the anchor atoms include Gly199, Glu200, Arg209, and Ala210.

2.11.7 Conclusions

Allostery, the fundamental process by which distant sites on a given protein are coupled, has been established as an efficient and ubiquitous mechanism for regulation of functional activity. The modes of action between orthosteric and allosteric drugs are significantly distinct. The main advantage of allosteric drugs is their higher specificity and lower toxicity. Despite the increasing popularity of using allosteric modulators as therapeutic agents, a long-standing challenge in the development of allosteric modulators is the discovery of allosteric sites in proteins of interest.[190–194] The identification of allosteric sites is a first step toward screening and optimizing allosteric modulators. Remarkably, in the last decade, the development of approaches for the finding of allosteric sites has considerable progress in many proteins,[195] such as enzymes and GPCRs, which provide novel opportunities to design allosteric modulators in more drug targets. Owing to the remarkable merits of allosteric modulators and the considerable interest invested in their development, we believe that the repertoire of allosteric modulators should be burgeoning in the pharmaceutical industry and drug discovery program.

Acknowledgments

We thank Prof. Ruth Nussinov at the National Cancer Institute, Frederick, for fruitful discussion. This work was supported by the National Basic Research Program of China (973 Program) (2015CB910403), National Natural Science Foundation of China (81322046, 81302698, and 81473137), Shanghai Rising-Star Program (13QA1402300), Shanghai Health and Family Planning Commission (20154Y0058), Program for Professor of Special Appointment (Eastern Scholar) at Shanghai Institutions of Higher Learning, and Program for New Century Excellent Talents in University (NCET-12-0355).

See also: 2.13. Small-Molecule Inhibitors of Protein–Protein Interactions. 5.01. Cancer Biology and the Principles of Targeted Cancer Drug Discovery. 5.03. Covalent Kinase Inhibitors for Cancer.

References

1. Nussinov, R.; Tsai, C.-J. *Cell* **2013,** *153,* 293–305.
2. Goodey, N. M.; Benkovic, S. J. *Nat. Chem. Biol.* **2008,** *4,* 474–482.
3. Changeux, J.-P.; Edelstein, S. J. *Science* **2005,** *308,* 1424–1428.
4. Fenton, A. W. *Trends Biochem. Sci.* **2008,** *33,* 420–425.
5. Otero, L. H.; Rojas-Altuve, A.; Llarrull, L. I.; Carrasco-López, C.; Kumarasiri, M.; Lastochkin, E.; Fishovitz, J.; Dawley, M.; Hesek, D.; Lee, M.; Johnson, J. W.; Fisher, J. F.; Chang, M.; Mobashery, S.; Hermoso, J. A. *Proc. Natl. Acad. Sci. U. S. A.* **2013,** *110,* 16808–16813.
6. Xiao, B.; Sanders, M. J.; Underwood, E.; Heath, R.; Mayer, F. V.; Carmena, D.; Jing, C.; Walker, P. A.; Eccleston, J. F.; Haire, L. F.; Saiu, P.; Howell, S. A.; Aasland, R.; Martin, S. R.; Carling, D.; Gamblin, S. J. *Nature* **2011,** *472,* 230–233.
7. Lin, K.; Lin, J.; Wu, W.-I.; Ballard, J.; Lee, B. B.; Gloor, S. L.; Vigers, G. P. A.; Morales, T. H.; Friedman, L. S.; Skelton, N.; Brandhuber, B. J. *Sci. Signal.* **2012,** *5,* ra37.
8. Ulaganathan, V.; Talapatra, S. K.; Rath, O.; Pannifer, A.; Hackney, D. D.; Kozielski, F. J. *Am. Chem. Soc.* **2013,** *135,* 2263–2272.
9. Raman, S.; Taylor, N.; Genuth, N.; Fields, S.; Church, G. M. *Trends Genet.* **2014,** *30,* 521–528.
10. Jiménez-Osés, G.; Osuna, S.; Gao, X.; Sawaya, M. R.; Gilson, L.; Collier, S. J.; Huisman, G. W.; Yeates, T. O.; Tang, Y.; Houk, K. N. *Nat. Chem. Biol.* **2014,** *10,* 431–436.
11. Moriconi, A.; Cunha, T. M.; Souza, G. R.; Lopes, A. H.; Cunha, F. Q.; Carneiro, V. L.; Pinto, L. G.; Brandolini, L.; Aramini, A.; Bizzarri, C.; Bianchini, G.; Beccari, A. R.; Fanton, M.; Bruno, A.; Costantino, G.; Bertini, R.; Galliera, E.; Locati, M.; Ferreira, S. H.; Teixeira, M. M.; Allegretti, M. *Proc. Natl. Acad. Sci. U. S. A.* **2014,** *111,* 16937–16942.
12. Monod, J.; Changeux, J.-P.; Jacob, F. J. *Mol. Biol.* **1963,** *6,* 306–329.
13. Cui, Q.; Karplus, M. *Protein Sci.* **2008,** *17,* 1295–1307.
14. Monod, J.; Wyman, J.; Changeux, J. P. J. *Mol. Biol.* **1965,** *12,* 88–118.
15. Koshland, D. E. J.; Nemethy, G.; Filmer, D. *Biochemistry* **1966,** *5,* 365–385.
16. Boehr, D. D.; Nussinov, R.; Wright, P. E. *Nat. Chem. Biol.* **2009,** *5,* 789–796.
17. Jaffe, E. K. *Trends Biochem. Sci.* **2005,** *30,* 490–497.
18. Selwood, T.; Jaffe, E. K. *Arch. Biochem. Biophys.* **2012,** *519,* 131–143.
19. Jaffe, E. K. *Curr. Top. Med. Chem.* **2013,** *13,* 55–63.
20. Tzeng, S.; Kalodimos, C. G. *Nat. Chem. Biol.* **2013,** *9,* 462–465.
21. Tzeng, S.-R.; Kalodimos, C. G. *Nature* **2009,** *462,* 368–372.
22. Tzeng, S.-R.; Kalodimos, C. G. *Nature* **2012,** *488,* 236–240.
23. Nussinov, R.; Tsai, C.-J. *Curr. Opin. Struct. Biol.* **2015,** *30,* 17–24.
24. Goncearenco, A.; Mitternacht, S.; Yong, T.; Eisenhaber, B.; Eisenhaber, F.; Berezovsky, I. N. *Nucleic Acids Res.* **2013,** *41,* W266–W272.
25. Kaya, C.; Armutlulu, A.; Ekesan, S.; Haliloglu, T. *Nucleic Acids Res.* **2013,** *41,* W249–W255.
26. Huang, W.; Lu, S.; Huang, Z.; Liu, X.; Mou, L.; Luo, Y.; Zhao, Y.; Liu, Y.; Chen, Z.; Hou, T.; Zhang, J. *Bioinformatics* **2013,** *29,* 2357–2359.
27. Huang, W.; Wang, G.; Shen, Q.; Liu, X.; Lu, S.; Geng, L.; Huang, Z.; Zhang, J. *Bioinformatics* **2015,** *31,* 2598–2600.
28. Dror, R. O.; Green, H. F.; Valant, C.; Borhani, D. W.; Valcourt, J. R.; Pan, A. C.; Arlow, D. H.; Canals, M.; Lane, J. R.; Rahmani, R.; Baell, J. B.; Sexton, P. M.; Christopoulos, A.; Shaw, D. E. *Nature* **2013,** *503,* 295–299.
29. Lu, S.; Deng, R.; Jiang, H.; Song, H.; Li, S.; Shen, Q.; Huang, W.; Nussinov, R.; Yu, J.; Zhang, J. *Structure* **2015,** *23,* 1725–1734.
30. Guo, J.; Pang, X.; Zhou, H.-X. *Structure* **2015,** *23,* 237–247.
31. Perilla, J. R.; Goh, B. C.; Cassidy, C. K.; Liu, B.; Bernardi, R. C.; Rudack, T.; Yu, H.; Wu, Z.; Schulten, K. *Curr. Opin. Struct. Biol.* **2015,** *31,* 64–74.
32. Wang, Q.; Qi, Y.; Yin, N.; Lai, L. *PLoS ONE* **2014,** *9,* e94829.
33. Qi, Y.; Wang, Q.; Tang, B.; Lai, L. J. *J. Chem. Theory Comput.* **2012,** *8,* 2962–2971.

34. Pei, J.; Yin, N.; Ma, X.; Lai, L. J. *Am. Chem. Soc.* **2014,** *136,* 11556–11565.
35. Panjkovich, A.; Daura, X. *BMC Bioinf.* **2012,** *13,* 273.
36. Panjkovich, A.; Daura, X. *Bioinformatics* **2014,** *30,* 1314–1315.
37. Greener, J. G.; Sternberg, M. J. *BMC Bioinf.* **2015,** *16,* 335.
38. Mitternacht, S.; Berezovsky, I. N. *PLoS Comput. Biol.* **2011,** *7,* e1002301.
39. Mitternacht, S.; Berezovsky, I. N. *Protein Eng. Des. Sel.* **2011,** *24,* 405–409.
40. De Ruvo, M.; Giuliani, A.; Paci, P.; Santoni, D.; Di Paola, L. *Biophys. Chem.* **2012,** *165–166,* 21–29.
41. Novinec, M.; Korenč, M.; Caflisch, A.; Ranganathan, R.; Lenarčič, B.; Baici, A. *Nat. Commun.* **2014,** *5,* 3287.
42. McLaughlin, R. N.; Poelwijk, F. J.; Raman, A.; Gosal, W. S.; Ranganathan, R. *Nature* **2012,** *491,* 138–142.
43. Reynolds, K. A.; McLaughlin, R. N.; Ranganathan, R. *Cell* **2011,** *147,* 1564–1575.
44. Smock, R. G.; Rivoire, O.; Russ, W. P.; Swain, J. F.; Leibler, S.; Ranganathan, R.; Gierasch, L. M. *Mol. Syst. Biol.* **2010,** *6,* 414.
45. Lee, J.; Natarajan, M.; Nashine, V. C.; Socolich, M.; Vo, T.; Russ, W. P.; Benkovic, S. J.; Ranganathan, R. *Science* **2008,** *322,* 438–442.
46. Häcker, H.-G.; Sisay, M. T.; Gütschow, M. *Pharmacol. Ther.* **2011,** *132,* 180–195.
47. Sadowsky, J. D.; Burlingame, M. A.; Wolan, D. W.; McClendon, C. L.; Jacobson, M. P.; Wells, J. A. *Proc. Natl. Acad. Sci. U. S. A.* **2011,** *108,* 6056–6061.
48. Murray, J.; Giannetti, A. M.; Steffek, M.; Gibbons, P.; Hearn, B. R.; Cohen, F.; Tam, C.; Pozniak, C.; Bravo, B.; Lewcock, J.; Jaishankar, P.; Ly, C. Q.; Zhao, X.; Tang, Y.; Chugha, P.; Arkin, M. R.; Flygare, J.; Renslo, A. R. *ChemMedChem* **2014,** *9,* 73–77.
49. Feldman, T.; Kabaleeswaran, V.; Jang, S. B.; Antczak, C.; Djaballah, H.; Wu, H.; Jiang, X. *Mol. Cell* **2012,** *47,* 585–595.
50. Urbaniak, M. D.; Collie, I. T.; Fang, W.; Aristotelous, T.; Eskilsson, S.; Raimi, O. G.; Harrison, J.; Navratilova, I. H.; Frearson, J. A.; van Aalten, D. M. F.; Ferguson, M. A. J. *ACS Chem. Biol.* **2013,** *8,* 1981–1987.
51. Brandt, P.; Geitmann, M.; Danielson, U. H. J. *Med. Chem.* **2011,** *54,* 709–718.
52. Saalau-Bethell, S. M.; Woodhead, A. J.; Chessari, G.; Carr, M. G.; Coyle, J.; Graham, B.; Hiscock, S. D.; Murray, C. W.; Pathuri, P.; Rich, S. J.; Richardson, C. J.; Williams, P. A.; Jhoti, H. *Nat. Chem. Biol.* **2012,** *8,* 920–925.
53. Haudecoeur, R.; Peuchmaur, M.; Ahmed-Belkacem, A.; Pawlotsky, J.-M.; Boumendjel, A. *Med. Res. Rev.* **2013,** *33,* 934–984.
54. Boehlein, S. K.; Shaw, J. R.; Stewart, J. D.; Hannah, L. C. *Plant Physiol.* **2008,** *146,* 289–299.
55. Boehlein, S. K.; Shaw, J. R.; Hannah, L. C.; Stewart, J. D. *Plant Physiol.* **2010,** *152,* 85–95.
56. Magnaghi, P.; D'Alessio, R.; Valsasina, B.; Avanzi, N.; Rizzi, S.; Asa, D.; Gasparri, F.; Cozzi, L.; Cucchi, U.; Orrenius, C.; Polucci, P.; Ballinari, D.; Perrera, C.; Leone, A.; Cervi, G.; Casale, E.; Xiao, Y.; Wong, C.; Anderson, D. J.; Galvani, A.; Donati, D.; O'Brien, T.; Jackson, P. K.; Isacchi, A. *Nat. Chem. Biol.* **2013,** *9,* 548–556.
57. Hamouda, A. K.; Jayakar, S. S.; Chiara, D. C.; Cohen, J. B. *J. Mol. Neurosci.* **2014,** *53,* 480–486.
58. Hamouda, A. K.; Stewart, D. S.; Chiara, D. C.; Savechenkov, P. Y.; Bruzik, K. S.; Cohen, J. B. *Mol. Pharmacol.* **2014,** *85,* 735–746.
59. Hardy, J. A.; Wells, J. A. *Curr. Opin. Struct. Biol.* **2004,** *14,* 706–715.
60. Tzeng, S.-R.; Kalodimos, C. G. *Curr. Opin. Struct. Biol.* **2011,** *21,* 62–67.
61. Tan, Q.; Zhu, Y.; Li, J.; Chen, Z.; Han, G. W.; Kufareva, I.; Li, T.; Ma, L.; Fenalti, G.; Li, J.; Zhang, W.; Xie, X.; Yang, H.; Jiang, H.; Cherezov, V.; Liu, H.; Stevens, R. C.; Zhao, Q.; Wu, B. *Science* **2013,** *341,* 1387–1390.
62. Wang, J.; Li, H.; Han, Z.; Zhang, H.; Wang, T.; Lin, G.; Chang, J.; Yang, W.; Chai, J. *Nature* **2015,** *525,* 265–268.
63. Zhang, D.; Gao, Z.-G.; Zhang, K.; Kiselev, E.; Crane, S.; Wang, J.; Paoletta, S.; Yi, C.; Ma, L.; Zhang, W.; Han, G. W.; Liu, H.; Cherezov, V.; Katritch, V.; Jiang, H.; Stevens, R. C.; Jacobson, K. A.; Zhao, Q.; Wu, B. *Nature* **2015,** *520,* 317–321.
64. Lee, C.-H.; Lü, W.; Michel, J. C.; Goehring, A.; Du, J.; Song, X.; Gouaux, E. *Nature* **2014,** *511,* 191–197.
65. Kunfermann, A.; Witschel, M.; Illarionov, B.; Martin, R.; Rottmann, M.; Höffken, H. W.; Seet, M.; Eisenreich, W.; Knölker, H.-J.; Fischer, M.; Bacher, A.; Groll, M.; Diederich, F. *Angew. Chem. Int. Ed. Engl.* **2014,** *53,* 2235–2239.
66. Wu, H.; Wang, C.; Gregory, K. J.; Han, G. W.; Cho, H. P.; Xia, Y.; Niswender, C. M.; Katritch, V.; Meiler, J.; Cherezov, V.; Conn, P. J.; Stevens, R. C. *Science* **2014,** *344,* 58–64.
67. Schneider, R.; Becker, C.; Simard, J. R.; Getlik, M.; Bohlke, N.; Janning, P.; Rauh, D. J. *Am. Chem. Soc.* **2012,** *134,* 9138–9141.
68. Wang, X.; Horswill, J. G.; Whalley, B. J.; Stephens, G. J. *Mol. Pharmacol.* **2011,** *2,* 758–767.
69. Wu, S.; Vysotskaya, Z. V.; Xu, X.; Xie, C.; Liu, Q.; Zhou, L. *Biophys. J.* **2011,** *100,* 1226–1232.
70. Huang, Z.; Zhu, L.; Cao, Y.; Wu, G.; Liu, X.; Chen, Y.; Wang, Q.; Shi, T.; Zhao, Y.; Wang, Y.; Li, W.; Li, Y.; Chen, H.; Chen, G.; Zhang, J. *Nucleic Acids Res.* **2011,** *39,* D663–D669.
71. Huang, Z.; Mou, L.; Shen, Q.; Lu, S.; Li, C.; Liu, X.; Wang, G.; Li, S.; Geng, L.; Liu, Y.; Wu, J.; Chen, G.; Zhang, J. *Nucleic Acids Res.* **2014,** *42,* D510–D516.
72. Shen, Q.; Wang, G.; Li, S.; Liu, X.; Lu, S.; Chen, Z.; Song, K.; Yan, J.; Geng, L.; Huang, Z.; Huang, W.; Chen, G.; Zhang, J. *Nucleic Acids Res.* **2016,** *44,* D527–D535.
73. Lamba, V.; Ghosh, I. *Curr. Pharm. Des.* **2012,** *18,* 2936–2945.
74. Nussinov, R.; Tsai, C. *Curr. Pharm. Des.* **2012,** *18,* 1311–1316.
75. Wu, P.; Nielsen, T. E.; Clausen, M. H. *Trends Pharmacol. Sci.* **2015,** *36,* 422–439.
76. Warne, T.; Serrano-Vega, M. J.; Baker, J. G.; Moukhametzianov, R.; Edwards, P. C.; Henderson, R.; Leslie, A. G. W.; Tate, C. G.; Schertler, G. F. X. *Nature* **2008,** *454,* 486–491.
77. Hudson, B. D.; Ulven, T.; Milligan, G. *Curr. Top. Med. Chem.* **2013,** *13,* 14–25.
78. Meharena, H. S.; Chang, P.; Keshwani, M. M.; Oruganty, K.; Nene, A. K.; Kannan, N.; Taylor, S. S.; Kornev, A. P. *PLoS Biol.* **2013,** *11,* e1001680.
79. Davis, M. I.; Hunt, J. P.; Herrgard, S.; Ciceri, P.; Wodicka, L. M.; Pallares, G.; Hocker, M.; Treiber, D. K.; Zarrinkar, P. P. *Nat. Biotechnol.* **2011,** *29,* 1046–1051.
80. Xie, L.; Xie, L.; Kinnings, S. L.; Bourne, P. E. *Annu. Rev. Pharmacol. Toxicol.* **2012,** *52,* 361–379.
81. Peters, J. *J. Med. Chem.* **2013,** *56,* 8955–8971.
82. Anighoro, A.; Rastelli, G. J. *Med. Chem.* **2014,** *57,* 7874–7887.
83. Duran-Frigola, M.; Mosca, R.; Aloy, P. *Chem. Biol.* **2013,** *20,* 674–684.
84. Chandramouly, G.; McDevitt, S.; Sullivan, K.; Kent, T.; Luz, A.; Glickman, J. F.; Andrake, M.; Skorski, T.; Pomerantz, R. T. *Chem. Biol.* **2015,** *22,* 1491–1504.
85. Kuhn, M.; Al Banchaabouchi, M.; Campillos, M.; Jensen, L. J.; Gross, C.; Gavin, A.-C.; Bork, P. *Mol. Syst. Biol.* **2013,** *9,* 663.
86. Wenthur, C. J.; Gentry, P. R.; Mathews, T. P.; Lindsley, C. W. *Annu. Rev. Pharmacol. Toxicol.* **2014,** *54,* 165–184.
87. Urwyler, S. *Pharmacol. Rev.* **2011,** *63,* 59–126.
88. Nussinov, R.; Tsai, C.-J. *Chem. Biol.* **2014,** *21,* 311–318.
89. Hoare, S. R. J. *Drug Discov. Today* **2005,** *10,* 417–427.
90. Gorre, M. E.; Mohammed, M.; Ellwood, K.; Hsu, N.; Paquette, R.; Rao, P. N.; Sawyers, C. L. *Science* **2001,** *293,* 876–881.
91. Shah, N. P.; Skaggs, B. J.; Branford, S.; Hughes, T. P.; Nicoll, J. M.; Paquette, R. L.; Sawyers, C. L. *J. Clin. Invest.* **2007,** *117,* 2562–2569.
92. Zhang, J.; Adrián, F. J.; Jahnke, W.; Cowan-Jacob, S. W.; Li, A. G.; Iacob, R. E.; Sim, T.; Powers, J.; Dierks, C.; Sun, F.; Guo, G.-R.; Ding, Q.; Okram, B.; Choi, Y.; Wojciechowski, A.; Deng, X.; Liu, G.; Fendrich, G.; Strauss, A.; Vajpai, N.; Grzesiek, S.; Tuntland, T.; Liu, Y.; Bursulaya, B.; Azam, M.; Manley, P. W.; Engen, J. R.; Daley, G. Q.; Warmuth, M.; Gray, N. S. *Nature* **2010,** *463,* 501–506.
93. Skora, L.; Mestan, J.; Fabbro, D.; Jahnke, W.; Grzesiek, S. *Proc. Natl. Acad. Sci. U. S. A.* **2013,** *110,* E4437–E4445.
94. Bennouar, K.-E.; Uberti, M. A.; Melon, C.; Bacolod, M. D.; Jimenez, H. N.; Cajina, M.; Kerkerian-Le Goff, L.; Doller, D.; Gubellini, P. *Neuropharmacology* **2013,** *66,* 158–169.

95. Lewis, J. A.; Lebois, E. P.; Lindsley, C. W. *Curr. Opin. Chem. Biol.* **2008,** *12,* 269–280.
96. Kew, J. N. C. *Pharmacol. Ther.* **2004,** *104,* 233–244.
97. Wilhelm, A.; Lopez-Garcia, L. A.; Busschots, K.; Fröhner, W.; Maurer, F.; Boettcher, S.; Zhang, H.; Schulze, J. O.; Biondi, R. M.; Engel, M. J. *Med. Chem.* **2012,** *55,* 9817–9830.
98. Changeux, J.-P. *Annu. Rev. Biophys.* **2012,** *41,* 103–133.
99. Seamon, K. J.; Hansen, E. C.; Kadina, A. P.; Kashemirov, B. A.; McKenna, C. E.; Bumpus, N. N.; Stivers, J. T. J. *Am. Chem. Soc.* **2014,** *136,* 9822–9825.
100. Ascenzi, P.; Bocedi, A.; Bolli, A.; Fasano, M.; Notari, S.; Polticelli, F. *Biochem. Mol. Biol. Educ.* **2005,** *33,* 169–176.
101. Katritch, V.; Fenalti, G.; Abola, E. E.; Roth, B. L.; Cherezov, V.; Stevens, R. C. *Trends Biochem. Sci.* **2014,** *39,* 233–244.
102. Fenalti, G.; Giguere, P. M.; Katritch, V.; Huang, X.-P.; Thompson, A. A.; Cherezov, V.; Roth, B. L.; Stevens, R. C. *Nature* **2014,** *506,* 191–196.
103. Motlagh, H. N.; Wrabl, J. O.; Li, J.; Hilser, V. J. *Nature* **2014,** *508,* 331–339.
104. Hilser, V. J. *Science* **2010,** *327,* 653–654.
105. Dunker, A. K.; Silman, I.; Uversky, V. N.; Sussman, J. L. *Curr. Opin. Struct. Biol.* **2008,** *18,* 756–764.
106. Dyson, H. J.; Wright, P. E. *Nat. Rev. Mol. Cell Biol.* **2005,** *6,* 197–208.
107. Krishnan, N.; Koveal, D.; Miller, D. H.; Xue, B.; Akshinthala, S. D.; Kragelj, J.; Jensen, M. R.; Gauss, C.-M.; Page, R.; Blackledge, M.; Muthuswamy, S. K.; Peti, W.; Tonks, N. K. *Nat. Chem. Biol.* **2014,** *10,* 558–566.
108. Li, X.; Chen, Y.; Lu, S.; Huang, Z.; Liu, X.; Wang, Q.; Shi, T.; Zhang, J. *J. Mol. Graph. Model.* **2013,** *40,* 30–39.
109. Yang, J.-S.; Seo, S. W.; Jang, S.; Jung, G. Y.; Kim, S. *PLoS Comput. Biol.* **2012,** *8,* e1002612.
110. Namboodiri, S.; Giuliani, A.; Nair, A. S.; Dhar, P. K. *J. Theor. Biol.* **2012,** *304,* 211–218.
111. Lu, S.; Huang, W.; Wang, Q.; Shen, Q.; Li, S.; Nussinov, R.; Zhang, J. *PLoS Comput. Biol.* **2014,** *10*, e1003831.
112. Buzko, O.; Shokat, K. M. *Bioinformatics* **2002,** *18,* 1274–1275.
113. Vulpetti, A.; Bosotti, R. *Farmaco* **2004,** *59,* 759–765.
114. Manning, G.; Whyte, D. B.; Martinez, R.; Hunter, T.; Sudarsanam, S. *Science* **2002,** *298,* 1912–1934.
115. Gao, M.; Skolnick, J. *Bioinformatics* **2013,** *29,* 597–604.
116. Wootten, D.; Christopoulos, A.; Sexton, P. M. *Nat. Rev. Drug Discov.* **2013,** *12,* 630–644.
117. Cawston, E. E.; Lam, P. C. H.; Harikumar, K. G.; Dong, M.; Ball, A. M.; Lou Augustine, M.; Akgün, E.; Portoghese, P. S.; Orry, A.; Abagyan, R.; Sexton, P. M.; Miller, L. J. *J. Biol. Chem.* **2012,** *287,* 18618–18635.
118. Abdul-Ridha, A.; Lane, J. R.; Sexton, P. M.; Canals, M.; Christopoulos, A. *Mol. Pharmacol.* **2013,** *83,* 521–530.
119. Willard, F. S.; Wootten, D.; Showalter, A. D.; Savage, E. E.; Ficorilli, J.; Farb, T. B.; Bokvist, K.; Alsina-Fernandez, J.; Furness, S. G. B.; Christopoulos, A.; Sexton, P. M.; Sloop, K. W. *Mol. Pharmacol.* **2012,** *82,* 1066–1073.
120. Wootten, D.; Savage, E. E.; Valant, C.; May, L. T.; Sloop, K. W.; Ficorilli, J.; Showalter, A. D.; Willard, F. S.; Christopoulos, A.; Sexton, P. M. *Mol. Pharmacol.* **2012,** *82,* 281–290.
121. Hollenberg, M. D.; Mihara, K.; Polley, D.; Suen, J. Y.; Han, A.; Fairlie, D. P.; Ramachandran, R. *Br. J. Pharmacol.* **2014,** *171,* 1180–1194.
122. Charfi, I.; Audet, N.; Bagheri Tudashki, H.; Pineyro, G. *Br. J. Pharmacol.* **2015,** *172,* 435–448.
123. Wisler, J. W.; Xiao, K.; Thomsen, A. R. B.; Lefkowitz, R. J. *Curr. Opin. Cell Biol.* **2014,** *27,* 18–24.
124. Shonberg, J.; Lopez, L.; Scammells, P. J.; Christopoulos, A.; Capuano, B.; Lane, J. R. *Med. Res. Rev.* **2014,** *34,* 1286–1330.
125. Gentry, P. R.; Sexton, P. M.; Christopoulos, A. J. *Biol. Chem.* **2015,** *290,* 19478–19488.
126. Sivertsen, B.; Holliday, N.; Madsen, A. N.; Holst, B. *Br. J. Pharmacol.* **2013,** *170,* 1349–1362.
127. Martí-Solano, M.; Guixà-González, R.; Sanz, F.; Pastor, M.; Selent, J. *Curr. Pharm. Des.* **2013,** *19,* 5156–5166.
128. Lamberts, J. T.; Traynor, J. R. *Curr. Pharm. Des.* **2013,** *19,* 7333–7347.
129. Shukla, A. K.; Singh, G.; Ghosh, E. *Trends Biochem. Sci.* **2014,** *39,* 594–602.
130. Michel, M. C.; Seifert, R. *Am. J. Physiol. Cell Physiol.* **2015,** *308,* C505–C520.
131. Brogi, S.; Tafi, A.; Désaubry, L.; Nebigil, C. G. *Front. Pharmacol.* **2014,** *5,* 255.
132. Halls, M. L.; Bathgate, R. A. D.; Sutton, S. W.; Dschietzig, T. B.; Summers, R. J. *Pharmacol. Rev.* **2015,** *67,* 389–440.
133. Leach, K.; Conigrave, A. D.; Sexton, P. M.; Christopoulos, A. *Trends Pharmacol. Sci.* **2015,** *36,* 215–225.
134. Van Westen, G. J. P.; Gaulton, A.; Overington, J. P. *PLoS Comput. Biol.* **2014,** *10*, e1003559.
135. Knox, C.; Law, V.; Jewison, T.; Liu, P.; Ly, S.; Frolkis, A.; Pon, A.; Banco, K.; Mak, C.; Neveu, V.; Djoumbou, Y.; Eisner, R.; Guo, A. C.; Wishart, D. S. *Nucleic Acids Res.* **2011,** *39,* D1035–D1041.
136. Wang, Q.; Zheng, M.; Huang, Z.; Liu, X.; Zhou, H.; Chen, Y.; Shi, T.; Zhang, J. *J. Mol. Graph. Model.* **2012,** *38,* 324–333.
137. Welsch, M. E.; Snyder, S. A.; Stockwell, B. R. *Curr. Opin. Chem. Biol.* **2010,** *14,* 347–361.
138. Polanski, J.; Kurczyk, A.; Bak, A.; Musiol, R. *Curr. Med. Chem.* **2012,** *19,* 1921–1945.
139. Kim, J.; Kim, H.; Park, S. B. J. *Am. Chem. Soc.* **2014,** *136,* 14629–14638.
140. Zhao, H.; Dietrich, J. *Expert Opin. Drug Discovery* **2015,** *10,* 781–790.
141. Kaushik, N. K.; Kaushik, N.; Attri, P.; Kumar, N.; Kim, C. H.; Verma, A. K.; Choi, E. H. *Molecules* **2013,** *18,* 6620–6662.
142. Zhang, M.-Z.; Chen, Q.; Yang, G.-F. *Eur. J. Med. Chem.* **2015,** *89,* 421–441.
143. Gagliardi, P. A.; di Blasio, L.; Primo, L. *Biochim. Biophys. Acta* **2015,** *1856,* 178–188.
144. Busschots, K.; Lopez-Garcia, L. A.; Lammi, C.; Stroba, A.; Zeuzem, S.; Piiper, A.; Alzari, P. M.; Neimanis, S.; Arencibia, J. M.; Engel, M.; Schulze, J. O.; Biondi, R. M. *Chem. Biol.* **2012,** *19,* 1152–1163.
145. Hindie, V.; Stroba, A.; Zhang, H.; Lopez-Garcia, L. A.; Idrissova, L.; Zeuzem, S.; Hirschberg, D.; Schaeffer, F.; Jørgensen, T. J. D.; Engel, M.; Alzari, P. M.; Biondi, R. M. *Nat. Chem. Biol.* **2009,** *5,* 758–764.
146. Stroba, A.; Schaeffer, F.; Hindie, V.; Lopez-Garcia, L.; Adrian, I.; Fröhner, W.; Hartmann, R. W.; Biondi, R. M.; Engel, M. J. *Med. Chem.* **2009,** *52,* 4683–4693.
147. Rettenmaier, T. J.; Fan, H.; Karpiak, J.; Doak, A.; Sali, A.; Shoichet, B. K.; Wells, J. A. J. *Med. Chem.* **2015,** *58,* 8285–8291.
148. Rettenmaier, T. J.; Sadowsky, J. D.; Thomsen, N. D.; Chen, S. C.; Doak, A. K.; Arkin, M. R.; Wells, J. A. *Proc. Natl. Acad. Sci. U. S. A.* **2014,** *111,* 18590–18595.
149. Stachulski, A. V.; Baillie, T. A.; Park, B. K.; Obach, R. S.; Dalvie, D. K.; Williams, D. P.; Srivastava, A.; Regan, S. L.; Antoine, D. J.; Goldring, C. E. P.; Chia, A. J. L.; Kitteringham, N. R.; Randle, L. E.; Callan, H.; Castrejon, J. L.; Farrell, J.; Naisbitt, D. J.; Lennard, M. S. *Med. Res. Rev.* **2013,** *33,* 985–1080.
150. Singh, J.; Petter, R. C.; Baillie, T. A.; Whitty, A. *Nat. Rev. Drug Discov.* **2011,** *10,* 307–317.
151. Hagel, M.; Niu, D.; Martin, T. S.; Sheets, M. P.; Qiao, L.; Bernard, H.; Karp, R. M.; Zhu, Z.; Labenski, M. T.; Chaturvedi, P.; Nacht, M.; Westlin, W. F.; Petter, R. C.; Singh, J. *Nat. Chem. Biol.* **2010,** *7,* 22–24.
152. Nussinov, R.; Tsai, C.-J. *Annu. Rev. Pharmacol. Toxicol.* **2015,** *55,* 249–267.
153. Weisner, J.; Gontla, R.; van der Westhuizen, L.; Oeck, S.; Ketzer, J.; Janning, P.; Richters, A.; Mühlenberg, T.; Fang, Z.; Taher, A.; Jendrossek, V.; Pelly, S. C.; Bauer, S.; van Otterlo, W. A. L.; Rauh, D. *Angew. Chem. Int. Ed. Engl.* **2015,** *54,* 10313–10316.
154. Cox, A. D.; Fesik, S. W.; Kimmelman, A. C.; Luo, J.; Der, C. J. *Nat. Rev. Drug Discov.* **2014,** *13,* 828–851.
155. Samatar, A. A.; Poulikakos, P. I. *Nat. Rev. Drug Discov.* **2014,** *13,* 928–942.

156. Zhou, Y.; Wong, C.-O.; Cho, K.; van der Hoeven, D.; Liang, H.; Thakur, D. P.; Luo, J.; Babic, M.; Zinsmaier, K. E.; Zhu, M. X.; Hu, H.; Venkatachalam, K.; Hancock, J. F. *Science* **2015,** *349,* 873–876.
157. Ostrem, J. M.; Peters, U.; Sos, M. L.; Wells, J. A.; Shokat, K. M. *Nature* **2013,** *503,* 548–551.
158. Valant, C.; Robert Lane, J.; Sexton, P. M.; Christopoulos, A. *Annu. Rev. Pharmacol. Toxicol.* **2012,** *52,* 153–178.
159. Lane, J. R.; Sexton, P. M.; Christopoulos, A. *Trends Pharmacol. Sci.* **2013,** *34,* 59–66.
160. Melancon, B. J.; Hopkins, C. R.; Wood, M. R.; Emmitte, K. A.; Niswender, C. M.; Christopoulos, A.; Conn, P. J.; Lindsley, C. W. J. *Med. Chem.* **2012,** *55,* 1445–1464.
161. Digby, G. J.; Noetzel, M. J.; Bubser, M.; Utley, T. J.; Walker, A. G.; Byun, N. E.; Lebois, E. P.; Xiang, Z.; Sheffler, D. J.; Cho, H. P.; Davis, A. A.; Nemirovsky, N. E.; Mennenga, S. E.; Camp, B. W.; Bimonte-Nelson, H. A.; Bode, J.; Italiano, K.; Morrison, R.; Daniels, J. S.; Niswender, C. M.; Olive, M. F.; Lindsley, C. W.; Jones, C. K.; Conn, P. J. *J. Neurosci.* **2012,** *32,* 8532–8544.
162. Steinfeld, T.; Mammen, M.; Smith, J. A. M.; Wilson, R. D.; Jasper, J. R. *Mol. Pharmacol.* **2007,** *72,* 291–302.
163. Antony, J.; Kellershohn, K.; Mohr-Andrä, M.; Kebig, A.; Prilla, S.; Muth, M.; Heller, E.; Disingrini, T.; Dallanoce, C.; Bertoni, S.; Schrobang, J.; Tränkle, C.; Kostenis, E.; Christopoulos, A.; Höltje, H.-D.; Barocelli, E.; De Amici, M.; Holzgrabe, U.; Mohr, K. *FASEB J.* **2009,** *23,* 442–450.
164. Mohr, K.; Schmitz, J.; Schrage, R.; Tränkle, C.; Holzgrabe, U. *Angew. Chem. Int. Ed. Engl.* **2013,** *52,* 508–516.
165. Keov, P.; López, L.; Devine, S. M.; Valant, C.; Lane, J. R.; Scammells, P. J.; Sexton, P. M.; Christopoulos, A. J. *Biol. Chem.* **2014,** *289,* 23817–23837.
166. Lane, J. R.; Donthamsetti, P.; Shonberg, J.; Draper-Joyce, C. J.; Dentry, S.; Michino, M.; Shi, L.; López, L.; Scammells, P. J.; Capuano, B.; Sexton, P. M.; Javitch, J. A.; Christopoulos, A. *Nat. Chem. Biol.* **2014,** *10,* 745–752.
167. Choy, M. S.; Hieke, M.; Kumar, G. S.; Lewis, G. R.; Gonzalez-DeWhitt, K. R.; Kessler, R. P.; Stein, B. J.; Hessenberger, M.; Nairn, A. C.; Peti, W.; Page, R. *Proc. Natl. Acad. Sci. U. S. A.* **2014,** *111,* 4097–4102.
168. Aeluri, M.; Chamakuri, S.; Dasari, B.; Guduru, S. K. R.; Jimmidi, R.; Jogula, S.; Arya, P. *Chem. Rev.* **2014,** *114,* 4640–4694.
169. Milroy, L.; Grossmann, T. N.; Hennig, S.; Brunsveld, L.; Ottmann, C. *Chem. Rev.* **2014,** *114,* 4695–4748.
170. Kitagishi, Y.; Nakanishi, A.; Ogura, Y.; Matsuda, S. *Alzheimers Res. Ther.* **2014,** *6,* 35.
171. Nussinov, R.; Tsai, C.-J.; Ma, B. *Annu. Rev. Biophys.* **2013,** *42,* 169–189.
172. Nussinov, R. *Phys. Biol.* **2013,** *10,* 045004.
173. Nussinov, R.; Tsai, C.-J.; Csermely, P. *Trends Pharmacol. Sci.* **2011,** *32,* 686–693.
174. Szilágyi, A.; Nussinov, R.; Csermely, P. *Curr. Top. Med. Chem.* **2013,** *13,* 64–77.
175. Csermely, P.; Korcsmáros, T.; Kiss, H. J. M.; London, G.; Nussinov, R. *Pharmacol. Ther.* **2013,** *138,* 333–408.
176. Engin, H. B.; Gursoy, A.; Nussinov, R.; Keskin, O. *Curr. Pharm. Des.* **2014,** *20,* 1201–1207.
177. Dowling, R. J. O.; Topisirovic, I.; Fonseca, B. D.; Sonenberg, N. *Biochim. Biophys. Acta* **2010,** *1804,* 433–439.
178. Dowling, R. J. O.; Topisirovic, I.; Alain, T.; Bidinosti, M.; Fonseca, B. D.; Petroulakis, E.; Wang, X.; Larsson, O.; Selvaraj, A.; Liu, Y.; Kozma, S. C.; Thomas, G.; Sonenberg, N. *Science* **2010,** *328,* 1172–1176.
179. Nagar, B.; Hantschel, O.; Young, M. A.; Scheffzek, K.; Veach, D.; Bornmann, W.; Clarkson, B.; Superti-Furga, G.; Kuriyan, J. *Cell* **2003,** *112,* 859–871.
180. Nagar, B.; Hantschel, O.; Seeliger, M.; Davies, J. M.; Weis, W. I.; Superti-Furga, G.; Kuriyan, J. *Mol. Cell* **2006,** *21,* 787–798.
181. Flaherty, K. T.; Infante, J. R.; Daud, A.; Gonzalez, R.; Kefford, R. F.; Sosman, J.; Hamid, O.; Schuchter, L.; Cebon, J.; Ibrahim, N.; Kudchadkar, R.; Burris, H. A.; Falchook, G.; Algazi, A.; Lewis, K.; Long, G. V.; Puzanov, I.; Lebowitz, P.; Singh, A.; Little, S.; Sun, P.; Allred, A.; Ouellet, D.; Kim, K. B.; Patel, K.; Weber, J. *N. Engl. J. Med.* **2012,** *367,* 1694–1703.
182. Long, G. V.; Stroyakovskiy, D.; Gogas, H.; Levchenko, E.; de Braud, F.; Larkin, J.; Garbe, C.; Jouary, T.; Hauschild, A.; Grob, J. J.; Chiarion Sileni, V.; Lebbe, C.; Mandalà, M.; Millward, M.; Arance, A.; Bondarenko, I.; Haanen, J. B. A. G.; Hansson, J.; Utikal, J.; Ferraresi, V.; Kovalenko, N.; Mohr, P.; Probachai, V.; Schadendorf, D.; Nathan, P.; Robert, C.; Ribas, A.; DeMarini, D. J.; Irani, J. G.; Casey, M.; Ouellet, D.; Martin, A.-M.; Le, N.; Patel, K.; Flaherty, K. *N. Engl. J. Med.* **2014,** *371,* 1877–1888.
183. Dong, Q.; Dougan, D. R.; Gong, X.; Halkowycz, P.; Jin, B.; Kanouni, T.; O'Connell, S. M.; Scorah, N.; Shi, L.; Wallace, M. B.; Zhou, F. *Bioorg. Med. Chem. Lett.* **2011,** *21,* 1315–1319.
184. Tsai, C.-J.; Nussinov, R. *PLoS Comput. Biol.* **2014,** *10,* e1003394.
185. Del Sol, A.; Tsai, C.-J.; Ma, B.; Nussinov, R. *Structure* **2009,** *17,* 1042–1450.
186. Nussinov, R.; Tsai, C.-J.; Xin, F.; Radivojac, P. *Trends Biochem. Sci.* **2012,** *37,* 447–455.
187. Nussinov, R.; Tsai, C.-J. *Trends Pharmacol. Sci.* **2014,** *35,* 256–264.
188. Nussinov, R.; Tsai, C.-J.; Liu, J. J. *Am. Chem. Soc.* **2014,** *136,* 17692–17701.
189. Badireddy, S.; Yunfeng, G.; Ritchie, M.; Akamine, P.; Wu, J.; Kim, C. W.; Taylor, S. S.; Qingsong, L.; Swaminathan, K.; Anand, G. S. *Mol. Cell. Proteomics* **2011,** *10.* M110.004390.
190. Guarnera, E.; Berezovsky, I. N. *Curr. Opin. Struct. Biol.* **2016,** *37,* 1–8.
191. Lu, S.; Huang, W.; Zhang, J. *Drug Discov. Today* **2014,** *19,* 1595–1600.
192. Feher, V. A.; Durrant, J. D.; Van Wart, A. T.; Amaro, R. E. *Curr. Opin. Struct. Biol.* **2014,** *25,* 98–103.
193. Hocker, H. J.; Rambahal, N.; Gorfe, A. A. *J. Chem. Inf. Model.* **2014,** *54,* 530–538.
194. Hocker, H. J.; Cho, K.-J.; Chen, C.-Y. K.; Rambahal, N.; Sagineedu, S. R.; Shaari, K.; Stanslas, J.; Hancock, J. F.; Gorfe, A. A. *Proc. Natl. Acad. Sci. U. S. A.* **2013,** *110,* 10201–10206.
195. Lu, S.; Li, S.; Zhang, J. *Med. Res. Rev.* **2014,** *34,* 1242–1285.

2.12 Novel Therapeutics Targeting Epigenetics

PM Woster, Medical University of South Carolina, Charleston, SC, United States

© 2017 Elsevier Ltd. All rights reserved.

2.12.1	**Introduction**	297
2.12.2	**Epigenetic Modulation via DNA Methylation/Demethylation**	298
2.12.3	**Epigenetic Control of Gene Expression via Histone Lysine and Histone Arginine PTM**	300
2.12.3.1	Histones and the Epigenetic Control of Gene Expression	300
2.12.3.2	Epigenetic Writers	301
2.12.3.2.1	Inhibitors of HATs	301
2.12.3.2.2	Inhibitors of histone methyltransferases (KMTs and protein arginine methyltransferases, PRMTs)	304
2.12.3.3	Epigenetic Erasers	309
2.12.3.3.1	HDACs	309
2.12.3.3.2	Histone demethylases (KDMs)	312
2.12.3.4	Agents Targeting Epigenetic Reader Proteins	318
2.12.4	**Conclusion**	320
References		322
Relevant Websites		328

2.12.1 Introduction

Epigenetic modulation of gene expression involves changes in gene expression and/or phenotype that are mediated by processes that do not involve alterations in the primary sequence of DNA. Epigenetic control of gene expression occurs in one of the three ways: (1) methylation of DNA at specific CpG dinucleotides in gene promoter regions, (2) recruitment of transcription factors that are incorporated into epigenetic complexes, and (3) covalent modification of histone proteins. These reversible chromatin remodeling modifications at promoter-specific chromatin marks determine, in part, whether specific genes are in an open/transcriptionally active conformation or a closed/transcriptionally repressed conformation,[1,2] and also solve the fundamental problem of storing approximately 2 m of DNA in a cell nucleus with an average diameter of 6 μm. Conceptually, enzymes that participate in epigenetic modulation of gene expression can be divided into three categories: writers, erasers, and readers.[1,3] In addition to methylation of DNA at CpG islands, the status of the epigenetic code is determined by the formation and breakdown of specific posttranslational modifications (PTMs) at histone lysine (acetylation, methylation, ubiquitination, sumoylation, crotonylation, butyrylation, and propionylation) and arginine (methylation, citrullination, and ADP-ribosylation) residues, as well as phosphorylation of serine, tyrosine, and threonine.[4–6] Taken together, CpG island methylation and histone PTMs at defined lysine and arginine residues make up an epigenetic "landscape" whereby cellular gene expression can be tightly and accurately controlled. Prior to 2004, the field of epigenetics was focused on two primary processes, histone acetylation/deacetylation[1,7] and DNA methylation.[8] At present, the epigenetic landscape is highly regulated by multiple enzymes, corepressor proteins, and transcription factors that form specific epigenetic complexes at a given promoter.

DNA methylation has been the most intensely studied of the epigenetic modulation processes, primarily in the context of DNA methylation changes that occur in cancer. These changes include hypermethylation of DNA at CpG dinucleotides in promoter regions and reduction of methylation in the body of the gene.[9–11] DNA methyltransferase (DNMT) inhibitors are well-known epigenetic modulators that have been used extensively in cancer chemotherapy.[12,13] Importantly, the process of DNA methylation is not an isolated event, and there are a number of functional links between changes in DNA methylation at CpG islands and alterations in the PTM of histone proteins.[14]

The process of histone lysine acetylation/deacetylation is the most extensively studied of the histone PTMs. The acetylation status of histones is controlled by opposing enzymes that covalently modify specific histone lysines. Histone acetyltransferases (HATs) promote histone hyperacetylation, which removes the positive charge on the ε-lysine and allows DNA to assume an open conformation known as euchromatin. In contrast, the histone deacetylases (HDACs), which catalyze acetyl group cleavage,[7,15] restore the lysine positive charge, which contracts DNA into a closed conformation known as heterochromatin. Normal mammalian cells efficiently control chromatin architecture in part by maintaining a balance between HAT and HDAC activities. Both the zinc-dependent[16,17] and sirtuin[18,19] classes of HDACs have been regarded as validated drug targets for a number of years, and four HDAC inhibitors have reached the market (vorinostat, panobinostat, belinostat, and romidepsin), with several other drug candidates in Phase II or III trials (**Table 1**).[20]

Historically, lysine methylation was thought to be a stable PTM that could only be reversed by the synthesis of new protein. Histone lysine methylation/demethylation was first described in 2004 with the identification of lysine specific demethylase 1 (LSD1),[21] but the value of LSD1 as a drug target for the treatment of cancer was not demonstrated until 2007.[22] To date, there are two known flavin-dependent histone demethylases, KDM1A and KDM1B, also known as LSD1 and LSD2, respectively.[23]

Table 1 Histone deacetylases involved in human chromatin remodeling

Zinc-dependent histone deacetylases		
HDAC	*Number of amino acids*	*Subcellular location*
Class I		
HDAC1	482	Nucleus
HDAC2	488	Nucleus
HDAC3	428	Nucleus
HDAC8	377	Nucleus
Class IIa		
HDAC4	1048	Nucleus/Cytoplasm
HDAC5	1122	Nucleus/Cytoplasm
HDAC7	855	Nucleus/Cytoplasm
HDAC9	1069	Nucleus/Cytoplasm
Class IIb		
HDAC6	1215	Cytoplasm
HDAC10	669	Cytoplasm
Class IV		
HDAC11	H3K9	Nucleus/Cytoplasm
NAD-dependent histone deacetylases (sirtuins)		
Class III		
SIRT1	747	Nucleus/Cytoplasm
SIRT2	352	Cytoplasm
SIRT3	399	Nucleus/Mitochondria
SIRT4	314	Mitochondria
SIRT5	310	Mitochondria
SIRT6	355	Nucleus
SIRT7	400	Nucleolus

Subsequently, five more families of histone demethylases that require Fe(II) and α-ketoglutarate as cofactors were identified, termed KDM2–6.[24] Because KDM26 share the common feature of possessing a Jmj domain, they are collectively termed Jumonji KDMs. To date, more than 30 Jumonji demethylases have been identified. The discussion in the following section will focus on drug development involving DNMT inhibitors and efforts targeting epigenetic histone writers, erasers, and readers.

2.12.2 Epigenetic Modulation via DNA Methylation/Demethylation

Methylation of DNA for the purpose of epigenetic control of gene expression occurs at specific cytosine residues. These cytosines are usually located in CpG islands, which are sequences of $\geq$200 base pairs with a GC percentage of 50% or greater. In human DNA, CpG dinucleotides are relatively rare, with the exception of gene promoters, which generally feature CpG islands.[25] The methylation/demethylation cycle for cytosines in CpG islands is shown in **Fig. 1**. A specific DNMT transfers a methyl group from *S*-adenosylmethionine (SAM) to the 5-position of the pyrimidine ring of cytosine, forming 5-methylcytosine. A total of eight DNMTs are known (DNMT1, DNMT1b, DNMT1o, DNMO1p, DNMT2, DNMT3A, DNMT3b, and DNMT3L), but only DNMT1, DNMT3A, and DNMT3b are important in epigenetic modulation.[26] Methylation can be either de novo when CpG on both strands receive a methyl group or maintenance when one strand is already methylated, and the DNMT uses the methylated strand to methylate the complementary strand. DNMT3A and DNMT3b are responsible for de novo methylation of DNA, and they play a major role during embryogenesis and genomic imprinting. DNMT1 can also perform de novo methylation but is largely responsible for maintenance methylation during epigenetic modulation.[27] In cancer, hypermethylation is observed at CpG islands, along with hypomethylation in the corresponding gene body.[26] These changes in DNA methylation lead to gene silencing, including tumor suppressor genes that play a role in preventing the development of cancer. For this reason, DNMT1 has long been regarded as a potential target for antitumor agents.

Although DNA methylation contributes to stable and heritable gene silencing, it is known that DNA demethylation can occur by one of the two routes.[28] During early development, DNA methylation patterns are set through de novo methylation at CpG islands. During replication, methylated DNA bases are restored in the hemimethylated copy by DNMT1, which uses the original strand as a methylation template. However, when DNMT1 is not present or is inhibited, 5-methylcytosine is replaced by cytosine in the copy, and thus replication dilutes methylation of DNA. DNA demethylation can also be catalyzed by specific enzymes, as shown in **Fig. 1**, and can proceed by either an oxidation or a deamination pathway.[27,28] The oxidative route is catalyzed by the ten-eleven translocation enzymes (TETs), proceeding in stepwise fashion to form 5-hydroxymethylcytosine, 5-formylcytosine, and then 5-carboxycytosine. Both 5-formylcytosine and 5-carboxycytosine can be converted to an abasic form by thymine-DNA glycosylase (TDG). In addition, 5-methylcytosine and 5-hydroxymethylcytosine can be deaminated by activation-induced deaminase (AID)

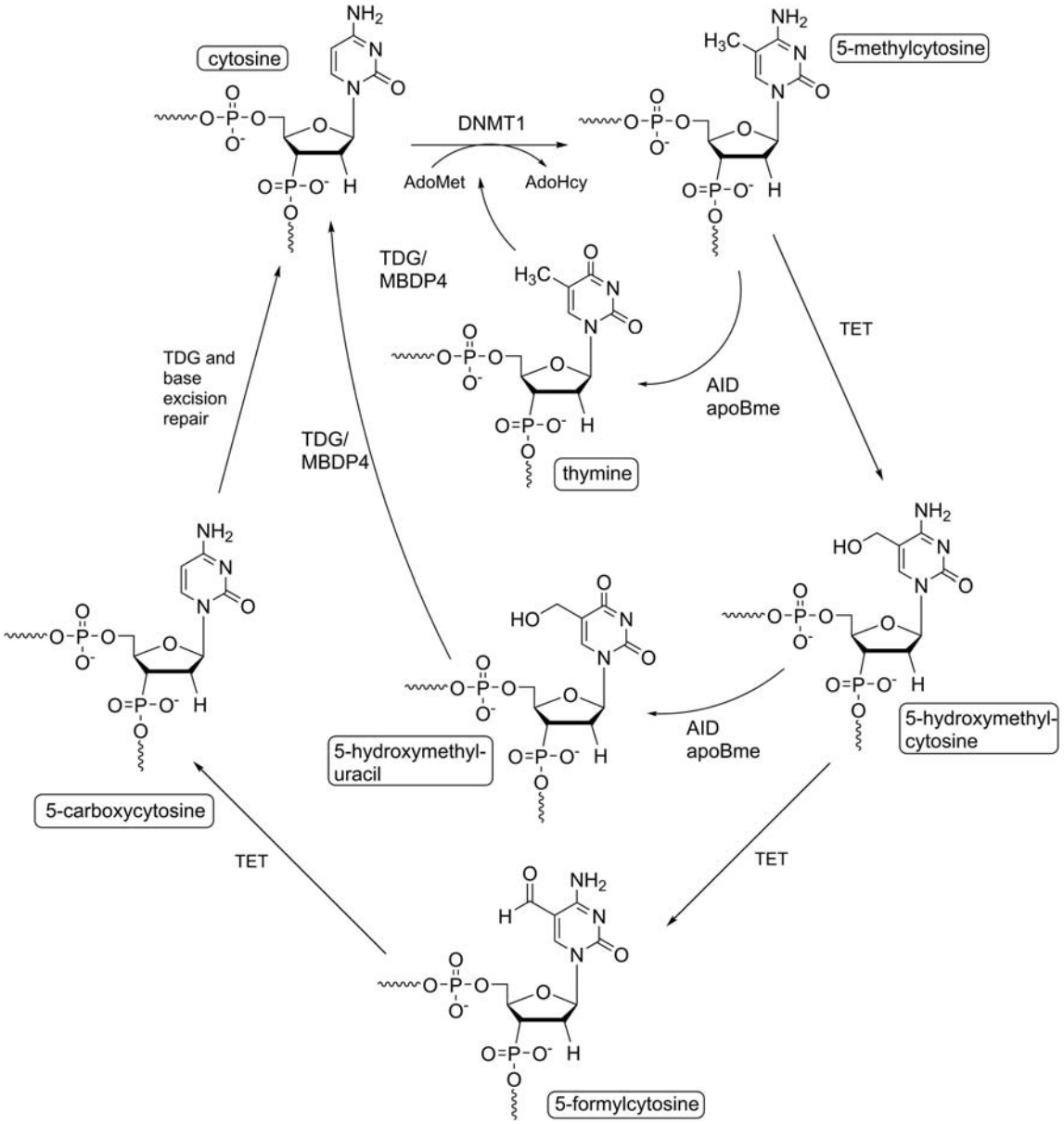

Fig. 1 The mammalian DNA methylation/demethylation cycle. *TET*, ten-eleven translocation enzymes; *AID*, activation-induced deaminase; *apoBme*, apolipoprotein B mRNA editing enzyme; *TDG*, thymine-DNA glycosylase; *MBDP4*, methyl-CpG binding domain protein 4 (MBDP4).

and apolipoprotein B mRNA editing enzyme (apoBme) to form thymine of 5-hydroxymethyluracil, respectively. These two deaminated species are recognized as a base mismatch and are converted to the abasic form by TDG and methyl-CpG binding domain protein 4 (MBD4). The abasic form is then replaced by base excision repair.

Hypermethylation of CpG islands is a hallmark of early-stage cancer and occurs in a gene- and cell-specific manner. DNMT inhibitors were first identified in the 1960s[29] and have emerged as effective cancer chemotherapeutics.[30,31] DNMT inhibitors fall into one of the two classes: nucleoside analogs and nonnucleoside compounds. Two nucleoside analogs, 5-azacytidine (5-AC) and 5-aza-2′-deoxycytidine (**Fig. 2**), have been approved for use in myelodysplastic syndrome and leukemia by the FDA.[32] These agents must be incorporated into DNA, where they serve as covalent inhibitors, such that a cysteine residue on the enzyme is appended to the 5-position of the analog.[33] However, 5-AC and 5-aza-2′-deoxycytidine exhibit poor chemical stability, a lack of specificity for DNMT1 in relation to other DNMTs, and they produce significant adverse side effects.[13,34] The deaminated analog of 5-AC, zebularine (**Fig. 2**), inhibits DNMT1 by promoting ubiquitin-targeted degradation of the enzyme.[35] It has increased stability and is relatively nontoxic; however, the high plasma concentrations required to produce adequate demethylation in vivo have hindered its clinical development.[36] The related pyrimidine-2-one nucleoside THU[37] and its analogs[38] are potent inhibitors of deoxycytidine deaminase. Two additional nucleoside-based inhibitors of DNMT, 5-fluoro-2′-deoxycytidine[39] and

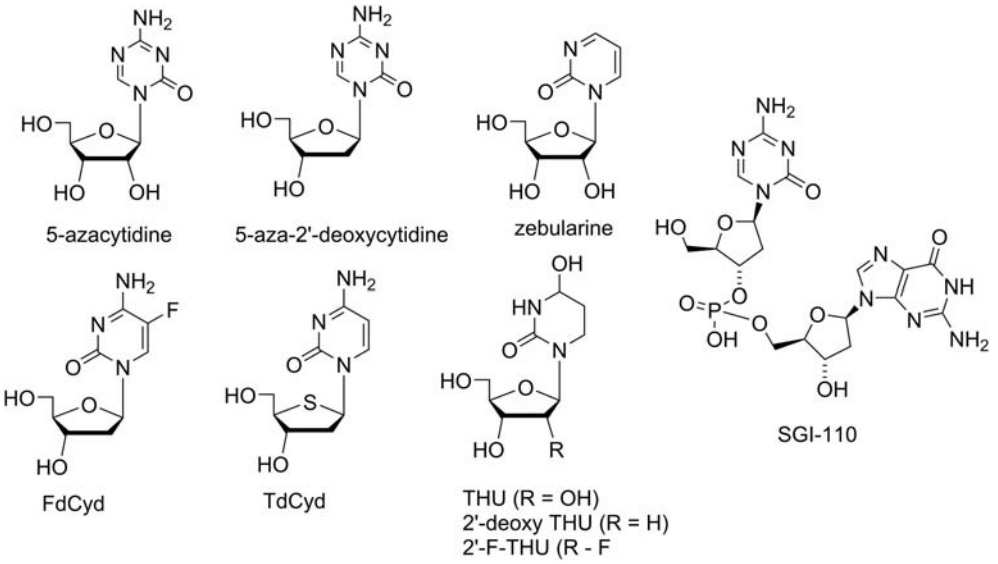

Fig. 2 Nucleoside-based DNMT1 and cytidine deaminase inhibitors.

4′-thio-2′-deoxycytidine (TdCyd)[40] (Fig. 2), have been entered into human clinical trials. TdCyd has been shown to be incorporated into DNA, where it acts as a potent inhibitor of DNMT. The CpG dinucleotide derivative SGI-110 is an efficient prodrug form of 5-aza-2′-deoxycytidine that exhibits increased resistance to cytidine deaminase, improved solubility, and enhanced cell penetration.[41]

Nonnucleoside inhibitors of DNMT (Fig. 3) constitute a structurally diverse group of compounds, and to date none of these have been particularly successful for a variety of reasons. However, nonnucleoside DNMT inhibitors do possess one advantage. Since they do not need to be incorporated into DNA, inhibitors selective toward each of the DNMT isoforms can ultimately be identified. Within this category, a number of known drugs can act as DNMT inhibitors. Examples include procainamide, which inhibits the hemimethylase activity of DNMT1,[42] and 6-mercaptopurine and 6-thioguanine, which like zebularine down regulate DNMT1 through ubiquitin-targeted degradation. The quinoline derivative SGI1027 acts as a hypomethylating agent and promotes the reexpression of tumor suppressor genes by blocking DNMT1 activity.[43] While more potent analogs related to SGI1027 have been synthesized, they still possess weak activity against DNMT1, especially in cell-based assays.[44] The polyphenol (−)-epigallocatechin-3-gallate was identified from a screen of 114 flavones and flavanones and found to be a high nanomolar inhibitor of DNMT1.[45] Also discovered in this initial screen was a series of 3-chloro-3-nitroflavones. Some of these nitroflavones were found to inhibit DNMT1. Additional screening by the same group resulted in the identification of diclone, a small halogenated naphthoquinone that is classically used as pesticide and fungicide. Diclone acted as a potent inhibitor of the DNMT3A/3L complex and was found to possess an EC_{50} of 460 nM against cultured DU145 prostate cells. Genistein has been shown to inhibit the hemimethylase activity of DNMT1, most likely by binding to the catalytic domain. Genistein also decreased CpG methylation in the promoter region of multiple tumor suppressor genes and increased the mRNA expression of these genes.[46] The rationally designed *N*-phthaloyl-L-tryptophan RG108, discovered through a virtual screen using a homology model derived from bacterial C5-DNMT, was shown to be a modest inhibitor of DNMT1, presumably by binding in the catalytic pocket.[47] Subsequently, analogs of RG108 that featured a substituted quinazoline-2,4(1H,3H)-dione in place of the phthalimido moiety showed enhanced activity against DNMT1. In particular, the 2-nitropyridylsulfenyl- and 2,4-dinitropyridylsulfenyl analogs produced the best inhibition (95%-98% inhibition at 500 μM).[48] Using a multistep docking approach of lead-like compounds with a homology model of the catalytic site of DNMT1, Kuck et al. identified seven new molecules with detectable DNMT1 inhibitory activity.[49] Six of these compounds appeared selective for DNMT1 and did not inhibit the DNMT3B methyltransferase. The most active in the series was the salicylic acid dimer NSC14778. The anthraquinone laccaic acid and several analogs were identified by high-throughput screening using a truncated form of DNMT.[50,51] Finally, using a scintillation proximity assay, a library of 180,000 compounds was screened against murine DNMT3A. The resulting 12 hits generated H_2O_2, and hence reactive oxygen species, and as such were not suitable for development. Further experiments revealed SW155246, did not generate peroxide, had an IC_{50} of 1.2 μM for DNMT1, and showed good selectivity for DNMT1 over DNMT3B/3L.

2.12.3 Epigenetic Control of Gene Expression via Histone Lysine and Histone Arginine PTM

2.12.3.1 Histones and the Epigenetic Control of Gene Expression

Histone proteins are octamers, consisting of one H_3-H_4 tetramer and two H_{2A}-H_{2B} dimers.[52] Histones are directed to DNA by their predominate positive charges[53] that interact with the negative charges on the DNA backbone. These proteins then interact with double-stranded DNA in such a way that a section of approximately 147 base pairs of DNA are wrapped around the histone

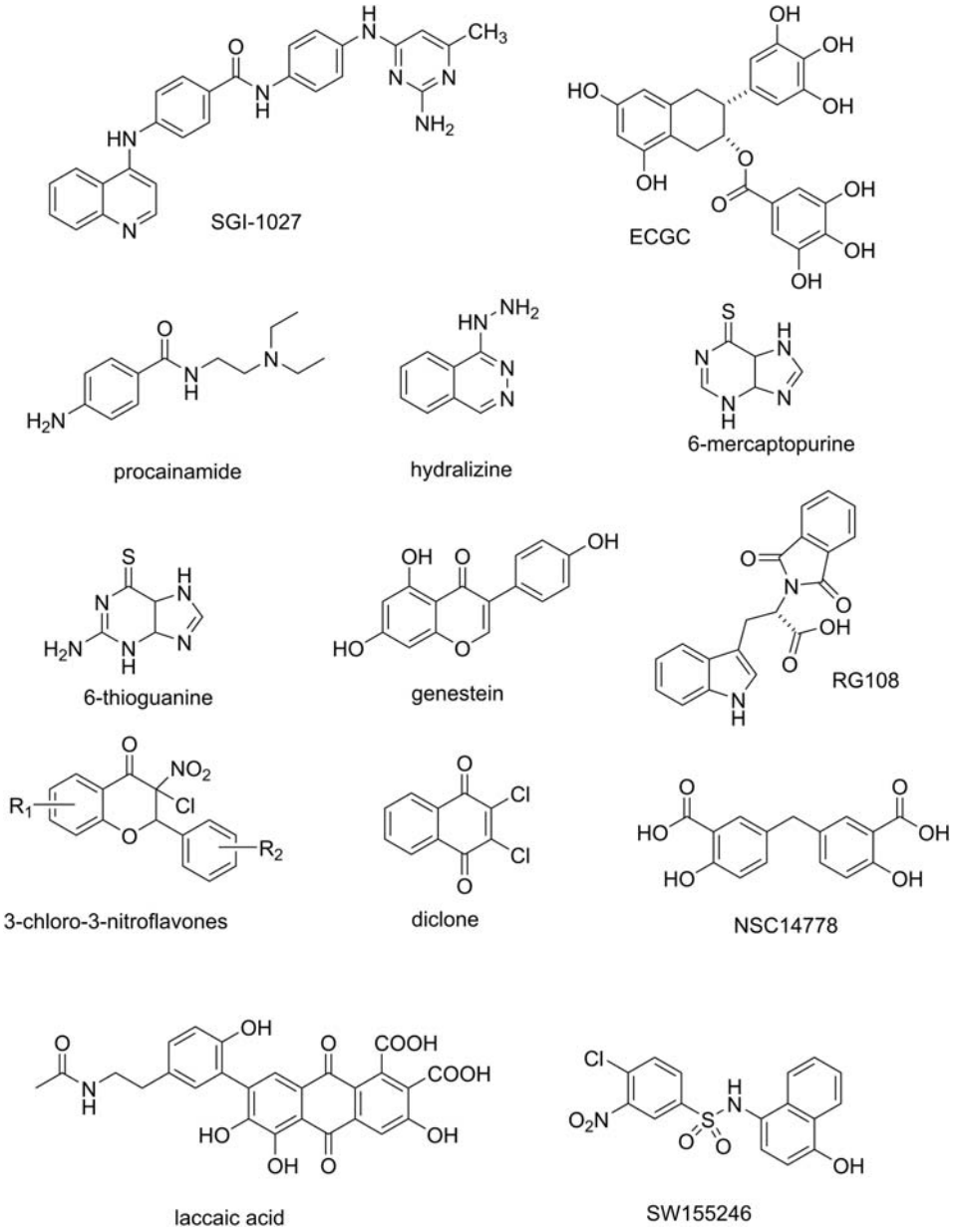

Fig. 3 Nonnucleoside inhibitors of DNMTs.

octamer, forming a structure known as a nucleosome (Fig. 4). As part of this structure, charged histone lysine tails protrude through the DNA strand and participate in the electrostatic binding of histones to DNA. Specific lysine and arginine residues on these histone tails become sites for chromatin PTMs, allowing for regional remodeling within higher order chromatin structure.[1]

As shown in Fig. 5, there are specific residues that undergo various PTMs, the most important of which are methylation at lysine and arginine, acetylation of lysine, phosphorylation of serine, and ubiquitination of histones H2A and H2B. The tail of histone H3 exhibits the highest number of PTM sites and can be methylated at R2, K4, K9, R17, R26, K27, K36, and K79 (K79 not shown); acetylated at K14, K18, and K23; and phosphorylated at S10 and S28. Histone H3 protein can also be methylated. The PTM sites on the tails of histones H4, H2A, and H2B are distinct from each other and from H4. It is notable that histones H2A and H2B can be ubiquinated.

2.12.3.2 Epigenetic Writers

2.12.3.2.1 Inhibitors of HATs

As stated earlier, histones can be posttranslationally modified by the addition of acetyl groups to lysine or by the addition of methyl groups to both lysine and arginine. These reactions are carried out by HATs or one of the several histone methyltransferases (KMTs),

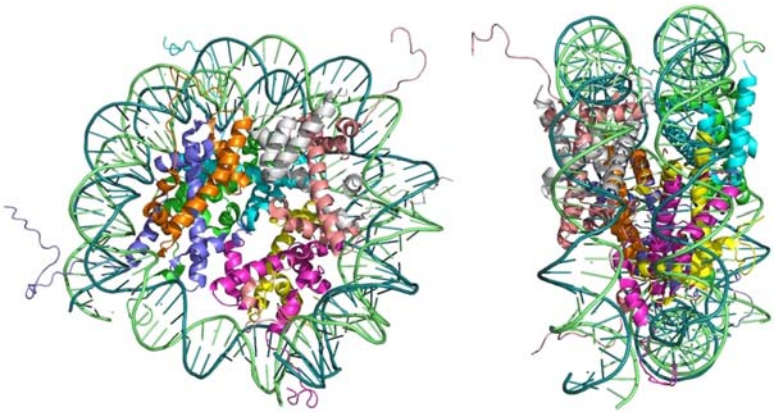

Fig. 4 The structure of the human nucleosome core particle in front and orthogonal views. Histone tails can be seen protruding from the histone proteins in the core. Adapted from Protein Data Bank structure PDB 3azh.

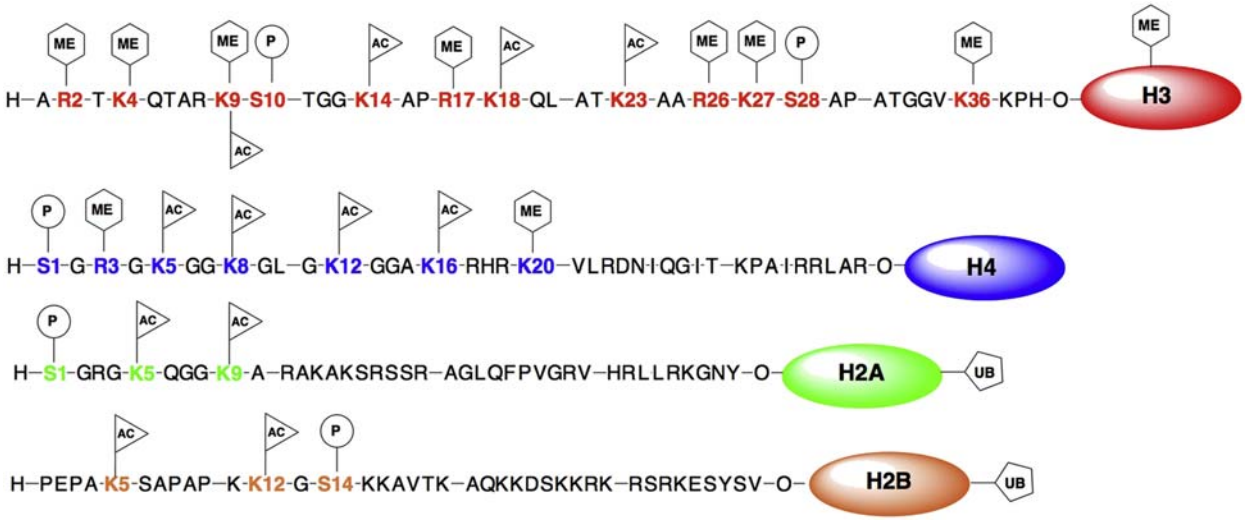

Fig. 5 Sites on histone tails for epigenetic posttranslational modifications on histones H3, H4, H2A, and H2B. *ME*, methyl; *AC*, acetyl; *P*, phosphoryl; *UB*, ubiquitinyl.

respectively. In the case of lysine acetylation, conversion of the terminal amino group of lysine to an amide serves two functions. Acetylation of the ε-amino groups of lysine cancels the positive charge, which allows DNA to assume a relaxed, transcriptionally accessible form (euchromatin).[1,7] This allows greater access to DNA by transcription factors and RNA polymerase and promotes regional gene expression. By contrast, deacetylation of histone lysine residues by HDACs restores the positive charge at ε-amino group, resulting in a densely packed form of chromatin (heterochromatin) that is transcriptionally inactive. Acetylated lysine residues also serve as recognition and binding sites for specific histone readers such as bromodomain-containing proteins (BCPs),[54,55] which will be discussed later in this chapter. The association of these reader proteins with an acetylated lysine on the histone tail also promotes transcription (Table 2).

Because nuclear-localized HATs acetylate a variety of nonhistone lysine residues,[56] they are more correctly referred to as lysine acetyltransferases (KATs). These enzymes are classified into five families based on structural homology and catalytic mechanism,[57,58] but only three of these constitute the major classes that are involved in chromatin remodeling: the GNAT superfamily (KAT1, KAT2A, KAT2B, and KAT9, formerly called HAT1, Gcn5, PCAF, and ELP3, respectively), the p300/CBP family (KAT3A and KAT3B, formerly called CBP and p300, respectively), and the MYST family (KAT5, KAT6A, KAT7, and KAT8, formerly called Tip60, MOZ, HBO1, and MOF, respectively).[59–62] These acetyltransferases can exhibit gene-specific or global effects on transcription, depending on their structure. They often participate in multisubunit protein complexes that determine substrate specificity. All KATs require acetyl CoA as a cosubstrate and despite having low sequence homology, they all exhibit a conserved acetyl CoA binding pocket.[57] The p300/CBP and GNAT family acetyltransferases appear to play a role in cancer, and elevated KAT activity has been observed in asthma and chronic obstructive pulmonary disease.[63] The levels of the acetyltransferase p300 have been suggested as biomarkers for prognosis in both lung and prostate cancers.[64,65] Mutations and/or deletions in the p300 or CBP genes

Table 2 Histone lysine and arginine methyltransferases involved in human chromatin remodeling

Histone lysine methyltransferases (KMTs)		
KMT	*Lysine mark*	*Methylation product*
SETD1A	H3K4	H3K4me, H3K4me2, H3K4me3
SETD1B	H3K4	H3K4me, H3K4me2, H3K4me3
	H3K9	H3K9me, H3K9me2, H3K9me3
ASH1L	H3K4	H3K4me, H3K4me3
MLL1 (KMT2A)	H3K4	H3K4me, H3K4me2, H3K4me3
MLL2	H3K4	H3K4me, H3K4me2, H3K4me3
MLL3	H3K4	H3K4me, H3K4me2, H3K4me3
MLL4	H3K4	H3K4me, H3K4me2, H3K4me3
SMYD3	H3K4	H3K4me2, H3K4me3
SETD7	H3K4	H3K4me3
PRMD9	H3K4	H3K4me3
SUV39H1 (KMT1A)	H3K9	H3K9me2, H3K9me3
SUV39H2	H3K9	H3K9me2, H3K9me3
G9A (KMT1C)	H3K9	H3K9me, H3K9me2
EHMT1	H3K9	H3K9me, H3K9me2
PRDM2	H3K9	H3K9me, H3K9me2, H3K9me3
EZH1	H3K27	H3K27me2, H3K27me3
EZH2 (KMT6)	H3K27	H3K27me2, H3K27me3
SETD2	H3K36	H3K36me, H3K36me2, H3K36me3
SMYD2	H3K36	H3K36me2
NSD1 (KMT3B)	H3K36	H3K36me, H3K36me2
NSD2	H3K36	H3K36me, H3K36me2
NSD3	H3K36	H3K36me, H3K36me2
DOT1L	H3K79	H3K79me, H3K79me2, H3K79me3
SUV420H1	H4K20	H4K20me2, H4K20me3
SUV420H2	H4K20	H4K20me2, H4K20me3
SETD8	H4K20	H4K20me
Protein arginine methyltransferases (PRMTs)		
PRMT	Arginine mark	Methylation product
CARM1 (PRMT4)	H3R2	H3R2me, H3R2me2
	H3R17	H3R17me, H3R17me2
	H3R26	H3R26me, H3R26me2
PRMT1	H4R3	H4R3me, H4R3me2
PRMT5	H3R2	H3R2me, H3R2me2
	H3R8	H3R8me, H3R2me2
	H4R3	H4R3me, H4R3me2
PRMT6	H3R2	H3R2me, H3R2me2
	H4R3	H4R3me, H4R3me2
PRMT7	H3R2	H3R2me, H3R2me2
	H4R3	H4R3me, H4R3me2

have been observed in several types of cancer and thus may play a role in tumorigenesis.[66–68] Acetyltransferases from the GNAT and MYST families have also been implicated in cancer through a variety of mechanisms, which have recently been reviewed.[62]

Only a handful of HAT inhibitors have been identified to date (**Fig. 6**) and were useful as chemical tools in delineating the enzyme mechanism and identifying the role of various KATs in cancer. These inhibitors are classified as bisubstrate analogs, natural products, or synthetic small molecules.[69] Lau et al. described the synthesis and application of a bisubstrate adduct between lysine and acetyl CoA, a potent ($IC_{50} = 500$ nM) and selective ($\sim$200-fold) bisubstrate inhibitor of KAT3B that displayed an unusual catalytic mechanism.[70] Interestingly, addition of a 20-mer peptide analogous to the sequence of the H3 lysine tail produces a compound that is selective for KAT2A ($IC_{50} = 300$ nM) and KAT2B over KAT3B.[71] A number of natural products such as curcumin (KAT3B inhibitor), garcinol (KAT3B inhibitor), and anacardic acid (nonselective KAT inhibitor) act as micromolar inhibitors of KATs.[63] Small molecule synthetic analogs of these natural product KAT inhibitors were also found to inhibit KATs. The most notable derivatives of anacardic acid reported by Eliseeva et al., which feature long-chain fatty acid moieties, produced HAT inhibition that correlates with its antiproliferative effects, and caused H4 hypoacetylation in MCF7 cells in vitro.[72] In addition, isothiazolone derivatives have been shown to inhibit the GNAT family acetyltransferase KAT2B,[73] while α-methylene-γ-butyrolactones described by Biel et al. have been shown to inhibit the GNAT family acetyltransferase KAT2A.[74] Gao et al. discovered the KAT3B inhibitor C646, which

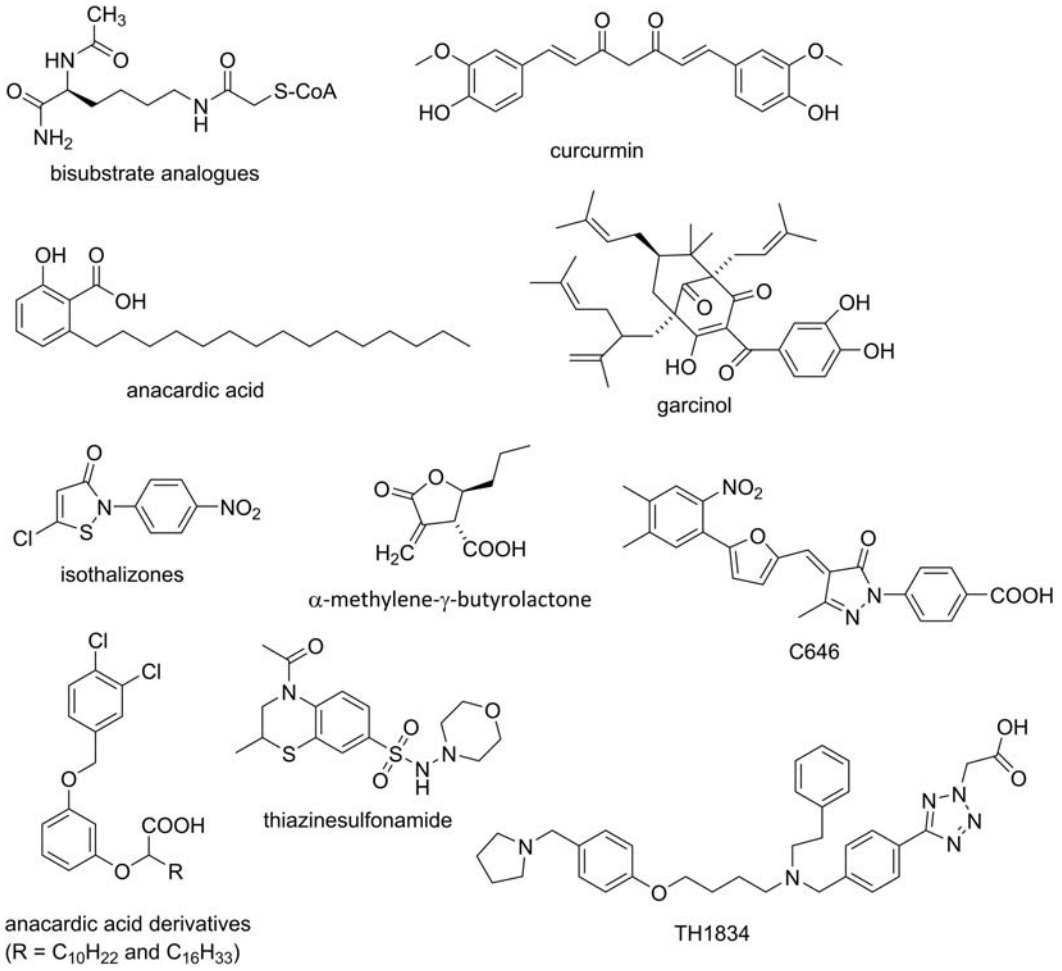

Fig. 6 Known inhibitors of histone acetyltransferases.

induces cell cycle arrest and apoptosis in AML1-ETO-positive acute myelocytic leukemia.[75] Finally, an inhibitor of KAT5 was recently reported[76] (TH1834) that reduced KAT5 activity by 60% at 500 μM.

2.12.3.2.2 Inhibitors of histone methyltransferases (KMTs and protein arginine methyltransferases, PRMTs)

Lysine residues on histone tails undergo methylation of the ε-nitrogen at specific histone lysine and arginine chromatin marks.[7,77] There are six lysine residues (histone 3 lysine 4, H3K4; H3 lysine 9, H3K9; H3K27; H3K36; H3K79; and H4K20) and five arginine residues (H3R2, H3R8, H3R17, H3R26, and H4R3) on histone protein tails that have been shown to undergo methylation[73] catalyzed by more than 50 lysine methyltransferases (KMTs)[78–80] and 11 PRMTs.[77,81,82] All KMTs and PRMTs require SAM as methyl donor and produce the by-product *S*-adenosylhomocysteine (SAH), which is recycled through salvage pathways. Histone KMTs generally target a specific lysine residue and can promote or repress transcription, depending on the lysine residue involved.[79,83,84] The eight classes of histone KMTs involved in chromatin remodeling include seven SET1 domain KMTs, five SET2 domain KMTs, six KMTs in the SUV39 group, EZH1 and 2, three KMTs in the PRDM group, four KMTs in the other-SET group, and one non-SET domain KMT.[85] Except for the nonSET KMT hDOT1L, all histone KMTs contain a conserved 130 amino acid SET (SU(VAR)3–9, enhancer-of-Zeste, Trihorax) domain that catalyzes the methyl transfer.[80,86,87] As shown in **Fig. 7A**, histone KMTs catalyze the stepwise conversion of unmethylated histone lysines to the mono-, di-, and trimethylated forms. There are also two separate groups of PRMTs, five Type I PRMTs and four Type II PRMTs. Type I PRMTs methylate arginine to produce *N*-monomethyl arginine (**Fig. 7B**). From there, a second methyl group can be added to the same carbon to form gem-*N*,*N*-dimethylarginine, or a Type II PRMT can methylate the second arginine nitrogen. Importantly, aberrant methylation of histone arginines and lysines is linked to carcinogenesis[88,89] and possibly to coronary disease.[90]

Although efforts to identify histone KMT and PRMT inhibitors are in early stages, a number of promising compounds have been discovered. Most of these histone methyltransferase inhibitors compete with either SAM or the histone substrate.

A large number of inhibitors of DOT1L has been reported by Epizyme,[91,92] of which the most noteworthy are EPZ04777 and EPZ5676 (**Fig. 8**). EPZ04777 is a potent, SAM-competitive inhibitor ($IC_{50} = 0.4$ nM) that selectively inhibits H3K79 methylation

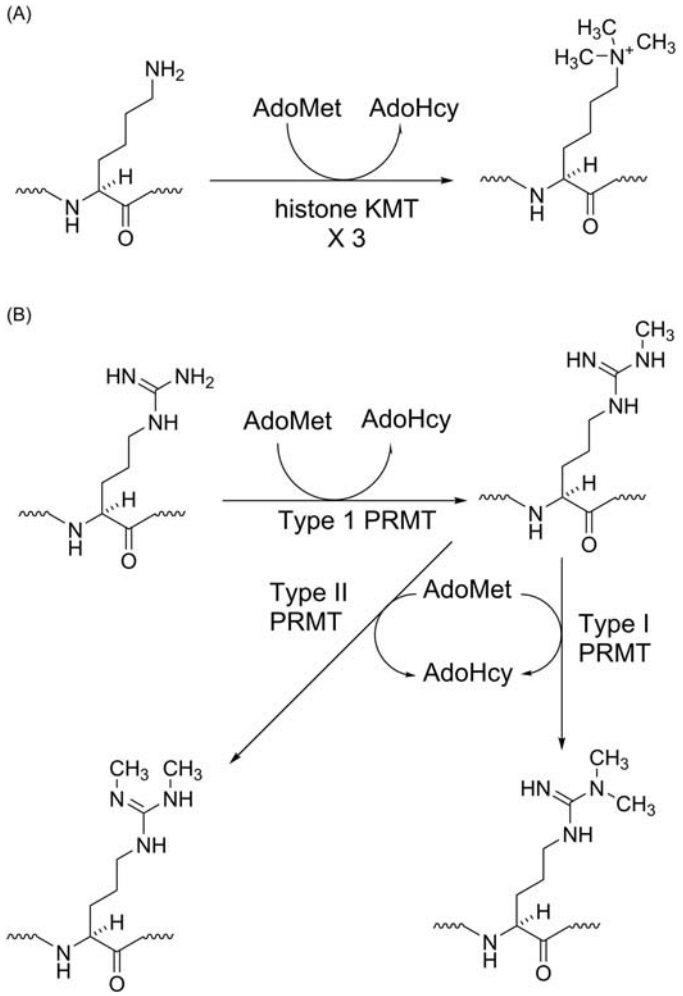

Fig. 7 The histone KMT and histone PRMT methylation reactions.

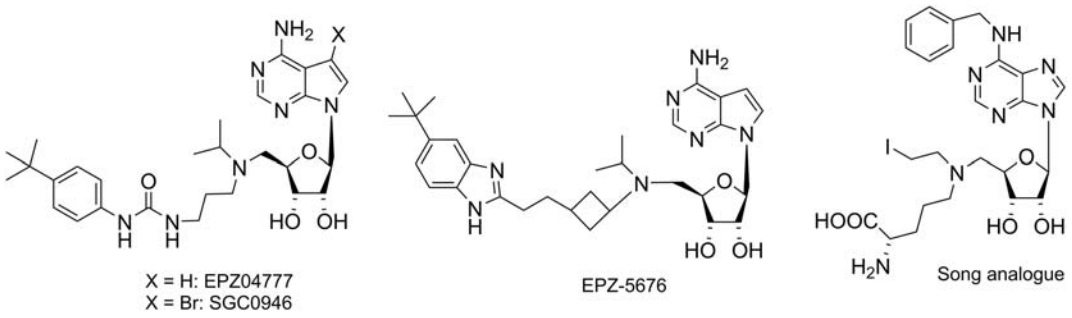

Fig. 8 Inhibitors of the KMT DOT1L.

and blocks expression of leukemogenic genes in MLL cells in vitro.[93] The efforts to improve the pharmacokinetic properties of EPZ04777 led to the synthesis of EPZ-5676 (pinometastat), a conformationally rigid analog of EPZ04777 that displayed improved potency ($K_i < 0.08$ nM) and selectivity for H3K79 (>37,000-fold).[94] A phase I clinical trial has been initiated for EPZ5676 to evaluate it as a therapy for acute leukemia bearing MLL-rearrangements. In an attempt to elucidate the mechanism, the 7-bromo analog of EP04777, SGC0946, was synthesized. SGC0946 is slightly more potent against DOT1L ($IC_{50} = 0.3$ nM, 100-fold selective), reduces H3K79 dimethylation, and selectively kills MLL cancer cells.[95] A series of inhibitors that resemble SAH were reported from Song's laboratory, and one of the most potent inhibitors, compound **10** ($IC_{50} = 38$ nM) reported by Yao et al., showed weak/no activity against other KMTs or PRMTs.[96] More recently, surface plasmon resonance was used to identify DC-L115, which exhibits an IC_{50} of 1.5 μM against DOT1L and selectively inhibits MLL-rearranged cell proliferation (IC_{50} 37.1 μM).[97]

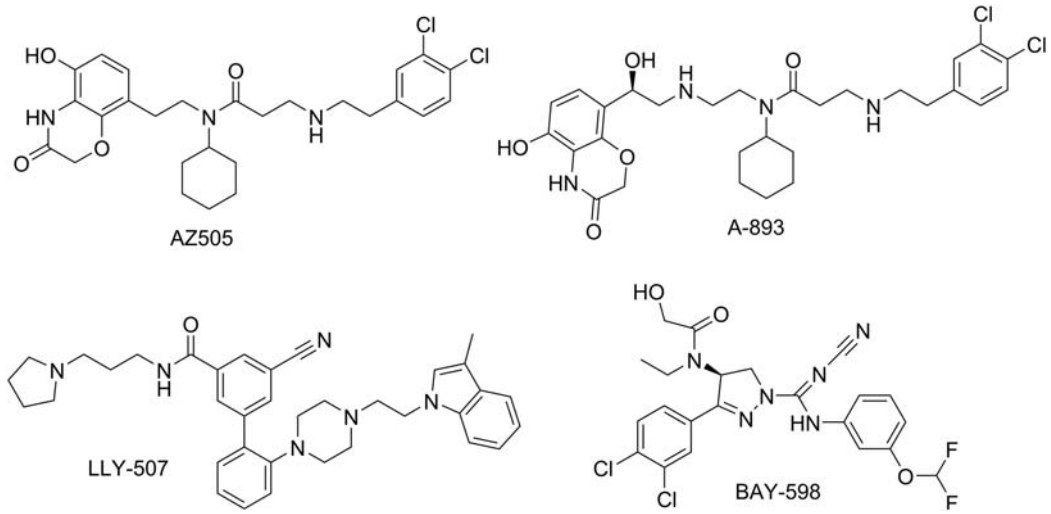

Fig. 9 Inhibitors of the KMT SMYD2.

AZ505 (Fig. 9) acts as a potent ($IC_{50} = 0.12$ μM) and selective inhibitor of SMYD2, the oncogenic protein that represses the functional activities of tumor suppressors such as p53 and Rb.[98] A cocrystal of SMYD2 with AZ505 showed that it is a substrate competitive inhibitor of the enzyme. Sweis et al. then developed AZ505 analogs with improved activity, including A-893, which exhibited an IC_{50} of 2 nM against SMYD2 and suppressed p53K570 methylation in the A549 lung carcinoma line. The compound known as LLY-507 (Fig. 9) acts as a potent and selective inhibitor of SMYD2, with an IC_{50} of 15 nM and 100-fold selectivity over the related family members, SUV420H1 and SUV420H2.[99] Most recently, the SMYD2 inhibitor BAY-598 was developed, which exhibits an IC_{50} of 27 nM against SMYD2 and can enhance the activity of doxorubicin in vivo.[100]

The mycotoxin chaetocin (Fig. 10) reported by Greiner et al. inhibits the KMT Su(var)3–9 from *Drosophila* ($IC_{50} = 0.8$ μM) and produces antitumor effects in vivo.[101] More recently, it was demonstrated that chaetocin causes a 25-fold induction of latent HIV-1 expression without activation of T-cells, suggesting that it may be useful in clearing latent HIV from infected cells.[102] The compound BIX-01294 reported by Kubicek et al. inhibits the G9a KMT and produces a reduction in histone H3K9 dimethylation (but not mono- or trimethylation) in several cell lines.[103] BIX-01294 and its homologs also exhibit potent antimalarial activity in both chloroquine-sensitive and -resistant strains, an effect that is mediated through histone KMT inhibition.[104] Liu et al. reported UNC0224 (Fig. 10), a potent G9a inhibitor with an IC_{50} of 15 nM. Structure-based lead optimization of UNC0224 led to the

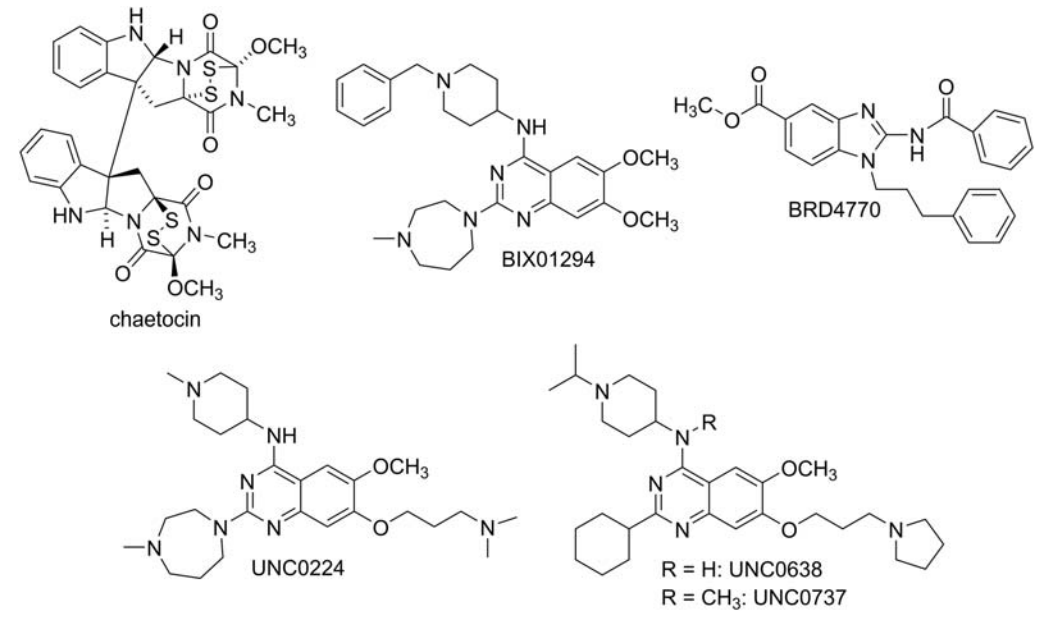

Fig. 10 Inhibitors of the KMT G9a.

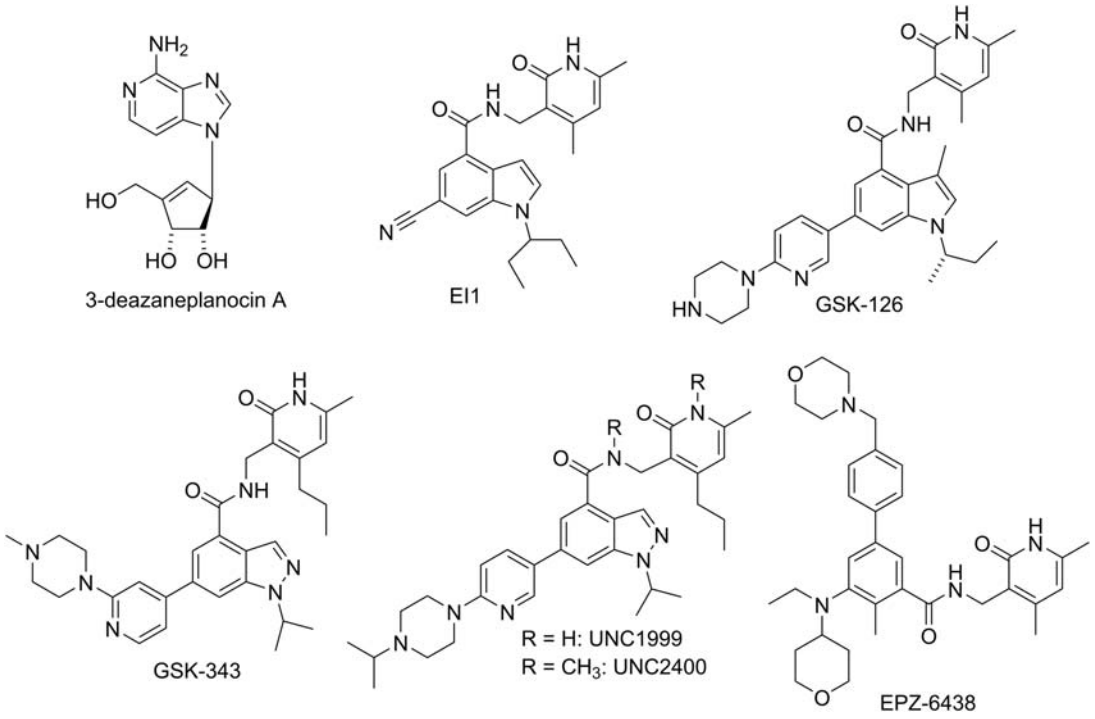

Fig. 11 Inhibitors of the KMT EZH2.

discovery of UNC0638 (R = H), a potent (IC_{50} for G9A = 15 nM and for GLP = 19 nM) inhibitor of histone KMTs G9a and GLP with excellent selectivity compared to numerous epigenetic and nonepigenetic targets.[105] Structure/activity studies revealed that conversion of the molecule to UNC0737 (R = CH_3) destroys the inhibitory activity of the analog, suggesting that H-bonding between Asp 1083 of G9a and the aminoquinazoline moiety in UNC0638 is required for binding to the active site of G9a. The purine analog BRD4770 (Fig. 10) inhibits the histone KMT G9a and induces senescence in pancreatic adenocarcinoma cells in vitro.[106]

EZH2 plays a significant role in a multitude of cancers including prostate, breast, and bladder, and thus became a target for the discovery of specific inhibitors. The EZH2 inhibitor 3-deazaneplanocin A (Fig. 11) depletes EZH2 levels while inhibiting the formation of K3K27me3 in acute myeloid leukemia (AML) cells.[107] Significant depletion of EZH2 activity was observed in cultured AML cells when 3-deazaneplanocin A was combined with panobinostat, a pan-HDAC inhibitor.[107] It was also reported that 3-deazaneplanocin A as a single agent inhibits tumor cell growth in nonsmall cell lung carcinoma in vitro through induction of a G1 cell cycle arrest.[108] Qi et al. carried out high-throughput screening against a recombinant PCR2 protein complex containing EZH2 that eventually resulted in the design of El1 (Fig. 11). This compound elicited potent inhibitory activity against both wild-type (IC_{50} = 15 nM) and Y641F mutant enzymes (IC_{50} = 13 nM).[109] In addition to being highly selective for EZH2 when compared with EZH1 (90-fold selectivity) or other HMTs (10,000-fold selectivity), EI1 inhibits H3K27 methylation, reduces cell proliferation, and initiates cell cycle arrest and apoptosis.

Based on a combination of high-throughput screening and subsequent lead optimization, McCabe et al. identified a series of novel, SAM-competitive indole-based EZH2 inhibitors.[110] The representative compound GSK-126 (Fig. 11) inhibited both wild-type and mutant EZH2 with similar potencies ($K_i^{app} = 0.5 - 3.0$ nM) and displayed 1000-fold selectivity over other methyltransferases and 150-fold selective over EZH1.[110] In addition, GSK-126 inhibited the proliferation of EZH2 mutants in both diffuse large B-cell lymphoma cell lines and xenografts. Through structural modification, Verma et al. discovered GSK-343 ($K_i^{app} = 1.2$ nM), in which an indazole moiety is substituted for the indole in GSK-126.[111] Both compounds GSK-126 and GSK-343 decreased H3K27me3 levels in a dose-dependent manner. Despite GSK-343 being more potent, it was precluded from advancement to clinical studies due to high clearance as suggested by rat pharmacokinetic studies.[111] Konze et al. later disclosed UNC1999, an orally bioavailable, SAM-competitive inhibitor that exhibited high in vitro potency (IC_{50} 45 nM) for wild-type and mutant EZH2 as well as the closely related H3K27 methyltransferase EZH1. UNC1999 potently reduced H3K27me3 with an IC_{50} of 124 nM in MCF7 cells. Interestingly, the close homolog UNC2400, in which a pair of N-methyl groups was added to UNC1999, was 1000-fold less potent than UNC1999 and did not show any activity in cell preparations. All of the compounds shown in Fig. 11 are in preclinical (3-deazaneplanocin, EI1, GSK-343, and UNC1999) or Phase I (GSK-126) clinical trials.

Through a combination of screening and iterative medicinal chemistry, Knutson et al. designed a novel class of pyridine-based EZH2 inhibitors. The SAM-competitive inhibitor EPZ6438 (tazemetostat, Fig. 11) displayed a K_i value of 2.5 nM and a selectivity index of 35-fold over EZH1 and >4500-fold over other PMTs.[112] EPZ6438 inhibited H3K27me3 levels leading to specific killing of

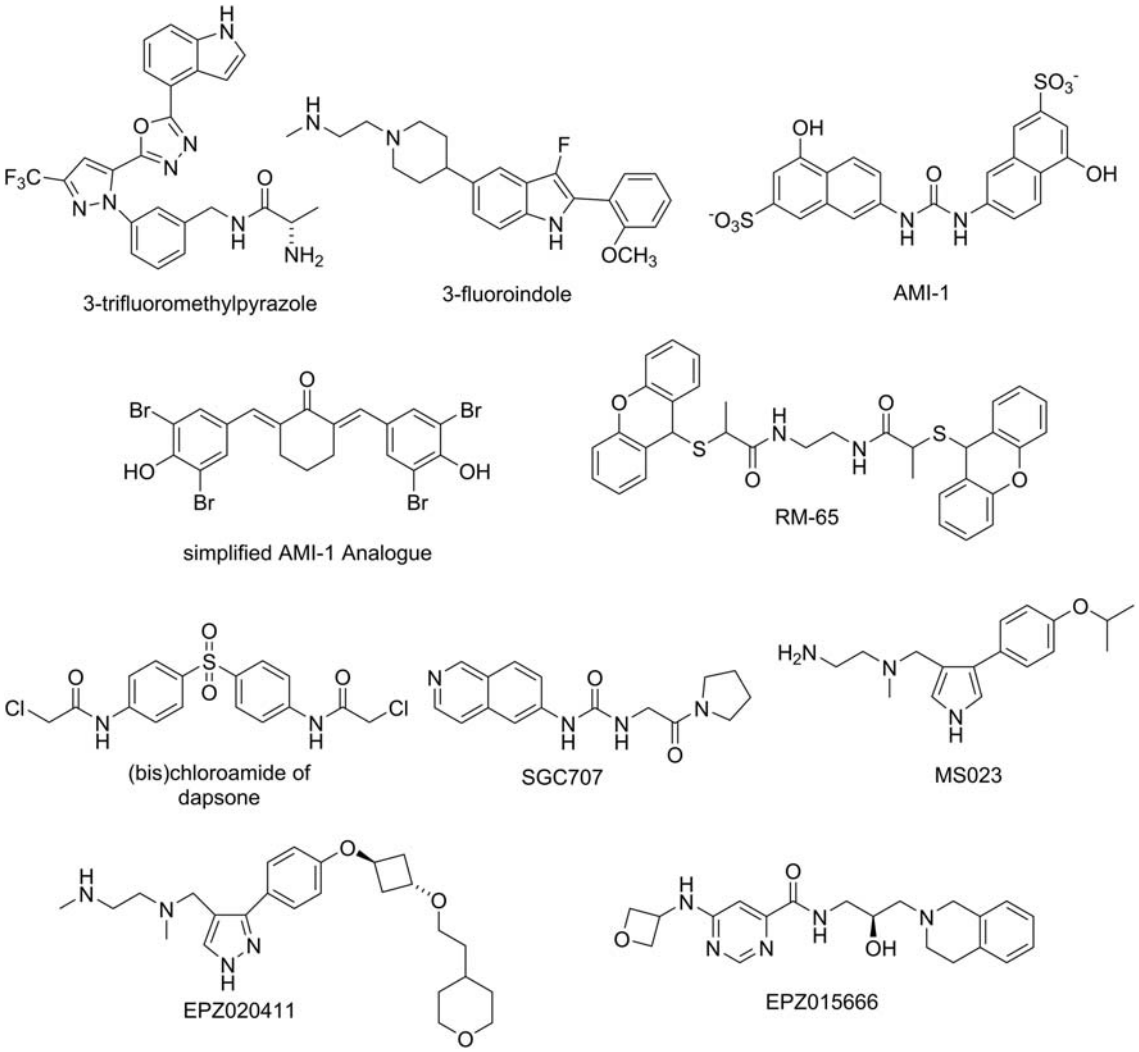

Fig. 12 Selected inhibitors of arginine methyltransferases (PRMTs).

lymphoma cell lines. Epizyme recently initiated a Phase I/II clinical trial to evaluate EPZ6438 as a treatment for nonHodgkin lymphoma in patients with EZH2 SET domain mutants.

A number of groups are involved in the design and synthesis of selective histone PRMT inhibitors (Fig. 12). A high-throughput screening using full-length coactivator-associated arginine methyltransferase 1 (CARM1, PRMT4) followed by hit-to-lead optimization results in a 3-trifluoropyrazole (Fig. 12) with an IC_{50} of 27 nM.[113] A 3-fluoroindole derivative was also identified with an IC_{50} of 30 nM against CARM1. Both compounds exhibited selectivity indices of >300-fold against PRMT1 and 3.[113] X-ray crystallography showed that the 3-fluoroindole analog occupies the substrate-binding pocket and the high selectivity arises from sequence differences between PRMT4 and PRMT1/3. A random screen of a compound library carried out by Cheng afforded nine PRMT inhibitors with structures related to AMI-1 ($IC_{50}=8.81$ μM).[114] Further studies have shown that AMI-1 is selective for PRMT over KMT and produced an in vivo effect on arginine methylation.[114] Subsequent studies revealed structure-optimized analogs with increased potency against PRMT1 and PRMT4 that modulated T-helper cell cytokine production.[115] Analogs of AMI-1 bearing 2-bromo- and 2,6-dibromophenol moieties linked through unsaturated cyclic spacers, such as the simplified AMI-1 analog shown in Fig. 12, equally inhibited PRMTs, HKMT, HAT, and SIRTs, thus behaving as multiple ligands for these epigenetic targets.[116] A related series of linear and cyclic urea analogs produced modest inhibition of PRMT1 and PRMT5.[117] Using a combination of pharmacophore-based virtual screening methods and radioactive methylation assays, Wang et al. identified compounds A9 and A36, which disrupted PRMT1 function by directly targeting the substrate H4 and that were more effective than AMI-1.[118] Dillon et al. used a high-throughput screening approach to identify two novel inhibitors selective for PRMT1 over other SAM-requiring protein methyltransferases.[119] Spannhoff et al. conducted a focused virtual screening of 9000 compounds and a subsequent optimization of a hit molecule that resulted in compound RM-65. This compound inhibited PRMTs RmtA ($IC_{50}=46$ μM) and PRMT1 ($IC_{50}=55$ μM) without affecting lysine methyltransferase SET7/9. In silico docking experiments suggested that RM-65 acts as a bisubstrate mimic occupying

both the arginine and SAM binding pockets.[120] Acylated derivatives of *p*-aminobenzenesulfonamides and the antileprosy drug dapsone also act as inhibitors of PRMT1.[121] The (bis)chloroacetyl amide of dapsone (Fig. 12) selectively inhibited human PRMT1 (IC_{50} 1.5 μM) and was selective for PRMT1 over the arginine methyltransferase CARM1 and the lysine methyltransferase Set7/9.[121] It also showed anticancer activity in MCF7a and LNCaP cells in vitro and blocked androgen-dependent transcription specifically in a reporter gene system.

The allosteric inhibitor SGC707 was shown to inhibit PRMT3 with an IC_{50} of 31 nM[122] but did not inhibit members of a panel of 27 protein methyltransferases. In an A549 cell preparation, SGC707 was able to reduce H4R3me2 with an EC_{50} of 225 nM. X-ray crystallographic studies of the complex between SGC707 and PRMT3 suggest that the inhibitor occupies a cavity >15 Å from the enzyme active site. EPZ020411 (Fig. 12) inhibits PRMT6 with an IC_{50} of 10 nM and exhibits good selectivity (>10-fold) against PRMT1 and 8.[123] In cellular assays, EPZ020411 produced a dose-dependent decrease of H3R2me2 (EC_{50} 640 nM). In contrast to the enzyme-specific inhibitors described earlier, MS023 is a pan-inhibitor of type I PRMTs.[124] It was designed based on the structures of the 3-trifluoromethylpyrazole PRMT4 and the PRMT6 inhibitor EPZ020411. MS023 exhibited an enzyme IC_{50} of 30, 119, 83, 4, and 5 nM against PRMT1, 3, 4, 6, and 8, respectively. Treatment of MCF7 cells with MS023 significantly decreased levels of H3R2me2 and H4R3me2 with EC_{50} values of 56 and 9 nM, respectively. Remarkably, if the primary nitrogen of MS023 is converted to a hydroxyl, then the resulting compound, MS094, is inactive against PRMTs. EPZ015666 acts as a potent and selective inhibitor of PRMT5 (IC_{50} = 22 nM)[125] and exhibited potent antiproliferative activity against Z-138 mantle cell lymphoma cell lines Z-138 and Maver-1 (EC_{50} = 96 and 450 nM, respectively). This potent cellular activity likely occurs because PRMT5 is dramatically overexpressed in this type of tumor. EPZ015666 also possessed in vivo antitumor activity in xenograft mouse models involving the Z-138 and Maver-1 cell lines.

2.12.3.3 Epigenetic Erasers

2.12.3.3.1 HDACs

As mentioned above, the acetylation status of histones is controlled by a balance between two enzymes, HAT, which promotes histone hyperacetylation, and the HDAC, which catalyzes acetyl group cleavage. Acetylation of the ε-amino groups of lysine residues located at N-termini removes the positive charge and loosens the tightly wound chromatin.[7,52,126] This allows greater access to DNA by transcription factors and RNA polymerase and promotes the expression of various transcriptional products. By contrast, transcriptional repression dominates at times when DNA methylation occurs at promoter CpG islands. Methylation of DNA results in the recruitment of HDACs and subsequent deacetylation of lysine tails restores the positive charge and thus promotes formation of closed chromatin (Fig. 13). The recruitment of HDAC activity by DNA methylation is an important event in epigenetic silencing.[127] Normal mammalian cells exhibit an exquisite level of control of chromatin architecture in part by maintaining a balance between HAT and HDAC activities. There are currently 11 known mammalian HDAC isoforms that can be divided into three structural classes: Class I HDACs[128] include HDAC isoforms 1, 2, 3, and 8. Class I HDAC proteins are characterized by a highly conserved catalytic site sequence homology and have molecular weights between 42 and 55 kDa. They contain a nucleus localization sequence (NLS) in addition to their catalytic domain. These enzymes catalyze histone deacetylation by a zinc-dependent mechanism.[129] Class II HDACs include HDACs 4, 5, 6, 7, 9, 10, and 11[130] and are characterized by their sequence homology in both the C-terminal catalytic domain and the N-terminal regulatory domain. Class II HDACs have molecular weights between 120 and 130 kDa and are also zinc-dependent deacetylases. Class II HDACs are further divided into Class IIa (HDAC 4, 5, 7, and 9), which feature an NLS, and Class IIb (HDAC 6 and 10), which lack an NLS, but feature a second catalytic domain that is active in HDAC6, but does not function in HDAC10. HDAC6 can also acetylate tubulin and contains a C-terminal zinc finger that has a very high affinity for free ubiquitin and ubiquitinated proteins. Structural comparisons among different Class I and II HDACs, as well as HDAC homologs from different species that share significant homology with human classical HDACs, reveal a conserved group of active site residues, suggesting a common mechanism for the metal-dependent hydrolysis of acetylated substrates. Class IV contains a single HDAC, 11, which is similar in size to Class I HDACs, but has low sequence homology. The Class III HDACs were identified based on their similarity to the NAD-dependent yeast transcriptional repressor protein Sir2.[131–133] Unlike Class I and II HDACs, Class III HDACs, which have not been well characterized in mammalian systems, do not require zinc and as such are unresponsive to known HDAC inhibitors (see below). Class III HDACs use NAD^+ as a reactant to deacetylate acetyl lysine residues of protein substrates forming nicotinamide, the deacetylated product, and the metabolite 2′-*O*-acetyl-ADP-ribose.

Overexpression of HDACs correlates positively with tumor growth by promoting silencing or abnormal transcription of crucial genes that control cell cycle regulation, apoptosis, DNA repair, and chromatin structure.[134] The irregularity in HDAC function thus contributes to the initiation and progress of several tumors. In some tumor cell types, excessive hypoacetylation of histones results in the under-expression of growth regulatory factors such as the cyclin-dependent kinase inhibitor $p21^{Waf1}$ and thus contributes to the development of cancer. Specific mutations can result in hypermethylation of DNA and formation of aberrant transcriptional proteins that recruit HDAC's, resulting in excessive deacetylation of lysine residues on histone tails. As a result, chromatin is condensed and transcription is repressed, causing inactivation of the tumor suppressors including $p21^{Waf1}$.[135] These results are typically seen in addition to a variety of cell signaling aberrations that occur in response to excessive histone deacetylation. These changes have the potential to produce a malignant phenotype resulting from a combination of genetic abnormalities and epigenetic modifications leading to dysregulation of critical genes controlling cell proliferation, differentiation, and death. These changes include modification of the histone code, including changes in histone acetylation, and alteration in DNA methylation patterns. Considerable data highlight the important role that methylation of cytosine residues in promoter regions plays in the

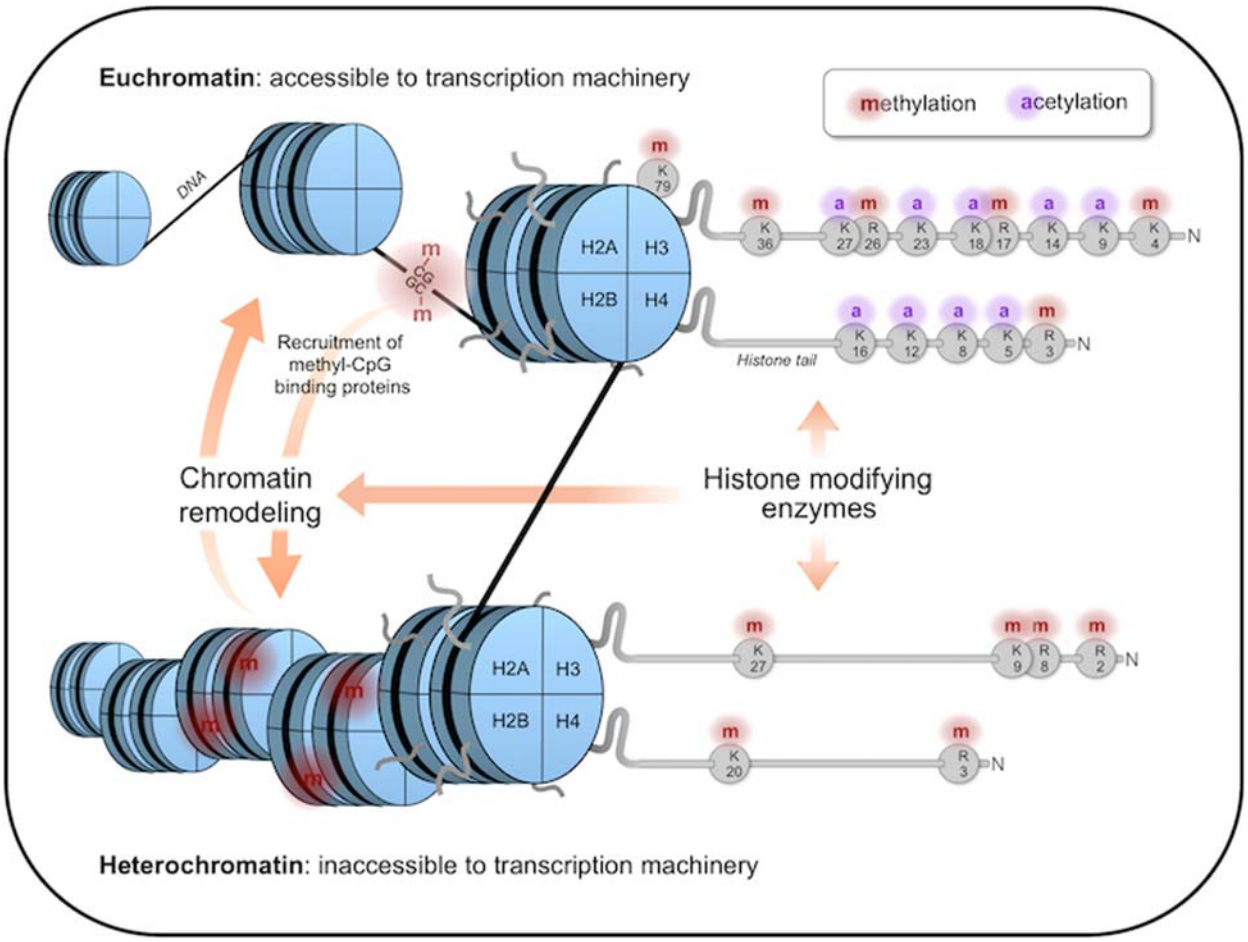

Fig. 13 Epigenetic regulation of gene expression wherein DNA alternates between euchromatin and heterochromatin via histone modifying enzymes. https://fortyfourandtwo.net/2016/08/08/the-chromatin-code.

transcriptional silencing of genes.[136] HDAC inhibitors suppress histone deacetylation and enhance gene expression by promoting the formation of euchromatin and reversing gene silencing.

Histone hyperacetylation caused by HDAC inhibitors such as trichostatin, MS-275, and SAHA (Fig. 14) can cause growth arrest in a wide range of transformed cells and can inhibit the growth of human tumor xenografts.[135,137–139] HDAC inhibitors restore normal cell cycle and apoptotic functions in human tumor cells. Known HDAC inhibitors fall into distinct structural classes (Fig. 14) including hydroxamic acids, benzamides, short-chain carboxylic acids, and cyclic peptides. A current effort in the design of additional HDAC inhibitors is the discovery of isoform-specific HDAC inhibitors. Such molecules would be of great value as chemical tools for elucidating the roles of HDAC isoforms in both normal and cancer cell lines.

Recent clinical studies have demonstrated that synergistic reexpression of genes that are silenced through promoter methylation can be achieved by the sequential application of DNMT inhibitors and HDAC inhibitors, resulting in an enhanced response to antitumor therapy.[140,141] However, clinical experience with MS-275 and other HDAC inhibitors demonstrate that step-down dosing of the HDAC inhibitors is often required to minimize toxicity. Consequently, effective HDAC inhibitors having minimal toxicity on their own may provide excellent candidates for combination with demethylating agent like 5-AC and 5-aza-2′-deoxycytidine.

There are thousands of papers that describe the efforts to develop HDAC inhibitors with enhanced efficacy, improved pharmacokinetic profiles, and significant isoform specificity. As such, a comprehensive review of HDAC drug discovery research is beyond the scope of this article, and therefore this article will focus on novel HDAC inhibitors published since 2010. Cho et al. synthesized a series of pyridone-based hydroxamic acids and evaluated the HDAC inhibition profile of the resulting compounds.[142] The most promising of these analogs (Fig. 15) produced potent HDAC inhibition (IC_{50} 0.07μM) and was highly selective for HDAC1 (Class I) and HDAC6 (Class II) enzymes. Using the conventional HDAC pharmacophore model, Marek et al. designed LMK235, which inhibited HDAC with an IC_{50} of 0.65 μM), a value comparable to vorinostat ($IC_{50}=0.53$ μM) against global cellular HDACs. LMK235 was also more cytotoxic to the human cancer cell lines A2780, Cal27, Kyse510, and MDA-MB231 than vorinostat[143] and produced a synergistic antitumor effect when combined with cisplatin. LMK235 exhibited a novel HDAC isoform selectivity profile and produced nanomolar inhibition of HDAC4 ($IC_{50}=12$ nM) and HDAC5 ($IC_{50}=4$ nM). It was also metabolically stable

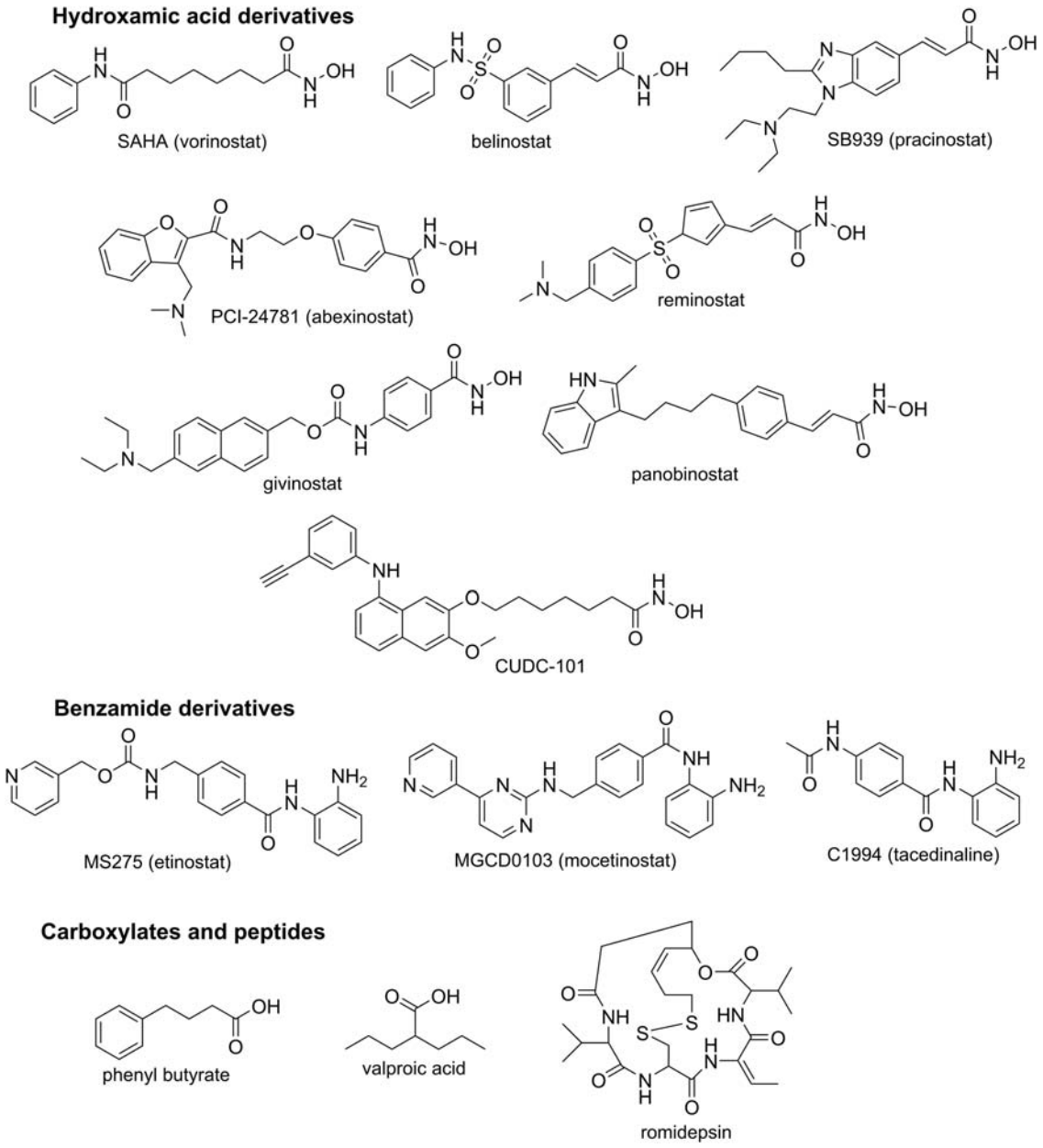

Fig. 14 HDAC inhibitors that are currently marketed or in human clinical trials.

in mouse liver microsomes and produced growth inhibition of various cancer cell lines. Giannini et al. described ST7612AA1, a thioacetate-ω(γ-lactam carboxamide) derivative that had an IC_{50} value of 70 nM against NCI-H460 lung cancer cells in vitro, was orally active and metabolically stable, and was more effective than carboplatin in limiting tumor volume in a xenograft model.[144] The benzamide MC2392 was found to induce caspase-8-dependent cell death accompanied by RIP1 induction and production of reactive oxygen species. Solid tumors and leukemia did not respond to MC2392, but in the presence of the PML-RARα repressive complex, it initiates cell death. The authors suggest a model in which MC2392 binds to the RARα moiety and inhibits the HDACs that are components of the repressive complex responsible for the transcriptional impairment in acute promyelocytic leukemia, suggesting a context-dependent targeted therapy.[145] There are numerous additional examples of novel HDAC inhibitors; the reader is directed to an excellent review on the subject.[139]

Although initially designed as antitumor agents, HDAC inhibitors are finding utility in a variety of noncancer disease states. By way of example, the HDAC3-selective inhibitor RGFP966 ($IC_{50} = 80$ nM) was found to persistently reduce cocaine-seeking behavior.[146] HDAC inhibitors can also cause increases in glucocerebrosidase activity in Gaucher's disease by modulating the levels of molecular chaperones. Other treatment applications for HDAC inhibitors include liver and kidney fibrosis,[147] encephalomyelitis,[148] stroke and neuroprotection,[149] Huntington's disease,[150] and a host of other applications. The NAD^+-dependent

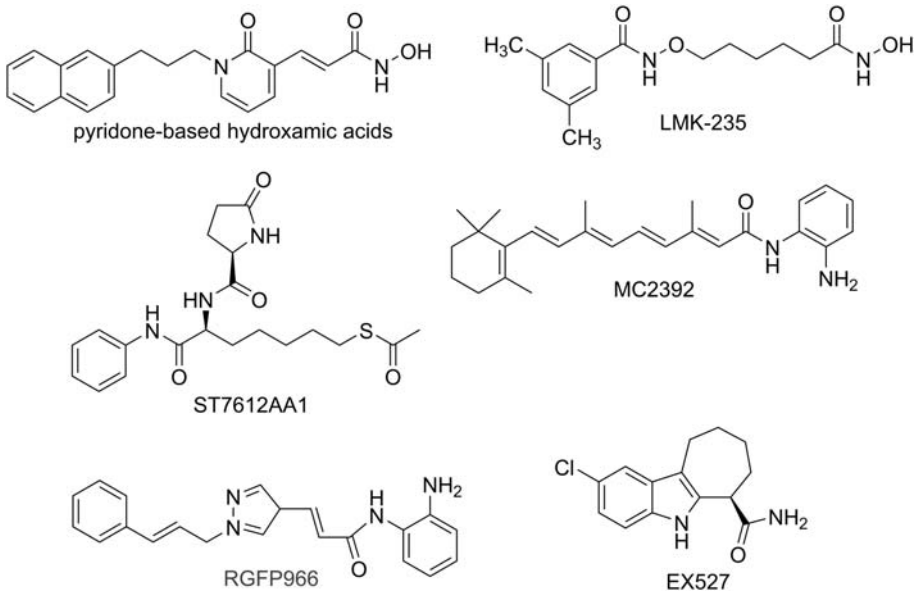

Fig. 15 Recent examples of novel HDAC inhibitors.

deacetylase SIRT1 regulates transcription via deacetylation of transcription factors such as PPARγ, NFκB, and the tumor suppressor protein p53. In the 2.5 Å crystal structure of the SIRT1 catalytic domain (residues 241–516) bound to NAD^+, EX527 ($IC_{50}=98$ nM) binds deep in the catalytic cleft, where it displaces NAD^+ and forces it into an extended conformation that sterically prevents substrate binding,[151] thus defining a novel mechanism of HDAC inhibition. Yu has identified a hydroxamate-based inhibitor of HDAC6 that is not toxic to cancer cells, but may serve as a lead for the treatment of sepsis or inflammation, since it produced a 40% improvement in survival in a lipopolysaccharide-induced mouse model of endotoxemia.[152] Recent research suggests that HDAC6 may play a significant role in a number of cellular processes. Ellis has demonstrated that HDAC6 may represent an optimal target for future immunosuppressant therapeutics with a particular role in organ transplantation.[153]

2.12.3.3.2 Histone demethylases (KDMs)

2.12.3.3.2.1 Histone lysine demethylases

Histone lysine and arginine methylation, formerly thought to be permanent PTMs, are not static modifications. This was validated when it was discovered that removal of methyl groups from H3K4 mono- and dimethyllysines was catalyzed by LSD1, (aka BHC110 or KDM1A) in a complex where it is associated with the CoREST protein.[21] Since histone 3 dimethyllysine 4 (H3K4me2) is a key chromatin mark found associated with promoters of active genes,[154,155] oxidative demethylation of histone 3 methyllysine 4 (H3K4me1) and H3K4me2 by LSD1 is associated with transcriptional repression. Overexpression of LSD1 results in aberrant demethylation of this mark and therefore silences tumor suppressor genes important in human cancer.[22] In light of this observation, LSD1 has become a validated target for the development of a new class of antitumor drugs that mediate their effects through inhibition of LSD1.[156] Interestingly, when LSD1 associates with the androgen receptor rather than CoREST, it becomes a specific demethylase for H3K9me and H3K9me2.[157] In addition, inhibitors of LSD1 unlock the all-trans-retinoic acid (ATRA)-driven therapeutic response in nonAPL AML through epigenetic reprogramming, suggesting that LSD1 may contribute to AML pathogenesis by inhibiting the normal prodifferentiative function of ATRA and paving the way for new combinatorial therapies for AML. A distinct form of LSD1, which was termed LSD2 or KDM1B,[158,159] has the same substrate specificity, but does not bind to CoREST, because it lacks the requisite tower domain necessary for CoREST binding. LSD2 appears to play a distinct epigenetic role from LSD1.

It is important to understand that chromatin-modifying enzymes do not function independently but rather exist as components of histone-modifying epigenetic protein complexes. For example, the LSD1/CoREST epigenetic complex is comprised of HDAC1, HDAC2, BRAF30, CoREST, and BCH80, while the LSD1 NURD complex contains HDAC1, HDAC2, Mi2, MBD, RbAp, and MTA proteins.[160] A number of other LSD1-containing complexes exist, including LSD1-AR/ER, MLL-UTX, and PRC2-RBBP2, to name but a few. It has recently been shown that silencing of the human gene that codes for γ-globin, a component of fetal hemoglobin, is mediated by the DRED complex, which forms early in life and silences the γ-globin gene.[161] In light of the importance of these epigenetic complexes, it is likely that inhibition of a given enzyme within an epigenetic complex may lead to alterations in gene expression due to disassembly of the complex.

Since the discovery of LSD1 in 2004, a number of additional histone lysine demethylases (KDMs) have been identified. Histone demethylases are classified in one of the six families termed KDM1–KDM6, as shown in **Table 3**. A discussion of the histone lysine substrate specificity, the effects they have on gene expression, and the roles they play in cancer and other diseases has recently been reviewed.[162–164] Briefly, the KDM1 family, consisting of LSD1 and 2, are flavin-dependent amine oxidases that show specificity for

Table 3 Histone demethylases involved in human chromatin remodeling

KDM	*Alternate names*	*Histone substrates*
Flavin-dependent histone demethylases		
KDM 1 family		
KDM1A	LSD1, BHC110	H3K4me, H3K4me2
	AOF2	H3K9me, H3K9me2
KDM1B	LSD2, AOF1	H3K4me, H3K4me2
Fe(II)/2-oxoglutarate-dependent histone demethylases		
KDM2 family		
KDM2A	JHDM1A	H3K36me, H3K36me2
	FBXL11	
KDM2B	JHDM1B	H3K36me, H3K36me2
	FBXL10	
KDM3 family		
KDM3A	JHDM2A, TSGA	H3K9me, H3K9me2
	JMJD1A	
KDM3B	JHDM2B, 5qNCA	H3K9me, H3K9me2
	JJMJD1B	
KDM3C	JHDM2C, TRIP8	H3K9me, H3K9me2
	JMJD1C	
KDM4 family		
KDM4A	JMJD2A, JHDM3A	H3K9me2, H3K9m
		H3K36me2, H3K36me3
KDM4B	JMJD2B, JHDM3B	H3K9me2, H3K9me
		H3K36me2, H3K36me3
KDM4C	JMJD2C, JHDM3C	H3K9me2, H3K9me3
	GASC1	H3K36me2, H3K36me3
KDM5 family		
KDM5A	JARID1A, RBP2	H3K4me2, H3K4me3
KDM5B	JARID1B, PLU-1	H3K4me2, H3K4me3
KDM5C	JARID1C, SMCX	H3K4me2, H3K4me3
KDM5D	JARID1D, SMCY	H3K4me2, H3K4me3
KDM6 family		
KDM6A	UTX	H3K27me2, H3K27me3
KDM6B	JMJD3	H3K27me2, H3K27me3

either H3K4 or H3K9. The catalytic mechanism for demethylation by LSD1 and 2 requires a protonated nitrogen moiety, and thus flavin-dependent histone demethylases can only demethylate monomethyl- and dimethyllysines. The histone demethylases in classes KDM2–KDM6 all utilize Fe(II) and 2-oxoglutarate cofactors and thus do not have the same substrate restriction.[165] They are able to demethylate the mono-, di-, and trimethylated forms of lysines H3K4, H3K9, H3K27, H3K36, and H1K26 on the histone tail. The 2-oxoglutarate-dependent histone demethylases are members of the Jumonji family; so named because they contain the JmjC (Jumonji) protein domain within their structure.[166] KDMs in classes 2–6 belong to six subfamilies termed JMJD1, JMJD2, JARID1, UTX/Y-JMJD3, PHF, and FXBL. However, to avoid confusion brought about by different names for each, the nomenclature is changed to KDM2–KDM6 enzymes (**Table 3**).

The KDM2 subfamily is comprised of two histone demethylases, KDM2A (JHDM1A, FBXL11)[167] and KDM2B (JHDM1B, FBXL10),[168] both of which are specific for H3K36me and H3K36me2, recognize unmethylated GpG island DNA, and target the polycomb repression system. The KDM3 subfamily contains three KDMs: KDM3A (JMJD1A, JH-DM2A, and TSGA),[169] KDM3B (JMJD1B, JHDM2B, and 5qNCA),[170] and KDM3C (JMJD1C, JHDM2C, and TRIP8).[171] The KDM3 subfamilies are specific for H3K9me and H3K9me2 and act as transcriptional activators. The KDM4 subfamily is comprised of KDM4A (JMJD2A and JHDM3A),[172] KDM4B (JMJD2B, JHDM3B),[173] and KDM4C (JMJD2C, JHDM3C, and GASC1).[174] KDM4s can demethylate H3K9me2 and H3K9me3, leading to the activation of transcription; or H3K36me2 and H3K36me3, leading to transcriptional repression. The KDM5s KDM5A, B, C, and D demethylate H3K4me2 and H3K4me3, leading to transcriptional repression, while KDM6A and B demethylate H3K27me2 and H3K27me3, promoting transcriptional activation.

It is now well established that H3K4 methylation mediated by LSD1 is one of the drivers in cancer initiation and progression. This observation has generated considerable interest in the design and development of novel LSD1 inhibitors for use as antitumor agents. These inhibitors can be broadly classified into at least four classes: (1) peptide-based inhibitors, (2) tranylcypromine (TCP) analogs, (3) oligoamines, and (4) other small molecule inhibitors.

Peptidic analogs of the 21 amino acid H3K4 substrate region of LSD1, aziridinyl-K4H3$_{1-21}$, propargyl-K4H3$_{1-21}$, and *N*-methylpropargyl-K4H3$_{1-21}$ (**Fig. 16**) were synthesized in an effort to identify novel active site-directed inhibitors of LSD1. The

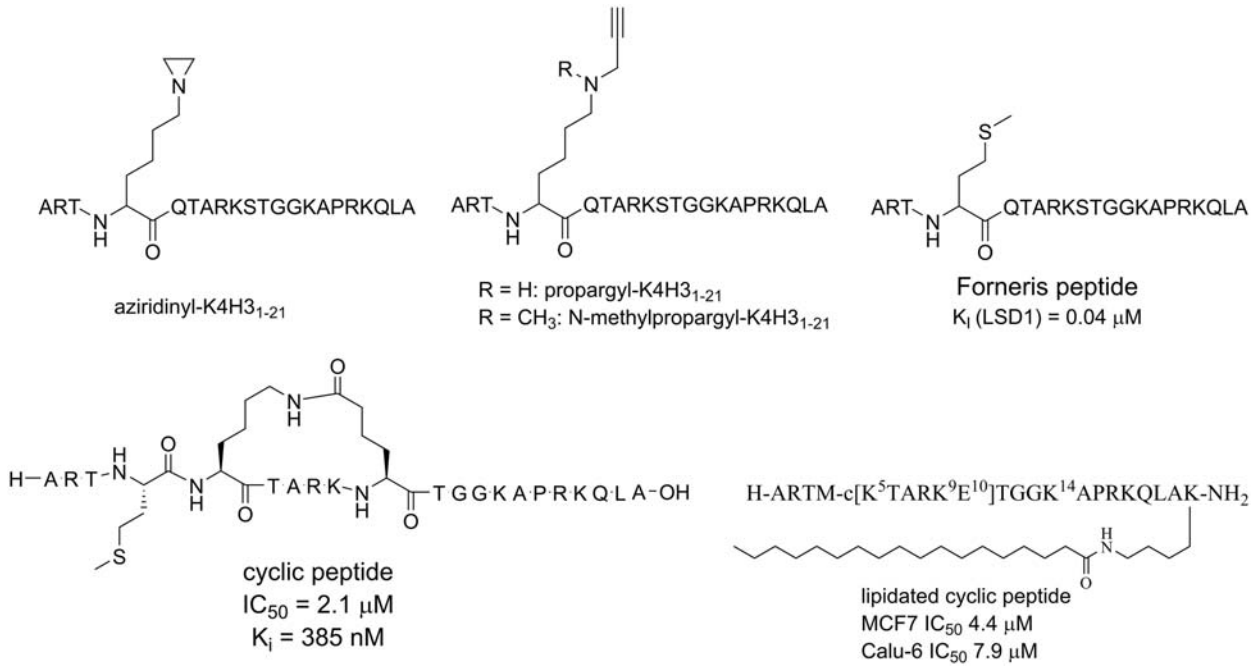

Fig. 16 Examples of peptide-based inhibitors of LSD1 (KDM1A).

aziridinyl derivative reversibly inhibited LSD1 with an IC_{50} of 15.6 μM, while propargyl-K4H3$_{1-21}$ produced time-dependent inactivation with a K_i of 16.6 μM.[175] The analogs propargyl-K4H3$_{1-21}$ and *N*-methylpropargyl-K4H3$_{1-21}$ were later shown to produce time-dependent inactivation of LSD1 through formation of a covalent adduct with the enzyme-bound flavin cofactor; thus these peptides were valuable as tools to elucidate the mechanism of LSD1.[176,177] Dancy et al. reported a number of peptide-based inhibitors that exhibited good LSD1 inhibition.[178] While these analogs acted as efficient probes to unravel the mechanism of LSD1, their poor bioavailability precluded their potential for further advancement.[178] Forneris et al. described a 21-mer peptide analogous to the H3K4 substrate region of LSD1, wherein Lys4 was replaced by a methionine. This linear peptide was a potent inhibitor of recombinant LSD1 with an K_i value of 0.04 μM and of LSD1 bound to CoREST with an K_i value of 0.05 μM.[179] The X-ray structure of this peptide bound to LSD1/CoRESt revealed that it assumed a cyclic orientation in the binding site. This crystal structure was used as a template to design cyclic peptide inhibitors of LSD1. Cyclic peptides are generally considered to be more stable against proteolytic enzymes than their linear counterparts[180] and can facilitate elucidation of bioactive conformations that are important for biological activity. Subsequently, a 21 amino acid cyclic peptide (Fig. 16) was synthesized and found to inhibit LSD1 with an IC_{50} of 2.1 μM and a K_i value of 385 nM.[181] This cyclic peptide was seven-fold more stable than the Forneris peptide in rat plasma. These cyclic peptides, although potent inhibitors of the purified enzyme, exhibited poor cell penetration. A lipidated version of the most active cyclic peptide (Fig. 16) retained the potency of the parent against the enzyme and had good antitumor activity in MCF7 and Calu-6 cell culture preparations. The lipidated compound also promoted a cellular increase in H3K4me2, as measured by PCR.

Because of the homology between LSD1 and monoamine oxidases (MAOs), classical MAO inhibitors such as pargyline and TCP were among the first small molecule LSD1 inhibitors that were tested and reported in the literature. The classical MAO inhibitors phenelzine and TCP are effective LSD1 inhibitors but act as pan-oxidase inhibitors that show no selectivity between LSD1 and MAO. A large number of inhibitors based on the TCP scaffold have been synthesized, and compounds in this class have been extensively reviewed elsewhere.[182] Johnson et al. disclosed novel LSD1 inhibitors containing piperidinyl analogs of phenyl cyclopropylamine.[183] A representative compound from this series was shown to be highly potent against LSD1 (mean $pIC_{50} = 8.3$) and very selective when compared to MAO-B ($pIC_{50} = 4.1$). Three TCP analogs from this series (Fig. 17) developed by GlaxoSmithKline (GSK2879552, GSK-LSD1, and GSK2699537) act as mechanism-based inhibitors of LSD1 and form adducts with the flavin ring of FAD. These compounds are highly specific for LSD1 and do not inhibit MAO-A or MAO-B. The clinical compound, GSK2879552, has a K_i^{app} of 1.7 μM and a k_{inact} value of 0.11 min^{-1}.[184] GSK2879552 entered phase I dose escalation study in subjects with AML. A similar TCP analog, ORY-1001,[185–187] is also in phase I/II clinical trials for AML through a collaboration between Oryzon and Roche. Neelamegam reported a series of brain-penetrating TCP analogs, the most promising of which is RN-1.[188] RN-1 inhibited LSD1 with an IC_{50} of 10–70 nM (depending on the assay used) and was highly selective for LSD1 over MAO-A and B. They used this compound to show that LSD1 inhibition can abolish long-term memory formation without affecting short-term memory, providing further evidence for the importance of reversible histone methylation in the function of the nervous system. A series of pyrrole and indole-containing TCP analogs have recently been described,[189,190] the most potent of which is shown in Fig. 17. This compound not only inhibited LSD1 with an IC_{50} of 40 nM, but also inhibited MAO-A (IC_{50} 160 nM).

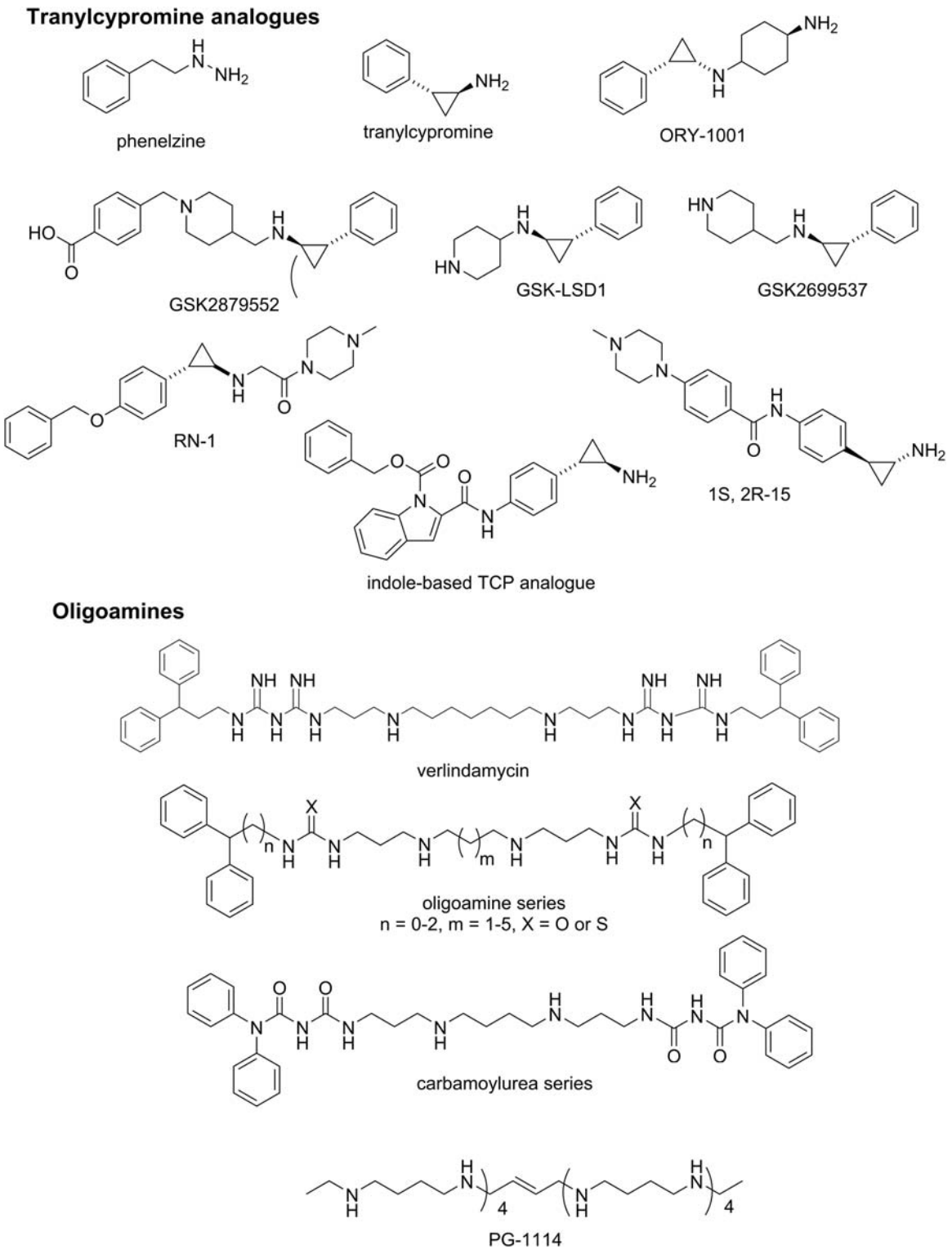

Fig. 17 Tranylcypromine- and oligoamine-based inhibitors of LSD1.

Vianello reported a TCP analog, compound 1S,2R-15 (Fig. 17), that inhibited LSD1 with an IC_{50} of 84 nM. The analog produced 85% growth inhibition in APL blast cells at 250 nM and 60% growth inhibition in THP1 cells at 500 nM. It also prolonged survival by 62% in a murine leukemia model, although at a relatively high oral dose (22.5 mg kg^{-1}).[191] For a comprehensive description of TCP-based LSD1 inhibitors, the reader is referred to the excellent review by McAllister et al.[192]

Due to the structural similarity between LSD1 and the polyamine-metabolic enzyme spermine oxidase, a series of (bis)guanidine and (bis)biguanude polyamine oxidase inhibitors were evaluated for activity against LSD1. This resulted in the identification of the first small molecule inhibitor of LSD1, the (bis)biguanide verlindamycin, which was reported in 2007. Verlindamycin was found to act as a noncompetitive inhibitor of LSD1 with a K_i value of 0.6 μM and caused a promoter-specific increase in H3K4me2 and the corresponding reexpression of silenced tumor suppressor genes (*SFRP*1, *SFRP*4, *SFRP*5, and *GATA*5) in HCT116 colon tumor cells.[22] Verlindamycin and the related oligoamine PG-11144 also had in vivo efficacy when combined with the deoxynucleotide methyltransferase (DNMT) inhibitor 5-AC in a mouse xenograft model.[193] Isosteric replacement of the biguanide moiety in verlindamycin with a urea, thiourea, or carbamoylurea resulted in the discovery of (bis)ureido- and (bis)-thioureido-oligamines and bis-substituted carbamoylureas (**Fig. 17**) that were more potent than verlindamycin with regard to LSD1 inhibition and reexpression of silenced tumor suppressor genes.[194] Subsequent SAR studies demonstrated that the most active epigenetic modulators were (bis) ureas or (bis)thioureas that had an $n=1$ and an $m=3$ or 4.[195] Three out of nine compounds with the 3-5-3 backbone produced >95% inhibition of the enzyme at 10 μM in a fluorimetric assay. The compound where $m=3$, X=S, and $n=2$ displayed potent LSD1 activity ($IC_{50}=5.5$ μM) and produced significant cytotoxicity in an MTS reduction assay ($IC_{50}=4$ μM). It also induced significant reexpression of aberrantly silenced tumor suppressors such as SFRP2, HCAD, GATA4, and p16 in Calu6 lung adenocarcinoma cells. Importantly, this analog was also found to be an effective growth inhibitor of the MCF7 estrogen receptor-positive breast tumor cell line ($IC_{50}=5.6$ μM) and the estrogen receptor negative MDA-MB-231 breast tumor line ($IC_{50}=9.2$ μM) in vitro, but was less effective against the MCF10A breast epithelial cell line ($IC_{50}=19$ μM). When evaluated in an Hs683 glioma xenograft, it was well tolerated and effective in limiting tumor growth without weight loss in combination with 5-AC but was less effective than 5-AC plus verlindamycin or PG-11144.

In addition to TCP analogs, which are all mechanism-based, irreversible inhibitors of LSD1, a number of reversible inhibitors have appeared (**Fig. 18**). As part of an effort to identify novel LSD1 inhibitor scaffolds, Hazeldine et al. carried out virtual screening of the Maybridge Hitfinder 5 compound library and identified a series of amidoxime as potential LSD1 inhibitors.[196] In this model, amidoxime A contained a hydrophilic moiety that appeared to be situated near the FAD cofactor and a hydrophobic substituent that was bound in the hydrophobic pocket. It was a weak inhibitor of LSD1 (11.4% at 10 μM) and promoted a 1.6-fold increase in global H3K4me2 levels in the Calu-6 lung tumor cell line. Optimization studies led to the identification of the ortho fluoro derivative amidoxime B, which was a modest inhibitor of LSD1, but produced a 12.4-fold increase in global H3K4 methylation at 10 μM and then to amidoxime C and related analogs. Compounds in this series served as epigenetic modulators that produced increases in H3K4 methylation as high as 3700-fold, including amidoxime C (39% inhibition of LSD1 at 10 μM with an accompanying 837-fold increase in global H3K4me2 levels). Under the same conditions, TCP and pargyline at 10 μM produced an 18.4% and 69.8% inhibition of LSD1. Recently, Abdulla et al. reported that, in a fluorimetric assay, various natural polyphenols such as resveratrol, curcumin, and quercetin were identified as LSD1 inhibitors.[197] Inhibition of LSD1 by resveratrol and curcumin appears to inhibit myogenesis in cell culture by inhibition of myogenic gene expression. These natural polyphenols have a novel mechanism that should be elucidated, since their inhibitory activity appears to be independent of their antioxidant properties.

By combining the key ligand attributes of oligoamines, MAO inhibitors, and a methionine-based LSD1 peptide inhibitor,[179] Dulla et al. reported a small series of phenyl oxazoles containing either amine or guanidine moiety.[198] The representative compound shown in **Fig. 18** displayed a good LSD1 inhibition profile (in vitro IC_{50} of 9.5 μM; cellular $IC_{50}=1.3$ μM in cultured MDA-MB-231 cells) and induced apoptosis in zebrafish embryos, suggesting the therapeutic potential of these compounds. Namoline, a γ-pyrone derivative, was shown by Willmann et al. to inhibit LSD1 ($IC_{50}=51$ μM) but not MAO-A and B.[199] Namoline caused increases in H3K4me2 and H3K4me, and it silenced androgen receptor-mediated gene expression, leading to reduced proliferation of LnCAP prostate tumor cells in vitro and in vivo. Schmitt and coworkers recently described a series of nonpeptidic propargylamine LSD1 inhibitors.[200] These compounds, which contained the propargyl and other warhead moieties, were only modestly potent ($IC_{50}=22.2$ μM for the compound shown in **Fig. 18**) and produced increases in H3K4me2 in MCF7 cells (1.6–1.7-fold) only at concentrations of ≥100 μM. Although these compounds contain a propargyl moiety that is present in previously described inactivators of LSD1, no enzyme kinetic data were presented.

Fiskus and coworkers reported a series of reversible benzohydrazide inhibitors such as SP-2509 (**Fig. 18**)[187,201] that attenuated the binding of LSD1 with CoREST, increased the transcription activating mark H3K4Me3 at target gene promoters, and increased the levels of p21, p27, and CCAAT/enhancer binding protein A in cultured AML cells. Coadministration of SP2509 and the HDAC inhibitor panobinostat in an immune-depleted mouse model of human AML afforded significantly better survival than either agent alone with minimal toxicity and represents a potential for cure of the immune-depleted mice engrafted with AML cells expressing NPM1 mutation. Kutz and coworkers recently described a series of potent LSD1 inhibitors based on a novel 3,5-diamino-1,2,4-triazole scaffold.[202] The two best inhibitors in the series, C1 and C15 (**Fig. 18**), act as potent LSD1 inhibitors, with IC_{50} values of 1.19 and 2.22 μM, respectively. Compound C1 is a competitive inhibitor of the enzyme, with a K_i of 2.2 μM. Both C1 and C15 show a high degree of specificity for LSD1 in vitro and do not inhibit MAO-A or MAO-B at concentrations up to 100 μM. Both cause significant increases in cellular levels of the transcription-activating mark H3K4me2. Importantly, these inhibitors exhibit low toxicity to mammalian cells in vitro, and thus they may show utility in the treatment of epigenetically based diseases where cell death is not a desired endpoint. The 1,2,3-triazole-dithiocarbamate hybrid shown in **Fig. 18** produced specific and robust inhibition of LSD1 (IC_{50} 2.1 μM) as well as inhibition of migration and invasion in the gastric cancer cell line MGC-823.[203] *N*′-(1-Phenylethylidene)-benzohydrazide is a potent and specific LSD1 inhibitor, but its activity in a xenograft of castration resistant prostate tumor appears to be due to cytotoxicity unrelated to LSD1 inhibition.[204,205] GSK354, a novel tricyclic pyridine analog, was

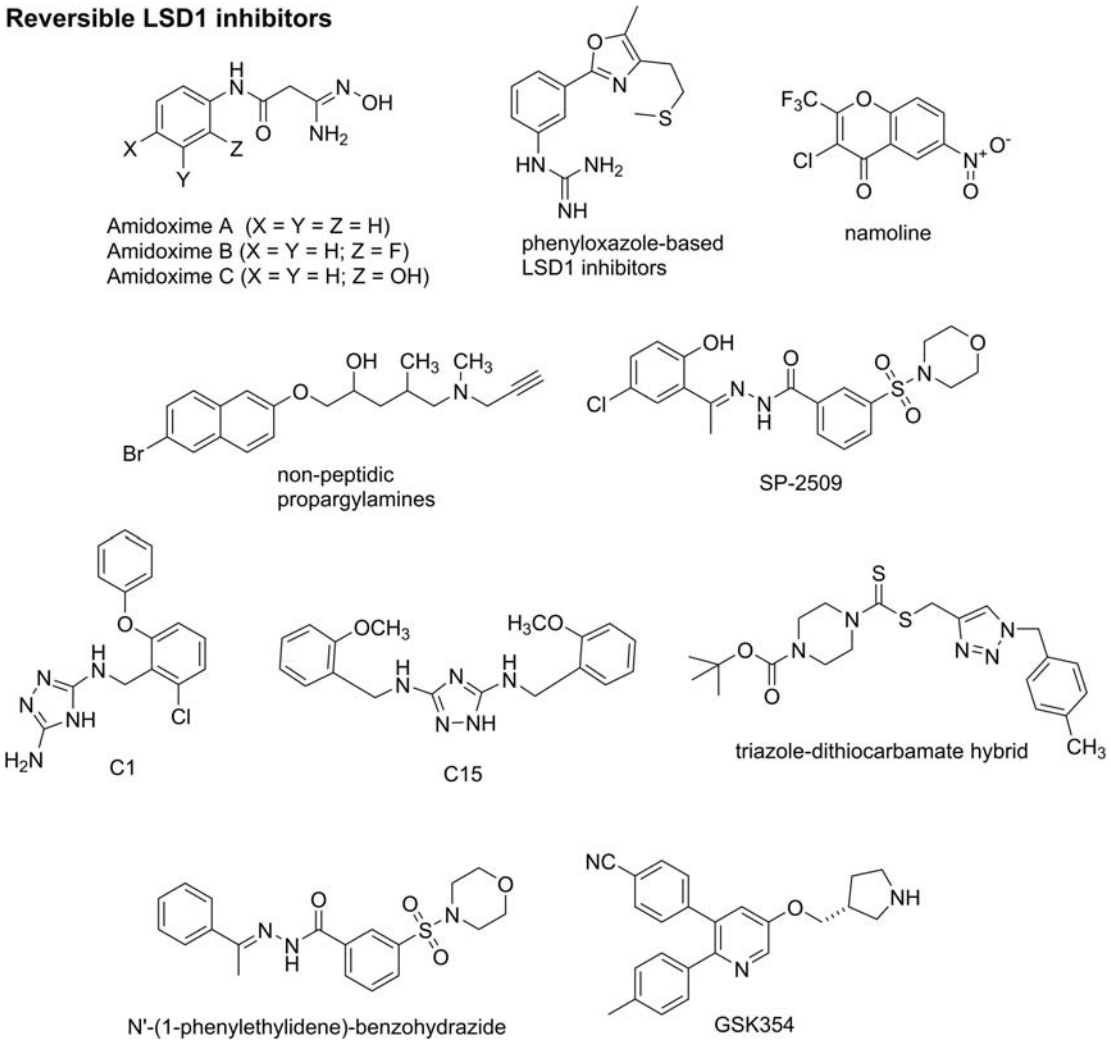

Fig. 18 Reversible inhibitors of LSD1.

found to be a potent LSD1 inhibitor ($IC_{50} \leq 100$ nM) and highly selective (MAO $IC_{50} \geq 200$ μM). This compound is not being developed but is considered a chemical probe suitable for use in biological function studies.[206]

Considering the importance of JmjC domain-containing demethylases in various cancers, intense inhibitor-design efforts were pursued to identify optimal compounds that elicit good activity and selectivity. These inhibitors (**Fig. 19**) are classified into at least five categories: (1) hydroxamic acids, (2) oxalyl derivatives, (3) pyridyl analogs, (4) flavanoids/catechols, and (5) hydroxyquinolines. A comprehensive review of inhibitors of JMJD demethylases has recently been published.[192]

It has been hypothesized that compounds that coordinate with Zn^{2+} (such as HDAC inhibitors) may also coordinate with the Fe^{2+} present in JmjC demethylases. However, when the known HDAC inhibitor SAHA was tested against JMJD2E, a weak inhibition was observed ($IC_{50} = 540$ μM) suggesting that it was not the case.[207] Subsequently, it was reported that hydroxamic acids linked to tertiary amines or cyclopropane groups through alkyl chains can efficiently inhibit KDM4 and KDM2A activities, respectively.[208] However, through screening and hit-to-lead optimization, the long-chain hydroxamic acid shown in **Fig. 19** was discovered. This compound exhibited an IC_{50} against KDM5A of 3.3 μM, and was reasonably selective over KDM4C and KDM3A. A number of other hydroxamates have been synthesized as jumonji demethylase inhibitors, and some success has been achieved with inhibitors selective for KDM2A. One of the potent hydroxamic acid inhibitors reported so far is 3-hydroxyphenyl hydroxamic acid ($IC_{50} = 28$ μM; 4.8 μM with preincubation against JMJD2E).

Rose et al. identified a series of metal-chelating inhibitor scaffolds that mimic the 2-oxoglutarate cofactor in Fe(II)-2-oxoglutarate-dependent histone demethylases.[207] *N*-Oxalyl glycine, R = H, displayed an IC_{50} of 78 μM when tested against JMJD2E. Interestingly, the IC_{50} dropped to 24 μM with 30 min preincubation. Several other derivatives of N-oxalylated D-amino acids were synthesized, the most active being an *N*-oxalylphenylalanine ($IC_{50} = 5.4$ μM) containing a *p*-bromobenzene sulfonyl substituent.

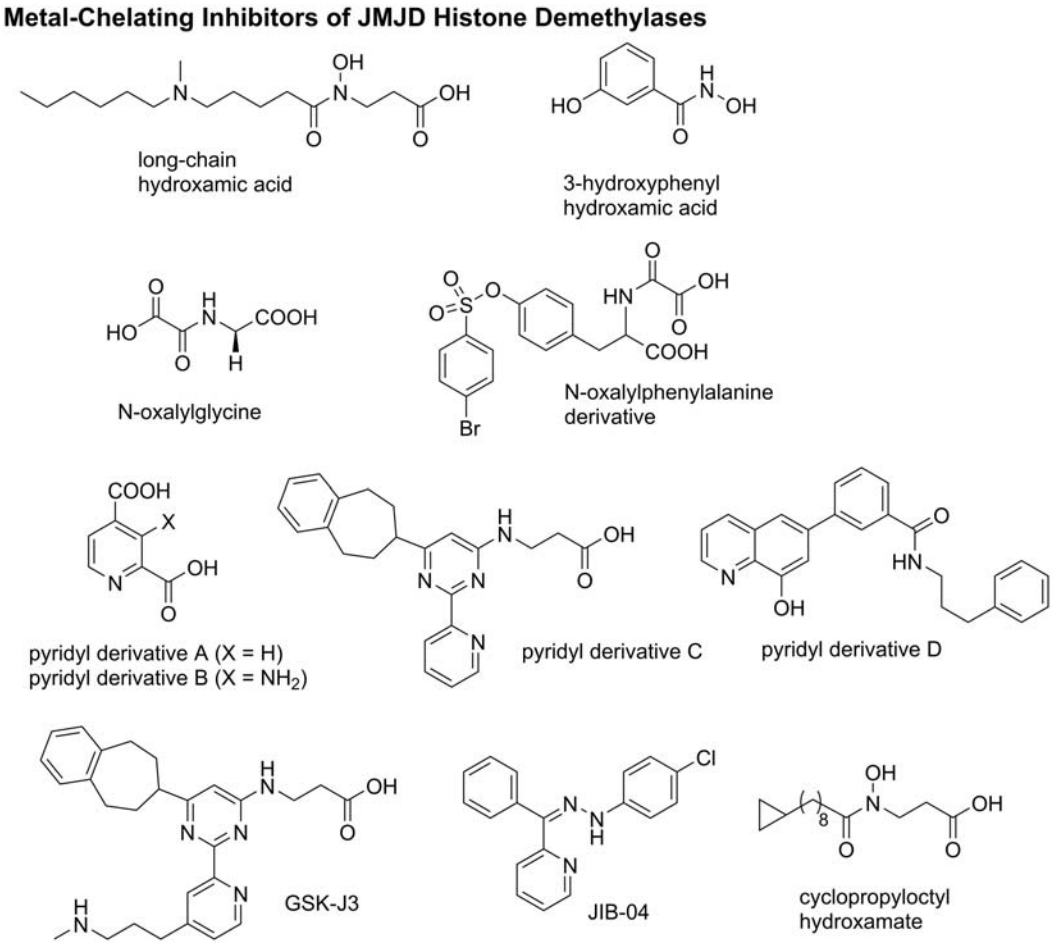

Fig. 19 Metal-chelating inhibitors of JMJD histone demethylases.

Thalhammer et al. tested the JMJD2E inhibition of pyridyl carboxylates (Fig. 19) that are known to interact with Fe^{2+} in collagen/hypoxia-inducible factor. Pyridyl derivative emerged as a good inhibitor with IC_{50} value of 1.4 μM. Continuing studies produced additional analogs such as pyridyl derivative B and C, with IC_{50} values of 0.11 and 2.5 μM, respectively, against JMJD2E.[209] More recently, hydroxyquinolines related to pyridyl derivative D have been discovered. This compound is a potent inhibitor of KDM4B (IC_{50} 10 nM), has low micromolar activity against KDM4A, 4C, and 5A, and does not inhibit LSD1. Pyridyl derivative D is cytotoxic against LNCaP cells in vitro with an IC_{50} of < 1 μM.[210]

Kruidenier et al. reported one of the most potent JMJD3 (KDM6) inhibitors thus far.[211,212] Based on a structure-based and chemoproteomics approach, they synthesized a series of beta-alanine derivatives containing 2-(pyridinyl)-4-pyrimidine moiety. One of the potent inhibitors in the series, GSK-J3, is highly active against JMJD3 ($IC_{50} = 60$ nM), shows no activity against a panel of other family members, and reduces lipopolysaccharide-induced proinflammatory cytokine (TNF-α) production by human macrophages, a process regulated by JMJD3 and UTX. The compound known as JIB-04 specifically inhibits the activity of the Jumonji family of histone demethylases in vitro, in cancer cells, and in tumors in vivo. Interestingly, it is not a competitive inhibitor of α-ketoglutarate. Studies show that JIB-04 alters transcriptional pathways, thus blocking cell viability, reducing tumor burden, and prolonging survival. The cyclopropyloctyl hydroxamate shown in Fig. 19 was found to be a potent inhibitor of KDM2A ($IC_{50} = 6.8$ μM), KDM7A ($IC_{50} = 0.2$ μM), and KDM7B ($IC_{50} = 1.2$ μM) but only produced modest increases in H3K27me2.[213] However, this analog showed antiproliferative activity against the KYSE150 esophageal squamous cell carcinoma line.

Sakurai et al. designed and implemented a robust and miniaturized high-throughput kinetic assay to identify JMJD2E inhibitors.[214] Naturally occurring flavonoids (such as myricetin, baicalein, and β-lapachone) and catechols (such as dopamine, (*S*)-carbidopa, and fenoldopam) were identified as hits with IC_{50} values ranging from 2 to 10 μM.

2.12.3.4 Agents Targeting Epigenetic Reader Proteins

Histone PTMs signal for changes in gene expression using specific reader proteins that either recruit or stabilize various components of the transcriptional machinery.[4] There are at least 26 families of reader proteins that function to interpret signals from methylated

Table 4 Epigenetic reader proteins and their recognized ligands

Reader protein	*Histone substrates*
Methylated lysine residues	
ADD	H3K9me3
Ankyrin	H3K9me, H3K9me2
BAH	H4K20me2
Chromobarrel	H3K36me2, H3K36me3, H4K20me1, H3K4me1
Chromodomains	H3K9me2, H3K9me3, H3K27me2, H3K27me3
DCD	H3K4me3, H3K4me2, H3K4me1
MBT	H3Kme1, H3Kme2, H4Kme1, H4Kme2
PHD	H3K4me2, H3K4me3, H3K9me3
PWWP	H3K36me3, H4K20me1, H4K20me3, H3K79me3
TTD	H3K4me3, H3K9me3, H4K20me2
Tudor	H3K36me3
WD40	H3K27me3, H3K9me3
zf-CW	H3K4me3
Methylated arginine residues	
ADD	H4R3me2 (symmetrical)
Tudor	H3Rme2, H4Rme2
WD-40	H3R2me2
Acetylated lysine residues	
Bromodomains	H3Kac, H4Kac, H2AKac, H2BKac
DBD	H3KacKac, H4KacKac
DPF	H3Kac
Double PH	H3K56ac

lysines and arginines, acetylated lysines, phosphorylated serines and threonines, and even unmodified histones (Table 4, Fig. 20). A complete discussion of these reader proteins, their specificities for histone PTMs, and their effects on transcription is not included in this article, since it is the subject of an excellent review.[4] The methyllysine reader group has been the most completely characterized, but bromodomains have received the most attention as drug targets.[215] The term bromodomain refers to the Bromodomain and Extra-Terminal (BET) family of human proteins (BRD2, BRD3, and BRD4), which feature two highly conserved N-terminal bromodomains as well as a C-terminal domain with potential for more divergence in sequence.[216,217] There are eight families of BCPs, and to date, 61 bromodomains have been identified as components of 46 large, multidomain protein BCPs. Within BCP reader proteins, bromodomains fold to form a highly conserved four-helix bundle structure, creating a deep hydrophobic cavity that recognizes and binds acetyllysine. Acetylated lysine makes several contacts with these hydrophobic residues, and the complex is stabilized by a hydrogen bond with a highly conserved asparagine. Lysine acetylation recruits transcriptional coactivators such as p300 and the bromodomain-containing cyclic AMP-responsive element binding protein (PCAF).[54,55] The bromodomain found in PCAF is one of the three known protein domains that act as acetylated lysine-binding elements [the other two are DPF and double pleckstrin

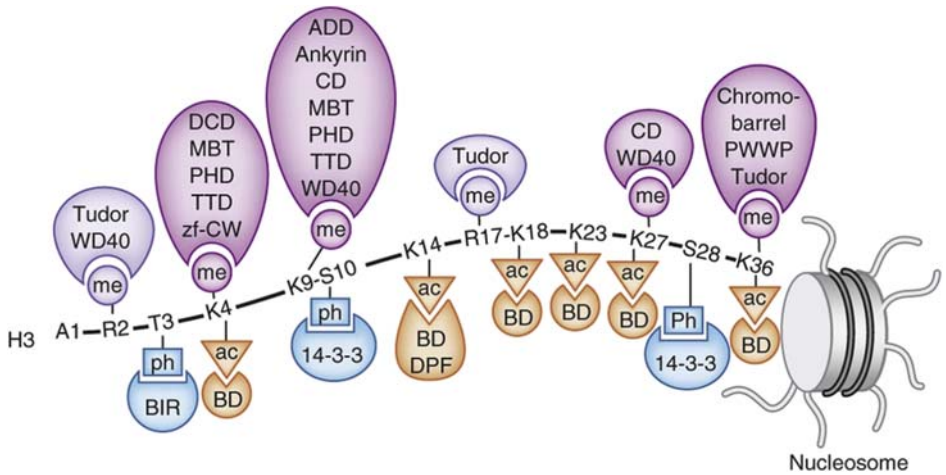

Fig. 20 Epigenetic reader proteins and their PTM ligands. From Musselman, C.A.; Lalonde, M.E.; Cote, J.; Kutateladze, T.G. Perceiving the Epigenetic Landscape Through Histone Readers. Adapted from Musselman et al. *Nat. Struct. Biol.* **2012**, *19* (12), 1218–1227.

homology (PH) domains].[215] These coactivators have inherent autocatalytic acetyltransferase activity, and also recruit transcription factors into a complex that promotes active gene transcription, and therefore play a key role in the activation of transcription.[7,218] Aberrant HDAC overexpression results in the reduction of acetylated lysine and the loss of BCPs, leading to transcriptional repression. HDAC inhibitors have been shown to synergize with p300 autoacetylation to restore acetyl lysine levels and the binding of bromodomain-containing transcription factors, activating transcription.[19] This series of events promotes the expression of various transcriptional products. Based on these facts, it is clear that small molecule inhibitors of the interaction of bromodomains with acetyllysines could serve as epigenetic modulators with therapeutic value. Because BET proteins can play a role in the development of cancer, they are a rational target for the discovery of antitumor agents. Specifically, BRD4 influences mitotic progression by binding to transcriptional start sites of genes and directing postmitotic transcription, mediates transcriptional elongation and has been linked to c-MYC dependent transcription as well as positive transcription elongation factor complex-induced increased growth promotion.[219,220]

Mujtaba et al. utilized an NMR-based screening approach to identify small molecules that could bind to the PCAF bromodomain and disrupt its function.[221] Although *N*-aminopropyl-2-nitro-4-methylaniline (**Fig. 21**, $IC_{50} = 1.6$ μM) disrupted the PCAF BRD/Tat-AcK50 protein/protein interaction,[222] it was found to bind to PCAF in the peptide-binding groove and not at the acetyllysine site. Subsequent efforts to design small molecule bromodomain inhibitors have focused largely on the BET family of bromodomains. Filippakopoulos et al. used structure-based design techniques to discover (+)JQ1, an optically active molecule that contains the thienodiazepine moiety that binds to BET bromodomain and disrupts the binding of acetyllysine to the BRD4 bromodomain. This interaction promotes cellular differentiation and growth inhibition in a NUT midline carcinoma cell line.[216] Nicoteme et al. performed a physical screen to identify molecules that can upregulate the ApoA1 reporter gene. They ultimately discovered GSK525762, a potent inhibitor containing the benzodiazepine moiety, that binds to the tandem bromodomains of BET with high affinity ($K_d = 50.5–61.3$ nM).[223] GSK525762 offers protection against LPS-induced endotoxic shock and bacteria-induced sepsis and is currently in clinical trials to evaluate efficacy in patients with NUT midline carcinoma and other cancers. The observation that the triazolodiazepine nucleus was a common structural feature in bromodomain inhibitors led to the discovery that clinically approved benzodiazepines, most notably alprazolam, had low micromolar affinity for the BRD4 bromodomain. The compound known as RVX-208 is an orally acting bromodomain inhibitor produced by Resverlogix Corporation. The quinazolinone analog RVX-208 is 15- to 30-fold more active against the BET family reader BRD2 compared to BRD1.[224] By contrast, diazobenzenes MS436[225] and olinone[226] preferentially bind to the BRD1 BET family proteins. RVX-208 removes atherosclerotic plaque via reverse cholesterol transport and is currently in Phase IIb trials.[227] Lastly, OTX-015, a novel orally acting BET bromodomain inhibitor produced by OncoEthix, induces potent antiproliferative effects that are associated with cell cycle arrest, cellular senescence, or apoptosis. The compound was in Phase I clinical trials where it is evaluated against acute leukemia and other hematological malignancies, but that trial was stopped after 1 year.[228] Incyte is also conducting a phase I/II clinical trial for patients with advanced malignancies, but the structure of the compound being evaluated, INCB054329, has not been disclosed.

A number of other bromodomain inhibitors with a variety of therapeutic properties have been reported. Hewings et al. used X-ray crystallographic structures to design a substituted 3,5-dimethylisoxazole A,[229] which had an IC_{50} of 4.8 μM against BRD4 and 1.6 μM against BRD2. A similar analog, 3,5-dimethylisoxazole B, was identified through focused fragment screening by Bamborough et al.[230] 3,5-dimethylisoxazole B exhibited enhanced water solubility and IC_{50} values of 0.5 μM against BRD2, BRD3, and BRD4. This molecule has been shown to possess antiinflammatory activity in a cellular assay system. Dawson et al. reported IBET-151, which inhibits transcription in MLL-fusion leukemia cells by inhibition of BRD3 ($K_d = 20$ nM) and BRD4 ($K_d = 100$ nM) binding to acetyllysine.[231] The benzimidazole analog BIC-1 (**Fig. 21**) was found to block the association of BRD2 with acetylated H3K12 with a dissociation constant of 28 μM.[232] Using structure-based fragment assessment and optimization, Fish et al. discovered PFI-1 (**Fig. 21**), a novel small-molecule that can be used as a chemical probe to study the BET family.[233] Wagner et al. pursued structure-based drug design strategy and reported the discovery of UNC669 ($IC_{50} = 6$ μM), a potent L3MBTL1 inhibitor that displayed fivefold increase in binding affinity compared to the native peptide H4K20me1. The same group also discovered UNC1215, the first potent L3BMTL3 antagonist ($K_d = 120$ nM) that is selective against other members of the MBT family as well as against other reader domains.[234,235] Two selective inhibitors recently developed by the SGC, SGC-CBP-30 and I-CBP112, have low nanomolar potencies for the CBP/EP300 bromodomains.[236] The literature has linked CBP/EP300 to a number of disorders, including (but not limited to) AML and a number of neurodegenerative diseases. The BAZ2B bromodomain inhibitor GSK2801 exhibits high affinity and selectivity for BAZ2B and the closely related protein BAZ2A (K_d of 136 and 257 nM, respectively).[238] Collectively, these studies indicate that specific inhibitors of bromodomain binding have promise for use as biological probes of bromodomain function and for development as novel therapeutic agents. In addition, at least five pharmaceutical companies have bromodomain inhibitors in phase I or II clinical trials.[236] There has been considerable progress in the identification of compounds that disrupt epigenetic reader protein binding to their corresponding epigenetic marks, but a full discussion of all such inhibitors is beyond the scope of this article. However, recent progress in this area has been reviewed.[239,240]

2.12.4 Conclusion

It is evident that the field of epigenetics is a rapidly evolving area of research and the amount of information regarding the topic is formidable and expanding. This article is meant to give the reader a broad view of the processes involved in the epigenetic control of

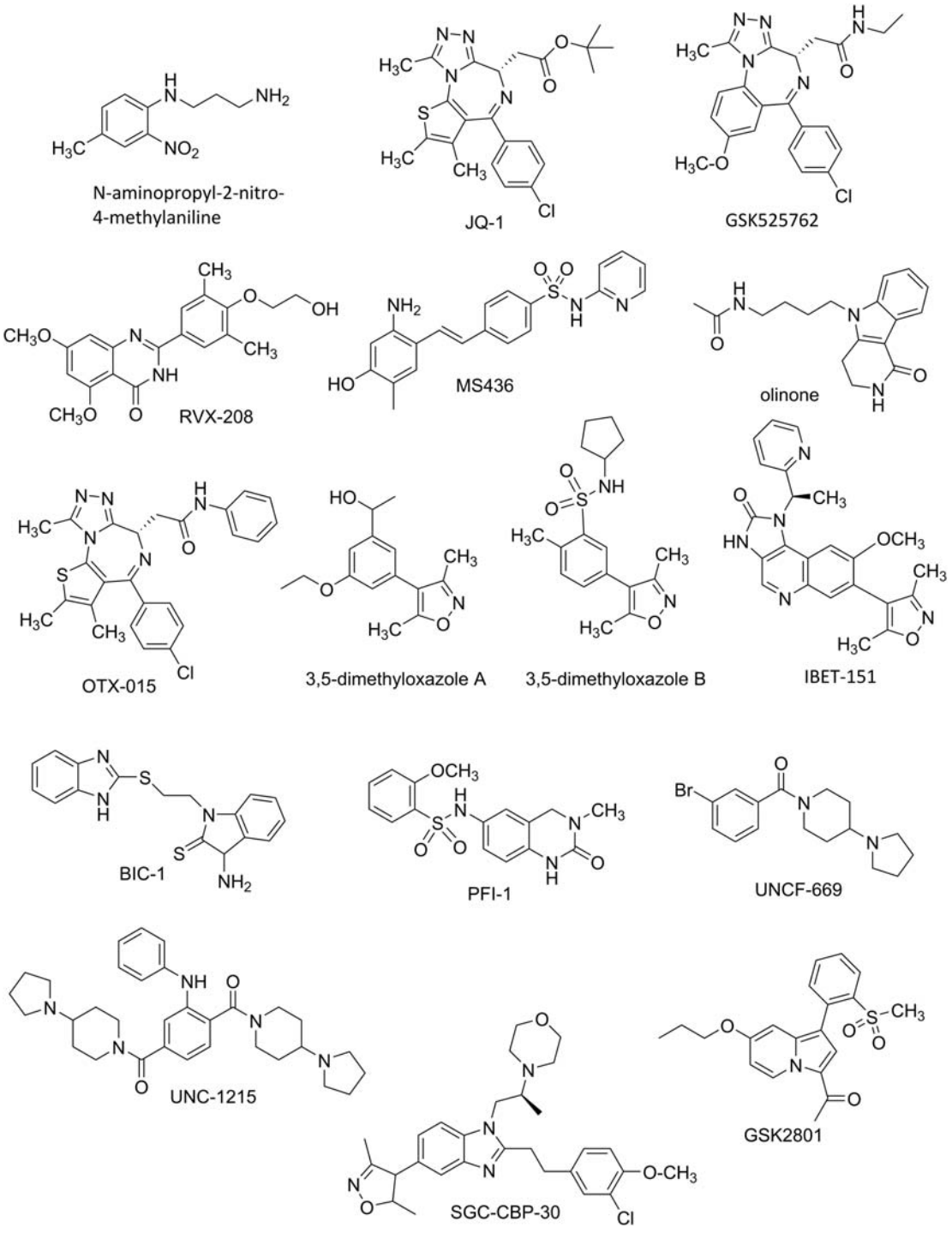

Fig. 21 Inhibitors of the interactions of bromodomain proteins with acetylated lysines.

gene expression, to define epigenetic enzymes and proteins that have become targets for drug discovery, and to provide examples of compounds developed to interact with various aspects of epigenetic modulation. As epigenetic research continues to expand, it will provide a more complete view of the epigenetic landscape and the interaction between various players involved. New targets for drug discovery will be identified and will ultimately result in an arsenal of therapeutic agents to treat diseases with an epigenetic basis. These agents will hopefully be useful for controlling the epigenetic processes that underlay a variety of important maladies and provide a new treatment paradigm for cancer and for a variety of other diseases.

See also: 5.01. Cancer Biology and the Principles of Targeted Cancer Drug Discovery. 5.08. Inhibitors of Epigenetic Regulation in Cancer.

References

1. Jenuwein, T.; Allis, C. D. Translating the Histone Code. *Science* **2001,** *293* (5532), 1074–1080.
2. Lachner, M.; O'Sullivan, R. J.; Jenuwein, T. An Epigenetic Road Map for Histone Lysine Methylation. *J. Cell Sci.* **2003,** *116* (Pt 11), 2117–2124.
3. Ruthenburg, A. J.; Allis, C. D.; Wysocka, J. Methylation of Lysine 4 on Histone H3: Intricacy of Writing and Reading a Single Epigenetic Mark. *Mol. Cell* **2007,** *25* (1), 15–30.
4. Musselman, C. A.; Lalonde, M. E.; Cote, J.; Kutateladze, T. G. Perceiving the Epigenetic Landscape Through Histone Readers. *Nat. Struct. Mol. Biol.* **2012,** *19* (12), 1218–1227.
5. Portela, A.; Esteller, M. Epigenetic Modifications and Human Disease. *Nat. Biotechnol.* **2010,** *28* (10), 1057–1068.
6. Rossetto, D.; Avvakumov, N.; Cote, J. Histone Phosphorylation: A Chromatin Modification Involved in Diverse Nuclear Events. *Epigenetics* **2012,** *7* (10), 1098–1108.
7. Johnstone, R. W. Histone-Deacetylase Inhibitors: Novel Drugs for the Treatment of Cancer. *Nat. Rev. Drug Discov.* **2002,** *1* (4), 287–299.
8. He, X. J.; Chen, T.; Zhu, J. K. Regulation and Function of DNA Methylation in Plants and Animals. *Cell Res.* **2011,** *21* (3), 442–465.
9. Baylin, S. B.; Jones, P. A. A Decade of Exploring the Cancer Epigenome—Biological and Translational Implications. *Nat. Rev. Cancer* **2011,** *11* (10), 726–734.
10. Hansen, K. D.; Timp, W.; Bravo, H. C.; Sabunciyan, S.; Langmead, B.; McDonald, O. G.; Wen, B.; Wu, H.; Liu, Y.; Diep, D.; Briem, E.; Zhang, K.; Irizarry, R. A.; Feinberg, A. P. Increased Methylation Variation in Epigenetic Domains Across Cancer Types. *Nat. Genet.* **2011,** *43* (8), 768–775.
11. Rodriguez-Paredes, M.; Esteller, M. Cancer Epigenetics Reaches Mainstream Oncology. *Nat. Med.* **2011,** *17* (3), 330–339.
12. Fahy, J.; Jeltsch, A.; Arimondo, P. B. DNA Methyltransferase Inhibitors in Cancer: A Chemical and Therapeutic Patent Overview and Selected Clinical Studies. *Expert Opin. Ther. Pat.* **2012,** *22* (12), 1427–1442.
13. Gros, C.; Fahy, J.; Halby, L.; Dufau, I.; Erdmann, A.; Gregoire, J. M.; Ausseil, F.; Vispe, S.; Arimondo, P. B. DNA Methylation Inhibitors in Cancer: Recent and Future Approaches. *Biochimie* **2012,** *94* (11), 2280–2296.
14. Ellis, L.; Atadja, P. W.; Johnstone, R. W. Epigenetics in Cancer: Targeting Chromatin Modifications. *Mol. Cancer Ther.* **2009,** *8* (6), 1409–1420.
15. Marks, P. A.; Richon, V. M.; Miller, T.; Kelly, W. K. Histone Deacetylase Inhibitors. *Adv. Cancer Res.* **2004,** *91,* 137–168.
16. Carafa, V.; Miceli, M.; Altucci, L.; Nebbioso, A. Histone Deacetylase Inhibitors: A Patent Review (2009–2011). *Expert Opin. Ther. Pat.* **2013,** *23* (1), 1–17.
17. Li, J.; Li, G.; Xu, W. Histone Deacetylase Inhibitors: An Attractive Strategy for Cancer Therapy. *Curr. Med. Chem.* **2013,** *20,* 1858–1886.
18. Chen, L. Medicinal Chemistry of Sirtuin Inhibitors. *Curr. Med. Chem.* **2011,** *18* (13), 1936–1946.
19. Stunkel, W.; Campbell, R. M. Sirtuin 1 (SIRT1): The Misunderstood HDAC. *J. Biomol. Screen.* **2011,** *16* (10), 1153–1169.
20. West, A. C.; Johnstone, R. W. New and Emerging HDAC Inhibitors for Cancer Treatment. *J. Clin. Invest.* **2014,** *124* (1), 30–39.
21. Shi, Y.; Lan, F.; Matson, C.; Mulligan, P.; Whetstine, J.; Cole, P.; Casero, R.; Shi, Y. Histone Demethylation Mediated by the Nuclear Amine Oxidase Homolog LSD1. *Cell* **2004,** *119* (7), 941–953.
22. Huang, Y.; Greene, E.; Stewart, T. M.; Goodwin, A. C.; Baylin, S. B.; Woster, P. M.; Casero, R. A. Inhibition of Lysine-Specific Demethylase 1 by Polyamine Analogues Results in Reexpression of Aberrantly Silenced Genes. *Proc. Natl. Acad. Sci. U.S.A.* **2007,** *104,* 8023–8028.
23. Marabelli, C.; Marrocco, B.; Mattevi, A. The Growing Structural and Functional Complexity of the LSD1/KDM1A Histone Demethylase. *Curr. Opin. Struct. Biol.* **2016,** *41,* 135–144.
24. Klose, R. J.; Kallin, E. M.; Zhang, Y. JmjC-Domain-Containing Proteins and Histone Demethylation. *Nat. Rev. Genet.* **2006,** *7* (9), 715–727.
25. Saxonov, S.; Berg, P.; Brutlag, D. L. A Genome-Wide Analysis of CpG Dinucleotides in the Human Genome Distinguishes Two Distinct Classes of Promoters. *Proc. Natl. Acad. Sci. U. S. A.* **2006,** *103* (5), 1412–1417.
26. Akhavan-Niaki, H.; Samadani, A. A. DNA Methylation and Cancer Development: Molecular Mechanism. *Cell Biochem. Biophys.* **2013,** *67* (2), 501–513.
27. Elhamamsy, A. R. DNA Methylation Dynamics in Plants and Mammals: Overview of Regulation and Dysregulation. *Cell Biochem. Funct.* **2016,** *34* (5), 289–298.
28. Wu, S. C.; Zhang, Y. Active DNA Demethylation: Many Roads Lead to Rome. *Nat. Rev. Mol. Cell Biol.* **2010,** *11* (9), 607–620.
29. Sorm, F.; Piskala, A.; Cihak, A.; Vesely, J. 5-Azacytidine, a New, Highly Effective Cancerostatic. *Experientia* **1964,** *20* (4), 202–203.
30. Xu, P.; Hu, G.; Luo, C.; Liang, Z. DNA Methyltransferase Inhibitors: An Updated Patent Review (2012–2015). *Expert Opin. Ther. Pat.* **2016,** *26,* 1–14.
31. Gnyszka, A.; Jastrzebski, Z.; Flis, S. DNA Methyltransferase Inhibitors and Their Emerging Role in Epigenetic Therapy of Cancer. *Anticancer Res.* **2013,** *33* (8), 2989–2996.
32. Esteller, M. Epigenetics in Cancer. *N. Engl. J. Med.* **2008,** *358* (11), 1148–1159.
33. Stresemann, C.; Bokelmann, I.; Mahlknecht, U.; Lyko, F. Azacytidine Causes Complex DNA Methylation Responses in Myeloid Leukemia. *Mol. Cancer Ther.* **2008,** *7* (9), 2998–3005.
34. Stresemann, C.; Lyko, F. Modes of Action of the DNA Methyltransferase Inhibitors Azacytidine and Decitabine. *Int. J. Cancer* **2008,** *123* (1), 8–13.
35. Flesner, B. K.; Kumar, S. R.; Bryan, J. N. 6-Thioguanine and Zebularine Down-Regulate DNMT1 and Globally Demethylate Canine Malignant Lymphoid Cells. *BMC Vet. Res.* **2014,** *10,* 290.
36. Flotho, C.; Claus, R.; Batz, C.; Schneider, M.; Sandrock, I.; Ihde, S.; Plass, C.; Niemeyer, C. M.; Lubbert, M. The DNA Methyltransferase Inhibitors Azacitidine, Decitabine and Zebularine Exert Differential Effects on Cancer Gene Expression in Acute Myeloid Leukemia Cells. *Leukemia* **2009,** *23* (6), 1019–1028.
37. Kim, C. H.; Marquez, V. E.; Mao, D. T.; Haines, D. R.; McCormack, J. J. Synthesis of Pyrimidin-2-One Nucleosides As Acid-Stable Inhibitors of Cytidine Deaminase. *J. Med. Chem.* **1986,** *29* (8), 1374–1380.
38. Barchi, J. J., Jr.; Cooney, D. A.; Hao, Z.; Weinberg, Z. H.; Taft, C.; Marquez, V. E.; Ford, H., Jr. Improved Synthesis of Zebularine [1-(Beta-D-ribofuranosyl)-dihydropyrimidin-2-one] Nucleotides As Inhibitors of Human Deoxycytidylate Deaminase. *J. Enzyme Inhib.* **1995,** *9* (2), 147–162.
39. Newman, E. M.; Morgan, R. J.; Kummar, S.; Beumer, J. H.; Blanchard, M. S.; Ruel, C.; El-Khoueiry, A. B.; Carroll, M. I.; Hou, J. M.; Li, C.; Lenz, H. J.; Eiseman, J. L.; Doroshow, J. H. A Phase I, Pharmacokinetic, and Pharmacodynamic Evaluation of the DNA Methyltransferase Inhibitor 5-Fluoro-2'-deoxycytidine, Administered With Tetrahydrouridine. *Cancer Chemother. Pharmacol.* **2015,** *75* (3), 537–546.
40. Thottassery, J. V.; Sambandam, V.; Allan, P. W.; Maddry, J. A.; Maxuitenko, Y. Y.; Tiwari, K.; Hollingshead, M.; Parker, W. B. Novel DNA Methyltransferase-1 (DNMT1) Depleting Anticancer Nucleosides, 4'-Thio-2'-deoxycytidine and 5-Aza-4'-thio-2'-deoxycytidine. *Cancer Chemother. Pharmacol.* **2014,** *74* (2), 291–302.
41. Chuang, J. C.; Warner, S. L.; Vollmer, D.; Vankayalapati, H.; Redkar, S.; Bearss, D. J.; Qiu, X.; Yoo, C. B.; Jones, P. A. S110, a 5-Aza-2'-deoxycytidine-Containing Dinucleotide, Is an Effective DNA Methylation Inhibitor *In Vivo* and Can Reduce Tumor Growth. *Mol. Cancer Ther.* **2010,** *9* (5), 1443–1450.
42. Lee, B. H.; Yegnasubramanian, S.; Lin, X.; Nelson, W. G. Procainamide Is a Specific Inhibitor of DNA Methyltransferase 1. *J. Biol. Chem.* **2005,** *280* (49), 40749–40756.
43. Datta, J.; Ghoshal, K.; Denny, W. A.; Gamage, S. A.; Brooke, D. G.; Phiasivongsa, P.; Redkar, S.; Jacob, S. T. A New Class of Quinoline-Based DNA Hypomethylating Agents Reactivates Tumor Suppressor Genes by Blocking DNA Methyltransferase 1 Activity and Inducing Its Degradation. *Cancer Res.* **2009,** *69* (10), 4277–4285.

44. Rilova, E.; Erdmann, A.; Gros, C.; Masson, V.; Aussagues, Y.; Poughon-Cassabois, V.; Rajavelu, A.; Jeltsch, A.; Menon, Y.; Novosad, N.; Gregoire, J. M.; Vispe, S.; Schambel, P.; Ausseil, F.; Sautel, F.; Arimondo, P. B.; Cantagrel, F. Design, Synthesis and Biological Evaluation of 4-Amino-*N*-(4-aminophenyl)benzamide Analogues of Quinoline-Based SGI-1027 As Inhibitors of DNA Methylation. *ChemMedChem* **2014,** *9* (3), 590–601.
45. Ceccaldi, A.; Rajavelu, A.; Champion, C.; Rampon, C.; Jurkowska, R.; Jankevicius, G.; Senamaud-Beaufort, C.; Ponger, L.; Gagey, N.; Ali, H. D.; Tost, J.; Vriz, S.; Ros, S.; Dauzonne, D.; Jeltsch, A.; Guianvarc'h, D.; Arimondo, P. B. C5-DNA Methyltransferase Inhibitors: From Screening to Effects on Zebrafish Embryo Development. *Chembiochem* **2011,** *12* (9), 1337–1345.
46. Xie, Q.; Bai, Q.; Zou, L. Y.; Zhang, Q. Y.; Zhou, Y.; Chang, H.; Yi, L.; Zhu, J. D.; Mi, M. T. Genistein Inhibits DNA Methylation and Increases Expression of Tumor Suppressor Genes in Human Breast Cancer Cells. *Genes Chromosomes Cancer* **2014,** *53* (5), 422–431.
47. Siedlecki, P.; Garcia Boy, R.; Musch, T.; Brueckner, B.; Suhai, S.; Lyko, F.; Zielenkiewicz, P. Discovery of Two Novel, Small-Molecule Inhibitors of DNA Methylation. *J. Med. Chem.* **2006,** *49* (2), 678–683.
48. Asgatay, S.; Champion, C.; Marloie, G.; Drujon, T.; Senamaud-Beaufort, C.; Ceccaldi, A.; Erdmann, A.; Rajavelu, A.; Schambel, P.; Jeltsch, A.; Lequin, O.; Karoyan, P.; Arimondo, P. B.; Guianvarc'h, D. Synthesis and Evaluation of Analogues of *N*-Phthaloyl-l-tryptophan (RG108) As Inhibitors of DNA Methyltransferase 1. *J. Med. Chem.* **2014,** *57* (2), 421–434.
49. Kuck, D.; Singh, N.; Lyko, F.; Medina-Franco, J. L. Novel and Selective DNA Methyltransferase Inhibitors: Docking-Based Virtual Screening and Experimental Evaluation. *Bioorg. Med. Chem.* **2010,** *18* (2), 822–829.
50. Fagan, R. L.; Cryderman, D. E.; Kopelovich, L.; Wallrath, L. L.; Brenner, C. Laccaic Acid A Is a direct, DNA-Competitive Inhibitor of DNA Methyltransferase 1. *J. Biol. Chem.* **2013,** *288* (33), 23858–23867.
51. Fagan, R. L.; Wu, M.; Chedin, F.; Brenner, C. An Ultrasensitive High Throughput Screen for DNA Methyltransferase 1-Targeted Molecular Probes. *PLoS One* **2013,** *8* (11), e78752.
52. Marks, P. A.; Miller, T.; Richon, V. M. Histone Deacetylases. *Curr. Opin. Pharmacol.* **2003,** *3* (4), 344–351.
53. Luger, K.; Mader, A. W.; Richmond, R. K.; Sargent, D. F.; Richmond, T. J. Crystal Structure of the Nucleosome Core Particle at 2.8 A Resolution. *Nature* **1997,** *389* (6648), 251–260.
54. Chen, J.; Ghazawi, F. M.; Li, Q. Interplay of Bromodomain and Histone Acetylation in the Regulation of p300-Dependent Genes. *Epigenetics* **2010,** *5* (6), 509–515.
55. Stiehl, D. P.; Fath, D. M.; Liang, D.; Jiang, Y.; Sang, N. Histone Deacetylase Inhibitors Synergize p300 Autoacetylation That Regulates Its Transactivation Activity and Complex Formation. *Cancer Res.* **2007,** *67* (5), 2256–2264.
56. Allis, C. D.; Berger, S. L.; Cote, J.; Dent, S.; Jenuwien, T.; Kouzarides, T.; Pillus, L.; Reinberg, D.; Shi, Y.; Shiekhattar, R.; Shilatifard, A.; Workman, J.; Zhang, Y. New Nomenclature for Chromatin-Modifying Enzymes. *Cell* **2007,** *131* (4), 633–636.
57. Furdas, S. D.; Kannan, S.; Sippl, W.; Jung, M. Small Molecule Inhibitors of Histone Acetyltransferases As Epigenetic Tools and Drug Candidates. *Arch. Pharm. (Weinheim)* **2012,** *345* (1), 7–21.
58. Roth, S. Y.; Denu, J. M.; Allis, C. D. Histone Acetyltransferases. *Annu. Rev. Biochem.* **2001,** *70,* 81–120.
59. Kouzarides, T. Chromatin Modifications and Their Function. *Cell* **2007,** *128* (4), 693–705.
60. Hodawadekar, S. C.; Marmorstein, R. Chemistry of Acetyl Transfer by Histone Modifying Enzymes: Structure, Mechanism and Implications for Effector Design. *Oncogene* **2007,** *26* (37), 5528–5540.
61. Trievel, R. C.; Rojas, J. R.; Sterner, D. E.; Venkataramani, R. N.; Wang, L.; Zhou, J.; Allis, C. D.; Berger, S. L.; Marmorstein, R. Crystal Structure and Mechanism of Histone Acetylation of the Yeast GCN5 Transcriptional Coactivator. *Proc. Natl. Acad. Sci. U. S. A.* **1999,** *96* (16), 8931–8936.
62. Di Martile, M.; Del Bufalo, D.; Trisciuoglio, D. The Multifaceted Role of Lysine Acetylation in Cancer: Prognostic Biomarker and Therapeutic Target. *Oncotarget* **2016,** *7* (34), 55789–55810.
63. Dekker, F. J.; Haisma, H. J. Histone Acetyl Transferases As Emerging Drug Targets. *Drug Discov. Today* **2009,** *14* (19–20), 942–948.
64. Isharwal, S.; Miller, M. C.; Marlow, C.; Makarov, D. V.; Partin, A. W.; Veltri, R. W. p300 (Histone Acetyltransferase) Biomarker Predicts Prostate Cancer Biochemical Recurrence and Correlates With Changes in Epithelia Nuclear Size and Shape. *Prostate* **2008,** *68* (10), 1097–1104.
65. Liu, Y.; Mayo, M. W.; Nagji, A. S.; Hall, E. H.; Shock, L. S.; Xiao, A.; Stelow, E. B.; Jones, D. R. BRMS1 Suppresses Lung Cancer Metastases Through an E3 Ligase Function on Histone Acetyltransferase p300. *Cancer Res.* **2012,** *73* (4), 1308–1317.
66. Kishimoto, M.; Kohno, T.; Okudela, K.; Otsuka, A.; Sasaki, H.; Tanabe, C.; Sakiyama, T.; Hirama, C.; Kitabayashi, I.; Minna, J. D.; Takenoshita, S.; Yokota, J. Mutations and Deletions of the CBP Gene in Human Lung Cancer. *Clin. Cancer Res.* **2005,** *11* (2 Pt 1), 512–519.
67. Gayther, S. A.; Batley, S. J.; Linger, L.; Bannister, A.; Thorpe, K.; Chin, S. F.; Daigo, Y.; Russell, P.; Wilson, A.; Sowter, H. M.; Delhanty, J. D.; Ponder, B. A.; Kouzarides, T.; Caldas, C. Mutations Truncating the EP300 Acetylase in Human Cancers. *Nat. Genet.* **2000,** *24* (3), 300–303.
68. Bryan, E. J.; Jokubaitis, V. J.; Chamberlain, N. L.; Baxter, S. W.; Dawson, E.; Choong, D. Y.; Campbell, I. G. Mutation Analysis of EP300 in Colon, Breast and Ovarian Carcinomas. *Int. J. Cancer* **2002,** *102* (2), 137–141.
69. Manzo, F.; Tambaro, F. P.; Mai, A.; Altucci, L. Histone Acetyltransferase Inhibitors and Preclinical Studies. *Expert Opin. Ther. Pat.* **2009,** *19* (6), 761–774.
70. Lau, O. D.; Kundu, T. K.; Soccio, R. E.; Ait-Si-Ali, S.; Khalil, E. M.; Vassilev, A.; Wolffe, A. P.; Nakatani, Y.; Roeder, R. G.; Cole, P. A. HATs Off: Selective Synthetic Inhibitors of the Histone Acetyltransferases p300 and PCAF. *Mol. Cell* **2000,** *5* (3), 589–595.
71. Zheng, Y.; Thompson, P. R.; Cebrat, M.; Wang, L.; Devlin, M. K.; Alani, R. M.; Cole, P. A. Selective HAT Inhibitors As Mechanistic Tools for Protein Acetylation. *Methods Enzymol.* **2004,** *376,* 188–199.
72. Eliseeva, E. D.; Valkov, V.; Jung, M.; Jung, M. O. Characterization of Novel Inhibitors of Histone Acetyltransferases. *Mol. Cancer Ther.* **2007,** *6* (9), 2391–2398.
73. Stimson, L.; Rowlands, M. G.; Newbatt, Y. M.; Smith, N. F.; Raynaud, F. I.; Rogers, P.; Bavetsias, V.; Gorsuch, S.; Jarman, M.; Bannister, A.; Kouzarides, T.; McDonald, E.; Workman, P.; Aherne, G. W. Isothiazolones As Inhibitors of PCAF and p300 Histone Acetyltransferase Activity. *Mol. Cancer Ther.* **2005,** *4* (10), 1521–1532.
74. Biel, M.; Kretsovali, A.; Karatzali, E.; Papamatheakis, J.; Giannis, A. Design, Synthesis, and Biological Evaluation of a Small-Molecule Inhibitor of the Histone Acetyltransferase Gcn5. *Angew. Chem. Int. Ed.* **2004,** *43* (30), 3974–3976.
75. Gao, X. N.; Lin, J.; Ning, Q. Y.; Gao, L.; Yao, Y. S.; Zhou, J. H.; Li, Y. H.; Wang, L. L.; Yu, L. A Histone Acetyltransferase p300 Inhibitor C646 Induces Cell Cycle Arrest and Apoptosis Selectively in AML1-ETO-Positive AML Cells. *PLoS One* **2013,** *8* (2), e55481.
76. Gao, C.; Bourke, E.; Scobie, M.; Famme, M. A.; Koolmeister, T.; Helleday, T.; Eriksson, L. A.; Lowndes, N. F.; Brown, J. A. Rational Design and Validation of a Tip60 Histone Acetyltransferase Inhibitor. *Sci. Rep.* **2014,** *4,* 5372.
77. Smith, B. C.; Denu, J. M. Chemical Mechanisms of Histone Lysine and Arginine Modifications. *Biochim. Biophys. Acta* **2009,** *1789* (1), 45–57.
78. Feng, Q.; Wang, H.; Ng, H. H.; Erdjument-Bromage, H.; Tempst, P.; Struhl, K.; Zhang, Y. Methylation of H3-Lysine 79 Is Mediated by a New Family of HMTases Without a SET Domain. *Curr. Biol.* **2002,** *12* (12), 1052–1058.
79. Zhang, Y.; Reinberg, D. Transcription Regulation by Histone Methylation: Interplay Between Different Covalent Modifications of the Core Histone Tails. *Genes Dev.* **2001,** *15* (18), 2343–2360.
80. Kaniskan, H. U.; Jin, J. Chemical Probes of Histone Lysine Methyltransferases. *ACS Chem. Biol.* **2015,** *10* (1), 40–50.
81. Krause, C. D.; Yang, Z.-H.; Kim, Y.-S.; Lee, J.-H.; Cook, J. R.; Pestka, S. Protein Arginine Methyltransferases: Evolution and Assessment of Their Pharmacological and Therapeutic Potential. *Pharmacol. Ther.* **2007,** *113* (1), 50–87.
82. Cha, B.; Jho, E. H. Protein Arginine Methyltransferases (PRMTs) As Therapeutic Targets. *Expert Opin. Ther. Targets* **2012,** *16* (7), 651–664.
83. Kouzarides, T. Histone Methylation in Transcriptional Control. *Curr. Opin. Genet. Dev.* **2002,** *12* (2), 198–209.
84. Martin, C.; Zhang, Y. The Diverse Functions of Histone Lysine Methylation. *Nat. Rev. Mol. Cell Biol.* **2005,** *6* (11), 838–849.

85. Li, K. K.; Luo, C.; Wang, D.; Jiang, H.; Zheng, Y. G. Chemical and Biochemical Approaches in the Study of Histone Methylation and Demethylation. *Med. Res. Rev.* **2012,** *32,* 815–867.
86. Jenuwein, T. Re-SET-Ting Heterochromatin by Histone Methyltransferases. *Trends Cell. Biol.* **2001,** *11* (6), 266–273.
87. Cheng, X.; Collins, R. E.; Zhang, X. Structural and Sequence Motifs of Protein (Histone) Methylation Enzymes. *Annu. Rev. Biophys. Biomol. Struct.* **2005,** *34,* 267–294.
88. Schneider, R.; Bannister, A. J.; Kouzarides, T. Unsafe SETs: Histone Lysine Methyltransferases and Cancer. *Trends Biochem. Sci.* **2002,** *27* (8), 396–402.
89. Spannhoff, A.; Hauser, A. T.; Heinke, R.; Sippl, W.; Jung, M. The Emerging Therapeutic Potential of Histone Methyltransferase and Demethylase Inhibitors. *ChemMedChem* **2009,** *4* (10), 1568–1582.
90. Chen, X.; Niroomand, F.; Liu, Z.; Zankl, A.; Katus, H. A.; Jahn, L.; Tiefenbacher, C. P. Expression of Nitric Oxide Related Enzymes in Coronary Heart Disease. *Basic Res. Cardiol.* **2006,** *101* (4), 346–353.
91. Chesworth, B.; Kuntz, K.W.; Olhava, E.J.; Patane, M.A. Preparation of Nucleosides As Modulators of Histone Methyltransferase. WO2011-US63309, **2012**.
92. Olhava, E.J.; Chesworth, R.; Kuntz, K.W.; Richon, V.M.; Pollock, R.M.; Daigle, S.R. Preparation of Susbtituted Purine and 7-Deazapurine Compounds As Modulators of Epigenetic Enzymes. WO 2011/US63314, **2012**.
93. Daigle, S. R.; Olhava, E. J.; Therkelsen, C. A.; Majer, C. R.; Sneeringer, C. J.; Song, J.; Johnston, L. D.; Scott, M. P.; Smith, J. J.; Xiao, Y.; Jin, L.; Kuntz, K. W.; Chesworth, R.; Moyer, M. P.; Bernt, K. M.; Tseng, J. C.; Kung, A. L.; Armstrong, S. A.; Copeland, R. A.; Richon, V. M.; Pollock, R. M. Selective Killing of Mixed Lineage Leukemia Cells by a Potent Small-Molecule DOT1L Inhibitor. *Cancer Cell* **2011,** *20* (1), 53–65.
94. Daigle, S. R.; Olhava, E. J.; Therkelsen, C. A.; Basavapathruni, A.; Jin, L.; Boriack-Sjodin, P. A.; Allain, C. J.; Klaus, C. R.; Raimondi, A.; Scott, M. P.; Waters, N. J.; Chesworth, R.; Moyer, M. P.; Copeland, R. A.; Richon, V. M.; Pollock, R. M. Potent Inhibition of DOT1L As Treatment of MLL-Fusion Leukemia. *Blood* **2013,** *122* (6), 1017–1025.
95. Yu, W.; Chory, E. J.; Wernimont, A. K.; Tempel, W.; Scopton, A.; Federation, A.; Marineau, J. J.; Qi, J.; Barsyte-Lovejoy, D.; Yi, J.; Marcellus, R.; Iacob, R. E.; Engen, J. R.; Griffin, C.; Aman, A.; Wienholds, E.; Li, F.; Pineda, J.; Estiu, G.; Shatseva, T.; Hajian, T.; Al-Awar, R.; Dick, J. E.; Vedadi, M.; Brown, P. J.; Arrowsmith, C. H.; Bradner, J. E.; Schapira, M. Catalytic Site Remodelling of the DOT1L Methyltransferase by Selective Inhibitors. *Nat. Commun.* **2012,** *3,* 1288.
96. Yao, Y.; Chen, P.; Diao, J.; Cheng, G.; Deng, L.; Anglin, J. L.; Prasad, B. V.; Song, Y. Selective Inhibitors of Histone Methyltransferase DOT1L: Design, Synthesis, and Crystallographic Studies. *J. Am. Chem. Soc.* **2011,** *133* (42), 16746–16749.
97. Chen, S.; Li, L.; Chen, Y.; Hu, J.; Liu, J.; Liu, Y. C.; Liu, R.; Zhang, Y.; Meng, F.; Zhu, K.; Lu, J.; Zheng, M.; Chen, K.; Zhang, J.; Jiang, H.; Yao, Z.; Luo, C. Identification of Novel Disruptor of Telomeric Silencing 1-Like (DOT1L) Inhibitors Through Structure-Based Virtual Screening and Biological Assays. *J. Chem. Inf. Model* **2016,** *56* (3), 527–534.
98. Ferguson, A. D.; Larsen, N. A.; Howard, T.; Pollard, H.; Green, I.; Grande, C.; Cheung, T.; Garcia-Arenas, R.; Cowen, S.; Wu, J.; Godin, R.; Chen, H.; Keen, N. Structural Basis of Substrate Methylation and Inhibition of SMYD2. *Structure* **2011,** *19* (9), 1262–1273.
99. Nguyen, H.; Allali-Hassani, A.; Antonysamy, S.; Chang, S.; Chen, L. H.; Curtis, C.; Emtage, S.; Fan, L.; Gheyi, T.; Li, F.; Liu, S.; Martin, J. R.; Mendel, D.; Olsen, J. B.; Pelletier, L.; Shatseva, T.; Wu, S.; Zhang, F. F.; Arrowsmith, C. H.; Brown, P. J.; Campbell, R. M.; Garcia, B. A.; Barsyte-Lovejoy, D.; Mader, M.; Vedadi, M. LLY-507, a Cell-Active, Potent, and Selective Inhibitor of Protein-Lysine Methyltransferase SMYD2. *J. Biol. Chem.* **2015,** *290* (22), 13641–13653.
100. Eggert, E.; Hillig, R. C.; Koehr, S.; Stockigt, D.; Weiske, J.; Barak, N.; Mowat, J.; Brumby, T.; Christ, C. D.; Ter Laak, A.; Lang, T.; Fernandez-Montalvan, A. E.; Badock, V.; Weinmann, H.; Hartung, I. V.; Barsyte-Lovejoy, D.; Szewczyk, M.; Kennedy, S.; Li, F.; Vedadi, M.; Brown, P. J.; Santhakumar, V.; Arrowsmith, C. H.; Stellfeld, T.; Stresemann, C. Discovery and Characterization of a Highly Potent and Selective Aminopyrazoline-Based In Vivo Probe (BAY-598) for the Protein Lysine Methyltransferase SMYD2. *J. Med. Chem.* **2016,** *59* (10), 4578–4600.
101. Greiner, D.; Bonaldi, T.; Eskeland, R.; Roemer, E.; Imhof, A. Identification of a Specific Inhibitor of the Histone Methyltransferase SU(VAR)3-9. *Nat. Chem. Biol.* **2005,** *1* (3), 143–145.
102. Bernhard, W.; Barreto, K.; Saunders, A.; Dahabieh, M. S.; Johnson, P.; Sadowski, I. The Suv39H1 Methyltransferase Inhibitor Chaetocin Causes Induction of Integrated HIV-1 Without Producing a T Cell Response. *FEBS Lett.* **2011,** *585* (22), 3549–3554.
103. Kubicek, S.; O'Sullivan, R. J.; August, E. M.; Hickey, E. R.; Zhang, Q.; Teodoro, M. L.; Rea, S.; Mechtler, K.; Kowalski, J. A.; Homon, C. A.; Kelly, T. A.; Jenuwein, T. Reversal of H3K9me2 by a Small-Molecule Inhibitor for the G9a Histone Methyltransferase. *Mol. Cell* **2007,** *25* (3), 473–481.
104. Malmquist, N. A.; Moss, T. A.; Mecheri, S.; Scherf, A.; Fuchter, M. J. Small-Molecule Histone Methyltransferase Inhibitors Display Rapid Antimalarial Activity Against All Blood Stage Forms in *Plasmodium falciparum*. *Proc. Natl. Acad. Sci. U. S. A.* **2012,** *109* (41), 16708–16713.
105. Vedadi, M.; Barsyte-Lovejoy, D.; Liu, F.; Rival-Gervier, S.; Allali-Hassani, A.; Labrie, V.; Wigle, T. J.; Dimaggio, P. A.; Wasney, G. A.; Siarheyeva, A.; Dong, A.; Tempel, W.; Wang, S. C.; Chen, X.; Chau, I.; Mangano, T. J.; Huang, X. P.; Simpson, C. D.; Pattenden, S. G.; Norris, J. L.; Kireev, D. B.; Tripathy, A.; Edwards, A.; Roth, B. L.; Janzen, W. P.; Garcia, B. A.; Petronis, A.; Ellis, J.; Brown, P. J.; Frye, S. V.; Arrowsmith, C. H.; Jin, J. A Chemical Probe Selectively Inhibits G9a and GLP Methyltransferase Activity in Cells. *Nat. Chem. Biol.* **2011,** *7* (8), 566–574.
106. Yuan, Y.; Wang, Q.; Paulk, J.; Kubicek, S.; Kemp, M. M.; Adams, D. J.; Shamji, A. F.; Wagner, B. K.; Schreiber, S. L. A Small-Molecule Probe of the Histone Methyltransferase G9a Induces Cellular Senescence in Pancreatic Adenocarcinoma. *ACS Chem. Biol.* **2012,** *7* (7), 1152–1157.
107. Fiskus, W.; Wang, Y.; Sreekumar, A.; Buckley, K. M.; Shi, H.; Jillella, A.; Ustun, C.; Rao, R.; Fernandez, P.; Chen, J.; Balusu, R.; Koul, S.; Atadja, P.; Marquez, V. E.; Bhalla, K. N. Combined Epigenetic Therapy With the Histone Methyltransferase EZH2 Inhibitor 3-Deazaneplanocin A and the Histone Deacetylase Inhibitor Panobinostat Against Human AML Cells. *Blood* **2009,** *114* (13), 2733–2743.
108. Kikuchi, J.; Takashina, T.; Kinoshita, I.; Kikuchi, E.; Shimizu, Y.; Sakakibara-Konishi, J.; Oizumi, S.; Marquez, V. E.; Nishimura, M.; Dosaka-Akita, H. Epigenetic Therapy With 3-Deazaneplanocin A, an Inhibitor of the Histone Methyltransferase EZH2, Inhibits Growth of Non-Small Cell Lung Cancer Cells. *Lung Cancer* **2012,** *78* (2), 138–143.
109. Qi, W.; Chan, H.; Teng, L.; Li, L.; Chuai, S.; Zhang, R.; Zeng, J.; Li, M.; Fan, H.; Lin, Y.; Gu, J.; Ardayfio, O.; Zhang, J. H.; Yan, X.; Fang, J.; Mi, Y.; Zhang, M.; Zhou, T.; Feng, G.; Chen, Z.; Li, G.; Yang, T.; Zhao, K.; Liu, X.; Yu, Z.; Lu, C. X.; Atadja, P.; Li, E. Selective Inhibition of Ezh2 by a Small Molecule Inhibitor Blocks Tumor Cells Proliferation. *Proc. Natl. Acad. Sci. U. S. A.* **2012,** *109* (52), 21360–21365.
110. McCabe, M. T.; Ott, H. M.; Ganji, G.; Korenchuk, S.; Thompson, C.; Van Aller, G. S.; Liu, Y.; Graves, A. P.; Della Pietra, A., III; Diaz, E.; LaFrance, L. V.; Mellinger, M.; Duquenne, C.; Tian, X.; Kruger, R. G.; McHugh, C. F.; Brandt, M.; Miller, W. H.; Dhanak, D.; Verma, S. K.; Tummino, P. J.; Creasy, C. L. EZH2 Inhibition As a Therapeutic Strategy For Lymphoma With EZH2-Activating Mutations. *Nature* **2012,** *492* (7427), 108–112.
111. Verma, S. K.; Tian, X.; LaFrance, L.; Duquenne, C.; Suarez, D. P.; Newlander, K. A.; Romeril, S. P.; Burgess, J. L.; Grant, S. W.; Brackley, J. A.; Graves, A. P.; Scherzer, D. A.; Shu, A.; Thompson, C.; Ott, H. M.; Van Aller, G. S.; Machutta, C. A.; Diaz, E.; Jiang, Y.; Johnson, N. W.; Knight, S. D.; Kruger, R. G.; McCabe, M. T.; Dhanak, D.; Tummino, P. J.; Creasy, C. L.; Miller, W. H. Identification of Potent, Selective, Cell-Active Inhibitors of the Histone Lysine Methyltransferase EZH2. *ACS Med. Chem. Lett.* **2012,** *3,* 1091–1096.
112. Knutson, S. K.; Warholic, N. M.; Wigle, T. J.; Klaus, C. R.; Allain, C. J.; Raimondi, A.; Porter Scott, M.; Chesworth, R.; Moyer, M. P.; Copeland, R. A.; Richon, V. M.; Pollock, R. M.; Kuntz, K. W.; Keilhack, H. Durable Tumor Regression in Genetically Altered Malignant Rhabdoid Tumors by Inhibition of Methyltransferase EZH2. *Proc. Natl. Acad. Sci. U. S. A.* **2013,** *110* (19), 7922–7927.
113. Sack, J. S.; Thieffine, S.; Bandiera, T.; Fasolini, M.; Duke, G. J.; Jayaraman, L.; Kish, K. F.; Klei, H. E.; Purandare, A. V.; Rosettani, P.; Troiani, S.; Xie, D.; Bertrand, J. A. Structural Basis for CARM1 Inhibition by Indole and Pyrazole Inhibitors. *Biochem. J.* **2011,** *436* (2), 331–339.
114. Cheng, D.; Yadav, N.; King, R. W.; Swanson, M. S.; Weinstein, E. J.; Bedford, M. T. Small Molecule Regulators of Protein Arginine Methyltransferases. *J. Biol. Chem.* **2004,** *279* (23), 23892–23899.
115. Bonham, K.; Hemmers, S.; Lim, Y. H.; Hill, D. M.; Finn, M. G.; Mowen, K. A. Effects of a Novel Arginine Methyltransferase Inhibitor on T-Helper Cell Cytokine Production. *FEBS J.* **2010,** *277* (9), 2096–2108.

116. Mai, A.; Cheng, D.; Bedford, M. T.; Valente, S.; Nebbioso, A.; Perrone, A.; Brosch, G.; Sbardella, G.; De Bellis, F.; Miceli, M.; Altucci, L. Epigenetic Multiple Ligands: Mixed Histone/Protein Methyltransferase, Acetyltransferase, and Class III Deacetylase (Sirtuin) Inhibitors. *J. Med. Chem.* **2008,** *51* (7), 2279–2290.
117. Fontan, N.; Garcia-Dominguez, P.; Alvarez, R.; de Lera, A. R. Novel Symmetrical Ureas As Modulators of Protein Arginine Methyl Transferases. *Bioorg. Med. Chem.* **2013,** *21* (7), 2056–2067.
118. Wang, J.; Chen, L.; Sinha, S. H.; Liang, Z.; Chai, H.; Muniyan, S.; Chou, Y. W.; Yang, C.; Yan, L.; Feng, Y.; Li, K. K.; Lin, M. F.; Jiang, H.; Zheng, Y. G.; Luo, C. Pharmacophore-Based Virtual Screening and Biological Evaluation of Small Molecule Inhibitors for Protein Arginine Methylation. *J. Med. Chem.* **2012,** *55* (18), 7978–7987.
119. Dillon, M. B.; Bachovchin, D. A.; Brown, S. J.; Finn, M. G.; Rosen, H.; Cravatt, B. F.; Mowen, K. A. Novel Inhibitors for PRMT1 Discovered by High-Throughput Screening Using Activity-Based Fluorescence Polarization. *ACS Chem. Biol.* **2012,** *7* (7), 1198–1204.
120. Spannhoff, A.; Machmur, R.; Heinke, R.; Trojer, P.; Bauer, I.; Brosch, G.; Schule, R.; Hanefeld, W.; Sippl, W.; Jung, M. A Novel Arginine Methyltransferase Inhibitor With Cellular Activity. *Bioorg. Med. Chem. Lett.* **2007,** *17* (15), 4150–4153.
121. Bissinger, E. M.; Heinke, R.; Spannhoff, A.; Eberlin, A.; Metzger, E.; Cura, V.; Hassenboehler, P.; Cavarelli, J.; Schule, R.; Bedford, M. T.; Sippl, W.; Jung, M. Acyl Derivatives of *p*-Aminosulfonamides and Dapsone As New Inhibitors of the Arginine Methyltransferase hPRMT1. *Bioorg. Med. Chem.* **2011,** *19* (12), 3717–3731.
122. Kaniskan, H. U.; Szewczyk, M. M.; Yu, Z.; Eram, M. S.; Yang, X.; Schmidt, K.; Luo, X.; Dai, M.; He, F.; Zang, I.; Lin, Y.; Kennedy, S.; Li, F.; Dobrovetsky, E.; Dong, A.; Smil, D.; Min, S. J.; Landon, M.; Lin-Jones, J.; Huang, X. P.; Roth, B. L.; Schapira, M.; Atadja, P.; Barsyte-Lovejoy, D.; Arrowsmith, C. H.; Brown, P. J.; Zhao, K.; Jin, J.; Vedadi, M. A Potent, Selective and Cell-Active Allosteric Inhibitor of Protein Arginine Methyltransferase 3 (PRMT3). *Angew. Chem. Int. Ed. Engl.* **2015,** *54* (17), 5166–5170.
123. Mitchell, L. H.; Drew, A. E.; Ribich, S. A.; Rioux, N.; Swinger, K. K.; Jacques, S. L.; Lingaraj, T.; Boriack-Sjodin, P. A.; Waters, N. J.; Wigle, T. J.; Moradei, O.; Jin, L.; Riera, T.; Porter-Scott, M.; Moyer, M. P.; Smith, J. J.; Chesworth, R.; Copeland, R. A. Aryl Pyrazoles As Potent Inhibitors of Arginine Methyltransferases: Identification of the First PRMT6 Tool Compound. *ACS Med. Chem. Lett.* **2015,** *6* (6), 655–659.
124. Eram, M. S.; Shen, Y.; Szewczyk, M. M.; Wu, H.; Senisterra, G.; Li, F.; Butler, K. V.; Kaniskan, H. U.; Speed, B. A.; dela Sena, C.; Dong, A.; Zeng, H.; Schapira, M.; Brown, P. J.; Arrowsmith, C. H.; Barsyte-Lovejoy, D.; Liu, J.; Vedadi, M.; Jin, J. A Potent, Selective, and Cell-Active Inhibitor of Human Type I Protein Arginine Methyltransferases. *ACS Chem. Biol.* **2016,** *11* (3), 772–781.
125. Chan-Penebre, E.; Kuplast, K. G.; Majer, C. R.; Boriack-Sjodin, P. A.; Wigle, T. J.; Johnston, L. D.; Rioux, N.; Munchhof, M. J.; Jin, L.; Jacques, S. L.; West, K. A.; Lingaraj, T.; Stickland, K.; Ribich, S. A.; Raimondi, A.; Scott, M. P.; Waters, N. J.; Pollock, R. M.; Smith, J. J.; Barbash, O.; Pappalardi, M.; Ho, T. F.; Nurse, K.; Oza, K. P.; Gallagher, K. T.; Kruger, R.; Moyer, M. P.; Copeland, R. A.; Chesworth, R.; Duncan, K. W. A Selective Inhibitor of PRMT5 With In Vivo and In Vitro Potency in MCL Models. *Nat. Chem. Biol.* **2015,** *11* (6), 432–437.
126. Seto, E.; Yoshida, M. Erasers of Histone Acetylation: The Histone Deacetylase Enzymes. *Cold Spring Harb. Perspect. Biol.* **2014,** *6* (4), a018713.
127. Robertson, K. D. DNA Methylation, Methyltransferases, and Cancer. *Oncogene* **2001,** *20* (24), 3139–3155.
128. Taunton, J.; Hassig, C. A.; Schreiber, S. L. A Mammalian Histone Deacetylase Related to the Yeast Transcriptional Regulator Rpd3p. *Science* **1996,** *272,* 408–411.
129. Grozinger, C. M.; Schreiber, S. L. Deacetylase Enzymes: Biological Functions and the Use of Small-Molecule Inhibitors. *Chem. Biol.* **2002,** *9* (1), 3–16.
130. Grozinger, C. M.; Hassig, C. A.; Schreiber, S. L. Three Proteins Define a Class of Human Histone Deacetylases Related to Yeast Hda1p. *Proc. Natl. Acad. Sci. U. S. A.* **1999,** *96* (9), 4868–4873.
131. Imai, S.; Armstrong, C. M.; Kaeberlein, M.; Guarente, L. Transcriptional Silencing and Longevity Protein Sir2 Is an NAD-Dependent Histone Deacetylase. *Nature* **2000,** *403* (6771), 795–800.
132. Jing, H.; Lin, H. Sirtuins in Epigenetic Regulation. *Chem. Rev.* **2015,** *115* (6), 2350–2375.
133. Kumar, A.; Chauhan, S. How Much Successful Are the Medicinal Chemists in Modulation of SIRT1: A Critical Review. *Eur. J. Med. Chem.* **2016,** *119,* 45–69.
134. Rajak, H.; Singh, A.; Raghuwanshi, K.; Kumar, R.; Dewangan, P. K.; Veerasamy, R.; Sharma, P. C.; Dixit, A.; Mishra, P. A Structural Insight Into Hydroxamic Acid Based Histone Deacetylase Inhibitors for the Presence of Anticancer Activity. *Curr. Med. Chem.* **2014,** *21* (23), 2642–2664.
135. Johnstone, R. W.; Licht, J. D. Histone Deacetylase Inhibitors in Cancer Therapy: Is Transcription the Primary Target? *Cancer Cell* **2003,** *4* (1), 13–18.
136. Herman, J. G.; Baylin, S. B. Gene Silencing in Cancer in Association With Promoter Hypermethylation. *N. Engl. J. Med.* **2003,** *349* (21), 2042–2054.
137. Marks, P.; Rifkind, R. A.; Richon, V. M.; Breslow, R.; Miller, T.; Kelly, W. K. Histone Deacetylases and Cancer: Causes and Therapies. *Nat. Rev. Cancer* **2001,** *1* (3), 194–202.
138. Weinmann, H.; Ottow, E. Recent Advances in the Medicinal Chemistry of Histone Deacetylase Inhibitors. *Annu. Rep. Med. Chem.* **2004,** *39,* 185–196.
139. Manal, M.; Chandrasekar, M. J.; Gomathi Priya, J.; Nanjan, M. J. Inhibitors of Histone Deacetylase As Antitumor Agents: A Critical Review. *Bioorg. Chem.* **2016,** *67,* 18–42.
140. Marchi, E.; Zullo, K. M.; Amengual, J. E.; Kalac, M.; Bongero, D.; McIntosh, C. M.; Fogli, L. K.; Rossi, M.; Zinzani, P. L.; Pileri, S. A.; Piccaluga, P. P.; Fuligni, F.; Scotto, L.; O'Connor, O. A. The Combination of Hypomethylating Agents and Histone Deacetylase Inhibitors Produce Marked Synergy in Preclinical Models of T-Cell Lymphoma. *Br. J. Haematol.* **2015,** *171,* 215–226.
141. Pathania, R.; Ramachandran, S.; Mariappan, G.; Thakur, P.; Shi, H.; Choi, J. H.; Manicassamy, S.; Kolhe, R.; Prasad, P. D.; Sharma, S.; Lokeshwar, B. L.; Ganapathy, V.; Thangaraju, M. Combined Inhibition of DNMT and HDAC Blocks the Tumorigenicity of Cancer Stem-Like Cells and Attenuates Mammary Tumor Growth. *Cancer Res.* **2016,** *76* (11), 3224–3235.
142. Cho, M.; Choi, E.; Yang, J. S.; Lee, C.; Seo, J. J.; Kim, B. S.; Oh, S. J.; Kim, H. M.; Lee, K.; Park, S. K.; Kwon, H. J.; Han, G. Discovery of Pyridone-Based Histone Deacetylase Inhibitors: Approaches for Metabolic Stability. *ChemMedChem* **2013,** *8* (2), 272–279.
143. Marek, L.; Hamacher, A.; Hansen, F. K.; Kuna, K.; Gohlke, H.; Kassack, M. U.; Kurz, T. Histone Deacetylase (HDAC) Inhibitors With a Novel Connecting Unit Linker Region Reveal a Selectivity Profile for HDAC4 and HDAC5 With Improved Activity Against Chemoresistant Cancer Cells. *J. Med. Chem.* **2013,** *56* (2), 427–436.
144. Giannini, G.; Vesci, L.; Battistuzzi, G.; Vignola, D.; Milazzo, F. M.; Guglielmi, M. B.; Barbarino, M.; Santaniello, M.; Fanto, N.; Mor, M.; Rivara, S.; Pala, D.; Taddei, M.; Pisano, C.; Cabri, W. ST7612AA1, a Thioacetate-Omega(Gamma-Lactam Carboxamide) Derivative Selected From a Novel Generation of Oral HDAC Inhibitors. *J. Med. Chem.* **2014,** *57* (20), 8358–8377.
145. De Bellis, F.; Carafa, V.; Conte, M.; Rotili, D.; Petraglia, F.; Matarese, F.; Francoijs, K. J.; Ablain, J.; Valente, S.; Castellano, R.; Goubard, A.; Collette, Y.; Mandoli, A.; Martens, J. H.; de The, H.; Nebbioso, A.; Mai, A.; Stunnenberg, H. G.; Altucci, L. Context-Selective Death of Acute Myeloid Leukemia Cells Triggered by the Novel Hybrid Retinoid-HDAC Inhibitor MC2392. *Cancer Res.* **2014,** *74* (8), 2328–2339.
146. Malvaez, M.; McQuown, S. C.; Rogge, G. A.; Astarabadi, M.; Jacques, V.; Carreiro, S.; Rusche, J. R.; Wood, M. A. HDAC3-Selective Inhibitor Enhances Extinction of Cocaine-Seeking Behavior in a Persistent Manner. *Proc. Natl. Acad. Sci. U. S. A.* **2013,** *110* (7), 2647–2652.
147. Van Beneden, K.; Mannaerts, I.; Pauwels, M.; Van den Branden, C.; van Grunsven, L. A. HDAC Inhibitors in Experimental Liver and Kidney Fibrosis. *Fibrogenesis Tissue Repair* **2013,** *6* (1), 1.
148. Ge, Z.; Da, Y.; Xue, Z.; Zhang, K.; Zhuang, H.; Peng, M.; Li, Y.; Li, W.; Simard, A.; Hao, J.; Yao, Z.; Zhang, R. Vorinostat, a Histone Deacetylase Inhibitor, Suppresses Dendritic Cell Function and Ameliorates Experimental Autoimmune Encephalomyelitis. *Exp. Neurol.* **2012,** *241C,* 56–66.
149. Chen, Y. T.; Zang, X. F.; Pan, J.; Zhu, X. L.; Chen, F.; Chen, Z. B.; Xu, Y. Expression Patterns of Histone Deacetylases in Experimental Stroke and Potential Targets for Neuroprotection. *Clin. Exp. Pharmacol. Physiol.* **2012,** *39* (9), 751–758.
150. Jia, H.; Pallos, J.; Jacques, V.; Lau, A.; Tang, B.; Cooper, A.; Syed, A.; Purcell, J.; Chen, Y.; Sharma, S.; Sangrey, G. R.; Darnell, S. B.; Plasterer, H.; Sadri-Vakili, G.; Gottesfeld, J. M.; Thompson, L. M.; Rusche, J. R.; Marsh, J. L.; Thomas, E. A. Histone Deacetylase (HDAC) Inhibitors Targeting HDAC3 and HDAC1 Ameliorate Polyglutamine-Elicited Phenotypes in Model Systems of Huntington's Disease. *Neurobiol. Dis.* **2012,** *46* (2), 351–361.
151. Zhao, X.; Allison, D.; Condon, B.; Zhang, F.; Gheyi, T.; Zhang, A.; Ashok, S.; Russell, M.; Macewan, I.; Qian, Y.; Jamison, J. A.; Luz, J. G. The 2.5 A Crystal Structure of the SIRT1 Catalytic Domain Bound to Nicotinamide Adenine Dinucleotide (NAD+) and an Indole (EX527 Analog) Reveals a Novel Mechanism of Histone Deacetylase Inhibition. *J. Med. Chem.* **2013,** *56* (3), 963–969.

152. Yoo, J.; Kim, S. J.; Son, D.; Seo, H.; Baek, S. Y.; Maeng, C. Y.; Lee, C.; Kim, I. S.; Jung, Y. H.; Lee, S. M.; Park, H. J. Computer-Aided Identification of New Histone Deacetylase 6 Selective Inhibitor With Anti-Sepsis Activity. *Eur. J. Med. Chem.* **2016,** *116,* 126–135.
153. Ellis, J. D.; Neil, D. A.; Inston, N. G.; Jenkinson, E.; Drayson, M. T.; Hampson, P.; Shuttleworth, S. J.; Ready, A. R.; Cobbold, M. Inhibition of Histone Deacetylase 6 Reveals a Potent Immunosuppressant Effect in Models of Transplantation. *Transplantation* **2016,** *100* (8), 1667–1674.
154. Liang, G.; Lin, J. C.; Wei, V.; Yoo, C.; Cheng, J. C.; Nguyen, C. T.; Weisenberger, D. J.; Egger, G.; Takai, D.; Gonzales, F. A.; Jones, P. A. Distinct Localization of Histone H3 Acetylation and H3-K4 Methylation to the Transcription Start Sites in the Human Genome. *Proc. Natl. Acad. Sci. U. S. A.* **2004,** *101* (19), 7357–7362.
155. Schneider, R.; Bannister, A. J.; Myers, F. A.; Thorne, A. W.; Crane-Robinson, C.; Kouzarides, T. Histone H3 Lysine 4 Methylation Patterns in Higher Eukaryotic Genes. *Nat. Cell Biol.* **2004,** *6* (1), 73–77.
156. Stavropoulos, P.; Hoelz, A. Lysine-Specific Demethylase 1 As a Potential Therapeutic Target. *Expert Opin. Ther. Targets* **2007,** *11* (6), 809–820.
157. Metzger, E.; Wissmann, M.; Yin, N.; Muller, J. M.; Schneider, R.; Peters, A. H.; Gunther, T.; Buettner, R.; Schule, R. LSD1 Demethylates Repressive Histone Marks to Promote Androgen-Receptor-Dependent Transcription. *Nature* **2005,** *437* (7057), 436–439.
158. Hou, H.; Yu, H. Structural Insights Into Histone Lysine Demethylation. *Curr. Opin. Struct. Biol.* **2010,** *20* (6), 739–748.
159. Karytinos, A.; Forneris, F.; Profumo, A.; Ciossani, G.; Battaglioli, E.; Binda, C.; Mattevi, A. A Novel Mammalian Flavin-Dependent Histone Demethylase. *J. Biol. Chem.* **2009,** *284* (26), 17775–17782.
160. Mosammaparast, N.; Shi, Y. Reversal of Histone Methylation: Biochemical and Molecular Mechanisms of Histone Demethylases. *Annu. Rev. Biochem.* **2010,** *79,* 155–179.
161. Shi, L.; Cui, S.; Engel, J. D.; Tanabe, O. Lysine-Specific Demethylase 1 Is a Therapeutic Target for Fetal Hemoglobin Induction. *Nat. Med.* **2013,** *19* (3), 291–294.
162. Rotili, D.; Mai, A. Targeting Histone Demethylases: A New Avenue for the Fight Against Cancer. *Genes Cancer* **2011,** *2* (6), 663–679.
163. Kooistra, S. M.; Helin, K. Molecular Mechanisms and Potential Functions of Histone Demethylases. *Nat. Rev. Mol. Cell Biol.* **2012,** *13* (5), 297–311.
164. Dimitrova, E.; Turberfield, A. H.; Klose, R. J. Histone Demethylases in Chromatin Biology and Beyond. *EMBO Rep.* **2015,** *16* (12), 1620–1639.
165. Loenarz, C.; Schofield, C. J. Expanding Chemical Biology of 2-Oxoglutarate Oxygenases. *Nat. Chem. Biol.* **2008,** *4* (3), 152–156.
166. Takeuchi, T.; Yamazaki, Y.; Katoh-Fukui, Y.; Tsuchiya, R.; Kondo, S.; Motoyama, J.; Higashinakagawa, T. Gene Trap Capture of a Novel Mouse Gene, Jumonji, Required for Neural Tube Formation. *Genes Dev.* **1995,** *9* (10), 1211–1222.
167. Zhou, J. C.; Blackledge, N. P.; Farcas, A. M.; Klose, R. J. Recognition of CpG Island Chromatin by KDM2A Requires Direct and Specific Interaction With Linker DNA. *Mol. Cell Biol.* **2012,** *32* (2), 479–489.
168. Farcas, A. M.; Blackledge, N. P.; Sudbery, I.; Long, H. K.; McGouran, J. F.; Rose, N. R.; Lee, S.; Sims, D.; Cerase, A.; Sheahan, T. W.; Koseki, H.; Brockdorff, N.; Ponting, C. P.; Kessler, B. M.; Klose, R. J. KDM2B Links the Polycomb Repressive Complex 1 (PRC1) to Recognition of CpG Islands. *Elife* **2012,** *1,* e00205.
169. Yamada, D.; Kobayashi, S.; Yamamoto, H.; Tomimaru, Y.; Noda, T.; Uemura, M.; Wada, H.; Marubashi, S.; Eguchi, H.; Tanemura, M.; Doki, Y.; Mori, M.; Nagano, H. Role of the Hypoxia-Related Gene, JMJD1A, in Hepatocellular Carcinoma: Clinical Impact on Recurrence After Hepatic Resection. *Ann. Surg. Oncol.* **2012,** *19* (Suppl 3), S355–S364.
170. Kim, J. Y.; Kim, K. B.; Eom, G. H.; Choe, N.; Kee, H. J.; Son, H. J.; Oh, S. T.; Kim, D. W.; Pak, J. H.; Baek, H. J.; Kook, H.; Hahn, Y.; Kook, H.; Chakravarti, D.; Seo, S. B. KDM3B is the H3K9 Demethylase Involved in Transcriptional Activation of Imo2 in Leukemia. *Mol. Cell Biol.* **2012,** *32* (14), 2917–2933.
171. Jin, G.; Sun, J.; Kim, S. T.; Feng, J.; Wang, Z.; Tao, S.; Chen, Z.; Purcell, L.; Smith, S.; Isaacs, W. B.; Rittmaster, R. S.; Zheng, S. L.; Condreay, L. D.; Xu, J. Genome-Wide Association Study Identifies a New Locus JMJD1C at 10q21 That May Influence Serum Androgen Levels in Men. *Hum. Mol. Genet.* **2012,** *21* (23), 5222–5228.
172. Berry, W. L.; Shin, S.; Lightfoot, S. A.; Janknecht, R. Oncogenic Features of the JMJD2A Histone Demethylase in Breast Cancer. *Int. J. Oncol.* **2012,** *41* (5), 1701–1706.
173. Antony, J.; Oback, F.; Chamley, L. W.; Oback, B.; Laible, G. Transient JMJD2B-Mediated Reduction of H3K9me3 Levels Improves Reprogramming of Embryonic Stem Cells Into Cloned Embryos. *Mol. Cell Biol.* **2012,** *33* (5), 974–983.
174. Berdel, B.; Nieminen, K.; Soini, Y.; Tengstrom, M.; Malinen, M.; Kosma, V. M.; Palvimo, J. J.; Mannermaa, A. Histone Demethylase GASC1—A Potential Prognostic and Predictive Marker in Invasive Breast Cancer. *BMC Cancer* **2012,** *12,* 516.
175. Culhane, J. C.; Szewczuk, L. M.; Liu, X.; Da, G.; Marmorstein, R.; Cole, P. A. A Mechanism-Based Inactivator for Histone Demethylase LSD1. *J. Am. Chem. Soc.* **2006,** *128* (14), 4536–4537.
176. Schmidt, D. M.; McCafferty, D. G. Trans-2-Phenylcyclopropylamine Is a Mechanism-Based Inactivator of the Histone Demethylase LSD1. *Biochemistry* **2007,** *46* (14), 4408–4416.
177. Szewczuk, L. M.; Culhane, J. C.; Yang, M.; Majumdar, A.; Yu, H.; Cole, P. A. Mechanistic Analysis of a Suicide Inactivator of Histone Demethylase LSD1. *Biochemistry* **2007,** *46,* 6892–6902.
178. Dancy, B. C.; Ming, S. A.; Papazyan, R.; Jelinek, C. A.; Majumdar, A.; Sun, Y.; Dancy, B. M.; Drury, W. J., III; Cotter, R. J.; Taverna, S. D.; Cole, P. A. Azalysine Analogues As Probes for Protein Lysine Deacetylation and Demethylation. *J. Am. Chem. Soc.* **2012,** *134* (11), 5138–5148.
179. Forneris, F.; Binda, C.; Adamo, A.; Battaglioli, E.; Mattevi, A. Structural Basis of LSD1-CoREST Selectivity in Histone H3 Recognition. *J. Biol. Chem.* **2007,** *282* (28), 20070–20074.
180. Hruby, V. J. Designing Peptide Receptor Agonists and Antagonists. *Nat. Rev. Drug Discov.* **2002,** *1* (11), 847–858.
181. Kumarasinghe, I. R.; Woster, P. M. Synthesis and Evaluation of Novel Cyclic Peptide Inhibitors of Lysine-Specific Demethylase 1. *ACS Med. Chem. Lett.* **2014,** *5* (1), 29–33.
182. Suzuki, T.; Miyata, N. Lysine Demethylases Inhibitors. *J. Med. Chem.* **2011,** *54* (24), 8236–8250.
183. Johnson, N.W.; Kasparec, J.; Miller, W.H.; Rouse, M.B.; Suarez, D.P.; Tian, X. Cyclopropylamines As LSD1 Inhibitors. WO/2012/135113A2, **2012**.
184. Mohammad, H. P.; Smitheman, K. N.; Kamat, C. D.; Soong, D.; Federowicz, K. E.; Van Aller, G. S.; Schneck, J. L.; Carson, J. D.; Liu, Y.; Butticello, M.; Bonnette, W. G.; Gorman, S. A.; Degenhardt, Y.; Bai, Y.; McCabe, M. T.; Pappalardi, M. B.; Kasparec, J.; Tian, X.; McNulty, K. C.; Rouse, M.; McDevitt, P.; Ho, T.; Crouthamel, M.; Hart, T. K.; Concha, N. O.; McHugh, C. F.; Miller, W. H.; Dhanak, D.; Tummino, P. J.; Carpenter, C. L.; Johnson, N. W.; Hann, C. L.; Kruger, R. G. A DNA Hypomethylation Signature Predicts Antitumor Activity of LSD1 Inhibitors in SCLC. *Cancer Cell* **2015,** *28* (1), 57–69.
185. Guibourt, N.; Ortega-Munoz, A.; Castro-Palomino Laria, J. US Patent Application 20120004262: Phenylcyclopropylamine Derivatives and Their Medical Use. **2012**.
186. Ortega-Munoz, A.; Castro-Palomino Laria, J.; Fyfe, M.C.T. Lysine-Specific Demethylase 1 Inhibitors and Their Use. **2011**.
187. Maes, T.; Carceller, E.; Salas, J.; Ortega, A.; Buesa, C. Advances in the Development of Histone Lysine Demethylase Inhibitors. *Curr. Opin. Pharmacol.* **2015,** *23,* 52–60.
188. Neelamegam, R.; Ricq, E. L.; Malvaez, M.; Patnaik, D.; Norton, S.; Carlin, S. M.; Hill, I. T.; Wood, M. A.; Haggarty, S. J.; Hooker, J. M. Brain-Penetrant LSD1 Inhibitors Can Block Memory Consolidation. *ACS Chem. Neurosci.* **2012,** *3* (2), 120–128.
189. Valente, S.; Rodriguez, V.; Mercurio, C.; Vianello, P.; Saponara, B.; Cirilli, R.; Ciossani, G.; Labella, D.; Marrocco, B.; Monaldi, D.; Ruoppolo, G.; Tilset, M.; Botrugno, O. A.; Dessanti, P.; Minucci, S.; Mattevi, A.; Varasi, M.; Mai, A. Pure Enantiomers of Benzoylamino-tranylcypromine: LSD1 Inhibition, Gene Modulation in Human Leukemia Cells and Effects on Clonogenic Potential of Murine Promyelocytic Blasts. *Eur. J. Med. Chem.* **2015,** *94,* 163–174.
190. Valente, S.; Rodriguez, V.; Mercurio, C.; Vianello, P.; Saponara, B.; Cirilli, R.; Ciossani, G.; Labella, D.; Marrocco, B.; Ruoppolo, G.; Botrugno, O. A.; Dessanti, P.; Minucci, S.; Mattevi, A.; Varasi, M.; Mai, A. Pure Diastereomers of a Tranylcypromine-Based LSD1 Inhibitor: Enzyme Selectivity and In-Cell Studies. *ACS Med. Chem. Lett.* **2015,** *6* (2), 173–177.
191. Vianello, P.; Botrugno, O. A.; Cappa, A.; Dal Zuffo, R.; Dessanti, P.; Mai, A.; Marrocco, B.; Mattevi, A.; Meroni, G.; Minucci, S.; Stazi, G.; Thaler, F.; Trifiro, P.; Valente, S.; Villa, M.; Varasi, M.; Mercurio, C. Discovery of a Novel Inhibitor of Histone Lysine-Specific Demethylase 1A (KDM1A/LSD1) As Orally Active Antitumor Agent. *J. Med. Chem.* **2016,** *59* (4), 1501–1517.
192. McAllister, T. E.; England, K. S.; Hopkinson, R. J.; Brennan, P. E.; Kawamura, A.; Schofield, C. J. Recent Progress in Histone Demethylase Inhibitors. *J. Med. Chem.* **2016,** *59* (4), 1308–1329.
193. Huang, Y.; Stewart, T. M.; Wu, Y.; Baylin, S. B.; Marton, L. J.; Perkins, B.; Jones, R. J.; Woster, P. M.; Casero, R. A., Jr. Novel Oligoamine Analogues Inhibit Lysine-Specific Demethylase 1 and Induce Reexpression of Epigenetically Silenced Genes. *Clin. Cancer Res.* **2009,** *15* (23), 7217–7228.

194. Sharma, S.; Wu, Y.; Steinbergs, N.; Crowley, M.; Hanson, A.; Casero, R. A. J.; Woster, P. (Bis)Urea and (bis)Thiourea Inhibitors of Lysine-Specific Demethylase 1 As Epigenetic Modulators. *J. Med. Chem.* **2010,** *53* (14), 5197–5212.
195. Nowotarski, S. L.; Pachaiyappan, B.; Holshouser, S. L.; Kutz, C. J.; Li, Y.; Huang, Y.; Sharma, S. K.; Casero, R. A., Jr.; Woster, P. M. Structure-Activity Study for (bis) Ureidopropyl- and (bis)Thioureidopropyldiamine LSD1 Inhibitors With 3-5-3 and 3-6-3 Carbon Backbone Architectures. *Bioorg. Med. Chem.* **2015,** *23,* 1601–1612.
196. Hazeldine, S.; Pachaiyappan, B.; Steinbergs, N.; Nowotarski, S.; Hanson, A. S.; Casero, R. A., Jr.; Woster, P. M. Low Molecular Weight Amidoximes That Act As Potent Inhibitors of Lysine-Specific Demethylase 1. *J. Med. Chem.* **2012,** *55* (17), 7378–7391.
197. Abdulla, A.; Zhao, X.; Yang, F. Natural Polyphenols Inhibit Lysine-Specific Demethylase-1. *J. Biochem. Pharmacol. Res.* **2013,** *1* (1), 56–63.
198. Dulla, B.; Kirla, K. T.; Rathore, V.; Deora, G. S.; Kavela, S.; Maddika, S.; Chatti, K.; Reiser, O.; Iqbal, J.; Pal, M. Synthesis and Evaluation of 3-Amino/Guanidine Substituted Phenyl Oxazoles As a Novel Class of LSD1 Inhibitors With Anti-Proliferative Properties. *Org. Biomol. Chem.* **2013,** *11* (19), 3103–3107.
199. Willmann, D.; Lim, S.; Wetzel, S.; Metzger, E.; Jandausch, A.; Wilk, W.; Jung, M.; Forne, I.; Imhof, A.; Janzer, A.; Kirfel, J.; Waldmann, H.; Schule, R.; Buettner, R. Impairment of Prostate Cancer Cell Growth by a Selective and Reversible Lysine-Specific Demethylase 1 Inhibitor. *Int. J. Cancer* **2012,** *131* (11), 2704–2709.
200. Schmitt, M. L.; Hauser, A. T.; Carlino, L.; Pippel, M.; Schulz-Fincke, J.; Metzger, E.; Willmann, D.; Yiu, T.; Barton, M.; Schule, R.; Sippl, W.; Jung, M. Nonpeptidic Propargylamines As Inhibitors of Lysine Specific Demethylase 1 (LSD1) With Cellular Activity. *J. Med. Chem.* **2013,** *56* (18), 7334–7342.
201. Fiskus, W.; Sharma, S.; Shah, B.; Portier, B. P.; Devaraj, S. G.; Liu, K.; Iyer, S. P.; Bearss, D.; Bhalla, K. N. Highly Effective Combination of LSD1 (KDM1A) Antagonist and Pan-Histone Deacetylase Inhibitor Against Human AML Cells. *Leukemia* **2014,** *28* (11), 2155–2164.
202. Kutz, C. J.; Holshouser, S. L.; Marrow, E. A.; Woster, P. M. 3,5-Diamino-1,2,4-triazoles As a Novel Scaffold for Potent, Reversible LSD1 (KDM1A) Inhibitors. *MedChemComm* **2014,** *5* (12), 1863–1870.
203. Zheng, Y. C.; Duan, Y. C.; Ma, J. L.; Xu, R. M.; Zi, X.; Lv, W. L.; Wang, M. M.; Ye, X. W.; Zhu, S.; Mobley, D.; Zhu, Y. Y.; Wang, J. W.; Li, J. F.; Wang, Z. R.; Zhao, W.; Liu, H. M. Triazole-Dithiocarbamate Based Selective Lysine Specific Demethylase 1 (LSD1) Inactivators Inhibit Gastric Cancer Cell Growth, Invasion, and Migration. *J. Med. Chem.* **2013,** *56,* 8543–8560.
204. Hitchin, J. R.; Blagg, J.; Burke, R.; Burns, S.; Cockerill, M. J.; Fairweather, E. E.; Hutton, C.; Jordan, A. M.; McAndrew, C.; Mirza, A.; Mould, D. P.; Thomson, G. J.; Waddella, I.; Ogilviea, D. J. Development and Evaluation of Selective, Reversible LSD1 Inhibitors Derived From Fragments. *MedChemComm* **2013,** *4,* 1513–1522.
205. Sorna, V.; Theisen, E. R.; Stephens, B.; Warner, S. L.; Bearss, D. J.; Vankayalapati, H.; Sharma, S. High-Throughput Virtual Screening Identifies Novel *N*′-(1-Phenylethylidene)-benzohydrazides As Potent, Specific, and Reversible LSD1 Inhibitors. *J. Med. Chem.* **2013,** *56* (23), 9496–9508.
206. Thinnes, C. C.; England, K. S.; Kawamura, A.; Chowdhury, R.; Schofield, C. J.; Hopkinson, R. J. Targeting Histone Lysine Demethylases—Progress, Challenges, and the Future. *Biochim. Biophys. Acta* **2014,** *1839* (12), 1416–1432.
207. Rose, N. R.; Ng, S. S.; Mecinovic, J.; Lienard, B. M.; Bello, S. H.; Sun, Z.; McDonough, M. A.; Oppermann, U.; Schofield, C. J. Inhibitor Scaffolds for 2-Oxoglutarate-Dependent Histone Lysine Demethylases. *J. Med. Chem.* **2008,** *51* (22), 7053–7056.
208. Hamada, S.; Suzuki, T.; Mino, K.; Koseki, K.; Oehme, F.; Flamme, I.; Ozasa, H.; Itoh, Y.; Ogasawara, D.; Komaarashi, H.; Kato, A.; Tsumoto, H.; Nakagawa, H.; Hasegawa, M.; Sasaki, R.; Mizukami, T.; Miyata, N. Design, Synthesis, Enzyme-Inhibitory Activity, and Effect on Human Cancer Cells of a Novel Series of Jumonji Domain-Containing Protein 2 Histone Demethylase Inhibitors. *J. Med. Chem.* **2010,** *53* (15), 5629–5638.
209. Thalhammer, A.; Mecinovic, J.; Loenarz, C.; Tumber, A.; Rose, N. R.; Heightman, T. D.; Schofield, C. J. Inhibition of the Histone Demethylase JMJD2E by 3-Substituted pyridine 2,4-dicarboxylates. *Org. Biomol. Chem.* **2011,** *9* (1), 127–135.
210. Rai, G.; Kawamura, A.; Tumber, A.; Liang, Y.; Vogel, J. L.; Arbuckle, J. H.; Rose, N. R.; Dexheimer, T. S.; Foley, T. L.; King, O. N.; Quinn, A.; Mott, B. T.; Schofield, C. J.; Oppermann, U.; Jadhav, A.; Simeonov, A.; Kristie, T. M.; Maloney, D. J. Discovery of ML324, a JMJD2 Demethylase Inhibitor With Demonstrated Antiviral Activity. In *Probe Reports From the NIH Molecular Libraries Program;* National Center for Biotechnology Information (US): Bethesda (MD), 2010.
211. Kruidenier, L.; Chung, C. W.; Cheng, Z.; Liddle, J.; Che, K.; Joberty, G.; Bantscheff, M.; Bountra, C.; Bridges, A.; Diallo, H.; Eberhard, D.; Hutchinson, S.; Jones, E.; Katso, R.; Leveridge, M.; Mander, P. K.; Mosley, J.; Ramirez-Molina, C.; Rowland, P.; Schofield, C. J.; Sheppard, R. J.; Smith, J. E.; Swales, C.; Tanner, R.; Thomas, P.; Tumber, A.; Drewes, G.; Oppermann, U.; Patel, D. J.; Lee, K.; Wilson, D. M. A Selective Jumonji H3K27 Demethylase Inhibitor Modulates the Proinflammatory Macrophage Response. *Nature* **2012,** *488* (7411), 404–408.
212. Atkinson, S.J.; Barker, M.D.; Campbell, M.; Humphreys, P.; Liddle, J.; Sheppard, R.J.; Wilson, D.M. N-2-(2-Pyridinyl)-4-pyrimidinyl-beta-alanine Derivatives As Inhibitors of Histone Demethylase JMJD3. WO/2012/052390, **2012**.
213. Suzuki, T.; Ozasa, H.; Itoh, Y.; Zhan, P.; Sawada, H.; Mino, K.; Walport, L.; Ohkubo, R.; Kawamura, A.; Yonezawa, M.; Tsukada, Y.; Tumber, A.; Nakagawa, H.; Hasegawa, M.; Sasaki, R.; Mizukami, T.; Schofield, C. J.; Miyata, N. Identification of the KDM2/7 Histone Lysine Demethylase Subfamily Inhibitor and Its Antiproliferative Activity. *J. Med. Chem.* **2013,** *56* (18), 7222–7231.
214. Sakurai, M.; Rose, N. R.; Schultz, L.; Quinn, A. M.; Jadhav, A.; Ng, S. S.; Oppermann, U.; Schofield, C. J.; Simeonov, A. A Miniaturized Screen for Inhibitors of Jumonji Histone Demethylases. *Mol. Biosyst.* **2010,** *6* (2), 357–364.
215. Sanchez, R.; Zhou, M. M. The Role of Human Bromodomains in Chromatin Biology and Gene Transcription. *Curr. Opin. Drug Discov. Devel.* **2009,** *12* (5), 659–665.
216. Filippakopoulos, P.; Qi, J.; Picaud, S.; Shen, Y.; Smith, W. B.; Fedorov, O.; Morse, E. M.; Keates, T.; Hickman, T. T.; Felletar, I.; Philpott, M.; Munro, S.; McKeown, M. R.; Wang, Y.; Christie, A. L.; West, N.; Cameron, M. J.; Schwartz, B.; Heightman, T. D.; La Thangue, N.; French, C. A.; Wiest, O.; Kung, A. L.; Knapp, S.; Bradner, J. E. Selective Inhibition of BET Bromodomains. *Nature* **2010,** *468* (7327), 1067–1073.
217. Zeng, L.; Zhou, M. M. Bromodomain: An Acetyl-Lysine Binding Domain. *FEBS Lett.* **2002,** *513,* 124–128.
218. Yang, X. J. Lysine Acetylation and the Bromodomain: A New Partnership for Signaling. *Bioessays* **2004,** *26* (10), 1076–1087.
219. Yang, Z.; He, N.; Zhou, Q. Brd4 Recruits P-TEFb to Chromosomes at Late Mitosis to Promote G1 Gene Expression and Cell Cycle Progression. *Mol. Cell Biol.* **2008,** *28,* 967–976.
220. Rahl, P. B.; Lin, C. Y.; Seila, A. C. c-MYC Regulates Transcriptional Pause Release. *Cell* **2010,** *141,* 4323–4445.
221. Mujtaba, S.; He, Y.; Zeng, L.; Farooq, A.; Carlson, J. E.; Ott, M.; Verdin, E.; Zhou, M. M. Structural Basis of Lysine-Acetylated HIV-1 Tat Recognition by PCAF Bromodomain. *Mol. Cell* **2002,** *9* (3), 575–586.
222. Zeng, L.; Li, J.; Muller, M.; Yan, S.; Mujtaba, S.; Pan, C.; Wang, Z.; Zhou, M. M. Selective Small Molecules Blocking HIV-1 Tat and Coactivator PCAF Association. *J. Am. Chem. Soc.* **2005,** *127* (8), 2376–2377.
223. Nicodeme, E.; Jeffrey, K. L.; Schaefer, U.; Beinke, S.; Dewell, S.; Chung, C. W.; Chandwani, R.; Marazzi, I.; Wilson, P.; Coste, H.; White, J.; Kirilovsky, J.; Rice, C. M.; Lora, J. M.; Prinjha, R. K.; Lee, K.; Tarakhovsky, A. Suppression of Inflammation by a Synthetic Histone Mimic. *Nature* **2010,** *468* (7327), 1119–1123.
224. Picaud, S.; Wells, C.; Felletar, I.; Brotherton, D.; Martin, S.; Savitsky, P.; Diez-Dacal, B.; Philpott, M.; Bountra, C.; Lingard, H.; Fedorov, O.; Muller, S.; Brennan, P. E.; Knapp, S.; Filippakopoulos, P. RVX-208, an Inhibitor of BET Transcriptional Regulators With Selectivity for the Second Bromodomain. *Proc. Natl. Acad. Sci. U. S. A.* **2013,** *110* (49), 19754–19759.
225. Zhang, G.; Plotnikov, A. N.; Rusinova, E.; Shen, T.; Morohashi, K.; Joshua, J.; Zeng, L.; Mujtaba, S.; Ohlmeyer, M.; Zhou, M. M. Structure-Guided Design of Potent Diazobenzene Inhibitors for the BET Bromodomains. *J. Med. Chem.* **2013,** *56* (22), 9251–9264.
226. Gacias, M.; Gerona-Navarro, G.; Plotnikov, A. N.; Zhang, G.; Zeng, L.; Kaur, J.; Moy, G.; Rusinova, E.; Rodriguez, Y.; Matikainen, B.; Vincek, A.; Joshua, J.; Casaccia, P.; Zhou, M. M. Selective Chemical Modulation of Gene Transcription Favors Oligodendrocyte Lineage Progression. *Chem. Biol.* **2014,** *21* (7), 841–854.
227. Nicholls, S. J.; Gordon, A.; Johannson, J.; Ballantyne, C. M.; Barter, P. J.; Brewer, H. B.; Kastelein, J. J.; Wong, N. C.; Borgman, M. R.; Nissen, S. E. ApoA-I Induction As a Potential Cardioprotective Strategy: Rationale for the SUSTAIN and ASSURE Studies. *Cardiovasc. Drugs Ther.* **2012,** *26* (2), 181–187.
228. Bonetti, P.; Boi, M.; Ponzoni, M.; Tibiletti, M.; Stahis, A.; Inghirami, G.; Noel, K.; Zucca, E.; Bertoni, F. The Brd-Inhibitor OTX015 Is Active in Pre-Clinical Models of Mature B-Cell Lymphoid Tumors. 54th ASH Annual Meeting and Exposition, Atlanta, GA (December 8–11, 2012).

229. Hewings, D. S.; Wang, M.; Philpott, M.; Fedorov, O.; Uttarkar, S.; Filippakopoulos, P.; Picaud, S.; Vuppusetty, C.; Marsden, B.; Knapp, S.; Conway, S. J.; Heightman, T. D. 3,5-Dimethylisoxazoles Act As Acetyl-Lysine-Mimetic Bromodomain Ligands. *J. Med. Chem.* **2011,** *54* (19), 6761–6770.
230. Bamborough, P.; Diallo, H.; Goodacre, J. D.; Gordon, L.; Lewis, A.; Seal, J. T.; Wilson, D. M.; Woodrow, M. D.; Chung, C. W. Fragment-Based Discovery of Bromodomain Inhibitors Part 2: Optimization of Phenylisoxazole Sulfonamides. *J. Med. Chem.* **2012,** *55* (2), 587–596.
231. Dawson, M. A.; Prinjha, R. K.; Dittmann, A.; Giotopoulos, G.; Bantscheff, M.; Chan, W. I.; Robson, S. C.; Chung, C. W.; Hopf, C.; Savitski, M. M.; Huthmacher, C.; Gudgin, E.; Lugo, D.; Beinke, S.; Chapman, T. D.; Roberts, E. J.; Soden, P. E.; Auger, K. R.; Mirguet, O.; Doehner, K.; Delwel, R.; Burnett, A. K.; Jeffrey, P.; Drewes, G.; Lee, K.; Huntly, B. J.; Kouzarides, T. Inhibition of BET Recruitment to Chromatin As an Effective Treatment for MLL-Fusion Leukaemia. *Nature* **2011,** *478* (7370), 529–533.
232. Ito, T.; Umehara, T.; Sasaki, K.; Nakamura, Y.; Nishino, N.; Terada, T.; Shirouzu, M.; Padmanabhan, B.; Yokoyama, S.; Ito, A.; Yoshida, M. Real-Time Imaging of Histone H4K12-Specific Acetylation Determines the Modes of Action of Histone Deacetylase and Bromodomain Inhibitors. *Chem. Biol.* **2011,** *18* (4), 495–507.
233. Fish, P. V.; Filippakopoulos, P.; Bish, G.; Brennan, P. E.; Bunnage, M. E.; Cook, A. S.; Federov, O.; Gerstenberger, B. S.; Jones, H.; Knapp, S.; Marsden, B.; Nocka, K.; Owen, D. R.; Philpott, M.; Picaud, S.; Primiano, M. J.; Ralph, M. J.; Sciammetta, N.; Trzupek, J. D. Identification of a Chemical Probe for Bromo and Extra C-Terminal Bromodomain Inhibition Through Optimization of a Fragment-Derived Hit. *J. Med. Chem.* **2012,** *55* (22), 9831–9837.
234. James, L. I.; Barsyte-Lovejoy, D.; Zhong, N.; Krichevsky, L.; Korboukh, V. K.; Herold, J. M.; MacNevin, C. J.; Norris, J. L.; Sagum, C. A.; Tempel, W.; Marcon, E.; Guo, H.; Gao, C.; Huang, X. P.; Duan, S.; Emili, A.; Greenblatt, J. F.; Kireev, D. B.; Jin, J.; Janzen, W. P.; Brown, P. J.; Bedford, M. T.; Arrowsmith, C. H.; Frye, S. V. Discovery of a Chemical Probe for the L3MBTL3 Methyllysine Reader Domain. *Nat. Chem. Biol.* **2013,** *9* (3), 184–191.
235. James, L. I.; Korboukh, V. K.; Krichevsky, L.; Baughman, B. M.; Herold, J. M.; Norris, J. L.; Jin, J.; Kireev, D. B.; Janzen, W. P.; Arrowsmith, C. H.; Frye, S. V. Small-Molecule Ligands of Methyl-Lysine Binding Proteins: Optimization of Selectivity for L3MBTL3. *J. Med. Chem.* **2013,** *56* (18), 7358–7371.
236. Smith, S. G.; Zhou, M. M. The Bromodomain: A New Target in Emerging Epigenetic Medicine. *ACS Chem. Biol.* **2016,** *11* (3), 598–608.
237. Chen, P.; Chaikuad, A.; Bamborough, P.; Bantscheff, M.; Bountra, C.; Chung, C. W.; Fedorov, O.; Grandi, P.; Jung, D.; Lesniak, R.; Lindon, M.; Muller, S.; Philpott, M.; Prinjha, R.; Rogers, C.; Selenski, C.; Tallant, C.; Werner, T.; Willson, T. M.; Knapp, S.; Drewry, D. H. Discovery and Characterization of GSK2801, a Selective Chemical Probe for the Bromodomains BAZ2A and BAZ2B. *J. Med. Chem.* **2016,** *59* (4), 1410–1424.
238. Romero, F. A.; Taylor, A. M.; Crawford, T. D.; Tsui, V.; Cote, A.; Magnuson, S. Disrupting Acetyl-Lysine Recognition: Progress in the Development of Bromodomain Inhibitors. *J. Med. Chem.* **2016,** *59* (4), 1271–1298.
239. Wadhwa, E.; Nicolaides, T. Bromodomain Inhibitor Review: Bromodomain and Extra-Terminal Family Protein Inhibitors As a Potential New Therapy in Central Nervous System Tumors. *Cureus* **2016,** *8* (5), e620.
240. Ferguson, F. M.; Fedorov, O.; Chaikuad, A.; Philpott, M.; Muniz, J. R.; Felletar, I.; von Delft, F.; Heightman, T.; Knapp, S.; Abell, C.; Ciulli, A. Targeting Low-Druggability Bromodomains: Fragment Based Screening and Inhibitor Design Against the BAZ2B Bromodomain. *J. Med. Chem.* **2013,** *56* (24), 10183–10187.

Relevant Websites

http://www.actrec.gov.in/histome/index.php—HIstome: The Histone Infobase.
http://www.activemotif.com/documents/1815.pdf—Histone modification guide.
https://www.cellsignal.com/contents/resources-reference-tables/histone-modification-table/science-tables-histone—Histone modification table.
https://en.wikipedia.org/wiki/Epigenetics—Epigenetics WIKI.

2.13 Small-Molecule Inhibitors of Protein–Protein Interactions

Z Liu, H Chen, EA Wold, and J Zhou, University of Texas Medical Branch, Galveston, TX, United States

© 2017 Elsevier Ltd. All rights reserved.

2.13.1	**Introduction**	331
2.13.2	**Critical Role of Protein–Protein Interactions in Various Diseases**	332
2.13.2.1	Cancer	332
2.13.2.2	Central Nervous System Disorders	332
2.13.2.3	Inflammation and Autoimmune Diseases	333
2.13.2.4	Cardiovascular Disease	333
2.13.2.5	Infectious Diseases	334
2.13.2.6	Other Diseases	334
2.13.3	**Protein–Protein Interactions as Drug Targets**	334
2.13.3.1	Hotspots and Allosteric Sites	334
2.13.3.2	Identification of Druggable Protein–Protein Interactions	335
2.13.3.3	Small Molecular Protein–Protein Interaction Inhibitors	336
2.13.4	**Strategies to Generate Protein–Protein Interaction Inhibitors**	336
2.13.4.1	Peptides and Peptidomimetics	336
2.13.4.2	High-Throughput Screening	336
2.13.4.3	Fragment-Based Drug Design	337
2.13.4.4	Virtual Screening	337
2.13.5	**Highlights on Recent Advances in Drug Discovery Targeting Protein–Protein Interactions**	338
2.13.5.1	Cancer	338
2.13.5.1.1	Bcl-2/Bcl-x_L–Bak	338
2.13.5.1.2	MDM2–p53	338
2.13.5.1.3	WDR5–MLL	339
2.13.5.1.4	Bromodomain–acetylated histone	341
2.13.5.2	Central Nervous System Disorders	342
2.13.5.2.1	PDZ Domain Interactions	342
2.13.5.2.2	α-Synuclein aggregation	343
2.13.5.3	Inflammation and Autoimmune Diseases	343
2.13.5.3.1	LFA-1–ICAM-1	343
2.13.5.3.2	Keap1–Nrf2	343
2.13.5.4	Cardiovascular Disease	344
2.13.5.5	Infectious Diseases	345
2.13.6	**Concluding Remarks and Future Prospects**	346
Acknowledgments		346
References		346
Relevant Websites		353

Abbreviations

A Ala
ACS Acute coronary syndrome
AD Alzheimer's disease
AKAP A-kinase anchor protein
Akt Protein kinase B
ALL Acute lymphoid leukemia
AMA1 Apical membrane antigen 1
AML Acute myeloid leukemia
AP1 Activator protein 1
APCs Antigen-presenting cells
ASH2L Absent small homeotic disks-2-like
Aβ Amyloid-β
Bad Bcl-2-associated death promoter
Bak Bcl-2 homologous antagonist killer
Bcl-2 B-cell lymphoma 2
Bcl-x_L B-cell lymphoma-extra large
BD Bromodomain
BET Bromodomain and extraterminal domain
BH Bcl-2 homology domains
BRD4 Bromodomain containing 4
CAM Cell adhesion molecules
cAMP Cyclic adenosine 3′,5′-monophosphate
CLL Chronic lymphocytic leukemia
CNS Central nervous system
CVB3 Human coxsackievirus B3
DLBCL Diffuse large B-cell lymphoma
DSF Differential scanning fluorimetry
E Glu

EGFR Epidermal growth factor receptor
F Phe
FBDD Fragment-based drug design
FDA US Food and Drug Administration
FGF14 The fibroblast growth factor 14
FP Fluorescence polarization
FRET Fluorescence resonance energy transfer
GM130 Golgi matrix protein 130
GP Platelet glycoprotein
GPCRs G-protein-coupled receptors
GSK3 Glycogen Synthase Kinase 3
H3K4 Histone H3 lysine 4
HDB High-dose bolus
HER2 Human epidermal growth factor receptor 2
HIV Human immunodeficiency virus type 1
Hsp Heat shock protein
HSQC Heteronuclear single-quantum coherence
HTRF Homogeneous time-resolved fluorescence
HTS High-throughput screening
IDAS I-Domain allosteric site
IKKγ IkB kinase γ
IL-2R Interleukin-2 receptor
ITC Isothermal calorimetry
JIP1 JNK-interacting protein-1
JNKs Jun N-terminal kinases
Keap1 Kelch-like ECH-associated protein 1
L Leu
LC Light chain
LE Higher ligand efficiency
LEDGF Lens epithelium-derived growth factor
LFA-1 Leukocyte function-associated antigen
LPS Lipopolysaccharide
MAGUK Membrane-associated guanylate kinases
MAPK Mitogen-activated protein kinases
Max Myc associated factor X
MCAO Middle cerebral artery occlusion
MCRs Multicomponent reactions
MDM2 Mouse double minute 2 homolog
MLL1 Mixed lineage leukemia 1
MLR Mixed lymphocyte reaction
MS Mass spectroscopy
Nav Voltage-gated sodium
NCI National Cancer Institute
NEMO Essential modulator
NF-kB Nuclear factor kappa B
NHL Non-Hodgkin's lymphoma
NMC NUT midline carcinoma
NMDAR *N*-methyl-D-aspartate receptor
NMR Nuclear magnetic resonance
nNOS Neuronal nitric oxide
NO Nitric oxide
Nrf2 Nuclear factor erythroid 2-related factor 2
PAQR3 Progestin and adipoQ receptors 3
PARP Poly(ADP-ribose)polymerase
PD Parkinson's disease
PDE4 Phosphodiesterase 4
PDZ The PSD95/DlgA/ZO-1 homology
PE Phosphatidylethanolamine
PfAtg8 *Plasmodium falciparum* Atg8
PKA Protein kinase A
PPIs Protein–protein interactions
PRISM PLATELET Receptor Inhibition in Ischemic Syndrome Management
PSA Polar surface area
PSD-95 Postsynaptic density protein 95
Q Gln
R Arg
RA Rheumatoid arthritis
RbBP5 Retinoblastoma-binding protein 5
RO3 Rule of three
RON2 Rhoptry neck protein 2
S Ser
SAA Serum amyloid A
SAR Structure–activity relationship
Scap SREBP cleavage-activating protein
SOS Son of sevenless
SPR Surface plasmon resonance
SREBP Sterol regulatory element-binding protein
ssNMR Solid-state nuclear magnetic resonance
T Thr
TAZ Transcriptional coactivator with PDZ-binding motif
TEAD Transcriptional enhancer associate domain
TFs Transcription factors
THIQ Tetrahydroisoquinoline
TNF Tumor necrosis factor
TNFRSFs TNF superfamily receptors
TNKS Tankyrase
TRAF6 TNF receptor-associated factor 6
TTR Transthyretin
Ubl Ubiquitin-like
VEGF Vascular endothelial growth factor
VEGFR VEGF receptors
VS Virtual screening
vwf von Willebrand factor
W Trp
WDR5 WD40 repeat protein 5
XIAP X-linked inhibitor of apoptosis
Y Tyr
YAP Yes associate protein

2.13.1 Introduction

Protein–protein interactions (PPIs), which refer to physical contacts between two or more proteins as a result of biochemical events and/or electrostatic forces, play an important role in human physiology and pathophysiology. The interactions of two or more proteins participate in virtually all cellular processes, including gene regulation, DNA replication, cell growth, cell differentiation, cell apoptosis, signal transduction, transcriptional activation, and many others. Abnormal PPIs either through the loss of an essential interaction or via the formation of a protein complex at an inappropriate time or location are associated with various human diseases, such as cancer and central nervous system (CNS) disorders.[1] While it is estimated that there are approximately 130,000 to 650,000 PPIs in the human interactome,[2,3] only a very limited number of them have been investigated for drug discovery. Construction of the interactome is considered as a critical step after the human genome project.[4] Systematically mapping gene and protein interactions will assist in understanding how genes are involved in various signaling pathways and how these pathways function in disease states. Therefore, PPIs represent a rich source of novel drug targets, which are substantially different from the traditional G-protein-coupled receptors (GPCRs), ion-channel, and enzyme target classes. Over the past two decades, PPIs have attracted increasing attention in the research field along with rapidly expanding studies of relevant strategies and technologies (Fig. 1).

Based on different standards of classifications, PPIs can be divided into homo-oligomers versus hetero-oligomers, stable interactions versus transient interactions, or covalent versus noncovalent interactions. Various PPIs can be identified by in vitro (eg, protein arrays, tandem affinity purification, affinity chromatography, coimmunoprecipitation, X-ray crystallography, and nuclear magnetic resonance (NMR) spectroscopy), in vivo (eg, yeast two-hybrid and synthetic lethality), and in silico methods (eg, computational PPI prediction methods).[5–10] Selectively abrogating these PPIs may provide a promising strategy for drug discovery. PPI inhibitors can be classified into two categories: antibodies (eg, Avastin[11] and Herceptin[12]) and small molecules, such as peptides, peptidomimetics, and nonpeptide small molecules, which are the major focus of this article. Small molecules modulate PPIs through at least three different mechanisms: orthosteric inhibition, allosteric modulation, and interfacial binding/stabilization.[13] Despite a number of challenges, research effort on finding small-molecule, protein–protein modulators has made significant progress over the past decade.[14] Some of these molecules have been advanced into different phases of human clinical trials and several of them have even reached the market (Table 1).

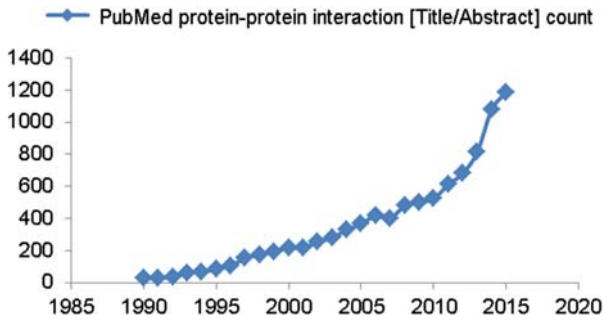

Fig. 1 Search results using the keyword "protein–protein interactions" in the title and abstract from PubMed on Nov. 19, 2015. *Horizontal axis*: publication year; *vertical axis*: numbers of publications having "protein–protein interactions" in the title and abstract.

Table 1 Selected small molecular PPI inhibitors in human clinical trials

Name	*Company*	*Clinical Phase*[a]	*Interactome*	*Indications*
Maraviroc	Pfizer	Launched	CCR5–gp120	HIV infection
Tirofiban	Merck	Launched	Fibrinogen–GPIIb/IIIa	Non-ST elevation acute coronary syndrome (ACS)
SAR1118	Sunesis	Phase III	LFA-1–ICAM-1	Dry eye; Keratoconjunctivitis sicca
Venetoclax	Abbvie	Phase III	Bcl-2/Bcl-x_L–Bak/Bad	Chronic lymphocytic leukemia
Tramiprosate	Neurochem	Phase III[b]	Amyloid-β aggregation	Alzheimer's disease
Tanespimycin	Bristol-Myers Squibb	Phase III	Hsp90–Src	Multiple myeloma; gastrointestinal stromal tumors; primary peritoneal cavity cancer; stage III/IV ovarian epithelial cancer
RVX-208	Resverlogix	Phase III	Bromodomain–acetylated histone	Type II diabetes; coronary artery disease; cardiovascular diseases
Navitoclax	Abbvie	Phase II	Bcl-2/Bcl-x_L–Bak/Bad	Chronic lymphocytic leukemia; prostate cancer
LCL161	Novartis	Phase II	XIAP–Caspase-9	Breast cancer; leukemia; recurrent plasma cell myeloma; refractory plasma cell myeloma
GSK525762	GSK	Phase I/II	Bromodomain– acetylated histone	Nut midline carcinoma; other cancer
RO5045337	Roche	Phase I	p53–MDM2	Neoplasms; sarcoma; myelogenous leukemia
AMG232	Amgen	Phase I	p53–MDM2	Advanced malignancy; advanced solid tumors; cancer

[a]For more information, see: https://clinicaltrials.gov/.
[b]Failed likely due to pharmacokinetics and tolerability issues.

In this article, we discuss the critical role of PPIs associated with various human diseases and different approaches to the identification of small molecular inhibitors targeting PPIs. The highlights on recent advances in developing such modulators as novel therapeutics are also presented.

2.13.2 Critical Role of Protein–Protein Interactions in Various Diseases

Aberrant PPIs may result in various human diseases. Numerous studies have identified and characterized specific interactions associated with a variety of disease systems, including cancer, CNS disorders, inflammation, and other human conditions.[15]

2.13.2.1 Cancer

PPIs form important signaling nodes and hubs in numerous signaling pathways that promote tumorigenesis, tumor progression, invasion, and metastasis. Thus, disruption of specific PPIs critical in cancer processes may provide an effective and novel therapy.[16]

B-cell lymphoma 2 (Bcl-2) family proteins regulate the mitochondrial signaling which is one of the two principal processes (intrinsic and extrinsic apoptotic signaling pathways) leading to apoptosis.[17–19] Interactions between the Bcl-2 family members decide the fate of cells—to die or to live. The antiapoptotic proteins like Bcl-2 and Bcl-x_L heterodimerize with the proapoptotic members, such as Bak, Bax, Bim, and Bad, through the conserved BH3 domain.[20] Overexpression of antiapoptotic Bcl-2 family proteins is implicated in both the pathology and drug resistance of various hematopoietic malignancies and solid tumors.[21,22] Targeting the BH3 domain or BH4 domain, where Bcl-2 interacts with Bcl-2 members or non-Bcl-2 family proteins, is a promising strategy for cancer therapy.[23–26]

The tumor suppressor p53 plays an important role in the regulation of cellular process and its inactivation is a frequent causal event in the development and progression of cancer.[27–29] One critical inhibitory mechanism is mediated by overexpression of mouse double minute 2 homolog (MDM2). MDM2 amplification has been found in about 11% of all tumors and is reported at higher levels in certain tumor types, including hepatocellular carcinoma (44%), osteosarcomas (20%), and soft tissue sarcomas (31%).[30,31] MDM2 binds to the p53 transactivation domain, blocking p53-dependent transcriptional activity. Disturbing the MDM2–p53 interaction can result in the release of p53 from MDM2, thereby restoring the tumor suppressor function of wild-type p53.

Mixed lineage leukemia 1 (MLL1), a histone H3 lysine 4 (H3K4) methyltransferase, is crucial for definitive hematopoiesis and embryonic development and has been implicated in a number of cancers.[32–34] Deregulation of MLL1 is associated with acute lymphoid leukemia (ALL) and acute myeloid leukemia (AML). MLL1 works optimally when in complex with other components: WD40 repeat protein 5 (WDR5), retinoblastoma-binding protein 5 (RbBP5), absent small homeotic disks-2-like (ASH2L), and DPY-30 (WRAD).[35] The MLL1/WDR5 PPI is essential for MLL1 enzymatic activity. Targeting the WDR5–MLL1 PPI is proven to be a practical approach to inhibiting the activity of MLL1 complex, providing a novel therapeutic strategy for acute leukemia harboring MLL1 fusion proteins.[36,37]

Yes associate protein (YAP) and transcriptional coactivator with PDZ-binding motif (TAZ) are targets and terminal effectors of Hippo pathway whose dysfunctions are involved in cancer development.[38] The Hippo pathway is a newly discovered functionally conserved signaling network that is critical for controlling organ size by modulating both cell proliferation and apoptosis.[39–41] Inhibition of this signaling induces YAP/TAZ translocation to the nucleus, where they would interact with other proteins, such as transcriptional enhancer associate domain (TEAD) transcription factors (TFs), triggering the expression of cell proliferation-promoting genes.[42]

A growing list of validated PPIs as targets for cancer therapeutic development has been reported, including S100B–p53,[43] XIAP–caspase,[44] Ras–SOS,[45] EGFR–HER2,[46] HER2–HER3,[47] Max–Myc,[48] Akt–Bad–14-3-3,[49] MLL–menin,[50] VEGF–VEGFR,[51] and bromodomain–acetylated histone.[52] A new concept of cancer genomics has led to the discovery of a number of genomic alternations that drive tumorigenesis and/or progression,[53,54] and contributed to the rapid development of protein interaction networks. The identification of cancer-specific onco-fusion proteins has increased knowledge of PPI-mediated epigenetic mechanisms and also revealed numerous PPIs that are directly associated with cancer pathology.[16]

2.13.2.2 Central Nervous System Disorders

PPIs are strikingly important for cellular processes in CNS including neurite outgrowth, synaptic formation and modulation, neurotransmission, signal transduction, and the induction of apoptosis.[55,56] Aggregation and/or misfolding of proteins, such as transthyretin (TTR), immunoglobulin light chain (LC), serum amyloid A (SAA), and amyloid-β (Aβ), may cause a number of neurodegenerative disorders.[57,58] It is reported that Aβ aggregates promote Alzheimer's disease (AD).[59–62]

The GPCR heteroreceptor complexes in the CNS are attracting more and more attention and have emerged as novel targets for the treatment of Parkinson's disease (PD), schizophrenia, drug addiction, anxiety, and depression, opening new avenues in neuropsychopharmacology.[63,64] The striatal adenosine A2A and dopamine D2 heteromeric receptor complexes exist in equilibrium with A2A and D2 homoreceptor complexes on the plasma membrane in the striato-pallidal GABAergic neurons where they strongly modulate excitability. This occurs via their ability to counteract the inhibitory D2R signaling to multiple effectors upon agonist

activation of the A2AR protomer.[65–67] These proteins may act as important antiparkinsonian targets based on the existence of antagonistic A2A–D2 receptor–receptor interactions within them.[68]

Glycogen Synthase Kinase 3 (GSK3) has important roles in neuronal polarity and synaptic plasticity, and it has been found dysfunctional in a plethora of brain disorders.[69–71] The fibroblast growth factor 14 (FGF14)-voltage-gated sodium (Nav) channel complex is identified as a new target of GSK3.[72] Inhibition of GSK3 reduces the assembly of the FGF14-Nav channel complex, modifies FGF14-dependent regulation of Na^+ currents, and induces dissociation and subcellular redistribution of the native FGF14–Nav channel complex in hippocampal neurons.

2.13.2.3 Inflammation and Autoimmune Diseases

The Kelch-like ECH-associated protein 1 (Keap1) and Nuclear factor erythroid 2-related factor 2 (Nrf2) pathway is one of the most important cytoprotective mechanisms acquired in vertebrates over the course of evolution. The Keap1–Nrf2 interaction plays a critical role in the protection of human body against drug toxicity and stress-induced diseases.[73] Direct and competitive Keap1–Nrf2 PPI inhibitors have been shown to be effective for enhancing Nrf2 activity, which has an important role in the protection against various diseases, including acute lung injury, chronic obstructive pulmonary diseases, autoimmune disease, inflammation, cancer, neurodegenerative disease, and cardiovascular disease.[74–78]

Nuclear factor kappa B (NF-kB) essential modulator (NEMO), also known as IkB kinase γ (IKKγ), is the regulatory subunit of the inhibitor of IKK complex, an essential component of the canonical NF-kB signaling pathway.[79–81] IKK complex, composed of NEMO and the catalytic alpha and beta subunits (IKKα and IKKβ), can activate NF-kB signaling, resulting in activation of genes involved in inflammation, immunity, cell survival, and other pathways. Thus, disruption of the NEMO–IKKα/β interaction that holds the complex together has emerged as a promising therapeutic target.[82]

Human coxsackievirus B3 (CVB3) causes a number of clinical manifestations including myocarditis, pancreatitis, and meningitis.[83–86] A recent study identified the host factor Golgi matrix protein 130 (GM130) as a novel target of CVB3, which may implicate in the pathogenesis of CVB3-induced acute pancreatitis.[87] The interaction of viral protein VP1 with GM130 disrupts GM130–GRASP65 complexes and may cause GM130 degradation, leading to disruption of the Golgi ribbon and development of acute pancreatitis in mice.

Tankyrase (TNKS), a member of the poly(ADP-ribose)polymerase (PARP) family, interacts with a variety of proteins involved in a wide range of biological functions.[88] In the case of adaptor protein 3BP2, mutations of the TNKS-binding motif underlie the human disease cherubism, a condition characterized by inflammatory lesions of the facial bone.[89]

Tumor necrosis factor (TNF) receptor-associated factor 6 (TRAF6) is a cytoplasmic protein that mediates signaling from the TNF superfamily receptors (TNFRSFs). The interactions between TRAF6 and TNFRSFs activate NF-kB family and activator protein 1 (AP1) family TFs, triggering immune and inflammatory responses and modulating bone homeostasis,[90] representing a promising target for the treatment of rheumatoid arthritis (RA).[91]

Blocking the IL-2/Interleukin-2-receptor (IL-2/IL-2R) interaction is important in suppression of immune responses.[92,93] The PPI between CD2 on T cells and CD58 on antigen-presenting cells(APCs) plays a significant role in the early stage of immune responses,[94] which are critically associated with inflammatory and autoimmune diseases.[95] CD40–TRAF6 interactions are also known to play an essential role in several inflammatory diseases.[96] More interactions remain to be elucidated.

2.13.2.4 Cardiovascular Disease

It is reported that a Golgi-localized membrane protein progestin and adipoQ receptors 3 (PAQR3) interacts with Scap and SREBP and tethers them to the Golgi to modulate cholesterol homeostasis.[97] Dysregulation of cholesterol homeostasis is closely associated with the pathogenesis of many human diseases, including atherosclerosis, myocardial infarction, and stroke.

Targeting PPIs, such as PDE4D5–β arrestin, PDE4–HSP20, and AKAP complexes within the cyclic adenosine 3′,5′-monophosphate (cAMP) signaling system, is a promising therapeutic strategy for cardiovascular disease.[98] cAMP participates in the fine control of excitation–contraction coupling in the heart, and thus dysfunction of this signaling cascade induces cardiac disease. The multifunctional scaffold protein β-arrestin orchestrates the dynamic redistribution of PDE4D5 in heart and airway cells, following the activation of the β2-adrenergic receptors.[99–101] An active pool of PDE4 is then recruited to the site of cAMP synthesis to initiate the desensitization process. AKAPs are important in the maintenance of distinct cAMP signaling compartments in cells.[102] Some AKAPs organize downstream cardiac signals that are driven by PKA via binding and anchoring PKA to sequester and localize the enzyme in the vicinity of its substrates and other signaling proteins. AKAPs are considered as a new and emerging target of drug development for chronic heart failure.[103] Small-molecule FMP-API-1 (**1**, **Fig. 2**), an inhibitor of AKAP–PKA interactions, was discovered to increase contractility of cultured rat cardiac myocytes and intact hearts.[104]

Besides the interactions mentioned earlier, a number of other PPIs related to cardiovascular disease are under investigation and will contribute to the discovery of new drugs in clinic. For example, inhibition of the complex formed by von Willebrand factor (vwf) and platelet glycoprotein (GP) Ib-V-IX is important for the development of antithrombotic agents.[105]

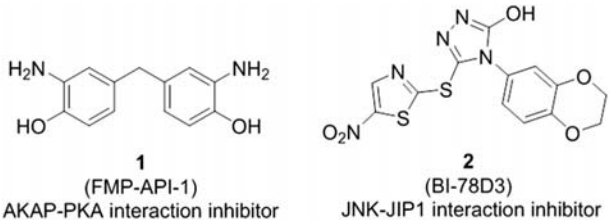

Fig. 2 Chemical structures of PPI inhibitors FMP-API-1 and BI-78D3.

2.13.2.5 Infectious Diseases

Many infectious diseases are results of abnormal PPIs involving endogenous proteins and proteins from pathogens. Atg8, the ubiquitin-like (Ubl) protein essential for formation and maturation of autophagosomes in autophagy in Eukarya, is partially conjugated to the membrane of the apicoplast under nonstarvation conditions in *Plasmodium*.[106–108] A second thioester intermediate formed by Atg8 transferred to its E2-like conjugating enzyme Atg3 and their noncovalent interaction are required for the lipidation of Atg8 to phosphatidylethanolamine (PE) in membranes in most eukaryotes. Inhibition of this PPI to prevent *Plasmodium falciparum* Atg8 (*Pf*Atg8) lipidation represents a promising strategy for antimalarial therapy.[109]

Viral E2 protein is critical for both replication and segregation of papilloma viruses which can cause warts and other diseases. It was reported that E2 protein interacts with C-terminus of bromodomain-containing protein 4 (BRD4) to form a physical tether between the viral plasmid and the host cell mitotic chromosomes.[110,111] Given that overexpression of C-terminus of BRD4 is enough to interrupt the interaction and stop the transmission of viral DNA into daughter cells, targeting E2-BRD4 interaction may be a promising therapeutic strategy for papilloma virus infection.

In addition, some other important PPIs, such as LEDGF–integrase interaction in HIV disease,[112] AMA1–RON2 interaction in malaria,[113] and ZipA–FtsZ interactions in bacterial infection,[114] have also demonstrated potential for developing new therapeutic interventions for infectious diseases.

2.13.2.6 Other Diseases

Jun N-terminal kinases (JNKs), serine threonine protein kinases, and members of the mitogen-activated protein kinases (MAPK) family, phosphorylate and activate a variety of cellular factors involved in various diseases including diabetes, atherosclerosis, and neurodegenerative diseases.[115] JNK-interacting protein-1 (JIP1) is a scaffolding protein that binds JNK via a specific, high-affinity D-domain. JIP1 can enhance JNK signaling by creating a proximity effect between JNK and upstream kinases.[116] JNK binding-domain of JIP1 acts as a competitive inhibitor of JNK signaling and restores normoglycemia in a mouse model of type 2 diabetes.[117–119] A screened compound BI-78D3 (**2**, **Fig. 2**) was shown to displace biotinylated JIP1 from GST-JNK1 and selectively inhibit JNK activity at nanomolar concentrations.[120] Moreover, BI-78D3 is effective for concanavalin A-induced liver damage in mice and restores insulin sensitivity in mouse model of type 2 diabetes in a few hours. Thus, JIP1 mimetic targeting JIP1–JNK interaction is feasible and effective, holding promise for new classes of JNK inhibitors.

Orally administered agonists of hormone erythropoietin (EPO) receptor are highly desired to replace the recombinant EPO to cure anemias caused by kidney failure through promoting the production of red blood cells.[121] Inhibitors of the SH2 domain as antiresorption agents may be used against osteoporosis.[122,123] More applications of PPI modulators remain to be explored in other human diseases in the future.

2.13.3 Protein–Protein Interactions as Drug Targets

Targeting PPIs by small molecules was once considered "undruggable" due to their large, flat interactive surfaces that lack apparently tractable cavities.[124,125] The average volume of pockets seen at protein–protein interfaces is only 54 Å, whereas traditional drug target proteins have one or two disproportionately large pockets with an average volume of 260 Å.[126] The interface contains six such small pockets on the average.[127] A small-molecule PPI inhibitor will likely target three to five small pockets in the protein–protein surface and take advantage of protein adaptability. In addition, unlike the traditional drug targets, PPIs do not have endogenous ligands that serve as potential starting points for medicinal chemists. As PPIs are largely dependent on hydrophobic contacts, such an inhibitor may suffer pharmacokinetic issues including poor solubility. Facilitated by the achievements in developing hotspots, screening techniques, and computational analyses, PPIs as drug targets now become possible and as a result, significant progress has been made in this field.

2.13.3.1 Hotspots and Allosteric Sites

Accumulating studies have shown that PPIs are critically dependent on some key residues ("hotspots") at the interface. Hotspots refer to a small subset of residues on the protein–protein interface contributing to the majority of the binding free energy.[128]

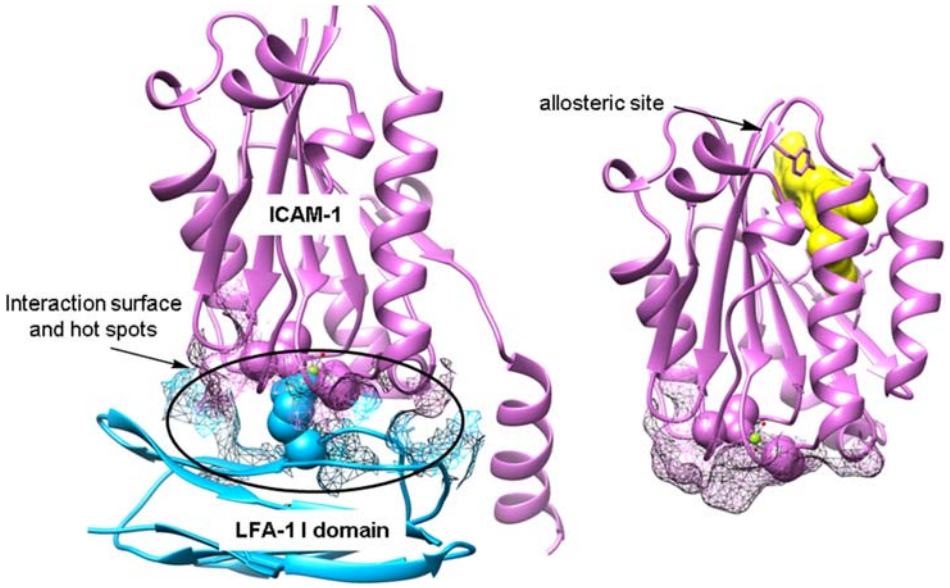

Fig. 3 Exemplary representation of interactive surface, hotspots, and allosteric site. *Left panel*: Complex of LFA I domain and ICAM-1 (PDB Code: 3BN3); Interaction surface and hotspots are depicted. *Right panel*: Complex of ICAM-1 with BMS-587101 (PDB Code: 2ICA); BMS-587101 is shown in *yellow*.

They are often surrounded by a ring of more polar residues that act as an "O-ring" to exclude bulk water from the immediate environment of the hotspots. Hotspots can also be considered as a site on a therapeutic target that has high propensity for ligand binding in the drug design. As an exemplary representation of the concept, the interaction surface and hotspots of LFA-1 complexed with ICAM-1 is depicted in **Fig. 3** (left panel). Hotspots are often identified by experimental methods (eg, alanine scanning, NMR, and crystallographic methods) or computational methods.[129,130] Substitution of a hotspot by an alanine leads to a significant decrease in the free energy of binding ($\Delta\Delta G_{binding} > 1.5$ kcal mol^{-1}).[128] Systematic analysis of alanine mutants on amino acid residues in protein–protein binding sites indicates that the amino acid composition of hotspots may be enriched in tryptophan (W), arginine (R), and tyrosine (Y).[131,132] NMR and crystallographic methods with mutational data provide useful information to define hotspots in 3D structures of protein complex. Also, computational methods have been developed to predict hotspots as a complementary method to the alanine scanning experiments, which may be faulted due to false positives and the possible omission of binding hotspots.[133] To date, a number of software programs, such as PredHS, iPred, and HotPoint,[134–136] are available for the identification of hotspots. Taking hotspots as the starting points for ligand identification is considered as an essential strategy for the development of PPIs.[137] No matter if it is the α-helix or nonlinear epitopes mediating the PPI, a mimetic that reproduces the key recognition features of the hotspots can act as a competitive inhibitor.[137–139]

Allosteric sites are where ligands bind to the target protein distinct from the protein–protein interface. Taking LFA-1 complexed with ICAM-1 as an example (**Fig. 3**, right panel), it is clear that the allosteric inhibitor BMS-587101 binds to a pocket that is distinct from their interactive surface. This kind of binding hinders the macromolecular interaction in an allosteric manner through inducing changes in either the static conformation or the dynamic properties of the target protein(s).[140–142] Disruption of a PPI occurs upon the binding of a ligand to a PPI allosteric site without competing with the binding protein partner. The primary advantages of developing allosteric modulators include the high level of control over the PPI modulation and often improved identification of the suitable allosteric sites.

2.13.3.2 Identification of Druggable Protein–Protein Interactions

The characteristics of a druggable PPI have been identified and explored.[143–145] The Vajda group found that the druggable PPI sites include a cluster of binding hotspots, which are distinguishable from other regions of the protein because of their concave topology combined with a pattern of hydrophobic and polar functionality.[146] Meanwhile, the hotspot pocket tends to undergo different induced-fit rearrangements when the target protein interacts with different protein partners and small-molecule ligands. The critical components of this adaptivity are largely local, involving primarily low energy side chain motions within 6 Å of a hotspot.[146] The druggability of a binding site increases logarithmically with total surface area and apolar contact area, while it decreases logarithmically with polar contact area, which plays a decisive role in recognizing drug-like small molecules.[147] Surface roughness and pocket shape are also crucial for the druggability of a protein pocket.[148] The amino acid residues around druggable PPI pockets (higher frequency of aromatic residues and methionine observed) are obviously different from that in the other areas on the protein surface.[149,150] An increasing number of charged residues can play a negative role on the druggability of a pocket.[143]

2.13.3.3 Small Molecular Protein–Protein Interaction Inhibitors

Small molecular PPI inhibitors can be classified as peptides, secondary structure mimetics, and nonpeptide small molecules. They have unique advantages and disadvantages different from those small molecules targeting traditional enzymes. It is a double-edged sword that typical PPI interfaces are usually very large. On the one hand, this large surface area is difficult to target, but on the other hand, it offers more room to encode selectivity compared with the conserved traditional substrate binding site.[151] Increased selectivity benefits the reduction of the likelihood of off-target toxicities. Meanwhile, in order to maximize the surface contact area, PPI inhibitors need to be large and lipophilic with more rings and fewer rotatable bonds. This brings about big challenges on optimizing ADME property and improving druggability. In addition, PPI inhibitors may reduce the susceptibility to resistance mutations because of the distinct structural features that underlie PPIs.[152] Meanwhile, it is more feasible to control the pharmacokinetic property of PPI inhibitors compared with the traditional active-site inhibitors as PPI inhibitors are prone to be more solvent exposed. It is also observed that the appearance of a nitro moiety is quite common in PPI modulators.[153] Proper replacements of such a group are needed, because aromatic nitro may be potentially toxic when it is metabolized in the body.[154]

2.13.4 Strategies to Generate Protein–Protein Interaction Inhibitors

Characterization of protein interaction interfaces is the first step to develop small-molecule inhibitors of PPIs. The understanding of the PPI interface provides strong support for the efforts to discover novel small-molecule PPI inhibitors.[155]

2.13.4.1 Peptides and Peptidomimetics

The easiest way to generate a PPI inhibitor is to cut out the amino acid sequence of an interacting epitope in a similar fashion to that we mentioned in the section of hotspots. A peptidomimetic is a small protein-like chain designed to mimic that peptide. In a broad sense, peptidomimetics include peptide backbone mimetics, functional mimetics, and topographical mimetics.[156] Native peptides are easily accessible in light of standard synthetic protocols and have a lot of advantages, such as high selectivity and specificity. But their developments are limited due to the intrinsic weaknesses including chemical/physical instability, tendency for aggregation, short half-life, fast elimination, and low membrane permeability.[157] To address these issues, various approaches are taken to design peptidomimetics. For example, peptide bonds can be replaced with other chemical scaffolds. Also, amino acid residues, which are prone to hydrolysis, can be changed into other kinds of amino acids or nonpeptide fragments to increase their stability. Cell-penetrating peptides, such as the transcription trans-activating (TAT) sequences, are developed to solve the problem of membrane permeability. TAT-$IDP_{DD/AA}$ is an analog of TAT-Pep2, which is a competitive inhibitor of the Bcl-2–IP3R interaction. Asp–Asp (DD), the aspartyl protease site in TAT-Pep2, was replaced with Ala–Ala in TAT-$IDP_{DD/AA}$. This strategy reduced proteolytic cleavage, increased cellular uptake, improved the stability, and ultimately reinforced the efficacy of TAT-$IDP_{DD/AA}$.[158] The critical sequence often exists in the form of an α-helix, or β-sheet when it is a part of a protein. Thus chemical modifications (eg, cyclic[159] and stapled[160] forms) are required to maintain its secondary structure as the peptide itself is usually a random coil in solution. Stabilizing of the secondary structure offers an opportunity for oral peptides and helps to improve patient convenience and compliance. Cyclization is the simplest way to introduce a conformational constraint often via connecting two suitable sites (head to tail, backbone to side chain, or side chain to side chain). The all-hydrocarbon staple is another kind of chemical interventions, conferring α-helical structure, protease resistance, cellular penetrance, and biological activity.[161] N-methylation, establishment of intramolecular hydrogen bonds, and building hydrophobic faces are all effective approaches to stabilizing secondary structure.[157] ATSP-7041 (**3**, **Fig. 4A**), a potent and selective stapled peptide reactivator of the wild-type p53 tumor suppressor protein, has shown great promise to enter clinical trials based on its preclinical results. ATSP-7041 targets the interactions of p53 with its major negative regulators MDM2 and MDMX, which are overexpressed in some cancers with equipotent nanomolar inhibitory activity. In addition, it suppresses tumor growth in animal models of multiple human xenograft models (eg, breast cancer and bone cancer).[162,163] Furthermore, it displays favorable drug-like and pharmacokinetic properties such as efficient cell membrane penetration and potential for once-weekly dosing. From the cocrystal structure of ATSP-7041 with MDMX (**Fig. 4B**, right panel), it is revealed that the peptidomimetic is bound in the p53 binding site of MDMX (**Fig. 4B**, left panel).

2.13.4.2 High-Throughput Screening

High-throughput screening (HTS) is a widely used method for discovering hits in traditional targets. When it is applied to PPIs, the first problem lies in low hit rates due to the different chemical space of PPIs from traditional compound libraries. The HTS hit rate is as low as 0.0001% in the identification of JIP-JNK inhibitors performed by Chen et al.[164] Tremendous efforts have been made to build new libraries suitable for PPIs such as peptide libraries,[165–167] α-helix mimetic library,[168] iPPI-DB,[169] and natural product libraries. The most widely used HTS techniques for PPIs include the two-hybrid assay, affinity purification, fluorescence polarization (FP), and fluorescence resonance energy transfer (FRET).[170–172] One of the advantages with HTS is that it works even when the structure information of a target protein is not available. In addition, HTS can also be applied to reveal inducible pockets in protein–protein interfaces, as well as allosteric modulators.[16] However, the limitations include the low hit rate due to incompatible libraries and the potential false positives, which need to be eliminated. The discovery of nutlins and benzodiazepinediones as p53–MDM2

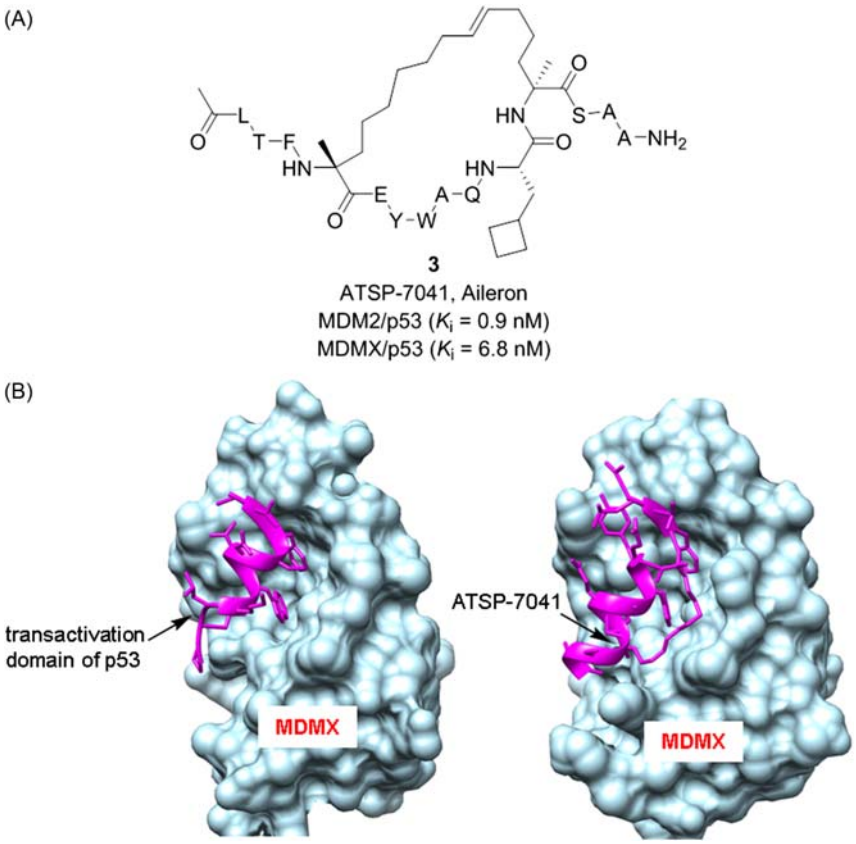

Fig. 4 (A) Chemical structure of PPI inhibitor ATSP-0741. *L*, Leu; *T*, Thr; *F*, Phe; *E*, Glu; *Y*, Tyr; *W*, Trp; *A*, Ala; *Q*, Gln; *S*, Ser. (B) *Left panel*: Structure of the human MDMX protein bound to the p53 tumor suppressor transactivation domain (PDB code: 3DAB). *Right panel*: Structure of ATSP-0741 bound to MDMX (PDB code: 4N5T).

inhibitors is one of the most successful examples in identifying PPI inhibitors through HTS.[173,174] RG7112, a nutlin derivative, is currently in Phase I clinical trials for the treatment of leukemia and solid tumors.[175,176]

2.13.4.3 Fragment-Based Drug Design

Fragment screening and fragment-based drug design (FBDD) are effective to discover protein–protein inhibitors. It is based on identifying small chemical fragment hits, which may bind only weakly to the biological target, and can be optimized via fragment linking, fragment evolution, fragment modification, and fragment self-assembly to produce a lead with a higher affinity.[153,177] A fragment is usually defined as a small organic molecule that follows the "rule of three" (RO3; the molecular weight of the compound $\leqslant$ 300, ClogP $\leqslant$ 3, the number of H-bond donors $\leqslant$ 3, the number of H-bond acceptors $\leqslant$ 3, the number of rotatable bonds $\leqslant$ 3, and polar surface area (tPSA) $\leqslant$ 60 Å^2).[178] It is suggested that some of these strict criteria should be compromised for fragments of PPIs.[179] There are a variety of methods to screen and validate the fragment hits including NMR, MS, X-ray crystallography, surface plasmon resonance (SPR) spectroscopy, tethering, differential scanning fluorimetry (DSF), and isothermal calorimetry (ITC).[177] Weak fragments bound to different hotspots can be connected by a linker and further optimized to generate a high-affinity lead with increased drug-likeness. Fragment screening has higher hit rates, higher ligand efficiency (LE; LE = 1.37 pIC_{50}/number of heavy atoms), and a larger chemical space compared to HTS. In the fragment screening of HIF–TACC3 inhibitors, the hit rate reached 2.3%.[180] Nevertheless, it also has high demands for detection equipment and specific expertise.[181] Meanwhile, it is not applicable for proteins whose structures are unclear. The development of ABT737 and its derivatives ABT263/ABT199 as Bcl-2 inhibitors are outstanding cases of application through FBDD. ABT199, currently in Phase III clinical trials, represents the most promising Bcl-2 inhibitor to be approved by US Food and Drug Administration (FDA) in the future.

2.13.4.4 Virtual Screening

Virtual screening (VS),[182] a computer-aided drug discovery approach comprising the in silico screening of a compound library, is a complementary method to HTS given the work burden of screening compound libraries. The ligand-based

(or pharmacophore-based) approach and structure-based VS are two general screening techniques used in VS.[183] The former model emphasizes the chemical features of compounds important for efficient protein binding.[184] The latter one depends on the structural information of the binding pocket on the target protein.[185] One of the most commonly applied VS methods is molecular docking, by which drug-like compounds are placed into the binding site on their receptor structure virtually, and the binding affinity is evaluated in terms of energy scoring function. Docking methods are used in different stages of identifying a lead compound, such as modeling the protein complex and screening for hotspots on the interactive surface and small molecular PPI modulators.[186] Because of protein flexibility, computational methods appear critically important to search the conformational space of the protein surface and druggable pockets. Though significant progress (eg, predefined structural ensembles[187]) on modeling induced fit effects has been made, two main barriers still remain: comprehensive sampling techniques and scoring.[151,188] As to the screening of small molecular inhibitors, the rule-of-five guideline may be inappropriate. A number of new rules have been developed to predict the physicochemical properties as well as toxicities of PPI inhibitors.[189–191] The hit rate of VS may also be higher than HTS. In the VS of IFN-α–IFNAR inhibitors, it is as high as 16.7%.[192] NSC 66811, a novel p53–MDM2 interaction inhibitor, was discovered via virtual database screening strategy with a hit rate of 14.9%. It mimics three p53 residues (Leu26, Trp23, and Phe19) critical for the interaction and binds to MDM2 with a K_i value of 120 nM.[193]

2.13.5 Highlights on Recent Advances in Drug Discovery Targeting Protein–Protein Interactions

2.13.5.1 Cancer

2.13.5.1.1 Bcl-2/Bcl-x_L–Bak

Developing BH3 mimetics, such as Bcl-2 inhibitors disturbing the interactions between Bcl-2 and proapoptotic proteins, has attracted tremendous attention over the past decade. The AbbVie researchers conducted an NMR-based screening and discovered two fragments (Compounds **4** and **5**, Fig. 5) bound with different sites of Bcl-x_L, with IC_{50} values of 300 and 4300 μM, respectively.[194] Through linking strategy, NMR-based structure information guided parallel synthesis, and reasonable optimization, a potent Bcl-2 inhibitor ABT-737 (Compound **6**, Fig. 5) was obtained. It effectively binds to Bcl-x_L, Bcl-2, and Bcl-w with K_i values less than 1 nM, rather than Bcl-B, Mcl-1, and A1 ($K_i = 0.46 \pm 0.11$ μM, >1 μM, and >1 μM, respectively).[195,196] ABT-737 was shown to disrupt an intracellular Bcl-2 family PPI via a mammalian two-hybrid system. It causes tumor regression in established human tumor xenograft models and displays synergistic cytotoxicity with chemotherapeutics and radiation. However, a major drawback of ABT-737 is its poor oral bioavailability. Thus, a second generation of Bcl-2 inhibitor **7** (ABT-263, Fig. 5A) was developed, with an oral bioavailability of 20% to 50% in preclinical animal models.[197] ABT-263 also displays high affinity for Bcl-x_L, Bcl-2, and Bcl-w and selectivity over Mcl-1 and A1. From the cocrystal structures, it clearly occupies the same pocket where BH3 domains of proapoptotic proteins bind to Bcl-x_L (Fig. 5B). With better PK profiles and effective preclinical in vivo tumor regression studies, ABT-263 was enrolled into clinical trials. However, concomitant on-target thrombocytopenia caused by Bcl-x_L inhibition limits its efficacy.[198] Therefore, a third generation of Bcl-2 inhibitor **8** (ABT-199, Fig. 5A), a selective Bcl-2 inhibitor, was created.[199] ABT-199 has a subnanomolar affinity for Bcl-2 with K_i value less than 0.01 nM, more than 1000-fold selectivity over Bcl-x_L ($K_i = 48$ nM) and Bcl-w ($K_i = 245$ nM) in a time-resolved FRET competition binding assay. It exhibits single-agent cell-killing activity against a number of non-Hodgkin's lymphoma (NHL) cell lines including diffuse large B-cell lymphoma (DLBCL). ABT-199 suppresses tumor growth in a variety of human hematological tumor xenografts as a single agent or in combination with other anticancer agents. More importantly, ABT-199 has obviously reduced effects on platelets compared with ABT-263 due to selective inhibition of Bcl-2. Currently, it is under Phase III clinical trials and has recently been granted breakthrough therapy designation for the treatment of 17p deletion relapsed-refractory chronic lymphocytic leukemia (CLL) (http://abbvie.mediaroom.com/).

2.13.5.1.2 MDM2–p53

RO5045337 (compound **9**, Fig. 6A) is the first clinical MDM2 inhibitor designed to occupy the p53-binding pocket of MDM2. It was derived from a series of *cis*-diphenyl substituted imidazoline-containing compounds known as "nutlins" screened by SPR.[173] RO5045337 shows high MDM2 affinity ($IC_{50} = 18$ nM) in a homogeneous time-resolved fluorescence (HTRF) assay that utilizes the N-terminal domain of recombinant human MDM2 protein and a peptide derived from the binding site of p53.[176] From the cocrystal structure (Fig. 6B), RO5045337 efficiently occupies the major three pockets P1, P2, and P3, which are originally filled with residues Leu26, Trp23, and Phe19 of p53. It effectively inhibits 15 different cancer cell lines expressing wild-type p53 with IC_{50} values in the range of 0.18–2.2 μM, while 5.7–20.3 μM inhibitory activity against cancer cell lines with p53 mutation. RO5045337 also displays favorable pharmacokinetic properties with an AUC value of 251.2 $\mu g \cdot h\ mL^{-1}$, C_{max} value of 15.5 $\mu g\ mL^{-1}$, and longer half-life ($t_{1/2} = 8.8$ h).[200] It effectively suppresses the growth of established tumor xenografts of SJSA1 and MHM osteosarcoma cell lines with MDM2 gene amplification and overexpression of MDM2 protein in nude mice. In clinical trials, it has been investigated against a wide range of cancers, such as sarcoma, myelogenous leukemia, and hematologic neoplasms. RO5045337 displays good human PK profile and signs of antitumor efficacy in patients; however, it has adverse events including neutropenia and thrombocytopenia.[175]

SAR405838 (**10**, Fig. 6A) was discovered by Wang group at the University of Michigan and advanced into phase I clinical trials in 2012.[201] It was optimized from a series of spirooxindoles designed using a structure-based approach to mimic the three key p53-binding residues: Phe19, Trp23, and Leu26.[202] SAR405838 has high affinity to MDM2 with an IC_{50} value of 0.88 nM. It is

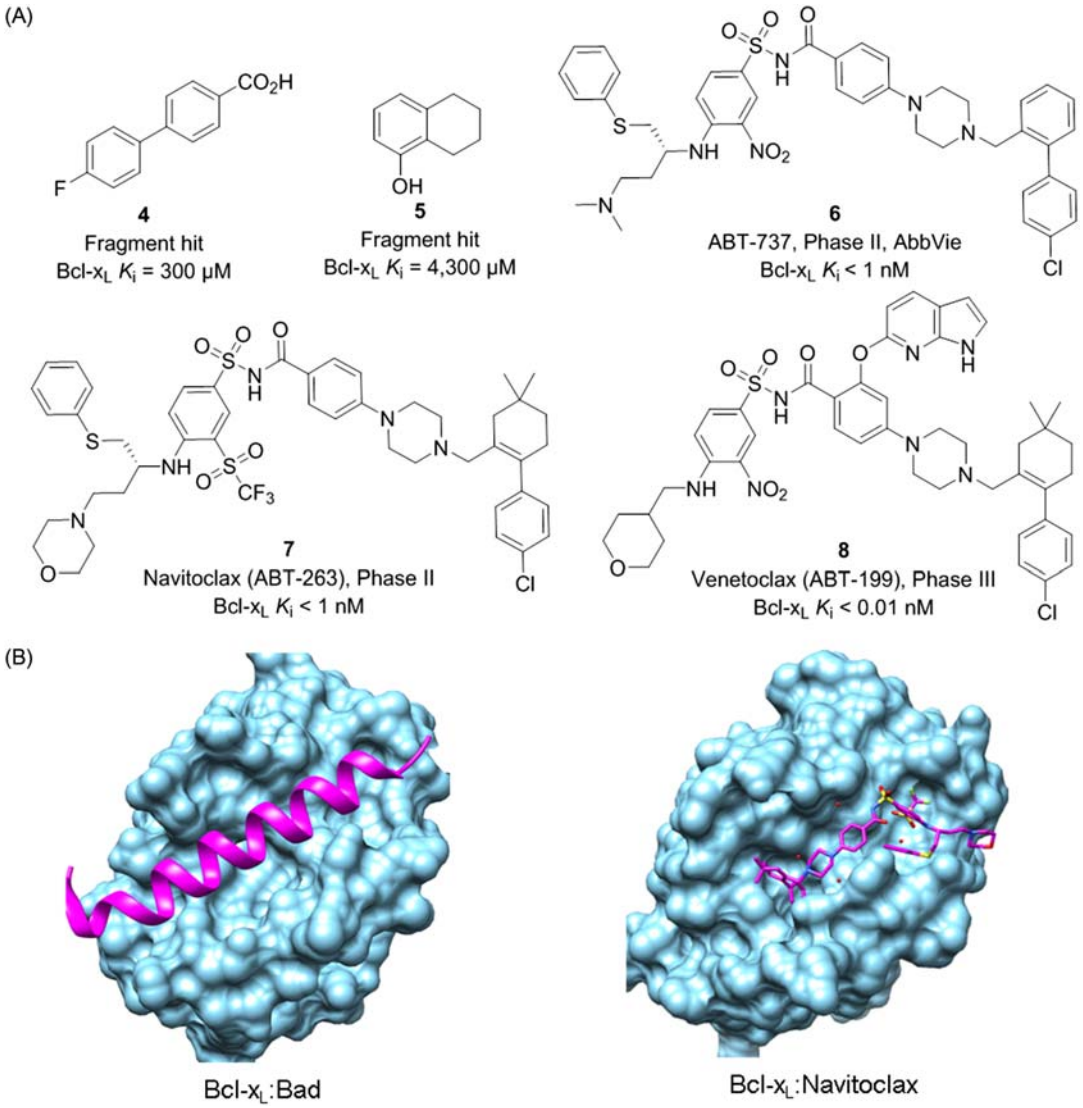

Fig. 5 (A) Chemical structures of selected Bcl-2 inhibitors. (B) *Left panel*: Cocrystal structure of Bcl-x_L and full length Bad (PDB code: 2BZW). *Right panel*: Complex of Bcl-x_L and ABT-263 (PDB code: 4LVT).

revealed by the cocrystal structure of MDM2/SAR405838 complex that SAR405838 not only occupies the pockets original filled by Phe19, Trp23, and Leu26, but also gains additional interactions including hydrophobic contacts of Cl with MDM2 and π–π stacking of 2-fluoro-3-chlorophenyl with the His96 of MDM2. Moreover, the N-terminus of MDM2 (residues 10–18) refolds and has extensive interactions with SAR405838 via Val14 and Thr16. SAR405838 potently inhibits cell growth in diverse cancer cell lines (eg, SJSA-1, RS4;11, LNCaP, and HCT-116) with wild-type p53 and displays high selectivity (>100-folds) over cancer cell lines with mutated or deleted p53. SAR405838 achieves either durable tumor regression or complete tumor growth inhibition in mouse xenograft models of SJSA-1 osteosarcoma, RS4;11 acute leukemia, LNCaP prostate cancer, and HCT-116 colon cancer.[201] Currently, it is under Phase I clinical trials to assess its safety, tolerability, and pharmacokinetics in patients with advanced stage cancer.

Several other MDM2 inhibitors targeting MDM2–p53 interactions are in Phase I human clinical trials such as AMG232 (compound **11**, Fig. 6) developed by Amgen.[203] They display promising implications for the treatment of human solid cancers and leukemia as a single agent or in combination with traditional chemotherapy agents and molecularly targeted agents.

2.13.5.1.3 WDR5–MLL

MM-102 (Compound **12**, Fig. 7) is a peptidomimetic to inhibit the MLL1–WDR5 interaction based on the binding motif derived from MLL1.[36] It binds to WDR5 with $K_i < 1$ nM and inhibits MLL1 activity potently in a fully reconstituted in vitro H3K4 methyltransferase assay. Cocrystal structure of MM-102 and WDR5 indicates that the Arg side chain of MM-102 inserts deeply into the central channel of WDR5 and all the nitrogen atoms in the molecule engage in either intra- or intermolecular hydrogen bonds.

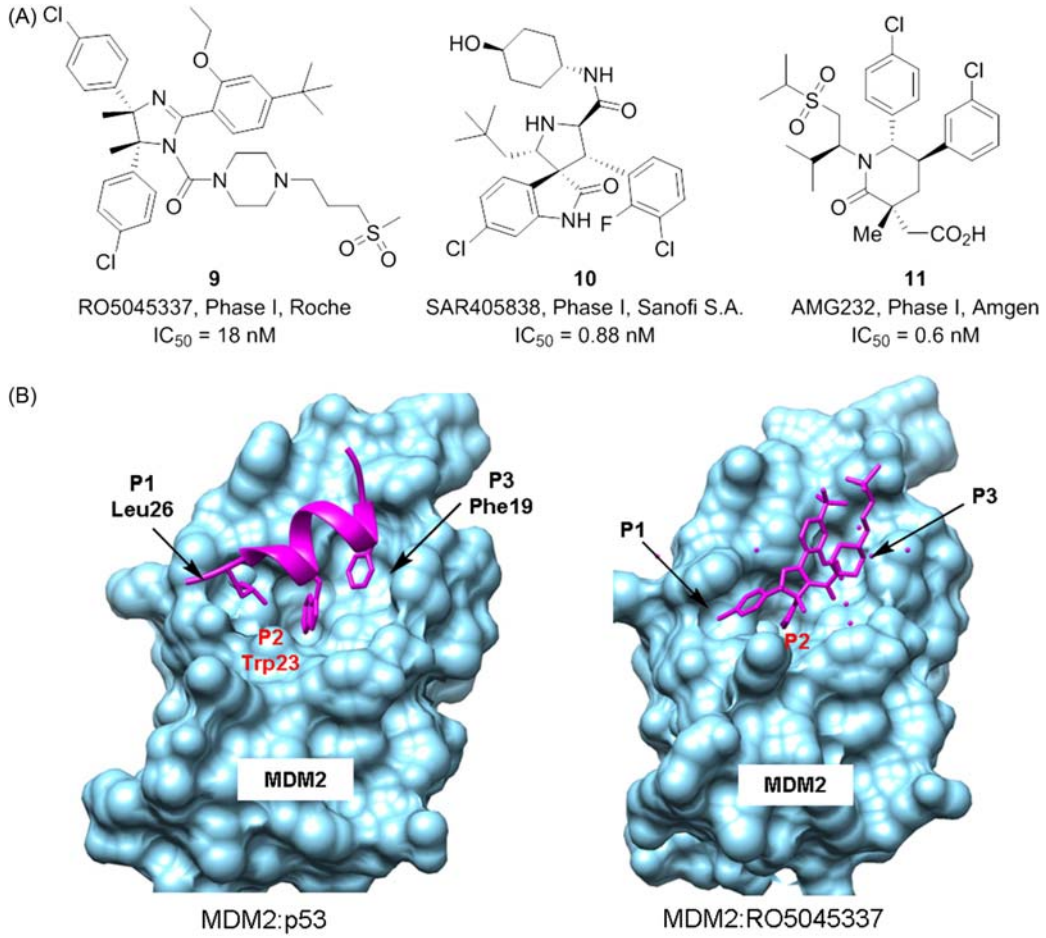

Fig. 6 (A) Chemical structures of selected MDM2 inhibitors. (B) *Left panel*: Cocrystal structure of MDM2 and p53 (PDB code: 1YCQ). *Right panel*: Cocrystal structure of MDM2 and RO5045337 (PDB code: 4IPF).

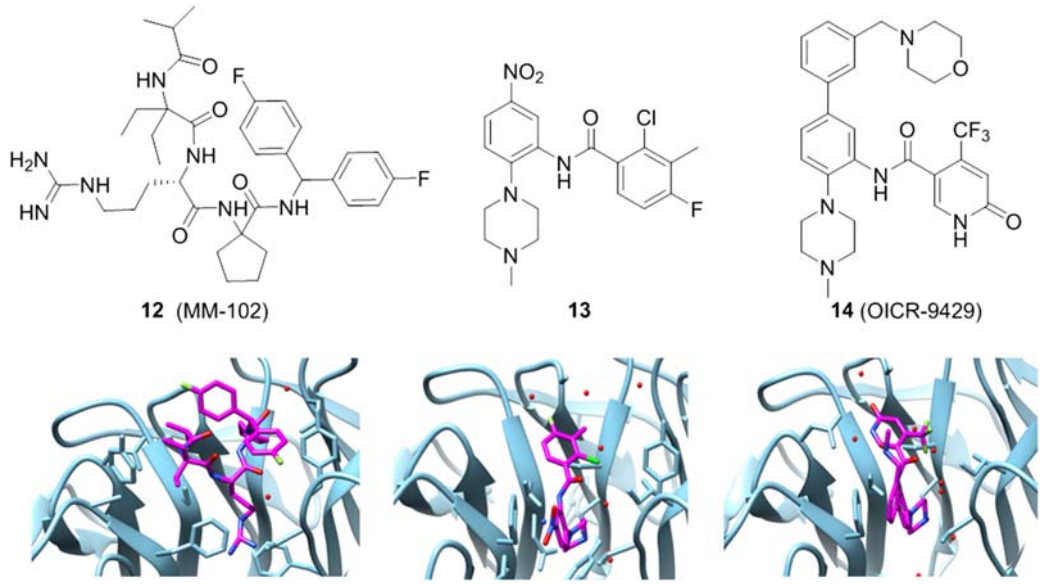

Fig. 7 Chemical structures of PPI inhibitors MM-102 (**12**), **13**, OICR-9429 (**14**) and their cocrystal structures with WDR5 (PDB codes: 4GM8, 4IA9, and 4QL1).

MM-102 effectively decreases the expression of two critical MLL1 target genes (HoxA9 and Meis-1) in bone marrow cells transduced with MLL1-AF9 fusion construct. It also specifically inhibits cell growth and induces apoptosis in leukemia cells harboring MLL1 fusion proteins.[36] Based on the screening result of an established assay that can detect displacement of a fluorescein-labeled WIN peptide (GSARAEVHLRKS) from its binding pocket in WDR5 using FP,[204,205] further optimization led to the discovery of compound **13** (**Fig. 7**).[37] It has a greater than 25-fold gain in potency compared to its parent compound. Further modification has resulted in a potent MLL–WDR5 interaction inhibitor OICR-9429 (Compound **14**, **Fig. 7**), which binds WDR5 with an IC_{50} of 93 nM. OICR-9429 selectively inhibits proliferation and induces differentiation in p30-expressing human AML cells, indicating that WDR5 is a promising therapeutic target in CEBPA-mutant AML.

2.13.5.1.4 Bromodomain–acetylated histone

BET (bromodomain and extraterminal domain) family is a class of well-known bromodomain proteins. Member proteins (eg, BRD2, BRD3, BRD4, and BRDT) binding to acetylated lysine residues in histone tails represents an activation marker of gene expression. Among them, BRD4 is reported to involve in the pathogenesis of various cancers including NUT midline carcinoma (NMC) and AML.[206–208] Since the discovery of (+)-JQ1, which binds tightly to the first and second bromodomains (BD1 and BD2) of BRD4 competing against acetylated histone, a number of novel inhibitors have been reported and several of them are enrolled into clinical trials. RVX-208 (**15**, **Fig. 8A**) is now in Phase II clinical trials with stable coronary artery disease. It is not a BRD4-specific inhibitor, but a pan-BET inhibitor and prefers BD2 of BET proteins. Cocrystal structures of RVX-208 with BRD4 BD1 and BRD2 BD2 are shown in the form of surface presentation (**Fig. 8B, i** and ii). I-BET762 (**16**) and OTX-015 (**17**),[209,210] analogs of benzodiazepine (BZD), are now in Phase I clinical trials for NMC and acute leukemia, respectively. BZD, a well-known privileged structure, is widely used in clinical drugs for anticonvulsant, sedative, and anxiolytic purposes working via the gamma-aminobutyric acid (GABA)-A receptor.[211] Repurposing of privileged structures is very popular in recent years,[212] and BZDs have been applied to

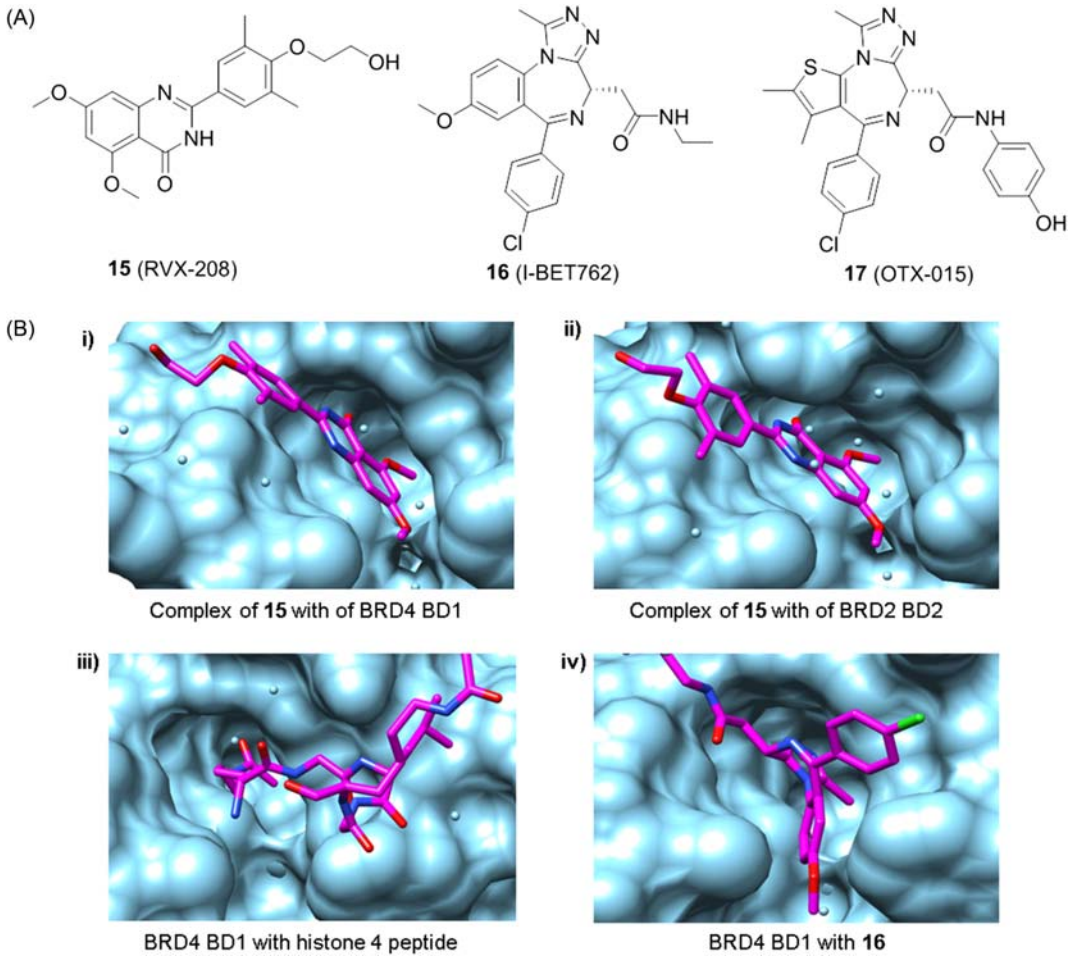

Fig. 8 (A) Chemical structures of bromodomain–acetylated histone inhibitors **15**–**17**. (B) Cocrystal structures of bromodomain–acetylated histone inhibitors. (i) Complex of **15** with BRD4 BD1 (PDB code: 4MR4). (ii) Complex of **15** with BRD2 BD2 (PDB code: 4J1P). (iii) Complex of BRD4 BD1 with histone 4 peptide (PDB code: 3UW9). (iv) Complex of BRD4 BD1 with **16** (PDB code: 4C66).

interactions with BET proteins by fusing to an isostere of benzene or thiophene starting from (+)-JQ1. Neither (+)-JQ1 nor I-BET762 shows interaction with the BZD binding site on the GABA receptor.[213,214] The tortuous BZD scaffold of I-BET762 helps it extend beyond the binding region that a lysine-acetylated histone would occupy (Fig. 8B, iii and iv).

2.13.5.2 Central Nervous System Disorders

2.13.5.2.1 PDZ Domain Interactions

The PSD95/DlgA/ZO-1 homology (PDZ) domain is involved in interactions between many different proteins in a variety of cellular contexts. Interaction of neuronal nitric oxide synthase (nNOS) with the protein postsynaptic density-95 (PSD-95) was reported to induce nitric oxide (NO) overproduction, neuronal injury,[215] and impaired regenerative repair after stroke in rats.[216] Given that the salt bridge (between Asp62 and Arg121, Fig. 9A, left panel) is structurally required and hydrophobic residues (Leu107 and Phe111, Fig. 9A, left panel) are crucial for the nNOS β-finger interacting with PSD-95, ZL006 (**18**, Fig. 9A, right panel) was designed by connecting a hydrophobic ring and a hydrophilic ring through a flexible linker. ZL006 not only selectively blocks the ischemia-induced nNOS–PSD-95 association, displaying potent neuroprotective activity in vitro, but also ameliorates focal cerebral ischemic damage in mice and rats subjected to middle cerebral artery occlusion (MCAO) and reperfusion, without inhibiting NMDAR function, catalytic activity of nNOS or spatial memory, indicating ZL006 may treat stroke without major side effects.[215] Another nNOS–PSD95 inhibitor IC87201 (**19**, Fig. 9A, right panel) was yielded by a high-throughput screen using in vitro binding assay. It reverses NMDA-induced thermal hyperalgesia in mice potently and reverses mechanical allodynia induced by chronic constriction of the sciatic nerve via intrathecal administration.[217]

PSD-95 and the related MAGUK proteins contain three consecutive PDZ domains, and thus trimeric ligand **20** (Fig. 9B) was designed to target all three PDZ domains by introducing a PDZ3-binding peptide moiety via a cysteine-derivatized NPEG linker.[218] It has optimal length for targeting the PDZ1–2–3 proteins of PSD-95 and high affinity with K_i value of 3.3 nM. Based on a series of indole analogues derived from peptide-mimetics of C-terminus of PDZ ligands,[219] compound **21** (Fig. 9B) was developed to disrupt the interaction between the PDZ protein PSD-95 and the C-terminal domain of the 5-HT_{2A} serotonin receptor.[220] Its inhibitory activity against interactions between PSD-95 and the 5-HT_{2A} receptor in vitro was confirmed by $^{1}H-^{15}N$ heteronuclear single-quantum coherence (HSQC) experiments. Compound **21** significantly suppresses mechanical hyperalgesia in an experimental model of traumatic neuropathic pain in the rat, which can be abolished by the coadministration of the 5-HT_{2A} receptor antagonist M100907.[220]

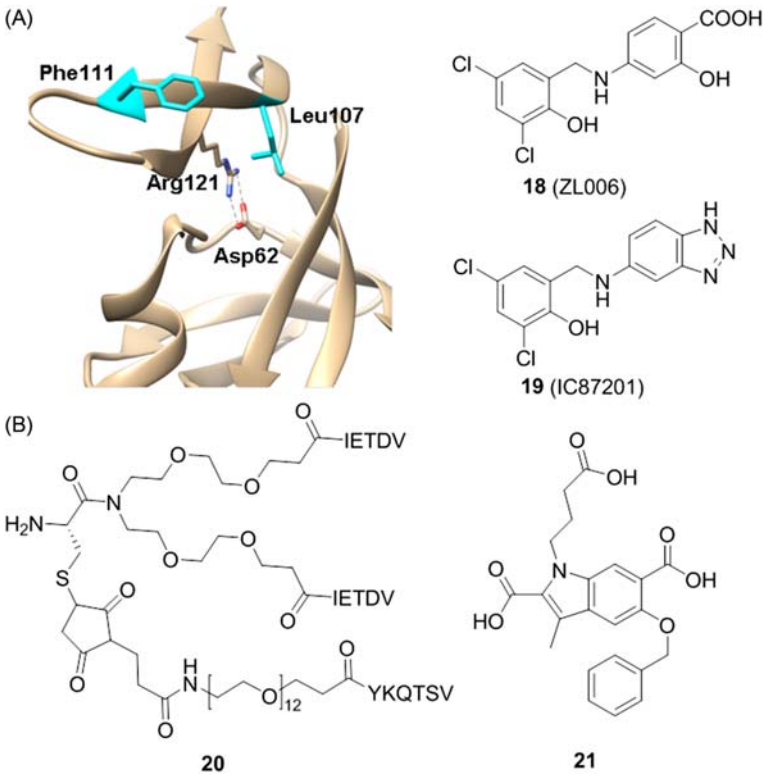

Fig. 9 (A) *Left panel*: Structure of extended nNOS-PDZ domain. *Right panel*: Chemical structures of PPI inhibitors **18** and **19**. (B) Chemical structures of PPI inhibitors **20** and **21**.

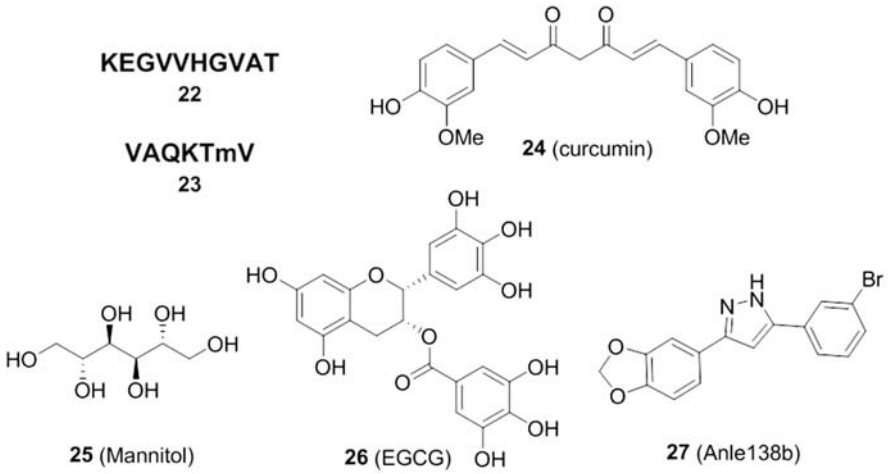

Fig. 10 Chemical structures of α-synuclein aggregation inhibitors **22**–**27**.

2.13.5.2.2 α-Synuclein aggregation

Targeting α-synuclein holds great promise for the treatment of PD.[221–223] Both peptides **22** and **23** (Fig. 10) are able to disrupt the aggregation of α-synuclein. Peptide **22** was generated from residues 45–54 (KEGVVHGVAT) where most early-onset mutations are located,[224] while peptide **23** was derived from residues 77–82 (VAQKTV), which is identified as key residues within amyloidogenic protein sequences by solid-state nuclear magnetic resonance (ssNMR).[225] Polyphenols including compounds **24**–**26** inhibit initiation and/or growth of α-synuclein fibrils. Compound **24** was shown to bind specifically to oligomeric intermediates instead of monomeric α-synuclein indicated by fluorescence and two-dimensional nuclear magnetic resonance (2D-NMR) data.[226] Mannitol (**25**), a blood–brain barrier (BBB) disrupter, interferes with α-synuclein aggregation in vitro and in vivo without adverse toxicity.[227] It reduces the amount of α-synuclein aggregates in a Parkinson drosophila model and the mThy1-human α-synuclein transgenic mouse model. EGCG (**26**) directly binds to unfolded polypeptide chains and inhibits β-sheet formation (an early event in the amyloid formation cascade) by redirecting aggregation prone polypeptides into off-pathway protein assemblies.[228,229] Anle138b (**27**), developed based on a logical HTS combined with medicinal chemistry modification, blocks the formation of α-synuclein aggregates in vitro and inhibits oligomer accumulation, neuronal degeneration, and disease progression in three different PD mouse models in vivo.[230]

2.13.5.3 Inflammation and Autoimmune Diseases

2.13.5.3.1 LFA-1–ICAM-1

Compound **28** (Fig. 11A) is an LFA-1 antagonist through blocking its binding of ICAM-1. It was generated by mimicking nonlinear protein epitopes of ICAM-1 (eg, E34, K39, M64, Y66, N68, and Q73), responsible for its association with LFA-1 (Fig. 11B, left panel).[138] Compound **28** exhibits potent inhibition of ICAM-1/LFA-1 binding, with an IC_{50} value of 1.4 nM in LFA-1 ELISA assay, inhibits mixed lymphocyte reaction (MLR) with an IC_{50} value of 3 nM, and also exhibits significant antiinflammatory effects in vivo. BMS-587101 (Compound **29**, Fig. 11A) was optimized from spirocyclic hydantoin based LFA-1 antagonists and is a potent inhibitor of LFA-1-mediated adhesion in the T-cell/HUVEC adhesion assay with an IC_{50} value of 20 nM. Also, it shows moderate potency in vitro mouse adhesion assay and good PK property in several preclinical species. Moreover, BMS-587101 displays efficacy in two different in vivo models of inflammation.[231] However, it was terminated in Phase II clinical trials likely owing to insufficient efficacy. A second generation ICAM-1/LFA-1 interaction inhibitor BMS-688521 (**30**) with an enhanced potency was obtained through exploring carboxylic acid substituted heterocycles appended to the pyrrolidine ring of the spirocyclic hydantoin core.[232] NMR and X-ray crystal structure (Fig. 11B, right panel) shows that this series of compounds bind to the I-Domain allosteric site (IDAS) of the I-Domain, which is distinct from the site LFA-1 I domain interacting with ICAM-1 (Fig. 11B, middle panel). Based on the pharmacophore analysis of screening hits with micromolar potency against the binding of LFA-1 to ICAM-1, A-286982 (**31**) was developed via searching different linkers to connect a piperazine to occupy a newly identified binding pocket.[233] It has IC_{50} values of 44 and 35 nM in an LFA-1/ICAM-1 binding assay and LFA-1-mediated cellular adhesion assay, respectively. Further optimization of A-286982 through fragment-based NMR screening led to compound **32**, with improved solubility and oral bioavailability. Tetrahydroisoquinoline (THIQ)-derived LFA-1/ICAM-1 antagonists were evolved from an analog of compound **28** by cyclization.[234,235] A systematic structure–activity relationship (SAR) study yielded SAR1118 (**33**), which is currently in Phase III clinical studies as an ophthalmic solution for treating dry eye.[236]

2.13.5.3.2 Keap1–Nrf2

Direct and competitive Keap1–Nrf2 PPI inhibitors have been shown to be effective for enhancing Nrf2 activity, which is important in the protection against various diseases, including acute lung injury, chronic obstructive pulmonary diseases, autoimmune

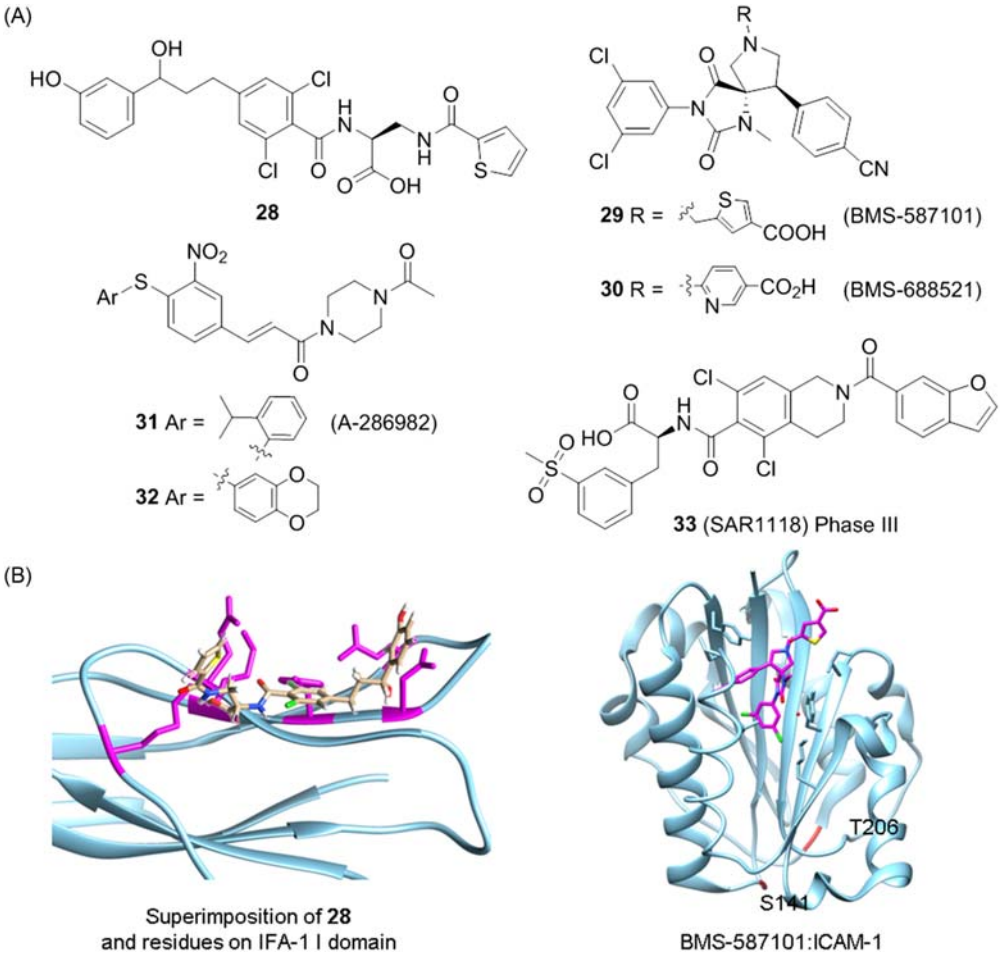

Fig. 11 (A) Chemical structures of PPI inhibitors **28**, BMS-587101, A-286982, and SAR1118. (B) *Left panel*: Superimposition of **28** and ICAM-1 epitope. *Right panel*: BMS-587101:ICAM-1 complex (PDB code: 2ICA).

disease, inflammation, cancer, neurodegenerative disease, and cardiovascular disease.[237] Both peptides (compounds **34** and **35**, Fig. 12A) that mimic Nrf2 and small-molecule Nrf2 activators (compounds **37**–**40**, Fig. 12A) have been reported to disrupt the Keap1–Nrf2 PPI. Compound **36** was identified by VS,[238] while compound **37** was discovered by HTS.[239] Structure-based design of the PPI Inhibitor of Nrf2–Keap1 led to compound **38**. It is the first compound that binds to Keap1 with K_D value of 3.59 nM at the single-digit nanomolar level.[240] Compound **38** cannot only disrupt the Nrf2–Keap1 interaction effectively ($EC_{50} = 28.6$ nM) in the FP assay but also activate the Nrf2 transcription activity in the cell-based ARE-luciferase reporter assay in a dose-dependent manner. Further chemical modification of this compound for improving the physicochemical properties (especially solubility) and in vivo inflammatory effects yielded compound **39** with *p*-acetamido substituents on the side chain of phenyl rings.[241] An exploratory in vivo experiment in a lipopolysaccharide (LPS)-challenged mouse model displayed that compound **39** could reduce the level of circulating proinflammatory cytokines induced by LPS and relieve the inflammatory response. Compound **40** was developed by taking advantage of the available crystal structures of the human Keap1 Kelch domain through an in silico fragment-based approach. It drives the formation of the "open" conformation of the Keap1–Nrf2 complex in a live cell-based imaging experiment.[75] RA839 (**41**), obtained by a screening effect, prevents the interaction of an Nrf2-derived peptide that includes the sequence of Keap1 binding ETGE motif with the Keap1 Kelch domain potently ($IC_{50} = 0.14 \pm 0.04$ μM, FP assay).[242] In mice, RA839 can acutely induce Nrf2-target gene expression in liver. Cocrystal structures of peptides derived from Nrf2, **37**, and RA839 with Keap1 (Fig. 12B) show overlapping binding sites of the ligands.

2.13.5.4 Cardiovascular Disease

Tirofiban (**42**, Fig. 13), an Arg-Gly-Asp (RGD) peptide mimetic, was designed via pharmacophore-based VS to disrupt the fibrinogen–glycoprotein (GP) IIb/IIIa (also known as integrin α_{IIb}/β_3) interaction, which bridges platelets together inducing platelet aggregation.[243] It is a reversible and selective antagonist of fibrinogen binding to the GP IIb/IIIa receptor, with a K_d value of 15 nM. It occupies the same pocket as fibrinogen peptide bound to GP IIb/IIIa (Fig. 13). Given the positive results of Platelet

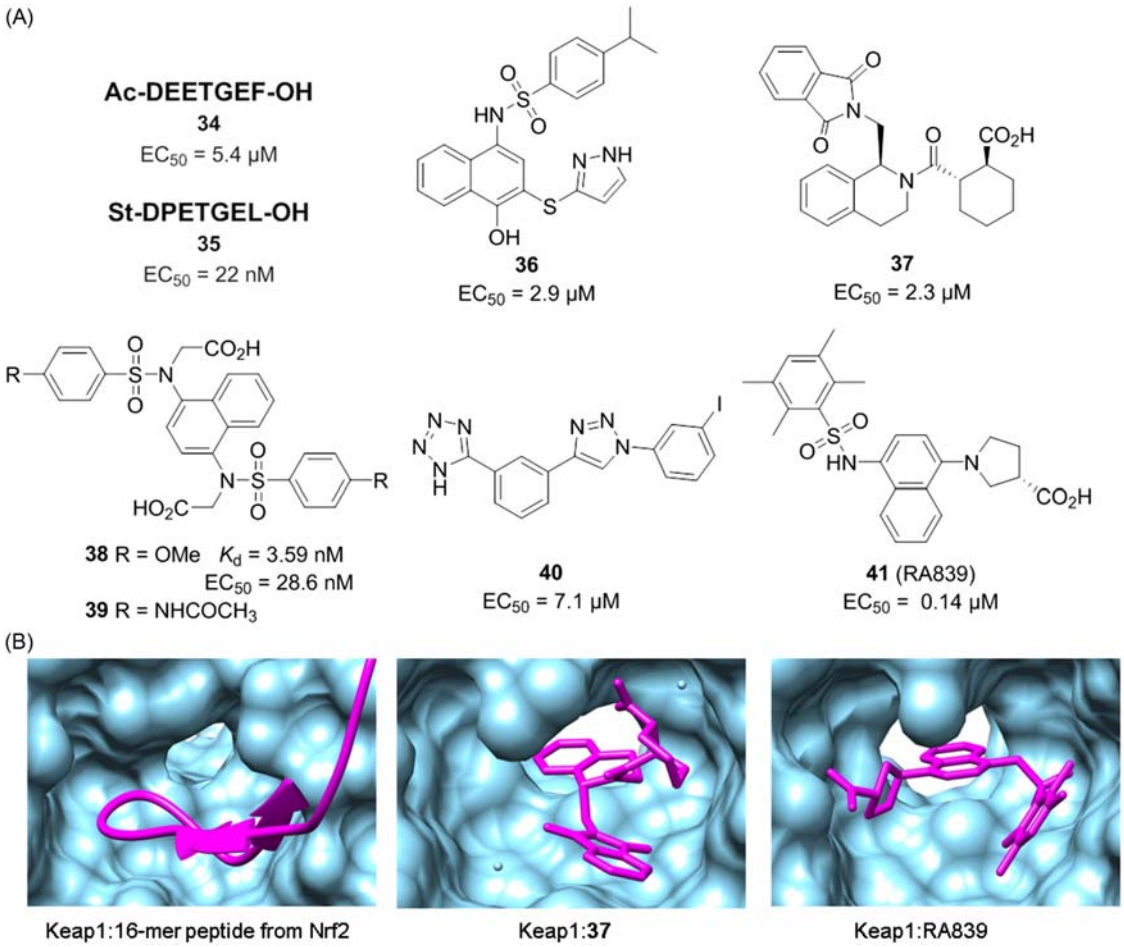

Fig. 12 (A) Chemical structures of PPI inhibitors **34**–**41**. (B) Cocrystal structure of Keap1 and Nrf2 (*left*, PDB code: 2FLU), **37** (*middle*, PDB code: 4L7B), and RA839 (*right*, PDB code: 5CGJ).

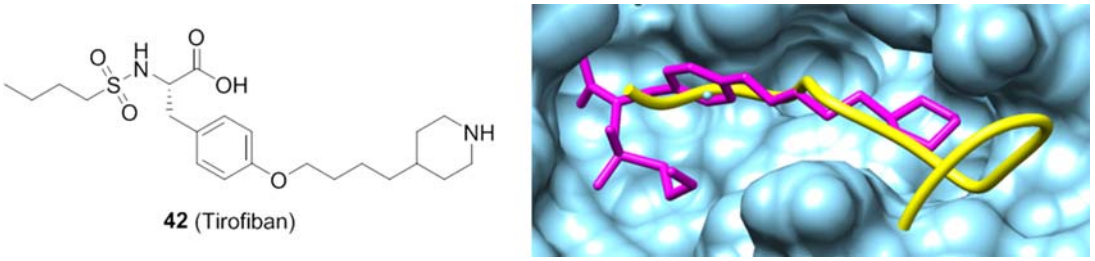

Fig. 13 *Left panel*: Chemical structure of tirofiban. *Right panel*: Overlay structure of fibrinogen peptide (*yellow*) and tirofiban (*magenta*) bound to GPIIb/IIIa (PDB codes: 2VDO and 2VDM).

Receptor Inhibition in Ischemic Syndrome Management (PRISM) clinical trials,[244,245] tirofiban was approved by FDA in 1998 for the treatment of acute coronary syndrome (ACS). From 1998 to 2000, it was the most widely used small-molecule GP IIb/IIIa inhibitor; however, it soon fell out of favor due to the inferiority of the original dosing regimen.[246] The high-dose bolus (HDB) regimen of tirofiban bounced back by achieving therapeutic platelet inhibition faster than that with the original dosing regimen and was subsequently approved by FDA in 2013.

2.13.5.5 Infectious Diseases

Modulating PPIs offers great potential to develop new drugs to treat various infectious diseases, such as HIV, bacterial infection. For instance, Maraviroc (**43**, Fig. 14), an allosteric modulator of the interaction between the chemokine receptor CCR5 and HIV-1

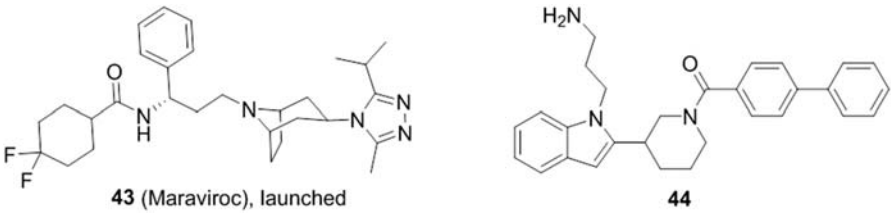

Fig. 14 Chemical structures of PPI inhibitors **43–44**.

gp120, was approved by FDA in 2007 to treat HIV infection.[247] Compound **44**, an inhibitor of cell division in *Escherichia coli* and *Bacillus subtilis*, binds to ZipA at FtsZ-binding site.[248]

2.13.6 Concluding Remarks and Future Prospects

Despite various challenges, developing small molecular PPI inhibitors has made great progress, with some of them available in the market and a number of them progressed into different phases of clinical trials. PPIs participate in virtually all cellular processes and are involved in a wide range of disease process, but only a limited of them are explored. Thus, developing modulators of PPIs including PPI inhibitors and stabilizers[249,250] holds promising therapeutic potential.

The understanding of protein–protein interactive interface provides strong support for the efforts to discover small-molecule PPI inhibitors. It is not necessary for the inhibitors to interact with all the residues on the large and flat interactive surface but simply the efficacious hotspots. The hotspot pocket then tends to undergo different induced-fit rearrangements when the target protein interacts with different protein partners and small-molecule ligands. Therefore, X-ray crystallography of the apoprotein structure may not provide druggable pockets directly. Computational methods may be enlisted in this effort to search the conformational space of the protein surface.

Currently, there are two general strategies to identify small molecules to inhibit PPI: screening and rational design. Because inhibitors targeting PPIs are usually large and more hydrophobic, and different from traditional inhibitors, the screening hit rates of PPI inhibitors are relatively low. New PPI focused libraries have been developed including natural products library, peptidomimetic library, multicomponent reactions (MCRs) developed library, etc. It is imperative to create new rules for PPI inhibitors. More libraries are in urgent need, possibly containing compounds outside the "Rule of Five" to increase the screening hit rates of PPIs. Peptides, peptidomimetics, and nonpeptides small molecules can be designed based on the analysis of interactive surface to mimic its partner. Peptides are believed to have higher selectivity which potentially leads to low toxicity, while the stability and permeability limit their development. Stapled peptides, cyclic peptides, and small molecules, which mimic protein secondary structures and have improved properties, may provide a wealth options. Nonpeptide small molecular disrupters of PPIs are usually large but more specific to their target. Different targets often require different chemotypes. To this end, fragment-based screening may be favorable, and more efficient than HTS.

The era of PPI-based drug discovery is coming with more and more knowledge and experience gained. It is reasonable to believe that targeting various PPIs through small-molecule drug discovery will bring more therapeutic benefits to patients in the future.

Acknowledgments

This work was supported by grants P30 DA028821 and R01 DA038446 from the National Institutes of Health, Cancer Prevention Research Institute of Texas (CPRIT) award, R. A. Welch Foundation Chemistry and Biology Collaborative Grant from the Gulf Coast Consortia (GCC), and a training fellowship from the Center for Addiction Research (NIDA grant T32 DA07287), John Sealy Memorial Endowment Fund, Institute for Translational Sciences (ITS), and the Center for Addiction Research at UTMB.

Conflict of Interest

The authors declare no competing financial interest.

See also: 5.06. Protein-Protein Interaction Inhibitors in Cancer.

References

1. Blazer, L. L.; Neubig, R. R. Small Molecule Protein–Protein Interaction Inhibitors as CNS Therapeutic Agents: Current Progress and Future Hurdles. *Neuropsychopharmacology* **2009,** *34,* 126–141.
2. Venkatesan, K.; Rual, J. F.; Vazquez, A.; Stelzl, U.; Lemmens, I.; Hirozane-Kishikawa, T.; Hao, T.; Zenkner, M.; Xin, X.; Goh, K. I.; Yildirim, M. A.; Simonis, N.; Heinzmann, K.; Gebreab, F.; Sahalie, J. M.; Cevik, S.; Simon, C.; de Smet, A. S.; Dann, E.; Smolyar, A.; Vinayagam, A.; Yu, H.; Szeto, D.; Borick, H.; Dricot, A.; Klitgord, N.; Murray, R. R.; Lin, C.; Lalowski, M.; Timm, J.; Rau, K.; Boone, C.; Braun, P.; Cusick, M. E.; Roth, F. P.; Hill, D. E.; Tavernier, J.; Wanker, E. E.; Barabasi, A. L.; Vidal, M. An Empirical Framework for Binary Interactome Mapping. *Nat. Methods* **2009,** *6,* 83–90.

3. Stumpf, M. P.; Thorne, T.; de Silva, E.; Stewart, R.; An, H. J.; Lappe, M.; Wiuf, C. Estimating the Size of the Human Interactome. *Proc. Natl. Acad. Sci. U. S. A.* **2008,** *105,* 6959–6964.
4. Bonetta, L. Protein–Protein Interactions: Interactome Under Construction. *Nature* **2010,** *468,* 851–854.
5. Berggard, T.; Linse, S.; James, P. Methods for the Detection and Analysis of Protein–Protein Interactions. *Proteomics* **2007,** *7,* 2833–2842.
6. Kotlyar, M.; Pastrello, C.; Pivetta, F.; Lo Sardo, A.; Cumbaa, C.; Li, H.; Naranian, T.; Niu, Y.; Ding, Z.; Vafaee, F.; Broackes-Carter, F.; Petschnigg, J.; Mills, G. B.; Jurisicova, A.; Stagljar, I.; Maestro, R.; Jurisica, I. In Silico Prediction of Physical Protein Interactions and Characterization of Interactome Orphans. *Nat. Methods* **2015,** *12,* 79–84.
7. Rao, V. S.; Srinivas, K.; Sujini, G. N.; Kumar, G. N. Protein–Protein Interaction Detection: Methods and Analysis. *Int. J. Proteomics* **2014,** *2014,* 147648.
8. Lin, S.; He, D.; Long, T.; Zhang, S.; Meng, R.; Chen, P. R. Genetically Encoded Cleavable Protein Photo-Cross-Linker. *J. Am. Chem. Soc.* **2014,** *136,* 11860–11863.
9. Gul, S.; Hadian, K. Protein–Protein Interaction Modulator Drug Discovery: Past Efforts and Future Opportunities Using a Rich Source of Low- and High-Throughput Screening Assays. *Expert Opin. Drug Discov.* **2014,** *9,* 1393–1404.
10. Barile, E.; Pellecchia, M. NMR-Based Approaches for the Identification and Optimization of Inhibitors of Protein–Protein Interactions. *Chem. Rev.* **2014,** *114,* 4749–4763.
11. Los, M.; Roodhart, J. M.; Voest, E. E. Target Practice: Lessons From Phase III Trials With Bevacizumab and Vatalanib in the Treatment of Advanced Colorectal Cancer. *Oncologist* **2007,** *12,* 443–450.
12. Hudis, C. A. Trastuzumab—Mechanism of Action and Use in Clinical Practice. *N. Engl. J. Med.* **2007,** *357,* 39–51.
13. Jin, L.; Wang, W.; Fang, G. Targeting Protein–Protein Interaction by Small Molecules. *Annu. Rev. Pharmacol. Toxicol.* **2014,** *54,* 435–456.
14. Aeluri, M.; Chamakuri, S.; Dasari, B.; Guduru, S. K.; Jimmidi, R.; Jogula, S.; Arya, P. Small Molecule Modulators of Protein–Protein Interactions: Selected Case Studies. *Chem. Rev.* **2014,** *114,* 4640–4694.
15. Ryan, D. P.; Matthews, J. M. Protein–Protein Interactions in Human Disease. *Curr. Opin. Struct. Biol.* **2005,** *15,* 441–446.
16. Ivanov, A. A.; Khuri, F. R.; Fu, H. Targeting Protein–Protein Interactions as an Anticancer Strategy. *Trends Pharmacol. Sci.* **2013,** *34,* 393–400.
17. Cory, S.; Adams, J. M. The Bcl2 Family: Regulators of the Cellular Life-or-Death Switch. *Nat. Rev. Cancer* **2002,** *2,* 647–656.
18. Danial, N. N.; Korsmeyer, S. J. Cell Death: Critical Control Points. *Cell* **2004,** *116,* 205–219.
19. Liu, Z.; Ding, Y.; Ye, N.; Wild, C.; Chen, H.; Zhou, J. Direct Activation of Bax Protein for Cancer Therapy. *Med. Res. Rev.* **2016,** *36,* 313–341.
20. Walensky, L. D. BCL-2 in the Crosshairs: Tipping the Balance of Life and Death. *Cell Death Differ.* **2006,** *13,* 1339–1350.
21. Galsky, M. D.; Vogelzang, N. J. Docetaxel-Based Combination Therapy for Castration-Resistant Prostate Cancer. *Ann. Oncol.* **2010,** *21,* 2135–2144.
22. Kang, M. H.; Reynolds, C. P. Bcl-2 Inhibitors: Targeting Mitochondrial Apoptotic Pathways in Cancer Therapy. *Clin. Cancer Res.* **2009,** *15,* 1126–1132.
23. Han, B.; Park, D.; Li, R.; Xie, M.; Owonikoko, T. K.; Zhang, G.; Sica, G. L.; Ding, C.; Zhou, J.; Magis, A. T.; Chen, Z. G.; Shin, D. M.; Ramalingam, S. S.; Khuri, F. R.; Curran, W. J.; Deng, X. Small-Molecule Bcl2 BH4 Antagonist for Lung Cancer Therapy. *Cancer Cell* **2015,** *27,* 852–863.
24. Czabotar, P. E.; Lessene, G.; Strasser, A.; Adams, J. M. Control of Apoptosis by the BCL-2 Protein Family: Implications for Physiology and Therapy. *Nat. Rev. Mol. Cell Biol.* **2014,** *15,* 49–63.
25. Liu, Z.; Wild, C.; Ding, Y.; Ye, N.; Chen, H.; Wold, E. A.; Zhou, J. BH4 domain of Bcl-2 as a novel target for cancer therapy. *Drug Discov. Today* **2015**. http://dx.doi.org/10.1016/j.drudis.2015.11.008. PMID: 26631752.
26. Xin, M.; Li, R.; Xie, M.; Park, D.; Owonikoko, T. K.; Sica, G. L.; Corsino, P. E.; Zhou, J.; Ding, C.; White, M. A.; Magis, A. T.; Ramalingam, S. S.; Curran, W. J.; Khuri, F. R.; Deng, X. Small-Molecule Bax Agonists for Cancer Therapy. *Nat. Commun.* **2014,** *5,* 4935.
27. Stiewe, T. The p53 Family in Differentiation and Tumorigenesis. *Nat. Rev. Cancer* **2007,** *7,* 165–168.
28. Brown, C. J.; Lain, S.; Verma, C. S.; Fersht, A. R.; Lane, D. P. Awakening Guardian Angels: Drugging the p53 Pathway. *Nat. Rev. Cancer* **2009,** *9,* 862–873.
29. Hardcastle, I. R.; Liu, J.; Valeur, E.; Watson, A.; Ahmed, S. U.; Blackburn, T. J.; Bennaceur, K.; Clegg, W.; Drummond, C.; Endicott, J. A.; Golding, B. T.; Griffin, R. J.; Gruber, J.; Haggerty, K.; Harrington, R. W.; Hutton, C.; Kemp, S.; Lu, X.; McDonnell, J. M.; Newell, D. R.; Noble, M. E.; Payne, S. L.; Revill, C. H.; Riedinger, C.; Xu, Q.; Lunec, J. Isoindolinone Inhibitors of the Murine Double Minute 2 (MDM2)-p53 Protein–Protein Interaction: Structure–Activity Studies Leading to Improved Potency. *J. Med. Chem.* **2011,** *54,* 1233–1243.
30. Oliner, J. D.; Kinzler, K. W.; Meltzer, P. S.; George, D. L.; Vogelstein, B. Amplification of a Gene Encoding a p53-Associated Protein in Human Sarcomas. *Nature* **1992,** *358,* 80–83.
31. Toledo, F.; Wahl, G. M. Regulating the p53 Pathway: in vitro Hypotheses, in vivo Veritas. *Nat. Rev. Cancer* **2006,** *6,* 909–923.
32. Lim, D. A.; Huang, Y. C.; Swigut, T.; Mirick, A. L.; Garcia-Verdugo, J. M.; Wysocka, J.; Ernst, P.; Alvarez-Buylla, A. Chromatin Remodelling Factor Mll1 Is Essential for Neurogenesis From Postnatal Neural Stem Cells. *Nature* **2009,** *458,* 529–533.
33. Rampalli, S.; Li, L.; Mak, E.; Ge, K.; Brand, M.; Tapscott, S. J.; Dilworth, F. J. p38 MAPK Signaling Regulates Recruitment of Ash2L-Containing Methyltransferase Complexes to Specific Genes During Differentiation. *Nat. Struct. Mol. Biol.* **2007,** *14,* 1150–1156.
34. Krivtsov, A. V.; Armstrong, S. A. MLL Translocations, Histone Modifications and Leukaemia Stem-Cell Development. *Nat. Rev. Cancer* **2007,** *7,* 823–833.
35. Ernst, P.; Vakoc, C. R. WRAD: Enabler of the SET1-Family of H3K4 Methyltransferases. *Brief. Funct. Genomics* **2012,** *11,* 217–226.
36. Karatas, H.; Townsend, E. C.; Cao, F.; Chen, Y.; Bernard, D.; Liu, L.; Lei, M.; Dou, Y.; Wang, S. High-Affinity, Small-Molecule Peptidomimetic Inhibitors of MLL1/WDR5 Protein–Protein Interaction. *J. Am. Chem. Soc.* **2013,** *135,* 669–682.
37. Bolshan, Y.; Getlik, M.; Kuznetsova, E.; Wasney, G. A.; Hajian, T.; Poda, G.; Nguyen, K. T.; Wu, H.; Dombrovski, L.; Dong, A.; Senisterra, G.; Schapira, M.; Arrowsmith, C. H.; Brown, P. J.; Al-Awar, R.; Vedadi, M.; Smil, D. Synthesis, Optimization, and Evaluation of Novel Small Molecules as Antagonists of WDR5–MLL Interaction. *ACS Med. Chem. Lett.* **2013,** *4,* 353–357.
38. Mo, J. S.; Park, H. W.; Guan, K. L. The Hippo Signaling Pathway in Stem Cell Biology and Cancer. *EMBO Rep.* **2014,** *15,* 642–656.
39. Halder, G.; Johnson, R. L. Hippo Signaling: Growth Control and Beyond. *Development* **2011,** *138,* 9–22.
40. Zhao, B.; Li, L.; Lei, Q.; Guan, K. L. The Hippo-YAP Pathway in Organ Size Control and Tumorigenesis: An Updated Version. *Genes Dev.* **2010,** *24,* 862–874.
41. Zhao, B.; Tumaneng, K.; Guan, K. L. The Hippo Pathway in Organ Size Control, Tissue Regeneration and Stem Cell Self-Renewal. *Nat. Cell Biol.* **2011,** *13,* 877–883.
42. Santucci, M.; Vignudelli, T.; Ferrari, S.; Mor, M.; Scalvini, L.; Bolognesi, M. L.; Uliassi, E.; Costi, M. P. The Hippo Pathway and YAP/TAZ-TEAD Protein–Protein Interaction as Targets for Regenerative Medicine and Cancer Treatment. *J. Med. Chem.* **2015,** *58,* 4857–4873.
43. Markowitz, J.; Chen, I.; Gitti, R.; Baldisseri, D. M.; Pan, Y.; Udan, R.; Carrier, F.; MacKerell, A. D., Jr.; Weber, D. J. Identification and Characterization of Small Molecule Inhibitors of the Calcium-Dependent S100B-p53 Tumor Suppressor Interaction. *J. Med. Chem.* **2004,** *47,* 5085–5093.
44. Flygare, J. A.; Beresini, M.; Budha, N.; Chan, H.; Chan, I. T.; Cheeti, S.; Cohen, F.; Deshayes, K.; Doerner, K.; Eckhardt, S. G.; Elliott, L. O.; Feng, B.; Franklin, M. C.; Reisner, S. F.; Gazzard, L.; Halladay, J.; Hymowitz, S. G.; La, H.; LoRusso, P.; Maurer, B.; Murray, L.; Plise, E.; Quan, C.; Stephan, J. P.; Young, S. G.; Tom, J.; Tsui, V.; Um, J.; Varfolomeev, E.; Vucic, D.; Wagner, A. J.; Wallweber, H. J.; Wang, L.; Ware, J.; Wen, Z.; Wong, H.; Wong, J. M.; Wong, M.; Wong, S.; Yu, R.; Zobel, K.; Fairbrother, W. J. Discovery of a Potent Small-Molecule Antagonist of Inhibitor of Apoptosis (IAP) Proteins and Clinical Candidate for the Treatment of Cancer (GDC-0152). *J. Med. Chem.* **2012,** *55,* 4101–4113.
45. Patgiri, A.; Yadav, K. K.; Arora, P. S.; Bar-Sagi, D. An Orthosteric Inhibitor of the Ras–Sos Interaction. *Nat. Chem. Biol.* **2011,** *7,* 585–587.
46. Banappagari, S.; Corti, M.; Pincus, S.; Satyanarayanajois, S. Inhibition of Protein–Protein Interaction of HER2–EGFR and HER2–HER3 by a Rationally Designed Peptidomimetic. *J. Biomol. Struct. Dyn.* **2012,** *30,* 594–606.
47. Kanthala, S.; Banappagari, S.; Gokhale, A.; Liu, Y. Y.; Xin, G.; Zhao, Y.; Jois, S. Novel Peptidomimetics for Inhibition of HER2:HER3 Heterodimerization in HER2-Positive Breast Cancer. *Chem. Biol. Drug Des.* **2015,** *85,* 702–714.

48. Jiang, H.; Bower, K. E.; Beusche, A. E. t.; Zhou, B.; Bobkov, A. A.; Olson, A. J.; Vogt, P. K. Stabilizers of the Max Homodimer Identified in Virtual Ligand Screening Inhibit Myc Function. *Mol. Pharmacol.* **2009,** *76,* 491–502.
49. Hennessy, B. T.; Smith, D. L.; Ram, P. T.; Lu, Y.; Mills, G. B. Exploiting the PI3K/AKT Pathway for Cancer Drug Discovery. *Nat. Rev. Drug Discov.* **2005,** *4,* 988–1004.
50. Kuhn, M. W.; Armstrong, S. A. Designed to Kill: Novel Menin-MLL Inhibitors Target MLL-Rearranged Leukemia. *Cancer Cell* **2015,** *27,* 431–433.
51. Gautier, B.; Miteva, M. A.; Goncalves, V.; Huguenot, F.; Coric, P.; Bouaziz, S.; Seijo, B.; Gaucher, J. F.; Broutin, I.; Garbay, C.; Lesnard, A.; Rault, S.; Inguimbert, N.; Villoutreix, B. O.; Vidal, M. Targeting the Proangiogenic VEGF–VEGFR Protein–Protein Interface With Drug-Like Compounds by In Silico and In Vitro Screening. *Chem. Biol.* **2011,** *18,* 1631–1639.
52. Romero, F. A.; Taylor, A. M.; Crawford, T. D.; Tsui, V.; Cote, A.; Magnuson, S. Disrupting Acetyl-Lysine Recognition: Progress in the Development of Bromodomain Inhibitors. *J. Med. Chem.* **2016,** *59,* 1271–1298.
53. Vogelstein, B.; Papadopoulos, N.; Velculescu, V. E.; Zhou, S.; Diaz, L. A., Jr.; Kinzler, K. W. Cancer Genome Landscapes. *Science* **2013,** *339,* 1546–1558.
54. Garraway, L. A.; Lander, E. S. Lessons From the Cancer Genome. *Cell* **2013,** *153,* 17–37.
55. Collins, M. O.; Grant, S. G. Supramolecular Signalling Complexes in the Nervous System. *Subcell. Biochem.* **2007,** *43,* 185–207.
56. Planas, A. M.; Gorina, R.; Chamorro, A. Signalling Pathways Mediating Inflammatory Responses in Brain Ischaemia. *Biochem. Soc. Trans.* **2006,** *34,* 1267–1270.
57. Sipe, J. D.; Benson, M. D.; Buxbaum, J. N.; Ikeda, S.; Merlini, G.; Saraiva, M. J.; Westermark, P. Nomenclature 2014: Amyloid Fibril Proteins and Clinical Classification of the Amyloidosis. *Amyloid* **2014,** *2014* (21), 221–224.
58. Eisele, Y. S.; Monteiro, C.; Fearns, C.; Encalada, S. E.; Wiseman, R. L.; Powers, E. T.; Kelly, J. W. Targeting Protein Aggregation for the Treatment of Degenerative Diseases. *Nat. Rev. Drug Discov.* **2015,** *14,* 759–780.
59. Oddo, S.; Caccamo, A.; Shepherd, J. D.; Murphy, M. P.; Golde, T. E.; Kayed, R.; Metherate, R.; Mattson, M. P.; Akbari, Y.; LaFerla, F. M. Triple-Transgenic Model of Alzheimer's Disease With Plaques and Tangles: Intracellular Abeta and Synaptic Dysfunction. *Neuron* **2003,** *39,* 409–421.
60. Knauer, M. F.; Soreghan, B.; Burdick, D.; Kosmoski, J.; Glabe, C. G. Intracellular Accumulation and Resistance to Degradation of the Alzheimer Amyloid A4/beta Protein. *Proc. Natl. Acad. Sci. U. S. A.* **1992,** *89,* 7437–7441.
61. Page, L. J.; Suk, J. Y.; Bazhenova, L.; Fleming, S. M.; Wood, M.; Jiang, Y.; Guo, L. T.; Mizisin, A. P.; Kisilevsky, R.; Shelton, G. D.; Balch, W. E.; Kelly, J. W. Secretion of Amyloidogenic Gelsolin Progressively Compromises Protein Homeostasis Leading to the Intracellular Aggregation of Proteins. *Proc. Natl. Acad. Sci. U. S. A.* **2009,** *106,* 11125–11130.
62. Ferretti, M. T.; Bruno, M. A.; Ducatenzeiler, A.; Klein, W. L.; Cuello, A. C. Intracellular Abeta-Oligomers and Early Inflammation in a Model of Alzheimer's Disease. *Neurobiol. Aging* **2012,** *33,* 1329–1342.
63. Fuxe, K.; Borroto-Escuela, D. O.; Romero-Fernandez, W.; Palkovits, M.; Tarakanov, A. O.; Ciruela, F.; Agnati, L. F. Moonlighting Proteins and Protein–Protein Interactions as Neurotherapeutic Targets in the G Protein-Coupled Receptor Field. *Neuropsychopharmacology* **2014,** *39,* 131–155.
64. George, S. R.; O'Dowd, B. F.; Lee, S. P. G-Protein-Coupled Receptor Oligomerization and Its Potential for Drug Discovery. *Nat. Rev. Drug Discov.* **2002,** *1,* 808–820.
65. Fuxe, K.; Marcellino, D.; Borroto-Escuela, D. O.; Guescini, M.; Fernandez-Duenas, V.; Tanganelli, S.; Rivera, A.; Ciruela, F.; Agnati, L. F. Adenosine–Dopamine Interactions in the Pathophysiology and Treatment of CNS Disorders. *CNS Neurosci. Ther.* **2010,** *16,* e18–e42.
66. Fuxe, K.; Marcellino, D.; Genedani, S.; Agnati, L. Adenosine A(2A) Receptors, Dopamine D(2) Receptors and Their Interactions in Parkinson's Disease. *Mov. Disord.* **2007,** *22,* 1990–2017.
67. Trifilieff, P.; Rives, M. L.; Urizar, E.; Piskorowski, R. A.; Vishwasrao, H. D.; Castrillon, J.; Schmauss, C.; Slattman, M.; Gullberg, M.; Javitch, J. A. Detection of Antigen Interactions Ex Vivo by Proximity Ligation Assay: Endogenous Dopamine D2–Adenosine A2A Receptor Complexes in the Striatum. *Biotechniques* **2011,** *51,* 111–118.
68. Fuxe, K.; Ferre, S.; Zoli, M.; Agnati, L. F. Integrated Events in Central Dopamine Transmission as Analyzed at Multiple Levels. Evidence for Intramembrane Adenosine A2A/Dopamine D2 and Adenosine A1/Dopamine D1 Receptor Interactions in the Basal Ganglia. *Brain Res. Brain Res. Rev.* **1998,** *26,* 258–273.
69. Li, X.; Jope, R. S. Is Glycogen Synthase Kinase-3 a Central Modulator in Mood Regulation? *Neuropsychopharmacology* **2010,** *35,* 2143–2154.
70. Peineau, S.; Taghibiglou, C.; Bradley, C.; Wong, T. P.; Liu, L.; Lu, J.; Lo, E.; Wu, D.; Saule, E.; Bouschet, T.; Matthews, P.; Isaac, J. T.; Bortolotto, Z. A.; Wang, Y. T.; Collingridge, G. L. LTP Inhibits LTD in the Hippocampus via Regulation of GSK3beta. *Neuron* **2007,** *53,* 703–717.
71. Wildburger, N. C.; Laezza, F. Control of Neuronal Ion Channel Function by Glycogen Synthase Kinase-3: New Prospective for an Old Kinase. *Front. Mol. Neurosci.* **2012,** *5,* 80.
72. Shavkunov, A. S.; Wildburger, N. C.; Nenov, M. N.; James, T. F.; Buzhdygan, T. P.; Panova-Elektronova, N. I.; Green, T. A.; Veselenak, R. L.; Bourne, N.; Laezza, F. The Fibroblast Growth Factor 14.Voltage-Gated Sodium Channel Complex Is a New Target of Glycogen Synthase Kinase 3 (GSK3). *J. Biol. Chem.* **2013,** *288,* 19370–19385.
73. Taguchi, K.; Motohashi, H.; Yamamoto, M. Molecular Mechanisms of the Keap1–Nrf2 Pathway in Stress Response and Cancer Evolution. *Genes Cells* **2011,** *16,* 123–140.
74. Suzuki, T.; Motohashi, H.; Yamamoto, M. Toward Clinical Application of the Keap1–Nrf2 Pathway. *Trends Pharmacol. Sci.* **2013,** *34,* 340–346.
75. Bertrand, H. C.; Schaap, M.; Baird, L.; Georgakopoulos, N. D.; Fowkes, A.; Thiollier, C.; Kachi, H.; Dinkova-Kostova, A. T.; Wells, G. Design, Synthesis, and Evaluation of Triazole Derivatives That Induce Nrf2 Dependent Gene Products and Inhibit the Keap1-Nrf2 Protein–Protein Interaction. *J. Med. Chem.* **2015,** *58,* 7186–7194.
76. Zhong, M.; Lynch, A.; Jehle, S.; Kozakov, D.; Vajda, S.; Allen, K.; Whitty, A. Fragment-Based Drug Discovery Targeting KEAP1/Nrf2 Binding. *FASEB J.* **2015,** *29.*
77. Bohanon, F. J.; Wang, X.; Ding, C.; Ding, Y.; Radhakrishnan, G. L.; Rastellini, C.; Zhou, J.; Radhakrishnan, R. S. Oridonin Inhibits Hepatic Stellate Cell Proliferation and Fibrogenesis. *J. Surg. Res.* **2014,** *190,* 55–63.
78. Bohanon, F. J.; Wang, X.; Graham, B. M.; Prasai, A.; Vasudevan, S. J.; Ding, C.; Ding, Y.; Radhakrishnan, G. L.; Rastellini, C.; Zhou, J.; Radhakrishnan, R. S. Enhanced Anti-Fibrogenic Effects of Novel Oridonin Derivative CYD0692 in Hepatic Stellate Cells. *Mol. Cell. Biochem.* **2015,** *410,* 293–300.
79. Gilmore, T. D. Introduction to NF-kappaB: Players, Pathways, Perspectives. *Oncogene* **2006,** *25,* 6680–6684.
80. Israel, A. The IKK Complex, a Central Regulator of NF-kappaB Activation. *Cold Spring Harb. Perspect. Biol.* **2010,** *2,* a000158.
81. Gautheron, J.; Courtois, G. "Without Ub I Am Nothing": NEMO as a Multifunctional Player in Ubiquitin-Mediated Control of NF-kappaB Activation. *Cell. Mol. Life Sci.* **2010,** *67,* 3101–3113.
82. Golden, M. S.; Cote, S. M.; Sayeg, M.; Zerbe, B. S.; Villar, E. A.; Beglov, D.; Sazinsky, S. L.; Georgiadis, R. M.; Vajda, S.; Kozakov, D.; Whitty, A. Comprehensive Experimental and Computational Analysis of Binding Energy Hot Spots at the NF-kappaB Essential Modulator/IKKbeta Protein–Protein Interface. *J. Am. Chem. Soc.* **2013,** *135,* 6242–6256.
83. Tracy, S.; Hofling, K.; Pirruccello, S.; Lane, P. H.; Reyna, S. M.; Gauntt, C. J. Group B Coxsackievirus Myocarditis and Pancreatitis: Connection Between Viral Virulence Phenotypes in Mice. *J. Med. Virol.* **2000,** *62,* 70–81.
84. Blay, R.; Simpson, K.; Leslie, K.; Huber, S. Coxsackievirus-Induced Disease. CD4+ Cells Initiate Both Myocarditis and Pancreatitis in DBA/2 Mice. *Am. J. Pathol.* **1989,** *135,* 899–907.
85. Chen, H.; Mrazek, A. A.; Wang, X.; Ding, C.; Ding, Y.; Porro, L. J.; Liu, H.; Chao, C.; Hellmich, M. R.; Zhou, J. Design, Synthesis, and Characterization of Novel Apigenin Analogues That Suppress Pancreatic Stellate Cell Proliferation In Vitro and Associated Pancreatic Fibrosis In Vivo. *Bioorg. Med. Chem.* **2014,** *22,* 3393–3404.
86. Mrazek, A. A.; Porro, L. J.; Bhatia, V.; Falzon, M.; Spratt, H.; Zhou, J.; Chao, C.; Hellmich, M. R. Apigenin Inhibits Pancreatic Stellate Cell Activity in Pancreatitis. *J. Surg. Res.* **2015,** *196,* 8–16.
87. Li, X.; Xia, Y.; Huang, S.; Liu, F.; Ying, Y.; Xu, Q.; Liu, X.; Jin, G.; Papasian, C. J.; Chen, J.; Fu, M.; Huang, X. Identification of the Interaction of VP1 With GM130 Which May Implicate in the Pathogenesis of CVB3-Induced Acute Pancreatitis. *Sci. Rep.* **2015,** *5,* 13324.
88. Guettler, S.; LaRose, J.; Petsalaki, E.; Gish, G.; Scotter, A.; Pawson, T.; Rottapel, R.; Sicheri, F. Structural Basis and Sequence Rules for Substrate Recognition by Tankyrase Explain the Basis for Cherubism Disease. *Cell* **2011,** *147,* 1340–1354.
89. Levaot, N.; Voytyuk, O.; Dimitriou, I.; Sircoulomb, F.; Chandrakumar, A.; Deckert, M.; Krzyzanowski, P. M.; Scotter, A.; Gu, S.; Janmohamed, S.; Cong, F.; Simoncic, P. D.; Ueki, Y.; La Rose, J.; Rottapel, R. Loss of Tankyrase-Mediated Destruction of 3BP2 Is the Underlying Pathogenic Mechanism of Cherubism. *Cell* **2011,** *147,* 1324–1339.
90. Kobayashi, T.; Walsh, M. C.; Choi, Y. The Role of TRAF6 in Signal Transduction and the Immune Response. *Microbes Infect.* **2004,** *6,* 1333–1338.

91. Moriya, J.; Takeuchi, K.; Tai, K.; Arai, K.; Kobayashi, N.; Yoneda, N.; Fukunishi, Y.; Inoue, A.; Kihara, M.; Murakami, T.; Chiba, K.; Shimada, I. Structure-Based Development of a Protein–Protein Interaction Inhibitor Targeting Tumor Necrosis Factor Receptor-Associated Factor 6. *J. Med. Chem.* **2015,** *58,* 5674–5683.
92. Waldmann, T. A. The IL-2/IL-2 Receptor System: A Target for Rational Immune Intervention. *Immunol. Today* **1993,** *14,* 264–270.
93. Emerson, S. D.; Palermo, R.; Liu, C. M.; Tilley, J. W.; Chen, L.; Danho, W.; Madison, V. S.; Greeley, D. N.; Ju, G.; Fry, D. C. NMR Characterization of Interleukin-2 in Complexes With the IL-2Ralpha Receptor Component, and With Low Molecular Weight Compounds That Inhibit the IL-2/IL-Ralpha Interaction. *Protein Sci.* **2003,** *12,* 811–822.
94. Chen, L.; Flies, D. B. Molecular Mechanisms of T Cell Co-Stimulation and Co-Inhibition. *Nat. Rev. Immunol.* **2013,** *13,* 227–242.
95. Raychaudhuri, S.; Thomson, B. P.; Remmers, E. F.; Eyre, S.; Hinks, A.; Guiducci, C.; Catanese, J. J.; Xie, G.; Stahl, E. A.; Chen, R.; Alfredsson, L.; Amos, C. I.; Ardlie, K. G.; Consortium, B.; Barton, A.; Bowes, J.; Burtt, N. P.; Chang, M.; Coblyn, J.; Costenbader, K. H.; Criswell, L. A.; Crusius, J. B.; Cui, J.; De Jager, P. L.; Ding, B.; Emery, P.; Flynn, E.; Harrison, P.; Hocking, L. J.; Huizinga, T. W.; Kastner, D. L.; Ke, X.; Kurreeman, F. A.; Lee, A. T.; Liu, X.; Li, Y.; Martin, P.; Morgan, A. W.; Padyukov, L.; Reid, D. M.; Seielstad, M.; Seldin, M. F.; Shadick, N. A.; Steer, S.; Tak, P. P.; Thomson, W.; van der Helm-van Mil, A. H.; van der Horst-Bruinsma, I. E.; Weinblatt, M. E.; Wilson, A. G.; Wolbink, G. J.; Wordsworth, P.; Consortium, Y.; Altshuler, D.; Karlson, E. W.; Toes, R. E.; de Vries, N.; Begovich, A. B.; Siminovitch, K. A.; Worthington, J.; Klareskog, L.; Gregersen, P. K.; Daly, M. J.; Plenge, R. M. Genetic Variants at CD28, PRDM1 and CD2/CD58 Are Associated With Rheumatoid Arthritis Risk. *Nat. Genet.* **2009,** *41,* 1313–1318.
96. Zarzycka, B.; Seijkens, T.; Nabuurs, S. B.; Ritschel, T.; Grommes, J.; Soehnlein, O.; Schrijver, R.; van Tiel, C. M.; Hackeng, T. M.; Weber, C.; Giehler, F.; Kieser, A.; Lutgens, E.; Vriend, G.; Nicolaes, G. A. Discovery of Small Molecule CD40-TRAF6 Inhibitors. *J. Chem. Inf. Model.* **2015,** *55,* 294–307.
97. Xu, D.; Wang, Z.; Zhang, Y.; Jiang, W.; Pan, Y.; Song, B. L.; Chen, Y. PAQR3 Modulates Cholesterol Homeostasis by Anchoring Scap/SREBP Complex to the Golgi Apparatus. *Nat. Commun.* **2015,** *6,* 8100.
98. Lee, L. C.; Maurice, D. H.; Baillie, G. S. Targeting Protein–Protein Interactions Within the Cyclic AMP Signaling System as a Therapeutic Strategy for Cardiovascular Disease. *Future Med. Chem.* **2013,** *5,* 451–464.
99. Perry, S. J.; Baillie, G. S.; Kohout, T. A.; McPhee, I.; Magiera, M. M.; Ang, K. L.; Miller, W. E.; McLean, A. J.; Conti, M.; Houslay, M. D.; Lefkowitz, R. J. Targeting of Cyclic AMP Degradation to Beta 2-Adrenergic Receptors by Beta-Arrestins. *Science* **2002,** *298,* 834–836.
100. Willoughby, D.; Baillie, G. S.; Lynch, M. J.; Ciruela, A.; Houslay, M. D.; Cooper, D. M. Dynamic Regulation, Desensitization, and Cross-Talk in Discrete Subcellular Microdomains During beta2-Adrenoceptor and Prostanoid Receptor cAMP Signaling. *J. Biol. Chem.* **2007,** *282,* 34235–34249.
101. Trian, T.; Burgess, J. K.; Niimi, K.; Moir, L. M.; Ge, Q.; Berger, P.; Liggett, S. B.; Black, J. L.; Oliver, B. G.; Trian, T.; Burgess, J. K.; Niimi, K.; Moir, L. M.; Ge, Q.; Berger, P.; Liggett, S. B.; Black, J. L.; Oliver, B. G. beta2-Agonist Induced cAMP Is Decreased in Asthmatic Airway Smooth Muscle due to Increased PDE4D. *PLoS One* **2011,** *6,* e20000.
102. McConnachie, G.; Langeberg, L. K.; Scott, J. D. AKAP Signaling Complexes: Getting to the Heart of the Matter. *Trends Mol. Med.* **2006,** *12,* 317–323.
103. Troger, J.; Moutty, M. C.; Skroblin, P.; Klussmann, E. A-Kinase Anchoring Proteins as Potential Drug Targets. *Br. J. Pharmacol.* **2012,** *166,* 420–433.
104. Christian, F.; Szaszak, M.; Friedl, S.; Drewianka, S.; Lorenz, D.; Goncalves, A.; Furkert, J.; Vargas, C.; Schmieder, P.; Gotz, F.; Zuhlke, K.; Moutty, M.; Gottert, H.; Joshi, M.; Reif, B.; Haase, H.; Morano, I.; Grossmann, S.; Klukovits, A.; Verli, J.; Gaspar, R.; Noack, C.; Bergmann, M.; Kass, R.; Hampel, K.; Kashin, D.; Genieser, H. G.; Herberg, F. W.; Willoughby, D.; Cooper, D. M.; Baillie, G. S.; Houslay, M. D.; von Kries, J. P.; Zimmermann, B.; Rosenthal, W.; Klussmann, E. Small Molecule AKAP-Protein Kinase A (PKA) Interaction Disruptors That Activate PKA Interfere With Compartmentalized cAMP Signaling in Cardiac Myocytes. *J. Biol. Chem.* **2011,** *286,* 9079–9096.
105. Ulrichts, H.; Silence, K.; Schoolmeester, A.; de Jaegere, P.; Rossenu, S.; Roodt, J.; Priem, S.; Lauwereys, M.; Casteels, P.; Van Bockstaele, F.; Verschueren, K.; Stanssens, P.; Baumeister, J.; Holz, J. B. Antithrombotic Drug Candidate ALX-0081 Shows Superior Preclinical Efficacy and Safety Compared With Currently Marketed Antiplatelet Drugs. *Blood* **2011,** *118,* 757–765.
106. Cervantes, S.; Bunnik, E. M.; Saraf, A.; Conner, C. M.; Escalante, A.; Sardiu, M. E.; Ponts, N.; Prudhomme, J.; Florens, L.; Le Roch, K. G. The Multifunctional Autophagy Pathway in the Human Malaria Parasite *Plasmodium falciparum*. *Autophagy* **2014,** *10,* 80–92.
107. Jayabalasingham, B.; Voss, C.; Ehrenman, K.; Romano, J. D.; Smith, M. E.; Fidock, D. A.; Bosch, J.; Coppens, I. Characterization of the ATG8-Conjugation System in 2 Plasmodium Species With Special Focus on the Liver Stage: Possible Linkage Between the Apicoplastic and Autophagic Systems? *Autophagy* **2014,** *10,* 269–284.
108. Eickel, N.; Kaiser, G.; Prado, M.; Burda, P. C.; Roelli, M.; Stanway, R. R.; Heussler, V. T. Features of Autophagic Cell Death in Plasmodium Liver-Stage Parasites. *Autophagy* **2013,** *9,* 568–580.
109. Hain, A. U.; Bartee, D.; Sanders, N. G.; Miller, A. S.; Sullivan, D. J.; Levitskaya, J.; Meyers, C. F.; Bosch, J. Identification of an Atg8-Atg3 Protein–Protein Interaction Inhibitor From the Medicines for Malaria Venture Malaria Box Active in Blood and Liver Stage *Plasmodium Falciparum* Parasites. *J. Med. Chem.* **2014,** *57,* 4521–4531.
110. Brannon, A. R.; Maresca, J. A.; Boeke, J. D.; Basrai, M. A.; McBride, A. A. Reconstitution of Papillomavirus E2-Mediated Plasmid Maintenance in Saccharomyces Cerevisiae by the Brd4 Bromodomain Protein. *Proc. Natl. Acad. Sci. U. S. A.* **2005,** *102,* 2998–3003.
111. You, J.; Croyle, J. L.; Nishimura, A.; Ozato, K.; Howley, P. M. Interaction of the Bovine Papillomavirus E2 Protein With Brd4 Tethers the Viral DNA to Host Mitotic Chromosomes. *Cell* **2004,** *117,* 349–360.
112. Le Rouzic, E.; Bonnard, D.; Chasset, S.; Bruneau, J. M.; Chevreuil, F.; Le Strat, F.; Nguyen, J.; Beauvoir, R.; Amadori, C.; Brias, J.; Vomscheid, S.; Eiler, S.; Levy, N.; Delelis, O.; Deprez, E.; Saib, A.; Zamborlini, A.; Emiliani, S.; Ruff, M.; Ledoussal, B.; Moreau, F.; Benarous, R. Dual Inhibition of HIV-1 Replication by Integrase-LEDGF Allosteric Inhibitors is Predominant at the Post-Integration Stage. *Retrovirology* **2013,** *10,* 144.
113. Pihan, E.; Delgadillo, R. F.; Tonkin, M. L.; Pugniere, M.; Lebrun, M.; Boulanger, M. J.; Douguet, D. Computational and Biophysical Approaches to Protein–Protein Interaction Inhibition of *Plasmodium falciparum* AMA1/RON2 Complex. *J. Comput. Aided Mol. Des.* **2015,** *29,* 525–539.
114. Tsao, D. H.; Sutherland, A. G.; Jennings, L. D.; Li, Y.; Rush, T. S., 3rd.; Alvarez, J. C.; Ding, W.; Dushin, E. G.; Dushin, R. G.; Haney, S. A.; Kenny, C. H.; Malakian, A. K.; Nilakantan, R.; Mosyak, L. Discovery of Novel Inhibitors of the ZipA/FtsZ Complex by NMR Fragment Screening Coupled With Structure-Based Design. *Bioorg. Med. Chem.* **2006,** *14,* 7953–7961.
115. Manning, A. M.; Davis, R. J. Targeting JNK for Therapeutic Benefit: From Junk to Gold? *Nat. Rev. Drug Discov.* **2003,** *2,* 554–565.
116. Whitmarsh, A. J.; Cavanagh, J.; Tournier, C.; Yasuda, J.; Davis, R. J. A Mammalian Scaffold Complex That Selectively Mediates MAP Kinase Activation. *Science* **1998,** *281,* 1671–1674.
117. Barr, R. K.; Kendrick, T. S.; Bogoyevitch, M. A. Identification of the Critical Features of a Small Peptide Inhibitor of JNK Activity. *J. Biol. Chem.* **2002,** *277,* 10987–10997.
118. Bonny, C.; Oberson, A.; Negri, S.; Sauser, C.; Schorderet, D. F. Cell-Permeable Peptide Inhibitors of JNK: Novel Blockers of Beta-Cell Death. *Diabetes* **2001,** *50,* 77–82.
119. Kaneto, H.; Nakatani, Y.; Miyatsuka, T.; Kawamori, D.; Matsuoka, T. A.; Matsuhisa, M.; Kajimoto, Y.; Ichijo, H.; Yamasaki, Y.; Hori, M. Possible Novel Therapy for Diabetes With Cell-Permeable JNK-Inhibitory Peptide. *Nat. Med.* **2004,** *10,* 1128–1132.
120. Stebbins, J. L.; De, S. K.; Machleidt, T.; Becattini, B.; Vazquez, J.; Kuntzen, C.; Chen, L. H.; Cellitti, J. F.; Riel-Mehan, M.; Emdadi, A.; Solinas, G.; Karin, M.; Pellecchia, M. Identification of a New JNK Inhibitor Targeting the JNK–JIP Interaction Site. *Proc. Natl. Acad. Sci. U. S. A.* **2008,** *105,* 16809–16813.
121. Boger, D. L.; Goldberg, J. Cytokine Receptor Dimerization and Activation: Prospects for Small Molecule Agonists. *Bioorg. Med. Chem.* **2001,** *9,* 557–562.
122. Shakespeare, W.; Yang, M.; Bohacek, R.; Cerasoli, F.; Stebbins, K.; Sundaramoorthi, R.; Azimioara, M.; Vu, C.; Pradeepan, S.; Metcalf, C., 3rd.; Haraldson, C.; Merry, T.; Dalgarno, D.; Narula, S.; Hatada, M.; Lu, X.; van Schravendijk, M. R.; Adams, S.; Violette, S.; Smith, J.; Guan, W.; Bartlett, C.; Herson, J.; Iuliucci, J.; Weigele, M.; Sawyer, T. Structure-Based Design of an Osteoclast-Selective, Nonpeptide src Homology 2 Inhibitor With In Vivo Antiresorptive Activity. *Proc. Natl. Acad. Sci. U. S. A.* **2000,** *97,* 9373–9378.
123. Violette, S. M.; Shakespeare, W. C.; Bartlett, C.; Guan, W.; Smith, J. A.; Rickles, R. J.; Bohacek, R. S.; Holt, D. A.; Baron, R.; Sawyer, T. K. A Src SH2 Selective Binding Compound Inhibits Osteoclast-Mediated Resorption. *Chem. Biol.* **2000,** *7,* 225–235.
124. Dixon, S. J.; Stockwell, B. R. Identifying Druggable Disease-Modifying Gene Products. *Curr. Opin. Chem. Biol.* **2009,** *13,* 549–555.
125. Hopkins, A. L.; Groom, C. R. The Druggable Genome. *Nat. Rev. Drug Discov.* **2002,** *1,* 727–730.

126. Berg, T. Small-Molecule Inhibitors of Protein–Protein Interactions. *Curr. Opin. Drug Discov. Devel.* **2008,** *11,* 666–674.
127. Fuller, J. C.; Burgoyne, N. J.; Jackson, R. M. Predicting Druggable Binding Sites at the Protein–Protein Interface. *Drug Discov. Today* **2009,** *14,* 155–161.
128. Clackson, T.; Wells, J. A. A Hot Spot of Binding Energy in a Hormone–Receptor Interface. *Science* **1995,** *267,* 383–386.
129. Wells, J. A. Systematic Mutational Analyses of Protein–Protein Interfaces. *Methods Enzymol.* **1991,** *202,* 390–411.
130. Van Petegem, F.; Duderstadt, K. E.; Clark, K. A.; Wang, M.; Minor, D. L., Jr. Alanine-Scanning Mutagenesis Defines a Conserved Energetic Hotspot in the CaValpha1 AID–CaVbeta Interaction Site That Is Critical for Channel Modulation. *Structure* **2008,** *16,* 280–294.
131. Bogan, A. A.; Thorn, K. S. Anatomy of Hot Spots in Protein Interfaces. *J. Mol. Biol.* **1998,** *280,* 1–9.
132. Hu, Z.; Ma, B.; Wolfson, H.; Nussinov, R. Conservation of Polar Residues as Hot Spots at Protein Interfaces. *Proteins* **2000,** *39,* 331–342.
133. Morrow, J. K.; Zhang, S. Computational Prediction of Protein Hot Spot Residues. *Curr. Pharm. Des.* **2012,** *18,* 1255–1265.
134. Deng, L.; Zhang, Q. C.; Chen, Z.; Meng, Y.; Guan, J.; Zhou, S. PredHS: A Web Server for Predicting Protein–Protein Interaction Hot Spots by Using Structural Neighborhood Properties. *Nucleic Acids Res.* **2014,** *42,* W290–W295.
135. Geppert, T.; Hoy, B.; Wessler, S.; Schneider, G. Context-Based Identification Of Protein–Protein Interfaces and "Hot-Spot" Residues. *Chem. Biol.* **2011,** *18,* 344–353.
136. Tuncbag, N.; Keskin, O.; Gursoy, A. HotPoint: Hot Spot Prediction Server for Protein Interfaces. *Nucleic Acids Res.* **2010,** *38,* W402–W406.
137. Azzarito, V.; Long, K.; Murphy, N. S.; Wilson, A. J. Inhibition of Alpha-Helix-Mediated Protein–Protein Interactions Using Designed Molecules. *Nat. Chem.* **2013,** *5,* 161–173.
138. Gadek, T. R.; Burdick, D. J.; McDowell, R. S.; Stanley, M. S.; Marsters, J. C., Jr.; Paris, K. J.; Oare, D. A.; Reynolds, M. E.; Ladner, C.; Zioncheck, K. A.; Lee, W. P.; Gribling, P.; Dennis, M. S.; Skelton, N. J.; Tumas, D. B.; Clark, K. R.; Keating, S. M.; Beresini, M. H.; Tilley, J. W.; Presta, L. G.; Bodary, S. C. Generation of an LFA-1 Antagonist by the Transfer of the ICAM-1 Immunoregulatory Epitope to a Small Molecule. *Science* **2002,** *295,* 1086–1089.
139. Hoggard, L. R.; Zhang, Y.; Zhang, M.; Panic, V.; Wisniewski, J. A.; Ji, H. Rational Design of Selective Small-Molecule Inhibitors for Beta-Catenin/B-Cell Lymphoma 9 Protein–Protein Interactions. *J. Am. Chem. Soc.* **2015,** *137,* 12249–12260.
140. Ding, C.; Bremer, N. M.; Smith, T. D.; Seitz, P. K.; Anastasio, N. C.; Cunningham, K. A.; Zhou, J. Exploration of Synthetic Approaches and Pharmacological Evaluation of PNU-69176E and Its Stereoisomer as 5-HT2C Receptor Allosteric Modulators. *ACS Chem. Neurosci.* **2012,** *3,* 538–545.
141. Chen, H.; Wang, C. Z.; Ding, C.; Wild, C.; Copits, B.; Swanson, G. T.; Johnson, K. M.; Zhou, J. A Combined Bioinformatics and Chemoinformatics Approach for Developing Asymmetric Bivalent AMPA Receptor Positive Allosteric Modulators as Neuroprotective Agents. *ChemMedChem* **2013,** *8,* 226–230.
142. Wild, C.; Cunningham, K. A.; Zhou, J. Allosteric Modulation of G Protein-Coupled Receptors: An Emerging Approach of Drug Discovery. *Austin J. Pharmacol. Ther.* **2014,** *2,* 3.
143. Hajduk, P. J.; Huth, J. R.; Fesik, S. W. Druggability Indices for Protein Targets Derived From NMR-Based Screening Data. *J. Med. Chem.* **2005,** *48,* 2518–2525.
144. Ulucan, O.; Eyrisch, S.; Helms, V. Druggability of Dynamic Protein–Protein Interfaces. *Curr. Pharm. Des.* **2012,** *18,* 4599–4606.
145. London, N.; Raveh, B.; Schueler-Furman, O. Druggable Protein–Protein Interactions—From Hot Spots to Hot Segments. *Curr. Opin. Chem. Biol.* **2013,** *17,* 952–959.
146. Kozakov, D.; Hall, D. R.; Chuang, G. Y.; Cencic, R.; Brenke, R.; Grove, L. E.; Beglov, D.; Pelletier, J.; Whitty, A.; Vajda, S. Structural Conservation of Druggable Hot Spots in Protein–Protein Interfaces. *Proc. Natl. Acad. Sci. U. S. A.* **2011,** *108,* 13528–13533.
147. Schmidtke, P.; Barril, X. Understanding and Predicting Druggability. A High-Throughput Method for Detection of Drug Binding Sites. *J. Med. Chem.* **2010,** *53,* 5858–5867.
148. Pettit, F. K.; Bowie, J. U. Protein Surface Roughness and Small Molecular Binding Sites. *J. Mol. Biol.* **1999,** *285,* 1377–1382.
149. Li, Y.; Liu, Z.; Han, L.; Li, C.; Wang, R. Mining the Characteristic Interaction Patterns on Protein–Protein Binding Interfaces. *J. Chem. Inf. Model.* **2013,** *53,* 2437–2447.
150. Soga, S.; Shirai, H.; Kobori, M.; Hirayama, N. Use of Amino Acid Composition to Predict Ligand-Binding Sites. *J. Chem. Inf. Model.* **2007,** *47,* 400–406.
151. Laraia, L.; McKenzie, G.; Spring, D. R.; Venkitaraman, A. R.; Huggins, D. J. Overcoming Chemical, Biological, and Computational Challenges in the Development of Inhibitors Targeting Protein–Protein Interactions. *Chem. Biol.* **2015,** *22,* 689–703.
152. Parai, M. K.; Huggins, D. J.; Cao, H.; Nalam, M. N.; Ali, A.; Schiffer, C. A.; Tidor, B.; Rana, T. M. Design, Synthesis, and Biological and Structural Evaluations of Novel HIV-1 Protease Inhibitors to Combat Drug Resistance. *J. Med. Chem.* **2012,** *55,* 6328–6341.
153. Valkov, E.; Sharpe, T.; Marsh, M.; Greive, S.; Hyvonen, M. Targeting Protein–Protein Interactions and Fragment-Based Drug Discovery. *Top. Curr. Chem.* **2012,** *317,* 145–179.
154. Boelsterli, U. A.; Ho, H. K.; Zhou, S.; Leow, K. Y. Bioactivation and Hepatotoxicity of Nitroaromatic Drugs. *Curr. Drug Metab.* **2006,** *7,* 715–727.
155. Guo, W.; Wisniewski, J. A.; Ji, H. Hot Spot-Based Design of Small-Molecule Inhibitors for Protein–Protein Interactions. *Bioorg. Med. Chem. Lett.* **2014,** *24,* 2546–2554.
156. Ripka, A. S.; Rich, D. H. Peptidomimetic Design. *Curr. Opin. Chem. Biol.* **1998,** *2,* 441–452.
157. Fosgerau, K.; Hoffmann, T. Peptide Therapeutics: Current Status and Future Directions. *Drug Discov. Today* **2015,** *20,* 122–128.
158. Zhong, F.; Harr, M. W.; Bultynck, G.; Monaco, G.; Parys, J. B.; De Smedt, H.; Rong, Y. P.; Molitoris, J. K.; Lam, M.; Ryder, C.; Matsuyama, S.; Distelhorst, C. W. Induction of Ca(2)+-Driven Apoptosis in Chronic Lymphocytic Leukemia Cells by Peptide-Mediated Disruption of Bcl-2–IP3 Receptor Interaction. *Blood* **2011,** *117,* 2924–2934.
159. Zhou, H.; Liu, L.; Huang, J.; Bernard, D.; Karatas, H.; Navarro, A.; Lei, M.; Wang, S. Structure-Based Design of High-Affinity Macrocyclic Peptidomimetics to Block the Menin-Mixed Lineage Leukemia 1 (MLL1) Protein–Protein Interaction. *J. Med. Chem.* **2013,** *56,* 1113–1123.
160. Schafmeister, C. E.; Po, J.; Verdine, G. L. An All-Hydrocarbon Cross-Linking System for Enhancing the Helicity and Metabolic Stability of Peptides. *J. Am. Chem. Soc.* **2000,** *122,* 5891–5892.
161. Walensky, L. D.; Bird, G. H. Hydrocarbon-Stapled Peptides: Principles, Practice, and Progress. *J. Med. Chem.* **2014,** *57,* 6275–6288.
162. Chang, Y. S.; Graves, B.; Guerlavais, V.; Tovar, C.; Packman, K.; To, K. H.; Olson, K. A.; Kesavan, K.; Gangurde, P.; Mukherjee, A.; Baker, T.; Darlak, K.; Elkin, C.; Filipovic, Z.; Qureshi, F. Z.; Cai, H.; Berry, P.; Feyfant, E.; Shi, X. E.; Horstick, J.; Annis, D. A.; Manning, A. M.; Fotouhi, N.; Nash, H.; Vassilev, L. T.; Sawyer, T. K. Stapled Alpha-Helical Peptide Drug Development: A Potent Dual Inhibitor of MDM2 and MDMX for p53-Dependent Cancer Therapy. *Proc. Natl. Acad. Sci. U. S. A.* **2013,** *110,* E3445–E3454.
163. Crunkhorn, S. Anticancer Drugs: Stapled Peptide Reactivates p53. *Nat. Rev. Drug Discov.* **2013,** *12,* 741.
164. Chen, T.; Kablaoui, N.; Little, J.; Timofeevski, S.; Tschantz, W. R.; Chen, P.; Feng, J.; Charlton, M.; Stanton, R.; Bauer, P. Identification of Small-Molecule Inhibitors of the JIP–JNK Interaction. *Biochem. J.* **2009,** *420,* 283–294.
165. Sun, Y.; Lu, G.; Tam, J. P. A Thioester Ligation Approach to Amphipathic Bicyclic Peptide Library. *Org. Lett.* **2001,** *3,* 1681–1684.
166. Heinis, C.; Rutherford, T.; Freund, S.; Winter, G. Phage-Encoded Combinatorial Chemical Libraries Based on Bicyclic Peptides. *Nat. Chem. Biol.* **2009,** *5,* 502–507.
167. Lian, W.; Upadhyaya, P.; Rhodes, C. A.; Liu, Y.; Pei, D. Screening Bicyclic Peptide Libraries for Protein–Protein Interaction Inhibitors: Discovery of a Tumor Necrosis Factor-Alpha Antagonist. *J. Am. Chem. Soc.* **2013,** *135,* 11990–11995.
168. Shaginian, A.; Whitby, L. R.; Hong, S.; Hwang, I.; Farooqi, B.; Searcey, M.; Chen, J.; Vogt, P. K.; Boger, D. L. Design, Synthesis, and Evaluation of an Alpha-Helix Mimetic Library Targeting Protein–Protein Interactions. *J. Am. Chem. Soc.* **2009,** *131,* 5564–5572.
169. Labbe, C. M.; Laconde, G.; Kuenemann, M. A.; Villoutreix, B. O.; Sperandio, O. iPPI-DB: A Manually Curated and Interactive Database of Small Non-Peptide Inhibitors of Protein–Protein Interactions. *Drug Discov. Today* **2013,** *18,* 958–968.
170. Mehla, J.; Caufield, J. H.; Uetz, P. The Yeast Two-Hybrid System: A Tool for Mapping Protein–Protein Interactions. *Cold Spring Harb. Protoc.* **2015,** *2015,* 425–430.
171. Du, Y.; Nikolovska-Coleska, Z.; Qui, M.; Li, L.; Lewis, I.; Dingledine, R.; Stuckey, J. A.; Krajewski, K.; Roller, P. P.; Wang, S.; Fu, H. A Dual-Readout F2 Assay That Combines Fluorescence Resonance Energy Transfer and Fluorescence Polarization for Monitoring Bimolecular Interactions. *Assay Drug Dev. Technol.* **2011,** *9,* 382–393.
172. Li, X.; Wang, W.; Chen, J. From Pathways to Networks: Connecting Dots by Establishing Protein–Protein Interaction Networks in Signaling Pathways Using Affinity Purification and Mass Spectrometry. *Proteomics* **2015,** *15,* 188–202.
173. Vassilev, L. T.; Vu, B. T.; Graves, B.; Carvajal, D.; Podlaski, F.; Filipovic, Z.; Kong, N.; Kammlott, U.; Lukacs, C.; Klein, C.; Fotouhi, N.; Liu, E. A. In Vivo Activation of the p53 Pathway by Small-Molecule Antagonists of MDM2. *Science* **2004,** *303,* 844–848.

174. Grasberger, B. L.; Lu, T.; Schubert, C.; Parks, D. J.; Carver, T. E.; Koblish, H. K.; Cummings, M. D.; LaFrance, L. V.; Milkiewicz, K. L.; Calvo, R. R.; Maguire, D.; Lattanze, J.; Franks, C. F.; Zhao, S.; Ramachandren, K.; Bylebyl, G. R.; Zhang, M.; Manthey, C. L.; Petrella, E. C.; Pantoliano, M. W.; Deckman, I. C.; Spurlino, J. C.; Maroney, A. C.; Tomczuk, B. E.; Molloy, C. J.; Bone, R. F. Discovery and Cocrystal Structure of Benzodiazepinedione HDM2 Antagonists That Activate p53 in Cells. *J. Med. Chem.* **2005,** *48,* 909–912.
175. Ray-Coquard, I.; Blay, J. Y.; Italiano, A.; Le Cesne, A.; Penel, N.; Zhi, J.; Heil, F.; Rueger, R.; Graves, B.; Ding, M.; Geho, D.; Middleton, S. A.; Vassilev, L. T.; Nichols, G. L.; Bui, B. N. Effect of the MDM2 Antagonist RG7112 on the P53 Pathway in Patients With MDM2-Amplified, Well-Differentiated or Dedifferentiated Liposarcoma: An Exploratory Proof-of-Mechanism Study. *Lancet Oncol.* **2012,** *13,* 1133–1140.
176. Tovar, C.; Graves, B.; Packman, K.; Filipovic, Z.; Higgins, B.; Xia, M.; Tardell, C.; Garrido, R.; Lee, E.; Kolinsky, K.; To, K. H.; Linn, M.; Podlaski, F.; Wovkulich, P.; Vu, B.; Vassilev, L. T. MDM2 Small-Molecule Antagonist RG7112 Activates p53 Signaling and Regresses Human Tumors in Preclinical Cancer Models. *Cancer Res.* **2013,** *73,* 2587–2597.
177. Chen, H.; Zhou, X.; Wang, A.; Zheng, Y.; Gao, Y.; Zhou, J. Evolutions in Fragment-Based Drug Design: The Deconstruction–Reconstruction Approach. *Drug Discov. Today* **2015,** *20,* 105–113.
178. Congreve, M.; Carr, R.; Murray, C.; Jhoti, H. A 'Rule of Three' for Fragment-Based Lead Discovery? *Drug Discov. Today* **2003,** *8,* 876–877.
179. Koster, H.; Craan, T.; Brass, S.; Herhaus, C.; Zentgraf, M.; Neumann, L.; Heine, A.; Klebe, G. A Small Nonrule of 3 Compatible Fragment Library Provides High hit Rate of Endothiapepsin Crystal Structures With Various Fragment Chemotypes. *J. Med. Chem.* **2011,** *54,* 7784–7796.
180. Guo, Y.; Partch, C. L.; Key, J.; Card, P. B.; Pashkov, V.; Patel, A.; Bruick, R. K.; Wurdak, H.; Gardner, K. H. Regulating the ARNT/TACC3 Axis: Multiple Approaches to Manipulating Protein/Protein Interactions With Small Molecules. *ACS Chem. Biol.* **2013,** *8,* 626–635.
181. Farmer, S. Fragment-Based Drug Discovery: What Really Works. An Interview With Sandy Farmer of Boehringer Ingelheim. *J. Comput. Aided Mol. Des.* **2011,** *25,* 599–605.
182. Braga, R. C.; Alves, V. M.; Silva, A. C.; Nascimento, M. N.; Silva, F. C.; Liao, L. M.; Andrade, C. H. Virtual Screening Strategies in Medicinal Chemistry: The State of the Art and Current Challenges. *Curr. Top. Med. Chem.* **2014,** *14,* 1899–1912.
183. McInnes, C. Virtual Screening Strategies in Drug Discovery. *Curr. Opin. Chem. Biol.* **2007,** *11,* 494–502.
184. Yang, S. Y. Pharmacophore Modeling and Applications in Drug Discovery: Challenges and Recent Advances. *Drug Discov. Today* **2010,** *15,* 444–450.
185. Zheng, X.; Gan, L.; Wang, E.; Wang, J. Pocket-Based Drug Design: Exploring Pocket Space. *AAPS J.* **2013,** *15,* 228–241.
186. Sable, R.; Jois, S. Surfing the Protein–Protein Interaction Surface Using Docking Methods: Application to the Design of PPI Inhibitors. *Molecules* **2015,** *20,* 11569–11603.
187. Korb, O.; Olsson, T. S.; Bowden, S. J.; Hall, R. J.; Verdonk, M. L.; Liebeschuetz, J. W.; Cole, J. C. Potential and Limitations of Ensemble Docking. *J. Chem. Inf. Model.* **2012,** *52,* 1262–1274.
188. Schneider, G. Designing the Molecular Future. *J. Comput. Aided Mol. Des.* **2012,** *26,* 115–120.
189. Doak, B. C.; Over, B.; Giordanetto, F.; Kihlberg, J. Oral Druggable Space Beyond the Rule of 5: Insights From Drugs and Clinical Candidates. *Chem. Biol.* **2014,** *21,* 1115–1142.
190. Hann, M. M.; Keseru, G. M. Finding the Sweet Spot: The Role of Nature and Nurture in Medicinal Chemistry. *Nat. Rev. Drug Discov.* **2012,** *11,* 355–365.
191. Taboureau, O.; Baell, J. B.; Fernandez-Recio, J.; Villoutreix, B. O. Established and Emerging Trends in Computational Drug Discovery in the Structural Genomics Era. *Chem. Biol.* **2012,** *19,* 29–41.
192. Geppert, T.; Bauer, S.; Hiss, J. A.; Conrad, E.; Reutlinger, M.; Schneider, P.; Weisel, M.; Pfeiffer, B.; Altmann, K. H.; Waibler, Z.; Schneider, G. Immunosuppressive Small Molecule Discovered by Structure-Based Virtual Screening for Inhibitors of Protein–Protein Interactions. *Angew. Chem.* **2012,** *51,* 258–261.
193. Lu, Y.; Nikolovska-Coleska, Z.; Fang, X.; Gao, W.; Shangary, S.; Qiu, S.; Qin, D.; Wang, S. Discovery of a Nanomolar Inhibitor of the Human Murine Double Minute 2 (MDM2)–p53 Interaction Through an Integrated, Virtual Database Screening Strategy. *J. Med. Chem.* **2006,** *49,* 3759–3762.
194. Petros, A. M.; Dinges, J.; Augeri, D. J.; Baumeister, S. A.; Betebenner, D. A.; Bures, M. G.; Elmore, S. W.; Hajduk, P. J.; Joseph, M. K.; Landis, S. K.; Nettesheim, D. G.; Rosenberg, S. H.; Shen, W.; Thomas, S.; Wang, X.; Zanze, I.; Zhang, H.; Fesik, S. W. Discovery of a Potent Inhibitor of the Antiapoptotic Protein Bcl-xL From NMR and Parallel Synthesis. *J. Med. Chem.* **2006,** *49,* 656–663.
195. Bruncko, M.; Oost, T. K.; Belli, B. A.; Ding, H.; Joseph, M. K.; Kunzer, A.; Martineau, D.; McClellan, W. J.; Mitten, M.; Ng, S. C.; Nimmer, P. M.; Oltersdorf, T.; Park, C. M.; Petros, A. M.; Shoemaker, A. R.; Song, X.; Wang, X.; Wendt, M. D.; Zhang, H.; Fesik, S. W.; Rosenberg, S. H.; Elmore, S. W. Studies Leading to Potent, Dual Inhibitors of Bcl-2 and Bcl-xL. *J. Med. Chem.* **2007,** *50,* 641–662.
196. Oltersdorf, T.; Elmore, S. W.; Shoemaker, A. R.; Armstrong, R. C.; Augeri, D. J.; Belli, B. A.; Bruncko, M.; Deckwerth, T. L.; Dinges, J.; Hajduk, P. J.; Joseph, M. K.; Kitada, S.; Korsmeyer, S. J.; Kunzer, A. R.; Letai, A.; Li, C.; Mitten, M. J.; Nettesheim, D. G.; Ng, S.; Nimmer, P. M.; O'Connor, J. M.; Oleksijew, A.; Petros, A. M.; Reed, J. C.; Shen, W.; Tahir, S. K.; Thompson, C. B.; Tomaselli, K. J.; Wang, B.; Wendt, M. D.; Zhang, H.; Fesik, S. W.; Rosenberg, S. H. An Inhibitor of Bcl-2 Family Proteins Induces Regression of Solid Tumours. *Nature* **2005,** *435,* 677–681.
197. Tse, C.; Shoemaker, A. R.; Adickes, J.; Anderson, M. G.; Chen, J.; Jin, S.; Johnson, E. F.; Marsh, K. C.; Mitten, M. J.; Nimmer, P.; Roberts, L.; Tahir, S. K.; Xiao, Y.; Yang, X.; Zhang, H.; Fesik, S.; Rosenberg, S. H.; Elmore, S. W. ABT-263: A Potent and Orally Bioavailable Bcl-2 Family Inhibitor. *Cancer Res.* **2008,** *68,* 3421–3428.
198. Wilson, W. H.; O'Connor, O. A.; Czuczman, M. S.; LaCasce, A. S.; Gerecitano, J. F.; Leonard, J. P.; Tulpule, A.; Dunleavy, K.; Xiong, H.; Chiu, Y. L.; Cui, Y.; Busman, T.; Elmore, S. W.; Rosenberg, S. H.; Krivoshik, A. P.; Enschede, S. H.; Humerickhouse, R. A. Navitoclax, a Targeted High-Affinity Inhibitor of BCL-2, in Lymphoid Malignancies: A Phase 1 Dose-Escalation Study of Safety, Pharmacokinetics, Pharmacodynamics, and Antitumour Activity. *Lancet Oncol.* **2010,** *11,* 1149–1159.
199. Souers, A. J.; Leverson, J. D.; Boghaert, E. R.; Ackler, S. L.; Catron, N. D.; Chen, J.; Dayton, B. D.; Ding, H.; Enschede, S. H.; Fairbrother, W. J.; Huang, D. C.; Hymowitz, S. G.; Jin, S.; Khaw, S. L.; Kovar, P. J.; Lam, L. T.; Lee, J.; Maecker, H. L.; Marsh, K. C.; Mason, K. D.; Mitten, M. J.; Nimmer, P. M.; Oleksijew, A.; Park, C. H.; Park, C. M.; Phillips, D. C.; Roberts, A. W.; Sampath, D.; Seymour, J. F.; Smith, M. L.; Sullivan, G. M.; Tahir, S. K.; Tse, C.; Wendt, M. D.; Xiao, Y.; Xue, J. C.; Zhang, H.; Humerickhouse, R. A.; Rosenberg, S. H.; Elmore, S. W. ABT-199, a Potent and Selective BCL-2 Inhibitor, Achieves Antitumor Activity While Sparing Platelets. *Nat. Med.* **2013,** *19,* 202–208.
200. Vu, B.; Wovkulich, P.; Pizzolato, G.; Lovey, A.; Ding, Q.; Jiang, N.; Liu, J. J.; Zhao, C.; Glenn, K.; Wen, Y.; Tovar, C.; Packman, K.; Vassilev, L.; Graves, B. Discovery of RG7112: A Small-Molecule MDM2 Inhibitor in Clinical Development. *ACS Med. Chem. Lett.* **2013,** *4,* 466–469.
201. Wang, S.; Sun, W.; Zhao, Y.; McEachern, D.; Meaux, I.; Barriere, C.; Stuckey, J. A.; Meagher, J. L.; Bai, L.; Liu, L.; Hoffman-Luca, C. G.; Lu, J.; Shangary, S.; Yu, S.; Bernard, D.; Aguilar, A.; Dos-Santos, O.; Besret, L.; Guerif, S.; Pannier, P.; Gorge-Bernat, D.; Debussche, L. SAR405838: An Optimized Inhibitor of MDM2–p53 Interaction That Induces Complete and Durable Tumor Regression. *Cancer Res.* **2014,** *74,* 5855–5865.
202. Ding, K.; Lu, Y.; Nikolovska-Coleska, Z.; Qiu, S.; Ding, Y.; Gao, W.; Stuckey, J.; Krajewski, K.; Roller, P. P.; Tomita, Y.; Parrish, D. A.; Deschamps, J. R.; Wang, S. Structure-Based Design of Potent Non-Peptide MDM2 Inhibitors. *J. Am. Chem. Soc.* **2005,** *127,* 10130–10131.
203. Sun, D.; Li, Z.; Rew, Y.; Gribble, M.; Bartberger, M. D.; Beck, H. P.; Canon, J.; Chen, A.; Chen, X.; Chow, D.; Deignan, J.; Duquette, J.; Eksterowicz, J.; Fisher, B.; Fox, B. M.; Fu, J.; Gonzalez, A. Z.; Gonzalez-Lopez De Turiso, F.; Houze, J. B.; Huang, X.; Jiang, M.; Jin, L.; Kayser, F.; Liu, J. J.; Lo, M. C.; Long, A. M.; Lucas, B.; McGee, L. R.; McIntosh, J.; Mihalic, J.; Oliner, J. D.; Osgood, T.; Peterson, M. L.; Roveto, P.; Saiki, A. Y.; Shaffer, P.; Toteva, M.; Wang, Y.; Wang, Y. C.; Wortman, S.; Yakowec, P.; Yan, X.; Ye, Q.; Yu, D.; Yu, M.; Zhao, X.; Zhou, J.; Zhu, J.; Olson, S. H.; Medina, J. C. Discovery of AMG 232, a Potent, Selective, and Orally Bioavailable MDM2–p53 Inhibitor in Clinical Development. *J. Med. Chem.* **2014,** *57,* 1454–1472.
204. Allali-Hassani, A.; Wasney, G. A.; Siarheyeva, A.; Hajian, T.; Arrowsmith, C. H.; Vedadi, M. Fluorescence-Based Methods for Screening Writers and Readers of Histone Methyl Marks. *J. Biomol. Screen.* **2012,** *17,* 71–84.
205. Senisterra, G.; Wu, H.; Allali-Hassani, A.; Wasney, G. A.; Barsyte-Lovejoy, D.; Dombrovski, L.; Dong, A.; Nguyen, K. T.; Smil, D.; Bolshan, Y.; Hajian, T.; He, H.; Seitova, A.; Chau, I.; Li, F.; Poda, G.; Couture, J. F.; Brown, P. J.; Al-Awar, R.; Schapira, M.; Arrowsmith, C. H.; Vedadi, M. Small-Molecule Inhibition of MLL Activity by Disruption of Its Interaction With WDR5. *Biochem. J.* **2013,** *449,* 151–159.

206. French, C. A.; Miyoshi, I.; Kubonishi, I.; Grier, H. E.; Perez-Atayde, A. R.; Fletcher, J. A. BRD4–NUT Fusion Oncogene: A Novel Mechanism in Aggressive Carcinoma. *Cancer Res.* **2003,** *63,* 304–307.
207. Zuber, J.; Rappaport, A. R.; Luo, W.; Wang, E.; Chen, C.; Vaseva, A. V.; Shi, J.; Weissmueller, S.; Fellmann, C.; Taylor, M. J.; Weissenboeck, M.; Graeber, T. G.; Kogan, S. C.; Vakoc, C. R.; Lowe, S. W. An Integrated Approach to Dissecting Oncogene Addiction Implicates a Myb-Coordinated Self-Renewal Program as Essential for Leukemia Maintenance. *Genes Dev.* **2011,** *25,* 1628–1640.
208. Dawson, M. A.; Prinjha, R. K.; Dittmann, A.; Giotopoulos, G.; Bantscheff, M.; Chan, W. I.; Robson, S. C.; Chung, C. W.; Hopf, C.; Savitski, M. M.; Huthmacher, C.; Gudgin, E.; Lugo, D.; Beinke, S.; Chapman, T. D.; Roberts, E. J.; Soden, P. E.; Auger, K. R.; Mirguet, O.; Doehner, K.; Delwel, R.; Burnett, A. K.; Jeffrey, P.; Drewes, G.; Lee, K.; Huntly, B. J.; Kouzarides, T. Inhibition of BET Recruitment to Chromatin as an Effective Treatment for MLL-Fusion Leukaemia. *Nature* **2011,** *478,* 529–533.
209. Mirguet, O.; Gosmini, R.; Toum, J.; Clement, C. A.; Barnathan, M.; Brusq, J. M.; Mordaunt, J. E.; Grimes, R. M.; Crowe, M.; Pineau, O.; Ajakane, M.; Daugan, A.; Jeffrey, P.; Cutler, L.; Haynes, A. C.; Smithers, N. N.; Chung, C. W.; Bamborough, P.; Uings, I. J.; Lewis, A.; Witherington, J.; Parr, N.; Prinjha, R. K.; Nicodeme, E. Discovery of Epigenetic Regulator I-BET762: Lead Optimization to Afford a Clinical Candidate Inhibitor of the BET Bromodomains. *J. Med. Chem.* **2013,** *56,* 7501–7515.
210. Odore, E.; Lokiec, F.; Cvitkovic, E.; Bekradda, M.; Herait, P.; Bourdel, F.; Kahatt, C.; Raffoux, E.; Stathis, A.; Thieblemont, C.; Quesnel, B.; Cunningham, D.; Riveiro, M. E.; Rezai, K. Phase I Population Pharmacokinetic Assessment of the Oral Bromodomain Inhibitor OTX015 in Patients With Haematologic Malignancies. *Clin. Pharmacokinet.* **2016,** *55,* 397–405.
211. Smith, S. G.; Sanchez, R.; Zhou, M. M. Privileged Diazepine Compounds and Their Emergence as Bromodomain Inhibitors. *Chem. Biol.* **2014,** *21,* 573–583.
212. Liu, Z.; Ai, J.; Peng, X.; Song, Z.; Wu, K.; Zhang, J.; Yao, Q.; Chen, Y.; Ji, Y.; Yang, Y.; Geng, M.; Zhang, A. Novel 2,4-Diarylaminopyrimidine Analogues (DAAPalogues) Showing Potent c-Met/ALK Multikinase Inhibitory Activities. *ACS Med. Chem. Lett.* **2014,** *5,* 304–308.
213. Filippakopoulos, P.; Qi, J.; Picaud, S.; Shen, Y.; Smith, W. B.; Fedorov, O.; Morse, E. M.; Keates, T.; Hickman, T. T.; Felletar, I.; Philpott, M.; Munro, S.; McKeown, M. R.; Wang, Y.; Christie, A. L.; West, N.; Cameron, M. J.; Schwartz, B.; Heightman, T. D.; La Thangue, N.; French, C. A.; Wiest, O.; Kung, A. L.; Knapp, S.; Bradner, J. E. Selective Inhibition of BET Bromodomains. *Nature* **2010,** *468,* 1067–1073.
214. Borea, P. A.; Bonora, A. Brain Receptor Binding and Lipophilic Character of Benzodiazepines. *Biochem. Pharmacol.* **1983,** *32,* 603–607.
215. Zhou, L.; Li, F.; Xu, H. B.; Luo, C. X.; Wu, H. Y.; Zhu, M. M.; Lu, W.; Ji, X.; Zhou, Q. G.; Zhu, D. Y. Treatment of Cerebral Ischemia by Disrupting Ischemia-Induced Interaction of nNOS With PSD-95. *Nat. Med.* **2010,** *16,* 1439–1443.
216. Luo, C. X.; Lin, Y. H.; Qian, X. D.; Tang, Y.; Zhou, H. H.; Jin, X.; Ni, H. Y.; Zhang, F. Y.; Qin, C.; Li, F.; Zhang, Y.; Wu, H. Y.; Chang, L.; Zhu, D. Y. Interaction of nNOS With PSD-95 Negatively Controls Regenerative Repair After Stroke. *J. Neurosci.* **2014,** *34,* 13535–13548.
217. Florio, S. K.; Loh, C.; Huang, S. M.; Iwamaye, A. E.; Kitto, K. F.; Fowler, K. W.; Treiberg, J. A.; Hayflick, J. S.; Walker, J. M.; Fairbanks, C. A.; Lai, Y. Disruption of nNOS-PSD95 Protein–Protein Interaction Inhibits Acute Thermal Hyperalgesia and Chronic Mechanical Allodynia in Rodents. *Br. J. Pharmacol.* **2009,** *158,* 494–506.
218. Nissen, K. B.; Haugaard-Kedstrom, L. M.; Wilbek, T. S.; Nielsen, L. S.; Aberg, E.; Kristensen, A. S.; Bach, A.; Jemth, P.; Stromgaard, K. Targeting Protein–Protein Interactions With Trimeric Ligands: High Affinity Inhibitors of the MAGUK Protein Family. *PLoS One* **2015,** *10,* e0117668.
219. Vogrig, A.; Boucherle, B.; Deokar, H.; Thomas, I.; Ripoche, I.; Lian, L. Y.; Ducki, S. NMR Evaluation of Interactions Between Substituted-Indole and PDZ1 Domain of PSD-95. *Bioorg. Med. Chem. Lett.* **2011,** *21,* 3349–3353.
220. Vogrig, A.; Dorr, L.; Bouzidi, N.; Boucherle, B.; Wattiez, A. S.; Cassier, E.; Vallon, G.; Ripoche, I.; Abrunhosa-Thomas, I.; Marin, P.; Nauton, L.; Thery, V.; Courteix, C.; Lian, L. Y.; Ducki, S. Structure-Based Design of PDZ Ligands as Inhibitors of 5-HT(2A) Receptor/PSD-95 PDZ1 Domain Interaction Possessing Anti-Hyperalgesic Activity. *ACS Chem. Biol.* **2013,** *8,* 2209–2216.
221. Goedert, M. NEURODEGENERATION. Alzheimer's and Parkinson's Diseases: The Prion Concept in Relation to Assembled Abeta, Tau, and Alpha-Synuclein. *Science* **2015,** *349,* 1255555.
222. Dehay, B.; Bourdenx, M.; Gorry, P.; Przedborski, S.; Vila, M.; Hunot, S.; Singleton, A.; Olanow, C. W.; Merchant, K. M.; Bezard, E.; Petsko, G. A.; Meissner, W. G. Targeting Alpha-Synuclein for Treatment of Parkinson's Disease: Mechanistic and Therapeutic Considerations. *Lancet Neurol.* **2015,** *14,* 855–866.
223. Reglodi, D.; Renaud, J.; Tamas, A.; Tizabi, Y.; Socias, B.; Del-Bel, E.; Raisman-Vozari, R. Novel Tactics for Neuroprotection in Parkinson's Disease: Role of Antibiotics, Polyphenols and Neuropeptides. *Prog. Neurobiol.* **2015;** http://dx.doi.org/10.1016/j.pneurobio.2015.10.004. PMID: 26542398.
224. Cheruvara, H.; Allen-Baume, V. L.; Kad, N. M.; Mason, J. M. Intracellular Screening of a Peptide Library to Derive a Potent Peptide Inhibitor of Alpha-Synuclein Aggregation. *J. Biol. Chem.* **2015,** *290,* 7426–7435.
225. Madine, J.; Doig, A. J.; Middleton, D. A. Design of an N-Methylated Peptide Inhibitor of Alpha-Synuclein Aggregation Guided by Solid-State NMR. *J. Am. Chem. Soc.* **2008,** *130,* 7873–7881.
226. Singh, P. K.; Kotia, V.; Ghosh, D.; Mohite, G. M.; Kumar, A.; Maji, S. K. Curcumin Modulates Alpha-Synuclein Aggregation and Toxicity. *ACS Chem. Neurosci.* **2013,** *4,* 393–407.
227. Shaltiel-Karyo, R.; Frenkel-Pinter, M.; Rockenstein, E.; Patrick, C.; Levy-Sakin, M.; Schiller, A.; Egoz-Matia, N.; Masliah, E.; Segal, D.; Gazit, E. A Blood–Brain Barrier (BBB) Disrupter Is Also a Potent Alpha-Synuclein (Alpha-syn) Aggregation Inhibitor: A Novel Dual Mechanism of Mannitol for the Treatment of Parkinson Disease (PD). *J. Biol. Chem.* **2013,** *288,* 17579–17588.
228. Ehrnhoefer, D. E.; Bieschke, J.; Boeddrich, A.; Herbst, M.; Masino, L.; Lurz, R.; Engemann, S.; Pastore, A.; Wanker, E. E. EGCG Redirects Amyloidogenic Polypeptides Into Unstructured, Off-Pathway Oligomers. *Nat. Struct. Mol. Biol.* **2008,** *15,* 558–566.
229. Bieschke, J.; Russ, J.; Friedrich, R. P.; Ehrnhoefer, D. E.; Wobst, H.; Neugebauer, K.; Wanker, E. E. EGCG Remodels Mature Alpha-Synuclein and Amyloid-Beta Fibrils and Reduces Cellular Toxicity. *Proc. Natl. Acad. Sci. U. S. A.* **2010,** *107,* 7710–7715.
230. Wagner, J.; Ryazanov, S.; Leonov, A.; Levin, J.; Shi, S.; Schmidt, F.; Prix, C.; Pan-Montojo, F.; Bertsch, U.; Mitteregger-Kretzschmar, G.; Geissen, M.; Eiden, M.; Leidel, F.; Hirschberger, T.; Deeg, A. A.; Krauth, J. J.; Zinth, W.; Tavan, P.; Pilger, J.; Zweckstetter, M.; Frank, T.; Bahr, M.; Weishaupt, J. H.; Uhr, M.; Urlaub, H.; Teichmann, U.; Samwer, M.; Botzel, K.; Groschup, M.; Kretzschmar, H.; Griesinger, C.; Giese, A. Anle138b: A Novel Oligomer Modulator for Disease-Modifying Therapy of Neurodegenerative Diseases Such as Prion and Parkinson's Disease. *Acta Neuropathol.* **2013,** *125,* 795–813.
231. Potin, D.; Launay, M.; Monatlik, F.; Malabre, P.; Fabreguettes, M.; Fouquet, A.; Maillet, M.; Nicolai, E.; Dorgeret, L.; Chevallier, F.; Besse, D.; Dufort, M.; Caussade, F.; Ahmad, S. Z.; Stetsko, D. K.; Skala, S.; Davis, P. M.; Balimane, P.; Patel, K.; Yang, Z.; Marathe, P.; Postelneck, J.; Townsend, R. M.; Goldfarb, V.; Sheriff, S.; Einspahr, H.; Kish, K.; Malley, M. F.; DiMarco, J. D.; Gougoutas, J. Z.; Kadiyala, P.; Cheney, D. L.; Tejwani, R. W.; Murphy, D. K.; McIntyre, K. W.; Yang, X.; Chao, S.; Leith, L.; Xiao, Z.; Mathur, A.; Chen, B. C.; Wu, D. R.; Traeger, S. C.; McKinnon, M.; Barrish, J. C.; Robl, J. A.; Iwanowicz, E. J.; Suchard, S. J.; Dhar, T. G. Discovery and Development of 5-[(5S,9R)-9-(4-Cyanophenyl)-3-(3,5-dichlorophenyl)-1-methyl-2,4-dioxo-1,3,7-tria Zaspiro[4.4]non-7-yl-methyl]-3-thiophenecarboxylic acid (BMS-587101)—A Small Molecule Antagonist of Leukocyte Function Associated Antigen-1. *J. Med. Chem.* **2006,** *49,* 6946–6949.
232. Watterson, S. H.; Xiao, Z.; Dodd, D. S.; Tortolani, D. R.; Vaccaro, W.; Potin, D.; Launay, M.; Stetsko, D. K.; Skala, S.; Davis, P. M.; Lee, D.; Yang, X.; McIntyre, K. W.; Balimane, P.; Patel, K.; Yang, Z.; Marathe, P.; Kadiyala, P.; Tebben, A. J.; Sheriff, S.; Chang, C. Y.; Ziemba, T.; Zhang, H.; Chen, B. C.; DelMonte, A. J.; Aranibar, N.; McKinnon, M.; Barrish, J. C.; Suchard, S. J.; Murali Dhar, T. G. Small Molecule Antagonist of Leukocyte Function Associated Antigen-1 (LFA-1): Structure–Activity Relationships Leading to the Identification of 6-((5S,9R)-9-(4-Cyanophenyl)-3-(3,5-dichlorophenyl)-1-methyl-2,4-dioxo-1,3,7-tria Zaspiro[4.4]nonan-7-yl)nicotinic acid (BMS-688521). *J. Med. Chem.* **2010,** *53,* 3814–3830.
233. Liu, G.; Link, J. T.; Pei, Z.; Reilly, E. B.; Leitza, S.; Nguyen, B.; Marsh, K. C.; Okasinski, G. F.; von Geldern, T. W.; Ormes, M.; Fowler, K.; Gallatin, M. Discovery of Novel p-Arylthio Cinnamides as Antagonists of Leukocyte Function-Associated Antigen-1/Intracellular Adhesion Molecule-1 Interaction. 1. Identification of an Additional Binding Pocket Based on an Anilino Diaryl Sulfide Lead. *J. Med. Chem.* **2000,** *43,* 4025–4040.

234. Zhong, M.; Shen, W.; Barr, K. J.; Arbitrario, J. P.; Arkin, M. R.; Bui, M.; Chen, T.; Cunningham, B. C.; Evanchik, M. J.; Hanan, E. J.; Hoch, U.; Huen, K.; Hyde, J.; Kumer, J. L.; Lac, T.; Lawrence, C. E.; Martell, J. R.; Oslob, J. D.; Paulvannan, K.; Prabhu, S.; Silverman, J. A.; Wright, J.; Yu, C. H.; Zhu, J.; Flanagan, W. M. Discovery of Tetrahydroisoquinoline (THIQ) Derivatives as Potent and Orally Bioavailable LFA-1/ICAM-1 Antagonists. *Bioorg. Med. Chem. Lett.* **2010,** *20,* 5269–5273.
235. Zhong, M.; Hanan, E. J.; Shen, W.; Bui, M.; Arkin, M. R.; Barr, K. J.; Evanchik, M. J.; Hoch, U.; Hyde, J.; Martell, J. R.; Oslob, J. D.; Paulvannan, K.; Prabhu, S.; Silverman, J. A.; Wright, J.; Yu, C. H.; Zhu, J.; Flanagan, W. M. Structure-Activity Relationship (SAR) of the Alpha-Amino Acid Residue of Potent Tetrahydroisoquinoline (THIQ)-Derived LFA-1/ICAM-1 Antagonists. *Bioorg. Med. Chem. Lett.* **2011,** *21,* 307–310.
236. Zhong, M.; Gadek, T. R.; Bui, M.; Shen, W.; Burnier, J.; Barr, K. J.; Hanan, E. J.; Oslob, J. D.; Yu, C. H.; Zhu, J.; Arkin, M. R.; Evanchik, M. J.; Flanagan, W. M.; Hoch, U.; Hyde, J.; Prabhu, S.; Silverman, J. A.; Wright, J. Discovery and Development of Potent LFA-1/ICAM-1 Antagonist SAR 1118 as an Ophthalmic Solution for Treating Dry Eye. *ACS Med. Chem. Lett.* **2012,** *3,* 203–206.
237. Copple, I. M. The Keap1-Nrf2 Cell Defense Pathway—A Promising Therapeutic Target? *Adv. Pharmacol.* **2012,** *63,* 43–79.
238. Zhuang, C.; Narayanapillai, S.; Zhang, W.; Sham, Y. Y.; Xing, C. Rapid Identification of Keap1–Nrf2 Small-Molecule Inhibitors Through Structure-Based Virtual Screening and Hit-Based Substructure Search. *J. Med. Chem.* **2014,** *57,* 1121–1126.
239. Jnoff, E.; Albrecht, C.; Barker, J. J.; Barker, O.; Beaumont, E.; Bromidge, S.; Brookfield, F.; Brooks, M.; Bubert, C.; Ceska, T.; Corden, V.; Dawson, G.; Duclos, S.; Fryatt, T.; Genicot, C.; Jigorel, E.; Kwong, J.; Maghames, R.; Mushi, I.; Pike, R.; Sands, Z. A.; Smith, M. A.; Stimson, C. C.; Courade, J. P. Binding Mode and Structure–Activity Relationships Around Direct Inhibitors of the Nrf2–Keap1 Complex. *ChemMedChem* **2014,** *9,* 699–705.
240. Jiang, Z. Y.; Lu, M. C.; Xu, L. L.; Yang, T. T.; Xi, M. Y.; Xu, X. L.; Guo, X. K.; Zhang, X. J.; You, Q. D.; Sun, H. P. Discovery of Potent Keap1–Nrf2 protein–protein Interaction Inhibitor Based on Molecular Binding Determinants Analysis. *J. Med. Chem.* **2014,** *57,* 2736–2745.
241. Hartman, G. D.; Egbertson, M. S.; Halczenko, W.; Laswell, W. L.; Duggan, M. E.; Smith, R. L.; Naylor, A. M.; Manno, P. D.; Lynch, R. J.; Zhang, G.; et al. Non-Peptide Fibrinogen Receptor Antagonists. 1. Discovery and Design of Exosite Inhibitors. *J. Med. Chem.* **1992,** *35,* 4640–4642.
242. The PURSUIT Trial Investigators. Inhibition of Platelet Glycoprotein IIb/IIIa With Eptifibatide in Patients With Acute Coronary Syndromes. Platelet Glycoprotein IIb/IIIa in Unstable Angina: Receptor Suppression Using Integrilin Therapy. *N. Engl. J. Med.* **1998,** *339,* 436–443.
243. Platelet Receptor Inhibition in Ischemic Syndrome Management (PRISM) Study Investigators. A Comparison of Aspirin Plus Tirofiban With Aspirin Plus Heparin for Unstable Angina. *N. Engl. J. Med.* **1998,** *338,* 1498–1505.
244. King, S.; Short, M.; Harmon, C. Glycoprotein IIb/IIIa Inhibitors: The Resurgence of Tirofiban. *Vascul. Pharmacol.* **2016,** *78,* 10–16.
245. MacArthur, R. D.; Novak, R. M. Reviews of Anti-Infective Agents: Maraviroc: The First of a New Class of Antiretroviral Agents. *Clin. Infect. Dis.* **2008,** *47,* 236–241.
246. Jennings, L. D.; Foreman, K. W.; Rush, T. S., 3rd; Tsao, D. H.; Mosyak, L.; Kincaid, S. L.; Sukhdeo, M. N.; Sutherland, A. G.; Ding, W.; Kenny, C. H.; Sabus, C. L.; Liu, H.; Dushin, E. G.; Moghazeh, S. L.; Labthavikul, P.; Petersen, P. J.; Tuckman, M.; Haney, S. A.; Ruzin, A. V. Combinatorial Synthesis of Substituted 3-(2-Indolyl)piperidines and 2-Phenyl Indoles as Inhibitors of ZipA–FtsZ Interaction. *Bioorg. Med. Chem.* **2004,** *12,* 5115–5131.
247. Zarzycka, B.; Kuenemann, M. A.; Miteva, M. A.; Nicolaes, G. A.; Vriend, G.; Sperandio, O. Stabilization of Protein–Protein Interaction Complexes Through Small Molecules. *Drug Discov. Today* **2016,** *21,* 48–57.
248. Milroy, L. G.; Grossmann, T. N.; Hennig, S.; Brunsveld, L.; Ottmann, C. Modulators of Protein–Protein Interactions. *Chem. Rev.* **2014,** *114,* 4695–4748.
249. Jiang, Z. Y.; Xu, L. L.; Lu, M. C.; Chen, Z. Y.; Yuan, Z. W.; Xu, X. L.; Guo, X. K.; Zhang, X. J.; Sun, H. P.; You, Q. D. Structure-Activity and Structure–property Relationship and Exploratory in vivo Evaluation of the Nanomolar Keap1-Nrf2 Protein–Protein Interaction Inhibitor. *J. Med. Chem.* **2015,** *58,* 6410–6421.
250. Winkel, A. F.; Engel, C. K.; Margerie, D.; Kannt, A.; Szillat, H.; Glombik, H.; Kallus, C.; Ruf, S.; Gussregen, S.; Riedel, J.; Herling, A. W.; von Knethen, A.; Weigert, A.; Brune, B.; Schmoll, D. Characterization of RA839, a Noncovalent Small Molecule Binder to Keap1 and Selective Activator of Nrf2 Signaling. *J. Biol. Chem.* **2015,** *290,* 28446–28455.

Relevant Websites

http://thebiogrid.org—BioGRID, a database of genetic and physical interactions.
http://www.ippidb.cdithem.fr/—iPPI-DB, inhibitors of protein–protein interaction database.
http://string-db.org/—STRING, Protein networks based on experimental data and predictions at EMBL.
http://www.ihop-net.org/UniPub/iHOP/—iHOP, Information Hyperlinked over Proteins. Protei n association network built by literature mining.
http://www.ebi.ac.uk/intact/—IntAct, protein–protein interaction database.
http://mentha.uniroma2.it/index.php—mentha, protein–protein interaction database.
http://kbdock.loria.fr/—KBDOCK, 3D database that defines and spatially clusters protein binding sites for knowledge-based protein docking.
http://www.bonvinlab.org/software/haddock2.2/haddock.html—HADDOCK, online protein–protein docking method.
http://ps2v3.life.nctu.edu.tw/—Dockscore, a webserver for ranking protein–protein docked poses.
http://centria.di.fct.unl.pt/∼ludi/bigger.html —BIGGER, protein–protein docking method.
http://strcomp.protein.osaka-u.ac.jp/homcos/—HOMCOS, homology modeling of protein complex structure.
http://bioinf.cs.ucl.ac.uk/psipred/—PSIPRED and HSPred, Hotspot predictions.
http://mordred.bioc.cam.ac.uk/timbal—TIMBAL, atomic interactions and profile of small molecules disrupting PPI interfaces.
http://brylinski.cct.lsu.edu/content/efindsiteppi-webserver?ticket=Pa7WBPClqB—eFindSite PPI, a tool detects protein binding sites and residues using meta-threading.
http://www.vls3d.com/—Vls3d, comprehensive list of drug design tools in the form of weblinks including protein–protein interactions.

2.14 Next Generation Sequencing Technologies

R Rajesh Singh, The University of Texas MD Anderson Cancer Center, Houston, TX, United States

© 2017 Elsevier Ltd. All rights reserved.

2.14.1	**Introduction**	354
2.14.2	**Second Generation or NGS Technologies**	354
2.14.2.1	Pyrosequencing-Based Optical NGS Technology	355
2.14.2.1.1	Optical sequencing using distinctly labeled fluorescent nucleotide	356
2.14.2.2	Nonoptical NGS	356
2.14.2.2.1	Semiconductor based nonoptical sequencing system	356
2.14.3	**Third Generation Genome Sequencing Technologies**	357
2.14.4	**Implementation of NGS Technologies for Clinical Applications**	357
2.14.5	**Clinical Utility of NGS Technology**	357
2.14.6	**NGS in Drug Discovery and Development**	359
References		360

2.14.1 Introduction

The ability to obtain the sequence of the genome, the "blueprint" of life, is of very high importance to understand the underlying biology. Consequently, this is of great interest and need in every field encompassing biology like medicine, pharmaceuticals, microbiology, agriculture, and farming. In medicine, the push towards identifying the causal genetic aberrations which drive the disease and tailoring the therapy to target it (targeted therapy) has gained high prominence. This places more emphasis on achieving genome sequencing with high accuracy and efficiency with regards to time and cost requirements.

Early technologies or the first generation genome sequencing technologies were revolutionary in formulating a practical way of gleaning the genome sequence. The pioneering technology was the chemical degradation or the chemical cleavage method from Maxam and Gilbert.[1] This method is based on selective cleavage of single-strands of DNA by a combination of chemicals like dimethylsulfoxide, hydrazine, and piperidine. This coupled with radiolabeling of DNA strands at the 5′-end, resulted in a DNA strand substrate which could be separated on acrylamide gels and identified by autoradiography. This method was effective and was used in pioneering genome sequencing studies.[2,3] However, it was cumbersome due to the compulsion to use harmful toxic chemicals, radioactivity, and acrylamide gels. These drawbacks were partially overcome by another method referred to sequencing by chain termination method or more famously known as Sanger Sequencing which completely revolutionized genome sequencing at large scale.[4] This method uses the sequencing by synthesis approach where a DNA strand to be sequenced is used as template over which a complementary strand is synthesized by Taq-DNA polymerase using a mixture of normal and dideoxy nucleotides. The incorporation of dideoxy nucleotides results in termination of the strand growth (hence the name "chain termination method"). Radiolabeling was used to tag the strands which when resolved on an acrylamide gels could provide the genomic sequence. Although radioactivity was used, the procedure eliminated the use of hazardous chemicals and being enzymatic was considerably more efficient than the chemical cleavage method and thus represented a major improvement. This technology was further improved and made safe with the use of distinct fluorescent-labeled dideoxy nucleotides which when incorporated in a growing strand resulted in distinct fluorescence. This, when coupled with separation of the DNA fragments using capillary electrophoresis and computerized base calling programs (referred as automated Sanger sequencing) drastically improved the efficiency and sequencing capacity of Sanger sequencing. Automated Sanger sequencing methodology has been a dominant force and resulted in an explosion of genomes being characterized and made it feasible for widespread use for routine genome sequencing for research and clinical use. It was also instrumental in achieving the first-ever completed sequence of the human genome.[5] However, Sanger sequencing still had drawbacks, such as low to medium throughput and relatively small size of the genomic areas which could be sequenced in a reasonable amount of time. A revolution in genome sequencing approach and analysis capabilities to deal with large amount of information was needed to take genome sequencing to the next level. This was possible by the onset of massively parallel sequencing technologies which are referred to as the second generation of "next generation sequencing" (NGS) technologies which have permanently changed the face of genome sequencing capability, cost, accessibility, and efficiency. The nature of these technologies, their advantages, and challenges for implementing them for routine clinical applications have been discussed in this chapter in detail.

2.14.2 Second Generation or NGS Technologies

The hallmark of the NGS technologies is the ability to perform massively parallel sequencing of millions of DNA strands simultaneously, which is coupled with the ability to collect, process, and analyze this information facilitated by the revolution in data

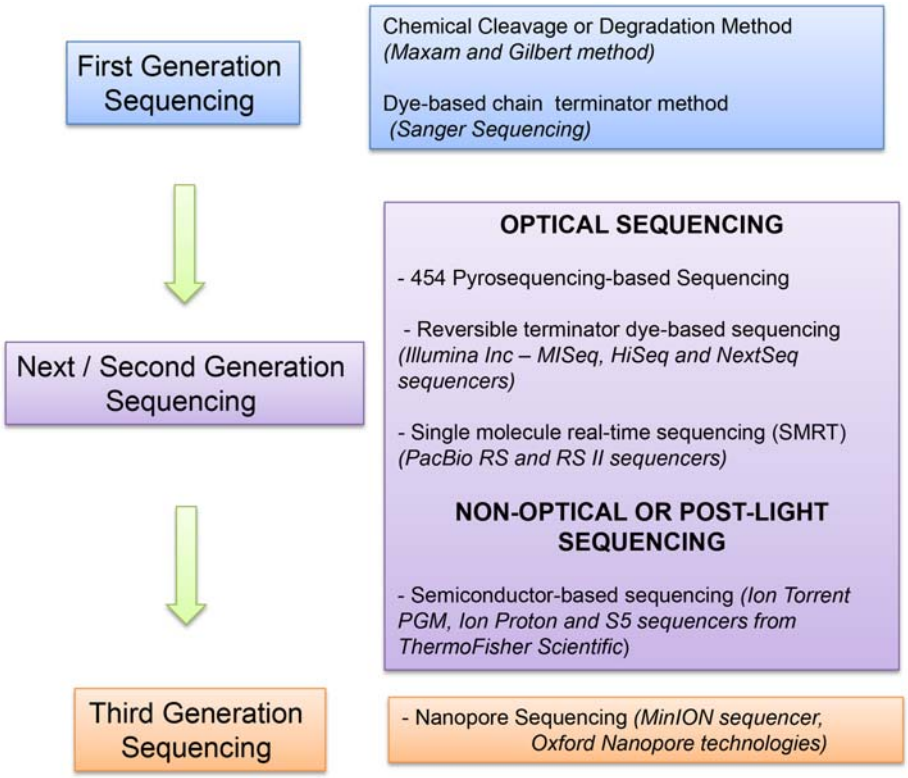

Fig. 1 Summary and evolution of sequencing technologies. A schematic diagram representing the onset of pioneering technologies of chemical cleavage and chain termination methods of genome sequencing followed by the massively parallel next generation sequencing platforms and the revolutionary third generation sequencing platforms which could be expected to appear as mainstream technologies.

processing and computing. The coming-of-age of these two capabilities (sequencing and data processing) created a perfect storm that helped in an explosion of the NGS technology innovation and implementation for diverse applications. Numerous excellent reviews and papers regarding the technologies, the fundamental basis of their technologies and their advantages have been published.[6–10] The following is a summary of the most commonly used NGS technologies along with their strengths and weaknesses and the challenges of validating them for routine clinical use.

The NGS technologies which proliferated immediately as successors of automated Sanger sequencing, utilized similar principles of using a DNA strand as a template to build a complementary DNA strand during sequencing (sequencing-by-synthesis or SBS) and optical detection. These are referred to as optical imaging or light-based NGS technologies. A detailed description of the light-based NGS technologies is provided below and summarized in Fig. 1.

2.14.2.1 Pyrosequencing-Based Optical NGS Technology

This technology uses the approach of pyrosequencing, where the DNA strand to be sequenced is used as template and the synthesis of the complementary strand is accomplished by flowing each deoxy nucleotide tri phosphate (dNTPs) one a time. If the dNTP introduced is complementary to the nucleotide in the template DNA strand, it is incorporated in the growing strand by the formation of a phospho-diester bond and the release of a pyrophosphate. The released pyrophosphate is coupled to a luciferase mediated enzymatic reaction which generates an optical signal each time a nucleotide is incorporated and hence the name pyrosequencing.[11] This technique was employed on a large scale in the Roche/454 sequencer to facilitate massive parallel sequencing. Here, the DNA strands to be sequenced were amplified on to microscopic beads by emulsion PCR and deposited into microscopic wells on PicoTitrePlates (PTPs). SBS is performed by flowing each nucleotide at a time along with other reagents necessary for DNA synthesis. The PTPs are coupled to a high-resolution camera to detect the light generated by the pyrophosphate-coupled luciferase activity on the incorporation of a nucleotide in the millions of strands tested simultaneously. This platform can generate sequencing reads of up to 700 bp but suffers from high sequencing error rates in the regions of homo-polymer stretches where the same nucleotides are repeated in the sequences (polyA, polyC, etc.). In these areas, when a nucleotide complementary to the homo-polymer stretch is released into the reaction mixture, it results in simultaneous incorporation of several nucleotides and generation of a light signal that may not be proportional to the number of nucleotides incorporated. This results in the calling of false mutations like deletions

(disproportionately lower optical signal to the total nucleotides incorporated) or false substitutions due to misalignment of sequence.

2.14.2.1.1 Optical sequencing using distinctly labeled fluorescent nucleotide

This is the most widely used model of optical sequencing currently and is characteristic of the sequencing platforms of various capacities from Illumina Inc. This technology also uses the SBS mode of using the DNA strand of interest as a template over which the complementary strand is synthesized using 3′-OH group blocked fluorescently labeled dNTPs. The sequencing is performed in a flow-cell which has a minute glass tubes or lanes on the internal surface of which individual DNA strands are clonally amplified to generate distinct clusters, which are used as templates for SBS. The sequencing reaction is started by introducing the polymerase and a mixture of four labeled dNTPs into the flow-cell. Once a complementary nucleotide is incorporated, further growth of the strand is arrested due to the unavailability of the free 3′-OH group. After each incorporation, the fluorescently labeled growing strands are imaged with high sensitivity cameras to get the information regarding the incorporated nucleotide in the millions of DNA strand clusters simultaneously thus achieving massive parallel sequencing. After imaging, the modification protecting the 3′-OH group is enzymatically cleaved making way for the incorporation of the next nucleotide and thus starting the next cycle of nucleotide incorporation, followed again by imaging. These successive repetitive steps are referred to as sequencing "cycles" and as the 3′-OH group blocking is reversible it is referred to as the "reversible terminator-based" sequencing methodology. As imaging is performed after each cycle of nucleotide incorporation and distinct fluorescent labeling of the nucleotides, the sequencing time is relatively long but is compensated or justified by the high quality of sequence obtained and low error rates. Also, the DNA strands in the clusters can be sequenced in one direction or in both directions, which is referred to as "single reads" or "paired-reads," respectively. Bi-directional sequencing is the preferred approach due to its high accuracy especially in applications that are used to screen for mutational changes in the DNA.

This methodology of sequencing forms the basis of all Illumina sequencers of different capacities like the table top medium-capacity MiSeq sequencer and a variety of high capacity HiSeq sequencers (HiSeq 2500, 3000, 4000, HiSeq Xten, etc.) which currently represent the most commonly used NGS-based sequencers for targeted small scale and comprehensive large scale genomic sequencing applications. Furthermore, a recently released Illumina sequencer called NextSeq uses a slightly different approach of using only two different fluorescent labels for sequencing. Here, two nucleotides (dATP and dCTP) have distinctly labeled fluorescent tags; dTTP has both of these tags and has an overlapping fluorescent signature whereas dGTP is unlabeled. This two-channel approach helps in decreasing the time required for sequencing in comparison to the four dye labeled workflow and thus increasing the efficiency. The NextSeq also has a sequencing capacity between MiSeq and a HiSeq and serves as the right platform for the medium–high throughput sequencing requirements.

2.14.2.1.1.1 Single molecule real-time sequencing technologies

This is a unique method of optical or light-based sequencing where SBS is used as the basis, but unlike the Illumina platforms, the sequencing of the DNA strand is gleaned continuously without interruption as the complementary strand is being synthesized and hence is also referred to as "real-time DNA sequencing." This technology is characteristic of the sequencer from Pacific Biosystems (PacBio RS and RS II sequencers).[6,12] Here, sequencing is performed in numerous units called as zero-mode waveguides at the bottom of which a single molecule of DNA polymerase is immobilized which binds to a DNA template strand to be sequenced and performs SBS using four distinct fluorescent-labeled dNTPs. As a single DNA strand is replicated the fluorescence from the labeled dNTPs being incorporated is imaged and recorded in real-time similar to a video recording, it is referred to as "single molecule real-time sequencing technology (SMRT). Consequently, this provides a high speed of DNA sequencing and as a single strand is used, it does not require PCR amplification of the DNA strands to be sequenced (thus eliminating PCR-based bias of target DNA to be sequenced) and sequencing of very long reads become possible. Generally, the strands used for sequencing are circular DNA strands obtained by incorporating hair-pins on either side and can be sequenced multiple times by the polymerase thus generating repeated sequencing of the same DNA strand. The most obvious advantage of the SMRT sequencing systems of PacBio is the long read lengths which can achieved. These range from 1500 bp to 60 kb and this ability represents a drastic advantage over other NGS technologies whose read lengths vary from 100 to 600 bp. Consequently, the SMRT sequencing sequencers are platforms of choice for genome assembly which is more accurate and efficient by using the long contiguous reads generated.[12–15] Due to its capability to sequence a single strand of DNA which is different from the typical NGS platforms where clonal clusters of PCR-amplified DNA strands of are sequenced SMRT sequencing is also considered as the third generation sequencing technology (akin to the nanopore-based sequencing platforms discussed later in this chapter).

2.14.2.2 Nonoptical NGS

The majority of the NGS platforms currently in widespread use are light or optical signal recording platforms. However, there are some sequencing platforms which are not light based and use drastically different and revolutionary technologies as described below.

2.14.2.2.1 Semiconductor based nonoptical sequencing system

This is a revolutionary NGS platform (referred to as postlight sequencing), which monitors and measures the protons from the 3′-OH group during the formation of phospho-diester bonds during SBS to sequence the DNA.[16] The approach used is similar

to pyrosequencing used in Roche/454 sequencer, where SBS is performed on microscopic beads with clonally amplified DNA strands using unlabeled dNTPs which are introduced one at a time in a predetermined order. These beads are deposited in microscopic wells, each large enough to accommodate one bead and SBS is performed and interfaced with a semiconductor chip. Incorporation of a nucleotide results in the release of a proton, which when occurring simultaneously on all clonal DNA strands on the bead results in millions of protons being released to proportionately decrease the pH of the well microenvironment, which is recorded by the semiconductor chip as a change of voltage. Each chip has millions of wells and with each flow of nucleotide across them results in simultaneous sequencing of strands clonally amplified on millions of beads thus facilitating massive parallel sequencing. This sequencing technology is used in the IonTorrent sequencing platforms from ThermoFisher Scientific (Ion Personal Genome Machine or Ion PGM, Ion Proton, and Ion S5 sequencers) that are finding wide use in low and medium throughput genome sequencing applications.[17–22]

Several studies pertaining to the performances of the optical and nonoptical sequencing technologies, and their comparison with respect to their sequencing capacity, accuracy, and the associated costs have been published and serve as valuable resources for laboratories to decide upon a choice of NGS technology and sequencer for implementation.[7,23–25]

2.14.3 Third Generation Genome Sequencing Technologies

These technologies represent recent advances of genome sequencing methodologies which are drastically different for the first and second generation sequencing platforms and represent radical changes and improvements. An example is the Nanopore sequencing technology, which is based upon sequencing single molecule of DNA by passing it through a nanoscale pore across which a small voltage is imposed. As the DNA molecule passes through the pore, it temporarily blocks the pore creating a nucleotide-specific change in the voltage which can be detected and correlated to glean the sequence.[26–28] As a variation, an exonuclease linked to the nanopore can cleave each nucleotide which passes to the pore. The identity of the nucleotide can be obtained by the signature alteration of the voltage across the pore resulting in the sequencing of DNA. This mode of sequencing can be used to generate sequence both small and very large DNA strands (as long as 50 kb) and could prove very valuable for both targeted or whole exome and genome sequencing applications. On the whole, the nanopore technology has a potential to decrease the costs drastically and time of large scale genome sequencing.[29] Currently, this mode of sequencing is being used in the MinION nanopore sequencer (Oxford Nanopore Technologies) and is being evaluated for various applications.[30]

2.14.4 Implementation of NGS Technologies for Clinical Applications

The capacity of NGS sequencing platforms to perform massively parallel sequencing of DNA and RNA is very desirable and valuable in routine clinical use for clinical purposes. They provide the capability of simultaneously sequencing a large volume of samples for multiple markers for a variety of genomic aberrations in a relatively short time at lower costs as compared to the traditional sequencing platforms. However, majority of the NGS platforms and the associated technologies are meant for research-use-only purposes and their implementation requires their vetting or thorough validation for routine clinical use. This is a very important prerequisite and NGS tests being more complex in comparison to the traditional tests, makes their thorough validation challenging. In recent years, in order to provide guidance, several regulatory agencies like the College of American Pathologists (CAP), Association for Molecular Pathology (AMP), American College of Medical Genetics, US Centers for Disease Control and Prevention (CDC) provide important reference and resource for a laboratory which intends to implement NGS technologies.[31–34]

The general approach for validation includes thorough testing and establishing the basic performance characteristics of the platform as defined by guidelines which have been in use for any high-complexity molecular test.[35] A list of these parameters and their significance has been provided in **Table 1** and summarized in **Fig. 2**. However, in comparison to the earlier sequencing and genotyping methodologies, the NGS technologies are associated with higher complexity at every level, be it wet bench preparation, sequencing, data interpretation, storage, and clinical reporting. This required reinterpretation and modification of the previous guidelines, and defining novel approaches to ensure adequate validation of the NGS platforms. This reinterpretation has been provided in guidelines proposed by several agencies as mentioned earlier. In addition to the published guidelines from agencies, several laboratories have published details of validating numerous NGS platforms which serve as a very important resource for the performance characteristics of the technologies and the associated challenges and advantages.[36–40] Reports of cross laboratory cost analysis for routine implementation of NGS tests are also available which are very helpful for the labs to consider the financial implications of NGS testing and choose the most well-suited platform and workflows.[41]

2.14.5 Clinical Utility of NGS Technology

The massively parallel sequencing capability of NGS technologies provides powerful solution for clinical screening of genomic in a clinical setup be it to screen for germ line aberrations of significance in hereditary medical syndromes, physical and mental health, somatic aberrations in cancers and characterization of microbial populations in infectious diseases. The ability of NGS to sequence multiple genomic areas in multiple samples simultaneously with a single input of DNA or RNA provides a crucial advantage in

Table 1 Performance parameters of NGS platforms for validation before clinical implementation[a]

Performance parameters	*Details*	*Significance/comments*
Analytical sensitivity	Number of samples positive for mutation and are classified as positives	Capacity to detect true sequence variants as detected by orthogonal gold standard technologies like Sanger Sequencing (false negative rate)
Analytical specificity	Number of samples conformed as negative for mutations and are classified as negative	Rate of mutations detected which are false positive
Accuracy	Concordance of sequence obtained by the NGS platform and the reference sequence	Error rates of the NGS technology
Precision or reproducibility	The capacity to achieve accurate results across many repeats performed by multiple users	Measure of reproducibility (interuser, instrument, and sequencing run reproducibility)
Limit-of-detection	The lower limit of mutation detection	Limit-of-detection for different variants (single and multinucleotide mutations, insertions, deletions, gene amplifications, and fusions)
Sequencing depth and allelic frequency cutoffs for detection	Minimum sequencing depth necessary for confident detection of mutations	To be individually established for each variant type

[a]As recommended by published studies.[31,35]

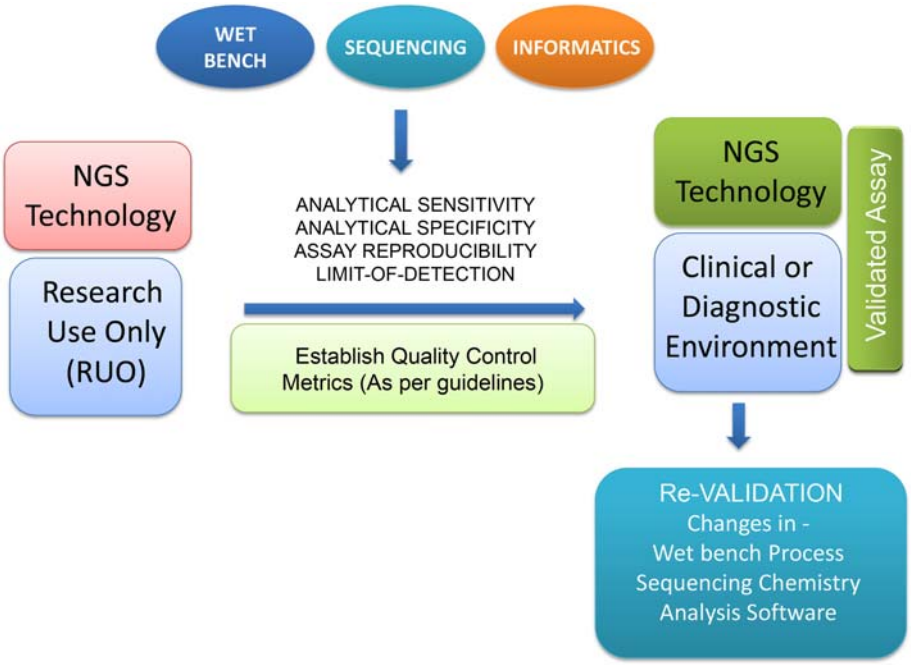

Fig. 2 NGS assay validation for clinical implementation. Assay performance parameters which need to be validated and established prior to implementation of NGS assay in a clinical laboratory as per guidelines are shown.

a clinical setup in order to screen for established markers in an accurate and timely manner. The impact of NGS for clinical genomic testing can be understood by better considering the example of routine screening of tumor samples for markers of prognostic and predictive significance. In a clinical setup, screening of solid tumors and hematological cancers needs screening of multiple markers for a variety of genomic aberrations like SNVs, insertions, deletions, gene copy number variations, and fusions from often very limited tumor material. This was a major challenge for the low and medium throughput classical sequencing technologies like Sanger and pyrosequencing. The advent of NGS technologies provided a feasible solution to meet these demands. Consequently, in a relatively short time, NGS has found active application in clinical diagnostic laboratories. For cancers, the early NGS tests implemented screened relatively limited regions of a limited number of markers of clinical significance.[37–39] During this crucial initial phase, the diagnostic community, which was used to simpler single-gene screening tests realized the challenges of analyzing, interpreting, reporting, and storing complex and sizeable NGS information and evolved to overcome them. The regulatory agencies also realized these challenges and provided timely guidelines for conducting, interpreting, and reporting NGS-based clinical tests which helped the diagnostic community with the technical and ethical challenges of extensive genomic testing.[31–33] Subsequently,

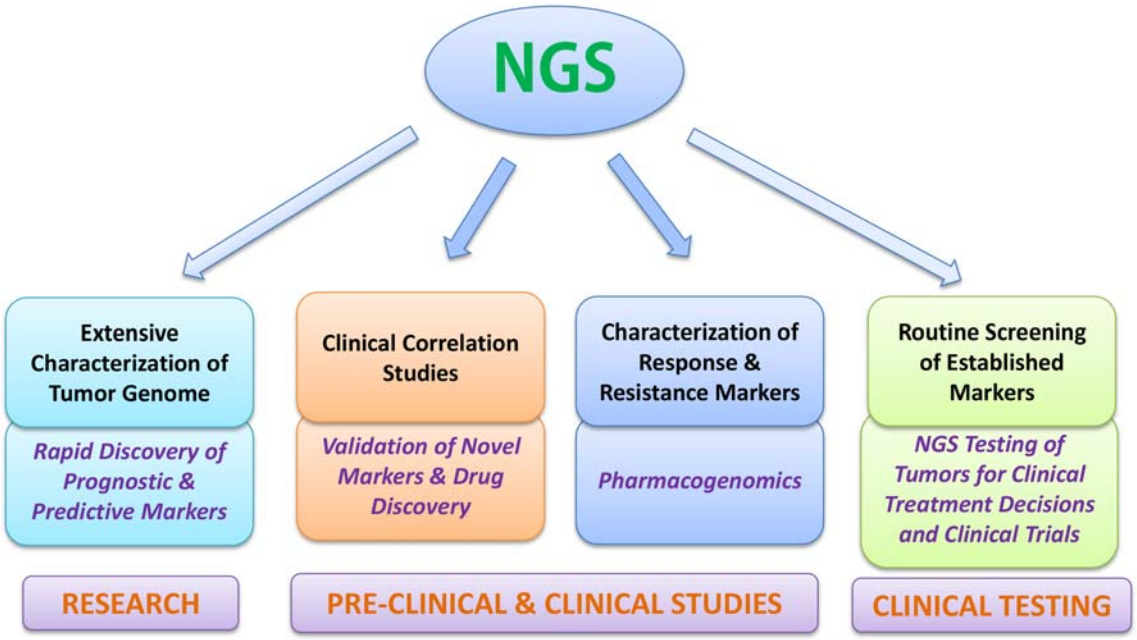

Fig. 3 The clinical utility of NGS. The implementation and utility of the massively parallel NGS technologies in every aspect of clinical workflow starting from discovery, characterization, and establishment of markers to drug discovery and routine screening of clinical samples has been depicted.

building on this initial experience and taking advantage of improving NGS and its technologies associated with the workflow starting from target capture, library preparation and informatics solutions for analysis and interpretation there has been a considerable surge in the implementation of more extensive NGS testing for clinical purposes. Consequently in a recent and relatively short time, there has been a surge in implementing clinical NGS tests ranging from targeted screening of hundreds of markers of clinical significance and extending into sequencing whole exome or genome.[40,42–44] More recently, the NGS technologies have started to make inroads into screening of nucleic acids in liquid biopsies, which is set to revolutionize precision medicine by providing minimally invasive option for early detection and monitoring of disease progression and response to therapies.[45] A schematic representation of the intimate involvement of NGS technology in every stage related to oncology is presented in **Fig. 3**.

In addition to routine screening of tumors, genome screening by NGS technology is also rapidly establishing as important component of clinical trials thus playing critical role as a link between initial discovery of a marker of clinical significance and establishing its targetability, clinical utility, and inducting as a marker to be screened for standard of care and precision medicine.[46,47] In comparison to earlier trials which utilized a single or a limited set of markers, NGS screening of patient samples facilitates screening a higher number of samples and variant types with very high sensitivity, which is very advantageous in order to simultaneously associate multiple treatment arms to a trial thus revolutionizing the approach.[47]

2.14.6 NGS in Drug Discovery and Development

Screening of cellular nucleic acids to understand their role and interactions with the cellular machinery forms a key aspect of understanding signaling and regulatory networks and key to identifying and establishing new targetable markers. NGS, with its capability to screen nucleic acids with high sensitivity is increasingly being used in several aspects associated with characterizing nucleic acids like identification of genomic mutations, gene copy number aberrations and fusions, characterizing modulation of gene expression by alteration of chromatin dynamics and RNA-seq to measure relative levels of gene expressions, and noncoding RNAs.[48] Subsequent to identification of targetable markers, NGS also plays a key role in discovery and development of relevant drugs and vaccines. The key areas include evaluation of genomic causes characterizing the absorption, metabolism, and excretion of the drug (pharmacokinetics), and the tolerance, toxicity, and resistance of drugs in an individual and tailoring the drugs and doses accordingly (pharmacogenomics).[48,49] This information is crucial in establishing population and individual-based drug tolerance, effectiveness, and resistance. In addition to this, NGS analysis is also extensively used for detection and characterization of diseases, host-pathogen interactions, evaluation of microbial population diversity, and evolving of strains and drug-resistance of pathogens with relation to infectious diseases caused by microorganisms.[50,51] Additionally, NGS is also extensively used for design of vaccines and facilitating screening of large number of longitudinal samples, characterization of interaction of the pathogen with the host, and characterization of the host immune response.[52–54]

To summarize, NGS technologies represent a major revolution in genome sequencing technologies which have provided unprecedented capacity for obtaining genome sequencing information for application in every branch of biological sciences. They are also characterized by unprecedented level of complexity of technology, volume of data output, difficulty of interpretation, and their ethical and economic consequences. They are also associated with a very rapid rate of progress and innovation resulting in an ever-changing landscape of sequencing technologies and their applications. With the expected onset and proliferation of the third and fourth generation sequencing technologies, this revolution is bound to gain momentum and has the potential to have major impact on precision medicine by revolutionizing disease characterization, drug design and discovery, and facilitation of personalized therapy.

See also: 2.02. Hit and Lead Generation Strategies. 2.17. Label-Free Screening Technologies.

References

1. Maxam, A. M.; Gilbert, W. *Proc. Natl. Acad. Sci. U. S. A.* **1977,** *74,* 560.
2. Jeffreys, A. J.; Flavell, R. A. *Cell* **1977,** *12,* 1097.
3. Breathnach, R.; Benoist, C.; O'Hare, K.; Gannon, F.; Chambon, P. *Proc. Natl. Acad. Sci. U. S. A.* **1978,** *75,* 4853.
4. Sanger, F.; Nicklen, S.; Coulson, A. R. *Proc. Natl. Acad. Sci. U. S. A.* **1977,** *74,* 5463.
5. International Human Genome Sequencing Consortium *Nature* **2004,** *431,* 931.
6. Metzker, M. L. *Nat. Rev. Genet.* **2010,** *11,* 31.
7. Quail, M. A.; Smith, M.; Coupland, P.; Otto, T. D.; Harris, S. R.; Connor, T. R.; Bertoni, A.; Swerdlow, H. P.; Gu, Y. *BMC Genomics* **2012,** *13,* 341.
8. Buermans, H. P.; den Dunnen, J. T. *Biochim. Biophys. Acta* **2014,** *1842,* 1932.
9. Mardis, E. R. *Annu. Rev. Anal. Chem. (Palo Alto, Calif)* **2013,** *6,* 287.
10. Mardis, E. R. *Annu. Rev. Genomics Hum. Genet.* **2008,** *9,* 387.
11. Harrington, C. T.; Lin, E. I.; Olson, M. T.; Eshleman, J. R. *Arch. Pathol. Lab. Med.* **2013,** *137,* 1296.
12. Rhoads, A.; Au, K. F. *Genomics, Proteomics Bioinf.* **2015,** *13,* 278.
13. Chaisson, M. J.; Huddleston, J.; Dennis, M. Y.; Sudmant, P. H.; Malig, M.; Hormozdiari, F.; Antonacci, F.; Surti, U.; Sandstrom, R.; Boitano, M.; Landolin, J. M.; Stamatoyannopoulos, J. A.; Hunkapiller, M. W.; Korlach, J.; Eichler, E. E. *Nature* **2015,** *517,* 608.
14. Koren, S.; Harhay, G. P.; Smith, T. P.; Bono, J. L.; Harhay, D. M.; McVey, S. D.; Radune, D.; Bergman, N. H.; Phillippy, A. M. *Genome Biol.* **2013,** *14,* R101.
15. Huddleston, J.; Ranade, S.; Malig, M.; Antonacci, F.; Chaisson, M.; Hon, L.; Sudmant, P. H.; Graves, T. A.; Alkan, C.; Dennis, M. Y.; Wilson, R. K.; Turner, S. W.; Korlach, J.; Eichler, E. E. *Genome Res.* **2014,** *24,* 688.
16. Rothberg, J. M.; Hinz, W.; Rearick, T. M.; Schultz, J.; Mileski, W.; Davey, M.; Leamon, J. H.; Johnson, K.; Milgrew, M. J.; Edwards, M.; Hoon, J.; Simons, J. F.; Marran, D.; Myers, J. W.; Davidson, J. F.; Branting, A.; Nobile, J. R.; Puc, B. P.; Light, D.; Clark, T. A.; Huber, M.; Branciforte, J. T.; Stoner, I. B.; Cawley, S. E.; Lyons, M.; Fu, Y.; Homer, N.; Sedova, M.; Miao, X.; Reed, B.; Sabina, J.; Feierstein, E.; Schorn, M.; Alanjary, M.; Dimalanta, E.; Dressman, D.; Kasinskas, R.; Sokolsky, T.; Fidanza, J. A.; Namsaraev, E.; McKernan, K. J.; Williams, A.; Roth, G. T.; Bustillo, J. *Nature* **2011,** *475,* 348.
17. Bertolini, F.; Geraci, C.; Schiavo, G.; Sardina, M. T.; Chiofalo, V.; Fontanesi, L. *Mar. Genomics* **2016,** *28,* 63.
18. Lacoste, C.; Desvignes, J. P.; Salgado, D.; Pecheux, C.; Villard, L.; Bartoli, M.; Beroud, C.; Levy, N.; Badens, C.; Krahn, M. *J. Genet.* **2016,** *95,* 203.
19. Zheng, H.; Wang, Y.; Tang, C.; Jones, L.; Ye, H.; Zhang, G.; Cao, W.; Li, J.; Liu, L.; Liu, Z.; Zhang, C.; Lou, F.; Liu, Z.; Li, Y.; Shi, Z.; Zhang, J.; Zhang, D.; Sun, H.; Dong, H.; Dong, Z.; Guo, B.; Yan, H. E.; Lu, Q.; Huang, X.; Chen, S. Y. *Cancer Genomics Proteomics* **2016,** *13,* 231.
20. Zhao, Y.; Cao, H.; Song, Y.; Feng, Y.; Ding, X.; Pang, M.; Zhang, Y.; Zhang, H.; Ding, J.; Xia, X. *Int. J. Mol. Med.* **2016,** *37,* 1511.
21. Salvianti, F.; Rotunno, G.; Galardi, F.; De Luca, F.; Pestrin, M.; Vannucchi, A. M.; Di Leo, A.; Pazzagli, M.; Pinzani, P. *Biomol. Detect. Quantif.* **2015,** *5,* 23.
22. Olson, N. D.; Lund, S. P.; Zook, J. M.; Rojas-Cornejo, F.; Beck, B.; Foy, C.; Huggett, J.; Whale, A. S.; Sui, Z.; Baoutina, A.; Dobeson, M.; Partis, L.; Morrow, J. B. *Biomol. Detect. Quantif.* **2015,** *3,* 17.
23. Suzuki, S.; Ono, N.; Furusawa, C.; Ying, B. W.; Yomo, T. *PLoS One* **2011,** *6,* e19534.
24. Liu, L.; Li, Y.; Li, S.; Hu, N.; He, Y.; Pong, R.; Lin, D.; Lu, L.; Law, M. *J. Biomed. Biotechnol.* **2012,** *2012,* 251364.
25. Koshimizu, E.; Miyatake, S.; Okamoto, N.; Nakashima, M.; Tsurusaki, Y.; Miyake, N.; Saitsu, H.; Matsumoto, N. *PLoS One* **2013,** *8,* e74167.
26. Branton, D.; Deamer, D. W.; Marziali, A.; Bayley, H.; Benner, S. A.; Butler, T.; Di Ventra, M.; Garaj, S.; Hibbs, A.; Huang, X.; Jovanovich, S. B.; Krstic, P. S.; Lindsay, S.; Ling, X. S.; Mastrangelo, C. H.; Meller, A.; Oliver, J. S.; Pershin, Y. V.; Ramsey, J. M.; Riehn, R.; Soni, G. V.; Tabard-Cossa, V.; Wanunu, M.; Wiggin, M.; Schloss, J. A. *Nat. Biotechnol.* **2008,** *26,* 1146.
27. Wang, Y.; Yang, Q.; Wang, Z. *Front. Genet.* **2014,** *5,* 449.
28. Yao, F.; Duan, J.; Wang, Y.; Zhang, Y.; Guo, Y.; Guo, H.; Kang, X. *Anal. Chem.* **2015,** *87,* 338.
29. Rosenstein, J. *IEEE Pulse* **2014,** *5,* 52.
30. Laver, T.; Harrison, J.; O'Neill, P. A.; Moore, K.; Farbos, A.; Paszkiewicz, K.; Studholme, D. J. *Biomol. Detect. Quantif.* **2015,** *3,* 1.
31. Gargis, A. S.; Kalman, L.; Berry, M. W.; Bick, D. P.; Dimmock, D. P.; Hambuch, T.; Lu, F.; Lyon, E.; Voelkerding, K. V.; Zehnbauer, B. A.; Agarwala, R.; Bennett, S. F.; Chen, B.; Chin, E. L.; Compton, J. G.; Das, S.; Farkas, D. H.; Ferber, M. J.; Funke, B. H.; Furtado, M. R.; Ganova-Raeva, L. M.; Geigenmuller, U.; Gunselman, S. J.; Hegde, M. R.; Johnson, P. L.; Kasarskis, A.; Kulkarni, S.; Lenk, T.; Liu, C. S.; Manion, M.; Manolio, T. A.; Mardis, E. R.; Merker, J. D.; Rajeevan, M. S.; Reese, M. G.; Rehm, H. L.; Simen, B. B.; Yeakley, J. M.; Zook, J. M.; Lubin, I. M. *Nat. Biotechnol.* **2012,** *30,* 1033.
32. Richards, S.; Aziz, N.; Bale, S.; Bick, D.; Das, S.; Gastier-Foster, J.; Grody, W. W.; Hegde, M.; Lyon, E.; Spector, E.; Voelkerding, K.; Rehm, H. L.; Committee, A. L. Q. A. *Genet. Med.* **2015,** *17,* 405.
33. Aziz, N.; Zhao, Q.; Bry, L.; Driscoll, D. K.; Funke, B.; Gibson, J. S.; Grody, W. W.; Hegde, M. R.; Hoeltge, G. A.; Leonard, D. G.; Merker, J. D.; Nagarajan, R.; Palicki, L. A.; Robetorye, R. S.; Schrijver, I.; Weck, K. E.; Voelkerding, K. V. *Arch. Pathol. Lab. Med.* **2015,** *139,* 481.
34. Schrijver, I.; Aziz, N.; Farkas, D. H.; Furtado, M.; Gonzalez, A. F.; Greiner, T. C.; Grody, W. W.; Hambuch, T.; Kalman, L.; Kant, J. A.; Klein, R. D.; Leonard, D. G.; Lubin, I. M.; Mao, R.; Nagan, N.; Pratt, V. M.; Sobel, M. E.; Voelkerding, K. V.; Gibson, J. S. *J. Mol. Diagn.* **2012,** *14,* 525.
35. Jennings, L.; Van Deerlin, V. M.; Gulley, M. L.; College of American Pathologists Molecular Pathology Resource, C. *Arch. Pathol. Lab. Med.* **2009,** *133,* 743.
36. Choudhary, A.; Mambo, E.; Sanford, T.; Boedigheimer, M.; Twomey, B.; Califano, J.; Hadd, A.; Oliner, K. S.; Beaudenon, S.; Latham, G. J.; Adai, A. T. *BMC Med. Genomics* **2014,** *7,* 62.
37. Beadling, C.; Neff, T. L.; Heinrich, M. C.; Rhodes, K.; Thornton, M.; Leamon, J.; Andersen, M.; Corless, C. L. *J. Mol. Diagn.* **2013,** *15,* 171.
38. Luthra, R.; Patel, K. P.; Reddy, N. G.; Haghshenas, V.; Routbort, M. J.; Harmon, M. A.; Barkoh, B. A.; Kanagal-Shamanna, R.; Ravandi, F.; Cortes, J. E.; Kantarjian, H. M.; Medeiros, L. J.; Singh, R. R. *Haematologica* **2014,** *99,* 465.

39. Singh, R. R.; Patel, K. P.; Routbort, M. J.; Reddy, N. G.; Barkoh, B. A.; Handal, B.; Kanagal-Shamanna, R.; Greaves, W. O.; Medeiros, L. J.; Aldape, K. D.; Luthra, R. *J. Mol. Diagn.* **2013,** *15,* 607.
40. Singh, R. R.; Patel, K. P.; Routbort, M. J.; Aldape, K.; Lu, X.; Manekia, J.; Abraham, R.; Reddy, N. G.; Barkoh, B. A.; Veliyathu, J.; Medeiros, L. J.; Luthra, R. *Br. J. Cancer* **2014,** *111,* 2014.
41. Sabatini, L. M.; Mathews, C.; Ptak, D.; Doshi, S.; Tynan, K.; Hegde, M. R.; Burke, T. L.; Bossler, A. D. *J. Mol. Diagn.* **2016,** *18,* 319.
42. Cheng, D. T.; Mitchell, T. N.; Zehir, A.; Shah, R. H.; Benayed, R.; Syed, A.; Chandramohan, R.; Liu, Z. Y.; Won, H. H.; Scott, S. N.; Brannon, A. R.; O'Reilly, C.; Sadowska, J.; Casanova, J.; Yannes, A.; Hechtman, J. F.; Yao, J.; Song, W.; Ross, D. S.; Oultache, A.; Dogan, S.; Borsu, L.; Hameed, M.; Nafa, K.; Arcila, M. E.; Ladanyi, M.; Berger, M. F. *J. Mol. Diagn.* **2015,** *17,* 251.
43. Van Allen, E. M.; Wagle, N.; Stojanov, P.; Perrin, D. L.; Cibulskis, K.; Marlow, S.; Jane-Valbuena, J.; Friedrich, D. C.; Kryukov, G.; Carter, S. L.; McKenna, A.; Sivachenko, A.; Rosenberg, M.; Kiezun, A.; Voet, D.; Lawrence, M.; Lichtenstein, L. T.; Gentry, J. G.; Huang, F. W.; Fostel, J.; Farlow, D.; Barbie, D.; Gandhi, L.; Lander, E. S.; Gray, S. W.; Joffe, S.; Janne, P.; Garber, J.; MacConaill, L.; Lindeman, N.; Rollins, B.; Kantoff, P.; Fisher, S. A.; Gabriel, S.; Getz, G.; Garraway, L. A. *Nat. Med.* **2014,** *20,* 682.
44. Foley, S. B.; Rios, J. J.; Mgbemena, V. E.; Robinson, L. S.; Hampel, H. L.; Toland, A. E.; Durham, L.; Ross, T. S. *EBioMedicine* **2015,** *2,* 74.
45. Ma, M.; Zhu, H.; Zhang, C.; Sun, X.; Gao, X.; Chen, G. *Ann. Transl. Med.* **2015,** *3,* 235.
46. Siu, L. L.; Conley, B. A.; Boerner, S.; LoRusso, P. M. *Clin. Cancer Res.* **2015,** *21,* 4536.
47. Conley, B. A.; Doroshow, J. H. *Semin. Oncol.* **2014,** *41,* 297.
48. Woollard, P. M.; Mehta, N. A.; Vamathevan, J. J.; Van Horn, S.; Bonde, B. K.; Dow, D. J. *Drug Discov. Today* **2011,** *16,* 512.
49. Gervasini, G.; Benitez, J.; Carrillo, J. A. *Eur. J. Clin. Pharmacol.* **2010,** *66,* 755.
50. Lefterova, M. I.; Suarez, C. J.; Banaei, N.; Pinsky, B. A. *J. Mol. Diagn.* **2015,** *17,* 623.
51. Lecuit, M.; Eloit, M. *Front. Cell. Infect. Microbiol.* **2014,** *4,* 25.
52. Luciani, F.; Bull, R. A.; Lloyd, A. R. *Trends Biotechnol.* **2012,** *30,* 443.
53. Proietti, C.; Doolan, D. L. *Front. Microbiol.* **2014,** *5,* 741.
54. Doolan, D. L.; Apte, S. H.; Proietti, C. *Int. J. Parasitol.* **2014,** *44,* 901.

2.15 Cellular Imaging in Drug Discovery: Imaging and Informatics for Complex Cell Biology

Z Li, ME Cvijic, and L Zhang, Bristol-Myers Squibb, Princeton, NJ, United States

© 2017 Elsevier Ltd. All rights reserved.

2.15.1	**Introduction**	362
2.15.2	**HCS and Complex Cell Biology**	363
2.15.2.1	Applications of HCS for Different Cellular Processes	363
2.15.2.2	Complex Cellular Models for HCS	363
2.15.2.2.1	Primary cells from human or rodents	363
2.15.2.2.2	Pathophysiologically-relevant cell lines: immortalized human cells, stem cells or iPSC-derived cells	364
2.15.2.2.3	Organoid and three-dimensional (3-D) cellular models	364
2.15.2.2.4	Methods for cellular models validation and quality controls	364
2.15.2.3	Complexity and Multiplicity of HCS Assay Readouts	365
2.15.2.3.1	Uniqueness of HCS assays and associated detection reagents	365
2.15.2.3.2	Multiplicity of HCS	365
2.15.2.3.3	Complexity of readout vs. stages of drug discovery	366
2.15.3	**Image Technologies and Instruments**	366
2.15.3.1	Wide Field Imagers	366
2.15.3.2	Confocal Imager	366
2.15.3.3	Laser Scanning Cytometers	367
2.15.3.4	HCS Instrument With Niches	367
2.15.4	**Image Acquisition and Analysis**	368
2.15.4.1	Image Acquisition	368
2.15.4.2	Screening Compatible Image Analysis Software	368
2.15.4.3	Image Analysis Algorithm Development	368
2.15.5	**HCS Data Workflow Management, Statistical Analysis and Informatics**	370
2.15.6	**Application of HCS in Various Therapeutic Areas and in Toxicity Studies**	371
2.15.6.1	Epithelial-Mesenchymal Transition (EMT)	371
2.15.6.2	Three-Dimensional Organotypic Culture Mimics Ovarian Cancer Microenvironment	371
2.15.6.3	Invadopodia and Cancer Invasion	372
2.15.6.4	Oligodendrocyte Progenitor Cell (OPC) Differentiation and Remyelination	373
2.15.6.5	Lipid Accumulation in Adipocytes	376
2.15.6.6	Lysosomal Storage Disease	377
2.15.6.7	Progeroid and Abnormal Nuclear Structures	377
2.15.6.8	Leishmanial Proliferation in Macrophage	379
2.15.6.9	Tubulin Polymerization and Redistribution	382
2.15.7	**Conclusions**	384
References		384
Relevant Websites		387

2.15.1 Introduction

High-content screening (HCS) or high-content analysis (HCA) encompasses highly multiplexed, microtiter plate amenable, and automated fluorescent microscopy-based measurement of biological activity at the organelle, cell, or organoid levels in response to treatment with chemical compounds or other substances. In contrast to conventional bioassay technologies, which have one or two readouts of activity per treatment, HCS allows scientists to measure the responses of an individual organelle, cell, or organoid to compound treatments using many features. The ability to simultaneously study many features and combinations of these features makes the HCS technology powerful yet challenging.[1–8] Enabled by more sophisticated image acquisition, analysis, and informatics technologies and driven by needs for complex cell biology studies, over the past two decades HCS has overcome many technical obstacles and gained broader acceptance across the entire drug discovery pipeline, including target validation, lead discovery, lead optimization, toxicity studies, drug delivery, and translational biomarkers.[9–21] This chapter will focus on lead discovery, lead optimization, and toxicity studies.

2.15.2 HCS and Complex Cell Biology

2.15.2.1 Applications of HCS for Different Cellular Processes

The ability of HCS to provide both spatial and temporal resolutions makes it an ideal assay technology for studying complex cell biology. Like standard high-resolution microscopes, HCS can be applied to study many cellular processes for both target-based and phenotype-based screening at higher throughput. Some of the events, such as protein expression, epigenetic modifications, and/or posttranslational modifications (acetylation, phosphorylation, citrullination, etc.), can be analyzed by conventional assay technologies, such as Western Blots or total immuno-fluorescent intensity readouts. However, HCS methods often use fewer cells with higher sensitivity and deliver more comprehensive information on a compound's effects on cells or organoids, not only for the intended targets or processes, but also for the entire cellular/tissue network, thus providing more insightful knowledge about the compound's efficacy and potential adverse effects.

The forte of HCS is its use of microscopy that can be applied to create enlarged views of single cells and associated subcellular structures with high resolution, such that one can analyze and visualize cellular processes otherwise intractable using conventional assay technologies. These cellular processes often play pivotal roles in diseases and understanding these processes is critical for the development of therapies. A particular HCS-based assay could be developed based on one of four basic types: intracellular protein translocations, cellular/organoid morphology alterations, organelle structure changes, and cell subpopulation redistributions; or based on combinations of these four basic types, making HCS versatile yet heavily reliant on sophisticated image analysis and informatics tools to interpret results.

The intracellular protein translocation assay is a hallmark of HCS. Examples are internalization of G-protein coupled receptors to start signal cascades, translocation of glucose transporter from cytoplasm to the cell surface to facilitate glucose uptake, tubulin polymerization and redistribution in response to cytotoxic compounds, and translocation of a transcription factor from the cytoplasm to the nucleus to initiate or modulate gene expression.[22–24] Cellular/organoid morphology alteration is another common assay for HCS. Examples are oligodendrocyte differentiation for myelin sheath production and neuron protection, neurite or axon outgrowth for central nervous system (CNS) regeneration, epithelial-mesenchymal transition (EMT) to initial cancer metastasis, and angiogenesis to support tumor growth. The size changes in tumor spheroids are often used to measure the potency of anticancer drugs.[25–29] The ability of HCS to create enlarged views of subcellular structures provides unmatched methods to study organelle structure changes. Micronucleus tests are often conducted in toxicological screening for potential genotoxic compounds. Mitochondrial structure assays have been used to identify genes that are associated with neurodegenerative diseases. Quantification of lipid droplets has been utilized to study mechanisms of metabolic diseases.[30–33] The ability to measure responses from different subpopulations of cells in a single well of a microtiter plate makes HCS an incomparable tool for studying rare cellular events, cellular heterogeneity, cocultures, and other complex biology. Examples are analysis of cell cycle, investigation of cell differentiation, characterization of immune cells in tumor microenvironments, and depiction of cell migration, and wound healing and fibrosis in fibroblast and epithelial cocultures.[34–42]

2.15.2.2 Complex Cellular Models for HCS

Many factors beyond pathophysiological relevance could contribute to decision-making on selection of cellular models. These factors include, but are not limited to, availability of cells, donor-to-donor variation, stability of cell lines, ease-of-handling for screening, cost, safety, and signal strength and variability. Balancing robustness of screening vs. mimicking of disease environment is important for conducting a successful HCS.

Early HCS campaigns reported in literature were often based on overexpressing target proteins in cancer cell lines, such as HeLa and U2OS. Except for cancer indications, most of these immortalized cancer cell lines lacked connectivity to the pathophysiology of diseases for which therapies were sought. To reduce bench-top-to-bedside translation risks, more pathophysiologically relevant and predictive cellular models have been characterized and applied in both target-based and phenotype-based HCS campaigns in recent years.[43–46]

2.15.2.2.1 Primary cells from human or rodents

Although primary cells from diseased human organs collected during surgical or postmortem procedures are considered as bona fide disease models for drug discovery, conducting high-throughput or medium-throughput HCS using human primary cells, from diseased or normal organs, face tremendous challenges. First, apart from serious ethical challenges, supplies of primary cells, such as primary and metastatic tumors, beta cells or islets, hepatocytes, adipose cells, kidney epithelial cells, and different types of brain cells, are scarce; these cells also have limited-to-zero capacity for proliferation. Second, donor-to-donor variation, including differences in genetics, medical history, and sample preparations, will make screening results very difficult to interpret. Third, diseased cells are surrounded by different cell types in the organ, and responses to external stimuli from these diseased cells in different locations of the organ could be variable due to tissue heterogeneity. Finally, access to human primary cells frequently requires strict Institutional Review Board (IRB) approvals, research collaborations, and complex material transfer agreements with hospitals or other institutions. These logistical challenges can be time-consuming and tedious. Therefore, in the foreseeable future, with the exception of blood cells, human primary cells are likely to be used primarily for lead discovery using a limited-size chemical library, and for lead optimization, toxicity, and translational biomarker studies. For these applications, imposing

limitations on donor demographics and/or prescreening of donor cells are valuable approaches for minimizing donor-to-donor variation.

The use of primary cells from animals—especially rodents—for HCS could be more feasible. Rodent-to-rodent variation could be minimized when rodents with identical genetic backgrounds are used for sample collection, and many on-site animal facilities can make sample preparation procedures more transparent. However, increasing evidence suggest that the biomedical translation between rodent and human is very limited. For example, the correlation between rodent in vivo models and clinical trials for immune-related diseases has been shown to be extremely poor.[47] It is also well-known that the homology between human and rodent proteins could be very limited, with additional significant interspecies differences in signaling pathways. Therefore, prior to using primary cells from rodents or other animal models for HCS-based drug discovery, one must rigorously validate if animal models mimic the biology and pathophysiology of human diseases. Furthermore, in the follow up studies, an assay using human cells must be conducted in parallel to confirm the translation between species.

2.15.2.2.2 Pathophysiologically-relevant cell lines: immortalized human cells, stem cells or iPSC-derived cells

Many well-studied immortalized human cell lines, derived from normal or diseased human tissues that retain characteristics of the original cell types, make excellent cellular models for drug screening. However, these immortalized cells may contain genetic and metabolic abnormalities due to their derivation. Therefore, during reagent validation and assay development, one should ensure that key pathways involved in targeted diseases are still active in the selected cell lines.

Recent developments in research involving adult stem cells and induced pluripotent stem cells (iPSCs) could provide predictive, stable, and scalable cellular models for drug screening. A range of adult stem cell types that can be differentiated into a variety of cellular lineages are available. For example, multipotent mesenchymal stem cells could be used to generate osteoblasts, chondrocytes, hepatocytes, adipocytes, and other cell types.[48] Because iPSCs are derived directly from the somatic tissues of normal persons or patients, this technology overcomes major ethical concerns that have afflicted the use of embryonic stem cells. Furthermore, iPSCs provide an unlimited source of proliferating cells, and when combined with new generation gene editing technologies such as Clustered regularly interspaced short palindromic repeats (CRISPR), iPSC has tremendous potential to become a versatile tool for generating disease relevant and scalable cells for HCS.[49] Many iPSC differentiation protocols for cardiomyocytes have been reported and validated. Protocols for other cell types in different organs have also been described. However, current differentiation protocols are not optimal. Even minor variations in protocols could result in altered degrees of differentiation, with assorted genetic and morphologic changes. Often, purification of partially differentiated cells is necessary in order to obtain meaningful screening outcomes. Significant investment in technology is needed in order to substantially improve differentiation protocols, thus providing disease-relevant cellular models truly amenable for HCS-based lead discovery.[50–54]

2.15.2.2.3 Organoid and three-dimensional (3-D) cellular models

A single cell type, grown in a two-dimensional (2-D) monolayer culture, frequently does not mimic the in vivo microenvironment, morphology, and physiology of diseased tissues. New molecular entities identified through 2-D cell culture models based on transformed cell lines have often failed in animal models or in expensive clinical trials. Recently, the number of publications on 3-D organoids, including microtissues, tissue explants, and tumor spheroids using various cell types has increased significantly, mainly with three types of approaches: (1) using physiologically-relevant primary cells and human tissue-derived cells to build the 3-D models; (2) using multiple types of cell lines that are derived from corresponding tissues and tumors; (3) fabricating an appropriate extracellular matrix (ECM) or micropattern to mimic the microenvironment; or combinations of these three approaches. HCS has played a pivotal role in applying 3-D cellular models for drug screening or toxicity studies, by providing readouts at whole organoid level using low magnification, or at single cell and subcellular resolution using more sophisticated *z*-stacking imaging acquisition method. When *z*-stack is performed, a set of confocal images are taken from the specimen so that the image area along the *x*- and *y*-axes remains the same but the distance from the objective (*z*-axis) is different for each image. As the distance between adjacent images is precisely controlled in the z-stack, it can be used to construct a 3-D image.[55–64]

The development of screening models using coculture of multiple cell types, or construction of 3-D organoids with multiple cell types, is driven by the hypothesis that when different cell types are placed together, they tend to self-assemble in an orderly manner. This order is based on specific interactions between surface proteins expressed on different types of cells, as well as the presence of secreted autocrine and paracrine factors, to support each other for growth and renewal. Thus, the in vitro multiple cell type 3-D organoids could reasonably—though not entirely—mimic the morphology, physiology, and in vivo environment. Such models could be significantly more predictive than those based on 2-D confluent monocultures. The major weakness of the in vitro 3-D cellular models is that the organoids grown using the three approaches described above lack vascular and lymphatic vessels. This inhibits circulation of nutrients, metabolites, and small molecules, and does not mimic host immune responses. Recent development of human organs-on-chips could circumvent this lack of circulation issue.[65]

2.15.2.2.4 Methods for cellular models validation and quality controls

It is imperative that all cellular models be validated prior to conducting drug screening. Genotyping is inexpensive, making it worth considering for any cell line that is acquired through a commercial source or a collaborator. mRNA profiling could be a first-line tool to ensure that key pathways involved in the targeted diseases are present in the cellular models. Biomarker or protein marker verification and/or metabolic profiling of relevant signaling pathways could be second-line tools to verify the activation of these key pathways. Functional responses, such as responses to insulin stimulation by pancreatic islets in a glucose-dependent manner, or

responses to chemokines by immune cells, are the ultimate tests needed to warrant the authenticity of the models. Furthermore, the maximum passage number of cells with acceptable functional responses must be determined prior to the start of screening, to ensure the quality of large-scale or long-term screening. Alternatively, protocols using cryopreserved cells could be considered to ensure run-to-run consistency. Finally, it is important to make sure that the use of cellular models complies with safety regulations, and that the cell lines to be used are mycoplasma free.

2.15.2.3 Complexity and Multiplicity of HCS Assay Readouts

2.15.2.3.1 Uniqueness of HCS assays and associated detection reagents

It is not a trivial task to develop HCS-based assays in the laboratory. A detailed description of the assay development steps can be found in the NIH Assay Guidance Manual.[3] Each complex cellular model would have its own unique proliferation, differentiation, and other stimulation conditions that could have been defined in literature. The uniqueness of HCS assays starts from cell plating. The ability to spread cells evenly in a well of microtiter plates for 2-D assays, or to form uniform 3-D structures in terms of both organoid size and intercellular microenvironment, is often determined by the plate types and cell culture media used. For example, 2-D epithelial cells could prefer collagen I-coated flat-bottom plates and 3-D tumor spheroids could have a preference for poly-hema coated U-bottom plates.[63] A comprehensive plate coating selection guide for different cell types can be found in https://www.corning.com/media/worldwide/cls/documents/CLS-C-DL-006.pdf

Live-cell kinetic imaging is commonly used for microscopy-based assays. However, for lead discovery, lead optimization, and toxicity study purposes, the most common HCS practices use end-point reading methods with fixed cells. Cell fixation and permeabilization usually are realized by using combinations of paraformaldehyde and/or methanol at different concentrations, incubation times, and temperatures, depending on the purpose of the study. For example, to determine protein trafficking to the cell surface, a gentle fixing condition typically would be used to minimize permeabilization of cell membrane, thus increasing the chances of antibodies to recognize cell surface proteins and limiting access of the antibodies to intracellular proteins.

Unlike bright-field imaging in which cell number, morphology, and migration are monitored using transmitted lights, fluorescent imaging relies on tagging different proteins or organelles with various fluorophores at distinguishable colors (wavelengths) to detect changes in cellular processes of interest. Several protein/mRNA/organelle labeling technologies based on different principles are commercially available. Intellectual property positions and costs of reagents could determine the selection of labeling methods. It is imperative to ensure that the labeling methods do not interfere with normal cell cycles, protein function, or with the cellular processes important for the studies.

Typically, protein and organelle labeling methods are based on (1) Immunofluorescence assays in which fluorescent-labeled specific antibodies are used to detect the expression levels, locations, and interactions of proteins of interest, (2) fluorescent proteins (Green fluorescent protein (GFP), Red fluorescent protein (RFP) and their variants), and alternatives such as SNAP-tag, Halo-tag, and fluorogen activating protein, as biosensors for protein expression and trafficking, and as fluorescent donor and acceptor pairs in fluorescence resonance energy transfer (FRET)-based protein–protein interaction assays, (3) organelle specific fluorescent dyes, such as dyes with high affinity for the nucleus, cell membrane, mitochondrion or lysosome, and (4) chemical probes. Examples are fluorescent dye or quantum dot labeled receptor ligands, enzyme substrates, and complementary nucleotides for DNA or RNA. Fluorophores which emit at the yellow wavelength region normally are brighter (have higher fluorescence quantum yields), but often are susceptible to interference from auto-fluorescence of cell or organoid, or from highly cell permeable and nonspecific compounds with strong fluorescent emission in the yellow region. To minimize interference from auto-fluorescence, red-shifted dyes are often used. However, most commercially available red-shifted dyes are not as bright as yellow ones. Therefore, many efforts have been dedicated to discover new generations of red-shifted dyes with higher quantum yield and better stability.[66] Even with very bright dyes, sometimes the expression levels of proteins of interest are too low to detect. To this end, several tactics to increase the payload of florescent dyes, such as the use of secondary and tertiary antibodies, branched DNA, and proximity-ligation assay methods could be used to amplify assay signals to improve the robustness of HCS assays.

A novel cellular and tissue imaging technology that could be applied for lead optimization and toxicity studies has recently emerged. This imaging mass cytometry technology uses rare-earth metals, instead of fluorescent dyes, to label antibodies that recognize proteins of interest, thus increasing multiplicity to greater than 40. Coupled with immunohistochemical and immunocytochemical-like data analysis methods, and enabled by high-resolution laser ablation for spatial recognition, rare-earth metal abundance measurement by time-of-flight mass spectroscopy method allows for the determination of expression of different proteins in tissues at individual cells.[67]

2.15.2.3.2 Multiplicity of HCS

The multiplicity of HCS is demonstrated in two categories. The first one is the ability to extract multiple features based on one simple fluorescent or bright-field readout. For example, a nuclear stain image would enable scientists to obtain information on cell numbers which are connected with apoptosis, necrosis, or cell proliferation, and on nuclear structures that are associated with toxicity, cell differentiation, or other cellular events. One bright-field image could be used for cell number, morphology, colony formation, and/or chemotaxis studies, though the bright-field image technology is not optimal for lead discovery because compounds with poor solubility often interfere with the readout method. The second one is the ability to read at multiple wavelengths, and to generate higher levels of information by combining multiple features extracted from images taken at different wavelengths. To balance multiplicity and throughput and to minimize cross-talk from different fluorophores for a given bioassay, most

HCS instruments acquire up to four images simultaneously at different fluorescent wavelengths, plus one bright-field image. Highly multiplexed assays are often used in lead optimization and in toxicity studies. In reality, the degree of multiplicity is also limited by availability of specific antibodies and their selectivity, the relative abundance of proteins of interest in the cells, kinetics of signaling cascades, and the compatibility among different detection reagents.

For cell-based HCS, because most cellular events are observed at the single cell level, to develop robust assays one must ensure that statistically significant number of cells is captured. Using microscopy objectives with magnifications of 4× to 10× normally allow for the capture of sufficient numbers of cells per well within a high-density microtiter plate (384- or 1536-well formats), but often at the cost of image resolution. For assays that require higher subcellular resolutions, such as assays for intracellular protein translocation and for subcellular structure changes, microscopy objectives with higher magnification (20×, 40× or higher) and higher numerical aperture (N.A.) should be used (see section "Image Technologies and Instruments"). In combination with acquiring images from multiple fields in a well, the requirements for significant cell numbers and for higher resolution could be met, yet screening throughput may be sacrificed. Overall, information content, cost, and throughput must be carefully balanced during HCS assay design and development.

The flexibility of HCS readout is built on the technology's ability to visualize subcellular structures and to distinguish subpopulations of cells. The images acquired thus contain an immense amount of information. However, in most HCS-related publications, only two to three features were used for assay quality control and positive hit identification, and most information about the cells/tissues and the compounds were not utilized. To maximize the benefits of HCS on complex cell biology, more sophisticated and user friendly statistical and informatics tools must be developed and applied to extract all relevant and nonparallel features. These features could be clustered into different measurements and used for assay QC and hit identification, and could be further grouped to define phenotypes of cells or mechanisms of action of compounds.[68,69]

2.15.2.3.3 Complexity of readout vs. stages of drug discovery

Not surprisingly, different stages of drug discovery have different emphasis on HCS assay readouts. Regardless of target-based or phenotype-based high-throughput screening approaches, to accommodate throughput requirements on image acquisition and process with constrained budget, HCS assays for lead discovery[70] purposes normally would be developed to answer limited questions such as if compounds modulate a specific function with selectivity, and if the compounds cause any significant cytotoxic effects. Consequently, most HCS assays for lead discovery use a few features during image acquisition and analysis for hit selection and compound ranking. Also, to accommodate throughput and cost requirements, scalability of cell production and pathophysiological relevancy of the cellular models are equally important for selecting cellular models. To this end, immortalized human cell lines and iPSC-derived physiologically-relevant cells are reasonable cellular models for lead discovery.

To maximize benefits from HCS technology, for lead optimization[71] and toxicity studies, more features are acquired and analyzed from HCS-based assays using more complex cellular systems that are physiologically and/or disease relevant. In addition to the structure–activity-relationship for primary targets or phenotypes, other features often acquired from HCS readouts are signaling pathways, selectivity against other targets, potential adverse effects on "untouchable" pathways, or simply cell health. For translational biomarker studies, human or animal tissues are often the subjects for study of interactions between malfunctioned cells and other cell types in a disease tissue microenvironment. Examples are interactions between cancer cells and immune cells, and epithelial cell-fibroblast interactions in lung fibrosis.

2.15.3 Image Technologies and Instruments

HCS is the application of automated microscopy and image analysis for cell-based or organoid-based assays. The fundamentals of image acquisition and image analysis of HCS are very similar to that of fluorescent microscopy. Several commercial and noncommercial websites offer extremely detailed information about microscopy, and readers are encouraged to visit these sites listed at the end of this chapter.

To meet throughput, resolution, flexibility, and information-rich requirements, an ideal HCS system should have the features summarized in **Table 1**.

The capabilities of commercially available instruments vary with particular emphasis.

2.15.3.1 Wide Field Imagers

HCS platforms with wide field imagers are the workhorses for studying various cellular processes to support lead discovery, lead optimization, and toxicity studies. These instruments are often built around inverted research microscopes from major vendors such as Nikon, Zeiss, Olympus, etc., and include both fluorescent and bright-field imaging capabilities. Commercially available wide field imagers frequently cited in literature are summarized in **Table 2**.

2.15.3.2 Confocal Imager

By adding a spatial pinhole at the confocal plane of the lens to eliminate out-of-focus light, confocal microscopy gains the optical resolution and contrast of a micrograph, which leads to sharper images that ease image analysis processes, and enable better z-

Table 1 An ideal HCS system for drug discovery

Optical requirements	Options to select fluorescence vs. transmitted light, and wide field vs. confocal.
	High-quality objectives for different resolution and sample type needs.
	Powerful and stable light sources to excite different fluorophores commonly used for bioimaging.
	Multiple fluorescent excitation and emission filter combinations to detect multiple fluorescent probes in one experiment without cross-talk.
	Large chip-size cameras with high sensitivity, high frame rates, large dynamic range, broad spectral sensitivity, and high resolution.
	Autofocus for fast image acquisition.
Automation requirement	Workflow-oriented and simple to navigate software for setting up interface between reader, robotic arm, and peripheral instruments (incubator, plate stacks, …)
	Compatibility with image acquisitions from microtiter plates with various densities (6, 24, 96, 384, and 1536-well format), tissue slides, and tissue microarrays
	Built-in liquid handling for investigating fast cellular events.
	Environmental controls for live-cell time course studies.
Image analysis	Intuitive graphical user interface to enable biologist users to rapidly set up image acquisition protocol and image analysis algorithm.
	Balances flexibility with ease-of-use
Data management	HCS data workflow management software to facilitate large-scale image storage, query, retrieval, analysis, and visualization.

Table 2 Commercially available HCS instrument

Manufacturer	*Wide field imagers*	*Confocal imager*
ThermoFisher/Cellomics	ArrayScan™ VTI Cellinsight™ CX5	Cellinsight™ CX7
Perkin Elmer	Operetta™	Opera™ Opera Phenix™
GE	InCell™ Analyzer 1000, 2000 and 2200	InCell™ Analyzer 6000
Molecular Devices	ImageXpress™ Micro	ImageXpress™ Ultra
BD	Pathway™ 435	Pathway™ 855
IDEA Bio-Medical	WiSCAN™	
MAIA	MIAS™	
Yokogawa		Cell Voyager™ CV7000

stacking for 3-D imaging.[64] But this comes at a cost of reduced light signal and limitation of sampling only from a single point in the specimen at any given moment. To overcome this problem, most HCS instruments with confocality use Nipkow spinning disk or laser scanning confocal microscope methodologies to increase illumination and the number of points in the specimen that can be imaged simultaneously. Because of these additional functions, confocal imaging is often more expensive, and takes longer to complete a screening compared to wide field imaging. Confocal HCS instruments are best used for determining small and complicated changes at subcellular levels, complex 3-D structures, or samples with high background fluorescence. Commercially available confocal imagers reported in literature are listed in Table 2.

2.15.3.3 Laser Scanning Cytometers

These cytometers use multiple laser beams at different colors to scan across the entire bottom of assay plates and detect fluorescent emissions using photomultiplier tubes. These imagers generate images equivalent to, at maximum, a low NA 20× objective of microscopy, often best used to detect protein expression levels, cell numbers, and cell morphology changes. However, the laser scanning cytometers can acquire images at very high speeds with large depth of fields (in the range of about 200 μm in *z*-axis), which enables whole-well image acquisitions at high speed, independent of plate well density, thus empowering imaging of simple spheroid and organoid size changes, or counting cell number changes in multiple cell layers, without the requirement of assembling images from different z-stacks.

Acumen™ e^{X3} by TTP Labtech, Velos™ laser Scanning cytometer by Molecular Devices, and Compucyte™ iCyte by Beckman Coulter, are examples of instrument in this category.

2.15.3.4 HCS Instrument With Niches

There are niche HCS instruments on the market. Although only possessing a few features as shown in the "ideal HCS" instrument list (Table 1), these instruments were built for specific purposes, and they perform their intended functions very well. For example, the

IncuCyte™ ZOOM system by Essen Bioscience consists of a microscope framework that can reside in a cell incubator, allowing live cell analysis in both bright-field and fluorescence modes. The Celigo™ S system by Nexcelom is often used for both bright-field and fluorescence-based analysis of tumor spheroids and stem cell colonies. The Amnis™ ImageStream X by Amnis provides combined Fluorescence-activated cell sorting (FACS) and HCS functions for single cell analysis by acquiring both stain intensity and images of cells passing through a flow cuvette. The ToxInsight™ IVT platform by Cellomics/Thermo Fisher is designed to specialize in identifying potential toxic liabilities in newly identified compound. Lastly, the Kinetic Image Cytometry™ by Vala Sciences has a built-in electric stimulation mechanism, allowing one to perform patch-clamp-like studies of ion channels, and can often be applied for cardiotoxicity studies.

2.15.4 Image Acquisition and Analysis

2.15.4.1 Image Acquisition

Capturing high-quality images of representative cellular processes of interest is essential for subsequent image analysis. For HCS-based lead discovery, lead optimization, and toxicity studies, it is important to balance screening speed with information content based on individual program needs. Assay plates containing baseline vs. induced or positive vs. negative control samples should be ready before setting image acquisition protocols. Image acquisition optimization often includes selection pixel resolution and magnification, weighting number of objects captured for analysis vs. details of cellular structures, balancing signal intensity vs. background and noise, choosing location of images and number of image fields per assay well, and determining frequency of autofocusing, time of exposure, and number of z-stacks needed for 3-D image, etc.[3]

2.15.4.2 Screening Compatible Image Analysis Software

Embedded computer software for automated image acquisition, analysis, and management is an instrumental component of HCS and is often the key factor that differentiates different HCS platforms. Most of the HCS platforms described in section "Image Technologies and Instruments" of this chapter come with image analysis software that runs in real time or immediately after the image acquisition. Greater than 80% of image analysis needs for complex cell biology processes described in this chapter could be accomplished by this platform-associated image analysis software, and vendors also provide thorough training for new users.

Platform-independent image analysis software is available in both free open source and commercially available formats. ImageJ and CellProfiler[71] are two popular open source softwares. The image analysis speed of these open source softwares is relatively slow, and often could be sped up using a computational system with multiple CPUs (central processing units). Commercially available and highly flexible software such as Definiens, Media Cybernetics, and MATLAB may be needed for very complicated cellular process analysis. Image analysis using these platform-independent software packages often requires very skilled programmers with essential biology knowledge.

2.15.4.3 Image Analysis Algorithm Development

The image analysis algorithm development is an iterative process (**Scheme 1**), and the quality of the algorithm is heavily dependent on the quality of the cellular assays, the sharpness of images acquired, and the depth of knowledge on disease biology and associated phenotypes. The NIH Assay Guidance Manual e-book on HCS[3] devotes one section to this topic and readers are encouraged to read the e-book.

After flat-field correction to remove artifacts from images that are caused by variations in the pixel-to-pixel sensitivity of the detector and/or by distortions in the optical path, image analysis normally starts with segmentation of images for object identification[68,69,72–80] (often cells, but could be organelles or tissues) based on a combination of fluorescent intensity thresholding and image area selection algorithm, followed by accurate extraction of features within, about, and among the identified objects. Hundreds of features can be extracted for each segmented object (e.g., intensity, size, shape, and texture), and many of the features are highly correlated. To reduce the dimensionality of the features, both supervised and unsupervised machine learning classification algorithms[81,82] can be applied to cluster features, and to group the clusters into different phenotypes. **Scheme 2** demonstrates one example of using a trained logistic regression model to discriminate cell populations based on the distribution of a GFP-tagged protein colocalized with nuclear (nuc) and/or mitochondrial (mit) in cells.[82] For complex cellular assays, the combinations of multiple features or clusters are often critical for establishing assay QC standards and for hit identification criteria.

Although high dimension features, clusters, or phenotypes could be generated from HCS campaigns, to balance information content and computation time needed, typically only features that are important for ranking compound potency, identifying false positives, and differentiating mechanisms of action would be extracted. Bioassay designer, algorithm developer, and disease biology expert must work together to determine key features to be captured and clustered during bioassay and algorithm development.

Before finalizing the newly developed image analysis algorithm, it is imperative to test the algorithm in a small trial, against relevant siRNA or small molecular collections, to verify the algorithm is capable of apprehending and discriminating important and relevant phenotypes, filtering out false positives and identifying compounds with undesirable adverse effects. Often, fine-tuning of algorithm is necessary prior to applying the algorithm for screening. After completing the entire HCS-based screening, adjustment of image analysis algorithm and reanalysis of images offline are often necessary under certain circumstances. For

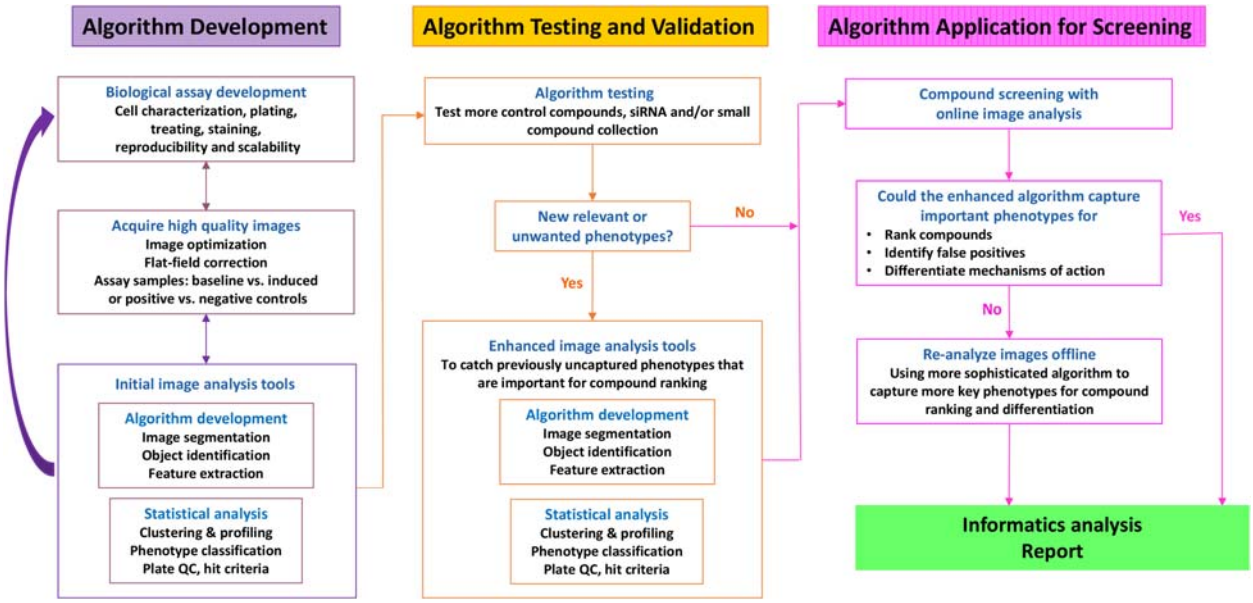

Scheme 1 A typical image acquisition and analysis workflow during assay development and screening.

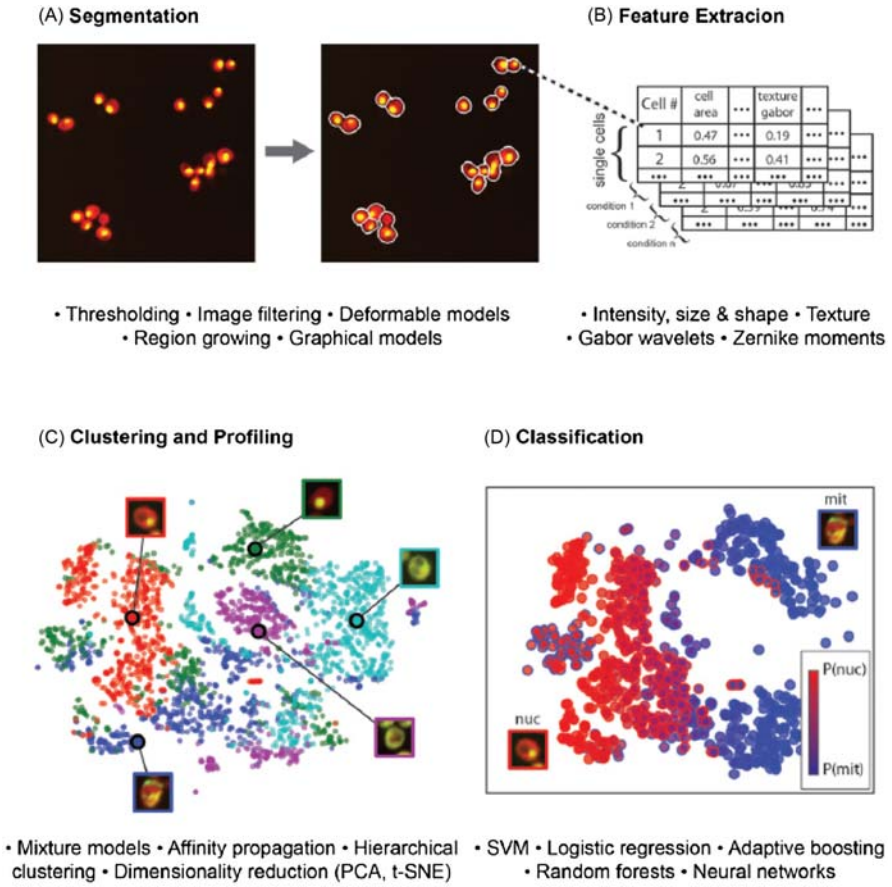

Scheme 2 Typical steps involved in analyzing microscopy images. From Kraus, O. Z.; Frey, B. J. Computer Vision for High Content Screening. *Crit. Rev. Biochem. Mol. Biol.* **2016**, *51*, 102–109, http://dx.doi.org/10.3109/10409238.2015.1135868, figure 1.

example, (1) a simplified algorithm was used during screening to reduce instrument time, but unwanted plate patterns were observed during screening QC inspection. Therefore, application of a normalization factor for result analysis is needed; (2) new phenotypes associated with important biological processes were observed upon manual inspection of hits, modification of algorithm could be necessary in order to capture or to differentiate these phenotypes. A highly effective and flexible HCS data management system would be needed in order to conduct large-scale image reanalysis (see section "HCS Data Workflow Management, Statistical Analysis and Informatics").

2.15.5 HCS Data Workflow Management, Statistical Analysis and Informatics

Although HCS provides richly-descriptive information, how to extract the most critical information for the disease-relevant cellular processes in a timely manner is still a challenge to the drug discovery institutions. A streamlined HCS image acquisition, storage, query, analysis, and retrieval workflow, coupled with sophisticated statistical and informatics tools is crucial to extract meaningful information from several to hundreds of gigabytes (GB) of data generated per HCS campaign. For small laboratories with a single HCS platform, the associated vendor's data management solution is a reasonable approach. For large institutions with multiple HCS platforms, it is worthwhile to build a centralized and unified HCS data management system to enable cross-platform and cross-program data mining, comparison, and information extraction.

HCS data management starts with image capture. The captured images, along with metadata, must be stored and registered in an overarching bioimaging repository with appropriate architectures, suitable for long-term storage and iterative retrieval and reanalysis. Image analysis numerical descriptors at the individual cell level, such as cell morphology, and protein abundance and location, must be linked to images and associated metadata. The metadata includes, but is not limited, to program information, compound structures, reagent information, image acquisition settings, plate barcodes, and well locations. Metadata is critical for meaningful statistical and informatics analysis. The repository must be accessible for platform-dependent and- independent image analysis software for interactive image/data exploration, as well as advanced statistical analysis and informatics tools for automated scoring of complex phenotypes. The automated scoring should be able to combine multiple extracted features per cell/well, and be performed in plate-batch manner for timely image analysis. Furthermore, the repository must be coupled to institutional central data repository to enable establishment of relationships with other information, such as gene expression, biomarkers, structures, in vivo results, safety, and clinical outcomes (**Scheme 3**). Finally, it is important to develop data retention policies for effective data management.

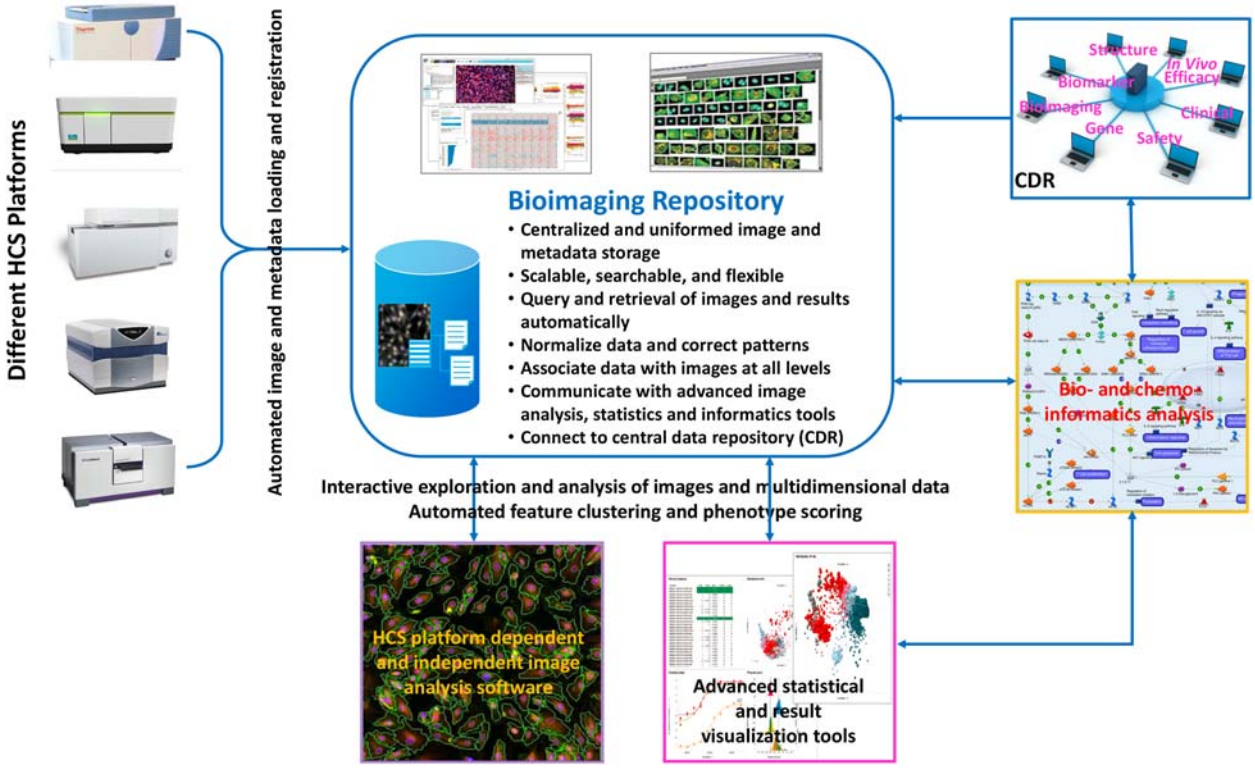

Scheme 3 A streamlined HCS data management workflow.

A picture is worth a thousand words. Often, numeric results calculated based on an initial image analysis algorithm do not capture all key aspects of the images. A bioimaging repository's capability to retrieve images associated with a set of compounds, and to present the images to downstream visualization tools such as SpotFire™, is a must for refining image analysis algorithms. Furthermore, the ability to generate on-the-fly summaries of millions of data points and to communicate these data points to downstream advanced statistical analysis (e.g., machine learning capability) and informatics tools is also required. Although software platforms, such as Phaedra by Johnson & Johnson, CellProfiler Analyst by Broad Institute, and OMERO by University of Dundee; and commercial software such as GeneData Screener for HCS by GeneData and Columbus by Perkin Elmer, have been reported to have both abilities mentioned here, most software for bioimaging repository applications still need major enhancements to meet speed, flexibility, and complexity requirements for HCS applications in lead discovery, lead optimization, and toxicity studies.[83–87]

Finally, to leverage rich information obtained via HCS campaigns and extract broadly impactful underlining disease knowledge across related therapeutic areas, more sophisticated bioinformatics tools are required for pathway mapping and mechanisms of action studies, and for establishment of holistic relationships with other information, such as proteomics, next gen sequence, in vivo results, and safety and clinical outcomes.

2.15.6 Application of HCS in Various Therapeutic Areas and in Toxicity Studies

HCS has been applied to almost all therapeutic areas and functional departments in both academic and industrial settings for drug discovery and development. This chapter will focus on recent applications related to complex cell biology in oncology, CNS, metabolic diseases, rare diseases, infectious diseases, and toxicity studies.

2.15.6.1 Epithelial-Mesenchymal Transition (EMT)

Despite advancements in therapies developed for the treatment of cancer, patient prognosis and mortality rates have improved insignificantly for patients with metastatic cancer. An underlying mechanism promoting metastasis in many types of cancer is EMT. EMT is now considered a valid target for drug development in cancer, as well as in fibrosis. EMT starts when epithelial cells are stressed by injury or inflammation and the cells lose their epithelial characteristics such as tight junction protein expression (e.g., ZO-1) and apical-basolateral polarity (Cobblestone shape for both cell and nucleus morphologies), and acquire a mesenchymal phenotype characterized by cadherin gene-expression shift and a clear front-rear polarity (elongated shape for both cell and nucleus morphologies) (Fig. 1A). The mesenchymal cells are then ready for migration and invasion.[88,89]

It is reasonable to assume that small molecules or other substances capable of inhibiting the loss of epithelial markers and/or the gain of mesenchymal markers could be used to antagonize EMT, and subsequently prevent cancer metastasis. HCS-based compound screening for EMT blockers has been reported. The HCS-based screening exemplified here was conducted in 2-D monolayer cell culture format using pooled human primary renal proximal tubule epithelial cells (RPTECs) seeded in collagen I-coated 96-well plates. The RPTEC of eight donors were evaluated separately for their suitability in a TGF-β1 induced EMT assay, quantified by a combination of three features derived from HCS results: cell morphology, nuclear morphology, and epithelial marker ZO-1. Cells from six donors were selected for High throughput screening (HTS). Each donor's cells could be proliferated up to four passages without sacrificing assay robustness. Compounds were incubated with the RPTEC in the presence of TGF-β1 for 72 h in serum free medium, followed by cell fixation and staining for nucleus, cytoplasm, and epithelial marker ZO-1. Positive hits were identified based on their ability to inhibit the TGF-β1 induced EMT by reversal of morphology from elongated to cobblestone for both cytoplasm and nucleus shapes, plus restoration of ZO-1 marker (Fig. 1B).[90] Compounds optimized based on hits identified via the screening have demonstrated efficacy in in vivo cancer models.

2.15.6.2 Three-Dimensional Organotypic Culture Mimics Ovarian Cancer Microenvironment

Ovarian cancer is highly aggressive. Metastatic ovarian cancer patients have less than 10% survival rate. Based on clinical observations, it is believed that ovarian cancer cells initially travel through the peritoneal fluid to the surface of other abdominal organs to start metastasis. Human omentum consists of well-organized mesothelial cells at the top, fibroblast cells as the basis, supported by ECM. When ovarian cancer cells reach the omentum surface, they will adhibit, invade and grow, thus initiating metastasis (Fig. 2A).

It was believed that creating a tumor microenvironment that accurately reflects the complex biology of ovarian cancer should help the medical community to understand the underlying mechanisms of metastasis, as well as to identify new therapeutics. To assemble a 3-D model, clinicians collected noncancerous omental tissue from consented patients undergoing abdominal surgery. In the laboratory, mesothelial cells and fibroblasts, two of the predominant cell types found in omental tissue, were isolated and cultured. In the presence of ECM proteins, these cells were then mixed and allowed to self-assemble for over 48 h into a multilayered cell culture model mimicking ovarian cancer microenvironment (Fig. 2B and C). The model was used in HTS to identify compounds that could inhibit ovarian cancer cell line SKOV3ip1–GFP adhesion, invasion, and growth in the 3-D organotypic culture, therefore having the potential to prevent human ovarian cancer metastasis. Specifically, compounds dissolved in Dimethyl sulfoxide (DMSO) were added to the organotypic culture immediately after SKOV3ip1–GFP cancer cells were added.

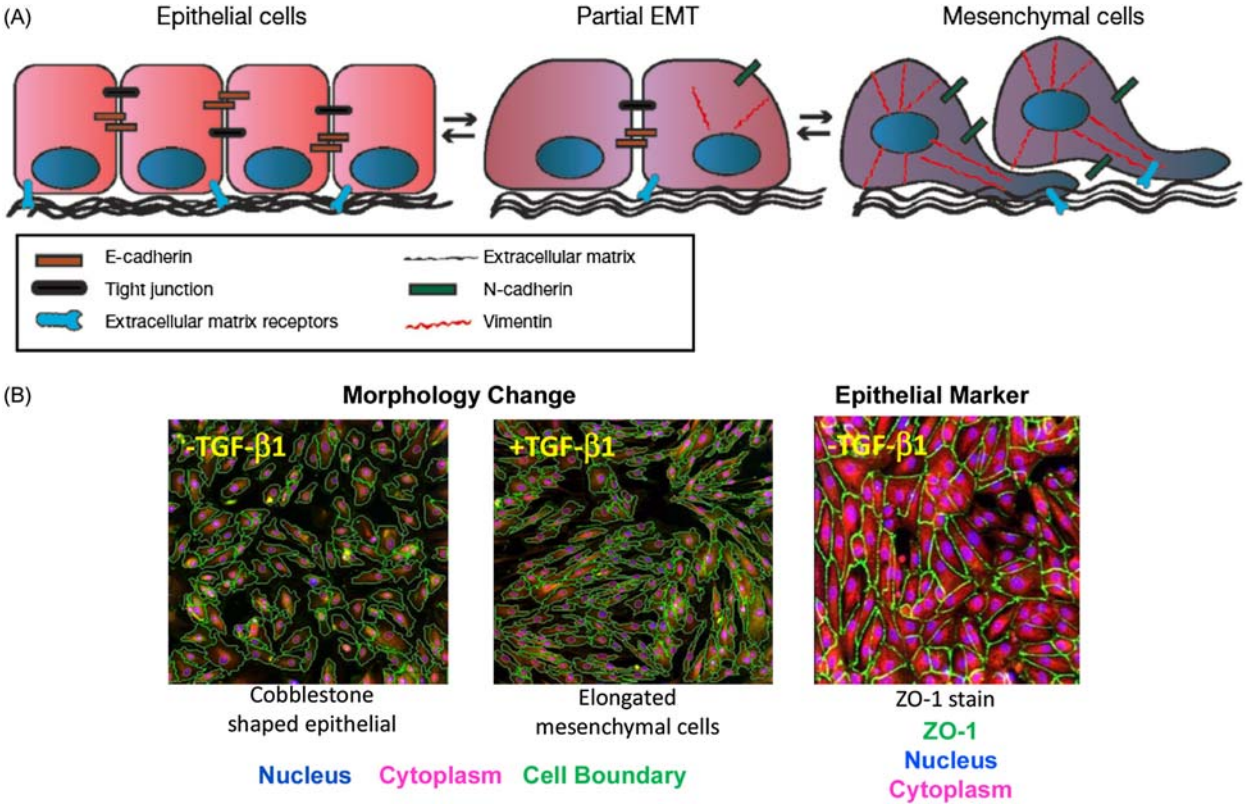

Fig. 1 Epithelial to mesenchymal transition (EMT). (A) EMT involves a cellular phenotypic shift. Epithelial cells are characterized by Cobblestone-like morphology, intact cell–cell contacts, expression of tight junction protein (e.g., ZO-1), barrier function, and lack of movement. During the EMT process, cells with partial EMT appear characterized by the incipient presence of a front-rear polarity and have leaky cell–cell contacts. At the same time upregulation of the mesenchymal markers vimentin, N-cadherin, ZEB1 and 2, SNAIL, SLUG, and matrix metalloproteinases begin. In addition, these partial EMT cells express lower amounts of E-cadherin and ZO-1 than epithelial cells. After finalization of EMT, the established mesenchymal cells have a clear front-rear polarity with no or few cell contacts. The expression of mesenchymal proteins is increased, and a cadherin gene-expression shift, most often from E-cadherin into N-cadherin expression. (B) High throughput high-content screening for specific small-molecule inhibitors of TGF-β1 induced EMT by following the reversal of morphology from elongated to cobblestone for both cytoplasm and nucleus shape, plus restoration of epithelial marker ZO-1 expression, using primary human epithelial cells. Fig 1A From Jakobsen, K. R.; Demuth, C.; Sorensen, B. S.; Nielsen, A. L. The Role of Epithelial to Mesenchymal Transition in Resistance to Epidermal Growth Factor Receptor Tyrosine Kinase Inhibitors in Non-Small Cell Lung Cancer. *Transl. Lung Cancer Res.* **2016**, *5*, 172–182, figure 1

After 18 h of incubation, cancer cells remaining in the cell culture medium were aspirated, and the organotypic culture was washed. Then Acumen, the HCS instrument with a large depth of field enabling image acquisition of multiple cell layers was used to count the SKOV3ip1–GFP cells that adhibited and/or invaded in the 3-D organotypic culture. Hits identified from the HTS screen were triaged, and selected compounds were tested in in vivo adhesion and invasion, prevention, and intra-ovarian intervention studies. Beta-escin and tomatine were selected as the lead compounds due to demonstrated efficacy in the three in vivo models described.[91]

2.15.6.3 Invadopodia and Cancer Invasion

The transition of cancer from benign to metastatic form requires the acquisition of various cellular properties, including migratory ability and invasiveness. Invasive characteristics facilitate tumor escape through the basement membrane barrier, as well as local invasion and remodeling of the tumor microenvironment in the primary and metastatic sites. Various studies have correlated the ability of cancer cells to form invadopodia with invasiveness. Invadopodia is an actin-rich cell membrane microstructure that can protrude into the ECM to start invasion (**Fig. 3A**).[92]

The mechanism of invadopodia formation is not well characterized. Therefore, a HCS-based assay was established and used to screen against the Library of Pharmacologically Active Compounds (LOPAC) for invadopodia modulators. For primary screening, NIH 3T3 cells transformed with activated Src (Src-3T3) were used. This cell line uniformly expresses many invadopodia per cell, which eases image acquisition and analysis. Src-3T3 cells were plated and grown in 384-well optical plates for 3 days, incubated with compounds for 16 h, then fixed and stained with 4′,6-Diamidino-2-Phenylindole, Dihydrochloride (DAPI) to visualize nuclei

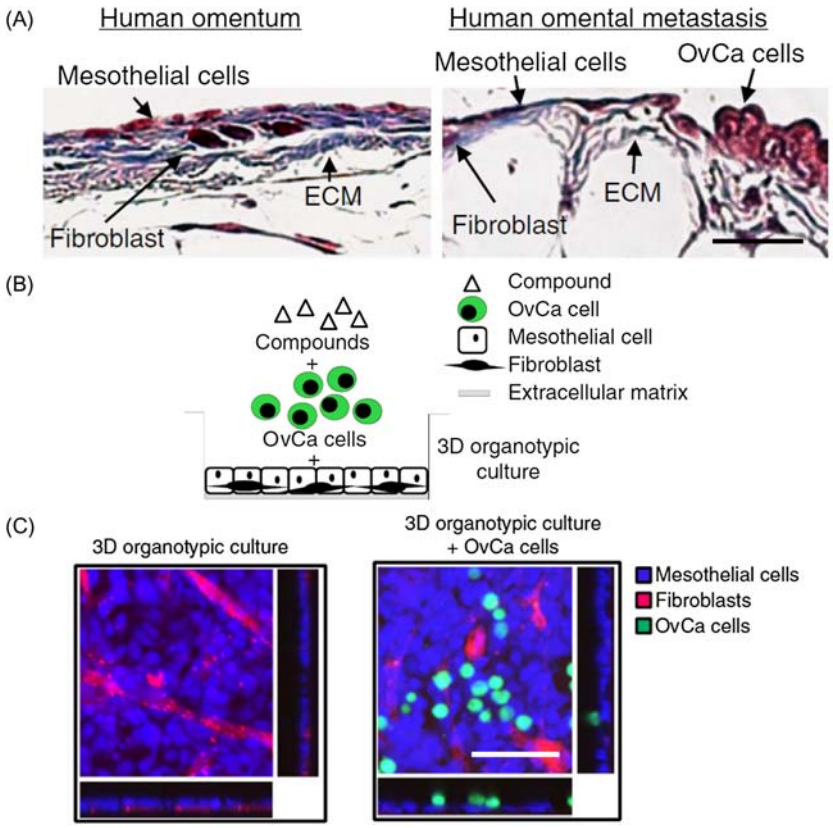

Fig. 2 3-D organotypic culture mimics ovarian cancer microenvironment. (A) Tissue images of human omentum, normal vs. with metastatic ovarian cancer cells. (B) Scheme on how 3-D organotypic culture was constructed. (C) Florescent image of the 3-D organotypic culture. Fibroblast, *red*; mesothelial cells, *blue*; ovarian cancer cells (SKOV3ip1–GFP), *green*. The *square images* were the views from the top of a well in 1536-well plates. The images on the sides were Z-plane reconstruction of optical sections with orthogonal view of maximum intensity. Scale bar indicates 100 μm. Modified from Kenny, H. A.; Lal-Nag, M.; White, E. A.; Shen, M.; Chiang, C.-Y.; Mitra, A. K.; Zhang, Y.; Curtis, M.; Schryver, E. M.; Bettis, S.; Jadhav, A.; Boxer, M. B.; Li, Z.; Ferrer, M.; Lengyel, E. Quantitative High Throughput Screening Using a Primary Human Three-Dimensional Organotypic Culture Predicts in vivo Efficacy. *Nat. Commun.* **2015**, *6*, 6220, figure 1.

and phalloidin for F-actin (Fig. 3B). The primary screening identified five invadopodia inhibitors and two activators. The ability of these seven compounds to decrease or increase gelatin degradation by Src-3T3 were confirmed using FITC-gelatin-coated glass coverslips observed under microscopy. In follow up studies, hits Purvalanol A and GCP74514A were shown to significantly reduce both the fraction of cells positive for invadopodia and the number of invadopodia per cell in human squamous cell carcinoma of the head and neck cells (SCC61). Hits Paclitaxel and Cantharidin, on the other hand, increased the number of invadopodia per cell. Furthermore, degradation of FITC-gelatin by invasive cancer cell lines SCC61, C8161.9 (melanoma), OVCAR8 (ovarian cancer), and NCIH460 (nonsmall cell lung cancer) can be prevented by Purvalanol A or GCP74514A, but enhanced by Cantharidin or Paclitaxel (Fig. 3C). Finally, in a subsequent mechanism study, Cdk5 was identified as the targeted protein for Purvalanol A and GCP74514A, and was confirmed to play a key role in invadopodia formation, therefore becoming a potential target for cancer therapy.[93]

2.15.6.4 Oligodendrocyte Progenitor Cell (OPC) Differentiation and Remyelination

Oligodendrocytes provide insulation for neurons by producing a myelin sheath around axons. It is believed that in multiple sclerosis (MS) patients, the myelin sheath is damaged by inflammation, which could cascade to axonal damage, disruption of neuronal signaling, and eventually oligodendrocyte and neuronal cell death (Fig. 4A). Standard MS therapies are aimed at preventing further immune-mediated damage of myelin. While these drugs have some disease modifying activity for patients, they fail to slow disease progression or prevent disability. Alternatively, experts in the field are considering drugs that would promote the enhanced differentiation and myelination capacity of resident OPCs, and consequently restoration of axonal conduction, based on the following observations: (1) OPCs constitute up to 5% of adult human brain cells and are the predominant source of myelinating oligodendrocytes in the CNS, (2) these resident OPCs have the capacity to differentiate into oligodendrocytes and remyelinate axons in response to damage caused by disease, aging, or injury. However, in many conditions, including MS, the

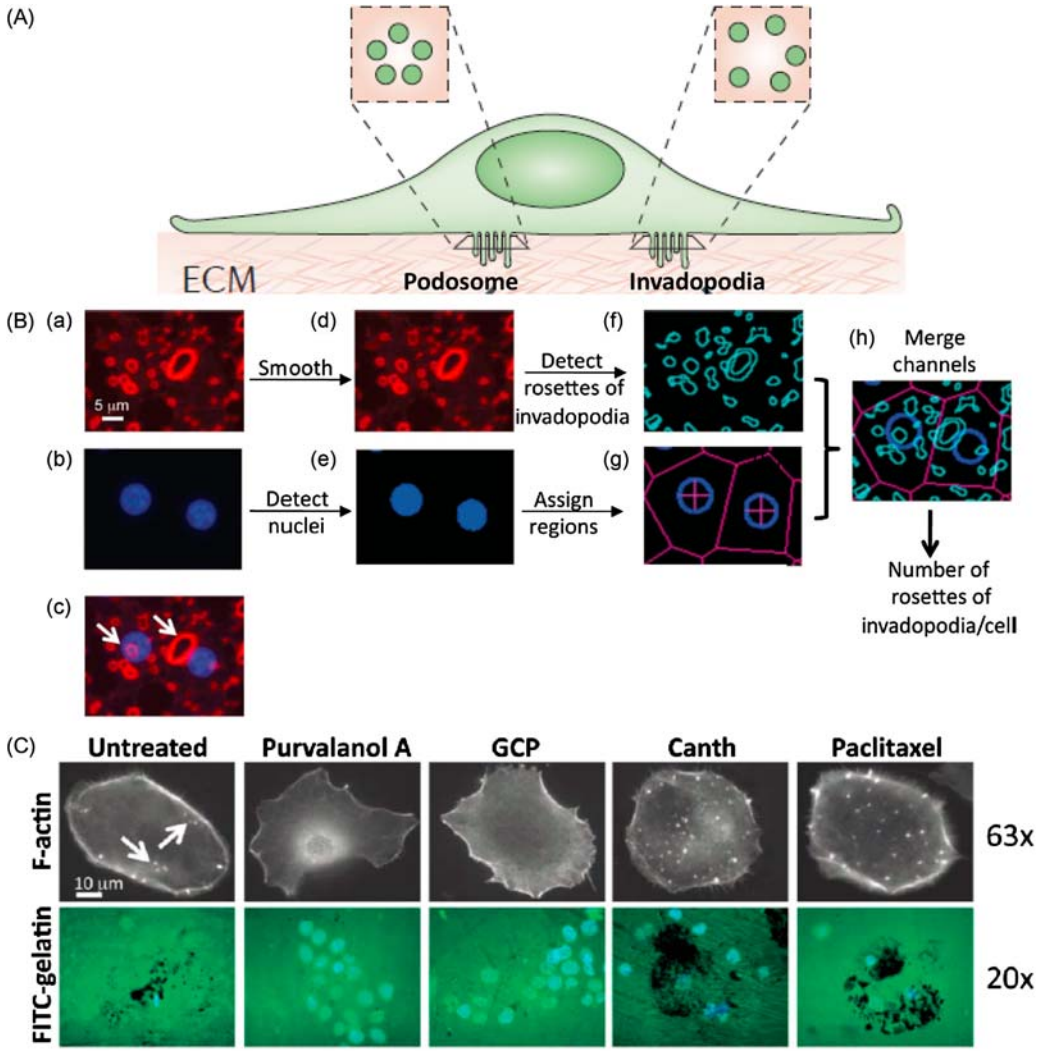

Fig. 3 Invadopodia and cancer invasion. (A) Depending on the cell type and stimuli provided, invadopodia and podosomes can form as individual puncta or as rosettes on cell surface membranes, both are actin-rich microstructures that protrude into the extracellular matrix (ECM), and could be used by cancer cells for invasion. (B) HCS Image analysis for invadopodia formation in Src-3T3 cells in 384-well plate. Cells stained with phalloidin for F-actin (*red*) (a) and with DAPI for nuclei (*blue*) (b). The overlay of both channels is displayed in (c). The image background for the red channel was subtracted and a 3-by-3 median filter was applied to smooth the image and remove fine actin fibers (c). Nuclei detection was applied (e) and nuclear parameters were extracted from the segmented DAPI image. From the nuclei masks (e), cellular regions were assigned to each nucleus (g). The red channel was segmented using fluorescence aggregate detection to find rosettes (f). Finally, the detected nuclei, assigned cellular regions, and detected rosettes were merged (h) and the number of detected rosettes was calculated on a cell-by-cell basis. (C) Effects of active compounds on invadopodia formation and cancer cell invasiveness. SCC61 cells were grown on FITC-gelatin coated coverslips; treated with DMSO control, 2 μM Purvalanol A, GCP74514A (GCP), Cantharidin (Canth), or Paclitaxel. It was then assayed for invadopodia formation (F-actin) and gelatin degradation (FITC-gelatin). Representative invadopodia are highlighted with *white arrows* in the upper left panel. (A) From Murphy, D. A.; Courtneidge, S. A. The "Ins" and "Outs" of Podosomes and Invadopodia: Characteristics, Formation and Function. *Nat. Rev. Mol. Cell Biol.* **2011**, *12*, 413–426, figure 2. (B) Modified from Quintavalle, M.; Elia, L.; Price, J. H.; Heynen-Genel, S.; Courtneidge, S. A. A Cell-Based High-Content Screening Assay Reveals Activators and Inhibitors of Cancer Cell Invasion. *Sci. Signal.* **2011**, *4*, ra49, figure 1. (C) From Quintavalle, M.; Elia, L.; Price, J. H.; Heynen-Genel, S.; Courtneidge, S. A. A Cell-Based High-Content Screening Assay Reveals Activators and Inhibitors of Cancer Cell Invasion. *Sci. Signal.* **2011**, *4*, ra49, figure 2.

resident OPCs ultimately fail to repair the myelin damage, leading to permanent functional deficits. Therefore, screening for compounds that can differentiate OPCs into oligodendrocytes is a reasonable approach to identify potential lead compounds for MS therapy.

A new method was developed to generate screening-scale OPCs from mouse stem cells. The mouse OPCs were thoroughly validated using gene array for genomic integrity, immuno-staining for key biomarkers, RNA-seq for gene expression and purity, and in vivo transplantation for myelinogenic functions. A HCS assay based on nuclear and antimyelin basic protein (MBP) stains

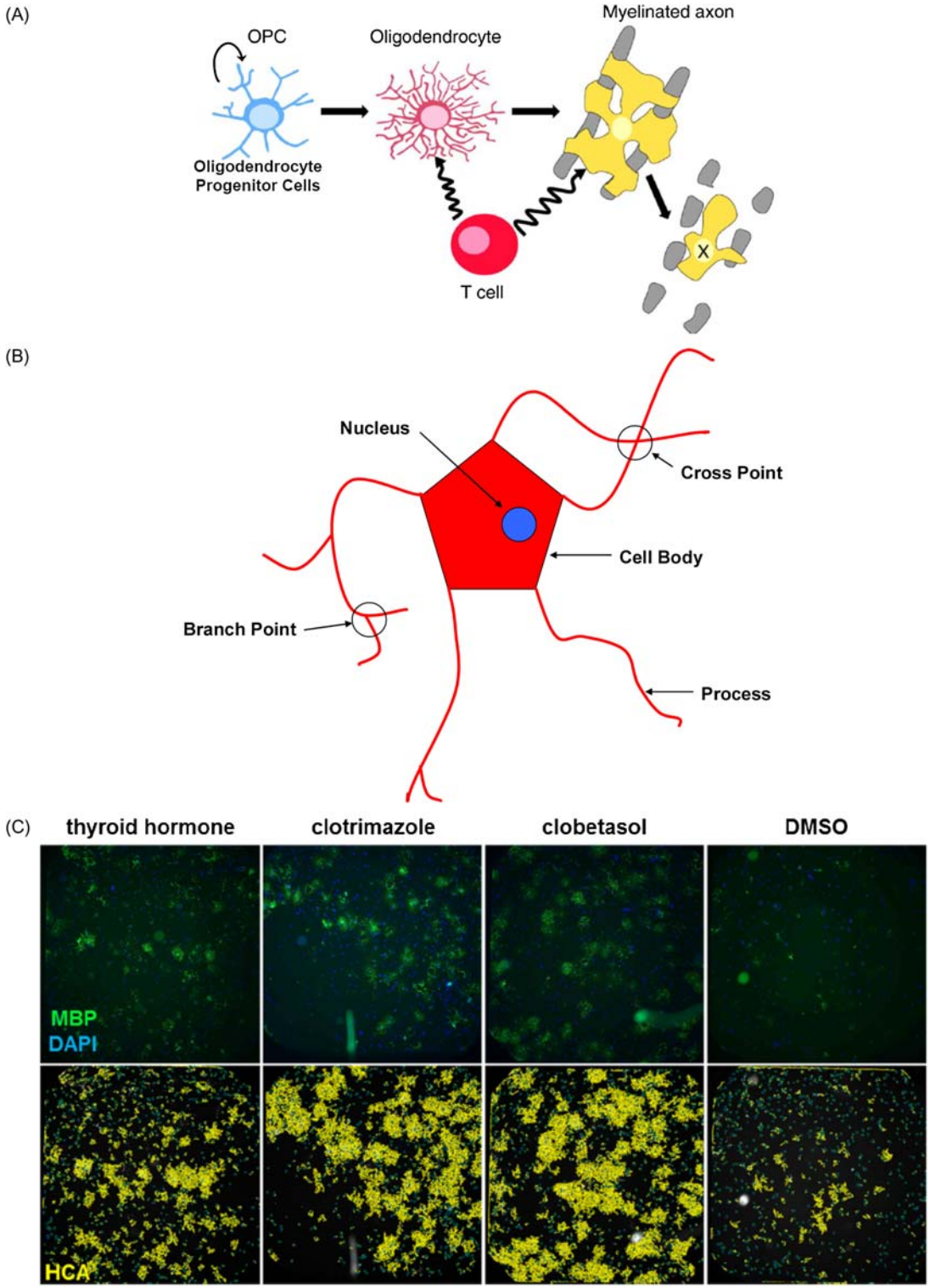

Fig. 4 Oligodendrocyte progenitor cell (OPC) differentiation and remyelination. (A) Cellular dynamics of multiple sclerosis (MS) pathology. OPCs could be differentiated into oligodendrocytes which produce myelin sheaths to protect axon. Overactive T cells of MS patients could damage the myelin sheaths and further destroy axons. (B) Typical cell morphology of OPC. (C) Images taken by InCell 2000 from a 1536-well plate, for OPCs treated with positive control compound thyroid hormone, negative control DMSO, and clotrimazole and clobetasol, two hits identified via screening. Nucleus, *blue*; MBP protein, *green*; oligodendrocyte processes identified via InCell 2000 software, *yellow lines*. Modified from Najm, F. J.; Madhavan, M.; Zaremba, A.; Shick, E.; Karl, R. T.; Factor, D. C.; Miller, T. E.; Nevin, Z. S.; Kantor, C.; Sargent, A.; Quick, K. L.; Schlatzer, D. M.; Tang, H.; Papoian, R.; Brimacombe, K. R.; Shen, M.; Boxer, M. B.; Jadhav, A.; Robinson, A. P.; Podojil, J. R.; Miller, S. D.; Miller, R. H.; and Tesar, P. J. Drug-Based Modulation of Endogenous Stem Cells Promotes Functional Remyelination In Vivo. *Nature* **2015**, *522*, 216–220, extended data figure 2.

was established to search for compounds that can differentiate mouse OPC into oligodendrocytes characterized by increased MBP protein expression and number of processes (Fig. 4B). Results from screening against FDA-approved drug collection were published, and 22 hits were identified based on EC50 and TC50 combination scores. Fig. 4C shows images taken by InCell 2000 from 1536-well plates. The 22 compounds were tested in human OPCs to ensure cross-species activities. Of these compounds, clobetasol and miconazole were prioritized for further characterization and both demonstrated efficacy in mouse ex vivo cerebellar slice cultures and in Lysophosphatidylcholine (LPC) lesion mouse model.[94]

2.15.6.5 Lipid Accumulation in Adipocytes

Phenotypic screening provides a nonbiased approach to chemically interrogate the proteome in its pathophysiologically-relevant environment, and accordingly increase the chances of revealing authentic disease mechanisms and identifying potential therapies. However, the biggest challenge of phenotypic screening is the identification of the molecular targets of bioactive hit compounds. Without a target (or targets), chemical optimization and preclinical toxicity studies on phenotypic screening hits are daunting tasks, and translation of potential drugs discovered by phenotypic screening into clinical applications would face significant obstacles.

In the study demonstrated here, a HCS-based phenotypic screening was conducted in preadipocytes against a focused small-molecule library of carbamates designed to inhibit the serine hydrolase enzyme super family. The extent of lipid accumulation and adipocyte differentiation were visualized by fluorescent lipid Nile Red (shown in green in Fig. 5A). Several carbamates including WWL 113 specifically promoted adipocyte differentiation and lipid storage in the fat cells. These molecules could be beneficial for obesity-linked insulin resistance patients, working to reduce levels of circulating free

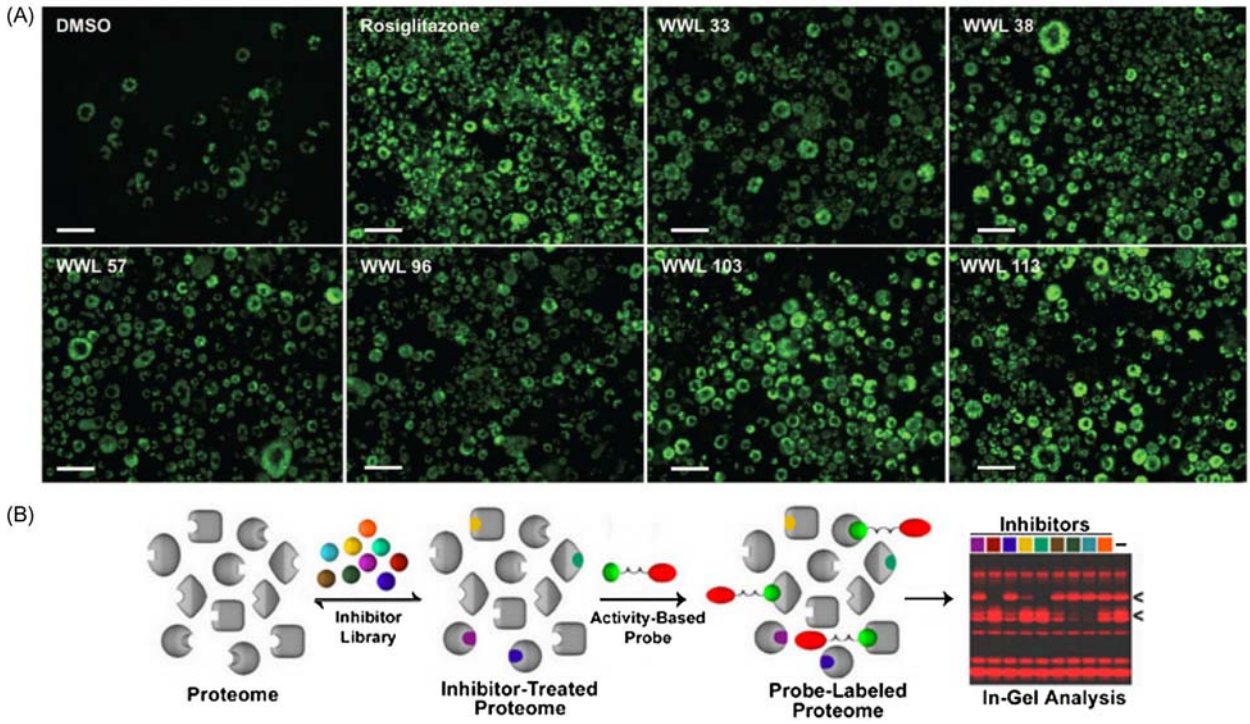

Fig. 5 Lipid accumulation in adipocytes. (A) A phenotypic screening against a focused set of bioactive compounds targeting serine hydrolase superfamily in 3T3-L1 cells was conducted. 3T3-L1 preadipocytes were induced to differentiate into adipocytes 2 days postconfluence in the presence of 10 μM individual compounds. Two days later, induction media was replaced with maintenance media and compounds refreshed. On day 7, the extent of lipid accumulation (marked by fluorescent lipid Nile Red, shown in *green*) and adipocyte differentiation was evaluated by HCS-based assay. WWL 113, along with other compounds, were identified as lipolysis inhibitors. Scale bar indicates 100 μm. (B) Competitive ABPP strategy was used to identify the molecular target(s) of WWL 113 in the cells. ABPP technology monitors changes in the functional state of serine hydrolases directly in the cells. ABPP probe includes three elements: an enzyme active-site directed reactive group, a linker and a fluorophore tag. For serine hydrolase superfamily, the reactive group is fluorophosphonates (FP), a near-universal activity probe for the enzyme family. The fluorophore tag allows visualization of probe-labeled proteins in the gel. In the competitive mode of ABPP technology, inhibitors will displace the probe associated with the enzymes, lead to the disappearance of protein band(s) in the gel. (A) From Dominguez, E.; Galmozzi, A.; Chang, J. W.; Hsu, K.-L.; Pawlak, J.; Li, W.; Godio, C.; Thomas, J.; Partida, D.; Niessen, S.; O'Brien, P. E.; Russell, A. P.; Watt, M. J.; Nomura, D. K.; Cravatt, B. F.; Saez, E. Integrated Phenotypic and Activity-Based Profiling Links Ces3 to Obesity and Diabetes. *Nat. Chem. Biol.* **2014**, *10*, 113–121, supplementary figure 1. (B) From http://www.scripps.edu/cravatt/research.html, figure 3.

fatty acids, restoring normal lipid partitions among tissues, potentiating adipocyte function, and subsequently enhancing systemic insulin action.[95]

In order to identify the molecular target(s) of WWL 113 and other hits obtained via the HCS-based phenotypic screening, a competitive activity-based protein profiling (ABPP) strategy was used. ABPP technology monitors changes in the functional state of enzyme families directly in the cells. An ABPP probe includes three elements: an enzyme active-site directed reactive group, a linker and a fluorophore tag. For the serine hydrolase superfamily, the reactive group is fluorophosphonates (FP), a near-universal activity probe for the enzyme family. The fluorophore tag allows visualization of probe-bound proteins in the gels. In the competitive mode of ABPP technology, inhibitors such as WWL 113 displace the probes associated with the proteins, leading to protein band(s) disappearing in the gel (**Fig. 5B**).[96] Next, the fluorophore tag of the ABPP probe was replaced by biotin, and used as a capture probe to separate probe-labeled proteins from unlabeled ones. WWL 113, as an inhibitor of the hydrolase enzyme, competed with the biotinylated probe, and consequently reduced the amount of proteins pulled down. The pulled down proteins were then subjected to tryptic digestion and mass spectroscopy analysis. Using this approach, two carboxylesterase enzymes, Ces3 and Ces1f, were identified as the molecular targets for WWL 113. Ces3 and Ces1f are endoplasmic reticulum glycoproteins that have been previously associated with adipocyte lipolysis. Treatment of two mouse models of obesity-diabetes with WWL 113 ameliorated multiple features of metabolic syndrome, validating the ABPP strategy described above for accelerating the identification of true therapeutic targets and the development of new therapies.[95]

2.15.6.6 Lysosomal Storage Disease

Niemann–Pick disease type C (NPC) is a rare autosomal recessive genetic disease caused by mutations in the NPC1 or NPC2 gene. The NPC genes encode proteins to regulate cholesterol transport from late endosomes-lysosomes to other intracellular compartments, such as the trans-Golgi network and plasma membrane caveolae. Deficiency in NPC1 or NPC2 proteins results in malfunction of intracellular cholesterol trafficking and lysosomal accumulation of unesterified cholesterols (**Fig. 6A**). This lysosomal lipid storage defect causes progressive neurodegeneration and eventually leads to disability and death of patients.

A number of agents have been reported to have therapeutic potential for treatment of NPC. Hydroxypropyl-β-cyclodextrin (HPBCD), methyl-β-cyclodextrin (MBCD), and δ-tocopherol are known to reduce brain cholesterol accumulation and increase life span in NPC1 mouse models. The effect of the three compounds on the reduction of lysosomal cholesterol accumulation has been confirmed in the NPC patient-derived fibroblasts and primary mouse neurons. However, these agents have not been directly evaluated in human NPC neuronal cells, the type of cells that are more relevant to the disease pathogenesis. Therefore, NPC patient iPSC-derived neuronal cells were generated and used for drug efficacy evaluation.

Fibroblasts from an NPC1 patient were reprogrammed to iPSCs using a commercially available virus reprogramming system that expresses Oct3/4, Sox2, Klf4, and cMyc factors. The pluripotency of patient iPSC thus generated was confirmed using immunofluorescence staining on Oct4, Sox2, SSEA4, and TRA-1-81, and similar patterns were observed and compared to iPSC generated from normal human fibroblasts. Further characterization of the patient iPSCs showed a normal karyotype, typical teratoma formation, and original NPC1 gene mutations.

Using commercial reagents, the NPC1 iPSC were first differentiated into neural stem cells (NSCs), expanded, and confirmed for expression of NSC markers nestin and Sox2 by fluorescent staining. The NPC1 NSC were then differentiated into neuronal cells, and neuronal phenotype was confirmed using Tuj1, Map2, and neurofilament markers. The time required for NPC1 neuron maturation, cell morphology changes, and expression of neural markers was similar to that of control wild type (WT) iPSC.

An enlarged lysosome with accumulated unesterified cholesterol is a major phenotype of the disease. Three dyes were used to characterize WT and NPC1 NSC and neuronal cells, and the phenotype was confirmed in NPC1 NSC and neuronal cells. The dyes used were: Filipin, a dye that stains unesterified cholesterols in cells; LysoTracker dye that locates cellular acidic compartment and could be used to observe lysosome size changes; and nuclear dye. **Fig. 6B** showed that upon increasing cellular cholesterol levels by exposing cells to a higher percentage of serum in culture media, the accumulation of unesterified cholesterols in NPC1 iPSC-derived neuronal cells was much faster and more significant compared to WT iPSC-derived neuronal cells, as evidenced by higher intensity of Filipin stain and larger lysosome body size. Finally, HPBCD, MBCD, and δ-tocopherol were used to treat both NPC1 iPSC-derived NSC and neuronal cells, and their ability to ameliorate cholesterol accumulation in lysosomes in these cells was confirmed (**Fig. 6C**). Therefore, the NPC1 patient iPSC-derived NSC and neuronal cells are appropriate models for efficacy evaluation on NPC disease modifying drugs.[97]

2.15.6.7 Progeroid and Abnormal Nuclear Structures

Hutchinson-Gilford progeria syndrome (HGPS) is caused by mutations in the LMNA gene encoding prelamin A and lamin C proteins. These mutations result in an internally truncated form of prelamin A (called progerin). Because of the truncation, its farnesylated carboxyl-terminal cannot be processed correctly, making the farnesylation permanent. Farnesylated progerin then accumulates at the nuclear rim, leading to abnormal nuclear shapes, compromised chromatin maintenance and DNA repair functions, and other unknown damages (**Fig. 7A**). These cause patient to age prematurely. Target-based drug discovery approaches failed, given that the abnormal cellular phenotypes make it difficult to determine whether progerin drives the HGPS phenotype or are only

bystanders. To circumvent this issue, a phenotypic screening assay was established and applied to identify leads for progerin therapies with potential novel mechanisms.

In phenotypic screening, the first and most important action is to select and validate appropriate cellular models. It was found that primary cells from HGPS patients were not suitable for HTS, because these cells were restricted in their in vitro growth, and showed considerable donor variability in phenotypes and responses. An inducible GFP-progerin cell line, along with two control cell lines, were engineered using human dermal fibroblasts and validated against patient cells prior to being used for HTS. Protein markers used to validate screening cell lines are: progerin—the disease causing protein; lamin B1 and LAP2—nuclear structure proteins; HP1g and H2K27-3M—chromatin structure proteins; gH2AX and 53BP1 foci—DNA damage activation markers (Fig. 7B).

Three different phenotypes were expected from three cell lines expressing different LMNA gene variants in human dermal fibroblasts; this hypothesis was confirmed experimentally. Normal Lamin A gene led to normal nuclear structure and low level of DNA damage. Progerin gene led to abnormal nuclear structure and high level of DNA damages. A mutation in progerin gene, C661S, protected progerin from being processed by farnesyltransferase, keeping progerin in the nucleus without destroying the nuclear structure (Fig. 7C).

The inducible GFP-progerin cell line was used for HCS-based screening in 384-well format. Four parameters were collected: cell number for toxicity, GFP-progerin for disease protein levels, Lamin B1 nuclear structure for early HGPS indication, and gH2AX DNA damage signal for late HGPS indication. L-744, 832 a farnesyltransferase inhibitor, was used as a positive control. Assay window was very small and multiparameter analysis was needed for assay quality controls and hit identification. NIH FDA-

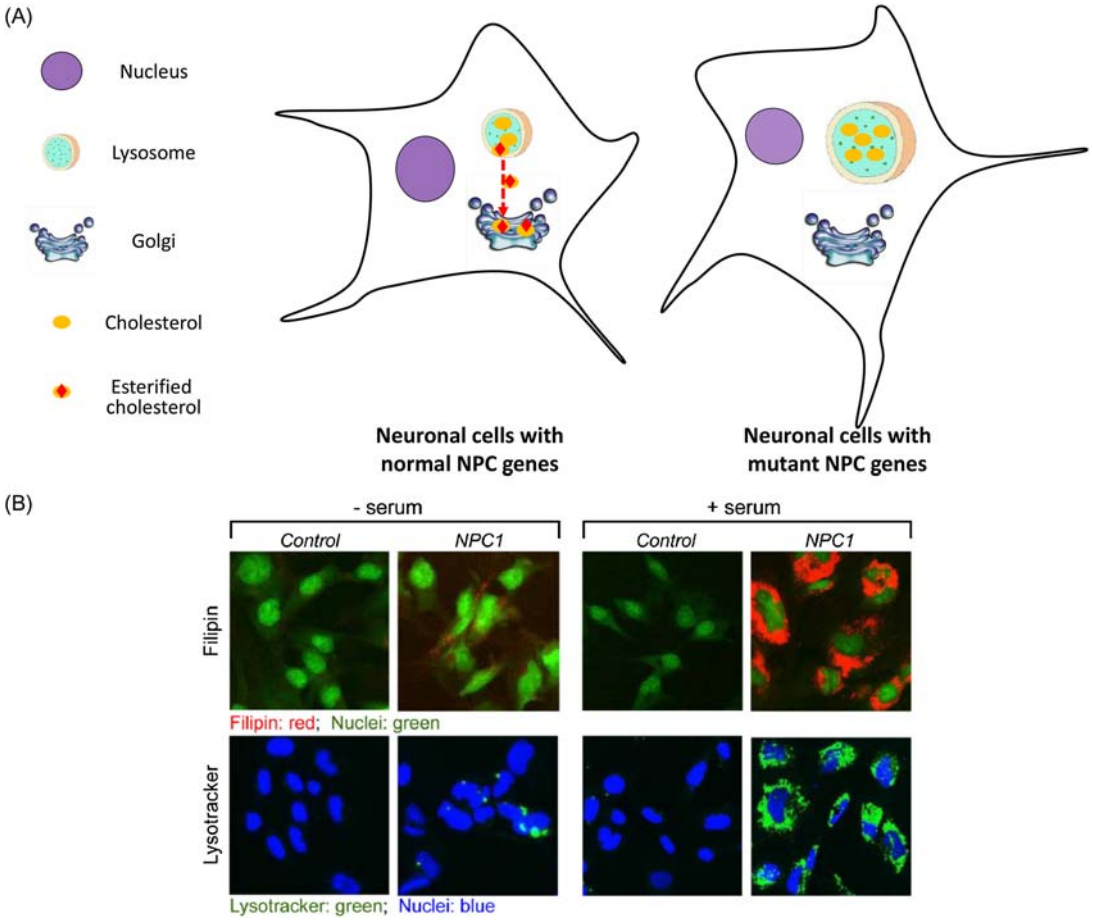

Fig. 6 Lysosomal storage disease. (A) NPC is a lysosomal storage disease associated with mutations in NPC1 and NPC2 genes. Deficiency in NPC1 or NPC2 protein results in malfunction of intracellular cholesterol trafficking and lysosomal accumulation of unesterified cholesterols. (B) Lysosomal cholesterol accumulation in NPC1 neuronal cells derived from NPC1 iPSC line. Filipin cholesterol staining and Lysotracker staining in the absence or presence of 10% serum in culture medium that provided additional cholesterol to cells.Controls: WT iPSC-derived neuronal cells. (C) Effects of HPBCD, MBCD, and δ-tocopherol on reducing the levels of cholesterol accumulation and the degree and/or number of enlarged lysosomes in NPC1 neuronal cells and NPC1 neural stem cells (B) and (C). From Yu, D.; Swaroop, M.; Wang, M.; Baxa, U.; Yang, R.; Yan, Y.; Coksaygan, T.; DeTolla, L.; Marugan, J. J.; Austin, C. P.; McKew, J. C.; Gong, D.-W.; Zheng, W. Niemann–Pick Disease Type C: Induced Pluripotent Stem Cell-Derived Neuronal Cells for Modeling Neural Disease and Evaluating Drug Efficacy. *J. Biomol. Screen.* **2014**, *19*, 1164–1173, (B) figure 3, (C) figure 4.

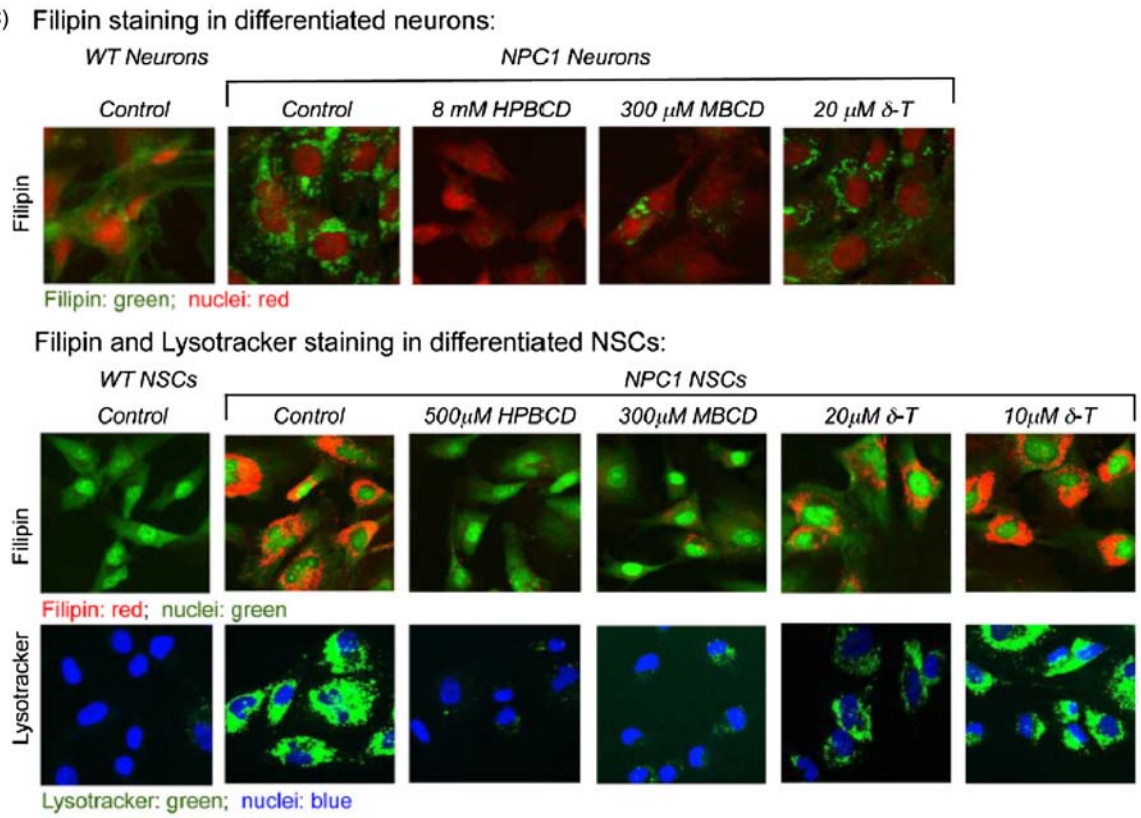

Fig. 6 (*continued*).

approved drug collection was screened at four concentrations. Hits were defined as compounds with at least two out of four concentrations having impacts on at least one protein readout. Twenty-seven compounds were confirmed as leads in HGPS patient primary cells, 11 of them corticoids, three phosphodiesterase inhibitors (PDEi), three adrenergic agonists, two retinoids, and eight others. Retinoids and corticoids were selected as candidates based on their capability to reduce DNA damage signs and GFP-progerin levels, and to restore nuclear and chromatin structures. Other analogs of retinoids demonstrated similar efficacy, in line with literature reports that retinoid bound nuclear receptor Retinoic acid receptors (RARs) can repress lamin A, progerin, and lamin C expression at the mRNA levels. PDEi and adrenergic agonists predominantly affected lamin B1 and/or gH2AX without affecting progerin levels.[98]

2.15.6.8 Leishmanial Proliferation in Macrophage

Leishmaniases are neglected parasitic diseases causing severe morbidity and mortality. They are caused by protozoan parasites that belong to the genus Leishmania. No vaccine exists against any form of leishmaniasis and most of the existing antileishmanial drugs have serious side effects.

Metacyclic promastigotes, the extracellular form in the life cycle of leishmania, are inoculated by the bite of an infected sandfly resulting in recruitment of neutrophils and uptake of parasites by neutrophils, dermal dendritic cells, and resident tissue macrophages. Promastigotes differentiate to amastigotes within macrophages and live within acidic phagolysosomes where they replicate, form parasitophorous vacuoles (PVs), and cause lesions either in the tissue site or in the systemic organs (Fig. 8A and B(a)). Since the innate immune cells are weakened by the parasites, the resolution of infection with all leishmania species will depend on effective responses from T cells and other adaptive immune cells, but the mechanisms are not well characterized.[99,100]

The assay illustrated here highly mimics the pathological conditions of leishmanial amazonensis infectious conditions. The highly virulent lesions-derived amastigotes of leishmanial amazonensis were genetically modified to stably express a DsRed2 fluorescent protein reporter, and propagated in Swiss nu/nu mice by subcutaneous injection. After 6–8 weeks, amastigote inoculation lesions were excised and amastigotes were purified from the lesions. Homogeneous populations of 6 day-old mouse macrophages differentiated from bone marrow progenitors were placed in 384-well plates and allowed to form monolayers. DsRed2-amastigotes freshly purified were then added to the macrophage monolayer at three amastigote per macrophage ratio. The amastigote-macrophage coculture was allowed to incubate for 48 h prior to the addition of 10 μM test compounds. Images of live infected

(A)

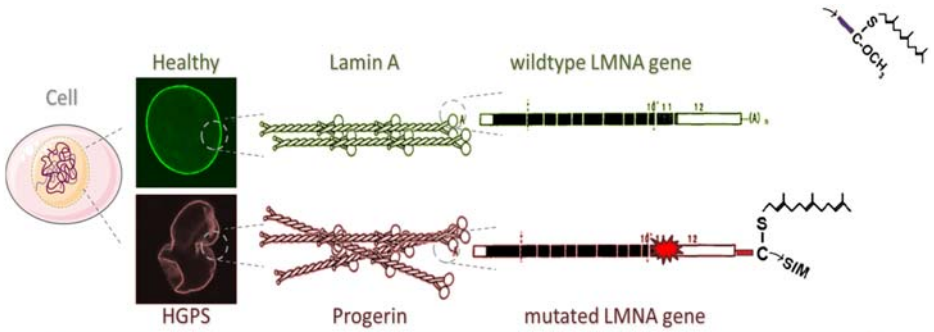

(B)

HGPS Markers Checked	Cellular Functions
Progerin	Disease protein
Lamin B1	Nuclear structure
LAP2	Nuclear structure
HP1γ	Chromatin structure
H3-K27-3M	Chromatin structure
γH2AX	Activation of DNA damage signaling
53BP1 foci	Activation of DNA damage signaling

(C)

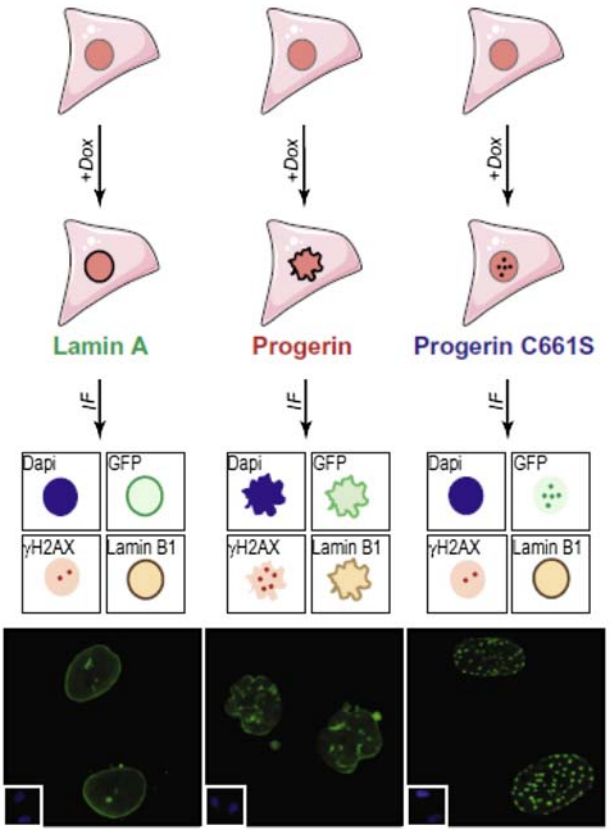

Fig. 7 Progeroid and abnormal nuclear structures. (A) Progerin disease. Mutations in LMNA gene cause prelamin A protein truncation and permanent farnesylation, which leads to abnormal nuclear shapes. (B) Protein markers used to characterize GFP-progerin cell lines engineered from human dermal fibroblasts. (C) Three different phenotypes were expected from three cell lines expressing different LMNA gene variants in human dermal fibroblasts, and the phenotypes were confirmed using HCS methods, *green*, GFP-tagged proteins, from left to right: lamin A, progerin, and progerin C661S. (A) Modified from Kubben, N.; Brimacombe, K. R.; Donegan, M.; Li, Z.; Misteli, T. A High-Content Imaging-Based Screening Pipeline for the Systematic Identification of Anti-Progeroid Compounds. *Methods* **2016**, *96*, 46–58, figure 1. (C) Adapted from Kubben, N.; Brimacombe, K. R.; Donegan, M.; Li, Z.; Misteli, T. A High-Content Imaging-Based Screening Pipeline for the Systematic Identification of Anti-Progeroid Compounds. *Methods* **2016**, *96*, 46–58, figure 1.

macrophage cultures preincubated 60 min with Hoechst nuclear dye and LysoTracker dye for PV were acquired on an HCS reader after 3 days of incubation with compounds. All incubation temperatures were at 34°C.

By allowing real-time monitoring of the live-interaction between virulent amastigote and primary macrophages, this approach offered many advantages over conventional assay methods. It allowed the identification of both fast-acting and slow-acting compounds, functioning via killing the amastigote inside the PV directly or by activation of microbicidal mechanisms of the host macrophage (Fig. 8B(b–c)). The assay also permitted monitoring the health status of host macrophages by visualizing their nuclear morphology with the permeant DNA probe Hoechst 33342. In the presence of a toxic compound like cycloheximide, dead macrophages were easily differentiated from healthy cells and identified by the loss of nuclear integrity (Fig. 8B(d)).

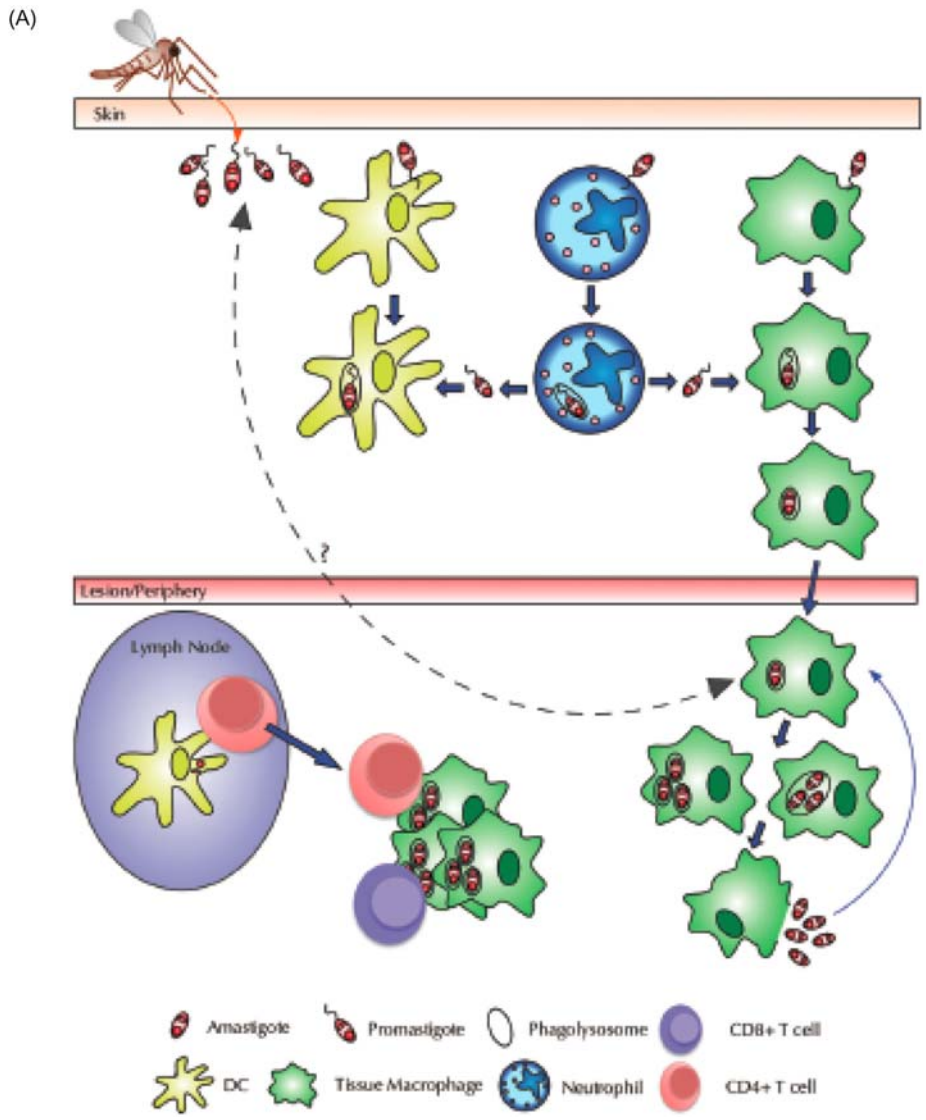

Fig. 8 Leishmanial proliferation in macrophage. (A) The life cycle of Leishmania parasites. Promastigotes are inoculated by the bite of an infected sandfly resulting in recruitment of neutrophils and uptake of parasites by neutrophils, dermal dendritic cells, and resident tissue macrophages. Promastigotes differentiate to amastigotes within macrophages and live within acidic phagolysosomes where they can replicate and cause lesions either in the tissue site or in the systemic organs. B. Leishmania amazonensis strain lodges and multiplies within acidic phagolysosomes of macrophages to form parasitophorous vacuole (PV). Six day-old macrophages were seeded into 384-well microplates and incubated with Leishmania amazonensis DsRed2 expressing amastigotes (red) for 48 h. (a) Phase contrast image demonstrates the lodging of the amastigotes within PV. (b to d) Images of living infected macrophage cultures pre-incubated 60 min with Hoechst nuclear dye (blue) and LysoTracker dye for PV (green) were acquired on a HCS Opera reader after 3 days of incubation with compounds. (b) 1% DMSO (negative control), (c) 0.5 mM Amphotericin B (anti Leishmania agent) and (d) 180 mM Cycloheximide (cytotoxic compound). A) From Cellular Microbiology **(2011)** *13*(11), 1659–1667, Figure 1. B) From PLoS Negl Trop Dis. **2013** Apr 4;*7*(4):e2154, figure 1.

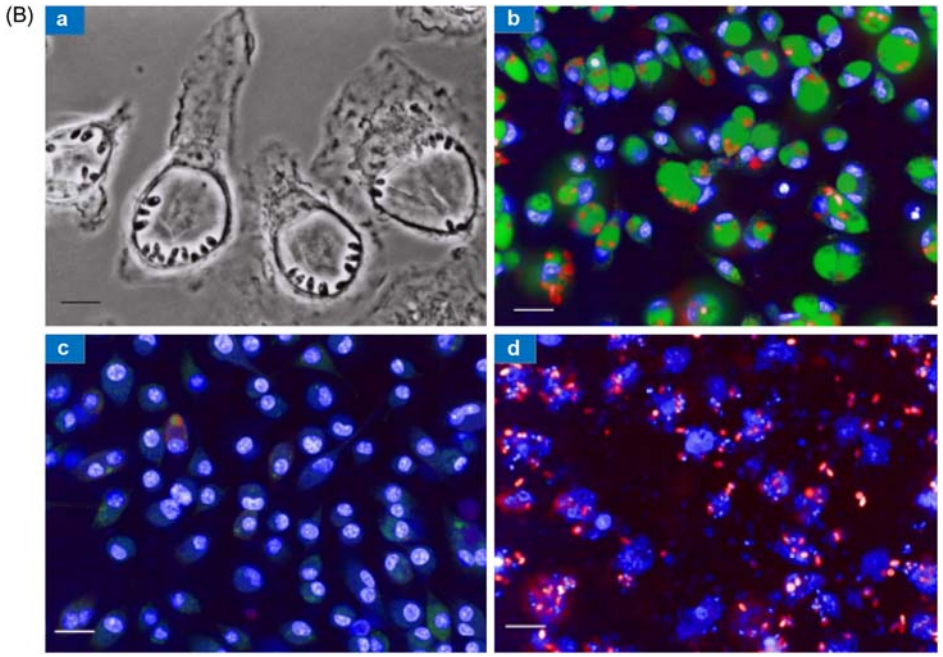

Fig. 8 (*continued*).

As a pathologically relevant model system, the amastigote-macrophage coculture also provides a powerful tool to further elucidate the cellular processes associated with intracellular infection and the host immune response to pathogen mechanisms, thus identifying new targets for more effective leishmanial therapies.[101]

2.15.6.9 Tubulin Polymerization and Redistribution

Microtubules are a component of the cytoskeleton. α,β-Tubulin heterodimers organize into structures called protofilaments. Ten to fifteen protofilaments associate to form the hollow cylindrical polymers of microtubules. The dynamics of microtubule assembly and disassembly play crucial roles in the development and maintenance of cell shape, in transportation of vesicles, mitochondria and other components throughout cells, in cell signaling, and in cell division and mitosis (**Fig. 9A**).[102]

A number of well characterized anticancer drugs have demonstrated cytotoxic effects by altering microtubule dynamics in cancer cells, consequently disrupting the formation of mitotic spindles and the progression of mitotic process. For example, paclitaxel binds to a pocket within β-tubulin that putatively counteracts the effect of Guanosine triphosphate (GTP) hydrolysis, resulting in stabilization of microtubule structure. Also vinblastine interferes with microtubule dynamics by causing tubulin depolymerization. The stabilization of microtubules or disruption of tubulin polymerization by these compounds leads to cell cycle arrest and cancer cell death. As a result, monitoring effects on microtubule polymerization is indispensable to understanding the mechanisms of action for cancer chemotherapy medications.[103,104] On the other hand, many other therapeutic approaches aim to avoid interference of tubulin dynamics, given that this may cause cytotoxicity. Therefore, an assay that can accurately monitor microtubule dynamics is broadly applicable to drug discovery programs seeking to optimize and progress lead compounds.

A HCS-based assay was established to systematically monitor tubulin polymerization in A549 cells in order to understand the mechanisms of action for anticancer drugs and to evaluate potential cytotoxicity on lead compounds or drug candidates for other disease indications. In examples illustrated in **Fig. 9B**, A549 cells were treated with DMSO control, 2 μM vinblastine or paclitaxel for 3, 6, or 18 h. Microtubule structure (green) was visualized by fluorescent labeling using anti-α-tubulin rat primary antibody followed by Alexa-488-labeled antirat antibody. Nuclei were counterstained using Hoechst 33342 (blue). Normal microtubule network structure was visible in the DMSO treated control cells. Stabilization of the microtubules by paclitaxel was evidenced by a thickening of the microtubule fiber that was most prominent at 18 h. Vinblastine caused disruption of the microtubule network, leading to a diffused staining of α-tubulin that was also visible after 3 h and lasted up to 18 h.

This HCS-based assay platform enables the monitoring of tubulin polymerization status by directly measuring the acute effects of drug candidates on the cellular tubulin network with the capability to dissect the mechanisms of action. It distinguishes in a quantitative manner between compounds that act as tubulin stabilizers vs. those that are tubulin destabilizers. In addition, using a multiplexed approach, this analysis also allows one to simultaneously monitor physiological cellular responses and associated cellular phenotypes. Understanding the mechanisms of action might lead to improved dosing regimens and allow for the design of combination therapies with other "molecularly targeted" drugs.[105]

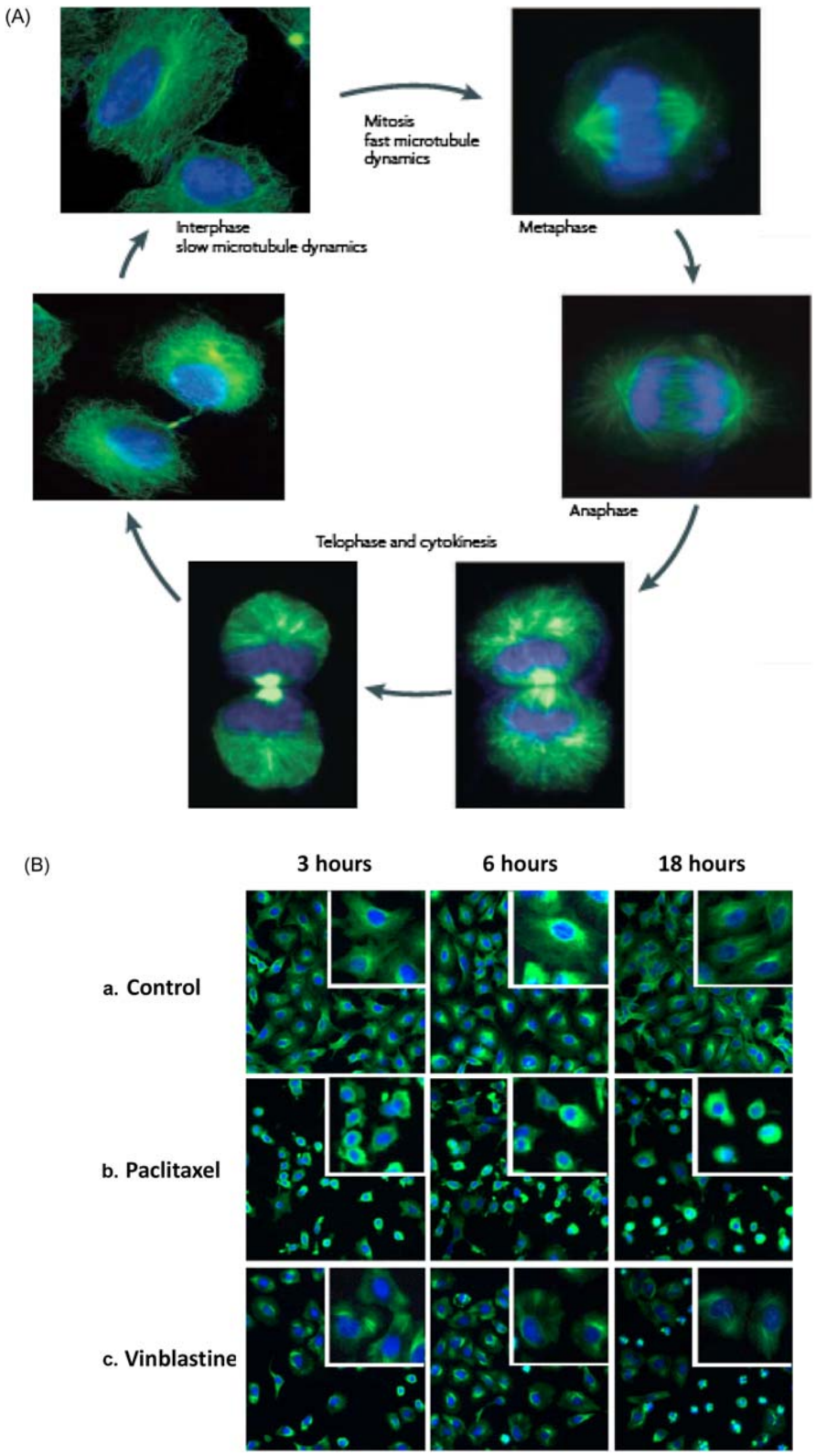

Fig. 9 Tubulin polymerization and redistribution. (A) Microtubule changes during the cell cycle. Microtubules are tubular polymers of tubulin proteins. Microtubule structures (shown in *green*) undergo marked morphological changes to mediate specific functions throughout the cell cycle. Microtubule dynamics vary during the cell cycle, being least dynamic in interphase cells and most dynamic during mitosis, making this an important target for anticancer drug design. DNA is shown in *blue*. (B) High-content images of fluorescently-labeled α-tubulin in A549 cells treated with tubulin-active compounds. A549 cells were treated with DMSO control, 2 μM vinblastine or paclitaxel for 3, 6, or 18 h. Microtubules were visualized by Alexa-488 labeled anti-α-tubulin antibody (*green*), nuclei were counterstained by Hoechst dye (*blue*). Enlarged images are shown in the inserts to further visualize the changes in microtubule network upon the different treatments. (A) Modified from Kavallaris, M. Microtubules and Resistance to Tubulin-Binding Agents. *Nat. Rev. Cancer* **2010**, *10*, 194–204, figure 1. (B) Modified from Sum, C. S.; Nickischer, D.; Lei, M.; Weston, A.; Zhang, L.; Schweizer, L. Establishing a High-Content Analysis Method for Tubulin Polymerization to Evaluate Both the Stabilizing and Destabilizing Activities of Compounds. *Curr. Chem. Genomics Transl. Med.* **2014**, *8*, 16–26, figure 1.

2.15.7 Conclusions

To increase the success rate of drug discovery, more predictive in vitro bioassays and in vivo disease and/or safety models are in demand. Due to its flexibility and information-rich nature, the bioimaging-based HCS assay technology, in combination with pathophysiologically-relevant complex cellular models, has demonstrated significant predictivity enhancement over conventional in vitro assay technologies, and has generated tremendous impact on drug discovery, ranging from target identification and validation, lead discovery and optimization, to translational medicine. In summary, there are three critical factors that determine the success of a HCS campaign. First, it is important to maintain balance between physiological relevancy and scalability of the complex cellular models, and balance between information content and screening throughput. In the early phase of drug discovery, utilizing immortalized human cell lines or iPSC-derived tissue relevant cells, and general and inclusive image acquisition protocols and analysis algorithms are reasonable approaches. In the late phase of drug discovery, more primary cells from normal or diseased tissues, or patient iPSC-derived cells are likely required, and more sophisticated image acquisition protocols and analysis algorithms allowing differentiation between different mechanisms of action would be necessary. Second, it is critical to establish an overarching bioimaging repository platform with appropriate architectures. This repository should facilitate interactive exploration and analysis of images and multidimensional data from different HCS reader platforms, automated feature clustering and phenotype scoring using more sophisticated statistical analysis tools, and pathway mapping and mechanisms of action studies using advance bioinformatics software. Third, the establishment of an interdisciplinary HCS core team is essential which could include highly skilled associates in cell biology, HCS assay technology, image analysis algorithm development, IT for HCS data management workflow, advanced statistical analysis, and informatics analysis. HCS technology has a steep learning curve. Integrating knowledge from the skilled associates from different disciplines would not only accelerate the assay development and screening process, but would also ensure that "fit-for-purpose" complex cellular models and image analysis algorithms are used to investigate the diseases of interest.

See also: 5.01. Cancer Biology and the Principles of Targeted Cancer Drug Discovery.

References

1. Giuliano, K. A.; Johnston, P. A.; Gough, A.; Taylor, D. L. Systems Cell Biology Based on High-Content Screening. *Methods Enzymol.* **2006,** *414,* 601–619.
2. Taylor, D. L. A Personal Perspective on High-Content Screening (HCS): From the Beginning. *J. Biomol. Screen.* **2010,** *15,* 720–725.
3. Buchsner, W.; Collins, M.; Garyantes, T.; Guha, R.; Haney, S.; Lemmon, V.; Li, Z.; Trask, O. J. *Assay Development Guidelines for Image-Based High Content Screening, High Content Analysis and High Content Imaging, NIH Assay Guideline Manual*. http://www.ncbi.nlm.nih.gov/books/NBK100913/, 2012.
4. Boutros, M.; Heigwer, F.; Laufer, C. Microscopy-Based High-Content Screening. *Cell* **2015,** *163,* 1314–1325.
5. Fraietta, I.; Gasparri, F. The Development of High-Content Screening (HCS) Technology and its Importance to Drug Discovery. *Expert Opin. Drug Discovery* **2016,** *11,* 501–514.
6. Li, Z. High Content Screening for Lead Identification and Optimization. *Curr. Chem. Genomics Transl. Med. Ed.* **2014,** *8,* 1–2.
7. Mattiazzi Usaj, M.; Styles, E. B.; Verster, A. J.; Friesen, H.; Boone, C.; Andrews, B. J. High-Content Screening for Quantitative Cell Biology. *Trends Cell Biol.* **2016,** *1–14.* http://www.sciencedirect.com/science/article/pii/S0962892416300010.
8. Nierode, G.; Kwon, P. S.; Dordick, J. S.; Kwon, S.-J. Cell-Based Assay Design for High-Content Screening of Drug Candidates. *J. Microbiol. Biotechnol.* **2015,** *26,* 213–225.
9. Ang, M. L. T.; Pethe, K. Contribution of High-Content Imaging Technologies to the Development of Anti-Infective Drugs. *Cytometry A* **2016;** http://dx.doi.org/10.1002/cyto.a.22885. http://onlinelibrary.wiley.com/doi/10.1002/cyto.a.22885/epdf.
10. Antczak, C.; Wee, B.; Radu, C.; Bhinder, B.; Holland, E. C.; Djaballah, H. A High-Content Assay Strategy for the Identification and Profiling of ABCG2 Modulators in Live Cells. *Assay Drug Dev. Technol.* **2014,** *12,* 28–42.
11. Hua, Y.; Shun, T. Y.; Strock, C. J.; Johnston, P. A. High-Content Positional Biosensor Screening Assay for Compounds to Prevent or Disrupt Androgen Receptor and Transcriptional Intermediary Factor 2 Protein–Protein Interactions. *Assay Drug Dev. Technol.* **2014,** *12,* 395–418.
12. Schweizer, L.; Zhang, L. Enhancing Cancer Drug Discovery Through Novel Cell Signaling Pathway Panel Strategy. *Cancer Growth Metastasis* **2013,** *6,* 53–59.
13. Reid, B. G.; Stratton, M. S.; Bowers, S.; Cavasin, M. A.; Demos-Davies, K. M.; Susano, I.; McKinsey, T. A. Discovery of Novel Small Molecule Inhibitors of Cardiac Hypertrophy Using High Throughput, High Content Imaging. *J. Mol. Cell. Cardiol.* **2016,** *97,* 106–113.
14. Thorne, N.; Malik, N.; Shah, S.; Zhao, J.; Class, B.; Aguisanda, F.; Southall, N.; Xia, M.; McKew, J. C.; Rao, M.; Zheng, W. High-Throughput Phenotypic Screening of Human Astrocytes to Identify Compounds That Protect Against Oxidative Stress. *Stem Cells Transl. Med.* **2016,** *5,* 613–627.
15. Sugarman, E.; Koo, A.; Suyama, E.; Ruidiaz, M. E.; Heynen-Genel, S.; Nguyen, K. H.; Vasile, S.; Soundarapandian, M. M.; Vega, R. B.; Kelly, D. P.; Smith, L. H.; Malany, S. Identification of Inhibitors of Triacylglyceride Accumulation in Muscle Cells: Comparing HTS Results From 1536-Well Plate-Based and High-Content Platforms. *J. Biomol. Screen.* **2014,** *19,* 77–87.
16. Tschapalda, K.; Zhang, Y.-Q.; Liu, L.; Golovnina, K.; Schlemper, T.; Eichmann, T. O.; Lal-Nag, M.; Sreenivasan, U.; McLenithan, J.; Ziegler, S.; Sztalryd, C.; Lass, A.; Auld, D.; Oliver, B.; Waldmann, H.; Li, Z.; Shen, M.; Boxer, M. B.; Beller, M. A Class of Diacylglycerol Acyltransferase 1 Inhibitors Identified by a Combination of Phenotypic High-Throughput Screening, Genomics, and Genetics. *EBioMedicine* **2016,** 1–11. http://www.ebiomedicine.com/article/S2352-3964(16)30149-9/pdf.
17. Tolosa, L.; Gómez-Lechón, M. J.; Donato, M. T. High-Content Screening Technology for Studying Drug-Induced Hepatotoxicity in Cell Models. *Arch. Toxicol.* **2015,** *89,* 1007–1022.
18. Pradip, A.; Steel, D.; Jacobsson, S.; Holmgren, G.; Ingelman-sundberg, M.; Björquist, P.; Johansson, I.; Edsbagge, J. High Content Analysis of Human Pluripotent Stem Cell Derived Hepatocytes Reveals Drug-Induced Steatosis and Phospholipidosis. *Stem Cells Int.* **2016;** http://dx.doi.org/10.1155/2016/2475631. http://www.ncbi.nlm.nih.gov/pmc/articles/PMC4736406/.
19. Delehanty, J. B.; Boeneman, K.; Bradburne, C. E.; Robertson, K.; Bongard, J. E.; Medintz, I. L. Peptides for Specific Intracellular Delivery and Targeting of Nanoparticles: Implications for Developing Nanoparticle-Mediated Drug Delivery. *Ther. Deliv.* **2010,** *1,* 411–433.
20. Rajendran, L.; Knölker, H. J.; Simons, K. Subcellular Targeting Strategies for Drug Design and Delivery. *Nat. Rev. Drug Discov.* **2010,** *9,* 29–42.
21. Falcon, B. L.; Stewart, J.; Ezell, S.; Hanson, J.; Wijsman, J.; Ye, X.; Westin, E.; Donoho, G.; Credille, K.; Uhlik, M. T. High-Content Multiplexed Tissue Imaging and Quantification for Cancer Drug Discovery. *Drug Discov. Today* **2013,** *18,* 510–522.

22. Hudson, C. C.; Oakley, R. H.; Sjaastad, M. D.; Loomis, C. R. High-Content Screening of Known G Protein-Coupled Receptors by Arrestin Translocation. *Methods Enzymol.* **2006,** *414,* 63–78.
23. Garippa, R. J.; Hoffman, A. F.; Gradl, G.; Kirsch, A. High-Throughput Confocal Microscopy for β-Arrestin-Green Fluorescent Protein Translocation G Protein-Coupled Receptor Assays Using the Evotec Opera. *Methods Enzymol.* **2006,** *414,* 99–120.
24. Baus, D.; Yan, Y.; Li, Z.; Garyantes, T.; de Hoop, M.; Tennagels, N. A Robust Assay Measuring GLUT4 Translocation in Rat Myoblasts Overexpressing GLUT4-myc and AS160_v2. *Anal. Biochem.* **2010,** *397,* 233–240.
25. Blackmore, M. G.; Moore, D. L.; Smith, R. P.; Goldberg, J. L.; Bixby, L.; Lemmon, V. P. Regulators of Axon Growth. *Mol. Cell* **2011,** *44,* 43–54.
26. Usher, L. C.; Johnstone, A. J.; Erturk, A.; Hu, Y.; Strikis, D.; Wanner, I. B.; Moorman, S.; Lee, J.; Min, J.; Ha, H.; Duan, Y.; Hoffman, S.; Goldberg, J. L.; Bradke, F.; Chang, Y.; Lemmon, V. P.; Bixby, J. L. A Chemical Screen Identifies Novel Compounds That Overcome Glial-Mediated Inhibition of Neuronal Regeneration. *J. Neurosci.* **2010,** *30,* 4693–4706.
27. Rudhard, Y.; Sengupta Ghosh, A.; Lippert, B.; Böcker, A.; Pedaran, M.; Krämer, J.; Ngu, H.; Foreman, O.; Liu, Y.; Lewcock, J. W. Identification of 12/15-Lipoxygenase as a Regulator of Axon Degeneration Through High-Content Screening. *J. Neurosci.* **2015,** *35,* 2927–2941.
28. Isherwood, B. J.; Walls, R. E.; Roberts, M. E.; Houslay, T. M.; Brave, S. R.; Barry, S. T.; Carragher, N. O. High-Content Analysis to Leverage a Robust Phenotypic Profiling Approach to Vascular Modulation. *J. Biomol. Screen.* **2013,** *18,* 1246–1259.
29. Dragunow, M. High-Content Analysis in Neuroscience. *Nat. Rev. Neurosci.* **2008,** *9,* 779–788.
30. Hasson, S. A.; Kane, L. A.; Yamano, K.; Huang, C.-H.; Sliter, D. A.; Buehler, E.; Wang, C.; Heman-Ackah, S. M.; Hessa, T.; Guha, R.; Martin, S. E.; Youle, R. J. High-Content Genome-Wide RNAi Screens Identify Regulators of Parkin Upstream of Mitophagy. *Nature* **2013,** *504,* 291–295.
31. Attene-Ramos, M. S.; Huang, R.; Sakamuru, S.; Witt, K. L.; Beeson, G. C.; Shou, L.; Schnellmann, R. G.; Beeson, C. S.; Tice, R. R.; Austin, C. P.; Xia, M. A Systematic Study of Mitochondrial Toxicity of Environmental Chemicals Using Quantitative High Throughput Screening. *Chem. Res. Toxicol.* **2013,** *26,* 1323–1332.
32. Zhang, L.; Yu, J.; Pan, H.; Hu, P.; Hao, Y.; Cai, W.; Zhu, H.; Yu, A. D.; Xie, X.; Ma, D.; Yuan, J. Small Molecule Regulators of Autophagy Identified by an Image-Based High-Throughput Screen. *Proc. Natl. Acad. Sci. U. S. A.* **2007,** *104,* 19023–19028.
33. Diaz, D.; Scott, A.; Carmichael, P.; Shi, W.; Costales, C. Evaluation of an Automated in vitro Micronucleus Assay in CHO-K1 Cells. *Mutat. Res. Genet. Toxicol. Environ. Mutagen.* **2007,** *630,* 1–13.
34. Gough, A.; Shun, T. Y.; Taylor, D. L.; Schurdak, M. A Metric and Workflow for Quality Control in the Analysis of Heterogeneity in Phenotypic Profiles and Screens. *Methods* **2016,** *2016* (96), 12–26.
35. Altschuler, S. J.; Wu, L. F. Cellular Heterogeneity: Do Differences Make a Difference? *Cell* **2010,** *141,* 559–563.
36. Li, Z.; Yan, Y.; Powers, E. A.; Ying, X.; Janjua, K.; Garyantes, T.; Baron, B. Identification of Gap Junction Blockers Using Automated Fluorescence Microscopy Imaging. *J. Biomol. Screen.* **2003,** *8,* 489–499.
37. Snijder, B.; Pelkmans, L. Origins of Regulated Cell-to-Cell Variability. *Nat. Rev. Mol. Cell Biol.* **2011,** *12,* 119–125.
38. Snijder, B.; Sacher, R.; Rämö, P.; Damm, E.-M.; Liberali, P.; Pelkmans, L. Population Context Determines Cell-to-Cell Variability in Endocytosis and Virus Infection. *Nature* **2009,** *461,* 520–523.
39. Kerz, M.; Folarin, A.; Meleckyte, R.; Watt, F. M.; Dobson, R. J.; Danovi, D. A Novel Automated High-Content Analysis Workflow Capturing Cell Population Dynamics from Induced Pluripotent Stem Cell Live Imaging Data. *J. Biomol. Screen.* **2016**. pii: http://dx.doi.org/1087057116652064.
40. Logan, D. J.; Shan, J.; Bhatia, S. N.; Carpenter, A. E. Quantifying Co-Cultured Cell Phenotypes in High-Throughput Using Pixel-Based Classification. *Methods* **2016,** *96,* 6–11.
41. Prasad, S.; Hogaboam, C. M.; Jarai, G. Deficient Repair Response of IPF Fibroblasts in a Co-Culture Model of Epithelial Injury and Repair. *Fibrogenesis Tissue Repair* **2014,** *7,* 7.
42. Trask, O. J.; Moore, A.; LeCluyse, E. L. A Micropatterned Hepatocyte Coculture Model for Assessment of Liver Toxicity Using High-Content Imaging Analysis. *Assay Drug Dev. Technol.* **2014,** *12,* 16–27.
43. Lee, J. A.; Berg, E. L. Neoclassic Drug Discovery: The Case for Lead Generation Using Phenotypic and Functional Approaches. *J. Biomol. Screen.* **2013,** *18,* 1143–1155.
44. Moffat, J. G.; Rudolph, J.; Bailey, D. Phenotypic Screening in Cancer Drug Discovery—Past, Present and Future. *Nat. Rev. Drug Discov.* **2014,** *13,* 588–602.
45. Vincent, F.; Loria, P.; Pregel, M.; Stanton, R.; Kitching, L.; Nocka, K.; Doyonnas, R.; Steppan, C.; Gilbert, A.; Schroeter, T.; Peakman, M. Developing predictive assays: the phenotypic screening "rule of 3". *Sci. Transl. Med.* **2015,** *7,* 293ps15.
46. Zhang, L.; Decicco, C. The Changing Face of Innovation in Drug Discovery. In *Collaborative Innovation in Drug Discovery;* Chaguturu, R., Ed.; John Wiley & Sons, Inc: Hoboken, NJ, 2014. http://dx.doi.org/10.1002/9781118778166.ch4.
47. Ioannidis, J. Extrapolating from Animals to Humans. *Sci. Transl. Med.* **2012,** *4,* 1–4.
48. Abdallah, B. M.; Kassem, M. Human Mesenchymal Stem Cells: From Basic Biology to Clinical Applications. *Gene Ther.* **2008,** *15,* 109–116.
49. Lin, J.; Musunuru, K. Genome Engineering Tools for Building Cellular Models of Disease. *FEBS J.* **2016;** http://dx.doi.org/10.1111/febs.13763.
50. Desbordes, S. C.; Placantonakis, D. G.; Ciro, A.; Socci, N. D.; Lee, G.; Djaballah, H.; Studer, L. High-Throughput Screening Assay for the Identification of Compounds Regulating Self-Renewal and Differentiation in Human Embryonic Stem Cells. *Cell Stem Cell* **2008,** *2,* 602–612.
51. Haston, K. M.; Finkbeiner, S. Clinical Trials in a Dish: The Potential of Pluripotent Stem Cells to Develop Therapies for Neurodegenerative Diseases. *Annu. Rev. Pharmacol. Toxicol.* **2016,** *56,* 489–510.
52. Lee, G.; Ramirez, C. N.; Kim, H.; Zeltner, N.; Liu, B.; Radu, C.; Bhinder, B.; Kim, Y. J.; Choi, I. Y.; Mukherjee-Clavin, B.; Djaballah, H.; Studer, L. Large-Scale Screening Using Familial Dysautonomia Induced Pluripotent Stem Cells Identifies Compounds That Rescue IKBKAP Expression. *Nat. Biotechnol.* **2012,** *30,* 1244–1248.
53. Leha, A.; Moens, N.; Meleckyte, R.; Culley, O. J.; Gervasio, M. K.; Kerz, M.; Reimer, A.; Cain, S. A.; Streeter, I.; Folarin, A.; Stegle, O.; Kielty, C. M.; Durbin, R.; Watt, F. M.; Danovi, D. A High-Content Platform to Characterise Human Induced Pluripotent Stem Cell Lines. *Methods* **2015,** *96,* 85–96.
54. Hattori, F.; Chen, H.; Yamashita, H.; Tohyama, S.; Satoh, Y.; Yuasa, S.; Li, W.; Yamakawa, H.; Tanaka, T.; Onitsuka, T.; Shimoji, K.; Ohno, Y.; Egashira, T.; Kaneda, R.; Murata, M.; Hidaka, K.; Morisaki, T.; Sasaki, E.; Suzuki, T.; Sano, M.; Makino, S.; Oikawa, S.; Fukuda, K. Nongenetic Method for Purifying Stem Cell-Derived Cardiomyocytes. *Nat. Methods* **2010,** *7,* 61–66.
55. Sandercock, A. M.; Rust, S.; Guillard, S.; Sachsenmeier, K. F.; Holoweckyj, N.; Hay, C.; Flynn, M.; Huang, Q.; Yan, K.; Herpers, B.; Price, L. S.; Soden, J.; Freeth, J.; Jermutus, L.; Hollingsworth, R.; Minter, R. Identification of Anti-Tumour Biologics Using Primary Tumour Models, 3-D Phenotypic Screening and Image-Based Multi-Parametric Profiling. *Mol. Cancer* **2015,** *14,* 147.
56. Ramachandran, K.; Peng, X.; Bokvist, K.; Stehno-Bittel, L. Assessment of Re-aggregated Human Pancreatic Islets for Secondary Drug Screening. *Br. J. Pharmacol.* **2014,** *171,* 3010–3022.
57. Hirschhaeuser, F.; Menne, H.; Dittfeld, C.; West, J.; Mueller-Klieser, W.; Kunz-Schughart, L. A. Multicellular Tumor Spheroids: An Underestimated Tool is Catching up Again. *J. Biotechnol.* **2010,** *148,* 3–15.
58. Wenzel, C.; Otto, S.; Prechtl, S.; Parczyk, K.; Steigemann, P. A Novel 3D High-Content Assay Identifies Compounds That Prevent Fibroblast Invasion into Tissue Surrogates. *Exp. Cell Res.* **2015,** *339,* 35–43.
59. LaBarbera, D. V.; Reid, B. G.; Yoo, B. H. The Multicellular Tumor Spheroid Model for High-Throughput Cancer Drug Discovery. *Expert Opin. Drug Discovery* **2012,** *7,* 819–830.
60. Fennema, E.; Rivron, N.; Rouwkema, J.; van Blitterswijk, C.; De Boer, J. Spheroid Culture as a Tool for Creating 3D Complex Tissues. *Trends Biotechnol.* **2013,** *31,* 108–115.
61. Monjaret, F.; Fernandes, M.; Duchemin-Pelletier, E.; Argento, A.; Degot, S.; Young, J. Fully Automated One-Step Production of Functional 3D Tumor Spheroids for High-Content Screening. *J. Lab. Autom.* **2016,** *21,* 268–280.

62. Krausz, E.; de Hoogt, R.; Gustin, E.; Cornelissen, F.; Grand-Perret, T.; Janssen, L.; Vloemans, N.; Wuyts, D.; Frans, S.; Axel, A.; Peeters, P. J.; Hall, B.; Cik, M. Translation of a Tumor Microenvironment Mimicking 3D Tumor Growth Co-culture Assay Platform to High-Content Screening. *J. Biomol. Screen.* **2012,** *18,* 1–13.
63. Ivascu, A.; Kubbies, M. Rapid Generation of Single-Tumor Spheroids for High-Throughput Cell Function and Toxicity Analysis. *J. Biomol. Screen.* **2006,** *11,* 922–932.
64. Pawley, J. B. *Ed; Handbook of Biological Confocal Microscopy,* 3rd ed.; Springer: Berlin, 2006.
65. Benam, K. H.; Villenave, R.; Lucchesi, C.; Varone, A.; Hubeau, C.; Lee, H.-H.; Alves, S. E.; Salmon, M.; Ferrante, T. C.; Weaver, J. C.; Bahinski, A.; Hamilton, G. A.; Ingber, D. E. Small Airway-on-a-Chip Enables Analysis of Human Lung Inflammation and Drug Responses In Vitro. *Nat. Methods* **2013,** *13,* 151–157.
66. Grimm, J. B.; English, B. P.; Chen, J.; Slaughter, J. P.; Zhang, Z.; Revyakin, A.; Patel, R.; Macklin, J. J.; Normanno, D.; Singer, R. H.; Lionnet, T.; Lavis, L. D. A General Method to Improve Fluorophores for Live-Cell and Single-Molecule Microscopy. *Nat. Methods* **2015,** *12,* 244–250.
67. Giesen, C.; Wang, H. A. O.; Schapiro, D.; Zivanovic, N.; Jacobs, A.; Hattendorf, B.; Schüffler, P. J.; Grolimund, D.; Buhmann, J. M.; Brandt, S.; Varga, Z.; Wild, P. J.; Günther, D.; Bodenmiller, B. Highly Multiplexed Imaging of Tumor Tissues With Subcellular Resolution by Mass Cytometry. *Nat. Methods* **2014,** *11,* 417–422.
68. Singh, S.; Carpenter, A. E.; Genovesio, A. Increasing the Content of High-Content Screening: An Overview. *J. Biomol. Screen.* **2014,** *19,* 640–650.
69. Cornelissen, F.; Cik, M.; Gustin, E. Phaedra, a Protocol-Driven System for Analysis and Validation of High-Content Imaging and Flow Cytometry. *J. Biomol. Screen.* **2012,** *17,* 496–506.
70. Macarron, R.; Banks, M. N.; Bojanic, D.; Burns, D. J.; Cirovic, D. A.; Garyantes, T.; Green, D. V. S.; Hertzberg, R. P.; Janzen, W. P.; Paslay, J. W.; Schopfer, U. Impact of High-Throughput Screening. *Nat. Rev. Drug Discov.* **2011,** *10,* 188–195.
71. Zhang, L.; Cvijic, M. E.; Lippy, J.; Myslik, J.; Brenner, S. L.; Binnie, A.; Houston, J. G. Case Study: Technology Initiative Led to Advanced Lead Optimization Screening Processes at Bristol-Myers Squibb, 2004–2009. *Drug Discov. Today* **2012,** *17,* 733–740.
72. Shariff, A.; Kangas, J.; Coelho, L. P.; Quinn, S.; Murphy, R. F. Automated Image Analysis for High-Content Screening and Analysis. *J. Biomol. Screen.* **2010,** *15,* 726–734.
73. Kümmel, A.; Gubler, H.; Gehin, P.; Beibel, M.; Gabriel, D.; Parker, C. N. Integration of Multiple Readouts into the z' Factor for Assay Quality Assessment. *J. Biomol. Screen.* **2010,** *15,* 95–101.
74. Erdmann, G.; Volz, C.; Boutros, M. Systematic Approaches to Dissect Biological Processes in Stem Cells by Image-Based Screening. *Biotechnol. J.* **2012,** *7,* 768–778.
75. Fischer, B.; Sandmann, T.; Horn, T.; Billmann, M.; Chaudhary, V.; Huber, W.; Boutros, M. A Map of Directional Genetic Interactions in a Metazoan Cell. *Elife* **2015,** 1–21.
76. Gorenstein, J.; Zack, B.; Marszalek, J. R.; Bagchi, A.; Subramaniam, S.; Carroll, P.; Elbi, C. Reducing the Multidimensionality of High-Content Screening Into Versatile Powerful Descriptors. *Biotechniques* **2010,** *49,* 663–665.
77. Haney, S. A. Increasing the Robustness and Validity of RNAi Screens. *Pharmacogenomics* **2007,** *8,* 1037–1049.
78. Li, L.; Zhou, Q.; Voss, T. C.; Quick, K. L.; LaBarbera, D. V. High-Throughput Imaging: Focusing in on Drug Discovery in 3D. *Methods* **2016,** *96,* 97–102.
79. Reid, B. G.; Jerjian, T.; Patel, P.; Zhou, Q.; Yoo, B. H.; Kabos, P.; Sartorius, C. A.; Labarbera, D. V. Live Multicellular Tumor Spheroid Models for High-Content Imaging and Screening In Cancer Drug Discovery. *Curr. Chem. Genomics Transl. Med.* **2014,** *8,* 27–35.
80. Gough, W.; Hulkower, K. I.; Lynch, R.; Mcglynn, P.; Uhlik, M.; Yan, L.; Lee, J. A. A Quantitative, Facile, and High-Throughput Image-Based Cell Migration Method is a Robust Alternative to the Scratch Assay. *J. Biomol. Screen.* **2011,** *16,* 155–163.
81. Sommer, C.; Gerlich, D. W. Machine Learning in Cell Biology—Teaching Computers to Recognize Phenotypes. *J. Cell Sci.* **2013,** *126,* 5529–5539.
82. Kraus, O. Z.; Frey, B. J. Computer Vision for High Content Screening. *Crit. Rev. Biochem. Mol. Biol.* **2016,** *51,* 102–109. http://dx.doi.org/10.3109/10409238.2015.1135868.
83. Collins, M. A. Generating "Omic Knowledge": The Role of Informatics in High Content Screening. *Comb. Chem. High Throughput Screen.* **2009,** *12,* 917–925.
84. Reisen, F.; Sauty de Chalon, A.; Pfeifer, M.; Zhang, X.; Gabriel, D.; Selzer, P. Linking Phenotypes and Modes of Action Through High-Content Screen Fingerprints. *Assay Drug Dev. Technol.* **2015,** *13,* 415–427.
85. Allan, C.; Burel, J.; Moore, J.; Blackburn, C.; Linkert, M.; Macdonald, D.; Moore, W. J.; Neves, C.; Patterson, A.; Porter, M.; Tarkowska, A.; Loranger, B.; Avondo, J.; Lianas, L.; Leo, S.; Hands, K.; Hay, R. T.; Best, C.; Kleywegt, G. J.; Zanetti, G.; Jason, R. Europe PMC Funders Group OME Remote Objects (OMERO): A Flexible, Model-Driven Data Management System for Experimental Biology. *Nat. Methods* **2012,** *9,* 245–253.
86. Li, S.; Besson, S.; Blackburn, C.; Carroll, M.; Ferguson, R. K.; Flynn, H.; Gillen, K.; Leigh, R.; Lindner, D.; Linkert, M.; Moore, W. J.; Ramalingam, B.; Rozbicki, E.; Rustici, G.; Tarkowska, A.; Walczysko, P.; Williams, E.; Allan, C.; Burel, J.-M.; Moore, J.; Swedlow, J. R. Metadata Management for High Content Screening in OMERO. *Methods* **2016,** *96,* 27–32.
87. Jones, T. R.; Kang, I. H.; Wheeler, D. B.; Lindquist, R. A.; Papallo, A.; Sabatini, D. M.; Golland, P.; Carpenter, A. E. Cell Profiler Analyst: Data Exploration and Analysis Software for Complex Image-Based Screens. *BMC Bioinf.* **2008,** *9,* 482.
88. Jakobsen, K. R.; Demuth, C.; Sorensen, B. S.; Nielsen, A. L. The Role of Epithelial to Mesenchymal Transition in Resistance to Epidermal Growth Factor Receptor Tyrosine Kinase Inhibitors in Non-Small Cell Lung Cancer. *Transl. Lung Cancer Res.* **2016,** *5,* 172–182.
89. Lovisa, S.; LeBleu, V. S.; Tampe, B.; Sugimoto, H.; Vadnagara, K.; Carstens, J. L.; Wu, C.-C.; Hagos, Y.; Burckhardt, B. C.; Pentcheva-Hoang, T.; Nischal, H.; Allison, J. P.; Zeisberg, M.; Kalluri, R. Epithelial-to-Mesenchymal Transition Induces Cell Cycle Arrest and Parenchymal Damage in Renal Fibrosis. *Nat. Med.* **2015,** *21,* 998–1009.
90. Li, Z. *Leveraging Innovation in High Content Screening: The Integration of Bioimaging, Informatics, and Data Management to Realize High Throughput High Content Screening Using Physiologically Relevant Cellular Models;* Society for Laboratory Automation and Screening: San Diego, CA, 2012.
91. Kenny, H. A.; Lal-Nag, M.; White, E. A.; Shen, M.; Chiang, C.-Y.; Mitra, A. K.; Zhang, Y.; Curtis, M.; Schryver, E. M.; Bettis, S.; Jadhav, A.; Boxer, M. B.; Li, Z.; Ferrer, M.; Lengyel, E. Quantitative High Throughput Screening Using a Primary Human Three-Dimensional Organotypic Culture Predicts In Vivo Efficacy. *Nat. Commun.* **2015,** *6,* 6220.
92. Murphy, D. A.; Courtneidge, S. A. The "Ins" and "Outs" of Podosomes and Invadopodia: Characteristics, Formation and Function. *Nat. Rev. Mol. Cell Biol.* **2011,** *12,* 413–426.
93. Quintavalle, M.; Elia, L.; Price, J. H.; Heynen-Genel, S.; Courtneidge, S. A. A Cell-Based High-Content Screening Assay Reveals Activators and Inhibitors of Cancer Cell Invasion. *Sci. Signal.* **2011,** *4,* ra49.
94. Najm, F. J.; Madhavan, M.; Zaremba, A.; Shick, E.; Karl, R. T.; Factor, D. C.; Miller, T. E.; Nevin, Z. S.; Kantor, C.; Sargent, A.; Quick, K. L.; Schlatzer, D. M.; Tang, H.; Papoian, R.; Brimacombe, K. R.; Shen, M.; Boxer, M. B.; Jadhav, A.; Robinson, A. P.; Podojil, J. R.; Miller, S. D.; Miller, R. H.; Tesar, P. J. Drug-Based Modulation of Endogenous Stem Cells Promotes Functional Remyelination In Vivo. *Nature* **2015,** *522,* 216–220.
95. Dominguez, E.; Galmozzi, A.; Chang, J. W.; Hsu, K.-L.; Pawlak, J.; Li, W.; Godio, C.; Thomas, J.; Partida, D.; Niessen, S.; O'Brien, P. E.; Russell, A. P.; Watt, M. J.; Nomura, D. K.; Cravatt, B. F.; Saez, E. Integrated Phenotypic and Activity-Based Profiling Links Ces3 to Obesity and Diabetes. *Nat. Chem. Biol.* **2014,** *10,* 113–121.
96. Hanash, S. Disease Proteomics. *Nature* **2003,** *422,* 226–232.
97. Yu, D.; Swaroop, M.; Wang, M.; Baxa, U.; Yang, R.; Yan, Y.; Coksaygan, T.; DeTolla, L.; Marugan, J. J.; Austin, C. P.; McKew, J. C.; Gong, D.-W.; Zheng, W. Niemann–Pick Disease Type C: Induced Pluripotent Stem Cell-Derived Neuronal Cells for Modeling Neural Disease and Evaluating Drug Efficacy. *J. Biomol. Screen.* **2014,** *19,* 1164–1173.
98. Kubben, N.; Brimacombe, K. R.; Donegan, M.; Li, Z.; Misteli, T. A High-Content Imaging-Based Screening Pipeline for the Systematic Identification of Anti-Progeroid Compounds. *Methods* **2016,** *96,* 46–58.
99. Beattie, L.; Kaye, P. M. Leishmania-Host Interactions: What has Imaging Taught Us? *Cell. Microbiol.* **2011,** *13,* 1659–1667.
100. Siqueira-Neto, J. L.; Moon, S.; Jang, J.; Yang, G.; Lee, C.; Moon, H. K.; Chatelain, E.; Genovesio, A.; Cechetto, J.; Freitas-Junior, L. H. An Image-Based High-Content Screening Assay for Compounds Targeting Intracellular Leishmania Donovani Amastigotes in Human Macrophages. *PLoS Negl. Trop. Dis.* **2012,** *6.*
101. Aulner, N.; Danckaert, A.; Rouault-Hardoin, E.; Desrivot, J.; Helynck, O.; Commere, P. H.; Munier-Lehmann, H.; Späth, G. F.; Shorte, S. L.; Milon, G.; Prina, E. High Content Analysis of Primary Macrophages Hosting Proliferating Leishmania Amastigotes: Application to Anti-Leishmanial Drug Discovery. *PLoS Negl. Trop. Dis.* **2013,** *7* (4), e2154. http://www.ncbi.nlm.nih.gov/pmc/articles/PMC3617141/.
102. Amos, L. A.; Löwe, J. How Taxol® Stabilises Microtubule Structure. *Chem. Biol.* **1999,** *6,* 65–69.

103. Jordan, M. A.; Wilson, L. Microtubules as a Target for Anticancer Drugs. *Nat. Rev. Cancer* **2004,** *4,* 253–265.
104. Kavallaris, M. Microtubules and Resistance to Tubulin-Binding Agents. *Nat. Rev. Cancer* **2010,** *10,* 194–204.
105. Sum, C. S.; Nickischer, D.; Lei, M.; Weston, A.; Zhang, L.; Schweizer, L. Establishing a High-Content Analysis Method for Tubulin Polymerization to Evaluate Both the Stabilizing and Destabilizing Activities of Compounds. *Curr. Chem. Genomics Transl. Med.* **2014,** *8*, 16–26.

Relevant Websites

http://cellprofiler.org/—Broad Institute, free open-access image analysis and data management software Cell Profiler, and Cell Profiler Analyst.
http://micro.magnet.fsu.edu/primer/index.html—Florida State University, Molecular Expressions website-Home.
https://www.biacore.com/high-content-analysis/applications/Publications_Database/index.html—GE Healthcare, Library of HCS publications related to InCell instruments.
https://www.moleculardevices.com/systems/high-content-imaging/imagexpress-micro-confocal-high-content-imaging-system—Molecular Devices, library of HCS publications related to Molecular Devices HCS instrument
http://www.ncbi.nlm.nih.gov/books/NBK100913/—NIH Assay Guidance Manual. Chapter—Assay Development Guidelines for Image-Based High Content Screening, High Content Analysis and High Content Imaging.
http://cellularimaging.perkinelmer.com/publications/featured.php—Perkin Elmer, library of HCS publications related to Perkin Elmer HCS instrument.
http://www.thermofisher.com/us/en/home/life-science/cell-analysis/cellular-imaging/high-content-screening/high-content-screening-instruments.html#pubs—Thermofisher/Cellomics, library of HCS publications related Cellomics instrument.
http://ttplabtech.com/resources/bibliography/ - acumen Cellista—TTP Labtech, library of HCS publications related to TTP Acumen.

2.16 3D High-Content Screening of Organoids for Drug Discovery

L Li and DV LaBarbera, University of Colorado Anschutz Medical Campus, Aurora, CO, United States

© 2017 Elsevier Ltd. All rights reserved.

2.16.1	**Introduction**	388
2.16.2	**High-Content Screening and Analysis**	389
2.16.2.1	HCS Assay Development	390
2.16.2.1.1	Assay plates	390
2.16.2.1.2	Automation	390
2.16.2.1.3	Fluorescent probes	391
2.16.2.2	Image Acquisition	391
2.16.2.3	Image Analysis	391
2.16.2.3.1	Image correction	391
2.16.2.3.2	Image segmentation	391
2.16.2.3.3	Object tracking	392
2.16.2.3.4	Feature extraction	392
2.16.2.3.5	Machine learning	392
2.16.2.4	Data Analysis	393
2.16.2.4.1	Statistical evaluation	393
2.16.2.4.2	Data normalization	394
2.16.2.4.3	Hit selection	395
2.16.2.4.4	Data visualization	395
2.16.2.4.5	Data reduction methods	395
2.16.3	**High-Throughput 3D Culture Technologies**	396
2.16.3.1	Traditional 3D Culture Techniques	397
2.16.3.1.1	Spinner flask and rotating wall vessel bioreactors	397
2.16.3.1.2	Solid scaffolds	397
2.16.3.1.3	Hydrogel	400
2.16.3.2	HCS Compatible 3D Cell Culture Platforms	400
2.16.3.2.1	The hanging drop method	401
2.16.3.2.2	The liquid overlay methods with non-adherent surface plates	401
2.16.3.2.3	Micropatterned plates	401
2.16.3.2.4	Magnetic levitation	401
2.16.3.2.5	Microfluidic devices	402
2.16.4	**Hardware and Software for 3D HCS**	402
2.16.4.1	HCS Hardware	402
2.16.4.1.1	Brightfield and widefield microscopy, and live-cell 3D imaging	402
2.16.4.1.2	Confocal microscopy	404
2.16.4.1.3	Two-photon microscopy	405
2.16.4.1.4	Light sheet fluorescence microscopy	405
2.16.4.1.5	Laser scanning cytometers	406
2.16.4.2	HCS Software	406
2.16.4.2.1	HCS image acquisition software	406
2.16.4.2.2	Deconvolution	408
2.16.4.2.3	HCS image visualizations and analysis software	408
2.16.4.2.4	HCS workflow platform	410
2.16.5	**Perspective of the Key Limitations of 3D HCA and HCS Technologies**	410
2.16.6	**Outlook and Conclusion**	410
References		410
Relevant Websites		415

2.16.1 Introduction

More than 90% of drugs that pass through preclinical studies fail to meet the desired efficacy or safety margins required in subsequent clinical trials. As a result, successful drug development requires decades of research that costs hundreds of millions to billions of dollars.[1–3] While there are many factors that contribute to the high attrition rate of drug candidates, it is reasonable to argue that our drug discovery models are a significant contributing factor due to their inability to identify drug leads that are safe and effective

in humans. In the modern era of drug discovery, two-dimensional (2D) cell-based assay models have been the dominant approach used to study cellular processes in human disease and for high-throughput drug discovery.[2] 2D-cell models are relatively cost-effective and highly amenable to high-throughput and high-content screening (HTS/HCS) drug discovery, but their cellular responses and phenotypes do not effectively recapitulate the pathology of human disease.[4] Once lead drug candidates are identified, they are assessed for toxicity and efficacy using animal models that provide a controllable experimental environment with complexities similar to those observed within human cells and organs. However, the use of animals in drug research is far from ideal as these models are expensive, time-consuming, low-throughput, vary widely in results among species, and limited by controversial ethical issues.[2] Although animal models remain an important component in the drug development pipeline, there is an unmet need for more predictive efficacy and toxicology models that are amenable to HTS/HCS drug discovery. Over the past decade there has been a boom in concerted multidisciplinary efforts by scientists and biomedical engineers with a vision of developing three-dimensional (3D) ex vivo tissue models of human organ function and other models of human anatomy and disease.[5,6] These 3D models are referred to as organoid, organotypic, or spheroid and are often used interchangeably within the collective literature.[5,7] In this book chapter we will utilize the term organoid for a simple yet elegant description of 3D tissue culture.

Organoids have the distinct feature of self-assembly when relevant microenvironment components are present such as extracellular matrix (ECM) proteins or fibroblast cells (mesenchyme components). Importantly, organoids can be generated from human primary tissues, induced pluripotent stem cells (iPSC), and from existing human cell lines (e.g., the multicellular tumor spheroid model, MCTS).[2,5–9] Various types of organoid models have been reported, including mammary gland, salivary gland, kidney, lung, small intestine, colon, liver, stomach, pancreas, prostate, optic cup, brain, blood vessels, and human tumors.[2,5–9] Importantly, organoids are superior to 2D cell culture models of human disease and function, and in some cases rival animal models, for example cerebral organoids.[10] Organoid models are built using formats that are highly amenable to HTS/HCS such as the liquid overlay, ECM embedded, mechanically supported culture systems, microfluidics, and microchip technologies. The adaptability to HTS/HCS drug and other therapeutic discovery methodologies will be critical to improving our developmental therapeutics pipeline and success rate. Organoids are poised to fill the unmet need to identify more effective therapies with improved clinical translation success rates; therefore, they can be considered as the future of biomedical research. The marriage of high-throughput technologies such as HCS applied to organoid research and therapeutic screening will be important to achieve the promise of precision medicine (Fig. 1).[11] Hence, this book chapter will focus on 3D organoids and technologies applied to high-content screening drug discovery.

2.16.2 High-Content Screening and Analysis

High-throughput screening (HTS) is a technology platform that enables researchers with the capacity for large-scale screening of compound libraries in a rapid and cost-effective manner. In the late 1990s, a more sophisticated HTS drug discovery platform,

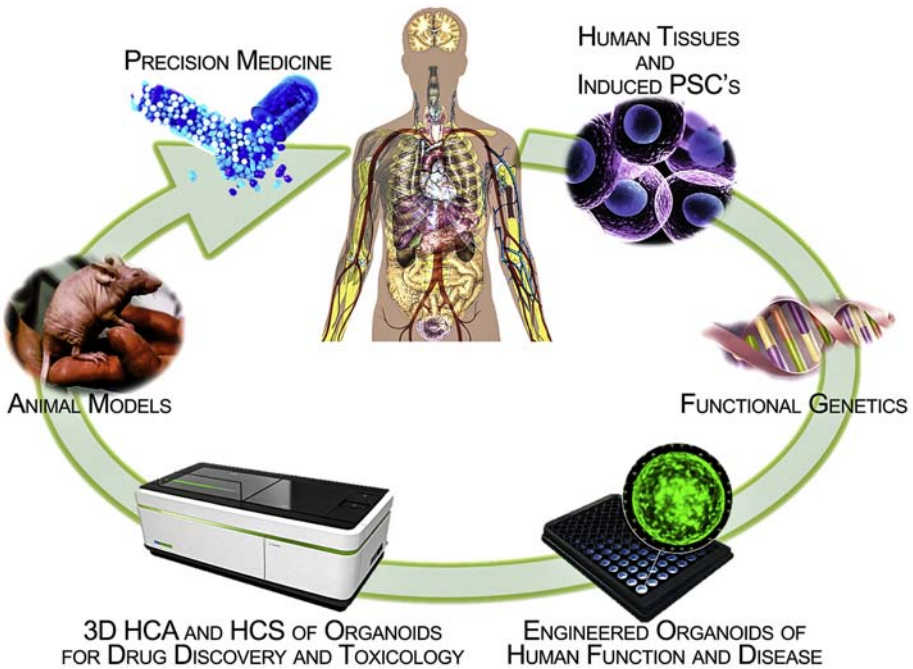

Fig. 1 The marriage of HCS with organoid models will be a key technology component to achieve more effective therapies and the promise of precision and personalized medicine for human disease.

known as high-content screening (HCS), emerged that combines HTS robotic handling technologies together with high-resolution microscopy and multiparametric acquisition and data analysis, also known as high-content analysis (HCA).[12,13] HCS and HCA technology has been quickly adopted by the pharmaceutical industry and government research institutions to characterize preclinical drug candidates and is now integrated into all aspects of contemporary drug discovery. Moreover, the growing availability of HCS instrumentation coupled with funding support from government agencies has spurred an emergence of academic HTS/HCS screening centers and core facilities, promoting worldwide applications of HCS in academia.

HCS image processing can be combined with machine learning to extract objects of interest from biological images and to subsequently analyze data derived from these collections of objects on a population level, constructing biologically meaningful conclusions. The ability to conduct multiple independent measurements simultaneously is one of the most powerful features of HCS. In contrast to traditional HTS, which has a single read out of activity, HCS is able to deliver many properties or features of individual cells or organisms in parallel. In addition to the target-specific fluorescence readouts, multiple parameters such as cytoplasm shape, size, area as well as information about nuclear intensity allow scientists to simultaneously monitor the temporal and spatial relationships between multiple cellular targets in an intact biological system. In addition to the increased content, sophisticated HCA in HCS provides information such as intracellular protein relocation or organelle quantification that is difficult to obtain by conventional methods. Owing to the multiplexing and multiparametric characteristics of HCA, HCS assays are considered to produce higher hit rates compared to conventional bioassays.[14] A typical flow chart for high-content screening experiment consists of four major stages: assay development, image acquisition, image analysis, and data analysis.

2.16.2.1 HCS Assay Development

Developing a high-content assay involves setting up a measurable and reliable reporter of a biological activity and converting it to a quantitative readout. A typical HCS assay consists of a biological sample (individual cells in culture, 3D organoids and tissue samples, or whole organisms) processed to extract a visible readout after appropriate reporter transduction or sample staining that is acquired through automated microscopy and quantified by image analysis. Factors such as the cell seeding density, plate type, plate layout, fluorescent probes, substrate concentrations, and assay kinetics require careful optimization for HCS.

2.16.2.1.1 Assay plates

The choice of assay plate is critical to a successful screening campaign, with advances in miniaturization and detection technologies; current HTS/HCS experiments are usually performed in a highly automated, standardized, and controlled fashion using 96- to 384- or 1536-well microtiter plates provided by suppliers such as Corning, ThermoFisher, and Greiner Bio-One. HCS plates must have excellent optical quality and provide a suitable environment for cellular growth to attain the maximal scan performance capability from high-content imaging systems. Clear flat bottom black plates are recommended for fluorescence-based reading technologies to achieve high quality images with lower background signal and minimal cross talk. The bottom material of an opaque plate is generally made of polystyrene or glass. Tissue culture-treated polystyrene plates with the ability to bind proteins and to support cell attachment are the most commonly used plate type in HTS and are suitable for many HCS applications. Glass is one of the flattest materials and exhibits excellent optical properties, but is less suitable for cell culture. Both glass and plastic bottoms can be coated with various biomolecules to improve the adherences of cells and/or mimic appropriate biological conditions of the assay. Synthetic polypeptide like Poly-D-Lysine (PDL) and a variety of ECM proteins including collagen, laminin, and fibronectin are available for this purpose. The thickness of the plate bottom is another important parameter of the imaging plates as it has implications for the choice of microscope objectives; thin-bottomed ($<200\ \mu m$) plates are recommended for high numerical aperture (NA) objectives as they typically have a short working distance. Thick bottom ($>250\ \mu m$) plates require the use of long working distance (WD) objectives, which typically have a lower numerical aperture.

2.16.2.1.2 Automation

Automation is essential for HTS/HCS; the core of the automated system resides in one or more automatic multichannel liquid handling instruments, which are crucial to the production of high quality data. High-content assays require a great deal of liquid handling since they typically have a relatively large number of steps, including aspirating, transferring, dispensing, and mixing liquids. Commercially available robotic liquid handlers and reagent dispensers can transfer or dispense volumes from the picoliter to milliliter range and greater. These fully automated liquid handling workstations can manage compound addition and dilutions, reformatting of reagent stocks, and complicated immunofluorescence staining protocols. Recent advances in acoustic dispensing have unlocked the potential of high-throughput dose matrix analysis, allowing the creation of efficient and flexible compound synergy assays.[15] Microplate washers tremendously improve the speed and accuracy of many different washing procedures and are particularly useful for high-content assay automation. In addition, most HCS assays use microtiter plates that have been standardized by the American National Standards Institute (ANSI) and Society for Laboratory Automation and Screening (SLAS),[16] which facilitates the use of microplates across plate-handling robots and liquid handling instruments. Robotic plate handling is the key to connecting individual workstations and creating an integrated screening laboratory. Robots and plate stacking arrays are highly amenable to high-content imaging systems, allowing automated integration and increased throughput.

2.16.2.1.3 Fluorescent probes

Labeling technologies have drastically expanded recently; an increasing variety of commercially available fluorescent antibodies and dyes has provided unprecedented insight into intricate cellular events. The most commonly used fluorescent labels are fluorescent proteins, fluorescent dyes, and antibodies.[17] For HCS assays, probes should accurately reflect the underlying biology and minimize the artifacts while avoiding cross talk. Multiplexed fluorescence labeling is one of the most important features in HCS, which involves the use of different sets of fluorescent probes, whose spectral properties are sufficiently distinct, to allow the discrimination of fluorescent signals related to different biosensors. There can be significant bleed through from one fluorescent probe to another due to their broad excitation and emission spectra. The excitation wavelengths chosen should take into account the peak properties of the fluorescent targets to minimize cross excitation. The filters in the emission path must be optimized to minimize cross talk between the different fluorescence emitters and that is directly dependent on the dichroic filter in the optical path. Cell staining simulation tool from Invitrogen,[18] and fluorescence spectrum viewer from Thermo Fisher Scientific,[19] Semlock,[20] and BD Biosciences[21] are useful online applications for choosing fluorescent dyes and assessing their compatibility.

2.16.2.2 Image Acquisition

With a robust assay in hand, the next step is for sophisticated image acquisition hardware. Imagers for HCS are microscopes that automatically capture and store fluorescent images from wells of microtiter plates. Much more than a standard microscope, a high-content imager could also incorporate an automated platform for plate handling and image processing software to quantify the data collected under specified parameters. Since the introduction of automated cell imager in 1997,[12] numerous technological advances and hardware improvements such as auto-focusing and sample positioning have spurred development of automated brightfield and confocal images and laser scanning cytometers. Lamp, light-emitting diodes (LEDs), and lasers are the three typical excitation light sources of HCS imagers. Xenon arc, metal-halide, and mercury lamps provide a broad spectrum to excite many fluorescent dyes and proteins. Lasers and LEDs are currently the optimal choices due to their stable, narrow light output and long lifespan.

Image acquisition is a crucial step for high-content screening as the image quality determines the overall screen quality. Proper selection of the exposure parameters (e.g., exposure time, imaging height), excitation filters, emission filters, and objectives of the microscope is essential to capture the subcellular details for the phenotype while providing sufficient cell counts for robust statistics. As out of focus or over exposure leads to loss of information in the fine structure of images and degradation in the performance of segmentation algorithms in the image processing step, care must be taken to minimize imaging artifacts during an HCS experiment.

2.16.2.3 Image Analysis

The automated image analysis process, or HCA, aims to extract numerical information from large sets of bioimages. Image analysis can be divided into four major steps, including image correction, image segmentation, object tracking, and feature extraction.

2.16.2.3.1 Image correction

Image correction serves to enhance image quality and create a more pronounced distinction between background signal and objects. Imperfections of the optical system (e.g., variation in the output from the light source, slight component misalignment, or even dust on lenses) and unequal excitation of the fluorophore could create nonuniform illumination of the sample and thus differences in signal. Compensation of uneven illumination of the sample during image acquisition is a common step to improve image quality. In addition, microscope systems often produce peripheral illumination as the light is channeled through the various lenses and apertures. Flat-field correction is a standard calibration procedure used to correct peripheral illumination artifacts and normalize signal intensity level, which consists of correcting raw images with a reference image containing no sample. Gray-level transformation and image filtering are other typical image processing techniques for converting an input image into a new image with better visibility.[22]

2.16.2.3.2 Image segmentation

Segmentation is the process of partitioning an image into multiple regions by assigning the same label to the pixels with common features; segmented objects or shapes are often called regions of interest (ROI). The function of image segmentation in an image analysis system for cellular and tissue engineering is to identify biologically meaningful objects such as a nucleus or another functional tissue region for further quantitative characterization.[23] Objects in biological images are often far more difficult to be recognized than typical daily-life images due to their ambiguous boundaries. This is the most challenging step of image analysis and often requires careful optimization of key parameters in order to identify the boundary of each cell and the subcellular compartments correctly so that subsequently extracted cellular features can correctly represent the cellular phenomenon of interest.

Segmentation algorithms consist of multiple image processing steps that either remove pixels or separate large objects from the underlying, closely spaced objects that represent the biological specimen. Image processing filters can be used to enhance general contrast of the images or shapes that have to be segmented. There are various predefined algorithms for segmentation, which are commonly used to identify targeted objects in HCS analysis. Due to its simplicity, thresholding is one of the most commonly used segmentation methods that compares the values of each image pixel to preset threshold values and to label pixels.[22] Values above the threshold are identified as objects and those values below the threshold are considered background. Edge detector or sharpen filters could be useful to detect objects and increase intensity separation with adjacent elements, making thresholding easier. More sophisticated methods including watershed transform, Markov random field (MRF), and model-evolution approaches help split overlapping objects and have been successfully applied to cell segmentation in microscopy.[22]

2.16.2.3.3 Object tracking

Object tracking is used to identify the motion traces of the objects of interest using time-lapse images. For cell-based assays, this refers to the process of identifying and linking segmented cells from frame to frame in the image sequence to obtain cell trajectories. Automated tracking of cells in time-lapse microscopy images enables high-throughput measurements of a range of dynamic cell behaviors, including cell cycle progression, migration and invasion, and apoptosis as well as the reconstruction of cell lineages (parent-daughter relationship). Traditional tracking approaches establish spatiotemporal correspondence between two neighboring time points based on their morphology, position, and motion.[24] More sophisticated algorithms solve this correspondence over multiple image frames simultaneously, achieving significantly better accuracy.[25,26]

2.16.2.3.4 Feature extraction

Once the segmentation process has been successful, the identified objects are used to extract quantifiable features from images. Unlike human eyes that are only sensitive to relative intensity values, computers can easily determine absolute intensity of regions within an image. This ability is used to categorize segmented objects into different features such as morphology, texture, and spatial distribution. These features are extracted from single or multiple fluorescence channels from the same field of view and are used to characterize the phenotypes encountered in each image.[27]

Intensity is the most basic measurement that comes from the image sensor and is related to the number of photons captured on the sensor during the exposure time. The total intensity, or integrated intensity, represents an aggregation of all the pixel intensities combined to make up the unit area. The intensity of a pixel is related to the amount of marker at that location; thus, the measured total intensity is proportional to the amount of substance labeled. The mean intensity feature is the average accumulation of pixel intensities per unit area.

Morphology features characterize the size and shape of an object of interest in the image.[28] For globular objects, the size measurements include area, radius, and perimeter while the shape is described by features such as length of the major and minor axes, orientation, compactness, symmetry, and roundness. Features like curvature, number of branch points, cross-link spaces, and cross-link densities are frequently used to describe tubular objects. Furthermore, the ratio of the same morphological feature from different biological structures can be used as a phenotype to reflect the relative morphological change between different objects. For instance, the ratio of the length and width of an object can serve as a measure of elongation, which may be of biological interest.

Texture is a property that represents the surface and structure of an image.[28] Texture descriptors characterize spatial smoothness and regularity for each marker, and are often used for characterizing the fine patterns of protein localization. Typical descriptions associated with image texture properties are smooth, rough, granular, spotty, fibrous, line patterns, etc. Texture analysis is a special technique that can be used to quantify biological effects, which makes use of the patterns or structures of the fluorescent region rather than using the average intensity or shape of the region.

2.16.2.3.5 Machine learning

Machine learning is a rich and rapidly advancing field of computer science and is widely used in HCS to classify biologically meaningful pattern features that are traced by fluorescent markers.[29] Machine learning is particularly superior to conventional image processing programs when it comes to solving complex multidimensional data analysis tasks that are not easily described by a few parameters. In general, machine-learning approaches can be broadly classified into two categories: supervised and unsupervised learning. Supervised machine learning methods aim to make accurate predictions of large sets of data samples based on a few training examples. These methods can be applied to cell phenotypic recognition and clustering on the basis of hundreds of quantitative nuclear features. In this approach, the user generates a training data set by annotating some representative examples according to predefined classes. The machine learning algorithm (e.g., support vector machines, adaptive boosting, and random forest) automatically infers the rules to discriminate the classes, which can then be applied to independent large data sets. Supervised machine learning has been an important backbone for analysis pipelines in many HCS projects.[30] Unsupervised learning, by contrast, extracts information from the data completely independent of prior user definition and enables the exploration of novel phenotypes. The goal of unsupervised machine learning is to group data points into clusters on the basis of a similarity measure or to facilitate data mining by reducing the complexity of the data. Unsupervised learning algorithm (e.g., k-means clustering, Gaussian mixture model, and hierarchical clustering) makes no initial assumptions about how the data are related and instead seeks to discover and characterize the hidden distribution of data. These methods are extremely useful to distinguish between image perturbations resulting from small molecules or RNA interferences in cases where the phenotype is unknown.

There has been tremendous growth in the computational methods for automated learning and discovery over the past three decades. Machine-learning tools such as CellProfiler Analyst,[31] CellOrganizer[32] and PerkinElmer's PhenoLOGIC plug-in can be trained to identify and count cells belonging to different subpopulations and have been optimized for the needs of large-scale microscopic image data. For example, the PhenoLOGIC plug-in provides advanced supervised machine learning technology for scientists to develop the image analysis algorithms for highly robust and statistically relevant classification of cells using a simple learn-by-example approach. After categorizing examples of objects or regions with a few clicks of the mouse, the software combines the most meaningful parameters to identify all similar objects or regions in all other images of the same experiment. Machine learning holds the potential to replace most manually programmed analysis pipelines eventually to facilitate assay development and increase processing throughput.[33]

2.16.2.4 Data Analysis

A central goal of image analysis is the conversion of microscopic images into biologically meaningful quantitative data. Recent development of quantitative HTS (qHTS) that performs multiple concentration experiments in a low-volume cellular system[34] and the increasing size of chemical and biological libraries used in HCS campaigns generate overwhelming amounts of complex multidimensional data sets in a short period of time. Mining these large HCS datasets relies heavily on computational approaches for efficient and unbiased quality assessment and interpretation. HCS, unlike HTS cell-based assays, often has large variability because of heterogeneous cellular populations in a given well. In practice, all HTS assays contain both random and systematic variability that contribute to the "noise" associated with the experimental data. HCS multiparametric assays also introduce several new sources of variability such as image acquisition parameters, size of the imaged area, and the data extraction algorithm.

2.16.2.4.1 Statistical evaluation

There are various biological, instrumental, and environmental factors that contribute to assay performance in HCS; thus, detecting systematic error is essential during assay validation and optimization of assays. Statistical evaluation of the assay performance is a very critical step to determine if the data collected from each plate meet the minimum quality requirements. A number of statistical parameters have been developed to evaluate the quality of HTS assays.[35] Statistical analysis is also pivotal in the hit selection process from primary screens and in the evaluation during confirmatory screens.

2.16.2.4.1.1 Signal to background ratio and signal to noise ratio

Signal-to-background ratio (S/B) is the simplest method for calculating assay performance, taking the ratio of the mean value of the positive control responses to the background or negative control responses (**Table 1**, entry 1), but it does not contain any information regarding data variability. Signal-to-noise ratio (S/N) is used in imaging as a physical measure of the sensitivity of an imaging system. S/N is defined as the ratio of the difference between the positive and negative controls to the variance of the negative controls (**Table 1**, entry 2); however, S/N only captures the variability of the negative controls group. Consequently, both S/B and S/N are considered weak parameters to represent the dynamic signal range for an HTS.

2.16.2.4.1.2 Z′-factor

The Z'-factor indicates how well separated the positive and negative controls are, given the variation present in both control populations. This dimensionless statistical parameter represents the ratio of the difference between the means and the standard deviations (SD) of the positive and negative populations (**Table 1**, entry 3) and proves to be very useful to capture and compare variability caused by assay biology and instrumentation.[36] The Z'-factor quantitatively estimates the robustness of a single data point assay by characterizing the screening window that could be used to identify hits. The highest possible value of Z'-factor and related robust Z-factor is 1; negative values indicate that distinguishing between positive and negative controls is not possible. In general, a Z'-factor of 0.5 or greater is considered an excellent assay for a high-throughput screen. For many large-scale multiple-parameter HCS campaigns it may be difficult to validate an assay using Z'-factor based on only one parameter,[37] but it is possible to improve Z'-factor analysis by combining data from multiple output parameters. The simple, easy-to-calculate Z' statistic is the most widely accepted measure of HTS/HCS assay performance.

2.16.2.4.1.3 V-factor

The V-factor complements the Z'-factor statistic in that it gives a more realistic measure of the overall assay performance by accounting for intermediate points in the dose–response curve that have higher variability due to effects of computation and

Table 1 Formulas of HTS quality control parameters

Entry	*Method*	*Formula*
1	Signal to background ratio	$S/B = \frac{Mean_{pos}}{Mean_{neg}}$
2	Signal-to-noise ratio	$S/N = \frac{\lvert Mean_{pos} - Mean_{neg} \rvert}{SD_{neg}}$
3	Z'-factor	$Z' = 1 - \frac{3\times(SD_{pos}+SD_{neg})}{\lvert Mean_{pos} - Mean_{neg} \rvert}$
4	V-factor	$V = 1 - 6 \times \frac{\sqrt{\frac{1}{n}\sum_1^n (f_{exp} - f_{pos})^2}}{\lvert Mean_{pos} - Mean_{neg} \rvert}$
5	SSMD	$\beta = \frac{Mean_{pos} - Mean_{neg}}{\sqrt{SD_{pos}{}^2 + SD_{neg}{}^2}}$

$Mean_{pos}$ and $Mean_{neg}$: mean of positive control and negative control; SD_{pos} and SD_{neg}: standard deviation of positive control and negative control; f_{exp} and f_{mod}: experimental and model values of the assay measure at a given concentration; n: the number of experimental points in the dose–response curve.

dispensing errors, rather than just the positive and negative controls alone. *V*-factor, proposed by Ilya Ravkin,[38] can be interpreted as the generalization of Z'-factor to the dose–response curve as it reverts to Z'-factor if there are only two dose points (**Table 1**, entry 4). *V*-factor can also be used to compare different image analysis algorithms.

2.16.2.4.1.4 Strictly standardized mean difference

Recently, strictly standardized mean difference (SSMD) has been proposed as a statistical parameter for the contrast analysis of two groups.[39] SSMD, denoted as β, is defined as the ratio between the difference of the means and the standard deviation of the difference between controls (**Table 1**, entry 5). SSMD differs from Z'- and *Z*-factor by its ability to handle controls with different effects, which enables the selection of multiple quality control criteria for assays. SSMD estimates tend to be closer to population values than the equivalent *t*-statistics. Due to its basis in probabilistic and statistical theories, SSMD is a better quality control parameter than the empirically derived Z'-factor. SSMD is developed primarily for accessing data quality in RNAi screenings as it anticipates unequal phenotypic variance in either the positive or negative controls, preventing either one from dominating the calculation.[40,41]

2.16.2.4.2 Data normalization

Normalization of raw screening data corrects systematic errors occurring in a plate-specific manner without disrupting the results in other plates, making measurements comparable across plates. There are two main approaches for normalizing HTS/HTS data: control-based and non-control-based.[35]

2.16.2.4.2.1 Control-based normalization methods

Positive controls and negative controls are commonly used in HTS to represent maximum and minimum assay readout signals. Control-based percent inhibition or activation is the most common and simple data normalization technique; it is defined as the ratio of the sample measurement to the mean value of negative controls within each plate (**Table 2**, entry 1).[42] Similarly, normalized percent inhibition process removes the plate-to-plate variability by subtracting the mean value of negative controls from raw sample data and dividing the absolute difference between the means of the positive and negative controls (**Table 2**, entry 2). The percent of control and normalized percent inhibition found in table 2, are data normalization methods that bring the assay readout values into a standardized numerical range (0–100% scale) for intuitive interpretation. Hit-identification can then be easily accomplished by assigning a percent cut-off value relative to the assay signal window. However, these two procedures do not incorporate any information regarding the distribution or variability of the controls.

2.16.2.4.2.2 Z-score and robust Z-score

The *Z*-score or standard score, which permits the comparison of scores among different plates, is a statistical score calculated from only the sample values (no controls) on plate-by-plate basis.[43] *Z*-score has the advantage of incorporating information regarding the variability of the control distribution and simply measures the effect of one perturbation normalized to the mean and standard deviation of the whole plate (**Table 2**, entry 3). *Z*-score is frequently used in HTS to indicate the extremity of the observation in relation to the control distribution, but while this method is accessible, it has a few limitations. First, both the mean and the standard deviation are sensitive to the number of outlying values of highly active compounds on the plate. Second, *Z*-score statistical method implicitly assumes that the vast majority of compounds on a plate is inactive and is only valid for normal of the phenotypic quantification, both of which are not always satisfied in practice, especially in cellular imaging assays. An alternative to the *Z*-score, robust *Z*-score, accounts for different variability effects across HTS plates to provide unbiased data normalization. It substitutes the

Table 2 Formulas of data normalization methods

Entry	Method	Formula	Notes
1	Percent of control	$\frac{X_i}{\text{Mean}_{\text{pos}}} \times 100$	X_i, raw measurement of the ith sample; Mean_{pos}, mean of positive control; Mean_{neg}, mean of negative control
2	Normalized percent inhibition	$\frac{X_i - \text{Mean}_{\text{neg}}}{\text{Mean}_{\text{pos}} - \text{Mean}_{\text{neg}}} \times 100$	X_i, raw measurement of the ith sample; Mean_{pos}, mean of positive control; Mean_{neg}, mean of negative control
3	*Z*-Score	$\frac{X_i - \text{Mean}_{\text{sample}}}{\text{SD}_{\text{sample}}}$	$\text{Mean}_{\text{sample}}$ and $\text{SD}_{\text{sample}}$ are the mean and standard deviation of all the sample measurements on a plate
4	Robust *Z*-Score	$\frac{X_i - \text{Median}_{\text{sample}}}{\text{MAD}}$ $\text{MAD} = 1.4826 \times \text{median}\left(\lvert X_i - \text{Median}_{\text{sample}}\rvert\right)$	$\text{Median}_{\text{sample}}$ is the median of all the sample measurements on a plate; MAD is the median absolute deviation
5	*B*-Score	$\frac{Y_{ijp}}{\text{MAD}_p}$ where, $Y_{ijp} = X_{ijp} - \text{Mean}_p - \text{Row}_{ip} - \text{Column}_{jp}$ and, $\text{MAD}_p = 1.4826 \times \text{median}\left(\lvert Y_{ijp} - \text{Median}_{\text{sample}}\rvert\right)$	Y_{ijp} (median polish) and X_{ijp} are the random error estimate and the sample value on the ith row and jth column of the pth plate. Mean_p is the plate average, Row_{ip} and Column_{jp} are the estimate systematic artifacts for the ith row and jth column of the pth plate. MAD_p is the median absolute deviation of the random error estimate on the pth plate

control mean and standard deviation with the control median and median absolute deviation (MAD) for outlier resistant dispersion estimates (Table 2, entry 4).[44]

2.16.2.4.2.3 B-score

The *B*-score or better-score is another non-control-based statistical normalization parameter designed to correct systematic biases. Better than *Z*-score, *B*-score uses iterative mathematical modeling to reduce the impact of systematic row, column, and plate artifacts in HTS data. The mathematical model of the *B*-score involves the residual values calculated from two-way median polish algorithm and the sample MAD to account for data variability (Table 2, entry 5).[45] The *B*-score adjusts for intra-plate variability, effectively normalizing observations for data that exhibit row and/or column effects. However, implementation of the *B*-score is not trivial, as the data must be processed using a programming language or sophisticated statistical software such as R or MATLAB. Therefore, while the *B*-score method offers a powerful tool for data processing, it also presents a formidable barrier to accessibility and understanding.

2.16.2.4.3 Hit selection

The major goal for HTS and HCS data analysis is to maximize the identification of biologically relevant hits from a large library (e.g., small molecules), while minimizing false positives that require expensive time-consuming follow-up assays to confirm the hits. In most cases, the most active samples will be selected as hits; however, the challenge lies in selecting the marginally active hits. Thus, it is crucial to select a reasonable cut-off value that will result in a manageable quantity of hits for secondary confirmatory assays while reducing the false positive hit rates. Combining a robust statistical method such as the *B*-score or *Z*-score with the control-based percent activity will facilitate the selection of the most appropriate threshold. A wide range of more sophisticated hit identification techniques is available to improve the quality of the results generated from HCS;[46] most of these hit identification methods can be defined as distance from the mean or the median that takes into account the variance. In addition, hit selection is frequently coupled with orthogonal methods to classify hits. In small molecule screens, the hits will be pooled by structural properties to identify common scaffolds. In RNA interference (RNAi) screens, enrichment analysis is needed to link identified gene sets of interest to significant biological pathways and process networks.

2.16.2.4.3.1 Mean ± standard deviations

Depending on the normalization method and the performance of the controls, a simple method of selecting a set of reasonably robust hits is to calculate the mean and standard deviation of the dataset; sample values that are two or three SD above the mean for activation assays or below the mean for inhibition assays can be identified as hit limits.[43]

2.16.2.4.3.2 Strictly standardized mean difference

SSMD is a robust parameter to capture the magnitude of the RNAi effects with various sample sizes. In addition to its role in defining the robustness of a screen (introduced in Section "**Strictly standardized mean difference**"), SSMD values calculated on individual wells can be used as a hit selection parameter in HTS/HCS data analysis due to its ability to account for the phenotypic variability that can occur for either the hits or controls in RNAi screens. The SSMD parameter used for primary screens without replicates holds a linear relationship with the *Z*-score method.

2.16.2.4.4 Data visualization

Data visualization is essential for understanding and interpreting complex data extracted from cellular images and is very effective for uncovering abnormalities and outliers. There are numerous multivariate graphical methods and tools commonly used for the visualization of the screening data in various formats such as bar charts, whisker plots or box plots, scatter and trellis plots, heat maps, and frequency plots. Box plots display multiple descriptive statistics and can help identify outliers within a distribution. Scatter plots are especially useful for visualizing correlations between replicates to assess reproducibility. Heat maps use a color scale to display the intensity of the readout from multivariate experiments. Hive network plots[47] and glyph-based PhenoPlots[48] are useful tools to represent multidimensional cellular measurements in an intuitive manner. TIBCO Spotfire® is a common visualization software platform that allows for integration of images with various plots, vital to the analysis and exploration of high-content data. High Content Profiler™ from PerkinElmer, an integrated solution within Spotfire environment, simultaneously supports multiple HCS data management systems and provides a one-stop solution for quality control analyses, data normalization, and data exploration with real-time multivariate visualization techniques. Genedata Screener offers a user-friendly solution to take full advantage of the rich volume of multiparametric data from HCS. The software allows review of images directly next to the calculated results, providing instant confirmation of phenotypic changes and biological events. Specific visualizers such as cell density plots, overlay plots, and compare plots also enable for quick overview to identify interesting results.

2.16.2.4.5 Data reduction methods

HCS is a technique that is designed to capture a vast number of features of individual cells in large data-rich files. However, the complexity and volume of the data are often the limiting factor in HCS data analysis. One solution for data reduction is to eliminate redundant feature collection while avoiding the loss of important details during HCA. Dimensionality reduction is a widely used machine learning method; it aims to transform very high dimensional data into a more compact, low-dimensional representation, while limiting the loss of information contained within the data. Dimensionality reduction can be classified into two branches: linear

and nonlinear. Nonlinear techniques include Laplacian Eigenmaps, local tangent space analysis (LTSA), local linear embedding (LLE), and diffusion maps.[49] Linear transformation techniques for dimension reduction include factor analysis,[50] linear discriminant analysis (LDA),[51] and the widely used principal component analysis (PCA).[52] Many dimensionality reduction methods have been successfully applied to HCS data analysis for image feature reduction.[53,54] By focusing on the relevant uncorrelated readouts, dimension reduction and feature selection will help efficiency and accuracy of the data analysis without losing essential biological information.

2.16.3 High-Throughput 3D Culture Technologies

Established 3D cell and tissue culture techniques (Table 3) can be divided into two main categories. The first category is macroscale 3D culture systems that are specifically designed to overcome the limitations of traditional 2D in vitro systems. The second category

Table 3 Summary of 3D culture methods

Methods	*Advantage*	*Disadvantage*	*Adaptable for HCS*
Spinner Flask	Simple Mass production of spheroids Long-term culture Perfusion of nutrients	Require special equipment No spheroid uniformity control Slow spheroid formation High shear force for cells	No
Rotating Wall Vessel Bioreactor	Low shear stress for cells Several options available Mass production of spheroids Long-term culture Perfusion of nutrients	Require expensive equipment No spheroid uniformity control Slow spheroid formation	No
Solid Scaffold	Simple Variety of available materials Customizable	Hard to recover products Possible scaffold-to-scaffold variation Biocompatibility and biodegradability issues of scaffold material	Limited
Naturally Derived Hydrogel	Biocompatible Mimicking native ECM Compatible with other 3D culture methods Can be mass produced	Batch-to-batch variation Constituent may interfere with downstream assay analysis Gelling mechanism Limited options for modification Hard to recover desired product	Limited
Synthetic Hydrogel	Functionalized easily Biocompatible Reproducible No animal trans-contamination Compatible with other 3D culture methods	Lack of cell type-specific niches and organ-specific structures May not be transparent Gelling mechanism Hard to recover product	Limited
Hanging Drop Plate	Uniform spheroid size Rapid and consistent spheroid formation No specialized equipment required Control over coculture patterns	Labor intensive and time consuming Low stability, droplet can detach from plate Long-term culture difficult Difficult to change growth media Not suitable for scale-up Need to transfer spheroids for analysis	Yes
Micropatterned Plate	Uniform spheroid size Customizable patterns for different cell types Consistent spheroid formation No specialized equipment required	Hard to retrieve spheroids Limited spheroid size Biocompatibility and biodegradability issues of scaffold material Cost	Yes
Non-adherent Surface Plate	Simple, easy to scale up Rapid and consistent spheroid formation No specialized equipment required	Nonuniform spheroid size Hard to defined coculture cellular composition	Yes
Magnetic Levitation	Uniform spheroid size Scaffold-free Rapid and consistent spheroid formation	Uncertain effect of magnetic nanoparticles Require magnetic holding drive Physiological changes to the cells caused by external forces are not well characterized	Yes
Microfluidic Device	In vitro organ-specific systems Perfusion of nutrients Uniform spheroid size Consistent spheroid formation Analysis may be integrated into the device	Material compatibility issue with hydrophobic compoundsHard to retrieve spheroids Long-term culture difficult Require expertise to operate	Yes

is 3D cell culture screening systems developed to increase the throughput capacity of traditional 3D cell culture systems. In recent years, advances in the establishment of organoid models have stimulated commercial activity around 3D-based technologies, resulting in a number of highly specialized solid scaffolds, hydrogels, bioreactors, and multiwell microplates, and other technologies have been commercialized (Table 4). These 3D models and products range in complexity and offer researchers an array of 3D cell and tissue culture tools and methods to fit their specific needs.

2.16.3.1 Traditional 3D Culture Techniques

Culture systems were initially developed for macroscale production of 3D models with in vivo like cell–cell and cell–matrix interactions independent of tissue culture plastic attachment. Macroscale 3D culture typically utilizes milliliters to liters of reagents using enclosed bioreactors or hundreds of microliters of reagents using multi-well plate formats. Some of the most commonly used 3D macroscale culture systems include rotating cell bioreactors, solid scaffolds, and natural and synthetic matrices. While most traditional mass production 3D culture methods are not directly applicable to HTS/HCS, there is great potential for these techniques to become applicable by developing automated technologies to harvest and transfer organoid structures to HTS/HCS platforms. In addition, technologies that would allow for cryogenic preservation of 3D structures such as those available for single-cell suspensions would also improve the supply and throughput necessary for HTS/HCS in 3D.

2.16.3.1.1 Spinner flask and rotating wall vessel bioreactors

Spinner flasks were first developed in the 1970s for culturing large amounts of 3D multicellular spheroids.[55] By continuously stirring cells in suspension with an impeller or magnetic stir bar, spinner flasks allow cells to naturally aggregate and then differentiate into robust 3D structures, typically forming multicellular spheroids. The rotation speed is properly controlled such that it is fast enough to prevent cell suspension from settling but slow enough to avoid cell damages due to shear forces from the moving fluid. The movement of fluid provides a controlled environment to transport nutrients and waste from the spheroid surface, mimicking the transport mechanism in tumors in vivo. However, although limited, a drawback of the spinner flask culture method is a relatively high shear stress resulting from the spinning impeller or stirring mechanism that may affect the cellular physiology. The rotating wall vessel (RWV) bioreactor, known commercially as the Rotary Cell Culture System (RCCS), was developed to address this limitation. The RCCS was originally invented at NASA Johnson Space Center in 1990s to simulate the microgravity conditions in space based on the principle of clinorotation[56]; it is a dynamic system that suspends cells in a low-shear stress, microgravity-mimicking environment. Instead of stirring the whole culture suspension with internal mechanical agitator as in the spinner flask bioreactor, the RCCS suspends cells without generating cell damaging mechanical forces. As the RWV rotates, culture fluid can reach a near-laminar flow condition, and cellular aggregates cultured in the fluid are in a state of free fall, but never reach the bottom of the vessel because of the constant rotation of the device. This mild fluid turbulence growth environment allows anchorage-dependent cells to readily aggregate and form into 3D organoids while simultaneously producing high mass transfer of nutrients and oxygen. Additionally, RCCS technology allows several cell types to be cocultured to generate relevant 3D tissues. The spinner flasks and rotating cell bioreactors prevent cells from adhering to the container walls by keeping cell suspensions in constant motion and are suitable for long-term culture and large-scale production. A major limitation of both systems is the variability of the size and shape of the 3D culture.

2.16.3.1.2 Solid scaffolds

Solid scaffolds of diverse size, structure, stiffness, porosity, permeability, and mechanical characteristics have been developed and fabricated for 3D cell culture.[57] These scaffolds are made of a broad range of materials, including metals, ceramics, glass, polymers, and composites. These inert matrices can be engineered into thin membranes that fit into conventional cell culture plasticware, ranging from Petri dishes to 384-well plates (Table 4). In particular, 3D insert scaffolds can be fabricated from both biodegradable (e.g., polycaprolactone, PCL) and nonbiodegradable polymers (e.g., polystyrene, PS). PCL is a biodegradable polymer used in many FDA-approved surgical implants and drug delivery devices for tissue engineering and regenerative medicine applications. Polystyrene is a non-cytotoxic polymer that is frequently used in the fabrication of various cell culture vessels; the transparency of the polystyrene 3D insert scaffold makes it easy for researchers to observe the cell growth directly using an inverted microscope. The scaffolds provide initial support to the seeded cells, localize the cells in the appropriate spaces, and provide physical and biological cues for adhesion, migration, proliferation, differentiation, and eventually formation of tissues and organoids. Currently, scaffolds have been used for model tissue architecture of bone, cartilage, ligament, cardiovascular system, nerve, skin, vascular, neural, and liver.[58]

The 3D precision microfabrication technology provides microfabricated scaffolds with well-defined pore sizes, ranging from 200 to 500 microns. Once scaffolds are inserted, cell treatment and assay component dispensing procedures are performed in a manner akin to that used with 2D cell culture, which means routine 2D cell culture protocols can easily be adapted to 3D cell culture without adding expensive instruments. Nutrients easily flow through the evenly spaced pores and channels, allowing cells to migrate and fill the spaces within the scaffold and form 3D structures. The arrangement of fibers and pores allows cells to remain close to nutrient sources, enabling exchange of nutrients, waste material, and gases mimicking in vivo function. One drawback of using solid scaffolds is the extensive separation steps associated with recovering desired products from the matrix. In addition, matrix stiffness, permeability, and the material used for constructing the scaffold can impact cell adhesion, growth, and behavior. Imaging may also become difficult depending on the scaffold size, transparency of material, and depth capacity of the microscope.

Table 4 Commercially available 3D culture products

Method	*Product*	*Company*
Solid Scaffold	3D Inserts, Hydroxyapatite disc, and β-TCP disc	3D Biotek
	AlgiMatrix 3D Cell Culture System	ThermoFisher
	3D Petri Dish	Microtissues
	Dot-Cult, Confo-Cult, and ECM Graft	ExCel Matrix Biologic Devices
	3D CelluSponge	InvitroCue
	Cellusponge, Cellusponge-Galactose, and Cellusponge-Collagen	Bio-Byblos Biomedical
	Alvetex Synthetic Scaffold and Well Insert	Reinnervate
	RAFT 3D Cell Culture System	Lonza
	SeedEZ and GradientEZ	Lena Biosciences
	Biomerix 3D Scaffold	Biomerix
	OptiMaix-3D	Matricel
	Nanobiomatrix Sheets, Discs, and Plates	Synthecon
	CellCream, CellCrown, and CellVessel	Scaffdex
	3D Aligned Nanofiber Inserts, and 3D Cell/Tissue-Based Models and Kits	Neuromics
	BIOFELT Bioabsorbable Scaffold	ETE Medical
	AK-Polyfibers	Akron Biotech
	Mimetix 3D Cell Culture Scaffolds, and Tissue Culture Plates	Electrospinning.
	Vers3D	Screvo
	MIGHTY Atelocollagen Sponge, and Atelocollagen Honeycomb Sponge	ReproCELL
	NanoAligned, and NanoECM 3D Cell Culture Scaffolds	Nanofiber Solutions
	IVS Inserts, and 3D Tissue Fabrication Kit	InvivoSciences
Bioreactor	ProCulture Spinner Flasks	Corning
	Magna-Flex and Celstir Spinner Flasks	Wheaton
	Bell-Flo Spinner Flasks	Bellco Glass
	Nalgene Polycarbonate Magnetic Culture Vessel	ThermoFisher
	Rotary Cell Culture System, and RCCMax Perfusion Systems	Synthecon
	Universal Turning Device miniPERM Bioreactor	Sarstedt
	U-CUP Perfusion Bioreactor with Ceramic and Collagen Scaffolds	Cellec Biotek
	3D Perfusion Bioreactor	3D Biotek
	Z®RP Bioreactor with Z®RP Sponceram	Glen Mills
	TissueFlex Microreactor	CN Bio Innovations
	DASGIP Benchtop Bioreactors for Cell Culture	Eppendorf
	ambr 250 bioreactor vessels	sartorius
	Alvetex Perfusion Plate	Reinnervate
	Nucleo Bioreactor Platform	ATMI LifeSciences
	VECELL Gas Permeable Plate and Petri Dish	Nacalai
	MicroBrx, Primer, Multi-6, AutovaxID, Maximizer, and Xcellerator Bioreactor	Biovest International
	Quasi-Vivo Products (QV500, QV600 and QV900)	Kirkstall
	BioSep Acoustic Perfusion System	Applikon Biotechnology
	3D Manufacturing Platform (Proprietary Bioreactor System)	Pluristem Therapeutics
	Quantum Cell Expansion System (3D Hollow Fiber Bioreactor)	Terumo BCT
	μ-Slide III 3D Perfusion	Ibidi
	Hollow Fiber Cell Perfused Bioreactor System	FiberCell Systems
	3D Perfusion Co-culture Models	KiYATEC
	BISS Bioreactor Systems	BISS TGT
Non-adherent Surface	Ultra-Low Attachment Surface Spheroid Microplates	Corning
	Cultrex Spheroid Formation and Invasion Plate	Trevigen
	Nunclon Sphera Surface	ThermoFisher
	CELLSTAR Cell Culture Vessel with Cell-Repellent Surface	Greiner Bio-One
	CellCarrier Spheroid Ultra Low Attachment Microplates	PerkimElmer
	Lipidure-COAT Plates	NOF
	Low Attachment Plates, and Happy Cell Advanced Suspension Medium	Happy Cell
	Non-Adherent Culture Dish	ExCel Matrix Biologic Devices
	PrimeSurface Low Cell Adhesion Products	Sumitomo Bakelite
	GravityTRAP Ultra-Low Attachment Plate	InSphero

Table 4 Commercially available 3D culture products—cont'd

Method	*Product*	*Company*
Hydrogel	Matrigel Matrix, PuraMatrix Peptide Hydrogel, and Cell Recovery Solution	Corning
	MaxGel Human ECM, HydroMatrix, and Upstate ECL Cell Attachment Matrix	MilliporeSigma
	PathClear 3D Culture Matrix, Organoid Qualified Basement Membrane Extracts	Trevige
	MAPTrix HyGel	Kollodis Biosciences
	HepatoCue	InvitroCue
	Gletrex, Laminin, Collagen, Fibronectin and Gelatin	ThermoFisher
	QGel Assay Kit	QGel
	Extracel, Mebiol Thermoreversible Hydrogel, and various 3D Matrix Products	CellSystems
	3D HuBiogel Culture System	Vivo Bioscience
	PGmatrix	PepGel
	Alginates, Chitosans and Sodium Hyaluronates	NovaMatrix
	Collagen I-3D Gelling Kit	ScienCell
	GrowDex Wood-based Cellulose Nanofibril Hydrogel	UPM Biochemicals
	Hystem Hydrogel Products, Glycosil and Heprasil Hyaluronan Acid	ESI BIO
	MyEZGel	Applied StemCell
	AlphaMax3D Human ECM, Collagel, and AlphaGEL3D Hydrogels	Neuromics
	ArtiGel Matrix	CELLON
	PureCol EZ Gel, VitroCol, Nutragen, and other ECM	Advance BioMatix
	CosiGel Hydrogel	Interchim
	FlowMatrics Liquid 3D Cell Culture Matrix	FlowMatrics
	PanaceaGel for 3D Cell Culture	Menicon Life Science
	Biogelx Powder	Biogelx
	AlphaBioGel, Collagel Hydrogel, and Bovine Base Hydrogel Coated Plate	Alphabioregen
	BIOMIMESYS, BIOMIMESYS Adipocyte and Hepatocyte	Celenys
	minisys G Hydrogel	irisbiosciences
	3-D Life Hydrogel and Hydrogel Component	Cellendes
Hanging Drop Plate	Perfecta3D Hanging Drop Plates, and Spheroid Transfer Tool	3D Biomatrix
	GravityPLUS 3D Hanging Drop Cell Culture Platform	InSphero
	96-Well Clear Polystyrene Hanging Drop Plates	TTP Labtech
	IMAPlate 5RC96	NCL New Concept Lab
Micropattened Plate	NanoCulture Plate, and NanoCulture Dish	SCIVAX
	Micropattened CYTOOplates and CYTOOchips, and OncoSphere System	CYTOO
	Elplasia Three-Dimensional Culture Plate	Kuraray
	Nanosurface ANFS Cell/Tissue Culture Dish and Plates	NanoSurface Biomedical
	AggreWell 400, 400Ex, and 800 Plate	StemCell
	HepatoPac Micropatterned Tissue Culture Plate	Hepregen
	Cell-able Plate	Toyo Gosei
Magnetic Levitation	Spheroid Bioprinting Kit, and NanoShuttle-PL	n3D Bioscience
	GEM Magnetic Alginate Microcarrier, BioLevitator	Global Cell Solutions
Microfluidic Device	iuvo Microchannel 5250 Microconduit Array Plate	BellBrook Labs
	CellDirector 3D	Gradientech
	OrganoPlates 9601	MIMETAS
	Droplet System with Mitos Duo XS-Pump	Dolomite
	CellASIC ONIX2 Microfluidic Platform, and M04S Microfluidic Plate	SigmaMillipore
Other 3D Cell and Tissue Culture Product	BioWiggler Magnetic Stirrer	Global Cell Solutions
	Seahorse XF^{e}96 Spheroid Microplates and FluxPaks for Metabolic Analysis	Agilent Technologies
	Cytodex Surface Microcarriers	GE Healthcare
	SoloHill Microcarriers	PALL
	HyQsphere Microcarriers	ThermoFisher
	Cell-in-a-Box Cell Encapsulation Kit	MillporeSigma (Austrianova)
	CnT-Prime Epithelial Culture Medium	CELLnTEC
	UpCell using Temperature Cell Harvest Technology	CellSeed
	ECM Coated 3D Cell Culture Systems using Stem Cells	Celprogen
	Oris 3D Embedded Invasion Assay	Platypus Technologies
	3D Collagen Cell Contraction Assay	Cambridge Bioscience
	CellTiter-Glo 3D Cell Viability Assay	Promega
	Various 3D Tissue Model Products	Alphabioregen
	3D Insight Human/Rat Liver, Human/Rat Islet, and HepG2 Tumor Microtissues	InSphero

2.16.3.1.3 Hydrogel

Unlike rigid scaffolds, hydrogels are comprised of networks of cross-linked polymer chains or complex proteinmolecules of natural or synthetic origin.[59] Hydrogels are highly absorbent and can contain as much as 99.9% water, providing them with a high degree of flexibility that displays solid-like material properties. These gels are sufficiently porous, to enable nutrient and waste exchange, and possess sufficient mechanical properties for self-supporting. Due to their significant water content, hydrogels possess biophysical characteristics very similar to natural tissues and serve as highly effective matrices for 3D cell culture. Hydrogels need to be dispensed at specific temperatures and concentration to prevent premature gelation, which may disqualify them from using with many liquid handling systems associated with HTS. The enormous versatility of hydrogel materials makes it possible to design scaffolds with predefined mechanical properties, as well as with desired biofunctionality. Hydrogels can be used as stand-alone 3D matrices or combined with other technologies, such as solid scaffolds, permeable supports, cellular microarrays, and microfluidics devices. Scaffolds derived from biological, synthetic, or natural sources have been widely used for the engineering of functional tissues and organs such as cartilage, skin, bone, bladder, blood vessels, heart, liver, and lung. Hydrogels can be employed in 3D culture systems in a variety of ways. They can be used as a coating reagent to embed cells within scaffold proteins in a liquid state. Alternatively, cells can be seeded either overlaying on top of polymerized ECM gels or sandwiched between layers of ECM hydrogels. Like all 3D culture models, the morphology, growth, and functionality within the hydrogel matrix depend on the physical properties such as permeability and stiffness as well as biophysical and biochemical component extracellular interactions and signals.

ECM from natural sources has served as an important tool for biologists and is most commonly used for applications of 3D cell culture due to its structural and mechanical similarity to native tissues. The inherently biocompatible and bioactive matrices not only provide a scaffold to which the cells can attach and reorganize into 3D structures but also deliver the correct microenvironment of soluble growth factors, hormones, and other molecules and components that cells interact with in an in vivo environment. Naturally derived hydrogels for cell culture are typically composed of common ECM proteins such as collagen, fibrin gel derived from thrombin cleavage of fibrinogen, stromal ECM synthesized by fibroblasts, and reconstituted basement membrane (e.g., Matrigel).[60] Collagen I, a fibrous protein found in connective tissues, is the most abundant protein in humans.[61] It is widely used as a thin layer on tissue-culture surfaces to enhance cell attachment and proliferation. In addition, type I collagen can self-assemble into a 3D supramolecular gel in vitro, making it a logical choice as a cell culture scaffold to promote more in vivo-like cellular morphology and function. Matrigel matrix is another ECM-based natural hydrogel that has been used extensively for 3D cell cultures in vitro and in vivo. Extracted from the Engelbreth-Holm-Swarm (EHS) mouse sarcoma, a tumor rich in ECM proteins, this reconstituted basement membrane contains laminin, collagen IV, entactin/nidogen, proteoglycans, and a number of growth factors. In addition, naturally derived polysaccharide alginate (extracted from brown seaweed algae) and chitosan (extracted from crab/shrimp shells) have been extensively used as hydrogel ECM for cell encapsulation, cell and drug delivery, and tissue engineering. Although natural matrices help recreate the in vivo environment by providing cells with the geometry, biochemistry, and signaling cues found in vivo, inherent batch-to-batch variability in composition and limited modification of biochemical and mechanical properties are considered limitations for obtaining consistent and reproducible outcomes.

Synthetic matrices closely mimic natural extracellular matrices while offering the flexibility for customization with growth factors, attachment factors, and proteins creating an ECM that can be optimized for specific 3D culture models. These materials typically possess a structural backbone, cell-binding ligands, and a cell-friendly crosslinking mechanism. The most common of these include polyethylene glycol (PEG)-based hydrogels and self-assembling peptides. Various bioactive components facilitating the release of biomolecules and morphogens from the extracellular microenvironment can be deposited in the hydrogel. Without the uncontrolled effects of unknown growth factors, such chemically defined synthetic scaffold materials have the advantage of improved reproducibility and reduced risk of animal transcontamination. Furthermore, synthetic matrices offer more defined properties than natural matrices by controlling adhesive moieties, proteolytic sites, and the mechanics of the material more precisely by modifying the polymer architecture. To more closely mimic the natural functions of an ECM, such hydrogels are covalently modified with cell adhesion peptides containing cell recognition motifs of ECM proteins and cell-degradable cross-linker molecules containing matrix metalloproteinase-cleavable peptides.[62]

2.16.3.2 HCS Compatible 3D Cell Culture Platforms

Traditional 3D culture systems require large volumes of reagents and cells, and are not compatible with HTS systems; in addition, the high costs associated with the reagents needed for these 3D culture methods have hindered the widespread adoption of these technologies. An ongoing challenge is to develop in vitro 3D organoid models that are compatible with industrial-scale applications and readily automated for HCS.[63] To increase the throughput of compound screening in 3D cell culture, assays are required to be compatible with robotic systems including liquid handling technologies, which are generally in a 96- to 1536-well microtiter plate format, which allows accurate aspiration and dispensing of assay reagents and screening compounds in a timely manner. Accordingly, there has been an increase in the design, development, and utilization of more in vivo like 3D culture systems with better functions, lower cost and labor, and enhanced throughput. Reproducible mass production of spheroids and organoids is a promising path in which 3D culture systems can be incorporated into mainstream drug development processes. Available high-throughput compatible 3D organoid screening platforms can be classified into five main categories: hanging drop plates, liquid overlay using non-adherent binding plates, micropatterned plates, magnetic levitation, and microfluidic devices.

2.16.3.2.1 The hanging drop method

The hanging drop method relies on gravity to promote self-assembly for spheroid formation; it was originally used by adding cell droplets to the inside of standard tissue culture lids.[29] This antiquated method has been adapted for HTS via the development of 96-well and 384-well arrayed microfluidic hanging drop plates.[64] Hanging drops of mono- or cocultures are created by dispensing small volumes of cell suspension into access holes on the top of the plate without the need for any support matrices. Spheroid size is controlled by the number of cells from as few as 50 cells to as many as 15,000 cells. The resulting suspended media droplets utilize gravitational force to aggregate cells over the course of hours to days allowing for spheroid formation. Different from traditional microtiter plates, the hanging drop plates are carefully designed to form a discrete droplet of media sufficient for cellular aggregation, while at the same time they are small enough to prevent the droplets from being dislodged during manipulation.[65] Reagents, drugs, and cells can be added to or removed from each hanging drop through the access hole in the plate by hand-held pipette or by robotic liquid handling equipment to ensure reliable media exchange and consistent and stable formation of the spheroids. Evaporation of medium from the hanging drop during spheroid maturation or long-term incubation in the drop can alter the ionic strength of the medium and impact the consistency of spheroid; commercialized handing drops plate system contains either a humidifier pad saturated with buffer (GravityPLUS™ from InSphero) or a complementary lid and tray as well as a water reservoir constructed around the periphery of the culture plate (Perfecta3D® from 3D Biomatrix) to minimize evaporation (**Table 4**). Spheroids generated with hanging drop method can also be embedded into biological scaffolds to mimic the ECM surrounding cancer tumors. The downside of this method is the relatively high cost of the plate, low stability of the droplets toward mechanical shocks, and plate movement. Hence, spheroid integrity may be compromised during media change or drug screening. In addition, handing drop plates require a transfer step of spheroids into a receiver plate for imaging and analysis.[66]

2.16.3.2.2 The liquid overlay methods with non-adherent surface plates

The formation of spheroids can also be achieved by modifying vessel surfaces with non-adherent natural polymers such as agarose and poly-2-hydroxyethyl methacrylate (polyHEMA) to prevent cells from adhering to any ECM while promoting cell-to-cell attachment.[67] Thus, non-adherent surfaces promote cells of mono- or cocultures into a suspended state that enables aggregation and 3D spheroid formation. Using this method, tumor spheroids of uniform sizes and morphologies can be obtained within 24 h, providing a relatively faster alternative to bioreactors. The ultra-low attachment surface is available in plates, dishes, and flasks, as well as 96-well and 384-well plates that are suitable for high-throughput spheroid production and screening applications (**Table 4**). Well bottoms of these HTS/HCS compatible plates usually possess either a round, tapered, or V-shaped geometries that facilitate single spheroid formation in the middle of the well, making it easier to find, image, measure, and analyze. In addition, this method represents a flexible and automation-friendly platform for the generation and long-term cultivation of organoids.[68]

2.16.3.2.3 Micropatterned plates

Micropatterned plates are a novel technology for 3D cell culture that combines the advantages of scaffold-based technologies with the ease of use found in other platforms to facilitate spheroid formation in a consistent and reproducible manner.[69,70] Each plate contains micrometer-sized patterns regularly arrayed on the bottom of each well that can be fabricated using several methods, including lithography, chemical and physical roughening, electrospinning, or electrospray (**Table 4**).[71] Patterns can be of various shapes, including square, round, or square with slits between the barriers of adjacent wells. The geometry of these patterns has been used to dictate the size and distribution of integrin-mediated adhesions, cell shape, and cytoskeletal architecture as well as multicellular organization. Wells can also be coated to create a low adhesion surface within each micro-space pattern to minimize cell adherence without altering the physical or chemical attributes of the microenvironment. In addition, the bottom of the plate is made of a thin, transparent film that is suitable for microscopic imaging of the cellular structures. Once seeded on the microtiter plate with micropatterns imprinted on its bottom, cells attach and stretch out over the non-adhesive surface and the geometric distribution of adhesive contacts between cells and substrate induces reproducible polarization of the cell machinery. Cell position, cell shape, cell polarity, and internal cell organization become normalized, which can facilitate reliable and sensitive quantitative analysis.

2.16.3.2.4 Magnetic levitation

Magnetic levitation can be used to spatially organize cells into useful 3D shapes and models by manipulating the magnetic fields.[72] The magnetic levitation method relies on biocompatible magnetic nanoparticles to be taken up by cells prior to 3D culture. Treated cells then become magnetic and can be manipulated with an external magnetic field that is strong enough to force cell aggregation that can promote organoid formation. In particular, when a magnetic field is applied above the culture plate, cells are levitated from the bottom surface, where they interact and aggregate with each other to form larger 3D cultures. Once magnetized cultures are generated, they become the building block material for the magnetic 3D bioprinting process. With magnetized spheroids, medium exchange is made easy by using magnetic force to hold them in a stationary position during aspiration, thereby minimizing spheroid loss. If necessary, spheroids can also be picked up and transferred between vessels with proper magnetic tools. The magnetic nanoparticles act at the cellular level, allowing for culture medium to be scaled down in size suitable for HTS.[73,74] This method has been shown to induce the formation of ECM within hours after levitation by the magnetic field and maintain cellular phenotype for days. The most basic application of the magnetic levitation method is to culture 3D cell cultures under different biochemical or environmental conditions and then analyze them using common biological research techniques. Even though magnetic nanoparticles have been shown to not affect macro cell functions such as proliferation, viability, metabolism,

and oxidative stress in short term,[75] their uncertain long term and other unknown effects are a significant shortcoming of this method. In addition, physiological changes to the cells caused by external forces are not well characterized. Overall, the magnetic external force works as an invisible scaffold that rapidly aggregates cells to induce cell–cell interactions and ECM synthesis, making magnetic levitation an effective tool to generate structurally and biologically representative 3D structures.

2.16.3.2.5 Microfluidic devices

Microfluidic devices, particularly organ-on-a-chip, are an emerging powerful technique that has been used for 3D cell culture on miniaturized chips, facilitating experiments on a small scale.[76] Various microfluidic devices fabricated with polydimethylsiloxane (PDMS) have been developed to culture spheroids in micro-wells, micro-chambers, or on micro-textured surfaces to overcome many challenges associated with 3D culture models. Microfluidic devices allow for high-throughput production and analysis of size-controlled spheroids. Many of these platforms are equipped with biosensors for real-time imaging and monitoring of the system (Table 4).[64] These devices allow for controllable culture by manipulating the flow of liquids and the precise placement of cells within geometrically confined micro-channels.[77] In addition, supporting ECM can also be added into these chambers to encourage ECM–cell interactions and promote their assembly into 3D structures. Microfluidic generation of cell-laden hydrogel beads has been demonstrated as a rapid fabrication method for multicellular three-dimensional tissue constructs.[78] Microfluidic-based technologies can be automated and are suitable for efficient screening of 3D spheroids and organoids under various conditions. Although microchips may be the next wave of 3D tools, many of the current versions require considerable expertise to operate and troubleshoot, limiting their widespread adoption.

2.16.4 Hardware and Software for 3D HCS

Incorporating 3D organoid culture models with HTS/HCS screening is essential, providing more relevant human disease platforms to survey compound libraries for drug discovery. However, moving from 2D to 3D adds not only one more dimension in terms of shape and volume, but also a higher level of complexity with respect to assay preparation, image acquisition, visualization, and data analysis, creating several technological challenges. The first and most obvious challenge of 3D optical imaging is that the resolution along the *Z*-axis of the microscope is poor compared to the resolution in the lateral dimensions due to the inherent limit imposed by the point spread function (PSF) in conventional microscopes. Other hurdles related to 3D imaging include light scattering, light absorption, and optical aberrations associated with tissue samples that are hundreds of micrometers thick, requiring more sophisticated fluorescence microscopy techniques normally applied to 2D cell imaging.[79] Meanwhile, the photobleaching and photodamage must also be low enough to allow live imaging at needed speed for an extended period of time. Furthermore, the complex structure of 3D tissues poses additional challenges not only for image acquisition but also for image analysis and quantification. Researchers and microscope makers alike are constantly striving to push the boundaries of resolution, speed, and sensitivity, the so-called eternal triangle of microscopy systems. Advances in imaging technology such as scientific complementary metal-oxide semiconductor (sCMOS) cameras and high numerical water immersion apertures, more powerful light sources, and higher throughput capability of the imaging systems over past decades have aided the rapid measurement and quality of in-depth imaging beyond a few millimeter thickness in tissues.[8,80] Powerful and user-friendly imaging analysis and mining software for high-content images are also rapidly evolving toward robust quantitative HCA of 3D organoids.

2.16.4.1 HCS Hardware

Live cell imaging with high- and super-resolution technologies now allows for the acquisition of data in a more biologically relevant context, providing greater insight into cellular function than what was previously been possible. Most commercially available high-content imaging systems (Table 5) are tailored for 2D monolayer cell models but are capable of acquiring image stacks with defined optical Z-plane sections that can be used to explore the complexities of 3D culture models, including organoids and primary human tissue slices. As with most technologies, there is no one-size-fits-all solution to support imaging of organoids in 3D. Therefore, each imaging modality has relative strengths and weaknesses that must be considered during HCS in 3D. Deploying an automated HCS system with a suitable microscopy technique will be a costly and time-consuming process with the abundant available options; it is therefore important to carefully compare key specifications like light source, illumination methods (optics), filter and objective options, field of view, spatial resolution, image stack recording rate, and built-in image acquisition and storage software along with factors such as technical support and customer service before making a final decision.[81]

2.16.4.1.1 Brightfield and widefield microscopy, and live-cell 3D imaging

The detection of white light transmitted through thin and transparent specimens, known as brightfield microscopy, is the most basic optical microscopy illumination technique.[82] Brightfield microscopy is widely used to characterize morphological or behavioral changes using whole organisms. However, exploiting brightfield microscopy for colorimetric analysis of 3D cellular or tissue sections is not ideal and will result in a low contrast image due to light absorption and light scattering. Widefield microscopy is a type of fluorescence imaging that relies on illumination of the entire field of view (width and depth) by exciting the florescent molecules of interest and simultaneous detecting the emitted fluorescence using the digital camera sensors such as charge-coupled device (CCD) or sCMOS.[83] Widefield imagers are faster and provide higher signal intensities when working with dimmer

Table 5 Available 3D high-content screening systems

3D HCS system	*Optics*	*Light source*	*Software*	*Company*
Opera Phenix	Confocal/Widefield	Laser	Harmony/Columbus	PerkinElmer
Operetta CLS	Confocal/Brightfield/Widefield	LED Lamp	Harmony/Columbus	PerkinElmer
Operetta	Confocal/Brightfield/Widefield	Xenon Lamp/LED	Harmony/Columbus	PerkinElmer
IN Cell Analyzer 6000	Confocal/Brightfield/Phase Contrast/DIC[a]	Laser/LED	IN Cell Investigator/Miner	GE Healthcare
ImageXpress Ultra	Confocal/Widefield	Laser	MetaXpress/AcuityXpress	Molecular Devices
ImageXpress Micro 4	Confocal/Widefield/Phase Contrast	LED	MetaXpress/AcuityXpress	Molecular Devices
Micro Confocal	Confocal/Widefield/Phase Contrast	LED	MetaXpress/AcuityXpress	Molecular Devices
Arrayscan XTI	Confocal/Brightfield/Widefield	LED	HCS Studio/Store	ThermoFisher
CellInsight CX7	Confocal/Brightfield/Widefield	LED	HCS Studio/Store	ThermoFisher
Cell Voyager 7000S	Confocal/Widefield/Phase Contrast	Laser	Yokogawa Analysis	Yokogawa Electric
CQ1	Confocal/Brightfield/Image Cytometer	Laser	Yokogawa Analysis	Yokogawa Electric
Acumen Cellista	Laser-Scanning Cytometer	Laser	Cellista Software	TTP LabTech
iCyte	Laser-Scanning Cytometer	Laser	iBrowser, iGeneration	ThorLabs
ImageXpress Micro XLS	Phase contrast/Widefield	Xenon Lamp	MetaMorph/MetaXpress	Molecular Devices
Celigo	Brightfield/Widefield	LED	Celigo Software	Nexcelom
Cytation 5	Brightfield/Widefield/Phase Contrast	Xenon Lamp	Gen5	Biotek
Cell^{3}iMager	Brightfield	LED	Cell^{3}iMager Software	InSphero
ScanR	Widefield	Xenon Lamp	ScanR Analysis Software	Olympus
WiScan Hermes	Brightfield/Widefield	LED	WiSoft	IDEA Bio-Medical
HCA System	Phase contrast/Fluorescence	Lamp/LED/Laser	NIS-Elements HC	Nikon Instruments
HDS-2500/5800	Brightfield/Darkfield	LED	Panasis	Huvitz
3D Microscope	Optics	Light source	Software	Company
A1 MP+/A1R MP+	Multiphoton/Confocal	Laser	NIS-Elements C	Nikon Instruments
ChromoFlex	Multiphoton	Laser	SciScan/ScanImage	Scientifica
LSM 510 META	Confocal	Laser	LSM Image Browser	ZEISS
FLUOVIEW FV1000	Confocal	Laser	FLUOVIEW Viewer	Olympus
Lightsheet Z.1	Light-Sheet Fluorescence	Laser	ZEN	ZEISS
TCS SP8 DLS	Light-Sheet/Confocal	Laser	LAS X	Leica
UltraMicroscope II	Light-Sheet Fluorescence	Laser	InspectorPro	LaVisionBioTec
UltraVIEW VoX 3D	Confocal/Brightfield	LED/Laser	Volocity	PerkinElmer
IncuCyte ZOOM	Phase contrast/Widefield	LED	IncuCyte ZOOM Software	Essen Bioscience
Bio Station CT/IM-Q	Phase contrast/Widefield	LED	CL-Quant/NIS-Elements	Nikon Instruments
EVOS FL Auto	Brightfield/Widefield	LED	EVOS FL Auto	ThermoFisher
Lionheart FX	Brightfield/Widefield/Phase Contrast	LED	Gen5	Biotek
BioRam	Raman/Brightfield/Widefield	Raman Laser	Innovative Software	CellTool
3D Cell Explorer	Tomography	Laser	STEVE Software	NanoLive
Nexus 128	Photoacoustic Tomography	Laser	Nexus Software	Endra Life Science
BioSorter/COPAS FP	Flow Cytometry	Laser	FlowPilot	Union Biometrica
DeltaVision OMX	3D SIM[b]/Brightfield	Laser	SoftWoRx/OMX Acquision	GE Healthcare

[a]DIC, Differential Interference Contrast.
[b]SIM, Structured Illumination Imaging.

samples. The depth of the field (DOF) or effective focus range of objective lens determines how much of the specimen appears in focus. In non-confocal (widefield) mode, emission light from the focal plane competes with fluorescence originating from outside the plane. Significant flaring and light scatter can occur, creating a blurry, low-contrast image. This will obscure the resolution of features and fine details that lie in the objective focal plate, especially in large specimens such as tissue or small organisms, and samples with a substantial fluorescence signal both within the cells and in the extracellular matrix. For instance, the depth of field for a 20× long WD objective with 0.45 NA is approximately 4.6 μm deep, if the sample thickness is around 138 μm, 30 sections of the images are needed to accurately capture the sample in its entirety. Widefield microscopy-based imaging can provide in-depth information about individual cell structure, function, and relative location as well as overall changes in the morphology and growth of the 3D structure. Therefore, widefield imaging is becoming a standard readout method by providing images of sufficient quality despite the lack of resolution on depth.

Live-cell 3D imaging is perhaps one of the most rewarding and challenging of microscopy applications.[84] In one way, 3D imaging of living cells gives researchers a more detailed and accurate spatial visualization of the interplay of cells and their components than was possible. On the other hand, overexposure may cause cellular damage that leads to altered biological behavior, negatively impacting experimental analysis, and interpretation. Effects of phototoxicity are cumulative and directly proportional to excitation light intensity and total photon load.[85] Therefore, balanced strategies to maximize light collection efficiency while minimizing excitation of the total sample volume are crucial in advancing non-invasive time-lapse 3D imaging. Intracellular staining options are limited in live cell work, as few dyes can cross cellular membranes. Other than utilizing genetically encoded fluorescent

proteins (i.e., green fluorescent protein, GFP and red fluorescent protein, RFP), transmitted light imaging techniques such as differential interference contrast (DIC) and phase contrast are widely used to visualize live cells independent of chemical staining. Automatic phase contrast and fluorescence imaging and analysis platforms such as the IncuCyte (Essen Bioscience) and BioStation CT (Nikon Instrument) offer a non-perturbing imaging approach to obtain detailed images of live cells with various filters and condensers. These imaging systems have been used to track the formation of 3D structures and quantify morphological drug responses with 3D organoids using time-lapse imaging.[86–88] The combination of resolution, depth, excellent contrast level, and fast imaging speed gives researchers the flexibility to view subtle and dynamic processes taking place deep within cells. These systems reside in a standard cell culture incubator with stable environment control of humidity, temperature, and CO_2 concentration. They are compatible with a variety of cell culture vessels including 96–384 well plates. All of the images are automatically collected according to a user-defined schedule and the imaging process is completely noninvasive and non-perturbing to cell health. In addition, conventional brightfield and widefield microscopies have also been used to image spheroids and time lapse has been used to view and quantify the self-assembled kinetics of spheroids and microtissues.[89,90] 3D images are analyzed with maximal projections in real time, providing deeper insight into active biological processes that is not possible using single-point and end-point measurements.

2.16.4.1.2 Confocal microscopy

Confocal microscopes provide better depth resolution and increased image contrast by using a light barrier via a fixed size slit, pinhole, or electronic shutter to reduce the amount of out-of-focus light reaching the detector.[91] Rather than uniformly illuminating the sample at the same time, a pinhole-sized point of excitation energy is projected into the sample in a point-scanning confocal microscope, and fluorescence from only this single point reaches back to the photomultiplier tube (PMT) detector. Light from above and below the plane of focus will not go through the pinhole; so most of the light reaching the detector is from the focused spot. The confocal image and related intensity data are captured point-by-point and computationally reconstructed after the completion of image acquisition. Point-scanning confocal systems also have variable pinhole and optical zoom, providing more flexibility. In particular, confocal high-content imaging systems are able to record the localization and intensity of multiple fluorescent reporters, providing a simple yet powerful technique for effective imaging of relatively thick specimens. In addition to help determine the optimal focus height for each spectral channel, Z-stacks or optical sections are predominantly used in conjunction with the confocal acquisition mode to obtain "depth-encoded" image sequences at different focal planes without actually cutting the 3D sample into thin slices (Fig. 2). These serial image sections can be stacked together to generate a 2D planar projection using Maximum Intensity Projection (MIP), which contains the features from all the image planes and displays the maximum values from the viewpoint to the plane of projection, or aligned and reconstructed to create a high-resolution 3D rendering of the sample and its interior to obtain detailed information regarding cellular phenotypes.

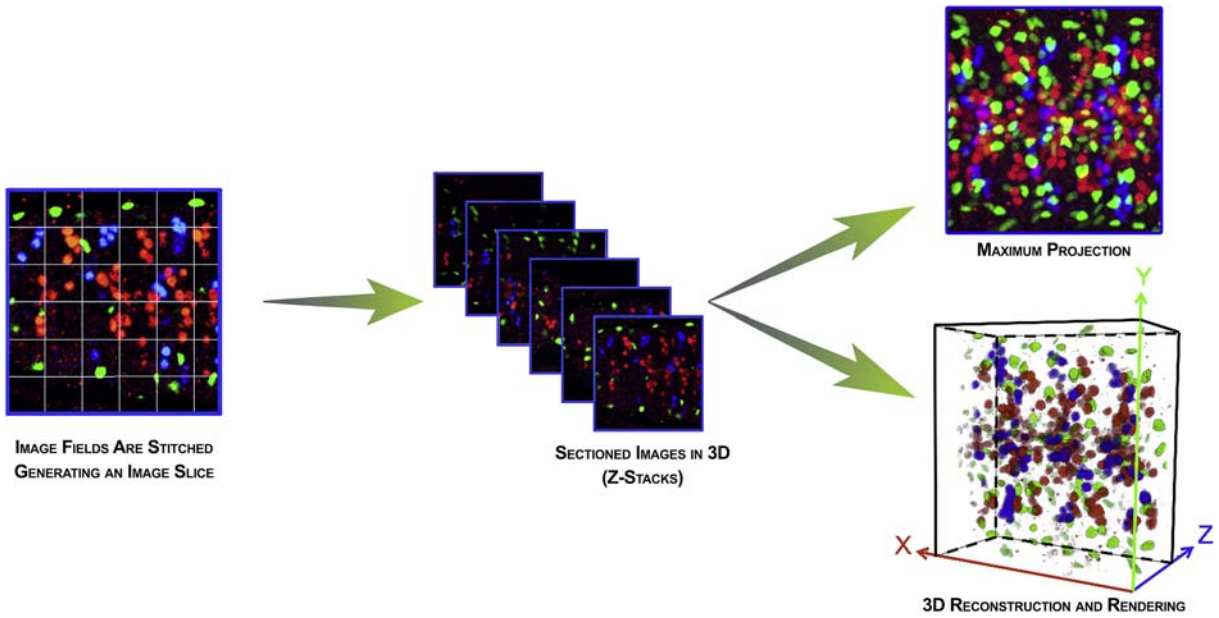

Fig. 2 A typical workflow of 3D image acquisition and visualization. In any given image slice, fields of view are stitched together. The resulting images are optically sectioned into Z-stacks that can be combined to generate a maximum intensity projection image. The Z-stacks can also be reconstructed to create a high-resolution 3D rendering of the image slices. The data above represent the late-embryonic-stage nervous system of *Drosophila* and were generated from a test dataset provided by Vaa3D open-source software developer (**Table 7**) using Fiji image processing software.[95] The 3D reconstructed image was generated from Vaa3D software with the same dataset.

However, by trading efficiency for clarity, most of the total excitation signal is intentionally blocked by the light barrier and excluded from measurement, resulting in dimmer emission signal and longer imaging times. One approach is to combine confocal imaging with high-power light pulses such as lasers or solid-state illuminators and water immersion lenses without paying the penalty of reduced sensitivity due to spectral cross talk;[123] laser scanning confocal microscopy (LSCM, also referred to as confocal laser scanning microscopy, CLSM) generates sharp images of 3D culture models necessary for further imaging analysis. An alternative solution to increase the speed of capture is to utilize multipoint Nipkow disk as in spinning disk confocal microscopy (SDCM) (e.g., Opera Phenix and Operetta from PerkinElmer, ImageXpress Micro Confocal and ImageXpress Micro 4 from Molecular Devices, and Cell Voyager 7000S from Yokogawa Electric, **Table 5**),[124] which has multiple small pinholes to increase the number of points in the specimen that can be imaged simultaneously. For example, the Operetta high-content imaging system, equipped with spinning disk confocal technology, has been used to image colorectal and breast cancer organoids.[125,126] Reid et al. used T47D luminal breast cancer organoids to specifically track and target a subpopulation of cancer stem cells that were marked by cytokeratin 5 (CK5) promoter-GFP (CK5Pro-GFP) reporter.[125] Using built-in Harmony software the authors developed an image analysis sequence to quantitate CK5Pro-GFP expression within Z-stack optical slices and the entire organoid using maximal projections. In yet another application, Zhou et al. utilized the Operetta to track the reversion of epithelial-mesenchymal transition (EMT) within colorectal cancer organoids using a fix and stain method to measure EMT biomarker expression.[126] By employing a software-controllable rolling shutter on an sCMOS camera, line-scanning confocal high-content imager (e.g., IN Cell Analyzer 6000 from GE Healthcare) is also able to acquire images through an adjustable aperture to fit different lighting conditions with tremendous sensitivity that is comparable to SDCM.[127] Issues such as phototoxicity toward live cells and photobleaching toward fluorescent molecules are drastically reduced in these systems, particularly when imaging multiple Z-sections, making them perfect fits for time-lapse live cell observation. In general, widely used confocal high-content imagers offer great image resolution with high sensitivity and flexibility for deep biological insights from cellular and tissue samples, becoming an integral tool for drug screening and life sciences research.

2.16.4.1.3 Two-photon microscopy

Multiphoton fluorescence microscopy is a powerful research tool that combines the advanced optical techniques of laser scanning microscopy with long wavelength multiphoton fluorescence excitation to capture high-resolution 3D images of samples tagged with highly specific fluorophores.[128] Although two-photon excitation (TPE) microscopy does not produce images with higher resolution than confocal microscopy, it does allow for increased depth of penetration into thick specimens. The penetration depth in confocal microscopy is limited by absorption of excitation energy throughout the beam path and by specimen scattering that affects the delivery of both the excitation and emission photons to the focus. Rather than exciting the fluorophore with one photon and generating fluorescence throughout the entire beam path, a fluorophore is excited by ultrafast laser via near-simultaneous absorption of two longer wavelengths and lower energy photons in two-photon microscopy,[129] which provides distinct advantages. The deep red and near-infrared radiation has orders of magnitude less absorption in biological specimens compared to UV or blue-green light used in one-photon microcopy. Furthermore, the long wavelength significantly reduced light scattering, and offers much better excitation beam penetration depth and enhanced *Z*-axial resolution compared to confocal microscopy.[130] More specifically, two-photon excitation occurs only at or near the focal plane where the laser light is most concentrated, restricting the emission to the narrow focal region and providing sectioning ability without the use of a pinhole. Furthermore, the limited excitation region greatly reduces phototoxicity because photobleaching is largely confined to the vicinity of the focal volume, resulting in increased viability of live cell culture during long-term imaging.[131] The multiphoton approach is a good alternative to confocal microscopy and is routinely applied to imaging experiments that require deep penetration into 3D samples such as intact tissues and animals.[132,133]

2.16.4.1.4 Light sheet fluorescence microscopy

Light sheet-based fluorescence microscopy (LSFM), also known as selective or single plane illumination microscopy (SPIM), has emerged as a versatile and indispensable microscopy technique for fast, high-resolution volumetric imaging of complex thick biological samples.[134,135] The excitation laser beam of LSFM is passed through a cylindrical lens becoming a thin sheet of light that illuminates the focal plane followed by detection in the direction perpendicular to excitation, requiring much less energy to illuminate samples compared to widefield and confocal fluorescence microscopy.[136] The thickness of the light sheet can range between 2 and 6 μm, but may also be thinner than the depth of field of the detection system. Thus, only fluorophores close to the focal plane of the detection system are excited, generating an inherently thin optical section. Another advantage of this method is that images are recorded from one plane at a time, boosting detection efficiency while reducing phototoxicity and photobleaching. LSFM can be used to image virtually any plane with multiple views obtained from different angles. In summary, with low and efficient energy light input, fast recording speed, high sectioning capability, reduced phototoxicity, and multichannel fluorescence imaging,[137] LSFM produces high quality, well-registered optical sections of complex and highly scattering specimens, representing a promising approach for 3D fluorescence microscopy.[138] LSFM has been used for high-resolution 3D imaging of multicellular specimens,[139–142] which has provided the opportunity to study subcellular or even cellular structural details of 3D tissues. For example, Wenzel et al. have reported an HCS assay model of breast cancer using T47D MCTS uniformly arrayed in 384-well plates to detect small molecules that specifically target quiescent cells.[142] 3D HCA was achieved using custom-built LSFM[143,144] and Imaris image analysis software. Light sheet microscope is commercially available from major optical manufacturers such as ZEISS,

LaVisionBioTec, and Leica (Table 5). In addition, a high-throughput imaging microscope for high-speed imaging of entire live embryos based on light-sheet microscopy has recently been developed,[145] demonstrating the future utility of light-sheet-based HCS instruments.

2.16.4.1.5 Laser scanning cytometers

In addition to microscopy, flow cytometry can be used to simultaneously measure multiple events within single cells and populations of cells.[146] It also has the ability to both analyze and sort large sized particles similar to 3D spheroid structures. For example, the BioSorter and COPAS platforms developed by Union Biometrica are fully automated systems for sorting and dispensing large particles ranging from 20 to 1500 microns in diameter. However, limitations of flow cytometry such as the lack of time-resolved measurements, the inability to analyze subcellular localization of fluorochromes, and the inability to analyze the same cell with multiple probes have spurred the development of the image cytometer by performing high-content assays providing both rich morphological and biochemical information.[147] Automated 2D image flow cytometers such as Amnis ImageStream^{x} Mark II from MilliporeSigma and iCyte from Throlabs (Table 5) combine the detailed imagery and functional insights of microscopy with speed, sensitivity, phenotyping abilities, and real-time population data analysis of flow cytometry in a single instrument, to produce high levels of information with minimal investigation time. This unique combination enables a broad range of applications that would be impossible using either technique alone.[148] The built-in software removes the adoption barriers associated with image analysis through a cytometric approach that is user friendly and provides full statistical analysis and composite imaging. Numerical data are displayed as bivariate scattergram plots or traditional cytometric histograms from the derived image data. An important extension of the image cytometry system is the addition of 3D resolution with the help of laser scanning imaging cytometry (LSC) that employs laser-spot scanning illumination.[149] The detection system, which combines PMTs for fluorescence detection and photodiodes for absorbance and scatter detection, offers excellent quantitative cytometric performance and imaging capabilities (field of view $\sim$400 mm^2, focal depth $\sim$200 μm). Furthermore, LSC can image the entire depth of a well without Z-stack assembly or changing focus height in a single scan, allowing differentiation between low and high concentration of signals in a short time frame.[150] This technology is effective for rapid high-throughput identification (quantity, area, and volume) of cells, colonies/spheroids, and model organisms, and particularly suited to the analysis of 3D cultures, as even large objects ($>$1 mm diameter) can be imaged without stitching multiple images. Commercial (i.e., Acumen Cellista from TTP Labtech) and custom-built high-throughput 3D image cytometer enables rapid detection of colony positive objects with predefined thresholds for 3D high-content analysis of spheroids without generating huge data output.[151–153] For example, Kenny et al. measured migratory fluorescent ovarian cancer within an organoid model of the ovary omentum and peritoneum.[153] The HCS assay was analyzed using a TTP Labtech Acumen eX3 fluorescent cytometer. Interestingly, this model was used in both 384-well and 1536-well plates, which gave comparable results despite the scale platform.

2.16.4.2 HCS Software

As the complexity of the biological systems continues to increase, from simple 2D cell cultures to more physiological 3D organoids, the size and complexity of acquired imaging data will continue to grow. With the technology to perform high-content image-based screenings now accessible to many labs, there are growing demands for powerful software tools that enable the acquisition, analysis and visualization, and management of large multidimensional image data sets.

2.16.4.2.1 HCS image acquisition software

In broad terms, there are two types of commercial software programs available for HCS image acquisition. The first one comes bundled with the imaging system and is tailor-made by the manufacturer to drive their own instruments (Table 5). However, built-in applications do not interact with devices from other companies. This type of software can range from the basic picture-taking packages designed for general digital microscopes to highly sophisticated applications that are capable of visualization and quantitative measurements of multidimensional images. The second type of customary proprietary image acquisition software packages are designed to work with most imaging platforms by third-party developers. These software applications such as ScanImage (Vidrio Technologies), SlideBook (Intelligent Imaging Innovations), and Image-Pro Insight (Media Cybernetics) provide their own image acquisition, processing, and analysis functions (Table 6). They are also compatible with a wide variety of motorized microscopes, scientific cameras, illuminators, and other microscope accessories from different manufacturers. Commercially available software packages usually have intuitive and easy-to-use graphical user interface (GUI) and do not require extensive computer skill to master. However, they lack flexibility and have limited opportunities for users to customize or extend their function. Commercial software is often expensive, and depending on the software maintenance agreement, typically there is an extra cost for the updates of the software offered by the respective vender. Open-source software, such as μManager and YouScope, is a cost-effective bioimage software option that not only is able to control many high-content imaging devices on the market but also numerous custom-built imaging systems.[154–156] These packages are free to download and are compatible with various computer operating systems. To take the advantage of the open-source model, the source code of the software is readily available for modification and can be further customized for those with computer programming expertise. For instance, μManager's intuitive graphical user interface and programming interface let anyone write code to control microscope related equipment, resulting in a large and growing list of supported equipment. In addition, μManager's plug-in capabilities allow new application-level functionality to be added for specialized techniques.

Table 6 HCS software for image acquisition, analysis, and data management

Types	*Name*	*Main features and related references*	*URL*	*Cost*
Image Acquisition	μManager	Complete image acquisition and microscope control package with HCS Site Generator plugin[154,155]	https://micro-manager.org https://open-imaging.com	Free/Commercial
	YouScope	Control automated microscopes. Generating protocols graphical interface[156]	http://langmo.github.io/youscope	Free
	ScanImage	Control of various microscopes for neuroscience imaging[157]	http://vidriotechnologies.com	Commercial
	SlideBook	Managing everything from instrument control to image processing and data analysis[158]	https://www.intelligent-imaging.com/slidebook.php	Commercial
	i-Solution	Streamline image capture, measurement, and enhancement process[159]	http://www.imt-digital.com	Commercial
	Image-Pro Insight	Advanced image acquisition software for scientific cameras[160]	http://www.mediacy.com/imageproinsight	Commercial
Image Analysis	Fiji/ImageJ	Bioimage analysis bundle with a broad collections of plugins[92–94]	http://fiji.sc http://imagej.net	Free
	CellProfiler	Interactive exploration and analysis of high-throughput image-based data[161,162]	http://cellprofiler.org	Free
	CellProfiler Analyst	Exploring and analyzing image-derived data. Machine learning tools for identifying complex and subtle phenotypes[31,163]	http://cellprofiler.org	Free
	ITK	Includes leading-edge algorithms for registering and segmenting multidimensional data[164]	https://itk.org	Free
	PhenoRipper	Image block-based tools for rapid exploration and interpretation of high-content microscopy data[165]	http://awlab.ucsf.edu/Web_Site/PhenoRipper/default.htm	Free
	ilastik	Interactive image classification, segmentation, and analysis[166]	http://ilastik.org	Free
	Cell Cognition	Cross platform high-content image analysis on the single cell level[167]	http://cellcognition.org	Free
	TLM-Tracker	Cell segmentation, tracking, and lineage analysis in time-lapse microscopy movies[168]	http://www.tlmtracker.tu-bs.de/index.php/Main_Page	Free
	CellOrganizer	Building accurate models of cell organization directly from microscope images[32]	http://cellorganizer.org	Free
	scikit-image	Image processing library that implements algorithms and utilities for research[169]	http://scikit-image.org	Free
	CellClassifier	Automated classification of single-cell phenotypes with supervised machine learning methods[170]	http://www.pelkmanslab.org/?page_id=63	Free
	Image-Pro Premier	Segment, count, classify, and analysis 2D image. Process and enhance image, data management[171]	http://www.mediacy.com/imageprepremier	Commercial
	DCILabs	Personalized packages such as Neurite Outgrowth and Cell Invasion Assay for HCA[172]	http://www.dcilabs.com/Software.php	Commercial
	Aphelion Dev	Object recognition and measurements, option for 3D image processing.[173,174]	http://www.adcis.net	Commercial
	GSA Image Analyser Batch	Object surface calculation, object length calculation and object counting of images in batch mode[175]	http://image.analyzer.batch.gsa-online.de	Commercial
Data and Workflow Management	KNIME	Integration scientific workflow systems for data analytics and reporting[176,177]	https://www.knime.org/knime	Free/Commercial
	openBIS for HCS and microscopy	Open platform for managing scientific information. Review, brows, annotate, visualize, and analysis images produced in HCS experiments[178]	https://sis.id.ethz.ch/software/openbis-screening.html	Free
	BisQue	Store, visualize, organize, and analyze images in the cloud[179]	http://bioimage.ucsb.edu/bisque	Free
	OMERO	Client–server software for management, visualization, and analysis of biological images[180,181]	https://www.openmicroscopy.org	Free
	Orange	Visual programming software for data mining, machine learning, and workflow management[182]	http://orange.biolab.si	Free
	Pipeline Pilot	Automation and standardization of data preparation and collation. Integrates image data to a unified Image Collection computing framework[176,183]	http://accelrys.com/products/collaborative-science/biovia-pipeline-pilot	Commercial

2.16.4.2.2 Deconvolution

Deconvolution is a computationally intensive image processing technique to reassign light back to its correct plane of focus, producing images with higher contrast and resolution.[184] By taking advantage of PSF that provides information about the microscope's optical characteristics such as the instrument modality and objective lens parameters, a mathematical model is generated to predict the distribution of out-of-focus light caused by the inherent optical limitations of the instrument. Out-of-focus light can then be compensated with iterative deblurring and restoration algorithms from the deconvolution software (Volocity from PerkinElmer, Huygens from Scientific Volume Imaging, etc.), which mathematically erase preexisting noise by redistributing every point of light back into its correct focal plane, resulting in a cleaner image. At the same time, the relative intensities in the image remain largely untouched after restoration, preserving the quantitative relationship in the image analysis.[185] Deconvolution can be used to increase the resolution of widefield and confocal images and is frequently used with 3D Z-stack images.[186] It can also increase the signal-to-noise ratio within the image, resulting in potentially better image segmentation results. However, due to the heavy computational requirements, deconvolved images cannot provide immediate feedback during an experiment.

2.16.4.2.3 HCS image visualizations and analysis software

As microscopy technology develops, images are carrying more and more information in the form of additional dimensions. The number of dimensions in an image is equal to the number of pieces of information needed to identify individual pixels. In a 2D image, a pixel is identified by its x and y coordinates. A voxel or volume element for 3D images is at location (x, y, z). In fluorescence microscopy, a four-dimensional (4D; x, y, z, λ) image is generated by inserting spectral channel λ that represents different imaging channels to an existing 3D image. In time-lapse fluorescence imaging, a voxel's location is specified as a spatiotemporal five-dimensional (5D) point, (x, y, z, λ, t). As dimensionality and size of image data sets continue to grow, visualization together with summarization of the results becomes more challenging, creating the need for software tools that can be used to explore multidimensional image data directly and efficiently.

One of the major advances in recent years is the development of proprietary and open-source bioimage informatics software packages (**Table 6**). These applications enable batch analysis of large data sets to better exploit the multiparametric nature of HCS.[187] Most HCS assays are currently analyzed using commercial instrumentation with bundled software to extract useful information from the phenotypes of interest. These dedicated software platforms have a sizable number of tools that a user can script together to form an image analysis workflow for high-throughput quantitative analysis of image datasets (**Table 5**). For example, an image analysis sequence of Harmony software (PerkinElmer) usually contains sections such as find objects (Find Nuclei, Find Cytoplasm, Find Spots, etc.), define regions of interest (Select Cell Region and Select Region), quantify properties in regions (Calculate Intensity, Morphology and Texture Properties), identify subpopulations (Filter by Property), and calculate readout values (Define Results) (**Fig. 3**). Third-party stand-alone software packages (e.g., Image-Pro Premier and Aphelion Dev) are not integrated with HCS instrumentation forcing image HCA to be done separate from image acquisition. Nonetheless, both integrated and third-party application platforms are flexible and can support sophisticated analyses. While commercial software applications offer more tools and features as well as support for biological visualization and image analysis, open-source software such as ImageJ/Fiji[92–94] and CellProfiler[161,162] prove to be a reliable and cost-effective alternative for postprocessing and management of HCS image sets. For example, Fiji software is a Java-based application for microscopy that provides the ability to write customized plug-ins.[92] Fiji supports a large collection of image formats used by the microscopy community and is compatible with Mac, Linux, and Windows computer operating systems. Most of the aforementioned software packages only provide functions to visualize and analyze 2D images.

While 2D HCS analysis software are well developed and user friendly, they are currently not translatable to more sophisticated 3D organoid models. Therefore, HCS industry developers and researchers are investing in software solutions that are compatible with 3D HCA.[8] Several commercial software applications such as Imaris (Bitplane), Amira (FEI), and ImagePro Premier 3D (Media Cybernetics) (**Table 7**) are becoming widely used for performing 3D image visualization and analysis tasks. Besides commercially available comprehensive tools, there are also numerous freely available open-access 3D imaging software packages (**Table 7**) that are shared and supported by a broad base of scientific community, designed for scientist with little or no programming knowledge. Most of these programs allow user to explore, rotate, and render 3D images in incredible detail and clarity. They also contain flexible

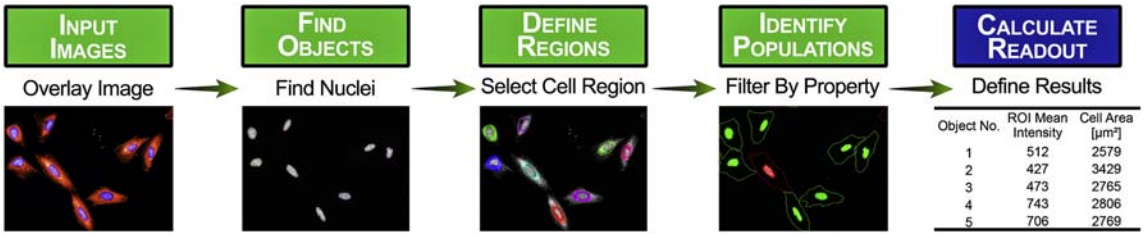

Fig. 3 A flowchart of an image analysis sequence using Harmony high-content imaging and analysis software (version 4.1, PerkinElmer). Fetal human lens epithelial FHL 124 cells were stained with Hoechst 33342 (*blue*) to detect nuclei and RFP (*red*) to detect α-smooth muscle actin (α-SMA) within cell images. Images were captured using a 20× long WD objective with a PerkinElmer Operetta High-Content Imaging System.

Table 7 Software for 3D image analysis and visualization

Name	*Main Features and Related References*	*URL*	*Cost*
Fiji/ImageJ	3D object counter, and 3D surface plot. Plug-ins such as 3D viewer, and image5D[92–94]	http://fiji.sc http://imagej.net	Free
Vaa3D	Interactive 3D/4D/5D image visualization and analysis of reconstructed 3D model[95,96]	http://home.penglab.com/proj/vaa3d/home/index.html	Free
MorphoGraphX	Accurately extract curved surface meshes from 3D volumetric data for image analysis[97,98]	www.morphographx.org	Free
Icy	Intuitive visualization in 3D, powerful plug-ins for 3D image processing and analysis[99]	http://icy.bioimageanalysis.org	Free
FARSight	Quantitative tools for studying complex and dynamic 4D/5D microscopy data[100]	http://www.farsight-toolkit.org	Free
Free-D	Automated 2D and 3D segmentation, and quantitative analysis of 3D reconstructed model[101]	http://free-d.versailles.inra.fr	Free
TANGO	High-throughput processing and quantitative analysis of 3D fluorescence microscopy images[102,103]	http://biophysique.mnhn.fr/tango/HomePage	Free
BioImageXD	Visualization of multichannel image stacks. Batch processor, deconvolution, and motion tracking[104]	http://www.bioimagexd.net	Free
VTK	Scientific visualization, volume rendering, and 3D annotation[105,106]	http://www.vtk.org	Free
Endrov	Design to handle complex 4D data schemes and unlimited number of channels[107]	http://www.endrov.net	Free
OsiriX	Visualization of multimodality and multidimensional images from medical equipment[108]	http://www.osirix-viewer.com	Free
SAMA	Quantitative 3D analysis of the shape of a population of structures in a 3D image[109]	http://montevil.theobio.org/content/sama	Free
ClearVolume	Live 3D visualization and GPU-based image processing for light-sheet microscopy[110]	http://clearvolume.github.io	Free
BioSig3D	Platform for HCA of 3D culture models. Visualization of raw and processed 3D volumetric data[111,112]	http://biosig.lbl.gov	Free
Volocity	Rendering, deconvolution, volumetric segmentation, and quantitative measurement for 3D analysis of fluorescence images[113,114]	http://cellularimaging.perkinelmer.com/downloads/detail.php?id=14	Commercial
arivis Vision4D	Acquisition, visualization, sharing, and analysis of high dimensional image data. High performance interactive 3D/4D rendering of volume data[115]	http://www.arivis.com/en/imaging-science/arivis-vision4d	Commercial
Imaris	Visualization and interpretation of multidimensional data sets. 4D object tracking[116,117]	http://www.bitplane.com	Commercial
Amira	3D image segmentation and reconstruction, 3D data visualization, processing, and analysis[118]	http://www.fei.com/software/amira-3d-for-life-sciences/	Commercial
NOCTY	Handling a large range of multichannel/temporal data with advanced editing and matching tools	http://www.noctylio.com	Commercial
BioVis3D	Visualize, manipulate, and analyze 3D models. Record movies and measure points of interest[119]	http://www.biovis3d.com	Commercial
Image-Pro Premier 3D	Measure complex 3D objects, 3D/4D visualization and data management, key frame animations[120]	http://www.mediacy.com/imagepropremier3d	Commercial
Huygens	Image deconvolution, volume visualization, and interactive analysis of 3D images[121,122]	https://svi.nl	Commercial

and sophisticated toolboxes to measure shapes, volumes, and distances of the 3D objects with precision. Open-sourced Visualization Toolkit (VTK) is a favorite choice for developing customized 3D visualization tools due to its extensive information visualization framework and 3D interaction widgets.[105,106] Similarly, Vaa3D is a cross platform software application geared toward biological visualization of multidimensional images.[95,96] In addition, Vaa3D can find, measure, track, and chart objects for accurate 3D quantitative measurements from single images or large data sets. Icy, funded by Institut Pasteur and France Bio Imaging, is another software application for bioimage informatics that provides a powerful platform for third-party developers to design specialized 3D plug-ins such as 3D-OrthoViewer, Active Cells 3D, Crop 5D, FastFilter3D, and Animation 3D.[99] Web-based BioSig3D is a computational platform that provides end-to-end solutions for HCS of 3D cell culture models.[111] It integrates advanced bioinformatic analysis and links visualized raw or processed 3D volumetric data with experimental variables for quality control. By employing one or more of these versatile image analysis packages (Table 7), visualization and on-the-fly analysis of MCTS and other 3D cell culture model can be accomplished faster and more efficiently, transitioning 3D HTS/HCS into a more quantitative and reproducible technique for drug discovery.

2.16.4.2.4 HCS workflow platform

HCS data contain a diversity of information from multiple sources, including details pertaining to screening libraries, acquired image stacks, HCA data, and quality control statistics and hit selection results. Many free and commercial software tools are now available to tackle the problems that occur in each step of bioimage analysis; however, large amounts of data are transferred manually between these applications, which is time-consuming and error-prone. To improve productivity and increase efficiency, it is crucial to utilize a workflow management software application that covers all aspects of these HCA functionalities to automate the image analysis and hit assessment during HCS. Flexible workflow systems such as KNIME and Pipeline Pilot (**Table 6**) are able to integrate diverse types of resources and facilitate data exchange during HCA. By seamlessly integrating existing software tools with ever-growing number of data sources, KNIME enables users to conveniently build and share specific data analysis pipelines (nodes).[176,177] The business model of KNIME involves licensing enterprise components that allow users to exchange workflows and build Web portals. The base product, KNIME Analytics Platform, is a free open-source package for integrated data access, data mining, statistics, visualization, and reporting. The KNIME Image Processing Extension provides connections to state-of-the-art bioimage analysis software packages, such as ImgLib2 (default programming framework for multidimensional image processing),[188] ImageJ, OMERO, and CellProfiler. KNIME Image Processing nodes can be combined with other available KNIME extensions (e.g., cheminformatics extensions) to generate a comprehensible HCA workflow.[189] Pipeline Pilot is BIOVIA's graphic workflow application that automates the scientific data flow. Pipeline Pilot has the ability to process and integrate all types of data including numerical, text, chemical structure, biological structure, and image data. Its Imaging Collection component enables researchers to process, segment, measure, export, apply advanced learning algorithms, and create custom interactive reports with image-data links. Complete image processing and analysis protocols can be created without ever performing complex scripting or programming, making the Pipeline Pilot a useful HCS informatics platform.[183,190]

2.16.5 Perspective of the Key Limitations of 3D HCA and HCS Technologies

As discussed throughout this chapter, 3D organoid models have superior advantages over traditional 2D cell culture methods. However, it must be recognized that major challenges remain, which limit the widespread use of organoids for HCA/HCS drug discovery. The major challenges identified from this chapter include: (1) the high cost of 3D cell-based imaging and screening compared to 2D. Specifically, everything from plates (e.g., hanging drop plate) to biological reagents (e.g., Matrigel) to high-content imaging acquisition (instrumentation time and custom features); (2) 3D organoid structures exhibit a higher degree of variability and heterogeneity compared to 2D systems. Therefore, every technical aspect in the assay protocols must be carefully optimized to minimize well-to-well and plate-to-plate variation; (3) Analyzing the vast amounts of data generated from 3D HCS poses other significant challenges due to the fact that most imaging analysis programs are tailored to meet the needs of 2D HCS. Currently, there is no single software package that covers all aspects of 3D HCA required for segmenting, tracking, visualizing, quantifying, and batch analyzing organoids. Finally, most 3D models remain relatively simplistic; however, this area of biomedical and tissue engineering research is progressing rapidly, which will likely yield more complex and sophisticated organoid models in the near future. Therefore, in addition to addressing the current challenges, imaging and software companies must anticipate, prepare for, and develop solutions to 3D imaging challenges that will arise from more complex organoid models.

2.16.6 Outlook and Conclusion

The development of safe and effective drug therapies to prevent or treat human disease is arguably one of the most challenging human pursuits. Tremendous resources and time are devoted to accomplish this pursuit by industry, government, and academia alike. Despite our success in the endeavor to provide safe and effective drug therapies, the drug discovery and development process has a remarkably low success rate and high financial cost. However, the future of the drug discovery and development pipeline is brighter than ever before due to our technological advances and ever improving understanding of human anatomy and disease on the cellular and biological level. We are now poised with the ability to reproduce complex human anatomy and disease, ex vivo, in the form of 3D organoid models that are uniformly scaled and adaptable for high-throughput drug discovery. The marriage of automated HCS with 3D models of human disease holds the potential to discover more effective drug therapies with improved translational clinical success rates. Moreover, organoids can be produced from primary human tissues and genetically functionalized to study individual human disease or even populations, providing a platform to develop precision medicines.

See also: 2.17. Label-Free Screening Technologies.

References

1. Kola, I.; Landis, J. Can the Pharmaceutical Industry Reduce Attrition Rates? *Nat. Rev. Drug Discov.* **2004,** *3*, 711–715.
2. LaBarbera, D. V.; Reid, B. G.; Yoo, B. H. The Multicellular Tumor Spheroid Model for High-Throughput Cancer Drug Discovery. *Expert Opin. Drug Dis.* **2012,** *7*, 819–830.

3. Hynds, R. E.; Giangreco, A. Concise Review: The Relevance of Human Stem Cell-Derived Organoid Models for Epithelial Translational Medicine. *Stem Cells* **2013,** *31,* 417–422.
4. Pampaloni, F.; Reynaud, E. G.; Stelzer, E. H. K. The Third Dimension Bridges the Gap Between Cell Culture and Live Tissue. *Nat. Rev. Mol. Cell Biol.* **2007,** *8,* 839–845.
5. Shamir, E. R.; Ewald, A. J. Three-Dimensional Organotypic Culture: Experimental Models of Mammalian Biology and Disease. *Nat. Rev. Mol. Cell Biol.* **2014,** *15,* 647–664.
6. Lancaster, M. A.; Knoblich, J. A. Organogenesis in a Dish: Modeling Development and Disease Using Organoid Technologies. *Science* **2014,** *345,* 1247125.
7. Fatehullah, A.; Tan, S. H.; Barker, N. Organoids as an in vitro Model of Human Development and Disease. *Nat. Cell Biol.* **2016,** *18,* 246–254.
8. Li, L.; Zhou, Q.; Voss, T. C.; Quick, K. L.; LaBarbera, D. V. High-Throughput Imaging: Focusing in on Drug Discovery in 3D. *Methods* **2016,** *96,* 97–102.
9. Yin, X.; Mead, B. E.; Safaee, H.; Langer, R.; Karp, J. M.; Levy, O. Engineering Stem Cell Organoids. *Cell Stem Cell* **2016,** *18,* 25–38.
10. Lancaster, M. A.; Renner, M.; Martin, C. A.; Wenzel, D.; Bicknell, L. S.; Hurles, M. E.; Homfray, T.; Penninger, J. M.; et al. Cerebral Organoids Model Human Brain Development and Microcephaly. *Nature* **2013,** *501,* 373–379.
11. Collins, F. S.; Varmus, H. A New Initiative on Precision Medicine. *N. Engl. J. Med.* **2015,** *372,* 793–795.
12. Giuliano, K. A.; DeBiasio, R. L.; Dunlay, R. T.; Gough, A.; Volosky, J. M.; Zock, J.; Pavlakis, G. N.; Taylor, D. L. High-Content Screening: A New Approach to Easing Key Bottlenecks in the Drug Discovery Process. *J. Biomol. Screen.* **1997,** *2,* 249–259.
13. Taylor, D. L. A Personal Perspective on High-Content Screening (HCS): From the Beginning. *J. Biomol. Screen.* **2010,** *15,* 720–725.
14. Bickle, M. The Beautiful Cell: High-Content Screening in Drug Discovery. *Anal. Bioanal. Chem.* **2010,** *398,* 219–226.
15. Chan, G. K.; Wilson, S.; Schmidt, S.; Moffat, J. G. Unlocking the Potential of High-Throughput Drug Combination Assays Using Acoustic Dispensing. *J. Lab. Autom.* **2016,** *21,* 125–132.
16. Astle, T. W. Microplate Standardization. *Mol. Online* **1997,** *1,* 106–113.
17. Lakowicz, J. R. Fluorophores. In *Principles of Fluorescence Spectroscopy;* Lakowicz, J. R., Ed.; Springer: Boston, MA, USA, 1999; pp 63–93.
18. https://www.thermofisher.com/us/en/home/life-science/lab-data-management-analysis-software/lab-apps/cell-staining-tool.html.
19. https://www.thermofisher.com/us/en/home/life-science/cell-analysis/labeling-chemistry/fluorescence-spectraviewer.html.
20. http://searchlight.semrock.com/.
21. http://m.bdbiosciences.com/us/s/spectrumviewer.
22. Uchida, S. Image Processing and Recognition for Biological Images. *Dev. Growth Differ.* **2013,** *55,* 523–549.
23. Shariff, A.; Kangas, J.; Coelho, L. P.; Quinn, S.; Murphy, R. F. Automated Image Analysis for High-Content Screening and Analysis. *J. Biomol. Screen.* **2010,** *15,* 726–734.
24. Jaqaman, K.; Loerke, D.; Mettlen, M.; Kuwata, H.; Grinstein, S.; Schmid, S. L.; Danuser, G. Robust Single-Particle Tracking in Live-Cell Time-Lapse Sequences. *Nat. Methods* **2008,** *5,* 695–702.
25. Maska, M.; Ulman, V.; Svoboda, D.; Matula, P.; Matula, P.; Ederra, C.; Urbiola, A.; Espana, T.; et al. A Benchmark for Comparison of Cell Tracking Algorithms. *Bioinformatics* **2014,** *30,* 1609–1617.
26. Matula, P.; Maska, M.; Sorokin, D. V.; Matula, P.; Ortiz-de-Solorzano, C.; Kozubek, M. Cell Tracking Accuracy Measurement Based on Comparison of Acyclic Oriented Graphs. *PLoS One* **2015,** *10,* e0144959.
27. Bradley, J.; Bowman, D.; Chakravarty, A. Image Processing. In *An Introduction to High Content Screening;* Haney, S. A., Bowman, D., Chakravarty, A., Eds.; John Wiley & Sons, Inc: Hoboken, New Jersey, USA, 2014; pp 47–61.
28. Shuoyu, X.; Piyushkumar, A. M.; Huipeng, L.; Shiwen, Z.; Roy, E. W.; Jagath, C. R. Image Analysis for Cellular and Tissue Engineering. In *Imaging in Cellular and Tissue Engineering;* Yu, H., Rahim, N. A. A., Eds.; CRC Press: Boca Raton, FL, 2013; pp 223–245.
29. Kelm, J. M.; Timmins, N. E.; Brown, C. J.; Fussenegger, M.; Nielsen, L. K. Method for Generation of Homogeneous Multicellular Tumor Spheroids Applicable to a Wide Variety of Cell Types. *Biotechnol. Bioeng.* **2003,** *83,* 173–180.
30. Millard, B. L.; Niepel, M.; Menden, M. P.; Muhlich, J. L.; Sorger, P. K. Adaptive Informatics for Multifactorial and High-Content Biological Data. *Nat. Methods* **2011,** *8,* 487–492.
31. Jones, T. R.; Carpenter, A. E.; Lamprecht, M. R.; Moffat, J.; Silver, S. J.; Grenier, J. K.; Castoreno, A. B.; Eggert, U. S.; et al. Scoring Diverse Cellular Morphologies in Image-Based Screens With Iterative Feedback and Machine Learning. *Proc. Natl. Acad. Sci. U. S. A.* **2009,** *106,* 1826–1831.
32. Murphy, R. F. Cell Organizer: Image-Derived Models of Subcellular Organization and Protein Distribution. *Methods Cell Biol.* **2012,** *110,* 179–193.
33. Sommer, C.; Gerlich, D. W. Machine Learning in Cell Biology—Teaching Computers to Recognize Phenotypes. *J. Cell Sci.* **2013,** *126,* 5529–5539.
34. Shockley, K. R. Quantitative High-Throughput Screening Data Analysis: Challenges and Recent Advances. *Drug Discov. Today* **2015,** *20,* 296–300.
35. Gubler, H. High-Throughput Screening Data Analysis. In *Nonclinical Statistics for Pharmaceutical and Biotechnology Industries;* Zhang, L., Ed.; Springer International Publishing: Switzerland, 2016; pp 83–139.
36. Zhang, J. H.; Chung, T. D.; Oldenburg, K. R. A Simple Statistical Parameter for Use in Evaluation and Validation of High Throughput Screening Assays. *J. Biomol. Screen.* **1999,** *4,* 67–73.
37. Majumdar, A.; Stock, D. Large Sample Inference for an Assay Quality Measure Used in High-Throughput Screening. *Pharm. Stat.* **2011,** *10,* 227–231.
38. Ravkin, I.; Temov, V.; Nelson, A. D.; Zarowitz, M. A.; Hoopes, M.; Verhovsky, Y.; Ascue, G.; Goldbard, S.; et al. Multiplexed High-Throughput Image Cytometry Using Encoded Carriers. *Proc. SPIE* **2004,** *5322,* 52–63.
39. Zhang, X. D. A Pair of New Statistical Parameters for Quality Control in RNA Interference High-Throughput Screening Assays. *Genomics* **2007,** *89,* 552–561.
40. Zhang, X. D.; Lacson, R.; Yang, R.; Marine, S. D.; McCampbell, A.; Toolan, D. M.; Hare, T. R.; Kajdas, J.; et al. The Use of SSMD-Based False Discovery and False Nondiscovery Rates in Genome-Scale RNAi Screens. *J. Biomol. Screen.* **2010,** *15,* 1123–1131.
41. Zhang, X. D. Illustration of SSMD, z Score, SSMD*, z* Score, and t Statistic for Hit Selection in RNAi High-Throughput Screens. *J. Biomol. Screen.* **2011,** *16,* 775–785.
42. Goktug, A. N.; Chai, S. C.; Chen, T. Data Analysis Approaches in High Throughput Screening. In *Drug Discovery;* El-Shemy, H. A., Ed.; INTECH Open Access Publisher, 2013.
43. Malo, N.; Hanley, J. A.; Cerquozzi, S.; Pelletier, J.; Nadon, R. Statistical Practice in High-Throughput Screening Data Analysis. *Nat. Biotechnol.* **2006,** *24,* 167–175.
44. Chung, N.; Zhang, X. D.; Kreamer, A.; Locco, L.; Kuan, P. F.; Bartz, S.; Linsley, P. S.; Ferrer, M.; et al. Median Absolute Deviation to Improve Hit Selection for Genome-Scale RNAi Screens. *J. Biomol. Screen.* **2008,** *13,* 149–158.
45. Brideau, C.; Gunter, B.; Pikounis, B.; Liaw, A. Improved Statistical Methods for Hit Selection in High-Throughput Screening. *J. Biomol. Screen.* **2003,** *8,* 634–647.
46. Caraus, I.; Alsuwailem, A. A.; Nadon, R.; Makarenkov, V. Detecting and Overcoming Systematic Bias in High-Throughput Screening Technologies: A Comprehensive Review of Practical Issues and Methodological Solutions. *Brief. Bioinform.* **2015,** *16,* 974–986.
47. Krzywinski, M.; Birol, I.; Jones, S. J. M.; Marra, M. A. Hive Plots-Rational Approach to Visualizing Networks. *Brief. Bioinform.* **2012,** *13,* 627–644.
48. Sailem, H. Z.; Sero, J. E.; Bakal, C. Visualizing Cellular Imaging Data Using PhenoPlot. *Nat. Commun.* **2015,** *6,* 5825.
49. De Backer, S.; Naud, A.; Scheunders, P. Non-Linear Dimensionality Reduction Techniques for Unsupervised Feature Extraction. *Pattern Recog. Lett.* **1998,** *19,* 711–720.
50. Young, D. W.; Bender, A.; Hoyt, J.; McWhinnie, E.; Chirn, G. W.; Tao, C. Y.; Tallarico, J. A.; Labow, M.; et al. Integrating High-Content Screening and Ligand-Target Prediction to Identify Mechanism of Action. *Nat. Chem. Biol.* **2008,** *4,* 59–68.
51. Ahn, H.; Moon, H. Classification: Supervised Learning With High-Dimensional Biological Data. In *Statistical Bioinformatics;* Lee, J. K., Ed.; John Wiley & Sons, Inc: Hoboken, New Jersey, USA, 2010; pp 129–156.
52. Yom-Tov, E. Machine Learning Techniques for Large Data. In *High-Throughput Image Reconstruction and Analysis;* Rao, A. R., Cecchi, G. A., Eds.; Artech House: Boston, 2009; pp 161–178.
53. Kummel, A.; Gubler, H.; Gehin, P.; Beibel, M.; Gabriel, D.; Parker, C. N. Integration of Multiple Readouts Into the Z' Factor for Assay Quality Assessment. *J. Biomol. Screen.* **2010,** *15,* 95–101.

54. Twarog, N. R.; Low, J. A.; Currier, D. G.; Miller, G.; Chen, T. S.; Shelat, A. A. Robust Classification of Small-Molecule Mechanism of Action Using a Minimalist High-Content Microscopy Screen and Multidimensional Phenotypic Trajectory Analysis. *PLoS One* **2016,** *11,* e0149439.
55. Sutherland, R. M.; Inch, W. R.; McCredie, J. A.; Kruuv, J. A Multi-Component Radiation Survival Curve Using an in vitro Tumour Model. *Int. J. Radiat. Biol. Relat. Stud. Phys. Chem. Med.* **1970,** *18,* 491–495.
56. Goodwin, T. J.; Prewett, T. L.; Wolf, D. A.; Spaulding, G. F. Reduced Shear Stress: A Major Component in the Ability of Mammalian Tissues to Form Three-Dimensional Assemblies in Simulated Microgravity. *J. Cell. Biochem.* **1993,** *51,* 301–311.
57. Levinger, I.; Ventura, Y.; Vago, R. Life Is Three Dimensional-as in vitro Cancer Cultures Should Be. *Adv. Cancer Res.* **2014,** *121,* 383–414.
58. Dhandayuthapani, B.; Yoshida, Y.; Maekawa, T.; Kumar, D. S. Polymeric Scaffolds in Tissue Engineering Application: A Review. *Int. J. Polym. Sci.* **2011,** *2011,* 290602.
59. Worthington, P.; Pochan, D. J.; Langhans, S. A. Peptide Hydrogels—Versatile Matrices for 3D Cell Culture in Cancer Medicine. *Front. Oncol.* **2015,** *5,* 92.
60. Frantz, C.; Stewart, K. M.; Weaver, V. M. The Extracellular Matrix at a Glance. *J. Cell Sci.* **2010,** *123,* 4195–4200.
61. Di Lullo, G. A.; Sweeney, S. M.; Korkko, J.; Ala-Kokko, L.; San Antonio, J. D. Mapping the Ligand-Binding Sites and Disease-Associated Mutations on the Most Abundant Protein in the Human, Type I Collagen. *J. Biol. Chem.* **2002,** *277,* 4223–4231.
62. Benton, J. A.; Fairbanks, B. D.; Anseth, K. S. Characterization of Valvular Interstitial Cell Function in Three Dimensional Matrix Metalloproteinase Degradable PEG Hydrogels. *Biomaterials* **2009,** *30,* 6593–6603.
63. Montanez-Sauri, S. I.; Beebe, D. J.; Sung, K. E. Microscale Screening Systems for 3D Cellular Microenvironments: Platforms, Advances, and Challenges. *Cell. Mol. Life Sci.* **2015,** *72,* 237–249.
64. Agastin, S.; Giang, U. B.; Geng, Y.; Delouise, L. A.; King, M. R. Continuously Perfused Microbubble Array for 3D Tumor Spheroid Model. *Biomicrofluidics* **2011,** *5,* 24110.
65. Hsiao, A. Y.; Tung, Y. C.; Kuo, C. H.; Mosadegh, B.; Bedenis, R.; Pienta, K. J.; Takayama, S. Micro-Ring Structures Stabilize Microdroplets to Enable Long Term Spheroid Culture in 384 Hanging Drop Array Plates. *Biomed. Microdevices* **2012,** *14,* 313–323.
66. Drewitz, M.; Helbling, M.; Fried, N.; Bieri, M.; Moritz, W.; Lichtenberg, J.; Kelm, J. M. Towards Automated Production and Drug Sensitivity Testing Using Scaffold-Free Spherical Tumor Microtissues. *Biotechnol. J.* **2011,** *6,* 1488–1496.
67. Friedrich, J.; Seidel, C.; Ebner, R.; Kunz-Schughart, L. A. Spheroid-Based Drug Screen: Considerations and Practical Approach. *Nat. Protoc.* **2009,** *4,* 309–324.
68. Li, Q.; Chen, C.; Kapadia, A.; Zhou, Q.; Harper, M. K.; Schaack, J.; LaBarbera, D. V. 3D Models of Epithelial-Mesenchymal Transition in Breast Cancer Metastasis: High-Throughput Screening Assay Development, Validation, and Pilot Screen. *J. Biomol. Screen.* **2011,** *16,* 141–154.
69. Ejiri, Y.; Yoshida, A.; Hosoda, M.; Kobayashi, K.; Chiba, K. Characterization of a Human Hepatocelluar Carcinoma Cell Line on Micro-Space Cell Culture Plate. *Drug Metab. Rev.* **2011,** *43,* 138–139.
70. Kobayashi, K.; Yoshida, A.; Ejiri, Y.; Takagi, S.; Mimura, H.; Hosoda, M.; Matsuura, T.; Chiba, K. Increased Expression of Drug-Metabolizing Enzymes in Human Hepatocarcinoma FLC-4 Cells Cultured on Micro-Space Cell Culture Plates. *Drug Metab. Pharmacokinet.* **2012,** *27,* 478–485.
71. Jeon, H.; Simon, C. G., Jr.; Kim, G. A Mini-Review: Cell Response to Microscale, Nanoscale, and Hierarchical Patterning of Surface Structure. *J. Biomed. Mater. Res. B Appl. Biomater.* **2014,** *102,* 1580–1594.
72. Souza, G. R.; Molina, J. R.; Raphael, R. M.; Ozawa, M. G.; Stark, D. J.; Levin, C. S.; Bronk, L. F.; Ananta, J. S.; et al. Three-Dimensional Tissue Culture Based on Magnetic Cell Levitation. *Nat. Nanotechnol.* **2010,** *5,* 291–296.
73. Timm, D. M.; Chen, J.; Sing, D.; Gage, J. A.; Haisler, W. L.; Neeley, S. K.; Raphael, R. M.; Dehghani, M.; et al. A High-Throughput Three-Dimensional Cell Migration Assay for Toxicity Screening With Mobile Device-Based Macroscopic Image Analysis. *Sci. Rep.* **2013,** *3,* 3000.
74. Tseng, H.; Gage, J. A.; Shen, T.; Haisler, W. L.; Neeley, S. K.; Shiao, S.; Chen, J.; Desai, P. K.; et al. A Spheroid Toxicity Assay Using Magnetic 3D Bioprinting and Real-Time Mobile Device-Based Imaging. *Sci. Rep.* **2015,** *5,* 13987.
75. Reddy, L. H.; Arias, J. L.; Nicolas, J.; Couvreur, P. Magnetic Nanoparticles: Design and Characterization, Toxicity and Biocompatibility, Pharmaceutical and Biomedical Applications. *Chem. Rev.* **2012,** *112,* 5818–5878.
76. Huh, D.; Hamilton, G. A.; Ingber, D. E. From 3D Cell Culture to Organs-on-Chips. *Trends Cell Biol.* **2011,** *21,* 745–754.
77. Tehranirokh, M.; Kouzani, A. Z.; Francis, P. S.; Kanwar, J. R. Microfluidic Devices for Cell Cultivation and Proliferation. *Biomicrofluidics* **2013,** *7,* 51502.
78. Alessandri, K.; Sarangi, B. R.; Gurchenkov, V. V.; Sinha, B.; Kiessling, T. R.; Fetler, L.; Rico, F.; Scheuring, S.; et al. Cellular Capsules as a Tool for Multicellular Spheroid Production and for Investigating the Mechanics of Tumor Progression In Vitro. *Proc. Natl. Acad. Sci. U. S. A.* **2013,** *110,* 14843–14848.
79. Ntziachristos, V. Going Deeper Than Microscopy: The Optical Imaging Frontier in Biology. *Nat. Methods* **2010,** *7,* 603–614.
80. Fischer, R. S.; Wu, Y.; Kanchanawong, P.; Shroff, H.; Waterman, C. M. Microscopy in 3D: A Biologist's Toolbox. *Trends Cell Biol.* **2011,** *21,* 682–691.
81. Furman, C.; Bowman, D.; Davies, A.; Shamu, C.; Haney, S. A. A General Guide to Selecting and Setting Up a High Content Imaging Platform. In *An Introduction to High Content Screening;* Haney, S. A., Bowman, D., Chakravarty, A., Eds.; John Wiley & Sons, Inc: Hoboken, New Jersey, USA, 2014; pp 65–79.
82. Bell, S.; Morris, K. Types of Microscopes. In *An Introduction to Microscopy;* Bell, S., Morris, K., Eds.; CRC Press: Boca Raton, FL, 2009; pp 17–30.
83. Jerome, W. G.; Price, R. L. Fluorescence Microscopy. In *Basic Confocal Microscopy;* Price, L. R., Jerome, W. G., Eds.; Springer: New York, NY, 2011; pp 29–59.
84. Stephens, D. J.; Allan, V. J. Light Microscopy Techniques for Live Cell Imaging. *Science* **2003,** *300,* 82–86.
85. Hoebe, R. A.; Van der Voort, H. T.; Stap, J.; Van Noorden, C. J.; Manders, E. M. Quantitative Determination of the Reduction of Phototoxicity and Photobleaching by Controlled Light Exposure Microscopy. *J. Microsc.* **2008,** *231,* 9–20.
86. Sakamoto, R.; Rahman, M. M.; Shimomura, M.; Itoh, M.; Nakatsura, T. Time-Lapse Imaging Assay Using the BioStation CT: A Sensitive Drug-Screening Method for Three-Dimensional Cell Culture. *Cancer Sci.* **2015,** *106,* 757–765.
87. Hongisto, V.; Jernstrom, S.; Fey, V.; Mpindi, J. P.; Kleivi Sahlberg, K.; Kallioniemi, O.; Perala, M. High-Throughput 3D Screening Reveals Differences in Drug Sensitivities Between Culture Models of JIMT1 Breast Cancer Cells. *PLoS One* **2013,** *8,* e77232.
88. Härmä, V.; Schukov, H. P.; Happonen, A.; Ahonen, I.; Virtanen, J.; Siitari, H.; Akerfelt, M.; Lotjonen, J.; et al. Quantification of Dynamic Morphological Drug Responses in 3D Organotypic Cell Cultures by Automated Image Analysis. *PLoS One* **2014,** *9,* e96426.
89. Achilli, T. M.; McCalla, S.; Tripathi, A.; Morgan, J. R. Quantification of the Kinetics and Extent of Self-Sorting in Three Dimensional Spheroids. *Tissue Eng. Part C Methods* **2012,** *18,* 302–309.
90. Vinci, M.; Gowan, S.; Boxall, F.; Patterson, L.; Zimmermann, M.; Court, W.; Lomas, C.; Mendiola, M.; et al. Advances in Establishment and Analysis of Three-Dimensional Tumor Spheroid-Based Functional Assays for Target Validation and Drug Evaluation. *BMC Biol.* **2012,** *10,* 29.
91. Muller, M. *Introduction to Confocal Fluorescence Microscopy,* 2nd ed.; SPIE press: Bellingham, Washington, USA, 2006.
92. Schindelin, J.; Arganda-Carreras, I.; Frise, E.; Kaynig, V.; Longair, M.; Pietzsch, T.; Preibisch, S.; Rueden, C.; et al. Fiji: An Open-Source Platform for Biological-Image Analysis. *Nat. Methods* **2012,** *9,* 676–682.
93. Schneider, C. A.; Rasband, W. S.; Eliceiri, K. W. NIH Image to ImageJ: 25 Years of Image Analysis. *Nat. Methods* **2012,** *9,* 671–675.
94. Schindelin, J.; Rueden, C. T.; Hiner, M. C.; Eliceiri, K. W. The ImageJ Ecosystem: An Open Platform for Biomedical Image Analysis. *Mol. Reprod. Dev.* **2015,** *82,* 518–529.
95. Peng, H.; Bria, A.; Zhou, Z.; Iannello, G.; Long, F. Extensible Visualization and Analysis for Multidimensional Images Using Vaa3D. *Nat. Protoc.* **2014,** *9,* 193–208.
96. Peng, H.; Tang, J.; Xiao, H.; Bria, A.; Zhou, J.; Butler, V.; Zhou, Z.; Gonzalez-Bellido, P. T.; et al. Virtual Finger Boosts Three-Dimensional Imaging and Microsurgery As Well As Terabyte Volume Image Visualization and Analysis. *Nat. Commun.* **2014,** *5,* 4342.
97. de Reuille, P. B.; Robinson, S.; Smith, R. S. Quantifying Cell Shape and Gene Expression in the Shoot Apical Meristem Using MorphoGraphX. *Methods Mol. Biol.* **2014,** *1080,* 121–134.
98. Barbier de Reuille, P.; Routier-Kierzkowska, A. L.; Kierzkowski, D.; Bassel, G. W.; Schupbach, T.; Tauriello, G.; Bajpai, N.; Strauss, S.; et al. MorphoGraphX: A Platform for Quantifying Morphogenesis in 4D. *Elife* **2015,** *4,* 05864.

99. de Chaumont, F.; Dallongeville, S.; Chenouard, N.; Hervé, N.; Pop, S.; Provoost, T.; Meas-Yedid, V.; Pankajakshan, P.; et al. Icy: An Open Bioimage Informatics Platform for Extended Reproducible Research. *Nat. Methods* **2012,** *9,* 690–696.
100. Luisi, J.; Narayanaswamy, A.; Galbreath, Z.; Roysam, B. The FARSIGHT Trace Editor: An Open Source Tool for 3-D Inspection and Efficient Pattern Analysis Aided Editing of Automated Neuronal Reconstructions. *Neuroinformatics* **2011,** *9,* 305–315.
101. Andrey, P.; Maurin, Y. Free-D: An Integrated Environment for Three-Dimensional Reconstruction From Serial Sections. *J. Neurosci. Methods* **2005,** *145,* 233–244.
102. Ollion, J.; Cochennec, J.; Loll, F.; Escudé, C.; Boudier, T. TANGO: A Generic Tool for High-Throughput 3D Image Analysis for Studying Nuclear Organization. *Bioinformatics* **2013,** *29,* 1840–1841.
103. Ollion, J.; Cochennec, J.; Loll, F.; Escude, C.; Boudier, T. Analysis of Nuclear Organization With TANGO, Software for High-Throughput Quantitative Analysis of 3D Fluorescence Microscopy Images. *Methods Mol. Biol.* **2015,** *1228,* 203–222.
104. Kankaanpää, P.; Paavolainen, L.; Tiitta, S.; Karjalainen, M.; Paivarinne, J.; Nieminen, J.; Marjomaki, V.; Heino, J.; et al. BioImageXD: An Open, General-Purpose and High-Throughput Image-Processing Platform. *Nat. Methods* **2012,** *9,* 683–689.
105. Taka, S. J.; Srinivasan, S. NIRViz: 3D Visualization Software for Multimodality Optical Imaging Using Visualization Toolkit (VTK) and Insight Segmentation Toolkit (ITK). *J. Digit. Imaging* **2011,** *24,* 1103–1111.
106. Wills, G. Visualization Toolkit Software. *Wiley Interdiscip. Rev. Comput. Stat.* **2012,** *4,* 474–481.
107. Henriksson, J.; Hench, J.; Tong, Y. G.; Johansson, A.; Johansson, D.; Burglin, T. R. Endrov: An Integrated Platform for Image Analysis. *Nat. Methods* **2013,** *10,* 454–456.
108. Rosset, A.; Spadola, L.; Ratib, O. OsiriX: An Open-Source Software for Navigating in Multidimensional DICOM Images. *J. Digit. Imaging* **2004,** *17,* 205–216.
109. Paulose, T.; Montevil, M.; Speroni, L.; Cerruti, F.; Sonnenschein, C.; Soto, A. M. SAMA: A Method for 3D Morphological Analysis. *PLoS One* **2016,** *11,* e0153022.
110. Royer, L. A.; Weigert, M.; Gunther, U.; Maghelli, N.; Jug, F.; Sbalzarini, I. F.; Myers, E. W. ClearVolume: Open-Source Live 3D Visualization for Light-Sheet Microscopy. *Nat. Methods* **2015,** *12,* 480–481.
111. Bilgin, C. C.; Fontenay, G.; Cheng, Q.; Chang, H.; Han, J.; Parvin, B. BioSig3D: High Content Screening of Three-Dimensional Cell Culture Models. *PLoS One* **2016,** *11,* e0148379.
112. Bilgin, C. C.; Kim, S.; Leung, E.; Chang, H.; Parvin, B. Integrated Profiling of Three Dimensional Cell Culture Models and 3D Microscopy. *Bioinformatics* **2013,** *29,* 3087–3093.
113. Shimosako, N.; Hadjieconomou, D.; Salecker, I. Flybow to Dissect Circuit Assembly in the Drosophila Brain. *Methods Mol. Biol.* **2014,** *1082,* 57–69.
114. Carmona, G.; Perera, U.; Gillett, C.; Naba, A.; Law, A. L.; Sharma, V. P.; Wang, J.; Wyckoff, J.; et al. Lamellipodin Promotes Invasive 3D Cancer Cell Migration via Regulated Interactions With Ena/VASP and SCAR/WAVE. *Oncogene* **2016,** *36,* 5155–5169. http://dx.doi.org/10.1038/onc.2016.1047.
115. Lee, E.; Choi, J.; Jo, Y.; Kim, J. Y.; Jang, Y. J.; Lee, H. M.; Kim, S. Y.; Lee, H. J.; et al. ACT-PRESTO: Rapid and Consistent Tissue Clearing and Labeling Method for 3-Dimensional (3D) Imaging. *Sci. Rep.* **2016,** *6,* 18631.
116. Lou, Y. R.; Kanninen, L.; Kaehr, B.; Townson, J. L.; Niklander, J.; Harjumaki, R.; Jeffrey Brinker, C.; Yliperttula, M. Silica Bioreplication Preserves Three-Dimensional Spheroid Structures of Human Pluripotent Stem Cells and HepG2 Cells. *Sci. Rep.* **2015,** *5,* 13635.
117. Widmer, C.; Heinrich, S.; Drewe, P.; Lou, X.; Umrania, S.; Ratsch, G. Graph-Regularized 3D Shape Reconstruction From Highly Anisotropic and Noisy Images. *Signal Image Video Process.* **2014,** *8,* 41–48.
118. Rühland, S.; Wechselberger, A.; Spitzweg, C.; Huss, R.; Nelson, P. J.; Harz, H. Quantification of in vitro Mesenchymal Stem Cell Invasion Into Tumor Spheroids Using Selective Plane Illumination Microscopy. *J. Biomed. Opt.* **2015,** *20,* 040501.
119. Schlomer, B. J.; Feretti, M.; Rodriguez, E., Jr.; Blaschko, S.; Cunha, G.; Baskin, L. Sexual Differentiation in the Male and Female Mouse From Days 0 to 21: A Detailed and Novel Morphometric Description. *J. Urol.* **2013,** *190,* 1610–1617.
120. Hellmer, C. B.; Zhou, Y.; Fyk-Kolodziej, B.; Hu, Z.; Ichinose, T. Morphological and Physiological Analysis of Type-5 and Other Bipolar Cells in the Mouse Retina. *Neuroscience* **2016,** *315,* 246–258.
121. Freeman, K.; Tao, W.; Sun, H.; Soonpaa, M. H.; Rubart, M. In Situ Three-Dimensional Reconstruction of Mouse Heart Sympathetic Innervation by Two-Photon Excitation Fluorescence Imaging. *J. Neurosci. Methods* **2014,** *221,* 48–61.
122. Barna, L.; Dudok, B.; Miczan, V.; Horvath, A.; Laszlo, Z. I.; Katona, I. Correlated Confocal and Super-Resolution Imaging by VividSTORM. *Nat. Protoc.* **2016,** *11,* 163–183.
123. Paddock, S. W.; Eliceiri, K. W. Laser Scanning Confocal Microscopy: History, Applications, and Related Optical Sectioning Techniques. In *Confocal Microscopy: Methods and Protocols;* Paddock, W. S., Ed.; Springer: New York, NY, USA, 2014; pp 9–47.
124. Oreopoulos, J.; Berman, R.; Browne, M. Spinning-Disk Confocal Microscopy: Present Technology and Future Trends. *Methods Cell Biol.* **2014,** *123,* 153–175.
125. Reid, B. G.; Jerjian, T.; Patel, P.; Zhou, Q.; Yoo, B. H.; Kabos, P.; Sartorius, C. A.; Labarbera, D. V. Live Multicellular Tumor Spheroid Models for High-Content Imaging and Screening in Cancer Drug Discovery. *Curr. Chem. Genom. Transl. Med.* **2014,** *8,* 27–35.
126. Zhou, Q.; Abraham, A. D.; Li, L.; Babalmorad, A.; Bagby, S.; Arcaroli, J. J.; Hansen, R. J.; Valeriote, F. A.; et al. Topoisomerase IIα Mediates TCF-Dependent Epithelial-Mesenchymal Transition in Colon Cancer. *Oncogene* **2016,** *35,* 4990–4999. http://dx.doi.org/10.1038/onc.2016.1029.
127. Mei, E.; Fomitchov, P. A.; Graves, R.; Campion, M. A Line Scanning Confocal Fluorescent Microscope Using a CMOS Rolling Shutter as an Adjustable Aperture. *J. Microsc.* **2012,** *247,* 269–276.
128. Denk, W.; Strickler, J. H.; Webb, W. W. Two-Photon Laser Scanning Fluorescence Microscopy. *Science* **1990,** *248,* 73–76.
129. Oheim, M.; Michael, D. J.; Geisbauer, M.; Madsen, D.; Chow, R. H. Principles of Two-Photon Excitation Fluorescence Microscopy and Other Nonlinear Imaging Approaches. *Adv. Drug Deliv. Rev.* **2006,** *58,* 788–808.
130. Gilbert, R. J.; Hoffman, M.; Capitano, A.; So, P. T. C. Imaging of Three-Dimensional Epithelial Architecture and Function in Cultured CaCo2a Monolayers With Two-Photon Excitation Microscopy. *Microsc. Res. Tech.* **2000,** *51,* 204–210.
131. Squirrell, J. M.; Wokosin, D. L.; White, J. G.; Bavister, B. D. Long-Term Two-Photon Fluorescence Imaging of Mammalian Embryos Without Compromising Viability. *Nat. Biotechnol.* **1999,** *17,* 763–767.
132. Zhang, H.; He, S.; Liu, S.; Xie, Y.; Chen, G.; Zhang, J.; Sun, S.; Liang, D.; et al. Measurement of in vivo Three-Dimensional Corneal Cell Density and Size Using Two-Photon Imaging in C57BL/6 Mice. *Curr. Eye Res.* **2016,** *41,* 448–455.
133. Kim, M. J.; Shin, Y. C.; Lee, J. H.; Jun, S. W.; Kim, C. S.; Lee, Y.; Park, J. C.; Lee, S. H.; et al. Multiphoton Imaging of Myogenic Differentiation in Gelatin-Based Hydrogels as Tissue Engineering Scaffolds. *Biomater. Res.* **2016,** *20,* 2.
134. de Medeiros, G.; Norlin, N.; Gunther, S.; Albert, M.; Panavaite, L.; Fiuza, U. M.; Peri, F.; Hiiragi, T.; et al. Confocal Multiview Light-Sheet Microscopy. *Nat. Commun.* **2015,** *6,* 8881.
135. Lim, J.; Lee, H. K.; Yu, W.; Ahmed, S. Light Sheet Fluorescence Microscopy (LSFM): Past, Present and Future. *Analyst* **2014,** *139,* 4758–4768.
136. Keller, P. J.; Schmidt, A. D.; Wittbrodt, J.; Stelzer, E. H. Reconstruction of Zebrafish Early Embryonic Development by Scanned Light Sheet Microscopy. *Science* **2008,** *322,* 1065–1069.
137. Pampaloni, F.; Stelzer, E. H. K; Masotti, A. Three-Dimensional Tissue Models for Drug Discovery and Toxicology. *Recent Pat. Biotechnol.* **2009,** *3,* 103–117.
138. Pampaloni, F.; Ansari, N.; Stelzer, E. H. K. High-Resolution Deep Imaging of Live Cellular Spheroids With Light-Sheet-Based Fluorescence Microscopy. *Cell Tissue Res.* **2013,** *352,* 161–177.
139. Pampaloni, F.; Richa, R.; Ansari, N.; Stelzer, E. H. K. Live Spheroid Formation Recorded With Light Sheet-Based Fluorescence Microscopy. *Methods Mol. Biol.* **2015,** *1251,* 43–57.
140. Pampaloni, F.; Berge, U.; Marmaras, A.; Horvath, P.; Kroschewski, R.; Stelzer, E. H. K. Tissue-Culture Light Sheet Fluorescence Microscopy (TC-LSFM) Allows Long-Term Imaging of Three-Dimensional Cell Cultures Under Controlled Conditions. *Integr. Biol.* **2014,** *6,* 988–998.

141. Fu, Q.; Martin, B. L.; Matus, D. Q.; Gao, L. Imaging Multicellular Specimens With Real-Time Optimized Tiling Light-Sheet Selective Plane Illumination Microscopy. *Nat. Commun.* **2016,** *7,* 11088.
142. Wenzel, C.; Riefke, B.; Gründemann, S.; Krebs, A.; Christian, S.; Prinz, F.; Osterland, M.; Golfier, S.; et al. 3D High-Content Screening for the Identification of Compounds That Target Cells in Dormant Tumor Spheroid Regions. *Exp. Cell Res.* **2014,** *323,* 131–143.
143. Verveer, P. J.; Swoger, J.; Pampaloni, F.; Greger, K.; Marcello, M.; Stelzer, E. H. K. High-Resolution Three-Dimensional Imaging of Large Specimens With Light Sheet-Based Microscopy. *Nat. Methods* **2007,** *4,* 311–313.
144. Keller, P. J.; Schmidt, A. D.; Santella, A.; Khairy, K.; Bao, Z.; Wittbrodt, J.; Stelzer, E. H. K. Fast, High-Contrast Imaging of Animal Development With Scanned Light Sheet-Based Structured-Illumination Microscopy. *Nat. Methods* **2010,** *7,* 637–642.
145. Tomer, R.; Khairy, K.; Amat, F.; Keller, P. J. Quantitative High-Speed Imaging of Entire Developing Embryos With Simultaneous Multiview Light-Sheet Microscopy. *Nat. Methods* **2012,** *9,* 755–763.
146. Edwards, B. S.; Sklar, L. A. Flow Cytometry: Impact on Early Drug Discovery. *J. Biomol. Screen.* **2015,** *20,* 689–707.
147. Cappella, P.; Gasparri, F. Highly Multiplexed Phenotypic Imaging for Cell Proliferation Studies. *J. Biomol. Screen.* **2014,** *19,* 145–157.
148. Basiji, D.; O'Gorman, M. R. Imaging Flow Cytometry. *J. Immunol. Methods* **2015,** *423,* 1–2.
149. Wylie, P. G.; Onley, D. J.; Hammerstein, A. F.; Bowen, W. P. Advances in Laser Scanning Imaging Cytometry for High-Content Screening. *Assay Drug Dev. Technol.* **2015,** *13,* 66–78.
150. Bowen, W. P.; Wylie, P. G. Application of Laser-Scanning Fluorescence Microplate Cytometry in High Content Screening. *Assay Drug Dev. Technol.* **2006,** *4,* 209–221.
151. Horman, S. R.; To, J.; Orth, A. P.; Slawny, N.; Cuddihy, M. J.; Caracino, D. High-Content Analysis of Three-Dimensional Tumor Spheroids: Investigating Signaling Pathways Using Small Hairpin RNA. *Nat. Methods* **2013,** *10,* v–vi.
152. Choi, H.; Wadduwage, D. N.; Tu, T. Y.; Matsudaira, P.; So, P. T. Three-Dimensional Image Cytometer Based on Widefield Structured Light Microscopy and High-Speed Remote Depth Scanning. *Cytometry A* **2015,** *87,* 49–60.
153. Kenny, H. A.; Lal-Nag, M.; White, E. A.; Shen, M.; Chiang, C. Y.; Mitra, A. K.; Zhang, Y.; Curtis, M.; et al. Quantitative High Throughput Screening Using a Primary Human Three-Dimensional Organotypic Culture Predicts in vivo Efficacy. *Nat. Commun.* **2015,** *6,* 6220.
154. Edelstein, A.; Amodaj, N.; Hoover, K.; Vale, R.; Stuurman, N. Computer Control of Microscopes Using μManager. *Curr. Protoc. Mol. Biol.* **2010,** 14.20.11–14.20.17.
155. Edelstein, A. D.; Tsuchida, M. A.; Amodaj, N.; Pinkard, H.; Vale, R. D.; Stuurman, N. Advanced Methods of Microscope Control Using μManager Software. *J. Biol. Methods* **2014,** *1,* e11.
156. Lang, M.; Rudolf, F.; Stelling, J. Use of YouScope to Implement Systematic Microscopy Protocols. *Curr. Protoc. Mol. Biol.* **2012**. Unit 14.21 01–23.
157. Pologruto, T. A.; Sabatini, B. L.; Svoboda, K. ScanImage: Flexible Software for Operating Laser Scanning Microscopes. *Biomed. Eng. Online* **2003,** *2,* 13.
158. Jain, P.; Worthylake, R. A.; Alahari, S. K. Quantitative Analysis of Random Migration of Cells Using Time-Lapse Video Microscopy. *J. Vis. Exp.* **2012;**, e3585.
159. Lee, I. C.; Ko, J. W.; Lee, S. M.; Kim, S. H.; Shin, I. S.; Moon, O. S.; Yoon, W. K.; Kim, H. C.; et al. Time-Course and Molecular Mechanism of Hepatotoxicity Induced by 1,3-dichloro-2-propanol in Rats. *Environ. Toxicol. Pharmacol.* **2015,** *40,* 191–198.
160. da Cunha, A. C.; Marquezan, M.; Lima, I.; Lopes, R. T.; Nojima, L. I.; Sant'Anna, E. F. Influence of Bone Architecture on the Primary Stability of Different Mini-Implant Designs. *Am. J. Orthod. Dentofacial Orthop.* **2015,** *147,* 45–51.
161. Carpenter, A. E.; Jones, T. R.; Lamprecht, M. R.; Clarke, C.; Kang, I. H.; Friman, O.; Guertin, D. A.; Chang, J. H.; et al. Cell Profiler: Image Analysis Software for Identifying and Quantifying Cell Phenotypes. *Genome Biol.* **2006,** *7,* R100.
162. Kamentsky, L.; Jones, T. R.; Fraser, A.; Bray, M. A.; Logan, D. J.; Madden, K. L.; Ljosa, V.; Rueden, C.; et al. Improved Structure, Function and Compatibility for Cell Profiler: Modular High-Throughput Image Analysis Software. *Bioinformatics* **2011,** *27,* 1179–1180.
163. Jones, T. R.; Kang, I. H.; Wheeler, D. B.; Lindquist, R. A.; Papallo, A.; Sabatini, D. M.; Golland, P.; Carpenter, A. E. Cell Profiler Analyst: Data Exploration and Analysis Software for Complex Image-Based Screens. *BMC Bioinformatics* **2008,** *9,* 482.
164. Johnson, H. J.; McCormick, M. M.; Ibanez, L. *The ITK Software Guide Book 2: Design and Functionality—Volume 2;* Kitware, Inc, 2015.
165. Rajaram, S.; Pavie, B.; Wu, L. F.; Altschuler, S. J. PhenoRipper: Software for Rapidly Profiling Microscopy Images. *Nat. Methods* **2012,** *9,* 635–637.
166. Sommer, C.; Straehle, C.; Koethe, U.; Hamprecht, F. A. Ilastik: Interactive Learning and Segmentation Toolkit. IEEE International Symposium on Biomedical Imaging: From Nano to Macro**;** 2011; pp 230–233.
167. Held, M.; Schmitz, M. H.; Fischer, B.; Walter, T.; Neumann, B.; Olma, M. H.; Peter, M.; Ellenberg, J.; et al. Cell Cognition: Time-Resolved Phenotype Annotation in High-Throughput Live Cell Imaging. *Nat. Methods* **2010,** *7,* 747–754.
168. Klein, J.; Leupold, S.; Biegler, I.; Biedendieck, R.; Munch, R.; Jahn, D. TLM-Tracker: Software for Cell Segmentation, Tracking and Lineage Analysis in Time-Lapse Microscopy Movies. *Bioinformatics* **2012,** *28,* 2276–2277.
169. van der Walt, S.; Schonberger, J. L.; Nunez-Iglesias, J.; Boulogne, F.; Warner, J. D.; Yager, N.; Gouillart, E.; Yu, T.; et al. scikit-Image: Image Processing in Python. *PeerJ* **2014,** *2,* e453.
170. Ramo, P.; Sacher, R.; Snijder, B.; Begemann, B.; Pelkmans, L. Cell Classifier: Supervised Learning of Cellular Phenotypes. *Bioinformatics* **2009,** *25,* 3028–3030.
171. Good, D. W.; Khan, A.; Hammer, S.; Scanlan, P.; Shu, W.; Phipps, S.; Parson, S. H.; Stewart, G. D.; et al. Tissue Quality Assessment Using a Novel Direct Elasticity Assessment Device (the E-Finger): A Cadaveric Study of Prostatectomy Dissection. *PLoS One* **2014,** *9,* e112872.
172. Krausz, E.; de Hoogt, R.; Gustin, E.; Cornelissen, F.; Grand-Perret, T.; Janssen, L.; Vloemans, N.; Wuyts, D.; et al. Translation of a Tumor Microenvironment Mimicking 3D Tumor Growth Co-Culture Assay Platform to High-Content Screening. *J. Biomol. Screen.* **2013,** *18,* 54–66.
173. Hemalatha, R.; Santhiyakumari, N.; Suresh, S. Implementation of Medical Image Segmentation Using Virtex FPGA Kit. International Conference on Signal Processing and Communication Engineering Systems (SPACES)**;** 2015; pp 358–362.
174. Varum, F. J.; Veiga, F.; Sousa, J. S.; Basit, A. W. Mucus Thickness in the Gastrointestinal Tract of Laboratory Animals. *J. Pharm. Pharmacol.* **2012,** *64,* 218–227.
175. Ortinau, S.; Schmich, J.; Block, S.; Liedmann, A.; Jonas, L.; Weiss, D. G.; Helm, C. A.; Rolfs, A.; et al. Effect of 3D-Scaffold Formation on Differentiation and Survival in Human Neural Progenitor Cells. *Biomed. Eng. Online* **2010,** *9,* 70.
176. Warr, W. A. Scientific Workflow Systems: Pipeline Pilot and KNIME. *J. Comput. Aided Mol. Des.* **2012,** *26,* 801–804.
177. Dietz, C.; Berthold, M. R. KNIME for Open-Source Bioimage Analysis: A Tutorial. *Adv. Anat. Embryol. Cell Biol.* **2016,** *219,* 179–197.
178. Bauch, A.; Adamczyk, I.; Buczek, P.; Elmer, F. J.; Enimanev, K.; Glyzewski, P.; Kohler, M.; Pylak, T.; et al. openBIS: A Flexible Framework for Managing and Analyzing Complex Data in Biology Research. *BMC Bioinformatics* **2011,** *12,* 468.
179. Kvilekval, K.; Fedorov, D.; Obara, B.; Singh, A.; Manjunath, B. S. Bisque: A Platform for Bioimage Analysis and Management. *Bioinformatics* **2010,** *26,* 544–552.
180. Allan, C.; Burel, J. M.; Moore, J.; Blackburn, C.; Linkert, M.; Loynton, S.; Macdonald, D.; Moore, W. J.; et al. OMERO: Flexible, Model-Driven Data Management for Experimental Biology. *Nat. Methods* **2012,** *9,* 245–253.
181. Li, S.; Besson, S.; Blackburn, C.; Carroll, M.; Ferguson, R. K.; Flynn, H.; Gillen, K.; Leigh, R.; et al. Metadata Management for High Content Screening in OMERO. *Methods* **2016,** *96,* 27–32.
182. Demšar, J.; Curk, T.; Erjavec, A.; Gorup, Č.; Hočevar, T.; Milutinovič, M.; Možina, M.; Polajnar, M.; et al. Orange: Data Mining Toolbox in Python. *J. Mach. Learn. Res.* **2013,** *14,* 2349–2353.
183. Paveley, R. A.; Mansour, N. R.; Hallyburton, I.; Bleicher, L. S.; Benn, A. E.; Mikic, I.; Guidi, A.; Gilbert, I. H.; et al. Whole Organism High-Content Screening by Label-Free, Image-Based Bayesian Classification for Parasitic Diseases. *PLoS Negl. Trop. Dis.* **2012,** *6*, e1762.
184. Biggs, D. S. 3D Deconvolution Microscopy. *Curr. Protoc. Cytom.* **2010,** *12.* Unit 12.19 01–20.
185. Swedlow, J. R. Quantitative Fluorescence Microscopy and Image Deconvolution. *Methods Cell Biol.* **2013,** *114,* 407–426.

186. Shaw, P. J. Comparison of Widefield/Deconvolution and Confocal Microscopy for Three-Dimensional Imaging. In *Handbook of Biological Confocal Microscopy;* Pawley, B. J., Ed.; Springer: Boston, MA, USA, 2006; pp 453–467.
187. Eliceiri, K. W.; Berthold, M. R.; Goldberg, I. G.; Ibanez, L.; Manjunath, B. S.; Martone, M. E.; Murphy, R. F.; Peng, H. C.; et al. Biological Imaging Software Tools. *Nat. Methods* **2012,** *9,* 697–710.
188. Pietzsch, T.; Preibisch, S.; Tomancak, P.; Saalfeld, S. ImgLib2—Generic Image Processing in Java. *Bioinformatics* **2012,** *28,* 3009–3011.
189. Saha, A. K.; Kappes, F.; Mundade, A.; Deutzmann, A.; Rosmarin, D. M.; Legendre, M.; Chatain, N.; Al-Obaidi, Z.; et al. Intercellular Trafficking of the Nuclear Oncoprotein DEK. *Proc. Natl. Acad. Sci. U. S. A.* **2013,** *110,* 6847–6852.
190. Rabal, O.; Link, W.; Serelde, B. G.; Bischoff, J. R.; Oyarzabal, J. An Integrated One-Step System to Extract, Analyze and Annotate All Relevant Information From Image-Based Cell Screening of Chemical Libraries. *Mol. Biosyst.* **2010,** *6,* 711–720.

Relevant Websites

https://www.highcontentreview.com—HCS basics.
http://3dcellculture.com/Home—3D Cell culture publication collection.
http://www.imagescience.org—Collections of imaging related websites.
https://www.thermofisher.com/us/en/home/life-science/cell-analysis/labeling-chemistry/fluorescence-spectraviewer.html—Fluorescence SpectraViewer.
http://www.broadinstitute.org/bbbc/index.html—Broad Bioimage Benchmark Collection.
http://zeiss-campus.magnet.fsu.edu/tutorials/index.html—Optical microscopy and digital imaging tutorials.
http://poster.sciencemag.org/confocal/content.html—The past, present and future of confocal microscopy.
3dbiomatrix, n.d https://3dbiomatrix.com/white-papers—3D cell culture white papers.
http://www.perkinelmer.com/category/high-content-screening-analysis—HCS instrument and application notes from PerkinElmer.
https://www.thermofisher.com/us/en/home/life-science/cell-analysis/cellular-imaging/high-content-screening/high-content-screening-instruments.html—HCS instrument and application notes from ThermoFisher
https://www.moleculardevices.com/applications/applications/cellular-imaging-and-analysis—HCS instrument and application notes from MolecularDevices.
http://www.biotek.com/resources/—3D Cell culture application note from Biotek.
https://www.corning.com/in/en/products/life-sciences/applications/cell-culture/3D-cell-culture.html—3D Cell culture application note from Corning.
http://www.sigmaaldrich.com/labware/labware-products.html?TablePage=108300502—3D Cell culture products from MilliporeSigma.
http://www.highcontentanalysis.com—High-content analysis and 3D screening conferences.

2.17 Label-Free Screening Technologies

Y Fang, Corning Incorporated, Corning, NY, United States

© 2017 Elsevier Ltd. All rights reserved.

2.17.1	**Introduction**	417
2.17.2	**Label-Free Screening Techniques**	418
2.17.2.1	Mass Spectrometry	418
2.17.2.2	Resonant Waveguide Grating Biosensor	419
2.17.2.3	Surface Plasmon Resonance	419
2.17.2.4	Electric Biosensor	420
2.17.2.5	Virtual Screening Techniques	420
2.17.2.6	Nuclear Magnetic Resonance	420
2.17.3	**Target Identification**	420
2.17.3.1	MS-Based Proteomics for Target Identification	420
2.17.3.2	Label-Free Cell Phenotypic Profiling for Target Identification	422
2.17.3.3	Ligand-Based Virtual Screening for Target Prediction	423
2.17.4	**High-Throughput Screening**	423
2.17.4.1	RWG Biosensor for (Ultra)HTS	423
2.17.4.2	Molecular Docking for Ultra-HTS	424
2.17.4.3	NMR Spectroscopy for Fragment Screening	424
2.17.5	**Lead Optimization**	425
2.17.5.1	LBVS to Expand Compound Library	425
2.17.5.2	RWG to Perform Quantitative Structure–Activity Analysis (SAR)	425
2.17.5.3	SPR to Characterize the Binding Kinetics of Lead-Like Compounds	425
2.17.5.4	Isothermal Titration Calorimetry to Characterize the Thermodynamics of Lead-Like Compounds	426
2.17.6	**Lead Selection**	427
2.17.6.1	Virtual Screening Techniques to Identify Potential off-Target Effects of Lead Molecules	427
2.17.6.2	RWG-Enabled Cell Phenotypic Profiling to Prioritize Lead Molecules	427
2.17.6.3	Microfluidics RWG to Elucidate the Biochemical MOA of Lead Molecules	427
2.17.6.4	Electric Biosensor to Assess Compound-Induced Toxicity	428
2.17.6.5	LC/MS to Detect the Metabolites of Lead Molecules	429
2.17.7	**Summary**	429
2.17.8	**Outlook**	429
References		429
Relevant websites		433

Abbreviations

ABPP Activity or affinity-based protein profiling
ADR Adverse drug reaction
AP-MS Affinity purification followed by MS
BLI Biolayer interferometry
DMR Dynamic mass redistribution
ESI Electrospray ionization
FT Fourier transform
GPCR G protein-coupled receptor
HTS High-throughput screening
iPOT Label-free integrative pharmacology on-target
ITC Isothermal titration calorimetry
LBVS Ligand-based virtual screening
LC Liquid chromatography
MALDI Matrix-assisted laser desorption/ionization
MOA Mechanism of action
MS Mass spectrometry
NMR Nuclear magnetic resonance
NOE Nuclear overhauser effect
RWG Resonant waveguide grating
SAR Structure–activity relationship
SBVS Structure-based virtual screening
SEA Similarity ensemble approach
SILAC Stable isotope labeling with amino acids in cell culture
SPR Surface plasmon resonance
TCM Traditional Chinese Medicine
TOF Time-of-flight
TPP Thermal proteome profiling

2.17.1 Introduction

The past decade has seen resurgence of label-free screening techniques for drug discovery driven by several important developments. First, the dominance of target-based approaches in drug discovery has been coincident with the steady decline in pharmaceutical research and development in the past decades.[1–3] Label-dependent target-based screens are found to be more productive for discovering follow-on drugs, but less so for first-in-class drugs than phenotypic screens.[4] Second, as growing efforts have been directed towards unmet therapeutic needs and unexploited biological mechanisms, pharmaceutical innovation has become increasingly challenging and a predetermined mechanism of action (MOA) for screening may be deemed to fail to deliver positive results.[5] MOA refers to the specific biochemical interaction through which a drug substance produces its biological or pharmacological effect. Third, drug pharmacology is much more complicated than initially thought. Numerous studies have shown that, although drugs are traditionally optimized against a single protein, many drugs display clinically relevant polypharmacology,[6,7] pathway-selective on-target pharmacology,[8,9] divergent phenotypic pharmacology,[10,11] and network pharmacology,[12,13] besides metabolism, which is a well-known complicating factor. Polypharmacology refers to the specific binding of a drug to more than one target, while on-target pharmacology is the biological activity of a drug after binding to a specific target; phenotypic pharmacology is the cell-/tissue-specific action of a drug, and network pharmacology is the action of a drug in which the drug modulates more than one target in a signaling network.[14] Fourth, binding affinity has been traditionally used as a primary surrogate for predicting the in vivo efficacy of drug molecules; however, recent studies suggest that the nonequilibrium biochemical MOA of drug molecules is advantageous for developing efficacious drugs.[15–18] Biochemical MOA describes the kinetics, in particular receptor residence time (the reciprocal of K_{off}), as related to the mechanism of drug action.[15] Fifth, as the centerpiece of target-based drug discovery, labeling techniques have advantages associated with high sensitivity, molecular specificity, and compatibility to high-throughput screening (HTS) or high content screening, but disadvantages related to label interferences,[19,20] cell alterations,[21] and constraints in target/MOA screened.[22] Label-free screening techniques overcome these limitations by offering unbiased approaches to investigate the binding and functions of drug–target interactions in native and physiologically relevant environments.[22] Advances in instrumentation and methodologies in the past decade have made various label-free techniques useful for drug discovery (**Table 1**).

In this article, the principles of these label-free screening techniques and how to best implement them in the workflow of drug discovery process are discussed (**Fig. 1**). Specifically, mass spectrometry (MS)-based proteomics is useful for target identification.[23,24] Proteomics is the systemic determination of gene and cellular function directly at the protein level. Resonant waveguide grating (RWG) biosensor is capable of HTS or even ultra-HTS using engineered or native cells,[25,26] while virtual screening based on protein structure has become a reality for screening tens of millions of compounds computationally.[27–29] Nuclear magnetic resonance (NMR) has found its role in fragment screening.[30,31] Surface plasmon resonance (SPR) has become the leading technique for kinetic profiling.[32] Both RWG and electric biosensors have been used for real-time cell phenotypic profiling of drug molecules, enabling high

Table 1 Label-free screening techniques used in drug discovery

Technique	*Key features*	*Key applications in drug discovery*
MS[a]	Molecular ions	On- and off-target identification Polypharmacology determination Drug metabolism determination
RWG	Direct binding DMR in living cells	Biochemical-based HTS Cell-based HTS Quantitative SAR Polypharmacology Lead prioritization Biochemical MOA assessment
SPR	Drug association and dissociation	Drug kinetics profiling
Electric biosensor	Cell-substrate impedance	Quantitative SAR Polypharmacology Toxicity assessment
LBVS	Ligand similarity	On- and off-target identification Chemical library expansion Ultra-HTS
SBVS	Molecular docking, X-ray structure, homology structure	Target druggability Ultra-HTS Bind mode determination
NMR	Chemical shifts, relaxation time, etc.	Fragment screening Bind mode determination
ITC	Heat	Thermodynamics profiling
BLI	Drug association and dissociation	Biologics kinetics profiling

[a]Abbreviations. *MS*, mass spectrometry; *RWG*, resonant waveguide grating; *SPR*, surface plasmon resonance; *DMR*, dynamic mass redistribution; *HTS*, high-throughput screening; *SAR*, structure–activity relationship; *LBVS*, ligand-based virtual screening; SBVS, structure-based virtual screening; *NMR*, nuclear magnetic resonance; *ITC*, isothermal titration calorimetry; *BLI*, biolayer interferometry; *MOA*, mechanism of action.

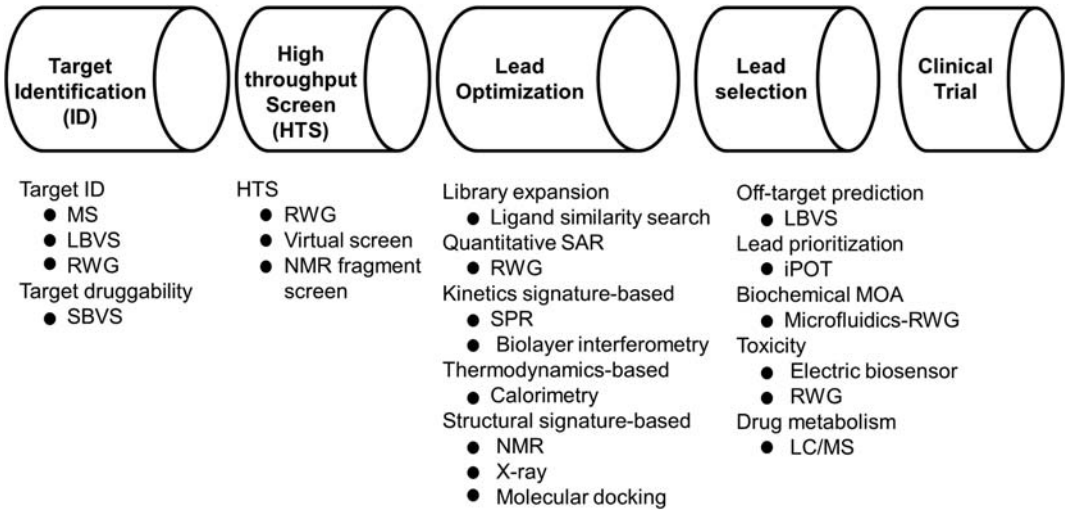

Fig. 1 Label-free screening techniques and how to best implement in drug discovery process. Mass spectrometry-based proteomics (*MS*), ligand-based virtual screening (*LBVS*), and resonant waveguide grating (*RWG*) biosensor are useful for target identification, while structure-based virtual screening (*SBVS*) is applicable to determine the druggability of targets. For high-throughput screening (*HTS*), three label-free techniques are RWG-based biochemical and cell assays, virtual screening, and NMR-based fragment screening. For lead optimization, ligand similarity searching can quickly expand the compound library, while RWG enables quantitative structure–activity relationship (*SAR*) analysis, surface plasmon resonance (*SPR*) and biolayer interferometry for kinetics profiling, calorimetry for thermodynamics profiling, and NMR, X-ray and molecular docking for the structural determination of drug–target interactions. For lead selection, LBVS is applicable to off-target prediction, while label-free integrative pharmacology on-target (*iPOT*) is suitable for lead prioritization, microfluidics RWG for biochemical mechanism of action (*MOA*) determination, RWG and electric biosensors for toxicity assessment, and liquid chromatography/MS (*LC/MS*) for drug metabolism profiling.

resolution mapping of divergent pharmacological activities of distinct drug molecules for a specific target, which is crucial to lead optimization and selection.[33,34] Label-free techniques are also useful for assessing drug safety. MS-based proteomics approaches[24] and chemical similarity analysis[29] are useful for identifying possible off-target effects, while RWG or electric biosensors are useful for assessing potential cardiotoxicity, neurotoxicity, or hepatotoxicity of lead candidate molecules using advanced cell models.[35]

2.17.2 Label-Free Screening Techniques

2.17.2.1 Mass Spectrometry

MS is well-known to accurately measure the weight of a molecule in terms of its mass-to-charge ratio (m/z) using a mass analyzer after the molecule in the gas phase is electrically charged using an ion source. The two common techniques to volatize and ionize proteins or peptides are electrospray ionization (ESI) and matrix-assisted laser desorption/ionization (MALDI). ESI ionizes the samples out of a solution, while MALDI ionizes the samples out of a dry, crystalline matrix via laser pulses.

There are four major types of MS analyzers; namely, ion trap, quadrupole, time-of-flight (TOF), and Fourier transform (FT) ion cyclotron analyzers, each with its own physical principle and analytical performance.[36] The ion trap analyzer uses a resonant electric field in a quadruple section to capture and excite ions. The quadrupole analyzer uses a time-varying electric field between four rods to create a stable trajectory to trap and excite ions. The TOF instrument uses a flight tube to accelerate ions to high kinetic energy and separate them based on arrival times at a detector as a result of different velocities. The FT-MS analyzer such as Orbitrap uses a strong magnetic field to trap ions. All these analyzers can scan different fragments in a sample to create a mass spectrum. Nowadays, hybrid instruments have been designed and widely used to combine the capabilities of different mass analyzers. Owing to its high accuracy in mass determination, Orbitrap is the most popular technique for proteomics applications.

With advances in instrumentation and methodologies, MS has been used to generate human proteome maps[37,38] and to characterize the expression, quantity, modification state, and interactions of the proteins that constitute a proteome using different strategies.[39,40] The most frequently used shotgun or discovery approach uses a liquid chromatography and MS (LC–MS) to detect precursor ions in a survey scan, so large sets of MS and tandem mass spectrometry (MS/MS) data are generated and used to identify vast numbers of proteins contained in biological samples based on characteristic peptide fragmentation patterns. For directed or targeted proteomics approaches, affinity purification of interaction partners or enrichment of specific organelles or protein modifications is performed upfront, so specific, predetermined segments of a proteome are identified and quantified. The most recent data-independent analysis approach can be used to identify all proteins in each sample. These approaches profile different subsets of the proteome with distinct comprehensiveness, reproducibility, selectivity, sensitivity, accuracy, and dynamic range.[41]

MS-based proteomics consists of several critical steps. Regardless of whether the protein complement of a sample is analyzed directly, fractionated, or affinity purified, proteins extracted from cells or tissues are first digested to peptides. Peptides in the mixture

are then separated, typically with a gradient of aqueous/organic solvent in high-performance LC. The peptides are then converted to gas phase ions mostly by ESI via direct on-line coupling of the effluent of the column, and transferred into the mass spectrometer, where peptide fragment ion spectra are recorded. The resulting fragment ion spectra are used to assign peptide sequences from which the corresponding proteins are inferred. The fragment ion spectra are also indicative of specific amino acid modifications, and quantity of a sample peptide or protein.[40]

For expression proteomics, both label-free and isotope-labeled approaches are used to determine quantitatively the changes in protein expression. Label-free quantification directly compares the signals of the same peptides in different experiments. Stable isotope-labeled approaches compare the signal of a peptide with that having a heavy version of specific amino acid residue, the incorporation of which is achieved either by chemical derivatization or by metabolic labeling. In metabolic labeling, stable isotope labeling with amino acids in cell culture (SILAC) is achieved by culturing one cell population in media containing only normal essential amino acids (eg, arginine or lysine), and another cell population in media containing only heavy forms of the amino acids.[42] SILAC labeling leads to a defined and easily recognizable mass difference.

For interaction proteomics analysis, affinity purification followed by MS (AP-MS) is the method of choice for studying protein–protein interactions, elucidating the composition and dynamics of biological networks, and correlating dynamic network rewiring with the cellular phenotype.[40] AP-MS uses the bait protein of interest to pull down its interacting proteins.

2.17.2.2 Resonant Waveguide Grating Biosensor

RWG belongs to a family of label-free optical biosensors, including grating coupler, photonic crystal biosensor, and optical waveguide lightmode spectroscopy, that use a diffractive nanograting waveguide structure to create a surface-bound electromagnetic wave, also known as evanescent wave, under light illumination for biosensing. The evanescent wave is sensitive to changes in local refractive index, a function of local mass density at the sensor surface.

RWG is the only label-free technique that is capable of screening drugs based on both the binding of drug molecules to receptors immobilized on the sensor surface[18] and the drug-induced dynamic mass redistribution (DMR) in living cells[34,43–47] (Fig. 2). RWG is made readily in microtiter plate formats (eg, 96-, 384-, and 1536-wells), the standard footprint for drug screening. Integrating a RWG system with automation enables HTS and even ultra-HTS.[25,26] Notably, the DMR signal of a drug molecule, recorded as the shift in resonant wavelength or angle using RWG systems, is a real-time cell phenotypic response that reflects the systems biology of the receptor(s) activated by the drug molecule,[48–51] as well as the systems pharmacology of the drug molecule in the cell tested.[52–54] Furthermore, owing to its noninvasiveness and high sensitivity in measurement, RWG enables screening of drugs using native and physiologically relevant cells including primary[55,56] and stem cells,[57] in addition to recombinant cell lines commonly used in conventional label-dependent screens.

2.17.2.3 Surface Plasmon Resonance

SPR employs light excited surface plasmon polaritons (SPP) to detect the binding of ligands to the receptors immobilized on a gold surface. Similar to RWG, SPP is also a surface-bound electromagnetic wave but arising from the interaction of light with mobile surface chargers in gold layer. Coupled with robust microfluidics to reliably control drug–target interactions, SPR has become the gold standard to characterize the kinetics of ligands binding to the receptors of interest.[58] The on and off rate constants are estimated by regression of the association and dissociation curves. Similar to RWG, SPR also detects changes in local refractive index. In the recent years, SPR has also been used for profiling the functional responses of drug–target interactions in living cells but with low throughput.[59] Interestingly, most SPR instruments operate in visible wavelength range. Switching to near- and mid-infrared wavelength range permits SPR to probe cellular responses with much longer sensing depth than conventional SPR or RWG (typically <200 nm).[60]

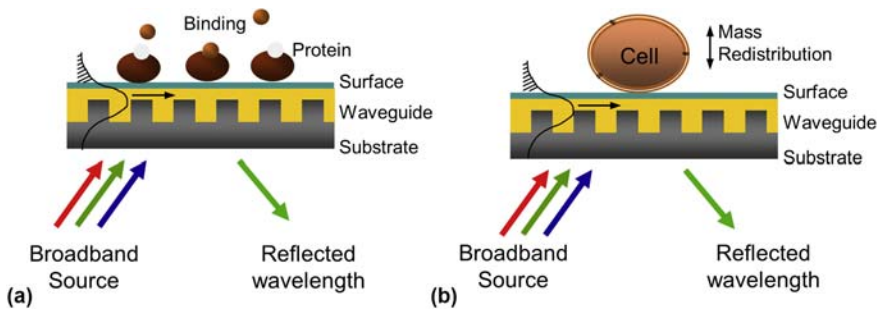

Fig. 2 Resonant waveguide grating (*RWG*) biosensor for both affinity biochemical assay (A) and functional cell-based assay (B). For biochemical assay, RWG measures the wavelength shift in the reflected light arising from the binding of small molecules to the proteins immobilized on the surface of the biosensor. For cell-based assay, RWG measures the wavelength shift in the reflected light arising from the drug-induced dynamic mass redistribution within the cells.

2.17.2.4 Electric Biosensor

Electric biosensor uses a low electrolyte interface to detect the impedance of the cell-electrode system under electric fields generated with sinusoidal voltages.[61] When the electric fields are applied, the cellular plasma membrane acts as an insulating barrier directing the current to flow between or beneath the cells, leading to extracellular and transcellular currents, respectively. The extracellular current (a function of the intercellular conduction) can be separated from the transcellular current (a function of cell-membrane capacitance) and is commonly used for cell-based assays. Here, cells are cultured onto a microelectrode array substrate and then exposed to sinusoidal voltages that are swept through a range of frequencies in a continuous wave mode. For cell assays, a reference impedance value is first obtained in the absence of cells. After cells are added, the changes of impedance relative to the reference impedance value are then calculated and recorded in real time as a unit-less cell index signal. The cell index signal is a function of changes in electrical conductivity or permeability of the cell layer arising from the morphological remodeling upon stimulation.[62]

2.17.2.5 Virtual Screening Techniques

Structure- and ligand-based virtual screening (SBVS and LBVS, respectively) are two primary computational approaches for screening. These approaches are considered to be label-free in broad terms, and can be integrated with other label-free screens. Unlike empirical and trial-and-error approaches, these computational techniques can be applied to maximally exploit the available chemical space at minimum cost to identify virtual hits that need to be experimentally confirmed.[63]

SBVS computationally screens compound library, often up to tens of millions of compounds, using known structures of protein targets.[27–29] Here, compounds from the database are docked into a known binding site of the targeted proteins to predict their binding potentials to form a stable complex. Hits are selected based on ranking using one or several scoring functions, and tested experimentally. For SBVS, it is necessary to have protein tertiary structure, ligand active conformation, and binding mode available before docking. Protein structures may be determined experimentally by X-ray crystallography or solution phase NMR, or predicted by homology modeling.

LBVS identifies key 2D or 3D chemical structures or molecular descriptors (a pharmacophore) of known active molecules (and sometimes inactive derivatives) for a target protein and uses them to query compounds in databases.[64–66] LBVS assumes similarity principle—similar compounds will be likely to have similar properties and will bind to the same group of proteins. Specifically, compounds are first annotated with a unique data (bit) string such as SMILES string. Compounds in the database are systematically compared with the query ligands at the pharmacophore level using a distance measure such as Tanimoto coefficient. The highest ranked molecules by similarity are predicted as the most likely candidate to bind, and are selected and tested experimentally. A pharmacophore is an abstract description of molecular features, which are necessary for molecular recognition of a ligand by the target protein.[67] The Tanimoto coefficient is the ratio of the number of features common to both molecules (the intersection of the data strings) to the total number of features (the union of the data strings), and gives values in the range of zero (no bits in common) to unity (all bits the same).[68] It is prerequisite for LBVS to have a relatively large set of known ligands for the target proteins.

2.17.2.6 Nuclear Magnetic Resonance

NMR spectroscopy is one of the most pivotal methods to study drug–target interactions in solution, because it is a robust technique to provide information on protein structure, dynamics, and interaction at an atomic level in solution, although it has the low absolute sensitivity. NMR spectroscopy parameters such as changes in chemical shift, nuclear Overhauser effects (NOEs), relaxation times, or diffusion constants can serve to interrogate molecular interactions and binding.

Two types of NMR experiments have been used in fragment-based drug discovery. Ligand-based NMR measures small molecule ligand resonance, while protein-based NMR measures the resonances of the isotopically labeled protein(s). When the size of the target protein allows, both NMR approaches can be used synergistically to provide a complete picture for an interaction.[69] Recently, there has been a strong emphasis on a broad range of ligand-based methods, such as diffusion experiments, saturation transfer difference, NOE pumping, water LOGSY, SALMON, and transferred NOE.[70,71] NMR-based experiments have key advantages associated with their ability to detect weak binders.

2.17.3 Target Identification

Crucial to drug discovery is to determine target engagement by a drug in cells or tissues. Most clinically available drugs achieve their therapeutic effect(s) necessarily through direct binding to one or a few target proteins.[72] However, target identification for small molecules is often the rate limiting step in drug discovery.[73] Several label-free screening techniques have been applied to identify primary and off-targets of drug molecules at an unprecedented scale, given that they offer unbiased means to survey drug–target interactions in cells.

2.17.3.1 MS-Based Proteomics for Target Identification

MS-based proteomics has been developed as an unbiased approach to elucidate the MOA of drug molecules in the context of the proteome as expressed in the targeted cell or tissue. There are three major chemical proteomics techniques, global proteomics, AP-MS, and activity- or affinity-based protein profiling (ABPP) approaches.[24]

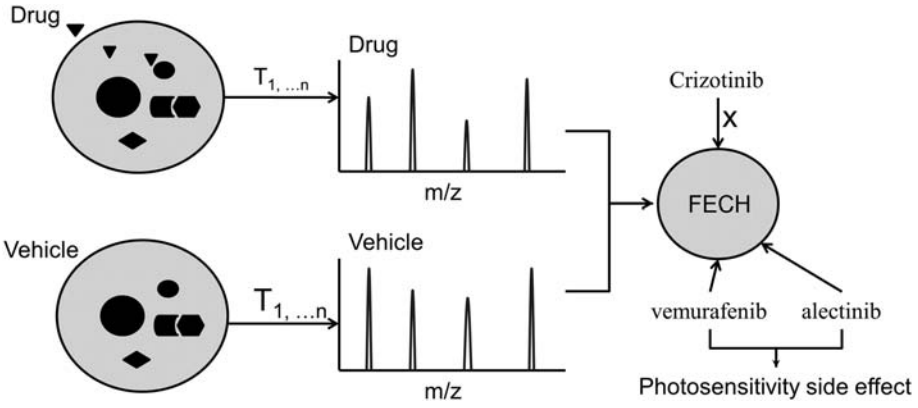

Fig. 3 A thermal proteome profiling (*TPP*) approach to identify off-target of drugs. Cells are cultured in the presence and absence of a drug (drug vs. vehicle). Samples of intact cells are then subjected to extraction with buffer. For each condition, the cell extract is divided into 10 aliquots, each followed by heating at a specific temperature. After digestion with trypsin, each sample is labeled with a different isotope tag, and analyzed by LC–MS/MS. The TPP of drugs in K562 cells led to identification of the enzyme FECH as an off-target of the two kinase drugs vemurafenib and alectinib, but not crizotinib. Schematic drawing based on the data reported in Ref.[75]

The global proteomics approaches compare the protein expression or posttranslational modifications of a drug treated cell, tissue, or animal sample with those of a control counterpart. Quantification of protein abundance and activation is achieved by either stable isotope labeling or spectral counting. These approaches have advantages in that they are unbiased and measure endogenous targets without drug modification. However, they also have disadvantages in that the observable changes are limited by the analysis depth and are often restricted to the most abundant proteins, since no target enrichment is used.[24] Recently, a MS-centric proteomics method based on ligand-induced stabilization of the target protein(s), termed cellular thermal shift assay[74] or thermal proteome profiling (TPP),[75] has been developed to directly monitor target engagement inside cells (**Fig. 3**). Savitski et al. performed thermal profiling using quantitative MS to study cancer drug pharmacology at the entire proteome.[75] They acquired quantitative thermal stability data for 5299 proteins (about 30% of the entire human proteome!) from human chronic myeloid leukemia K562 cell, and delineated 51 kinase targets and 2 heme biosynthesis enzymes including coproporphyrinogen-III oxidase and ferrochelatase (FECH) for the pan-specific kinase inhibitor staurosporine. They also found FECH as an off-target of several kinase inhibitors including vemurafenib and alectinib, but not crizotinib. FECH deficiency is genetically linked to protoporphyria, suggesting that the photosensitivity induced by vemurafenib and other drugs is mediated by FECH. Of note, they did not detect the majority of high-affinity targets for dasatinib. These results suggest that although it will miss proteins due to insufficient abundance and/or solubility or the absence of a significant ligand thermal effect, the TPH approach is useful in analyzing the on- and off-targets of drug molecules.

The AP-MS approaches employ a ligand conjugated solid substrate (eg, resin or bead) to capture and purify the interacting proteins in a sample, which are then subjected to the LC–MS/MS analysis. This type of approaches has been widely used to identify on- and off-targets of many kinase inhibitors, a family of ligands that are known to display polypharmacology.[76] For instance, using an affinity resin having seven kinase inhibitors immobilized ("kinobeads"), Bantscheff et al. found that the kinobeads can capture 307 nonredundant kinases in total as well as other ATP- and purine-binding proteins from 14 different human and mouse cell lines.[77] They further applied the kinobeads to the quantitative profiling of three tyrosine kinase ABL inhibitors, bosutinib, imatinib, and dasatinib, and found that in K562 cells imatinib binds to 13 proteins including ABL/BCR-ABL, ARG, and two novel targets (DDR1 and quinone oxidoreductase NQO2), while dasatinib and bosutinib have broad target profiles (39 and 53 kinases, respectively) including the three imatinib targets BCR-ABL, ARG, and DDR1. Interestingly, they also identified five downstream signaling pathway targets that underwent substantial downregulation of their phosphorylation status in response to imatinib.

The ABPP approaches employ activity-based chemical probes to covalently capture and subsequently purify one class of biological targets. Recently, Frei et al.[78] designed and synthesized a biocompatible chemoproteomic probe incorporating three independent functionalities: an *N*-hydroxysuccinimide ester for conjugating the reagent to a ligand containing a free amino group, a protected hydrazine that reacts with aldehydes in carbohydrates on glycoprotein receptors after exposure the cells to gentle oxidizations with sodium metaperiodate, and a biotin group for the affinity purification of the captured glycopeptides for mass spectrometric analysis. They used this probe to label intact mature vaccinia viruses, and found the cell surface proteins AXL, M6PR, DAG1, CSPG4, and CDH13 as binding factors on human cells.

Although certain protein classes (kinases and proteases in particular) can be profiled using a plethora of probes, there are few ways to assess drug binding of other families such as G protein-coupled receptors (GPCRs), ion channels, or solute carriers. Recently, Niphakis et al.[79] described a set of lipid-based chemical proteomic probes and their global interaction map in mammalian cells. They found in HEK293T cells that these probes gave rise to distinct protein labeling profiles; for instance, the fatty-acid-amide-based probe (AEA-DA) showed substantial labeling of both soluble and membrane proteins. From HEK293T and Neuro2a cells these lipid probes were found to be able to enrich more than 1000 proteins in total, of which primarily involve in protein transport,

lipid metabolism, and host–virus interactions. Furthermore, they confirmed the MOA of the dual PTGS1/2 inhibitor (±)-flurbiprofen and the selective PTGS2 inhibitor rofecoxib. Beside the known interactions with PTGS, rofecoxib-, but not (±)-flurbiprofen, was found to interact with aldose reductase-related protein 2 (AKR1B8).

2.17.3.2 Label-Free Cell Phenotypic Profiling for Target Identification

RWG measures DMR, while electric biosensor measures impedance signals arising from cell morphological change-related ionic redistribution in living cells.[33] Both DMR and impedance signals can be viewed as kinetics cell phenotypic responses of compounds, which contain target- and pathway-specific information.[34] Therefore, label-free cell phenotypic profiling approaches have advantages for target identification over traditional phenotypic approaches, which mostly rely on discrete, descriptive, empirical, and endpoint results using isolated tissues or animals, which, by themselves and individually, may offer little insights about the MOA of drugs.[80]

For label-free inhibitor screens, target hypothesis is predefined by the reference agonist cognate to the receptor of interest, so target interactions can be confirmed using direct binding assays or conventional pharmacological tools. For label-free cell phenotypic profiling that directly monitors the cellular responses of compounds, target hypothesis can be generated through similarity analysis, which compares the phenotypic profiles of compounds to those of known reference (probe) molecules.[14,25,26] For instance, Abassi et al. used the kinetic impedance profiling technique to monitor the impact of compounds in a library on the entire life cycle of cancer cell lines.[81,82] Through comparison with the kinetic profiles of marketed drugs and other probe molecules with known MOAs, they identified and deconvoluted targets for multiple classes of cell growth-inhibitory natural products and discovered novel mechanisms for existing drugs (eg, monastrol as a calcium channel inhibitor).[82]

Label-free cell phenotypic profiling can be combined with chemical biology and/or genetic manipulation techniques (eg, RNA interference (RNAi), clustered regularly interspaced short palindromic repeats-mediated gene deletion or editing) to deconvolute targets/pathways. Recently, our DMR agonist profiling of a library of 72 ion channel ligands had shown that pinacidil, a known K_{ATP} channel opener, triggered a robust negative DMR in A431, A549, HT29, and HepG2C3A, but not HepG2 cells[83] (Fig. 4). Given that the expression and function of K_{ATP} channel in the liver cell line HepG2C3A is unknown, we applied RNAi knockdown of known K_{ATP} channel component and pathway proteins to decode the pinacidil activated channel to be a SUR2-containing K_{ATP} channel, whose activation triggers signaling through Rho kinase (ROCK) and Janus kinase-2 (JAK2) and JAK3. Follow-up pharmacological assays using known probes further confirmed these results.

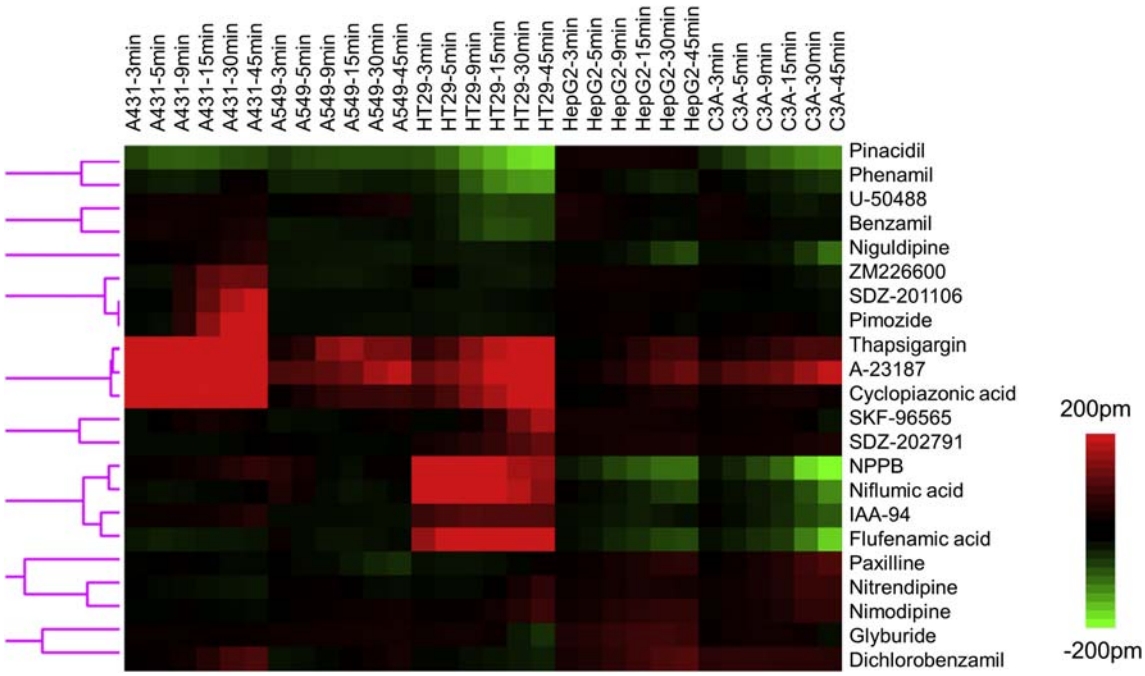

Fig. 4 Label-free cell phenotypic profiling for identifying mechanism of action of drugs in cells. DMR heat map of ion channel ligands that are active in five cell lines, A431, A549, HT29, HepG2, and C3A. This heat map was obtained using clustering analysis of the DMR profiles of the ion channel ligands in the five cell lines. For each ligand, the real responses at six discrete time points post stimulation (3, 5, 9, 15, 30, 45 min) in each cell line were used for the cluster analysis. Only ligands that led to a DMR greater than 50 pm or less than −50 pm in at least one cell line were included in this analysis. Reproduced from Sun, H.; Wei, Y.; Xiong, Q.; Li, M.; Lahiri, J.; Fang, Y. Label-Free Cell Phenotypic Profiling Decodes the Composition and Signaling of an Endogenous ATP-Sensitive Potassium Channel. *Sci. Rep.* **2014**, *4*, 4934. with through the Creative Commons Attribution License.

2.17.3.3 Ligand-Based Virtual Screening for Target Prediction

LBVS uses the known pharmacophores of targets that are well annotated with ligands to compute and predict the on- and off-targets of compounds from databases. One of the productive techniques is similarity ensemble approach (SEA), which combines statistical models derived from the BLAST algorithms with chemical similarity.[64–66] SEA predicts a likely target for a compound when the known ligands for a target resemble the "bait" compound much more closely than would be expected at random. Using this method, Shoichet et al. had discovered novel targets for over 30 drugs.[64,65,84] The most notable is their discovery of primary targets of seven orphan drugs including σ-receptor for three antitussives clemastine, cloperastine, and nepinalone; dopamine D_2 receptor for the antiemetic benzquinamide; muscarinic M_1, M_2, and M_3 receptors for the muscle relaxant cyclobenzaprine; three aminergic transporters (SERT, NET, and DAT) and $5HT_2$ receptors for the analgesic nefopam; and cyclooxygenase-2 for the immunomodulator lobenzarit.[84]

2.17.4 High-Throughput Screening

The identification of hits in the early stage of drug discovery has relied heavily on HTS. In the past decade, four major types of label-free techniques have been attempted for HTS and even ultra-HTS. RWG has been used in (ultra)HTS for hit identification using both biochemical and cell-based assays, while NMR has been used for fragment screening, and computational approaches for predicting the binding potential of millions of compounds to target proteins that are well annotated with structures or ligands. Generally, unlike labeled techniques that are often limited to detect compounds competing with the same binding site of the labeled probe used, label-free can detect hits for all possible binding sites of the target protein.

2.17.4.1 RWG Biosensor for (Ultra)HTS

RWG enables affinity-based HTS using purified proteins, where the proteins are immobilized onto the biosensor surface via either covalent bonding or high-affinity biotin–avidin interaction, and compound binding is detected directly. For instance, Wells et al. used the RWG to screen inhibitors that perturb the interaction between $G_{\beta\gamma}$ protein and SNARE (soluble *N*-ethylmaleimide-sensitive factor attachment protein receptors).[85] They identified both inhibitors and enhancers for the $G_{\beta\gamma}$–SNARE interaction, a downstream event of voltage-dependent calcium channels and signaling mediated through $G_{i/o}$-coupled presynaptic GPCRs such as dopamine D_2 receptor, $5HT_1$ serotonin receptors, M_4 muscarinic receptor, and $GABA_b$ receptors. Geschwindner et al. compared several different assay formats afforded by the RWG including direct binding, surface competitive binding, inhibition in solution and protease degradation assays for their performance in screening fragments for the protease trypsin I.[86] They found that the inhibition in solution assay delivered hits similar to NMR-based counter screen. Here, the binding of a compound to the target protein occurs free in solution, and a reference compound is tethered onto the biosensor surface and serves as the probe to determine the change of free target protein concentration in the presence of the compound.

RWG also enables HTS and even ultra-HTS using native cells including both adherent and suspension cells, primary and stem cells.[25,26] RWG-enabled HTS using living cells has several advantages. First, it is unbiased and thus permits the identification of distinct classes of ligands for the receptor of interest, such as antagonists, agonists, and allosteric modulators. For instance, Gitschier et al.[87] developed a triple-addition RWG cellular assay for simultaneously screening agonists, allosteric potentiators, and antagonists for muscarinic M_1 receptor. Here, the screen is performed in three sequential steps, and measures the DMR at 14 min of compounds, the DMR at 30 min of acetylcholine at its EC_{20} dose, and finally the DMR at 30 min of acetylcholine at its EC_{80} dose. Acetylcholine is the nonselective, orthosteric muscarinic receptor agonist. They used this assay to screen a library of approximately 180,000 compounds and found that out of all compounds screened, 0.6% were identified as hits in agonist mode, 0.05% as hits in potentiator mode, and 3% as hits in antagonist mode. Follow-up study confirmed 675 to be agonists, and 45 to be positive allosteric modulators.

Second, RWG enables multitarget screen. The agonist screen that identifies compounds to trigger detectable DMR is multitarget by nature. For instance, Zhang et al.[88] screened 320 fractions from two Traditional Chinese Medicinal (TCM) plants using three cell lines A431, A549, and HT29 and identified multiple fractions to be active at GPR35, a poorly characterized GPCR, as well as niacin that activates an endogenous GPR109A in A431 cells. Similarly, the antagonist screen also enables multitarget screens. For instance, we had developed a duplexed assay to screen both agonists and antagonists for histamine H_1 and β_2-adrenergic receptors (β_2-AR), both endogenously expressed in A431.[89] Out of 1280 compounds screened, we found that the agonism screen correctly identified all known agonists for several endogenous GPCRs including H_1, P2Y, adenosine, and β_2 receptors (**Fig. 5**), while the antagonism screen identified 77 apparent ligands for the β_2-AR, and 51 apparent antagonists for the H_1 receptor. Correlating the agonism profile with the antagonism profile of each compound further segregated the hit compounds into both receptor-specific agonists and antagonists, and pathway modulators.

Third, RWG enables HTS with relatively low false positives and negatives, compared to conventional secondary messenger assays (eg, Ca^{2+} mobilization).[90] Conventional label-dependent screens are known to generally result in high negative rates (mostly due to the bias defined by the molecular hypothesis for the screen) and high false positive rates (mostly related to the chemo-physical properties such as aggregation, colors, or fluorescence of compounds, and the presence of compensatory targets/pathways).[91]

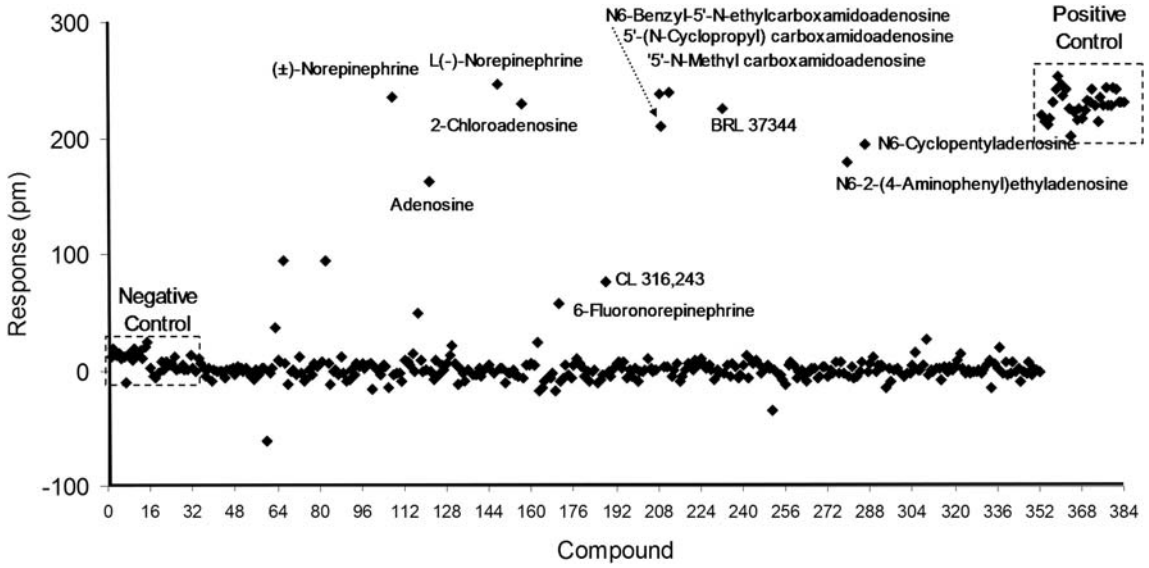

Fig. 5 RWG enables multitarget agonist screening. A hit map example from a single 384-well RWG plate shows the DMR amplitude at 50 min as a function of compounds. The positive hits for both the β_2-adrenergic and adenosine receptors were indicated. Reproduced with permission from Tran, E.; Fang, Y. Duplexed Label-Free G Protein-Coupled Receptor Assays for High Throughput Screening. *J. Biomol. Screen.* **2008**, *13*(10), 975–985.

2.17.4.2 Molecular Docking for Ultra-HTS

Molecular docking or SBVS has become an indispensable ultra-HTS technique and has started making an impact on drug discovery and development, in part due to increasing numbers of X-ray structures of proteins, in particular ligand-bound proteins, and in part due to well-annotated databases such as PubChem, ChEMBL, ZINC, and DrugBank, which provide public access to the structures and biological activities of millions of chemicals.[29]

SBVS assumes that the structures of a target will provide a template to predict the binding of compounds. The accuracy of SBVS-based prediction can be improved by using ligand-bound receptor structures, thus reducing false positives and negatives. SBVS has two clear advantages. First, it has theoretically ultra-high throughput with low cost, enabling sampling of a much larger number of compounds. Second, SBVS often results in true hit rates significantly greater than empirical HTS.[92–95] Although SBVS is mostly limited to targets with known structure and hits identified in a virtual screen still need experimental confirmation, SBVS can be used as a complementary technique to empirical screen.

One of the most exciting developments in SBVS is the recently available over 200 X-ray structures of GPCRs, many of which are in complex with ligands of varied pharmacology, peptides, antibodies, or G protein.[96,97] GPCRs are one of the most important classes of drug targets. These structures offer an unprecedented opportunity to discover new drug candidate molecules. Kolb et al. used molecular docking to virtually screen a library of close to one million commercially available, "lead-like" molecules against the inverse agonist carazolol-bound β_2-AR structure, and predicted and confirmed using a radiobinding assay 5 novel inverse agonists and 1 antagonist, the best of which has a K_i of 9 nM.[98] This study suggests that SBVS can be effective for discovering high quality hits, but the docking hits apparently bias toward the conformation stabilized by the bound ligand. SBVS has been used to identify novel ligands against X-ray or homology models of many other GPCRs, such as adenosine A_{2A} receptor, D_3 dopamine receptor, and CXCR4 receptor. It is worthy to note that SBVS is mostly limited to protein targets with known structure, while LBVS is limited to a small set of drug targets that are well annotated with known ligands.[29] Combining SBVS with LBVS, together with improved chemical similarity analysis tools, could further boost the productivity of virtual screening for drug discovery.[99,100]

2.17.4.3 NMR Spectroscopy for Fragment Screening

NMR spectroscopy, as a highly versatile structure analysis tool, is useful for fragment screening, as well as validating hits and assessing target druggability.[30,31] Many different NMR techniques including reporters, spin labels, monitoring methyl group resonances, and affinity tags have been developed to improve sensitivity and/or throughput. NMR is unique in many aspects. First, unlike many ligand-binding techniques, NMR is applicable to any class of compounds with a broad range of affinity from covalent to millimolar. NMR can reliably detect binding up to single digit millimolar K_d values, often the only hits found for challenging targets.[101] Second, NMR is applicable to almost all soluble proteins, natively unstructured proteins, and membrane proteins. Third, unlike other techniques except for X-ray crystallography, NMR can be used to determine the binding sites of fragments and modes of binding. Fourth, unlike labeled techniques, NMR detects binding directly so it does not usually suffer from false positives. Fifth, NMR detects all possible binding sites including novel binding "hot spots" such as allosteric sites and sites that result from protein conformational changes.

NMR-based fragment screening does not require a priori knowledge of protein function or endogenous binding partners as needed in many other types of assay. There are numerous successful examples illustrating the power of NMR-based fragment discovery in the literature (reviewed in Ref.[69]). For instance, Wu et al. described a HTS by combining NMR with the basic principle of combinatorial chemistry to screen a large library of fragments ($>10^5$ compounds) on a common backbone, and identified novel ligands for the ligand-binding domain of the EphA4 receptor with good binding affinity and selectivity.[102] This approach seems particularly suited to target large protein–protein interaction surfaces. EphA4 receptor is a protein-tyrosine kinase belonging to the ephrin receptor subfamily, and is implicated in mediating developmental events and linked to the neurodegenerative disease Amyotrophic lateral sclerosis.

2.17.5 Lead Optimization

Hits identified in a screen are first confirmed using a series of testing including dose response curves using the same assay for screening; orthogonal testing with different assay(s); secondary screening using functional assay(s); medicinal chemistry evaluation of synthetic tractability; hit ranking and clustering; freedom to operate evaluation; preliminary assessment of drug-likeness; and early assessment of toxicity, metabolism, and stability-related risks. Once hits are confirmed, next critical step is to expand hits by synthesis of analogs and to generate and optimize lead candidate compounds with a goal to improve potency, reduce off-target activities, and achieve desired physicochemical/metabolic properties. Label-free screening techniques have played an essential role in lead optimization, since they have been used to determine almost every important aspect of drug–target interactions starting from affinity to kinetics, structure, and thermodynamics.

2.17.5.1 LBVS to Expand Compound Library

To initiate lead optimization, several compound clusters are usually chosen from the hits identified based on a number of parameters including ligand efficiency and lipophilic efficiency, and used to expand the compound library for lead generation. Instead of custom chemical synthesis using classical organic, combinatorial, or high-throughput chemistry approach, searching for molecules based on similarity or substructure from public and private compound databases is an effective means to rapidly expand chemical library so analogs can be quickly obtained and novel and highly potent lead-like compounds can be identified. In the recent years, there are increasing number of public chemical databases including PubChem,[103] ChemBank,[104] DrugBank,[72] ChemBL,[105] and ZINC[106]; these databases contain millions of compounds annotated with biological and pharmacological activities.

2.17.5.2 RWG to Perform Quantitative Structure–Activity Analysis (SAR)

RWG can be used to perform quantitative structure–activity relationship (SAR) analysis for lead candidate compounds. This can be done using both bio-affinity binding and cell-based assays. RWG-enabled cell assay has advantages in rich information content, real-time kinetics, highly flexible assay formats, and high throughput, wide pathway coverage, and ability in multitarget profiling and screening.[25,26] Therefore, SAR analysis using RWG can provide information regarding the efficacy, potency, mode of action, and off-target effects of lead-like compounds.

Recently, we had combined the RWG-enabled cell phenotypic profiling technique with a chemical similarity search approach to discover different classes of ligands for GPR35 (Fig. 6). DMR screening of an internal chemical library of 660 compounds, originally synthesized for applications in nonlinear optics and organic field-effect transistors, led us to identify several 2-(4-methylfuran-2(5*H*)-ylidene)malononitrile compounds to be GPR35 agonists.[107] Considering the similarity of these compounds with tyrphostins, which are tyrosine analogs designed as the first generation of tyrosine kinase inhibitors, we hypothesized and confirmed that a group of tyrphostins such as tyrphostin-25[108] and multiple tyrosine metabolites including 5,6-dihydroxyindole-2-carboxylic acid (DHICA) and 3-Nitro-L-tyrosine are GPR35 agonists.[109,110] Our DMR screening of a library of 880 natural products also identified 13 natural phenols as GPR35 agonists.[111] Searching substructures of active compounds from the DrugBank led us to identify the fragment compound catechol and pyrogallol,[112] and a group of nitrophenol containing drugs such as entacapone, tolcapone, and nitecapone as GPR35 agonists, among which 4,4′-(2,2-dichloroethene-1,1-diyl)bis(2,6-dinitrophenol) displays high potency with an EC_{50} of 6 nM.[113]

2.17.5.3 SPR to Characterize the Binding Kinetics of Lead-Like Compounds

Binding kinetics is concerned with the rate constants of ligand association (k_{on}) and dissociation (k_{off}); and the ratio of the two defines the equilibrium dissociation constant ($K_d = k_{off}/k_{on}$). Compared to binding affinity, the kinetics, in particular receptor residence time, of a drug has found to be better correlated with its clinical efficacy, safety, duration of action, tolerability, indication, and therapeutic differentiation.[15,16] For instance, drugs with slower off-rates give longer duration of action, more likely leading to a once-a-day dosing. For instance, the long lasting anti-bronchiodilatation drug tiotropium dissociates 10 times slower from its primary target, muscarinic M_3 receptor, than from M_1 and M_2 receptors, resulting in an improved selectivity for this drug over other mixed $M_1/M_2/M_3$ antagonists.[114] Tiotropium exhibits similar binding affinity at both M_2 and M_3 receptors; the M_3 receptor in airway tissues is the primary target for its efficacy, while the M_2 receptor in body is responsible for its cardiovascular side effects.

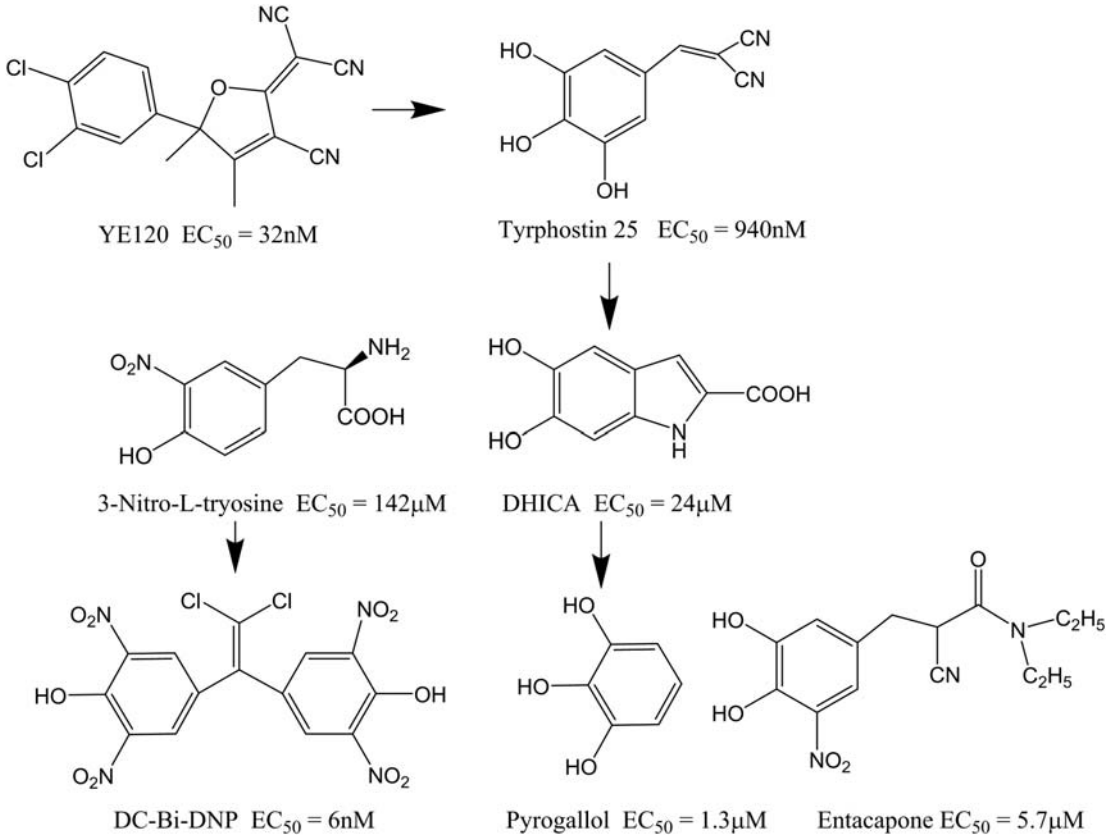

Fig. 6 Combining label-free cell-based screen with chemical similarity search quickly identifies native and novel ligands. YE120 was first identified as a full agonist for GPR35 in HT29 from our label-free screen. SAR results led us to search for and profile known malononitrile-containing compounds from public database, yielding a family of tyrphostins (eg, tyrphostin-25) and multiple tyrosine metabolites (eg, DHICA and 3-nitro-L-tyrosine) as GPR35 agonists. Substructure search of active hits identified from public database yielding DC-Bi-DNP as one of the most potent agonist known for GPR35, and nitrophenol containing drugs such as entacapone as GPR35 agonists. EC50 values reported were obtained using dynamic mass redistribution assays in HT29 cells.

The drugs such as tiotropium that work well because of kinetic differences were not designed that way. Thus, understanding kinetics earlier prospectively would be of great value, since it gives access to more diverse chemical space, more scope for intellectual property, and better defined biology. SPR is the standard technique now routinely used in laboratories for characterizing the affinity and kinetics of drugs binding to target proteins in vitro. SPR is applicable for a wide range of protein classes, particularly soluble proteins including enzymes, kinases, and proteases. However, applying SPR to GPCRs has been slow.[115] Recently, the use of thermostablized or tagged wild-type GPCRs has made it possible to use SPR to characterize ligand–GPCR interactions including adenosine A_{2A} receptor[116] and β_1-AR,[117] both of which contain a number of point mutations to improve thermostability and are further stabilized in a specific conformation in complex with a specific ligand.

Biolayer interferometry (BLI) is an alternative for profiling binding kinetics, mostly for antibodies. Instead of microfluidics used in SPR, BLI dips optical microfibres directly into the wells of standard plates for kinetic measurements with relatively higher throughput.[118] Given that there is plentiful evidence showing that compounds with the same affinity but different on- and off-rates can have a very different biological activity profile, there is a strong demand for high-throughput kinetic profiling techniques.

2.17.5.4 Isothermal Titration Calorimetry to Characterize the Thermodynamics of Lead-Like Compounds

Thermodynamic binding is influenced by multiple factors, including hydrogen bonding, hydrophobic interactions, desolvation, residual mobility, dynamics, and the local water structure, all of which contribute to the binding.[119] Ligand binding occurs only when it is associated with a negative Gibbs free binding energy ΔG, which is the sum of two energetic terms, an enthalpic term (ΔH) and an entropic term ($-T\Delta S$); $\Delta G = \Delta H - T\Delta S$. The equilibrium dissociation constant K_d is related to ΔG; $K_d = e^{\Delta G/RT}$, where R is the universal gas constant and T the absolute temperature.

There are three ways to medicinal chemistry optimization based on binding thermodynamics. The most common strategy is to optimize ΔG,[120] but it can be difficult primarily due to the frequently observed enthalpy–entropy compensation for drug–target binding.[121] Alternatively, leads can be optimized by decreasing ΔH to dominate over disfavored ΔS changes, or by increasing

ΔS to compensate for ΔH penalties.[122] Therefore, discriminating enthalpic from entropic term is useful for medicinal chemistry optimization purpose.

Isothermal titration calorimetry (ITC), as a label-free homogenous solution-based assay, is the most common approach to determine the binding thermodynamics. Current ITC can use a small cell volume ($\sim$200 μL) to detect binding-induced heat by stepwise adding a ligand solution (each about 1.4 μL). The binding isotherm obtained is then used to calculate binding constant K_d, ΔH, and ΔS. The differences in entropic and enthalpic contributions reflect different binding modes, making it possible to distinguish ligands with similar binding affinity. However, ITC has low throughput and sensitivity, requires large sample volumes, and generally is rather limited to highly potent and entropy-driven ligands. Compared to conventional ITC, the recently developed enthalpic array technique has higher throughput using as little as $\sim$500 nL of sample.[123]

Thermodynamic profiling has been used to guide lead optimization. Geschwindner et al.[124] recently reviewed their thermodynamics profiling guided efforts in optimizing inhibitors for β-site APP cleaving enzyme 1 (BACE1), a key player in the production of toxic amyloid beta clusters in brain. These inhibitors span a K_D range from about 10 μM to 10 nM, with ΔH_{obs} values from -11 to $+1$ kcal mol^{-1} and ΔS_{obs} values from -8 to $+3$ kcal mol^{-1}, typical for a hit identification–early lead optimization campaign. These studies confirmed the quite common occurrence of enthalpy entropy compensation for binding, and thermodynamics properties are well correlated with lipophilic ligand efficiency—a common metric often used to estimate the specificity of binding and can generally be written as $-$Log(potency) $-$ Log(partition coefficient).

2.17.6 Lead Selection

Following lead optimization, drug discovery projects then prioritize and select appropriate lead candidate molecules for animal and preclinical testing. Label-free screening techniques have a role to play in lead selection ranging from on- and off-target identification to biochemical MOA determination to drug safety assessment. Effective lead prioritization and selection is essential for controlling the costs of drug discovery.

2.17.6.1 Virtual Screening Techniques to Identify Potential off-Target Effects of Lead Molecules

The efficacy of a drug is critically dependent on the extent of its engagement at primary target; however, adverse drug reactions (ADRs) are often due to excessive binding of the drug in toxicity prone cells or its off-target interactions. Animal and clinical studies over the past century have established the association of over 70 protein targets with ADRs.[125] Both SBVS and LBVS are capable of identifying potential off-target effects of lead-like molecules, which is important to derisking toxicological liabilities in drug discovery. Lounkine et al. applied LBVS to predict the activity of 656 marketed drugs on 73 unintended "side-effect" targets.[66] They established several new ADR associations; for instance, the abdominal pain side effect of the synthetic estrogen chlorotrianisene was mediated through its inhibition of the enzyme cyclooxygenase-1.

2.17.6.2 RWG-Enabled Cell Phenotypic Profiling to Prioritize Lead Molecules

Typical screening campaigns screen millions of compounds, leading to identification of tens of thousands of hits. After optimization, about 100 lead-like molecules are selected for animal testing. Current approaches to prioritize and select lead molecules for in vivo testing are mostly idiosyncratic and unpredictable. Recently, we developed a RWG-based label-free integrative pharmacology on-target (iPOT) approach to analyze a family of ligands with diverse modes of action for β_2-AR,[11,126] and another for μ-, δ2-, and k-opioid receptors.[127,128] This approach leverages the power of RWG to detect functional receptome in living cells, as well as the sensitivity of drug-induced DMR to pathway intervention by small molecules or genetic manipulation. The iPOT can be performed using a panel of probe molecule-modulated cells, or a panel of different recombinant or disease relevant cell lines. We found that the iPOT is capable of generating self-referenced pharmacological activity map, enabling the classification of lead-like molecules into distinct clusters, each of which may share a common molecular MOA, so representative lead-like molecules from each cluster shall be selected for in vivo testing.

2.17.6.3 Microfluidics RWG to Elucidate the Biochemical MOA of Lead Molecules

Elucidating the biochemical MOA of drug candidate molecules is a critical step in drug discovery. The label-free cell phenotypic signals, measured by either DMR or impedance, were found to be influenced by the molecular or biochemical MOA of drugs, such as biased agonism,[54] binding kinetics,[129,130] binding orientation,[131] and transport mechanisms.[132] The biased agonism describes ligand-dependent selectivity for a specific signal transduction pathway over others downstream the same receptor, and is common to GPCRs and potentially other classes of receptors.[14] Although there was a positive correlation between the efficacy and receptor residence time of ligands for adenosine A_{2A} receptor[129] or M_3 muscarinic receptor,[130] the label-free profiling in living cells under static conditions often does not directly manifest the biochemical MOA of drugs.

Microfluidics RWG is the best suited to elucidate the biochemical MOA of a family of ligands having different binding kinetics for a specific receptor. Microfluidics is the most effective means to control the duration of a ligand exposed to the cells, so it is possible to determine whether the effect of the ligand is short or long acting. Using microfluidics RWG, we found that the activation

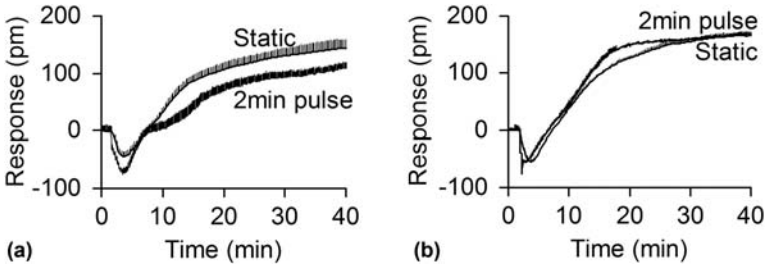

Fig. 7 Microfluidics RWG to elucidate the biochemical mechanism of action of drugs. The DMR signals induced by distinct β_2-AR agonists, (A) 2 nM salbutamol and (B) 5 nM pindolol, under the 2 min pulse stimulation in comparison with the sustained stimulation (static) conditions. Salbutamol is a short acting agonist, while pindolol is a moderately long acting partial agonist. Data represents mean + s.d. ($n = 3$). Reproduced from Goral, V.; Jin, Y.; Sun, H.; Ferrie, A. M.; Wu, Q.; Fang, Y. Agonist-Directed Desensitization of the b2-Adrenergic Receptor. *PLoS One* **2011**, *6*, e19282. with through the Creative Commons Attribution License.

of the β_2-AR in A431 with a pulse of its agonists as short as 1 min is sufficient to trigger a sustained response, whose sustainability is dependent on the receptor residence time of the agonist (Fig. 7),[133] as well as the concentration and stimulation duration of the agonist.[134] For antagonists, DMR profiling using microfluidics RWG also allowed estimation of the residence times of different antagonists acting at M_3 receptor in native cells.[135]

The cell-membrane permeability and transport mechanism are important for the efficacy of drugs acting at intracellular targets. Recently, using microfluidics RWG we found that the efficacy of inhibitors to block epidermal growth factor receptor signaling is mostly related to cellular uptake and efflux via efflux transporter such as breast cancer resistance protein (BCRP/ABCG2), instead of receptor residence time.[132] Furthermore, microfluidics RWG can also be used to detect ligand-directed desensitization and resensitization.[133,136,137]

2.17.6.4 Electric Biosensor to Assess Compound-Induced Toxicity

Drug toxicity/safety assessment is essential to drug discovery and development. Drug-induced toxicities in liver, heart, kidney, and brain currently account for more than 70% of drug attrition and drug withdrawal.[138] Label-free techniques including RWG and electric biosensors can be used to assess compound-induced cardiotoxicity,[139,140] skeletal muscle hypertrophy,[141] hepatotoxicity, and neurotoxicity.[35]

Drug-induced cardiovascular toxicity remains one of the most common causes for attrition of drugs, creating a need for using better, more predictive in vitro models and high-throughput techniques to assess cardiotoxicity early in drug discovery process. Stem cell-derived cardiomyocytes represent highly physiologically relevant and robust systems to assess accurately compound-induced cardiotoxicity. The recently developed high frequency electric impedance biosensor system has been used to detect compound-induced cardiotoxicity by monitoring the effect of drugs on the beating patterns of primary or stem cell-derived cardiomyocytes. This system was found to be able to recapitulate known effects of various known modulators of cardiac function.[139] We recently also developed a high frequency RWG imager to measure the compound-induced cardiotoxicity (Fig. 8).[140] Results showed that, after culture for 11 days, induced pluripotent stem cell-derived cardiomyocytes form a monolayer on the biosensor surface and

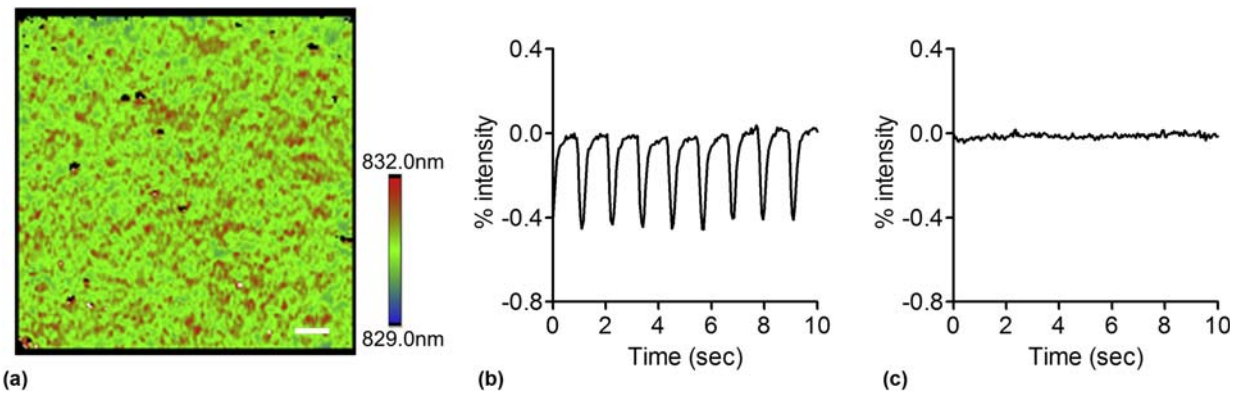

Fig. 8 High frequency resonant waveguide grating system for detecting compound-induced cardiotoxicity. (A) A resonant wavelength image of a biosensor covered with human-induced pluripotent stem cell-derived cardiomyocytes after cultured for 11 days at 37 °C. (B and C) The intensity modulation pattern before (B) and 1 min (C) after treatment with 10 μM isradipine.

beat in a synchronized fashion, resulting in a regular beating pattern consisting of a series of minimal valleys. The treatment of cardiomyocytes with isradipine, a known toxic compound, for 1 min completely stopped their beating.

Recently, Rakhilin et al.[141] applied an electric biosensor to demonstrate that the changes in electrical impedance as a function of cellular adhesion in real time correlate well with variation in myotube thickness caused by atrophy or hypertrophy agents, suggesting that impedance can be used as a reliable and sensitive biomarker for myotube atrophy or hypertrophy.

2.17.6.5 LC/MS to Detect the Metabolites of Lead Molecules

Detecting metabolites of lead molecules is critical to appreciate their bioavailability, pharmacokinetics, and pharmacodynamics. Certain drug metabolites may display biological activities different from the drug itself. For instance, aspirin exerts its clinical efficacy primarily through cyclooxygenases 1/2, but we found that several of its metabolites display agonistic activity at GPR35.[142,143] LC/MS emerged as a powerful means to study drug metabolism.[144] Lead molecules having at least one easily ionizable functional group can be routinely analyzed with LC/MS using ESI, while less polar compounds such as steroids can be analyzed using atmospheric pressure chemical ionization or atmospheric pressure photoionization. Combining LC/MS with in vitro drug metabolism systems such as hepatocytes or liver microsomal fractions can be fruitful for detecting drug metabolites.

2.17.7 Summary

Recent advances in instrumentation and methodology have made several label-free screening techniques applicable to different stages of drug discovery. Depending on the objectives of specific screening campaigns, different label-free strategies can be used to facilitate drug discovery. For follow-on drug discovery, the molecular mechanism of action (MMOA) sought is known, label-free can be implemented in a way similar to conventional label-dependent screens, and lead-like molecules can be optimized and advanced based on binding affinity and efficacy. On the other hand, for first-in-class drug discovery, the desired MMOA is unknown, label-free should be combined with labeling techniques to provide systematic comprehension of the druggability of the target and lead-like molecules. Label-free screening techniques have a bright future in drug discovery and development.

2.17.8 Outlook

The past decade has seen dramatic expansion of label-free techniques, ranging from electronic biosensors (eg, semiconducting silicon nanowires, carbon nanotubes, and electrochemical impedance spectroscopy) to mechanical biosensors (eg, quartz crystal microbalance, integrated surface acoustic wave biosensors, and microcantilevers) to photonic biosensors (eg, optical microcavity sensors, whispering gallery mode biosensors, and liquid-core optical rings resonators). Many of these biosensors have not been used in drug discovery, while some (eg, SPR, RWG, and impedance biosensor) have found limited applications. Any label-free techniques have to address four critical questions in order to be adopted in drug discovery; namely, throughput, information content, practicability in daily operation, and compatibility to current workflow. Drug discovery demands label-free with high throughput, high information content (eg, kinetics in binding or cells or tissues), and high temporal and spatial resolution.[145] On the other hand, label-free cell-based assays generally have caveats associated with low molecular specificity and unclear cellular mechanisms for the signals obtained. Elucidating the contextual relevance of label-free cell profiles of drug molecules to cell biology and signal transduction is essential to advance and drive the wide adoption of label-free technologies.[14]

See also: 2.02. Hit and Lead Generation Strategies. 2.16. 3D High-Content Screening of Organoids for Drug Discovery. 3.16. Empirical and Physics-Based Calculations of Physical–Chemical Properties.

References

1. Pammolli, F.; Magazzini, L.; Riccaboni, M. The Productivity Crisis in Pharmaceutical R&D. *Nat. Rev. Drug Discov.* **2011,** *10* (6), 428–438.
2. Scannell, J. W. Diagnosing the Decline in Pharmaceutical R&D Efficiency. *Nat. Rev. Drug Discov.* **2012,** *11* (3), 191–200.
3. Hay, M.; Thomas, D. W.; Craighead, J. L.; Economides, C.; Rosenthal, J. Clinical Development Success Rates for Investigational Drugs. *Nat. Biotechnol.* **2014,** *32* (1), 40–51.
4. Swinney, D. C.; Anthony, J. How Were New Medicines Discovered? *Nat. Rev. Drug Discov.* **2011,** *10* (7), 507–519.
5. Rask-Andersen, M.; Almén, M. S.; Schiöth, H. B. Trends in the Exploitation of Novel Drug Targets. *Nat. Rev. Drug Discov.* **2011,** *10* (8), 579–590.
6. Paolini, G. V.; Shapland, R. H.; van Hoorn, W. P.; Mason, J. S.; Hopkins, A. L. Global Mapping of Pharmacological Space. *Nat. Biotechnol.* **2006,** *24* (7), 805–815.
7. Yildirim, M. A.; Goh, K. I.; Cusick, M. E.; Barabási, A. L.; Vidal, M. Drug–Target Network. *Nat. Biotechnol.* **2007,** *25* (10), 1119–1126.
8. Kenakin, T.; Miller, L. J. Seven Transmembrane Receptors as Shapeshifting Proteins: The Impact of Allosteric Modulation and Functional Selectivity on New Drug Discovery. *Pharmacol. Rev.* **2010,** *62* (2), 265–304.
9. Choi, J. H.; Banks, A. S.; Kamenecka, T. M.; Busby, S. A.; Chalmers, M. J.; Kumar, N.; Kuruvilla, D. S.; Shin, Y.; He, Y.; Bruning, J. B.; Marciano, D. P.; Cameron, M. D.; Laznik, D.; Jurczak, M. J.; Schürer, S. C.; Vidović, D.; Shulman, G. I.; Spiegelman, B. M.; Griffin, P. R. Anti-Diabetic Actions of a Non-Agonist PPARγ Ligand Blocking Cdk5-Mediated Phosphorylation. *Nature* **2011,** *477* (7465), 477–481.

10. Nelson, C. P.; Challiss, R. A. "Phenotypic" Pharmacology: The Influence of Cellular Environment on G Protein-Coupled Receptor Antagonist and Inverse Agonist Pharmacology. *Biochem. Pharmacol.* **2007,** *73* (6), 737–751.
11. Ferrie, A. M.; Sun, H.; Zaytseva, N.; Fang, Y. Divergent Label-Free Cell Phenotypic Pharmacology of Ligands at the Overexpressed β_2-Adrenergic Receptors. *Sci. Rep.* **2014,** *4,* 3828.
12. Hopkins, A. L. Network Pharmacology: The Next Paradigm in Drug Discovery. *Nat. Chem. Biol.* **2008,** *4* (11), 682–690.
13. Dar, A. C.; Das, T. K.; Shokat, K. M.; Cagan, R. L. Chemical Genetic Discovery of Targets and Anti-Targets for Cancer Polypharmacology. *Nature* **2012,** *486* (7401), 80–84.
14. Fang, Y. Troubleshooting and Deconvoluting Label-Free Cell Phenotypic Assays in Drug Discovery. *J. Pharmacol. Toxical. Methods* **2013,** *67* (2), 69–81.
15. Swinney, D. C. Biochemical Mechanisms of Drug Action: What Does It Take for Success? *Nat. Rev. Drug Discov.* **2004,** *3* (9), 801–808.
16. Copeland, R. A.; Pompliano, D. L.; Meek, T. D. Drug–Target Residence Time and Its Implications for Lead Optimization. *Nat. Rev. Drug Discov.* **2006,** *5* (9), 730–739.
17. Singh, J.; Petter, R. C.; Baillie, T. A.; Whitty, A. The Resurgence of Covalent Drugs. *Nat. Rev. Drug Discov.* **2011,** *10* (4), 307–317.
18. Fang, Y. Ligand–Receptor Interaction Platforms and Their Applications for Drug Discovery. *Exp. Opin. Drug Discov.* **2012,** *7* (10), 969–988.
19. Pacholec, M.; Bleasdale, J. E.; Chrunyk, B.; Cunningham, D.; Flynn, D.; Garofalo, R. S.; Griffith, D.; Griffor, M.; Loulakis, P.; Pabst, B.; Qiu, X.; Stockman, B.; Thanabal, V.; Varghese, A.; Ward, J.; Withka, J.; Ahn, K. SRT1720, SRT2183, SRT1460, and Resveratrol Are Not Direct Activators of SIRT1. *J. Biol. Chem.* **2010,** *285* (11), 8340–8351.
20. Hu, H.; Deng, H.; Fang, Y. Label-Free Phenotypic Profiling Identified D-Luciferin as a GPR35 Agonist. *PLoS One* **2012,** *7,* e34934.
21. Macarron, R.; Banks, M. N.; Bojanic, D.; Burns, D. J.; Cirovic, D. A.; Garyantes, T.; Green, D. V.; Hertzberg, R. P.; Janzen, W. P.; Paslay, J. W.; Schopfer, U.; Sittampalam, G. S. Impact of High-Throughput Screening in Biomedical Research. *Nat. Rev. Drug Discov.* **2011,** *10* (3), 188–195.
22. Fang, Y. Are Label-Free Investigations the Best Approach to Drug Discovery? *Future Med. Chem.* **2015,** *7* (12), 1561–1564.
23. Aebersold, R.; Mann, M. Mass Spectrometry-Based Proteomics. *Nature* **2003,** *422* (6928), 198–207.
24. Bantscheff, M.; Scholten, A.; Heck, A. J. Revealing Promiscuous Drug–Target Interactions by Chemical Proteomics. *Drug Discov. Today* **2009,** *14* (21–22), 1021–1029.
25. Fang, Y. Label-Free Drug Discovery. *Front. Pharmacol.* **2014,** *5,* 52.
26. Fang, Y. Label-Free Cell Phenotypic Drug Discovery. *Comb. Chem. High Throughput Screen.* **2014,** *17* (7), 566–578.
27. Blundell, T. L.; Jhoti, H.; Abell, C. High-Throughput Crystallography for Lead Discovery in Drug Design. *Nat. Rev. Drug Discov.* **2002,** *1* (1), 45–54.
28. Shoichet, B. K.; Kobilka, B. K. Structure-Based Drug Screening for G-Protein-Coupled Receptors. *Trends Pharmacol. Sci.* **2012,** *33* (5), 268–272.
29. Fang, Y. Combining Label-Free Cell Phenotypic Profiling With Computational Approaches for Novel Drug Discovery. *Exp. Opin. Drug Discov.* **2015,** *10* (4), 331–343.
30. Pellecchia, M.; Bertini, I.; Cowburn, D.; Dalvit, C.; Giralt, E.; Jahnke, W.; James, T. L.; Homans, S. W.; Kessler, H.; Luchinat, C.; Meyer, B.; Oschkinat, H.; Peng, J.; Schwalbe, H.; Siegal, G. Perspectives on NMR in Drug Discovery: A Technique Comes of Age. *Nat. Rev. Drug Discov.* **2008,** *7* (9), 738–745.
31. Dalvit, C. NMR Methods in Fragment Screening: Theory and a Comparison With Other Biophysical Techniques. *Drug Discov. Today* **2009,** *14* (21–22), 1051–1057.
32. Huber, W.; Mueller, F. Biomolecular Interaction Analysis in Drug Discovery Using Surface Plasmon Resonance Technology. *Curr. Pharm. Des.* **2006,** *12* (31), 3999–4021.
33. Fang, Y. Label-Free Receptor Assays. *Drug Discov. Today Technol.* **2010,** *7,* e5–e11.
34. Fang, Y. The Development of Label-Free Cellular Assays for Drug Discovery. *Expert Opin. Drug Discov.* **2011,** *6* (12), 1285–1298.
35. Fang, Y., Ed. *Label-Free Biosensor Methods in Drug Discovery;* Springer: New York, 2015.
36. Han, X.; Aslanian, A.; Yates, J. R. I. I. I. Mass Spectrometry for Proteomics. *Curr. Opin. Chem. Biol.* **2008,** *12* (5), 483–490.
37. Kim, M. S.; Pinto, S. M.; Getnet, D.; Nirujogi, R. S.; Manda, S. S.; Chaerkady, R.; Madugundu, A. K.; et al. A Draft Map of the Human Proteome. *Nature* **2014,** *509* (7502), 575.
38. Wilhelm, M.; Schlegl, J.; Hahne, H.; Moghaddas Gholami, A.; Lieberenz, M.; Savitski, M. M.; Ziegler, E.; Butzmann, L.; Gessulat, S.; Marx, H.; Mathieson, T.; Lemeer, S.; Schnatbaum, K.; Reimer, U.; Wenschuh, H.; Mollenhauer, M.; Slotta-Huspenina, J.; Boese, J. H.; Bantscheff, M.; Gerstmair, A.; Faerber, F.; Kuster, B. Mass-Spectrometry-Based Draft of the Human Proteome. *Nature* **2014,** *509* (7502), 582.
39. Cox, J.; Mann, M. Quantitative, High-Resolution Proteomics for Data-Driven Systems Biology. *Annu. Rev. Biochem.* **2011,** *80,* 273–299.
40. Bensimon, A.; Heck, A. J. R.; Aebersold, R. Mass Spectrometry-Based Proteomics and Network Biology. *Annu. Rev. Biochem.* **2012,** *81,* 379–405.
41. Ahrens, C. H.; Brunner, E.; Qeli, E.; Basler, K.; Aebersold, R. Generating and Navigating Proteome Maps Using Mass Spectrometry. *Nat. Rev. Mol. Cell Biol.* **2010,** *11* (11), 789–801.
42. Ong, S. E.; Blagoev, B.; Kratchmarova, I.; Kristensen, D. B.; Steen, H.; Pandey, A.; Mann, M. Stable Isotope Labeling by Amino Acids in Cell Culture, SILAC, as a Simple and Accurate Approach to Expression Proteomics. *Mol. Cell. Proteomics* **2002,** *1* (5), 376.
43. Fang, Y.; Ferrie, A. M.; Fontaine, N. H.; Mauro, J.; Balakrishnan, J. Resonant Waveguide Grating Biosensor for Living Cell Sensing. *Biophys. J.* **2006,** *91* (5), 1925–1940.
44. Fang, Y. Label-Free Cell-Based Assays With Optical Biosensors in Drug Discovery. *Assay Drug Dev. Technol.* **2006,** *4* (5), 583–595.
45. Shamah, S. M.; Cunningham, B. T. Label-Free Cell-Based Assays Using Photonic Crystal Optical Biosensors. *Analyst* **2011,** *136* (6), 1090–1102.
46. Fang, Y. Label-Free Biosensors for Cell Biology. *Int. J. Electrochem.* **2011,** *2011,* e460850.
47. Li, G.; Ferrie, A. M.; Fang, Y. Label-Free Profiling of Endogenous G Protein-Coupled Receptors Using a Cell-Based High Throughput Screening Technology. *J. Assoc. Lab. Automat.* **2006,** *11,* 181–187.
48. Fang, Y.; Ferrie, A. M.; Fontaine, N. H.; Yuen, P. K. Characteristics of Dynamic Mass Redistribution of EGF Receptor Signaling in Living Cells Measured With Label Free Optical Biosensors. *Anal. Chem.* **2005,** *77* (17), 5720–5725.
49. Fang, Y.; Li, G.; Peng, J. Optical Biosensor Provides Insights for Bradykinin B2 Receptor Signaling in A431 Cells. *FEBS Lett.* **2005,** *579* (28), 6365–6374.
50. Tran, E.; Fang, Y. Label-Free Optical Biosensor for Probing Integrative Role of Adenylyl Cyclase in G Protein-Coupled Receptor Signaling. *J. Recept. Signal Transduct. Res.* **2009,** *29* (3–4), 154–162.
51. Verrier, F.; An, S.; Ferrie, A. M.; Sun, H.; Kyoung, M.; Fang, Y.; Benkovic, S. J. GPCRs Regulate the Assembly of a Multienzyme Complex for Purine Biosynthesis. *Nat. Chem. Biol.* **2011,** *7* (12), 909–915.
52. Fang, Y.; Li, G.; Ferrie, A. M. Non-Invasive Optical Biosensor for Assaying Endogenous G Protein-Coupled Receptors in Adherent Cells. *J. Pharmacol. Toxical. Methods* **2007,** *55* (3), 314–322.
53. Schröder, R.; Janssen, N.; Schmidt, J.; Kebig, A.; Merten, N.; Hennen, S.; Müller, A.; Blättermann, S.; Mohr-Andrä, M.; Zahn, S.; Wenzel, J.; Smith, N. J.; Gomeza, J.; Drewke, C.; Milligan, G.; Mohr, K.; Kostenis, E. Deconvolution of Complex G Protein-Coupled Receptor Signaling in Live Cells Using Dynamic Mass Redistribution Measurements. *Nat. Biotechnol.* **2010,** *28* (9), 943–949.
54. Fang, Y.; Ferrie, A. M. Label-Free Optical Biosensor for Ligand-Directed Functional Selectivity Acting on β2-Adrenoceptor in Living Cells. *FEBS Lett.* **2008,** *582,* 558–564.
55. Hennen, S.; Wang, H.; Peters, L.; Merten, N.; Simon, K.; Spinrath, A.; Blättermann, S.; Akkari, R.; Schrage, R.; Schröder, R.; Schulz, D.; Vermeiren, C.; Zimmermann, K.; Kehraus, S.; Drewke, C.; Pfeifer, A.; König, G. M.; Mohr, K.; Gillard, M.; Müller, C. E.; Lu, Q. R.; Gomeza, J.; Kostenis, E. Decoding Signaling and Function of the Orphan G Protein-Coupled Receptor GPR17 With a Small-Molecule Agonist. *Sci. Signal.* **2013,** *6,* ra93.
56. Carter, R. L.; Grisanti, L. A.; Yu, J. E.; Repas, A. A.; Woodall, M.; Ibetti, J.; Koch, W. J.; Jacobson, M. A.; Tilley, D. G. Dynamic Mass Redistribution Analysis of Endogenous β-Adrenergic Receptor Signaling in Neonatal Rat Cardiac Fibroblasts. *Pharmacol. Res. Perspect.* **2014,** *2,* 24.
57. Pai, S.; Verrier, F.; Sun, H.; Hu, H.; Ferrie, A. M.; Eshraghi, A.; Fang, Y. Dynamic Mass Redistribution Assay Decodes Differentiation of a Neural Progenitor Stem Cell. *J. Biomol. Screen.* **2012,** *17* (9), 1180–1191.
58. Rich, R. L.; Myszka, D. G. Higher-Throughput, Label-Free, Real-Time Molecular Interaction Analysis. *Anal. Biochem.* **2007,** *361* (1), 1–6.
59. Bourassa, P.; Tudashki, H. B.; Pineyro, G.; Grandbois, M.; Gendron, L. Label-Free Monitoring of μ-Opioid Receptor-Mediated Signaling. *Mol. Pharmacol.* **2014,** *86* (2), 138–149.

60. Ziblat, R.; Lirtsman, V.; Davidov, D.; Aroeti, B. Infrared Surface plasmon Resonance: A Novel Tool for Real Time Sensing of Variations in Living Cells. *Biophys. J.* **2006,** *90* (7), 2592–2599.
61. McGuinness, R. Impedance-Based Cellular Assay Technologies: Recent Advances, Future Promise. *Curr. Opin. Pharmacol.* **2007,** *7* (5), 535–540.
62. Atienza, J. M.; Yu, N.; Kirstein, S. L.; Xi, B.; Wang, X.; Xu, X.; Abassi, Y. A. Dynamic and Label-Free Cell-Based Assays Using the Real-Time Cell Electronic Sensing System. *Assay Drug Dev. Technol.* **2006,** *4* (5), 597–607.
63. Bajorath, J. Integration of Virtual and High-Throughput Screening. *Nat. Rev. Drug Discov.* **2002,** *1* (11), 882–894.
64. Keiser, M. J.; Roth, B. L.; Armbruster, B. N.; Ernsberger, P.; Irwin, J. J.; Shoichet, B. K. Relating Protein Pharmacology by Ligand Chemistry. *Nat. Biotechnol.* **2007,** *25* (2), 197–206.
65. Keiser, M. J.; Setola, V.; Irwin, J. J.; Laggner, C.; Abbas, A. I.; Hufeisen, S. J.; Jensen, N. H.; Kuijer, M. B.; Matos, R. C.; Tran, T. B.; Whaley, R.; Glennon, R. A.; Hert, J.; Thomas, K. L.; Edwards, D. D.; Shoichet, B. K.; Roth, B. L. Predicting New Molecular Targets for Known Drugs. *Nature* **2009,** *462* (7270), 175–181.
66. Lounkine, E.; Keiser, M. J.; Whitebread, S.; Mikhailov, D.; Hamon, J.; Jenkins, J. L.; Lavan, P.; Weber, E.; Doak, A. K.; Côté, S.; Shoichet, B. K.; Urban, L. Large-Scale Prediction and Testing of Drug Activity on Side-Effect Targets. *Nature* **2012,** *486* (7403), 361–367.
67. McGregor, M. J.; Muskal, S. M. Pharmacophore Fingerprinting 1. Application to QSAR and Focused Library Design. *J. Chem. Inf. Comput. Sci.* **1999,** *39* (3), 569–574.
68. Willett, P. Similarity-Based Virtual Screening Using 2D Fingerprints. *Drug Discov. Today* **2006,** *11* (23–24), 1046–1053.
69. Dias, D. M.; Ciulli, A. NMR Approaches in Structure-Based Lead Discovery: Recent Developments and New Frontiers for Targeting Multi-Protein Complexes. *Prog. Biophys. Mol. Biol.* **2014,** *116* (2–3), 101–112.
70. Ludwig, C.; Guenther, U. L. Ligand Based NMR Methods for Drug Discovery. *Front. Biosci.* **2009,** *14,* 4565–4574.
71. Barile, E.; Pellecchia, M. NMR-Based Approaches for the Identification and Optimization of Inhibitors of Protein–Protein Interactions. *Chem. Rev.* **2014,** *114* (9), 4749–4763.
72. Wishart, D. S.; Knox, C.; Guo, A. C.; Cheng, D.; Shrivastava, S.; Tzur, D.; Gautam, B.; Hassanali, M. DrugBank: A Knowledgebase for Drugs, Drug Actions and Drug Targets. *Nucleic Acids Res.* **2008,** *36* (Database issue), D901–906.
73. Simon, G. M.; Niphakis, M. J.; Cravatt, B. F. Determining Target Engagement in Living Systems. *Nat. Chem. Biol.* **2013,** *9* (4), 200–205.
74. Martinez Molina, D.; Jafari, R.; Ignatushchenko, M.; Seki, T.; Larsson, E. A.; Dan, C.; Sreekumar, L.; Cao, Y.; Nordlund, P. Monitoring Drug Target Engagement in Cells and Tissues Using the Cellular Thermal Shift Assay. *Science* **2013,** *341* (341), 84–87.
75. Savitski, M. M.; Reinhard, F. B.; Franken, H.; Werner, T.; Savitski, M. F.; Eberhard, D.; Martinez Molina, D.; Jafari, R.; Dovega, R. B.; Klaeger, S.; Kuster, B.; Nordlund, P.; Bantscheff, M.; Drewes, G. Tracking Cancer Drugs in Living Cells by Thermal Profiling of the Proteome. *Science* **2014,** *346* (346), 1255784.
76. Daub, H. Quantitative Proteomics of Kinase Inhibitor Targets and Mechanisms. *ACS Chem. Biol.* **2015,** *10* (1), 201–212.
77. Bantscheff, M.; Eberhard, D.; Abraham, Y.; Bastuck, S.; Boesche, M.; Hobson, S.; Mathieson, T.; Perrin, J.; Raida, M.; Rau, C.; Reader, V.; Sweetman, G.; Bauer, A.; Bouwmeester, T.; Hopf, C.; Kruse, U.; Neubauer, G.; Ramsden, N.; Rick, J.; Kuster, B.; Drewes, G. Quantitative Chemical Proteomics Reveals Mechanisms of Action of Clinical ABL Kinase Inhibitors. *Nat. Biotechnol.* **2007,** *25* (9), 1035–1044.
78. Frei, A. P.; Jeon, O. Y.; Kilcher, S.; Moest, H.; Henning, L. M.; Jost, C.; Plückthun, A.; Mercer, J.; Aebersold, R.; Carreira, E. M.; Wollscheid, B. Direct Identification of Ligand-Receptor Interactions on Living Cells and Tissues. *Nat. Biotechnol.* **2012,** *30* (10), 997–1001.
79. Niphakis, M. J.; Lum, K. M.; Cognetta, A. B., 3rd; Correia, B. E.; Ichu, T. A.; Olucha, J.; Brown, S. J.; Kundu, S.; Piscitelli, F.; Rosen, H.; Cravatt, B. F. A Global Map of Lipid-Binding Proteins and Their Ligandability in Cells. *Cell* **2015,** *161* (7), 1668–1680.
80. Feng, Y.; Mitchison, T. J.; Bender, A.; Young, D. W.; Tallarico, J. A. Multi-Parameter Phenotypic Profiling: Using Cellular Effects to Characterize Small-Molecule Compounds. *Nat. Rev. Drug Discov.* **2009,** *8* (7), 567–578.
81. Abassi, Y. A.; Xi, B.; Zhang, W.; Ye, P.; Kirstein, S. L.; Gaylord, M. R.; Feinstein, S. C.; Wang, X.; Xu, X. Kinetic Cell-Based Morphological Screening: Prediction of Mechanism of Compound Action and Off-Target Effects. *Chem. Biol.* **2009,** *16* (7), 712–723.
82. Fu, H.; Fu, W.; Sun, M.; Shou, Q.; Zhai, Y.; Cheng, H.; Teng, L.; Mou, X.; Li, Y.; Wan, S.; Zhang, S.; Xu, Q.; Zhang, X.; Wang, J.; Zhu, J.; Wang, X.; Xu, X.; Lv, G.; Jin, L.; Guo, W.; Ke, Y. Kinetic Cellular Phenotypic Profiling: Prediction, Identification, and Analysis of Bioactive Natural Products. *Anal. Chem.* **2011,** *83* (17), 6518–6526.
83. Sun, H.; Wei, Y.; Xiong, Q.; Li, M.; Lahiri, J.; Fang, Y. Label-Free Cell Phenotypic Profiling Decodes the Composition and Signaling of an Endogenous ATP-Sensitive Potassium Channel. *Sci. Rep.* **2014,** *4,* 4934.
84. Gregori-Puigjané, E.; Setola, V.; Hert, J.; Crews, B. A.; Irwin, J. J.; Lounkine, E.; Marnett, L.; Roth, B. L.; Shoichet, B. K. Identifying mechanism-of-action targets for drugs and probes. *Proc. Natl. Acad. Sci. U. S. A.* **2012,** *109* (28), 11178–11183.
85. Wells, C. A.; Betke, K. M.; Lindsley, C. W.; Hamm, H. E. Label-Free Detection of G Protein-SNARE Interactions and Screening for Small Molecule Modulators. *ACS Chem. Neurosci.* **2012,** *3* (1), 69–78.
86. Geschwindner, S.; Carlsson, J. F.; Knecht, W. Application of Optical Biosensors in Small-Molecule Screening Activities. *Sensors* **2012,** *12* (4), 4311–4323.
87. Gitschier, H. J.; Bergeron, A. B.; Randle, D. H.; Bacon, C. E.; Baez, M.; Yang, P.; Broad, L. M.; Goldsmith, P. J.; Felder, C. C.; Schober, D. A. Triple-Addition Label-Free Assays for High-Throughput Screening of Muscarinic m1 Receptor Agonists, Antagonists, and Allosteric Modulators. *Methods Pharmacol. Toxical.* **2015,** *53,* 197–214.
88. Zhang, X.; Deng, H.; Xiao, Y.; Xue, X.; Ferrie, A. M.; Tran, E.; Liang, X.; Fang, Y. Label-Free Cell Phenotypic Profiling Identifies Pharmacologically Active Compounds in Two Traditional Chinese Medicinal Plants. *RSC Adv.* **2014,** *4* (50), 26368–26377.
89. Tran, E.; Fang, Y. Duplexed Label-Free G Protein-Coupled Receptor Assays for High Throughput Screening. *J. Biomol. Screen.* **2008,** *13* (10), 975–985.
90. Dodgson, K.; Gedge, L.; Murray, D. C.; Coldwell, M. A 100 K Well Screen for a Muscarinic Receptor Using the Epic Label-Free System—A Reflection on the Benefits of the Label-Free Approach to Screening Seven-Transmembrane Receptors. *J. Recept. Signal Transduct. Res.* **2009,** *29* (3–4), 163–172.
91. Malo, N.; Hanley, J. A.; Cerquozzi, S.; Pelletier, J.; Nadon, R. Statistical Practice in High-Throughput Screening Data Analysis. *Nat. Biotechnol.* **2006,** *24* (2), 167–175.
92. Shoichet, B. K. Virtual Screening of Chemical Libraries. *Nature* **2004,** *432* (7019), 862–865.
93. Polgar, T.; Baki, A.; Szendrei, G. I.; Keseru, G. M. Comparative Virtual and Experimental High-Throughput Screening for Glycogen Synthase Kinase-3β Inhibitors. *J. Med. Chem.* **2005,** *48* (25), 7946–7959.
94. Klebe, G. Virtual Ligand Screening: Strategies, Perspectives and Limitations. *Drug Discov. Today* **2006,** *11* (13–14), 580–594.
95. Babaoglu, K.; Simeonov, A.; Irwin, J.; Nelson, M. E.; Feng, B.; Thomas, C. J.; Cancian, L.; Costi, M. P.; Maltby, D. A.; Jadhav, A.; Inglese, J.; Austin, C. P.; Shoichet, B. K. Comprehensive Mechanistic Analysis of Hits From High-Throughput and Docking Screens Against β-Lactamase. *J. Med. Chem.* **2008,** *51* (8), 2502–2511.
96. Congreve, M.; Langmead, C. J.; Mason, J. S.; Marshall, F. H. Progress in Structure Based Drug Design for G Protein-Coupled Receptors. *J. Med. Chem.* **2011,** *54* (13), 4283–4311.
97. Ghosh, E.; Kumari, P.; Jaiman, D.; Shukla, A. K. Methodological Advances: The Unsung Heroes of the GPCR Structural Revolution. *Nat. Rev. Mol. Cell Biol.* **2015,** *16* (2), 69–81.
98. Kolb, P.; Rosenbaum, D. M.; Irwin, J. J.; Fung, J. J.; Kobilka, B. K.; Shoichet, B. K. Structure-Based Discovery of β2-Adrenergic Receptor Ligands. *Proc. Natl. Acad. Sci. U. S. A.* **2009,** *106* (16), 6843–6848.
99. Broccatelli, F.; Brown, N. Best of Both Worlds: On the Complementarity of Ligand-Based and Structure-Based Virtual Screening. *J. Chem. Inf. Model.* **2014,** *54* (6), 1634–1641.
100. Venkatraman, V.; Pérez-Nueno, V. I.; Mavridis, L.; Ritchie, D. W. Comprehensive Comparison of Ligand-Based Virtual Screening Tools Against the DUD Data Set Reveals Limitations of Current 3D Methods. *J. Chem. Inf. Model.* **2010,** *50* (12), 2079–2093.
101. Carr, R. A.; Congreve, M.; Murray, C. W.; Rees, D. C. Fragment-Based Lead Discovery: Leads by Design. *Drug Discov. Today* **2005,** *10* (14), 987–992.
102. Wu, B.; Zhang, Z.; Noberini, R.; Barile, E.; Giulianotti, M.; Pinilla, C.; Houghten, R. A.; Pasquale, E. B.; Pellecchia, M. HTS by NMR of Combinatorial Libraries: A Fragment-Based Approach to Ligand Discovery. *Chem. Biol.* **2013,** *20* (1), 19–33.

103. Wang, Y.; Xiao, J.; Suzek, T. O.; Zhang, J.; Wang, J.; Bryant, S. H.; Wang, Y.; Xiao, J.; Suzek, T. O.; Zhang, J.; Wang, J.; Bryant, S. H.; Wang, Y.; Xiao, J.; Suzek, T. O.; Zhang, J.; Wang, J.; Bryant, S. H. PubChem: A Public Information System for Analyzing Bioactivities of Small Molecules. *Nucleic Acids Res.* **2009,** *37* (Web Server issue), W623–W633.
104. Seiler, K. P.; George, G. A.; Happ, M. P.; Bodycombe, N. E.; Carrinski, H. A.; Norton, S.; Brudz, S.; Sullivan, J. P.; Muhlich, J.; Serrano, M.; Ferraiolo, P.; Tolliday, N. J.; Schreiber, S. L.; Clemons, P. A. ChemBank: A Small-Molecule Screening and Cheminformatics Resource Database. *Nucleic Acids Res.* **2008,** *36* (database issue), D351–D359.
105. Gaulton, A.; Bellis, L. J.; Bento, A. P.; Chambers, J.; Davies, M.; Hersey, A.; Light, Y.; McGlinchey, S.; Michalovich, D.; Al-Lazikani, B.; Overington, J. P. ChEMBL: A Large-Scale Bioactivity Database for Drug Discovery. *Nucleic Acids Res.* **2012,** *40* (database issue), D1100–D1107.
106. Irwin, J. J.; Shoichet, B. K. ZINC—A Free Database of Commercially Available Compounds for Virtual Screening. *J. Chem. Inf. Model.* **2005,** *45* (1), 177–182.
107. Deng, H.; Hu, H.; He, M.; Hu, J.; Niu, W.; Ferrie, A. M.; Fang, Y. Discovery of 2-(4-Methylfuran-2(5H)-ylidene)malononitrile and thieno[3,2-b]thiophene-2-carboxylic Acid Derivatives as G Protein-Coupled Receptor-35 (GPR35) Agonists. *J. Med. Chem.* **2011,** *54* (20), 7385–7396.
108. Deng, H.; Hu, H.; Fang, Y. Tyrphostin Analogs are GPR35 Agonists. *FEBS Lett.* **2011,** *585* (12), 1957–1962.
109. Deng, H.; Hu, H.; Fang, Y. Multiple Tyrosine Metabolites are GPR35 Agonists. *Sci. Rep.* **2012,** *2,* 373.
110. Deng, H.; Fang, Y. Synthesis and Agonistic Activity at the GPR35 of 5,6-Dihydroxyindole-2-carboxylic Acid Analogs. *ACS Med. Chem. Lett.* **2012,** *3* (7), 550–554.
111. Deng, H.; Hu, H.; Ling, S.; Ferrie, A. M.; Fang, Y. Discovery of Natural Phenols as G Protein-Coupled Receptor-35 (GPR35) Agonists. *ACS Med. Chem. Lett.* **2012,** *3* (2), 165–169.
112. Deng, H.; Fang, Y. The Three Catecholics Benserazide, Catechol and Pyrogallol Are GPR35 Agonists. *Pharmaceuticals* **2013,** *6* (4), 500–509.
113. Deng, H.; Fang, Y. Discovery of Nitrophenols as GPR35 Agonists. *MedChemComm* **2012,** *3,* 1270–1274.
114. Disse, B.; Speck, G. A.; Rominger, K. L.; Witek, T. J., Jr.; Hammer, R. Tiotropium (Spiriva): Mechanistical Considerations and Clinical Profile in Obstructive Lung Disease. *Life Sci.* **1999,** *64* (6–7), 457–464.
115. Shepherd, C. A.; Hopkins, A. L.; Navratilova, I. Fragment Screening by SPR and Advanced Application to GPCRs. *Prog. Biophys. Mol. Biol.* **2014,** *116* (2–3), 113–123.
116. Congreve, M.; Rich, R. L.; Myszka, D. G.; Figaroa, F.; Siegal, G.; Marshall, F. H. Fragment Screening of Stabilized G-Protein-Coupled Receptors Using Biophysical Methods. *Methods Enzymol.* **2011,** *493,* 115–136.
117. Christopher, J. A.; Brown, J.; Dore, A. S.; Errey, J. C.; Koglin, M.; Marshall, F. H.; Myszka, D. G.; Rich, R. L.; Tate, C. G.; Tehan, B.; Warne, T.; Congreve, M. Biophysical Fragment Screening of the b1-Adrenergic Receptor: Identification of High Affinity Arylpiperazine Leads Using Structure-Based Drug Design. *J. Med. Chem.* **2013,** *56* (9), 3446–3455.
118. Estep, P.; Reid, F.; Nauman, C.; Liu, Y.; Sun, T.; Sun, J.; Xu, Y. High Throughput Solution-Based Measurement of Antibody-Antigen Affinity and Epitope Binning. *MAbs* **2013,** *5* (2), 270–278.
119. Klebe, G. Applying Thermodynamic Profiling in Lead Finding and Optimization. *Nat. Rev. Drug Discov.* **2015,** *14* (2), 95–110.
120. Bissantz, C.; Kuhn, B.; Stahl, M. A Medicinal Chemist's Guide to Molecular Interactions. *J. Med. Chem.* **2010,** *53* (14), 5061–5084.
121. Whitesides, G. M.; Krishnamurthy, V. M. Designing Ligands to Bind Proteins. *Q. Rev. Biophys.* **2005,** *38* (4), 385–395.
122. Ferenczy, G. G.; Keseru, G. M. Thermodynamics Guided Lead Discovery and Optimization. *Drug Discov. Today* **2010,** *15* (21–22), 919–932.
123. Torres, F. E.; Recht, M. I.; Coyle, J. E.; Bruce, R. H.; Williams, G. Higher Throughput Calorimetry: Opportunities, Approaches and Challenges. *Curr. Opin. Struct. Biol.* **2010,** *20* (5), 598–605.
124. Geschwindner, S.; Ulander, J.; Johansson, P. Ligand Binding Thermodynamics in Drug Discovery: Still a Hot Tip? *J. Med. Chem.* **2015,** *58* (16), 6321–6335.
125. Azzaoui, K.; Hamon, J.; Faller, B.; Whitebread, S.; Jacoby, E.; Bender, A.; Jenkins, J. L.; Urban, L. Modeling Promiscuity Based on in vitro Safety Pharmacology Profiling Data. *ChemMedChem* **2007,** *2* (6), 874–880.
126. Ferrie, A. M.; Sun, H.; Fang, Y. Label-Free Integrative Pharmacology On-Target of Drugs at the β2-Adrenergic Receptor. *Sci. Rep.* **2011,** *1,* 33.
127. Morse, M.; Tran, E.; Levension, R. L.; Fang, Y. Ligand-Directed Functional Selectivity at the Mu Opioid Receptor Revealed by Label-Free on-Target Pharmacology. *PLoS One* **2011,** *6,* e.25643.
128. Morse, M.; Sun, H.; Tran, E.; Levenson, R. L.; Fang, Y. Label-Free Integrative Pharmacology Ontarget of Opioid Ligands at the Opioid Receptor Family. *BMC Pharmacol. Toxical.* **2013,** *14,* 17.
129. Guo, D.; Mulder-Krieger, T.; Ijzerman, A. P.; Heitman, L. H. Functional Efficacy of Adenosine A_2A Receptor Agonists is Positively Correlated to Their Receptor Residence Time. *Br. J. Pharmacol.* **2012,** *166* (6), 1846–1859.
130. Deng, H.; Sun, H.; Fang, Y. Label-Free Cell Phenotypic Assessment of the Biased Agonism and Efficacy of Agonists at the Endogenous Muscarinic M3 Receptors. *J. Pharmacol. Toxical. Methods* **2013,** *68* (3), 323–333.
131. Bock, A.; Chirinda, B.; Krebs, F.; Messerer, R.; Bätz, J.; Muth, M.; Dallanoce, C.; Klingenthal, D.; Tränkle, C.; Hoffmann, C.; De Amici, M.; Holzgrabe, U.; Kostenis, E.; Mohr, K. Dynamic Ligand Binding Dictates Partial Agonism at a G Protein-Coupled Receptor. *Nat. Chem. Biol.* **2014,** *10* (1), 18–20.
132. Deng, H.; Wang, C.; Fang, Y. Label-Free Cell Phenotypic Assessment of the Molecular Mechanism of Action of Epidermal Growth Factor Receptor Inhibitors. *RSC Adv.* **2013,** *3,* 10370–10378.
133. Goral, V.; Jin, Y.; Sun, H.; Ferrie, A. M.; Wu, Q.; Fang, Y. Agonist-Directed Desensitization of the β2-Adrenergic Receptor. *PLoS One* **2011,** *6,* e.19282.
134. Ferrie, A. M.; Wang, C.; Deng, H.; Fang, Y. Label-Free Optical Biosensor With Microfluidics Identifies an Intracellular Signalling Wave Mediated Through the β2-Adrerengic Receptor. *Integr. Biol.* **2013,** *5* (10), 1253–1261.
135. Deng, H.; Wang, C.; Su, M.; Fang, Y. Probing Biochemical Mechanisms of Action of Muscarinic M3 Receptor Antagonists With Label-Free Whole-Cell Assays. *Anal. Chem.* **2012,** *84* (19), 8232–8239.
136. Goral, V.; Wu, Q.; Sun, H.; Fang, Y. Label-Free Optical Biosensor With Microfluidics for Sensing Ligand-Directed Functional Selectivity on Trafficking of Thrombin Receptor. *FEBS Lett.* **2011,** *585* (7), 1054–1060.
137. Zaytseva, N.; Miller, W.; Goral, V.; Hepburn, J.; Fang, Y. Microfluidic Resonant Waveguide Grating Biosensor System for Whole Cell Sensing. *Appl. Phys. Lett.* **2011,** *96,* 163703.
138. Wilke, R. A.; Lin, D. W.; Roden, D. M.; Watkins, P. B.; Flockhart, D.; Zineh, I.; Giacomini, K. M.; Krauss, R. M. Identifying Genetic Risk Factors for Serious Adverse Drug Reactions: Current Progress and Challenges. *Nat. Rev. Drug Discov.* **2007,** *6* (11), 904–916.
139. Abassi, Y. A.; Xi, B.; Li, N.; Ouyang, W.; Seiler, A.; Watzele, M.; Kettenhofen, R.; Bohlen, H.; Ehlich, A.; Kolossov, E.; Wang, X.; Xu, X. Dynamic Monitoring of Beating Periodicity of Stem Cell-Derived Cardiomyocytes as a Predictive Tool for Preclinical Safety Assessment. *Br. J. Pharmacol.* **2012,** *165* (5), 1424–1441.
140. Ferrie, A. M.; Wu, Q.; Deichmann, O.; Fang, Y. High Frequency Resonant Waveguide Grating Imager for Assessing Drug-Induced Cardiotoxicity. *Appl. Phys. Lett.* **2014,** *104,* 183702.
141. Rakhilin, S.; Turner, G.; Katz, M.; Warden, R.; Irelan, J.; Abassi, Y. A.; Glass, D. J. Electrical Impedance as a Novel Biomarker of Myotube Atrophy and Hypertrophy. *J. Biomol. Screen.* **2011,** *16* (6), 565–574.
142. Deng, H.; Fang, Y. Aspirin Metabolites Are GPR35 Agonists. *Naunyn-Schmiedeberg's Arch Pharmacol.* **2012,** *385* (7), 729–737.
143. Deng, H.; Fang, Y. Anti-Inflammatory Gallic Acid and Wedelolactone Are G Protein-Coupled Receptor-35 Agonists. *Pharmacology* **2012,** *89* (3–4), 211–219.
144. Tolonen, A.; Turpeinen, M.; Pelkonen, O. Liquid Chromatography-Mass Spectrometry in in vitro Drug Metabolite Screening. *Drug Discov. Today* **2009,** *14* (3–4), 120–133.
145. Fang, Y. Label-Free Chemical and Phenotypic Profiling of Living Cells. *Sci. Lett.* **2015,** *4,* 156.

Relevant websites

http://www.drugbank.ca/–DrugBank: a public bioinformatics and cheminformatics resource that combines drug data with comprehensive drug target information.
https://pubchem.ncbi.nlm.nih.gov/–PubChem: a public database of bioassays, compounds, and substance.
https://www.ebi.ac.uk/chembl/–ChemBL: the world's most comprehensive, freely available and up-to-date databases of bioassays and compounds.
http://chembank.broadinstitute.org/–ChemBank: a public, web-based informatics environment.
http://zinc.docking.org/–ZINC: a free database of commercially-available compounds for virtual screening.

2.18 Systems Biology: Methods and Applications

B Titz, A Knorr, A Sewer, F Martin, NV Ivanov, M Talikka, I Gonzalez Suarez, MC Peitsch, and J Hoeng, Quai Jeanrenaud 5, Neuchatel, Switzerland

© 2017 Elsevier Ltd. All rights reserved.

2.18.1	**Introduction**	436
2.18.2	**Experimental Technologies**	436
2.18.2.1	Transcriptomics	436
2.18.2.1.1	Microarray technology	436
2.18.2.1.2	RNA-sequencing	437
2.18.2.1.3	MicroRNA expression	437
2.18.2.1.4	Single-cell transcriptomics	438
2.18.2.1.5	Quantitative and digital PCR	439
2.18.2.2	Identification of Adduct Formation by Sequencing	439
2.18.2.3	Proteomics	440
2.18.2.3.1	Protein expression profiling	440
2.18.2.3.2	Spatial proteomics	442
2.18.2.3.3	Proteome synthesis and degradation	442
2.18.2.3.4	Protein phosphorylation profiling	443
2.18.2.3.5	Proteome activity profiling	444
2.18.2.3.6	Protein interaction profiling	444
2.18.2.3.7	Special considerations and outlook	445
2.18.2.4	Metabolomics	445
2.18.2.4.1	Methods and recent developments	446
2.18.2.4.2	Mass spectrometric platforms for metabolomics	447
2.18.2.4.3	Structure identification	449
2.18.2.4.4	Metabolomics data evaluation	450
2.18.2.4.5	Special considerations and outlook	450
2.18.3	**Network-Based Modeling Approaches for Systems Biology**	450
2.18.3.1	Literature-Driven Network Model Building	451
2.18.3.2	Data-Driven Interaction Network Inference	452
2.18.3.2.1	The goal of network inference	452
2.18.3.2.2	Experimental data	453
2.18.3.2.3	Inferring edges using pairwise measures	453
2.18.3.2.4	Algorithms tailored to time-series data	454
2.18.3.3	Scoring of Causal Biological Network Models	454
2.18.3.4	Mathematical Models for Network Biology	456
2.18.3.4.1	From interaction network to mathematical dynamic model	457
2.18.3.4.2	Stochastic versus deterministic models	458
2.18.3.4.3	Enzyme kinetics	458
2.18.3.4.4	Model parameter fitting	458
2.18.3.4.5	Model simplification: S-systems	459
2.18.3.4.6	Model analysis and validation	459
2.18.3.4.7	Model usage in systems research	459
2.18.4	**Systems Biology Applications**	460
2.18.4.1	Systems Pharmacology	461
2.18.4.1.1	Target identification	461
2.18.4.1.2	Adverse drug reactions	461
2.18.4.2	Systems Toxicology	461
2.18.4.2.1	Systems toxicology use case: assessment of nutraceuticals	462
2.18.4.3	Systems Medicine: Diagnostics	462
2.18.4.3.1	Personalized medicine	463
2.18.4.3.2	Translational systems biology	464
2.18.4.4	Cross-Species Translation	464
2.18.5	**Special Considerations**	464
2.18.5.1	Experimental Design and Data Production	464
2.18.5.2	Data Evaluation	465

2.18.5.3 Data Standards and Sharing 465
2.18.5.3.1 Standardization in transcriptomics 466
2.18.5.3.2 Standardization in proteomics 466
2.18.5.3.3 Standardization in metabolomics 466
2.18.5.4 Systems Biology Verification 467
2.18.5.5 Education on Systems Biology 467
2.18.5.6 Current Status of Systems Biology in Industry 467
2.18.6 Conclusions 469
Acknowledgments 469
References 469

Abbreviations

ACD Advanced Chemistry Development Inc.
ADRs Adverse drug reactions
ARACNE Algorithm for the Reconstruction of Accurate Cellular Networks
BEL Biological Expression Language
cDNA Complementary DNA
CE-MS Capillary electrophoresis coupled to MS
CI Chemical ionization
CID Collision-induced dissociation
COSMOS COordination of Standards In MetabOlomicS
CpG Regions of DNA where a cytosine nucleotide is followed by a guanine nucleotide in the linear sequence of bases along its $5' \rightarrow 3'$ direction
CycIF Cyclic immunofluorescence
DIA Data-independent
dPCR Digital PCR
DPI Data-processing inequality
DREAM Dialogue for Reverse Engineering Assessment and Method
EGFR Epidermal growth factor
ePD Enhanced PD
ESI Electrospray ionization
ETH Eidgenössische Technische Hochschule
FDA Food and Drug Administration
GC Gas chromatography
GC × GC-TOF MS Two-dimensional gas chromatography coupled with time-of-flight mass spectrometry
GMD Golm Metabolome Database
HCA Hierarchical clustering analysis
HCD Higher-energy collisional dissociation
HIF Hypoxia-inducible transcription factors
iTRAQ Isobaric-tag-based quantification
KEGG Kyoto encyclopedia of genes and genomes
KI Kovats Index
LC–MS/MS Liquid chromatography–tandem mass spectrometry
MAQC Microarray Quality Control
MIAME Minimal Information about a Microarray Experiment
MIAPE Minimum information about a proteomics experiment
miRNAs MicroRNAs
MRM Multiple reaction monitoring
MS Mass spectrometry
MS^2 Fragmentation experiments
NGS Next-generation sequencing
NMR Nuclear magnetic resonance
NPAs Network perturbation amplitudes
ODE Ordinary differential equation
O-PLS-DA Orthogonal PLS-DA
P4 Predictive, Personalized, Preventive, and Participatory
PBPK Physiologically based pharmacokinetics
PCA Principle component analysis
PCR Polymerase chain reaction
PD Pharmacodynamics
PK Pharmacokinetics
PLS-DA Partial least-square discriminant analysis
PRM Parallel reaction monitoring
PSI Proteomics Standards Initiative
qPCR Quantitative PCR
QSPR Quantitative structure–property relationship
RKIP Raf kinase inhibitor protein
RNA-seq RNA-sequencing
SBVImprover Systems Biology Verification project
scRNA-seq Single-cell transcriptomic sequencing
SEQC Sequencing Quality Control
SH2 Src homology 2
STOMP Spatially targeted optical microproteomics
SVMs Support vector machines
TD Toxicodynamics
TMT Tandem mass tag
XML Extensible Markup Language
Y2H Yeast two-hybrid

2.18.1 Introduction

Life science research is focused on linking molecules and signaling pathways to biological phenomena such as the emergence of adverse events and disease. Undoubtedly, traditional approaches have provided many valuable insights and will continue to do so. However, the reductionist understanding of the behavior of individual elements or specific interactions in isolation is not always sufficient, because biological systems are dynamic, and are composed of many parts that interact with each other in a regulated manner. The complex networks of interactions between the many diverse molecular and cellular entities of an organism are ultimately responsible for maintaining tissue homeostasis and driving adaptive responses to the environment. It is the perturbation of these networks of interactions that lead to adverse outcomes and disease.[1]

Systems biology is a highly interdisciplinary approach that integrates many levels of knowledge. It combines experimental approaches with computational methods to study the dynamic interactions between the diverse molecular and cellular entities within a biological system. Systems biology aims to consider the biological system as a whole. As described in this article (section "Experimental Technologies"), systems biology depends on data produced by rapidly developing -omics technologies, such as transcriptomics, metabolomics, and proteomics. In the early days, when high-throughput omics technologies emerged, it was customary to analyze lists of differentially expressed molecular entities using dedicated web applications to identify affected pathways.[2,3] Today's analytical methods are far more sophisticated as computational scientists have developed ways to reduce the complexity and distil information from huge amounts of data produced by high-throughput measurement technologies. These include algorithms to probe for causal inferences from molecular patterns, and the use of a priori knowledge represented as biological network models that can be used to filter the data based on biological context.

In this article, we also summarize applications that showcase how systems-based approaches impact drug discovery,[4] pharmacology and toxicology,[5,6] and medicine.[7] Finally, we touch upon the many challenges faced by systems biology when dealing with large amounts of heterologous data.

2.18.2 Experimental Technologies

2.18.2.1 Transcriptomics

Genome-wide omics methods play critical roles in basic and translational research and are now making their way into the clinic. The methods reviewed here embrace "global" approaches to biological studies. Microarrays pioneered studies on the expression of thousands of genes in parallel, instead of just a handful of genes at a time. This concept has been extended further with the introduction of newer technologies, most notably next-generation sequencing (NGS), to dramatically increase our understanding of biological pathways and networks. Emerging single-cell technologies have greatly improved our ability to understand diverse cellular interactions by separating out the functional characteristics of individual cell types. Importantly, all of the methods reviewed here have radically increased the amounts and types of data that must be comprehensively analyzed and evaluated. Bioinformatics is now accepted as a critical component of modern science because adequate computational infrastructure and expertise are required to fully interpret the mass of information. The modern scientific community recognizes the value of interpreting data holistically, because this is how biology works. Indeed, the genome, transcriptome, and all the other "-omes" work together, and we are beginning to see technologies that can integrate multiple datasets, together with the development of statistical and algorithmic approaches to make sense of the data. This overview provides a top-level summary of several excellent reviews of this field. Throughout the article, the reader is directed to the relevant reviews for in-depth descriptions of methodological details and applications.

2.18.2.1.1 Microarray technology

Examining gene expression is central to understanding gene function. Many of the initial molecular biology methods to study gene expression, such as the Northern blot, were applicable to known genes and were limited to examining a handful of genes or samples in a single run. The desire to examine thousands of genes in parallel led to the development of microarrays in the 1990s. The earliest microarrays were produced by robotically depositing probes on glass microscope slides.[8,9] The probes were typically complementary DNAs (cDNAs) hundreds of bases long, and were limited to genes that had been cloned. In the 1980s and 1990s, when little genome sequence information was available, microarray density was limited because relatively few probes could be generated.

High-density arrays became available when Affymetrix pioneered photolithography synthesis methods, as used in the semiconductor industry, for fine-detailed printing of 25-mer oligonucleotides.[8,9] In contrast to the two-color dye approach of spotted microarrays, these microarrays used one fluorescent dye.[9] The high-tech production method meant these arrays were relatively expensive, prohibiting large-scale studies. Specialized setups were required and image acquisition demanded a proprietary Affymetrix scanner. However, as costs and printing quality improved, Affymetrix became the clear leader in microarray technology. Despite the success of this technology platform, Affymetrix microarrays were only available for a limited number of species.

Microarray experiments generated a substantial amount of data, which required the development of new bioinformatics algorithms and statistical methods to assign hybridization signals to the correct genes, based largely on annotations supplied by the commercial vendor or through academic efforts. Scientists using early microarray technologies also needed to consider the

evolving annotation efforts at the time. For example, probes had multiple names or were sometimes mislabeled, complicating data analysis. Significant annotation efforts by the academic and commercial sectors have dramatically improved annotations. However, the substantial increase in genomic and transcriptomic sequencing efforts in recent years means that potential issues in gene/protein annotations should still be considered.

Data analyses and statistical methods for large-scale datasets have advanced substantially in recent years. Many early microarray studies suffered from inadequate statistical rigor, and the importance of applying rigorous statistical analysis to microarray data is now widely recognized. Because of the variety of microarray platforms and technologies originally available, a coalition of scientists was formed to provide standardized protocols and quality control metrics. Data reporting standards should now adhere to the Minimal Information about a Microarray Experiment (MIAME), which has led to consistent documentation of experimental parameters and data analysis. Another consortium effort, the Microarray Quality Control (MAQC), examined microarray reproducibility across labs and provided a valuable reference dataset to understand sources of error. Despite the advent of NGS technology, which generates comparable biological information[10,11] and reveals substantial additional biological insights, Affymetrix microarray technology remains a mature platform of choice with high reproducibility. This platform is ideally suited to experiments where comparability with studies carried out in the past decade is crucial.

2.18.2.1.2 RNA-sequencing

Traditional microarray technologies, like single and dual channel microarrays, are quickly being surpassed by RNA-sequencing (RNA-seq)[11] as the preferred approach for large-scale transcriptomic analysis, particularly as sequencing costs rapidly decrease. The advantages of RNA-seq over microarrays include de novo transcript and gene discovery, and deep (high coverage) sequencing that allows researchers to detect rare variants. The sample preparation and processing steps for RNA-seq are similar to those used for traditional microarray technologies: that is, RNA extraction, RNA fragmentation, and cDNA synthesis, followed by library construction, with the added component of high-throughput sequencing.[12] Millions or billions of reads can be generated, assigned quality scores, aligned to reference genomes, and indexed to coding regions/exons/junctions to identify transcripts of interest. Once the transcript's identity is known or reasonably assigned, the data can be examined for differential gene expression, pathway analysis, or integration with epigenomic, proteomic, or other types of data. These bioinformatics steps require sophisticated open source or commercial bioinformatics applications, and significant in-house investment in personnel with the necessary data analysis expertise.

The major NGS platforms differ in their costs, run times, read sizes, error rates, and computational resource requirements. Illumina uses sequence-by-synthesis technology, whereas Ion Torrent relies on proton detection to decipher sequences. Although the sequencing cost per gigabase varies among sequencing instruments, Illumina sequencing is typically cheaper than other platforms, and thus is widely viewed as the industry leader. Read length is another important difference between platforms, because shorter reads are more challenging to assemble and consume more computational resources.

Sequence data analysis is an essential part of RNA-seq experiments because billions of short reads are generated, and the downstream data analysis is complex. Most NGS platforms have similar postprocessing steps once the raw sequence data are available: read mapping, read counting, normalization to account for process bias, and statistical tests to distinguish true signals from noise (e.g., to detect differential gene expression).[13] Read-quality and read-mapping algorithms are fairly well established. Briefly, assessing read quality begins by removing adaptor sequences, known contaminants, low-quality bases, and over-represented sequences. The remaining reads are considered to be high quality and are appropriate for mapping to a reference genome(s). In contrast, computational approaches to detect differential gene expression, splice variants, and allele-specific expression continue to evolve. The sheer number of bioinformatics options can be overwhelming for those not well-versed in scientific programming and scripting. Organizations often underestimate the level of resources (i.e., bioinformatics personnel) required to set up, develop, maintain, and manage bioinformatics resources. Indeed, Han et al.[12] described 54 distinct programs developed solely for RNA-seq processing and analysis, each with their own specific advantages and disadvantages (some significant and some subtle).

2.18.2.1.3 MicroRNA expression

MicroRNAs (miRNAs) are short noncoding RNAs that regulate gene expression and target essentially all coding transcripts. Because they can silence gene expression, there has been tremendous interest in their use as molecular tools to explore biological processes and pathways. Despite their promise, miRNAs present unique challenges for research, including their short-length, sequence homology within families, inaccurate prediction algorithms, multiple target sequences, and the difficulty in identifying mature miRNAs from pre-miRNAs.[14]

Several technologies have been developed that take advantage of the unique characteristics of miRNAs, particularly their utility in modulating or inhibiting gene expression.[15] These methods, which can be broadly divided into miRNA/non-miRNA-specific, and gene/non-gene-specific, have enabled a wide variety of experimental manipulations in basic research and drug discovery applications, and miRNAs themselves are potential biomarkers. For example, the miRNA expression profile associated with melanoma was reported,[16] and several studies have shown the potential of miRNAs as biomarkers of multiple sclerosis.[17]

Profiling-based methods for identifying miRNA targets span a variety of approaches.[18] Briefly, they can be categorized as protein arrays, microarrays/RNA-seq, proteome profiling, and ribosome mapping. These methods can generally be applied to any type of sample, although the proteome profiling methods require expensive mass spectrometry (MS) and bioinformatics infrastructure and expertise.

Like RNA-seq, the analysis of miRNAs poses several analytical challenges because of the peculiar structure of miRNAs. Thus, identifying miRNA–target interactions remains a key focus of many of the available bioinformatics prediction algorithms, most of which are web-based.[18] Typically, miRNAs have multiple targets and the known and/or putative interactions are recorded in databases such as miRTarbase (experimentally identified interactions) and miRecords (experimentally identified and predicted interactions).[19,20]

2.18.2.1.4 Single-cell transcriptomics

A major challenge in many biological studies is to identify the functional contributions of specific cell types in heterogeneous tissues. The development of methods to isolate single cells and construct libraries from them has led to discoveries that would not have been possible using traditional transcriptomic approaches. The advantage of single-cell transcriptomic sequencing (scRNA-seq, see Fig. 1A) is that it allows researchers to determine the functional contribution of individual cell types to the biological system. This method can also determine how specific cell types contribute to processes such as splicing, allele-specific expression, and cellular signaling.

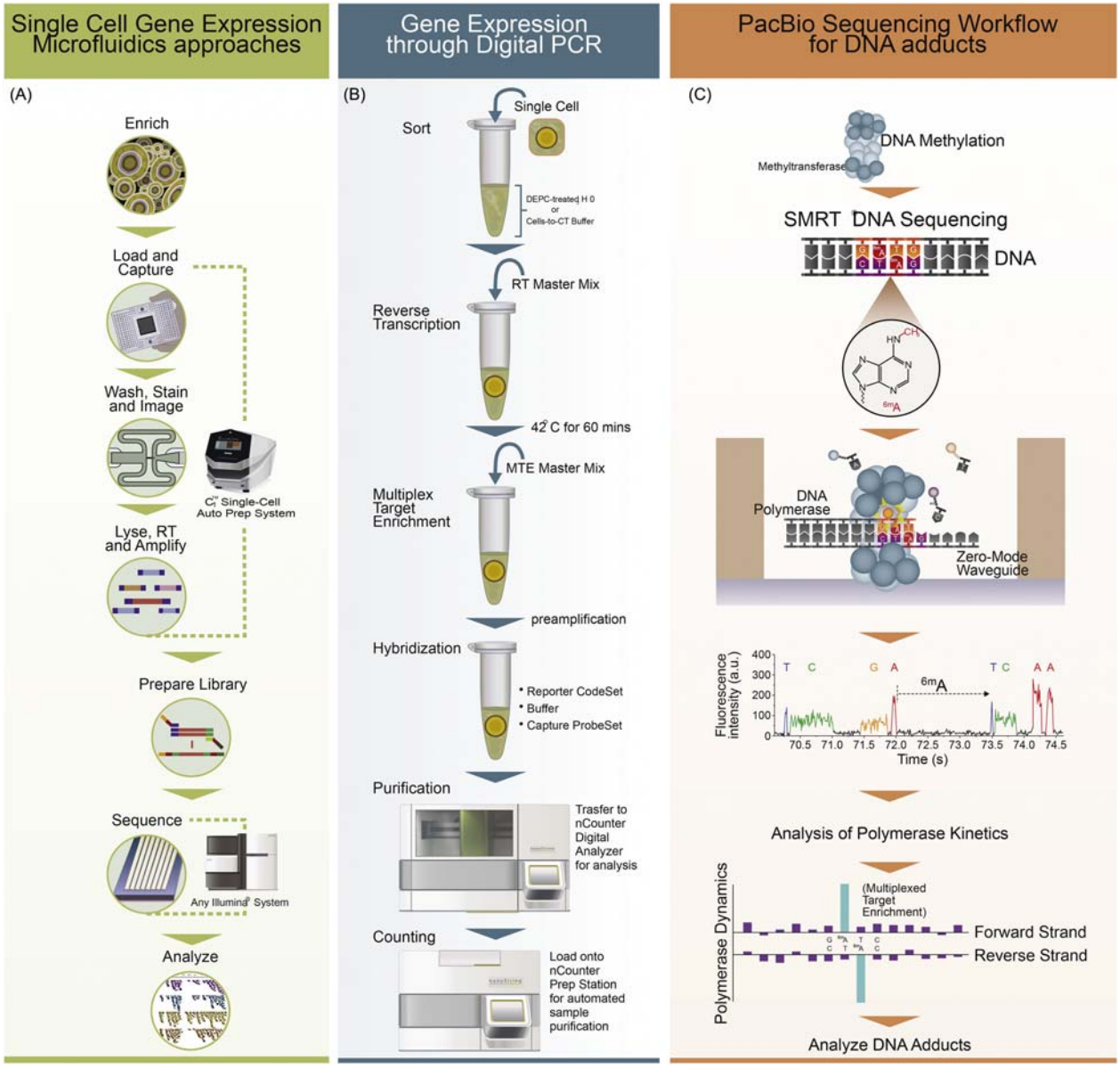

Fig. 1 Some -omics technologies. *Panel* (A) shows the workflow for the next-generation sequencing technology applied to the gene expression measurements in a single cell using microfluidic approaches. *Panel* (B) describes one of the "digital PCR" approaches that counts the gene transcripts directly without using PCR amplification. *Panel* (C) outlines measurements of DNA adducts including DNA methylation using third-generation sequencer RSII from Pacific Biosciences Inc.

Individual cells must be isolated based on their cellular phenotype and/or cell surface markers using methods that maintain the cell in its native state. Commonly used methods include mechanical dispersion followed by enzymatic treatment and subsequent isolation by fluorescence-activated cell sorting, micromanipulation, and laser-capture microdissection.[21] Notably, spatial information about isolated cells as they existed in three-dimensional space is lost, and this may affect the outcomes being explored. Because a single human cell contains 10–30 pg total RNA, amplification by several hundred-thousand-fold, usually by multiple displacement analysis, polymerase chain reaction (PCR), or multiple annealing and looping-based amplification cycles, is required to generate sufficient material for analysis.

Several methods of single-cell analysis have been reviewed by Zhang et al.[21] Single-cell whole genome sequencing is an effective method to screen for copy number variants and single nucleotide variants. However, since the exome encompasses ~1% of the whole genome, yet contains ~85% of variants implicated in disease, single-cell whole exome sequencing often provides sufficiently rich information to examine coding sequences. Other studies have used state-of-the art methods to examine the single-cell genome and transcriptome simultaneously. The scRNA-seq approach has all the advantages of RNA-seq (i.e., it provides a snapshot of the global transcriptome) and offers additional capabilities. For example, emerging protocols have allowed researchers to better understand heterogeneous cell populations by examining cell-to-cell variation and expression level heterogeneity.[22]

Single-cell analytical methods are rapidly evolving. Most single-cell isolation protocols published to date have focused on messenger RNAs, leaving substantial opportunities to develop new methods,[23] such as those to analyze noncoding RNA species. Although isolation protocols and technologies continue to improve, they are labor intensive and require specialized and expensive equipment. In addition, the current protocols result in poor yields, with an estimated recovery of ~10% of the transcriptome, generally resulting in poor sensitivity. Thus, detecting low-abundance transcripts has proven difficult because such transcripts often are at or below the noise level. Several technological improvements are expected in the near future that will further facilitate the effective use of single-cell sequencing approaches, including improved microfluidic cell-isolation systems, amplification methods, and normalization methods.[24,25]

2.18.2.1.5 Quantitative and digital PCR

The PCR method is essential for amplifying nucleic acid sequences, and novel chemistries, instrumentation, and detection methods are still being introduced. Real-time quantitative PCR (qPCR) has been used in numerous research and clinical settings. The qPCR detection methods may be categorized according to the method used to detect the amplified DNA.[26] Intercalating dyes have been available for many years and are inexpensive, but they do not typically distinguish between specific and nonspecific amplified products. Probes that combine donor and acceptor moieties (with different excitation and emission spectra) in the same molecule are also available, but each has unique advantages and disadvantages.

Digital PCR (dPCR, **Fig. 1B**) enables the parallel processing of millions or billions of individual PCR reactions in tiny droplets, facilitating transcriptomic and genomic analyses. For example, combining the advantages of dPCR with NGS provided enhanced and sensitive detection of very-low-level residual chronic myeloid leukemia.[27] That study used the Fludigm (R) platform, one of the first dPCR systems to be developed. A more recently developed direct digital transcript counting system known as the nCounter Gene Expression Assay (NanoString Technologies, Inc.) does not use PCR because of its well-known amplification bias. Instead, nCounter digitally monitors up to 800 different nucleotide probes simultaneously. Because of the complex nature of dPCR experiments, these systems require sophisticated statistical methods for data analysis.[28]

2.18.2.2 Identification of Adduct Formation by Sequencing

Methylation of DNA occurs in all organisms[29,30] and plays an important role in many biological processes. Methylated DNA can be detected using a variety of methods, including immunoprecipitation, bisulfite conversion-based methods, and microarrays. Some methods are better designed to examine genome-wide methylation and are useful to discover methylation events, whereas other methods are better suited to examine methylation events in specific regulatory regions or at loci of interest. Kurdyukov et al. provide a comprehensive overview of methods for analyzing differentially methylated DNA regions.[31] The amount of sample required and CpG (cytosine nucleotide followed by a guanine nucleotide) coverage vary significantly among methods, and both parameters are important considerations when developing experimental strategies. Currently, the leading method to detect the DNA methylation is whole genome bisulfite sequencing, which provides 100% CpG coverage and requires 50–100 ng DNA.

A detailed illustration of the technical and mechanistic differences among genome-wide DNA methylation mapping methods and descriptions of their advantages and disadvantages are provided by Marzese et al.[30] and Olkhov-Mitsel et al.[32] Several methods have been validated in hundreds of publications, and some methods are still evolving as protocols are improved. Nevertheless, there are several robust methods available for use in genome-wide and targeted methylation studies, such as those used by Illumina or Pacific Biosciences RSII sequencing protocols (**Fig. 1**).

Examination of additional types of DNA modifications, beyond just CpG methylation, is collectively referred to as DNA adductomics, or the study of the "exposome." These modifications/adducts arise from chemical and environmental insults and are studied using a variety of methods, especially MS-based methods.[33]

2.18.2.3 Proteomics

Proteins are the workhorses in biological networks. They define biological structures, mediate biological activities, and compute and transmit information among different biological entities. The proteome is the complement of all proteins in a biological system, including their posttranslational modifications, localizations, and specific functional states. Proteomics subsumes a broad range of protein analytical methods that are designed to identify and quantify a large number of proteins simultaneously. Most importantly, these methods have been designed to address central scientific questions in the field, for example, how the proteome of a cell or tissue enables specific biological processes and how these are affected by different disease states. In the systems biology context, the questions are similar, but their emphasis is often shifted toward a more quantitative—and possibly more predictive—understanding of how proteins interact to facilitate the emergent properties of complex adaptive biological systems.

To unravel this complexity, a broad range of complementary proteomics methods are needed to fully capture the functional proteome of a biological system. In the following sections, we discuss the main proteomics methods that are used in systems biology studies to measure (1) protein expression, (2) protein localization, (3) protein translation and degradation, (4) protein modification, (5) protein activity, and (6) protein interactions.

2.18.2.3.1 Protein expression profiling

How the expression level (i.e., abundance) of proteins changes under different conditions or compares across different biological systems is among the most basic information on the functional involvement of proteins in a biological process. There are several alternative methods to profile protein expression, which can be broadly classified as affinity-reagent and MS-based methods.

Antibodies are the classical affinity reagents used to profile protein expression. Currently, and despite its limitations, the western blot is still the most commonly used assay to measure changes in protein expression. High-throughput versions have been developed[34,35]; for example, Ciaccio et al. developed microwestern arrays that were used to reconstruct the epidermal growth factor (EGFR) signaling network.[34] However, due to their dimension, even these miniaturized western blot methods are limited to a few target proteins. Protein arrays, which are extensions of classical enzyme-linked immunosorbent assays, allow for higher throughput and more sensitive protein quantification.[36] For these assays, antibodies are spotted at defined positions onto a solid support, the generated array is incubated with the protein sample to be tested, and binding to the spotted antibodies is measured—usually with another pool of detection antibodies. For example, Straussman et al. used antibody arrays to discover the role of hepatocyte growth factor signaling in the innate resistance of melanomas to targeted inhibitor treatment.[37] Alternatively, for reverse-phase protein arrays, the protein samples to be profiled are spotted onto a solid support (e.g., a slide) and are then directly probed with labeled antibodies against the targets of interest.[36]

In addition to antibodies, alternative affinity probes offer specific analytical benefits. For example, aptamers are DNA or RNA molecules that can form secondary or tertiary structures capable of specifically binding to proteins and other cellular targets.[38] Considered as the chemical equivalent to antibodies, aptamers can be used in a microarray format to profile protein expression.[39] Another advantage is that they can support hybridization to DNA microarrays.[40] For example, this method was used recently to identify protein markers of aging.[41]

Affinity-reagent-based methods are also used to profile protein expression, but these methods critically depend on the availability of high-quality affinity reagents.[42–44] For example, one study tested 49 commercially available antibodies against 19 signaling receptors, and found that most of them bound to more than one target.[45] Another study showed that approximately one-quarter of 246 antibodies used in epigenetic studies lacked specificity.[46]

Methods based on MS are gaining popularity for protein expression profiling.[47] This is mainly due to their high specificity and the ability to conduct experiments without predefined target lists (untargeted approaches). The data from such analyses can then be complemented with highly specific and quantitative MS-based targeted assays in the follow-up studies. Such MS-based methods are further facilitated by recent developments in instrumentation and methodology that increase the depth and sensitivity of proteome analyses.[48–50]

MS-based protein profiling can be performed as either a top-down approach, where intact proteins are analyzed directly, or more commonly as a "bottom-up" or "shotgun" approach. In the latter case, the isolated proteins are first cleaved into peptides with a specific protease (most commonly, trypsin and Lys-C) and subsequent (chromatographic) separations, identifications, and quantifications are conducted at the peptide level.[51]

While this "divide and conquer" approach eases the analytical steps, it requires specific tools to reassemble peptide information into protein information, and to prevent the loss of correlations between different regions of the same protein. Peptide identification is at the core of "bottom-up" approaches. Commonly, the peptides injected into the mass spectrometer are identified based on two levels of information: the molecular weight of the peptide, and its fragmentation pattern. For identification, the experimental peptide fragmentation pattern is matched to all theoretical fragmentation patterns of the peptides encoded in the genome of the studied organism. Statistical methods are used to calculate the probability of wrong assignments, which yields highly reliable peptide identification (e.g., Refs. 52,53).

Peptide/protein quantification is the next critical component of protein profiling approaches. The available methods differ in their quantitative accuracy and ease of implementation. Generally, MS-based quantification methods are divided into those that work on native peptides (label-free methods) and those that require peptide modification (label-based methods). The simplest label-free quantification method is spectral counting.[54] It relies on the fact that peptide identification in the "bottom-up" workflow represents a statistical sampling procedure in which the probability of identifying a peptide is proportional to its abundance. In this

rather coarse quantification method, the number of identifications assigned to a given protein is used as a measure of its abundance. More recent label-free quantification approaches rely on integrating the signals of the peptide elution peaks as the measure of abundance—essentially, as a measure of the total number of ions detected for a given peptide.[55] Recently, label-free quantification approaches have improved significantly and are gaining popularity, especially because of their ease of implementation.

Label-based methods require modification of the sample before analysis. The main objective is to make peptides derived from different samples distinguishable, which then allows for multiplexed analysis of different samples. The advantage is that the concurrent processing and analysis of these multiplexed samples ensures that the quantities of derived peptide are directly comparable by removing the variability that is introduced by separate analytical steps. Commonly, these label-based methods rely on the use of heavy isotopes to introduce a mass shift between the different multiplexed samples. One commonly used method is stable isotope labeling in cell culture.[56] In the original implementation of this method, specific isotope-labeled amino acids are incorporated into the whole proteome of a cell culture. Cell cultures that are experimentally compared (e.g., control vs. treatment) are labeled with isotope-labeled amino acids with a different mass for each condition. After the experiment, the samples to be compared are mixed and analyzed using the conventional label-free workflow. Because the peptides derived from the different conditions are shifted in mass, the elution peaks can be integrated separately and directly compared among multiplexed samples.

In other label-based quantification methods, the peptide modifications are introduced at a later step and do not require metabolic labeling. This is crucial when metabolic labeling is not possible, for example, in the case of most clinical samples. Isobaric-tag-based quantification (e.g., iTRAQ® and tandem mass tag (TMT) labeling) relies on chemical modification of the isolated peptides after the protease digestion step (**Fig. 2**).[57–59] Again, different samples are labeled with different tags, pooled, and analyzed together by MS. Currently, this method allows for multiplexing of up to 10 samples; that is, the use of up to 10 distinguishable tags. In these methods, "isobaric" indicates that each tag of a series has the same total mass; that is, a given tagged peptide derived from different multiplexed samples is indistinguishable at the level of the whole peptide. Only during the peptide fragmentation step are reporter ions with specific masses released from each sample. The intensity ratios between these reporter ions are used for relative quantification. Of note for systems biology applications, these isobaric-tag methods are especially good for detecting statistical differences in protein expression, but tend to underestimate the ratios between reporter ions.[60,61]

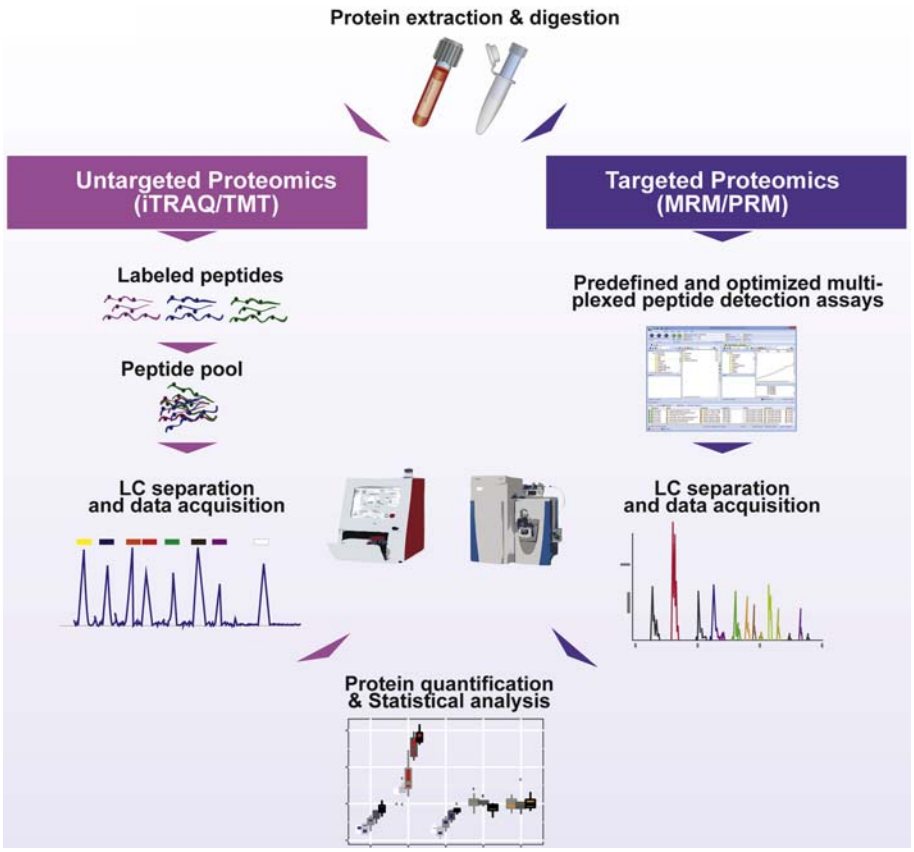

Fig. 2 Mass spectrometry-based proteomics workflows. (*Left*) Untargeted proteomics workflow with isobaric-tag based quantification (iTRAQ or TMT). (*Right*) Targeted proteomics workflow with multiple reaction monitoring (MRM) or parallel reaction monitoring (PRM). The untargeted (isobaric-tag) workflow allows for multiplexed analyses of peptide sample pools with different chemical tags/labels for each sample. The targeted workflow allows for more accurate quantification of a (smaller) predefined set of peptides/proteins.

All of these methods were established for untargeted analyses of proteomes. They work without predefining or optimizing assays for a specific set of peptides/proteins. However, as these methods rely on statistical sampling of the proteome, consistency of the measurements across MS runs is not always guaranteed, and it is difficult to validate assays for specific peptide sets. This is why "shotgun" proteomics methods are usually complemented by targeted proteomics methods, especially for clinical applications or to establish systems biology models.[62,63] While the general detection and quantification principles are similar, targeted proteomics—for example, the multiple reaction monitoring (MRM) and parallel reaction monitoring (PRM) methods—relies on predefined (and optimized) specific multiplexed peptide detection assays (see **Fig. 2** for details). To further increase the accuracy of quantification, a heavy-isotope-labeled internal standard peptide is commonly included for each quantified peptide. This strategy supports robust quantification, even among different laboratories.[64]

Finally, data-independent (DIA) acquisition methods are becoming increasingly popular. These methods are conceptually located between untargeted and targeted proteomics approaches and combine untargeted acquisition with targeted computational analyses of the proteome.[52] In these methods, the mass spectrometer is programmed to acquire the fragmentation patterns (and possibly peptide masses) of a large fraction of the proteome. Then, specific spectral libraries are used to deconvolute these complex fragmentation datasets and compute the quantities of peptides and proteins. The advantages of these methods include their high quantification accuracy with broad proteome coverage, the ease of comparisons across MS runs with limited missing values, and the ability for targeted reanalysis of the same data sets for different target sets.[49,52]

2.18.2.3.2 Spatial proteomics

The functions of proteins strongly depend on their localization in the cell and tissues. For example, translocation of transcription factors to the nucleus is a common regulatory mechanism that is also a central element of several systems biology models of signal transduction.[65]

Antibody-based assays to determine the localization of proteins, using either colorimetric or immunofluorescence visualization, are a mainstay of cellular biology.[66] More recently, these techniques have been adapted to characterize the localization of larger sets of proteins. For example, Uhlen et al. generated a map of the human tissue proteome that provided spatial localization of proteins from the tissue level to the single-cell level.[67] For this purpose, the authors combined RNA-seq and an extensive immunohistochemistry data set (more than 13 million images annotated by pathologists). The results of this *tour de force* are available at www.proteinatlas.org. In a related project, Stadler et al. conducted a large-scale subcellular localization study for more than 500 human proteins, which were detected by visualizing antibody-based immunofluorescence and expressed fluorescent fusion proteins.[68] These two studies represent large-scale projects that rely on extensive infrastructure, and will likely be out of reach for individual labs. Recently, however, a relatively simple protocol for multiplexed immunofluorescence analysis was described.[69] Named cyclic immunofluorescence (CycIF), this method makes use of alternating antibody staining and bleaching cycles. In the initial report, CycIF allowed for simultaneous expression profiling of up to 15 targets in a cellular population. A similar approach was taken by Gerdes et al. for the multiplexed single-cell analysis of formalin-fixed, paraffin-embedded cancer tissue.[70]

Alternatively, MS-based methods are also available to characterize the localization of proteins. Commonly, these rely on a combination of fractionation methods (e.g., of subcellular compartments or cell types), with MS-based identification and quantification of the differentially enriched proteome fractions as described in the "**Protein expression profiling**" section. Boisvert et al. used this approach to analyze the proteome response to DNA damage in three different cellular compartments: the cytoplasm, the nucleus, and the nucleolus.[71] An interesting result was that DNA damage triggered the relocation of proteasomal components into the nucleus, which was likely related to changes in their intricate intracellular dynamics under different cellular states and responses.[72] Recently, Christoforou et al. further refined this approach to analyze the spatial proteome of mouse pluripotent stem cells.[73] For this, digested proteins from 10 differentially enriched subcellular fractions (cytosol, chromatin-enriched, and eight density-gradient fractions) were labeled with 10-plex isobaric TMT and then identified and quantified by liquid chromatography coupled with MS (LC–MS/MS). These analyses provided detailed localization information for more than 5000 proteins and yielded insights into organelle structures, protein complex localizations, and the localization of protein isoforms.

Other methods combine MS with imaging approaches to reveal the localization of proteins. In matrix-assisted laser desorption/ionization imaging MS, ion spectra of a tissue slice are spatially resolved.[74] Tissue sections are placed on a solid support and coated with a chemical matrix that supports desorption and ionization of molecules when irradiated by a laser. During the experiment, the tissue is scanned by a laser and the ion spectra that are measured for each x,y-coordinate are compiled into a two-dimensional map of ion intensities. However, identification of proteins from the obtained complex ion spectra remains a challenge.[75] An alternative with a much lower spatial resolution is the combination of laser-capture microdissection with LC–MS/MS-based expression proteomics.[76] Recently, this technique was used to analyze protein expression in neurons from the temporal cortex of patients with Alzheimer's disease.[77] Finally, the spatially targeted optical microproteomics (STOMP) method has been developed to provide a higher resolution analysis.[78] In this method, two-photon laser scanning microscopy is used for specific affinity photo-labeling of proteins in a selected tissue region. This allows for specific enrichment and MS-based identification of the photo-labeled proteins in the selected tissue region. In the test case, STOMP was able to identify known and novel amyloid plaque components from Alzheimer's disease samples.

2.18.2.3.3 Proteome synthesis and degradation

Protein levels are regulated both at the level of protein synthesis and degradation. The hypoxia-inducible transcription factors (HIF) are key regulators of the hypoxic stress response, and are examples of proteins with tightly regulated degradation.[79] Under normoxic

conditions, HIFs are rapidly degraded by a mechanism that involves hydroxylation of key proline residues by members of the oxygen-sensitive prolyl hydroxylase enzyme family.[80] By contrast, low-oxygen conditions prevent hydroxylation and protein degradation, resulting in rapidly increasing levels of the HIFs that trigger the activation of hypoxic stress-response programs. As this hypoxic stress response is central to several biological processes including cancer development, systems biology models have been devised to better understand this response. For example, Nguyen et al. derived a mathematical model of HIF-1a regulation by hypoxia, which was able to confirm the overall network topology and provided insights into the complexity of the regulation of HIf-1a degradation during the hypoxic stress response.[81]

More tools to measure degradation and synthesis rates at the proteome-scale are needed to expand our knowledge of the role of regulated protein degradation and synthesis.[82] Several MS-based methods have been devised, which combine isotope labeling and/or pharmacological inhibition of translation with quantitative LC–MS/MS-based proteomics measurements. For example, Schwannhauser et al. developed a method for the global analysis of protein translation using pulsed addition of heavy-isotope-labeled amino acids to a cell culture.[83] The labeled amino acids are taken up by the cells and incorporated into newly synthesized proteins. Subsequently, MS-based proteomics analyses allow for proteome-wide measurement of the incorporation of these isotope-labeled amino acids into newly synthesized proteins, yielding estimates of relative protein translation rates. Using this approach, Selbach et al. demonstrated the global but relatively mild effects of miRNAs on protein synthesis.[84] To measure protein degradation rates, Larance et al. globally blocked translation with the inhibitor cycloheximide and measured the amounts of remaining proteins by LC–MS/MS-based proteomics.[85] This analysis reemphasized the importance of regulated protein degradation in regulating the cell cycle.

To complement these analyses, proteomics methods that support the global analysis of protein ubiquitination have been devised. Polyubiquitination of proteins serves as a specific tag to target proteins for proteasomal degradation, and a whole machinery of specific and well-regulated ubiquitin ligases controls this process.[86] Upon oxidative stress, the ubiquitin ligase adaptor protein Keap1 is inactivated, which stabilizes its substrate Nrf2—a key transcriptional regulator of the oxidative stress response.[87] Proteomics studies to measure global protein ubiquitination commonly rely on an affinity-enrichment strategy for ubiquitinated peptides.[88] To enrich ubiquitinated peptides, Kim et al. used a monoclonal antibody that recognizes diglycine-containing isopeptides. These isopeptides are generated when ubiquitinated proteins are digested during sample processing for LC–MS/MS-based quantitative proteomics analysis.[89] This strategy quantified 19,000 ubiquitinated peptides in approximately 5000 proteins.

2.18.2.3.4 Protein phosphorylation profiling

As already discussed for protein ubiquitination, specific protein modifications are central to the regulation of protein levels and activities.[90] Phosphorylation—likely the best understood protein modification—regulates enzymatic activity, stability, complex formation, and localization. All of these cellular processes are tightly regulated by the opposing activities of kinases and phosphatases, which are organized into intricate phosphorylation networks that function as sophisticated signal processing units to elicit specific cellular responses.[91]

Quantitative phosphorylation profiling by MS is a well-established technique.[92] Analogous to the protein ubiquitination analysis, after digestion of proteins into peptides, phosphorylated peptides are enriched before being identified and quantified by MS. Several different phospho-peptide enrichment methods are available. Because of the availability of high-affinity antibodies for tyrosine (Tyr)-phosphorylated proteins, antibody affinity enrichment has been the centerpiece for phospho-profiling studies focused on the effects on phospho-Tyr-signaling. For example, Rubbi et al. conducted a phospho-Tyr profiling study to dissect the regulatory interactions between the BCR-ABL1 oncogene and Src-family kinases in leukemia.[93] Drake et al. also used this approach to identify druggable kinases in prostate cancer tissue samples.[94] Antibody-based enrichment to profile serine and threonine phosphorylation is hampered by the lack of highly specific anti-phospho-serine/threonine antibodies, although phosphorylation-motif-specific antibodies have recently become available (e.g., for the AKT kinase phosphorylation motif).[95,96] Thus, metal-based affinity enrichment is most commonly used for global phospho-profiling of phospho-serine/-threonine/-Tyr peptides. Titanium dioxide and immobilized iron ions are commonly used as affinity reagents because of their strong affinity for phosphorylated peptides (e.g., Refs. 97–100). Of note, because of the lower abundance of phospho-Tyr residues, their coverage can be limited and the combination of antibody- and metal-based affinity-enrichment approaches can be beneficial.[101]

A common challenge encountered with these phospho-profiling methods is that they require a relatively large sample input (sometimes in the milligram range) and have a low throughput. To allow for high-throughput analyses of phospho-proteomes, Humphrey et al. recently described a scalable phosphoproteomics platform that can quantify hundreds of phospho-proteomes at a depth of $>10{,}000$ phosphorylation sites.[102] This was achieved through streamlined protocols and parallel processing in 96-well plates. In the initial study, this method was used to characterize the phospho-proteome response of mouse liver to insulin stimulation at a high temporal resolution (starting <15 s after insulin stimulation) and depth ($>25{,}000$ phosphorylation sites). Another recent study demonstrated that phospho-peptide enrichment coupled with targeted MS can accurately quantify signaling networks, such as the DNA damage signaling network.[103] Clearly, while providing lower coverage (107 phospho-sites in that case), such targeted and well-validated quantification methods are well suited to generate data for cellular dynamics models and for use in a clinical setting.

Beyond phospho-profiling, related affinity-enrichment and MS assays have been developed for various other protein modifications, including acetylation,[104] methylation,[105] O-linked β-*N*-acetylglucosamine modification,[106] and lipid modification.[107]

2.18.2.3.5 Proteome activity profiling

Several proteomics methods can either measure protein activity directly or provide readouts that depend on the activity state of the proteins. Kinase inhibitor profiling with "kinobeads" is an example of the latter.[108] In this chemical proteomics approach, a collection of nonselective kinase inhibitors is immobilized onto beads ("kinobeads"). Because these kinase inhibitors target the active sites of a broad collection of kinases, the beads can be used as affinity reagents before the LC–MS/MS analysis of the kinome; that is, the set of all (bound) kinases. Importantly, because the active sites are targeted, binding of other active site inhibitors will interfere with binding and deplete the targeted kinases in this experiment. In their original report on this method, Bantscheff et al. used it to characterize kinase inhibitor profiles for leukemia and identified the kinases DDR1 and the oxidoreductase NQO2 as novel targets of the BCRABL1 inhibitor imatinib.[108]

Active site probes can assess the activities of enzymes in the proteome more directly.[109] At the core of this technology lie chemical probes that are designed to covalently bind to the active site of the enzyme class of interest. These probes carry tags that, for example, allow for affinity purification of the modified proteins/peptides and their subsequent identification and quantification by LC–MS/MS (or western blot). Probes are available for a broad range of enzyme classes including serine hydrolases, cysteine proteases, metallohydrolases, kinases, and other nucleotide-binding proteins. A protocol has been established to quantify proteasome activity in living cells.[110] This protocol was used to demonstrate that interferon gamma rapidly induced immunoproteasome activities in respiratory cells of the lung. This result demonstrated that nonimmune cells can contribute to the adaptive immune response to intracellular infections.[111]

Even more direct proteomics assays to profile enzyme activities have been devised, including peptide microarrays to profile kinase activities.[112,113] For this, a large collection of peptides with kinase recognition sites are synthesized and arrayed on a microarray slide. To measure kinase activities, these chips are incubated with purified kinases or cellular lysates and fluorescently tagged with anti-phospho-peptide antibodies. Alternatively, phospho-specific affinity reagents are used to produce a readout of the kinase activities (i.e., phosphorylation levels). Similar peptide microarrays have been developed to quantify the activities of other enzymes. For example, Rauh et al. developed a peptide microarray to characterize the activity of protein deacetylases.[114] Kubota et al. also devised a MS-based strategy to measure kinase activities.[115] In this assay, synthesized peptide libraries with a preselected distribution of kinase recognition sites are incubated with cellular lysates. Phosphorylation of these peptides is then quantitatively assessed using LC–MS/MS and kinase activity patterns are compared among samples.

2.18.2.3.6 Protein interaction profiling

Proteins function in the context of complex biological networks. Unraveling these interactions is at the core of systems biology research, and several approaches have been devised to analyze interactions among proteins on a large scale.[116,117]

Functional genomics approaches to detect protein interactions rely on the engineered expression of potentially interacting molecules in a cell. Such systems are designed in a way that interacting molecules result either in cell survival or the expression of a detectable marker. The yeast two-hybrid (Y2H) system is the best-known assay to detect protein interactions. In the classical Y2H assay, the two proteins to be tested are coexpressed in yeast cells, one fused to the DNA-binding domain and the other to the transactivation domain of a transcription factor. If the two proteins interact, a functionally active transcription factor is reconstituted, which then mediates the expression of a reporter gene that either allows the yeast colonies to grow in the presence of a toxicant, or that can be detected with a colorimetric assay. Large-scale versions of this assay have been devised, in which many interactions between many protein pairs are tested in an array format. The growth or specific color-staining of yeast colonies in the array indicate specific protein–protein interactions (PPIs). Genome-scale Y2H approaches have been used to define PPI networks in viruses, bacteria, and human cells (e.g., Refs. 118–121).

Protein and peptide arrays have also been used to characterize protein interaction networks. In an early study, Jones et al. constructed protein microarrays comprising nearly all Src homology 2 (SH2) and phosphotyrosine-binding domains of the human genome, and probed them to detect binding to 61 Tyr-phosphorylated peptides from the EGFR receptor family.[122] Measuring the equilibrium dissociation constants of all these interactions allowed for quantitative comparisons of the binding specificities among the various family members—with potential implications for their roles as oncogenic drivers. More recently, Yu et al. established "self-assembly" protein arrays with 10,000 human proteins, and identified their interactions with two effector proteins (SidM and LidA) from the bacterium *Legionella pneumophila*.[123] To assemble the human protein array, the authors used the "nucleic acid-programmable protein array" approach, in which DNA encoding human genes is spotted onto a microarray slide, and then proteins are synthesized in situ through in vitro transcription/translation. Because the translated proteins carry a tag, they are directly captured on the array by cospotted anti-tag antibodies, and can then be probed by bacterial effector proteins. This assay was able to reproduce 18 of the 20 known targets for these effectors and revealed three novel host interaction proteins.

Protein microarrays are complemented by peptide microarrays. Peptide microarrays are limited to the detection of interactions with linear epitopes, but are easier to produce and allow for more control over the spotted peptide sequences, including their post-translational modifications. Recently, Tinti et al. used this technology to profile the binding landscape of SH2 domains to the human phospho-Tyr peptidome. In total, 6202 phosphopeptides with phospho-Tyr in the center position were synthesized and spotted in triplicate onto a microarray slide. Afterward, these chips were probed with a collection of 99 human SH2 domains. The data obtained supported the creation of a probabilistic interaction network for SH2 domains and suggested intriguing biological links; for example, between the Tyr-phosphatase SHP2 and the phosphorylated Tyr in the extracellular signal-regulated kinase activation loop in growth factor signaling.

Affinity purification of protein complexes coupled with identification of complex components by LC–MS/MS is an effective and proven method to characterize protein interaction networks.[124] These approaches are based on classical protein pulldown and coimmunoprecipitation protocols, but LC–MS/MS is used instead of western blots to identify and quantify the components of the protein complex. The main challenge of these approaches is that they require high-affinity binding reagents for the proteins of interest. Commonly, this challenge is circumvented by engineered expression of proteins with a tag for which high-affinity purification reagents are readily available. For example, an early affinity purification study on yeast used a library of yeast strains that were engineered to express each yeast gene as an affinity-tagged fusion protein.[125] For mammalian systems, viral delivery systems, bacterial artificial chromosome transgenics,[126] and most recently, genome engineering[127] have been used to express tagged proteins for affinity purification. Another common challenge is how to distinguish true from false-positive interactions. For this, quantitative MS can distinguish between specific and unspecific binders.[128,129] Recently, Hein et al. used a protein complex and an LC–MS/MS enrichment approach to define an extensive human interaction network of 5400 proteins and 28,500 interactions.[130] The authors expressed 1330 GFP-tagged proteins under the control of their native promoter in a human cell line, affinity-enriched the protein complexes with anti-GFP antibodies, and then conducted label-free quantification of these protein complexes. Importantly, this quantitative approach provided measures of the specificity, stoichiometry, and abundance of human protein complexes, and demonstrated that protein networks are dominated by weak interactions, with only a few stable complexes with balanced protein stoichiometry.

Beyond PPIs, proteomics methods have been developed to characterize protein binding to other classes of molecules. This includes methods to identify targets for pharmacological inhibitors,[131] natural products,[132] and toxicants.[133]

2.18.2.3.7 Special considerations and outlook

Systems biology is about understanding how biological functions and responses emerge from the complex, dynamic interactions in biological networks. Proteomics methods cover a broad range of the proteomic space, from expression levels, to modifications, to activities, to interactions. Beyond providing insights into the roles of individual proteins, proteomics approaches have demonstrated their value to further our understanding of systems-level properties—for example, how robustness is built into biological networks,[134] how modularity is used as a basic building principle to structure biological functions,[125,128] how complex interactions within signaling networks govern cellular responses,[135] and how complex signatures can identify diseases.[136]

Clearly, different systems-level questions will benefit from different proteomics methods. When the protein properties of interest (e.g., localization, posttranslational modification) have been selected, the main consideration is the potential tradeoff between quantitative accuracy and sample throughput. As discussed earlier, protein quantification is constantly improving, allowing for larger numbers of proteins to be quantified with high accuracy. Protein and peptide array methods are high-throughput, but rely on the availability of highly specific affinity reagents. Targeted proteomics methods are best suited for MS-based assays if precise quantification of a few proteins is required (e.g., for pharmacodynamics, PD modeling approaches).[103] If global network dynamics is the topic of interest, then nontargeted methods are better suited. DIA MS forms a middle ground between the two classical extremes and has the potential to combine the advantages of both worlds toward broad and accurate quantification of proteome responses.[137]

Proteomics instrumentation and methods are still rapidly evolving. It is expected that these improved and more accessible "third-generation" proteomics tools will be indispensable in cell biology and molecular medicine in the future.[138] Such methods will allow us to reach a true systems-level understanding of dynamic physiological and disease processes. Clearly, to this end, integration of proteomics data with other data modalities presented in this article is the key to gaining a comprehensive understanding of biological systems.[139,140]

2.18.2.4 Metabolomics

Metabolomics aims to provide a comprehensive description of the metabolome representing all cellular metabolites in one living system at a specific time. With respect to systems biology approaches, metabolomics adds to the classical -omics technologies (i.e., transcriptomics and proteomics) for a complementary and holistic understanding of the behavior of a living system within its environment. The characterization of the cellular metabolome represents the intermediates and end-products of all enzymatic reactions in a biological cell. This information allows for the evaluation of the cell's biochemical activity and, furthermore, its biochemical networks, which predict the organism's molecular physiology and changes in phenotype.[141,142] In addition to metabolomics terminology focusing on endogenous metabolites alone, metabonomics includes the characterization of metabolites related to external stimuli, like xenobiotic metabolites, dietary metabolites, responses to disease, or extragenomic factors such as gut microflora. Besides unbiased hypothesis-free nontargeted approaches, several hypothesis-directed approaches have been also established. These include metabolic profiling[143–145] focused on predefined metabolites related to specific pathways of interest, and metabolic fingerprinting[143] to provide rapid, high-throughput sample classification information and metabolite target analysis for quantitative analysis of a limited number of metabolites for specific pathways. As a result of rapidly growing interest from academia, industry, and government, metabolomics has been a part of the National Institute for Health road map initiative since 2003.[146] Along with the immense growth in metabolomics technologies, this broad interest has led to strong positioning of this field in the life sciences.

Metabolomics covers a wide range of research areas, including plant biology,[142,147] biotechnology industrial processes,[148] toxicology,[149] drug development,[150] clinical diagnostics,[143,151] biomedical research[152] including diagnostic and prognostic

biomarkers, responses to medical treatment,[146] and environmental factors impacting human health. Specific examples of how this and other -omics technologies can advance different fields are discussed elsewhere in the article.

2.18.2.4.1 Methods and recent developments

Despite the tremendous progress in instrumentation technologies, no single analytical technology can cover the metabolome comprehensively. Usually, multiple methods with complementary characteristics are used. Nuclear magnetic resonance (NMR) and MS techniques are most commonly used in metabolomics research,[153,154] while different separation techniques coupled to MS platforms are chosen if greater sensitivity is required.[155] Shotgun approaches that avoid separating the sample matrix before MS were established some time ago for high-throughput lipidomics.[156] Researchers from Eidgenössische Technische Hochschule (ETH) Zurich recently developed a shotgun approach for real-time metabolome profiling of about 300 metabolites to monitor metabolite dynamics.[157] Separation techniques are required for comprehensive metabolome characterization because of the complex nature of the cellular matrix. Gas chromatography (GC) and LC coupled to MS (GC/MS and LC/MS, respectively) are widely used in combination because of their complementary coverage of the range of metabolites. Each of them provides a multiplicity of methods to analyze different metabolite classes. A typical workflow is shown in Fig. 3.

Complex sample preparation procedures represent a high risk of changing the sample composition. Therefore, sample preparation is generally kept as simple as possible, and is preferably limited to quenching of metabolism and metabolite extraction using the crude extract for analyses.[158] Nevertheless, more complex sample preparation procedures are sometimes unavoidable. Such procedures include protein precipitation, solvent changes for GC/MS analysis due to incompatibility of aqueous media, and/or derivatization procedures. Recently, scientists developed a technique for direct injection of aqueous media samples from incubated microsomal or S9 fractions, cell culture media, or smoke-bubbled phosphate buffered saline in two-dimensional GC coupled with time-of-flight MS (GC × GC-TOF MS).[159,160]

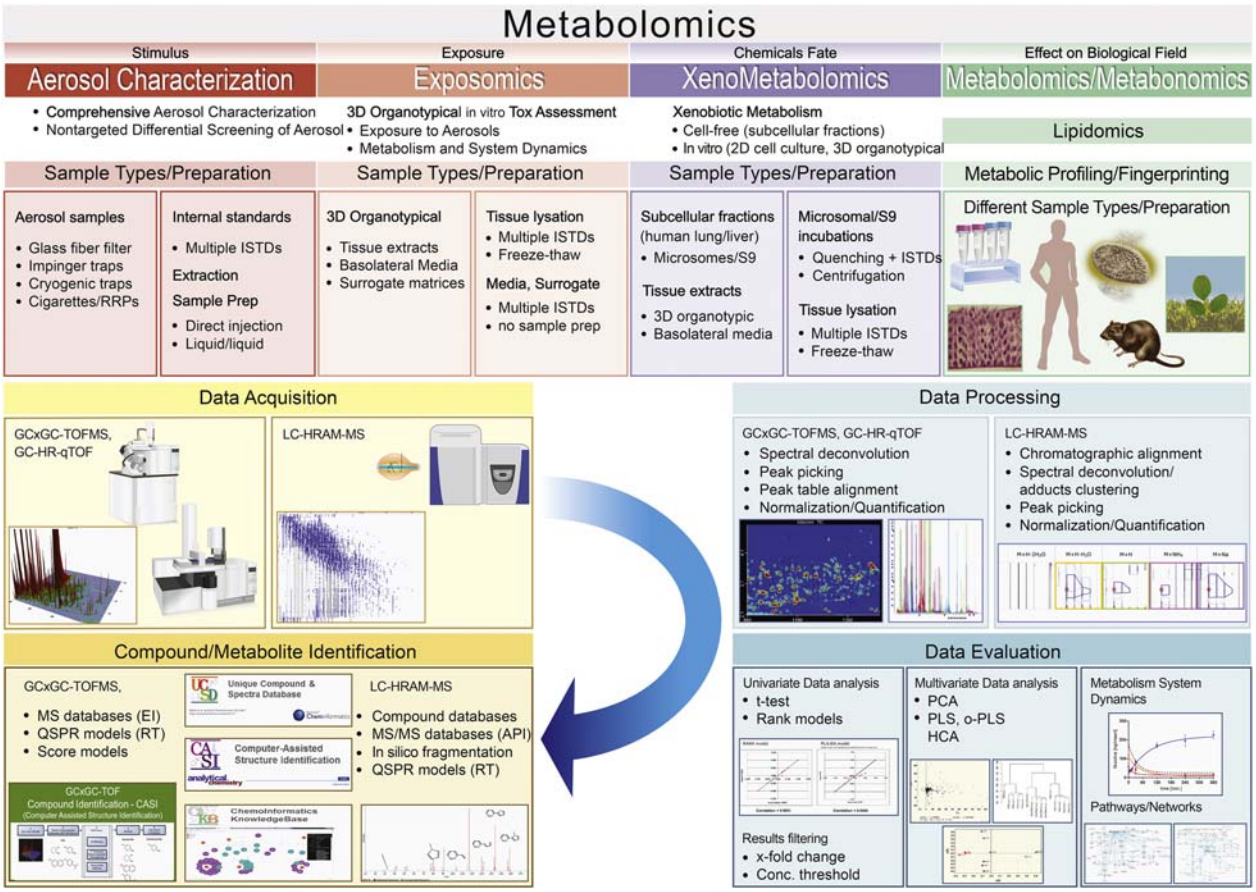

Fig. 3 Metabolomics workflows. Metabolomics applications and typical workflows including comprehensive characterization of the stimulus (e.g., aerosol or smoke with complex chemical composition) test system exposure, metabolism, and kinetics. *API*, atmospheric pressure ionization; *CASI*, computer-assisted structure identification; *GCxGC-TOFMS*, two-dimensional gas chromatography coupled to time-of-flight mass spectrometry; *GC-HR-qTOF*, gas chromatography coupled to high-resolution time-of-flight mass spectrometry combined with quadrupole and collision cell; *HCA*, hierarchical clustering; *ISTDs*, internal standards; *LC–HRAM-MS*, liquid chromatography coupled to high-resolution accurate mass spectrometry; *o-PLS*, orthogonal partial least squares; *PCA*, principal component analysis; *PLS*, partial least squares; *QSPR*, quantitative structure–property relationships.

2.18.2.4.2 Mass spectrometric platforms for metabolomics

Many separation and MS methodologies have been established for each instrument platform. Most often, multiple complementary methods are used within a platform to achieve the most comprehensive metabolome coverage. In addition to the key LC/MS and GC/MS platforms, capillary electrophoresis coupled to MS (CE-MS) has recently been established in the metabolomics research. This technique is relevant for the metabolomics research because of its complementary character, in that it allows for analyses of ionic and highly polar metabolites.[161,162]

2.18.2.4.2.1 LC/MS

LC-based separations for nontargeted analyses are usually based on reversed-phase chromatography, hydrophilic interaction chromatography, or ion exchange chromatography.[163–165] Developments in column stationary phases have provided a tremendous diversity of separation properties. New polymer-coated core shell stationary phases provide stability and robustness for large sample series, and well-defined small particles enlarge the surface area for analyte-to-stationary phase interactions, which are beneficial for effective separation. The high pressure stability of modern stationary phases increases the sensitivity and decreases the separation times of modern Ultra Performance Liquid Chromatography applications, allowing for high-throughput capabilities. The combination of MS and LC has evolved dramatically, especially in life science research. The traditional LC–MS/MS triple-quadrupole instrumentation has largely been replaced by accurate mass analyzers. The TOF mass analyzers that provide sufficient mass resolution and mass accuracy are frequently combined with a quadrupole mass filter and a collision cell in the front end, allowing for collision-induced dissociation (CID) fragmentation experiments (MS^2). The obtained fragmentation mass spectra are a valuable tool for metabolite confirmation and, to some extent, metabolite identification. Recent revolutionary MS concepts based on Thermo Electron Corporation's Orbitrap technology provide unprecedented mass accuracy, resolution, and fragmentation capabilities for MS^n experiments, combined with high sensitivity and robustness.[165,166] Different ionization techniques are often used to broaden the metabolite coverage. Commonly used ionization techniques include atmospheric pressure ionization using electrospray ionization (ESI) in positive and negative modes, as well as atmospheric pressure chemical ionization (CI) to complement the ESI data.

In addition to the classical approach of acquiring data in full-scan mode followed by, or combined with, data-dependent MS^2, several MS-based generic substance class screening approaches have been established. These focus on specific metabolite classes using either diagnostic fragment ions; for example, glycerophospholipid classes of phosphatidylcholine (m/z 184), phosphatidylethanolamine (m/z 141), and phosphatidylinositol (m/z 241), or characteristic neutral losses of the head group of phosphatidylserine (loss of m/z 185).[167] Traditional approaches to screen glutathione adducts use the characteristic neutral loss of pyroglutamate (m/z 129) and the diagnostic precursor ion in negative ionization mode (m/z 272).[168] Recent improvements to stable isotope-dilution techniques for generic screening of glutathione adducts have increased the comprehensiveness, selectivity, and sensitivity of these methods.[169,170] A mixture of stable isotope-labeled and nonlabeled glutathione is applied as a nucleophile to conjugate electrophilic compounds or metabolites, for example, in microsomal bioactivation experiments. High-resolution accurate MS is then carried out to screen the resulting specific isotopic fingerprint of the conjugates. Scientists at Philip Morris International have established a generic stable isotope-dilution-based glutathione adducts screening method to identify electrophilic smoke constituents and metabolites, including downstream reduction metabolites, derived from bioactivation of smoke compounds using microsomal and S9 fractions.[171] This method was compared with those using different nucleophiles to screen generic electrophilic compounds.[172]

2.18.2.4.2.2 GC/MS

For decades, GC/MS has been a well-known technology in metabolomics research. Various stationary phase materials covering a wide range of polarities are available for separation. These materials are based on chemically immobilized modified silicon oil, poly ethylene glycol, and recently developed ionic liquids.[173] Mass spectrometers have evolved from traditional unit mass resolution single-quadrupole or triple-quadrupole technologies toward TOF analyzers with fast data acquisition rates, accurate mass and high resolution, often combined with MS^2 capabilities, and finally toward the recently introduced GC-coupled Orbitrap technology.[174,175] Newly developed GC × GC-TOF MS methods provide comprehensive chemical characterization in metabolomics. These techniques are capable of chromatographically resolving highly complex matrices and thus, represent a standard technique in GC/MS-based metabolomics approaches.[176,177] Such methods will further benefit from recently introduced GC × GC high-resolution accurate mass TOF technology.[178] The most common ionization technique in GC/MS-based metabolomics is electron ionization (EI), which provides standardized high-energy fragmentation mass spectra that allow for simple and fast structure identification based on comparisons of the mass spectra with those in commercial databases. The structural identification of compounds that are not present in commercial databases requires additional information (besides manual interpretation of EI mass spectra) derived from low-energy ionization techniques like CI in positive and negative ionization modes. In CI, different gases (e.g., methane, isobutene, or ammonia) are used to adduct charged CI molecules to the analyte. Information on the molecular mass of the adduct provides the elemental composition. Further information on compound substructures can be obtained by CID fragmentation with different collision energies.

2.18.2.4.2.3 Spectral processing

Metabolomics studies yield highly complex data with respect to chemical composition. Typically, several thousand compounds can be separated and detected with a specific method. However, the huge number of samples that are needed to address biological

variance require advanced spectral processing strategies. Spectral processing aims to reproducibly and sensitively quantify of all the detectable features (information subsets; e.g., a specific ion intrinsically related to a metabolite) in the complete sample set while reducing the number of false positives, including system-immanent features, often referred to as noise reduction. Huge metabolomics datasets require data reduction strategies that do not significantly reduce the information content (e.g., conversion of accurate MS profile data into centroidic data).

Spectral processing strategies for MS generally consist of multiple processing steps that can differ slightly according to the data-processing software. Spectral preprocessing typically includes spectral deconvolution, peak detection and integration, and peak alignment and normalization.[153,179,180]

The aim of spectral preprocessing is to separate sample-related spectral information from systemic noise, thereby increasing spectral quality. Strategies for noise reduction include simple baseline subtraction or more sophisticated spectral deconvolution algorithms. The LC/MS mass spectra acquired in the ESI mode often produce multiple additional adducts like sodium, potassium, and ammonia adducts next to the protonated molecular ion, thereby complicating the data analysis. Modern LC/MS metabolomics software therefore includes automated adduct- and isotope-clustering algorithms to reduce data complexity.

Peak or feature detection, often referred to as peak-picking procedures, screens the whole dataset to detect analytical signals that reflect the applied peak-picking parameters. Typically, a huge dynamic range in peak abundance (sometimes up to 50 or 60) needs to be considered, which represents a significant challenge for robust peak detection and integration, especially for poorly separated peaks or small peaks close to major ones. The GC × GC-TOF MS data are often processed using the vendor software package ChromaTOF,[176] which includes an algorithm for peak picking based on unique masses. This algorithm is suitable for discriminating analytical signals related to a true peak from the background noise. Strategies based on binning of spectral data to process huge datasets with limited computational performance have been complemented by peak-based approaches that use several different strategies like wavelet-transformation, and recursive threshold or local maxima peak detectors.[181–183] The disadvantages of binning approaches (e.g., the occurrence of peaks masses at bin borders and subsequent rejection or splitting between bins) have been overcome by overlapping bins followed by a postprocessing step to remove double findings from overlapping bins.[184]

Peak alignment of metabolomics datasets is an essential processing step to generate a high-quality results matrix. Huge analytical datasets inherently produce variations upon data acquisition. The analyzed sample matrix can affect the column material in both LC/MS and GC/MS platforms, resulting in continuous peak shifts or modified separation characteristics such as broadened peak width. Such peak shifts and modifications in separation characteristics have different effects depending on the metabolite class.[185,186] Although analytical-quality samples can, to a certain extent, ensure controlled data acquisition, it is not practically possible to maintain the relevant criteria for all observed peaks. Chromatographic shifts and peak broadening can occur in a linear, that is, small changes in carrier-gas flow in GC, or nonlinear manner, that is, matrix–stationary phase interaction in LC can change analyte–stationary phase interactions for specific compounds, like phenolic, acidic, or basic compounds depending on the nature of interaction and compounds physicochemical properties, that is, pK_a/pK_b. Shifting of the mass accuracy over time appears in systemic drifts in most cases.[187] A common obstacle for GC/MS is the accumulation of matrix-related components, like nonvolatized or thermally degraded components (often referred to as "dirt" in the injection system). These substances can result in the disappearance of small peaks over time because of their increasing adsorptive effects within the injection system, that is, accumulation of wax compounds like long-chained fatty alcohols, lipids in plant extracts, or carbohydrates introduced into a hot injection system resulting in a multiplicity of reaction products critical for maintaining inertness of the injection system.

Various peak alignment strategies have been established. These strategies can be classified into linear methods or nonlinear warping methods.[183,188] Both strategies try to maximize the correlation between the whole spectra set and the complete dataset. A common strategy in GC/MS-based methods is the concept of linear retention indices introduced by Kovats, known as the Kovats Index (KI).[189] Typically, a set of *n*-alkanes are used as retention index markers for nonpolar analytical columns to transform absolute retention times into an index system that adapts to chromatographic shifts. Different retention index systems have been established depending on column characteristics. For example, a retention index based on free fatty acid methyl esters is often used for polar columns. Linear retention index systems represent a powerful approach to correct for chromatographic shifts, and often are used to construct retention index prediction models for structure identification.[172,190,191] Nevertheless, such approaches have limited applicability for aligning shifts related to individual substance classes. To align individual shifts related to individual compounds, nonlinear warping techniques based on physicochemical properties have been developed. They are most commonly used in LC/MS-based approaches because of the higher complexity of compound interactions, and because this separation system favors individual compound shifts over systematic linear shifts.[188] The nonlinear warping techniques include segmental correlation optimized warping or dynamic time warping.[153]

Normalization of the analytical dataset is a crucial step for metabolite quantification and the accurate evaluation of relative differences (x-fold changes). Normalization can be performed according to endogenous stable metabolites (e.g., creatinine in urine), total peak areas, or by the addition of stable isotope-labeled internal standards to the sample. Selecting an internal standard that is structurally closely related to the metabolite of interest generally results in the most accurate concentration estimates. Advanced approaches that use metabolite clustering to determine the structural similarity to a set of internal standards can provide good concentration estimates for a wider range of metabolite classes. In LC/MS, ion suppression or enhancement effects in soft ionization techniques can significantly affect semiquantification, particularly if the chromatographic environment (matrix composition, and/or embedding of a metabolite) changes between samples.

2.18.2.4.3 Structure identification

Compound identification is widely recognized as a major bottleneck in metabolomic approaches and high-throughput nontargeted characterization of complex matrices. The most straightforward strategy to identify metabolites is to compare experimental mass spectra with those in commercially or publicly available mass spectra databases. The highly standardized mass spectra generated by electron impact ionization used in GC/MS has led to the establishment of huge commercial databases like the NIST14[192] and Wiley mass spectra libraries,[193] which together contain >950,000 mass spectra of 760,000 unique compounds. Mass spectra information is also housed in specialized libraries like the Maurer/Pfleger/Weber[194] or Golm Metabolome Databases (GMDs),[195] which cover several hundred thousand MS spectra of chemicals. These databases and libraries have enabled GC/MS to become a powerful structure identification tool. Nevertheless, the metabolite coverage is small compared with the total number of estimated metabolites within biological systems. For example, less than 10% of the known metabolites present in compound databases like the Human Metabolome Database (HMDB)[196] and Metabolomics Database, METLIN[197] are linked to mass spectral data. Because the majority of MS databases for GC/MS include only unit mass-resolved mass spectra, additional accurate mass measurements obtained using modern high-resolution instruments are not sufficiently utilized.

There is a low level of confidence in the proposed structures of resolved components if the structures are purely based on simple mass spectral library queries. To increase the level of confidence, manual verification and interpretation of the mass spectral library search must be carried out. While commonly used search algorithms for EI mass spectra like implemented in the NIST spectral database collection represents powerful tools to preselect possible structural candidates, the MS scientist can interpret based on expert knowledge the relevance of sometimes small fragments compared with the overall spectrum, providing essential information for the absence or presence of molecular substructures to help for the decision process on the proposed structural candidates. Finally, for unequivocal compound identification, confirmation with reference standards is required. Additional parameters (orthogonal information) derived from chromatographic analyses, such as the retention time or KI, can improve the level of confidence in structures proposed from mass spectral library searches. Also, addition of prediction model parameters such as KI can dramatically improve the confidence of compound identification. Several models that predict KI values based on molecular structures and properties, known as quantitative structure–property relationship (QSPR) models, have been developed.[191] Similarly, second-dimension retention times from GC × GC-TOF MS can provide additional information.

Computer-assisted structure identification approaches combine chromatographic and mass spectral data to accelerate and standardize the identification of compound structures. An automated platform for high-throughput identification of small molecules by GC × GC-TOF MS was recently developed and validated. This method is based on matching experimental MS data, first-dimension separation KI, second-dimension separation relative retention time, and the KI-correlated boiling point with MS databases, and includes QSPR-based models of the other parameters. The match factor of each parameter is combined to give an overall score, which corresponds to the confidence for the proposed structure.[198]

The use of high-resolution instrumentation for GC/MS means that elemental composition can be derived from accurate mass and isotope profile analyses. Combined with soft ionization techniques like CI, these methods allow for the establishment of compound database-type approaches to identify the structures of metabolites that are not present in MS databases.

Many commercially or publicly available in silico mass spectral prediction software tools have been introduced to simulate mass spectral fragmentation of EI spectra. Such software packages include MOLGEN-MSF (University Bayreuth), ACD/MS Fragmenter (Advanced Chemistry Development Inc.), and Mass Frontier (HighChem Ltd.). However, because of the complexity of fragmentation pathways in high-energy EI, in silico prediction software still provide inconsistent prediction quality, limiting their use for structural identification.[199]

Historically, structure identification by LC/MS was driven by analyzing classical target reference compounds and generating individual user mass spectral fragmentation databases. Fragmentation mass spectra in LC/MS were far from being standardized, because they were strongly affected by the diversity of instrument types, fragmentation energies, and collision cell design. More recently, generic structural identification approaches in LC/MS have become more focused on accurate mass instrumentation combined with compound-centric databases, like METLIN,[197,200] ChemSpider,[200,201] GMD,[195] HMDB,[196] and PubChem,[202] or pathway-centric databases, like the Kyoto Encyclopedia of Genes and Genomes (KEGG),[203] WikiPathways,[204] and BioCyc.[205] Recent attempts to standardize experimentally derived fragmentation mass spectra have been very successful; for example, ramped or stepped collision energies for classical CID or kinetic excitation combined with collision (linear ion trap hybrid instruments).[206] Other recent developments include higher-energy collisional dissociation (HCD, specific to Orbitrap-type instruments), where fragmentation is performed after ion transfer from the C-trap to an external HCD cell, and the option of stepped normalized collision energies.[207] A comparison between ramped or stepped CID fragmentation and stepped HCD could demonstrate sufficient similarity, which would be the first step toward building a standardized fragmentation mass spectral library for LC/MS. Consequently, an increasing number of fragmentation mass spectra have been included in compound-centric databases.[208] Methods for using in silico mass spectral fragmentation data in generic structure identification workflows are much more evolved in LC/MS than in GC/MS. Scheubert et al.[209] classified in silico fragmentation approaches into two types of methods: rule-based approaches using fragmentation rules that were extracted from the MS literature; and combinatorial approaches that generically dissect a compound into hypothetical fragments. The best-known examples of rule-based approaches are Mass Frontier and ACD MS Fragmenter. Among the combinatorial approaches, MetFrag results in high-quality predictions. MetFrag has recently been included in METLIN.[210,211]

2.18.2.4.4 Metabolomics data evaluation

Data evaluation procedures are as diverse as other focus areas, and a multitude of scientific groups are working on this topic. Different approaches are discussed in detail in a recent review by Alonso et al.[153] In general, data evaluation approaches can be classified into univariate analysis methods, like Student's *t*-test and analysis of variance, or multivariate analysis methods, like principle component analysis (PCA), partial least-squares discriminant analysis (PLS-DA), orthogonal PLS-DA (O-PLS-DA), support vector machines (SVMs), and hierarchical clustering analysis (HCA). Univariate analyses are often used to compare a limited number of sample groups with or without the use of correction methods for type I (false positive) or type II (false negative) errors. Multivariate approaches can be divided into unsupervised methods, like PCA or HCA, and supervised methods, like PLS-DA, O-PLS-DA, and SVMs. While unsupervised methods are frequently used to gain a rapid overview of group classification, supervised methods are used to identify the metabolites that make the greatest contribution to variance among sample groups (e.g., loadings). The O-PLS-DA method further emphasizes the contribution of the variable of interest while separating it from uncorrelated variables (orthogonal components). Performance of the models is usually assessed by receiver operating characteristics curves, where an area under the curve value greater than 0.7 indicates a good predictive model.

Pathway analysis and network integration are other essential steps in interpreting metabolomics data. Their integration in systems biology or systems toxicology is discussed in section "**Network-based modeling approaches for systems biology**."

2.18.2.4.5 Special considerations and outlook

Analytical approaches covering a huge number of metabolites have been available for biological research since the early 1970s. However, metabolomics is still seen as an emerging technique with much room for further development. Unlike other -omes, the metabolome is not composed of multiple combinations of a limited number of building blocks (like amino acids), which simplifies analytical approaches, but in fact the huge chemical diversity of the metabolome complicates analytical strategies. The components of the metabolome have an extensive range of physicochemical properties, huge ranges in concentrations, and limited stability. The metabolic profile of a biological system requires the investigation of kinetics because of its highly dynamic nature. Metabolites are often involved in multiple pathways (influenced by feedback regulation) and can serve as substrates, intermediates, and products, which complicates the interpretation of observed results. Additional analyses (e.g., mass flux balance analysis supported by advanced mathematical models and high-performance computing) may be required to interpret metabolomic data. Biological variances cause similar difficulties to those inherent to other -omics technologies. Depending on the types of biological samples and focus of the research, huge sample numbers must be analyzed to obtain significant results.

Although there are many obstacles, there is a rapidly growing metabolomics community that is facing the huge challenges in metabolomics studies. There is also continuously growing interest from academia, industry, and government to drive technological development. Developments in instrumentation such as high-performance accurate mass spectrometers, rapidly growing coverage of the metabolome and its mass spectra in databases, and improvements to in silico fragmentation algorithms are key factors for improving the quality of metabolomics research. The availability of reference compounds for confirmation or quantitative purposes has been improved by complementing classical organic synthesis with genetic engineering. The integration of metabolomics with the other -omics techniques is leading to a holistic and rapidly evolving systems biology approach.

2.18.3 Network-Based Modeling Approaches for Systems Biology

In previous sections, we discussed the numerous high-throughput technologies to measure the contents of various molecular species (transcripts, proteins, or metabolites) in biological samples. These technologies have provided large amounts of data, which have fueled the iterative discovery cycle underlying systems biology (**Fig. 4A**). That is, experimental data are fed into computational models that are then explored to extract hypotheses to be tested in new experiments. These experiments then provide new data to restart the discovery cycle.[212] These iterative processes naturally bring us to this section's topic, which deals with quantitative modeling approaches and how to integrate systems-wide data into an interpretable biological context. As a note to the reader, we will not cover the "standard" computational biology approaches involving statistical models that are used to detect significant abundance changes at molecular levels,[213] nor will we discuss the interpretation of their results in terms of predefined lists of protein-coding genes.[214] Instead, we focus on approaches that use network models to capture the complexity of biological systems and their behaviors under different conditions.[215] Networks explicitly encode the interactions among relevant molecular entities. Such interactions have turned out to be the key for understanding the variety of observed phenotypes. Indeed, the sequencing of the human genome has revealed a lower number of protein-coding genes than initially expected (approximately 20,000), and has highlighted the importance of other mechanisms for generating biological diversity.[216] Together with alternative splicing and posttranslational modifications, the ability to precisely regulate the expression of the protein-coding genes is the most relevant of these mechanisms. This regulation of expression levels mainly results from the interactions among genes themselves. This fact provides the ideal starting point for the network-based modeling approaches used in systems biology.

In this section, we first describe how typical network models are constructed either by mining the scientific literature or by using molecular expression data. Then, we describe two examples of network-based methodologies that address concrete biomedical problems using a systems biology approach.

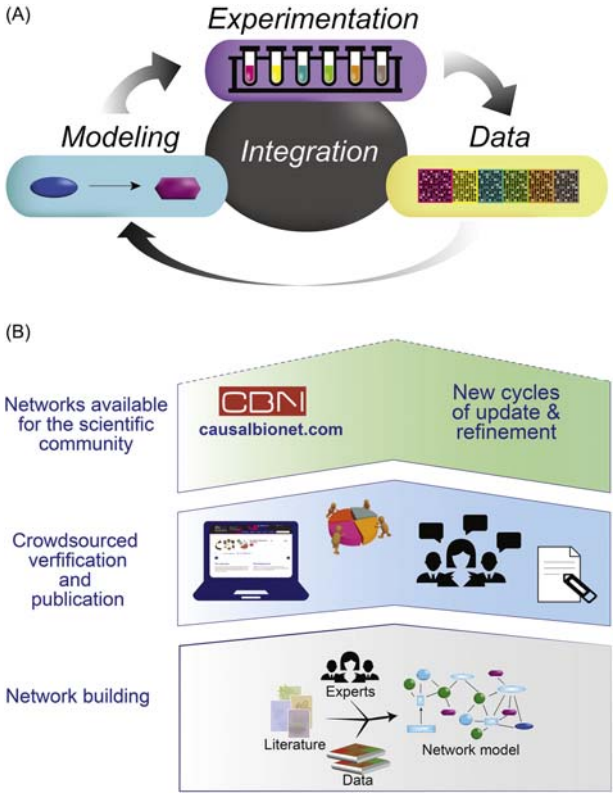

Fig. 4 Network models for systems biology. (A) Discovery cycle in Systems Biology: high-throughput -omics data provide untargeted comprehensive information about the system, enabling exploration of many different aspects using quantitative modeling. This can lead to novel hypotheses to be experimentally tested. (B) Flowchart for assembling and maintaining causal network models: to ensure their scientific acceptability, multiple steps are necessary to preserve their quality and objectivity, especially when some of the mechanisms are still incompletely understood.

2.18.3.1 Literature-Driven Network Model Building

The scientific literature contains much information about gene interactions, and modern search tools allow researchers to efficiently retrieve specific pieces of information. However, to achieve a satisfactory systems biology-based description of a given biological process, large-scale mining of hundreds of scientific articles is required. The results usually consist of a collection of pathways or networks that bring together genes involved in similar biological functions. Typical examples of such collections are the KEGG database or the WikiPathways resource.[204,217] The main advantage of literature-based network models is the quality of their content, as their assembly involves human curation and uses reliable "raw" material. Their main disadvantage is that they do not include all ~20,000 protein-coding genes, since the coverage of the genes is far from uniform and literature-mining efforts must be selective to be efficient. In the context of the aforementioned iterative discovery cycle underlying systems biology, the main application of these network models is to enable the interpretation and the integration of systems-wide -omics data.

In the following section, we focus on a specific type of literature-based network model that will appear several times later in this article: the causal network model. Essentially, causal network models represent more refined and more comprehensive versions of the familiar biological pathway models (e.g., describing the regulation of proliferation by kinase signaling) that makes them more suitable for computational analyses.

For clarity, we restrict the discussion to a "steady state" modeling approach, where time dependence is deliberately ignored. Although this might appear to be an oversimplification, this approach works well when using these networks with experimental -omics data. This is because -omics data are generated by merging the molecular content of millions of cells, and thus, represent a temporal average over the fastest time scales of the system. In other words, the experimental -omics data effectively measure a "quasi-steady state." A dedicated discussion of time-dependent modeling is given in section "Mathematical Models for Network Biology."

The specificity of causal network models is then given by both:

1. the nodes, which are quantifiable biological entities such as protein abundances, transcript levels, protein phosphorylation sites, and protein activities.
2. the edges, which describe direct and signed cause-and-effect relationships supported by evidence in the literature, for example, activity of a transcription factor increases abundance of its regulated transcripts and activity of a kinase increases the phosphorylation of its targets.

It is also important to note that "causal" does not necessarily mean "direct" in a physicochemical sense. A causal relationship can also be indirect and, if supported by the literature, it can be included in causal network models. The main feature of the causal network models discussed here is that they are genuinely mechanistic. That is, their nodes correspond to biological functions or activities at molecular or cellular levels, and they are not limited to transcript levels or protein abundance, like other network types used in systems biology.

Another important feature is the semantics of their node and edge labels, which is based, in our case, on the Biological Expression Language (BEL), a programming language that allows for a flexible representation of biological processes in a computable format (http://www.openbel.org/). The BEL statements are extracted from the Selventa Knowledgebase (http://selventa.com), which stores the results of mining of selected scientific literature and the contents of public and proprietary databases. This knowledgebase contains 1.5 million nodes (biological concepts and entities) and more than 7.5 million edges (connections between nodes). The knowledgebase must be licensed, like similar sources of curated biological knowledge that require extensive mining of the scientific literature (e.g., Biobase and Ingenuity Pathway Analysis[218]). However, the openBEL portal contains an increasing amount of publically available material extracted from the Selventa Knowledgebase, such as the "BEL Large Corpus" (http://www.openbel.org/).

The design and assembly of causal network models have been an iterative multistep process complemented by a crowdsourcing initiative (**Fig. 4B**). The biological boundaries of each network were first defined by a team of discipline-specific experts, who were guided by a literature survey of the relevant signaling pathways related to the process of interest. The BEL-encoded causal relationships that described the pathways covered by the biological boundaries of the network were extracted from the Selventa Knowledgebase. These relationships were assembled to populate the "literature network model" with causal relationships within the boundaries of tissue context and biological mechanisms. The content of the literature network model was augmented by a data-driven step based on relevant context-specific transcriptomics datasets available from public data repositories.[219] For this purpose, discipline-specific scientific experts conducted a terminal manual review, thus refining the content and connectivity of the integrated network model. The resulting causal network model was then submitted to a peer-reviewed open-access publication, where reviewers helped to improve the quality of its content.[220] A further curation step took place in the framework of the Network Verification Challenge of the Systems Biology Verification project (SBVImprover).[221] This challenge was based on an innovative crowdsourcing approach where a large community (>50) of contributors were allowed to vote on various edges and nodes of the networks via a dedicated web interface. A "moderator" supervised the votes for each model and, together with a panel of experts, made decisions to include or exclude node and edges based on the community's choices.

The design and assembly process described earlier has been repeated for approximately 50 networks, each of them first defined by its biological boundaries. The purpose of these definitions was not only to match the high-level biological functions described by the single network, but also to cover globally the essential biological processes and responses of healthy lung tissues.[220] As a result, a hierarchical organization was chosen with five main network families on the top—each with a subset of the approximately 50 causal network models: cell proliferation,[222] cellular stress,[223] cell fate,[224] pulmonary inflammation,[225] and tissue repair and angiogenesis.[226]

Systems biology, and network approaches in particular, exploits large amounts of biological knowledge to accurately interpret the results of -omics analyses. Biological curation, "biocuration," aims to harness and preserve biological insights in databases in a format that can be used in computational approaches. It organizes biological information into well-annotated, computable statements that can be visualized as a model describing certain area of biology.[227] Since manual curation can be extremely labor- and time-intensive, computational approaches are being developed to extract causal relationships from the scientific literature. One such workflow combines text mining with expert reviews by scientists for accurate and easy conversion of scientific text into a computable form.[228]

2.18.3.2 Data-Driven Interaction Network Inference

While "literature-driven network model building" can yield high-quality representations of the known biology, it is labor intensive and limited by the availability of relevant publications. Fortunately, with the advance of omics technologies, increasing amounts of data are available in clearly defined and specific experimental contexts. This has attracted the interest of the systems biology community, and many approaches have been developed to reconstruct networks from the available data, a process known as "reverse engineering of networks."

2.18.3.2.1 The goal of network inference

These network inference approaches start with a given set of molecular entities (nodes, say $X_1,\ldots,X_n$), which, for example, can be genes, proteins, or metabolites. Data involving these molecular entities are available and the goal is now to effectively leverage these data to infer the connections between those entities (**Fig. 5A** and **C**).

Several types of interaction networks are commonly studied: gene networks (or gene regulatory networks) are representations of gene–gene regulation; protein functional networks describe the interplay of proteins or protein activities[229]; while PPI networks describe physical interactions between proteins that form complexes.[230] Experimental techniques can provide information on network structures (chip-on-chip data for transcription factors, Y2H,[231] or affinity purification/MS for PPI networks)[232] (see Methods section). However, these methods are labor intensive and costly, can produce false positives and false negatives, and do not necessarily reveal the functional relevance of the detected interactions. Thus, even with these experimental data available

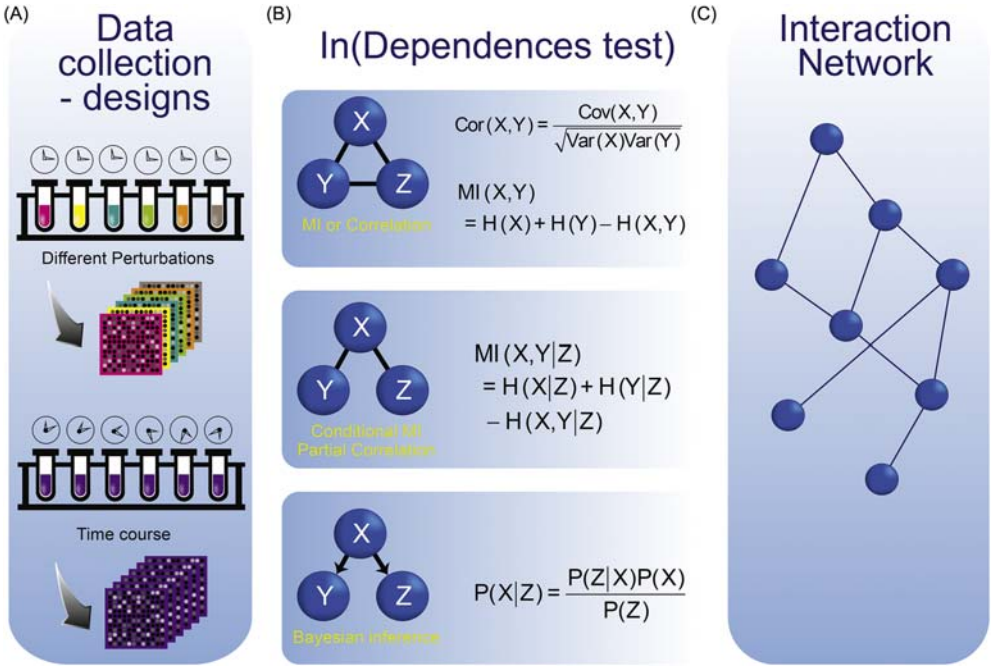

Fig. 5 High-level description of the interaction network inference problem. (A) Experimental data are gathered following a specific experimental design. (B) Method and statistical measure of interaction between the measured molecules are selected depending on the scope and goal of (C) the network model.

(as structural network templates), data-driven network reconstruction is still necessary to complement the results and to extract functionally relevant models that predict relevant biological phenotypes.

The use of these in silico methods for inferring interaction networks based on omics data, such as transcriptomics or proteomics, has grown rapidly. The development of algorithms to address this challenging task has been at the heart of the Dialogue for Reverse Engineering Assessment and Method (DREAM) challenges (http://dreamchallenges.org).[233] In these challenges, the participants were asked to reconstruct a genome-scale regulatory network from a large collection of microarray data sets to predict a PPI network of 47 proteins and predict the genes for transcription factor binding (DREAM2); infer a signaling network from flow cytometry data (DREAM 3); infer simulated gene regulation networks and predict gene expression measurements (DREAM 4); and infer simulated and in vivo gene regulation networks (DREAM5). More recently, the participants were asked to predict outcomes of perturbations in systems biology models after being given the complete and incomplete structures of the model for a gene regulatory network (DREAM7).[233–237]

2.18.3.2.2 Experimental data

The choice of a computational method depends not only on the scope of the biology to capture (e.g., genome-wide vs. biological process specific), but also on the experimental design underlying the collected omics data (**Fig. 5A**). Longitudinal (time-series) data require the algorithm to be tailored toward dynamic responses and can leverage differential equations describing the (bio-) chemical reactions occurring over time. Perturbation or gene silencing data are also appropriate for inferring networks (http://dreamchallenges.org/).[233] Factorial designs can be leveraged to infer networks.[238] Finally, large compendiums of data have been used[239] to infer genome-wide networks related to a specific tissue or disease.

2.18.3.2.3 Inferring edges using pairwise measures

Independent of the type of data at hand, different computational approaches may lead to very different interpretations of the resulting network (**Fig. 5B**)—for example, as discussed here for "relevance networks," "Markov networks," and "Bayesian networks."

Relevance networks, for example, rely only on the correlation structure (or the mutual information, MI) between the molecular entities: an edge between a pair of entities $\{X_i, X_j\}$ (e.g., two genes) is defined, if these show statistically significant correlation in the data. For longitudinal data additional computing steps (e.g., dynamic correlation[240]) are used to account for the time-dependent nature of the data, or time-delayed gene regulation can be inferred based on cross-correlation and network deconvolution.[241] While these approaches are straightforward and applicable at a large scale, the resulting networks cannot describe causalities.[242] Indeed, if (gene) A regulates both (genes) B and C, but B and C do not interact with each other (**Fig. 5B**, bottom), then it is likely that all the edges among A, B, and C will appear in the (correlation-based) relevance network (**Fig. 5B**, top). Consequently, relevance networks capture community structures between genes but cannot unravel the true nature of the underlying causal mechanisms. The solution

to this problem relies on the concept of conditional independence between molecular entities leading, for example, to Markov[243] or Bayesian networks.[244]

For Markov networks, which are undirected networks (Fig. 5B, middle), the key quantity considered for each interaction is the conditional MI: $MI(X_i, X_j|X_1,\ldots X_{i-1},X_{i+1},\ldots,X_{j-1},X_{j+1},\ldots X_n)$.[245] The MI is an information theory measure for the dependence of two random variables and the conditional MI is 0 if and only if X_i and X_j are independent conditional on all the other variables. Therefore, we could theoretically infer a network structure where an edge is present whenever the above quantity is significantly nonzero. Unfortunately, testing conditional independence usually requires too much data and is computationally intractable. However, when the variables X_i are assumed to be multivariate Gaussian, the conditional MI is equivalent to the partial correlation, which is easier to estimate. This approach, called Gaussian graphical modeling, has been successfully applied to small problems (a few dozen nodes). For larger problems, approximation to the full conditional independence can be achieved by considering all the kth order conditional MI: $MI(X_i, X_j|X_s)$, where s is any subset of indices of size k not containing i and j. This strategy is at the heart of the path-consistency algorithm PC,[246] which has been adapted to MI, and was validated in the benchmark gene regulatory networks in the DREAM challenge.[247]

Additional approaches to distinguish direct from indirect interactions have been developed. In the method called Algorithm for the Reconstruction of Accurate Cellular Networks (ARACNE), triangles in the relevance network inferred from MI are further tested using data-processing inequality (DPI).[245] The DPI states that if $X \rightarrow Y \rightarrow Z$ is a Markov chain then $MI(X,Y) \geq MI(X,Z)$. Consequently, the algorithm removes edges with lower MI value. Alternatively, in the so-called Minimum Redundancy Network approach, the principle of maximum relevance/minimum redundancy[248] is used to distinguish direct from indirect interactions.[249] In a nutshell, for each entity of the network X_i, its potential regulators are sequentially ranked according to the score defined as the MI with X_i (maximum relevance) minus the average MI with the other potential regulators (minimum redundancy). An edge is deleted if the minimum of the score obtained when ranking according to X_i, and X_j is below a given threshold.

Bayesian networks have also been used to derive causal interaction networks because they rely on the conditional independence concept (Fig. 5B, bottom). The structure of the network can be inferred by maximizing the full posterior distribution, but this problem is usually intractable even for moderately sized problems. Therefore, sampling methods such as Markov chain Monte Carlo have been proposed, and structure-learning algorithms relying on scores such as Bayesian information criteria have been developed. Bayesian networks can also be used to model time-series data; these are known as dynamic Bayesian networks.[250]

2.18.3.2.4 Algorithms tailored to time-series data

The inference of interaction networks from time-series data (longitudinal design) can benefit from specific model representations and methods. A common approach is to assume that the data are observed from a generative model which is a set ordinary differential equation (ODE) (see e.g., Ref.251). The ODE describes how the system, in its current state and under predefined parameters, changes over time. The simplest way to describe the temporal behavior of a system is to perform a first-order approximation of the dynamic of that system. This involves linear equations of the form:

$$\frac{dX_i}{dt}(t) = a_i + \sum_{j \neq i} b_j^i X_j(t)$$

where the coefficients b_k are nonzero only for the regulators of X_i. Using the fact that data are collected in a time-series $x_i(t_1),\ldots,x_i(t_n)$, the derivatives at t_k are approximated by $X_i(t_{k+1}) - X_i(t_k)/t_{k+1} - t_k$. Finally, $X_i(t_{k+1}) - X_i(t_k)/\ t_{k+1} - t_k$ is regressed against the potential regulators: $a_i + \sum_{j \neq i} b_j^i X_j(t)$. Fitting procedures such as LASSO,[252] elastic net,[253] or any other approach leading to a sparse solution can then be used to discover the regulator set of X_i. The nonzero coefficients serve to build the interaction network by defining an edge (and its sign) between X_i and X_j if the coefficient b_j^i is nonzero (or above a given threshold). For example, the best performer in the DREAM3 challenge used the elastic net as a fitting procedure.[254]

Finally, a network inference method can be a hybrid method, in the sense that it can leverage both data and knowledge from the literature in a supervised manner. For example, SIRENE[255] leverages both transcription factor target knowledge and gene expression data by learning a supervised model—it trains a binary classifier to discriminate between genes known to be regulated and genes known not to be regulated by the transcription factor, based on the expression data. The classifiers associated with the set of transcription factors are then applied to each gene not used during training. The obtained scores are then combined across all different models to rank the candidate transcription factor–gene interactions. In Ref.256, this supervised approach was shown to outperform unsupervised ones such as ARACNE, providing promising results.

In conclusion, reverse engineering of the interactions among molecular species based on experimental data remains a difficult problem. Many challenges remain and as pointed out in the DREAM challenges, the network reconstruction task remains unsolved.[257] Despite this, it is a key approach to understand molecular species as a whole.

2.18.3.3 Scoring of Causal Biological Network Models

Given the systems-wide -omics data and the causal network models discussed earlier in this article, our goal is to integrate these two elements to gain mechanistic insights that enable a systems biology-based interpretation of the underlying experiment. As briefly mentioned at the beginning of this section, computational biology methods allow researchers to quantify changes in abundance at

the molecular level and to test their statistical significance. Analogously, the "network-scoring" approach presented later allows researchers to:

1. quantify changes in activity or "perturbation amplitudes" for network nodes describing molecular mechanisms (not only molecular abundance).
2. quantify network perturbation amplitudes (NPAs) obtained by aggregating the corresponding node-level values to assess changes in the activity of high-level biological function described by the network.

The scoring of causal network models ultimately reduces system complexity by replacing approximately 20,000 protein-coding genes with approximately 2000 nodes distributed in about 50 causal network models (Fig. 6). Such a feature offers a valuable advantage from the point of view of biological understanding, given that the interpretation of molecular-level -omics data requires significant efforts in terms of data processing and integration of existing biological knowledge.[258–260] As discussed in the next section, the scoring of causal network models has opened the door to a variety of applications and opportunities in contexts ranging from individual-based diagnostics to mechanism-based evaluation of toxicants.

In essence, the network-scoring approach is based on the earlier-mentioned NPA concept, which was introduced to assess the biological impact of an exposure to a biologically active substance, and which was expected to be useful in pharmacology or toxicology contexts.[261] At the time of its development, most existing approaches for network-based analyses of -omics data focused on evaluating statistical significance based on *P*-values, which were obtained by testing the distribution of changes in the gene

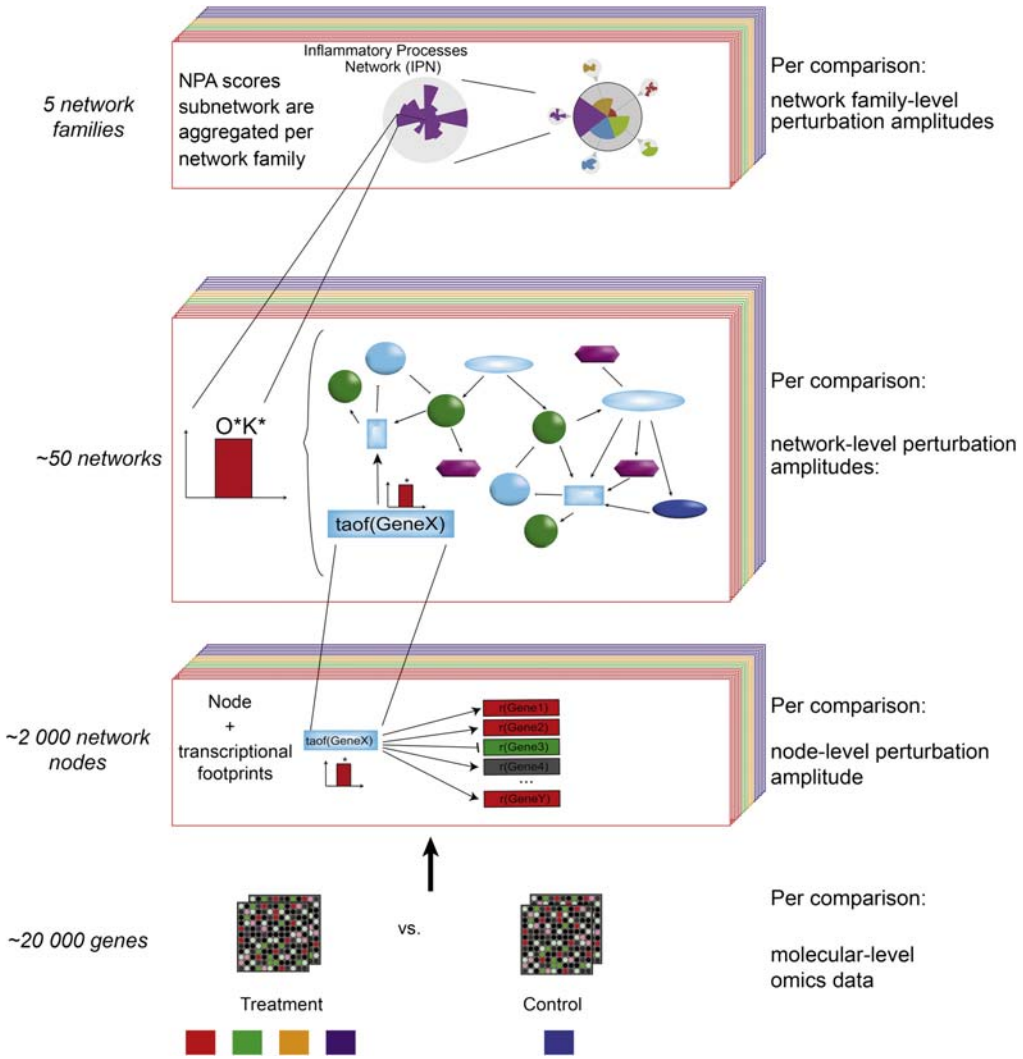

Fig. 6 Schematic representation of the network perturbation amplitude (NPA) methodology. The hierarchical structure of the causal network models (nodes → networks → network families) is completed by the corresponding transcriptional footprints matching the experimental data measuring treatment-induced changes in transcript abundance. Changes in the activities of higher-level network model entities are calculated by the NPA method and allow seamless bottom-up examinations of treatment effects at various levels of mechanistic precision and data complexity.

abundance in the considered network.[262] The main purpose of NPA quantification was to derive an authentic amplitude of the effect, as opposed to a significance *P*-value or an abstract score. This amplitude would be used not only for comparison with other treatments (other doses, exposure durations, etc.), but also for comparison with phenotypic endpoints associated with a network that can be experimentally measured independently of -omics data. This feature would provide the connection between molecular-level -omics data and phenotypic measurements, which fits well with the guidelines of 21st century toxicology, see what follows.[263,264]

From the details described earlier, it became clear that molecular-level -omics data and causal network models are the two main inputs for a network-scoring NPA calculation. The description in the previous subsection "Literature-Based Network Model Building" mentioned the hierarchical organization of the approximately 50 networks. When taken together, these networks cover the essential biological processes and responses of healthy lung tissues (see, e.g., Hoeng et al.[265] and Phillips et al.[266]). To safely apply the NPA method and obtain biologically sound results, careful a priori network selection needs to be done to match the cellular content of the experimental samples that yielded from -omics data. This is particularly true for the pulmonary inflammation network family, which contains many cell-specific networks such as "macrophage signaling" or "mast cell activation."

A further essential aspect of the causal network models is the way they integrate molecular-level -omics data. In the case of transcriptomics, most network nodes can be attached to a set of causal edges ending exclusively in transcript nodes. These end nodes constitute the "transcriptional footprint" of the biological entity described by the common start node of the edges. The biological meaning of a transcriptional footprint is straightforward when the start node describes the activity of a transcription factor protein—detecting changes in the abundance of its regulated transcripts provides indirect information about changes in the activity of the transcription factor itself. This idea can be generalized to any biological activity as long as their transcriptional footprints are available, as it is the case in the Selventa Knowledgebase. Typically, the size of these transcriptional footprints ranges from a lower limit of five to an upper limit of several hundred, depending on the types of methods that were used to experimentally validate the tested causal relationships, and the "depth" of the scientific literature mining used to build the Selventa Knowledgebase. The integration of other types of -omics data is possible in principle, especially proteomics data, as long as causal relationships between the changes in the corresponding molecular entities can be retrieved from the scientific literature. However, it is practically more difficult, because the Selventa Knowledgebase used to build the networks does not yet contain enough causal edges ending with measurable molecular entities that are not transcriptomic.

The actual NPA calculation consists of a series of steps that follow the arrows of the augmented network structure sketched above: from transcriptional footprints (genes) to network nodes to networks to network families (Fig. 6).

- The first step is to calculate the node-level perturbation amplitudes. This is achieved by aggregating the changes in abundance of all the genes contained in the transcriptional footprint of the considered node, multiplied by the sign of the corresponding edge.[267] The result is accompanied by two statistics quantifying (1) its 95% confidence interval, which should not contain 0 to have an effect, and (2) its specificity *P*-value, which is deduced from its comparison with the null distribution of perturbation amplitudes of the same node when assigned randomized transcriptional footprints.
- The second step is to calculate the network-level perturbation amplitudes. This calculation requires more advanced graph-theoretical concepts (e.g., the signed Laplacian matrix of the network). It provides a global score aggregating over the network an edge-based measure of sign coherence between the perturbation amplitudes of the edge start and end nodes.[268] A network-based interpolation procedure is first used to ensure that perturbation amplitudes are defined for all nodes, even those without transcriptional footprints. The result is accompanied by three statistics quantifying (1) its 95% confidence interval, which should not contain 0 to have an effect, (2) its *O*-specificity, which is deduced from its comparison with the null distribution of the perturbation amplitudes obtained for adequately randomized versions of the network transcriptional footprints, and (3) its *K*-specificity, which is deduced from its comparison with the null distribution of the perturbation amplitudes obtained for adequately randomized versions of the network itself.
- The third step is to derive perturbation amplitudes for a network family, which requires that at least two abundance change calculations, or "contrasts," are contained in the transcriptomics dataset. One of them is considered as the "reference" according to the experimental design. The calculation aggregates only the significant perturbation amplitudes of the networks contained in the network family; that is, only those that satisfy the three statistics described earlier (confidence interval, *O*- and *K*-specificities). To make the results comparable across multiple contrasts and possibly network families, normalization to the value of the reference contrast is performed.[265] When there is a large difference in network sizes within one family, additional normalization schemes might be used.[269]

Performed in the order nodes → networks → network families, the three steps provide perturbation amplitude values at three levels of reducing mechanistic complexity (Fig. 6). As the changes in transcript abundance constitute the initial and most complex data, they are suitably positioned at the bottom of the NPA values. When available, the accompanying statistics allow the researcher to prioritize investigations on the entities yielding the strongest signals. Practically, the top-down approach is very appealing for data interpretation and provides a rapid overview of the structure of systems behavior under various treatments by collecting the associated "mechanistic fingerprints."[270] In the "Application" section, several examples of the use of NPA methodology are discussed.

2.18.3.4 Mathematical Models for Network Biology

In sections "Literature-Driven Network Model Building" and "Data-Driven Interaction Network Inference," we discussed the inference of network structures from literature and data, and in section "Scoring of Causal Biological Network Models" we

described how this information can be combined with experimental -omics data to gain mechanistic insights from a systems biology perspective. Although we used causal network models that contain the idea of temporal order, the actual time evolution of the system has never been considered explicitly. This is because -omics data captures the systems in a "quasi-steady state" that is sufficient to reflect the causal relationships contained in the network models. However, in further modeling steps, it makes sense to address the time evolution aspect and to develop a modeling framework in which networks can be used to predict the dynamic behavior of the system based on the interactions between its nodes. The ultimate goal of network reverse engineering is not only to infer the network's structure, but also to model its dynamic behavior by modeling the evolution of every species over time. The laws of enzyme and chemical kinetics must be described in ODE systems with sufficient detail to reproduce time-course experimental data and to predict the network outcome.

2.18.3.4.1 From interaction network to mathematical dynamic model

The models of cellular behavior and phenomena are conveniently represented as schematic diagrams of the interactions among the involved species to describe the reactions of the network. Generally, these interactions correspond to those discussed in section "Scoring of Causal Biological Network Models." However, some fine-tuning is often required during the development of these mathematical models, for example, taking into account the following nonexhaustive list of considerations.

For open systems, arrows without parents and arrows without children are drawn to represent the exchange of material with the outside environment (dashed arrows in Fig. 7A). This is not incompatible with the interaction network described previously—the decision to treat the system as open or closed affects mainly the equation rates, and this decision is made before writing the set of equations.

Inhibition can be represented as arrows from the inhibitor molecule to a reaction between two other molecules (edge starting at "E" in Fig. 7A). This specific aspect is usually not captured when inferring the interaction network as the majority of the algorithms will output a negative edge between "E" and "B," but will usually be unable to distinguish the inhibition of the reactions "A → B" and "F → B" (Fig. 7A).

Not every species in a model can be or has been measured. For example, phosphorylation events might be included in the model but not appear in data-driven interaction networks, or may require the addition of intermediate molecules.

Some reactions are considered instantaneous and related equations can be simplified (also known as the rapid equilibrium assumption) to describe the dynamic on a given time scale.

If all dynamic reactions linked to species A occurs on a fast timescale (compared with those of other species), an algebraic (as opposed to differential) equation may be used to model the system. This situation is called the quasi-steady-state assumption.

The goal of such models is to predict the temporal evolution of the species concentration starting from initial concentrations in a fixed volume via various reaction rates. The reaction rates may depend on the concentration of the reactant and also on the physicochemical conditions (pH, temperature).

Some additional assumptions can be made to make the problem tractable. A typical assumption is that the reactant is homogeneously distributed throughout the volume, in which case the reaction volume is said to be well stirred. This implies that the rates are constant in space.

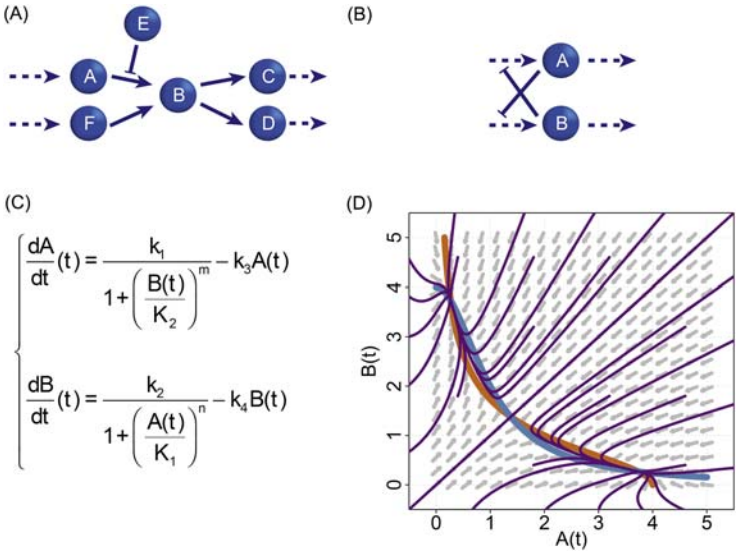

Fig. 7 (A) Typical diagram describing a dynamic network, whereby the production rate of B from A is inhibited by E; (B) a simple system of dual inhibition; (C) ordinary differential equations (ODE) associated with the system in B); (D) flow field (*gray arrows*), trajectories (*purple curves*), and nullclines (*orange curve* for A and *blue curve* for B). Nullcline intersections indicate steady states of the system. For lower k_1 there would be only one steady state (the "low A and high B"); for higher k_1 only the steady state for "high A and low B" would remain.

2.18.3.4.2 Stochastic versus deterministic models

A model is said to be deterministic if its trajectories are reproducible. That is, once the conditions and parameters are set, the behavior is determined unambiguously. In contrast, a stochastic model is a model in which randomness plays a role in determining the output of the system. A well-known example is the Lotka–Volterra prey–predator model where stochastic and deterministic models differ significantly. This typically happens in systems biology either when there are few available molecules (typically in a gene transcription and translation model) or when thermal agitation of individual molecules induces randomness. When many molecules are assumed to be present all the time, the concentrations are considered to vary continuously, as opposed to an integer value of molecule abundance. Deterministic models lead to differential equations while stochastic models rely on the description of continuous time stochastic processes, such as Markov processes described by the master equation.[271] The latter relies on stochastic mass action kinetics, whereby the probability of a reaction occurring is proportional to the probability that the reactants meet. In contrast, (continuous) mass action kinetics assume that the rate of a chemical reaction is proportional to the product of the concentrations of the reactants. Each reactant appears with the power equal to its molecularity in the reaction.

The application of mass action will lead to an ODE system describing the time evolution of the concentration of each species as follows: $\mathrm{d}x/\mathrm{d}t = S\nu(x)$, where S is the stoichiometric matrix of the system. This applies to chemical reactions but also to enzyme kinetics.

2.18.3.4.3 Enzyme kinetics

Enzymatic reactions follow the classical "lock-and-key" model, where the free enzyme E binds to its substrate S to form the enzyme–substrate complex (C1), which is then catalyzed into the enzyme–product complex (C2) from which the free enzyme and product are released: $\mathrm{S}+\mathrm{E} \leftrightarrow \mathrm{C}_1 \leftrightarrow \mathrm{C}_2 \rightarrow \mathrm{P}+\mathrm{E}$. This model represents the vast majority of the reactions that occur in a cell. Enzyme-catalyzed reaction rates can be modeled by Michaelis–Menten kinetics, assuming that:

- the timescale for conversion of the enzyme–substrate complex to the enzyme–product complex is faster than those of other reactions, hence the reaction becomes $\mathrm{S}+\mathrm{E} \leftrightarrow \mathrm{C} \rightarrow \mathrm{P}+\mathrm{E}$.
- the product never binds to the free enzyme.
- the substrate is far more abundant than the enzyme, $\mathrm{S} \gg \mathrm{E}$ (implying that the complex C is in a quasi-steady state). This assumption typically does not hold when modeling PPIs in signaling cascades.
- the total enzyme concentration is constant (conserved moiety) because it is not consumed by the reaction.

Putting all those arguments together and applying the law of mass action, the rate of $\mathrm{S} \rightarrow \mathrm{P}$ is represented as follows: $V_{\max}\mathrm{s}/K_{\mathrm{M}} + \mathrm{s}$.

Enzymatic activity is tightly regulated in the cell by different mechanisms[272] such as competitive inhibition, noncompetitive inhibition, mixed inhibition, allosteric inhibition, and cooperativity. Each of those mechanisms has specific kinetic rates and equations. Table 1 shows some common examples.

2.18.3.4.4 Model parameter fitting

Obviously, understanding each type of reaction in the model is not sufficient to predict its output. One quickly realizes that, even for systems involving only a few reactions, the number of parameters can increase rapidly, leading to serious difficulties. Some of the kinetic constants might be known, some others could be measured in vitro, but generally these constants are unknown to the modeler. A classical approach is to generate time-series data for some of the species involved in the model, for the time scale under study. Then, the parameters are fitted to the experimental output, typically using a maximum likelihood or least-squares formulation. As opposed to a problem that can be solved with simple optimization techniques (e.g., convex problems), this approach leads to nonconvex optimization problems that require advanced optimization solvers. For global optimization methods, the computational cost usually increases exponentially with the number of free parameters. Therefore, advanced global

Table 1 Common types of enzymatic reactions and their associated rates

Name	*Reaction scheme*	*Rate*
No inhibition (Michaelis–Menten)	$\mathrm{S}+\mathrm{E} \leftrightarrow \mathrm{C} \rightarrow \mathrm{P}+\mathrm{E}$	$\nu = V_{\max}\mathrm{S}/\mathrm{S} + K_{\mathrm{m}}$
Competitive inhibition	$\mathrm{S}+\mathrm{E} \leftrightarrow \mathrm{C} \rightarrow \mathrm{P}+\mathrm{E}$ $\mathrm{I}+\mathrm{E} \leftrightarrow \mathrm{C}_{\mathrm{I}}$	$\nu = \frac{V_{\max}\mathrm{S}}{\mathrm{S}+K_{\mathrm{m}}\left(1+\frac{I}{K_{\mathrm{I}}}\right)}$
Allosteric (noncompetitive) inhibition	$\mathrm{S}+\mathrm{E} \leftrightarrow \mathrm{ES} \rightarrow \mathrm{P}+\mathrm{E}$ $\mathrm{I}+\mathrm{E} \leftrightarrow \mathrm{EI}$ $\mathrm{I}+\mathrm{ES} \leftrightarrow \mathrm{ESI}$ $\mathrm{S}+\mathrm{EI} \leftrightarrow \mathrm{ESI}$	$\nu = \frac{V_{\mathrm{m}}\mathrm{S}}{(\mathrm{S}+K_{\mathrm{m}})\left(1+\frac{I}{K_{\mathrm{I}}}\right)}$
Hill cooperativity (X molecule binding to protein P)	$\mathrm{P}+\mathrm{X} \leftrightarrow \mathrm{P}X_1$ $\mathrm{P}X_1+\mathrm{X} \leftrightarrow \mathrm{P}X_2$ $\mathrm{P}X_{n-1}+\mathrm{X} \leftrightarrow \mathrm{P}X_n$	$\nu = X^n/K^n + X^n$

Rates are valid under the same assumptions as those for Michaelis–Menten kinetics.

optimization methods (such as generalized simulated annealing, particle swarm optimization, or genetic algorithms) have to be used. The computational optimization of the parameters in a systems biology model can easily be underdetermined. If some initial guesses are available, then restricting the search space around those values may help avoid over-fitting. In the Biomodel database,[273] the median size of the network model is about a dozen reactions, which highlights the difficulty in estimating all kinetic constants.

2.18.3.4.5 Model simplification: S-systems

A simplified parameters search was proposed by Michael Savageau:[274] all production (respectively, consumption) terms are lumped together into a single power-law as follows:

$$\frac{dx_i}{dt} = \theta_i \prod_j x_j^{\alpha_{ij}} - \mu_i \prod_j x_j^{\beta_{ij}}$$

where the signs of the exponents are positive except for inhibition and the θ and μ values are positive. This dramatically reduces the number of parameters[275] and has led to the development of several parameter-optimization methodologies.[276] Another approach to reduce the number of parameters is to consult the literature to identify key parameters that have been confirmed experimentally.

2.18.3.4.6 Model analysis and validation

Nonlinear dynamic systems show a wide range of behaviors. A global behavior analysis can, however, be overwhelming. Hence, focusing the analysis near a particular operating point is a common approach. An advantage of the local analysis of a system is that it allows for a linear approximation over a small domain. The stability around steady states is analyzed by evaluating the eigenvalues of the Jacobian matrix (containing all the partial derivatives) of that system. Visualization of the phase plane (e.g., with direction fields) and nullclines (i.e., coordinates where time derivatives are 0) can also provide information on the type of dynamic behavior and help detect, for example, limit cycles.

Another important aspect is a sensitivity analysis; that is, how sensitive the solutions or steady state are to changes in different parameters. A sensitivity analysis is usually applied to study local sensitivity, to determine the effect of *small* changes in parameters on the global solution. For example, a change in parameter values can lead to a qualitative change in long-term dynamic behavior (i.e., changes in the number of steady states or their stability). The parameter values at which this happens are known as bifurcation points. Some simple systems exhibit bi-stable behavior, and a bifurcation analysis can show how the system can abruptly change from one basin of attraction to another (i.e., switch its steady state). Despite this apparently complex behavior, even very simple systems can show bi-stabilities.[277] The system described in Ref. 278 (**Fig. 7B** and **C**) is one such example. While the constant k_1 increases (**Fig. 7C**), the system becomes bi-stable as shown by the three intersections of the nullclines (the nullcline for $X_i(t)$ is the solution to $dX_i/dt(t) = 0$ solved for X_j) (**Fig. 7D**). Bi-stability is an essential property of the apoptotic machinery, as the status "alive" must be stable and resistant toward minor accidental trigger signals. Bi-stable behaviors have been proven both experimentally and theoretically to be governed by several signal transduction pathways leading to cell fate decision. A typical example is the bi-stability of receptor-induced apoptosis through the caspase cascade.[279] In Ref. 280, the pathway of caspase activation was shown to be essential for apoptosis induction by various stimuli, including cytotoxic stress. Depending on the context, a caspase is activated either gradually or in a switch-like fashion, and this determines whether caspase activation irreversibly leads to cell apoptosis. By analyzing a quantitative kinetic model, the authors showed that inhibition of Casp3 and Casp9 by apoptosis inhibitors resulted in implicit positive feedback that induced bi-stability.

Last but not least, model validation is of prime importance. A common way to validate a model is to apply it to "hold-out" data, which is a subset of data not used for fitting purposes. The modeler checks the accuracy of the predictions to assess the quality of the model. This procedure can be repeated many times by randomly selecting the "hold-out" data. However, this can lead to over-optimism if not performed properly (see e.g., Ref.281). Another proposed approach is to compare the hold-out data predictions to a completely unsupervised solution.[282]

In conclusion, mathematical models describing the dynamic of biological processes can serve as predictive tools to provide information on various aspects, such as biological robustness, drug efficacy, and response to toxicants.

2.18.3.4.7 Model usage in systems research

PD is the study of the effects of a drug once it reaches the site of action, and toxicodynamics (TD) is the study of the effects of exposure to a toxicant. In PD/TD studies, common concepts are maximum effect (E_{max}), and the dose at which 50% of the maximum effect is reached (EC_{50}). For a drug, the therapeutic index is defined as the relationship between concentrations causing adverse effects and concentrations causing desired effects: EC_{50} (adverse effect)/EC_{50} (desired effect). Consequently, drugs with a high therapeutic index are desirable in practice. For a toxicant, its potency (the dose at which EC_{50} is reached) is the quantity of interest. While this curve can be determined by measuring a biomarker of effect, PD also focuses on ligand–receptor affinities and inhibitions. When there is competitive inhibition, where another ligand "competes" with the primary drug, a higher dose of the drug is needed to obtain the desired effect, while E_{max} can still be achieved. When there is noncompetitive inhibition, E_{max} is lowered by reducing the number of functional receptors and is not reversed by increasing the drug concentration. Enhanced PD (ePD)[283,284] refers to the concept where systems biology mathematical models and PD meet. In this context, the drug target network is modeled taking into account not only enzymatic and metabolic reactions but also epigenetic and genetic factors and

posttranslational characteristics. ePD allows researchers to predict drug responses for individual subjects with different genetic and epigenetic backgrounds.

Similarly, enhanced TD can be defined in the context of toxicology. The ePD model discussed in Iyengar et al. addresses the effect of an EGFR inhibitor (e.g., *gefitinib*®) on tumor growth. The model is a simple linear pathway: the tumor growth response is mediated through SHC1/SOS1/GBR2, KRAS, RAF1, MEK1/2, MAPK1/2 RPS6KA1, JUN, CCND1, CDK4/6, and proliferation. An additional single coherent feed-forward motif from EGFR to Raf kinase inhibitor protein (RKIP) and RAF1 is added. Finally, factors such as an activation mutation in the *EGFR* gene, hyper/hypo-methylation of the *RASAL1* promoter, and/or changes in the microRNA miR-221 (which inhibits CDKN1B, in turn inhibiting CDK4/6) are added. Then, different patient characteristics are used to predict drug efficacy: a patient with a hyper-methylated *RASAL1* gene and no other RKIP changes or miR-221 will be resistant to the therapy. In contrast, a patient with a normal *RASALP1* gene, a single nucleotide polymorphism in the *RKIP/PEPB* gene that produces a hyperactive RKIP (which inhibits RAF1), and a decreased amount of miR-221 is predicted to be highly responsive to the therapy.

When modeling all the relevant regulatory pathways, the initial conditions of the model of drug availability are crucial to make realistic predictions. In this context, ePD intimately relies on the pharmacokinetics (PK) of the drug. PK and physiologically based pharmacokinetics (PBPK)[285] aim to model drug absorption, distribution, metabolism, and excretion principle. PK models help to elucidate a drug's half-life and its distribution in the body. In particular, these models can quantify the drug concentration at its site of action, which is the initial concentration needed in an ePD model. Additional examples on how systems toxicology can be used in these areas are discussed later.

2.18.4 Systems Biology Applications

Systems biology is a powerful tool to generate hypotheses, and provides an unbiased approach to identify the components responsible for biological phenomena. High-throughput technologies are used to identify groups of molecules that are regulated similarly and that may not have been linked to the biological phenomenon previously (Fig. 8A). The network approach described earlier allows researchers to trace the network perturbation back to the individual components responsible for the observed impact and, similar to gene sets and pathways, identify known and novel mechanisms of perturbation. Importantly, this approach can draw special attention to single molecules that do not belong to any specific or known biological pathway. This allows researchers to design targeted experiments to further verify and extend the insights obtained using high-throughput approaches. Such findings can be further corroborated by research groups with long-standing expertise in investigating specific molecules and pathways identified (or not) by systems biology approaches. Likewise, network approaches can be used to unravel novel interactions among known molecular pathways, thus expanding the knowledge on how a cell or tissue functions as a whole. By profiling the molecular response when a key element is disrupted in a relevant experimental system, the network around the molecule of interest can be expanded (Fig. 8B). Undoubtedly, basic research as we know it has been, and will continue to be, revolutionized by systems biology.

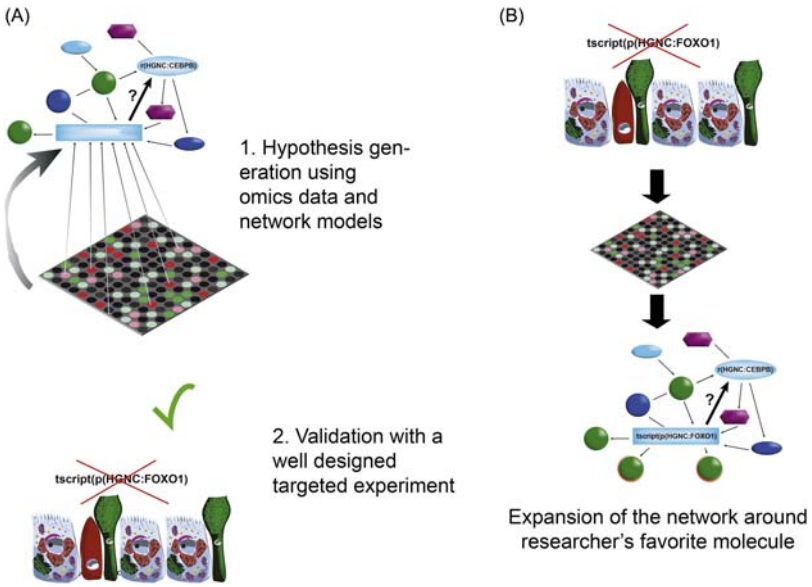

Fig. 8 Systems biology in basic research. (A) Systems biology is a powerful tool for hypothesis generation and (B) the identification of novel molecular networks.

2.18.4.1 Systems Pharmacology

2.18.4.1.1 Target identification

Systems biology approaches can be leveraged for drug development, and are then referred to as systems pharmacology. During the early stages of drug development, chemo-informatics has been commonly used for target prediction by grouping drugs based on their chemical structure,[286] and to predict off-target effects (and to identify additional targets). According to the classical view, drugs usually interact not only with their intended target but also with other molecules, "off-targets," causing potential side effects.[287,288] Moreover, while intended drug-induced effects are by definition localized, adverse, and/or off-target effects can be either local or systemic.

Consequently, systems pharmacology considers the system as a whole to predict not only how a drug may interact with its targets, but also how the drug target interacts with its network as well as how gene variants may alter the system's response to the drug.[289] Frequently used methods include chemical compound, protein structure, PPI, signaling, gene interaction, and metabolic network approaches.[290] Although networks built using a priori knowledge cover genome-scale biological detail, they usually do not cover dose- and time-dependent responses. Kinetic models, on the other hand, can rank drug targets based on their quantitative effects and simulate a drug's mode of action, even though they encompass more limited biology.[291] Moreover, even if a network can accurately predict the response to a given drug, the network is assumed to adapt when drug targets change as the network adapts.[291] A typical example is the multidrug resistance that results when a drug is transported out of the target cell.[292]

2.18.4.1.2 Adverse drug reactions

Even with well-defined targets and off-targets, some drugs can have unwanted effects or cause adverse drug reactions (ADRs). Many models have been developed to elucidate and predict adverse drug effects. For example, drugs can be grouped based on their clinical side effects,[293] and the use of different data sets and analyses of multiple side effects has been shown to improve this approach.[294] Modeling of the physiochemical characteristics of the drug with the target protein network can help connect targets and side effects by the drugs they share.[295] The topological properties of PPI networks for ADR-related proteins can predict the involvement of proteins in modulating ADRs.[296] Finally, multilevel process drug side-effect networks combine drug side effects with drug-biological process networks[297] or drug targets with drug side-effect relations.[298]

Demonstrating the power of the network approach, Zhao and colleagues derived a global concordance score and predicted biological fingerprints for 726 drugs approved by the Food and Drug Administration (FDA) based on correlations observed in pharmacological and genomic spaces.[299] Possibly the most powerful predictions are the approaches that integrate multiple similarity measures from various data types, including chemical, biological, phenotypic, and therapeutic.[300–302]

ADRs can also occur when individual characteristics disrupt the mechanism of action of a drug. Many different data types (microbiome, metabolome, lifestyle, nutrition, and genome, including transcriptome and proteome) need to be considered to fully appreciate the likelihood of an adverse effect. Integrated analyses of these data allow researchers to predict an individual's risk of an adverse response to a given drug, allowing certain at-risk individuals to be excluded from clinical trials and/or drug treatments.[286] This provides the foundation for systems pharmacology-based predictions of drug safety.

2.18.4.2 Systems Toxicology

Similar to pharmacology, the field of toxicology is progressively being "systemized." The 21st century toxicity paradigm initiated this change by recommending the inclusion of PK/PD modeling, omics data, and high-throughput technologies to assess the toxicity of potentially harmful compounds.[264] In its simplest form, the combination of high-throughput molecular profiling and computational approaches can derive signatures that describe similar behaviors of molecular species, and pathways that were not previously linked to these species. Now, -omics signatures can be viewed on their own as biomarkers of an exposure response (e.g., to cigarette smoke), as well as markers of effects of interactions between an individual's genetic background and exposure levels.[303,304] Molecular profiling can also help identify the mode of action of compounds whose health impacts are poorly understood.

Equally relevant in the context of toxicological assessment is the concept of the exposome. It refers to all of the exposures a human faces during his or her lifetime, and encompasses both external exposures to chemicals in the environment as well as internal conditions that are defined by the unique characteristics of the individual. While it will be difficult to cover all exposures simultaneously, even limited insights into the exposome will benefit the management of human well-being.[305] In particular, the serum exposome studied in the exposome-wide-association study provided the means to identify and validate markers of exposure and to distinguish between disease markers and simple exposure markers.[306] High-resolution metabolomics has been used for high-throughput relative quantification of thousands of chemicals and metabolites that activate biological pathways.[307] A more detailed review is provided in Ref.308.

The "Human Toxome" project (http://humantoxome.com/) aspires to identify pathways of toxicity by using untargeted methods instead of existing pathway knowledge. The approach is based on two types of -omics technologies: (i) transcriptomics, which is considered as a mature technology; and (ii) metabolomics, which probably best reflects actual phenotypic changes. The project seeks to establish the reproducibility of results obtained at different sites and using different technologies.[309] In the endocrine disruptor project, two independent laboratories produced high-throughput data from a breast cancer cell line treated with known endocrine disruptors. These data will be used to infer pathways of toxicity.[310] For this purpose, the consortium running the project

developed a range of bioinformatics methods to analyze the transcriptional events induced by estradiol treatment. These include the clustering of genes based on the topology of a weighted correlation network[311] as well as a new sensitive gene-enrichment method that creates a gene list ordered by expression values (as opposed to differential gene expression).[312]

Beyond toxicity pathways and molecular signatures or pathway analyses, systems toxicology combines large-scale molecular measurements with classical toxicology endpoints across multiple levels of biological organization.[6] High-throughput technologies have been used in toxicity assessments to compare the impact of tobacco products administered in vivo via the inhalation route[266,313] and in vitro.[314,315] These studies combined the traditional toxicity/disease endpoints with extensive molecular measurements. The causal biological network models described earlier were scored with transcriptomics data for quantitative impact assessment, combined with either proteomics and lipidomics analyses[266,313] or high-content-screening-based assays.[314,315] The following subsection includes another example of how systems biology can be applied to toxicological assessment.

2.18.4.2.1 Systems toxicology use case: assessment of nutraceuticals

The old saying "we are what we eat" emphasizes that dietary habits affect human health. Excessive consumption of salt, refined sugars, or saturated fats is known to increase the risk of cardiovascular and neurodegenerative diseases, as well as different types of cancer. Conversely, a higher dietary intake of fish, fruits, and vegetables seems to protect against these diseases.[316–318] Over the last two decades, several food components have been proposed to be responsible for the health benefits associated with certain dietary habits. Collectively known as nutraceuticals, these food constituents comprise multiple types of chemicals, such as polyunsaturated fatty acids (i.e., omega-3), polyphenols, isoflavones, carotenoids, and many more. Nutraceuticals have a wide range of biological effects including antioxidant, antiinflammatory, and antiproliferative properties.[319–324] Although most of these effects have been observed only in vitro, these studies suggested that nutraceuticals could protect against cancer and other diseases. However, current clinical and epidemiological data does not support these health claims.[319,321]

The apparent discrepancies between in vitro and epidemiological studies can be explained, at least partly, by some of the intrinsic characteristics of nutraceuticals. First, they have generally low-to-moderate biological activity at typical dietary doses. As a result, any potential effect could only be observed after long-term consumption. Also, they often result in a subtle (although highly desirable) beneficial effect not easily detectable in short-term clinical studies. Second, the systemic bioavailability of nutraceuticals is generally low. Thus, it is unlikely that they will reach target organs and tissues at pharmacologically relevant concentrations unless the level of exposure is very high. This is in contrast to pharmaceutical drugs, which are designed to reach target organs and exert an effect in much smaller timescales and at lower concentrations. Third, it is likely that any beneficial effect associated with a particular dietary habit results from the combined action of multiple bioactive constituents. Furthermore, other parameters (i.e., smoking status, body mass index, and age) can modulate the effects of nutraceuticals. Therefore, it is very challenging to detect the biological effects of a single constituent, even if the experimental design is adequate.[321,325,326]

Despite the lack of robust scientific evidence, nutraceuticals are generally perceived as beneficial and are widely consumed as dietary supplements at much higher doses than those naturally present in food. This, however, raises toxicological concerns. Nutraceuticals are considered as safe at dietary doses and no adverse effects are observed in standard toxicity assays. However, the consumption of supplements can result in much higher levels of exposure. Moreover, studies have shown that some of their effects are due to transcriptional and epigenetic regulation of gene expression.[327–329] These genomic effects can occur at relatively low concentrations,[329] and their potential consequences may not be detected easily in traditional toxicity assays.

Recently, we used a combination of gene expression data and high-content imaging-based endpoints to investigate the biological effects of a selected group of nutraceuticals in two in vitro cellular models: human primary endothelial cells and cryopreserved hepatocytes.[314] All of the tested compounds showed cytotoxicity in the different cell types, although the effects were observed only at doses well above dietary levels. However, we also observed significant gene expression changes in pathways regulating cell and oxidative stress responses at considerably lower doses. These effects were consistent with previous reports that nutraceuticals at high doses have a pro-oxidant effect.[330,331] Moreover, this study clearly showed how systems toxicology approaches can be useful for the toxicological assessment of nutraceuticals.

2.18.4.3 Systems Medicine: Diagnostics

By definition, a diagnostic biomarker objectively classifies subjects into groups based on phenotype, such as healthy versus sick, or early versus late stage of disease. Since the genetic makeup of an individual cannot fully explain and predict phenotypes, and since single-gene disorders are rare, measurement of individual markers has limited value in modern diagnostics. Systems biology acknowledges that disease represents the disturbance of many biological networks, and is not due to the erratic behavior of a single molecule.

As in toxicology, molecular signatures derived from high-throughput technologies can be used to classify subject groups. Such examples include genetic and epigenetic alterations,[332,333] gene expression changes (including miRNA profiles),[334] as well as proteomic and metabolic changes[335] that can be linked to phenotypes. Although molecular signatures are useful for diagnostic purposes, they are usually only correlative, and cannot provide deep insights into the complex biology underlying a disease.

Instead of considering single molecules as biomarkers, network models that consist of causal molecular interactions representing cellular processes based on prior knowledge provide static and mechanistic views of the disease state. A comprehensive network-based human disease model views the phenotype as the consequence of genetic and environmental perturbations causing specific PPIs that are linked to genome, epigenome, transcriptome, proteome, and metabolome.[336] Dynamic network biomarkers can be used to follow the disease over time and to separate the disease into different stages.[336]

Metabolomics is one of the promising technologies in cancer research[337,338] for early detection and diagnosis,[339] to search for biomarkers and altered metabolic pathways—for example, the tendency of cancer cells to rely on glycolysis and lactic acid generation rather than on full oxidation through oxidative phosphorylation (Warburg effect)—and to evaluate the efficacy of cancer treatments. Another important application is screening of newborns for inborn metabolic disorders[340–342] (e.g., fatty acid oxidation defects, organic acidemia, amino acid metabolism, and urea cycle defects), which can lead to the development of new diagnostic tests. Lipidomics techniques have been established to detect and monitor the development of cardiovascular disease,[343–345] diabetes,[346,347] inflammatory diseases,[348,349] Alzheimer's disease,[350,351] and many cancers.[352,353]

2.18.4.3.1 Personalized medicine

The contribution of systems biology to personalized medicine is undeniable. Network approaches, in particular, may provide a more elegant way to stratify subjects and explain different responses to individual drugs, and to identify the best combination of drugs to treat each patient[280] by comparisons with molecular signatures. When the key players are more or less known for a disease or treatment effect, it may make more sense to build more focused, signaling-pathway-specific network models, rather than models that encompass large biological processes (as described in section "**Systems Biology Applications**") to elucidate treatment failures in response to specific drugs. Such an approach was tested using a public dataset from patients suffering from ulcerative colitis who did not respond to anti-tumor necrosis factor (anti-TNF) treatment. Transcriptomics data from the affected tissue analyzed in the context of a network model containing three signaling pathways leading to NFκB activation, TNF-IL1α-TLR-NFκB model, allowed the identification of crucial biology to distinguish responders from nonresponders, but did not explain the treatment outcome, and others that could predict as well as explain the treatment outcome. The analysis suggested that MYD88 and TLR family members might be more important than TNF signaling to distinguish the nonresponders from the responders.[268] Without any knowledge on the genomic makeup, the approach could help in stratifying subjects and predict treatment outcomes.

It makes sense to build biomarkers and diagnostic predictors using multiple levels of data.[354] Subject stratification using multi-omics data may be the only way to manage complex diseases,[355] as proposed in the molecular-data-first approach for autism.[356] The establishment of integrative personal -omics profiles is important to ensure timely patient diagnosis, to provide personalized therapy to those who need it and will respond to it, and to follow therapeutic responses.[357–359] This new era in medicine centers around the term "Predictive, Personalized, Preventive, and Participatory (P4) medicine,"[232] which is the true medical application of systems biology[360] (**Fig. 9**). Under the P4 approach, concepts such as "biomedicalization," "quaternary prevention," "holistic medicalization," and "technoscientific transformations of health" are becoming increasingly popular. They all refer to the integration of biology, medicine, technology, and computation.[360] In his review on P4 medicine, Leroy Hood predicted that, "In 10 years each individual will be surrounded by a virtual cloud of billions of data points…"[361] Powerful, systems-based candidate biomarkers

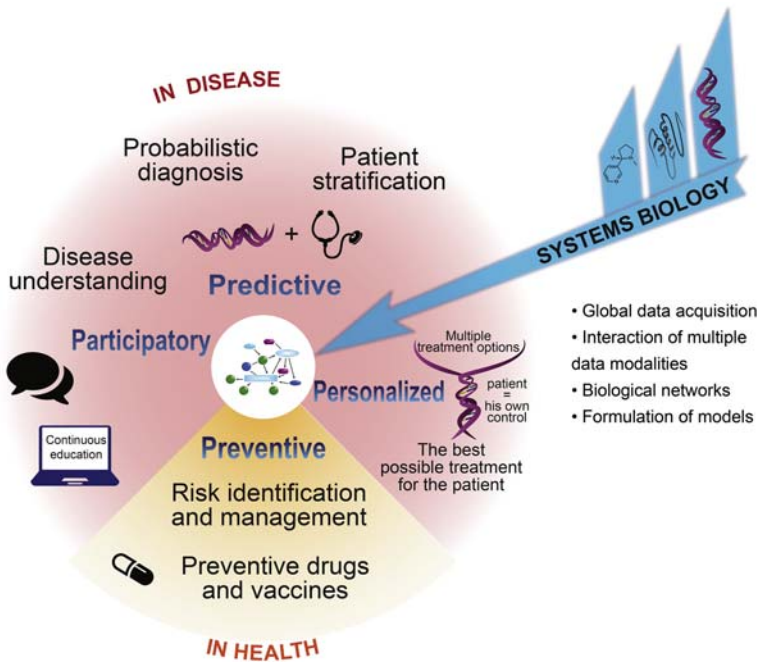

Fig. 9 Systems biology can serve many areas of P4 medicine that uses integrated personal -omics profiling to prevent disease as well as predict disease outcomes and treatment response.

for diagnostics and patient care should be verified and validated using hundreds of samples to ensure reproducibility, specificity, and sensitivity until they are sufficient to replace existing clinical tests.[332]

2.18.4.3.2 Translational systems biology

Translational medicine aims to convert information gained from basic research into human applications.[362] With a systems approach, this can be accelerated by combining insights gained from clinical trials and laboratory experiments using simplified systems.[363] Introducing higher-level biology using network biology may be a more reliable way to translate findings in preclinical systems to humans, compared with single-molecule measurements. Computational network models can be used to align preclinical in vitro and clinical findings. This approach has been demonstrated for the xenobiotic response to cigarette smoke exposure in organotypic tissue culture systems and human subjects.[364] A quantitative systems-level approach showed that the correlations of the transcriptomic response using the xenobiotic metabolism network model allowed for a robust comparison of datasets generated from in vivo samples and in vitro organotypic models. Quantification of the response in different model systems is accompanied by mechanistic insights when a network is analyzed at the level of key contributors.[364] This is relevant for translational research and could possibly be used to estimate effective doses in in vivo and in vitro systems.

Molecular profiling and detailed clinical measurements of subjects undergoing drug treatments can identify elements that are part of the same functional network. These elements can then be further investigated in simple well-controlled experimental systems to extract mechanistic features that explain the clinical symptoms. This involves systematic interference with the biological system and comparison of the unperturbed and perturbed states. The differences are considered as the in vivo functional network, the components of which can be investigated in controlled settings using in vivo, ex vivo, and in vitro approaches.[365]

The ultimate goal of translational medicine is to revisit clinical practice for more efficient patient diagnosis and better care.

2.18.4.4 Cross-Species Translation

In vivo rodent models are valuable tools to mimic human diseases and responses to treatments.[366] However, there can be substantial difficulties in translating research findings across species, and sometimes correlations are less than adequate.[367] Excluding poorly conducted large animal studies,[368] poor translatability can be due to discrepancies between human and mouse orthologous genes,[369] the failure to translate gene orthologues to biological function,[369] divergence in tissue-specific gene regulation among species,[370] and/or large differences in overall physiology.[371]

Using cultured human and rat airway cells, the species translation challenge conducted by the sbvIMPROVER Project[372] sets out to understand the limits of species-to-species translatability. The results showed that, at the cellular level, computational methods can be used to translate some specific stimuli and biological processes between rat and human based on phosphoproteomics, transcriptomics, and cytokine data.[373,374]

Future effective and robust species translation approaches will likely depend on a detailed mechanistic understanding of biological processes and how their components and parameters differ among species. The PBPK models (section "**Mathematical Models for Network Biology**") are designed to capture the adsorption, distribution, metabolism, and excretion of drugs in deep mechanistic detail—including, for example, drug-specific permeability coefficients and metabolic kinetic rates.[375] Several authors have argued that these mechanistic models are especially well suited for cross-species translation.[376–379] Some species-specific parameters can be replaced directly (e.g., blood flows and organ volumes), well-established scaling relations or predictions can be used for other parameters (e.g., permeability coefficients), and the remaining parameters can be obtained by direct measurements or fitting procedures (e.g., enzymatic rates and plasma protein binding). For example, recently, Thiel et al. systematically evaluated the translatability of PBPK models for 10 drugs between mouse and human.[380] The PBPK models were translatable between species, but the translation accuracy strongly depended on the availability of translatable model parameters—including kinetic rates and the abundance of metabolic enzymes.

Therefore, in addition to the development of well-characterized in vitro systems in relevant species, increasing modeling know-how will be a crucial part in translating preclinical findings into clinical research.

2.18.5 Special Considerations

2.18.5.1 Experimental Design and Data Production

Systems biology has initiated a new era in drug discovery, diagnostics, and toxicology, but it will take time until it will be fully accepted and leveraged. Rightfully so, because the workflows that provide information based on the analyses of thousands of data points must be well controlled, since there are many instances where bias and errors can inadvertently be introduced during data interpretation as listed in **Fig. 10** and described later.

There can be large variability among measurements, which calls for careful calculations beforehand to ensure that there is a sufficient number of biological replicates to obtain robust and useful data.[381–383] Some data modalities are also very sensitive to sample type, quality, and processing, and subject-related factors such as genetics, gender, environment, and nutrition. Such factors can drastically sway the molecular profiles. In the context of metabolomics, Courant et al. have listed several aspects that need to be taken into account to design studies involving the analysis of thousands of data points.[384] Another example describes how a routine proteomics analysis can vary among laboratories.[385]

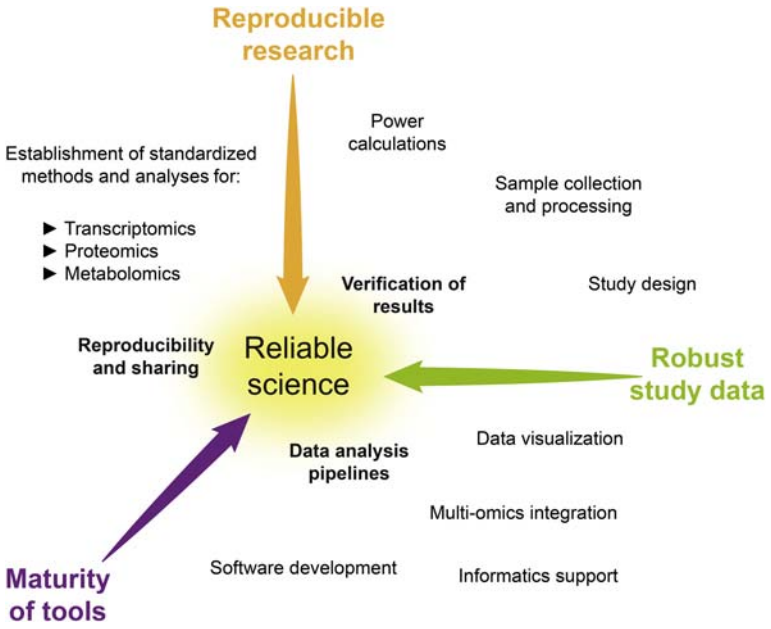

Fig. 10 Special considerations in systems biology. The figure summarizes aspects that should be taken into account to establish reproducible and reliable science. It starts with appropriate study designs and sample analysis, continues with the development of standard data analysis workflows and methods to integrate -omics data types. Finally, global data standards guarantee open data sharing and assessment of reproducibility.

Even at the same institute, with the same personnel handling the samples, there can be batch effects and/or variations related to changes in laboratory conditions, reagent lots, and individuals handling samples.[386] For gene expression profiling, the MAQC project sets out to assess the intra- and interplatform variability in microarray experiments.[387] Similar initiatives have been started around high-throughput sequencing of RNA (RNA-seq). The Sequencing Quality Control is the third phase of MAQC, and the project goal was to assess the reproducibility and comparability of RNA-seq methods by evaluating different sequencing platforms in real-world use cases.[388]

2.18.5.2 Data Evaluation

Even when there is an adequate experimental design, there are many sources of bias when handling big data. For all -omics analyses, the workflows need to be well defined and validated. Working instructions and standard operating procedures must be established, and reproducibility should be assessed using internal controls. Even so, results are not always reproducible when data are reanalyzed at different sites, partly because of differences in personal workflows and challenges in data sharing, as demonstrated in The Human Toxome Project.[310] Moreover, rapidly moving algorithm and software development requires constant bioinformatics support and specialized infrastructure to process, secure, and store the massive amounts of data that are produced.[389]

Omics technologies provide an extensive collection of distinct data at different levels (genome, transcriptome, proteome, and metabolome) that support and complement each other. The challenge lies in integrating these data types into a comprehensive analysis, and understanding the many relationships among the -omics datatypes for easier interpretation. In essence, the data from different technologies can be integrated in several ways. The data can be analyzed independently and then an explanation is formulated based on the results. Alternatively, the data can be integrated statistically by searching for associations or by using preexisting biological models to gain mechanistic insights.[390,391] Statistical and computational integration methods are still under development, and related challenges in data integration have been described.[392,393]

2.18.5.3 Data Standards and Sharing

To ensure reproducible science, which is a substantial difficulty in research today, total transparency with data-sharing and collaborative tools is needed. Experiments are often described in diverse ways with different levels of detail, sometimes purposely vague and even with incorrect descriptions. Every experiment has critical parts that need to be identified and properly annotated for full sample traceability and data reuse. Standards for experimental description and execution, terminology, data analysis, and data exchange are crucial if the data is to be shared in public repositories.[394] Without proper standards the valuable -omics data produced will remain largely unused.[395]

2.18.5.3.1 Standardization in transcriptomics

For transcriptomics, MIAME specifies the minimum requirements for experimental design, description protocols, and sample annotation, as well as raw and processed data.[396,397] However, it lacks guidelines for the terminology that should be used when describing experiments. Gene Expression-Tabular, MAGE-TAB, and MicroArray are simple, spreadsheet-based data description formats that are easily read by researchers.[398] The hierarchical Investigation-Study-Assay-Tab is a generic format for experimental representations. This initiative also develops and provides open-access tools, including conversion tools to other data formats, to aid data reporting for -omics technologies.[385,399] There are many other proposed formats, some no longer in use and some supported only by certain data repositories. However, with all the different initiatives, global standards are missing; for transcriptomics alone, there are at least 10 proposed standards and no real agreement among researchers on what constitutes a standard.[400] To address this problem, BioSharing offers a web interphase for sharing policy documents and information about the available standards as well as the possibility to register new standard initiatives.[401] The state of standards is discussed in detail in Ref. 400.

2.18.5.3.2 Standardization in proteomics

Proteomics is a rapidly maturing field, whose diversity reflects the complexity inherent in protein regulation and function. As we have seen, proteomics methods cover a wide range of protein properties including expression levels, modifications, and interactions. Each subfield has numerous sample preparation and analytical methods and instrumentation (e.g., mass spectrometers based on different principles and from different vendors). At the same time, the recent improvements in coverage and the accuracy of quantification strongly encourage the reuse of published proteomics data sets to gain deeper biological insights and to refine clinical applications. Common standards that capture the diversity of proteomics experiments are the key to facilitate effective reuse and to ensure the highest impact of proteomics in (systems) biology and medicine.

The Proteomics Standards Initiative (PSI)—an initiative formed by the Human Proteome Organization in 2002—has been the main driving force for the development and implementation of standards in the proteomics field.[402] The PSI is tasked to advance standardization in five areas: minimum information guidelines, data formats, controlled vocabularies, resources and software tools, and dissemination.

Minimum information guidelines define the minimum information that is required to understand how the study was conducted and how it can be reproduced. The first guideline, developed in 2006, is the minimum information about a proteomics experiment (MIAPE) guideline,[403] which was devised with a modular structure to allow for the diverse requirements of different proteomics experiments: MIAPE-CC describes column chromatography;[404] MIAPE-GE describes gel electrophoresis;[405] MIAPE-MS describes the generation of raw MS data;[406] MIAPE-Metabolomics Standards Initiative (MSI) describes informatics analysis workflows;[407] and MIAPE-Quan—the most recent addition—describes quantitative proteomics methods.[408]

The interoperability of data-sharing and analysis software depends on the availability of common data standards. The PSI defines two types of standard formats: Extensible Markup Language (XML) formats for computational processing; and tabular text formats for more lightweight reporting. Again, to address the diversity of proteomics methods, these formats must cover a broad range of analytical and processing results. The PSI has created XML-based file formats to store raw MS data (mzML),[409] input lists for targeted MS experiments (TraML),[410] peptide identification from MS experiments (mzIdentML),[411] and results from quantitative MS experiments (mzQuantML).[412] To promote the use of these formats, the latter two are complemented by the tabular mzTab format, which captures high-level information from both mzIdentML and mzQuantML, but is easier to work with.[413] As an important element of these formats, the PSI has also developed several controlled vocabularies to consistently and systematically capture the required information (e.g., sample types, instruments, and processing).[414]

These standardized formats and descriptions facilitate data sharing, which the PSI supports most directly through proteomics databases. The ProteomeXchange consortium provides an integrated framework for the submission and dissemination of MS proteomics data[415] and includes the PRIDE (untargeted proteomics data),[416] PeptideAtlas (targeted proteomics data),[417] and MassIVE (untargeted proteomics data, http://massive.ucsd.edu) databases.

These efforts to facilitate data sharing are very important, but are insufficient to bring proteomics into a clinical setting. To achieve this goal, standardization and understanding of the intra- and interlaboratory variability of proteomics assays is essential.[418] For example, Percy et al. developed reference kits and standardized protocols for targeted measurement of plasma proteins. This has allowed reproducible measurement of 22 plasma proteins across instruments and laboratories.[419]

Despite these advances, the translation of proteomics results into clinical practice is very limited. To date, only one proteomic biomarker assay—the OVA1 ovarian cancer test[420]—has been cleared by the FDA. With more robust and reproducible proteomics methods now available, we realize that more general factors of proteomics studies are hampering progress. Such factors include underpowered study designs, inadequate sample quality, and lack of validation.[421] We hope that the standardization initiatives will have broad impacts on the field of systems biology, leading to better overall study designs, and consequently, more robust translatability into a clinical setting.

2.18.5.3.3 Standardization in metabolomics

There are many metabolomics applications that offer a huge diversity of approaches designed to address individual scientific questions, and standardization based on common techniques is continuously progressing. Under the auspices of the Metabolomics

Society, the leading organization for promoting the growth, use, and understanding of metabolomics in the life sciences, the MSI has been formed with the goal to find a consensus for a minimum core set of necessary data (e.g., with respect to best practices in selecting and analyzing biological samples, chemical analysis, data analysis, ontology, data exchange standards, and reporting standards).[422] The MSI is organized by an oversight committee chaired by Oliver Fiehn and several subchairs according to the areas identified as being most important for describing metabolomics experiments.[423] A recent outcome is the global effort COSMOS (COordination of Standards In MetabOlomicS) for free and open sharing of metabolomics data. The metabolomics data can be in different data exchange formats, and include raw MS and NMR data, metabolite quantification and identification, and experimental metadata. Coordinated by the European Bioinformatics Institute—COSMOS has brought together European metabolomics data providers including universities and industry partners to establish and promote community standards. Open-access and exchange repositories for metabolomics experiments like MetaboLights (www.ebi.ac.uk/metabolights), Metabolomic Repository Bordeaux (http://metabolomexchange.org/rss/search/mwbs), and Metabolomics Workbench (http://www.metabolomicsworkbench.org/) have become the standards for e-infrastructures. For example, MetaboLights is a cross-species, cross-technique database that includes metabolite structures and their reference spectra as well as their biological roles, locations, and concentrations, and experimental data from metabolic experiments.[424]

Cross-platform comparisons for metabolomics methods provide valuable insights for the expected quality of analytical results, and have been established to compare quantitative metabolomics data related to primary metabolism obtained using GC/MS, LC/MS, and CE-MS platforms.[425] The outcome of such studies can be leveraged for recommendations on preferred analytical platforms for a specific research area and are very valuable to the metabolomics community.

While waiting for the establishment of standards covering all of the -omics platforms, transparent data sharing is still essential in research. Even though it is common sense to share data, it does not happen routinely, even in high impact journals, only a fraction of which enforce free data sharing.[426] Journals such as Scientific Data and its primary article type, the Data Descriptor, are dedicated to publishing scientifically valuable datasets (http://www.nature.com/sdata/). The production of data needs to be well described and annotated to allow others to reuse the data and verify conclusions.[427] A recent example is an inhalation study that was described in great detail to allow data sharing and reuse.[428]

2.18.5.4 Systems Biology Verification

Reproducible science is the key for all research areas. It can, however, not be taken for granted. While crucially important, there are many issues with the current peer review system.[429] Several aspects regarding its fairness and transparency are currently being discussed and include the anonymity of both authors and reviewers, and the compromised confidentiality of data and findings.[430] There are also criticism regarding the speed and cost of the current system.[431] One solution could be the F1000Research open science platform that proposes an open peer review to enforce open collaboration within the research community.[216] Systems biology faces special challenges in this regard, as research conclusions are always accompanied by high volumes of data that need to be analyzed with suitable expertise. The first level of systems biology verification relies on data publication that should follow the same transparency that allows independent verification, as alluded to in the previous sections.[432]

Even in the presence of the best of standards and open sharing of the omics data, significant effort should be assigned for comprehensive verification of results and methods used in systems biology. To complement the peer review system, several initiatives, such as CASP, BioCreAtIvE,[433] DREAM (discussed in more detail elsewhere in the article),[233] PROTEINCHALLENGE,[434] and sbvIMPROVER,[372] have been launched to verify methods of protein structure prediction, information extraction, gene network inference, proteomics analysis, and software development, as well as entire systems biology research workflows, respectively. Rather than relying on peer review by journals that publish results and methods, these initiatives engage crowds to evaluate existing and to contribute in developing new methods. Such innovation and verification of computational approaches could be considered as the second level of verification in systems biology.

As the third layer of verification, panels of scientific experts could be engaged to review comprehensive datasets for study design, technical aspects, as well as data analysis and interpretation. While the open peer review platform offered by F1000Research has its advantages, it may hinder honest review due to pressure by strong opinions in the field. Independent parties, such as the SciPinion (https://scipinion.com/) as the mediators of expert review, may provide the final layer of multilevel verification of systems biology research.

2.18.5.5 Education on Systems Biology

The overwhelming number of data points handled with the most sophisticated algorithms does not mean much until fully understood, accepted, and interpreted by specialized investigators. Such researchers have the knowledge and experience to crack the details of the all-encompassing information provided by systems biology. To inspire confidence in systems research, there are several initiatives that aim to educate researchers in various disciplines of systems biology (**Table 2**).

2.18.5.6 Current Status of Systems Biology in Industry

To make systems biology approaches relevant for industry in the long run, it is crucial that the data production and interpretation processes are at a level that is expected and accepted by regulatory agencies. Only then systems biology data can directly enable new

Table 2 List of online biology programs offered by universities across Europe, Asia, and North America

Institution	*Location*	*URL*	*Focus*	*Since*
Free University of Amsterdam	Amsterdam, The Netherlands	http://www.vu.nl/en/programmes/international-masters/programmes/a-b/bioinformatics-msc/index.aspx	Masters Program	2010
University of Vienna	Vienna, Austria	https://www.univie.ac.at/mosys/	Masters and PhD programs	N/A
Flanders Institute for Biotechnology	Flanders, Belgium	http://www.vib.be/en/research/departments/Pages/VIB-Department-of-Plant-Systems-Biology-UGent.aspx	PhD and postdoctoral programs	N/A
Technical University of Denmark	Kongens Lyngby, Denmark	http://www.dtu.dk/english/Education/msc/Programmes/systems_biology	Masters and PhD programs	N/A
University of Copenhagen	Copenhagen, Denmark	http://www.cpr.ku.dk/staff/385200/	Masters and PhD programs	N/A
Institut Curie	Paris, France	http://u900.curie.fr/en/equipe/Bioinformatics%20and%20computational%20systems%20biology%20of%20cancer	Masters, PhD, and postdoctoral programs	N/A
Max Planck Institute	Munich, Germany	http://www.molgen.mpg.de/en/bioinformatics	PhD program	N/A
Gebze Technical University	Gebze, Turkey	http://www.systemsbiology.info.tr/	Summer internships, Masters, and PhD programs	2016
Oxford University	Oxford, United Kingdom	http://www.sysbiodtc.ox.ac.uk/	PhD program	N/A
ETH Zurich	Zurich, Switzerland	http://www.imsb.ethz.ch/education.html	Masters and PhD programs	N/A
Humboldt University	Berlin, Germany	http://www.berlin-csb.de/	PhD program	N/A
Free University of Brussels	Brussels, Belgium	http://www.vub.ac.be/en/study/biomedical-engineering/programme/r/master-of-science-in-biomedical-engineering	Masters Program	N/A
University of Tokyo	Tokyo, Japan	http://www.cbms.k.u-tokyo.ac.jp/english/index.html	Internships, Masters, and PhD programs	N/A
Kyoto University	Kyoto, Japan	http://www.kuicr.kyoto-u.ac.jp/	Internships, Masters, and PhD programs	2001
University of Tokyo	Tokyo, Japan	http://www.ims.u-tokyo.ac.jp/imsut/en/lab/hgclink/	Internships, Masters, and PhD programs	N/A
Keio University	Tsuruoka/Tokyo, Japan	http://www.iab.keio.ac.jp/en/content/blogsection/14/74/	Masters/PhD and Post-Doctoral programs	2001
Jawaharlal Nehru University	Delhi, India	http://www.jnu.ac.in/scis/	Masters and PhD programs	2001
University of Toronto	Toronto, Canada	http://www.sgs.utoronto.ca/prospectivestudents/Pages/Programs/Cell-and-Systems-Biology.aspx	Masters and PhD programs	N/A
Boston University	Boston, United States	http://www.bu.edu/bioinformatics/travel-fellowships/international-bioinformatics-and-systems-biology-research-and-training-program/	Masters and PhD programs	2001
Harvard	Boston, United States	https://sysbio.med.harvard.edu/	PhD program	N/A
Stanford	Stanford, United States	https://chemsysbio.stanford.edu/	PhD and Post-Doctoral programs	N/A
California Institute of Technology	Pasadena, United States	http://www.sysbio.caltech.edu/	PhD and Post-Doctoral programs	N/A
Columbia University	New York, United States	https://systemsbiology.columbia.edu/graduate-education	PhD program	N/A
CSBi (Massachusetts Institute of Technology)	Cambridge, United States	http://csbi.mit.edu/education/phd.html	PhD program	N/A
Georgia Institute of Technology	Atlanta, United States	http://www.biology.gatech.edu/graduate/computational-biology-and-bioinformatics	Masters and PhD programs	1999

This list provides examples only, and is not a comprehensive list of all available courses and programs.

targeted treatments and support the biological safety of new drugs or other consumer products. Several points discussed in this article, especially those relating to standardization and validation of methods and analysis approaches, are key toward this important goal. Importantly, regulatory agencies—with the FDA at the forefront—have already taken action and support the development of highly reliable and robust systems biology technologies that can enable regulatory decision-making.[435] For example, the FDA has already implemented a Voluntary eXploratory Data Submission program, which enables the sponsor of an application to include omics data in a regulatory submission.[436] The idea of this program is for the FDA to learn how omics data can effectively be used in regulatory submissions. Also, to actively contribute to the development of robust omics technologies, the FDA is leading the MAQC, which aims to address technological challenges such as reproducibility, precision, specificity/sensitivity,

and data interpretation. For example, recently, in a project focused on NGS, the consortium demonstrated that RNA-seq can reliably and accurately measure relative gene expression across laboratories.[435] Importantly, initiatives focused on data generation need to be flanked by initiatives that are focused on robust and reproducible computational approaches. For example, recently, several of these computational challenges have been discussed during the Global Summit on Regulatory Science 2015, including the need for validated computational tools, validated analysis processes, and storage solutions that ensure data integrity.[437]

Despite advances, not many diagnostic or therapeutic options that are based on systems medicine have made it to the clinic. Mechanisms of the Development of ALLergy (MeDALL) was one of the first EU projects to implement a systems medicine approach for the understanding of complex chronic disease. By harvesting epidemiological, clinical and basic research data into a knowledge management platform, and by developing the allergen microarray chip combined with machine-learning methods to identify novel phenotypes, MeDALL's goal is to empower the patients themselves to know their disease.[438] Other success stories in systems medicine and network pharmacology are the multiple drugs targeting the cyclic GMP[439] as well as the inclusion of exome and genome sequencing for the diagnosis of neurodevelopmental disorders in children.[440]

All in all, the use of systems medicine in real life is not yet fully established. In their review, Mc Shane et al. list the criteria that should be used for omics-based predictors in National Cancer Institute-supported clinical trials. These criteria focus on the availability and quality of clinical specimens, issues with assays, model evaluation, clinical trial design, as well as ethical, legal, and regulatory issues.[441] In addition to these issues, depending on the diagnostic purpose, there may be differences which combinations of omics data are the most appropriate. Moreover, large-scale training of medical staff and the evaluation of the cost-effectiveness of each method are needed.[442] Nine tests that use gene expression profiling and expanded immunohistochemistry to guide the use of adjuvant chemotherapy in breast cancer management have been tested for cost-effectiveness by systematic review of evidence. While OncotypeDX was considered to be the most robust, the study stated the gaps in the evidence base and heterogeneity of patient cohorts as a weakness for such analysis.[443]

2.18.6 Conclusions

Biological systems are inherently complex. They typically contain a large number of components that interact with each other in a regulated manner. It is the sum of all the interactions between multiple components that are responsible for phenotypic plasticity. In this context, systems biology offers an unparalleled opportunity to investigate the global effects of a specific chemical (i.e., a drug or a toxicant) in a particular biological system (i.e., a cell, a tissue, or an organ). Systems biology comprises both experimental approaches that generate large amounts of data and the computational tools that enable the extraction of relevant mechanistic information from that data. Omics technologies offer nearly limitless possibilities to identify the molecular interactions in a complex system. In particular, the combination of multiple omics-based approaches results in complementary layers of information that can be integrated to provide a more accurate description of a biological system.

During the past two decades, systems-wide approaches have progressively become more common in biomedical research. Systems biology is currently used in many areas, including modern toxicology, pharmacology, and medicine, because it allows to investigate multiple biological processes that can occur simultaneously. At the same time, as with any powerful approach, there are still many challenges that need to be addressed to enable science and to fully benefit from this approach.

Acknowledgments

The authors would like to thank Dr. Stéphanie Boué and Ms. Samantha Elmhurst for the illustrations in this article.

See also: 1.05. Nutraceuticals. 2.19. Systems Chemical Biology: Integrating Medicinal Chemistry and Systems Biology for Drug Discovery. 3.20. An Introduction to Systems Biology and Quantitative Systems Pharmacology. 4.11. Genetic Toxicology. 5.01. Cancer Biology and the Principles of Targeted Cancer Drug Discovery. 5.07. Targeting Protein Synthesis, Folding, and Degradation Pathways in Cancer.

References

1. Peitsch, M. C.; De Graaf, D. A Decade of Systems Biology: Where Are We and Where Are We Going to. *Drug Discov. Today* **2013**.
2. Dennis, G., Jr.; Sherman, B. T.; Hosack, D. A.; Yang, J.; Gao, W.; Lane, H. C.; Lempicki, R. A. DAVID: Database for Annotation, Visualization, and Integrated Discovery. *Genome Biol.* **2003,** *4* (5), P3.
3. Subramanian, A.; Tamayo, P.; Mootha, V. K.; Mukherjee, S.; Ebert, B. L.; Gillette, M. A.; Paulovich, A.; Pomeroy, S. L.; Golub, T. R.; Lander, E. S.; Mesirov, J. P. Gene Set Enrichment Analysis: A Knowledge-Based Approach for Interpreting Genome-Wide Expression Profiles. *Proc. Natl. Acad. Sci. U. S. A.* **2005,** *102* (43), 15545–15550.
4. Cho, C. R.; Labow, M.; Reinhardt, M.; van Oostrum, J.; Peitsch, M. C. The Application of Systems Biology to Drug Discovery. *Curr. Opin. Chem. Biol.* **2006,** *10* (4), 294–302.
5. Bai, J. P.; Abernethy, D. R. Systems Pharmacology to Predict Drug Toxicity: Integration Across Levels of Biological Organization. *Annu. Rev. Pharmacol. Toxicol.* **2013,** *53*, 451–473.

6. Sturla, S. J.; Boobis, A. R.; FitzGerald, R. E.; Hoeng, J.; Kavlock, R. J.; Schirmer, K.; Whelan, M.; Wilks, M. F.; Peitsch, M. C. Systems Toxicology: From Basic Research to Risk Assessment. *Chem. Res. Toxicol.* **2014,** *27* (3), 314–329.
7. Hood, L.; Flores, M. A Personal View on Systems Medicine and the Emergence of Proactive P4 Medicine: Predictive, Preventive, Personalized and Participatory. *New Biotechnol.* **2012,** *29* (6), 613–624.
8. Ahmed, F. E. Microarray RNA Transcriptional Profiling: Part I. Platforms, Experimental Design and Standardization. *Expert. Rev. Mol. Diagn.* **2006,** *6* (4), 535–550.
9. Mandruzzato, S. Technological Platforms for Microarray Gene Expression Profiling. *Adv. Exp. Med. Biol.* **2007,** *593,* 12–18.
10. Malone, J. H.; Oliver, B. Microarrays, Deep Sequencing and the True Measure of the Transcriptome. *BMC Biol.* **2011,** *9,* 34.
11. Sirbu, A.; Kerr, G.; Crane, M.; Ruskin, H. J. RNA-Seq vs. Dual- and Single-Channel Microarray Data: Sensitivity Analysis for Differential Expression and Clustering. *PLoS One* **2012,** *7* (12), e50986.
12. Han, Y.; Gao, S.; Muegge, K.; Zhang, W.; Zhou, B. Advanced Applications of RNA Sequencing and Challenges. *Bioinform. Biol. Insights* **2015,** *9* (Suppl. 1), 29–46.
13. Finotello, F.; Di Camillo, B. Measuring Differential Gene Expression With RNA-seq: Challenges and Strategies for Data Analysis. *Brief Funct. Genomics* **2015,** *14* (2), 130–142.
14. Kaeuferle, T.; Bartel, S.; Dehmel, S.; Krauss-Etschmann, S. MicroRNA Methodology: Advances in miRNA Technologies. *Methods Mol. Biol.* **2014,** *1169,* 121–130.
15. Wang, Z. Chapter 2 mIRNA Interference Technologies: An Overview. In *MicroRNA Interference Technologies;* Wang, Z., Ed.; Springer: Berlin, 2009.
16. Leidinger, P.; Keller, A.; Borries, A.; Reichrath, J.; Rass, K.; Jager, S. U.; Lenhof, H. P.; Meese, E. High-Throughput miRNA Profiling of Human Melanoma Blood Samples. *BMC Cancer* **2010,** *10,* 262.
17. Guerau-de-Arellano, M.; Alder, H.; Ozer, H. G.; Lovett-Racke, A.; Racke, M. K. miRNA Profiling for Biomarker Discovery in Multiple Sclerosis: From Microarray to Deep Sequencing. *J. Neuroimmunol.* **2012,** *248* (1–2), 32–39.
18. Steinkraus, B. R.; Toegel, M.; Fulga, T. A. Tiny Giants of Gene Regulation: Experimental Strategies for microRNA Functional Studies. *Wiley Interdiscip. Rev. Dev. Biol.* **2016,** *5* (3), 311–362.
19. Chou, C.-H.; Chang, N.-W.; Shrestha, S.; Hsu, S.-D.; Lin, Y.-L.; Lee, W.-H.; Yang, C.-D.; Hong, H.-C.; Wei, T.-Y.; Tu, S.-J. miRTarBase 2016: Updates to the Experimentally Validated miRNA-Target Interactions Database. *Nucleic Acids Res.* **2016,** *44* (D1), D239–D247.
20. Xiao, F.; Zuo, Z.; Cai, G.; Kang, S.; Gao, X.; Li, T. miRecords: An Integrated Resource for microRNA–Target Interactions. *Nucleic Acids Res.* **2009,** *37* (Suppl. 1), D105–D110.
21. Zhang, X.; Marjani, S. L.; Hu, Z.; Weissman, S. M.; Pan, X.; Wu, S. Single-Cell Sequencing for Precise Cancer Research: Progress and Prospects. *Cancer Res.* **2016,** *76* (6), 1305–1312.
22. Kolodziejczyk, A. A.; Kim, J. K.; Svensson, V.; Marioni, J. C.; Teichmann, S. A. The Technology and Biology of Single-Cell RNA Sequencing. *Mol. Cell* **2015,** *58* (4), 610–620.
23. Liu, S.; Trapnell, C. Single-Cell Transcriptome Sequencing: Recent Advances and Remaining Challenges. *F1000Res.* **2016,** *5.*
24. Stegle, O.; Teichmann, S. A.; Marioni, J. C. Computational and Analytical Challenges in Single-Cell Transcriptomics. *Nat. Rev. Genet.* **2015,** *16* (3), 133–145.
25. Gawad, C.; Koh, W.; Quake, S. R. Single-Cell Genome Sequencing: Current State of the Science. *Nat. Rev. Genet.* **2016,** *17* (3), 175–188.
26. Navarro, E.; Serrano-Heras, G.; Castano, M. J.; Solera, J. Real-Time PCR Detection Chemistry. *Clin. Chim. Acta* **2015,** *439,* 231–250.
27. Alikian, M.; Ellery, P.; Forbes, M.; Gerrard, G.; Kasperaviciute, D.; Sosinsky, A.; Mueller, M.; Whale, A. S.; Milojkovic, D.; Apperley, J.; Huggett, J. F.; Foroni, L.; Reid, A. G. Next-Generation Sequencing-Assisted DNA-Based Digital PCR for a Personalized Approach to the Detection and Quantification of Residual Disease in Chronic Myeloid Leukemia Patients. *J. Mol. Diagn.* **2016,** *18* (2), 176–189.
28. Jung, S. H.; Sohn, I. Statistical Issues in the Design and Analysis of nCounter Projects. *Cancer Inform.* **2014,** *13* (Suppl. 7), 35–43.
29. Chen, P.; Jeannotte, R.; Weimer, B. C. Exploring Bacterial Epigenomics in the Next-Generation Sequencing Era: A New Approach for an Emerging Frontier. *Trends Microbiol.* **2014,** *22* (5), 292–300.
30. Marzese, D. M.; Hoon, D. S. Emerging Technologies for Studying DNA Methylation for the Molecular Diagnosis of Cancer. *Expert. Rev. Mol. Diagn.* **2015,** *15* (5), 647–664.
31. Kurdyukov, S.; Bullock, M. DNA Methylation Analysis: Choosing the Right Method. *Biology* **2016,** *5* (1), 3.
32. Olkhov-Mitsel, E.; Bapat, B. Strategies for Discovery and Validation of Methylated and Hydroxymethylated DNA Biomarkers. *Cancer Med.* **2012,** *1* (2), 237–260.
33. Balbo, S.; Turesky, R. J.; Villalta, P. W. DNA Adductomics. *Chem. Res. Toxicol.* **2014,** *27* (3), 356–366.
34. Ciaccio, M. F.; Wagner, J. P.; Chuu, C. P.; Lauffenburger, D. A.; Jones, R. B. Systems Analysis of EGF Receptor Signaling Dynamics With Microwestern Arrays. *Nat. Methods* **2010,** *7* (2), 148–155.
35. Hughes, A. J.; Herr, A. E. Microfluidic Western Blotting. *Proc. Natl. Acad. Sci. U. S. A.* **2012,** *109* (52), 21450–21455.
36. Sutandy, F.; Qian, J.; Chen, C. S.; Zhu, H. Overview of Protein Microarrays. *Curr. Protoc. Protein Sci.* **2013,** 27.1.1–27.1.16.
37. Straussman, R.; Morikawa, T.; Shee, K.; Barzily-Rokni, M.; Qian, Z. R.; Du, J.; Davis, A.; Mongare, M. M.; Gould, J.; Frederick, D. T. Tumour Micro-Environment Elicits Innate Resistance to RAF Inhibitors Through HGF Secretion. *Nature* **2012,** *487* (7408), 500–504.
38. Ellington, A. D.; Szostak, J. W. In Vitro Selection of RNA Molecules That Bind Specific Ligands. *Nature* **1990,** *346* (6287), 818–822.
39. McCauley, T. G.; Hamaguchi, N.; Stanton, M. Aptamer-Based Biosensor Arrays for Detection and Quantification of Biological Macromolecules. *Anal. Biochem.* **2003,** *319* (2), 244–250.
40. Keeney, T. R.; Bock, C.; Gold, L.; Kraemer, S.; Lollo, B.; Nikrad, M.; Stanton, M.; Stewart, A.; Vaught, J. D.; Walker, J. J. Automation of the SomaLogic Proteomics Assay: A Platform for Biomarker Discovery. *J. Assoc. Lab. Autom.* **2009,** *14* (6), 360–366.
41. Menni, C.; Kiddle, S. J.; Mangino, M.; Viñuela, A.; Psatha, M.; Steves, C.; Sattlecker, M.; Buil, A.; Newhouse, S.; Nelson, S. Circulating Proteomic Signatures of Chronological Age. *J. Gerontol. Ser. A Biol. Med. Sci.* **2015,** *70* (7), 809–816.
42. Vicari, K. Targeted Proteomics. *Nat. Methods* **2013,** *10* (1), 19.
43. Aebersold, R.; Burlingame, A. L.; Bradshaw, R. A. Western Blots Versus Selected Reaction Monitoring Assays: Time to Turn the Tables? *Mol. Cell. Proteomics* **2013,** *12* (9), 2381–2382.
44. Baker, M. Blame It on the Antibodies. *Nature* **2015,** *521* (7552), 274–276.
45. Michel, M. C.; Wieland, T.; Tsujimoto, G. How Reliable Are G-Protein-Coupled Receptor Antibodies? *Naunyn Schmiedebergs Arch. Pharmacol.* **2009,** *379* (4), 385–388.
46. Egelhofer, T. A.; Minoda, A.; Klugman, S.; Lee, K.; Kolasinska-Zwierz, P.; Alekseyenko, A. A.; Cheung, M.-S.; Day, D. S.; Gadel, S.; Gorchakov, A. A. An Assessment of Histone-Modification Antibody Quality. *Nat. Struct. Mol. Biol.* **2011,** *18* (1), 91–93.
47. Bensimon, A.; Heck, A. J.; Aebersold, R. Mass Spectrometry-Based Proteomics and Network Biology. *Annu. Rev. Biochem.* **2012,** *81,* 379–405.
48. Lesur, A.; Domon, B. Advances in High-Resolution Accurate Mass Spectrometry Application to Targeted Proteomics. *Proteomics* **2015,** *15* (5–6), 880–890.
49. Bruderer, R.; Bernhardt, O. M.; Gandhi, T.; Miladinović, S. M.; Cheng, L.-Y.; Messner, S.; Ehrenberger, T.; Zanotelli, V.; Butscheid, Y.; Escher, C. Extending the Limits of Quantitative Proteome Profiling With Data-Independent Acquisition and Application to Acetaminophen-Treated Three-Dimensional Liver Microtissues. *Mol. Cell. Proteomics* **2015,** *14* (5), 1400–1410.
50. Eliuk, S.; Makarov, A. Evolution of Orbitrap Mass Spectrometry Instrumentation. *Annu. Rev. Anal. Chem.* **2015,** *8,* 61–80.
51. Titz, B.; Elamin, A.; Martin, F.; Schneider, T.; Dijon, S.; Ivanov, N. V.; Hoeng, J.; Peitsch, M. C. Proteomics for Systems Toxicology. *Comput. Struct. Biotechnol. J.* **2014,** *11* (18), 73–90.
52. Gillet, L. C.; Navarro, P.; Tate, S.; Röst, H.; Selevsek, N.; Reiter, L.; Bonner, R.; Aebersold, R. Targeted Data Extraction of the MS/MS Spectra Generated by Data-Independent Acquisition: A New Concept for Consistent and Accurate Proteome Analysis. *Mol. Cell. Proteomics* **2012,** *11* (6), O111. 016717.
53. Marx, H.; Lemeer, S.; Schliep, J. E.; Matheron, L.; Mohammed, S.; Cox, J.; Mann, M.; Heck, A. J.; Kuster, B. A Large Synthetic Peptide and Phosphopeptide Reference Library for Mass Spectrometry-Based Proteomics. *Nat. Biotechnol.* **2013,** *31* (6), 557–564.
54. Lundgren, D. H.; Hwang, S.-I.; Wu, L.; Han, D. K. Role of Spectral Counting in Quantitative Proteomics. *Expert Rev. Proteomics* **2010,** *7* (1), 39–53.
55. Nahnsen, S.; Bielow, C.; Reinert, K.; Kohlbacher, O. Tools for Label-Free Peptide Quantification. *Mol. Cell. Proteomics* **2013,** *12* (3), 549–556.

56. Ong, S.-E.; Blagoev, B.; Kratchmarova, I.; Kristensen, D. B.; Steen, H.; Pandey, A.; Mann, M. Stable Isotope Labeling by Amino Acids in Cell Culture, SILAC, As a Simple and Accurate Approach to Expression Proteomics. *Mol. Cell. Proteomics* **2002,** *1* (5), 376–386.
57. Titz, B.; Schneider, T.; Elamin, A.; Martin, F.; Dijon, S.; Ivanov, N.; Hoeng, J.; Peitsch, M. Analysis of Proteomic Data for Toxicological Applications. In *Computational Systems Toxicology;* Springer: New York, 2015; pp 257–284.
58. Wiese, S.; Reidegeld, K. A.; Meyer, H. E.; Warscheid, B. Protein Labeling by iTRAQ: A New Tool for Quantitative Mass Spectrometry in Proteome Research. *Proteomics* **2007,** *7* (3), 340–350.
59. Thompson, A.; Schäfer, J.; Kuhn, K.; Kienle, S.; Schwarz, J.; Schmidt, G.; Neumann, T.; Hamon, C. Tandem Mass Tags: A Novel Quantification Strategy for Comparative Analysis of Complex Protein Mixtures by MS/MS. *Anal. Chem.* **2003,** *75* (8), 1895–1904.
60. Ohlmeier, S.; Mazur, W.; Linja-Aho, A.; Louhelainen, N.; Ronty, M.; Toljamo, T.; Bergmann, U.; Kinnula, V. L. Sputum Proteomics Identifies Elevated PIGR Levels in Smokers and Mild-to-Moderate COPD. *J. Proteome Res.* **2012,** *11* (2), 599–608.
61. Williamson, J. C.; Edwards, A. V.; Verano-Braga, T.; Schwämmle, V.; Kjeldsen, F.; Jensen, O. N.; Larsen, M. R. High-Performance Hybrid Orbitrap Mass Spectrometers for Quantitative Proteome Analysis: Observations and Implications. *Proteomics* **2016,** *16* (6), 907–914.
62. Gillette, M. A.; Carr, S. A. Quantitative Analysis of Peptides and Proteins in Biomedicine by Targeted Mass Spectrometry. *Nat. Methods* **2013,** *10* (1), 28–34.
63. Carr, S. A.; Abbatiello, S. E.; Ackermann, B. L.; Borchers, C.; Domon, B.; Deutsch, E. W.; Grant, R. P.; Hoofnagle, A. N.; Hüttenhain, R.; Koomen, J. M. Targeted Peptide Measurements in Biology and Medicine: Best Practices for Mass Spectrometry-Based Assay Development Using a Fit-for-Purpose Approach. *Mol. Cell. Proteomics* **2014,** *13* (3), 907–917.
64. Addona, T. A.; Abbatiello, S. E.; Schilling, B.; Skates, S. J.; Mani, D.; Bunk, D. M.; Spiegelman, C. H.; Zimmerman, L. J.; Ham, A.-J. L.; Keshishian, H. Multi-Site Assessment of the Precision and Reproducibility of Multiple Reaction Monitoring-Based Measurements of Proteins in Plasma. *Nat. Biotechnol.* **2009,** *27* (7), 633–641.
65. Hao, N.; Budnik, B. A.; Gunawardena, J.; O'Shea, E. K. Tunable Signal Processing Through Modular Control of Transcription Factor Translocation. *Science* **2013,** *339* (6118), 460–464.
66. Katikireddy, K. R.; O'Sullivan, F. Immunohistochemical and Immunofluorescence Procedures for Protein Analysis. *Methods Mol. Biol.* **2011,** *784,* 155–167.
67. Uhlén, M.; Fagerberg, L.; Hallström, B. M.; Lindskog, C.; Oksvold, P.; Mardinoglu, A.; Sivertsson, Å.; Kampf, C.; Sjöstedt, E.; Asplund, A. Tissue-Based Map of the Human Proteome. *Science* **2015,** *347* (6220), 1260419.
68. Stadler, C.; Rexhepaj, E.; Singan, V. R.; Murphy, R. F.; Pepperkok, R.; Uhlén, M.; Simpson, J. C.; Lundberg, E. Immunofluorescence and Fluorescent-Protein Tagging Show High Correlation for Protein Localization in Mammalian Cells. *Nat. Methods* **2013,** *10* (4), 315–323.
69. Lin, J. R.; Fallahi-Sichani, M.; Sorger, P. K. Highly Multiplexed Imaging of Single Cells Using a High-Throughput Cyclic Immunofluorescence Method. *Nat. Commun.* **2015,** *6,* 8390.
70. Gerdes, M. J.; Sevinsky, C. J.; Sood, A.; Adak, S.; Bello, M. O.; Bordwell, A.; Can, A.; Corwin, A.; Dinn, S.; Filkins, R. J.; Hollman, D.; Kamath, V.; Kaanumalle, S.; Kenny, K.; Larsen, M.; Lazare, M.; Li, Q.; Lowes, C.; McCulloch, C. C.; McDonough, E.; Montalto, M. C.; Pang, Z.; Rittscher, J.; Santamaria-Pang, A.; Sarachan, B. D.; Seel, M. L.; Seppo, A.; Shaikh, K.; Sui, Y.; Zhang, J.; Ginty, F. Highly Multiplexed Single-Cell Analysis of Formalin-Fixed, Paraffin-Embedded Cancer Tissue. *Proc. Natl. Acad. Sci. U. S. A.* **2013,** *110* (29), 11982–11987.
71. Boisvert, F.-M.; Lam, Y. W.; Lamont, D.; Lamond, A. I. A Quantitative Proteomics Analysis of Subcellular Proteome Localization and Changes Induced by DNA Damage. *Mol. Cell. Proteomics* **2010,** *9* (3), 457–470.
72. Chowdhury, M.; Enenkel, C. Intracellular Dynamics of the Ubiquitin-Proteasome-System. *F1000Res.* **2015,** *4,* 367.
73. Christoforou, A.; Mulvey, C. M.; Breckels, L. M.; Geladaki, A.; Hurrell, T.; Hayward, P. C.; Naake, T.; Gatto, L.; Viner, R.; Arias, A. M.; Lilley, K. S. A Draft Map of the Mouse Pluripotent Stem Cell Spatial Proteome. *Nat. Commun.* **2016,** *7,* 9992.
74. Gessel, M. M.; Norris, J. L.; Caprioli, R. M. MALDI Imaging Mass Spectrometry: Spatial Molecular Analysis to Enable a New Age of Discovery. *J. Proteomics* **2014,** *107,* 71–82.
75. Diehl, H. C.; Beine, B.; Elm, J.; Trede, D.; Ahrens, M.; Eisenacher, M.; Marcus, K.; Meyer, H. E.; Henkel, C. The Challenge of On-Tissue Digestion for MALDI MSI—A Comparison of Different Protocols to Improve Imaging Experiments. *Anal. Bioanal. Chem.* **2015,** *407* (8), 2223–2243.
76. Wiśniewski, J. R.; Duś, K.; Mann, M. Proteomic Workflow for Analysis of Archival Formalin-Fixed and Paraffin-Embedded Clinical Samples to a Depth of 10 000 Proteins. *Proteomics Clin. Appl.* **2013,** *7* (3–4), 225–233.
77. Drummond, E. S.; Nayak, S.; Ueberheide, B.; Wisniewski, T. Proteomic Analysis of Neurons Microdissected From Formalin-Fixed, Paraffin-Embedded Alzheimer's Disease Brain Tissue. *Sci. Rep.* **2015,** *5,* 15456.
78. Hadley, K. C.; Rakhit, R.; Guo, H.; Sun, Y.; Jonkman, J. E.; McLaurin, J.; Hazrati, L.-N.; Emili, A.; Chakrabartty, A. Determining Composition of Micron-Scale Protein Deposits in Neurodegenerative Disease by Spatially Targeted Optical Microproteomics. *eLife* **2015,** *4,* e09579.
79. Semenza, G. L. Hypoxia-Inducible Factors in Physiology and Medicine. *Cell* **2012,** *148* (3), 399–408.
80. Schofield, C. J.; Ratcliffe, P. J. Oxygen Sensing by HIF Hydroxylases. *Nat. Rev. Mol. Cell Biol.* **2004,** *5* (5), 343–354.
81. Nguyen, L. K.; Cavadas, M. A.; Scholz, C. C.; Fitzpatrick, S. F.; Bruning, U.; Cummins, E. P.; Tambuwala, M. M.; Manresa, M. C.; Kholodenko, B. N.; Taylor, C. T. A Dynamic Model of the Hypoxia-Inducible Factor 1α (HIF-1α) Network. *J. Cell Sci.* **2013,** *126* (6), 1454–1463.
82. Vogel, C.; Marcotte, E. M. Insights Into the Regulation of Protein Abundance From Proteomic and Transcriptomic Analyses. *Nat. Rev. Genet.* **2012,** *13* (4), 227–232.
83. Schwanhäusser, B.; Gossen, M.; Dittmar, G.; Selbach, M. Global Analysis of Cellular Protein Translation by Pulsed SILAC. *Proteomics* **2009,** *9* (1), 205–209.
84. Selbach, M.; Schwanhäusser, B.; Thierfelder, N.; Fang, Z.; Khanin, R.; Rajewsky, N. Widespread Changes in Protein Synthesis Induced by microRNAs. *Nature* **2008,** *455* (7209), 58–63.
85. Larance, M.; Ahmad, Y.; Kirkwood, K. J.; Ly, T.; Lamond, A. I. Global Subcellular Characterization of Protein Degradation Using Quantitative Proteomics. *Mol. Cell. Proteomics* **2013,** *12* (3), 638–650.
86. Hochstrasser, M. Ubiquitin-Dependent Protein Degradation. *Annu. Rev. Genet.* **1996,** *30* (1), 405–439.
87. Kobayashi, A.; Kang, M.-I.; Watai, Y.; Tong, K. I.; Shibata, T.; Uchida, K.; Yamamoto, M. Oxidative and Electrophilic Stresses Activate Nrf2 Through Inhibition of Ubiquitination Activity of Keap1. *Mol. Cell. Biol.* **2006,** *26* (1), 221–229.
88. Beaudette, P.; Popp, O.; Dittmar, G. Proteomic Techniques to Probe the Ubiquitin Landscape. *Proteomics* **2016,** *16* (2), 273–287.
89. Kim, W.; Bennett, E. J.; Huttlin, E. L.; Guo, A.; Li, J.; Possemato, A.; Sowa, M. E.; Rad, R.; Rush, J.; Comb, M. J. Systematic and Quantitative Assessment of the Ubiquitin-Modified Proteome. *Mol. Cell* **2011,** *44* (2), 325–340.
90. Olsen, J. V.; Mann, M. Status of Large-Scale Analysis of Post-Translational Modifications by Mass Spectrometry. *Mol. Cell. Proteomics* **2013,** *12* (12), 3444–3452.
91. Fisher, D.; Krasinska, L.; Coudreuse, D.; Novák, B. Phosphorylation Network Dynamics in the Control of Cell Cycle Transitions. *J. Cell Sci.* **2012,** *125* (20), 4703–4711.
92. Jünger, M. A.; Aebersold, R. Mass Spectrometry-Driven Phosphoproteomics: Patterning the Systems Biology Mosaic. *Wiley Interdiscip. Rev. Dev. Biol.* **2014,** *3* (1), 83–112.
93. Rubbi, L.; Titz, B.; Brown, L.; Galvan, E.; Komisopoulou, E.; Chen, S. S.; Low, T.; Tahmasian, M.; Skaggs, B.; Müschen, M. Global Phosphoproteomics Reveals Crosstalk Between Bcr-Abl and Negative Feedback Mechanisms Controlling Src Signaling. *Sci. Signaling* **2011,** *4* (166), ra18.
94. Drake, J. M.; Graham, N. A.; Lee, J. K.; Stoyanova, T.; Faltermeier, C. M.; Sud, S.; Titz, B.; Huang, J.; Pienta, K. J.; Graeber, T. G. Metastatic Castration-Resistant Prostate Cancer Reveals Intrapatient Similarity and Interpatient Heterogeneity of Therapeutic Kinase Targets. *Proc. Natl. Acad. Sci. U. S. A.* **2013,** *110* (49), E4762–E4769.
95. Ducommun, S.; Deak, M.; Sumpton, D.; Ford, R. J.; Nunez Galindo, A.; Kussmann, M.; Viollet, B.; Steinberg, G. R.; Foretz, M.; Dayon, L.; Morrice, N. A.; Sakamoto, K. Motif Affinity and Mass Spectrometry Proteomic Approach for the Discovery of Cellular AMPK Targets: Identification of Mitochondrial Fission Factor As a New AMPK Substrate. *Cell. Signalling* **2015,** *27* (5), 978–988.

96. Moritz, A.; Li, Y.; Guo, A.; Villen, J.; Wang, Y.; MacNeill, J.; Kornhauser, J.; Sprott, K.; Zhou, J.; Possemato, A.; Ren, J. M.; Hornbeck, P.; Cantley, L. C.; Gygi, S. P.; Rush, J.; Comb, M. J. Akt-RSK-S6 Kinase Signaling Networks Activated by Oncogenic Receptor Tyrosine Kinases. *Sci. Signaling* **2010,** *3* (136), ra64.
97. Ruprecht, B.; Koch, H.; Medard, G.; Mundt, M.; Kuster, B.; Lemeer, S. Comprehensive and Reproducible Phosphopeptide Enrichment Using Iron Immobilized Metal Ion Affinity Chromatography (Fe-IMAC) Columns. *Mol. Cell. Proteomics* **2015,** *14* (1), 205–215.
98. Zarei, M.; Sprenger, A.; Metzger, F.; Gretzmeier, C.; Dengjel, J. Comparison of ERLIC–TiO2, HILIC–TiO2, and SCX–TiO2 for Global Phosphoproteomics Approaches. *J. Proteome Res.* **2011,** *10* (8), 3474–3483.
99. Villén, J.; Gygi, S. P. The SCX/IMAC Enrichment Approach for Global Phosphorylation Analysis by Mass Spectrometry. *Nat. Protoc.* **2008,** *3* (10), 1630–1638.
100. Zimman, A.; Chen, S. S.; Komisopoulou, E.; Titz, B.; Martínez-Pinna, R.; Kafi, A.; Berliner, J. A.; Graeber, T. G. Activation of Aortic Endothelial Cells by Oxidized Phospholipids: A Phosphoproteomic Analysis. *J. Proteome Res.* **2010,** *9* (6), 2812–2824.
101. Di Palma, S.; Zoumaro-Djayoon, A.; Peng, M.; Post, H.; Preisinger, C.; Munoz, J.; Heck, A. J. Finding the Same Needles in the Haystack? A Comparison of Phosphotyrosine Peptides Enriched by Immuno-Affinity Precipitation and Metal-Based Affinity Chromatography. *J. Proteomics* **2013,** *91,* 331–337.
102. Humphrey, S. J.; Azimifar, S. B.; Mann, M. High-Throughput Phosphoproteomics Reveals In Vivo Insulin Signaling Dynamics. *Nat. Biotechnol.* **2015,** *33* (9), 990–995.
103. Kennedy, J. J.; Yan, P.; Zhao, L.; Ivey, R. G.; Voytovich, U. J.; Moore, H. D.; Lin, C.; Pogosova-Agadjanyan, E. L.; Stirewalt, D. L.; Reding, K. W.; Whiteaker, J. R.; Paulovich, A. G. Immobilized Metal Affinity Chromatography Coupled to Multiple Reaction Monitoring Enables Reproducible Quantification of Phospho-Signaling. *Mol. Cell. Proteomics* **2016,** *15* (2), 726–739.
104. Lundby, A.; Lage, K.; Weinert, B. T.; Bekker-Jensen, D. B.; Secher, A.; Skovgaard, T.; Kelstrup, C. D.; Dmytriyev, A.; Choudhary, C.; Lundby, C. Proteomic Analysis of Lysine Acetylation Sites in Rat Tissues Reveals Organ Specificity and Subcellular Patterns. *Cell Rep.* **2012,** *2* (2), 419–431.
105. Guo, A.; Gu, H.; Zhou, J.; Mulhern, D.; Wang, Y.; Lee, K. A.; Yang, V.; Aguiar, M.; Kornhauser, J.; Jia, X.; Ren, J.; Beausoleil, S. A.; Silva, J. C.; Vemulapalli, V.; Bedford, M. T.; Comb, M. J. Immunoaffinity Enrichment and Mass Spectrometry Analysis of Protein Methylation. *Mol. Cell. Proteomics* **2014,** *13* (1), 372–387.
106. Hahne, H.; Sobotzki, N.; Nyberg, T.; Helm, D.; Borodkin, V. S.; van Aalten, D. M.; Agnew, B.; Kuster, B. Proteome Wide Purification and Identification of O-GlcNAc-Modified Proteins Using Click Chemistry and Mass Spectrometry. *J. Proteome Res.* **2013,** *12* (2), 927–936.
107. Broncel, M.; Serwa, R. A.; Ciepla, P.; Krause, E.; Dallman, M. J.; Magee, A. I.; Tate, E. W. Multifunctional Reagents for Quantitative Proteome-Wide Analysis of Protein Modification in Human Cells and Dynamic Profiling of Protein Lipidation During Vertebrate Development. *Angew. Chem. Int. Ed.* **2015,** *54* (20), 5948–5951.
108. Bantscheff, M.; Eberhard, D.; Abraham, Y.; Bastuck, S.; Boesche, M.; Hobson, S.; Mathieson, T.; Perrin, J.; Raida, M.; Rau, C. Quantitative Chemical Proteomics Reveals Mechanisms of Action of Clinical ABL Kinase Inhibitors. *Nat. Biotechnol.* **2007,** *25* (9), 1035–1044.
109. Cravatt, B. F.; Wright, A. T.; Kozarich, J. W. Activity-Based Protein Profiling: From Enzyme Chemistry to Proteomic Chemistry. *Annu. Rev. Biochem.* **2008,** *77,* 383–414.
110. Li, N.; Kuo, C.-L.; Paniagua, G.; van den Elst, H.; Verdoes, M.; Willems, L. I.; van der Linden, W. A.; Ruben, M.; van Genderen, E.; Gubbens, J. Relative Quantification of Proteasome Activity by Activity-Based Protein Profiling and LC-MS/MS. *Nat. Protoc.* **2013,** *8* (6), 1155–1168.
111. Keller, I. E.; Vosyka, O.; Takenaka, S.; Kloß, A.; Dahlmann, B.; Willems, L. I.; Verdoes, M.; Overkleeft, H. S.; Marcos, E.; Adnot, S. Regulation of Immunoproteasome Function in the Lung. *Sci. Rep.* **2015,** *5,* 10230.
112. Houseman, B. T.; Huh, J. H.; Kron, S. J.; Mrksich, M. Peptide Chips for the Quantitative Evaluation of Protein Kinase Activity. *Nat. Biotechnol.* **2002,** *20* (3), 270–274.
113. Han, X.; Katayama, Y. A Peptide Microarray for Detecting Protein Kinase Activity in Cell Lysates. In *Small Molecule Microarrays: Methods and Protocols;* Humana Press, 2010; pp 183–194. vol. 669.
114. Rauh, D.; Fischer, F.; Gertz, M.; Lakshminarasimhan, M.; Bergbrede, T.; Aladini, F.; Kambach, C.; Becker, C. F.; Zerweck, J.; Schutkowski, M. An Acetylome Peptide Microarray Reveals Specificities and Deacetylation Substrates for all Human Sirtuin Isoforms. *Nat. Commun.* **2013,** *4,* 2327.
115. Kubota, K.; Anjum, R.; Yu, Y.; Kunz, R. C.; Andersen, J. N.; Kraus, M.; Keilhack, H.; Nagashima, K.; Krauss, S.; Paweletz, C. Sensitive Multiplexed Analysis of Kinase Activities and Activity-Based Kinase Identification. *Nat. Biotechnol.* **2009,** *27* (10), 933–940.
116. Titz, B.; Schlesner, M.; Uetz, P. What Do We Learn From High-Throughput Protein Interaction Data? *Expert Rev. Proteomics* **2004,** *1* (1), 111–121.
117. De Las Rivas, J.; Fontanillo, C. Protein–Protein Interactions Essentials: Key Concepts to Building and Analyzing Interactome Networks. *PLoS Comput. Biol.* **2010,** *6* (6), e1000807.
118. Rajagopala, S. V.; Sikorski, P.; Kumar, A.; Mosca, R.; Vlasblom, J.; Arnold, R.; Franca-Koh, J.; Pakala, S. B.; Phanse, S.; Ceol, A. The Binary Protein–Protein Interaction Landscape of *Escherichia coli*. *Nat. Biotechnol.* **2014,** *32* (3), 285–290.
119. Titz, B.; Rajagopala, S. V.; Goll, J.; Häuser, R.; McKevitt, M. T.; Palzkill, T.; Uetz, P. The Binary Protein Interactome of *Treponema pallidum*—The Syphilis Spirochete. *PLoS One* **2008,** *3* (5), e2292.
120. Uetz, P.; Dong, Y.-A.; Zeretzke, C.; Atzler, C.; Baiker, A.; Berger, B.; Rajagopala, S. V.; Roupelieva, M.; Rose, D.; Fossum, E. Herpesviral Protein Networks and Their Interaction With the Human Proteome. *Science* **2006,** *311* (5758), 239–242.
121. Rolland, T.; Taşan, M.; Charloteaux, B.; Pevzner, S. J.; Zhong, Q.; Sahni, N.; Yi, S.; Lemmens, I.; Fontanillo, C.; Mosca, R. A Proteome-Scale Map of the Human Interactome Network. *Cell* **2014,** *159* (5), 1212–1226.
122. Jones, R. B.; Gordus, A.; Krall, J. A.; MacBeath, G. A Quantitative Protein Interaction Network for the ErbB Receptors Using Protein Microarrays. *Nature* **2006,** *439* (7073), 168–174.
123. Yu, X.; Decker, K. B.; Barker, K.; Neunuebel, M. R.; Saul, J.; Graves, M.; Westcott, N.; Hang, H.; LaBaer, J.; Qiu, J.; Machner, M. P. Host-Pathogen Interaction Profiling Using Self-Assembling Human Protein Arrays. *J. Proteome Res.* **2015,** *14* (4), 1920–1936.
124. Rigaut, G.; Shevchenko, A.; Rutz, B.; Wilm, M.; Mann, M.; Séraphin, B. A Generic Protein Purification Method for Protein Complex Characterization and Proteome Exploration. *Nat. Biotechnol.* **1999,** *17* (10), 1030–1032.
125. Gavin, A.-C.; Aloy, P.; Grandi, P.; Krause, R.; Boesche, M.; Marzioch, M.; Rau, C.; Jensen, L. J.; Bastuck, S.; Dümpelfeld, B. Proteome Survey Reveals Modularity of the Yeast Cell Machinery. *Nature* **2006,** *440* (7084), 631–636.
126. Poser, I.; Sarov, M.; Hutchins, J. R.; Hériché, J.-K.; Toyoda, Y.; Pozniakovsky, A.; Weigl, D.; Nitzsche, A.; Hegemann, B.; Bird, A. W. BAC TransgeneOmics: A High-Throughput Method for Exploration of Protein Function in Mammals. *Nat. Methods* **2008,** *5* (5), 409–415.
127. Dalvai, M.; Loehr, J.; Jacquet, K.; Huard, C. C.; Roques, C.; Herst, P.; Cote, J.; Doyon, Y. A Scalable Genome-Editing-Based Approach for Mapping Multiprotein Complexes in Human Cells. *Cell Rep.* **2015,** *13* (3), 621–633.
128. Titz, B.; Low, T.; Komisopoulou, E.; Chen, S.; Rubbi, L.; Graeber, T. The Proximal Signaling Network of the BCR-ABL1 Oncogene Shows a Modular Organization. *Oncogene* **2010,** *29* (44), 5895–5910.
129. Kaake, R. M.; Wang, X.; Huang, L. Profiling of Protein Interaction Networks of Protein Complexes Using Affinity Purification and Quantitative Mass Spectrometry. *Mol. Cell. Proteomics* **2010,** *9* (8), 1650–1665.
130. Hein, M. Y.; Hubner, N. C.; Poser, I.; Cox, J.; Nagaraj, N.; Toyoda, Y.; Gak, I. A.; Weisswange, I.; Mansfeld, J.; Buchholz, F. A Human Interactome in Three Quantitative Dimensions Organized by Stoichiometries and Abundances. *Cell* **2015,** *163* (3), 712–723.
131. Daub, H. Quantitative Proteomics of Kinase Inhibitor Targets and Mechanisms. *ACS Chem. Biol.* **2015,** *10* (1), 201–212.
132. Cassiano, C.; Casapullo, A.; Tosco, A.; Monti, M. C.; Riccio, R. In Cell Interactome of Oleocanthal, an Extra Virgin Olive Oil Bioactive Component. *Nat. Prod. Commun.* **2015,** *10* (6), 1013–1016.
133. Tuo, X.; Chen, J.; Zhao, S.; Xie, P. Chemical Proteomic Analysis of the Potential Toxicological Mechanisms of Microcystin-RR in Zebrafish (Danio Rerio) Liver. *Environ. Toxicol.* **2015**.
134. Jarnuczak, A. F.; Eyers, C. E.; Schwartz, J. M.; Grant, C. M.; Hubbard, S. J. Quantitative Proteomics and Network Analysis of SSA1 and SSB1 Deletion Mutants Reveals Robustness of Chaperone HSP70 Network in *Saccharomyces cerevisiae*. *Proteomics* **2015,** *15* (18), 3126–3139.

135. Gajadhar, A. S.; White, F. M. System Level Dynamics of Post-Translational Modifications. *Curr. Opin. Biotechnol.* **2014,** *28,* 83–87.
136. Vachani, A.; Pass, H. I.; Rom, W. N.; Midthun, D. E.; Edell, E. S.; Laviolette, M.; Li, X.-J.; Fong, P.-Y.; Hunsucker, S. W.; Hayward, C. Validation of a Multiprotein Plasma Classifier to Identify Benign Lung Nodules. *J. Thorac. Oncol.* **2015,** *10* (4), 629–637.
137. Doerr, A. DIA Mass Spectrometry. *Nat. Methods* **2015,** *12* (1), 35.
138. Lamond, A. I.; Uhlen, M.; Horning, S.; Makarov, A.; Robinson, C. V.; Serrano, L.; Hartl, F. U.; Baumeister, W.; Werenskiold, A. K.; Andersen, J. S.; Vorm, O.; Linial, M.; Aebersold, R.; Mann, M. Advancing Cell Biology Through Proteomics in Space and Time (PROSPECTS). *Mol. Cell. Proteomics* **2012,** *11* (3), O112 017731.
139. Gomez-Cabrero, D.; Abugessaisa, I.; Maier, D.; Teschendorff, A.; Merkenschlager, M.; Gisel, A.; Ballestar, E.; Bongcam-Rudloff, E.; Conesa, A.; Tegnér, J. Data Integration in the Era of Omics: Current and Future Challenges. *BMC Syst. Biol.* **2014,** *8* (Suppl. 2), I1.
140. Gligorijević, V.; Pržulj, N. Methods for Biological Data Integration: Perspectives and Challenges. *J. R. Soc. Interface* **2015,** *12* (112), 20150571.
141. Baker, M. Metabolomics: From Small Molecules to Big Ideas. *Nat. Methods* **2011,** *8,* 117–121.
142. Fiehn, O. Metabolomics—The Link Between Genotypes and Phenotypes. *Plant Mol. Biol.* **2002,** *48* (1–2), 155–171.
143. Ellis, D. I.; Dunn, W. B.; Griffin, J. L.; Allwood, J. W.; Goodacre, R. Metabolic Fingerprinting As a Diagnostic Tool. *Pharmacogenomics* **2007,** *8* (9), 1243–1266.
144. Robinson, A. B.; Robinson, N. E. Origins of Metabolic Profiling. *Methods Mol. Biol.* **2011,** *708,* 1–23.
145. Shaham, O. Metabolic Profiling of the Human Response to a Glucose Challenge Reveals Distinct Axes of Insulin Sensitivity. *Mol. Syst. Biol.* **2008,** *4,* 214.
146. Zerhouni, E. Medicine. The NIH Roadmap. *Science* **2003,** *302* (5642), 63–72.
147. Jorge, T. F.; Rodrigues, J. A.; Caldana, C.; Schmidt, R.; van Dongen, J. T.; Thomas-Oates, J.; Antonio, C. Mass Spectrometry-Based Plant Metabolomics: Metabolite Responses to Abiotic Stress. *Mass Spectrom. Rev.* **2015**.
148. Okazaki, Y.; Saito, K. Recent Advances of Metabolomics in Plant Biotechnology. *Plant Biotechnol. Rep.* **2012,** *6* (1), 1–15.
149. Nicholson, J. K.; Connelly, J.; Lindon, J. C.; Holmes, E. Metabonomics: A Platform for Studying Drug Toxicity and Gene Function. *Nat. Rev. Drug Discov.* **2002,** *1,* 153–161.
150. Rabinowitz, J. D.; Purdy, J. G.; Vastag, L.; Shenk, T.; Koyuncu, E. Metabolomics in Drug Target Discovery. *Cold Spring Harbor Symp. Quant. Biol.* **2011,** *76,* 235–246.
151. Gowda, G. A.; Zhang, S.; Gu, H.; Asiago, V.; Shanaiah, N.; Raftery, D. Metabolomics-Based Methods for Early Disease Diagnostics. *Expert. Rev. Mol. Diagn.* **2008,** *8* (5), 617–633.
152. Suhre, K. Human Metabolic Individuality in Biomedical and Pharmaceutical Research. *Nature* **2011,** *477,* 54–60.
153. Alonso, A.; Marsal, S.; Julia, A. Analytical Methods in Untargeted Metabolomics: State of the Art in 2015. *Front. Bioeng. Biotechnol.* **2015,** *3,* 23.
154. Dieterle, F.; Riefke, B.; Schlotterbeck, G.; Ross, A.; Senn, H.; Amberg, A. NMR and MS Methods for Metabonomics. *Methods Mol. Biol.* **2011,** *691,* 385–415.
155. Veenstra, T. D. Metabolomics: The Final Frontier? *Genome Med.* **2012,** *4* (4), 40.
156. Han, X.; Gross, R. W. Shotgun Lipidomics: Electrospray Ionization Mass Spectrometric Analysis and Quantitation of Cellular Lipidomes Directly From Crude Extracts of Biological Samples. *Mass Spectrom. Rev.* **2005,** *24,* 367–412.
157. Link, H.; Fuhrer, T.; Gerosa, L.; Zamboni, N.; Sauer, U. Real-Time Metabolome Profiling of the Metabolic Switch Between Starvation and Growth. *Nat. Methods* **2015,** *12* (11), 1091–1097.
158. Kim, S.; Lee do, Y.; Wohlgemuth, G.; Park, H. S.; Fiehn, O.; Kim, K. H. Evaluation and Optimization of Metabolome Sample Preparation Methods for *Saccharomyces cerevisiae*. *Anal. Chem.* **2013,** *85* (4), 2169–2176.
159. Martin Almstetter, A. K.; Debrick, A.; Dutertre, Q.; Bentley, M. Screening of Aqueous Media Using GC×GC-TOF-MS. *Metabolomics Society 2013 Conference Glasgow, Scotland*.
160. Dutertre, Q.; Knorr, A.; Debrick, A.; Almstetter, M.; Martin, E.; Bentley, M. Ionic Liquid GCxGC-TOF-MS Approach for Generic Screening of Aerosol Constituents in Aqueous Tobacco Aerosol Fractions and Analysis of Microsomal Incubates, Drug Metabolism Reviews. In Informa Healthcare Telephone House: 69-77 Paul Street, London EC2A 4LQ, England, 2014; p 38.
161. Ramautar, R.; Somsen, G. W.; de Jong, G. J. CE-MS in Metabolomics. *Electrophoresis* **2009,** *30* (1), 276–291.
162. Garcia-Perez, I.; Lindon, J. C.; Minet, E. Application of CE-MS to a Metabonomics Study of Human Urine From Cigarette Smokers and Non-Smokers. *Bioanalysis* **2014,** *6* (20), 2733–2749.
163. Berg, M.; Vanaerschot, M.; Jankevics, A.; Cuypers, B.; Breitling, R.; Dujardin, J. C. LC-MS Metabolomics From Study Design to Data-Analysis—Using a Versatile Pathogen As a Test Case. *Comput. Struct. Biotechnol. J.* **2013,** *4,* e201301002.
164. Patti, G. J. Separation Strategies for Untargeted Metabolomics. *J. Sep. Sci.* **2011,** *34,* 3460–3469.
165. Ramautar, R.; de Jong, G. J. Recent Developments in Liquid-Phase Separation Techniques for Metabolomics. *Bioanalysis* **2014,** *6* (7), 1011–1026.
166. Hu, Q.; Noll, R. J.; Li, H.; Makarov, A.; Hardman, M.; Graham Cooks, R. The Orbitrap: A New Mass Spectrometer. *J. Mass Spectrom.* **2005,** *40* (4), 430–443.
167. Han, X.; Gross, R. W. Global Analyses of Cellular Lipidomes Directly From Crude Extracts of Biological Samples by ESI Mass Spectrometry: A Bridge to Lipidomics. *J. Lipid Res.* **2003,** *44* (6), 1071–1079.
168. Jian, W.; Liu, H. F.; Zhao, W.; Jones, E.; Zhu, M. Simultaneous Screening of Glutathione and Cyanide Adducts Using Precursor Ion and Neutral Loss Scans-Dependent Product Ion Spectral Acquisition and Data Mining Tools. *J. Am. Soc. Mass Spectrom.* **2012,** *23* (5), 964–976.
169. Blair, I. A. Analysis of Endogenous Glutathione-Adducts and Their Metabolites. *Biomed. Chromatogr.* **2010,** *24* (1), 29–38.
170. Ciccimaro, E.; Blair, I. A. Stable-Isotope Dilution LC-MS for Quantitative Biomarker Analysis. *Bioanalysis* **2010,** *2* (2), 311–341.
171. Knorr, A.; Dutertre, Q.; Almstetter, M.; Martin, E.; Bentley, M.; Vanscheeuwijck, P. Bioactivation of Furans by Human Lung and Liver Microsomes and S9, Drug Metabolism Reviews. In Taylor & Francis Ltd: 4 Park Square, Milton Park, Abingdon OX14 4RN, Oxon, England, 2015; pp 136–137.
172. Knorr, A.; Debrick, A.; Dutertre, Q.; Almstetter, M.; Bentley, M. In *Applicability of Different Soft Nucleophiles for Screening Reactive Metabolites Resulting from Microsomal Activation of Furan Mixtures and Cigarette Smoke, Drug Metabolism Reviews;* Informa Healthcare Telephone House: 69-77 Paul Street, London EC2A 4LQ, England, 2014; pp 33–34.
173. Armstrong, D. W.; He, L.; Liu, Y. S. Examination of Ionic Liquids and Their Interaction With Molecules, When Used As Stationary Phases in Gas Chromatography. *Anal. Chem.* **1999,** *71* (17), 3873–3876.
174. Peterson, A. C.; Hauschild, J. P.; Quarmby, S. T.; Krumwiede, D.; Lange, O.; Lemke, R. A.; Grosse-Coosmann, F.; Horning, S.; Donohue, T. J.; Westphall, M. S.; Coon, J. J.; Griep-Raming, J. Development of a GC/Quadrupole-Orbitrap Mass Spectrometer, Part I: Design and Characterization. *Anal. Chem.* **2014,** *86* (20), 10036–10043.
175. Peterson, A. C.; Balloon, A. J.; Westphall, M. S.; Coon, J. J. Development of a GC/Quadrupole-Orbitrap Mass Spectrometer, Part II: New Approaches for Discovery Metabolomics. *Anal. Chem.* **2014,** *86* (20), 10044–10051.
176. Shellie, R. A.; Welthagen, W.; Zrostlikova, J.; Spranger, J.; Ristow, M.; Fiehn, O.; Zimmermann, R. Statistical Methods for Comparing Comprehensive Two-Dimensional Gas Chromatography-Time-of-Flight Mass Spectrometry Results: Metabolomic Analysis of Mouse Tissue Extracts. *J. Chromatogr. A* **2005,** *1086* (1–2), 83–90.
177. Welthagen, W.; Shellie, R. A.; Spranger, J.; Ristow, M.; Zimmermann, R.; Fiehn, O. Comprehensive Two-Dimensional Gas Chromatography–Time-of-Flight Mass Spectrometry (GC × GC-TOF) for High Resolution Metabolomics: Biomarker Discovery on Spleen Tissue Extracts of Obese NZO Compared to Lean C57BL/6 Mice. *Metabolomics* **2005,** *1* (1), 65–73.
178. Alonso, D. E.; Binkley, J. E. Effective Comparison of Yeast Extracts Using High Resolution GC and GCxGC-HRTOFMS. *ISCC 2015*.
179. Gurdeniz, G.; Kristensen, M.; Skov, T.; Dragsted, L. O. The Effect of LC-MS Data Preprocessing Methods on the Selection of Plasma Biomarkers in Fed vs. Fasted Rats. *Metabolites* **2012,** *2* (1), 77–99.
180. Katajamaa, M.; Oresic, M. Processing Methods for Differential Analysis of LC/MS Profile Data. *BMC Bioinformatics* **2005,** *6,* 179.
181. Katajamaa, M.; Miettinen, J.; Oresic, M. MZmine: Toolbox for Processing and Visualization of Mass Spectrometry Based Molecular Profile Data. *Bioinformatics* **2006,** *22,* 634–636.

182. Pluskal, T.; Castillo, S.; Villar-Briones, A.; Oresic, M. MZmine 2: Modular Framework for Processing, Visualizing, and Analyzing Mass Spectrometry-Based Molecular Profile Data. *BMC Bioinformatics* **2010,** *11,* 395.
183. Smith, C. A.; Want, E. J.; O'Maille, G.; Abagyan, R.; Siuzdak, G. XCMS: Processing Mass Spectrometry Data for Metabolite Profiling Using Nonlinear Peak Alignment, Matching, and Identification. *Anal. Chem.* **2006,** *78,* 779–787.
184. Krishnan, S.; Vogels, J. T.; Coulier, L.; Bas, R. C.; Hendriks, M. W.; Hankemeier, T.; Thissen, U. Instrument and Process Independent Binning and Baseline Correction Methods for Liquid Chromatography-High Resolution-Mass Spectrometry Deconvolution. *Anal. Chim. Acta* **2012,** *740,* 12–19.
185. Burton, L.; Ivosev, G.; Tate, S.; Impey, G.; Wingate, J.; Bonner, R. Instrumental and Experimental Effects in LC-MS-Based Metabolomics. *J. Chromatogr. B Anal. Technol. Biomed. Life Sci.* **2008,** *871* (2), 227–235.
186. Wang, S. Y.; Kuo, C. H.; Tseng, Y. J. Batch Normalizer: A Fast Total Abundance Regression Calibration Method to Simultaneously Adjust Batch and Injection Order Effects in Liquid Chromatography/Time-of-Flight Mass Spectrometry-Based Metabolomics Data and Comparison With Current Calibration Methods. *Anal. Chem.* **2013,** *85* (2), 1037–1046.
187. Scheltema, R. A.; Kamleh, A.; Wildridge, D.; Ebikeme, C.; Watson, D. G.; Barrett, M. P.; Jansen, R. C.; Breitling, R. Increasing the Mass Accuracy of High-Resolution LC-MS Data Using Background Ions: A Case Study on the LTQ-Orbitrap. *Proteomics* **2008,** *8* (22), 4647–4656.
188. Lange, E.; Tautenhahn, R.; Neumann, S.; Gropl, C. Critical Assessment of Alignment Procedures for LC-MS Proteomics and Metabolomics Measurements. *BMC Bioinformatics* **2008,** *9,* 375.
189. Kováts, E. Gas-Chromatographische Charakterisierung Organischer Verbindungen. Teil 1: Retentionsindices Aliphatischer Halogenide, Alkohole, Aldehyde und Ketone. *Helv. Chim. Acta* **1958,** *41* (7), 1915–1932.
190. Garkani-Nejad, Z.; Karlovits, M.; Demuth, W.; Stimpfl, T.; Vycudilik, W.; Jalali-Heravi, M.; Varmuza, K. Prediction of Gas Chromatographic Retention Indices of a Diverse Set of Toxicologically Relevant Compounds. *J. Chromatogr. A* **2004,** *1028* (2), 287–295.
191. Mihaleva, V. V.; Verhoeven, H. A.; de Vos, R. C.; Hall, R. D.; van Ham, R. C. Automated Procedure for Candidate Compound Selection in GC-MS Metabolomics Based on Prediction of Kovats Retention Index. *Bioinformatics* **2009,** *25* (6), 787–794.
192. Stein, S.E. NIST Standard Reference Database 1A. http://www.nist.gov/srd/nist1a.cfm.
193. Wiley Wiley Registry 10th Edition.
194. Maurer, H. H.; Pfleger, K.; Weber, A. A. *Mass Spectral Library of Drugs, Poisons, Pesticides, Pollutants and Their Metabolites 2011;* Wiley-VCH, 2011.
195. Kopka, J.; Schauer, N.; Krueger, S.; Birkemeyer, C.; Usadel, B.; Bergmuller, E.; Dormann, P.; Weckwerth, W.; Gibon, Y.; Stitt, M.; Willmitzer, L.; Fernie, A. R.; Steinhauser, D. GMD@CSB.DB: The Golm Metabolome Database. *Bioinformatics* **2005,** *21* (8), 1635–1638.
196. Wishart, D. S. HMDB: A Knowledgebase for the Human Metabolome. *Nucleic Acids Res.* **2009,** *37,* D603–D610.
197. Smith, C. A. METLIN: A Metabolite Mass Spectral Database. *Ther. Drug Monit.* **2005,** *27,* 747–751.
198. Knorr, A.; Monge, A.; Stueber, M.; Stratmann, A.; Arndt, D.; Martin, E.; Pospisil, P. Computer-Assisted Structure Identification (CASI)—An Automated Platform for High-Throughput Identification of Small Molecules by Two-Dimensional Gas Chromatography Coupled to Mass Spectrometry. *Anal. Chem.* **2013,** *85* (23), 11216–11224.
199. Schymanski, E. L.; Meringer, M.; Brack, W. Matching Structures to Mass Spectra Using Fragmentation Patterns: Are the Results as Good as They Look? *Anal. Chem.* **2009,** *81* (9), 3608–3617.
200. Little, J. L.; Williams, A. J.; Pshenichnov, A.; Tkachenko, V. Identification of "Known Unknowns" Utilizing Accurate Mass Data and ChemSpider. *J. Am. Soc. Mass Spectrom.* **2012,** *23* (1), 179–185.
201. Williams, A. J. Public Chemical Compound Databases. *Curr. Opin. Drug Discov. Devel.* **2008,** *11* (3), 393–404.
202. Wang, Y.; Xiao, J.; Suzek, T. O.; Zhang, J.; Wang, J.; Bryant, S. H. PubChem: A Public Information System for Analyzing Bioactivities of Small Molecules. *Nucleic Acids Res.* **2009,** *37* (Web Server issue), W623–W633.
203. Ogata, H.; Goto, S.; Sato, K.; Fujibuchi, W.; Bono, H.; Kanehisa, M. KEGG: Kyoto Encyclopedia of Genes and Genomes. *Nucleic Acids Res.* **1999,** *27* (1), 29–34.
204. Kelder, T.; van Iersel, M. P.; Hanspers, K.; Kutmon, M.; Conklin, B. R.; Evelo, C. T.; Pico, A. R. WikiPathways: Building Research Communities on Biological Pathways. *Nucleic Acids Res.* **2012,** *40* (Database issue), D1301–D1307.
205. Fiehn, O.; Barupal, D. K.; Kind, T. Extending Biochemical Databases by Metabolomic Surveys. *J. Biol. Chem.* **2011,** *286* (27), 23637–23643.
206. Collings, B. A. Fragmentation of Ions in a Low Pressure Linear Ion Trap. *J. Am. Soc. Mass Spectrom.* **2007,** *18* (8), 1459–1466.
207. Eliuk, S.; Makarov, A. Evolution of Orbitrap Mass Spectrometry Instrumentation. *Annu. Rev. Anal. Chem.* **2015,** *8,* 61–80.
208. Vinaixa, M.; Schymanski, E. L.; Neumann, S.; Navarro, M.; Salek, R. M.; Yanes, O. Mass Spectral Databases for LC/MS- and GC/MS-Based Metabolomics: State of the Field and Future Prospects. *TrAC Trends Anal. Chem.* **2016,** *78,* 23–35.
209. Scheubert, K.; Hufsky, F.; Bocker, S. Computational Mass Spectrometry for Small Molecules. *J. Cheminform.* **2013,** *5* (1), 12.
210. Wolf, S.; Schmidt, S.; Muller-Hannemann, M.; Neumann, S. In Silico Fragmentation for Computer Assisted Identification of Metabolite Mass Spectra. *BMC Bioinformatics* **2010,** *11,* 148.
211. Tautenhahn, R.; Cho, K.; Uritboonthai, W.; Zhu, Z.; Patti, G. J.; Siuzdak, G. An Accelerated Workflow for Untargeted Metabolomics Using the METLIN Database. *Nat. Biotechnol.* **2012,** *30* (9), 826–828.
212. Kitano, H. Systems Biology: A Brief Overview. *Science* **2002,** *295* (5560), 1662–1664.
213. Steinhoff, C.; Vingron, M. Normalization and Quantification of Differential Expression in Gene Expression Microarrays. *Brief. Bioinform.* **2006,** *7* (2), 166–177.
214. Hung, J.-H.; Yang, T.-H.; Hu, Z.; Weng, Z.; DeLisi, C. Gene Set Enrichment Analysis: Performance Evaluation and Usage Guidelines. *Brief. Bioinform.* **2011,** bbr049.
215. Barabasi, A.-L.; Oltvai, Z. N. Network Biology: Understanding the Cell's Functional Organization. *Nat. Rev. Genet.* **2004,** *5* (2), 101–113.
216. Pray, L. Eukaryotic Genome Complexity. *Nat. Educ.* **2008,** *1* (1), 96.
217. Kanehisa, M.; Goto, S. KEGG: Kyoto Encyclopedia of Genes and Genomes. *Nucleic Acids Res.* **2000,** *28* (1), 27–30.
218. Kupershmidt, I.; Su, Q. J.; Grewal, A.; Sundaresh, S.; Halperin, I.; Flynn, J.; Shekar, M.; Wang, H.; Park, J.; Cui, W. Ontology-Based Meta-Analysis of Global Collections of High-Throughput Public Data. *PLoS One* **2010,** *5* (9), e13066.
219. Catlett, N. L.; Bargnesi, A. J.; Ungerer, S.; Seagaran, T.; Ladd, W.; Elliston, K. O.; Pratt, D. Reverse Causal Reasoning: Applying Qualitative Causal Knowledge to the Interpretation of High-Throughput Data. *BMC Bioinformatics* **2013,** *14* (1), 340.
220. Boué, S.; Talikka, M.; Westra, J. W.; Hayes, W.; Di Fabio, A.; Park, J.; Schlage, W. K.; Sewer, A.; Fields, B.; Ansari, S. Causal Biological Network Database: A Comprehensive Platform of Causal Biological Network Models Focused on the Pulmonary and Vascular Systems. *Database* **2015,** *2015,* bav030.
221. Boue, S.; Fields, B.; Hoeng, J.; Park, J.; Peitsch, M. C.; Schlage, W. K.; Talikka, M.; Binenbaum, I.; Bondarenko, V.; Bulgakov, O. V. Enhancement of COPD Biological Networks Using a Web-Based Collaboration Interface. *F1000Res.* **2015,** *4,* 32.
222. Westra, J. W.; Schlage, W. K.; Frushour, B. P.; Gebel, S.; Catlett, N. L.; Han, W.; Eddy, S. F.; Hengstermann, A.; Matthews, A. L.; Mathis, C.; Lichtner, R. B.; Poussin, C.; Talikka, M.; Veljkovic, E.; Van Hooser, A. A.; Wong, B.; Maria, M. J.; Peitsch, M. C.; Deehan, R.; Hoeng, J. Construction of a Computable Cell Proliferation Network Focused on Non-Diseased Lung Cells. *BMC Syst. Biol.* **2011,** *5* (1), 105.
223. Schlage, W. K.; Westra, J. W.; Gebel, S.; Catlett, N. L.; Mathis, C.; Frushour, B. P.; Hengstermann, A.; Van Hooser, A.; Poussin, C.; Wong, B.; Lietz, M.; Park, J.; Drubin, D.; Veljkovic, E.; Peitsch, M. C.; Hoeng, J.; Deehan, R. A Computable Cellular Stress Network Model for Non-Diseased Pulmonary and Cardiovascular Tissue. *BMC Syst. Biol.* **2011,** *5,* 168.
224. Gebel, S.; Lichtner, R. B.; Frushour, B.; Schlage, W. K.; Hoang, V.; Talikka, M.; Hengstermann, A.; Mathis, C.; Veljkovic, E.; Peck, M.; Peitsch, M. C.; Deehan, R.; Hoeng, J.; Westra, J. W.; Gebel, S.; Lichtner, R. B.; Frushour, B.; Schlage, W. K.; Hoang, V.; Talikka, M.; Hengstermann, A.; Mathis, C.; Veljkovic, E.; Peck, M.; Peitsch, M. C.; Deehan, R.; Hoeng, J.; Westra, J. W. Construction of a Computable Network Model for DNA Damage, Autophagy, Cell Death, and Senescence. *Bioinform. Biol. Insights* **2013,** *7* (11154 Additional Files), 97–117.

225. Westra, J. W.; Schlage, W. K.; Hengstermann, A.; Gebel, S.; Mathis, C.; Thomson, T.; Wong, B.; Hoang, V.; Veljkovic, E.; Peck, M.; Lichtner, R. B.; Weisensee, D.; Talikka, M.; Deehan, R.; Hoeng, J.; Peitsch, M. C. A Modular Cell-Type Focused Inflammatory Process Network Model for Non-Diseased Pulmonary Tissue. *Bioinform. Biol. Insights* **2013,** *7,* 167–192.
226. Park, J.; Schlage, W.; Frushour, B.; Talikka, M.; Toedter, G. Construction of a Computable Network Model of Tissue Repair and Angiogenesis in the Lung. *J. Clin. Toxicol.* **2013,** *S12,* 002. http://dx.doi.org/10.4172/2161-0495.
227. Howe, D.; Costanzo, M.; Fey, P.; Gojobori, T.; Hannick, L.; Hide, W.; Hill, D. P.; Kania, R.; Schaeffer, M.; St Pierre, S. Big Data: The Future of Biocuration. *Nature* **2008,** *455* (7209), 47–50.
228. Szostak, J.; Ansari, S.; Madan, S.; Fluck, J.; Talikka, M.; Iskandar, A.; De Leon, H.; Hofmann-Apitius, M.; Peitsch, M. C.; Hoeng, J. Construction of Biological Networks From Unstructured Information Based on a Semi-Automated Curation Workflow. *Database* **2015,** *2015,* bav057.
229. Szklarczyk, D.; Franceschini, A.; Wyder, S.; Forslund, K.; Heller, D.; Huerta-Cepas, J.; Simonovic, M.; Roth, A.; Santos, A.; Tsafou, K. P. STRING v10: Protein–Protein Interaction Networks, Integrated Over the Tree of Life. *Nucleic Acids Res.* **2014,** *43* (D1), D447–D452.
230. Pagel, P.; Kovac, S.; Oesterheld, M.; Brauner, B.; Dunger-Kaltenbach, I.; Frishman, G.; Montrone, C.; Mark, P.; Stümpflen, V.; Mewes, H.-W. The MIPS Mammalian Protein–Protein Interaction Database. *Bioinformatics* **2005,** *21* (6), 832–834.
231. Uetz, P.; Giot, L.; Cagney, G.; Mansfield, T. A.; Judson, R. S.; Knight, J. R.; Lockshon, D.; Narayan, V.; Srinivasan, M.; Pochart, P. A Comprehensive Analysis of Protein–Protein Interactions in *Saccharomyces cerevisiae*. *Nature* **2000,** *403* (6770), 623–627.
232. Rao, V. S.; Srinivas, K.; Sujini, G.; Kumar, G. Protein–Protein Interaction Detection: Methods and Analysis. *Int. J. Proteomics* **2014,** *2014,* 147648.
233. Stolovitzky, G.; Monroe, D.; Califano, A. Dialogue on Reverse-Engineering Assessment and Methods. *Ann. N. Y. Acad. Sci.* **2007,** *1115* (1), 1–22.
234. Greenfield, A.; Madar, A.; Ostrer, H.; Bonneau, R. DREAM4: Combining Genetic and Dynamic Information to Identify Biological Networks and Dynamical Models. *PLoS One* **2010,** *5* (10), e13397.
235. Meyer, P.; Cokelaer, T.; Chandran, D.; Kim, K. H.; Loh, P.-R.; Tucker, G.; Lipson, M.; Berger, B.; Kreutz, C.; Raue, A. Network Topology and Parameter Estimation: From Experimental Design Methods to Gene Regulatory Network Kinetics Using a Community Based Approach. *BMC Syst. Biol.* **2014,** *8* (1), 13.
236. Prill, R. J.; Saez-Rodriguez, J.; Alexopoulos, L. G.; Sorger, P. K.; Stolovitzky, G. Crowdsourcing Network Inference: The DREAM Predictive Signaling Network Challenge. *Sci. Signaling* **2011,** *4* (189), mr7.
237. Stolovitzky, G.; Prill, R. J.; Califano, A. Lessons From the DREAM2 Challenges. *Ann. N. Y. Acad. Sci.* **2009,** *1158* (1), 159–195.
238. Xiang, Y.; Kogel, U.; Gebel, S.; Peck, M. J.; Peitsch, M. C.; Akmaev, V. R.; Hoeng, J. Discovery of Emphysema Relevant Molecular Networks From an A/J Mouse Inhalation Study Using Reverse Engineering and Forward Simulation (REFS™). *Gene Regul. Syst. Biol.* **2013,** *8,* 45–61.
239. Belcastro, V.; di Bernardo, D. Reverse Engineering Transcriptional Gene Networks. *Gene Funct. Anal.* **2014,** *1101,* 179–196.
240. Opgen-Rhein, R.; Strimmer, K. Using Regularized Dynamic Correlation to Infer Gene Dependency Networks From Time-Series Microarray Data. Proceedings of the 4th International Workshop on Computational Systems Biology (WCSB 2006), Tampere, 2006; pp 73–76.
241. Chen, H.; Mundra, P. A.; Zhao, L. N.; Lin, F.; Zheng, J. Highly Sensitive Inference of Time-Delayed Gene Regulation by Network Deconvolution. *BMC Syst. Biol.* **2014,** *8* (Suppl. 4), S6.
242. Pearl, J. Causality: Models, Reasoning and Inference. *Economet. Theor.* **2003,** *19,* 675–685.
243. Rue, H.; Held, L. *Gaussian Markov Random Fields: Theory and Applications;* CRC Press, 2005.
244. Scutari, M.; Denis, J.-B. *Bayesian Networks: With Examples in R;* CRC Press, 2014.
245. Cover, T. M.; Thomas, J. A. *Elements of Information Theory;* John Wiley & Sons, 2012.
246. Kalisch, M.; Bühlmann, P. Estimating High-Dimensional Directed Acyclic Graphs With the PC-Algorithm. *J. Mach. Learn. Res.* **2007,** *8,* 613–636.
247. Zhang, X.; Zhao, X.-M.; He, K.; Lu, L.; Cao, Y.; Liu, J.; Hao, J.-K.; Liu, Z.-P.; Chen, L. Inferring Gene Regulatory Networks From Gene Expression Data by Path Consistency Algorithm Based on Conditional Mutual Information. *Bioinformatics* **2012,** *28* (1), 98–104.
248. Peng, H.; Long, F.; Ding, C. Feature Selection Based on Mutual Information Criteria of Max-Dependency, Max-Relevance, and Min-Redundancy. *IEEE Trans. Pattern Anal. Mach. Intell.* **2005,** *27* (8), 1226–1238.
249. Meyer, P. E.; Kontos, K.; Lafitte, F.; Bontempi, G. Information-Theoretic Inference of Large Transcriptional Regulatory Networks. *EURASIP J. Bioinform. Syst. Biol.* **2007,** *2007* (1), 1–9.
250. Perrin, B.-E.; Ralaivola, L.; Mazurie, A.; Bottani, S.; Mallet, J.; d'Alche–Buc, F. Gene Networks Inference Using Dynamic Bayesian Networks. *Bioinformatics* **2003,** *19* (Suppl. 2), ii138–ii148.
251. Greenfield, A.; Hafemeister, C.; Bonneau, R. Robust Data-Driven Incorporation of Prior Knowledge Into the Inference of Dynamic Regulatory Networks. *Bioinformatics* **2013,** *29* (8), 1060–1067.
252. Tibshirani, R. Regression Shrinkage and Selection via the Lasso. *J. R. Stat. Soc. B. Methodol.* **1996,** *58,* 267–288.
253. Zou, H.; Hastie, T. Regularization and Variable Selection via the Elastic Net. *J. R. Stat. Soc. Series B Stat. Methodol.* **2005,** *67* (2), 301–320.
254. Gustafsson, M.; Hörnquist, M. Gene Expression Prediction by Soft Integration and the Elastic Net—Best Performance of the DREAM3 Gene Expression Challenge. *PLoS One* **2010,** *5* (2), e9134.
255. Mordelet, F.; Vert, J.-P. SIRENE: Supervised Inference of Regulatory Networks. *Bioinformatics* **2008,** *24* (16), i76–i82.
256. Madhamshettiwar, P. B.; Maetschke, S. R.; Davis, M. J.; Reverter, A.; Ragan, M. A. Gene Regulatory Network Inference: Evaluation and Application to Ovarian Cancer Allows the Prioritization of Drug Targets. *Genome Med.* **2012,** *4* (5), 1–16.
257. Prill, R. J.; Marbach, D.; Saez-Rodriguez, J.; Sorger, P. K.; Alexopoulos, L. G.; Xue, X.; Clarke, N. D.; Altan-Bonnet, G.; Stolovitzky, G. Towards a Rigorous Assessment of Systems Biology Models: The DREAM3 Challenges. *PLoS One* **2010,** *5* (2), e9202.
258. Alyass, A.; Turcotte, M.; Meyre, D. From Big Data Analysis to Personalized Medicine for All: Challenges and Opportunities. *BMC Med. Genomics* **2015,** *8* (1), 33.
259. Mardis, E. R. The $1,000 Genome, the $100,000 Analysis. *Genome Med.* **2010,** *2* (11), 84.
260. Tong, W.; Ostroff, S.; Blais, B.; Silva, P.; Dubuc, M.; Healy, M.; Slikker, W. Genomics in the Land of Regulatory Science. *Regul. Toxicol. Pharmacol.* **2015,** *72* (1), 102–106.
261. Hoeng, J.; Deehan, R.; Pratt, D.; Martin, F.; Sewer, A.; Thomson, T. M.; Drubin, D. A.; Waters, C. A.; de Graaf, D.; Peitsch, M. C. A Network-Based Approach to Quantifying the Impact of Biologically Active Substances. *Drug Discov. Today* **2012,** *17* (9), 413–418.
262. Khatri, P.; Sirota, M.; Butte, A. J. Ten Years of Pathway Analysis: Current Approaches and Outstanding Challenges. *PLoS Comput. Biol.* **2012,** *8* (2), e1002375.
263. Krewski, D.; Acosta, D., Jr.; Andersen, M.; Anderson, H.; Bailar, J. C., III; Boekelheide, K.; Brent, R.; Charnley, G.; Cheung, V. G.; Green, S., Jr. Toxicity Testing in the 21st Century: A Vision and a Strategy. *J. Toxicol. Environ. Health Part B* **2010,** *13* (2–4), 51–138.
264. Hartung, T. Toxicology for the Twenty-First Century. *Nature* **2009,** *460* (7252), 208–212.
265. Hoeng, J.; Talikka, M.; Martin, F.; Sewer, A.; Yang, X.; Iskandar, A.; Schlage, W. K.; Peitsch, M. C. Case Study: The Role of Mechanistic Network Models in Systems Toxicology. *Drug Discov. Today* **2014,** *19* (2), 183–192.
266. Phillips, B.; Veljkovic, E.; Peck, M. J.; Buettner, A.; Elamin, A.; Guedj, E.; Vuillaume, G.; Ivanov, N. V.; Martin, F.; Boué, S. A 7-Month Cigarette Smoke Inhalation Study in C57BL/6 Mice Demonstrates Reduced Lung Inflammation and Emphysema Following Smoking Cessation or Aerosol Exposure From a Prototypic Modified Risk Tobacco Product. *Food Chem. Toxicol.* **2015,** *80,* 328–345.
267. Martin, F.; Thomson, T. M.; Sewer, A.; Drubin, D. A.; Mathis, C.; Weisensee, D.; Pratt, D.; Hoeng, J.; Peitsch, M. C. Assessment of Network Perturbation Amplitudes by Applying High-Throughput Data to Causal Biological Networks. *BMC Syst. Biol.* **2012,** *6* (1), 54.
268. Martin, F.; Sewer, A.; Talikka, M.; Xiang, Y.; Hoeng, J.; Peitsch, M. C. Quantification of Biological Network Perturbations for Mechanistic Insight and Diagnostics Using Two-Layer Causal Models. *BMC Bioinformatics* **2014,** *15* (1), 1.

269. Thomson, T. M.; Sewer, A.; Martin, F.; Belcastro, V.; Frushour, B. P.; Gebel, S.; Park, J.; Schlage, W. K.; Talikka, M.; Vasilyev, D. M. Quantitative Assessment of Biological Impact Using Transcriptomic Data and Mechanistic Network Models. *Toxicol. Appl. Pharmacol.* **2013,** *272* (3), 863–878.
270. Gonzalez-Suarez, I.; Sewer, A.; Walker, P.; Mathis, C.; Ellis, S.; Woodhouse, H.; Guedj, E.; Dulize, R.; Marescotti, D.; Acali, S. Systems Biology Approach for Evaluating the Biological Impact of Environmental Toxicants In Vitro. *Chem. Res. Toxicol.* **2014,** *27* (3), 367–376.
271. Wilkinson, D. J. *Stochastic Modelling for Systems Biology;* CRC press: Boca Raton, Florida, 2011.
272. Sauro, H. M. *Enzyme Kinetics for Systems Biology;* Future Skill Software: Pasadena, California, 2012.
273. Li, C.; Donizelli, M.; Rodriguez, N.; Dharuri, H.; Endler, L.; Chelliah, V.; Li, L.; He, E.; Henry, A.; Stefan, M. I. BioModels Database: An Enhanced, Curated and Annotated Resource for Published Quantitative Kinetic Models. *BMC Syst. Biol.* **2010,** *4* (1), 92.
274. Savageau, M. A. *Biochemical Systems Analysis: A Study of Function and Design in Molecular Biology;* Addison-Wesley, 1976.
275. Voit, E. O. *Computational Analysis of Biochemical Systems: A Practical Guide for Biochemists and Molecular Biologists;* Cambridge University Press, 2000.
276. Kikuchi, S.; Tominaga, D.; Arita, M.; Takahashi, K.; Tomita, M. Dynamic Modeling of Genetic Networks Using Genetic Algorithm and S-System. *Bioinformatics* **2003,** *19* (5), 643–650.
277. Wilhelm, T. The Smallest Chemical Reaction System With Bistability. *BMC Syst. Biol.* **2009,** *3* (1), 1.
278. Ingalls, B. *Mathematical Modelling in Systems Biology: An Introduction;* MIT Press: Massachusetts, 2013. Internet.[cited at p. 117].
279. Eissing, T.; Conzelmann, H.; Gilles, E. D.; Allgöwer, F.; Bullinger, E.; Scheurich, P. Bistability Analyses of a Caspase Activation Model for Receptor-Induced Apoptosis. *J. Biol. Chem.* **2004,** *279* (35), 36892–36897.
280. Legewie, S.; Blüthgen, N.; Herzel, H. Mathematical Modeling Identifies Inhibitors of Apoptosis As Mediators of Positive Feedback and Bistability. *PLoS Comput. Biol.* **2006,** *2* (9), e120.
281. Hasdemir, D.; Hoefsloot, H. C.; Smilde, A. K. Validation and Selection of ODE Based Systems Biology Models: How to Arrive at More Reliable Decisions. *BMC Syst. Biol.* **2015,** *9* (1), 1.
282. Hasdemir, D.; Hoefsloot, H. C.; Westerhuis, J. A.; Smilde, A. K. How Informative Is Your Kinetic Model?: Using Resampling Methods for Model Invalidation. *BMC Syst. Biol.* **2014,** *8* (1), 1.
283. Iyengar, R.; Zhao, S.; Chung, S.-W.; Mager, D. E.; Gallo, J. M. Merging Systems Biology With Pharmacodynamics. *Sci. Transl. Med.* **2012,** *4* (126), 126ps7.
284. Panetta, J. C.; Sparreboom, A.; Pui, C.-H.; Relling, M. V.; Evans, W. E. Modeling Mechanisms of In Vivo Variability in Methotrexate Accumulation and Folate Pathway Inhibition in Acute Lymphoblastic Leukemia Cells. *PLoS Comput. Biol.* **2010,** *6* (12), e1001019.
285. Peters, S. A. Physiologically-Based Pharmacokinetic (PBPK) Modeling and Simulations: Principles, Methods, and Applications in the Pharmaceutical Industry. *John Wiley & Sons* **2012**.
286. Boland, M. R.; Jacunski, A.; Lorberbaum, T.; Romano, J. D.; Moskovitch, R.; Tatonetti, N. P. Systems Biology Approaches for Identifying Adverse Drug Reactions and Elucidating Their Underlying Biological Mechanisms. *Wiley Interdiscip. Rev. Syst. Biol. Med.* **2015**.
287. Hopkins, A. L. Network Pharmacology. *Nat. Biotechnol.* **2007,** *25* (10), 1110.
288. Hopkins, A. L. Network Pharmacology: The Next Paradigm in Drug Discovery. *Nat. Chem. Biol.* **2008,** *4* (11), 682–690.
289. Xie, L.; Xie, L.; Bourne, P. E. Structure-Based Systems Biology for Analyzing Off-Target Binding. *Curr. Opin. Struct. Biol.* **2011,** *21* (2), 189–199.
290. Csermely, P.; Korcsmáros, T.; Kiss, H. J.; London, G.; Nussinov, R. Structure and Dynamics of Molecular Networks: A Novel Paradigm of Drug Discovery: A Comprehensive Review. *Pharmacol. Ther.* **2013,** *138* (3), 333–408.
291. Haanstra, J. R.; Bakker, B. M. Drug Target Identification Through Systems Biology. *Drug Discov. Today Technol.* **2015,** *15,* 17–22.
292. Wu, Q.; Yang, Z.; Nie, Y.; Shi, Y.; Fan, D. Multi-Drug Resistance in Cancer Chemotherapeutics: Mechanisms and Lab Approaches. *Cancer Lett.* **2014,** *347* (2), 159–166.
293. Ye, H.; Liu, Q.; Wei, J. Construction of Drug Network Based on Side Effects and Its Application for Drug Repositioning. *PLoS One* **2014,** *9* (2), e87864.
294. Atias, N.; Sharan, R. An Algorithmic Framework for Predicting Side Effects of Drugs. *J. Comput. Biol.* **2011,** *18* (3), 207–218.
295. Pérez-Nueno, V. I.; Souchet, M.; Karaboga, A. S.; Ritchie, D. W. GESSE: Predicting Drug Side Effects From Drug–Target Relationships. *J. Chem. Inf. Model.* **2015,** *55* (9), 1804–1823.
296. Jiang, Y.; Li, Y.; Kuang, Q.; Ye, L.; Wu, Y.; Yang, L.; Li, M. Predicting Putative Adverse Drug Reaction Related Proteins Based on Network Topological Properties. *Anal. Methods* **2014,** *6* (8), 2692–2698.
297. Lee, S.; Lee, K. H.; Song, M.; Lee, D. Building the Process-Drug–Side Effect Network to Discover the Relationship Between Biological Processes and Side Effects. *BMC Bioinformatics* **2011,** *12* (2), 1.
298. Kuhn, M.; Al Banchaabouchi, M.; Campillos, M.; Jensen, L. J.; Gross, C.; Gavin, A. C.; Bork, P. Systematic Identification of Proteins That Elicit Drug Side Effects. *Mol. Syst. Biol.* **2013,** *9* (1), 663.
299. Zhao, S.; Li, S. Network-Based Relating Pharmacological and Genomic Spaces for Drug Target Identification. *PLoS One* **2010,** *5* (7), e11764.
300. Cao, D. S.; Xiao, N.; Li, Y. J.; Zeng, W. B.; Liang, Y. Z.; Lu, A. P.; Xu, Q. S.; Chen, A. Integrating Multiple Evidence Sources to Predict Adverse Drug Reactions Based on a Systems Pharmacology Model. *CPT Pharmacometrics Syst. Pharmacol.* **2015,** *4* (9), 498–506.
301. Cheng, F.; Li, W.; Wang, X.; Zhou, Y.; Wu, Z.; Shen, J.; Tang, Y. Adverse Drug Events: Database Construction and In Silico Prediction. *J. Chem. Inf. Model.* **2013,** *53* (4), 744–752.
302. Liu, M.; Wu, Y.; Chen, Y.; Sun, J.; Zhao, Z.; Chen, X.-W.; Matheny, M. E.; Xu, H. Large-Scale Prediction of Adverse Drug Reactions Using Chemical, Biological, and Phenotypic Properties of Drugs. *J. Am. Med. Inform. Assoc.* **2012,** *19* (e1), e28–e35.
303. Benet, M.; Moya, M.; Donato, M. T.; Lahoz, A.; Hervás, D.; Guzmán, C.; Gómez-Lechón, M. J.; Castell, J. V.; Jover, R. A Simple Transcriptomic Signature Able to Predict Drug-Induced Hepatic Steatosis. *Arch. Toxicol.* **2014,** *88* (4), 967–982.
304. Martin, F.; Talikka, M.; Hoeng, J.; Peitsch, M. Identification of Gene Expression Signature for Cigarette Smoke Exposure Response—From Man to Mouse. *Hum. Exp. Toxicol.* **2015,** *34* (12), 1200–1211.
305. Wild, C. P. The Exposome: From Concept to Utility. *Int. J. Epidemiol.* **2012,** *41* (1), 24–32.
306. Rappaport, S. M. Biomarkers Intersect With the Exposome. *Biomarkers* **2012,** *17* (6), 483–489.
307. Go, Y.-M.; Walker, D. I.; Liang, Y.; Uppal, K.; Soltow, Q. A.; Tran, V.; Strobel, F.; Quyyumi, A. A.; Ziegler, T. R.; Pennell, K. D. Reference Standardization for Mass Spectrometry and High-Resolution Metabolomics Applications to Exposome Research. *Toxicol. Sci.* **2015,** *148* (2), 531–543.
308. Athersuch, T. Metabolome Analyses in Exposome Studies: Profiling Methods for a Vast Chemical Space. *Arch. Biochem. Biophys.* **2016,** *589,* 177–186.
309. Bouhifd, M.; Hogberg, H. T.; Kleensang, A.; Maertens, A.; Zhao, L.; Hartung, T. Mapping the Human Toxome by Systems Toxicology. *Basic Clin. Pharmacol. Toxicol.* **2014,** *115* (1), 24–31.
310. Fasani, R. A.; Livi, C. B.; Roy Choudhury, D.; Kleensang, A.; Bouhifd, M.; Pendse, S. N.; McMullen, P. D.; Anderson, M. E.; Hartung, T.; Rosenberg, M. The Human Toxome Collaboratorium: A Shared environment for Multi-Omic Computational Collaboration Within a Consortium. *Front. Pharmacol.* **2015,** *6,* 322.
311. Maertens, A.; Luechtefeld, T.; Kleensang, A.; Hartung, T. MPTP's Pathway of Toxicity Indicates Central Role of Transcription Factor SP1. *Arch. Toxicol.* **2015,** *89* (5), 743–755.
312. Pendse, S. N.; Maertens, A.; Rosenberg, M.; Roy, D.; Fasani, R. A.; Vantangoli, M. M.; Madnick, S. J.; Boekelheide, K.; Fornace, A. J.; Yager, J. D. Information-Dependent Enrichment Analysis Reveals Time-Dependent Transcriptional Regulation of the Estrogen Pathway of Toxicity. *Arch. Toxicol.* **2016,** 038570.
313. Phillips, B.; Veljkovic, E.; Boué, S.; Schlage, W. K.; Vuillaume, G.; Martin, F.; Titz, B.; Leroy, P.; Buettner, A.; Elamin, A. An 8-Month Systems Toxicology Inhalation/Cessation Study in Apoe −/− Mice to Investigate Cardiovascular and Respiratory Exposure Effects of a Candidate Modified Risk Tobacco Product, THS 2.2, Compared With Conventional Cigarettes. *Toxicol. Sci.* **2015,** kfv243.

314. Gonzalez-Suarez, I.; Martin, F.; Marescotti, D.; Guedj, E.; Acali, S.; Johne, S.; Dulize, R.; Baumer, K.; Peric, D.; Goedertier, D.; Frentzel, S.; Ivanov, N. V.; Mathis, C.; Hoeng, J.; Peitsch, M. C. In Vitro Systems Toxicology Assessment of a Candidate Modified Risk Tobacco Product Shows Reduced Toxicity Compared to That of a Conventional Cigarette. *Chem. Res. Toxicol.* **2016,** *29* (1), 3–18.
315. Kogel, U.; Gonzalez Suarez, I.; Xiang, Y.; Dossin, E.; Guy, P. A.; Mathis, C.; Marescotti, D.; Goedertier, D.; Martin, F.; Peitsch, M. C.; Hoeng, J. Biological Impact of Cigarette Smoke Compared to an Aerosol Produced From a Prototypic Modified Risk Tobacco Product on Normal Human Bronchial Epithelial Cells. *Toxicol. In Vitro* **2015,** *29* (8), 2102–2115.
316. WHO Healthy diet: Fact sheet no 394. http://www.who.int/mediacentre/factsheets/fs394/en/ (accessed 12 February 2015).
317. Mandair, D. S.; Rossi, R. E.; Pericleous, M.; Whyand, T.; Caplin, M. The Impact of Diet and Nutrition in the Prevention and Progression of Hepatocellular Carcinoma. *Expert Rev. Gastroenterol. Hepatol.* **2014,** *8* (4), 369–382.
318. Aragon, F.; Perdigon, G.; de Moreno de LeBlanc, A. Modification in the Diet Can Induce Beneficial Effects Against Breast Cancer. *World J. Clin. Oncol.* **2014,** *5* (3), 455–464.
319. Ahmad, A.; Ginnebaugh, K. R.; Li, Y.; Padhye, S. B.; Sarkar, F. H. Molecular Targets of Naturopathy in Cancer Research: Bridge to Modern Medicine. *Nutrients* **2015,** *7* (1), 321–334.
320. Enns, J. E.; Yeganeh, A.; Zarychanski, R.; Abou-Setta, A. M.; Friesen, C.; Zahradka, P.; Taylor, C. G. The Impact of Omega-3 Polyunsaturated Fatty Acid Supplementation on the Incidence of Cardiovascular Events and Complications in Peripheral Arterial Disease: A Systematic Review and Meta-Analysis. *BMC Cardiovasc. Disord.* **2014,** *14,* 70.
321. Espin, J. C.; Garcia-Conesa, M. T.; Tomas-Barberan, F. A. Nutraceuticals: Facts and Fiction. *Phytochemistry* **2007,** *68* (22–24), 2986–3008.
322. Gylling, H.; Plat, J.; Turley, S.; Ginsberg, H. N.; Ellegard, L.; Jessup, W.; Jones, P. J.; Lutjohann, D.; Maerz, W.; Masana, L.; Silbernagel, G.; Staels, B.; Boren, J.; Catapano, A. L.; De Backer, G.; Deanfield, J.; Descamps, O. S.; Kovanen, P. T.; Riccardi, G.; Tokgozoglu, L.; Chapman, M. J. Plant Sterols and Plant Stanols in the Management of Dyslipidaemia and Prevention of Cardiovascular Disease. *Atherosclerosis* **2014,** *232* (2), 346–360.
323. Jang, M.; Cai, L.; Udeani, G. O.; Slowing, K. V.; Thomas, C. F.; Beecher, C. W.; Fong, H. H.; Farnsworth, N. R.; Kinghorn, A. D.; Mehta, R. G.; Moon, R. C.; Pezzuto, J. M. Cancer Chemopreventive Activity of Resveratrol, a Natural Product Derived From Grapes. *Science* **1997,** *275* (5297), 218–220.
324. Mecocci, P.; Tinarelli, C.; Schulz, R. J.; Polidori, M. C. Nutraceuticals in Cognitive Impairment and Alzheimer's Disease. *Front. Pharmacol.* **2014,** *5,* 147.
325. Benetou, V.; Orfanos, P.; Lagiou, P.; Trichopoulos, D.; Boffetta, P.; Trichopoulou, A. Vegetables and Fruits in Relation to Cancer Risk: Evidence From the Greek EPIC Cohort Study. *Cancer Epidemiol. Biomarkers Prev.* **2008,** *17* (2), 387–392.
326. Freedman, N. D.; Park, Y.; Subar, A. F.; Hollenbeck, A. R.; Leitzmann, M. F.; Schatzkin, A.; Abnet, C. C. Fruit and Vegetable Intake and Head and Neck Cancer Risk in a Large United States Prospective Cohort Study. *Int. J. Cancer* **2008,** *122* (10), 2330–2336.
327. Byrne, M. M.; Murphy, R. T.; Ryan, A. W. Epigenetic Modulation in the Treatment of Atherosclerotic Disease. *Front. Genet.* **2014,** *5,* 364.
328. Boesch-Saadatmandi, C.; Loboda, A.; Wagner, A. E.; Stachurska, A.; Jozkowicz, A.; Dulak, J.; Doring, F.; Wolffram, S.; Rimbach, G. Effect of Quercetin and Its Metabolites Isorhamnetin and Quercetin-3-glucuronide on Inflammatory Gene Expression: Role of miR-155. *J. Nutr. Biochem.* **2011,** *22* (3), 293–299.
329. Chin, Y. T.; Hsieh, M. T.; Yang, S. H.; Tsai, P. W.; Wang, S. H.; Wang, C. C.; Lee, Y. S.; Cheng, G. Y.; HuangFu, W. C.; London, D.; Tang, H. Y.; Fu, E.; Yen, Y.; Liu, L. F.; Lin, H. Y.; Davis, P. J. Anti-Proliferative and Gene Expression Actions of Resveratrol in Breast Cancer Cells In Vitro. *Oncotarget* **2014,** *5* (24), 12891–12907.
330. Wang, C. T.; Chang, H. H.; Hsiao, C. H.; Lee, M. J.; Ku, H. C.; Hu, Y. J.; Kao, Y. H. The Effects of Green Tea (-)-Epigallocatechin-3-Gallate on Reactive Oxygen Species in 3T3-L1 Preadipocytes and Adipocytes Depend on the Glutathione and 67 kDa Laminin Receptor Pathways. *Mol. Nutr. Food Res.* **2009,** *53* (3), 349–360.
331. Isbrucker, R. A.; Bausch, J.; Edwards, J. A.; Wolz, E. Safety Studies on Epigallocatechin Gallate (EGCG) Preparations. Part 1: Genotoxicity. *Food Chem. Toxicol.* **2006,** *44* (5), 626–635.
332. Nishida, N.; Goel, A. Genetic and Epigenetic Signatures in Human Hepatocellular Carcinoma: A Systematic Review. *Curr. Genomics* **2011,** *12* (2), 130–137.
333. da Costa, A. N.; Herceg, Z. Detection of Cancer-Specific Epigenomic Changes in Biofluids: Powerful Tools in Biomarker Discovery and Application. *Mol. Oncol.* **2012,** *6* (6), 704–715.
334. Katoh, M. Cardio-miRNAs and Onco-miRNAs: Circulating miRNA-Based Diagnostics for Non-Cancerous and Cancerous Diseases. *Front. Cell Dev. Biol.* **2014,** *2,* 61.
335. Bujak, R.; Struck-Lewicka, W.; Markuszewski, M. J.; Kaliszan, R. Metabolomics for Laboratory Diagnostics. *J. Pharm. Biomed. Anal.* **2015,** *113,* 108–120.
336. Chen, H.; Zhu, Z.; Zhu, Y.; Wang, J.; Mei, Y.; Cheng, Y. Pathway Mapping and Development of Disease-Specific Biomarkers: Protein-Based Network Biomarkers. *J. Cell. Mol. Med.* **2015,** *19* (2), 297–314.
337. Beger, R. D. A Review of Applications of Metabolomics in Cancer. *Metabolites* **2013,** *3* (3), 552–574.
338. Vermeersch, K. A.; Styczynski, M. P. Applications of Metabolomics in Cancer Research. *J. Carcinog.* **2013,** *12,* 9.
339. Golman, K.; Zandt, R. I.; Lerche, M.; Pehrson, R.; Ardenkjaer-Larsen, J. H. Metabolic Imaging by Hyperpolarized 13C Magnetic Resonance Imaging for In Vivo Tumor Diagnosis. *Cancer Res.* **2006,** *66,* 10855–10860.
340. Shetty, K. T. Metabolomics: Impact on Diagnosis and Monitoring of 'Inborn'/'Acquired' Metabolic Disorders. *Indian J. Clin. Biochem.* **2007,** *22* (2), 3–5.
341. Miller, M. J.; Kennedy, A. D.; Eckhart, A. D.; Burrage, L. C.; Wulff, J. E.; Miller, L. A.; Milburn, M. V.; Ryals, J. A.; Beaudet, A. L.; Sun, Q.; Sutton, V. R.; Elsea, S. H. Untargeted Metabolomic Analysis for the Clinical Screening of Inborn Errors of Metabolism. *J. Inherit. Metab. Dis.* **2015,** *38* (6), 1029–1039.
342. Scolamiero, E.; Cozzolino, C.; Albano, L.; Ansalone, A.; Caterino, M.; Corbo, G.; di Girolamo, M. G.; Di Stefano, C.; Durante, A.; Franzese, G.; Franzese, I.; Gallo, G.; Giliberti, P.; Ingenito, L.; Ippolito, G.; Malamisura, B.; Mazzeo, P.; Norma, A.; Ombrone, D.; Parenti, G.; Pellecchia, S.; Pecce, R.; Pierucci, I.; Romanelli, R.; Rossi, A.; Siano, M.; Stoduto, T.; Villani, G. R.; Andria, G.; Salvatore, F.; Frisso, G.; Ruoppolo, M. Targeted Metabolomics in the Expanded Newborn Screening for Inborn Errors of Metabolism. *Mol. BioSyst.* **2015,** *11* (6), 1525–1535.
343. Stegemann, C.; Pechlaner, R.; Willeit, P.; Langley, S. R.; Mangino, M.; Mayr, U.; Menni, C.; Moayyeri, A.; Santer, P.; Rungger, G.; Spector, T. D.; Willeit, J.; Kiechl, S.; Mayr, M. Lipidomics Profiling and Risk of Cardiovascular Disease in the Prospective Population-Based Bruneck Study. *Circulation* **2014,** *129* (18), 1821–1831.
344. De Leon, H.; Boue, S.; Szostak, J.; Peitsch, M. C.; Hoeng, J. Systems Biology Research Into Cardiovascular Disease: Contributions of Lipidomics-Based Approaches to Biomarker Discovery. *Curr. Drug Discov. Technol.* **2015,** *12* (3), 129–154.
345. Hinterwirth, H.; Stegemann, C.; Mayr, M. Lipidomics: Quest for Molecular Lipid Biomarkers in Cardiovascular Disease. *Circ. Cardiovasc. Genet.* **2014,** *7* (6), 941–954.
346. Meikle, P. J.; Wong, G.; Barlow, C. K.; Kingwell, B. A. Lipidomics: Potential Role in Risk Prediction and Therapeutic Monitoring for Diabetes and Cardiovascular Disease. *Pharmacol. Ther.* **2014,** *143* (1), 12–23.
347. Gross, R. W.; Han, X. Lipidomics in Diabetes and the Metabolic Syndrome. *Methods Enzymol.* **2007,** *433,* 73–90.
348. Fan, F.; Mundra, P. A.; Fang, L.; Galvin, A.; Moore, X. L.; Weir, J. M.; Wong, G.; White, D. A.; Chin-Dusting, J.; Sparrow, M. P.; Meikle, P. J.; Dart, A. M. Lipidomic Profiling in Inflammatory Bowel Disease: Comparison Between Ulcerative Colitis and Crohn's Disease. *Inflamm. Bowel Dis.* **2015,** *21* (7), 1511–1518.
349. Arita, M. Mediator Lipidomics in Acute Inflammation and Resolution. *J. Biochem.* **2012,** *152* (4), 313–319.
350. Touboul, D.; Gaudin, M. Lipidomics of Alzheimer's Disease. *Bioanalysis* **2014,** *6* (4), 541–561.
351. Wood, P. L. Lipidomics of Alzheimer's Disease: Current Status. *Alzheimers Res. Ther.* **2012,** *4* (1), 5.
352. Hilvo, M.; Denkert, C.; Lehtinen, L.; Muller, B.; Brockmoller, S.; Seppanen-Laakso, T.; Budczies, J.; Bucher, E.; Yetukuri, L.; Castillo, S.; Berg, E.; Nygren, H.; Sysi-Aho, M.; Griffin, J. L.; Fiehn, O.; Loibl, S.; Richter-Ehrenstein, C.; Radke, C.; Hyotylainen, T.; Kallioniemi, O.; Iljin, K.; Oresic, M. Novel Theranostic Opportunities Offered by Characterization of Altered Membrane Lipid Metabolism in Breast Cancer Progression. *Cancer Res.* **2011,** *71* (9), 3236–3245.
353. Zhou, X.; Mao, J.; Ai, J.; Deng, Y.; Roth, M. R.; Pound, C.; Henegar, J.; Welti, R.; Bigler, S. A. Identification of Plasma Lipid Biomarkers for Prostate Cancer by Lipidomics and Bioinformatics. *PLoS One* **2012,** *7* (11), e48889.
354. Maguire, G. Using a Systems-Based Approach to Overcome Reductionist Strategies in the Development of Diagnostics. *Expert. Rev. Mol. Diagn.* **2013,** *13* (8), 895–905.
355. Sun, Y. V.; Hu, Y. J. Integrative Analysis of Multi-Omics Data for Discovery and Functional Studies of Complex Human Diseases. *Adv. Genet.* **2016,** *93,* 147–190.

356. Higdon, R.; Earl, R. K.; Stanberry, L.; Hudac, C. M.; Montague, E.; Stewart, E.; Janko, I.; Choiniere, J.; Broomall, W.; Kolker, N. The Promise of Multi-Omics and Clinical Data Integration to Identify and Target Personalized Healthcare Approaches in Autism Spectrum Disorders. *OMICS* **2015,** *19* (4), 197–208.
357. Caberlotto, L.; Lauria, M. Systems Biology Meets-Omic Technologies: Novel Approaches to Biomarker Discovery and Companion Diagnostic Development. *Expert. Rev. Mol. Diagn.* **2015,** *15* (2), 255–265.
358. Chen, R.; Snyder, M. Systems Biology: Personalized Medicine for the Future? *Curr. Opin. Pharmacol.* **2012,** *12* (5), 623–628.
359. Collins, F. S.; Varmus, H. A New Initiative on Precision Medicine. *N. Engl. J. Med.* **2015,** *372* (9), 793–795.
360. Vogt, H.; Hofmann, B.; Getz, L. The New Holism: P4 Systems Medicine and the Medicalization of Health and Life Itself. *Med. Health Care Philos.* **2016,** *19* (2), 1–17.
361. Hood, L. Systems Biology and p4 Medicine: Past, Present, and Future. *Rambam Maimonides Med. J.* **2013,** *4* (2), e0012.
362. Wehling, M. Translational Medicine: Can It Really Facilitate the Transition of Research "From Bench to Bedside"? *Eur. J. Clin. Pharmacol.* **2006,** *62* (2), 91–95.
363. Ideker, T.; Galitski, T.; Hood, L. A New Approach to Decoding Life: Systems Biology. *Annu. Rev. Genomics Hum. Genet.* **2001,** *2* (1), 343–372.
364. Iskandar, A. R.; Martin, F.; Talikka, M.; Schlage, W. K.; Kostadinova, R.; Mathis, C.; Hoeng, J.; Peitsch, M. C. Systems Approaches Evaluating the Perturbation of Xenobiotic Metabolism in Response to Cigarette Smoke Exposure in Nasal and Bronchial Tissues. *Biomed. Res. Int.* **2013,** *2013,* 512086.
365. Bielekova, B.; Vodovotz, Y.; An, G.; Hallenbeck, J. How Implementation of Systems Biology Into Clinical Trials Accelerates Understanding of Diseases. *Front. Neurol.* **2014,** *5,* 102.
366. Frick, A.; Suzuki, O.; Butz, N.; Chan, E.; Wiltshire, T. In Vitro and In Vivo Mouse Models for Pharmacogenetic Studies. *Methods Mol. Biol.* **2013,** 263–278.
367. Seok, J.; Warren, H. S.; Cuenca, A. G.; Mindrinos, M. N.; Baker, H. V.; Xu, W.; Richards, D. R.; McDonald-Smith, G. P.; Gao, H.; Hennessy, L. Genomic Responses in Mouse Models Poorly Mimic Human Inflammatory Diseases. *Proc. Natl. Acad. Sci. U. S. A.* **2013,** *110* (9), 3507–3512.
368. Green, S. B. Can Animal Data Translate to Innovations Necessary for a New Era of Patient-Centred and Individualised Healthcare? Bias in Preclinical Animal Research. *BMC Med. Ethics* **2015,** *16* (1), 1.
369. Gharib, W. H.; Robinson-Rechavi, M. When Orthologs Diverge Between Human and Mouse. *Brief. Bioinform.* **2011,** *12* (5), 436–441.
370. Odom, D. T.; Dowell, R. D.; Jacobsen, E. S.; Gordon, W.; Danford, T. W.; MacIsaac, K. D.; Rolfe, P. A.; Conboy, C. M.; Gifford, D. K.; Fraenkel, E. Tissue-Specific Transcriptional Regulation Has Diverged Significantly Between Human and Mouse. *Nat. Genet.* **2007,** *39* (6), 730–732.
371. Suo, J.; Ferrara, D. E.; Sorescu, D.; Guldberg, R. E.; Taylor, W. R.; Giddens, D. P. Hemodynamic Shear Stresses in Mouse Aortas Implications for Atherogenesis. *Arterioscler. Thromb. Vasc. Biol.* **2007,** *27* (2), 346–351.
372. Meyer, P.; Alexopoulos, L. G.; Bonk, T.; Califano, A.; Cho, C. R.; de la Fuente, A.; de Graaf, D.; Hartemink, A. J.; Hoeng, J.; Ivanov, N. V. Verification of Systems Biology Research in the Age of Collaborative Competition. *Nat. Biotechnol.* **2011,** *29* (9), 811.
373. Poussin, C.; Mathis, C.; Alexopoulos, L. G.; Messinis, D. E.; Dulize, R. H.; Belcastro, V.; Melas, I. N.; Sakellaropoulos, T.; Rhrissorrakrai, K.; Bilal, E. The Species Translation Challenge—A Systems Biology Perspective on Human and Rat Bronchial Epithelial Cells. *Sci. Data* **2014,** *1,* 140009.
374. Rhrissorrakrai, K.; Belcastro, V.; Bilal, E.; Norel, R.; Poussin, C.; Mathis, C.; Dulize, R. H.; Ivanov, N. V.; Alexopoulos, L.; Rice, J. J. Understanding the Limits of Animal Models As Predictors of Human Biology: Lessons Learned From the sbv IMPROVER Species Translation Challenge. *Bioinformatics* **2014,** btu611.
375. Ferl, G. Z.; Theil, F. P.; Wong, H. Physiologically-Based Pharmacokinetic Models of Small Molecules and Therapeutic Antibodies: Mini-Review on Fundamental Concepts and Applications. *Biopharm. Drug Dispos.* **2015**.
376. Caruso, A.; Frances, N.; Meille, C.; Greiter-Wilke, A.; Hillebrecht, A.; Lavé, T. Translational PK/PD Modeling for Cardiovascular Safety Assessment of Drug Candidates: Methods and Examples in Drug Development. *J. Pharmacol. Toxicol. Methods* **2014,** *70* (1), 73–85.
377. Zhao, J.; Cao, Y.; Jusko, W. J. Across-Species Scaling of Monoclonal Antibody Pharmacokinetics Using a Minimal PBPK Model. *Pharm. Res.* **2015,** *32* (10), 3269–3281.
378. Wang, X.; Santostefano, M. J.; DeVito, M. J.; Birnbaum, L. S. Extrapolation of a PBPK Model for Dioxins Across Dosage Regimen, Gender, Strain, and Species. *Toxicol. Sci.* **2000,** *56* (1), 49–60.
379. Hall, C.; Lueshen, E.; Mošat, A.; Linninger, A. A. Interspecies Scaling in Pharmacokinetics: A Novel Whole-Body Physiologically Based Modeling Framework to Discover Drug Biodistribution Mechanisms In Vivo. *J. Pharm. Sci.* **2012,** *101* (3), 1221–1241.
380. Thiel, C.; Schneckener, S.; Krauss, M.; Ghallab, A.; Hofmann, U.; Kanacher, T.; Zellmer, S.; Gebhardt, R.; Hengstler, J. G.; Kuepfer, L. A Systematic Evaluation of the Use of Physiologically Based Pharmacokinetic Modeling for Cross-Species Extrapolation. *J. Pharm. Sci.* **2015,** *104* (1), 191–206.
381. Hoeng, J.; Talikka, M.; Martin, F.; Ansari, S.; Drubin, D.; Elamin, A.; Gebel, S.; Ivanov, N.; Kenny, R.; Koegel, U. *Toxicopanomics: Applications of Genomics, Transcriptomics, Proteomics and Lipidomics in Predictive Mechanistic Toxicology;* CRC Press: Boca Raton, FL, 2014.
382. Mayer, G.; Heinze, G.; Mischak, H.; Hellemons, M. E.; Heerspink, H. J. L.; Bakker, S. J.; de Zeeuw, D.; Haiduk, M.; Rossing, P.; Oberbauer, R. Omics–Bioinformatics in the Context of Clinical Data. *Methods Mol. Biol.* **2011,** 479–497.
383. Krzywinski, M.; Altman, N. Points of Significance: Power and Sample Size. *Nat. Methods* **2013,** *10* (12), 1139–1140.
384. Courant, F.; Antignac, J. P.; Dervilly-Pinel, G.; Le Bizec, B. Basics of Mass Spectrometry Based Metabolomics. *Proteomics* **2014,** *14* (21–22), 2369–2388.
385. Rocca-Serra, P.; Brandizi, M.; Maguire, E.; Sklyar, N.; Taylor, C.; Begley, K.; Field, D.; Harris, S.; Hide, W.; Hofmann, O. ISA Software Suite: Supporting Standards-Compliant Experimental Annotation and Enabling Curation at the Community Level. *Bioinformatics* **2010,** *26* (18), 2354–2356.
386. Leek, J. T.; Scharpf, R. B.; Bravo, H. C.; Simcha, D.; Langmead, B.; Johnson, W. E.; Geman, D.; Baggerly, K.; Irizarry, R. A. Tackling the Widespread and Critical Impact of Batch Effects in High-Throughput Data. *Nat. Rev. Genet.* **2010,** *11* (10), 733–739.
387. Shi, L.; Reid, L. H.; Jones, W. D.; Shippy, R.; Warrington, J. A.; Baker, S. C.; Collins, P. J.; De Longueville, F.; Kawasaki, E. S.; Lee, K. Y. The MicroArray Quality Control (MAQC) Project Shows Inter-and Intraplatform Reproducibility of Gene Expression Measurements. *Nat. Biotechnol.* **2006,** *24* (9), 1151–1161.
388. Consortium, S. M.-I. A Comprehensive Assessment of RNA-seq Accuracy, Reproducibility and Information Content by the Sequencing Quality Control Consortium. *Nat. Biotechnol.* **2014,** *32* (9), 903–914.
389. Marx, V. Biology: The Big Challenges of Big Data. *Nature* **2013,** *498* (7453), 255–260.
390. Cavill, R.; Jennen, D.; Kleinjans, J.; Briedé, J. J. Transcriptomic and Metabolomic Data Integration. *Brief. Bioinform.* **2015,** bbv090.
391. Choi, H.; Pavelka, N. When One and One Gives More Than Two: Challenges and Opportunities of Integrative Omics. *Front. Genet.* **2011,** *2* (105), 105.
392. Palsson, B.; Zengler, K. The Challenges of Integrating Multi-Omic Data Sets. *Nat. Chem. Biol.* **2010,** *6* (11), 787–789.
393. Bersanelli, M.; Mosca, E.; Remondini, D.; Giampieri, E.; Sala, C.; Castellani, G.; Milanesi, L. Methods for the Integration of Multi-Omics Data: Mathematical Aspects. *BMC Bioinformatics* **2016,** *17* (2), 167.
394. Chervitz, S. A.; Deutsch, E. W.; Field, D.; Parkinson, H.; Quackenbush, J.; Rocca-Serra, P.; Sansone, S.-A.; Stoeckert, C. J.; Taylor, C. F.; Taylor, R. Data Standards for Omics Data: the Basis of Data Sharing and Reuse. *Methods Mol. Biol.* **2011,** 31–69.
395. Vaudel, M.; Verheggen, K.; Csordas, A.; Ræder, H.; Berven, F. S.; Martens, L.; Vizcaíno, J. A.; Barsnes, H. Exploring the Potential of Public Proteomics Data. *Proteomics* **2016,** *16* (2), 214–225.
396. Brazma, A. Minimum Information About a Microarray Experiment (MIAME)—Successes, Failures, Challenges. *Sci. World J.* **2009,** *9,* 420–423.
397. Brazma, A.; Hingamp, P.; Quackenbush, J.; Sherlock, G.; Spellman, P.; Stoeckert, C.; Aach, J.; Ansorge, W.; Ball, C. A.; Causton, H. C. Minimum Information About a Microarray Experiment (MIAME)—Toward Standards for Microarray Data. *Nat. Genet.* **2001,** *29* (4), 365–371.
398. Rayner, T. F.; Rocca-Serra, P.; Spellman, P. T.; Causton, H. C.; Farne, A.; Holloway, E.; Irizarry, R. A.; Liu, J.; Maier, D. S.; Miller, M. A Simple Spreadsheet-Based, MIAME-Supportive Format for Microarray Data: MAGE-TAB. *BMC Bioinformatics* **2006,** *7* (1), 1.
399. Sansone, S.-A.; Rocca-Serra, P.; Field, D.; Maguire, E.; Taylor, C.; Hofmann, O.; Fang, H.; Neumann, S.; Tong, W.; Amaral-Zettler, L. Toward Interoperable Bioscience Data. *Nat. Genet.* **2012,** *44* (2), 121–126.
400. Tenenbaum, J. D.; Sansone, S.-A.; Haendel, M. A Sea of Standards for Omics Data: Sink or Swim? *J. Am. Med. Inform. Assoc.* **2014,** *21* (2), 200–203.

401. Field, D.; Sansone, S.; DeLong, E. F.; Sterk, P.; Friedberg, I.; Gaudet, P.; Lewis, S.; Kottmann, R.; Hirschman, L.; Garrity, G. Meeting Report: BioSharing at ISMB 2010. *Stand. Genomic Sci.* **2010,** *3* (3), 254–258.
402. Deutsch, E. W.; Albar, J. P.; Binz, P.-A.; Eisenacher, M.; Jones, A. R.; Mayer, G.; Omenn, G. S.; Orchard, S.; Vizcaíno, J. A.; Hermjakob, H. Development of Data Representation Standards by the Human Proteome Organization Proteomics Standards Initiative. *J. Am. Med. Inform. Assoc.* **2015,** *22* (3), 495–506.
403. Taylor, C. F. Minimum Reporting Requirements for Proteomics: A MIAPE Primer. *Proteomics* **2006,** *6* (Suppl. 2), 39–44.
404. Jones, A. R.; Carroll, K.; Knight, D.; Maclellan, K.; Domann, P. J.; Legido-Quigley, C.; Huang, L.; Smallshaw, L.; Mirzaei, H.; Shofstahl, J.; Paton, N. W. Guidelines for Reporting the Use of Column Chromatography in Proteomics. *Nat. Biotechnol.* **2010,** *28* (7), 654.
405. Hoogland, C.; O'Gorman, M.; Bogard, P.; Gibson, F.; Berth, M.; Cockell, S. J.; Ekefjard, A.; Forsstrom-Olsson, O.; Kapferer, A.; Nilsson, M.; Martinez-Bartolome, S.; Albar, J. P.; Echevarria-Zomeno, S.; Martinez-Gomariz, M.; Joets, J.; Binz, P. A.; Taylor, C. F.; Dowsey, A.; Jones, A. R. Guidelines for Reporting the Use of Gel Image Informatics in Proteomics. *Nat. Biotechnol.* **2010,** *28* (7), 655–656.
406. Taylor, C. F.; Binz, P. A.; Aebersold, R.; Affolter, M.; Barkovich, R.; Deutsch, E. W.; Horn, D. M.; Huhmer, A.; Kussmann, M.; Lilley, K.; Macht, M.; Mann, M.; Muller, D.; Neubert, T. A.; Nickson, J.; Patterson, S. D.; Raso, R.; Resing, K.; Seymour, S. L.; Tsugita, A.; Xenarios, I.; Zeng, R.; Julian, R. K., Jr. Guidelines for Reporting the Use of Mass Spectrometry in Proteomics. *Nat. Biotechnol.* **2008,** *26* (8), 860–861.
407. Binz, P. A.; Barkovich, R.; Beavis, R. C.; Creasy, D.; Horn, D. M.; Julian, R. K., Jr.; Seymour, S. L.; Taylor, C. F.; Vandenbrouck, Y. Guidelines for Reporting the Use of Mass Spectrometry Informatics in Proteomics. *Nat. Biotechnol.* **2008,** *26* (8), 862.
408. Martinez-Bartolome, S.; Deutsch, E. W.; Binz, P. A.; Jones, A. R.; Eisenacher, M.; Mayer, G.; Campos, A.; Canals, F.; Bech-Serra, J. J.; Carrascal, M.; Gay, M.; Paradela, A.; Navajas, R.; Marcilla, M.; Hernaez, M. L.; Gutierrez-Blazquez, M. D.; Velarde, L. F.; Aloria, K.; Beaskoetxea, J.; Medina-Aunon, J. A.; Albar, J. P. Guidelines for Reporting Quantitative Mass Spectrometry Based Experiments in Proteomics. *J. Proteomics* **2013,** *95,* 84–88.
409. Deutsch, E. mzML: A Single, Unifying Data Format for Mass Spectrometer Output. *Proteomics* **2008,** *8* (14), 2776–2777.
410. Deutsch, E. W.; Chambers, M.; Neumann, S.; Levander, F.; Binz, P. A.; Shofstahl, J.; Campbell, D. S.; Mendoza, L.; Ovelleiro, D.; Helsens, K.; Martens, L.; Aebersold, R.; Moritz, R. L.; Brusniak, M. Y. TraML—A Standard Format for Exchange of Selected Reaction Monitoring Transition Lists. *Mol. Cell. Proteomics* **2012,** *11* (4). R111 015040.
411. Jones, A. R.; Eisenacher, M.; Mayer, G.; Kohlbacher, O.; Siepen, J.; Hubbard, S. J.; Selley, J. N.; Searle, B. C.; Shofstahl, J.; Seymour, S. L.; Julian, R.; Binz, P. A.; Deutsch, E. W.; Hermjakob, H.; Reisinger, F.; Griss, J.; Vizcaino, J. A.; Chambers, M.; Pizarro, A.; Creasy, D. The mzIdentML Data Standard for Mass Spectrometry-Based Proteomics Results. *Mol. Cell. Proteomics* **2012,** *11* (7).
412. Walzer, M.; Qi, D.; Mayer, G.; Uszkoreit, J.; Eisenacher, M.; Sachsenberg, T.; Gonzalez-Galarza, F. F.; Fan, J.; Bessant, C.; Deutsch, E. W.; Reisinger, F.; Vizcaino, J. A.; Medina-Aunon, J. A.; Albar, J. P.; Kohlbacher, O.; Jones, A. R. The mzQuantML Data Standard for Mass Spectrometry-Based Quantitative Studies in Proteomics. *Mol. Cell. Proteomics* **2013,** *12* (8), 2332–2340.
413. Griss, J.; Jones, A. R.; Sachsenberg, T.; Walzer, M.; Gatto, L.; Hartler, J.; Thallinger, G. G.; Salek, R. M.; Steinbeck, C.; Neuhauser, N.; Cox, J.; Neumann, S.; Fan, J.; Reisinger, F.; Xu, Q. W.; Del Toro, N.; Perez-Riverol, Y.; Ghali, F.; Bandeira, N.; Xenarios, I.; Kohlbacher, O.; Vizcaino, J. A.; Hermjakob, H. The mzTab Data Exchange Format: Communicating Mass-Spectrometry-Based Proteomics and Metabolomics Experimental Results to a Wider Audience. *Mol. Cell. Proteomics* **2014,** *13* (10), 2765–2775.
414. Mayer, G.; Jones, A. R.; Binz, P. A.; Deutsch, E. W.; Orchard, S.; Montecchi-Palazzi, L.; Vizcaino, J. A.; Hermjakob, H.; Oveillero, D.; Julian, R.; Stephan, C.; Meyer, H. E.; Eisenacher, M. Controlled Vocabularies and Ontologies in Proteomics: Overview, Principles and Practice. *Biochim. Biophys. Acta* **2014,** *1844* (1 Pt A), 98–107.
415. Vizcaino, J. A.; Deutsch, E. W.; Wang, R.; Csordas, A.; Reisinger, F.; Rios, D.; Dianes, J. A.; Sun, Z.; Farrah, T.; Bandeira, N.; Binz, P. A.; Xenarios, I.; Eisenacher, M.; Mayer, G.; Gatto, L.; Campos, A.; Chalkley, R. J.; Kraus, H. J.; Albar, J. P.; Martinez-Bartolome, S.; Apweiler, R.; Omenn, G. S.; Martens, L.; Jones, A. R.; Hermjakob, H. ProteomeXchange Provides Globally Coordinated Proteomics Data Submission and Dissemination. *Nat. Biotechnol.* **2014,** *32* (3), 223–226.
416. Vizcaíno, J. A.; Côté, R. G.; Csordas, A.; Dianes, J. A.; Fabregat, A.; Foster, J. M.; Griss, J.; Alpi, E.; Birim, M.; Contell, J. The PRoteomics IDEntifications (PRIDE) Database and Associated Tools: Status in 2013. *Nucleic Acids Res.* **2013,** *41* (D1), D1063–D1069.
417. Farrah, T.; Deutsch, E. W.; Kreisberg, R.; Sun, Z.; Campbell, D. S.; Mendoza, L.; Kusebauch, U.; Brusniak, M. Y.; Huttenhain, R.; Schiess, R.; Selevsek, N.; Aebersold, R.; Moritz, R. L. PASSEL: The PeptideAtlas SRMexperiment Library. *Proteomics* **2012,** *12* (8), 1170–1175.
418. Ivanov, A. R.; Colangelo, C. M.; Dufresne, C. P.; Friedman, D. B.; Lilley, K. S.; Mechtler, K.; Phinney, B. S.; Rose, K. L.; Rudnick, P. A.; Searle, B. C. Interlaboratory Studies and Initiatives Developing Standards for Proteomics. *Proteomics* **2013,** *13* (6), 904–909.
419. Percy, A. J.; Chambers, A. G.; Yang, J.; Jackson, A. M.; Domanski, D.; Burkhart, J.; Sickmann, A.; Borchers, C. H. Method and Platform Standardization in MRM-Based Quantitative Plasma Proteomics. *J. Proteomics* **2013,** *95,* 66–76.
420. Zhang, Z.; Chan, D. W. The Road From Discovery to Clinical Diagnostics: Lessons Learned From the First FDA-Cleared In Vitro Diagnostic Multivariate Index Assay of Proteomic Biomarkers. *Cancer Epidemiol. Biomarkers Prev.* **2010,** *19* (12), 2995–2999.
421. Heegaard, N. H.; Østergaard, O.; Bahl, J.; Overgaard, M.; Beck, H. C.; Rasmussen, L. M.; Larsen, M. R. Important Options Available—From Start to Finish—for Translating Proteomics Results to Clinical Chemistry. *Proteomics Clin. Appl.* **2015,** *9* (1–2), 235–252.
422. Sumner, L. W.; Amberg, A.; Barrett, D.; Beale, M. H.; Beger, R.; Daykin, C. A.; Fan, T. W.; Fiehn, O.; Goodacre, R.; Griffin, J. L.; Hankemeier, T.; Hardy, N.; Harnly, J.; Higashi, R.; Kopka, J.; Lane, A. N.; Lindon, J. C.; Marriott, P.; Nicholls, A. W.; Reily, M. D.; Thaden, J. J.; Viant, M. R. Proposed Minimum Reporting Standards for Chemical Analysis Chemical Analysis Working Group (CAWG) Metabolomics Standards Initiative (MSI). *Metabolomics* **2007,** *3* (3), 211–221.
423. Sansone, S. A.; Fan, T.; Goodacre, R.; Griffin, J. L.; Hardy, N. W.; Kaddurah-Daouk, R.; Kristal, B. S.; Lindon, J.; Mendes, P.; Morrison, N.; Nikolau, B.; Robertson, D.; Sumner, L. W.; Taylor, C.; van der Werf, M.; van Ommen, B.; Fiehn, O. The Metabolomics Standards Initiative. *Nat. Biotechnol.* **2007,** *25* (8), 846–848.
424. Haug, K.; Salek, R. M.; Conesa, P.; Hastings, J.; de Matos, P.; Rijnbeek, M.; Mahendraker, T.; Williams, M.; Neumann, S.; Rocca-Serra, P.; Maguire, E.; Gonzalez-Beltran, A.; Sansone, S. A.; Griffin, J. L.; Steinbeck, C. MetaboLights—An Open-Access General-Purpose Repository for Metabolomics Studies and Associated Meta-Data. *Nucleic Acids Res.* **2013,** *41* (Database issue), D781–D786.
425. Buscher, J. M.; Czernik, D.; Ewald, J. C.; Sauer, U.; Zamboni, N. Cross-Platform Comparison of Methods for Quantitative Metabolomics of Primary Metabolism. *Anal. Chem.* **2009,** *81,* 2135–2143.
426. Alsheikh-Ali, A. A.; Qureshi, W.; Al-Mallah, M. H.; Ioannidis, J. P. Public Availability of Published Research Data in High-Impact Journals. *PLoS One* **2011,** *6* (9), e24357.
427. Waller, L. A.; Miller, G. W. More Than Manuscripts: Reproducibility, Rigor, and Research Productivity in the Big Data Era. *Toxicol. Sci.* **2016,** *149* (2), 275–276.
428. Ansari, S.; Baumer, K.; Boué, S.; Dijon, S.; Dulize, R.; Ekroos, K.; Elamin, A.; Foong, C.; Guedj, E.; Hoeng, J. Comprehensive Systems Biology Analysis of a 7-Month Cigarette Smoke Inhalation Study in C57BL/6 Mice. *Sci. Data* **2016,** *3,* 150077.
429. Manchikanti, L.; Kaye, A.; Boswell, M.; Hirsch, J. Medical Journal Peer Review: Process and Bias. *Pain Physician* **2014,** *18* (1), E1–E14.
430. Gebel, S.; Lichtner, R. B.; Frushour, B.; Schlage, W. K.; Hoang, V.; Talikka, M.; Hengstermann, A.; Mathis, C.; Veljkovic, E.; Peck, M.; Peitsch, M. C.; Deehan, R.; Hoeng, J.; Westra, J. W. Construction of a Computable Network Model for DNA Damage, Autophagy, Cell Death, and Senescence. *Bioinform. Biol. Insights* **2013,** *7,* 97–117.
431. Smith, R. Peer Review: A Flawed Process at the Heart of Science and Journals. *J. R. Soc. Med.* **2006,** *99* (4), 178–182.
432. Kratz, J.; Strasser, C. Data Publication Consensus and Controversies. *F1000Res.* **2014,** *3,* 94.
433. Hirschman, L.; Yeh, A.; Blaschke, C.; Valencia, A. Overview of BioCreAtIvE: Critical Assessment of Information Extraction for Biology. *BMC Bioinformatics* **2005,** *6* (Suppl. 1), S1.
434. Martin, S. F.; Falkenberg, H.; Dyrlund, T. F.; Khoudoli, G. A.; Mageean, C. J.; Linding, R. PROTEINCHALLENGE: Crowd Sourcing in Proteomics Analysis and Software Development. *J. Proteomics* **2013,** *88,* 41–46.
435. Xu, J.; Thakkar, S.; Gong, B.; Tong, W. The FDA's Experience With Emerging Genomics Technologies-Past, Present, and Future. *AAPS J.* **2016,** *18* (4), 814–818.

436. Goodsaid, F. M.; Amur, S.; Aubrecht, J.; Burczynski, M. E.; Carl, K.; Catalano, J.; Charlab, R.; Close, S.; Cornu-Artis, C.; Essioux, L.; Fornace, A. J., Jr.; Hinman, L.; Hong, H.; Hunt, I.; Jacobson-Kram, D.; Jawaid, A.; Laurie, D.; Lesko, L.; Li, H. H.; Lindpaintner, K.; Mayne, J.; Morrow, P.; Papaluca-Amati, M.; Robison, T. W.; Roth, J.; Schuppe-Koistinen, I.; Shi, L.; Spleiss, O.; Tong, W.; Truter, S. L.; Vonderscher, J.; Westelinck, A.; Zhang, L.; Zineh, I. Voluntary Exploratory Data Submissions to the US FDA and the EMA: Experience and Impact. *Nat. Rev. Drug Discov.* **2010,** *9* (6), 435–445.
437. Healy, M. J.; Tong, W.; Ostroff, S.; Eichler, H. G.; Patak, A.; Neuspiel, M.; Deluyker, H.; Slikker, W., Jr. Regulatory Bioinformatics for Food and Drug Safety. *Regul. Toxicol. Pharmacol.* **2016,** *80,* 342–347.
438. Bousquet, J.; Anto, J.; Akdis, M.; Auffray, C.; Keil, T.; Momas, I.; Postma, D.; Valenta, R.; Wickman, M.; Cambon-Thomsen, A. Paving the Way of Systems Biology and Precision Medicine in Allergic Diseases: The MeDALL Success Story. *Allergy* **2016,** *71* (11), 1513–1525.
439. Oettrich, J.; Dao, V.; Frijhoff, J.; Kleikers, P.; Casas, A.; Hobbs, A.; Schmidt, H. Clinical Relevance of Cyclic GMP Modulators: A Translational Success Story of Network Pharmacology. *Clin. Pharmacol. Ther.* **2016,** *99* (4), 360–362.
440. Soden, S. E.; Saunders, C. J.; Willig, L. K.; Farrow, E. G.; Smith, L. D.; Petrikin, J. E.; LePichon, J.-B.; Miller, N. A.; Thiffault, I.; Dinwiddie, D. L. Effectiveness of Exome and Genome Sequencing Guided by Acuity of Illness for Diagnosis of Neurodevelopmental Disorders. *Sci. Transl. Med.* **2014,** *6* (265), 265ra168.
441. McShane, L. M.; Cavenagh, M. M.; Lively, T. G.; Eberhard, D. A.; Bigbee, W. L.; Williams, P. M.; Mesirov, J. P.; Polley, M.-Y. C.; Kim, K. Y.; Tricoli, J. V. Criteria for the Use of Omics-Based Predictors in Clinical Trials: Explanation and Elaboration. *BMC Med.* **2013,** *11* (1), 1.
442. Benson, M. Clinical Implications of Omics and Systems Medicine: Focus on Predictive and Individualized Treatment. *J. Int. Med.* **2015**.
443. Ward, S.; Scope, A.; Rafia, R.; Pandor, A.; Harnan, S.; Evans, P.; Wyld, L. Gene Expression Profiling and Expanded Immunohistochemistry Tests to Guide the Use of Adjuvant Chemotherapy in Breast Cancer Management: A Systematic Review and Cost-Effectiveness Analysis. *Health Technol. Assess.* **2013,** *17* (44), 1–302.

2.19 Systems Chemical Biology: Integrating Medicinal Chemistry and Systems Biology for Drug Discovery

R-S Wang and J Loscalzo, Harvard Medical School, Boston, MA, United States

© 2017 Elsevier Ltd. All rights reserved.

2.19.1	**Introduction**	481
2.19.2	**Data Integration in Systems Chemical Biology**	482
2.19.3	**Computational Methodologies in Systems Chemical Biology**	483
2.19.3.1	Data Mining and Machine Learning	484
2.19.3.2	Dynamic Modeling	484
2.19.3.3	Network Analysis and Graph Theory	485
2.19.3.4	Data Integration	485
2.19.4	**Drug–Target Identification and Prioritization**	485
2.19.5	**Drug Repositioning and Drug Combination**	487
2.19.6	**ADE Prediction**	488
2.19.7	**Systems Chemical Biology for Personalized Medicine**	490
2.19.8	**Conclusions**	490
Acknowledgments		491
References		491
Relevant Websites		494

2.19.1 Introduction

Although there is no consistent definition, chemical biology is a discipline spanning several fields, including chemistry, biology, and physics.[1] It aims to study and manipulate biological systems through chemical techniques, tools, and analyses. Medicinal chemistry is a research domain within chemical biology that links various scientific disciplines for discovery and development of new drugs.[2–4] One of the main goals of chemical biology and medicinal chemistry is to study how various small molecules affect biological systems. Recently, chemical biology has begun to use an emerging systematic screening strategy to obtain large collections of small molecules and explore their interactions with genes and proteins, a field now denoted chemogenomics, or chemical genomics.[5,6] Chemogenomics combines the latest tools of genomics and chemistry to conduct systematic screening of large-scale chemical libraries of small molecules against selected target families with the ultimate goal of identifying a small molecule that binds to and modulates the target proteins. With a one-ligand–one-target mind-set, chemogenomics is expected to validate therapeutic targets and identify drug candidates quickly and efficiently.[7]

During the past several decades, drug discovery and development have produced many effective therapeutic agents with a specific protein as a target. However, adverse side effects of drugs remain a major problem, and many drugs fail in clinical trials as a consequence of their previously unrecognized side effects.[8] One of the main reasons for this problem is that the traditional one-ligand–one-target drug design model does not consider the complex context of the *in vivo* environment, whereas multiple-target drugs may have a better opportunity to affect the key pathways and minimize toxicity issues.[9,10] Drug development should be based on the operational principles of biological systems. Biological processes are highly complex, with many components interacting with each other. Drugs exert their effects by modulating signaling networks in biological systems rather than affecting a single specific target in isolation. It is, therefore, of great importance to design network-based drugs. Indeed, for this reason, drug discovery is now moving from the conventional drug design model to a systems biology paradigm.[11–13]

Different from chemical biology and conventional reductionism, systems biology aims to describe and understand complex biological processes from a systems perspective and develop predictive models of biological systems by integrating high-throughput omics data and computational methods. Taking advantage of multidisciplinary collaboration, systems biology has developed many tools and approaches that have the potential to make a significant impact in biomedical science, including the field of drug discovery and development.[14,15] Massive amounts of omics data generated using systems biology techniques allow a comparison of gene or protein activities under different conditions and uncover global network structures. However, there is little awareness of chemistry in current systems biology studies. Integration of biological networks with large collections of small chemical entities is not only promising for target identification but also useful for understanding the mechanisms of action of drugs and identifying adverse effects.[16]

Both chemical biology and systems biology have had an increasing impact on drug discovery and drug design. Although these two disciplines have largely evolved in parallel in the recent past, there is an increasing need to integrate them to obtain a more complete picture of the way small molecules affect biological systems, which led to the emergence of a new field—systems chemical biology (SCB).[17] Systems chemical biology integrates large-scale heterogeneous data from chemical space and biological space and

provides a platform for understanding how small molecules affect biological systems with the aid of computational methods and quantitative modeling. This new discipline will not only offer new insights into biological systems but also have important applications in biomedicine. In addition, systems chemical biology provides new opportunities for drug discovery and development through systems-level research. In this article, we review the methodologies of systems chemical biology and discuss their impact on drug discovery and development.

2.19.2 Data Integration in Systems Chemical Biology

A biological system consists of a few essential elements, such as components (e.g., genes, proteins, and metabolites), their activities, and the connectivity relationships between them. Thanks to high-throughput technologies in chemical biology and systems biology, an increasing accumulation of various chemical and omics data is available on these elements of the system. Systems biology utilizes the massive omics data to reveal the entire network structure of biological systems, whereas chemical biology is focused on pairing individual compounds and targets through large-scale screening that may be real or virtual. How to store, integrate, and transform the data into translational knowledge is critical for the success of systems chemical biology.

High-throughput data from chemical space include the structure of small molecules, their activity assays, and ligand–target interactions. Advances in biotechnologies have resulted in numerous cell-based assays that are used to discover biologically active small chemical entities. The high-throughput screening commonly used in chemical biology can typically screen around 2–3 log orders of small molecules for an effect on a biological process of interest.[18] Many such data are now freely available in a variety of public databases. For example, ChEMBL is a database containing binding and functional information for a large number of drug-like bioactive compounds.[19] PubChem is a database of chemical molecules and their activities in biological assays which are maintained by the National Center for Biotechnology Information (NCBI).[20,21] ChemBank, developed through a collaboration at the Broad Institute of MIT and Harvard, is a web-based informatics environment storing data on small molecules and small-molecule screens.[22] ChemProt is a disease chemical biology database compiling annotated and predicted chemical–protein interactions, as well as disease-associated protein–protein interactions.[23] In addition, the data on ligand–target interactions have been steadily accumulated in publicly available databases. For example, STITCH is a database integrating various databases of biological pathways, drug–target relationships, and binding affinities, including BindingDB and PharmGKB.[24–26] **Table 1** lists some select chemical database resources that are publicly available and can be used for data integration in systems chemical biology.

Biological components include genes, proteins, small molecules, and metabolites. Thus far, many databases have been developed in which to deposit information on individual biological components. For example, Entrez Gene is NCBI's database for gene-specific information, which focuses on genomes that have been completely sequenced.[27] UniProtKB is the central hub for the collection of functional information on proteins.[28] There are also some databases with specific types of proteins, for example, BRENDA is a main source of functional enzyme data.[29] The Human Metabolome Database (HMDB) is an electronic database containing detailed information about small-molecule metabolites found in humans.[30] These databases provide acquisition sources for the components of biological systems relevant to systems chemical biology. Perturbations of biological systems by small molecules (drugs) lead to changes in the activities of biological components. The bioactivity of small molecules and macromolecules is commonly assessed by measuring gene expression, metabolite abundance, and protein concentration. Gene Expression Omnibus (GEO) stores massive microarray- and sequence-based gene expression datasets representing gene activities under different conditions.[31] The Human Protein Atlas (HPA) is a database containing protein expression and localization profiles for a large majority of

Table 1 Select publicly available chemical database resources for data integration in systems chemical biology

Databases	*Descriptions*	*Web links*
ChEMBL	A large-scale bioactivity database of more than 1 million compounds and 10,000 protein targets	https://www.ebi.ac.uk/chembl
PubChem	A database of small chemical molecules and their activities in biological assays maintained by NCBI	https://pubchem.ncbi.nlm.nih.gov/
ChemBank	A web-based informatics environment storing data on small molecules and small-molecule screens	http://chembank.broadinstitute.org
ChemProt	A resource of annotated and predicted chemical–protein interactions	http://www.cbs.dtu.dk/services/ChemProt/
ChemSpider	A chemical structure database providing fast text and structure search access to over 43 million structures from hundreds of data sources	http://www.chemspider.com/
DrugBank	A cheminformatics resource that combines detailed drug data with comprehensive drug–target information	http://www.drugbank.ca/
PharmGKB	A comprehensive resource that curates knowledge about the impact of genetic variation on drug response for clinicians and researchers	https://www.pharmgkb.org/
BindingDB	A database of measured binding affinities, focusing chiefly on the interactions of protein targets with small molecules	https://www.bindingdb.org
STITCH 4	An interaction database for small molecules and proteins	http://stitch.embl.de/

Table 2 Select publicly available database resources of bioactivity and biochemical pathways for systems chemical biology

Databases	*Descriptions*	*Web links*
HMDB	An electronic database containing detailed information on small-molecule metabolites found in humans	http://www.hmdb.ca/
GEO	A functional genomic data repository supporting MIAME-compliant array- and sequence-based data submissions	http://www.ncbi.nlm.nih.gov/geo/
HPA	A database with millions of high-resolution images showing the spatial distribution of proteins in many tissues and cell types	http://www.proteinatlas.org/
KEGG Pathway	A collection of manually drawn pathway maps representing the molecular interaction and reaction networks for metabolism, cellular processes, and human diseases	http://www.genome.jp/kegg/pathway.html
MetaCyc	A comprehensive curated database describing experimentally determined small-molecule metabolic pathways and enzymes from over 2500 organisms	http://metacyc.org/
Reactome	A curated and peer-reviewed pathway database	http://www.reactome.org/
Pathway Commons	A network biology resource providing access to biological pathway information collected from different pathway databases	http://www.pathwaycommons.org/about/
MSigDB	A comprehensive collection of annotated gene sets for doing gene set enrichment analysis	http://software.broadinstitute.org/gsea/msigdb/

all human protein-coding genes based on both RNA and protein data.[32] In addition to metabolite information, HMDB also stores in situ metabolite concentration data submitted by different research laboratories.[30] **Table 2** lists select database resources of bioactivity information relevant to systems chemical biology.

Small molecules (drugs) may also affect the connectivity relationships among biological components of a biological system as they modulate signaling pathways rather than a single specific target. Data on molecular interactions, signaling pathways, and biochemical pathways under healthy and diseased conditions have also been complied. Molecular interactions that can be generated in a high-throughput manner include protein–DNA interactions,[33] protein–protein interactions,[34,35] and kinase–substrate interactions.[36] Signaling pathways transmit information through dynamic protein interaction networks. An automated high-throughput technology, luminescence-based mammalian interactome mapping, was developed for mapping dynamic signaling networks in mammalian cells.[37] KEGG Pathway is a collection of manually drawn pathway maps describing the molecular interaction and reaction networks for metabolism, cellular processes, and human diseases.[38] In addition to KEGG Pathway, there are other databases for biochemical pathways, such as MetaCyc[39] and Reactome.[40] Pathway Commons provides a network biology resource for accessing biological pathway information collected from public pathway databases.[41] The Molecular Signatures Database (MSigDB) is a collection of annotated gene sets for use in gene set enrichment analysis.[42,43] These gene sets can be divided into eight categories, including coherently expressed gene signatures representing well-defined biological states or processes, curated gene sets from online pathway databases and literature, genes annotated by the same GO terms, and genes with conserved cis-regulatory motifs. The public availability of various pathway databases facilitates mapping large-scale omics datasets and chemical datasets to signaling and biochemical pathways for biological interpretation of systems-level mechanisms. These databases and their web links are summarized in **Table 2**.

Systems biology and chemical biology have largely evolved in parallel in the past two decades. These two disciplines share many commonalities and also have unique complementary domains. As shown in **Fig. 1**, both of these disciplines have begun using high-throughput technologies to generate large-scale datasets, although for different purposes. Systems biology uses high-throughput techniques to generate massive amounts of genomic, transcriptomic, proteomic, and metabolomic data and aims to reveal the systems-level mechanisms of biology processes by data integration. Chemical biology utilizes high-throughput screens to generate large-scale chemical structures and bioactivity information of small molecules and aims to pair ligands and targets. The increasing accumulation of omics data and their modulation by small molecules make it critical to integrate chemical biology and systems biology and develop the new field of systems chemical biology.[17,44] Systems chemical biology relies on high-level integration of chemical, biological, and interactome databases using sophisticated computational methods and mathematical modeling, with an ultimate goal of understanding how small molecules manipulate a biological system as a whole, not simply individual drug targets. Systems chemical biology, therefore, will not only offer new unique insights into biological systems but also have significant impact on various aspects of drug discovery and development.

2.19.3 Computational Methodologies in Systems Chemical Biology

Computational methodologies are not only the important elements of systems biology but also an essential part of chemical biology. Systems chemical biology benefits from collaborations and interactions from multidisciplinary fields. In the development process of systems chemical biology, computational methodologies, such as data mining, machine learning, and dynamic

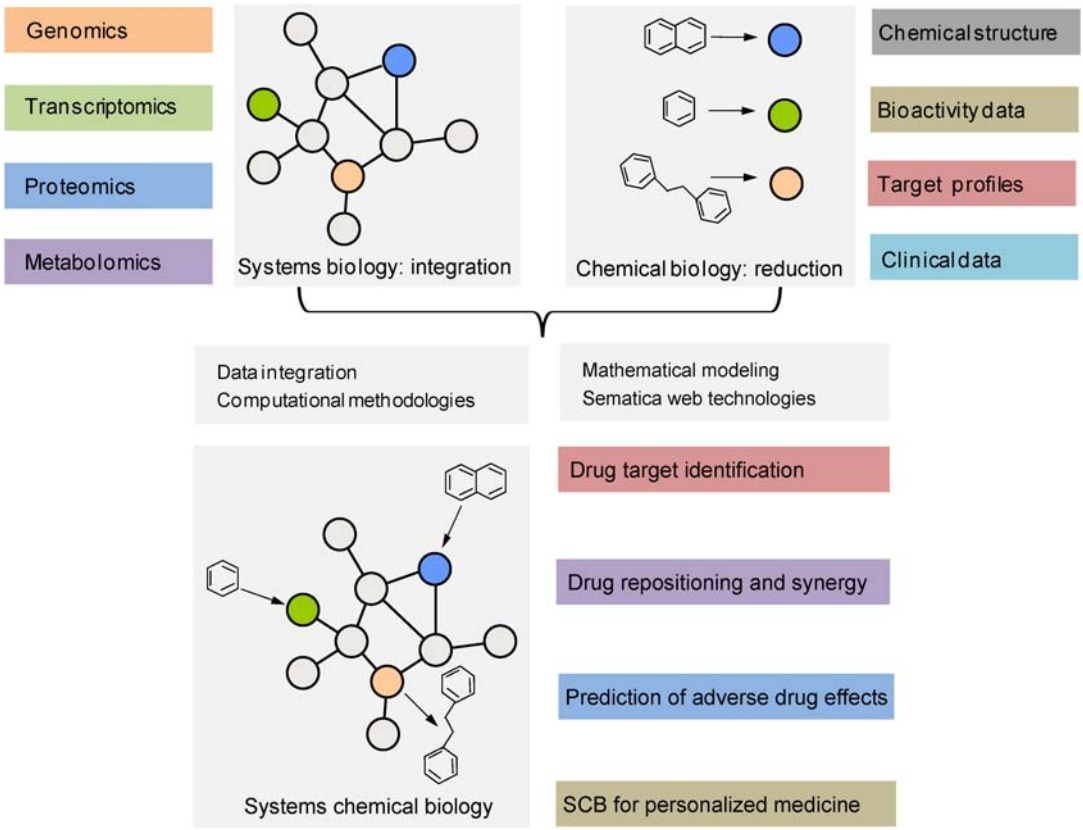

Fig. 1 Integration of systems biology and chemical biology for drug discovery.

modeling, cannot be ignored. In addition, network science and graph theory are indispensable as the topology of biological systems can be represented by an interaction network that is itself quantitatively tractable. Various data integration approaches and semantic web technologies are also very useful in this field. With the aid of these methodologies, systems chemical biology can facilitate efficient and highly predictable drug discovery.

2.19.3.1 Data Mining and Machine Learning

The explosive growth of chemical and biological data drives drug discovery from individual similarity searching using reference compounds toward automatic large-scale predictions using data mining and machine-learning approaches.[45] Such methods usually require a representative training set on which to base the models, learn model parameters, and derive a robust predictive model with good generalizability. The application of machine learning in drug discovery is extensive, including drug–target prediction, drug repositioning, and adverse drug event (ADE) prediction. For example, drug–drug chemical similarity and target–target sequence similarity represent core concepts in the chemical space and genomic space, respectively, and can be used as features of machine-learning models for predicting new drug–target interactions.[46] A unique advantage of machine-learning methods is their ability to integrate and fuse information from multiple resources and transform the data into meaningful knowledge. For example, Napolitano et al.[47] integrated data sources from drug–drug chemical similarity, target–target closeness in the protein interaction network, and correlations between drug-induced gene expression profiles into a support vector machine (SVM) classifier whose outcome is a therapeutic class for a given drug. The classifier achieves promising high-level accuracy and has the potential to affect drug discovery. Data mining and machine-learning methodologies have also been similarly applied to prediction of ADEs.[48]

2.19.3.2 Dynamic Modeling

Biological systems are not static, but are highly dynamic. Dynamic modeling is, therefore, an essential computational approach in systems chemical biology. It can simulate how a variety of perturbations of a biological system induced by a small molecule affect the behavior of the system. Such simulations are very helpful for deriving mechanistic insights about the system. Discrete logical modeling simplifies biological reality, ignores quantitative kinetic parameters, and, thus, can make qualitative (or semiquantitative) dynamic predictions of system behaviors. Flobak et al.[49] developed a dynamical logical model representing a cell fate decision network in the AGS gastric cancer cell line based on knowledge extracted from the literature and databases for discovering drug

synergy. With the aid of the software GINsim, the model can cope with the vast state space, simulate the perturbations of the network caused by anticancer drug combinations, and predict the synergistic growth-inhibitory action of some combinations of drugs. In addition, molecular dynamics simulations play an increasingly important role in drug discovery. For example, atomistic dynamic simulations of protein receptors and their small-molecule ligands are very useful in computer-aided drug discovery,[50] including virtual compound screening, identification of binding sites (both orthosteric and allosteric), and prediction of binding energies. Okimoto et al.[51] conducted a computational screen of compounds by combining molecular docking with massive-scale molecular dynamics simulations. This screening method has a much higher enrichment performance than molecular docking alone. Lastly, when specific kinetic and binding constants are known and extracellular species concentration can be calculated, forward dynamic modeling by ordinary differential equations, stochastic differential equations, or mixed models can be used to determine the combinations of drugs that maximize pathway effects and minimize ADEs.[52]

2.19.3.3 Network Analysis and Graph Theory

Biological molecules and their dynamic interactions determine the function of a complex biological system. These interactions form different types of molecular networks with characteristic topology[53] that are indispensable for understanding the systems-level mechanisms of drug action. Systems pharmacology aims to combine network analyses with pharmacokinetic and pharmacodynamic models in order to understand drug action at the systems level.[54] In addition, network modeling provides a powerful method to investigate drug discovery-related problems. One pioneering work in this regard is the contribution of a drug–target network in which FDA-approved drugs and proteins are linked by drug–target binary associations to form a bipartite graph.[55] Topological analyses of this network indicate that drugs of similar types cluster together and that newer drugs tend to target already targeted proteins. Cami et al.[56] constructed a bipartite network representation of existing drug–ADE associations and incorporated the topological features of nodes into a logistic regression model to predict new drug–ADE relationships. A chemical similarity network capturing drug–drug similarity has aided in new target prediction, as well.[57] In addition, network pharmacology approaches have also been used to map the unexplored target space and therapeutic potential of natural products, providing a systematic means by which to extend the druggable space of proteins implicated in complex diseases.[58]

2.19.3.4 Data Integration

As mentioned earlier, one unique feature of systems chemical biology is the massive accumulation of data from multiple experimental spaces. Therefore, effective integration of heterogeneous data and knowledge from different sources will be crucial for future drug discovery.[59] Data integration techniques include ensemble methods, multiple kernel learning, and information fusion. A few integrative methods have been applied in drug discovery to date. For example, a kernel regression model-based method that integrates heterogeneous data sources from the chemical space and the biological space was developed to predict potential side-effect profiles of drugs.[60] Cao et al.[61] developed a multiple evidence fusion method integrating multiple similarity measures from various data types for large-scale prediction of adverse drug reactions (ADRs). In a recent study, Zheng et al.[62] developed a weighted ensemble similarity algorithm based on ligand structural features for predicting drug targets and potential drug repositioning. In addition, semantic web technologies are highly useful for data integration in systems chemical biology as searching multiple datasets through a single framework is much more convenient than searching those datasets individually. A variety of semantic languages and tools have been designed for searching and mining large heterogeneous datasets from chemistry and biology, which have become technical enablers of systems chemical biology.[63]

Traditional drug discovery involves cell-based or target-focused screening of chemical compounds in a very expensive and lengthy process. By contrast, many drugs exert effects by modulating biological pathways rather than individual targets. With the aid of the computational methodologies described earlier, systems chemical biology approaches that integrate increasingly available data on drugs, proteins, and diseases will be beneficial to drug discovery, drug repurposing, drug side-effect prediction, and personalized medicine.[12,64]

2.19.4 Drug–Target Identification and Prioritization

High-throughput screening of biological systems has identified many biologically active small molecules. Follow-up studies typically focus on determining their precise protein targets. There are two fundamental methods in chemical genetics by which to understand the action of small molecules on biological systems: forward chemical genetics and reverse chemical genetics.[16] The former directly tests the impact of small molecules on a biological process and then follows with target identification to determine the protein responsible for the phenotype. Starting with a protein target, the latter conducts a high-throughput screen to identify candidate small molecules and then exposes biological systems to those candidates to determine compound-induced phenotypes. Some biochemical methods, such as biochemical affinity purification, can directly find target proteins that bind small molecules of interest.[65] Genetic-based target identification methods determine protein targets by performing large-scale modifications and measurements of DNA or RNA. For example, Eggert et al.[66] conducted parallel testing of both small-molecule screens and genome-wide-scale RNAi perturbation to enable identification of cytokinesis inhibitors and their targets.[66] Castoreno et al.[67] developed a RNAi-sensitized small-molecule screen to target small molecules toward a specific pathway. With these types of advances in

high-throughput technologies for systems chemical biology, large-scale genomic and chemical data have increasingly accumulated and provide unprecedented platforms for drug–target identification by computational inference and prediction. Thus far, many analytic methods have been proposed to predict new drug targets or drug–target interactions. We are particularly interested in those that utilize chemical information of drugs or small molecules, as these methods serve as the basis for systems-centric structure-based drug design as reviewed recently by Pei et al.[68]

Computational methods can be used to predict protein targets of drugs and small molecules based on data from chemogenomics and systems biology studies. One class of methods is to identify new targets of existing drugs based on the similarity of bioactivity profiles of drugs. The principle underlying these methods is that compounds with the same mechanisms of action tend to have similar chemical structure or activities across different biological assays. For example, Keiser et al.[69] developed a statistics-based chemoinformatics approach that explores the chemical similarities between drug and ligand sets to predict thousands of unanticipated drug–target interactions. From a more granular perspective, bioorthogonal or orthogonal bioorthogonal chemistries can be used to determine the targets of specific drug molecules and their interaction partners in complex networks in situ, respectively.[70] Target prioritization and drug–target identification methodologies have rarely taken the cellular interaction environment into account in conventional pharmacology. It is necessary and beneficial to consider cellular context as many phenotypes are caused by the effects of ligand on multiple-target proteins. Yamanish et al.[71] performed a novel analysis that revealed significant correlations between drug structure similarity, target sequence similarity, and the drug–target interaction network topology and subsequently integrated chemical and genomic spaces into a pharmacological space to predict drug–target interactions using supervised learning for a bipartite graph. They further incorporated pharmacological effects into the prediction algorithm as they found drug–target interactions better correlate with pharmacological effect similarity than with chemical structure similarity.[72] A recent study presented a new computational target identification method called Chemical Similarity Network Analysis Pulldown (CSNAP) that utilizes chemical similarity networks for large-scale drug–target profiling.[57] CSNAP clusters diverse chemical structures into distinct subnetworks representing consensus chemical patterns, which likely target common proteins.

Some methods complement existing chemical structure-based and ligand-based target prediction methods. Drug targets may display unique topological features in the human interactome. Mitsopoulos et al.[73] presented a systematic computational analysis of topological parameters of the human interactome and identified several distinctive topological patterns that distinguish druggable proteins in cellular networks.[73] Advances in biotechnologies make it possible to collect genome-wide responses to genetic and chemical perturbations. A massive number of somatic mutations have been accumulated as a result of these technologies. Some proteins may contain 'driver' mutations that are critical for the pathogenesis of a complex disease and, thus, could be potential drug targets. Zhao et al.[74] hypothesized that mutations at protein–ligand binding-site residues are likely to be druggable targets and developed a structural genomics-based Bayesian inference method incorporating the somatic missense mutations into protein–ligand binding-site residues to prioritize druggable mutations. Currently, information about drugs and drug targets in publicly available online databases is biased toward established drugs and drug–target interactions. Rask-Andersen et al.[75] collected a data set of clinical trial drug–target interactions based on CenterWatch's Drugs in Clinical Trials Database and identified 475 potentially novel clinical trial drug targets.

Systems chemical biology integrates data from chemical, genomic, and phenotypic spaces and uses network-based approaches and systematic strategies to prioritize and predict drug targets (**Fig. 2**). Incorporation of chemical structure and activity information into drug–target identification can make the prediction more accurate. Such computational prediction can provide useful target candidates that are subject to validation using biochemical methods or chemical genetics methods. In addition, systems chemical biology approaches not only provide drug–target candidates but also offer novel insights into the systems-level mechanisms of drug action derived from omics data. Systems chemical biology is expected to have a significant impact on virtual screening of chemical libraries and increase research productivity in drug discovery in the future.

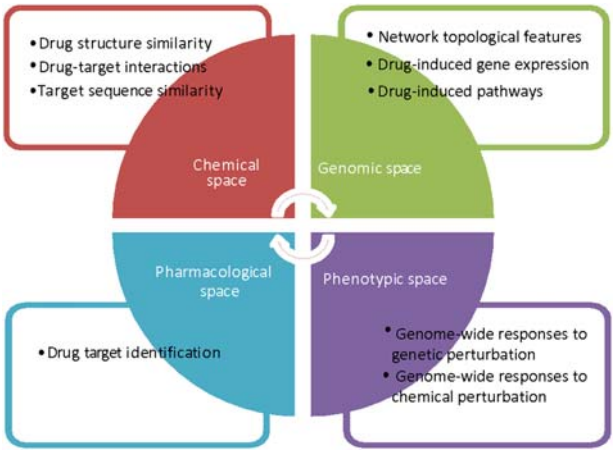

Fig. 2 Integration of heterogeneous data from different spaces for drug–target identification.

2.19.5 Drug Repositioning and Drug Combination

Pharmaceutical research and development (R&D) reports show that the number of approved new drugs has declined in the past two decades, although investment in pharmaceutical R&D has increased substantially.[76] Moreover, the average development time of drugs has increased significantly, urging researchers to seek more efficient solutions. Drug repositioning or drug repurposing, which aims to find new uses for known drugs, can narrow down drug candidates and, thus, shorten the development time, offering a promising alternative to *de novo* drug discovery. A variety of methods have been developed for drug repositioning. Computational strategies can predict new therapeutic indications for existing FDA-approved drugs that are subject to clinical trials. One of the great benefits of drug repositioning is that the pharmacokinetics and safety of known drugs do not need to be reassessed. Here, we focus on network-based drug repositioning methods relevant to systems chemical biology.

Core concepts that support drug repurposing using network strategies include drug–target interactions, target–disease associations, and drug–indication associations. As shown in **Fig. 3A**, a drug may have multiple targets, and identification of a new drug target that connects with causal genes for another disease may be helpful for drug repositioning. In addition, a new indication can be predicted by revealing new target–disease associations, that is, new associations of an existing drug target with another disease. For example, Sawada et al.[77] developed a target-based drug repositioning method to predict potential drug targets and new drug indications based on chemical structural similarity and phenotypic effect similarity derived from large-scale chemical–protein interaction data. A comprehensive drug–target–disease association network of over 8000 drugs and 1400 diseases has been constructed in this study, providing insights into the mechanisms of the predicted new drug indications. Zhao and Li presented a comodule approach to describing drug–gene–disease relationships. In this study, network-based gene closeness profiles are constructed to relate drugs to diseases, and a Bayesian partition method is then used to identify drug–gene–disease comodules.[78] Napolitano et al.[47] adopted a machine-learning approach integrating multiple layers of information including the similarity of chemical structures of drugs and the closeness of drug targets within the protein–protein interaction network for drug repositioning.

Drug-induced gene expression data have rich information for systematic drug repositioning, as illustrated in **Fig. 3B**. To discover the functional connections among diseases, genetic perturbation, and drug action, Lamb et al.[79] created a reference collection of gene expression profiles from cultured human cells treated with bioactive small molecules. This Connectivity Map (CMap) can be used to find connections among small molecules sharing a mechanism of action and is a useful resource for drug repositioning. One of the successful applications of CMap was conducted by Iorio et al.[80] In this study, the similarities in phenotypic effects and modes of action of drugs are calculated based on the similarity in gene expression profiles following drug treatment. A drug network displaying similarities of pairs of drugs was next constructed and partitioned into densely interconnected modules. A drug can be repositioned based on the drug modules to which it belongs. The mode of action for nine anticancer compounds was correctly predicted, and an unreported effect for a well-known drug, fasudil (a Rho-kinase inhibitor), was discovered using this network approach.[81] In the study conducted by Iskar et al.,[81] a large set of drug-induced transcriptional modules was identified using CMap data. Based on conserved and cell type-specific drug-induced modules, they further predicted gene functions of some regulators and revealed new mechanisms of action for existing drugs, providing a starting point for drug repositioning. Sirota et al.[82] integrated gene expression measurements from diseases with the CMap data and successfully predicted the new therapeutic effects of drugs based on the correlation scores between drugs and disease gene signatures. The assumption underlying this method is that a drug has the potential to have a therapeutic effect on a disease if exposure to this drug can reverse the disease state signified by a specific set of gene expression changes. More drug repositioning methods can be found in a recent comprehensive review.[83]

Drug combination strategies, which refer to the use of two or more drugs administered to a patient, can also be used as a rational therapeutic intervention. A drug combination therapy may have higher efficacy, fewer side effects, and less toxicity

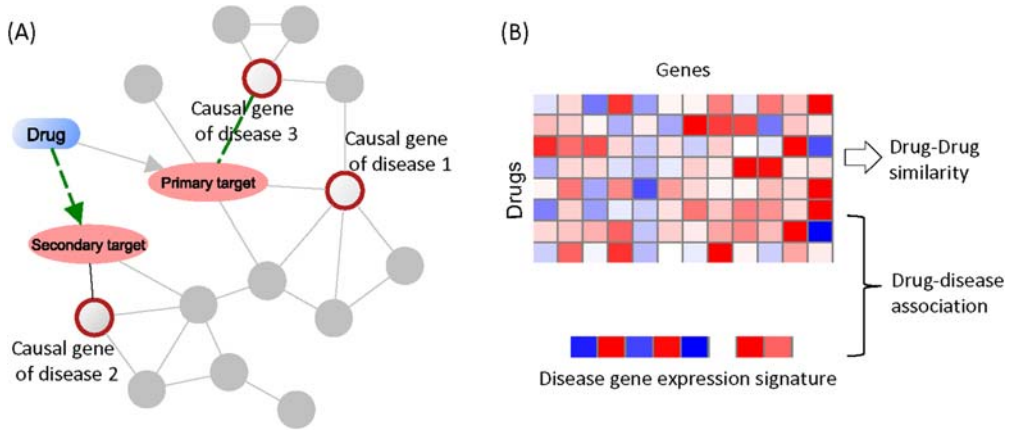

Fig. 3 Examples of network-based drug repositioning. (A) Drug repositioning based on new drug–target interactions and new target–disease associations. (B) Drug repositioning based on correlation of the drug-induced gene expression profiles.

compared to single-drug treatment due to additive or ideally synergistic effects among different drugs.[84,85] Some drug combinations have been used in treating complex diseases, such as cancer and cardiovascular diseases. For example, it has been demonstrated that the combination of aspirin and dipyridamole is more effective than aspirin alone in reducing the risk of stroke and other serious vascular events.[86] Experimental screening of drug combinations, however, is very costly and often only identifies a small number of synergistic combinations owing to the large search space and the difficulties in quantifying drug synergy.[87,88] With the exponential growth of molecular data available, systems chemical biology approaches can be used to filter this experimental search space and predict novel synergistic drug combinations with the aid of computational methods and mathematical models.[52] As in drug repositioning, drug-induced gene expression profiles can capture the complex dependencies of drugs and provide rich information for drug combination identification. A community computational challenge was launched to develop computational methods for ranking compound pairs based on gene expression profiles of human cells treated with individual compounds at multiple time points and concentrations.[89] Four of the 32 submitted methods performed significantly better than random guessing, indicating that computational prediction of optimal drug combinations is possible. In a recent study, Sun et al.[90] established a semisupervised learning model called the Ranking-system of Anti-Cancer Synergy to predict the synergistic potential of the available anticancer drugs by combining features of targeting networks and transcriptomic profiles. The model first does a preliminary ranking by calculating the synergistic potential for queried drug pairs and then refines the rankings based on gene expression correlations between individual drugs. In addition, a framework based on differential coexpression and Pareto optimization has been developed to mine drug-induced high-throughput transcriptomic data for predicting targeted drug combinations.[91] Drug combinations not only can achieve higher efficacy but also can reduce side effects. For example, rosiglitazone is an antidiabetic drug with cardiovascular side effects including myocardial infarction (MI). Zhao et al.[92] searched for the usage of a second drug in the FDA's Adverse Event Reporting System (FAERS) that could mitigate the risk of rosiglitazone-associated MI and found that the combination of rosiglitazone with exenatide significantly reduces rosiglitazone-associated MI.[92] Next-generation high-throughput technologies that enable the measurement of millions of cellular data points simultaneously also provide a great opportunity for systems chemical biology to identify more synergistic drug combinations.[85]

2.19.6 ADE Prediction

In Europe, nearly 200,000 people die every year from ADRs according to estimates from the European Commission. Taken together, about 328,000 patients in the United States and Europe die from prescription drugs each year. ADEs or ADRs have posed serious challenges to public health.[93,94] Therefore, early and accurate prediction of ADEs is critically important for reducing the event rates and has direct impact on drug safety and public health. Thus far, there has been a wide range of methods developed to detect or predict ADEs. Approaches from systems chemical biology integrating technologies from biological, chemical, and quantitative sciences can elucidate and predict adverse drug effects from cellular to whole-systems levels. These approaches, which integrate large-scale data related to drugs, proteins, and biological pathways, not only enhance our ability to assess the side effects of small molecules with higher accuracy than traditional toxicity studies but also provide mechanistic insights leading to ADRs.[95] In addition to data from genomics, chemistry, and systems biology, there are a few public data sources for drug safety and drug toxicity that can be utilized in early identification of ADRs through computational inference. **Table 3** summarizes some relevant data sources for this purpose.

Table 3 Select publicly available data sources for prediction of ADEs

Databases	*Descriptions*	*Web links*
FAERS	An information database designed to support the FDA postmarketing safety surveillance program for all approved drug and therapeutic biological products	http://www.fda.gov/Drugs/default.htm
SIDER	A side-effect database that contains information on 1430 marketed drugs and their recorded adverse reactions	http://sideeffects.embl.de/
CTD	A database that provides manually curated information about chemical–protein interactions, chemical–disease relationships, and gene–disease relationships	http://ctdbase.org/
DrugMatrix	A toxicology reference database that stores the results of thousands of highly controlled and standardized toxicological experiments	https://ntp.niehs.nih.gov/drugmatrix
Open TG-GATEs	A toxicogenomic database developed to store data on observed gene expression and toxicity in rats and humans after exposure to 150 compounds	http://toxico.nibiohn.go.jp/english/
ToxRefDB	A database capturing thousands of in vivo animal toxicity studies on hundreds of chemicals	http://www.epa.gov/comptox/toxrefdb/
DSSTox	A high-quality chemistry resource for supporting improved predictive toxicology	https://www.epa.gov/chemical-research/distributed-structure-searchable-toxicity-dsstox-database

As shown in Fig. 4, the datasets that provide relevant information for drug side-effect prediction are diverse, including similarity of drug or target structure, drug–ADR relationships, drug–target relationships, and drug–drug interactions. In addition, knowledge of the affected biological pathways of drugs and the gene ontology (GO) annotations of drug targets is useful in drug safety prediction. Xie et al.[96] generated protein–ligand binding profiles on a genome-wide scale by comparing ligand-binding sites with known protein structures and elucidated the molecular mechanisms associated with the adverse drug effects of CETP inhibitors for the treatment of cardiovascular diseases. The serious side effects of one CETP inhibitor, torcetrapib, were explained using this systems chemical biology approach by recognizing that torcetrapib, in addition to other members of the class of compounds, activates the renin–angiotensin system increasing blood pressure with its attendant cardiovascular risks. Based on chemical structure similarities between drugs and those molecules that lead to specific side effects, Lounkine et al.[97] used a molecular fingerprint strategy to screen computationally the 656 drugs against the 339-target panel and predict their activities on 73 unintended 'side-effect' targets. An association metric was then developed to prioritize those new off-targets and created a drug–target–ADR network. Cami et al.[56] constructed a bipartite network representation of existing drug–ADE associations called predictive pharmacosafety networks on the basis of a widely used drug safety database, defined nine network covariates and taxonomic covariates, and then used a logistic regression model to predict whether a given drug–ADE pair has a relationship or not. A recent study presented a new method to predict potential side effects of drugs from their drug–target relationships. This approach uses a canonical correlation analysis of the full drug–target and drug–ADE matrices and then calculates the probability that each drug has a given side effect using a Bayesian discriminant analysis technique.[98]

Other studies utilized complementary methods to predict the side effects of drugs. The data in spontaneous reporting systems may have many uncharacterized confounding factors, such as concomitant medications, patient demographics, and patient medical histories that interfere with statistical analysis. Tatonetti et al.[99] presented an adaptive data-driven approach for correcting some of these factors and created comprehensive database of drug effects (OFFSIDES) and a database of drug–drug interaction side effects (TWOSIDES). Brouwers et al.[100] mapped drug targets to protein–protein interaction networks and found that network neighbors of drug targets contribute to the similarity of drug side effects. Recently, a community-based DREAM challenge was launched to predict the toxicity of environmental compounds on human health.[3] The given data are the cytotoxicity of 156 compounds in human cell lines for which genotype and transcriptional data are available. The challenge participants were asked to develop algorithms to predict interindividual variability in toxic response based on genomic and transcriptional profiles and predict population-level cytotoxicity based on the structural attributes of the compounds.[3]

Cardiotoxicity is one of the major causes for drug withdrawals, and many drugs can induce irreversible cardiotoxicity.[101] Huang et al.[102] developed a network biology method integrating clinical observation data with drug–target data, protein–protein interaction networks, and GO annotations to predict drug side effects by using the combination of SVM and logistic regression. Using cardiotoxicity as a case study, they demonstrated that biomolecular networks and gene annotation information can significantly improve the predictive accuracy of ADRs of drugs. Incorporating drug chemical structures is also informative for drug safety prediction.[103] Ivanov et al.[104] developed a computational approach for identifying drug-induced MI-related proteins by predicting drug–target interactions based on the chemical structural similarity of the compounds. Drug-induced gene expression profiles can also provide insights into the similarity of drug side effects. Wang et al.[105] explored the prediction of ADRs based on the drug-induced gene expression profiles from CMap. They found that drugs inducing comparable ADRs tend to lead to similar CMap

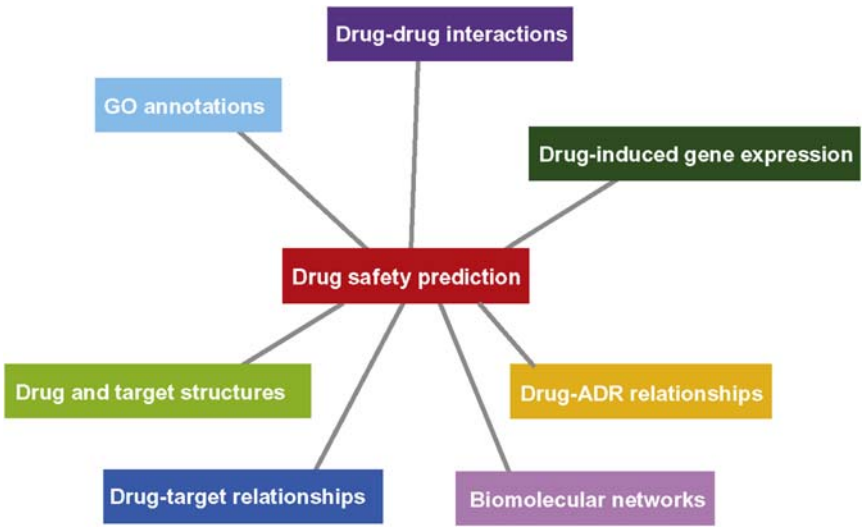

Fig. 4 Diverse datasets that can be used in drug safety prediction.

expression profiles. Based on such correlations, predictive models were constructed for various ADRs, including severe myocardial and infectious events. More systems biology approaches to understanding cardiotoxicity in cancer treatments can be found in a recent review.[101]

There is still a long way to go for reliable drug safety prediction, but systems chemical biology offers new avenues for investigating this critical area of drug development. Different from conventional drug design models, systems chemical biology combines the biological and chemical characteristics of drug targets and small molecules and considers system-wide side effects that cause the drug to fail. The approaches of systems chemical biology allow us to develop the hypotheses about drug side effects by understanding the signaling pathways underlying drug toxicity. We expect that systems chemical biology will have an increasing impact on drug safety prediction in the future.

2.19.7 Systems Chemical Biology for Personalized Medicine

Clearly, the high rate of ADRs is a major challenge in drug development. The one-size-fits-all drug model that ignores individual differences is often a primary cause of the ADRs. Personalized medicine puts aside the time-honored one-size-fits-all drug model and aims to provide an individual patient with tailored treatments based on his or her genetic profiles. The chemical biology community has successfully adapted high-throughput screening methodologies to facilitate the discovery of targeted therapeutics for personalized medicine. For example, chronic myeloid leukemia (CML) is characterized by a reciprocal translocation between chromosomes 9 and 22 that results in the constitutive activation of the tyrosine kinase enzyme BCR-ABL. A compound identified by *in vitro* screening for tyrosine kinase inhibitors, imatinib, was developed to act on cancers where BCR-ABL is stuck in the "ON" position.[106] This is one of the first cancer therapies that shows the potential for targeted treatment and has been widely used in the treatment of CML, gastrointestinal stromal tumors, and a number of other "unrelated" malignant tumors with this translocation. Since then, an increasing list of molecularly targeted therapeutics has been developed by similar approaches to drug discovery and target validation,[107–109] demonstrating the great potential of personalized medicine.

By contrast, systems biology has had many successes in utilizing high-throughput omics technologies to illuminate potential targets for disease intervention. With the increasing accumulation of next-generation sequencing and DNA variation array data, personalized medicine takes advantage of the great opportunity and is making promising progress. For example, The Cancer Genome Atlas (TCGA) is a publically funded project that aims to catalog and identify cancer-causing somatic variants in DNA, chromatin, and RNA of cancer genomes. Thus far, TCGA research team has analyzed large cohorts of over 30 human tumors through latest large-scale genome sequencing technologies and sophisticated multidimensional analytic methods.[110,111] The results are expected to provide rich information for personalized drug design. Chen et al.[112] combined different high-throughput technologies to present an integrative personal omics profile analysis that integrates genomic, transcriptomic, proteomic, metabolomic, and autoantibody profiles from a single individual over a 14-month period. This longitudinal analysis assessed disease risks and monitored disease states and trajectories for some complex diseases, such as type 2 diabetes, rhinovirus infection, and respiratory syncytial virus infection, demonstrating the possibility of personalized medicine enabled by systems chemical biology.

Personalized medicine focuses on personalized benefits, that is, improving a drug's potential to benefit a particular patient based on that patient's genetic makeup. A recent study demonstrated that it is possible for personalized medicine to predict a drug's downside risk as well, that is, a drug's side effects.[113] This study collected omics data from individuals and constructed data-driven personalized whole-cell kinetic models of metabolism to identify individuals at risk for a drug side effect. Although personalized medicine models have not yet been fully realized, the availability of large-scale genomic data and chemical data has revolutionized how biomedical scientists understand and explore biological systems. It has long been recognized that genetics may contribute to variability in drug action.[114] Exploration of available genomic sequencing data allows us to understand the variability of drug responses in different people. Systems chemical biology integrating genomics and other types of omics data with small molecule–target interaction profiles provides unprecedented opportunities for targeted therapeutic agents and new diagnostics. The contributions of system chemical biology to personalized medicine will become increasingly important and will urge new strategies not only for drug discovery but also for clinical trial design.[115,13]

2.19.8 Conclusions

Systems chemical biology is an emerging field that spans multiple disciplines including chemical biology, medicinal chemistry, systems biology, and computational science. By integrating heterogeneous chemical data and omics data using computational modeling, systems chemical biology could alter our way of thinking about biological systems and offers new avenues for understanding how small molecules perturb biological systems as a whole. A higher-level understanding of perturbation mechanisms of biological systems can guide researchers in the potential therapeutic impact of a small molecule on a signaling pathway and further affect the field of drug discovery. We anticipate more discoveries and applications in the field of systems chemical biology in the near future.

Acknowledgments

The authors would like to acknowledge the support of their studies from NIH grants (HL61795, HL108630 (MAPGen Consortium), and HL048743 to JL).

See also: 1.02. Drug Repurposing Review. 2.18. Systems Biology: Methods and Applications. 2.20. Translational Aspects in Drug Discovery. 3.17. Predicting Target and Chemical Druggability. 3.20. An Introduction to Systems Biology and Quantitative Systems Pharmacology. 4.08. A Comprehensive Overview of the Current Status and Application of Predictive ADMET: Introduction and Overview.

References

1. Anon. Voices of Chemical Biology. *Nat. Chem. Biol.* **2015,** *11* (6), 378–379.
2. Patrick, G. L. *An Introduction to Medicinal Chemistry,* 5th ed.; Oxford University Press: Oxford, 2013.
3. Lombardino, J. G.; Lowe, J. A., III The Role of the Medicinal Chemist in Drug Discovery—Then and Now. *Nat. Rev. Drug Discov.* **2004,** *3* (10), 853–862.
4. Stevens, E. *Medicinal Chemistry: The Modern Drug Discovery Process Pearson,* 1st ed.; Pearson: Boston, 2013.
5. Bredel, M.; Jacoby, E. Chemogenomics: An Emerging Strategy for Rapid Target and Drug Discovery. *Nat. Rev. Genet.* **2004,** *5* (4), 262–275.
6. Kawasumi, M.; Nghiem, P. Chemical Genetics: Elucidating Biological Systems With Small-Molecule Compounds. *J. Invest. Dermatol.* **2007,** *127* (7), 1577–1584.
7. Caron, P. R.; Mullican, M. D.; Mashal, R. D.; Wilson, K. P.; Su, M. S.; Murcko, M. A. Chemogenomic Approaches to Drug Discovery. *Curr. Opin. Chem. Biol.* **2001,** *5* (4), 464–470.
8. Peterson, R. T. Chemical Biology and the Limits of Reductionism. *Nat. Chem. Biol.* **2008,** *4* (11), 635–638.
9. Csermely, P.; Agoston, V.; Pongor, S. The Efficiency of Multi-Target Drugs: The Network Approach Might Help Drug Design. *Trends Pharmacol. Sci.* **2005,** *26* (4), 178–182.
10. Zimmermann, G. R.; Lehar, J.; Keith, C. T. Multi-Target Therapeutics: When the Whole Is Greater Than the Sum of the Parts. *Drug Discov. Today* **2007,** *12* (1-2), 34–42.
11. Csermely, P.; Korcsmaros, T.; Kiss, H. J.; London, G.; Nussinov, R. Structure and Dynamics of Molecular Networks: A Novel Paradigm of Drug Discovery: A Comprehensive Review. *Pharmacol. Ther.* **2013,** *138* (3), 333–408.
12. Hopkins, A. L. Network Pharmacology: The Next Paradigm in Drug Discovery. *Nat. Chem. Biol.* **2008,** *4* (11), 682–690.
13. Antman, E.; Weiss, S.; Loscalzo, J. Systems Pharmacology, Pharmacogenetics, and Clinical Trial Design in Network Medicine. *Wiley Interdiscip. Rev. Syst. Biol. Med.* **2012,** *4* (4), 367–383.
14. Butcher, E. C.; Berg, E. L.; Kunkel, E. J. Systems Biology in Drug Discovery. *Nat. Biotechnol.* **2004,** *22* (10), 1253–1259.
15. Wang, R. S.; Maron, B. A.; Loscalzo, J. Systems Medicine: Evolution of Systems Biology From Bench to Bedside. *Wiley Interdiscip. Rev. Syst. Biol. Med.* **2015,** *7* (4), 141–161.
16. Schenone, M.; Dancik, V.; Wagner, B. K.; Clemons, P. A. Target Identification and Mechanism of Action in Chemical Biology and Drug Discovery. *Nat. Chem. Biol.* **2013,** *9* (4), 232–240.
17. Oprea, T. I.; Tropsha, A.; Faulon, J. L.; Rintoul, M. D. Systems Chemical Biology. *Nat. Chem. Biol.* **2007,** *3* (8), 447–450.
18. Mayr, L. M.; Bojanic, D. Novel Trends in High-Throughput Screening. *Curr. Opin. Pharmacol.* **2009,** *9* (5), 580–588.
19. Gaulton, A.; Bellis, L. J.; Bento, A. P.; Chambers, J.; Davies, M.; Hersey, A.; Light, Y.; McGlinchey, S.; Michalovich, D.; Al-Lazikani, B.; Overington, J. P. ChEMBL: A Large-Scale Bioactivity Database for Drug Discovery. *Nucleic Acids Res.* **2012,** *40* (Database issue), D1100–D1107.
20. Wang, Y.; Suzek, T.; Zhang, J.; Wang, J.; He, S.; Cheng, T.; Shoemaker, B. A.; Gindulyte, A.; Bryant, S. H. PubChem Bioassay: 2014 Update. *Nucleic Acids Res.* **2014,** *42* (Database issue), D1075–D1082.
21. Kim, S.; Thiessen, P. A.; Bolton, E. E.; Chen, J.; Fu, G.; Gindulyte, A.; Han, L.; He, J.; He, S.; Shoemaker, B. A.; Wang, J.; Yu, B.; Zhang, J.; Bryant, S. H. PubChem Substance and Compound Databases. *Nucleic Acids Res.* **2016,** *44* (D1), D1202–D1213.
22. Seiler, K. P.; George, G. A.; Happ, M. P.; Bodycombe, N. E.; Carrinski, H. A.; Norton, S.; Brudz, S.; Sullivan, J. P.; Muhlich, J.; Serrano, M.; Ferraiolo, P.; Tolliday, N. J.; Schreiber, S. L.; Clemons, P. A. ChemBank: A Small-Molecule Screening and Cheminformatics Resource Database. *Nucleic Acids Res.* **2008,** *36* (Database issue), D351–D359.
23. Taboureau, O.; Nielsen, S. K.; Audouze, K.; Weinhold, N.; Edsgard, D.; Roque, F. S.; Kouskoumvekaki, I.; Bora, A.; Curpan, R.; Jensen, T. S.; Brunak, S.; Oprea, T. I. ChemProt: A Disease Chemical Biology Database. *Nucleic Acids Res.* **2011,** *39* (Database issue), D367–D372.
24. Kuhn, M.; Szklarczyk, D.; Pletscher-Frankild, S.; Blicher, T. H.; von Mering, C.; Jensen, L. J.; Bork, P. STITCH 4: Integration of Protein–Chemical Interactions With User Data. *Nucleic Acids Res.* **2014,** *42* (Database issue), D401–D407.
25. Gilson, M. K.; Liu, T.; Baitaluk, M.; Nicola, G.; Hwang, L.; Chong, J. BindingDB in 2015: A Public Database for Medicinal Chemistry, Computational Chemistry and Systems Pharmacology. *Nucleic Acids Res.* **2016,** *44* (D1), D1045–D1053.
26. Thorn, C. F.; Klein, T. E.; Altman, R. B. PharmGKB: The Pharmacogenetics and Pharmacogenomics Knowledge Base. *Methods Mol. Biol.* **2005,** *311,* 179–191.
27. Maglott, D.; Ostell, J.; Pruitt, K. D.; Tatusova, T. Entrez Gene: Gene-Centered Information at NCBI. *Nucleic Acids Res.* **2011,** *39* (Database issue), D52–D57.
28. Wu, C. H.; Apweiler, R.; Bairoch, A.; Natale, D. A.; Barker, W. C.; Boeckmann, B.; Ferro, S.; Gasteiger, E.; Huang, H.; Lopez, R.; Magrane, M.; Martin, M. J.; Mazumder, R.; O'Donovan, C.; Redaschi, N.; Suzek, B. The Universal Protein Resource (UniProt): An Expanding Universe of Protein Information. *Nucleic Acids Res.* **2006,** *34* (Database issue), D187–D191.
29. Scheer, M.; Grote, A.; Chang, A.; Schomburg, I.; Munaretto, C.; Rother, M.; Sohngen, C.; Stelzer, M.; Thiele, J.; Schomburg, D. BRENDA, the Enzyme Information System in 2011. *Nucleic Acids Res.* **2011,** *39* (Database issue), D670–D676.
30. Wishart, D. S.; Jewison, T.; Guo, A. C.; Wilson, M.; Knox, C.; Liu, Y.; Djoumbou, Y.; Mandal, R.; Aziat, F.; Dong, E.; Bouatra, S.; Sinelnikov, I.; Arndt, D.; Xia, J.; Liu, P.; Yallou, F.; Bjorndahl, T.; Perez-Pineiro, R.; Eisner, R.; Allen, F.; Neveu, V.; Greiner, R.; Scalbert, A. HMDB 3.0: The Human Metabolome Database in 2013. *Nucleic Acids Res.* **2013,** *41,* D801–D807.
31. Barrett, T.; Edgar, R. Gene Expression Omnibus: Microarray Data Storage, Submission, Retrieval, and Analysis. *Methods Enzymol.* **2006,** *411,* 352–369.
32. Uhlen, M.; Oksvold, P.; Fagerberg, L.; Lundberg, E.; Jonasson, K.; Forsberg, M.; Zwahlen, M.; Kampf, C.; Wester, K.; Hober, S.; Wernerus, H.; Bjorling, L.; Ponten, F. Towards a Knowledge-Based Human Protein Atlas. *Nat. Biotechnol.* **2010,** *28* (12), 1248–1250.
33. Landt, S. G.; Marinov, G. K.; Kundaje, A.; Kheradpour, P.; Pauli, F.; Batzoglou, S.; Bernstein, B. E.; Bickel, P.; Brown, J. B.; Cayting, P.; Chen, Y.; DeSalvo, G.; Epstein, C.; Fisher-Aylor, K. I.; Euskirchen, G.; Gerstein, M.; Gertz, J.; Hartemink, A. J.; Hoffman, M. M.; Iyer, V. R.; Jung, Y. L.; Karmakar, S.; Kellis, M.; Kharchenko, P. V.; Li, Q.; Liu, T.; Liu, X. S.; Ma, L.; Milosavljevic, A.; Myers, R. M.; Park, P. J.; Pazin, M. J.; Perry, M. D.; Raha, D.; Reddy, T. E.; Rozowsky, J.; Shoresh, N.; Sidow, A.; Slattery, M.; Stamatoyannopoulos, J. A.; Tolstorukov, M. Y.; White, K. P.; Xi, S.; Farnham, P. J.; Lieb, J. D.; Wold, B. J.; Snyder, M. ChIP-seq Guidelines and Practices of the ENCODE and modENCODE Consortia. *Genome Res.* **2012,** *22* (9), 1813–1831.

34. Rolland, T.; Tasan, M.; Charloteaux, B.; Pevzner, S. J.; Zhong, Q.; Sahni, N.; Yi, S.; Lemmens, I.; Fontanillo, C.; Mosca, R.; Kamburov, A.; Ghiassian, S. D.; Yang, X.; Ghamsari, L.; Balcha, D.; Begg, B. E.; Braun, P.; Brehme, M.; Broly, M. P.; Carvunis, A. R.; Convery-Zupan, D.; Corominas, R.; Coulombe-Huntington, J.; Dann, E.; Dreze, M.; Dricot, A.; Fan, C.; Franzosa, E.; Gebreab, F.; Gutierrez, B. J.; Hardy, M. F.; Jin, M.; Kang, S.; Kiros, R.; Lin, G. N.; Luck, K.; MacWilliams, A.; Menche, J.; Murray, R. R.; Palagi, A.; Poulin, M. M.; Rambout, X.; Rasla, J.; Reichert, P.; Romero, V.; Ruyssinck, E.; Sahalie, J. M.; Scholz, A.; Shah, A. A.; Sharma, A.; Shen, Y.; Spirohn, K.; Tam, S.; Tejeda, A. O.; Trigg, S. A.; Twizere, J. C.; Vega, K.; Walsh, J.; Cusick, M. E.; Xia, Y.; Barabasi, A. L.; Iakoucheva, L. M.; Aloy, P.; De Las Rivas, J.; Tavernier, J.; Calderwood, M. A.; Hill, D. E.; Hao, T.; Roth, F. P.; Vidal, M. A Proteome-Scale map of the Human Interactome Network. *Cell* **2014,** *159* (5), 1212–1226.
35. Ewing, R. M.; Chu, P.; Elisma, F.; Li, H.; Taylor, P.; Climie, S.; McBroom-Cerajewski, L.; Robinson, M. D.; O'Connor, L.; Li, M.; Taylor, R.; Dharsee, M.; Ho, Y.; Heilbut, A.; Moore, L.; Zhang, S.; Ornatsky, O.; Bukhman, Y. V.; Ethier, M.; Sheng, Y.; Vasilescu, J.; Abu-Farha, M.; Lambert, J. P.; Duewel, H. S.; Stewart, I. I.; Kuehl, B.; Hogue, K.; Colwill, K.; Gladwish, K.; Muskat, B.; Kinach, R.; Adams, S. L.; Moran, M. F.; Morin, G. B.; Topaloglou, T.; Figeys, D. Large-Scale Mapping of Human Protein–Protein Interactions by Mass Spectrometry. *Mol. Syst. Biol.* **2007,** *3,* 89.
36. Smith, M. G.; Ptacek, J.; Snyder, M. Kinase Substrate Interactions. *Methods Mol. Biol.* **2011,** *723,* 201–212.
37. Barrios-Rodiles, M.; Brown, K. R.; Ozdamar, B.; Bose, R.; Liu, Z.; Donovan, R. S.; Shinjo, F.; Liu, Y.; Dembowy, J.; Taylor, I. W.; Luga, V.; Przulj, N.; Robinson, M.; Suzuki, H.; Hayashizaki, Y.; Jurisica, I.; Wrana, J. L. High-Throughput Mapping of a Dynamic Signaling Network in Mammalian Cells. *Science* **2005,** *307* (5715), 1621–1625.
38. Kanehisa, M.; Goto, S. KEGG: Kyoto Encyclopedia of Genes and Genomes. *Nucleic Acids Res.* **2000,** *28* (1), 27–30.
39. Caspi, R.; Billington, R.; Ferrer, L.; Foerster, H.; Fulcher, C. A.; Keseler, I. M.; Kothari, A.; Krummenacker, M.; Latendresse, M.; Mueller, L. A.; Ong, Q.; Paley, S.; Subhraveti, P.; Weaver, D. S.; Karp, P. D. The MetaCyc Database of Metabolic Pathways and Enzymes and the BioCyc Collection of Pathway/Genome Databases. *Nucleic Acids Res.* **2016,** *44* (D1), D471–D480.
40. Fabregat, A.; Sidiropoulos, K.; Garapati, P.; Gillespie, M.; Hausmann, K.; Haw, R.; Jassal, B.; Jupe, S.; Korninger, F.; McKay, S.; Matthews, L.; May, B.; Milacic, M.; Rothfels, K.; Shamovsky, V.; Webber, M.; Weiser, J.; Williams, M.; Wu, G.; Stein, L.; Hermjakob, H.; D'Eustachio, P. The Reactome Pathway Knowledgebase. *Nucleic Acids Res.* **2016,** *44* (D1), D481–D487.
41. Cerami, E. G.; Gross, B. E.; Demir, E.; Rodchenkov, I.; Babur, O.; Anwar, N.; Schultz, N.; Bader, G. D.; Sander, C. Pathway Commons, a Web Resource for Biological Pathway Data. *Nucleic Acids Res.* **2011,** *39* (Database issue), D685–D690.
42. Liberzon, A.; Birger, C.; Thorvaldsdottir, H.; Ghandi, M.; Mesirov, J. P.; Tamayo, P. The Molecular Signatures Database (MSigDB) Hallmark Gene set Collection. *Cell Syst.* **2015,** *1* (6), 417–425.
43. Subramanian, A.; Tamayo, P.; Mootha, V. K.; Mukherjee, S.; Ebert, B. L.; Gillette, M. A.; Paulovich, A.; Pomeroy, S. L.; Golub, T. R.; Lander, E. S.; Mesirov, J. P. Gene Set Enrichment Analysis: A Knowledge-Based Approach for Interpreting Genome-Wide Expression Profiles. *Proc. Natl. Acad. Sci. U. S. A.* **2005,** *102* (43), 15545–15550.
44. Oprea, T. I.; May, E. E.; Leitao, A.; Tropsha, A. Computational Systems Chemical Biology. *Methods Mol. Biol.* **2011,** *672,* 459–488.
45. Lavecchia, A. Machine-Learning Approaches in Drug Discovery: Methods and Applications. *Drug Discov. Today* **2015,** *20* (3), 318–331.
46. Ding, H.; Takigawa, I.; Mamitsuka, H.; Zhu, S. Similarity-Based Machine Learning Methods for Predicting Drug-Target Interactions: A Brief Review. *Brief. Bioinform.* **2014,** *15* (5), 734–747.
47. Napolitano, F.; Zhao, Y.; Moreira, V. M.; Tagliaferri, R.; Kere, J.; D'Amato, M.; Greco, D. Drug Repositioning: A Machine–Learning Approach Through Data Integration. *J. Chem. Theory Comput.* **2013,** *5* (1), 30.
48. Harpaz, R.; DuMouchel, W.; Shah, N. H.; Madigan, D.; Ryan, P.; Friedman, C. Novel Data-Mining Methodologies for Adverse Drug Event Discovery and Analysis. *Clin. Pharmacol. Ther.* **2012,** *91* (6), 1010–1021.
49. Flobak, A.; Baudot, A.; Remy, E.; Thommesen, L.; Thieffry, D.; Kuiper, M.; Laegreid, A. Discovery of Drug Synergies in Gastric Cancer Cells Predicted by Logical Modeling. *PLoS Comput. Biol.* **2015,** *11* (8), e1004426.
50. Durrant, J. D.; McCammon, J. A. Molecular Dynamics Simulations and Drug Discovery. *BMC Biol.* **2011,** *9,* 71.
51. Okimoto, N.; Futatsugi, N.; Fuji, H.; Suenaga, A.; Morimoto, G.; Yanai, R.; Ohno, Y.; Narumi, T.; Taiji, M. High-Performance Drug Discovery: Computational Screening by Combining Docking and Molecular Dynamics Simulations. *PLoS Comput. Biol.* **2009,** *5* (10), e1000528.
52. Garmaroudi, F. S.; Handy, D. E.; Liu, Y.-Y.; Loscalzo, J. Systems Pharmacology and Rational Polypharmacy: Nitric Oxide-Cyclic GMP Signaling Pathway as an Illustrative Example and Derivation of the General Case. *PLoS Comput. Biol.* **2016,** *12* (3), e1004822.
53. Barabasi, A. L.; Oltvai, Z. N. Network Biology: Understanding the Cell's Functional Organization. *Nat. Rev. Genet.* **2004,** *5* (2), 101–113.
54. Zhao, S.; Iyengar, R. Systems Pharmacology: Network Analysis to Identify Multiscale Mechanisms of Drug Action. *Annu. Rev. Pharmacol. Toxicol.* **2012,** *52,* 505–521.
55. Yildirim, M. A.; Goh, K. I.; Cusick, M. E.; Barabasi, A. L.; Vidal, M. Drug–Target Network. *Nat. Biotechnol.* **2007,** *25* (10), 1119–1126.
56. Cami, A.; Arnold, A.; Manzi, S.; Reis, B. Predicting Adverse Drug Events Using Pharmacological Network Models. *Sci. Transl. Med.* **2011,** *3* (114), 114ra127.
57. Lo, Y. C.; Senese, S.; Li, C. M.; Hu, Q.; Huang, Y.; Damoiseaux, R.; Torres, J. Z. Large-Scale Chemical Similarity Networks for Target Profiling of Compounds Identified in Cell-Based Chemical Screens. *PLoS Comput. Biol.* **2015,** *11* (3), e1004153.
58. Kibble, M.; Saarinen, N.; Tang, J.; Wennerberg, K.; Makela, S.; Aittokallio, T. Network Pharmacology Applications to Map the Unexplored Target Space and Therapeutic Potential of Natural Products. *Nat. Prod. Rep.* **2015,** *32* (8), 1249–1266.
59. Searls, D. B. Data Integration: Challenges for Drug Discovery. *Nat. Rev. Drug Discov.* **2005,** *4* (1), 45–58.
60. Yamanishi, Y.; Pauwels, E.; Kotera, M. Drug Side-Effect Prediction Based on the Integration of Chemical and Biological Spaces. *J. Chem. Inf. Model.* **2012,** *52* (12), 3284–3292.
61. Cao, D. S.; Xiao, N.; Li, Y. J.; Zeng, W. B.; Liang, Y. Z.; Lu, A. P.; Xu, Q. S.; Chen, A. F. Integrating Multiple Evidence Sources to Predict Adverse Drug Reactions Based on a Systems Pharmacology Model. *CPT Pharmacometrics Syst. Pharmacol.* **2015,** *4* (9), 498–506.
62. Zheng, C.; Guo, Z.; Huang, C.; Wu, Z.; Li, Y.; Chen, X.; Fu, Y.; Ru, J.; Ali Shar, P.; Wang, Y. Large-Scale Direct Targeting for Drug Repositioning and Discovery. *Sci. Rep.* **2015,** *5,* 11970.
63. Wild, D. J.; Ding, Y.; Sheth, A. P.; Harland, L.; Gifford, E. M.; Lajiness, M. S. Systems Chemical Biology and the Semantic Web: What They Mean for the Future of Drug Discovery Research. *Drug Discov. Today* **2012,** *17* (9-10), 469–474.
64. Brown, J. B.; Okuno, Y. Systems Biology and Systems Chemistry: New Directions for Drug Discovery. *Chem. Biol.* **2012,** *19* (1), 23–28.
65. Lomenick, B.; Olsen, R. W.; Huang, J. Identification of Direct Protein Targets of Small Molecules. *ACS Chem. Biol.* **2011,** *6* (1), 34–46.
66. Eggert, U. S.; Kiger, A. A.; Richter, C.; Perlman, Z. E.; Perrimon, N.; Mitchison, T. J.; Field, C. M. Parallel Chemical Genetic and Genome-Wide RNAi Screens Identify Cytokinesis Inhibitors and Targets. *PLoS Biol.* **2004,** *2* (12), e379.
67. Castoreno, A. B.; Smurnyy, Y.; Torres, A. D.; Vokes, M. S.; Jones, T. R.; Carpenter, A. E.; Eggert, U. S. Small Molecules Discovered in a Pathway Screen Target the Rho Pathway in Cytokinesis. *Nat. Chem. Biol.* **2010,** *6* (6), 457–463.
68. Pei, J.; Yin, N.; Ma, X.; Lai, L. Systems Biology Brings new Dimensions for Structure-Based Drug Design. *J. Am. Chem. Soc.* **2014,** *136* (33), 11556–11565.
69. Keiser, M. J.; Setola, V.; Irwin, J. J.; Laggner, C.; Abbas, A. I.; Hufeisen, S. J.; Jensen, N. H.; Kuijer, M. B.; Matos, R. C.; Tran, T. B.; Whaley, R.; Glennon, R. A.; Hert, J.; Thomas, K. L.; Edwards, D. D.; Shoichet, B. K.; Roth, B. L. Predicting New Molecular Targets for Known Drugs. *Nature* **2009,** *462* (7270), 175–181.
70. Patterson, D. M.; Prescher, J. A. Orthogonal Bioorthogonal Chemistries. *Curr. Opin. Chem. Biol.* **2015,** *28,* 141–149.
71. Yamanishi, Y.; Araki, M.; Gutteridge, A.; Honda, W.; Kanehisa, M. Prediction of Drug–Target Interaction Networks From the Integration of Chemical and Genomic Spaces. *Bioinformatics* **2008,** *24* (13), i232–i240.
72. Yamanishi, Y.; Kotera, M.; Kanehisa, M.; Goto, S. Drug–Target Interaction Prediction from Chemical, Genomic and Pharmacological Data in an Integrated Framework. *Bioinformatics* **2010,** *26* (12), i246–i254.

73. Mitsopoulos, C.; Schierz, A. C.; Workman, P.; Al-Lazikani, B. Distinctive Behaviors of Druggable Proteins in Cellular Networks. *PLoS Comput. Biol.* **2015,** *11* (12), e1004597.
74. Zhao, J.; Cheng, F.; Wang, Y.; Arteaga, C. L.; Zhao, Z. Systematic Prioritization of Druggable Mutations in Approximately 5000 Genomes Across 16 Cancer Types Using a Structural Genomics-Based Approach. *Mol. Cell. Proteomics* **2016,** *15* (2), 642–656.
75. Rask-Andersen, M.; Masuram, S.; Schioth, H. B. The Druggable Genome: Evaluation of Drug Targets in Clinical Trials Suggests Major Shifts in Molecular Class and Indication. *Annu. Rev. Pharmacol. Toxicol.* **2014,** *54,* 9–26.
76. Pammolli, F.; Magazzini, L.; Riccaboni, M. The Productivity Crisis in Pharmaceutical R&D. *Nat. Rev. Drug Discov.* **2011,** *10* (6), 428–438.
77. Sawada, R.; Iwata, H.; Mizutani, S.; Yamanishi, Y. Target-Based Drug Repositioning Using Large-Scale Chemical-Protein Interactome Data. *J. Chem. Inf. Model.* **2015,** *55* (12), 2717–2730.
78. Zhao, S.; Li, S. A co-Module Approach for Elucidating Drug-Disease Associations and Revealing Their Molecular Basis. *Bioinformatics* **2012,** *28* (7), 955–961.
79. Lamb, J.; Crawford, E. D.; Peck, D.; Modell, J. W.; Blat, I. C.; Wrobel, M. J.; Lerner, J.; Brunet, J. P.; Subramanian, A.; Ross, K. N.; Reich, M.; Hieronymus, H.; Wei, G.; Armstrong, S. A.; Haggarty, S. J.; Clemons, P. A.; Wei, R.; Carr, S. A.; Lander, E. S.; Golub, T. R. The Connectivity Map: Using Gene-Expression Signatures to Connect Small Molecules, Genes, and Disease. *Science* **2006,** *313* (5795), 1929–1935.
80. Iorio, F.; Bosotti, R.; Scacheri, E.; Belcastro, V.; Mithbaokar, P.; Ferriero, R.; Murino, L.; Tagliaferri, R.; Brunetti-Pierri, N.; Isacchi, A.; di Bernardo, D. Discovery of Drug Mode of Action and Drug Repositioning From Transcriptional Responses. *Proc. Natl. Acad. Sci. U. S. A.* **2010,** *107* (33), 14621–14626.
81. Iskar, M.; Zeller, G.; Blattmann, P.; Campillos, M.; Kuhn, M.; Kaminska, K. H.; Runz, H.; Gavin, A. C.; Pepperkok, R.; van Noort, V.; Bork, P. Characterization of Drug-Induced Transcriptional Modules: Towards Drug Repositioning and Functional Understanding. *Mol. Syst. Biol.* **2013,** *9,* 662.
82. Sirota, M.; Dudley, J. T.; Kim, J.; Chiang, A. P.; Morgan, A. A.; Sweet-Cordero, A.; Sage, J.; Butte, A. J. Discovery and Preclinical Validation of Drug Indications Using Compendia of Public Gene Expression Data. *Sci. Transl. Med.* **2011,** *3* (96), 96ra77.
83. Jin, G.; Wong, S. T. Toward Better Drug Repositioning: Prioritizing and Integrating Existing Methods Into Efficient Pipelines. *Drug Discov. Today* **2014,** *19* (5), 637–644.
84. Fitzgerald, J. B.; Schoeberl, B.; Nielsen, U. B.; Sorger, P. K. Systems Biology and Combination Therapy in the Quest for Clinical Efficacy. *Nat. Chem. Biol.* **2006,** *2* (9), 458–466.
85. Sun, X.; Vilar, S.; Tatonetti, N. P. High-Throughput Methods for Combinatorial Drug Discovery. *Sci. Transl. Med.* **2013,** *5* (205), 205.
86. Verro, P.; Gorelick, P. B.; Nguyen, D. Aspirin Plus Dipyridamole Versus Aspirin for Prevention of Vascular Events After Stroke or TIA: A Meta-Analysis. *Stroke* **2008,** *39* (4), 1358–1363.
87. Tallarida, R. J. An Overview of Drug Combination Analysis With Isobolograms. *J. Pharmacol. Exp. Ther.* **2006,** *319* (1), 1–7.
88. Lehar, J.; Krueger, A. S.; Avery, W.; Heilbut, A. M.; Johansen, L. M.; Price, E. R.; Rickles, R. J.; Short, G. F., 3rd; Staunton, J. E.; Jin, X.; Lee, M. S.; Zimmermann, G. R.; Borisy, A. A. Synergistic Drug Combinations Tend to Improve Therapeutically Relevant Selectivity. *Nat. Biotechnol.* **2009,** *27* (7), 659–666.
89. Bansal, M.; Yang, J.; Karan, C.; Menden, M. P.; Costello, J. C.; Tang, H.; Xiao, G.; Li, Y.; Allen, J.; Zhong, R.; Chen, B.; Kim, M.; Wang, T.; Heiser, L. M.; Realubit, R.; Mattioli, M.; Alvarez, M. J.; Shen, Y.; Gallahan, D.; Singer, D.; Saez-Rodriguez, J.; Xie, Y.; Stolovitzky, G.; Califano, A. A Community Computational Challenge to Predict the Activity of Pairs of Compounds. *Nat. Biotechnol.* **2014,** *32* (12), 1213–1222.
90. Sun, Y.; Sheng, Z.; Ma, C.; Tang, K.; Zhu, R.; Wu, Z.; Shen, R.; Feng, J.; Wu, D.; Huang, D.; Fei, J.; Liu, Q.; Cao, Z. Combining Genomic and Network Characteristics for Extended Capability in Predicting Synergistic Drugs for Cancer. *Nat. Commun.* **2015,** *6,* 8481.
91. Penrod, N. M.; Greene, C. S.; Moore, J. H. Predicting Targeted Drug Combinations Based on Pareto Optimal Patterns of Coexpression Network Connectivity. *Genome Med.* **2014,** *6* (4), 33.
92. Zhao, S.; Nishimura, T.; Chen, Y.; Azeloglu, E. U.; Gottesman, O.; Giannarelli, C.; Zafar, M. U.; Benard, L.; Badimon, J. J.; Hajjar, R. J.; Goldfarb, J.; Iyengar, R. Systems Pharmacology of Adverse Event Mitigation by Drug Combinations. *Sci. Transl. Med.* **2013,** *5* (206), 206ra140.
93. Onakpoya, I. J.; Heneghan, C. J.; Aronson, J. K. Post-Marketing Withdrawal of 462 Medicinal Products Because of Adverse Drug Reactions: A Systematic Review of the World Literature. *BMC Med.* **2016,** *14* (1), 10.
94. Rawson, N. S. Drug Safety: Withdrawn Medications Are Only Part of the Picture. *BMC Med.* **2016,** *14* (1), 28.
95. Wang, R. S.; Loscalzo, J. Illuminating Drug Action by Network Integration of Disease Genes: A Case Study of Myocardial Infarction. *Mol. Biosyst.* **2016,** *12* (5), 1653–1666.
96. Xie, L.; Li, J.; Bourne, P. E. Drug Discovery Using Chemical Systems Biology: Identification of the Protein–Ligand Binding Network to Explain the Side Effects of CETP Inhibitors. *PLoS Comput. Biol.* **2009,** *5* (5), e1000387.
97. Lounkine, E.; Keiser, M. J.; Whitebread, S.; Mikhailov, D.; Hamon, J.; Jenkins, J. L.; Lavan, P.; Weber, E.; Doak, A. K.; Cote, S.; Shoichet, B. K.; Urban, L. Large-Scale Prediction and Testing of Drug Activity on Side-Effect Targets. *Nature* **2012,** *486* (7403), 361–367.
98. Perez-Nueno, V. I.; Souchet, M.; Karaboga, A. S.; Ritchie, D. W. GESSE: Predicting Drug Side Effects From Drug-Target Relationships. *J. Chem. Inf. Model.* **2015,** *55* (9), 1804–1823.
99. Tatonetti, N. P.; Ye, P. P.; Daneshjou, R.; Altman, R. B. Data-Driven Prediction of Drug Effects and Interactions. *Sci. Transl. Med.* **2012,** *4* (125), 125ra31.
100. Brouwers, L.; Iskar, M.; Zeller, G.; van Noort, V.; Bork, P. Network Neighbors of Drug Targets Contribute to Drug Side-Effect Similarity. *PLoS ONE* **2011,** *6* (7), e22187.
101. Brown, S. A.; Sandhu, N.; Herrmann, J. Systems Biology Approaches to Adverse Drug Effects: The Example of Cardio-Oncology. *Nat. Rev. Clin. Oncol.* **2015,** *12* (12), 718–731.
102. Huang, L. C.; Wu, X.; Chen, J. Y. Predicting Adverse Side Effects of Drugs. *BMC Genomics* **2011,** *12* (Suppl 5), S11.
103. Huang, L. C.; Wu, X.; Chen, J. Y. Predicting Adverse Drug Reaction Profiles by Integrating Protein Interaction Networks With Drug Structures. *Proteomics* **2013,** *13* (2), 313–324.
104. Ivanov, S. M.; Lagunin, A. A.; Pogodin, P. V.; Filimonov, D. A.; Poroikov, V. V. Identification of Drug-Induced Myocardial Infarction-Related Protein Targets Through the Prediction of Drug–Target Interactions and Analysis of Biological Processes. *Chem. Res. Toxicol.* **2014,** *27* (7), 1263–1281.
105. Wang, K.; Weng, Z.; Sun, L.; Sun, J.; Zhou, S. F.; He, L. Systematic Drug Safety Evaluation Based on Public Genomic Expression (Connectivity Map) Data: Myocardial and Infectious Adverse Reactions as Application Cases. *Biochem. Biophys. Res. Commun.* **2015,** *457* (3), 249–255.
106. Druker, B. J.; Talpaz, M.; Resta, D. J.; Peng, B.; Buchdunger, E.; Ford, J. M.; Lydon, N. B.; Kantarjian, H.; Capdeville, R.; Ohno-Jones, S.; Sawyers, C. L. Efficacy and Safety of a Specific Inhibitor of the BCR-ABL Tyrosine Kinase in Chronic Myeloid Leukemia. *N. Engl. J. Med.* **2001,** *344* (14), 1031–1037.
107. Lynch, T. J.; Bell, D. W.; Sordella, R.; Gurubhagavatula, S.; Okimoto, R. A.; Brannigan, B. W.; Harris, P. L.; Haserlat, S. M.; Supko, J. G.; Haluska, F. G.; Louis, D. N.; Christiani, D. C.; Settleman, J.; Haber, D. A. Activating Mutations in the Epidermal Growth Factor Receptor Underlying Responsiveness of Non-Small-Cell Lung Cancer to Gefitinib. *N. Engl. J. Med.* **2004,** *350* (21), 2129–2139.
108. Garber, K. Cancer Research: Melanoma Drug Vindicates Targeted Approach. *Science* **2009,** *326,* 1619.
109. Vassilev, L. T.; Vu, B. T.; Graves, B.; Carvajal, D.; Podlaski, F.; Filipovic, Z.; Kong, N.; Kammlott, U.; Lukacs, C.; Klein, C.; Fotouhi, N.; Liu, E. A. In Vivo Activation of the p53 Pathway by Small-Molecule Antagonists of MDM2. *Science* **2004,** *303* (5659), 844–848.
110. Weinstein, J. N.; Collisson, E. A.; Mills, G. B.; Shaw, K. R.; Ozenberger, B. A.; Ellrott, K.; Shmulevich, I.; Sander, C.; Stuart, J. M. The Cancer Genome Atlas Pan-Cancer Analysis Project. *Nat. Genet.* **2013,** *45* (10), 1113–1120.
111. Gonzalez de Castro, D.; Clarke, P. A.; Al-Lazikani, B.; Workman, P. Personalized Cancer Medicine: Molecular Diagnostics, Predictive Biomarkers, and Drug Resistance. *Clin. Pharmacol. Ther.* **2013,** *93* (3), 252–259.

112. Chen, R.; Mias, G. I.; Li-Pook-Than, J.; Jiang, L.; Lam, H. Y.; Miriami, E.; Karczewski, K. J.; Hariharan, M.; Dewey, F. E.; Cheng, Y.; Clark, M. J.; Im, H.; Habegger, L.; Balasubramanian, S.; O'Huallachain, M.; Dudley, J. T.; Hillenmeyer, S.; Haraksingh, R.; Sharon, D.; Euskirchen, G.; Lacroute, P.; Bettinger, K.; Boyle, A. P.; Kasowski, M.; Grubert, F.; Seki, S.; Garcia, M.; Whirl-Carrillo, M.; Gallardo, M.; Blasco, M. A.; Greenberg, P. L.; Snyder, P.; Klein, T. E.; Altman, R. B.; Butte, A. J.; Ashley, E. A.; Gerstein, M.; Nadeau, K. C.; Tang, H.; Snyder, M. Personal Omics Profiling Reveals Dynamic Molecular and Medical Phenotypes. *Cell* **2012,** *148* (6), 1293–1307.
113. Bordbar, A.; McCloskey, D.; Zielinski, D. C.; Sonnenschein, N.; Jamshidi, N.; Palsson, B. O. Personalized Whole-Cell Kinetic Models of Metabolism for Discovery in Genomics and Pharmacodynamics. *Cell Syst.* **2015,** *1* (4), 283–292.
114. Roden, D. M.; George, A. L., Jr. The Genetic Basis of Variability in Drug Responses. *Nat. Rev. Drug Discov.* **2002,** *1* (1), 37–44.
115. Silverman, E. K.; Loscalzo, J. Developing New Drug Treatments in the Era of Network Medicine. *Clin. Pharmacol. Ther.* **2013,** *93* (1), 26–28.

Relevant Websites

116. http://www.drugs.com/—This website contains comprehensive information about drugs, including drug categories, drug side effects, and dosage guide.
117. http://www.fda.gov/Drugs/—The website provides information about drug approvals, drug-related databases, drug safety and availability, and other aspects of drugs.
118. http://www.genome.jp/kegg/drug/—KEGG Drug is a comprehensive drug information resource for approved drugs in Japan, USA, and Europe.
119. https://clinicaltrials.gov/—This website is a registry and results database of publicly and privately supported clinical studies of human participants conducted around the world.
120. http://www.centerwatch.com/—This is a website for collecting information on clinical trials and related drugs for both clinical research professionals and patients.
121. http://cdb.ics.uci.edu/—A website that provides the most diverse and useful set of chemoinformatics tools and applications available to the public.
122. http://www.cbs.dtu.dk/services/NutriChem-1.0/—NutriChem is a systems chemical biology resource generated by text mining of MEDLINE abstracts to explore the medicinal value of plant-based foods by linking them with their small molecule components and human disease phenotypes.

2.20 Translational Aspects in Drug Discovery

L Detalle*, K Vanheusden*, and ML Sargentini-Maier*, Ablynx Technologiepark, Zwijnaarde, Belgium
T Stöhr*, A2M Pharma GmbH, Monheim, Germany

© 2017 Elsevier Ltd. All rights reserved.

2.20.1 Introduction 496
2.20.2 Biomarkers 497
2.20.2.1 Definition 497
2.20.2.2 Types 497
2.20.2.2.1 Pharmacodynamic biomarkers 497
2.20.2.2.2 Efficacy biomarkers 498
2.20.2.2.3 Stratification and predictive biomarkers 498
2.20.2.2.4 Safety biomarkers 498
2.20.2.2.5 Competitive biomarkers 499
2.20.2.2.6 Pharmaco-economic biomarkers 499
2.20.2.3 Use of Biomarkers 499
2.20.2.4 Assays/Methods 499
2.20.2.4.1 Enzyme-linked immunosorbent assay 500
2.20.2.4.2 Multiplex assays 500
2.20.2.4.3 Mass spectrometry 500
2.20.2.5 Validation and Qualification 501
2.20.2.5.1 Validation 501
2.20.2.5.2 Qualification 503
2.20.3 Modeling and Simulations 503
2.20.3.1 Introduction 503
2.20.3.2 From Empirical to Mechanistic Pharmacokinetic/Pharmacodynamic Models 504
2.20.3.3 From Mechanistic Models to System Biology Models 505
2.20.3.4 Examples of Applications of Empirical, Mechanistic, and System Biology Models 507
2.20.3.4.1 Empirical Pharmacokinetic/Pharmacodynamic models—effect-compartment model 507
2.20.3.4.2 Mechanistic Pharmacokinetic/Pharmacodynamic models—selection of starting dose for first-in-human studies 507
2.20.3.4.3 PBPK models—drug–drug interactions consequent to drug-mediated cytokine elevations 508
2.20.3.4.4 System biology models—identification of optimal combinations of molecular targeted drugs in oncology 508
2.20.3.4.5 System biology models—a mathematical model for rheumatoid arthritis 509
2.20.3.5 Conclusion 509
2.20.4 Animal Model 510
2.20.4.1 Generalities 510
2.20.4.2 How to Improve Animal Models? 510
2.20.4.2.1 Multisite animal model trials 510
2.20.4.2.2 Enhance variability and reduce standardization 510
2.20.4.2.3 Design the animal model concurrent with the design recommended for a pivotal clinical trial 511
2.20.4.2.4 Humanize animal models 511
2.20.4.2.5 Introduce more relevant clinical endpoints 512
2.20.4.2.6 Ensure proper validation of animal models 512
2.20.4.3 How to Implement Animal Models Into a Translational Strategy? 512
2.20.4.3.1 Design an animal model strategy with a high translational value 512
2.20.4.3.2 Back-translate clinical trial findings into animal models 513
2.20.5 Imaging 514
2.20.5.1 Types and Technologies 514
2.20.5.1.1 Radiography 514
2.20.5.1.2 Computed tomography 514
2.20.5.1.3 Magnetic resonance imaging 515
2.20.5.1.4 Positron emission tomography 515
2.20.5.1.5 Optical imaging 515
2.20.5.2 Uses 515
2.20.5.2.1 Application of radiography in drug development 515
2.20.5.2.2 Application of CT in drug development 515

*All authors contributed equally.

2.20.5.2.3 Application of MRI in drug development 516
2.20.5.2.4 Application of PET in drug development 516
2.20.6 Strategy and Integration 517
2.20.6.1 Design of Translation Strategies 517
2.20.6.1.1 Introduction 517
2.20.6.1.2 Stroke TM strategies 517
2.20.6.1.3 ALX-0171 translational strategy 519
2.20.6.1.4 Tocilizumab translation in Crohn's disease 520
2.20.6.2 Integrative Thinking 520
2.20.6.2.1 Introduction 520
2.20.6.2.2 Bedside back to bench 520
2.20.6.2.3 Integrative thinking in oncology 521
2.20.6.3 Combination of Technologies 523
2.20.7 Conclusions 524
References 524

Abbreviations

ADME Absorption distribution metabolism and excretion
BQRT Biomarker qualification review team
CNS Central nervous system
COU Context of use
CRP C-reactive protein
CT Computed tomography
CYP Cytochrome P450
ELISA Enzyme-linked immunosorbent assay
EMA European Medicines Agency
FDA Food and Drug Administration
LOI Letter of intent
mAb Monoclonal antibody
MABEL Minimum anticipated biological effect level
MCA Middle cerebral artery
MRD Minimum required dilution
MRI Magnetic resonance imaging
MS Mass spectrometry
MSRD Maximally required starting dose
NIR Near infrared
NOD Nonobese diabetic
NSCLC Nonsmall cell lung cancer
PBPK Physiology based pharmacokinetic
PD Pharmacodynamic
PET Positron emission tomography
PK Pharmacokinetics
POC Proof of concept
QC Quality control
QoL Quality of life
(p)RCT (Preclinical) randomized clinical trial
RO Receptor occupancy
RSV Respiratory syncytial virus
RT Room temperature
SmPC Summary of product characteristic
SPECT Single photon emission computed tomography
TBI Traumatic brain injury
TCI Target controlled infusion
TM Translational medicine
WM White matter

2.20.1 Introduction

The efficiency of drug development has seen a constant decline. For instance, during the past 65 years, the number of drugs approved per billion US dollar investment has halved every 9 years.[1] This observation is somewhat paradoxical since during the same time there have been huge advancements in drug discovery and development technologies that made it much cheaper, faster, and easier to identify new drug targets and new drug molecules. The number of drug-like molecules that can be synthesized by one chemist, for example, has increased from 1 per week by about three orders of magnitude since the early 1990s.

Translational Science or Translational Medicine (TM) has arisen as an important discipline in modern drug discovery and development. It was triggered by the recognition of the so-called valley of death[2,3] where despite the huge advances in drug discovery technologies that resulted in the discovery of large amounts of new drug targets as well as the development of promising biological and small molecule drugs modulating these targets, many of these drugs failed in clinical trials. The challenge was thus to enhance the predictivity of the preclinical models and to design exploratory clinical trial designs and methodologies to test promising molecules earlier and faster.

Despite some advances, the number of drugs that finally receive regulatory approval is still low, and those drugs that make it to the market are often improved versions of older drugs (me-better drugs such as new formulations or new chemical entities targeting

known modes of action). The main reason for this drug failure rate was a lack of efficacy observed in clinical trials of drug candidates that showed great promise in drug discovery.

There may be two main factors responsible for this:

1. The industrialization of drug discovery and development led to huge specialized departments that operate in isolation, often distributed over different countries, continents, and time zones. A lack of communication between the relevant disciplines within a company or academic institution but also with other key stakeholders, for example, patients, prescribers, regulators, and payers, is thus probably one of the key factors. While each discipline was probably able to produce highly sophisticated work, there was not sufficient interaction and alignment as well as limited integration of knowledge during the whole drug development process.
2. Tools for successful translational research have only been developed in the last one or two decades. Among those tools are biomarkers that can help (if used wisely) to achieve more efficient translation between in vitro findings, animal model results, and clinical trial endpoints. Another opportunity is represented by the increased bioinformatics capabilities and the greater predictive power of in silico methods enabling evaluation of likely benefit/risk profiles for future drug candidates.[4] Other tools that have become available or that have been greatly advanced during the last years are animal models, modeling and simulation as well as imaging technologies.

In this article, we will describe the tools used in translational research, that is, biomarkers, animal models, imaging, in silico modeling and simulations. Their use will be illustrated with examples and specific tips and tricks of how to implement those into daily project work. We believe, however, that TM is more than these tools and technologies—it is not yet another discipline or department, it is a way of thinking that should become part of every discipline involved in drug development. Thus, in addition to describing the tools and how best to use them, we will elaborate on how to design a translational research strategy and exemplify with some case studies as to how this has been successfully implemented in the past.

2.20.2 Biomarkers

2.20.2.1 Definition

"Biomarkers" or "biological markers" are biological measures of biological processes. In Dec. 1998, the National Institutes of Health Biomarkers Definitions Working group defined a biomarker as "a characteristic that is objectively measured and evaluated as an indicator of normal biological processes, pathogenic processes, or pharmacologic responses to a therapeutic intervention."[5] Biomarkers can take many shapes or forms and in essence any biological marker that objectively quantifies a certain disease process or engagement of a drug to its target and has the potential to correlate statistically to clinical outcomes falls in this category. Depending on how a specific biomarker is measured, it will be subdivided into "wet biomarker" or "dry biomarker." Examples of wet biomarkers include soluble markers (in plasma, urine, or any other biological matrix) and genomics (gene expression patterns, genotyping), whereas examples of dry biomarkers include imaging (computed tomography (CT), positron emission tomography (PET), X-ray, magnetic resonance image (MRI)), scoring systems, questionnaires, etc.[6]

There is no well-established categorization system for biomarkers, but typically the following classes are frequently used based on the purpose for which they are destined: pharmacodynamic (PD) biomarkers, efficacy biomarkers, safety biomarkers, stratification and predictive biomarkers, competitive biomarkers, prognostic biomarkers, and pharmaco-economic biomarkers. It is important to bear in mind that for any classification system, classes are not discrete and/or mutually exclusive, that is, one biomarker can belong to either one or several classes based on the intended "purpose" of the biomarker. For instance, insulin sensitivity can serve as an efficacy biomarker in the context of type II diabetes[7] and a safety biomarker for the assessment of an antipsychotic drug.[8]

2.20.2.2 Types

2.20.2.2.1 Pharmacodynamic biomarkers

PD biomarkers are markers of a certain pharmacological response that is directly linked to engagement of the primary molecular target by the drug. As such, PD markers intervene upstream in the cascade of events that ultimately lead to the disease and are thus also referred to as proximal biomarkers as opposed to distal biomarkers (or efficacy biomarkers). Importantly, PD markers are modulated by drug treatment in a drug concentration-dependent manner and hence, correlate drug concentration to target occupancy when not at saturation. These biomarkers are crucial in gaining insight into disease mechanisms for first-in-class drugs with a novel nonvalidated mechanism of action. For example, if the PD biomarker indicates a strong target engagement but this relates to a lack of clinical effect, it is very likely that the biological process that is modulated does not play a prominent role in the pathophysiology leading to the disease, or that the patient population was inadequately selected. Ideally, a suitable PD biomarker should therefore be identified early on in the drug development process before or during proof-of-efficacy animal studies. The translatability of the PD biomarker from animal models to humans is critical such that any findings from preclinical studies can be appropriately bridged to the clinical setting. For example, the robustness and suitability of soluble IL-6 receptor levels as a PD biomarker for anti-IL-6 receptor biologics (ALX-0061 and tocilizumab) has been shown both nonclinically[9] and clinically.[10]

2.20.2.2.2 Efficacy biomarkers

Efficacy biomarkers (or distal biomarkers) typically are situated further downstream in the biological cascade that leads to the clinical disease in contrast to the PD biomarkers (or proximal biomarkers) that intervene more upstream. The separation between PD biomarkers and efficacy biomarkers can be very thin and in practice the term "efficacy biomarkers" is used for surrogate, predictive, and PD alike. In this section, efficacy biomarkers are seen as a specific class and are modulated by drug treatment in a dose-dependent manner, which correlates with a favorable efficacy, clinically meaningful response, or outcome and can range from more proximal PD biomarkers, to the most distal markers. As such, efficacy markers measure effects that are indirectly linked or are secondary to the drug binding to its target. A small proportion of efficacy biomarkers are validated and are accepted as surrogate endpoints for regulatory approval such as arterial blood pressure as a surrogate for heart failure, blood glucose levels as a surrogate for survival, and/or complications in diabetes mellitus, prostate-specific antigen response for survival in prostate cancer, forced expiratory volume (FEV1) in 1 second for lung function.

2.20.2.2.3 Stratification and predictive biomarkers

Stratification biomarkers are typically pretreatment markers (i.e., baseline markers) or signatures associated with a specific anticipated beneficial response (or safety concern) or lack of response to a particular therapy in that population. In other words, the stratification biomarkers are used in the context of a clinical trial and in daily clinical practice to select patients who are eligible to a certain treatment and whose response to that treatment is predictable, while patients who are unlikely to benefit or who are at risk of developing adverse reactions to the given treatment can be excluded. This stratification of patients upfront mainly serves two important purposes: firstly, because of the selection of more homogenous patient subpopulations, clinical effects will be augmented which will increase the success rate of drug approvals; secondly, the number of patients at risk of side effects who would likely only partially respond to treatment is minimized. More broadly, stratification biomarkers are also useful in routine clinical practice as they can assist physicians in making initial treatment decisions (e.g., selecting treatment options) for their patients or in identifying patients with different disease subtypes. Predictive biomarkers, although often used interchangeably with stratification biomarkers, are associated with a response or lack of response to a particular therapy. In contrast to stratification biomarkers that are typically pretreatment markers, predictive biomarkers can be measured throughout the treatment course and allow to adapt or adjust the treatment of a patient as early as possible and to predict long-term effects based on an early change in predictive biomarker signatures. For example, V-Ki-ras2 Kirsten rat sarcoma viral oncogene homolog (KRAS) and v-raf murine sarcoma viral oncogene homolog B1 (BRAF) are currently under focus as useful predictive biomarkers in patients with metastatic diseases treated with antiepidermal growth factor receptor monoclonal antibodies (mAbs), such as cetuximab and panitumumab.[11]

It is important to note the difference between "prognostic" and "predictive" biomarkers. A prognostic biomarker provides information on the clinical outcome of a disease in the absence of therapy, and is in essence a measure of its natural history. A predictive biomarker in contrast provides information on the likely outcome of treatment. For example, there is a weak but significant association between poor clinical outcome (i.e., poor prognosis) and overexpression of the oncogene Her2, as seen in approximately 15% of invasive breast cancers. In addition, Her2 overexpression predicts that those patients will likely not respond to cytotoxic chemotherapies (e.g., the combination of cytoxan methotrexate-5-fluoracil) but will likely respond to others (e.g., anthracyclines, taxanes, and trastuzumab). As such, Her2 expression status is both a prognostic and a predictive biomarker.[12] In contrast, the expression levels of both the estrogen receptor-α and the progesterone receptor have a relatively weak prognostic value but a very strong predictive value for response to hormonal therapies, such as tamoxifen.[12]

The use of stratification biomarkers or predictive biomarkers in clinical trials requires the development of a companion diagnostic in parallel to drug development. The Food and Drug Administration (FDA) has drafted in 2014 a guideline to facilitate companion diagnostic development.[13] It defines what a companion diagnostic is and various scenarios for use, and describes FDA policies for approval and labeling. Regulatory approvals of the device and drug should be contemporaneous. European Medicines Agency (EMA) published some reflection papers, still mostly focused on pharmacogenomics biomarkers to provide guidance.[14–18] Although companion diagnostics are a natural consequence of the flow toward a more personalized medicine, it comes with an extra burden during drug development.

2.20.2.2.4 Safety biomarkers

Safety biomarkers are markers that predict or diagnose clinically relevant adverse outcomes in response to a drug treatment or therapy. As this class of biomarkers is of prime importance to guarantee drug safety, the selection of safety biomarkers should be based on robust preclinical data, previous studies, or literature data. Ideally, these biomarkers should be specific and sensitive markers of early clinical injury and of high predictive value. This predictive value of a specific biomarker depends on the temporal relationship between the change in the biomarker and the occurrence of the adverse event. If the change in the biomarker occurs before the adverse event has occurred, the biomarker will be truly predictive and referred to as a "predictive safety biomarker." For example, QT wave interval prolongation on electrocardiograms is used as a surrogate marker for a particular type of cardiac arrhythmias, that is, torsades de pointes in drug development.[19] If the change in biomarker occurs concomitantly or after an adverse event (but before the appearance of the clinical manifestations), the biomarker will be referred to as a "diagnostic safety biomarker." The aim of safety biomarkers is primarily to identify and assess the risk for adverse effects and, as a result, increase drug safety but they are also used to increase drug development cost-effectiveness/success rate by identifying early those drugs that display acceptable safety profiles and by stopping early the development of those drugs that show an unacceptable safety profile. In addition safety

biomarkers help guide the selection of the starting dose for clinical studies or aid in the identification of patients that are at risk of developing adverse events to the drug (see also stratification biomarkers).

Several safety biomarkers have been developed and accepted over the years, such as alanine aminotransferase and aspartate aminotransferase that can detect toxicity in the liver. The predictive nature of these two biomarkers is rather weak as they are reflective of ongoing liver toxicity when tissue damage has already occurred but are not predictive of liver function. Several other biomarkers of liver toxicity that are being evaluated include glutamate dehydrogenase, malate dehydrogenase, paraoxonase/arylesterase 1, purine nucleoside phosphorylase, arginase, sorbitol dehydrogenase, and glutathione *S*-transferase.[20] Biomarkers for drug-induced renal damage and nephrotoxicity such as urinary protein biomarkers include Kim-1, albumin, total protein, β2-microglobulin, cystatin C, clusterin, and trefoil factor-3.[21,22]

2.20.2.2.5 Competitive biomarkers

Competitive biomarkers are used to assess whether or not a treatment has a competitive benefit versus a comparator (competitor, benchmark, standard of care therapy). This benefit can be on safety, efficacy, cost, etc. These competitive biomarkers aid in guiding strategic decisions and clinical trial designs, specifically when performing a head-to-head clinical trial with the benchmark or comparator drug. Go/no go decisions can be taken on the basis of the competitive biomarker data which provides an insight into the competitive edge of the investigational drug versus the benchmark. The use of such competitive biomarkers is especially important for a drug being developed in a "saturated indication" where a lack of competitive edge would allow early decision making and decrease drug attrition rates. For example, changes in HbA1c (glycated hemoglobin) levels were used to indirectly estimate the comparative efficacies of two dipeptidyl peptidase-4 inhibitors (sitagliptin and linagliptin) for the treatment of type II diabetes mellitus.[23] While often the competitiveness is either for efficacy or safety (i.e., the competitive biomarkers would overlap with those biomarkers) those could also include markers for speed of onset of action. When selecting a competitive biomarker, one should keep in mind that this biomarker does not need to be the best efficacy or safety biomarker, but should be selected to provide the best possible or most meaningful differentiation.

2.20.2.2.6 Pharmaco-economic biomarkers

One factor that drives increasing failure rates of approvals and reimbursement of drugs, besides a lack of efficacy or safety concerns, is the increasing awareness of many regulatory authorities and payers about the cost-effectiveness of a drug, specifically for "life-style drugs" that would a priori not obtain reimbursement (e.g., urinary incontinence, sexual dysfunction). Pharmaco-economic biomarkers are used to assess the pharmaco-economic value of a new drug and to compare the cost-effectiveness versus the standard of care. In essence, the assessment of pharmaco-economic biomarkers enables the analysis of the affordability of a drug. In the current healthcare system environment, which is becoming more and more cost sensitive, it is essential to include early measures to quantify patient benefits and potential cost savings in other areas (e.g., number of days in hospital). Even if a drug receives regulatory approval, the payers may decide not to reimburse the costs or to a level that would not be sufficient to compensate the costs of its development. Increased safety or efficacy by its own may not be sufficient for a premium price versus generic competitors but if there are quantifiable savings in other health care costs, for example, less surgeries or doctor visits this may support a higher than generic drug price.

2.20.2.3 Use of Biomarkers

Over recent years there has been a decline in drug approval and an increase in the attrition rate of compounds in late clinical development resulting in increased drug development costs.[24] As a consequence, the use of biomarkers as key components of translational strategies in drug development and clinical practice is encouraged by the US FDA.[25] Incorporating biomarkers into drug development at preclinical and clinical stages serves several objectives. Their use aids in appropriate decision making throughout the development process such as "go/no go" decisions, lead candidate selection, defining optimal dose regimens for efficacy and safety, and for guiding treatment decisions. They also provide valuable information on the disease mechanism and ultimately allow patient stratification which is core in a personalized medicine approach or to be used as a surrogate endpoint for clinical effect or clinical safety. Recommendations to improve the decisions about incorporation of biomarker studies in early investigational drug trials have been published.[26]

2.20.2.4 Assays/Methods

As mentioned previously, there is a clear incentive by regulatory bodies (FDA and EMA) to include biomarkers in translational strategies. As a consequence, the reliable and quantitative measurements of a large number of biomarkers are warranted. As biomarkers can take numerous and ever expanding forms, it is not the intent of this section to list all possible methods here but to focus on the methods currently most frequently used for quantitative biomarkers and their advantages and disadvantages. For the sake of this article, this will focus on peptide biomarkers. For the validation of other methods to assess biomarkers, there is less guidance available and this is thus on a fit-for-purpose approach. While it is impossible to give advice on the validation of all kinds of assays and measurements, the criteria given further below can serve as guidance for the validation of other assays.

Currently, there are two approaches for absolute quantification: antibody-based assays and mass spectrometry (MS)-based assays.[27] Although the current standard for biomarker quantification is the classical enzyme-linked immunosorbent assay (ELISA),

Table 1 Advantages and disadvantages of analytical methods

Assay type	*Advantages*	*Disadvantages*
Mass spectrometry MRM/SRM	● Eliminates analytical interferences (e.g., nonspecific antibody binding, matrix effects) ● Allows the analysis of a wide variety of compounds, even across different compound classes ● Antibody-free detection ● Linear response over a wide dynamic range ● Increased sensitivity for targeted methods	● Impeded by lack of sensitivity and its nonquantitative nature for untargeted methods ● Requires prior knowledge of protein mass/sequence ● SRM is currently limited to the targeted measurements of up to 100 proteins per run versus thousands for untargeted approach
Immunoassays		
Singleplex ELISA	● High selectivity, sensitivity, and assay versatility	● Requires relatively large sample volumes ● Requires the use of high-quality antibody pairs ● Narrow dynamic range ● Immobilization of antigen to the solid matrix can cause issues with accuracy and reproducibility
Multiplex assays	● Multiple analytes measured in the same run from the same sample (limits freeze/thaw cycles, reduces sample storage space, etc.) ● Reasonable sensitivity, reproducibility, and broad assay dynamic range (pg mL^{-1} to ng mL^{-1}) ● High-throughput nature ● Requirement for smaller sample volume ● Time/cost efficiency ● Reagent costs substantially reduced	● Requires the use of high-quality antibody pairs ● Resources needed to develop multiplex assays as frequently hampered by lack of adequate selectivity and specificity ● Extensive validation

alternative methods such as multiplex assays and MS-based quantification assays are gaining in importance. Singleplex assays, of which the ELISA is the best example, have one important shortcoming in that one single analyte is measured at a time. In view of the integration of biomarkers in translational strategies and the requirement for high-throughput screening, singleplex assays are ill-suited for the quantification of a large number of candidate biomarker proteins. In contrast, multiplex assays (such as Luminex, bead arrays, etc.) allow the quantification of multiple analytes at once but will require extensive development (Table 1).

2.20.2.4.1 Enzyme-linked immunosorbent assay

ELISA is a solid-phase enzyme immunoassay and is the most widely used method for biomarker detection and quantification. It offers high selectivity, sensitivity, and assay versatility; however, it presents certain limitations such as a narrow dynamic range, low throughput, modest reproducibility due to its numerous wash steps, and the requirement of antibodies with high-specificity against each targeted protein or peptide of interest. ELISA assays also have limited multiplexing capabilities which can render the quantification of multiple biomarkers costly and time-consuming. In addition, higher sample volumes would be required to allow sequential analysis of various biomarkers. This would particularly pose a problem during clinical studies in certain patient populations (e.g., infants) or with particular matrices (e.g., synovial fluid) where the collected amount of biological material will be limited.

2.20.2.4.2 Multiplex assays

Due to the shortcomings of the singleplex assays, multiplex assays have gained importance over the years as they allow the quantification of multiple analytes in a single step and are often used for high-throughput screening.[28] Antibody-based multiplex assays offer significant advantages with regards to time, cost, sample volume, and storage requirements, and the amount of data that can be generated in a short timeframe. Multiple platforms are available which rely either on microbeads for the in-solution format (such as Luminex) or microspot array for the planar format (such as Luminex, MesoScale Discovery, and Fast Quant).[27] The main hurdle of multiplex assays is the requirement for extensive development and validation in order to minimize assay imprecision and inaccuracy (see section "Validation").

2.20.2.4.3 Mass spectrometry

MS is a widely used analytical technique in the physical and chemical sciences to quantify low molecular weight compounds (~200 Da or less). Over the past 30 years, the use of MS technology in bio-specimen analysis has grown and its use is currently widespread in clinical reference and referral laboratories.[29] The advances in MS, bioinformatics tools, and related proteomic technology have made it possible to identify thousands of proteins from a single sample.[27] In these proteomic studies, the common approach used is generally what is referred to as the "shotgun" or untargeted approach, in which the sample proteins are enzymatically degraded to peptides, which are then analyzed by MS operated in data-dependent acquisition mode, in an attempt to cover as many proteins as possible in the hope of revealing promising biomarker candidates.[30] This shotgun approach is a powerful tool for

high-throughput screening of peptides and their relative quantification, but is unsuitable for absolute quantification or for the targeting of specific proteins because of the limited sensitivity and poor reproducibility of target selection. Selected reaction monitoring (SRM) or multiple reaction monitoring (MRM) measurement platforms allow multiplexed analysis using tandem MS for targeted proteomics and allows the reliable quantification of low abundance analytes in complex matrices. The high sensitivity of this technique complements the untargeted shotgun methods.[30–32]

2.20.2.5 Validation and Qualification

The terms "biomarker validation" and "biomarker qualification" are regularly used interchangeably in the literature despite the fact that both terms mean different things. Whereas validation is the assessment of the performance characteristics of the biomarker measurement, qualification, however, is the evidentiary process of providing a linkage between the biomarker and a clinical endpoint such that it can be used as a surrogate endpoint.[33]

2.20.2.5.1 Validation

As reliable and accurate data are crucial for sound decision making, biomarker assays must be validated in a manner that enables the generation of such data. Validation is the process of evaluating the biomarker and its measurement performance characteristics and determining the range of conditions under which the biomarker will give reproducible and accurate data.[34,35] It is a necessary component to deliver high-quality research data for effective use of biomarkers. Depending on the intended use of the biomarker and the nature of the technology utilized, the extent of validation can differ in a "fit-for-purpose" approach[36] (**Fig. 1**). During preclinical and clinical development, biomarkers can be used for decision-making purposes or can be rather supportive or exploratory. Validation of the assays needs to be tailored to their intended use. The further along the spectrum toward a surrogate endpoint or decision making diagnostic the biomarker is positioned, the greater the degree of thoroughness necessary to validate the biomarker assay is[36–38] (**Fig. 1**). A noncomprehensive list of definitions linked to bioanalytical method validation is represented in **Table 2**.

For supportive and exploratory biomarkers, a *limited validation* might suffice, while for decision-making biomarkers (e.g., for patient stratification) a *full validation* is required (**Table 3**). Both types of validation are dependent on acceptance criteria which are set up front. The most extensive set of parameters which can be evaluated are listed and briefly discussed here. This set is applicable in the setting of a quantitative ELISA or multiplex assay but by no means applies to all platforms and biomarker types. An example of "deviating platform" is flow cytometry where the accuracy of a certain biomarker is seldom being determined due to a lack of established standards to do so.[39] An example of a type of biomarker very different with respect to validation in comparison to an ELISA is a questionnaire or an index like the EULAR Sjogren's Syndrome Patient Reported Index. This index is based on three questionnaires designed to measure patients' symptoms in primary Sjogren's syndrome and for which a prospective international 6-month duration validation study was conducted in 15 countries to conclude that it had good construct validity and sensitivity.[40,41]

The validation of an assay follows the initial stage of method development, where the global purpose of the assay is being defined, where the selection of the assay setup and conditions occurs and during which the strategy for method validation is being designed (adapted from Ref. 36). After method development, exploratory validation and prevalidation follows. During this phase, the dynamic range is established and the selectivity and specificity of the candidate assay is tested. When this is successful, effective validation takes place during which the assay performance is characterized. This validation ultimately evaluates and concludes whether the assay is fit-for-purpose. Validation results are recorded in a method validation report and a working protocol, rendering the assay ready for in-study target population sample analysis. Further evaluation of the "fit-for-purposeness" occurs with the true study samples during "in-study validation." This entails parallelism testing on study samples, incurred sample reanalysis, and trending of low–medium–

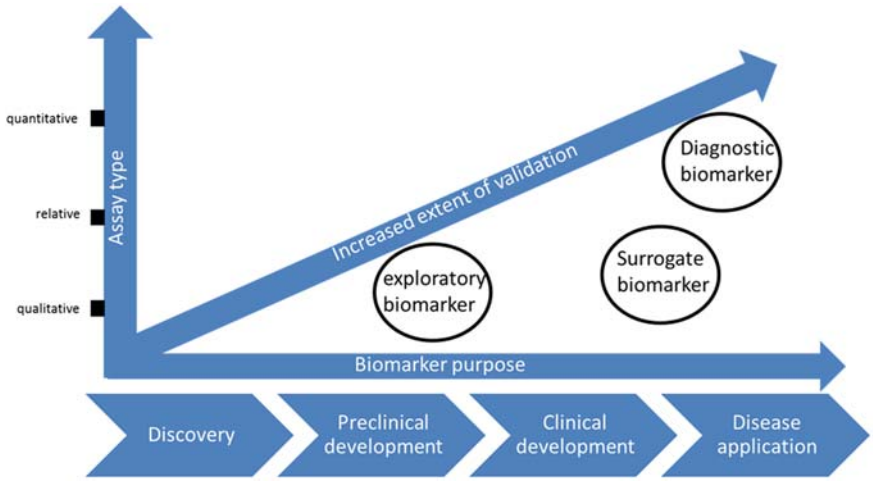

Fig. 1 Link between biomarker validation, assay type, and biomarker qualification.

Table 2 Noncomprehensive overview of definitions valid in the context of bioanalytical methods

Accuracy	The accuracy of an analytical method describes the closeness of mean test results (calculated concentration) obtained by the method to the theoretical value (nominal concentration in case of spiked samples) or target value (defined in target definition runs in case of endogenous samples) o f the analyte. This is also referred to as bias or relative error
Dilutional linearity	Dilutional linearity implies a test to demonstrate that the analyte of interest, when present in concentrations above the dynamic range, can be diluted to bring the analyte concentrations into the dynamic range for analysis by the method
Dynamic range	The interval between the upper and lower sample analyte concentration for which the assay has been demonstrated to have an acceptable level of precision and accuracy
HiQC/VS	High concentration quality control sample or validation sample
Incurred sample	Study sample
LoQC/VS	Low concentration quality control sample or validation sample
Matrix effect	Direct or indirect change in signal of the analyte by the presence of unwanted components or other interfering substances in the processed sample
MeQC/VS	Medium concentration quality control sample or validation sample
MRD	Minimum required dilution: the minimum dilution required to dilute out matrix interference in the sample
Parallelism	Parallelism documents that the concentration/response relationship of the endogenous analyte in the sample matrix from the study population is sufficiently similar and proportional to the reference material in the (substitute) matrix
Precision	Precision of an analytical method describes the closeness of individual measures of an analyte when the procedure is applied repeatedly to multiple aliquots of a single homogeneous volume of biological matrix. Precision is usually expressed as standard deviation (SD) and coefficient of variation (CV). This may be considered at the repeatability (=intra-assay precision) level
Quality controls (=QCs)	A set of sample, preferably endogenous analyte or alternatively recombinant analyte prepared in the intended biological matrix with concentrations that span the dynamic range. QCs are used in each sample analysis run to monitor assay performance for batch acceptance (in-study run acceptance). Three levels are used: LoQC, MeQC, and HiQC. These samples are the same as the validation samples and are called QCs once the precision and accuracy assessment is successfully finished. The target concentration of the QC samples will be calculated using the concentrations obtained in the three target definition runs and the six precision and accuracy runs
Selectivity	The ability of the method to measure the analyte unequivocally in the presence of other components in the assay matrix
Sensitivity	The lowest concentration of analyte that an analytical method can reliably differentiate from background
Specificity	The ability of the assay reagents to bind the antigen of interest without cross reactivity with variant forms of the analyte or other structurally related compounds that might be present in the sample
Target range	Range of analyte concentrations wherein the study samples are expected to fall
Validation	The confirmation via extensive laboratory investigations that the performance characteristics of an assay are suitable and reliable for the intended analytical use
Validation samples (VSs)	A set of sample, preferably endogenous analyte or alternatively spiked recombinant analyte prepared in the intended biological matrix with concentrations that span the dynamic range. Validation samples are used in each prevalidation and in the first validation runs to evaluate assay performance. The target concentration of the VSs will be calculated using the concentrations obtained in the three target definition runs. After the accuracy and precision runs of the validation, these samples can become the quality controls (QCs)

Table 3 Overview different steps of limited and full validation (based on Cummings et al.[36] and Lee et al.[35])

Exploratory validation	1. Theoretical establishment of target range, sensitivity, and acceptance criteria 2. Choice of calibrators and establishment of working range 3. Initial choice of appropriate working regression model 4. Choice of matrix for validation samples	
Prevalidation	1. Minimum required dilution 2. Establishment of limit of detection 3. Establishment of assay dynamic range and limits of quantification 4. Parallelism	
Validation	Limited validation 1. Intra- and interassay accuracy and precision calibrators based on three runs 2. Intra- and interassay accuracy and precision–validation samples based on three runs 3. In-study validation	Full validation 1. Intra- and interassay accuracy and precision calibrators based on six runs 2. Intra- and interassay accuracy and precision-validation samples based on six runs 3. Spike recovery 4. Stability 5. In-study validation

high-quality control (QC) samples. After successful "in-study validation," the assay may enter into routine use, while continuously monitoring the behavior of the assay QCs and evaluating the effect of reagent batch to batch differences.

For an *exploratory validation* (Table 3) the following parameters are being defined: (1) the theoretical potential target range, the required sensitivity, and acceptance criteria; (2) the selection of calibrators and the establishment of the working range; (3) the appropriate working regression model; and (4) the choice of validation samples. During *prevalidation* (Table 3) the following attributes are being defined: (1) the minimum required dilution (MRD) of the samples; (2) the limit of detection; (3) the assay dynamic range and limits of quantification; and (4) parallelism (which evaluates whether the concentration/response relationship of the endogenous analyte in the sample matrix from the study population is sufficiently similar and proportional to the reference material in the substitute matrix).

For a *limited validation* (Table 3), three runs are sufficient to determine intra- and interassay accuracy and precision of both calibrators and validation samples. For a *full validation* (Table 3), at least six runs are required to determine intra- and interassay accuracy and precision of both calibrators and validation samples, as well as the assessment of whole plate uniformity, spike recovery, and stability. Spike recovery is used to determine whether analyte detection is affected by the biological sample matrix. Stability testing evaluates to what extent the conditions under which study samples will be collected, stored, and processed (RT, freezing, long-term storage, etc.) could affect the stability of the biomarker.

However, if certain effects are expected (e.g., if the selected matrix affects biomarker stability), these parameters for limited validation should be extended to meet the fit-for-purpose quality evaluation.

2.20.2.5.2 Qualification

Biomarker qualification is an official evidence-based development process which provides a framework for scientific development and regulatory acceptance of biomarkers for use in drug development.[42] The biomarker qualification process consists of three major stages: initiation, consultation, and advice and review. The first stage consists in the submission, by the submitter, of a letter of intent (LOI) which contains a description of the potential biomarkers with their proposed context of use (COU) and a rationale to support qualification. In order to reduce the time taken by the applicant to prepare LOIs and to facilitate parallel submissions to the EMA and to the US FDA, the two agencies launched a joint LOI in Dec. 2014 which allows the two agencies to share scientific perspectives and advice.[43] This COU is the most important part of the qualification discussion as it identifies the boundaries of known reliability as shown by evidence and should clearly describe how a biomarker should be used such that the results enable decision making in drug development. For example, it defines how the biomarker should be sampled and analyzed and what decisions will be made based on the gathered data. The FDA then evaluates the potential and scientific merit of the proposal and decides whether the biomarker submission is accepted or not into the biomarker qualification program. If accepted, the consultation and advice stage begins with the assembly of an interdisciplinary working team (Biomarker Qualification Review Team—BQRT or QT) that will guide the submitter toward further biomarker development (e.g., additional studies to be conducted as needed) to support the proposed COU, and will review the complete evidence. The BQRT will provide the submitter with instructions for submission of the full qualification package when it determines that no critical gaps in knowledge remain and when the data are considered sufficient to initiate a review. Following the submission of the full data package by the submitter, the review stage, which consists of an evaluation of the full qualification package, can start. After complete review of the package, qualification recommendations are generated and, if positive, formal qualification is granted which indicates that the gathered data on the biomarker supports its use within a specified COU. The qualification statements are then made public on the FDA and EMA website first as a "draft guidance" and later finalized after a public comment period. The qualified biomarker can then be used by drug developers for the qualified context in regulatory submissions without the Center for Drug Evaluation and Research or the Committee for Medicinal Products for Human Use having to re-review or reconsider the suitability of the biomarker.[44–46]

2.20.3 Modeling and Simulations

2.20.3.1 Introduction

For a long time PKs (pharmacokinetics) and PDs have been considered as two independent disciplines of pharmacology, and in the past PK studies, evaluating the time course of drug levels, were mostly focused on meeting regulatory requirements. However, when considered separately from PDs, PKs are of limited information, and provide only summary drug characteristics for observed levels of systemic drug exposure.

Given the limited regulatory requirements, there has been little motivation for companies to invest in intensive efforts in linking PKs to PDs. In addition, drug development has usually relied on observed effects at a certain dose of the drug without understanding how systemic drug exposure is linked to the observed effects. This knowledge gap has been considered one of the factors impacting the attrition rate in drug development,[24] and companies are now encouraged by regulatory agencies to invest in quantitative methods to explain dose/exposure/response relationships allowing more informed/less risky decisions during drug development. It is proposed to use the advances in informatics technologies and the increased computational power[4,47] as tools for making, testing, and confirming hypotheses, which might be revisited in case of unexpected findings,[48] thus increasing the knowledge on the drug, eliminate less promising candidates, and focus on those with higher probability of success.

2.20.3.2 From Empirical to Mechanistic Pharmacokinetic/Pharmacodynamic Models

The activity of a drug depends on its concentration at the effect sites, but often these are of difficult access. Traditional PKs assume that changes in systemic exposure reflect changes in drug concentrations at the effect site(s), although this might not always hold true.

After administration, the drug undergoes several processes occurring concomitantly or in parallel at different rates. These processes are generally referred to as absorption, distribution, metabolism, and excretion (ADME). In vitro "ADME studies" can focus on each of these processes specifically, whereas in in vivo studies, mostly referred to as "PK studies," the resultant time-course drug concentration profiles result from the integration of the different ADME processes. These latter can be represented through mathematical functions including "PK parameters" characteristic of the drug under study. Mathematical models representing simplifications of body structures (*compartmental models*) can be used to describe the observed drug levels. These models are empirical because the observed data determine the type of model required to describe the data themselves. The compartments used to describe a drug's behavior do not represent real physiologic spaces, rather groups of organs/tissues in which the drug has similar distribution characteristics: the highly perfused or central compartment (blood, heart, liver, kidney, lung) and the peripheral compartment (including fat, muscle, cerebrospinal fluid, skin, etc.). A classical two-compartmental model is shown in Fig. 2.

If adequate for extrapolation of other dosing regimens under certain conditions, the value of empirical models is limited for translational purposes (across different species, populations, disease states, etc.). In these cases, mechanistic models with a more accurate representation of anatomic and physiological functions are needed.[49–53] Physiologically based pharmacokinetic (PBPK) models use several differential equations parametrized using not only physicochemical parameters, characteristic of the drug (size, solubility, effective permeability, etc.), but also known physiologic and anatomical parameters of the "system" to which the drug is administered (organ volumes, blood flows, etc.) (Fig. 3). If the drug characteristics remain identical across species, populations, and disease states, the system parameters can be scaled or adjusted, allowing a reliable extrapolation of the drug behavior in other animal species, disease states, or general conditions. PBPK models can also predict drug exposure in inaccessible tissues where the drug acts or exerts its desired or undesired effects. The shortcoming of the PBPK approach is that it relies heavily on systems of differential equations involving a large number of parameters from different research fields, and often from in vitro experiments and summarized literature data (for drug-related and system-specific parameters, respectively), always carrying a certain degree of error due to the uncertainty of in vitro results or in vivo reported parameters. Hence PBPK models have often to be confirmed with real data, so that a "data-driven" refinement of certain parameters can be done for further use of the model. The PBPK modeling has also been extensively used by regulatory agencies in the last decade for regulatory review or labeling claims[54–57] to evaluate the effect of intrinsic (age, gender, race, weight, height, disease, genetic polymorphism, pregnancy, and organ dysfunction) and extrinsic (drugs, herbal products, diet, smoking, and alcohol use) factors affecting the response (safety/efficacy) to the administered drug. An example is the dose-adjustment based on individual patient factors in the FDA labeling of rosuvastatin. The effects of the concomitant use of other drugs, ethnic factors, renal and hepatic impairment on the exposure to rosuvastatin have been investigated through a PBPK model, including the available information on the metabolism and transporter kinetics of the drug, and the label has been accepted after review of the results of these investigations in various clinical pharmacology documents.[31]

As previously mentioned, if not linked to the effects, PK models are of limited use. Linking PKs to PDs through mathematical Pharmacokinetic/Pharmacodynamic (PK/PD) models moves the focus on the driver of effects from the dose/administration site to the exposure at the site of effect. The use of integrated PK/PD models enables the prediction of desired and undesired effects, allowing the optimization of study designs to maximize efficacy while minimizing toxicity. These models are widely used for comparison and selection of lead drug candidates, starting doses for human studies, risk/benefit evaluations, and drug benchmarking.

As for PK models, a distinction between empirical and mechanistic models exists for PK/PD models. An assumption of descriptive PK compartmental models is that systemic drug levels reflect drug levels at the site of action. However, for numerous drugs the distribution into organs/tissues can represent a rate-limiting step for the onset of the effect. This delay has been accounted for in empirical PK/PD models with the addition of an "effect compartment"[58,59] into which the drug would distribute in minimal amount without perturbation of the overall PKs (Fig. 4). These empirical PK/PD effect-compartment models have been frequently used to predict steady-state timecourse of effects from non-steady-state data, but their predictability becomes less reliable when perturbations of the "system" occur, such as a change in the equilibration of the drug levels consequent to a reduced blood flow, or a change in permeability of a tissue in a diseased state, etc. For translational purposes, mechanistic PK/PD[60–62] models demonstrate much improved properties. As for their PK analogs, mechanistic PK/PD models include parameters describing drug-specific properties (e.g., target affinity, intrinsic efficacy) constant across species/individuals and biological system-specific properties (e.g., time-dependent transduction factors, homeostatic feedback mechanisms) with species-dependent intra- and inter-individual variability (Fig. 5).

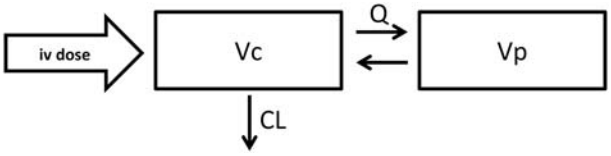

Fig. 2 Two-compartment model. V_c is the central compartment and V_p the peripheral compartment. The drug is cleared from the central compartment, the elimination being characterized by a clearance CL. The drug also distributes to peripheral organs/tissues, and the mass transfer is characterized by an intercompartmental clearance Q.

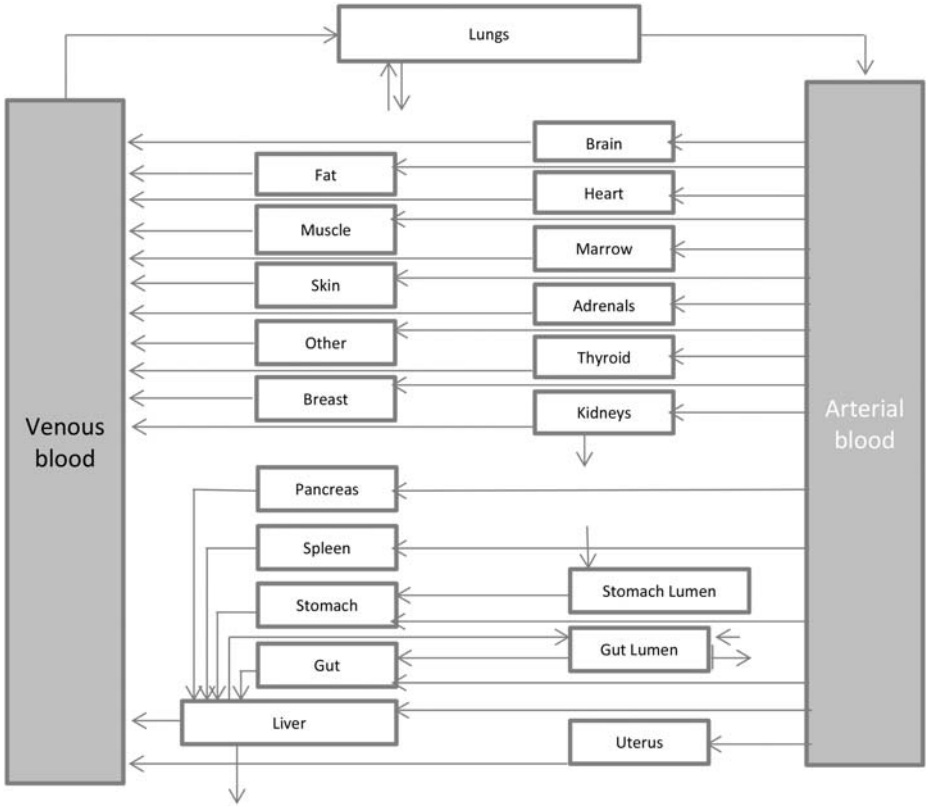

Fig. 3 A whole-body physiologically based pharmacokinetic model.

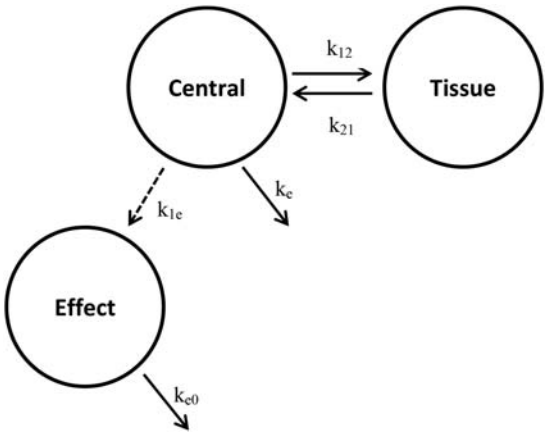

Fig. 4 Effect-compartment PK/PD model. Hypothetical effect compartment, connected to central through k_{1e}, very small relative to other rate constants of PK model. k_{e0}, the rate constant of drug removal from the effect compartment, characterizes the temporal aspects of equilibration between drug concentrations in the central compartment and the effect.

2.20.3.3 From Mechanistic Models to System Biology Models

If mechanistic models appear as more complex than simple empirical compartmental models, an even higher degree of complexity would be needed to address different important questions for selection of new drug candidates, such as "which target to hit" and "which would be the most relevant biomarkers to follow in preclinical/clinical studies for safety/efficacy evaluation" or "which drug candidate would have characteristics closer to the defined target product profile, TPP." In this case, mathematical models are built on hypothetical pathways and expression profile data linking the different components of the system of interest. This is what is known as "bottom-up modeling," in contrast to the "top-down modeling" based on the clinical data from an overall integrated system, as with compartmental models. A hypothetical example of a very small signaling cascade is the one indicated in Fig. 6.

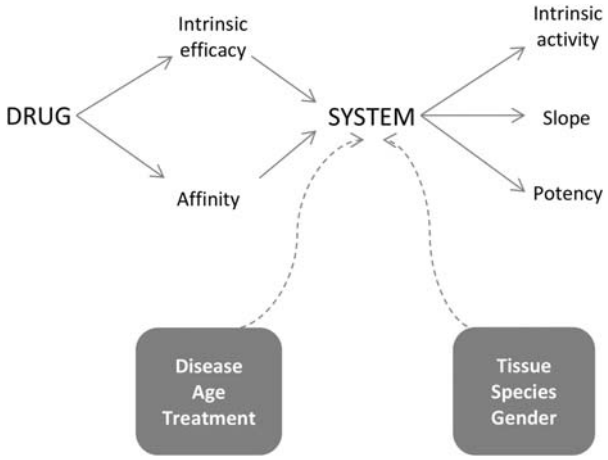

Fig. 5 Shape and location of in vivo drug concentration–effect relationships is determined by drug-specific (affinity, intrinsic efficacy) and biological system-specific (transducer function relating receptor activation to effect) properties. Adapted from Van der Graaf, P.H.; Danhof, M. Analysis of drug-receptor interactions in vivo: a new approach in pharmacokinetic-pharmacodynamic modelling. *Int. J. Clin. Pharmacol. Ther.* **1997**, *35*, 442–446.

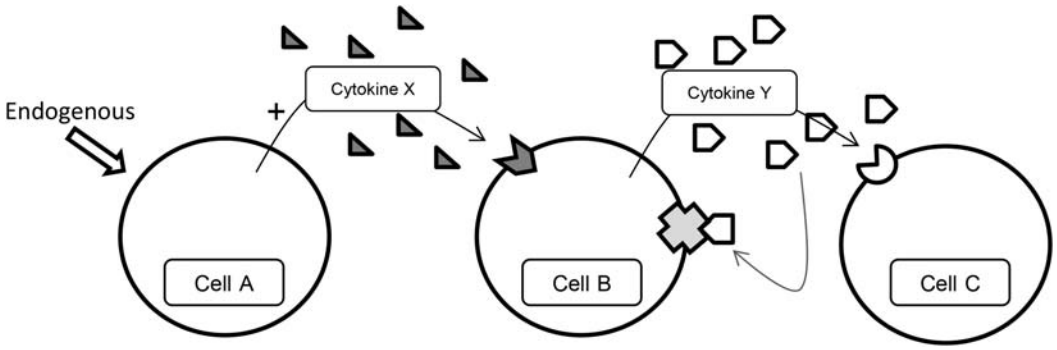

Fig. 6 Hypothetical signaling cascade. Cell A is inappropriately activated by an endogenous signal, which results in the upregulation (+) of the expression and secretion of cytokine X, which in turn stimulates cell B to upregulate the expression of cytokine Y and its autocrine receptor. Cytokine Y signals cell C to produce deleterious effect.

Here, a cell A is inappropriately activated by an endogenous signal to secrete cytokine X, which in turn stimulates the production of cytokine Y from cell B. Cytokine Y could stimulate the autocrine receptor on cell B as well as another receptor present on cell C initiating a deleterious effect. If the objective would be to interfere with this cascade of events to counter the deleterious effect, potential target processes to hit would be the activation of cell B by cytokine X, or of the stimulation of the autocrine receptor on cell B by cytokine Y, or the final activation of cell C. What is not known is which of these processes would be the most influential one on the deleterious effect. In silico models based in this case on in vitro data would allow through simulations to determine the relative importance of the different processes accounted for in the cascade of events and provide information on the most promising target to select. The previous simple example could be extended by integrating a wide variety of data, providing insight into how complex biological systems are regulated in both healthy and diseased conditions. These large-scale biosimulation models often involving disciplines like genomics, bioinformatics, and proteomics are referred to as *system biology models*, and can predict in a very early phase of development the overall clinical effect of modulating individual pathways or targets in terms of efficacy and side effects. Based on databases including literature, public and proprietary data and integrated information collected from experts in the medical areas of interest, clinical outcomes are related to biological mechanisms which in turn are dissected to unravel the underlying cellular and molecular processes that allow to quantify clinical and subclinical outcomes. If assumptions are not confirmed, gaps in the knowledge of the observed effects can be identified and further investigation steps to fill them can be planned. This provides new insights into complex mechanisms of action that determine the direction of program and study strategies. In silico simulations enabling a better understanding of protocol parameters contributing more to expected effects provide also an opportunity to explore different possible study designs, thus reducing the uncertainty on the outcomes, resulting in a faster and more efficient development of the drug. The complexity of these models, based on hundreds of equations and parameters, require extensive time and human resources for their building and testing.[63–66]

2.20.3.4 Examples of Applications of Empirical, Mechanistic, and System Biology Models

The models summarily described in the previous paragraph have a different degree of complexity and the choice of the model is dictated by the specific objective(s) of the modeling exercise. We give hereafter some examples of applications.

2.20.3.4.1 Empirical Pharmacokinetic/Pharmacodynamic models—effect-compartment model

Empirical models were first developed by anesthesiologists under the need to adjust doses of anesthetics using target controlled infusion (TCI) devices.[59,67] Most anesthetics have a narrow therapeutic index, and a precise control of the anesthetic effect requires a good understanding of the dose-effect relationship. As these drugs act in the brain, plasma concentrations do not reflect the extent of the effect, and a certain delay between maximal plasma concentration and maximal effect can be observed. "Effect compartment models" account for this delay through a parameter k_{e0} which can also be expressed as a half-time k_{e0}, directly corresponding to the time of equilibration between the central compartment and the effect site. The faster k_{e0} is, the faster the maximal effect will be attained (Fig. 7, left). In anesthesia, the dose to be given to achieve the target concentration will depend upon the PK characteristics of the drug (distribution properties to the site of action), and when using TCI it is usual to set a higher initial dose (infusion rate or concentration) to reach the desired effect more rapidly. The lower the k_{e0} value is, the higher will be the initial plasma overshoot (Fig. 7, right). At equilibrium, infusion conditions are maintained constant.

2.20.3.4.2 Mechanistic Pharmacokinetic/Pharmacodynamic models—selection of starting dose for first-in-human studies

The selection of the starting dose for human studies followed in the past the recommendations of an FDA guidance[68] on a maximal recommended starting dose selection. This guidance suggests how to determine the highest dose which can be considered safe, rather than the lowest dose which can be considered active. It is based on doses rather than exposures which are allometrically scaled from animals to humans. Unfortunately, the lack of integration of pharmacology, safety, and efficacy data of this approach revealed its limits when it was applied to the CD28 agonist antibody TGN1412.[69] In the volunteers, the selected starting dose was associated with life-threatening events related to the pharmacology of the mAb, not predicted from the toxicology studies performed in monkeys. The dose selection approach in the new EMA guidance[70] recommends to integrate all pharmacological, toxicological, and efficacy knowledge gathered in in vitro/in vivo preclinical studies to determine a minimum anticipated biological effect level (MABEL). The use of a simple formula to calculate the receptor occupancy (RO) has been suggested to determine a MABEL[71] (Fig. 8A), but a more accurate evaluation can be done through mechanistic PK/PD models,[72,73] accounting not only for the affinity of the drug to the target, but also for the turnover of the target (the balance of its formation and elimination rates) (Fig. 8B). Applied to the TGN1412 example, these equations predict a RO of $>90\%$ for the selected starting human dose. The model-predicted human

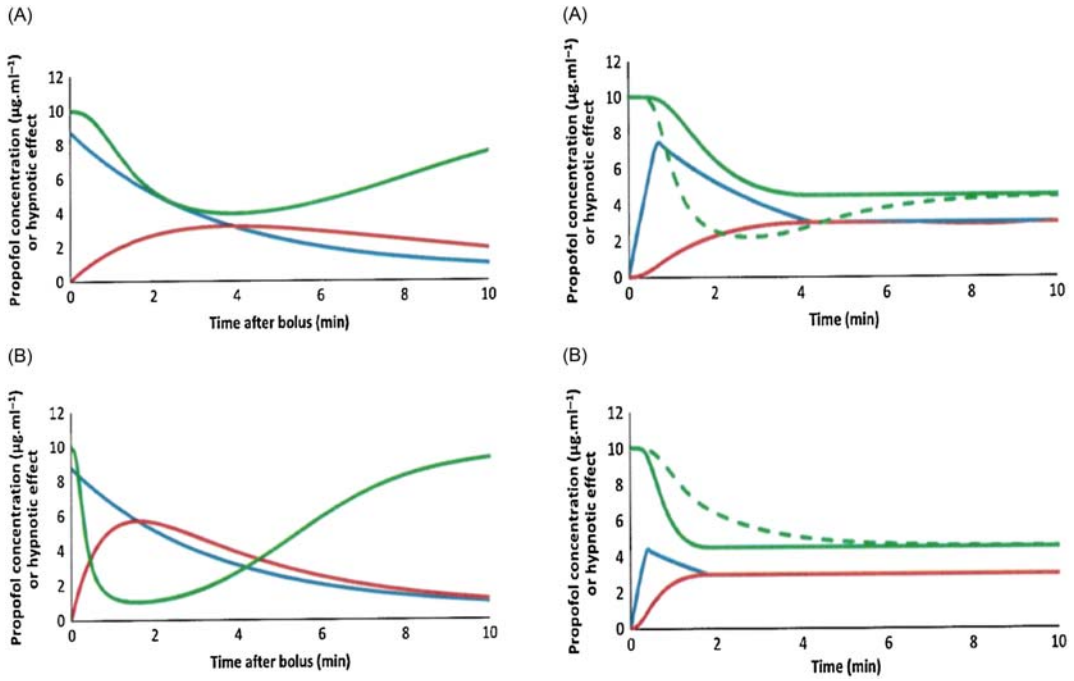

Fig. 7 Left: Effect of k_{e0}: low versus high k_{e0}, time plots of plasma concentration, effect site concentration and effect (left top: propofol model with slow k_{e0}; left bottom: propofol model with rapid k_{e0}). Right: effect of plasma overshoot, higher loading for slower k_{e0} (right top: propofol model with slow k_{e0}; right bottom: propofol model with rapid k_{e0}). *Blue,* plasma concentrations; *red,* effect site concentrations; *green,* effect. From Cortinez, L. I. What Is the ke0 and What Does It Tell Me About Propofol? *Anaesthesia* 2014, 69(5), 399–402. [AF].

(A)

$$RO = \frac{[mAb]}{K_D + [mAb]}$$

for TGN1412 K_D: equilibrium dissociation constant, 1.88 nM; [mAb]: 0.1mg/kg of 150 kDa IgG in 2.5L plasma of a 70 kg human

(B)

$$complex = \frac{(K_D + TD + TT) - \sqrt{(K_D + TD + TT)^2 - 4 \cdot TD \cdot TT}}{2}$$

TD=[MAb]+[Cpx]

TT=[Ag]+[Cpx]

for TGN1412 TT: total target 150 000 receptors/T-lymphocyte and 1.3x109 T-lymphocytes/L blood; K_D: equilibrium dissociation constant, 1.88 nM; TD: total drug 0.1mg/kg of 150 kDa IgG in 2.5L plasma of a 70 kg human

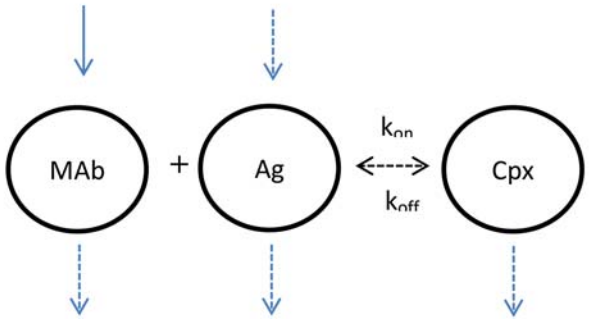

Fig. 8 Equations for calculating receptor occupancy: (A) when [mAb] ≫ [TT], (B) accounting for target expression.

dose corresponding to a minimal RO (10%) would be 100 times lower (i.e., 1.5 μg kg^{-1}) than the one selected based on the MSRD approach (i.e., 0.1 mg kg^{-1}).

2.20.3.4.3 PBPK models—drug–drug interactions consequent to drug-mediated cytokine elevations

Very often applied in the design of pediatric studies or to anticipate the impact of pharmacogenomics or race, physiological states (i.e., pregnancy, etc.)/diseases, and uncommon administration routes on drug exposure, PBPK modeling is widely used to study drug–drug interactions. Blinatumomab is a bispecific T cell engager antibody which, when binding to T cells, redirects them to B cell malignant cells.[74] Transient elevation of cytokines generally takes place on the first day of treatment, returning to normal by the second day. Proinflammatory cytokines are known to suppress cytochrome P450 (CYP) activities and consequently decrease the clearance of drugs metabolized through them. An effective antiinflammatory treatment would be expected to reestablish the normal CYP activity: this is critical for patients under chronic concomitant medications as the systemic exposure to these latter can be affected. PBPK modeling has therefore been used to prospectively predict the effect of the transient increase of IL-6 levels, consequent to blinatumomab treatment, on known drug-metabolizing enzymes (CYP3A4, CYP2C9, and CYP1A2), using simvastatin and midazolam, theophylline and caffeine, and (*S*)-warfarin as respective substrates in the simulations. The parameters and data used to predict the expected change in the substrate levels were IL-6 profiles from patients receiving blinatumomab, in vitro IL-6 parameters for enzyme suppression, such as E_{min} (minimum CYP enzyme activity, i.e., the maximum enzyme suppression) and EC_{50}, and the system parameters available for the degradation constant (k_{deg}) of CYP3A4, CYP1A2, and CYP2C9 in the liver and intestine. Simulations suggested that changes in exposure to substrates of the CYPs under study are expected to be less than twofold with the magnitude of the CYP suppression being highly dependent on the duration of the cytokine elevation. Drug monitoring is thus recommended in patients under concomitant treatments with narrow therapeutic index.[75]

2.20.3.4.4 System biology models—identification of optimal combinations of molecular targeted drugs in oncology

Targeted treatments in cancer research are very promising, but the inhibition/activation of specific pathways can be compensated by regulatory loops or bypass mechanisms. A system biology model, built to study the insulin-like growth factor (IGF) signaling network in the MDA-MB231 breast cancer cell line, demonstrated that the most straightforward strategy, consisting in the inhibition

of the input source for signal transduction (inhibition of insulin-like growth factor receptor (IGFR)), would not be the most successful for a selective reduction of tumor cell proliferation which is caused by p-mitogen-activated protein kinase activation through K-Ras and B-Raf mutations. A more effective inhibition of aberrant signaling would be accomplished through multiple combined inhibitions of targeted molecules such as mitogen-activated protein kinase (MPAK) and phosphoinositide-3-kinase/protein kinase B (PI3K/AKT).[76] The proposed computational approach is more and more used to identify and validate drug combinations that can inhibit aberrant networks in a panel of human cancer cell lines.

2.20.3.4.5 System biology models—a mathematical model for rheumatoid arthritis

A large-scale mathematical model of rheumatoid arthritis has been constructed with the Entelos® PhysioLab platform, mechanistically linking cellular and cytokine components of the pathophysiology across multiple compartments, including synovial lining, cartilage, and bone to patient-level measures. The scope of the biology represented in the Entelos RA PhysioLab platform is summarized in Fig. 9. This model has been used to explore new critical pathways and targets for intervention, to investigate and compare the potential of new drug candidates, and to test the expected outcomes for different virtual patient phenotypes and study designs.[77,78]

2.20.3.5 Conclusion

The scope of the basic PK science has broadened in the recent years from that of a descriptive science to an instrumental tool in support of drug discovery and development. No model is better than others, if its purpose and objective(s) are not clearly stated upfront. Hence the choice of the use of empirical, mechanistic, or system biology models, more and more complex and time-consuming, is dictated by the specific question to be answered. The concept of "quantitative pharmacology" relies on their use for making decisions on the future of the drug candidate, by increasing the understanding of its action, and the expected benefit/risk profile in the target patient population.

Hence, system biology models that provide better and more realistic insights into disease processes and drug mechanisms can help identify disease-specific molecules and drug-specific targets and biomarkers for safety/efficacy and patient stratification.

Once the target is selected, mechanistic models can hint to gaps in the knowledge of the PKs or PDs of the drug, so that its properties can be modulated to achieve the best possible ones described in the best possible wished product characteristics TPP.

Another important benefit of these models is that they may be scalable from preclinical species to humans, from healthy to diseased patients and support labeling claims on drug interactions and dose adjustments in special populations.

The early availability of PK/PD models also allows a more informed drug development strategy building and enables the evaluation of different scenarios for study designs, including the test of different doses, dose regimens, statistical tests, sampling/observation times, duration of treatment, study subpopulations, etc.

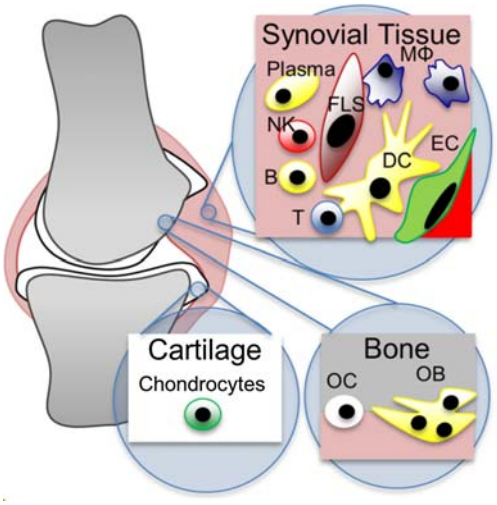

Fig. 9 Biology represented in the biosimulation platform (adapted from Schmidt, B. J., et al. Alternate Virtual Populations Elucidate the Type I Interferon Signature Predictive of the Response to Rituximab in Rheumatoid Arthritis. *BMC Bioinformatics* **2013**, *14*, 221). In the synovial tissue, the activity of fibroblast-like synoviocytes (FLS), B cells (B), plasma cells, natural killer cells (NK), macrophages (MΦ), and endothelial cells (EC) are modeled. T cells (T) are modeled with distinct CD4 and CD8 T cell subpopulations. CD4 T cells are further divided into Th1, Th2, Th17, and Treg subpopulations, as well as a CD28-subset that has lost the requirement for costimulation. Antigen presentation by dendritic cells (DCs) is also represented. Bone remodeling by osteoclasts (OC) and osteoblasts (OB) as well as cartilage remodeling by chondrocytes and MMPs is included.

2.20.4 Animal Model

2.20.4.1 Generalities

Animal models are a core tool for TM research, since they can be used to bridge in vitro research to clinical testing, for example, the generation of new potential therapeutic molecules or novel drug targets. More specifically, animal models can help to:

(i) Predict the efficacy of a potential novel therapy: new potential drug targets are often identified in screening efforts using omics technologies (e.g., genomics or proteomics) that can yield numerous targets in a short period of time. However, these potential targets often lack sufficient validation to be tested directly in pivotal clinical trials. Animal models can help in providing a certain level of validation or at least give a certain ranking of more or less promising targets. For this, several approaches are possible besides the direct testing of a drug candidate such as the use of transgenic animals with a changed expression of the target of interest or the use of siRNA or antisense.

(ii) Predict the safety of a potential new therapy: new targets come with largely unknown adverse event risks. Such adverse events might be specific or be more prominent in subjects suffering from the disease that is to be treated. Thus, in addition to classical safety pharmacology or toxicology studies that use healthy animals, animal models can also give important information as to the adverse event profile that can be expected under the disease condition and to the associated safety margin. For instance, patients suffering from type II diabetes have an increased risk for cardiovascular adverse drug reactions by sodium channel blockers.[79]

(iii) Dosing prediction for initial clinical trials: in order to be efficacious, drugs need to interact with a sufficient number of target molecules in the tissue of interest. For instance, in order to provide antipsychotic activity at least 50% of dopamine receptors need to be blocked by a drug.[80,81] Animal model studies can support predictions relating to the dose level and the administration scheme needed for a particular effect.

(iv) Competitive advantages: many new drugs are developed in areas for on which there is a standard therapy available (often as a generic drug). Thus, in order to provide a pharmaco-economic advantage, the new investigational drug must demonstrate a competitive advantage in order to be reimbursed. Animal models may provide early evidence for such competitive advantage (or the lack thereof) and thus reduce costly failures of drug development programs in late-stage clinical trials.

Despite their broad utility, the predictions of animal models often are not confirmed in large-scale clinical trials (see section "**Radiography**" and "**Stroke TM strategies**" for an example). This lack of predictivity can be multifactorial: (i) the design of the animal models was insufficient to support the prediction, (ii) the wrong prediction was drawn from the animal model results, or (iii) the animal model had no predictive validity.

There is numerous literature available on the correct design of animal model experiments such as: including sample size calculations (many experiments are underpowered), blinding, and randomization to reduce biases[82] and selection of the appropriate dosing and treatment schedule. Thus, instead of reiterating the importance of a correct experimental design, this section will focus on new developments to improve animal models and how to implement animal model testing into a translational strategy.

2.20.4.2 How to Improve Animal Models?

2.20.4.2.1 Multisite animal model trials

One major problem with the current use of animal models is the lack of reproducibility. This can be due to specific conductance or design of animal experiments in the laboratory that reports the results or even characteristics of the experimenter[83]: experimental conditions such as the lighting of the experimental room, the housing, and handling of the animals, the provider of the animals, or the gender of the experimenter. Such differences between laboratories influencing the outcome of an animal experiment can be overcome by multisite trials. The concept is well established in the clinical arena but has been recently introduced into animal research. A recent publication reports the outcome of a multisite randomized controlled animal model trial that investigated the efficacy of an anti-CD49d antibody in two models for stroke. This is a way to overcome the limitations of a single animal experiment in an isolated laboratory, that is, the small number of subjects and the lack of variability in experimental conditions that mirrors the variability that is present in clinical practice. Ideally, such multisite preclinical trials are conducted by consortia of academic centers under a central organization to ensure homogenous study design, central statistical analysis, definition of key primary and secondary endpoints. Another example is on the use of patient-derived xenograft models for the screening of potential oncology drug combinations for clinical efficacy. For this, researchers have used tumor material derived from patients and transplanted this to immunocompromised mice in a design whereby each mouse received material from a different patient. With that they mimicked the variability one would expect from a clinical trial in an animal model.

2.20.4.2.2 Enhance variability and reduce standardization

Standardization has been regarded key for the establishment of experimental methods in each laboratory. This standardization often includes the use of well-defined subjects (strain, breeder, gender, body weight), the housing conditions (light, temperature, food), their handling, and the exact experimental conditions. While this standardization certainly helps to reduce the variability within one experiment and therefore increases the power and allows for the detection of significant effects with lesser subjects, this may also cause problems. Richter and coworkers examined the reproducibility of behavioral parameters for experiments that were highly standardized and found that this was considerably lower than those for experiments where higher variability

was allowed.[84,85] A classical example for the application is in oncology animal studies. Originally one animal study was always performed with all mice receiving the same tumor cell line. More recently with the advent of patient-derived xenograft model each mouse in a given preclinical trial can receive the tumor material of different patients thereby reinstating the natural patient variability.[86] Perceivably, the number of animals needed to reach statistical significance in one experiment is larger. This may be seen in contrast to the 3R principle (reduce, refine, replace) of ethics in the use of experimental animals.[87,88] On the other hand, often several experiments are performed in order to support initiation of clinical trials and by increasing the meaningfulness of individual experiments this number could be reduced.

2.20.4.2.3 Design the animal model concurrent with the design recommended for a pivotal clinical trial

Where guidance is available with respect to the recommended design of a pivotal clinical trial in the same indication, the key recommendations should also be implemented in the animal model testing. A disease that has seen many discovery and early development programs fail during late-stage clinical trials is rheumatoid arthritis. One of the reasons might be that often the design and the endpoints of the animal models do not represent those of the pivotal clinical trials. Collagen-induced arthritis in rodents is used as an animal model to assess the efficacy of antirheumatic drugs. In the past the design has often involved the start of treatment early after induction of the disease and the evaluation of efficacy via the pain response toward evoked pain or the post-mortem joint histology. A more sophisticated approach has been taken by Bender et al.[89] who has enriched this classical mouse model for rheumatoid arthritis with clinically meaningful biomarkers and imaging to enhance its translational value. First of all they used radiographic analysis of joint morphology in their mouse experiment since this is the gold standard for the clinical assessment of disease progression. Secondly, they chose to initiate treatment in one group of mice late in the disease process since this normally is the point in time that patients would receive an experimental drug and would thus enter potential clinical trials. The aim of the work by Bender and colleagues[89] aimed at assessing the potential therapeutic utility of an EP4 receptor antagonist and predict its efficacy in a clinical trial. While this mode of action may be most relevant during the phases of the disease where inflammatory cells infiltrate the joint, the efficacy of the compound may strongly depend on whether or not an individual patient has a weaker or stronger ongoing local inflammatory response. Thus, this was monitored via bioluminescence imaging to provide a potential PD biomarker that could be directly translated to clinical trials with the potential to act as a stratification biomarker as well.

2.20.4.2.4 Humanize animal models

Although mammals share overall genetic similarity, there are important differences between, for example, mice and man, particularly in the immune system. Thus, for instance, many mAbs targeting immunological molecules in man are not cross-reactive to the mouse counterpart protein. In the simplest manner of mouse humanization, a mouse protein is replaced by its human homolog in order to allow for testing a human mAb targeting this protein in a mouse model. This has for instance been achieved for CD3, a protein that forms part of the T cell receptor complex and which is a potential target for drugs against type 1 diabetes. Human mAb targeting CD3 such as teplizumab or otelixizumab do not cross-react with mouse CD3 and could thus not be evaluated in mouse models of type 1 diabetes such as the nonobese diabetic (NOD) mouse. One approach would have been to create a mouse cross-reactive mAb against CD3 as a surrogate and to assess this in a mouse model. While this would allow for a general proof-of-principle for the target, it is virtually impossible to create a surrogate antibody that has exactly the same characteristics in mice than the parent antibody in man. Thus, the approach was to replace the mouse CD3 protein by its human homolog. This has allowed for a successful evaluation of a human anti-CD3 mAb in the NOD mouse model.[90] Importantly while the clinical trials already showed a potential therapeutic benefit of anti-CD3 antibodies against type 1 diabetes, the same trials showed the safety margin to be very small. Therefore, going back to an animal model allowed for an evaluation of different dosing strategies in order to improve the benefit risk ratio.

Humanization of animal models has a long history in oncology: anticancer compounds have for a long-time been assessed in xenograft models where mice receive subcutaneous implants of cell lines originally derived from human tumors. This requires mice deficient in their own immune response such as the nude or Severe combined immunodeficiency (SCID) mutant mice. While this approach has yielded some novel anticancer drugs, it remained largely unsuccessful mostly because the "human tumor" grows isolated from its mouse host, that is, creating a petri-dish on four paws and because the cell lines, originally isolated from human tumors, were used over decades and hundreds of generations, thereby loosing many of the original features. Thus, more sophisticated approaches use patient-derived tumor material that has undergone little manipulation in the laboratory setting thereby retaining its original heterogeneity. Such patient-derived tumor models allow for a phase 2 like preclinical testing of new anticancer drugs in mice.[91] Other attempts have been the creation of mice displaying some characteristics of the human immune system.[92]

While many organ systems show remarkable similarity between rodents and humans, the immune system is significantly different. Such differences make the assessment of immune-related phenomena in rodents difficult. That is why attempts have been made to reproduce a human immune system in mice by first ablating their own immune response and subsequently adding human immunocompetent cells.[92,93] Such models have helped to develop more representative cancer models that allow not only human cancer cells to form tumors in rodents but also for the established tumors to interact with the humanized immune system.[94,95] These models have enabled the development of the immune-oncological therapies that have great promise as novel anticancer therapies. One of the greatest debacles of modern drug development was the so-called Tegenero incident in which human volunteers treated with the experimental antibody TGN1412 experienced a severe cytokine storm. Such an effect has not been observed even at high doses when tested in nonhuman primates (NHPs). Recently a mouse model was created by reconstitution of human peripheral blood mononuclear cells in immunodeficient NRG (NOD-Rag1^{null} IL2rγ^{null}) double mutant mice in

which this effect could for the first time be replicated in an animal model.[96] Although these mice did not express all relevant human cytokines (IL-2, IL-4) and others to a much lesser extent, the mice responded to an injection of TGN1412 with a cytokine release storm including lymphopenia, release of interferon-gamma, tumor necrosis factor α, and several interleukins as well as behavioral signs indicative of severe illness.

Although humanization of animal models will always (by definition) remain imperfect, such models may certainly help to answer specific questions. The challenges with such humanized models are that on the one hand there is often an overlap between the original host species biology with the human biology that was introduced, for example, in the case of immunodeficient mice there is always part of the mouse immune system left. On the other hand, human receptors or signaling molecules expressed by the host species may not naturally interact with the respective host ligand or receptor systems. A profound knowledge of the target physiology is therefore essential for a proper interpretation of the results obtained with humanized animal models.

2.20.4.2.5 Introduce more relevant clinical endpoints

Animal models often use endpoints that are different than those used in clinical trials, especially the primary clinical endpoints. One of the prime examples for this is pain research. While many animal models naturally focus on an objective assessment of the pain response, the clinical endpoints accepted by regulatory agencies focus on subjective responses and more broadly on quality of life (QoL) rather than on pain itself. Analgesic drug development has has, as a consequence, seen many late-stage clinical failures due to lack of efficacy. Consequently, animal models have been enriched with more meaningful endpoints. Many of the simple pain measurements include reflex withdrawals in response to painful stimuli. This may be appropriate to assess a pain threshold under baseline conditions but ignores the potentially more important affective component. Moreover, for patients suffering from chronic pain, the nonevoked, that is, spontaneous pain is more debilitating than the evoked pain and thus potentially contributes more to the clinical assessment of pain, for example, via patient rating scales. Recently, an assessment of the facial expression in rodents revealed that the so-called grimace scale can provide a reliable and valid assessment of spontaneous pain in rats.[97]

Another example of a recent attempt to introduce more meaningful and sophisticated endpoints into animal models is the more detailed assessment of motor behavior. Many chronic diseases have a motor component, for example, arthritis pain, movement disorders such as Parkinson's disease or amyotrophic lateral sclerosis. Former methods to assess movement disability and its potential reversal included, for instance, wheel running which provides an easy quantitative assessment of gross motor but is confounded by motivational influences and provides little information on more subtle qualitative changes. A so-called CatWalk system has been developed for a detailed analysis of the rodent gait such as symmetry of foot prints, body weight distribution, or walking patterns.[98]

QoL is probably the single most important clinical endpoint for most, especially chronic, disorders. This is especially true in the light of an increased need for cost efficiency in the health care system and the request of the reimbursement agencies for pharmacoeconomic measures which often include QoL. While QoL assessment is nowadays regularly used in clinical assessments of new therapies, this endpoint is still rarely used in animal models. Such measures can include relatively simple parameters such as body weight development or food intake. More sophisticated QoL endpoints need to be assessed more continuously by observation in the home cage of the animals which is technically more challenging but such technologies have become available, (for example, video observation systems, telemetry, or implantable chips). With such new technologies at hand, circadian rhythms, quality of sleep, social behavior, or grooming can be assessed. Most often QoL of patients is assessed by questionnaires, a methodology that obviously cannot be used in experimental animals. However, there are recent attempts to model questionnaires which serve as primary outcome measures in clinical trials, for example, for pain in animals. For instance, the human brief pain inventory was successfully modeled in dogs suffering from cancer pain.[99]

2.20.4.2.6 Ensure proper validation of animal models

Validation of models is a complex process and classically involves the assessment of face-, construct-, and predictive validity.[100] Face validity refers to the similarity between the symptoms observed in the model with the clinical signs typical for the human disease. Construct validity has to do with the plausibility that links the design of the animal model with the human disease and is perceivably the most difficult of the three criteria. Most often applied, especially when animal models are to be used for drug discovery and development, is the criterion of predictive validity, which means that clinically used treatments should have comparable beneficial effects in the animal model. Although most often used, the latter criterion has an inherent problem and may be the cause of limited innovation: if existing drugs are used to optimize animal models, these models may not be well suited to discover completely novel drugs. Thus, the emphasis should be to apply the criteria of face and construct validity more stringently.

Models, by definition, do not claim to fully reproduce the human condition but rather represent certain aspects of it. The fit-for-purpose concept applies to validation of animal models as well, i.e. that the particular use of the model determines the required validation. For instance, if one is interested in either the manic or the depressive phase of bipolar disorder it might be sufficient to model either one of the endophenotypes. If however there is a need to assess the effects of a drug on the disease, it may be needed to reproduce the cyclic nature of the human disease in the animal model.[101]

2.20.4.3 How to Implement Animal Models Into a Translational Strategy?

2.20.4.3.1 Design an animal model strategy with a high translational value

A model is a simple representation of a complex system. Consequently, an animal model for a human disease is by no means attempting to reproduce the human disease with all its complexities in an animal but rather to model specific aspects of a disease.

Whenever using an animal model, it is of utmost importance to address a specific question and to ensure that the chosen model is appropriate to provide an answer to this specific question. Since the type of question changes during a drug discovery and development process there is, in many cases, not one model that has a high validity throughout. Consequently it may be appropriate to select different models along the development path.

While a model is not a perfect replication of the clinical condition, not all criteria can be met in a single model. However, a combination of different models can eventually come closer to the clinical situation as a single, even highly sophisticated model. But what is an optimal combination of models? Frank Sams-Dodd has proposed a model validity scoring system of which an extended version is shown in **Table 4**.[102]

This scoring system uses five different criteria:

Species: The closer a species is to human (from a genetic point of view), the more likely it is that the pathophysiology of the disease is similar to that of humans.

Complexity: Test systems on a molecular level, for example, comprise enzyme inhibition or radioligand binding assays. Cellular assays use whole cell systems and assess endpoints like apoptosis or Ca-influx. Tissue assays investigate drug effects on whole tissues such as cardiac contraction. At the highest level, in vivo tests look at drug effects in living individuals, for example, locomotion or cognitive performance.

Disease simulation: Current models use different principles to induce the disease of interest. The simplest models do not even attempt to induce a disease but simply look at a measure in healthy individuals that is disturbed in a disease. Antipsychotic drugs, for example, are assessed in auditory gating models in healthy animals and humans, as auditory gating is impaired in schizophrenic patients.[103] Somewhat more complex is the use of drugs to induce disease symptoms such as phencyclidine or amphetamine to elicit psychotic like symptoms. For most central nervous system (CNS) disorders the etiology has not been fully elucidated which means that a true disease simulation, as for instance in infectious diseases, is not possible. However, models are available that model in a complex manner the disease pathophysiology. For example, hippocampal deficits, which are most probably induced during early development are, known for schizophrenic patients. An animal model has been developed based on these findings, which induces an early hippocampal lesion in rats, mimics several symptoms and recapitulates the characteristic time course of schizophrenia (disease onset after puberty).[104]

Predictivity: A drug effect in an experimental model can, in principle, be observed in two different manners: a quantal (all or none) or a graded response. A quantal response does just indicate as to whether a drug is active or not. A graded response, however, allows to distinguish between drugs/doses with higher and lower activity. Such models allow the comparison of different drugs and may help to decide as to whether an experimental compound is similarly or even superior to the existing gold standard of therapy.

Face validity: This criterion can be further differentiated depending on whether just one symptom of a disease is modeled or a set of symptoms and whether this includes core symptoms or rather minor symptoms.

This scoring system can be of dual purpose. First it can help to compare different models regarding their validity. The apomorphine screening test for screening potential antipsychotics with antidopaminergic activity, for example, scores lower than the neonatal hippocampal lesion model for schizophrenia. But probably more importantly, the scoring system can help to assemble a screening cascade/combination of models which altogether has maximal validity. For example, the neonatal hippocampal lesion model for schizophrenia scores high for all criteria other than "species" and could thus be ideally complemented by a relatively simple human model.[105]

2.20.4.3.2 Back-translate clinical trial findings into animal models

Often clinical findings are at odds with the results of an animal model experiment and often, the conclusion is that the human clinical trial is right and the animal model wrong. An alternative view that may be more productive in the refinement of the translational drug development process is to consider both are right to some extent but the question is being viewed from different angles.

Table 4 Proposed validity scoring system

Criterion	*Value*	*Score*	*Criterion*	*Value*	*Score*
Species	Human	4	Complexity	In vivo	4
	Nonhuman primate	3		Tissue	3
	Nonhuman mammal	2		Cellular	2
	Nonmammal	1		Subcellular/molecular	1
Disease simulation	True	4	Predictivity	Graded for all pharmacological principles	4
	Complex	3		Graded for certain pharmacological principles	3
	Pharmacological	2		All or none for certain pharmacological principles	2
	No	1		No or not shown	1
Face validity	>1 core symptom	4			
	1 core symptom	3			
	1 symptom	2			
	No	1			

Translational research is often seen as a methodology to increase the probability that research findings generated at one level (e.g., animal model) can be reproduced at the next level (e.g., clinical trial). This forward translation is certainly the ultimate goal of translational research. However, this translation will never be perfect in that predictions generated at one level will not be verified at the next higher level of research. One could simply accept these failures, but in order to fully exploit the potential of the translational research spirit, a back translation of the discrepant findings at one level with the ones generated at an earlier level can be beneficial.

As mentioned earlier, the assessment of pain in experimental animals often involves the measurement of provoked pain responses. Many different pain responses have been established in animals such as the response to heat and cold but also different types of mechanical and chemical stimuli. In order to enhance the translatability of pain research in animals, attempts were made to establish the same measurements in clinical studies. This improved the translation from animal studies to clinical trials. However, when conventional and generally accepted pain assessments were run side-by-side with the evoked pain measures, the effects of (potential) analgesics were not always congruent on both sets of parameters. The failure of a number of initially very promising pain therapies in late-stage clinical trials has consequently led to the back translation of pain measures used in clinical trials into animal models (see the earlier text).

Another example of successful reverse translation of clinical findings into the improvement of preclinical models is in the field of multiple sclerosis research. Experimental autoimmune encephalitis is the gold standard model for screening drugs for potential therapeutic value for multiple sclerosis. While this model helped to identify and characterize some of the current treatment options for multiple sclerosis patients, the list of drugs that were found positive in the model but did not demonstrate therapeutic value in clinical trials is even longer.[106] This has led to controversies over the usefulness of this model in the research and development of therapies for multiple sclerosis and other demyelinating disorders.[107,108] Although many of the arguments put forward by the opponents of this model are well taken, there are virtually no alternatives for experimental multiple sclerosis research. Thus, a pragmatic approach forward is to back translate the findings of clinical trials into the model in order to improve the design and conduct of experiments and/or to understand the differences in the pathophysiology in the model versus the human disease.[109,110] Another interesting aspect of reverse translation comes from human genetic association studies, for example, in multiple sclerosis. Such studies often identify hundreds, if not thousands, of potential genes and it is virtually impossible to understand their relevance and function in human studies. For this purpose, the human findings can again be reverse translated in animal models to identify the genes and pathways with the potentially highest relevance for the human disease.[111]

2.20.5 Imaging

Most biomarkers, such as "wet biomarkers" which have biophysical properties allowing their quantification in biological samples such as urine, plasma, serum, cerebrospinal fluid, synovial fluids, etc. (e.g., cytokines), or in biopsies (e.g., gene expression profiles), are referred to as "molecular biomarkers" or "nonimaging biomarkers." In practice obtaining biological samples in which to quantify these molecular biomarkers can often prove to be difficult due to the frequency of sampling, volume needed, or to the relative invasiveness of the sampling techniques (specifically in the case of synovial fluid collection, for example, or blood collection in a neonate). In contrast, imaging biomarkers are measured using imaging techniques which quantify changes in anatomic, physiologic, biochemical, or molecular parameters[112] such as conventional radiography, CT, MRI, ultrasound, PET, single photon emission computed tomography, optical imaging, light microscopy, MR elastography, and spectroscopy.[112–114] These imaging-based biomarkers can provide objective measures in a reasonable time frame, potentially nonbiased by the act of taking a biopsy and usually in a noninvasive and painless manner. Although these imaging techniques tend to be expensive, they can be cost-effective when used in well-defined situations where subjective assessment has been the only approach available.[115]

2.20.5.1 Types and Technologies

2.20.5.1.1 Radiography

Radiography uses ionizing electromagnetic radiation (X-rays) to produce an image of an internal body structure. These X-rays are produced in a tube via an energy conversion that takes place when an electrical current accelerates electrons from a heated tungsten filament cathode to an anode. As it passes through the body of the patient, a fraction of the X-ray beam is absorbed by the different tissues and body structures, while the rest of the beam is captured by a detector which can be either a photographic film or a digital detector. The obtained image is therefore the sum of the various body densities that the beam has passed through.

2.20.5.1.2 Computed tomography

A major disadvantage of conventional radiography (X-ray) is that it reproduces a 3D structure into a 2D image. Although based on X-ray imaging, CT scan, also called X-ray computed tomography (X-ray CT) or computed axial tomography, provides a different type of imaging known as cross-sectional imaging. In the data acquisition phase, a fan-shaped beam of X-rays is emitted from a source that rotates around the inside of a circular opening and used to irradiate a section of the patient's body. Detectors on the opposite side of the emitting source measure the attenuation of the X-rays as they pass through the body at a given angle. Multiple 2D views or "snapshots" are collected and reconstructed by a computer into a cross-sectional image (or slice) during the image reconstruction phase allowing 3D imaging when the slices are assembled. "Multi-slice" or "multi-detector" technology allows up to 640 slices to be

taken at a time for the most recent scanners. Although the resolution of CT scans is lower than conventional radiography, it has extremely good low contrast resolution which enables the detection of very small changes in tissue type and gives accurate diagnostic information about the distribution of structures inside the body.

2.20.5.1.3 Magnetic resonance imaging

MRI scanners differ from X-ray and CT scanners in that they do not use ionizing radiation but instead use radio waves and a powerful magnetic field. The intense magnetic field forces the protons within hydrogen nuclei contained in water molecules to align with that field. When a pulse of radiofrequency wave is applied, the protons are stimulated and are knocked out of alignment, absorbing energy in the process. When the radiofrequency field is turned off, the MRI sensors are able to detect the energy released as the protons realign with the magnetic field. As each tissue has a different water content, the protons will realign with the magnetic field at different rates and release different amounts of energy which are used to create the image.[116]

2.20.5.1.4 Positron emission tomography

PET imaging relies on the detection of two simultaneously released gamma rays resulting from the annihilation of a positron (antiparticle to the electron) with an electron in tissue. This positron originates from a compound labeled with a positron-emitting radioisotope that was introduced into the body, usually by intravenous injection prior to the procedure, and that accumulates in regions with high metabolic activity for the most frequently used PET tracer—the glucose analog [^{18}F]2-fluoro-2-deoxy-D-glucose (^{18}FDG-PET). PET imaging provides a highly sensitive and accurate measure of the in vivo concentration of the radiotracer due to the physics of the emission, and the detection of the coincident gamma rays. In contrast to MRI and CT scans that show the structure of, and blood flow to and from organs, a PET scan measures important body functions, such as blood flow, oxygen use, and sugar (glucose) metabolism.[117,118]

2.20.5.1.5 Optical imaging

Optical imaging uses light to visualize cellular and molecular function or track molecules in the living body in a fast, sensitive, and cost-effective way. Images are generated by using photons of light in the wavelength range from ultraviolet to near infrared (NIR). Upon excitation of a target molecule with a light source such as a laser or by the use of a natural light-emitting protein such as luciferase, the photons that are emitted are captured by a detector. As the radiation used is nonionizing, optical imaging is appealing in many settings as it reduces costs and infrastructure requirements, such as shielded rooms. The technique exploits contrast that is derived through the use of either endogenous molecules with optical signatures (e.g., hemoglobin, collagen), exogenous agents that provide a signal (e.g., dyes or fluorescent probes) or reporter genes.

The intrinsic fluorescence of many substances such as keratin, elastin, collagen cross-links, phospholipids, tryptophan, retinol, lipofuscin, and metabolites nicotinamide adenine dinucleotide and flavin adenine dinucleotide as well as the differential absorption properties of oxy- and deoxy-hemoglobin, lipids, and water can provide information about both the structure and function of living tissue. In addition to this endogenous contrast present in many organisms, exogenous contrast can further add to the possibilities of optical in vivo imaging and consists in the in vivo injection of fluorescently labeled targeting agents (peptides or proteins), inorganic dyes, nanoparticles, and more complex constructs that exploit properties such as Förster resonance energy transfer (FRET).[119,120] NIR probes, in contrast to those that emit light at visible wavelengths, offers the advantage that biological tissues have a reduced absorption of NIR light. This feature allows NIR light to penetrate deeper into tissue than light at visible wavelengths. Another advantage of NIR probes is that it reduces the masking effect on the signal from the optical probe by intrinsic autofluorescence as less autofluorescence is present at the NIR, thus enabling higher signal-to-background ratios.[121]

2.20.5.2 Uses

2.20.5.2.1 Application of radiography in drug development

Radiography is currently used as the first choice imaging technique for the diagnosis and follow-up of rheumatoid arthritis[122] as it is cheap, easily reproducible, and provides a permanent record with which the disease can be serially evaluated. An additional advantage of radiographs is that they can be randomized and blinded for standardized scoring with radiographic scoring methods such as Kellgren, Sharp, Larsen, van der Heijde, etc. The main disadvantage, however, is the absence of hallmark radiographic findings of bony erosions and joint space narrowing relatively early in the disease course and these may only occur late in the pathophysiology of the disease. In contrast, MRI provides a more accurate assessment, as well as earlier detection of lesions. Radiography is also frequently used to assess the severity and progression of Rheumatoid arthritis (RA) during drug treatment, for example, in clinical studies evaluating anakinra, leflunomide, etanercept, and infliximab.[125]

2.20.5.2.2 Application of CT in drug development

CT scans are often used to evaluate metastatic liver disease and to assess the tumor response to therapy (e.g., cytotoxic chemotherapy,[126] trastuzumab[112]) with the efficacy endpoint being the reduction in tumor volume. CT imaging was also shown to be a useful technique for the in vivo evaluation of the PKs of platinated agents.[127]

2.20.5.2.3 Application of MRI in drug development

As MRI is being widely used in the clinical setting, it has also become an increasingly important tool for small animal imaging at multiple levels of preclinical research. Its applications cover the cardiovascular, neurovascular, and renal disease fields. For example, MRI enables in vivo assessments of renal perfusion or cardiac morphology and function; in vivo visualization of neuroinflammatory lesions in animal models of multiple sclerosis, of cerebrovascular dysfunction in animal models of cerebral amyloid angiopathies or angiogenesis and neovascularization in animal tumor models.[128] It can also play a pivotal role in the evaluation of neuroprotective agents in animal models of perinatal brain injury[129,130] or investigate multiple aspects of small animal vasculature and obtain hemodynamic and structural information in small animal peripheral artery disease models.[131]

2.20.5.2.4 Application of PET in drug development

PET has been widely used in the recent years by pharmaceutical companies, especially in the fields of oncology and neurosciences, to assess drug distribution to tissues of interest in microdosing studies,[132,133] to measure RO (as a surrogate biomarker of efficacy),[134–142] and to assess disease progression and pathological changes induced by the drug in the region of interest.[143,144]

2.20.5.2.4.1 Assessing drug distribution with PET in microdosing studies

PET has proven its effectiveness in assessing drug concentration–time profiles in body tissues targeted for treatment. Microdosing of carbon-11 or fluorine-18-labeled drugs allowed fast evaluation of PK properties of anticancer and CNS drugs. For example, brain exposure of ^{11}C-labeled CNS drugs has been compared in cynomolgus monkeys after PET microdosing, and the extent of P-glycoprotein mediated transport of ^{11}C-verapamil at the blood–brain barrier (BBB) has been characterized after administration of PET tracers at therapeutic doses and microdoses, demonstrating that the exchange of radioactivity between plasma and brain was not different after a microdose or a therapeutic dose, despite the differences in other PK parameters.[145] Microdosing data after ^{11}C-docetaxel PET can be used to predict tumor uptake of docetaxel to predict patients' responsiveness to chemotherapy.[146]

2.20.5.2.4.2 Measuring RO with PET

The assessment of RO has been widely used in TM for the dose selection in proof-of-concept (POCs) studies of drugs with relatively tight therapeutic margins, such as antipsychotics, anxiolytics, and antidepressants. Systemic kinetics can indeed not reflect the kinetics at the effect site, due to distribution delays and the dynamic interactions with the target. Furthermore, there can be significant differences between in vitro and in vivo results of RO assays, mainly due to the PK properties of the drug (distribution and metabolism). If in preclinical studies the target organ(s)/tissue(s) can be sampled at necropsy, this is not feasible in human, and PET provides an elegant noninvasive alternative for collecting useful information on the availability of the drug at the effect site. From PK/RO relationships established in preclinical species, human PK/RO profiles can be predicted after adjustments for cross-species differences in protein-binding and physiological parameters such as organ of interest blood flow and vascular/extravascular volume for different drug doses/regimens. A preliminary PET study in human allows the confirmation of the dose(s) to be selected for the POC study in patients. A prerequisite of these studies is the availability of a suitable radioligand[147–150] binding the receptor of interest. Often, regions devoid of the target receptor are taken as reference (to correct for a specific binding), and a ratio of radioactivity in the target/nontarget areas represents the signal. The assessment of RO is done in two steps:

1. the radioligand is administered by iv bolus or infusion at baseline (predose), PET scans are collected after an adequate lag-time, and the baseline target/not-target ratio(s) is(are) measured
2. the same radioligand is administered after treatment with the unlabeled drug, competing with the radioligand for the receptors of interest. The percent reduction in the target/nontarget ratio represents the fraction of total receptor occupied by the unlabeled drug.

2.20.5.2.4.3 Assessing pathological changes with PET

The use of PET scanning has a great potential for a more accurate and earlier diagnosis of degenerative disorders, such as Alzheimer's disease (AD). Currently, the definitive diagnosis of AD is possible histologically only by post-mortem observation of Aβ plaques and tau neurofibrillary tangles.[151] The use of PET neuroimaging together with radiotracers enabling the exploration/monitoring of specific mechanisms of dysregulation potentially causing AD (visualization of histone deacetylase (HDACs) activity, DNA methylation, Amyloid, tau protein) has revealed very promising for an improved prevention and treatment for AD.[143]

Functional imaging has been demonstrated invaluable in oncology, as metabolic changes in tissue usually precede structural changes detected via other imaging techniques such as CT and MRI, enabling detection of malignant disease at an earlier stage of development. For oncological PET studies, the most extensively used radiotracer is [^{18}F]-FDG-PET, with improved specificity and sensitivity versus structural imaging. However, coupling functional and structural imaging, as with PET/CT oncologic imaging, allows the accurate structure localization and intervention, as in the evaluation of mass lesions, staging and restaging of cancer, planning of radiotherapy treatments, and detection of cancer recurrence.[152]

In clinical practice, [^{18}F]-FDG-PET and integrated [^{18}F]-FDG-PET/CT are increasingly used to assess the therapeutic effect of drugs in tumor patients or to diagnose recurrence in curatively treated patients with head and neck cancer[153] and esophageal cancer.[154] These imaging techniques, however, have not yet been sufficiently validated to be accepted as a surrogate endpoint for clinical studies by regulatory agencies. Currently, a multicenter qualification study of [^{18}F]-FDG-PET/CT as a predictive marker of tumor response and patient outcome in patients with nonsmall cell lung cancer (NSCLC) has been initiated by the American College of Radiology Imaging Network.[155]

2.20.6 Strategy and Integration

2.20.6.1 Design of Translation Strategies

2.20.6.1.1 Introduction

The best translational tool is of limited value if not used as part of a translational strategy. Thus, at the beginning of each translational research project, a strategy should be designed that helps to select the best tools that are fit-for-purpose. This is best done by thinking backwards from the goal that is to be achieved. For a drug development project, this is normally the target package insert, the summary of product characteristics (SmPC), or the TPP. The most important features can then be back-translated, for example, if the key differentiating feature is an improved safety margin versus a competitor drug, one can think of the most appropriate endpoints in the various preclinical experiments and clinical trials and how those can best be translated from one step to the next. In reality, one rarely has a detailed SmPC at the beginning of a drug discovery project. Nevertheless, it is helpful to have a core of the TPP rather early on in the process and slowly develop this further during the discovery and development process. Alternatively one can work along a set of questions to identify the key focus points of the translational strategy:

1. What are the efficacy endpoints that the drug needs to meet? What are the primary endpoints that would be acceptable for the regulatory agencies and which endpoints would matter most for patients?
2. Which safety issues could arise based on the mode of action and based on the chemistry of the drug molecule?
3. Is there an important competitor drug? What is the competitive advantage of the drug in development over the competitor? Normally this is either efficacy or safety or a combination of both but it is not always the primary efficacy or safety endpoints that are key for differentiation.
4. What will be the pharmaco-economic case presented to the reimbursement bodies? While improved safety and efficacy is key for the regulatory agencies, the reimbursement bodies such as the British National Institute for Health and Care Excellence or the German Institut für Qualität und Wirtschaftlichkeit im Gesundheitswesen are keen to see a cost-benefit such as a reduction in other health care spending or an overall increase in the QoL.

It may be important to assign priorities to these various questions that need to be addressed during the course of drug development. For instance, for a life-threatening orphan disease with no marketed therapy, the competition and the pharmaco-economic case are less relevant than for a drug that is about to enter a market with strong generic competition. For the key arguments of highest priority it makes particular sense to back translate the criteria and desired results to allow for a project progress assessment throughout the life-time of the project. For this purpose, it is essential that the criteria and tools used are translatable from one step to the next.

2.20.6.1.2 Stroke TM strategies

Development of drugs for brain disorders has proven to be very challenging. More than 40 large clinical trials have failed to promote recovery from traumatic brain injury (TBI) and, similarly for stroke, over 1000 agents have been successfully tested preclinically but failed in clinical trials. In fact, only the thrombolytic agent tissue plasminogen activator (rtPA) and thrombectomy with a retriever stent have been approved so far for the treatment of ischemic stroke.[156,157]

Undoubtedly, stroke is a challenging and complex disorder as it is characterized by induction of a secondary neuronal injury by brain leukocyte infiltration after an acute brain lesion which might be categorized as an ischemic, hemorrhagic, or a transient ischemic attack. Only recently the involvement of the white matter (WM) has been acknowledged to play an important role in stroke.[158] It is the injury of the WM that is the major cause of paresis in all types of stroke and it is both the size of the infarct and, more importantly, the location that determines the functional outcome after stroke.[159] Hence in the field of neuropathology, a clear focus exists on the induction of WM lesions, the mechanisms involved in its pathophysiology, and the improvement of WM damage.[160]

As in all therapeutic domains, the success of translational research relies on target validation, use of predictive animal models, well-designed clinical trials, and inclusion of relevant biomarkers throughout the development of the drug. Improved translational research will let less drugs end in the drug graveyard and prevent more patients from receiving ineffective or even harmful drugs.

The pathophysiology and mechanisms of this injury in its different phases have not been fully elucidated, triggering the need for relevant animal models. Recently, WM has been recognized as playing a crucial role for functional recovery and post-stroke rehabilitation, based on clinical and preclinical data.[161,162] Clearly, differences in the architecture of the brain exist between rodents and humans, predominantly in the ratio of WM to gray matter, and the injury to WM can be induced by different agents and to different locations in the brain. All these parameters have a vast impact on the kind of induced lesion and hence caution is needed in translating results from preclinical models to a certain type of stroke or to a certain aspect of stroke amelioration. Obviously, current animal models do not reproduce all the clinical hallmarks of WM disease and support mostly the unraveling of the different mechanisms of damage induction and the potential interference of drugs in this process.

Improvement of the translation of animal models of stroke can be exerted at the level of the animal study (1) by selecting the right model to answer the particular question of interest, (2) by ensuring a sufficiently powered study, (3) by repeating the model in different centers, (4) by better mimicking a clinical trial in patients, (5) by a standardization of methods over the different centers involved, (6) by the implementation of relevant biomarkers in these studies, and (7) by the translation and interpretation of the results to the right patient population.

A good example of an improved preclinical strategy is the setup of a preclinical randomized controlled international multicenter trial (pRCT) to test anti-CD49d antibodies as stroke therapy.[163] Six independent European research centers investigated the efficacy

of anti-CD49d antibodies in two different mouse models of stroke in a centrally coordinated, randomized, and blinded approach, to better mimic the design of a randomized controlled clinical trial and avoid the confounding effects of bias. Maximum harmonization of the methods, used in the different centers, was pursued for the pRCT, as this is generally standard practice in a clinical trial. The multicenter approach facilitated achieving sufficient numbers to power the study and increase the sensitivity of outcome measures such as the infarct volume in the middle cerebral artery (MCA) occlusion model.

Before this cooperation, several smaller studies had been conducted by different laboratories, with conflicting results.[164,165] By performing the pRCT, the researchers could conclude that the benefit of anti-CD49d antibodies may depend on the severity and localization of the infarct as the reduction of lesion size was observed after the permanent distal occlusion of the MCA where a small cortical infarction was created, but not after transient proximal occlusion of the MCA, which induced larger lesions.

The power of a single study can be augmented as well by a meta-analysis of similar studies. Whereas the concept of meta-analyses is very common for clinical trials, it is very scarce for preclinical research in neurological disorders.[166,167] The major advantage of the pRCT, however, is the harmonization of protocols and the centralized analysis, which will substantially reduce intersite variation, while still capturing to some extent the intersite variation which might truthfully reflect variation in a multicenter clinical trial. In addition, prior to the actual pRCT, it might be optimal to run a pretrial to validate the methods which will be used, assess the level of harmonization in-between study centers, and possibly evaluate different drug doses. Confirmation of the predictive nature of a preclinical trial will ultimately require comparison of the results of the clinical trials with the results of their preceding pRCTs.

Several international research consortia have been established, including the European Union-funded Multicenter Preclinical Animal Research Team (Multi-PART) consortium for stroke research and the National Institutes of Health-funded Consortium for preclinical assESsment of cARdioprotective therapies (CAESAR) consortium for cardiovascular research to aid in the improvement of preclinical trial design, statistical analysis, and adequate reporting. Also the "Stroke Therapy Industry Roundtable" has proposed guidelines for the robust preclinical evaluation of neuroprotective drugs for ischemic stroke to improve the successful translation of neuroprotective agents.[168]

Improvement on the side of clinical trials depends on a better quality of trial design, well-selected outcome measures, adequate trial planning, homogeneous patient selection, and inclusion of reliable biomarkers that complement the clinical outcome measures.

Progesterone had consistently demonstrated a potentially neuroprotective effect in a vast number of experimental animal studies for brain disorders, including TBI and ischemic stroke[169,170] and the benefit was further supported by the findings in small phase 2 trials in TBI patients.[171,172] Two large, multicenter, randomized, and placebo-controlled phase 3 trials, named ProTECT III and SyNAPSE, however could not confirm its efficacy in TBI.[173,174] Critical comments about these trials included a different mode of administration than in the preclinical studies, a potentially suboptimal clinical dose setting and inadequate treatment duration, a presumed negative effect caused by abrupt discontinuation of treatment and inclusion of low sensitivity and low predictivity biomarkers like the Glasgow Coma Scale and Extended Glasgow Outcome Scale (GOS-E) for the evaluation of such a heterogeneous condition as TBI. Hence, a clear mismatch and failure in the translation of the preclinical knowledge to clinical studies of progesterone neuroprotection after TBI can be observed, of which some might have been caused by timing issues, preventing inclusion of the preclinical findings in the clinical trial design. As such, the failure of progesterone as neuroprotective agent after TBI represents another example of the exceptionally high attrition rate in drug development for CNS disorders.

Besides better design of preclinical and clinical studies and a thorough translational strategy that links, confirms, and improves the knowledge of both the disease and the drug throughout development, a higher success rate might be achieved by implementation of a pathoanatomically based classification system. The current thinking supports classification and treatment of TBI and stroke patients based on the pathoanatomic injury, that is, the abnormality to be targeted by the treatment; and less on the clinical symptoms the patients present.[175] Both in TBI and stroke, neurological assessments, brain imaging, and blood biomarkers may improve diagnosis, patient stratification, and clinical outcome evaluation.

As stroke is a very heterogeneous disorder in etiology, symptoms, severity, and recovery, there is a clear need for guidance in the selection of appropriate scales to assess recovery in stroke, both from a physical, psychometric, and a QoL perspective. Different clinical-rated and patient-reported outcome measures exist like the Stroke Rehabilitation Assessment of Movement, the Chedoke Arm and Hand Inventory, ABILHAND, Fugl-Meyer Assessment (FMA), and Action Research Arm Test (ARA).[176] Currently there is no general consensus on the scales that should be used, the required level of effect and the most appropriate timing both in clinical stroke trials and clinical practice. Attempts for the improvement of clinical measures in stroke have been reported and are being extended.[176–179]

Imaging helps unravel the role of WM in acute neurologic conditions and the mechanisms associated with WM injuries and hence the selection of a more homogeneous patient population.[180] Different modalities of MRI are being used to visualize brain lesions. Perfusion-weighted imaging and diffusion-weighted imaging identify the area of acute ischemia in acute stroke; diffusion tensor imaging measures the degree of diffusion anisotropy in the brain and enables a more thorough investigation of the WM.[181,182] The result is a visualization of the structural integrity of brain WM tracts, potentially serving as a predictive biomarker for motor recovery which can aid in a personalized and optimal rehabilitation regime.[183]

Overall, the arrival of such imaging techniques has significantly improved both the diagnostics of WM injury and the monitoring of structural changes in the brain. Lesion mapping has identified that the hemispheric WM is preferentially affected in patients with major MCA stroke as compared to patients with lesion regression[184] and that patients unresponsive to rtPA and without recanalization of the MCA showed larger brain lesions with greater hemispheric WM damage than those who experienced successful thrombolysis.[185]

Obviously, biomarkers complementary to imaging and neurological assessments, for example, metabolic, anatomical, immunological, and genetic characteristics can further improve diagnosis, stratification, and evaluation of clinical efficacy.[186]

It is critical for patients to be rapidly diagnosed and considered for acute therapy. The development of diagnostic blood biomarkers for stroke, which might help distinguish stroke from mimics, is being complicated by the heterogeneity of stroke, the complexity of brain injury involving excitotoxicity, oxidative stress, inflammation, BBB dysfunction, apoptosis, etc.[186] Overall, the biomarkers related to these processes might be applicable for the prediction, diagnosis, assessment, prognosis, or treatment of stroke. Whereas individual markers have lacked sufficient sensitivity and specificity for stroke diagnosis, panels of biomarkers (like a composite score of matrix metalloproteinase 9 (MMP-9), brain natriuretic factor, d-dimer, and S-100beta) may hold greater promise and are actively being evaluated.[187,188]

In addition to diagnosis, biomarkers might assist with the identification of stroke mechanism and aid in prevention and treatment strategies, once validated.[186]

In summary, approval of drugs for neurological disorders like stroke has proven to be very challenging. This is caused by the complexity and heterogeneity of these diseases, the incomplete understanding of the different pathophysiological processes leading to brain injury, and the lack of biomarkers to describe these pathways and diagnose and monitor the neuronal damage. In addition, preclinical studies of therapeutic agents have had some limitations and flaws, as was the case for the clinical trials in this domain. Better understanding of the pathophysiology will help improve current clinical diagnosis, assessment, prognosis, and therapy. Inclusion of biomarkers reflecting relevant events of the pathophysiological processes in clinical trials as well as implementation of optimized clinical scales to measure QoL, physical, and psychometric patient characteristics and new imaging techniques will hopefully further advance and multiply the treatment options for patients suffering from these complex neurological disorders.

2.20.6.1.3 ALX-0171 translational strategy

Human respiratory syncytial virus (RSV) is the most important viral pathogen causing acute lower respiratory tract infections in infants with clinical signs ranging from mild upper respiratory tract illness to severe lower respiratory tract infections, including pneumonia and bronchiolitis. ALX-0171 is a trivalent Nanobody which is designed to target the RSV F-protein for delivery via inhalation.[189] It is currently in clinical development for the treatment of RSV lower respiratory tract infections in infants.[190]

Based on project goals and the defined target population for which the drug is being developed, a TM strategy should be laid out and documented in a TM plan. Implementing such a TM strategy in drug discovery and clinical development is key, as it integrates all TM aspects for a particular project and provides clarity on the objectives and how those objectives are going to be reached. As a starting point in building such a TM strategy, critical points and/or issues of the project need to be identified.

In the case of ALX-0171, the following aspects were considered as key points.

2.20.6.1.3.1 Efficacy

Infants with RSV disease typically develop clinical manifestations such as bronchiolitis and pneumonia that both result in significant hypoxia. Hallmark symptoms of bronchiolitis include wheezing, rales, rhonchi, increased respiratory rates, and signs of air trapping with flaring of nasal passages and intercostal muscle retractions.[191,192] In fact most clinicians recognize bronchiolitis as a constellation of clinical symptoms and signs[193] with a high heterogeneity in disease severity likely due to a combination of host and viral factors.[194] As such, there is a high need for a valid and reliable scoring instrument that could be used as a measure to evaluate the efficacy of clinical interventions in randomized controlled trials.[195] Such lack of clinically validated scores makes translatability of any preclinical results to the clinical setting difficult. To overcome such a hurdle it was considered important to identify biomarkers which could support efficacy in addition to the clinical endpoints. A logical example for an antiviral drug would be to assess the effect of treatment on viral loads both preclinically and clinically. In this respect, it has been shown that viral load consistently correlated with increases in multiple different disease measurements (symptoms, physical examination, and amount of nasal mucus) in a human challenge study,[196] and predicts disease severity in previously healthy infants.[197,198] It is therefore possible that reducing the RSV burden of infected infants at the time of hospital admission results in clinical benefit.

Many animal models of RSV disease, including NHPs, calves, lambs, mice, guinea pigs, ferrets, hamsters, and cotton rats, have been described.[199,200] However, all these animal models have limitations and should be selected appropriately based on the study objectives. For example, mice are not natural hosts of RSV and therefore require high viral inocula for an effective infection but are easy to handle and many transgenic and knockout strains are available. Cotton rats are 100-fold more permissive to RSV infection and the viral kinetics are closer to that in humans than for mice but the disease still does not sufficiently parallel events in the infant disease.[201] As colostrum-deprived neonatal lambs are naturally susceptible to RSV disease, share anatomical, physiological, and developmental similarities to that of human infants[202–205] and develop mild clinical symptoms such as expiratory efforts, fever, tachypnea, wheeze, malaise, and listlessness when experimentally infected with RSV,[206–208] this model was selected to assess the PK/PD properties of ALX-0171.

2.20.6.1.3.2 Efficiency of administration and dose predictions

As RSV is an acute disease, it is expected that a rapid delivery of high concentrations of drug within the respiratory tract would allow rapid viral neutralization and consequently a shortened disease time course.[209] For these reasons, the inhalation route was selected for delivery of ALX-0171.

The first issue with this administration route is that the drug is submitted to high shear forces during the aerosol generation that could induce physicochemical degradation or protein fragmentation and could potentially result in loss of biological activity, toxicity, and/or immunogenicity.[209,210] The second issue is that drug deposition within the airways is highly dependent on particle size distribution, airway anatomy, respiratory parameters, and gas volume in the lungs[211] which can be quite different between not

only different animal species but also between human adults and infants. As a consequence, the translatability of dose predictions from the preclinical setting to the clinical setting needs to be multifaceted. One important consideration is that the target concentration in the epithelial lining fluid needs to be defined appropriately. As infants are not small adults with regards to the development of organ systems, ideally modeling approaches need to take the differences in anatomy/physiology into account as these parameters can possibly result in changes in drug disposition in infants as compared to the adult situation. A PBPK model as the one developed for ALX-0171[212] is a good example of such a model and is further described in section "**From Empirical to Mechanistic Pharmacokinetic/Pharmacodynamic Models**." This model, however, describes the PK behavior of the drug once it has reached the lower lung but does not provide insight in the dose that needs to be nebulized in order to reach the required lung deposited dose. Additional models such as the in vitro Sofia Anatomical Infant Nose and Throat model (SAINT)[213] or the Multiple-Path Particle Dosimetry (MPPD) computational model are useful to study aerosol deposition in the respiratory tract of infants and thus can further complement the PBPK model for dose selection.

2.20.6.1.4 Tocilizumab translation in Crohn's disease

System biology can be applied to scale across different indications. Dwivedi[214] published an elegant example of a multiscale systems model developed to describe IL-6-mediated immune modulation in Crohn's disease, to assess and compare the expected performance of intervention on different potential targets.

Crohn's disease is a chronic inflammatory disorder, caused by a combination of environmental, immune, and bacterial factors in genetically susceptible individuals, in which the body's immune system attacks the gastrointestinal tract possibly directed at microbial antigens.

Further to other cytokines, IL-6 is increased in the intestinal mucosa and in the peripheral blood of patients diagnosed with Crohn's disease. IL-6 signaling can occur through membrane-bound IL-6 receptor (mIL-6R) or soluble IL-6 receptor (sIL-6R). The complex IL-6/IL-6R can recruit a membrane-bound gp130 coreceptor, forming a trimer which subsequently dimerizes to form a hexameric complex, and triggers the phosphorylation of gp-130-bound Janus kinase proteins. IL-6 signaling results in an increased expression of acute-phase proteins such as C-reactive protein (CRP), as also reported in Crohn's disease. Hence, the development of a system biology model describing the IL-6-mediated immune signaling pathway at the cellular level, and target organs relevant in Crohn's disease can contribute to the evaluation of the most sensitive target to hit in Crohn's disease. The model was based in previous in vitro knowledge and in vivo information gathered in another patient population. CRP data from a previously published pilot clinical trial of the anti-IL-6R mAb Tocilizumab were used to qualify the model.

Based on the model, the effects of IL-6 or IL-6R inhibition and a fusion protein combining the extracellular portion of gp130 with the Fc region of human IgG1, sgp130Fc on PD serum and gastrointestinal tract (GI) tract biomarkers (CRP and pSTAT3 activity) have been compared. The predicted profiles of the PD biomarkers suggest that the best targets would be IL-6 and sIL-6R, whereas the sgp130 therapy will likely be less effective. The model also allowed the comparison of expected dose–response curves for IL6 or IL-6R inhibition, appearing different in shape: IL-6 inhibition is characterized by a smooth dose–response until saturation at high doses, whereas the interference with the IL-6R leads to an abrupt increase in the response. The different behavior is explained by the very different levels of free IL-6 and soluble (s)IL-6R. The different levels of IL-6 and sIL-6R confer different profiles to antibodies targeting them, and a greater dose-dependent modulation of the effects is predicted for anti-IL-6 than for anti-anti-IL-6R antibodies, so that targeting IL-6 would require lower and less frequent dosing compared to an anti-IL-6R, to achieve similar reduction of the effects of the IL-6 signaling. On the other hand, the very high baseline level of sgp130 compared to free IL-6 and complex makes it relatively insensitive to small changes in its concentrations. This hypothesis needs, however, further clinical validation.

2.20.6.2 Integrative Thinking

2.20.6.2.1 Introduction

The rapid evolutions in new technologies have opened up a lot of opportunities for basic and clinical research and diagnostics. In addition, elements from different sciences and technology branches are more frequently being combined. These developments are more and more being fed in clinical settings (TM from bench to bedside), while also the bedside to bench translation can be very informative and expedite finding of new or better therapies. Last but not least, integrative thinking in TM also refers to integration of knowledge within a particular field and over different fields, for example, the research that is concentrated in societies or other programs that integrate the experiences and requirements of researchers, clinicians, and health care providers.[215]

2.20.6.2.2 Bedside back to bench

Integrative thinking also entails learning from failed therapies, whether caused by safety or lack of efficacy reasons. By trying to elucidate failures and by reporting on failures, important knowledge is being captured that can in turn save a follow-up molecule from the clinical graveyard. One of the many drugs that was discontinued during phase I clinical trials due to safety concerns is the anti-CD40L mAb ruplizumab (h5C8, Biogen). Thromboembolic (TE) events occurred in several ruplizumab trials: in a lupus nephritis trial, two patients suffered a myocardial infarction[216] and in a transplant trial, one obese, bedridden woman died from pulmonary embolism.[217] In addition, during a Phase II study receiving another CD40L-targeting compound toralizumab (IDEC-131), a Crohn's disease patient developed a blood clot in the leg.[217] The mechanism of the safety findings was further investigated and reported and this facilitated the development of Dapirolizumab Pegol (CDP7657, UCB).[218,219]

CD40L is a costimulatory molecule expressed on activated T cells which signals to professional antigen-presenting cells,[220] but it is also expressed on platelets and monocytes, natural killer (NK) cells, mast cells, and basophils under inflammatory conditions. For almost two decades, CD40L was an inaccessible target due to the TE events that occurred in several clinical and preclinical trials with anti-CD40L compounds.[217,221] At the time, these adverse events could not readily be explained. As CD40L is also expressed on platelets, anti-CD40L drugs could have bound and activated platelets. This was extensively investigated and by now, evidence has been generated that immune complexes comprised of CD40L (a trimer) and antibodies are able to activate platelets and induce platelet aggregation in vitro, predominantly by cross-linking of FcgRIIs on the platelet membrane. Either CD40 or CD40L can act as docking station on the platelets for the immune complexes, resulting in FcgRII-mediated platelet activation.[222–225] This hypothesis was further strengthened by the results obtained in a hu FcgRIIa transgenic mouse model and the findings reported in NHP safety studies. The transgenic mouse model was developed to facilitate the binding of a human mAb-Fc to transgenic Fc receptors expressed on murine platelets.[223] Injection of preformed complexes of recombinant soluble CD40L and anti-CD40L antibody in these mice caused thrombocytopenia and intravascular microthrombi. In addition, two safety studies in NHP confirmed the dependence on the Fc part of the anti-CD40L mAbs to induce thrombo-embolism in these animals: TE were quantified in rhesus monkeys treated with either ruplizumab[221] or the follow-up molecule CDP7657,[218] a PEGylated anti-CD40L Fab fragment. Extensive immunohistochemical analysis of the lungs revealed a lower prevalence of microthrombi in the lungs of rhesus monkeys treated with CDP7657 as compared to ruplizumab and a similar number for the CDP7657-treated animals compared to the number in vehicle-treated animals and historical controls. Importantly, the same holds true for variants of ruplizumab without effector function such as the aglycosylated version of the mAb and its di-Fab fragment. Two trials have been completed in meanwhile with CDP7657: a Phase I study in both healthy individuals and patients with systemic lupus erythematosus (SLE)[219] (ClinicalTrials.gov Identifier: NCT01093911) and one in patients with SLE (ClinicalTrials.gov Identifier: NCT01764594). No TE events were reported in the report of the first trial.[219] In the latter, safety and tolerability was assessed and in addition, disease activity measures were explored using the British Isles Lupus Activity Group (BILAG)-based Composite Lupus Assessment and the Systemic Lupus Responder Index.[226] Preliminary and cautious enthusiasm exists as exploratory analyses show greater improvement in clinical measures of disease activity in the CDP7657 group versus placebo. More importantly, however, no serious treatment emergent adverse events and no deaths occurred.

As such, the CD40L story is a good illustration of how the failure of two drugs, when well investigated may aid the development of a third one and facilitate better patient care.

2.20.6.2.3 Integrative thinking in oncology

The field of Oncology is moving fast forward and this movement is being supported by strong integrative thinking in different areas: (1) treatment strategies focus both on the tumor and the immune system; (2) combination therapy is the future and requires excellent knowledge of the action of the different single therapies and the potential interactions thereof, and (3) a more profound characterization of the patient, both with respect to tumor and immune characteristics, will improve patient stratification and combination therapy (Fig. 10).

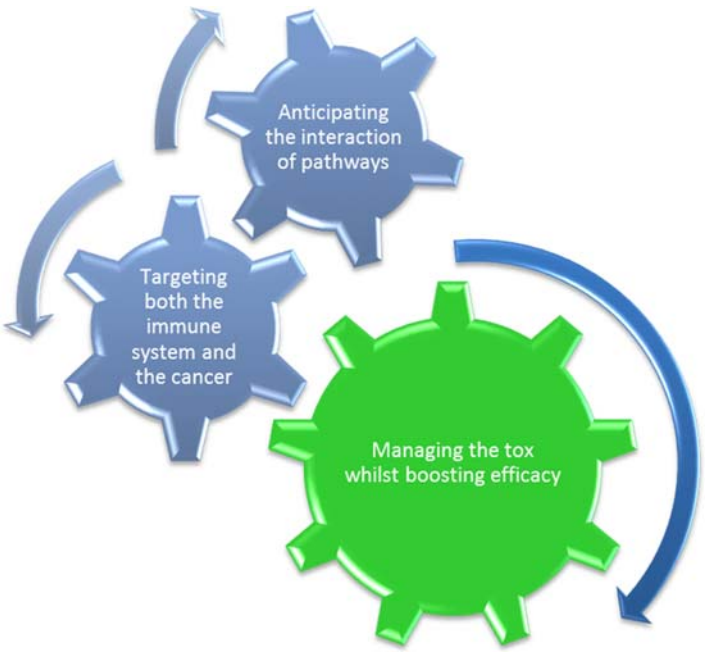

Fig. 10 The future of oncology is about combining.

2.20.6.2.3.1 Importance of both tumor and immune system (or immune contexture)

Before 2005, cancer therapy was focused on the tumor cells using antigen-targeted therapies, chemotherapy, radiotherapy, and kinase-targeted therapy. The treatment was mainly determined based on the characteristics of the tumor or the cancer (stage tumor lymph nodes metastasis (TNM), invasion status (L, V, Pn), grading (differentiated or not), mutations, histological subtype). This paradigm has changed by the rapidly advancing field of cancer immunology: now the focus is on the impact of the immune system and how this may be prompted to eradicate the cancer cells.[227] Insufficient immune-surveillance as well as the multiple immune suppressing mechanisms induced by the tumor might relate to the difficulty to recognize tumor as nonself and the subsequent elimination of tumor cells by the immune system. Many escape mechanisms are being exerted by cancer cells: (1) reduced expression of tumor/foreign antigens on their surface, (2) expression of immune suppressing proteins both on the tumor cell surface (e.g., Crry) and released in the tumor microenvironment (e.g., NO, IDO, and TGF-beta 1), and (3) the presence of multiple suppressing cell types like myeloid-derived suppressor cells (MDSCs), regulatory T cells (Tregs), etc. Hence, immunotherapy is focused on stimulating the immune system either by impairing the induction of tolerance (e.g., via PD-1, PD-L1, CTLA-4, LAG-3, TIM-3) or further strengthening the activating signals (e.g., via 4-1BB (CD-137), OX40 (CD134), and CD-27 agonists). As an example, tumors use checkpoint inhibitors,[228] which limit the strength and duration of normal immune responses to induce tolerance. Blocking the action of these checkpoint inhibitors has proven highly effective in multiple types of cancer and has led to the approval of ipilimumab (anti-CTLA4[229]), nivolumab and pembrolizumab (both anti-PD-1[230,231]), while many more are being evaluated and developed.[232,233] Durable tumor regression was most notable in melanoma and lung cancers, and favorable activity has been demonstrated in bladder cancer, head and neck cancer, renal cell carcinoma, ovarian cancer, and hematologic malignancies.[234–237] The importance of the immune system in cancer has been further highlighted by the predictive power of the immunoscore. This score, which is an assessment of infiltration of T cells in the tumor, has proven to be a strong prognostic marker and the most predictive parameter for overall and disease free survival (DFS) in colorectal cancer.[238,239] This immunoscore is in fact further complemented by the immunologic constant of rejection, which determines the functional orientation of the immune response (e.g., a predominantly Th1 driven cytotoxic response). Together they are referred to as the immune contexture. As a last example of the importance of the immune system in the control of cancer, it has been demonstrated in melanoma[240] and NSCLC[241] that more immunogenic tumors respond better to immunotherapy than cancers with a low mutational burden.

Although great leaps forward have been taken in cancer therapy, and more patients are experiencing durable long-term survival in certain cancer types, the majority of patients however remain unresponsive or relapse, warranting new drug combinations and further research both on tumor, tumor environment, and immune system.

2.20.6.2.3.2 Integration by combination of therapies: combination and sequencing

Tumors are in fact complex and heterogeneous tissues comprised of neoplastic cells interwoven with tumor-associated stroma cells. Targeted therapy, the former holy grail in the field of oncology, is susceptible to failure or relapse as the heterogeneity of the tumor warrants that a combination of targeted therapies will be necessary to achieve successful and sustained clinical benefit, as can be supported by the more favorable effect of the combination of a BRAF and (Mitogen-Activated Protein) Kinase/ERK (Extracellular Signal-Regulated Kinase) Kinase (MEK) inhibitor in BRAF mutation positive melanoma patients when compared to monotherapy.[242,243]

Further optimization of the potential of the immune system in cancer lies in (1) generation of sufficient numbers of antitumor T cells in the lymphoid compartment; (2) effective migration of T cells out to the lymphoid tissue into the tumor microenvironment; and (3) T cell effector function within the tumor microenvironment, characterized by the ability to bypass all aforementioned immune suppressing mechanisms.[244] Given the extensive toolbox that is currently available for cancer therapy, many combinations seem attractive from a theoretical point of view, to boost the immune response against the tumor cells. However, dose and dosing schedule, the optimal or even required order of the different treatments and even more importantly toxicity of a combination therapy render this approach a hazardous and difficult endeavor. Examples of potential combinations are a combination of an immune checkpoint inhibitor with a costimulatory receptor agonist[245]; or with radiation therapy,[246] chemotherapy,[247] or enhancement of innate immunity[248]; or with a second checkpoint inhibitor[249] or even with targeted therapy (NCT01454102, NCT0208812). Chemotherapy and radiotherapy form interesting combinations with checkpoint inhibitors as, in addition to the actual tumor cell killing, they both may indirectly release tumor-associated antigens, rendering the tumor more immunogenic for the immunotherapy as well as enhance costimulatory signals on antigen-presenting cells. Again, the sequence and the dose of this adjuvant therapy are crucial[250,251] and also here toxicity remains a concern.

2.20.6.2.3.3 Moving toward a multidisciplinary patient characterization will lead to more profound understanding of cancer progression and ultimately to better patient stratification

To identify the best treatment for a cancer patient, information from a multidisciplinary team should be assembled and interlinked[252]: the immune phenotype (e.g., expression of tolerance inducing signals; the T cell repertoire), the localization of the immune cells (infiltrating in the tumor or not), the genetic major histocompatibility complex (MHC) background, the tumor specific mutations and resistance mechanisms, and tumor staging and grading. These data may improve understanding of why a certain therapy is effective in some patients but not in others with the same type and even stage of cancer and more importantly if a patient is not responding, which therapy or combination of therapies would be more appropriate.

Comprehensive genomic characterization has identified molecular subgroups and consequently potentially actionable genomic alterations. Lung-MAP (SWOG S1400)[253] is a fine example of how state-of-the-art genomic profiling efficiently can be employed for drug development and does this in a very cost-efficient way: lung-MAP is a biomarker-driven squamous cell lung cancer clinical trial study design which is multidrug and multiarm. It uses a targeted screening approach, with state-of-the-art genomic profiling of neoplastic cells to match patients with substudies testing investigational new drugs and immunotherapies, based on their unique tumor profiles. Because a broad next-generation sequencing (NGS) platform is being used and tissue and blood is being banked, a lot of data will be generated that hopefully will lead to better understanding of responsive geno/phenotypes. A systematic tumor genomic profiling before treatment and after relapse is evidently very useful to identify acquired resistance mechanisms and to help predict the outcome with a similar therapy in other patients with the same tumor genotype.[242] Whole exome sequencing has deduced that a higher mutational load is correlated with better response to checkpoint inhibitors in melanoma and NSCLC[254,255] and immunohistochemistry has revealed that PD-L1 expression is being linked with improved clinical outcomes for anti-PD-1 or PD-L1 treatment.[256] However, the fact that the latter is not an exclusionary predictive biomarker as exemplified in NSCLC, metastatic renal cell carcinoma (mRCC), colorectal, and anal cancer still warrants better understanding of the host immune system as well as the tumor microenvironment.[239] Indeed, the presence and phenotype of immune cells both in the center of the tumor and the invasive margin is very informative. The immunoscore, as developed by Galon et al.,[257] depends on the number and localization of cytotoxic T cells in the tumor and is the strongest prognostic factor for DFS and overall survival in colorectal cancer (CRC). Although first described in CRC, the impact of the immunoscore has been demonstrated in many other human tumors and appears to be a general phenomenon.[258,259] Also the presence of Tregs,[260] tumor-associated macrophages,[261] and MDSC[262] might help clarify why a certain treatment is not efficacious, while indicating that the immune suppressive environment in the tumor is too strong.

During the last decade, biomedical technologies have undergone an explosive evolution. The widespread availability of next-generation genomic sequencing has opened the door to the development of precision oncology. Steadily, cellular and molecular mechanisms of tumorigenesis are being unraveled and the relevance of the microenvironment in the primary tumor is being acknowledged and understood leading to the clinical trial design with incorporation of more biomarkers, a more widespread use of NGS[263] and implementation of new (molecular) imaging technologies and immunohistochemistry (IHC) on tumor biopsies.[264]

2.20.6.3 Combination of Technologies

In the preceding sections we have highlighted important tools in translation research, for example, biomarkers, imaging, or animal models. While each of these tools helps to enhance translatability of findings from the preclinical to the clinical stage, it is the combination of these technologies that is really powerful.

Imaging has shown its power in translational research since it allows for visualization and quantification of (patho)physiological processes in vivo across species. However, the quality of the information obtained through imaging highly depends on the setting from which it was derived. For instance, many animal imaging studies are performed with anesthetized animals, well knowing that anesthesia by itself may have profound effects on general brain activity. An NHP study has demonstrated that the effects of buprenorphine in a nonanesthetized monkey were comparable to that seen clinically while in an anesthetized animal there was hardly any effect visible.[265] More importantly, the quality of imaging depends strongly on the validation of the imaging markers used. While a poorly validated marker may translate well from animals to human, the qualitative information may still be poor in both the animal and the clinical setting. Thus, it is the combination of a well-validated animal model and imaging that yields translatable and meaningful information.

Imaging and biomarkers are particularly useful especially when combined in an animal model to qualify markers for the discovery and development of new therapies.[266] Brain tumors are notoriously difficult to treat and few therapeutic approaches evaluated in animals have translated into successful therapies. One of the inherent problems of a brain disease is the difficulty to directly measure the pathophysiological processes and disease progression/attenuation in an organ that is probably the least accessible organ of the human body.

Parkinson's disease is one of the most common neurodegenerative disorders affecting up to 2% of the elderly population. A number of symptomatic therapies are available which have mostly been identified and developed with the help of the 6-OHDA model, one of the oldest animal models in neuroscience.[267–269] Since the model involves the destruction of dopaminergic neurons in the nigro-striatal system, all drugs developed so far are dopamine agonists that substitute for the loss of dopamine in the model. While these drugs show some symptomatic efficacy in the model, little progress has been made clinically since the initial introduction of the first of these drugs, L-DOPA, about half a century ago. Most importantly, no drug has yet been identified that affects the progression of the disease or could provide a cure. To overcome the vicious circle whereby validation of an animal model with existing drugs can lead to identification of drugs that are relatively similar thus providing little progress, new models have been developed that include additional markers beyond behavioral parameters.[270] Imaging and biomarkers have been established in animal models and in humans to assess disease severity and progression to higher precision and the hope is that with these combination of translational tools (animal models with imaging and biomarkers), disease modifying therapies can be identified.[271]

2.20.7 Conclusions

In the preceding sections, we have highlighted the various tools that are important for translational research and gave examples on how they have helped others to achieve drug development successes. Furthermore, we have highlighted that these tools need to be part of a strategy rather than to be used in isolation. The most important TM tool is integrative thinking. To summarize we have tried to formulate the key points into the 10 golden rules of TM.

1. Think through your translational research project from the end: what exactly do the results need to be in order to make it a success.
2. Back-translate your ultimate goals into intermediate objectives: what are the key results you need to achieve in order to be reassured that further investments are warranted. For instance, what results need to be achieved in the animal model to be convinced that the following clinical trial will be successful.
3. Select the tools carefully, making sure that they are qualified for the purpose. A biomarker, for instance, can be qualified as a general efficacy marker for a certain disease (e.g., amyloid beta for Alzheimer's disease) but still not be qualified for a specific purpose (e.g., cognitive function in Alzheimer's patients).
4. Assure sufficient qualification of the tool methodology: the best biomarker is useless if you cannot be assured that the way it is measured is reliable.
5. Keep consistency across the different steps: if progression-free survival is to be the main endpoint in a clinical trial, the assessment of tumor size in the animal model as primary endpoint may not be appropriate.
6. Use modeling and simulations in order to use the available results is redundant to create concrete hypothesis for the next stage.
7. Combine tools to evaluate a question based on different biomarkers, with different orthogonal methodologies.
8. Acquire knowledge in the pathophysiological interaction of key players and how one player influences the other, in the context of the expected outcome of a single treatment or the added value of combinations.
9. Get buy-in from all disciplines involved.
10. Learn from failures, that is, if something did not work out as foreseen, for example, a clinical trial endpoint did not show an effect while the animal model correlate did, it might be worthwhile to find out why. It might be that the disease pathophysiology is different or that the endpoint is not equivalent. The failure of one project may become the cornerstone of a successful one.

See also: 2.18. Systems Biology: Methods and Applications. 2.21. Companion Diagnostics: From Biomarkers to Diagnostics. 4.04. Human Pk Prediction and Modeling. 4.15. Emerging Translatable Safety Biomarkers.

References

1. Scannell, J. W.; et al. Diagnosing the Decline in Pharmaceutical R&D Efficiency. *Nat. Rev. Drug Discov.* **2012,** *11* (3), 191–200.
2. Coller, B. S.; Califf, R. M. Traversing the Valley of Death: A Guide to Assessing Prospects for Translational Success. *Sci. Transl. Med.* **2009,** *1* (10), 10cm9.
3. Butler, D. Translational Research: Crossing the Valley of Death. *Nature* **2008,** *453* (7197), 840–842.
4. PriceWaterhouseCoopers. *Pharma 2005—Silicon Rally: The Race to e-R&D,* 2005 (cited Jan 9, 2016). Available from: http://www.pwc.com/gx/en/pharma-life-sciences/pdf/silicon_rally.pdf.
5. Group, B. D. W. Biomarkers and Surrogate Endpoints: Preferred Definitions and Conceptual Framework. *Clin. Pharmacol. Ther.* **2001,** *69* (3), 89–95.
6. Kraus, V. B.; et al. Application of Biomarkers in the Development of Drugs Intended for the Treatment of Osteoarthritis. *Osteoarthr. Cartil.* **2011,** *19* (5), 515–542.
7. Ceriello, A.; et al. Comparison of Effect of Pioglitazone With Metformin or Sulfonylurea (Monotherapy and Combination Therapy) on Postload Glycemia and Composite Insulin Sensitivity Index During an Oral Glucose Tolerance Test in Patients With Type 2 Diabetes. *Diabetes Care* **2005,** *28* (2), 266–272.
8. Teff, K. L.; et al. Antipsychotic-Induced Insulin Resistance and Postprandial Hormonal Dysregulation Independent of Weight Gain or Psychiatric Disease. *Diabetes* **2013,** *62* (9), 3232–3240.
9. Van Roy, M.; et al. The Preclinical Pharmacology of the High Affinity Anti-IL-6R Nanobody(R) ALX-0061 Supports Its Clinical Development in Rheumatoid Arthritis. *Arthritis Res. Ther.* **2015,** *17,* 135.
10. Nishimoto, N.; et al. Mechanisms and Pathologic Significances in Increase in Serum Interleukin-6 (IL-6) and Soluble IL-6 Receptor After Administration of an Anti-IL-6 Receptor Antibody, Tocilizumab, in Patients With Rheumatoid Arthritis and Castleman Disease. *Blood* **2008,** *112* (10), 3959–3964.
11. Yokota, T. Are KRAS/BRAF Mutations Potent Prognostic and/or Predictive Biomarkers in Colorectal Cancers? *Anti Cancer Agents Med. Chem.* **2012,** *12* (2), 163–171.
12. Allred, D. C. Issues and Updates: Evaluating Estrogen Receptor-Alpha, Progesterone Receptor, and HER2 in Breast Cancer. *Mod. Pathol.* **2010,** *23* (Suppl. 2), S52–S59.
13. FDA. *Guidance for Industry and Food and Drug Administration Staff—In Vitro Companion Diagnostic Devices,* 2014 (cited Apr 29, 2016). Available from: http://www.fda.gov/downloads/MedicalDevices/DeviceRegulationandGuidance/GuidanceDocuments/UCM262327.pdf.
14. Reflection Paper on Pharmacogenomic Samples, Testing and Data Handling. EMEA/CHMP/PGxWP/201914/2006, 2006.
15. European Medicines Agency.; Committee for Human Medicinal Products. *Reflection Paper on Pharmacogenomics in Oncology (Draft);* The Agency: London, 2008.
16. European Medicines Agency.; Committee for Human Medicinal Products. *Reflection Paper on Methodological Issues With Pharmacogenomic Biomarkers in Relation to Clinical Development and Patient Selection (Draft);* The Agency: London, 2011, 2011 June. Report No: EMA/446337/2011.
17. European Medicines Agency.; Committee for Human Medicinal Products. *Reflection Paper on Co-Development of Pharmacogenomic Biomarkers and Assays in the Context of Drug Development (Draft);* The Agency: London, 2010, 2010 June. Report No.: EMA/CHMP/641298/2008.
18. European Medicines Agency.; Oncology Working Party. *Guideline on the Evaluation of Anticancer Medicinal Products in Man;* The Agency: London, 2012, 2012 December. Report No.: EMA/CHMP/205/95/Rev.
19. FDA. *Guidance for Industry—E14 Clinical Evaluation of QT/QTc Interval Prolongation and Proarrhythmic Potential for Non-Antiarrhythmic Drugs,* 2005 (cited Apr 29, 2016). Available from: http://www.fda.gov/downloads/drugs/guidancecomplianceregulatoryinformation/guidances/ucm073153.pdf.
20. Campion, S.; et al. The Current Status of Biomarkers for Predicting Toxicity. *Expert Opin. Drug Metab. Toxicol.* **2013,** *9* (11), 1391–1408.

21. Fuchs, T. C.; Hewitt, P. Biomarkers for Drug-Induced Renal Damage and Nephrotoxicity—An Overview for Applied Toxicology. *AAPS J.* **2011,** *13* (4), 615–631.
22. FDA. *Review of Qualification Data for Biomarkers of Nephrotoxicity Submitted by the Predictive Safety Testing Consortium,* 2009 (cited Apr, 29, 2016). Available from: http://www.fda.gov/downloads/Drugs/DevelopmentApprovalProcess/DrugDevelopmentToolsQualificationProgram/UCM382536.pdf.
23. Gross, J. L.; et al. A Novel Model-Based Meta-Analysis to Indirectly Estimate the Comparative Efficacy of Two Medications: An Example Using DPP-4 Inhibitors, Sitagliptin and Linagliptin, in Treatment of Type 2 Diabetes Mellitus. *BMJ Open* **2013,** *3* (3), e001844.
24. FDA. *Innovation or Stagnation: Challenge and Opportunity on the Critical Path to New Medical Products,* 2004 (cited Dec 15, 2015). Available from: http://www.fda.gov/ScienceResearch/SpecialTopics/CriticalPathInitiative/CriticalPathOpportunitiesReports/ucm077262.htm.
25. Amur, S.; et al. Integration and Use of Biomarkers in Drug Development, Regulation and Clinical Practice: A US Regulatory Perspective. *Biomark. Med* **2008,** *2* (3), 305–311.
26. Dancey, J. E.; et al. Guidelines for the Development and Incorporation of Biomarker Studies in Early Clinical Trials of Novel Agents. *Clin. Cancer Res.* **2010,** *16* (6), 1745–1755.
27. Fu, Q.; et al. Multiplex Assays for Biomarker Research and Clinical Application: Translational Science Coming of Age. *Proteomics Clin. Appl.* **2010,** *4* (3), 271–284.
28. Kingsmore, S. F. Multiplexed Protein Measurement: Technologies and Applications of Protein and Antibody Arrays. *Nat. Rev. Drug Discov.* **2006,** *5* (4), 310–320.
29. Grebe, S. K.; Singh, R. J. LC-MS/MS in the Clinical Laboratory—Where to From Here? *Clin. Biochem. Rev.* **2011,** *32* (1), 5–31.
30. Lange, V.; et al. Selected Reaction Monitoring for Quantitative Proteomics: A Tutorial. *Mol. Syst. Biol.* **2008,** *4,* 222.
31. Picotti, P.; Aebersold, R. Selected Reaction Monitoring-Based Proteomics: Workflows, Potential, Pitfalls and Future Directions. *Nat. Methods* **2012,** *9* (6), 555–566.
32. Manes, N. P.; Mann, J. M.; Nita-Lazar, A. Selected Reaction Monitoring Mass Spectrometry for Absolute Protein Quantification. *J. Vis. Exp.* **2015,** *102,* e52959.
33. Hunter, D. J.; et al. A Pathway and Approach to Biomarker Validation and Qualification for Osteoarthritis Clinical Trials. *Curr. Drug Targets* **2010,** *11* (5), 536–545.
34. Wagner, J. A. Overview of Biomarkers and Surrogate Endpoints in Drug Development. *Dis. Markers* **2002,** *18* (2), 41–46.
35. Lee, J. W.; et al. Fit-for-Purpose Method Development and Validation for Successful Biomarker Measurement. *Pharm. Res.* **2006,** *23* (2), 312–328.
36. Cummings, J.; Ward, T. H.; Dive, C. Fit-for-Purpose Biomarker Method Validation in Anticancer Drug Development. *Drug Discov. Today* **2010,** *15* (19–20), 816–825.
37. Wang, J.; et al. "Fit-for-Purpose" Method Validation and Application of a Biomarker (C-Terminal Telopeptides of Type 1 Collagen) in Denosumab Clinical Studies. *AAPS J.* **2009,** *11* (2), 385–394.
38. Bleavins, M. R., Rahbari, R., Jurima-Romet, M., Carini, C., Eds. *Biomarkers in Drug Development: A Handbook of Practice, Application, and Strategy;* John Wiley and Sons, Inc: Hoboken, NJ, 2010.
39. O'Hara, D. M.; et al. Recommendations for the Validation of Flow Cytometric Testing During Drug Development: II Assays. *J. Immunol. Methods* **2011,** *363* (2), 120–134.
40. Seror, R.; et al. EULAR Sjogren's Syndrome Patient Reported Index (ESSPRI): Development of a Consensus Patient Index for Primary Sjogren's Syndrome. *Ann. Rheum. Dis.* **2011,** *70* (6), 968–972.
41. Seror, R.; et al. Validation of EULAR Primary Sjogren's Syndrome Disease Activity (ESSDAI) and Patient Indexes (ESSPRI). *Ann. Rheum. Dis.* **2015,** *74* (5), 859–866.
42. FDA. Biomarker Qualification Program. (cited Jan 11, 2016). Available from: http://www.fda.gov/Drugs/DevelopmentApprovalProcess/DrugDevelopmentToolsQualificationProgram/ucm284076.htm.
43. EMA. Qualification of Novel Methodologies for Medicine Development. (cited Apr 29, 2016). Available from: http://www.ema.europa.eu/ema/index.jsp?curl=pages/regulation/document_listing/document_listing_000319.jsp.
44. Amur, S. G.; et al. Building a Roadmap to Biomarker Qualification: Challenges and Opportunities. *Biomark. Med.* **2015,** *9* (11), 1095–1105.
45. FDA. *Guidance for Industry and FDA Staff—Qualification Process for Drug Development Tools,* 2014. Available from: http://www.fda.gov/downloads/drugs/guidancecomplianceregulatoryinformation/guidances/ucm230597.pdf.
46. EMA. *Qualification of Novel Methodologies for Drug Development: Guidance to Applicants,* 2014 (cited Apr 29, 2016). Available from: http://www.ema.europa.eu/docs/en_GB/document_library/Regulatory_and_procedural_guideline/2009/10/WC500004201.pdf.
47. FDA. *Innovation or Stagnation. Critical Path Opportunities List,* 2006 (cited Jan 9, 2016). Available from: http://www.fda.gov/downloads/ScienceResearch/SpecialTopics/CriticalPathInitiative/CriticalPathOpportunitiesReports/UCM077258.pdf.
48. Sheiner, L. B. Learning Versus Confirming in Clinical Drug Development. *Clin. Pharmacol. Ther.* **1997,** *61* (3), 275–291.
49. Aarons, L. Physiologically Based Pharmacokinetic Modelling: A Sound Mechanistic Basis Is Needed. *Br. J. Clin. Pharmacol.* **2005,** *60* (6), 581–583.
50. Espie, P.; et al. Physiologically Based Pharmacokinetics (PBPK). *Drug Metab. Rev.* **2009,** *41* (3), 391–407.
51. Tsamandouras, N.; Rostami-Hodjegan, A.; Aarons, L. Combining the 'Bottom Up' and 'Top Down' Approaches in Pharmacokinetic Modelling: Fitting PBPK Models to Observed Clinical Data. *Br. J. Clin. Pharmacol.* **2015,** *79* (1), 48–55.
52. Poggesi, I.; Snoeys, J.; Van Peer, A. The Successes and Failures of Physiologically Based Pharmacokinetic Modeling: There Is Room for Improvement. *Expert Opin. Drug Metab. Toxicol.* **2014,** *10* (5), 631–635.
53. Jones, H. M.; Mayawala, K.; Poulin, P. Dose Selection Based on Physiologically Based Pharmacokinetic (PBPK) Approaches. *AAPS J.* **2013,** *15* (2), 377–387.
54. Zhao, P.; et al. Applications of Physiologically Based Pharmacokinetic (PBPK) Modeling and Simulation During Regulatory Review. *Clin. Pharmacol. Ther.* **2011,** *89* (2), 259–267.
55. Huang, S. M.; Rowland, M. The Role of Physiologically Based Pharmacokinetic Modeling in Regulatory Review. *Clin. Pharmacol. Ther.* **2012,** *91* (3), 542–549.
56. Zhao, P.; Rowland, M.; Huang, S. M. Best Practice in the Use of Physiologically Based Pharmacokinetic Modeling and Simulation to Address Clinical Pharmacology Regulatory Questions. *Clin. Pharmacol. Ther.* **2012,** *92* (1), 17–20.
57. Wagner, C.; et al. Application of Physiologically Based Pharmacokinetic (PBPK) Modeling to Support Dose Selection: Report of an FDA Public Workshop on PBPK. *CPT Pharmacometrics Syst. Pharmacol.* **2015,** *4* (4), 226–230.
58. Segre, G. Kinetics of Interaction Between Drugs and Biological Systems. *Farmaco Sci.* **1968,** *23* (10), 907–918.
59. Sheiner, L. B.; et al. Simultaneous Modeling of Pharmacokinetics and Pharmacodynamics: Application to d-Tubocurarine. *Clin. Pharmacol. Ther.* **1979,** *25* (3), 358–371.
60. Meibohm, B.; Derendorf, H. Basic Concepts of Pharmacokinetic/Pharmacodynamic (PK/PD) Modelling. *Int. J. Clin. Pharmacol. Ther.* **1997,** *35* (10), 401–413.
61. Danhof, M.; et al. Mechanism-Based Pharmacokinetic-Pharmacodynamic Modeling: Biophase Distribution, Receptor Theory, and Dynamical Systems Analysis. *Annu. Rev. Pharmacol. Toxicol.* **2007,** *47,* 357–400.
62. Danhof, M.; et al. Mechanism-Based Pharmacokinetic-Pharmacodynamic (PK-PD) Modeling in Translational Drug Research. *Trends Pharmacol. Sci.* **2008,** *29* (4), 186–191.
63. Shoda, L.; et al. The Type 1 Diabetes PhysioLab Platform: A Validated Physiologically Based Mathematical Model of Pathogenesis in the Non-Obese Diabetic Mouse. *Clin. Exp. Immunol.* **2010,** *161* (2), 250–267.
64. Geerts, H.; Roberts, P.; Spiros, A. Assessing the Synergy Between Cholinomimetics and Memantine As Augmentation Therapy in Cognitive Impairment in Schizophrenia. A Virtual Human Patient Trial Using Quantitative Systems Pharmacology. *Front. Pharmacol.* **2015,** *6,* 198.
65. Legendre, A.; et al. *An In Silico Simulator to Study Oscillopathies and Drug Effects in Various Neurologic Disorders. Society for Neuroscience Meeting 2014:* Washington DC. http://www.rhenovia.com/docs/Poster%20SFN%202014-RHENOVIA%20Oscillopathies.pdf.
66. Baillie, R.; et al. Pediatric PK, PhysioPD™ Modeling Analysis of Ursodiol in a Neonate Clinical Trial. *Poster Presentation American Conference on Pharmacometrics (ACOP)* 2011: San Diego, CA.
67. Cortinez, L. I. What is the ke0 and What Does It Tell Me About Propofol? *Anaesthesia* **2014,** *69* (5), 399–402.
68. FDA. *Guidance for Industry: Estimating the Maximum Safe Starting Dose in Initial Clinical Trials for Therapeutics in Adult Healthy Volunteers,* 2005. Available from: http://www.fda.gov/downloads/Drugs/…/Guidances/UCM078932.pdf.
69. Nada, A.; Somberg, J. First-in-Man (FIM) Clinical Trials Post-Tegenero: A Review of the Impact of the TeGenero Trial on the Design, Conduct, and Ethics of FIM Trials. *Am. J. Ther.* **2007,** *14* (6), 594–604.

70. EMEA. *Guideline on Strategies to Identify and Mitigate Risks for First-in-Human Clinical Trials With Investigational Medicinal Products,* 2007. Available from: http://www.ema.europa.eu/docs/en_GB/document_library/Scientific_guideline/2009/09/WC500002988.pdf.
71. Duff, G. W. *Expert Scientific Group on Phase One Clinical Trials: Final Report,* 2006. Available from: http://webarchive.nationalarchives.gov.uk/20130107105354/http:/www.dh.gov.uk/prod_consum_dh/groups/dh_digitalassets/@dh/@en/documents/digitalasset/dh_073165.pd.
72. Lowe, P. J.; et al. On the Anticipation of the Human Dose in First-in-Man Trials From Preclinical and Prior Clinical Information in Early Drug Development. *Xenobiotica* **2007,** *37* (10–11), 1331–1354.
73. Agoram, B. M. Use of Pharmacokinetic/Pharmacodynamic Modelling for Starting Dose Selection in First-in-Human Trials of High-Risk Biologics. *Br. J. Clin. Pharmacol.* **2009,** *67* (2), 153–160.
74. Xu, Y.; et al. Physiologically Based Pharmacokinetic Model to Assess the Influence of Blinatumomab-Mediated Cytokine Elevations on Cytochrome P450 Enzyme Activity. *CPT Pharmacometrics Syst. Pharmacol.* **2015,** *4* (9), 507–515.
75. FDA. Labeling Information Blincyto. Available from: http://www.accessdata.fda.gov/drugsatfda_docs/label/2014/125557lbl.pdf.
76. Iadevaia, S.; et al. Identification of Optimal Drug Combinations Targeting Cellular Networks: Integrating Phospho-Proteomics and Computational Network Analysis. *Cancer Res.* **2010,** *70* (17), 6704–6714.
77. Rullmann, J. A.; et al. Systems Biology for Battling Rheumatoid Arthritis: Application of the Entelos PhysioLab Platform. *Syst. Biol.* **2005,** *152* (4), 256–262.
78. Schmidt, B. J.; et al. Alternate Virtual Populations Elucidate the Type I Interferon Signature Predictive of the Response to Rituximab in Rheumatoid Arthritis. *BMC Bioinformatics* **2013,** *14,* 221.
79. Mahgoub, M. A.; Abd-Elfattah, A. S. Diabetes Mellitus and Cardiac Function. *Mol. Cell. Biochem.* **1998,** *180* (1–2), 59–64.
80. Graff-Guerrero, A.; et al. Evaluation of Antipsychotic Dose Reduction in Late-Life Schizophrenia: A Prospective Dopamine D2/3 Receptor Occupancy Study. *JAMA Psychiatry* **2015,** *72* (9), 927–934.
81. Agid, O.; et al. Striatal vs. Extrastriatal Dopamine D2 Receptors in Antipsychotic Response—A Double-Blind PET Study in Schizophrenia. *Neuropsychopharmacology* **2007,** *32* (6), 1209–1215.
82. Macleod, M. R.; et al. Risk of Bias in Reports of In Vivo Research: A Focus for Improvement. *PLoS Biol.* **2015,** *13* (10), e1002273.
83. Sorge, R. E.; et al. Olfactory Exposure to Males, Including Men, Causes Stress and Related Analgesia in Rodents. *Nat. Methods* **2014,** *11* (6), 629–632.
84. Richter, S. H.; Garner, J. P.; Wurbel, H. Environmental Standardization: Cure or Cause of Poor Reproducibility in Animal Experiments? *Nat. Methods* **2009,** *6* (4), 257–261.
85. Richter, S. H.; et al. Effect of Population Heterogenization on the Reproducibility of Mouse Behavior: A Multi-Laboratory Study. *PLoS One* **2011,** *6* (1), e16461.
86. Gao, H.; et al. High-Throughput Screening Using Patient-Derived Tumor Xenografts to Predict Clinical Trial Drug Response. *Nat. Med.* **2015,** *21* (11), 1318–1325.
87. Richmond, J. Refinement, Reduction, and Replacement of Animal Use for Regulatory Testing: Future Improvements and Implementation Within the Regulatory Framework. *ILAR J.* **2002,** *43* (Suppl.), S63–S68.
88. Leist, M.; Kadereit, S.; Schildknecht, S. Food for Thought… on the Real Success of 3R Approaches. *ALTEX* **2008,** *25* (1), 17–32.
89. Bender, A. T.; et al. Evaluation of a Candidate Anti-Arthritic Drug Using the Mouse Collagen Antibody Induced Arthritis Model and Clinically Relevant Biomarkers. *Am. J. Transl. Res.* **2013,** *5* (1), 92–102.
90. Kuhn, C.; et al. Human CD3 Transgenic Mice: Preclinical Testing of Antibodies Promoting Immune Tolerance. *Sci. Transl. Med.* **2011,** *3* (68), 68ra10.
91. Siolas, D.; Hannon, G. J. Patient-Derived Tumor Xenografts: Transforming Clinical Samples Into Mouse Models. *Cancer Res.* **2013,** *73* (17), 5315–5319.
92. Shultz, L. D.; et al. Humanized Mice for Immune System Investigation: Progress, Promise and Challenges. *Nat. Rev. Immunol.* **2012,** *12* (11), 786–798.
93. Gonzalez, L.; Strbo, N.; Podack, E. R. Humanized Mice: Novel Model for Studying Mechanisms of Human Immune-Based Therapies. *Immunol. Res.* **2013,** *57* (1–3), 326–334.
94. Zhou, Q.; et al. Humanized NOD-SCID IL2rg −/− Mice As a Preclinical Model for Cancer Research and Its Potential Use for Individualized Cancer Therapies. *Cancer Lett.* **2014,** *344* (1), 13–19.
95. Jin, K.; et al. Patient-Derived Human Tumour Tissue Xenografts in Immunodeficient Mice: A Systematic Review. *Clin. Transl. Oncol.* **2010,** *12* (7), 473–480.
96. Weissmuller, S.; et al. TGN1412 Induces Lymphopenia and Human Cytokine Release in a Humanized Mouse Model. *PLoS One* **2016,** *11* (3), e0149093.
97. Oliver, V.; et al. Psychometric Assessment of the Rat Grimace Scale and Development of an Analgesic Intervention Score. *PLoS One* **2014,** *9* (5), e97882.
98. Vrinten, D. H.; Hamers, F. F. 'CatWalk' Automated Quantitative Gait Analysis As a Novel Method to Assess Mechanical Allodynia in the Rat; A Comparison With von Frey Testing. *Pain* **2003,** *102* (1–2), 203–209.
99. Brown, D. C.; et al. A Novel Approach to the Use of Animals in Studies of Pain: Validation of the Canine Brief Pain Inventory in Canine Bone Cancer. *Pain Med.* **2009,** *10* (1), 133–142.
100. Willner, P. Validation Criteria for Animal Models of Human Mental Disorders: Learned Helplessness As a Paradigm Case. *Prog. Neuro-Psychopharmacol. Biol. Psychiatry* **1986,** *10* (6), 677–690.
101. Malkesman, O.; et al. Reverse Translational Strategies for Developing Animal Models of Bipolar Disorder. *Dis. Model Mech.* **2009,** *2* (5–6), 238–245.
102. Sams-Dodd, F. Drug Discovery: Selecting the Optimal Approach. *Drug Discov. Today* **2006,** *11* (9–10), 465–472.
103. Braff, D. L.; et al. Impact of Prepulse Characteristics on the Detection of Sensorimotor Gating Deficits in Schizophrenia. *Schizophr. Res.* **2001,** *49* (1–2), 171–178.
104. Lillrank, S. M.; Lipska, B. K.; Weinberger, D. R. Neurodevelopmental Animal Models of Schizophrenia. *Clin. Neurosci.* **1995,** *3* (2), 98–104.
105. Geyer, M. A. Developing Translational Animal Models for Symptoms of Schizophrenia or Bipolar Mania. *Neurotox. Res.* **2008,** *14* (1), 71–78.
106. Robinson, A. P.; et al. The Experimental Autoimmune Encephalomyelitis (EAE) Model of MS: Utility for Understanding Disease Pathophysiology and Treatment. *Handb. Clin. Neurol.* **2014,** *122,* 173–189.
107. Behan, P. O.; Chaudhuri, A. EAE Is Not a Useful Model for Demyelinating Disease. *Mult. Scler. Relat. Disord.* **2014,** *3* (5), 565–574.
108. Sriram, S.; Steiner, I. Experimental Allergic Encephalomyelitis: A Misleading Model of Multiple Sclerosis. *Ann. Neurol.* **2005,** *58* (6), 939–945.
109. t Hart, B. A. Reverse Translation of Failed Treatments Can Help Improving the Validity of Preclinical Animal Models. *Eur. J. Pharmacol.* **2015,** *759,* 14–18.
110. Hart, B. A.; et al. Improvement of Preclinical Animal Models for Autoimmune-Mediated Disorders via Reverse Translation of Failed Therapies. *Drug Discov. Today* **2014,** *19* (9), 1394–1401.
111. Guerreiro-Cacais, A. O.; et al. Translational Utility of Experimental Autoimmune Encephalomyelitis: Recent Developments. *J. Inflamm. Res.* **2015,** *8,* 211–225.
112. Smith, J. J.; Sorensen, A. G.; Thrall, J. H. Biomarkers in Imaging: Realizing Radiology's Future. *Radiology* **2003,** *227* (3), 633–638.
113. Prescott, J. W. Quantitative Imaging Biomarkers: The Application of Advanced Image Processing and Analysis to Clinical and Preclinical Decision Making. *J. Digit. Imaging* **2013,** *26* (1), 97–108.
114. Radiology, E. S.o. White Paper on Imaging Biomarkers. *Insights Imaging* **2010,** *1* (2), 42–45.
115. Bleavins, M. R.; et al. Biomarkers. In *Pharmaceutical Sciences Encyclopedia*; vol. 37; John Wiley & Sons: New York, NY, 2010, ; pp 1–18.
116. Bioengineering, N.I.o.B.I.a. Magnetic Resonance Imaging (MRI) (cited Apr 29, 2016). Available from: https://www.nibib.nih.gov/science-education/science-topics/magnetic-resonance-imaging-mri.
117. Vaquero, J. J.; Kinahan, P. Positron Emission Tomography: Current Challenges and Opportunities for Technological Advances in Clinical and Preclinical Imaging Systems. *Annu. Rev. Biomed. Eng.* **2015,** *17,* 385–414.
118. Cherry, S. R.; Gambhir, S. S. Use of Positron Emission Tomography in Animal Research. *ILAR J.* **2001,** *42* (3), 219–232.
119. Hillman, E. M.; et al. In Vivo Optical Imaging and Dynamic Contrast Methods for Biomedical Research. *Philos. Trans. A Math. Phys. Eng. Sci.* **2011,** *369* (1955), 4620–4643.
120. Hillman, E. M. Optical Brain Imaging In Vivo: Techniques and Applications From Animal to Man. *J. Biomed. Opt.* **2007,** *12* (5), 051402.
121. Zhang, X.; et al. Near-Infrared Molecular Probes for in vivo Imaging. *Curr. Protoc. Cytom.* **2012,** Unit12 27. Editorial board, Paul Robinson, J.; managing editor… [et al.], (Chapter 12).

122. Sommer, O. J.; et al. Rheumatoid Arthritis: A Practical Guide to State-of-the-Art Imaging, Image Interpretation, and Clinical Implications. *Radiographics* **2005,** *25* (2), 381–398.
123. Boini, S.; Guillemin, F. Radiographic Scoring Methods As Outcome Measures in Rheumatoid Arthritis: Properties and Advantages. *Ann. Rheum. Dis.* **2001,** *60* (9), 817–827.
124. Guermazi, A.; et al. Imaging of Bone Erosion in Rheumatoid Arthritis. *Semin. Musculoskelet. Radiol.* **2004,** *8* (4), 269–285.
125. Ory, P. A. Interpreting Radiographic Data in Rheumatoid Arthritis. *Ann. Rheum. Dis.* **2003,** *62* (7), 597–604.
126. He, H.; et al. Contrast-Enhanced Computed Tomography Evaluation of Hepatic Metastases in Breast Cancer Patients Before and After Cytotoxic Chemotherapy or Targeted Therapy. *Can. Assoc. Radiol. J.* **2015,** *66* (4), 356–362.
127. Salem, K. A.; et al. X-Ray Computed Tomography Methods for In Vivo Evaluation of Local Drug Release Systems. *IEEE Trans. Med. Imaging* **2002,** *21* (10), 1310–1316.
128. Niendorf, T.; et al. Advancing Cardiovascular, Neurovascular, and Renal Magnetic Resonance Imaging in Small Rodents Using Cryogenic Radiofrequency Coil Technology. *Front. Pharmacol.* **2015,** *6,* 255.
129. Lodygensky, G. A.; Inder, T. E.; Neil, J. J. Application of Magnetic Resonance Imaging in Animal Models of Perinatal Hypoxic-Ischemic Cerebral Injury. *Int. J. Dev. Neurosci.* **2008,** *26* (1), 13–25.
130. van de Looij, Y.; et al. Advanced Magnetic Resonance Spectroscopy and Imaging Techniques Applied to Brain Development and Animal Models of Perinatal Injury. *Int. J. Dev. Neurosci.* **2015,** *45,* 29–38.
131. Lin, J. B.; et al. Imaging of Small Animal Peripheral Artery Disease Models: Recent Advancements and Translational Potential. *Int. J. Mol. Sci.* **2015,** *16* (5), 11131–11177.
132. Wagner, C. C.; Langer, O. Approaches Using Molecular Imaging Technology—Use of PET in Clinical Microdose Studies. *Adv. Drug Deliv. Rev.* **2011,** *63* (7), 539–546.
133. Schou, M.; et al. Large Variation in Brain Exposure of Reference CNS Drugs: A PET Study in Nonhuman Primates. *Int. J. Neuropsychopharmacol.* **2015,** *18* (10), pyv036.
134. Falcoz, C.; et al. *PKPD Modeling of Brain Receptor Occupancy From Animal to Man for Establishing the Clinical Dose of the NK-1 Antagonist LY686017. Poster Presentation in Pharmacokinetics UK Meeting 2008*: London, UK. http://www.pharsight.com/library/Falcoz-Kielbasa%20Poster%20PKUK%202008%20%5BNK1%5D.pdf.
135. van Waarde, A. Measuring Receptor Occupancy With PET. *Curr. Pharm. Des.* **2000,** *6* (16), 1593–1610.
136. Zhang, Y.; Fox, G. B. PET Imaging for Receptor Occupancy: Meditations on Calculation and Simplification. *J. Biomed. Res.* **2012,** *26* (2), 69–76.
137. Lim, K. S.; et al. Modeling of Brain D2 Receptor Occupancy-Plasma Concentration Relationships With a Novel Antipsychotic, YKP1358, Using Serial PET Scans in Healthy Volunteers. *Clin. Pharmacol. Ther.* **2007,** *81* (2), 252–258.
138. Zamuner, S.; et al. Adaptive-Optimal Design in PET Occupancy Studies. *Clin. Pharmacol. Ther.* **2010,** *87* (5), 563–571.
139. Abanades, S.; et al. Prediction of Repeat-Dose Occupancy From Single-Dose Data: Characterisation of the Relationship Between Plasma Pharmacokinetics and Brain Target Occupancy. *J. Cereb. Blood Flow Metab.* **2011,** *31* (3), 944–952.
140. Fischer, K.; et al. Noninvasive Nuclear Imaging Enables the in vivo Quantification of Striatal Dopamine Receptor Expression and Raclopride Affinity in Mice. *J. Nucl. Med.* **2011,** *52* (7), 1133–1141.
141. Johnson, M.; et al. Mechanism-Based Pharmacokinetic-Pharmacodynamic Modeling of the Dopamine D2 Receptor Occupancy of Olanzapine in Rats. *Pharm. Res.* **2011,** *28* (10), 2490–2504.
142. Kozielska, M.; et al. Pharmacokinetic-Pharmacodynamic Modeling of the D(2) and 5-HT (2A) Receptor Occupancy of Risperidone and Paliperidone in Rats. *Pharm. Res.* **2012,** *29* (7), 1932–1948.
143. Couto, P. J.; Millis, R. M. PET Imaging of Epigenetic Influences on Alzheimer's Disease. *Int. J. Alzheimers Dis.* **2015,** *2015,* 575078.
144. Waldron, A. M.; et al. In Vivo Molecular Neuroimaging of Glucose Utilization and Its Association With Fibrillar Amyloid-Beta Load in Aged APPPS1-21 Mice. *Alzheimers Res. Ther.* **2015,** *7* (1), 76.
145. Wagner, C. C.; et al. A Combined Accelerator Mass Spectrometry-Positron Emission Tomography Human Microdose Study With 14C- and 11C-Labelled Verapamil. *Clin. Pharmacokinet.* **2011,** *50* (2), 111–120.
146. van der Veldt, A. A.; et al. Toward Prediction of Efficacy of Chemotherapy: A Proof of Concept Study in Lung Cancer Patients Using [(1)(1)C]Docetaxel and Positron Emission Tomography. *Clin. Cancer Res.* **2013,** *19* (15), 4163–4173.
147. Plisson, C.; et al. 11C-GSK189254: A Selective Radioligand for in vivo Central Nervous System Imaging of Histamine H3 Receptors by PET. *J. Nucl. Med.* **2009,** *50* (12), 2064–2072.
148. Ashworth, S.; et al. Evaluation of 11C-GSK189254 As a Novel Radioligand for the H3 Receptor in Humans Using PET. *J. Nucl. Med.* **2010,** *51* (7), 1021–1029.
149. Brooks, D. J. Positron Emission Tomography and Single-Photon Emission Computed Tomography in Central Nervous System Drug Development. *NeuroRx* **2005,** *2* (2), 226–236.
150. Agdeppa, E. D.; Spilker, M. E. A Review of Imaging Agent Development. *AAPS J.* **2009,** *11* (2), 286–299.
151. Wang, C.; Schroeder, F. A.; Hooker, J. M. Visualizing Epigenetics: Current Advances and Advantages in HDAC PET Imaging Techniques. *Neuroscience* **2014,** *264,* 186–197.
152. Jennings, M.; Marcu, L. G.; Bezak, E. PET-Specific Parameters and Radiotracers in Theoretical Tumour Modelling. *Comput. Math. Methods Med.* **2015,** *2015,* 415923.
153. Sheikhbahaei, S.; et al. Diagnostic Accuracy of Follow-Up FDG PET or PET/CT in Patients With Head and Neck Cancer After Definitive Treatment: A Systematic Review and Meta-Analysis. *AJR Am. J. Roentgenol.* **2015,** *205* (3), 629–639.
154. Goense, L.; et al. Diagnostic Performance of (1)(8)F-FDG PET and PET/CT for the Detection of Recurrent Esophageal Cancer After Treatment With Curative Intent: A Systematic Review and Meta-Analysis. *J. Nucl. Med.* **2015,** *56* (7), 995–1002.
155. ESR. White Paper on Imaging Biomarkers. *Insights imaging* **2010,** *1* (2), 42–45.
156. Berkhemer, O. A.; et al. A Randomized Trial of Intraarterial Treatment for Acute Ischemic Stroke. *N. Engl. J. Med.* **2015,** *372* (1), 11–20.
157. Smith, W. S. Safety of Mechanical Thrombectomy and Intravenous Tissue Plasminogen Activator in Acute Ischemic Stroke. Results of the Multi Mechanical Embolus Removal in Cerebral Ischemia (MERCI) Trial, Part I. *AJNR Am. J. Neuroradiol.* **2006,** *27* (6), 1177–1182.
158. Catani, M.; ffytche, D. H. The Rises and Falls of Disconnection Syndromes. *Brain* **2005,** *128* (Pt. 10), 2224–2239.
159. Binkofski, F.; et al. Thalamic Metabolism and Corticospinal Tract Integrity Determine Motor Recovery in Stroke. *Ann. Neurol.* **1996,** *39* (4), 460–470.
160. Ahmad, A. S.; et al. Considerations for the Optimization of Induced White Matter Injury Preclinical Models. *Front. Neurol.* **2015,** *6,* 172.
161. Hedna, V. S.; et al. Mechanisms of Arm Paresis in Middle Cerebral Artery Distribution Stroke: Pilot Study. *J. Rehabil. Res. Dev.* **2013,** *50* (8), 1113–1122.
162. Shibata, M.; et al. White Matter Lesions and Glial Activation in a Novel Mouse Model of Chronic Cerebral Hypoperfusion. *Stroke* **2004,** *35* (11), 2598–2603.
163. Llovera, G.; et al. Results of a Preclinical Randomized Controlled Multicenter Trial (pRCT): Anti-CD49d Treatment for Acute Brain Ischemia. *Sci. Transl. Med.* **2015,** *7* (299), 299ra121.
164. Liesz, A.; et al. Inhibition of Lymphocyte Trafficking Shields the Brain Against Deleterious Neuroinflammation After Stroke. *Brain* **2011,** *134* (Pt 3), 704–720.
165. Langhauser, F.; et al. Blocking of Alpha4 Integrin Does Not Protect From Acute Ischemic Stroke in Mice. *Stroke* **2014,** *45* (6), 1799–1806.
166. Strom, J. O.; et al. Method Parameters' Impact on Mortality and Variability in Rat Stroke Experiments: A Meta-Analysis. *BMC Neurosci.* **2013,** *14,* 41.
167. Peng, W.; et al. The Efficacy of Erythropoietin in Treating Experimental Traumatic Brain Injury: A Systematic Review of Controlled Trials in Animal Models. *J. Neurosurg.* **2014,** *121* (3), 653–664.
168. Fisher, M.; et al. Update of the Stroke Therapy Academic Industry Roundtable Preclinical Recommendations. *Stroke* **2009,** *40* (6), 2244–2250.
169. Gibson, C. L.; et al. Progesterone for the Treatment of Experimental Brain Injury; A Systematic Review. *Brain* **2008,** *131* (Pt 2), 318–328.
170. Schumacher, M.; et al. Revisiting the Roles of Progesterone and Allopregnanolone in the Nervous System: Resurgence of the Progesterone Receptors. *Prog. Neurobiol.* **2014,** *113,* 6–39.
171. Shakeri, M.; et al. Effect of Progesterone Administration on Prognosis of Patients With Diffuse Axonal Injury Due to Severe Head Trauma. *Clin. Neurol. Neurosurg.* **2013,** *115* (10), 2019–2022.

172. Xiao, G.; et al. Improved Outcomes From the Administration of Progesterone for Patients With Acute Severe Traumatic Brain Injury: A Randomized Controlled Trial. *Crit. Care* **2008,** *12* (2), R61.
173. Wright, D. W.; et al. Very Early Administration of Progesterone for Acute Traumatic Brain Injury. *N. Engl. J. Med.* **2014,** *371* (26), 2457–2466.
174. Skolnick, B. E.; et al. A Clinical Trial of Progesterone for Severe Traumatic Brain Injury. *N. Engl. J. Med.* **2014,** *371* (26), 2467–2476.
175. Saatman, K. E.; et al. Classification of Traumatic Brain Injury for Targeted Therapies. *J. Neurotrauma* **2008,** *25* (7), 719–738.
176. Baker, K.; Cano, S. J.; Playford, E. D. Outcome Measurement in Stroke: A Scale Selection Strategy. *Stroke* **2011,** *42* (6), 1787–1794.
177. Salter, K.; Richardson, M.; Mehta, S.; Jutai, J.; Zettler, L.; Moses, M.; McClure, A.; Mays, R.; Foley, N.; Teasell, R. *Outcome Measures in Stroke Rehabilitation,* 2013. www.ebrsr.com.
178. Harrison, J. K.; McArthur, K. S.; Quinn, T. J. Assessment Scales in Stroke: Clinimetric and Clinical Considerations. *Clin. Interv. Aging* **2013,** *8,* 201–211.
179. Kahle, M. P.; Bix, G. J. Successfully Climbing the "STAIRs": Surmounting Failed Translation of Experimental Ischemic Stroke Treatments. *Stroke Res. Treat.* **2012,** *2012,* 374098.
180. Seitz, R. J.; Robert, L. Impact of White Matter Damage After Stroke. In *Neuroimaging—Methods;* 2012.
181. Beaulieu, C. The Basis of Anisotropic Water Diffusion in the Nervous System—A Technical Review. *NMR Biomed.* **2002,** *15* (7–8), 435–455.
182. Song, S. K.; et al. Diffusion Tensor Imaging Detects and Differentiates Axon and Myelin Degeneration in Mouse Optic Nerve After Retinal Ischemia. *NeuroImage* **2003,** *20* (3), 1714–1722.
183. Song, J.; et al. DTI Measures Track and Predict Motor Function Outcomes in Stroke Rehabilitation Utilizing BCI Technology. *Front. Hum. Neurosci.* **2015,** *9,* 195.
184. Stoeckel, M. C.; et al. Pattern of Cortex and White Matter Involvement in Severe Middle Cerebral Artery Ischemia. *J. Neuroimaging* **2007,** *17* (2), 131–140.
185. Seitz, R. J.; et al. Lesion Patterns in Successful and Failed Thrombolysis in Middle Cerebral Artery Stroke. *Neuroradiology* **2009,** *51* (12), 865–871.
186. Guo, Y.; Li, P.; Guo, Q.; Shang, K.; Yan, D.; Du, S.; Lu, Y. Pathophysiology and Biomarkers in Acute Ischemic Stroke—A Review. *Trop. J. Pharm. Res.* **2013,** *12* (6), 1097–1105.
187. Kaplan, R. C.; et al. Inflammation and Hemostasis Biomarkers for Predicting Stroke in Postmenopausal Women: The Women's Health Initiative Observational Study. *J. Stroke Cerebrovasc. Dis.* **2008,** *17* (6), 344–355.
188. Laskowitz, D. T.; et al. Clinical Usefulness of a Biomarker-Based Diagnostic Test for Acute Stroke: The Biomarker Rapid Assessment in Ischemic Injury (BRAIN) Study. *Stroke* **2009,** *40* (1), 77–85.
189. Detalle, L.; et al. Generation and Characterization of ALX-0171, a Potent Novel Therapeutic Nanobody for the Treatment of Respiratory Syncytial Virus Infection. *Antimicrob. Agents Chemother.* **2015,** *60* (1), 6–13.
190. Health, U.S.N.I.o. A Multicentre Study in Otherwise Healthy Infants and Toddlers Hospitalised for and Diagnosed With RSV Lower Respiratory Tract Infection to Evaluate the Safety, Tolerability, and Clinical Activity of ALX-0171. 2014 (Dec 1, 2015; Jan 22, 2016). Available from: https://www.clinicaltrials.gov/ct2/show/NCT02309320?term=ALX-0171&rank=4.
191. Friedman, J. N.; Rieder, M. J.; Walton, J. M. Bronchiolitis: Recommendations for Diagnosis, Monitoring and Management of Children One to 24 Months of Age. *Paediatr. Child Health* **2014,** *19* (9), 485–498.
192. Eiland, L. S. Respiratory Syncytial Virus: Diagnosis, Treatment and Prevention. *J. Pediatr. Pharmacol. Ther.* **2009,** *14* (2), 75–85.
193. American Academy of Pediatrics Subcommittee on Diagnosis and Management of Bronchiolitis. Diagnosis and Management of Bronchiolitis. *Pediatrics* **2006,** *118* (4), 1774–1793.
194. Devincenzo, J. P. Natural Infection of Infants With Respiratory Syncytial Virus Subgroups A and B: A Study of Frequency, Disease Severity, and Viral Load. *Pediatr. Res.* **2004,** *56* (6), 914–917.
195. van Miert, C.; et al. Development and Validation of the Liverpool Infant Bronchiolitis Severity Score: A Research Protocol. *J. Adv. Nurs.* **2014,** *70* (10), 2353–2362.
196. DeVincenzo, J. P.; et al. Viral Load Drives Disease in Humans Experimentally Infected With Respiratory Syncytial Virus. *Am. J. Respir. Crit. Care Med.* **2010,** *182* (10), 1305–1314.
197. DeVincenzo, J. P.; El Saleeby, C. M.; Bush, A. J. Respiratory Syncytial Virus Load Predicts Disease Severity in Previously Healthy Infants. *J. Infect. Dis.* **2005,** *191* (11), 1861–1868.
198. Buckingham, S. C.; Bush, A. J.; Devincenzo, J. P. Nasal Quantity of Respiratory Syncytical Virus Correlates With Disease Severity in Hospitalized Infants. *Pediatr. Infect. Dis. J.* **2000,** *19* (2), 113–117.
199. Byrd, L. G.; Prince, G. A. Animal Models of Respiratory Syncytial Virus Infection. *Clin. Infect. Dis.* **1997,** *25* (6), 1363–1368.
200. Bem, R. A.; Domachowske, J. B.; Rosenberg, H. F. Animal Models of Human Respiratory Syncytial Virus Disease. *Am. J. Physiol. Lung Cell. Mol. Physiol.* **2011,** *301* (2), L148–L156.
201. Pickles, R. J.; DeVincenzo, J. P. Respiratory Syncytial Virus (RSV) and Its Propensity for Causing Bronchiolitis. *J. Pathol.* **2015,** *235* (2), 266–276.
202. Scheerlinck, J. P.; et al. Biomedical Applications of Sheep Models: From Asthma to Vaccines. *Trends Biotechnol.* **2008,** *26* (5), 259–266.
203. Meeusen, E. L.; et al. Sheep As a Model Species for the Study and Treatment of Human Asthma and Other Respiratory Diseases. *Drug Discov. Today* **2009,** *6* (4), 101–106.
204. Society, A. T. Mechanisms and Limits of Induced Postnatal Lung Growth. *Am. J. Respir. Crit. Care Med.* **2004,** *170* (3), 319–343.
205. Derscheid, R. J.; Ackermann, M. R. Perinatal Lamb Model of Respiratory Syncytial Virus (RSV) Infection. *Viruses* **2012,** *4* (10), 2359–2378.
206. Derscheid, R. J.; et al. Human Respiratory Syncytial Virus Memphis 37 Causes Acute Respiratory Disease in Perinatal Lamb Lung. *Biores. Open Access* **2014,** *3* (2), 60–69.
207. Larios Mora, A.; et al. Kinetics of Respiratory Syncytial Virus (RSV) Memphis Strain 37 (M37) Infection in the Respiratory Tract of Newborn Lambs As an RSV Infection Model for Human Infants. *PLoS One* **2015,** *10* (12), e0143580.
208. Olivier, A.; et al. Human Respiratory Syncytial Virus A2 Strain Replicates and Induces Innate Immune Responses By Respiratory Epithelia of Neonatal Lambs. *Int. J. Exp. Pathol.* **2009,** *90* (4), 431–438.
209. Van Heeke, G.; et al. Nanobodies® As Inhaled Biotherapeutics for Lung Diseases. *Pharmacol. Ther.* **2016,** *16,* 30102–30104.
210. McElroy, M. C.; et al. Inhaled Biopharmaceutical Drug Development: Nonclinical Considerations and Case Studies. *Inhal. Toxicol.* **2013,** *25* (4), 219–232.
211. Heyder, J.; Svartengren, M. U. Basic Principles of Particle Behavior in the Human Respiratory Tract. In *Drug Delivery to the Lung;* Bisgaard, H., O'Callaghan, C., Smaldone, G. C., Eds.; Marcel Dekker: New York, NY, 2002.
212. Germani, M.; et al. *A Physiologically-Based Pharmacokinetic (PB-PK) Model to Explore ALX-0171 PK in Infants Following Inhalation.* Poster Presentation American Conference on Pharmacometrics (ACOP) 2014: Las Vegas, Nevada, United States. http://www.ablynx.com/uploads/data/files/poster_pbpk_acop2014.pdf.
213. Janssens, H. M.; et al. The Sophia Anatomical Infant Nose-Throat (Saint) Model: A Valuable Tool to Study Aerosol Deposition in Infants. *J. Aerosol Med.* **2001,** *14* (4), 433–441.
214. Dwivedi, G.; et al. A Multiscale Model of Interleukin-6-Mediated Immune Regulation in Crohn's Disease and Its Application in Drug Discovery and Development. *CPT Pharmacometrics Syst. Pharmacol.* **2014,** *3,* e89.
215. Horig, H.; Marincola, E.; Marincola, F. M. Obstacles and Opportunities in Translational Research. *Nat. Med.* **2005,** *11* (7), 705–708.
216. Boumpas, D. T.; et al. A Short Course of BG9588 (Anti-CD40 Ligand Antibody) Improves Serologic Activity and Decreases Hematuria in Patients With Proliferative Lupus Glomerulonephritis. *Arthritis Rheum.* **2003,** *48* (3), 719–727.
217. Couzin, J. Drug Discovery. Magnificent Obsession. *Science* **2005,** *307* (5716), 1712–1715.
218. Shock, A.; et al. CDP7657, an Anti-CD40L Antibody Lacking an Fc Domain, Inhibits CD40L-Dependent Immune Responses Without Thrombotic Complications: An In Vivo Study. *Arthritis Res. Ther.* **2015,** *17,* 234.
219. Tocoian, A.; et al. First-in-Human Trial of the Safety, Pharmacokinetics and Immunogenicity of a PEGylated Anti-CD40L Antibody Fragment (CDP7657) in Healthy Individuals and Patients With Systemic Lupus Erythematosus. *Lupus* **2015,** *24* (10), 1045–1056.

220. van Kooten, C.; Banchereau, J. CD40-CD40 Ligand. *J. Leukoc. Biol.* **2000,** *67* (1), 2–17.
221. Wakefield, I.; et al. An Assessment of theThromboembolic Potential of CDP7657, a Monovalent Fab' PEG Anti-CD40L Antibody, in Rhesus Macaques. *Arthritis Rheum.* **2010,** *62,* 1243. http://dx.doi.org/10.1002/art.29009.
222. Langer, F.; et al. The Role of CD40 in CD40L- and Antibody-Mediated Platelet Activation. *Thromb. Haemost.* **2005,** *93* (6), 1137–1146.
223. Robles-Carrillo, L.; et al. Anti-CD40L Immune Complexes Potently Activate Platelets in vitro and Cause Thrombosis in FCGR2A Transgenic Mice. *J. Immunol.* **2010,** *185* (3), 1577–1583.
224. Mirabet, M.; et al. Platelet Pro-Aggregatory Effects of CD40L Monoclonal Antibody. *Mol. Immunol.* **2008,** *45* (4), 937–944.
225. Deambrosis, I.; et al. Inhibition of CD40-CD154 Costimulatory Pathway By a Cyclic Peptide Targeting CD154. *J. Mol. Med.* **2009,** *87* (2), 181–197.
226. Chamberlain, C.; Soranson, J.; Watling, M.; Colman, P.; Harari, O.; Dorner, T.; Hiepe, F. Repeated Administration of Dapirolizumab Pegol (DZP) Appears Safe and Well Tolerated in Patients With Systemic Lupus Erythematosus (SLE) and Is Accompanied By an Improvement in Disease Activity: Results From a Phase 1 Study. *ACR/ARHP Annual Meeting Abstracts*.
227. Galon, J.; et al. The Continuum of Cancer Immunosurveillance: Prognostic, Predictive, and Mechanistic Signatures. *Immunity* **2013,** *39* (1), 11–26.
228. Leach, D. R.; Krummel, M. F.; Allison, J. P. Enhancement of Antitumor Immunity by CTLA-4 Blockade. *Science* **1996,** *271* (5256), 1734–1736.
229. Delyon, J.; Maio, M.; Lebbe, C. The Ipilimumab Lesson in Melanoma: Achieving Long-Term Survival. *Semin. Oncol.* **2015,** *42* (3), 387–401.
230. Ivashko, I. N.; Kolesar, J. M. Pembrolizumab and Nivolumab: PD-1 Inhibitors for Advanced Melanoma. *Am. J. Health Syst. Pharm.* **2016,** *73* (4), 193–201.
231. Khoja, L.; et al. Pembrolizumab. *J. Immunother. Cancer* **2015,** *3,* 36.
232. Ito, A.; et al. Clinical Development of Immune Checkpoint Inhibitors. *Biomed. Res. Int.* **2015,** *2015,* 605478.
233. Marquez-Rodas, I.; et al. Immune Checkpoint Inhibitors: Therapeutic Advances in Melanoma. *Ann. Transl. Med.* **2015,** *3* (18), 267.
234. Garon, E. B.; et al. Pembrolizumab for the Treatment of Non-Small-Cell Lung Cancer. *N. Engl. J. Med.* **2015,** *372* (21), 2018–2028.
235. Ansell, S. M.; et al. PD-1 Blockade With Nivolumab in Relapsed or Refractory Hodgkin's Lymphoma. *N. Engl. J. Med.* **2015,** *372* (4), 311–319.
236. Hamanishi, J.; et al. Safety and Antitumor Activity of Anti-PD-1 Antibody, Nivolumab, in Patients With Platinum-Resistant Ovarian Cancer. *J. Clin. Oncol.* **2015,** *33* (34), 4015–4022.
237. Segal, N.; et al. Preliminary Data From a Multi-Arm Expansion Study of MEDI4736, an Anti-PD-L1 Antibody. *J. Clin. Oncol.* **2014,** *32* (Suppl. 5s; abstr 3002), 36–144.
238. Angell, H.; Galon, J. From the Immune Contexture to the Immunoscore: The Role of Prognostic and Predictive Immune Markers in Cancer. *Curr. Opin. Immunol.* **2013,** *25* (2), 261–267.
239. Galon, J.; et al. Towards the Introduction of the 'Immunoscore' in the Classification of Malignant Tumours. *J. Pathol.* **2014,** *232* (2), 199–209.
240. Snyder, A.; Chan, T. A. Immunogenic Peptide Discovery in Cancer Genomes. *Curr. Opin. Genet. Dev.* **2015,** *30,* 7–16.
241. Rizvi, N. A.; et al. Cancer Immunology. Mutational Landscape Determines Sensitivity to PD-1 Blockade in Non-Small Cell Lung Cancer. *Science* **2015,** *348* (6230), 124–128.
242. Wagle, N.; et al. Dissecting Therapeutic Resistance to RAF Inhibition in Melanoma By Tumor Genomic Profiling. *J. Clin. Oncol.* **2011,** *29* (22), 3085–3096.
243. Long, G. V.; et al. Combined BRAF and MEK Inhibition Versus BRAF Inhibition Alone in Melanoma. *N. Engl. J. Med.* **2014,** *371* (20), 1877–1888.
244. Tchekmedyian, N.; et al. Propelling Immunotherapy Combinations Into the Clinic. *Oncology* **2015,** *29* (12), 214814.
245. Ansell, S.; Northfelt, D.; Flinn, I.; Burris, H.; Dinner, S.; Villalobos, V.; Sikic, B.; Pilja, L.; Yellin, M.; Keler, T.; Davis, T. A Phase I Study of an Agonist Anti-CD27 Human Antibody (CDX-1127) in Patients With Advanced Hematologic Malignancies or Solid Tumors. *J. Immunother. Cancer* **2013,** *1* (Suppl. 1), P259.
246. Tang, C.; et al. Combining Radiation and Immunotherapy: A New Systemic Therapy for Solid Tumors? *Cancer Immunol. Res.* **2014,** *2* (9), 831–838.
247. Lynch, T. J.; et al. Ipilimumab in Combination With Paclitaxel and Carboplatin As First-Line Treatment in Stage IIIB/IV Non-Small-Cell Lung Cancer: Results From a Randomized, Double-Blind, Multicenter Phase II Study. *J. Clin. Oncol.* **2012,** *30* (17), 2046–2054.
248. Fong, L.; et al. Potentiating Endogenous Antitumor Immunity to Prostate Cancer Through Combination Immunotherapy With CTLA4 Blockade and GM-CSF. *Cancer Res.* **2009,** *69* (2), 609–615.
249. Wolchok, J. D.; et al. Nivolumab Plus Ipilimumab in Advanced Melanoma. *N. Engl. J. Med.* **2013,** *369* (2), 122–133.
250. Pendergrast, W. J., Jr.; Drake, W. P.; Mardiney, M. R., Jr. A Proper Sequence for the Treatment of B16 Melanoma: Chemotherapy, Surgery, and Immunotherapy. *J. Natl. Cancer Inst.* **1976,** *57* (3), 539–544.
251. Drake, C. G. Combination Immunotherapy Approaches. *Ann. Oncol.* **2012,** *23* (Suppl. 8), viii41-6.
252. European Partnership Action Against Cancer consensus group; Josep, M.; Borras, J. M.; Albreht, T.; Audisio, R.; Briers, E.; Casali, P.; Esperou, H.; Grube, B.; Hamoir, M.; Henning, G.; Kelly, J.; Knox, S.; Nabal, M.; Pierotti, M.; Lombardo, C.; van Harten, W.; Poston, G.; Prades, J.; Sant, M.; Travado, L.; Valentini, V.; van de Velde, C.; van den Bogaert, S.; van den Bulcke, M.; van Hoof, E.; van den Neucker, I.; Wilson, R. Policy Statement on Multidisciplinary Cancer Care. *Eur. J. Cancer* **2014,** *50* (3), 475–480.
253. Herbst, R. S.; et al. Lung Master Protocol (Lung-MAP)—A Biomarker-Driven Protocol for Accelerating Development of Therapies for Squamous Cell Lung Cancer: SWOG S1400. *Clin. Cancer Res.* **2015,** *21* (7), 1514–1524.
254. Snyder, A.; et al. Genetic Basis for Clinical Response to CTLA-4 Blockade in Melanoma. *N. Engl. J. Med.* **2014,** *371* (23), 2189–2199.
255. Govindan, R.; et al. Genomic Landscape of Non-Small Cell Lung Cancer in Smokers and Never-Smokers. *Cell* **2012,** *150* (6), 1121–1134.
256. Patel, S. P.; Kurzrock, R. PD-L1 Expression As a Predictive Biomarker in Cancer Immunotherapy. *Mol. Cancer Ther.* **2015,** *14* (4), 847–856.
257. Galon, J.; et al. Cancer Classification Using the Immunoscore: A Worldwide Task Force. *J. Transl. Med.* **2012,** *10,* 205.
258. Ascierto, M. L.; et al. An Immunologic Portrait of Cancer. *J. Transl. Med.* **2011,** *9,* 146.
259. Pages, F.; et al. Immune Infiltration in Human Tumors: A Prognostic Factor That Should Not Be Ignored. *Oncogene* **2010,** *29* (8), 1093–1102.
260. Nishikawa, H.; Sakaguchi, S. Regulatory T Cells in Cancer Immunotherapy. *Curr. Opin. Immunol.* **2014,** *27,* 1–7.
261. Chavez-Galan, L.; et al. Much More Than M1 and M2 Macrophages, There Are Also CD169(+) and TCR(+) Macrophages. *Front. Immunol.* **2015,** *6,* 263.
262. Motallebnezhad, M.; et al. The Immunobiology of Myeloid-Derived Suppressor Cells in Cancer. *Tumour Biol.* **2016,** *37* (2), 1387–1406.
263. Redman, M. W.; Allegra, C. J. The Master Protocol Concept. *Semin. Oncol.* **2015,** *42* (5), 724–730.
264. Miyahira, A. K.; et al. Multidisciplinary Intervention of Early, Lethal Metastatic Prostate Cancer: Report From the 2015 Coffey-Holden Prostate Cancer Academy Meeting. *Prostate* **2016,** *76* (2), 125–139.
265. Seah, S.; et al. Investigation of Cross-Species Translatability of Pharmacological MRI in Awake Nonhuman Primate—A Buprenorphine Challenge Study. *PLoS One* **2014,** *9* (10), e110432.
266. Moffat, B. A.; Galban, C. J.; Rehemtulla, A. Advanced MRI: Translation From Animal to Human in Brain Tumor Research. *Neuroimaging Clin. N. Am.* **2009,** *19* (4), 517–526.
267. Tranzer, J. P.; Thoenen, H. An Electron Microscopic Study of Selective, Acute Degeneration of Sympathetic Nerve Terminals After Administration of 6-Hydroxydopamine. *Experientia* **1968,** *24* (2), 155–156.
268. Ungerstedt, U. 6-Hydroxy-dopamine Induced Degeneration of Central Monoamine Neurons. *Eur. J. Pharmacol.* **1968,** *5* (1), 107–110.
269. Ungerstedt, U.; Arbuthnott, G. W. Quantitative Recording of Rotational Behavior in Rats After 6-Hydroxy-Dopamine Lesions of the Nigrostriatal Dopamine System. *Brain Res.* **1970,** *24* (3), 485–493.
270. Yun, J. W.; Ahn, J. B.; Kang, B. C. Modeling Parkinson's Disease in the Common Marmoset (*Callithrix jacchus*): Overview of Models, Methods, and Animal Care. *Lab. Anim. Res.* **2015,** *31* (4), 155–165.
271. Kalia, L. V.; Kalia, S. K.; Lang, A. E. Disease-Modifying Strategies for Parkinson's Disease. *Mov. Disord.* **2015,** *30* (11), 1442–1450.

2.21 Companion Diagnostics: From Biomarkers to Diagnostics

JT Jørgensen, Dx-Rx Institute, Fredensborg, Denmark
KB Nielsen, Agilent Technologies Inc, Glostrup, Denmark

© 2017 Elsevier Ltd. All rights reserved.

2.21.1	**Introduction**	530
2.21.2	**Companion Diagnostics**	531
2.21.2.1	Terminology and Definitions	531
2.21.2.2	Historical Aspects	531
2.21.3	**Biomarker Discovery**	532
2.21.4	**Assay Development**	532
2.21.4.1	Assay Methodology	533
2.21.4.2	Prototype Assays	533
2.21.4.3	Assay Verification	534
2.21.4.4	Assay Validation	534
2.21.5	**Clinical Development**	535
2.21.5.1	Cutoff Selection	535
2.21.5.2	Clinical Validation	535
2.21.5.2.1	The clinical study design	536
2.21.5.2.2	Basket and umbrella studies	538
2.21.6	**Regulatory Aspects**	539
2.21.6.1	US Regulatory Requirements	540
2.21.6.2	EU Regulatory Requirements	540
2.21.7	**The Impact of the Drug–Diagnostic Codevelopment Model**	540
2.21.8	**Future Trends and Conclusion**	542
References		544

2.21.1 Introduction

Optimally, any drug-development project should rely on an in-depth understanding of the disease biology and the drug mechanism of action. However, we are not there yet, but within a disease area like oncology, the advances in molecular medicine have given us sufficient insight to allow us to practice a more rational drug-development process, which has led to the development of companion diagnostic (CDx) assays. These assays hold the promise of improving the predictability of the drug-development process and being an important tool for the clinical use of the drugs after their approval. For some drugs, the CDx assays have taken up a central role in the development process, and the success of this type of drugs largely depends on the performance of these assays. The CDx assays have the individual patient as a point of reference, and they will be decisive for the move toward a more precise and individualized pharmacotherapy.[1,2]

There is a crucial need for an improvement in the success rate of drug development. The likelihood of regulatory approval for a drug entering phase I seems to be no more than 10%, however, with some variability as regards to disease areas. For infectious diseases, the likelihood of approval has been estimated to 16.7% but is as low as 6.7% for oncology.[3] Such figures greatly influence the productivity of the research and development (R&D) activities in pharma and biotech companies. Based on the low productivity, the head of the European Medicines Agency (EMA), a few years ago, estimated that around 60 billion USD of the 85 billion USD spent on pharmaceutical R&D globally each year was more or less wasted due to the high drug failure rate.[4]

When it comes to the clinical use of drugs, we have recognized that the treatment outcome is subject to great inherent patient variability, which often seems to be of a significant magnitude. Over the last couple of decades, we have learned that drugs are not always as effective as they ought to be and that pharmacotherapy needs to be individualized in order to achieve an improved treatment outcome.[5,6] These considerations have led to an increased focus on "personalized medicine," and the US president Barack Obama's recent announcement of the national Precision Medicine Initiative should be seen in this context.[7]

A CDx is an assay linked to a specific drug, and it is often during the drug discovery phase that the biomarker candidates are identified, which will be tested for their predictive potential later on in the clinical drug-development phases. In this article, we will discuss the individual steps in the development of a CDx assay, from the discovery phase over assay development to analytic and clinical validation. In the last part of the article, we will also discuss the regulatory aspects of CDx and the impact they have had on the drug-development process. However, when it comes to the development of CDx assays, there is one disease area that has been in the forefront, and that is oncology. This will also be reflected in this article as most of the examples given will come from this disease area.

2.21.2 Companion Diagnostics

The term companion diagnostics appears for the first time in the literature in an article published in 2006.[8] This article discussed the state of immunohistochemistry (IHC) and devices available for a quantitative assessment of the human epidermal growth factor receptor 2 (HER2) expression. In this paragraph, we will discuss the different terms and definitions used in relation to CDx assays and briefly touch upon some few historical aspects.

2.21.2.1 Terminology and Definitions

A prerequisite for a CDx assay is the predictive biomarker, so let us start by defining what a biomarker is. In 2001, the Biomarkers Definitions Working Group came up with the following definition: "A characteristic that is objectively measured and evaluated as an indicator of normal biological processes, pathogenic processes, or pharmacological responses to a therapeutic intervention."[9] It is especially the last part of this definition saying that a biomarker can be an objective measure for a pharmacological response to a therapeutic intervention, which is of interest when discussing CDx assays. The predictive property of a biomarker is the key to a CDx assay.

When it comes to the name that describes the predictive biomarker assay developed in parallel to a specific drug and used for preselection of likely responding patients, consensus seems to be lacking. In the literature and guidelines, different names are used, such as pharmacodiagnostics, theranostics, pharmacogenomic biomarkers, and companion diagnostics. However, within the last 5–6 years, the name companion diagnostics is being used more and more frequently. This term was first adapted by the US FDA and subsequently also by EMA and other regulatory agencies.[2,10,11]

In 2014, the US FDA issued a guidance document on *In Vitro Companion Diagnostics Devices* in which a CDx is defined.[12] According to this definition, a CDx assay is an in vitro diagnostic (IVD) device that provides information that is essential for the safe and effective use of a corresponding therapeutic product. Furthermore, the US FDA specifies four areas where a CDx assay could be essential: (1) to identify patients who are most likely to benefit from the therapeutic product; (2) to identify patients likely to be at increased risk of serious adverse reactions as a result of treatment with the therapeutic product; (3) to monitor response to treatment with the therapeutic product for the purpose of adjusting treatment (e.g., schedule, dose, and discontinuation) to achieve improved safety or effectiveness; and finally (4) to identify patients in the population for whom the therapeutic product has been adequately studied and found safe and effective, that is, there is insufficient information about the safety and effectiveness of the therapeutic product in any other population. Overall, these different areas in the US FDA's definition can be summarized as outcome prediction (efficacy and safety) and therapy monitoring. The fourth aspect mentioned in the definition can be regarded as a kind of disclaimer and is related to the type of study design most often used in the clinical validation of the CDx assays, the enrichment study design, which will be discussed later on in this article.

In the European Union (EU), the legal framework for IVD medical devices is under revision, and this also includes CDx assays. In the proposal issued in 2012, CDx is defined as a device specifically intended to select patients with a previously diagnosed condition or predisposition as eligible for a targeted therapy.[13] However, during a revision of the proposed legal framework by the Council of EU Ministers in 2015, this definition was changed, so it is now almost identical to the definition used by the US FDA.[14] If we look at how CDx assays have been used so far, especially the predictive role in relation to drug efficacy has dominated. A definition, proposed already in 2008, which has this focus and is making a link to "personalized medicine," reads as follows: "A pretreatment test performed in order to determine whether or not a patient is likely to respond to a given therapy. This type of test is classified as a predictive test and is a prerequisite for implementation of stratified and personalized medicine."[15]

2.21.2.2 Historical Aspects

Looking at the history of drug development, the first time we see molecular testing becoming an integrated part of the development process was in the 1970s. When the selective estrogen receptor modulator (SERM) tamoxifen (Nolvadex, AstraZeneca) was developed for the treatment of advanced breast cancer, data on estrogen receptor (ER) status were correlated with the treatment outcome. Based on data from a phase II study in patients with metastatic breast cancer, published in 1976, the investigators concluded "a high degree of correlation between response and positive estrogen receptor assay suggests the value of the diagnostic test as a means to select patients for tamoxifen treatment."[2,16] At that time, ER receptor status was measured by a biochemical assay and not as today with the simpler IHC test. With the development of the IHC test, determination of ER status became standard for all patients diagnosed with breast cancer, and today, it is a prerequisite for initiation of endocrine treatment with a SERM or an aromatase inhibitor. Although molecular testing in relation to the development of tamoxifen clearly identified a group of responders, that is, patients with a positive ER status, it was not until the 1990s that the drug–diagnostic codevelopment model really proved its value.

When Genentech developed the monoclonal antibody trastuzumab (Herceptin, Roche/Genentech) for treatment of women with advanced breast cancer who overexpressed HER2, they also developed an IHC assay that could determine the level of HER2 expression in the tumors. During the clinical development phases, this assay was used to preselect the patients for treatment with trastuzumab and, in fact, formed the basis for the enrichment study design as we know it today. The diagnostic company Dako further improved the IHC assay known as HercepTest. On the same day in Sep. 1998, the US FDA, in a new coordinated approval process, approved both the drug and the diagnostic assay simultaneously.[17] HercepTest became the first CDx assay linked to the use

of a specific drug, and the way that Genentech did the parallel development of drug and diagnostic has served as an inspiration to a number of other pharmaceutical and biotech companies and regulatory agencies. When the US FDA issued the concept paper on drug–diagnostic codevelopment in 2005, the inspiration was likewise clear.[18]

2.21.3 Biomarker Discovery

The prerequisite for the drug–diagnostic codevelopment model, as outlined in Fig. 1, is a thorough molecular knowledge of the disease mechanisms and of how the targeted drug in question interacts with these mechanisms. The drug discovery process is often sequential, starting with a characterization and understanding of the disease mechanisms, followed by target identification and then finally lead compound development. However, due to the large amount of data generated during this process, drug discovery has slowly become a nonlinear and iterative process, which can also involve preclinical and even different types of clinical data in a kind of "system pharmacological" approach. Both genetic and nongenetic data can be part of these integrated analyses. The genetic data will often originate from high-throughput technologies, such as next-generation sequencing (NGS), but also phenotypic data and other types of data are used. This type of dataset is often referred to as "big data." It is typically during this process that potential biomarker candidates will be identified, which have to be tested for their predictive potential later on during the preclinical and early clinical phases.[19]

Targeted drugs are designed to interact with or block specific molecular or intracellular pathways often driven by genetic changes of heritable or somatic nature, as we know it from cancer. The success of the drug–diagnostic codevelopment model very much depends on how well these mechanisms are understood and on the strength of the biomarker hypotheses that can be deduced from the knowledge generated mainly during the drug discovery and preclinical phases.[10] During the discovery phase, we often see several different parallel analysis methods applied; however, it is important to notice that the methods used during biomarker discovery are not always the same as the ones used later on in the clinic. Once the biomarkers are identified and characterized, often the simpler and more cost-effective methods will be applied to the samples in the clinic.[20] As stated earlier, it might be not only one hypothesis that is tested through a prototype assay but also sometimes several hypotheses. These hypotheses will then be investigated in parallel using different analytic platforms as described in the next paragraph.

2.21.4 Assay Development

In the former paragraph, we discussed biomarker discovery and underlined the importance of a strong biomarker hypothesis. However, a strong biomarker hypothesis is worthless if the CDx assay does not measure the biomarker in question correctly. In this paragraph, we will discuss assay development from choice of platform, development of prototype assays, and, finally, assay verification and validation. This is done to ensure that the CDx assay is robust and reliable before it undergoes clinical testing.

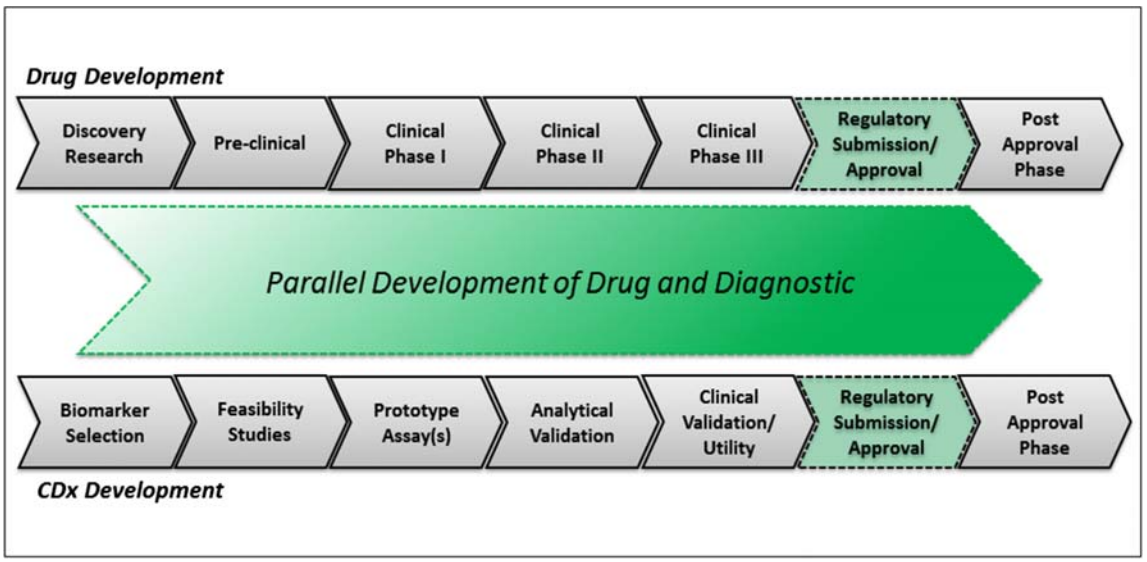

Fig. 1 The drug–diagnostic codevelopment model illustrating the parallel development of drug and CDx with an aligned regulatory submission and approval at the end of phase III.

2.21.4.1 Assay Methodology

The selection of the assay methodology is biomarker-dependent, and the method selected must be relevant for the predictive biomarker in question. The FDA-approved CDx assays analyze variations in the sequence, structure, or expression of deoxyribonucleic acid (DNA) and ribonucleic acid (RNA) or profiling protein expression. The first ER assay used to select a group of breast cancer patients for treatment with tamoxifen was a biochemical assay, as mentioned previously, but this has now been substituted by an IHC assay. The first FDA-approved CDx, HercepTest, was also an IHC assay, but since then, a few other technologies have been used as analytic method for CDx assays. So far, the methods that have been used as CDx assays to identify genetic or protein alterations/abnormalities in human diseases are polymerase chain reaction (PCR), fluorescence in situ hybridization (FISH), DNA sequencing, or IHC. Whereas the IHC assays identify protein expression, the remaining methods are used to analyze various nucleic acid compositions or alterations. The FISH and the IHC methods are semipreservative regarding the tissue morphology and make it possible to evaluate individual cells, whereas the other methods are disruptive to the tissue as some degree of nucleic acid extraction is needed to obtain a result. Both the IHC and FISH methods are single analyses with limited opportunities to multiplex in contrast to the methods based on nucleic acid extraction that can be run as multiplex analyses.

The antibodies used in the IHC assays must be specific and sensitive in recognizing the protein of interest. These antibodies can, for example, target a membrane protein such as HER2 or, more generally, identify the presence of a protein, as seen for other IHC assays.[17,21] The scoring criteria for these assays vary; in one instance, it can be identification of the percentage of positively stained cells and in other instances to identify the presence of a specific protein at a clinically relevant cut point. A pathologist normally performs the scoring of the IHC stained slides, and the method as such is considered to be quantitative or semiquantitative depending on the scoring method and reporting result.

FISH probes can be designed as a copy number evaluating assay such as *HER2* IQFISH pharmDx (Dako) where the gene of interest is targeted by a DNA-specific probe, or it can be used to identify changes on the gene or chromosome level as for the Vysis *ALK* Break Apart FISH probe kit (Abbott Molecular).[22,23] The *HER2* IQFISH pharmDx assay contains both a gene probe that targets the *HER2* gene and a centromeric probe that targets the centromeric region on chromosome 17. The cutoff for the assay is defined as the ratio between the gene copy number and the number of centromeric signals (*HER2*/CEN-17). For the *HER2* IQFISH pharmDx assay, cases with a ratio ≥ 2 are defined as being *HER2* amplified. The break-apart probe uses two probes labeled with different fluorophores (red and green); one probe is targeting the gene in question, whereas the other is targeting a sequence in close proximity to the gene. Under normal conditions, these signals will be close to each other and will appear yellow, but in case of rearrangement, the red and green signal will be identifiable as separate signals. In both types of assays, the specific gene and centromeric signals are enumerated, and the test can be considered quantitative. In case of the copy number enumeration, the ratio is translated into binary results as either positive (ratio greater or equal to the cutoff) or negative (below the cutoff). The *HER2* IQFISH pharmDx assay is linked to the use of the HER2-targeted drugs trastuzumab and in the United States also to the use of pertuzumab (Perjeta, Roche/Genentech) and ado-trastuzumab emtansine (Kadcyla, Roche/Genentech). The Vysis ALK Break Apart FISH probe kit is linked to the use of the ALK inhibitor crizotinib (Xalkori, Pfizer).

PCR is used for mutation analysis as in the case of the Cobas 4800 *BRAF V600* Mutation Test (Roche Molecular Diagnostics).[24] This test will identify if a *BRAF V600E* gene mutation is present or not. The Cobas 4800 *BRAF V600* Mutation Test is linked to the use of the BRAF inhibitor vemurafenib (Zelboraf, Roche/Genentech). The BRACAnalysis CDx (Myriad Genetic Laboratories) uses Sanger sequencing in combination with quantitative PCR to detect single-nucleotide variations and small deletions in the *BRCA1* and *BRCA2* genes.[25] The BRACAnalysis CDx assay is linked to the use of the PARP inhibitor olaparib (Lynparza, AstraZeneca).

The aforementioned methodologies include those that the US FDA have currently approved as CDx, but other methodologies such as immunoassays, enzyme-linked immunosorbent assay (ELISA), and fluorescence-activated cell sorting (FACS) are being tested in clinical settings in the attempt to generate a CDx.[26] Along with PCR, these techniques are becoming key in the process of generating CDx within circulating tumor cells (CTC) as exemplified by the immunoassay Kit CELLSEARCH Circulating Tumor Cell, which is currently the only cleared US FDA method for the clinical detection of CTC for patients with breast, colon, and prostate cancer.[27] The techniques are currently facing difficulties with the heterogeneity of the CTC within individuals, which is a big challenge in the process of analytic validation of the assays.[28]

WILEX has developed a HER-2/neu ELISA assay that has been US FDA-cleared as an IVD blood test for quantifying the serum HER-2/neu level in women with metastatic breast cancer as a criterion for a suitable therapy.[29,30]

2.21.4.2 Prototype Assays

When the assay methodology has been decided, feasibility of the selected CDx assay must be tested to document that the alterations in sequence, structure, or expression profile of the biomarker can be correctly identified. The first and foremost question to be answered is whether or not it is possible to develop a CDx assay for the selected biomarker.

This work includes selection of suitable antibodies, probes, primers, or sequences depending on selected assay methodology. Part of this is testing the assay's ability to identify the biomarker in a reliable way in all clinically relevant sample types. Also, the sampling and the potential method of fixation of tissue are being tested as these preanalytic processes can have large impact on the performance of the assay. Another important aspect of the initial phases of the CDx development is to establish the assay sensitivity and specificity for the detection of the relevant biomarker in patient specimens. The other part of the feasibility phase is to

demonstrate that the biomarker is relevant for predicting the efficacy of the drug in patients. This requires a thorough understanding of the biology of the disease and drug mechanism of action—as described in the previous paragraph. The design control is also established during the feasibility testing.

Once the characterization of the assay feasibility has been established, a prototype assay can be developed. The assay protocol should include all information on how to perform the test, including how to obtain and prepare the patient samples, test parameter setting, interpretation, and documentation of assay results. Additionally, the shelf lives and storage conditions must also be tested and documented for all kit components including both chemicals and biologicals. The acceptable ranges for pH, concentrations, temperatures, and reaction times also need to be established. If automation is being applied, the performance of the assay on the equipment must be described in detail, including operational specifications and calibration.

These activities are generated under design control to ensure that the documentation of the assay development process is captured and documented correctly. As a minimum, the assay design specifications should include the definitions of sensitivity and specificity, the disease in question, tissue type, and interpretation guidelines and/or scoring criteria. Furthermore, potential positive and negative controls should be tested and established. The purpose of these controls is to identify whether or not the assay performance is acceptable. The controls can be internal or external controls depending on the selected method. A data report form is established to ensure that the intended data is collected during the testing phases and when the prototype assay later on is applied to the patient samples in the clinical trials.

2.21.4.3 Assay Verification

The next phase of the prototype assay development is the analytic verification, which is performed to test the assay parameters that were identified during the feasibility phase. A number of assay robustness studies are conducted including assay stability (accelerated), reproducibility, and repeatability. The main parts of these studies are performed following development of the analytically validated assay. The outcome of the verification phase is a set of test parameters that are used to confirm or revise the assays' Instructions for Use.

During analytic verification, the prototype assay is tested, and the range for a positive test result is identified. The knowledge generated during the verification process serve as the basis for the transfer of the assay into the large-scale production environment. A prototype assay can be used in early clinical trials either retrospectively or prospectively depending on the amount of documentation available on its performance.

2.21.4.4 Assay Validation

According the US FDA, validation of a medical device means confirmation by examination and provision of objective evidence that the particular requirements for a specific intended use can be consistently fulfilled.[31] Before the analytic validation of a CDx assay can be initiated, there is an important task that needs to be clarified, which is the selection of the clinical cutoff. This is needed for the final configuration of the assay, which also includes potential positive and negative controls. The cutoff, or decision point for the identification of biomarker-positive or biomarker-negative patients, is based on outcome data obtained in earlier stage clinical trials and must be linked to the efficacy of the drug. The cutoff is also needed prior to entering the final clinical validation of the CDx assay as described in more details in the next paragraph. Furthermore, if a CDx assay is used prospectively for the selection of patients in a phase II or III pivotal trial, it is strongly recommended that it has been analytically validated.

The final configured assay must be produced under good manufacturing practice where the processes used to manufacture the assay have been through process validation.[31–33] This is to ensure that the assay produced in the new environment meets the predetermined product specifications. The analytic validation of the assay is performed in order to establish objective evidence that the specifications conform to the user needs and the intended use(s).[31] The final assay configuration and design are validated through generation of data on accuracy, technical sensitivity and specificity, robustness (tolerance), and precision/internal reproducibility (intra-assay, inter-assay, interlot variability, interreader variability, and interinstrumentation variability). Finally, an external analytic validation study is performed to document reproducibility (day-to-day, interreader, and interlaboratory) at clinical laboratories representing the end user sites.

The sensitivity and specificity testing of the assay is performed in order to confirm absence of cross-reactivity to closely related targets and its ability to identify the specified biomarker in both patient samples and samples from healthy subjects. If the assay is to be released as an IVD test, the shelf life of the assay/kit will be tested during real-time stability.[18] Furthermore, the individual kit components are tested for working stability along with the potential onboard instrument stability. The different analytic and process validation activities are critical to perform in order to ensure that the CDx assay meets its specification requirements; thus, it can be deployed in a safe and effective manner in the clinical setting.

An IVD test can also be developed for use within a single laboratory. This type of assay is called a laboratory-developed test (LDT), and supposing this is a CDx assay, often, it will not have undergone clinical validation, which could be critical in relation to its accuracy. Over the years, the US FDA has identified a number of problems with some high-risk LDTs, including situations where healthcare providers initiated unnecessary treatment or delayed treatment for serious health conditions. Based on this and on other problems identified by the US FDA, they have recently suggested a new framework for approval of high-risk LDTs such as those intended for assessment of treatment eligibility.[34]

2.21.5 Clinical Development

Seen from the CDx assays' point of view, the three most important elements in the drug–diagnostic codevelopment model are (1) the biomarker hypothesis, (2) the analytic validation, and (3) the clinical validity. In this paragraph, we will discuss the clinical development aspects, which will include cutoff selection and the strategies for clinical validation and the demonstration of clinical utility.

2.21.5.1 Cutoff Selection

In the former paragraph, we described how prototype assays were developed in order to test the biomarker hypotheses raised mainly during the discovery and research phases of the drug-development process. These assays will subsequently be tested in preclinical and/or early clinical phase studies in order to get an impression of the predictive potential. If one or more of these hypotheses appear promising, the next step will normally be to finalize the analytic validation of the CDx assay. However, before the analytic validation can start and the pivotal phase II/III studies can be initiated, the clinical cutoff must be selected. The assay cutoff will define what a positive test result and negative test result are and will transform the CDx assay into a clinical useful tool, which enables it to distinguish between likely responders and nonresponders to the drug under development.[10,18]

The selection of the assay cutoff is normally based on the test results and clinical outcome data generated in early phase I and II studies. To establish the cutoff for a CDx assay is often a challenging process due to the limited number of data available at this relatively early stage of the clinical development of the drug. One method often used to select an appropriate cutoff is the receiver operating characteristic (ROC) curves, where sensitivity (true positivity) is plotted against 1-specificity (false positivity) for a number of different preliminary selected cutoff points. Subsequently, the area under the curve (AUC) is calculated for the different cutoff points, and the one giving the largest AUC will normally be selected as the final clinical cutoff for the assay.[18] This method was used for selection of the cutoff for the PD-L1 IHC 22C3 pharmDx (Dako) assay, which is the CDx assay for the PD-1 checkpoint inhibitor pembrolizumab (Keytruda, Merck Sharp & Dohme).[35]

The dataset used for the selection of the cutoff for the PD-L1 IHC 22C3 pharmDx assay came from the KEYNOTE-001 study, which was the first larger data set to demonstrate a positive correlation between programmed death-ligand 1 (PD-L1) expression and the outcome following treatment with pembrolizumab in patients with advanced nonsmall cell lung cancer (NSCLC). The KEYNOTE-001 study was a large-scale phase I study aimed to evaluate the safety and efficacy of pembrolizumab in patients with NSCLC and to clinically validate the PD-L1 IHC 22C3 pharmDx assay. The study enrolled a little >500 patients of whom approximately one-third were assigned to a training group and two-thirds to a validation group. The data from the training group were used to define the clinical cutoff for the PD-L1 assay. Based on ROC analyses, a proportion score of $\geq 50\%$ was selected, which corresponds to a PD-L1 membrane expression in at least 50% of the tumor cells. When the treatment outcome data from the validation group were analyzed, applying the selected cutoff value, the results showed that patients with a proportion score $\geq 50\%$ had a higher objective response rate and also longer progression-free and overall survival than patients with a proportion score $<50\%$.[35,36]

The way that the selection of the clinical cutoff for the PD-L1 IHC 22C3 pharmDx assay was done, using data from the KEYNOTE-001 study, is an excellent example of how such an analysis should be performed. The initial relationship between PD-L1 expression and the objective repose rate following treatment with pembrolizumab was established using data from the training group, and based on these data, a cutoff was selected. In order to avoid overfitting, the selected cutoff was then applied on an independent patient dataset from the validation group.

2.21.5.2 Clinical Validation

The main aim of the clinical validation is to demonstrate that the CDx assay is able to detect the biomarkers of interest and to select the patient population of interest. Another aspect, very closely linked to the clinical validation, is the clinical utility, that is, the assay's ability to select a patient population that will experience an improved benefit/risk ratio of the drug in question.[18] In most situations, the clinical studies designed to evaluate the clinical validation of the CDx assay also support its clinical utility.

When the cutoff has been selected, the analytic validation of the CDx assay can be finalized, and subsequently, the pivotal clinical studies can be initiated. The reason why it is important to use the "final version" of the assay for the pivotal clinical studies is that the analytic validation is deemed to assure a correct performance of the assay. However, due to challenges with the alignment and timing of the development of the drug and the CDx assay, it is sometimes tempting to start the clinical study with a prototype assay and then replace it with the analytically validated version later on during the study. Unfortunately, such a strategy is not recommendable as it makes it difficult to interpret the results from the clinical study since it divides the patient into two subpopulations: one population selected with the prototype assay and another selected with the final analytically validated version of the assay. If different versions of the assay have been used in the clinical validation studies, a subsequent bridging study will be needed, which is both resource- and time-demanding. A kind of "golden rule" for the final clinical validation of a CDx assay is to use only *one* version of the assay, which must be the final analytically validated version, and, furthermore, only to use *one* testing site in order to reduce possible interlaboratory variability.[10,37,38]

In the drug–diagnostic codevelopment model, the pivotal phase II and III studies are aimed not only to demonstrate safety and efficacy of the drug but also to clinically validate the CDx assay. In these studies, it must be demonstrated that the assay, with

a relatively high probability, is able to select the responding patients. In this respect, the clinical diagnostic accuracy of the CDx assay is important, and in relation to the individual clinical study designs, the diagnostics metrics such as clinical sensitivity, specificity, positive predictive value (PPV), and negative predictive value (NPV) must be considered. For the drug–diagnostic codevelopment model, several study designs have been proposed; however, not all of them make it possible to calculate these diagnostic metrics.[10] The knowledge about these different metrics is important in order to assess the clinical value of a CDx assay. A low accuracy will lead to a suboptimal selection of the patient population that might benefit from the drug that is linked to the CDx assay. Assay accuracy has also been central in the recent discussion of the predictive value of PD-L1 expression in NSCLC for the selection of patients for treatment with PD-1 checkpoint inhibitors.[36,39]

2.21.5.2.1 The clinical study design

Looking at the list of CDx assays that have been approved through the US FDA premarket approval application (PMA) process, most of these have used the enrichment study design for the clinical validation.[40] Originally, this design is built on the traditional randomized controlled clinical study, however, with an extra step included in relation to the patient selection process. The enrichment design should only be applied if there is clear evidence of a strong relationship between a positive CDx status and the treatment outcome of the new drug under development, for example, from previous conducted preclinical and clinical studies. With this study design, all patients are tested with the CDx assay, but only the CDx-positive patients are enrolled in the study and subsequently randomized to the new drug or the "standard" treatment as outlined in **Fig. 2**.[10]

The advantage of the enrichment study design is that it generally requires a smaller number of patients compared with the traditional randomized study with an all-comers design. The reason for this is that only patients who have a CDx-positive status are enrolled in the trial, thus making the study population more homogeneous by reducing the variability that originate from the nonresponding patients. However, this design allows only the PPV to be calculated and not sensitivity, specificity and NPV, which is definitely a limitation of this design.[10,18] This study design was the one used for the approval of trastuzumab and its corresponding CDx assay. Here, 469 HER2-positive women with metastatic breast cancer where enrolled in a phase III study and then randomized to receive trastuzumab plus chemotherapy or chemotherapy alone.[41] The randomized enrichment study has subsequently been used for the approval of other targeted cancer drugs, such as vemurafenib (Zelboraf, Roche/Genentech) and pertuzumab (Perjeta, Roche/Genentech).

Within the last few years, an even simpler version of the enrichment design has been used in relation to the clinical development of drug–diagnostic combinations, which is the nonrandomized enrichment study as shown in **Fig. 3**.

When crizotinib (Xalkori, Pfizer) was under development for treatment of *ALK*-positive metastatic NSCLC, together with its corresponding CDx assay, the Vysis *ALK* Break Apart FISH probe kit (Abbott Molecular), this very simple clinical study design was used and proved to be successful. When the US FDA approved crizotinib in 2011, it was based on efficacy data from only 255 *ALK*-positive patients with metastatic NSCLC, who were enrolled in two nonrandomized phase I/II studies based on a preselection using the Abbott *ALK* FISH assay.[2,42] The approval of the drug was based on a quite impressive clinical efficacy of crizotinib in the selected *ALK*-positive patients. In the US FDA's medical review, the following was stated: "This new drug application is supported by two single-arm studies (Study A and Study B). Response rate of 50% in Study A and 61% in Study B is higher than any approved single and/or combined chemotherapeutic agent for the treatment of NSCLC along with a favorable safety profile compared to these chemotherapeutic agents is the basis for approval for this application."[43] Even when such a simple study design is used, as the nonrandomized enrichment study, it seems to be acceptable for the clinical evaluation of the CDx assay, if the drug that is linked to its use is sufficiently effective in the selected patient population. However, in cases where the number of patients in the clinical

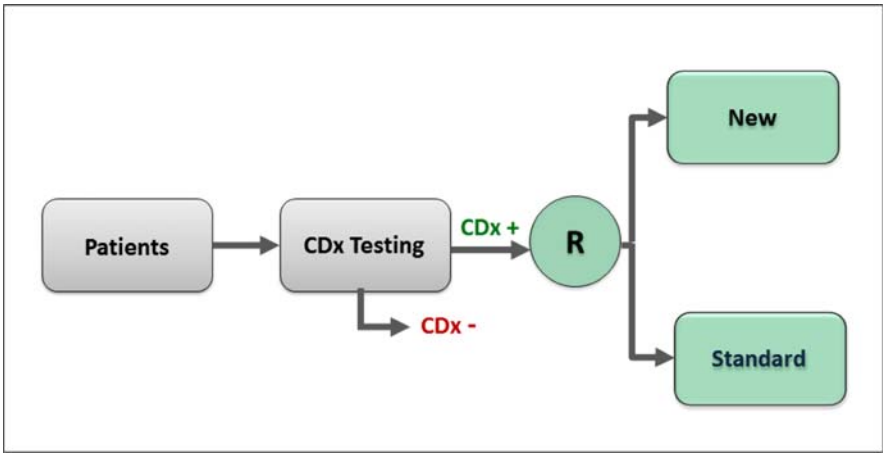

Fig. 2 The randomized enrichment study design. All patients tested positive (CDx+) are randomized (R) to one of the two treatment arms. CDx+ = test-positive patients; CDx− = test-negative patients.

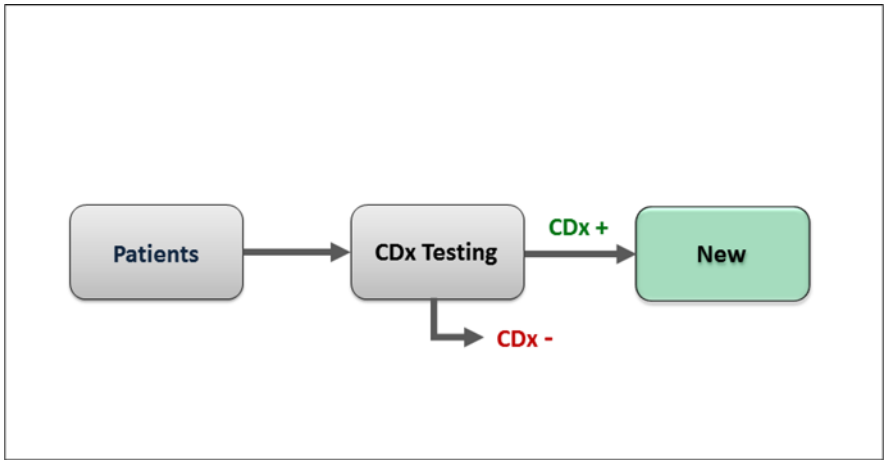

Fig. 3 The nonrandomized enrichment study design. All patients tested positive (CDx+) are treated with the new drug. CDx+=test-positive patients; CDx−=test-negative patients.

development program is as low as it was for crizotinib and the Abbott *ALK* FISH assay, it is reasonable that the regulators require data from the postapproval phase, which was also the case here.[2]

After the regulatory approval of crizotinib, a couple of other ALK inhibitors have achieved US FDA approval based on similar simple study designs in populations of *ALK*-positive patients with metastatic NSCLC. This is the ALK inhibitors ceritinib (Zykadia, Novartis) and alectinib (Alecensa, Roche/Genentech), which were both approved based on efficacy data from <250 patients. For ceritinib, the number of patients was 163, and for alectinib, it was 225.[44,45]

One of the drawbacks of the enrichment study design is that it provides no insight into the efficacy of the drug in the patients who are tested negative with the CDx assay. As previously mentioned, this is also the reason why this design should only be used if there are data available to support a strong relationship between a CDx-positive status and efficacy of the drug. If this type of evidence is weak or nonexisting, an all-comers or a stratified study design should be used.

The all-comers study design, as shown in Fig. 4, does not have positive CDx assay results as part of the inclusion criteria. Both test-positive and test-negative patients are allowed into the study and will be allocated to the two treatment arms as in the traditional randomized controlled study. Most often, this study design is used in phase I or early phase II where there is uncertainty about the link between drug efficacy and the biomarker status. There are both pros and cons in relation to the use of the all-comers study design. One of the positive aspects of this design is that it allows for calculation of the different diagnostic metrics, such as sensitivity, specificity, PPV, and NPV. However, there is also one significant drawback. If the prevalence of test-positive patients is low, it will require a large sample size to reach a conclusion about the predictive potential of the CDx assay.[46]

With the stratified study design, the patients are allocated into a CDx-positive or CDx-negative group based on the assay result and then subsequently randomized to either the new drug or the "standard" treatment as illustrated in Fig. 5. This design is more or less similar to conducting two independent randomized studies, one in the CDx-positive patients and one in the CDx-negative

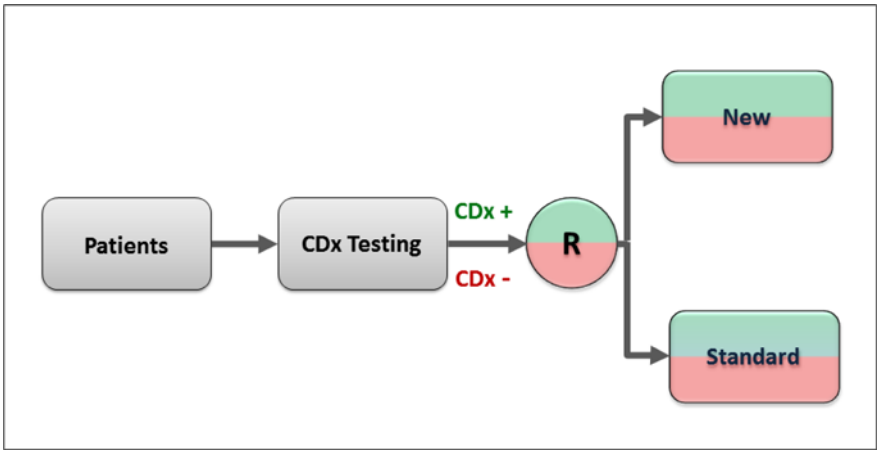

Fig. 4 The all-comers study design. All patients are enrolled in the study independent of a positive or negative CDx status and randomized (R) to one of the two treatment arms. CDx+=test-positive patients; CDx−=test-negative patients.

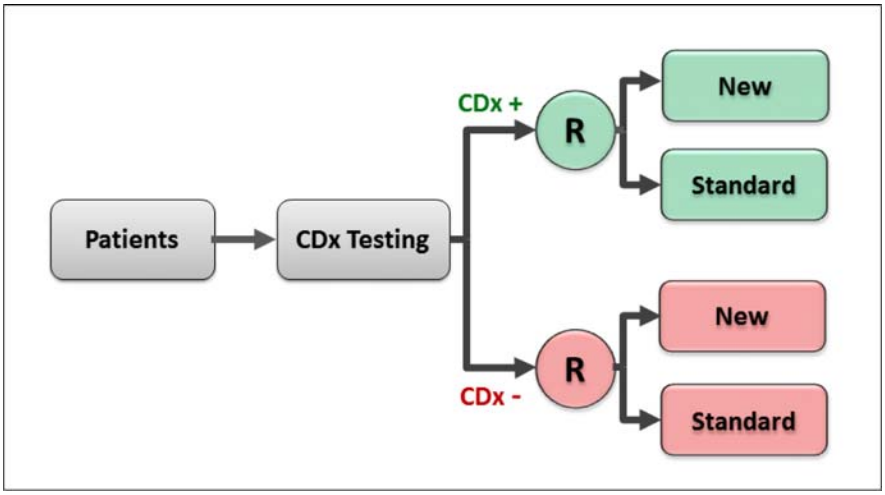

Fig. 5 The stratified study design. All patients are stratified based on the result of the CDx assay and subsequently randomized (R) to one of the two treatment arms. CDx+ = test-positive patients; CDx− = test-negative patients.

patients. However, these studies are conducted simultaneously as one logistic unit. Compared with the all-comers design, it is easier here to manage possible prevalence differences in the test-positive and test-negative patient groups, as they belong to different arms of the study. Furthermore, as for the all-comers study, it is possible to calculate the different diagnostic metrics for the CDx assay.[18,46]

2.21.5.2.2 Basket and umbrella studies

The advances in molecular medicine have provided an increased understanding of the molecular basis for a number of diseases, and especially within cancer, it has led to the development of new drug–diagnostic study designs. Traditionally, cancer diseases have mainly been classified according to the location in body and the histological characteristics; however, the progress within molecular diagnostic and tumor biology has taught us that the same targetable molecular aberration can be detected across different tumor types.[47] An example of this is HER2 overexpression and *BRAF* mutation, which is found in several cancer diseases.[48,49]

The basket study design should be seen as a direct consequence of the evolving new molecular understanding and disease classification within oncology. The assumption for using this study design is that the molecular characteristics prevail over tumor location and histology when it comes to the efficacy of the drug. In this basket study design, the purpose is to test the effect of a single drug related to a single biomarker, measured by a CDx assay, in multiple cancer types. This design allows a simultaneous evaluation of the effect of a specific drug in multiple cancer types with the same specific molecular characteristic, as it is shown in Fig. 6. Such

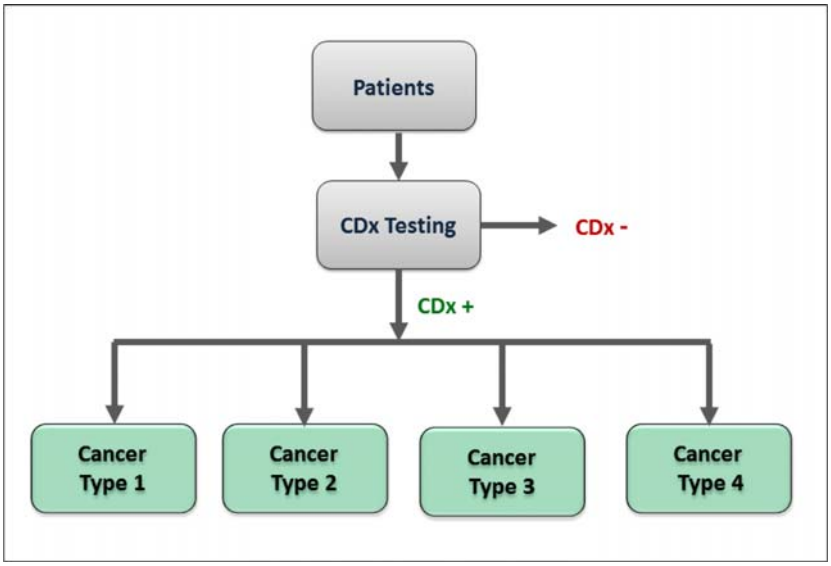

Fig. 6 The basket study design. Testing of one drug in multiple cancer types with one specific molecular characteristic measured by a CDx assay. CDx+ = test-positive patients; CDx− = test-negative patients.

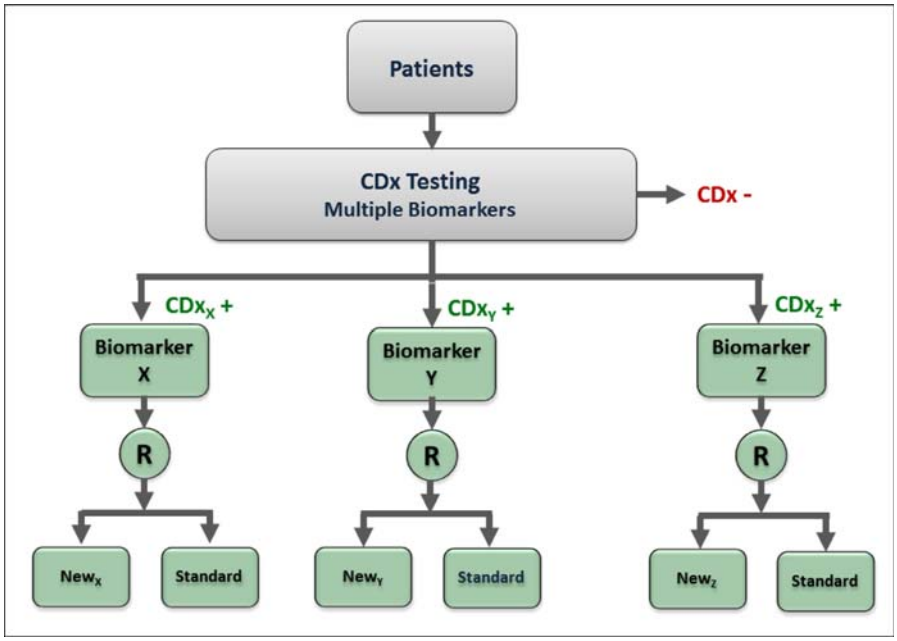

Fig. 7 The umbrella study design. Testing of multiple drugs in a single cancer type with different molecular characteristics measured by different CDx assays. CDx+=test-positive patients; CDx−=test-negative patients.

a study design would be useful in an early explorative phase of the clinical development of a new drug. An example of such study was recently published with the selective BRAF V600 kinase inhibitor, vemurafenib, which was originally developed for treatment of melanoma.[49] In this study, a number of nonmelanoma *BRAF V600* mutation-positive cancer patients were treated with vemurafenib, and the results showed that specifically patients with NSCLC and Erdheim–Chester disease responded to the drug with objective response rates above 40%.

Another new study design that will be described here is the umbrella study. Here, multiple drugs are tested in one cancer type, which is the opposite of the basket study where the effect of one drug is tested in multiple cancer types. To each of the drugs tested in an umbrella study, a specific CDx assay will be used to preselect the patients treated in the different arms of the study as illustrated in Fig. 7. An example of an umbrella study is the National Lung Matrix Trial, which is conducted by Cancer Research UK. In this study, a number of targeted drugs are tested in patients with NSCLC.[50]

2.21.6 Regulatory Aspects

The main purpose of developing a CDx assay in a drug research program is to have a test that can predict whether a patient is likely to benefit from the drug in question. For many of the new cancer drugs that have been developed within the last decade, the CDx assays have taken up a central role as an important stratification factor, both during development and subsequently also after approval when the drug is used routinely in the clinic. For the individual patient, this type of assays has become a kind of "gatekeeper" for the treatment decision.[2,10] However, if a CDx assay measures a specific biomarker but it turns out that it is insufficiently correlated with the clinical state or outcome, it will not provide meaningful results. Such an erroneous test result could lead to either a false-positive or false-negative result, which potentially may cause risk and harm to the patient. For example, a false-positive result could lead to treatment with a drug where the biological condition for a positive outcome is missing, and consequently, the patient will be put at risk due to potential toxic side effects from an ineffective treatment. Similarly, a false-negative test result could withhold a potentially beneficial treatment and thus also bring the patient at risk.[10,31] In oncology, an early and correct diagnosis and intervention are two elements of key importance when treating patients. In case of a wrong treatment decision, the cancer disease may become disseminated with no or very low chances of cure.[10]

With this central role of the CDx assay in mind, it has been argued that the regulatory requirements for these assays should be at the same level as for drugs.[2,51] This was also stressed recently in the interview with professor Daniel Hayes, University of Michigan Comprehensive Cancer Center, a biomarker pioneer, when he stated "a bad tumor biomarker test is as bad as a bad drug." In the same interview, he also expressed that people need to value biomarker tests as much as they value drugs and that researchers should do biomarker studies with the same amount of rigor as therapeutic trials.[52] The critical role of CDx assays in relation to both drug development and the clinical use after approval has also caught the attention of the regulatory authorities. Especially the US FDA has been at the forefront with respect to developing regulatory standards and guidelines for CDx assays and drug–diagnostic codevelopment.[10]

2.21.6.1 US Regulatory Requirements

In the United States, CDx assays are classified as IVD class III products, which according to the regulations are medical devices that usually support or sustain human life, are of substantial importance in preventing impairment of human health, or present a potential, unreasonable risk of illness or injury.[53] Furthermore, an IVD class III product normally requires a PMA application, in order to secure a high standard for both the analytic and clinical performance of the assays. Compared with other types of IVD submissions, the PMA requires the most comprehensive documentation level. The way that CDx assays are classified by the US FDA underlines their central and critical role with regard to the treatment decision for the individual patient.

Over the years, the US FDA has issued several important documents defining the requirements for development of CDx assays. One document, which has already been mentioned in this article, is the *Drug-Diagnostic Co-Development Concept Paper* that was issued already in 2005. This paper must be regarded as a landmark in relation to the drug–diagnostic codevelopment model, and it has served as guidance and inspiration for most CDx assays developed over the past decade.[18] This document was a kind of discussion paper, and on several occasions, the US FDA has announced that they would follow up with a real guideline, but in the beginning of 2016, such a guideline has still not been issued. While anticipating this guideline, the US FDA issued a guidance document on *In vitro Companion Diagnostics Devices* in 2014.[12] However, this guidance document should not be seen as a replacement for the concept paper that came in 2005, but rather an operational guide for pharma and diagnostic companies involved in codevelopment of drugs and diagnostics. This document defined what a CDx assay is and suggested possible regulatory pathways and labeling and other regulatory requirements.[10]

2.21.6.2 EU Regulatory Requirements

The regulatory framework for CDx assays in the EU is the IVD directive 98/79/EC issued in 1998.[54] However, this directive does not mention CDx assays in the definition of an IVD, and likewise, the classification system does not consider CDx assays at all, which, of course, has to do with the age of the directive. Currently, any CDx assay entering the EU market is classified as general IVD, which means low-risk devices, based on an assessment of conformity according to the IVD directive. The manufacturer itself, through the so-called self-certification procedure, performs this conformity assessment and subsequent CE marking. Compared with the PMA approval process in the United States, the EU self-certification procedure must be considered a very different regulatory pathway, which does not to the same extent take into consideration the critical role of the CDx assay in the treatment decision for the individual patient.[10]

In 2012, the European Commission proposed a new regulatory framework that will be more up-to-date with the current thinking when it comes to safety and effectiveness of medical devices, including CDx assays.[13,14] An important change in the proposed legislation is that CDx assays will no longer be considered as low-risk devices and likewise self-certification will no longer be a possibility. According to the new proposal, CDx assays will be classified as class C, which means a high individual risk or moderate public health risk, where an erroneous result would put the patient in an imminent life-threatening situation or would have major negative impact on outcome. It has also been proposed that evidence of the clinical utility of the device for the intended use should be required for CDx assays. Furthermore, it will also be required that the conformity assessment should be performed by an independent notified body and that this notified body also has to consult the EMA or one of the medical product national competent authorities.[11,13,14] Despite the fact that this proposal for a new legislation was put forward in 2012, it has still not been decided when it should be fully implemented, but it is likely to happen before 2020.

2.21.7 The Impact of the Drug–Diagnostic Codevelopment Model

Within oncology, the drug–diagnostic codevelopment model has produced a number of targeted drugs, which has demonstrated surprisingly high efficacy rates in the selected patient populations. In **Table 1** are listed some of these drugs that all have obtained approval within the past 15 years for different advanced or metastatic cancer indications. The objective response rates listed in the table are extracted from the prescribing information available to healthcare professionals in the United States.[55] The majority of the drugs listed in **Table 1** are not classified as chemotherapeutics but rather as targeted drugs, either monoclonal antibodies or small molecules, predominantly tyrosine kinase inhibitors. If these drugs are broken down according to whether they have a CDx assay linked to their use or not, there is a clear trend toward a somewhat higher response rate for the group of drugs with a CDx.[6] The response rates for this group range from 41.0% to 80.2%, while for the group of drugs that have no CDx assay linked to their use, the range is 6.8–45.0%.

It is clear that the drug–diagnostic codevelopment model has produced a number of effective drugs within several cancer diseases with great unmet medical needs, but there seem to be other benefits in relation to use a CDx assay in the drug-development process. When the drug–diagnostic codevelopment model was in its early implementation phase, 8–10 years ago, there was speculation that it could have a major impact on the different aspects of the drug-development process such as success rate, development time, and cost.[56]

One of the first to discuss the potential benefits of the drug–diagnostic codevelopment model and the clinical enrichment study design was Dr. Richard Simon at the US National Cancer Institute, Maryland. In an article published in 2004, he used the pivotal phase III study with trastuzumab, conducted in the late 1990s, to underline the power of the enrichment design.[34,57,58] In this

Table 1 Objective response rates for anticancer drugs with and without a CDx assay linked to their use[a]

Drug	*Indication and biomarker*	*CDx*	*Response rate (%)*
Pertuzumab (Perjeta)	Breast cancer (HER2+)	Yes	80.2
Crizotinib (Xalkori)	NSCLC (*ALK*+)	Yes	65.0
Erlotinib (Tarceva)	NSCLC (*EGFR*+)	Yes	65.0
Cetuximab (Erbitux)	Colorectal cancer (EGFR+/*KRAS*)	Yes	57.0
Imatinib mesylate (Gleevec)	GIST (CD117+)	Yes	53.9
Dabrafenib (Tafinlar)	Melanoma (*BRAF*+)	Yes	52.0
Vemurafenib (Zelboraf)	Melanoma (*BRAF*+)	Yes	48.4
Ado-trastuzumab emtansine (Kadcyla)	Breast cancer (HER2+)	Yes	43.6
Pembrolizumab (Keytruda)	NSCLC (PD-L1+)	Yes	41.0
Bevacizumab (Avastin)	Colorectal cancer	No	45.0
Ixabepilone (Ixempra)	Breast cancer	No	34.7
Paclitaxel protein-bound particles (Abraxane)	NSCLC	No	33.0
Pemetrexed (Alimta)	NSCLC	No	27.1
Pembrolizumab (Keytruda)	Melanoma	No	24.0
Ziv-aflibercept (Zaltrap)	Colorectal cancer	No	19.8
Eribulin mesylate (Halaven)	Breast cancer	No	11.0
Ipilimumab (Yervoy)	Melanoma	No	10.9
Sunitinib malate (Sutent)	GIST	No	6.8

[a]The indications mentioned in the table are for metastatic and/or advanced-stage disease. All drugs listed in the table have obtained FDA approval after 2000.[55]

article, the strength of preselecting patients by means of a CDx assay was illustrated by sample size calculations performed on two alternative clinical study designs—the enrichment and the traditional randomized design or all-comers design.[59] In the pivotal phase III study with trastuzumab, only HER2-positive breast cancer patients were randomized to receive chemotherapy with and without trastuzumab. A total of 469 patients were enrolled, and the result was statistically significant in favor of the trastuzumab arm with regard to 1-year survival.[41] Without the use of a CDx assay for preselection of the patients, a much larger study would have been needed in order to detect the same survival benefit as observed in the phase III study. Dr. Simon used two alternative scenarios of the traditional randomized study design to demonstrate this. In the first one, it was assumed that the effect of trastuzumab in the HER2-negative patients was half the effect observed in HER2-positive patients. The sample size calculation for this scenario showed that the number of patients needed in order to show a significant difference in 1-year survival was 1254 patients. A second scenario was calculated, and again, the traditional randomized study design was used with no preselection with a CDx assay, and the assumption here was that the assay-negative patients had no benefit from treatment with trastuzumab. The sample size needed for this scenario was 8050 patients, which were 17.2 times more patients than were enrolled in the original phase III study.[59] These sample size calculations clearly showed that the number of patients needed would have been dramatically higher, if Genentech had used the traditional randomized study design. It is obvious that the HER2 IHC assay played a critical role in the development of trastuzumab and, in fact, there was speculation that in absence of this assay, we would probably have been without this effective drug today.[59]

Drug development related to HER2-positive breast cancer has also been used to determine the success rate of new drug approvals.[58] A retrospective analysis has looked at industry-sponsored drug-development programs for HER2-positive patients and compared them with programs for patients that either had failed or had been exposed to an anthracycline or taxane. For the period from 1998 to 2012, a number of breast cancer drugs were identified; 29 for HER2-positive patients and 28 for anthracycline/taxane-exposed patients met the inclusion criteria for the analysis. The result of the analysis showed that the overall success rate of drug development in the anthracycline/taxane patients was 15%, while it was 23% in the HER2-positive patients. Furthermore, the analysis also showed that the use of a validated biomarker assay reduced the clinical trial risk by as much as 50%, which could be transformed to a cost saving of 27%.[60]

The impact of the drug–diagnostic codevelopment model on the success rate of drug development has also been demonstrated for other than the HER2-targeted drugs. Similar analyses have been performed on drugs for treatment of metastatic melanoma and NSCLC.[61,62] **Fig. 8** shows the cumulative success rates of the clinical development for melanoma and NSCLC, for drugs with or without a CDx assay linked to their use. The cumulative success rate represents the product of the probability for passing each of the prior phases, from phase I to III, and obtains regulatory approval. The data used in the analyses for melanoma were collected during the period from 1998 to 2013 and for NSCLC from 1998 to 2012.

As it appears from **Fig. 8**, the cumulative success rates for both advanced melanoma and NSCLC are many folds higher for drugs with a CDx compared with the drugs that have entered the clinical development without a CDx assay. The analysis performed in relation to NSCLC lung cancer also looked at the clinical development costs.[62] Here, it was estimated that the risk-adjusted costs for NSCLC clinical development were calculated to be 1.89 billion USD, but this was decreased substantially to 1.40 billion USD if conducted with a CDx assay. Furthermore, the researchers that performed the analysis put forward that the savings could be more significant if the combination of drug and diagnostics could decrease the number of clinical studies needed to obtain marketing approval. This was the situation when the ALK inhibitor crizotinib (Xalkori, Pfizer), which was discussed earlier, obtained

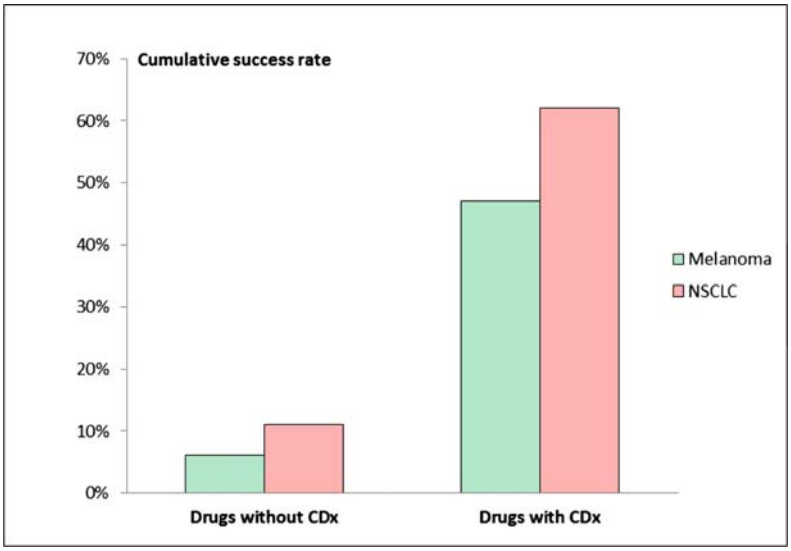

Fig. 8 The cumulative clinical development success rate in advanced melanoma and NSCLC for drugs with and without a CDx assay. The cumulative success rate represents the product of the probability for passing each of the clinical development phases (phases I–III).[60,61]

US FDA approval based on 255 patients from two phase I/II single-arm studies. Based on information from the clinical development program for crizotinib, it was estimated that the cost was between 500 and 600 million USD, which is less than a third of the estimated average cost for the clinical development of NSCLC drugs.[62] Furthermore, it should be added that the development time for crizotinib was extremely short, <4 years.[63] Subsequently, we have witnessed a couple of similar examples of drugs for treatment of advanced NSCLC. As also mentioned previously in this article, these are the ALK inhibitors ceritinib and alectinib, which have recently obtained US FDA approval based on efficacy data from nonrandomized studies with <250 patients. For ceritinib, the data originated from one early-phase study with only 163 patients and for alectinib from two studies with totally 225 patients.[44,45]

To some extent, it seems as if the drug–diagnostic codevelopment model has delivered on some of the expected promises, such as increased development success rates, shorter development times, and decreased costs. However, having said that, the number of drugs that have used the drug–diagnostic codevelopment model is still relatively small, so some reservation is needed in relation to the current data, but in spite of this, there seems to be basis for optimism in relation to the importance of using CDx assays in clinical drug development.

2.21.8 Future Trends and Conclusion

Based on the examples we have from oncology, CDx assays seem to hold the promise in relation to improving the predictability of the drug-development process and to become an important tool for the physician in relation to the choice of treatment for the individual patient as well. As described in this article, a number of drug–diagnostic codevelopment projects have already been completed successfully, and the prescription of a number of targeted cancer drugs is now guided by the result from a CDx assay. Many of the targeted drugs have shown significantly higher response rates and prolonged progression-free survival in selected groups of cancer patients. However, for all these drugs, resistance will develop at some point in time resulting in disease progression. For this reason, it is unlikely that the current approach of single biomarker detection and treatment with one specific drug will achieve long-lasting remission, and most likely, we will need to move away from the "one biomarker–one drug" scenario toward a more complex multimodal approach.[10] This new approach will need to integrate multiple biomarkers and multiple targeted cancer drugs used simultaneously or in sequence in order to block alternative signal pathways and thus prevent resistance to develop. For the CDx assays, this will mean development of specifically designed multiplex assays most likely based on technologies such as gene expression arrays or NGS.[10,64] Another area where the NGS technology will undoubtedly play a role is in relation to "liquid biopsies" and the analysis of freely circulating tumor DNA (ctDNA). Recent research has shown that ctDNA detected in plasma can indicate development of resistance to an ongoing treatment.[65] Similarly, measurement of ctDNA might also be used for monitoring of relapse, as was shown recently in breast cancer.[66]

To some extent, NGS has already moved in the direction toward being a CDx platform. By the end of 2013, the US FDA granted marketing authorization for the Illumina MiSeqDx platform for screening and diagnosis of cystic fibrosis. This platform can also be used to identify cystic fibrosis patients with specific mutations in the cystic fibrosis transmembrane conductance regulator gene that might be eligible for treatment with ivacaftor (Kalydeco, Vertex Pharmaceuticals).[67,68] NGS may also play a role for a group of drugs like antibiotics. Here, antimicrobial susceptibility testing based on detection of phenotypic resistance by measuring bacterial growth

has been used for decades. However, new knowledge with regard to the molecular determinants of antibiotic resistance has facilitated the development of a number of new methods, based on technologies like NGS, PCR, microarray, and mass spectrometry.[69] These new methods are likely to play a critical role in relation to cope with the increasing global problem with antibiotic resistance and in relation to the development of new antiinfectives. Another area outside oncology where we will probably see CDx assay development will be in relation to treatment of rheumatoid arthritis (RA) and other autoimmune diseases. For a disease like RA, early diagnosis and an effective and correct therapy are crucial in order to prevent joint destruction and functional disability. The use of biological targeted agents, such as anti-TNF-α drugs, has significantly improved the outcome for RA patients but approximately one-third of the patients do not respond adequately. A CDx assay that could stratify RA patients into likely responders or nonresponders to the different anti-TNF-α drugs is needed.[1] In the United Kingdom, such an assay is currently under development. It is based on a multiplex platform, and hopefully, it will be able to demonstrate clinical utility and be of benefit to the RA patients.[70]

In order to achieve a more effective and safe pharmacotherapy, we need to individualize the treatment much more than we do today. Today, the prescription of most drugs is essentially based on a trial-and-error approach, and far from all patients respond adequately.[6,71] Especially for patients with severe chronic diseases, this situation needs improvement. Besides the relatively few CDx assays approved by the US FDA for oncology indications, there is a list containing more than 120 additional drugs that have pharmacogenomic biomarker information included in the drug labeling.[72] A large number of these drugs are indicated for severe chronic conditions within cardiology, endocrinology, infectious diseases, neurology, psychiatry, and more. This information could be important in relation to both identifying drug response and avoiding side effects in the individual patient. However, the assays needed for these pharmacogenomic biomarkers are seldom clinically accessible to the same extent as the CDx assays for the oncology drugs, and their application in standard care is still a long way off.[6]

In 1999, Robert Langreth and Michael Waldholz published an article entitled "New Era of Personalized Medicine—Targeting Drugs for Each Unique Genetic Profile" in The Wall Street Journal, which started the discussion on individualizing pharmacotherapy.[73] Now, more than 15 years down the road, we know that it was a new era that started, and we have already seen the first important results.[74] Especially within oncology, we have witnessed a number of breakthrough drugs that have been developed through the drug–diagnostic codevelopment model and where the prescriptions of these drugs now are based on the result from a CDx assay. The efficacy of these drugs clearly outnumbers the more traditional drugs where the prescriptions are based on nonmolecular data, but we also have to realize that there is still a long way to go before the vision of "personalized medicine" will be realized.[6] The development toward a more individualized pharmacotherapy will continue in the decades to come, and "personalized medicine" will be one of the biggest challenges for the pharmaceutical companies and the healthcare system in the 21st century. The promise of "targeting drugs for each unique genetic profile" is still far from being fulfilled, and what we see right now with regard to the implementation of "personalized medicine" is a stepwise approach, and the first step we have named "stratified medicine" or "precision medicine." Here, drug and CDx are very closely linked together, and the test result is used to stratify the patient to the most optimal treatment.[15] The development we have seen within oncology in the last 10–20 years is a clear example of "precision medicine." The move from "blockbuster medicine" toward "personalized medicine" that we currently experience can be illustrated by a staircase as shown in Fig. 9. Currently, we are slowly moving up the staircase toward the middle step, which is "precision medicine." However, the next step toward "personalized medicine" will be much more challenging, and when it comes to CDx assays, it will involve multiplex assays, which will most likely comprise both proteomic and genomic technologies.

In the years to come, we will likely see CDx assays used in relation to other therapeutic areas than oncology, and one of the first new areas is probably the autoimmune diseases. Furthermore, the way that the CDx assays are currently developed is likely to change, both in relation to the discovery phase, where "system pharmacology" and "big data" approaches will be used, and in the development phase where we will see the new clinical study designs gain ground.

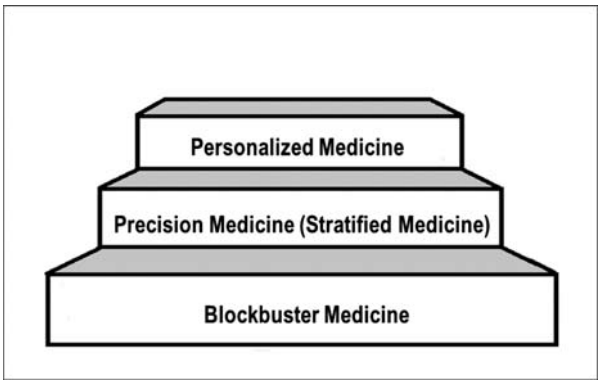

Fig. 9 The move from "blockbuster medicine" toward "personalized medicine" will be stepwise. We are currently on the first step moving toward "precision medicine."

See also: 2.17. Label-Free Screening Technologies. 2.20. Translational Aspects in Drug Discovery. 4.15. Emerging Translatable Safety Biomarkers.

References

1. Jørgensen, J. T. Companion Diagnostics: The Key to Personalized Medicine. *Expert Rev. Mol. Diagn.* **2015,** *15* (2), 153–156.
2. Jørgensen, J. T. Companion Diagnostics in Oncology—Current Status and Future Aspects. *Oncology* **2013,** *85* (1), 59–68.
3. Hay, M.; Thomas, D. W.; Craighead, J. L.; Economides, C.; Rosenthal, J. Clinical Development Success Rates for Investigational Drugs. *Nat. Biotechnol.* **2014,** *32* (1), 40–51.
4. Lancet Editorial: Where Will New Drugs Come From? *Lancet* **2011,** *377* (9760), 97.
5. Schork, N. J. Personalized Medicine: Time for One-Person Trials. *Nature* **2015,** *520* (7549), 609–611.
6. Jørgensen, J. T. Clinical Application of Companion Diagnostics. *Trends Mol. Med.* **2015,** *21* (7), 405–407.
7. Collins, F. S.; Varmus, H. A new Initiative on Precision Medicine. *N. Engl. J. Med.* **2015,** *372* (9), 793–795.
8. Cregger, M.; Berger, A. J.; Rimm, D. L. Immunohistochemistry and Quantitative Analysis of Protein Expression. *Arch. Pathol. Lab. Med.* **2006,** *130* (7), 1026–1030.
9. Biomarkers Definitions Working Group. Biomarkers and Surrogate Endpoints: Preferred Definitions and Conceptual Framework. *Clin. Pharmacol. Ther.* **2001,** *69* (3), 89–95.
10. Olsen, D.; Jørgensen, J. T. Companion Diagnostics for Targeted Cancer Drugs—Clinical and Regulatory Aspects. *Front. Oncol.* **2014,** *4* (105), 1–8.
11. Pignatti, F.; Ehmann, F.; Hemmings, R.; Jonsson, B.; Nuebling, M.; Papaluca-Amati, M.; Posch, M.; Rasi, G. Cancer Drug Development and the Evolving Regulatory Framework for Companion Diagnostics in the European Union. *Clin. Cancer Res.* **2014,** *20* (6), 1458–1468.
12. US FDA. *Guidance for Industry and Food and Drug Administration Staff. in vitro Companion Diagnostic Devices.* August 6, 2014. http://www.fda.gov/downloads/MedicalDevices/DeviceRegulationandGuidance/GuidanceDocuments/UCM262327.pdf (accessed Dec 29, 2015).
13. European Commission. *Proposal for a Regulation of the European Parliament and of the Council on in vitro Diagnostic Medical Devices.* September 26, 2012. http://eur-lex.europa.eu/LexUriServ/LexUriServ.do?uri=COM:2012:0541:FIN:EN:PDF (accessed Dec 29, 2015).
14. European Commission. *Proposal for a Regulation of the European Parliament and of the Council on in vitro Diagnostic Medical Devices.* June 12, 2015. http://data.consilium.europa.eu/doc/document/ST-9770-2015-INIT/en/pdf (accessed April 6, 2016).
15. Jørgensen, J. T. Are We Approaching the Post-Blockbuster Era? Pharmacodiagnostics and Rational Drug Development. *Expert Rev. Mol. Diagn.* **2008,** *8* (6), 689–695.
16. Lerner, H. J.; Band, P. R.; Israel, L.; Leung, B. S. Phase II Study of Tamoxifen: Report of 74 Patients With Stage IV Breast Cancer. *Cancer Treat. Rep.* **1976,** *76* (60), 1431–1435.
17. Jørgensen, J. T.; Winther, H. The Development of the HercepTest—From Bench to Bedside. In *Molecular Diagnostics—The Key Driver of Personalized Cancer Medicine;* Jørgensen, J. T., Winther, H., Eds.; Pan Stanford: Singapore, 2010; pp 43–60.
18. US FDA. *Drug-Diagnostic Co-Development Concept Paper. Draft.* April 2005. http://www.fda.gov/downloads/Drugs/ScienceResearch/ResearchAreas/Pharmacogenetics/ucm116689.pdf (accessed Dec 29, 2015).
19. Anderson, D. C.; Kodukula, K. Biomarkers in Pharmacology and Drug Discovery. *Biochem. Pharmacol.* **2014,** *87* (1), 172–188.
20. Scaros, O.; Fisler, R. Biomarker Technology Roundup: From Discovery to Clinical Applications, a Broad Set of Tools is Required to Translate From the Lab to the Clinic. *Biotechniques* **2005,** *38* (S4), S30–S32.
21. Phillips, T.; Simmons, P.; Inzunza, H. D.; Cogswell, J.; Novotny, J., Jr.; Taylor, C.; Zhang, X. Development of an Automated PD-L1 Immunohistochemistry (IHC) Assay for Non-Small Cell Lung Cancer. *Appl. Immunohistochem. Mol. Morphol.* **2015,** *23* (8), 541–549.
22. Franchet, C.; Filleron, T.; Cayre, A.; Mounié, E.; Penault-Llorca, F.; Jacquemier, J.; Macgrogan, G.; Arnould, L.; Lacroix-Triki, M. Instant-Quality Fluorescence In-Situ Hybridization as a New Tool for HER2 Testing in Breast Cancer: A Comparative Study. *Histopathology* **2014,** *64* (2), 274–283.
23. Shaw, A. T.; Solomon, B.; Kenudson, M. M. Crizotinib and Testing for ALK. *J. Natl. Compr. Canc. Netw.* **2011,** *9* (12), 1335–1341.
24. Halait, H.; Demartin, K.; Shah, S.; Soviero, S.; Langland, R.; Cheng, S.; Hillman, G.; Wu, L.; Lawrence, H. J. Analytical Performance of a Real-Time PCR-Based Assay for V600 Mutations in the BRAF Gene, Used as the Companion Diagnostic Test for the Novel BRAF Inhibitor Vemurafenib in Metastatic Melanoma. *Diagn. Mol. Pathol.* **2012,** *21* (1), 1–8.
25. Gunderson, C. C.; Moore, K. N. BRACAnalysis CDx as a Companion Diagnostic Tool for Lynparza. *Expert Rev. Mol. Diagn.* **2015,** *15* (9), 1111–1116.
26. Meadows, N. A.; Morrison, A.; Brindley, D. A.; Schuh, A.; Barker, R. W. An Evaluation of Regulatory and Commercial Barriers to Stratified Medicine Development and Adoption. *Pharmacogenomics J.* **2015,** *15* (1), 6–12.
27. Negin, B. P.; Cohen, S. J. Circulating Tumor Cells in Colorectal Cancer: Past, Present, and Future Challenges. *Curr. Treat. Options Oncol.* **2010,** *11* (1–2), 1–13.
28. Danila, D. C.; Pantel, K.; Fleisher, M.; Scher, H. I. Circulating Tumors Cells as Biomarkers: Progress Toward Biomarker Qualification. *Cancer J.* **2011,** *17* (6), 438–450.
29. Tchou, J.; Lam, L.; Li, Y. R.; Edwards, C.; Ky, B.; Zhang, H. Monitoring Serum HER2 Levels in Breast Cancer Patients. *Springerplus* **2015,** *4,* 237.
30. Carney, W. P.; Bernhardt, D.; Jasani, B. Circulating HER2 Extracellular Domain: A Specific and Quantitative Biomarker of Prognostic Value in All Breast Cancer Patients? *Biomark. Cancer* **2013,** *5,* 31–39.
31. US FDA. *Code of Federal Regulations. Subchapter H—Medical Devices. Definitions. 21CFR820.3.* April 2015. http://www.accessdata.fda.gov/scripts/cdrh/cfdocs/cfCFR/CFRSearch.cfm?fr=820.3 (accessed Feb 29, 2016).
32. US FDA. *Code of Federal Regulations. Subchapter H—Medical Devices. Process Validation. 21CFR820.75.* April 2015. http://www.accessdata.fda.gov/scripts/cdrh/cfdocs/cfcfr/cfrsearch.cfm?fr=820.75 (accessed Feb 29, 2016).
33. ISO. *Medical Devices—Quality Management Systems—Requirements for Regulatory Purposes.* ISO 13485:2003(E).
34. US FDA. *Laboratory Developed Tests.* http://www.fda.gov/MedicalDevices/ProductsandMedicalProcedures/InVitroDiagnostics/ucm407296.htm (accessed May 25, 2016).
35. Garon, E. B.; Rizvi, N. A.; Hui, R.; Leighl, N.; Balmanoukian, A. S.; Eder, J. P.; Patnaik, A.; Aggarwal, C.; Gubens, M.; Horn, L.; Carcereny, E.; Ahn, M. J.; Felip, E.; Lee, J. S.; Hellmann, M. D.; Hamid, O.; Goldman, J. W.; Soria, J. C.; Dolled-Filhart, M.; Rutledge, R. Z.; Zhang, J.; Lunceford, J. K.; Rangwala, R.; Lubiniecki, G. M.; Roach, C.; Emancipator, K.; Gandhi, L.; KEYNOTE-001 Investigators. Pembrolizumab for the Treatment of Non-Small-Cell Lung Cancer. *N. Engl. J. Med.* **2015,** *372* (21), 2018–2028.
36. Jørgensen, J. T. Companion Diagnostic Assays for PD-1/PD-L1 Checkpoint Inhibitors in NSCLC. *Expert Rev. Mol. Diagn.* **2016,** *16* (2), 131–133.
37. US FDA. *Paving the Way for Personalized Medicine: FDA's Role in a New Era of Medical Product Development.* http://www.fda.gov/downloads/ScienceResearch/SpecialTopics/PersonalizedMedicine/UCM372421.pdf (accessed Jan 2, 2016).
38. Roscoe, D. M.; Hu, Y. F.; Philip, R. Companion Diagnostics: A Regulatory Perspective From the Last 5 Years of Molecular Companion Diagnostic Approvals. *Expert Rev. Mol. Diagn.* **2015,** *15* (7), 869–880.
39. Kerr, K. M.; Hirsch, F. R. Programmed Death Ligand-1 Immunohistochemistry: Friend or Foe? *Arch. Pathol. Lab. Med.* **2016,** *140* (4), 326–331.
40. US FDA. *Companion Diagnostic Devices: In vitro and Imaging Tools.* Updated: December 21, 2015. http://www.fda.gov/MedicalDevices/ProductsandMedicalProcedures/InVitroDiagnostics/ucm301431.htm (accessed Jan 2, 2016).
41. Slamon, D. J.; Leyland-Jones, B.; Shak, S.; Fuchs, H.; Paton, V.; Bajamonde, A.; Fleming, T.; Eiermann, W.; Wolter, J.; Pegram, M.; Baselga, J.; Norton, L. Use of Chemotherapy Plus a Monoclonal Antibody Against HER2 for Metastatic Breast Cancer That Overexpresses HER2. *N. Engl. J. Med.* **2001,** *344* (11), 783–792.
42. Ou, S. H. Crizotinib: A Novel and First-in-Class Multitargeted Tyrosine Kinase Inhibitor for the Treatment of Anaplastic Lymphoma Kinase Rearranged Non-Small Cell Lung Cancer and Beyond. *Drug Des. Devel. Ther.* **2001,** *5,* 471–485.

43. US FDA Center for Drug Evaluation and Research. *Medical Review*. Application Number 202370Orig1s000. August 12, 2011. http://www.accessdata.fda.gov/drugsatfda_docs/nda/2011/202570Orig1s000MedR.pdf (accessed Jan 3, 2016).
44. US FDA. *Prescribing Information for Zykadia (Ceritinib) Capsules, for Oral Use*. April 2014. http://www.accessdata.fda.gov/drugsatfda_docs/label/2014/205755lbl.pdf (accessed Jan 3, 2016).
45. US FDA. *Prescribing Information for Alecensa (Alectinib) Capsules, for Oral Use*. December 2015. http://www.accessdata.fda.gov/drugsatfda_docs/label/2015/208434s000lbl.pdf (accessed Jan 3, 2016).
46. Jørgensen, J. T. Companion Diagnostics and the Drug-Diagnostic Co-Development Model. *Drug Dev. Res.* **2012,** *73*, 390–397.
47. Menis, J.; Hasan, B.; Besse, B. New Clinical Research Strategies in Thoracic Oncology: Clinical Trial Design, Adaptive, Basket and Umbrella Trials, New End-Points and New Evaluations of Response. *Eur. Respir. Rev.* **2014,** *23* (133), 367–378.
48. Jørgensen, J. T. Role of Human Epidermal Growth Factor Receptor 2 in Gastric Cancer: Biological and Pharmacological Aspects. *World J. Gastroenterol.* **2014,** *20* (16), 4526–4535.
49. Hyman, D. M.; Puzanov, I.; Subbiah, V.; Faris, J. E.; Chau, I.; Blay, J. Y.; Wolf, J.; Raje, N. S.; Diamond, E. L.; Hollebecque, A.; Gervais, R.; Elez-Fernandez, M. E.; Italiano, A.; Hofheinz, R. D.; Hidalgo, M.; Chan, E.; Schuler, M.; Lasserre, S. F.; Makrutzki, M.; Sirzen, F.; Veronese, M. L.; Tabernero, J.; Baselga, J. Vemurafenib in Multiple Nonmelanoma Cancers With BRAF V600 Mutations. *N. Engl. J. Med.* **2015,** *373* (8), 726–736.
50. Middleton, G.; Crack, L. R.; Popat, S.; Swanton, C.; Hollingsworth, S. J.; Buller, R.; Walker, I.; Carr, T. H.; Wherton, D.; Billingham, L. J. The National Lung Matrix Trial: Translating the Biology of Stratification in Advanced Non-Small-Cell Lung Cancer. *Ann. Oncol.* **2015,** *26* (12), 2464–2469.
51. Hayes, D. F.; Allen, J.; Compton, C.; Gustavsen, G.; Leonard, D. G.; McCormack, R.; Newcomer, L.; Pothier, K.; Ransohoff, D.; Schilsky, R. L.; Sigal, E.; Taube, S. E.; Tunis, S. R. Breaking a Vicious Cycle. *Sci. Transl. Med.* **2013,** *5* (196), 196cm6.
52. Hayes, D.; Raison, C. Lessons for Tumor Biomarker Trials: Vicious Cycles, Scientific Method & Developing Guidelines. *Expert Rev. Mol. Diagn.* **2015,** *15* (2), 165–169.
53. US FDA. *Guidance for Industry and FDA Staff. in vitro Diagnostic (IVD) Device Studies—Frequently Asked Questions*. June 25, 2010. http://www.fda.gov/downloads/MedicalDevices/.../ucm071230.pdf (accessed Jan 6, 2016).
54. *Directive 98/79/EC of the European Parliament and of the Council of 27 October 1998 on in vitro Diagnostic Medical Devices*. http://eur-lex.europa.eu/LexUriServ/LexUriServ.do?uri=OJ:L:1998:331:0001:0037:EN:PDF (accessed Jan 6, 2016).
55. US FDA. *Drugs@FDA*, 2014. http://www.accessdata.fda.gov/scripts/cder/drugsatfda/ (accessed Jan 7, 2016).
56. Trusheim, M. R.; Berndt, E. R.; Douglas, F. L. Stratified Medicine: Strategic and Economic Implications of Combining Drugs and Clinical Biomarkers. *Nat. Rev. Drug Discov.* **2007,** *6* (4), 287–293.
57. Simon, R.; Maitournam, A. Evaluating the Efficiency of Targeted Designs for Randomized Clinical Trials. *Clin. Cancer Res.* **2004,** *10* (20), 6759–6763.
58. Correction-Article on Evaluating the Efficiency of Targeted Designs. *Clin. Cancer Res.* **2006,** *12* (10), 3229.
59. Winther, H.; Jørgensen, J. T. Drug-Diagnostic Co-Development in Cancer. *Pharm. Med.* **2010,** *24* (6), 363–375.
60. Parker, J. L.; Lushina, N.; Bal, P. S.; Petrella, T.; Dent, R.; Lopes, G. Impact of Biomarkers on Clinical Trial Risk in Breast Cancer. *Breast Cancer Res. Treat.* **2012,** *136* (1), 179–185.
61. Rubinger, D. A.; Hollmann, S. S.; Serdetchnaia, V.; Ernst, D. S.; Parker, J. L. Biomarker Use is Associated With Reduced Clinical Trial Failure Risk in Metastatic Melanoma. *Biomark. Med.* **2015,** *9* (1), 13–23.
62. Falconi, A.; Lopes, G.; Parker, J. L. Biomarkers and Receptor Targeted Therapies Reduce Clinical Trial Risk in Non-Small-Cell Lung Cancer. *J. Thorac. Oncol.* **2014,** *9* (2), 163–169.
63. Gandhi, L.; Jänne, P. A. Crizotinib for ALK-Rearranged Non-Small Cell Lung Cancer: A New Targeted Therapy for a New Target. *Clin. Cancer Res.* **2012,** *18* (14), 3737–3742.
64. Jørgensen, J. T. A Changing Landscape for Companion Diagnostics. *Expert Rev. Mol. Diagn.* **2013,** *13* (7), 667–669.
65. Murtaza, M.; Dawson, S. J.; Tsui, D. W.; Gale, D.; Forshew, T.; Piskorz, A. M.; Parkinson, C.; Chin, S. F.; Kingsbury, Z.; Wong, A. S.; Marass, F.; Humphray, S.; Hadfield, J.; Bentley, D.; Chin, T. M.; Brenton, J. D.; Caldas, C.; Rosenfeld, N. Non-Invasive Analysis of Acquired Resistance to Cancer Therapy by Sequencing of Plasma DNA. *Nature* **2014,** *497* (7447), 108–112.
66. Garcia Murillas, I.; Schiavon, G.; Weigelt, B.; Ng, C.; Hrebien, S.; Cutts, R. J.; Cheang, M.; Osin, P.; Nerurkar, A.; Kozarewa, I.; Garrido, J. A.; Dowsett, M.; Reis-Filho, J. S.; Smith, I. E.; Turner, N. C. Mutation Tracking in Circulating Tumor DNA Predicts Relapse in Early Breast Cancer. *Sci. Transl. Med.* **2015,** *7* (302), 302ra133.
67. Grosu, D. S.; Hague, L.; Chelliserry, M.; Kruglyak, K. M.; Lenta, R.; Klotzle, B.; San, J.; Goldstein, W. M.; Moturi, S.; Devers, P.; Woolworth, J.; Peters, E.; Elashoff, B.; Stoerker, J.; Wolff, D. J.; Friedman, K. J.; Highsmith, W. E.; Lin, E.; Ong, F. S. Clinical Investigational Studies for Validation of a Next-Generation Sequencing in vitro Diagnostic Device for Cystic Fibrosis Testing. *Expert Rev. Mol. Diagn.* **2014,** *14* (5), 605–622.
68. US FDA. *Prescribing Information for Kalydeco (Ivacaftor) Tablets, for Oral Use*. December 2014. http://www.accessdata.fda.gov/drugsatfda_docs/label/2015/203188s017lbl.pdf (accessed Jan 9, 2016).
69. Pulido, M. R.; García-Quintanilla, M.; Martín-Peña, R.; Cisneros, J. M.; McConnell, M. J. Progress on the Development of Rapid Methods for Antimicrobial Susceptibility Testing. *J. Antimicrob. Chemother.* **2013,** *68* (12), 2710–2717.
70. Gibson, D. S.; Bustard, M. J.; McGeough, C. M.; Murray, H. A.; Crockard, M. A.; McDowell, A.; Blayney, J. K.; Gardiner, P. V.; Bjourson, A. J. Current and Future Trends in Biomarker Discovery and Development of Companion Diagnostics for Arthritis. *Expert Rev. Mol. Diagn.* **2015,** *15* (2), 219–234.
71. Schork, N. J. Time for One-Person Trials. *Nature* **2015,** *520* (7549), 609–611.
72. US FDA. *Table of Pharmacogenomic Biomarkers in Drug Labeling*. http://www.fda.gov/%20drugs/scienceresearch/researchareas/pharmacogenetics/ucm083378.htm (accessed May 16, 2016).
73. Langreth, R.; Waldholz, M. New Era of Personalized Medicine—Targeting Drugs for Each Unique Genetic Profile. *Oncologist* **1999,** *4* (5), 426–427.
74. Jørgensen, J. T. New Era of Personalized Medicine: A 10-Year Anniversary. *Oncologist* **2009,** *14* (5), 557–558.

This page intentionally left blank

COMPREHENSIVE MEDICINAL CHEMISTRY III

This page intentionally left blank

COMPREHENSIVE MEDICINAL CHEMISTRY III

EDITORS-IN-CHIEF

Samuel Chackalamannil
Rutgers University, Piscataway, NJ, United States

David Rotella
Montclair State University, Montclair, NJ, United States

Simon E. Ward
University of Sussex, Brighton, United Kingdom

VOLUME 3

IN SILICO DRUG DISCOVERY TOOLS

VOLUME EDITORS

Andrew M. Davis
AstraZeneca R&D Gothenburg, Gothenburg, Sweden

Colin Edge
GlaxoSmithKline Medicines Research Centre, Stevenage, United Kingdom

ELSEVIER

Elsevier
Radarweg 29, PO Box 211, 1000 AE Amsterdam, The Netherlands
The Boulevard, Langford Lane, Kidlington, Oxford OX5 1GB, United Kingdom
50 Hampshire Street, 5th Floor, Cambridge, MA 02139, United States

Copyright © 2017 Elsevier Ltd. All rights reserved

No part of this publication may be reproduced or transmitted in any form or by any means, electronic or mechanical, including photocopying, recording, or any information storage and retrieval system, without permission in writing from the publisher. Details on how to seek permission, further information about the Publisher's permissions policies and our arrangements with organizations such as the Copyright Clearance Center and the Copyright Licensing Agency, can be found at our website: www.elsevier.com/permissions.

This book and the individual contributions contained in it are protected under copyright by the Publisher (other than as may be noted herein).

Notices
Knowledge and best practice in this field are constantly changing. As new research and experience broaden our understanding, changes in research methods, professional practices, or medical treatment may become necessary.

Practitioners and researchers may always rely on their own experience and knowledge in evaluating and using any information, methods, compounds, or experiments described herein. In using such information or methods they should be mindful of their own safety and the safety of others, including parties for whom they have a professional responsibility.

To the fullest extent of the law, neither the Publisher nor the authors, contributors, or editors, assume any liability for any injury and/or damage to persons or property as a matter of products liability, negligence or otherwise, or from any use or operation of any methods, products, instructions, or ideas contained in the material herein.

Library of Congress Cataloging-in-Publication Data
A catalog record for this book is available from the Library of Congress

British Library Cataloguing-in-Publication Data
A catalogue record for this book is available from the British Library

ISBN 978-0-12-803200-8

For information on all publications visit our website at
http://store.elsevier.com

Working together
to grow libraries in
developing countries
www.elsevier.com • www.bookaid.org

Publisher: Oliver Walter
Acquisition Editor: Rachel Gerlis
Content Project Manager: Gemma Tomalin
Associate Content Project Manager: Marise Willis
Designer: Mark Rogers

Printed and bound in the United Kingdom

PREFACE

Previous editions of *Comprehensive Medicinal Chemistry*, published in 1990 and 2006, provided an integrated reference source that encompassed all major aspects of drug discovery research. The third edition follows this tradition and considerably expands its scope and content.

The trailblazing scientific discoveries of the 21st century have brought new opportunities for drug discovery research. The discipline of medicinal chemistry continues to evolve as it adapts to these new opportunities and strives to solve new challenges. Covered in the new edition are not only the breakthrough therapies of the past decade in cancer, hepatitis C, heart failure, dyslipidemia, cystic fibrosis, multiple sclerosis, HIV, etc., but also extensive discussion of new business models in drug discovery research, shifting industry demographics, emerging technologies, *in silico* drug discovery tools, experimental ADME and toxicology, and biologics medicine. The tone of this edition is prospective in which contributors identify outstanding issues and paths forward in their area of expertise. The aim is to provide drug discovery scientists in industry, government, academia, and research organizations with a contemporary global perspective on the field that includes a look ahead in selected areas.

The eight individual volumes fulfill these objectives and include extensive discussion of biomolecular therapeutics, drug targeting and delivery, development of chemical biology tools, data collection and analysis, *in silico* models as predictors for biological properties, identification/validation of new targets, approaches to quantify target engagement, new methods for synthesis of drug candidates such as green chemistry, development of novel scaffolds for drug discovery, and the role of regulatory agencies in drug discovery.

The individual volume editors have done an outstanding job to identify topics and contributors to meet these goals and we thank them for their hardwork and diligence. In volume 1, Ana Martinez and Carmen Gil recruited an international group of contributors who provide chapters on the emerging role of organizations other than traditional pharmaceutical companies in drug discovery, the evolving science of chemical biology, and new organic chemistry contributions to the discipline. In volume 2, Helmut Buschmann, Norbert Handler, and Andrea Wolkerstorfer have accomplished a seemingly impossible task and attracted world-leading experts across the wide field of drug discovery enabling technologies, covering contemporary thinking in a wide range of key disciplines that enable modern medicinal chemistry and drug discovery and development. The computational enabling technologies are the focus of volume 3, in which Andy Davis and Colin Edge have assembled chapters covering both ligand-based and protein structure–based advances as well as exciting new methodologies and case studies exploiting these. Alan Wilson identified experts in the fields of pharmacokinetics and toxicology who describe a wide range of contemporary advances in prediction and analysis of pharmaceutical properties and drug safety in volume 4. In volume 5, Ian Collins, Louis Lombardo, and Will Watkins have assembled leading experts to discuss high impact drug discovery accomplishments over the past decade in cancer chemotherapeutics, immunology and inflammation, and infectious diseases therapeutic areas. Ved Srivastava edited volume 6 on biologic medicines, a significant and rapidly evolving area where medicinal chemistry plays an important role. The chapters in this volume provide timely information on not only protein-based drugs, such as monoclonal antibodies and therapeutic proteins, but also peptides and nucleic acid–based therapeutics. Volume 7, edited by Adrian Hall, Santhosh Neelamkavil, and Rob Jones, presents a detailed account of the major advances in CNS, metabolic, and cardiovascular fields over the past decade and the promising new opportunities. Joerg Holenz edited volume 8 that presents case histories of successful drug discovery and strategic differentiation that have resulted in commercialized drugs and candidates in advanced clinical trials.

We are truly grateful to the publishing team at Elsevier that includes Gemma Tomalin, Rachel Gerlis, Marise Willis, and Sean Simms for their assistance and support throughout the process. With their expertise, this project became what we believe is a noteworthy and valuable resource for the discipline of medicinal chemistry. We look forward to the response and feedback of our colleagues who will use this information in their own work.

Samuel Chackalamannil, David P. Rotella, and Simon E. Ward

EDITORS-IN-CHIEF: BIOGRAPHIES

Dr. Samuel Chackalamannil

Dr. Chackalamannil obtained his PhD in chemistry from Yale University in 1984 and subsequently worked in drug discovery research at Schering-Plough Corporation and Merck Research Laboratories, where he was a distinguished fellow when he left in 2011. Since then, he has been teaching at Ernest Mario School of Pharmacy, Rutgers University, New Jersey.

Dr. Chackalamannil has significant accomplishments in the discovery of new medicines. He led the discovery of vorapaxar (Zontivity®), an FDA-approved antiplatelet drug for the prevention of heart attack and stroke. His group also discovered a PDE-5 inhibitor clinical candidate dasantafil and an adenosine A2a antagonist clinical candidate for the treatment of Parkinson's disease. Altogether, he was responsible for the discovery of nine development candidates in cardiovascular, central nervous system, and metabolic disease areas.

Dr. Chackalamannil is a coinventor of 62 allowed US patents and numerous patent applications worldwide. He has published 81 peer-reviewed articles and has coauthored a book. He has also given numerous lectures at international meetings and academic institutions.

Dr. Chackalamannil is a two-time recipient of the Thomas Alva Edison Award for Emerging Technology Patent and a two-time recipient of the Presidential Award for Discovery at Schering-Plough Research Institute. He has chaired several sessions at American Chemical Society national meetings and Gordon Research Conference on Medicinal Chemistry and was an organizer for Chemistry as a Life Science Symposium.

Dr. David Rotella

Dr. Rotella earned a PhD in medicinal chemistry from The Ohio State University and carried out postdoctoral research in organic chemistry at Penn State University. He joined the faculty at Montclair State University in July 2011 as the Margaret and Herman Sokol Professor of medicinal chemistry after a successful career in the pharmaceutical industry. He is an expert in the discovery and optimization of small molecule drug candidates for use in metabolic, cardiovascular, cancer, and central nervous system diseases. His current research is focused on discovering new lead compounds for use in parasitic and central nervous system diseases. He has coedited the seventh edition of *Burger's Medicinal Chemistry* and is a senior editor for the Royal Society of Chemistry's Drug Discovery book series. He has authored over 40 peer-reviewed articles, is an inventor on 8 issued US patents, and has contributed 10 book chapters.

Simon E. Ward

Simon Ward has an MA in natural sciences and PhD in synthetic organic chemistry from Cambridge University, UK. He has a wide-ranging experience of drug discovery in both large and small companies (GlaxoSmithKline, Knoll Pharmaceuticals, Vernalis, Chiroscience, BioCrea) and specialist experience of discovering and developing drugs for central nervous system indications. He has led multidisciplinary project teams and medicinal chemistry groups from target identification through to early clinical studies, delivering multiple clinical development candidates across indications. He is a fellow of the Royal Society of Chemistry. He is currently a professor of medicinal chemistry at the University of Sussex, UK, and the director of the Sussex Drug Discovery Centre, which he established within the University of Sussex in 2010.

This page intentionally left blank

CONTRIBUTORS TO VOLUME 3

Y A Abramov
Pfizer Worldwide Research and Development, Groton, CT, United States

M Aldeghi
University of Oxford, Oxford, United Kingdom

D Bajusz
Research Institute for Natural Sciences, Hungarian Academy of Sciences, Budapest, Hungary

I I Baskin
M.V. Lomonosov Moscow State University, Moscow, Russia

P C Biggin
University of Oxford, Oxford, United Kingdom

A Bortolato
Heptares Therapeutics, BioPark, Hertfordshire, United Kingdom

G Brown
Heptares Therapeutics, BioPark, Hertfordshire, United Kingdom

J Cole
Cambridge Crystallographic Data Centre, Cambridge, United Kingdom

M Congreve
Heptares Therapeutics, BioPark, Hertfordshire, United Kingdom

R M Cooke
Heptares Therapeutics, BioPark, Hertfordshire, United Kingdom

A M Davis
AstraZeneca R&D Gothenburg, Mölndal, Sweden

E Davis
The Cambridge Crystallographic Data Centre Inc, Piscataway, NJ, United States

A G Dossetter
MedChemica Limited, Macclesfield, United Kingdom

C M Edge
GlaxoSmithKline Medicines Research Centre, Stevenage, United Kingdom

C Estarellas
University of Barcelona, Barcelona, Spain

M V Fedorov
Skolkovo Institute of Science and Technology, Moscow, Russia; and University of Strathclyde, Glasgow, United Kingdom

F L Gervasio
University College London, London, United Kingdom

B C Gomes
Pharmacometrics Modeling and Simulation, Novartis, Cambridge, MA, United States

E J Griffen
MedChemica Limited, Macclesfield, United Kingdom

C Hasselgren
PureInfo Discovery, Albuquerque, NM, United States

K Héberger
Research Institute for Natural Sciences, Hungarian Academy of Sciences, Budapest, Hungary

G Jones
Arena Pharmaceuticals, San Diego, CA, United States

E J M Lang
University of Bristol, Bristol, United Kingdom

A G Leach
Liverpool John Moores University, Liverpool, United Kingdom; and MedChemica Limited, Macclesfield, United Kingdom

A R Leach
European Bioinformatics Institute, Hinxton, United Kingdom and GSK, Stevenage, United Kingdom

R A Lewis
Novartis Pharma AG, Basel, Switzerland

D J Livingstone
ChemQuest, Isle of Wight, United Kingdom

I Lukac
Liverpool John Moores University, Liverpool, United Kingdom

M Mackey
Cresset, Litlington, United Kingdom

A J Mulholland
University of Bristol, Bristol, United Kingdom

T I Oprea
University of New Mexico School of Medicine, Albuquerque, NM, United States

A Rácz
Research Institute for Natural Sciences, Hungarian Academy of Sciences, Budapest, Hungary; and Szent István University, Budapest, Hungary

E L Ratkova
Institute of Structural Biology, Neuherberg, Germany

C R Sage
Arena Pharmaceuticals, San Diego, CA, United States

G Saladino
University College London, London, United Kingdom

F Sirockin
Novartis Pharma AG, Basel, Switzerland

C Southan
University of Edinburgh, Edinburgh, United Kingdom

C J Swain
Cambridge MedChem Consulting, Cambridge, United Kingdom

Robin Taylor
Cambridge Crystallographic Data Centre, Cambridge, United Kingdom

I V Tetko
Institute of Structural Biology, Neuherberg, Germany; and BIGCHEM GmbH, Neuherberg, Germany

P J Thomas
European Bioinformatics Institute, Hinxton, United Kingdom and GSK, Stevenage, United Kingdom

P Tosco
Cresset, Litlington, United Kingdom

A Warshel
University of Southern California, Los Angeles, CA, United States

M Withnall
Institute of Structural Biology, Neuherberg, Germany

C Yan
University of Missouri, Columbia, MO, United States

H Yoon
University of Southern California, Los Angeles, CA, United States

J M Zarnecka
Liverpool John Moores University, Liverpool, United Kingdom

X Zou
University of Missouri, Columbia, MO, United States

CONTENTS OF VOLUME 3

Preface *v*

Editors-in-Chief: Biographies *vii*

Contributors to Volume 3 *ix*

Editorial Board *xiii*

Survival of the Fittest Computational Chemists, Computers, and Reference Works (Over a 30-Year Period) *xv*

3.01 Perspective on Calculations of Binding Free Energies 1
H Yoon and A Warshel

3.02 Advances in Molecular Simulation 14
M Aldeghi and P C Biggin

3.03 Recent Progress in Free Energy Methods 34
G Saladino, C Estarellas, and F L Gervasio

3.04 Molecular Dynamics, Quantum Mechanics, and Combined Quantum Mechanics/Molecular Mechanics Methods for Drug Discovery and Development 51
E J M Lang and A J Mulholland

3.05 Progress in the Understanding of Traditional and Nontraditional Molecular Interactions 67
Robin Taylor

3.06 Using 3D Structural Information in Computational Design 101
A M Davis and C M Edge

3.07 Protein Structure Prediction and Homology Modeling 120
A R Leach and P J Thomas

3.08 Modeling and Design for Membrane Protein Targets 145
M Congreve, A Bortolato, G Brown, and R M Cooke

3.09 2/3D Pharmacophore Definitions and Their Application 189
R A Lewis and F Sirockin

3.10 Matched Molecular Pair Analysis 221
A G Leach, I Lukac, J M Zarnecka, A G Dossetter, and E J Griffen

3.11 Lessons and Successes in the Use of Molecular Fields 253
P Tosco and M Mackey

3.12 Molecular Docking—A Solved Problem? 297
J Cole, E Davis, G Jones, and C R Sage

3.13 Modeling Protein Flexibility in Molecular Docking 319
C Yan and X Zou

3.14 Chemical Data Formats, Fingerprints, and Other Molecular Descriptions for Database Analysis and Searching 329
D Bajusz, A Rácz, and K Héberger

3.15 Quantitative Structure—Activity Relationships 379
A M Davis

3.16 Empirical and Physics-Based Calculations of Physical—Chemical Properties 393
E L Ratkova, Y A Abramov, I I Baskin, D J Livingstone, M V Fedorov, M Withnall, and I V Tetko

3.17 Predicting Target and Chemical Druggability 429
T I Oprea and C Hasselgren

3.18 Data Analysis and Visualization Tools 440
C J Swain

3.19 Examples of SAR-Centric Patent Mining Using Open Resources 464
C Southan

3.20 An Introduction to Systems Biology and Quantitative Systems Pharmacology 488
B C Gomes

EDITORIAL BOARD

EDITORS-IN-CHIEF

Samuel Chackalamannil
Rutgers University, Piscataway, NJ, United States

David Rotella
Montclair State University, Montclair, NJ, United States

Simon E. Ward
University of Sussex, Brighton, United Kingdom

VOLUME 1
GENERAL PERSPECTIVE - THE FUTURE OF DRUG DISCOVERY

VOLUME EDITORS

Ana Martinez
Centro de Investigaciones Biologicas-CSIC, Madrid, Spain

Carmen Gil
Centro de Investigaciones Biologicas-CSIC, Madrid, Spain

VOLUME 2
DRUG DISCOVERY TECHNOLOGIES

VOLUME EDITORS

Helmut Buschmann
Savira Pharmaceuticals GmbH, Vienna, Austria

Norbert Handler
Savira Pharmaceuticals GmbH, Vienna, Austria

Andrea Wolkerstorfer
Baxalta Innovations GmbH — Now part of Shire, Vienna, Austria

VOLUME 3
IN SILICO DRUG DISCOVERY TOOLS

VOLUME EDITORS

Andrew M. Davis
AstraZeneca R&D Gothenburg, Gothenburg, Sweden

Colin Edge
GlaxoSmithKline Medicines Research Centre, Stevenage, United Kingdom

VOLUME 4
EXPERIMENTAL ADME AND TOXICOLOGY

VOLUME EDITOR

Alan G. E. Wilson
Lexicon Pharmaceuticals, The Woodlands, TX, United States

VOLUME 5
CANCER, IMMUNOLOGY AND INFLAMMATION, AND INFECTIOUS DISEASE

VOLUME EDITORS

Ian Collins
The Institute of Cancer Research, London, United Kingdom

William Watkins
Gilead Sciences, Foster City, CA, United States

Louis J. Lombardo
Bristol-Myers Squibb Research and Development, Princeton, NJ, United States

VOLUME 6
BIOLOGICS MEDICINE

VOLUME EDITOR

Ved Srivastava
Intarcia Therapeutics, Durham, NC, United States

VOLUME 7
CNS, PAIN, METABOLIC SYNDROME, CARDIOVASCULAR, TISSUE FIBROSIS AND URINARY INCONTINENCE

VOLUME EDITORS

Adrian Hall
UCB BioPharma SPRL, Brussels, Belgium

Santhosh Neelamkavil
Merck Research Laboratories, Kenilworth, NJ, United States

Rob Jones
BlackThorn Therapeutics, San Francisco, CA, United States

VOLUME 8
CASE HISTORIES IN RECENT DRUG DISCOVERY

VOLUME EDITOR

Joerg Holenz
R&D Neurosciences TAU, GSK, PA, United States

Survival of the Fittest Computational Chemists, Computers, and Reference Works (Over a 30-Year Period)

AM Davis, AstraZeneca R&D Gothenburg, Gothenburg, Sweden
CM Edge, GSK Medicines Research Centre, Stevenage, United Kingdom

© 2017 Elsevier Ltd. All rights reserved.

Computational Methods in Materials Science xviii
Advances in Understanding of Receptor Thermodynamics xviii
Receptor Kinetics xviii
Design of Experiments in Drug Design xix
Design of Screening Libraries xix
References xxi

As editors of this volume, we two are very complementary. We are of a similar age, both in 50s, and have spent our careers in two of Europe's notable pharmaceutical companies, GSK and AstraZeneca. AD has spent his career as a physical organic chemist specializing in physical properties and quantitative structure–activity relationship (QSAR), and CE has spent his time as a computational chemist. So, together we span the worlds of empirical- and physics-based modeling, which make up our discipline of computational chemistry. Throughout this period we have known of each other's work and admired each other's craft, from afar, and so it is a joy that we have finally been able to work together on this volume. (But enough self-indulgent back-slapping, let's get on to why we agreed to edit this book…)

We are successes in the limited sense that we are Darwin's successes. In a field where we have seen attrition in terms of compounds, companies, and colleagues, we have survived, through a natural selection process of good decisions and blind luck. (Whether we should be aligned to a successful, ubiquitous design like the dragonfly, or a lucky niche-survivor like the coelacanth, we shall let the reader decide.) At the time we didn't know what we were doing, although looking back we can identify some of our successful traits. We hope to share these with you, through these chapters and this introduction, discussing some of the science topics we hold dear and which we think have been the tools of our survival, and hoping to highlight how the science itself has evolved and adapted to the environment we have experienced.

We remember the early days of our career, fresh from University, and the many visits to the company libraries to search through the shelves of *Chemical Abstracts* and its indices and the aisles of bound paper journals, and the Chemistry Bibles of *Beilstein*, *Organic Syntheses*, and the newly published encyclopedic *Comprehensive Medicinal Chemistry*. These were the condensed fountains of knowledge from which we learned our craft. (Although come to think of it, they were not so condensed—even then *CMC*1 was six volumes, and *Chemical Abstracts* filled a wall.) Since those days, while we have developed influential careers, the bound copies of *Chemical Abstracts* have been sent to paper recycling and replaced by access to a web page, https://scifinder.cas.org. Meanwhile, *Comprehensive Medicinal Chemistry* has grown into this third edition eight-volume hardcopy set. It was an honor to be asked to edit the volume on "*In Silico* Tools", the first update for 10 years.

As we reflect on our changing careers, we also remember how our tools and science have progressed. In 1990 our first word processors were IBM PS2s or early Macintoshes and in computational chemistry the display of chemical structures was done on devices such as the Evans and Sutherland PS300, with calculations on mainframe VAXes and the incoming MicroVax, all now dead. Today we have phones many times more powerful than our first desk computer with 200 times the storage capacity, and mobile tablets can render and rotate complex 3-D structures better than those half-million dollar Evans and Sutherland beasts. Indeed Moore's law continues to operate. We now have practically unlimited storage, and huge calculation capacity, and what in 1988 may have taken weeks or months to compute can now be done in real time. But despite all the change we have experienced, some things have remained largely unchanged. A time traveler from 1990 would recognize the science if not the software, with free energy perturbation (FEP) theory, molecular dynamics, quantum mechanics (QM), fingerprints, pharmacophores, and QSAR all mature theories 26 years ago. The big difference is the amount of data, and of course the aforementioned continued to increase in performance of modern computers.

To continue the evolutionary theme, one might wonder how *Comprehensive Medicinal Chemistry* has survived, and whether students of today respect it in much the same way we do. After all, up-to-date authoritative reviews on virtually any subject close to our hearts are available at our fingertips through the World Wide Web, and a visit to a library with real books is such a rare experience. How could a wieldy eight-volume hardcopy set survive? Many research centers no longer have libraries at all. Of course *Comprehensive Medicinal Chemistry* has moved with the times, as PDF chapters are available online for purchase. But out-of-date online reviews cannot be the reason for its survival. So what is the role of *Comprehensive Medicinal Chemistry* today? Maybe it has survived because it is indeed *comprehensive*.

As invited editors, the responsibility of carrying the title weighed heavily us. Our scientific naivety gave us hope we could aspire toward Comprehensiveness. But there is always something left behind, particularly when commercial publishing deadlines meet busy scientists. While the modern world of e-publications would be flexible about late-breaking chapters, the call of the printing presses could not be ignored. So for reasons of time we were doomed as scientist idealists to disappoint the advertised title of Comprehensive, and leave some chapters behind to wither and die under the pressure of selection of the fittest. We have unfortunately had to leave behind such topics as binding thermodynamics, screening libraries, and experimental design. We also wanted to pick up on some of the newer peripheral areas that are expanding toward medicinal chemistry territory, such as solid-state modeling, polymorph risk assessment, large-scale systems, and multicomponent assemblies. Sadly we failed to get chapters completed for these in the time available.

If *Comprehensive Medicinal Chemistry* could not be comprehensive, then for a volume updated every 10 years to be a Darwin success, we believe it is its ability to be deep, reflective, and provocative to judge progress and to look to the future. This became our focus for the volume. We asked our authors to consider the context of their discipline and to look at what has happened and how the discipline could change and thrive. Our authors have delivered. The chapters in this *In Silico* volume are a joy to read, written as they are by some of our industry's leading thinkers, writers, and doers. We relished editing every last one of the 25,000 or so words per chapter.

The first chapter in this volume is one that we are immensely proud of. One of the Nobel Laureates in our field, Arieh Warshel, graciously agreed to write a Perspective on Calculations of Binding Free Energies. This is a great introduction to a field that has been around for years, but is rapidly becoming relevant for medicinal chemists, because of technological advances in computer speed and memory. Yoon and Warshel (University of Southern California) provide a personal journey from rigorous but slow microscopic methods, through to simplified models of electrostatics. They then discuss the pros and cons of using different strategies to apply the models, such as FEP and linear response approximation (LRA) methods. It is interesting to see their view on the "disappointing performance of FEP, even with a polarizable force field," since FEP is being touted quite heavily by some software manufacturers. (Although to be fair, Yoon and Warshel go on to suggest a water flooding method that seems to improve the performance of any free energy method.)

The baton is picked up by Matteo Aldeghi and Phil Biggin (Oxford) in their chapter on "Advances in Molecular Simulation." This has some overlap with Warshel's chapter, but spends more time on the "nuts and bolts," such as processors, algorithms, and molecular mechanics force fields. They then go on to discuss the latest simulation approaches such as Markov state models (MSMs) and replica exchange (RE) methods, which can be used to improve sampling—one of the bugbears of the science. Put simply, we are millisecond animals consisting of huge ensembles of molecules, but we can simulate one or a few systems for nanoseconds. They then go on to discuss methods such as metadynamics, which explore the complex conformational options of a macromolecular system by "filling in" the energy wells that have been found, encouraging the system to explore other conformational states. One comment that struck us when reviewing this chapter was that simulations were starting to be run on the same timescale as some experimental techniques and that we were bound to see more convergence in the future. This is exciting, since the combination of theory and experiment always strengthens theory and sometimes supplants experiment. (Take aeronautical design as an example.)

The third chapter on simulations also takes its lead from Arieh Warshel and discusses FEP methods in more depth. Francesco Gervasio (UCL) gives an introduction to the basic "alchemical" approaches of FEP and thermodynamic integration (TI), when one atom or small functional group is transmuted to another, giving an estimation of a difference in free energy ($\Delta\Delta G$) between two molecular systems. He then goes on to describe various enhanced sampling collective variable methods followed by variable-free methods. This chapter will take you deeper into the mechanics of these methods and point you at some seminal papers.

Another area with a venerable tradition is QM. Graham Richards' influential book, *Quantum Pharmacology*, was one of the reasons that we entered the pharmaceutical industry in the first place. Predicting the properties of molecules from the wave function was cutting edge (and admittedly largely science fiction) in the 1980s, but we could see where QM was going. Many of the leading lights in pharmaceutical computational chemistry passed through Graham's lab. Adrian Mulholland is one such and is now a renowned expert on quantum mechanics/molecular mechanics (QM/MM) hybrid methods. He and Eric Johnson (Bristol) have provided us with an overview of QM at a time when it is really becoming mainstream again, because of the availability of cheap computer power.

One of our favorite chapters is the deceptively simple one on "Molecular Interactions" by Robin Taylor. He delighted us with his update on the state of understanding of drug–receptor interactions. His voice of authority and experience, together with an easy writing style, was a joy to read. This is a discussion of all the intermolecular interactions you will come across as a medicinal chemist, plus some you shouldn't believe, such as fluorine as a halogen bond donor. The author has spent a large part of his career at the Cambridge Crystallographic Data Centre, looking at interactions in crystals, and this chapter is essentially his distilled wisdom on the subject, backed up by lots of examples. This work is highly recommended for those who want to get more from their crystal structures, whether small molecule or protein ligand.

Many computational chemists utilize X-ray structures as the basis for structure-based campaigns or even for validating new computational code. Useful guidance on using X-ray crystal structures in computational programs is given by the editors' own chapter, calling on highly cited reviews they have been contributors to over the last 10 years.

Oftentimes, you are unlucky and there is no structural model available for your target macromolecule. In this situation you may be able to build a homology model. If that is the case, you have two options: send the sequence to one of the automatic model building web sites on the Web, or put some effort in yourself to build the model. Andrew Leach (EBI) and Pamela Thomas (GSK) take you through the steps of building such a model. Crucially, they identify the risks and pitfalls along the way. Even if you have no intention of building a model yourself, this chapter will help you have the right level of appreciation and skeptic doubt about any model you acquire.

While some subjects are welcome refreshes and updates of evolving science, some chapters are new and reflect the way our thinking and capabilities are developing. Miles Congreve et al. give us an insight into drug design using membrane protein structures according to Heptares, surely one of the most innovative high-end science companies of the last 10 years, with science that was virtually unthinkable when the last edition of *Comprehensive Medicinal Chemistry* was rushing to press ink to paper. Membrane-associated targets such as G protein–coupled receptors (GPCRs) continue to be underrepresented in the PDB. Structural models of these targets are still "special" compared to those of soluble monomeric proteins. The chapter tells of a fast-paced discipline where almost every structure was significant in moving the science onward. Will solving membrane-associated structures become routine within the next 10 years? We suspect, "yes and no." Some class A GPCRs are already routine in the hands of experts such as Heptares, but larger many-helix transporters may require us to move away from X-ray diffraction methods to, say, 3-D electron microscopy (3DEM) methods.

Another way to distil knowledge from structure—and then do something with it—is to build a pharmacophore. Richard Lewis and Finton Sirockin of Novartis have provided us with an authoritative chapter on what seemed to us to be a rather stagnant field. How wrong we were! They have shown us that in some ways, pharmacophores are the original and most robust form of medicinal chemistry, in that "they are a property of the training set of molecules rather than the target" and so fall neatly in with medicinal chemistry concepts such as R-group substitution, homologous series, molecular similarity, and the like. Indeed the pharmacophore has the power to transcend these and arrive at truly novel molecules with completely different scaffolds.

An important subset of pharmacophore- or similarity-based approaches is the matched molecular pair analysis (MMPA). Andrew Leach (Liverpool John Moores) was one of the pioneers of this analysis method. He and his colleagues have offered us a history of MMPA from the coining of the term onward and then into the future. This is an excellent treatise on molecular matched pairs, reminiscent of an old style QSAR method—but it's very much a drug design tool of the modern age, being dependent as it does on large-scale cheminformatics structure-matching and statistical data analysis. Again this is a technique that should appeal to any medicinal chemist and it aligns well with R-group analysis and (in some implementations) with scaffold hopping. It is a relatively recent development, so there is still excitement over the next steps, such as expanding MMPA into three dimensions or being used to anonymously compare compound sets between organizations.

The use of molecular interaction fields (MIFs) in computational chemistry goes back to the eighties with developments such as GRID and CoMFA. Nowadays these techniques have had a new lease of life in areas as diverse as water mapping and crystal structure quality assessment. Paolo Tosco and Mark Mackey (Cresset) are world experts in these methods and have continued to develop the XED-based fields pioneered by Andy Vinter. Their chapter is a tour through the how and why of MIFs, from simple alignment and pose prediction through to recent developments such as activity cliff identification and water placement. Although these methods are not as alluring to some as simulation-based methods such as WaterMap, they are quick, simple, and easily interpretable and surely must act as a baseline method in which the likes of WaterMap and SZMAP must strive to outperform. In our experience, MIFs work very well in the cases that do not involve force field complications such as high charge gradients (metals, phosphates in the binding site) and are therefore the first choice.

One area of computational chemistry that we thought had slowed down in the last 10 years was molecular docking, the practice of suggesting poses for ligands within a target site. We cheekily suggested the title, "Molecular Docking – a Solved Problem?" and to their credit, Jason Cole and Erin Davis (CCDC) and Gareth Jones and Carleton Sage (Arena) gamely agreed to write it. The generation of poses does seem to be remarkably successful, as one can see by looking at the docking challenges. The "right" pose is almost always on the list. However, the ranking of poses is by no means a solved problem, as this pose can be far down the ranking. This chapter discusses the reasons why this is the case: there is much work to be done in affinity prediction and coping with protein flexibility. The chapter is written in a very engaging style and is full of hints and tips for the uninitiated and the old lag.

The assumption of a rigid receptor is a risky assumption made by computational chemists using X-ray structures. Protein flexibility is the subject of a chapter by Chengfei Yan and Xiaoquin Zou (Missouri). This develops further some of the ideas in the chapter of Cole et al. It describes some of the tactics and techniques used to try to accommodate the inconvenient motion of the target site when presented with a ligand. These include soft docking, induced fit docking, and ensemble docking as ways to ameliorate poor interactions during a pose calculation. The authors also discuss postdocking methods to address steric clashes or flexible amino acid side chains, such as relaxation methods.

Molecules need descriptors. Dávid Bajusz, Anita Rácz, and Károly Héberger (Budapest) will tell you how to describe them. This chapter is a "comprehensive and reasonably compact" tour through the many ways to represent a molecule in a computer and how those representations can be used. As a bonus, they also discuss the online databases that medicinal chemists might use. Their outlook for the future is interesting. It seems we may have more or less peaked in the number of molecular descriptors available, but the number of ways of manipulating those descriptors continues to grow. More complex manipulations (consensus modeling, multi-y optimization, etc.) have become popular. This is partly due to the improvement in computational power, but just as much

due to helpful toolkits such as MySQL, R, RDKIT, and Python modules focused on cheminformatics. The area will continue to grow, as long as "Big Data" remains popular.

Physical property calculations are equally a critical part of the computational chemistry armory and deserve a place within this volume. So much has happened in the past 10 years to physical property calculations and their applications, and Igor Tetko (GmbH) brings us up to date, while Tudor Oprea (New Mexico) gives us a perspective on the last 10 years focus on compound quality.

While the focus of the volume is on heavy physics, visualization has always been important, and talk of toolkits and descriptors brings us on to Chris Swain's chapter on online databases. You have all these data, but how are you going to organize it and analyze it? Welcome to the world of "data analysis and visualization tools." These range from expensive, monolithic, multipurpose program suites sold by companies such as Schrodinger and Chemical Computing Group down to apps on your smartphone. In between is the hinterland of open-source programs. Chris gives us a summary of data-mining and visualization tools for the practising medicinal chemist with useful web links, case studies, and examples. More recent disciplines such as bioinformatics rely for the most part on free software, much of it also open source. We wondered whether it was possible to run a medicinal chemistry program with no software budget. This chapter suggests that this might be possible in the near future and is possible in some subdisciplines, such as cheminformatics, right now.

Cheminformatics and online databases have also enabled the field of open-source patent informatics, which is neatly reviewed by Chris Southan (Edinburgh). This is a great resource for anyone wondering what they can do with patent data, the most neglected source of free, open information. Chris takes the reader through the various online resources and shows what can be accomplished using fairly simple search techniques and focusing on extracting SAR. The birth of this chapter is very much of the modern age, as it was conceived during a Twitter conversation, and written against very tight deadlines.

Finally we have a chapter where everything is brought together into one huge model. With the recognition that failure in translational science is a major source of attrition, and also therefore a key for future success, Bruce Gomes' (Novartis) chapter on Systems Biology feels very timely in this volume. Systems biology is a very structured way of assembling your biology story. It provides project biology with a formal mathematical framework, and can help with both assays development and clinical trial design, especially when the relationship between mechanism and endpoint is not direct. Systems biology is moving away from toy systems where almost any change in output was judged to be "emergent activity" to models of PK/PD behavior that are genuinely useful. On top of this, the development of huge multicomponent models of, say, the heart or lung is being attempted. Bruce has provided a thought-provoking look at the current state of the art. It makes us wonder, will this be the norm in 10 years' time? It seems too soon, but we anticipate that more and more complex models of physiological behavior will become available at some point.

Where we have had to leave behind some chapters and topics, we can at least point you toward recent authoritative reviews on these many subjects, and isn't that one of the definitions of a great resource?—a pointer to other great resources, and isn't that the definition of a great review?—one that summarizes succinctly key knowledge so you can quickly find what you need to make discoveries of your own… So we can save you a few chapters of 25,000 words each, with a few hints, tips, and key references in a mere fraction of the 25,000 words per chapter—and be as quick and succinct as our tablet computer is compared to our old Evans and Sutherland. So what are the topics not covered in this volume?

Computational Methods in Materials Science

For up-to-date information on the impact of computational methods in materials science, we point you to a number of excellent reviews by Docherty and colleagues,[1–3] They are pioneers of a physics-based approach to materials engineering and if you follow their published work, it will give you a good basis for further exploration of this important field for crystal engineering, polymorph prediction, dissolution, particle flow, aerodynamics for inhaled drugs, and solid-state stability among other material properties.

Advances in Understanding of Receptor Thermodynamics

This is a big subject, and somewhat covered by Robin Taylor's chapter on progress in the understanding of traditional and nontraditional molecular interactions. As editors we were keen to probe the insight gained from measurements of on- and off-rates, and the deconvolution of free energy into measurements of enthalpy and entropy changes on binding of a drug to its target, and how this information has impacted computational chemistry and compound design.

Receptor Kinetics

In many systems, we measure at steady state, so even if the on-rate is slow, we set up assays to measure at equilibrium. Slow receptor binding often indicates conformation change, or changes in solvation, or both. Receptor kinetics can be measured biochemically, with washout experiments, although this is rather laborious. Nowadays Biacore technology allows receptor kinetics to be measured

directly. A number of drugs claim to benefit from slow receptor kinetics, although the off-rate would need to approach the dosing interval to contribute to pharmacodynamics duration. Tiotropium, the long acting M3 antagonist, has a slow receptor off-rate, and this is claimed to contribute toward its pharmacodynamic half-life, but its pharmacokinetic half-life is also long. There has been a long-term literature debate about the molecule driver for the long pharmacodynamic half-life of the β2 agonist salmeterol. Early papers suggested it was due to slow receptor off-rate due to an exo-site binding. Other studies suggested it may also be driven by its lipophilicity and membrane affinity. A recent receptor kinetic study appears to support this pharmacokinetic explanation as its off-rate measurements cannot explain its long pharmacodynamics off-rate.[4] But it is likely that slow receptor off-rate, if slow enough, could contribute to a pharmacodynamic half-life of drugs, after all irreversible compounds are just an extreme case of a slow off-rate. A review by Dahl and Akerud shows that for many drugs with long drug–target residence times, they also have even longer pharmacokinetic half-lives, so the residence time is not the "rate-determining step" for their pharmacodynamics duration.[5] A good start point for those interested in the role of slow receptor kinetics would be David Swinney's review.[6] A recent review by Klebe is also worth a read, which is also a segue into our next and related topic.[7]

The prospective design of slow off-rate compounds may be an area for the future of computational chemistry design. But design of irreversible compounds is already enabled, as exampled by a number of drug introductions, including ibrutinib, carfilzomib, rociletinib, not to mention the older classics such as clopidogrel, omeprazole, penicillin, and aspirin. For recent reviews we point readers to recent reviews by Gonzalez-Bello,[8] Singh,[9] and the article on structure-based design of EGFR T790M mutant irreversible inhibitors.[10]

One other aspect of receptor thermodynamics that has generated a lot of interest, but so far confusing impact, is the deconvolution of free energy changes into the fundamental enthalpy and entropy contributions. While biologists in general measure free energy changes, computational chemists generally estimate enthalpy changes. It would seem logical therefore that the partitioning of free energy into ΔH and TΔS contributions should aid computational approaches to understanding binding, as the entropy term can be considered separately. Indeed Biacore and isothermal titration calorimetry (ITC) enable the measurements to be easily made for amenable systems. Amenable for ITC means if the binding kinetics are fast enough, the protein can be expressed in large enough amounts and is soluble enough to be studied in the calorimeter. For Biacore amenable means if the protein or the ligand can be immobilized on a chip to measure the binding event.

So far the analysis of ΔH and TΔS changes has only confused and complicated the picture rather than aiding it. It has been proposed that best-in-class drugs are more ΔH driven than first in class drugs[11] and that thermodynamic signatures should be used to choose lead series. This is an excellent review, and while it may have some truth, that best-in-class drugs may be more enthalpically driven, this may be more likely a consequence of better control over ligand lipophilic efficiency rather than a fundamental principle of the receptor thermodynamics. A recent analysis of fragment binding to the S1 pocket in thrombin suggests fragments can be either more enthalpy driven or entropy driven.[12] Over congeneric series, ΔG can show a comparatively smooth transition, but a number of examples show that ΔH and TΔS can vary widely and in opposing directions, due to enthalpy–entropy compensation. Prospectively using ΔH and TΔS in drug design can be completely baffling. Many publications have appeared by rather bemused authors, in some high impact journals.[13] Interpretation can often only be made retrospectively, with reference to high-resolution X-ray crystal structures, and water rearrangements, as well as protein and ligand movements are often major contributors.[14] Independent changes to the ligand, such as increasing hydrophobicity and introduction of hydrogen bonds, can also cause cooperative changes in ΔH and TΔS. Increasing hydrophobicity can affect the strength of hydrogen bonds, and vice versa.[15] We believe the deconvolution of free energy into ΔH and TΔS is uncovering complexity and subtlety of drug–receptor interactions that is important information, and reminds us of the complexity of what we are trying to do. But it seems too early to be sure how computational chemistry should or could use ΔH and TΔS measurements prospectively. It seems too complex, and we should stick with ΔG for design. Further work is required in this discipline, and continuing thermodynamic profiling is recommended, alongside the developments in our computational discipline. The editors recommend the readers continue to follow the publications of Ladbury, Frere, and Klebe over the next few years, and see how this field develops.

Design of Experiments in Drug Design

Experimental design was another desired chapter, but it appears that little has happened in this area to justify a chapter on its own. Experimental design and design of experiments has always been important in designing *in vivo* experiments, reaction optimization, protein crystallization, formulation, and other areas of pharmaceutical research, but it has not evolved further as a technique for QSAR and drug design in the past 10 years. A search of SciFinder for the terms "design of experiments" or "experimental design" and "QSAR" only identified six publications since 2004.[16–21] If you are interested in experimental design, read these citations. Multiparameter optimization also continues to be of interest.[22]

Design of Screening Libraries

Finally we dearly wanted to discuss library design. This was a big subject in the second edition of *Computational Medicinal Chemistry*, covered by two chapters. This is not a static area and the design of screening libraries themselves continues to be a focus for drug

discovery. Supplementation of the HTS screening deck by new chemical libraries, or selecting subsets from it,[23–25] continues to be an important topic. Most companies developing HTS screening libraries have computational prescreens to remove ugly and unwanted compounds from compound acquisition activities, or to filter them from hit lists if the compounds are already in the HTS collection.[26] The Leadlike paradigm[27] has had a profound influence on the design of HTS screening collections and stimulated the field of fragment-based drug discovery. Fragment screens (by X-ray or NMR screening) are typically only a few thousand members, and hence design of the best few thousand members has also been a hot topic.[28] HTS is limited to 1–2 million structures, but the use of DNA encoding has allowed the screening of libraries of billions of small molecules, or up to 10^{18} member peptide libraries. The highest cited review on DNA-encoded library design is by Clark.[29] Now virtual screening is taking the numbers game to the next level. Pfizer have constructed a 10^{13} virtual library available for screening of every compound they could make with their available reagents and known reactions.[30,31] Lilly have recently published on their own synthesizable virtual library.[32] The chemical space project has now fully enumerated every compound up to 17 atoms of C, N, O, S, and halogens, a library of 116 billion members, and developed tools to virtual screen it. Clearly library design is still an exciting and developing field, driving the development of new enumeration and screening methodologies, and facilitated by the massive improvement in computational power that is now at our fingertips.

Now for the fun bit. This is where we make predictions about the next 10 years. This is not easy and no doubt there will be howls of derision at what we missed, but we shall have a go anyway. Anyone who knows the science fiction film genre will recognize that predictions have a strong grounding in current culture (e.g., miniskirts in *Star Trek*, phone boxes in *Blade Runner*). We are talking to you from the dying days of 2016, a time of Big Data, Cloud Computing, and gaming-sourced GPU processors. We've seen this before. The rise of Silicon Graphics and Netscape in the early 1990s was based on the supplanting of old technology (Cray, VAX, VMS, Teletype terminals) by parallel hardware and new display technology. The essence of the age was to dispense with experimental design and "just make everything." This is doomed to fail unless you can make some limits to your chemical space (i.e., put back in the design element). Even the 10^{18} and 10^{13} libraries mentioned above are tiny compared to the estimated "druglike" universe of about 10^{60}. After all, $10^{60}–10^{18} = 10^{60}$, to many significant figures, so we are nowhere near full coverage. We are hoping that we do not see a return to brute force methods and have concentrated our predictions elsewhere.

There has been a renewed effort on molecular mechanics force fields in recent years. These seem to have been stuck in the Doldrums since the Merck Molecular Force Field was published in 1996.[33] However, there is a renewed interest in polarizable force fields for proteins and a notable recent contribution is the AMOEBA force field.[34] This extends the charge representation from a simple atom-centered monopole expansion of so-called point charges to a quadrupole at each atom. The advantage is that the constructed atomic model should behave in a more realistic way in high dielectrics, such as water and when in highly charged environments, such as metal and phosphate sites. Although AMOEBA is still being tested, it seems to be an important step forward and other groups are working on extensions to existing force fields such as AMBER.[35] We can expect to see these force fields in routine use in the next 10 years.

One might also expect to see this resurgence of force field development to carry over into the more complex world of druglike molecules, where we need many more parameters than for proteins and oligosaccharides. We are not so sure. Of course, some common atom types that are not seen in proteins will be parameterized, for instance, pyridine nitrogens. However, we wonder whether the march of Moore's law and the cheapness of gaming graphics cards will mean that QM/MM methods will become routine. In a couple of years it wouldn't require that much effort to build a desk-side PC or even a laptop with enough memory and GPU power to run calculations on smallish enzymes with a quantum mechanical treatment of the whole active site and a surrounding shell of molecular mechanics. This is already routine on multithread Linux computers. The advantage of this technique is that the parameterization is limited to the choice of basis set and theoretical model, so we do not need to parameterize new ligands (provided they contain relatively common atoms). Admittedly, this provides a relatively static view of the binding site, consisting of transition states and energy minima, as we don't expect quantum dynamics solutions to be accessible. There are hybrid solutions where one runs alternate phases of molecular dynamics and QM/MM that might become popular.

Like QM, which was used a lot in drug discovery in the 1980s and early 1990s, another technique that we see reestablishing itself is QSAR analysis. This dates back to the work of Hansch in the 1960s and 1970s but fell out of favor somewhat at the turn of the century. This was partly due to the influence of the "we'll make everything so we don't need to design anything" gung-ho spirit of combinatorial chemistry and partly due to the replacement of cheminformatics by molecular simulation at many university departments. There was also the draw of Wall Street. If one is reasonably numerate and understands a little statistics, why get a job predicting the logD of a molecule when you can earn 10 times the amount analyzing stock trends? Anyway, QSAR has been under the radar for a number of years, except in a few very important areas. It has established a preeminent position in ADMET prediction in most large pharmaceutical companies, where various risks can be estimated before molecules are made. For instance, at GSK, we have a complete panel of liability assays, such as CYP450 inhibition, that have been provided as simple web services that can be called from an Excel spreadsheet. We see this influence extending back into lead optimization efforts and perhaps supplanting docking in some cases. This is because there are now simple systems such as Biovia's QSAR Workbench (QSAR-WB) that automatically build and test a huge number of QSAR models, including regression, recursive partitioning, neural networks, random forests, and so on. The results are presented in an intuitive way so you do not need a deep expert in statistics to wade through them. (For instance, it is easy to see overfitting of neural network models.)

The next prediction is the renaissance of structure-based *de novo* design methods. This is another area where disappointing results in synthetic prediction methods and poor scoring functions led to its almost complete abandonment in the early 2000s. (We could not find anyone to write a chapter on *de novo* design for this book; try doing a literature search for *de novo* design

from 2005 onward…) De novo design was replaced by systems using known building blocks and known chemistry to devise large (but relatively limited) chemistry spaces that could be explored using either computational or experimental methods. Yet, there is much more synthetic chemistry literature now, so a Google-like data-driven approach to synthetic accessibility might work. Besides, there are also newer synthetic prediction programs arriving on the scene. We can see a time in the next few years where *de novo* design systems are run on good resolution target structures and provide new designs with a good chance of actual synthesis.

Automation continues to impact on all aspects of our lives, and while it removes the drudgery, so the editors' dishwashers free us up to watch the aforementioned old Star Trek and Blade Runner movies, automation also brings objectivity. We have seen how the Protein Data Bank is encouraging crystallographers to minimize subjectivity in determining X-ray structures, and automated QSAR modeling is removing the subjectivity from QSAR model building. Maybe more automation is also a trend we should encourage as much as possible in the wider computational chemistry discipline.

Ultimately, computational chemists (and those who depend on them) should remember that they are merely purveyors of opinion. We don't make anything nor test anything nor create primary data. This sounds like a bleak message in a book on the use of *in silico* tools. Yet, we have shown that computational chemistry has had an impact for years and it would be an odd drug discovery effort that did not use some sort of computational prediction. The main and perhaps only real job of a computational chemist is to provide testable hypotheses, via a mixture of routine computational methods and some personal inspiration (the equivalent of the chemist's "gut feeling index"). We see the role becoming even more so. If automated systems such as the QSAR-WB take away some of the tedium and QM methods and improved force fields provide better scoring of docking poses, then the job will become even more to do with devising molecules to address issues and optimize potency. That is, if we are not drowning under a sea of output from huge simulation runs and massive lists of alternate molecules…

So that's the end of the introduction from Darwin's survivors, and the start of the book. Natural selection has chosen us three old dinosaurs/dragonflies/coelacanths, and may we continue to roar/buzz/burble(?) for a few years more. It's hard to say which of us Darwin successes will be around in 10 years' time, we hope we are all still deep, reflective, and provocative and that this will help our survival, but our money is on *Comprehensive Medicinal Chemistry IV*.

References

1. Materials science. Solid Form Design and Crystallisation Process Development Roberts, Kevin; Docherty, Robert; Taylor. *Stefan RSC Drug Discovery Series* **2011,** *9,* 286–316 (Pharmaceutical Process Development).
2. Docherty, R.; Clear, N. In *Handbook of Medicinal Chemistry;* Davis, A. M., Ward, S., Eds.; RSC Publishing, 2014.
3. Feeder, N.; Pidcock, E.; Reilly, A. M.; Sadiq, G.; Doherty, C. L.; Back, K. R.; Meenan, P.; Docherty, R. The Integration of Solid-Form Informatics into Solid-Form Selection. *J. Pharm. Pharmacol.* **2015,** *67* (6), 857–868.
4. Sykes, D. A.; Charlton, S. J. Slow Receptor Dissociation Is Not a Key Factor in the Duration of Action of Inhaled Long-Acting 2-Adrenoceptor Agonists. *Br. J. Pharmacol.* **2012,** *165* (8), 2672–2683.
5. Dahl, G.; Akerud, T. Pharmacokinetics and the Drug-Target Residence Time Concept. *Drug Discovery Today* **2013,** *18* (15–16), 697–707.
6. Swinney, D. C. The Role of Binding Kinetics in Therapeutically Useful Drug Action. *Curr. Opin. Drug Discovery Dev.* **2009,** *12* (1), 31–39.
7. Klebe, G. The Use of Thermodynamic and Kinetic Data in Drug Discovery: Decisive Insight or Increasing the Puzzlement? *ChemMedChem* **2015,** *10* (2), 229–231.
8. Gonzalez-Bello, C. Designing Irreversible Inhibitors-Worth the Effort? *ChemMedChem* **2016,** *11* (1), 22–30.
9. Singh, P. K.; Singh, H.; Silakari, O. Kinases Inhibitors in Lung Cancer: From Benchside to Bedside. *Biochim. Biophys. Acta Rev. Cancer* **2016,** *1866* (1), 128–140.
10. Hennessy, E. J.; Chuaqui, C.; Ashton, S.; Colclough, N.; Cross, D. A. E.; Debreczeni, J. E.; Eberlein, C.; Gingipalli, L.; Klinowska, T. C. M.; Orme, J. P.; et al. Utilization of Structure-based Design to Identify Novel, Irreversible Inhibitors of EGFR Harboring the T790M Mutation. *ACS Med. Chem. Lett.* **2016,** *7* (5), 514–519.
11. Ladbury, J. E.; Klebe, G.; Freire, E. Adding Calorimetric Data to Decision Making in Lead Discovery: A Hot Tip. *Nat. Rev. Drug Discovery* **2010,** *9* (1), 23–27.
12. Ruehmann, E.; Betz, M.; Heine, A.; Klebe, G. Fragment Binding Can Be Either More Enthalpy-Driven or Entropy-Driven: Crystal Structures and Residual Hydration Patterns Suggest Why. *J. Med. Chem.* **2015,** *58* (17), 6960–6971.
13. Krishnamurthy, V. M.; Bohall, B. R.; Semetey, V.; Whitesides, G. M. The Paradoxical Thermodynamic Basis for the Interaction of Ethylene Glycol, Glycine, and Sarcosine Chains with Bovine Carbonic Anhydrase II: An Unexpected Manifestation of Enthalpy/Entropy Compensation. *J. Am. Chem. Soc.* **2006,** *128* (17), 5802–5812.
14. Krimmer, S. G.; Betz, M.; Heine, A.; Klebe, G. Methyl, Ethyl, Propyl, Butyl: Futile but Not for Water, as the Correlation of Structure and Thermodynamic Signature Shows in a Congeneric Series of Thermolysin Inhibitors Quick View Other Sources. *ChemMedChem* **2014,** *9* (4), 833–846.
15. Klebe, G. Applying Thermodynamic Profiling in Lead Finding and Optimization. *Nat. Rev. Drug Discovery* **2015,** *14* (2), 95–110.
16. Brandmaier, S.; Sahlin, U.; Tetko, I. V.; Oberg, T. Pls-optimal: a Stepwise D-optimal Design Based on Latent Variables. *J. Chem. Inf. Model.* **2012,** *52* (4), 975–983.
17. Tye, H. Application of Statistical 'design of Experiments' Methods in Drug Discovery. *Drug Discovery Today* **2004,** *9* (11), 485–491.
18. Brandmaier, S.; Tetko, I. V.; Oeberg, T. An Evaluation of Experimental Design in QSAR Modelling Utilizing the K-medoid Clustering. *J. Chemom.* **2012,** *26* (10), 509–517.
19. Sahariah, P.; Snorradottir, B. S.; Hjalmarsdottir, M. A.; Sigurjonsson, O. E.; Masson, M. Experimental Design for Determining Quantitative Structure Activity Relationship for Antibacterial Chitosan Derivatives. *J. Mater. Chem. B Mater. Biol. Med.* **2016,** *4* (27), 4762–4770.
20. Maciejewski, M.; Wassermann, A. M.; Glick, M.; Lounkine, E. Experimental Design Strategy: Weak Reinforcement Leads to Increased Hit Rates and Enhanced Chemical Diversity. *J. Chem. Inf. Model.* **2015,** *55* (5), 956–962.
21. Giannetti, A. M. From Experimental Design to Validated Hits: A Comprehensive Walk-through of Fragment Lead Identification Using Surface Plasmon Resonance. *Methods Enzymol.* **2011,** *493,* 169–218 (Fragment-Based Drug Design).
22. Segall, M. D.; Champness, E. J. The Challenges of Making Decisions Using Uncertain Data. *J. Comp. Aided Mol. Design* **2015,** *29* (9), 809–816.
23. Bell, A. S.; Bradley, J.; Everett, J. R.; Loesel, J.; McLoughlin, D.; Mills, J.; Peakman, M.-C.; Sharp, R. E.; Williams, C.; Zhu, H. Plate-based Diversity Subset Screening Generation 2: an Improved Paradigm for High-throughput Screening of Large Compound Files. *Mol. Diversity* **2016**. Ahead of Print.
24. Paricharak, S.; Ijzerman, A. P.; Bender, A.; Nigsch, F. Analysis of Iterative Screening with Stepwise Compound Selection Based on Novartis In-house HTS Data. *ACS Chem. Biol.* **2016,** *11* (5), 1255–1264.

25. Macarron, R. Chemical Libraries How Dark Is HTS Dark Matter? *Nat. Chem. Biol.* **2015,** *11* (12), 904–905.
26. Cumming, J. G.; Davis, A. M.; Muresan, S.; Haeberlein, M.; Chen, H. Chemical Predictive Modelling to Improve Compound Quality. *Nat. Rev. Drug Discovery* **2013,** *12* (12), 948–962.
27. Teague, S. J.; Davis, A. M.; Leeson, P. D.; Oprea, T. The Design of Leadlike Combinatorial Libraries. *Angew. Chem. Int. Ed.* **1999,** *38* (24), 3743–3748.
28. Erlanson, D. A.; Fesik, S. W.; Hubbard, R. E.; Jahnke, W.; Jhoti, H. Twenty Years on: the Impact of Fragments on Drug Discovery. *Nat. Rev. Drug Discovery* **2016,** *15* (9), 605–619.
29. Clark, M. A.; Acharya, R. A.; Arico-Muendel, C. C.; Belyanskaya, S. L.; Benjamin, D. R.; Carlson, N. R.; Centrella, P. A.; Chiu, C. H.; Creaser, S. P.; Cuozzo, J. W.; et al. Design, Synthesis and Selection of DNA-Encoded Small-Molecule Libraries. *Nat. Chem. Biol.* **2009,** *5* (9), 647–654.
30. Hu, Q.; Peng, Z.; Kostrowicki, J.; Kuki, A. LEAP into the Pfizer Global Virtual Library (PGVL) Space: Creation of Readily Synthesizable Design Ideas Automatically. *Methods Mol. Biol. (New York, NY, United States)* **2011,** *685,* 253–276 (Chemical Library Design).
31. Hu, Q.; Peng, Z.; Sutton, S. C.; Na, J.; Kostrowicki, J.; Yang, B.; Thacher, T.; Kong, X.; Mattaparti, S.; Zhou, J. Z.; et al. Pfizer Global Virtual Library (PGVL): A Chemistry Design Tool Powered by Experimentally Validated Parallel Synthesis Information. *ACS Comb. Sci.* **2012,** *14* (11), 579–589.
32. Nicolaou, C. A.; Watson, I. A.; Hu, H.; Wang, J. The Proximal Lilly Collection: Mapping, Exploring and Exploiting Feasible Chemical Space. *J. Chem. Inf. Model.* **2016,** *56* (7), 1253–1266.
33. Halgren, T. Merck Molecular Force Field. I. Basis, Form, Scope, Parameterization, and Performance of MMFF94. *J. Comp. Chem.* **1996,** 17.
34. Shi, Y.; et al. The Polarizable Atomic Multipole-Based AMOEBA Force Field for Proteins. *J. Chem. Theory Comput.* **2013,** *9* (9), 4046–4063.
35. Salomon-Ferrer, R.; Case, D. A.; Walker, R. C. An Overview of the Amber Biomolecular Simulation Package. *Wiley Interdiscip. Rev. Comput. Mol. Sci.* **2013,** *3* (2), 198–210.

PERMISSION ACKNOWLEDGMENTS

The following material is reproduced with kind permission of Taylor & Francis

Scheme 2 Cellular Imaging in Drug Discovery: Biomolecular Imaging and Informatics (HCS, HCA, HCI)
Figure 2 Past Present Future
Figure 5 Past Present Future
Figure 6 Past Present Future
www.taylorandfrancisgroup.com

The following material is reproduced with kind permission of Oxford University press

Table 1 Targeting G-quadruplex Nucleic Acids for Cancer Therapy
Table 2 Targeting G-quadruplex Nucleic Acids for Cancer Therapy
Figure 1 Protein Structure Prediction and Homology Modelling
www.oup.com

The following material is reproduced with kind permission of American Association for the Advancement of Science

Figure 3b,c Cellular Imaging in Drug Discovery: Biomolecular Imaging and Informatics (HCS, HCA, HCI)
www.aaas.org

The following material is reproduced with kind permission of Nature Publishing Group

Table 4 Use of Stem Cells in Toxicology
Table 6 Use of Stem Cells in Toxicology
Figure 17 Strategy and Tactics for Designing Analogs; Biochemical Characterization of the Large Molecules
Figure 30 Strategy and Tactics for Designing Analogs; Biochemical Characterization of the Large Molecules
Figure 2 Cellular Imaging in Drug Discovery: Biomolecular Imaging and Informatics (HCS, HCA, HCI)
Figure 3a Cellular Imaging in Drug Discovery: Biomolecular Imaging and Informatics (HCS, HCA, HCI)
Figure 4 Cellular Imaging in Drug Discovery: Biomolecular Imaging and Informatics (HCS, HCA, HCI)
Figure 5a Cellular Imaging in Drug Discovery: Biomolecular Imaging and Informatics (HCS, HCA, HCI)
Figure 9a Cellular Imaging in Drug Discovery: Biomolecular Imaging and Informatics (HCS, HCA, HCI)
Figure 20 Epigenetics: Novel Therapeutics Targeting Epigenetics
Figure 1 UCB5857
Figure 6 Empirical and Physics Based Calculations of Physical Properties
Figure 4 Progress and Challenges in the Development if PET Ligands to Aid CNS Drug Discovery
http://www.nature.com

3.01 Perspective on Calculations of Binding Free Energies

H Yoon and A Warshel, University of Southern California, Los Angeles, CA, United States

© 2017 Elsevier Ltd. All rights reserved.

3.01.1	**Introduction**	1
3.01.2	**Computational Strategies**	1
3.01.2.1	Rigorous but Slowly Converging Calculations by All-Atom Models	1
3.01.2.2	Using Simplified Electrostatic Models	4
3.01.3	**Calculating Binding Free Energies by Different Strategies**	5
3.01.3.1	Studies of Drug Binding by FEP Approaches	5
3.01.3.2	Evaluation of Absolute Binding Energies by the LRA and LIE Approaches	6
3.01.3.3	Semimacroscopic and Macroscopic Calculations of Ligand Binding	6
3.01.3.4	Protein–Protein Interactions	6
3.01.3.5	Binding Entropy Calculations	8
3.01.4	**Perspectives**	8
Acknowledgment		11
References		12

3.01.1 Introduction

The ability to correlate the structure of protein–ligand complexes with their binding affinity is a challenge of major practical and fundamental importance. A clear example is the need for effective tools in rational design of drugs that would block the activity of proteins that are involved in specific diseases. Thus, reaching accurate prediction in calculations of binding energies is one of the most important aims of computational biology. The starting point for addressing this challenge is the progress in structural evaluations of protein–ligand complexes by X-ray crystallography and NMR spectroscopy. The Protein Data Bank (PDB)[1] continues to grow at an accelerated rate. The enormous structural advances call for a corresponding progress in the use of computer modeling in analyzing the energetics of protein–ligand complexes. An obvious step in such studies is the ability to search for optimal docking of proteins and different drug candidates. Several effective programs have been developed for this purpose (e.g., Glide,[2] GOLD,[3] FlexX,[4] and DOCK[5]). For review see Refs. 6–8. However, this issue is out of the scope of the present review (except in using the docking programs in finding starting points for calculations of binding free energies). Here, we provide some perspective on calculations of binding free energies emphasizing the progress made after our last review.[9] In particular, we will emphasize approaches that are based on "first-principle" free energy estimates.

As far as rational drug design is concerned, the role of first-principle binding calculations is mainly in ranking sets of reasonable candidates, which are obtained from more qualitative approaches. Unfortunately, the advance in the more quantitative direction is still far from being satisfactory. However, at some stage (which might be coming relatively soon), we expect calculations of binding free energies and in particular the corresponding electrostatic contributions should become a major quantitative tool in rational drug design.

3.01.2 Computational Strategies

The key to energy-based drug design is the ability to obtain reliable free energy results in calculations of protein–ligand interactions. Accomplishing this task is, however, far from simple, due to inherent convergence problems and to inconsistencies of some approaches. In this review, we consider different strategies for evaluations of binding free energies. In doing so, we pay major attention to calculations of electrostatic contributions to the overall binding free energy, since we consider this effect to be the most important contribution. However, we will also consider approaches that evaluate all other contributions in the following sections.

3.01.2.1 Rigorous but Slowly Converging Calculations by All-Atom Models

Thermodynamic cycles of the same type as used in chemistry textbooks can describe many biochemical processes. Such cycles allow one to replace the very challenging direct calculations of physical processes by calculations of much simpler either physical or nonphysical processes. The use of thermodynamic cycles in microscopic calculations of free energies of biological processes had been introduced in the early 1980s.[10] These studies focused on the evaluation of the difference between the pK_a of acids in proteins and in water, by considering the nonphysical process of "mutating" the protonated acid to its ionized form in the protein and in water, instead of calculating the binding energies of the protonated and ionized forms of the acid.[10] Another example has been provided by studies of enzyme catalysis[10,11] (see discussion in Ref. 12). Related cycles for studies of ligand binding have been

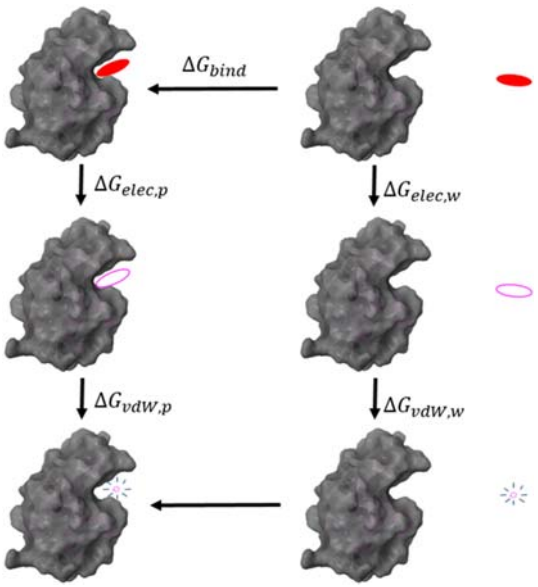

Fig. 1 A schematic description of the free energy cycle for protein–ligand binding. The ligand on the right changes from being polar to nonpolar and to nothing. The cycle is divided into electrostatic and nonelectrostatic parts.

introduced in Ref. 13. At any rate, thermodynamic cycles have become a major part of many approaches in free-energy calculations of biological processes (e.g., Refs. 13–15).

In principle, we can evaluate binding free energies using the cycle of Fig. 1

Of course, the key issue in the evaluation of thermodynamic cycles is the ability to evaluate the relevant free energies. Unfortunately, doing so by statistical mechanical approaches and microscopic simulations is extremely time consuming, owing to the difficulties of sampling the relevant conformational space. We will consider later some approaches that allow one to evaluate the energies in the cycle. Before doing so, it is useful to clarify that the upper part of the cycle can be evaluated by a direct approach (Fig. 2), but the evaluation of the corresponding potential of mean force (PMF) is extremely challenging, since it should reflect the equilibration of the surrounding water molecules during the penetration of the substrate to the active site.

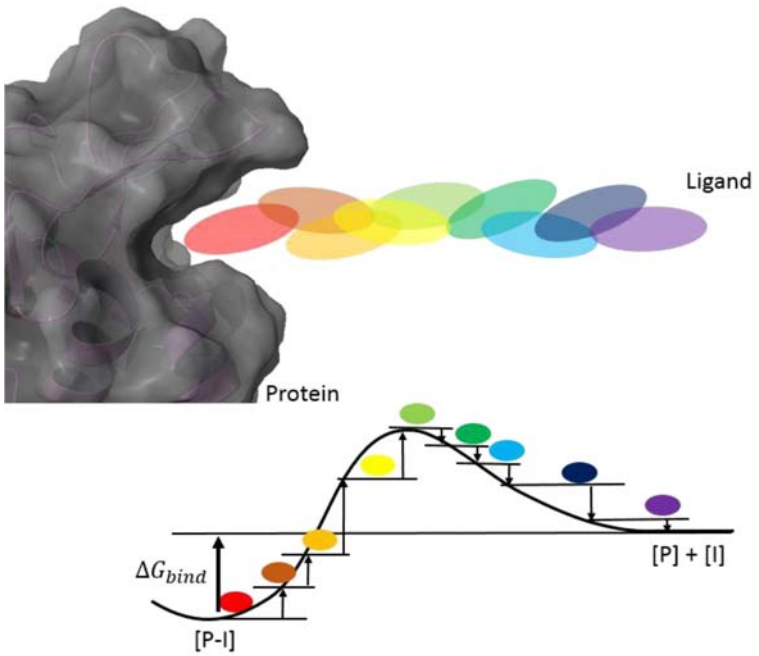

Fig. 2 Showing a direct approach of evaluating the binding free energy by evaluating the corresponding PMF.

To avoid the PMF calculations we can start by considering the thermodynamic cycle of Fig. 1

These contributions can be evaluated in principle by the free-energy perturbation (FEP) method[16,17] and the related umbrella sampling method.[17] The FEP method evaluates the free energy associated with the change of the potential surface from U_1 to U_2 by gradually changing the potential surface using the relationship

$$U_m(\lambda_m) = U_1(1-\lambda_m) + U_2\lambda_m \tag{1}$$

where λ_m is a parameter that changes between $(0 \le \lambda_m \le 1)$. The free-energy increment, associated with the change of U_m, can be obtained by[17]

$$exp\{-\delta G(\lambda_m \rightarrow \lambda_{m'})\beta\} = \langle exp\{-(U_{m'} - U_m)\beta\}\rangle_m \tag{2}$$

where $\langle\rangle_m$ indicates that the given average is evaluated by propagating trajectories over U_m. The overall free-energy change is now obtained by changing λ_m in n increments and evaluating the sum of the corresponding δG:

$$\Delta G(U_1 \rightarrow U_2) = \sum_{m=0}^{n-1} \delta G(\lambda_m \rightarrow \lambda_{m+1}) \tag{3}$$

The FEP approach has been used extensively in studies of free energies of biological systems (e.g., Refs. 14,18) and has been introduced quite early[19] in studies of electrostatic free energies in proteins.

In many cases, it is very hard to perform converging FEP calculations (e.g., binding of large ligands). In such cases, it is very useful to estimate the free energy of biological processes by an equation derived by Lee et al.[20,21] and used in studies of ligand binding to proteins. This equation expresses the free energy associated with changing the potential of the system from U_1 to U_2 by

$$\Delta G(U_1 \rightarrow U_2) = \frac{1}{2}\left(\langle U_2 - U_1\rangle_1 + \langle U_2 - U_1\rangle_2\right) \tag{4}$$

where $\langle\rangle_i$ designates an average over molecular dynamics (MD) trajectories obtained with $U = U_i$. The derivation of this equation was based on the assumption that the linear response approximation (LRA)[22] is valid. Namely, the protein and solvent environments respond linearly to the force associated with the given process. This assumption is, in fact, the basis of macroscopic theory where the free energy of charging a positive ion is given by the well-known result $\Delta G = \S U(Q=1)$, where U is the electrostatic potential of the given charge (Q).[23] Although it is hard to accept that the LRA can provide a reliable way of describing the energetics of macromolecules or of realistic molecular systems, it was found by simulation studies that it is a reasonable approximation, in particular for processes that depend on electrostatic effects.[24–27]

In cases when the nonelectrostatic contribution (the lower part of Fig. 1) is important, we need to augment the LRA, and some ways of doing so are described later.

The FEP and PMF evaluations can be performed by approaches that are rigorous in principle. However, it must be emphasized that the convergence of such approaches is extremely slow and that even a perfect convergence does not guarantee proper results. For example, FEP calculations using models with improper long-range treatments cannot provide proper electrostatic energy. This issue is discussed in great detail in Ref. 28 and can only be appreciated by trying to evaluate known electrostatic free energies like pK_as. Interestingly, the PMF approach, which has the appearance of the most rigorous approach (here one simply pulls the ligand to the active site), may make one "blind" to problems with the simulation model. For example, PMF studies of ion penetration in ion channels do not tell us about the absolute energy of moving the ion from water to the given channel site. Thus, one might tend to believe that the electrostatic model is correct even if the absolute energies are entirely incorrect (see discussion in Ref. 29).

In calculations of binding free energies, it is recommended to use specialized spherical models[30–32] and to avoid the use of the periodic Ewald method[33–35] in estimating long-range corrections (see discussion in Ref. 28). The slow realization that proper treatments of long-range effects are crucial for proper modeling of protein functions is still a major problem in the field. Apparently, many workers still emphasize the length of the simulations and the number of atoms in the simulation system instead of validating the calculated electrostatic free energies.

The convergence problem becomes more serious when we are trying to evaluate van der Waals (vdW) contributions (the transition from the middle stage to the lower stage in Fig. 1). This stage involves mutating the nonpolar substrate from its current size to a dummy atom of a zero size. A direct FEP mutation leads to a convergence catastrophe since the motion on the end point with zero vdW can lead to infinite values for the real potential.[36–38] Several ways have been provided to resolve this problem by replacing the zero vdW potential of the dummy atom by a finite potential[39–41] (see also later).

Another major problem is the evaluation of the effect of water penetration. That is, not only is it hard in such cases to identify the position of the water molecules, but also this position changes drastically during the binding process. In principle, one can try to insert water molecules in a grand canonical Monte Carlo (MC) treatment, but the chance of a water molecule being accepted is extremely small since in most insertion attempts, we will not have a large enough cavity in the protein site. Our strategy for this challenging problem is the water flooding (WF) approach,[42] where (see Fig. 3) we insert clusters of water molecules into the active site, relax and optimize the energy of the cluster, and then use the LRA approach to estimate the energy of each of the internal water molecules in the cluster. Next we take the LRA-estimated energies of the internal water and evaluate the probability that a water molecule will be inside the protein by running an external MC program that postprocesses the energetics by simply iterating on the LRA run relative to the energy of inserting water in aqueous solution (where the free energy is around -6 kcal/mol). Our

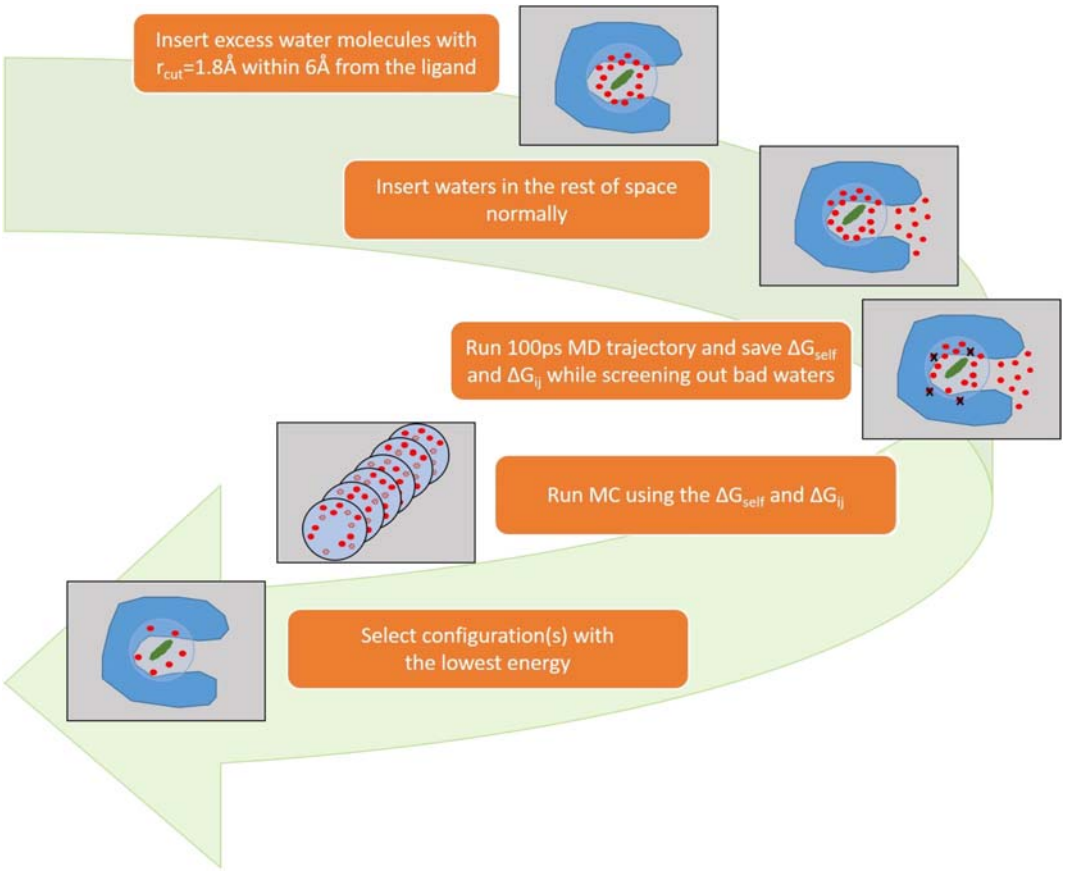

Fig. 3 Illustrating the water flooding procedure.

postprocessing approach means that instead of running MC on actual water insertion we already have energies for inserted water molecules and the MC is performed on these energies.

In concluding this section, we note that despite the early emergence of FEP calculations of electrostatic energies in proteins (e.g., Refs. 19,43), there are still major convergence problems in both FEP- and LRA-type studies (e.g., Refs. 44,45).

Some of these convergence problems can be reduced by the vdW calculations and the WF approach.

3.01.2.2 Using Simplified Electrostatic Models

Calculations of electrostatic energies provide one of the most effective correlations between the structure and function of proteins (e.g., Ref. 23). As explained in Ref. 28 the first consistent treatment of electrostatic energies in proteins[46] represented all the relevant electrostatic interactions microscopically but used a simplified model of Langevin-type dipoles on a grid to represent the solvent. This protein dipoles Langevin dipoles (PDLD) model facilitated studies of the role of electrostatic energies in protein function with the limited computer power of the mid-1970s (see Ref. 23). Such studies considered microscopically the shape of the protein and its local polarity as well as the effect of the solvent around the protein and to a limited extent the effect of the protein reorganization (which was modeled by energy minimization). The subsequent advance in Poisson–Boltzmann (PB)-type models has allowed macroscopic continuum approaches to take into account the shape of the protein.[47,48] Early discretized continuum models involved some of the inconsistencies of the Tanford–Kirkwood (TK) model (see discussion in Ref.28). However, recent PB models have represented these dipoles explicitly, and became increasingly semimacroscopic.[49]

In many cases, one finds that macroscopic and semimacroscopic models give more stable results than the corresponding microscopic models. This interesting feature is due to the fact that the microscopic models involve compensation of large numbers while the macroscopic models assume implicitly that the compensation exists by using a protein dielectric constant, ε_p. Thus, PB models give excellent results when dealing with surface groups but become more problematic when one deals with groups in the protein interiors. Here the problem is that the results depend strongly on the assumed ε_p, which apparently has little to do with the actual protein dielectric but merely with the contributions that are treated implicitly (see Refs. 50,51).

An effective way to exploit the stability of the semimacroscopic models, and yet to keep a clear physical picture, is the semimacroscopic version of the PDLD model (the PDLD/S model[43]). The PDLD/S model takes the PDLD model and scales the

corresponding contributions by assuming that the protein has a dielectric constant, ε_p. Now, in order to reduce the unknown factors in ε_p, it is useful to move to the PDLD/S-LRA model, where the PDLD/S energy is evaluated within the LRA approximation of Eq. (6) with an average on the configurations generated by MD simulation of the charged and the uncharged states (see Refs. 44,51,52). Since the protein reorganization is considered explicitly, we have less uncertainty with ε_p.

In deriving the PDLD/S-LRA binding expression, we note that the cycle of Fig. 1 is composed of electrostatic and nonelectrostatic components and expresses the binding free energy as

$$\Delta G_{\text{bind}} = \frac{1}{2}\left[\left\langle U^{p}_{\text{elec},\ell}\right\rangle_{\ell} + \left\langle U^{p}_{\text{elec},\ell}\right\rangle_{\ell'} - \left\langle U^{w}_{\text{elec},\ell}\right\rangle_{\ell} - \left\langle U^{w}_{\text{elec},\ell}\right\rangle_{\ell'}\right] + \Delta G^{\text{nonelec}}_{\text{bind}} \tag{5}$$

where $U^{p}_{\text{elec},\ell}$ is the electrostatic contribution for the interaction between the ligand and its surroundings, p and w designate protein and water, respectively, and ℓ and ℓ' designate the ligand in its actual charged form and the "nonpolar" ligand where all the residual charges are set to zero. In this expression, the terms $\langle U_{\text{elec},\ell} - U_{\text{elec},\ell'}\rangle$, which are required by Eq. (4), are replaced by $\langle U_{\text{elec},\ell}\rangle$ since $U_{\text{elec},\ell'} = 0$. Now, the evaluation of the nonelectrostatic contribution $\Delta G^{\text{nonelec}}_{\text{bind}}$ is still very challenging, since these contributions might not follow the LRA. A useful option, which was used in Refs. 20 and 53 is to evaluate the contribution to the binding free energy from hydrophobic effects, vdW, and water penetration. Another powerful option is the so-called linear interaction energy (LIE) approach.[26,54] This approach adopts the LRA approximation for the electrostatic contribution but neglects the $\langle U_{\text{elec},\ell}\rangle_{\ell'}$ terms. If we use the PDLD/S approach and the Us that correspond to this approach (see Ref. 55), we can write the binding energy using

$$\Delta G^{\text{elec/PDLD/S-LRA}}_{\text{bind}} = \frac{1}{2}\left\{\left[\left\langle \bar{U}^{p}_{\text{elec},l}\right\rangle_{l'} + \left\langle \bar{U}^{p}_{\text{elec},l}\right\rangle_{l}\right] - \left[\left\langle \bar{U}^{w}_{\text{elec},l}\right\rangle_{l'} + \left\langle \bar{U}^{w}_{\text{elec},l}\right\rangle_{l}\right]\right\} \tag{6}$$

$$\Delta G^{\text{PDLD/S-LRA}/\beta}_{\text{bind}} = \Delta G^{\text{elec/PDLD/S-LRA}}_{\text{bind}} + \beta\left(\left\langle U^{\beta}_{\text{vdw},\ell}\right\rangle_{\ell} - \left\langle U^{w}_{\text{vdw},\ell}\right\rangle_{\ell}\right) \tag{7}$$

where β is an empirical parameter that scales the vdW component of the protein–ligand interaction. A careful analysis of the relationship between the LRA and LIE approaches and the origin of the α and β parameters is given in Ref. 53

It is also important to mention that the increasingly popular molecular mechanics PB surface area (MM/PBSA) model,[56] and the related molecular mechanics-generalized Born surface area MM/GBSA are apparently inconsistent adaptations of the PDLD/S-LRA idea of MD generation of configurations for implicit solvent calculations, while only calculating the average over the configurations generated with the charged solute (the first term of Eq. 6). More importantly, the MM/PBSA and MM/GBSA are problematic on other key levels. The first problem is that the model uses $\varepsilon_p = 1$ without sufficient relaxation, this means that the interaction between ionized groups is overestimated in a major way. The model uses entropy estimates that are simply incorrect (see Ref. 55) and finally it uses a vdW term that sometimes compensates for the error in the other terms. The problems with the (MM/PBSA) have been quantified and demonstrated clearly in Ref. 55.

3.01.3 Calculating Binding Free Energies by Different Strategies

Armed with the computational approaches described in the "Computational Strategies" section, we may now examine different strategies for the calculation of binding free energies.

3.01.3.1 Studies of Drug Binding by FEP Approaches

In principle, we can evaluate binding energies by the two paths depicted in Fig. 1 and Fig. 2. The path of Fig. 2 involves a direct PMF calculation but such a strategy still involves major convergence problems in trying to capture the solvent protein rearrangements associated with the transfer of the ligand from the bulk water to the protein-binding site. The path of Fig. 1 involves a cycle that can be evaluated by the FEP approach. This approach gives reasonable results in studies of differences in binding due to small "mutations" of the given ligand[13,14,57] (e.g., replacement of NH_2 by OH) but it involves major convergence problems when one tries to evaluate the absolute binding free energy of medium-size ligands. In such cases, one has to "mutate" the ligand to "nothing," and at present, the reported results are quite disappointing except in cases of small ligands. Nevertheless, this approach can be used in some well-defined test cases of polar or charged ligands (e.g., Refs. 20,58,59) and it can be considered, at least in principle, as the "cleanest" approach for calculations of absolute binding energies. At any rate, the constant increase of computer power makes FEP calculations more and more practical and thus we try to consider here the current performance. A good example is provided by a case where a careful benchmark of Ref. 60 encountered large deviation and was forced to scale the ligand charge. Our study includes WF and the move from nonpolarized to polarized force field (see Table 1) and showed significant improvement upon moving to polarized force field. Our finding can serve as a useful example for the advantages of using polarizable force field.

Interestingly, as will be shown in the following section, the PDLD/S gives better results than the present FEP calculations. Thus, we leave the more systematic exploration of the current problems of the FEP approach to subsequent studies.

Table 1 The trend in FEP calculations of binding energies of a challenging cases[a]

Ligand	*PDB*	*Experimental (kcal/mol)*	*FEP (kcal/mol)*	*FEP/induced (kcal/mol)*
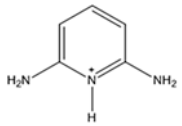	4JM8	−5.8	−15.6	−3.9
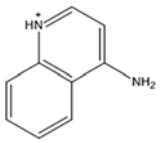	4JQJ	−5.8	−18.7	−9.5
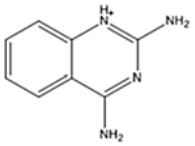	4JPT	−5.7	−14.3	−7.9
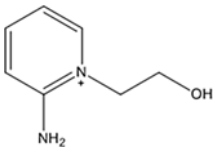	4JQK	−4.7	−13.0	−4.8

[a]The benchmark considered includes cases where Ref. 60 found large deviations for charged drugs.

3.01.3.2 Evaluation of Absolute Binding Energies by the LRA and LIE Approaches

In the general case of large ligands, it is not obvious that the FEP approach is the optimal option and the best alternative is probably provided by the PDLD/S-LRA β method of Eq. (7). This approach is particularly effective in calculating the electrostatic contribution to the binding energy.[20,53]

The idea that conformational averaging is useful for free energy calculations seems quite obvious, generally understood, and widely used.[56,61] What is much less understood, and somehow still ignored by a large part of the computational community, is that a proper LRA treatment requires averaging on both the charged (or polar) and nonpolar states of the ligand. The frequently neglected average on the nonpolar state (the second term of Eq. 6) plays a crucial role in proteins as it reflects the effect of the protein preorganization. The role of this term in binding calculations has been discussed in Ref. 53 and its importance has been illustrated in an impressive way in studies of the fidelity of DNA polymerase.[62] This study found that the crucial process of discrimination between correct and incorrect bases is determined to a significant extent by the preorganization of the binding site plus the template.

A systematic study[55] of the performance of the LIE and LRA β considered the benchmark of **Fig. 4**.

The results of the study are given in **Fig. 5** and show a very reasonable agreement between the calculated free energy and observed results.

3.01.3.3 Semimacroscopic and Macroscopic Calculations of Ligand Binding

As pointed out earlier, although microscopic models are rigorous in principle they may involve major convergence problems and thus it may be useful to explore binding energies by semimacroscopic and macroscopic approaches. This includes the use of Eq. (5) and the PDLD/S-LRA β model of Eq. (7), as well as other approaches mentioned in the "**Using Simplified Electrostatic Models**" section. The electrostatic contribution of the PDLD/S-LRA β is quite rigorous since it considers explicitly the protein reorganization and thus allows one to use less arbitrary ε_p than the one used by more macroscopic approaches. The more *ad hoc* nonelectrostatic term also seems to be quite effective with the proper scaling. An example of the performance of the PDLD/S-LRA β-type approach in binding calculations is given in **Fig. 5**.

Another validation has been obtained recently and is summarized in **Table 2**. In this case, we consider the very challenging benchmark of Refs. 60 and 63 comparing the FEP calculations reported in this works to the PDLD/S-LRA β results.

3.01.3.4 Protein–Protein Interactions

One of the most exciting aspects of rational drug design involves the search for drugs that would disrupt the interaction between proteins that transmit different signals in the cell cycle. Here, the hope is that understanding the nature of the interaction between two proteins will allow one to design drugs that would exploit the same type of interactions, and thus will bind to one of the proteins and compete with the binding between these proteins. An example of this idea is given in **Figs. 6** and **7**.

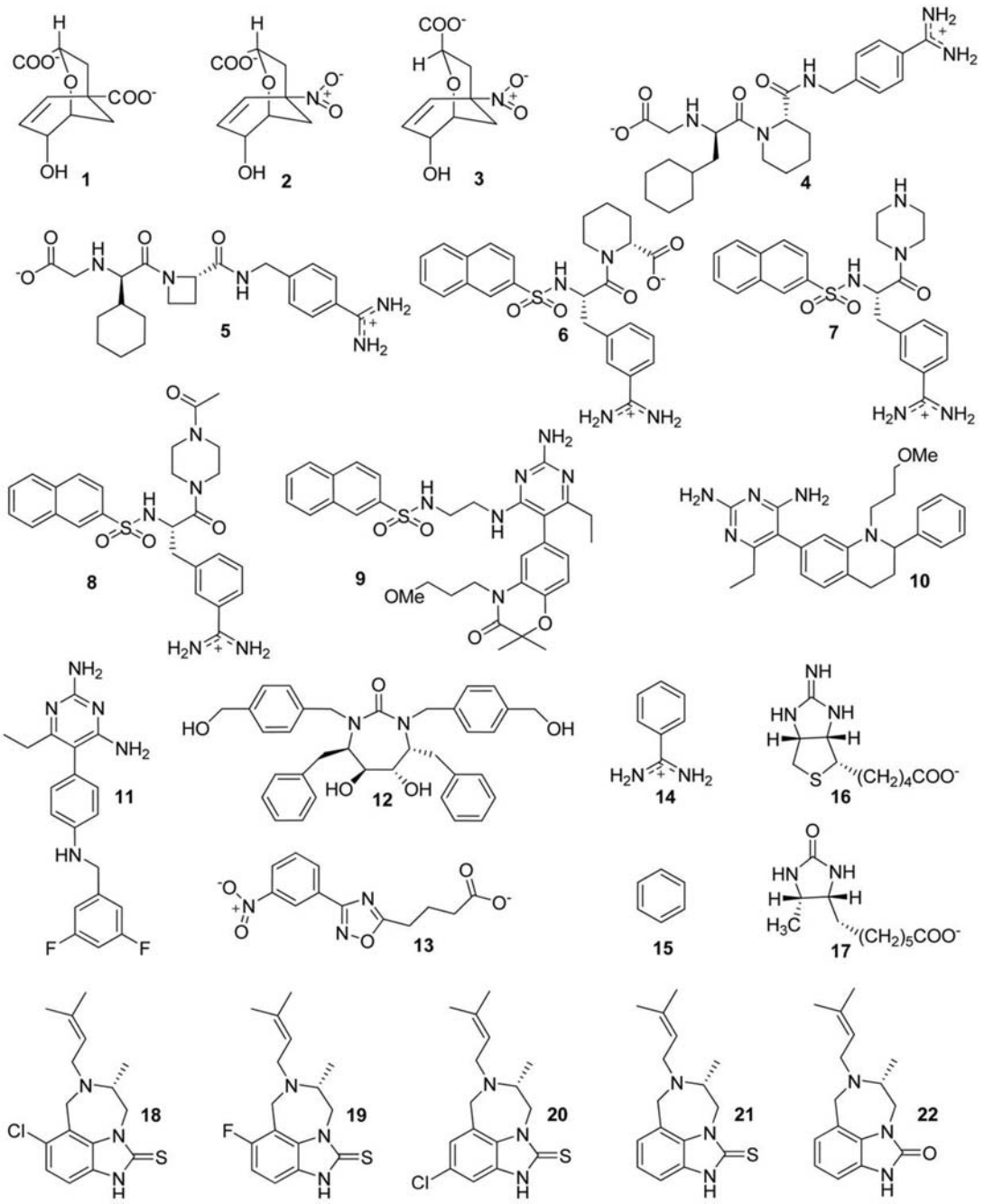

Fig. 4 The benchmark used for the binding calculations of Ref. 55.

Muegge et al. ([64]) explored carefully the effect of the protein reorganization in the Ras/Raf complex. Several approaches and several levels of the PDLD/S-LRA model were explored. However, disappointing results were obtained from the formally most rigorous treatments that consider explicitly the reorganization of the proteins during the binding process while using small ε_p. The most promising results were obtained by using the PDLD/S with $\varepsilon_p = 4$ for dipoles interactions and the simple coulomb charge—charge with large dielectric ($\varepsilon_{eff} = 23$ for charge–charge interaction). This approach was found to be effective in both predicting the effects of mutations on the protein–protein binding energy and in estimating the overall absolute binding energies. Thus, the use of small ε_p for dipole and large ε_{eff} for charge–charge interaction can be quite effective in providing estimates of the contributions of different residues to protein–protein interactions. These types of calculations can be quite useful for designing drugs that would disrupt the binding of Ras and Raf and help fight cancer (see Fig. 6).

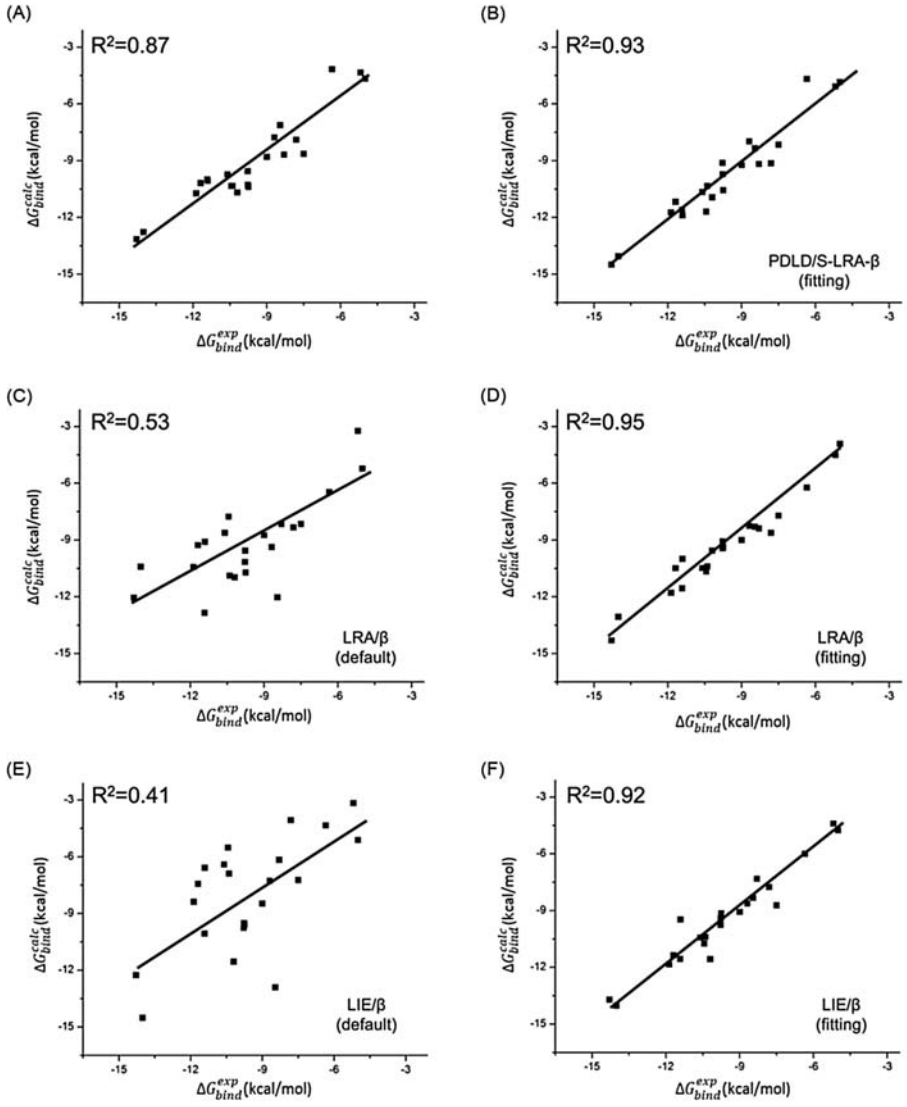

Fig. 5 The correlation between the calculated and observed values for different approaches. Taken from Singh, N.; Warshel, A. Absolute Binding Free Energy Calculations: On the Accuracy of Computational Scoring of Protein–Ligand Interactions. *Proteins: Struct., Funct., Bioinf.* **2010**, *78*, 1705–1723.

3.01.3.5 Binding Entropy Calculations

One of the greater challenges in studies of binding energies is the evaluation of binding entropies. Here, it was realized that the frequently used harmonic or quasiharmonic approximations[65,66] are unlikely to give quantitative results. In a search for a more quantitative model, we adopted our early idea[67] and developed a variational restraint release (RR) approach, which is described in detail elsewhere.[68] This approach was used recently[69] in evaluation of the binding entropy of benzene to bacteriophage T4-lysozyme, and the corresponding thermodynamic cycle is depicted in Fig. 8.

3.01.4 Perspectives

The calculations of binding energies have advanced enormously since pioneering studies that did not include the solvent.[70] However, despite the qualitative and semiquantitative advances in calculation of binding energies, the progress in getting actual quantitative predictions has been quite slow. A part of the problem may have been associated with the belief that approaches that are formally rigorous may have enormous difficulties in converging. This problem has been enhanced by the fact that very few workers tried to validate their approach by comparing the calculated and observed results of challenging benchmarks (see the "Semimacroscopic and Macroscopic Calculations of Ligand Binding" section). Here, as stated earlier, the discrimination between the binding affinities of different ligands in the 2 kcal/mol limit has been disappointing. Our early attempts to evaluate

Table 2 Comparisons of the accuracy of binding energy calculations[a]

Ligand	Exp	FEP	PDLD/S-LRA β			PDLD/S-LRA β with water flooding		
			Intrinsic	Elec	Total	Intrinsic	Elec	Total
(PDB:4JQM)	−7.1	−4.2[60]	−4.6	−6.1	−10.7	−3.6	−5.2	−8.8
(PDB:4JPU)	−6.6	−3.3[60]	−6.7	−6.1	−12.7	−2.1	−6.2	−8.2
(PDB:4JQK)	−4.7	−2.3[60]	5.4	−4.9	0.5	0.4	−3.2	−2.8
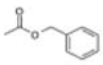 (PDB:3HUK)	−4.5	−1.3[63]	−3.6	0.0	−3.6	−3.4	−0.3	−3.7

[a]Only the cases where Refs. 60 and 63 obtained poor agreement were considered. Apparently the PDLD/S-LRA β results are more reliable than the FEP results for charged ligands. "Intrinsic" designates the results when the charges of the protein ionizable residues are set to zero and "elect" is the change in the binding energies when the effect of the ionizable residues is added by using a charge–charge interaction at dielectric of 40.

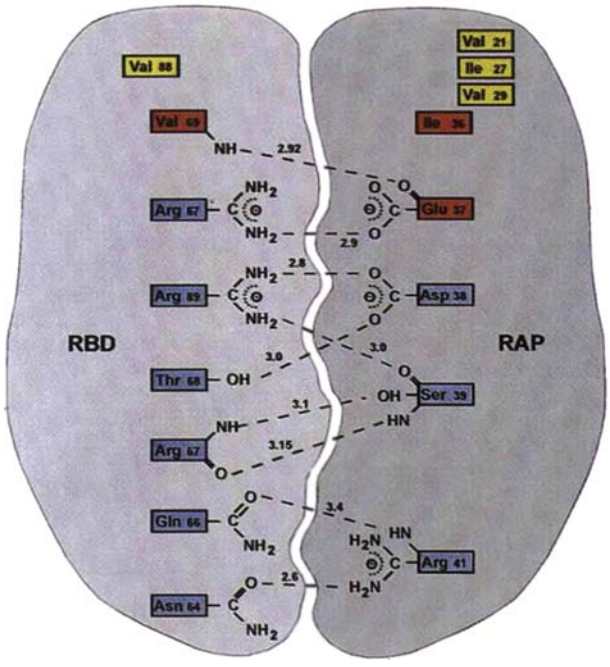

Fig. 6 Showing the residues involved in the Rap/Raf interaction. Taken from Kamerlin, S. C. L., et al. Why Nature Really Chose Phosphate. *Quart. Rev. Biophys.* **2013**, *46*, 1–132.

the binding free energies by the fully microscopic FEP approach were disappointing even with the use of a polarizable force field and the use of proper long-range treatments. Note, however, that the calculations did not include the WF treatment.

As an instructive example it is useful to consider the benchmark of chorismate mutase,[71] where we considered a highly charged active site and ligands in three different charged states (see Fig. 9). Our attempts to use the PDLD/S-LRA semimacroscopic approach were reasonably successful (see Fig. 9), but still far from being satisfactory. In the fully microscopic cycle, we must have significant convergence problems. What comes to mind are the incomplete protein reorganization and water penetration that seems to lead to a major overestimate of charge–charge interactions.[64,72] In dealing with the semimacroscopic estimate, we can handle the

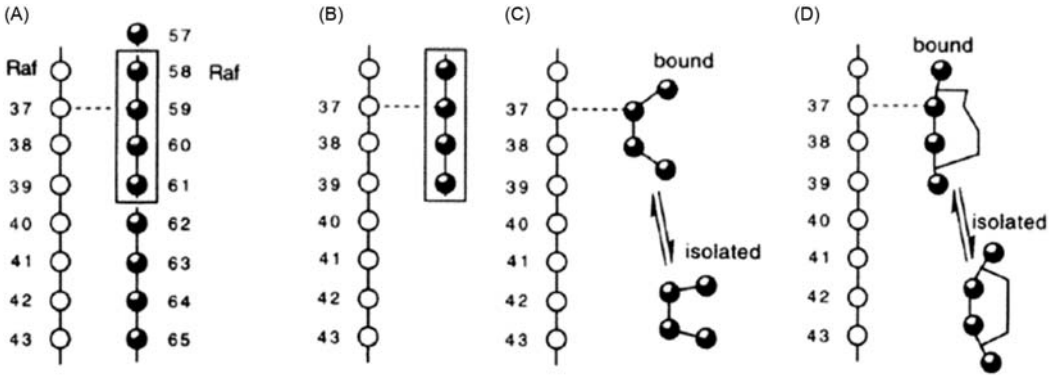

Fig. 7 Fighting Ras/Raf interaction. Outlining a way for exploiting structural information from the Ras/Raf interface, for designing drugs that deactivate defected Ras. In this strategy we (A) identify the regions in Raf with strong contribution to binding, (B, C) examine if the corresponding short peptides also bind strongly, (D) and then examine if cyclic analogues of those peptides also retain strong binding. The resulting constructs would be good drug candidates. Taken from Kamerlin, S. C. L., et al. Why Nature Really Chose Phosphate. *Quart. Rev. Biophys.* **2013**, *46*, 1–132.

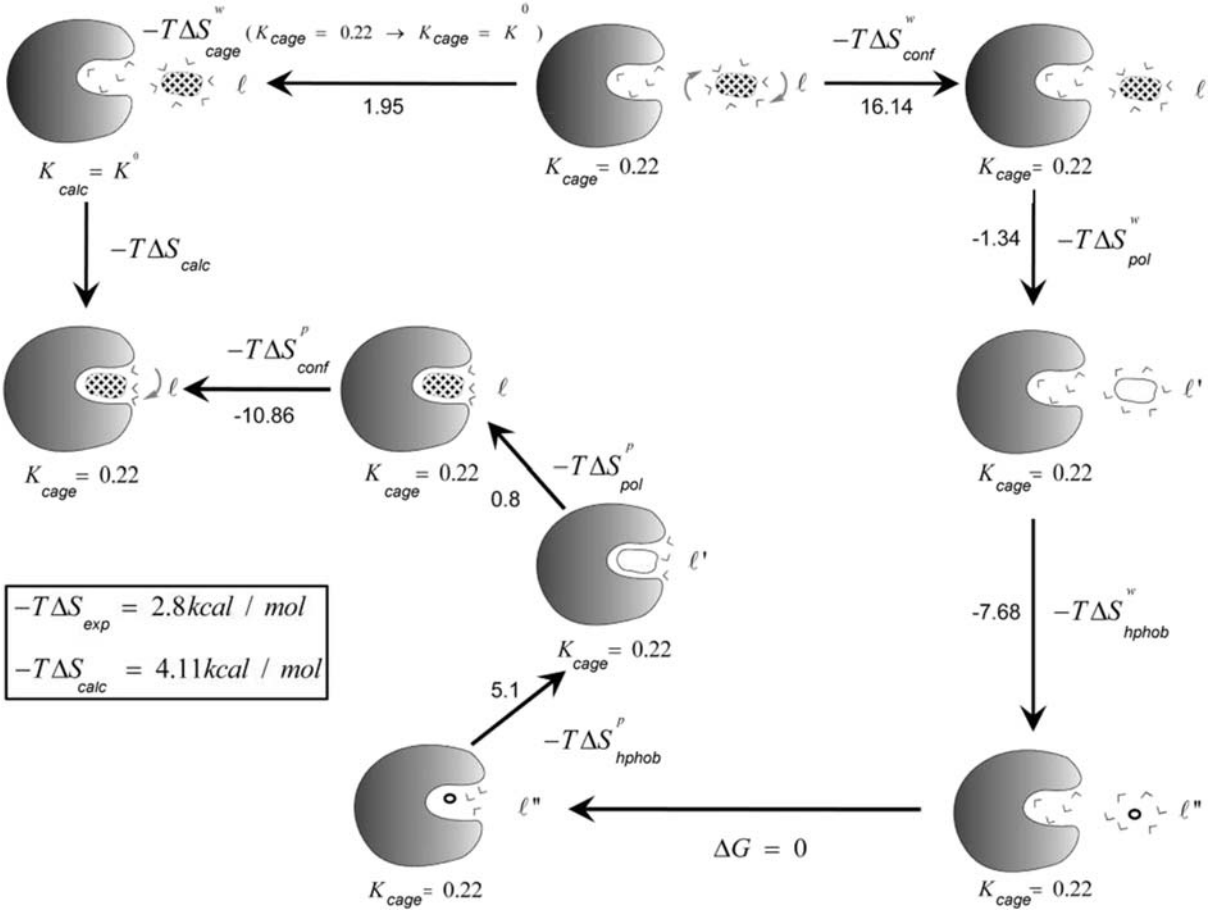

Fig. 8 The thermodynamic cycle used to calculate the overall binding entropy of binding of benzene to bacteriophage T4-lysozyme. ℓ(⬬) and ℓ'(⬭) represent the charged and uncharged (where all of the residual charges of the ligand were set to zero) forms of the ligand, respectively, while ℓ''(○) represents the ligand being reduced to "nothing." "*p*" and "*w*" designate protein and water, respectively. K_{cons} = large designates a large constraint on the molecule(s) for which RR energy is being calculated. The calculations use $K_{cage} = 0.22$ kcal mol^{-1} Å^{-2} and $K^0 = 0.026$ kcal mol^{-1} Å^{-2}, which correspond to a molar volume (1660 Å^2) in the indicated steps. Also, note that the calculations of the polarization and hydrophobic entropies involve a strong constraint on the ligand. The figure does not describe the freezing of the ligands or the solvent molecules explicitly, as this will require more steps.

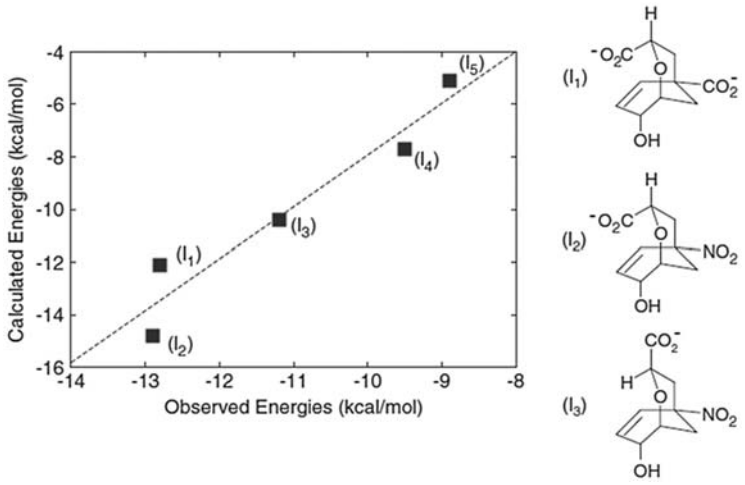

Fig. 9 Calculated and observed binding energies of different ligands of CM. Taken from Kato, M.; Braun-Sand, S.; Warshel, A. Challenges and Progresses in Calculations of Binding Free Energies – What Does It Take to Quantify Electrostatic Contributions to Protein–Ligand Interactions? In *Computational and Structural Approaches to Drug Discovery*; RSC Publishing, 2008; pp. 268–292.

electrostatic problem by using a proper effective dielectric constant for charge–charge interactions, but the nonelectrostatic term still presents a problem.

The difficulties in obtaining reliable results, in fact, an opportunity since they provide clear benchmarks that must be resolved unless one believes in metaphysical missing effects. That is, one can and should require that the PDLD/S-LRA β and the microscopic simulations will both converge to the experimental results. Note that at present only the PDLD/S-LRA formulation can provide a clear bridge between the semimacroscopic and microscopic models.[51] At any rate, requiring that the microscopic and macroscopic simulations will give the same results for each part of the overall thermodynamic cycle should give eventually clear clues about the origin of the problems with these approaches.

One of the most serious problems in obtaining a converging result in calculations of binding free energies is the fact that the binding process involves a change in the number of internal water molecules and that this process is probably associated with a slow relaxation time. In order to overcome this challenge, we introduced the WF approach. This type of treatment is expected to provide a clearer insight into the nature of β and significantly improve the microscopic results.

Despite the earlier and current problems, there is no doubt that computer-aided free energy calculations will eventually become the key quantitative tool in rational drug design. It is also clear that quantitative evaluation of electrostatic free energies will be one of the most important factors in advancing reliable calculations of ligand binding to proteins. Once a more quantitative level is achieved, we can see several promising directions. For example, it will be possible to augment automated screening procedures and to refine the final drug candidates. Here, the ability to understand what interactions are responsible to the optimal binding may help in advancing better ideas about new drugs that were not included in the original refinement process.

Another promising direction where computational approaches can in fact compete with combinatorial drug screening is the fight against drug resistance. Here, the challenge is to anticipate the mutations that will be developed by the resistant strain (e.g., the HIV virus) and design a drug that will still be bound strongly despite the emergence of new mutations. A preliminary advance in this direction has been made in our lab by calculating the so-called vitality value ($\gamma = (k_{cat}/K_M) \times K_i$), which expresses the competition between the attempt of the mutated virus to increase K_i and the requirement that the specific protein (e.g., an HIV protease) will still perform its usual catalytic function. Evaluating simultaneously the PDLD/S contribution of each residue to k_{cat}/K_M (the binding energy of the transition state) for the natural substrate and the K_i for the given drug produces the corresponding contribution to the vitality factor.[73,74] With this predicted value, one can look for mutations that will maximize γ, and thus predict the optimal drug resistance process. Once the next move of the virus is anticipated, the problem is reduced to the design of drugs that will bind strongly to the new, predicted mutants. Examples of proof of principle are given in Refs. 73,74 Other major advances in computer-aided drug design will clearly emerge in the future and the only question is how long it would take to make such approaches fully quantitative. Here, we believe that approaches that would go below the 1 kcal/mol error could be considered as sufficiently quantitative approaches and advance us to a new era in computer-aided drug design. It is quite possible that approaches that involve direct calculations of the PMF for binding will start to be effective with sufficiently long simulation time.

Acknowledgment

This work was supported by NIH Grants GM 24492, GM 40283, and U19CA105010, and NSF grant MCB-1243719. We thank the High Performance Computing Center (HPCC) at the University of Southern California (USC) for computer time. We also thank Extreme Science and Engineering Discovery Environment (XSEDE) (which are supported by National Science Foundation grant number ACI-1053575) for computer time.

References

1. Berman, H.; Henrick, K.; Nakamura, H. Announcing the Worldwide Protein Data Bank. *Nat. Struct. Biol.* **2003,** *10* (12), 980.
2. Friesner, R. A.; et al. Extra Precision Glide: Docking and Scoring Incorporating a Model of Hydrophobic Enclosure for Protein-Ligand Complexes. *J. Med. Chem.* **2006,** *49* (21), 6177–6196.
3. Jones, G.; et al. Development and Validation of a Genetic Algorithm for Flexible Ligand Docking. *Abstr. Pap. Am. Chem. Soc.* **1997,** *214.* 154-Comp.
4. Rarey, M.; et al. A Fast Flexible Docking Method Using an Incremental Construction Algorithm. *J. Mol. Biol.* **1996,** *261* (3), 470–489.
5. Ewing, T. J. A.; Kuntz, I. D. Critical Evaluation of Search Algorithms for Automated Molecular Docking and Database Screening. *J. Comput. Chem.* **1997,** *18* (9), 1175–1189.
6. Muegge, I.; Rarey, M. Small Molecule Docking and Scoring. In *Reviews in Computational Chemistry;* Lipkowitz, K. B., Boyd, D. B., Eds.; Wiley-VCH, John Wiley and Sons: New York, 2001; pp 1–60.
7. Gohlke, H.; Klebe, G. Approaches to the Description and Prediction of the Binding Affinity of Small-Molecule Ligands to Macromolecular Receptors. *Angew. Chem. Int. Ed.* **2002,** *41* (15), 2645–2676.
8. Brooijmans, N.; Kuntz, I. D. Molecular Recognition and Docking Algorithms. *Annu. Rev. Biophys. Biomol. Struct.* **2003,** *32,* 335–373.
9. Kato, M.; Braun-Sand, S.; Warshel, A. Challenges and Progresses in Calculations of Binding Free Energies – What Does It Take to Quantify Electrostatic Contributions to Protein–Ligand Interactions?. In *Computational and Structural Approaches to Drug Discovery, Ligand Protein Interactions;* Stroud, R. M., finer-Moore, J., Eds.; England: Royal Society of Chemistry, 2008; pp 268–292.
10. Warshel, A. Calculations of Enzymic Reactions: Calculations of pK_a, Proton Transfer Reactions, and General Acid Catalysis Reactions in Enzymes. *Biochemistry* **1981,** *20,* 3167–3177.
11. Warshel, A. Simulating the Energetics and Dynamics of Enzymatic Reactions. In *Specificity in Biological Interactions*; . 1984, vol. 55 **1984,** *vol. 55. Pontificiae Academiae Scientiarum Scripta Varia D. Reidel publishing company, Dordrecht, Netherlands.*
12. Warshel, A. Computer Simulations of Enzymatic Reactions. *Curr. Opin. Struct. Biol.* **1992,** *2,* 230–236.
13. Wong, C. F.; McCammon, J. A. Dynamics and Design of Enzymes and Inhibitors. *J. Am. Chem. Soc.* **1986,** *108,* 3830–3832.
14. Kollman, P. Free Energy Calculations: Applications to Chemical and Biochemical Phenomena. *Chem. Rev.* **1993,** *93,* 2395–2417.
15. Shurki, A.; Warshel, A. Structure/Function Correlations of Proteins Using MM, QM/MM and Related Approaches; Methods, Concepts, Pitfalls and Current Progress. *Adv. Protein Chem.* **2003,** *66,* 249–312.
16. Zwanzig, R. W. High-Temperature Equation of State by a Perturbation Method. I. Nonpolar Gases. *J. Chem. Phys.* **1954,** *22,* 1420.
17. Valleau, J. P.; Torrie, G. M. A Guide to Monte Carlo for Statistical Mechanics. 2. Byways. In *Modern Theoretical Chemistry;* Berne, B. J., Ed.; vol. 5; Plenum Press: New York, 1977.
18. Warshel, A.; Åqvist, J. Electrostatic Energy and Macromolecular Function. *Annu. Rev. Biophys. Chem.* **1991,** *20,* 267–298.
19. Warshel, A.; Sussman, F.; King, G. Free Energy of Charges in Solvated Proteins: Microscopic Calculations Using a Reversible Charging Process. *Biochemistry* **1986,** *25,* 8368–8372.
20. Lee, F. S.; et al. Calculations of Antibody-Antigen Interactions: Microscopic and Semi-Microscopic Evaluation of the Free Energies of Binding of Phosphorylcholine Analogs to McPC603. *Protein Eng.* **1992,** *5,* 215–228.
21. Hummer, G.; Szabo, A. Calculation of Free Energy Differences from Computer Simulations of Initial and Final States. *J. Chem. Phys.* **1996,** *105* (5), 2004–2010.
22. Kubo, R.; Toda, M.; Hashitsume, N. *Statistical Physics II: Nonequilibrium Statistical Mechanics;* Springer-Verlag: Berlin, 1985.
23. Warshel, A.; Russell, S. T. Calculations of Electrostatic Interactions in Biological Systems and in Solutions. *Q. Rev. Biophys.* **1984,** *17,* 283–421.
24. Hwang, J.-K.; Warshel, A. Microscopic Examination of Free Energy Relationships for Electron Transfer in Polar Solvents. *J. Am. Chem. Soc.* **1987,** *109,* 715–720.
25. Kuharski, R. A.; et al. Molecular Model for Aqueous Ferrous Ferric Electron Transfer. *J. Chem. Phys.* **1988,** *89,* 3248–3257.
26. Åqvist, J.; Hansson, T. On the Validity of Electrostatic Linear Response in Polar Solvents. *J. Phys. Chem.* **1996,** *100,* 9512–9521.
27. Morreale, A.; et al. Partition of Protein Solvation into Group Contributions From Molecular Dynamics Simulations. *Proteins: Struct., Funct., Bioinf.* **2005,** *58* (1), 101–109.
28. Warshel, A.; et al. Modeling electrostatic effects in proteins. *Biochim. Biophys. Acta* **2006,** *1764* (11), 1647–1676.
29. Burykin, A.; et al. Simulations of Ion Current in Realistic Models of Ion Channels: The KcsA Potassium Channel. *Proteins: Struct., Funct., Bioinf.* **2002,** *47,* 265–280.
30. Warshel, A. Calculations of Chemical Processes in Solutions. *J. Phys. Chem.* **1979,** *83,* 1640–1650.
31. King, G.; Warshel, A. A Surface Constrained All-Atom Solvent Model for Effective Simulations of Polar Solutions. *J. Chem. Phys.* **1989,** *91* (6), 3647–3661.
32. Lee, F. S.; Warshel, A. A Local Reaction Field Method for Fast Evaluation of Long-Range Electrostatic Interactions in Molecular Simulations. *J. Chem. Phys.* **1992,** *97,* 3100–3107.
33. Figueirido, F.; Del Buono, G. S.; Levy, R. M. On the Finite Size Corrections to the Free Energy of Ionic Hydration. *J. Phys. Chem. B* **1997,** *101* (29), 5622–5623.
34. Bogusz, S.; Cheatham, T. E., III; Brooks, B. R. Removal of Pressure and Free Energy Artifacts in Charged Periodic Systems via Net Charge Corrections to the Ewald Potential. *J. Chem. Phys.* **1998,** *108,* 7070–7084.
35. Hummer, G.; Pratt, L. R.; Garcia, A. E. Free Energy of Ionic Hydration. *J. Phys. Chem.* **1996,** *100,* 1206–1215.
36. Mezei, M.; Beveridge, D. L. Free Energy Simulations. *Ann. N. Y. Acad. Sci.* **1986,** *482,* 1–23.
37. Cross, A. J. Influence of Hamiltonian Parameterization on Convergence of Kirkwood Free-Energy Calculations. *Chem. Phys. Lett.* **1986,** *128* (2), 198–202.
38. Mruzik, M. R.; et al. Monte-Carlo Study of Ion-Water Clusters. *J. Chem. Phys.* **1976,** *64* (2), 481–491.
39. Beutler, T. C.; et al. Avoiding Singularities and Numerical Instabilities in Free-Energy Calculations Based on Molecular Simulations. *Chem. Phys. Lett.* **1994,** *222* (6), 529–539.
40. Zacharias, M.; Straatsma, T. P.; Mccammon, J. A. Separation-Shifted Scaling, a New Scaling Method for Lennard-Jones Interactions in Thermodynamic Integration. *J. Chem. Phys.* **1994,** *100* (12), 9025–9031.
41. Steinbrecher, T.; Joung, I.; Case, D. A. Soft-Core Potentials in Thermodynamic Integration: Comparing One- and Two-Step Transformations. *J. Comput. Chem.* **2011,** *32* (15), 3253–3263.
42. Chakrabarty, S.; Warshel, A. Capturing the Energetics of Water Insertion in Biological Systems: The Water Flooding Approach. *Proteins: Struct., Funct., Bioinf.* **2013,** *81* (1), 93–106.
43. Aqvist, J.; Warshel, A. Calculations of Free-Energy Profiles for the Staphylococcal Nuclease Catalyzed Reaction. *Biochemistry* **1989,** *28* (11), 4680–4689.
44. Sham, Y. Y.; Chu, Z. T.; Warshel, A. Consistent Calculations of pK_a's of Ionizable Residues in Proteins: Semi-Microscopic and Macroscopic Approaches. *J. Phys. Chem. B* **1997,** *101,* 4458–4472.
45. Buono, G. S.; Figueirido, F. E.; Levy, R. M. Intrinsic pK_a's of Ionizable Residues in Proteins: An Explicit Solvent Calculation for Lysozyme. *Proteins: Struct., Funct., Bioinf.* **1994,** *20,* 85–97.
46. Warshel, A.; Levitt, M. Theoretical Studies of Enzymic Reactions: Dielectric, Electrostatic and Steric Stabilization of the Carbonium Ion in the Reaction of Lysozyme. *J. Mol. Biol.* **1976,** *103,* 227–249.
47. Warwicker, J.; Watson, H. C. Calculation of the Electric Potential in the Active Site Cleft due to Alpha-Helix Dipoles. *J. Mol. Biol.* **1982,** *157,* 671–679.
48. Sharp, K. A.; Honig, B. Electrostatic Interactions in Macromolecules: Theory and Applications. *Annu. Rev. Biophys. Biophys. Chem.* **1990,** *19,* 301–332.
49. Warshel, A.; Papazyan, A. Electrostatic Effects in Macromolecules: Fundamental Concepts and Practical Modeling. *Curr. Opin. Struct. Biol.* **1998,** *8,* 211–217.
50. King, G.; Lee, F. S.; Warshel, A. Microscopic Simulations of Macroscopic Dielectric Constants of Solvated Proteins. *J. Chem. Phys.* **1991,** *95,* 4366–4377.
51. Schutz, C. N.; Warshel, A. What Are the Dielectric "Constants" of Proteins and How to Validate Electrostatic Models. *Proteins: Struct., Funct., Bioinf.* **2001,** *44,* 400–417.

52. Lee, F. S.; Chu, Z. T.; Warshel, A. Microscopic and Semimicroscopic Calculations of Electrostatic Energies in Proteins by the POLARIS and ENZYMIX Programs. *J. Comput. Chem.* **1993,** *14,* 161–185.
53. Sham, Y. Y.; et al. Examining Methods for Calculations of Binding Free Energies: LRA, LIE, PDLD-LRA, and PDLD/S-LRA Calculations of Ligands Binding to an HIV Protease. *Proteins: Struct., Funct., Bioinf.* **2000,** *39,* 393–407.
54. Aqvist, J.; Luzhkov, V. B.; Brandsdal, B. O. Ligand Binding Affinities from MD Simulations. *Acc. Chem. Res.* **2002,** *35* (6), 358–365.
55. Singh, N.; Warshel, A. Absolute Binding Free Energy Calculations: On the Accuracy of Computational Scoring of Protein-Ligand Interactions. *Proteins: Struct., Funct., Bioinf.* **2010,** *78* (7), 1705–1723.
56. Kollman, P. A.; et al. Calculating Structures and Free Energies of Complex Molecules: Combining Molecular Mechanics and Continuum Models. *Acc. Chem. Res.* **2000,** *33,* 889–897.
57. Graffner-Nordberg, M.; et al. Computational Predictions of Binding Affinities to Dihydrofolate Reductase: Synthesis and Biological Evaluation of Methotrexate Analogues. *J. Med. Chem.* **2000,** *43* (21), 3852–3861. FIELD Publication Date:2000 Oct 19, FIELD Reference Number: FIELD Journal Code:9716531 FIELD Call Number.
58. Florian, J.; Goodman, M. F.; Warshel, A. Free-Energy Perturbation Calculations of DNA Destabilization by Base Substitutions: The Effect of Neutral Guanine Thymine, Adenine Cytosine and Adenine Difluorotoluene Mismatches. *J. Phys. Chem. B* **2000,** *104* (43), 10092–10099.
59. Dolenc, J.; et al. Molecular Dynamics Simulations and Free Energy Calculations of Netropsin and Distamycin Binding to an AAAAA DNA Binding Site. *Nucleic Acids Res.* **2005,** *33* (2), 725–733.
60. Rocklin, G. J.; et al. Blind Prediction of Charged Ligand Binding Affinities in a Model Binding Site. *J. Mol. Biol.* **2013,** *425* (22), 4569–4583.
61. You, T. J.; Bashford, D. Conformation and Hydrogen Ion Titration of Proteins: A Continuum Electrostatic Model with Conformational Flexibility. *Biophys. J.* **1995,** *69,* 1721–1733.
62. Florian, J.; Goodman, M. F.; Warshel, A. Theoretical Investigation of the Binding Free Energies and Key Substrate-Recognition Components of the Replication Fidelity of Human DNA Polymerase b. *J. Phys. Chem. B* **2002,** *106,* 5739–5753.
63. Boyce, S. E.; et al. Predicting Ligand Binding Affinity with Alchemical Free Energy Methods in a Polar Model Binding Site. *J. Mol. Biol.* **2009,** *394* (4), 747–763.
64. Muegge, I.; Schweins, T.; Warshel, A. Electrostatic Contributions to Protein-Protein Binding Affinities: Application to Rap/Raf Interaction. *Proteins: Struct., Funct., Bioinf.* **1998,** *30,* 407–423.
65. Bakowies, D.; van Gunsteren, W. F. Simulations of Apo and Holo-Fatty Acid Binding Protein: Structure and Dynamics of Protein, Ligand and Internal Water. *J. Mol. Biol.* **2002,** *315* (4), 713–736.
66. Karplus, M.; Kushick, J. N. Method for Estimating the Configurational Entropy of Macromolecules. *Macromolecules* **1981,** *14* (2), 325–332.
67. Warshel, A. Computer Simulation of Chemical Reactions in Synthetic Model Compounds and Genetically Engineered Active Sites. Proposal to the Office of Naval Research. Award Number N00014-91-J-1318.
68. Strajbl, M.; et al. Calculations of Activation Entropies of Chemical Reactions in Solution. *J. Phys. Chem.* **2000,** *104,* 4578–4584.
69. Singh, N.; Warshel, A. A Comprehensive Examination of the Contributions to the Binding Entropy of Protein-Ligand Complexes. *Proteins: Struct., Funct., Bioinf.* **2010,** *78* (7), 1724–1735.
70. Platzer, K. E. B.; Momany, F. A.; Scheraga, H. A. Conformational Energy Calculations of Enzyme-Substrate Interactions. 2. Computation of Binding-Energy for Substrates in Active-Site of Alpha-Chymotrypsin. *Int. J. Pept. Protein Res.* **1972,** *4* (3), 201.
71. Mandal, A.; Hilvert, D. Charge Optimization Increases the Potency and Selectivity of a Chorismate Mutase Inhibitor. *J. Am. Chem. Soc.* **2003,** *125* (19), 5598–5599.
72. Johnson, E. T.; Parson, W. W. Electrostatic Interactions in an Integral Membrane Protein. *Biochemistry* **2002,** *41,* 6483–6494.
73. Singh, N.; Frushicheva, M. P.; Warshel, A. Validating the Vitality Strategy for Fighting Drug Resistance. *Proteins: Struct., Funct., Bioinf.* **2012,** *80* (4), 1110–1122.
74. Ishikita, H.; Warshel, A. Predicting drug-resistant mutations of HIV protease. *Angewandte Chemie-International Edition* **2008,** *47* (4), 697–700.

3.02 Advances in Molecular Simulation

M Aldeghi and PC Biggin, University of Oxford, Oxford, United Kingdom

© 2017 Elsevier Ltd. All rights reserved.

3.02.1	**Hardware and Software Advances**	14
3.02.1.1	Special-Purpose Machines	14
3.02.1.2	Graphics Processing Units	15
3.02.1.3	Cloud and Distributed Computing	16
3.02.1.4	Novel Algorithms and Parallelization	16
3.02.2	**Force Field Advances**	17
3.02.2.1	Protein Force Fields	18
3.02.2.2	Organic Molecule Force Fields	18
3.02.2.3	Force Fields for Other Species: Nucleic Acids, Lipids, Sugars, and Water	19
3.02.2.4	Polarizable Force Fields	19
3.02.2.5	Coarse-Grained Force Fields	21
3.02.3	**Novel Simulation Approaches and Trends**	22
3.02.3.1	Parallel and Enhanced Sampling	22
3.02.3.1.1	Markov state models	22
3.02.3.1.2	Replica exchange methods	24
3.02.3.1.3	Bias potential methods: Metadynamics	25
3.02.3.2	Simulation of Large Systems	26
3.02.4	**Conclusion**	27
References		27

3.02.1 Hardware and Software Advances

The main obstacles to the progress in application of molecular dynamics (MD) to drug discovery have been the computational cost of the simulations, leading to precision and convergence issues, and inaccuracies of the underlying physical model used. Problems with convergence arise from incomplete sampling of all accessible configurations. As the properties of interest often depend on an average of all ensemble conformations, it will not be possible to have a converged estimate of those properties until the simulation has sampled all, or at least many, such conformations. Issues with the physical model arise on the other hand from the assumptions and simplifications made with respect to the classical treatment of atoms and molecules, as well as inaccuracies in the derivation of parameters. The two problems are however interconnected, because in order to be able to rigorously test a physical model and improve upon it, it is necessary to be able to compute the quantities of interest with a precision similar to the experimental counterpart. For the most part this necessitates access to the relevant space- and timescales.

There has, however, been a steady increase in the scales accessible by molecular dynamics simulations over the past few decades. This has arisen, at least in part, from a direct consequence of Moore's Law for semiconductors and computing, which observes that the number of transistors on CPUs and the consequent computer power approximately doubles every 2 years.[1] However, algorithmic advances have also played an important role in expanding simulations capabilities, in particular by maximizing the opportunities presented by new hardware technologies such as graphical processing units (GPUs) for example. In fact, simulation speed has been growing faster than Moore's Law,[2] suggesting that hardware and software innovations have worked in synchrony to deliver necessary improvements in simulation performance as witnessed by both the scale[3] and timescales[4] of simulation now achievable.

3.02.1.1 Special-Purpose Machines

Among the most notable hardware advances since the turn of the century is the development of Anton, a specialized machine designed specifically to accelerate MD simulations, by D.E. Shaw Research.[5] Previous efforts in this direction were not particularly successful due to the fact the production of specialized chips is demanding and, without adequate resources, too slow to keep up with the pace of general-purpose processors. Yet, D.E. Shaw Research managed to develop a parallel machine, based on 512 specialized nodes that interact in a tightly coupled manner through a dedicated high-speed communication network, which performs simulations at about two orders of magnitude of the speed of standard hardware.[5] In the years following its release, Anton allowed ground-breaking simulations of milliseconds in length, two orders of magnitude longer than the lengthiest simulation performed before,[6] which permitted the observation of phenomena such as the folding of small proteins into their native structure,[7] or the unbiased binding of a drug into a binding pocket.[8]

Lindorff-Larsen et al.[9] reported the folding of 12 diverse small proteins through simulation on the Anton chip. The authors observed at least ten folding and unfolding events for each of these proteins using simulations of length between 0.1 and 1 ms. Other than proving how relatively simple physics-based models are able to fold proteins into their native structure, the work suggested the existence of a preferential folding route for the studied systems. The ability to simulate and study protein folding pathways will impact our understanding of misfolding diseases such as Alzheimer's and Parkinson's, and possibly on our ability to develop strategies to tackle such illnesses.

The same year, Shan et al.[10] showed how long unbiased molecular dynamics simulations were able to capture the binding process and final (crystallographically observed) pose of two Src kinase inhibitors; PP1 and dasatinib. These results are potentially significant for drug discovery, as the methodology does not assume any prior knowledge of the binding location and pose. Thus it is conceivable that this approach might be applied to the discovery of allosteric inhibitors targeting previously unknown binding sites. Moreover, it allows the elucidation of the binding pathway, which can significantly affect the binding kinetics. Longer timescales not only allow us to access biologically relevant timescales, but also provide the fundamental framework necessary to test the validity of the force fields, as it will be discussed later.[11–13]

Currently, an upgraded version of this machine (Anton-2) is in use at D.E. Shaw Research, while the previous version was donated to the Pittsburgh Supercomputer Centre for noncommercial use. This new machine achieves the impressive performance of 85 μs/day on dihydrofolate reductase (DHFR), a standard benchmark system of 23,558 atoms and breaks the 1 μs/day barrier on million-atom systems; for instance, using all 512 nodes (33,792 processors) a performance of 3.6 μs/day is achievable for a ribosome system containing 2.2 million atoms.[14]

3.02.1.2 Graphics Processing Units

While special-purpose architectures can deliver extraordinary performances as described above, they are not widely available as a significant investment in human and financial resources is necessary for their continuous development. Recently however, another avenue for simulation acceleration has become available that is much cheaper, namely GPUs. Driven by a $100 billion interactive entertainment industry, large and sustained investments in GPU development have resulted in steady increases in performance alongside decreasing costs.[15]

When rendering graphics, many of the operations required are simple but large amounts of data need to be handled. GPUs have thus been designed with a large number (hundreds or thousands) of simple processors that work in parallel. GPUs are basically a specialized circuit, built in order to perform a large number of floating-point operations per video frame (Fig. 1). Some of the calculations performed during a molecular simulation are of similar nature to the ones that GPUs can accelerate, such as the computing of the nonbonded pair interactions between a large number of atoms, which is typically the most expensive calculation during a simulation.[15,16] It thus became clear that such computations could be solved faster with the use of GPUs, improving the simulation throughput.[16,17]

In the late 2000s, comprehensive MD engines such as ACEMD[18] and OpenMM[19] have been developed specifically to take advantage of the acceleration provided by widely available GPUs. At the time of publication, in 2009, ACEMD using 3 GPUs

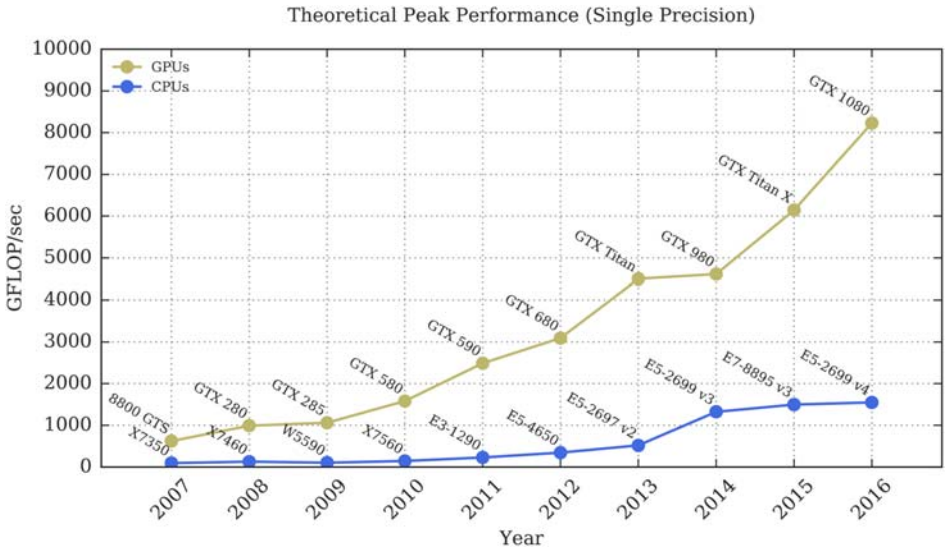

Fig. 1 Performance improvements of CPUs and GPUs in the last decade. The plot compares the GeForce series of Nvidia consumer graphics card with high-end Intel Xeon processors by launch year. Performance for GPUs was taken from https://en.wikipedia.org/wiki/List_of_Nvidia_graphics_processing_units, and for CPU was calculated from data available at https://en.wikipedia.org/wiki/List_of_Intel_Xeon_microprocessors and http://ark.intel.com.

and 3 CPU cores showed a performance on the DHFR benchmark that was roughly equivalent to that of GROMACS on 20 CPU cores.[18] Using ACEMD and a GPU cluster, Buch et al.[20] carried out 50 μs of aggregate simulated time and reconstructed the binding of benzamidine to trypsin. In 2015, the same group carried out similar unbiased simulations for 42 fragments and the protein serine protease factor Xa, for a total of 2.1 ms simulated time and managed to recapitulate binding poses, affinities, and kinetics for a number of the ligands studied.[21] In both cases the use of GPUs enabled such extensive sampling.

Nowadays, most widely used MD software can take advantage of available GPUs to significantly improve simulation throughput and cost-efficiency. Some packages, such as GROMACS, CHARMM, and NAMD, use GPUs in an off-loading approach where the short-range nonbonded interactions are sent to the GPU, while the rest of the calculation is borne by the CPU; in other packages, such as ACEMD or AMBER, almost all of the computation is performed on the GPU. Kutzner et al.[22] recently evaluated a number of hardware setups with GROMACS 4.6 in terms of pure simulation performance, but also performance-to-price ratio, taking also into account the energy consumption of the hardware. From a purely performance perspective, they noted that GPUs increase the speed of a compute node by a factor of 1.7–3.8, with inexpensive GeForce consumer cards also providing a 2–3 factor increase in performance-to-price ratio. As an example, a single node comprising two Intel Xeon E5-2680v2 processors (10 cores each) offered 26.8 ns/day of simulation on a membrane protein system of 81,743 atoms. At the time of their study in 2014 this setup would have cost about 4400€. However, when adding a single Nvidia GeForce GTX 980 card, the performance doubled to 52.0 ns/day, against an extra cost of only ~450€. The peak performance of 66.9 ns/day was obtained with four GTX 980 cards, however, adding the third and fourth GPU improved performance only marginally as the simulation became CPU-bound, consequently not improving the cost-efficiency of the setup. When considering energy consumption, nodes with one or two GPUs have an increased power draw and energy cost, yet still produce from 1.5 to 2 times the MD trajectory per € invested than CPU-only nodes. The authors also remarked that the energy efficiency improvement of the newer Maxwell architecture as compared to the Kepler one, results in a ~20% reduction of trajectory costs. With AMBER14, a soluble test system of 90,906 atoms provided an output of 4.5 ns/day on two E5-2650v3 processors (10 cores each), going to 34.6 ns/day when using one GTX 980 card (almost a 8× speedup) and up to 50.2 ns/day with two GTX 980 cards. It is interesting to note that since the code barely uses the CPU, the performance does not become CPU-bound when using more GPUs, reaching an output of 90.0 ns/day when using four GTX Titan X cards.

3.02.1.3 Cloud and Distributed Computing

In addition to new hardware and faster and larger supercomputers, recent years have seen the rise of cloud and distributed computing.[23–25] Cloud computing involves the use of a network of remote servers to process and store the data[23] and allows access to large computer power with flexible pay-as-you-go pricing schemes. Some private vendors such as Amazon Elastic Compute Cloud (EC2; https://aws.amazon.com/ec2/) or IBM Platform Computing (http://www-03.ibm.com/systems/uk/platformcomputing/solutions/hpccloud.html) have started providing services on the cloud specifically for HPC. Google have instead been supplying computing facilities for academic research for free, but based on a competitive application process. In its first year in 2013, it provided about 1 billion core-hours for projects covering a wide range of science and engineering challenges including antibiotic resistance, drug discovery,[26] and protein structure prediction and design. As a consequence of this trend, software to facilitate the execution of ensemble of simulation on remote cloud services has been developed.[27]

Distributed computing projects such as Folding@Home or Rosetta@Home rely instead on the unused power of volunteers' personal computers, where anyone can contribute by downloading a software client.[25,28] This creates a large network of heterogeneous hardware that is available to the researcher for performing molecular dynamics simulations. Presently, more than 100,000 users are contributing to the Folding@Home project, providing over 20 petaflops of computing power, comparable to the peak performance of IBM Sequoia, the third most powerful supercomputer as of late 2015 (see https://www.top500.org). Since the early 2000s, such computing power has been employed for many important computational studies on protein folding and design.[29–37] Similarly, GPUGRID.net was released in 2007 and uses the graphics cards of volunteers in order to pursue scientific research in cancer, HIV, and neural disorders through the use of simulations.[38–41]

Cloud and distributed computing provide much raw power at low cost. However, they do not provide the same communication and I/O performance as supercomputing. The strength of distributed systems is that they are cheaper than supercomputers, as they tend to use off-the-shelf computers for processors and memory, which also require minimal cooling costs. However, high-speed network and storage, and tight connections between nodes, mean that many nodes of supercomputers such as Tianhe-2, Titan, or Sequoia, can work together on the same tasks since data can move between processors rapidly. Supercomputers are therefore still more suited for highly-complex, real-time applications. For molecular dynamics simulations specifically, it means that running a very large simulation consisting of millions of atoms would perform better on an HPC facility. On the other hand, running thousands of small simulations on cloud/distributed computing would be more cost effective without suffering much performance loss. Moreover, the analysis of large amounts of data also benefits from the communication hardware provided by HPC facilities. The data need to be read in (often as whole data sets) and processed. Consequently, aspects such as data I/O, CPU speed, and node communication become important factors.

3.02.1.4 Novel Algorithms and Parallelization

Hardware advances need to be combined with new and improved software and algorithms in order to maximize any potential benefits that arise. GPUs have provided probably the most significant step change in recent years; since the introduction of general

GPU programming platforms, such as NVIDIA's CUDA in 2006 or OpenCL in 2009, the use of the new hardware for scientific applications has become much more accessible. Prior to these developments, graphics specific application programming interface (APIs) such as OpenGL had to be used in order to perform calculations that were not related to the rendering of vector graphics, making the development of new code time consuming. Similarly, the availability of tools like MPI and OpenMP have allowed the implementation of parallel algorithms for multicore machines, including large supercomputing clusters, greatly increasing the performance of MD codes. As a result, all widely used MD codes have substantially improved their parallel performance in the last decade. For instance, as part of the Blue Gene project, scientists at IBM have been exploring parallel strategies in order to achieve strong scaling for their Blue Matter simulation code; in 2006 they reported continued speedup to fewer than three atoms per node.[42] Scaling is important as the number of cores available increases; there will be the issue of using efficiently a large number of cores for small and medium size systems.

MD algorithms have been constantly refined in order to decrease the communication requirements between processors, resulting in decreased latency. Interprocessor communication is necessary on parallel machines when evaluating forces on interacting particles. In early designs, because of its simplicity and the fact that it was fairly efficient over a limited number of cores, particle decomposition was the main method employed to distribute the computation of near interactions across the available processors.[43,44] In this scheme, at the beginning of the simulation each particle in the box is assigned to a processor, which then computes its interactions at each time step. However, this method does not scale well with system size and number of cores: since the decomposition is static, but the particles diffuse through the simulation box, the interaction partners of a specific particle will be distributed across the whole box and many of the CPUs will be involved in the computation, resulting in a large communication volume.[43]

Spatial decomposition methods on the other hand can really take advantage of the locality of the interactions, by dividing the space of the simulation into a number of cells and dynamically assigning particles to processors based on the location of each particle. In this way, particles in a cell will interact only with other ones in the same cell or in the neighboring cells, improving data locality and minimizing interprocessor communication requirements despite the additional book-keeping necessary to keep track of particles moving between cells. In addition, many modern parallel machines (e.g., Blue Gene/L and Cray's T3D, T3E, and XT3 systems) have networks with toroidal topology, so that spatial decomposition allows matching the box grid to the network grid for faster data exchange.[45]

A number of spatial decomposition methods have been developed during the years, but more recently the so-called "neutral territory" methods have provided a significant reduction in the amount of data that needs to be exchanged between cores.[45–47] Due to particle diffusion across spatial domains of inhomogeneous systems, load imbalance between processors can be an issue as the number and type of particles in each domain determine the load. The issue is however easily solved by dynamically balancing the load on the cores by shifting the boundaries of the domains.[43] For a more in-depth review on a number of decomposition methods see Refs.[43–45]

Other algorithmic advances have been related to the acceleration of floating-point calculations, for instance by the development of custom math functions: Enenkel et al. reported a number of functions optimized for MD, improving floating-point efficiency.[48] Alternatives to the widely used Particle Mesh Ewald (PME) method for the computation of long-range electrostatic interactions have been proposed: the multilevel (or multigrid) summation method provides similar speed and accuracy to the traditional PME, but it can also be used for semiperiodic and nonperiodic systems.[49–52] Semiperiodicity might be useful for the simulation of different solvent conditions across a membrane for instance. Such a method has also been shown to provide improved parallel scalability over PME as implemented in NAMD for a system of size <100 K atoms simulated on over a thousand cores.[50] A number of improved implementations of the traditional bonds constraint method SHAKE have been proposed,[53–56] as well as alternative methodologies that are more easily parallelizable for global constraints such as LINCS.[57,58]

3.02.2 Force Field Advances

In the last decade the trend of force field improvement continued. While their functional forms have remained unvaried, their parameters have been modified in order to better match experimental and quantum mechanical data. One concern that has only recently been addressed, is to what extent force field parameters reproduce longer-timescale properties. In 2012, Lindorff-Larsen et al.[11] used Anton to access long timescale simulations and assessed the performance of a number of modern force fields from the AMBER, OPLS, and CHARMM families through comparison with experimental data. The test evaluated the ability of the force fields to reproduce folded protein structure and fluctuations from NMR data, secondary structure content, and to correctly fold small proteins into their native structure. The results indicated that the force fields considered showed steady improvement during the previous decade, with the most recent versions providing the most accurate descriptions of different protein structural and dynamical properties.

However, despite years of optimization and steady improvement, current models are still far from perfect and there is still plenty of room for improvement. In fact, the same study mentioned above also identified some deficiencies; in particular, the force fields did not manage to capture the temperature dependency of the secondary structure propensities. Piana et al.[13] used the fast-folding variant of the villin headpiece as a test case in order to assess the ability of four force fields to fold the protein into its native structure. While they observed that all force fields correctly folded the protein with rates in agreement to experiment, it was noticed that the folding mechanism and the properties of the unfolded states strongly depended on the force field employed. Rauscher et al.[59] have

instead recently studied the structural ensembles generated with μs-long simulations for intrinsically disordered proteins (IDPs). The group compared eight different force fields for a total simulation time of almost a millisecond, and found that different force fields yielded markedly different ensembles that differed in chain dimensions, hydrogen bonding, and secondary structure content. While IDPs are highly sensitive to force field parameters given their rugged energy landscape, the observation that changing the force field had a larger effect on secondary structure content than changing the entire peptide sequence points to clear limitations in the physical model.

Here, we will focus mainly on some of the most popular fixed-charge all-atom force fields, while an overview of recent developments on polarizable and coarse-grained force fields will be given too. Notable exclusions from this review are improvements on united-atom force fields (such as the improvements to the GROMOS force field[60]), universal force fields,[61,62] reactive force fields,[63,64] and force fields with more complex functional form such as the Merck Molecular Force Fields.[65]

3.02.2.1 Protein Force Fields

A number of researchers noticed that the AMBER ff94 and ff99 energy functions produced an imbalanced proportion of secondary structure elements with over-stabilization of α-helices. In 2006 the backbone dihedrals of the AMBER ff99 force field were improved by fitting the energies of multiple conformation of glycine and alanine tetra-peptides to high-level ab initio quantum mechanical data.[66] Additional backbone torsion improvements by Best and Hummer to correct the α-helical propensity of the model resulted in the ff99SB* and ff03* force fields in 2009.[67] Lindorff-Larsen and coworkers introduced ff99SB-ILDN in 2010, which improved side chain torsions, by fitting energies to QM calculations and comparing microsecond-long MD simulations to NMR data.[12] Other enhanced versions of ff99SB were the ff99SB-nmr by Li and Brüschweiler[68] and ff99SB-phi by Nerenberg and Head-Gordon.[69] At the time of writing, the latest AMBER force field available is ff14SB, which is a result of a complete refit of all amino acid side chain torsions. The work also included multidimensional dihedrals scans to improve the parameter transferability. Additional empirical adjustments were made to protein backbone dihedral parameters in order to better reproduce NMR scalar coupling data.[70]

Analogous backbone dihedral issues have been found for other force fields too. In 2004 MacKerrel and coworkers used QM and crystallographic data to improve the peptide-backbone parameters of CHARMM22, introducing the CHARM22/CMAP[71] force field. Despite some degree of success for protein folding applications,[72] flaws were still present as indicated by the misfolding observed in long simulations of the fast-folding WW domain[73,74] and the discrepancy of the folding mechanism of the villin headpiece subdomain between simulations and experiment.[72] Piana et al.[13] tackled the issue of α-helical over-stabilization[75] by replacing the CMAP correction with new backbone torsion terms, which resulted in a force field they named CHARM22*. A substantial revision of the CHARMM force field parameters by the MacKerell lab, trying to address the above shortcomings, resulted in 2012 in the improved CHARMM36 force field.[76]

Another popular protein force field that has undergone constant refinement in the last 20 years since its initial introduction is the OPLS-AA force field.[77] The nonbonded interactions in OPLS-AA are parameterized in order to reproduce properties of pure organic liquids, such as heat of vaporization, densities, and hydration free energies, while torsional parameters are fit to available experimental or QM data. The original torsion scans were performed at the Hartree-Fock (HF) level of theory with a small basis set due to the computational limitations at the time, but a revised OPLS-AA/L was presented in 2001 where single point energies of HF geometry optimized structures were obtained using local MP2 calculations and a larger basis set.[78] In 2015, the torsional parameters were revised, performing torsional scans with modern hybrid density functionals[79,80] which has resulted in the latest OPLS-AA/M force field.[81]

3.02.2.2 Organic Molecule Force Fields

If simulations are to be used for drug discovery, it is necessary to have a good physical model for small organic molecules in addition to proteins. However, while the chemical space covered by polypeptides has clear boundaries, this is not the case for small organic molecules. The drug-like space is vast with a huge number of possible atom combinations. Even though there are many stable chemical groups in which a molecule can be broken down in to, the properties of such groups can change drastically depending on the neighboring chemical moieties. For instance, the electrostatic properties of an aromatic ring such as benzene depend strongly on its substituents and their relative positions. As a consequence, the development of a general yet accurate organic molecule force field is a difficult task.

Due to the increasing interest in the use of modeling and simulation for drug discovery, since the mid-2000s there has been increasing effort in developing organic molecule parameter sets that are consistent with existing (typically protein) force fields. While OPLS was considered from the beginning as a force field for both organic and biological molecules, others such as AMBER or CHARMM had mainly focussed on proteins. In 2004, the General AMBER Force Field (GAFF) was introduced by Wang et al.[82] and is meant to be compatible with the AMBER family of protein force fields. Since then, the force field has been regularly updated to improve many of the parameters, with these improvements incorporated into each new release (see http://www.ambermd.org).

Following a philosophy that focuses on quality at the expense of transferability, Vanommeslaeghe et al. developed a CHARMM-compatible organic molecule force field, named the general CHARMM force field (CGenFF).[83] CGenFF is actively maintained and constantly being improved.[84] As manual assignment of parameters is cumbersome, prone to errors, and prevents task automation, algorithms for automated atom typing have been developed for both the general AMBER and CHARMM force fields.[85–87] In

addition, due to the fact that encountering missing or imprecise parameters is relatively common given the diversity of existing drug-like species, tools to aid the users in the derivation of new parameters have been developed.[88–91]

Also of note is the proprietary OPLS force field developed by Schrödinger Inc. for proteins and organic molecules. OPLS_2005, OPLS2.1 and the most recent OPLS3 have been developed in order to have a broader coverage of medicinal chemical space and support their free energy perturbation suite for binding affinity prediction.[92,93] In OPLS3, the reparameterization of peptide dihedral angles and the inclusion of off-atom charge sites to better represent halogen bonding and aryl nitrogen lone pairs resulted in more accurate binding free energy calculations.[92] The work reminds us how it is not only the ligand, but also the protein parameters, and how they interplay with each other, that have a substantial effect on modeling approaches to drug design. Overall, it appears that across the different small molecule force fields there has been a focus on the improvement of dihedral parameters and partial charges due to their limited transferability across different chemical species.[94–97]

3.02.2.3 Force Fields for Other Species: Nucleic Acids, Lipids, Sugars, and Water

While proteins represent the majority of current drug targets, there is clearly an interest to model and simulate nucleic acids too. Nucleic acid force fields have historically lagged behind protein force fields; nonetheless, in the last decade there had been significant improvements in the availability of force fields for DNA and RNA simulations. In the early 2000s, the CHARMM27 force field for nucleic acids was released and has been recently updated.[98,99] At the same time, when 50–100 ns long simulation times became available, deficiencies in the AMBER force field for nucleic acids were observed, in particular in the sampling of backbone populations.[100,101] Pérez et al. have provided the improved set of parameters ff99-bsc0[102] and work by Yildirim and coworkers focussed on reparameterizing the RNA chi torsional angles.[103–105] Additional recent work focussed on the derivation of specific improved parameters for both RNA[106,107] and DNA.[108,109] Testing and benchmarking of all these parameter modifications and extensions is still very much an on-going exercise.

With increasing interest in the study of membrane properties and the role of lipids in the modulation of protein functions, dedicated lipid parameter sets that are compatible with other protein force fields are increasingly becoming available and accurate. In 2005, a revised version of CHARMM27 with optimized parameters for aliphatic tails was published and termed CHARMM27r.[110] Later in 2010, the CHARMM 36 lipid FF was developed by improving the parameters of the headgroups and ester links.[111] On the other hand, AMBER had not had support for lipid parameters until 2012, when Lipid11 and GAFF lipid were released.[112,113] Lipid14 was later released in 2014 as a significant advance over the previous AMBER lipid force fields[114] and allowed the artificial surface tension term that was previously required to keep the correct phase to be dropped. Lipid14 compared favorably with a number of experimental properties, such as area/volume per lipid, bilayer thickness, NMR order parameters, scattering data, and lipid lateral diffusion. In 2015, the first example of spontaneous lipid bilayer formation during unbiased all-atom simulations was presented using both the CHARMM36 lipid FF and AMBER Lipid14.[115]

Carbohydrates are fundamental building blocks in biology and have important roles in many cellular processes. Moreover, carbohydrate-based structures are of interest for drug design purposes.[116,117] However, the modeling of carbohydrates presents a distinct set of challenges due to their particular structural and electronic properties. The high number of chiral centers, rotatable bonds, and linkages between units, results in a large number of complex structures. In addition to the high number of polar groups, peculiarities such as the anomeric effect cause complex charge distributions around the molecule, contributing to the difficulty to derive adequate fixed partial charges. As a consequence, carbohydrate force fields are currently not as mature as force fields for other biological small molecules such as lipids and it may well be that more complex functional forms are required to fully capture the properties of carbohydrates properly.[118,119] The main carbohydrate atomistic force fields currently available are GLYCAM06[120,121] and CHARMM36.[122–125] In particular GLYCAM06, which is compatible with the AMBER force field, supports a large collection of carbohydrates with parameters for both anomeric and enantiomeric forms of the compounds. An OPLS version for carbohydrates dates back to 2002,[126] and there have also been contributions to the GROMOS force field.[127]

The quality of the solvent model is fundamental too, as properties such as partition coefficients and binding affinities depend strongly on the solute–solvent interactions. Water models are also deeply entrenched in the fabric of all solute force fields, so that it is difficult to replace water models straightforwardly. However, the prevalent models of liquid water were developed decades ago[128] despite computational advances and larger availability of experimental data. This motivates the development of new models showing better agreement with experiment.[129] Among recent developments on fixed-charge water models, there is the 4-point Optimal Point Charge (OPC) water model, which showed an improved performance for a number of different bulk properties as compared to other popular models such as TIP3P, SPC/E, TIP4P-Ew, and TIP5P.[129] The authors also suggest an improved performance in the results of hydration free energy calculation for small molecules. Similarly, new TIP3P and TIP4P parameters (termed TIP3P-FB and TIP4P-FB) were derived using an automated force field optimization program, and showed much better agreement with bulk properties than the original water models.[130]

3.02.2.4 Polarizable Force Fields

The lack of explicit polarization has long been recognized as one of the crudest simplifications of traditional fixed-charge force fields.[131,132] Indeed, it is known that the environment has a large effect of the electronic distribution of a molecule; for instance, the charge distribution around a peptide depends upon its conformation[133] and that of a ligand changes between the bound and unbound states.[134] Such effects cannot be captured with a fixed-charge model. There have therefore been efforts to develop

polarizable force fields for decades now. However, it has only been recently that there has been an increased interest in these models, facilitated by the computer power now available along with efforts to include them in widely used simulation software such as GROMACS, NAMD, AMBER, and CHARMM. A few different theoretical methods with different degrees of rigor have been explored in order to model atom polarization during molecular simulations.

One such approach is the "fluctuating charge" model, in which the partial charge of each atom is placed on their nucleus but the magnitude of each charge can change during the simulation.[135] Charges are transferred between atoms in a way that equalizes the electronegativities, where the instantaneous electronegativity on an atomic site depends upon the atom's type, charge, and the electrostatic potential it experiences due to its neighboring particles.[135] While it does not require any more interaction terms than classical force fields, it can easily represent polarization that occurs in the direction of atomic bonds.[131] The most extensively applied fluctuating charge model so far has been the charge equilibration (CHEQ) force field developed within the CHARMM program.[136,137]

Another popular method is based on classical Drude oscillators, where a pair of point charges represents each polarizable atom. While the first charge is positioned on the nucleus like in typical fixed-charge force fields, the second charge is attached to the nucleus via a spring as a massless (Drude) particle. The two particles can therefore be considered as representing the nucleus and electron cloud of the atom, and the total partial charge for the atom is the sum of the charges of these two particles. The mimicking of polarization is due to the fact that the second particle is free to move around the nucleus responding to the external field and creating an induced dipole moment.[138–140]

This approach too is easily implemented within already existing force fields and simulation codes. On the other hand it involves a substantially larger amount of charges present in the system, so that many more interactions need to be calculated at each time step. The Drude-2013 model by MacKerell, Roux and coworkers, where Drude particles are added to all nonhydrogen atoms, is currently the most widely adopted for simulation of biomolecules.[141–144] Extra point charges, representing lone pairs and an anisotropic form of polarizability, have been introduced in order to better represent hydrogen-bond acceptors.[145] Lemkul et al.[145] have recently published a comprehensive review on this model and we redirect the readers to it for a more in-depth treatment of the subject.

In the inducible dipole methodology, inducible point dipoles are assigned to each atomic site. The field due to the explicit charges alone is calculated first, and then dipoles are calculated as the field multiplied by the local polarizability, resulting in a new electric field.[133] Dipoles are therefore usually calculated with an iterative procedure to convergence, and the electrostatic energy derived from charge–charge, charge–dipole, and dipole–dipole interactions.[145,146] Such an approach was used with the AMBER ff02 force field and AMBER simulation package.[82,147] A more rigorous approach that includes multipoles up to quadrupoles is employed in the AMOEBA force field.[148–152] Contrary to all the other approaches discussed above, AMOEBA takes into account anisotropic polarization through permanent multipole moments and does not need additional point charges in order to represent anisotropy due to lone pairs. In addition, other instances of anisotropy such as pi-clouds or sigma-holes are naturally taken into account too.[131,153–156]

Most parameterization efforts for polarizable force fields for biomolecules have focussed on proteins (indeed, all of the above-mentioned force fields include parameters for proteins). Polarizability is also expected to have a strong impact on nucleic acids, firstly because they are highly charged and contain a large number of hydrogen bonds, but secondly their high charge density means they are highly polarizing themselves. Amber ff02 and Drude-2013 both contain parameters for nucleic acids. Parameters for lipids and carbohydrates, while highly desirable, are still limited, with the CHARMM Drude and CHEQ force field providing only partial coverage for these species.[131] A broad set of parameters for arbitrary organic molecules is not available yet, but would be extremely desirable in the context of drug design. At present, it is clear that there is a huge potential for polarizable force fields, but much work is still needed to develop and validate them. Consequently, fixed-charge force fields are still very much the standard for molecular simulations of protein-ligand complexes.

While simulations using polarizable force fields tend to be computationally more intensive and used to be limited to very short timescales, there are now instances of simulations with lengths in the tens to hundreds of nanosecond in length. The Drude-2013 force field has been used for simulations of proteins with up to 224 residues and for 100–200 ns,[144] while for smaller proteins simulations of even up to the microsecond timescale have been run.[157] The more expensive AMOEBA force field was used in 2013 with optimized parameters for 30 ns long simulations of 10 different proteins in solution. The simulations showed how the structures were stable with good agreement of the calculated order parameters with NMR data. In addition, the force field showed a correlation coefficient of 0.998 between the x, y, and z components of the gas phase dipole moments obtained with AMOEBA and high-level QM calculation for each amino acid dipeptide at multiple conformations, which is an unprecedented level of accuracy in reproducing the electrostatic properties of peptides using a molecular mechanics based force field.[148] Jiao et al., using the same force field, also found good quantitative agreement between calculated and experimental binding free energies for a series of benzamidine-like ligands binding to trypsin.[158,159] Often, however, polarizable force fields are found to perform just as well as classical force fields. Nevertheless, classical force fields have gone through much more extensive optimization. Assuming the same extent of scrutiny and development will be achieved for polarizable force fields within a few years, we can expect these to yield a more accurate representation of molecular interactions in the near future.

One of the perceived disadvantages of polarizable force fields is the fact that they are slower than fixed-charge force fields. However, this is expected given the higher complexity of the functional form, and once fully developed the more appropriate question will probably be: what level of physical detail of the system do I need in order to study the process/property I am interested in? Conventional additive force fields will likely always provide longer trajectories given the same amount of computation, trading-off accuracy in the electrostatic description of interactions for speed. Therefore, researchers will have to weigh the

advantages of a longer timescale versus greater accuracy and decide which one is more important for the problem at hand. Similar considerations already apply when deciding whether to use an all-atom force field versus a coarse-grained model, or even versus a quantum mechanical treatment of the system. Computational demands notwithstanding, advances in polarizable force fields are among the most promising developments toward the goal of more accurate force fields.

3.02.2.5 Coarse-Grained Force Fields

Despite the increase of computational power available and efficiency of simulation algorithms, the large spatiotemporal jump between the atomistic and mesoscopic scales calls for coarser physical models in order to describe many biologically relevant properties. In fact, important phenomena, such as complex self-assembly or macromolecular crowding, only start to emerge at the mesoscale, where systems are typically of μm in length and several seconds in time. In addition, depending on the scientific question asked, the level of detail provided by atomistic simulations might not be necessary, and sometimes not even desirable considering the computational burden. With access to longer simulation time and space scales we can begin to address more biologically relevant scales, and to have broad overlap with experiments, which is important not only for validation but also for prospective use of such simulations. Coarse-grained (CG) models therefore provide a much-needed representation of biological and chemical systems that bridge the gap between atomistic and continuum models.

In most forms of coarse-graining, groups of atoms are clustered into a lower number of CG beads. There are therefore many different levels of coarse-graining, from models that cluster only a few atoms into one bead, to ones that represent a whole protein with one bead. One challenge when developing a coarse-grained model is therefore to determine the appropriate mapping of atoms on the CG sites for the problem to be studied; too much detail might result in useless additional computation and thus limit accessible spatiotemporal scales, while too little detail might average out useful information about the properties of the systems we are interested into. Thus, Einstein's advice to "make everything as simple as possible, but not simpler" applies here too. The other chief challenge in the development of CG models in general, is to obtain a potential energy function that is able to approximate the atomistic one.[160] Coarse-graining is effectively a dimensionality reduction process, in which atomic interactions are renormalized into a coarser representation. This process results in a smoother free energy landscape where the kinetics is typically accelerated, yet as much of the underlying physics as possible has been retained.

While Levitt and Warshel performed possibly the first CG simulation of protein folding over 40 years ago,[161] it is in the last 10 years or so that the CG field started expanding rapidly, allowing the application of MD to a number of new biological problems. One CG force field that has become popular is the MARTINI model.[162–166] This force field is based on relatively high-resolution models where typically four heavy atoms are mapped to one CG particle, allowing computational efficiency while retaining some chemical relevance (see Fig. 2). The CG beads are of four types (polar, nonpolar, apolar, and charged), where each type

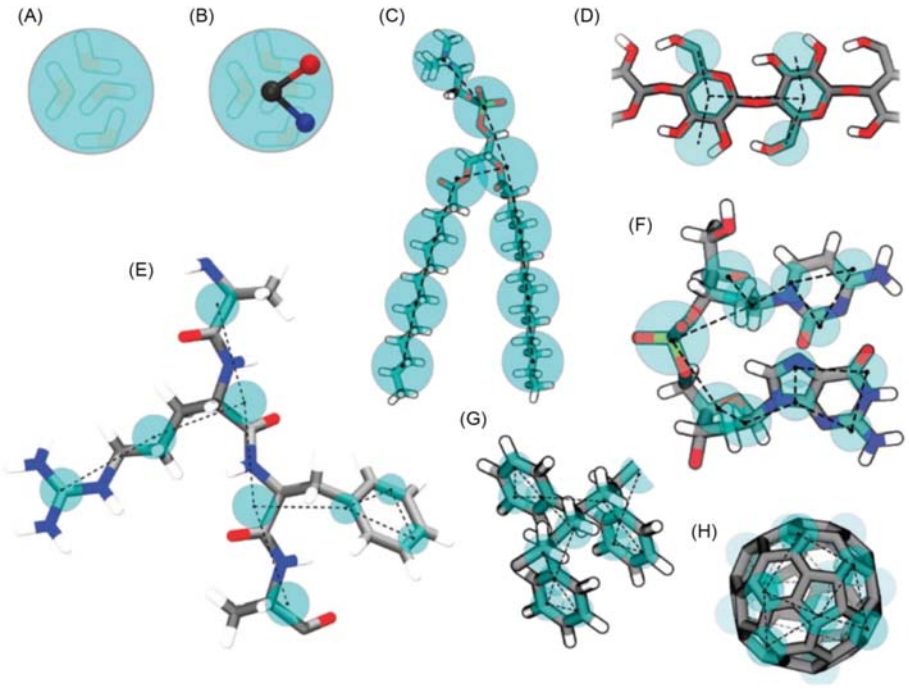

Fig. 2 Martini mapping examples of selected molecules. (A) Standard water particle representing four water molecules. (B) Polarizable water molecule with embedded charges. (C) DMPC lipid. (D) Polysaccharide fragment. (E) Peptide. (F) DNA fragment. (G) Polystyrene fragment. (H) Fullerene molecule. In all cases Martini CG beads are shown as cyan transparent beads overlaying the atomistic structure. From Marrink, S. J.; Tieleman, D. P. *Chem. Soc. Rev.* **2013**, *42*, 6801, reproduced with permission from the Royal Society of Chemistry.

can have different hydrogen-bonding capabilities (donor, acceptor, both, or none) and degree of polarity (from 1 = low to 5 = high polarity), forming a total of 18 fundamental bead types. The nonbonded interaction for the CG particles are based on the standard 12-6 Lennard-Jones potential, with Coulombic interaction too for the charged bead type, where parameters are derived empirically from experimental thermodynamic data such as free energies of hydration, vaporization, and partitioning between water and organic phases.[167] Such a top-down approach, where the model is calibrated based on experimental properties, coupled with the high-resolution of the model, means that MARTINI manages to be quite transferable between different systems. Such transferability and the availability in a number of simulation packages (GROMACS, NAMD, GROMOS, Desmond) have made MARTINI one of the most popular CG models for the simulation of biological systems.[167–179]

Voth and coworkers adopted a different philosophy for the development of their multiscale coarse-graining (MS-CG) methodology. In this bottom-up approach, forces from atomistic simulations are variationally mapped onto the CG potential, with no fitting to experimental data.[160,180–182] Since the approach relies on a variational principle, it allows for a rigorous derivation of CG force field parameters from a corresponding all-atom system. The broad applicability of the approach has resulted in its use for a number of different applications; from the study of simple and complex liquids[183] to nanoparticles,[184] lipid bilayers,[185,186] and proteins.[187,188] On the other hand, being derived for specific systems and conditions, MS-CG potentials might not be easily transferred to others. However, transferability is, in general, inherently reduced in all coarse-graining procedures, due to the simplified representation of a system that causes loss of information.

Multiscale methods that integrate atomistic and CG models in a single simulation are now starting to appear, either in a static[189] or adaptive fashion,[190–193] where the resolution of the molecule depends on its position in space. Some of the main challenges in this case are the parameterization of the interaction between atomistic and CG particles, and the appropriate mapping between all-atom and CG representations.[160,194–196] An alternative approach, termed resolution exchange, is based on the replica exchange methodology and allows Monte Carlo swaps between replicas at different resolutions.[197,198] While this approach avoids the problem of interactions between all-atom and CG particles, the on-the-fly mapping between the two resolutions still needs to be addressed efficiently. So far, however, the most common approach to mix CG and atomistic scales has been to use CG for enhanced sampling and then to convert certain configurations to an all-atom representation[199] that is a reasonable starting point for additional, more detailed, simulations.[194,200–206] A few tools to back-map all-atoms particles onto CG beads have been developed. Stansfeld and Sansom[199] described a fragment-based protocol for the conversion of lipid and proteins from CG to all-atom resolution in 2011. Wassenaar et al.[207] later proposed a general approach based on a geometric projection followed by force field-based relaxation.

3.02.3 Novel Simulation Approaches and Trends

The hardware and force field advances have been complemented in recent years by the development and application of new simulation approaches, some of which we highlight in this final section. We also draw attention to the types of problems that these approaches can begin to address that were not conceivable just 10 years ago.

3.02.3.1 Parallel and Enhanced Sampling

With increasing availability of a large number of processors to the researcher through large-scale facilities or distributed computing, the question of how to exploit most efficiently such computing power arises. In fact, in recent years, while Moore's law still applied, there has been a barrier to increased clock speed due to heat dissipation issues and vendors have rather focussed on increasing the number of cores on chips.[208,209] This means that larger and larger systems can be studied, however a point might be reached where "standard" systems of up to 100 K atoms will not benefit any more from a larger number of cores due to limits in parallelization. In addition, since during an MD simulation a large amount of time is spent sampling the low energy states, the relevant states and transition the researcher is interested in might not be sampled within the timescales currently achievable with MD. Therefore, a number of techniques that aim at accelerating the sampling of a single simulation or at combining information from parallel independent simulations have been pursued. Here we review some of these approaches that in our opinion have made significant progress in the last decade and have started being adopted by the broader MD community. Due to the limitation in space we are not reviewing comprehensively all such methods; we apologize in advance for the inevitable omissions in that regard.

3.02.3.1.1 Markov state models

Perfect parallelism that would make an efficient use of a large number of processors could be achieved by running multiple independent simulations. However, the process of interest might often occur on timescales longer than the individual simulations. Therefore, the challenge becomes to meaningfully combine the data so as to correctly extract information about the long timescale dynamics of the system. For instance, while one might run efficiently a thousand 1 μs long simulations on a supercomputer with enough CPU/GPU power, can we extrapolate information about events happening in the millisecond timescale? Another question that follows immediately is how to process the data in such a way that the results are easily interpretable. Discrete state kinetic models, such as Markov Models, are statistical approaches that have recently been very successful at addressing the above challenges.[210–212] While the theoretical framework has been available for many years, application to biological systems has only really appeared in the last 10–15 years. The increase in popularity in Markov state models (MSM) and hidden MSMs is in part

due to the development of freely available tools[213,214] that allow the user to build such models in a relatively straightforward manner, despite the complexity of the underlying statistical methods.

The idea behind such analysis is to cluster an ensemble of structures from MD simulations based on kinetic rather than on geometric distance, and to derive transition rates between all these states from the simulation data.[210,213,214] In practice, a typical workflow would start with the definition of a set of observables that will be used for analysis. However, in contrast to other techniques we will describe in the next sections, this set does not need to be system-specific, so that there is no need to know a priori the reaction coordinate that best describes, for instance, the opening of a channel or the loop movement of a kinase. These variables could be the Cartesian coordinates of a group of atoms, certain angles and torsions, as well as the distance between all Cα atoms, or contacts between any residues.[213]

Since a large number of variables can be selected in such a way, some of which might be redundant, potentially resulting in an inefficient discretization of the high-dimensional space, a dimensionality reduction is generally performed first. The time-lagged independent component analysis (TICA) has become the standard dimensionality reduction technique employed for the construction of MSM. This is because as opposed to methods using orthogonal transformations such as principal component analysis (PCA), which maximize the variance of the transformed coordinates, TICA maximizes their autocorrelation, that is it finds the slowest-relaxing degrees of freedom.[215–218] This is important because we are interested in studying the kinetics of the system, identifying, for example, metastable states and rare transitions, rather than finding the most similar/different conformations. The transformed input is then discretized into a number of microstates using clustering methods such as k-means, and conditional probabilities of transitioning between these microstates within a certain time-lag are estimated from the MD data.[213,219,220] Such probabilities are the basis for the estimation of the MSM (or the hidden MSM). Using the MSM model one can then estimate equilibrium expectations of observable, free energy surfaces (FES), relaxation timescales that can be compared to experiment, or metastable states. In addition, using transition path theory one can compute fluxes between sets of states and recover the mechanism and kinetics of going from state A to state B.[221–223] Since thousands of states are hard to visualize and hardly comprehensible, kinetically related microstates can be clustered into a few relevant macrostates in order to have a coarser, more interpretable, view of the configurational space and its kinetics.[224]

MSMs have rapidly become widespread and their application to diverse biological problems has been demonstrated in a number of noteworthy studies. Voelz et al.[225] employed MSM to study the folding pathway of the millisecond folder NTL9(1–39). The authors used adaptive resampling techniques in order to improve the sampling of metastable basins and transitions between them. The simulations, revealing a network of possible paths with different likelihoods, identified numerous folding pathways (see **Fig. 3**).

Kohlhoff et al.[26] used Google servers in order to run a large number of simulations of the active and inactive structures of the β_2-adrenergic receptor for a total of 2.15 ms of MD, and then used MSM in order to combine all the trajectories and study the activation mechanism of this G-protein coupled receptor (GPCR). Again, many parallel pathways rather than a single dominant

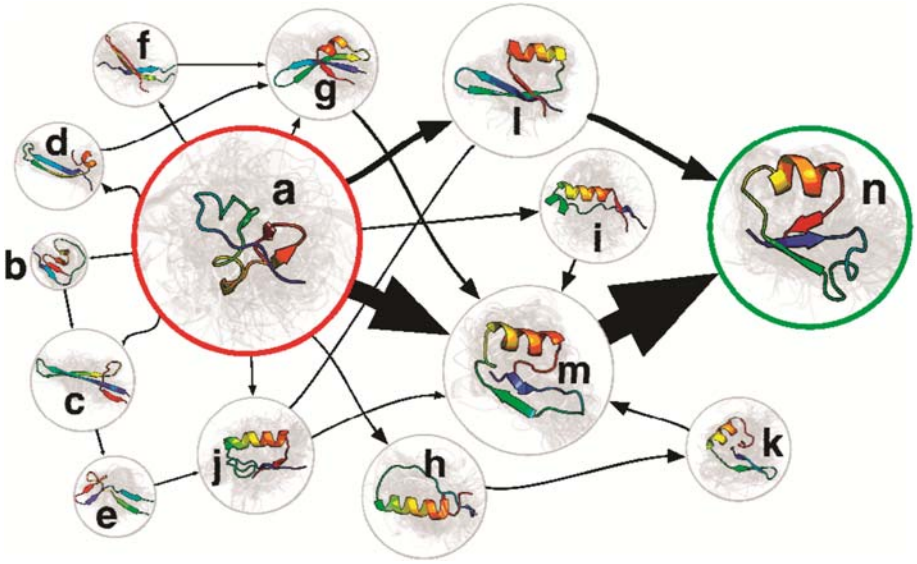

Fig. 3 Schematic representation of a MSM. A 2000-state Markov state model (MSM) was built using a lag time of 12 ns. Shown is the superposition of the top 10 folding fluxes, calculated by a greedy backtracking algorithm. These pathways account for only ~25% of the total flux and transit only 14 of the 2000 macrostates (shown labeled a–n, for convenient discussion). The visual size of each state is proportional to its free energy, and arrow size is proportional to the interstate flux. Reprinted with permission from Voelz, V. A.; Singh, V. R.; Wedemeyer, W. J.; Lapidus, L. J.; Pande, V. S. Unfolded-State Dynamics and Structure of Protein L Characterized by Simulation and Experiment. *J. Am. Chem. Soc.* **2010**, *132*, 4702–4709. Copyright 2010 American Chemical Society.

one were observed. In addition, it was shown how ligands modulate the activity of the receptor by affecting its probability of accessing the active state. Finally, different receptor states along the activation pathways were used for docking, resulting in the enrichment of different chemotypes for different receptor conformations, showing how the use of intermediate states might be beneficial for hit discovery.

Shukla et al.[226] used MSMs, transition pathways, and adaptive sampling techniques on distributed computing in order to study the activation pathways of Src kinase. In such a way they provided a thermodynamic and kinetic description of the activation mechanism of the kinase at atomistic detail. In addition, novel intermediates states that could be targeted by allosteric inhibitors have been identified. Plattner and Noé[227] have instead employed MSMs to study the binding mechanism of benzamidine to trypsin, and in particular the role of protein conformational plasticity in ligand binding. Six different slowly-interconverting (of the order of tens of microseconds) apo-state conformations have been found, with one additional conformation that was accessible only to the bound state. The binding kinetics observed, exhibited both conformational selection and induced fit features. The study showed how conformation and binding kinetics are closely coupled, and how various trypsin conformations can be accessed and stabilized both by ligand binding or protein mutations.

Overall, the use of MSM results in a number of benefits for molecular simulations. First of all, as mentioned previously, the approach provides a means to perfect parallelization, and also takes advantage of the direction of recent hardware trends towards higher number of cores on chips rather than increased speeds of single processors. Moreover, adaptive sampling coupled with MSM should provide more effective sampling of rare events. In fact, many biological systems are characterized by rugged energy landscapes that result in the presence of several metastable states separated by high-energy barriers. As a consequence, most of the time in a conventional MD simulation is spent sampling a few low energy states due to kinetic bottlenecks, and the exploration of transition events or other metastable states is limited. Adaptive sampling would allow one to focus the computational effort into phase space areas that have not been extensively sampled yet by the simulations. In addition, MSMs provide a framework for the study of the kinetics of molecular events such as drug binding and protein conformational change. Last but not least, MSMs allow a human-readable interpretation of large amounts of data thanks to the kinetic clustering and coarse-graining procedures.

3.02.3.1.2 Replica exchange methods

Replica exchange molecular dynamics (REMD) methods enhance sampling by running multiple simulations of the same system in parallel at different thermodynamic states. In the first use of the method, Swendsen and Wang used multiple Monte Carlo replicas at different temperatures to speedup sampling.[228] Sugita and Okamoto later proposed a similar framework for MD.[229] This is often called "parallel tempering" or "temperature replica exchange" (T-REMD), and the idea is to run simulations at higher temperatures than the one of interest in order to explore larger volumes of phase space thanks to the Arrhenius law.[230–232]

A set of simulations with increasing temperatures $T_0 < T_1 < T_2 < T_M$ is prepared, where T_0 is the thermodynamic state we are interested in. All the simulations are run in parallel and the system configurations (i.e., the positions of the particles) are allowed to swap between replicas according to a Metropolis criterion that depends on the potential energy difference between replicas. The exchange probability between replicas i and j is $p(i \to j) = \min(1, e^{\Delta_{ij}})$, where for parallel tempering $\Delta_{ij} = [(\beta_i - \beta_j)(U(r_i) - U(r_j))]$, with β being $1/kT$, and U the potential energy of the configuration r.[232,233] In such a way, energetic barriers are more easily overcome thanks to the larger kinetic energy at higher temperatures, while providing a correct ensemble of conformations at T_0. The acceptance criterion implies that swaps between replicas occur frequently only if the energetic overlap between replicas is sufficient, which affects the number and temperatures of replicas needed for a specific system.[232] Typically, swaps are allowed only between neighboring replicas (e.g., between T_0 and T_1, or T_1 and T_2), however, it is possible to swap configurations across all replicas leading to improved mixing between states.[234] More generally, replica exchange belongs to the group of techniques referred to as *generalized ensembles*, among which are also *expanded ensemble* methods, a serial equivalent of replica exchange.[235–237]

It soon became clear that temperature is not the only alteration between replicas that can be used, and several variants of the original T-REMD have been implemented and widely used in the last decade. Hamiltonian replica exchange (H-REMD) is a more general form of REMD where it is possible to enhance sampling by using parameters other than temperature.[238–241] Interaction energies can be scaled between replicas for example, and as such H-REMD can be used for free energy perturbation calculations, where two systems (e.g., two protein mutants, or the apo and holo forms of a protein) are interpolated by a coupling parameter λ, and the replicas correspond to the two end states plus a number of intermediate ones.[242–245] In replica exchange with solute tempering (REST) the system is divided into two parts, the solute and the solvent, so that the potential energy of the system can be described by three terms: the internal energy of the solute, the one of the solvent, and the interaction energy between the two. As the temperature increases on the replica ladder, the internal energy of the solvent and the solute-solvent interaction energy are scaled, while that of the solute is not. The effect is similar to that of raising the temperature of the solute while keeping the temperature of the solvent constant. This trick removes the dependence of the exchange acceptance probability on the number of waters in the system, which often causes poor scaling with system size. Thus, with REST fewer replicas are needed to explore a certain temperature range.[246,363] In addition, different flavors of multidimensional REMD where replicas are swapped in more than one dimension have been developed, and have been successfully applied, for instance, in free energy calculations.[247–249]

Thanks to its robust implementation in mainstream MD packages,[239,250–252] replica exchange has become a standard technique to accelerate sampling and aid convergence. It has found many applications for the study of protein dynamics and folding,[253–263] free energy calculations,[242,264–268] as well as ligand binding site and pose identification,[269,270] and constant pH simulations.[271–275] The computational cost of replica exchange grows proportionally with the number of replicas, however, it has become accepted that

the sampling obtained is more efficient than can be obtained from a single (long) simulation. In addition, the computational overhead due to the swaps and the Monte Carlo move is negligible, considering that the potential energies of the systems are evaluated anyway for the calculation of the forces. These facts have contributed in making replica exchange methods a standard instrument in the modeler's current toolbox.

3.02.3.1.3 Bias potential methods: Metadynamics

Bias potential methods facilitate the exploration of the FES by introducing additional potential energy terms that encourage the system to move out of free energy minima.[233] Typically, such methods act on a small number of degrees of freedom, often called *collective variables* (CVs). Many methods that fall in this category have been developed, including umbrella sampling,[276] local elevation,[277] adaptive force bias,[278] accelerated molecular dynamics,[279,280] conformational flooding,[281,282] and steered MD.[283] Here, however, we will focus only on metadynamics,[284–287] one of the most popular bias potential approaches, thanks in part to its availability across multiple MD packages (AMBER,[288] GROMACS,[251] NAMD,[252] LAMMPS[289]) through the PLUMED code.[290,291]

Metadynamics allows accelerated exploration of phase space and reconstruction of the FES along selected CVs by adding a history-dependent bias potential.[284–287,292] Such bias is a function of the chosen CVs. Therefore, the choice of CVs is an important step in the setup of the simulations and has important consequences on the ability to enhance sampling and the convergence of the free energy estimates. A CV is a function of the microscopic coordinates of the system, and a wide choice of CVs is available to the researcher. Typical CVs are distances, angles, or dihedrals, as well as the number of hydrogen bonds, radius of gyration, or dipole moments.[290,291] The CVs that best describe the reaction coordinate of interest should be chosen for the bias potential to be added. Broadly speaking, CVs should allow one to distinguish between the initial and final state, describe all relevant intermediates, and include all the slow modes of the system. Moreover, it is suggested that the number of CVs is kept as low as possible (usually not more than three), since higher dimensionality comes with considerable computational cost, in addition to the fact that the interpretation of high-dimensional surfaces can become difficult.[284–287] The a priori choice of CVs is far from trivial. Often, machine learning or dimensionality reduction is performed on preliminary MD runs, in order to identify the most relevant degrees of freedom for the process of interest.[293–298] Knowledge of the physical and chemical behavior of the system can go a long way in the identification of the most suitable CVs for the problem at hand.

Once a set of CVs is determined, the metadynamics simulation biases the potential energy function along the chosen CVs so that configurations that have been visited already are discouraged. The bias potential that is added to the force field-based potential energy can be described by a sum of Gaussians.[284–287,292] **Fig. 4**, adapted from the original metadynamics paper,[287] exemplifies the basic idea behind the approach. In this example a one-dimensional potential energy surface (PES) with three minima is considered. The thick black line represents the shape of the potential surface along a general CV, which is unknown, and the simulation is in fact used to explore it. However, if we start a conventional MD simulation from basin B, the system would remain stuck in this minimum if the barriers are larger than thermal fluctuations. On the other hand, adding the bias potential during the course of the simulation we modify the shape of the PES. At step = 10 the depth of the basin is reduced, but a minimum is still present; at step = 20 the energy minimum is filled by the bias potential and the system can fall into the local minimum A; at step = 40 the bias potential now starts filling basin A; continuing to deposit Gaussian-shaped potentials along the CV, the point where the global minimum C is explored is reached at step = 160; eventually, the PES becomes flat and the system evolution resembles a random walk after step = 320. Once a flat PES is obtained, the bias potential can be used to recover the negative image of the underlying free energy.[287,292,299] Since in a single run the bias potential tends to oscillate around (rather than converge to) the free energy, the well-tempered variant of metadynamics method, in which the bias deposition rate decreases over time, has been developed to address the issue.[300,301]

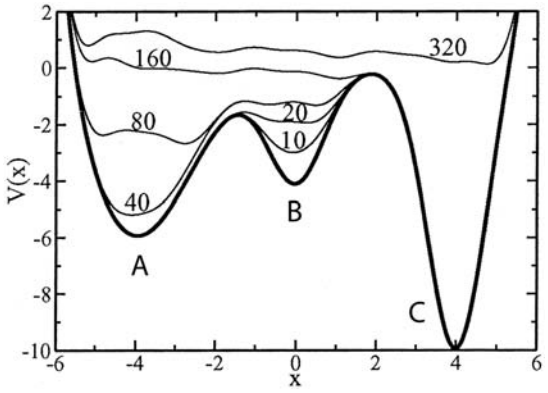

Fig. 4 Time evolution of the sum of a one-dimensional model potential $V(\sigma)$ and accumulating Gaussian terms. The dynamic evolution *(thin lines)* is labeled by the number of dynamical iterations. The starting potential *(thick line)* has three minima and the dynamics is initiated in the second minimum. Adapted from Laio, A.; Parrinello, M. Escaping Free-Energy Minima. *Proc. Natl. Acad. Sci. U. S. A.* **2002**, *99*, 12562–12566.

As compared to replica exchange approaches, metadynamics allows us to overcome larger energy barriers. On the other hand, it acts only on a few selected CVs, which, if inadequate, might provide nonconverged or misleading estimates of the energy barriers between minima.[285,301] The two methods are therefore complementary and can in fact be combined.[302] In such a way, while parallel tempering allows us to cross moderate free energy barriers on all degrees of freedom, metadynamics allows us to cross larger barriers on the specified CVs.[303,304] Alternatively, replica exchange can be used in order to bias different sets of CVs in a number of parallel simulations while allowing exchanges between them, in a paradigm called *bias exchange*. A reweighting procedure that is specific to bias exchange can be used in order to recover the FES as a function of part of the set of CVs.[305,306]

Metadynamics has been used quite extensively in biomolecular dynamics and protein-ligand association.[303,307–321] As an example applied to drug discovery, Limongelli et al.[318] have studied the full dissociation process of SC-558, a highly selective cyclooxygenase-2 (COX-2) inhibitor, through the use of metadynamics calculations based on a distance and a torsional angle as the two CVs. They discovered an alternative binding mode to the one observed experimentally, and suggested this as the reason behind the selectivity and the long residence time of the inhibitor for this isoform. In fact, when simulating the dissociation of SC-558 from COX-1, only one energy minimum, that is, a single binding mode, was observed in the protein binding site. This binding mode was very close to the crystallographically observed pose in COX-2 for the same inhibitor. On the other hand, the simulations with COX-2 revealed a second energy minimum in the binding site, in which the ligand also engages in additional hydrophobic contacts with the protein. Lanzo et al.[322] had previously shown with fluorescence quenching experiments that an analogue of SC-558 would bind to COX-1 in a two-step process, but an additional unidentified step was required to bind to COX-2. The authors also reported slower dissociation kinetics from COX-2 as compared to COX-1 (several hours versus 1 min). Limongelli et al.[318] suggested that the alternative binding pose observed in their simulation is what causes the detection of an additional binding step in the fluorescence experiments.

Grazioso et al.[316] used a similar method to study glutamate uptake from the synaptic cleft and its release into the intracellular medium. The authors managed to describe the opening mechanism, which involved a large-scale hairpin motion, and the associated free energy profile. Herbert et al.[315] reported the discovery of the first extracellular inhibitor of the fibroblast growth factor receptor, a tyrosine kinase receptor involved in cell growth, proliferation, and survival. In this study, bias exchange metadynamics was used in order to study the ligand's mode of action. Experimental methods had hitherto been unsuccessful in identifying the inhibitor's binding site. The simulations correctly predicted the dissociation constant of the inhibitor, as well as for other lower potency analogues, validating the in-silico analysis.

3.02.3.2 Simulation of Large Systems

As we enter an era of exascale computing with highly optimized MD codes, larger and larger systems are starting to be studied through simulation, both in all-atom and coarse-grained detail. Accessing greater spatial scales is important in order to probe the function of biological machineries, which often operate on scales spanning hundreds of nanometers to micrometers.[3] Simulations of viruses,[323] the ribosome,[324] large membranes,[325] and small organelles[326] contain millions of atoms and require highly scalable software.[3] Such systems present both opportunities and challenges for high-performing computing and molecular modeling, and hold the promise to contribute to a deeper level of understanding of living organisms and their behavior at the mesoscale. This, in turn, would enable the design of new therapeutics based on small molecules and engineered biologics with the aid of computation.

Due to the large size of viruses for MD simulations, most initial studies on viruses focused on isolated proteins or fragments of the viral capsid.[327] However, in 2006, Freddolino et al.[328] simulated for the first time a complete virion (capsid and genetic material) atomistically, despite some approximations in the RNA genome structure. The authors simulated the entire virion and both the capsid and RNA core alone of the satellite tobacco mosaic virus for a total of 50 ns of MD. The systems contained about 1 million atoms, and the simulations demonstrated the stability of the virion and RNA core, while showing instability for the capsid without RNA. Since then, other large and complex viral components of, for instance, Poliovirus,[329] Dengue,[330] influenza,[331] and HIV-1,[201,332] have been studied by means of simulation. Reddy et al.[331] reported the microsecond-long CG (Martini) simulations of an influenza A virion. The authors showed how the presence of the Forssman glycolipid altered the mobility of bilayer species, and suggested that the viral spike proteins do not aggregate and are thus competent for IgG antibody binding. In other studies, the spontaneous assembly of the viral capsid, a fundamental step in the replication cycle of the virus, has been studied by simulation at different levels of coarse-graining.[329,333–336]

Through Brownian dynamics, it was shown how the optimal configuration of viral genome is essential for the correct assembly of the capsid.[333,334] Recently, electron microscopy has been integrated with molecular dynamics flexible fitting (MDFF)[337] in order to elucidate the structure of complex viral capsids in atomic detail and in their native environments. Zhao et al.[332] obtained an 8 Å cryo-EM structure of the mature HIV-1 native capsid, a polymorphic capsid with no apparent symmetry; they then docked atomic NMR and X-ray structures of capsid proteins into the density map, modeled the linker and missing loops, and finally refined the model by MDFF to obtain an atomistic representation of the virus. The final model contained 64 million atoms and was simulated in explicit solvent for 100 ns, and demonstrated the importance of the placement of capsid protein pentamers in the structure. Other multimillion simulations of viral structures, such as in the case of the Rabbit hemorrhagic disease virus (RHDV),[338] have been successfully employed in the refinement of crystal structures fitting into cryo-EM densities.[339,340]

The ribosome is an obvious antibacterial target, and in the last decade an increasing amount of experimental data has become available. Consequently, a number of researchers have started simulating the ribosome with MD, trying to bridge the gap between

its structure and dynamics.[324] Similar to viruses, the first ribosome simulations focussed on selected regions due to the computational expense of million-atom simulations.[341,342] However, with increasing computing power available, simulations of the entire ribosome became viable.[343] Recently, Bock et al.[344] performed MD simulations of 13 intermediate translocation states of an entire bacterial ribosome. Such systems comprised ~2.2 million atoms and were simulated for a total of more than 1.8 μs, revealing a description of the time-resolved translocation in atomic detail. Kinetic information was extracted from the simulations and it was found that tRNA motions govern the transition rates within the pretranslocation and posttranslocation states. On the other hand, faster submicrosecond rates were observed for intersubunit rotations and L1-stalk motion. Overall, the results added the time dimension to the structural data available, providing information on transition rates, molecular forces, and correlated functional motions that could not have been obtained otherwise.

Whitford et al.[345] also carried out microsecond MD simulations of a complete ribosome, identifying reaction coordinates for the subunit rotation that were used to estimate free energy barriers associated with the translocation. Given its role as a pharmaceutical target, a number of MD simulations of the ribosome in the presence of antibiotics have been performed in order to elucidate the mode of action of small molecules.[346–350] For instance, Sothiselvam et al.[346] used both biochemical methods and molecular dynamics to show how erythromycin, a macrolide antibiotic, allosterically predisposes the ribosome to translational arrest, without necessarily forming extensive contacts with the nascent peptide in the exit tunnel as previously suggested. MD, in particular, hypothesized the base flipping of specific nucleotides in the catalytic center, which were later confirmed by cryo-EM data.[346,351] With the increasing availability of ribosome structures, including human ribosomes,[352–354] and computer power, molecular simulations have the opportunity to significantly contribute towards the understanding of drug action on the ribosome and to the next generation of much-needed antibiotics.[355–357]

Large membrane bilayers have been simulated at increasing degrees of chemical detail and complexity, trying to include as many lipid species as possible in order to reproduce compositions found in living cells.[3,170,325,358–360] Marrink and coworkers used the Martini coarse-grained model to simulate a large plasma membrane containing 63 different lipid species.[325] The 71 × 71 nm patch included about 20,000 lipids, which with water and ion beads totalled almost half a million particles, and was simulated for 40 μs. The study provided a high-resolution view of the cell membrane and showed an asymmetrical distribution of cholesterol with enrichment in the outer leaflet. Moreover, transient domains with liquid-ordered character were observed to appear and disappear in the microsecond timescale.[325] Similarly, Koldsø and Sansom[170] simulated a complex and large (>100 nm) plasma membrane also using CG MD, where they introduced two types of crowded membrane proteins in order to study the interplay between lipids and proteins in determining mesoscale fluctuations of the bilayer and clustering of receptors. Closing the gap between experiments and simulations in terms of membrane complexity and spatial scales, the study showed good agreement with the dynamical behavior of lipids observed in living cells.[361,362]

3.02.4 Conclusion

In this chapter we have tried to summarize the main advances in molecular simulation in the past decade or so. Progress in both hardware and algorithm design have construed to make it possible to explore length and timescales that are now within the regimen of several experimental techniques. In the next decade we can expect this overlap to be extended. The resulting integration between experiment and simulation will become a powerful way to understand many underlying biophysical principles as well as improve our prospects for the design of new therapeutic approaches.

References

1. Heath, M. T. *Int. J. High Perform. Comput. Appl.* **2015,** *29,* 320.
2. Perez, A.; Morrone, J. A.; Simmerling, C.; Dill, K. A. *Curr. Opin. Struct. Biol.* **2016,** *36,* 25.
3. Perilla, J. R.; Goh, B. C.; Cassidy, C. K.; Liu, B.; Bernardi, R. C.; Rudack, T.; Yu, H.; Wu, Z.; Schulten, K. *Curr. Opin. Struct. Biol.* **2015,** *31,* 64.
4. Klepeis, J. L.; Lindorff-Larsen, K.; Dror, R. O.; Shaw, D. E. *Curr. Opin. Struct. Biol.* **2009,** *19,* 120.
5. Shaw, D. E.; Deneroff, M. M.; Dror, R. O.; Kuskin, J. S.; Larson, R. H.; Salmon, J. K.; Young, C.; Batson, B.; Bowers, K. J.; Chao, J. C.; Eastwood, M. P.; Gagliardo, J.; Grossman, J. P.; Ho, C. R.; Ist, D. J. I. *Commun. ACM* **2008,** *51,* 91.
6. Shaw, D. E.; Dror, R. O.; Salmon, J. K.; Grossman, J. P.; Mackenzie, K. M.; Bank, J. A.; Young, C.; Deneroff, M. M.; Batson, B.; Bowers, K. J.; Chow, E.; Eastwood, M. P.; Ierardi, D. J.; Klepeis, J. L.; Kuskin, J. S.; Larson, R. H.; Lindorff-Larsen, K.; Maragakis, P.; Moraes, M. A.; Piana, S.; Shan, Y.; Towles, B. Proc. *Conf. High Perform. Comput. Net. Stor. Anal*; ACM: Portland, OR, 2009; p 1.
7. Shaw, D. E.; Maragakis, P.; Lindorff-Larsen, K.; Piana, S.; Dror, R. O.; Eastwood, M. P.; Bank, J. A.; Jumper, J. M.; Salmon, J. K.; Shan, Y.; Wriggers, W. *Science* **2010,** *330,* 341.
8. Dror, R. O.; Pan, A. C.; Arlow, D. H.; Borhani, D. W.; Maragakis, P.; Shan, Y.; Xu, H.; Shaw, D. E. *Proc. Natl. Acad. Sci. U. S. A.* **2011,** *108,* 13118.
9. Lindorff-Larsen, K.; Piana, S.; Dror, R. O.; Shaw, D. E. *Science* **2011,** *334,* 517.
10. Shan, Y.; Kim, E. T.; Eastwood, M. P.; Dror, R. O.; Seeliger, M. A.; Shaw, D. E. *J. Am. Chem. Soc.* **2011,** *133,* 9181.
11. Lindorff-Larsen, K.; Maragakis, P.; Piana, S.; Eastwood, M. P.; Dror, R. O.; Shaw, D. E. *PLoS One* **2012,** *7.*
12. Lindorff-Larsen, K.; Piana, S.; Palmo, K.; Maragakis, P.; Klepeis, J.; Dror, R.; Shaw, D. *Proteins Struct. Funct. Genet.* **2010,** *78,* 1950.
13. Piana, S.; Lindorff-Larsen, K.; Shaw, D. E. *Biophys. J.* **2011,** *100,* L47.
14. Shaw, D. E.; Grossman, J. P.; Bank, J. A.; Batson, B.; Butts, J. A.; Chao, J. C.; Deneroff, M. M.; Dror, R. O.; Even, A.; Fenton, C. H.; Forte, A.; Gagliardo, J.; Gill, G.; Greskamp, B.; Ho, C. R.; Ierardi, D. J.; Iserovich, L.; Kuskin, J. S.; Larson, R. H.; Layman, T.; Lee, L.-S.; Lerer, A. K.; Li, C.; Killebrew, D.; Mackenzie, K. M.; Mok, S. Y.-H.; Moraes, M. A.; Mueller, R.; Nociolo, L. J.; Peticolas, J. L.; Quan, T.; Ramot, D.; Salmon, J. K.; Scarpazza, D. P.; Schafer, U. B.; Siddique, N.; Snyder, C. W.; Spengler, J.; Tang, P. T. P.; Theobald, M.; Toma, H.; Towles, B.; Vitale, B.; Wang, S. C.; Young, C. Proceedings of the International Conference for High Performance Computing, Networking, Storage and Analysis; IEEE Press: Orleans, LA, 2014; p 41.

15. Xu, D.; Williamson, M. J.; Walker, R. C. In *Ann. Rep. Comp. Chem.,* vol. 6, Ralph, A. W., Ed.; Elsevier: Amsterdam, 2010; p 2.
16. Stone, J. E.; Phillips, J. C.; Freddolino, P. L.; Hardy, D. J.; Trabuco, L. G.; Schulten, K. *J. Comput. Chem.* **2007,** *28,* 2618.
17. Yang, J.; Wang, Y.; Chen, Y. *J. Comp. Physiol.* **2007,** *221,* 799.
18. Harvey, M. J.; Giupponi, G.; Fabritiis, G. D. *J. Chem. Theory Comput.* **2009,** *5,* 1632.
19. Eastman, P.; Friedrichs, M. S.; Chodera, J. D.; Radmer, R. J.; Bruns, C. M.; Ku, J. P.; Beauchamp, K. A.; Lane, T. J.; Wang, L.-P.; Shukla, D.; Tye, T.; Houston, M.; Stich, T.; Klein, C.; Shirts, M. R.; Pande, V. S. *J. Chem. Theory Comput.* **2013,** *9,* 461.
20. Buch, I.; Giorgino, T.; De Fabritiis, G. *Proc. Natl. Acad. Sci. U. S. A.* **2011,** *108,* 10184.
21. Ferruz, N.; Harvey, M. J.; Mestres, J.; De Fabritiis, G. *J. Chem. Inf. Model.* **2015,** *55,* 2200.
22. Kutzner, C.; Páll, S.; Fechner, M.; Esztermann, A.; de Groot, B. L.; Grubmüller, H. *J. Comput. Chem.* **2015,** *36,* 1990.
23. Hellerstein, J. L.; Kohlhoff, K. J.; Konerding, D. E. *IEEE Internet Comput.* **2012,** *16,* 64.
24. Schatz, M. C.; Langmead, B.; Salzberg, S. L. *Nat. Biotechnol.* **2010,** *28,* 691.
25. Shirts, M.; Pande, V. S. *Science* **2000,** *290,* 1903.
26. Kohlhoff, K. J.; Shukla, D.; Lawrenz, M.; Bowman, G. R.; Konerding, D. E.; Belov, D.; Altman, R. B.; Pande, V. S. *Nat. Chem.* **2014,** *6,* 15.
27. Harvey, M. J.; De Fabritiis, G. *J. Chem. Inf. Model.* **2015,** *55,* 909.
28. Das, R.; Qian, B.; Raman, S.; Vernon, R.; Thompson, J.; Bradley, P.; Khare, S.; Tyka, M. D.; Bhat, D.; Chivian, D.; Kim, D. E.; Sheffler, W. H.; Malmström, L.; Wollacott, A. M.; Wang, C.; Andre, I.; Baker, D. *Proteins Struct. Funct. Genet.* **2007,** *69,* 118.
29. Lange, O. F.; Rossi, P.; Sgourakis, N. G.; Song, Y.; Lee, H.-W.; Aramini, J. M.; Ertekin, A.; Xiao, R.; Acton, T. B.; Montelione, G. T.; Baker, D. *Proc. Natl. Acad. Sci. U. S. A.* **2012,** *109,* 10873.
30. Koday, M. T.; Nelson, J.; Chevalier, A.; Koday, M.; Kalinoski, H.; Stewart, L.; Carter, L.; Nieusma, T.; Lee, P. S.; Ward, A. B..; Wilson, I. A.; Dagley, A.; Smee, D. F.; Baker, D.; Fuller, D. H. *PLoS Pathog.* **2016,** *12.*
31. Brunette, T. J.; Parmeggiani, F.; Huang, P.-S.; Bhabha, G.; Ekiert, D. C.; Tsutakawa, S. E.; Hura, G. L.; Tainer, J. A.; Baker, D. *Nature* **2015,** *528,* 580.
32. Lawrenz, M.; Shukla, D.; Pande, V. S. *Sci. Rep.* **2015,** *5,* 7918.
33. Koga, N.; Tatsumi-Koga, R.; Liu, G.; Xiao, R.; Acton, T. B.; Montelione, G. T.; Baker, D. *Nature* **2012,** *491,* 222.
34. Beauchamp, K. A.; Lin, Y.-S.; Das, R.; Pande, V. S. *J. Chem. Theory Comput.* **2012,** *8,* 1409.
35. Bowman, G. R.; Pande, V. S. *Proc. Natl. Acad. Sci. U. S. A.* **2010,** *107,* 10890.
36. Zagrovic, B.; Pande, V. S. *Nat. Struct. Mol. Biol.* **2003,** *10,* 955.
37. Snow, C. D.; Nguyen, H.; Pande, V. S.; Gruebele, M. *Nature* **2002,** *420,* 102.
38. Stanley, N.; Esteban-Martín, S.; De Fabritiis, G. *Nat. Commun.* **2014,** 5.
39. Dainese, E.; De Fabritiis, G.; Sabatucci, A.; Oddi, S.; Angelucci, C. B.; Di Pancrazio, C.; Giorgino, T.; Stanley, N.; Del Carlo, M.; Cravatt, B. F.; Maccarrone, M. *Biochem. J.* **2014,** *457,* 463.
40. Sadiq, S. K.; Noé, F.; De Fabritiis, G. *Proc. Natl. Acad. Sci. U. S. A.* **2012,** *109,* 20449.
41. Buch, I.; Harvey, M. J.; Giorgino, T.; Anderson, D. P.; De Fabritiis, G. *J. Chem. Inf. Model.* **2010,** *50,* 397.
42. Fitch, B. G.; Rayshubskiy, A.; Eleftheriou, M.; Ward, T. J. C.; Giampapa, M.; Zhestkov, Y.; Pitman, M. C.; Suits, F.; Grossfield, A.; Pitera, J.; Swope, W.; Zhou, R.; Feller, S.; Germain, R. S. In Alexandrov, V. N., van Albada, G. D., Sloot, P. M. A., Dongarra, J., EdsComputational Science—ICCS 2006: 6th International Conference, Reading, UK, May 28–31, 2006. Proceedings, Part II; Springer: Berlin, Heidelberg, 2006; p 846.
43. Larsson, P.; Hess, B.; Lindahl, E. *Comput. Mol. Sci.* **2011,** *1,* 93.
44. Heffelfinger, G. S. *Comput. Phys. Commun.* **2000,** *128,* 219.
45. Bowers, K. J.; Dror, R. O.; Shaw, D. E. *J. Comput. Phys.* **2007,** *221,* 303.
46. Bowers, K. J.; Dror, R. O.; Shaw, D. E. *J. Phys. Conf. Ser.* **2005,** *16,* 300.
47. Bowers, K. J.; Dror, R. O.; Shaw, D. E. *J. Chem. Phys.* **2006,** 124.
48. Enenkel, R. F.; Fitch, B. G.; Germain, R. S.; Gustavson, F. G.; Martin, A.; Mendell, M.; Pitera, J. W.; Pitman, M. C.; Rayshubskiy, A.; Suits, F.; Swope, W. C.; Ward, T. J. C. *IBM J. Res. Dev.* **2005,** *49,* 465.
49. Sagui, C.; Darden, T. *J. Chem. Phys.* **2001,** *114,* 6578.
50. Hardy, D. J.; Wu, Z.; Phillips, J. C.; Stone, J. E.; Skeel, R. D.; Schulten, K. *J. Chem. Theory Comput.* **2015,** *11,* 766.
51. Hardy, D. J.; Stone, J. E.; Schulten, K. *Parallel Comput.* **2009,** *35,* 164.
52. Skeel, R. D.; Tezcan, I.; Hardy, D. J. *J. Comput. Chem.* **2002,** *23,* 673.
53. Gonnet, P. *J. Comput. Phys.* **2007,** *220,* 740.
54. Krautler, V.; Van Gunsteren, W. F.; Hunenberger, P. H. *J. Comput. Chem.* **2001,** *22,* 501.
55. Eastman, P.; Pande, V. S. *J. Chem. Theory Comput.* **2010,** *6,* 434.
56. Bailey, A. G.; Lowe, C. P. *J. Comput. Chem.* **2009,** *30,* 2485.
57. Hess, B. *J. Chem. Theory Comput.* **2008,** *4,* 116.
58. Hess, B.; Bekker, J.; Berendsen, H. J. C.; Fraaije, J. G. E. M. *J. Comput. Chem.* **1997,** *18,* 1463.
59. Rauscher, S.; Gapsys, V.; Gajda, M. J.; Zweckstetter, M.; de Groot, B. L.; Grubmüller, H. *J. Chem. Theory Comput.* **2015,** *11,* 5513.
60. Oostenbrink, C.; Villa, A.; Mark, A.; Van Gunsteren, W. *J. Comput. Chem.* **2004,** *25,* 1656.
61. Rappe, A. K.; Casewit, C. J.; Colwell, K. S.; Goddard, W. A.; Skiff, W. M. *J. Am. Chem. Soc.* **1992,** *114,* 10024.
62. Addicoat, M. A.; Vankova, N.; Akter, I. F.; Heine, T. *J. Chem. Theory Comput.* **2014,** *10,* 880.
63. van Duin, A. C. T.; Dasgupta, S.; Lorant, F.; Goddard, W. A. *J. Phys. Chem. A* **2001,** *105,* 9396.
64. Liang, T.; Shin, Y. K.; Cheng, Y.-T.; Yilmaz, D. E.; Vishnu, K. G.; Verners, O.; Zou, C.; Phillpot, S. R.; Sinnott, S. B.; van Duin, A. C. T. *Annu. Rev. Mater. Res.* **2013,** *43,* 109.
65. Halgren, T. A. *J. Comput. Chem.* **1996,** *17,* 490.
66. Hornak, V.; Abel, R.; Okur, A.; Strockbine, B.; Roitberg, A.; Simmerling, C. *Proteins: Struct., Funct., Bioinf.* **2006,** *65,* 712.
67. Best, R. B.; Hummer, G. *J. Phys. Chem. B* **2009,** *113,* 9004.
68. Li, D.-W.; Brüschweiler, R. *Angew. Chem., Int. Ed.* **2010,** *49,* 6778.
69. Nerenberg, P. S.; Head-Gordon, T. *J. Chem. Theory Comput.* **2011,** *7,* 1220.
70. Maier, J. A.; Martinez, C.; Kasavajhala, K.; Wickstrom, L.; Hauser, K. E.; Simmerling, C. *J. Chem. Theory Comput.* **2015,** *11,* 3696.
71. Mackerell, A. D.; Feig, M.; Brooks, C. L. *J. Comput. Chem.* **2004,** *25,* 1400.
72. Freddolino, P. L.; Schulten, K. *Biophys. J.* **2009,** *97,* 2338.
73. Freddolino, P. L.; Park, S.; Roux, B.; Schulten, K. *Biophys. J.* **2009,** *96,* 3772.
74. Freddolino, P. L.; Liu, F.; Gruebele, M.; Schulten, K. *Biophys. J.* **2008,** *94,* L75.
75. Best, R. B.; Buchete, N.-V.; Hummer, G. *Biophys. J.* **2008,** *95,* L07.
76. Best, R. B.; Zhu, X.; Shim, J.; Lopes, P. E. M.; Mittal, J.; Feig, M.; MacKerell, A. D. *J. Chem. Theory Comput.* **2012,** *8,* 3257.
77. Jorgensen, W. L.; Maxwell, D. S.; Tirado-Rives, J. *J. Am. Chem. Soc.* **1996,** *118,* 11225.
78. Kaminski, G. A.; Friesner, R. A.; Tirado-Rives, J.; Jorgensen, W. L. *J. Phys. Chem. B* **2001,** *105,* 6474.
79. Chai, J.-D.; Head-Gordon, M. *Phys. Chem. Chem. Phys.* **2008,** *10,* 6615.

80. Grimme, S. *J. Comput. Chem.* **2006,** *27,* 1787.
81. Robertson, M. J.; Tirado-Rives, J.; Jorgensen, W. L. *J. Chem. Theory Comput.* **2015,** *11,* 3499.
82. Wang, J.; Wolf, R. M.; Caldwell, J. W.; Kollman, P. A.; Case, D. A. *J. Comput. Chem.* **2004,** *25,* 1157.
83. Vanommeslaeghe, K.; Hatcher, E.; Acharya, C.; Kundu, S.; Zhong, S.; Shim, J.; Darian, E.; Guvench, O.; Lopes, P.; Vorobyov, I.; Mackerell, A. D. *J. Comput. Chem.* **2010,** *31,* 671.
84. Yu, W.; He, X.; Vanommeslaeghe, K.; MacKerell, A. D. *J. Comput. Chem.* **2012,** *33,* 2451.
85. Vanommeslaeghe, K.; Raman, E. P.; MacKerell, A. D. *J. Chem. Inf. Model.* **2012,** *52,* 3155.
86. Vanommeslaeghe, K.; MacKerell, A. D. *J. Chem. Inf. Model.* **2012,** *52,* 3144.
87. Wang, J.; Wang, W.; Kollman, P. A.; Case, D. A. *J. Mol. Graph. Model.* **2006,** *25,* 247.
88. Huang, L.; Roux, B. *J. Chem. Theory Comput.* **2013,** 9. http://dx.doi.org/10.1021/ct4003477.
89. Mayne, C. G.; Saam, J.; Schulten, K.; Tajkhorshid, E.; Gumbart, J. C. *J. Comput. Chem.* **2013,** *34,* 2757.
90. Betz, R. M.; Walker, R. C. *J. Comput. Chem.* **2015,** *36,* 79.
91. Lundborg, M.; Lindahl, E. *J. Phys. Chem. B* **2015,** *119,* 810.
92. Harder, E.; Damm, W.; Maple, J.; Wu, C.; Reboul, M.; Xiang, J. Y.; Wang, L.; Lupyan, D.; Dahlgren, M. K.; Knight, J. L.; Kaus, J. W.; Cerutti, D. S.; Krilov, G.; Jorgensen, W. L.; Abel, R.; Friesner, R. A. *J. Chem. Theory Comput.* **2016,** *12,* 281.
93. Wang, L.; Wu, Y.; Deng, Y.; Kim, B.; Pierce, L.; Krilov, G.; Lupyan, D.; Robinson, S.; Dahlgren, M. K.; Greenwood, J.; Romero, D. L.; Masse, C.; Knight, J. L.; Steinbrecher, T.; Beuming, T.; Damm, W.; Harder, E.; Sherman, W.; Brewer, M.; Wester, R.; Murcko, M.; Frye, L.; Farid, R.; Lin, T.; Mobley, D. L.; Jorgensen, W. L.; Berne, B. J.; Friesner, R. A.; Abel, R. *J. Am. Chem. Soc.* **2015,** *137,* 2695.
94. Jakalian, A.; Bush, B. L.; Jack, D. B.; Bayly, C. I. *J. Comput. Chem.* **2000,** *21,* 132.
95. Dahlgren, M. K.; Schyman, P.; Tirado-Rives, J.; Jorgensen, W. L. *J. Chem. Inf. Model.* **2013,** *53,* 1191.
96. Huang, L.; Roux, B. *J. Chem. Theory Comput.* **2013,** *9,* 3543.
97. Jakalian, A.; Jack, D. B.; Bayly, C. I. *J. Comput. Chem.* **2002,** *23,* 1623.
98. MacKerell, A. D.; Banavali, N.; Foloppe, N. *Biopolymers* **2000,** *56,* 257.
99. Denning, E. J.; Priyakumar, U. D.; Nilsson, L.; Mackerell, A. D. J. *J. Comput. Chem.* **2011,** *32,* 1929.
100. Špačková, N. A.; Cheatham, T. E.; Ryjáček, F.; Lankaš, F.; van Meervelt, L.; Hobza, P.; Šponer, J. *J. Am. Chem. Soc.* **2003,** *125,* 1759.
101. Varnai, P.; Djuranovic, D.; Lavery, R.; Hartmann, B. *Nucleic Acids Res.* **2002,** *30,* 5398.
102. Pérez, A.; Marchán, I.; Svozil, D.; Sponer, J.; Cheatham Iii, T. E.; Laughton, C. A.; Orozco, M. *Biophys. J.* **2007,** *92,* 3817.
103. Yildirim, I.; Kennedy, S. D.; Stern, H. A.; Hart, J. M.; Kierzek, R.; Turner, D. H. *J. Chem. Theory Comput.* **2012,** *8,* 172.
104. Yildirim, I.; Stern, H. A.; Tubbs, J. D.; Kennedy, S. D.; Turner, D. H. *J. Phys. Chem. B* **2011,** *115,* 9261.
105. Yildirim, I.; Stern, H. A.; Kennedy, S. D.; Tubbs, J. D.; Turner, D. H. *J. Chem. Theory Comput.* **2010,** *6,* 1520.
106. Zgarbová, M.; Otyepka, M.; Šponer, J.; Mládek, A.; Banáš, P.; Cheatham, T. E.; Jurečka, P. *J. Chem. Theory Comput.* **2011,** *7,* 2886.
107. Banáš, P.; Hollas, D.; Zgarbová, M.; Jurečka, P.; Orozco, M.; Cheatham, T. E.; Šponer, J.; Otyepka, M. *J. Chem. Theory Comput.* **2010,** *6,* 3836.
108. Zgarbová, M.; Luque, F. J.; Šponer, J.; Cheatham, T. E.; Otyepka, M.; Jurečka, P. *J. Chem. Theory Comput.* **2013,** *9,* 2339.
109. Krepl, M.; Zgarbová, M.; Stadlbauer, P.; Otyepka, M.; Banáš, P.; Koča, J.; Cheatham, T. E.; Jurečka, P.; Šponer, J. *J. Chem. Theory Comput.* **2012,** *8,* 2506.
110. Klauda, J. B.; Brooks, B. R.; MacKerell, A. D.; Venable, R. M.; Pastor, R. W. *J. Phys. Chem. B* **2005,** *109,* 5300.
111. Klauda, J. B.; Venable, R. M.; Freites, J. A.; O'Connor, J. W.; Tobias, D. J.; Mondragon-Ramirez, C.; Vorobyov, I.; MacKerell, A. D.; Pastor, R. W. *J. Phys. Chem. B* **2010,** *114,* 7830.
112. Dickson, C. J.; Rosso, L.; Betz, R. M.; Walker, R. C.; Gould, I. R. *Soft Matter* **2012,** *8,* 9617.
113. Skjevik, Å. A.; Madej, B. D.; Walker, R. C.; Teigen, K. *J. Phys. Chem. B* **2012,** *116,* 11124.
114. Dickson, C. J.; Madej, B. D.; Skjevik, Å. A.; Betz, R. M.; Teigen, K.; Gould, I. R.; Walker, R. C. *J. Chem. Theory Comput.* **2014,** *10,* 865.
115. Skjevik, A. A.; Madej, B. D.; Dickson, C. J.; Teigen, K.; Walker, R. C.; Gould, I. R. *Chem. Commun.* **2015,** *51,* 4402.
116. Klyosov, A. A.; *Glycobiology and Drug Design,* vol. 1102; American Chemical Society: Washington, DC, 2012; p 3.
117. Fadda, E.; Woods, R. J. *Drug Discov. Today* **2010,** *15,* 596.
118. Foley, B. L.; Tessier, M. B.; Woods, R. J. *Wiley Interdiscip. Rev.: Comput. Mol. Sci.* **2012,** *2,* 652.
119. Xiong, X.; Chen, Z.; Cossins, B. P.; Xu, Z.; Shao, Q.; Ding, K.; Zhu, W.; Shi, J. *Carbohydr. Res.* **2015,** *401,* 73.
120. Tessier, M. B.; DeMarco, M. L.; Yongye, A. B..; Woods, R. J. *Mol. Simul.* **2008,** *34,* 349.
121. Kirschner, K. N.; Yongye, A. B..; Tschampel, S. M.; González-Outeiriño, J.; Daniels, C. R.; Foley, B. L.; Woods, R. J. *J. Comput. Chem.* **2008,** *29,* 622.
122. Patel, D. S.; Pendrill, R.; Mallajosyula, S. S.; Widmalm, G.; MacKerell, A. D. *J. Phys. Chem. B* **2014,** *118,* 2851.
123. Guvench, O.; Mallajosyula, S. S.; Raman, E. P.; Hatcher, E.; Vanommeslaeghe, K.; Foster, T. J.; Jamison, F. W.; MacKerell, A. D. *J. Chem. Theory Comput.* **2011,** *7,* 3162.
124. Hatcher, E.; Säwén, E.; Widmalm, G.; MacKerell, A. D. *J. Phys. Chem. B* **2011,** *115,* 597.
125. Raman, E. P.; Guvench, O.; MacKerell, A. D. *J. Phys. Chem. B* **2010,** *114,* 12981.
126. Kony, D.; Damm, W.; Stoll, S.; Van Gunsteren, W. F. *J. Comput. Chem.* **2002,** *23,* 1416.
127. Pol-Fachin, L.; Rusu, V. H.; Verli, H.; Lins, R. D. *J. Chem. Theory Comput.* **2012,** *8,* 4681.
128. Jorgensen, W. L.; Chandresekhar, J.; Madura, J. D.; Impey, R. W.; Klein, M. L. *J. Chem. Phys.* **1983,** *79,* 926.
129. Izadi, S.; Anandakrishnan, R.; Onufriev, A. V. *J. Phys. Chem. Lett.* **2014,** *5,* 3863.
130. Wang, L.-P.; Martinez, T. J.; Pande, V. S. *J. Phys. Chem. Lett.* **2014,** *5,* 1885.
131. Baker, C. M. *Wiley Interdiscip. Rev.: Comput. Mol. Sci.* **2015,** *5,* 241.
132. Halgren, T. A.; Damm, W. *Curr. Opin. Struct. Biol.* **2001,** *11,* 236.
133. Williams, D. E. *Biopolymers* **1990,** *29,* 1367.
134. Hensen, C.; Hermann, J. C.; Nam, K.; Ma, S.; Gao, J.; Höltje, H.-D. *J. Med. Chem.* **2004,** *47,* 6673.
135. Mortier, W. J.; Ghosh, S. K.; Shankar, S. *J. Am. Chem. Soc.* **1986,** *108,* 4315.
136. Lucas, T. R.; Bauer, B. A.; Patel, S. *Biochim. Biophys. Acta Biomembr.* **2012,** *1818,* 318.
137. Bauer, B. A.; Patel, S. *Theor. Chem. Acc.* **2012,** *131,* 1.
138. Yu, H.; van Gunsteren, W. F. *Comput. Phys. Commun.* **2005,** *172,* 69.
139. Lamoureux, G.; MacKerell, A. D.; Roux, B.t. *J. Chem. Phys.* **2003,** *119,* 5185.
140. Lamoureux, G.; Roux, B.t. *J. Chem. Phys.* **2003,** *119,* 3025.
141. Yu, W.; Lopes, P. E. M.; Roux, B.; MacKerell, A. D. *J. Chem. Phys.* **2013,** *138,* 034508.
142. Chowdhary, J.; Harder, E.; Lopes, P. E. M.; Huang, L.; MacKerell, A. D.; Roux, B. *J. Phys. Chem. B* **2013,** *117,* 9142.
143. Savelyev, A.; MacKerell, A. D. *J. Comput. Chem.* **2014,** *35,* 1219.
144. Lopes, P. E. M.; Huang, J.; Shim, J.; Luo, Y.; Li, H.; Roux, B.; MacKerell, A. D. *J. Chem. Theory Comput.* **2013,** *9,* 5430.
145. Lemkul, J. A.; Huang, J.; Roux, B.; MacKerell, A. D. *Chem. Rev.* **2016,** *116,* 4983.
146. Davis, M. E.; McCammon, J. A. *Chem. Rev.* **1990,** *90,* 509.
147. Cieplak, P.; Caldwell, J.; Kollman, P. *J. Comput. Chem.* **2001,** *22,* 1048.

148. Shi, Y.; Xia, Z.; Zhang, J.; Best, R.; Wu, C.; Ponder, J. W.; Ren, P. *J. Chem. Theory Comput.* **2013,** *9,* 4046.
149. Ponder, J. W.; Wu, C.; Ren, P.; Pande, V. S.; Chodera, J. D.; Schnieders, M. J.; Haque, I.; Mobley, D. L.; Lambrecht, D. S.; DiStasio, R. A.; Head-Gordon, M.; Clark, G. N. I.; Johnson, M. E.; Head-Gordon, T. *J. Phys. Chem. B* **2010,** *114,* 2549.
150. Ren, P.; Ponder, J. W. *J. Phys. Chem. B* **2003,** *107,* 5933.
151. Kuyucak, S.; Chung, S. H. *Biophys. Chem.* **1994,** *51,* 15.
152. Brenner, S. *Genetics* **1974,** *77,* 71.
153. Cardamone, S.; Hughes, T. J.; Popelier, P. L. A. *Phys. Chem. Chem. Phys.* **2014,** *16,* 10367.
154. Hashimoto, K.; Fukushima, T.; Shimizu, E.; Komatsu, N.; Watanabe, H.; Shinoda, N.; Nakazato, M.; Kumakiri, C.; Okada, S.-I.; Hasegawa, H.; Imai, K.; Iyo, M. *Arch. Gen. Psychiatry* **2003,** *60,* 573.
155. Gilson, M. K.; Rashin, A.; Fine, R.; Honig, B. *J. Mol. Biol.* **1985,** *183,* 503.
156. Fukami-Kobayashi, K.; Tateno, Y.; Nishikawa, K. *J. Mol. Biol.* **1999,** *286,* 279.
157. Huang, J.; Lopes, P. E. M.; Roux, B.; MacKerell, A. D. *J. Phys. Chem. Lett.* **2014,** *5,* 3144.
158. Jiao, D.; Zhang, J.; Duke, R. E.; Li, G.; Schnieders, M. J.; Ren, P. *J. Comput. Chem.* **2009,** *30,* 1701.
159. Jiao, D.; Golubkov, P. A.; Darden, T. A.; Ren, P. *Proc. Natl. Acad. Sci. U. S. A.* **2008,** *105,* 6290.
160. Saunders, M. G.; Voth, G. A. *Annu. Rev. Plant Physiol. Plant Mol. Biol.* **2013,** *42,* 73.
161. Levitt, M.; Warshel, A. *Nature* **1975,** *253,* 694.
162. Uusitalo, J. J.; Ingólfsson, H. I.; Akhshi, P.; Tieleman, D. P.; Marrink, S. J. *J. Chem. Theory Comput.* **2015,** *11,* 3932.
163. de Jong, D. H.; Singh, G.; Bennett, W. F. D.; Arnarez, C.; Wassenaar, T. A.; Schäfer, L. V.; Periole, X.; Tieleman, D. P.; Marrink, S. J. *J. Chem. Theory Comput.* **2013,** *9,* 687.
164. Monticelli, L.; Kandasamy, S. K.; Periole, X.; Larson, R. G.; Tieleman, D. P.; Marrink, S.-J. *J. Chem. Theory Comput.* **2008,** *4,* 819.
165. Marrink, S. J.; Risselada, H. J.; Yefimov, S.; Tieleman, D. P.; de Vries, A. H. *J. Phys. Chem. B* **2007,** *111,* 7812.
166. Marrink, S. J.; de Vries, A. H.; Mark, A. E. *J. Phys. Chem. B* **2004,** *108,* 750.
167. Marrink, S. J.; Tieleman, D. P. *Chem. Soc. Rev.* **2013,** *42,* 6801.
168. Domański, J.; Marrink, S. J.; Schäfer, L. V. *Biochim. Biophys. Acta Biomembr.* **2012,** *1818,* 984.
169. Parton, D. L.; Klingelhoefer, J. W.; Sansom, M. S. P. *Biophys. J.* **2011,** *101,* 691.
170. Koldsø, H.; Sansom, M. S. P. *J. Am. Chem. Soc.* **2015,** *137,* 14694.
171. Sørensen, J.; Periole, X.; Skeby, K. K.; Marrink, S.-J.; Schiøtt, B. *J. Phys. Chem. Lett.* **2011,** *2,* 2385.
172. Louhivuori, M.; Risselada, H. J.; van der Giessen, E.; Marrink, S. J. *Proc. Natl. Acad. Sci. U. S. A.* **2010,** *107,* 19856.
173. Wong-Ekkabut, J.; Baoukina, S.; Triampo, W.; Tang, I. M.; Tieleman, D. P.; Monticelli, L. *Nat. Nanotechnol.* **2008,** *3,* 363.
174. Baoukina, S.; Tieleman, D. P. *Biophys. J.* **2011,** *100,* 1678.
175. Risselada, H. J.; Kutzner, C.; Grubmüller, H. *ChemBioChem* **2011,** *12,* 1049.
176. Hedger, G.; Sansom, M. S. P.; Koldsø, H. *Sci. Rep.* **2015,** *5,* 9198.
177. Leung, A. K. K.; Hafez, I. M.; Baoukina, S.; Belliveau, N. M.; Zhigaltsev, I. V.; Afshinmanesh, E.; Tieleman, D. P.; Hansen, C. L.; Hope, M. J.; Cullis, P. R. *J. Phys. Chem. C* **2012,** *116,* 18440.
178. Frederix, P. W. J. M.; Ulijn, R. V.; Hunt, N. T.; Tuttle, T. *J. Phys. Chem. Lett.* **2011,** *2,* 2380.
179. Lee, O.-S.; Cho, V.; Schatz, G. C. *Nano Lett.* **2012,** *12,* 4907.
180. Noid, W. G.; Liu, P.; Wang, Y.; Chu, J.-W.; Ayton, G. S.; Izvekov, S.; Andersen, H. C.; Voth, G. A. *J. Chem. Phys.* **2008,** *128,* 244115.
181. Noid, W. G.; Chu, J.-W.; Ayton, G. S.; Krishna, V.; Izvekov, S.; Voth, G. A.; Das, A.; Andersen, H. C. *J. Chem. Phys.* **2008,** *128,* 244114.
182. Izvekov, S.; Voth, G. A. *J. Phys. Chem. B* **2005,** *109,* 2469.
183. Wang, Y.; Voth, G. A. *J. Am. Chem. Soc.* **2005,** *127,* 12192.
184. Izvekov, S.; Violi, A.; Voth, G. A. *J. Phys. Chem. B* **2005,** *109,* 17019.
185. Izvekov, S.; Voth, G. A. *J. Phys. Chem. B* **2009,** *113,* 4443.
186. Lu, L.; Voth, G. A. *J. Phys. Chem. B* **2009,** *113,* 1501.
187. Pfaendtner, J.; Voth, G. A. *Biophys. J.* **2008,** *95,* 5324.
188. Shi, Q.; Izvekov, S.; Voth, G. A. *J. Phys. Chem. B* **2006,** *110,* 15045.
189. Rzepiela, A. J.; Louhivuori, M.; Peter, C.; Marrink, S. J. *Phys. Chem. Chem. Phys.* **2011,** *13,* 10437.
190. Zavadlav, J.; Podgornik, R.; Praprotnik, M. *J. Chem. Theory Comput.* **2015,** *11,* 5035.
191. Zavadlav, J.; Melo, M. N.; Marrink, S. J.; Praprotnik, M. *J. Chem. Phys.* **2015,** *142,* 244118.
192. Praprotnik, M.; Matysiak, S.; Site, L. D.; Kremer, K.; Clementi, C. *J. Phys. Condens. Matter* **2007,** *19,* 292201.
193. Praprotnik, M.; Delle Site, L.; Kremer, K. *J. Chem. Phys.* **2005,** *123,* 224106.
194. Stansfeld, P. J.; Jefferys, E. E.; Sansom, M. S. P. *Structure* **2013,** *21,* 810.
195. Chu, J. W.; Ayton, G. S.; Izvekov, S.; Voth, G. A. *Mol. Phys.* **2007,** *105,* 167.
196. Nielsen, S. O.; Bulo, R. E.; Moore, P. B.; Ensing, B. *Phys. Chem. Chem. Phys.* **2010,** *12,* 12401.
197. Lyman, E.; Ytreberg, F. M.; Zuckerman, D. M. *Phys. Rev. Lett.* **2006,** *96,* 028105.
198. Christen, M.; Van Gunsteren, W. F. *J. Chem. Phys.* **2006,** *124,* 154106.1.
199. Stansfeld, P. J.; Sansom, M. S. P. *J. Chem. Theory Comput.* **2011,** *7,* 1157.
200. Perlmutter, J. D.; Sachs, J. N. *Biophys. J.*, *100*, **2011**, 640a.
201. Ayton, G. S.; Voth, G. A. *Biophys. J.* **2010,** *99,* 2757.
202. Kalli, A. C.; Sansom, M. S. P.; Reithmeier, R. A. F. *PLoS Comput. Biol.* **2015,** *11*, e1004123.
203. Kalli, A. C.; Hall, B. A.; Campbell, I. D.; Sansom, M. S. P. *Structure* **2011,** *19,* 1477.
204. Wei, P.; Xu, L.; Li, C.-D.; Sun, F.-D.; Chen, L.; Tan, T.; Luo, S.-Z. *PLoS One* **2014,** *9*, e105560.
205. Lonsdale, R.; Rouse, S. L.; Sansom, M. S. P.; Mulholland, A. J. *PLoS Comput. Biol.* **2014,** *10*, e1003714.
206. Stansfeld, P. J.; Goose, J. E.; Caffrey, M.; Carpenter, E. P.; Parker, J. L.; Newstead, S.; Sansom, M. S. P. *Structure* **2015,** *23,* 1350.
207. Wassenaar, T. A.; Pluhackova, K.; Böckmann, R. A.; Marrink, S. J.; Tieleman, D. P. *J. Chem. Theory Comput.* **2014,** *10,* 676.
208. Waldrop, M. M. *Nature* **2016,** *530,* 144.
209. Larsson, P.; Hess, B.; Lindahl, E. *Wiley Interdiscip. Rev.: Comput. Mol. Sci.* **2011,** *1,* 93.
210. Pande, V. S.; Beauchamp, K.; Bowman, G. R. *Methods* **2010,** *52,* 99.
211. Chodera, J. D.; Noé, F. *Curr. Opin. Struct. Biol.* **2014,** *25,* 135.
212. Shukla, D.; Hernández, C. X.; Weber, J. K.; Pande, V. S. *Acc. Chem. Res.* **2015,** *48,* 414.
213. Scherer, M. K.; Trendelkamp-Schroer, B.; Paul, F.; Pérez-Hernández, G.; Hoffmann, M.; Plattner, N.; Wehmeyer, C.; Prinz, J.-H.; Noé, F. *J. Chem. Theory Comput.* **2015,** *11,* 5525.
214. Beauchamp, K. A.; Bowman, G. R.; Lane, T. J.; Maibaum, L.; Haque, I. S.; Pande, V. S. *J. Chem. Theory Comput.* **2011,** *7,* 3412.
215. Noé, F.; Nüske, F. *SIAM Multiscale Model. Simul.* **2012,** *11,* 1.
216. Nüske, F.; Keller, B. G.; Pérez-Hernández, G.; Mey, A. S. J. S.; Noé, F. *J. Chem. Theory Comput.* **2014,** *10,* 1739.

217. Schwantes, C. R.; Pande, V. S. *J. Chem. Theory Comput.* **2013,** *9,* 2000.
218. Pérez-Hernández, G.; Paul, F.; Giorgino, T.; De Fabritiis, G.; Noé, F. *J. Chem. Phys.* **2013,** *139,* 015102.
219. Arthur, D.; Vassilvitskii, S. In *Proc. Eighteenth Annu. ACM-SIAM Symp. Discret. Algorithms,* 8; 2007; p 1027.
220. Lloyd, S. P. *IEEE Trans. Inf. Theory* **1982,** *28,* 129.
221. Berezhkovskii, A.; Hummer, G.; Szabo, A. *J. Chem. Phys.* **2009,** *130,* 205102.
222. Metzner, P.; Schütte, C.; Vanden-Eijnden, E. *Multiscale Model. Simul.* **2009,** *7,* 1192.
223. Weinan, E.; Vanden-Eijnden, E. *J. Stat. Phys.* **2006,** *123,* 503.
224. Röblitz, S.; Weber, M. *Adv. Data Anal. Classif.* **2013,** *7,* 147.
225. Voelz, V. A.; Bowman, G. R.; Beauchamp, K.; Pande, V. S. *J. Am. Chem. Soc.* **2010,** *132,* 1526.
226. Shukla, D.; Meng, Y.; Roux, B.; Pande, V. S. *Nat. Commun.* **2014,** 5.
227. Plattner, N.; Noe, F. *Nat. Commun.* **2015,** 6.
228. Swendsen, R. H.; Wang, J. S. *Phys. Rev. Lett.* **1986,** *57,* 2607.
229. Sugita, Y.; Okamoto, Y. *Chem. Phys. Lett.* **1999,** *314,* 141.
230. Okamoto, Y. *J. Mol. Graph. Model.* **2004,** *22,* 425.
231. Bernardi, R. C.; Melo, M. C. R.; Schulten, K. *Biochim. Biophys. Acta* **2015,** *1850,* 872.
232. Earl, D. J.; Deem, M. W. *Phys. Chem. Chem. Phys.* **2005,** *7,* 3910.
233. Abrams, C.; Bussi, G. *Entropy* **2014,** *16,* 163.
234. Chodera, J. D.; Shirts, M. R. *J. Chem. Phys.* **2011,** *2011,* 194110.
235. Li, H.; Fajer, M.; Yang, W. *J. Chem. Phys.* **2007,** *126,* 024106.
236. Lyubartsev, A. P.; Martsinovski, A. A.; Shevkunov, S. V.; Vorontsov-Velyaminov, P. N. *J. Chem. Phys.* **1992,** *96,* 1776.
237. Marinari, E.; Parisi, G. *Europhys. Lett.* **1992,** *19,* 451.
238. Faraldo-Gómez, J. D.; Roux, B. *J. Comput. Chem.* **2007,** *28,* 1634.
239. Bussi, G. *Mol. Phys.* **2014,** *112,* 379.
240. Ostermeir, K.; Zacharias, M. *Biochim. Biophys. Acta* **2013,** *1834,* 847.
241. Roe, D. R.; Bergonzo, C.; Cheatham, T. E. *J. Phys. Chem. B* **2014,** *118,* 3543.
242. Jiang, W.; Roux, B. *J. Chem. Theory Comput.* **2010,** *6,* 2559.
243. Woods, C. J.; Essex, J. W.; King, M. A. *J. Phys. Chem. B* **2003,** *107,* 13711.
244. Hritz, J.; Oostenbrink, C. *J. Chem. Phys.* **2008,** *128,* 144121.
245. Bitetti-Putzer, R.; Yang, W.; Karplus, M. *Chem. Phys. Lett.* **2003,** *377,* 633.
246. Liu, P.; Kim, B.; Friesner, R. A.; Berne, B. J. *Proc. Natl. Acad. Sci. U. S. A.* **2005,** *102,* 13749.
247. Sugita, Y.; Kitao, A.; Okamoto, Y. *J. Chem. Phys.* **2000,** *113,* 6042.
248. Yan, Q.; de Pablo, J. J. *J. Chem. Phys.* **2000,** *113,* 1276.
249. Yan, Q.; de Pablo, J. J. *J. Chem. Phys.* **1999,** *111,* 9509.
250. Jiang, W.; Phillips, J. C.; Huang, L.; Fajer, M.; Meng, Y.; Gumbart, J. C.; Luo, Y.; Schulten, K.; Roux, B. *Comput. Phys. Commun.* **2014,** *185,* 908.
251. Pronk, S.; Páll, S.; Schulz, R.; Larsson, P.; Bjelkmar, P.; Apostolov, R.; Shirts, M. R.; Smith, J. C.; Kasson, P. M.; van der Spoel, D.; Hess, B.; Lindahl, E. *Bioinformatics* **2013,** *29,* 845.
252. Phillips, J. C.; Braun, R.; Wang, W.; Gumbart, J.; Tajkhorshid, E.; Villa, E.; Chipot, C.; Skeel, R. D.; Kale, L.; Schulten, K. *J. Comput. Chem.* **2005,** *26,* 1781.
253. Zerze, G. H.; Uz, B.; Mittal, J. *Proteins: Struct., Funct., Bioinf.* **2015,** *83,* 1307.
254. Fan, H.; Periole, X.; Mark, A. E. *Proteins: Struct., Funct., Bioinf.* **2012,** *80,* 1744.
255. Chu, W.-T.; Zhang, J.-L.; Zheng, Q.-C.; Chen, L.; Zhang, H.-X. *PLoS One* **2013,** *8,* e64886.
256. Chen, A. A.; García, A. E. *Proc. Natl. Acad. Sci. U. S. A.* **2013,** *110,* 16820.
257. Baillod, P.; Garrec, J.; Tavernelli, I.; Rothlisberger, U. *Biochemistry* **2013,** *19,* 8518.
258. Ning, L.; Wang, Q.; Zheng, Y.; Liu, H.; Yao, X. *Mol. Biosyst.* **2015,** *11,* 647.
259. Swails, J. M.; Roitberg, A. E. *J. Chem. Theory Comput.* **2012,** *8,* 4393.
260. Xue, X.; Yongjun, W.; Zhihong, L. *J. Theor. Biol.* **2015,** *365,* 265.
261. Patel, S.; Vierling, E.; Tama, F. *Biophys. J.* **2014,** *106,* 2644.
262. Ostermeir, K.; Zacharias, M. *Proteins* **2014,** *82,* 3410.
263. Jiang, F.; Wu, Y. D. *J. Am. Chem. Soc.* **2014,** *136,* 9536.
264. Nguyen, T. H.; Minh, D. D. L. *J. Chem. Theory Comput.* **2016,** *12,* 2154.
265. Mentes, A.; Deng, N. J.; Vijayan, R. S.; Xia, J.; Gallicchio, E.; Levy, R. M. *J. Chem. Theory Comput.* **2016,** *12,* 2459.
266. Meng, Y.; Dashti, D. S.; Roitberg, A. E. *J. Chem. Theory Comput.* **2011,** *7,* 2721.
267. Wang, L.; Deng, Y.; Knight, J. L.; Wu, Y.; Kim, B.; Sherman, W.; Shelley, J. C.; Lin, T.; Abel, R. *J. Chem. Theory Comput.* **2013,** *9,* 1282.
268. Jiang, W.; Hodoscek, M.; Roux, B. *J. Chem. Theory Comput.* **2009,** *5,* 2583.
269. Luitz, M. P.; Zacharias, M. *J. Chem. Inf. Model.* **2014,** *54,* 1669.
270. Wang, K.; Chodera, J. D.; Yang, Y.; Shirts, M. R. *J. Comput. Aided Mol. Des.* **2013,** *27,* 989.
271. Itoh, S. G.; Damjanović, A.; Brooks, B. R. *Proteins: Struct., Funct., Bioinf.* **2011,** *79,* 3420.
272. Swails, J. M.; York, D. M.; Roitberg, A. E. *J. Chem. Theory Comput.* **2014,** *10,* 1341.
273. Sabri Dashti, D.; Meng, Y.; Roitberg, A. E. *J. Phys. Chem. B* **2012,** *116,* 8805.
274. Meng, Y.; Roitberg, A. E. *J. Chem. Theory Comput.* **2010,** *6,* 1401.
275. Lee, J.; Miller, B. T.; Damjanović, A.; Brooks, B. R. *J. Chem. Theory Comput.* **2014,** *10,* 2738.
276. Torrie, G. M.; Valleau, J. P. *J. Comput. Phys.* **1977,** *23,* 187.
277. Huber, T.; Torda, A. E.; van Gunsteren, W. F. *J. Comput. Aided Mol. Des.* **1994,** *8,* 695.
278. Darve, E.; Pohorille, A. *J. Chem. Phys.* **2001,** *115,* 9169.
279. Miao, Y.; Feher, V. A.; McCammon, J. A. *J. Chem. Theory Comput.* **2015,** *11,* 3584.
280. Hamelberg, D.; McCammon, J. A. *J. Am. Chem. Soc.* **2004,** *126,* 7683.
281. Müller, E. M.; de Meijere, A.; Grubmüller, H. *J. Chem. Phys.* **2002,** *116,* 897.
282. Grubmüller, H. *Phys. Rev. E* **1995,** *52,* 2893.
283. Park, S.; Schulten, K. *J. Chem. Phys.* **2004,** *120,* 5946.
284. Laio, A.; Gervasio, F. L. *Rep. Prog. Phys.* **2008,** *71,* 126601.
285. Valsson, O.; Tiwary, P.; Parrinello, M. *Annu. Rev. Phys. Chem.* **2016,** *67,* 040215.
286. Barducci, A.; Bonomi, M.; Parrinello, M. *Wiley Interdiscip. Rev.: Comput. Mol. Sci.* **2011,** *1,* 826.
287. Laio, A.; Parrinello, M. *Proc. Natl. Acad. Sci. U. S. A.* **2002,** *99,* 12562.

288. Case, D. A.; Cheatham, T. E.; Darden, T. O. M.; Gohlke, H.; Luo, R. A. Y.; Merz, K. M.; Onufriev, A.; Simmerling, C.; Wang, B.; Woods, R. J. *J. Comput. Chem.* **2005,** *26,* 1668.
289. Plimpton, S. *J. Comput. Phys.* **1995,** *117,* 1.
290. Bonomi, M.; Branduardi, D.; Bussi, G.; Camilloni, C.; Provasi, D.; Raiteri, P.; Donadio, D.; Marinelli, F.; Pietrucci, F.; Broglia, R. A.; Parrinello, M. *Comput. Phys. Commun.* **2009,** *180,* 1961.
291. Tribello, G. A.; Bonomi, M.; Branduardi, D.; Camilloni, C.; Bussi, G. *Comput. Phys. Commun.* **2014,** *185,* 604.
292. Laio, A.; Rodriguez-Fortea, A.; Gervasio, F. L.; Ceccarelli, M.; Parrinello, M. *J. Phys. Chem. B* **2005,** *109,* 6714.
293. Chen, M.; Yu, T.-Q.; Tuckerman, M. E. *Proc. Natl. Acad. Sci. U. S. A.* **2015,** *112,* 3235.
294. Gasparotto, P.; Ceriotti, M. *J. Chem. Phys.* **2014,** *141,* 174110.
295. Rohrdanz, M. A.; Zheng, W.; Clementi, C. *Annu. Rev. Phys. Chem.* **2013,** *64,* 295.
296. Ceriotti, M.; Tribello, G. A.; Parrinello, M. *Proc. Natl. Acad. Sci. U. S. A.* **2011,** *108,* 13023.
297. Tribello, G. A.; Ceriotti, M.; Parrinello, M. *Proc. Natl. Acad. Sci. U. S. A.* **2010,** *107,* 17509.
298. Spiwok, V.; Lipovová, P.; Králová, B. *J. Phys. Chem. B* **2007,** *111,* 3073.
299. Bussi, G.; Laio, A.; Parrinello, M. *Phys. Rev. Lett.* **2006,** *96,* 090601.
300. Bonomi, M.; Parrinello, M. *Phys. Rev. Lett.* **2010,** *104,* 190601.
301. Barducci, A.; Bussi, G.; Parrinello, M. *Phys. Rev. Lett.* **2008,** *100,* 020603.
302. Sutto, L.; Marsili, S.; Gervasio, F. L. *Wiley Interdiscip. Rev.: Comput. Mol. Sci.* **2012,** *2,* 771.
303. Bussi, G.; Gervasio, F. L.; Laio, A.; Parrinello, M. *J. Am. Chem. Soc.* **2006,** *128,* 13435.
304. Camilloni, C.; Provasi, D.; Tiana, G.; Broglia, R. A. *Proteins: Struct., Funct., Bioinf.* **2008,** *71,* 1647.
305. Marinelli, F.; Pietrucci, F.; Laio, A.; Piana, S. *PLoS Comput. Biol.* **2009,** *5*, e1000452.
306. Piana, S.; Laio, A. *J. Phys. Chem. B* **2007,** *111,* 4553.
307. Di Leva, F. S.; Novellino, E.; Cavalli, A.; Parrinello, M.; Limongelli, V. *Nucleic Acids Res.* **2014,** *424,* 5447–5455.
308. Vargiu, A. V.; Ruggerone, P.; Magistrato, A.; Carloni, P. *Nucleic Acids Res.* **2008,** *36,* 5910.
309. Sutto, L.; Gervasio, F. L. *Proc. Natl. Acad. Sci. U. S. A.* **2013,** *110,* 10616.
310. Berteotti, A.; Cavalli, A.; Branduardi, D.; Gervasio, F. L.; Recanatini, M.; Parrinello, M. *J. Am. Chem. Soc.* **2009,** *131,* 244.
311. Gervasio, F. L.; Laio, A.; Parrinello, M. *J. Am. Chem. Soc.* **2005,** *127,* 2600.
312. Bonomi, M.; Branduardi, D.; Gervasio, F. L.; Parrinello, M. *J. Am. Chem. Soc.* **2008,** *130,* 13938.
313. Pfaendtner, J.; Branduardi, D.; Parrinello, M.; Pollard, T. D.; Voth, G. A. *Proc. Natl. Acad. Sci. U. S. A.* **2009,** *106,* 12723.
314. Pietrucci, F.; Marinelli, F.; Carloni, P.; Laio, A. *J. Am. Chem. Soc.* **2009,** *131,* 11811.
315. Herbert, C.; Schieborr, U.; Saxena, K.; Juraszek, J.; De Smet, F.; Alcouffe, C.; Bianciotto, M.; Saladino, G.; Sibrac, D.; Kudlinzki, D.; Sreeramulu, S.; Brown, A.; Rigon, P.; Herault, J.-P.; Lassalle, G.; Blundell, T. L.; Rousseau, F.; Gils, A.; Schymkowitz, J.; Tompa, P.; Herbert, J.-M.; Carmeliet, P.; Gervasio, F. L.; Schwalbe, H.; Bono, F. *Cancer Cell* **2013,** *23,* 489.
316. Grazioso, G.; Limongelli, V.; Branduardi, D.; Novellino, E.; De Micheli, C.; Cavalli, A.; Parrinello, M. *J. Am. Chem. Soc.* **2012,** *134,* 453.
317. Troussicot, L.; Guillière, F.; Limongelli, V.; Walker, O.; Lancelin, J.-M. *J. Am. Chem. Soc.* **2015,** *137,* 1273.
318. Limongelli, V.; Bonomi, M.; Marinelli, L.; Gervasio, F. L.; Cavalli, A.; Novellino, E.; Parrinello, M. *Proc. Natl. Acad. Sci. U. S. A.* **2010,** *107,* 5411.
319. De Vivo, M.; Masetti, M.; Bottegoni, G.; Cavalli, A. *J. Med. Chem.* **2016,** *59,* 4035.
320. Cavalli, A.; Spitaleri, A.; Saladino, G.; Gervasio, F. L. *Acc. Chem. Res.* **2015,** *48,* 277.
321. Limongelli, V.; Bonomi, M.; Parrinello, M. *Proc. Natl. Acad. Sci. U. S. A.* **2013,** *110,* 6358.
322. Lanzo, C. A.; Sutin, J.; Rowlinson, S.; Talley, J.; Marnett, L. *J. Biochem.* **2000,** *39,* 6228.
323. Reddy, T.; Sansom, M. S. P. *Biochim. Biophys. Acta* **2016,** *1858,* 1610.
324. Sanbonmatsu, K. Y. *Curr. Opin. Struct. Biol.* **2012,** *22,* 168.
325. Ingólfsson, H. I.; Melo, M. N.; van Eerden, F. J.; Arnarez, C.; Lopez, C. A.; Wassenaar, T. A.; Periole, X.; de Vries, A. H.; Tieleman, D. P.; Marrink, S. J. *J. Am. Chem. Soc.* **2014,** *136,* 14554.
326. Chandler, D. E.; Strümpfer, J.; Sener, M.; Scheuring, S.; Schulten, K. *Biophys. J.* **2014,** *106,* 2503.
327. Roos, W. H.; Bruinsma, R.; Wuite, G. J. L. *Nat. Phys.* **2010,** *6,* 733.
328. Freddolino, P. L.; Arkhipov, A. S.; Larson, S. B.; McPherson, A.; Schulten, K. *Structure* **2006,** *14,* 437.
329. Arkhipov, A.; Freddolino, P. L.; Schulten, K. *Structure* **2006,** *14,* 1767.
330. Reddy, T.; Sansom, M. S. P. *Structure* **2016,** *24,* 375.
331. Reddy, T.; Shorthouse, D.; Parton, D. L.; Jefferys, E.; Fowler, P. W.; Chavent, M.; Baaden, M.; Sansom, M. S. P. *Structure* **2015,** *3,* 584.
332. Zhao, G.; Perilla, J. R.; Yufenyuy, E. L.; Meng, X.; Chen, B.; Ning, J.; Ahn, J.; Gronenborn, A. M.; Schulten, K.; Aiken, C.; Zhang, P. *Nature* **2013,** *497,* 643.
333. Perlmutter, J. D.; Perkett, M. R.; Hagan, M. F. *J. Mol. Biol.* **2014,** *426,* 3148.
334. Perlmutter, J. D.; Qiao, C.; Hagan, M. F. *eLife* **2013,** *2,* e00632.
335. Nguyen, H. D.; Reddy, V. S.; Brooks, C. L. *Nano Lett.* **2007,** *7,* 338.
336. Hagan, M. F.; Chandler, D. *Biophys. J.* **2006,** *91,* 42.
337. Trabuco, L. G.; Villa, E.; Schreiner, E.; Harrison, C. B.; Schulten, K. *Methods* **2009,** *49,* 174.
338. Wang, X.; Xu, F.; Liu, J.; Gao, B.; Liu, Y.; Zhai, Y.; Ma, J.; Zhang, K.; Baker, T. S.; Schulten, K.; Zheng, D.; Pang, H.; Sun, F. *PLoS Pathog.* **2013,** *9,* e1003132.
339. Schur, F. K. M.; Hagen, W. J. H.; Rumlova, M.; Ruml, T.; Muller, B.; Krausslich, H.-G.; Briggs, J. A. G. *Nature* **2015,** *517,* 505.
340. Bharat, T. A. M.; Castillo Menendez, L. R.; Hagen, W. J. H.; Lux, V.; Igonet, S.; Schorb, M.; Schur, F. K. M.; Kräusslich, H.-G.; Briggs, J. A. G. *Proc. Natl. Acad. Sci. U. S. A.* **2014,** *111,* 8233.
341. Li, W.; Ma, B.; Shapiro, B. A. *Nucleic Acids Res.* **2003,** *31,* 629.
342. Sanbonmatsu, K. Y.; Joseph, S. *J. Mol. Biol.* **2003,** *328,* 33.
343. Sanbonmatsu, K. Y.; Joseph, S.; Tung, C.-S. *Proc. Natl. Acad. Sci. U. S. A.* **2005,** *102,* 15854.
344. Bock, L. V.; Blau, C.; Schröder, G. F.; Davydov, I. I.; Fischer, N.; Stark, H.; Rodnina, M. V.; Vaiana, A. C.; Grubmüller, H. *Nat. Struct. Mol. Biol.* **2013,** *20,* 1390.
345. Whitford, P. C.; Blanchard, S. C.; Cate, J. H. D.; Sanbonmatsu, K. Y. *PLoS Comput. Biol.* **2013,** *9,* e1003003.
346. Sothiselvam, S.; Liu, B.; Han, W.; Ramu, H.; Klepacki, D.; Atkinson, G. C.; Brauer, A.; Remm, M.; Tenson, T.; Schulten, K.; Vázquez-Laslop, N.; Mankin, A. S. *Proc. Natl. Acad. Sci. U. S. A.* **2014,** *111,* 9804.
347. Small, M. C.; Lopes, P.; Andrade, R. B.; MacKerell, A. D., Jr. *PLoS Comput. Biol.* **2013,** *9,* e1003113.
348. Vaiana, A. C.; Sanbonmatsu, K. Y. *J. Mol. Biol.* **2009,** *386,* 648.
349. Aleksandrov, A.; Simonson, T. *Biochemistry* **2008,** *47,* 13594.
350. Meroueh, S. O.; Mobashery, S. *Chem. Biol. Drug Des.* **2007,** *69,* 291.
351. Arenz, S.; Meydan, S.; Starosta, A. L.; Berninghausen, O.; Beckmann, R.; Vázquez-Laslop, N.; Wilson, D. N. *Mol. Cell* **2014,** *56,* 446.
352. Khatter, H.; Myasnikov, A. G.; Natchiar, S. K.; Klaholz, B. P. *Nature* **2015,** *520,* 640.
353. Amunts, A.; Brown, A.; Toots, J.; Scheres, S. H. W.; Ramakrishnan, V. *Science* **2015,** *348,* 95.

354. Anger, A. M.; Armache, J.-P.; Berninghausen, O.; Habeck, M.; Subklewe, M.; Wilson, D. N.; Beckmann, R. *Nature* **2013,** *497,* 80.
355. Blair, J. M. A.; Webber, M. A.; Baylay, A. J.; Ogbolu, D. O.; Piddock, L. J. V. *Nat. Rev. Microbiol.* **2015,** *13,* 42.
356. Lewis, K. *Nat. Rev. Drug Discov.* **2013,** *12,* 371.
357. Payne, D. J.; Gwynn, M. N.; Holmes, D. J.; Pompliano, D. L. *Nat. Rev. Drug Discov.* **2007,** *6,* 29.
358. Yu, H.; Schulten, K. *PLoS Comput. Biol.* **2013,** *9,* e1002892.
359. Rassam, P.; Copeland, N. A.; Birkholz, O.; Toth, C.; Chavent, M.; Duncan, A. L.; Cross, S. J.; Housden, N. G.; Kaminska, R.; Seger, U.; Quinn, D. M.; Garrod, T. J.; Sansom, M. S. P.; Piehler, J.; Baumann, C. G.; Kleanthous, C. *Nature* **2015,** *523,* 333.
360. Hedger, G.; Sansom, M. S. P. *Biochim. Biophys. Acta*, **2016**, *1858*, 2390–2400.
361. Eggeling, C.; Ringemann, C.; Medda, R.; Schwarzmann, G.; Sandhoff, K.; Polyakova, S.; Belov, V. N.; Hein, B.; von Middendorff, C.; Schonle, A.; Hell, S. W. *Nature* **2009,** *457,* 1159.
362. Mueller, V.; Ringemann, C.; Honigmann, A.; Schwarzmann, G.; Medda, R.; Leutenegger, M.; Polyakova, S.; Belov, V. N.; Hell, S. W.; Eggeling, C. *Biophys. J.* **2011,** *101,* 1651.
363. Wang, L.; Friesner, R. A.; Berne, B. J. Replica exchange with solute scaling: a more efficient version of replica exchange with solute tempering (REST2). *J Phys Chem B* **2011,** *115,* 9431–9438.

3.03 Recent Progress in Free Energy Methods

G Saladino, University College London, London, United Kingdom
C Estarellas, University of Barcelona, Barcelona, Spain
FL Gervasio, University College London, London, United Kingdom

© 2017 Elsevier Ltd. All rights reserved.

3.03.1	**An Introduction to Free Energy Methods**	34
3.03.2	**Alchemical Methods**	35
3.03.2.1	Thermodynamic Integration Versus Free Energy Perturbation	35
3.03.2.2	Evolution of the Alchemical Methods	36
3.03.3	**ES Algorithms**	38
3.03.3.1	CVs-Based Methods	39
3.03.3.2	Optimal Choice of the CVs	39
3.03.3.3	Umbrella Sampling	41
3.03.3.4	Metadynamics	41
3.03.3.5	Steered MD	42
3.03.4	**Other Methods**	43
3.03.4.1	Replica Exchange	43
3.03.4.2	Accelerated MD	43
3.03.5	**Combining Different Methods**	44
3.03.5.1	Successful Applications of ES Techniques	44
3.03.6	**Binding Kinetics**	45
3.03.7	**Conclusions**	46
References		46

3.03.1 An Introduction to Free Energy Methods

Since the very first molecular dynamics (MD) simulation of a protein by Karplus and McCammon[1] it was clear that physics-based atomistic simulations held great promise for structure-based drug discovery, due to their ability to track the behavior of ligand–target interactions with atomic precision across different time scales. Indeed, MD allows the understanding and quantification of ligand–target binding events in unprecedented details, with a significant potential on preclinical drug discovery, ranging from understanding how new hits modulate their target biomolecules, to guiding the rational design of more potent derivatives in the hit-to-lead phase. An example of this was the success of the MD-based design of new HIV-integrase inhibitors. Using MD simulations, a new transient binding "trench" was discovered,[2] not observed in crystallographic structures, which led to the development of more effective inhibitors.[3] However, the promise of MD has been long held back by the insufficient accuracy of the available force fields, the limited computer power available and above all, the short time scales accessible. Thus, the articles reporting a successful, prospective use of atomistic MD simulations in drug discovery are still few compared with those relying on more approximate methods.

But there is a general consensus that a number of recent developments will change the situation for the better. The use of graphics processing units (GPUs) as programmable co-processors,[4] the development of highly parallel supercomputers and, more recently, specialized hardware for MD[5,6] finally allows extremely long MD simulations, ranging from hundreds of microseconds up to a few milliseconds. Long MD running on the new hardware were able to sample the reversible folding of a number of small proteins[7,8] and the spontaneous binding of ligand to pharmaceutically relevant targets.[9–11] The possibility of performing very long MD simulations has also had a positive effect on the accuracy of the force fields. Long simulations can be more easily compared with experimental results, leading to better parameterization.[12–17] Still, even on specialized hardware such as Anton,[5,6] specifically designed to run MD and several times faster than conventional supercomputers, it is usually not possible to observe a statistically relevant number of binding and unbinding events. Indeed, the residence time of most drugs is very long (from hours to days) and the observation of a few binding events are surely not sufficient to sample all the relevant conformations and calculate the binding rates and free energies. The accurate prediction of protein–ligand free energies of binding is a fundamental goal of computational chemistry and computer-aided drug design (CADD).[18] The limitations of standard MD with respect to free energy calculations have been historically addressed by a number of "free energy methods" that rely on various MD-based algorithms to compute the free energy of binding $\Delta G^{\text{bind}} = \langle G^{\text{PL}} \rangle - \langle G^{\text{P}} \rangle - \langle G^{\text{L}} \rangle$ where the P, L, and PL superscripts stand for protein, ligand, and their complex, respectively.[19,20]

A reliable, and possibly fast, evaluation of the binding free energy together with a molecular understanding of the features of the ligand and the target contributing to its potency is very useful in the early phases of drug discovery. In particular in the hit-to-lead

phase, predicting the binding free energy of various derivatives and understanding the role of different substituents can speed-up the development of clinical candidates.[18] This vital step has been often delegated to more approximated approaches such as docking, with variable degrees of success.[21,22] Thanks to the aforementioned technical progress in computing power,[4] algorithms,[23] and force fields,[12–17] it can now be routinely performed by more rigorous MD-based free energy methods.

Of the plethora of different algorithms that have been developed in the last decades to allow the calculations of free energies here we focus on those that have passed the test of time by continuous improvements, or have been recently developed. Free energy methods broadly fall into two separate categories. The first class, "end point" methods, are aimed at computing the relative free energy of the bound and unbound states, without trying to compute the full free energy profile along the binding coordinate. These include free energy perturbation (FEP), thermodynamic integration (TI), λ-dynamics, linear interaction energy, WaterSwap, and those which combine molecular mechanics with Poisson-Boltzmann (or generalized Born) implicit solvation and surface areas calculations (MM-PBSA and MM-GBSA).[24–27] These approaches often involve the use of an "alchemical transformation," where the identity of the atoms in the models will change, making them appear, disappear, or change to a different atom during the process. This is achieved computationally by progressively shifting the Hamiltonian of the system H is to a different H' passing through a series of, often unphysical, intermediates. The second class includes methods aimed at calculating the full binding free energy profile along a physical pathway. These classes of methods generally work by enhancing the sampling of standard MD through different approaches, and are often referred to as "enhanced sampling" (ES) methods. End point approaches are generally less computationally intensive (as they focus on the bound and unbound states and in some instances use implicit solvent models), but they do not deliver the same amount of information of the full binding free energy profile, including the binding mechanism, on-path intermediates, and transition states (TS), which have the potential to unleash crucial insight for the design of small molecules. Thus, the two types of methods are complementary and the choice of one versus the other depends on the specific application at hand. Moreover, the boundary between the two approaches is increasingly blurred as many methods combining them are being successfully used in CADD.

3.03.2 Alchemical Methods

Alchemical binding free energy calculations are one of the most established and useful "accurate" computational techniques in CADD. Their advantage with respect to faster and more approximate techniques is that, in principle, they include all the important thermodynamic contributions to the free energy, such as the conformational entropy (for small conformational changes), the discrete nature of the solvent, and are able to include the effect of protonation states or tautomer distributions, all of which are neglected in most fast screening techniques routinely used in drug design. Indeed, these crucial, but often neglected effects are the main responsible of the lack of effectiveness and inaccuracies in many computational predictions.[28] Alchemical methods can be used to compute either absolute binding free energies or relative binding free energies (the difference between the binding free energies of two or more, usually related ligands). Although the statistical mechanic relations used in alchemical methods have been introduced a long time ago[29,30] it was only at the beginning of the 1980s, with the increase in available computational resources, made their use possible with molecular simulations. One of the first examples of their application was the study of proton transfer in lysozymes by Hwang and Warshel.[31] In the same period, a paper by McCammon and coworkers reported the relative binding free energies of a number of congeneric ligands to receptor.[32] These approaches, usually referred to as "alchemical transformations" due to the fact that one ligand is "transmutated" to another one or to a noninteracting "dummy" molecule through a series of "nonphysical" intermediates steps, have now been established as the standard procedure to obtain accurate relative free energy differences by a number of groups, including McCammon's, Warshel's, and their coworkers.[19,33,34]

3.03.2.1 Thermodynamic Integration Versus Free Energy Perturbation

TI and FEP are among the most widely used alchemical methods using explicit solvent simulations.

TI is a classical alchemical method in which the free energy between the end points (e.g., bound and unbound states) is calculated by taking the derivative of the free energy with respect to a continuous parameter λ describing a series of intermediate nonphysical (alchemical) states and computing the average of the derivative from $\lambda = 0$ to $\lambda = 1$

$$\frac{dG}{d\lambda} = \frac{d}{d\lambda}\int e^{-\beta H(\lambda,x)}dx = \left\langle \frac{dH(\lambda,x)}{d\lambda} \right\rangle_{\lambda}$$

$$\Delta G = \int_0^1 \left\langle \frac{dH(\lambda,x)}{d\lambda} \right\rangle_{\lambda}$$

For alchemical changes that result in smooth curves for $\left\langle \frac{dH}{d\lambda} \right\rangle$, TI can provide quite accurate estimates using a relatively small number of intermediate points. However, if the curvature becomes large, as can be the case in alchemical simulations where the molecule "disappears" by turning the Lennard–Jones potentials off, then the error introduced by discretization of the integral can become large.[35] Thus the choice of the alchemical pathway is fundamental to achieve sufficient accuracy.[36,37] Once an optimal alchemical pathway has been devised, the total free energy difference is computed from the individual simulations at different λ

values by using a numerical integration of the integral. To this end, a number of numerical techniques have been applied, ranging from the simple trapezoidal rule to high order integration methods. Higher order integration methods often allow a larger distance between integration points, but are more sensitive to the value of the derivatives of the function, which can become large, especially close to end points.[38]

The term "perturbation" in FEP refers to the alchemical changes in the atom identities, such as bromine to a methyl group. Usually FEP is used to refer specifically to the application of the Zwanzig relationship[30] in which the free energy difference between two Hamiltonians $H_0(x)$ and $H_1(x)$ is calculated as:

$$\Delta G = -kT \ln \left\langle \exp^{-\beta[H_1(x)-H_0(x)]} \right\rangle_0$$

In recent years, FEP calculations have greatly benefited from the improved force fields and the combination with new sampling algorithms.[18,39,40] Historically, FEP had difficulties in converging the free energy of systems undergoing complex conformational changes between the initial and final conformations. However, nowadays, the difference between FEP and TI methods depends basically on the formula used. While FEP uses an exact formula, the TI approach uses a discretized version of the formula, although both are a priori equivalent. Most probably, today, the advantage of FEP with respect to TI is the widespread adoption of the multistate Bennett acceptance ratio (MBAR) approach and the use of discrete points, which allows to (i) equilibrate each point, (ii) add extra points a posteriori if needed, and (iii) apply independent spacing pattern between different λ points to improve the efficiency of the method and minimizing the convergence error.[41] Even so, the use of one technique versus the other depends basically of the kind of simulation protocol used by the researcher.

3.03.2.2 Evolution of the Alchemical Methods

The continuous progress in alchemical free energy calculations is due to several factors. The initial results obtained at the end of 1980s and their comparison with experiment resulted in many early technical improvements.[42] The enormous increase in available computer time due to Moore's law allowed much longer simulations and made it clear that, to obtain a consistent result, significantly longer simulations than those feasible in the 1980s were necessary. The algorithms have been continuously improved during the last 20 years and, more recently, they have been effectively combined with other ES techniques, increasing the accuracy of the results and their use in academic and industrial environments. Finally, the availability of much cheaper high performance computing resources and of automatic setup interfaces made the often complex setup and interpretation of the results more accessible, and allowed the avoidance of a number of common mistakes that marred the results in many past calculations.[40,43–48] In more detail, one of the most common problems in the "alchemical transformations" methods is related to the appearing and disappearing atoms during the transformation of the ligands. This introduces a numerical problem related to the repulsive term in the Lennard–Jones potential. In order to solve this problem, soft-core potentials have been introduced.[49,50] Another important issue is related to the sampling at end points and of different conformations. The dynamics of the system can be unstable due to the vanishing of the atoms especially at the end points of the simulations ($\lambda = 0$ and $\lambda = 1$). This problem was also addressed by the use of soft-core potentials. The exploration of different conformational states by MD simulations is a more complex problem. In most cases, it is the responsibility of the slow (or no) convergence of the methods. For instance, the conformational changes of the target due to the binding of a ligand can be very complex in nature and, due to high free energy barriers, require extremely long simulation to be sufficiently sampled. If the ligand is forced in the binding cavity without the needed conformational changes occurring first, the resulting free energy differences will be wrong.[51] This issue can also explain the dependency of the results from the starting structure. This is a significant issue, since the conformations observed in the X-ray structure of the unbound target can be very far from those needed for binding. Thus the exploration of the correct conformation often requires very long MD simulations or the combination of the alchemical algorithms with ES approaches.[52–55] Similarly, when multiple binding modes are accessible to the ligand, the sampling needed to converge the free energy will greatly increase.[56] These phenomena can easily lead to wrong relative free energy differences, and together with some systematic inaccuracies in the force fields explain most of the observed discrepancies between simulated and experimental results.

These points have been discussed in detail in the review by Chodera et al. focused on the challenges facing the use of alchemical calculations in drug discovery.[26] An interesting observation is that, when validating the calculated free energy results with experimental binding affinities obtained by biophysical procedures, one needs to keep in mind that also the experimental results are affected by significant uncertainties and often contain systematic errors. Thus, the error bars on both the predicted and experimental binding energies limit their correlation. In order to further improve the accuracy of predicted binding free energies high quality experimental data is needed.[57]

The first application of alchemical free energy methods was reported by Tembe and McCammon at the beginning of the 1980s.[32] Later, the success obtained by Wong and McCammon[19] in computing the free energy of three different inhibitors of trypsin and the accurate binding free energies of xenon atoms in myoglobin reported by Herman[58] promoted the use of alchemical applications, with a number of papers appearing at the end of 1980s and at the beginning of the 1990s. However, the abovementioned deficiencies in the methodology and the prohibitive computational cost on the supercomputers then available postponed a widespread use of these techniques until the beginning of the 2000s, when the newly available computational resources and methodological progress heralded the "coming of age" of alchemical transformations.[59] Traditionally the alchemical free energy methods are used in the calculation of relative binding free energy. However, recently a number of successful

examples of the application of alchemical transformations to the calculation of absolute binding free energies[60,61,62] and solvation free energies have been reported.[61,63]

Below, we discuss in some detail a number of interesting examples of alchemical transformations in the calculation of relative binding free energy, which involves the "nonphysical" transformation of one ligand in another one based on the appropriate thermodynamic cycle.

One of the most successful and complete examples was reported by Jorgensen and coworkers and is related to the nonnucleoside reverse transcriptase inhibitors (NNRTIs) of the HIV-1.[64] The HIV-1 reverse transcriptase (HIVRT) enzyme is a critical system to the retrovirus since it is responsible for the conversion of the viral RNA into DNA to incorporate the viral genes into the host cell. Therefore, the NNRTIs have a crucial role in inhibiting this enzyme. However, the HIVRT mutates rapidly, resulting in drug resistance to the NNRTIs, which requires a fast development of new and more potent inhibitors to address the new drug-resistance-inducing mutations. In 2000 there were three drugs approved by the FDA against the HIVRT called Nevirapine, Delavarine, and Sustiva. Two point mutations of HIVRT, V106A and Y181C, result in an increased resistance to the known drugs, with the exception of Sustiva. To understand the causes of this interesting effect, explain the resistance, and thus the effectiveness of Sustiva in countering the mutations, Jorgensen and coworkers used a combination of docking and FEP calculations.[64] Since the X-ray structure of the HIVRT with Sustiva bound to the active site was not available, they first performed docking calculations to determine the probable structural location of Sustiva in the binding site, taking into consideration other available HIVRT–ligand X-ray structures. The best-docked poses provided a plausible structural explanation of the mode of action of Sustiva in the mutated HIVRT. A specific hydrogen bond interaction between the ligand and Lys101, as well as the aryl-π interactions with Tyr181 and Tyr188, favorably contributed to the binding. The thermodynamic cycle considering the wild-type (WT) and mutated enzyme and two inhibitor drugs validated the structural model obtained from docking and provided a quantitative estimate of the resistance. The results obtained were in good agreement with the experimental results, validating the qualitative picture obtained from docking and revealed why Sustiva is the only ligand that effectively inhibits the mutant protein. The calculations also provided a number of specific structural interactions engaged by Sustiva with the mutant protein that can be used in the design of novel inhibitors. In 2004, following a similar computational strategy, the same group studied another crucial drug-resistance-inducing mutation in HIVRT, K103N.[65] It was observed that Efavirenz had a higher potency toward the mutant protein. In this case two crystal structures of the ligand-bound protein were available. However, the orientation of the side chain of Tyr181, a crucial residue for the binding, was different in the two structures. Therefore, the FEP calculations were used not only to clarify the structural origins of the K103N-induced resistance, but also which of the two available structures were in better agreement with the activity data. The calculations showed that only the structure with the conventional orientation of Y181 ("up") in both the WT and K103N mutant provide free energy differences in qualitative agreement with the experimental results. These results reaffirm the importance of a careful preliminary analysis and selection of the available crystal structures for the accuracy of the free energy calculations. They also explain the increased accuracy of combined algorithms, where FEP together with other ES approaches is able to sample different conformations of the target protein that might contribute to the binding free energy. The resistance observed in the K103N mutant enzyme toward most drugs was explained in terms of specific interactions in the holo and apo enzyme. The quinazolinone analogs of Efavirenz present higher activity in the mutated enzyme due to a hydrogen bond network formed between these inhibitors and several water molecules located at the binding site. Finally, a new and more effective NNRTI, Etravirine, was designed with the help of the novel insights and approved in 2008. The problem of the drug-resistance-inducing mutations in HIVRT requires sustained and continuous efforts from the drug design community. To this end the use of FEP calculations to understand the molecular mechanism of drug resistance played a crucial role in guiding lead optimization and the development of new lead ligands.[66] Through the judicious use of alchemical free energy calculations, Jorgensen and coworkers were able to convert the inactive core of a building block in an inhibitor against HIVRT with a potency of 10–20 nM.

Erion[67] used FEP calculations to design a series of inhibitors of fructose 1,6-biphosphatase (FBPase). The AMP inhibits FBPase, which is a potential target for diabetes type II. In a preliminary work,[68] the authors used the FEP calculations to determine the contributions of the individual heteroatoms of AMP toward the inhibition. Later,[67] they predicted the structure–activity relationship (SAR) of AMP analogs taking into consideration the solvation and the binding free energies with the goal of designing potent inhibitors against FBPase. These analyses are very useful since in some cases the desolvation energy cost reduces the binding affinity considerably, while in others the group associated with the high desolvation energy cost also formed strong favorable interactions with the protein compensating the cost of desolvation and leading to a higher binding affinity. Another example of interest was the case of human neutrophil elastase (HNEs).[53] HNEs specifically cleaves small aliphatic amino acids, hydrolyzing the proteins which confers elasticity to the skin. Unregulated HNE activity plays a role in a number of diseases, including cystic fibrosis or pulmonary emphysema. In order to design more effective inhibitors, Streibencher et al. applied TI to a number of bornyl caffenate derivative ligands, showing a promising binding affinity. The combination of ligand docking, with MM-PBSA and explicit solvent TI calculations showed that specific hydrogen bonds formed by the ligand and the placement of the hydrophobic moiety into the S1 binding site of the protein crucially contribute to the binding affinity.

Another interesting study showing the value of alchemical free energy calculations is related to the F1F0-ATP synthase. This enzyme is responsible for most of the ATP synthesis in living organisms.[69] From F1F0 complex, the catalytic subunit F1, which is able to hydrolyze the ATP, is formed alternating 3-α and 3-β subunits located around the γ subunit. The γ subunit is asymmetric and their rotation alters the conformations of the three β subunits of the catalytic subunit for the substrates and products. It is known that the ligand is bound with higher affinity to one of these three subunits, however, the relationship between the binding affinities and the different conformations of the β subunit was not clear. In the first X-ray structure obtained, each β subunit was

crystallized with different analogs, that is, one subunit contains an analog of ATP (ANP) and was called a β_{TP}, another with ADP, called β_{DP} and the third subunit was called β_E because was empty in the crystal structure. However, this subunit in a second X-ray structure obtained was called β_{HC} (from half-closed). It was not clear which of the β_{TP} and β_{DP} subunits had the highest affinity to the ligand. In order to shed some light, Karplus and coworkers computed the free energy differences using TI of the hydrolysis of ATP from both crystal structures.[70,71] The results of the calculations suggest that the binding site with the highest affinity for ATP is found in β_{TP}. These results are also confirmed by the structural information of the binding sites. The charged residues found in the β subunits together with the Mg^{2+} cation contribute to the difference in the binding between the subunits. The presence of these residues stabilizes ATP versus ADP due to the stronger interactions of γ-phosphate of ATP in β_{TP} than in β_{DP}. The calculations clarified the relation between the structural features of the different catalytic sites with the experimental binding affinities. Another interesting and challenging example is related to the 8-oxoguanine DNA glycosylase I (hOGG1), which is able to distinguish between guanine (G) and the mutagenic 8-oxoguanine (oxoG). The question here was how the hOGG1 enzyme is able to discern between these two very similar nucleobases. In order to elucidate the structural features that contribute to the binding, Karplus and coworkers[72] performed free energies calculations with the G and oxoG in the binding site and in the exo sites. The calculations suggest that the binding of oxoG toward hOGG1 is favored in both normal and exo site. The FEP analysis indicates that the change of the lone pair in N7 of the guanine by the N7H in the oxoG favors the hydrogen bond with the carbonylic oxygen of Gly42 backbone, which despite the presence of other repulsive interactions, make a net contribution of 3.5 kcal/mol to the binding.

Very recently, a systematic application of a combination of FEP with an enhanced sampling protocol to a large number of ligand–target systems, has shown such a level of high predictive accuracy and robustness to make it ripe for its routine use industrial drug discovery environments.[15] The protocol builds on the significant improvement in the sampling due to the use of combined algorithms and the concomitant increase in the accuracy of the force fields due to a painstaking reparameterization work of the ligand force field performed in the last years.[15,18,39,40,73,74] The authors demonstrate the effectiveness of this protocol testing $\simeq$ 200 ligands and 10 different targets. Only nine of the predicted free energies deviated more than 2 kcal/mol from the experiment. They addressed most of the challenges discussed earlier.[26] The combination of an improved version of the force field Optimized Potentials for Liquid Simulations (OPLS),[75] with the extensive sampling of the conformational space by the combined FEP/replica exchange with solute tempering[55,76,77] was fundamental to address that aim the implementation of these algorithms into the fast MD package Desmond, made its use computationally feasible.[78] Moreover, the implementation of the algorithms in a package with a robust interface simplified several aspects such as (i) the selection of a specific region of the system where sampling at a higher temperature can be useful, focusing the sampling where it is needed to cross the conformational barriers[55] or (ii) avoiding the problem of torsional barriers limiting the ergodicity of the system (that torsional barriers do not limit the complete sampling of the system over the timecourse of the MD). Moreover, an automatic way to generate the perturbations pathways through a variant of the LOMAP algorithm was implemented.[55] In that way, it was possible to set up 16 independent calculations in approximately 30 min, making it faster and devoid of possible human errors. Finally, the algorithms were implemented on GPUs, with a speed-up of FEP calculation of 5–10 in comparison to running on CPUs. The results obtained show not only an improved scoring with respect to other methodologies like SAR or MM-GB/SA, but also the usefulness of the knowledge of the different physical phenomena involved in the binding that free energy calculations can accurately describe. For instance, this methodology is able to capture the changes in the hydrophobic interactions, hydrogen bonding interactions or solvent effects due to the transmutation of one ligand to another one, providing a very useful chemical insight in the hit-to-lead phase of CADD.

These encouraging results show that the widespread application of combined alchemical/ES approaches together with better ligand force field might have a significant impact on CADD. Although the specific FEP/REST implementation requires special care in the selection of the REST region and the OPLS 3 force field is currently only available in very expensive proprietary software packages, this will undoubtedly change as other, more universally accessible, ligand force fields are improved and alchemical methods are combined with a number of other enhanced sampling approaches.

Therefore, the evolution of the alchemical methodologies in the last 30 years and their combination with other ES algorithms shows real promise, and although there are still a number of open challenges to be addressed, their routine application in drug discovery as one of the accurate computational tool of choice is increasingly feasible and justified.

3.03.3 ES Algorithms

The general aim of ES methods is to speed-up the sampling of relevant areas of the phase space by MD using ad hoc algorithms. ES algorithms are able to explore "rare events" taking place on time scales that are much longer than those typically accessible to MD. By sampling multiple times different conformations these approaches are able not only to provide an insight on possible binding mechanisms and allosteric effects, but also provide an estimate of the free energy landscape (**Fig. 1**). A large number of ES algorithms have been developed, and an in depth discussion of their characteristics and of the many applications they have in a number of fields is the argument of numerous books and reviews.[23,25,79] Three different subclasses of ES can be broadly defined. (1) Methods based on "collective variables" (CVs) (i.e., a combination of variables approximating the reaction coordinate (RC)) that add an external potential to favor a more effective exploration of the relevant regions of the conformational landscape. (2) Methods that do not make an explicit use of CVs, such as Markov state models (MSMs)[80] and multiple replica approaches (parallel tempering (PT),[81] Hamiltonian replica exchange,[82] etc.). (3) A large class of methods based on a "path" linking initial and final states (such as transition path sampling[83] or milestoning[84]). Approaches in the first class have been most extensively used in

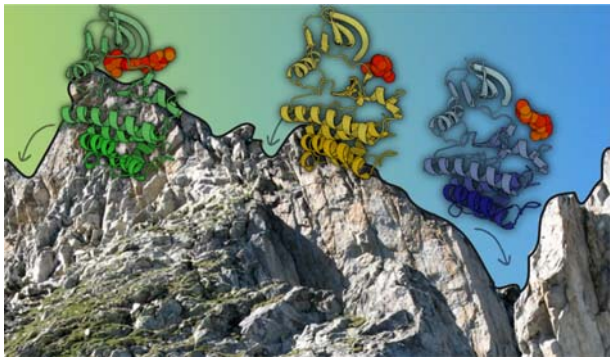

Fig. 1 Pictorial representation of the binding landscape. Methods that rely on a physical pathway are able to predict the full free energy profile of the (un)binding process, revealing transition states and metastable states.

CADD. They require the a priori knowledge and definition of a "collective variable" that approximates more or less precisely the RC. An example of a CV often used to study ligand binding is the distance of the ligand from the binding cavity. Methods from the second class do not need the definition a priori of a precise RC, and are thus at the same time more general (e.g., do not need the knowledge of the binding cavity) and often more computationally expensive. Finally, methods based on paths, which usually require the knowledge of the initial and final states and a guess path linking the two. These path-based approaches have been used less often in CADD as they tend to be very computationally demanding, but they are in principle able to provide accurate binding rates in addition to binding affinities. A common observation is that the more knowledge of the system is available and used to direct the sampling, the more efficient is the reconstruction of the free energy landscape.

3.03.3.1 CVs-Based Methods

Most CV-based methods make use of an external potential to enhance the exploration of the conformational landscape and reconstruct the free energy landscape. For this potential to be effective, it needs to favor the transition to new regions of the free energy surface (FES) that would normally not be sampled due to high free energy barriers or slow diffusion. To maximize the efficiency, the bias potential should act only on the atoms involved in the transition and push the system along the RC of the transition under study. Thus, M "collective variables" $\mathbf{s} = (s_1(\mathbf{R})\ldots s_M(\mathbf{R}))$, function of the relevant atomic coordinates and approximating the real RC are introduced. By acting on these CVs, the bias potential will not affect all the degrees of freedom indistinguishably, but will be instead only focused on those contributing to the transition. Once the relevant degrees of freedom have been extensively explored, it is possible to get a reconstruction of the free energy profile (or of the multidimensional FES). Indeed, the free energy profile as a function of the RC can be written as:

$$F(s) = -k_{\mathrm{B}}T\ln\langle\delta(s(\mathbf{R}) - s)\rangle$$

where the Dirac delta function maps the $\mathbf{R}$ coordinates onto the CV space, that is, all the configurations $\mathbf{R}$ which realize the same CV value s are counted together. The dynamics of the system is biased by the introduction of a potential $V^*(\mathbf{R}) = V^*(s(\mathbf{R}))$ which is a function of the defined CVs, to the real potential $V(\mathbf{R})$.

3.03.3.2 Optimal Choice of the CVs

The efficiency of CV-based methods in reconstructing the FES strongly depends on the choice of optimal CVs. An optimal set of CVs not only has to distinguish between the initial and final state, but also include most slow degrees of freedom involved in the transition. If important (slow) degrees of freedom are omitted, the free energy reconstruction might fail, suffer from hysteresis or take a considerable time to converge. This is due to the fact that the neglected, slow orthogonal degrees of freedom are not biased and are in principle explored as slow as in a standard MD run. A typical example of this is the case of ligand binding mechanisms requiring significant conformational changes. If the chosen CVs do not describe the conformational change, the reconstructed free energy might be wrong or very slowly converging. This was observed in the case of a ligand binding to the deep gorge of human acetyl cholinesterase (AChE). An ES method, metadynamics, was run initially with one CV, the distance between ligand and the deeply buried binding pocket. However, it was soon evident that a couple of aromatic residues lining the gorge blocked the translocation of the ligand. The reconstructed free energy suffered from hysteresis since, depending on the state of the "gate" formed by the aromatic residues, predicted a higher (open state) or lower (closed state) barrier. When a new CV describing the orientation of the aromatic residues was introduced, it was possible to get a well-converged free energy reconstruction in a fraction of the time that would have been needed without it.[85]

The most common choices of CVs for ligand binding applications are simple geometric functions of the coordinates, as distances, angles, and dihedrals formed by atoms or group of atoms. Typically, when computing binding free energies along

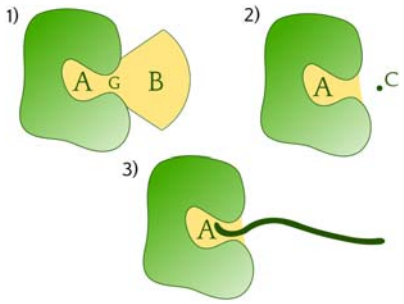

Fig. 2 Optimal choice of collective variables to study ligand binding to a target of interest. *A* is the binding cavity, *G* is the entrance gate, *B* is the bulk solution, and *C* is a point outside the cavity. In (1) an ES simulation is run using a distance and an angle as CV; in (2) the free energy difference between the bound pose and a point just outside the cavity is calculated using a distance and other geometric variables; in (3) an optimal path collective variables (PCV) describes the physical (un)binding mechanism using a series of snapshots along a low free energy pathway.

a physically meaningful association/dissociation path, one distance is used to define the position of the ligand from the target and one or two angles or dihedrals are used to describe its orientation. An additional variable can be used to explore conformational changes of the target. Geometric CVs are both easy to define and to implement in MD codes and have been successfully used together with ES approaches such as umbrella sampling (US) and metadynamics to compute a number of binding free energy profiles.[86–91]

An important issue to consider when computing the binding free energy landscape with CVs based on distances is the need to reduce the amount of sampling needed by limiting the range of distances explored (see Fig. 2). This can be achieved, for instance, by using various restraining potentials ("walls"), a common practice when using metadynamics. Indeed, in most cases, sampling all the possible orientations and positions of a ligand both in the bulk solvent and all possible nonspecific binding sites on the surface of the target is impractical. To this aim, various kinds of more or less complex restraints and walls have been introduced. These range from simply introducing a harmonic restraint acting above a set maximum distance[86] up to inverse-funnel-shaped restraints on the position of the ligand.[92] When computing absolute free energy distances in the presence of such boundaries, a simple correction needs to be applied to take into account the effective volume accessible to the ligand compared to that accessible on average to a ligand at a standard concentration.[40]

For more complex mechanisms (e.g., binding events requiring significant conformational changes of the target), geometric CVs might provide a suboptimal description.[23] In these cases CVs such as the root mean square deviation (RMSD) from a specific conformation or the changes in the target contact map have been successfully used.[93,94]

To tackle this problem, significant efforts have been devoted to develop optimal CVs and CV combinations that are generally applicable to ligand binding to flexible ligands, capturing all the important degrees of freedom involved in a transition. These include, among others, CV based on linear and nonlinear dimensionality reduction techniques such as principal component analysis vectors[95] and path collective variables (PCVs).[96] PCVs are a particularly effective choice to compute ligand binding free energies and (in combination with a path-sampling method) to compute binding kinetics (Fig. 2). PCVs are based on the idea that the main pathway used by the ligand to reach the binding pocket on its target can be described explicitly as a curvilinear path, defined by a series of snapshots along the path itself. In this way, even very complex association paths, that cannot be described by simple geometric CVs as the ligand–protein distance, can be efficiently sampled. Thus, in PCV, the configuration sampled by the ligand is described in relation to the defined path, as the progression along the path $s(\mathbf{R})$, that is, where the configuration is respective to the bound and unbound states, and the distance from the path $z(\mathbf{R})$, that is, how far from the path described in the PCV the configuration explored is. Having a series of snapshots describing the initial path, PCV are defined as

$$s(\mathbf{R}) = \frac{\sum_{i=1}^{N} i \cdot e^{-\lambda \|\mathbf{R}-\mathbf{R}_i\|}}{\sum_{i=1}^{N} e^{-\lambda \|\mathbf{R}-\mathbf{R}_i\|}} \quad z(\mathbf{R}) = -\frac{1}{\lambda} \ln \sum_{i=1}^{N} e^{-\lambda \|\mathbf{R}-\mathbf{R}_i\|}$$

where

$$\lambda = \frac{2.3 \times (N-1)}{\sum_{i=1}^{N-1} \|\mathbf{R}_i - \mathbf{R}_{i+1}\|}$$

and the distance metric $\| \ldots \|$ can be arbitrarily defined. In the software PLUMED2,[97] a plug-in compatible with many MD engines that implements metadynamics and other methods together with a wide range of CVs, the RMSD, the RMSD of distances, and the difference between contact map matrices are the available options for the distance metric. While having a good initial path for the construction of PCVs provides a considerable boost in efficiency, an approximate "guess" path can also be used. Paths obtained through preliminary ES simulations, for example, using steered MD (SMD) or metadynamics[98,99] (see later), are reported in the literature as paths constructed by interpolation of the initial and final states.[100]

3.03.3.3 Umbrella Sampling

The US approach was developed by Torrie and Valleau in 1977[101] and is based on the idea of introducing an external potential to favor the exploration of all the regions of interest (e.g., bound and unbound states of our complex), which will normally be difficult to sample in a single simulation due to high free energy barriers. Introducing the bias potential $V^*(s)$, the system evolves under the action of a modified potential $V' = V(\mathbf{R}) + V^*(s(\mathbf{R}))$ and sample a biased probability distribution $P'(s)$. The effect of the added potential $V^*(s)$ is that of adding an additional weight $e^{-\beta V^*(s)}$ to the Boltzmann weight of every state. Knowing this, and the external potential $V^*(s)$, the real probability distribution $P(s)$ can be recovered as

$$P(s) = \langle \delta(s(\mathbf{R}) - s) \rangle = \frac{\left\langle \delta(s(\mathbf{R}) - s) \cdot e^{\beta V^*(s(\mathbf{R}))} \right\rangle_{V'}}{\left\langle e^{\beta V^*(s(\mathbf{R}))} \right\rangle_{V'}}$$

where the subscript indicates that the averaging $\langle \rangle_{V'}$ is done in a simulation governed by V'. Thus, *Vsr* could be chosen so that the biased distribution $P'(s)$ is uniform and each region of the CV space is equally explored. The efficiency and convergence of the resulting free energy profile depend dramatically on the choice of the applied potential. Generally, the US bias potential is expressed as

$$V^*_{\mathrm{US}} = \frac{k}{2} \cdot (s(\mathbf{R}) - \hat{s})^2$$

that is, as an harmonic potential centered in $\hat{s}$. In most practical cases, however, it is difficult to achieve the desired sampling using a single bias potential. For this reason, it is common to perform US using "windows," each with a different value of $\hat{s}$

$$V^*_i = \frac{k_i}{2} \cdot (s(\mathbf{R}) - \hat{s}_i)^2$$

to cover the entire CV space. The free energy in each window will have an arbitrary offset, so that a matching of the separate segments of the profile is needed. Provided that the different windows have a certain degree of overlap, the statistic from each of them can be combined using the weighted histogram analysis method[102] or the umbrella integration technique.[103]

Different values have been used in the literature for both the number of windows and the force constant k, and, even if attempts to give some sensible guidelines have been made,[104] the choice remains system-dependent. Kästner and Mascarenhas[105] studied the binding of maltose to the maltose-binding protein and the conformational change between the open and close state of the protein using US. They used the distance between the centers of mass of the ligand and of the binding cite as CV and a total of 41 windows covering the CV range between 0.4 and 4.7 nm. However, the final setup was the result of a constant tweaking of the parameters. The authors started with 21 windows with a spacing of roughly 0.2 nm between each window. Later, to increase the overlap and decrease the noise of the free energy profile, they included an additional 20 windows, with a final separation of approximately 0.05 nm between each of them. A similar trial and error procedure was used for the force constant, which was initially set at 1000 kJ mol^{-1} nm^{-2} and increased to 2000 kJ mol^{-1} nm^{-2}, with one window having a k of 3000 kJ mol^{-1} nm^{-2}. Also the length of the simulations, which needs to be sufficient to equilibrate the transverse degrees of freedom not included in the CV, was evaluated for each window independently, monitoring the change in the force over 10 ns in intervals of 1 ns. Thanks to these procedures, the authors achieved a smooth free energy profile and a remarkable agreement between their ΔG^{bind} estimate (-46.1 ± 4.4 kJ mol^{-1}) and the experimental value of -49.1 kJ mol^{-1}. Moreover, they revealed important details regarding the binding mechanism, which they describe as a mixed model, involving both conformational selection and induced fit. Vargiu et al.[106] used US to describe the sliding of two drugs, duocarmycin and anthramycin, along the minor groove of DNA, using 23 windows along the selected CV, the distance between the reactive atoms of the drug and the DNA base. The separation of the windows along the CV in this case was around 0.035 nm. A complex profile characterized by different intermediates states was obtained, and interesting differences were observed for the two drugs.

3.03.3.4 Metadynamics

As discussed above, a bias potential $V^*(s(\mathbf{R}))$ can be used to "flatten" the FES and favor a more homogeneous exploration. The most homogeneous sampling is generally realized for $V^*(s) = -F(s)$, as the bias potential $V^*(s)$ compensates the underlying free energy and allows the system to diffuse freely in the CV space. While devising such a potential would require knowing a priori the $F(s)$ (which we are trying to calculate), several methods have been developed around the concept of an "adaptive" potential that try to "locally" compensate the free energy on the fly. These include Tabu search,[107,108] *local elevation*,[109] *conformational flooding*,[110] and the widely used *metadynamics*.[79,111] Metadynamics was developed by Laio and Parrinello in 2001 and, while it shares several traits with other "self-healing" approaches, it was the first to be used to reconstruct binding free energy landscapes and has a number of advantages over similar approaches. In metadynamics a history-dependent bias potential $V^*(s(\mathbf{R}))$ is built on the fly during the simulation and, as it flattens the local FES it helps overcoming free energy barriers and favors a uniform exploration of the conformational space described by the chosen CVs.[111] $V^*(s(\mathbf{R}))$ has been described in a review by Laio and Gervasio[79] as "computational sand" filling the crevasses and basins of a rough free energy landscape resulting in an easy to explore flat FES. The main idea is that, even without knowing the overall shape of $F(s)$, we can compensate the free energy landscape progressively, so that for a long

simulation, $V^*(s)$ will in time grow to be equal to $-F(s)$. To do so, metadynamics introduces a history-dependent bias potential defined as a sum of small Gaussians

$$V^*_{\text{meta}}(s,t) = h \cdot \sum_{t=\tau,2\tau,\ldots} e^{\frac{-(s(\mathbf{R})-s(t))^2}{2\delta s^2}}$$

where $s(\mathbf{R})$ is the instantaneous value of the CV and $s(t)$ is the value of the CV at time t and τ is the interval between the addition of Gaussians. While in the original algorithm the height h of the Gaussians was kept constant, the well-tempered formulation of metadynamics[112] introduces variable-height Gaussians that decrease their height throughout the simulation according to

$$h = h_0 \cdot \tau \cdot e^{\frac{-V^*(s,t)}{\Delta T}}$$

thus ensuring that for an arbitrary long time the $V(s)$ will not oscillate around the correct free energy, but converge to it, that is,

$$V^*(s, t \to \infty) = -\frac{\Delta T}{\Delta T + T} \cdot F(s)$$

where the first term takes into account the scaling factor ΔT. Thus, at the end of a metadynamics simulation, the added bias provides an estimate of the free energy profile. It is important to know that, at difference with a number of more or less similar approaches, the well-tempered formulation of metadynamics has been mathematically proven to converge to the "real" FES.[113]

Several examples of the use of metadynamics in drug binding are reported in the literature, and have been described in a recent review.[23] The first simulations, carried out by Gervasio et al., correctly predicted the binding pose for several protein–ligand complexes and were found to be able to reconstruct a full FES faster than US. The predicted binding free energies were surprisingly similar to the experimental ones.[86]

This was probably due in part to a cancellation of errors, as the use of simple geometric CVs, a suboptimal ligand force field and the very short length of the simulations impacted the convergence of the reconstructed FES. The importance of selecting an optimal set of CVs was further shown in the study of Branduardi et al.[85] on the binding mechanism of the tetramethylammonium ion into human AChE, as discussed earlier.

As aforementioned, the selection of proper CVs in ligand (un)binding is further complicated by the features of the unbound state, that is, by the large conformational space available to the ligand in the bulk solvent. This translates into a flat and diffusive region in the free energy landscape that is difficult to sample thoroughly. Masetti et al.[88] address this issue assessing how metadynamics performs when the ligand is not allowed to fully explore the unbound state. Indeed, exploration is allowed only as far as the main exit barrier (TS) and thus remains circumscribed to the protein internal cavity. Nevertheless, this approach, denominated "coarse-metadynamics," could successfully rank series of congeneric compounds. An alternative, frequently used in the first binding studies, is introducing restraints on the explored bulk area. This way, the "reduced" unbound state can be easily sampled and the convergence of FESs is faster. The binding free energy can then be corrected for the real bulk volume available to the ligand. The restraints range from simple "wall" potentials on the maximum/minimum value of the CVs, to more complex potential, as funnel-shaped ones.[92] A different approach, which has been applied extensively in the context of metadynamics, is the use of the aforementioned PCVs. Using the PCV, Fidelak et al.[90] studied a congeneric series of CDK2 inhibitors and were able to rank correctly the compounds, obtaining free energies in remarkable agreement with the experimental ones. Using a similar strategy, Provasi and coauthors used the PCV to study the binding mechanism of various ligands to the β2-adrenergic receptor. Several efforts have also been devoted to develop semiautomatic protocols for ligand scoring in a pharmaceutical setup. Saladino et al.[98] correctly ranked a series of p38 inhibitors frequently used to assess the performance of end point methods and scoring functions, running unsupervised metadynamics with PCV and a minimal semiautomatic setup. Mason et al. at Heptares Therapeutics used a combination of adiabatic biased MD and short well-tempered metadynamics runs with PCV to devise a fast and successful protocol to assess the druggability and effect of mutations on the binding of ligands to GPCRs. The approach named "MetaScore" uses the adiabatic biased MD simulations to define an initial binding path and then computes the binding free energy profiles along this path to the WT and mutant proteins with well-tempered metadynamics and PCV.[114]

3.03.3.5 Steered MD

Inspired by the pulling experiments of atomic force microscopy, Grubmüller et al.,[115] pioneered the calculation from MD of the work W needed to pull a molecule out if its binding site. To do so, the authors applied a spring-like potential of the form

$$V^*_{\text{pull}} = \frac{k}{2} \cdot (s(\mathbf{R}) - \hat{s}(t))^2$$

where the center of the potential is moved according to $\hat{s}(t) = s_0 + v_{\text{pull}} \cdot t$, to one of the atoms of the ligand. Similar approaches were later used by Schulten and coworkers[116] and became known as steered molecular dynamics. Conceptually, SMD could be thought as a continuous version of US where the harmonic potential is moved along the RC. The main difference is that, unless the work is performed reversibly and, thus, infinitely slow, the simulation is out of equilibrium. Recovering an equilibrium property, like the free energy, from nonequilibrium simulations, however, has been made possible by the work of Jarzynski.[117] Provided that the simulations are all started from an equilibrium distribution, he demonstrated that $e^{-\beta\Delta G} = \langle e^{-\beta W} \rangle$. Thus, a free energy can be

obtained by exponential average of the work values of multiple SMDs. As high-energy pathways will contribute very little to the average, convergence of the ΔG strongly depends on how far from equilibrium the simulations are and will be considerably slower for higher pulling speeds.

3.03.4 Other Methods

One of the main disadvantages of the methods in the previous section is that their efficiency relies on the choice of the CVs used. When the selected variables are not a good approximation of the RC and, in particular, do not take into account important degrees of freedom, convergence of the free energy profile can be problematic. Due to the inherent difficulty of defining a good set of CVs for complex systems, great effort has been devoted to the development of general methods that do not require an a priori knowledge of an approximated RC. This type of methods will be discussed in this section.

3.03.4.1 Replica Exchange

Free energy landscapes are smoother at high temperature and it is easier for a system to escape local minima and cross energy barriers. Several methods, indeed, have been developed in which sampling is enhanced using simulations at higher temperature. Borrowing some ideas from Monte Carlo methods, Sugita and Okamoto developed replica exchange molecular dynamics (REMD). In PT,[118] the most popular variant of REMD, different replicas of the system are run at different temperatures and exchanges of conformations between neighboring replicas are occasionally attempted. To ensure that each replica samples the correct Boltzmann distribution, exchanges are accepted automatically when the potential energy of the higher temperature replica is lower than the one of the colder replica. When this condition is not satisfied, an exchange can still occur with probability

$$p = e^{-\Delta} \quad \Delta = (\beta_i - \beta_j)\cdot(E_j - E_i)$$

where $\beta = \frac{1}{k_B T}$ and the i and j subscript are used to indicate the energy E and β of two neighboring replica. Other variants of REMD have been developed using different parameters other than temperature, for example, the *Hamiltonian replica exchange*.

Hamiltonian replica exchange MD (H-REMD) has been successfully used in the identification of ligand binding sites, thus improving the predictive value of molecular docking calculations as reported by Luitz and Zacharias[119] and to finding hidden (cryptic) binding pockets.[120] H-REMD allows the sampling of the conformational space around docking sites, using less replicas that the T-REMD approach. Indeed, since the scaling of the Hamiltonian can be applied to specific and small portions of the system, it accelerates the transitions in a more efficient way than T-REMD that increases the temperature of the whole system, including that of the many water molecules. The application of this technique to the analysis of ligand binding sites has been shown to improve the misplaced ligand–receptor complexes obtained by classical docking techniques. Obviously, this combined technique does not replace a standard docking protocol, since it is much more computationally expensive, but it can be very useful in refining selected docking poses and in difficult cases where a significant conformational change is involved or the binding cavity is not visible in the apo structure (cryptic pockets).[120]

3.03.4.2 Accelerated MD

Accelerated molecular dynamics (aMD), developed by Hamelberg et al.,[121] is based on ideas similar to US and metadynamics, that is, on the introduction of a bias potential, but dispenses the requirement for the definition of a CV. The system is simulated under the action of the modified potential $V'(\mathbf{R})$

$$V'(\mathbf{R}) = \begin{cases} V(\mathbf{R}) & V(\mathbf{R}) \geq E \\ V(\mathbf{R}) + V^*(\mathbf{R}) & V(\mathbf{R}) < E \end{cases}$$

where $V(\mathbf{R})$ is the real potential and $V^*(\mathbf{R})$ is a "boost" potential introduced by aMD. Hence, when $V(\mathbf{R})$ is lower than a certain energy value E (called "boost energy"), for example, when the system is in a stable minimum, the current conformation is disfavored by the additional potential $V^*(\mathbf{R})$. Regions where the energy is higher than E, for example, barrier regions, are not affected and the system is simulated under the action of the real potential $V(\mathbf{R})$. The "boost potential" $V^*(\mathbf{R})$ is generally defined as

$$V^*(\mathbf{R}) = \frac{(E - V(\mathbf{R}))^2}{\alpha + (E - V(\mathbf{R}))}$$

where α is a tuning parameter. The boost $V^*(\mathbf{R})$ can be applied on any term of the potential energy function and "dihedral aMD" have been used to enhance the sampling of protein conformations. Boosting of the total potential energy has also been reported in the literature, and the "dual boost" formulation is combined with a separate dihedral boosting.

The main drawback of aMD is that a high boost potential might prevent the reweighting of the different conformations[122] and, consequently, the calculations of a full FES. Other procedures, however, such as restarting multiple MDs from the different conformations explored and using MM-PBSA,[123] have been used to obtain a free energy estimate.

3.03.5 Combining Different Methods

The various methods described in the previous sections have unique advantages and disadvantages and are more or less effective depending on the specific system and the questions that need to be addressed. As also discussed earlier, often the best results are obtained when methods from different classes are combined (e.g., FEP with REST). The use of replica exchange, indeed, can be highly beneficial in cases where optimal CVs (e.g., describing complex conformational changes) are difficult to identify and, more generally, to sample the orthogonal degrees of freedom not included in the CVs and relieve from the eventual omission of important ones. One of the first successful examples is parallel tempering metadynamics (PT-MetaD),[124] which combines the CV-based metadynamics[111] with PT.[81,118] Thanks to the excursion in temperature introduced by PT, hidden degrees of freedom are sampled and the convergence of the FES is significantly improved. Conversely, metadynamics allows sampling of higher energy regions that would not be properly sampled in standard PT, such as TS.

PT-MetaD has been successfully used to compute the free energy landscape associated with the flip of the conserved "DFG" motif in a number of tyrosine kinases.[125] Type II kinase inhibitors, including the successful antileukemic drug Imatinib, selectively bind to a subset of tyrosine kinases by taking advantage of the different free energy penalty associated with the "flip" of the conserved DFG motif. Free energy calculations with PT-MetaD have not only been used to understand the molecular binding mechanism,[125] but also to clarify how drug resistance-causing mutations affect the conformational change.[126] The results of these accurate calculations have been subsequently confirmed by NMR and surface plasmon resonance (SPR) experiments.[99] An approach similar to PT-MetaD that allows the use of many CVs was proposed by Piana and Laio in the form of bias exchange metadynamics (BEMD).[127] Instead of having multiple simulations of the systems running at different temperatures as in PT-MetaD, in BEMD each replica is biased with a different CV. This allows for a more flexible number of replicas and for a higher number of CVs, without degrading the performance of metadynamics. Both methods have been used to investigate the mode of action of SSR128129E (hereafter referred to as SSR), a newly developed inhibitor of the fibroblast growth factor receptor (FGFR),[128,129] and the first inhibitor discovered to bind extracellularly. FGFR is a receptor tyrosine kinase involved in cellular processes, such as cell growth, proliferation, and survival. SSR was discovered by high-throughput screening, but several experimental techniques, including X-ray crystallography and NMR, failed to identify the binding site for the compound. Using BEMD, Herbert and coworkers were able to test a wide range of CVs and to observe the binding of SSR to the D3 domain of FGFR. Interestingly, a conformational change that elongates a small α-helix in the D3 domain was needed to open the binding pocket and for SSR to dock into the receptor. This is a typical case in which the use of combined approaches can help, as the CV is difficult to guess and there are unknown degrees of freedom (such as those involved in the unexpected conformational change) that need to be sampled.

While BEMD allows the use a larger number of CVs than PT-MetaD, it does not improve the sampling of degrees of freedom that are not explicitly included and thus might still suffer from convergence problems due to the omission of an important variable, at difference with PT-MetaD. Thus, several approaches have been developed to contain the demanding computational cost of PT-MetaD (or standard PT). An example of this is constituted by the well-tempered ensemble approach (WTE) developed by Bonomi et al.[130] In the WTE approach, a preliminary metadynamics is run using the potential energy as CV, which has the effect of broadening the potential energy distributions. This way, the overlap between the distributions of neighboring replicas is enhanced and PT-MetaD (or standard PT) can be performed using a significantly lower number of replicas.

Several examples of the use of PT-MetaD together with WTE are reported in the literature.

3.03.5.1 Successful Applications of ES Techniques

ES techniques have been successfully used to study ligand binding and conformational changes in targets of therapeutic interest. ES techniques are able to describe the complete mechanism of the process analyzed, such as the binding/unbinding of a ligand to a specific protein system. This provides relevant information that cannot be obtained from high-resolution structural techniques such as X-ray, or where only a static snapshot of the system is provided. What is more, these techniques allow us to study spontaneous target conformational changes which can take from microseconds to hundreds of seconds, and it would be impossible to study in detail with standard MD simulations. A nice example of a complex binding mechanism revealed by ES techniques (WTE metadynamics) is that of ligand binding to different isoforms of the cyclooxygenase enzyme. The cyclooxygenase enzymes (COXs) are relevant inflammation drug targets that are inhibited by the nonsteroidal antiinflammatory drugs. These drugs block the entrance of the endogenous ligand, arachidonic acid. An important consideration in the targeting of COX enzymes is the existence of two different isoforms (COX1 and COX2), one involved in the therapeutic effect and the other in side effects and toxicity. Thus there is a need for selective inhibition. Interestingly some ligands are able to differentiate between the two isoforms by means of different binding kinetics. The crystallographic data shows that the pocket of COX2 is slightly wider than the binding site pocket of COX1, and this was thought to be involved in the differential binding affinity of the selective inhibitors in COX-2 with respect to COX1. However, the molecular mechanism underlying the selectivity was not clear. Limongelli et al.[92] used well-tempered metadynamics to study the binding free energy profile of a COX2-selective inhibitor, SC-558, in COX2 and COX1. The simulations show that, while in COX1, SC-558 can be only bound to one binding site, in the case of COX2 it can bind both to the "standard" crystallographic binding site and to an "alternative" binding cavity, which had not been reported until that moment. This fact, later confirmed by crystallographic data, explains why the residence time of the inhibitor in COX2 is much longer than in COX1. These results allow the rational design of novel inhibitors with specific selectivity profiles by increasing or reducing the contact with the two binding sites (standard or alternative), producing inhibitors with fine-tuned residence times and kinetics. This work displays

how the use of ES techniques can provide useful mechanistic insights in the ligand binding mechanism, that are usually not available to any other technique.

Another interesting example was reported by Favia et al.[131] They combined metadynamics with SMD simulations in order to predict the binding path and the associated free energy of the type I 11-β-hydroxysteroid dehydrogenase (11 β-HSD-1) with its substrate. The study of the binding/unbinding processes, allowed the clarification of the residues that form the gate, the role of waters and the key role of Y177 in the ligand recognition. Moreover, they observed multiple energy basins corresponding to different conformations, and thus understood the complex interplay between the protein and its ligand.

Combined ES approaches such as PT-MetaD discussed earlier are very effective in exploring complex conformational changes, such as the activation of kinases. As discussed earlier, PT-MetaD has been used to clarify the selectivity of an anticancer drug that binds to a specific inactive conformation.[126] Interestingly PT-MetaD has also been used to clarify the mode of action of cancer-causing and drug-resistance-inducing mutations in the epidermal growth factor receptor (EGFR) tyrosine kinase.[94] Activating and drug-resistance-inducing mutations in EGFR are frequently found in many cancers, including lung cancer. Their mode of action was not clear. It had been suggested that either changes in the equilibrium between its active and inactive conformations or disorder at the dimerization interface were linked to their oncogenic potential.[132] In the paper by Sutto and Gervasio[94] PT-MetaD with CVs based on contact maps was used to quantify the effects of some of the most common single (L858R and T790M) and double (T790M-L858R) oncogenic and drug-resistance-inducing mutations on the conformational free energy landscape of the EGFR kinase domain. The result reconciled a previous proposal showing that, the L858R mutation stabilizes the active conformation at the expense of the inactive conformation and rigidifies the αC-helix at the dimerization interface. Moreover it was shown that the drug-resistance-inducing T790M gatekeeper mutant favors activation by stabilizing a cluster of hydrophobic residues.

A similar approach was used to study the effect of a single mutation (V600E) on the conformational landscape of the B-RAF kinase. This mutation is found in more than 50% of all malignant melanomas. The free energy landscapes of the WT and the V600E mutant reconstructed with PT-MetaD and a contact-map-based CV showed that mutation increases the barrier of the active to inactive transition, trapping B-Raf in the active state and increases the flexibility of the activation loop speeding-up the rate-limiting step of phosphorylation.

3.03.6 Binding Kinetics

In recent years, a lot of emphasis has been put on drug binding kinetics, with many reviews stressing the importance of predicting rates early in the drug discovery pipeline.[133–140] During the different phases of drug development, binding affinity is highly optimized, under the assumption that it constitutes a good proxy for the in vivo efficacy. However, in vivo, the concentration of a drug changes over time as a consequence of the complex physiological mechanisms of adsorption, distribution, and excretion, globally known as pharmacokinetics and the residence time (τ_{off}), that is, the time that a drug spends bound to its target, has emerged as a better indicator of a drug's efficacy.[133,136] The "optimization" of binding rates also offers new attractive opportunities to fine tune selectivity, for example, achieving longer residence times for the desired target even when the affinity for other receptors is comparable, and minimize toxicity, for example, having a faster dissociation in the case of on-target toxicity, such as in the case of dopamine receptor antagonists.[141] While experimental techniques, such as SPR, are able to measure binding rates of a drug dissociation (and association), tuning these rates would require knowledge about the structure and energy of the TS, whose limited lifetime makes it elusive to most experimental techniques. Computational tools are thus the main avenue to achieve kinetically optimized compounds.

Ideally, being able to run arbitrarily long MD simulations, the rates of drug (un)binding could be derived by simply averaging the dissociation/association time over multiple events directly observed in a simulation. Notwithstanding advancements in computer hardware, MD remains too computationally expensive to reach timescales where most biomolecular processes could be observed spontaneously. Purpose-built machines, such as Anton,[5,6] while accurately predicting association rates, still struggle to observe spontaneous dissociation of drugs from their target, for which typical residence times are in the order of seconds to hours, or even days. Thus the calculation of drug binding rates cannot forgo, generally, the use of some kind of "enhanced sampling" technique, able to speed-up the simulations.

Interestingly, while the ecosystem of computational methods for the estimation of molecular rates is flourishing, very few applications to drug binding are reported in the literature and most of these cases are confined to very simple systems, like the binding of benzamidine to the serine protease Trypsin.

De Fabritiis and coworkers[11] used the ACEMD software[142] and a GPU-based distributed computing grid to obtain around 500 short trajectories (100 ns each, for an aggregate time of 50 μs) for the aforementioned benzamidine–trypsin system. They were able to observe numerous binding and unbinding events thanks to the fast kinetics (and limited affinity, around -6.2 kcal mol^{-1}) of benzamidine. Using a MSM[80] they reconstructed a full free energy profile and characterized the binding mechanism in details, identify several metastable states were benzamidine makes weaker interactions with the protein. This also allowed them to infer the on and off rates for the binding, which were predicted to be $k_{on} = (1.5 \pm 0.2) \times 10^8$ M^{-1} s^{-1} and $k_{off} = (9.5 \pm 3.3) \times 10^4$ s^{-1}, both deviating at least an order of magnitude from the experimental results, 2.9×10^7 M^{-1} s^{-1} and 6×10^2 s^{-1}, respectively. The authors associated the large errors to the inherent difficulty of extracting long-time rates from a collection of shorter trajectories and to the lack of sampling of full unbinding events, leading to higher uncertainty for the k_{off}. Noé and Plattner[143] revisited the same system with a similar approach, generating 543 MD trajectories with an aggregate time of nearly 150 μs and using MSM to derive

Table 1 Benzamidine-trypsin binding kinetics: experimental values compared to Markov State Models and Metadynamics predictions

Method	k_{on} ($M^{-1} s^{-1}$)	k_{off} (s^{-1})	*References*
Exp.	2.9	6	
MSM	15 ± 2	950 ± 330	De Fabritiis et al.[11]
MSM	6.4 ± 1.6	131 ± 109	Noé and Plattner[143]
Metadynamics	1.2 ± 1	0.91 ± 0.25	Tiwary et al.[144]

kinetic parameters. While a remarkable agreement was obtained for the $k_{on} = (6.4 \pm 1.6) \times 10^7\ M^{-1}\ s^{-1}$, the dissociation rate was overestimated as in the work of De Fabritiis and coworkers[11] with a predicted value of $(131 \pm 109) \times 10^2\ s^{-1}$, due to the poorly sampled dissociation events. Nonetheless, the authors were able to give a compelling description of the binding pathway and mechanism, which includes features typical of "conformational selection" and "induced fit" models. Tiwary et al.[144] calculated the on and off rates for the same system using a new method based on "infrequent biasing" metadynamics.[145] A summary of the results, compared to those obtained by previous works, is reported in **Table 1**.

An aggregate time of 5 μs of biased simulations were needed to calculate rates, but resulted in a better agreement between the predicted kinetics parameters and experiments.

The prediction of binding rates for more complex systems was recently attempted by Morando et al.[99] who studied the binding of the antileukemic drug Gleevec to the c-Src tyrosine kinase. Using a new method, transition state-partial path transition interface sampling, which combine the free energy calculated by metadynamic with a transmission coefficient obtained through path sampling, the authors obtained a remarkable agreement between the calculated k_{off} ($0.0114\ s^{-1}$) and the experimental results, which they measured using SPR ($0.024–0.19\ s^{-1}$). Using scaled potentials, which enhance the transitions between different minima, Mollica et al.[146] were able to calculate *relative* off rates for several complexes of pharmaceutical interest. This way, the authors were able to rank different congeneric compounds predicting the k_{off} ratio with respect to a reference ligand–target complex, achieving regression correlation coefficients in the 0.85–0.95 range. While being more approximate and providing only partial information, the method is more straightforward and easy to implement, in addition to requiring fewer computational resources.

In summary, recent years have seen significant advancements in the prediction of association and dissociation rates by MD simulations. The field remains, however, in its infancy and, with a limited number of examples reported in the literature, the suitability of the different methods for the prediction of binding rates in a pharmaceutical setup remains an open question.

3.03.7 Conclusions

The accuracy and usefulness of free energy methods have greatly improved in recent years. This, together with significantly improved protein and ligand force fields and the availability of low-cost high-performance computing resources provided by graphics processing units and cloud computing, concur to make free energy methods a fundamental tool in CADD. In this article, we have discussed a number of recent and recently improved algorithms as well as a range of interesting applications reported in the literature. Free energy methods can now not only compute accurate relative and absolute binding free energies, but also conformational free energy landscapes, cryptic binding pockets, binding mechanisms, and (in combination with other approaches) binding kinetics.

See also: 3.01. Perspective on Calculations of Binding Free Energies.

References

1. McCammon, J. A.; Gelin, B. R.; Karplus, M. Dynamics of Folded Proteins. *Nature* **1977,** *267,* 585–590.
2. Schames, J. R.; Henchman, R. H.; Siegel, J. S.; Sotriffer, C. A.; Ni, H.; McCammon, J. A. Discovery of a Novel Binding Trench in HIV Integrase. *J. Med. Chem.* **2004,** *47,* 1879–1881.
3. Summa, V.; et al. Discovery of Raltegravir, a Potent, Selective Orally Bioavailable HIV-Integrase Inhibitor for the Treatment of HIV-AIDS Infection. *J. Med. Chem.* **2008,** *51,* 5843–5855.
4. Buch, I.; Harvey, M. J.; Giorgino, T.; Anderson, D. P.; De Fabritiis, G. High-Throughput All-Atom Molecular Dynamics Simulations Using Distributed Computing. *J. Chem. Inf. Model.* **2010,** *50,* 397–403.
5. Shaw, D. E.; et al. Millisecond-Scale Molecular Dynamics Simulations on Anton. Proc. Conf. High Perform. Comput. Networking, Storage Anal. – SC '09, ACM Press: New York, 2009; p 1.
6. Shaw, D. E.; et al. Anton 2: Raising the Bar for Performance and Programmability in a Special-Purpose Molecular Dynamics Supercomputer. In SC14 Int. Conf. High Perform. Comput. Networking, Storage Anal, 2014; pp 41–53.
7. Shaw, D. E.; et al. Atomic-Level Characterization of the Structural Dynamics of Proteins. *Science* **2010,** *330,* 341–346.
8. Chung, H. S.; Piana-Agostinetti, S.; Shaw, D. E.; Eaton, W. A. Structural Origin of Slow Diffusion in Protein Folding. *Science* **2015,** *349,* 1504–1510.

9. Shan, Y.; Kim, E. T.; Eastwood, M. P.; Dror, R. O.; Seeliger, M. A.; Shaw, D. E. How Does a Drug Molecule Find Its Target Binding Site? *J. Am. Chem. Soc.* **2011,** *133,* 9181–9183.
10. Dror, R. O.; Pan, A. C.; Arlow, D. H.; Borhani, D. W.; Maragakis, P.; Shan, Y.; Xu, H.; Shaw, D. E. Pathway and Mechanism of Drug Binding to G-Protein-Coupled Receptors. *Proc. Natl. Acad. Sci. U. S. A.* **2011,** *108,* 13118–13123.
11. Buch, I.; Giorgino, T.; De Fabritiis, G. Complete Reconstruction of an Enzyme-Inhibitor Binding Process by Molecular Dynamics Simulations. *Proc. Natl. Acad. Sci. U. S. A.* **2011,** *108,* 10184–10189.
12. Lindorff-Larsen, K.; Piana, S.; Palmo, K.; Maragakis, P.; Klepeis, J. L.; Dror, R. O.; Shaw, D. E. Improved Side-Chain Torsion Potentials for the Amber Ff99SB Protein Force Field. *Proteins* **2010,** *78,* 1950–1958.
13. Best, R. B.; Hummer, G. Optimized Molecular Dynamics Force Fields Applied to the Helix-Coil Transition of Polypeptides. *J. Phys. Chem. B* **2009,** *113,* 9004–9015.
14. Best, R. B.; Zhu, X.; Shim, J.; Lopes, P. E. M.; Mittal, J.; Feig, M.; MacKerell, A. D., Jr. Optimization of the Additive CHARMM All-Atom Protein Force Field Targeting Improved Sampling of the Backbone Φ, Ψ and Side-Chain X 1 and X 2 Dihedral Angles. *J. Chem. Theory Comput.* **2012,** *8,* 3257–3273.
15. Wang, L.; et al. Accurate and Reliable Prediction of Relative Ligand Binding Potency in Prospective Drug Discovery by Way of a Modern Free-Energy Calculation Protocol and Force Field. *J. Am. Chem. Soc.* **2015,** *137,* 2695–2703.
16. Maier, J. A.; Martinez, C.; Kasavajhala, K.; Wickstrom, L.; Hauser, K. E.; Simmerling, C. Ff14SB: Improving the Accuracy of Protein Side Chain and Backbone Parameters From Ff99SB. *J. Chem. Theory Comput.* **2015,** *11,* 3696–3713.
17. Robertson, M. J.; Tirado-Rives, J.; Jorgensen, W. L. Improved Peptide and Protein Torsional Energetics With the OPLSAA Force Field. *J. Chem. Theory Comput.* **2015,** *11,* 3499–3509.
18. Jorgensen, W. L. Efficient Drug Lead Discovery and Optimization. *Acc. Chem. Res.* **2009,** *42,* 724–733.
19. Wong, C. F.; Mccammon, J. A. Dynamics and Design of Enzymes and Inhibitors. *J. Am. Chem. Soc.* **1986,** *108,* 3830–3832.
20. Kollman, P. Free Energy Calculations: Applications to Chemical and Biochemical Phenomena. *Chem. Rev.* **1993,** *93,* 2395–2417.
21. Liu, J.; Wang, R. Classification of Current Scoring Functions. *J. Chem. Inf. Model.* **2015,** *55,* 475–482.
22. Steinbrecher, T. B.; Dahlgren, M.; Cappel, D.; Lin, T.; Wang, L.; Krilov, G.; Abel, R.; Friesner, R.; Sherman, W. Accurate Binding Free Energy Predictions in Fragment Optimization. *J. Chem. Inf. Model.* **2015,** *55,* 2411–2420.
23. Cavalli, A.; Spitaleri, A.; Saladino, G.; Gervasio, F. L. Investigating Drug-Target Association and Dissociation Mechanisms Using Metadynamics-Based Algorithms. *Acc. Chem. Res.* **2015,** *48,* 277–285.
24. Homeyer, N.; Stoll, F.; Hillisch, A.; Gohlke, H. Binding Free Energy Calculations for Lead Optimization: Assessment of Their Accuracy in an Industrial Drug Design Context. *J. Chem. Theory Comput.* **2014,** *10,* 3331–3344.
25. Chipot, C.; Pohorille, A. *Free Energy Calculations: Theory and Applications in Chemistry and Biology;* Springer: Berlin and Heidelberg, 2007. Vol. 86.
26. Chodera, J. D.; Mobley, D. L.; Shirts, M. R.; Dixon, R. W.; Branson, K.; Pande, V. S. Alchemical Free Energy Methods for Drug Discovery: Progress and Challenges. *Curr. Opin. Struct. Biol.* **2011,** *21,* 150–160.
27. Woods, C. J.; Malaisree, M.; Hannongbua, S.; Mulholland, A. J. A Water-Swap Reaction Coordinate for the Calculation of Absolute Protein-Ligand Binding Free Energies. *J. Chem. Phys.* **2011,** *134,* 054114.
28. Schneider, G. Virtual Screening: An Endless Staircase? *Nat. Rev. Drug Discov.* **2010,** *9,* 273–276.
29. Kirkwood, J. G. Statistical Mechanics of Fluid Mixtures. *J. Chem. Phys.* **1935,** *3,* 300–313.
30. Zwanzig, R. W. High-Temperature Equation of State by a Perturbation Method. I. Nonpolar Gases. *J. Chem. Phys.* **1954,** *22,* 1420–1426.
31. Warshel, A. Simulating the Energetics and Dynamics of Enzymatic Reactions. *Pontif. Acad. Sci. Scr. Varia* **1984,** *55,* 60–81.
32. Tembre, B. L.; McCammon, J. A. Ligand-Receptor Interactions. *Comput. Chem.* **1984,** *8,* 281–283.
33. Bash, P. A.; Singh, U. C.; Brown, F. K.; Langridge, R.; Kollman, P. A. Calculation of the Relative Change in Binding Free Energy of a Protein-Inhibitor Complex. *Science* **1987,** *235,* 574–576.
34. Hwang, J. K.; Warshel, A. Semiquantitative Calculations of Catalytic Free Energies in Genetically Modified Enzymes. *Biochemistry* **1987,** *26,* 2669–2673.
35. Steinbrecher, T.; Mobley, D. L.; Case, D. A. Nonlinear Scaling Schemes for Lennard–Jones Interactions in Free Energy Calculations. *J. Chem. Phys.* **2007,** *127,* 214108.
36. Blondel, A. Ensemble Variance in Free Energy Calculations by Thermodynamic Integration: Theory, Optimal "Alchemical" Path, and Practical Solutions. *J. Comput. Chem.* **2004,** *25,* 985–993.
37. Merz, K. M., Jr.; Ringe, D.; Reynolds, C. H. Drug Design: Structure-and Ligand-Based Approaches. In Cambridge University Press: Cambridge, 2010.
38. Resat, H.; Mezei, M. Studies on Free Energy Calculations. I. Thermodynamic Integration Using a Polynomial Path. *J. Chem. Phys.* **1993,** *99,* 6052.
39. Gallicchio, E.; Levy, R. M. Advances in All Atom Sampling Methods for Modeling Protein-Ligand Binding Affinities. *Curr. Opin. Struct. Biol.* **2011,** *21,* 161–166.
40. Deng, Y.; Roux, B. Computations of Standard Binding Free Energies With Molecular Dynamics Simulations. *J. Phys. Chem. B* **2009,** *113,* 2234–2246.
41. Brandsdal, B. O.; Österberg, F.; Almlöf, M.; Feierberg, I.; Luzhkov, V. B.; Åqvist, J. Free Energy Calculations and Ligand Binding. *Adv. Protein Chem.* **2003,** *66,* 123–158.
42. Pearlman, D. A. Free Energy Calculations in Rational Drug Design. In Kluwer Academic/Plenum Publishers: New York, 2001.
43. Aleksandrov, A.; Thompson, D.; Simonson, T. Alchemical Free Energy Simulations for Biological Complexes: Powerful but Temperamental. *J. Mol. Recognit.* **2010,** *23,* 117–127.
44. Shirts, M. R.; Mobley, D. L.; Brown, S. P. Free-Energy Calculations in Structure-Based Drug Design. In *Drug Design Structure- and Ligand-Based Approaches;* Cambridge University Press: Cambridge and New York, 2010. Chapter 5.
45. Michel, J.; Essex, J. W. Prediction of Protein–Ligand Binding Affinity by Free Energy Simulations: Assumptions, Pitfalls and Expectations. *J. Comput. Aided Mol. Des.* **2010,** *24,* 639–658.
46. Christ, C. D.; Mark, A. E.; van Gunsteren, W. F. Basic Ingredients of Free Energy Calculations: A Review. *J. Comput. Chem.* **2010,** *31,* 1569–1582.
47. Pohorille, A.; Jarzynski, C.; Chipot, C. Good Practices in Free-Energy Calculations. *J. Phys. Chem. B* **2010,** *114,* 10235–10253.
48. Shenfeld, D. K.; Xu, H.; Eastwood, M. P.; Dror, R. O.; Shaw, D. E. Minimizing Thermodynamic Length to Select Intermediate States for Free-Energy Calculations and Replica-Exchange Simulations. *Phys. Rev. E Stat. Nonlinear Soft Matter Phys.* **2009,** *80,* 046705.
49. Beutler, T. C.; Mark, A. E.; van Schaik, R. C.; Gerber, P. R.; van Gunsteren, W. F. Avoiding Singularities and Numerical Instabilities in Free Energy Calculations Based on Molecular Simulations. *Chem. Phys. Lett.* **1994,** *222,* 529–539.
50. Zacharias, M.; Straatsma, T. P.; McCammon, J. A. Separation-Shifted Scaling. A New Scaling Method for Lennard–Jones Interactions in Thermodynamic Integration. *J. Chem. Phys.* **1994,** *100,* 9025–9031.
51. Mobley, D. L.; Chodera, J. D.; Dill, K. A. The Confine-and-Release Method: Obtaining Correct Binding Free Energies in the Presence of Protein Conformational Change. *J. Chem. Theory Comput.* **2007,** *3,* 1231–1235.
52. Boyce, S. E.; Mobley, D. L.; Rocklin, G.; Graves, A. P.; Dill, K. A.; Shoichet, B. K. Predicting Ligand Binding Affinity With Alchemical Free Energy Methods in a Polar Model Binding Site. *J. Mol. Biol.* **2009,** *394,* 747–763.
53. Steinbrecher, T.; Case, D. A.; Labahn, A. A Multistep Approach to Structure-Based Drug Design: Studying Ligand Binding at the Human Neutrophil Elastase. *J. Med. Chem.* **2006,** *49,* 1837–1844.
54. Oostenbrink, C.; van Gunsteren, W. F. Free Energies of Binding of Polychlorinated Biphenyls to the Estrogen Receptor From a Single Simulation. *Proteins* **2004,** *54,* 237–246.

55. Wang, L.; Berne, B. J.; Friesner, R. A. On Achieving High Accuracy and Reliability in the Calculation of Relative Protein–Ligand Binding Affinities. *Proc. Natl. Acad. Sci. U. S. A.* **2012,** *109,* 1937–1942.
56. Mobley, D. L.; Dill, K. A. Binding of Small-Molecule Ligands to Proteins: "What You See" Is Not Always "What You Get". *Structure* **2009,** *17,* 489–498.
57. Brown, S. P.; Muchmore, S. W.; Hajduk, P. J. Healthy Skepticism: Assessing Realistic Model Performance. *Drug Discov. Today* **2009,** *14,* 420–427.
58. Hermans, J.; Shankar, S. The Free Energy of Xenon Binding to Myoglobin From Molecular Dynamics Simulation. *Isr. J. Chem.* **1986,** *27,* 225–227.
59. Chipot, C. Free Energy Calculations in Biomolecular Simulations: How Useful Are They in Practice?. In *Lecture Notes in Computational Science and Engineering: New Algorithms for Molecular Simulations;* Leimkuhler, B., Chipot, C., Elber, R., Laaksonen, A., Mark, A. E. S. T., Schütte, C., Skeel, R., Eds.; Springer: New York, 2005 . vol. 49; pp 183–209.
60. Mobley, D. L.; Graves, A. P.; Chodera, J. D.; McReynolds, A. C.; Shoichet, B. K.; Dill, K. A. Predicting Absolute Ligand Binding Free Energies to a Simple Model Site. *J. Mol. Biol.* **2007,** *371,* 1118–1134.
61. Mobley, D. L.; Dumont, E.; Chodera, J. D.; Dill, K. A. Comparison of Charge Models for Fixed-Charge Force Fields: Small-Molecule Hydration Free Energies in Explicit Solvent. *J. Phys. Chem. B* **2007,** *111,* 2242–2254.
62. Aldeghi, M.; Heifetz, A.; Bodkin, M. J.; Stefan Knapp, S.; Biggin, P. C. Accurate calculation of the absolute free energy of binding for drug molecules. *Chem. Sci* **2016,** *7,* 207–218.
63. Nicholls, A.; Mobley, D. L.; Guthrie, J. P.; Chodera, J. D.; Bayly, C. I.; Cooper, M. D.; Pande, V. S. Predicting Small-Molecule Solvation Free Energies: An Informal Blind Test for Computational Chemistry. *J. Med. Chem.* **2008,** *51,* 769–779.
64. Rizzo, R. C.; Wang, D.-P.; Tirado-Rives, J.; Jorgensen, W. L. Validation of a Model for the Complex of HIV-1 Reverse Transcriptase With Sustiva Through Computation of Resistance Profiles. *J. Am. Chem. Soc.* **2000,** *122,* 12898–12900.
65. Udier-Blagovic, M.; Tirado-Rives, J.; Jorgensen, W. L. Structural and Energetic Analyses of the Effects of the K103N Mutation of HIV-1 Reverse Transcriptase on Efavirenz Analogues. *J. Med. Chem.* **2004,** *47,* 2389–2392.
66. Zeevaart, J. G.; Wang, L.; Thakur, V. V.; Leung, C. S.; Tirado-Rives, J.; Bailey, C. M.; Domaoal, R. A.; Anderson, K. S.; Jorgensen, W. L. Optimization of Azoles as Anti-Human Immunodeficiency Virus Agents Guided by Free-Energy Calculations. *J. Am. Chem. Soc.* **2008,** *130,* 9492–9499.
67. Reddy, M. R.; Erion, M. D. Calculation of Relative Binding Free Energy Differences for Fructose 1,6-Biphosphatase Inhibitors Using the Thermodynamic Cycle Perturbation Approach. *J. Am. Chem. Soc.* **2001,** *123,* 6246–6252.
68. Erion, M. D.; van Poelje, P. D.; Reddy, M. R. Computer-Assisted Scanning of Ligand Interactions: Analysis of the Fructose 1,6-Bisphosphatase-AMP Complex Using Free Energy Calculations. *J. Am. Chem. Soc.* **2000,** *122,* 6114–6115.
69. Yang, W.; Gao, Y. Q.; Cui, Q.; Ma, J.; Karplus, M. The Missing Link Between Thermodynamics and Structure in F1-ATPase. *Proc. Natl. Acad. Sci. U. S. A.* **2003,** *100,* 874–879.
70. Braig, K.; Menz, R. I.; Montgomery, M. G.; Leslie, A. G.; Walker, J. E. Structure of Bovine Mitochondrial F(1)-ATPase Inhibited by Mg(2+) ADP and Aluminium Fluoride. *Structure* **2000,** *8,* 567–573.
71. Menz, R. I.; Walker, J. E.; Leslie, A. G. W. Structure of Bovine Mitochondrial F1-ATPase With Nucleotide Bound to All Three Catalytic Sites. *Cell* **2001,** *106,* 331–341.
72. Banerjee, A.; Yang, W.; Karplus, M.; Verdine, G. L. Structure of Repair Enzyme Interrogating Undamaged DNA Elucidates Recognition of Damaged DNA. *Nature* **2005,** *434,* 612–618.
73. Durrant, J. D.; McCammon, J. A. Molecular Dynamics Simulations and Drug Discovery. *BMC Biol.* **2011,** *9,* 71.
74. Michel, J.; Essex, J. W. Hit Identification and Binding Mode Predictions by Rigorous Free Energy Simulations. *J. Med. Chem.* **2008,** *51,* 6654–6664.
75. Harder, E.; Damm, W.; Maple, J.; Wu, C.; Reboul, M.; Xiang, J. Y.; Wang, L.; Lupyan, D.; Dahlgren, M. K.; Knight, J. L.; Kaus, J. W.; Cerutti, D. S.; Krilov, G.; Jorgensen, W. L.; Abel, R.; Friesner, R. A. OPLS3: A Force Field Providing Broad Coverage of Drug-Like Small Molecules and Proteins. *J. Chem. Theory Comput.* **2016,** *12,* 281–296.
76. Liu, P.; Kim, B.; Friesner, R. A.; Berne, B. J. Replica Exchange With Solute Tempering: A Method for Sampling Biological Systems in Explicit Water. *Proc. Natl. Acad. Sci. U. S. A.* **2005,** *102,* 13749–13754.
77. Wang, L.; Friesner, R. A.; Berne, B. J. Replica Exchange With Solute Scaling: A More Efficient Version of Replica Exchange With Solute Tempering (REST2). *J. Phys. Chem. B* **2011,** *115,* 9431–9438.
78. Bowers, K. J.; et al. Scalable Algorithms for Molecular Dynamics Simulations on Commodity Clusters. In *Proceedings of the ACM/IEEE Conference on Supercomputing (SC06)*, 2006; p 84.
79. Laio, A.; Gervasio, F. L. Metadynamics: A Method to Simulate Rare Events and Reconstruct the Free Energy in Biophysics, Chemistry and Material Science. *Rep. Prog. Phys.* **2008,** *71,* 126601.
80. Chodera, J. D.; Noe, F. Markov State Models of Biomolecular Conformational Dynamics. *Curr. Opin. Struct. Biol.* **2014,** *25,* 135–144.
81. Sugita, Y.; Okamoto, Y. Replica-Exchange Molecular Dynamics Method for Protein Folding. *Chem. Phys. Lett.* **1999,** *314,* 141–151.
82. Sugita, Y.; Okamoto, Y. Replica-Exchange Multicanonical Algorithm and Multicanonical Replica-Exchange Method for Simulating Systems With Rough Energy Landscape. *Chem. Phys. Lett.* **2000,** *329,* 261–270.
83. Dellago, C.; Bolhuis, P. G.; Csajka, F. S.; Chandler, D. Transition Path Sampling and the Calculation of Rate Constants. *J. Chem. Phys.* **1998,** *108,* 1964–1977.
84. Faradjian, A. K.; Elber, R. Computing Time Scales From Reaction Coordinates by Milestoning. *J. Chem. Phys.* **2004,** *120,* 10880.
85. Branduardi, D.; Gervasio, F. L.; Cavalli, A.; Recanatini, M.; Parrinello, M. The Role of the Peripheral Anionic Site and Cation-pi Interactions in the Ligand Penetration of the Human AChE Gorge. *J. Am. Chem. Soc.* **2005,** *127,* 9147–9155.
86. Gervasio, F. L.; Laio, A.; Parrinello, M. Flexible Docking in Solution Using Metadynamics. *J. Am. Chem. Soc.* **2005,** *127,* 2600–2607.
87. Lee, M. S.; Olson, M. A. Calculation of Absolute Protein-Ligand Binding Affinity Using Path and Endpoint Approaches. *Biophys. J.* **2006,** *90,* 864–877.
88. Masetti, M.; Cavalli, A.; Recanatini, M.; Gervasio, F. L. Exploring Complex Protein-Ligand Recognition Mechanisms With Coarse Metadynamics. *J. Phys. Chem. B* **2009,** *113,* 4807–4816.
89. Pietrucci, F.; Marinelli, F.; Carloni, P.; Laio, A. Substrate Binding Mechanism of HIV-1 Protease From Explicit-Solvent Atomistic Simulations. *J. Am. Chem. Soc.* **2009,** *131,* 11811–11818.
90. Fidelak, J.; Juraszek, J.; Branduardi, D.; Bianciotto, M.; Gervasio, F. L. Free-Energy-Based Methods for Binding Profile Determination in a Congeneric Series of CDK2 Inhibitors. *J. Phys. Chem. B* **2010,** *114,* 9516–9524.
91. Limongelli, V.; Bonomi, M.; Marinelli, L.; Gervasio, F. L.; Cavalli, A.; Novellino, E.; Parrinello, M. Molecular Basis of Cyclooxygenase Enzymes (COXs) Selective Inhibition. *Proc. Natl. Acad. Sci. U. S. A.* **2010,** *107,* 5411–5416.
92. Limongelli, V.; Bonomi, M.; Parrinello, M. Funnel Metadynamics as Accurate Binding Free-Energy Method. *Proc. Natl. Acad. Sci. U. S. A.* **2013,** *110,* 6358–6363.
93. Bui, J. M.; Mccammon, J. A. Protein Complex Formation by Acetylcholinesterase and the Neurotoxin Fasciculin-2 Appears to Involve an Induced-Fit Mechanism. *Proc. Natl. Acad. Sci. U. S. A.* **2006,** *103,* 15451–15456.
94. Sutto, L.; Gervasio, F. L. Effects of Oncogenic Mutations on the Conformational Free-Energy Landscape of EGFR Kinase. *Proc. Natl. Acad. Sci. U. S. A.* **2013,** *110,* 10616–10621.
95. Sutto, L.; D'Abramo, M.; Gervasio, F. L. Comparing the Efficiency of Biased and Unbiased Molecular Dynamics in Reconstructing the Free Energy Landscape of Met-Enkephalin. *J. Chem. Theory Comput.* **2010,** *6,* 3640–3646.
96. Branduardi, D.; Gervasio, F. L.; Parrinello, M. From A to B in Free Energy Space. *J. Chem. Phys.* **2007,** *126,* 054103.

97. Tribello, G. A.; Bonomi, M.; Branduardi, D.; Camilloni, C.; Bussi, G. PLUMED 2: New Feathers for an Old Bird. *Comput. Phys. Commun.* **2014,** *185,* 604–613.
98. Saladino, G.; Gauthier, L.; Bianciotto, M.; Gervasio, F. L. Assessing the Performance of Metadynamics and Path Variables in Predicting the Binding Free Energies of P38 Inhibitors. *J. Chem. Theory Comput.* **2012,** *8,* 1165–1170.
99. Morando, M. A.; Saladino, G.; D'Amelio, N.; Pucheta-Martinez, E.; Lovera, S.; Lelli, M.; López-Méndez, B.; Marenchino, M.; Campos-Olivas, R.; Gervasio, F. L. Conformational Selection and Induced Fit Mechanisms in the Binding of an Anticancer Drug to the C-Src Kinase. *Sci. Rep.* **2016,** *6,* 24439.
100. Berteotti, A.; Cavalli, A.; Branduardi, D.; Gervasio, F. L.; Recanatini, M.; Parrinello, M. Protein Conformational Transitions: The Closure Mechanism of a Kinase Explored by Atomistic Simulations. *J. Am. Chem. Soc.* **2009,** *131,* 244–250.
101. Torrie, G. M.; Valleau, J. P. Nonphysical Sampling Distributions in Monte Carlo Free-Energy Estimation: Umbrella Sampling. *J. Comput. Phys.* **1977,** *23,* 187–199.
102. Kumar, S.; Rosenberg, J. M.; Bouzida, D.; Swendsen, R. H.; Kollman, P. A. The Weighted Histogram Analysis Method for Free-Energy Calculations on Biomolecules. I. The Method. *J. Comput. Chem.* **1992,** *13,* 1011–1021.
103. Kästner, J.; Thiel, W. Bridging the Gap Between Thermodynamic Integration and Umbrella Sampling Provides a Novel Analysis Method: "Umbrella integration". *J. Chem. Phys.* **2005,** *123,* 144104.
104. Beutler, T. C.; van Gunsteren, W. F. The Computation of a Potential of Mean Force: Choice of the Biasing Potential in the Umbrella Sampling Technique. *J. Chem. Phys.* **1994,** *100,* 1492.
105. Mascarenhas, N. M.; Kästner, J. How Maltose Influences Structural Changes to Bind to Maltose-Binding Protein: Results From Umbrella Sampling Simulation. *Proteins* **2013,** *81,* 185–198.
106. Vargiu, A. V.; Ruggerone, P.; Magistrato, A.; Carloni, P. Sliding of Alkylating Anticancer Drugs Along the Minor Groove of DNA: New Insights on Sequence Selectivity. *Biophys. J.* **2008,** *94,* 550–561.
107. Glover, F. Tabu Search—Part I. *ORSA J. Comput.* **1989,** *1,* 190–206.
108. Cvijovic, D.; Klinowski, J. Taboo Search: An Approach to the Multiple Minima Problem—ProQuest. *Science* **1995,** *267,* 664–666.
109. Huber, T.; Torda, A. E.; van Gunsteren, W. F.; Gunsteren, W. F. Local Elevation: A Method for Improving the Searching Properties of Molecular Dynamics Simulation. *J. Comput. Aided Mol. Des.* **1994,** *8,* 695–708.
110. Grubmüller, H. Predicting Slow Structural Transitions in Macromolecular Systems: Conformational Flooding. *Phys. Rev. E Stat. Phys. Plasmas Fluids Relat. Interdiscip. Top.* **1995,** *52,* 2893–2906.
111. Laio, A.; Parrinello, M. Escaping Free-Energy Minima. *Proc. Natl. Acad. Sci. U. S. A.* **2002,** *99,* 12562–12566.
112. Barducci, A.; Bussi, G.; Parrinello, M. Well-Tempered Metadynamics: A Smoothly Converging and Tunable Free-Energy Method. *Phys. Rev. Lett.* **2008,** *100,* 020603.
113. Dama, J. F.; Parrinello, M.; Voth, G. A. Well-Tempered Metadynamics Converges Asymptotically. *Phys. Rev. Lett.* **2014,** *112,* 240602.
114. Mason, J.; Bortolato, A.; Weiss, D.; Deflorian, F. High End GPCR Design: Crafted Ligand Design and Druggability Analysis Using Protein Structure, Lipophilic Hotspots and Explicit Water Networks. *In Silico Pharmacol.* **2013,** *1,* 1–23.
115. Grubmüller, H.; Heymann, B.; Tavan, P.; Grubmüller, H. Ligand Binding: Molecular Mechanics Calculation of the Streptavidin-Biotin Rupture Force. *Science* **1996,** *271,* 997–999.
116. Izrailev, S.; Stepaniants, S.; Balsera, M.; Oono, Y.; Schulten, K. Molecular Dynamics Study of Unbinding of the Avidin-Biotin Complex. *Biophys. J.* **1997,** *72,* 1568–1581.
117. Jarzynski, C. Nonequilibrium Equality for Free Energy Differences. *Phys. Rev. Lett.* **1997,** *78,* 2690–2693.
118. Hansmann, U. H. E. Parallel Tempering Algorithm for Conformational Studies of Biological Molecules. *Chem. Phys. Lett.* **1997,** *281,* 140–150.
119. Luitz, M. P.; Zacharias, M. Protein-Ligand Docking Using Hamiltonian Replica Exchange Simulations With Soft Core Potentials. *J. Chem. Inf. Model.* **2014,** *54,* 1669–1675.
120. Oleinikovas, V.; Saladino, G.; Cossins, B. P.; Gervasio, F. L. Understanding cryptic pocket formation in protein targets by enhanced sampling simulations. *J. Am. Chem. Soc.* **2016,** *138,* 14257–14263.
121. Hamelberg, D.; Mongan, J.; McCammon, J. A. Accelerated Molecular Dynamics: A Promising and Efficient Simulation Method for Biomolecules. *J. Chem. Phys.* **2004,** *120,* 11919–11929.
122. Wereszczynski, J.; McCammon, J. A. Accelerated Molecular Dynamics in Computational Drug Design. In *Methods;* Baron, R., Ed.; Vol. 819; Springer: New York, 2012; pp 515–524.
123. Markwick, P. R. L.; Cervantes, C. F.; Abel, B. L.; Komives, E. A.; Blackledge, M.; McCammon, J. A. Enhanced Conformational Space Sampling Improves the Prediction of Chemical Shifts in Proteins. *J. Am. Chem. Soc.* **2010,** *132,* 1220–1221.
124. Bussi, G.; Gervasio, F. L.; Laio, A.; Parrinello, M. Free-Energy Landscape for Beta Hairpin Folding From Combined Parallel Tempering and Metadynamics. *J. Am. Chem. Soc.* **2006,** *128,* 13435–13441.
125. Lovera, S.; Sutto, L.; Boubeva, R.; Scapozza, L.; Dölker, N.; Gervasio, F. L. The Different Flexibility of C-Src and C-Abl Kinases Regulates the Accessibility of a Druggable Inactive Conformation. *J. Am. Chem. Soc.* **2012,** *134,* 2496–2499.
126. Lovera, S.; Morando, M.; Pucheta-Martinez, E.; Martinez-Torrecuadrada, J. L.; Saladino, G.; Gervasio, F. L. Towards a Molecular Understanding of the Link Between Imatinib Resistance and Kinase Conformational Dynamics. *PLoS Comput. Biol.* **2015,** *11,* 1004578.
127. Piana, S.; Laio, A. A Bias-Exchange Approach to Protein Folding. *J. Phys. Chem. B* **2007,** *111,* 4553–4559.
128. Bono, F.; et al. Inhibition of Tumor Angiogenesis and Growth by a Small-Molecule Multi-FGF Receptor Blocker With Allosteric Properties. *Cancer Cell* **2013,** *23,* 477–488.
129. Herbert, C.; et al. Molecular Mechanism of SSR128129E, an Extracellularly Acting, Small-Molecule, Allosteric Inhibitor of FGF Receptor Signaling. *Cancer Cell* **2013,** *23,* 489–501.
130. Bonomi, M.; Parrinello, M. Enhanced Sampling in the Well-Tempered Ensemble. *Phys. Rev. Lett.* **2010,** *104,* 1–4.
131. Favia, A. D.; Masetti, M.; Recanatini, M.; Cavalli, A. Substrate Binding Process and Mechanistic Functioning of Type 1 11-Beta-Hydroxysteroid Dehydrogenase From Enhanced Sampling Methods. *PLoS One* **2011,** *6,* 25375.
132. Shan, Y.; Eastwood, M. P.; Zhang, X.; Kim, E. T.; Arkhipov, A.; Dror, R. O.; Jumper, J.; Kuriyan, J.; Shaw, D. E. Oncogenic Mutations Counteract Intrinsic Disorder in the EGFR Kinase and Promote Receptor Dimerization. *Cell* **2012,** *149,* 860–870.
133. Copeland, R. A.; Pompliano, D. L.; Meek, T. D. Drug–Target Residence Time and Its Implications for Lead Optimization. *Nat. Rev. Drug Discov.* **2006,** *5,* 730–739.
134. Copeland, R. A. The Dynamics of Drug-Target Interactions: Drug-Target Residence Time and Its Impact on Efficacy and Safety. *Expert Opin. Drug Discovery* **2010,** *5,* 305–310.
135. Copeland, R. A. The Drug–Target Residence Time Model: A 10-Year Retrospective. *Nat. Rev. Drug Discov.* **2015,** *15,* 87–95.
136. Swinney, D. C. The Role of Binding Kinetics in Therapeutically Useful Drug Action. *Curr. Opin. Drug Discov. Dev.* **2009,** *12,* 31–39.
137. Swinney, D. C. Applications of Binding Kinetics to Drug Discovery Therapeutic Responses. *Pharm. Med.* **2008,** *22,* 23–34.
138. Swinney, D. C.; Anthony, J. How Were New Medicines Discovered? *Nat. Rev. Drug Discov.* **2011,** *10,* 507–519.
139. Vauquelin, G.; Charlton, S. J. Long-Lasting Target Binding and Rebinding as Mechanisms to Prolong In Vivo Drug Action. *Br. J. Pharmacol.* **2010,** *161,* 488–508.
140. Zhang, R.; Monsma, F. The Importance of Drug-Target Residence Time. *Curr. Opin. Drug Discov. Dev.* **2009,** *12,* 488–496.
141. Guo, D.; Hillger, J. M.; IJzerman, A. P.; Heitman, L. H. Drug-Target Residence Time—A Case for G Protein-Coupled Receptors. *Med. Res. Rev.* **2014,** *34,* 856–892.
142. Harvey, M. J.; Giupponi, G.; De Fabritiis, G. ACEMD: Accelerating Biomolecular Dynamics in the Microsecond Time Scale. *J. Chem. Theory Comput.* **2009,** *5,* 1632–1639.

143. Plattner, N.; Noé, F. Protein Conformational Plasticity and Complex Ligand-Binding Kinetics Explored by Atomistic Simulations and Markov Models. *Nat. Commun.* **2015,** *6,* 7653.
144. Tiwary, P.; Limongelli, V.; Salvalaglio, M.; Parrinello, M. Kinetics of Protein–Ligand Unbinding: Predicting Pathways, Rates, and Rate-Limiting Steps. *Proc. Natl. Acad. Sci. U. S. A.* **2015,** *112,* 386.
145. Tiwary, P.; Parrinello, M. From Metadynamics to Dynamics. *Phys. Rev. Lett.* **2013,** *111,* 230602.
146. Mollica, L.; Decherchi, S.; Zia, S. R.; Gaspari, R.; Cavalli, A.; Rocchia, W. Kinetics of Protein-Ligand Unbinding via Smoothed Potential Molecular Dynamics Simulations. *Sci. Rep.* **2015,** *5,* 11539.

3.04 Molecular Dynamics, Quantum Mechanics, and Combined Quantum Mechanics/Molecular Mechanics Methods for Drug Discovery and Development

EJM Lang and AJ Mulholland, University of Bristol, Bristol, United Kingdom

© 2017 Elsevier Ltd. All rights reserved.

3.04.1	**Introduction**	51
3.04.2	**Theoretical Background**	52
3.04.2.1	About MD	52
3.04.2.2	A Brief Overview of the Foundations of Quantum Chemistry	53
3.04.2.3	Hybrid QM/MM Simulations	53
3.04.3	**Accurate, Reliable, Fast, and Easy to Use Methods for Drug Discovery and Development**	54
3.04.3.1	Recent Advances in MD Simulations	54
3.04.3.2	Determination of the Thermodynamics Properties of Protein-Ligand Association	55
3.04.3.3	Chemical Accuracy in QM/MM Calculations: High-Level Ab Initio QM/MM Methods	55
3.04.4	**Examples of Applications**	56
3.04.4.1	Deciphering the Effects of Influenza Virus Mutations on Antiviral Efficiency	56
3.04.4.2	Improving the Design of Covalent Inhibitors	57
3.04.4.3	Tackling Antibiotic Resistance	58
3.04.4.4	Supporting Sustainable Processes in Drug Development and Manufacturing	59
3.04.4.5	Predicting Drug Metabolism	61
3.04.5	**Conclusions**	62
Acknowledgments		63
References		63
Relevant Websites		66

3.04.1 Introduction

Among the computational methods used in drug discovery, virtual screening is probably the most popular approach and has received considerable publicity.[1–3] Yet, despite being an extremely powerful method for screening many compounds in a minimum amount of time, the actual number of projects in which virtual screening has been a key factor in the discovery of a new drug are relatively limited.[4] Several factors might explain this, among which the most critical are perhaps the tendency of users to rely on static models for the receptor and even for the ligands and the fact that virtual screening is plagued by the lack of accuracy in determining the relative binding free energy of a ligand along with the associated entropic and enthalpic contributions.[4,5]

Taking into account protein flexibility is fundamental when attempting to discover potent and selective molecules that can either deactivate or activate a particular protein. Indeed, proteins are dynamic entities and their dynamic behavior is intimately linked to their function.[6,7] Therefore when modeling the affinity of a ligand for a protein, one needs to go past the historical lock-and-key model,[8] which is based on the assumption that proteins are rigid bodies, and account for the dynamics of the binding site (see, e.g., Ref.[9] and references therein). Similarly, when it comes to understanding enzyme catalysis at a molecular level, the effect of dynamics needs to be taken into account.[10–14] For example, an enzymatic reaction can proceed via a high-energy conformation different from the predominant enzyme-ligand complex, that stabilizes greatly the transition state (TS) of the reaction and that is accessible thanks to the enzyme structural fluctuations.[15,16] It is, therefore, crucial to account for protein dynamics when studying protein-ligand binding, enzymatic reactions, or any other processes relevant to drug discovery.

Computational methods such as Molecular Dynamics (MD), Free Energy Perturbation (FEP), Quantum Mechanics (QM), and hybrid Quantum Mechanical/Molecular Mechanical (QM/MM) methods are able to account for protein dynamics and also to provide thermodynamics data that are far more accurate than those obtained from virtual screening or molecular docking. This increased accuracy, however, comes at the cost of an increased computational burden, and thus these methods were often disregarded in drug discovery and development. However, considerable progress in both hardware and software[17–23] make the use of these computational approaches much more amenable to the typical time frame of a computer-aided drug discovery project. Moreover, unlike virtual screening, these methods are not limited to studying ligand binding but can deliver extremely valuable information at the atomic level on the mechanisms involved with specific protein functions, thereby providing the necessary framework for the discovery, design, and improvement of active pharmaceutical ingredients.

In this article, we will first briefly review the theoretical underpinning of MD, QM, and QM/MM and then provide an overview of the recent methodological advances that have increased the accuracy, ease of use, and rapidity of these techniques and that could benefit drug discovery. We will then present a number of case studies that highlight the power of these methods in drug discovery

and development. Since the use of MD and molecular mechanics (MM) based free energy methods in drug discovery has been reviewed in great detail elsewhere (see, e.g., Refs.[17,24–31]), here only a few examples of these approaches will be presented and the focus will be primarily made on the applicability of QM/MM methods. Specifically, we will discuss the use of MD and free energy calculations to deciphering antiviral resistance mechanisms, the application of QM/MM to fighting antimicrobial resistance and designing covalent inhibitors, as well as the use of computational methods to predict drug metabolism and to support sustainable drug development processes. We will then conclude by discussing the advantages and limitations of MD, QM, and QM/MM approaches in drug discovery and development.

3.04.2 Theoretical Background

3.04.2.1 About MD

MD simulation is one of the few techniques able to provide direct information on protein dynamics and has been referred to as the "computational microscope" of biochemistry.[32] Several books and reviews present MD in great detail and describe how this technique is implemented in a computationally efficient and robust manner (see, e.g., Ref.[33–36] and references therein). Here, only the theoretical basis of MD will be summarized.

The central concept of MD simulation relies on Newton's second law:

$$\boldsymbol{F}_i = m_i \boldsymbol{a}_i \tag{1}$$

which states that it is possible to determine the acceleration $\boldsymbol{a}_i$ of a particle i of mass m_i by knowing the force $\boldsymbol{F}_i$ applied on it. Since the force acting on each atom of a macromolecule can be expressed as the first derivative of the potential energy V of the system with respect to the atom position $\boldsymbol{r}_i$, and the acceleration corresponds to the second derivative of the atomic position with respect to the time, Eq. (1) can be rewritten in its differential form as:

$$-\frac{\mathrm{d}V}{\mathrm{d}\boldsymbol{r}_i} = m_i \frac{\mathrm{d}^2 \boldsymbol{r}_i}{\mathrm{d}t^2} \tag{2}$$

For atoms with positions $\boldsymbol{r}_i$ at a specific time t, the position a small time step Δt later is given by a second order Taylor expansion.

$$\boldsymbol{r}_i(t + \Delta t) = \boldsymbol{r}_i(t) + \boldsymbol{v}_i(t)\,\Delta t + \frac{1}{2}\boldsymbol{a}_i(t)\,\Delta t^2 \tag{3}$$

This enables the atomic positions to be calculated numerically after a small time step knowing the position, velocity, and acceleration at time t, the acceleration being obtained with Newton's second law. Therefore, starting from an initial atomic model prepared from X-ray crystallography or NMR data, and from initial velocities obtained from a Boltzmann distribution at a given temperature, a trajectory can be calculated by derivation of the potential energy function with respect to the three-dimensional position of each atom.

However, Eq. (3) is, in fact, a truncated version of the Taylor expansion, which includes higher order terms. These terms cannot be simply ignored, as it would lead to important errors. One computationally efficient way to overcome this is to use the Verlet algorithm or one of its variants. Presently the velocity Verlet algorithm is used in most of the MD simulation packages owing to its improvement over the classical Verlet algorithm and its leap-frog variant. Indeed, the Verlet algorithm uses no explicit velocities and lack of precision, whereas in the leapfrog variant, velocities are explicitly calculated but they are not calculated at the same time as the positions. In contrast, the velocity Verlet algorithm does not compromise on precision and velocities, accelerations, and positions are calculated at the same time t by relying on Eq. (3) and also on Eq. (4), which gives the velocities $\boldsymbol{v}_i$ at a specific time t plus a small time step Δt later.

$$\boldsymbol{v}_i(t + \Delta t) = \boldsymbol{v}_i(t) + \frac{1}{2}[\boldsymbol{a}_i(t) + \boldsymbol{a}_i(t + \Delta t)]\,\Delta t^2 \tag{4}$$

The only missing piece is the potential energy of the system to retrieve the acceleration. Even though potential energy can be calculated using QM in order to take into account electronic effects, this is only possible for small molecules due to the computational resources required. For proteins, the potential energy can be calculated by empirical energy functions based on classical mechanics. Both the energy arising from bonded and from non-bonded interactions should be taken into account as shown in the simplified, typical potential energy function described (adapted from Ref.[28]). Bonded interactions, bond stretching, and angle bending are modeled using harmonic potentials, while the steric barriers (as well as electronic effects, depending on the force field) between atoms separated by three bonds are modeled by a torsion angle potential. Non-bonded interactions are composed of van der Waals interactions, modeled by the Lennard-Jones 6–12 potential, and of electrostatic interactions represented by a Coulomb potential. Parameters used in the potential energy function are determined using both quantum mechanical calculations on small systems and experimental data. The potential energy equation and its parameters are collectively referred to as a force field. Several force fields are available, the most common associated with the simulation packages AMBER,[37] CHARMM,[38] and GROMOS;[39] it is important to distinguish between the force field (parameter set) and the simulation package (which may have similar names). Several generations of forcefields associated with each package have been developed, and can be used with different simulation programs.

$$E_{\text{Total}} = \sum_{\text{Bonds}} K_r\left(r - r_{\text{eq}}\right)^2 + \sum_{\text{Angles}} K_\theta\left(\theta - \theta_{\text{eq}}\right)^2 + \sum_{\text{Dihedrals}} \frac{V_n}{2}\left[1 + cos(n\phi - \gamma)\right] + \sum_{\text{Non-bonded}} \left[\frac{A_{ij}}{R_{ij}^{12}} - \frac{B_{ij}}{R_{ij}^{6}} + \frac{q_i q_j}{\varepsilon R_{ij}}\right] \tag{5}$$

The trajectory of each atom can then be solved numerically using a MD software package such as AMBER,[40] CHARMM,[41] GROMACS,[42,43] GROMOS,[44] or NAMD,[45] all of which are specifically designed to run MD simulations on supercomputer clusters. In addition, MD codes allow the microscopic data (atom positions, velocities, etc.) obtained from the simulation to be linked to macroscopic observables (energy, temperature, pressure, etc.), using statistical mechanics. At this point, it is important to note that MD simulations calculate time averages while the macroscopic observables are assumed to be an ensemble average, therefore, to link the results of a MD simulation to macroscopic data, one should rely on the ergodic hypothesis which states that ensemble average equals time average. To satisfy this equality, MD simulations should be sufficiently long to sample enough representative conformations.

3.04.2.2 A Brief Overview of the Foundations of Quantum Chemistry

The theoretical underpinning and computational implementation of quantum chemistry have been detailed in several classical textbooks (see, e.g., Refs.[33,46,47] and references therein) and here only some of the key concepts are introduced.

Quantum chemistry is typically based on the time-independent Schrödinger equation, which requires a number of approximations to be applied in order to find a solution. The first one, the Born-Oppenheimer approximation, consists in considering the nuclei as fixed in space. Indeed, due to the difference in mass between nuclei and electrons, the electrons will move faster and thus their motion can be considered as being instantaneously equilibrated at each nuclear displacement. This approximation helps to greatly simplify the Schrödinger equation but is not sufficient. The next approximation, the orbital approximation, consists of considering the wave function of a many-electron system as the product of one-electron wave functions called orbitals. In the third approximation, each orbital can be described by a linear combination of a set of atomic orbitals that form a basis set.

These approximations form the basis of the Hartree-Fock (HF) method. HF, however, does not take into account electron correlation, that is, the tendency of electrons to avoid each other, and this omission can lead to significant errors. To overcome this problem, other ab initio methods, such as the second order Møller-Plesset (MP2) method, take into account electron correlation at the cost of an increased computational burden. Density functional theory methods (DFT) have been developed with the objective of approaching the accuracy of the post-HF ab initio methods at a lower computational cost. These methods rely on the electron density distribution instead of the wave function in order to calculate the (ground state) energy. However, the functional linking electron density and energy is not known and the different DFT methods seek to approximate it. Several functionals have been developed, among which B3LYP is probably the most famous. Semi-empirical methods (such as MNDO, AM1, PM3, PM6, DFTB etc.), are the least computationally demanding methods. MNDO-types methods are based on a simplification of the HF method whereas DFTB is based on DFT. Semi-empirical methods are typically the least accurate and rely on experimental correction to improve accuracy. However, utilization of a semi-empirical method on a reaction for which the method has been correctly parameterized can lead to results that approach the reliability of a fraction.

3.04.2.3 Hybrid QM/MM Simulations

QM calculations are particularly intensive from a computational point of view and the required computational power increases significantly with the size of the system. It is therefore typically not feasible to model a complete protein (and surrounding solvent) with QM. However, changes occurring during catalysis are usually confined to a small region of the enzyme with only a few residues directly involved. Therefore, a very powerful approach to study enzymatic reactions is to use a hybrid QM/MM scheme in which the active site and substrates are modeled using a QM level of theory, whereas the rest of the solvated enzyme is modeled at the MM level of theory (Fig. 1). This approach enables to model in a computationally efficient manner the reactions taking place within the active site of an enzyme or any other phenomena in which electrons or polarization are important. QM/MM methods are particularly useful in studies of enzyme-catalyzed reaction mechanisms, but are increasingly also finding application in drug discovery and the award of the 2013 Nobel Prize in Chemistry to Martin Karplus, Michael Levitt, and Arieh Warshel, recognized the importance of QM/MM methods in understanding biological function.[48–50]

QM/MM methods have been presented in great detail in various excellent reviews (see, e.g., Refs.[51–56] and references therein) and we focus here on some of the key aspects of QM/MM.

Hybrid QM/MM approaches for modeling enzyme reactions are based on using a QM method to describe the substrates as well as the residues involved in the reaction and an MM force field to describe the rest of the system. The size of the QM region, that is, which atoms are treated by QM, is a trade-off between accuracy and computational cost: the more atoms added the longer the calculations, but the better the accuracy might be. Usually, the substrates, the residues participating in the reactions (in most of the cases their side chain only) as well as other molecules that might be directly involved in the reaction (metal ions, water molecules, inorganic ions, etc.) are included in the QM region.

The total energy of the system can be expressed as follows in the case of the additive QM/MM approach:

$$E_{\text{Total}} = E_{\text{QM}} + E_{\text{MM}} + E_{\text{QM/MM}} + E_{\text{Boundary}} \tag{6}$$

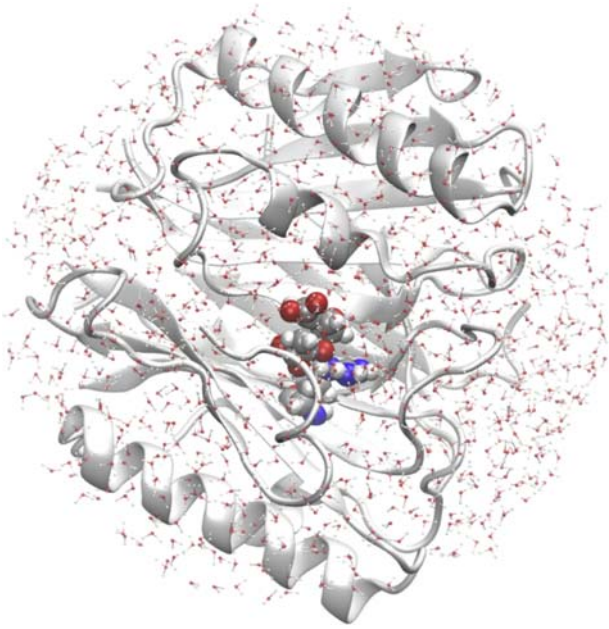

Fig. 1 Typical QM/MM partitioning, illustrated here for chorismate mutase. The protein and water molecules, shown in a *cartoon* and a *balls and sticks* representation respectively, are treated with classical MM, whereas the substrates and relevant active site residues, represented with *spheres*, are treated with QM.

where E_{QM} corresponds to the energy of the QM region, E_{MM} to the energy of the MM region, $E_{Boundary}$ arises from the finite number of atoms in the simulation, and $E_{QM/MM}$ describes the interactions between the QM and MM regions. This term accounts for the electrostatic "embedding" of the QM region within the MM region, allowing the QM region to be affected by the charges of the atoms in the MM region. It also includes van der Waals interactions between QM and MM atoms as well as bounding terms arising when the separation between QM and MM region "cut" a covalent bond (e.g., when only the side chain of a residue is included in the QM region). In this case, the most common approach consists in creating a fictitious link atom (usually a hydrogen atom), which is added along the covalent bond that crosses the QM-MM boundary, so the valence of the QM atom is satisfied. It is important to note that one should avoid "cutting" polar covalent bonds and, when possible, a good choice consists in cutting a C-C bond distant from any functional groups or from the backbone atoms.

There are two main types of QM/MM approaches to model reactions. The first one, adiabatic mapping, essentially relies on performing energy minimization at different values of a reaction coordinate to reconstruct the potential energy surface. The advantage of this approach is that high-level QM methods can be used (ab initio, DFT). The main drawbacks are that the energy minimization can lead to local minima (and thus conformational changes during the reaction cannot be correctly modeled) and the calculations lead to a potential energy profile and not a free energy profile, although the free energy profile can, for example, be estimated by performing frequency calculations in order to include an approximated entropy contribution. The second approach is similar but consists in running MD simulations, more specifically umbrella sampling along the chosen reaction coordinate (QM/MM-MD approach). This has the advantage that it leads to a free energy profile after statistical reweighting of the umbrella sampling trajectories using, for example, the Weighted Histogram Analysis Method, and to a more accurate exploration of the phase space. However, this method requires a large number of calculations of the energy (one per MD step) so only less accurate, semi-empirical methods (e.g., AM1, PM6, SCC-DFTB, etc.) can be used. This can be partially solved by including single point energy calculations along the reaction pathway at a high-level of QM, thereby improving the accuracy of the method.

As conformational and catalytic landscapes are linked and different conformations can lead to different energy profiles of reactions,[10,57,58] it is important several QM/MM calculations starting from slightly different conformations are performed (e.g., obtained from MD simulations) to account for the fact that, in reality, the reactions do not start from a single structure but instead from an ensemble of structures.

3.04.3 Accurate, Reliable, Fast, and Easy to Use Methods for Drug Discovery and Development

3.04.3.1 Recent Advances in MD Simulations

One of the main limitations of MD is the sampling problem: has the simulation run for long enough? If the simulation were to be run for longer, would the results be different? Fortunately, there are various ways to get around this problem. One of the most commonly used approaches is to run several shorter MD simulations starting with different atomic velocities instead of a single

longer simulation. Due to the chaotic nature of MD, these small velocity changes are sufficient to generate completely different trajectories and ultimately lead to a much better sampling of the free energy landscape than a single trajectory.[59]

Another approach, designed to adequately sample the free energy landscape is to run numerous very short simulations, each sampling different parts of the free energy landscape and then to reconstruct the whole process using Markov state models (MSMs).[18,60,61]

Classical all-atom MD can also be modified to access long timescales or sample rare events with reasonable computational resources. These techniques are based on an enhanced sampling of the free energy landscape via various means and include, for example, accelerated MD,[62] metadynamics,[63] or temperature replica-exchange MD[64] among many others.

Methods and protocols designed to address the sampling problems are not the only advances that could benefit drug discovery, the continuous improvements of the various force fields[65–68] with the inclusion of an ever growing number of biologically relevant small molecules, carbohydrates, lipids, and peptides,[69–71] as well as the tools designed to rapidly, automatically, and accurately parameterize any sort of ligands[72–77] can make major differences in the accuracy of MD calculations. In addition, the development of polarizable force fields[78–80] enables to account for the polarizability of molecules in a purely molecular mechanical framework.

3.04.3.2 Determination of the Thermodynamics Properties of Protein-Ligand Association

Free energy calculations[81–83] are an essential element of the molecular modeler toolbox and are used for a wide variety of applications such as calculating solvation energy, binding thermodynamics, or energy changes associated with conformational changes.[84] Of particular interest to drug discovery is the study of molecular recognition and binding using free energy methods that rely on MD, Monte Carlo (MC), or QM/MM for an improved accuracy compared with standard docking experiments that are associated with large errors due to the fact that they do not account for entropy, water effects, electrostatics, and protein flexibility (with the exception of induced fit docking which accounts for some degree of binding site plasticity).

One of the easiest approaches to include protein flexibility is to rely on ensemble-based screening methods in which, for a given protein, an ensemble of structures obtained from MD or MC simulations, NMR experiments, or other approaches are used to dock the compounds of interest.[85–87] This method presents a clear advantage when compared with single conformation docking, but cannot lead to reliable free energy estimates due to the limitations of the scoring functions used in docking. A more accurate estimation of the binding free energies can be obtained using MM combined with continuum solvation models such as Poisson-Boltzmann or generalized Born surface area.[88–90] These approaches are the fastest MD-based methods that provide a fair precision, but they are limited by the large errors on the entropy term which is approximated by normal mode analysis frequency calculations. Alchemical FEP[91,92] (and related free energy methods such as thermodynamic integration) and adaptive biasing force[93] are among the most accurate approaches that can be used in estimating binding free energies and correlate very well with experimental results. In order to facilitate the use and improve even more the accuracy of these high-level free energy simulations, a set of good practices has been proposed,[71,94,95] including the addition of specific geometrical restraints that alleviate the sampling limitations of MD.[96,97] Finally, tools like the Sire molecular simulation package (siremol.org), FESetup[98] that permits a fast and automated setup of the calculations or WaterSwap[99] which enables the calculation of absolute free energies with high accuracy in a simple and efficient way, provide the users with a powerful yet simple framework for running high-level free energy calculations.

Further improvements in terms of accuracy of the free energy methods come from the use of QM and QM/MM approaches[100,101] that enable to account for charge transfer or polarization of the protein-ligand complex. Free energy calculations can now be carried out in a reasonable amount of time with high-level QM/MM methods.[102]

Another approach for studying ligand-protein association consists in running multiple MD simulations in which the ligand is allowed to diffuse without constraints into and from the binding site of the protein and to reconstruct the binding mechanism using MSM.[103,104] This approach is particularly demanding computationally but provides invaluable information on the ligand binding and unbinding pathways as well as on the kinetic and thermodynamic parameters of the phenomenon. Metadynamics has also been successfully used to study binding and unbinding mechanisms and, by following the binding process along representative coordinates and using carefully chosen restraints such as a funnel-shaped harmonic potential, greatly reduces the computational cost of simulations (when compared with unbiased MD binding simulations) while providing detailed mechanistic and thermodynamic insights[105,106] and even recover unbiased kinetic information.[107]

3.04.3.3 Chemical Accuracy in QM/MM Calculations: High-Level Ab Initio QM/MM Methods

Recent progress made in the field of QM/MM makes it possible to predict energy barriers of enzyme-catalyzed reactions with unprecedented accuracy and leads to results in excellent agreement with experimental data.[108] In particular, state-of-the-art QM/MM calculations on chorismate mutase (CM) and *para*-hydroxybenzoate hydroxylase (PHBH)[109] resulted in a calculated activation free energy at 300 K of 13.7 kcal mol^{-1} for PHBH whereas experimental values range between 14 and 15 kcal mol^{-1}, and for CM an activation enthalpy at 300 K of 13.1 kcal mol^{-1} and an entropic contribution of 2.5 kcal mol^{-1}, compared with experimental values of 12.7 and 2.7 kcal mol^{-1} respectively.

In addition, recent pure QM calculations (using linear-scaling DFT) of the reaction catalyzed by CM was in excellent agreement with DFT-based QM/MM calculations for the same reaction,[110] highlighting the fact that QM/MM methods can deliver results similar to large scale QM calculations for a fraction of the computational burden. This work also showed that the MM treatment

of the residues and water molecules, not directly involved in a reaction, correctly approximate the effect of these residues on the reaction.

Methodological developments such as the projector-embedding approach can be applied in combination with QM/MM calculations,[111] and promise an attractive approach for calculations on large biomolecular systems, and makes highly accurate ab initio (e.g. CCSD(T)) calculations of reaction energies and barriers, and other electronic properties.

3.04.4 Examples of Applications

3.04.4.1 Deciphering the Effects of Influenza Virus Mutations on Antiviral Efficiency

Response to the pandemic H1N1-2009 influenza virus led to the massive use of the neuraminidase inhibitors oseltamivir (commercialized under the trade name Tamiflu) and zanamivir (commercialized under the trade name Relenza) which precipitated the appearance of drug-resistant strains of the virus.[112] In order to maintain an arsenal of potent antiviral agents for future pandemics, an in-depth understanding of such resistance mechanisms was required.

Using MD simulations, Woods et al.[113] investigated the molecular basis of drug resistance for neuraminidase mutant I222R and double mutant I223R/H274Y (using N2 numbering, corresponding to H275Y and I223R in the original paper, **Fig. 2**) which dramatically reduce the effectiveness of oseltamivir and to a lesser extend zanamivir.[114,115] Results of this study indicated that while oseltamivir can maintain the 150-loop in a closed conformation in the wild type and I222R mutant, in the I222R/H274Y double mutant, the loss of a key hydrogen bond between the 150-loop and the inhibitor led to the opening of the binding site. The resulting modification of the electrostatic environment that follows this conformational change results in a lower affinity of oseltamivir for its target. It was also shown that the I222R mutation brings about a competitive hydrogen bond that reduces binding affinity. Zanamivir, however, is able to compensate for this by forming a strong hydrogen bond with a neighboring residue thanks to its guanidinium group. The authors then suggested that by designing inhibitors capable of forming strong hydrogen bonds with the 150-loop or with R222, thereby maintaining the closed conformation in the presence of inhibitor, this resistance mechanism should be overcome.

Independently, Chipot and co-workers[116] used FEP calculations to determine the molecular basis of drug resistance in three H1N1-2009 neuraminidase single mutants H274Y, N294S, and Y252H (**Fig. 2**). They found that the resistance in these mutants is caused by water molecules entering the binding site and reorganizing the residues surrounding the active site, thus perturbing the electrostatic environment of the active site. Because of its increased polarity compared with oseltamivir as well as its larger size impeding the entrance of water molecules into the active site, the authors argued that zanamivir is able to maintain a better selectivity toward the mutants than oseltamivir. Finally, the calculated differences in relative binding energy of oseltamivir and zanamivir between the wild-type enzyme and each mutant were in very good agreement with the experimental values, confirming the ability of FEP to provide accurate estimates of free energy changes upon mutation.

The role of water was later confirmed and refined by Woods et al.[117] who ran 500 ns MD simulations of the wild-type, three single mutants (H274Y I222R and S246N) and two double mutants (I222R/H274Y and S246N/H274Y), all complexed with oseltamivir (**Fig. 2**). In the case of the mutants, multiple unbinding and rebinding events took place over the course of the simulations.

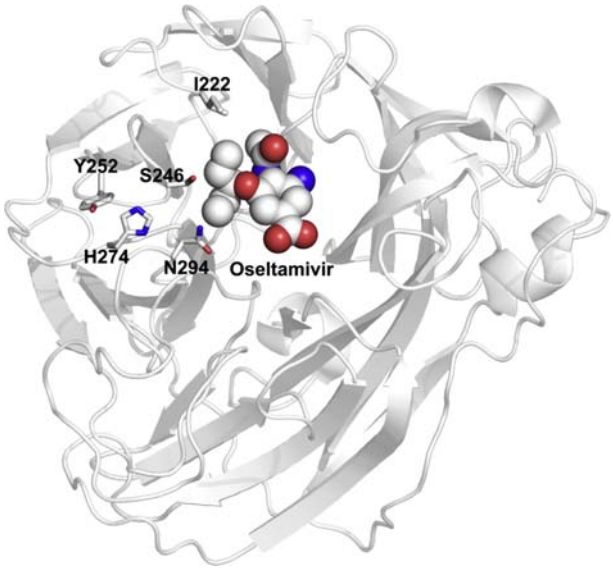

Fig. 2 Monomeric unit of neuraminidase from H1N1-2009 in complex with oseltamivir (represented with *spheres*) PDB ID: 3TI6. Residues which are discussed here are represented with *sticks*.

Careful examination of these unbinding events revealed that the mutations lead to conformational changes that enable bulk water to infiltrate the binding pocket, thereby displacing the drug. In addition, the simulations exposed the role of tightly bound water molecules, in a pocket underneath oseltamivir, as being essential for the binding of the drug. Rebinding kinetic was shown to be strongly affected by the diffusion of excess water molecules out of this pocket, demonstrating the general importance of water in binding and unbinding events. Finally, the study further clarified the role of the 150-loop since the loop opening and closing motions were concomitant with the unbinding and rebinding of oseltamivir respectively. Because oseltamivir resembles the TS of neuraminidase, the authors suggested that the movement of this loop is likely to be functionally important, enabling binding of the substrate and release of the product.

In order to determine whether or not the tightly bound water molecules underneath oseltamivir should be targeted for displacement during ligand design, the absolute QM/MM binding free energy of these water molecules to neuraminidase/ligand complexes (i.e., the free energy difference between the complex containing the water molecule and the complex with an unoccupied water binding site) were calculated. These water molecules being conserved in a range of neuraminidases, the calculations were performed in the N9 variant of neuraminidase[118] for which simulation data of the enzyme in complex with oseltamivir, peramivir (commercialized under the trade name Rapivab), sialic acid, TS analog DANA, and ligand G28 were readily available. QM/MM binding free energy calculations were performed using a MC replica exchange thermodynamic integration QM/MM[102] which enables to greatly improve the treatment of electrostatics when compared to MM approaches. Enzyme and ligands were treated with the AMBER99 force field[119] and the Generalized AMBER Force Field[37] respectively, whereas the QM/MM calculations for the water molecules were performed at the BLYP/aug-cc-pVDZ level for QM and TIP4P[120] level for the MM. Compared to MM free energy calculations, the QM/MM calculations were found to predict a tighter binding of the water molecules, a consequence of the more accurate treatment of electrostatics with QM. Comparison with the same perturbation in solution demonstrated that this effect is important for binding affinity. This study confirmed the importance of a water molecule which presents a strong electrostatic interaction with the protein and thus highlights the importance of taking it into account when designing neuraminidase inhibitors. Moreover, the authors used this as a case study to demonstrate the efficiency and applicability of the used protocol for calculating precise QM/MM binding free energy.

The protocol used to study antiviral resistance in H1N1-2009 proved itself to be extremely valuable to assay the effects of mutation during the H7N9 avian influenza outbreak in 2013. The Effect of the mutation R292K on the binding of oseltamivir, zanamivir, and peramivir was calculated within 2 weeks of H7N9 sequence's availability. MD simulations showed that the R292K mutation altered-drug binding, and WaterSwap[99] calculations confirmed a reduction in absolute binding free energy of the three antivirals for the R292K mutant. The results, submitted 2 months after the first H7N9 cases were reported by the Chinese authorities, compared very well with the experimental results published later that found a weakened binding affinity of all three drugs in the R292K mutants.[121]

3.04.4.2 Improving the Design of Covalent Inhibitors

Despite having a proven track-record of success for a variety of indications, there is a tendency to avoid covalent inhibitors in drug discovery programs, owing to concerns about toxicity, long-lasting effects, and extremely high potency.[122,123] Covalent inhibitors present, however, a number of key advantages over reversible-inhibitors[123,124] and the development of strategies that address the safety and selectivity issues associated with this mode of action has led to the resurgence of covalent inhibitors as drug candidates.[122,125,126]

In order to design highly selective covalent inhibitors, it is crucial to understand the reaction mechanisms, and also the binding modes, of these agents, in particular, the relative orientation between the nucleophilic side chain involved in the covalent bond and the ligand.[126] This sort of information can be provided with great accuracy using QM/MM as it enables the bond formation between the enzyme and the inhibitor to be modeled.

The case of fatty acid amide hydrolase (FAAH) is a striking example of how QM/MM can improve the design of covalent inhibitors. FAAH is responsible for the deactivating hydrolysis of lipid amides and is a promising drug target.[127,128] Carbamic acids, such as URB524 and URB597 (**Fig. 3A**),[129] are potent covalent FAAH inhibitors that react with the active site nucleophile Ser241 (**Fig. 3B**). The exact mechanism by which URB524 and its derivatives are able to carbamoylate Ser241 was, however, unknown. In particular, URB524 can be docked in two possible orientations and previous studies failed to identify the actual biologically relevant binding mode. Lodola et al.[130] investigated the binding mode of URB524 using QM/MM at the PM3/CHARMM22 level and correcting the potential energy by running gas phase QM calculations at the B3LYP/6-31+G(d) level of theory. The resulting B3LYP/6-31+G(d)//PM3-CHARMM22 energy profile showed that only one of the two conformations of URB524 was favorable for the carbamoylation of Ser241, the other conformation leading to higher energy barriers and to an unstable product. This prediction was later confirmed by the crystallographic structure of the FAAH-URB597 carbamoylated adduct,[131] demonstrating the reliability of this QM/MM approach.

In another study on the covalent inhibition of FAAH, Mulholland and co-workers[132] used the same level of QM/MM theory to rationalize experimental results suggesting that FAAH is insensitive to the electron donor effect of conjugated substituents on the biphenyl scaffold of URB524. For the three inhibitors tested in this study, the QM/MM calculations showed that the rate limiting step was always the deprotonation of Ser241 which leads to the formation of a tetrahedral intermediate, that is, the first step of the three-step mechanism characterizing the carbamoylating reaction of Ser241. Electron-donor substituents do not affect significantly the TS of this step as the TS structure is dominated by the proton transfer between Ser241 and Ser217 (**Fig. 3B**). Differential

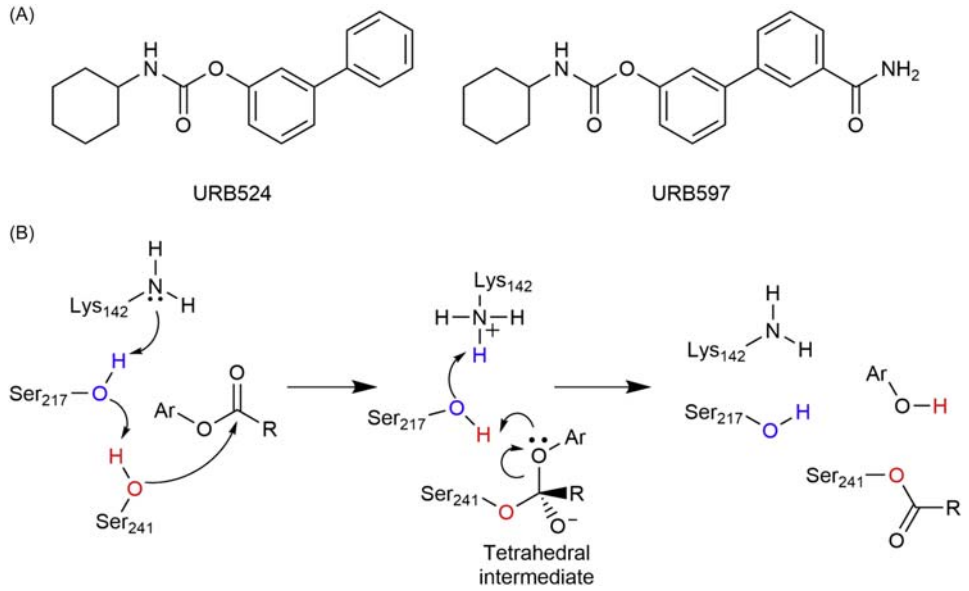

Fig. 3 (A) Structure of carbamic acids URB524 and URB597. (B) Reaction mechanism of Ser241 carbomoylation in FAAH.

transition state stabilization (DTSS), which consists of assessing the contribution of each residue surrounding the TS to its stability,[133,134] performed at the MP2/6-31+G(d) level of theory, revealed that the stabilization of the TS is mainly due to residues involved in the proton transfer reaction. Using QM/MM, the authors were able to demonstrate that the energy barrier of the rate limiting step is not affected by substitutions that greatly affect the pharmacokinetic properties of the carbamates derivatives, thereby opening a new avenue for the development of potent and selective inhibitors presenting an improved absorption, distribution, metabolism, and excretion (ADME) profile.

Further study of the rate limiting step revealed that the tetrahedral intermediate formation in the enzyme (studied at the B3LYP/6-31+G(d)//PM3-CHARMM22 level of QM/MM theory) presents an energy barrier 6 kcal mol^{-1} lower than the reaction in water (studied at the B3LYP/6-31+G(d) level of QM theory). DTSS, at the MP2/6-31+G(d) level of theory, was used to further analyses the active site residues and water molecules responsible for this stabilizing effect. Thr236, Ser218 as well as a conserved water molecule were identified as being the main contributors to TS stabilization. A number of additional residues were found to have a smaller contribution. Multiple sequence alignment confirmed that the key stabilizing residues are also very well conserved across the amidase family. This analysis, which supports the conclusions from QM/MM calculations, revealed that the active site interactions are predominantly electrostatic. Because of this dominance of electrostatic effects, a catalytic field approach[134] was used to identify the regions where significant charge redistribution occurs. These regions, that correspond to the alkyl substituent at the nitrogen atom and the distal phenyl ring, are the most important for modulating the interactions between FAHH and the carbamate derivatives, providing valuable insights for the design of future potent FAAH inhibitors.

Mor and co-workers[135] studied the reactivation mechanism and energetic profile of carbamoylated FAAH using QM/MM calculations at the SCC-DFTB/CHARMM27 level of theory with corrections at the B3LYP/6-31+G(d) level. The authors calculated that decarbamoylation of the covalent FAAH-URB597 adduct involved energy barriers of 28.9 kcal mol^{-1}, to be compared with the 16.6 kcal mol^{-1} barrier calculated for decarbamoylation of FAAH and its oleamide substrate, explaining the irreversible nature of the FAAH inhibition by carbamate derivatives. The authors also found that the secondary carbamic portion of the FAAH-URB597 adduct reduces the active site electrostatic stabilization of the TSs and intermediates, increasing significantly the energy barrier of the reactivation. These results, once again, greatly support the design of novel covalent FAAH inhibitors.

3.04.4.3 Tackling Antibiotic Resistance

Antimicrobial resistance is a global threat to public health and the dramatic increase in the number of bacterial pathogens resistant to multiple antimicrobial agents witnessed over the past decade urges the scientific and medical communities to rapidly identify countermeasures to stop this pandemic.[136–138] Fighting antimicrobial resistance, however, requires a detailed understanding, at a molecular level, of the involved mechanisms, including how drug-resistant pathogens are able to enzymatically alter antimicrobial agents, and QM/MM methods, in particular, can provide extremely valuable insights into these mechanisms. The recent work on carbapenemases provides an excellent illustrative example of how QM/MM can be used to address the antimicrobial resistance problem.

Carbapenems are the most recent class of β-lactam antibiotics and are considered as "last resort" antimicrobial agents for many multi-drug resistant bacterial pathogens, owing to their potency, broad spectrum, and relative stability toward hydrolysis by

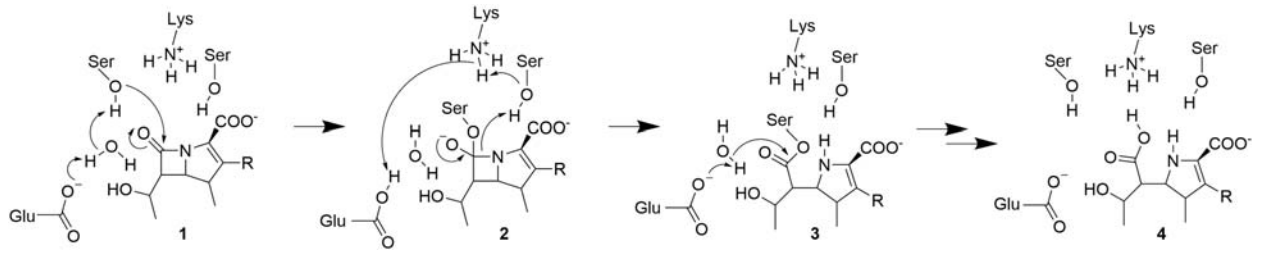

Fig. 4 Reaction mechanism of carbapenems with Class A β-lactamases. Carbapenem (**1**) acylates an active site serine to form the acylenzyme (**3**) via a tetrahedral intermediate (**2**). The acylenzyme can then be broken down via the nucleophilic attack of a deacylating water to release hydrolyzed carbapenems (**4**). Adapted from Fonseca, F., et al. The Basis for Carbapenem Hydrolysis by Class A ß-Lactamases: A Combined Investigation Using Crystallography and Simulations. *J. Am. Chem. Soc.* **2012**, *134* (44), 18275–18285.

β-lactamases. Of particular concern, however, carbapenem-hydrolyzing β-lactamases (carbapenemases) are now spreading among bacteria,[139] threatening to overthrow this last line of defense. The hydrolysis of β-lactam antibiotics in class A β-lactamases takes place firstly via a nucleophilic attack of an active site serine upon the β-lactam amide bond to form a tetrahedral intermediate that yields the acylenzyme.[140] This is then followed by a deacylation step involving the nucleophilic attack of a water molecule activated by an active site glutamate (**Fig. 4**).[141] The acylenzyme is a long-lived species in carbapenem-inhibited β-lactamases,[142] whereas the deacylation occurs rapidly in carbapenem-hydrolyzing β-lactamases. The lack of structural differences that could distinguish carbapenemases from carbapenem-inhibited enzymes prevent the identification of carbapenemases solely based on structural information and requires other approaches to better understand carbapenemase activity in β-lactamases.[143]

Using hybrid QM/MM umbrella sampling calculations, Chudyk et al.[144] have developed a protocol that enables prediction of carbapenemase activity in class A β-lactamases. Starting from the crystal structure of the enzyme, the acylenzyme is modeled based on the acylenzyme complex between carbapenemase SFC-1 and the carbapenem meropenem which has recently been crystallized.[143] Using the AMBER ff12SB/SCC-DFTB[145] level of QM/MM theory, the system is heated, equilibrated and 300 ps of unrestrained QM/MM MD are run from which starting structures for umbrella sampling are extracted using specific criteria that rely partly on previous observations.[143] The QM region consists of the common carbapenem scaffold, the water molecule responsible for the nucleophilic attack, as well as the side chains of the glutamate residue that activate the water and the serine residue covalently bond to the carbapenem moiety. QM/MM umbrella sampling is then performed along two reaction coordinates that capture the proton transfer between the water molecule and the active site glutamate as well as the nucleophilic attack of this water molecule on the carbonyl of the acylenzyme (**Fig. 5**) to generate a two-dimensional free energy surface from which the activation free energy is calculated after identification of the minimum energy path for the reaction. A total of eight different class A β-lactamases were tested using this method and it was found, based on the predicted reaction barriers, that the β-lactamases fell into two distinct groups: one group with energy barriers of about 10 kcal mol^{-1} and a second with barriers around 17–18 kcal mol^{-1}. The lower the activation energy, the more facile the deacylation is, whereas higher barriers indicate long-lived acylenzymes and thus poor carbapenemase activity. Moreover, the calculated energy barriers were in good agreement with experimental data despite a tendency to underestimate barriers, which is a common feature of SCC-DFTB. Overall this method provides a robust computational approach to predict carbapenemase activity in class A β-lactamases and illustrates how QM/MM methods can be used to assay and predict biological activity.

3.04.4.4 Supporting Sustainable Processes in Drug Development and Manufacturing

Over the past decade, the trend in the pharmaceutical industry has increasingly been toward the use of more sustainable methods in drug discovery, development, and manufacturing.[146–148] This approach not only greatly reduces the impact of the pharmaceutical processes on the environment, but it also permits significant cost reductions and improved safety. One of the pillars of green chemistry is to rely when possible on enzyme catalysis,[149–151] however in order to further the use of biocatalysts in the pharmaceutical industry, it is essential to both fully understand the catalytic function of industrially relevant classes of enzymes and be able to design, whenever required, enzymes able to perform a specific reaction. Computational chemistry, in particular, QM and hybrid QM/MM methods, are particularly well suited for these tasks.

In a recent example, hybrid QM/MM modeling was instrumental in identifying for the first time the mechanism of a bona fide natural Diels-Alderase enzyme at the molecular level of details.[152] The Diels-Alder reaction, the [4 + 2] cycloaddition of a conjugated diene to a dienophile that yields a cyclohexene, is one of the most well-known reactions in organic chemistry and has been used in numerous pharmaceuticals, agrochemicals, and fine chemicals manufacturing routes.[153] Nonetheless, despite its potential, Diels-Alder reaction remains underused in the pharmaceutical industry for the development of drug candidates,[154] likely due to the safety challenges that can arise during the scale up of this reaction.[155,156] Therefore, identifying natural enzymes capable of catalyzing Diels-Alder reactions is of prime interest as it would enable to carry out this reaction in a safer and more sustainable way.

Byrne et al.[152] used a combination of experimental and computational methods to demonstrate that the spirotetronate cyclase AbyU catalyzes a Diels-Alder reaction. In order to establish the catalytic mechanism of AbyU, the authors performed an initial

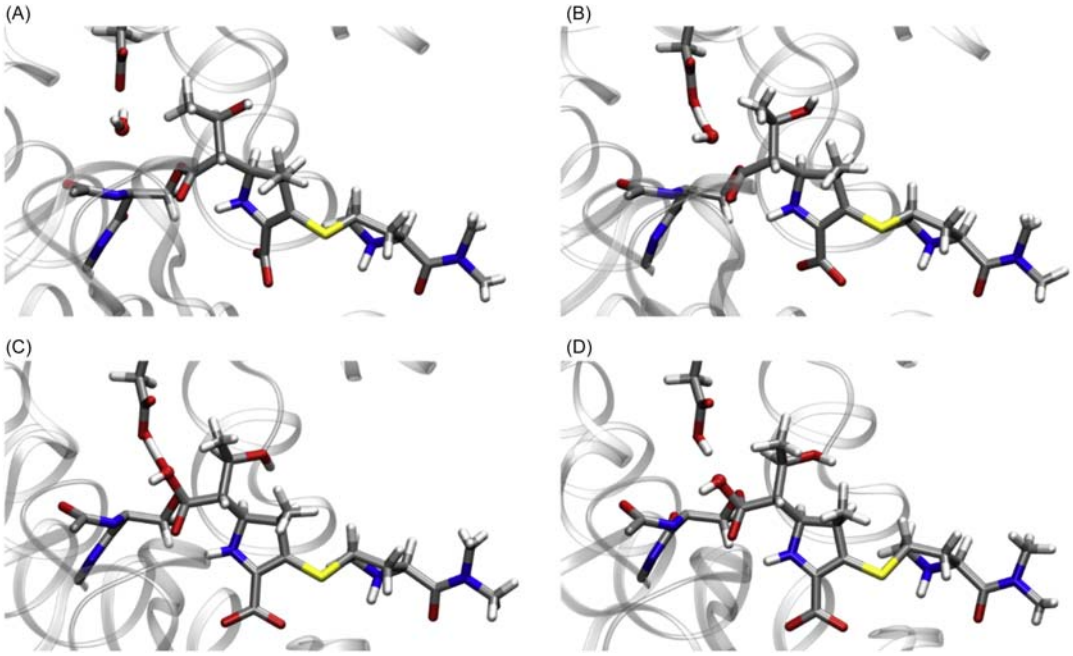

Fig. 5 QM/MM simulation of a molecule of meropenem being broken down by KPC-2 (Class A carbapenemase from *Klebsiella pneumoniae*). (A) An active site glutamate, meropenem, and the deacylating water are represented with *sticks* and the rest of the protein with *ribbons*. The proton transfer from the deacylating water to the active site gultamate (B) is concerted with the nucleophilic attack of this water on the acylenzyme. Transition state is shown in (C) and the resulting tetrahedral intermediate is shown in (D). Adapted from Chudyk, E.I., et al. QM/MM Simulations As an Assay for Carbapenemase Activity in Class A Beta-Lactamases. *Chem. Commun.* **2014**, *50*(94), 14736–14739.

docking of the substrate and product in the crystal structure of the enzyme, demonstrating that the enzyme is able to accommodate the substrate in a reactive conformation. The stability of the binding modes obtained from docking were then confirmed by running MD simulations of the apo, substrate-bound, and product-bound enzyme. QM/MM umbrella sampling simulations at the SCC-DFTB/AMBER f14SB level of theory were then carried out, starting from the product and modeling the reaction in the reverse direction, to investigate the reaction mechanism. Four binding poses were used in the calculation, and for each pose, eight different snapshots obtained from unrestrained QM/MM MD simulations were used to start the umbrella sampling simulations. The results showed that the reaction proceeds via a concerted, asynchronous Diels-Alder mechanism in which one of the C-C bond formation occurs first and represents the energy barrier, whereas the second bond formation occurs essentially after the crossing this energy barrier.

To confirm the TS geometry, electronic structure, and order of bond formation, higher-level DFT calculations were performed in the gas phase. Firstly, the potential energy surface for the reaction in gas phase was obtained following the minimum energy path at the B97D/6-31G(d,p) level of theory, followed by single point energy calculations at the M06-2X/6-31G(d,p) and SCC-DFTB level of theory. High-level DFT calculations (M06-2X/6-31G(d,p)) confirmed the results of the QM/MM simulations and indicated that SCC-DFTB underestimates the energy barrier of the reaction by approximately 7.3 kcal mol^{-1}. The similarity between the gas phase and enzymatic TS suggested that the enzyme essentially orientates the substrate in a reactive conformation allowing the Diels-Alder reaction to proceed via a relatively low free energy barrier. The authors also showed that the enzyme was able to work with non-natural, more stable substrates, and this relative promiscuity coupled with the simplicity of the enzyme makes it an ideal starting point for engineering potent Diels-Alderases.

Another example relevant to industrial biocatalysis is the study by Rommel et al. of the radical reaction catalyzed by glutamate mutase.[157] Using QM/MM at the M06/CHARMM22 level of theory, the authors were able to decipher the mechanism involved in the conversion of glutamate to methylaspartate. They showed that the reaction proceeds via a fragmentation-recombination mechanism involving a rate-limiting hydrogen transfer. By comparing the enzymatic reaction with the solution and gas phase reactions, the authors found that the enzyme influences the reaction electrostatically and, to a lesser extent, sterically and has a stronger impact on the hydrogen transfer steps than on the carbon skeleton rearrangements.

QM and QM/MM methods provide a powerful way to understand reaction mechanisms in known enzyme at a molecular level, but can also be used to engineer enzymes de novo. A good example of such an application is the computational design by Baker and co-workers[158] of an enzyme that catalyzes the Kemp elimination, for which no known naturally occurring enzyme exists. The protocol used by the authors consists in relying on QM calculations to model the theoretical active site which consists in the TS and the catalytic residues that will be the most effective at stabilizing it. Then, using RosettaMatch,[159] the PDB[160] is searched to identify a template that could accommodate the idealized active site. Finally, residues surrounding the TS are mutated and

optimized using RosettaDesign to maximize the stability of the active site and the affinity for the TS. This approach has been successfully applied to various enzymes[161] and represents an attractive and effective way to design de novo enzymes.

3.04.4.5 Predicting Drug Metabolism

Drug metabolism is a key process in which a particular set of enzymes works at deactivating and removing drugs from the organism. This process takes place in two phases, first, the solubility of the drug is increased via the addition of polar groups and is usually carried out by the cytochrome P450 family of enzymes, then an ionizable bulky group is added to the molecule, finishing the deactivation, and making the excretion of the metabolites possible. However, during the first phase of the metabolism, the cytochrome P450 enzymes can generate toxic metabolites that can lead to serious side effects. Similarly, concomitant administration of other drugs or specific food intakes can inhibit the activity of particular P450 enzymes, leading to the detrimental accumulation of an active pharmaceutical ingredient in the organism. It is therefore of crucial, when designing new active pharmaceutical ingredients, to test their ADME properties and computational approaches that can be reliability used to predict drug metabolism are of prime importance. In particular, QM and hybrid QM/MM methods have been successfully used to model the metabolism of several active pharmaceutical ingredients, and to understand the selectivity observed experimentally.[162]

For example, Bathelt et al.[163] used a realistic porphyrin model system to study the mechanism of cytochrome P450 mediated hydroxylation of aromatics compound using the B3LYP level of theory. The authors found that the rate-limiting step was the addition of an aromatic carbon to Compound I (Cpd I, the highly reactive species in P450s capable of oxidizing unactivated C-H bonds and which corresponds to an iron(IV)-oxo porphyrin species, shown in Fig. 6) via a TS with mixed radical and cationic character, whereas the subsequent products formations occur with low energy barriers. In addition, the authors demonstrated that the effect of an aromatic substitution could be predicted thanks to the correlation between the activation energy for Cpd I addition and a combination of radical and cationic Hammett σ-constants.

Bathelt et al.[164] also studied benzene hydroxylation in the more realistic enzyme environment of CYP2C9 using QM/MM at the B3LYP/CHARMM22 level of theory, leading to a calculated energy barrier for the addition of Cpd I to benzene in very good agreement with experimental data. In contrast with gas-phase QM models, the inclusion of the protein environment indicated that face-on and side-on geometries compete during the aromatic addition step. The authors found that in the face-on pathway epoxide and ketone products are formed with comparable ease whereas the side-on pathway tends to favor epoxide formation, providing a good example of the ability of a given CYP enzyme to catalyze different reaction depending on the substrate.[165]

In another example, Lonsdale et al. used QM/MM at the B3LYP-D/CHARM27 level of theory to investigate the CYP-catalyzed hydroxylation of primary amines using the N-hydroxylation of anti-arrhythmic (R)-mexiletine in CYP1A2 as a model reaction.[166] The two potential mechanisms, that is, the direct N-oxidation and the hydrogen abstraction followed by rebound, were modeled for the doublet and quartet spin states of Cpd I. A dispersion correction was added to the B3LYP functional as it was shown to lead to more accurate energy barriers.[167] The calculated barriers indicate that the direct N-oxidation is the preferred mechanism. Moreover, MD simulations revealed that, although not directly involved in the reaction mechanism, a water molecule is particularly important in maintaining (R)-mexiletine in a reactive conformation.

To rationalize experimental results and further the theoretical understanding of selectivity in cytochrome P450s, Mulholland and co-workers explored the oxidation of (S)-ibuprofen, diclofenac, and (S)-warfarin (Fig. 7) by CYP2C9 at different metabolism sites using QM/MM at the B3LYP-D/CHARM27 level of theory.[168] In the case of (S)-ibuprofen, the lower activation barrier was found to be for a hydrogen abstraction at the C3 position rather than at the C2 position, consistent with experimental results. For this

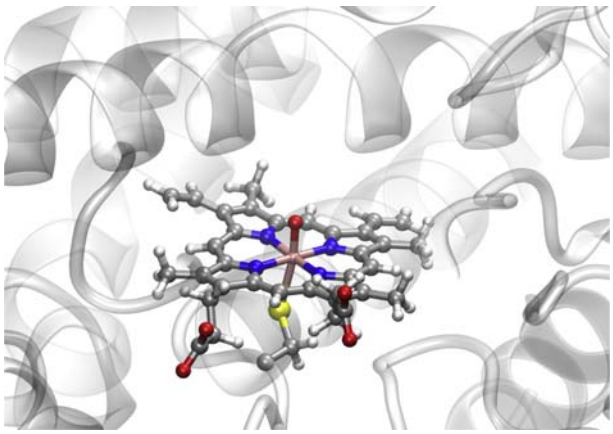

Fig. 6 Compound I modeled in the Cytochrome $P450_{cam}$ from soil bacterium *Pseudomonas putida* (PDB ID: 1DZ9). Compound I and its tethering cysteine residue are represented with *balls* and *sticks*.

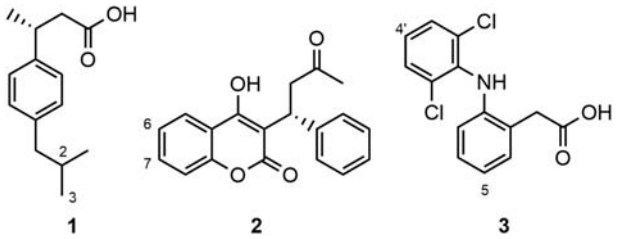

Fig. 7 Structures of (S)-ibuprofen (**1**), (S)-warfarin (**2**), and diclofenac (**3**). Carbon positions discussed in the main text are numbered on each structure.

aliphatic hydroxylation, the role of the enzyme is to promote the regioselectivity of the reaction by restricting the orientation of the substrate and placing C3 at an optimal position and angle for the hydroxylation to take place. In the case of (S)-warfarin, QM/MM calculations predict an aromatic hydroxylation at C7 to be favored, again in agreement with experimental data. As for ibuprofen, the active site residues orient warfarin in a position that promotes the C7 attack, despite C6 being slightly more reactive toward Cpd I. QM/MM study of the hydroxylation of diclofenac suggests an addition in C5, in contrast with experimental results demonstrating a C4′ hydroxylation. This difference was suggested to arise from the fact that the difference in binding energies for the two possible orientations of the substrate is not accounted for in the QM/MM calculations. This hypothesis is supported by the role of Arg108 in stabilizing the binding conformation favoring the C4′ hydroxylation. QM/MM calculations clearly outperformed the QM calculations performed without accounting for the protein, revealing the importance of the active site residues in controlling the selectivity of CYP2C9.

3.04.5 Conclusions

MD simulation, free energy calculations, QM and hybrid QM/MM methods are now well established computational approaches to study protein function and regulation and are becoming increasingly important in drug discovery, design, and development. Software and hardware advances make the use of these methods possible within the timeframe of a typical drug discovery project and new enhanced sampling approaches enable one to access rare events at a fraction of the computational cost previously required to access long timescale dynamics. Improvements in the user-friendliness and methodology of free energy calculations make it a much more accessible tool, enabling one to perform routinely and time-efficiently accurate free energy calculations and to assess the contribution of entropy and enthalpy to the binding free energy. Finally, QM/MM methods have proved to be extremely powerful techniques and highly accurate QM methods can now be applied in QM/MM calculations on enzymes in order to reach "chemical accuracy."

The examples of application presented here provide only a glimpse at the ever growing body of simulations relevant to drug discovery and development. Yet, they demonstrate how MD, free energy, QM and QM/MM methods can be applied in a time-effective and robust manner to support the design of new pharmaceutical agents or to shed light on the molecular mechanisms that govern therapeutically relevant biological processes.

QM/MM methods, in particular, have sometimes been underappreciated in the past. The award of the 2013 Nobel prize in Chemistry, however, has contributed to a renewed interest in this type of multiscale modeling and the advantages QM/MM calculations offer over standard QM or MM approaches have been illustrated above through a number of examples. QM/MM methods can indeed model bond breaking and making, determine likely enzyme mechanisms, identify catalytic and binding interactions, contribute to structure-based design, model covalent inhibition, and drug metabolism and provide more accurate information on binding affinity by taking into account polarization effects.

Computational methods such as those described in this article are not devoid of limitations. It is, for example, almost impossible to sample, using conventional MD, events that take place at the millisecond timescale or above. Drawing conclusions from an under-sampled phase space is also a common error. The number of methods available to compute binding free energy can be daunting and obtaining precise and reliable results that compare well with experimental data requires lengthy calculations. QM/MM methods are limited by the level of QM theory used, and certain methods can yield misleading energy barriers that might lead to qualitatively wrong mechanistic conclusions.

In spite of these limitations, computational modeling using MD, free energy, and/or QM/MM methods is now mature enough to generate invaluable insights into the functionally relevant molecular mechanisms of pharmaceutical targets and provide a clear competitive advantage for the discovery and development of new drugs. As for all computational approaches, these methods can only reach their full potential by being combined with experiment, and it is via the cross-fertilization between molecular modeling and experimental chemistry, biophysics, and biochemistry as well as genetics and molecular biology that the development of the next generation of pharmaceutical compounds will thrive.

Acknowledgments

This work was supported by BBSRC and EPSRC through the BrisSynBio Synthetic Biology Research Centre(BB/L01386X/1). The authors would like to thank Dr Kara Ranaghan, Dr Marc van der Kamp and Dr Christopher Woods for useful discussions regarding the work described here and for their help in preparing some of the figures.

References

1. Kitchen, D. B.; et al. Docking and Scoring in Virtual Screening for Drug Discovery: Methods and Applications. *Nat. Rev. Drug Discov.* **2004,** *3* (11), 935–949.
2. Alvarez, J.; Shoichet, B. *Virtual Screening in Drug Discovery;* CRC Press: Boca Raton, Florida, 2005.
3. Evanthia, L.; et al. Structure-Based Virtual Screening for Drug Discovery: Principles, Applications and Recent Advances. *Curr. Top. Med. Chem.* **2014,** *14* (16), 1923–1938.
4. Schneider, G. Virtual Screening: An Endless Staircase? *Nat. Rev. Drug Discov.* **2010,** *9* (4), 273–276.
5. Forli, S. Charting a Path to Success in Virtual Screening. *Molecules* **2015,** *20* (10), 18732.
6. Henzler-Wildman, K.; Kern, D. Dynamic Personalities of Proteins. *Nature* **2007,** *450* (7172), 964–972.
7. Wei, G.; et al. Protein Ensembles: How Does Nature Harness Thermodynamic Fluctuations for Life? The Diverse Functional Roles of Conformational Ensembles in the Cell. *Chem. Rev.* **2016,** *116* (11), 6516–6551.
8. Fischer, E. Einfluss der Configuration auf die Wirkung der Enzyme. *Ber. Dtsch. Chem. Ges.* **1894,** *27* (3), 2985–2993.
9. Stank, A.; et al. Protein Binding Pocket Dynamics. *Acc. Chem. Res.* **2016,** *49* (5), 809–815.
10. Swint-Kruse, L.; Fisher, H. F. Enzymatic Reaction Sequences As Coupled Multiple Traces on a Multidimensional Landscape. *Trends Biochem. Sci.* **2008,** *33* (3), 104–112.
11. Hammes-Schiffer, S. Catalytic Efficiency of Enzymes: A Theoretical Analysis. *Biochemistry* **2012,** *52* (12), 2012–2020.
12. Glowacki, D. R.; Harvey, J. N.; Mulholland, A. J. Taking Ockham's Razor to Enzyme Dynamics and Catalysis. *Nat. Chem.* **2012,** *4* (3), 169–176.
13. Villali, J.; Kern, D. Choreographing an Enzyme's Dance. *Curr. Opin. Chem. Biol.* **2010,** *14* (5), 636–643.
14. McGeagh, J. D.; Ranaghan, K. E.; Mulholland, A. J. Protein Dynamics and Enzyme Catalysis: Insights From Simulations. *Biochim. Biophys. Acta* **2011,** *1814* (8), 1077–1092.
15. Lodola, A.; et al. Conformational Effects in Enzyme Catalysis: Reaction via a High Energy Conformation in Fatty Acid Amide Hydrolase. *Biophys. J.* **2007,** *92* (2), L20–L22.
16. Lodola, A.; et al. Structural Fluctuations in Enzyme-Catalyzed Reactions: Determinants of Reactivity in Fatty Acid Amide Hydrolase From Multivariate Statistical Analysis of Quantum Mechanics/Molecular Mechanics Paths. *J. Chem. Theory Comput.* **2010,** *6* (9), 2948–2960.
17. Borhani, D. W.; Shaw, D. E. The Future of Molecular Dynamics Simulations in Drug Discovery. *J. Comput. Aided Mol. Des.* **2012,** *26* (1), 15–26.
18. Harvey, M. J.; De Fabritiis, G. High-Throughput Molecular Dynamics: The Powerful New Tool for Drug Discovery. *Drug Discov. Today* **2012,** *17* (19–20), 1059–1062.
19. Harvey, M. J.; De Fabritiis, G. A Survey of Computational Molecular Science Using Graphics Processing Units. *Wiley Interdiscip. Rev. Comput. Mol. Sci.* **2012,** *2* (5), 734–742.
20. Lawrenz, M.; Shukla, D.; Pande, V. S. Cloud Computing Approaches for Prediction of Ligand Binding Poses and Pathways. *Sci. Rep.* **2015,** *5,* 7918.
21. Kohlhoff, K. J.; et al. Cloud-Based Simulations on Google Exacycle Reveal Ligand Modulation of GPCR Activation Pathways. *Nat. Chem.* **2014,** *6* (1), 15–21.
22. Sweet, J. C.; et al. Long Timestep Molecular Dynamics on the Graphical Processing Unit. *J. Chem. Theory Comput.* **2013,** *9* (8), 3267–3281.
23. Luehr, N.; Ufimtsev, I. S.; Martínez, T. J. Dynamic Precision for Electron Repulsion Integral Evaluation on Graphical Processing Units (GPUs). *J. Chem. Theory Comput.* **2011,** *7* (4), 949–954.
24. De Vivo, M.; et al. Role of Molecular Dynamics and Related Methods in Drug Discovery. *J. Med. Chem.* **2016,** *59* (9), 4035–4061.
25. Jorgensen, W. L. Efficient Drug Lead Discovery and Optimization. *Acc. Chem. Res.* **2009,** *42* (6), 724–733.
26. Zhao, H.; Caflisch, A. Molecular Dynamics in Drug Design. *Eur. J. Med. Chem.* **2015,** *91,* 4–14.
27. Mortier, J.; et al. The Impact of Molecular Dynamics on Drug Design: Applications for the Characterization of Ligand–Macromolecule Complexes. *Drug Discov. Today* **2015,** *20* (6), 686–702.
28. Durrant, J.; McCammon, J. A. Molecular Dynamics Simulations and Drug Discovery. *BMC Biol.* **2011,** *9* (1), 71.
29. Salsbury, F. R., Jr. Molecular Dynamics Simulations of Protein Dynamics and Their Relevance to Drug Discovery. *Curr. Opin. Pharmacol.* **2010,** *10* (6), 738–744.
30. Stephen John, F.; et al. The Multifaceted Roles of Molecular Dynamics Simulations in Drug Discovery. *Curr. Pharm. Des.* **2016,** *22* (23), 3585–3600.
31. Stanley, N.; De Fabritiis, G. High Throughput Molecular Dynamics for Drug Discovery. *In Silico Pharmacol.* **2015,** *3* (1), 1–4.
32. Dror, R. O.; et al. Biomolecular Simulation: A Computational Microscope for Molecular Biology. *Annu. Rev. Biophys.* **2012,** *41,* 429–452.
33. Jensen, F. *Introduction to Computational Chemistry;* John Wiley & Sons: Chichester, 2006.
34. Adcock, S. A.; McCammon, J. A. Molecular Dynamics: Survey of Methods for Simulating the Activity of Proteins. *Chem. Rev.* **2006,** *106* (5), 1589–1615.
35. Leach, A. *Molecular Modelling: Principles and Applications,* 2nd ed.; Prentice Hall, 2001.
36. Frenkel, D.; Smit, B. *Understanding Molecular Simulation;* Academic Press, Inc: Orlando, FL, 2001, 638.
37. Wang, J.; et al. Development and Testing of a General Amber Force Field. *J. Comput. Chem.* **2004,** *25* (9), 1157–1174.
38. MacKerell, A. D., Jr.; et al. All-Atom Empirical Potential for Molecular Modeling and Dynamics Studies of Proteins. *J. Phys. Chem. B* **1998,** *102* (18), 3586–3616.
39. Oostenbrink, C.; et al. A Biomolecular Force Field Based on the Free Enthalpy of Hydration and Solvation: The GROMOS Force-Field Parameter Sets 53A5 and 53A6. *J. Comput. Chem.* **2004,** *25* (13), 1656–1676.
40. Case, D. A.; et al. The Amber Biomolecular Simulation Programs. *J. Comput. Chem.* **2005,** *26* (16), 1668–1688.
41. Brooks, B. R.; et al. CHARMM: A Program for Macromolecular Energy, Minimization, and Dynamics Calculations. *J. Comput. Chem.* **1983,** *4* (2), 187–217.
42. Hess, B.; et al. GROMACS 4: Algorithms for Highly Efficient, Load-Balanced, and Scalable Molecular Simulation. *J. Chem. Theory Comput.* **2008,** *4* (3), 435–447.
43. van der Spoel, D.; et al. GROMACS: Fast, Flexible, and Free. *J. Comput. Chem.* **2005,** *26* (16), 1701–1718.
44. Christen, M.; et al. The GROMOS Software for Biomolecular Simulation: GROMOS05. *J. Comput. Chem.* **2005,** *26* (16), 1719–1751.
45. Phillips, J. C.; et al. Scalable Molecular Dynamics With NAMD. *J. Comput. Chem.* **2005,** *26* (16), 1781–1802.
46. Cramer, C. J. *Essentials of Computational Chemistry: Theories and Models,* 2nd ed.; John Wiley & Sons: Chichester, UK; Hoboken, USA, 2004.
47. Hinchliffe, A. *Molecular Modelling for Beginners;* Wiley: Weinheim, 2008.
48. Karplus, M. Development of Multiscale Models for Complex Chemical Systems: From H + H2 to Biomolecules (Nobel Lecture). *Angew. Chem. Int. Ed.* **2014,** *53,* 9992–10005.
49. Levitt, M. Birth and Future of Multiscale Modeling for Macromolecular Systems (Nobel Lecture). *Angew. Chem. Int. Ed.* **2014,** *53,* 10006–10018.
50. Warshel, A. Multiscale Modeling of Biological Functions: From Enzymes to Molecular Machines (Nobel Lecture). *Angew. Chem. Int. Ed.* **2014,** *53* (38), 10020–10031.
51. Lonsdale, R.; Ranaghan, K. E.; Mulholland, A. J. Computational Enzymology. *Chem. Commun.* **2010,** *46* (14), 2354–2372.
52. Ranaghan, K. E.; Mulholland, A. J. Investigations of Enzyme-Catalysed Reactions With Combined Quantum Mechanics/Molecular Mechanics (QM/MM) Methods. *Int. Rev. Phys. Chem.* **2010,** *29* (1), 65–133.
53. Lonsdale, R.; Harvey, J. N.; Mulholland, A. J. A Practical Guide to Modelling Enzyme-Catalysed Reactions. *Chem. Soc. Rev.* **2012,** *41* (8), 3025–3038.
54. van der Kamp, M. W.; Mulholland, A. J. Combined Quantum Mechanics/Molecular Mechanics (QM/MM) Methods in Computational Enzymology. *Biochemistry* **2013,** *52* (16), 2708–2728.
55. Senn, H.; Thiel, W. In *QM/MM Methods for Biological Systems;* Reiher, M., Ed.; Springer: Berlin, Heidelberg, 2007; pp 173–290.

56. Gao, J.; Truhlar, D. G. Quantum Mechanical Methods for Enzyme Kinetics. *Annu. Rev. Phys. Chem.* **2002,** *53* (1), 467–505.
57. Glowacki, D. R.; Harvey, J. N.; Mulholland, A. J. Taking Ockham's Razor to Enzyme Dynamics and Catalysis. *Nat. Chem.* **2012,** *4* (3), 169–176.
58. Benkovic, S. J.; Hammes, G. G.; Hammes-Schiffer, S. Free-Energy Landscape of Enzyme Catalysis. *Biochemistry* **2008,** *47* (11), 3317–3321.
59. Caves, L. S. D.; Evanseck, J. D.; Karplus, M. Locally Accessible Conformations of Proteins: Multiple Molecular Dynamics Simulations of Crambin. *Protein Sci.* **1998,** *7* (3), 649–666.
60. Klenin, K.; et al. Modelling Proteins: Conformational Sampling and Reconstruction of Folding Kinetics. *Biochim. Biophys. Acta* **2011,** *1814* (8), 977–1000.
61. Zwier, M. C.; Chong, L. T. Reaching Biological Timescales With All-Atom Molecular Dynamics Simulations. *Curr. Opin. Pharmacol.* **2010,** *10* (6), 745–752.
62. Hamelberg, D.; Mongan, J.; McCammon, J. A. Accelerated Molecular Dynamics: A Promising and Efficient Simulation Method for Biomolecules. *J. Chem. Phys.* **2004,** *120* (24), 11919–11929.
63. Barducci, A.; Bonomi, M.; Parrinello, M. Metadynamics. *Wiley Interdiscip. Rev. Comput. Mol. Sci.* **2011,** *1* (5), 826–843.
64. Sugita, Y.; Okamoto, Y. Replica-Exchange Molecular Dynamics Method for Protein Folding. *Chem. Phys. Lett.* **1999,** *314* (1–2), 141–151.
65. Huang, J.; MacKerell, A. D. CHARMM36 All-Atom Additive Protein Force Field: Validation Based on Comparison to NMR Data. *J. Comput. Chem.* **2013,** *34* (25), 2135–2145.
66. Zhu, X.; Lopes, P. E. M.; MacKerell, A. D. Recent Developments and Applications of the CHARMM Force Fields. *Wiley Interdiscip. Rev. Comput. Mol. Sci.* **2012,** *2* (1), 167–185.
67. Wang, Q.; et al. General Model for Treating Short-Range Electrostatic Penetration in a Molecular Mechanics Force Field. *J. Chem. Theory Comput.* **2015,** *11* (6), 2609–2618.
68. Betz, R. M.; Walker, R. C. Paramfit: Automated Optimization of Force Field Parameters for Molecular Dynamics Simulations. *J. Comput. Chem.* **2015,** *36* (2), 79–87.
69. Vanommeslaeghe, K.; et al. CHARMM General Force Field: A Force Field for Drug-Like Molecules Compatible With the CHARMM All-Atom Additive Biological Force Fields. *J. Comput. Chem.* **2010,** *31* (4), 671–690.
70. Jämbeck, J. P. M.; Lyubartsev, A. P. Update to the General Amber Force Field for Small Solutes With an Emphasis on Free Energies of Hydration. *J. Phys. Chem. B* **2014,** *118* (14), 3793–3804.
71. Wang, L.; et al. Accurate and Reliable Prediction of Relative Ligand Binding Potency in Prospective Drug Discovery by Way of a Modern Free-Energy Calculation Protocol and Force Field. *J. Am. Chem. Soc.* **2015,** *137* (7), 2695–2703.
72. Zoete, V.; et al. SwissParam: A Fast Force Field Generation Tool for Small Organic Molecules. *J. Comput. Chem.* **2011,** *32* (11), 2359–2368.
73. Yesselman, J. D.; et al. MATCH: An Atom-Typing Toolset for Molecular Mechanics Force Fields. *J. Comput. Chem.* **2012,** *33* (2), 189–202.
74. Vanommeslaeghe, K.; MacKerell, A. D. Automation of the CHARMM General Force Field (CGenFF) I: Bond Perception and Atom Typing. *J. Chem. Inf. Model.* **2012,** *52* (12), 3144–3154.
75. Vanommeslaeghe, K.; Raman, E. P.; MacKerell, A. D., Jr. Automation of the CHARMM General Force Field (CGenFF) II: Assignment of Bonded Parameters and Partial Atomic Charges. *J. Chem. Inf. Model.* **2012,** *52* (12), 3155–3168.
76. Mayne, C. G.; et al. Rapid Parameterization of Small Molecules Using the Force Field Toolkit. *J. Comput. Chem.* **2013,** *34* (32), 2757–2770.
77. Huang, L.; Roux, B. Automated Force Field Parameterization for Nonpolarizable and Polarizable Atomic Models Based on Ab Initio Target Data. *J. Chem. Theory Comput.* **2013,** *9* (8), 3543–3556.
78. Baker, C. M. Polarizable Force Fields for Molecular Dynamics Simulations of Biomolecules. *Wiley Interdiscip. Rev. Comput. Mol. Sci.* **2015,** *5* (2), 241–254.
79. Shi, Y.; et al. Polarizable Atomic Multipole-Based AMOEBA Force Field for Proteins. *J. Chem. Theory Comput.* **2013,** *9* (9), 4046–4063.
80. Lemkul, J. A.; et al. An Empirical Polarizable Force Field Based on the Classical Drude Oscillator Model: Development History and Recent Applications. *Chem. Rev.* **2016,** *116* (9), 4983–5013.
81. Kollman, P. Free Energy Calculations: Applications to Chemical and Biochemical Phenomena. *Chem. Rev.* **1993,** *93* (7), 2395–2417.
82. Christ, C. D.; Mark, A. E.; van Gunsteren, W. F. Basic Ingredients of Free Energy Calculations: A Review. *J. Comput. Chem.* **2010,** *31* (8), 1569–1582.
83. van Gunsteren, W. F.; Daura, X.; Mark, A. E. Computation of Free Energy. *Helv. Chim. Acta* **2002,** *85* (10), 3113–3129.
84. Hansen, N.; van Gunsteren, W. F. Practical Aspects of Free-Energy Calculations: A Review. *J. Chem. Theory Comput.* **2014,** *10* (7), 2632–2647.
85. Wereszczynski, J.; McCammon, J. A. Statistical Mechanics and Molecular Dynamics in Evaluating Thermodynamic Properties of Biomolecular Recognition. *Q. Rev. Biophys.* **2012,** *45* (01), 1–25.
86. Feixas, F.; et al. Exploring the Role of Receptor Flexibility in Structure-Based Drug Discovery. *Biophys. Chem.* **2014,** *186,* 31–45.
87. von Grafenstein, S.; Fuchs, E. J.; Liedl, R. K. (How to) Profit From Molecular Dynamics-Based Ensemble Docking. In *Application of Computational Techniques in Pharmacy and Medicine;* Gorb, L., Kuz'min, V., Muratov, E., Eds.; Springer: Netherlands, Dordrecht, 2014; pp 501–538.
88. Rastelli, G.; et al. Fast and Accurate Predictions of Binding Free Energies Using MM-PBSA and MM-GBSA. *J. Comput. Chem.* **2010,** *31* (4), 797–810.
89. Junmei, W.; Tingjun, H.; Xiaojie, X. Recent Advances in Free Energy Calculations With a Combination of Molecular Mechanics and Continuum Models. *Curr. Comput. Aided-Drug Des.* **2006,** *2* (3), 287–306.
90. Kollman, P. A.; et al. Calculating Structures and Free Energies of Complex Molecules: Combining Molecular Mechanics and Continuum Models. *Acc. Chem. Res.* **2000,** *33* (12), 889–897.
91. Chodera, J. D.; et al. Alchemical Free Energy Methods for Drug Discovery: Progress and Challenges. *Curr. Opin. Struct. Biol.* **2011,** *21* (2), 150–160.
92. Mobley, D. L.; Klimovich, P. V. Perspective: Alchemical Free Energy Calculations for Drug Discovery. *J. Chem. Phys.* **2012,** *137* (23), 230901–230912.
93. Comer, J.; et al. The Adaptive Biasing Force Method: Everything You Always Wanted to Know but Were Afraid to Ask. *J. Phys. Chem. B* **2015,** *119,* 1129–1151.
94. Chipot, C. Frontiers in Free-Energy Calculations of Biological Systems. *Wiley Interdiscip. Rev. Comput. Mol. Sci.* **2014,** *4* (1), 71–89.
95. Pohorille, A.; Jarzynski, C.; Chipot, C. Good Practices in Free-Energy Calculations. *J. Phys. Chem. B* **2010,** *114* (32), 10235–10253.
96. Gumbart, J. C.; Roux, B.; Chipot, C. Standard Binding Free Energies From Computer Simulations: What Is the Best Strategy? *J. Chem. Theory Comput.* **2012,** *9* (1), 794–802.
97. Gumbart, J. C.; Roux, B.; Chipot, C. Efficient Determination of Protein–Protein Standard Binding Free Energies From First Principles. *J. Chem. Theory Comput.* **2013,** *9* (8), 3789–3798.
98. Loeffler, H. H.; Michel, J.; Woods, C. FESetup: Automating Setup for Alchemical Free Energy Simulations. *J. Chem. Inf. Model.* **2015,** *55* (12), 2485–2490.
99. Woods, C. J.; et al. A Water-Swap Reaction Coordinate for the Calculation of Absolute Protein–Ligand Binding Free Energies. *J. Chem. Phys.* **2011,** *134* (5), 054114.
100. Shaw, K. E.; et al. QM and QM/MM Approaches to Evaluating Binding Affinities. In *Burger's Medicinal Chemistry and Drug Discovery;* John Wiley & Sons, Inc: Hoboken, NJ, 2003.
101. Ryde, U.; Söderhjelm, P. Ligand-Binding Affinity Estimates Supported by Quantum-Mechanical Methods. *Chem. Rev.* **2016,** *116* (9), 5520–5566.
102. Woods, C. J.; Manby, F. R.; Mulholland, A. J. An Efficient Method for the Calculation of Quantum Mechanics/Molecular Mechanics Free Energies. *J. Chem. Phys.* **2008,** *128* (1), 014109.
103. Buch, I.; Giorgino, T.; De Fabritiis, G. Complete Reconstruction of an Enzyme-Inhibitor Binding Process by Molecular Dynamics Simulations. *Proc. Natl. Acad. Sci.* **2011,** *108* (25), 10184–10189.
104. Plattner, N.; Noé, F. Protein Conformational Plasticity and Complex Ligand-Binding Kinetics Explored by Atomistic Simulations and Markov Models. *Nat. Commun.* **2015,** *6,* 7653.
105. Limongelli, V.; et al. Sampling Protein Motion and Solvent Effect During Ligand Binding. *Proc. Natl. Acad. Sci.* **2012,** *109* (5), 1467–1472.
106. Limongelli, V.; Bonomi, M.; Parrinello, M. Funnel Metadynamics As Accurate Binding Free-Energy Method. *Proc. Natl. Acad. Sci.* **2013,** *110* (16), 6358–6363.
107. Tiwary, P.; et al. Kinetics of Protein–Ligand Unbinding: Predicting Pathways, Rates, and Rate-Limiting Steps. *Proc. Natl. Acad. Sci.* **2015,** *112* (5), E386–E391.
108. Mulholland, A. J. Chemical Accuracy in QM/MM Calculations on Enzyme-Catalysed Reactions. *Chem. Cent. J.* **2007,** *1* (1), 1–5.
109. Claeyssens, F.; et al. High-Accuracy Computation of Reaction Barriers in Enzymes. *Angew. Chem. Int. Ed.* **2006,** *45* (41), 6856–6859.

110. Lever, G.; et al. Large-Scale Density Functional Theory Transition State Searching in Enzymes. *J. Phys. Chem. Lett.* **2014,** *5* (21), 3614–3619.
111. Bennie, S. J.; et al. A Projector-Embedding Approach for Multiscale Coupled-Cluster Calculations Applied to Citrate Synthase. *J. Chem. Theory Comput.* **2016,** *12* (6), 2689–2697.
112. Hurt, A. C.; et al. Antiviral Resistance During the 2009 Influenza A H1N1 Pandemic: Public Health, Laboratory, and Clinical Perspectives. *Lancet Infect. Dis.* **2012,** *12* (3), 240–248.
113. Woods, C. J.; et al. Long Time Scale GPU Dynamics Reveal the Mechanism of Drug Resistance of the Dual Mutant I223R/H275Y Neuraminidase From H1N1-2009 Influenza Virus. *Biochemistry* **2012,** *51* (21), 4364–4375.
114. van der Vries, E.; Stelma, F. F.; Boucher, C. A. B. Emergence of a Multidrug-Resistant Pandemic Influenza A (H1N1) Virus. *N. Engl. J. Med.* **2010,** *363* (14), 1381–1382.
115. Nguyen, H. T.; et al. Recovery of a Multidrug-Resistant Strain of Pandemic Influenza A 2009 (H1N1) Virus Carrying a Dual H275Y/I223R Mutation From a Child After Prolonged Treatment With Oseltamivir. *Clin. Infect. Dis.* **2010,** *51* (8), 983–984.
116. Vergara-Jaque, A.; et al. Molecular Basis of Drug Resistance in A/H1N1 Virus. *J. Chem. Inf. Model.* **2012,** *52* (10), 2650–2656.
117. Woods, C. J.; et al. Analysis and Assay of Oseltamivir-Resistant Mutants of Influenza Neuraminidase via Direct Observation of Drug Unbinding and Rebinding in Simulation. *Biochemistry* **2013,** *52* (45), 8150–8164.
118. Woods, C. J.; Shaw, K. E.; Mulholland, A. J. Combined Quantum Mechanics/Molecular Mechanics (QM/MM) Simulations for Protein–Ligand Complexes: Free Energies of Binding of Water Molecules in Influenza Neuraminidase. *J. Phys. Chem. B* **2015,** *119* (3), 997–1001.
119. Wang, J.; Cieplak, P.; Kollman, P. A. How Well Does a Restrained Electrostatic Potential (RESP) Model Perform in Calculating Conformational Energies of Organic and Biological Molecules? *J. Comput. Chem.* **2000,** *21* (12), 1049–1074.
120. Jorgensen, W. L.; et al. Comparison of Simple Potential Functions for Simulating Liquid Water. *J. Chem. Phys.* **1983,** *79* (2), 926–935.
121. Yen, H.-L.; et al. Resistance to Neuraminidase Inhibitors Conferred by an R292K Mutation in a Human Influenza Virus H7N9 Isolate Can Be Masked by a Mixed R/K Viral Population. *mBio* **2013,** *4* (4), e00396–e00413.
122. Singh, J.; et al. The Resurgence of Covalent Drugs. *Nat. Rev. Drug Discov.* **2011,** *10* (4), 307–317.
123. Kalgutkar, A. S.; Dalvie, D. K. Drug Discovery for a New Generation of Covalent Drugs. *Expert Opin. Drug Discovery* **2012,** *7* (7), 561–581.
124. Bauer, R. A. Covalent Inhibitors in Drug Discovery: From Accidental Discoveries to Avoided Liabilities and Designed Therapies. *Drug Discov. Today* **2015,** *20* (9), 1061–1073.
125. Johnson, D. S.; Weerapana, E.; Cravatt, B. F. Strategies for Discovering and Derisking Covalent, Irreversible Enzyme Inhibitors. *Future Med. Chem.* **2010,** *2* (6), 949–964.
126. Mah, R.; Thomas, J.; Shafer, C. Drug Discovery Considerations in the Development of Covalent Inhibitors. *Bioorg. Med. Chem. Lett.* **2014,** *24* (1), 33–39.
127. Cravatt, B. F.; Lichtman, A. H. Fatty Acid Amide Hydrolase: An Emerging Therapeutic Target in the Endocannabinoid System. *Curr. Opin. Chem. Biol.* **2003,** *7* (4), 469–475.
128. Piomelli, D. The Molecular Logic of Endocannabinoid Signalling. *Nat. Rev. Neurosci.* **2003,** *4* (11), 873–884.
129. Piomelli, D.; et al. Pharmacological Profile of the Selective FAAH Inhibitor KDS-4103 (URB597). *CNS Drug Rev.* **2006,** *12* (1), 21–38.
130. Lodola, A.; et al. Identification of Productive Inhibitor Binding Orientation in Fatty Acid Amide Hydrolase (FAAH) by QM/MM Mechanistic Modelling. *Chem. Commun.* **2008,** *2,* 214–216.
131. Mileni, M.; et al. Crystal Structure of Fatty Acid Amide Hydrolase Bound to the Carbamate Inhibitor URB597: Discovery of a Deacylating Water Molecule and Insight Into Enzyme Inactivation. *J. Mol. Biol.* **2010,** *400* (4), 743–754.
132. Lodola, A.; et al. Understanding the Role of Carbamate Reactivity in Fatty Acid Amide Hydrolase Inhibition by QM/MM Mechanistic Modelling. *Chem. Commun.* **2011,** *47* (9), 2517–2519.
133. Szefczyk, B.; et al. Differential Transition-State Stabilization in Enzyme Catalysis: Quantum Chemical Analysis of Interactions in the Chorismate Mutase Reaction and Prediction of the Optimal Catalytic Field. *J. Am. Chem. Soc.* **2004,** *126* (49), 16148–16159.
134. Sokalski, W. A. The Physical Nature of Catalytic Activity Due to the Molecular Environment in Terms of Intermolecular Interaction Theory: Derivation of Simplified Models. *J. Mol. Catal.* **1985,** *30* (3), 395–410.
135. Lodola, A.; et al. Quantum Mechanics/Molecular Mechanics Modeling of Fatty Acid Amide Hydrolase Reactivation Distinguishes Substrate From Irreversible Covalent Inhibitors. *J. Med. Chem.* **2013,** *56* (6), 2500–2512.
136. Levy, S. B.; Marshall, B. Antibacterial Resistance Worldwide: Causes, Challenges and Responses. *Nat. Med.* **2004,** *10,* S122–S129.
137. Roca, I.; et al. The Global Threat of Antimicrobial Resistance: Science for Intervention. *New Microbes New Infect.* **2015,** *6,* 22–29.
138. Holmes, A. H.; et al. Understanding the Mechanisms and Drivers of Antimicrobial Resistance. *Lancet* **2016,** *387* (10014), 176–187.
139. World Health Organziation (WHO): Antimicrobial Resistance: Global Report on Surveilance. **2014**.
140. Hermann, J. C.; et al. High Level QM/MM Modeling of the Formation of the Tetrahedral Intermediate in the Acylation of Wild Type and K73A Mutant TEM-1 Class A Beta-Lactamase. *J. Phys. Chem. A* **2009,** *113* (43), 11984–11994.
141. Hermann, J. C.; et al. Molecular Mechanisms of Antibiotic Resistance: QM/MM Modelling of Deacylation in a Class A Beta-Lactamase. *Org. Biomol. Chem.* **2006,** *4* (2), 206–210.
142. Mourey, L.; et al. Inhibition of the NMC-A Beta-Lactamase by a Penicillanic Acid Derivative and the Structural Bases for the Increase in Substrate Profile of This Antibiotic Resistance Enzyme. *J. Am. Chem. Soc.* **1998,** *120* (36), 9382–9383.
143. Fonseca, F.; et al. The Basis for Carbapenem Hydrolysis by Class A Beta-Lactamases: A Combined Investigation Using Crystallography and Simulations. *J. Am. Chem. Soc.* **2012,** *134* (44), 18275–18285.
144. Chudyk, E. I.; et al. QM/MM Simulations As an Assay for Carbapenemase Activity in Class A Beta-Lactamases. *Chem. Commun.* **2014,** *50* (94), 14736–14739.
145. Elstner, M.; et al. Self-Consistent-Charge Density-Functional Tight-Binding Method for Simulations of Complex Materials Properties. *Phys. Rev. B* **1998,** *58* (11), 7260–7268.
146. Dunn, P. J.; Wells, A.; Williams, M. T. *Green Chemistry in the Pharmaceutical Industry;* John Wiley & Sons, 2010.
147. Tucker, J. L. Green Chemistry, a Pharmaceutical Perspective. *Org. Process Res. Dev.* **2006,** *10* (2), 315–319.
148. Tucker, J. L.; Faul, M. M. Industrial Research: Drug Companies Must Adopt Green Chemistry. *Nature* **2016,** *534* (7605), 27–29.
149. Wohlgemuth, R. Biocatalysis—Key to Sustainable Industrial Chemistry. *Curr. Opin. Biotechnol.* **2010,** *21* (6), 713–724.
150. Dunn, P. J. The Importance of Green Chemistry in Process Research and Development. *Chem. Soc. Rev.* **2012,** *41* (4), 1452–1461.
151. Woodley, J. M. New Opportunities for Biocatalysis: Making Pharmaceutical Processes Greener. *Trends Biotechnol.* **2008,** *26* (6), 321–327.
152. Byrne, M. J.; et al. The Catalytic Mechanism of a Natural Diels–Alderase Revealed in Molecular Detail. *J. Am. Chem. Soc.* **2016,** *138* (19), 6095–6098.
153. Funel, J.-A.; Abele, S. Industrial Applications of the Diels–Alder Reaction. *Angew. Chem. Int. Ed.* **2013,** *52* (14), 3822–3863.
154. Carey, J. S.; et al. Analysis of the Reactions Used for the Preparation of Drug Candidate Molecules. *Org. Biomol. Chem.* **2006,** *4* (12), 2337–2347.
155. Funel, J.-A.; Schmidt, G.; Abele, S. Design and Scale-Up of Diels–Alder Reactions for the Practical Synthesis of 5-Phenylbicyclo[2.2.2]oct-5-en-2-one. *Org. Process Res. Dev.* **2011,** *15* (6), 1420–1427.
156. Abele, S.; et al. Safety Assessment of Diels–Alder Reactions With Highly Reactive Acrylic Monomers. *Org. Process Res. Dev.* **2012,** *16* (12), 2015–2020.
157. Rommel, J. B.; Kästner, J. The Fragmentation–Recombination Mechanism of the Enzyme Glutamate Mutase Studied by QM/MM Simulations. *J. Am. Chem. Soc.* **2011,** *133* (26), 10195–10203.
158. Rothlisberger, D.; et al. Kemp Elimination Catalysts by Computational Enzyme Design. *Nature* **2008,** *453* (7192), 190–195.
159. Zanghellini, A.; et al. New Algorithms and an In Silico Benchmark for Computational Enzyme Design. *Protein Sci.* **2006,** *15* (12), 2785–2794.
160. Berman, H. M.; et al. The Protein Data Bank. *Nucleic Acids Res.* **2000,** *28* (1), 235–242.
161. Kiss, G.; et al. Computational Enzyme Design. *Angew. Chem. Int. Ed.* **2013,** *52* (22), 5700–5725.
162. Lonsdale, R.; Mulholland, A. J. QM/MM Modelling of Drug-Metabolizing Enzymes. *Curr. Top. Med. Chem.* **2014,** *14* (11), 1339–1347.

163. Bathelt, C. M.; et al. Mechanism and Structure-Reactivity Relationships for Aromatic Hydroxylation by Cytochrome P450. *Org. Biomol. Chem.* **2004,** *2* (20), 2998–3005.
164. Bathelt, C. M.; Mulholland, A. J.; Harvey, J. N. QM/MM Modeling of Benzene Hydroxylation in Human Cytochrome P450 2C9. *J. Phys. Chem. A* **2008,** *112* (50), 13149–13156.
165. Harvey, J. N.; Bathelt, C. M.; Mulholland, A. J. QM/MM Modeling of Compound I Active Species in Cytochrome P450, Cytochrome C Peroxidase, and Ascorbate Peroxidase. *J. Comput. Chem.* **2006,** *27* (12), 1352–1362.
166. Lonsdale, R.; et al. Quantum Mechanics/Molecular Mechanics Modeling of Drug Metabolism: Mexiletine N-Hydroxylation by Cytochrome P450 1A2. *Chem. Res. Toxicol.* **2016,** *29* (6), 963–971.
167. Rydberg, P.; et al. Trends in Predicted Chemoselectivity of Cytochrome P450 Oxidation: B3LYP Barrier Heights for Epoxidation and Hydroxylation Reactions. *J. Mol. Graph. Model.* **2014,** *52,* 30–35.
168. Lonsdale, R.; et al. Quantum Mechanics/Molecular Mechanics Modeling of Regioselectivity of Drug Metabolism in Cytochrome P450 2C9. *J. Am. Chem. Soc.* **2013,** *135* (21), 8001–8015.

Relevant Websites

http://siremol.org/—Sire: An advanced, multiscale, molecular simulation framework—Includes WaterSwap and QM/MM free energy calculations packages.
http://www.hecbiosim.ac.uk/fesetup#fes—FESetup—A tool to easily setup alchemical free energy perturbation calculations.
http://www.nobelprize.org/nobel_prizes/chemistry/laureates/2013/—Nobel Prize in Chemistry 2013—More information on the Nobel prize winners.
http://www.alchemistry.org/wiki/Main_Page—Alchemistry wiki—Useful information on MM alchemical free energy calculations.

3.05 Progress in the Understanding of Traditional and Nontraditional Molecular Interactions

Robin Taylor, Cambridge Crystallographic Data Centre, Cambridge, United Kingdom

© 2017 Elsevier Ltd. All rights reserved.

3.05.1	**Introduction**	68
3.05.2	**Background**	68
3.05.2.1	Methods	68
3.05.2.2	The Components of a Molecular Interaction	70
3.05.2.3	Water Is the Driving Force of All Nature	70
3.05.2.4	Enthalpy–Entropy Compensation	71
3.05.3	**Molecular Interactions or Emperor's New Clothes?**	71
3.05.3.1	The Diversification of the Hydrogen Bond	71
3.05.3.2	Every Atom Has to Be Somewhere	72
3.05.3.3	Assessing the Relative Importance of Molecular Interactions	72
3.05.4	**The Major Types of Molecular Interactions**	73
3.05.4.1	An Abridged Guide to Hydrogen Bonding	73
3.05.4.2	Interactions Involving Aromatic Rings	74
3.05.4.2.1	The instructive example of the benzene dimer	74
3.05.4.2.2	The interaction formerly known as π-stacking	75
3.05.4.2.3	Stacking of aromatic rings with amide groups	77
3.05.4.2.4	Aromatic-ring interactions with halogens	77
3.05.4.2.5	Cation–π interactions	78
3.05.4.2.6	Aromatic rings as hydrogen bond acceptors	79
3.05.4.2.7	Anion–π: An interaction in search of a medicinal role	80
3.05.4.2.8	CH$\cdots\pi$ interactions	81
3.05.4.3	The Occupation of Nonpolar Pockets by Ligand Hydrophobic Groups	82
3.05.4.4	Halogen Bonding	83
3.05.4.4.1	Background	83
3.05.4.4.2	Fluorine as a halogen-bond donor	84
3.05.4.4.3	Halogen-bond geometries	84
3.05.4.4.4	Halogen bonds in protein–ligand complexes	84
3.05.4.4.5	Halogen-enriched fragment libraries	86
3.05.4.4.6	Halogen bonding in drug development	86
3.05.4.4.7	The skeptical chemist's view of halogen bonding	86
3.05.4.5	Fluorine, the Little Atom That Couldn't	87
3.05.4.6	Carbonyl-Group Interactions	88
3.05.4.7	Sulfur Interactions	89
3.05.4.7.1	Sulfur interactions to nonpolar groups	89
3.05.4.7.2	Hydrogen bonds involving sulfur	90
3.05.4.7.3	Chalcogen bonding	90
3.05.4.7.4	Sulfur as a halogen bond acceptor	91
3.05.5	**Molecular Interactions and the Pharmaceutical Crystal Form**	91
3.05.5.1	Background	91
3.05.5.2	Hydrogen-Bond Patterns and Crystal Form Stability	92
3.05.5.3	Impact of Crystal-Structure Interactions on Physical Properties	94
3.05.6	**Summary**	94
Acknowledgment		95
References		95
Relevant Websites		100

3.05.1 Introduction

The pivotal role of noncovalent molecular interactions in biological chemistry has been recognized since Emil Fischer's *Schlüssel-Schloss Prinzip*, which proposed that a substrate fits into an enzyme active site as does a key into a lock.[1] This notion naturally suggested that another molecule of the same shape as the substrate might also fit into the active site and thereby disrupt the enzyme's function. Fischer's principle has been elaborated over the years. Proteins are flexible, as are most of the small molecules that bind to them, so hand-in-glove might be a better analogy than key-in-lock. And crucially, it is not as simple as matching shapes. Some atoms like to be close to each other and some do not, so even a perfect steric match may be insufficient to yield a high binding affinity. The complexity of optimizing atom–atom contacts is one of the many reasons why drug discovery is dreadfully difficult.

So chemists desiring to invent molecules that will bind to pharmaceutically relevant proteins have long been interested in which molecular interactions are favorable and which are not. Enormous efforts have been made to extend our knowledge of the subject but there remains much to learn. Interactions between aromatic groups are particularly difficult to predict because they are very sensitive to substituents and ring heteroatoms, and the reason for this is still a matter of debate. Halogen bonding has become increasingly *à la mode* over the past few years but doubts remain about the substance behind the hype. Weak interactions such as CH···O, CH···F, and CH···π are viewed as hydrogen bonds by some and of questionable significance by others. Then there are cation–π and anion–π interactions. They sound like opposites; how can they both be stabilizing? The thermodynamics of protein–ligand binding now appears much more complicated than it once did. Hydrogen bonding can be entropically driven, while the displacement of water molecules from a protein cavity by a hydrophobic ligand group can be driven by enthalpy, in contrast to the traditional viewpoint.

Twenty years ago, a chapter like this would have been directed exclusively to those interested in protein–ligand binding. But now molecular interactions have attracted the attention of another group of pharmaceutical scientists, those involved in drug formulation. Their burgeoning interest in crystal forms is motivated both by fear (of metastable polymorphs) and fervor (about the potential advantages of cocrystals). The interactions between molecules in crystals are now just as important to the pharmaceutical industry as those between inhibitors and enzymes.

This article is not a balanced account of molecular interactions; if it were, it would mostly be about hydrogen bonding. Less space is devoted to mature aspects of the subject so that more can be given to those that are still a matter of debate or even controversy, and which have therefore received particular attention over the past 10 years. In order that the article can be read in stand-alone fashion by chemists without a particular knowledge of the subject. The "**Background**" section briefly covers some of the basics—what an interaction is, how interactions may be studied, and so on. The importance of water and entropy is touched upon. The section "**Molecular Interactions or Emperor's New Clothes?**" takes an overview of the multitude of interaction types—strong hydrogen bonds, weak hydrogen bonds, halogen and chalcogen bonds, etc.—and asks whether their relative importance can be assessed in an objective and statistically rigorous manner. The bulk of the article is devoted to a more detailed consideration of each of the major types of interaction. Then the focus turns to the pharmaceutical crystal form: does the consideration of molecular interactions make it possible to spot a metastable crystal-packing arrangement, or help in the design of a cocrystal? The article concludes with a short summary.

3.05.2 Background

3.05.2.1 Methods

Most of our knowledge of molecular interactions comes from three sources: crystallography, measurements in solution (usually spectroscopic or calorimetric), and theoretical calculations. The first of these is the most important for medicinal chemists because of the widespread use of protein–ligand crystal structures in structure-based drug design. Its value is greatly enhanced by the existence of the two main crystallographic databases, the Protein Data Bank (PDB)[2] and the Cambridge Structural Database (CSD),[3] together with the derived knowledge-base IsoStar.[4] The latter is a library of three-dimensional plots, each of which shows the observed distribution of one type of chemical group around another in crystal structures from the CSD or PDB. For example, the plot of OH and NH groups around oxazole (**Fig. 1**) reveals that the nitrogen atom accepts hydrogen bonds much more commonly than the oxygen atom.[5] There are several programs and adjunct databases for use alongside the PDB. They include the search and analysis systems, Proasis3,[6] Relibase+,[7] and the PDBbind database,[8] which stores experimentally measured ligand binding affinities.

It is easy to forget the shortcomings of crystallographic data. In the PDB, the chief problem is the comparatively low observation/parameter ratios of all but the highest resolution structures. This results in relatively low precision and the danger of overfitting, so protein structures must always be interpreted with care.[9,10] Water positions are particularly uncertain but, worse, it is possible for ligand structures to be grossly in error.[11,12] The Uppsala electron density server enables calculation and display of the electron density of PDB crystal structures and is a good tool for spotting poorly fitted ligands and side chains.[13] Other systems provide a variety of options for validation and re-refinement of protein structures.[14–16] These days, structures are usually determined at low temperature to reduce radiation damage, which improves precision but may restrict flexible side chains to a subset of the conformations they can adopt in vivo.[17,18] Temperature also affects pK_a and can therefore alter the protonation states of ionizable side chains.

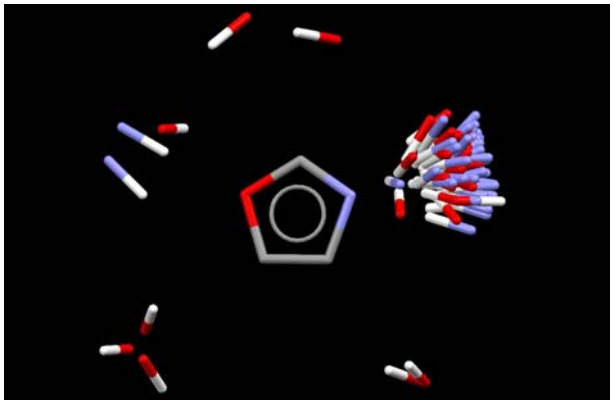

Fig. 1 IsoStar plot showing the observed distribution of OH and NH groups around oxazole rings in crystal structures from the CSD. Only contacts shorter than the sum of van der Waals radii minus 0.3 Å are shown.

The small-molecule crystal structures in the CSD are usually of high precision, bond lengths typically being determined with uncertainties of only a few thousandths of an Ångström. However, there are some systematic differences between the intermolecular contacts seen in small-molecule structures and those in protein–ligand complexes. Interaction geometries in the former can be influenced by the type of symmetry operator relating the interacting molecules. This occasionally results in a bias toward geometries that are favored by common symmetry elements, notably inversion. For example, antiparallel stacking of carbonyl groups (see "**Carbonyl-Group Interactions**") is much more common when the interacting groups are symmetry related by a crystallographic inversion center than when they are not symmetry related.[19] Therefore, this interaction is more often seen in the CSD, where structures with inversion centers are commonplace, than in protein–ligand complexes. Also, inspection of radial density distributions showed that small-molecule crystal structures favor hydrophobic C···C contacts to a lesser degree than do protein–ligand complexes.[20] The result cannot be explained by differences in stoichiometry. Its cause has not been established but may be related to desolvation effects, given that many structures in the CSD were determined using crystals grown from organic solvents.

Moving to solution measurements, a seminal contribution was made by Abraham et al., who measured the equilibrium constants for 1:1 hydrogen-bonding complexation of a large number of compounds with standard hydrogen-bond donor or acceptor molecules. This enabled them to derive parameters similar to substituent constants that measure the capacity of functional groups to accept or donate hydrogen bonds.[21] Similar methodology is being pursued by others.[22–24] These more recent measurements use Fourier transform infrared spectrometry, which often allows deconvolution of overlapping bands in the spectrum. This makes it possible to estimate the individual strengths of the separate acceptor sites in a polyfunctional molecule. Another important technique is isothermal titration calorimetry (ITC). Its application to protein–ligand complexation is giving fascinating and often surprising information about the relative importance to binding free energy of enthalpy and entropy (see "**Water is the Driving Force of All Nature**" and "**Enthalpy–Entropy Compensation**").[25,26] Efforts have been made to capture the results of ITC experiments on proteins in database form.[27]

The use of model systems such as supramolecular assemblies[28] and molecular torsion balances has proved valuable for studying molecular interactions in solution. A supramolecular assembly is a complex of two or more molecules held together by noncovalent interactions. The degree of molecular association can be measured by a range of titration techniques (potentiometric, NMR, fluorescence, calorimetric, etc.).[29] Complexation of guest molecules into cage-like hosts has given insight into how molecular cavities are optimally occupied (see "**The Occupation of Nonpolar Pockets by Ligand Hydrophobic Groups**").[30] Molecular torsion balances are molecules designed to have a limited degree of flexibility, which allows a particular intramolecular interaction to occur when the molecule adopts a folded conformation but not when the conformation is extended. The ratio of folded to extended conformers is measured by NMR, allowing the strength of the interaction to be estimated. The technique has been applied to CH···O, aryl–alkyl, aryl–halogen, aryl–aryl stacking, and aryl–aryl edge-to-face interactions, among others.[31] Its principal drawback is that interactions other than the one of interest might significantly affect the conformational equilibrium. However, the use of chemical double-mutant cycles enables secondary effects to be canceled out so that the energy due to the interaction of interest can be isolated.[32]

Quantum-mechanical calculations can provide invaluable insights into molecular interactions but suffer from two significant problems, basis set superposition error (BSSE) and the difficulty of accounting for electron correlation. The former arises when the basis set used for a molecule (the set of mathematical functions that are combined to represent molecular orbitals) is inadequate; sadly, this is always. When two molecules approach, each makes some use of the other's basis set to help compensate for the deficiencies of its own. This gives rise to an apparent but artifactual charge transfer stabilization, the BSSE. It can be partly corrected by use of the "counterpoise" method but the best defense is to improve the basis set by adding more functions. There is a bewildering variety of basis sets in common use. No doubt with their tongues in their cheeks, Dunitz and Gavezzotti pragmatically advised nonexperts to assume that the longer the name of the basis set, the better it is likely to be.[33]

The Hartree–Fock approximation, which might be described as the entry-level ab initio methodology,[34] fails to reproduce electron correlation effects because it assumes that each electron experiences the average field created by the others. This is disastrous when studying molecular interactions because electron correlation is responsible for dispersion, an important contributor to noncovalent interaction energies (see "The Components of a Molecular Interaction"). There are several higher-level ("post-Hartree–Fock") approximations that can take account of electron correlation with varying degrees of accuracy, but their computational costs escalate at a frightening rate. For example, the compute requirements of the MP2, CCSD, and CCSD(T) methods are dependent on the fifth, sixth, and seventh powers, respectively, of the size of the system being studied. CCSD(T)/CBS has come to be regarded as the "gold standard," being capable of predicting interaction enthalpies to an accuracy of about 1.5%, but at high cost.[35] Lower-level approximations (MP2, CCSD) are less accurate but can be usefully applied to larger systems.[36] Perturbation theory methods such as the widely used symmetry-adapted perturbation theory (SAPT) can also give very good results and have the additional advantage that they decompose molecular interaction energies into their component terms.[37] Unfortunately, the popular and relatively fast density functional theory (DFT) methods are difficult to apply to molecular interactions. Nevertheless, they can sometimes give excellent results when used with dispersion corrections.[38] In summary, while it is easy to get numbers out of a quantum-mechanical program, selection of appropriate methods and interpretation of results require considerable expertise.

3.05.2.2 The Components of a Molecular Interaction

The enthalpy of interaction between two molecules in the gas-phase is comprised of five components: electrostatic, polarization (also called induction), dispersion, charge transfer, and exchange repulsion. The electrostatic term is due to the interaction between the permanent charge distributions of the two molecules and may be energetically favorable or unfavorable. It is often the most important contributor to interaction energy, particularly for hydrogen bonds. Polarization is the interaction of the permanent charge distribution of one molecule with an induced change in the charge distribution of the other. Although it is usually small, it can sometimes have significant effects. For example, when a hydroxyl group donates its hydrogen to a hydrogen-bond acceptor, the electron density on the hydrogen atom is decreased and that on the donor oxygen is increased. This induced change makes the donor oxygen a better acceptor. In consequence, the hydrogen bonds in an ···OH···OH···OH··· chain act cooperatively, each being much stronger than an isolated OH···OH bond.[39] Dispersion (the London force) is due to electron correlation: a momentary dipole in the electron distribution of an atom in one molecule induces an opposite dipole in an atom of the other. Like polarization, it is necessarily energetically favorable. An individual atom···atom dispersion interaction is proportional to the product of the atom polarizabilities and the inverse sixth power of the interatomic distance, and is invariably small. However, the total dispersion interaction of two molecules, being the sum over all atom pairs, can be large enough to have a significant role in determining both protein–ligand binding affinities and optimum molecular arrangements in the crystal structures of organic molecules.[40] Charge transfer is the transfer of electron density from one molecule to the other. If it occurs, there is a degree of covalency in the molecular interaction. It is rarely significant in protein–ligand binding. Finally, exchange repulsion is a quantum chemical effect that causes a rise in energy when the electron densities of nonbonded atoms overlap. It is invariably small, for the simple reason that the energy increase is so steep when molecules approach too closely that in practice they do not. This can sometimes conceal problems from the drug designer. A molecule slightly too large to fit optimally into a protein binding site might still bind, the protein relaxing slightly to relieve the close contact(s). The resulting strain energy is dissipated imperceptibly over the binding site residues, hiding the design fault.

3.05.2.3 Water Is the Driving Force of All Nature[41]

Life for the drug designer would be much easier without water.[42] Firstly, its ubiquitous presence makes it difficult to assess how much free energy will be gained (or lost) by forming a hydrogen bond between protein and ligand, since this can only be done by first desolvating the groups involved. Water is a good hydrogen-bond donor and acceptor, so the outcome of swapping protein–water and ligand–water for protein–ligand and water–water hydrogen bonds is uncertain. In a classic experiment, Fersht et al. demonstrated by protein engineering that hydrogen bonds between tyrosyl-tRNA synthetase and its substrate contribute only modest amounts to binding affinity unless they involve charged groups.[43]

Next on the list is the problem of water molecules that are so strongly bound to the protein that they are hard or impossible to displace when ligands bind. They are not always easy to recognize. Given sufficient crystal structures of the same protein complexed with different ligands, conserved water molecules can be seen by overlaying the binding sites. For example, phosphodiesterase 10 contains two water molecules that are hydrogen-bonded to each other, and to two and three protein residues, respectively. The former was displaced in 1 of 15 ligand series, while the latter could not be displaced at all.[44] Several computational methods have been devised to assess which water molecules can be displaced,[45,46] but the problem is difficult and cannot yet be considered solved. Persch et al. offer a pleasingly simple rule of thumb: ordered water molecules that undergo four bonding interactions to the protein cannot be displaced; those that form three close contacts are very difficult to remove; those that form two can be replaced, but the gain in free enthalpy might be small; those that form one are easily replaceable and can offer substantial enthalpic gains.[47]

A particularly challenging problem is to understand the so-called hydrophobic effect. It is well known that occupying nonpolar binding site pockets with ligand hydrophobic groups is a good way of improving binding affinity. The reason is less clear. It is unlikely to be due to the strength of hydrophobic interactions per se: calculations on the methane dimer suggest an interaction enthalpy of only about -0.5 kcal mol^{-1} at best.[48] The traditional explanation is that water molecules surrounding a hydrophobic

surface form a "cage," which restricts their rotational freedom compared with their behavior in bulk water.[49] Hence, a hydrophobic ligand group that displaces water molecules from a nonpolar pocket results in an increase in entropy and thereby improves the free energy of binding. It transpires, however, that the truth is rather more complicated. Diederich et al. recounted their introduction to the "nonclassical hydrophobic effect."[50] They used calorimetry to investigate the thermodynamics of host–guest complexation between cyclophanes and *para*-disubstituted benzenes. To their surprise, formation of the complexes was driven by enthalpy, partly offset by an unfavorable entropic term. This is the opposite of what the classical hydrophobic effect would have led them to expect. On searching the literature, they found several similar examples. The nonclassical hydrophobic effect is rationalized as follows: (1) stronger water–water hydrogen bonds are formed in bulk solvent than by water molecules at a hydrophobic surface (there is some spectroscopic evidence for this[51]); (2) dispersion interactions between hydrophobic groups are enthalpically more favorable than those between a hydrophobic group and water, because water is less polarizable; (3) entropy is lost when the guest binds tightly to the host. So current thinking is that there is more than one "hydrophobic effect."[52,53] The balance between enthalpy and entropy when a hydrophobic ligand group binds into a lipophilic protein pocket is influenced by several factors, including the degree of protein flexibility, the size and curvature of the pocket, and the extent to which the pocket is hydrated before the ligand binds.

Some particularly fascinating studies have looked at the relationship between binding affinities and the structure of water networks at binding sites. A large difference in potency between two very similar chloro-aromatic fragments binding at the S1 pocket of thrombin was ascribed to the local water networks. The more potent fragment bound with an additional water molecule that incorporated Glu192 in the binding.[54] Attempts to fill a hydrophobic pocket in tRNA-guanine transglycosylase failed to produce the expected gains in binding energy because the ligands disturbed water molecules around two aspartate residues.[55] A pronounced nonadditivity of substituent effects on the binding of four thermolysin ligands was rationalized in terms of the surrounding water network. Three of the ligands allowed a continuously connected network to form between protein and ligand. In the fourth, the network was ruptured and the binding affinity was unexpectedly low.[56] Crystallographic and calorimetric investigations of another series of thermolysin inhibitors also provided instructive results. The inhibitors differed only in the nature of a hydrophobic side chain, and it was found that the addition or rearrangement of even one methyl group could significantly alter the geometry of the water network at the solvent-exposed surface of the complex. This, in turn, affected binding affinities and the enthalpy–entropy signatures of binding;[57] which takes us to the issue of enthalpy–entropy compensation (EEC).

3.05.2.4 Enthalpy–Entropy Compensation

The phenomenon of EEC is often observed in ITC studies of protein–ligand binding. Within a series of ligands with similar free energies of binding (ΔG), the enthalpic (ΔH) and entropic ($T\Delta S$) contributions can vary significantly but in an opposing manner. As an example, a series of trypsin inhibitors with constant structure except for a variable side chain, R, were found to have ΔG values in a narrow range but greatly differing enthalpic and entropic terms.[58] For instance, at 20°C the inhibitors with R = methyl, propyl, and *n*-hexyl had, respectively, $\Delta G = -27.5, -25.7, -28.9$; $\Delta H = -16.7, -9.7, -6.6$; $T\Delta S = 10.8, 16.0, 22.2$ kcal mol^{-1}. The most common explanation for EEC focuses on ligand and protein flexibility: stronger binding (greater enthalpic contribution) is tighter binding, meaning less mobility, hence less entropy. In the case of the trypsin inhibitors, the entropic contribution becomes more favorable as the *R* group increases in length, suggesting that the more flexible alkyl chains retain greater mobility when bound, but in consequence form weaker interactions with the protein pocket. However, EEC can also be connected to differences in the structure of water networks around bound ligands.[59,60]

It should be noted that there is a question mark over the evidence for EEC. Results from ITC experiments can have large unreported errors. In a test, identical aliquots of protein–ligand preparations were sent to 14 laboratories; the resulting ΔH values had a root-mean-square error of 24%![61] Further, the propagation of errors in ITC is such that errors in ΔG tend to be smaller than those in ΔH, which can give the appearance of EEC even when none is present.[62] In a careful study, Olsson et al. modeled the effects of these experimental constraints on 32 ITC data sets relating to diverse proteins.[63] They concluded that the tendency for EEC is strong, but by no means universal. It can be weak, and it is occasionally observed that enthalpic and entropic binding contributions move in the same rather than opposing directions. Overall, theoretical studies have focused on explaining a stronger tendency for EEC than appears to exist. It remains to be seen why some changes to ligands result in compensation and others do not.

3.05.3 Molecular Interactions or Emperor's New Clothes?

3.05.3.1 The Diversification of the Hydrogen Bond

Once upon a time there was the hydrogen bond and that was that. It was acknowledged that molecules interact in a general sort of way through van der Waals (vdw) forces,[64] but the hydrogen bond was the only specific, directional, noncovalent interaction worthy of a name. Its unique influence on physical properties and its role in determining small-molecule crystal structures were soon recognized. As far as biological chemists were concerned, hydrogen bonds could involve only two types of donors, OH or NH, and two types of acceptors, oxygen or nitrogen. That was enough for Pauling to predict the α-helix and for Watson and Crick to solve the structure of DNA.

The first crack in this simple edifice was the suggestion that CH groups could also act as hydrogen-bond donors.[65] Initially dismissed,[66] the idea was resurrected[67] and then enthusiastically evangelized.[68] Not everyone was convinced. From the group of the famous organometallic chemist Al Cotton came this complaint: "While the literature contains numerous allusions to C–H···N

'hydrogen bonds' there seems little if any reason to accept this description. Or, to invoke the parable of the emperor's new clothes, the question of why many people seem to find the emperor well dressed despite any persuasive evidence that he isn't naked, arises."[69] Cotton's disapprobation was countered by Steiner and Desiraju on the not entirely compelling grounds that CH···O interactions tend to become more linear at the hydrogen atom as the polarization of the CH bond increases.[70] Thereafter, an increasingly diverse array of interactions attracted the terminology "hydrogen bond." They included some very weak interactions indeed: CH···F–C,[71] CH···Cl–C,[72] and CH···π.[73] Eventually, IUPAC set up a task force, which proposed a new definition of the hydrogen bond.[74,75] An initial comparison of definitions old and new leaves one wondering what the difference is but, on closer inspection, it is clear that the intent of the new definition is to encompass much weaker interactions (down to 0.5 kcal mol^{-1}). Cotton is no doubt turning in his grave.

Does the new definition add to or clarify our understanding of molecular interactions? No. But the process by which it was arrived at was useful. It highlighted the possibility that even weak interactions may have a significant influence on how molecules associate with one another. The new definition does, however, have a clear disadvantage: it covers such as wide range of interaction energies that, in discussing hydrogen bonds, we must now specify what type we mean. Jeffrey recommended the terms "strong," "moderate," and "weak" for hydrogen bonds with energies in the ranges of 15–40, 4–15, and <4 kcal mol^{-1}, respectively.[76] For present purposes, this effectively means that strong hydrogen bonds involve charged donors or acceptors; moderate are of the type (O,N)H···(O,N); weak is everything else, but most importantly CH···O, CH···N, and NH···π.

3.05.3.2 Every Atom Has to Be Somewhere

While the hydrogen bond was adding new donors and acceptors to its portfolio, other molecular interactions were being discovered, rediscovered, or otherwise promoted. They included halogen bonds,[77] chalcogen and pnicogen bonds,[78] π–π interactions,[79] cation–π interactions,[80] and anion–π interactions.[81] The poor medicinal chemist, staring at an enzyme active site on the computer screen and wondering how to design a new inhibitor, might be forgiven a degree of confusion. Are all these interactions important?

The Irish comedian Spike Milligan once remarked that "Everybody's got to be somewhere."[82] By the same token, every atom has to be somewhere. Further, in organic condensed phases, every atom has to be somewhere near an atom in another molecule unless it is buried inside the molecule to which it belongs. We pay close attention to the idea that short intermolecular contacts might be indicative of stabilizing interactions, but rarely contemplate the possibility that two atoms might be forced into close mutual proximity against their will (if the reader will forgive the anthropomorphism). This argument applies particularly to contacts involving hydrogen, as pointed out by Dunitz and Gavezzotti: "Only atoms on the outer surfaces of molecules can come into contact with atoms of other molecules. Since these are usually hydrogen atoms, CH···X contacts in organic crystals are almost unavoidable. One must therefore be very careful about their significance as main contributors to intermolecular stabilization."[33] The argument could also be applied, of course, to protein–ligand complexes.

These doubts were reiterated recently. Bader's "atoms in molecules" approach[83] argues that, for two atoms to be covalently bonded, there must be a $(3, -1)$ bond critical point. This is a point between the atomic nuclei where the electron density is at minimum along one axis, the bond path, and at a maximum along any direction perpendicular to that axis. The bond path is the line followed by the ridge of electron density between the two atoms. It is often argued that a similar criterion should apply to intermolecular "bonds."[84,85] Dunitz recently questioned whether the condition is fulfilled even by medium-strength hydrogen bonds, let alone weaker interactions.[86] Others made haste to reply,[87,88] contending that criteria based on the atoms-in-molecules approach clearly support the stabilizing nature of many types of weak interactions, including halogen and chalcogen bonds, CH···O, and CH···F–C. We may assume that the matter is not considered settled.

3.05.3.3 Assessing the Relative Importance of Molecular Interactions

Prompted by the argument that CH···X contacts in organic crystals are almost unavoidable, a recent study assessed whether they occur significantly more often, in a statistical sense, than would be expected by chance.[89] They and other types of intermolecular atom···atom interactions in organic crystal structures were ranked on the ratio (R_F) of their observed frequency of occurrence to the frequency expected at random. Expected frequencies were calculated from binomial statistics, assuming that the probability of a given atom forming its shortest (relative to vdw radii) line-of-sight contact to an atom of type X equals SA_X/SA_{TOTAL}, where SA_{TOTAL} is the total surface area of the molecules in the crystallographic unit cell, and SA_X is the surface area contributed by atoms of type X. A line-of-sight contact is one in which the two atoms "see" each other because no third atom intrudes between them. 95% confidence limits for R_F values were determined by bootstrapping, so it was possible to establish whether the R_F of a given type of interaction was significantly greater than 1. If so, the interaction occurs significantly more often than would be expected by chance and is therefore associated with energetically favorable molecular arrangements. Conversely, the importance of an interaction with R_F significantly less than 1 is open to serious doubt. The greater the amount by which an interaction's R_F value exceeds 1, the more influential the interaction can be assumed to be in determining how small molecules pack in the crystalline state.[90]

As would be expected, the interactions with the highest R_F values are strong and moderate hydrogen bonds, which typically occur 5–10 times more often than would be expected at random (some example R_F values are given in **Table 1**). At about the same level is I···N, which is a halogen bond. Other halogen bonds involving iodine or bromine come lower in the ranking, but still have R_F comfortably greater than 1. However, Cl···O and Cl···N interactions have $R_F \approx 1$, which raises doubts about their importance in influencing crystal-packing arrangements. CH···O interactions have R_F significantly greater than 1, the value of the parameter rising

Table 1 R_F values of some intermolecular interactions, with 95% confidence limits[89]

Interaction[a]	R_F	*95% confidence limits*
O(carbonyl)···H(polar)	9.2	7.9–11.2
O(hydroxyl)···H(polar)	5.9	5.2–7.1
O(ether)···H(polar)	4.0	3.6–4.7
N···H(polar)	5.7	4.9–6.9
C–I···N	6.5	5.7–7.6
C–I···O	2.7	2.5–3.1
C–Br···N	1.8	1.5–2.0
C–Br···O	1.5	1.3–1.7
C–Cl···N	0.9	0.7–1.1
C–Cl···O	1.0	0.8–1.2
C(sp)–H···O	5.2	4.5–5.9
C(aromatic)–H···O	2.3	2.2–2.3
C(methyl)–H···O	1.5	1.5–1.6
C–F···H–C	1.7	1.5–1.9
C–Cl···H–C	1.3	1.0–1.6

[a]H(polar) indicates H covalently bonded to O, N, or S; N excludes quaternary and trigonal planar nitrogen.
For a given interaction, *X*···*Y*, R_F is the ratio of the observed number of *X*···*Y* contacts in organic crystal structures to the number expected if determined solely by surface area considerations.
Reproduced from Taylor, R. *CrystEngComm* **2014**, *16*, 6852–6865 with permission from the Royal Society of Chemistry.

as the intramolecular environment of the hydrogen becomes more electron withdrawing; indeed, the acetylenic C(sp)–H···O interaction has the remarkably high value of $R_F = 5.2$. The C–F···HC and C–Cl···HC interactions also have $R_F > 1$. The point raised by Dunitz and Gavezzoti—that one would expect many CH···X contacts given the high surface exposure of hydrogen atoms—is comprehensively answered. These contacts occur significantly more often than can be explained by surface area considerations alone. The emperor is clothed, after all.

3.05.4 The Major Types of Molecular Interactions

3.05.4.1 An Abridged Guide to Hydrogen Bonding

Of all molecular interactions, the hydrogen bond is by far the most important. It is also the most studied, the most reviewed, and the best understood. It therefore presents some difficulty here: what is worth saying in the small space available when so much has already been said? Some of the lesser-known aspects of hydrogen bonding (to π-systems, to halogens, involving sulfur) are dealt with elsewhere in this article but, for the familiar interaction involving OH or NH donating to oxygen or nitrogen, brevity would seem to be in order. Hence, the facts of most relevance in medicinal chemistry are listed below with little amplification. Where references are not explicitly cited, further information can be found in standard text books and reviews.[76,91–93]

1. Charged groups form stronger hydrogen bonds than uncharged.
2. Hydrogen-bond donor and acceptor strengths do not correlate particularly well with acidities and basicities, as measured by pK_a values. For example, thiols are more acidic than alcohols but poorer hydrogen-bond donors.
3. In general, uncharged OH is a stronger donor than uncharged NH.
4. The strengths of uncharged acceptors decrease in the approximate order N-oxide > sulfoxide > amide ≈ pyridine > ketone > nitrile ≈ alcohol ≈ ester carbonyl > alkyl ether > phenol > diaryl ether.[22]
5. The strength of a donor or acceptor group can be strongly dependent on its intramolecular environment.
6. Nearby electron-withdrawing groups increase the strengths of donors.
7. Conversely, electron-donating groups increase the strength of an acceptor, while electron-withdrawing groups decrease it. For example, the acceptor strengths of the nitrogen atoms in 4-ethylpyridine, pyridine, and 4-chloropyridine are, respectively, 2.07, 1.86, and 1.54, as measured by the pK_{BHX} hydrogen-bond basicity scale (higher values indicate better acceptors).[22]
8. Conjugated oxygen atoms (in furan, oxazole, ester, etc.) are very weak acceptors and prefer to form contacts with CH groups rather than OH or NH (**Fig. 1**).[5,94,95]
9. The ability of a 3-coordinate nitrogen atom to accept a hydrogen bond depends on its geometry. It can be a good acceptor if pyramidal; a weak acceptor if slightly pyramidal, as in aniline; and cannot accept if planar, as in an amide group.
10. Bifurcated hydrogen bonds, in which the donor hydrogen interacts with two acceptors, are relatively common.[96,97] By necessity, at least one of the components of a bifurcated interaction must be appreciably nonlinear (D–H···A ≪ 180 degree, where D and A represent donor and acceptor, respectively).
11. Trifurcated bonds are rare, probably for steric reasons.

Table 2 Numbers of hydrogen bonds accepted by various groups[a]

Acceptor group	N*(1)*	N*(2)*	N*(> 2)*	*%(1)*	*%(2)*	*%(> 2)*
Nitrile nitrogen	1399	215	75	82.8	12.7	4.4
Pyridyl nitrogen	5757	285	12	95.1	4.7	0.2
Carbonyl oxygen	32,038	7964	2738	75.0	18.6	6.4
Phosphate and phosphonate oxygen	10	48	211	3.7	17.8	78.4

[a]*N*(*n*) and %(*n*) = number and percentage of groups in CSD that accept *n* hydrogen bonds. Statistics based on 2015 version of CSD, using only nondisordered organic structures with *R*-factor ≤ 5%, hydrogen covalent bond distances normalized to average neutron-diffraction values. Hydrogen bonds restricted to NH or OH donors with D–H···A ≥ 90 degree and H···A ≤ sum of vdw radii plus 0.2 Å.

12. Acceptor groups can interact with more than one OH or NH donor. The ability to do so can be roughly correlated with the number of available lone pairs, so carbonyl groups often accept two donors and phosphate oxygen can accept three, whereas pyridine nitrogen rarely accepts more than one (Table 2). Steric accessibility is also relevant, so nitrile nitrogen is more likely to accept > 1 hydrogen bond than pyridyl nitrogen.
13. H···A distances are almost always shorter than the sum of vdw radii, often by 0.5 Å or more. The corresponding D···A distances are usually shorter than the sum of vdw radii. Stronger donors and acceptors tend to form shorter bonds.[93]
14. Hydrogen-bond distances are easily influenced by their environment. Hydrogen-bond distance distributions typically have 95% limits spanning 0.4 to 0.5 Å.[93]
15. Unless the bond is bifurcated, D–H···A angles usually exceed 150 degree and the energy becomes very small below 120 degree.[98]
16. Shorter hydrogen bonds tend to have larger D–H···A angles.
17. Directional preferences at the acceptor atom are discernible but rather weak.
18. Carbonyl oxygen atoms prefer to form hydrogen bonds in or close to the carbonyl-group plane. However, there is only a slight tendency for the interactions to form in the lone-pair directions within that plane. The tendency may be steric rather than electrostatic in origin.[99]
19. Hydrogen bonds to ether oxygen atoms have no preference for hydrogen bonding in the sp^3 lone-pair directions, but there is a strong preference for the plane bisecting the C–O–C angle.
20. Pyridyl and other sp^2 nitrogen atoms have a tendency to accept from donors positioned approximately along the lone-pair direction.
21. Hydrogen bonds can show cooperativity (two or more proximal bonds strengthening one another).[100]
22. They may also be anticooperative. For example, the dipolar interaction between two donor groups hydrogen bonding to the same carbonyl oxygen atom is unfavorable.
23. Intramolecular hydrogen bonds in conjugated systems are often described as "resonance assisted" but the extent to which this is the case is open to question.[101]
24. NH and OH groups in proteins are almost invariably donated in hydrogen bonds to good oxygen or nitrogen acceptors. This can, of course, include water.
25. Oxygen and nitrogen acceptors are usually hydrogen-bonded to OH or NH groups, but it is also common for them to form contacts only to CH groups.
26. The contribution of protein–ligand hydrogen bonds to binding energy is variable and difficult to predict, but often small because of desolvation costs.[102] It is possible for a hydrogen bond between protein and ligand to be entropy-driven rather than enthalpy-driven.[103]
27. Desolvating a protein donor group without forming a compensatory hydrogen bond to the ligand is almost certain to have a highly unfavorable impact on binding affinity. Acceptors may be more forgiving.[44]

CH···O and CH···N hydrogen bonds have been extensively dealt with in the literature,[104] so, again, the discussion here will be brief. Donor strengths tend to decrease in the order C(sp)–H > C(sp^2)–H > C(sp^3)–H, but even methyl groups are capable of forming stabilizing interactions. Electron-withdrawing groups promote donor ability—for example, the CH groups at the 6-position of uracil and the 2-position of imidazole and imidazolium are better donors than most other CH groups. Hydrogen bonds with CH donors tend to be longer than their OH and NH analogs, with H···O and H···N distances that sometimes exceed the sum of vdw radii. Directional preferences are much weaker, both at the hydrogen atom[98] and at the acceptor. Although they are weak, CH···O hydrogen bonds can be numerous and hence significant in protein–ligand binding[105,106] (eg, in kinases[107]). It has been claimed that they are comparable to NH···O interactions in the context of the forces that hold together the adjacent strands of β-sheets.[108]

3.05.4.2 Interactions Involving Aromatic Rings

3.05.4.2.1 The instructive example of the benzene dimer

Apart from strong and moderate hydrogen bonds, the molecular interactions of most importance in rational drug design are probably those involving aromatic rings. This is partly because of the popularity of phenyl groups and aromatic heterocycles in medicinal

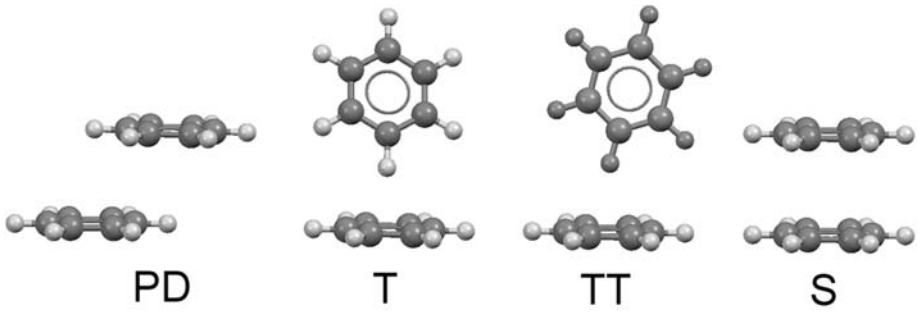

Fig. 2 Four important benzene dimer geometries.

chemistry and also, of course, because phenylalanine, tyrosine, and tryptophan side chains are often present in binding pockets. It is ironic, then, that these interactions have proved particularly difficult to understand and predict. Moreover, the experts' view of them has changed significantly over the past 10 years.

Most reviews of aromatic interactions begin with the benzene dimer, and rightly so, because it is a highly instructive system. It has been studied extensively, both experimentally and computationally, but both approaches have been problematic. The main difficulty with theoretical methods is that much of the stabilization energy of the dimer is due to dispersion. Approaches such as Hartree–Fock and what we might call "vanilla" DFT completely fail to reproduce this physical effect, so higher-level methods are necessary. Computationally, they are much more expensive. In consequence, it has been impossible until comparatively recently to fully explore the potential energy hypersurface of the dimer at an adequate level of approximation.[109–113] The results provided new insights. Until 2006, it had been thought that the two most stable arrangements were the parallel-displaced (PD) and the symmetric T-shaped (T) geometries (Fig. 2). However, SAPT calculations indicated that the T geometry is at a saddle point on the potential energy hypersurface.[111] The global minimum is similar to the T arrangement but with a tilt that improves dispersion interactions (TT; Fig. 2). The PD, T, and TT geometries are similar in energy, all three falling in the range -2.6 to -2.8 kcal mol^{-1}. In contrast, the classic "π-stacked" sandwich arrangement (S) is significantly less stable at -1.8 kcal mol^{-1}. The other recent theoretical studies referenced above differ in matters of detail, but confirm the overall picture of a rather flat potential energy hypersurface with PD, T, and TT geometries most favored, and S distinctly less so. Rotational spectroscopy indicated the presence of tilted T-shaped geometries in the gas-phase.[114] The crystal structure of benzene at normal pressure has pairs of neighboring molecules with geometries approximating TT.[115]

These results might seem irrelevant to medicinal chemists, whose interest in aromatic rings lies exclusively in the substituted variety. And substitution certainly has an effect on optimum geometries: Calculations on the toluene dimer, for example, suggest that the introduction of the methyl group makes the PD geometry more stable than the T arrangement.[116] But three important conclusions can be drawn from the benzene dimer system. Firstly, it is only during the past few years that theoretical methods have become capable of delivering reliable results on this system (and, therefore, on other aromatic complexes). Secondly, the benzene dimer can adopt a range of geometries that are approximately isoenergetic (T, TT, PD), so it is to be expected that the introduction of substituents onto one or both rings may swing the balance in favor of one geometry and against others. This is the main reason why the interactions of aryl groups have proved so difficult to understand. Thirdly, the sandwich geometry is energetically accessible but *not* the favored geometry, despite the assumptions of many that it is.

3.05.4.2.2 The interaction formerly known as π-stacking

An early attempt to understand the effect of substitution on aromatic-ring stacking (the S and PD geometries of Fig. 2) was made by Cozzi, Siegel, and coworkers.[117,118] They used NMR to measure the barrier to rotation about the aryl–naphthalene bonds in variously substituted 1,8-diaryl-naphthalene molecules. For steric reasons, the minimum-energy conformation has both aryl rings approximately perpendicular to the naphthalene system and therefore in a stacked geometry with respect to each other. It was argued that the rotation barrier is a measure of the strength of the aryl–aryl stacking energy. When only one of the rings was substituted, there was an approximately linear correlation between rotation barrier and Hammett substituent constant,[119] the barrier increasing as the substituent became more electron withdrawing. When both rings were substituted, the rotation barrier correlated with the sum of the Hammett constants. The stacking interaction was most favorable when both rings bore electron-withdrawing substituents, and least favorable when they had electron-donating substituents. While stacking produces a favorable dispersion interaction between the phenyl rings, there is also an unfavorable electrostatic term. It was concluded that electron-withdrawing groups reduce the π-electron density and thereby lower electrostatic repulsion between the stacked rings. Electron donors have the opposite effect.

In a seminal paper, Hunter and Sanders presented a similar though not identical argument.[120] Benzene has a large negative quadrupole moment (δ^+ around the edges of the ring, δ^- above and below the ring).[121] The sandwich (S) arrangement is therefore electrostatically unfavorable, T-shaped and PD geometries being preferable. However, if the aromatic system is polarized by substituents or heteroatoms, the strength of sandwich and near-sandwich stacked arrangements is affected. Rings with electron-donating

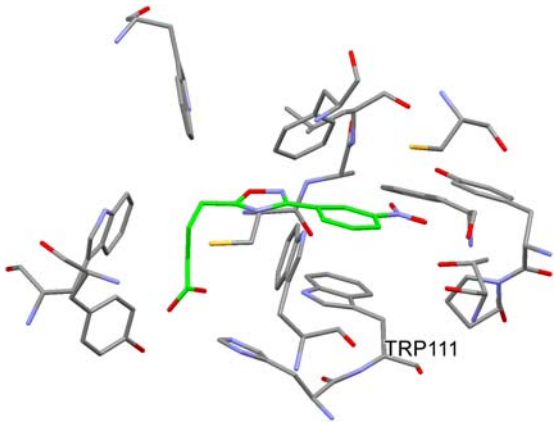

Fig. 3 Stacking of an inhibitor nitrophenyl ring with a tryptophan side chain in an aldose reductase complex (PDB code 2IKG).

substituents such as $-NMe_2$ will have increased negative quadrupole moments and will stack less favorably with benzene than an unsubstituted ring because of a larger electrostatic repulsion. Electron-withdrawing substituents such as $-NO_2$ will have the opposite effect. An example relevant to medicinal chemistry is provided by the aldose reductase complex shown in **Fig. 3**.[122] The *m*-nitrophenyl of the inhibitor stacks with the indole ring of Trp111 and the ligand lacking the nitro group show an activity drop of an order of magnitude. Two π-systems polarized in opposite directions will attract. This explains, for example, the crystal structures of the complexes of perfluorobenzene with methyl-substituted benzenes such as *p*-xylene.[123] They contain stacks of alternating molecules, radically different from the structure of benzene itself.

Both the Cozzi–Siegel and Hunter–Sanders models rationalize substituent effects in terms of the polarization of π-clouds, and this has become the standard viewpoint over the last two decades. However, a radically different explanation has now been put forward that dismisses the significance of π-cloud effects. Doubts about the π-polarization model arose when several theoreticians calculated that all substituents make stacking more favorable compared with the unsubstituted benzene dimer, irrespective of whether they are electron withdrawing or donating.[110,124–126] Further, it was concluded that substituent effects on stacking energy are additive.[127] This is hard to rationalize by π-polarization arguments because the polarizing influence of substituents would be expected to attenuate as more are introduced onto the ring. Also, Dunitz pointed out that 1,3,5-trifluorobenzene has no appreciable quadrupole moment, yet its crystal structure contains stacks of alternating molecules similar to those seen in the cocrystal of benzene and perfluorobenzene, which were rationalized on the basis of negative quadrupole/positive quadrupole attraction.[128]

Then came a short but notable paper that delivered a hammer blow to the π-polarization model.[129] The authors first calculated the energies of 24 dimers of general formula $C_6H_6\cdots C_6H_5X$, all in a stacked (S) arrangement, with optimized monomer geometries and inter-ring distances. The resulting dimer energies could be linearly correlated with Hammett sigma *meta* constants ($r=0.91$), which in itself is unsurprising. All of the complexes with $X \neq H$ had more favorable dimerization energies than that of the benzene dimer itself, supporting the notion that any substituent will stabilize stacking. This is most easily explained by the additional dispersion interactions that take place between the substituent and the unsubstituted ring. In the crucial part of the study, the authors then performed analogous calculations on the systems $C_6H_6\cdots HX$; in other words, the phenyl group of the substituted molecule is replaced by hydrogen. The hydrogen was placed along the original C–X bond direction. Remarkably, the resulting energies showed the same trend. The energies of $C_6H_6\cdots C_6H_5X$ and $C_6H_6\cdots HX$ differed, but the two sets of energies were strongly correlated ($r=0.91$). In other words, the effect of X on interaction energy is more or less the same whether the number of π-systems present is one or two. This implies that π-polarization effects need not be invoked to explain the effects of substituents on stacking energies. Rather, the reason for the energy variations seems to lie in the interaction with the unsubstituted ring of the substituent itself and the dipole associated with its covalent bond.

In a later paper,[130] Wheeler went one stage further and showed that energies of the simpler system propene$\cdots$HX also correlate closely with those of $C_6H_6\cdots C_6H_5X$ ($r=0.94$, excluding two outliers discussed in the paper). He concluded that substituent effects on stacking interactions depend largely on the direct, localized interaction of the substituent and its covalent bond with the closest vertex of the neighboring ring, the remainder of the ring being relatively unimportant. Further evidence was presented to support this contention. He summarized thus: "substituent effects arise from the interaction of the local dipole (or higher-order multipole) associated with the substituent (including the first polarized σ-bond) with the nearby local C–H dipoles of the other ring. As a result, substituent effects are insensitive to changes to the distal side of either the substituted or unsubstituted ring. In cases where both rings bear substituents, our local, direct interaction model predicts that substituents will operate independently as long as they are not in close proximity."[131] Similar arguments have been made for substituent effects on edge-to-face (T-shaped), cation–π, and anion–π interactions.[132–134] Stacking of nucleic acid bases has also been rationalized in terms of local electrostatic interactions between bond dipoles, coupled with dispersion interactions.[135]

If it stands the test of time, the localized substituent effect model should have profound implications for structure-based drug design, with a move away from looking at rings as a whole toward consideration of interactions directly involving substituents and

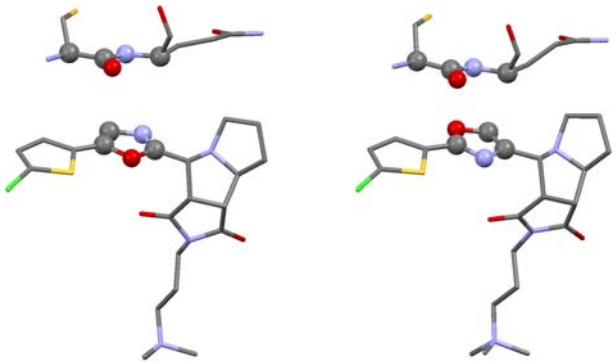

Fig. 4 Binding site detail in two factor Xa complexes. Both have a stacking interaction between the ligand oxazole ring and a protein peptide linkage (relevant atoms shown as spheres). The dipole moments associated with the stacked groups are approximately antiparallel in the tighter binding complex (*left*: PDB code 2Y5G, $K_i = 146$ nM) and parallel in the other (*right*: PDB code 2Y5H, $K_i = 1620$ nM).[140]

heteroatoms. One particular methodological issue is the use of electrostatic potentials. Proponents of the localized substituent effect model argue that, while this is valid for analyzing cation–π interactions,[136] it is of limited use for assessing whether two aromatic groups are mutually complementary and therefore likely to stack with each other. This is because changes in the electrostatic potential above an aryl group do not necessarily indicate a change in π-electron density but may be due to the through-space effect of substituents.[137]

One side-effect of the recent work on stacking is the suggestion in two papers that the terms "π-stacking" and "π–π interactions" are of limited validity.[138,139] It is argued that they imply (1) that aromatic face-to-face stacking is generally favored, which it is not, and (2) that when stacking does occur, the stabilization is primarily due to interactions of the π-systems, which is extremely arguable. Your present author agrees. The terms are confusing at best, misleading at worst, and should be consigned to history; "aromatic-ring stacking" is neutral about the cause of the interaction and is to be preferred.

3.05.4.2.3 Stacking of aromatic rings with amide groups

The amide group is known for forming hydrogen bonds but it can also form less polar interactions above and below the amide plane, including stacking interactions with aromatic heterocycles. This is relevant in drug design, since amide groups from the protein backbone or glutamine and asparagine side chains are often exposed at binding sites. The point was made and exemplified recently by Harder et al.,[140] who concluded that stacking interactions between aromatic rings and backbone peptide groups are important for ligand binding in cathepsin L,[141] phosphodiesterase 10,[142] and factor Xa complexes.[143] The latter example is particularly instructive. Two inhibitors with very similar structures were observed to bind in almost the same way to the protein, both with an oxazole ring stacked over a backbone peptide group (Fig. 4). Since the oxazole was 2,5-linked in one inhibitor and 2,4-linked in the other, the orientation of the ring, and therefore its dipole, with respect to the peptide group dipole was different in the two complexes. It was to this that the 11-fold difference in binding affinities was tentatively ascribed. In the better inhibitor, the oxazole and peptide dipoles were antiparallel, which would be expected to be electrostatically optimum.

In the same study, a series of quantum-mechanical calculations was performed on the dimers between *N*-methylacetamide and a variety of aromatic heterocycles. It was concluded that the stacking energy is indeed optimized when amide and heterocycle dipoles are antiparallel. The most favorable energies were with heterocycles that had large dipole moments; pyridazine and 2-pyridone were the best. It was also established that, in crystal structures containing ligand pyridyl groups stacked on backbone amide groups, there is a tendency toward the geometry corresponding to antiparallel dipoles.

3.05.4.2.4 Aromatic-ring interactions with halogens

Interactions between aromatic rings and halogen atoms were highlighted by Matter et al. in the context of factor Xa.[144] The authors' interest was provoked by the excellent K_i values (3 and 13 nM) of two inhibitors binding with a *p*-chlorophenyl group occupying the S1 pocket of the enzyme. Similar levels of binding were obtained with the *p*-bromo derivatives. By comparison, the unsubstituted molecules bound much less tightly ($K_i = 204$, 478 nM). Crystallography showed that the halo-substituents were pointed toward the face of the Tyr288 aromatic ring, leading the authors to hypothesize that C–Cl···π and C–Br···π interactions can make an important contribution to protein–ligand binding.

Both these authors and other groups have performed CSD searches to characterize the radial distribution of halogen atoms (X) around phenyl rings.[44,145,146] Somewhat ironically, given the interest in halogen···π interactions, all the studies agree that by far the most likely geometry is with the halogen at the edge of the ring, where it can interact with ring hydrogen atoms (Fig. 5). The preference for this position decreases in the order F > Cl > Br > I, and can readily be explained on the basis of electrostatic attraction, $H^{\delta+}\cdots X^{\delta-}$. A similar situation is found in the PDB. In over 2000 PDB complexes involving halogenated ligands, only 189 distinct X···π interactions were found; this contrasts with 1420 C–X···H contacts in 72 NMR and high-quality X-ray structures of protein complexes with halogenated ligands (although many of the latter will be to alkyl hydrogens).[147] The same study

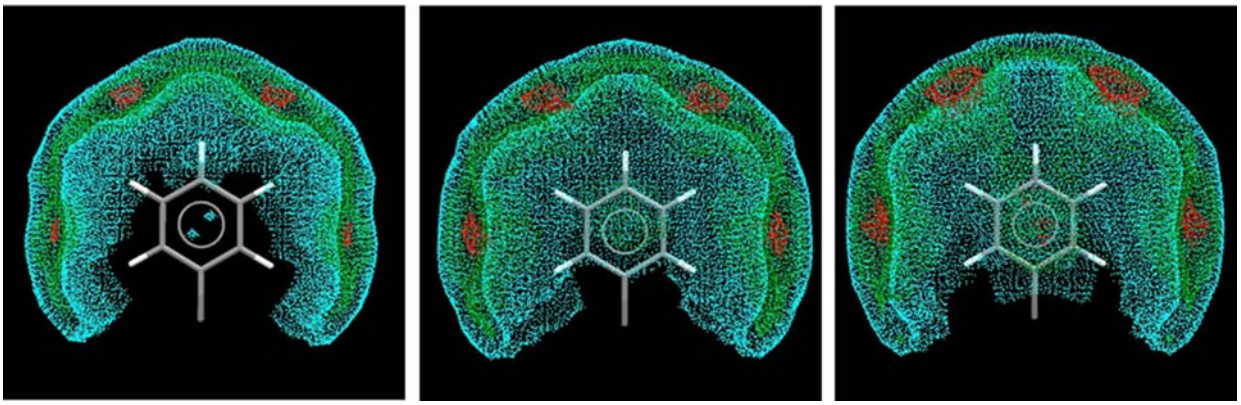

Fig. 5 IsoStar plots showing the density distributions of C–F (*left*), C–Cl (*center*), and C–Br (*right*) halogen atoms around phenyl groups in crystal structures from the CSD. The density levels *red*, *green*, and *cyan* show, respectively, regions where halogen atom density is four, two, and one times the value expected at random, given the stoichiometries of the crystal structures contributing to the plots.[4]

found the mean angles at hydrogen of CH···X contacts to be 119.5, 112.6, 96.8, and 101.7 degrees for X = F, Cl, Br, I, respectively. The interactions show only weak directional preferences, but there is evidence that H···F contacts below 2.6 Å only occur when C–H···F > 120 degrees.[44]

Despite the preference for C–H···X contacts, the radial distribution plots also do show many halogen atoms positioned over the ring and therefore interacting with the aromatic π-system; not for fluorine, but certainly for the heavier halogens (Fig. 5). The nature of these interactions is not entirely clear. Bissantz et al. noted that most of the contacts involving halogens bonded to aromatic rings are clearly the side-effects of aromatic-ring stacking.[44] However, there remain many other X···π contacts to rationalize. Some have argued that they are halogen bonds, stabilized by electrostatic attraction between the negative π-system and the positive area of electrostatic potential along the extension of the C–X bond (the "σ hole"; see halogen-bonding "Background" section). This is supported by a clear preference of C–Cl and C–Br vectors to be perpendicular to the aromatic-ring plane at the closest observed distances from the ring centroid (< 3.4 Å for Cl, < 3.5 Å for Br).[44] However, theoretical work suggests a different explanation. Calculations were performed at various levels of approximation on the T-shaped complexes between *p*-cresol and chlorobenzene and bromobenzene (ie, the geometries with the halogen atoms pointing at the cresol π-system). The higher-level approximations predicted interaction energies in the range −1.6 to −2.2 kcal mol^{-1} for the chlorobenzene complex, and between −2.7 and −2.8 kcal mol^{-1} for the bromobenzene complex. But, crucially, two methods incapable of reproducing electron correlation effects predicted no attractive interaction at all. This strongly suggests that dispersion rather than electrostatics is the dominant cause of stabilization.[148] Matter et al. concurred.[144] They performed calculations showing that the energy of the C–Cl···π interaction has very little angular dependence. This suggests that the major source of attraction is dispersion, since any electrostatic interaction between the halogen σ hole and the aromatic π-system would be expected to have strong directional preferences.

3.05.4.2.5 Cation–π interactions

The cation–π interaction[50,79,80,149] is the interaction between the π-system of an aromatic group and a metal or organic cation. There is general consensus that it is predominately electrostatic in nature,[150,151] the electronegative π-system attracting the electropositive cation. Polarization is also known to play a significant role.[152] The strength of the interaction was investigated in a biological context by Diederich et al., using two pairs of factor Xa inhibitors.[153,154] The S4 pocket of this enzyme is an "aromatic box" defined by the side chains of Tyr99, Phe174, and Trp215. The inhibitors in the first pair were identical except that where one had a *t*-butyl group, the other had a trimethylammonium. Their binding constants were 29 and 0.28 μM, respectively. Crystallography established that the $-NMe_3^+$ group occupies the S4 pocket, as expected (Fig. 6). Since the two groups have virtually identical volumes, the difference in binding affinities can be ascribed to the cation–π effect. It corresponds to a ΔΔG of 2.8 kcal mol^{-1}, equivalent to an average contribution of about 0.9 kcal mol^{-1} for each of the three aromatic side chains. The second pair of inhibitors also differed by the $-CMe_3$/$-NMe_3^+$ replacement. Again, the cationic group gave much better binding, 550 versus 9 nM. This corresponds to ΔΔG = 2.5 kcal mol^{-1}, an average contribution of 0.8 kcal mol^{-1} per ring, pleasingly consistent with the result from the first pair. The authors also established that increasing methylation of the ammonium group has an enormous effect on binding; the K_i values for inhibitors with $-NH_3^+$, $-NH_2Me^+$, $-NHMe_2^+$, and $-NMe_3^+$ groups were 9800, 911, 56, and 9 nM, respectively. This can presumably be ascribed to the high cost of desolvating N^+–H protons.

Dougherty et al. performed an interesting series of experiments in which aromatic residues in binding sites were changed to their fluorinated analogs: for example, tryptophan to 4,5,6,7-tetrafluorotryptophan. They argued that this completely removes the electrostatic component of any cation–π interactions that the residue forms when a cationic ligand binds. Solvent effects are minimized because the ligand itself is not changed. Fluorination reduced the binding affinity of acetylcholine to various proteins by factors of 50 to 500. A ratio of over 10,000 was observed for the binding of glycine to its cognate receptor.[80,155,156]

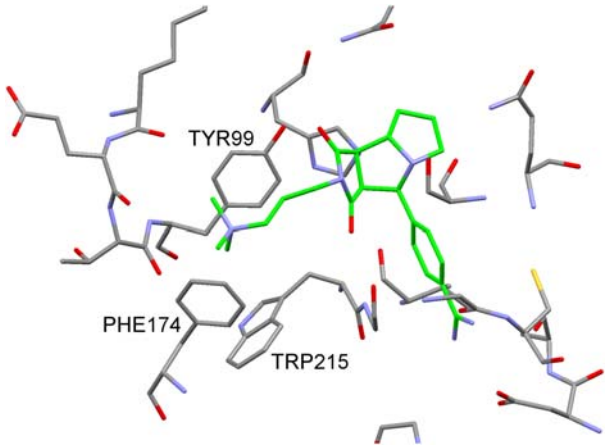

Fig. 6 Cation–π interaction between a ligand $-NMe_3^+$ group and an "aromatic box" defined by three protein side chains of factor Xa (PDB code 2BOK).

Cation–π interactions in protein–ligand complexes can utilize any of the three naturally occurring aromatic amino acid side chains, though there is evidence that tryptophan is most commonly involved (presumably because it has the most electron-rich π-system).[157,158] The aromatic box motif, mentioned above in the context of factor Xa, is found in many unrelated proteins. This has been ascribed to convergent evolution.[159] The motif does not always involve the same number or types of aromatic side chains. The most famous example is probably in acetylcholinesterase (AChE), where it has evolved to bind the $-NMe_3^+$ group of acetylcholine. The binding of this cationic group in a hydrophobic pocket was a surprise to almost everyone when the first AChE crystal structure was solved,[160] the prevailing view at the time being that an anionic site would be needed. The triumphant exceptions were Dougherty and Stauffer, who had correctly predicted the truth a year earlier.[161] In addition to molecules containing $-NMe_3^+$ groups, AChE binds a wide variety of inhibitors, including tetrahydroaminoacridinium and the natural products galantamine and huperzine. They are structurally very diverse, but most have large, electron-deficient hydrophobic groups that can interact with the active-site aromatic side chains, particularly the key tryptophan residue.[162] Enzymes that contain aromatic boxes therefore offer excellent opportunities for designing patent-busting leads with novel scaffolds. Salonen et al. make the point that quaternary ammonium ions do not cross biological membranes but unionized tertiary amines do. In the factor Xa study discussed earlier, binding affinity was reduced by changing $-NMe_3^+$ to $-NHMe_2^+$, but not catastrophically (9 to 56 nM).[79] Therefore, use of weakly basic tertiary amines may give acceptable transport properties in the neutral form combined with the ability, after protonation, to form cation–π interactions at the binding site.

Cation–π interactions that involve guanidinium groups deserve particular mention because of the presence of this group in arginine. In a survey of 83 protein structures, Flocco and Mowbray found that the parallel stacked arrangement, in which arginine guanidinium groups are positioned directly over the center of the rings of aromatic side chains, occurs much more frequently than would be expected by chance. This is particularly so in functionally important regions of proteins. The arrangement leaves all three guanidinium nitrogen atoms free to donate hydrogen bonds, and it was therefore hypothesized that it provides conformational tethering of the arginine side chain while still allowing it to bind ligands. The aromatic ring might also tune the pK_a of the arginine hydrogen bond partner.[163] Arginine is commonly used for suppressing protein aggregation. Mass spectrometry on model peptides suggests that the guanidinium group preferentially binds to aromatic residues and it is hypothesized that this disrupts the aromatic–aromatic interactions that are known to drive aggregation.[164]

In conclusion, the cation–π interaction is seen in many protein–ligand complexes and can be an extremely useful design tool that offers the possibility of scaffold hopping. It is also implicated in protein–protein binding: in a survey, about half of protein complexes were found to contain at least one intermolecular cation–π pair.[165]

3.05.4.2.6 Aromatic rings as hydrogen bond acceptors

There is no doubt that aromatic rings can accept hydrogen bonds from XH donors (X = O, N). This is illustrated by the IsoStar plot showing the distribution of XH groups around indole rings in the CSD (Fig. 7). Many clear examples of nitrogen or oxygen atoms positioned above the center of one or other of the rings, particularly the 6-membered ring, can be seen. A rather old but still definitive study of XH···π hydrogen bonds in the CSD adds considerable detail.[166] The authors searched for XH contacts to substituted and unsubstituted phenyl groups in good-quality organic structures and categorized them by geometry. A minority had the XH group positioned above the ring with the X–H···RC angle greater than 150 degrees (RC = ring centroid). This geometry was more commonly seen for NH groups than for OH. A more common geometry had the XH group above the ring but tilted so that the hydrogen atom pointed toward one of the ring carbon atoms. The most common arrangement had the XH group positioned not over the ring but to one side of it, with the hydrogen pointing at a ring carbon. This was overwhelmingly the preferred

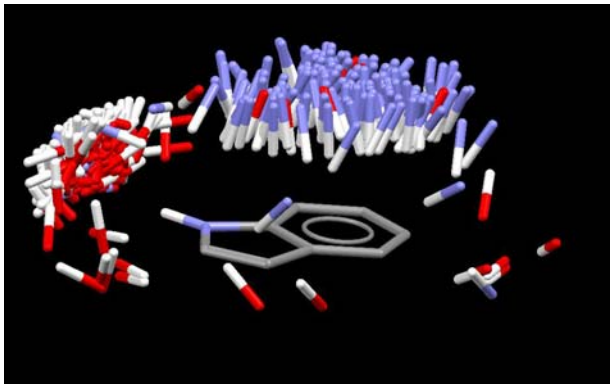

Fig. 7 IsoStar plot showing the observed distribution of OH and NH groups around indole rings in crystal structures from the CSD. Only contacts shorter than the sum of van der Waals radii minus 0.4 Å are shown. The cluster of predominately NH groups above the ring are forming XH···π hydrogen bonds, whereas the OH groups near the indole NH are accepting NH···O hydrogen bonds.

arrangement for OH groups and the authors suggested that these contacts may actually be C(phenyl)–H···OH hydrogen bonds, albeit with very bent C–H···O angles. Their conclusion was supported by a more recent CSD survey.[167]

Calculations on the water–benzene and ammonia–benzene hydrogen-bonded complexes gave interaction energies of −3.0 and −2.2 kcal mol^{-1}, respectively.[168] More recently, calculations on the alanine–benzene system gave a range of energies for the alanine–OH···π and alanine–NH···π hydrogen bonds, depending on the theoretical model used, but they were broadly in line with the earlier results. Using MP2, for example, the OH and NH interactions were calculated to have energies of −3.2 and −1.1 kcal mol^{-1}, respectively.[169] It has been shown experimentally that the stabilization energy of the OH···π hydrogen bonds is primarily electrostatic in origin and can be as large as −3 kcal mol^{-1}. As expected, the strength of the electrostatic interaction decreases in the order OH > NH > SH.[170,171]

A survey of 592 high-resolution protein crystal structures found 1311 putative XH···π hydrogen bonds (X = N, O, S) and concluded that the best of the aromatic acceptors, tryptophan, accepts one hydrogen bond per 5.7 residues.[172] However, the geometric criteria used to define the XH···π hydrogen bond were relatively lax. Further, and crucially, no checks were made that the XH group was not donating to a conventional (oxygen or nitrogen) acceptor. This leaves the possibility that the XH···π contact may be little more than incidental. And an even bigger snag: despite all the evidence that aromatic rings can act as hydrogen-bond acceptors, it is unusual to find convincing examples of NH···π or OH···π hydrogen bonding between proteins and ligands. There are a few, such as the complex of human cartilage glycoprotein-39 and chitotetraose (Fig. 8).[173] The reason for their scarcity is not hard to find: OH and NH groups form much stronger hydrogen bonds to water than they do to aromatic rings. Therefore, the desolvation cost will rarely make protein–ligand XH···π hydrogen bonding a viable proposition and the interaction is consequently of little use to the drug designer.

3.05.4.2.7 Anion–π: An interaction in search of a medicinal role

As noted earlier (see "The interaction formerly known as π-stacking"), the electrostatic potential above and below aromatic rings loaded with electron-withdrawing substituents is positive, in contrast to most aromatic systems; hexafluorobenzene is the classic example. The same can occur in rings with several heteroatoms, such as triazine.[174] The "anion–π" interaction occurs between

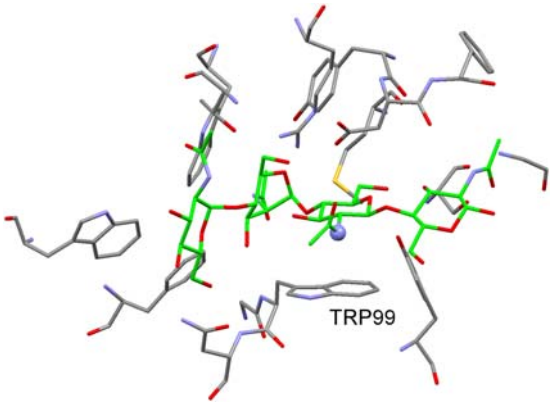

Fig. 8 A rare example of an NH···π hydrogen bond between a ligand and a protein (PDB code 1NWU; donor nitrogen shown as sphere).

a positively polarized ring such as C_6F_6 or triazine and an anion (halide, perchlorate, phosphate, etc.) positioned more or less centrally over the ring. It owes its stability principally to electrostatic attraction, although polarization and dispersion also contribute.[175] The term "anion–π" is misleading, suggesting as it does that π-electrons are important: it is positive rather than negative potential above the ring that is required for the interaction to occur. Theoretical calculations suggest that the interaction energies can be comparable with those of cation–π interactions—perhaps weaker when the aromatic ring is charge neutral but stronger with positively charged rings.[176] Despite some skepticism,[177] it is clear that the interaction has been frequently observed in small-molecule crystal structures, and also in solution and the gas-phase.[176,178,179] It has been exploited in the design of synthetic anion receptors.[180]

How relevant the interaction is in biology is uncertain. It may be implicated in chloride ion transport. As a proof-of-concept, model "anion–π slides" have been synthesized that successfully transport halide ions along electron-deficient aromatic oligomers.[181] Short contacts between anions and aromatic rings have been found in surveys of crystal structures in the PDB, though whether these are anion–π interactions is open to question.[178,182] Moreover, of the aromatic systems found in naturally occurring amino acids, only the protonated form of histidine is electron deficient and therefore suitable for anion–π interactions. This and the requirement for an anionic ligand would seem to limit the potential value of anion–π interactions in drug design. There is more hope, perhaps, in the nucleic acid area, since nucleotide bases contain electron-withdrawing heteroatoms. It has been suggested that interactions between oxygen lone pairs and protonated nucleobases could be significantly stabilizing.[183] For now, though, it seems unlikely that the anion–π interaction will ever be as useful to the medicinal chemist as its cousin, the cation–π.

3.05.4.2.8 CH···π interactions

This section covers all types of CH interactions with aromatic π-systems, including those in which the CH group itself belongs to an aromatic group. The latter are effectively T- or TT-shaped (edge-to-face) aromatic–aromatic interactions (see "**The instructive example of the benzene dimer**"), which some authors prefer to consider separately.

The CH···π interaction is weak but not insignificant. In the gas-phase, the energy of the methane–benzene cluster was measured spectroscopically as -1.03 to -1.13 kcal mol^{-1}.[184] High-quality CCSD(T) calculations on other benzene–alkane clusters showed that the optimum geometries of the dimers invariably have one of the CH groups pointing toward the benzene π-system. After correction for zero-point vibrational energy, binding energies were computed as -1.62, -2.49, -2.63, -2.45, and -2.59 kcal mol^{-1} for ethane, propane, *n*-butane, *iso*-butane, and cyclohexane, respectively.[185] In all of the dimers, the dominant contribution to the interaction energy comes from dispersion, due mainly to the relatively polarizable carbon atoms. There is a monotonic correlation between alkane size and binding energy until the benzene–cyclohexane complex, which is no more favorable than the *n*-butane complex. This suggests that only the closest four carbon atoms of the alkane make a significant contribution to the interaction energy.

However, electrostatics can also play a role. It is accepted that the CH···π interaction becomes stronger as the acidity of the hydrogen atom increases.[186–188] Gas-phase measurements on the benzene–ethylene and benzene–acetylene clusters gave association energies of -1.4 and -2.7 kcal mol^{-1}.[189] The former is not appreciably different from that of benzene–ethane (mentioned previously) but the latter is substantially more favorable, as would be expected from the greater acidity of the acetylenic hydrogen atom. The benzene–dichloromethane and benzene–chloroform dimers are even more stable: -3.8 and -5.2 kcal mol^{-1}, respectively, as measured by two-color ionization spectroscopy.[190] Theoretical calculations by the same authors gave results consistent with the experimental measurements. It was concluded that the benzene complexes with the haloalkanes are stabilized not only by dispersion but also by significant electrostatic attraction between the acidic hydrogen atom and the benzene π system.

On the basis of these and other results, and particularly because of the importance of dispersion, Tsuzuki argues that most CH···π interactions should not be classed as hydrogen bonds, though the descriptor might perhaps be applicable to the interactions formed by unusually acidic CH groups.[188] Other scientists take an opposing view and routinely use the term "CH···π hydrogen bond".[73] For what it is worth, your present author is persuaded by Tsuzuki's arguments.

It is clear both from solution measurements and crystal structures that CH···π interactions are influenced by aromatic-ring substitution patterns. Chemical double-mutant cycles on zipper complexes were used to quantify CH···π interactions of the edge-to-face type (ie, the CH group is part of an aromatic ring). Interaction energies depended on the substituents present on the rings, varying from $+0.2$ to -1.2 kcal mol^{-1}.[191] The energies correlated with Hammett substituent constants, tending to become more favorable with electron-withdrawing substituents on the CH donor ring and electron-donating groups on the ring providing the π system. Cole et al. used the IsoStar database to investigate the spatial distribution of C(sp^3)–H groups around phenyl, *p*-methoxyphenyl, *p*-tolyl, *p*-nitrophenyl, pentafluorophenyl, and 3,5-dinitrophenyl groups in small-molecule crystal structures.[192] As the ring substitution became more electron withdrawing, the density of CH hydrogens above the aromatic ring was observed to decrease. Ring heteroatoms had a similar effect, the CH density being high above indole ring systems and low above pyridine rings (and, in the latter case, displaced from the ring center toward the ring nitrogen).

In another CSD study, Takahashi et al. determined the mean distance between the hydrogen atom and the aromatic-ring plane for contacts involving various types of CH groups.[193] As would be expected, the distance becomes progressively longer as the acidity of the hydrogen atom decreases: 2.53, 2.62, 2.61, 2.72, and 2.75 Å for Cl_3C–H, Cl_2HC–H, C(sp)–H, C(sp^2)–H, and C(sp^3)–H, respectively. CSD analysis also showed that the CH group has a distinct tendency to interact with the center of the ring; this is clearly discerned after correction for a geometric factor.[194] If CP is the closest point on the ring plane to the hydrogen atom, the C–H···CP angle can be very nonlinear, the mode of its distribution being about 140 degrees. In other words, there is not a strong propensity for the CH group vector to be perpendicular to the ring plane.[73]

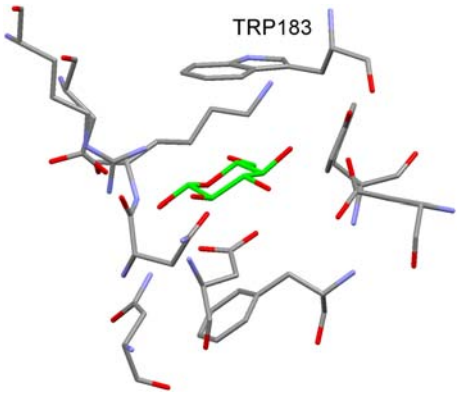

Fig. 9 A common sugar binding motif: the pyranose ring forms C–H···π interactions by stacking with a tryptophan side chain (galactose binding protein; PDB code 2HPH).

There is substantial evidence that CH···π interactions influence protein structures.[73] For example, it has been known for many years that aromatic–aromatic side chain interactions show a preference for edge-to-face orientations.[195,196] From a considerable body of more recent work, three examples will further illustrate the point. The first relates to the 35-residue peptide α_2D, which folds as a dimeric four-helix bundle with two stacked Phe–Phe pairs buried in the hydrophobic core. When one of the phenylalanine residues of each pair was mutated to cyclohexylalanine, the resulting complex was found to be more stable than the original system. This was ascribed to cyclohexyl–phenyl stacking, with the three axial CH groups on one face of the saturated ring pointing toward the π-cloud of the aromatic ring. The stabilization amounted to about 0.7 kcal mol^{-1} per CH···π interaction.[197] Proton NMR studies on short peptides show that the Pro–Pro peptide bond in Pro–Pro–Phe adopts *cis* and *trans* geometries about equally, with the former stabilized by CH···π interactions between the terminal proline and phenylalanine side chains.[198] The stabilization of *cis*-peptide geometries by proline–aromatic interactions is more effective with tyrosine and tryptophan than phenylalanine, suggesting an electronic effect, and the *cis*/*trans* ratio can be tuned by inserting electron-withdrawing or -donating substituents onto the 4-position of the phenyl group.[199]

Of greatest importance to medicinal chemistry is the extent to which CH···π interactions are involved in the binding of protein ligands. Small sugar molecules, for example, often bind by stacking with aromatic residues, particularly with tryptophan (Fig. 9).[200,201] The CH groups on pyranose rings are polarized by the proximal oxygen atoms and therefore well suited to the formation of CH···π interactions. Although many AChE inhibitors bind via cation–π interactions, there are others which bind to the same aromatic residues by means of CH···π interactions involving (relatively) unpolarized CH groups.[202] Changing the morpholine group of a factor Xa inhibitor into morpholin-3-one improved the IC_{50} from 43 to 0.7 nM. The extra carbonyl group did not interact directly with the protein, the inference therefore being drawn that it improves binding by polarizing a ring CH_2 group that is positioned above the face of a tryptophan side chain.[44,203] Similarly, in a series of steroid dehydrogenase inhibitors, binding was improved from 110 to 17 nM by introducing a fluoro substituent between two CH groups in contact with a tyrosine ring.[44,204]

In summary, CH···π interactions are among the most important for medicinal chemistry simply because the participating groups are so common. Although weak, they offer the possibility of being strengthened by introducing appropriate substituents, and several CH···π interactions can add up to a useful amount of binding energy. However, it is rarely appropriate to regard them as hydrogen bonds.

3.05.4.3 The Occupation of Nonpolar Pockets by Ligand Hydrophobic Groups

A classic result from host–guest chemistry was obtained by Mecozzi and Rebek, who determined that optimum binding of a hydrophobic guest is obtained if it occupies about 55% of the volume of the cavity in the host.[30] While this conclusion was based on synthetic host–guest systems, a similar figure has been arrived at for some protein–ligand complexes.[55] A nonpolar side chain in a series of plasmepsin inhibitors was systematically varied in size, ranging from *n*-butyl to *n*-undecyl. The volume of the pocket that the side chain occupied was computed from the X-ray structure and the ratios PC = (volume of side chain)/(volume of pocket) were calculated. A plot of IC_{50} against PC showed a bell-shape curve. At one end of the PC range was the *n*-butyl derivate, with PC = 30%, IC_{50} = 4190 nM; at the other extreme was *n*-undecyl, with PC = 75%, IC_{50} = 1950 nM; the optimum was obtained with 4-isopropylbutyl and 3-cyclopentylpropyl, for which PC = 50, 52% and IC_{50} = 30 nM. Kashiwagi et al. got similar results on the vitamin D receptor, their best in vitro agonist having a PC value of 56%.[205]

While these results are nicely consistent, the full truth is unlikely to be that simple. Although rare exceptions are known,[206] nonpolar cavities in uncomplexed proteins are almost invariably hydrated, and it is often the enthalpic and entropic consequences of displacing the water that drive cavity–ligand binding.[207,208] If the ligand is a little too small, the possibility exists of trapping a water molecule with deleterious entropic consequences. Once the ligand is large enough to displace all the water in the cavity, further size increases may give little or no improvement to binding affinity, and must eventually become counterproductive. The

optimum percentage occupancy of any particular cavity must depend on the nature of the water network within it. One thing is clear: binding affinity can be very sensitive to even small changes in the volume occupancy of a nonpolar pocket. A good example is provided by the S1 pocket of dipeptidyl peptidase IV. An inhibitor pair differing only by a single *meta* methyl substituent on the phenyl group occupying this pocket had K_i values of 200 and 4.6 nM for the unsubstituted and methylated compounds, respectively.[209]

In their perspective on the art of filling apolar pockets, Zürcher and Diederich contrast two enzymes, IspE and IspF, in the non-mevalonate pathway of isoprenoid biosynthesis.[55] The active site of the latter contains a small, hydrophobic pocket that is evidently flexible, since its conformation changes from one crystal structure to the next. Occupation of this pocket yielded little if any gain in binding affinity. IspE, on the other hand, contains a small but much less flexible ("preorganized") pocket. Optimal filling of this pocket delivers an inhibitor with $K_i = 0.29$ μM, compared with 2.6 μM when the pocket is largely unoccupied. The authors conclude that large affinity gains can be obtained by filling preorganized pockets, but the occupancy of very flexible pockets results either in poor enthalpic interactions or a loss of protein flexibility with a consequential entropic penalty.[210]

3.05.4.4 Halogen Bonding

3.05.4.4.1 Background

The strangest thing about the halogen bond is that it has been known for a long time. Perhaps, it just needed some good public relations before it was taken seriously. Whatever the reason, the growth in interest in the interaction over the past few years has been explosive.[211] It is truly the bee's knees, the cat's pajamas, the must-have interaction for the contemporary drug designer.

The first evidence for halogen bonding actually dates back a century and a half, to Guthrie's 1863 preparation (on the island of Mauritius) of the adduct of iodine and ammonia.[212] A considerable time later, Hassel and Hvoslef solved the beautiful crystal structure of the bromine–dioxane complex (**Fig. 10**), which shows the short contact distance (2.72 Å) and the close-to-linear angle of approach (Br–Br···O = 178 degrees) that we now know to be so characteristic of halogen bonds.[213] The authors observed that the geometry indicated "a very strong interaction between the bromine and oxygen atoms." In due course, a succession of CSD surveys and some quantum-mechanical calculations established a number of basic facts. In addition to the dihalogens, carbon-bound halogen atoms (C–X, X = Cl, Br, I) can also form the interaction. While nucleophiles (Nu) preferentially approach with C–X···Nu angles of 165 degrees or more, electrophiles (E) favor C–X···E angles of around 100 degrees. It is the former interaction that is termed the "halogen bond." The attractive nature of C–X···Nu is primarily due to electrostatic effects. X···Nu distances can be much shorter than the sum of vdw radii.[214–217] Subsequent work has not altered this picture to any significant extent, although considerable detail has been added.

The nature of halogen bonding has been widely studied by theoreticians.[218–220] The electrostatic potential around carbon-bound chlorine, bromine, and iodine atoms is not uniformly negative, even though halogens are electronegative elements. In CH_3Br, CBr_4, and CCl_4, for example, the potential is positive in the region along the extension of the C–X bond; elsewhere, it is negative. In CH_3F, on the other hand, it is negative throughout.[221] The positive area is called the "σ hole." Its origins are explained rather nicely by Clark et al.[222] in terms of the hybridization of the bonding and lone-pair orbitals of the halogen atom. Two of the halogen unshared electron pairs occupy p orbitals perpendicular to the C–X direction, resulting in a high electron density and negative electrostatic potential in a belt around the C–X axis. The halogen atom's contribution to the C–X σ bond is predominately a p orbital, meaning that the third lone pair has mainly s-orbital character and is rather diffuse. The consequence is that the nuclear charge is poorly shielded along the extension of the C–X bond, resulting in the σ hole. A nucleophile approaching with C–X···Nu close to 180 degrees therefore feels an electrostatic attraction—the halogen bond. The effect is enhanced by polarization of the X atom if the other groups on the C–X carbon atom are electron withdrawing.

A range of groups can play the role of nucleophile, including carbonyl and ether oxygen, pyridine and other sp^2-hybridized nitrogen atoms, amine nitrogen, and perhaps—but very arguably—the π-systems of aromatic groups (see "**Aromatic-ring interactions with halogens**").[223,224] Some calculated interaction energies are given in **Table 3**, together with those of typical strong,

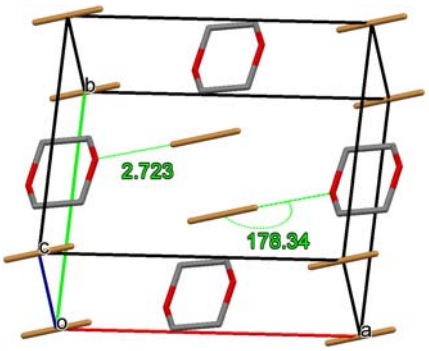

Fig. 10 Crystal structure of the bromine–dioxane complex (CSD code DOXABR).

Table 3 CCSD(T)/CBS calculated energies of some illustrative halogen bonds and hydrogen bonds

Type	*Donor*[a]	*Acceptor*[a]	ΔE *(kcal mol*$^{-1}$*)*[b]	*Ref.*
Hydrogen bonds				
OH···O=C	Formic acid	Formic acid	−9.31[c]	[36]
NH···O=C	Formamide	Formamide	−7.98[c]	[36]
OH···N	Water	Ammonia	−6.49	[35]
OH···O	Water	Water	−5.01	[35]
OH···π	Water	Ethene	−2.56	[35]
CH···π	Ethyne	Ethyne	−1.52	[35]
Halogen bonds				
C(sp^3)–Cl···O	Chloromethane	Formaldehyde	−1.17	[225]
C(sp^2)–Cl···O	Chlorobenzene	Acetone	−1.49	[225]
C(sp^3)–Br···O	Bromomethane	Formaldehyde	−1.72	[225]
C(sp^2)–Br···O	Bromobenzene	Acetone	−2.43	[225]
C(sp^3)–I···O	Iodomethane	Formaldehyde	−2.38	[225]
C(sp^2)–I···O	Iodobenzene	Acetone	−3.46	[225]
C(sp^2)–I···S	Iodobenzene	Methanethiol	−3.08	[225]
C(sp^2)–I···N	Iodobenzene	Trimethylamine	−5.81	[225]

[a]Somewhat confusingly, the halogen atom (the electron acceptor) is conventionally termed the *donor* of a halogen bond while the electron donor (oxygen, nitrogen, or whatever) is the *acceptor*. Think of it as donating or accepting the σ hole.
[b]Calculated interaction enthalpy.
[c]Dimer contains two hydrogen bonds, so value given is half the dimerization energy.

moderate, and weak hydrogen bonds for comparison. Iodine generally forms stronger halogen bonds than bromine, which in turn tends to form stronger bonds than chlorine. As a general rule, halogen-bond energies are comparable with those of weak hydrogen bonds, although they can be stronger in exceptional circumstances. Solution calorimetry was used to determine the enthalpy of formation of the 1:1 complex between iodo-perfluorocyclohexane and 2,2,6,6,-tetramethylpiperidine.[226] With such a highly polarized iodine, the result, −7.5 kcal mol^{-1}, is about as strong as a halogen bond gets. Other experimental data on strong halogen-bond donors are available; for example, association constants of fluorinated iodoalkanes and iodoarenes with a range of acceptors have been measured in solution by NMR titration.[227,228]

While most regard halogen bonding as primarily an electrostatic interaction, this is not a unanimous view. In a recent paper, it was suggested that charge transfer plays a significant role,[229] with donation of electron density from the nucleophile lone pair into the relatively low-lying C–X σ^* antibonding orbital.

3.05.4.4.2 Fluorine as a halogen-bond donor

It isn't. Or at least, only so weakly and in circumstances sufficiently exceptional that the possibility need not trouble the medicinal chemist.[230,231]

3.05.4.4.3 Halogen-bond geometries

The geometric preferences of halogen bonds are well established, both from X-ray data[217] and theoretical calculations.[217–219] Halogen···acceptor distances tend to be short and can be less than the sum of the atoms' vdw radii by 0.3 Å or more. As noted earlier, the most striking feature is the preference for a linear or near-linear geometry at the halogen. Deviations of 25–30 degrees from the linear C–X···acceptor arrangement reduce interaction energies by about 50%.[232] If the deviation is 40 degrees or more, it is doubtful whether an interaction should be called a halogen bond. Calculations on model complexes between bromobenzenes or bromopyrimidines and acetone indicate that a Br···O=C angle of 120 degrees or slightly higher is optimum,[219] corresponding to approach of the halogen along an oxygen lone-pair direction. However, there is evidence from the PDB that halogen atoms can approach carbonyl oxygen atoms from a direction approximately orthogonal to the C=O plane, corresponding to interaction with the carbonyl π-electron density.[233] This is supported by the higher-precision structural data in the CSD. For example, the structure shown in Fig. 11 contains a clear-cut Br···O halogen bond (short Br···O distance, near-linear C–Br···O angle) in a near-orthogonal geometry.[234]

3.05.4.4.4 Halogen bonds in protein–ligand complexes

In an interesting case study, the influence of halogen bonding on the binding affinities of ligands to human cathepsin L was examined.[141] A series of covalently bound ligands was positioned with a phenyl group occupying the S3 pocket of the enzyme. Substituents at the *para* position of the phenyl were suitably located to interact with the backbone carbonyl oxygen atom of Gly61. The IC_{50} value of the unsubstituted phenyl derivative was 0.29 μM, whereas those of the *para* methyl-, fluoro-, chloro-, bromo-, and iodophenyl analogs were 0.13, 0.34, 0.022, 0.012, and 0.0065 μM, respectively. The similar sizes of methyl and chlorine argue against a steric effect. It is therefore reasonable to argue that the increase in affinity along the series H ≈ Me ≈ F < Cl ≈ Br < I is due to halogen bonding, remembering that the C=O···X interaction becomes stronger as the atomic number of *X* increases. The low

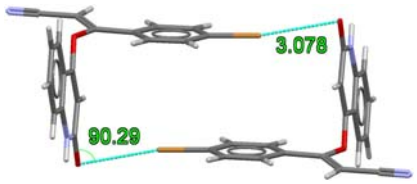

Fig. 11 Br···O═C halogen bonds formed approximately orthogonally to the carbonyl-group plane (CSD structure IDOZAD).

affinity of the fluoro compound can be ascribed to O···F electrostatic repulsion. Other ligand series, with additional substitution of the phenyl ring or its replacement with pyridyl or thienyl, showed similar trends. Crystal structures of some of the complexes established that the halo-substituents were in the correct position for the halogen bond. As the authors pointed out, however, halogen bonding might not be the only factor in play. The complexes may also be stabilized by CH···X interactions, and halo-substitution might affect the stacking energy between the aromatic ring and a proximal section of the protein backbone. Moreover, affinities were little altered by the introduction of electron-withdrawing substituents at other positions on the aromatic ring, although it might have been expected that this would strengthen halogen bonding through polarization.

The halogen bond in the cathepsin L complexes occurs in a polar, solvent accessible region of the protein. In contrast, ligands of MEK1 kinase have been shown to form halogen bonds in a predominately apolar pocket.[235] Again, the acceptor is a carbonyl oxygen atom (of Val127) and the donors are *para* substituents on a phenyl ring. Binding affinity improves as the substituent is varied along the series F (IC_{50} = 0.12 μM), H (0.052 μM), Cl (0.026 μM), Br (0.0077 μM), and I (0.0020 μM). Crystallography on the iodo-derivative confirmed the presence of the halogen bond, with the substituent pointing directly at the oxygen atom. All the other contacts in the pocket are hydrophobic. That the improvement is only modest when changing –H to –Cl was ascribed to a longer than optimal Cl···O distance, a problem not present with the heavier halo-derivatives, where the C-halogen bond lengths are longer and the halogen atoms bigger (note, however, the comments on Cl···O halogen bonds in "**The skeptical chemist's view of halogen bonding**").

There have accumulated numerous other instances of the use of halogen bonding in ligand design, some more convincing than others. As expected, affinity improvements depend on the halogen and the interaction geometry, with iodine being particularly effective. For example, changing –H for –I in a series of adenosine kinase inhibitors improves activity by over two orders of magnitude.[236] In contrast, introduction of an iodo substituent in a series of β-secretase inhibitors resulted in only a modest 26-fold increase in affinity.[237] The I···O distance is very long (4.2 Å) and the C–I···O angle very small (139 degrees), so it is probable that the increased binding is less due to a σ-hole interaction than to dispersion.[232] Several authors have reviewed other examples of halogen bonding in protein–ligand complexes.[44,232,238,239] The importance of halogen bonds involving chlorine is open to doubt (see "**The skeptical chemist's view of halogen bonding**") However, the antibacterial molecule triclosan binds with one of its three chlorine atoms forming a reasonably convincing interaction to a backbone carbonyl oxygen atom at the mouth of the binding site. Although Cl···O interactions are weak, binding affinity could not be improved by replacing this chlorine with hydrophobic or hydrogen-bond donor groups.[240]

Of particular interest is a complex of HIV reverse transcriptase, in which an iodine atom of the inhibitor interacts with the backbone carbonyl oxygen of Tyr188 in a direction approximately orthogonal to the carbonyl plane, allowing the oxygen to maintain a β-sheet hydrogen bond to Tyr181 (**Fig. 12**).[241] This nicely supports the argument of Voth et al. that carbonyl acceptors can accommodate both halogen and hydrogen donors because the former can interact with the C═O π-orbital, leaving the oxygen lone pairs for the hydrogen-bonding group.[233]

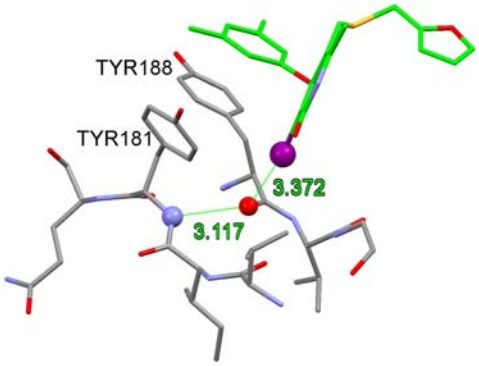

Fig. 12 Halogen bond to the carbonyl oxygen atom of Tyr188 in HIV reverse transcriptase (PDB code 2BE2). The direction of the interaction leaves the oxygen atom free also to form a structural hydrogen bond to Tyr181.

In their extensive review of halogen bonding in medicinal chemistry, Wilcken et al. point out that proteins have other potential acceptors for halogen bonds apart from backbone carbonyl oxygen.[232] They give examples of protein–ligand complexes with halogen contacts to aspartate carboxylate and tyrosine hydroxyl oxygen atoms.

3.05.4.4.5 Halogen-enriched fragment libraries

In a lead generation exercise targeted at the p53 cancer mutation Y220C, Wilcken et al. designed a fragment library enriched in compounds containing the heavier halogens.[242] They had noticed that a drugable surface crevice of the protein contains a backbone carbonyl group suitably positioned to accept halogen bonds. The fragment library was designed using standard criteria but setting an upper limit on the number of heavy atoms rather than a molecular-weight limit. All molecules were required to contain a heavy halogen. Of 79 compounds screened, the best was a di-iodophenol, which bound with a dissociation constant of 184 ± 23 μM. Crystal-structure analysis showed that one of the iodine atoms forms the expected I···O halogen bond to the targeted carbonyl group. Optimization of this lead resulted in a series of iodophenols with binding modes retaining the I···O halogen bond and having significantly improved binding affinities.

3.05.4.4.6 Halogen bonding in drug development

Xu et al. defined the ratio X/F as the number of chemical entities at a given stage of the drug development process that contain X (chlorine, bromine, or iodine) to the number that contain fluorine.[243] They reasoned that X/F might say something about the possible importance of halogen bonding in drug development, since X atoms can form the interaction and F atoms cannot. An interesting result came out of this: the X/F ratios at drug discovery, clinical stage I, stage II, stage III, pre-registration/registered, and launched are, respectively, 0.9, 0.9, 0.8, 1.0, 1.4, and 1.7. The overall percentage of molecules containing one or more X atoms rose from 44.0% at stage II to 63.3% at launch. It appeared that molecules containing X atoms are less likely to fail. The authors suggested that halogen bonding might play a role in tuning ADME/T properties, for example, by enhancing binding to plasma transport proteins. On the other hand, the numbers of molecules in the study with X = Br or I—the halogens best able to form halogen bonds—were small, so the conclusions drawn must be regarded as tentative.

3.05.4.4.7 The skeptical chemist's view of halogen bonding

Halogen bonding has attracted so much attention in recent years that cynics may be tempted to wonder how much of it is justified. After all, if the interaction is genuinely useful in ligand design, why did it take so long to be recognized and exploited? But even for a confirmed skeptic like your author, there is too much evidence to sustain disbelief—from crystallography, theoretical calculations, and protein–ligand binding affinity studies. The halogen bonds formed by iodine and bromine can be useful tools for structure-based design, and, as the Roche group noted, they have the advantage of a lower desolvation cost than classical hydrogen bonds.[44]

Chlorine, however, is another matter, and of 1574 drugs surveyed in 2012, 14.7% contained chlorine, compared with only 1.5% for bromine and 1.1% for iodine.[232] Chlorine forms very weak halogen bonds. This is illustrated not only by the data in **Table 3** but also by the observation that Cl···O and Cl···N contacts in organic crystal structures are no more common than would be expected by chance (see "**Assessing the Relative Importance of Molecular Interactions**"). Only when it is in a highly polarizing environment—for example, at the 2-position of an imidazole ring—does chlorine form significant numbers of these contacts.[89] Theoretical calculations also indicate that polarization is critical. For example, chlorine in CH_3COCl has a positive region on its electrostatic surface, but in CH_3Cl it does not.[244] When analyzing protein–ligand crystal structures, it is debatable whether a Cl···O contact should be assumed important to binding unless the chlorine is in an electron-withdrawing environment and, even then, only if the C–Cl···O angle exceeds 150 degrees.

Some researchers have compared halogen bonds to the hydrogen bonds formed by OH and NH groups as they can both be accepted by oxygen or nitrogen and are both highly directional. Nevertheless, there are important differences: in their relative energies, of course, and also in the extent to which the donor groups are discriminating in the interactions they form. **Fig. 13** shows the relative frequencies with which bromine, iodine, and OH/NH hydrogen atoms form their shortest (relative to vdw radii)

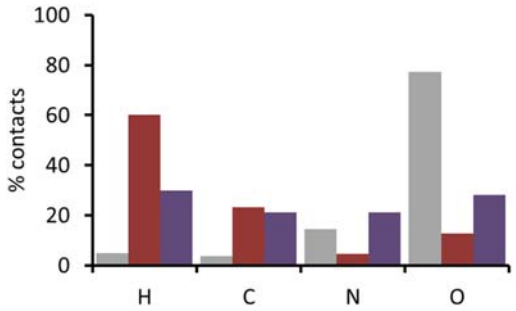

Fig. 13 Relative frequencies with which OH and NH hydrogen (*gray bars*), bromine (*brown bars*), and iodine (*purple bars*) atoms form their primary intermolecular contacts to hydrogen, carbon, nitrogen, or oxygen. Statistics based on well-refined (R-factor $\leq 5\%$, no disorder, all atoms located) organic crystal structures in the 2015 version of the CSD.

intermolecular, line-of-sight contacts to H, C, N, or O in CSD organic crystal structures. The hydrogen atoms overwhelmingly prefer to interact with N or O—in other words, form hydrogen bonds—whereas the halogens frequently interact with H or C rather than N or O. Hence, the halogens are much less discriminating in their interactions than the hydrogen atoms. This conclusion is consistent with a recent experimental study that indicated that hydrogen bonds are more important than halogen bonds in determining packing arrangements in crystal structures.[245]

3.05.4.5 Fluorine, the Little Atom That Couldn't

The importance of fluorine in medicinal chemistry hardly needs elaboration.[246] By 2014, it was estimated to occur in 25% of drugs.[247] It is used for a multitude of purposes: to block oxidative and hydrolytic metabolism, to improve bioavailability by tuning lipophilicity and the pK_a values of neighboring nitrogen atoms, to inhibit racemization, to reduce activity at the hERG channel, and so on.[248–250] As it is so common, it is particularly important to understand the interactions it makes at protein binding sites. They are dictated by the unusual properties of the fluorine atom: small, very electronegative, and difficult to polarize. Hence, although fluorine has similarities with the other halogens, it deserves its own little section in this article. The discussion is confined to fluorine atoms that are covalently bonded to carbon. The title of the section was provoked by a 2005 paper with the arresting title "Fluorine in crystal engineering—'the little atom that could'".[251] The approach preferred here is to focus first on the things that fluorine cannot do. For practical purposes, it cannot act as the donor in halogen bonds; it does not interact favorably with electronegative atoms or π-systems[252]; and it cannot compete with oxygen or nitrogen as an acceptor of hydrogen bonds from OH and NH donors. Between them, these constraints rather restrict what fluorine *can* do.

The last of the three constraints deserves discussion. Two papers in the 1990s both concluded that C–F···H–(O,N) hydrogen bonds hardly ever occur, either in small-molecule or macromolecular crystal structures.[253,254] At first sight this is rather surprising because of the electronegativity of fluorine. It was ascribed to two factors. First, fluorine has a low proton affinity due to its low-lying lone-pair orbitals and tightness of its electron shell. Second, it is unable to modify this by intramolecular electron delocalization or intermolecular cooperative effects. Subsequently, some researchers were at pains to prove that these hydrogen bonds can occur, providing theoretical,[255] spectroscopic,[256] and crystallographic evidence.[257] In fact, this rather misses the point: it was never argued that the hydrogen bonds *cannot* form, simply that they only do so rarely. Fluorine is a much weaker acceptor than sp^2 hybridized nitrogen and virtually all types of oxygen, and hence is out-competed. The best estimate of the energy of the fluoromethane···methanol hydrogen bond is -3.89 kcal mol^{-1},[225] which ,is less favorable than typical hydrogen bonds involving OH or NH donating to common oxygen or nitrogen acceptors.[258]

It is true that C–F···H–(O,N) interactions are occasionally associated with an increase in protein–ligand binding affinity.[44] Further, the authors of a 2004 PDB study concluded that 10% of ligand C–F groups form close contacts to OH or NH groups.[259] However, the mean H···F distance (hydrogen atoms were added in calculated positions) was 2.313 Å. This is much longer than average O···H and N···H hydrogen-bond distances,[93] implying that the interactions are weak. Also, it is not clear how many of the contacts were components of bifurcated interactions, in which the donor group also hydrogen bonds to an oxygen or nitrogen acceptor. From the donor's point of view, an interaction with fluorine alone is a poor option, but a bifurcated interaction with fluorine and oxygen or nitrogen is better. An example is provided by the thrombin complex shown in **Fig. 14**.[260] A backbone NH clearly interacts with a C–F group but the backbone conformation at that point allows an additional (albeit very nonlinear) hydrogen-bonding contact to the carbonyl oxygen of the next residue.

So what does a C–F group do when it is thrown into the milieu of a protein binding site? It is likely to be out-muscled by oxygen or nitrogen acceptors in the competition to interact with OH or NH donor groups. Close contacts to oxygen atoms or π-systems are electrostatically unfavorable. The most viable option, and by far the one most commonly observed,[261] is to interact with carbon-

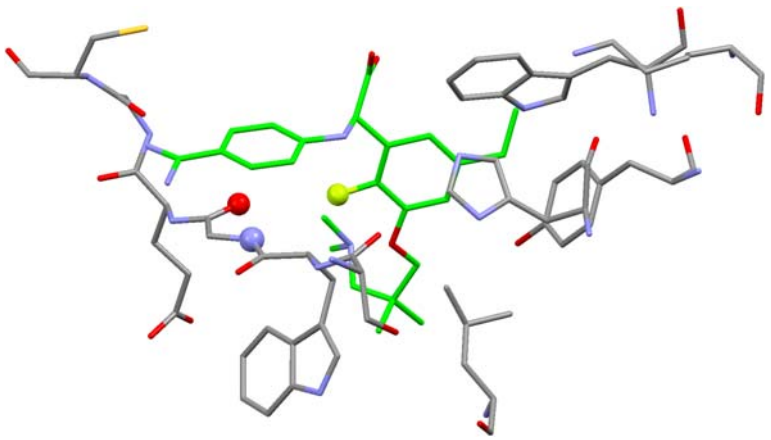

Fig. 14 Bifurcated hydrogen-bonding interaction in a thrombin complex (PDB code 2V3O). The atoms involved are shown as spheres.

bound hydrogen atoms. They are plentiful, accessible, and almost always slightly electropositive. The situation is similar to that seen in small-molecule crystal structures, where C–F···HC has an R_F value of 1.7, indicating that interactions of this type occur almost twice as often as would be expected by chance (see "Assessing the Relative Importance of Molecular Interactions").[89] Intriguingly, the R_F of C–F···HC is significantly higher than that of C–Br···O, although it is undoubtedly the weaker interaction. This can plausibly be explained by remembering that every atom in a crystal structure has to be near an atom in a neighboring molecule. Bromine can form energetically acceptable contacts to a range of atom types. Fluorine, on the other hand, is a fussy sort of atom: carbon-bound hydrogen is one of the few neighbors with which it is comfortable. Hence, there are lots of CH···F contacts. Another possible factor is that C–Br···O interactions have strong directional preferences whereas C–F···HC interactions do not, so it may be more difficult to find molecular arrangements that will accommodate the former.

Another interaction is worth mentioning, less common than C–F···HC but certainly stabilizing. It has been established that C–F groups can interact with carbonyl carbon atoms (which of course carry a net electropositive charge) from a direction approximately perpendicular to the carbonyl plane.[262] This and similar interactions are further discussed in the next section.

3.05.4.6 Carbonyl-Group Interactions

In addition to its more familiar interactions (hydrogen bonds, halogen bonds), a carbonyl group can interact favorably with a polar bond such as C–F, C–Cl, or C=O positioned above the carbonyl-group plane. The best known interaction of this type is between two carbonyl groups. It was first studied in detail by Allen et al.[263] By searching the CSD, they identified three main types of geometry (Fig. 15): a slightly sheared, "stacked" motif with the C=O dipoles antiparallel (observed on 630 occasions); a highly sheared motif with the bond dipoles parallel (130 occurrences); and a motif in which the C=O vectors are mutually perpendicular (116 occurrences). In all three motifs, at least one of the carbonyl carbon atoms forms a close contact to the oxygen atom of the other group in a direction approximately perpendicular to the carbonyl-group plane. The stacked geometry is likely to be overrepresented in small-molecule crystal structures compared to protein–ligand complexes because of crystal-packing effects.[19] The highly sheared geometry is usually seen when the carbonyl groups are bonded to C(sp^2) atoms and the carbonyl–carbonyl interaction is part of a more extended stacking arrangement. A 2002 search for interactions between protein carbonyl groups and ligand ketones found roughly equal numbers of the stacked and perpendicular geometries (13 and 8, respectively) and no examples of the highly sheared, parallel arrangement.[264]

Turning to C–X···C=O (X = F, Cl), the IsoStar plots in Fig. 16 show the density distributions of fluorine and chlorine atoms around peptide linkages in PDB complexes. They clearly reveal a preference for the halogen atom to lie above and below the carbonyl carbon atom. (The secondary maximum in the C–Cl plot is partly due to large series of factor Xa and thrombin complexes, but may also indicate some halogen bonding contacts.) Searches of the CSD confirm that C–F···C=O and C–Cl···C=O contacts are numerous. The X···C=O angle tends to be close to 90 degrees but the C–X···C angle is highly variable and does not correlate with the X···C distance.[265] A histogram of the F···C=O angle and a scatterplot of the F···C distance against the C–F···C angle are given in Fig. 17.

Both the carbonyl–carbonyl and the halogen–carbonyl interactions are widely viewed as being mainly electrostatic in nature,[262] but with dispersion also making a significant contribution.[266] However, some theoreticians maintain that amide carbonyl–carbonyl interactions are stabilized by charge transfer.[267,268] Estimates of interaction energies vary widely. Intermolecular perturbation theory (IMPT) gave energies of -5.3 and -1.8 kcal mol^{-1} for the carbonyl–carbonyl interaction in the stacked antiparallel and orthogonal geometries, respectively.[263] Chemical double-mutant cycles on model systems suggested a free enthalpy of between -0.29 and -0.65 kcal mol^{-1}, depending on solvent, for the orthogonal interaction of two amide carbonyl groups.[266] The same authors calculated lower (more stabilizing) energies using IMPT. However, it was argued that the calculated values will never be achieved in crystal structures or solutions because of packing forces, steric constraints, and solvent effects. The interaction was considered

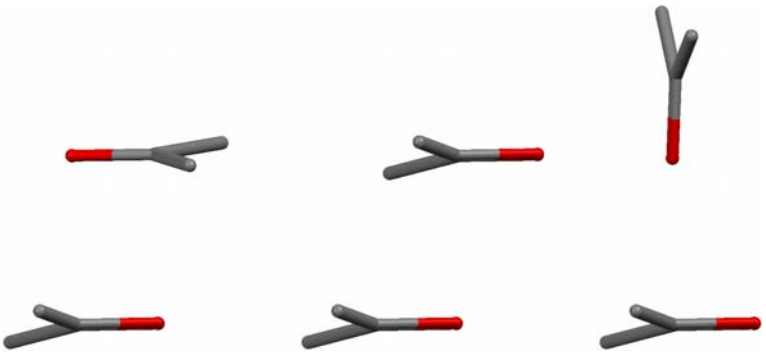

Fig. 15 Schematic representation of the three main types of carbonyl–carbonyl arrangement: stacked antiparallel (*left*), sheared parallel (*center*), and perpendicular (*right*).

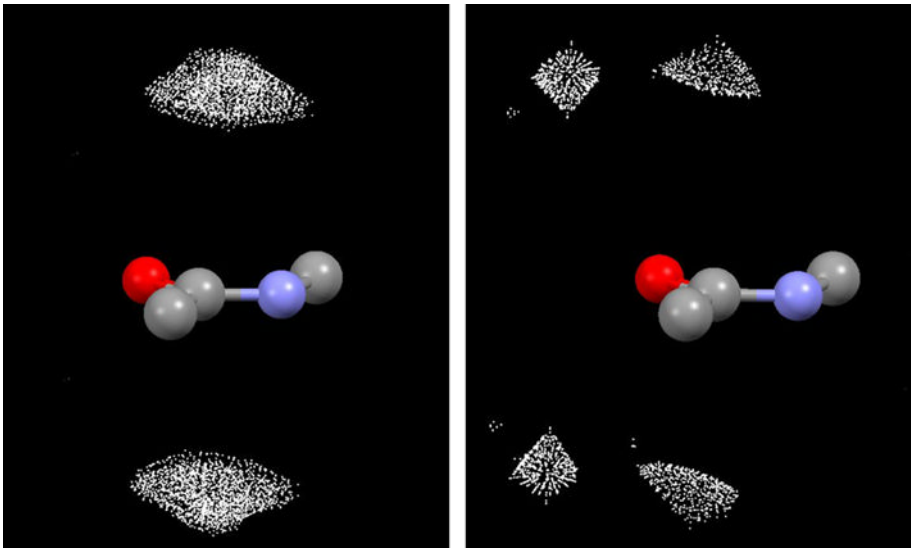

Fig. 16 IsoStar plots showing the density distributions of C–F (*left*) and C–Cl (*right*) halogen atoms around peptide linkages in PDB crystal structures.

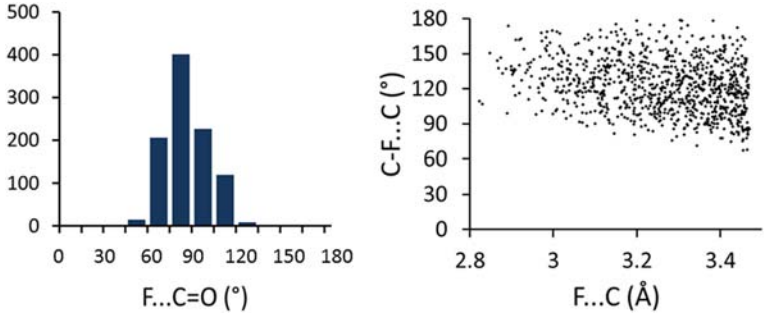

Fig. 17 Histogram of the F···C═O angle and scatterplot of the F···C distance against the C–F···C(carbonyl) angle for C–F···C═O contacts in the CSD.[265]

comparable in strength to aromatic–aromatic CH···π interactions. Other double-mutant cycles showed that a C–F···C═O interaction improves binding free enthalpy by 0.2 to 0.3 kcal mol^{-1} in an apolar environment.[269,270]

Several examples of these interactions have been found in PDB protein–ligand complexes.[262] The Bcr-Abl tyrosine kinase inhibitor nilotinib, for example, forms both carbonyl–carbonyl and C–F···C═O interactions at the binding site, and replacement of its $-CF_3$ group by methyl reduces activity in an autophosphorylation assay by more than 5-fold.[44,271] Of course, the interaction is weak, so the extent to which it causes the enhanced activity is uncertain. Pollock et al. introduced trifluoromethyl groups into thienopyrimidine menin–MLL inhibitors with the specific intention of creating molecules that would form C–F···C═O interactions at the binding site, and thereby obtained activity improvements of up to 5- to 10-fold.[272] Carbonyl–carbonyl interactions have been implicated in stabilizing some protein structural features: the right-handed twist found in most β-strands,[273] and partially allowed Ramachandran conformations of asparagine and aspartic acid residues.[274]

This section has focused on the carbonyl group because of its importance in protein–ligand binding, but similar interactions can be formed by other dipolar groups, such as nitriles. They have been generically termed "orthogonal multipolar interactions" and were reviewed by Paulini et al.[262]

3.05.4.7 Sulfur Interactions

3.05.4.7.1 Sulfur interactions to nonpolar groups

Because of its high polarizability, sulfur is, in its noncovalent interactions, the most versatile of the elements relevant to medicinal chemistry. Depending on its intramolecular environment, it may be capable of donating or accepting hydrogen bonds, forming attractive S···O and S···N contacts, or accepting halogen bonds. Most commonly, though, thioether, thioamide, sulfoxide, and other types of sulfur interact with hydrophobic groups. It is clear from several PDB surveys, which are well summarized in a recent

review,[275] that methionine and cysteine side chains interact favorably with aromatic rings. These interactions can be of various types and geometries, involving either the face or the edge of the ring: S–CH_3···π, S···π, S–H···π and S···HC.[79] Bissantz et al. concluded from PDB and CSD searches that the interaction with the edge of the ring is the more common and pointed out that several other authors agreed.[44] However, other workers have emphasized the importance of methionine interactions with the aromatic-ring face. For this orientation, they performed quantum-mechanical calculations on model dimers between dimethylthioether and benzene, phenol, and indole. The results suggested that the dimers are more favorable than the corresponding propane–aromatic systems by up to about 1.5 kcal mol^{-1}.[276] The stabilization is primarily due to dispersion rather than electrostatics. Methionine is frequently present at adenine binding sites, with the side chain positioned above the adenine ring system.[44] However, interactions are certainly not confined to aromatic groups: Imai et al. found that the most common intermolecular contact formed by methionine sulfur in PDB structures is to the hydrogen atoms of methylene groups.[277]

Sulfur interactions with hydrophobic groups have been shown to contribute to protein–ligand binding affinity on several occasions.[79,275] An instructive example is provided by three inhibitors of tRNA-guanine transglycosylase.[278] The inhibitors differ only in the nature of a side chain, which is either –OPh, –CH_2Ph, or –SPh. They have K_i values of 5600, 3600 and 100 nM, respectively. The superior activity of the sulfur analog was ascribed to several factors. The sulfur-containing molecule is the most lipophilic and therefore partitions more efficiently from solution into the hydrophobic enzyme pocket where it binds. Sulfur is highly polarizable and therefore forms stronger dispersion interactions in the pocket. Finally, the conformational preferences of the sulfur derivative were more favorable for binding than those of the oxygen and methylene analogs. In the same study, two other S/O inhibitor pairs were found with large binding affinity differences in favor of the sulfur analog.

3.05.4.7.2 Hydrogen bonds involving sulfur

The hydrogen-bonding properties of sulfur have been well characterized by surveys of the CSD and PDB. While sulfur is a much weaker donor than nitrogen or oxygen, sulfhydryl groups are often involved in hydrogen bonds. In a set of 753 proteins containing cysteine, there were 314 SH···O=C hydrogen bonds to backbone carbonyl groups.[279] Of these, about a third occurred in α-helices between the –SH group of cysteine residue i and the carbonyl oxygen of residue $i-4$. In a survey of CSD crystal structures, about 70% of SH groups were donated to acceptors, mainly O=C and S=C groups.[280] SH···π hydrogen bonds are possible, and it has been claimed on the basis of gas-phase spectroscopic measurements that "sulfur is not too far behind oxygen, nitrogen, and carbon in regard to forming the π-type hydrogen bond".[281] However, there is no doubt that SH is a much weaker donor than OH or NH.

The ability of sulfur to accept hydrogen bonds is critically dependent on its intramolecular environment. In small-molecule crystal structures, thioether sulfur has a very low propensity to accept hydrogen bonds from OH and NH groups. A CSD search found that only 86 of 1811 (=4.8%) Y–S–Z fragments (Y, Z=C, N, O, or S) formed intermolecular hydrogen bonds of this type with the S···H distance shorter than sum of vdw radii.[280] With a much more liberal distance criterion (S···H shorter than sum of vdw radii + 0.3 Å; S···H–O,N ≥ 90 degrees) the ratio is still only 16.4%.[282] The picture is similar in protein structures, where sulfur atoms rarely accept hydrogen bonds from OH and NH groups.[279] Double-bonded sulfur is rather different. In thioamides and thioureas, electron delocalization from the nitrogen lone pair into the C=S π* orbital induces a significant $C^{\delta+}=S^{\delta-}$ dipole. A 2008 survey of the CSD found that these groups often form C=S···H–(O, N) hydrogen bonds. In contrast, none were found to aliphatic thiones. After correction for vdw radii, the thioamide and thiourea hydrogen bonds were typically about 0.25 Å longer than those formed by amides and ureas, implying that the thio groups are poorer acceptors than their oxygen analogs. The directional preferences at the acceptor atom are also different, C=S···H angles falling in the range 102–109 degrees, and C=O···H in the range 127–140 degrees. IMPT calculations were consistent with these results, suggesting that the interaction energies to sulfur are less favorable than those to oxygen by about 3 kcal mol^{-1}.[283]

3.05.4.7.3 Chalcogen bonding

In a classic early CSD study, Rosenfield et al. showed that divalent sulfur atoms have different directional preferences in their interactions with nucleophiles and electrophiles.[284] Electrophiles tend to form contacts in a direction approximately 20 degrees from the perpendicular to the Y–S–Z plane, whereas nucleophiles (Nu) tend to lie in that plane and along the extension of the Y–S or Z–S covalent bond. The latter interaction is called the "chalcogen bond"[285] and is the Group 16 equivalent of the halogen bond (the Group 15 version is the "pnicogen bond"). Chalcogen bonds are stabilized by dispersion, by electron transfer from a lone-pair orbital on the nucleophile into a low-lying Y–S or Z–S σ* orbital, and by electrostatic attraction between the nucleophile (typically oxygen or nitrogen) and a localized patch of electropositive potential on the sulfur atom (the σ hole; see halogen-bonding "**Background**" section). The balance between these effects depends on the intramolecular environment of the sulfur atom. The interactions tend to be more favorable when the sulfur is strongly polarized by nearby electron-withdrawing atoms, as in, for example, thiazole, isothiazole, and thiadiazole. These matters are surveyed in the extensive review by Beno et al., which also contains numerous examples.[275] These authors argue that the interaction is primarily useful for conformational control, since attractive S···O and S···N contacts are most commonly intramolecular and can strongly influence torsional preferences.[286]

The predominance of intramolecular interactions suggests that steric factors may often prevent close intermolecular approach of oxygen or nitrogen atoms to divalent sulfur in the direction required for chalcogen bonding. Nevertheless, it is not hard to find intermolecular chalcogen bonds. A search of the 2015 CSD for thiophene intermolecular S···O or S···N interactions (C–S···O,N ≥ 160 degrees; S···O,N < sum of vdw radii) found 242 examples in the 5132 structures in which the interaction is theoretically possible, a hit rate of 4.7%. Corresponding figures for thiazole are 93 interactions in 1002 structures (9.3%). The higher ratio for thiazole can be ascribed to the polarizing influence on the sulfur atom of the ring nitrogen. Accordingly, the ratio is even higher

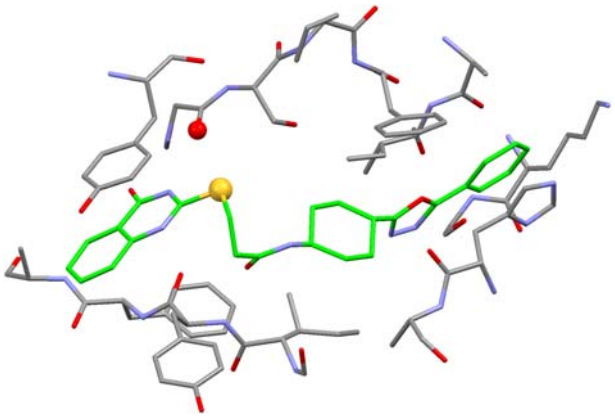

Fig. 18 S···O interaction in a tankyrase complex; atoms involved shown as spheres (PDB code 4MSG).

for 1,3,4-thiadiazole (13.5%; 67 interactions in 496 structures) and higher still in thiazolium (31.4%; 32 in 102). A previous CSD study suggested that, in S···O=C interactions, the sulfur atom can lie either in the carbonyl plane or approximately perpendicular to it, the latter being preferred for amides.[287] This suggests that amides can simultaneously form hydrogen bonds and chalcogen bonds. S···O interactions between ligand sulfur atoms and backbone amide groups have been observed in CHK1 kinase[288,289] and tankyrase (Fig. 18).[290] As expected, the sulfur atoms involved are in polarizing environments.

3.05.4.7.4 Sulfur as a halogen bond acceptor

In the 2015 version of the CSD, there are 186 structures that contain a C–X group (X = Br, I) and a sulfur atom from an aliphatic thioether, thiol, or disulfide. In 24 of these (12.9%), the sulfur atom forms a contact with the halogen with C–X···S ≥ 160 degrees and X···S < sum of vdw radii. Surprisingly, the analogous searches for the oxygen analogs find 284 of 4647 structures containing C–X···O halogen bonds, a lower percentage (6.1%). In only three of the sulfur contacts might the directionality of the contact at the sulfur atom suggest chalcogen bonding; the rest appear to be halogen bonds. C=S···I halogen bonding has been shown to occur predictably in a series of thioamide cocrystals with 1,4-diiodotetrafluorobenzene.[291] Quantum-mechanical calculations on model systems gave energy for the methionine–iodobenzene halogen bond of about -4.3 kcal mol^{-1}, which is quite substantial, with a strong preference for linearity at iodine (C–I···S > 150 degrees). The preferred direction of approach of the iodine is perpendicular, or approximately so, to the C–S–C plane, which is the direction expected for electrophiles (see "Chalcogen bonding"). Interactions with bromine and chlorine are much weaker.[292] Overall, the results suggest that methionine and cysteine sulfur atoms in proteins should be capable of accepting halogen bonds from ligands containing iodine or bromine.

3.05.5 Molecular Interactions and the Pharmaceutical Crystal Form

3.05.5.1 Background

The crystal forms in which active pharmaceutical ingredients (APIs) are delivered became a subject of intense interest following the astonishing events of 1998 surrounding Abbott's antiretroviral drug ritonavir.[293] Almost two decades later, the story still seems more like science fiction than fact. After 2 years on the market, the crystal form of the drug spontaneously changed at the US manufacturing plant. Shortly thereafter, following a visit to the company's Italian site by scientists from the United States, the same happened there. The original Form I could no longer be made at either plant. The new Form II was thermodynamically more stable and less soluble, reducing oral bioavailability and forcing Abbot temporarily to withdraw their oral capsule at eye-watering cost. The difference in physical properties of the two forms—or "polymorphs" to use the crystallographic jargon—must arise from their different crystal-packing arrangements. Form II, being the more stable, must have more favorable molecular interactions. If only it had been possible to spot that there was something suboptimal about the interactions in Form I! Similar problems have since occurred with other drugs, including rotigotine and the blood-pressure medication Avalide.[294] It now appears that many—perhaps most—organic molecules can exhibit polymorphism.[295] Polymorphs may differ in a wide range of physical and thermodynamic properties and are patentable. Hence, it is necessary to perform experimental polymorph screening, varying crystallization conditions such as solvent and evaporation rate in an attempt to find all possible crystal forms of the API.[296]

Almost as important as polymorphism is the possibility of optimizing formulations by delivering APIs as cocrystals, which can improve a variety of properties: dissolution rate, thermodynamic stability, hydration propensity, tableting behavior, and so on.[297,298] Simply expressed, a cocrystal is a crystal which contains two (or more) chemically different molecules—in the present context, the API and another molecule, the "coformer." (The official definition of a cocrystal has been the subject of vigorous and widespread debate but need not concern us here.[299]) Like polymorphs, cocrystals are patentable.[300] Finding a suitable cocrystal

involves two steps: searching for molecules that will act as coformers and characterizing the physical properties of the resulting crystals. Once again, recourse must be taken to extensive crystallization experiments.[301]

Such experiments, whether aimed at polymorphs or cocrystals, are time-consuming and nonexhaustive. In an ideal world, they would be guided or even rendered superfluous by computational crystal-structure prediction (CSP), using accurate energy calculations on a massive number of candidate molecular packing arrangements. Sadly, this is out of reach. In 1994, Gavezzotti brought a wry smile to the readers of his paper, "Are crystal structures predictable?" by starting with the single word "No."[302] The answer was still "No" in 2003, but with some qualifications.[303] And it is "No" today, but with even more qualifications because the occasional crystal structure can now be predicted by the occasional research group, including structures of drug-like molecules.[304–306] There are two main problems. Firstly, and surprisingly, the typical finding for an organic molecule is that there are several possible crystal-packing arrangements with very similar energies. Therefore, it is hard to discriminate between them. Secondly, and crucially, it is clear that kinetic, entropic, and solvent effects are very important and they are horrendously difficult to model. Indeed, the very existence of polymorphism is evidence that the nucleation and growth of crystals is generally under kinetic control. There has been a case in which all three known polymorphs of a molecule were predicted by energy calculations (ie, were calculated to be the three most stable forms). It was argued that previous failures on the molecule were therefore due to inaccuracies in the force fields used rather than the kinetics of crystallization.[307] But even if true for that particular molecule, there is no reason to assume it will be universally the case.

Given, then, that reliable CSP is not yet possible, simpler if less rigorous approaches have been developed to help direct the efforts of the experimentalists. Most commonly, they rely on knowledge extracted from the CSD about how molecules interact, particularly through hydrogen bonding, in known crystal structures. The basic idea is that a crystal structure containing an unusual hydrogen-bond pattern might be a metastable polymorph. And that is where the pharmaceutical crystal form intersects with the subject matter of this article.

3.05.5.2 Hydrogen-Bond Patterns and Crystal Form Stability

In 1990, Etter put forward three general rules about hydrogen bonding in organic crystal structures: (1) All good proton donors and acceptors are used; (2) six-membered intramolecular hydrogen-bond rings form in preference to intermolecular hydrogen bonds; and (3) the best donors pair with the best acceptors.[308] The seminal importance of these rules lies not so much in their accuracy (which is limited) but on the extent to which they galvanized interest in the analysis of hydrogen-bond patterns in crystal structures. Exceptions to the first rule are quite easy to find. For example, in 12 of 50 crystal structures containing carbamazepine, one of the amide NH groups does not form a hydrogen bond. More generally across the CSD, 2.5% of good hydrogen bond donors (NH or OH groups) have no good acceptor within the sum of vdw radii plus 0.3 Å and with the donor-hydrogen-acceptor angle at least 90 degrees. The relatively high proportion of carbamazepine structures containing an NH group that does not hydrogen bond was ascribed to poor steric accessibility of the relevant hydrogen atom (**Fig. 19**).[309] The suggestion was strongly supported by a CSD survey which showed that, in organic structures containing both donors and acceptors, two-thirds of the donors or acceptors which do not hydrogen bond are sterically crowded by neighboring atoms in the same molecule. The cases where the donor or acceptor was sterically accessible but not hydrogen-bonded to a good complementary group were more difficult to rationalize. In some cases, donors were hydrogen-bonded to π-systems instead of conventional acceptors.[310] Other studies have looked at the numbers of hydrogen-bonding contacts formed by different types of chemical groups in organic crystal structures.[311,312] Water, for example, most commonly donates two and accepts one hydrogen bond (39.1% of water molecules surveyed), and almost as often donates two and accepts two (37.4%). Empirical functions have been derived to predict these "hydrogen-bond coordination numbers" for various donor and acceptor groups.[313]

Turning to Etter's second rule, Bilton et al. found all intramolecular hydrogen-bonded ring motifs in the CSD that contain <20 atoms, NH or OH donors, and nitrogen or oxygen acceptors. The different motifs were ranked on the ratio of the number of times the motif was observed to occur to the number of times it could possibly have occurred (P_m).[314] The 12 most common motifs were all planar, 6-membered rings stabilized by a conjugated π-system. Their P_m values ranged from 1.0 to 0.86. In contrast, saturated 6-membered rings had $P_m < 0.2$. Conjugated 5-membered rings were also found to be favorable, but motifs involving 7-membered rings and above are relatively rare. A more recent survey, focusing particularly on intramolecular, hydrogen-bonded rings of medicinal chemistry interest, came to similar conclusions.[315]

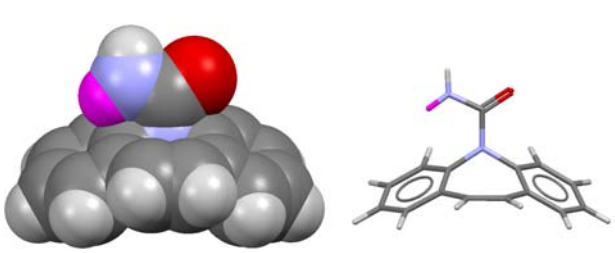

Fig. 19 The sterically crowded hydrogen atom in carbamazepine (colored magenta) is disinclined to form a hydrogen bond.

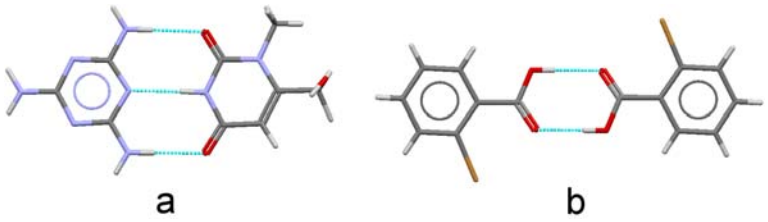

Fig. 20 Examples of (A) the most favored intermolecular hydrogen-bond motif in organic crystal structures, as judged by the P_m statistic;[321] (B) the well-known but much less favored carboxylic acid dimer motif (CSD structures AFABOZ, BRBZAC01).

The intramolecular motifs are interesting, but it is intermolecular hydrogen-bond motifs that have attracted more attention. They were first examined seriously by crystal engineers, who pointed out they could be used to design, or "synthesize", crystal structures with predictable architectures. For this reason, the motifs are often referred to as "synthons" in the crystal engineering community.[316,317] That they might be relevant to CSP and related problems was highlighted in a paper by Sarma and Desiraju.[318] They argued that CSP algorithms based on theoretical energy calculations only take enthalpy into account. Kinetic information is implicitly contained in the CSD, since a motif that is commonly observed is likely to be favored kinetically and, indeed, may play a key role in the process of crystal nucleation. If a CSP algorithm predicts several structures, those containing hydrogen-bond motifs commonly observed in the CSD are therefore the more credible.

Intermolecular hydrogen-bond motifs can have three basic topologies: rings, chains, or discrete dimers.[308] Some common motifs have been well known for decades, including those between carboxylic acid groups[319] and between amide groups.[320] In a study paralleling the intramolecular survey described above, all intermolecular cyclic motifs of ring size <20 were found and ranked on the P_m statistic.[321] The most favored motif (Fig. 20A) had $P_m = 0.97$; in other words, in 97% of the cases where it could have occurred, it did occur. However, this was very much an exception. Most P_m values were much lower, with only eight motifs having $P_m > 0.5$. Even the cyclic carboxylic acid dimer motif (Fig. 20B), commonly assumed to be one of the most reliable synthons, only had $P_m = 0.33$. Recent work has shown that carboxylic acid groups can hydrogen bond to each other in many diverse arrangements.[322]

The most important factor lowering the P_m value of the cyclic carboxylic acid dimer is probably the presence of competing donors and acceptors. Steiner surveyed crystal structures containing the carboxylic acid group and at least one other acceptor group, A. He found many in which OH···A was formed instead of OH···O=C(acid), even for acceptors weaker than acid carbonyl—for example, when A was an ether oxygen.[323] This, of course, is in violation of Etter's third rule (the best donors pair with the best acceptors), which Steiner concluded was only a *tendency*. He suggested that the weaker acceptor is most commonly preferred when the acid group is carried on an awkwardly shaped molecule. The sensitivity of hydrogen-bond patterns to steric factors has also been indicated by other work. Cruz-Cabeza et al. found that even minor changes to the carbamazepine molecule can radically change the crystal-structure hydrogen bonding, and ascribed it to differences in the molecular shapes.[324] Infantes and Motherwell showed that the steric accessibilities of hydrogen-bonding atoms influence the motif adopted in pyrazole and oxime crystal structures.[325] It has also been suggested that hydrogen bonds may form to weak acceptors rather than strong acceptors if there are more of the former in the molecule.[326]

So it appears that motifs are rather difficult to predict after all. The information in the CSD about known hydrogen-bond patterns *can* be used to help discriminate between likely and unlikely molecular packing arrangements, but not simply by looking at synthon probabilities. More sophisticated methods must be used. One such method is the logit hydrogen-bond propensity (LHP) model.[327,328] Given a molecule containing a hydrogen-bond donor *X*, an acceptor *Y*, and other donors and/or acceptors, the propensity for an *X*···*Y* hydrogen bond to form when the molecule crystallizes is estimated by an empirical function. The variables of the function include the chemical identities of *X* and *Y*, those of the competing donors and acceptors, the steric accessibilities of *X* and *Y*, and the aromaticity of the molecule. The function is parameterized by surveying the hydrogen bonds that occur in known crystal structures of similar molecules. LHP predicts a low propensity (0.11) for one of the hydrogen bonds observed in the metastable form I of ritonavir, whereas all those occurring in form II have propensities greater than 0.3.[328] In principle, therefore, the method might have been able to alert development chemists to the problem with form I. A weakness of the method is that it will give identical results for two polymorphs that contain the same hydrogen bonds, a situation that can certainly occur.[329–331]

The LHP approach may also be applied to cocrystal design. Given two molecules A and B, their likelihood of forming a cocrystal is estimated by the difference between the propensity of the best hetero hydrogen bond and that of the best homo hydrogen bond. A hetero hydrogen bond involves a group in A interacting with one in B, a homo interaction is between two A molecules or two B molecules. A high propensity difference in favor of the hetero interaction is taken as indicating that cocrystallization is probable. The method was moderately successful in predicting the outcomes of paracetamol coformer screening experiments.[332] An alternative method for assessing hetero versus homo interactions uses electrostatic potential surfaces, pairing the most positive point on one molecule with the most negative point on the other, then the next most extreme pair, and so on in implicit compliance with Etter's third rule.[333,334] However, the most common approach for prioritizing cocrystallization experiments is to look for molecules with functional groups that are complementary to those on the API, such that a well-known hydrogen-bond motif may be expected to form between them.[335,336] All of these methods ignore factors known to be important, such as molecular shape,[337,338] but more sophisticated approaches, even if effective, are likely to be too slow for practical applications.

3.05.5.3 Impact of Crystal-Structure Interactions on Physical Properties

Aqueous solubility is a function not just of molecular properties but also of the intermolecular interactions that occur in the crystalline state: Strongly cohesive interactions that increase lattice energy result in lower solubility. A 2011, paper described a proof-of-concept study on the benzodiazepine molecule nordiazepam, the crystal structure of which contains a hydrogen-bonded lactam dimer motif and a CH···O hydrogen bond. Solubility was improved by a factor of about eight by adding substituents that prevented the formation of these interactions.[339] The log *D* value was virtually unchanged. Of course, this approach is only viable if the molecular changes do not seriously compromise other properties, most obviously biological activity, but such situations do occur, as the following examples will demonstrate. A group from AstraZeneca improved both activity and solubility in a series of G protein coupled receptor 119 agonists. The changes they made included introduction of an axial methyl group, which disrupted aromatic stacking interactions in the crystalline state, and replacement of a methyl sulfone by a 3-cyanopyridyl group, which removed a CH···O═S interaction.[340] In a second example, stacking and CH···π interactions were disturbed to obtain an approximately four-fold solubility improvement without compromising activity in a series of kinesin spindle protein inhibitors.[341] Introduction of a methyl group on an inhibitor of the phosphoinositide kinase PI3Kβ achieved a remarkable 100-fold increase in solubility by disrupting indoline ring stacking interactions; biological activity was retained.[342]

The interactions of chemical groups exposed on crystal faces are important in the prediction and optimization of physical properties such as morphology[343] and surface adhesion and tableting behavior.[344,345]

3.05.6 Summary

The years since the last edition of *Comprehensive Medicinal Chemistry* have seen substantial changes in our perception of noncovalent molecular interactions. The halogen bond has emerged from relative obscurity and is now regarded as a useful interaction in structure-based drug design. Which it is, but as the halogens most widely used in medicinal chemistry do not form, or form only weak, halogen bonds (fluorine and chlorine, respectively), its value is somewhat limited. A wider appreciation of the chalcogen bond (attractive S···O and S···N interactions) is surely not far away; likewise, the use of sulfur as an acceptor of halogen bonds from iodo- or bromo-substituents on ligands. Statistical analysis of small-molecule crystal structures confirms the significant influence of CH···O, CH···N, and CH···F interactions on molecular packing arrangements. Quantum-mechanical calculations have given new insights into the interactions between aromatic rings, suggesting that they can be rationalized in terms of the localized, through-space interactions of the rings' substituents and heteroatoms. The significance of the electrostatic potential associated with the ring π-systems is questioned. Results from ITC experiments challenge our understanding of the hydrophobic effect and emphasize the importance of the geometry and continuity of the water networks that exist at protein binding sites. Hydrogen-bond interactions in the crystal forms of development candidates have moved into the limelight as researchers strive to relate them to stability and physical properties such as solubility. Interest in cocrystals and the interactions therein has grown at an exponential rate.[346]

It is a human instinct to name things, so there is now an extensive catalog of molecular interactions. Are all the different labels necessary? It would not be a heinous offense if we talked of electrostatic interactions instead of halogen bonds and chalcogen bonds and cation–π interactions and anion–π interactions, etc. Admittedly, dispersion and polarization and, very occasionally, charge transfer make contributions too, and the anisotropy of the electrostatic potential around some atoms has to be borne in mind. But there is an underlying simplicity, a unifying theme: electropositive atoms attract electronegative atoms.

But while molecular interactions are simpler than their nomenclature might suggest, they are also far more complex. The reason can be given in two words: water; entropy. ITC shows us that the classical hydrophobic effect is hopelessly inadequate to explain what goes on in and around nonpolar pockets at protein binding sites. Changes to the environment of an individual water molecule or a cluster of waters can cause substantial nonadditivity of substituent effects on binding free energy. No wonder that structure–activity relationships are a nightmare. Within a series of closely analogous protein–ligand complexes, the relative importance of enthalpy and entropy can swing wildly from one ligand to the next. No wonder that, for all we know about molecular interactions, we are useless at predicting protein–ligand binding affinities.[347]

Still, we *do* know a lot about molecular interactions. The last few years have brought many new insights and so will the next few, particularly given the growing power of the tools at our disposal: quantum-mechanical calculations such as CCSD(T) that are now up to the job; methods such as ITC that can probe the thermodynamics of binding; and the continued growth of the invaluable crystallographic databases, now containing in excess of 750,000 (CSD) and 100,000 (PDB) structures.

But to conclude, some words of caution. Many people believe they are destined to pick the slowest queue in supermarkets. Actually, they only notice the occasions when they do. Cognitive scientists call it confirmation bias. There is a real danger that the same error can influence our perception of molecular interactions. Once we notice an interesting interatomic contact, we are attuned to spotting it again. And, as Dunitz and Gavezzotti commented, the CSD and PDB are so huge that we can find examples of any contact we like.[348] The problem is exacerbated by the exigencies of scientific publishing. When writing a paper on the *X*···*Y* interaction, it is unwise to choose the title "No conclusive evidence that *X*···*Y* interactions significantly influence protein–ligand binding." To get the manuscript accepted, it may be necessary to maintain a position of cautious optimism: "The *X*···*Y* interaction: a new tool in drug design?" The overwhelming majority of scientists are scrupulously honest, so the results presented will remain the same, but the more positive spin can create a climate in which people accept rather than doubt. All of the interactions discussed in this article are real and have been characterized by high-quality scientific work, but most are weak. What we must not lose is our sense of

perspective. Protein–ligand binding is dominated by OH···O, NH···O, OH···N, and NH···N hydrogen bonds and the burial of hydrophobic groups. The importance of all other interactions pales in comparison.

Acknowledgment

Colin Groom of the Cambridge Crystallographic Data Centre is thanked for commenting with his usual perspicacity on a preliminary draft of this article.

References

1. Fischer, E. *Ber. Dtsch. Chem. Ges.* **1894,** *27,* 2985–2993.
2. Rose, P. W.; Beran, B.; Bi, C.; Bluhm, W. F.; Dimitropoulos, D.; Goodsell, D. S.; Prlić, A.; Quesada, M.; Quinn, G. B.; Westbrook, J. D.; Young, J.; Yukich, B.; Zardecki, C.; Berman, H. M.; Bourne, P. E. *Nucleic Acids Res.* **2011,** *39,* D392–D401.
3. Groom, C. R.; Allen, F. H. *Angew. Chem. Int. Ed.* **2014,** *53,* 662–671.
4. Bruno, I. J.; Cole, J. C.; Lommerse, J. P. M.; Rowland, R. S.; Taylor, R.; Verdonk, M. L. *J. Comput.-Aided Mol. Des.* **1997,** *11,* 525–537.
5. Böhm, H.-J.; Brode, S.; Hesse, U.; Klebe, G. *Chem. Eur. J.* **1996,** *2,* 1509–1513.
6. http://www.desertsci.com/proasis3proteinstructuredatabase.html.
7. Günther, J.; Bergner, A.; Hendlich, M.; Klebe, G. *J. Mol. Biol.* **2003,** *326,* 621–636.
8. Liu, Z.; Li, Y.; Han, L.; Li, J.; Liu, J.; Zhao, Z.; Nie, W.; Liu, Y.; Wang, R. *Bioinformatics* **2015,** *31,* 405–412.
9. Wlodawer, A.; Minor, W.; Dauter, Z.; Jaskolski, M. *FEBS J.* **2008,** *275,* 1–21.
10. Davis, A. M.; St-Gallay, S. A.; Kleywegt, G. J. *Drug Discov. Today* **2008,** *13,* 831–841.
11. Kleywegt, G. J. *Acta Crystallogr. D Biol. Crystallogr.* **2007,** *63,* 94–100.
12. Liebeschuetz, J.; Hennemann, J.; Olsson, T.; Groom, C. R. *J. Comput. Aided Mol. Des.* **2012,** *26,* 169–183.
13. Kleywegt, G. J.; Harris, M. R.; Zou, J.; Taylor, T. C.; Wählby, A.; Jones, T. A. *Acta Crystallogr. D Biol. Crystallogr.* **2004,** *60,* 2240–2249.
14. Chen, V. B.; Arendall, W. B. I. I. I.; Headd, J. J.; Keedy, D. A.; Immormino, R. M.; Kapral, G. J.; Murray, L. W.; Richardson, J. S.; Richardson, D. C. *Acta Crystallogr. D Biol. Crystallogr.* **2010,** *66,* 12–21.
15. Read, R. J.; Adams, P. D.; Arendall, W. B. I. I. I.; Brunger, A. T.; Emsley, P.; Joosten, R. P.; Kleywegt, G. J.; Krissinel, E. B.; Lütteke, T.; Otwinowski, Z.; Perrakis, A.; Richardson, J. S.; Sheffler, W. H.; Smith, J. L.; Tickel, I. J.; Vriend, G.; Zwart, P. H. *Structure* **2011,** *19,* 1395–1412.
16. Joosten, R. P.; Salzemann, J.; Bloch, V.; Stockinger, H.; Berglund, A.-C.; Blanchet, C.; Bongcam-Rudloff, E.; Combet, C.; Da Costa, A. L.; Deleage, G.; Diarena, M.; Fabbretti, R.; Fettahi, G.; Flegel, V.; Gisel, A.; Kasam, V.; Kervinen, T.; Korpelainen, E.; Mattila, K.; Pagni, M.; Reichstadt, M.; Breton, V.; Tickle, I. J.; Vriend, G. *J. Appl. Crystallogr.* **2009,** *42,* 376–384.
17. Fraser, J. S.; van den Bedem, H.; Samelson, A. J.; Lang, P. T.; Holton, J. M.; Echols, N.; Alber, T. *Proc. Natl. Acad. Sci. U. S. A.* **2011,** *108,* 16247–16252.
18. Keedy, D. A.; van den Bedem, H.; Sivak, D. A.; Petsko, G. A.; Ringe, D.; Wilson, M. A.; Fraser, J. S. *Structure* **2014,** *22,* 899–910.
19. Taylor, R.; Allen, F. H.; Cole, J. C. *CrystEngComm* **2015,** *17,* 2651–2666.
20. Verdonk, M. L.; Cole, J. C.; Taylor, R. *J. Mol. Biol.* **1999,** *289,* 1093–1099.
21. Abraham, M. H.; Platts, J. A. J. *Org. Chem.* **2001,** *66,* 3484–3491.
22. Laurence, C.; Brameld, K. A.; Graton, J.; Le Questel, J.-Y.; Renault, E. *J. Med. Chem.* **2009,** *52,* 4073–4086.
23. Laurence, C.; Graton, J.; Berthelot, M.; Besseau, F.; Le Questel, J.-Y.; Luçon, M.; Ouvrard, C.; Planchat, A.; Renault, E. J. *Org. Chem.* **2010,** *75,* 4105–4123.
24. Graton, J.; Besseau, F.; Brossard, A.-M.; Charpentier, E.; Deroche, A.; Le Questel, J.-Y. *J. Phys. Chem. A* **2013,** *117,* 13184–13193.
25. Ladbury, J. E. *Biochem. Soc. Trans.* **2010,** *38,* 888–893.
26. Klebe, G. *Nat. Rev. Drug Discov.* **2015,** *14,* 95–110.
27. Olsson, T. S. G.; Williams, M. A.; Pitt, W. R.; Ladbury, J. E. *J. Mol. Biol.* **2008,** *384,* 1002–1017.
28. Schneider, H.-J. *Angew. Chem. Int. Ed.* **2009,** *48,* 3924–3977.
29. Steed, J. W.; Atwood, J. L. *Supramolecular Chemistry;* Wiley: Chichester, UK, 2013.
30. Mecozzi, S.; Rebek, J., Jr. *Chem. Eur. J.* **1998,** *4,* 1016–1022.
31. Mati, I. K.; Cockroft, S. L. *Chem. Soc. Rev.* **2010,** *39,* 4195–4205.
32. Cockroft, S. L.; Hunter, C. A. *Chem. Soc. Rev.* **2007,** *36,* 172–188.
33. Dunitz, J. D.; Gavezzotti, A. *Chem. Soc. Rev.* **2009,** *38,* 2622–2633.
34. For accurate work on molecular interactions, lower-level approximations such as force fields and semi-empirical methods are wholly unsuitable.
35. Řezáč, J.; Hobza, P. *J. Chem. Theory Comput.* **2013,** *9,* 2151–2155.
36. Hobza, P. *Acc. Chem. Res.* **2012,** *45,* 663–672.
37. Stone, A. J. *The Theory of Intermolecular Forces;* Oxford University Press: Oxford, 2013.
38. Černý, J.; Hobza, P. *Phys. Chem. Chem. Phys.* **2007,** *9,* 5291–5303.
39. Kleeberg, H.; Klein, D.; Luck, W. A. P. J. *Phys. Chem.* **1987,** *91,* 3200–3203.
40. Kitaigorodsky, A. I. *Organic Chemical Crystallography;* Consultants Bureau: New York, 1961.
41. A typically prescient observation by Leonardo da Vinci.
42. It is acknowledged that there would be some attendant difficulties.
43. Fersht, A. R.; Shi, J.-P.; Knill-Jones, J.; Lowe, D. M.; Wilkinson, A. J.; Blow, D. M.; Brick, P.; Carter, P.; Waye, M. M. Y.; Winter, G. *Nature* **1984,** *314,* 235–238.
44. Bissantz, C.; Kuhn, B.; Stahl, M. *J. Med. Chem.* **2010,** *53,* 5061–5084.
45. Yang, Y.; Lightstone, F. C.; Wong, S. E. *Expert Opin. Drug Discovery* **2013,** *8,* 277–287.
46. Bayden, A. S.; Moustakas, D. T.; Joseph-McCarthy, D.; Lamb, M. L. *J. Chem. Inf. Model.* **2015,** *55,* 1552–1565.
47. Persch, E.; Dumele, O.; Diederich, F. *Angew. Chem. Int. Ed.* **2015,** *54,* 3290–3327.
48. Li, A. H.-T.; Chao, S. D. *J. Chem. Phys.* **2006,** *125,* 094312.
49. Tanford, C. *The Hydrophobic Effect: Formation of Micelles and Biological Membranes;* Wiley: New York, 1973.
50. Meyer, E. A.; Castellano, R. K.; Diederich, F. *Angew. Chem. Int. Ed.* **2003,** *42,* 1210–1250.
51. Scatena, L. F.; Brown, M. G.; Richmond, G. L. *Science* **2001,** *292,* 908–912.
52. Snyder, P. W.; Lockett, M. R.; Moustakas, D. T.; Whitesides, G. M. *Eur. Phys. J. Spec. Top.* **2014,** *223,* 853–891.
53. Biedermann, F.; Nau, W. M.; Schneider, H.-J. *Angew. Chem. Int. Ed.* **2014,** *53,* 11158–11171.

54. Rühmann, E.; Betz, M.; Heine, A.; Klebe, G. *J. Med. Chem.* **2015,** *58,* 6960–6971.
55. Zürcher, M.; Diederich, F. J. *Org. Chem.* **2008,** *73,* 4345–4361.
56. Biela, A.; Betz, M.; Heine, A.; Klebe, G. *ChemMedChem* **2012,** *7,* 1423–1434.
57. Krimmer, S. G.; Betz, M.; Heine, A.; Klebe, G. *ChemMedChem* **2014,** *9,* 833–846.
58. Talhout, R.; Villa, A.; Mark, A. E.; Engberts, J. B. F. N. *J. Am. Chem. Soc.* **2003,** *125,* 10570–10579.
59. Breiten, B.; Lockett, M. R.; Sherman, W.; Fujita, S.; Al-Sayah, M.; Lange, H.; Bowers, C. M.; Heroux, A.; Krilov, G.; Whitesides, G. M. *J. Am. Chem. Soc.* **2013,** *135,* 15579–15584.
60. Geschwindner, S.; Ulander, J.; Johansson, P. *J. Med. Chem.* **2015,** *58,* 6321–6335.
61. Myszka, D. G.; Abdiche, Y. N.; Arisaka, F.; Byron, O.; Eisenstein, E.; Hensley, P.; Thomson, J. A.; Lombardo, C. R.; Schwarz, F.; Stafford, W.; Doyle, M. L. *J. Biomol. Tech.* **2003,** *14,* 247–269.
62. Chodera, J. D.; Mobley, D. L. *Annu. Rev. Biophys.* **2013,** *42,* 121–142.
63. Olsson, T. S. G.; Ladbury, J. E.; Pitt, W. R.; Williams, M. A. *Protein Sci.* **2011,** *20,* 1607–1618.
64. In other words, dispersion plus exchange repulsion.
65. Sutor, D. J. *Nature* **1962,** *195,* 68–69.
66. Donohue, J. In *Structural Chemistry and Molecular Biology;* Rich, A., Davidson, N., Eds.; San Francisco: Freeman, 1968; pp 459–463.
67. Taylor, R.; Kennard, O. *J. Am. Chem. Soc.* **1982,** *104,* 5063–5070.
68. Desiraju, G. R. *Acc. Chem. Res.* **1991,** *24,* 290–296.
69. Cotton, F. A.; Daniels, L. M.; Jordan, G. T., IV; Murillo, C. A. *Chem. Commun.* **1997,** 1673–1674.
70. Steiner, T.; Desiraju, G. R. *Chem. Commun.* **1998,** 891–892.
71. Thalladi, V. R.; Weiss, H.-C.; Bläser, D.; Boese, R.; Nangia, A.; Desiraju, G. R. *J. Am. Chem. Soc.* **1998,** *120,* 8702–8710.
72. Aakeröy, C. B.; Evans, T. A.; Seddon, K. R.; Pálinkó, I. *New J. Chem.* **1999,** *23,* 145–152.
73. Nishio, M.; Umezawa, Y.; Honda, K.; Tsuboyama, S.; Suezawa, H. *CrystEngComm* **2009,** *11,* 1757–1788.
74. Arunan, E.; Desiraju, G. R.; Klein, R. A.; Sadlej, J.; Scheiner, S.; Alkorta, I.; Clary, D. C.; Crabtree, R. H.; Dannenberg, J. J.; Hobza, P.; Kjaergaard, H. G.; Legon, A. C.; Mennucci, B.; Nesbitt, D. J. *Pure Appl. Chem.* **2011,** *83,* 1637–1641.
75. The new definition is: "The hydrogen bond is an attractive interaction between a hydrogen atom from a molecule or a molecular fragment X-H in which X is more electronegative than H, and an atom or a group of atoms in the same or a different molecule, in which there is evidence of bond formation."
76. Jeffrey, G. A. *An Introduction to Hydrogen Bonding;* Oxford University Press: Oxford, 1997.
77. Metrangolo, P.; Pilati, T.; Resnati, G. *CrystEngComm* **2006,** *8,* 946–947.
78. Bauzá, A.; Quiñonero, D.; Deyà, P. M.; Frontera, A. *CrystEngComm* **2013,** *15,* 3137–3144.
79. Salonen, L. M.; Ellermann, M.; Diederich, F. *Angew. Chem. Int. Ed.* **2011,** *50,* 4808–4842.
80. Dougherty, D. A. *Acc. Chem. Res.* **2013,** *46,* 885–893.
81. de Hoog, P.; Gamez, P.; Mutikainen, I.; Turpeinen, U.; Reedijk, J. *Angew. Chem.* **2004,** *116,* 5939–5941.
82. When playing the character Eccles in the last ever episode of a famous British radio series, *The Goons.*
83. Bader, R. F. W. *Atoms in Molecules: A Quantum Theory;* Clarendon: Oxford, 1990.
84. Johnson, E. R.; Keinan, S.; Mori-Sánchez, P.; Contreras-García, J.; Cohen, A. J.; Yang, W. *J. Am. Chem. Soc.* **2010,** *132,* 6498–6506.
85. Contreras-García, J.; Johnson, E. R.; Keinan, S.; Chaudret, R.; Piquemal, J.-P.; Beratan, D. N.; Yang, W. *J. Chem. Theory Comput.* **2011,** *7,* 625–632.
86. Dunitz, J. D. *IUCrJ* **2015,** *2,* 157–158.
87. Lecomte, C.; Espinosa, E.; Matta, C. F. *IUCrJ* **2015,** *2,* 161–163.
88. Thakur, T. S.; Dubey, R.; Desiraju, G. R. *IUCrJ* **2015,** *2,* 159–160.
89. Taylor, R. *CrystEngComm* **2014,** *16,* 6852–6865.
90. Extension of the methodology to interactions in protein-ligand complexes is non-trivial but should be possible. However, nothing has yet been published.
91. Jeffrey, G. A.; Saenger, W. *Hydrogen Bonding in Biological Structures;* Springer Verlag: Berlin, 1994.
92. Gilli, G.; Gilli, P. *The Nature of the Hydrogen Bond: Outline of a Comprehensive Hydrogen Bond Theory;* Oxford University Press: Oxford, 2009.
93. Steiner, T. *Angew. Chem. Int. Ed.* **2002,** *41,* 48–76.
94. Nobeli, I.; Price, S. L.; Lommerse, J. P. M.; Taylor, R. *J. Comput. Chem.* **1997,** *18,* 2060–2074.
95. Lommerse, J. P. M.; Price, S. L.; Taylor, R. *J. Comput. Chem.* **1997,** *18,* 757–774.
96. Preissner, R.; Egner, U.; Saenger, W. *FEBS Lett.* **1991,** *288,* 192–196.
97. Feldblum, E. S.; Arkin, I. T. *Proc. Natl. Acad. Sci. U. S. A.* **2014,** *111,* 4085–4090.
98. Wood, P. A.; Allen, F. H.; Pidcock, E. *CrystEngComm* **2009,** *11,* 1563–1571.
99. Mitchell, J. B. O.; Price, S. L. *Chem. Phys. Lett.* **1989,** *154,* 267–272.
100. Karpfen, A. *Adv. Chem. Phys.* **2002,** *123,* 469–510.
101. Góra, R. W.; Maj, M.; Grabowski, S. J. *Phys. Chem. Chem. Phys.* **2013,** *15,* 2514–2522.
102. Freire, E. *Drug Discov. Today* **2008,** *13,* 869–874.
103. Yin, F.; Cao, R.; Goddard, A.; Zhang, Y.; Oldfield, E. *J. Am. Chem. Soc.* **2006,** *128,* 3524–3525.
104. Desiraju, G. R.; Steiner, T. *The Weak Hydrogen Bond in Structural Chemistry and Biology;* Oxford University Press: Oxford, 2001.
105. Panigrahi, S. K.; Desiraju, G. R. *Proteins: Struct., Funct., Bioinf.* **2007,** *67,* 128–141.
106. Toth, G.; Bowers, S. G.; Truong, A. P.; Probst, G. *Curr. Pharm. Des.* **2007,** *13,* 3476–3493.
107. Pierce, A. C.; Sandretto, K. L.; Bemis, G. W. *Proteins: Struct., Funct., Bioinf.* **2002,** *49,* 567–576.
108. Scheiner, S. *Phys. Chem. Chem. Phys.* **2011,** *13,* 13860–13872.
109. Pitoňák, M.; Neogrády, P.; Řezáč, J.; Jurečka, P.; Urban, M.; Hobza, P. *J. Chem. Theory Comput.* **2008,** *4,* 1829–1834.
110. Sinnokrot, M. O.; Sherrill, C. D. *J. Phys. Chem. A* **2006,** *110,* 10656–10668.
111. Podeszwa, R.; Bukowski, R.; Szalewicz, K. *J. Phys. Chem. A* **2006,** *110,* 10345–10354.
112. DiStasio, R. A., Jr.; von Helden, G.; Steele, R. P.; Head-Gordon, M. *Chem. Phys. Lett.* **2007,** *437,* 277–283.
113. Ninković, D. B.; Janjić, G. V.; Veljković, D.Ž.; Sredojević, D. N.; Zarić, S. D. *ChemPhysChem* **2011,** *12,* 3511–3514.
114. Schnell, M.; Erlekam, U.; Bunker, P. R.; von Helden, G.; Grabow, J.-U.; Meijer, G.; van der Avoird, A. *Angew. Chem. Int. Ed.* **2013,** *52,* 5180–5183.
115. Bacon, G. E.; Curry, N. A.; Wilson, S. A. *Proc. R. Soc. London, Ser. A* **1964,** *279,* 98–110.
116. Tsuzuki, S.; Honda, K.; Uchimaru, T.; Mikami, M. *J. Chem. Phys.* **2005,** *122,* 144323.
117. Cozzi, F.; Cinquini, M.; Annunziata, R.; Dwyer, T.; Siegel, J. S. *J. Am. Chem. Soc.* **1992,** *114,* 5729–5733.
118. Cozzi, F.; Cinquini, M.; Annunziata, R.; Siegel, J. S. J. *Am. Chem. Soc.* **1993,** *115,* 5330–5331.
119. Hansch, C.; Leo, A.; Taft, R. W. *Chem. Rev.* **1991,** *91,* 165–195.
120. Hunter, C. A.; Sanders, J. K. M. *J. Am. Chem. Soc.* **1990,** *112,* 5525–5534.
121. Battaglia, M. R.; Buckingham, A. D.; Williams, J. H. *Chem. Phys. Lett.* **1981,** *78,* 421–423.
122. Steuber, H.; Heine, A.; Klebe, G. *J. Mol. Biol.* **2007,** *368,* 618–638.

123. Dahl, T. *Acta Chem. Scand., Ser. A* **1975,** *29,* 170–174.
124. Sinnokrot, M. O.; Sherrill, C. D. *J. Phys. Chem. A* **2003,** *107,* 8377–8379.
125. Lee, E. C.; Kim, D.; Jurečka, P.; Tarakeshwar, P.; Hobza, P.; Kim, K. S. *J. Phys. Chem. A* **2007,** *111,* 3446–3457.
126. Grimme, S.; Antony, J.; Schwabe, T.; Mück-Lichtenfeld, C. *Org. Biomol. Chem.* **2007,** *5,* 741–758.
127. Ringer, A. L.; Sinnokrot, M. O.; Lively, R. P.; Sherrill, C. D. *Chem. Eur. J.* **2006,** *12,* 3821–3828.
128. Dunitz, J. D. *ChemBioChem* **2004,** *5,* 614–621.
129. Wheeler, S. E.; Houk, K. N. *J. Am. Chem. Soc.* **2008,** *130,* 10854–10855.
130. Wheeler, S. E. *J. Am. Chem. Soc.* **2011,** *133,* 10262–10274.
131. Wheeler, S. E. *Acc. Chem. Res.* **2013,** *46,* 1029–1038.
132. Wheeler, S. E.; Houk, K. N. *Mol. Phys.* **2009,** *107,* 749–760.
133. Wheeler, S. E.; Houk, K. N. *J. Am. Chem. Soc.* **2009,** *131,* 3126–3127.
134. Wheeler, S. E.; Houk, K. N. *J. Phys. Chem. A* **2010,** *114,* 8658–8664.
135. Šponer, J.; Šponer, J. E.; Mládek, A.; Jurečka, P.; Banás, P.; Otyepka, M. *Biopolymers* **2013,** *99,* 978–988.
136. Mecozzi, S.; West, A. P., Jr.; Dougherty, D. A. *Proc. Natl. Acad. Sci. U. S. A.* **1996,** *93,* 10566–10571.
137. Wheeler, S. E.; Houk, K. N. *J. Chem. Theory Comput.* **2009,** *5,* 2301–2312.
138. Grimme, S. *Angew. Chem. Int. Ed.* **2008,** *47,* 3430–3434.
139. Martinez, C. R.; Iverson, B. L. *Chem. Sci.* **2012,** *3,* 2191–2201.
140. Harder, M.; Kuhn, B.; Diederich, F. *ChemMedChem* **2013,** *8,* 397–404.
141. Hardegger, L. A.; Kuhn, B.; Spinnler, B.; Anselm, L.; Ecabert, R.; Stihle, M.; Gsell, B.; Thoma, R.; Diez, J.; Benz, J.; Plancher, J.-M.; Hartmann, G.; Banner, D. W.; Haap, W.; Diederich, F. *Angew. Chem. Int. Ed.* **2011,** *50,* 314–318.
142. Helal, C. J.; Kang, Z.; Hou, X.; Pandit, J.; Chappie, T. A.; Humphrey, J. M.; Marr, E. S.; Fennell, K. F.; Chenard, L. K.; Fox, C.; Schmidt, C. J.; Williams, R. D.; Chapin, D. S.; Siuciak, J.; Lebel, L.; Menniti, F.; Cianfrogna, J.; Fonseca, K. R.; Nelson, F. R.; O'Connor, R.; MacDougall, M.; McDowell, L.; Liras, S. *J. Med. Chem.* **2011,** *54,* 4536–4547.
143. Salonen, L. M.; Holland, M. C.; Kaib, P. S. J.; Haap, W.; Benz, J.; Mary, J.-L.; Kuster, O.; Schweizer, W. B.; Banner, D. W.; Diederich, F. *Chem. Eur. J.* **2012,** *18,* 213–222.
144. Matter, H.; Nazaré, M.; Güssregen, S.; Will, D. W.; Schreuder, H.; Bauer, A.; Urmann, M.; Ritter, K.; Wagner, M.; Wehner, V. *Angew. Chem. Int. Ed.* **2009,** *48,* 2911–2916.
145. Matter, H.; Nazaré, M.; Güssregen, S. In *The Importance of Pi-Interactions in Crystal Engineering: Frontiers in Crystal Engineering;* Tiekink, E. R., Zuckerman-Schpector, J., Eds.; Wiley: Chichester, UK, 2012; pp 187–232.
146. Mooibroek, T. J.; Gamez, P. *CrystEngComm* **2013,** *15,* 1802–1805.
147. Lu, Y.; Wang, Y.; Zhu, W. *Phys. Chem. Chem. Phys.* **2010,** *12,* 4543–4551.
148. Wallnoefer, H. G.; Fox, T.; Liedl, K. R.; Tautermann, C. S. *Phys. Chem. Chem. Phys.* **2010,** *12,* 14941–14949.
149. Ma, J. C.; Dougherty, D. A. *Chem. Rev.* **1997,** *97,* 1303–1324.
150. Caldwell, J. W.; Kollman, P. *J. Am. Chem. Soc.* **1995,** *117,* 4177–4178.
151. Mecozzi, S.; West, A. P., Jr.; Dougherty, D. A. *J. Am. Chem. Soc.* **1996,** *118,* 2307–2308.
152. Tsuzuki, S. *Struct. Bond. (Berlin)* **2005,** *115,* 149–193.
153. Schärer, K.; Morgenthaler, M.; Paulini, R.; Obst-Sander, U.; Banner, D. W.; Schlatter, D.; Benz, J.; Stihle, M.; Diederich, F. *Angew. Chem. Int. Ed.* **2005,** *44,* 4400–4404.
154. Salonen, L. M.; Bucher, C.; Banner, D. W.; Haap, W.; Mary, J.-L.; Benz, J.; Kuster, O.; Seiler, P.; Schweizer, W. B.; Diederich, F. *Angew. Chem. Int. Ed.* **2009,** *48,* 811–814.
155. Beene, D. L.; Brandt, G. S.; Zhong, W.; Zacharias, N. M.; Lester, H. A.; Dougherty, D. A. *Biochemistry* **2002,** *41,* 10262–10269.
156. Tavares, X. D. S.; Blum, A. P.; Nakamura, D. T.; Puskar, N. L.; Shanata, J. A. P.; Lester, H. A.; Dougherty, D. A. *J. Am. Chem. Soc.* **2012,** *134,* 11474–11480.
157. Gallivan, J. P.; Dougherty, D. A. *Proc. Natl. Acad. Sci. U. S. A.* **1999,** *96,* 9459–9464.
158. Dougherty, D. A. *J. Nutr.* **2007,** *137,* 15045–15085.
159. Haga, K.; Knuse, A. C.; Asada, H.; Yurugi-Kobayashi, T.; Shiroishi, M.; Zhang, C.; Weis, W. I.; Okada, T.; Kobilka, B. K.; Haga, T.; Kobayashi, T. *Nature* **2012,** *482,* 547–551.
160. Sussman, J. L.; Harel, M.; Frolow, F.; Oefner, C.; Goldman, A.; Toker, L.; Silman, I. *Science* **1991,** *253,* 872–879.
161. Dougherty, D. A.; Stauffer, D. A. *Science* **1990,** *250,* 1558–1560.
162. Khan, M. T. H. *New Biotechnol.* **2009,** *25,* 331–346.
163. Flocco, M. M.; Mowbray, S. L. *J. Mol. Biol.* **1994,** *235,* 709–717.
164. Shah, D.; Li, J.; Shaikh, A. R.; Rajagopalan, R. *Biotechnol. Prog.* **2012,** *28,* 223–231.
165. Crowley, P. B.; Golovin, A. *Proteins: Struct., Funct., Bioinf.* **2005,** *59,* 231–239.
166. Malone, J. F.; Murray, C. M.; Charlton, M. H.; Docherty, R.; Lavery, A. J. *J. Chem. Soc. Faraday Trans.* **1997,** *93,* 3429–3436.
167. Mooibroek, T. J.; Gamez, P. *CrystEngComm* **2012,** *14,* 8462–8467.
168. Tsuzuki, S.; Honda, K.; Uchimaru, T.; Mikami, M.; Tanabe, K. *J. Am. Chem. Soc.* **2000,** *122,* 11450–11458.
169. Mohan, N.; Vijayalakshmi, K. P.; Koga, N.; Suresh, C. H. *J. Comput. Chem.* **2010,** *31,* 2874–2882.
170. Saggu, M.; Levinson, N. M.; Boxer, S. G. *J. Am. Chem. Soc.* **2011,** *133,* 17414–17419.
171. Saggu, M.; Levinson, N. M.; Boxer, S. G. *J. Am. Chem. Soc.* **2012,** *134,* 18986–18997.
172. Steiner, T.; Koellner, G. *J. Mol. Biol.* **2001,** *305,* 535–557.
173. Fusetti, F.; Pijning, T.; Kalk, K. H.; Bos, E.; Dijkstra, B. W. *J. Biol. Chem.* **2003,** *278,* 37753–37760.
174. Wheeler, S. E.; Bloom, J. W. G. *Chem. Commun.* **2014,** *50,* 11118–11121.
175. Quiñonero, D.; Garau, C.; Frontera, A.; Ballester, P.; Costa, A.; Deyà, P. M. *Chem. Phys. Lett.* **2002,** *359,* 486–492.
176. Frontera, A.; Gamez, P.; Mascal, M.; Mooibroek, T.; Reedijk, J. *Angew. Chem. Int. Ed.* **2011,** *50,* 9564–9583.
177. Hay, B. P.; Custelcean, R. *Cryst. Growth Des.* **2009,** *9,* 2539–2545.
178. Robertazzi, A.; Krull, F.; Knapp, E.-W.; Gamez, P. *CrystEngComm* **2011,** *13,* 3293–3300.
179. Schottel, B. L.; Chifotides, H. T.; Dunbar, K. R. *Chem. Soc. Rev.* **2008,** *37,* 68–83.
180. Gale, P. A.; Busschaert, N.; Haynes, C. J. E.; Karagiannidis, L. E.; Kirby, I. L. *Chem. Soc. Rev.* **2014,** *43,* 205–241.
181. Gorteau, V.; Bollot, G.; Mareda, J.; Matile, S. *Org. Biomol. Chem.* **2007,** *5,* 3000–3012.
182. Chakravarty, S.; Sheng, Z.-Z.; Iverson, B.; Moore, B. *FEBS Lett.* **2012,** *586,* 4180–4185.
183. Egli, M.; Sarkhel, S. *Acc. Chem. Res.* **2007,** *40,* 197–205.
184. Shibasaki, K.; Fujii, A.; Mikami, N.; Tsuzuki, S. *J. Phys. Chem. A* **2006,** *110,* 4397–4404.
185. Fujii, A.; Hayashi, H.; Park, J. W.; Kazama, T.; Mikami, N.; Tsuzuki, S. *Phys. Chem. Chem. Phys.* **2011,** *13,* 14131–14141.
186. Nishio, M.; Umezawa, Y.; Fantini, J.; Weiss, M. S.; Chakrabarti, P. *Phys. Chem. Chem. Phys.* **2014,** *16,* 12648–12683.
187. Takahashi, O.; Kohno, Y.; Nishio, M. *Chem. Rev.* **2010,** *110,* 6049–6076.
188. Tsuzuki, S. *Annu. Rep. Prog. Chem., Sect. C: Phys. Chem.* **2012,** *108,* 69–95.
189. Shibasaki, K.; Fujii, A.; Mikami, N.; Tsuzuki, S. *J. Phys. Chem. A* **2007,** *111,* 753–758.
190. Fujii, A.; Shibasaki, K.; Kazama, T.; Itaya, R.; Mikami, N.; Tsuzuki, S. *Phys. Chem. Chem. Phys.* **2008,** *10,* 2836–2843.
191. Carver, F. J.; Hunter, C. A.; Livingstone, D. J.; McCabe, J. F.; Seward, E. M. *Chem. Eur. J.* **2002,** *8,* 2847–2859.
192. Cole, J. C.; Taylor, R.; Verdonk, M. L. *Acta Crystallogr. D Biol. Crystallogr.* **1998,** *54,* 1183–1193.

193. Takahashi, O.; Kohno, Y.; Iwasaki, S.; Saito, K.; Iwaoka, M.; Tomoda, S.; Umezawa, Y.; Tsuboyama, S.; Nishio, M. *Bull. Chem. Soc. Jpn.* **2001,** *74,* 2421–2430.
194. Ciunik, Z.; Desiraju, G. R. *Chem. Commun.* **2001,** 703–704.
195. Burley, S. K.; Petsko, G. A. *Science* **1985,** *229,* 23–28.
196. Singh, J.; Thornton, J. M. *FEBS Lett.* **1985,** *191,* 1–6.
197. Pace, C. J.; Kim, D.; Gao, J. *Chem. Eur. J.* **2012,** *18,* 5832–5836.
198. Dasgupta, B.; Chakrabarti, P.; Basu, G. *FEBS Lett.* **2007,** *581,* 4529–4532.
199. Zondlo, N. J. *Acc. Chem. Res.* **2013,** *46,* 1039–1049.
200. Quiocho, F. A. *Annu. Rev. Biochem.* **1986,** *55,* 287–315.
201. Mason, P. E.; Lerbret, A.; Sabougni, M.-L.; Neilson, G. W.; Dempsey, C. E.; Brady, J. W. *Proteins: Struct., Funct., Bioinf.* **2011,** *79,* 2224–2232.
202. Umezawa, Y.; Nishio, M. *Biopolymers* **2005,** *79,* 248–258.
203. Roehrig, S.; Straub, A.; Pohlmann, J.; Lampe, T.; Pernerstorfer, J.; Schlemmer, K.-H.; Reinemer, P.; Perzborn, W. *J. Med. Chem.* **2005,** *48,* 5900–5908.
204. Yuan, C.; St. Jean, D. J.; Liu, Q.; Cai, L.; Li, A.; Han, N.; Moniz, G.; Askew, B.; Hungate, R. W.; Johansson, L.; Tedenborg, L.; Pyring, D.; Williams, M.; Hale, C.; Chen, M.; Cupples, R.; Zhang, J.; Jordan, S.; Bartberger, M. D.; Sun, Y.; Emery, M.; Wang, M.; Fotsch, C. *Bioorg. Med. Chem. Lett.* **2007,** *17,* 6056–6061.
205. Kashiwagi, H.; Ono, Y.; Ohta, M.; Morikami, K.; Takahashi, T. *Bioorg. Med. Chem.* **2012,** *20,* 4495–4506.
206. Qvist, J.; Davidovic, M.; Hamelberg, D.; Halle, B. *Proc. Natl. Acad. Sci. U. S. A.* **2008,** *105,* 6296–6301.
207. Baron, R.; Setny, P.; McCammon, J. A. *J. Am. Chem. Soc.* **2010,** *132,* 12091–12097.
208. Hummer, G. *Nat. Chem.* **2010,** *2,* 906–907.
209. Boehringer, M.; Fischer, H.; Hennig, M.; Hunziker, D.; Huwyler, J.; Kuhn, B.; Loeffler, B. M.; Luebbers, T.; Mattei, P.; Narquizian, R.; Sebokova, E.; Sprecher, U.; Wessel, H. P. *Bioorg. Med. Chem. Lett.* **2010,** *20,* 1106–1108.
210. Wand, A. J. *Curr. Opin. Struct. Biol.* **2013,** *23,* 75–81.
211. Metrangolo, P.; Resnati, G. *Cryst. Growth Des.* **2012,** *12,* 5835–5838.
212. Guthrie, F. *J. Chem. Soc.* **1863,** *16,* 239–244.
213. Hassel, O.; Hvoslef, J. *Acta Chem. Scand.* **1954,** *8,* 873.
214. Murray-Rust, P.; Motherwell, W. D. S. *J. Am. Chem. Soc.* **1979,** *101,* 4374–4376.
215. Nyburg, S. C.; Faerman, C. H. *Acta Crystallogr. B* **1985,** *41,* 274–279.
216. Ramasubbu, N.; Parthasarathy, R.; Murray-Rust, P. *J. Am. Chem. Soc.* **1986,** *108,* 4308–4314.
217. Lommerse, J. P. M.; Stone, A. J.; Taylor, R.; Allen, F. H. *J. Am. Chem. Soc.* **1996,** *118,* 3108–3116.
218. Politzer, P.; Murray, J. S.; Clark, T. *Phys. Chem. Chem. Phys.* **2010,** *12,* 7748–7757.
219. Riley, K. E.; Murray, J. S.; Politzer, P.; Concha, M. C.; Hobza, P. *J. Chem. Theory Comput.* **2009,** *5,* 155–163.
220. Mohajeri, A.; Pakiari, A. H.; Bagheri, N. *Chem. Phys. Lett.* **2009,** *467,* 393–397.
221. Brink, T.; Murray, J. S.; Politzer, P. *Int. J. Quantum Chem. Quant. Biol. Symp.* **1992,** *44,* 57–64.
222. Clark, T.; Hennemann, M.; Murray, J. S.; Politzer, P. J. *J. Mol. Model.* **2007,** *13,* 291–296.
223. Zhang, Y.; Ji, B.; Tian, A.; Wang, W. *J. Chem. Phys.* **2012,** *136,* 141101.
224. Gao, H. Y.; Shen, Q. J.; Zhao, X. R.; Yan, X. Q.; Pang, X.; Jin, W. J. *J. Mater. Chem.* **2012,** *22,* 5336–5343.
225. Řezáč, J.; Riley, K. E.; Hobza, P. *J. Chem. Theory Comput.* **2012,** *8,* 4285–4292.
226. Corradi, E.; Meille, S. V.; Messina, M. T.; Metrangolo, P.; Resnati, G. *Angew. Chem. Int. Ed.* **2000,** *30,* 1782–1786.
227. Cabot, R.; Hunter, C. A. *Chem. Commun.* **2009,** 2005–2007.
228. Sarwar, M. G.; Dragisic, B.; Salsberg, L. J.; Gouliaras, C.; Taylor, M. S. *J. Am. Chem. Soc.* **2010,** *132,* 1646–1653.
229. Wang, C.; Danovich, D.; Mo, Y.; Shaik, S. *J. Chem. Theory Comput.* **2014,** *10,* 3726–3737.
230. Metrangolo, P.; Murray, J. S.; Pilati, T.; Politzer, P.; Resnati, G.; Terraneo, G. *Cryst. Growth Des.* **2011,** *11,* 4238–4246.
231. Metrangolo, P.; Murray, J. S.; Pilati, T.; Politzer, P.; Resnati, G.; Terraneo, G. *CrystEngComm* **2011,** *13,* 6593–6596.
232. Wilcken, R.; Zimmermann, M. O.; Lange, A.; Joerger, A. C.; Boeckler, F. M. *J. Med. Chem.* **2013,** *56,* 1363–1388.
233. Voth, A. R.; Khuu, P.; Oishi, K.; Ho, P. S. *Nat. Chem.* **2009,** *1,* 74–79.
234. Cruz, S.; de la Torre, J. M.; Cobo, J.; Low, J. N.; Glidewell, C. *Acta Crystallogr. Sect. E: Struct. Rep. Online* **2006,** *62,* o3056–o3058.
235. Hardegger, L. A.; Kuhn, B.; Spinnler, B.; Anselm, L.; Ecabert, R.; Stihle, M.; Gsell, B.; Thoma, R.; Diez, J.; Benz, J.; Plancher, J.-M.; Hartmann, G.; Isshiki, Y.; Morikami, K.; Shimma, N.; Haap, W.; Banner, D. W.; Diederich, F. *ChemMedChem* **2011,** *6,* 2048–2054.
236. Iltzsch, M. H.; Uber, S. S.; Tankersley, K. O.; el Kouni, M. H. *Biochem. Pharmacol.* **1995,** *49,* 1501–1512.
237. Maillard, M. C.; Hom, R. K.; Benson, T. E.; Moon, J. B.; Mamo, S.; Bienkowski, M.; Tomasselli, A. G.; Woods, D. D.; Prince, D. B.; Paddock, D. J.; Emmons, T. L.; Tucker, J. A.; Dappen, M. S.; Brogley, L.; Thorsett, E. D.; Jewett, N.; Sinha, S.; John, V. *J. Med. Chem.* **2007,** *50,* 776–781.
238. Lu, Y.; Liu, Y.; Xu, Z.; Li, H.; Liu, H.; Zhu, W. *Expert Opin. Drug Discovery* **2012,** *7,* 375–383.
239. Scholfield, M. R.; Vander Zanden, C. M.; Carter, M.; Ho, P. S. *Protein Sci.* **2013,** *22,* 139–152.
240. Freundlich, J. S.; Anderson, J. W.; Sarantakis, D.; Shieh, H.-M.; Yu, M.; Valderramos, J.-C.; Lucumi, E.; Kuo, M.; Jacobs, W. R., Jr.; Fidock, D. A.; Schiehser, G. A.; Jacobus, D. P.; Sacchettini, J. C. *Bioorg. Med. Chem. Lett.* **2005,** *15,* 5247–5252.
241. Himmel, D. M.; Das, K.; Clark, A. D., Jr.; Hughes, S. H.; Benjahad, A.; Oumouch, S.; Guillemont, J.; Coupa, S.; Poncelet, A.; Csoka, I.; Meyer, C.; Andries, K.; Nguyen, C. H.; Grierson, D. S.; Arnold, E. *J. Med. Chem.* **2005,** *48,* 7582–7591.
242. Wilcken, R.; Liu, X.; Zimmermann, M. O.; Rutherford, T. J.; Fersht, A. R.; Joerger, A. C.; Boeckler, F. M. *J. Am. Chem. Soc.* **2012,** *134,* 6810–6818.
243. Xu, Z.; Yang, Z.; Liu, Y.; Lu, Y.; Chen, K.; Zhu, W. *J. Chem. Inf. Model.* **2014,** *54,* 69–78.
244. Politzer, P.; Murray, J. S.; Lane, P. *Int. J. Quantum Chem.* **2007,** *107,* 3046–3052.
245. Aakeröy, C.; Spartz, C. L.; Dembowski, S.; Dwyre, S.; Desper, J. *IUCrJ* **2015,** *2,* 498–510.
246. Gillis, E. P.; Eastman, K. J.; Hill, M. D.; Donnelly, D. J.; Meanwell, N. A. *J. Med. Chem.* **2015,** *58* (21), 8315–8359.
247. Wang, J.; Sánchez-Roselló, M.; Aceña, J. L.; del Pozo, C.; Sorochinsky, A. E.; Fustero, S.; Soloshonok, V. A.; Liu, H. *Chem. Rev.* **2014,** *114,* 2432–2506.
248. Purser, S.; Moore, P. R.; Swallow, S.; Gouverneur, V. *Chem. Soc. Rev.* **2008,** *37,* 320–330.
249. Jamieson, C.; Moir, E. M.; Rankovic, Z.; Wishart, G. *J. Med. Chem.* **2006,** *49,* 5029–5046.
250. Hagmann, W. K. *J. Med. Chem.* **2008,** *51,* 4359–4369.
251. Reichenbächer, K.; Süss, H. I.; Hulliger, J. *Chem. Soc. Rev.* **2005,** *34,* 22–30.
252. DiMagno, S. G.; Sun, H. *Curr. Top. Med. Chem.* **2006,** *6,* 1473–1482.
253. Howard, J. A. K.; Hoy, V. J.; O'Hagan, D.; Smith, G. T. *Tetrahedron* **1996,** *52,* 12613–12622.
254. Dunitz, J. D.; Taylor, R. *Chem. Eur. J.* **1997,** *3,* 89–98.
255. Rosenberg, R. E. *J. Phys. Chem. A* **2012,** *116,* 10842–10849.
256. Dalvit, C.; Invernizzi, C.; Vulpetti, A. *Chem. Eur. J.* **2014,** *20,* 11058–11068.
257. Struble, M. D.; Kelly, C.; Siegler, M. A.; Lectka, T. *Angew. Chem. Int. Ed.* **2014,** *53,* 8924–8928.
258. Řezáč, J.; Riley, K. E.; Hobza, P. *J. Chem. Theory Comput.* **2011,** *7,* 2427–2438.
259. Carosati, E.; Sciabola, S.; Cruciani, G. *J. Med. Chem.* **2004,** *47,* 5114–5125.

260. Müller, K.; Faeh, C.; Diederich, F. *Science* **2007,** *317,* 1881–1886.
261. Zhou, P.; Zou, J.; Tian, F.; Shang, Z. *J. Chem. Inf. Model.* **2009,** *49,* 2344–2355.
262. Paulini, R.; Müller, K.; Diederich, F. *Angew. Chem. Int. Ed.* **2005,** *44,* 1788–1805.
263. Allen, F. H.; Baalham, C. A.; Lommerse, J. P. M.; Raithby, P. R. *Acta Crystallogr. B* **1998,** *54,* 320–329.
264. Bergner, A.; Günther, J.; Hendlich, M.; Klebe, G.; Verdonk, M. *Biopolymers* **2002,** *61,* 99–110.
265. Based on the 2015 version of the CSD, using non-disordered, non-polymeric, organic structures with R-factor $\leq$ 7.5%, powder structures and structures marked as being in error excluded. Searches were for X···C(═O) contacts shorter than sum of vdw radii plus 0.3 Å.
266. Fischer, F. R.; Wood, P. A.; Allen, F. H.; Diederich, F. *Proc. Natl. Acad. Sci. U. S. A.* **2008,** *105,* 17290–17294.
267. Adhikari, U.; Scheiner, S. *J. Phys. Chem. A* **2013,** *117,* 489–496.
268. Newberry, R. W.; VanVeller, B.; Guzei, I. A.; Raines, R. T. *J. Am. Chem. Soc.* **2013,** *135,* 7843–7846.
269. Hof, F.; Scofield, D. M.; Schweizer, W. B.; Diederich, F. *Angew. Chem. Int. Ed.* **2004,** *43,* 5056–5059.
270. Fischer, F. R.; Schweizer, W. B.; Diederich, F. *Angew. Chem. Int. Ed.* **2007,** *46,* 8270–8273.
271. Cowan-Jacob, S. W.; Fendrich, G.; Floersheimer, A.; Furet, P.; Liebetanz, J.; Rummel, G.; Rheinberger, P.; Centeleghe, M.; Fabbro, D.; Manley, P. W. *Acta Crystallogr., Sect. D: Biol. Crystallogr.* **2007,** *63,* 80–93.
272. Pollock, J.; Borkin, D.; Lund, G.; Purohit, T.; Dyguda-Kazimierowicz, E.; Grembecka, J.; Cierpicki, T. *J. Med. Chem.* **2015,** *58* (18), 7465–7474.
273. Maccallum, P. H.; Poet, R.; Milner-White, E. J. *J. Mol. Biol.* **1995,** *248,* 374–384.
274. Deane, C. M.; Allen, F. H.; Taylor, R.; Blundell, T. L. *Protein Eng.* **1999,** *12,* 1025–1028.
275. Beno, B. R.; Yeung, K.-S.; Bartberger, M. D.; Pennington, L. D.; Meanwell, N. A. *J. Med. Chem.* **2015,** *58,* 4383–4438.
276. Valley, C. C.; Cembran, A.; Perlmutter, J. D.; Lewis, A. K.; Labello, N. P.; Gao, J.; Sachs, J. N. *J. Biol. Chem.* **2012,** *287,* 34979–34991.
277. Imai, Y.; Inoue, Y.; Yamamoto, Y. *J. Med. Chem.* **2007,** *50,* 1189–1196.
278. Meyer, E. A.; Brenk, R.; Castellano, R. K.; Furler, M.; Klebe, G.; Diederich, F. *ChemBioChem* **2002,** *3,* 250–253.
279. Zhou, P.; Tian, F.; Lv, F.; Shang, Z. *Proteins: Struct., Funct., Bioinf.* **2009,** *76,* 151–163.
280. Allen, F. H.; Bird, C. M.; Rowland, R. S.; Raithby, P. R. *Acta Crystallogr. B* **1997,** *53,* 696–701.
281. Biswal, H. S.; Wategaonkar, S. *J. Phys. Chem. A* **2009,** *113,* 12774–12782.
282. Based on the 2015 version of the CSD using organic structures with *R*-factor $\leq$ 5% and containing both Y–S–Z and H–(O, N) groups. Hydrogen atom positions were adjusted to make H–(O, N) distances equal to average neutron diffraction values.
283. Wood, P. A.; Pidcock, E.; Allen, F. H. *Acta Crystallogr. B* **2008,** *64,* 491–496.
284. Rosenfield, R. E., Jr.; Parthasarathy, R.; Dunitz, J. D. *J. Am. Chem. Soc.* **1977,** *99,* 4860–4862.
285. Politzer, P.; Murray, J. S.; Clark, T. *Phys. Chem. Chem. Phys.* **2013,** *15,* 11178–11189.
286. Lupyan, D.; Abramov, Y. A.; Sherman, W. *J. Comput. Aided Mol. Des.* **2012,** *26,* 1195–1205.
287. Iwaoka, M.; Takemoto, S.; Tomoda, S. *J. Am. Chem. Soc.* **2002,** *124,* 10613–10620.
288. Huang, X.; Cheng, C. C.; Fischmann, T. O.; Duca, J. S.; Yang, X.; Richards, M.; Shipps, G. W., Jr. *ACS Med. Chem. Lett.* **2012,** *3,* 123–128.
289. Huang, X.; Cheng, C. C.; Fischmann, T. O.; Duca, J. S.; Richards, M.; Tadikonda, P. K.; Reddy, P. A.; Zhao, L.; Siddiqui, M. A.; Parry, D.; Davis, N.; Seghezzi, W.; Wiswell, D.; Shipps, G. W., Jr. *Bioorg. Med. Chem. Lett.* **2013,** *23,* 2590–2594.
290. Hua, Z.; Bregman, H.; Buchanan, J. L.; Chakka, N.; Guzman-Perez, A.; Gunaydin, H.; Huang, X.; Gu, Y.; Berry, V.; Liu, J.; Teffera, Y.; Huang, L.; Egge, B.; Emkey, R.; Mullady, E. L.; Schneider, S.; Andrews, P. S.; Acquaviva, L.; Dovey, J.; Mishra, A.; Newcomb, J.; Saffran, D.; Serafino, R.; Strathdee, C. A.; Turci, S. M.; Stanton, M.; Wilson, C.; DiMauro, E. F. *J. Med. Chem.* **2013,** *56,* 10003–10015.
291. Eccles, K. S.; Morrison, R. E.; Sinha, A. S.; Maguire, A. R.; Lawrence, S. E. *Cryst. Growth Des.* **2015,** *15,* 3442–3451.
292. Wilcken, R.; Zimmermann, M. O.; Lange, A.; Zahn, S.; Kirchner, B.; Boeckler, F. M. *J. Chem. Theory Comput.* **2011,** *7,* 2307–2315.
293. Datta, S.; Grant, D. J. W. *Nat. Rev. Drug Discov.* **2004,** *3,* 42–57.
294. Lee, A. Y.; Erdemir, D.; Myerson, A. S. *Annu. Rev. Chem. Biomol. Eng.* **2011,** *2,* 259–280.
295. Stahly, G. P. *Cryst. Growth Des.* **2007,** *7,* 1007–1026.
296. Hilfiker, R. *Polymorphism in the Pharmaceutical Industry;* Wiley-VCH: Weinheim, 2006.
297. Brittain, H. G. *J. Pharm. Sci.* **2013,** *102,* 311–317.
298. Steed, J. W. *Trends Pharmacol. Sci.* **2013,** *34,* 185–193.
299. Aitipamula, S.; Banerjee, R.; Bansal, A. K.; Biradha, K.; Cheney, M. L.; Choudhury, A. R.; Desiraju, G. R.; Dikundwar, A. G.; Dubey, R.; Duggirala, N.; Ghogale, P. P.; Ghosh, S.; Goswami, P. K.; Goud, N. R.; Jetti, R. R. K. R.; Karpinski, P.; Kaushik, P.; Kumar, D.; Kumar, V.; Moulton, B.; Mukherjee, A.; Mukherjee, G.; Myerson, A. S.; Puri, V.; Ramanan, A.; Rajamannar, T.; Reddy, C. M.; Rodriguez-Hornedo, N.; Rogers, R. D.; Row, T. N. G.; Sanphui, P.; Shan, N.; Shete, G.; Singh, A.; Sun, C. C.; Swift, J. A.; Thaimattam, R.; Thakur, T. S.; Thaper, R. K.; Thomas, S. P.; Tothadi, S.; Vangala, V. R.; Variankaval, N.; Vishweshwar, P.; Weyna, D. R.; Zaworotko, M. J. *Cryst. Growth Des.* **2012,** *12,* 2147–2152.
300. Trask, A. V. *Mol. Pharm.* **2007,** *4,* 301–309.
301. Morissette, S. L.; Almarsson, Ö.; Peterson, M. L.; Remenar, J. F.; Read, M. J.; Lemmo, A. V.; Ellis, S.; Cima, M. J.; Gardner, C. R. *Adv. Drug Deliv. Rev.* **2004,** *56,* 275–300.
302. Gavezzotti, A. *Acc. Chem. Res.* **1994,** *27,* 309–314.
303. Dunitz, J. D. *Chem. Commun.* **2003,** 545–548.
304. Bardwell, D. A.; Adjiman, C. S.; Arnautova, Y. A.; Bartashevich, E.; Boerrigter, S. X. M.; Braun, D. E.; Cruz-Cabeza, A. J.; Day, G. M.; Della Valle, R. G.; Desiraju, G. R.; van Eijck, B. P.; Facelli, J. C.; Ferraro, M. B.; Grillo, D.; Habgood, M.; Hofmann, D. W. M.; Hofmann, F.; Jose, K. V. J.; Karamertzanis, P. G.; Kazantsev, A. V.; Kendrick, J.; Kuleshova, L. N.; Leusen, F. J. J.; Maleev, A. V.; Misquitta, A. J.; Mohamed, S.; Needs, R. J.; Neumann, M. A.; Nikylov, D.; Orendt, A. M.; Pal, R.; Pantelides, C. C.; Pickard, C. J.; Price, L. S.; Price, S. L.; Scheraga, H. A.; van de Streek, J.; Thakur, T. S.; Tiwari, S.; Venuti, E.; Zhitkov, I. K. *Acta Crystallogr. B* **2011,** *67,* 535–551.
305. Thakur, T. S.; Dubey, R.; Desiraju, G. R. *Annu. Rev. Phys. Chem.* **2015,** *66,* 21–42.
306. Price, S. L. *Chem. Soc. Rev.* **2014,** *43,* 2098–2111.
307. Chan, H. C. S.; Kendrick, J.; Leusen, F. J. J. *Angew. Chem. Int. Ed.* **2011,** *50,* 2979–2981.
308. Etter, M. C. *Acc. Chem. Res.* **1990,** *23,* 120–126.
309. Childs, S. L.; Wood, P. A.; Rodríguez-Hornedo, N.; Reddy, L. S.; Hardcastle, K. I. *Cryst. Growth Des.* **2009,** *9,* 1869–1888.
310. Wood, P. A.; Galek, P. T. A. *CrystEngComm* **2010,** *12,* 2485–2491.
311. Gillon, A. L.; Feeder, N.; Davey, R. J.; Storey, R. *Cryst. Growth Des.* **2003,** *3,* 663–673.
312. Infantes, L.; Motherwell, W. D. S. *Chem. Commun.* **2004,** 1166–1167.
313. Galek, P. T. A.; Chisholm, J. A.; Pidcock, E.; Wood, P. A. *Acta Crystallogr. B* **2014,** *70,* 91–105.
314. Bilton, C.; Allen, F. H.; Shields, G. P.; Howard, J. A. K. *Acta Crystallogr. B* **2000,** *56,* 849–856.
315. Kuhn, B.; Mohr, P.; Stahl, M. *J. Med. Chem.* **2010,** *33,* 2601–2611.
316. Desiraju, G. R. *Angew. Chem. Int. Ed. Engl.* **1995,** *34,* 2311–2327.
317. Desiraju, G. R.; Vittal, J. J.; Ramanan, A. *Crystal Engineering;* World Scientific: Singapore, 2011.
318. Sarma, J. A. R. P.; Desiraju, G. R. *Cryst. Growth Des.* **2002,** *2,* 93–100.
319. Leiserowitz, L. *Acta Crystallogr. B* **1976,** *32,* 775–802.

320. Leiserowitz, L.; Tuval, M. *Acta Crystallogr. B* **1978,** *34,* 1230–1247.
321. Allen, F. H.; Motherwell, W. D. S.; Raithby, P. R.; Shields, G. P.; Taylor, R. *New J. Chem.* **1999,** *23,* 25–34.
322. D'Ascenzo, L.; Auffinger, P. *Acta Crystallogr. B* **2015,** *71,* 164–175.
323. Steiner, T. *Acta Crystallogr. B* **2001,** *57,* 103–106.
324. Cruz-Cabeza, A. J.; Day, G. M.; Motherwell, W. D. S.; Jones, W. *Cryst. Growth Des.* **2007,** *7,* 100–107.
325. Infantes, L.; Motherwell, S. *Struct. Chem.* **2004,** *15,* 173–184.
326. Rathore, R. S.; Alekhya, Y.; Kondapi, A. K.; Sathiyanarayanan, K. *CrystEngComm* **2011,** *13,* 5234–5238.
327. Galek, P. T. A.; Fábián, L.; Motherwell, W. D. S.; Allen, F. H.; Feeder, N. *Acta Crystallogr. B* **2007,** *63,* 768–782.
328. Galek, P. T. A.; Allen, F. H.; Fábián, L.; Feeder, N. *CrystEngComm* **2009,** *11,* 2634–2639.
329. Nauha, E.; Bernstein, J. *Cryst. Growth Des.* **2014,** *14,* 4364–4370.
330. Nauha, E.; Bernstein, J. *J. Pharm. Sci.* **2015,** *104,* 2056–2061.
331. Abramov, Y. A. *Org. Process Res. Dev.* **2013,** *17,* 472–485.
332. Wood, P. A.; Feeder, N.; Furlow, M.; Galek, P. T. A.; Groom, C. R.; Pidcock, E. *CrystEngComm* **2014,** *16,* 5839–5848.
333. Grecu, T.; Adams, H.; Hunter, C. A.; McCabe, J. F.; Portell, A.; Prohens, R. *Cryst. Growth Des.* **2014,** *14,* 1749–1755.
334. Politzer, P.; Murray, J. S. *Cryst. Growth Des.* **2015,** *15,* 3767–3774.
335. Friščić, T.; Jones, W. *Faraday Discuss.* **2007,** *136,* 167–178.
336. Shattock, T. R.; Arora, K. K.; Vishweshwar, P.; Zaworotko, M. J. *Cryst. Growth Des.* **2008,** *8,* 4533–4545.
337. Fábián, L. *Cryst. Growth Des.* **2009,** *9,* 1436–1443.
338. Issa, N.; Barnett, S. A.; Mohamed, S.; Braun, D. E.; Copley, R. C. B.; Tocher, D. A.; Price, S. L. *CrystEngComm* **2012,** *14,* 2454–2464.
339. Briggner, L.-E.; Hendrickx, R.; Kloo, L.; Rosdahl, J.; Svensson, P. H. *ChemMedChem* **2011,** *6,* 60–62.
340. Scott, J. S.; Birch, A. M.; Brocklehurst, K. J.; Broo, A.; Brown, H. S.; Butlin, R. J.; Clarke, D. S.; Davidsson, Ő.; Ertan, A.; Goldberg, K.; Groombridge, S. D.; Hudson, J. A.; Laber, D.; Leach, A. G.; MacFaul, P. A.; McKerrecher, D.; Pickup, A.; Schofield, P.; Svensson, P. H.; Sörme, P.; Teague, J. *J. Med. Chem.* **2012,** *55,* 5361–5379.
341. Takeuchi, T.; Oishi, S.; Kaneda, M.; Ohno, H.; Nakamura, S.; Nakanishi, I.; Yamane, M.; Sawada, J.; Asai, A.; Fujii, N. *ACS Med. Chem. Lett.* **2014,** *5,* 566–571.
342. Certal, V.; Carry, J.-C.; Halley, F.; Virone-Oddos, A.; Thompson, F.; Filoche-Rommé, B.; El-Ahmad, Y.; Karlsson, A.; Charrier, V.; Delorme, C.; Rak, A.; Abecassis, P.-Y.; Amara, C.; Vincent, L.; Bonnevaux, H.; Nicolas, J.-P.; Mathieu, M.; Bertrand, T.; Marquette, J.-P.; Michot, N.; Benard, T.; Perrin, M.-A.; Lemaitre, O.; Guerif, S.; Perron, S.; Monget, S.; Gruss-Leleu, F.; Doerflinger, G.; Guizani, H.; Brollo, M.; Delbarre, L.; Bertin, L.; Richepin, P.; Loyau, V.; Garcia-Echeverria, C.; Lengauer, C.; Schio, L. *J. Med. Chem.* **2014,** *57,* 903–920.
343. Rosbottom, I.; Roberts, K. J.; Docherty, R. *CrystEngChem* **2015,** *17,* 5768–5788.
344. Ramachandran, V.; Murnane, D.; Hammond, R. B.; Pickering, J.; Roberts, K. J.; Soufian, M.; Forbes, B.; Jaffari, S.; Martin, G. P.; Collins, E.; Pencheva, K. *Mol. Pharm.* **2015,** *12,* 18–33.
345. Waknis, V.; Chu, E.; Schlam, R.; Sidorenko, A.; Badawy, S.; Yin, S.; Narang, A. S. *Pharm. Res.* **2014,** *31,* 160–172.
346. Aakeröy, C. *Acta Crystallogr. B* **2015,** *71,* 387–391.
347. Perhaps this remark may offend those developing high-level methods for calculating such affinities, but in the context of day-to-day drug discovery, where predictions must be accurate and delivered quickly and cheaply, it is surely justified.
348. Dunitz, J. D.; Gavezzotti, A. *Angew. Chem. Int. Ed.* **2005,** *44,* 1766–1787.

Relevant Websites

http://www.rcsb.org/pdb/home/home.do and http://www.ebi.ac.uk/pdbe/—Portals to the Protein Data Bank.
http://www.ccdc.cam.ac.uk/pages/Home.aspx—Cambridge Crystallographic Data Centre, distributors of the Cambridge Structural Database.

3.06 Using 3D Structural Information in Computational Design

AM Davis, AstraZeneca R&D Gothenburg, Gothenburg, Sweden
CM Edge, GlaxoSmithKline Medicines Research Centre, Stevenage, United Kingdom

© 2017 Elsevier Ltd. All rights reserved.

3.06.1	**Introduction**	101
3.06.2	**A Brief History of Protein Structure Determination**	102
3.06.3	**A Brief History of the Use of X-Ray Structures in Structure-Based Drug Design**	103
3.06.4	**Limitations and Lessons in Using X-Ray Crystal Structures**	105
3.06.5	**Where Experts Can Be Fooled, Chemists Should Always Be Extra Wary**	106
3.06.6	**Uncertainties in Using X-Ray Crystal Structures**	106
3.06.6.1	Crystallization Conditions May Not Be Relevant for the Target Biology	108
3.06.6.2	Identification of Water Molecules in the Electron-Density Maps Can Be a Problem	108
3.06.6.3	The Effects of Protein Flexibility Are Small or At Least Understood	108
3.06.7	**Validation of X-Ray Crystal Structures**	109
3.06.8	**Using X-Ray Crystal Structures in Docking and Scoring Validation Studies**	109
3.06.9	**Fitting to Coordinate Versus Fitting to Electron Density**	113
3.06.10	**Using Electron Microscopy Structures**	114
3.06.10.1	Use and Limitations of Electron Microscopy	114
3.06.11	**Summary**	116
Acknowledgment		116
References		117

3.06.1 Introduction

Computational design based on three-dimensional (3D) protein structural information is now fully embedded in the drug discovery process, with structure-based drug design playing a critical part in many well-known marketed drug stories.[1] The 3D structure information may have come from an X-ray crystal structure, a homology model based on a similar protein, an NMR-derived structure, or more recently from electron cryo-microscopy (3DEM). Other new techniques such as hydrogen deuterium exchange mass spectrometry can also provide complementary information on the location of ligand binding sites, the impact of ligand binding on solvent accessibility, and changes in protein flexibility. However, X-ray crystallography remains the dominant source of 3D data (Fig. 1).

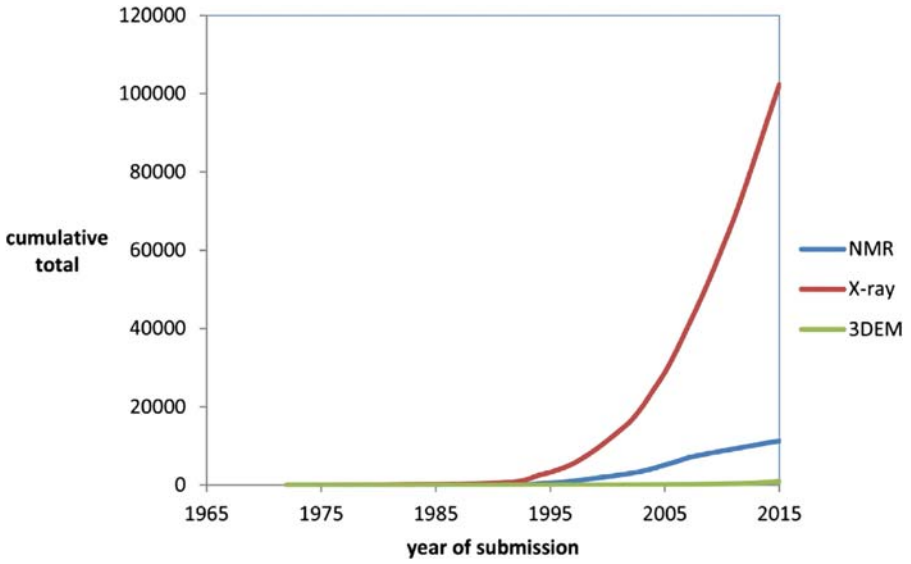

Fig. 1 PDB cumulative deposition by year for NMR, X-ray, and 3DEM structures.

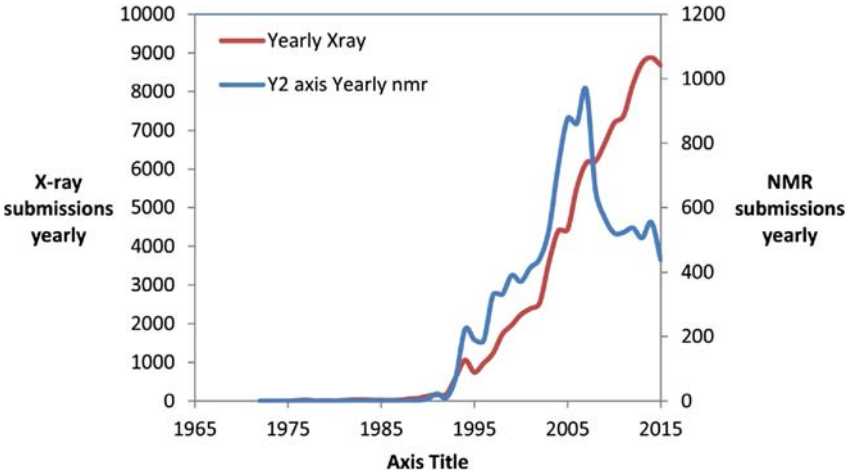

Fig. 2 X-ray and NMR submissions per year to the PDB.

3.06.2 A Brief History of Protein Structure Determination

The first X-ray structure of globular proteins were myoglobin and hemoglobin in 1958, for which Kendrew and Perutz were awarded the Nobel Prize in Chemistry in 1962. This was the result of over 20 years' effort, began by Perutz in 1927 starting with hemoglobin. By the time the Protein Database was established in 191 it contained seven X-ray structures, and by the time of the first PDB newsletter in 1974, 12 had been deposited. The deposition rates increased year-on-year in an almost exponential fashion until 2008, and by 2016, over 120,000 protein structures had been deposited.

In comparison protein structure determination by NMR is a much newer technique. Wüthrich had been working on NMR of proteins since 1967, and the first de novo 3-D protein structure was solved by NMR in 1984.[2] Through the 1990s the number of 3D structures derived by NMR began to increase. It reached a zenith in 2007 with 965 NMR structures deposited that year in PDB. Since then the number of NMR-derived structures has been falling, Fig. 2. Even though NMR hardware and software have undoubtedly improved over the past 10 years, the inherent limitations to relatively small proteins, Fig. 3, the requirement for large amounts of multiply labeled protein and access to expensive high-field NMR machines, have limited the numbers of NMR-derived structures. X-ray crystallography on the other hand, continued an unbroken year on year rise in protein structures deposited to the PDB from 1995 to 2014. The last full year, 2015 showed a significant drop on 2013, and we await what 2016 brings to see if this is a blip, a saturation of delivery from the method, or a reaction to some other global change. The statistics of course do not include the large numbers of X-ray crystal structures (of the most interesting drug targets) that sit behind the firewalls of pharmaceutical companies. Few NMR-determined protein structures exist behind those same firewalls, where NMR, it seems, based on the authors own experiences, has been relegated to fragment-based screening duties.

So far, fewer than 1000 3DEM models have been deposited to the PDB, although the Electron Microscopy Data Bank (EMDB) contains over 4000 volume maps. The resolution achievable with 3DEM has been limiting, but with the introduction of direct electron detectors, this situation is rapidly improving and 3DEM may well be the method of the future even for protein–ligand structure determination.

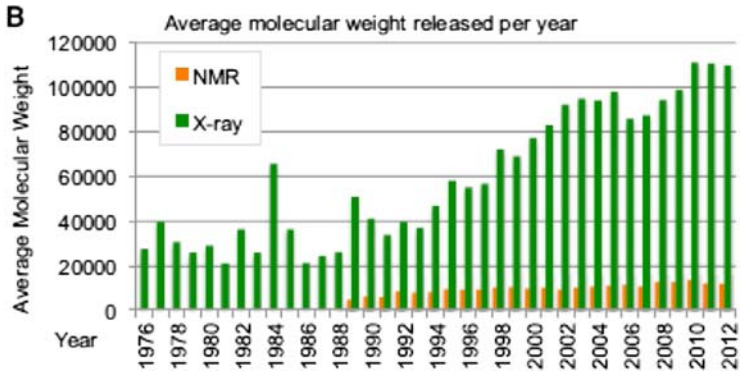

Fig. 3 The average molecular weight of protein structures determined by X-ray crystallography and NMR by year of deposition in PDB.[3]

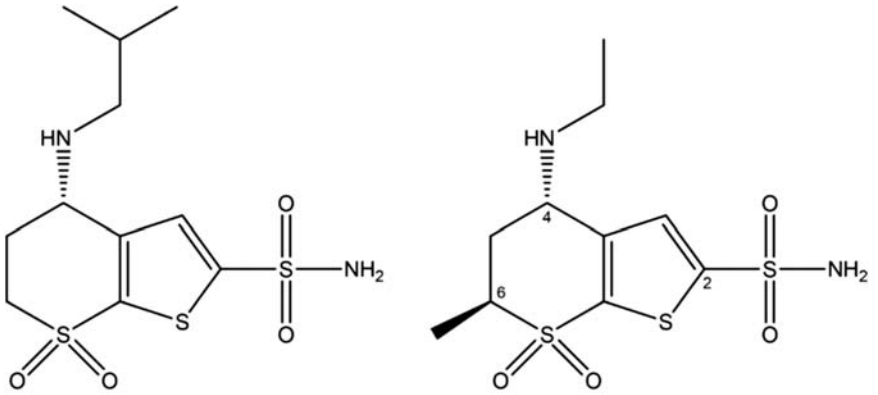

Fig. 4 MK-417, the subject of structural studies and MK-507, the resulting designed molecule.

With the widespread availability of good quality X-ray structures one might think that homology modeling has become rather sidelined. Many drug targets, particularly membrane protein targets are not yet amenable to routine iterative crystallography, although for G protein-coupled receptors (GPCRs) at least, companies such as Heptares are opening up the field.[4,5] So homology modeling still has a role in the arsenal of the computational chemist involved in structure-based drug design, and is reviewed within this volume.

3.06.3 A Brief History of the Use of X-Ray Structures in Structure-Based Drug Design

When we started working in the pharmaceutical business, we were frequently asked what drugs computational chemistry had ever discovered. Thirty years later, "comp. chem." is mainstream and an integral part of most drug discovery efforts. (In fact one could argue that many scientists are too ready to believe whatever numbers are spat out of a computer program.) This section reviews some of the original history of structure-based drug design (SBDD) and tries to draw out lessons for future medicinal and computational chemistry programs.

One of the first SBDD successes was the discovery of dorzolamide by Merck researchers, Fig. 4. They had access to X-ray crystal structures of MK-417 and its enantiomer, both bound to carbonic anhydrase.[6] Both molecules coordinated with zinc in the enzyme active site via the sulfonamide group, but the constraints of the site forced the (*S*)-enantiomer to adopt a conformation with the isobutylamino group in a pseudo-axial position. Ab initio molecular orbital calculations of the isolated ligand confirmed that this was less favorable than the pseudo-equatorial form seen for the (*R*)-enantiomer. More importantly, this led to the hypothesis that a 6-substitution, such as (*S*)-6-Me, would stabilize the favored conformation, leading to MK-0507, (dorzolamide), an antiglaucoma treatment.[7] This is an instructive example, because, although this seems like a small change in structure, the team went to the considerable trouble of calculating quantum mechanics energetics using a 1980s computer, adding evidence to a simple theory of how to stabilize the desired conformation.

Another case that is often cited as an early success of SBDD is that of zanamivir (Relenza), Fig. 5. Glaxo and a group from Monash University, Victoria were interested in neuraminidase as a target for influenza, as it is responsible for the cleavage of mature

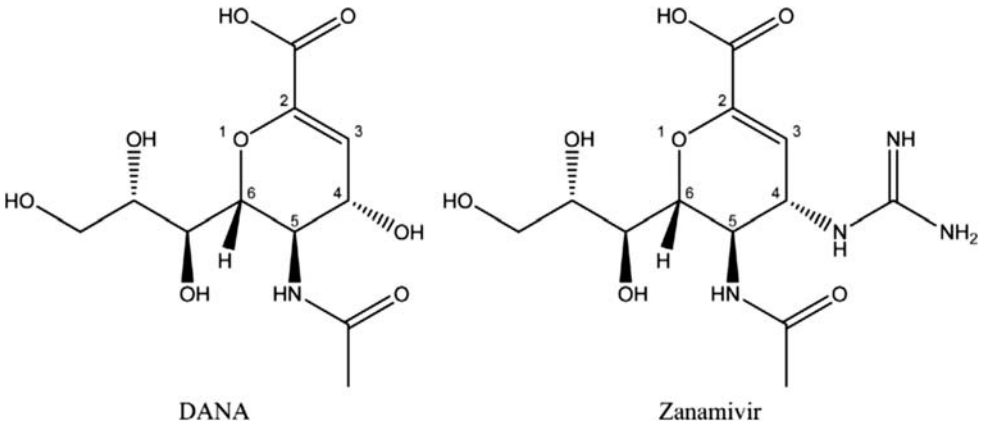

Fig. 5 The prototypical inhibitor, DANA and the designed drug, zanamivir.

viral particles from the host cell. The team had a crystal structure of neuraminidase with a substrate analog 2-deoxy-2,3-dehydro-*N*-acetylneuraminic acid bound in the active site. Although the crystal structure had a number of questionable features by today's standards, it provided a reliable enough template for the use of molecular field analysis, using the GRID program.[8] This allowed the team to identify the 4-hydroxyl group as a candidate for replacement by amino and ultimately guanidino groups, giving orders of magnitude more binding affinity than the natural substrate. The amine and guanidine groups made better hydrogen bonds than the hydroxyl, but optimizing hydrogen bonding is not often a route to markedly better binding, since water itself is such a good hydrogen bonding medium. Subsequent crystallographic and theoretical studies have shown that the key in this case is the water in the region of the 4-position. This makes one hydrogen bond rather than the more usual two or three and is thus a good candidate for substitution by the ligand.[9,10] Two of the guanidino nitrogens also occupy loci of water oxygens in the pocket. It seems that these waters are interconnected in that both positions are favorable sites for water, but only one at a time (J.W. Essex, personal communication). The guanidine nitrogens can occupy both loci simultaneously and "free" the water to return to bulk solvent, thus providing a large binding energy effect.

Another fruitful avenue for SBDD has been inhibition of various proteases. Many groups have used molecular modeling of crystal structures along with ancillary calculations (or just "eyeballing" structures) to design more potent or more selective ligands. The calculations are not only grid-based, like the zanamivir story above, but also include other scoring methods, such as molecular mechanics force field energies, docking scores, and simple steric bump checks. Examples of this type of work include the discovery of aliskiren, a renin inhibitor[11] and boceprevir, an inhibitor of NS3-NS4A HCV serine protease.[12] In both these cases SBDD methods were acknowledged as being at the forefront of the design process.

In the case of aliskiren, **Fig. 6**, the design strategy was to target a particular kind of binding mode, that is, to go for novel S1 to S3 pocket binders rather than the more "traditional" P1 to P4 backbone skeletons that were prevalent in the literature. A hydroxyethylene framework was chosen as a transition state mimetic and a pharmacophore was derived for the P1 to P3 region. The program GRASP was used to characterize the binding pocket and a particular hydrophobic patch ("S3 superpocket") discovered in a crystal structure was targeted for interaction. The eventual design spanned the P3 to P2′ substrate equivalent rather than the P4 to P1, so fit the initial design intentions.[13]

The Schering Plough team who discovered boceprevir resorted to rational design because they had failed to identify any decent leads from screening libraries of compounds.12 (This was a common complaint in the late 1990s and early 2000s, as many corporate screening collections were stuffed with rather unattractive, but easily made combinatorial libraries.) They took

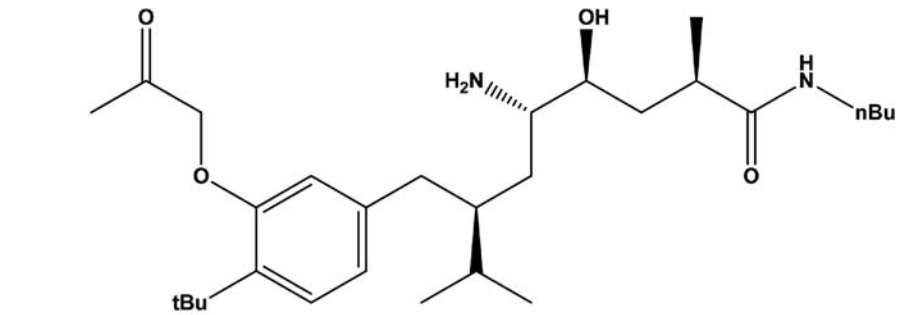

Hit molecule

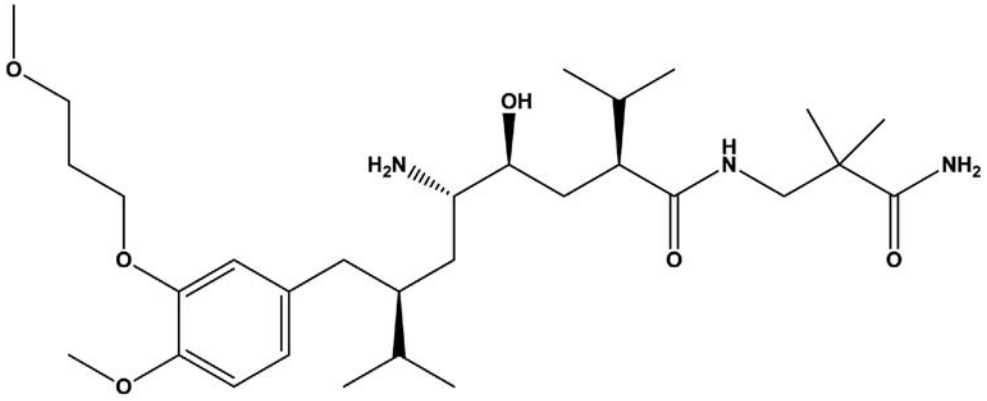

Aliskiren

Fig. 6 Renin inhibitor Aliskiren and its starting point.

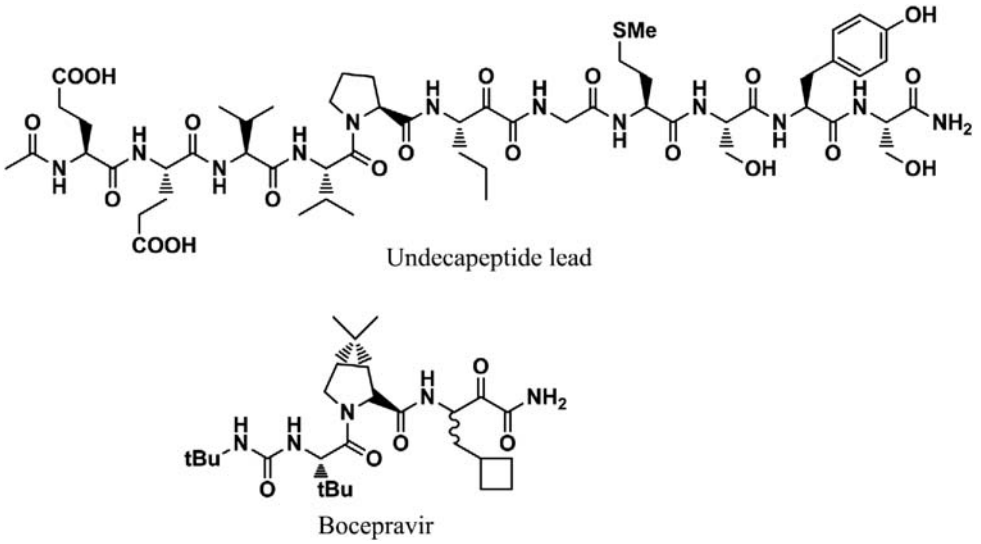

Fig. 7 The original undecapeptide lead, spanning P6 to P5′ and the final designed drug, bocepravir.

a large undecapeptide, which spanned from P6 to P5′(!), and modified it using computational and medicinal chemistry. These included SAR at particular pocket loci, macrocyclic "depeptidation," truncation, and examination of what crystal structures were available. The end result was a reduction in span from P6 to P5′ to P3 to P1, with a drop in Ki from 1.9 to 25 nM, but with far superior PK properties, such as oral bioavailability, Fig. 7.

There are other well-known examples of drug discovery with a computational component that tell similar stories. The interested reader should take a look at an excellent review of structure-based drug design successes (up to 2010) by Talele et al. in *Current Topics in Medicinal Chemistry*.[14] This discusses the above cases in more detail as well as some others. A recent issue of *Trends in Pharmacological Sciences* (33(5), 2012) was dedicated to structure-based drug design and contains articles on recent attempts and successes in areas such as kinase inhibition[15] and G protein-coupled receptors.[16]

Although there is now a good body of success stories in the literature, we are perhaps more interested in cases where things go wrong. We still regularly come across papers in the literature containing words like "surprising," "unanticipated," and especially "unexpected binding." Examples include: unexpected binding modes for JNK3,[17] thrombin,[18] factor VIIa,[19] IspE,[20] IMPCH,[21] NS5A,[22] and BACE,[23,24]; unexpected conformations of Aurora B kinase,[25] the cSrc gatekeeper methionine,[26] human neutrophil elastase,[27] BoNT/A-LC,[28] BpML1,[29] and 15S-LOX.[30] The final case is actually a 2008 rerefinement of a 1997 15S-lipoxygenase crystal structure which seemed to be badly disordered in three segments, suggesting large-scale mobility of helix 2. The refinement, however, assumed that the original crystalline sample was twinned and produced two conformationally distinct LOX molecules contacting in the crystal. Even in this case, the authors were "surprised" to find that only one of the molecules had a bound inhibitor, while the other was empty.

What does all this surprise and unexpectedness mean? Some is obviously just a way to make the story look more interesting to journal editors, but most of the above examples do genuinely contain structures that the authors did not expect. While many computational chemists would argue that pose prediction in docking is a solved problem (but ranking the poses is not), many structural scientists seem to be unearthing structures with issues, such as unanticipated crystal twinning, flipped binding modes, and flexible regions previously thought to be rigid. So while the computational tools may be improving, they are dependent upon the accuracy and precision of the structural model on which they base their work.

3.06.4 Limitations and Lessons in Using X-Ray Crystal Structures

With over 120,000 structures available, and 40 years of experience, one might expect we have become rather good at using X-ray structures in computational design. On the contrary, we are still learning to cope with its strengths and limitations, and learning lessons, structure by structure, and project by project. In 2002 some of these limitations and lessons learned across many projects and protein targets were highlighted to medicinal chemists in a review by Kleywegt, Teague, and Davis.[31]

The three authors, practitioners in crystallography, medicinal chemistry, and computational chemistry respectively, realized that important information was often lost, overlooked, or misinterpreted between the core disciplines which drive structure-based design. The review, targeted at medicinal and computational chemists, built upon the robust literature and self-critique of the X-ray crystallography community, but which had largely failed to permeate into the hands, or should we say the minds, of users of such information, the computational chemists. The review reminded readers that an X-ray crystal structure *"is one crystallographer's subjective interpretation of an observed electron-density map expressed in terms of an atomic model."* The authors went

on to state that "Some published protein models appear to have been more determined by the crystallographer's imagination than by any experimental data."

3.06.5 Where Experts Can Be Fooled, Chemists Should Always Be Extra Wary

The difference between experimental data and imagination can sometimes be hard to distinguish, even by experts. In 2006, it became apparent that a structure of human C3b complement system component[32] from a lab at the University of Alabama may have been based on fabricated "experimental" data. A subsequent 2-year investigation by the university concluded in 2009 that this structure and 10 others were "more likely than not falsified and/or fabricated" by one of the authors.[33] Apparently two of the structures had even been selected as targets for a dengue fever global virtual screening initiative. The journalists at Nature, not known for use of hyperbole, reported the story in 2009 with the headline "Fraud rocks the protein community."[34] For all its condemnation, it was not until 2016 that Nature finally retracted the original paper published in its journal.[35]

In Apr. 2008, the wwPDB had already established an X-ray validation task force (VTF) consisting of experts in the field, to advise wwPDB on approaches to validate structures on deposition. The recommendations and detailed analyses were published in 2011,[36] (with recommendations for 3EDM structures following in 2012 and NMR structures in 2013[37]).

The result was the development by wwPDB of a validation pipeline for X-ray structures incorporating community-consensus methods and software. The pipeline can be used through a stand-alone anonymous server and is also used during deposition and annotation of structures to the PDB. The official validation reports obtained after annotation can be submitted to journals to accompany manuscripts in which structures are described, and several journals have made this a mandatory requirement for manuscript submission. As of 2016, the wwPDB validation pipeline and server can handle structures determined by all current methods, and validation reports for all structures in the PDB are available for download and through the wwPDB partner websites.

The recommendations led to the provision of validation tools that were evaluated on the whole PDB. This in turn led to the provision of diagnostics alongside the structure in PDB, and a validation report on every structure.[38] The tools used in the PDB validation reports are listed within the PDB validation report documentation.[39]

Guides to the validation reports for X-ray structures,[39] NMR structures[40], and 3DEM structures[41] are available. The wwPDB team is working on an application programming interface (API) which will soon be made available so that anyone can access the tools programmatically. The hope is that the API will be integrated in the standard structure determination packages so the users can access it during structure determination and refinement.[42]

While examples of outright fraud may be rare, the human C3b complement system component example highlights how difficult it can be for even crystallography experts to separate and identify reality from imagination, fact from fiction, reliable from unreliable, when examining the beauty of an atomic coordinate model. If experts can be fooled, chemists should always be extra wary.

The advice in Teague, Davis, and Kleywegt's 2002 review is as relevant today as it was 14 years ago. A chemist using an X-ray crystal atomic model should examine it together with the crystallographer and discuss its strengths and weaknesses, areas of confidence, and uncertainty. Put simply, "examine the atomic model with the electron density, and where there is no density, there are no electrons, and where there are no electrons there are no atoms," as an eminent crystallographer once put it. Sounds easy, but it was not until 2008 that deposition of structure factors with the atomic coordinates became mandatory in PDB.[43] On the other hand, thanks to the rapid growth of the archive, the fraction of legacy entries for which the experimental data are not available (and presumably lost for all eternity) is becoming smaller and smaller (as of 2016, approximately 1 in 6 X-ray entries has no experimental data). At least inside pharma companies chemists have the opportunity to work closely with the originating crystallographer, but even so, there still exists plenty of opportunity for misinterpretations, misunderstandings, and over-interpretations to be made.

3.06.6 Uncertainties in Using X-Ray Crystal Structures

Kleywegt, Teague, and Davis highlighted the following uncertainties,[31] among others.

> (Nearly) Isoelectronic atoms and ions cannot be directly distinguished from the electron density, so it can be difficult to determine the relative orientation of the δN and δO of glutamine and γN and γO of asparagine.

If a conscious decision is made over the position of the N and O it is often by inspection of local hydrogen bond patterns, although sometimes before waters have been added to the structure. The switch from a strong donor to a strong acceptor, by the uncertainty of the position of N and O could make a drastic difference to a putative docked ligand interacting with this residue.

A more recent review by Dauter provides a nice example of N/O of asparagine being incorrectly placed. Of the 15 crystal structure depositions for savinase (subtilisin from *Bacillus lentus*), there are three, 1svn, 1tk2, and 3bx1, in which the amide N atom of an asparagine is in the immediate vicinity of the Ca^{2+} ion in the calcium binding site, instead of the O atom. This is not chemically sensible as the amide NH_2 is not a ligand for calcium coordination[44] (Fig. 8).

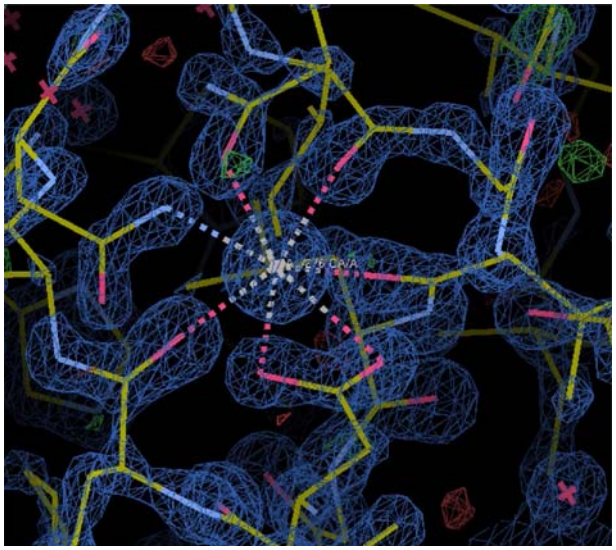

Fig. 8 1svn 1.4 Å structure of savinase 2Fo-Fc map (*blue*) showing the chemically unreasonable asparagine NH_2 pointing directed toward the calcium ion. Also showing the Fo-Fc map with *green* showing positive density (density not described by the model) and *red* showing negative density (features in the model that may be just noise).

Similar uncertainties apply to small molecules bound to the protein, for example, the position of the nitrogen in pyridines can be difficult to determine from the density. As hydrogens are not observed, the tautomeric state of histidines cannot be determined. Similarly the ionization state of the ligand or protein side chains cannot be determined directly, only inferred. Because of the local microenvironment of the protein active site, the pK_as of ionizable groups can be markedly perturbed.

Again Dauter provides a recent example. Inspection of the vicinity of the residue His91 in 3unr shows that its $N^{\delta 1}$ atom and the peptide N atom of Ser93 form a favorable hydrogen bond at 2.97 Å but, curiously, both N atoms are protonated. Since the peptide group undoubtedly has the N—H form, the His91 residue must be neutral, with only one hydrogen attached to its $N^{\epsilon 2}$ atom (Fig. 9).

The assignment of protonation states of ionisable residues can be problematic, as the microenvironment within the protein may perturb their pK_as from their common values. Hydrogen atomic positions are generally only inferred in X-ray crystal structures, as they almost never can be seen in X-ray crystal structure even at the highest resolution. Hence the protonation state of any particular residue is an uncertainty when using an X-ray crystal structure for drug design. Neutron diffraction though provides a means to see hydrogen atoms when resolution is high, and exchange for deuterium atoms makes visualization even clearer, and has been used to determine the protonation states in the active site of HIV protease, *b*-lactamase, dihydrofolate reductase, carbonic anhydrase, and

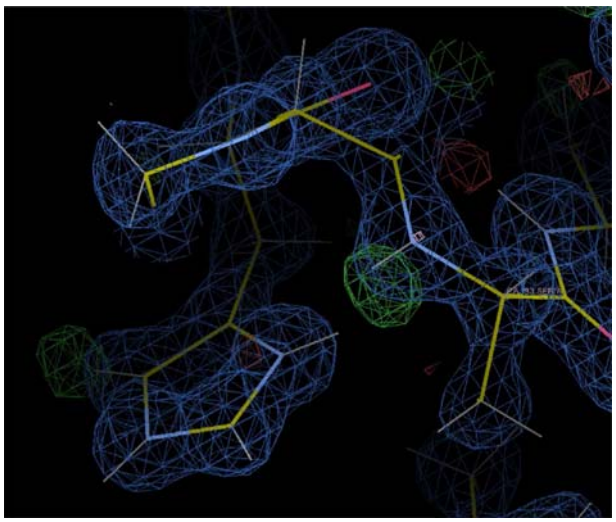

Fig. 9 3 unr trypsin at 1.2 Å 2Fo-Fc map (*blue*) and the Fo-Fc map with *green* showing positive density (density not described by the model) and *red* showing negative density (features in the model that may be just noise).

xylose isomerase.[45,46] The neutron diffraction crystal structure of human farnesyl pyrophosphate in complex with the clinical inhibitor risdronate demonstrated that as expected the pyridine nitrogen of risdronate is protonated and this proton forms a bifurcated hydrogen bond with Lys 200 and Thr 201. However what was surprising was that both risdronate phosphonate groups are deprotonated when bound to FFPS, despite the last deprotonation of the risdronate phosphonates having a $pK_a > 10.5$.

Neutron diffraction has a number of technical hurdles, not least the requirement for large crystals, the limitations of the flux of current beamlines, and the requirement for deuterium incorporation. So far PDB records only 105 structures, based in part at least on neutron diffraction data.[47] NMR can also be used to identify the protonation states of key residues, but requires proteins that are stable to pH titration and the results can be complicated by local environmental changes which may complicate chemical shift assignments and pK_a determinations.

Uncertainties can exist at the level of side chains, loops, or whole stretches of a protein if they are very mobile or otherwise disordered, and hence diffract so weakly as to have no discernible electron density. Obviously, the crystallographer knows they are there from the sequence of the sample and will model them in what appear to be sensible positions and conformations.

Looking at the structure with the electron density map is the clearest way of picking out these problems. At the level of side chains, real space density fits show that the most poorly defined residues are in order of improving average fit to the density Lys<Glu<Arg, Gln<Asp, Asn. [31] Lamb and colleagues in their paper, "You are lost without a map: Navigating the sea of protein structures," provide an illustrative example of an arginine residue in MppR, where the average B factor of the beta carbon is comparable with the main chain atoms, while the guanidinium group has only a "small scrap" of density centered upon the guanidinium group's central carbon.[48]

A further complexity occurs when alternative conformations are possible from the density, as most software will only display one of the possible positions of side chains. For example, Davis, Kleywegt, and Teague[31] cite the example disorder observed in both the nitrite and active site asparagine residues in the mutant Asp98Asn for of *Alcaligenes faecalis* S-6 nitrite reductase.[49]

3.06.6.1 Crystallization Conditions May Not Be Relevant for the Target Biology

In order to get the protein to crystallize, pH or salt conditions far from the physiological state may have been chosen, which can have dramatic consequences on the bound conformation of the ligand and/or protein. In a later review, Kleywegt, Davis, and St-Gallay[50] cite the example of the crystal structure of *Escherichia coli* ketopantoate reductase in complex with 20-phospho-ADP-ribose (a fragment of $NADP^+$ that lacks the nicotinamide ring). In an attempt to crystallize the ternary complex of the enzyme with pantoate and NADPH, crystals were obtained but the density showed no traces of pantoate and only a fragment of NADPH could be located. This fragment was confirmed to be 20-phospho-ADP-ribose by mass-spectrometry experiments. Compared with the complex with $NADP^+$, the ligand binds in the opposite orientation. Isothermal titration calorimetry with several mutants showed that the unusual binding mode is caused by changes in the protonation state of binding groups at low pH. The implication of this observation for fragment-based approaches to ligand design is that a binding mode may be altered profoundly by variations in crystallization conditions as well as by (unexpected or intentional) modifications of ligands.

3.06.6.2 Identification of Water Molecules in the Electron-Density Maps Can Be a Problem

Water molecules are a particular problem. Even at high resolution the presence of a water molecule may be uncertain, as the electron density may be indistinguishable from noise (or other unmodeled moieties that were in the crystallization solution), and thus their placement becomes quite subjective. As water is the third partner in the protein ligand binding interaction, confidence in their presence becomes rather critical. The observation of a density feature across serial X-ray structures provides confidence in the positioning of critical water molecules. Computational water placement algorithms, such as WaterMap[51] and SZMAP,[52] have been developed, and their impact on drug design was recently reviewed by Bodnarchuk.[53]

Subsequent reviews have reinforced these and other solvent ambiguities. For instance Lamb[48] highlighted that many proteins are crystallized from solutions containing polyethylene glycol or ammonium sulfate. Considering that ammonium sulfate contains two ammoniums for each sulfate, while about a quarter of all crystal structures contain sulfate, this is about 2 orders of magnitude more common than ammonium. But many water molecules adjacent to sulfate may in fact be ammonium, and the crystallographer and chemist should be open minded that a solvent molecule identified in the PDB entry could be something other than water. As NH_4^+, Na^+, and Mg^{2+} are all isoelectronic with water, assignment cannot be made on the basis of electron density alone.

Up to 2% of all crystal structures deposited in the PDB contain significant regions of unidentified density, which rises to nearly 6% of all unique structures.[54]

3.06.6.3 The Effects of Protein Flexibility Are Small or At Least Understood

Davis and Teague's review on protein flexility[55] gave many examples where the assumption of a rigid receptor is an unsafe assumption, and indicated that protein flexibility should be considered the norm, not the exception. While there are many surprises, one of

the most impactful was the change induced by oseltamivir on the active site of neuraminidase, which enabled it to supplant zanamivir as the neuraminidase inhibitor of choice for the antiinfluenza market. Oseltamivir replaces a strong guanidinium salt bridge interaction described above as critical for the binding of zanamivir, by an isopentyl chain, accommodated by an induced conformational change of the active site Glu276. This change not only gave similar affinity but also drastically modified the physical properties, and allowed oseltamivir, as a methyl ester prodrug, to become the first oral neuraminidase antiinfluenza treatment. The more favorable oral delivery route of oseltamivir over the inhaled zanamivir made it the influenza treatment of choice, and oseltamivir quickly supplanted zanamivir as the marketed neuraminidase inhibitor of choice.

Deller and Rupp highlight additional factors to be considered,[56]

- consideration of crystal packing, particularly if the ligand is close to the packing interface,
- consideration of the relevance of the asymmetric unit to the biology, as it is possible that a monomer pair in a dimer may not sit in the same asymmetric unit
- consideration of the B-factor of the ligand relative to the protein, or even different parts of the ligand, as ligand occupancy is never perfect

Their review also provides a good summary of validation software, including that used by the wwPDB.

Ligand geometries are a particular problem in protein crystallography and many examples of unusual or unrealistic bond lengths, angles, torsions or conformations can be found for small molecules in protein structures.[50] The problem is that whereas high-quality dictionaries of acceptable bond lengths, angles, and torsions are available for amino and nucleic acids in model refinement, the same is not true for complexed ligands. This is because of the huge diversity of small molecules compared to amino and nucleic acids. Even a ligand as common and well understood as ATP shows a surprisingly wide variety of bond lengths and angles. A review by Leibeschuetz based on years before 2000, 2006, and 2009 showed that up to 70% of the more recent structures could have been improved with better restraints, and 25% had errors that would have lead to misleading interpretation of binding interactions.[57] While computational chemists can postprocess a particular protein crystal structure to remove some of the issues with the ligand, such as QM refinement to reduce ligand strain, Reynolds recommends the problem is dealt with during structure determination.[58]

3.06.7 Validation of X-Ray Crystal Structures

Since the recommendations of the wwPDB X-ray VTF in 2011,[36] an officially watermarked wwPDB Validation Report is issued after annotation by the wwPDB curation staff. A similar report can be generated prior to submission using the wwPDB Validation Server.[59] For ligands, the wwPDB Validation Report includes geometrical and model fit diagnostic information.

The outcome of the first wwPDB/CCDC/D3R Ligand Validation Workshop in 2015 was recently published in Structure and made a number of recommendations to wwPDB for best practices for PDB archive deposition of cocrystal structure data:[60] The workshop also recommended that journals should require submission of the officially watermarked wwPDB validation reports and supplementary material to accompany all manuscripts describing macromolecular structure determinations, and that at least one referee has the technical expertise to evaluate in full the validation report. The group also considered what to do with PDB structures whose report flags unusual features. They not only hoped that original contributors would be motivated to correct entries, but also recognized that for many entries, the original depositors would not be in a position to make corrections. For these, the task force recommended that following a reasonable interval for self-correction, community experts could apply targeted corrections to any remaining PDB entries with poor validation outcomes, particularly for bound ligands of significant bio-medical interest. Indeed *PDBREDO* holds rerefined, and often improved, copies of all structures solved by X-ray, if the experimental data had also been deposited.[61,62]

3.06.8 Using X-Ray Crystal Structures in Docking and Scoring Validation Studies

The PDB provides a rich source of X-ray crystal structures for docking study validation, or even for training of new docking and scoring algorithms. Many datasets have been compiled focusing on size and diversity such as the 780 complexes in SB2010[63] and its update containing 1042 protein–ligand complexes SB2012. Even larger validation sets have been compiled, but the need for curation has been highlighted in a number of reviews. For example, the tetrahedral aromatic carbon in the 3-phenyl propylamine ligand in 1TNK, or the uncertain position of oleic acid in 1ICN, or the chemically unlikely flat methanesulfonyl group in 1PME, which were present within the FLEX-X validation set.[64]

With a focus on quality, a number of "clean sets" have been defined for validation purposes including Astex-85[65] and IRIDIUM.[66] In their validation of OMEGA, Warren and colleagues rigorously reviewed three previous validation sets to define 197 cocrystal structures.[67] Their selections, from others' selections, considered nominal resolution, structure factors that must be present, globally well fit models (Rfree-R must be <0.05), average positional errors assessed using the diffraction-component index (DPI <0.42 Å), poor fits of the ligand to its density [RSCC >0.9, RSR <0.2, OWAB <50, from the Uppsala Electron Density Server (EDS)], no intermolecular clashes, inappropriate physical properties, and structural dissimilarity (pairwise LINGOS similarity <0.9). They highlighted that resolution alone is not enough of a criterion, and provides two 2 Å structures, 1NHU and 1IY7, as comparisons, Figs. 10 and 11. In 1IY7 there is clearly a good fit of the ligand to the density, while in 1NHU, only partial density was observed for the ligand. They also cited two further sub-2 Å structures, 1ATL and 1ETA, where there was apparently no density supporting ligand placement at all (Fig. 12).

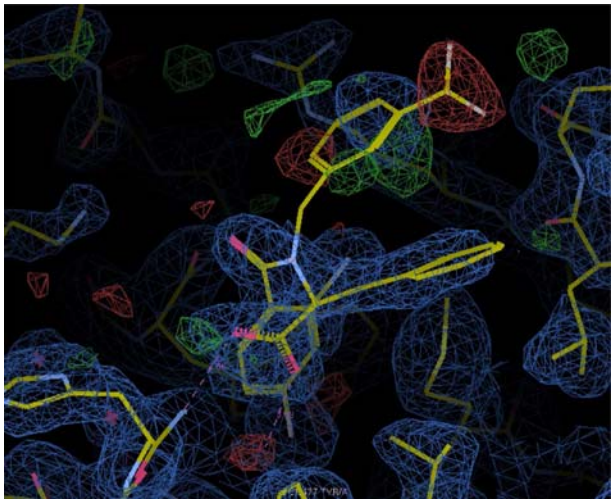

Fig. 10 1nhu, 2 Å structure of Hepatitis C virus RNA polymerase in complex with (2*S*)-2-[(2,4-dichloro-benzoyl)-(3-trifluoromethyl-benzyl)-amino]-3-phenyl-propionic acid 2Fo-Fc map (*blue*) together with Fo-Fc map with *green* showing positive density (density not described by the model) and *red* showing negative density (features in the model that may be just noise).

The DUD-E[68] database focuses on quality, and also includes a database of decoy binders to test docking protocols based on enrichment of true actives. Other validation sets have been compiled for specific purposes such as the LEADS-PEP[69] for peptide docking and the recently published docking validation set for GPCR structures.[70] Montez has recently reviewed the historical development of benchmarking sets for both ligand-based and structure-based virtual screening purposes.[71] PDB codes for the chosen protein–ligand structures in selected validation sets mentioned are shown in **Table 1**. The GPCR workbench set is shown in **Table 2**

Deller and Rupp[56] in their recent review highlight that it is difficult to anticipate every specific use of protein–ligand models, and one may need to define a particular validation set for a particular validation problem. They suggest a number of key questions that need to be considered. Their advice is to follow a three-step validation protocol covering validation of the ligand electron density, validation of the ligand stereochemistry, and validation of the protein and ligand environment. They provide a useful flow chart to follow, including recommendations for validation software for Inspection fit to electron density (**Fig. 13**).

EDS[72]
Twilight[73]
VHElibs[74]
ValLigURL[75]
wwPDB[76]
Coot[77] and Pymol[78]

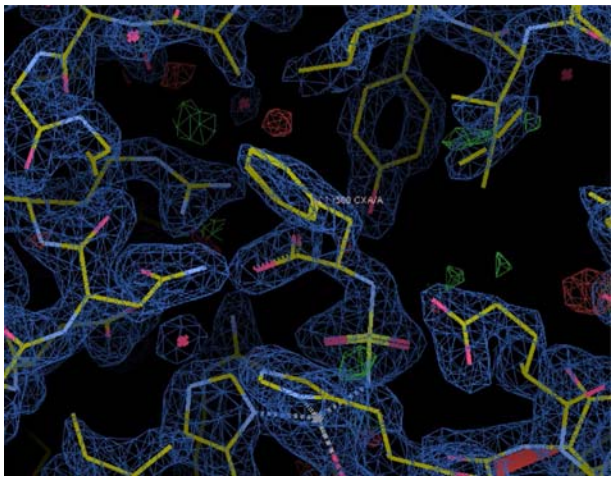

Fig. 11 1iy7 2 Å crystal structure of carboxypeptidase A and phenylalanine-*N*-sulfonamide inhibitor complex 2Fo-Fc map *blue* together with Fo-Fc map with *green* showing positive density (density not described by the model) and *red* showing negative density (features in the model that may be just noise).

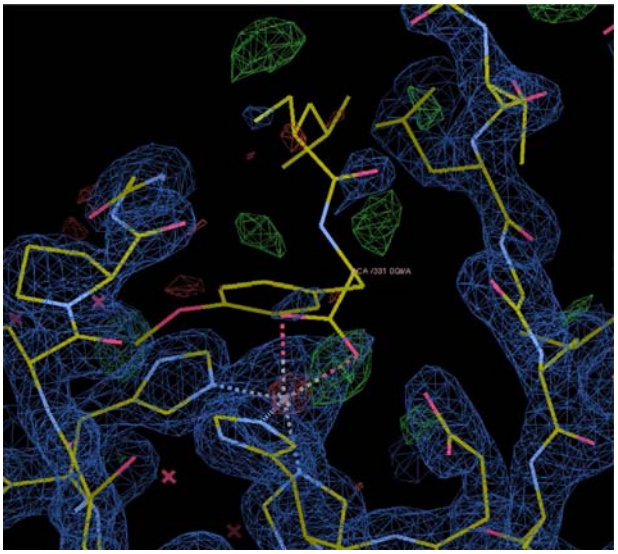

Fig. 12 1atl 1.8 Å resolution venom metalloproteinase, atrolysin C(form D) complexed with *O*-methyl-*N*-[(2*S*)-4-methyl-2-(sulfanylmethyl)pentanoyl]-L-tyrosine.

Table 1 The PDB identifiers for some recent docking validation sets, showing the structures unique to each collection and the overlap between them

Data set	*Number*	*PDB identifiers*
Astex-85 unique	28	1gkc 1ia1 1ig3 1j3j 1jje 1kzk 1meh 1n46 1opk 1q4g 1r1h 1r55 1s3v 1sg0 1sqn 1t40 1t46 1t9b 1tz8 1u1c 1v48 1v4s 1vcj 1xoz 1y6b 1ygc 2bm2 2bsm
CASF-2013 unique	185	10gs 1a30 1bcu 1f8b 1f8c 1f8d 1h23 1hfs 1igj 1jyq 1kel 1lbk 1lol 1loq 1lor 1nvq 1o3f 1o5b 1os0 1p1q 1ps3 1q8t 1q8u 1qi0 1r5y 1sln 1sqa 1u1b 1u33 1uto 1w3k 1w3l 1w4o 1xd0 1yc1 1zea 2brb 2cbj 2cet 2d1o 2d3u 2fvd 2g70 2gss 2hb1 2iwx 2j62 2j78 2jdm 2jdu 2jdy 2obf 2ole 2p4y 2pq9 2qbp 2qbr 2qft 2qmj 2r23 2v00 2v7a 2vl4 2vo5 2vot 2vvn 2vw5 2w66 2wbg 2wca 2weg 2wtv 2x00 2x0y 2x8z 2x97 2xb8 2xbv 2xdl 2xhm 2xnb 2xy9 2xys 2y5h 2yfe 2yge 2yki 2ymd 2zcq 2zcr 2zjw 2zwz 2zx6 2zxd 3acw 3ag9 3ao4 3b3s 3b3w 3b68 3bfu 3bkk 3bpc 3cft 3cj2 3coy 3cyx 3d4z 3dd0 3dxg 3e93 3ebp 3ehy 3ejr 3f17 3f3a 3f3c 3f3e 3f80 3fcq 3fk1 3fv1 3g0w 3g2n 3g2z 3gbb 3gcs 3ge7 3gnw 3gy4 3huc 3i3b 3imc 3ivg 3jvs 3k5v 3kgp 3kv2 3kwa 3l3n 3l4u 3l4w 3l7b 3lka 3mfv 3mss 3muz 3myg 3n7a 3n86 3nox 3nq3 3nw9 3oe5 3ov1 3owj 3ozt 3pe2 3pww 3pxf 3s8o 3su2 3su3 3su5 3u9q 3udh 3ueu 3uex 3uo4 3uri 3utu 3vd4 3vh9 3zso 3zsx 4de1 4de2 4des 4dew 4djr 4djv 4g8m 4gid 4gqq 4tmn
DUD-E unique	96	1bcd 1c8k 1d3g 1h00 1j4h 1kvo 1li4 1lru 1mv9 1njs 1q4x 1qw6 1s3b 1sqt 1syn 1udt 1uyg 1w7x 1xl2 1ype 1zw5 2aa2 2am9 2ayw 2azr 2b8t 2cnk 2e1w 2etr 2fsz 2gtk 2h7l 2hv5 2hzi 2i0e 2i78 2ica 2nnq 2of2 2oi0 2oj9 2ojg 2owb 2oyu 2p2i 2p54 2qd9 2rgp 2v3f 2vt4 2zdt 2zec 2znp 3bgs 3biz 3bkl 3bqd 3bwm 3bz3 3c4f 3ccw 3chp 3cjo 3cqw 3d0e 3d4q 3e37 3el8 3eml 3eqh 3f07 3f9m 3frj 3g0e 3g6z 3hl5 3hmm 3kba 3kgc 3kl6 3krj 3l3m 3l5d 3lan 3ln1 3lpb 3lq8 3m2w 3max 3nf7 3nxo 3nxu 3ny8 3odu 3pbl 830c
IRIDIUM-HT unique	65	1a28 1ai5 1azm 1b9v 1br6 1c1b 1ctr 1cvu 1cx2 1d3h 1dd7 1dds 1eoc 1exa 1ezq 1f0s 1f0t 1f0u 1fcx 1fcz 1fh8 1fh9 1fhd 1fjs 1fl3 1fm6 1fm9 1fq5 1frp 1fvt 1gwx 1h1p 1h1s 1hdy 1hgg 1hgh 1hgi 1hgj 1ivb 1ivd 1ive 1ivf 1iy7 1k1j 1lqd 1mbi 1ml1 1mts 1pbd 1pso 1qhi 1rob 1ukz 1ulb 1ydr 1yds 1ydt 2ack 2ctc 2mcp 2tmn 3ptb 4aah 4cox 4ts1
Astex-85 and CASF-2013	2	1gpk, 1hnn, 1n1m, 1n2v, 1oyt, 1z95
Astex-85 and DUD-E	1	1l2s, 1r9o,1sj0
Astex-85, CASF-2013, and IRIDIUM-HT	4	1hnn 1n1m 1n2v 1oyt
Astex-85, DUD-E, and IRIDIUM-HT	2	1l2s 1r9o
Astex-85 and IRIDIUM-HT	48	1g9v 1gm8 1hp0 1hq2 1hvy 1hwi 1hww 1jd0 1jla 1k3u 1ke5 1l7f 1lpz 1lrh 1m2z 1mmv 1mzc 1n2j 1nav 1of1 1of6 1oq5 1owe 1p2y 1p62 1pmn 1q1g 1q41 1r58 1s19 1sq5 1tow 1tt1 1u4d 1uml 1unl 1uou 1v0p 1w1p 1w2g 1x8x 1xm6 1xoq 1yqy 1yv3 1yvf 1ywr 2br1
CASF-2013 and DUD-E	2	1e66 1vso
CASF-2013 and IRIDIUM-HT	2	1mq6 2pcp

Table 2 The PDB identifiers for the GPCR workbench set

Data set	*Number*	*PDB identifiers*
GPCR-workbench unique	28	4IAR 4IB4 3UON 4DAJ 2VT4 2RH1 3PBL 3 RZE 4EIY 4NTJ 4MBS 3ODU 4EJ4 4DJH 4DKL 4EA3 4S0V 3VW7 4PHU 3V2Y 4K5Y 4OR2 4OO9 4KJV

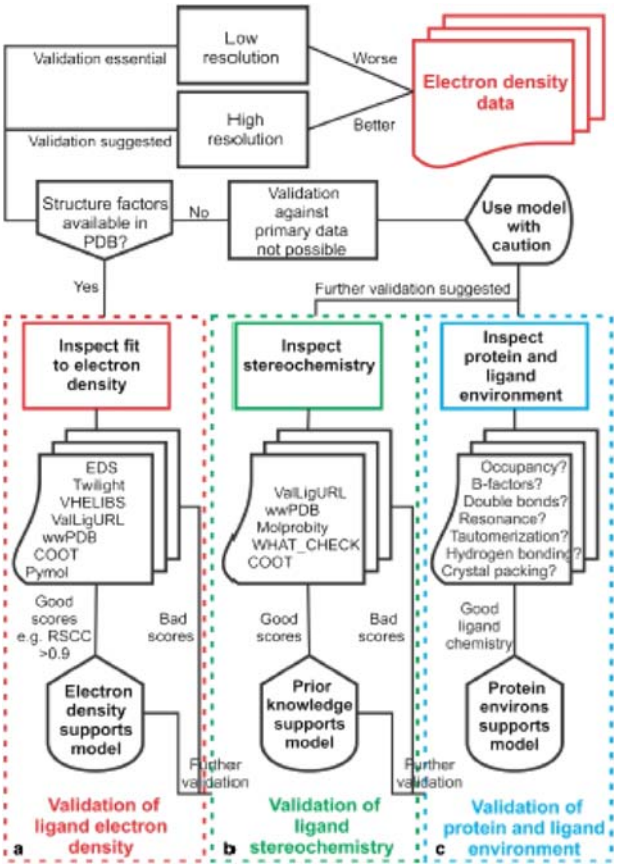

Fig. 13 3-step validation protocol covering validation of the ligand electron density, validation of the ligand stereochemistry, and validation of the protein and ligand environment. Reproduced from Deller, M.C.; Bernhard, R. Models of Protein–Ligand Crystal Structures: Trust, But Verify. *J. Comput. Aided Mol. Des.* **2015**, 29, 817–836.

Inspection of stereochemistry

ValLigURL[75]
wwPDB[79]
MolProbity[80]
WHAT_CHECK[81]
COOT

Inspection of the protein–ligand environment to consider

Occupancy,
B-factors,
double bonds,
resonance,
tautomerism,
H-bonding,
and crystal packing

3.06.9 Fitting to Coordinate Versus Fitting to Electron Density

The coordinates of the atomic model are often used to assess docking algorithms, where RMSD deviations from the X-ray-observed poses are typically used as success criteria. But as the atomic coordinates of the X-ray pose are themselves a model, and not the experimental data, this led Yusuf, Davis, Kleywegt, and Schmitt to propose using the electron density as the target to assess the fit.[82] RMSD to atomic positions had a number of drawbacks. First they ignore the protein environment of the docked pose, as low RMSD values can be achieved even when essential binding features are absent in the docked pose. Second, high RMSD values can be obtained even when essential binding features are identified correctly but a group that is unimportant to the binding mode such as a solvent-exposed group deviates substantially from the crystal structure. To overcome these limitations, Yusuf et al. recommended comparison of the docked pose to the crystallographic electron density maps instead of comparing the nonhydrogen atom coordinates from a docking pose against those of the atomic model. In doing so, any ambiguous features of a particular ligand orientation in a binding site environment and alternative placements or conformations are implicitly accounted for. As validation they compared three well-known docking algorithms [Gold (CCDC),Glide (Schrödinger), and Fred (OpenEye)]. As a quantitative definition of fit for the comparison of docking poses against electron densities they proposed the real space R-factor (RSR), which is routinely used in crystallography and measures the compatibility of an experimental electron density map and a group of atoms (here, the ligand atoms). They found that RMSD and RSR were nonredundant measures of fit. Of particular interest were examples with high RMSDs and low RSRs and those with lower RMSD and high RSRs. Inspection of the higher RSMD and low RSR examples showed that they can still be classified as correct when judged by the electron density (i.e., they are false negatives by the RMSD criterion). In many cases, the high RMSD value is caused by a substantial conformational difference in part of the ligand for which there is no convincing electron density.

Where they found RMSD was high but the RSR value low, there were also cases in which the ligand density was ambiguous. In such cases, the crystallographer had made a particular interpretation of the density in terms of the atomic model of the ligand. The docking pose then shows an alternative binding mode that explains the density just as well (or just as poorly) as the crystal structure but emphasizes alternative binding features.

They also found that there are quite a few cases of poses with low RMSD and high RSR. This suggested that there are cases (false positives) in which poses are classified as docking successes by the RMSD criterion even though they apparently do not fit the experimental electron density particularly well. Some of the cases involved ligands that were quite small so that even a moderate displacement could lead to a poor fit with the density. The majority of cases in which the docking solutions have low RMSD values but high RSR values were due to differences in the ligand conformations (in particular, of ring systems). The sampling of ligand conformations in docking calculations is sometimes sparse due to speed considerations and usually aims to produce low-energy conformations. During crystal-structure determination, on the other hand, energetic considerations usually take a lower priority than the need to explain the observed electron density in terms of an atomic model. This often leads to strained ligand conformations that explain the density and that may or may not be accurate representations of the true structures. In such cases, docking programs are unlikely to sample conformations identical or similar to that of the model in the crystal structure. Even if the docking procedure places the ligand in the binding site so that there is good overall agreement with the crystal structure in terms of atomic positions, interactions, and molecular shape, this does not guarantee that it will fit the electron density as well as the "hand-crafted" model produced by the crystallographer. In such cases, ostensibly small differences can result in high RSR values.

The use of the "fit to density" measures RSR and real space correlation coefficient (RSCC) has been investigated in a number of other docking evaluations compared to the more traditional, and philosophically inferior fit to coordinates RMSD measures. During the evaluation of the expert system DOCK Blaster, Shoichet and colleagues used three high-quality X-ray crystal sets developed for docking evaluations, the ASTEX-87 set, the GOLD-114 set, and the DUD set.[83] They found common failures of docking assessment using RMSD, including (a) insufficient conformational sampling of the ligand, particularly of aliphatic ring puckering; (b) symmetric or pseudosymmetric molecule; (c) critical missing water molecules; and (d) ligand pose dominated by electronic (orbital) effects. They also found that semisymmetric molecules gave poorer performance that would be better treated with a density-based pose assessment.

In the Community Structure Activity Resource Benchmark (CSAR) Exercise 2011–2012, RSR and RSSR were considered as an evaluation metric, as comparing back to the experimental data, however the metrics were not reproducible between different versions of the CCP4 (4.1.2 and 4.2.0) and they were not able to reproduce the reported value on the Uppsala Electron Density Server of the original crystal structure, so the method was not used. OpenEye evaluated cognate docking performance of their own software against a high-quality dataset prepared by themselves, called Iridium-HT which contained 121 ligand complexes with 208 separate ligand instances. They found that fit to the density proved a rather fragile measure with large differences in RSR or RSSR for small changes in geometry. They conclude that while fit to the density is scientifically more correct, the methods currently available for comparing density are unsuitable, but further work should be undertaken.

It is now mandated that protein structures deposited in the PDB must also contain the structure factors, so the model can always be checked versus the diffraction data. Some have gone further to suggest that even this is not enough and that raw diffraction images are also needed.[84] After all, even electron density maps and structure factors are derived data, as the raw data are the diffraction patterns. The reinterpretation of crystallographic data collected on the mammalian 15-S lipoxygenase is a cited case in point.[85] The originally deposited structure was solved and modeled on space group R32, but when the structure factors were reindexed to another space group and the structure was rebuilt, the size and shape of the binding site had changed so much that it was no longer able to accommodate the ligands proposed to fit. This is up to this point a still unresolved story and one which

cannot be further checked as only the structure factors were retained. There must be some unwittingly confused chemists out there, as 1LOX and 2P0M have each been downloaded over 34,000 times.[86] The community have been considering the infrastructure required for storing the diffraction data, and what criteria would be applied to decide when and where not to store images or whether it would just be cheaper to store everything.[87] A number of initiatives are now underway including TARDIS http://www.tardis.edu.au, a network of federated repositories at a national (Australian) level,[88] Ecrystals from the University of Southhampton,[89] NIH Big Data to Knowledge (BD2K) initiative,[90] and Structural Biology Data Grid (SBDG; data.sbgrid.org).[91]

While computational chemists wish to base their modeling hypotheses on the best available 3D models, which intuitively may appear to be X-ray crystal structures, all the aforementioned discussion should lead them to be cautious. 3D QSAR in techniques such as CoMFA can integrate the 3D chemistry information with biology measurements to quantitatively predictive models. Cramer and Vend built CoMFA and ComSIA models from datasets where the alignment of the compounds was entirely experimentally derived ligand poses from X-ray crystallography to those where the alignment was generated from ligand-centric template CoMFA.[92] They found that the fluctuations in the positions and conformations of compounds dominate X-ray-based alignments and can yield poorer predictions than those from the self-consistent template CoMFA alignments. Also, when there exist multiple different binding modes, structural interpretation in terms of binding site constraints can often be simpler with template-based alignments than with X-ray-based alignments.

3.06.10 Using Electron Microscopy Structures

3.06.10.1 Use and Limitations of Electron Microscopy

In 2015, a shouty title appeared in Nature, *The Revolution Will Not Be Crystallized*.[93] This promoted 3D-electron microscopy (3DEM) as the coming thing, pointing to a recent publication by groups from Cambridge and Beijing.[94] The collaboration had resulted in an atomic resolution model of gamma secretase, a well-targeted subject of Alzheimer's research. The resolution was quoted as 3.4 A for 1542 residues and was the result of image processing of 1.8 million particles picked from 2925 micrographs [PDB:5A63]. Perhaps more exciting is a subsequent publication by the Beijing group in which different conformational states of the secretase seem to be evident. The second and sixth helices of presenilin—one of the secretase complex components—are claimed to be mobile in some states but immobilized by an inhibitor, DAPT.[95] Thus, in the best cases to date, 3DEM can provide something that X-ray crystallography cannot—the simultaneous examination of discrete populations of conformations or states or assemblies.

Another remarkable recent paper is that by Bartesaghi et al., in which β-galactosidase and its inhibitor (PETG) are modeled at a resolution of 2.2 A, using 3DEM [PDB:5A1A].[96] **Fig. 1** of that paper shows that at this resolution, the EM density even shows a hole in the phenyl ring of Phe627, as can be seen in high-quality X-ray diffraction structures, **Fig. 14**. In addition to the enzyme, the authors identified about 800 water molecules, many of which corresponded to the previously published X-ray diffraction crystal structure model [PDB:1DB0].[97] It is arguable whether the 3DEM structure advances the knowledge of galactosidases that much, but there are some important points to be made. Thus 3DEM acts as a complementary/supporting technique to X-ray crystallography. For instance, the placement of many of the water molecules in the X-ray structure is confirmed in the 3DEM, thus suggesting

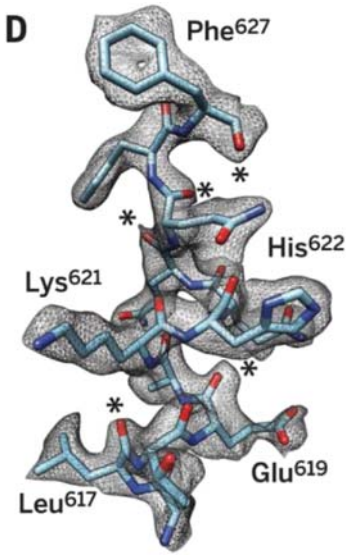

Fig. 14 3DEM density map for Phe627 of *b*-galactosidase, showing reduction of density in the center of the phenyl ring. Reproduced from Bartesaghi, A. 2.2 Å Resolution 3DEM Structure of *b*-Galactosidase in Complex With a Cell-Permeant Inhibitor. *Science.* **2015**, 348(6239), 1147–1151.

that the waters are not crystallographic artifacts, but a representation of the hydration shell. (The 3DEM samples were plunge-frozen direct from solution.) In the case of this paper, the authors are developing earlier 3DEM work by improving specimen selection rather than image collection and processing technology. They thus argue that 3DEM is now becoming a mature structure determination technique, limited by sample preparation rather than technology.

Another possible advantage of 3DEM over X-ray crystallography is that it can be used for the structures of protein assemblies. This is not to say that X-ray diffraction methods cannot; after all, Nobel Prizes have been awarded for crystallography of molecular assemblies such as the photosynthetic reaction center and the ribosome. However, 3DEM holds the promise of routine determination of such complex entities in drug design.[98] The results are not always that interpretable or convincing, though. An interesting recent example is the model of the LRRK2 protein, which has a genetic linkage to Parkinson's disease.[99] An impressive collaboration of scientists from 15 institutions used data from mass spectrometry, chemical cross-linking, X-ray scattering, and electron microscopy to build a model of the LRRK2 dimer. LRRK2 consists of seven domains: Armadillo, Ankyrin, and Leucine-rich repeat (LRR) scaffolds, followed by a Roc-COR dimerization unit, then a kinase domain and finally a WD40 scaffold unit. The authors succeeded in building a plausible model from the experimental data that offers new hypotheses for the functional mechanism of this protein. For instance, the proximity of the ankyrin and LRR domains to the kinase suggests for the first time (we think) that these domains are involved in regulation of the biological activity of LRRK2, rather than just being a framework skeleton for the assembly. Nevertheless, one can quibble with details of the model. Almost everyone who looks at the final model superimposed on the EM map immediately notices two "horns" growing from to structure that have no equivalent in the molecular model, **Fig. 15**. (We leave the readers to test their own perceptions.) Are these features that have not been modeled correctly, or are they artifacts of the EM process? Such features are often seen on EM reconstructions, where the atomic model is unable to completely fill or overfills the EM volume. Of course, this does not invalidate EM methods, but it does strain the credibility of the method as far as some medicinal chemists are concerned.

3D Electron microscopy has been around for years and has made an impact on drug discovery before. One can think of Richard Henderson's important work on the structure of bacteriorhodopsin as a paralogue for GPCRs.[100] This resulted in a number of speculative models of human rhodopsin being built in both industry and academia. These were then used to construct models of therapeutically relevant GPCRs, such as adrenergic, serotonin, and dopamine receptors. Although these models were crude, they gave rise to testable hypotheses for antagonist binding modes that were only improved on by subsequent crystallography work. In this case, crystallography has been used to refine the earlier 3DEM work. One wonders whether the latest generation 3DEM will supplant atomic resolution X-ray and neutron diffraction crystallography or will once again be superseded. The answer is probably, "yes and no." We anticipate that X-ray diffraction methods will remain valuable for ligand–protein pairings of monomeric, dimeric, and simple assemblies—particularly those amenable to crystal soaks for rapid determination of ligand-binding modes. However, where we are interested in larger, more complex assemblies or heterogeneous populations of conformational states, 3DEM will be the method of choice. For those interested in exploring this field more, we recommend the recent review by Bai et al.,[101] Kuehlbrandt,[102] and Milne et al.[103]

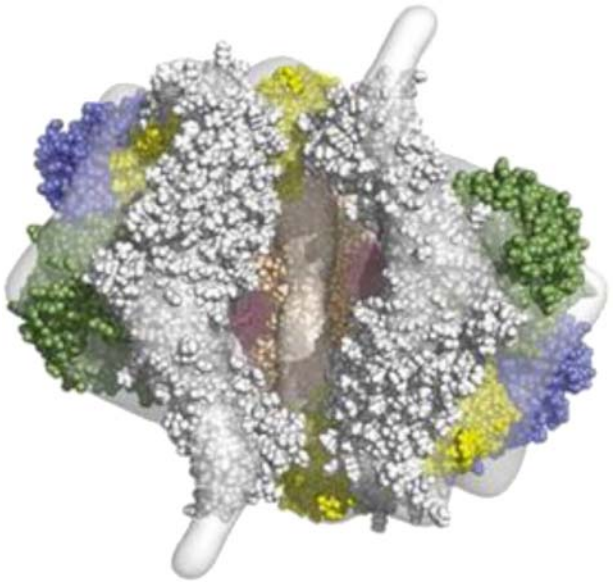

Fig. 15 A final LRRK2 model fitted to the EM density. Reproduced from Guaitoli, G., et al., Structural Model of the Dimeric Parkinson's Protein LRRK2 Reveals a Compact Architecture Involving Distant Interdomain Contacts. *Proc. Natl. Acad. Sci. U. S. A.* **2016**, 113(30), E4357–E4366.

3.06.11 Summary

The PDB continues to develop, based on a collaboration between its partners from the United States (http://rcsb.org), Japan (http://pdbj.org), and Europe (http://pdbe.org). They collaborate on everything related to getting the information into the single archive, for example, formats, policies, interactions with journals, and validation. But in the original 2003 wwPDB memorandum of understanding between its constituent members, it was agreed that members would compete with one another to offer different kinds of services and features. The RSCB has extensive search and reporting together with an education portal. PDBe has multiple search and browse capabilities with analysis and bioinformatics tools, and places an emphasis on validation, visualization, experimental data, and integration with other archives (UniProt, GO, Pfam, CATH, ChEMBL, etc.).[104] PDBj also supports browsing in multiple Asian languages. The BioMagResBank has many specialist capabilities to support the NMR community. The PDB archive contains information derived from X-ray/neutron/electron crystallography, NMR spectroscopy, and 3D electron microscopy. A workshop held in 2005 led to the policy that pure in silico models should not be part of the PDB,[105] and instead a separate portal should be established. The Protein Modelling Portal was established in 2007.[106]

The wwPDB are continuing to address validation and quality of 3D structure models, but it is user beware, as for all the best will in the world by the 3D structure community, one cannot mandate how a model will be used or by whom. For the moment X-ray crystallography remains the dominant source of 3D models. 3DEM is a fast up-and-coming technique, and certainly offers opportunities. More and more hybrid application of all these methods are being used,[107,108] and the caveats of the models will become more complex.

All the careful validation work such as the curation of docking validation sets and the scoring of PDB submissions is worthless unless someone (you?) takes advantage of it. If you are in a well-funded pharmaceutical company with its own structural scientists, then you should discuss new structures carefully with them. Remember that it is not just you who is under severe work pressure. They are committed to their work, but sometimes corners are cut, or at least they make assumptions that are logical to structural biologists but not so obvious to computational chemists. Many structures in the pharmaceutical proprietary collections are not of publication quality, because that is not the first priority. For instance, if you have a well-behaved system that is amenable to crystal soaks, then each successive ligand–protein structure will be solved by molecular replacement and any original anomalies will be carried through to new structures and new anomalies might arise too. The density around the ligand binding pocket will be examined closely, but it is unlikely that the whole structure will be rerefined.

If you are in a smaller organization with remote collaborators or outsource partners, then you will have to work harder to ensure the quality of the structures that you are using. If your structure is nonconfidential, the first thing you should do is avail yourself of the excellent tools at the wwPDB validation server. If you have access to Mercury, run it on the ligand to check if there are unusual geometric parameters. These steps are usually enough to catch atom hybridization errors, such as sp^3 benzene and sp^2 cyclohexanes. If you use commercial molecular modeling software such as MOE or Maestro, then run the protein preparation or protein health tools. These overlap somewhat with the wwPDB assessment, but can sometimes identify extra issues to consider. Any issues that do arise should be discussed with the structural scientist, if possible.

The same standard of rigor should be applied to homology models built by computational chemists. You should be aware of weaknesses and ambiguities in the model, such as where the "indels" (insertions and deletions in the sequence alignment) are. Indels are a major source of strain in the internal geometry of a model unless carefully resolved, as they are regions where the homology model deviates the most from the template structure. Just like the industry crystallographers, homology model builders must make a call on what parts of the model need their full attention and what bits can be built to a lower standard. The solution is often that binding sites are carefully built but other parts are left with holes or overlapping atoms. This is fine if the model is only used for docking ligands that are of similar size, shape, and chemistry to an original ligand, but is not good enough for more modern workflows, such as FEP simulations. Be wary of picking up a homology model from a computer disk or corporate database, unless you know its story or are willing to do some quality assessment.

Does this mean we are cautioning against the use of structure models and homology models? Far from it. George Box said, "all models are wrong, but some are useful." This is the case in protein models too. The best models are extremely useful. The reader is directed to look at the work done by the Heptares group, and Miles Congreves's chapter in this volume. They have carefully teased out high-quality X-ray crystal structures of several GPCRs and have also built homology models of others. These are of sufficient quality to run molecular dynamics, WaterMap and FEP simulations on.

The use of 3D structural information by computational chemists is not unlike using any other experimental data on which we base models. We would have the best understanding possible of the data we are using in our models. Equally the medicinal chemists should be aware of the risks they are taking in using our computational models. Dialog between discipline experts remains pivotal in the appropriate use of experimental data in computational chemistry, and computational models in drug design. We all take risks using any experimental or computational data on which we base decisions; we should just be aware of what risks we are taking.

Acknowledgment

We would like to thank Gerard Kleywegt (EMBL/EBI) for many helpful comments and detailed review of the manuscript.

See also: 1.15. Structural Chemogenomics Databases to Navigate Protein–Ligand Interaction Space. 2.06. High-Throughput Crystallography and Its Applications in Drug Discovery.

References

1. Davis, A. M., Blaney, J., Eds. *Handbook of Medicinal Chemistry—Principles and practice;* Royal Society of Chemistry: London, 2014; p p96.
2. Wüthrich, K. The Way to NMR Structures of Proteins. *Nat. Struct. Biol.* **2001,** *8,* 923–925.
3. http://www.rcsb.org/pdb/static.do?p=general_information/pdb_statistics/index.html.
4. Jazayeri, A.; Dias, J. M.; Marshall, F. H. From G Protein-Coupled Receptor Structure Resolution to Rational Drug Design. *J. Biol. Chem.* **2015,** *290* (32), 19489–19495.
5. Dore, A. S.; Robertson, N.; Errey, J. C.; Ng, I.; Hollenstein, K.; Tehan, B.; Hurrell, E.; Bennett, K.; Congreve, M.; Magnani, F.; et al. Structure of the Adenosine A2A Receptor in Complex With ZM241385 and the Xanthines XAC and Caffeine. *Structure, Cambridge, MA* **2011,** *19* (9), 1283–1293.
6. Baldwin, J. J.; Ponticello, G. S.; Anderson, P. S.; Christy, M. E.; Murcko, M. A.; Randall, W. C.; Schwam, H.; Sugrue, M. F.; Springer, J. P.; Gautheron, P.; Grove, J.; Mallorga, P.; Viader, M. P.; McKeever, B. M.; Navia, M. A. Thienothiopyran-2-sulfonamides: Novel Topically Active Carbonic Anhydrase Inhibitors for the Treatment of Glaucoma. *J. Med. Chem.* **1989,** *32* (12), 2510–2513.
7. Blacklock, T. J.; Sohar, P.; Butcher, J. W.; Lamanec, T.; Grabowski, E. J. J. An Enantioselective Synthesis of the Topically-Active Carbonic Anhydrase Inhibitor MK-0507: 5, g-Dihydro-(*S*)-4-(ethylamino)-(*S*)-6-methyl-4H-thieno[2,3-b]thiopyran-2-sulfonamide 7,7-Dioxide Hydrochloride. *J. Org. Chem.* **1993,** *58,* 1672–1679.
8. Von Itzstein, M.; Wu, W. Y.; Kok, G. B.; Pegg, M. S.; Dyason, J. C.; Jin, B.; Phan, T. V.; Mythe, M. L.; White, H. F.; Oliver, S. W.; Colman, P. M.; Varghese, J. N.; Ryan, D. M.; Woods, J. M.; Bethell, R. C.; Hotham, V. J.; Cameron, J. M.; Penn, C. R. Rational Design of Potent Sialidase-Based Inhibitors of Influenza Virus Replication. *Nature* **1993,** *363,* 418.
9. Barillari, C.; et al. Classification of Water Molecules in Protein Binding Sites. *J. Am. Chem. Soc.* **2007,** *129* (9), 2577–2587.
10. Cossins, B. P.; Foucher, S.; Edge, C. M.; Essex, J. W. Protein-Ligand Binding Affinity by Nonequilibrium Free Energy Methods. *J. Phys. Chem. B* **2008,** *112,* 14985–14992.
11. Wood, J. M.; et al. Structure-Based Design of Aliskiren, a Novel Orally Effective Renin Inhibitor. *Biochem. Biophys. Res. Commun.* **2003,** *308* (4), 698–705.
12. Venkatraman, S.; Bogen, S. L.; Arasappan, A.; Bennett, F.; Chen, K.; Jao, E.; Liu, Y.-T.; et al. Discovery of (1R,5*S*)-*N*-[3-Amino-1-(cyclobutylmethyl)-2,3-dioxopropyl]-3-[2(*S*)-[[[(1,1-dimethylethyl)amino]carbonyl]amino]-3,3-dimethyl-1-oxobutyl]-6,6-dimethyl-3-azabicyclo[3.1.0]hexan-2(*S*)-carboxamide (SCH 503034), a Selective, Potent, Orally Bioavailable Hepatitis C Virus NS3 Protease Inhibitor: A Potential Therapeutic Agent for the Treatment of Hepatitis C Infection. *J. Med. Chem.* **2006,** *49,* 6074–6086.
13. Rahuel, J.; Rasetti, V.; Maibaum, J.; Rüeger, H.; Göschke, R.; Cohen, N.-C.; Stutz, S.; Cumin, F.; Fuhrer, W.; Wood, J. M.; Grütter, M. G. Structure-Based Drug Design: The Discovery of Novel Nonpeptide Orally Active Inhibitors of Human Renin. *Chem. Biol.* **2000,** *7,* 493–504.
14. Talele, T. T.; Khedkar, S. A.; Rigby, A. C. Successful Applications of Computer Aided Drug Discovery: Moving Drugs From Concept to the Clinic. *Curr. Top. Med. Chem.* **2010,** *10* (1), 127–141.
15. Norman, R. A.; Toader, D.; Ferguson, A. D. Structural Approaches to Obtain Kinase Selectivity. *Trends Pharmacol. Sci.* **2012,** *33* (5), 273–278.
16. Shoichet, B. K.; Kobilka, B. K. Structure-Based Drug Screening for G-Protein-Coupled Receptors. *Trends Pharmacol. Sci.* **2012,** *33* (5), 268–272.
17. Jiang, R.; et al. 3,5-Disubstituted Quinolines as Novel c-Jun N-Terminal Kinase Inhibitors. *Bioorg. Med. Chem. Lett.* **2007,** *17* (22), 6378–6382.
18. Karle, M.; Knecht, W.; Xue, Y. Discovery of Benzothiazole Guanidines as Novel Inhibitors of Thrombin and Trypsin IV. *Bioorg. Med. Chem. Lett.* **2012,** *22* (14), 4839–4843.
19. Kadono, S.; et al. Structure-Based Design of P3 Moieties in the Peptide Mimetic Factor VIIa Inhibitor. *Biochem. Biophys. Res. Commun.* **2005,** *327* (2), 589–596.
20. Sgraja, T.; et al. Characterization of *Aquifex aeolicus* 4-Diphosphocytidyl-2C-methyl-D-erythritol Kinase—Ligand Recognition in a Template for Antimicrobial Drug Discovery. *FEBS J.* **2008,** *275* (11), 2779–2794.
21. Xu, L.; et al. Structure-Based Design, Synthesis, Evaluation, and Crystal Structures of Transition State Analogue Inhibitors of Inosine Monophosphate Cyclohydrolase. *J. Biol. Chem.* **2007,** *282* (17), 13033–13046.
22. Nettles, J. H.; et al. Asymmetric Binding to NS5A by Daclatasvir (BMS-790052) and Analogs Suggests Two Novel Modes of HCV Inhibition. *J. Med. Chem.* **2014,** *57* (23), 10031–10043.
23. Hanessian, S.; et al. Structure-Based Design and Synthesis of Macroheterocyclic Peptidomimetic Inhibitors of the Aspartic Protease β-Site Amyloid Precursor Protein Cleaving Enzyme (BACE). *J. Med. Chem.* **2006,** *49* (15), 4544–4567.
24. Hanessian, S.; et al. Structure-Based Design and Synthesis of Novel P2/P3 Modified, Non-Peptidic Beta-Secretase (BACE-1) Inhibitors. *Bioorg. Med. Chem. Lett.* **2010,** *20* (6), 1924–1927.
25. Elkins, J. M.; et al. Crystal Structure of Human Aurora B in Complex With INCENP and VX-680. *J. Med. Chem.* **2012,** *55* (17), 7841–7848.
26. Getlik, M.; et al. Hybrid Compound Design to Overcome the Gatekeeper T338M Mutation in cSrc. *J. Med. Chem.* **2009,** *52* (13), 3915–3926.
27. Hansen, G.; et al. Unexpected Active-Site Flexibility in the Structure of Human Neutrophil Elastase in Complex With a New Dihydropyrimidone Inhibitor. *J. Mol. Biol.* **2011,** *409* (5), 681–691.
28. Silvaggi, N. R.; et al. Structures of *Clostridium Botulinum* Neurotoxin Serotype A Light Chain Complexed With Small-Molecule Inhibitors Highlight Active-Site Flexibility. *Chem. Biol.* **2007,** *14* (5), 533–542.
29. Norville, I. H.; et al. The Structure of a Burkholderia Pseudomallei Immunophilin-Inhibitor Complex Reveals New Approaches to Antimicrobial Development. *Biochem. J.* **2011,** *437* (3), 413–422.
30. Choi, J.; et al. Conformational Flexibility in Mammalian 15S-Lipoxygenase: Reinterpretation of the Crystallographic Data. *Proteins* **2008,** *70* (3), 1023–1032.
31. Davis, A. M.; Teague, S. J.; Kleywegt, G. J. Application and Limitations of X-Ray Crystallographic Data in Structure-Based Ligand and Drug Design. *Angew. Chem. Int. Ed.* **2003,** *42* (24), 2718–2736.
32. Abdul Ajees, A.; Gunasekaran, K.; Volanakis, J. E.; Narayana, S. V. L.; Kotwal, G. J.; Krishna Murthy, H. M. The Structure of Complement C3b Provides Insights into Complement Activation and Regulation. *Nature* **2006,** *444,* 221–225.
33. http://www.uab.edu/reporterarchive/71570-uab-statement-on-proteindata-bank-issues.
34. Brendan, B. Fraud Rocks Protein Community. *Nature* **2009,** *462* (7276), 970.
35. Abdul Ajees, A.; Gunasekaran, K.; Volanakis, J. E.; NarayanaGirish, S. V. L.; Kotwal, J.; Krishna Murthy, H. M. Retraction: The Structure of Complement C3b Provides Insights into Complement Activation and Regulation. *Nature* **2016,** *532,* 268.
36. Read, R. J.; Adams, P. D.; Arendall, W. B., III; Brunger, A. T.; Emsley, P.; Joosten, R. P.; Kleywegt, G. J.; Krissinel, E. B.; Luetteke, T.; Otwinowski, Z.; et al. A New Generation of Crystallographic Validation Tools for the Protein Data Bank. *Structure* **2011,** *19* (10), 1395–1412 (Cambridge, MA, United States).
37. Montelione, G. T.; Nilges, M.; Bax, A.; Guntert, P.; Herrmann, T.; Richardson, J. S.; Schwieters, C. D.; Vranken, W. F.; Vuister, G. W.; Wishart, D. S.; et al. Recommendations of the wwPDB NMR Validation Task Force. *Structure* **2013,** *21* (9), 1563–1570 (Oxford, United Kingdom).
38. http://www.wwpdb.org/news/news?year=2013#02-August-2013.
39. http://www.wwpdb.org/validation/2016/XrayValidationReportHelp.
40. http://www.wwpdb.org/validation/2016/NMRValidationReportHelp.

41. http://www.wwpdb.org/validation/2016/EMValidationReportHelp.
42. Personal communication, Sameer Velankar, European Bioinformatics Institute.
43. Berman, H. M.; Kleywegt, G. J.; Nakamura, H.; Markley, J. L. How Community Has Shaped the Protein Data Bank. *Structure* **2013 Sep 3,** *21* (9), 1485–1491.
44. Zbigniew, D.; Alexander, W.; Wladek, M.; Mariusz, J.; Bernhard, R. Avoidable Errors in Deposited Macromolecular Structures: An Impediment to Efficient Data Mining. *IUCrJ* **2014,** *1* (Pt 3), 179–193.
45. O'Dell, W. B.; Bodenheimer, A. M.; Meilleur, F. Neutron Protein Crystallography: A Complementary Tool for Locating Hydrogens in Proteins. *Arch. Biochem. Biophys.* **2016,** *602,* 48–60.
46. Golden, E. A.; Vrielink, A. Looking for Hydrogen Atoms: Neutron Crystallography Provides Novel Insights Into Protein Structure and Function. *Aust. J. Chem.* **2014,** *67* (12), 1751–1762.
47. This link will provide an up-to-date search of PDB for structures, based at least in part, on neutron diffraction data http://www.ebi.ac.uk/pdbe/entry/search/index?status:REL&experimental_method:%22Neutron%20Diffraction%22
48. Lamb, A. L.; Kappock, T. J.; Silvaggi, N. R. You Are Lost Without a Map: Navigating the Sea of Protein Structures. *Biochim. Biophys. Acta, Proteins Proteomics* **2015,** *1854* (4), 258–268.
49. Boulanger, M. J.; Murphy, M. E. P. Alternate Substrate Binding Modes to Two Mutant (D98N and H255N) Forms of Nitrite Reductase From Alcaligenes Faecalis S-6: Structural Model of a Transient Catalytic Intermediate. *Biochemistry* **2001,** *40* (31), 9132–9141.
50. Davis, A. M.; St-Gallay, S. A.; Kleywegt, G. J. Limitations and Lessons in the Use of X-Ray Structural Information in Drug Design. *Drug Discov. Today* **2008,** *13* (19/20), 831–841.
51. Repasky, M. P.; Murphy, R. B.; Banks, J. L.; Greenwood, J. R.; Tubert-Brohman, I.; Bhat, S.; Friesner, R. A. Docking Performance of the Glide Program as Evaluated on the Astex and DUD Datasets: A Complete Set of Glide SP Results and Selected Results for a New Scoring Function Integrating WaterMap and Glide. *J. Comput. Aided Mol. Des.* **2012,** *26* (6), 787–799.
52. https://docs.eyesopen.com/szmap/.
53. Bodnarchuk, M. S. Water, Water, Everywhere… It's Time to Stop and Think. *Drug Discov. Today* **2016,** *21* (7), 1139–1146.
54. Zheng, H.; Hou, J.; Zimmerman, M. D.; Wlodawer, A.; Minor, W. The Future of Crystallography in Drug Discovery. *Expert Opin. Drug Discovery* **2014,** *9* (2), 125–137.
55. Davis, A. M.; Teague, S. J. Hydrogen Bonding, Hydrophobic Interactions, and Failure of the Rigid Receptor Hypothesis. *Angew. Chem. Int. Ed.* **1999,** *38* (6), 736–749.
56. Deller, M. C.; Rupp, B. Models of Protein–Ligand Crystal Structures: Trust, But Verify. *J. Comput. Aided Mol. Des.* **2015,** *29,* 817–836.
57. Liebeschuetz, J.; Hennemann, J.; Olsson, T.; Groom, C. R. The Good, the Bad and the Twisted: A Survey of Ligand Geometry in Protein Crystal Structures. *J. Comput. Aided Mol. Des.* **2012,** *26* (2), 169–183.
58. Reynolds, C. H. Protein-Ligand Cocrystal Structures: We Can Do Better. *ACS Med. Chem. Lett.* **2014,** *5* (7), 727–729.
59. http://wwpdb-validation.wwpdb.org/.
60. Adams, P. D.; Aertgeerts, K.; Bauer, C.; Bell, J. A.; Berman, H. M.; Bhat, T. N.; Blaney, J. M.; Bolton, E.; Bricogne, G.; Brown, D.; et al. Outcome of the First wwPDB/CCDC/D3R Ligand Validation Workshop. *Structure* **2016,** *24* (4), 502–508 (Oxford, United Kingdom).
61. Joosten, R. P.; Salzemann, J.; Bloch, V.; Stockinger, H.; Berglund, A. C.; Blanchet, C.; Bongcam-Rudloff, E.; Combet, C.; Da Costa, A. L.; Deleage, G.; et al. PDBREDO: Automated Re-Refinement of X-Ray Structure Models in the PDB. *J. Appl. Crystallogr.* **2009,** *42* (3), 376–384.
62. Joosten, R. P.; te Beek, T. A. H.; Krieger, E.; Hekkelman, M. L.; Hooft, R. W. W.; Schneider, R.; Sander, C.; Vriend, G. A Series of PDB Related Databases for Everyday Needs. *Nucleic Acids Res.* **2011,** *39* (Suppl. 1), D411–D419.
63. Mukherjee, S.; Balius, T. E.; Rizzo, R. C. Docking Validation Resources: Protein Family and Ligand Flexibility Experiments. *J. Chem. Inf. Model.* **2010,** *50* (11), 1986–2000.
64. Boström, J. *J. Comput. Aided Mol. Des.* **2001,** *15,* 1137–1152.
65. Hartshorn, M. J.; Verdonk, M. L.; Chessari, G.; Brewerton, S. C.; Mooij, W. T. M.; Mortenson, P. N.; Murray, C. W. Diverse, High-Quality Test Set for the Validation of Protein-Ligand Docking Performance. *J. Med. Chem.* **2007,** *50* (4), 726–741.
66. Warren, G. L.; Do, T. D.; Kelley, B. P.; Nicholls, A.; Warren, S. D. Essential Considerations for Using Protein-Ligand Structures in Drug Discovery. *Drug Discov. Today* **2012,** *17* (23–24), 1270–1281.
67. Hawkins, P. C. D.; Skillman, A. G.; Warren, G. L.; Ellingson, B. A.; Stahl, M. T. Conformer Generation With OMEGA: Algorithm and Validation Using High Quality Structures From the Protein Databank and Cambridge Structural Database. *J. Chem. Inf. Model.* **2010,** *50* (4), 572–584.
68. Mysinger, M. M.; Carchia, M.; Irwin, J. J.; Shoichet, B. K. Directory of Useful Decoys, Enhanced (DUD-E): Better Ligands and Decoys for Better Benchmarking. *J. Med. Chem.* **2012,** *55* (14), 6582–6594.
69. Hauser, A. S.; Windshuegel, B. LEADS-PEP: A Benchmark Data Set for Assessment of Peptide Docking Performance. *J. Chem. Inf. Model.* **2016,** *56* (1), 188–200.
70. Weiss, D. R.; Bortolato, A.; Tehan, B.; Mason, J. S. GPCR-Bench: A Benchmarking Set and Practitioners' Guide for G Protein-Coupled Receptor Docking. *J. Chem. Inf. Model.* **2016,** *56* (4), 642–651.
71. Lagarde, N.; Zagury, J.-F.; Montes, M. Benchmarking Data Sets for the Evaluation of Virtual Ligand Screening Methods: Review and Perspectives. *J. Chem. Inf. Model.* **2015,** *55* (7), 1297–1307.
72. http://bit.ly/1Ddnlkg.
73. http://bit.ly/1shcwu4.
74. http://bit.ly/1t5szxl.
75. http://bit.ly/1v80yoS.
76. http://bit.ly/1xdfoZN.
77. http://bit.ly/1wJNWBy.
78. Emsley, P.; Lohkamp, B.; Scott, W. G.; Cowtan, K. Features and Development of Coot. *Acta Crystallogr. Sect. D* **2010,** *66,* 486–501. http://bit.ly/1wJNWBy.
79. http://bit.ly/1xdfoZN and http://bit.ly/1si1ZeL.
80. http://bit.ly/1o1PuHW.
81. http://bit.ly/1F0j19Y.
82. Yusuf, D.; Davis, A. M.; Kleywegt, G. J.; Schmitt, S. An Alternative Method for the Evaluation of Docking Performance: RSR vs. RMSD. *J. Chem. Inf. Model.* **2008,** *48* (7), 1411–1422.
83. Irwin, J. J.; Shoichet, B. K.; Mysinger, M. M.; Huang, N.; Colizzi, F.; Wassam, P.; Cao, Y. Automated Docking Screens: A Feasibility Study. *J. Med. Chem.* **2009,** *52* (18), 5712–5720.
84. Jovine *J. Appl. Crystallogr.* **2008,** *41,* 659.
85. Dauter, Z.; Wlodawer, A.; Minor, W.; Jaskolski, M.; Rupp, B. Avoidable Errors in Deposited Macromolecular Structures: An Impediment to Efficient Data Mining. *IUCrJ* **2014,** *1* (3), 179–193.
86. Zheng; et al. *Expert Opin. Drug Discovery* **2014,** *9,* 125.
87. Guss, J. M.; McMahon, B. How to Make Deposition of Images a Reality. *Acta Crystallogr. D Biol. Crystallogr.* **2014 Oct 1,** *70* (Pt 10), 2520–2532.
88. Androulakis, S.; et al. *Acta Crystallogr.* **2008,** *D64,* 810–814.
89. http://ecrystals.chem.soton.ac.uk/.

90. Minor, W.; Dauter, Z.; Helliwell, J. R.; Jaskolski, M.; Wlodawer, A. Safeguarding Structural Data Repositories Against Bad Apples. *Structure* **2016,** *24* (2), 216–220 (Oxford, United Kingdom).
91. Meyer, P. A.; Socias, S.; Key, J.; Ransey, E.; Tjon, E. C.; Buschiazzo, A.; Lei, M.; Botka, C.; Withrow, J.; Neau, D.; et al. Data Publication With the Structural Biology Data Grid Supports Live Analysis. *Nat. Commun.* **2016,** *7,* 10882.
92. Wendt, B.; Cramer, R. D. Challenging the Gold Standard for 3D-QSAR: Template CoMFA Versus X-Ray Alignment. *J. Comput. Aided Mol. Des.* **2014,** *28* (8), 803–824.
93. Callaway. The Revolution Will Not Be Crystallized. *Nature* **2015,** *525.*
94. Bai, X. C.; et al. An Atomic Structure of Human Gamma-Secretase. *Nature* **2015,** *525* (7568), 212–217.
95. Bai, X. C.; et al. Sampling the Conformational Space of the Catalytic Subunit of Human Gamma-Secretase. *eLife* **2015,** *4.*
96. Bartesaghi, A. 2.2 Å Resolution 3DEM Structure of *b*-Galactosidase in Complex With a Cell-Permeant Inhibitor. *Science* **2015,** *348* (6239), 1147–1151.
97. Juers, D. H.; Jacobson, R. H.; Wigley, D.; Zhang, X.; Huber, R. E.; Tronrud, D. E.; Matthews, B. W. High Resolution Refinement of *b*-Galactosidase in a New Crystal Form Reveals Multiple Metal-Binding Sites and Provides a Structural Basis for a-Complementation. *Protein Sci.* **2000,** *9,* 1685–1699.
98. Subramaniam, S.; et al. Resolution Advances in 3DEM Enable Application to Drug Discovery. *Curr. Opin. Struct. Biol.* **2016,** *41,* 194–202.
99. Guaitoli, G.; et al. Structural Model of the Dimeric Parkinson's Protein LRRK2 Reveals a Compact Architecture Involving Distant Interdomain Contacts. *Proc. Natl. Acad. Sci. U. S. A.* **2016,** *113* (30), E4357–E4366.
100. Henderson, R.; Baldwin, J. M.; Ceska, T. A.; Zemlin, F.; Beckman, E.; Downing, K. H. Model for the Structure of Bacteriorhodopsin Based on High-Resolution Electron Cryo-Microscopy. *J. Mol. Biol.* **1990,** *213,* 899–929.
101. Bai, X. C.; McMullan, G.; Scheres, S. H. How 3DEM Is Revolutionizing Structural Biology. *Trends Biochem. Sci.* **2015,** *40* (1), 49–57.
102. Kuhlbrandt, W. 3DEM Enters a New Era. *Elife* **2014,** *3,* e03678.
103. Milne, J. L.; et al. Cryo-Electron Microscopy—a Primer for the Non-Microscopist. *FEBS J.* **2013,** *280* (1), 28–45.
104. Velankar, S.; van Ginkel, G.; Alhroub, Y.; Battle, G. M.; Berrisford, J. M.; Conroy, M. J.; Dana, J. M.; Gore, S. P.; Gutmanas, A.; Haslam, P.; et al. PDBe: Improved Accessibility of Macromolecular Structure Data From PDB and EMDB. *Nucleic Acids Res.* **2016,** *44* (D1), D385–D395.
105. Berman, H. M.; Burley, S. K.; Chiu, W.; Sali, A.; Adzhubei, A.; Bourne, P. E.; Bryant, S. H.; Dunbrack, R. L., Jr.; Fidelis, K.; Frank, J.; et al. Outcome of a Workshop on Archiving Structural Models of Biological Macromolecules. *Structure* **2006,** *14,* 1211–1217.
106. Haas, J.; Roth, S.; Arnold, K.; Keifer, F.; Schmidt, T.; Bordoli, L.; Schwede, T. The Protein Model Portal—a Comprehensive Resource for Protein Structure and Model Information. *Database (Oxford)* **2013,** *2013,* bat031.
107. Byeon, I. J.; Louis, J. M.; Gronenborn, A. M. A Captured Folding Intermediate Involved in Dimerization and Domain-Swapping of GB1. *J. Mol. Biol.* **2004,** *340,* 615–625.
108. Ward, A. B.; Sali, A.; Wilson, I. A. Biochemistry. Integrative Structural Biology. *Science* **2013,** *339,* 913–915.

3.07 Protein Structure Prediction and Homology Modeling

AR Leach and PJ Thomas, European Bioinformatics Institute, Hinxton, United Kingdom and GSK, Stevenage, United Kingdom

© 2017 Elsevier Ltd. All rights reserved.

3.07.1	**Introduction**	120
3.07.1.1	The Drive to Use 3D Protein Structures in Drug Discovery and Design	120
3.07.1.2	Quantifying the Need for Protein Structure Prediction Methods	121
3.07.1.3	Why Is the Number of Protein Folds Important?	122
3.07.1.4	The Uses and Limitations of Models in Protein Structure Analysis and Drug Discovery	123
3.07.1.5	Additional Challenges and Considerations When Using Protein Structures	124
3.07.1.6	A Timeline of Protein Structure Prediction and Protein Modeling	124
3.07.2	**How Is Protein Structure Information Used in Drug Discovery?**	124
3.07.2.1	How Accurate Does a Protein Model Need to be?	125
3.07.2.2	Protein Structure and Protein Models in Small Molecule Drug Discovery	126
3.07.2.3	Target Tractability and Ligandability	127
3.07.2.4	Synthetic Biology and Synthetic Biochemistry	128
3.07.2.5	Modeling Guiding Experiment: Construct Design and Side-Directed Mutagenesis	128
3.07.2.6	The Design of New Protein Therapeutics	128
3.07.2.7	Predicting Protein Function	129
3.07.3	**How Are Protein Models Built?**	129
3.07.3.1	Sequence and Structural Analysis	130
3.07.3.1.1	Fold identification: Identifying homologues of known structure	130
3.07.3.1.2	Generating the critical sequence-structure alignment	133
3.07.3.2	Building and Refining the Model	133
3.07.3.2.1	Model building directly from template structures	134
3.07.3.2.2	Segment matching	134
3.07.3.2.3	Modeling using spatial restraints	135
3.07.3.3	Loop Modeling	135
3.07.3.4	Side Chain Assignment	137
3.07.3.5	Structure Refinement Methods in Protein Modeling	137
3.07.3.6	Model Validation and Sources of Error	138
3.07.3.7	Evaluating Protein Model Building Methods: The CASP Experiments	139
3.07.4	**Current Status of the Protein Modeling Field and Future Directions**	139
Acknowledgments		141
References		141
Relevant Websites		144

3.07.1 Introduction

3.07.1.1 The Drive to Use 3D Protein Structures in Drug Discovery and Design

Ever since the very first atomic resolution structures of proteins were revealed, drug designers have sought to exploit this information in the design of new therapeutics. Perhaps the first practical example of such structure-based drug discovery was the pioneering work of Beddell, Goodford, and colleagues at the Wellcome Research Laboratories who in the mid-1970s used the hemoglobin X-ray structure to design compounds that bound to and stabilized the deoxy conformation, thereby promoting oxygen liberation.[1] In the subsequent years, the use of protein structure in drug discovery has become well established and pivotal to the discovery of many clinical candidates and a growing number of marketed medicines.[2–4] Further, the opportunity to exploit protein structure for drug discovery has over the past decades provided a major impetus for the development of new experimental techniques in protein structure determination and in the computational tools and techniques that use such structures for the design of new medicines.

Nevertheless, despite significant progress there remain major challenges, both in our ability to generate structural information from experiment and in our computational structure-based design tools and approaches. Unfortunately, there is no guarantee that an experimental structure can be obtained of the specific protein of interest. Given these practical challenges, limitations, and uncertainties, there has evolved a parallel area of science that is the focus of this chapter, which is on methods for the computational modeling and prediction of 3-dimensional (3D) protein structures that are of sufficient accuracy and precision to be of practical value in drug design and discovery.

The chapter is organized as follows: First, we introduce the field, placing protein modeling in the broader context of the biological data explosion. We then summarize the various and changing ways in which protein structural information is used in drug

discovery. The core of the chapter is concerned with an overview of the methodologies that are most commonly used for building and validating protein models within the context of drug discovery applications, including the significant efforts made by the community to objectively assess and compare these methods. Finally, we provide some reflections on the current state of the art and indicate potential future directions. It is not our aim to provide a comprehensive review of the field. Rather, our goal is to provide an accessible introduction for non-experts, who we hope will then be better placed to engage productively and critically with protein modeling experts among their colleagues and will have sufficient background knowledge to access the relevant literature. Our emphasis will be on those applications and problems likely to be of most interest to medicinal chemists and others actively involved in "real world" drug and therapeutic discovery. At the same time, we recognize that this is a broad field whose scope continues to expand in many areas of both fundamental and applied science. We will assume a degree of familiarity with the basic principles of protein structure and function.[5] There are also many reviews of the protein modeling field[6–11] and an ever-growing list of resources freely available on the web.

3.07.1.2 Quantifying the Need for Protein Structure Prediction Methods

Recent years have seen a revolution in the provision of data in the biological and medical sciences, driven initially by the sequencing of the human genome and the subsequent dramatic reduction in cost that has brought the era of the sub-$1000 genome. While DNA sequencing continues to attract the headlines, technological advances are also occurring in many other areas of biology. Fig. 1 shows how the volumes of data held in databases at the European Bioinformatics Institute (EBI) from various "omics" technologies (e.g., DNA sequencing, transcriptomics, proteomics, and metabolomics) have increased in recent years.[12] Nor are these advances in technology and data generation limited to "omics" methods; imaging techniques, to take just one example, are also undergoing rapid technology change and data growth. Pertinent to this chapter is the sobering comparison between the growth in the numbers of deposited protein sequences and the corresponding growth in protein structure data. Fig. 2 shows a comparison between the entries contained in the UniProt/SwissProt and UniProt/Trembl databases[13,14] of curated protein sequences and the worldwide Protein Data Bank (PDB) of 3D structures.[15,16] Both sequence and structure databases continue to show exponential growth but there is a significant gap between the sequence data and the corresponding structural data. In practice this means that there is a large and growing number of proteins whose 3D structure is not known and where some form of predictive computational modeling currently provides the only available option.

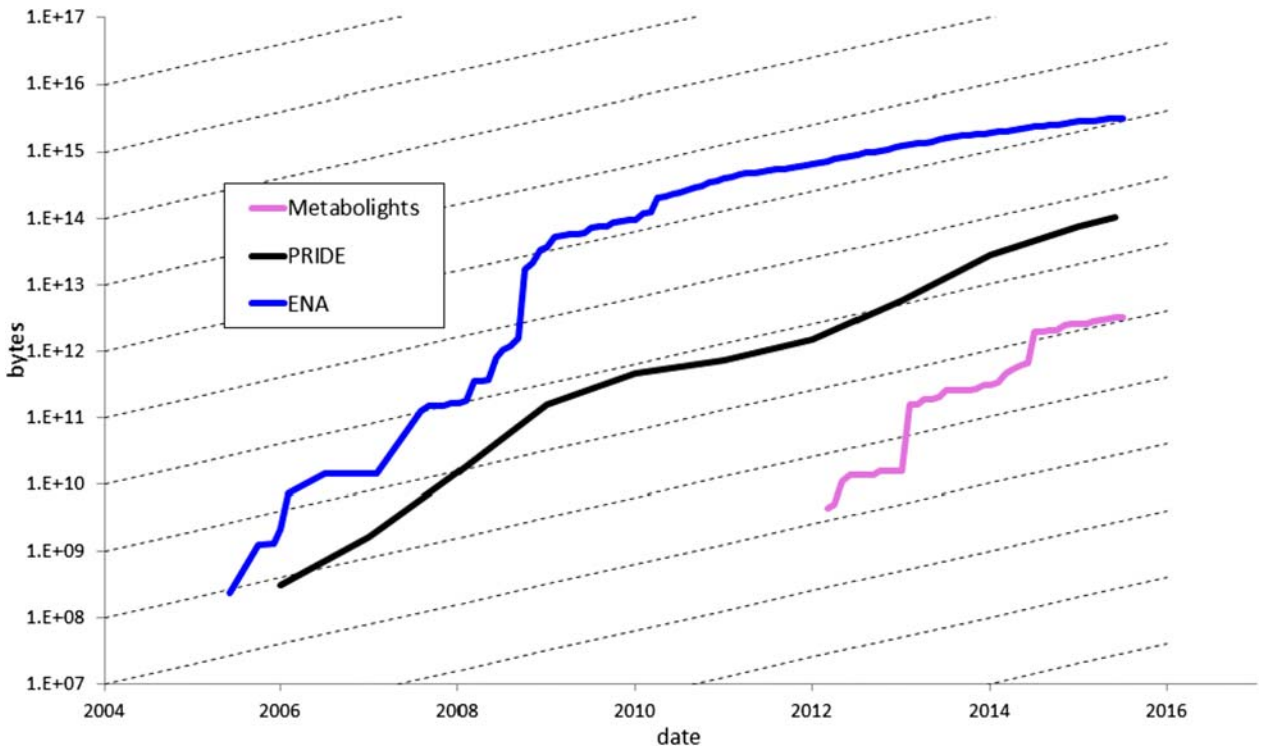

Fig. 1 Growth in data storage for selected resources at the European Bioinformatics Institute (EBI). *ENA*, European Nucleotide Archive; *PRIDE*, proteomics data; *Metabolights*, metabolomics data; The *dashed lines* correspond to a 12-month doubling rate. Adapted with permission from Cook, C. E.; Bergman, M. T.; Finn, R. D.; Cochrane, G.; Birney, E.; Apweiler, R. The European Bioinformatics Institute in 2016: Data Growth and Integration. Nucleic Acids Res. **2016**, *44*, D20–D26.

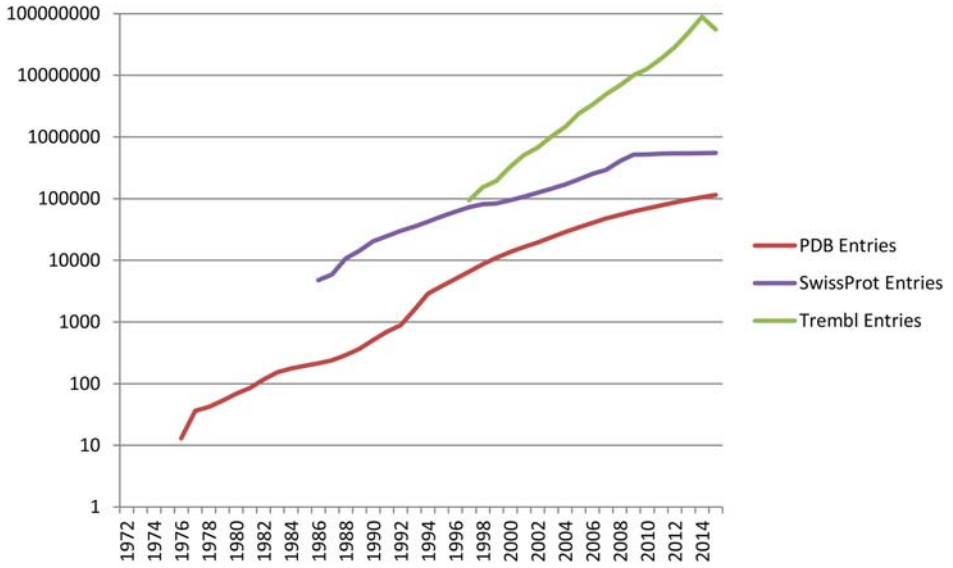

Fig. 2 Growth in deposited protein sequence data and corresponding protein structure data. PDB corresponds to the worldwide Protein Data Bank, SwissProt to curated protein sequences and Trembl to uncurated protein sequences. Note the logarithmic scale on the Y-axis.

3.07.1.3 Why Is the Number of Protein Folds Important?

This oft-quoted comparison between the growth in protein sequence and protein structure data is however only part of the story. A key observation made using the very earliest protein structures was that proteins with similar sequences had similar 3D structures. The pioneering work of Chothia and Lesk quantified the relationship between the degree of conservation of structure relative to sequence, and established the general principle that structure tends to be more highly conserved than sequence.[17] As we will discuss in more detail later, the most commonly used approach to protein model building for drug discovery applications (*comparative modeling*) seeks to identify proteins of known structure that would be expected to adopt the same overall conformation (or *fold*) as the unknown protein (henceforth referred to as the *target protein*). These proteins of known structure thus provide one or more 3D *templates* that can be used as the starting point to construct a structure of the unknown target protein. We also note that the older term *homology modeling* is frequently used interchangeably with comparative modeling; homologous proteins for the purposes of this chapter are those which have similar sequences, structures, or functions according to the context.

More relevant to the problem of protein model building therefore than the absolute number of available protein structures (which in any case includes many copies of some proteins, for example, with different ligands bound) is the number of distinct 3D protein folds that represent the currently known "universe" of protein conformations. Put more specifically, for the target protein that is of (therapeutic) interest to me, are there available experimental structures of proteins from the same fold family from which I can build a sufficiently accurate model?

As we have seen from Fig. 2 the numbers of both protein sequences and protein structures continue to grow rapidly. A key question for protein modeling is: how many different protein folds are there? The CATH[18,19] and SCOP[20,21] databases are widely used resources that characterize experimental structures from the Protein Data Bank into different fold families. They use somewhat different algorithms and strategies to define what differentiates a fold but are broadly similar in scope and intent. A year-by-year analysis of the numbers of new protein folds as new structures are added to the PDB is shown in Fig. 3. As can be seen, until around 1990 there was a slow growth in both the number of protein structures reported and the number of new folds. After 1990 the numbers of structures and folds underwent a huge increase. A practical consequence of this growth in the number of distinct folds over the last 25 years means that it is now much more likely that a 3D template will be available to enable comparative modeling for a new target protein. Indeed, although the number of structures has continued to rise steadily in recent years, no new folds have been reported since 2008, at least according to the CATH/SCOP definitions. This naturally raises the question as to whether we are reaching the point at which all viable folds have been discovered and that we are only limited by our ability to predict which fold a protein will adopt. Of course, this analysis is restricted to the structural data represented in the PDB; certain families such as membrane-bound proteins are underrepresented due to the experimental challenges of obtaining structural data.

A significant proportion of the increase in structural diversity in recent years is a consequence of the various structural genomics initiatives.[22] Recent studies have tried to quantify the impact of these large-scale programs, with one such analysis suggesting that the "structural coverage" for known protein sequences is currently approximately 40%, a value that had increased from 30% between 2000 and 2012.[23] This was a relatively simple calculation, based purely on sequence comparisons of the known sequences, against the sequences of proteins deposited in the Protein Data Bank. When broken down by organism type (eukaryotes, bacteria, viruses, etc.) it was found that viral proteins had the highest structure coverage at almost 60% whereas eukaryotic proteins were the

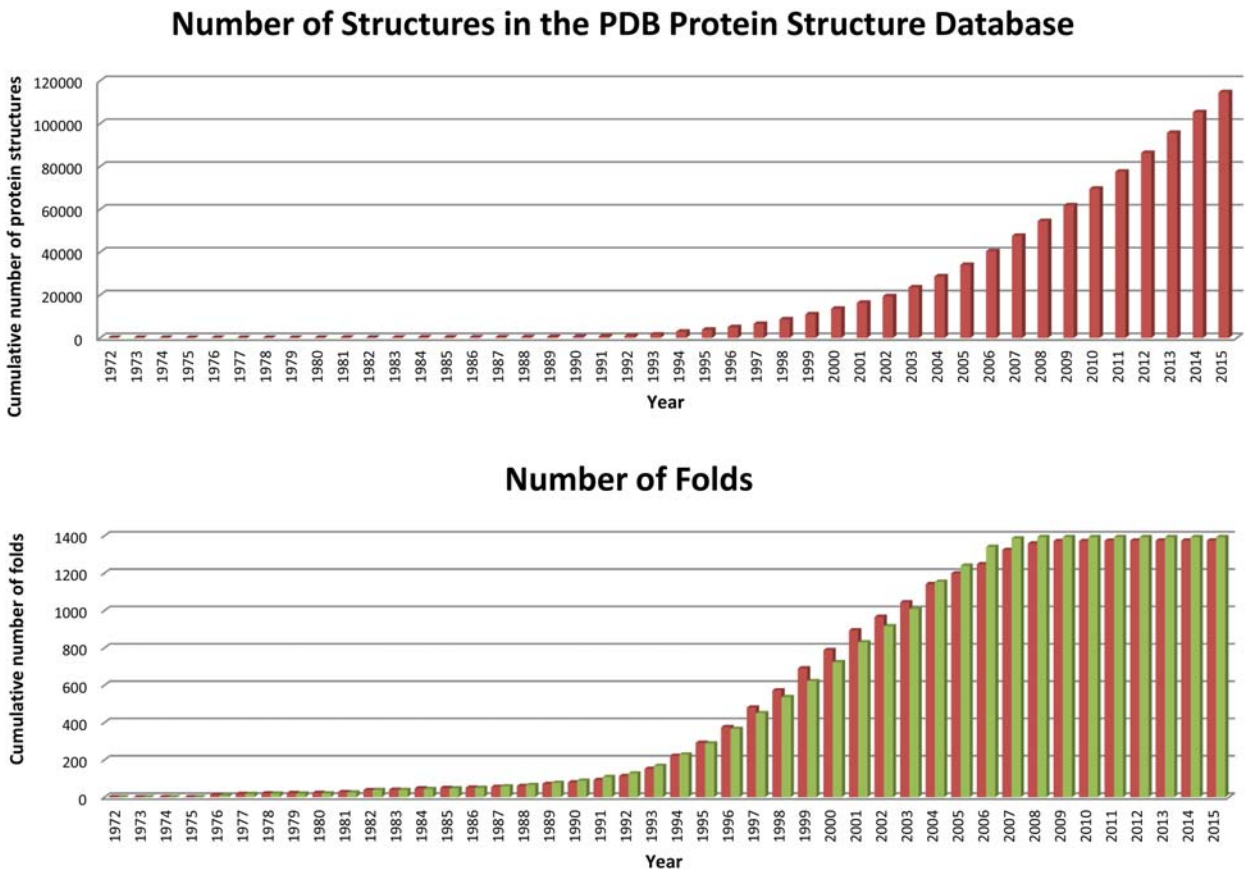

Fig. 3 Comparison of the growth in the number of structures in the wwPDB (*top*) with the number of folds (*bottom*), according to SCOP (in *green*) and CATH (in *red*).

lowest at approximately 30%. This latter figure had changed little in the previous decade and was ascribed to the challenges of generating sufficient material of the right quality for experimental structural studies of eukaryotic proteins. Finally, in addition to all the above considerations it is important to recognize that some proteins are in whole or part natively unfolded[24] although some may fold when complexed with partner proteins. Clearly, our ability to understand the function of these proteins through current approaches to protein modeling will be limited.

3.07.1.4 The Uses and Limitations of Models in Protein Structure Analysis and Drug Discovery

It is tempting to make a distinction between the data and results obtained from experimental sources and outputs from purely computational methods. Experimental results are often considered "definitive" outputs against which computational modeling approaches and predictions are to be compared. However, almost all experimental approaches themselves involve some form of model-building. A data point as apparently simple as an IC50 value is the result of fitting a particular predefined equation to a series of concentration-varying inhibition data. The generation of experimental protein structures involves extensive use of model building techniques.

Historically, the most commonly used and still the "gold standard" method for the determination of protein structures is *X-ray crystallography*, representing around 90% of all structures deposited in the Protein Data Bank. A key step in the crystallographic workflow involves fitting a 3D atomic model to the experimentally determined electron density.[25–29] *Nuclear Magnetic Resonance* (*NMR*) experiments have to date provided the second highest proportion of structures in the Protein Data Bank (approximately 10%). Here again, model building is a key aspect of the workflow, with 3D models being built to satisfy the experimental restraints (for example, distance restraints between pairs of atoms).[30,31] *cryo Electron Microscopy* (*cryo-EM*), limited for many years to depicting proteins as "blobs," is currently undergoing a "resolution revolution"[32–34] as a result of dramatic improvements in microscopes, detectors, and image processing techniques. This has led to a rapidly growing number of structures at 3 Å resolution or better, which enables more detailed information to be resolved than at lower resolution, such as the conformations of protein side chains. Again, model building is a crucial component of the cryo-EM workflow. Other experimental techniques such as hydrogen–deuterium exchange, small-angle X-ray scattering, chemical cross-linking, and light scattering can also provide information that may assist in the

construction and validation of protein structural models even though in general the lower resolution information from these methods cannot be used directly to generate a 3D structure.

Later in this chapter we will discuss briefly the potential sources of errors in protein models and validation procedures to help identify them. It is important to realize that experimental models also can be subject to errors, mistakes and over-interpretation.[35,36] It is therefore important to carefully scrutinize all experimental data prior to use and not to assume that an experimental result is necessarily definitive. On a more positive note, there are clear opportunities for productive synergies between experiment and theory in the area of protein structure analysis, prediction, and modeling. In some cases it is possible to incorporate experimental information (potentially from more than one experimental approach) directly into the model building process, and so deliver structures that take this information and knowledge into account. In other cases the experimental information can be used to filter a number of different possible models in order to identify those which are most consistent with the experiment.

3.07.1.5 Additional Challenges and Considerations When Using Protein Structures

A number of additional caveats should be borne in mind when using protein structural information, data, and models. Three of the most important relate to protein dynamics, solvation, and multicomponent complexes. Proteins in their natural environment are dynamic entities. By contrast, most "experimental" protein structures from X-ray crystallography are represented as static 3D models. In some cases conformational flexibility is explicitly captured (e.g., the different conformations of individual side chains), and certain other aspects of the experiment provide information on protein dynamics (e.g., temperature or B factors). However, such static representations are far removed from the true dynamical nature of proteins. Very similar arguments can be made about solvation and the critical role of water in protein structure and dynamics. Computational techniques such as molecular dynamics simulations may provide insights into dynamics and solvation but rarely capture the "true" environment within the cell and are often unable to run the calculations long enough to reach the timescales of biological processes. A third challenge arises from the fact that many proteins function as part of much larger complexes comprising multiple domains. Although the structures of some very large proteins and protein complexes have been solved, for practical drug discovery projects it is much more common to focus on single, isolated domains as these are more likely to be amenable to the production of diffracting crystals for X-ray crystallography or below the typical upper limit of $\sim$50kDa for NMR. The advent of high-resolution cryo-EM may change the situation as this method is more suited to the study of larger systems. Notwithstanding these caveats, the use of single protein domains that are treated as static entities with minimal account of solvent is still the norm in computational drug discovery. Nevertheless, experienced users of X-ray structures will be aware of these limitations and will take appropriate action when setting up and analyzing calculations.

3.07.1.6 A Timeline of Protein Structure Prediction and Protein Modeling

Ever since the very first experimental protein structures were determined it was recognized that proteins with different amino acid sequences can adopt the same fold.[17] This naturally led to an interest in methods for predicting their 3D structures in order to better understand the critical role that proteins play in driving many biological processes. From a practical drug discovery perspective the driver has often been to make use of the atomic resolution structural information in compound design. More broadly, protein structure prediction has been for many years one of the key unsolved problems in biology: starting from just the amino acid sequence of a protein is it possible to predict its structure? Closely related to this is the protein folding problem: how do proteins form such complex 3D structures when going from random polypeptide chain to complex 3D protein structure?

Some of the landmarks in the history and evolution of protein structure prediction are indicated in **Fig. 4**, including important breakthroughs, the creation of resources such as the PDB, and the introduction of key methodologies. We will touch on many of these innovations throughout the chapter. While the "holy grail" of being able to accurately predict the structure of any protein purely from its sequence remains unsolved, significant progress has been made not only in the fundamental science but also in the influence and impact of the field on experimental approaches, in computational science, and in engaging the scientific community and the general public.

3.07.2 How Is Protein Structure Information Used in Drug Discovery?

The close relationship between protein structure and biological function has a long and illustrious history with many landmarks and the award of a significant number of Nobel prizes. There are in addition numerous ways in which the 3D structure of a protein may be of value in the discovery of new therapeutic agents. The first, and still the most common, is in the design of small "drug-like" molecules that interact via a desired mode of action with the target protein. Closely related to this is the use of structure to design compounds that have no or reduced binding to that protein, for example, because it is a selectivity or liability target. While these two scenarios continue to be the most common for the practising medicinal chemist, there are nevertheless other uses of protein structures in drug discovery. The goal of a *ligandability assessment* is to predict the feasibility of identifying drug-like small molecules that bind to the target protein. *Construct design* involves the prediction of domain boundaries, sites of post-translational modification, and the overall properties of isolated domains in amino acid sequences in order to generate stable protein, often to optimize the likelihood of crystallization. *Synthetic biochemistry* is a relatively new area where, for example, it is desired to optimize the catalytic

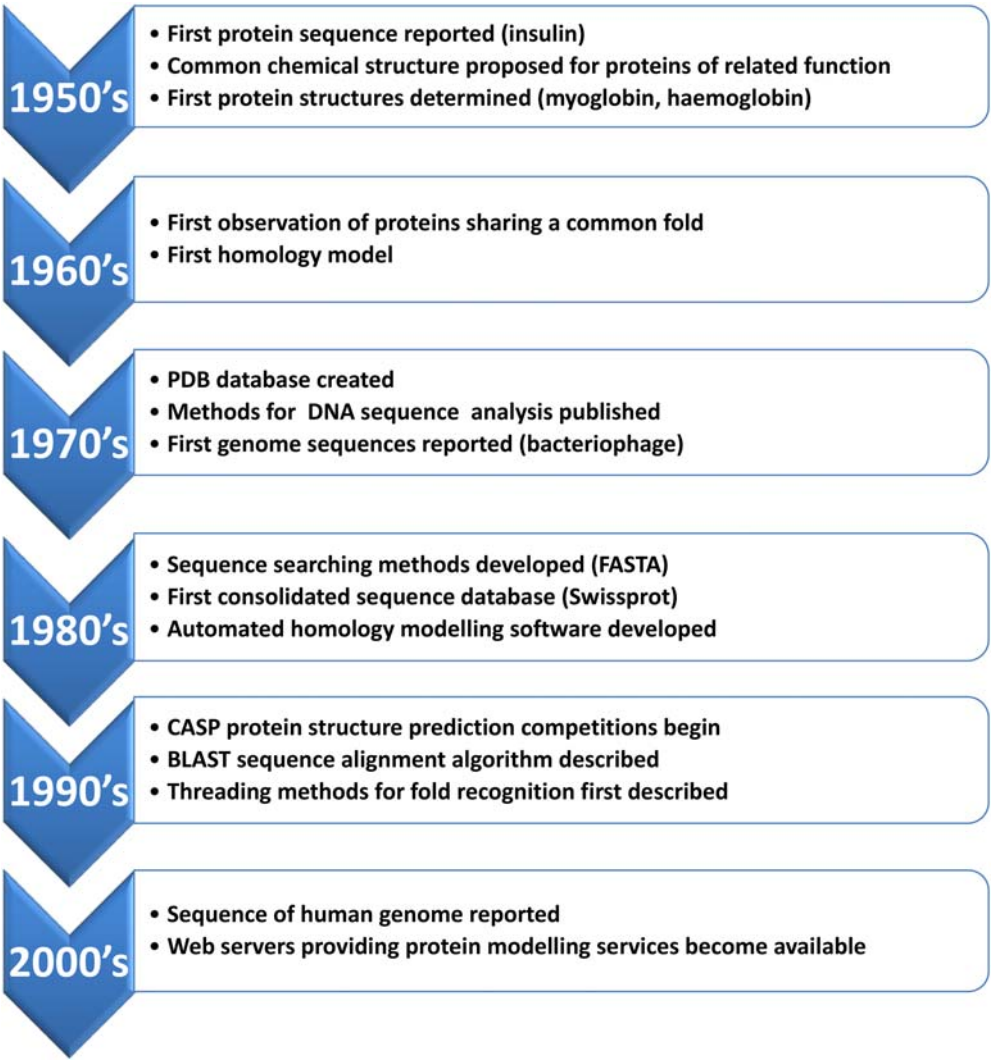

Fig. 4 Timeline showing some of the major landmarks in protein structure determination and protein modeling.

properties of an enzyme, to drive a desired chemical reaction under particular conditions (as might, for example, be required for the "green" synthesis of a drug or chemical). Beyond "small molecule" drug discovery there are increasingly important opportunities to exploit structural knowledge, for example, in the design of protein therapeutics such as antibodies and vaccines.

3.07.2.1 How Accurate Does a Protein Model Need to be?

An important factor when considering practical applications of predictive protein modeling is to have a general appreciation of the level of accuracy that is required of the protein model in order to be useful. The accuracy of a protein model can be assessed in many different ways. The most common method in the protein modeling community is to calculate the "Cα-RMSD" value between the model and the experimentally determined structure. This corresponds to the root-mean-square deviation (RMSD) when the alpha carbon atoms (Cα) of the protein backbone of the model and the experimental structure are optimally superimposed. This metric is straightforward, quantitative, and well understood. However, it may not be the most appropriate measure in practice and a host of alternatives have been developed. These include the "global distance test (GDT)," defined as the largest set of alpha carbon atoms in the model structure that fall within a defined distance cutoff of their position in the experimental structure. It was introduced[37] to address the fact that the RMSD metric for an otherwise correct model can be skewed toward a poor value due to inaccurate predictions in just small parts of the model. A practical limitation with the RMSD, GDT, and similar measures is that these metrics can only be calculated once the experimental structure is available (which in turn is often the reason for building a model in the first place). A further caveat is that measures of overall structure accuracy may not be the most relevant for drug discovery, because only a part of the structure is of practical interest. In small molecule applications it is often the binding site that is most relevant; a model that on the basis of an overall RMSD appears of lower quality can nevertheless be very useful if the binding region is well defined and vice

versa. Further, a very approximate model may be able to provide key insights that are pivotal for progress in one molecular design project whereas a highly accurate model (or indeed a highly accurate experimental structure) may not in practice help another project progress at all, for example because the issues are not related to protein–ligand interactions but rather another aspect such as pharmacokinetics, toxicity, or physical form. Some general guidelines based on practical experience are nevertheless illustrated in Fig. 5.

3.07.2.2 Protein Structure and Protein Models in Small Molecule Drug Discovery

Structure-based design methods are used in both the hit generation and lead optimization phases of small molecule drug discovery. In hit generation the most common use is for *virtual screening*, where the target protein structure is used to search compound databases to identify a subset of compounds for (physical) screening in some form of biological assay.[38–40] In the lead optimization phase, structure-based methods are often a key part of the iterative design, synthesize, and test cycle to enhance interactions with the target protein and in some cases to build in selectivity or eliminate off-target binding properties of the molecular series.

Central to many structure-based design strategies is *molecular docking*, the goal of which is to predict the binding mode of a molecular ligand when bound to its target protein. Many docking algorithms have been developed since the very first methods were introduced in the late 1980s.[41–43] Docking involves two core components. First, a method to explore the conformational and orientational space of the protein–ligand system in order to generate trial docking poses. Second, a method to score these poses such that the closer a pose is to the true binding mode, the more favorable is the score. The relative performance of docking programs is a topic of perennial interest and the field has benefitted significantly from the publication of highly curated, published training sets that have enabled a more consistent and thorough evaluation of docking performance.[44–48] Contemporary docking

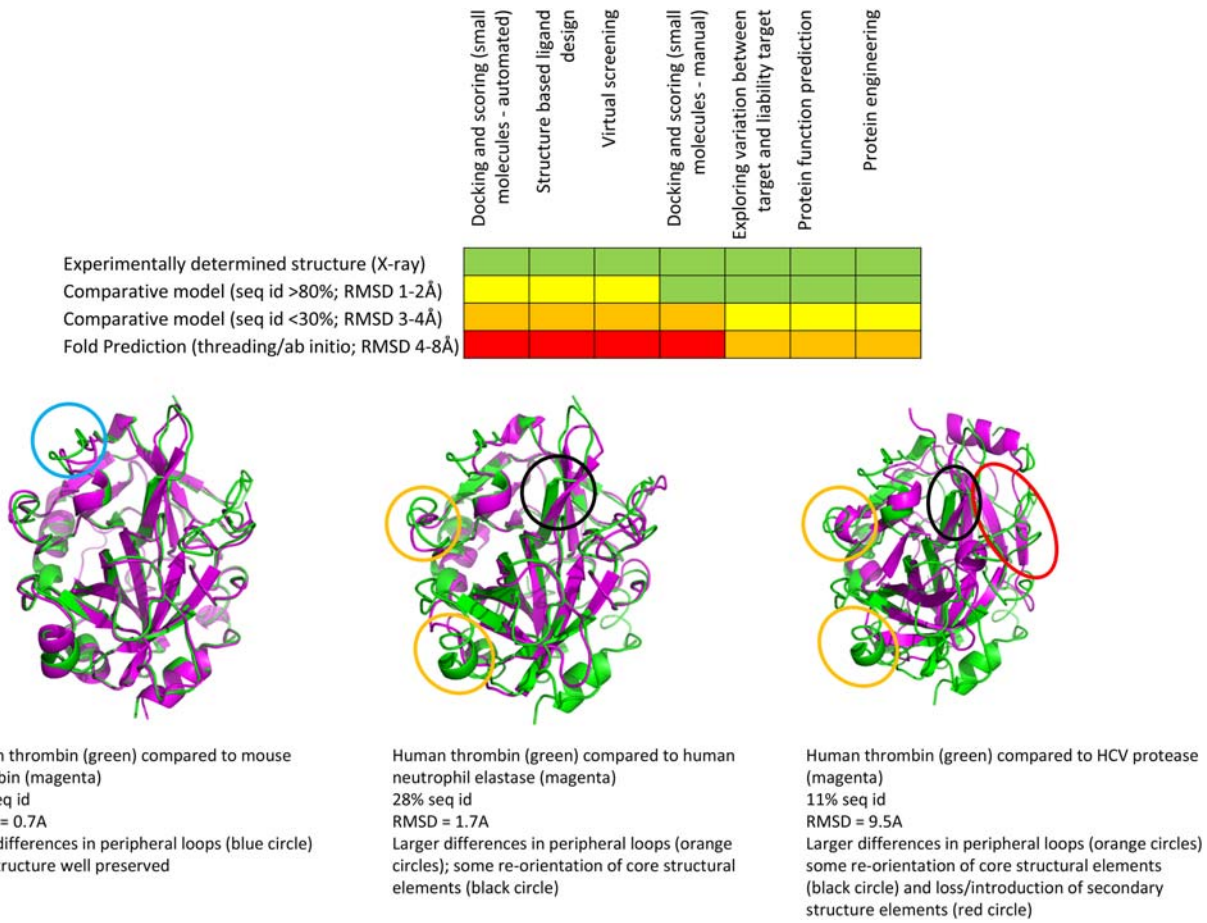

Fig. 5 Top: schematic illustration of the level of accuracy (as measured by RMSD to the experimental structure) required in a model to enable different applications. Color coding from *green* (likely to be useful) to *red* (very limited or no use for this application). "seq id" (sequence identity) is the percentage of amino acids common to two aligned protein sequences, i.e., the target protein being modeled and the 3D template from which that model is built (see Section "**Sequence and Structural Analysis**" for more details). The RMSD values are indicative of the likely accuracy that might be expected for each scenario. Bottom: examples to illustrate the practical comparison between human thrombin and three other proteins with varying RMSD. Protein structure images created using the PyMOL Molecular graphics system, Version 1.7.6.6 Schrodinger LLC.

programs are able to predict the binding mode of a ligand in about 70% of cases, a figure that has changed little over recent years. While clearly important, docking performance on a large, diverse test set is just one of several factors that should be taken into account when selecting a docking method. Other considerations include performance on the specific system(s) of interest, the ability (if required) to handle certain types of ligands (e.g., covalent binders), speed, and usability. Many algorithms are still not able to adequately take account of small or large movements in protein structures that can occur on ligand binding and the development of scoring functions that properly quantify the balance of ligand strain, fit to site, and solvation/desolvation effects continues to be an area of active research. An in-depth analysis and summary of molecular docking methods can be found elsewhere in this volume.

Molecular docking is usually performed using experimentally determined protein structures, but there has nevertheless been interest in using 3D protein models where an experimental structure is not available.[49–52] The literature contains a growing number of examples where protein models have been used successfully in virtual screening applications (i.e., "active" compounds were discovered when the compounds were screened in the biological assay). Of course, success cannot be guaranteed, and we should always be aware that the literature tends to record just those cases that were successful. Several studies have sought to compare the virtual screening performance of protein models relative to the use of a crystal structure. G-coupled protein receptors in particular have been a popular target family for such studies[53–58] but there are also comparisons for other protein families such as kinases.[59]

One might ask why virtual screening should work at all when using a computational predictive model? It should first be recalled that docking and scoring methods are approximate, and that even when using a high-resolution crystal structure for virtual screening there is a natural limitation on performance. Conversely, it may be sufficient for a model to capture just the key elements of the protein active site in order to identify molecules that are active when screened. Further, protein models may access regions of conformational space not explicitly captured in the static snapshots provided by experimental structures. An extension of these ideas involves the integration of structure-based design and ligand-based design methods. The latter encompass approaches such as 3D pharmacophore methods and molecular similarity calculations; ligand-based design is traditionally applied where there are known ligands but no structure of the biological target. Extracting the key features from a protein model for use in a ligand-based workflow may provide an effective strategy that addresses some of the inherent inaccuracies and approximations in protein models. Some groups have developed more approximate representations of a protein binding site (often termed *pseudoreceptors*).[60,61] Finally, a growing trend is for ligand structure–activity data to be used in the construction and (in particular) the validation of protein models, a development that has been much facilitated by the availability of structure-activity relationship (SAR) data from public databases such as ChEMBL.[62]

During lead optimization the focus shifts to the iterative design of compounds from the hit chemical series in order to achieve an appropriate balance of properties (e.g., potency at the target, selectivity, safety, pharmacokinetics, etc.). A wide variety of computational methods may be applied, depending on the particular aspects being addressed. Common examples include: modifying and extending the current chemical series to pick up further interactions with the target to improve potency; improving selectivity over homologous proteins by capitalizing on differences in their protein structures; interaction analysis to identify potential bioisosteric replacements. In contrast to a typical virtual screening protocol used for hit generation, the numbers of structures that need to be processed and modeled in lead optimization are often far fewer. This means that greater use of hands-on modeling approaches becomes possible and can often be successful, particularly if close attention is paid to ensuring that the model continues to be refined in order to remain consistent with the ligand SAR.

3.07.2.3 Target Tractability and Ligandability

Target tractability is often considered synonymous with the term "druggability." There is neither formal definition nor recognized quantification of these terms, but the general concept is based on the idea that not all proteins are linked to disease nor are they necessarily amenable to intervention by small molecule therapies. The link between target and disease is an area of considerable interest, with a particular focus in recent years on the exciting opportunities offered by genetics. Having a highly validated target with regard to disease linkage constitutes only a part of the bigger picture; it is also necessary for that target to be amenable to intervention by a therapeutic agent, traditionally a "drug-like" small molecule. This second, *ligandability*, component aims to characterize, and in some cases quantify, the likelihood that a target protein can bind small "drug-like" molecules with a sufficiently strong interaction. The concept gained particular prominence following the sequencing of the human genome and the recognition that not all of the expressed proteins would necessarily be viable drug targets. This led to the concept of the "druggable genome".[63] Various methods are available for assessing the ligandability of a target. The simplest are based on precedence: if some members of a protein family have been "drugged" then it is assumed that other members of the family will also be tractable to small, drug-like molecules. More complex computational methods for assessing the likely ligandability of a protein from its 3D structure (which may be derived from experiment or from modeling) have also been developed.[64–66] These variously aim to identify, characterize, and assess the putative binding site. Geometrical characteristics such as size and shape can be calculated; sites that are reasonably enclosed with a high degree of concavity are in general considered to be more tractable toward small drug-like molecules than large, flat regions. It is also possible to quantify a binding site's potential for making favorable binding interactions by considering the characteristics of its defining atoms. Machine learning techniques may be used in conjunction with such descriptors to develop mathematical models for quantifying a site's ligandability. There has also been interest in the identification and characterization of allosteric and/or cryptic sites[67]; these may not be visible in the crystal structure, particularly of the apo protein, but are revealed

following conformational change. In all cases, it should be borne in mind that to have any useful (i.e., disease modifying) effect a ligand must do more than bind to the target protein; the binding event must also result in relevant functional consequences.

3.07.2.4 Synthetic Biology and Synthetic Biochemistry

Synthetic biology seeks to design and create new and artificial biological systems with a particular emphasis on the use of engineering principles. It covers an extremely wide range of opportunities and potential applications.[68–70] One application of practical relevance from the perspective of the medicinal chemist is the prospect of using engineered enzymes to catalyze chemical reactions. These may be reactions that are difficult to achieve using traditional organic synthetic methods (for example because the reactants are sensitive to the conditions employed) or may be very costly (due to the use of expensive catalysts or at an industrial level because of poor yields). A more general driver for the use of synthetic biochemistry is the desire to adopt a "green agenda" with the goals of reducing waste and energy.

The advantages of enzymes for catalysis are well known and include the following: (1) the reactions can be performed at ambient temperatures and pressures, (2) reactions can be performed using water as a solvent, and (3) no need for expensive, rare, and potentially toxic metal catalysts. However, many naturally occurring enzymes have limited substrate specificity and may therefore not be suitable for the specific transformation of interest. It may also be desired to enhance the properties of a naturally occurring enzyme such as the need for greater stability or specificity. To engineer a modified enzyme invariably requires amino acid changes to be incorporated into the protein sequence. There are a number of strategies and approaches that can be used to tackle this problem.[71–74] Structural information about the enzyme can be used with knowledge about the enzymatic reaction to suggest suitable modifications. Such structural information can be derived from experiment or a protein modeling approach, though the complexities of enzyme reactions and the modeling thereof may require a very accurate model for any computational work to be successful.

3.07.2.5 Modeling Guiding Experiment: Construct Design and Side-Directed Mutagenesis

A common theme through the history of protein modeling (as indeed is the case in many areas of science) has been the tight interaction and interplay between theory and experiment. In the earliest days, the information flow tended to be in one direction, from experiment to theory, as the modeling community developed new techniques for evaluation against experiment or extracted rules and knowledge from the databases of experimental protein structures. However, the methods and results from protein modeling are increasingly of value when designing better and more effective experiments. Two areas where this interplay can be particularly fruitful are in the design of constructs for X-ray crystallography and to guide side-directed mutagenesis experiments. In construct design, models can provide useful information where one or more domains need to be excised from a larger multidomain protein. Models can help to determine the minimum length of the construct and for the visualization of features such as exposed hydrophobic patches that may compromise protein expression and production. They can be useful in designing mutations to alter protein properties such as oligomerization. Models can also be used to identify and characterize ligand binding sites and then to identify residues within those sites that upon mutation should alter ligand affinity. Matching mutation and SAR data can provide confidence in a model and the ligand binding modes, which in turn can facilitate ligand design.

3.07.2.6 The Design of New Protein Therapeutics

Protein therapeutics broadly covers two areas: antibodies and vaccines. Therapeutic antibodies provide an alternative to traditional small molecules; following direct administration the antibody interacts with the biological target to produce the desired therapeutic response. Vaccines by contrast involve administration of the antigen (e.g., an inactivated virus or a recombinant protein subunit) which stimulates the body's immune response to provide long-term protection from the pathogen.

The numbers and commercial value of new therapeutic antibodies have grown dramatically since the first product came to market in 1986 with more than 50 products approved and many more in clinical development.[75,76] Antibodies have been the topic of protein modeling studies[77,78]; their structures follow a well-understood set of rules that were devised following the earliest crystallographic studies in the 1980s, as we shall discuss briefly later in this chapter.

The development of vaccines is considered one of the most significant developments in the history of human health, with the potential in some cases to completely eradicate major diseases. Nevertheless, there remain many conditions that have hitherto proved intractable to current vaccine approaches or where there is room for improvement. In recent years the opportunity to use protein structural information and knowledge in vaccine design has been recognized,[79,80] with a particular focus on engineering modified antigens that have the potential to elicit a much stronger immune response. One rationale for this approach is that most current vaccine antigens are derived from the natural pathogen which have evolved to evade rather than induce immunity. Knowledge of antigen 3D structures and in particular the potential recognition motifs enables the design of modified antigens with improved properties such as stability and ease of production, and enhanced immunological performance. One example that illustrates this strategy is the development of a single factor H-binding protein antigen from meningitis B.[81] This particular protein has over 500 sequence variants that fall into three groups. An effective vaccine requires antigens specific for all three variants to be included, making the manufacturing process complex and expensive. Having solved the X-ray structure of H-binding protein, the epitopes for each of the three variants were mapped onto the 3D surface. These in turn resulted in a set of protein designs for

further evaluation, which ultimately provided a single protein molecule able to induce immunity against all antigenic variants. In this particular case it proved important to take account of the entire protein surface, rather than just a small number of isolated amino acid changes. The use of structural biology and protein modeling techniques in vaccine design is still relatively new but we can anticipate significant advances in the future.

3.07.2.7 Predicting Protein Function

The landmark publication in 2001 of the sequence of the human genome has in the subsequent few years led to an explosion in the amount of sequence data. The genomes of many thousands of organisms have now been determined and the numbers continue to grow rapidly. From the DNA sequence it is then possible to determine the set of proteins believed to be expressed by that organism (i.e., its proteome). Elucidating the functions of these proteins is a key precursor to improved understanding at the molecular, cellular, organ, and organism levels which in turn may lead *inter alia* to the identification of potential targets for drug discovery. However, experimental determination of protein function is a time-consuming process, providing a clear driver for the use of predictive computational techniques. The development, validation, and application of such computational methods is an active area of research. Many approaches are based on the use of protein sequence information alone, on the basis that proteins with similar sequences possess similar functions. Other methods however make use of 3D structural information, given the higher degree of evolutionary conservation of protein structure when compared to sequence. Some of the early genome-scale annotation experiments helped drive the development of automated workflows that enabled the processing of thousands of protein sequences and the development of databases for depositing protein models for wider community access.[82–86] When a structure is available a more recent development has been to use this in conjunction with virtual screening, to identify potential ligands and substrates that may in turn suggest possible function. A nice example of this approach is described by the Enzyme Function Initiative,[87] a consortium that seeks to assign functions to enzymes from bacterial genomes using a combination of both experimental and computational methodologies (it should be noted that of the approximately 45,000 proteomes currently available more than 40,000 are bacterial in origin, with just under 1000 eukaryotes and just over 3000 viruses). In a specific example, a series of 3D protein models were constructed for an amidohydrolase from a newly sequenced bacterium (Agrobacterium radiobacter K84) and used in docking experiments against a library of more than 57,000 high energy intermediate forms of 6440 metabolites. The hit lists from the docking experiments were observed to contain multiple pterin-containing molecules. This provided the impetus for a series of experiments that confirmed this molecular class as deaminase substrates for this particular enzyme.[88]

3.07.3 How Are Protein Models Built?

To the non-expert, there is a bewildering range of software and algorithms for building protein models and an extensive and growing literature. Given the visibility and importance of the protein folding problem and the new opportunities afforded by the data explosion in biology it is also unsurprising that the field continues to be very active. Broadly speaking, the methods for building protein models fall into two categories. As we have already indicated, *comparative modeling* methods (also referred to as *homology modeling* methods) rely upon sequence analysis methods to detect at least one related (i.e., homologous) protein of known structure that provides a starting point (i.e., a *template*) for building a 3D model of the unknown protein. By contrast, the second category of methods (variously referred to as nontemplate, ab initio, or new fold methods) do not explicitly rely upon the known structure of a related protein but construct the model "from scratch."[89,90] As such, ab initio methods are in principle more generally applicable. However, the ab initio prediction of whole protein structures purely from first principles is an exceedingly challenging problem. The most physically realistic approach to this problem involves the use of computer simulation techniques (typically molecular dynamics simulations) to fold an extended polypeptide chain into the native protein conformation in an effort to replicate as closely as possible the "real" folding event. However, the enormous computational demands of these calculations, particularly if performed using a full atomic representation including solvent, has limited their current applicability to small proteins. Developments in computer hardware and more efficient simulation methods have in recent years enabled more systems to be studied with some promising results, though for practical purposes this approach is currently a largely academic pursuit.[91,92] One particular advantage of the explicit simulation approach is the detailed insights provided into the actual dynamics and mechanisms of protein folding; this can lead to some particularly fruitful synergies with relevant experimental methods. Given these computational challenges and in order to make the problem of ab initio protein folding more tractable, simpler representations of protein structure and energetics have also been developed. Lattice models are a good example of such simpler representations that have provided significant insights into the protein folding problem and have also inspired much method development.[93] Currently, some of the most successful and practical approaches to ab initio structure generation are based around the use of fragments taken from known protein structures. These fragments are then built up into the structure of the target protein, guided by an appropriate energy function.[94] Notwithstanding the many contributions that ab initio methods have made to the protein structure prediction field, from a practical and contemporary drug discovery perspective, such approaches are not generally applicable to a sufficiently wide range of proteins of pharmaceutical interest nor can they yet routinely provide structures of sufficient accuracy for most applications.

From the practical drug discovery perspective, that is the focus of this chapter, the models most likely to be of practical utility are still overwhelmingly built using comparative modeling. There are a number of reasons for this, as we have already alluded. The most

important reason is that, as we have seen, there are now many more protein folds available from experimental studies, making it much more likely that a reasonable template can be found from the Protein Data Bank. Second, drug discovery often focuses on families of related proteins. Familiar examples are kinases, G protein-coupled receptors, proteases, and more recently the various epigenetic proteins such as the bromodomains. The growth of knowledge on a particular family often has a leveraging or catalytic effect, by providing essential "know how" to facilitate subsequent experimental studies and also in providing the knowledge base so essential for computational approaches such as protein modeling. There has in particular been considerable excitement at recent progress determining structures of GPCRs and other integral membrane proteins, discussed elsewhere in this volume. Third, the development of enhanced methods and algorithms and more accessible user interfaces have driven many aspects of comparative modeling, as we will now discuss.

There are three general stages involved in building a comparative model. The first stage involves sequence and structural analysis to identify homologous proteins of known structure that will provide the 3D template(s) upon which the model of the target protein will be constructed. The output of this first step is an alignment of the target sequence to these known structure(s). It has been shown many times that getting this alignment correct is critical for building an accurate model. The second stage involves the actual construction and refinement of the model, based upon this alignment, to give a set of 3D coordinates for the target. The final stage is the validation and evaluation of the model including an assessment of which regions are likely to be predicted with higher confidence.

3.07.3.1 Sequence and Structural Analysis

Where there is detectable homology between two or more protein sequences it can be inferred that these sequences will share the same protein fold. The converse, however, is not true—proteins with the same fold do not always show detectable homology between their amino acid sequences. This then is the first, and often the most important, challenge in comparative modeling—how to unambiguously assign the sequence of the unknown target protein to a fold family. This in turn allows one or more template structures to be identified upon which the physical model can be built. Here, identifying the best alignment between the target protein and a template is key to constructing the most accurate comparative model possible. If the alignment is incorrect then the model will have significant local or global errors depending on the location and type of errors in the alignment. That said, it is important to understand that meaningful alignments in poorly conserved regions of sequences and structures may be difficult or impossible to achieve. In such circumstances, and if these regions are of interest, then it may be possible to generate multiple models for assessment against relevant experimental data where available. Unsurprisingly, it is generally the case that a comparative model-built on a closely related template structure is more likely to be more accurate (all things being equal) than one built on a remote homologue. This relationship between sequence and structural similarity is also shown by the experimental data; as the similarity between two sequences decreases the RMSD between their experimental structures tends to increase, as shown in Fig. 6.[17] More recent studies have probed further this relationship in the context of the type of protein structure and in particular its secondary structural elements.[95]

3.07.3.1.1 Fold identification: Identifying homologues of known structure

The simplest method for finding one or more potential structural homologues of the unknown target protein is to use its amino acid sequence as a query to search the amino acid sequences of known experimental structures from the Protein Data Bank (and

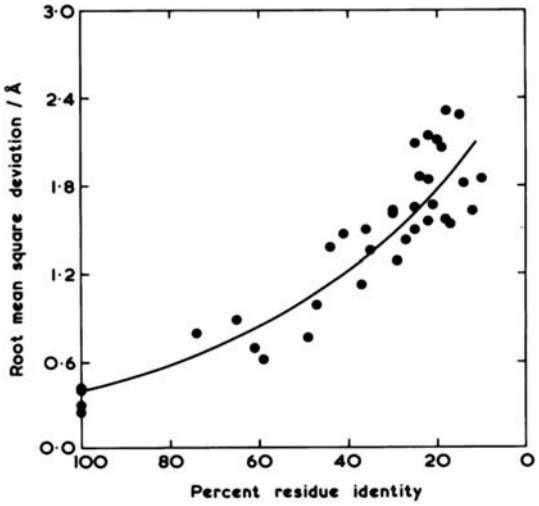

Fig. 6 Relationship between sequence similarity (given by the percentage sequence identity, see text for definition) and RMSD over C alpha atoms. From Chothia, C.; Lesk, A. M. The Relation Between the Divergence of Sequence and Structure in Proteins. EMBO J. **1986**, *5* (4), 823–826.

proprietary structures where available) using a *sequence to sequence matching algorithm*. These methods compare the query sequence of the target protein to each of the entries in a sequence database in order to identify the "best" matches, as determined by a scoring scheme. The score should allow a user to determine if the alignment is significant or not. The simplest and most easily understood metric used to report the degree of similarity between two aligned sequences is the *percentage sequence identity*. This gives the proportion of amino acids that are identical when the two sequences are matched. A simple example of two aligned sequences is shown in Fig. 7. This example also illustrates that to achieve the best alignment it is usually necessary for amino acids to be inserted or deleted in one or other sequence (often referred to as *gaps*).

Many computational algorithms have been devised to achieve the "best" alignment between two sequences. A detailed description of these methods is beyond our scope,[96] but there are some key features common to most of these procedures that it is useful to be aware of as they can impact and influence the results obtained. The comparison of two sequences is usually achieved using a matrix in which each element has a score for the similarity of the corresponding pair of amino acids, one from each sequence. Visual inspection of such a matrix reveals for two related sequences high-scoring diagonals which are the regions where the sequences are aligned. Breaks in the diagonals correspond to gaps where amino acids are inserted or deleted, as illustrated in Fig. 7.

The scores used for the amino acid pairs reflect the probability that one amino acid can be replaced by another. These propensities are typically represented as 20×20 substitution matrices, an example being shown in Fig. 7 for the widely used BLOSUM62 matrix.[97] The values in this matrix are determined from an analysis of alignments of conserved regions in known proteins, with a positive number in the substitution matrix meaning that there is a higher probability of that particular amino acid change occurring randomly and a negative number implying a lower probability. The substitution matrix, when combined with a *gap penalty* for insertions and deletions, enables different alignments to be scored in order to find the "best" match.

Some sequence matching methods guarantee to identify the optimal or best-scoring alignment, given a particular substitution matrix and gap penalty. The most common methods in this category use a technique called *dynamic programming*.[98,99] These are the methods of choice to derive the definitive alignment prior to the model building phase, but they are in general too slow for searching the very large sequence databases currently available. This led to the development of *heuristic methods* for sequence matching. These methods do not guarantee to find the globally optimal solution. However, in practice they rarely miss an important match and are sufficiently fast in execution to enable large database searching. The heuristic methods achieve their improvements in speed by identifying small high-scoring lengths of sequence matches which are then extended locally to generate a longer alignment. The best-known heuristic methods are BLAST[100] and FASTA[101,102]; the former in particular in its PSI-BLAST variant is probably the most widely used tool for searching sequence databases.

When the percent sequence identity is above 30–40%, the most commonly used sequence-to-sequence alignment algorithms are usually able to identify the most appropriate match or matches from the sequence database. More advanced metrics, such as E values that indicate the number of hits one would expect to see by chance when searching a database of a particular size, can in some cases help resolve the significance of matches below this threshold. Unfortunately, when the percent identity is low, the

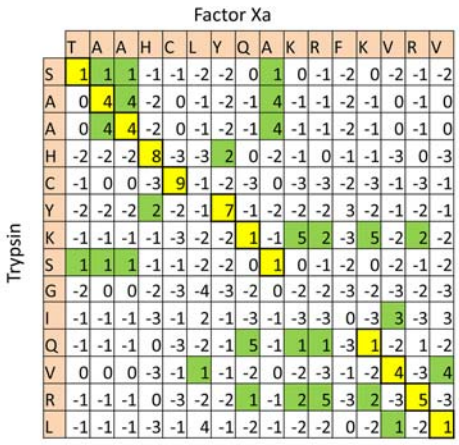

Fig. 7 Illustration of alignment algorithm operation using partial thrombin and trypsin sequences. A scoring matrix such as BLOSUM62 determines the score for each pair of amino acids. High-scoring diagonals (in *yellow*) indicate regions of aligned sequences. The alignment obtained from a sequence comparison is shown together with the corresponding alignment derived from overlaying the two structures in 3D space. As can be seen, there are some differences between the alignments obtained from the two methods, particularly in regions of insertion and deletion.

true hits may lie among other false positive matches and further work to confirm the significance of the match will be required. The phrase "twilight zone"[103] was introduced to refer to those situations where the percent sequence identity is less than around 30%, to indicate the challenges associated with identifying the correct fold (a sequence identity less than 10% is sometimes further described as the "midnight zone"). Alternative methodologies have been developed to address this sensitivity issue in order to identify positive matches, even at low levels of percentage sequence identity.

When comparing just two sequences it is possible that some misleading chance correspondence may occur. This can be in part addressed using a *multiple sequence alignment*, by enabling consensus features and trends to be detected with greater confidence across a whole family of related proteins. The most common way to construct a multiple alignment is by a *progressive alignment method*.[104,105] Here, the first step is a pairwise comparison of all of the sequences to be aligned. This enables a tree to be constructed that defines the relationships of the sequences to one another and can be used to iteratively construct the multiple alignment, starting with the most similar pair. Each step involves combining two sequences, a sequence to an alignment or two alignments, as illustrated in Fig. 8.

Accounting for the variation which occurs across the family provides a way to achieve greater search sensitivity during the fold recognition step. Position-specific scoring matrices (PSSMs)[106] and Hidden Markov Models (HMMs)[107–109] use *sequence profiles* that intrinsically capture the allowed amino acid variance at each position within the family and can be derived from a multiple sequence alignment. A target sequence can be searched against a database of precompiled profiles for known protein families, or conversely a profile can be used to search for new matching sequences. Where a sequence is used to search a database of profiles it may not be immediately clear whether a match to a profile includes a match to a known structure. However, databases such as PFAM[110] include links between profiles and structural information; it is then straightforward to determine if 3D structures are known for members of the family when a significant match is identified. The widely used PSI-BLAST method[111] uses an iterative approach involving multiple applications of the basic BLAST algorithm. The significant matches found at each iteration are used to calculate a position-sensitive score matrix for use in the next iteration, a process that continues until no new sequences are added.

Yet more sensitivity than the sequence-to-profile methods can be obtained by comparing profiles to profiles or HMMs to HMMs.[112,113] A profile or HMM is constructed for the target sequence by finding significant homologues, creating a multiple alignment and then deriving the profile from that alignment. This target profile is then searched against a database of profiles or HMMs as appropriate to determine significant matches. These methods further improve the detection of remote homologues.

The final fold identification method we will discuss is *threading*. Here, a target sequence is fitted to a library of protein folds. A key feature of threading is that 3D information is taken into account during the analysis. This comparison may be achieved by comparing the target sequence to a profile for each fold that includes information derived from the 3D nature of the fold such as secondary structure type and residue burial/exposure. Alternatively, the target sequence can be fitted (or threaded, hence the name) onto the 3D fold itself and an energy function used to score the fit of the sequence to the fold.[114] The fold or folds with the lowest energy value(s) then become potential candidates for that particular target sequence. Threading methods may be combined to obtain the best consensus result as used by the LOMETS methodology in the I-TASSER suite.[115]

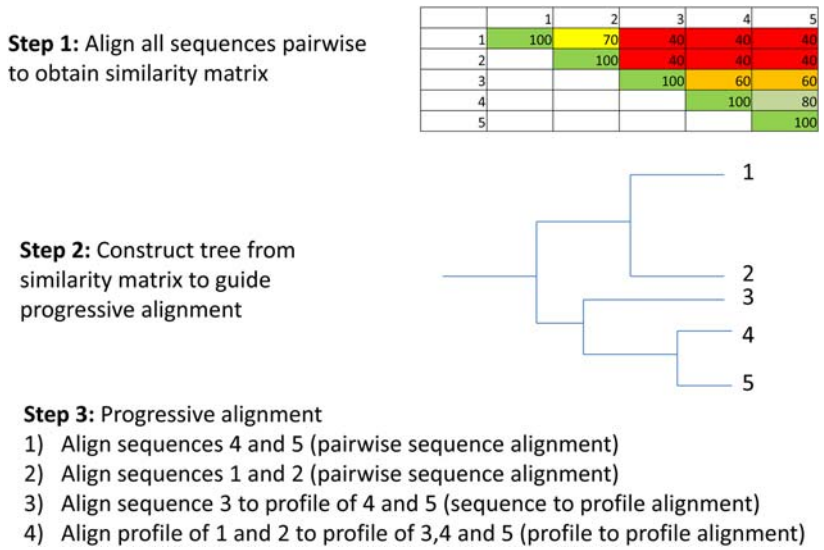

Fig. 8 Steps involved in creating a multiple sequence alignment using a progressive alignment method in which sequences are iteratively added to build upon the final result.

3.07.3.1.2 Generating the critical sequence-structure alignment

The methods used for fold identification will often provide the detailed set of amino acid matches between the target and any potential template(s). As we have indicated, alignments from sequence-to-profile and profile-to-profile searches in general would be expected to be better starting points than those from sequence-to-sequence searches since these also include information from the alignment of family members. It is always a good investment to construct a multiple alignment of the target and its significantly related sequences and the template(s) and its/their related sequences and structures. Many alignment programs are available, but for the purposes of comparative modeling and particularly for drug discovery applications the best tools are often those that allow manual editing of an alignment and visualization of structures in the alignment, or at the very least key structural features such as the location of secondary structural elements. Inspection of the alignment and known structures can uncover features which might indicate alterations in secondary structures such as a local disruption to a helix which may not be present in the potential template structures. Where there is a choice of template structures such visualization capabilities may suggest that one template is a better choice than another even if the homology appears lower.

The finished alignment will generally show two types of regions (Fig. 9). The first of these are blocks of the alignment where there are no insertions and deletions, relatively high conservation between all the sequences and structures used in the alignment and where the local RMSD between the overlaid template structures is low. These are the *structurally conserved regions* (SCRs) that lie at the heart of the comparative model. The SCRs taken from the template structure(s) provide the starting point for modeling the target. By contrast, the second type of region is characterized by insertions or deletions between sequences and/or where the overlaid structures show a high local RMSD. These regions are frequently referred to as *loops* or *structurally variable regions* (SVRs). As we will discuss in the next section, loops are often treated differently during the actual model building process.

3.07.3.2 Building and Refining the Model

The earliest published methods for constructing 3D comparative models broke the problem down into the following distinct steps: (1) construction of the backbone for the core conserved regions, (2) loop modeling, (3) adding side chains, and (4) refinement. This sequential workflow is still commonly encountered; it also provides opportunities for the user to intervene at each point in order to adjust the evolving model if appropriate. Indeed, many of the most widely used software packages provide the user with significant

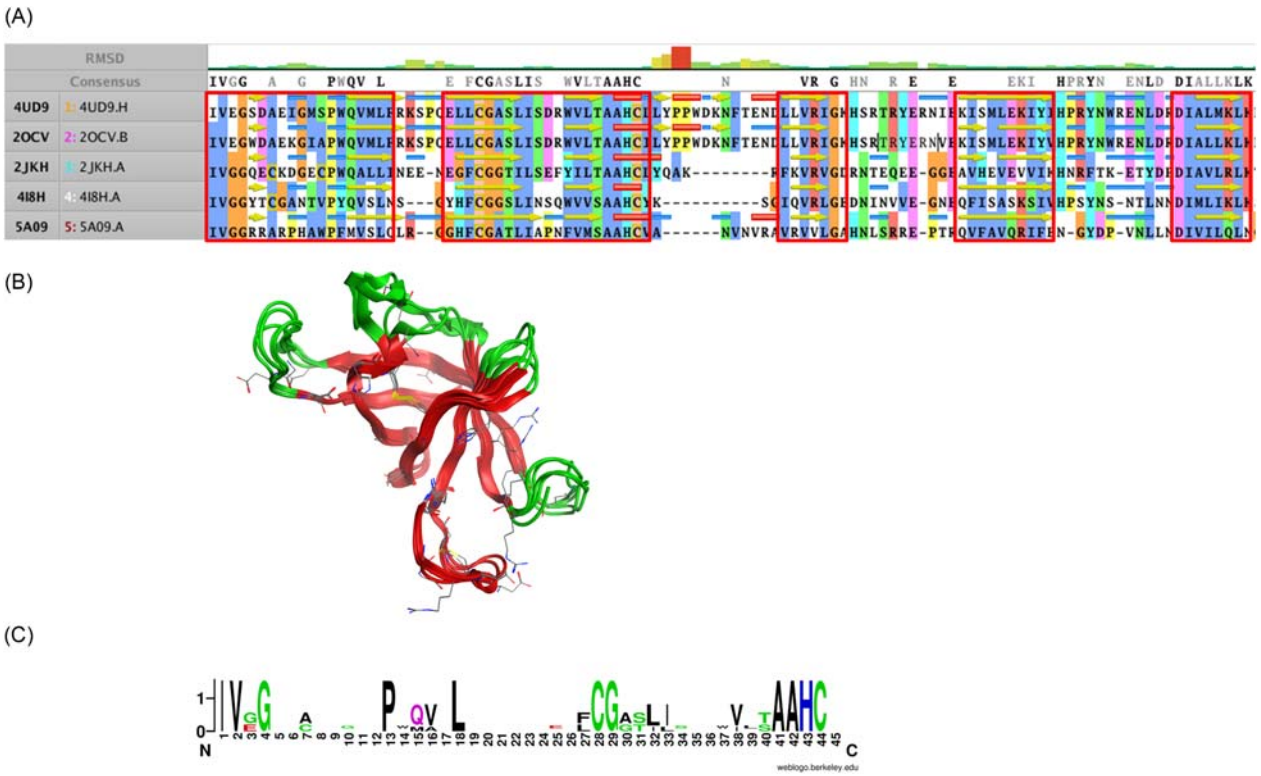

Fig. 9 (A) Section of an alignment of human thrombin (PDB code 4UD9), mouse thrombin (2OCV), Factor Xa (2JKH), bovine trypsin (4I8H), and human neutrophil elastase (5A09) with conserved blocks (*red boxes*) and variable regions (*no box*). Figure created using MOE.[116] (B) set of partial structures with SCRs (*red ribbon*) and loops (*green ribbon*) marked. (C) Weblogo[117] representation of part of the alignment which highlights regions of the sequence where there is absolute conservation, conservative substitution, and no conservation. This type of representation can be thought of as a form of visual profile for the alignment.

flexibility, for example providing direct programmatic access to specific components such as loop modeling or to enable bespoke workflows to be constructed for specific problems. In practice, many drug discovery applications of protein modeling employ a mix of automated, semiautomated, and hands-on modeling techniques, though the development of automated web servers and workflows that can take a protein sequence and produce a 3D model have provided access to a much larger user base. First we will outline the three types of methods used to construct the conserved regions and then discuss loop modeling, side chain addition, and model refinement.

3.07.3.2.1 Model building directly from template structures

One of the very earliest examples of comparative modeling serves to illustrate the basic principles involved when building models directly from the template structures. In 1981 Greer published a sequence and structure analysis of the mammalian serine proteases,[118] at a time when just three structures had been determined experimentally (those of chymotrypsin, trypsin, and elastase). This analysis then formed the basis for a model of the blood clotting protein factor Xa.[119] First, the three experimental structures were superimposed in 3D space. This enabled those regions where there was clear structural conservation to be determined based on the RMSD of Cα atoms in the superposed structures. The location of these conserved structural regions was then mapped onto the corresponding multiple sequence alignment. An additional eight mammalian serine proteases, whose structures were then not available, were then incorporated into the sequence alignment as a means of obtaining the best alignment between factor Xa and the known structures. As discussed earlier the complete alignment allowed the regions corresponding to the SCRs to be identified. The model of factor Xa was constructed by first assigning coordinates for the backbone atoms in the SCRs, taken in this case from the corresponding atoms in the elastase structure. Coordinates for the amino acid side chains in these conserved regions were also assigned where a match could be found from one of the known experimental structures. The variable regions were constructed by identifying which of the experimentally determined structures had a sequence of the same length and transferring those coordinates. This enabled 9 out of 12 variable regions to be constructed. The remaining three variable regions were not included in the reported model; as these loops were distant from the active site it was not considered essential for them to be physically constructed.

While such a model building exercise might be considered trivial today (and in contrast to the largely hands-on approach used by Greer would likely be performed using much more automated tools) nevertheless this early study captures many of the key components of comparative modeling. In particular, the importance of getting the alignment as accurate as possible, of building first those parts of the model where one has the greatest confidence and then continuing to those parts that are less well defined and being mindful of the question(s) the model will be used to answer. Note also the use of multiple experimental structures to build the model of the unknown target protein, with different parts of the model being derived from different experimental structures according to their similarity. There are now many experimental structures of factor Xa and the other mammalian serine proteases that confirm the high degree of structural similarity between the members of this family. Nevertheless, even today there are some protein families of intense biological and pharmacological interest where our structural knowledge does not necessarily extend to every family member. The protein kinases are generally accepted to fall into this category; these also present some additional modeling challenges due to the conformational changes that accompany phosphorylation/dephosphorylation of the activation loop. One example that illustrates the utility of even a straightforward modeling study is provided by Nichols et al.[120] who constructed a model of the LRRK2 kinase domain as part of a wider series of investigations into this Parkinson's disease-related protein. In this case the LRRK2 homology model was built using a single homologous protein kinase, ROCK1. This protein was chosen as the template due to the similar activity profiles of some inhibitors against both ROCK1 and LRRK2. This example also nicely illustrates that the template should be selected bearing in mind how the model will be used. In this case the focus was on ligand binding and design, and so a protein that also binds the same series of ligands is a good choice, even if there were other proteins that might have a higher overall degree of sequence identity. A comparison of key active site residues not only for the LRRK2 and ROCK1 wild-type proteins but also for LRRK2 mutants and other kinases such as protein kinase A provided further confidence in the model when assessed against compound SARs.

3.07.3.2.2 Segment matching

The very earliest protein structures revealed that a significant proportion of the overall conformation was constructed from common 3D structural features such as the well-known elements of secondary structure as well as features such as β-turn motifs. It was subsequently discovered, initially by Jones and Thirup,[121] that there were many more examples of common local structure beyond these established structural elements. This observation was put to practical use in their program Frodo, at the time widely used by protein crystallographers for building 3D models into electron density maps. The program would search a database of peptide fragments (typically containing 5–7 amino acids) that had been extracted from known protein structures, in order to find the best match for a particular stretch of electron density. This work not only had immediate practical application in protein crystallography but also acted as a catalyst for the development of some of the most successful methodologies in protein modeling.

Most practical implementations of segment matching define a set of non-redundant fragment structures extracted from an analysis over the whole PDB, with an emphasis on fragments from structures of the highest resolution. The use of a non-redundant set minimizes the numbers of fragments that need to be stored and searched while still ensuring appropriate coverage of the conformational space. One of the earliest of the segment matching algorithms was the work of Levitt[122] who developed a program based on this approach that automatically constructs a detailed 3D protein model by combining such fragments (also known as segments, hence the name) onto an initial alpha carbon backbone structure derived for example from the structure of a template protein. The

use of such fragments is also central to the widely used Rosetta suite[123–125] that has found particular application in ab initio structure prediction where fragments are built up from scratch. The group subsequently introduced the RosettaCM algorithm[126] (CM stands for comparative modeling) which aims to combine the advantages of the template-based approach with the complementary benefits of the fragment and torsional modification algorithms in Rosetta. The latter provide a way to deal with unknown parts of the structure and to explore conformational space. Such an approach is a good illustration of how current methodologies will often seek to combine a variety of different approaches in order to benefit from the advantages of each, a strategy that at least in the case of RosettaCM delivered more accurate models than alternative approaches.

3.07.3.2.3 Modeling using spatial restraints

The basis of the spatial restraint method is that a protein's 3D structure can be determined by first defining and then satisfying a set of geometric conditions. The MODELLER program is the best-known example of this approach.[127–129] In MODELLER the restraints are expressed as *probability density functions* (pdfs). The pdfs provide a general way to capture the preferred distributions of various types of geometric features in proteins. Some of these features such as bond lengths and bond angles are straightforward and can be taken from tables of standard geometries. Other features are derived by analyzing known protein structures[130] and in particular by examining specific information in the template proteins. For example, the distances between alpha carbon atoms in pairs of residues along the sequence can provide long-range information that is characteristic of the overall fold. The nature of the pdf specifies how closely a particular distance in the target protein structure needs to match the corresponding (known) distance in the template. In turn this depends on a number of parameters, derived from an analysis of known protein structures. For example, it is observed that the distances between corresponding pairs of amino acids in highly homologous structures tend to be close when their sequences are very similar and the amino acids are buried in the core of the protein. By contrast, if the sequences have a lower percent identity and/or the amino acids are solvent exposed then the corresponding distances are observed to deviate more. These two situations would be represented by the Gaussian probability distribution functions shown in Fig. 10; the more sharply peaked pdf means that the particular distance in the calculated model should be very close to the corresponding value in the template whereas the broader pdf will permit more latitude in the range of distances. For a typical protein, many thousands of such restraints can be defined. Starting from an initial arbitrary 3D conformation of the protein an optimization procedure is then used to derive a 3D structure that best satisfies the combined restraints. By providing the optimization process with different starting conformations (derived for example by adding a random amount to the initial coordinates derived from the template(s) structure(s)) it is possible to derive a number of solutions, from which the best may be selected for visual inspection or further refinement. The methodology is very general and can be used to model complete or partial protein structures and is also able to incorporate many types of experimental data, where these are also converted into appropriate pdf.

3.07.3.3 Loop Modeling

Loops can be important for determining a protein's specificity and function and in differentiating between the various members of a particular fold family. A good example is provided by the so-called ECL2 (extra-cellular loop 2) that links helices 4 and 5 in G protein-coupled receptors.[131] This loop has historically presented a particular challenge for protein modeling due (A) to its role in binding site formation as it often folds deep into the *trans*-membrane core (Fig. 11) and (B) the wide variability in both length and sequence composition. In other systems, loops might be considered less important from a modeling perspective. For example, the loop may be far from the active site or not relevant to the question being asked of the model. Further, some loops are clearly very dynamic with no real structure. In such cases there may be little value in expending a lot of time and energy trying to define an accurate conformation of the loop.

Where there is a high degree of overall sequence identity between the target protein and others from the fold family it may be possible to extract a viable conformation of the loop directly from a known structural homologue. As we have seen, this was the case

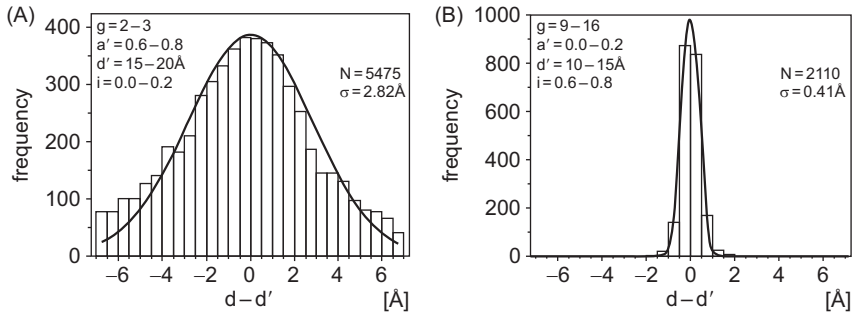

Fig. 10 Showing probability density functions (pdfs) for Cα-Cα distances. (A) The pdf where the residues have high solvent accessibility and there is overall low sequence identity shows a broad distribution of permitted distances. (B) The pdf for buried residues with high sequence identity is much more sharply peaked. From Sali, A.; Blundell, T.L. Comparative Protein Modelling by Satisfaction of Spatial Restraints. J. Mol. Biol. **1993**, *234* (3), 779–815.

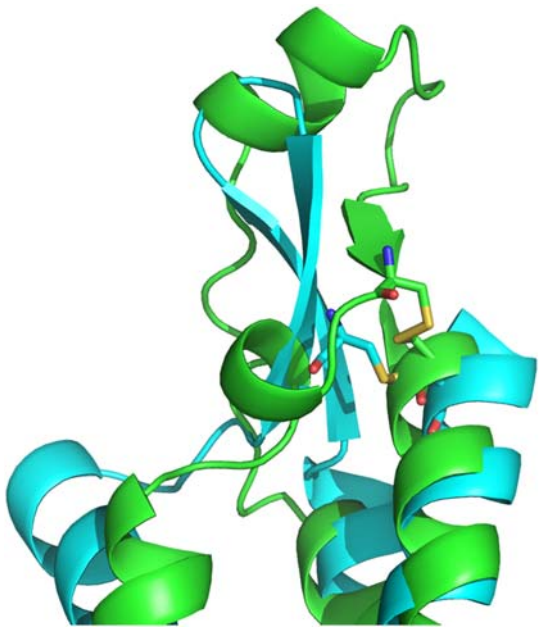

Fig. 11 Showing the different conformations for the ECL2 loop in the mu opioid receptor (PDB code 5CIM, *cyan*) and the adenosine A2A receptor (2YDV, *green*). ECL2 adopts a beta hairpin-like structure in the mu receptor; in the A2A receptor the loop contains alpha helices but is overall less structured. Protein structure images created using the PyMOL Molecular graphics system, Version 1.7.6.6 Schrodinger LLC.

for the early modeling studies on the mammalian serine proteases. However, the addition or deletion of just one amino acid can have a significant impact on the overall conformation of a loop. Moreover, stretches of amino acids can adopt different conformations in different proteins.[132] These features can make loop modeling a challenging problem and there has been a significant effort on the development of relevant techniques.

An obvious practical factor to consider when modeling loops is that they are constrained in space, not only because they need to fit with the leading and following SCRs of the model but also because they need to fit within the bulk of the remainder of the protein. Two general approaches to loop modeling have been developed by the protein modeling community. The first makes use of a database of loop conformations, extracted from known protein structures. For a given loop the database is searched to identify potential conformations of the required sequence length, where there is a geometric match to the ends of the leading and trailing conserved regions and reasonable steric complementarity with the rest of the model. Depending on the number of potential matches the putative loop conformations may be assessed according to these criteria together with others such as the degree of sequence homology or positions of residues such as proline or glycine that have particular influences on backbone conformation. If there are many possibilities for the loop conformation it may be productive to cluster the options into structural families. The highest ranked suggestions are then subjected to further refinement to optimize their conformation. The database approach can work very well where the loop would be expected to adopt a common and well-defined conformation such as a beta turn, for which there are many examples in the PDB. The approach works less well as the size of the loop grows and for which there are fewer examples in known structures.

The alternative to the database approach is to generate conformation(s) of the loop ab initio. The loop modeling problem then reduces to a constrained conformational search of the relevant polypeptide sequence, with the goal being to find one or more low-energy conformations that also satisfy the geometric and spatial requirements imposed by the ends of the conserved regions and the rest of the protein. Just as there are many algorithms for small molecule conformational analysis, so there are many methods in the literature for the ab initio prediction of loop structures. These methods can be characterized by the algorithm used to search the conformational space (examples include systematic and random search approaches, molecular dynamics, and using known torsion distributions from crystal structures) and the method used to characterize the energy of each conformation. The earliest attempts to tackle this problem were limited in particular by the then available computational performance; as computational power has increased it has been possible to introduce more refined conformational search protocols (e.g., that use a finer search grid for a systematic search or more iterations when using a random search or Monte Carlo method) and more complex and detailed energy assessment and optimization schemes. By way of illustration of a contemporary approach, the loop modeling method of Jacobson and colleagues[133] combines a number of such ideas. It first generates a set of initial structures using a hierarchical method for efficiently building up loops in torsion angle space. These initial structures are then clustered to remove duplicates and to select the best candidates for progression. Side chains are added and then each is energy minimized using an energy function with the important inclusion of a solvation contribution.

One final cautionary point applies to those algorithms that add loops one by one to an evolving model. In this case there may be an order dependence in the final results. Thus, the first loop to be added is not influenced by those yet to be built but as more and more loops are added the constraints on those that are unbuilt may increase and consign the last loops to be added to regions of space that they may not naturally explore.

Antibody proteins are a good example where loop modeling plays a particularly crucial role. The familiar "Y" structure of an antibody comprises two Fab antigen-binding regions and the tail Fc region. Each Fab fragment in turn consists of a core region onto which are grafted six so-called Complementarity Determining Regions(CDRs). A large number of Fab fragment structures are known. The SAbDab database[134] has 2553 antibody entries as of November 2016. This means that a suitable structural framework for the core region of a Fab fragment is likely to be available; it is important to carefully choose a pairing of the constituent light and heavy domains in the correct orientation since the antigen-binding site is formed at the interface of these two regions.[135,136] Antibody CDRs also represent a special case for loop modeling. Chothia and Lesk observed[137] that five of the six CDRs in a Fab fragment had a small repertoire of structures dictated by length and the presence of key amino acids, a finding further investigated by others.[138] The exception is CDR H3. These observations simplify the problem of building models for antibodies; from the antibody sequence it is possible to predict which of the canonical forms of five of the CDRs will be present and so select a template structure for the loop appropriately. The main challenge in modeling antibodies is then to obtain a good model for CDR H3 which is important as this loop is often involved in binding interactions with the antigen. Many homology modeling programs have separate antibody modeling modules and in recent years the antibody modeling assessment (AMA) competition has assessed the performance of programs in this particular branch of homology modeling.[139]

3.07.3.4 Side Chain Assignment

The assignment of side chain conformations is a common requirement in many protein modeling methods. Even when there is a high degree of sequence identity between the target protein and its structural homologue(s), there will invariably be some positions where the amino acids differ and so minimally these will need to be assigned.

When the conformations of amino acid side chains in experimentally determined structures are analyzed it is observed that they tend to adopt distinct families of conformations, often referred to as *rotamers*.[140] This observation is often exploited in the methods used to assign side chain conformations for protein modeling, by limiting the conformations permitted to a given side chain to those from a predefined rotamer library. It has further been shown that side chain conformations can also be dependent upon the local backbone structure, an observation exploited in backbone-dependent rotamer libraries[141,142] which further limits the available options for a given side chain.

In the most straightforward cases where there is a high degree of sequence identity between the target protein and one or more known experimental structures it may be possible to assign many of the side chains directly from the structure of the homologous protein(s) or from a rotamer library. Indeed, a number of homology modeling tools assume that where a residue is identical between target and template, the rotameric state will also be identical. More generally, it will be necessary to take account of potential interactions between the side chains, as the conformation adopted by one side chain will influence and impact on the conformational space available to its neighbors. The requirement then is to search the space of potential side chain conformations in order to identify the "optimal" combination of side chains, often determined using an energy function. This is a challenging combinatorial search problem where the total number of potential solutions can be very large. Even for a small loop with a few amino acids there may be tens of thousands of potential combinations; for a whole protein the number can become astronomically large. Nevertheless, methods have been developed that can efficiently explore this space to identify optimal or near-optimal combinations of side chain conformations. One popular approach is to initially assign each of the side chains to a randomly selected rotamer from the library. The side chains are then taken in turn and its rotamers are explored to find the optimal conformation as assessed by the energy function, while keeping all other side chains fixed. This process is applied iteratively until no further changes in side chain conformation occur. Other methods aim to identify the globally optimal solution through the use of specialist graph searching methods. The widely used SCWRL series of programs[143,144] incorporate many features designed to make the calculation run as quickly as possible without sacrificing accuracy, including a highly refined backbone-dependent rotamer library, methods to quickly and efficiently determine whether the side chains of two amino acids are potential interaction partners, a bespoke energy function comprising attractive and repulsive nonbonded terms, and a hydrogen bonding term.

3.07.3.5 Structure Refinement Methods in Protein Modeling

The nature of the algorithms used by many protein modeling approaches means that the initial 3D model will often not be perfect. For example, there may be deviations from the preferred values of bond lengths and angles where a loop has been inserted into an existing template. There may be pairs of atoms closer than the preferred nonbonded distances due to the use of a side chain rotamer library. A simple goal of structure refinement is to "clean up" the initial structure to remove such deviations. A more general objective of the structure refinement step is to generate a final structure that better reflects the balance of interactions in the target sequence, when compared for example to the template structure(s) from which it was built. Structure refinement methods are often performed as the final step in building the model, but in some cases they may be incorporated iteratively into the actual model building process or applied to specific parts of the model such as the loops.

The simplest approach to structure refinement uses energy minimization with a standard protein molecular mechanics force field to drive the conformation to the nearest local energy minimum.[145] This approach is very accessible, being an integral part of most modeling packages with several widely used force fields that are tailored for protein applications. Another popular approach is to use molecular dynamics simulations.[146,147] These enable the structure to explore the conformational space more thoroughly in the vicinity of the initial model. Snapshots may be taken from along the molecular dynamics trajectory for subsequent energy minimization. The temperature of the simulation may be gradually decreased to give a *simulated annealing protocol*; the initial high temperature enables higher-energy barriers and a broader search of conformational space to be performed with a more localized search at lower temperatures.

When structure refinement methods were first incorporated into model building protocols it was often found that the "refined" model was further away from the experimentally determined structure than the initial unrefined structure. Put another way, the energy functions were unable to discriminate native from non-native conformations. Various strategies have been developed to try and address these shortcomings. These include the incorporation of additional terms into standard force fields (such as terms that better represent solvation effects) or to use additional terms that restrain the more highly conserved parts of a model close to their starting locations.

An alternative to using a traditional molecular mechanics force field in protein modeling calculations is to use a *statistical potential* (also known as knowledge-based potentials of mean force) as the energy function. Here, the various contributions are derived from an analysis of experimental structures.[148,149] The basic idea is that features such as torsion angle distributions, levels of solvent exposure, and (particularly) the pairwise distances between amino acids or their constituent atoms all contribute to the overall free energy of a given protein structure, and that the quantitative contribution from each of these features can be determined from an analysis of known experimental protein structures. There are many different functional forms and derivations for protein statistical potentials; to illustrate the concept we will outline the "low-resolution" energy function from the Rosetta suite.[124,150] Here, amino acid side chains are represented as single particles, located at the side chain center of mass. Contributions are included to represent solvation, electrostatics, hydrogen bonding, and steric clashes. As noted, the parameters for each of these terms are derived from a statistical analysis of protein structures in the PDB. For example, the electrostatic contribution due to a particular pair of amino acid residues corresponds to the probability that the centroids of those amino acids are observed at the specific distance separation in experimental structures. The function is designed to provide a smooth energy surface to enable larger-scale exploration of conformational space. As a consequence, structures close to the true global energy minimum have a low calculated energy even if they contain local defects that with a regular force field would result in a high energy. In addition, the smaller number of interaction centers enables the calculations to be performed much more rapidly and a more efficient search of conformational space. Rosetta also includes a complementary high-resolution energy function; this is designed for use in more detailed modeling and uses an all-atom representation of the protein. Not only is the functional form of the high-resolution energy function more akin to a traditional force field, but also some of the parameters are so derived, together with terms obtained from structural analysis. As the energy functions have improved, attention has focused on how thoroughly the conformational space is being explored; the Rosetta group for example have used their comprehensive Monte Carlo search methods to tackle the problem of crystal-structure refinement.[151,152]

3.07.3.6 Model Validation and Sources of Error

Errors can arise at the different stages involved in building a protein model. The purpose of *model validation* is to help identify potential errors and thereby provide information about which parts of a model are likely to be reliable and which parts should be treated with a degree of caution. This can be very important in guiding any subsequent design work or predictions that may be based on the model. Some of the more common sources of error are:

Alignment errors, which may be local (i.e., may only affect a small number of residues) or global. These errors will result in residues being incorrectly located in the model. Some of these may be straightforward to identify if they result in residues being in the wrong environment. Small local errors may be ignored if they are in parts of the model remote from the region of interest. Global errors however cannot be ignored as they render the entire model uninterpretable.

Errors building the conserved regions may arise for example due to poor fitting of peptide fragments to the template. This may disrupt favorable interactions between sections of the core. For example, if two adjacent beta strands are misplaced relative to each another then the hydrogen bonds formed between them may be lost. This type of error is particularly likely to occur where fragments from different family members are used to build a single model.

Many protein modeling methods require different fragments to be joined together in order to create a single polypeptide chain and this can give rise to *fragment joining errors*. A common consequence of such errors is the creation of high-energy hotspots in the model which can be problematic for some refinement approaches unless care is taken to ensure that the structure does not "blow up" due to the large initial force from the hotspot region(s).

The use of fixed-conformation rotamer libraries for side chains can lead to *sub-optimal side chain packing*. This also can lead to energy hotspots. It may be possible to relieve these problems by rebuilding some of the side chains or using an appropriate refinement protocol. However, where an error in the backbone conformation also contributes to poor side chain packing, larger-scale revisions may be required.

There are broadly three types of validation checks that can be performed on the protein model. First, does the geometry of the model conform to the norms for experimentally determined protein structures? Second, do the amino acids occupy an appropriate environment? Third, is the model consistent with the experimental information known about the target or its close homologues?

For the first two categories software tools are widely available[153–156] and should be applied as a matter of routine. A growing number of web servers are also available to validate models.[157–159]

The simplest validation checks compare geometrical features such as bond lengths, angles, dihedrals in the modeled protein structure with the corresponding distributions of values obtained from analyses of non-redundant high-resolution X-ray structures. Many programs also look for significant steric clashes. In practice, small local deviations from normal may be acceptable. A *Ramachandran plot* can be used to assess the overall quality of the fold of a protein. This plot reveals whether the conformations of the constituent amino acids lie in allowed regions of conformational space or not. Large numbers of residues outside allowed regions are indicative of problems in the fold of the model.

An *environment check* on a protein structure evaluates the fitness and compatibility of each residue in the structure to the environment in which it is found. A straightforward way of checking this is to examine the solvent accessible surface area of each residue in the model. Most of the hydrophobic residues in a protein structure are expected to be buried with a low solvent accessible area ($< 10\%$). Hydrophilic residues will typically be exposed or, if buried, will be involved in hydrogen bonds or salt bridges. These characteristics are the norm for most globular, non-membrane-associated proteins. If a model contains significant numbers of amino acid residues in an unexpected environment then this may indicate a misalignment between target and template sequences or poor choices of loop structures. One caveat to bear in mind when modeling a single domain is that if this is normally part of a multidomain protein, then hydrophobic residues may be exposed that would normally be buried in the full length protein due to domain–domain packing.

If a model passes the first two checks then further validation, including against experimental criteria and other features related to the protein's biological function, can be undertaken. Here, there are many possible options depending on the amount of information available and the system being studied. For example, where the protein contains a metal binding site or a catalytic core then are the key residues correctly positioned? Where a disulfide bond is known to form, are the relevant cysteine residues appropriately oriented? Are the locations and orientations of residues consistent with available data on protein mutants? Is the model consistent with known ligand SAR?

Validation checks can help to identify potential issues with a protein model. It is nevertheless possible for a model to appear perfectly acceptable and yet to have major flaws. This is because many validation procedures test only for local factors and may not, for example, reveal a more fundamental problem such as selecting the wrong fold.

3.07.3.7 Evaluating Protein Model Building Methods: The CASP Experiments

The protein modeling community has been a pioneer in the concept of "blinded" challenges. The basic idea is very simple: structural biology laboratories make available to the wider community sequence information on proteins that are in the process of being solved; modeling groups generate 3D structural prediction(s) for these sequences; the experimental structure is published and compared to the predictions; a scientific conference is organized where the community comes together to discuss the outcomes and to assess progress; the detailed results and conclusions are published in the literature. The CASP (Critical Assessment of protein Structure Prediction) series of experiments was launched in 1994[160–162] and has been organized every 2 years since. In recognition of the diverse and evolving nature of the protein structure prediction field, different types of problems are typically defined for each round. For example, the very first CASP was subdivided into three categories: comparative modeling, fold recognition by threading, and ab initio structure prediction. These categories represented the status of protein structural biology and the protein modeling community at the time (threading was a "hot topic" in the early 1990s). The 11th CASP in 2014 had nine categories including template-based and template-free modeling approaches, the evaluation of refinement protocols, the inclusion of limited experimental information on long-range contacts, and methods to evaluate how factors other than alignment correctness impact on model accuracy.

3.07.4 Current Status of the Protein Modeling Field and Future Directions

A casual perusal of the literature might suggest that the protein modeling methods most frequently used in practical drug discovery have changed relatively little over the past 10–20 years. Many of the key methodologies and software in use today were first described in the 1990s or even in the late 1980s. For small molecule drug discovery applications the emphasis remains on comparative modeling, where the core algorithms and workflows are well understood and robust software packages have been developed and subsequently refined over many years. Critical to success continues to be the availability of a suitable template (or templates) from a known experimental structure, assigning the correct fold to the target sequence and then getting the best detailed sequence alignment. In this regard, the amounts of data now available, of course, have made a significant impact on the field.

That the key methods are now reasonably mature does not mean that the field is stagnant or irrelevant. The biannual CASP experiments, mentioned earlier, provide the community with a regular opportunity to come together and assess the current state of the art in a scientifically rigorous and challenging yet supportive environment where established groups and newcomers are all able to participate on an equal footing. The summary reports of the various CASP meetings over the years provide an excellent overview of how the field has evolved to reflect the changing nature of the science and the wider environment. A good example is the contrast between the emphasis on ab initio folding methods in the first CASP competition, where the number of experimental structures and folds was very limited, to the current situation where the number of experimentally determined folds has increased dramatically,

making comparative modeling a much more viable prospect than was the case previously. These changes have been reflected in the areas of focus for CASP, a good example being the assessment of methods for the refinement of initial models, once it had been established that the commonly used approaches at the time were not providing the desired results. At the same time, it is perhaps inevitable that as a field evolves and matures, so the focus tends toward more detailed and specific aspects of the subject where the emphasis is on "marginal gains" that may be of interest primarily to experts in the field.

There is now much wider access to software for protein modeling, with a variety of options available. Commercial software packages provide a reliable way to access established protein modeling methods and workflows, albeit at a cost (though it should be noted that the methods are often available at no or minimal cost to academic users). Another major feature of the protein modeling field is the creation and availability of web servers that provide facile access to good-quality and validated methodologies for building basic models.[163–165] Indeed, the protein modeling community has been a pioneer in the provision of free-to-access web servers. The advantages of such websites are clear: they alleviate the need to install and maintain often complex software on a local computer system, will often provide a good-quality result without the need for access to a local human expert, and are continually refined and upgraded through the active efforts of the host group. Many web servers also provide access to more than one approach for some of the key steps (for example, sequence alignment); this then permits the use of so-called consensus approaches where greater weight can be placed on a result that is obtained from several different approaches when compared to what may be an outlier from just a single method. The I-TASSER server[166,167] has been a consistent high performer in the "server" section in recent CASP rounds and provides a good illustration of the capabilities that can now be provided to a wide audience. As indicated earlier, I-TASSER uses threading algorithms to identify likely folds and potential templates. Continuous stretches of polypeptide chain are then excised from relevant template structures, with unaligned parts of the target protein such as loops being built initially using a 3D lattice-based method that enables an efficient search of conformational space. Subsequent steps gradually refine the putative models so produced, ultimately giving a small number of low-energy models at atomic resolution.

Of course such web servers also have drawbacks: there may be relatively little flexibility over the methodologies and workflows used, and they may not be considered appropriate for confidential work. Nevertheless, they provide a very useful service and will often enable a good-quality initial model to be generated for minimal cost, a model that of course can then be further refined and modified within the context of a medicinal chemistry program, for example.

As with so many other areas of the biological and biomedical sciences the impact of gene sequencing is being felt in protein modeling, not only in providing the challenge of functional annotation but also in catalyzing new methodology developments. One example of this is the development of *evolutionary co-variance methods*.[168,169] The basic principle here is that whenever there is a change in an amino acid at a particular location this will often be accompanied by a complementary change in a neighboring residue in order to maintain the overall 3D structure of a protein (and thus function). Given a sufficiently large set of aligned sequences and appropriate statistical analysis methods it is possible to identify pairs of residues that are predicted to be close in 3D space. This information constitutes a set of constraints that can be used with appropriate conformational search and optimization methods to derive a predicted 3D structure. It is noteworthy that this approach does not make use of any known structures or structural motifs. Encouraging initial results have been obtained with the method alone, generating structures with RMSD errors over the alpha carbons between 2.7 and 4.8 Å relative to the observed structure, over at least two-thirds of the protein. As we have discussed, this level of accuracy may not be sufficient for detailed ligand design applications, but it certainly demonstrates the potential for the approach, particularly if combined with other methodologies.

There are excellent opportunities for continued if not enhanced synergy between experimental techniques that provide information on protein structure and the complementary modeling techniques. The "gold standard" technique of X-ray crystallography looks set for continued evolution with the development of techniques such as the free-electron laser together with progress against more challenging targets such as membrane-bound proteins. Experimental techniques such as cryo-EM and hydrogen-deuterium exchange have experienced significant technology advances in recent years and offer real opportunities for even greater synergy with protein modeling. Cryo-EM in particular is widely considered to offer the greatest opportunities to deliver high-resolution structural data, enabling not only targets that have proved challenging for traditional crystallographic approaches but also insights into higher-order, multidomain structure. Exciting though the highest resolution cryo-EM structures will continue to be, the opportunities for even closer interaction between experiment and theory are perhaps greatest at lower resolutions, where the inclusion of information from experiment may lead to a significant improvement in the accuracy of the predictions, and so make them of practical value in a wider range of drug discovery applications. Moreover, different experimental techniques often provide complementary information; the integration of data from different experiments can in favorable cases be expected to further drive overall performance. In addition to experimental approaches that provide information directly related to protein structure, other types of data can also be valuable when building and validating a model. In particular, the ever-growing volume of small molecule SAR data via resources such as ChEMBL represents a valuable resource for the protein modeling community. Such SAR data can be used for model validation and in some cases more directly as part of the model building processes to guide the search toward models consistent with the binding data.

The synergy between experiment and theory extends far beyond the goal of building and validating protein models. There is a distinct trend toward collaborations that not only enable prospective evaluation and validation of model-building approaches but also represent wholly new areas of scientific investigation in which computational science plays a critical and integral part. The burgeoning area of synthetic biology provides some excellent illustrations of how experiment guided by theory can provide new insights into the design of new proteins.[170,171] The use of structural data in the design of protein therapeutics has the potential to transform this critically important area for tackling unmet medical need. Protein modeling has also been at the forefront of new

computational paradigms, such as the web servers for automated model building and the use of large-scale distributed computing such as folding@home.[172] This latter application uses "spare compute cycles" donated by members of the public to help understand protein folding and misfolding. The Foldit challenge[173,174] recasts the protein folding problem as a computer game, accessible to non-experts, that attracted thousands of users and generated results that in some cases outperformed the best computer algorithms.

The central role of proteins in biology is so dependent upon their 3D structures that we can anticipate continued strong interest in methods for structural biology and protein modeling. The field has benefitted from the development of algorithms and tools that are now quite mature, with understood strengths and limitations. From a practical drug discovery perspective there are well-established workflows and methodologies that when used with care can deliver models that can be of significant value in driving projects forward. It is always important to bear in mind the problem(s) that the model is designed to tackle, to be aware of the potential errors and limitations in the model, and to continue to challenge and refine (and indeed be prepared to discard) the model using available data. The "grand challenge" of predicting ab initio the structure of any protein remains unsolved though there are encouraging signs from recent work that significant progress may be anticipated in the near future.

Acknowledgments

We would like to thank Colin Edge, Paul Bamborough, and Alan Lewis for their comments and helpful suggestions on earlier versions of the manuscript and Guy Cochrane and Mary Todd Bergman from the European Bioinformatics Institute for assistance with Fig. 1.

References

1. Beddell, C. R.; Goodford, P. J.; Norrington, F. E.; Wilkinson, S.; Wootton, R. Compounds Designed to Fit a Site of Known Structure in Human Haemoglobin. *Br. J. Pharmacol.* **1976,** *57* (2), 201–209.
2. Talele, T. T.; Khedkar, S. A.; Rigby, A. C. Successful Applications of Computer Aided Drug Discovery: Moving Drugs From Concept to the Clinic. *Curr. Top. Med. Chem.* **2010,** *10* (1), 127–141.
3. Hardy, L. W.; Malikayil, A. The Impact of Structure-Guided Drug Design on Clinical Agents. *Curr. Drug Discov. Technol.* **2003,** *3,* 15–20.
4. Lounnas, V.; Ritschel, T.; Kelder, J.; McGuire, R.; Bywater, R. P.; Foloppe, N. Current Progress in Structure-Based Rational Drug Design Marks a New Mindset in Drug Discovery. *Comput. Struct. Biotechnol. J.* **2013,** *5* (6), e201302011.
5. Brandon, C. I.; Tooze, J. *Introduction to Protein Structure,* 2nd ed.; Garland Science: New York, 1998.
6. Hillisch, A.; Pineda, L. F.; Hilgenfeld, R. Utility of Homology Models in the Drug Discovery Process. *Drug Discov. Today* **2004,** *9* (15), 659–669.
7. Liu, T.; Tang, G. W.; Capriotti, E. Comparative Modeling: The State of the Art and Protein Drug Target Structure Prediction. *Comb. Chem. High Throughput Screen.* **2011,** *14* (6), 532–547.
8. Schwede, T. Protein Modeling: What Happened to the "Protein Structure Gap"? *Structure* **2013,** *21* (9), 1531–1540.
9. Zhang, Y. Progress and Challenges in Protein Structure Prediction. *Curr. Opin. Struct. Biol.* **2008,** *18* (3), 342–348.
10. Cavasotto, C. N.; Phatak, S. S. Homology Modeling in Drug Discovery: Current Trends and Applications. *Drug Discov. Today* **2009,** *14* (13-14), 676–683.
11. Baker, D.; Sali, A. Protein Structure Prediction and Structural Genomics. *Science* **2001,** *294* (5540), 93–96.
12. Cook, C. E.; Bergman, M. T.; Finn, R. D.; Cochrane, G.; Birney, E.; Apweiler, R. The European Bioinformatics Institute in 2016: Data Growth and Integration. *Nucleic Acids Res.* **2016,** *44,* D20–D26.
13. UniProt Consortium. UniProt: A Hub for Protein Information. *Nucleic Acids Res.* **2015,** *43* (Database issue), D204–D212.
14. Boeckmann, B.; Blatter, M. C.; Famiglietti, L.; Hinz, U.; Lane, L.; Roechert, B.; Bairoch, A. Protein Variety and Functional Diversity: Swiss-Prot Annotation in Its Biological Context. *C.R. Biol.* **2005,** *328* (10-11), 882–899.
15. Berman, H.; Henrick, K.; Nakamura, H. Announcing the Worldwide Protein Data Bank. *Nat. Struct. Biol.* **2003,** *10* (12), 980.
16. Berman, H. M.; Kleywegt, G. J.; Nakamura, H.; Markley, J. L. How Community Has Shaped the Protein Data Bank. *J. Struct. Des.* **2013,** *21* (9), 1485–1491.
17. Chothia, C.; Lesk, A. M. The Relation Between the Divergence of Sequence and Structure in Proteins. *EMBO J.* **1986,** *5* (4), 823–826.
18. Orengo, C. A.; Michie, A. D.; Jones, S.; Jones, D. T.; Swindells, M. B.; Thornton, J. M. CATH—A Hierarchic Classification of Protein Domain Structures. *Structure* **1997,** *5* (8), 1093–1108.
19. Sillitoe, I.; Lewis, T. E.; Cuff, A. L.; Das, S.; Ashford, P.; Dawson, N. L.; Furnham, N.; Laskowski, R. A.; Lee, D.; Lees, J.; Lehtinen, S.; Studer, R.; Thornton, J. M.; Orengo, C. A. CATH: Comprehensive Structural and Functional Annotations for Genome Sequences. *Nucleic Acids Res.* **2015,** *43* (Database issue), D376–D381.
20. Murzin, A. G.; Brenner, S. E.; Hubbard, T.; Chothia, C. SCOP: A Structural Classification of Proteins Database for the Investigation of Sequences and Structures. *J. Mol. Biol.* **1995,** *247,* 536–540.
21. Andreeva, A.; Howorth, D.; Chothia, C.; Kulesha, E.; Murzin, A. G. SCOP2 Prototype: A New Approach to Protein Structure Mining. *Nucleic Acids Res.* **2014,** *42* (D1), 310–314.
22. Montelione, G. T. The Protein Structure Initiative: Achievements and Visions for the Future. *F1000 Biol. Rep.* **2012,** *4,* 7.
23. Khafizov, K.; Madrid-Aliste, C.; Almo, S. C.; Fiser, A. Trends in Structural Coverage of the Protein Universe and the Impact of the Protein Structure Initiative. *Proc. Natl. Acad. Sci. U. S. A.* **2014,** *111* (10), 3733–3738.
24. Uversky, V. N.; Oldfield, C. J.; Midic, U.; Xie, H.; Xue, B.; Vucetic, S.; Iakoucheva, L. M.; Obradovic, Z.; Dunker, A. K. Unfoldomics of Human Diseases: Linking Protein Intrinsic Disorder With Diseases. *BMC Genomics* **2009,** *10* (Suppl. 1), S7.
25. Rupp, B. *Biomolecular Crystallography: Principles, Practice, and Application to Structural Biology;* Garland Science: New York, 2009.
26. Wlodawer, A.; Minor, W.; Dauter, Z.; Jaskolski, M. Protein Crystallography for Non-Crystallographers, or How to Get the Best (But Not More) From Published Macromolecular Structures. *FEBS J.* **2008,** *275* (1), 1–21.
27. Zheng, H.; Hou, J.; Zimmerman, M. D.; Wlodawer, A.; Minor, W. The Future of Crystallography in Drug Discovery. *Expert Opin. Drug Discovery* **2014,** *9* (2), 125–137.
28. Shi, Y. Review A Glimpse of Structural Biology through X-Ray Crystallography. *Cell* **2014,** *159* (5), 995–1014.
29. Perutz, M. *Protein Structure: New Approaches to Disease and Therapy;* Freeman: New York, 1992.
30. Wüthrich, K. The Way to NMR Structures of Proteins. *Nat. Struct. Biol.* **2001,** *8* (11), 923–925.
31. Cavanagh, J.; Fairbrother, W. J.; Palmer, A. G., III; Skelton, N. J.; Rance, M. *Protein NMR Spectroscopy: Principles and Practice,* 2nd ed.; Academic Press: New York, 2006.
32. Callaway, E. The Revolution Will Not Be Crystallized: A New Method Sweeps Through Structural Biology. *Nature* **2015,** *525* (7568), 172–174.

33. Nogales, E. The Development of Cryo-EM Into a Mainstream Structural Biology Technique. *Nat. Methods* **2016,** *13* (1), 24–27.
34. Glaeser, R. M. How Good Can Cryo-EM Become? *Nat. Methods* **2016,** *13* (1), 28–32.
35. Davis, A. M.; Teague, S. J.; Kleywegt, G. J. Application and Limitations of X-Ray Crystallographic Data in Structure-Based Ligand and Drug Design. *Angew. Chem. Int. Ed. Engl.* **2003,** *42* (24), 2718–2736.
36. Petsko, G. A. And the Second Shall Be First. *Genome Biol.* **2007,** *8* (2), 103.
37. Zemla, A.; Venclovas, Č.; Moult, J.; Fidelis, K. Processing and Analysis of CASP3 Protein Structure Predictions. *Proteins: Struct., Funct., Bioinf.* **1999,** *37* (S3), 22–29.
38. Kalyaanamoorthy, S.; Chen, Y. P. P. Structure-Based Drug Design to Augment Hit Discovery. *Drug Discov. Today* **2011,** *16* (17-18), 831–839.
39. Klebe, G. Virtual Ligand Screening: Strategies, Perspectives and Limitations. *Drug Discov. Today* **2006,** *11* (13-14), 580–594.
40. Scior, T.; Bender, A.; Tresadern, G.; Medina-franco, J. L.; Mart, K.; Langer, T.; Cuanalo-contreras, K.; Agrafiotis, D. K. Recognizing Pitfalls in Virtual Screening: A Critical Review. *J. Chem. Inf. Model* **2012,** *52* (4), 867–881.
41. Leach, A. R.; Shoichet, B. K.; Peishoff, C. E. Prediction of Protein-Ligand Interactions. Docking and Scoring: Successes and Gaps. *J. Med. Chem.* **2006,** *49* (20), 5851–5855.
42. Taylor, R. D.; Jewsbury, P. J.; Essex, J. W. A Review of Protein-Small Molecule Docking Methods. *J. Comput. Aided Mol. Des.* **2002,** *16* (3), 151–166.
43. Sousa, S. F.; Ribeiro, A. J. M.; Coimbra, J. T. S.; Neves, R. P. P.; Martins, S. A.; Moorthy, N. S. H. N.; Fernandes, P. A.; Ramos, M. J. Protein-Ligand Docking in the New Millennium—A Retrospective of 10 Years in the Field. *Curr. Med. Chem.* **2013,** *20* (18), 2296–2314.
44. Nissink, J. W. M.; Murray, C.; Hartshorn, M.; Verdonk, M. L.; Cole, J. C.; Taylor, R. A New Test Set for Validating Predictions of Protein-Ligand Interaction. *Proteins* **2002,** *49* (4), 457–471.
45. Huang, N.; Shoichet, B. K.; Irwin, J. J. Benchmarking Sets for Molecular Docking. *J. Med. Chem.* **2006,** *49* (23), 6789–6801.
46. Jones, G.; Willett, P.; Glen, R. C.; Leach, A. R.; Taylor, R. Development and Validation of a Genetic Algorithm for Flexible Docking. *J. Mol. Biol.* **1997,** *267* (3), 727–748.
47. Hartshorn, M. J.; Verdonk, M. L.; Chessari, G.; Brewerton, S. C.; Mooij, W. T. M.; Mortenson, P. N.; Murray, C. W. Diverse, High-Quality Test Set for the Validation of Protein − Ligand Docking Performance. *J. Med. Chem.* **2007,** *50* (4), 726–741.
48. Cole, J. C.; Murray, C. W.; Nissink, J. W.; Taylor, R. D.; Taylor, R. Comparing Protein-Ligand Docking Programs is Difficult. *Proteins* **2005,** *60* (3), 325–332.
49. Kairys, V.; Fernandes, M. X.; Gilson, M. K. Screening Drug-Like Compounds by Docking to Homology Models: A Systematic Study. *J. Chem. Inf. Model.* **2006,** *46* (1), 365–379.
50. Novoa, E. M.; Ribas de Pouplana, L.; Barril, X.; Orozco, M. Ensemble Docking From Homology Models. *J. Chem. Theory Comput.* **2010,** *6* (8), 2547–2557.
51. Fan, H.; Irwin, J. J.; Sali, A. Virtual Ligand Screening Against Comparative Protein Structure Models. *Methods Mol. Biol.* **2012,** *819,* 105–126.
52. Jacobson, M.; Sali, A. Comparative Protein Structure Modeling and Its Applications to Drug Discovery. *Annu. Rep. Med. Chem.* **2004,** *39,* 259–276.
53. Evers, A.; Klebe, G. Ligand-Supported Homology Modeling of G-Protein-Coupled Receptor Sites: Models Sufficient for Successful Virtual Screening. *Angew. Chem. Int. Ed.* **2004,** *43,* 248–251.
54. Evers, A.; Klebe, G. Successful Virtual Screening for a Submicromolar Antagonist of the Neurokinin-1 Receptor Based on a Ligand-Supported Homology Model. *J. Med. Chem.* **2004,** *47,* 5381–5392.
55. Evers, A.; Klabunde, T. Structure Based Drug Discovery Using GPCR Homology Modeling: Successful Virtual Screening for Antagonists of the Alpha1A Adrenergic Receptor. *J. Med. Chem.* **2005,** *48,* 1088–1097.
56. Huang, X. P.; Karpiak, J.; Kroeze, W. K.; Zhu, H.; Chen, X.; Moy, S. S.; Saddoris, K. A.; Nikolova, V. D.; Farrell, M. S.; Wang, S.; Mangano, T. J.; Deshpande, D. A.; Jiang, A.; Penn, R. B.; Jin, J.; Koller, B. H.; Kenakin, T.; Shoichet, B. K.; Roth, B. L. Allosteric Ligands for the Pharmacologically Dark Receptors GPR68 and GPR65. *Nature* **2015,** *527* (7579), 477–483.
57. Costanzi, S. On the Applicability of GPCR Homology Models to Computer-Aided Drug Discovery: A Comparison Between in Silico and Crystal Structures of the β2-Adrenergic Receptor. *J. Med. Chem.* **2008,** *51* (10), 2907–2914.
58. Shoichet, B. K.; Kobilka, B. K. Structure-Based Drug Screening for G-Protein-Coupled Receptors. *Trends Pharmacol. Sci.* **2012,** *33* (5), 268–272.
59. Tuccinardi, T.; Botta, M.; Giordano, A.; Martinelli, A. Protein Kinases: Docking and Homology Modeling Reliability. *J. Chem. Inf. Model.* **2010,** *50* (8), 1432–1441.
60. Schafferhansa, A.; Klebe, G. Docking Ligands Onto Binding Site Representations Derived From Proteins Built by Homology Modelling. *J. Mol. Biol.* **2001,** *307* (1), 407–427.
61. Tanrikulu, Y.; Schneider, G. Pseudoreceptor Models in Drug Design: Bridging Ligand- and Receptor-Based Virtual Screening. *Nat. Rev. Drug Discov.* **2008,** *7,* 667–677.
62. Bento, A. P.; Gaulton, A.; Hersey, A.; Bellis, L. J.; Chambers, J.; Davies, M.; Krüger, F. A.; Light, Y.; Mak, L.; McGlinchey, S.; Nowotka, M.; Papadatos, G.; Santos, R.; Overington, J. P. The ChEMBL Bioactivity Database: An Update. *Nucleic Acids Res.* **2014,** *42* (Database issue), D1083–D1090.
63. Hopkins, A. L.; Groom, C. R. The Druggable Genome. *Nat. Rev. Drug Discov.* **2002,** *1* (9), 727–730.
64. Henrich, S.; Salo-Ahen, O. M.; Huang, B.; Rippmann, F. F.; Cruciani, G.; Wade, R. C. Computational Approaches to Identifying and Characterizing Protein Binding Sites for Ligand Design. *J. Mol. Recognit.* **2010,** *23* (2), 209–219.
65. Trosset, J. Y.; Vodovar, N. Structure-Based Target Druggability Assessment. *Methods Mol. Biol.* **2013,** *986,* 141–164.
66. Kozakov, D.; Hall, D. R.; Napoleon, R. L.; Yueh, C.; Whitty, A.; Vajda, S. New Frontiers in Druggability. *J. Med. Chem.* **2015,** *58* (23), 9063–9088.
67. Cimermancic, P.; Weinkam, P.; Rettenmaier, T. J.; Bichmann, L.; Keedy, D. A.; Woldeyes, R. A.; Schneidmann, D.; Demerdash, O. N. A.; Mitchell, J. C.; Wells, J. A.; Fraser, J. S.; Sali, A. CryptoSite: Expanding the Druggable Proteome by Characterization and Prediction of Cryptic Binding Sites. *J. Mol. Biol.* **2016,** *2016,* 1–11.
68. Benner, S. A.; Sismoor, A. M. Synthetic Biology. *Nat. Rev. Genet.* **2005,** *6,* 533–543.
69. Khalil, A. S.; Collins, J. J. Synthetic Biology: Applications Come of Age. *Nat. Rev. Genet.* **2010,** *11,* 367–379.
70. Keasling, J. D. Synthetic Biology for Synthetic Chemistry. *ACS Chem. Biol.* **2008,** *3* (1), 64–76.
71. Davids, T.; Schmidt, M.; Bo, D. Strategies for the Discovery and Engineering of Enzymes for Biocatalysis. *Curr. Opin. Chem. Biol.* **2013,** *17* (2), 215–220.
72. Turner, N. J. Directed Evolution Drives the Next Generation of Biocatalysts. *Nat. Chem. Biol.* **2009,** *5* (8), 567–573.
73. Bornscheuer, U. T.; Huisman, G. W.; Kazlauskas, R. J.; Lutz, S.; Moore, J. C.; Robins, K. Engineering the Third Wave of Biocatalysis. *Nature* **2012,** *485* (7397), 185–194.
74. Kries, H.; Blomberg, R.; Hilvert, D. De. Novo Enzymes by Computational Design. *Curr. Opin. Chem. Biol.* **2013,** *17* (2), 221–228.
75. Reichert, J. M. Marketed Therapeutic Antibodies Compendium. *MAbs* **2012,** *4* (3), 413–415.
76. Dübel, S.; Reichert, J. M. *Handbook of Therapeutic Antibodies;* Wiley-Blackwell: Hoboken, New Jersey, 2014.
77. Kuroda, D.; Shirai, H.; Jacobson, M. P.; Nakamura, H. Computer-Aided Antibody Design. *Protein Eng. Des. Sel.* **2012,** *25* (10), 507–521.
78. Lippow, S. M.; Wittrup, K. D.; Tidor, B. Computational Design of Antibody-Affinity Improvement Beyond In Vivo Maturation. *Nat. Biotechnol.* **2007,** *25* (10), 1171–1176.
79. Dormitzer, P. R.; Ulmer, J. B.; Rappuoli, R. Structure-Based Antigen Design: A Strategy for Next Generation Vaccines. *Trends Biotechnol.* **2008,** *26* (12), 659–667.
80. Kulp, D. W.; Schief, W. R. Advances in Structure-Based Vaccine Design. *Curr. Opin. Virol.* **2013,** *3* (3), 322–331.
81. Dormitzer, P. R.; Grandi, G.; Rappuoli, R. Structural Vaccinology Starts to Deliver. *Nat. Rev. Microbiol.* **2012,** *10* (12), 807–813.
82. Ovchinnikov, S.; Kinch, L.; Park, H.; Liao, Y.; Pei, J.; Kim, D. E.; Kamisetty, H.; Grishin, N. V.; Baker, D. Large-Scale Determination of Previously Unsolved Protein Structures Using Evolutionary Information. *Elife* **2015,** *4,* 1–25.
83. Lewis, T. E.; Sillitoe, I.; Andreeva, A.; Blundell, T. L.; Buchan, D. W. A.; Chothia, C.; Cuff, A.; Dana, J. M.; Filippis, I.; Gough, J.; Hunter, S.; Jones, D. T.; Kelley, L. A.; Kleywegt, J.; Minneci, F.; Mitchell, A.; Murzin, A. G.; Ochoa-Montaño, B.; Rackham, O. J. L.; Smith, J.; Sternberg, M. J. E. Genome3D: A UK Collaborative Project to Annotate Genomic Sequences With Predicted 3D Structures Based on SCOP and CATH Domains. *Nucleic Acids Res.* **2013,** *41,* 499–507.
84. Chance, M. R.; Fiser, A.; Sali, A.; Pieper, U.; Eswar, N.; Xu, G.; Fajardo, J. E.; Radhakannan, T.; Marinkovic, N. High-Throughput Computational and Experimental Techniques in Structural Genomics. *Genome Res.* **2004,** *14* (10B), 2145–2154.
85. Martí-Renom, M. A.; Stuart, A. C.; Fiser, A.; Sánchez, R.; Melo, F.; Sali, A. Comparative Protein Structure Modeling of Genes and Genomes. *Annu. Rev. Biophys. Biomol. Struct.* **2000,** *29,* 291–325.

86. Pieper, U.; Eswar, N.; Braberg, H.; Madhusudhan, M. S.; Davis, F. P.; Stuart, A. C.; Mirkovic, N.; Rossi, A.; Marti-renom, M. A.; Fiser, A.; Webb, B.; Greenblatt, D.; Huang, C. C.; Ferrin, T. E.; Sali, A. MODBASE, a Database of Annotated Comparative Protein Structure Models, and Associated Resources. *Nucleic Acids Res.* **2004,** *32* (Database issue), D217–D222.
87. Gerlt, J. A.; Allen, K. N.; Almo, S. C.; Armstrong, R. N.; Babbitt, P. C.; Cronan, J. E.; Dunaway-mariano, D.; Imker, H. J.; Jacobson, M. P.; Minor, W.; Poulter, C. D.; Raushel, F. M.; Sali, A.; Shoichet, B. K.; Sweedler, J. V. The Enzyme Function Initiative. *Biochemistry* **2011,** *50* (46), 9950–9962.
88. Fan, H.; Hitchcock, D. S.; Ii, R. D. S.; Hillerich, B.; Lin, H.; Almo, S. C.; Sali, A.; Shoichet, B. K.; Raushel, F. M. Assignment of Pterin Deaminase Activity to an Enzyme of Unknown Function Guided by Homology Modeling and Docking. *J. Am. Chem. Soc.* **2013,** *135* (2), 795–803.
89. Lee, J.; Wu, S.; Zhang, Y. Ab Initio Protein Structure Prediction. From Protein Structure to Function With Bioinformatics. In Rigden, D. J., Ed.; Elsevier, 2009; pp 3–25.
90. Helles, G. A Comparative Study of the Reported Performance of Ab Initio Protein Structure Prediction Algorithms. *J. R. Soc. Interface* **2008,** *5* (21), 387–396.
91. Piana, S.; Lindorff-Larsen, K.; Shaw, D. E. Protein Folding Kinetics and Thermodynamics From Atomistic Simulation. *Proc. Natl. Acad. Sci. U. S. A.* **2012,** *109* (44), 17845–17850.
92. Piana, S.; Klepeis, J. L.; Shaw, D. E. Assessing the Accuracy of Physical Models Used in Protein-Folding Simulations: Quantitative Evidence From Long Molecular Dynamics Simulations. *Curr. Opin. Struct. Biol.* **2014,** *24,* 98–105.
93. Dill, K. A.; Maccallum, J. L.; Folding, P. The Protein-Folding Problem, 50 Years On. *Science* **2012,** *338* (6110), 1042–1046.
94. Bradley, P.; Misura, K. M.; Baker, D. Toward High-Resolution de Novo Structure Prediction for Small Proteins. *Science* **2005,** *309* (5742), 1868–1871.
95. Williams, S. G.; Lovell, S. C. The Effect of Sequence Evolution on Protein Structural Divergence. *Mol. Biol. Evol.* **2009,** *26* (5), 1055–1065.
96. Leach, A. R. *Molecular Modelling: Principles and Applications;* Prentice Hall: New Jersey, 2001.
97. Henikoff, S.; Henikoff, J. G. Amino Acid Substitution Matrices From Protein Blocks. *Proc. Natl. Acad. Sci. U. S. A.* **1992,** *89* (22), 10915–10919.
98. Needleman, S. B.; Wunsch, C. D. A General Method Applicable to the Search for Similarities in the Amino Acid Sequence of Two Proteins. *J. Mol. Biol.* **1970,** *48* (3), 443–453.
99. Smith, T. F.; Waterman, M. S. Identification of Common Molecular Subsequences. *J. Mol. Biol.* **1981,** *147* (1), 195–197.
100. Altschul, S. F.; Gish, W.; Miller, W.; Myers, E. W.; Lipman, D. J. Basic Local Alignment Search Tool. *J. Mol. Biol.* **1990,** *215,* 403–410.
101. Pearson, W. R. Rapid and Sensitive Sequence Comparison With FASTP and FASTA. *Methods Enzymol.* **1990,** *183,* 63–98.
102. Lipman, D. J.; Pearson, W. R. Rapid and Sensitive Protein Similarity Searches. *Science* **1985,** *227* (4693), 1435–1441.
103. Rost, B. Twilight Zone of Protein Sequence Alignments. *Protein Eng.* **1999,** *12* (2), 85–94.
104. Edgar, R. C.; Batzoglou, S. Multiple Sequence Alignment. *Curr. Opin. Struct. Biol.* **2006,** *16* (3), 368–373.
105. Thompson, J. D.; Higgins, D. G.; Gibson, T. J. CLUSTAL W: Improving the Sensitivity of Progressive Multiple Sequence Alignment Through Sequence Weighting, Position-Specific Gap Penalties and Weight Matrix Choice. *Nucleic Acids Res.* **1994,** *22* (22), 4673–4680.
106. Gribskov, M.; McLachlan, A. D.; Eisenberg, D. Profile Analysis: Detection of Distantly Related Proteins. *Proc. Natl. Acad. Sci. U. S. A.* **1987,** *84* (13), 4355–4358.
107. Krogh, A.; Brown, M.; Mian, I. S.; Sjölander, K.; Haussler, D. Hidden Markov Models in Computational Biology. Applications to Protein Modeling. *J. Mol. Biol.* **1994,** *235* (5), 1501–1531.
108. Eddy, S. R. Profile Hidden Markov Models. *Bioinformatics* **1998,** *14,* 755–763.
109. Eddy, S. R. What Is a Hidden Markov Model? *Nat. Biotechnol.* **2004,** *22* (10), 1315–1316.
110. Finn, R. D.; Coggill, P.; Eberhardt, R. Y.; Eddy, S. R.; Mistry, J.; Mitchell, A. L.; Potter, S. C.; Punta, M.; Qureshi, M.; Sangrador-Vegas, A.; Salazar, G. A.; Tate, J.; Bateman, A.; Acids Res, Nucleic. The Pfam Protein Families Database: Towards a More Sustainable Future. *Nucleic Acids Res.* **2015,** *44,* D279–D285.
111. Altschul, S. F.; Madden, T. L.; Schäffer, A. A.; Zhang, J.; Zhang, Z.; Miller, W.; Lipman, D. J. Gapped BLAST and PSI-BLAST: A New Generation of Protein Database Search Programs. *Nucleic Acids Res.* **1997,** *25,* 3389–3402.
112. Ohlson, T.; Wallner, B.; Elofsson, A. Profile-Profile Methods Provide Improved Fold-Recognition: A Study of Different Profile-Profile Alignment Methods. *Proteins* **2004,** *57* (1), 188–197.
113. Ye, X.; Wang, G.; Altschul, S. F. An Assessment of Substitution Scores for Protein Profile—Profile Comparison. *Biogeosciences* **2011,** *27* (24), 3356–3363.
114. Jones, D. T.; Taylor, W. R.; Thornton, J. M. A New Approach to Protein Fold Recognition. *Nature* **1992,** *358* (6381), 86–89.
115. Yang, J.; Yan, R.; Roy, A.; Xu, D.; Poisson, J.; Zhang, Y. The I-TASSER Suite: Protein Structure and Function Prediction. *Nat. Methods* **2015,** *12* (1), 7–8.
116. Molecular Operating Environment (MOE), 2013.08; Chemical Computing Group Inc., 1010 Sherbooke St. West, Suite #910, Montreal, QC, Canada, H3A 2R7, 2016.
117. Crooks, G. E.; Hon, G.; Chandonia, J. M.; Brenner, S. E. WebLogo: A Sequence Logo Generator. *Genome Res.* **2004,** *14,* 1188–1190.
118. Greer, J. Comparative Model-Building of the Mammalian Serine Proteases. *J. Mol. Biol.* **1981,** *153* (4), 1027–1042.
119. Greer, J. Model of a Specific Interaction: Salt-Bridges Form Between Prothrombin and Its Activating Enzyme Blood Clotting Factor Xa. *J. Mol. Biol.* **1981,** *153* (4), 1043–1053.
120. Nichols, R. J.; Dzamko, N.; Hutti, J. E.; Cantley, L. C.; Deak, M.; Moran, J.; Bamborough, P.; Reith, A. D.; Alessi, D. R. NIH Public Access. Substrate Specificity and Inhibitors of LRRK2, a Protein Kinase Mutated in Parkinson's Disease. *Biochem. J.* **2013,** *424* (1), 47–60.
121. Jones, T. A.; Thirup, S. Using Known Substructures in Protein Model Building and Crystallography. *EMBO J.* **1986,** *5* (4), 819–822.
122. Levitt, M. Accurate Modeling of Protein Conformation by Automatic Segment Matching. *J. Mol. Biol.* **1992,** *226* (2), 507–533.
123. Kaufmann, K. W.; Lemmon, G. H.; Deluca, S. L.; Sheehan, J. H.; Meiler, J. Practically Useful: What the Rosetta Protein Modeling Suite Can Do for You. *Biochemistry* **2010,** *49* (14), 2987–2998.
124. Rohl, C. A.; Strauss, C. E.; Misura, K. M.; Baker, D. Protein Structure Prediction Using Rosetta. *Methods Enzymol.* **2004,** *383,* 66–93.
125. Das, R.; Baker, D. Macromolecular Modeling With Rosetta. *Annu. Rev. Biochem.* **2008,** *77,* 363–382.
126. Song, Y.; DiMaio, F.; Wang, R. Y.; Kim, D.; Miles, C.; Brunette, T.; Thompson, J.; Baker, D. High-Resolution Comparative Modeling With RosettaCM. *Structure* **2013,** *21* (10), 1735–1742.
127. Sali, A.; Blundell, T. L. Comparative Protein Modelling by Satisfaction of Spatial Restraints. *J. Mol. Biol.* **1993,** *234* (3), 779–815.
128. Webb, B.; Sali, A. *Comparative Protein Structure Modeling Using Modeller. Current Protocols in Bioinformatics;* John Wiley & Sons: Hoboken, NJ, 2014.
129. Fiser, R. K. Do; Sali, A. Modeling of Loops in Protein Structures. *Protein Sci.* **2000,** *9,* 1753–1773.
130. Sali, A.; Overington, J. P. Derivation of Rules for Comparative Protein Modeling From a Database of Protein Structure Alignments. *Protein Sci.* **1994,** *3* (9), 1582–1596.
131. Rosenbaum, D. M.; Rasmussen, S. G. F.; Kobilka, B. K. The Structure and Function of G-Protein-Coupled Receptors. *Nature* **2009,** *459* (7245), 356–363.
132. Jacoboni, I.; Martelli, P. L.; Fariselli, P.; Compiani, M.; Casadio, R. Predictions of Protein Segments With the Same Amino acid Sequence and Different Secondary Structure: A Benchmark for Predictive Methods. *Proteins* **2000,** *41* (4), 535–544.
133. Jacobson, M. P.; Pincus, D. L.; Rapp, C. S.; Day, T. J. F.; Honig, B.; Shaw, D. E.; Friesner, R. A. A Hierarchical Approach to All-Atom Protein Loop Prediction. *Proteins* **2004,** *55,* 351–367.
134. Dunbar, J.; Krawczyk, K.; Leem, J.; Baker, T.; Fuchs, A.; Georges, G.; Shi, J.; Deane, C. M. SAbDab: The Structural Antibody Database. *Nucleic Acids Res.* **2014,** *42,* D1140–D1146.
135. Teplyakov, A.; Obmolova, G.; Malia, T.; Gillil, G. Antigen Recognition by Antibody C836 Through Adjustment of V(L)/V(H) Packing. *Acta Crystallogr. Sect. F: Struct. Biol. Cryst. Commun.* **2011,** *67,* 1165–1167.
136. Bujotzek, A.; Dunbar, J.; Lipsmeier, F.; Schafer, W.; Antes, I.; Deane, C. M.; Georges, G. Prediction of VH-VL Domain Orientation for Antibody Variable Domain Modelling. *Proteins* **2015,** *83,* 681–695.
137. Chothia, C.; Lesk, A. M. Canonical Structures for the Hypervariable Regions of Immunoglobulins. *J. Mol. Biol.* **1987,** *196* (4), 901–917.
138. Al-Lazikani, B.; Lesk, A. M.; Chothia, C. Standard Conformations for the Canonical Structures of Immunoglobulins. *J. Mol. Biol.* **1997,** *273* (4), 927–948.

139. Almagro, J. C.; Teplyakov, A.; Luo, J.; Sweet, R. W.; Kodangattil, S.; Hernandez-Guzman, F.; Gilliland, G. L. Second Antibody Modeling Assessment (AMA-II). *Proteins* **2014,** *82,* 1553–1562.
140. Ponder, J. W.; Richards, F. M.; Haven, N. Tertiary Templates for Proteins Use of Packing Criteria in the Enumeration of Allowed Sequences for Different Structural Classes. *J. Mol. Biol.* **1987,** *193* (4), 775–791.
141. Dunbrack, R. L., Jr.; Karplus, M. A Backbone Dependent Rotamer Library for Proteins: Application to Sidechain Prediction. *J. Mol. Biol.* **1993,** *230,* 543–571.
142. Dunbrack, R. L., Jr. Rotamer Libraries in the 21st Century. *Curr. Opin. Struct. Biol.* **2002,** *12,* 431–440.
143. Wang, Q.; Canutescu, A. A.; Dunbrack, R. L., Jr. SCWRL and MolIDE: Computer Programs for Side-Chain Conformation Prediction and Homology Modeling. *Nat. Protoc.* **2008,** *3* (12), 1832–1847.
144. Krivov, G. G.; Shapovalov, M. V.; Dunbrack, R. L., Jr. Improved Prediction of Protein Side-Chain Conformations With SCWRL4. *Proteins* **2009,** *77* (4), 778–795.
145. Summa, C. M.; Levitt, M. Near-Native Structure Refinement Using in Vacuo Energy Minimization. *Proc. Natl. Acad. Sci. U. S. A.* **2007,** *104* (9), 3177–3182.
146. Raval, A.; Piana, S.; Eastwood, M. P.; Dror, R. O.; Shaw, D. E. Refinement of Protein Structure Homology Models Via Long, All-Atom Molecular Dynamics Simulations. *Proteins* **2012,** *80* (8), 2071–2079.
147. Feig, M.; Mirjalili, V. Protein Structure Refinement via Molecular-Dynamics Simulations: What Works and What Does Not? *Proteins* **2016,** *84* (Suppl. 1), 282–292 http://dx.doi.org/10.1002/prot.24871.
148. Sippl, M. J. Calculation of Conformational Ensembles From Potentials of Mean Force. An Approach to the Knowledge-Based Prediction of Local Structures in Globular Proteins. *J. Mol. Biol.* **1990,** *213,* 859–883.
149. Shen, M.; Sali, A. Statistical Potential for Assessment and Prediction of Protein Structures. *Protein Sci.* **2006,** *15* (11), 2507–2524.
150. Simons, K. T.; Kooperberg, C.; Huang, E.; Baker, D. Assembly of Protein Tertiary Structures From Fragments With Similar Local Sequences Using Simulated Annealing and Bayesian Scoring Functions. *J. Mol. Biol.* **1997,** *268* (1), 209–225.
151. Park, H.; Dimaio, F.; Baker, D. CASP11 Refinement Experiments With ROSETTA. *Proteins* **2016,** *84* (Suppl. 1), 314–322. http://dx.doi.org/10.1002/prot.24862.
152. Misura, K. M.; Baker, D. Progress and Challenges in High-Resolution Refinement of Protein Structure Models. *Proteins* **2005,** *59* (1), 15–29.
153. Davis, I. W.; Leaver-Fay, A.; Chen, V. B.; Block, J. N.; Kapral, G. J.; Wang, X.; Murray, L. W.; Arendall, W. B.; Snoeyink, J.; Richardson, J. S.; Richardson, D. C. MolProbity: All-Atom Contacts and Structure Validation for Proteins and Nucleic Acids. *Nucleic Acids Res.* **2007,** *35* (Suppl. 2), 375–383.
154. Laskowski, R. A.; MacArthur, M. W.; Moss, D. S.; Thornton, J. M. PROCHECK: A Program to Check the Stereochemical Quality of Protein Structures. *J. Appl. Crystallogr.* **1993,** *26,* 283–291.
155. Lüthy, R.; Bowie, J. U.; Eisenberg, D. Assessment of Protein Models With Three-Dimensional Profiles. *Nature* **1992,** *356* (6364), 83–85.
156. Eisenberg, D.; Luthy, R.; Bowie, J. U. VERIFY3D: Assessment of Protein Models With Three-Dimensional Profiles. *Methods Enzymol.* **1997,** *277,* 396–404.
157. Willard, L.; Ranjan, A.; Zhang, H.; Monzavi, H.; Boyko, R. F.; Sykes, B. D.; Wishart, D. S. VADAR: A Web Server for Quantitative Evaluation of Protein Structure Quality. *Nucleic Acids Res.* **2003,** *31* (13), 3316–3319.
158. Pugalenthi, G.; Shameer, K.; Srinivasan, N. Sowdhamini HARMONY: A Server for the Assessment of Protein Structures. *Nucleic Acids Res.* **2006,** *34,* W231–W234.
159. Wiederstein, M.; Sippl, M. J. ProSA-Web: Interactive Web Service for the Recognition of Errors in Three-Dimensional Structures of Proteins. *Nucleic Acids Res.* **2007,** *35,* W407–W410.
160. Moult, J.; Pedersen, J. T.; Judson, R.; Fidelis, K. A Large-Scale Experiment to Assess Protein Structure Prediction Methods. *Proteins* **1995,** *23* (3), ii–v.
161. Moult, J. A Decade of CASP: Progress, Bottlenecks and Prognosis in Protein Structure Prediction. *Curr. Opin. Struct. Biol.* **2005,** *15* (3), 285–289.
162. Moult, J.; Fidelis, K.; Kryshtafovych, A.; Schwede, T.; Tramontano, A. Critical Assessment of Methods of Protein Structure Prediction (CASP) - Round X. *Proteins Struct. Funct. Bioinforma.* **2014,** *82* (Suppl. 2), 1–6.
163. Guex, N.; Peitsch, M. C.; Schwede, T. SWISS-MODEL: An Automated Protein Homology-Modeling Server. *Nucleic Acids Res.* **2003,** *31* (13), 3381–3385.
164. Kim, D. E.; Chivian, D.; Baker, D. Protein Structure Prediction and Analysis Using the Robetta Server. *Nucleic Acids Res.* **2004,** *32* (Web Server issue), W526–W531.
165. Kelley, L. A.; Mezulis, S.; Yates, C. M.; Wass, M. N.; Sternberg, M. J. E. The Phyre2 Web Portal for Protein Modeling. Prediction and Analysis. *Nat. Protoc.* **2015,** *10* (6), 845–858.
166. Yang, J.; Yan, R.; Roy, A.; Xu, D.; Poisson, J.; Zhang, Y. The I-TASSER Suite: Protein Structure and Function Prediction. *Nat. Publ. Group* **2015,** *12* (1), 7–8.
167. Roy, A.; Kucukural, A.; Zhang, Y. I-TASSER: A Unified Platform for Automated Protein Structure and Function Prediction. *Nat. Protoc.* **2010,** *5* (4), 725–738.
168. Marks, D. S.; Hopf, T. A.; Sander, C. Protein Structure Prediction From Sequence Variation. *Nat. Biotechnol.* **2012,** *30* (11), 1072–1080.
169. Marks, D. S.; Colwell, L. J.; Sheridan, R.; Hopf, T. A.; Pagnani, A.; Zecchina, R.; Sander, C. Protein 3D Structure Computed From Evolutionary Sequence Variation. *PLoS ONE* **2011,** *6* (12). e28766.
170. Dahiyat, B. I.; De Mayo, S. L. Novo Protein Design: Fully Automated Sequence Selection. *Science* **1997,** *278* (5335), 82–87.
171. Kuhlman, B.; Dantas, G.; Ireton, G. C.; Varani, G.; Stoddard, B. L.; Baker, D. Design of a Novel Globular Protein Fold With Atomic-Level Accuracy. *Science* **2003,** *302,* 1364–1369.
172. Lane, T. J.; Shukla, D.; Beauchamp, K. A.; Pande, V. S. To Milliseconds and Beyond: Challenges in the Simulation of Protein Folding. *Curr. Opin. Struct. Biol.* **2013,** *23* (1), 58–65.
173. Khatib, F.; Cooper, S.; Tyka, M. D.; Xu, K.; Makedon, I.; Popovi, Z. Algorithm Discovery by Protein Folding Game Players. *Proc. Natl. Acad. Sci. U. S. A.* **2011,** *108* (47), 18949–18953.
174. Eiben, C. B.; Siegel, J. B.; Bale, J. B.; Cooper, S.; Khatib, F.; Shen, B. W.; Players, F.; Stoddard, B. L.; Popovic, Z.; Baker, D. Increased Diels-Alderase Activity through Backbone Remodeling Guided by Foldit Players. *Nat. Biotechnol.* **2012,** *30* (2), 190–192.

Relevant Websites

http://predictioncenter.org/ Portal for the CASP project for protein structure prediction. Contains links to past and future CASP events, results, publications and more.
http://www.wwpdb.org/ Website of the worldwide Protein Data Bank (wwPDB). The wwPDB comprises four members who together manage the archive, ensure it is made freely available to the community and provide tools for searching, analyzing and visualizing the archive. These four members are:
http://www.bmrb.wisc.edu/ the Biological Magnetic Resonance Databank focuses on data from NMR experiments.
http://www.ebi.ac.uk/pdbe/ The Protein Data Bank in Europe (PDBe).
http://pdbj.org/ The Protein Data Bank Japan (PDBj).
http://www.rcsb.org/pdb/home/home.do The Research Collaboratory for Structural Bioinformatics Protein Data Bank (RCSB-PDB).
https://salilab.org/modeller/ home page for the MODELLER program.
http://modbase.compbio.ucsf.edu/modbase-cgi/index.cgi ModBase: a database of protein models calculated using MODELLER.
https://www.rosettacommons.org/ entry point for the Rosetta software suite.
http://zhanglab.ccmb.med.umich.edu/I-TASSER/ entry point for the I-TASSER modelling suite, highly ranked in recent CASP competitions.
http://swissmodel.expasy.org/ home of the SWISS-MODEL suite for automated modeling.

3.08 Modeling and Design for Membrane Protein Targets

M Congreve, A Bortolato, G Brown, and RM Cooke, Heptares Therapeutics, BioPark, Hertfordshire, United Kingdom

© 2017 Elsevier Ltd. All rights reserved.

3.08.1	**Introduction**	145
3.08.1.1	Classes of Membrane Proteins	145
3.08.1.2	The Emergence of High-Resolution Structures of Membrane Proteins	146
3.08.1.2.1	GPCRs	146
3.08.1.2.2	Membrane transporters	147
3.08.1.2.3	Ion channels	148
3.08.2	**Novel Structural Understanding of Membrane Proteins Focused on GPCRs**	151
3.08.2.1	From Structure to Function	151
3.08.2.2	Binding Site Analysis	153
3.08.3	**GPCR Ligand Design**	155
3.08.3.1	Hit Finding	155
3.08.4	**GPCR Computational Simulation**	156
3.08.4.1	Molecular Dynamics Simulations	156
3.08.4.2	Binding Free Energy and Binding Kinetics Predictions	160
3.08.5	**Applications of in Silico Design for Membrane Protein Targets**	163
3.08.5.1	Orthosteric GPCR Ligands	164
3.08.5.1.1	Class A GPCR aminergic	164
3.08.5.1.2	Class A GPCR peptidergic	170
3.08.5.1.3	Class A GPCR purinergic	171
3.08.5.1.4	Class A GPCR lipid receptors	176
3.08.5.1.5	Class A GPCR chemokine	176
3.08.5.2	Allosteric GPCR Ligands	179
3.08.6	**Conclusions**	180
References		181
Relevant Websites		187

Generic GPCR residue numbering.[1] The generic GPCR residue numbering system used throughout this article includes two numbers (XN); the first (1–7) denotes the transmembrane helix, and the following number indicates the residue position relative to the most conserved amino acid in the helix (which is assigned the number 50). Different schemes are available for the different GPCR families: Ballesteros-Weinstein (class A),[2] Wootten (class B),[3] Pin (class C),[4] and Wang (class F).[5] A letter (a, b, c, or f) can be included to specify the numbering scheme used. For example, 3.52b indicates the second residue after the most conserved amino acid in class B TM3. If an amino acid is followed by its residue number, the generic GPCR residue numbering is included as superscript (e.g., Tyr109$^{3.28a}$). Where GPCR crystal structure superposition shows a numbering offset due to helical bulges or constrictions, a structure-based number can be appended separated by an $\times$, for example, 5.42×43, or used as a substitute, for example, 5×43.[1]

3.08.1 Introduction

3.08.1.1 Classes of Membrane Proteins

Integral membrane proteins account for approximately 30% of the human genome but represent almost 50% of the targets of pharmaceutical agents.[6,7] Compounds modulating ion channels, transporters, or G protein-coupled receptors (GPCRs) have routinely been among the most widely prescribed therapies for several decades. There are multiple reasons for this, including not only the involvement of membrane proteins in many disease-related regulatory processes but also their inherent druggability arising from binding sites which have evolved to recognize small molecules.

Despite their popularity as drug targets, membrane proteins have consistently been poorly represented in collections of X-ray structures of proteins, primarily due to difficulties in purifying sufficient quantities of high-quality protein stable enough to form regular crystals. Examples were until relatively recently limited to a handful of heroic efforts, such as the photosystem complex.[8] However, between 1998 and 2002, breakthrough structures (described below) were achieved for ion channels, transporters, and GPCRs. A consistent theme for each of these classes of proteins has been the focus on particular family members, which, while still challenging, yielded valuable information before progressing to more difficult examples.

In this section, we will introduce the main classes of membrane proteins, which have been the focus of structural biology efforts. It is not possible to give a comprehensive analysis of the field in a single article; instead, we give an outline of the progress for each major target families here.

3.08.1.2 The Emergence of High-Resolution Structures of Membrane Proteins

3.08.1.2.1 GPCRs

GPCRs transmit signals across the cell membrane by activating G proteins bound to the intracellular face of the receptor. The GPCRs exist in inactive and active conformations, with the degree of signaling dependent on the proportion of each. In the simplest model, agonists stabilize active conformations, inverse agonists stabilize inactive conformations, partial agonists (in which the level of receptor activity when saturated with ligand is less than for a full agonist) bind to both conformations but prefer the active form, and neutral antagonists stabilize both active and inactive conformations in the same proportion as in the absence of the ligand.[9] The structural differences between active and inactive forms and how these relate to recognition of ligands with different pharmacologies have been key questions in understanding the mechanism of GPCR signaling.

The first breakthrough in GPCR structural biology came in 2000 with the solution of the structure of bovine rhodopsin.[10] This confirmed the presence of a bundle of seven transmembrane helices surrounding the retinal-binding site, which is located toward the extracellular surface, and an eighth helix, roughly perpendicular to the others. The conformation of the protein corresponded to the inactive form of the receptor, and while the details of the conformational changes required for activation could only be surmised, it gave a boost for homology modeling of many receptors of therapeutic interest. The rhodopsin used for crystallization was generated from a relatively abundant non-recombinant source of protein (bovine retinas), and it encouraged efforts to produce sufficient quantities of stable protein suitable for crystallization for other receptors. These efforts took until 2007 to yield success, with structures reported for the β_2, β_1, and A_{2A} receptors.[11–13] Each was in the inactive form, with ligand density clearly visible in the presumed orthosteric site. Since then, the number of receptors for which structures have been reported has increased dramatically, with over 25 now being available.[14]

While the first structures solved were for class A GPCRs, the most common, structures have now been solved for classes B,[15,16] C,[17,18] and F.[19] The details of ligand recognition vary considerably, with class A ligands being highly diverse and including small amines, fatty acids, peptides, and globular proteins such as chemokines, all seemingly engaging directly with the helical bundle; class B receptors bind peptides, which span from the helical bundle to an extracellular domain at the N-terminus end of the receptor; class C receptors are active as dimers and bind small neurotransmitters such as glutamate in an N-terminus domain, structurally distinct from the transmembrane region; class F receptors recognize lipoglycoproteins such as Wnt. However, all the structures solved so far are consistent with the hypothesis that the transmembrane region of each GPCRs is designed to exist in multiple conformations, with the inactive, resting state different from the agonist-bound conformation, which favors G protein binding and activation. Hence, for the class C receptors, while agonists bind to the N-terminus domain, allosteric modulation can be achieved by binding to the transmembrane domain and promoting or restricting activation.

Importantly, a number of class A receptor structures are available in inactive and active conformations, allowing visualization of the structural differences between them. Although the details vary considerably, the binding of agonists generally leads to a contraction of the ligand-binding pocket and movement of the intracellular end of TM6 away from the rest of the helical bundle, with a helix from the G protein taking its place.[20] Although the details of ligand binding differ in other classes of GPCRs, the same general conformational changes, allowing engagement of the G protein, are also anticipated. Activation is thus accompanied by changes in the ligand-binding pocket within the helical bundle (described later); hence, when this is the binding site for agonists or antagonists, the structural differences are critical determinants of ligand pharmacology. There is a long history of small changes to GPCR ligands causing a switch between antagonism and agonism,[21] and comparisons between X-ray structures of related ligands with different pharmacologies can explain the structural basis for this.[22] In addition to aiding the understanding of ligand pharmacological preferences, structures of related receptors can explain ligand selectivity profiles. For the 5-HT_{1B} and 5-HT_{2B} receptors, ergotamines such as LSD can bind to both, while the selectivity of most triptans for 5-HT_{1B} can be explained by helix 5 creating a narrower pocket in 5-HT_{2B}, which can only be accessed by those molecules with a flexible linker.[23]

The structures have also revealed the diversity of binding modes possible for GPCR ligands. As the natural agonists for some GPCRs are proteins in their own right, the binding surface can be extensive, and the range of potential locations where antagonists may bind is large, with the location of atoms in antagonists of the class F smoothened receptor spanning approximately 28 Å.[5] An extended binding mode was also observed for the GPR40 agonist TAK835,[24] which was found to occupy the "classical" site between the helices, but it also passes between two of the helices, with part of the ligand projecting into what would be the lipid bilayer. Allosteric ligands are also known for many other GPCRs, with binding sites so far revealed ranging from somewhat anticipated to the totally unexpected. The positive allosteric modulator LY2119620 sits above the orthosteric site of the M_2 receptor,[25] closing a cage of tyrosines around the agonist and blocking its dissociation, while the CRF1 antagonist CP-376395 binds deep inside the receptor, below the orthosteric pocket, and appears to function by blocking the movement of helices required for activation. The $P2Y_1$ structure[26] revealed a "conventional" binding mode between the helices for a nucleotide antagonist, while in contrast, a different chemotype binds in a completely unexpected site on the outside of the helical bundle.

The atomic detail provided by the structures of the receptors, in particular the locations of ligand-binding pockets and details of agonist or antagonist recognition, provides opportunities for structure-based design approaches for these receptors and better starting points for the modeling of related receptors. The number of reports in which receptor structures are used to support drug discovery is rapidly increasing and is reviewed later in this article.

3.08.1.2.2 Membrane transporters

Membrane transporters facilitate the transport of molecules across cell membranes either in response to or against a concentration gradient, with the latter being driven by the simultaneous transport of another molecule down its own concentration gradient. Unlike the ion channels discussed later, which, when open, allow a near-continuous flow of ions, transporters are generally considered to operate on a slower, substrate by substrate basis. This involves a mechanism in which the transporter is initially open to one side of the membrane and closed to the other. Following substrate binding, the transporter flips conformation and is open to the other side of the membrane, allowing the substrate to be released.

The transmembrane region of a transporter is typically composed of two domains, each of which contains five or six helices. The first high-resolution structure that revealed this topology was that of BtuCD,[27] a member of the ATP-binding cassette (ABC) family of primary active transporters (**Fig. 1A**), which are now more commonly regarded as membrane pumps. BtuCD is a vitamin B pump from *E. coli*, where each chain consists of a transmembrane domain attached to a nucleotide-binding domain. Two protein monomers form a symmetrical dimer, with a cavity between them of appropriate size to accommodate the vitamin B, and the two copies of the turn between TM4 and TM5 create a gate at the cytosolic surface. The structure also provided insights into how the energy from ATP hydrolysis could be coupled with transport of vitamin B and refinement of models of the conformational changes that happen during transport. Structures of the sugar transporters LacY and GlpT revealed similar arrangements[28,29] (**Fig. 1B**), with each protein organized into two domains of six transmembrane helices, with N- and C-termini in the cytosol. The substrate

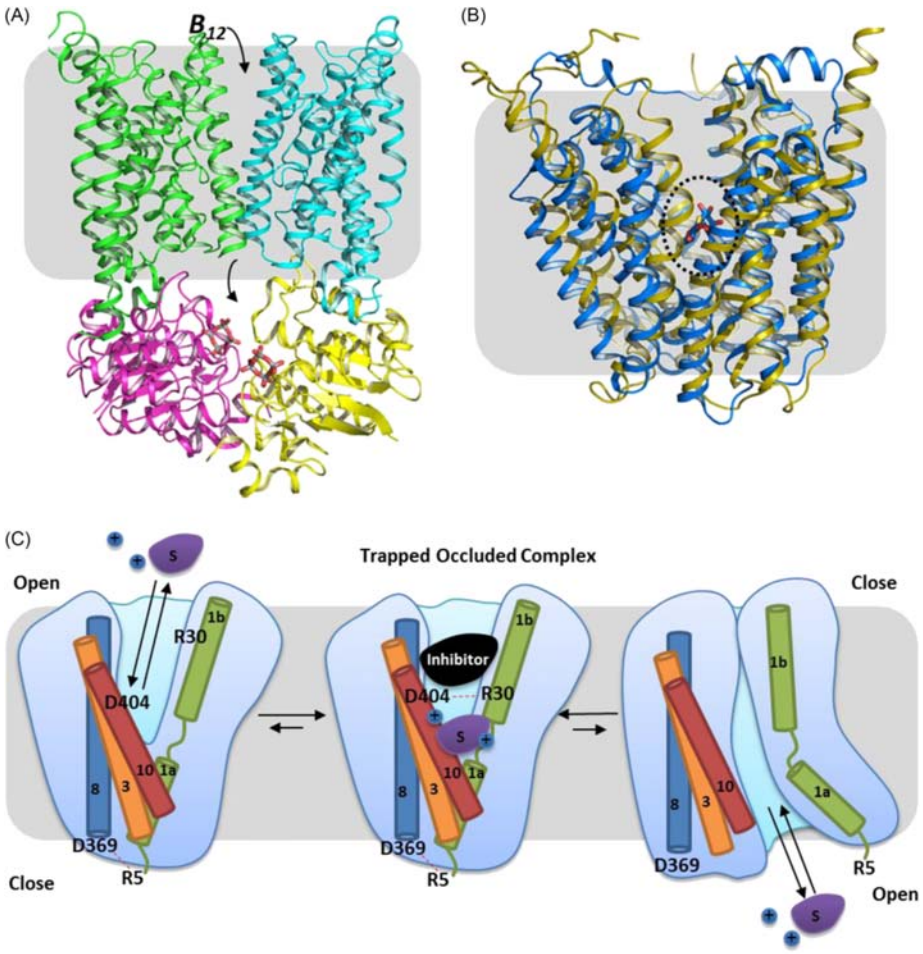

Fig. 1 Examples of transporter structures. (A) Ribbon diagram of BtuCD protein structure (PDB ID, 1L7V[27]) composed by two transmembrane chains (*green* and *cyan*) and two ABC cassettes BtuC subunits (*magenta* and *yellow*). Two arrows indicate the path followed by vitamin B_{12}. ATP-binding sites are occupied by cyclotetravanadate molecules shown as sticks. (B) Ribbon representation of the structures of the sugar transporters LacY (*blue*, PDB ID, 1PV7[28]) and GlpT (*yellow*, PDB ID, 1PW4[29]). The position of the LacY-bound lactose homolog, beta-D-galactopyranosyl-1-thio-beta-D-galactopyranoside, is shown in stick inside a dashed circle. (C) Proposed transporter mechanism (modified from[30]). The substrate (S in *purple*) and ions (*blue* circles) can bind the protein open toward the extracellular side (*left* panel) and progress toward the occluded state (*central* panel). When a noncompetitive inhibition is bound to this state, the substrate is trapped and cannot progress any further toward the intracellular cytosol (*right* panel). In all panels, the membrane region is indicated in gray, with the extracellular side and the intracellular side on the top and on the bottom, respectively.

binding site is located between the two domains, and particularly, enlightening was the fact that the site is approximately halfway across the TM region, consistent with an alternating access mechanism in which the substrate is effectively moved from one side of the membrane to the other by protein helices rearranging around a fixed substrate position.

The most revealing model structure, in terms of relevance for existing drug targets, has been that of the bacterial leucine transporter LeuT, which was solved at a very high resolution of 1.6 Å.[31] This was the first structure to be solved for the sodium symporter family, which includes the monoamine transporters for serotonin, dopamine, and norepinephrine (SERT, DAT, and NET, respectively), which are the targets of many therapeutic agents and drugs of abuse such as cocaine. In the case of LeuT, five transmembrane segments form each of the two domains, but as before, the substrate is bound approximately halfway across the transmembrane region, this time along with two sodium ions that are transported with the amino acid (**Fig. 1C**). The disposition of the helices appears to represent an outward-facing form, but a salt bridge makes a gate separating the leucine and the sodium ions from the extracellular matrix.

A better understanding of the structures of different states of LeuT was achieved with the use of antibody fragments to stabilize the inward- and outward-facing forms in the absence of leucine.[32] Large conformational rearrangements are observed between the outward- and inward-facing forms, as expected, and the gate that had previously formed around the leucine is absent. Sodium ions were bound to the Leu-free form of the protein for the outward-facing state only, with conformational changes in the inward-facing site disrupting their sites, explaining their transport into the cell (**Fig. 1C**). Particularly revealing was a structure with tryptophan, which binds in the same site as leucine, and although the protein adopts an outward-facing conformation, tryptophan sterically blocks formation of the gate, acting as an inhibitor rather than a substrate. Collectively, the structures allow proposals of a general alternating access model in which transport requires an intermediate state with both inward and outward faces blocked. Substrates are accommodated within such an occluded site, while inhibitors can occupy the site when open, but not when occluded (**Fig. 1C**). The model also covers all forms of transport, including cotransport of ions in either the same (symport) or opposite (antiport) direction as the substrate.[33] The sodium/galactose symporter from *Vibrio*, a model for the human diabetes target SGLT2, crystallized in an inward-facing form but with features recognizably similar to LeuT,[34] while the structure of PepT, a member of the major facilitator superfamily of transporters and a bacterial homologue of di- and tripeptide transporters, revealed an occluded state.[35] This was thought to be close to intermediate between inward- and outward-facing states, fully consistent with the alternating access mechanism.

The similarity of LeuT to monoamine transporters prompted investigations of the modes of binding of several drug molecules, with mixed results. The tricyclic antidepressants clomipramine and desipramine bind to LeuT in the presence of leucine, in a vestibule on the extracellular side of the leucine site,[36,37] seemingly inhibiting transport by locking shut the gate on the extracellular side of the leucine site, in a manner that is noncompetitive with leucine and sodium binding (**Fig. 1C**). Mutagenesis experiments on the human serotonin and dopamine transporters suggested that they contain equivalent vestibules and tricyclic binding sites.[37] Further work with three SSRIs showed they also bound in roughly the same pocket of LeuT as the tricyclics but made different interactions with the protein,[38] and substitutions in this region correlated with different selectivity profiles between the transporters for the tricyclics and the SSRIs.

Concerns as to the reliability of LeuT as a model of ligand binding to monoamine transporters prompted investigations in which mutations were added to increase the similarity of the former to the latter. Solving structures of the modified protein with four classes of antidepressants revealed that, like leucine, they each bound to the central cavity and identified three subsites, which the different classes of compounds could occupy differently.[39] They all, however, appeared to lock the transporter into an outward-facing conformation (**Fig. 1C**). This mode of binding and inhibition was also seen with the solution of the X-ray structure of the dopamine transporter from *Drosophila* with the tricyclic antidepressant nortriptyline,[40] where some subtle differences between the protein topologies of LeuT and DAT were revealed. Subsequent structures with a series of DAT ligands, including the substrates dopamine and amphetamines, and inhibitors including cocaine revealed that each bound to the same general central cavity, but conformational plasticity in the protein enabled specific recognition of the diverse range of chemotypes.[41] The substrates promoted formation of the occluded conformation, equivalent to that seen with leucine in LeuT, while inhibitors appeared to be wedging the protein into a fixed conformation, which would prevent the movements required for transport.

Despite the limitations described earlier in using the prokaryotic proteins to model the ligand-binding properties of eukaryotic counterparts, a number of authors have successfully used the structures to generate models of eukaryotic proteins and, by concentrating on the substrate binding site, have successfully identified novel ligands through virtual screening approaches[42,43] demonstrating their potential for drug discovery.

3.08.1.2.3 Ion channels

Ion channels allow the flow of anions or cations across a membrane in response to the electrochemical gradient of the ion, usually at much higher flux than transporters. They are thus key determinants of the electric potential difference across cell membranes, underlying activation processes for electrically excitable cells such as nerves and muscle. A channel can exist in states that are closed or open to the passage of ions, and the two predominant means of controlling this have led to the primary classification of channels as being gated by voltage or ligands. Understanding the interplay between the voltage and ligand sensor, the opening and closing of the channel, and the pore that allows passage of the required ion and selects others has been a driving force behind structural studies.

As for GPCRs and transporters, progress with ion channel structural biology has been enabled through the use of model systems, but in line with the greater diversity of the ion channel family, alternative approaches have also been utilized. In particular, studies of

isolated regulatory domains other than the transmembrane region have been useful. Although initial studies concentrated on how the structure of the ion channel pore allows conductance of some ions and not others, subsequent studies have addressed questions as to how the channels are themselves regulated, including identifying and characterizing the binding sites of some pharmaceutically important ligands.[44]

The first breakthrough structure for the ion channel field was that of the bacterial potassium channel KcsA.[45] Efforts to solve the structure of this channel were prompted by sequence similarities, which suggested it contains a structural motif that represents the fundamental pore domain found in many other channels, meaning the structure would be of high value as a model. The structure revealed a tetrameric arrangement of subunits, with each monomer composed of two transmembrane helices, and a shorter helix leading toward the pore formed by the well-conserved TVGYG sequence (**Fig. 2A**). The oxygen atoms presented by the four copies of this sequence (one from each monomer) coordinate dehydrated potassium ions at four sequential positions as they travel through the pore. The immediate focus of attention arising from this structure was how the channel achieves such high selectivity for potassium over the only slightly smaller sodium ions, with the initial suggestion being that the pore cannot contract enough for the TVGYG sequences to coordinate sodium ions. This hypothesis, however, is not the only one. The nonselective channel NaK, which normally contains two sequential cation-binding sites, was modified to contain one or two additional sites. It was found that only the protein with four binding sites was selective for potassium over sodium; those with two and three sites are nonselective, despite all proteins having pore dimensions equivalent to that of KcsA.[53]

The pores of most other ion channels are recognizably similar to that of KcsA, with notable exceptions being the voltage-gated chloride channels.[54] Structures of voltage-gated (Kv) and inward-rectifying (Kir) potassium channels revealed pores generated by tetrameric assemblies of transmembrane helices and selectivity sequences similar to KcsA, although with additional elements allowing for functions such as voltage sensing or regulation by ligands (**Fig. 2B**).

A fourfold repeat of the motif is observed in eukaryotic sodium channels, although in this case it arises from a single polypeptide chain containing 24 transmembrane helices, arranged in four bundles of six transmembrane helices. In contrast, the structure of Orai,[55] which forms the pore of the calcium release-activated calcium channel (CRAC), reveals a sixfold arrangement of bundles of four helices, with residues from the M1 helix coordinating cations as they pass through the pore. Although once again it appears the ions occupy a sequential set of binding sites as they pass through the channel, the means by which this is regulated and selectivity is achieved appear to be different compared with the potassium channels. In this case, a ring of basic residues near the intracellular surface possibly constitutes a site for negative regulation by anions and hindering the progress of sodium and potassium while allowing calcium to pass through slowly, probably driven by a gradient of approximately 40,000-fold across the membrane.[55]

Fourfold symmetry was also predicted in the ionotropic glutamate class of ligand-gated ion channels (LGICs). The transmembrane region forming the pore was predicted to resemble an inverted potassium channel and is attached to two extracellular domains forming the glutamate binding site. Initial X-ray structural studies focused on the glutamate binding domains, revealing details of the ligand-binding site.[56] These are most expanded in the apo state; slightly contracted in the presence of an antagonist, more with a partial agonist; and most contracted with agonists bound.[57] Although the conformational differences revealed in these structures could be seen as providing a mechanism for opening and closing the pore, formation of symmetrical dimers between domains from two of the four chains from the receptor appeared incompatible with a fourfold symmetry for the pore. The structure of a near full-length AMPA receptor revealed that a symmetry mismatch does occur, with the extracellular domains with twofold symmetry attached to a fourfold symmetrical pore[47] (**Fig. 2C**).

In contrast, a fivefold arrangement of subunits is observed in the Cys-loop class of ligand-gated ion channels. Members of the Cys-loop family can be selective for either cations or anions, with the former including members that are regulated by serotonin and acetylcholine while the latter including receptors for glycine and γ-aminobutyric acid. Each subunit is composed of a large extracellular domain and a transmembrane domain, and the pentamer can be composed of identical monomers or different but related subunits. The first detailed structural information was obtained for the nicotinic acetylcholine receptor. X-ray structures of pentameric acetylcholine-binding proteins from molluscs and annelids[58] have been used as the model for the extracellular domains, which include the nicotine binding sites, and structures with the partial agonist varenicline have been described.[59] Electron microscopy studies of the full receptor from the electric organ of the torpedo fish[48] at 4 Å resolution gave insights into the overall topology of the pentameric complex (**Fig. 2D**). It was not until 2008 when an X-ray structure of a bacterial homologue ELIC[60] showed the detailed arrangement of the pore formed by the five copies of the M2 helix. The absence of a ligand for ELIC caused a switch to another bacterial homologue, the proton-gated GLIC, for which subsequent structural studies elucidated the structural differences between open and closed states of the pore[61,62] and led to structures with propofol and desflurane, revealing a general anesthetic binding site in the upper part of the transmembrane domain[49] (**Fig. 2E**).

The first high-resolution view of a eukaryotic Cys-loop receptor came with the glutamate-gated chloride channel α (GluCl),[63] which contains three distinct binding sites for the endogenous neurotransmitter glutamate, the allosteric agonist ivermectin, and the channel blocker picrotoxin. The X-ray structure of the mouse serotonin $5HT_3$ receptor[64] subsequently highlighted details of the ion conductance path, the neurotransmitter binding site, and the relative arrangement of subunits. Interestingly, despite the fact that a potent inhibitor was used to obtain the structure, the features revealed were not conclusively of an open or closed state. The structure of another Cys-loop receptor, the pentameric human $GABA_A$ receptor,[50] gave the first high-resolution view of this chloride channel, which has been frequently targeted for drug discovery (**Fig. 2F**). Along with explaining a mechanistic role for disease-associated mutations, it showed benzamidine, a previously unknown agonist, bound in the neurotransmitter site, identifying opportunities to develop a new class of $GABA_A$ modulators by structure-based drug design. The structure of the glycine receptor a3 with

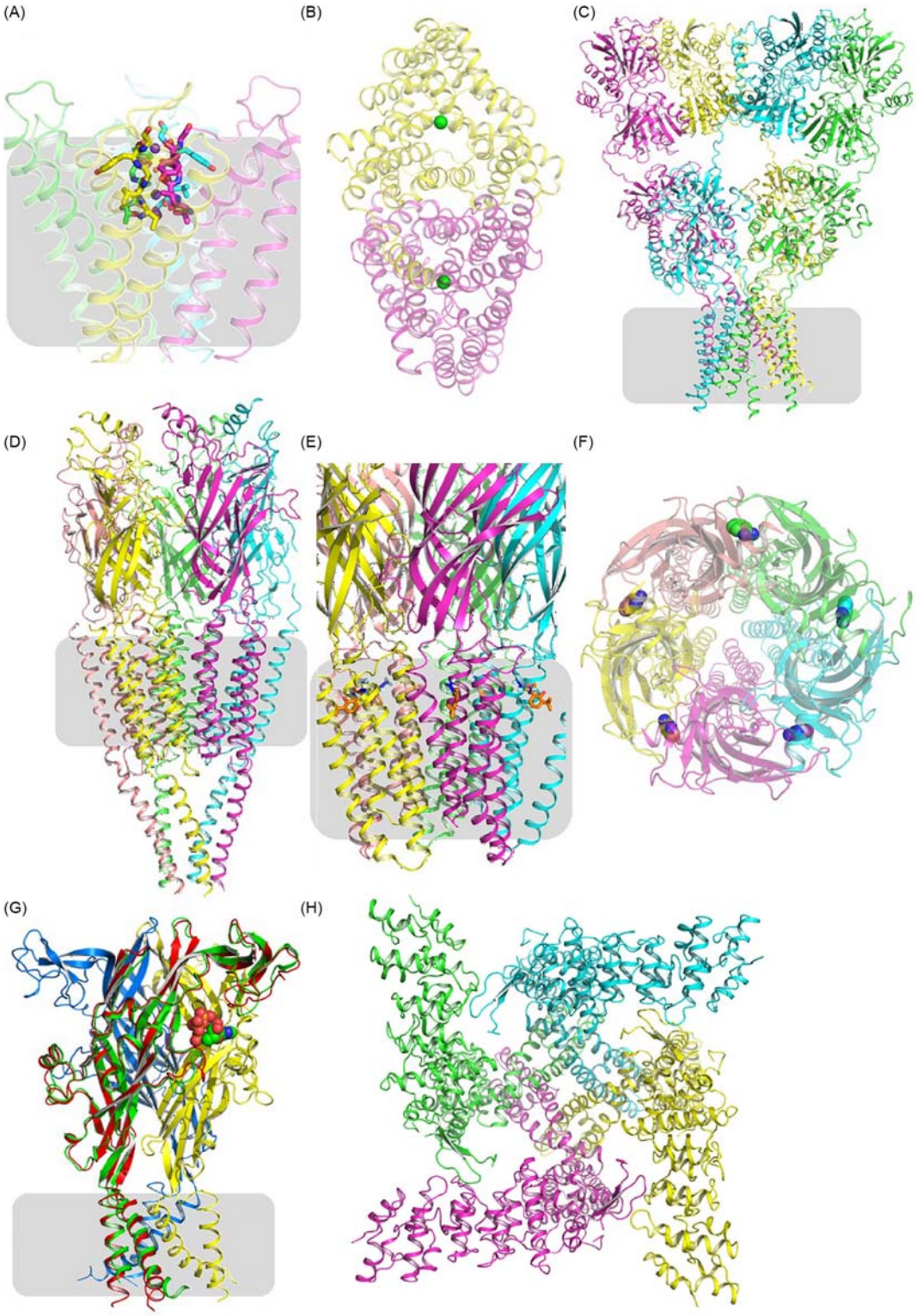

Fig. 2 Examples of ion channel structures. (A) Extracellular view of the crystal structure of the KcsA tetramer (PDB ID, 1BL8[45]) colored by chain. For every chain, the TVGYG motif is represented in stick and the potassium ions and a water molecule as spheres. (B) Extracellular view of StClC dimer (PDB ID, 1PKL[46]) colored by chain. Cl^- ions in the selectivity filters are represented as green spheres. (C) Side view of the crystal structure of the AMPA-sensitive, homotetrameric, rat GluA2 receptor (PDB ID, 3KG2[47]) colored by chain. (D) Side view of the crystal structure of the nicotinic acetylcholine receptor of the torpedo fish (PDB ID, 2BG9[48]) colored by chain. Membrane region and extracellular and intracellular sides are indicated. (E) Side view of part of the crystal structure of the pentameric ligand-gated ion channel GLIC (PDB ID, 3P4W[49]) colored by chain. Molecules of desflurane (from the PDB ID, 3P4W) and propofol (PDB ID, 3P50) are shown, respectively, as blue and orange sticks.[49] (F) Extracellular view of the

strychnine bound[65] added weight to the proposal of a general mechanism in which antagonists expand the orthosteric site and cause closure of the pore in the transmembrane domain.

A more complicated mechanism of ion conductance has been made apparent from the recent 3.1 Å resolution structure of the P2X4 ATP-gated sodium channel. The sodium ions appear to need to pass through a series of vestibules in the large extracellular domain, the conformation of which needs to be regulated by the binding of ATP to a site which is 45 Å distant from the pore domain. Subsequent comparisons of apo- and ATP-bound receptors revealed that ATP induces widening of several of the vestibules in the extracellular and transmembrane domains (**Fig. 2G**).[51]

X-ray structures of the TREK potassium channel[66] have revealed sizable rearrangements of helices in the transmembrane region. One of these structures included norfluoxetine, the active metabolite of fluoxetine (Prozac), which is a state-dependent blocker of the channel. The ligand was observed to bind to the transmembrane region adjacent to the pore filter, revealing a binding site that could be the basis of future structure-guided medicinal chemistry.

A recent development in structural biology of membrane proteins is illustrated from the structure of the VR1 potassium channel, obtained using single-particle cryo-electron microscopy methods. Recent advances in cryo-electron microscopy have enabled structures to be determined at resolutions near those obtainable with X-rays. This represents a very exciting development in the structural biology of membrane proteins.[67] Structures of TRPV1 in the unliganded, closed state[52] (**Fig. 2H**) and activator-bound open states[68] have resolutions of up to 3.4 Å and allowed observation of rearrangements to the outer pore helix and selectivity filter and relaxation of a hydrophobic constriction further into the pore, suggesting ion transport may be controlled at two sites. Subsequently, the cryo-EM structure of the TrpA1 channel at approximately 4 Å[69] revealed structural features of channel blocking and an antagonist binding site within the transmembrane region of the receptor, near the ion gate.

The structural information now available for ion channels and transporters is starting to be translated into structure-based drug design applications.[70] One example, reported by Schlessinger et al.,[70] is a remarkable use of structure-based drug design, which illustrates the future potential in the field. The authors created a homology model of the norepinephrine transporter (NET) using LeuT as a template. They then applied molecular docking to screen more than 6000 drugs in silico. Among them, 10 out of 18 high-scoring ligands were found to be NET inhibitors. Overall, our understanding of ion channels and transporter structural biology is evolving steadily, but, due to their added complexity, at a much slower pace compared with the SBDD revolution started in 2007 for the GPCRs with the β_2-adrenergic receptor noted earlier.[11]

3.08.2 Novel Structural Understanding of Membrane Proteins Focused on GPCRs

In the earlier section, the progress in our understanding of the structural biology of the key membrane protein families has been introduced. To date, for transporters and ion channels, despite the number of ligands and also drugs known that act at these targets and the recent increase in our knowledge of how some of these molecules bind to their protein partners, the know-how has just started to be translated to structure-based drug design (SBDD) applications. As such, the remainder of this article, which is focused on case studies of drug design, is largely limited to a discussion of GPCRs. This membrane protein family then serves as an example of how SBDD methods can be applied to the discovery of new ligands and lead compounds. In this section, we discuss in some detail the structural features of GPCRs that relate to their function, influenced by ligand binding. We describe briefly here examples of hit generation using in silico approaches in the various subfamilies of this system and also computational approaches to understanding ligand binding, unbinding, and kinetics for GPCR targets.

3.08.2.1 From Structure to Function

Based on the multiple available GPCR crystal structures, we can define broadly three distinct conformations these receptors can adopt: (I) an *inactive state* when the receptor is crystallized in complex with an antagonist or inverse agonist, (II) an *agonist-bound state*, and (III) an *active state* resulting from a ternary complex composed by the receptor, an agonist, and an intracellular protein (the G protein, a G protein surrogate, or arrestin). Most likely, less stable intermediate conformations link these three states. Overall, these conformations have distinct structural features resulting from differences in the chemical structure of the bound ligand.[71] The mechanisms that control GPCR receptor activation upon ligand binding are highly complex and in the past have been hindered by a lack of structural knowledge. For ligand design, an understanding of what governs the activation process is likely to be very important to relate the features of the ligand to agonism versus antagonism or to allow the in silico prediction of the structure of an agonist form of a receptor from an antagonist structure (or vice versa).

crystal structure of the human $GABA_A$ homopentamer receptor (PDB ID, 4COF[50]) colored by chain. In every chain, benzamidine is shown as spheres. (G) Side view of the crystal structure of the trimer ATP-gated P2X4 ion channel in the closed apo state (PDB ID, 4DW0[51]) colored by chain in *red*, *yellow*, and *blue*. The structural alignment of one monomer of the open ATP-bound P2X4 channel (PDB ID, 4DW1[51]) is included in *green* as ribbon with the ATP ligand as sphere representation. (H) Extracellular view of the structure of TRPV1 ion channel determined by single-particle electron cryo-microscopy (PDB ID, 3J5P[52]) colored by chain. In Figs. A, C, D, E, and G, the membrane region is indicated in gray, with the extracellular side and the intracellular side on the top and on the bottom, respectively.

Of significance, several pairs of active and inactive GPCR structures have recently been solved enabling detailed structural insight into the activation process of GPCRs. Combined with structural analyses, they have enabled Tehan and colleagues[72] to examine several different theories[20,73] proposed for GPCR activation. The authors proposed activation steps that are intrinsically related through their effect on the central hydrophobic core of GPCRs. Transmembrane helix 3 (TM3) and TM6 are at the heart of the common activation pathway thanks to the direct contacts with every other helix except TM1.[74] GPCR activation affects TM3 and TM6 to impart these common movements[75] seen within the active and inactive pairs available to date. These include (**Fig. 3A**) (I) the movement of TM5, (II) the upward movement of TM3, (III) the rotation of TM6, and (IV) the inward movements of TM7 and TM1. The rearrangement of the hydrophobic residues between TM3 and TM6 in the core of the receptor consists primarily of L3.43a, F6.44a, X6.40a (where X is a bulky hydrophobic residue, I, L, V, or M), and to a lesser extent X6.41a (**Fig. 3B**). The rearrangement of these contacts seen in the active-state structures allows for the gross TM movements, which opens a water channel through the hydrophobic core (**Fig. 3C and D**). The active conformation is transiently stabilized by the interactions with the water molecules allowing the creation of an H-bonding network from the extracellular side of the receptor to the intracellular side. The overall result is the opening of the cytoplasmic face of the receptor where G proteins interact. Crystallographic data of the β_2-adrenergic receptor (β_2AR), the M_2 muscarinic receptor, and the μ-opioid receptor (μOR) support that this extensive polar network between the ligand-binding pocket and the cytoplasmic domains has a central role in signal propagation.[78]

The importance of these key residues implicated in the proposed class A GPCR activation process is supported by in-depth conservational analysis and studies resulting in constitutively active mutants.[72] From the comparison of classes A, B, and F, the hydrophobic core residues appear to create very similar, but not identical contacts among the different subfamilies.[79] TM3 is always at the center of the contact network and may be a structural and functional hub, while TM6 is thought to be creating the most distinct network of interactions in the transmembrane domain among the subfamilies. Additionally, class B GPCR activation is likely affected by the presence of large extracellular domains (ECDs). A combination of structural biology approaches now suggests, for example, that the apo glucagon receptor (GCGR) can adopt both an open and a closed conformations associated with extensive contacts between the ECD and transmembrane domain.[80] The peptide hormone agonist acts to stabilize the open state by both interacting with the ECD and also triggering the activation by inducing conformational changes through contacts within the orthosteric site.

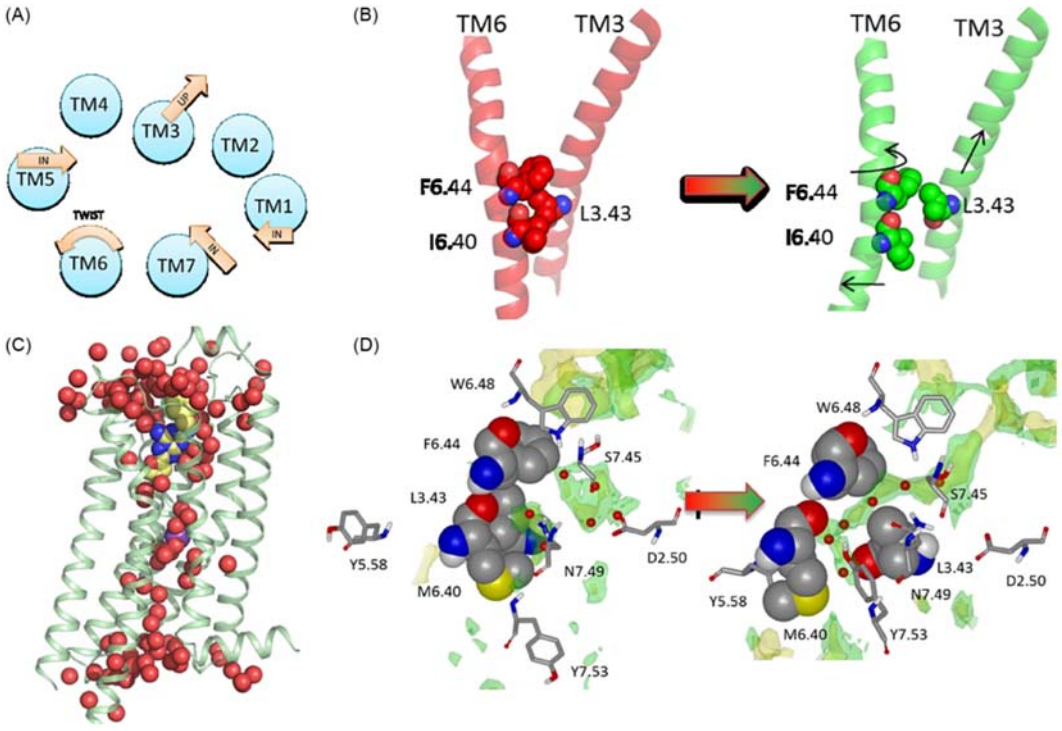

Fig. 3 GPCR activation conformational changes. (A) Arrows indicate the key movements of the transmembrane helices (TM1–7) from an extracellular view point. (B) Conformational changes of hydrophobic core residues in TM6 and TM3 of the β_2AR from the inactive (*red*) to active (*green*) conformation. (C) High-resolution X-ray crystal structure of the adenosine A_{2A} receptor (in *green* ribbon, PDB ID, 4EIY[76]) in complex with ligand ZM-241385 (sphere representation). The fusion protein is not shown. Water molecules linking the extracellular orthosteric site and the intracellular G protein-binding region are shown as red spheres. (D) Comparison of hydrophobic core region in the inactive (*left*) and active (*right*) rhodopsin X-ray crystal structures. The water molecules (*red* spheres) create a continuous water channel only in the active state, which is broken by the hydrophobic core residues (shown in spheres) in the inactive state. Other residues are shown in stick, and the hydrophobic and hydrophilic hot spot regions are included as transparent surfaces, respectively, *yellow* and *green*. These have been calculated using the GRID software,[77] using the OH2 water probe contoured at used −5.0 kcal/mol and the C1 = aromatic carbon probe contoured at −2.5 kcal/mol.

Recently, the publication of the neurotensin receptor NTSR1 structures has provided insight into mechanistic details of an active-like, agonist-occupied peptide GPCR.[81] The binding of the agonist peptide near the receptor surface results in the conserved W321$^{6.48a}$ adopting a conformation parallel to the membrane plane sealing the top of a collapsed Na^+ ion-binding pocket. This movement creates the conformational changes of the hydrophobic core residues (discussed earlier) in the inner half of NTSR1 promoting the productive interaction with G_q protein. The comparison of the X-ray crystal structure of the agonist-bound μOR in complex with a G protein mimetic with other active-state structures additionally reveals a common rearrangement in the packing of three conserved amino acids: I3.40a, P5.50a, and F6.44a.[78] Molecular dynamics simulations illustrate how the ligand-binding pocket is conformationally linked to this conserved triad that may initiate the cascade of structural changes involved in activation.[78]

It is now believed that GPCRs allosterically activate heterotrimeric G proteins and trigger GDP release through a highly conserved mechanism.[82] GPCRs create key contacts with the C-terminus and αN–β1 hinge region of the Gα subunit enabling the transfer of conformational changes to the nucleotide-binding pocket of the Gα subunit.[83,84] The interaction specificity between the G protein and the GPCRs results from disorder-to-order transitions of G protein regions important for the interactions with the receptors. This might explain how the GPCR-Gα system diversified rapidly while conserving the allosteric activation mechanism. Application of solution-state NMR to examine the process of μOR activation showed that the conformational changes in TM5 and TM6 required both the agonist ligand and the G protein.[85] The orthosteric site is likely only weakly coupled to the G protein-binding region, while the intracellular loop 1 and helix 8 may play a role in the initial interaction with the G protein that could be important for coupling specificity. Thanks to the recent rhodopsin–arrestin complex crystal structure, it is now possible to extend this structure-based analysis to arrestins. The structure reveals that the arrangement of TM helices is similar to that in the G protein-bound β_2AR complex, even if the TM6 outward movement is less pronounced.[86] With only four subtypes in vertebrates, arrestins are highly conserved, while the cytoplasmic interfaces of GPCRs are mainly nonconserved. However, electrostatic complementarity has been proposed to be an adaptive mechanism for arrestins to pair promiscuously with the large number of GPCRs in the family.

Agonists and antagonists or inverse agonists can often be identified within the same chemical class, and relatively small changes to the chemical structure can cause a change in the pharmacology (sometimes termed "mode switching"). A very recent review examines in some detail these examples of the structure–activity relationships (SAR) that relate to changes in ligand pharmacology for GPCR targets, and the reader is referred to this paper to explore this topic in more detail.[21]

3.08.2.2 Binding Site Analysis

GPCR X-ray crystal structures provide a crucial insight into the complexity of this protein family. They demonstrate the large diversity of regions in the receptor transmembrane domain that can be targeted with small molecules to affect protein function (**Fig. 4A**). The majority of class A ligands crystallized bind to the orthosteric site in the extracellular half of the receptor, inside the helical bundle, and below the extracellular loops not interacting with TM1. The precise location is highly variable, and as expected, it is linked to the specific properties of the binding site. Interesting exceptions are the GPR40 agonist TAK-875[24] and the negative allosteric modulator BPTU[26] crystallized in quite unexpected binding modes (**Fig. 4B**). The first binds between TM3 and TM4 to some extent near the orthosteric site and partially outside the helical bundle in the membrane. BPTU instead interacts only with the membrane-exposed extracellular side of TM1, TM2, and TM3. They together highlight the complexity and the multiple potential binding regions exploitable in GPCR structure-based drug discovery. This is even more evident when we extend the analysis beyond class A. The negative allosteric modulator (NAM) CP-376395 binds the class B CRF_1 receptor deep in the core of the receptor in a mainly hydrophobic site located among TM3, TM5, and TM6.[15] Class C NAM ligands like mavoglurant[18] bind in a region located between the class A orthosteric site and CRF_1 small-molecule binding pocket (**Fig. 4A**). In contrast, class F ligand binding seems to involve extensive interactions with the receptor extracellular face and loops.[19]

The novel structural information now available allows a detailed computational analysis of the chemical and physical properties of the binding sites and an estimation of the binding site water molecules' relative free energies.[93] These methods have been used to evaluate binding site druggability. Ligands tend to bind to highly specific regions of the protein characterized by a combination of hydrophilic and lipophilic/hydrophobic features, compatible with balanced small-molecule properties in best cases (**Fig. 2C**). Of particular interest are subregions of the binding site with mixed hydrophobic and hydrophilic properties occupied by displaceable water molecules predicted to have a free energy higher than bulk solvent. These areas are often exploited by high-affinity ligands to create productive interactions with the receptors resulting in significant free energy of binding gain. The orthosteric site of the A_{2A} receptor represents an excellent example of a druggable pocket (**Fig. 4C**, PDB ID, 3UZC[87]): the ligand **4g** binding mode allows effective interactions with key lipophilic/hydrophobic regions of the pocket displacing high-energy waters. Interestingly, the high chemical diversity among GPCR antagonists significantly correlates with the binding site hydrophobicity and negatively correlates with the number of hydrogen bond donors in the binding site.[94] In addition, as noted by Levit et al., there seems to be a link between the number of disulfide bridges in the extracellular region of a receptor and the range of molecular weights of antagonists that bind, suggesting the importance of the "entrance pathway" to the orthosteric site in determining the size selectivity for GPCR antagonists.[94]

The increasing number of GPCR crystal structures allows us now to combine experimental ligand binding and functional activity data with high-resolution structural analyses of GPCR–ligand interactions[95]. Potentially, this approach, together with receptor mutagenesis studies, amino acid sequence analyses, and novel insight into GPCR conformational changes upon activation, enables the identification of the molecular and structural determinants of ligand affinity, functional activity, and selectivity.[96,97] Although in its infancy, the observed contraction of the binding site upon activation (**Fig. 4D–G**) allows the use of putative ligand-docking modes to be applied to the active and inactive-state crystal structures to help understand their functional activity and allow an in silico assessment

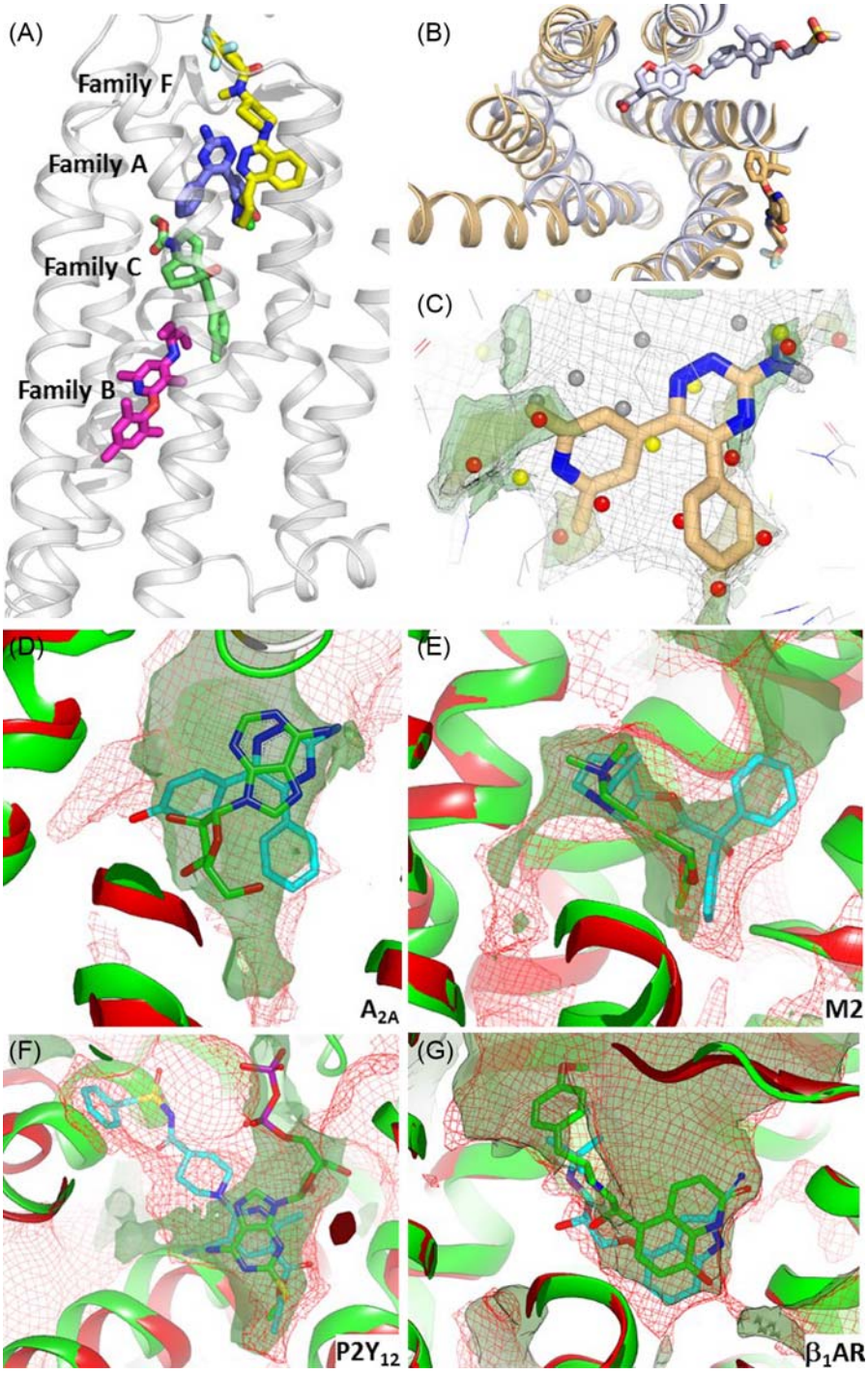

Fig. 4 Small-molecule binding sites in the GPCR transmembrane region. (A) Comparison of the crystallographic ligand-binding site locations for class A (ligand **4e** in *purple*, PDB ID, 3UZC[87]), B (ligand CP-376395 in *magenta*, PDB ID, 4K5Y[15]), C (ligand mavoglurant in *green*, PDB ID, 4OO9[18]), and F (ligand LY2940680 in *yellow*, PDB ID, 4JKV[19]) in a representative helical bundle shown as ribbon (A_{2A} receptor). (B) Binding modes of the allosteric modulators TAK-875 (shown as *light blue* spheres) to GPR40 receptor (shown as *light blue* ribbon, PDB ID, 4PHU[24]) and BPTU (shown as *light orange* spheres) to $P2Y_1$ receptor (shown as *light orange* ribbon, PDB ID, 4XNV[26]). (C) Adenosine A_{2A} receptor binding site druggability analysis based on GRID[77] and WaterMap.[88] Hydrophobic and hydrophilic hot spot regions are included as transparent surfaces, respectively, yellow (C1 = carbon sp^2 probe contoured at −2.8 kcal/mol) and green (OH2 water probe contoured at −5.0 kcal/mol). The shape of the pocket is shown as gray mesh (C3 carbon sp^3 probe contoured at used 1 kcal/mol). The triazine **4g** antagonist (PDB ID, 3UZA)[87] is shown as stick, the protein as line, and the apo WaterMap waters as small sphere color-coded according to their predicted free energy (*red* if $\Delta G > 3.5$ kcal/mol, *yellow* if ΔG between 2.5 and 3.5 kcal/mol, *blue* if $\Delta G < -1$ kcal/mol, and gray in the other cases). (D–G) Active site contraction upon receptor activation. Comparison of the inactive (protein and ligand in *red*) and active (protein in *green* and ligand in *cyan*) ligand-binding site of adenosine A_{2A} (D, PDB ID, 3UZC[87] and

of ligand pharmacology.[9] Ligands with the same functional activity can then be efficiently classified on the basis of their protein–ligand interaction profile. The use of protein–ligand interaction fingerprints derived from ligand-bound crystal structures with known agonists or antagonists may give effective tools to postprocess docking poses to identify ligands with a specific functional effect.[98]

Molecular modeling using the available X-ray GPCR structures is also beginning to be applied to predict GPCR polypharmacology using a structure-based approach to provide a consistent understanding of ligand recognition.[99] However, the use of structure-based methods to discover agonists has so far perhaps been hampered by limited atomic-level understanding of the activation mechanism (described earlier) and a chemical bias toward antagonists in the screening libraries.[100] High ligand complexity is often required for receptor activation, and a library of commercially available small molecules may not be suitable for agonist identification in many cases. Virtual screening to identify antagonist and agonist hits is discussed in more detail in the following section.

3.08.3 GPCR Ligand Design

3.08.3.1 Hit Finding

Virtual screening (VS) represents a widely used approach in modern drug discovery, playing an important role in the identification of novel hit molecules. In general, the approach consists of a fast in silico evaluation of the probability of a molecule having a desired biological activity. The method is typically applied to a large database of ligands, and the output is a ranked list based on the likelihood of relevant activity. VS techniques can be broadly divided in two families: (I) structure-based, taking advantage of known protein target coordinates, and (II) ligand-based, exploiting only the information derived from one or more active ligands. Breakthroughs in membrane protein crystallography have had a crucial impact in computational approaches used in GPCR virtual screening shifting the interest toward SBDD approaches. Before 2007, GPCR VS was mainly ligand-based or using homology models derived from the rhodopsin X-ray data (discussed earlier). Now, the available structural information includes 26 class A, 2 class B, 2 class C, and 1 class F GPCRs (Figs. 5–7). Class A X-ray diffraction crystals currently publicly available consist of eight aminergic, eight peptide, three protein (one is an NMR structure), three lipid, one sensory, and three nucleotide receptors. There is still no structural information for melatonin, steroid, ali carboxyl acids (including hydroxycarboxylic acid, oxoglutarate, and succinate receptors), adhesion, and orphan receptors.

The application of SBDD methods relying on the coordinates of GPCR targets can be further expanded by using homology modeling (HM) techniques. We broadly consider 30% sequence identity between template X-ray data and a target GPCR, the minimum threshold to apply this approach. Based on this general definition, we can divide GPCRs in three main groups: (I) those with experimental structural information, (II) those suitable for homology modeling, and (III) those thought challenging to be evaluated using a structure-based approach (Figs. 5–7). In addition, the success of using a homology modeling approach for VS is directly linked to the ability to improve, optimize, and validate the 3-D model using available experimental data.[103–107] When an X-ray structure is not available, another strategy to increase the success rate of an homology model-based VS depends on the creation of a complex hybrid protocol combining molecular docking with ligand-based approaches. Several examples of VS on GPCRs are reported in Table 1. They include broadly four different strategies: (I) structure-based VS, (II) homology model-based VS, (III) ligand-based VS, and (IV) hybrid protocols involving HM and ligand-based techniques. These studies must be compared with care since there are important differences, for example, protocols/software used, the general druggability of the target GPCR, the conformation of the receptor (active/inactive), important subjective choices in the ligand selection criteria, and the selection of the library for screening. In some cases, the library is restricted to fragment-sized molecules (e.g., <300 Da in size). Not surprisingly, the resulting hit rates are variable (Fig. 8A) but seem overall to support an important positive effect on the hit rate performance coming from the use of an X-ray structure.

When in silico screening millions of molecules, it is only possible to visually analyze the result for a small percent (typically a few hundred) of the top-ranked list. Molecular docking software aims to find the best compromise between speed and accuracy. These methods use efficient algorithms to explore the conformational space accessible to the ligand in the binding site and then evaluate the poses using simple scoring functions estimating the ligand–protein interactions. The so-called enrichment is generally linked to the ability to detect and give a low score to a ligand not able to bind the protein target. The top-scoring ligands will include a high number of false positives that an expert user can often identify and discard. The selection of compounds from a 3-D analysis of hits in a binding site is of course highly subjective and biased, but it represents a crucial part of a virtual screening campaign. Another important aspect often oversimplified in the literature is the preparation of the database used for the VS. Accurate preparation can dramatically reduce the number of false positives that would need to be discarded during the visual inspection step. An example of a protocol to prepare a database for VS and library design is illustrated in Fig. 8B.

It is not possible here to describe each example listed in the table nor is the Table 1 completely comprehensive. Instead, in later sections, we give a number of examples of SBDD efforts where hits have been developed into more advanced hit series or to lead compounds.

2YDO[22]), muscarinic M_2 (E, PDB ID, 3UON[89] and 4MQT[25]), $P2Y_{12}$ (F, PDB ID, 4NTJ[90] and 4PXZ[91]), and β_1AR (G, PDB ID, 2VT4[11] and 2Y02[92]) receptors. Receptors are shown in ribbon, ligands in sticks, and the pocket shape calculated using GRID (using the C3 probe with an interaction energy threshold of 1 kcal/mol) in mesh (inactive states) or transparent filled surface (active states).

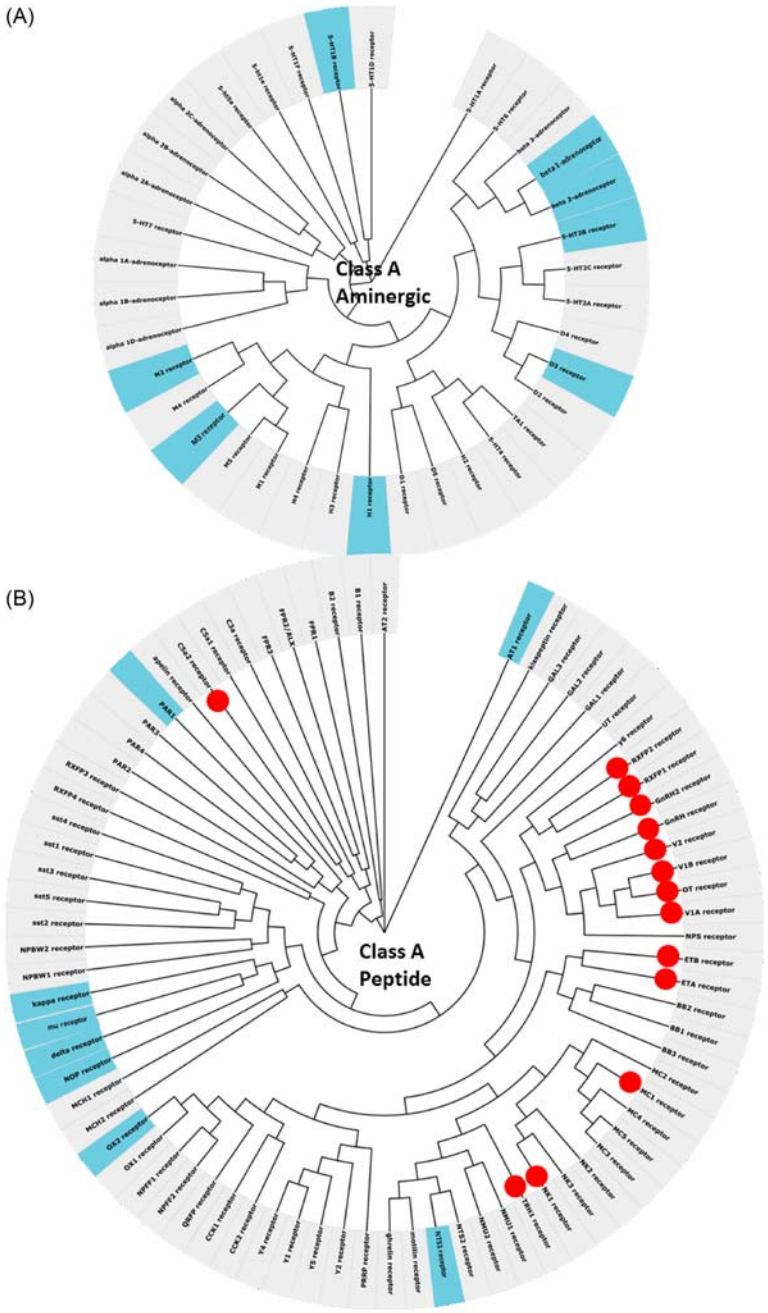

Fig. 5 Phylogenetic tree for class A GPCR aminergic (A) and peptide (B) receptors. Analysis created using the tools available in the GPCRDB.[101] GPCRs with available crystal structure in the Protein Data Bank[102] are highlighted in blue. Red circles highlight GPCRs for which the creation of a homology model can be particularly challenging. For these receptors, only low (less than 30%) sequence identity templates are available.

3.08.4 GPCR Computational Simulation

3.08.4.1 Molecular Dynamics Simulations

The structural plasticity of GPCRs is directly linked to their versatile functional activity.[147] The conformational space accessible to the receptor can be represented as a very rugged energy landscape. It corresponds to a multidimensional hypersurface with a very large number of valleys (stable conformations) and peaks (energy barriers).[148,149] The description of these energy levels can be evaluated more accurately in statistical terms. During that time, the GPCR will follow a temperature-dependent exploration of the different states. GPCR crystal structures represent a static low-energy snapshot of the conformational complexity of the protein.

Recent improvements in the computational algorithms, hardware, and underlying physical models[150] have allowed atomic-level molecular dynamics simulations of GPCRs to reach timescales as long as milliseconds. The full-atomic detailed MD including an

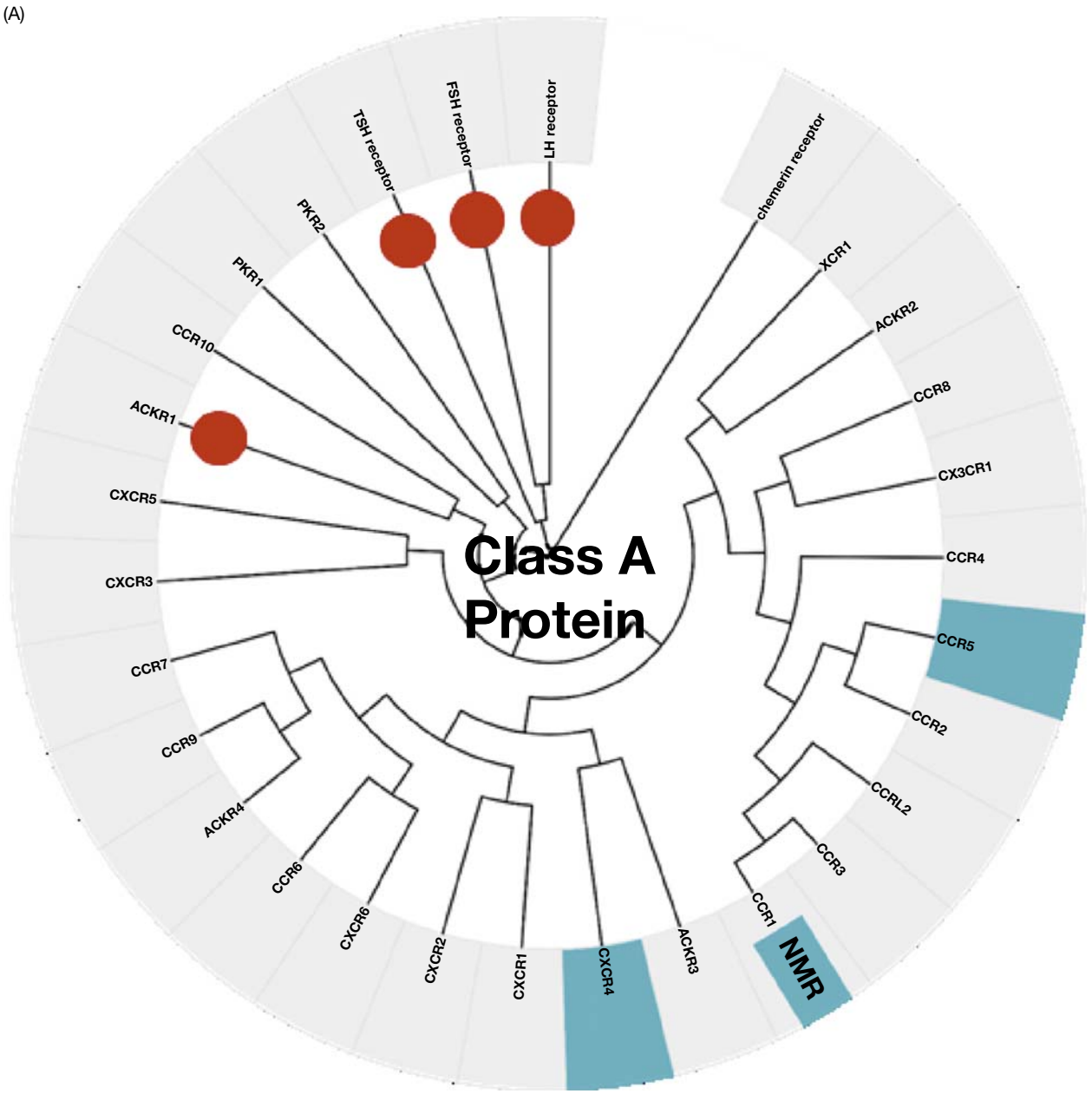

Fig. 6 Phylogenetic tree for class A GPCR protein (A), lipid (B), melatonin/nucleotide/steroid/ali carboxyl (C), and sensory (D) receptors. Analysis created using the tools available in the GPCRDB.[101] GPCRs with available crystal structure in the Protein Data Bank[102] are highlighted in *blue*. *Red* circles highlight GPCRs for which the creation of a homology model can be particularly challenging. For these receptors, only low (less than 30%) sequence identity templates are available.

explicit representation of solvent and the membrane environment can now capture the behavior of biological macromolecules in unprecedented detail.[151] Key aspects that can be investigated include conformational changes critical to protein function and ligand binding. The GPCR energy landscape can be modulated by ligands resulting in direct effects on the conformational equilibrium between the active and inactive states.[148] The overall changes in enthalpy and entropy of the system are affected by the ligand resulting in changes in population and amplitude of motion of given states, suggesting a complex landscape of states and substrates.[152] Indeed, NMR spectroscopy studies support the heterogeneity of conformational states present in agonist-bound and inverse agonist-bound conformations.[153] These states are not necessarily observed in crystal structures suggesting that the link between the orthosteric pocket and the G protein-binding site is not rigid and may be important for GPCRs' ability to engage multiple signaling and regulatory proteins. As such, when considering SBDD optimization of a ligand series based on X-ray data, we need to always take into account that the protein is actually quite mobile and the affinity and potency of a compound are not fully described in any given protein–ligand X-ray data set.

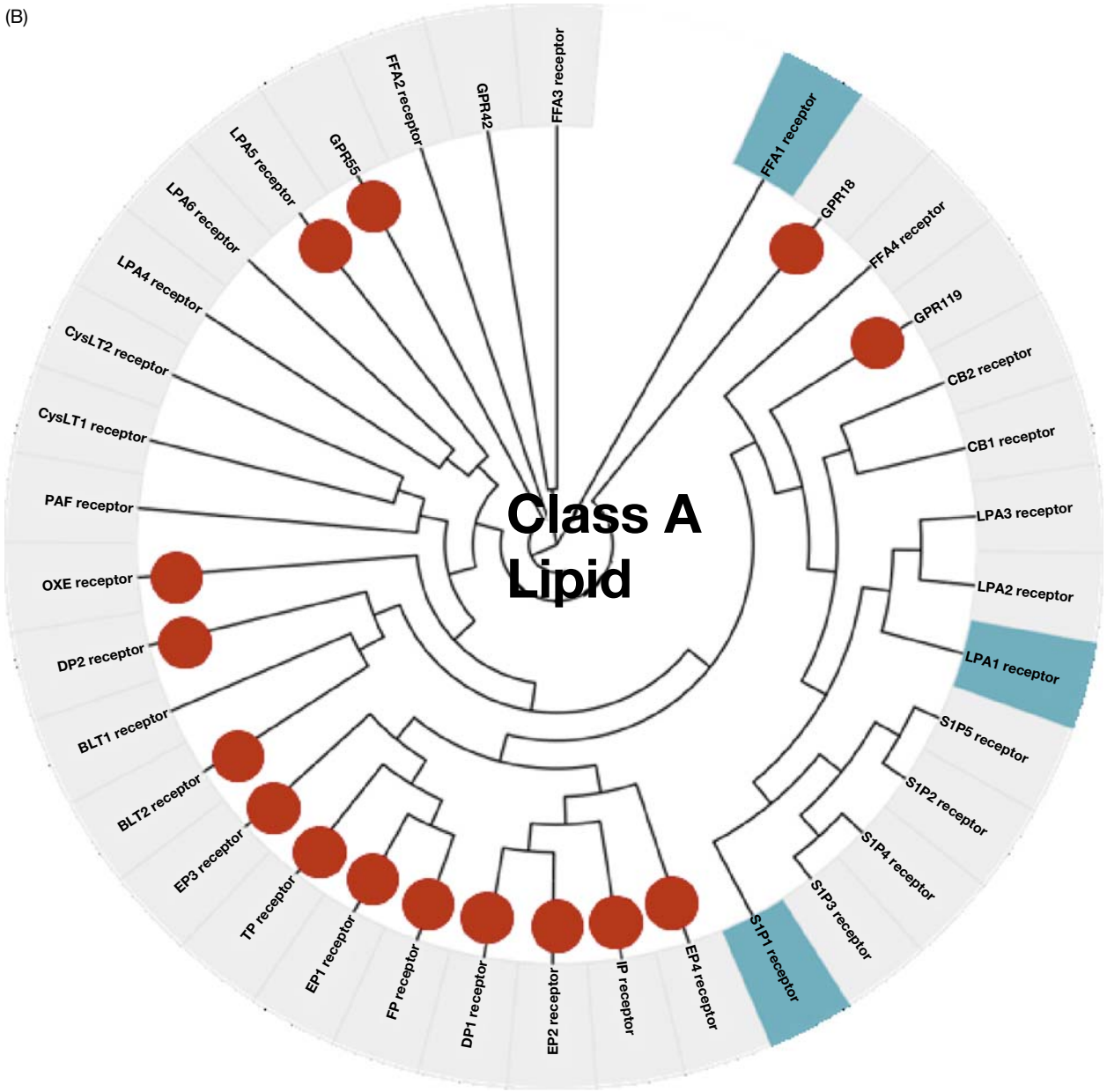

Fig. 6 (*continued*).

MD can now be used to incorporate protein flexibility to improve the virtual screening enrichments for GPCRs.[154] This approach has so far been applied to four GPCRs, and results suggest that selected frames from the MD trajectory can outperform X-ray structures and homology models in terms of enrichment factor and AUC values.[154] The best MD frame improved the early enrichment factor (EF1%) compared with the crystal structures of CXCR4, dopamine D_3, histamine H_4, and also homology models of 5-HT_6, respectively, from 0 to 6.7, from 0.32 to 3.5, from 13.3 to 26.7, and from 0 to 14.1. MD simulation seemed to capture protein conformations representing the key interacting points of the receptor but was less biased toward one specific chemotype. MD simulations have also been applied to evaluate the stability of ligand-binding modes predicted using molecular docking for the adenosine A_{2A} receptor. The proposed protocol successfully combined the rapid sampling of ligand poses into the binding site, typical of docking algorithms, with the thermodynamic accuracy of MD simulations in describing, at the molecular level, the stability of a GPCR–ligand complex embedded into an explicit lipid–water environment.[155] MD allows the simulation of the spontaneous association of ligands to GPCRs achieving final poses in some cases proved to closely match those determined crystallographically.[156] The analysis of the predicted binding event using this approach with several antagonists and agonists of the β_1-adrenergic receptor (β_1AR) and β_2AR shows that ligands follow the same well-defined binding pathway. Initially, ligands have to overcome the largest energy barrier to create initial contacts with a "vestibule"

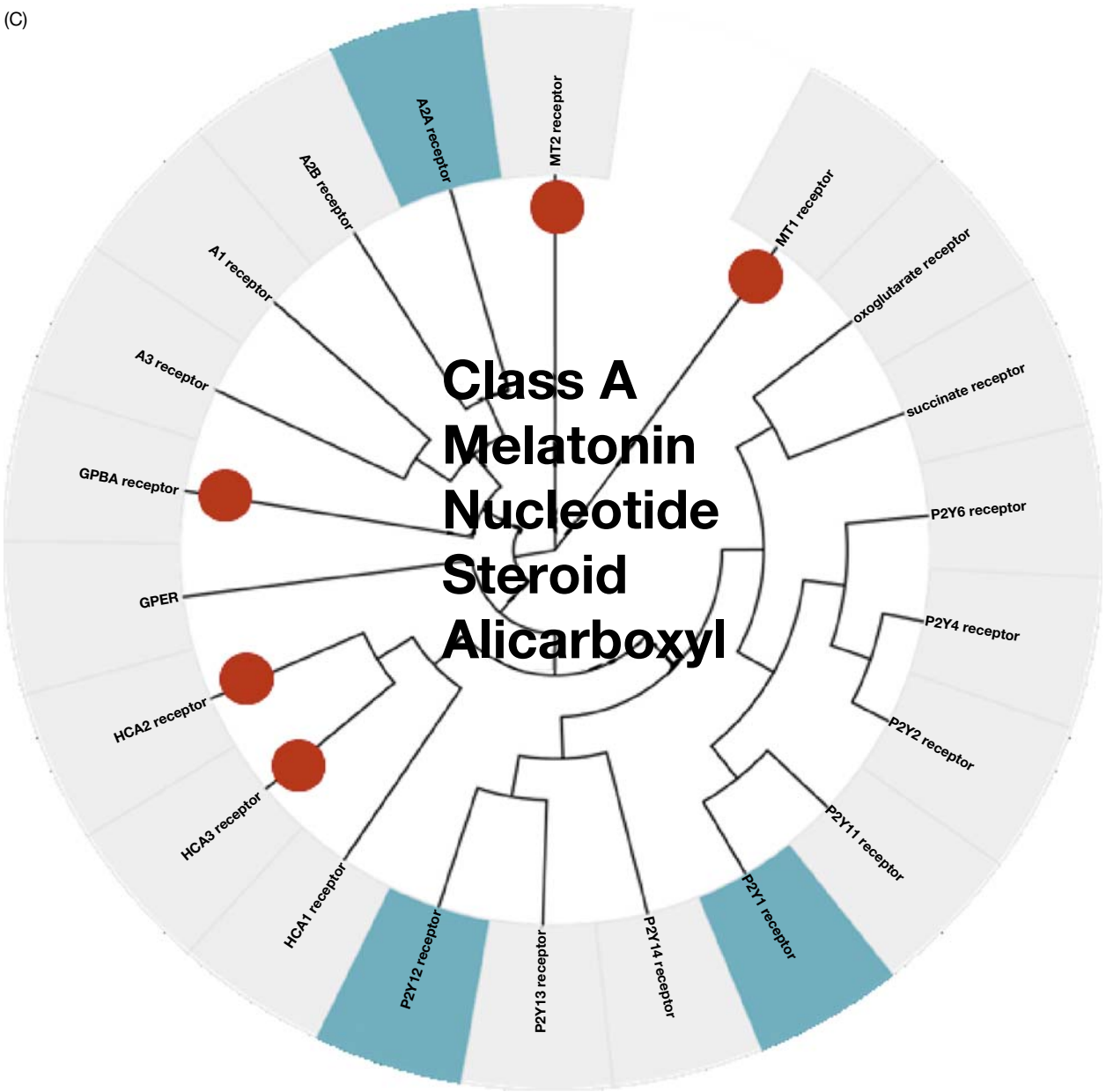

Fig. 6 (*continued*).

region in the extracellular side of the receptor at 15 Å from the final binding site. This early barrier is linked to the desolvation of the ligand and the protein.[156] The understanding of the ligand-binding event at a molecular level potentially provides opportunities for the design of novel ligands and allosteric modulators. MD simulation studies of different muscarinic M_2 allosteric modulator ligands show that they spontaneously associate with the receptor in the extracellular vestibule region forming cation–π interactions with clusters of aromatic residues.[157] Conformational changes and electrostatic interactions between ligands and the receptor revealed mechanisms that seemed to contribute to positive and negative allosteric modulation of classical ligand binding.

Recently, atomic-level simulations have been applied to elucidate the nucleotide release mechanism from the heterotrimeric G protein. The spontaneous opening of the α subunit Ras and the helical domains seems not sufficient for nucleotide release. MD simulation, confirmed by double electron–electron resonance spectroscopy and protein engineering, showed that GPCR binding is required for the structural rearrangements of the Ras domain necessary for rapid nucleotide release.[158] The same computational methods have been exploited to propose a mechanistic model for the sodium/potassium/calcium voltage-gated ion channel superfamily.[159] Again, MD highlighted important molecular switches between activated and deactivated states; on deactivation, the pore hydrophobic collapse rapidly halts ion flow involving an inward S4-helix motion; on activation, S4 moves outward, and fluctuations allow water and then potassium ions to enter the pore.

(D)

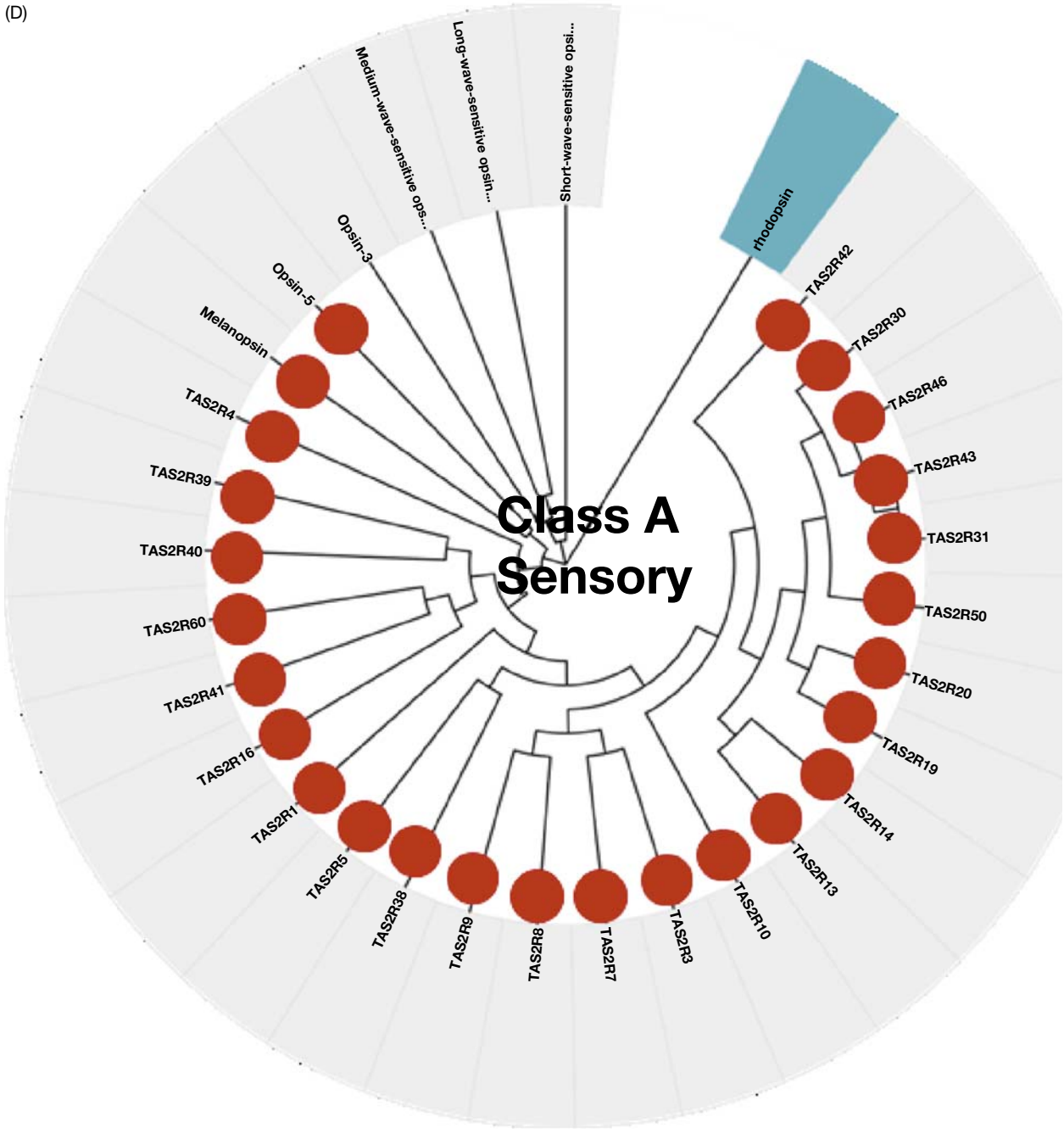

Fig. 6 (*continued*).

3.08.4.2 Binding Free Energy and Binding Kinetics Predictions

Computational predictions of ligand–protein affinity and kinetics of binding represent a key component of SBDD. The thermodynamics of ligand–protein binding (ΔG_{bind}) corresponds to the difference in free energy between the unbound species and the bound state, while the kinetics of the ligand-binding event is characterized by association and dissociation constants. Ligand-binding free energy predictions still remain a challenge for modern computational chemistry, in particular at the level of accuracy needed to guide lead optimization. Recent efforts in structure-based drug design have aimed to improve both the protocols and the force fields used in free energy perturbation calculations.[160] Retrospective results on soluble proteins covering 200 ligands and 330 chemical perturbations resulted in an average ΔG_{bind} root mean square error of 1 kcal/mol. The approach has then been tested in prospective drug discovery projects and fragment optimization[160,161] with similar results. Preliminary results of this approach in the GPCR field are promising; for example, Goldfeld et al. have used free energy perturbation calculations to provide evidence for the mechanism of interaction between ligands and kappa-opioid receptor.[162] They proposed a scoring model (WScore) for the binding

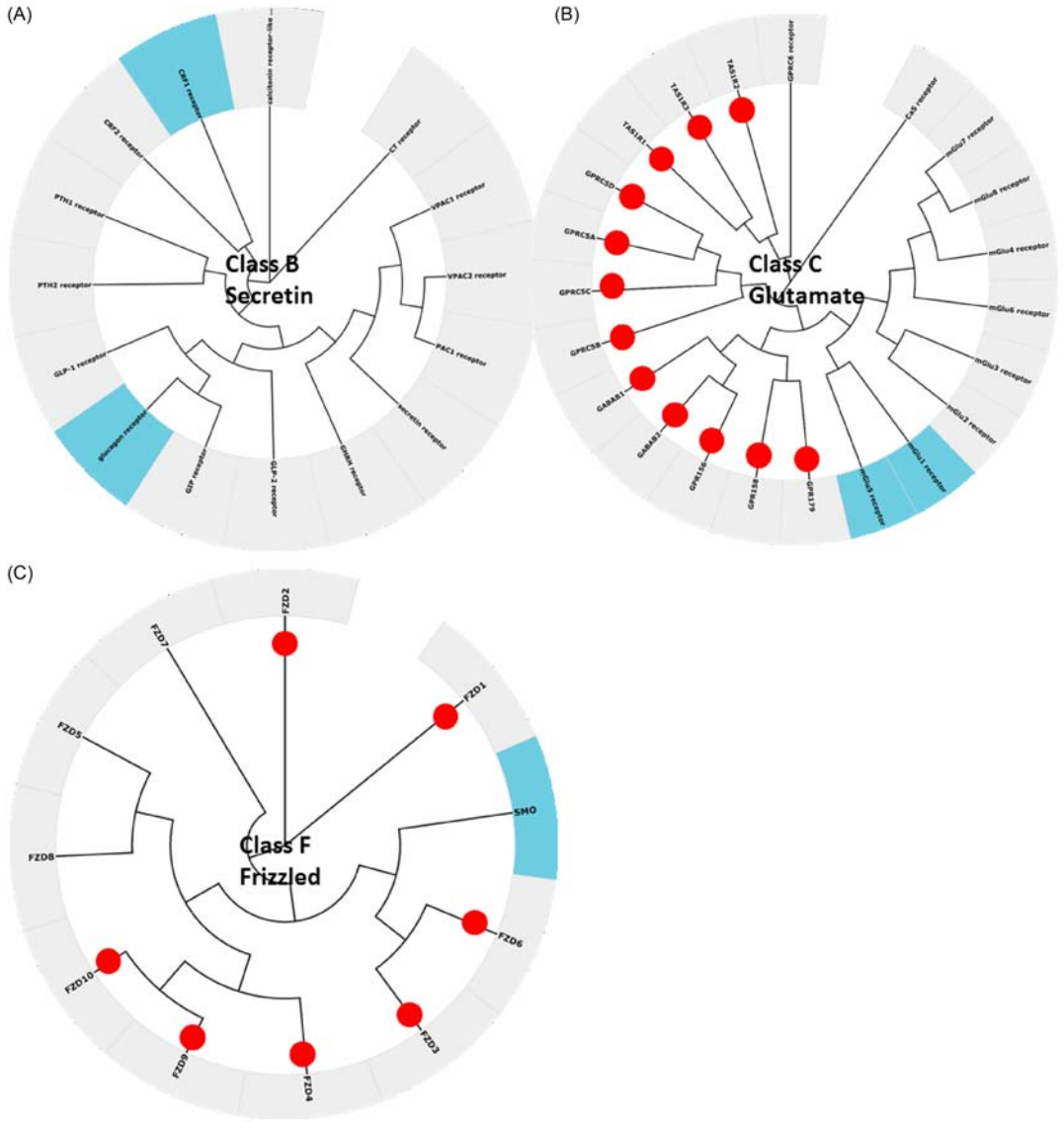

Fig. 7 Phylogenetic tree for class B GPCR secretin (A), class C glutamate (B), and class F frizzled receptors. Analysis created using the tools available in the GPCRDB.[101] GPCRs with available crystal structure in the Protein Data Bank[102] are highlighted in *blue*. *Red* circles highlight GPCRs for which the creation of a homology model can be particularly challenging. For these receptors, only low (less than 30%) sequence identity templates are available.

to this receptor based on the location of the water molecules in its binding site. WScore used with the docking program Glide resulted in better virtual screening enrichment on this target compared with an older generation of Glide scoring functions. Free energy calculations have been applied also to evaluate single-point mutations and their effect on ligand binding.[163,164] When applied to the adenosine A_{2A} receptor, the predictions were in agreement with the experimental effect of the point mutation on the binding affinity of a potent agonist.

The effect of ligand binding on the thermodynamics of GPCR conformational equilibria takes place on timescales that are not conveniently accessible to standard MD.[165] Enhanced molecular dynamics methods have been applied to GPCRs to study ligand recognition, ligand binding and unbinding pathways, receptor activation, and oligomerization (reviewed in Ref. [147]). Evaluation of the dynamic mechanisms by which ligands bind and unbind GPCRs can be a crucial aspect in lead optimization to understand binding kinetics and selectivity. Residence time, typically expressed as the inverse of the dissociation rate, has been shown in different studies to be important to evaluate GPCR ligand activity.[166] These included, for example, angiotensin II AT_1 receptor antagonists,[167] M_3 muscarinic agonists,[168] μ-opioid receptor ligands,[169] and dopamine D_2 receptor antagonists.[170,171] Enhanced sampling algorithms[172] like metadynamics (MetaD) or the construction of Markov state models (reviewed respectively in Refs. [173,174]) can be useful to evaluate ligand kinetics.[175] Another method uses a multiple-replica scaled molecular dynamics protocol with suitably defined harmonic restraints to accelerate the unbinding events.[176] This approach was able to rank adenosine A_{2A} receptor ligands according to the mean observed scaled unbinding time. Other computational methods available include fast protocols evaluating the role of the binding site water molecules in

Table 1 Performance of published prospective ligand- and structure-based virtual screenings on GPCR targets

GPCR target	*Approach*	*Protocol*	*Library size*	*Hit rate*	*Activity*	*Ref.*
$A_{2A}AR$	Molecular docking of small molecules	Inactive conformation X-ray	4 M	41%—23/56	Antagonists	108
$A_{2A}AR$	Molecular docking of small molecules	Inactive conformation X-ray	1 M	35%—7/20	Antagonists	109
$A_{2A}AR$	Molecular docking of fragments	Inactive conformation X-ray	328 K	63%—14/22	Antagonists	110
$A_{2A}AR$	Proteochemometric modeling	Protein and ligand fingerprints	791 K	11%—6/54	Antagonists	111
$A_{2A}AR$	Molecular docking of small molecules	Active-like conformation X-ray	6.7 M	45%—9/20	Antagonists	100
$A_{2A}AR$	Molecular docking of small molecules	Homology model	545 K	9%—20/230	Antagonists	112
$A_{2A}AR$	Structure-based pharmacophores and ligand-based chemogenomic approach	Inactive conformation X-ray	50 K	2%—18/900	Antagonists	113
$A_{2A}AR$	Virtual library molecular docking	Active-like conformation X-ray	2 K	94%—15/16	Agonists	114
$A_{2A}AR$	Ligand-based screening	Substructure mining	60 K	22%—8/36	Antagonists	115
$A_{2A}AR$	Similarity search	Ligand-based SHED descriptors	1.5 K	50%—2/4	Antagonists	116
A_3AR	Molecular docking of fragments	Homology models	$>$500 K	38%—8/21	Antagonists	117
β_2AR	Molecular docking of small molecules	Inactive conformation X-ray	4.4 M	21%—31/150	Antagonists	118
β_2AR	Molecular docking of small molecules	Inactive conformation X-ray	1 M	24%—6/25	Inverse agonists	119
β_2AR	Molecular docking of small molecules	Active conformation X-ray	3.1 M	27%—6/22	Agonist	120
β_2AR	Structure-based pharmacophores and ligand-based chemogenomic approach	Inactive conformation X-ray	50 K	0.7%—6/900	Antagonists	113
D_3R	Molecular docking of small molecules	Inactive conformation X-ray	4.1 M	56%—14/25	Antagonists	121
D_3R	Molecular docking of small molecules	Inactive conformation X-ray	4.1 M	32%—8/25	Allosteric modulators	121
D_3R	Molecular docking of fragments	Inactive conformation X-ray	12.9 K	18%—9/50	Binders	122
D_3R	Molecular docking of fragments	Ensemble docking on MD snapshots from X-ray	12.9 K	32%—18/56	Binders	122
D_3R	Molecular docking of fragments	Homology model	3.6 M	23%—6/23	Antagonists	123
D_3R	Molecular docking of small molecules	Inactive conformation X-ray	3.6 M	20%—5/25	Four antagonists, one partial agonist	123
D_3R	Molecular docking and pharmacophore search	Homology model	250 K	60%—12/20	Antagonists	124
H_1R	Docking of fragments, 3-D ligand fingerprints	Inactive conformation X-ray	108.8 K	73%—19/26	Antagonists	125
H_3R	Molecular docking of fragments	Homology model	156 K	62%—18/29	Antagonists	126
H_4R	Molecular docking of fragments	Homology model	12.9 K	22%—11/50	Binders	122
H_4R	Molecular docking of small molecules	Homology model	8.7 M	6%—16/255	Antagonists	127
H_4R	Molecular docking of fragments	Ensemble docking on MD snapshots from homology model	12.9 K	16%—8/50	Binders	122
$S1P_1R$	Structure-based pharmacophores and ligand-based chemogenomic approach	Active homology model	50 K	0.3%—3/900	Antagonists	113
CXCR4	Molecular docking of small molecules	Inactive conformation X-ray	4.2 M	17%—4/23	Allosteric modulators	128
CXCR4	Molecular docking of small molecules	Homology model	3.3 M	4%—1/25	Allosteric modulators	128
CXCR4 CXCR3	Molecular docking of small molecules	Inactive conformation X-ray and homology model	2.4 M	57%—4/7	NAMs	129
CXCR4 CXCR3	Molecular docking of small molecules	Inactive conformation X-ray and homology model	2.4 M	75%—3/4	PAMs and NAMs	129
CXCR4 CXCR3	Molecular docking of small molecules	Inactive conformation X-ray and homology model	2.4 M	50%—3/6	Mostly NAMs	129
M_2R	Molecular docking of small molecules and fragments	Inactive conformation X-ray	3 M	61%—11/18	Antagonists	130

Table 1 Performance of published prospective ligand- and structure-based virtual screenings on GPCR targets—cont'd

GPCR target	*Approach*	*Protocol*	*Library size*	*Hit rate*	*Activity*	*Ref.*
M_3R/M_2R	Molecular docking of small molecules and fragments	Inactive conformation X-ray	3 M	50%—8/16	seven antagonists, one selective partial agonist	130
k-OR	Molecular docking of small molecules	Inactive conformation X-ray	4.5 M	18%—4/22	Three antagonists, one selective agonist	131
$5\text{-}HT_{1B}$ $5\text{-}HT_{2B}$	Molecular docking of small molecules	Active-like conformation X-ray	1.3 M	50%—11/22	Binders and agonists, nine selective	132
$5\text{-}HT_{2B}$	Molecular docking of small molecules	Optimized crystal structure	100.4 K	70%—7/10	Antagonists	133
GPR34	Molecular docking of small molecules	Homology model	1.25 M	0.17%—5/2954	Inverse agonists	134
GPR17	Molecular docking of small molecules	Homology model	130 K	100%—5/5	Agonists and partial agonists	135
GPR40	Molecular docking, pharmacophore search and 2-D similarity	Homology model	2.6 M	11%—6/52	Full and partial agonists	136
MCH_1	Molecular docking, pharmacophore search and 2-D similarity	Homology model	615 K	2.8%—31/1096	Antagonists	137
MCH_1	Molecular docking	Homology model	187 K	11.8%—6/129	Antagonists	138
NK_1R	Molecular docking, pharmacophore search and 2-D similarity	Homology model	827 K	14%—1/7	Binders	139
FPR1	3-D pharmacophore search	Homology model	480 K	1.2%—52/4324	Antagonists, four weak partial agonists	140
GCGR	Similarity, molecular docking, interaction fingerprints	Homology model	1.9 M	8.7%—2/23	Antagonists	141
α1AR	Pharmacophore search, molecular docking	Homology model	23 K	46.2%—37/80	Antagonists	142
CB_2R	Pharmacophore search, molecular docking	Homology model	55.6 K	1.1%—1/86	Agonists	143
CCR5	Pharmacophore search, molecular docking	Homology model	1.6 M	17%—10/59	Mostly agonists	144
TRH_1R/TRH_2R	Molecular docking, 3-D pharmacophore	Homology model	1 M	5%—5/100	Antagonists	145
GPR68	Molecular docking	Homology model	3.1 M	23.5%—4/17	PAM	105
GPR65	Molecular docking	Homology model	3.1 M	35.5%—16/45	NAMs and one PAM	105

affecting the ligand residence times.[177] Shielding hydrogen bond interactions between the ligand and the protein from water molecules results in an increase in the ligand unbinding transition state energy barrier.[177,178] In addition, fast on-rates can be related to replacement of protein H bonds from waters to polar ligand atoms. Fast off-rates instead can be associated with limited displacement of unstable hydration sites.[178] Trapped unstable waters between the protein and triazine-based ligands have been highlighted as important in limiting ligand residence times for the adenosine A_{2A} receptor.[179,180] Another fast approach (aMetaD) uses a combination of adiabatic bias molecular dynamics and metadynamics to simulate the start of the ligand–protein unbinding event.[181] MD trajectories are automatically analyzed and translated into atomic solvation factor values representing the water dynamics during the unbinding event. Using a physics-based and fully flexible ligand scoring function, the aMetaD approach evaluates the maximum energy required to move the ligand from the bound-state energy basin to the next. This scoring scheme has been used successfully to classify the residence time of ligands of the muscarinic M_3, the adenosine A_{2A}, and CRF_1 receptors.

3.08.5 Applications of in Silico Design for Membrane Protein Targets

In the remainder of this article, progress with ligand design using computational methods and SBDD will be highlighted by focusing on a number of examples from the literature. The previous discussion has outlined progress with X-ray structure determination and SBDD methodology for several different protein targets covering GPCRs, ion channels, and transporters. In addition, in silico approaches applied to GPCR hit discovery and to an understanding of how ligands bind to GPCRs have been described in some detail. The scope of the rest of the article is limited to selected examples either where the design process uses the X-ray structure of the target protein itself in the relevant conformation or where homology modeling is used starting from a very similar protein structure (receptor subtype or the same receptor in another conformation, i.e., agonist or antagonist). In addition, due to the recent availability of multiple GPCR ligand–protein X-ray cocomplexes suitable for SBDD, the examples covered will focus on GPCR targets. The authors have attempted to use these examples to outline how SBDD methods can be readily applied to receptors and that many of the lessons learned from soluble targets can be successfully implemented. At the same time, there are some differences between

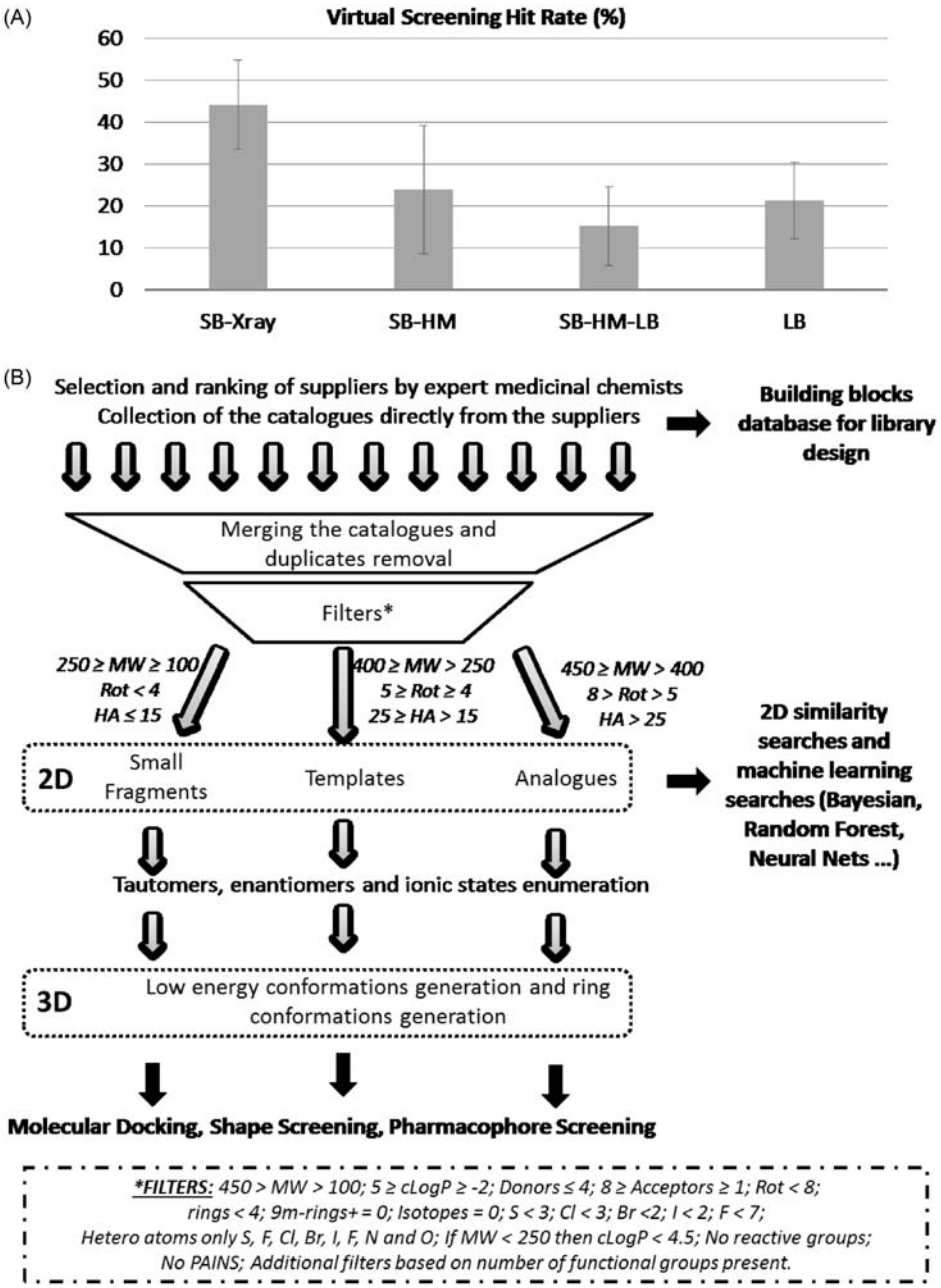

Fig. 8 (A) Average virtual screening hit rate (%) from the published prospective studies included in **Table 1** divided in four categories: structure-based using crystallographic information (SB-X-ray), structure-based using a homology model (SB-HM), combination of ligand-based and structure-based approach using a homology model (SB-HM-LB), and ligand-based virtual screening (LB). (B) Protocol used to generate Heptares' supplier databases of commercially available small molecules for virtual screening applications. The following abbreviations are used: MW, molecular weight; cLog P, predicted Log P (daylight); donors, number of H-bonding donors; acceptors, number of H-bonding acceptors; Rot, rotatable bonds; rings, number of rings; 9m-rings+, 9 or more ring atoms; PAINS, pan-assay interference compounds.[146]

GPCRs and soluble targets in compound binding and molecular properties, particularly if the ligand is bound deep within the protein in regions that are embedded in the cell membrane. We attempt to highlight the impact of these differences on the design process.

3.08.5.1 Orthosteric GPCR Ligands

3.08.5.1.1 Class A GPCR aminergic

α-Adrenergic receptors. The binding pose of a series of α_2-AR antagonists based on the pyridinoguanidine and pyridino-2-aminoimidazoline scaffolds has been elucidated using homology models of α_{2A}-AR and α_{2C}-AR derived from the β_2-AR

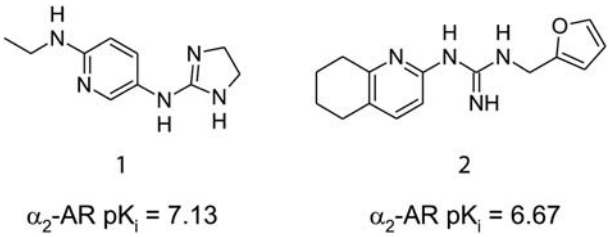

Scheme 1 α_2-AR antagonists **1** and **2** in which the cationic group interacts with the Asp113.

structure.[182] For the monosubstituted derivatives within these series, the cationic group interacts with two residues implicated in catechol ligand binding and receptor activation, derived from the understanding provided by the crystal structure of activated β_2-AR (Ser200$^{5.42a}$ and Ser204$^{5.46a}$ of the α_{2A}-AR and Ser214$^{5.42a}$ and Ser218$^{5.46a}$ of the α_{2C}-AR). Exceptions to this are the ethylamino pyridine derivatives, such as compound **1** in **Scheme 1**, which orientate the cationic group to interact with the Asp113$^{3.32a}$ (Asp131$^{3.32a}$ of the α_{2C}-AR) and fill the Ser200$^{5.42a}$/Ser204$^{5.46a}$ region of the receptor with the pyridyl core. The cationic group of the disubstituted guanidines and 1,4-dihydroquinazolines, such as compound **2**, within this series of compounds is also predicted to interact with Asp113$^{3.32a}$ of the α_{2A}-AR (Asp131$^{3.32a}$ of the α_{2C}-AR) in the homology model, and the substituent on the cationic group is thought to bind in a lipophilic pocket made up of aromatic residues from TM3 and TM7 (Tyr109$^{3.28a}$, Phe412$^{7.39a}$, and Tyr416$^{7.43a}$ of the α_{2A}-AR and Tyr127$^{3.28a}$, Phe423$^{7.39a}$, and Tyr427$^{7.43a}$ of the α_{2C}-AR). This overall binding pose explains the antagonist activity observed for these compounds because the cationic group is not able to interact with Ser200$^{5.42a}$/Ser204$^{5.46a}$ of the α_{2A}-AR (Ser214$^{5.42a}$/Ser218$^{5.46a}$ of the α_{2C}-AR) and causes receptor activation. This binding pose can be used to help in future design of new α_2-AR antagonists useful for the treatment of depression and schizophrenia.

β-Adrenergic receptors. In addition to the docking and virtual screening included in **Table 1**, SBDD has been applied to β-adrenergic receptors (β-AR). Hattori et al. have used structure-driven modifications in a series of biphenyl analogs containing acylsulfonamide substitution to obtain potent and selective β_3AR agonists.[183] The predicted binding pose was used to rationalize both selectivity and potency. A series of high-efficacy β_2AR agonists that are analogs of the known compound sibenadet, lacking the usual benzylic alcohol group found in most potent agonists, were generated by Stocks et al.[184] An induced fit was proposed in which Trp286$^{6.48a}$ moves to produce a new lipophilic pocket that can accommodate the ligand. Soriano-Ursúa et al. have designed boron-containing analogs of β_2AR agonists using the β_2 receptor X-ray structure.[185] Interestingly, one analog had higher potency than the corresponding diol (the usual pharmacophore) in a functional assay. Other analogs were shown to be competitively antagonized by β_2AR antagonists.

Christopher et al. have used the antagonist-stabilized β_1AR (StaR β_1AR; StaR is used to describe a receptor stabilized using mutagenesis) for fragment screening and then subsequently for X-ray crystallographic studies of analogs of the fragment hits.[186] Small phenyl piperazine hits such as **3**, **Scheme 2**, were identified using surface plasmon resonance (SPR) screening of the StaR immobilized on a chip. This is an unusual example of a biophysical screening approach being applied to a GPCR, facilitated by the additional stability introduced into the protein by mutagenesis. A modeling analysis was carried out to suggest binding modes for a number of related hits, which had affinities in the range of 1–50 μM, **4**, at the wild-type (WT) receptor. This led to subsequent purchasing of selected analogs for further screening. Of note, an indole-containing derivative, **5**, was prioritized due to a predicted additional interaction with the OH of Ser 211$^{5.42a}$. Upon screening, this compound was shown to have a significantly improved affinity of approximately 60 nM (assessed using a radioligand binding assay). Crystal structures of two fragment-sized molecules were then solved, confirming the modeling hypothesis and establishing the basis for further possible optimization. Overall, this case study demonstrates that the principles of fragment-based drug discovery can be applied to GPCRs.

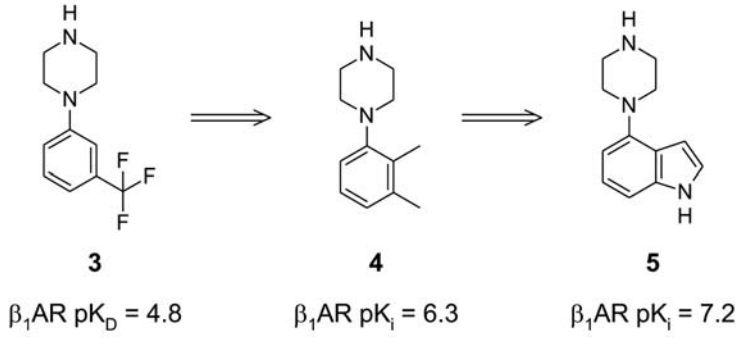

Scheme 2 β_1-AR antagonists SPR fragment hits **3** and **4**, and selected analogue **5**.

Dopamine receptors. There are five reported dopamine receptors subtypes (D_1, D_2, D_3, D_4, and D_5), and the pharmacological targeting of these receptors in the CNS has proved to be a very effective approach for the treatment of several pathological conditions. Both agonists and antagonists have been investigated clinically to treat a range of disease states such as Parkinson's disease, schizophrenia, bipolar disorder, and depression.

Using a homology model of the D_2 receptor (based on the published crystal structure of the D_3 receptor) and in comparison with the crystal structure of the 5-HT_{2B} receptor in complex with the biased agonist ergotamine, a range of biased D_2 receptor agonists have been rationally designed. Gmeiner et al.[187] have reported a series of D_2-biased ligands that incorporate a pyrazolopyridine-derived headgroup and an enyne motif (as an atypical bioisostere replacement of the catechol group found in dopamine itself). These ligands are predicted to bind in an extended binding site, and interestingly, the docking poses contained ligand–protein interactions in the identical positions as those observed within the crystal structure of the 5-HT_{2B} receptor in complex with the biased agonist ergotamine. This potentially indicates the presence of conserved receptor microdomains at the entrance to the orthosteric pocket that are involved in ligand bias.

Gmeiner et al.[188] then expanded upon this methodology with the discovery of **(*S*)-6**, Scheme 3, which contains an oxaenyne headgroup as an atypical bioisostere replacement of the catechol group and is a biased agonist that displays a strong preference for $G_{\alpha o}$ activation. It has been proposed that the activation of $G_{\alpha o}$ subunits will stimulate outgrowth of neuronal cells and promote synaptic plasticity, which in turn will impact the positive symptoms of schizophrenia.[189,190] Taking this further, using a classical catechol bioisostere replacement led to design of compound **(*R*)-7**, which showed β-arrestin recruitment while being a weak partial agonist for $G_{\alpha o}$ activation and an antagonist for $G_{\alpha i}$. Intriguingly, a β-arrestin-biased ligand could have clinical relevance for the treatment of antipsychotic symptoms in schizophrenia.[191]

Christopoulos and Lane et al.[192] have used a homology model of the D_2 receptor based on the crystal structure of the D_3 receptor to determine the binding mode of the ligand **SB-269652**, which is a bitopic negative allosteric modulator of the D_2 receptor. Bitopic is a term used in some of the literature to describe ligands that bind to two adjacent or contiguous binding sites in class A GPCRs, the deep orthosteric site usually occupied by the endogenous agonist and a "vestibule" site at the entrance to the binding pocket. The 1*H*-indole-2-carboxamide moiety of **SB269652** extends into this secondary pocket between the extracellular ends of TM2 and TM7, while the 7-cyano-1,2,3,4-tetrahydroisoquinoline headgroup occupies the orthosteric binding site.[192] Fragmentation of **SB-269652** led to *N*-isopropyl-1*H*-indole-2-carboxamide **8**, Scheme 4, which was the smallest fragment to still contain allosteric pharmacology. Structure–activity relationship studies based on **8** identified *N*-butyl-1*H*-indole-2-carboxamide, **9**, which had increased D_2 affinity and shows negative cooperativity.[193] Combining this active fragment with the 7-cyano-1,2,3,4-tetrahydroisoquinoline headgroup gave a highly active bitopic negative allosteric modular (NAM) **10**.

Utilizing the D_3 crystal structure and a structural hybridization approach incorporating dopaminergic dipropylamines and arene-carboxamides, Gaimer and coworkers[194] have described an enantiomerically pure biphenylcarboxamide D_3 receptor agonist, **(*S*)-11**, Scheme 5, with a very high binding affinity of 27 pM and good selectivity for the D_3 receptor over the D_2 subtype. AUTODOCK4 was used to dock a range of hybridized molecules into the D_3 crystal structure; the docking pose of **(*S*)-8** showed the expected polar interaction between $Asp110^{3.32a}$ in TM3 and the protonated central ammonium group and the tetrahydropyrazolopyridine headgroup forming a hydrophobic interaction with the amino acid residues $Val111^{3.33a}$, $Ser196^{5.46a}$, $Phe345^{6.51a}$, $Phe346^{6.52a}$, and $His349^{6.55a}$. The propyl group was predicted to bind into a pocket created by $Asp110^{3.32a}$, $Trp342^{6.48a}$, and $Thr369^{7.39a}$ between TM3, TM2, and TM7, while the endocyclic nitrogen of the tetrahydropyrazolopyridine group of **(*S*)-11** forms a hydrogen bond with the side chain of $Ser192^{5.42a}$, a proposal that was supported by site-directed mutagenesis (SDM) experiments. The N-butylbiphenylcarboxamide portion of **(*S*)-11** binds in a pocket created by TM2 and TM3, which is thought responsible for

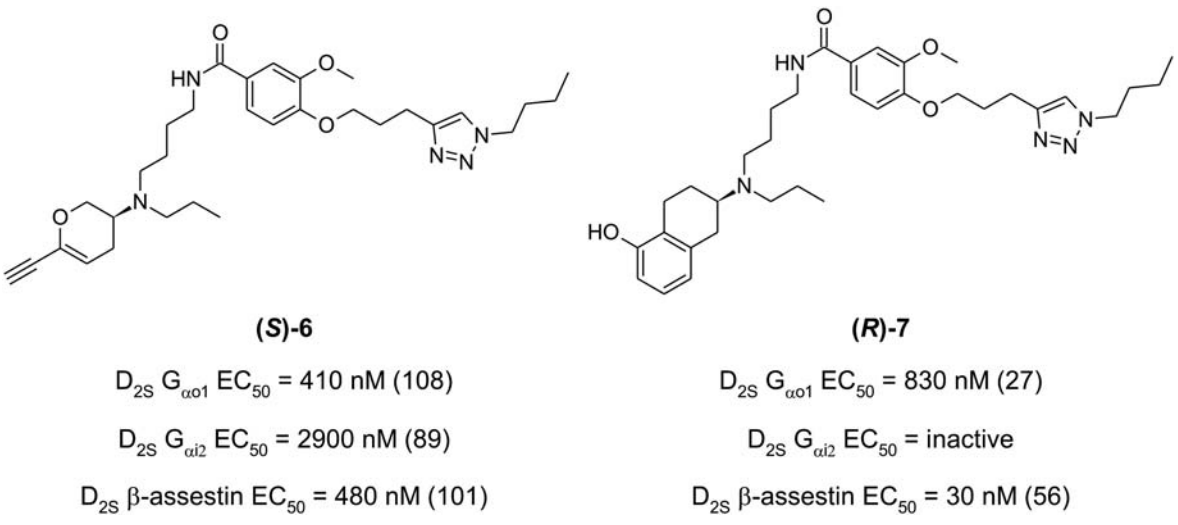

Scheme 3 D_2-biased receptor agonists **(*S*)-6** and **(*R*)-7**.

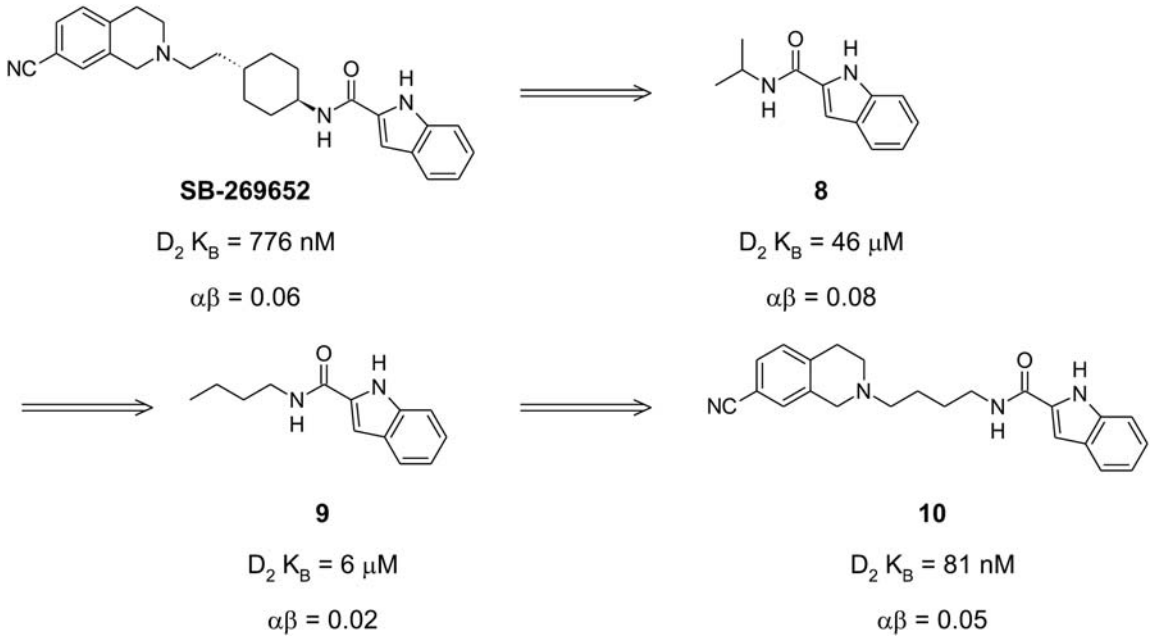

Scheme 4 Development of a bitopic D_2 NAM **10** from **SB-269652**.

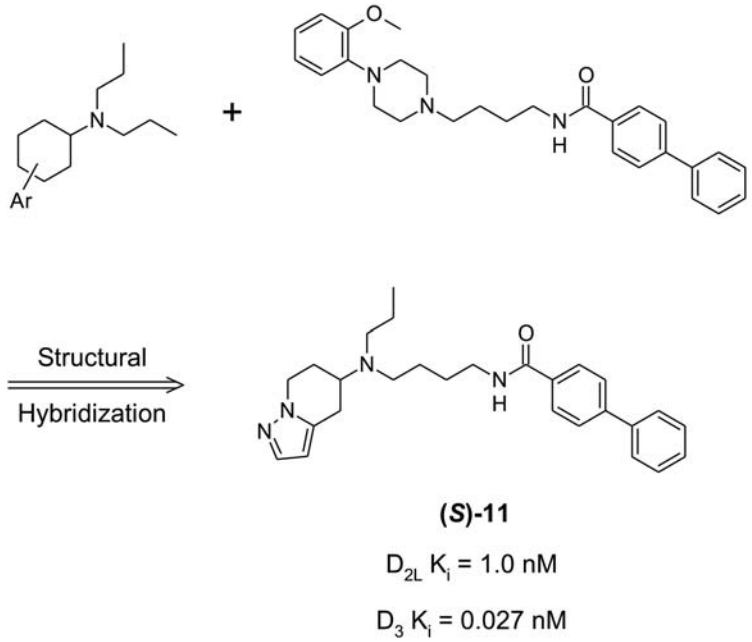

Scheme 5 Structural hybridization approach to give the D_3 receptor agonist **(S)-11**.

subtype selectivity. **(*S*)-11** was shown to have biased signaling with significant preference for [^{3}H]-thymidine incorporation compared with cAMP accumulation.

More recently, Ananthan et al.[195] have reported the discovery of a series of acylaminobutylpiperazines, Scheme 6, as antagonists or partial agonists of the dopamine D_3 receptor, which have subtype selectivity over D_2. Docking of this series of compounds into the reported D_3 crystal structure and a D_2 homology model provided an understanding of the compound attributes, which were contributing to binding selectivity and affinity of these compounds. Selectivity for the D_3 receptor was likely obtained via interactions of the imidazo[1,2-*a*]pyridine group with the tyrosine residue (Tyr365$^{7.35a}$) at the extracellular end of TM7; this region is significantly different in the D_2 and D_3 receptors. **SR21502**, Scheme 6, was assessed in rat in vivo models of cocaine self-administration and conditioned place preference. The compound was shown to be effective at significantly attenuating cocaine reward, cocaine self-administration, cue-induced reinstatement of cocaine-seeking, and blocking cocaine-induced place preference.

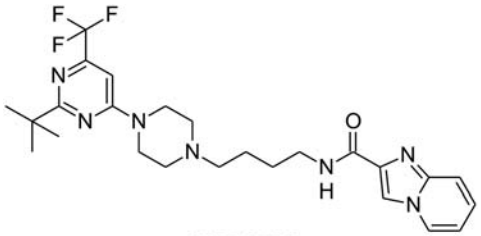

SR21502

D_2 K_i = 511 nM

D_3 K_i = 4.2 nM

Scheme 6 D_3 selective antagonist **SR21502**.

Serotonin receptors. There are seven reported families of the serotonin (5-hydroxytryptamine, 5-HT) receptors (5-HT_1, 5-HT_2, 5-HT_3, 5-HT_4, 5-HT_5, 5-HT_6, and 5-HT_7), which all belong to the GPCR superfamily except 5-HT_3 that is a ligand-gated ion channel. For several of these proteins, various subtypes of receptors have been described, namely, 5-$HT_{1A\text{-}F}$, 5-$HT_{2A\text{-}C}$, and 5-$HT_{5A\text{-}B}$. Serotonin receptors are distributed in the central and peripheral nervous systems, the gastrointestinal tract, the cardiovascular system, and the immune cells. Both agonists and antagonists have been developed for this receptor class including various antipsychotic, antidepressant, and antiemetic drugs. However, as the various 5-HT receptors were identified, it became apparent that many of these drugs lack receptor selectivity, making it difficult to determine the specific role of each receptor in these disease settings from the clinical findings.

As GPCR X-ray data have become available in recent years, there have been a number of reports in the literature focusing on 5-HT ligand–protein binding and SBDD efforts. Liégeois et al.[196] have used a homology model of the 5-HT_{1A} based on the published turkey β_1-adrenergic receptor structure to derive a series of carboxamide and sulfonamide alkyl piperazine analogs as exemplified by **12**, Scheme 7. The proposed docking pose of **12** into the orthosteric site was very similar to that found for the full and potent agonist R-8-OH-DPAT. The basic center of the compound was proposed to make an ionic interaction with $Asp116^{3.32a}$ and the 2-methoxyphenyl-piperazine portion of the molecule to interact with the aromatic residues $Phe361^{6.51a}$ and $Phe362^{6.52a}$. The oxygen of the methoxy group was suggested to form hydrogen bonds with $Ser199^{5.42a}$ and $Thr200^{5.43a}$. The naphthalene ring in the ligand was proposed to bind in a lipophilic aromatic pocket formed by the residues $Tyr96^{2.64a}$, $Trp387^{7.40a}$, and $Tyr390^{7.43a}$. Finally, the amide group seemed to form a hydrogen bond with $Asn386^{7.39a}$. Electrophysiological experiments were performed with compound **12** to investigate the effect on the firing rate of serotonergic neurons of the dorsal raphe nucleus (DR) in rat brain slices, and **12** was demonstrated to induce a concentration-dependent decrease in the firing rate of DR serotonergic neurons with an IC_{50} of 179 nM.

Huang et al.[133] have carried out a structure-based virtual screening campaign to identify novel 5-HT_{2B} receptor antagonists by using an induced-fit 5-HT_{2B} receptor antagonist model based on the reported agonist X-ray structure of the 5-HT_{2B} receptor. A series of *N*2-aryl-6,6-disubstituted-1,6-dihydro-1,3,5-triazine-2,4-diamines were identified from this initial screen, and these molecules adopted a similar binding mode in the induced-fit model. Further structure–activity relationship (SAR) studies were performed to identify **13**, Scheme 8, a promising candidate with high binding affinity and high selectivity for the 5-HT_{2B} receptor over eleven other 5-HT receptors. A 30 mg/kg oral dose of **13** produced significant reduction of visceral hypersensitivity in a rat model of irritable bowel syndrome (IBS). This series of compounds employs a protonated triazine ring to form hydrogen bonds with the $Asn344^{6.55a}$ residue and a salt bridge interaction with the carboxylate group of $Asp135^{3.32a}$ in the binding site.

The discovery of **PF-4479745** and **PF-4522654**, Scheme 9, as potent, selective 5-HT_{2C} receptor partial agonists based on the 4-substituted pyrimido[4,5-d]azepines scaffold has been reported by Storer et al.[197] **PF-4479745** and **PF-4522654** have no

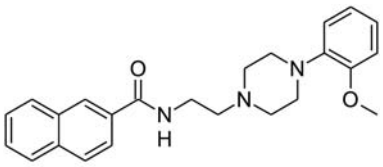

12

5-HT_{1A} K_i = 1.7 nM

Scheme 7 5-HT_{1A} agonist **12**, a carboxamide alkyl piperazine analog.

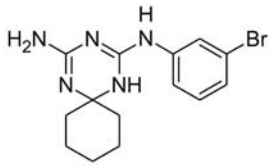

13

5-HT$_{2B}$ IC_{50} = 33.4 nM

5-HT$_{2B}$ K_i = 6 nM

5-HT$_{1A}$ K_i = 320 nM, 5-HT$_{1B}$ K_i > 10000 nM

5-HT$_{1D}$ K_i = 2904 nM, 5-HT$_{1E}$ K_i > 10000 nM

5-HT$_{2A}$ K_i = 211 nM , 5-HT$_{2C}$ K_i = 156 nM, 5-HT$_3$ K_i > 10000 nM

5-HT$_{5A}$ K_i = 227 nM, 5-HT$_6$ K_i = 3031 nM, 5-HT$_{7A}$ K_i = 401 nM

Scheme 8 5-HT$_{2B}$ receptor antagonist **13**.

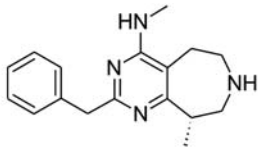

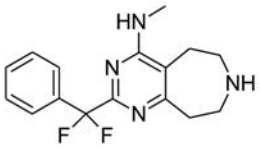

PF-4479745

5-HT$_{2C}$ EC_{50} = 21 nM (67)

5-HT$_{2C}$ K_i = 15 nM

5-HT$_{2B}$ EC_{50} > 10000 nM

PF-4522654

5-HT$_{2C}$ EC_{50} = 16 nM (58)

5-HT$_{2C}$ K_i = 8 nM

5-HT$_{2B}$ EC_{50} > 10000 nM

Scheme 9 5-HT$_{2C}$ receptor partial agonists **PF-4479745** and **PF-4522654**.

measurable functional agonism at 5-HT$_{2A}$ and 5-HT$_{2B}$ in relevant tissue-based assay systems. Both these compounds displayed in vivo efficacy in a canine peak urethral pressure model of stress urinary incontinence and potentially have desirable human pharmacokinetic profiles based on the measured human liver microsomal (HLM) and human hepatocyte clearances. Homology models derived from site-directed mutagenesis (SDM) data and crystal structures of the active and inactive β_2-adrenergic receptor were used to generate an inactive-state 5-HT$_{2C}$ homology model and an active-state 5-HT$_{2C}$ homology model. These models were used to rationalize the binding pose, affinity, and agonist efficacy of this series of molecules.

Kozikowski et al.[198] have reported a series of potent, selective 5-HT$_{2C}$ receptor agonists based on the 2-phenylcyclopropylmethylamine scaffold. Optimization of this series has led to the discovery of **(+)-14**, Scheme 10, which

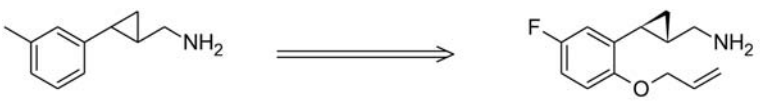

(+)-14

5-HT$_{2A}$ EC_{50} = 374 nM (56)

5-HT$_{2B}$ inactive

5-HT$_{2C}$ EC_{50} = 4.2 nM (87)

Scheme 10 Selective 5-HT$_{2C}$ receptor agonist **(+)-14**.

has an EC_{50} value of 4.2 nM at 5-HT_{2C}, has no significant activity at 5-HT_{2B}, and was 89-fold-selective against 5-HT_{2A}. At a dose of 20 mg/kg in a mouse schizophrenia in vivo model **(+)-14** completely reversed amphetamine-induced hyperactivity while showing no significant influence on the spontaneous activity of the tested animals. Two homology models were generated to predict the binding pose of this series of compounds. An inactive-state 5-HT_{2C} homology model derived from the inactive-state structure of β_2-adrenergic receptor and an active-state 5-HT_{2C} homology model based on a combination of the solved structure of 5-HT_{2B} in complex with ergotamine and the β_2-AR in its fully active state were developed. Major differences were observed between the binding poses of compound **(+)-14** with the inactive and active homology models. In the active-state homology model, the phenyl ring of **(+)-14** docks into a binding pocket lined by aromatic residues (Phe214$^{5.38a}$, Trp324$^{6.48a}$, Phe327$^{6.51a}$, Phe328$^{6.52a}$, and Tyr358$^{7.43a}$) deeper in the binding site, which creates a network of π–π stacking interactions. The ether bridge was proposed to be involved in two possible H bonds with Ser219$^{5.43a}$ and Asn331$^{6.55a}$ and the alkenyl tail π–π stacking with Phe214$^{5.38a}$. These predicted binding poses allow hypotheses to be developed for further compound design in this series of molecules.

3.08.5.1.2 Class A GPCR peptidergic

Opioid receptors. Opioids exert their function through interacting with one or more of the four opioid GPCRs, designated as the mu-opioid receptor (MOR), the kappa-opioid receptor (KOR), the delta-opioid receptor (DOR), and the nociception receptor (NOP). In recent years, a number of liganded X-ray structures have been published giving the opportunity for SBDD for these important pain targets.[199]

Zhang et al.[200] used a MOR homology model to design three generations of heteroaromatic-substituted naltrexone (antagonist) derivatives. These compounds were evaluated as potential MOR-selective ligands. The first-generation ligands appeared to be MOR-selective, whereas the second and the third generation ones showed MOR/KOR dual selectivity. Docking of MOR-selective and MOR/KOR dual-selective ligands into the three opioid receptor crystal structures revealed a nonconserved residue$^{2.63}$, which appears to facilitate a hydrogen-bonding network and might be responsible for the distinctive selectivity profiles. Overall, one antagonist was identified as a novel lead to develop MOR/KOR dual-selective ligands, which might possess therapeutic value for opioid addiction treatment.

Studies to understand the structure-based SAR of endomorphin analogs have been carried out by a number of groups reporting their results in the recent literature. The MOR endogenous tetrapeptides, endomorphin-1 (**EM-1**, H-Tyr-Pro-Trp-Phe-NH_2), Scheme 11, and endomorphin-2 (**EM-2**, H-Tyr-Pro-Phe-Phe-NH_2), Scheme 12, were originally isolated from the bovine brain and the human cortex. These peptides exhibit high affinity for the MOR and high selectivity over DOR. Wang et al.[201] rationalized the pharmacology of **EM-1** analogs, such as **15**, using flexible dockings into a model of human MOR, and then, the resultant poses were further optimized with molecular dynamics. The poses generated were supported by SDM experiments, and the results were compared with the crystal structure of the antagonist β-FNA in MOR. The study identified some promising new peptides modified with unnatural amino acids, suitable for further optimization. Sacchetti et al.[202] characterized potent analogs of **EM-2**, such as **16**, using a combination of proton nuclear magnetic resonance (NMR) conformational analysis, molecular dynamics, and docking studies into a model of MOR. In solution, the structures showed extended conformations, which were in agreement with the commonly accepted pharmacophore model for **EM-2**. The docking studies used an active form MOR model and generated a credible picture of how the active compounds were binding in a sensible ligand conformation. Again, the results were consistent with SDM experiments. Building confidence in the ligand conformation is particularly important in peptidomimetic drug discovery due to the potentially flexible nature of the peptide scaffolds; in practice, there tends to be only a small number of well-populated conformations in solution and a single form bound to the target receptor for any given analog.

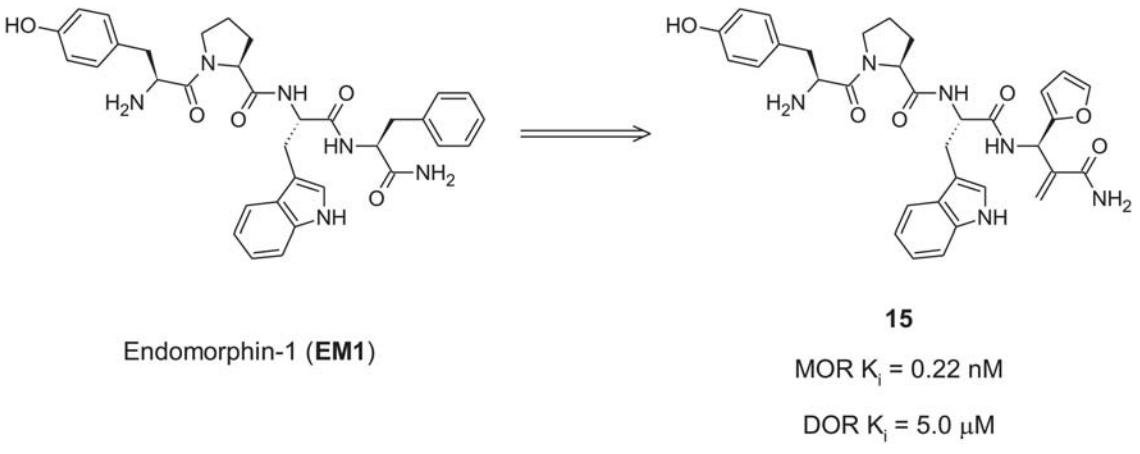

Endomorphin-1 (**EM1**)

15

MOR K_i = 0.22 nM

DOR K_i = 5.0 μM

Scheme 11 Selective endomorphin-1 peptidomimetic **15**.

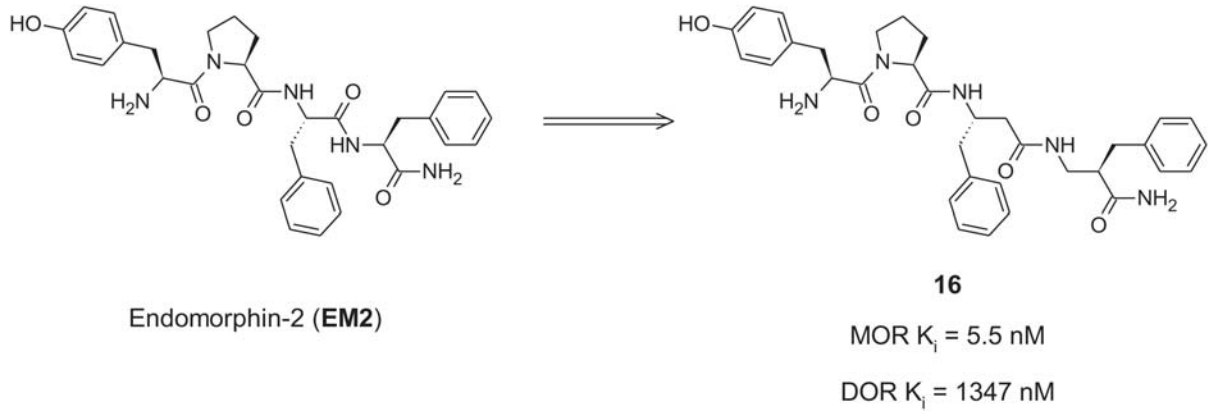

Scheme 12 Selective endomorphin-2 peptidomimetic **16**.

3.08.5.1.3 Class A GPCR purinergic

Adenosine receptors. The adenosine receptor family (A_1, A_{2A}, A_{2B}, and A_3) has been extensively researched over many years with a number of agents (both agonists and antagonists) being investigated clinically for the treatment of cardiovascular disease, renal disorders, asthma, Parkinson's disease, and cognitive disorders.[203] Antagonists of the adenosine A_{2A} receptor have also been more recently implicated in cancer immunotherapy.[204] There are now multiple published crystal structures of the adenosine A_{2A} receptor bound to small-molecule ligands in both antagonist and agonist receptor conformations, and this gives the opportunity for a new generation of adenosine receptor agonists and antagonists to be created. Indeed, SBDD approaches to adenosine receptors are the subject of a number of recent reviews.[205–207] Earlier in this article, we outlined some of the in silico studies carried out on this receptor and discussed how certain compounds bind and examined the opportunities for virtual screening.

The availability of stable purified protein has also meant that adenosine A_{2A} has been a work-horse system for fragment screening approaches over the last 5 years. Although not SBDD studies in themselves, fragment screening studies provide low-molecular-weight start points for the development of new series, and in fragment-based drug discovery, SBDD methodology is generally utilized. For example, target-immobilized NMR screening (TINS) is a methodology used to detect relatively weak interactions between proteins and small molecules. The technique uses changes in the NMR spectrum of the ligand upon its binding to the target protein due to a change in the speed with which it is tumbling through solution. The A_{2A} receptor has been stabilized using Heptares' StaR technology to give protein (A_{2A} StaR2) that could be successfully immobilized on Sepharose resin and then screened using the TINS method. A library of 531 fragment-sized molecules was analyzed at 500 μM.[208] After further characterization, five competitive orthosteric ligands with varied chemical structures were identified, with IC_{50} values ranging between 70 and 1880 μM in concentration-response studies with [^{3}H]-ZM-241385. This and other biophysical methods not discussed here have been successfully applied to stabilized GPCR proteins such as adenosine A_{2A}, demonstrating that fragment screening using direct-binding methodologies, previously applied only to soluble targets, has potential to facilitate GPCR drug discovery.

In a follow-up to the NMR fragment screen (in the aforementioned text), Siegal and Carlsson et al.[110] carried out docking studies of the fragment hits to try to predict their binging modes to the adenosine A_{2A} receptor. Molecular docking was able to predict four out of the five orthosteric ligands discovered by NMR among the top 5% of the ranked library, suggesting that structure-based methods could be used to prioritize among primary hits from biophysical screens. In addition, three fragments that were top-ranked by molecular docking, but had not been picked up by the NMR-based method, were demonstrated to be A_{2A} receptor ligands. Encouraged by these results, the authors carried out a virtual screen of a much larger library of commercially available fragments (328,000 compounds). Fourteen new active compounds were identified from biological testing of 22 purchased fragments and preliminary SAR established by screening of analogs of some of the more promising hits.

As noted earlier, the newly available A_{2A}R protein–ligand structures are being extensively applied to ligand design. There is an increasing understanding of the requirements of the pocket for potency, the roles of water molecules in the binding site, and the areas of the pocket important for selectivity for one receptor subtype over the others in the family. In addition, the availability of both antagonist and agonist forms of the receptor gives an insight into the mechanisms of receptor activation for these receptors and is aiding the design of new generations of selective agonists.

Pastorin et al. have reported a number of triazolotriazine derivatives as antagonists binding to the A_{2A} receptor and for which docking experiments using the GOLD software in the A_{2A}R crystal structure were studied.[209] Homology modeling was also carried out for the closely related A_3R to try to study selectivity. The structure–activity relationship for the series of compounds was then rationalized, and it was suggested that the presence of a relatively less bulky amino acid (Val169) in the ECL2 of the adenosine A_3 receptor might be important to affect potency and selectivity for the A_{2A} receptor versus the A_3 subtype. The molecules were then further optimized using SBDD in a separate publication, identifying the best vector to append aqueous solubilizing groups. This overcame some issues with poor solubility in the heterocyclic template itself and successfully generated highly potent and very soluble lead compounds.[210] In a chemically related series, Higgs et al. have investigated the SAR of a series of low-molecular-weight

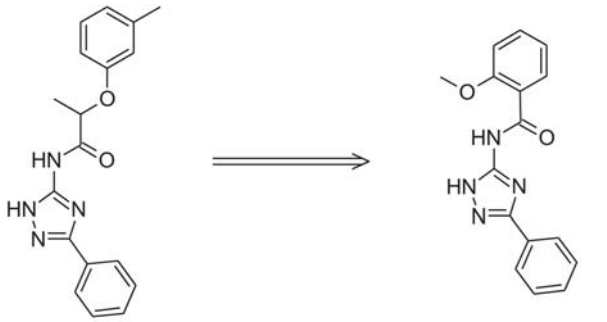

Scheme 13 Development of a series of 1,2,4-triazoles A_{2A} receptor antagonists.

triazolylpurines as adenosine A_{2A} antagonists. The importance of the role of water molecules in the binding site was investigated using the software WaterMap and using the crystal structure PDB ID, 3EML.[12] Interestingly, the SAR could be rationalized in that small substituents were proposed to occupy a region containing stable waters, while larger groups accessed a subpocket to displace unstable waters.

Carlsson and coworkers have investigated virtual screening of the adenosine A_{2A} receptor in the antagonist conformation in a number of contributions to the literature (in the aforementioned text and **Table 1**). In one report, the SAR across a series of 1,2,4-triazoles has been further investigated, again using modeling information.[211] Thirty-three analogs were tested in adenosine A_1, A_{2A}, and A_3 receptor radioligand binding assays and in functional assays for the A_{2B} receptor subtype. Surprisingly, a series of closely related analogs of the initial lead **17**, **Scheme 13**, did not display improved binding affinity or selectivity. Further molecular docking studies were used to guide the selection of more distantly related molecules resulting in the discovery of **18**, a submicromolar adenosine A_{2A} receptor antagonist (K_i 200 nM) with high ligand efficiency but lacking selectivity over the A_3 receptor. The polar core of **18** was proposed to form hydrogen-bonding interactions with Asn253$^{6.55a}$ and Glu169 (ECL2).

Volpini and coworkers have described the synthesis and biological evaluation at the four human adenosine receptor subtypes of a series of 9-substituted 8-(2-furyl)adenine derivatives.[212] Results showed that 8-(2-furyl)-9-methyladenine has high affinity at the A_{2A} subtype. Further modification of this compound with introduction of arylacetyl or arylcarbamoyl groups in the N^6-position modified the selectivity versus the other three adenosine receptor subtypes. A molecular modeling analysis at three different A_{2A} receptor crystal structures provided a preliminary interpretation of the obtained biological results. The authors went on to describe further studies of these 9-propyladenines this time bearing a phenylalkylamino group in the 2-position or a phenylalkyl chain in the N^6-position.[213] One analog 2-benzylamino-8-furyl-9-propyladenine was more active than the parent 8-furyl-9-propyladenine at A_{2A} and A_3 adenosine receptors (K_i A_{2A} = 6.6 nM and K_i A_3 = 29 nM compared with K_i A_{2A} = 18 nM and K_i A_3 = 790 nM). Molecular modeling studies again gave some explanation of the different activities of the compounds at the A_{2A} receptor. In particular, the findings suggested that the introduction of a phenylalkylamino chain in the 2- or 6-positions of 9-alkyl purine derivatives favors the interaction of the resulting compounds with the A_{2A} subtype providing further suggestions for the synthesis of new antagonists of this receptor.

In a recent contribution to the literature, Colotta and Moro et al. identified a promising phenylpropyl-substituted pyrazolopyrimidine derivative as a dual adenosine A_1/A_{2A} receptor antagonist, showing high affinity for both the receptor subtypes, compound **19**, **Scheme 14**.[214] Also described were some highly potent and selective antagonists for the adenosine A_1 receptor with low

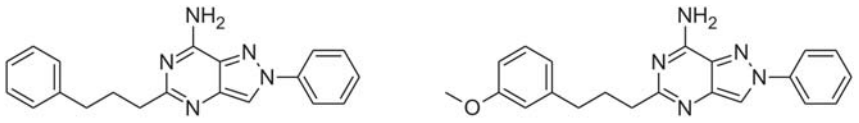

Scheme 14 Dual adenosine A_1/A_{2A} receptor antagonists **19** and **20**.

nanomolar affinity, such as **20**. Molecular modeling studies indicated that the selected compounds might adopt a placement in the adenosine A_1 and A_{2A} receptor binding clefts that resembles the crystallographic binding mode of X-ray cocomplex ligand **ZM-241385**. It was rationalized that stabilizing interactions, not shown at the A_{2A} receptor, with Thr270$^{7.35a}$, Tyr271$^{7.36a}$, Ser267$^{7.32a}$, or Glu170^{EL2a} residues might account for the enhanced adenosine A_1 affinity of ortho- and metasubstituted derivatives. These additional electrostatic interactions are either weaker or not detected for the parasubstituted derivatives, consistently with their lower affinity for both the subtypes.

The first GPCR structure-based drug design case study in which crystal structures of analogs were solved and used as part of the lead optimization process was targeted at identification of adenosine A_{2A} antagonists. Congreve et al. described the identification and derivatization of 1,2,4-triazine derivatives targeting the orthosteric site of the receptor.[87] The original highly potent but nonselective hit **21**, **Scheme 15**, was discovered using virtual screening against a homology model of the receptor optimized and enhanced using site-directed mutagenesis data.[112] The various hit series were next characterized using a method called Biophysical Mapping™. SDM in the binding site was carried out in the background of the stabilized receptor, followed by physical capture of each mutated protein sample onto a chip format. A biophysical technique, SPR screening, was then used to study the binding properties of the compounds versus each modified receptor.[215] In this way, a map of the binding site was produced correlating the changes made to amino acid side chains within the binding site and the SAR of the compound series. Using this analysis, the hit **21** (**Scheme 15**) was redesigned and simplified to an alternative regiochemistry aiming to more optimally fit the binding site. This led to identification of hit scaffold **22**.[87] Although less potent than **21**, simple optimization to better fill the binding pocket rapidly delivered potent compounds. Crystal structures of two analogs were presented in the article and illustrated that the molecules bind more deeply inside the orthosteric binding cavity than most other classes of A_{2A}R antagonists creating the opportunity to produce smaller and more drug-like molecules. The X-ray data also indicated that 3,5-disubstitution of one of the aryl rings was likely to be the driver of improved selectivity over the A_1 receptor, due to small differences between the receptors in the part of the binding pocket that this ring occupies. An optimized analog **23** was described in some detail and is a potent, ligand-efficient, 10-fold-selective, and orally efficacious compound representing a good lead compound. These results suggested further progression of the series of compounds. Indeed, Heptares Therapeutics has recently publically announced the selection of a clinical candidate HTL1071 that is being explored for the potential treatment of cancers in collaboration with AstraZeneca.

In a follow-on study, a series of chromone derivatives optimized using SBDD methods as antagonists of the adenosine A_{2A} receptor have been described by Andrews et al.[216] Again, the original hit **24**, **Scheme 16**, was derived from a virtual screening campaign versus a homology model of the receptor.[112] After consideration of the docking poses of the hit compound and in particular the polar interactions present between the ligand and the receptor, further analogs were purchased and screened. For example, removal of the carboxylic acid led to **25** with improved affinity and ligand efficiency. Using a druggability analysis of the binding site, a lipophilic hotspot was identified with a GRID aromatic CH (C1=) probe in a pocket lined by Ile66$^{2.64a}$ and Tyr271$^{7.36a}$. This led to the design of compounds with lipophilic groups at the C-6 of the chromone core. With this modification and the further addition of an acetyl group on the phenol derivative, **26** was designed resulting in very high affinity versus the receptor. Interestingly, in a related compound, removal of the methyl group from the thiazole ring system produced a significant reduction in affinity, and this was

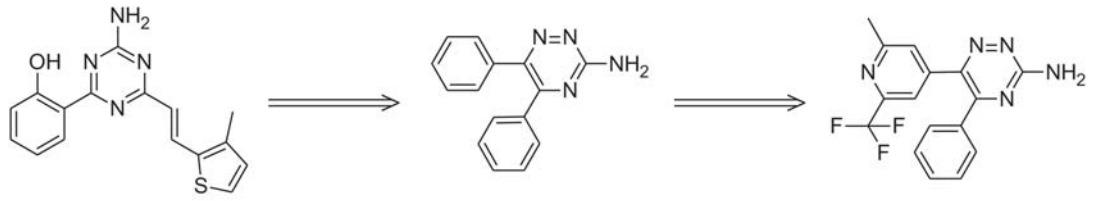

Scheme 15 Identification and optimisation of a series of 1,2,4-triazine A_{2A} receptor antagonists.

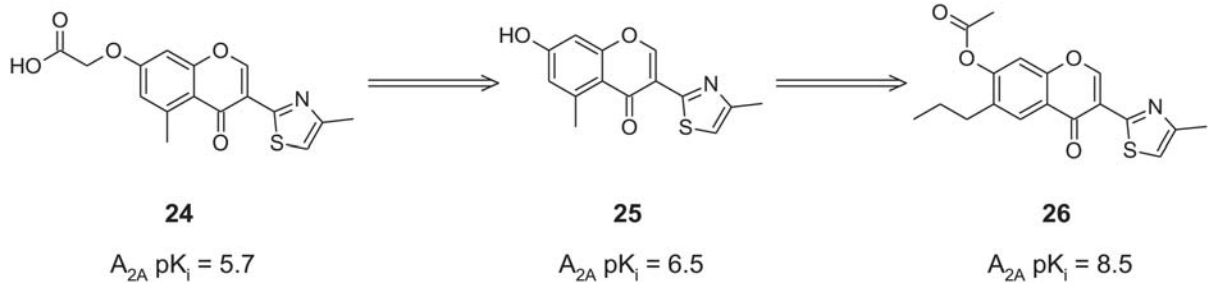

Scheme 16 SBDD optimisation of a series of chromone A_{2A} receptor antagonists.

rationalized to be because the methyl group displaces a water molecule trapped at the bottom of the binding site, and when the methyl is absent, this water is then present in an unfavorable lipophilic environment. Examples from the series were screened versus the other adenosine receptor subtypes and shown to have good selectivity for the adenosine A_{2A} receptor.

In addition to the examples described earlier of antagonists of the adenosine A_{2A} receptor, there have been many reports of studies on the other adenosine subfamily members. Included below are some selected examples targeting the adenosine A_3 receptor using homology modeling and starting from A_{2A}R crystal structures. The adenosine A_3 receptor is closely related to adenosine A_{2A} making the modeling of its binding site possible with a good degree of confidence.

Catarzi et al. have investigated a series of pyrazoloquinazoline adenosine A_3 receptor antagonists and carried out docking studies to rationalize the SAR and overall binding modes of the best compounds.[217] A number of docking proposals were considered, each with the tricyclic core interacting with Asn250$^{6.55a}$ and π-stacking with the Phe168^{ECL2}. Despite being a bulky rigid scaffold, a number of proposals appeared credible due to the large cavity predicted for the orthosteric site of the receptor. However, the detailed SAR for the derivatives was used to provide evidence for a preferred pose and allowed for the design of simplified analogs in the compound series, which maintained submicromolar receptor potency. This work has been extended in a recent publication, describing further optimization of related analogs with high selectivity for the A_3 receptor over the A_{2A} receptor.[218]

Pastorin, Spalluto, Colotta, and Moro et al. have extended their work (described earlier) on adenosine receptor antagonist ligands by developing pyrazolo-triazolo-pyrimidines and related compounds focusing on selective adenosine A_3 antagonists.[219–221] For example, using a combination of SAR and molecular modeling-driven hypotheses, a subnanomolar and highly selective adenosine A_3 antagonist has been identified that also lacks the furan ring system present in many adenosine receptor antagonists.[219] The furan ring is a possible source of reactive metabolites in vivo and therefore a potential toxicophore. The selectivity of the new lead compound was proposed to be derived from a significant rotation of the molecule within the A_{2A} binding site relative to the A_3 receptor perturbing the key H-bonding interactions with the critical polar residue Asn$^{6.55a}$. This appeared to be due to interaction with the molecule with Val169 (ECL2) in A_3 versus Glu169 (ECL2) in A_{2A} and that this was causing the change in binding pose in the A_{2A} subtype.

Gutiérrez-de-Terán et al. describe the synthesis and SAR of a series of aminopyrimidine adenosine A_3 antagonists, developed using SBDD.[222] A number of highly potent and selective molecules were identified. Using a homology model of the A_3 receptor, a binding pose for the series was optimized considering the SAR and selectivity. The core polar heterocycle and amide substituent were proposed to interact with Asn250$^{6.55a}$; an overlay of 62 examples was used to develop a 3-D QSAR model, and a detailed rationalization of the selectivity and potency was provided with careful consideration given to residues lining the binding sites in the various receptor subtypes. The robustness and predictive capabilities of the model were then validated by designing further compounds, such as **ISVY130**, **Scheme 17**, that explored new alkyl residues at one of the vectors from the chemical scaffold and that showed high affinity and selectivity profiles for the A_3 receptor.

Baraldi and Preti et al. have reported a new series of 2-heterocyclyl-imidazo[2,1-*i*]purin-5-one derivatives as adenosine receptor antagonists.[223] The 2-heterocyclyl substitution proved to induce excellent affinity and selectivity toward the adenosine A_3 subtype. Molecular modeling studies were helpful in rationalizing the observed SAR along with the selectivity profiles of the new series of ligands. In particular, docking of the most potent compound provided a credible binding mode of the newly described derivatives. A number of the adenosine A_3 antagonists showed good potency and selectivity and were thought suitable for further investigation. The same team has also published a follow-on paper in which urea-based derivatives were reported.[224]

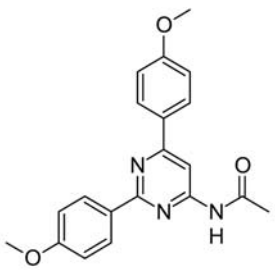

ISVY130

A_1 pK_i = 1% inhibition at 1 μM

A_{2A} pK_i = 10% inhibition at 1 μM

A_{2B} pK_i = 4% inhibition at 1 μM

A_3 pK_i = 3.6 nM

Scheme 17 A_3 receptor antagonist **ISVY130**.

The availability of agonist-bound structures of the adenosine A_{2A} receptor has precipitated a number of studies to reevaluate adenosine-derived small-molecule agonists. In fact, adenosine analogs have been studied for many years as agonists of adenosine receptors, and now, the binding modes and molecular interactions are finally being understood.[203]

Soon after the structures became available, Deflorian et al. compared previous docking studies of molecules into homology models of the receptor with dockings of each compound into X-ray structures of **UK-432,097** and **NECA**.[225] The purine base of the agonists overlays with the heterocyclic portion of antagonist ligands as perhaps might be expected. However, there are key differences between agonists and antagonists caused by the ribose moiety found in the agonists that forms additional important polar interactions with Thr88$^{3.36a}$, His250$^{6.52a}$, Ser277$^{7.42a}$, and His278$^{7.43a}$, which are largely absent in antagonists. Jacobson et al. have reported a number of subsequent studies on adenosine agonists using SBDD, for example, rationally designing adenosine analogs leading to a highly potent and selective adenosine A_3 agonist, demonstrating the high value of the new agonist-bound X-ray structures.[226]

Jacobson and Katritch et al. went on to use the agonist-bound A_{2A} crystal structures to directly design modifications to the ribose motif and create new agonist analogs.[114] The optimization process used in silico design and docking to modify substituents on the carboxylate functional group of the ribose, which is positioned deep in the bottom of the binding pocket of the receptor. In this way, a number of potent analogs were identified, derived from the nonselective ligand **NECA**. Interestingly, some of the new compounds showed differing patterns of selectivity across the closely related adenosine A_{2A}, A_1, and A_3 receptors and also varying degrees of partial to full agonism. For example, compound **27** in Scheme 18 is a potent and selective partial agonist at the adenosine A_1 receptor.

Jacobson et al. have also worked on structure-based optimization of (*N*)-methanocarba nucleosides, in which the ribose sugar has been altered to a carbocyclic ring system.[227] Efforts led to rational design of MRS5474, a moderately selective adenosine A_1 full agonist in which the N^6-substituent of the base had been modified. The compound showed efficacy in a relevant in vivo model. Nucleoside docking into an A_1 receptor homology model characterized distinct hydrophobic subpockets for the new substituents, the larger forming contacts with Thr270$^{7.35a}$, Tyr271$^{7.36a}$, Ile274$^{7.39a}$, and carbon chains of glutamates (EL2) and the smaller subpocket forming contacts between TM6 and TM7. In a related study, (*N*)-methanocarba(bicyclo[3.1.0]hexane)adenosine derivatives containing charged sulphonate substituents have been rationally designed as peripherally restricted adenosine A_3 agonists.[228] The rational design approach based on A_3 homology models successfully predicted sites for sulfonate incorporation, producing compounds designed to delineate adenosine's CNS versus peripheral actions.

Lavecchia and Cappellacci et al. have recently reported dual adenosine A_1/A_3 nucleoside agonists for potential treatment of glaucoma.[229] The ribose ring was substituted by a tetrazole ring rather than the usual amide (e.g., in **NECA** in the aforementioned text). N^6-substitued analogs were prepared and the SAR rationalized in silico using homology models of the receptors, providing a credible interpretation of the data. Example compounds described in the article are **28** and **29**, Scheme 19.

In a recent addition to the field, Louvel et al. report a series on nonnucleoside adenosine A_1 receptor full and partial agonists.[230] The ligands were derived from simplification and recombination of known scaffolds from the patent literature, and example compounds were shown to be relatively selective adenosine A_1 agonists compared with literature standards. Although the putative binding modes of the compounds were only briefly discussed, of interest is that the kinetic binding parameters were included and showed a wide range of on- and off-rates. The structure–kinetic relationships (SKRs) of a series of compounds are an important consideration in GPCR drug design, and yet, data are rarely reported. As the availability of biophysical characterization, such as SPR, becomes increasingly available, we would expect consideration of on- and off-rates will become more common and start to be used more frequently as part of the medicinal chemists compound design process.

Finally, in a recent and elegant study, Baraldi and Cosconati et al. designed hybrid or merged ligands incorporating the features of the selective A_{2A} antagonist **ZM-241385** and the nucleotide agonist **NECA**.[231] The ligands were directly inspired by the crystal structures of these two ligands and subsequent in silico optimization. The extended ligands maintained agonist pharmacology, and a highly potent and a selective A_{2A} agonist, **30**, was identified (A_{2A} $K_i = 4.8$ nM and A_{2A} $EC_{50} = 4.9$ nM), Scheme 20.

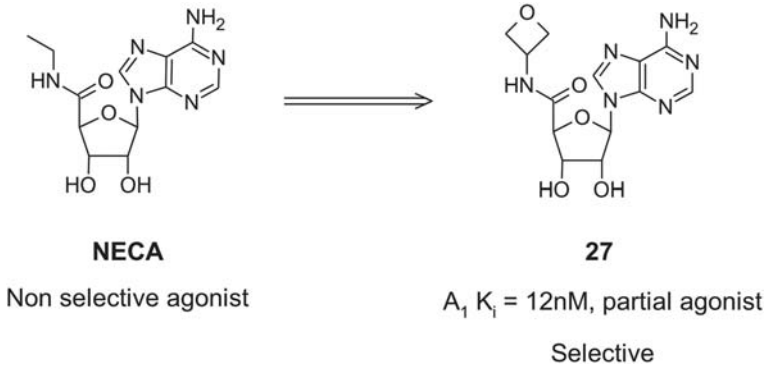

Scheme 18 A_1 partial agonist **27** derived from **NECA**.

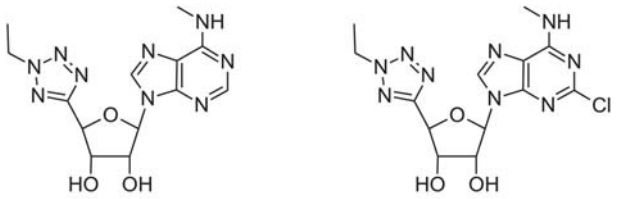

28

A_1 K_i = 3.56 nM

A_{2A} K_i = 778 nM

A_3 K_i = 0.48 nM

29

A_1 K_i = 8.59 nM

A_{2A} K_i = 3350 nM

A_3 K_i = 0.43 nM

Scheme 19 Dual adenosine A_1/A_3 agonists **29** and **29**.

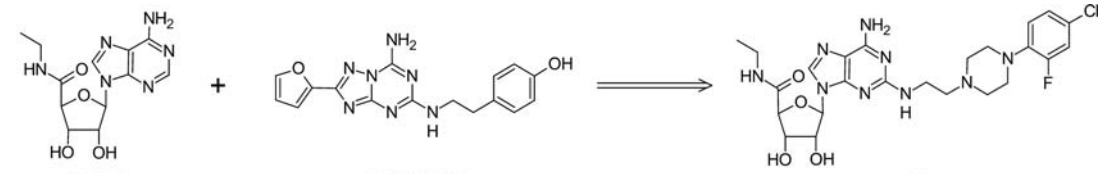

NECA

Non selective agonist

ZM-241385

A_{2A} selective antagonist

30

A_1 K_i > 10000 nM

A_{2A} K_i = 4.8 nM

A_{2A} EC_{50} = 4.9 nM

A_{2B} K_i > 10000 nM

A_3 K_i = 1487 nM

Scheme 20 Hybridization of **NECA** and **ZM-241385** to identify **30** A_{2A} receptor agonist.

3.08.5.1.4 Class A GPCR lipid receptors

GPR40. GPR40 agonists are being investigated clinically as one novel approach to the treatment of diabetes. GPR40 is a G_q protein-coupled receptor preferentially expressed in pancreatic β-cells, and medium- and long-chain free fatty acids have been found to activate the receptor as the natural ligands. GPR40 agonists stimulate insulin secretion only in the presence of high glucose concentrations. Based on this mechanism, GPR40 agonists are promising novel insulin secretagogues with low risk of hypoglycemia. The crystal structure of the GPR40 receptor in complex with a small-molecule agonist TAK-875 has now been described and was discussed earlier.[24]

In a recent publication from Takano and Toda et al., the optimizations of 3-aryl-3-ethoxypropanoic acids were performed leading to the identification of a new agent **DS-1558**, (3*S*)-3-ethoxy-3-(4-{[(1*R*)-4-(trifluoromethyl)-2,3-dihydro-1*H*-inden-1-yl]oxy}phenyl)propanoic acid, which had efficacy on glucose-dependent insulin secretion after intravenous glucose injection in SD rats.[232] Notably, an induced-fit docking study of **DS-1558** was carried out using the X-ray structure of GPR40, in which the molecule docked very well to the same binding site with a slightly rotated side chain of Trp174. The model was thought to explain the series SAR reasonably well. As might be expected, the carboxylic acid moiety in the compounds was highly coordinated by the key basic residues Arg183$^{5.39a}$ and Arg258$^{7.35a}$ forming a strong anchor point. The trifluoromethyl group on the indane moiety had hydrophobic interactions with both protein and hydrophobic portion of the lipid bilayer where the ligand exits the receptor. The (more active) *R* stereochemistry of the indane moiety was more favorable than the *S* form in the binding cavity, especially when there was a substituent on the 4-position, due to steric hindrance with the protein. Interestingly, the ethoxy moiety extending from the propanoic acid side chain was well accommodated in a small side pocket not utilized by TAK-875. Although retrospective, the study highlights further opportunities for the next generation of design of GPR40 agonists. TAK-875 is no longer in development, leaving an opportunity for the identification of new drugs.

3.08.5.1.5 Class A GPCR chemokine

Chemokines are a family of signaling proteins secreted by cells that induce directed chemotaxis in nearby responsive cells so that they are overall chemotactic cytokines. Chemokines are approximately 8–10 kDa in mass and have four cysteine residues in conserved locations that are key to forming their three-dimensional shape. Some chemokines act as pro-inflammatory agents and may be released during an immune response to recruit cells to a site of infection. Other classes of chemokines are considered

homeostatic and seem to be involved in controlling the migration of cells during normal processes of tissue maintenance or sometimes development. There are four main subfamilies, CXC, CC, CX3C, and XC, all of which exert their biological effects by interacting with GPCR receptors (chemokine receptors).

There are approximately 19 different chemokine receptors which have been characterized to date that are divided into four families: CXCR that binds CXC chemokines, CCR that binds CC chemokines, CX3CR1 that binds the sole CX3C chemokine (CX3CL1), and XCR1 that binds the two XC chemokines (XCL1 and XCL2). Chemokine receptors have overall typical GPCR structural features, being ~350 amino acids in length and seven helical transmembrane domains with three intracellular and three extracellular hydrophilic loops. They typically have a short, acidic *N*-terminus and an intracellular *C*-terminus containing serine and threonine residues important for receptor regulation.

There has been a great deal of interest and effort within the pharmaceutical industry to find drugs that bind as antagonists of chemokine receptors. Many compounds have entered clinical trials for a variety of indications with only limited success, and progress in the area has been comprehensibly reviewed.[233] There appears to have been two main challenges in the field. Firstly, there is a very complex interaction between the chemokine ligands and their receptors with many ligands binding to more than one receptor such that inhibition of one receptor pathway may not be sufficient to produce the anticipated effect. The situation is made even more complex by species differences in the chemokine system making the prediction of efficacy in humans challenging. Secondly, the chemokine ligands bind very tightly as agonists to their target receptors, and small-molecule antagonists therefore need to be extremely potent and have a long-lasting in vivo effect driven either by excellent exposure after dosing or due to insurmountable receptor kinetics or both to be efficacious.

Despite these issues, two drugs have been so far successfully launched that target chemokine receptors: plerixafor (AMD3100) that targets the CXCR4 receptor and is used for stem cell mobilization, approved by the FDA in 2008 to treat non-Hodgkin lymphoma and multiple myeloma, and maraviroc (UK-427,857) that targets the CCR5 receptor, which is an entry factor for macrophage-tropic strains of HIV-1, approved by the FDA in 2007 for the treatment of HIV infection.

In 2010, the complex of a small-molecule inhibitor IT1t and a number of peptide inhibitors with CXCR4 was published by Wu et al.[234] These data have been very informative for medicinal and computational chemists showing how completely different types of molecule that do not share the same pharmacophoric features can bind to the same receptor. In particular, the interactions of the small molecule appear dominated by hydrophobic contacts, sitting high in the large orthosteric binding site, surrounded by bulk water. The location of this site would have been extremely difficult to predict in the absence of the X-ray data, as docking programs will fit molecules more deeply inside a binding site rather than leave space between the molecules surface and the protein. Consideration of the water-molecule network and energies can help to rationalize the binding, and this type of methodology can now be used to attempt to predict small-molecule binding in other chemokine receptors.[93] In our own laboratories, we have found analysis of the energetics, and placement of binding site water molecules can have a significant role in both the interpretation of why a molecule binds to a GPCR as it does and to inform further rational design.

More recently, the structure of CXCR4 in complex with the viral chemokine antagonist vMIP-II has been revealed.[234] vMIP-II is a CC chemokine encoded by Kaposi's sarcoma-associated herpesvirus. vMIP-II functions as a broad-spectrum antagonist of many human CKRs and helps the virus to escape the host immune response. The protein–protein interaction has a 1:1 stoichiometry with a more extensive binding interface than was anticipated. The structure also helps rationalize a large body of mutagenesis data and in tandem with modeling provides insights into CXCR4 interactions with its endogenous ligand CXCL12, its ability to recognize diverse ligands, and the specificity of CC and CXC receptors for their respective chemokines.

As noted earlier, the CXCR4 receptor has been linked with promotion of metastasis, angiogenesis, and tumor growth.[235,236] Additionally, CXCR4 has been implicated in HIV pathogenesis as a coreceptor for viral cell entry.[237] The crystal structures of both small-molecule and peptide ligands highlighted earlier are starting to impact ligand design for this target, which is a good example of a GPCR with relatively low tractability for drug design. Mungalpara et al. have carried out peptide SAR analysis and computational studies to attempt to rationally design conformationally constrained cyclopentapeptide antagonists of CXCR4.[238] In silico docking into the X-ray structure of CXCR4 in complex with the 16-mer peptide antagonist CVX15 (PDB ID, 3OE0) was undertaken using induced-fit docking protocols. This resulted in a binding pose overall consistent with the SAR. A number of new molecules were designed and synthesized that had increased activity at the target, consistent with the design hypothesis.

Cyclotides are globular microproteins (28–37 amino acids) stabilized by three intramolecular disulfide bonds. These peptides provide a rigid molecular scaffold with improved metabolic stability compared with typical peptides in vivo. Aboye et al. have designed novel cyclotides to target the CXCR4 receptor using the peptide CXCR4 X-ray data as a starting point.[239] The most potent cyclotide was significantly more stable than the peptide antagonist CVX15.

In a recent publication from the Liotta group at Emory University, the United States, a novel series of CXCR4 antagonists containing substituted piperazines were described starting from **TIQ-15**,[240] **Scheme 21**. These compounds showed micromolar to nanomolar potency in CXCR4-mediated functional and HIV assays, such as inhibition of X4 HIV-1_{IIIB} virus in MAGI-CCR5/CXCR4 cells and also inhibition of SDF-1-induced calcium release in Chem-1 cells. Structure–activity relationship studies led to the identification of a series of *N*-aryl piperazines as the most interesting compounds, exemplified by **31**. The SAR examined the optimum type and position of the aromatic ring and linker and stereochemistry. A credible binding pose consistent with the SAR was produced for the lead molecules binding to the CXCR4 small-molecule binding pocket, giving the possibility of further structure-based optimization of the series. Interestingly, the molecules were predicted to overlap with both the **IT1t** and part of the cyclic peptide **CVX15** binding regions discussed earlier. Profiling of several lead compounds showed that one molecule **32** had the best overall profile and drug-like properties when considering both SDF-1 and HIV potencies (6–20 nM). In a further paper

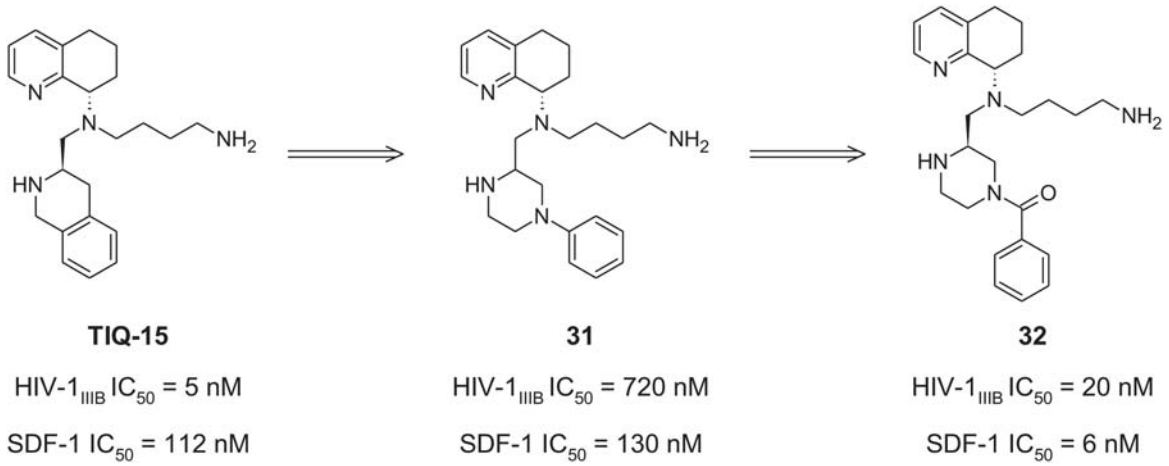

Scheme 21 Identification and optimisation of a series of CXCR4 antagonists based on **TIQ-15**.

by the same team, a series of simplified derivatives composed of a pyrazole-piperidine core have been described that had activity versus both CXCR4 and CCR5 receptors.[241]

In 2013, the crystal structure of a complex of maraviroc with the CCR5 receptor was published by Tan et al.[242] The structure reveals a ligand-binding site that appears to be distinct from the proposed recognition site for chemokines themselves and from the viral glycoprotein gp120. This allosteric binding mode gives an insight into the mechanism of the noncompetitive inhibition of chemokine signaling and viral entry by small molecules. Interestingly, maraviroc has a very slow off-rate from the receptor, which almost certainly contributes to its ability to inhibit viral entry, and the X-ray structure helps to rationalize this being deep inside the 7TM bundle of the receptor below the protein–protein interaction site.

There has so far been limited application of the CCR5 receptor structure reported; however, in a fascinating new paper, Akgün and Portoghese et al. investigated dimeric ligands targeting both CCR5 and MOR (discussed earlier). Chemokine release promotes cross talk between opioid and chemokine receptors that is thought to reduce the efficacy of morphine in the treatment of chronic pain. On the basis of the possibility that an MOR-CCR5 heteromer is involved in such cross talk, the authors synthesized bivalent ligands that contain mu-opioid agonist and CCR5 antagonist pharmacophores linked through homologous spacers (14–24 atoms, Scheme 22). When tested in vivo in mice treated with lipopolysaccharide to induce inflammation, a member of the series (**MCC22**)

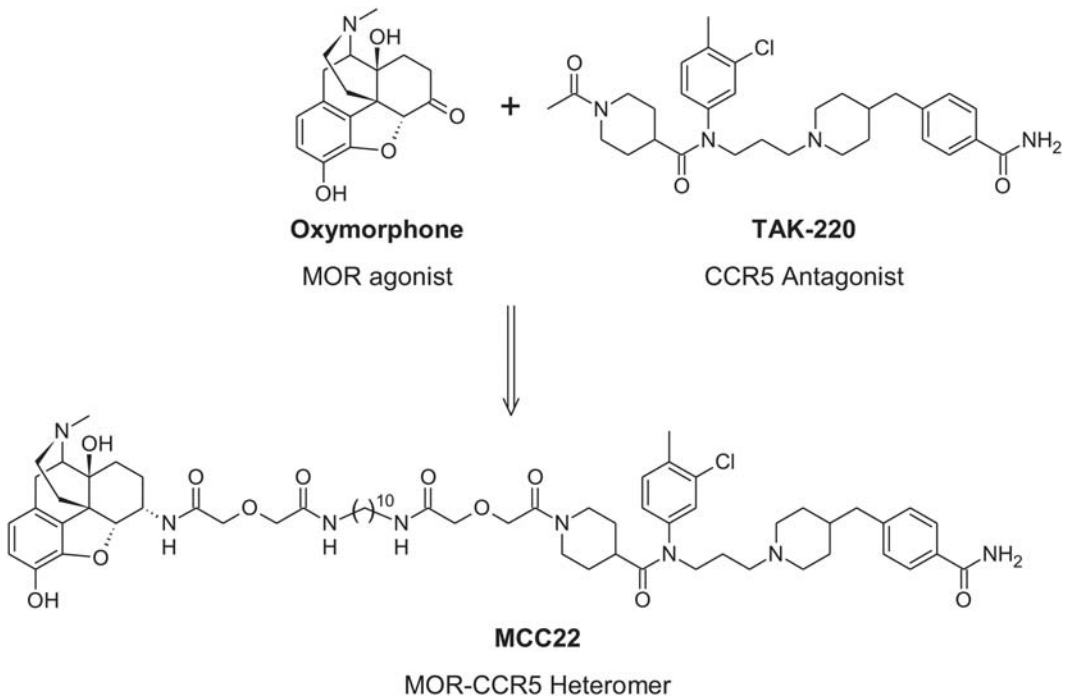

Scheme 22 Development of a **MCC22** a dual MOR agonist CCR5 antagonist.

with a 22-atom spacer exhibited profound antinociception (i.e., $ED_{50} = 0.0146$ pmol/mouse) that was 2000× greater than morphine. Moreover, **MCC22** was ~3500× more potent than a mixture of MOR agonist and CCR5 antagonist monovalent ligands given together in the same in vivo model. These data strongly suggested that **MCC22** has its action by bridging the protomers of a MOR-CCR5 heteromer. Molecular simulation studies were described and were consistent with this hypothesis of such bridging and supported the notion that the MOR-CCR5 heteromer is a novel target for the treatment of chronic pain.

In another recent publication, the structure of the human chemokine ligand CX3CL1 (fractalkine) has been solved in complex with the viral chemokine receptor US28 from cytomegalovirus.[243] This structure has the GPCR in its agonist conformation, providing information of this conformational state for a chemokine receptor for the first time. The globular body of CX3CL1 is perched on top of the US28 extracellular face, whereas its amino terminus projects into the central core of US28. Interestingly, the amino terminus projection occupies a similar location to maraviroc in the CCR5 complex noted earlier, suggesting a binding site for small molecules to interact with US28.

SBDD studies are beginning to extend to other chemokine receptors, building on the protein–ligand complexes now available. Blockade of undesired neutrophil migration to sites of inflammation remains an area of interest as an approach to treatment of inflammatory diseases. One long-standing therapeutic target is antagonism of the chemokine receptor CXCR2. Maeda et al. have reported the discovery of 6-(2-boronic acid-5-trifluoromethoxy-benzylsulfanyl)-*N*-(4-fluoro-phenyl)-nicotinamide, an antagonist with activity at both CXCR1 and CXCR2 receptors (IC_{50} values 31 and 21 nM, respectively).[244] The agent exhibited potent blockade of neutrophil influx in a rat in vivo model of pulmonary inflammation. Interestingly, the authors provided the hypothesis that the molecule interacts with a unique intracellular binding site on CXCR2.[245] The compound contains a boronic acid functional group known to be a potential covalent "warhead" reacting with activated nucleophiles on proteins, and the proposal has this group in close proximity to $Cys230^{5.57a}$ in the proposed binding site, although the authors do not propose that a covalent bond is formed. This compound **SX-576** is undergoing further investigation as a potential therapy for pulmonary inflammation.

3.08.5.2 Allosteric GPCR Ligands

Allosteric binding sites on GPCRs are a long-standing opportunity to address drug discovery to more challenging targets where the orthosteric site is highly challenging due to the nature of the natural ligand or due to difficulties in identifying selective ligands.[246] Allosterism also gives the opportunity to modulate the natural ligand in a positive or negative sense (positive allosteric modulators or negative allosteric modulators, PAMs and NAMs) giving drugs with potentially different pharmacological consequences to those targeting the orthosteric site.[247] This is a large field of interest with many contributions to the literature, and here, we focus on just two examples where X-ray structures of allosteric ligands are now available.

$mGlu_5$ receptor. Glutamate, a major excitatory neurotransmitter of the brain, mediates its activities via ion channels and through a family of eight metabotropic glutamate receptors (mGlu) that are part of the GPCR superfamily (class C). The $mGlu_5$ receptor is highly expressed in the basal ganglia, lateral septum, cortex, and hippocampus and has a key role regulating the activity of *N*-methyl-D-aspartate (NMDA) receptors. As such, modulation of the activation of this receptor is implicated in a range of CNS diseases including depression and anxiety.[248] The X-ray structure of the $mGlu_5$ receptor in complex with a negative allosteric modulator (NAM) mavoglurant has recently been published, and the implications of this structure were discussed earlier.[18]

Christopher et al. followed up on the publication of this X-ray complex with a description of the discovery of an $mGlu_5$ NAM HTL14242 (Fig. 9) using fragment- and structure-based approaches.[249] A fragment screening campaign using high-concentration

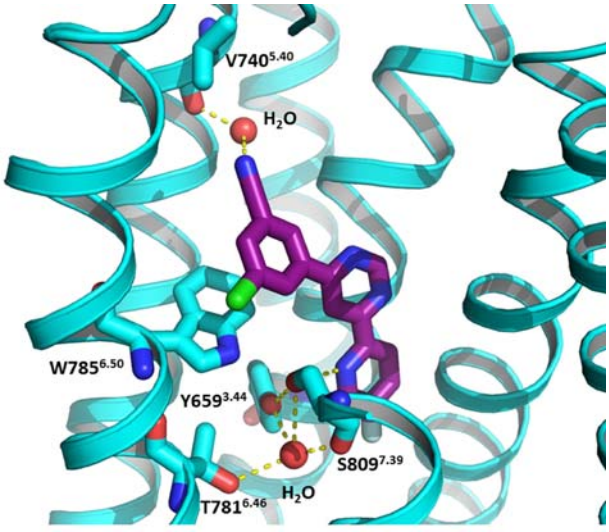

Fig. 9 X-ray crystal structure of HTL14242 bound to the $mGlu_5$ receptor. The allosteric modulator binds deeply in the center of the TM bundle of the receptor in an induced hydrophobic binding cavity. The nitrile group, which is essential for high affinity, binds to $Val740^{5.40c}$ via a water-mediated hydrogen bond. The pyridine ring forms the only direct H bond to the receptor to $Ser809^{7.39c}$.

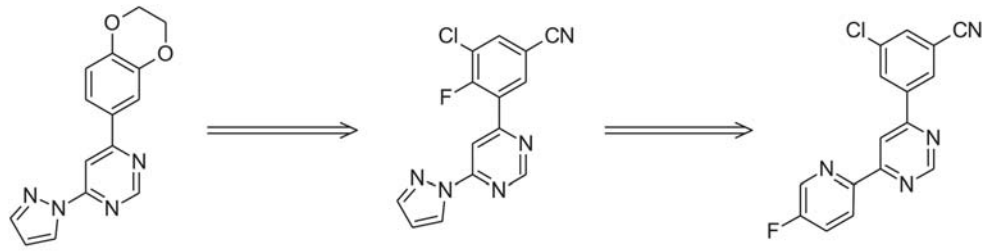

Scheme 23 Identification of HTL14242 an $mGlu_5$ NAM from a fragment screening hit **33**.

radioligand binding identified a number of hits with low micromolar activity including **33**, Scheme 23. Initially, testing a range of hypotheses of how the fragments might bind in comparison with literature ligands via docking into a homology model of the receptor led to compounds such as **34**. A number of X-ray structures were solved during the course of the subsequent lead optimization campaign clearly explaining the structure-based SAR of the series and the critical interactions required for affinity (Fig. 9). The clinical candidate **HTL14242** then emerged as the best molecule not only in terms of its affinity and potency but also based on the pharmacokinetic parameters needed for a CNS drug.

CRF_1 receptor. Corticotropin-releasing factor receptor 1 (CRF_1), a class B GPCR, is thought to play a potential role in the treatment of depression and anxiety. The structure of the CRF_1 receptor has been solved in complex with an allosteric antagonist CP-376395.[15] The molecule binds in the CRF_1 receptor site in an induced-fit pocket much deeper inside the 7TM bundle compared with any class A receptor ligand-binding site. These findings have helped to rationalize the SAR of CRF_1 antagonist small molecules and the slow off-rate kinetics of binding of some of these molecules.[250] In an interesting study by Yao et al., the escape pathway of the ligand has been predicted using molecular dynamics simulations, dynamic network analysis, random acceleration molecular dynamics (RAMD) simulations, and adaptive biasing force (ABF) calculations.[251] The results of dynamic network analysis indicated that TM7 of the CRF_1 receptor has the "strongest edges" during MD simulation. The kink in TM7 formed a pocket with $Gly356^{7.50b}$. $Asn283^{5.50b}$ had high hydrogen bond occupancy during 100 ns MD simulations and was likely the key interaction residue with the antagonist. RAMD simulation identified several possible pathways for CP-376395 to escape from the binding pocket. In the most promising pathway, the free energy was calculated by using ABF simulations. Two energy barriers were found along the reaction coordinates. Residues $Leu323^{6.49b}$, $Asn283^{5.50b}$, and $Met206^{3.47b}$ contributed to the steric hindrance for the first energy barrier, and residues $His199^{3.40b}$ and $Gln355^{7.49b}$ contributed to the second energy barrier through the hydrogen-bonding interactions between the ligand and the receptor. The results overall provide useful information to understand the interaction mechanisms between CP-376395 and CRF_1. These types of studies inform future drug design for the CRF_1 receptor and also give insights potentially useful for the design of allosteric modulators of other class B receptors.

3.08.6 Conclusions

In this article, we have attempted to introduce the findings from the structural biology breakthroughs for the major classes of membrane proteins that have emerged in recent years. The fascinating machinery involved in these pivotal proteins is starting to be uncovered in terms of how they function to engage with a diverse range of physiological molecules and synthetic ligands and how they modulate the function of cells. In a single article, we can only scratch the surface of the field and provide a brief introduction to the major topics. We have also tried to give the reader some insight into the rapidly developing in silico methodology now available to use the new X-ray data for drug design, not only uncovering the interactions made by small molecules with their target receptor (including the role of water molecules) but also considering how they engage with and exit their binding sites and the energetics involved in the binding and unbinding events. Finally, focusing on GPCRs where there is now a wealth of SBDD examples, we have illustrated how these methods are being applied in the design of ligands and potentially new therapeutic agents. Again, we cannot hope to be comprehensive and have selected the studies to showcase a range of approaches.

It is clear that the use of SBDD for membrane proteins and particularly GPCRs is a fruitful and evolving field, despite the relative difficulty of solving the first X-ray structure of each subfamily of receptor. Docking and prediction of binding poses for ligands are still challenging, but structure-based SAR can be carefully developed building confidence in the medicinal chemistry being pursued. Virtual screening is uncovering new classes of compounds, even for very well-worked targets that have been the subject of empirical design for many years, showing that SBDD has good potential under these circumstances. Today, there are still few published examples of new chemotypes being identified for poorly tractable targets; however, the recent publications of several allosteric modulator X-ray structures (discussed earlier) give potential for finding novel druggable binding sites where the orthosteric binding pocket has

poor properties for discovery of small-molecule drugs. Overall, we can expect many more exciting new discoveries in the structural biology and medicinal chemistry of membrane receptor targets in the next few years as the exponential rate of progress seems set to continue.

References

1. Isberg, V.; de Graaf, C.; Bortolato, A.; Cherezov, V.; Katritch, V.; Marshall, F. H.; Mordalski, S.; Pin, J.-P.; Stevens, R. C.; Vriend, G. Generic GPCR Residue Numbers—Aligning Topology Maps While Minding the Gaps. *Trends Pharmacol. Sci.* **2015,** *36,* 22–31.
2. Ballesteros, J. A.; Weinstein, H. Integrated Methods for the Construction of Three-Dimensional Models and Computational Probing of Structure-Function Relations in G Protein-Coupled Receptors. *Methods Neurosci.* **1995,** *25,* 366–428.
3. Wootten, D.; Simms, J.; Miller, L. J.; Christopoulos, A.; Sexton, P. M. Polar Transmembrane Interactions Drive Formation of Ligand-Specific and Signal Pathway-Biased Family B G Protein-Coupled Receptor Conformations. *Proc. Natl. Acad. Sci. U. S. A.* **2013,** *110,* 5211–5216.
4. Pin, J.-P.; Galvez, T.; Prézeau, L. Evolution, Structure, and Activation Mechanism of Family 3/C G-Protein-Coupled Receptors. *Pharmacol. Ther.* **2003,** *98,* 325–354.
5. Wang, C.; Wu, H.; Evron, T.; Vardy, E.; Han, G. W.; Huang, X.-P.; Hufeisen, S. J.; Mangano, T. J.; Urban, D. J.; Katritch, V.; Cherezov, V.; Caron, M. G.; Roth, B. L.; Stevens, R. C. Structural Basis for Smoothened Receptor Modulation and Chemoresistance to Anticancer Drugs. *Nat. Commun.* **2014,** *5,* 4355–4366.
6. Overington, J. P.; Al-Lazikani, B.; Hopkins, A. L. How Many Drug Targets Are There? *Nat. Rev. Drug Discov.* **2006,** *5,* 993–996.
7. Bakheet, T. M.; Doig, A. J. Properties and Identification of Human Protein Drug Targets. *Bioinformatics* **2009,** *25,* 451–457.
8. Deisenhofer, J.; Epp, O.; Miki, K.; Huber, R.; Michel, H. Structure of the Protein Subunits in the Photosynthetic Reaction Centre of Rhodopseudomonas Viridis at 3 Å Resolution. *Nature* **1985,** *318,* 618–624.
9. Bennett, K. A.; Tehan, B.; Lebon, G.; Tate, C. G.; Weir, M.; Marshall, F. H.; Langmead, C. J. Pharmacology and Structure of Isolated Conformations of the Adenosine A2A Receptor Define Ligand Efficacy. *Mol. Pharmacol.* **2013,** *83,* 949–958.
10. Palczewski, K.; Kumasaka, T.; Hori, T.; Behnke, C. A.; Motoshima, H.; Fox, B. A.; Le Trong, I.; Teller, D. C.; Okada, T.; Stenkamp, R. E.; Yamamoto, M.; Miyano, M. Crystal Structure of Rhodopsin: A G Protein-Coupled Receptor. *Science* **2000,** *289,* 739–745.
11. Cherezov, V.; Rosenbaum, D. M.; Hanson, M. A.; Rasmussen, S. G. F.; Thian, F. S.; Kobilka, T. S.; Choi, H.-J.; Kuhn, P.; Weis, W. I.; Kobilka, B. K.; Stevens, R. C. High-Resolution Crystal Structure of an Engineered Human Beta2-Adrenergic G Protein-Coupled Receptor. *Science* **2007,** *318,* 1258–1265.
12. Warne, T.; Serrano-Vega, M. J.; Baker, J. G.; Moukhametzianov, R.; Edwards, P. C.; Henderson, R.; Leslie, A. G. W.; Tate, C. G.; Schertler, G. F. X. Structure of a Beta1-Adrenergic G-Protein-Coupled Receptor. *Nature* **2008,** *454,* 486–491.
13. Jaakola, V.-P.; Griffith, M. T.; Hanson, M. A.; Cherezov, V.; Chien, E. Y. T.; Lane, J. R.; Ijzerman, A. P.; Stevens, R. C. The 2.6 Angstrom Crystal Structure of a Human A2A Adenosine Receptor Bound to an Antagonist. *Science* **2008,** *322,* 1211–1217.
14. Cooke, R. M.; Brown, A. J. H.; Marshall, F. H.; Mason, J. S. Structures of G Protein-Coupled Receptors Reveal New Opportunities for Drug Discovery. *Drug Discov. Today* **2015,** *20,* 1355–1364.
15. Hollenstein, K.; Kean, J.; Bortolato, A.; Cheng, R. K. Y.; Doré, A. S.; Jazayeri, A.; Cooke, R. M.; Weir, M.; Marshall, F. H. Structure of Class B GPCR Corticotropin-Releasing Factor Receptor 1. *Nature* **2013,** *499,* 438–443.
16. Siu, F. Y.; He, M.; de Graaf, C.; Han, G. W.; Yang, D.; Zhang, Z.; Zhou, C.; Xu, Q.; Wacker, D.; Joseph, J. S.; Liu, W.; Lau, J.; Cherezov, V.; Katritch, V.; Wang, M.-W.; Stevens, R. C. Structure of the Human Glucagon Class B G-Protein-Coupled Receptor. *Nature* **2013,** *499,* 444–449.
17. Wu, H.; Wang, C.; Gregory, K. J.; Han, G. W.; Cho, H. P.; Xia, Y.; Niswender, C. M.; Katritch, V.; Meiler, J.; Cherezov, V.; Conn, P. J.; Stevens, R. C. Structure of a Class C GPCR Metabotropic Glutamate Receptor 1 Bound to an Allosteric Modulator. *Science* **2014,** *344,* 58–64.
18. Doré, A. S.; Okrasa, K.; Patel, J. C.; Serrano-Vega, M.; Bennett, K.; Cooke, R. M.; Errey, J. C.; Jazayeri, A.; Khan, S.; Tehan, B.; Weir, M.; Wiggin, G. R.; Marshall, F. H. Structure of Class C GPCR Metabotropic Glutamate Receptor 5 Transmembrane Domain. *Nature* **2014,** *511,* 557–562.
19. Wang, C.; Wu, H.; Katritch, V.; Han, G. W.; Huang, X.-P.; Liu, W.; Siu, F. Y.; Roth, B. L.; Cherezov, V.; Stevens, R. C. Structure of the Human Smoothened Receptor Bound to an Antitumour Agent. *Nature* **2013,** *497,* 338–343.
20. Rasmussen, S. G. F.; DeVree, B. T.; Zou, Y.; Kruse, A. C.; Chung, K. Y.; Kobilka, T. S.; Thian, F. S.; Chae, P. S.; Pardon, E.; Calinski, D.; Mathiesen, J. M.; Shah, S. T. A.; Lyons, J. A.; Caffrey, M.; Gellman, S. H.; Steyaert, J.; Skiniotis, G.; Weis, W. I.; Sunahara, R. K.; Kobilka, B. K. Crystal Structure of the β2 Adrenergic Receptor-Gs Protein Complex. *Nature* **2011,** *477,* 549–555.
21. Dosa, P. I.; Amin, E. A. Tactical Approaches to Interconverting GPCR Agonists and Antagonists. *J. Med. Chem.* **2015,** *59,* 810–840.
22. Lebon, G.; Warne, T.; Edwards, P. C.; Bennett, K.; Langmead, C. J.; Leslie, A. G. W.; Tate, C. G. Agonist-Bound Adenosine A2A Receptor Structures Reveal Common Features of GPCR Activation. *Nature* **2011,** *474,* 521–525.
23. Wang, C.; Jiang, Y.; Ma, J.; Wu, H.; Wacker, D.; Katritch, V.; Han, G. W.; Liu, W.; Huang, X.-P.; Vardy, E.; McCorvy, J. D.; Gao, X.; Zhou, X. E.; Melcher, K.; Zhang, C.; Bai, F.; Yang, H.; Yang, L.; Jiang, H.; Roth, B. L.; Cherezov, V.; Stevens, R. C.; Xu, H. E. Structural Basis for Molecular Recognition at Serotonin Receptors. *Science* **2013,** *340,* 610–614.
24. Srivastava, A.; Yano, J.; Hirozane, Y.; Kefala, G.; Gruswitz, F.; Snell, G.; Lane, W.; Ivetac, A.; Aertgeerts, K.; Nguyen, J.; Jennings, A.; Okada, K. High-Resolution Structure of the Human GPR40 Receptor Bound to Allosteric Agonist TAK-875. *Nature* **2014,** *513,* 124–127.
25. Kruse, A. C.; Ring, A. M.; Manglik, A.; Hu, J.; Hu, K.; Eitel, K.; Hübner, H.; Pardon, E.; Valant, C.; Sexton, P. M.; Christopoulos, A.; Felder, C. C.; Gmeiner, P.; Steyaert, J.; Weis, W. I.; Garcia, K. C.; Wess, J.; Kobilka, B. K. Activation and Allosteric Modulation of a Muscarinic Acetylcholine Receptor. *Nature* **2013,** *504,* 101–106.
26. Zhang, D.; Gao, Z.-G.; Zhang, K.; Kiselev, E.; Crane, S.; Wang, J.; Paoletta, S.; Yi, C.; Ma, L.; Zhang, W.; Han, G. W.; Liu, H.; Cherezov, V.; Katritch, V.; Jiang, H.; Stevens, R. C.; Jacobson, K. A.; Zhao, Q.; Wu, B. Two Disparate Ligand-Binding Sites in the Human P2Y1 Receptor. *Nature* **2015,** *520,* 317–321.
27. Locher, K. P.; Lee, A. T.; Rees, D. C.; The, E. Coli BtuCD Structure: A Framework for ABC Transporter Architecture and Mechanism. *Science* **2002,** *296,* 1091–1098.
28. Abramson, J.; Smirnova, I.; Kasho, V.; Verner, G.; Kaback, H. R.; Iwata, S. Structure and Mechanism of the Lactose Permease of Escherichia Coli. *Science* **2003,** *301,* 610–615.
29. Huang, Y.; Lemieux, M. J.; Song, J.; Auer, M.; Wang, D.-N. Structure and Mechanism of the Glycerol-3-Phosphate Transporter from Escherichia Coli. *Science* **2003,** *301,* 616–620.
30. Singh, S. K. LeuT: A Prokaryotic Stepping Stone on the Way to a Eukaryotic Neurotransmitter Transporter Structure. *Channels* **2008,** *2,* 380–389.
31. Yamashita, A.; Singh, S. K.; Kawate, T.; Jin, Y.; Gouaux, E. Crystal Structure of a Bacterial Homologue of Na+/Cl—Dependent Neurotransmitter Transporters. *Nature* **2005,** *437,* 215–223.
32. Krishnamurthy, H.; Gouaux, E. X-Ray Structures of LeuT in Substrate-Free Outward-Open and Apo Inward-Open States. *Nature* **2012,** *481,* 469–474.
33. Forrest, L. R.; Rudnick, G. The Rocking Bundle: A Mechanism for Ion-Coupled Solute Flux by Symmetrical Transporters. *Physiology* **2009,** *24,* 377–386.
34. Faham, S.; Watanabe, A.; Besserer, G. M.; Cascio, D.; Specht, A.; Hirayama, B. A.; Wright, E. M.; Abramson, J. The Crystal Structure of a Sodium Galactose Transporter Reveals Mechanistic Insights into Na+/Sugar Symport. *Science* **2008,** *321,* 810–814.
35. Newstead, S.; Drew, D.; Cameron, A. D.; Postis, V. L. G.; Xia, X.; Fowler, P. W.; Ingram, J. C.; Carpenter, E. P.; Sansom, M. S. P.; McPherson, M. J.; Baldwin, S. A.; Iwata, S. Crystal Structure of a Prokaryotic Homologue of the Mammalian Oligopeptide-Proton Symporters, PepT1 and PepT2. *EMBO J.* **2011,** *30,* 417–426.

36. Singh, S. K.; Yamashita, A.; Gouaux, E. Antidepressant Binding Site in a Bacterial Homologue of Neurotransmitter Transporters. *Nature* **2007,** *448,* 952–956.
37. Zhou, Z.; Zhen, J.; Karpowich, N. K.; Goetz, R. M.; Law, C. J.; Reith, M. E. A.; Wang, D.-N. LeuT-Desipramine Structure Reveals How Antidepressants Block Neurotransmitter Reuptake. *Science* **2007,** *317,* 1390–1393.
38. Zhou, Z.; Zhen, J.; Karpowich, N. K.; Law, C. J.; Reith, M. E. A.; Wang, D.-N. Antidepressant Specificity of Serotonin Transporter Suggested by Three LeuT-SSRI Structures. *Nat. Struct. Mol. Biol.* **2009,** *16,* 652–657.
39. Wang, H.; Goehring, A.; Wang, K. H.; Penmatsa, A.; Ressler, R.; Gouaux, E. Structural Basis for Action by Diverse Antidepressants on Biogenic Amine Transporters. *Nature* **2013,** *503,* 141–145.
40. Penmatsa, A.; Wang, K. H.; Gouaux, E. X-Ray Structure of Dopamine Transporter Elucidates Antidepressant Mechanism. *Nature* **2013,** *503,* 85–90.
41. Wang, K. H.; Penmatsa, A.; Gouaux, E. Neurotransmitter and Psychostimulant Recognition by the Dopamine Transporter. *Nature* **2015,** *521,* 322–327.
42. Schlessinger, A.; Khuri, N.; Giacomini, K. M.; Sali, A. Molecular Modeling and Ligand Docking for Solute Carrier (SLC) Transporters. *Curr. Top. Med. Chem.* **2013,** *13,* 843–856.
43. Mortensen, O. V.; Kortagere, S. Designing Modulators of Monoamine Transporters Using Virtual Screening Techniques. *Front. Pharmacol.* **2015,** *6,* 223–231.
44. Bagal, S. K.; Brown, A. D.; Cox, P. J.; Omoto, K.; Owen, R. M.; Pryde, D. C.; Sidders, B.; Skerratt, S. E.; Stevens, E. B.; Storer, R. I.; Swain, N. A. Ion Channels as Therapeutic Targets: A Drug Discovery Perspective. *J. Med. Chem.* **2013,** *56,* 593–624.
45. Doyle, D. A.; Morais Cabral, J.; Pfuetzner, R. A.; Kuo, A.; Gulbis, J. M.; Cohen, S. L.; Chait, B. T.; MacKinnon, R. The Structure of the Potassium Channel: Molecular Basis of K+ Conduction and Selectivity. *Science* **1998,** *280,* 69–77.
46. Rigden, D. J.; Phillips, S. E.; Michels, P. A.; Fothergill-Gilmore, L. A. The Structure of Pyruvate Kinase from Leishmania Mexicana Reveals Details of the Allosteric Transition and Unusual Effector Specificity. *J. Mol. Biol.* **1999,** *291,* 615–635.
47. Sobolevsky, A. I.; Rosconi, M. P.; Gouaux, E. X-Ray Structure, Symmetry and Mechanism of an AMPA-Subtype Glutamate Receptor. *Nature* **2009,** *462,* 745–756.
48. Unwin, N. Refined Structure of the Nicotinic Acetylcholine Receptor at 4A Resolution. *J. Mol. Biol.* **2005,** *346,* 967–989.
49. Nury, H.; Van Renterghem, C.; Weng, Y.; Tran, A.; Baaden, M.; Dufresne, V.; Changeux, J.-P.; Sonner, J. M.; Delarue, M.; Corringer, P.-J. X-Ray Structures of General Anaesthetics Bound to a Pentameric Ligand-Gated Ion Channel. *Nature* **2011,** *469,* 428–431.
50. Miller, P. S.; Aricescu, A. R. Crystal Structure of a Human GABAA Receptor. *Nature* **2014,** *512,* 270–275.
51. Hattori, M.; Gouaux, E. Molecular Mechanism of ATP Binding and Ion Channel Activation in P2X Receptors. *Nature* **2012,** *485,* 207–212.
52. Liao, M.; Cao, E.; Julius, D.; Cheng, Y. Structure of the TRPV1 Ion Channel Determined by Electron Cryo-Microscopy. *Nature* **2013,** *504,* 107–112.
53. Derebe, M. G.; Sauer, D. B.; Zeng, W.; Alam, A.; Shi, N.; Jiang, Y. Tuning the Ion Selectivity of Tetrameric Cation Channels by Changing the Number of Ion Binding Sites. *Proc. Natl. Acad. Sci. U. S. A.* **2011,** *108,* 598–602.
54. Dutzler, R.; Campbell, E. B.; Cadene, M.; Chait, B. T.; MacKinnon, R. X-Ray Structure of a ClC Chloride Channel at 3.0 A Reveals the Molecular Basis of Anion Selectivity. *Nature* **2002,** *415,* 287–294.
55. Hou, X.; Pedi, L.; Diver, M. M.; Long, S. B. Crystal Structure of the Calcium Release-Activated Calcium Channel Orai. *Science* **2012,** *338,* 1308–1313.
56. Armstrong, N.; Sun, Y.; Chen, G. Q.; Gouaux, E. Structure of a Glutamate-Receptor Ligand-Binding Core in Complex With Kainate. *Nature* **1998,** *395,* 913–917.
57. Armstrong, N.; Gouaux, E. Mechanisms for Activation and Antagonism of an AMPA-Sensitive Glutamate Receptor: Crystal Structures of the GluR2 Ligand Binding Core. *Neuron* **2000,** *28,* 165–181.
58. Brejc, K.; van Dijk, W. J.; Klaassen, R. V.; Schuurmans, M.; van Der Oost, J.; Smit, A. B.; Sixma, T. K. Crystal Structure of an ACh-Binding Protein Reveals the Ligand-Binding Domain of Nicotinic Receptors. *Nature* **2001,** *411,* 269–276.
59. Rucktooa, P.; Haseler, C. A.; van Elk, R.; Smit, A. B.; Gallagher, T.; Sixma, T. K. Structural Characterization of Binding Mode of Smoking Cessation Drugs to Nicotinic Acetylcholine Receptors Through Study of Ligand Complexes With Acetylcholine-Binding Protein. *J. Biol. Chem.* **2012,** *287,* 23283–23293.
60. Hilf, R. J. C.; Dutzler, R. X-Ray Structure of a Prokaryotic Pentameric Ligand-Gated Ion Channel. *Nature* **2008,** *452,* 375–379.
61. Corringer, P.-J.; Baaden, M.; Bocquet, N.; Delarue, M.; Dufresne, V.; Nury, H.; Prevost, M.; Van Renterghem, C. Atomic Structure and Dynamics of Pentameric Ligand-Gated Ion Channels: New Insight From Bacterial Homologues. *J. Physiol.* **2010,** *588,* 565–572.
62. Sauguet, L.; Shahsavar, A.; Poitevin, F.; Huon, C.; Menny, A.; Nemecz, À.; Haouz, A.; Changeux, J.-P.; Corringer, P.-J.; Delarue, M. Crystal Structures of a Pentameric Ligand-Gated Ion Channel Provide a Mechanism for Activation. *Proc. Natl. Acad. Sci. U. S. A.* **2014,** *111,* 966–971.
63. Hibbs, R. E.; Gouaux, E. Principles of Activation and Permeation in an Anion-Selective Cys-Loop Receptor. *Nature* **2011,** *474,* 54–60.
64. Hassaine, G.; Deluz, C.; Grasso, L.; Wyss, R.; Tol, M. B.; Hovius, R.; Graff, A.; Stahlberg, H.; Tomizaki, T.; Desmyter, A.; Moreau, C.; Li, X.-D.; Poitevin, F.; Vogel, H.; Nury, H. X-Ray Structure of the Mouse Serotonin 5-HT3 Receptor. *Nature* **2014,** *512,* 276–281.
65. Huang, X.; Chen, H.; Michelsen, K.; Schneider, S.; Shaffer, P. L. Crystal Structure of Human Glycine Receptor-α3 Bound to Antagonist Strychnine. *Nature* **2015,** *526,* 277–280.
66. Dong, Y. Y.; Pike, A. C. W.; Mackenzie, A.; McClenaghan, C.; Aryal, P.; Dong, L.; Quigley, A.; Grieben, M.; Goubin, S.; Mukhopadhyay, S.; Ruda, G. F.; Clausen, M. V.; Cao, L.; Brennan, P. E.; Burgess-Brown, N. A.; Sansom, M. S. P.; Tucker, S. J.; Carpenter, E. P. K2P Channel Gating Mechanisms Revealed by Structures of TREK-2 and a Complex With Prozac. *Science* **2015,** *347,* 1256–1259.
67. Henderson, R. Overview and Future of Single Particle Electron Cryomicroscopy. *Arch. Biochem. Biophys.* **2015,** *581,* 19–24.
68. Cao, E.; Liao, M.; Cheng, Y.; Julius, D. TRPV1 Structures in Distinct Conformations Reveal Activation Mechanisms. *Nature* **2013,** *504,* 113–118.
69. Paulsen, C. E.; Armache, J.-P.; Gao, Y.; Cheng, Y.; Julius, D. Structure of the TRPA1 Ion Channel Suggests Regulatory Mechanisms. *Nature* **2015,** *520,* 511–517.
70. Schlessinger, A.; Geier, E.; Fan, H.; Irwin, J. J.; Shoichet, B. K.; Giacomini, K. M.; Sali, A. Structure-Based Discovery of Prescription Drugs That Interact with the Norepinephrine Transporter, NET. *Proc. Natl. Acad. Sci. U. S. A.* **2011,** *108,* 15810–15815.
71. Warne, T.; Tate, C. G. The Importance of Interactions with Helix 5 in Determining the Efficacy of beta-Adrenoceptor Ligands. *Biochem. Soc. Trans.* **2013,** *41,* 159–165.
72. Tehan, B. G.; Bortolato, A.; Blaney, F. E.; Weir, M. P.; Mason, J. S. Unifying Family A GPCR Theories of Activation. *Pharmacol. Ther.* **2014,** *143,* 51–60.
73. Standfuss, J.; Edwards, P. C.; D'Antona, A.; Fransen, M.; Xie, G.; Oprian, D. D.; Schertler, G. F. X. The Structural Basis of Agonist-Induced Activation in Constitutively Active Rhodopsin. *Nature* **2011,** *471,* 656–660.
74. Venkatakrishnan, A. J.; Deupi, X.; Lebon, G.; Tate, C. G.; Schertler, G. F.; Babu, M. M. Molecular Signatures of G-Protein-Coupled Receptors. *Nature* **2013,** *494,* 185–194.
75. Doré, A. S.; Robertson, N.; Errey, J. C.; Ng, I.; Hollenstein, K.; Tehan, B.; Hurrell, E.; Bennett, K.; Congreve, M.; Magnani, F.; Tate, C. G.; Weir, M.; Marshall, F. H. Structure of the Adenosine A2A Receptor in Complex With ZM241385 and the Xanthines XAC and Caffeine. *Structure* **2011,** *19,* 1283–1293.
76. Liu, W.; Chun, E.; Thompson, A. A.; Chubukov, P.; Xu, F.; Katritch, V.; Han, G. W.; Roth, C. B.; Heitman, L. H.; IJzerman, A. P.; Cherezov, V.; Stevens, R. C. Structural Basis for Allosteric Regulation of GPCRs by Sodium Ions. *Science* **2012,** *337,* 232–236.
77. Goodford, P. J. A Computational Procedure for Determining Energetically Favorable Binding Sites on Biologically Important Macromolecules. *J. Med. Chem.* **1985,** *28,* 849–857.
78. Huang, W.; Manglik, A.; Venkatakrishnan, A. J.; Laeremans, T.; Feinberg, E. N.; Sanborn, A. L.; Kato, H. E.; Livingston, K. E.; Thorsen, T. S.; Kling, R. C.; Granier, S.; Gmeiner, P.; Husbands, S. M.; Traynor, J. R.; Weis, W. I.; Steyaert, J.; Dror, R. O.; Kobilka, B. K. Structural Insights Into μ-Opioid Receptor Activation. *Nature* **2015,** *524,* 315–321.
79. Bortolato, A.; Doré, A. S.; Hollenstein, K.; Tehan, B. G.; Mason, J. S.; Marshall, F. H. Structure of Class B GPCRs: New Horizons for Drug Discovery. *Br. J. Pharmacol.* **2014,** *171,* 3132–3145.

80. Yang, L.; Yang, D.; de Graaf, C.; Moeller, A.; West, G. M.; Dharmarajan, V.; Wang, C.; Siu, F. Y.; Song, G.; Reedtz-Runge, S.; Pascal, B. D.; Wu, B.; Potter, C. S.; Zhou, H.; Griffin, P. R.; Carragher, B.; Yang, H.; Wang, M.-W.; Stevens, R. C.; Jiang, H. Conformational States of the Full-Length Glucagon Receptor. *Nat. Commun.* **2015,** *6,* 7859–7872.
81. Krumm, B. E.; White, J. F.; Shah, P.; Grisshammer, R. Structural Prerequisites for G-Protein Activation by the Neurotensin Receptor. *Nat. Commun.* **2015,** *6,* 7895–7905.
82. Flock, T.; Ravarani, C. N. J.; Sun, D.; Venkatakrishnan, A. J.; Kayikci, M.; Tate, C. G.; Veprintsev, D. B.; Babu, M. M. Universal Allosteric Mechanism for Gα Activation by GPCRs. *Nature* **2015,** *524,* 173–179.
83. Preininger, A. M.; Meiler, J.; Hamm, H. E. Conformational Flexibility and Structural Dynamics in GPCR-Mediated G Protein Activation: A Perspective. *J. Mol. Biol.* **2013,** *425,* 2288–2298.
84. Duc, N. M.; Kim, H. R.; Chung, K. Y. Structural Mechanism of G Protein Activation by G Protein-Coupled Receptor. *Eur. J. Pharmacol.* **2015,** *763,* 214–222.
85. Sounier, R.; Mas, C.; Steyaert, J.; Laeremans, T.; Manglik, A.; Huang, W.; Kobilka, B. K.; Déméné, H.; Granier, S. Propagation of Conformational Changes During μ-Opioid Receptor Activation. *Nature* **2015,** *524,* 375–378.
86. Kang, Y.; Zhou, X. E.; Gao, X.; He, Y.; Liu, W.; Ishchenko, A.; Barty, A.; White, T. A.; Yefanov, O.; Han, G. W.; Xu, Q.; Waal, P. W. de; Ke, J.; Tan, M. H. E.; Zhang, C.; Moeller, A.; West, G. M.; Pascal, B. D.; Eps, N. V.; Caro, L. N.; Vishnivetskiy, S. A.; Lee, R. J.; Suino-Powell, K. M.; Gu, X.; Pal, K.; Ma, J.; Zhi, X.; Boutet, S.; Williams, G. J.; Messerschmidt, M.; Gati, C.; Zatsepin, N. A.; Wang, D.; James, D.; Basu, S.; Roy-Chowdhury, S.; Conrad, C. E.; Coe, J.; Liu, H.; Lisova, S.; Kupitz, C.; Grotjohann, I.; Fromme, R.; Jiang, Y.; Tan, M.; Yang, H.; Li, J.; Wang, M.; Zheng, Z.; Li, D.; Howe, N.; Zhao, Y.; Standfuss, J.; Diederichs, K.; Dong, Y.; Potter, C. S.; Carragher, B.; Caffrey, M.; Jiang, H.; Chapman, H. N.; Spence, J. C. H.; Fromme, P.; Weierstall, U.; Ernst, O. P.; Katritch, V.; Gurevich, V. V.; Griffin, P. R.; Hubbell, W. L.; Stevens, R. C.; Cherezov, V.; Melcher, K.; Xu, H. E. Crystal Structure of Rhodopsin Bound to Arrestin by Femtosecond X-Ray Laser. *Nature* **2015,** *523,* 561–567.
87. Congreve, M.; Andrews, S. P.; Doré, A. S.; Hollenstein, K.; Hurrell, E.; Langmead, C. J.; Mason, J. S.; Ng, I. W.; Tehan, B.; Zhukov, A.; Weir, M.; Marshall, F. H. Discovery of 1,2,4-Triazine Derivatives as Adenosine A(2A) Antagonists Using Structure Based Drug Design. *J. Med. Chem.* **2012,** *55,* 1898–1903.
88. Abel, R.; Young, T.; Farid, R.; Berne, B. J.; Friesner, R. A. Role of the Active-Site Solvent in the Thermodynamics of Factor Xa Ligand Binding. *J. Am. Chem. Soc.* **2008,** *130,* 2817–2831.
89. Haga, K.; Kruse, A. C.; Asada, H.; Yurugi-Kobayashi, T.; Shiroishi, M.; Zhang, C.; Weis, W. I.; Okada, T.; Kobilka, B. K.; Haga, T.; Kobayashi, T. Structure of the Human M2 Muscarinic Acetylcholine Receptor Bound to an Antagonist. *Nature* **2012,** *482,* 547–551.
90. Zhang, K.; Zhang, J.; Gao, Z.-G.; Zhang, D.; Zhu, L.; Han, G. W.; Moss, S. M.; Paoletta, S.; Kiselev, E.; Lu, W.; Fenalti, G.; Zhang, W.; Müller, C. E.; Yang, H.; Jiang, H.; Cherezov, V.; Katritch, V.; Jacobson, K. A.; Stevens, R. C.; Wu, B.; Zhao, Q. Structure of the Human P2Y12 Receptor in Complex With an Antithrombotic Drug. *Nature* **2014,** *509,* 115–118.
91. Zhang, J.; Zhang, K.; Gao, Z.-G.; Paoletta, S.; Zhang, D.; Han, G. W.; Li, T.; Ma, L.; Zhang, W.; Müller, C. E.; Yang, H.; Jiang, H.; Cherezov, V.; Katritch, V.; Jacobson, K. A.; Stevens, R. C.; Wu, B.; Zhao, Q. Agonist-Bound Structure of the Human P2Y12 Receptor. *Nature* **2014,** *509,* 119–122.
92. Warne, T.; Moukhametzianov, R.; Baker, J. G.; Nehmé, R.; Edwards, P. C.; Leslie, A. G. W.; Schertler, G. F. X.; Tate, C. G. The Structural Basis for Agonist and Partial Agonist Action on a β(1)-Adrenergic Receptor. *Nature* **2011,** *469,* 241–244.
93. Mason, J. S.; Bortolato, A.; Congreve, M.; Marshall, F. H. New Insights From Structural Biology Into the Druggability of G Protein-Coupled Receptors. *Trends Pharmacol. Sci.* **2012,** *33,* 249–260.
94. Levit, A.; Beuming, T.; Krilov, G.; Sherman, W.; Niv, M. Y. Predicting GPCR Promiscuity Using Binding Site Features. *J. Chem. Inf. Model.* **2014,** *54,* 184–194.
95. Congreve, M.; Dias, J. M.; Marshall, F. H. Structure-Based Drug Design for G Protein-Coupled Receptors. *Prog. Med. Chem.* **2014,** *53,* 1–63.
96. Kooistra, A. J.; Kuhne, S.; de Esch, I. J. P.; Leurs, R.; de Graaf, C. A Structural Chemogenomics Analysis of Aminergic GPCRs: Lessons for Histamine Receptor Ligand Design. *Br. J. Pharmacol.* **2013,** *170,* 101–126.
97. Gutiérrez-de-Terán, H.; Keränen, H.; Azuaje, J.; Rodríguez, D.; Åqvist, J.; Sotelo, E. Computer-Aided Design of GPCR Ligands. *Methods Mol. Biol.* **2015,** *1272,* 271–291.
98. Kooistra, A. J.; Leurs, R.; de Esch, I. J. P.; de Graaf, C. Structure-Based Prediction of G-Protein-Coupled Receptor Ligand Function: A β-Adrenoceptor Case Study. *J. Chem. Inf. Model.* **2015,** *55,* 1045–1061.
99. Jacobson, K. A.; Costanzi, S.; Paoletta, S. Computational Studies to Predict or Explain G Protein Coupled Receptor Polypharmacology. *Trends Pharmacol. Sci.* **2014,** *35,* 658–663.
100. Rodríguez, D.; Gao, Z.-G.; Moss, S. M.; Jacobson, K. A.; Carlsson, J. Molecular Docking Screening Using Agonist-Bound GPCR Structures: Probing the A2A Adenosine Receptor. *J. Chem. Inf. Model.* **2015,** *55,* 550–563.
101. Horn, F.; Bettler, E.; Oliveira, L.; Campagne, F.; Cohen, F. E.; Vriend, G. GPCRDB Information System for G Protein-Coupled Receptors. *Nucleic Acids Res.* **2003,** *31,* 294–297.
102. Berman, H. M.; Westbrook, J.; Feng, Z.; Gilliland, G.; Bhat, T. N.; Weissig, H.; Shindyalov, I. N.; Bourne, P. E. The Protein Data Bank. *Nucleic Acids Res.* **2000,** *28,* 235–242.
103. Beuming, T.; Sherman, W. Current Assessment of Docking into GPCR Crystal Structures and Homology Models: Successes, Challenges, and Guidelines. *J. Chem. Inf. Model.* **2012,** *52,* 3263–3277.
104. Stevens, R. C.; Abagyan, R.; Kufareva, I.; Katritch, V.; Participants of GPCR Dock. Advances in GPCR Modeling Evaluated by the GPCR Dock 2013 Assessment: Meeting New Challenges. *Structure* **2013,** *2014* (22), 1120–1139.
105. Huang, X.-P.; Karpiak, J.; Kroeze, W. K.; Zhu, H.; Chen, X.; Moy, S. S.; Saddoris, K. A.; Nikolova, V. D.; Farrell, M. S.; Wang, S.; Mangano, T. J.; Deshpande, D. A.; Jiang, A.; Penn, R. B.; Jin, J.; Koller, B. H.; Kenakin, T.; Shoichet, B. K.; Roth, B. L. Allosteric Ligands for the Pharmacologically Dark Receptors GPR68 and GPR65. *Nature* **2015,** *527,* 477–483.
106. Norn, C.; Hauge, M.; Engelstoft, M. S.; Kim, S. H.; Lehmann, J.; Jones, R. M.; Schwartz, T. W.; Frimurer, T. M. Mutation-Guided Unbiased Modeling of the Fat Sensor GPR119 for High-Yield Agonist Screening. *Struct. Bond. (Berlin)* **2015,** *23,* 2377–2386.
107. Rodríguez, D.; Ranganathan, A.; Carlsson, J. Strategies for Improved Modeling of GPCR-Drug Complexes: Blind Predictions of Serotonin Receptors Bound to Ergotamine. *J. Chem. Inf. Model.* **2014,** *54,* 2004–2021.
108. Katritch, V.; Jaakola, V.-P.; Lane, J. R.; Lin, J.; Ijzerman, A. P.; Yeager, M.; Kufareva, I.; Stevens, R. C.; Abagyan, R. Structure-Based Discovery of Novel Chemotypes for Adenosine A(2A) Receptor Antagonists. *J. Med. Chem.* **2010,** *53,* 1799–1809.
109. Carlsson, J.; Yoo, L.; Gao, Z.-G.; Irwin, J. J.; Shoichet, B. K.; Jacobson, K. A. Structure-Based Discovery of A2A Adenosine Receptor Ligands. *J. Med. Chem.* **2010,** *53,* 3748–3755.
110. Chen, D.; Ranganathan, A.; IJzerman, A. P.; Siegal, G.; Carlsson, J. Complementarity between In Silico and Biophysical Screening Approaches in Fragment-Based Lead Discovery against the A(2A) Adenosine Receptor. *J. Chem. Inf. Model.* **2013,** *53,* 2701–2714.
111. Van Westen, G. J. P.; van den Hoven, O. O.; van der Pijl, R.; Mulder-Krieger, T.; de Vries, H.; Wegner, J. K.; Ijzerman, A. P.; van Vlijmen, H. W. T.; Bender, A. Identifying Novel Adenosine Receptor Ligands by Simultaneous Proteochemometric Modeling of Rat and Human Bioactivity Data. *J. Med. Chem.* **2012,** *55,* 7010–7020.
112. Langmead, C. J.; Andrews, S. P.; Congreve, M.; Errey, J. C.; Hurrell, E.; Marshall, F. H.; Mason, J. S.; Richardson, C. M.; Robertson, N.; Zhukov, A.; Weir, M. Identification of Novel Adenosine A(2A) Receptor Antagonists by Virtual Screening. *J. Med. Chem.* **2012,** *55,* 1904–1909.
113. Sanders, M. P. A.; Roumen, L.; van der Horst, E.; Lane, J. R.; Vischer, H. F.; van Offenbeek, J.; de Vries, H.; Verhoeven, S.; Chow, K. Y.; Verkaar, F.; Beukers, M. W.; McGuire, R.; Leurs, R.; Ijzerman, A. P.; de Vlieg, J.; de Esch, I. J. P.; Zaman, G. J. R.; Klomp, J. P. G.; Bender, A.; de Graaf, C. A Prospective Cross-Screening Study on G-Protein-Coupled Receptors: Lessons Learned in Virtual Compound Library Design. *J. Med. Chem.* **2012,** *55,* 5311–5325.
114. Tosh, D. K.; Phan, K.; Gao, Z.-G.; Gakh, A. A.; Xu, F.; Deflorian, F.; Abagyan, R.; Stevens, R. C.; Jacobson, K. A.; Katritch, V. Optimization of Adenosine 5'-Carboxamide Derivatives as Adenosine Receptor Agonists Using Structure-Based Ligand Design and Fragment Screening. *J. Med. Chem.* **2012,** *55,* 4297–4308.

115. Van der Horst, E.; van der Pijl, R.; Mulder-Krieger, T.; Bender, A.; Ijzerman, A. P. Substructure-Based Virtual Screening for Adenosine A2A Receptor Ligands. *ChemMedChem* **2011,** *6,* 2302–2311.
116. Areias, F.; Costa, M.; Castro, M.; Brea, J.; Gregori-Puigjané, E.; Proença, M. F.; Mestres, J.; Loza, M. I. New Chromene Scaffolds for Adenosine A(2A) Receptors: Synthesis, Pharmacology and Structure-Activity Relationships. *Eur. J. Med. Chem.* **2012,** *54,* 303–310.
117. Ranganathan, A.; Stoddart, L. A.; Hill, S. J.; Carlsson, J. Fragment-Based Discovery of Subtype-Selective Adenosine Receptor Ligands From Homology Models. *J. Med. Chem.* **2015,** *58,* 9578–9590.
118. Sabio, M.; Jones, K.; Topiol, S. Use of the X-Ray Structure of the Beta2-Adrenergic Receptor for Drug Discovery. Part 2: Identification of Active Compounds. *Bioorg. Med. Chem. Lett.* **2008,** *18,* 5391–5395.
119. Kolb, P.; Rosenbaum, D. M.; Irwin, J. J.; Fung, J. J.; Kobilka, B. K.; Shoichet, B. K. Structure-Based Discovery of Beta2-Adrenergic Receptor Ligands. *Proc. Natl. Acad. Sci. U. S. A.* **2009,** *106,* 6843–6848.
120. Weiss, D. R.; Ahn, S.; Sassano, M. F.; Kleist, A.; Zhu, X.; Strachan, R.; Roth, B. L.; Lefkowitz, R. J.; Shoichet, B. K. Conformation Guides Molecular Efficacy in Docking Screens of Activated β-2 Adrenergic G Protein Coupled Receptor. *ACS Chem. Biol.* **2013,** *8,* 1018–1026.
121. Lane, J. R.; Chubukov, P.; Liu, W.; Canals, M.; Cherezov, V.; Abagyan, R.; Stevens, R. C.; Katritch, V. Structure-Based Ligand Discovery Targeting Orthosteric and Allosteric Pockets of Dopamine Receptors. *Mol. Pharmacol.* **2013,** *84,* 794–807.
122. Vass, M.; Schmidt, É.; Horti, F.; Keserű, G. M. Virtual Fragment Screening on GPCRs: A Case Study on Dopamine D3 and Histamine H4 Receptors. *Eur. J. Med. Chem.* **2014,** *77,* 38–46.
123. Carlsson, J.; Coleman, R. G.; Setola, V.; Irwin, J. J.; Fan, H.; Schlessinger, A.; Sali, A.; Roth, B. L.; Shoichet, B. K. Ligand Discovery From a Dopamine D3 Receptor Homology Model and Crystal Structure. *Nat. Chem. Biol.* **2011,** *7,* 769–778.
124. Varady, J.; Wu, X.; Fang, X.; Min, J.; Hu, Z.; Levant, B.; Wang, S. Molecular Modeling of the Three-Dimensional Structure of Dopamine 3 (D3) Subtype Receptor: Discovery of Novel and Potent D3 Ligands Through a Hybrid Pharmacophore- and Structure-Based Database Searching Approach. *J. Med. Chem.* **2003,** *46,* 4377–4392.
125. De Graaf, C.; Kooistra, A. J.; Vischer, H. F.; Katritch, V.; Kuijer, M.; Shiroishi, M.; Iwata, S.; Shimamura, T.; Stevens, R. C.; de Esch, I. J. P.; Leurs, R. Crystal Structure-Based Virtual Screening for Fragment-Like Ligands of the Human Histamine H(1) Receptor. *J. Med. Chem.* **2011,** *54,* 8195–8206.
126. Sirci, F.; Istyastono, E. P.; Vischer, H. F.; Kooistra, A. J.; Nijmeijer, S.; Kuijer, M.; Wijtmans, M.; Mannhold, R.; Leurs, R.; de Esch, I. J. P.; de Graaf, C. Virtual Fragment Screening: Discovery of Histamine H3 Receptor Ligands Using Ligand-Based and Protein-Based Molecular Fingerprints. *J. Chem. Inf. Model.* **2012,** *52,* 3308–3324.
127. Kiss, R.; Kiss, B.; Könczöl, A.; Szalai, F.; Jelinek, I.; László, V.; Noszál, B.; Falus, A.; Keseru, G. M. Discovery of Novel Human Histamine H4 Receptor Ligands by Large-Scale Structure-Based Virtual Screening. *J. Med. Chem.* **2008,** *51,* 3145–3153.
128. Mysinger, M. M.; Weiss, D. R.; Ziarek, J. J.; Gravel, S.; Doak, A. K.; Karpiak, J.; Heveker, N.; Shoichet, B. K.; Volkman, B. F. Structure-Based Ligand Discovery for the Protein-Protein Interface of Chemokine Receptor CXCR4. *Proc. Natl. Acad. Sci. U. S. A.* **2012,** *109,* 5517–5522.
129. Schmidt, D.; Bernat, V.; Brox, R.; Tschammer, N.; Kolb, P. Identifying Modulators of CXC Receptors 3 and 4 With Tailored Selectivity Using Multi-Target Docking. *ACS Chem. Biol.* **2015,** *10,* 715–724.
130. Kruse, A. C.; Weiss, D. R.; Rossi, M.; Hu, J.; Hu, K.; Eitel, K.; Gmeiner, P.; Wess, J.; Kobilka, B. K.; Shoichet, B. K. Muscarinic Receptors as Model Targets and Antitargets for Structure-Based Ligand Discovery. *Mol. Pharmacol.* **2013,** *84,* 528–540.
131. Negri, A.; Rives, M.-L.; Caspers, M. J.; Prisinzano, T. E.; Javitch, J. A.; Filizola, M. Discovery of a Novel Selective Kappa-Opioid Receptor Agonist Using Crystal Structure-Based Virtual Screening. *J. Chem. Inf. Model.* **2013,** *53,* 521–526.
132. Rodríguez, D.; Brea, J.; Loza, M. I.; Carlsson, J. Structure-Based Discovery of Selective Serotonin 5-HT(1B) Receptor Ligands. *Struct. Bond. (Berlin)* **2014,** *22,* 1140–1151.
133. Zhou, Y.; Ma, J.; Lin, X.; Huang, X.-P.; Wu, K.; Huang, N. Structure-Based Discovery of Novel and Selective 5-Hydroxytryptamine 2B Receptor Antagonists for the Treatment of Irritable Bowel Syndrome. *J. Med. Chem.* **2016,** *59* (2), 707–720.
134. Diaz, C.; Bouteiller, L.; Yvon, S.; Cambon-Kernëis, A.; Roasio, A.; Jamme, M.; Aries, A.; Feuillerat, C.; Perret, E.; Guette, F. A Strategy Combining Differential Low-Throughput Screening and Virtual Screening (DLS-VS) Accelerating the Discovery of New Modulators for the Orphan GPR34 Receptor. *Mol. Inf.* **2013,** *32,* 213–229.
135. Eberini, I.; Daniele, S.; Parravicini, C.; Sensi, C.; Trincavelli, M. L.; Martini, C.; Abbracchio, M. P. In Silico Identification of New Ligands for GPR17: A Promising Therapeutic Target for Neurodegenerative Diseases. *J. Comput. Aided Mol. Des.* **2011,** *25,* 743–752.
136. Tikhonova, I. G.; Sum, C. S.; Neumann, S.; Engel, S.; Raaka, B. M.; Costanzi, S.; Gershengorn, M. C. Discovery of Novel Agonists and Antagonists of the Free Fatty Acid Receptor 1 (FFAR1) Using Virtual Screening. *J. Med. Chem.* **2008,** *51,* 625–633.
137. Clark, D. E.; Higgs, C.; Wren, S. P.; Dyke, H. J.; Wong, M.; Norman, D.; Lockey, P. M.; Roach, A. G. A Virtual Screening Approach to Finding Novel and Potent Antagonists at the Melanin-Concentrating Hormone 1 Receptor. *J. Med. Chem.* **2004,** *47,* 3962–3971.
138. Cavasotto, C. N.; Orry, A. J. W.; Murgolo, N. J.; Czarniecki, M. F.; Kocsi, S. A.; Hawes, B. E.; O'Neill, K. A.; Hine, H.; Burton, M. S.; Voigt, J. H.; Abagyan, R. A.; Bayne, M. L.; Monsma, F. J. Discovery of Novel Chemotypes to a G-Protein-Coupled Receptor Through Ligand-Steered Homology Modeling and Structure-Based Virtual Screening. *J. Med. Chem.* **2008,** *51,* 581–588.
139. Evers, A.; Klebe, G. Successful Virtual Screening for a Submicromolar Antagonist of the Neurokinin-1 Receptor Based on a Ligand-Supported Homology Model. *J. Med. Chem.* **2004,** *47,* 5381–5392.
140. Edwards, B. S.; Bologa, C.; Young, S. M.; Balakin, K. V.; Prossnitz, E. R.; Savchuck, N. P.; Sklar, L. A.; Oprea, T. I. Integration of Virtual Screening with High-Throughput Flow Cytometry to Identify Novel Small Molecule Formylpeptide Receptor Antagonists. *Mol. Pharmacol.* **2005,** *68,* 1301–1310.
141. De Graaf, C.; Rein, C.; Piwnica, D.; Giordanetto, F.; Rognan, D. Structure-Based Discovery of Allosteric Modulators of Two Related Class B G-Protein-Coupled Receptors. *ChemMedChem* **2011,** *6,* 2159–2169.
142. Evers, A.; Klabunde, T. Structure-Based Drug Discovery Using GPCR Homology Modeling: Successful Virtual Screening for Antagonists of the alpha1A Adrenergic Receptor. *J. Med. Chem.* **2005,** *48,* 1088–1097.
143. Salo, O. M. H.; Raitio, K. H.; Savinainen, J. R.; Nevalainen, T.; Lahtela-Kakkonen, M.; Laitinen, J. T.; Järvinen, T.; Poso, A. Virtual Screening of Novel CB2 Ligands Using a Comparative Model of the Human Cannabinoid CB2 Receptor. *J. Med. Chem.* **2005,** *48,* 7166–7171.
144. Kellenberger, E.; Springael, J.-Y.; Parmentier, M.; Hachet-Haas, M.; Galzi, J.-L.; Rognan, D. Identification of Nonpeptide CCR5 Receptor Agonists by Structure-Based Virtual Screening. *J. Med. Chem.* **2007,** *50,* 1294–1303.
145. Engel, S.; Skoumbourdis, A. P.; Childress, J.; Neumann, S.; Deschamps, J. R.; Thomas, C. J.; Colson, A.-O.; Costanzi, S.; Gershengorn, M. C. A Virtual Screen for Diverse Ligands: Discovery of Selective G Protein-Coupled Receptor Antagonists. *J. Am. Chem. Soc.* **2008,** *130,* 5115–5123.
146. Baell, J. B.; Holloway, G. A. New Substructure Filters for Removal of Pan Assay Interference Compounds (PAINS) from Screening Libraries and for Their Exclusion in Bioassays. *J. Med. Chem.* **2010,** *53,* 2719–2740.
147. Johnston, J. M.; Filizola, M. Beyond Standard Molecular Dynamics: Investigating the Molecular Mechanisms of G Protein-Coupled Receptors With Enhanced Molecular Dynamics Methods. *Adv. Exp. Med. Biol.* **2014,** *796,* 95–125.
148. Deupi, X.; Kobilka, B. K. Energy Landscapes as a Tool to Integrate GPCR Structure, Dynamics, and Function. *Phys. Chem. Chem. Phys.* **2010,** *25,* 293–303.
149. Vaidehi, N.; Kenakin, T. The Role of Conformational Ensembles of Seven Transmembrane Receptors in Functional Selectivity. *Curr. Opin. Pharmacol.* **2010,** *10,* 775–781.
150. Dror, R. O.; Dirks, R. M.; Grossman, J. P.; Xu, H.; Shaw, D. E. Biomolecular Simulation: A Computational Microscope for Molecular Biology. *Annu. Rev. Biophys.* **2012,** *41,* 429–452.
151. Cournia, Z.; Allen, T. W.; Andricioaei, I.; Antonny, B.; Baum, D.; Brannigan, G.; Buchete, N.-V.; Deckman, J. T.; Delemotte, L.; Del Val, C.; Friedman, R.; Gkeka, P.; Hege, H.-C.; Hénin, J.; Kasimova, M. A.; Kolocouris, A.; Klein, M. L.; Khalid, S.; Lemieux, M. J.; Lindow, N.; Roy, M.; Selent, J.; Tarek, M.; Tofoleanu, F.; Vanni, S.; Urban, S.; Wales, D. J.; Smith, J. C.; Bondar, A.-N. Membrane Protein Structure, Function, and Dynamics: A Perspective from Experiments and Theory. *J. Membr. Biol.* **2015,** *248,* 611–640.

152. Kim, T. H.; Chung, K. Y.; Manglik, A.; Hansen, A. L.; Dror, R. O.; Mildorf, T. J.; Shaw, D. E.; Kobilka, B. K.; Prosser, R. S. The Role of Ligands on the Equilibria between Functional States of a G Protein-Coupled Receptor. *J. Am. Chem. Soc.* **2013,** *135,* 9465–9474.
153. Nygaard, R.; Zou, Y.; Dror, R. O.; Mildorf, T. J.; Arlow, D. H.; Manglik, A.; Pan, A. C.; Liu, C. W.; Fung, J. J.; Bokoch, M. P.; Thian, F. S.; Kobilka, T. S.; Shaw, D. E.; Mueller, L.; Prosser, R. S.; Kobilka, B. K. The Dynamic Process of β(2)-Adrenergic Receptor Activation. *Cell* **2013,** *152,* 532–542.
154. Tarcsay, A.; Paragi, G.; Vass, M.; Jójárt, B.; Bogár, F.; Keserű, G. M. The Impact of Molecular Dynamics Sampling on the Performance of Virtual Screening Against GPCRs. *J. Chem. Inf. Model.* **2013,** *53,* 2990–2999.
155. Sabbadin, D.; Ciancetta, A.; Moro, S. Bridging Molecular Docking to Membrane Molecular Dynamics to Investigate GPCR-Ligand Recognition: The Human A2A Adenosine Receptor as a Key Study. *J. Chem. Inf. Model.* **2014,** *54,* 169–183.
156. Dror, R. O.; Pan, A. C.; Arlow, D. H.; Borhani, D. W.; Maragakis, P.; Shan, Y.; Xu, H.; Shaw, D. E. Pathway and Mechanism of Drug Binding to G-Protein-Coupled Receptors. *Proc. Natl. Acad. Sci. U. S. A.* **2011,** *108,* 13118–13123.
157. Dror, R. O.; Green, H. F.; Valant, C.; Borhani, D. W.; Valcourt, J. R.; Pan, A. C.; Arlow, D. H.; Canals, M.; Lane, J. R.; Rahmani, R.; Baell, J. B.; Sexton, P. M.; Christopoulos, A.; Shaw, D. E. Structural Basis for Modulation of a G-Protein-Coupled Receptor by Allosteric Drugs. *Nature* **2013,** *503,* 295–299.
158. Dror, R. O.; Mildorf, T. J.; Hilger, D.; Manglik, A.; Borhani, D. W.; Arlow, D. H.; Philippsen, A.; Villanueva, N.; Yang, Z.; Lerch, M. T.; Hubbell, W. L.; Kobilka, B. K.; Sunahara, R. K.; Shaw, D. E. Signal Transduction. Structural Basis for Nucleotide Exchange in Heterotrimeric G Proteins. *Science* **2015,** *348,* 1361–1365.
159. Jensen, M.Ø.; Jogini, V.; Borhani, D. W.; Leffler, A. E.; Dror, R. O.; Shaw, D. E. Mechanism of Voltage Gating in Potassium Channels. *Science* **2012,** *336,* 229–233.
160. Wang, L.; Wu, Y.; Deng, Y.; Kim, B.; Pierce, L.; Krilov, G.; Lupyan, D.; Robinson, S.; Dahlgren, M. K.; Greenwood, J.; Romero, D. L.; Masse, C.; Knight, J. L.; Steinbrecher, T.; Beuming, T.; Damm, W.; Harder, E.; Sherman, W.; Brewer, M.; Wester, R.; Murcko, M.; Frye, L.; Farid, R.; Lin, T.; Mobley, D. L.; Jorgensen, W. L.; Berne, B. J.; Friesner, R. A.; Abel, R. Accurate and Reliable Prediction of Relative Ligand Binding Potency in Prospective Drug Discovery by Way of a Modern Free-Energy Calculation Protocol and Force Field. *J. Am. Chem. Soc.* **2015,** *137,* 2695–2703.
161. Steinbrecher, T. B.; Dahlgren, M.; Cappel, D.; Lin, T.; Wang, L.; Krilov, G.; Abel, R.; Friesner, R.; Sherman, W. Accurate Binding Free Energy Predictions in Fragment Optimization. *J. Chem. Inf. Model.* **2015,** *55,* 2411–2420.
162. Goldfeld, D. A.; Murphy, R.; Kim, B.; Wang, L.; Beuming, T.; Abel, R.; Friesner, R. A. Docking and Free Energy Perturbation Studies of Ligand Binding in the Kappa Opioid Receptor. *J. Phys. Chem. B* **2015,** *119,* 824–835.
163. Keränen, H.; Åqvist, J.; Gutiérrez-de-Terán, H. Free Energy Calculations of A(2A) Adenosine Receptor Mutation Effects on Agonist Binding. *Chem. Commun.* **2015,** *51,* 3522–3525.
164. Keränen, H.; Gutiérrez-de-Terán, H.; Åqvist, J. Structural and Energetic Effects of A2A Adenosine Receptor Mutations on Agonist and Antagonist Binding. *PLoS One* **2014,** *9,* e108492.
165. Pan, A. C.; Borhani, D. W.; Dror, R. O.; Shaw, D. E. Molecular Determinants of Drug-Receptor Binding Kinetics. *Drug Discov. Today* **2013,** *18,* 667–673.
166. Guo, D.; Hillger, J. M.; IJzerman, A. P.; Heitman, L. H. Drug-Target Residence Time—A Case for G Protein-Coupled Receptors. *Med. Res. Rev.* **2014,** *34,* 856–892.
167. Verheijen, I.; Vanderheyden, P. M. L.; De Backer, J. P.; Vauquelin, G. AT1 Receptor Antagonists. *Curr. Med. Chem. Cardiovasc. Hematol. Agents* **2004,** *2,* 69–77.
168. Dowling, M. R.; Charlton, S. J. Quantifying the Association and Dissociation Rates of Unlabelled Antagonists at the Muscarinic M3 Receptor. *Br. J. Pharmacol.* **2006,** *148,* 927–937.
169. Yassen, A.; Olofsen, E.; Romberg, R.; Sarton, E.; Danhof, M.; Dahan, A. Mechanism-Based Pharmacokinetic-Pharmacodynamic Modeling of the Antinociceptive Effect of Buprenorphine in Healthy Volunteers. *Anesthesiology* **2006,** *104,* 1232–1242.
170. Kapur, S.; Seeman, P. Antipsychotic Agents Differ in How Fast They Come off the Dopamine D2 Receptors. Implications for Atypical Antipsychotic Action. *J. Psychiatry Neurosci.* **2000,** *25,* 161–166.
171. Seeman, P. Targeting the Dopamine D2 Receptor in Schizophrenia. *Expert Opin. Ther. Targets* **2006,** *10,* 515–531.
172. Mitsutake, A.; Mori, Y.; Okamoto, Y. Enhanced Sampling Algorithms. *Methods Mol. Biol.* **2013,** *924,* 153–195.
173. Cavalli, A.; Spitaleri, A.; Saladino, G.; Gervasio, F. L. Investigating Drug-Target Association and Dissociation Mechanisms Using Metadynamics-Based Algorithms. *Acc. Chem. Res.* **2015,** *48,* 277–285.
174. Shukla, D.; Hernández, C. X.; Weber, J. K.; Pande, V. S. Markov State Models Provide Insights into Dynamic Modulation of Protein Function. *Acc. Chem. Res.* **2015,** *48,* 414–422.
175. Tiwary, P.; Limongelli, V.; Salvalaglio, M.; Parrinello, M. Kinetics of Protein-Ligand Unbinding: Predicting Pathways, Rates, and Rate-Limiting Steps. *Proc. Natl. Acad. Sci. U. S. A.* **2015,** *112,* E386–E391.
176. Mollica, L.; Decherchi, S.; Zia, S. R.; Gaspari, R.; Cavalli, A.; Rocchia, W. Kinetics of Protein-Ligand Unbinding via Smoothed Potential Molecular Dynamics Simulations. *Sci. Rep.* **2015,** *5,* 11539.
177. Schmidtke, P.; Luque, F. J.; Murray, J. B.; Barril, X. Shielded Hydrogen Bonds as Structural Determinants of Binding Kinetics: Application in Drug Design. *J. Am. Chem. Soc.* **2011,** *133,* 18903–18910.
178. Pearlstein, R. A.; Hu, Q.-Y.; Zhou, J.; Yowe, D.; Levell, J.; Dale, B.; Kaushik, V. K.; Daniels, D.; Hanrahan, S.; Sherman, W.; Abel, R. New Hypotheses about the Structure-Function of Proprotein Convertase Subtilisin/kexin Type 9: Analysis of the Epidermal Growth Factor-like Repeat A Docking Site Using WaterMap. *Proteins* **2010,** *78,* 2571–2586.
179. Bortolato, A.; Tehan, B. G.; Bodnarchuk, M. S.; Essex, J. W.; Mason, J. S. Water Network Perturbation in Ligand Binding: Adenosine A 2A Antagonists as a Case Study. *J. Chem. Inf. Model.* **2013,** *53,* 1700–1713.
180. Sabbadin, D.; Ciancetta, A.; Moro, S. Perturbation of Fluid Dynamics Properties of Water Molecules during G Protein-Coupled Receptor-Ligand Recognition: The Human A2A Adenosine Receptor as a Key Study. *J. Chem. Inf. Model.* **2014,** *54,* 2846–2855.
181. Bortolato, A.; Deflorian, F.; Weiss, D. R.; Mason, J. S. Decoding the Role of Water Dynamics in Ligand-Protein Unbinding: CRF1R as a Test Case. *J. Chem. Inf. Model.* **2015,** *55,* 1857–1866.
182. Kelly, B.; McMullan, M.; Muguruza, C.; Ortega, J. E.; Meana, J. J.; Callado, L. F.; Rozas, I. α2-Adrenoceptor Antagonists: Synthesis, Pharmacological Evaluation, and Molecular Modeling Investigation of Pyridinoguanidine, Pyridino-2-Aminoimidazoline and Their Derivatives. *J. Med. Chem.* **2015,** *58,* 963–977.
183. Hattori, K.; Orita, M.; Toda, S.; Imanishi, M.; Itou, S.; Nakajima, Y.; Tanabe, D.; Washizuka, K.; Araki, T.; Sakurai, M.; Matsui, S.; Imamura, E.; Ueshima, K.; Yamamoto, T.; Yamamoto, N.; Ishikawa, H.; Nakano, K.; Unami, N.; Hamada, K.; Matsumura, Y.; Takamura, F. Discovery of Highly Potent and Selective Biphenylacylsulfonamide-Based beta3-Adrenergic Receptor Agonists and Molecular Modeling Based on the Solved X-Ray Structure of the beta2-Adrenergic Receptor: Part 6. *Bioorg. Med. Chem. Lett.* **2009,** *19,* 4679–4683.
184. Stocks, M. J.; Alcaraz, L.; Bailey, A.; Bonnert, R.; Cadogan, E.; Christie, J.; Connolly, S.; Cook, A.; Fisher, A.; Flaherty, A.; Hill, S.; Humphries, A.; Ingall, A.; Jordan, S.; Lawson, M.; Mullen, A.; Nicholls, D.; Paine, S.; Pairaudeau, G.; St-Gallay, S.; Young, A. Design Driven HtL: The Discovery and Synthesis of New High Efficacy β2-Agonists. *Bioorg. Med. Chem. Lett.* **2011,** *21,* 4027–4031.
185. Soriano-Ursúa, M. A.; Correa-Basurto, J.; Valencia-Hernández, I.; Amezcua-Gutiérrez, M. A.; Padilla-Martínez, I. I.; Trujillo-Ferrara, J. G. Design, Synthesis and in vitro Evaluation of (R)-4-(2-(tert-Butylamino)-1-Hydroxyethyl)-2-(hydroxymethyl)phenyl Hydrogen Phenylboronate: A Novel Salbutamol Derivative With High Intrinsic Efficacy on the β2 Adrenoceptor. *Bioorg. Med. Chem. Lett.* **2010,** *20,* 5623–5629.
186. Christopher, J. A.; Brown, J.; Doré, A. S.; Errey, J. C.; Koglin, M.; Marshall, F. H.; Myszka, D. G.; Rich, R. L.; Tate, C. G.; Tehan, B.; Warne, T.; Congreve, M. Biophysical Fragment Screening of the β1-Adrenergic Receptor: Identification of High Affinity Arylpiperazine Leads Using Structure-Based Drug Design. *J. Med. Chem.* **2013,** *56,* 3446–3455.

187. Hiller, C.; Kling, R. C.; Heinemann, F. W.; Meyer, K.; Hübner, H.; Gmeiner, P. Functionally Selective Dopamine D2/D3 Receptor Agonists Comprising an Enyne Moiety. *J. Med. Chem.* **2013,** *56,* 5130–5141.
188. Weichert, D.; Banerjee, A.; Hiller, C.; Kling, R. C.; Hübner, H.; Gmeiner, P. Molecular Determinants of Biased Agonism at the Dopamine D2 Receptor. *J. Med. Chem.* **2015,** *58,* 2703–2717.
189. Nakata, H.; Kozasa, T. Functional Characterization of Galphao Signaling Through G Protein-Regulated Inducer of Neurite Outgrowth 1. *Mol. Pharmacol.* **2005,** *67,* 695–702.
190. Bromberg, K. D.; Iyengar, R.; He, J. C. Regulation of Neurite Outgrowth by G(i/o) Signaling Pathways. *Front. Biosci.* **2008,** *13,* 4544–4557.
191. Allen, J. A.; Yost, J. M.; Setola, V.; Chen, X.; Sassano, M. F.; Chen, M.; Peterson, S.; Yadav, P. N.; Huang, X.; Feng, B.; Jensen, N. H.; Che, X.; Bai, X.; Frye, S. V.; Wetsel, W. C.; Caron, M. G.; Javitch, J. A.; Roth, B. L.; Jin, J. Discovery of β-Arrestin-Biased Dopamine D2 Ligands for Probing Signal Transduction Pathways Essential for Antipsychotic Efficacy. *Proc. Natl. Acad. Sci. U. S. A.* **2011,** *108,* 18488–18493.
192. Lane, J. R.; Donthamsetti, P.; Shonberg, J.; Draper-Joyce, C. J.; Dentry, S.; Michino, M.; Shi, L.; López, L.; Scammells, P. J.; Capuano, B.; Sexton, P. M.; Javitch, J. A.; Christopoulos, A. A New Mechanism of Allostery in a G Protein-Coupled Receptor Dimer. *Nat. Chem. Biol.* **2014,** *10,* 745–752.
193. Mistry, S. N.; Shonberg, J.; Draper-Joyce, C. J.; Klein Herenbrink, C.; Michino, M.; Shi, L.; Christopoulos, A.; Capuano, B.; Scammells, P. J.; Lane, J. R. Discovery of a Novel Class of Negative Allosteric Modulator of the Dopamine D2 Receptor Through Fragmentation of a Bitopic Ligand. *J. Med. Chem.* **2015,** *58,* 6819–6843.
194. Tschammer, N.; Elsner, J.; Goetz, A.; Ehrlich, K.; Schuster, S.; Ruberg, M.; Kühhorn, J.; Thompson, D.; Whistler, J.; Hübner, H.; Gmeiner, P. Highly Potent 5-Aminotetrahydropyrazolopyridines: Enantioselective Dopamine D3 Receptor Binding, Functional Selectivity, and Analysis of Receptor-Ligand Interactions. *J. Med. Chem.* **2011,** *54,* 2477–2491.
195. Ananthan, S.; Saini, S. K.; Zhou, G.; Hobrath, J. V.; Padmalayam, I.; Zhai, L.; Bostwick, J. R.; Antonio, T.; Reith, M. E. A.; McDowell, S.; Cho, E.; McAleer, L.; Taylor, M.; Luedtke, R. R. Design, Synthesis, and Structure-Activity Relationship Studies of a Series of [4-(4-Carboxamidobutyl)]-1-Arylpiperazines: Insights Into Structural Features Contributing to Dopamine D3 versus D2 Receptor Subtype Selectivity. *J. Med. Chem.* **2014,** *57,* 7042–7060.
196. Dilly, S.; Scuvée-Moreau, J.; Wouters, J.; Liégeois, J.-F. The 5-HT(1A) Agonism Potential of Substituted Piperazine-Ethyl-Amide Derivatives Is Conserved in the Hexyl Homologues: Molecular Modeling and Pharmacological Evaluation. *J. Chem. Inf. Model.* **2011,** *51,* 2961–2966.
197. Storer, R. I.; Brennan, P. E.; Brown, A. D.; Bungay, P. J.; Conlon, K. M.; Corbett, M. S.; DePianta, R. P.; Fish, P. V.; Heifetz, A.; Ho, D. K. H.; Jessiman, A. S.; McMurray, G.; de Oliveira, C. A. F.; Roberts, L. R.; Root, J. A.; Shanmugasundaram, V.; Shapiro, M. J.; Skerten, M.; Westbrook, D.; Wheeler, S.; Whitlock, G. A.; Wright, J. Multiparameter Optimization in CNS Drug Discovery: Design of pyrimido[4,5-D]azepines as Potent 5-Hydroxytryptamine 2C (5-HT2C) Receptor Agonists With Exquisite Functional Selectivity Over 5-HT2A and 5-HT2B Receptors. *J. Med. Chem.* **2014,** *57,* 5258–5269.
198. Cheng, J.; Giguère, P. M.; Onajole, O. K.; Lv, W.; Gaisin, A.; Gunosewoyo, H.; Schmerberg, C. M.; Pogorelov, V. M.; Rodriguiz, R. M.; Vistoli, G.; Wetsel, W. C.; Roth, B. L.; Kozikowski, A. P. Optimization of 2-Phenylcyclopropylmethylamines as Selective Serotonin 2C Receptor Agonists and Their Evaluation as Potential Antipsychotic Agents. *J. Med. Chem.* **2015,** *58,* 1992–2002.
199. Shang, Y.; Filizola, M. Opioid Receptors: Structural and Mechanistic Insights Into Pharmacology and Signaling. *Eur. J. Pharmacol.* **2015,** *763,* 206–213.
200. Yuan, Y.; Zaidi, S. A.; Elbegdorj, O.; Aschenbach, L. C. K.; Li, G.; Stevens, D. L.; Scoggins, K. L.; Dewey, W. L.; Selley, D. E.; Zhang, Y. Design, Synthesis, and Biological Evaluation of 14-Heteroaromatic-Substituted Naltrexone Derivatives: Pharmacological Profile Switch From Mu Opioid Receptor Selectivity to Mu/kappa Opioid Receptor Dual Selectivity. *J. Med. Chem.* **2013,** *56,* 9156–9169.
201. Wang, Y.; Xing, Y.; Liu, X.; Ji, H.; Kai, M.; Chen, Z.; Yu, J.; Zhao, D.; Ren, H.; Wang, R. A New Class of Highly Potent and Selective Endomorphin-1 Analogues Containing A-Methylene-B-Aminopropanoic Acids (map). *J. Med. Chem.* **2012,** *55,* 6224–6236.
202. Lesma, G.; Salvadori, S.; Airaghi, F.; Murray, T. F.; Recca, T.; Sacchetti, A.; Balboni, G.; Silvani, A. Structural and Biological Exploration of phe(3)-phe(4)-Modified Endomorphin-2 Peptidomimetics. *ACS Med. Chem. Lett.* **2013,** *4,* 795–799.
203. De Lera Ruiz, M.; Lim, Y.-H.; Zheng, J. Adenosine A2A Receptor as a Drug Discovery Target. *J. Med. Chem.* **2014,** *57,* 3623–3650.
204. Leone, R. D.; Lo, Y.-C.; Powell, J. D. A2aR Antagonists: Next Generation Checkpoint Blockade for Cancer Immunotherapy. *Comput. Struct. Biotechnol. J.* **2015,** *13,* 265–272.
205. Jacobson, K. A. Structure-Based Approaches to Ligands for G-Protein-Coupled Adenosine and P2Y Receptors, From Small Molecules to Nanoconjugates. *J. Med. Chem.* **2013,** *56,* 3749–3767.
206. Jacobson, K. A. Crystal Structures of the A2A Adenosine Receptor and Their Use in Medicinal Chemistry. *In Silico Pharmacol.* **2013,** *1,* 22–27.
207. Andrews, S. P.; Tehan, B. Stabilised G Protein-Coupled Receptors in Structure-Based Drug Design: A Case Study with Adenosine A2A Receptor. *Med. Chem. Commun.* **2013,** *4,* 52–67.
208. Chen, D.; Errey, J. C.; Heitman, L. H.; Marshall, F. H.; Ijzerman, A. P.; Siegal, G. Fragment Screening of GPCRs Using Biophysical Methods: Identification of Ligands of the Adenosine A(2A) Receptor With Novel Biological Activity. *ACS Chem. Biol.* **2012,** *7,* 2064–2073.
209. Pastorin, G.; Federico, S.; Paoletta, S.; Corradino, M.; Cateni, F.; Cacciari, B.; Klotz, K.-N.; Gao, Z.-G.; Jacobson, K. A.; Spalluto, G.; Moro, S. Synthesis and Pharmacological Characterization of a New Series of 5,7-Disubstituted-[1,2,4]triazolo[1,5-a][1,3,5]triazine Derivatives as Adenosine Receptor Antagonists: A Preliminary Inspection of Ligand-Receptor Recognition Process. *Bioorg. Med. Chem.* **2010,** *18,* 2524–2536.
210. Federico, S.; Paoletta, S.; Cheong, S. L.; Pastorin, G.; Cacciari, B.; Stragliotto, S.; Klotz, K. N.; Siegel, J.; Gao, Z.-G.; Jacobson, K. A.; Moro, S.; Spalluto, G. Synthesis and Biological Evaluation of a New Series of 1,2,4-triazolo[1,5-A]-1,3,5-Triazines as Human A(2A) Adenosine Receptor Antagonists With Improved Water Solubility. *J. Med. Chem.* **2011,** *54,* 877–889.
211. Carlsson, J.; Tosh, D. K.; Phan, K.; Gao, Z.-G.; Jacobson, K. A. Structure–Activity Relationships and Molecular Modeling of 1,2,4-Triazoles as Adenosine Receptor Antagonists. *ACS Med. Chem. Lett.* **2012,** *3,* 715–720.
212. Dal Ben, D.; Buccioni, M.; Lambertucci, C.; Thomas, A.; Klotz, K.-N.; Federico, S.; Cacciari, B.; Spalluto, G.; Volpini, R. 8-(2-Furyl)adenine Derivatives as A2A Adenosine Receptor Ligands. *Eur. J. Med. Chem.* **2013,** *70,* 525–535.
213. Lambertucci, C.; Buccioni, M.; Dal Ben, D.; Kachler, S.; Marucci, G.; Spinaci, A.; Thomas, A.; Klotz, K.-N.; Volpini, R. New Substituted 9-Propyladenine Derivatives as A 2A Adenosine Receptor Antagonists. *Med. Chem. Commun.* **2015,** *6,* 963–970.
214. Squarcialupi, L.; Colotta, V.; Catarzi, D.; Varano, F.; Betti, M.; Varani, K.; Vincenzi, F.; Borea, P. A.; Porta, N.; Ciancetta, A.; Moro, S. 7-Amino-2-phenylpyrazolo[4,3-D] pyrimidine Derivatives: Structural Investigations at the 5-Position to Target Human A1 And A(2A) Adenosine Receptors. Molecular Modeling and Pharmacological Studies. *Eur. J. Med. Chem.* **2014,** *84,* 614–627.
215. Zhukov, A.; Andrews, S. P.; Errey, J. C.; Robertson, N.; Tehan, B.; Mason, J. S.; Marshall, F. H.; Weir, M.; Congreve, M. Biophysical Mapping of the Adenosine A2A Receptor. *J. Med. Chem.* **2011,** *54,* 4312–4323.
216. Andrews, S. P.; Mason, J. S.; Hurrell, E.; Congreve, M. Structure-Based Drug Design of Chromone Antagonists of the Adenosine A2A Receptor. *Med. Chem. Commun.* **2014,** *5,* 571–575.
217. Catarzi, D.; Colotta, V.; Varano, F.; Poli, D.; Squarcialupi, L.; Filacchioni, G.; Varani, K.; Vincenzi, F.; Borea, P. A.; Dal Ben, D.; Lambertucci, C.; Cristalli, G. Pyrazolo[1,5-C] quinazoline Derivatives and Their Simplified Analogues as Adenosine Receptor Antagonists: Synthesis, Structure-Affinity Relationships and Molecular Modeling Studies. *Bioorg. Med. Chem.* **2013,** *21,* 283–294.
218. Catarzi, D.; Varano, F.; Poli, D.; Squarcialupi, L.; Betti, M.; Trincavelli, L.; Martini, C.; Dal Ben, D.; Thomas, A.; Volpini, R.; Colotta, V. 1,2,4-triazolo[1,5-A]quinoxaline Derivatives and Their Simplified Analogues as Adenosine A3 Receptor Antagonists. Synthesis, Structure-Affinity Relationships and Molecular Modeling Studies. *Bioorg. Med. Chem.* **2015,** *23,* 9–21.
219. Cheong, S. L.; Dolzhenko, A.; Kachler, S.; Paoletta, S.; Federico, S.; Cacciari, B.; Dolzhenko, A.; Klotz, K.-N.; Moro, S.; Spalluto, G.; Pastorin, G. The Significance of 2-Furyl Ring Substitution with a 2-(para-Substituted) Aryl Group in a New Series of Pyrazolo-Triazolo-Pyrimidines as Potent and Highly Selective hA(3) Adenosine Receptors Antagonists: New Insights into Structure-Affinity Relationship and Receptor-Antagonist Recognition. *J. Med. Chem.* **2010,** *53,* 3361–3375.

220. Federico, S.; Ciancetta, A.; Sabbadin, D.; Paoletta, S.; Pastorin, G.; Cacciari, B.; Klotz, K. N.; Moro, S.; Spalluto, G. Exploring the Directionality of 5-Substitutions in a New Series of 5-alkylaminopyrazolo[4,3-e]1,2,4-triazolo[1,5-C]pyrimidine as a Strategy to Design Novel Human a(3) Adenosine Receptor Antagonists. *J. Med. Chem.* **2012,** *55,* 9654–9668.
221. Squarcialupi, L.; Colotta, V.; Catarzi, D.; Varano, F.; Filacchioni, G.; Varani, K.; Corciulo, C.; Vincenzi, F.; Borea, P. A.; Ghelardini, C.; Di Cesare Mannelli, L.; Ciancetta, A.; Moro, S. 2-Arylpyrazolo[4,3-D]pyrimidin-7-Amino Derivatives as New Potent and Selective Human A3 Adenosine Receptor Antagonists. Molecular Modeling Studies and Pharmacological Evaluation. *J. Med. Chem.* **2013,** *56,* 2256–2269.
222. Yaziji, V.; Rodríguez, D.; Gutiérrez-de-Terán, H.; Coelho, A.; Caamaño, O.; García-Mera, X.; Brea, J.; Loza, M. I.; Cadavid, M. I.; Sotelo, E. Pyrimidine Derivatives as Potent and Selective A3 Adenosine Receptor Antagonists. *J. Med. Chem.* **2011,** *54,* 457–471.
223. Baraldi, P. G.; Preti, D.; Zaid, A. N.; Saponaro, G.; Tabrizi, M. A.; Baraldi, S.; Romagnoli, R.; Moorman, A. R.; Varani, K.; Cosconati, S.; Di Maro, S.; Marinelli, L.; Novellino, E.; Borea, P. A. New 2-Heterocyclyl-imidazo[2,1-l]purin-5-One Derivatives as Potent and Selective Human A3 Adenosine Receptor Antagonists. *J. Med. Chem.* **2011,** *54,* 5205–5220.
224. Baraldi, P. G.; Saponaro, G.; Romagnoli, R.; Aghazadeh Tabrizi, M.; Baraldi, S.; Moorman, A. R.; Cosconati, S.; Di Maro, S.; Marinelli, L.; Gessi, S.; Merighi, S.; Varani, K.; Borea, P. A.; Preti, D. Water-Soluble pyrazolo[4,3-e][1,2,4]triazolo[1,5-C]pyrimidines as Human A3 Adenosine Receptor Antagonists. *J. Med. Chem.* **2012,** *55,* 5380–5390.
225. Deflorian, F.; Kumar, T. S.; Phan, K.; Gao, Z.-G.; Xu, F.; Wu, H.; Katritch, V.; Stevens, R. C.; Jacobson, K. A. Evaluation of Molecular Modeling of Agonist Binding in Light of the Crystallographic Structure of an Agonist-Bound A2A Adenosine Receptor. *J. Med. Chem.* **2012,** *55,* 538–552.
226. Tosh, D. K.; Deflorian, F.; Phan, K.; Gao, Z.-G.; Wan, T. C.; Gizewski, E.; Auchampach, J. A.; Jacobson, K. A. Structure-Guided Design of A(3) Adenosine Receptor-Selective Nucleosides: Combination of 2-Arylethynyl and bicyclo[3.1.0]hexane Substitutions. *J. Med. Chem.* **2012,** *55,* 4847–4860.
227. Tosh, D. K.; Paoletta, S.; Deflorian, F.; Phan, K.; Moss, S. M.; Gao, Z.-G.; Jiang, X.; Jacobson, K. A. Structural Sweet Spot for A1 Adenosine Receptor Activation by Truncated (N)-Methanocarba Nucleosides: Receptor Docking and Potent Anticonvulsant Activity. *J. Med. Chem.* **2012,** *55,* 8075–8090.
228. Paoletta, S.; Tosh, D. K.; Finley, A.; Gizewski, E. T.; Moss, S. M.; Gao, Z.-G.; Auchampach, J. A.; Salvemini, D.; Jacobson, K. A. Rational Design of Sulfonated A3 Adenosine Receptor-Selective Nucleosides as Pharmacological Tools to Study Chronic Neuropathic Pain. *J. Med. Chem.* **2013,** *56,* 5949–5963.
229. Petrelli, R.; Torquati, I.; Kachler, S.; Luongo, L.; Maione, S.; Franchetti, P.; Grifantini, M.; Novellino, E.; Lavecchia, A.; Klotz, K.-N.; Cappellacci, L. 5'-C-Ethyl-Tetrazolyl-N(6)-Substituted Adenosine and 2-Chloro-Adenosine Derivatives as Highly Potent Dual Acting A1 Adenosine Receptor Agonists and A3 Adenosine Receptor Antagonists. *J. Med. Chem.* **2015,** *58,* 2560–2566.
230. Louvel, J.; Guo, D.; Agliardi, M.; Mocking, T. A. M.; Kars, R.; Pham, T. P.; Xia, L.; de Vries, H.; Brussee, J.; Heitman, L. H.; Ijzerman, A. P. Agonists for the Adenosine A1 Receptor With Tunable Residence Time. A Case for Nonribose 4-Amino-6-Aryl-5-Cyano-2-Thiopyrimidines. *J. Med. Chem.* **2014,** *57,* 3213–3222.
231. Preti, D.; Baraldi, P. G.; Saponaro, G.; Romagnoli, R.; Aghazadeh Tabrizi, M.; Baraldi, S.; Cosconati, S.; Bruno, A.; Novellino, E.; Vincenzi, F.; Ravani, A.; Borea, P. A.; Varani, K. Design, Synthesis, and Biological Evaluation of Novel 2-((2-(4-(substituted)phenylpiperazin-1-Yl)ethyl)amino)-5'-N-Ethylcarboxamidoadenosines as Potent and Selective Agonists of the A2A Adenosine Receptor. *J. Med. Chem.* **2015,** *58,* 3253–3267.
232. Takano, R.; Yoshida, M.; Inoue, M.; Honda, T.; Nakashima, R.; Matsumoto, K.; Yano, T.; Ogata, T.; Watanabe, N.; Hirouchi, M.; Kimura, T.; Toda, N. Optimization of 3-Aryl-3-Ethoxypropanoic Acids and Discovery of the Potent GPR40 Agonist DS-1558. *Bioorg. Med. Chem.* **2015,** *23,* 5546–5565.
233. Pease, J.; Horuk, R. Chemokine Receptor Antagonists. *J. Med. Chem.* **2012,** *55,* 9363–9392.
234. Qin, L.; Kufareva, I.; Holden, L. G.; Wang, C.; Zheng, Y.; Zhao, C.; Fenalti, G.; Wu, H.; Han, G. W.; Cherezov, V.; Abagyan, R.; Stevens, R. C.; Handel, T. M. Structural Biology. Crystal Structure of the Chemokine Receptor CXCR4 in Complex With a Viral Chemokine. *Science* **2015,** *347,* 1117–1122.
235. Hu, F.; Miao, L.; Zhao, Y.; Xiao, Y.-Y.; Xu, Q. A Meta-Analysis for C-X-C Chemokine Receptor Type 4 as a Prognostic Marker and Potential Drug Target in Hepatocellular Carcinoma. *Drug Des. Dev. Ther.* **2015,** *9,* 3625–3633.
236. Zhang, C.; Li, J.; Han, Y.; Jiang, J. A Meta-Analysis for CXCR4 as a Prognostic Marker and Potential Drug Target in Non-Small Cell Lung Cancer. *Drug Des. Dev. Ther.* **2015,** *9,* 3267–3278.
237. Naif, H. M. Pathogenesis of HIV Infection. *Infect. Dis. Rep.* **2013,** *5*, e6.
238. Mungalpara, J.; Thiele, S.; Eriksen, Ø.; Eksteen, J.; Rosenkilde, M. M.; Våbenø, J. Rational Design of Conformationally Constrained Cyclopentapeptide Antagonists for C-X-C Chemokine Receptor 4 (CXCR4). *J. Med. Chem.* **2012,** *55,* 10287–10291.
239. Aboye, T. L.; Ha, H.; Majumder, S.; Christ, F.; Debyser, Z.; Shekhtman, A.; Neamati, N.; Camarero, J. A. Design of a Novel Cyclotide-Based CXCR4 Antagonist with Anti-Human Immunodeficiency Virus (HIV)-1 Activity. *J. Med. Chem.* **2012,** *55,* 10729–10734.
240. Zhao, H.; Prosser, A. R.; Liotta, D. C.; Wilson, L. J. Discovery of Novel N-Aryl Piperazine CXCR4 Antagonists. *Bioorg. Med. Chem. Lett.* **2015,** *25,* 4950–4955.
241. Cox, B. D.; Prosser, A. R.; Sun, Y.; Li, Z.; Lee, S.; Huang, M. B.; Bond, V. C.; Snyder, J. P.; Krystal, M.; Wilson, L. J.; Liotta, D. C. Pyrazolo-Piperidines Exhibit Dual Inhibition of CCR5/CXCR4 HIV Entry and Reverse Transcriptase. *ACS Med. Chem. Lett.* **2015,** *6,* 753–757.
242. Tan, Q.; Zhu, Y.; Li, J.; Chen, Z.; Han, G. W.; Kufareva, I.; Li, T.; Ma, L.; Fenalti, G.; Li, J.; Zhang, W.; Xie, X.; Yang, H.; Jiang, H.; Cherezov, V.; Liu, H.; Stevens, R. C.; Zhao, Q.; Wu, B. Structure of the CCR5 Chemokine Receptor-HIV Entry Inhibitor Maraviroc Complex. *Science* **2013,** *341,* 1387–1390.
243. Burg, J. S.; Ingram, J. R.; Venkatakrishnan, A. J.; Jude, K. M.; Dukkipati, A.; Feinberg, E. N.; Angelini, A.; Waghray, D.; Dror, R. O.; Ploegh, H. L.; Garcia, K. C. Structural Biology. Structural Basis for Chemokine Recognition and Activation of a Viral G Protein-Coupled Receptor. *Science* **2015,** *347,* 1113–1117.
244. Maeda, D. Y.; Peck, A. M.; Schuler, A. D.; Quinn, M. T.; Kirpotina, L. N.; Wicomb, W. N.; Fan, G.-H.; Zebala, J. A. Discovery of 2-[5-(4-Fluorophenylcarbamoyl)pyridin-2-Ylsulfanylmethyl]phenylboronic Acid (SX-517): Noncompetitive Boronic Acid Antagonist of CXCR1 and CXCR2. *J. Med. Chem.* **2014,** *57,* 8378–8397.
245. Maeda, D. Y.; Peck, A. M.; Schuler, A. D.; Quinn, M. T.; Kirpotina, L. N.; Wicomb, W. N.; Auten, R. L.; Gundla, R.; Zebala, J. A. Boronic Acid-Containing CXCR1/2 Antagonists: Optimization of Metabolic Stability, in vivo Evaluation, and a Proposed Receptor Binding Model. *Bioorg. Med. Chem. Lett.* **2015,** *25,* 2280–2284.
246. Jacobson, K. A. New Paradigms in GPCR Drug Discovery. *Biochem. Pharmacol.* **2015,** *98,* 541–555.
247. Gentry, P. R.; Sexton, P. M.; Christopoulos, A. Novel Allosteric Modulators of G Protein-Coupled Receptors. *J. Biol. Chem.* **2015,** *290,* 19478–19488.
248. Jazayeri, A.; Marshall, F. Implications of Metabotropic Glutamate Receptor Structures for Drug Discovery in Neurotherapeutics. *Expert. Rev. Neurother.* **2015,** *15,* 123–125.
249. Christopher, J. A.; Aves, S. J.; Bennett, K. A.; Doré, A. S.; Errey, J. C.; Jazayeri, A.; Marshall, F. H.; Okrasa, K.; Serrano-Vega, M. J.; Tehan, B. G.; Wiggin, G. R.; Congreve, M. Fragment and Structure-Based Drug Discovery for a Class C GPCR: Discovery of the mGlu5 Negative Allosteric Modulator HTL14242 (3-Chloro-5-[6-(5-Fluoropyridin-2-Yl)pyrimidin-4-Yl]benzonitrile). *J. Med. Chem.* **2015,** *58,* 6653–6664.
250. Xu, J.; Wang, Z.; Liu, P.; Li, D.; Lin, J. An Insight Into Antagonist Binding and Induced Conformational Dynamics of Class B GPCR Corticotropin-Releasing Factor Receptor 1. *Mol. Biosyst.* **2015,** *11,* 2042–2050.
251. Bai, Q.; Shi, D.; Zhang, Y.; Liu, H.; Yao, X. Exploration of the Antagonist CP-376395 Escape Pathway for the Corticotropin-Releasing Factor Receptor 1 by Random Acceleration Molecular Dynamics Simulations. *Mol. Biosyst.* **2014,** *10,* 1958–1967.

Relevant Websites

http://gpcrdb.org/—GPCRdb offers reference data and easy-to-use web tools and diagrams for a multidisciplinary audience investigating GPCR function, drug design or evolution.
http://www.guidetopharmacology.org/—Wellcome Trust funded portal to pharmacological information.
http://www.rcsb.org/pdb/home/home.do—The Protein Data Bank (PDB) archive is the single worldwide repository of information about the 3D structures of large biological molecules, including proteins and nucleic acids.

https://www.ebi.ac.uk/chembl/—ChEMBL or ChEMBLdb is a manually curated chemical database of bioactive molecules with drug-like properties. It is maintained by the European Bioinformatics Institute (EBI), of the European Molecular Biology Laboratory (EMBL).
http://gpcr-modsim.org/—Server to generate a homology-based 3D model of your query GPCR sequence, and/or further equilibrate your GPCR structure with an all-atom Molecular Dynamics simulation protocol
http://zhanglab.ccmb.med.umich.edu/GPCR-EXP/—Database with the list of GPCR crystal structures available.
http://blanco.biomol.uci.edu/mpstruc/—Database of membrane proteins of known 3D structure.
http://sbcb.bioch.ox.ac.uk/memprotmd/beta/—A database of membrane proteins embedded in lipid bilayers.

3.09 2/3D Pharmacophore Definitions and Their Application

RA Lewis and F Sirockin, Novartis Pharma AG, Basel, Switzerland

© 2017 Elsevier Ltd. All rights reserved.

3.09.1	**Introduction**	190
3.09.2	**The Biological Context of Pharmacophores**	191
3.09.3	**Pharmacophore Elucidation**	191
3.09.3.1	Feature Representation	192
3.09.3.2	Feature Definition	193
3.09.3.3	Tautomers	193
3.09.3.3.1	Hydrogen-bond donor features	193
3.09.3.3.2	Hydrogen-bond acceptor features	194
3.09.3.3.3	Halogens	194
3.09.3.3.4	Donor/acceptor feature point positioning	194
3.09.3.3.5	Positive and negative features	194
3.09.3.3.6	Excluded volumes	195
3.09.3.3.7	Hydrophobic features	196
3.09.3.3.8	Customized features	197
3.09.3.4	Field-Based Pharmacophores	197
3.09.3.5	Searching for Candidate Alignments	198
3.09.3.5.1	Algorithms using pregenerated conformers	199
3.09.3.5.2	Algorithms that alter conformations on the fly	200
3.09.3.6	Scoring	200
3.09.3.7	Evaluation of Pharmacophore Methods	201
3.09.3.8	Causes of Underperformance in the Pharmacophore Concept	203
3.09.3.9	Practical Aspects and Applications	204
3.09.3.10	3D Database Searching	205
3.09.3.10.1	Database generation	205
3.09.3.10.2	Feature Matching	206
3.09.3.10.3	Geometry matching	206
3.09.3.10.4	Post-processing	207
3.09.4	**Pharmacophore Keys**	207
3.09.4.1	2D Pharmacophores	207
3.09.4.2	3D Pharmacophores	207
3.09.5	**3D Pharmacophores and Protein Structure**	208
3.09.5.1	Pharmacophores and 3D QSAR Methods	210
3.09.5.2	Exemplar Applications of 3D Pharmacophore Methods	211
3.09.5.3	Counterscreening and Target Identification	212
3.09.6	**Discussion and Future Directions**	213
3.09.6.1	The Challenge of Molecular Alignment	213
3.09.6.1.1	Alignment of ligands for 3D QSAR	213
3.09.6.1.2	Rationalization of the shared activity of two different types of ligands	214
3.09.6.1.3	Analysis of hits from a random screen	214
3.09.6.2	Validation Standards	215
3.09.6.3	Pharmacophore Feature Representation	215
3.09.6.4	Variable Binding Modes	216
3.09.6.5	The Future: Maximizing the Value of Pharmacophore Methods	216
Acknowledgments		216
References		216

Abbreviations

D Donor
GA Genetic algorithm
GKSST Greene, Kahn, Savoj, Sprague, Teig
GPCR G-protein coupled receptor
H Hydrophobe
HTS High-throughput screening
MD Molecular Dynamics
MEP Molecular electrostatic potential
MIF Molecular interaction field
PDB Protein data bank

RMSD Root mean-square deviation
QSAR Quantitative structure-activity relationship
SAR Structure–activity relationship
SIFt Structural interaction fingerprint
XED Extended electron distribution

3.09.1 Introduction

The term pharmacophore has been used in medicinal chemistry for many years, often to describe different concepts. (The true origins of the term pharmacophore have been investigated by Van Drie,[1] who credits Kier with the introduction of the concept in a series of publications in the late 1960s and the early 1970s.[2–5] Ehrlich is said to have coined the term toxicophore,[6] which is a forebear of our term.) In this article, we will cover many of these variations, but we start with the official 1998 IUPAC definition,[7] which is as follows:

> A pharmacophore is the ensemble of steric and electronic features that is necessary to ensure the optimal supramolecular interactions with a specific biological target structure and to trigger (or to block) its biological response.

The variations in this concept, as seen through many examples of incorrect usage in the medicinal chemistry literature, are implied in the notes that accompany the above definition:

> A pharmacophore does not represent a real molecule or a real association of functional groups, but a purely abstract concept that accounts for the common molecular interaction capacities of a group of compounds towards their target structure. The pharmacophore can be considered as the largest common denominator shared by a set of active molecules. This definition discards a misuse often found in the medicinal chemistry literature which consists of naming as pharmacophores simple chemical functionalities such as guanidines, sulphonamides or dihydroimidazoles (formerly imidazolines), or typical structural skeletons such as flavones, phenothiazines, prostaglandins or steroids.

The primary tenet of the pharmacophore concept is the idea that the molecular recognition, or strong binding, of a biological target by a group of (dissimilar) compounds can be ascribed to a (small) set of common features that interact with a set of complementary sites on the biological target. General features such as hydrogen-bond donors, hydrogen-bond acceptors, positively and negatively charged groups, and hydrophobic regions are typically used. As such, there is a close link between the pharmacophore concept and the widely used principles of bioisosterism. We will show that this concept is useful but may not always hold, even in seemingly ideal cases. High-affinity binding is not a direct consequence of the presence of a pharmacophore feature; rather the absence of such a feature has a very negative effect on the affinity.

The next pillar of the pharmacophore concept concerns the three-dimensional (3D) nature of molecular interactions, that is, 3D pharmacophore methods in which the spatial relationship between the pharmacophore features is also specified. Appreciation of the importance of molecular conformation grew during the 1970s and the 1980s, spurred by the increased availability of relevant experimental data (e.g., via the Cambridge Structural Database[8]) and the development of new computational methods for the calculation and visualization of stable molecular conformations. Marshall and colleagues in particular recognized the challenge of identifying the binding conformation from amongst the potentially very large number of accessible structures through their development of the "active analog" approach.[9,10] In addition, it was also recognized that many intermolecular interactions have preferred geometries.[11] This is the idea that not only does a compound need to express a pharmacophore, it should do it without incurring significant penalty, either through internal strain or poor intermolecular interactions (leading to desolvation penalties). This is the concept that a pharmacophore is a necessary but not sufficient condition for activity. We will explore this issue in more detail later.

The early pharmacophore studies were typically performed using small number of compounds in which the key features required for activity could be readily identified by visual inspection of the molecular structure(s). Such molecules also tended to possess limited conformational flexibility and/or limited functionality. These restrictions significantly limited the space of available solutions, possibly down to a single unique pharmacophore. It was thus generally possible to deduce the pharmacophore manually, possibly assisted through the use of interactive molecular graphics visualization programs. The diversity and complexity of molecular structures that characterize drug discovery today have led to the development of sophisticated computer algorithms for the elucidation, manipulation, and use of pharmacophore models. Many possible pharmacophore models may exist for a given training set, and need further work to remove redundancy. Despite this, the basic concept of a pharmacophore as a simple geometric representation of the key molecular interactions remains unchanged. Pharmacophores have found widespread use in medicinal chemistry both for hit and lead identification and during the subsequent lead optimization as counter-screens. The simplicity of the pharmacophore representation, inherent in the coarseness of the feature descriptions, does also inevitably mean that it cannot explain everything; understanding the limitations of the concept is essential to a successful application. This will also be a topic for further discussion. It is worth reiterating the role of

pharmacophore modeling with drug design: it can be used to enrich significantly screening hit rates, particularly in new chemotypes. Its speed lends itself to massive virtual screening campaigns; applying a pharmacophore as a filter can also greatly triage datasets before application of more expensive docking techniques. It can be used in ligand-based drug design, as a precursor to more sophisticated 3D Quantitative structure-activity relationship (QSAR) methods to generate alignments. It can also form the basis for the enrichment of corporate libraries, a topic we will also cover later.

We will start by looking at the biological context of pharmacophores, and the interplay between evolution, endogenous ligands, affinity, and function of targets, to understand when the pharmacophore concept can be usefully applied and when not. Then, we provide an overview of the computational pharmacophore methods most commonly used in drug discovery. We will break down the process into steps: feature definition, conformational analysis, and model selection. The combination of these steps leads to tools for pharmacophore elucidation: the identification, from a set of active molecules and their biological activities, of the key common features and their relative orientations (also called pharmacophore mapping). From this core concept has arisen a number of other widely used techniques, which we also review in outline. These include the use of 3D pharmacophore databases in focused screening, pharmacophore fingerprints, the derivation and application of pharmacophore information from protein structures and application to screening set design, the use of molecular fields as an alternative form of feature representation, and 3D QSAR methods. It is outside of our scope to provide a detailed survey of all recent developments, or a comprehensive historical review, which can be found elsewhere.[2,12–16] Space prevents us from providing much more than outline information on the various algorithms and software approaches; there are many particular details to a tool that are best appreciated by reading the primary literature. Our goal is to provide the interested reader with a fair assessment of the pharmacophore-based methods that in our experience are most widely used, and have the most value, in real drug discovery projects. We will cover both the practical aspects and some of the inherent limitations of such methods.

3.09.2 The Biological Context of Pharmacophores

A question that is often left unanswered in discussions of pharmacophores is whether evolution has needed to recognize one ligand very specifically, for example, in the monoamine G-protein-coupled receptors. These receptors can distinguish between highly similar ligands, to enable highly selective signaling. 5HT receptors do not recognize noradrenaline, for example. Cytochrome p450's, on the other hand, are evolved to metabolize xenobiotics, so driven by parsimony, they have evolved to be not very specific. Other systems, for example, the human Ether-à-go-go-Related Gene (hERG) channel have large binding sites but no known endogenous ligand, so again the binding site is promiscuous. From simple consideration of the function of a target, one can infer whether a well-defined pharmacophore should exist. The observation that these systems cannot distinguish enantiomer pairs[17] indicates that the pharmacophore concept is very weak in this case. Targets in the first category, that have evolved to recognize a very small number of chemotypes ought to yield a good model, if the training set is also of good quality; conversely a poor model might indicate problems in the training set or assay results. A caveat to this is the case when the endogenous ligand has low affinity, that is, the number of recognition elements is also reduced. Targets in the second category ought not to yield a good model, because there are multiple chemotypes that can bind to them, and probably also multiple binding modes. Pharmacophore models that have good statistics against these targets probably suffer from an artificially constrained training set and hence a limited domain of applicability. Users of such models are advised to exercise caution. It is instructive to consider the work of Kratz et al.[18] in building pharmacophore models for hERG. A set of models were built using patch clamp and clinical data. They recognized that the compounds in the training set were likely to have different binding modes, so seven complementary models were built and used. In validation work, the models could pick out the actives from the decoys very effectively. However, in a prospective study in which the models were used to search for hERG inhibitors from untested compounds, there were a large number of false positive structures as well as some hits in the patch clamp assay. In a similar context, methods that employ binding or efficacy data to score pharmacophores should also be viewed with care if the data is not direct, that is, from a biochemical binding study. Data from cellular assays may be confounded by the requirements of permeability, effects of the free drug concentration and so on. We return to this topic in the section on 3D QSARs.

3.09.3 Pharmacophore Elucidation

Pharmacophore elucidation can be formulated as a molecular alignment problem, the aim being to superimpose a set of active ligands, all of which bind in the same way to the same protein of unknown 3D structure, so that the features they have in common become evident. Variants of the problem in which the set of ligands includes inactives as well as actives, and/or the 3D structure of the binding site is known, are considered later. To illustrate the basic concept, we show in **Fig. 1** a series of structures together with the corresponding 3D pharmacophore.[19] The main focus of this article will be on 3D pharmacophores, that is, the combination of features with geometry to form a consistent alignment across a series of active molecules. It is possible to approximate geometry via bond counts, that is, a donor and an acceptor four bonds apart. This approach has value in the generation of pharmacophore keys for very large databases (see later), as one does not need to perform expensive conformational analyses. The main advantage is in speed and simplicity for comparison of datasets rather than in the elucidation of models that can be used for virtual screening. As the descriptors are discrete, they can also be used as descriptors for classical QSAR models and for scaffold hopping.[20]

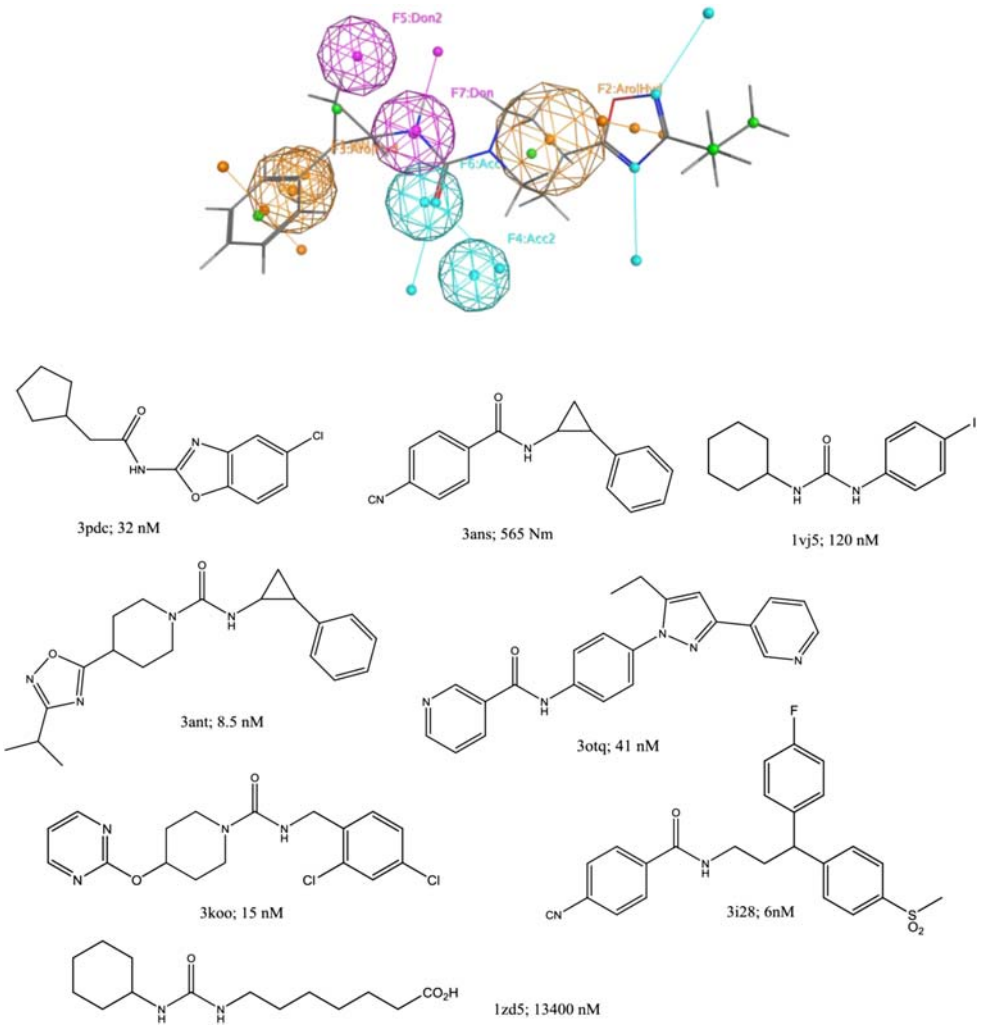

Fig. 1 An illustration of the basic pharmacophore concept. The soluble epoxide hydrolase inhibitors illustrated can be aligned[19] from their crystal structure conformations to generate a 3D pharmacophore model shown with the following color coding: H-bond acceptor *(cyan)*, H-bond donor *(magenta)*, and hydrophobic *(tan)*.

A number of programs for pharmacophore elucidation are widely used due largely to their availability in commercial software packages. These include CATALYST,[21] GALAHAD,[22] GASP,[23] the pharmacophore module of MOE,[24] FLAPpharm,[25] and PHASE.[26] Despite the maturity of these programs, many other pharmacophore elucidation/molecule alignment algorithms have been described, several of which have been published in the last few years or so.[14,27–36] This demonstrates that the problem is not considered adequately solved. Its difficulty stems from two sources. First, the calculation is compute-intensive because it involves searching the conformational space of flexible molecules and finding matching subsets of feature points from the different molecules. We will deal with each of these topics in its own right. Neither has a proven universal solution; the combination of possibilities is therefore formidable. Secondly, identifying the correct solution, if such a solution exists, can be extremely difficult (we return to this point later). In addition, for an algorithm to be useful, it must be able to align nontrivial sets of ligands that have no obvious common core. This might go without saying were it not that pharmacophore elucidation programs are occasionally "validated" by their authors on series of ligands that any competent modeler could mentally overlay in a few seconds.[37,38]

The key and necessary elements of any pharmacophore elucidation algorithm must include methods for: (1) representing the ligands (i.e., placing points on or around the molecules to represent the various pharmacophoric features they contain), (2) searching for candidate alignments, and (3) scoring those alignments. These aspects are considered separately.

3.09.3.1 Feature Representation

This involves two steps. First, the molecule must be partitioned into a set of features, each capable of representing a particular type of intermolecular interaction with the protein. Second, each feature must be represented by one or more points (or volumes) that can

be used for least-squares fitting of one molecule onto another. Greene et al. (henceforth "GKSST") wrote an influential paper describing how these steps were accomplished in the CATALYST program.[39] Many of the popular pharmacophore elucidation methods in use today employ a similar approach to feature representation,[40] and so we use their recommendations as a basis for discussion. In the discussion that follows, we talk about feature definitions in terms of functional groups or substructures. This is easy to understand but implies a hierarchy of detection. For example, the SMARTS query (OH) could match an alcohol or acid function, so the more exacting definition must come first. Later, we will discuss alternative methods based around field or molecular interaction field (MIF) formalisms.

3.09.3.2 Feature Definition

An implicit assumption of pharmacophore modeling is that there is a 1:1 mapping of features to recognition elements in the binding site. It has been known for a long time that for H-bonds, there is a balance between the number formed between the ligand and the solute, and the ligand, and the protein.[41] Certainly an imbalance in the number of interactions would usually have a strong negative effect on binding. We also point out that solubilizing groups (e.g., in many kinase active site ligands) may be necessary for activity not to be limited by solubility, but are not, per se, part of the interaction pharmacophore. Many approaches use feature descriptions that make binary assignments: H-bond acceptor, yes or no? This is one of the advantages of the pharmacophore method over 2D similarity, in that scaffold hopping is encouraged. However, the strength of the interaction is ignored. Should a urea carbonyl H-bond acceptor really be in the same class as an aniline? Clark et al.[42] and Kenny[43] have devised and applied H-bond acceptor strengths, but this has not permeated deeply into pharmacophore methodology. The MOE software offers a scheme for feature definition, which is based on extended Huckel theory[44] to compute an interaction type and a strength, allowing features to be customized by this descriptor. Likewise, the field of docking is starting to quantify the effect of desolvation on scores,[45–48] to change the nature of the best hits. This poses an unsolved problem: either the number of feature classes can be increased (to reflect the gradation of H-bonding strength) but at the cost of diminished scaffold-hopping power, or we need to relate the strengths of a feature with the observed activity (moderate strength H-bond acceptors have more potency than strong or weak ones in a particular training set). This internal weighting of a feature is not the same as weighting of the importance of a feature within the whole pharmacophore. In a thought experiment, it is easy to see that increasing the number of feature classes will reduce their membership, and eventually tend to similar results as obtained with 2D similarity metrics. One way forward might be to apply the concept of matched molecular pairs[49] to look at the differences in activity within the scope of a feature definition. This might give one an indication of the sensitivity of the model to the feature.

3.09.3.3 Tautomers

The assignment of the correct, or the most populated states of protonation or tautomerization, is very difficult,[50–52] but misassignment will have a profound effect on the pharmacophoric signature, turning donors into acceptors and vice versa[53] (**Fig. 2**). An edition of the *Journal of Computer-Aided Molecular Design* has been devoted entirely to the issue of tautomerization.[54–57] One important point is that different software programs employ different business rules for assignment, so that it is quite possible that, for the same query, different hits will be found by different programs. It may even depend on the primary source used to construct the database, making searches across different sources an issue. For this reason, we recommend that common tautomer business rules are described and used to prepare all structures used in query definition and searching. Normally, this is standard procedure in database creation, but the same rules may not be used in manual construction of a query from a set of ligands.

3.09.3.3.1 Hydrogen-bond donor features

Greene, Kahn, Savoj, Sprague, Teig (GKSST) define hydroxyl groups, nitrogen-bound hydrogens, thiols, and acetylenic CH groups as donors. The last two are controversial and many workers exclude them as being too weak. Conversely, some argue that other types of CH, in addition to acetylenes should be considered donors, for example, CH groups are posited to interact with O to form stabilizing interactions.[58] Ionization complicates the picture. GKSST exclude the hydroxyl of $-CO_2H$ as a donor because the acid is likely to be ionized at physiological pH, whereas basic amines (e.g., RCH_2NMe_2) are included because it is reasoned they will be protonated. One approach is to define explicitly all the variants in which hydrogen-bonding groups might be presented to the pharmacophore elucidation program (e.g., the use of a Daylight SMARTS string[55] that matches both RCH_2NMe_2 and $RCH_2NHMe_2^+$ could be used to ensure that both will be counted as donors). Many programs provide algorithms for "cleansing" ligand structures according to a set of business rules in order to achieve compatibility with the subsequent stages of pharmacophore generation and application. Alternatively, the assumption can be made that molecules will be presented to the pharmacophore elucidation program in their

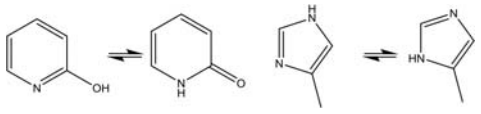

Fig. 2 Two examples of common heterocycles, whose pharmacophore character can be affected by tautomer state or protonation: pyridine and imidazole.

appropriate protonation states, thus delegating the entire problem to specialist ionization-state- and tautomer-prediction programs. The substructural definitions of hydrogen-bonding features then become much simpler. The recommendation here is not to "mix and match" between cleaning or preparation protocols, but to use the one specifically associated with the later pharmacophore elucidation program. The protocol should also match, as far as possible, the protocol and definitions used to build the database if virtual screening is the intended use of the model.

3.09.3.3.2 Hydrogen-bond acceptor features

GKSST define any N, O, or S with at least one available (i.e., nondelocalized) lone pair as an acceptor. There is a strong argument for excluding some types of oxygen atoms, for example, those in rings such as furan and oxazole, which theoretical and crystallographic evidence indicate are very weak acceptors.[59] Despite concern about metabolites, nitrile groups are becoming more common in approved drugs.[60] The nitrile group is a good acceptor group, and can be used as an isostere for hydroxyl or carbonyl. It is also claimed as a pseudo-halogen, through its electrostatic profile. This ambiguity would argue for finer division of pharmacophore feature space, with the counterargument that such divisions only show benefit in retrospective studies, where the interaction motif is shown.

3.09.3.3.3 Halogens

Halogens are not part of GKSST, or most other feature definitions. Surveys of F-containing ligands[61] have shown that C—F interacts with the C of carbonyl and amide groups. Wilcken et al.[62,63] have shown that the sigma-hole on higher aryl halogens could be used as an interaction partner with carbonyl backbone groups. They also describe the geometry and strength of such interactions, and propose them as viable pharmacophore features. While we agree with these findings that aryl hydrogens do constitute viable interaction partners, we return to our concerns with granularity and equivalence. Is a halogen–carbonyl bond worth the same as another donor–acceptor pair (corrected for solvation effects), and how often is this pairing a part of the ligand–protein interaction profile, as opposed to performing some other function? As Wilcken et al. observe, none of the common tools employ this feature, but it might be a very interesting customization when the halogen is known to play a crucial role (e.g., in the Factor Xa complex[64,65]).

3.09.3.3.4 Donor/acceptor feature point positioning

It is not sufficient merely to identify which features are present in each ligand molecule; it is also necessary to determine the locations of the associated feature points that will be overlaid in the resulting pharmacophore, reflecting the directionality of these interactions. Most programs in common use today associate donor and acceptor features not only with the corresponding ligand atoms but also with the presumed location(s) of the complementary protein atom involved in the interaction. For example, GKSST place feature points 3 Å from the heavy atom in the direction(s) of the donor hydrogen or acceptor lone pair(s), provided they are surface exposed. This strategy has the advantage that it permits the overlay of two ligands that form hydrogen bonds to the same protein atom but from different locations and directions (e.g., two ligand acceptors bonding to different H's of a putative amine sidechain,[66] see **Fig. 3A**, or an observed case based on binding to neprilysin, **Fig. 3B**). However, it implicitly makes assumptions about the directionality of hydrogen bonding and, if these assumptions are untrue, the points may be placed at inappropriate positions and the probability of generating a correct overlay reduced. Surveys of nonbonded interaction pairs in the protein data bank (PDB) have been performed, and for the common pairs, the statistics for the preferred H-bond directionality and distance can be obtained. This has been encoded into the ISOSTAR program.[67] Every feature should be characterized using maps generated by an ISOSTAR-like functionality, to see if the directionality is strongly defined, or if a wider spread of distances and angles are observed. This can be used to set tolerances for matches, and whether the ligand atom, the projection or both need to matched. One way of relaxing the directionality assumptions is to place points not only along lone-pair directions but also at intermediate positions (e.g., along the extension of the C═O bond of a carbonyl group). Alternatively, points can be placed on donor-hydrogen and "lone-pair positions" (typically chosen to be 1 Å from the acceptor atom), therefore reducing the leverage the points have when least-squares fitting or on the donor- or acceptor heavy-atom positions. One advantage of the latter is that it reduces the total number of feature points, which simplifies the search space.

GKSST account for the possibility of bond rotation in, for example, an R—OH group, by placing points at intervals on the circle swept out as the R—O bond rotates. This stratagem is unnecessary if hydroxyl groups are explicitly rotated during pharmacophore elucidation. Similar considerations apply to the lone-pair or virtual points associated with, for example, the oxygen atoms of an ionized phosphate.

3.09.3.3.5 Positive and negative features

GKSST define atoms bearing formal charges (taking into account probable ionization states in vivo) as positive or negative features unless they are bonded to an atom with the opposite charge. Delocalized groups bearing a net formal charge are also counted as positive or negative features. Feature points are placed on the centroid of the hetero-atoms of the group (e.g., the centroid of the two oxygen atoms of $-CO_2^-$). Some authors are careful to refer specifically to *ionizable* positive and negative features, emphasizing, for example, that they count RNH_3^+ as a positive feature but not $RNMe_3^+$. This makes sense because the intermolecular interactions of these two groups are very different: the former can donate very strong hydrogen bonds, the latter at best, only very weak hydrogen bonds.

Although most pharmacophore programs offer positive and negative features, it is arguable whether they are necessary. The underlying assumption is that a particular part of a protein binding site will accommodate either an ionized hydrogen-bonding

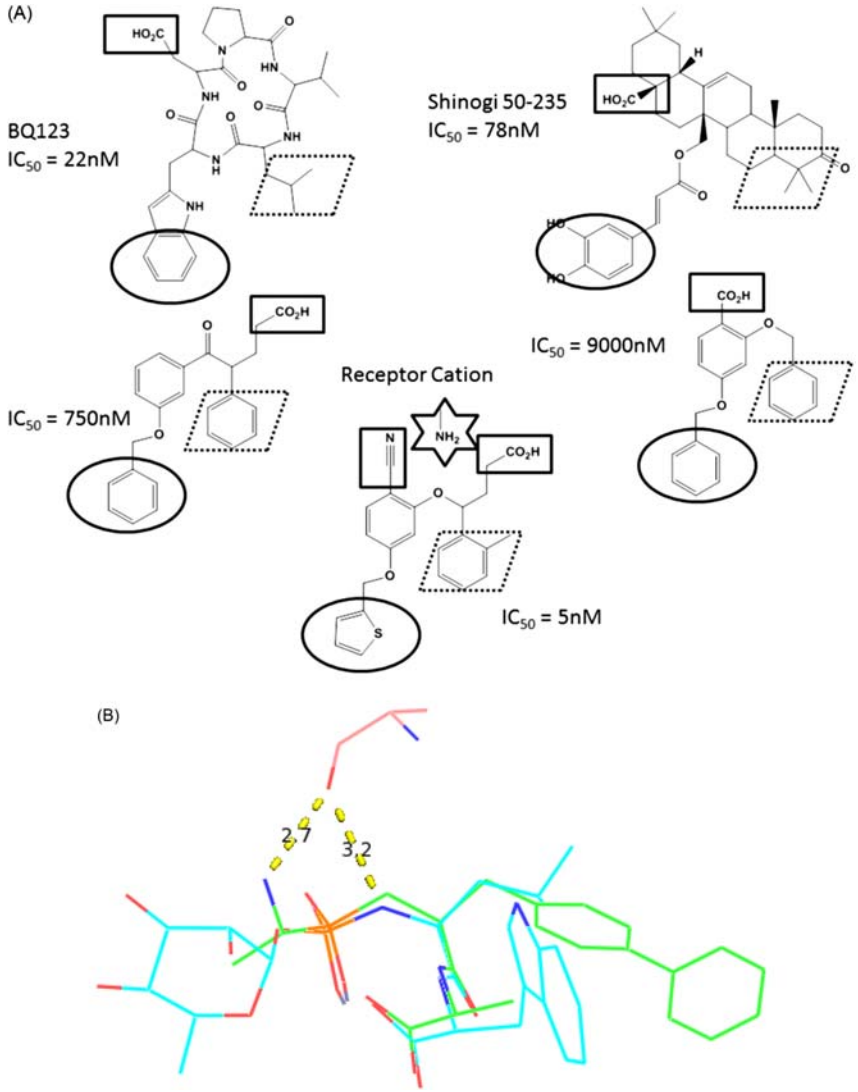

Fig. 3 (A) The derivation of a pharmacophore-based on structures binding to endothelin A, leading to a putative common acceptor-base interaction.[66] (B) Two neprilysin ligands from PDB structures 1r1h (ligand carbon atoms colored *green*) and 1dmt (*cyan* carbons) showing an observed common interaction approached from different recognition events. The $-NH_3^+$ nitrogen of the former and the amidophosphate nitrogen of the latter both donate hydrogen bonds to the backbone carbonyl oxygen of Ala543, but they interact with different lone pairs, so occupy very different positions in the binding site.

group or an unionized group, but not both. In practice, there are certainly exceptions to this rule. An alternative approach is to dispense with positive and negative features and use instead the concept of *hydrogen-bond similarity*. Each donor or acceptor group is assigned a strength (ionized groups having higher strengths than unionized); when subsequently scoring an overlay greater credit is given if groups of similar strength are overlaid on one another.[68–70] Of course, one should always be aware that the specific system under study may not necessarily conform to the general rule, due to the complex interplay between protein–ligand interactions and solvation/desolvation effects.

3.09.3.3.6 Excluded volumes

Excluded volumes are not really features themselves, but instead mark regions in which any structure matching the necessary pharmacophore must not place atoms. This is the natural extension of the concept that the pharmacophore is mapping out intermolecular interactions. A molecule making a potential salt bridge to a protein sidechain should not occupy the same volume as the side chain would. Excluded volumes are very useful if the protein binding site is known, and this topic is covered in more detail later. Even if the binding site is not known, excluded volumes can be used to explain the structure–activity relationship (SAR) between closely related analogs with very different activities.[71]

3.09.3.3.7 Hydrophobic features

Deciding which atoms, or which groups of atoms, should be considered hydrophobic is not straightforward. For example, a peptide linkage, though not at first sight a hydrophobe, often forms contacts to hydrophobic residues above and below the plane of the peptide atoms. The GKSST algorithm for placing hydrophobic feature points first assigns a hydrophobicity value to each atom, using a set of empirical rules based on the judgments of medicinal chemists. For example, a carbon atom three bonds from a double-bonded oxygen is assigned a hydrophobicity of 0.6. Each atom's hydrophobicity is modified to take account of its solvent accessibility (hence the algorithm is conformation dependent; many other programs neglect the solvent accessibility check to avoid this complication and use a set of substructure definitions). Finally, neighboring atoms with sufficiently large hydrophobicity values are clustered together into groups and a feature point placed at the centroid of each. The algorithm looks first for rings (weighting the centroid by the hydrophobicities of the ring atoms), then for groups such as $-CF_3$, then for chains. Chains are divided into contiguous, small groups of atoms. Many other programs in common use (e.g., PHASE and MOE) implement similar procedures, though they vary in detail.[31] Some programs, for example, QUASI,[32] place feature points on all atoms that are not donors or acceptors, which has the merit of being simple and producing a fine-grained representation of molecular shape. These feature points are classified in QUASI as "steric" rather than "hydrophobic," which emphasizes that there are two distinct, albeit closely related, aims: to get a good match of hydrophobic regions of molecules, and to achieve a good steric match. This distinction is explicit in the approach of Cheeseright et al. which has both van der Waals points and hydrophobic points.[72] The role of hydrophobicity is related to the role of solvent, but the methods cannot capture this level of detail. The effect of a hydrophobic point on activity is often to do with displacing (or even trapping, for a deleterious effect) water in the binding site, rather than forming direct interactions per se. Aromatic stacking is the exception rather than the rule here. Ultimately, there is no "right" way of placing the points since the hydrophobic regions of different ligands may not overlay in a tidy group-on-group fashion. For example, a common strategy is to place points at the centers of aromatic rings, but experimentally observed overlays (e.g., **Fig. 4**) do not necessarily have such rings neatly positioned on top of one another. Many programs represent certain types of hydrophobes, notably aromatic rings, by vectors rather than points so that directional interactions like π stacking can be taken into account when overlaying. In general, however, hydrophobic interactions are often not as well-defined geometrically as hydrogen bonds, and so are hard to localize to a small region of a molecule. It is also hard to quantify the relative energetic importance of a match to a hydrophobe feature, whereas the omission of an H-bond feature is usually fatal.

The most important purpose of features is to enable molecules to be overlaid in a sensible way, by least-squares fitting of feature points. In addition, feature points may be used in scoring, that is, the quality of an overlay might be judged by computing the root mean-square deviation (RMSD) between matched feature points. However, scoring can also be done without reference to the feature points, or with reference only to points relating to certain types of features. The placement of feature points is more critical if they are used both for generating and scoring an overlay, rather than just the former. A balance needs to be achieved between including all possible features and having sufficient to give a meaningful and parsimonious model. In particular, if there are many more hydrophobes than other features then these may dominate the alignment, just as putting six features on a carboxylate will do.[73] While this may give a better model according to scoring metrics, as it will be able to easily distinguish the training set from decoys, the model itself might be less useful for further work, as it will be poorer at finding new chemotypes and the domain of applicability will be small. This is similar to overfitting in QSAR modeling.

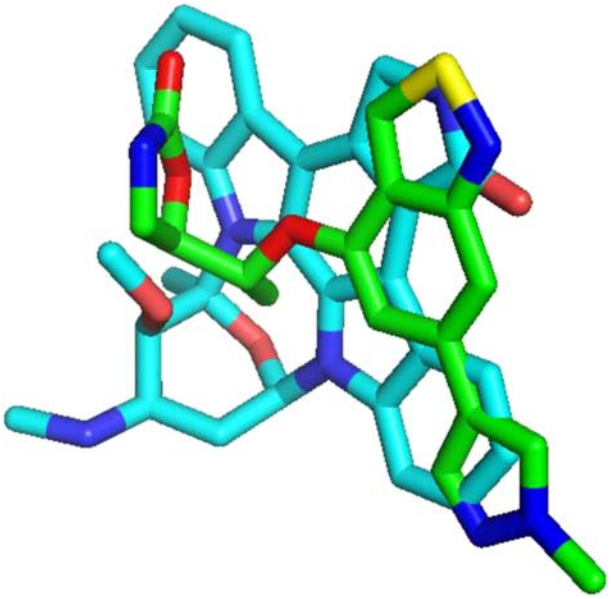

Fig. 4 Experimentally observed overlay of two SYK kinase ligands, from PDB structures 1xbc (carbon atoms colored *green*) and 5cy3 (carbons *green*), showing a poor match of ring centers.

3.09.3.3.8 Customized features

It is unlikely that there is a universally "best" set of feature types, though most would agree on an irreducible minimum of hydrogen-bond donor, hydrogen-bond acceptor and hydrophobe. Depending on the problem, other desirable types might include positive and negative centers, metal coordinators and different types of hydrophobes (e.g., aromatic and aliphatic). Interactions involving halogen atoms have been the subject of recent studies and may in some cases be usefully incorporated into a pharmacophore model.[63,74,75] Further, the user may wish to define a very specific type of feature to exploit a known SAR. For example, a chemist working on carbonic anhydrase II inhibition, aware that most known inhibitors have a terminal sulphonamide or sulphamate group, might wish to define a feature of precisely this type. As a consequence, many programs allow user-defined feature types; this is very useful in screening and selecting from large virtual libraries built around a central feature as a warhead or anchor point.[76]

Another adjustable parameter is feature separation (the minimum distance between two features for both to be counted). Does a carboxamide count as both donor and acceptor, and does phenol count as both aromatic/hydrophobe and donor/acceptor? While these two cases argue for a small separation, does a carboxylate count for two acceptor atoms, or worse four virtual points? This can lead to overweighting of certain functional groups in the model, which is particularly harmful if the main function of the functional group is to improve the properties of the molecule (e.g., solubility) rather than to interact with the protein. The feature separation distance is the same for all pairs of features so cannot be tailored during generation of a model. In the final model, features can be edited out if the user believes that over-emphasis has occurred.

3.09.3.4 Field-Based Pharmacophores

The pharmacophore generation methods described so far are based on the assignment of features to functional groups within the molecules and are, therefore, essentially atom based. An alternative approach is to base the alignment on the molecular fields exhibited by the molecules, recognizing that the interactions between molecules are governed by their overall electrostatic and van der Waals properties. Field-based approaches[77] thus aim to describe what the receptor "sees" in terms of charge distribution and shape rather than focusing on the underlying structural skeleton.

The molecular electrostatic potential (MEP) around a molecule depends on the distribution of atomic charge and is often modeled on a 3D grid or surface. The MEP at each grid point surrounding a molecule is calculated using Coulomb's law as the interaction between a probe atom of unit positive charge (a proton) and partial charges which are centered on the atoms. The resulting grids typically consist of a large number of data points so that direct alignment of the grids themselves is generally considered too compute-intensive to be feasible. However, Nicholls et al.[78] showed that the MEP can be modeled using atom-centered Gaussian functions; these provide an elegant way of overcoming the problem of handling the large number of data points in a grid. The Gaussian approximation allows the rapid comparison of the similarity of two fields using the cosine similarity coefficient. Such a similarity can then be used as the function to be maximized in an optimization of the alignment using, for example, a gradient-based method or a genetic algorithm (GA).

The MIFs produced by the GRID program[71] can be used to represent small molecules. However, MIF fields are not straightforward to model using Gaussians[79] so that identifying the optimum alignment of such fields remains a challenging task. One approach to using GRID fields that obviates the need for alignment is the GRIND method,[80,81] in which extrema in the field are identified and mapped to a fingerprint, to give a vector representation that can then be used in similarity searching as for the pharmacophore fingerprints described previously. It is not trivial, however, to determine which of the grid points should be included in the descriptor and the original GRIND approach requires that the user define the number of points that are extracted. More recently, an automated method for extracting hot spots from a field has been developed, which avoids the need for parameterization.[82] The probes can be of many different characters to reflect the different features driving recognition, but H, O, N1, and DRY probes are recognized as the basic minimal basis set. The MIFs can be combined with volumes and atom-centered features to give a more complete representation of the molecular recognition features.[25]

The use of atom-centered charges can lead to an inadequate representation of the MEP. For example, a carbonyl oxygen will give rise to a single field maximum extended outwards from the C=O double bond. The extended electron distribution (XED) force field attempts to model a quantum orbital description of the distribution of charge.[83] In XED, the charge on electronegative and π atoms is extended away from the nucleus of the atom to give rise to multipoles. For example, the carbonyl oxygen is modeled by two field maxima, which correspond to the positions of the lone pairs. The XED force field is the basis of a method to generate a pairwise alignment of two molecules based on the extrema (called field points) in their respective fields[84] (**Fig. 5**). Four types of field points can be calculated: positive, negative; hydrophobic, and van der Waals, depending on the potential used. Clique detection based on the field points is then used to find starting points for the alignment, which are optimized using a simplex algorithm. Similarity is measured by using the field points in each molecule to sample the whole field in the other, with the size of a "point" determined by the depth of the energy well, to give a more accurate reflection of the field than simply using the points themselves. Using such a multistage algorithm enables large databases to be searched in a reasonable time period.

As with the atom-based pharmacophore elucidation methods, conformational flexibility is most often handled using the ensemble approach in which conformers are precomputed and handled one at a time. It is also possible to vary conformation on-the-fly, usually under the assumption that the partial charges on the atoms are invariant to conformation, so that it is only necessary to recalculate the fields for different conformers.[85]

The most common application of field-based alignment has been to virtual screening where the molecules in a database are aligned, one at a time, to a query compound and scored. Usually, a single conformer of the query (the presumed bioactive conformation)

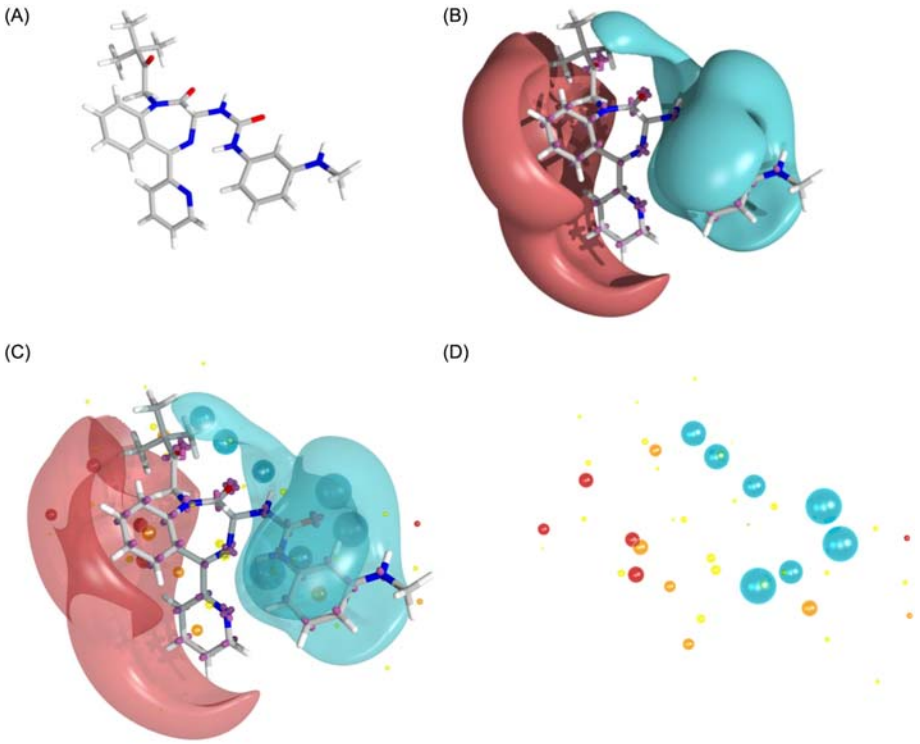

Fig. 5 The steps involved in generating field points around a molecule using the method of Cheeseright et al.[84] (A) a molecular conformation; (B) the electrostatic potential map calculated using XED (C) field points superimposed onto (B); (D) the final set of field points including electrophilic *(red)*, nucleophilic *(blue)*, van der Waals attractive *(yellow)*, and hydrophobic *(orange)* points. Reproduced with permission from Cheeseright, T.; Mackey, M.; Rose, S.; Vinter, A. Molecular Field Extrema as Descriptors of Biological Activity: Definition and Validation. *J. Chem. Inf. Model.* **2006**, *46* (2), 665–676.

is considered with the molecules in the database treated as flexible. Field-based methods have also been used to align multiple molecules. The simplest way to achieve this is to use a single molecule as the template or reference molecule,[86] but this approach is unlikely to lead to an optimal alignment. An improved approach is to first identify an overlay of two molecules by considering all pairwise alignments of the respective sets of conformers.[87] High scoring conformer pairs that share common fields can then be extended to a third, fourth, etc., molecule to give a multiconformer alignment. Such an alignment can then be used as a field-template for database screening.

3.09.3.5 Searching for Candidate Alignments

This is the most difficult part of the methodology to review because of the great diversity of published approaches. Ensuring that the bioactive conformations of the compounds are sampled is a major challenge since, in most cases, the precise form of the bioactive conformation is not known experimentally and most compounds can exist in a large number of conformations. The bioactive conformation does not always correspond to an energy minimum of the ligand in its unbound form. We make the assumption that ligands with strong affinity for their receptor do not have to channel much energy into accessing a high energy conformation. In absolute terms, this would be <2 kcal mol^{-1}, but most force fields are not accurate to this level, nor is the role of solvent taken into account, so a more pragmatic limit of 5 kcal mol^{-1} is usually taken as an upper bound over the lowest energy conformation. This again varies by force field and is one of the parameters that will control the elucidation and use of pharmacophore models. This line of reasoning can be extended to database searching as well: it is better to find matches for a pharmacophore amongst compounds in a very low energy conformation than ones that are strained, so that a first search is often performed against databases containing only a single conformer of a molecule. Obviously, this must be balanced against the number of hits desired. To reiterate: alignment can be conceptually divided into a feature matching problem and a conformational search problem. Perhaps the most telling difference between algorithms is how they deal with molecular flexibility: in particular, whether they operate on a pregenerated set of conformations for each ligand or, alternatively, alter ligand conformations on the fly during the alignment process. (Strangely, few programs do both—i.e., start with a set of pregenerated conformers but then tweak them to optimize the alignment.) Wolber et al. argue in favor of the former[88]: "Methods that tweak the molecule while fitting must dramatically reduce the search space while aligning in order to stay efficient and therefore bear the danger of falling into a local minimum." However, using precomputed conformations is itself a reduction in search space, especially for highly flexible molecules when the granularity of the conformational sampling is likely to be coarse. Thus, the possibility exists that the true answer will not be found because it lies between the conformations available to the algorithm. The ability of widely used programs to search conformational space has been extensively examined in recent years.[89–94]

Some of these studies have also investigated the conformational energy landscape and the strain energy of bound ligand conformations.[44,46] These studies provide useful guidelines for use not only in pharmacophore elucidation but also in applications such as database searching (see later). An important practical point is that whilst most pharmacophore elucidation programs contain their own conformer search procedures they do also permit the import of conformations generated with an external specialized conformer search procedure. Such flexibility provides the user with the ability to choose the best method for each distinct task in the pharmacophore elucidation process. Again, it must be emphasized that the protocols used to generate conformations for model elucidation must be the same as the ones used to generate or search any database. It is worthwhile to use a tool such as Mogul[95] to check the structures in the model as there is an assumption that active compounds will have minimal strain. Reproduction of the conformation observed in an X-ray complex as a criterion for success is more dubious, as many do contain levels of strain.[96] It should also be noted that there can be an order-dependence in the alignment, that is, B may align well to A, and C may align well to B, but C may not align well to A. Each molecule should be used as the base template for alignment to find the best global alignment.

3.09.3.5.1 Algorithms using pregenerated conformers

To avoid confusion, we use consistently the terms defined by Barnum et al.[21]: a *configuration* is a set of points in 3D space, each associated with a type of feature; a *partition* is an object associated with all configurations of a particular type, for example, the DHH partition is associated with all configurations consisting of one hydrogen-bond donor (D) feature and two hydrophobic (H) features. If two molecules both contain a configuration that belongs to the same partition, and which can be superimposed, one onto the other, within a specified threshold RMSD, this configuration is *common* to those molecules.

The classic way to identify common pharmacophore alignments from precomputed conformations is to use clique detection, first employed in the DISCO program,[97] and a mainstay of more recently published algorithms. However, the CATALYST/HipHop algorithm has probably been more widely used than any other. It operates on precomputed conformers and works by finding small common configurations and then attempting to enlarge them. The authors describe it as a "pruned exhaustive search." To begin, one or more molecules in the set to be aligned are chosen as *reference molecules*. All 2-point configurations in all conformations of the reference molecules are found. Configurations are rejected if either of the features is not surface accessible or if the interfeature distance is below a user-specified limit (this is to encourage diversity amongst the final answers). For each of the survivors, a search of the conformations of all the other molecules is performed to see whether the configuration is common to all ligands. If so, it is kept. Eventually, then, a list of all common 2-point configurations is compiled.

The algorithm then enumerates all 3-point configurations in the reference molecule(s). Any such configuration contains within it three 2-point configurations (e.g., a configuration belonging to the partition DHH will contain two DH configurations and one HH configuration). It can be rapidly ascertained (by checking the list of common 2-point configurations) whether these three 2-point configurations are common to all ligands. If this is not the case, the 3-point configuration is rejected (this is the pruning step). Otherwise, the remaining molecules are checked to see whether the 3-point configuration is common to all and a list of common 3-point configurations is built up.

Repetition of the procedure allows increasingly large common configurations to be found until no further increase in size is possible. As well as pruning, computer time is also saved by using a two-step procedure to ascertain whether a given configuration is present in a molecule. First, a precomputed list of all the interfeature distances in the molecule is checked to see whether the configuration might be present. Only if this filter is passed, will a final least-squares fit of feature points be performed as confirmation. Least-squares fitting is used in almost all pharmacophore programs as the final arbiter of whether a configuration is common to two molecules, since it distinguishes mirror images.

The claim that the algorithm is exhaustive is debatable. First, the number of solutions found depends on the granularity of the conformations presented to the algorithm. Second, the decision on whether a configuration is common or not depends on the threshold RMSD. Third, the algorithm will, if the user requests, allow certain molecules to miss a feature in a "common" configuration, provided the total number of such molecules remains below a specified limit. This is a highly desirable option, since such situations occur frequently in reality, but it again means that the number of solutions produced by the algorithm depends on a user-chosen parameter. In truth, no pharmacophore elucidation algorithm is exhaustive, despite occasional claims to the contrary.

The PHASE algorithm employs a tree-based partitioning method that rapidly groups together similar configurations according to their interpoint distances. For each conformer of each molecule, the program determines all k-point configurations that are present. Each configuration is represented by its vector of $n = k(k-1)/2$ interpoint distances. Each interpoint distance is filtered through a binary tree to assign it to a particular distance range. Once all n distances have been filtered, the configuration has effectively been assigned to an n-dimensional box whose sides are equal in length to the range corresponding to the bottom of the decision tree. Now, if two molecules each have, say, a 4-point configuration belonging to the same partition (say, 2 Donors and 2 Hydrophobes or DDHH) and falling in the same box, that configuration might be common to those molecules. (In addition, it is necessary to consider neighboring boxes, since similar distances may happen to fall either side of a box boundary; Wolber et al.[88] and Zhu and Agrafiotis[98] describe methods for circumventing this troublesome problem.) Potential common configurations of various sizes are therefore identified rapidly. A least-squares fit is then performed to determine which of these are truly common. A given k-point configuration is only accepted if it occurs in a user-specified minimum number of molecules. Open3DALIGN[99] is open source code that relies on conformations generated via quenched molecular dynamics (MD) or one of the many standard conformer generators.[94,100] Alignments are generated and scored using an atom-based cost function, which means that the alignment is unsupervised; this is a very useful tool for academics. FLAPpharm[25] takes an even simpler approach of using fingerprints to identify the consensus features that then drive the alignment.

3.09.3.5.2 Algorithms that alter conformations on the fly

An early but instructive example of this type of algorithm is GASP,[23] which uses a GA to optimize an initial population of random overlays. The ligand with the smallest number of features is chosen as a reference molecule. Each population member is represented by a chromosome containing (1) columns specifying torsion-angle values for all the rotatable bonds in all of the molecules, and (2) "mapping columns," which define pairings between features of each nonreference molecule and features of the reference molecule. This is enough information to generate a molecular overlay, by setting each molecule to the conformation defined by the appropriate torsion-angle columns and then least-squares fitting using the feature point pairings in the mapping columns. A scoring function is used to estimate the fitness of each overlay, taking into account the quality of geometric matching between paired feature points, the extent of volume overlap, and the ligand strain energies. In each step of the GA, mutation of one parent chromosome (changing either a torsion-angle or a mapping column) or crossover of two is used to generate a child (two children in the case of crossover), which, if sufficiently fit, can be used to replace the least-fit member(s) of the population.

The successor to GASP, viz. GALAHAD,[17] divides the problem into two steps. In stage one, which operates solely in ligand torsional space (i.e., the ligands are never actually overlaid), the GA is used to find a set of ligand conformations that tend to have large common volume and low steric energy, and are similar in the feature configurations they contain. The latter is determined by generating fingerprints for the ligands that capture the various triplets, quadruplets, etc., of features and their interfeature distances. Stage two employs an algorithm from image recognition to produce the final alignment of the ligands, held rigid in their conformations from the first step.

In summary, while the diversity of approaches defies easy classification, some common characteristics can be identified. Most algorithms have strategies for reducing compute time, most commonly the use of pruning or fingerprints. These may become of lesser importance as we gain access to faster larger computers with more memory. A good example of a fingerprint strategy is the CSD-Crossminer program[101] that allows interactive manipulation of pharmacophore models, which are then converted to fingerprints leading to real-time retrieval of hits. The final refined model can then be used for a more rigorous search. The use of clique detection and search techniques such as GAs are common. Least-squares fitting of matched feature points is almost always used to produce the final alignments.

3.09.3.6 Scoring

Most algorithms rank candidate overlays by means of a scoring function containing some or all of the following terms: feature matching, volume overlap, strain energy, and selectivity. Some of these terms have an underlying physical rationale; others are more subjective, being included to increase the score of the more "relevant" pharmacophores. Often, a particular molecule in the overlay, the *reference*, has a special status in the scoring procedure. The reference may be chosen arbitrarily, or its selection biased toward particularly active or less flexible molecules.

Catalyst/HypoGen takes activity data into account and uses both active and inactive compounds in an attempt to identify hypotheses that are common among the active compounds but not among the inactives. HypoGen builds hypotheses in three steps: a constructive step, a subtractive step, and an optimization step. The constructive step identifies pharmacophore candidates that are present in the most active set of compounds. The subtractive phase then eliminates configurations that are also present in at least half of the inactive compounds. This step needs to be considered carefully. Inactivity may stem from a number of reasons unrelated to the presence or absence of pharmacophore features. Visual inspection of the training set is vital to ensure that the set of inactives really does contain meaningful information that discriminates the causes of activity, and not just the absence of a solubilizing group. Subtraction does add value, if it can be used to eliminate trivial features from the final molecule (for instance hydrophobes). The final optimization step attempts to improve the score of the remaining hypotheses by applying small perturbations. HypoGen, thus, attempts to build hypotheses or SARs that correlate estimated activities with experimental activities and can be used subsequently to predict the activities of new compounds. The cleanest experimental data comes from a binding assay that returns K_d values. This is closest to the isolated recognition event that the pharmacophore is trying to model. Data from cellular assays contain other influences (solubility, permeability, and partitioning) and should be avoided when possible.

HypoGen ranks the hypotheses on their cost value; this consists of three components, namely, the weight cost, the error cost, and the configuration cost. The weight component increases in a Gaussian form as the feature weight deviates from the idealized value of 2.0. The error cost increases as the RMSD between the estimated and the measured activities for the training set increases. The configuration cost represents the complexity or the entropy of the hypothesis space being optimized and is constant for a given data set.

Catalyst first calculates the costs of two theoretical hypotheses, namely, the ideal hypothesis (fixed cost) and the null hypothesis. The ideal hypothesis has a minimal error cost and the slope of the activity correlation is one. The null hypothesis has a maximal error cost and the slope of the activity correlation is zero. Together they represent the upper and lower bounds on cost for the hypotheses that are generated. The greater the difference between them, the greater is the likelihood that a meaningful hypothesis can be found. The closer the cost of the generated hypothesis is to that of the ideal hypothesis, the higher the probability that the generated hypothesis represents a true correlation in the data. The hypothesis with the least cost ideally would map to all the features of the most active compounds in the training set. The cost is reported in bits and a difference of about 50–60 bits between the generated hypotheses and the null hypothesis suggests that the correlation may be significant, which in turn requires a difference of about 60–70 bits between the costs of the ideal and null hypotheses.

Three correlation coefficients are also used to evaluate the hypotheses: the Catalyst correlation score, Pearson's correlation coefficient, and Spearman's rank correlation coefficient. The Catalyst correlation score is derived from the simple linear regression

between the experimental and the estimated activities. The correlation coefficient can range from -1 to $+1$, with positive values indicating a direct linear relationship between the two variables, that is, the experimental and estimated values. Pearson's correlation coefficient indicates the degree of co-variation of two variables and was used to compare the estimated values with the experimental values. The closer they are, the better the correlation. Spearman's correlation coefficient measures the relationship between the relative ranks of the variable values.

The function used in PHASE, which may be written as:

$$\text{Score} = F + w_v V - w_e E + w_m^{M-1} + w_s S$$

serves as a typical example of a scoring function, where w_v, w_e, w_m, and w_s are user-defined weights. F measures the quality of alignment of features in the reference molecule with the corresponding matched features in each other molecule. Two criteria, appropriately weighted, are used: the RMSD of the matched feature points and the average cosine of the angles formed by matched pairs of vector features (e.g., aromatic rings). V is the average over the nonreference molecules of their volume overlap with the reference, measured as (intersection volume)/(union volume). E is the strain energy of the reference ligand conformer from which the pharmacophore is derived. PHASE allows configurations to be found that are common to some but not all of the molecules. M in the term w_m^{M-1} is the number of molecules that contain the configuration; so, depending on the user-chosen value of w_m, this term can be used to reward overlays in which M is large. S is a measure of selectivity, that is, an estimate of the fraction of molecules in a random database likely to match the common configuration of the overlaid molecules. The smaller this fraction is (i.e., the more unusual the arrangement of features in the common configuration), the larger S will be. The logic behind this term is that if the common configuration is unusual, it is reasonable to conclude that it occurs in the overlaid molecules *because it is a requirement of their activity*. It is too time-consuming to estimate S by searching a large database for the common configuration; Dixon et al.[26] and Barnum et al.[21] describe how it may be approximated.

Labute et al. describe a scoring mechanism based on the use of Gaussian functions.[102] In their formalism, all properties to be considered in the scoring (molecular volume, distribution within the molecule of hydrogen-bond donor and acceptor groups, etc.) are described in a consistent manner. Thus, for a given conformation of a molecule, the density of a property P at a point in space x is described by the equation:

$$f_P(x,\ x_1\ \ldots\ x_n) = \sum \left\{ (w_i/n)\left(a^2/2\pi {r_i}^2\right)^{3/2} exp\left(-a^2[x-x_i]^2/2{r_i}^2\right) \right\}$$

where $(x_1 \ldots x_n)$ are the positions of the n atoms of the ligand, r_i is the van der Waals radius of atom i, a is an empirical parameter, w_i is the weight of property P at x_i, and the summation is over the n atoms. For example, if property P is hydrogen-bond donor ability, then w_i could be set to one if atom i is a donor and zero if it is not.

The degree of overlap of property P for a pair of overlaid molecules can thus be calculated rapidly as a sum-of-Gaussians density in the interatomic distances. The degree of overlap of several properties is a weighted summation of the individual property-overlap equations, the weights reflecting the relative contribution of each property to the overall score. The consistent manner in which properties are treated lends itself to programming simplicity and makes it easy to add new properties to the scoring function.

A problem with the scoring methods described so far is that they require weights to be assigned to the different terms, and these weights are inevitably arbitrary. Some programs avoid the problem by Pareto ranking,[36,103] which produces a population of possible overlays, each representing a different compromise between conflicting criteria (e.g., ligand strain energy, volume overlap, and feature matching). Specifically, the aim is to converge on a set of *nondominated* overlays, such that, for any given overlay, there is no other overlay in the set that scores better against all criteria. The approach therefore recognizes that it is impossible to predict, for any given set of ligands, which criterion will be most important.

3.09.3.7 Evaluation of Pharmacophore Methods

The historic lack of good data sets where the "true" pharmacophore is known has meant that the evaluation of new pharmacophore generation methods has tended to be less rigorous than programs in other areas such as protein–ligand docking. Very often, programs have been evaluated on a small number of test cases (sometimes only one) and few comparative studies of different programs have been carried out. While such a situation is natural as a field develops, pharmacophore generation has now reached a state of maturity where more rigorous evaluations are appropriate.

The earliest automated pharmacophore generation methods tended to be evaluated by comparing the generated pharmacophores to those previously published in the literature that had been hand-crafted and/or were amply supported by experimental data. An alternative approach has been to fit compounds that are known to be active but that were not included in model generation to the pharmacophore. Ideally the model should also explain inactive molecules as well; for example, to determine whether the inactive compounds occupy regions outside the common volume of the pharmacophore.

The development of 3D database searching techniques made it possible to evaluate pharmacophore hypotheses in retrospective virtual screening experiments. A database of compounds can be spiked with compounds that share the same activity as those used to construct the pharmacophore. The database can then be either partitioned into those that match the pharmacophore and those that do not, or alternatively the compounds may be scored and ranked on their fit to the pharmacophore. Ideally, all active compounds will be retrieved or appear high in the ranked list.

A common approach to validate a pharmacophore hypothesis is to create a set of known actives and decoys, and look at the enrichment and area under the curve for ROC plots.[104] If the decoys are not chosen properly, this can give a misleadingly good impression. Decoys should be matched on pharmacophore features. If the model requires a basic center, and the decoys only contain such a feature rarely, the enrichment will always be good, and does not tell you if the model can truly distinguish actives from near-inactives. Likewise, a model with 4+ features is probably too specific and will show great enrichment, but be worse at scaffold hopping.

Validation statistics may also not discriminate well between models that can explain the same training set. This can be seen by a study that tried to rebuild pharmacophore models published in good peer-reviewed journals.[105] One factor for this was that key parameters were inadvertently omitted from the methods, the other was that there were several equally good models that could be generated: this is normally the case if there is no potent rigid molecule to act as a defining template. The differences arise not just from the positioning of the features, but in their number and type as well. Pharmacophore analysis is an underdetermined problem and it is very important that authors of new models describe the method appropriately as suggested below.

A template for pharmacophore model description.

	Requirement
1	Complete specification of all stereochemistry and how chiral molecules are treated, and the same for tautomer and protonation states
2	Program version and CPU platform
3	Contents of the feature/parameter file must be declared to be standard, or any changes described
4	Complete details of the conformational analysis technique used including: the technique for initial conformer generation, energy cutoff, the number of conformers generated, issues with stereochemistry, any other preferences
5	The uncertainty value must be given
6	Any feature changes to the standard dictionary must be specified
7	The choice and number of features used in the hypothesis construction, that is, 2*HBA and 5*PI
8	Settings for hypothesis generation, including: weight variation, variable tolerance, spacing, minimum number of total features, minimum numbers of particular features, Mapping coefficient, Feature Misses, Superposition error, check superposition tolerance factor, and other parameters particular to the method
9	The source of all activity data must be specified accurately
10	The number, type, weighting, tolerance, and separation of features in a resulting hypothesis should be given
11	The predicted activity values should be given
12	An independent test set should be used to assess the model

Database searching can also be used to choose between alternative hypotheses that may have been generated. Pharmacophore queries do, however, tend to produce large numbers of false positive hits, especially if used without additional features such as excluded volumes. There has been much discussion in the literature concerning the "proper" ways to perform such retrospective virtual screening evaluations.[106–111] From a practical drug discovery perspective the most important consideration is whether the search provides novel chemotypes that provide a new direction for a project to explore.

The DUD dataset,[112,113] is commonly used for validation, but this is not the correct and original intention of the authors, which was to provide decoys for assessing docking programs. A decoy set can be readily assembled for any set of input ligands.[114] Decoys are selected on the basis of matching physicochemical profiles and 2D similarity to the set of known active ligands. When applied to pharmacophores, it can give over-optimistic results, as ligands similar to the active chemotypes are removed (a particular issue if the pharmacophore training set is based on a single chemotype), and because pharmacophore methods are not as sensitive to the effects of molecular weight as some docking programs are. It would be better to match on a profile of pharmacophore features. The Maximum Unbiased Validation (MUV) dataset[115] is designed to eliminate analog bias, and so gives a better picture of how well a method can retrieve novel chemotypes. It contains less than two compounds per scaffold class. Pradon et al.[116] used this resource to compare the performance of MOE and PHASE methods for effective pharmacophore generation. Their work provides a good framework for comparison, even though the results were specific to the versions of the software at their disposal. They looked at overall retrieval rates, as well as initial enrichments (which may be more important if screening capacity is limited). The use of several models in addition to the top-ranked model was found to increase the overall retrieval rates, but at the expense of the initial enrichment. MOE seemed to perform well using default setting, whereas PHASE could be reliably tuned by addition of diverse models to the best model. Other workers[117] have shown that differences in feature definition (i.e., charged guanidinium groups), exclusion spheres (absolute barrier or only for atom centers and not bonds) treatment of tautomers, and the search strategies lead to different hit lists; these lists should be combined to maximize the effectiveness of scaffold hopping. It also highlights the difficulties in performing any type of comparison in absolute terms, and on the inadvisability of transferring any model generated using one approach to another program.

When the pharmacophore generation method is linked to the building of a 3D QSAR, as is possible in the CATALYST and PHASE programs, the pharmacophores can be evaluated on the statistical quality of the resulting models. In many cases, models have been evaluated on their internal predictivities but, as with all QSAR methods, a more rigorous evaluation involves the assessment of an external test set. In a recent comparison of PHASE and CATALYST, eight series of compounds with known activities against different targets were divided into training and test sets. The compounds in the training sets were used to generate pharmacophore hypotheses which were then tested on their abilities to predict the activities of compounds in the test sets.[118] Acceptable models

were found for only four of the data sets. Moreover, in some cases the programs were found to be highly sensitive to the chosen parameters, as has been found in other comparative studies.[105] Furthermore, the models with the highest predictivity did not correspond to the hypotheses that were scored highest by the programs, suggesting that such scores should be treated with caution.

The increased numbers and diversity of X-ray structures of protein–ligand complexes over the last decade has led to the development of test sets for the evaluation of protein–ligand docking programs. Performance is measured by the ability to reproduce the ligand binding modes. The initial test sets were of limited quality and diversity but these are now of a much higher quality with the data carefully examined for accuracy.[119] The availability of a wide diversity of protein–ligand complexes also provides opportunities for the development of test sets for pharmacophore methods, although this is a more complex task than for docking since each test case requires the identification of diverse ligands bound to the same protein target. Having identified such a set of ligands it is then necessary to superimpose the complexes based on the active site residues in order to generate an alignment of the ligands. Finally, the common features that comprise the pharmacophore can be identified, typically through visual inspection. This was the approach taken by Patel et al. in their evaluation of the programs CATALYST, DISCO, and GASP[120] which involved five protein targets (DHFR, thrombin, CDK2, thermolysin, and HIV reverse transcriptase) with up to 10 ligands for each target. The complexes were visually analyzed to identify the "true" pharmacophore and the three programs were evaluated on their ability to reproduce it. One outcome of this study was that the assessment of the generated pharmacophores is nontrivial. The ultimate goal is clear: the predicted 3D pharmacophore should consist of the X-ray conformation of each ligand superimposed exactly as seen in the crystal structure alignment. However, the definition of an acceptable solution is less clear. How should a pharmacophore be rated that contains the correct feature points (configuration) but the "wrong" conformations? What is an acceptable RMSD on the pharmacophoric distances (and conformations)? What if the variation in conformation is in a region of the ligand that is exposed to the solvent and not directly involved in the pharmacophore? What if most of the ligands are aligned correctly but one does not fit the pharmacophore? Multiple criteria were thus devised for the evaluation of the programs. The results, however, were rather disappointing, demonstrating several inadequacies of the existing programs and also the need for more rigorous evaluations.

Patel's dataset was perhaps the first attempt to develop a standard test set for pharmacophore elucidation and it has subsequently been used by other groups to evaluate new methods. As with the early attempts to develop test sets for docking, careful examination of these initial pharmacophore data sets by other authors revealed some errors (i.e., in protonation states of the ligands) which were subsequently corrected. Thus, as for the docking test sets, it is important that careful consideration is given to issues such as tautomerism, protonation state, and fit to electron density when identifying the true pharmacophore. Furthermore, the small size of the Patel data set leads to a real risk of programs being overtrained on a few examples. Cross et al.[25] used the Patel dataset to validate the FLAPpharm method and showed that they could get better chemotype enrichment rates, even when starting with only the 2D structures rather than the crystallographic poses, probably due to the richer description of the pharmacophore they employ. There is a clear need for the further development of such datasets that are accepted within the community as the minimum required for the evaluation of any new pharmacophore elucidation program. The Cruciani group[121] has attempted to answer this need with the PharmBench data set. The PharmBench validation suite consists of 81 datasets, with 960 ligands that can be aligned from their protein cocrystal complexes (which also have electron density maps available for further validation). The ligands and their conformers should be generated starting from the 2D structures, to avoid any transfer bias, before use as a validation test. With this information, one can test to see if the bioactive conformation is sampled, whether a correct alignment can be generated based on these conformations, and the overall similarity of the model to the X-ray alignment. Applying FLAPpharm to this set, reasonable alignments were found, but which had poorer RMSD statistics, which shows the danger of using distance-based metrics alone as a quality measure. These misses are caused by cases of poorly defined "tail" conformations, something that also affects docking programs. The alignments and the bioactive conformations generated from the proteins could also be suspect, so that a miss is not a disaster but a cause for further investigation, particularly using the electron density maps and the local resolution. Further datasets have been curated and published. The AstraZeneca set[122] includes an interesting assignment of the difficulty of each alignment set, so that one can get an impression not only of the overall performance, but the performance of a method on hard problems, which is really the key factor. The authors used their set to assess the CSD-based alignment tool[36] and found that it could reproduce the "easy" alignments 95% of the time, 73% of the moderate cases, and 39% of the hard cases. There are also infeasible cases, where any alignment is probably more a chance event, for example, when the ligands occupy different parts of the binding site as is the case of the endothiapepsin set. This study clearly shows where a method might fail, and for what reasons. They also introduce a metric for assessing the training set based on the degree of shape and electrostatic similarity and structural diversity. A training set containing molecules with low similarity and high diversity is likely to be hard to model.

3.09.3.8 Causes of Underperformance in the Pharmacophore Concept

There are many reasons why the assumptions behind the pharmacophore concept break down. The pitfalls that are faced by pharmacophore modeling are not markedly different to other methods for virtual screening. These have been well reviewed elsewhere[123] and are only repeated here in brief. Training a pharmacophore model to maximize the retrieval of known actives can compromise the discovery of scaffold hops. It would be unusual to find a new highly potent hit from a pharmacophore screen, as the model is underdefined and assumes a commonality of binding models that might not true. The pitfalls in feature definition and in conformational coverage have already been discussed. There is also the implicit assumption that the binding site is relatively constant, leading to a consistent binding mode. This ignores any possible role of water networks, protein flexibility, and induced fit. If two active ligands interact with the water network in different modes, one by stabilizing it with an H-bonding group, another

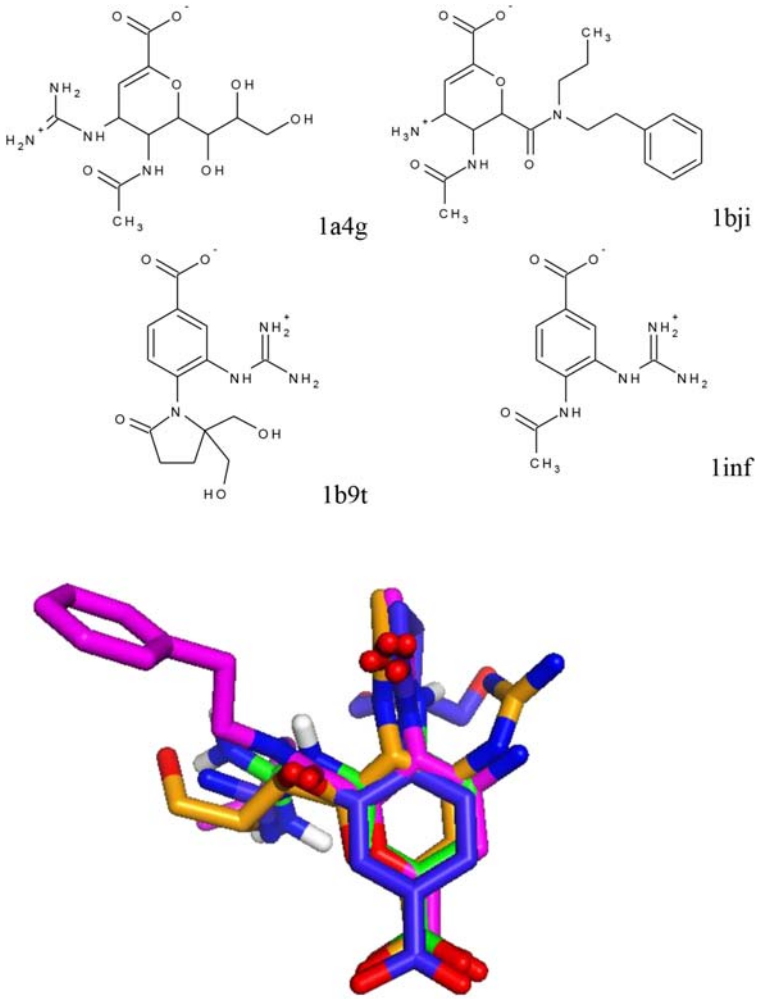

Fig. 6 Four ligands superimposed according to their binding mode to neuraminidase. Whilst the ring systems and the carboxylate group overlay, two ligands align their basic functional group to the west (1ifn in *green*, 1b9t in *blue*), two to the eastern domain (1a4g in *orange*, 1bji in *magenta*). A pharmacophore approach would treat all groups equally and produce an alignment that does not match the X-ray.

by displacing a water with a hydrophobe to form a new network, it will be very difficult to find a common pharmacophore. Likewise for a feature that may only tangentially interact with a binding site and whose main role is to confer improved properties such as solubility. This promotes the idea that pharmacophores should also be tested using feasible compounds that lack one or more of the features, to provide supporting evidence that the feature is important. It is also known that sidechains may take very different conformations even within highly homologous ligand series. A pharmacophore that does not reproduce the crystallographically observed binding mode is not necessarily a failure, but reflects the underdetermined nature of models based only on ligands (Fig. 6). This is very true for ligands with under three recognition features, such as fragment-like ligands. Pharmacophore scores have been used as surrogates for affinity. This is dangerous, as affinity is the balance of interactions in the complex and with the solvent.[41] The absence of a feature might be more important than its presence, but even within features there are changes in this balance that are not reliably predictable.[45,124] Even with the benefits of X-ray structures, free energy of binding is very hard to predict, so one should not hold pharmacophore models to the same standard. As a benchmark, a study[125] found that addition of a single methyl group to a lead structure caused a 10-fold jump in activity in 8% of the 2000 cases examined, and a 100-fold jump in 0.5% of the cases. Apart from conformational effects, this small change of an additional methyl would not be detected in most pharmacophore elucidation methods. Good enrichment of screens should be the primary goal, and that means performing a good deal of experimental validation.

3.09.3.9 Practical Aspects and Applications

It is to the credit of software developers that pharmacophore elucidation methods are no longer limited to a small number of expert computational chemistry practitioners but are much more widely accessible. However, it would be unfortunate when the reader to

assume that such methods have reached a degree of accuracy that they can be used "blind." Software programs such as these are no different to a sensitive instrument that requires knowledge and expertise to obtain the maximum benefit. As we have already indicated many programs contain a number of user-selectable parameters that govern (sometimes dramatically so) the amount and quality of output produced.

Three main stages can be identified in the elucidation of a pharmacophore. First, prepare the data set. Second, generate possible pharmacophores. Third, validate the pharmacophore(s). The compounds used to construct a 3D pharmacophore should all have the same mechanism of action (e.g., agonist, antagonist, inhibitor, and binder) and should preferably have a high affinity as measured in an appropriate biological assay (e.g., full-curve dose response from a binding assay). If a competitive binding assay is available then this may provide additional confidence that the ligands bind in the same region, though it cannot guarantee that they share a common binding mode. Data from cellular assays are less desirable, as the results can be influenced by factors outside of the pharmacophoric concept (solubility, permeability, partitioning, or stability). The ideal data set contains ligands from a number of different chemical series having limited conformational flexibility and without too many hetero-atoms. Each molecule should be inspected to ensure that it is represented as the appropriate tautomer and that the appropriate ionization state is used; depending on the software used these aspects may have a significant impact on the quality of conformations generated. It is also important to check the output from any cleansing procedures that may be applied to the input ligand structures. As the typical pharmacophore elucidation data set contains a relatively small number of molecules it should not be necessary to sacrifice speed for quality; it is also advisable to visually inspect the conformations for potential issues such as *cis* amides, high-energy axial ring substituents, and close contacts. Most pharmacophore generation programs will produce a number of results and will attempt to score them as outlined earlier. These scores can be a useful guide, but it is important to check for the quality of fit of each molecule to the pharmacophore, for a sensible common volume overlap and to ensure that the pharmacophore is consistent with the known SAR. Stereoisomers that show different activities can be very informative in helping to distinguish between possible pharmacophores. Inactive molecules can also be very useful. For example, if an inactive molecule gives a good match to the pharmacophore, then this may help to identify excluded regions. Sometimes it proves impossible to derive a satisfactory pharmacophore model. Clearly this may happen if the fundamental principle of a common binding mode does not apply. It may also be helpful to check the structures for functional groups that may not be involved in molecular recognition with the biological target (e.g., are solubilizing groups). Other strategies include relaxing various criteria (permitting partial matches). Ignoring the inactive compounds on the basis that a pharmacophore is a necessary but not sufficient requirement for activity may also help.

As will be discussed in the next section, 3D pharmacophores are widely used for virtual screening of databases in order to identify new lead series. They also have significant utility in other areas, particularly when no detailed structural information on the biological target is available. Thus a pharmacophore can help guide the design of focused arrays, can help to rationalize the SAR of a chemical series and can enable different chemical series to be combined and information transferred from one series to another. In these and other applications, the ability to visualize a 3D pharmacophore is an especially useful aspect. In all such uses however one should always remember that a pharmacophore is only a hypothesis that should be continually tested, refined, and possibly rejected.

3.09.3.10 3D Database Searching

One of the common purposes of making pharmacophore models is to search for novel chemical matter (scaffold hopping). At the time that the first pharmacophore searching algorithms were implemented in the early 1990s the discovery landscape was quite different. X-ray structures of proteins were relatively rare, and it was much more common to work with leads derived from endogenous ligands or from the literature. At the same time, the first generation of screening and compound handling robots were being developed, together with electronic databases of corporate archives. Most chemists are familiar with 2D substructure-based searches, but these typically find only compounds with similar scaffolds or members of the same structural family. The pharmacophore represents an abstraction that can be used to find alternate chemotypes (i.e., chemical series with a different underlying framework, scaffold, or common moiety). All that matters is the disposition of molecular recognition features, not the underlying pattern of atoms and bonds. The stage was therefore set to search large databases for compounds (both "real" and "virtual") that could exhibit the desired pharmacophore and thus (hopefully) have the same biological activity.[2,126,127] Depending on the precision of the query, one can find numbers of hits from 10s to 1000s, which was in line with the screening capacities available at the time. Many will be false positives and show no activity in the screen, but generally, the hit rates from pharmacophore searches are much higher than from random screening. The hits can also sample very novel and diverse chemotypes, allowing the medicinal chemist the luxury of pursuing the series with the best overall profile. Today, it can be equally cost effective to screen the whole corporate collection as to screen a significant subset. Thus the main role of pharmacophore searching in industry has changed, with a principal emphasis being on the creation of small focused sets for low throughput, higher quality assays to enhance the lead identification process in parallel with high-throughput screening (HTS). The sources of the compounds in such focused sets can be both internal and external (i.e., compound vendor). In academia, pharmacophore searching still plays a useful role in reducing screening set size to manageable proportions due to assay throughput; moreover, the main source of compounds is from commercial catalogs.

3.09.3.10.1 Database generation

All the issues highlighted previously now return in starker form, when a 3D pharmacophore is used as a search query for a large corporate database. It would be desirable to build the database so that it can be used generally, without further modification. The more the information that can be precomputed, the faster the search will be, but the larger the database will also become.

However, if the hard-coded parameters used to build the database do not match those used ad hoc to build the query, the retrieval rates will be greatly reduced. The key parameters to be considered are: tautomerism, stereochemistry, conformational sampling, and feature definition. As the usual approach is to capture as many actives as possible, even if that means more false positives, most databases are built to include all possibilities, that is, all tautomer and stereoisomer forms are added as duplicates. Conformational sampling is a particular headache, due to the trade-off between coverage and size of the database/search time. Broadly, there are two strategies: compute the conformations on the fly, or precompute and store. One can also use single conformer databases; if a good quality structure generation program is used, the single conformer ought to be close to, or even at, the global energy minimum. If this conformation can match the pharmacophore without further adjustment, the physical interpretation is that no strain energy is present, thus improving the energetics of binding. This low-energy match should have a better chance of translating into an experimentally active compound. However, the hit rate using flexible searching has been found to be 2–10 times higher.[56] The business rules used to construct the database need to be clearly documented for subsequent users, so that the pharmacophore queries can be adapted accordingly. The basic workflow involves two key steps: for each structure in the database, determine if the structure contains a predefined number of features from the query, and if it does, can the structure be made to display those features in the right geometry, within a defined tolerance?

3.09.3.10.2 Feature Matching

Feature definition is generally hard-coded, leading to very fast search times; one can prune any molecule from the search that does not contain the partition, before searching for the configuration. The feature definitions are encoded in a dictionary; when the database is built, the type and number of features in each molecule can be determined and stored. The same is done for the query, and only molecules with the same number (or more) and type of features are retained for the time-consuming next step. However, this can lead to a loss of applicability, if the pharmacophore query uses even slightly nonstandard definitions. The alternative approach of making the features very wide-ranging will reduce the power of a query to effectively discriminate between true hits and false positives. In the event that no matches are found, there is often the option of allowing partial matches (e.g., to match four out of five features). This assumes that the missing features can be designed in later (or perhaps sufficient activity can be obtained even with a partial match). Some programs allow relative weighting of features. This facility permits you to designate which features contribute most to the SAR, for example, the basic nitrogen for serotonin mimetics. This can also be done after the search of the final hit list. Feature matching can give high screen-out rates (80–100%), depending on the complexity of the query.

3.09.3.10.3 Geometry matching

Once the structures that might match the query are found, the next step is to examine the conformations of those structures to see if the geometric disposition of the features can be matched. Note also that a pure distance comparison cannot distinguish enantiomers; for this an actual fit (in 3D space) to the query is required. The goodness of fit to the query is defined by the tolerance allowed in the match between features. One might be looking for a donor–acceptor pair separated by 5 Å, but you are prepared to accept a value between 4 and 6 Å. Not all interfeature tolerances need to be the same: they should be set using knowledge of the SAR. Matching of the features should be possible without introducing undue strain into the structure. This is another parameter that can be defined. It is not possible to give specific rules, as the acceptable limit is force field dependent, but a strain energy of more than a few kcal/mol will lead to many false positives. Features can also be negative, for example, excluded volumes. Here the aim is to avoid rather than match. Inclusion volumes, for example, derived from the ensemble of aligned active ligands, can also be incorporated. Conformational analysis of all but the simplest structures quickly becomes very computationally expensive. Three strategies can be used, each with their good and bad points. The first strategy is used in UNITY,[128] which stores single conformers and uses the directed tweak algorithm[129] to perform flexible searches. The query is mapped onto the molecule, feature by feature, and a minimization in torsion space is conducted to satisfy each interfeature distance. The results are then checked for steric clashes. This is important to avoid unreasonable conformations with high internal energy. Multiple mappings of the query are possible, but once one good match is found, the search can be terminated. Essentially, the molecule is pulled by the query into the right shape, so the strain energy is the key parameter. Screen-out rates are lower than for the other methods, but with any rise in true hits found, there will also be a rise in false positives. This is a strategic decision that should be made in the wider context of the project. The second strategy is adopted by MOE, CATALYST, and PHASE, which all use a database of conformations. Each conformation can be quickly matched as a rigid body to the query, and if it does not fit, it is discarded. The strain energy can be preset so that all conformations are reasonable. The disadvantage is that normally only a relatively small number of conformations per structure can be stored (typically 250 or fewer). The selection of conformers may be performed using a poling approach to ensure "conformational diversity,"[130,131] and predefined preferences, for example, *cis*/*trans* ratios for carboxamides, or axial/equatorial ratios for saturated rings. The key issue here is whether the conformational sampling is of sufficient resolution to be useful, especially for more flexible molecules. In the third approach, compounds that pass the feature mapping stage, are subjected to conformational analysis on the fly according to a preset recipe (typically a rule-based enumeration that uses a predefined number of torsional increments for each type of rotatable bond). For each conformation, a rigid body match is performed as before, and the analysis aborted once a fit is found. Only the torsions that can affect the interfeature distances are analyzed. If the query is only loosely defined (few features, wide tolerance allowed in the fit), this approach can be very time consuming. A sensible upper limit for the number of rotatable bonds is usually defined to prevent the search time being dominated by the matching of just a few very flexible structures. The directed tweak can produce strained conformations (leading to a higher false positive rates), but the other approaches can fail to generate the matching conformation (higher false negative rate). This is the reason why it is not possible to say that one strategy is superior to the other: so much will depend on the query and the database

and the nature of the decoys. A final variant used by CATALYST is its BEST option, which is to take structures that nearly match the query, then to tweak them.

A very important test is that the search procedure should find the molecules used to build the original pharmacophore; failure to do so is an excellent way of losing any credibility! As with pharmacophore elucidation, there are a number of locally adjustable parameters. These include the tolerance allowed in the fit, and the number of features which can be skipped; naturally, loosening the search will increase the number of hits returned, so the capacity of the biological screen should be carefully kept in mind. Validation of the search parameters is a very valuable exercise that can be performed on a small test database, seeded with known actives and decoys, to see how changes to the query can change the enrichment statistics. It is strongly recommended to tune a query this way before running the main search.

3.09.3.10.4 Post-processing

A hit list of molecules that match the pharmacophore query should be post-processed. Highly flexible, feature-rich molecules such as peptides can match most queries. Parsimonious matches might be more promising. Where the information exists, exclusion, or inclusion volumes are often used; this will be discussed further in the section on using protein structures. Alternatively, simple measures of how much of the molecule falls within the pharmacophore, and how much outside, can be used to prioritize the virtual hits for inclusion in the final set for screening. Using the same scoring function as that used to create the query is possible, but given the inaccuracy of the scoring function, visual inspection is often a better guide. The simplest score is the RMSD fit to the query. One can also filter using physicochemical criteria (i.e., only returning hits that are druglike or leadlike in nature). However, a drawback of pruning too severely at this early stage is that novel chemical matter that could subsequently be modified to give a viable lead series would be lost.

3.09.4 Pharmacophore Keys

3.09.4.1 2D Pharmacophores

The archetype of a 2D pharmacophore is the Ftrees fingerprint,[132] which has been adapted by Gillet,[133] and in the ErG methodology of Stiefl[20] and others. Features are defined by substructural rules, to capture donors, acceptors, rings, and hydrophobes, under physiological protonation states. Features are joined into a simple tree using bond connectivity as the edge criteria, so that no conformational analysis needs to be performed, and then turned into a fingerprint using length functions. The Ftrees fingerprints can be combined to provide a consensus fingerprint or used to search large databases very quickly to provide possible scaffold hops, based on degree of similarity. It is recommended that the Ftrees matches are used to drive a 3D alignment to verify that the match is sensible, as artifacts can arise due to the abstract nature of the fingerprint. As the fingerprint gives very good screen-out rates, this is justified. In comparison with pure substructural fingerprints, ErG fingerprints could achieve similar rates of retrieval and better scaffold hopping behavior. The only case when the 2D pharmacophore fingerprint performed worse was when there was no clear consensus pattern, but a clearer substructure match. Just as 3D pharmacophore searches are a good prefilter for docking, 2D pharmacophore fingerprints can be a very fast prefilter for pharmacophore searches. The properties of the fingerprints can also be used to perform diversity comparisons during the prioritization of compounds to be added to corporate screening collections.

3.09.4.2 3D Pharmacophores

A 3D pharmacophore key is a binary descriptor of the partitions and configurations accessible to the molecule. Such a key (also called a fingerprint) is generated by performing a conformational analysis for each molecule and abstracting the interfeature geometries for each conformation sampled. Configurations are handled by binning the distances, for example one specific bit in the fingerprint is set if a donor and acceptor can be positioned 4–6 Å apart. By analogy with the use of the 2D fingerprints used in substructure and similarity searching the pharmacophore key can provide a way to improve search speeds for pharmacophore searches of 3D databases: the first phase of searching becomes a simple AND operation such that only molecules that pass this filter are matched further. 2-Center pharmacophore keys, in which bits are assigned to pairs of features, are probably not specific enough. If we consider seven features (i.e., donor, acceptor, hydrophobe, aromatic, positive, negative, and donor/acceptor) and 17 distance bins, the key would contain $7 \times 6 \times 17 = 714$ bits, and many bits would be turned on. The ability to discriminate between the known actives and inactive decoys is diminished. A 3-center key, in which each bit represents a triplet of features needs to be 184,884 bits long. This type of key is sparse, and so much more selective. In addition to binary keys, one can also count the frequency that a triplet is found during the analysis of a structure. 4-Center keys are even larger.[134] Using 6 feature types and 10 distance bins leads to 24 million distinct quadruplets, or tetrahedra. An example of this is the FLAP fingerprint.[135] The advantage is that such keys are now able to distinguish chirality. In contrast to database generation, feature matching is done at generation time rather than at query time. Parameters such as feature separation distances are hard-coded into the keys, so a common workflow for key generation is essential.

Pharmacophore keys capture information about shape and intermolecular interaction propensity. In contrast to the "traditional" pharmacophores described thus far they do not directly identify the particular arrangement(s) of features required for a specific biological activity. They can be a very useful prescreen to identify and prioritize putative alignment, and thus serve to speed up the full rigorous alignment process greatly.[136] The authors of this method use a neat trick of having two fingerprints with overlapping distance bins, to avoid edge effects at the bin boundaries. Pharmacophore keys are also whole-molecule descriptors that

have been used for a variety of similarity and diversity applications, driven in particular by the needs of technologies such as HTS and combinatorial chemistry where the number of chemicals to be processed is very large, for example, screening decks, or virtual combinatorial libraries. In library design one might like to answer the question, if I add this reagent, or remove that reagent, will the properties of my library improve? For example, in designing a library of type I kinase inhibitors, one will want to improve the overlap to the type I pharmacophore whereas if the library is being designed for more general enrichment purposes, one may want to minimize the overlap with the current screening deck, but maximize the overlap with the space of known drugs. Pairwise alignment of even a small library of 1000 compounds against a deck of 10^6 is not generally practical, even if it is feasible. Pharmacophore keys offer an alternate approach for the process of assessing diversity in a corporate archive. The drawback is the presence in the key of many unhelpful partitions, such as Hydrophobe-Hydrophobe-Hydrophobe separated by 12 Å, which probably do not merit a deliberate action to find molecules that fill this bin. We return to this topic in the section on pockets.

Ranking a set of compounds in a database according to their similarity to a query molecule is perhaps the most straightforward application of pharmacophore keys. New and modified similarity metrics have been developed to deal with the particular requirements of the pharmacophore key, which is in general larger and more sparse than a standard 2D fingerprint.[55] Flexophore[137] is an example of this approach. The Flexophore descriptor is constructed as a graph with the nodes as the features and the edge as frequency histograms of the feature separation. MM2 atom types are used to describe the pharmacophore features during the conformational analysis. A customized similarity function to compare the node types and the histogram results was devised: in enrichment studies the Flexophore descriptor did as well as 2D fingerprints at straight retrieval, and much better at scaffold hopping to molecules not in the training chemotypes. The union of the pharmacophore keys for a collection of molecules provides an overall profile that can be considered a diversity metric and can also be used to assess the extent to which the set adds new pharmacophores to an existing collection when purchasing compounds or in library design.[138] A pharmacophore key can also be used as a descriptor vector in QSAR modeling.[139,140] Here, the bits provide the basis of discriminating between actives and inactives. The nature of the pharmacophore key means that such models can in principle deal with multiple binding modes. Depending on the model building technique used it may also be possible to interrogate the resulting model to determine which pharmacophore(s) are responsible for the activity. As always, it is important to ensure that such models are robust and do not suffer from overfitting.

3.09.5 3D Pharmacophores and Protein Structure

Pharmacophores can be derived from the binding site of a protein. This is particularly relevant as the number of protein structures has greatly increased not only in simple numerical terms but also with regard to the breadth of coverage of gene families of interest to drug discovery. Moreover, the distinction between "structure-based" and "ligand-based" drug design methods is now much more diffuse and the judicious use of traditional ligand-based methods such as 3D pharmacophores can greatly enhance the efficiency and effectiveness of structure-based design.

The most straightforward way to derive a 3D pharmacophore from a protein structure is through the direct observation of specific interactions between protein and ligand(s). Such a pharmacophore can then be used in the usual way, for example to search a 3D database in order to identify compounds for focused screening. Database searching methods based on 3D pharmacophores are in general much faster than structure-based methods such as docking and so this can be a more effective way to screen very large databases. Alternatively, the 3D pharmacophore search can act as the first stage in a docking workflow. A large database can be prescreened using a pharmacophore query, to create a much smaller subset for docking. A pharmacophore, if properly constructed, will give very few false negatives (false negatives might arise from different binding modes or poor feature definition). The scores of docked hits may then become more useful.

Knowledge of the protein structure enables the pharmacophore to incorporate more detailed information about regions that are not accessible to the ligand. This is most commonly achieved through the use of exclusion volumes and/or inclusion regions.[141,142] An illustration of how a 3D pharmacophore can be enhanced by the addition of such information, especially when the site might have few discriminating features, or the features do not confer selectivity is given in **Fig. 7** for the development of a pharmacophore to identify inhibitors of liver X receptor agonists.[143] Models that could identify known selective agonists for the A isoform were chosen from the larger set of possible models and were used to screen the Specs virtual library of 202k entries.[144] When used for database searching such pharmacophore queries have the distinct advantage of finding hits that not only contain the key binding elements but are also able to fit into the active site, thereby reducing the false positive rate. In addition, the ligand shape itself was used as a Shape query. Three hits showing some selectivity were found, and there was not complete overlap between hits from the pharmacophore model and the shape query, again indicating the inherent fuzziness of both approaches. The extent to which an ensemble of excluded volumes can represent the atomic detail of a protein structure is obviously limited (though one should remember that proteins can be flexible, so the apparent precision of an atomic-resolution protein structure may be illusory). In addition, the widespread use of a two-stage algorithm further limits their utility. In this approach matches to the underlying pharmacophore features are first identified. The matching conformation is then tested for violation of the exclusion or inclusion criteria, often without any attempt to modify the conformation to fit these constraints. This can lead to potential hits being missed even though a relatively simple bond rotation could alleviate a clash. Conversely, the use of a limited number of exclusion volumes to represent an entire protein active site can result in "holes" through which a ligand may protrude. We also note that widely used shape searching methods provide an alternative way to tackle this problem.[78] Methods based purely on shape have found it expedient to incorporate elements of pharmacophore recognition in order to improve the efficiency and sensitivity of their algorithms.

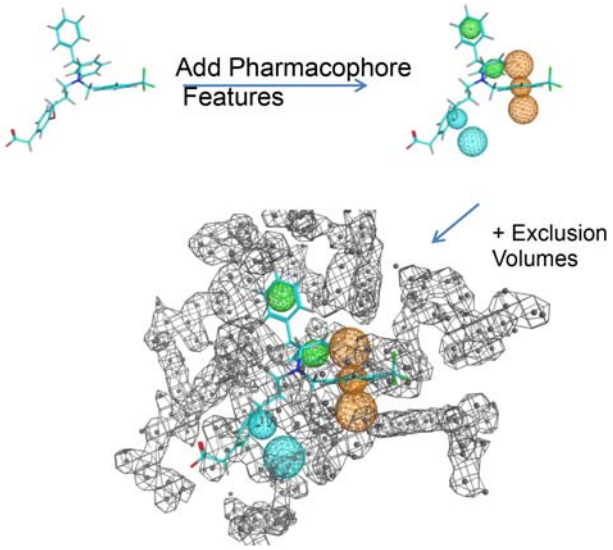

Fig. 7 Illustration of how a 3D pharmacophore can be enhanced by the addition of shape and excluded volume information, to identify inhibitors of liver X receptor agonists. The exclusion volumes are drawn at a reduced radius of 1.2 Å for clarity.

Structure-based 3D pharmacophores derived solely on the interactions observed in known protein–ligand complexes may be unnecessarily restrictive. An alternative is to define pharmacophores based on an analysis of the "hot spots" in the active site. A number of methods can in principle be used to identify such hot spots (or site points). These include programs such as FLAP[145] that probe the site with small molecules or functional groups and calculate the enthalpy of the interaction between the probe and the protein atoms at points on a grid lattice to generate an MIF. These fields can then be contoured by energy to find the most favorable regions for an acceptor or a donor (or any other type of feature) to interact with the protein. Programs such as SuperStar[146] use a knowledge-based approach in which rules are used to generate a set of interaction sites for each atom or functional group of the protein that is capable of participating in a nonbonded contact. The rules are largely based on statistical analysis of experimental structures from the PDB or small molecule crystal structures and take into account the chemical nature of the atoms as well as the directional preferences of features such as hydrogen-bond donors/acceptors. From the locations of the site points it is then necessary to construct one or more 3D pharmacophores. The simplistic approach would be to combine all such points into a single pharmacophore but the resulting query would typically be matched (if at all) only by a molecule filling the entire active site. Rather, all possible 3D pharmacophores (containing 3, 4, or more features) are enumerated from the set of site points. The most important step in such a procedure is to triage the set of pharmacophore queries. Commercially available programs such as LigandScout[147] can perform the entire process from site to pharmacophores. The question is then which features are key, and it is quite possible to select too many or too few. To deal with this issue, it is possible to analyze a trajectory file from a molecular dynamics run of a protein–ligand complex.[148,149] This function is available in LigandScout. This information can help identify stable features that persist throughout the simulation and more transient interactions. Features such as ring normals might rotate but the centroid remains. This type of analysis also protects against over-reliance on the X-ray structures, which might have artifactual interactions, and gives a frequency based score of the relative importance of the feature to the pharmacophore. This analysis can also assist when the interactions involve water. Hu and Lill[150] hypothesized that water molecules that are displaced upon ligand binding can significantly contribute to the free energy of binding depending on the free energy benefit of their release in bulk solvent; they developed a method based on thermodynamic analysis of MD trajectories to compute the free energy of water released. The protein-derived pharmacophore constraints are defined using short (50 ps) apo simulation to simulate limited conformational changes, then interaction potentials for hydrophobic and hydrogen-bonding probes are computed on a 3D grid and finally clustered. Pharmacophoric constraints are then associated with the clusters centers. The protein-derived pharmacophore types associated with the localization of waters that exhibit favorable free energy are selected to generate a reduced pharmacophore model. When compared with full protein-derived pharmacophore queries for three test cases (factor Xa, HIV protease, and pc-dihydrofolate reductase), the authors did not find a significant improvement in enrichment for their reduced pharmacophore but they could observe a sizeable improvement in screening speed, by a factor of 200–500, allowing for screening of very large libraries.

The combination of pharmacophore keys and techniques for site analysis allows one to avoid making (possibly subjective) choices about which features are important, or even which model of the active site is the bioactive form. The 3-center or 4-center key from a binding site is less sparse than the key of a ligand, but is still discriminating enough to be useful; it captures the overall character of the pocket. A comparison between the key of a protein and a ligand can quickly highlight common triples or tetrahedra, allowing fast alignment between the two objects. In the FLAP program,[145] 4-point pharmacophore fingerprints are derived from a GRID analysis of a protein active site and combined with a shape-based description of the binding site. When combined with a set of ligand pharmacophore fingerprints this provides an efficient way to perform structure-based virtual screening. Another well-known

application of this technique is embodied in the Metasite program.[151] Here, binding sites of cytochrome P450s have been characterized using the GRID approach and the key fields selected on the basis of experimentally determined sites of oxidation in substrates. New molecules are aligned to the pharmacophore keys to see which C–H bonds can come close to the oxidation center, and the results can be further ranked according to the reactivity of the C–H bond. In tests, the actual site of metabolism was in the top three predictions over 80% of the time. However, similar results can be obtained using just the reactivity concept embodied in the SmartCyp program,[152] indicating that the discriminatory power of any pharmacophore model is secondary to bond lability in this case, as the cytochromes go about their garbage collection business.

An obvious extension to searching for ligands is to compare site-based pharmacophore keys across proteins. If there is a high degree of similarity, the pockets are likely to bind the same type of chemical moiety. In addition to the CavBase program,[153] Nussinov et al.[154] have developed a much faster method, based in essence on pharmacophore triplets. Desaphy et al.[155] have proposed a method for binding sites comparisons that relies on the assignment of pharmacophore annotation to grid points evenly distributed around ligands complexed to proteins and on gaussian-based shape alignments. After two cavities have been shape aligned, pharmacophore types are assigned to grid cubes in the same framework; matching of the grid cube fingerprint is evaluated by a classical Tversky index. In theory, this pharmacophoric description of the cavity could be used for ligand-based screening and retrieval. Campagna-Slater et al.[156] proposed a method to screen the PDB for cavities similar to known methyl-lysine binding domains. They used a combination of biased pocket detection and protein-based limited pharmacophore assignment focused on the aromatic cage system. The pocket detection algorithm implemented in ICM[157] is focused on pockets exhibiting a specified set of aromatic and acidic residues the authors judged necessary to identify binding sites similar to methyl-lysine binding domains. The resulting set is then classically queried by pharmacophore screening, focusing on aromatic and one acidic pharmacophore type, and finally filtered by a combination of geometric and annotation consideration to prune small surface pockets. The authors could retrieve most of the methyl-lysine binding pockets, but also nonrelated aromatic cages and arginine binding sites, and allosteric pockets on known epigenetic targets. Despite the very specific focus of this work, it can be extended to more general searches by widening the pharmacophoric types used to characterize pockets. As always, there is a balance between speed and resolution, and the pharmacophore features are crude, and not influenced by any local electrostatic perturbations.

Another recent structure-based fingerprint is the structural interaction fingerprint (SIFt),[158,159] in which each residue in the binding site is represented by a 7-bit descriptor that characterizes whether (1) it is in contact with the ligand, (2) any main chain atom is involved in the contact, (3) any side chain atom is involved in the binding, (4) a polar interaction is involved, (5) a nonpolar interaction is involved, (6) the residue provides hydrogen-bond acceptor(s), and (7) the residue provides hydrogen-bond donors. The whole interaction fingerprint is constructed by concatenating these residue bitstrings together according to their sequence order. The SIFts have been used for a number of purposes. One straightforward application is to compare sets of docking results by calculating pairwise similarities between the fingerprints followed by a cluster analysis. This enables distinct groups of docking poses to be easily identified. By comparing the interaction fingerprints from docking results with the fingerprints for known protein–ligand complexes it was possible to achieve enrichments in virtual screening experiments that were superior to those obtained with commonly used scoring functions. Other variations and extensions to the SIFt concept include the use of weighted profile-like fingerprints that represent the interactions of multiple complexes[160] and encoding more detailed information about hydrogen-bonding strengths and geometries.[161] Finally, SIFts and other protein structural fingerprints can be used to cluster and compare the structures of different proteins across a gene family, most notably within the kinases. As with the ligand-based pharmacophore fingerprints the structural fingerprints enable complex data to be stored and manipulated efficiently using well-understood algorithms, albeit with some information loss.

Pharmacophores and shape: We have discussed the use of excluded volumes as a means of improving the selectivity of a pharmacophore model. These volumes may also be derived from the common volume overlap of the actives minus the common volume overlap of the inactives, assuming that the inactives have a full feature match. If there is a good set of actives but no obvious common pharmacophore, then methods for shape-based searching might be of use. This is beyond the scope of this article and the reader is referred elsewhere.[78]

Pharmacophores in de novo design: Pharmacophores can also be used as a constraint in de novo design.[162] In this case, one is searching virtual space rather than databases of known compounds. The construction method is based on the BRICS rules[163] applied to create fragment libraries. Molecules assembled using these rules should at least be feasible to synthesize. The scoring section involves fitting to the pharmacophore, including modification and geometric adjustment to optimize the score, which is a measure of the fit to the model. Pharmacophore features in the generated molecule that do not contribute to the fit are removed. The performance of this approach cannot be validated statistically per se, as one is trying to generate unknown molecules, so should be seen as an idea generator for medicinal chemists. In some well studied pharmacophore models (COX-2, BCR-Abl), the method was able to recapitulate most of the known topologies of active chemotypes.

3.09.5.1 Pharmacophores and 3D QSAR Methods

Field-based approaches have been widely used to generate 3D QSAR models from sets of aligned molecules, for example, in the widely used CoMFA program. In this case, a variety of different methods can be used to generate the alignment prior to model building, including overlays based on a 3D pharmacophore. In addition, some of the more commonly used pharmacophore methods also use 3D QSAR methods to refine their models or closely integrate the two techniques. In the HypoGen algorithm in CATALYST the degree to which each molecule matches the query (in a geometrical sense) is assumed to correlate with the observed activity. The PHASE program also provides a facility for constructing 3D QSAR models. These models can be atom-based

(i.e., taking all of the atoms in each ligand into account) or pharmacophore-based (i.e., only the features involved in matching the common pharmacophore are used). A rectangular grid is defined to surround the molecules aligned to match the pharmacophore. Each cube in this grid is then characterized according to the atoms or pharmacophore features that fall within it, resulting in a set of binary strings (one per molecule). Partial least squares regression applied to these bit strings helps to identify which features at which locations lead to an increase or decrease in activity.

3D QSAR presents challenges even beyond traditional pharmacophore elucidation methods, though in some cases they can clearly provide additional (and useful) information. In particular, the ability to incorporate inactive molecules is very appealing, though this should be done with great care; molecules can be inactive for a variety of reasons too subtle to be captured in the model, and they may only serve to add noise rather than signal. Any 3D QSAR protocol can be used to examine alignments, but bear in mind that pharmacophore models are underdetermined and using powerful statistical tools, it is easy to find patterns in the data that are not physically real and therefore have no utility to find novel active ligands.[164] As with a pharmacophore model, the output of a 3D QSAR protocol can be interpreted as a pseudo-receptor, or as a more refined pharmacophore query. In either case, one should complete a cycle of experimental validation to see if the models find new hits or explain existing unseen experimental data rather than relying only on statistical validation criteria. There is also a paradox between the pharmacophore alignment and the way in which 3D QSAR models are set up. A pharmacophore will emphasize the points of commonality: therefore, the variation in the fields around the common features will be low, so that these descriptor points can be removed from the QSAR model.

3.09.5.2 Exemplar Applications of 3D Pharmacophore Methods

Many applications of 3D pharmacophore methods can be found in the literature. In addition, several reviews and summaries of literature applications are available, often providing a useful practical perspective.[165–168] Here we highlight a very limited number of applications from the recent literature to illustrate some of the main ways in which 3D pharmacophore models are used in contemporary drug discovery.

A major use of 3D pharmacophore methods is for the identification of new hits and leads via 3D database searching. Such applications fall into two broad categories depending on whether the pharmacophore incorporates protein structural information or not. Pavadai and colleagues recently described the development of a *Plasmodium falciparum* dihydroorotate dehydrogenase inhibitor pharmacophore model from eight known active compounds[169] using the CATALYST method. The resulting pharmacophore contained four features. When used to search the NCI compound collection of approximately 265,000 structures almost 3590 hits were obtained, using a strict acceptance level. The authors also found nine other models of varying quality and comment that their models differ from those obtained by another group using a different training set.[170] This is a common occurrence, and underlines the concept that the pharmacophore is more a property of the training set than the target. The authors also describe in some detail how they subsequently reduced this large hit list down to a more manageable size (62 compounds) using a combination of docking scores and cluster analysis. A number of active compounds were identified, four of which had an activity (K_i) of under 10 μM (Fig. 8). The enrichment factor was estimated to be at least fivefold and the substructural similarity of the hits to the training set was also low. This shows the two strengths of pharmacophores as a VS technique, strong enrichment, and novel chemotypes.

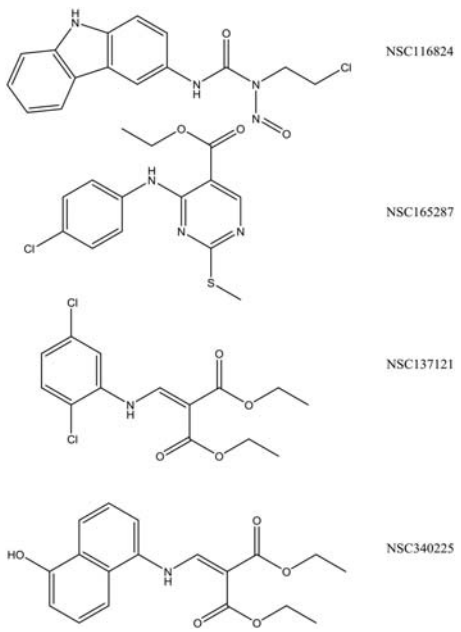

Fig. 8 Four new compounds that showed <12 μM IC_{50} against *Plasmodium falciparum* dihydroorotate dehydrogenase.

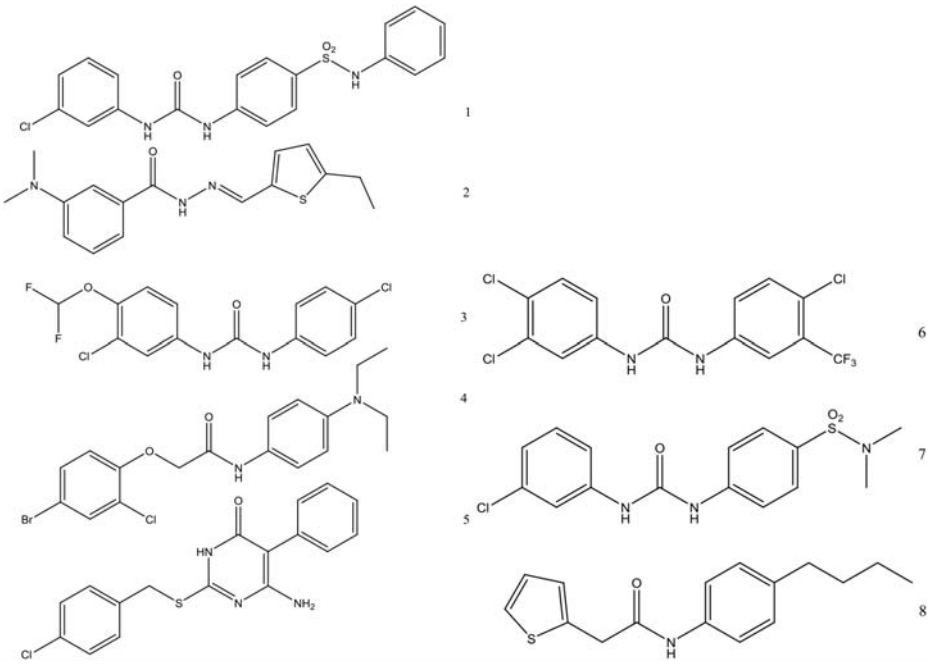

Fig. 9 The chemical structures of eight novel and highly active sEH inhibitors (<10% activity at 10 μM) identified using pharmacophore screens.

The work of Waltenberger et al.[19] to discovery novel soluble epoxide (sEH) inhibitors further illustrates the point made in the previous case study. Their training set came from both protein–ligand complexes and unbound but potent inhibitors. They also had a set of 192 confirmed inactive compounds as decoys. Models were built using LigandScout[147] and DiscoveryStudio (Catalyst[171]) methodology; the CATALYST model is illustrated in Fig. 1. They recognized that there was no one single model that retrieved all the known actives, so they built a series of models to be used in consensus. The six models with the highest combined enrichment were then used to screen the Specs database.[144] Even then, some known actives were missed, indicating again that a pharmacophore is not a unique object associated with a target. Two modeling packages were used as it is known that this will lead to an increased number of active chemotypes.[117] In biological validation of the chosen hits, a hit rate of 40% was obtained, including some novel low to moderate nanomolar inhibitors (Fig. 9). This demonstrates the key role of pharmacophores in finding new chemical matter with good enrichment, even for well studied targets such as sEH.

An example of hit identification using a structure-based pharmacophore comes from the work of Astles and colleagues[66] using the structures of just two structurally distinct and conformationally restricted inhibitors of endothelin A receptor. This provided the pharmacophore illustrated in Fig. 3A. A hit series was obtained with weak 1 μM activity and the model was used to optimize the activity by improving the fit to the model through geometry and conformational restriction, resulting in a final activity of 5 nM. The model required the use of a projected H-bond acceptor point to explain all the SARs; the positions of the H-bond acceptor atoms do not align and using this feature would have hindered the discovery of the pharmacophore model. The next example illustrates the use of pharmacophore models in lead optimization and comes from work to identify nonsteroidal glucocorticoid (GR) agonists.[172] A docking model of an established series of GR agonists was used to define a pharmacophore model. The model was used as a fast screen for screening 20k monomers to identify replacements for a metabolically labile benzoxazinone moiety. A three-step procedure was used for the selection process. First, a large 20k set of potential building blocks was identified and combined with the core template to generate an enumerated library. The virtual products were filtered using modified Lipinski criteria. The remaining structures were then converted to a 3D database and searched using the pharmacophore query. This process resulted in 200 compounds for synthesis, some of which did indeed show activity in a GR binding assay. It is important to note the role of pharmacophores in hit finding. Using these models as a filter during lead optimization is more problematic, as the SAR and the model might diverge, and using a pharmacophore model as a filter would eliminate many structures that would inform the SAR; this is said to be the case in the optimization of Liver Carnitine Palmitoyltransferase.[173]

3.09.5.3 Counterscreening and Target Identification

Pharmacophore models have also been used as counterscreens, to flag structures that might have undesirable activity, for example hERG inhibition or binding to CYP450s (as discussed earlier), or for target identification. Significant care and caution must be applied in these cases. As discussed earlier, a view needs to be taken on whether the target is capable of expressing a well-defined robust

pharmacophore. In the two cases given, many papers have been published claiming a model but it is not general in nature. The best results have been obtained using a number of complementary models to capture the different binding modes.[18] In a prospective study, these models gave a hit rate of 40% (or a false positive rate of 60%). The domain of applicability of a pharmacophore model is hard to describe, in the same sense as one would do for a 2D QSAR model.[174] Hence a match to a countertarget model should be used to promote a binding experiment to that target as first priority, to protect against the high number of false positives expected from this approach. Batteries of pharmacophore models[99] have also been used to suggest likely targets for ligands active in phenotypic screens. Again the results of such models should be seen not as confident predictions but as a means to prioritize experimental testing. Wang et al.[175] recognized the pitfalls in using fit scores to judge likelihood of actual affinity. They have adapted their PharmMapper web service to use *Z*-scores, that is, the chance of binding over random, rather than the absolute score. This works against promiscuous pharmacophores giving too many false positives. There are 7300 models corresponding to over 1500 targets in their system, and they are built using knowledge of the active sites (excluded volumes). Using the adjusted *Z*-scores, they could improve on the enrichment of actives over inactives, and identify with more certainty possible off-target interactions.

3.09.6 Discussion and Future Directions

In this final section, we focus on a small number of issues that seem to us particularly important: the difficulty of aligning molecules and its consequences; the need to improve validation standards; limitations in the way features are typically represented; the growing emphasis on the development of algorithms that take account of the possibility of multiple binding modes; and our views on how pharmacophore methods are most likely to be of value in the next few years. It is helpful to start with a simple summary of the key messages before going into detail later.

In the absence of protein–ligand X-ray data:

1. The pharmacophore is more a property of the training set of molecules than the target, and may have no physicochemical meaning when compared to the X-ray binding mode.
2. The pharmacophore models discovered are dependent on the features, the weight of the features and the conformational analysis method. Pharmacophores derived from the same rigid ligand starting point using different software tools will generate different hit lists.
3. It is not necessary to assume that there is only one possible pharmacophore model, especially for targets that are promiscuous, for example hERG. Consensus models might be better.
4. One should not look for pharmacophore models that are optimized to explaining known data; often this leads to a decrease in their ability to find novel chemical matter, which is still one of the main uses. It is more important to find new chemotypes when pharmacophores are being used for virtual screening, and better enrichment comes with an increase in the fuzziness of the description. However, the false positive rate will also increase, so the two factors are in balance.
5. The use of activity data for building pharmacophores is widespread but should be used with caution, to check that the fit to the model does correlate with the experimental observations, and not some other factor such as solubility or lipophilicity.

3.09.6.1 The Challenge of Molecular Alignment

Sadly, it is almost impossible to predict with confidence the correct way of overlaying a set of ligands that bind to a protein of unknown 3D structure (except perhaps in trivial cases involving small numbers of ligands that share a large common substructure). A typical protein binding site contains many surface exposed functional groups, and different ligands frequently interact with different selections of those groups. In addition, some of the interactions may be mediated by water molecules and the protein may be flexible. Overlaying ligands is especially difficult when the binding is largely driven by hydrophobic interactions, due to the weaker directional preferences than for hydrogen bonds. We discuss below how these problems are manifested in three different situations.

3.09.6.1.1 Alignment of ligands for 3D QSAR

In principle, this is the easiest case as the molecules are likely to be fairly close analogs. A study of protein–ligand complexes found that structurally similar ligands generally exhibit a high degree of structural conservation; changes are more likely to be found in water molecule architecture and/or side-chain movements.[176] Indeed, one might reasonably question whether it is necessary to use a computer program in such cases. Nevertheless, difficulties can arise due to local symmetry or approximate symmetry in the ligand structures. Consider the neuraminidase ligands in Fig. 6 (from PDB structures 1a4g, 1a4q, 1b9t, 1inf). The obvious (and indeed correct) way of aligning these is to superimpose the carboxylate groups and the ring atoms. However, each of the rings has two possible orientations (i.e., can be flipped to place the guanidinium or ammonium group on the "left" or "right" side). Consequently, there is a significant number of permutations from which to choose. Moreover, as is often the case, the correct answer is not obvious: two of the guanidinium groups lie on one side, the remaining guanidinium and the ammonium group on the other. The problem is exacerbated by the fact that substituents on synthetic ligands may have been introduced to moderate physical properties and may not form significant binding interactions with the protein.

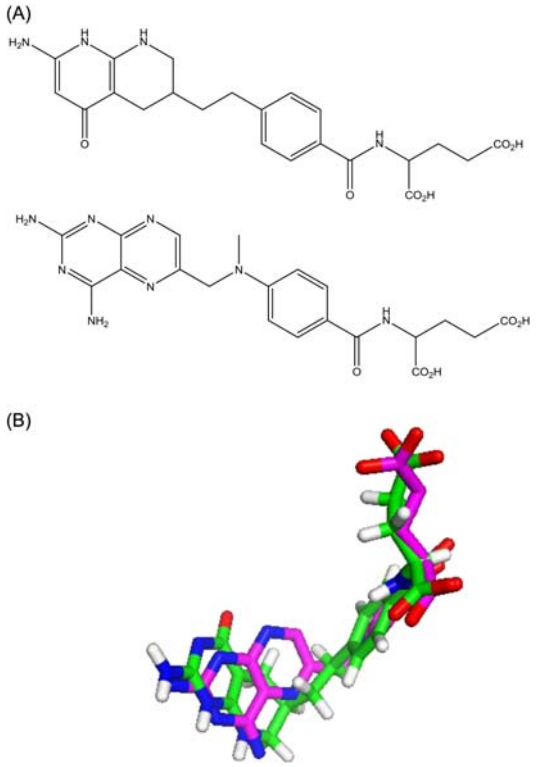

Fig. 10 The heterocyclic moieties of two dihydrofolate reductase ligands (A) do not overlay to maximize steric/substructural complementarity but rather align (B) to optimize the overlap of similar hydrogen-bonding functions (taken from 5ccc in *green*, 4qi9 in *magenta*). The glutamate tails are well aligned but do not contribute strongly to the pharmacophore as they are solvated and do not take part in a specific recognition event.

3.09.6.1.2 Rationalization of the shared activity of two different types of ligands

A frequent requirement is to overlay molecules that fall into distinct structural types in order to understand their common activity against the same target protein. An example is the pair of dihydrofolate reductase ligands shown in Fig. 10 (from PDB structures 1drf, 1mvt), the heterocyclic portions of which famously do not overlay in the way that maximizes steric complementarity but instead align so as to optimize the overlap of similar hydrogen-bonding functions. If the binding site structure were unknown, there would be no reason to favor the correct heterocycle overlay over the incorrect; both would be perfectly feasible given that some of the hydrogen-bonding groups might be solvent exposed.

3.09.6.1.3 Analysis of hits from a random screen

Overlaying a set of diverse molecules (e.g., hits from a random screen) is highly challenging. Consider the four DPP-IV ligands in Fig. 11 (from PDB structures 5ism, 5i7u, 3w2t, and 4a5s). Overlaying these ligands is quite hard as the consensus pharmacophore of the bioactive forms is limited to three features at the center of the overlay, with many other features only partially matched by two out of four ligands, despite the ligands having strong affinity. (We are aware of the argument that the correct pharmacophore can sometimes be predicted even if the correct overlay is not: but getting the right answer for the wrong reason makes us uneasy.)

In addition to the breakdown of the "single binding mode" assumption, it can also be shown that small changes to the parameters chosen for conformational analysis, feature definition, or even, sadly, the order in which ligands are considered and the version of software used, can lead to alternative, equally convincing, pharmacophore models. In one study[99] several published data sets were taken, and attempts were made to reproduce the pharmacophore models, with only limited success. This highlights the dangers of using models without follow-up experimental validation.

Despite these challenges, pharmacophore methods can—and do—make significant contributions to the advancement of drug discovery projects. Our point is that any attempt to rank a set of overlays with the expectation that the top-ranked one will be correct is unduly optimistic, not because of deficiencies in the algorithm but because the problem is underdetermined. We are better off acknowledging this unfortunate reality and accepting that multiple hypotheses must be generated, regarded as equally likely, and challenged experimentally. In the absence of a crystal structure, any pharmacophore model is more a property of the training set than the target.

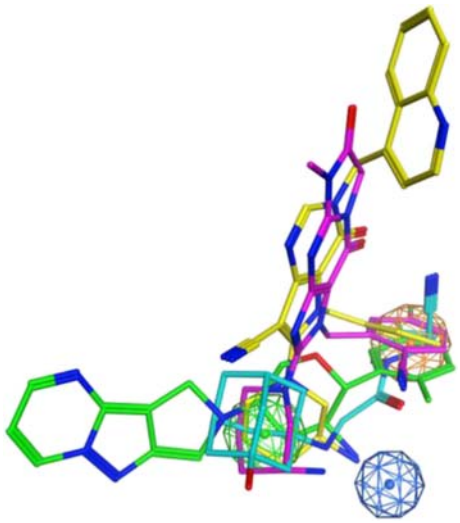

Fig. 11 Overlay of four DPP-IV inhibitors, taken from 5ism *(green)*, 5i7u *(magenta)*, 3w2t *(cyan)*, and (4a5s); only two hydrogen-bonding interactions and one hydrophobe are common to all four ligands. The set of ligands is from the category of moderate difficulty.[36]

3.09.6.2 Validation Standards

The standard sets discussed before are a good starting point but there is still more to be done. In stark contrast to protein–ligand docking, where construction of ever-more exacting test sets is almost a cottage industry, pharmacophore elucidation programs are typically validated on inadequate numbers of ligands, often with large common substructures. Sufficient protein–ligand series now exist in the PDB for this to be no longer excusable.[121,122] Admittedly, test-set construction is a harder task than for docking, since the detailed protein–ligand interactions in each test complex must be identified and properly understood. Nevertheless, test sets of reasonable size can and should be achieved. Of course, the obvious limitation of a validation protocol based on protein–ligand structures means that certain gene families of significant pharmaceutical interest (notably G-protein coupled receptor (GPCRs), ion channels, and transporters) will be under-represented, at least at present. The alternative approach, validation based on retrospective virtual screening experiments, is therefore very popular. As evidenced from the surfeit of papers on this topic there continues to be much debate concerning the "best" way to perform such experiments, from construction of the data set to what performance metric to employ. One major drawback of such studies compared to validation based on 3D structure is that they are indirect; the right answer may be found for the wrong reasons. The challenge is that "real" drug discovery is not so easily quantified and that true success (i.e., that a compound identified by virtual screening leads to a development candidate, let alone a marketed drug) is extremely rare.

3.09.6.3 Pharmacophore Feature Representation

Feature representation has probably had less attention recently than it deserves. With the exception of field-based methods, most programs use features that differ little from those described over a decade ago by Greene et al.[30] While acknowledging the seminal nature of that work, some questions can be posed. Some programs perform a surface-accessibility check before placing hydrophobic points, making the algorithm conformation dependent and hence slower. Is the extra computation justified? Most programs offer positive and negative feature types. Is this necessary, or is the hydrogen-bond similarity method of Jones et al.[18] or the EHT model[44] a better alternative? How important is it to align aromatic ring normals, and, if it is important, is it equally vital to achieve coplanarity of peptide and other groups that are hydrophobic in some directions but not in others (or is that achieved as a by-product of matching the hydrogen-bonding features of such groups)? Is it sensible to generate alignments by least-squares superposition of virtual points, placed along lone-pair or donor-hydrogen directions at the "expected" positions of the complementary protein atoms? It may assume greater hydrogen-bond directionality than exists in practice, especially given that the protein may flex a little from one ligand complex to another. Also, the situation that virtual points aim to deal with (**Fig. 3A**) may be quite rare.

One important observation in protein–ligand docking is that greatly improved results can often be obtained if the user's knowledge of the problem in hand can be exploited (e.g., by allowing constraints to be set). The same tactic can be similarly advantageous in pharmacophore analysis. For example, most programs do not have a separate "metal-coordinator" feature type, effectively assuming that the hydrogen-bond acceptor feature will be a suitable proxy. This assumption can break down, as in the case of the thiol-containing ligands. Thiol is a very weak hydrogen-bond acceptor but a good coordinator of zinc, which normally induces it to deprotonate. A user, aware that the target protein contains zinc, will obtain better results by overriding the usual program behavior and ensuring that the importance of this group is taken properly into account. This customization is becoming easier and more common.

One problem with ad hoc feature definition is that it causes difficulty at the searching stage, since databases are normally constructed with precomputed features, and screens based on those features. These are likely to be rendered useless if the query

contains features assigned according to different rules. Nevertheless, on-the-fly feature assignment on large databases, and searches of unscreened or poorly screened databases, are not impossible. It is perhaps better to get a good answer slowly than a bad answer quickly.

3.09.6.4 Variable Binding Modes

One limitation of the pharmacophore elucidation programs in common use is the assumption of a common binding mode for the ligands in the data set. Some relaxation of this requirement may be permitted (e.g., some compounds can match a subset of the common features) but data sets where the ligands correspond to two or more nonoverlapping pharmacophores will prove difficult or impossible. In addition, the nature of the algorithms can restrict the application of current methods to rather small data sets. Insofar as this may therefore result in a careful examination of the ligand structures, their activities and mechanism of action, such limitations may be considered valuable. However, in an era when large volumes of data can be generated using automated screening technologies it is useful to have tools that can not only deal with larger sets but can also cope with the possibility of multiple binding modes. Some of the QSAR methods, particularly those based on pharmacophore keys, are able in part to accommodate such situations; more recent pharmacophore elucidation methods are also designed to deal with multiple binding modes whilst also retaining the link to the underlying 3D models.

3.09.6.5 The Future: Maximizing the Value of Pharmacophore Methods

We have alluded to a number of challenges in the course of this article and have highlighted some areas for improvement. Nevertheless, it is undoubtedly true that the pharmacophore concept has proved to be an extremely useful one over the past 40 or so years. In part this is due to its simplicity, enabling the complexities of the molecular interaction between ligand and receptor (with attendant solvent, ions, cell membranes, etc.) to be reduced to a handful of features in a geometrical relationship. As such, it is perhaps surprising that it works at all. Pharmacophore methods are now commonly used as part of more complex workflows, for example as a prefilter prior to protein–ligand docking. The development of MD-based pharmacophores is particularly exciting.[149,150] Such workflows will continue to be further refined, driven by the continued growth in the number of protein structures of pharmaceutical relevance. It should also not be forgotten that integral membrane proteins (GPCRs, ion channels, and transporters) constitute many of the targets where pharmacophore analysis has been successfully applied for many years. Recent advances in X-ray structure determination for these families of proteins are providing new insights but it is likely to take some years before we achieve sufficient breadth of coverage and depth of understanding (especially of the more complex mechanisms of action) that will truly enable structure-based design techniques. Until then, simpler models as embodied in the pharmacophore concept will continue to play a key role.

So far as lead discovery is concerned, why not just use HTS? There can be a naïve expectation that HTS will return all known actives. However, HTS will miss some compounds for a number of good experimental reasons. It may also return too many false positives. Pharmacophore analysis is more hypothesis-driven and is intended to target small regions of chemical space for novel chemical matter; this can be of particular value when trying to accelerate lead discovery (e.g., by screening a small focused set prior to running a HTS) or when the available assay has low throughput. More importantly, pharmacophore methods can be used to search virtual chemical space, both in the form of known but not yet executed chemistry[177] and in the form of compounds unavailable in-house but (for example) accessible from a compound vendor. It can also be used to suggest focused screens after an HTS campaign. Corporate archives have a significant turnover of compounds over time. If the issues of a chemotype undergoing optimization only come to light years after the HTS campaign, pharmacophore models can be very useful to identify novel chemical matter to be screened in the lower capacity project-based screens.

It is now 4 decades since the modern-day concept of 3D pharmacophores was first introduced as a concept to explain SARs. It did not take long for scientists to appreciate the potential applications in drug discovery,[178] since when there has been a continuous stream of publications describing its use in the selection and design of new chemical entities with interesting pharmacological properties, a trend that continues until the present day. It is truly a concept that has stood the test of time, and one that is likely to play an important role in drug discovery for many more years to come.

Acknowledgments

We would like to thank our many colleagues in Novartis who have discussed, read, and commented on this manuscript.

References

1. Van Drie, J. H. Monty Kier and the Origin of the Pharmacophore Concept. *Int. Electron. J. Mol. Des.* **2007,** *6* (9), 271–279.
2. Mason, J. S.; Good, A. C.; Martin, E. J. 3-D Pharmacophores in Drug Discovery. *Curr. Pharm. Des.* **2001,** *7* (7), 567–597.
3. Kier, L. B. Molecular Orbital Calculation of Preferred Conformations of Acetylcholine, Muscarine, and Muscarone. *Mol. Pharmacol.* **1967,** *3* (5), 487–494.
4. Kier, L. B. The Preferred Conformations of Ephedrine Isomers and the Nature of the Alpha Adrenergic Receptor. *J. Pharmacol. Exp. Ther.* **1968,** *164* (1), 75–81.
5. Kier, L. B.; Danielli, J. F.; Moran, J. F.; Triggle, D. J. *Fundamental Concepts in Drug-Receptor Interactions;* Academic Press: New York, 1970.

6. Ehrlich, P. Über Den Jetzigen Stand Der Chemotherapie. *Ber. Dtsch. Chem. Ges.* **1909,** *42* (1), 17–47.
7. Wermuth, C. G.; Ganellin, C. R.; Lindberg, P.; Mitscher, L. A. Glossary of Terms Used in Medicinal Chemistry (IUPAC Recommendations 1998). *Pure Appl. Chem.* **1998,** *70* (5), 1129–1143.
8. Allen, F. H. The Cambridge Structural Database: A Quarter of a Million Crystal Structures and Rising. *Acta Crystallogr. Sect. B: Struct. Sci.* **2002,** *58,* 380–388.
9. Marshall, G. R.; Barry, C. D.; Bosshard, H. E.; Dammkoehler, R. A.; Dunn, D. A. The Conformational Parameter in Drug Design: The Active Analog Approach. In *Computer–Assisted Drug Design;* American Chemical Society: Columbus, OH, 1979; pp 205–226.
10. Mayer, D.; Naylor, C. B.; Motoc, I.; Marshall, G. R. A Unique Geometry of the Active Site of Angiotensin-Converting Enzyme Consistent With Structure-Activity Studies. *J. Comput. Aided Mol. Des.* **1987,** *1* (1), 3–16.
11. Bissantz, C.; Kuhn, B.; Stahl, M. A Medicinal Chemist's Guide to Molecular Interactions. *J. Med. Chem.* **2010,** *53,* 5061–5084.
12. van Drie, J. H. Pharmacophore Discovery—Lessons Learned. *Curr. Pharm. Des.* **2003,** *9,* 1649–1664.
13. Langer, T.; Laggner, C.; Rollinger, J. M.; Stuppner, H. Pharmacophore-Based Screening for the Successful Identification of Bio-Active Natural Products. *Chimia* **2007,** *61,* 350–354.
14. Cho, S. J.; Sun, Y. X. FLAME: A Program to Flexibly Align Molecules. *J. Chem. Inf. Model.* **2006,** *46* (1), 298–306.
15. Martin, Y. C. Pharmacophore Modeling: 1 —Methods. In *Comprehensive Medicinal Chemistry II, Computer-Assisted Drug Design,* Vol. 4, Mason, J. S., Ed.; Elsevier: Amsterdam, 2007; pp 119–147.
16. Martin, Y. C. Pharmacophore Modeling: 2 —Applications. In *Comprehensive Medicinal Chemistry II, Computer-Assisted Drug Design,* Vol. 4, Mason, J. S., Ed.; Elsevier: Amsterdam, 2007; pp 515–536.
17. Bagdanoff, J. T.; Xu, Y.; Dollinger, G.; Martin, E. Effect of Chirality on Common in vitro Experiments: An Enantiomeric Pair Analysis. *J. Med. Chem.* **2015,** *58* (15), 5781–5788.
18. Kratz, J. M.; Schuster, D.; Edtbauer, M.; Saxena, P.; Mair, C. E.; Kirchebner, J.; Matuszczak, B.; Baburin, I.; Hering, S.; Rollinger, J. M. Experimentally Validated hERG Pharmacophore Models as Cardiotoxicity Prediction Tools. *J. Chem. Inf. Model.* **2014,** *54* (10), 2887–2901.
19. Waltenberger, B.; Garscha, U.; Temml, V.; Liers, J.; Werz, O.; Schuster, D.; Stuppner, H. Discovery of Potent Soluble Epoxide Hydrolase (sEH) Inhibitors by Pharmacophore-Based Virtual Screening. *J. Chem. Inf. Model.* **2016,** *56* (4), 747–762.
20. Stiefl, N.; Watson, T. A.; Baumann, K.; Zaliani, A. ErG: 2D Pharmacophore Descriptions for Scaffold Hopping. *J. Chem. Inf. Model.* **2006,** *46* (1), 208–220.
21. Barnum, D.; Greene, J.; Smellie, A.; Sprague, P. Identification of Common Functional Configurations Among Molecules. *J. Chem. Inf. Comput. Sci.* **1996,** *36,* 563–571.
22. Richmond, N. J.; Abrams, C. A.; Wolohan, P. R. N.; Abrahamian, E.; Willett, P.; Clark, R. D. GALAHAD: 1. Pharmacophore Identification by Hypermolecular Alignment of Ligands in 3D. *J. Comput. Aided Mol. Des.* **2006,** *20,* 567–587.
23. Jones, G.; Willett, P.; Glen, R. C. GASP: Genetic Algorithm Superimposition Program. In vol. 2; International University Line: La Jolla, CA, 2000; pp 85–107.
24. *MOE*; Chemical Computing Group: 1010 Sherbrooke St. W, Suite 910 Montreal, Quebec, Canada.
25. Cross, S.; Baroni, M.; Goracci, L.; Cruciani, G. GRID-Based Three-Dimensional Pharmacophores I: FLAPpharm, A Novel Approach for Pharmacophore Elucidation. *J. Chem. Inf. Model.* **2012,** *52* (10), 2587–2598.
26. Dixon, S. L.; Smondyrev, A. M.; Knoll, E. H.; Rao, S. N.; Shaw, D. E.; Friesner, R. A. PHASE: A New Engine for Pharmacophore Perception, 3D QSAR Model Development, and 3D Database Screening: 1. Methodology and Preliminary Results. *J. Comput. Aided Mol. Des.* **2006,** *20* (10–11), 647–671.
27. Anghelescu, A. V.; DeLisle, R. K.; Lowrie, J. F.; Klon, A. E.; Xie, X.; Diller, D. J. Technique for Generating Three-Dimensional Alignments of Multiple Ligands From One-Dimensional Alignments. *J. Chem. Inf. Model.* **2008,** *48* (5), 1041–1054.
28. Feng, J.; Sanil, A.; Young, S. S. PharmID: Pharmacophore Identification Using Gibbs Sampling. *J. Chem. Inf. Model.* **2006,** *46* (3), 1352–1359.
29. Marialke, J.; Korner, R.; Tietze, S.; Apostolakis, J. Graph-Based Molecular Alignment (GMA). *J. Chem. Inf. Model.* **2007,** *47* (2), 591–601.
30. Zhu, F.; Agrafiotis, D. K. Recursive Distance Partitioning Algorithm for Common Pharmacophore Identification. *J. Chem. Inf. Model.* **2007,** *47* (4), 1619–1625.
31. Podolyan, Y.; Karypis, G. Common Pharmacophore Identification Using Frequent Clique Detection Algorithm. *J. Chem. Inf. Model.* **2009,** *49* (1), 13–21.
32. Todorov, N. P.; Alberts, I. L.; de Esch, I. J. P.; Dean, P. M. QUASI: A Novel Method for Simultaneous Superposition of Multiple Flexible Ligands and Virtual Screening Using Partial Similarity. *J. Chem. Inf. Model.* **2007,** *47* (3), 1007–1020.
33. Dai, S.-X.; Li, G.-H.; Gao, Y.-D.; Huang, J.-F. Pharmacophore-Map-Pick: A Method to Generate Pharmacophore Models for All Human GPCRs. *Mol. Inf.* **2015,** *35* (2), 81–91.
34. Fidom, K.; Isberg, V.; Hauser, A. S.; Mordalski, S.; Lehto, T.; Bojarski, A. J.; Gloriam, D. E. A New Crystal Structure Fragment-Based Pharmacophore Method for G Protein-Coupled Receptors. *Methods* **2015,** *71,* 104–112.
35. Moser, D.; Wittmann, S. K.; Kramer, J.; Blöcher, R.; Achenbach, J.; Pogoryelov, D.; Proschak, E. PENG: A Neural Gas-Based Approach for Pharmacophore Elucidation. Method Design, Validation, and Virtual Screening for Novel Ligands of LTA4H. *J. Chem. Inf. Model.* **2015,** *55* (2), 284–293.
36. Giangreco, I.; Olsson, T. S. G.; Cole, J. C.; Packer, M. J. Assessment of a Cambridge Structural Database-Driven Overlay Program. *J. Chem. Inf. Model.* **2014,** *54* (11), 3091–3098.
37. Martins, J. P. A.; Barbosa, E. G.; Pasqualoto, K. F. M.; Ferreira, M. M. C. LQTA-QSAR: A New 4D-QSAR Methodology. *J. Chem. Inf. Model.* **2009,** *49* (6), 1428–1436.
38. Taminau, J.; Thijs, G.; De Winter, H. Pharao: Pharmacophore Alignment and Optimization. *J. Mol. Graph. Model.* **2008,** *27* (2), 161–169.
39. Greene, J.; Kahn, S.; Savoj, H.; Sprague, P.; Teig, S. Chemical Function Queries for 3D Database Search. *J. Chem. Inf. Comput. Sci.* **1994,** *34* (6), 1297–1308.
40. Wolber, G.; Seidel, T.; Bendix, F.; Langer, T. Molecule-Pharmacophore Superpositioning and Pattern Matching in Computational Drug Design. *Drug Discov. Today* **2008,** *13* (1), 23–29.
41. Fersht, A. *Structure and Mechanism in Protein Science: A Guide to Enzyme Catalysis and Protein Folding;* W. H. Freeman and Company: New York, 1999.
42. Kerdawy, A. El; Tautermann, C. S.; Clark, T.; Fox, T. Economical and Accurate Protocol for Calculating Hydrogen-Bond-Acceptor Strengths. *J. Chem. Inf. Model.* **2013,** *53* (12), 3262–3272.
43. Kenny, P. W.; Montanari, C. A.; Prokopczyk, I. M.; Ribeiro, J. F. R.; Sartori, G. R. Hydrogen Bond Basicity Prediction for Medicinal Chemistry Design. *J. Med. Chem.* **2016,** *59* (9), 4278–4288.
44. Gerber, P. R. Charge Distribution From a Simple Molecular Orbital Type Calculation and Non-Bonding Interaction Terms in the Force Field MAB. *J. Comput. Aided Mol. Des.* **1998,** *12* (1), 37–51.
45. Schneider, N.; Hindle, S.; Lange, G.; Klein, R.; Albrecht, J.; Briem, H.; Beyer, K.; Claußen, H.; Gastreich, M.; Lemmen, C. Substantial Improvements in Large-Scale Redocking and Screening Using the Novel HYDE Scoring Function. *J. Comput. Aided Mol. Des.* **2012,** *26* (6), 701–723.
46. Abel, R.; Young, T.; Farid, R.; Berne, B. J.; Friesner, R. A. Role of the Active-Site Solvent in the Thermodynamics of Factor Xa Ligand Binding. *J. Am. Chem. Soc.* **2008,** *130* (9), 2817–2831.
47. Bayden, A. S.; Moustakas, D. T.; Joseph-McCarthy, D.; Lamb, M. L. Evaluating Free Energies of Binding and Conservation of Crystallographic Waters Using SZMAP. *J. Chem. Inf. Model.* **2015,** *55* (8), 1552–1565.
48. Bortolato, A.; Tehan, B. G.; Bodnarchuk, M. S.; Essex, J. W.; Mason, J. S. Water Network Perturbation in Ligand Binding: Adenosine A2A Antagonists as a Case Study. *J. Chem. Inf. Model.* **2013,** *53* (7), 1700–1713.
49. Hu, X.; Hu, Y.; Vogt, M.; Stumpfe, D.; Bajorath, J. MMP-Cliffs: Systematic Identification of Activity Cliffs on the Basis of Matched Molecular Pairs. *J. Chem. Inf. Model.* **2012,** *52* (5), 1138–1145.
50. Milletti, F.; Vulpetti, A. Tautomer Preference in PDB Complexes and Its Impact on Structure-Based Drug Discovery. *J. Chem. Inf. Model.* **2010,** *50,* 1062–1074.
51. Milletti, F.; Storchi, L.; Sforna, G.; Cross, S.; Cruciani, G. Tautomer Enumeration and Stability Prediction for Virtual Screening on Large Chemical Databases. *J. Chem. Inf. Model.* **2009,** *49* (1), 68–75.
52. Milletti, F.; Storchi, L.; Sforna, G.; Cruciani, G. New and Original pK(a) Prediction Method Using Grid Molecular Interaction Fields. *J. Chem. Inf. Model.* **2007,** *47,* 2172–2181.

53. Oellien, F.; Cramer, J.; Beyer, C.; Ihlenfeldt, W. D.; Selzer, P. M. The Impact of Tautomer Forms on Pharmacophore-Based Virtual Screening. *J. Chem. Inf. Model.* **2006,** *46* (6), 2342–2354.
54. Martin, Y. C. Overview of the Perspectives Devoted to Tautomerism in Molecular Design. *J. Comput. Aided Mol. Des.* **2010,** *24* (6), 473–474.
55. Katritzky, A. R.; Hall, C. D.; El-Gendy, B. E.-D. M.; Draghici, B. Tautomerism in Drug Discovery. *J. Comput. Aided Mol. Des.* **2010,** *24* (6), 475–484.
56. Sayle, R. A. So You Think You Understand Tautomerism? *J. Comput. Aided Mol. Des.* **2010,** *24* (6), 485–496.
57. Sitzmann, M.; Ihlenfeldt, W.-D.; Nicklaus, M. C. Tautomerism in Large Databases. *J. Comput. Aided Mol. Des.* **2010,** *24* (6), 521–551.
58. Yesselman, J. D.; Horowitz, S.; Brooks, C. L.; Trievel, R. C. Frequent Side Chain Methyl Carbon-Oxygen Hydrogen Bonding in Proteins Revealed by Computational and Stereochemical Analysis of Neutron Structures. *Proteins: Struct., Funct., Bioinf.* **2015,** *83* (3), 403–410.
59. Bohm, H. J.; Brode, S.; Hesse, U.; Klebe, G. Oxygen and Nitrogen in Competitive Situations—Which Is the Hydrogen-Bond Acceptor. *Chem. Eur. J.* **1996,** *2* (12), 1509–1513.
60. Fleming, F. F.; Yao, L.; Ravikumar, P. C.; Funk, L.; Shook, B. C. Nitrile-Containing Pharmaceuticals: Efficacious Roles of the Nitrile Pharmacophore. *J. Med. Chem.* **2010,** *53* (22), 7902–7917.
61. Dalvit, C.; Vulpetti, A. Fluorine-Protein Interactions and 19F NMR Isotropic Chemical Shift: An Empirical Correlation. *ChemMedChem* **2011,** *6,* 104–114.
62. Wilcken, R.; Zimmermann, M. O.; Lange, A.; Zahn, S.; Boeckler, F. M. Using Halogen Bonds to Address the Protein Backbone: A Systematic Evaluation. *J. Comput. Aided Mol. Des.* **2012,** *26* (8), 935–945.
63. Wilcken, R.; Zimmermann, M. O.; Lange, A.; Joerger, A. C.; Boeckler, F. M. Principles and Applications of Halogen Bonding in Medicinal Chemistry and Chemical Biology. *J. Med. Chem.* **2013,** *56* (4), 1363–1388.
64. Choi-Sledeski, Y. M.; Kearney, R.; Poli, G.; Pauls, H.; Gardner, C.; Gong, Y.; Becker, M.; Davis, R.; Spada, A.; Liang, G.; Chu, V.; Brown, K.; Collussi, D.; Leadley, R.; Rebello, S.; Moxey, P.; Morgan, S.; Bentley, R.; Kasiewski, C.; Maignan, S.; Guilloteau, J. P.; Mikol, V. Discovery of an Orally Efficacious Inhibitor of Coagulation Factor Xa Which Incorporates a Neutral P-1 Ligand. *J. Med. Chem.* **2003,** *46,* 681–684.
65. Maignan, S.; Guilloteau, J. P.; Choi-Sledski, Y. M.; Becker, M. R.; Ewing, W. R.; Pauls, H. W.; Spada, A. P.; Mikol, V. Molecular Structures of Human Factor Xa Complexed With Ketopiperazine Inhibitors: Preference for a Neutral Group in the S1 Pocket. *J. Med. Chem.* **2003,** *46* (5), 685–690.
66. Astles, P. C.; Brown, T. J.; Halley, F.; Handscombe, C. M.; Harris, N. V.; Majid, T. N.; McCarthy, C.; McLay, I. M.; Morley, A.; Porter, B.; Roach, A. G.; Sargent, C.; Smith, C.; Walsh, R. J. Selective ET(A) Antagonists. 5. Discovery and Structure-Activity Relationships of Phenoxyphenylacetic Acid Derivatives. *J. Med. Chem.* **2000,** *43* (5), 900–910.
67. Bruno, I. J.; Cole, J. C.; Lommerse, J. P. M.; Rowland, R. S.; Taylor, R.; Verdonk, M. L. Isostar—A Library of Information About Nonbonded Interactions. *J. Comput. Aided Mol. Des.* **1997,** *11,* 525–537.
68. Chau, P. L.; Dean, P. M. Electrostatic Complementarity Between Proteins and Ligands. 2. Ligand Moieties. *J. Comput. Aided Mol. Des.* **1994,** *8,* 527–544.
69. Abraham, M. H.; Ibrahim, A.; Zissimos, A. M.; Zhao, Y. H.; Comer, J.; Reynolds, D. P. Application of Hydrogen Bonding Calculations in Property Based Drug Design. *Drug Discov. Today* **2002,** *7* (20), 1056–1063.
70. Laurence, C.; Brameld, K. A.; Graton, J.; Le Questel, J.-Y.; Renault, E. The pKBHX Database: Toward a Better Understanding of Hydrogen-Bond Basicity for Medicinal Chemists. *J. Med. Chem.* **2009,** *52* (14), 4073–4086.
71. Ahmed, A.; Choo, H.; Cho, Y. S.; Park, W.-K.; Pae, A. N. Identification of Novel Serotonin 2C Receptor Ligands by Sequential Virtual Screening. *Bioorg. Med. Chem.* **2009,** *17* (13), 4559–4568.
72. Cheeseright, T. J.; Mackey, M. D.; Melville, J. L.; Vinter, J. G. FieldScreen: Virtual Screening Using Molecular Fields. Application to the DUD Data Set. *J. Chem. Inf. Model.* **2008,** *48* (11), 2108–2117.
73. Martin, Y. C. DISCO: What We Did Right and What We Missed. In *Pharmacophore Perception, Development, and Use in Drug Design;* International University Line: La Jolla, CA, 2000; pp 51–66.
74. Lu, Y.; Shi, T.; Wang, Y.; Yang, H.; Yan, X.; Luo, X.; Jiang, H.; Zhu, W. Halogen Bonding—A Novel Interaction for Rational Drug Design? *J. Med. Chem.* **2009,** *52* (9), 2854–2862.
75. Xu, Z.; Liu, Z.; Chen, T.; Chen, T.; Wang, Z.; Tian, G.; Shi, J.; Wang, X.; Lu, Y.; Yan, X.; Wang, G.; Jiang, H.; Chen, K.; Wang, S.; Xu, Y.; Shen, J.; Zhu, W. Utilization of Halogen Bond in Lead Optimization: A Case Study of Rational Design of Potent Phosphodiesterase Type 5 (PDE5) Inhibitors. *J. Med. Chem.* **2011,** *54* (15), 5607–5611.
76. Markt, P.; McGoohan, C.; Walker, B.; Kirchmair, J.; Feldmann, C.; Martino, G. D.; Spitzer, G.; Distinto, S.; Schuster, D.; Wolber, G.; Laggner, C.; Langer, T. Discovery of Novel Cathepsin S Inhibitors by Pharmacophore-Based Virtual High-Throughput Screening. *J. Chem. Inf. Model.* **2008,** *48* (8), 1693–1705.
77. Cross, S.; Cruciani, G. Molecular Fields in Drug Discovery: Getting Old or Reaching Maturity? *Drug Discov. Today* **2010,** *15,* 23–32.
78. Nicholls, A.; McGaughey, G. B.; Sheridan, R. P.; Good, A. C.; Warren, G.; Mathieu, M.; Muchmore, S. W.; Brown, S. P.; Grant, J. A.; Haigh, J. A.; Nevins, N.; Jain, A. N.; Kelley, B. Molecular Shape and Medicinal Chemistry: A Perspective. *J. Med. Chem.* **2010,** *53* (10), 3862–3886.
79. Nissink, J. W. M.; Verdonk, M. L.; Klebe, G. Simple Knowledge-Based Descriptors to Predict Protein-Ligand Interactions. Methodology and Validation. *J. Comput. Aided Mol. Des.* **2000,** *14* (8), 787–803.
80. Pastor, M.; Cruciani, G.; McLay, I.; Pickett, S.; Clementi, S. GRid-INdependent Descriptors (GRIND): A Novel Class of Alignment-Independent Three-Dimensional Molecular Descriptors. *J. Med. Chem.* **2000,** *43* (17), 3233–3243.
81. Cratteri, P.; Romanelli, M. N.; Cruciani, G.; Bonaccini, C.; Melani, F. GRIND-Derived Pharmacophore Model for a Series of Alpha-Tropanyl Derivative Ligands of the Sigma-2 Receptor. *J. Comput. Aided Mol. Des.* **2004,** *18* (5), 361–374.
82. Durán, Á.; Martínez, G. C.; Pastor, M. Development and Validation of AMANDA, A New Algorithm for Selecting Highly Relevant Regions in Molecular Interaction Fields. *J. Chem. Inf. Model.* **2008,** *48* (9), 1813–1823.
83. Vinter, J. G. Extended Electron Distributions Applied to the Molecular Mechanics of Some Intermolecular Interactions. *J. Comput. Aided Mol. Des.* **1994,** *8* (6), 653–668.
84. Cheeseright, T.; Mackey, M.; Rose, S.; Vinter, A. Molecular Field Extrema as Descriptors of Biological Activity: Definition and Validation. *J. Chem. Inf. Model.* **2006,** *46* (2), 665–676.
85. Thorner, D. A.; Wild, D. J.; Willett, P.; Wright, P. M. Similarity Searching in Files of Three-Dimensional Chemical Structures: Flexible Field-Based Searching of Molecular Electrostatic Potentials. *J. Chem. Inf. Comput. Sci.* **1996,** *36* (4), 900–908.
86. Jewell, N. E.; Turner, D. B.; Willett, P.; Sexton, G. J. Automatic Generation of Alignments for 3D QSAR Analyses. *J. Mol. Graph. Model.* **2001,** *20* (2), 121.
87. Cheeseright, T.; Mackey, M.; Rose, S.; Vinter, A. Molecular Field Technology Applied to Virtual Screening and Finding the Bioactive Conformation. *Expert Opin. Drug Discovery* **2007,** *2* (1), 131–144.
88. Wolber, G.; Dornhofer, A. A.; Langer, T. Efficient Overlay of Small Organic Molecules Using 3D Pharmacophores. *J. Comput. Aided Mol. Des.* **2006,** *20* (12), 773–788.
89. Bostrom, J.; Greenwood, J. R.; Gottfries, J. Assessing the Performance of OMEGA With Respect to Retrieving Bioactive Conformations. *J. Mol. Graph. Model.* **2003,** *21* (5), 449–462.
90. Perola, E.; Charifson, P. S. Conformational Analysis of Drug-Like Molecules Bound to Proteins: An Extensive Study of Ligand Reorganization Upon Binding. *J. Med. Chem.* **2004,** *47* (10), 2499–2510.
91. Agrafiotis, D. K.; Gibbs, A. C.; Zhu, F.; Izrailev, S.; Martin, E. Conformational Sampling of Bioactive Molecules: A Comparative Study. *J. Chem. Inf. Model.* **2007,** *47* (3), 1067–1086.
92. Chen, I.-J.; Foloppe, N. Drug-Like Bioactive Structures and Conformational Coverage With the LigPrep/ConfGen Suite: Comparison to Programs MOE and Catalyst. *J. Chem. Inf. Model.* **2010,** *50* (5), 822–839.
93. Chen, I.-J.; Foloppe, N. Conformational Sampling of Druglike Molecules With MOE and Catalyst: Implications for Pharmacophore Modeling and Virtual Screening. *J. Chem. Inf. Model.* **2008,** *48* (9), 1773–1791.
94. Riniker, S.; Landrum, G. A. Better Informed Distance Geometry: Using What We Know to Improve Conformation Generation. *J. Chem. Inf. Model.* **2015,** *55* (12), 2562–2574.

95. Taylor, R.; Cole, J.; Korb, O.; McCabe, P. Knowledge-Based Libraries for Predicting the Geometric Preferences of Druglike Molecules. *J. Chem. Inf. Model.* **2014,** *54* (9), 2500–2514.
96. Liebeschuetz, J.; Hennemann, J.; Olsson, T.; Groom, C. R. The Good, the Bad and the Twisted: A Survey of Ligand Geometry in Protein Crystal Structures. *J. Comput. Aided Mol. Des.* **2012,** *26* (2), 169–183.
97. Martin, Y. C.; Bures, M. G.; Danaher, E. A.; Delazzer, J.; Lico, I.; Pavlik, P. A. A Fast New Approach to Pharmacophore Mapping and Its Application to Dopaminergic and Benzodiazepine Agonists. *J. Comput. Aided Mol. Des.* **1993,** *7,* 83–102.
98. Agrafiotis, D. K. A Constant Time Algorithm for Estimating the Diversity of Large Chemical Libraries. *J. Chem. Inf. Comput. Sci.* **2001,** *41* (1), 159–167.
99. Tosco, P.; Balle, T.; Shiri, F. Open3DALIGN: An Open-Source Software Aimed at Unsupervised Ligand Alignment. *J. Comput. Aided Mol. Des.* **2011,** *25* (8), 777–783.
100. Ebejer, J.-P.; Morris, G. M.; Deane, C. M. Freely Available Conformer Generation Methods: How Good Are They? *J. Chem. Inf. Model.* **2012,** *52* (5), 1146–1158.
101. Korb, O.; Kuhn, B.; Hert, J.; Taylor, N.; Cole, J.; Groom, C.; Stahl, M. Interactive and Versatile Navigation of Structural Databases. *J. Med. Chem.* **2016,** *59* (9), 4257–4266.
102. Labute, P.; Williams, C.; Feher, M.; Sourial, E.; Schmidt, J. M. Flexible Alignment of Small Molecules. *J. Med. Chem.* **2001,** *44* (10), 1483–1490.
103. Cottrell, S. J.; Gillet, V. J.; Taylor, R. Incorporating Partial Matches Within Multiobjective Pharmacophore Identification. *J. Comput. Aided Mol. Des.* **2006,** *20* (12), 735–749.
104. McGann, M.; Nicholls, A.; Enyedy, I. The Statistics of Virtual Screening and Lead Optimization. *J. Comput. Aided Mol. Des.* **2015,** *29* (10), 923–936.
105. Kristam, R.; Gillet, V. J.; Lewis, R. A.; Thorner, D. Comparison of Conformational Analysis Techniques to Generate Pharmacophore Hypotheses Using Catalyst. *J. Chem. Inf. Model.* **2005,** *45* (2), 461–476.
106. Jain, A. N.; Nicholls, A. Recommendations for Evaluation of Computational Methods. *J. Comput. Aided Mol. Des.* **2008,** *22* (3), 133–139.
107. Hawkins, P. C. D.; Warren, G. L.; Skillman, A. G.; Nicholls, A. How to Do an Evaluation: Pitfalls and Traps. *J. Comput. Aided Mol. Des.* **2008,** *22* (3), 191–192.
108. Good, A. C.; Oprea, T. I. Optimization of CAMD Techniques 3. Virtual Screening Enrichment Studies: A Help or Hindrance in Tool Selection? *J. Comput. Aided Mol. Des.* **2008,** *22* (3), 169–178.
109. Truchon, J. F.; Bayly, C. I. Evaluating Virtual Screening Methods: Good and Bad Metrics for the "Early Recognition" Problem. *J. Chem. Inf. Model.* **2007,** *47* (2), 488–508.
110. Good, A. C.; Hermsmeier, M. A.; Hindle, S. A. Measuring CAMD Technique Performance: A Virtual Screening Case Study in the Design of Validation Experiments. *J. Comput. Aided Mol. Des.* **2004,** *18* (7), 529–536.
111. Mackey, M. D.; Melville, J. L. Better than Random? The Chemotype Enrichment Problem. *J. Chem. Inf. Model.* **2009,** *49* (5), 1154–1162.
112. Huang, N.; Shoichet, B. K.; Irwin, J. J. Benchmarking Sets for Molecular Docking. *J. Med. Chem.* **2006,** *49* (23), 6789–6801.
113. Mysinger, M. M.; Carchia, M.; Irwin, J. J.; Shoichet, B. K. Directory of Useful Decoys, Enhanced (DUD-E): Better Ligands and Decoys for Better Benchmarking. *J. Med. Chem.* **2012,** *55* (14), 6582–6594.
114. A Database of Useful Decoys—Enhanced. http://dude.docking.org/.
115. Rohrer, S. G.; Baumann, K. Maximum Unbiased Validation (MUV) Data Sets for Virtual Screening Based on PubChem Bioactivity Data. *J. Chem. Inf. Model.* **2009,** *49* (2), 169–184.
116. Pradon, J. A. New Approach for Chemotype Enrichment in Ligand Based Design. http://www.ukqsar.org/slides/JuliettePradon_A2010.pdf.
117. Spitzer, G. M.; Heiss, M.; Mangold, M.; Markt, P.; Kirchmair, J.; Wolber, G.; Liedl, K. R. One Concept, Three Implementations of 3D Pharmacophore-Based Virtual Screening: Distinct Coverage of Chemical Search Space. *J. Chem. Inf. Model.* **2010,** *50* (7), 1241–1247.
118. Evans, D. A.; Doman, T. N.; Thorner, D. A.; Bodkin, M. J. 3D QSAR Methods: Phase and Catalyst Compared. *J. Chem. Inf. Model.* **2007,** *47* (3), 1248–1257.
119. Hartshorn, M. J.; Verdonk, M. L.; Chessari, G.; Brewerton, S. C.; Mooij, W. T. M.; Mortenson, P. N.; Murray, C. W. Diverse, High-Quality Test Set for the Validation of Protein-Ligand Docking Performance. *J. Med. Chem.* **2007,** *50* (4), 726–741.
120. Patel, Y.; Gillet, V. J.; Bravi, G.; Leach, A. R. A Comparison of the Pharmacophore Identification Programs: Catalyst, DISCO and GASP. *J. Comput. Aided Mol. Des.* **2002,** *16* (8–9), 653–681.
121. Cross, S.; Ortuso, F.; Baroni, M.; Costa, G.; Distinto, S.; Moraca, F.; Alcaro, S.; Cruciani, G. GRID-Based Three-Dimensional Pharmacophores II: PharmBench, a Benchmark Data Set for Evaluating Pharmacophore Elucidation Methods. *J. Chem. Inf. Model.* **2012,** *52* (10), 2599–2608.
122. Giangreco, I.; Cosgrove, D. A.; Packer, M. J. An Extensive and Diverse Set of Molecular Overlays for the Validation of Pharmacophore Programs. *J. Chem. Inf. Model.* **2013,** *53* (4), 852–866.
123. Scior, T.; Bender, A.; Tresadern, G.; Medina-Franco, J. L.; Martínez-Mayorga, K.; Langer, T.; Cuanalo-Contreras, K.; Agrafiotis, D. K. Recognizing Pitfalls in Virtual Screening: A Critical Review. *J. Chem. Inf. Model.* **2012,** *52* (4), 867–881.
124. Schneider, N.; Lange, G.; Hindle, S.; Klein, R.; Rarey, M. A Consistent Description of Hydrogen Bond and Dehydration Energies in Protein–Ligand Complexes: Methods Behind the HYDE Scoring Function. *J. Comput. Aided Mol. Des.* **2013,** *27* (1), 15–29.
125. Leung, C. S.; Leung, S. S. F.; Tirado-Rives, J.; Jorgensen, W. L. Methyl Effects on Protein–Ligand Binding. *J. Med. Chem.* **2012,** *55* (9), 4489–4500.
126. Martin, Y. C. 3D Database Searching in Drug Design. *J. Med. Chem.* **1992,** *35* (12), 2145–2154.
127. Clark, D. E.; Westhead, D. R.; Sykes, R. A.; Murray, C. W. Active-Site-Directed 3D Database Searching: Pharmacophore Extraction and Validation of Hits. *J. Comput. Aided Mol. Des.* **1996,** *10* (5), 397–416.
128. *Unity*; Tripos, Inc.: 1699 South Hanley Road, Suite 303, St Louis, MO 63144, 2003.
129. Hurst, T. Flexible 3D Searching: The Directed Tweak Technique. *J. Chem. Inf. Comput. Sci.* **1994,** *34* (1), 190–196.
130. Smellie, A.; Kahn, S. D.; Teig, S. L. Analysis of Conformational Coverage. 1. Validation and Estimation of Coverage. *J. Chem. Inf. Comput. Sci.* **1995,** *35* (2), 285–294.
131. Smellie, A.; Kahn, S. D.; Teig, S. L. Analysis of Conformational Coverage. 2. Applications of Conformational Models. *J. Chem. Inf. Comput. Sci.* **1995,** *35* (2), 295–304.
132. Rarey, M.; Dixon, J. S. Feature Trees: A New Molecular Similarity Measure Based on Tree Matching. *J. Comput. Aided Mol. Des.* **1998,** *12* (5), 471–490.
133. Barker, E. J.; Gardiner, E. J.; Gillet, V. J.; Kitts, P.; Morris, J. Further Development of Reduced Graphs for Identifying Bioactive Compounds. *J. Chem. Inf. Comput. Sci.* **2003,** *43* (2), 346–356.
134. Mason, J. S.; Morize, I.; Menard, P. R.; Cheney, D. L.; Hulme, C.; Labaudiniere, R. F. New 4-Point Pharmacophore Method for Molecular Similarity and Diversity Applications: Overview of the Method and Applications, Including a Novel Approach to the Design of Combinatorial Libraries Containing Privileged Substructures. *J. Med. Chem.* **1994,** *42,* 3251–3264.
135. Perruccio, F.; Mason, J. S.; Sciabola, S.; Baroni, M. FLAP: 4-Point Pharmacophore Fingerprints From GRID. In *Molecular Interaction Fields;* Wiley-VCH Verlag GmbH: Weinheim, 2005; pp 83–102.
136. Taylor, R.; Cole, J. C.; Cosgrove, D. A.; Gardiner, E. J.; Gillet, V. J.; Korb, O. Development and Validation of an Improved Algorithm for Overlaying Flexible Molecules. *J. Comput. Aided Mol. Des.* **2012,** *26* (4), 451–472.
137. von Korff, M.; Freyss, J.; Sander, T. Flexophore, a New Versatile 3D Pharmacophore Descriptor That Considers Molecular Flexibility. *J. Chem. Inf. Model.* **2008,** *48* (4), 797–810.
138. Good, A. C.; Lewis, R. A. New Methodology for Profiling Combinatorial Libraries and Screening Sets: Cleaning Up the Design Process With HARPick. *J. Med. Chem.* **1997,** *40* (24), 3926–3936.
139. McGregor, M. J.; Muskal, S. M. Pharmacophore Fingerprinting. 1. Application to QSAR and Focused Library Design. *J. Chem. Inf. Comput. Sci.* **1999,** *39* (3), 569–574.
140. Deanda, F.; Stewart, E. L. Application of the PharmPrint Methodology to Two Protein Kinases. *J. Chem. Inf. Comput. Sci.* **2004,** *44* (5), 1803–1809.
141. Greenidge, P. A.; Carlsson, B.; Bladh, L.-G.; Gillner, M. Pharmacophores Incorporating Numerous Excluded Volumes Defined by X-Ray Crystallographic Structure in Three-Dimensional Database Searching: Application to the Thyroid Hormone Receptor. *J. Med. Chem.* **1998,** *41* (14), 2503–2512.
142. Tintori, C.; Corradi, V.; Magnani, M.; Manetti, F.; Botta, M. Targets Looking for Drugs: A Multistep Computational Protocol for the Development of Structure-Based Pharmacophores and Their Applications for Hit Discovery. *J. Chem. Inf. Model.* **2008,** *48* (11), 2166–2179.

143. Temml, V.; Voss, C. V.; Dirsch, V. M.; Schuster, D. Discovery of New Liver X Receptor Agonists by Pharmacophore Modeling and Shape-Based Virtual Screening. *J. Chem. Inf. Model.* **2014,** *54* (2), 367–371.
144. Specs compound library, http://www.specs.net.
145. Baroni, M.; Cruciani, G.; Sciabola, S.; Perruccio, F.; Mason, J. S. A Common Reference Framework for Analyzing/Comparing Proteins and Ligands. Fingerprints for Ligands and Proteins (FLAP): Theory and Application. *J. Chem. Inf. Model.* **2007,** *47* (2), 279–294.
146. Verdonk, M. L.; Cole, J. C.; Watson, P.; Gillet, V.; Willett, P. SuperStar: Improved Knowledge-Based Interaction Fields for Protein Binding Sites. *J. Mol. Biol.* **2001,** *307* (3), 841–859.
147. Wolber, G.; Langer, T. LigandScout: 3-D Pharmacophores Derived From Protein-Bound Ligands and Their Use as Virtual Screening Filters. *J. Chem. Inf. Model.* **2005,** *45* (1), 160–169.
148. Choudhury, C.; Priyakumar, U. D.; Sastry, G. N. Dynamics Based Pharmacophore Models for Screening Potential Inhibitors of Mycobacterial Cyclopropane Synthase. *J. Chem. Inf. Model.* **2015,** *55* (4), 848–860.
149. Wieder, M.; Perricone, U.; Boresch, S.; Seidel, T.; Langer, T. Evaluating the Stability of Pharmacophore Features Using Molecular Dynamics Simulations. *Biochem. Biophys. Res. Commun.* **2016,** *470* (3), 685–689.
150. Hu, B.; Lill, M. A. Protein Pharmacophore Selection Using Hydration-Site Analysis. *J. Chem. Inf. Model.* **2012,** *52* (4), 1046–1060.
151. Cruciani, G.; Carosati, E.; De, B. B.; Ethirajulu, K.; Mackie, C.; Howe, T.; Vianello, R. MetaSite: Understanding Metabolism in Human Cytochromes From the Perspective of the Chemist. *J. Med. Chem.* **2005,** *48* (22), 6970–6979.
152. Rydberg, P.; Rostkowski, M.; Gloriam, D. E.; Olsen, L. The Contribution of Atom Accessibility to Site of Metabolism Models for Cytochromes P450. *Mol. Pharm.* **2013,** *10* (4), 1216–1223.
153. Kuhn, D.; Weskamp, N.; Schmitt, S.; Hüllermeier, E.; Klebe, G. From the Similarity Analysis of Protein Cavities to the Functional Classification of Protein Families Using Cavbase. *J. Mol. Biol.* **2006,** *359* (4), 1023–1044.
154. Shatsky, M.; Shulman-Peleg, A.; Nussinov, R.; Wolfson, H. J. The Multiple Common Point Set Problem and Its Application to Molecule Binding Pattern Detection. *J. Comput. Biol.* **2006,** *13* (2), 407–428.
155. Desaphy, J.; Azdimousa, K.; Kellenberger, E.; Rognan, D. Comparison and Druggability Prediction of Protein–Ligand Binding Sites From Pharmacophore-Annotated Cavity Shapes. *J. Chem. Inf. Model.* **2012,** *52* (8), 2287–2299.
156. Campagna-Slater, V.; Arrowsmith, A. G.; Zhao, Y.; Schapira, M. Pharmacophore Screening of the Protein Data Bank for Specific Binding Site Chemistry. *J. Chem. Inf. Model.* **2010,** *50* (3), 358–367.
157. Kufareva, I.; Ilatovskiy, A. V.; Abagyan, R. Pocketome: an encyclopedia of small-molecule binding sites in 4D. *Nucl. Acids Res.* **2012,** *40* (D1), D535–D540.
158. Deng, Z.; Chuaqui, C.; Singh, J. Structural Interaction Fingerprint (SIFt): A Novel Method for Analyzing Three-Dimensional Protein-Ligand Binding Interactions. *J. Med. Chem.* **2004,** *47* (2), 337–344.
159. Brewerton, S. C. The Use of Protein-Ligand Interaction Fingerprints in Docking. *Curr. Opin. Drug Discovery Dev.* **2008,** *11* (3), 356–364.
160. Chuaqui, C.; Deng, Z.; Singh, J. Interaction Profiles of Protein Kinase-Inhibitor Complexes and Their Application to Virtual Screening. *J. Med. Chem.* **2005,** *48* (1), 121–133.
161. Kelly, M. D.; Mancera, R. L. Expanded Interaction Fingerprint Method for Analyzing Ligand Binding Modes in Docking and Structure-Based Drug Design. *J. Chem. Inf. Comput. Sci.* **2004,** *44* (6), 1942–1951.
162. Lippert, T.; Schulz-Gasch, T.; Roche, O.; Guba, W.; Rarey, M. De. Novo Design by Pharmacophore-Based Searches in Fragment Spaces. *J. Comput. Aided Mol. Des.* **2011,** *25* (10), 931–945.
163. Degen, J.; Wegscheid-Gerlach, C.; Zaliani, A.; Rarey, M. On the Art of Compiling and Using "Drug-Like" Chemical Fragment Spaces. *ChemMedChem* **2008,** *3* (10), 1503–1507.
164. Johnson, S. R. The Trouble With QSAR (or How I Learned to Stop Worrying and Embrace Fallacy). *J. Chem. Inf. Model.* **2008,** *48* (1), 25–26.
165. Schneider, G.; Schneider, P.; Renner, S. Scaffold-Hopping: How Far Can You Jump? *QSAR Comb. Sci.* **2006,** *25* (12), 1162–1171.
166. Clark, D. E. What Has Virtual Screening Ever Done for Drug Discovery? *Expert Opin. Drug Discovery* **2008,** *3* (8), 841–851.
167. Green, D. V. Virtual Screening of Chemical Libraries for Drug Discovery. *Expert Opin. Drug Discovery* **2008,** *3* (9), 1011–1026.
168. Sun, H. Pharmacophore-Based Virtual Screening. *Curr. Med. Chem.* **2008,** *15* (10), 1018–1024.
169. Pavadai, E.; El Mazouni, F.; Wittlin, S.; de Kock, C.; Phillips, M. A.; Chibale, K. Identification of New Human Malaria Parasite Plasmodium Falciparum Dihydroorotate Dehydrogenase Inhibitors by Pharmacophore and Structure-Based Virtual Screening. *J. Chem. Inf. Model.* **2016,** *56* (3), 548–562.
170. Aher, R. B.; Roy, K. Understanding the Structural Requirements in Diverse Scaffolds for the Inhibition of *P. Falciparum* Dihydroorotate Dehydrogenase (PfDHODH) Using 2D-QSAR, 3D-Pharmacophore and Structure-Based Energy-Optimized Pharmacophore Models. *Comb. Chem. High Throughput Screen.* **2015,** *18* (2), 217–226.
171. Accelrys Software. *Catalyst, Release 4.11;* Accelrys Software: San Diego, 2005.
172. Clackers, M.; Coe, D. M.; Demaine, D. A.; Hardy, G. W.; Humphreys, D.; Inglis, G. G. A.; Johnston, M. J.; Jones, H. T.; House, D.; Loiseau, R.; Minick, D. J.; Skone, P. A.; Uings, I.; McLay, I. M.; Macdonald, S. J. F. Non-Steroidal Glucocorticoid Agonists—The Discovery of Aryl Pyrazoles as A-Ring Mimetics. *Bioorg. Med. Chem. Lett.* **2007,** *17* (17), 4737–4745.
173. Kuhn, B.; Guba, W.; Hert, J.; Banner, D.; Bissantz, C.; Ceccarelli, S.; Haap, W.; Körner, M.; Kuglstatter, A.; Lerner, C.; Mattei, P.; Neidhart, W.; Pinard, E.; Rudolph, M. G.; Schulz-Gasch, T.; Woltering, T.; Stahl, M. A Real-World Perspective on Molecular Design. *J. Med. Chem.* **2016,** *59* (9), 4087–4102.
174. Carrió, P.; Pinto, M.; Ecker, G.; Sanz, F.; Pastor, M. Applicability Domain Analysis (ADAN): A Robust Method for Assessing the Reliability of Drug Property Predictions. *J. Chem. Inf. Model.* **2014,** *54* (5), 1500–1511.
175. Wang, X.; Pan, C.; Gong, J.; Liu, X.; Li, H. Enhancing the Enrichment of Pharmacophore-Based Target Prediction for the Polypharmacological Profiles of Drugs. *J. Chem. Inf. Model.* **2016,** *56* (6), 1175–1183.
176. Bostrom, J.; Hogner, A.; Schmitt, S. Do Structurally Similar Ligands Bind in a Similar Fashion? *J. Med. Chem.* **2006,** *49* (23), 6716–6725.
177. Lessel, U.; Wellenzohn, B.; Lilienthal, M.; Claussen, H. Searching Fragment Spaces With Feature Trees. *J. Chem. Inf. Model.* **2009,** *49* (2), 270–279.
178. Martin, Y. C.; Jarboe, C. H.; Krause, R. A.; Lynn, K. R.; Dunnigan, D.; Holland, J. B. Potential Anti-Parkinson Drugs Designed by Receptor Mapping. *J. Med. Chem.* **1973,** *16* (2), 147–150.

3.10 Matched Molecular Pair Analysis

AG Leach, Liverpool John Moores University, Liverpool, United Kingdom; and MedChemica Limited, Macclesfield, United Kingdom
I Lukac and JM Zarnecka, Liverpool John Moores University, Liverpool, United Kingdom
AG Dossetter and EJ Griffen, MedChemica Limited, Macclesfield, United Kingdom

© 2017 Elsevier Ltd. All rights reserved.

3.10.1 What Is Matched Molecular Pair Analysis? 221
3.10.2 How to Find Matched Molecular Pairs 222
3.10.2.1 Supervised 223
3.10.2.2 Unsupervised 223
3.10.2.2.1 Fragment and index 223
3.10.2.2.2 Maximum common substructure 226
3.10.2.2.3 Comparisons: The influence of settings 227
3.10.2.3 Context Dependence: Set Size Versus Specificity 227
3.10.2.4 Available Software 229
3.10.2.5 Recommendations 229
3.10.2.6 Dataset Selection and Preparation 230
3.10.2.6.1 Chemical structure 230
3.10.2.6.2 Measured property data 231
3.10.3 Example Applications of MMPA 231
3.10.3.1 Specific Structures 231
3.10.3.1.1 Substituents on aromatic rings 231
3.10.3.1.2 Oxadiazole regioisomers 232
3.10.3.1.3 Enantiomers 232
3.10.3.2 Specific Properties 232
3.10.3.2.1 Primary potency 232
3.10.3.2.2 In vivo pharmacokinetics 235
3.10.3.2.3 Metabolism 235
3.10.3.2.4 Permeability and efflux 238
3.10.3.2.5 Toxicity 239
3.10.3.2.6 Solubility 241
3.10.3.2.7 Melting point 244
3.10.3.2.8 Plasma protein binding 244
3.10.3.2.9 Lipophilicity (logD) 245
3.10.3.3 Sharing Data Among Pharmaceutical Companies 245
3.10.3.4 Elucidating Relationships in 3-D 246
3.10.3.5 Elucidating Pharmacophores 247
3.10.3.6 Matched Series 248
3.10.4 Related Approaches 249
3.10.4.1 Activity Cliffs 249
3.10.4.2 Bioisosteres 249
3.10.4.3 QSAR 249
3.10.5 Summary and Outlook 250
References 250
Relevant Websites 252

3.10.1 What Is Matched Molecular Pair Analysis?

A decade ago, a summary of how matched molecular pair analysis (MMPA) operated was proffered as "identifying every pair of molecules that differ only by a particular, well-defined, structural transformation in a database of measured properties and computing the corresponding change in property."[1] This definition still remains a good one for the scope of the analytic approach. However, it has become clear in recent years that many of those using MMPA have come to see it defined more by the way that they find the pairs than by this more general definition. Although a number of algorithms have been developed, one in particular has come to define the pairs. Thus, many now view MMPA as being about the effect of changing specific groups that arise out of fragmenting molecules according to the protocol outlined by Hussain and Rea.[2] This is unfortunate because, although this algorithm is

extremely powerful (as discussed later), it is not the only way of finding matched molecular pairs. It remains our contention that there is not a single correct way to find matched molecular pairs and some analyses that cannot be achieved (such as the study of enantiomeric pairs) by certain pair finding approaches are highlighted in order to emphasize this.[3,4]

The great power of matched molecular pairs is that they reflect the situation faced by most medicinal chemists seeking to optimize a lead compound in order to transform it into a candidate drug: a molecule that has many desirable properties must be changed structurally in order to reduce or eliminate undesirable properties. In both cases, it is about understanding and predicting what effect changing the structure will have on the properties, ideally retaining or enhancing the desirable properties while reducing the undesirable. Although MMPA as a distinct type of analysis was only introduced in the publication of Kenny and Sadowski in 2005,[5] medicinal chemists have been thinking about the relationship between changes in structure and changes in property for many decades, with notable linked approaches being those of Free and Wilson, who outlined a method to analyze how changes in structure at certain positions change activity, and Topliss, who suggested a set of structural motifs that could be made in a given series in order to probe the link between structure and properties.[6–8]

It is one of the key underlying principles of MMPA that the difference in properties is more easily and accurately predicted than the absolute value of properties. In this sense, it is reminiscent of perturbation theory in quantum chemistry or free-energy perturbation in the simulation field, which seeks to take a calculated value and then makes a small change to obtain more accurate values. In MMPA, the analogy is that the simplest way to predict the property of a compound is to find a similar compound and to assume that the compounds have the same property. Thus, in Fig. 1, P(**A**) is a property of interest of compound **A** and P(**B**), the corresponding property of **B**, where **B** is a compound that has either not yet been made or not yet had property P measured. In order to predict P(**B**), the simplest approach would be to assume that P(**B**) = P(**A**). This is the basis of a *k*-nearest neighbor approach in which $k = 1$. The perturbation to this prediction that would make it more accurate would be to find every previous occasion in which the structural feature represented by the green square had been substituted for the feature represented by the red circle and to compute an average change observed in this set. This difference ($\triangle$) can then be added such that the best prediction is that P(**B**) = P(**A**) + $\triangle$. Although this concept is straightforward, it can be implemented in a number of different ways, and these will be explored in the various sections in the succeeding text.

A further advantage that most MMPA approaches have is that they use only real data. There are no modeling and no extrapolation. Indeed, in its purest form, MMPA is actually just a mechanism for presenting historical data to chemists in a way that helps them to predict what the properties of future molecules might be. As such, one of the important areas of research and development has been devoted to finding good ways to present the output. It is inevitable that each end user and every application might have different requirements; some of the advances in presenting the output of MMPA will also be highlighted in this article.

One of the most important roles of MMPA is to discover new effects and provide insights. For the most part, such scientific breakthroughs are happy coincidences of applying the methods. By focusing on differences in structure and the link to differences in properties, new insights can be provided that would otherwise be challenging. For instance, when modeling human ether-a-go-go-related gene (hERG) blockers with a proposed structure of the channel, relating changes in potency of blockers to docking results was successful where comparing docking scores to IC50s would not have been.[9] Furthermore, the insights can be communicated in a much clearer fashion than having to explain how all parts of a molecule contribute to give the overall binding affinity. A consequence of looking at pairs of molecules and the change in structure between them is that the change in structure and change in property do not reveal anything that undermines patentability and therefore allows sharing of information anonymously.[10,11] Furthermore, as will be discussed, significant benefits can accrue from sharing.

MMPA has inspired people to think about medicinal chemistry differently. For instance, a number of reported lead generation campaigns have deliberately set out to generate and profile compounds that are MMPs.[12,13] Lead optimization chemists have incorporated MMPA into their design process such that compounds are now starting to emerge, which represent real tests of the predictive ability of MMPA as a tool both to design better compounds and to predict the properties of compounds before they are made.[14–17]

3.10.2 How to Find Matched Molecular Pairs

There are two broad classes of methods for identifying matched molecular pairs. These depend upon whether the pairs are found using manual intervention or automatically. Initial work in the area relied upon users encoding the structural change that defined the matched pairs and were usually designed to address the link between specific structural changes and specific properties; that is to say, they were driven by a scientific hypothesis or question. As the technique developed, it became clear that it produced valuable

Fig. 1 Conceptual matched molecular pairs.

insights but that this was limited by the imagination of those who defined the pairs. A new approach was needed in which matched pairs could be identified automatically. Two algorithmic approaches emerged: one based on fragmenting molecules (at selected acyclic single bonds) and indexing the resulting fragments and the other requiring the maximum common substructure (MCSS) between two molecules to be deduced. In both cases, the type of molecules that get paired depend upon the settings used and will be discussed. It has also been made clear that the amount of chemical structure that is used to define the context in which a structural transformation takes place can be important. Chemically more specific transformations can provide a higher fidelity and more relevant view of the effect of a structural change than more general structural contexts, but there is inevitably a trade-off between the specificity and dataset size. Recent years have also seen recommendations published concerning the preparation of datasets and about which types of data can be compared with one another. All of these aspects of how matched pairs are identified will be discussed.

3.10.2.1 Supervised

It is often the case that specific queries or hypotheses can be tested by MMPA. In such cases, the user is likely to have specific chemical structure types in mind, which are defined at a particular level of specificity. This would mean that the user can encode the change in structure and the informatics approaches to doing this are quite well developed; the SMARTS and SMIRKS nomenclatures in particular lend themselves well to this.[18] Such approaches require significant manual input and intellectual oversight, and as such, we classify them as supervised approaches.

The original publication in MMPA described how a molecular editor could be used to identify matched molecular pairs in which substituents are added to a benzene-like ring.[5] The effect of these structural changes on solubility was identified (**Fig. 22**). All compounds (encoded as SMILES strings) that had the substituent of interest on an appropriate ring were found. The molecular editor then deleted the substituent (one at a time in molecules that had more than one of the same type of substituent), and the SMILES string for the unsubstituted example was then used as a search in the original database to discover if the paired compound also existed and had measured solubility data. The editing was encoded using SMARTS strings and implemented in the molecular editor Leatherface.[5] SMARTS strings have the great advantage that they can be encoded to be extremely specific or general but provide exquisite control in terms of chemical structure. The software has now been superseded by the molecular editor MUDO that is provided as source code and has a similar basis but that exploits the advances in the underlying informatics in order to permit the editing of molecules in three dimensions, for instance.[19] The same approach to matched-pair finding was subsequently applied by Leach et al. who expanded the set of structural transformation types that were explored.[1] Specific queries were also implemented as part of a study of reactivity for some covalent binding of nitriles,[20] potency, and some physical properties for glycogen phosphorylase inhibitors.[21] A SMARTS-based approach was also adopted by Dossetter when searching for changes to aromatic rings and methylene carbon atoms.[13,22,23] Gleeson also used a manual encoding of sets of substituents in order to identify matched pairs differing only by the addition or interchange of those substituents.[24]

In a related approach, Lewis and Cucurull-Sanchez encoded the structural transformations linking two members of a matched pair in the RXN format.[25] This permits them to be applied to a set of compounds as reactions, the products of these reactions can then be searched for, and if present, the matched pairs can be identified.

The same approach has, in more recent years, been implemented using SMIRKS to encode structural transformations. In one of the first such publications, Hajduk and Sauer identified a set of 828 substituents present in databases of potency data using the Daylight findsub method.[26] These were transformed into SMIRKS strings that encode the addition of each of the substituents. These could then be applied to a database of SMILES strings, and the product SMILES strings searched against the original database in order to identify pairs that are present and that differ only by addition of one of the substituents. Boström and coworkers used SMIRKS to encode the interchange of oxadiazole regioisomers and Stepan and coworkers to study the variation between cyclic ethers.[27,28]

3.10.2.2 Unsupervised

Naturally, supervised approaches to finding matched pairs have many limitations; notably, the amount of human time required to encode the pairs can be excessive, but, more importantly, the pairs that are found are limited by the imagination of the user. Therefore, a number of unsupervised approaches have also been developed. These have broadly fallen into two conceptual classes: fragment and index or MCSS. In the first, each molecule is first fragmented, and the fragments are compared with those for other molecules. Molecules for which all fragments apart from one are the same can be considered pairs. In the second approach, two molecules are compared by computing their MCSS; if this is large enough, then the remainder of each molecule defines the difference between them. These two approaches will be discussed in more detail. An early first attempt encoded molecules as fingerprints and identified sets of pairs in which the change in fingerprint was the same.[29] This approach does not seem to have been taken forward.

3.10.2.2.1 Fragment and index

Although it was not the first publication to describe a fragment and index approach, the definitive paper in this area came from Hussain and Rea.[2] They highlight the limitation of systems that require the user to define the pairs and propose an alternative: the fragment and index approach.

In the first step, each molecule is fragmented, by breaking selected bonds. Hussain and Rea achieve this by defining the bonds to be broken using a SMARTS pattern. They aim to have this pattern be specific to acyclic single bonds. The SMARTS pattern suggested is "[*]!@!=[*]" that signifies an atom type joined to any atom type by neither a bond that is in a ring nor a double bond. Refinements to this definition have been proposed and are discussed in the following section.

Bonds are broken one at a time, and the resulting fragments are then stored as SMILES strings, which can be manipulated as text. This is the great advantage of the approach: after an initial fragmentation, which requires chemically aware software and time-consuming processing of molecules, all subsequent steps toward the identification of matched pairs involve only rapid text processing that does not require any chemoinformatics technology.

The SMILES strings of the fragments correspond either to the fixed part or to the changing part. Different terminology is used by different scientists to describe these components and is usually influenced by what they are trying to describe. In particular, the fixed part is often called the index, because it is the component in the database that is used to look up pairs. It can also be called the core when changes of substituent are being considered or vice versa. The terms fixed and changing emphasize the link to the matched pair itself in which the difference between the two molecules is defined by the changing part, and the fixed part is what brings that particular pair together. In general, it would be possible for each fragment to be considered the changing part with the remainder defining the fixed part. However, it is frequently the case that chemists expect the fixed part that is shared between two molecules in a pair to be of a certain size before they would consider two molecules to be a pair. If the changing part is very large, then it may be that the molecules might not be considered to be pairs. Similarly, if the two fragments in the changing part of each member of the pair differ in size too much, it may be considered that the change is unlikely to be well characterized by MMPA. All of these considerations have caused a number of limitations to be imposed upon the fragment and index approach. Hussain and Rea only allowed the changing part to contain up to 10 heavy atoms and only allowed up to three bonds to be fragmented. Others have imposed variations on these restrictions.

The fragmentation is illustrated in Fig. 2 for a hydrocarbon. There are two acyclic single bonds, which are fragmented in turn during the single fragmentation phase. Each of the resulting fragments can be considered as a candidate for the fixed part and the changing part. When a double fragmentation is considered, only one is possible, and it can only be considered when the disconnected fragments become the fixed part; otherwise, it would permit changes at more than one point, which defies the usual definition of matched molecular pairs in the fragment and index approach.

Having identified fragments, the indexed entries can then be compared in order to find pairs that are entries that have the same fixed part and different changing parts. Single-bond cuts will tend to identify the sort of pairs that might be considered as variations in substituents as shown in the first example in Fig. 3. In this example, the right-hand side of the two molecules shown is the same and is identified as such when both generate the same fixed part. The variation on the left-hand side is then captured as the changing parts. By contrast, when double fragmentation takes place, the pair type identified tends to be core changes. For instance, as shown in Fig. 3 ("core changes"), the two molecules differ in the central ring but have identical left and right groups. The double cut generates the same two disconnected fragments as a fixed part, and the core change from phenyl to pyridyl is captured in the changing part, which defines the matched-pair type. It should be noted that using this fragment and index approach, it is challenging to distinguish this change from that that leads to the alternative regioisomer shown at the bottom of the picture. The approach also precludes this example from being analyzed as part of a more general query concerning the transposition of an aromatic carbon to an aza nitrogen.

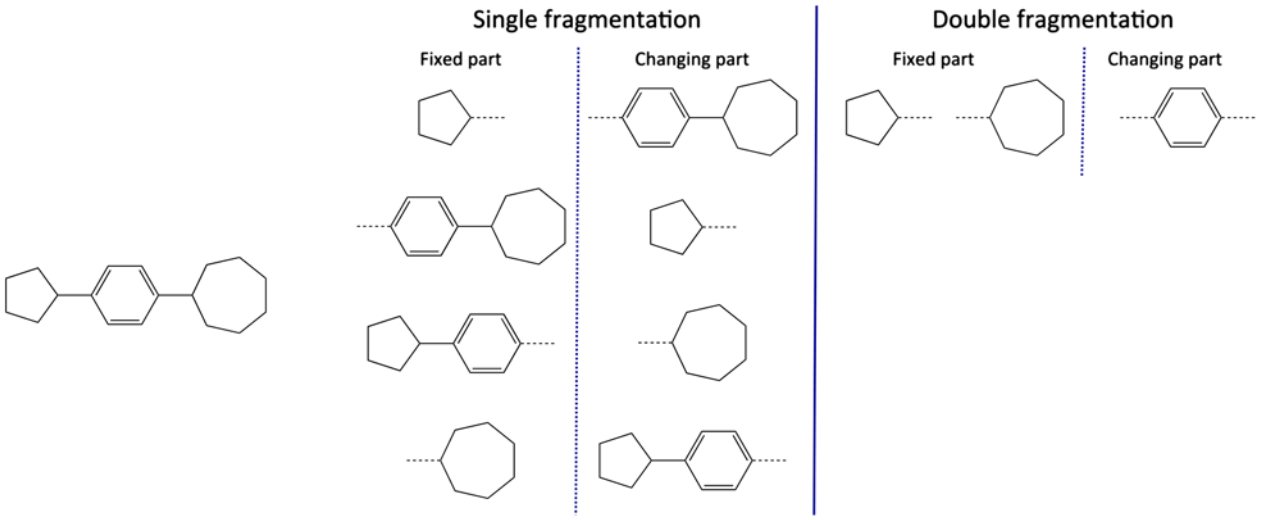

Fig. 2 The fragmentation and indexing output.

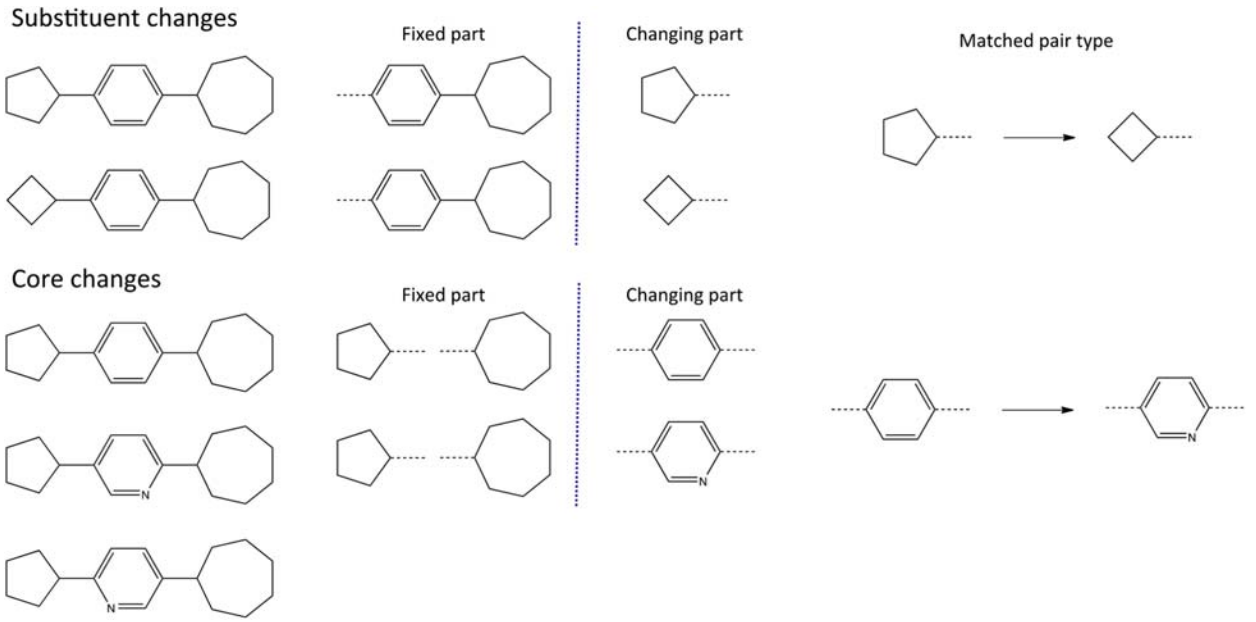

Fig. 3 Combining fragment and index data to identify matched molecular pairs.

When more than two fragmentations are considered, this can be thought of as involving more complicated, more highly substituted cores being changed. It is often the case that chemists find that increasing the number of fragmentations beyond about three or four leads to overly complicated transformations.

Hussain and Rea discuss the particular challenge posed by hydrogen atoms in this approach. Hydrogen is usually implicit in the structures that are stored in databases. SMILES strings require chemoinformatics software to interpret them in order to correctly assign hydrogens. This problem is solved in a subsequent, inelegant, but pragmatic step. Hydrogens are added to the position at which each fragmentation has taken place and the database searched in order to identify if the unsubstituted compound was present.

The output from the analysis can be encoded in many ways, which need not be chemoinformatic. The text corresponding to the two changing parts is sufficient to define the pair. However, Hussain and Rea generate a SMIRKS pattern that has the advantage that it can then be applied as a chemical transformation in order to translate the knowledge gained from the analysis into suggested molecules that are worth making. This is rather similar to the Drug Guru approach advocated by workers from Abbott.[30]

Hussain and Rea applied this technique to the NIH Molecular Libraries Small Molecule Repository, which at that time contained 333,332 compounds that passed their medicinal chemistry filters. The fragmentation took 501 min and led to 21.7 million fragmentations. Indexing took 356 min and identified 5.3 million pairs, which represented 2.6 million different sets of pairs (where a set of pairs represent all pairs corresponding to a given structural change). They discovered that matched pairs tend to have frequencies that follow a Zipfian distribution. That is to say that most sets (78%) of matched pairs have only one example in the database. There is a long tail in which sets containing large numbers of examples are rare.

The first publication to have suggested a fragment and index kind of approach came from Haubertin and Bruneau,[31] who were interested in using MMPA as a tool to aid in lead optimization. They applied only single fragmentations to molecules and so focused on substituent interchanges. The approach was applied in a slightly different way but with the same outcome as Hussain and Rea. They fragmented the AstraZeneca database using a variation of the RECAP protocol in order to identify all of the side chains that are represented.[32] The database was then searched in order to identify compounds that contained these side chains. This provided an interesting comparison with previous studies that assessed the frequency with which certain side chains are used in medicinal chemistry.[33,34]

Many others have subsequently used the Hussain and Rea approach. It has been implemented as a freely available piece of software through RDkit.[35] It is also used to generate analysis in the online chemical modeling environment (OCHEM).[36] The chemoinformatics providers, OpenEye, have encoded a version of the fragment and index approach as part of their toolkit, and MedChemica has incorporated fragment and index alongside the MCSS approach (described in the following section) in their software MCpairs.[37] The approach has been applied in many ways, which are discussed elsewhere in this article.[12,38–54]

One of the great advantages of the fragment and index approach is that once a molecule has been fragmented and added to the database, it is available for matching to any new molecule that is added.

Among the limitations of the fragment and index approach to finding matched pairs are that small changes to rings cannot be identified as pairs, highly substituted core changes are limited by the number of fragmentations considered, and the diversity of the structural changes can be limited by the restrictions that are imposed (usually heavy atom counts or ratios). One specific set of

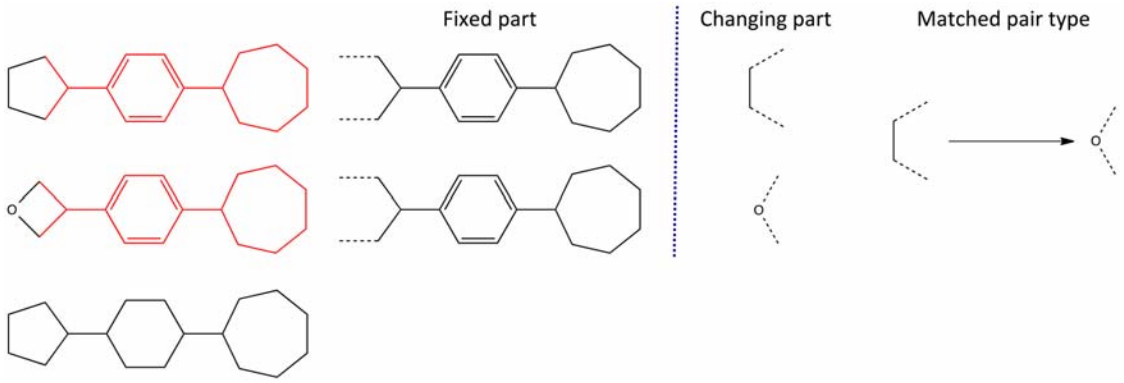

Fig. 4 The maximum common substructure approach to finding matched pairs.

changes that are not readily identified is modifications to macrocylic rings. The SMARTS definition that identifies which bonds are to be fragmented also is not ideal and can lead to fragmentations and grouping into sets of pairs that chemists would not normally consider to be chemically sensible. For instance, fragmentation of the single bond in amides, esters, or sulfonamides and acyclic triple bonds would happen if the original SMARTS proposed by Hussain and Rea was to be applied. Consequently, a refined SMARTS definition has been proposed by Wirth and coworkers and is "[#6+0;!$(*=,#[!#6&!R])]!@!#!=[*]." They also proposed a second rule that allows fragmentations of exocyclic double bonds: "[#6+0;R]=[#7&!R,#8&!R,#16&!R,#6+0&!R]." This definition signifies any atom type connected via a bond that is neither in a ring nor double nor triple to a carbon atom that is not charged and that in turn is not double- or triple-bonded to an atom of any element other than carbon (unless that atom is in a ring).

3.10.2.2.2 Maximum common substructure

An alternative unsupervised approach to finding matched pairs has also been proposed, which uses the MCSS between two molecules to define the fixed part. The first step in the approach is to compare two molecules using a MCSS algorithm. The same molecules as described earlier for the fragment and index approach are shown in Fig. 4 with the MCSS highlighted in red. This becomes the fixed part and the remainder of the molecule the changing part. This means that structural change in this case is then the change from CH_2CH_2 to O. There are a number of MCSS algorithms available, which permit different types of comparisons to be made. For instance, some allow disconnected common substructures, while others limit them to substructures of atoms that are contiguous.[55] The nature of the algorithm is important because it governs the kind of matched molecular pairs that can be identified. An algorithm that only allows contiguous common substructures would not find the most interesting link between the molecules at the top and bottom of Fig. 4 in which the phenyl ring has been replaced by cyclohexyl.

The key paper that sets out a protocol for accomplishing MMPA with an MCSS approach is from Warner and coworkers at AstraZeneca.[56] In an approach that they call WizePairZ, they employ OpenEye's molecular graph encoding.[57] This converts molecules into graphs, which are then amenable to the informatics techniques for processing graphs, many of which represent extremely rapid means to identify commonalities between molecules (subgraphs within graphs). As with the fragment and index approach, the outcome of the MCSS approach is governed by the choices made about deciding what to classify as a pair. Warner et al. elected to use a fast graph comparison technique that does not permit disconnected substructures to be generated and chose to limit the changing part of the molecule to be less than 10% of the fixed part.

As with the Hussain and Rea approach, Warner et al. encoded the output from their pair finding as SMIRKS that permits any structural changes identified as being of interest to be applied to molecules to which they may be relevant. In order to enhance the relevance of their findings, they also encoded the structural context for the transformation. This is discussed in more detail in the relevant section in the succeeding text. The approach was applied to a small library of 13 inhibitors of histone deacetylase. Two examples were excluded to serve as a test set. The remaining molecules were then analyzed with the MCSS algorithm. Pairs were identified and encoded as 68 SMIRKS. These SMIRKS were then applied to all the molecules in the database. This led to the suggestion of 15 new molecules. Of these suggestions, 12 were in the original set. The two test-set compounds were produced. In addition, three completely new compounds were suggested. The analysis was also used to predict the potency of the test-set compounds and was found to give excellent agreement; both were accurate to the first decimal place in terms of predicting a pIC_{50} value. Some of the same scientists also reported the use of the MCSS approach WizePairZ in a study that demonstrated the value of MMPA for designing out off-target effects.[58]

Unlike the fragment and index approach, one algorithm has not become the generally accepted standard that is widely available. Others have reported the use of MCSS approaches. These include Papadatos et al. who increased the speed of pair finding by reducing the number of pairwise comparisons that must be made. They only considered molecules that had a Tanimoto between their Daylight fingerprints of >0.75 and by only considering pairs that have a difference between their number of heavy atoms that is less than or equal to 15. They also require that the fixed part is as big as or bigger than the changing part. They discovered in their

analysis that when they used this approach and a fragment and index approach, they obtained very similar sets of pairs but that the fragment and index approach was significantly faster (it took 8 h as compared with 4.5 days for the MCSS approach).

Subsequently, Weber et al. have reported an MCSS approach that allows them to identify matched molecular pairs in the ChEMBL and PDBbind databases.[59] In particular, they identify pairs that share MCSS with a ligand of known binding mode. The changing part is required to be no more than half as small as the fixed part. The shared substructure is presumed to retain its binding position. Pose refinement in MOE (Molecular Operating Environment from Chemical Computing Group) and conformational sampling were used to position the changing part for the molecule that does not have a crystal structure. This permits matched pairs to be placed in a three-dimensional context. The shared substructure has a dual purpose: facilitating both pair finding and overlaying. The method has since been extended to provide a Web server implementation.[60]

The key limitations of the MCSS approach are (1) that the substructure comparison is slow and (2) that most algorithms for finding the MCSS require all of the atoms to be contiguous and therefore prevent pairs in which linkers change from being found. There are alternative algorithms available that permit disconnected substructures to be identified, but these will generally slow the comparison down further. This area has seen a number of recent technical and algorithmic advances, which hold out the prospect of improvements.[61]

3.10.2.2.3 Comparisons: The influence of settings

Many of the key considerations for the two approaches (fragment and index or MCSS) for finding matched molecular pairs have been outlined earlier, but there are certain factors that become clear when considering them in comparison to one another. A very practical one concerns the computational workload when the two methods are applied to large datasets. MedChemica has applied both methods during the compilation of their database, which is a very large analysis of data from three pharmaceutical companies.[10] They found that, as expected, the fragment and index approach is indeed quick to generate fragments. However, this was offset by the generation of extremely large sets of fragments for indexing. The capacity to store this intermediate information can become limiting quite quickly. There are many molecules that will have 10 breakable bonds, which will lead to more than 50 different fragmentations, even if only three fragmentations are considered. Meanwhile, also as expected, the MCSS suffers from a slow step generating the all-by-all comparison using the MCSS algorithm. Once the MCSS comparisons have been made, the set is reduced, and subsequent steps both are fast and require much less storage capacity than the fragment and index approach. Thus, the trade-off is between large storage requirements or slow comparisons. We note that whereas the processing can be parallelized, file storage is not easily divided up.

In order to characterize the difference between the methods, we have performed an analysis of the ChEMBL dataset of 1010 compounds with measured K_i for inhibition of the epidermal growth factor (EGF) receptor tyrosine kinase enzyme. Typical settings were selected such that (a) for the fragment and index approach, the ratio of the number of heavy atoms in the changing and fixed parts must be less than 0.3 and the changing part must be smaller than 10 heavy atoms and (b) for the MCSS approach, the MCSS must include at least 90% of the heavy atoms. The number of compound pairs that were found by the two methods is illustrated in the Venn diagram in Fig. 5. In Fig. 5A, the individual compound pairings are compared and show that the fragment and index (F+I) approach finds the most sets of pairs and the MCSS finds about 30% less pairs. The two methods pair many compounds in common, but it is striking that the two approaches find many unique compound pairings. In Fig. 5B, the number of pair types that are identified by each method is shown. The fragment and index approach can fragment each molecule in many ways, and so each pair of compounds that involves molecules with many fragmentable bonds will generate many pairs. By contrast, the MCSS finds the single simplest description of the change between molecules; each approach has its merit, but one consequence of this behavior is a very large storage requirement for the fragment and index approach when the number of compounds increases. In Fig. 5C, two pairs are given that are only found by each method and that illustrate some salient considerations. The requirement for the MCSS to be 90% of the substructure prevents the first set of compounds from being paired; this setting will tend to exclude small compounds from the set. The inability of the fragment and index method to fragment rings and study changes in them is illustrated by the second pair, which is nonetheless found by the MCSS approach.

3.10.2.3 Context Dependence: Set Size Versus Specificity

The chemical context in which structural changes are made can have an influence upon the change in properties that they cause. In their investigation of solubility and plasma protein binding, Leach et al. identified some outliers in the distributions for the addition of small substituents to aromatic rings and found that these were dominated by changes adjacent to amide or biphenyl linkages (Fig. 6).[1] They attributed this to the conformational change caused by substituting at these positions. Similarly, Haubertin and Bruneau used the atom to which substituents are attached to separate the context of the change into crude categories such as aliphatic carbon, aromatic carbon, and aliphatic nitrogen.[31]

This approach was formalized by Papadatos et al. who analyzed hERG pIC_{50}, log(solubility), and logD data in a categorical fashion by assigning changes of +0.3 or greater to the category "increase," −0.3 or lower to the category "decrease," and those in between to the category "no change." Multinomial tests were then used to identify the significance of any changes or chi-squared tests for larger sets of pairs (63 or more pairs in a set). The "no change" category is generally dominant.

They used a number of methods for subsetting by context: the fixed part was encoded as reduced graphs, Murcko scaffolds, and Daylight fingerprints. A similar set of local descriptors were used in which only the attachment point was described: its reduced graph description as SYBYL atom types and those of atoms up to three bonds away provide a compact description of the local

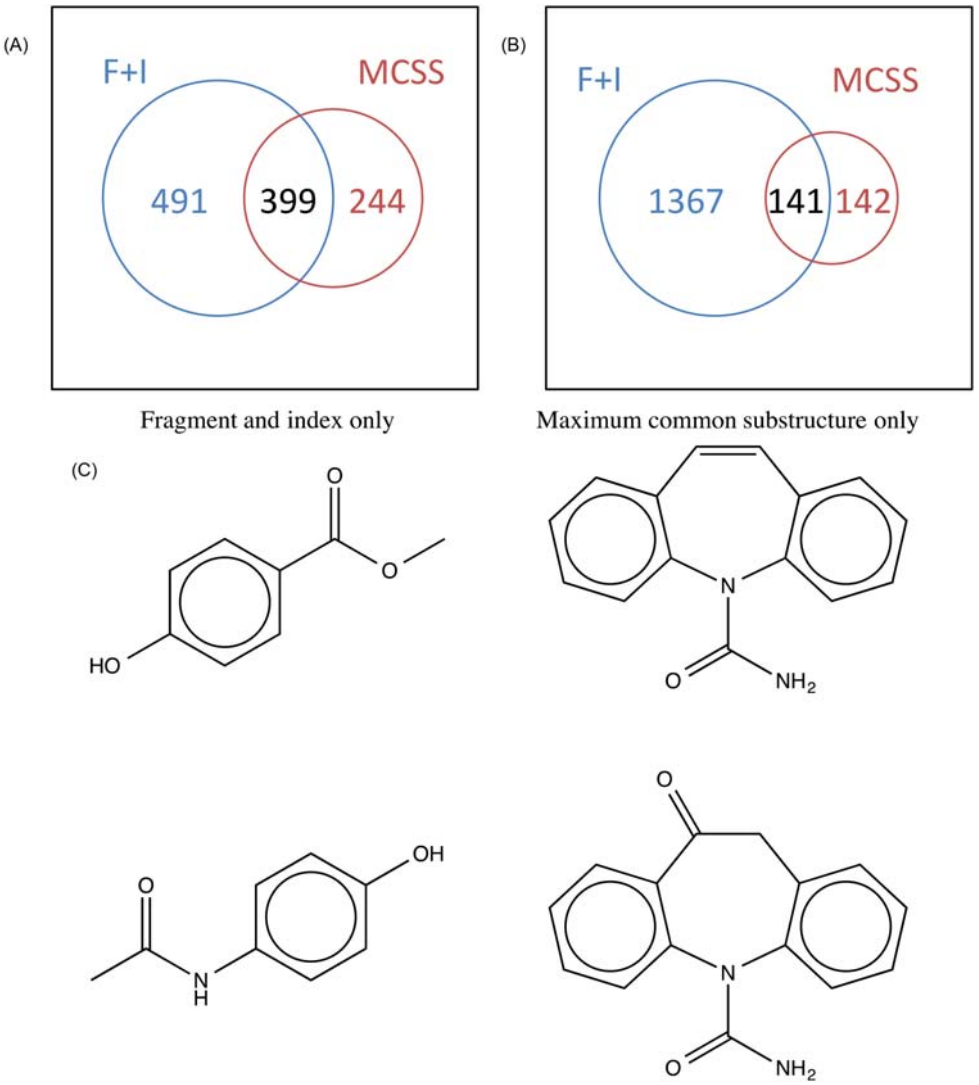

Fig. 5 Venn diagrams for (A) the number of compounds that are found as pairs by the fragment and index (F + I) method and the maximum common substructure (MCSS) method, (B) the number of pair set types that are identified by the same two approaches, and (C) examples of compounds that are paired only by the fragment and index method and only by the maximum common substructure method.

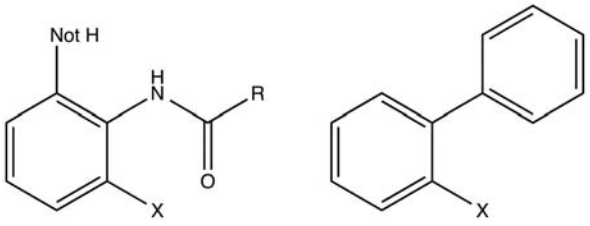

Fig. 6 Matched pairs in which groups added at X are often outliers.

environment. Each of these encodings can be considered a description of the chemical context in which a change in structure takes place. A number of subsets are identified in which the change in property for a subset defined by chemical context is statistically distinct from that for the rest of the set. Some of these changes are described in the relevant sections in the succeeding text. Chemical considerations do not play a part in identifying subsets so it is interesting and powerful that the method provides chemical insights. For instance, chemical contexts are found in which conformational changes occur, or an important pK_a is modified, or other electronics defy the dependence upon lipophilicity. This publication demonstrated that context can provide a great deal of added value but was applied after (and not during) matched-pair identification.

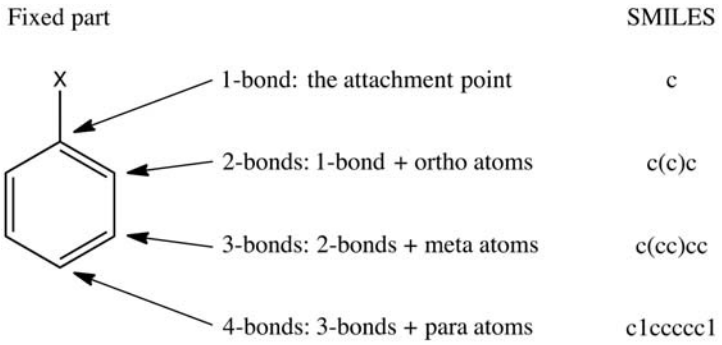

Fig. 7 The encoding of chemical context in the WizePairz approach.

In their publication describing the WizePairZ algorithm, Warner et al. describe how they encode the context of matched pairs directly such that interesting subsets can be identified readily. They chose to encode context using the SMILES for the atoms in the fixed part that are connected to the changing part (**Fig. 7**). They encode four levels of the context: 1-bond context is just the attachment point, 2-bond context is the attachment point plus the atoms attached to it, and 3-bond contexts are those plus the atoms attached to them. They selected to encode as far as four bonds in order to capture some information about positions of substituents around aromatic rings. These contexts were translated into the SMIRKS that they used to describe the change and that can therefore be used to apply context-specific information to only those molecules to which it is relevant.

More recently, Ritchie et al. have highlighted the importance of matched pairs that occur in specific contexts in which the change in structure interferes with intramolecular hydrogen-bonding motifs.[43]

The chemical context can also relate to the position that certain groups are likely to be in when molecules are in a protein-binding site. This aspect of context dependency has been emphasized in a number of the recent publications that have sought to incorporate three-dimensional information into MMPA.[49,59]

An extension of the idea of context was also provided by O'Boyle et al. who identified matched series in which a set of molecules with a common fixed part are linked together.[52] This broader context for each pair allows it to be viewed in a different way in which expectations can be set based on the broader structure–activity information that is available across the matched series.

It is clear that the idea of subsetting groups of matched pairs according to their context has gained a great deal of traction. Many scientists are seeking new ways to do this. Those that have been exemplified thus far include statistically led, chemical structure-led, protein binding site-led, and broader series SAR-led. Doubtless further context divisions will be identified in future. All suffer from the same dilemma: MMPA relies upon sufficient molecules being grouped into a set to permit statistically sound deductions to be made. The more the sets are divided up by context, the smaller the sets must inevitably be and therefore the statistical power must be reduced. This makes it very difficult to extract contextualized information without compromising statistical power. We have recently discovered that the dilemma can be viewed quantitatively. In an analysis of hERG data in Medchemica's very large database, each set of pairs was categorized according to a binomial analysis analogous to the detection of biased coins: heads correspond to an increase in potency, tails to a decrease. Biased sets of matched pairs correspond to ones that are certain (at 95% confidence) to change the potency in one direction or another. Those sets of pairs for which a bias could not be detected were classified as no effect determined (NED); these may be structural changes that cause no change in potency or pairs for which there are not yet enough data to detect the effect. Having established the behavior of the whole set of pairs, the change in the mean pIC_{50} as pairs are added sequentially to the set could be calculated. The value of the mean change above which an increase in potency is the most likely outcome for the group could then be computed for sets with two pairs, three pairs, four pairs, etc. These are then divided into context levels 1–4, as illustrated in **Fig. 7**. This is summarized in **Fig. 8**, which shows that a set of five pairs that are at context level 4 (the most specific) are equivalent to a set of about eight pairs at context level 1. The statistical challenge can actually be reduced when pairs are divided up by context.

3.10.2.4 Available Software

There are a number of software packages that are available to implement the various matched-pair approaches that have been discussed. The molecular editing software introduced by Kenny and Sadowski (Leatherface) is not itself available but has recently been updated and made available as MUDO.[19] An implementation of the F + I approach is available via RDkit and as a KNIME node.[35,62] Several software vendors also have implementations of MMPA and related approaches. In addition, a number of Web services provide access to MMPA such as VAMMPIRE and SwissBioisostere.[54,63]

3.10.2.5 Recommendations

As part of the development of their data-sharing consortium detailed in the succeeding text, MedChemica has created a software suite that is capable of generating matched pairs using either the fragment and index or the MCSS method. In each case, the resulting

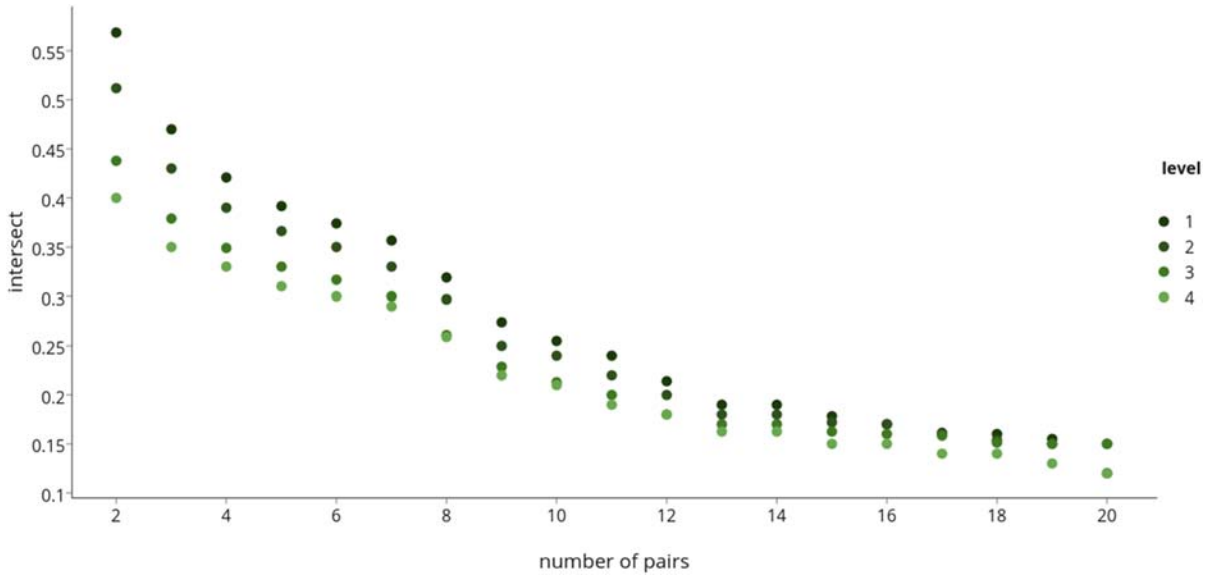

Fig. 8 The value of the average change in pIC_{50} above which a group of pairs is most likely to have a real bias to increase hERG channel block.

pairs are encoded in an identical fashion. As discussed earlier, the settings selected have a significant impact upon the pairs that are found. Determining a priori what the optimum settings are for each method for the question at hand is not currently possible. However, it is clear that the two methods can provide complementary sets of matched pairs. Given the wide availability of significant processor power and storage capacity, it seems to us that the best approach to finding matched pairs is to use both methods and to combine the output in order to gain the best chance of covering chemical scope and revealing the most useful insights that a dataset can provide. Given how much experimental effort goes in to generating the data that are analyzed, it is a false economy not to perform the best analysis that is possible. It is also clear that the more chemically specific a set of pairs is, the more likely it is that the matched-pair set will make a correct prediction and the smaller the set of pairs that is required in order to acquire that correct prediction. As such, it is recommended that context incorporation should be a required part of any matched pair finding algorithm.

3.10.2.6 Dataset Selection and Preparation

The data that are input into matched-pair analysis are of two kinds: the chemical structure and the measured properties. There are a number of considerations when preparing this combination of data for analysis.

3.10.2.6.1 Chemical structure

In this section, discussion is limited to those matched-pair studies that are taking molecular structure input in two dimensions. There are a number of matched-pair studies that are extending into three dimensions, and these are discussed in the relevant section. When handling the structures that are input to MMPA, there are a number of concerns, but most can be reduced to the question of which molecular structures should be considered the same and which should be different. One of the issues that is most commonly experienced and that is reported as troublesome in many of the publications cited in this article is the problem of stereochemistry. Sometimes, the stereochemistry of two molecules can be the same but registered in subtly different ways in a database. A strict matching routine in either the fragment and index or MCSS approach will therefore fail to make connections. For this reason, some methods drop stereochemistry when considering molecules for pairing. This can mean that molecules with different stereochemistry may be paired. This may not be the desired outcome. Further complication arises when the stereochemistry is destroyed upon bond breakage during the fragment and index method; this can be avoided in principle if a marker for the specific position of the break point is retained.

A further consideration that can complicate pair finding is the position of hydrogens. There are two chemical problems: tautomerism and ionization. A further problem is chemoinformatic: SMILES strings do not explicitly capture the position of hydrogens and rely on models to determine aromaticity. Among the chemical problems, the critical issue is that two molecular fragments, which must be found to be identical in order to match, should be represented identically. This requires each molecule to be transformed into a standard tautomer that will always present each fragment in the same form. Unfortunately, while this can be achieved for most cases, there will always be structures in which two tautomerizations interact and where one will perturb the other if only one representation is adopted. This can be avoided by enumerating all tautomeric possibilities, but this will make the task of pair finding much more challenging. Alternative chemoinformatics approaches to avoiding the problem of tautomerism are still being developed and are likely to be impactful in the area of MMPA. A similar challenge is raised by ionization and, as with

tautomers, requires structures that should be matched to be represented in the same way in the input. This is usually simpler than for tautomers. One representational problem that is not commonly understood is that certain functional groups, particularly those that have unusual valencies, can be represented in different ways and again must be standardized to the same form. An example of this is that the nitro group might be represented as $N^{+}(=O)O^{-}$ or as the chemoinformatically simpler but chemically problematic N(=O)=O. Once again, the representation selected is not important, but standardization is required. This is particularly important when taking data from a range of sources that have not used a set of rules to determine how they represent structures.

The chemoinformatic challenge posed by the absence of most hydrogen atoms in SMILES strings can complicate the treatment of tautomers.[5,64–66] Also, subtle changes can cause representation of structures that ought to be paired to be different. This can be particularly the case when the perception of whether a group of atoms are aromatic or nonaromatic differs. This is generally not a problem for smaller delocalized systems but can become a problem when three or more potentially delocalized systems are contiguous.

3.10.2.6.2 Measured property data

As discussed for chemical structure earlier, the key requirement for processed data is that only values that the user is happy to have compared are permitted to be compared. This is relatively easy to achieve for the small-scale manual studies that began the field of MMPA but is more challenging once the scale is increased and unsupervised methods are employed.

In general, MMPA subtracts the value of a property for one member of a pair from that for the other. Therefore, any properties that should usually be compared as ratios should be transformed logarithmically. These include equilibrium constants (such as K_i), IC_{50}s (or similar values), solubility, CL_{int}, P_{app}, and rate constants. Failure to make this transformation leads to the observation of pair sets such as those described by Keefer as multiplicative in which any useful insights are lost because of the nonlinearity of the scale.[39] Some thought also needs to be given about how to summarize the data when a compound has been studied several times and has more than one measurement. This is complicated if one or more of these measurements fall outside the range of the assay. In such cases, it is usually best to work with those who generated the data in order to determine, on an assay-by-assay basis, what the most appropriate means to process the data is. As mentioned in the section on melting point in the succeeding text, the highest T_m is likely the most appropriate one given that the most stable polymorph is usually the one of most interest; by analogy, the lowest solubility is often the best value to use.

The key consideration is to work out which sets of data should be compared. The most important contribution in this area has been from Kramer et al. who studied hERG inhibition as measured in an assay within Novartis and as reported in the ChEMBL database.[38] They emphasized the value of the paired *t*-test for MMPA because of its natural fit with the sort of comparisons being made, although it does require a normal distribution of data, which is not always observed. They demonstrate that matched pairs from the same assay (homogeneous pairs) are to be favored over pairs in which the two measurements come from different assays (heterogeneous pairs). They compute the difference in pIC_{50} that would be required in order to be detected as significantly different from zero within sets of heterogeneous pairs for different levels of experimental variability. They find that very large differences (2–8 log units) might be required for sets of two pairs, but this falls to 0.2 log units or less for sets of 100 pairs. This requirement is much lower for homogeneous pairs where the amount of broadening due to experimental variability is less. They advise that adding heterogeneous pairs only makes sense when adding a very large number of pairs because otherwise the amount of noise that is added outweighs any added signal. The rule of thumb they suggest is that there need to be twice as many heterogeneous pairs as the homogeneous pairs to which they are being added in order for it to be worth adding them. They also compute the number of pairs that are likely to be required in order to determine the effect for a structurally specific pair with 0.1 log units. They suggest that an average of 46 homogeneous pairs is required but that 200–400 heterogeneous pairs would be required.

ChEMBL records the assay that values were measured in, and this can be used to identify homogeneous sets. In their studies of the ChEMBL dataset, Kramer et al. also find that most pairs that fall into significant sets tend to have been measured in the same assay (homogeneous). By carefully analyzing the variation that they expect between pairs, they are able to detect compound pairs where the distribution is wider than expected. They find that this can sometimes be ascribed to the chemical context and note that the transformation from Me to Ph demonstrates this effect, whereas the transformation from F to Cl does not, suggesting that this transformation will cause the expected change regardless of context. They also find that outliers are more often database errors than real outliers and therefore demonstrate one of the unintended consequences of MMPA: by setting expectations of what is to be expected, unusual data points are flagged up, and these can be checked and will often turn out to be incorrect entries (either there was a problem with the experiment or the values have been incorrectly transcribed into the database). The final source of wider-than-expected variation they ascribe to chemical effects is the steric size of a group becoming large enough that it cannot be tolerated and the perturbation of pK_as.

3.10.3 Example Applications of MMPA

3.10.3.1 Specific Structures

3.10.3.1.1 Substituents on aromatic rings

The first publication in the area of MMPA described the addition of some common substituents to aromatic rings and the corresponding change in solubility.[5] The same structural change and its link to solubility, plasma protein binding, and in vivo exposure were explored by Leach et al.[1] An alternative approach to studying the addition of commonly occurring substituents was presented

by Haubertin and Bruneau for solubility, plasma protein binding, logD, and calculated properties.[31] They used a precompiled database of substituents as part of their analysis, which permitted them to explore the frequency of occurrence of these groups. A number of investigations have computed the effect of aromatic ring substitution patterns upon metabolism as measured in human liver microsomes.[23,25] Brown et al. looked at the effect of adding chlorine at different positions around a ring and also the effect of moving the chlorine around the ring in order to investigate the predominance of the para isomer in medicinal chemistry. They investigated potency, hERG, logD, solubility, Cl_{int} in microsomal assays, and permeability in Caco2 assays.

3.10.3.1.2 Oxadiazole regioisomers

Boström and coworkers performed a fascinating and detailed study of the effect of changing the position of the heteroatoms in oxadiazoles.[27] In particular, they investigated the exchange of 1,2,4-oxadiazoles with 1,3,4-oxadiazoles. They showed that the 1,2,4-oxadiazoles have a higher logD by about 1.2 log units(which is not always predicted correctly by logP calculators). Linked to this observation, they find that the 1,2,4-oxadiazoles have lower solubility, slightly higher Cl_{int} in human liver microsomes, slightly enhanced inhibition of the cytochromes P450 (particularly 1A2 and 3A4), and higher affinity for the hERG channel. They ascribe this to changes in the dipole moment of the two ring types and compute hydrogen-bond acceptor strength. The work was discussed by Muller in a commentary that highlighted Boström et al.'s work as a great example of MMPA in action and highlighted it as a useful lesson for medicinal chemists.[67] Related studies found that these general effects hold true in a specific example from a drug discovery program.[68]

3.10.3.1.3 Enantiomers

One of the more challenging structural changes to study is that of inversion of chirality. There are several challenges that make most of the matched pair finding methods ineffectual. The most important problem is that most methods require the pair to be defined as one specific structure type being converted into a second specific structure type. This would require a degree of specification of the chiral center that is usually impossible. Even the labels *R* and *S* are not generalizable because of their susceptibility to changes when the detailed nature of substituents changes. Also, many of the implementations of pair finding deliberately neglect stereochemistry. A further problem is that for molecules that contain more than one chiral center, inversion of overall chirality requires inversion of every stereocenter. As a consequence of all of these problems, the two reports concerning the influence of inverting stereochemistry upon properties have used nonstandard approaches to identifying pairs. Leach and coworkers identified enantiomeric pairs by transposing every occurrence of "@" and every occurrence of "@@" in the SMILES strings and then comparing the resulting SMILES string with the original database.[3] Bagdanoff et al., by contrast, used indexing based on structures with chirality flags removed in order to identify potential pairs in a first filtering step.[4] They subsequently inverted each stereocenter in the structures including chiral flags in order to verify which of the pairs correspond to inversion of chirality. Both studies examined solubility, permeability in Caco2 cells, cytochrome P450 inhibition, metabolism in microsomes, and hERG block. In addition, Leach et al. studied in vivo pharmacokinetic parameters, plasma protein binding, metabolism in hepatocytes, permeability in MDCK cells, and logD, and Bagdanoff et al. studied isocitrate dehydrogenase inhibition as an example of a potency target. Both approaches found that stereochemistry has no measurable effect on logD, solubility, permeability, and efflux. Meanwhile, in vivo pharmacokinetics, in vitro metabolism, hERG block, plasma protein binding, cytochrome P450 inhibition, and isocitrate dehydrogenase all have a dependency that can be detected although in some cases, Bagdanoff et al. suggest that the difference is too small to be of practical importance.

3.10.3.2 Specific Properties

Reports of MMPA now include studies of a great range of different endpoints of interest to compound designers. These have been divided into a number of categories.

3.10.3.2.1 Primary potency

Drug discovery projects typically aim to discover enzyme inhibitors (or activators), ion-channel blockers, receptor agonists, or antagonists. Examples of MMPA in this area are naturally therefore diverse, but progress could impact positively upon every drug discovery project. One of the earliest such studies, from Birch et al., describes the analysis of inhibition of glycogen phosphorylase.[21] As shown in Fig. 9, the effect of changing between the cores of some of the series of interest was examined for their effect upon pIC50 for inhibition, solubility and plasma protein binding.

Warner and coworkers examined effects on two ion channels, one of which (hKCNQ1) was the primary target and the other (hKCNE1) an undesired off-target.[58] They compared predictions made by examining similar compounds (near neighbors) with those made using MMPA and show a reduced RMSE for MMPA-based predictions compared with near-neighbor predictions; RMSEs of 0.33 and 0.39, respectively, were obtained. Predictions made by quantitative structure–activity relationships (QSAR) were less accurate with an RMSE of 0.40. They suggest that MMPA is a more effective means to avoid off-target effects than the other methods that were examined.

An example of MMPA taken from a real drug discovery program was provided by Waring et al. who were seeking activators of glucokinase of the type shown in Fig. 10.[14] They made matched pairs a central consideration in the selection of compounds that were to be made. All structural changes were exemplified as matched triplicates, which is to say that each structural change is very quickly represented as a set of three matched pairs such that MMPA can be performed immediately that the measured data are available. This permitted them to study the effect of structural changes upon pEC50 values for glucokinase activation, logD, and hERG

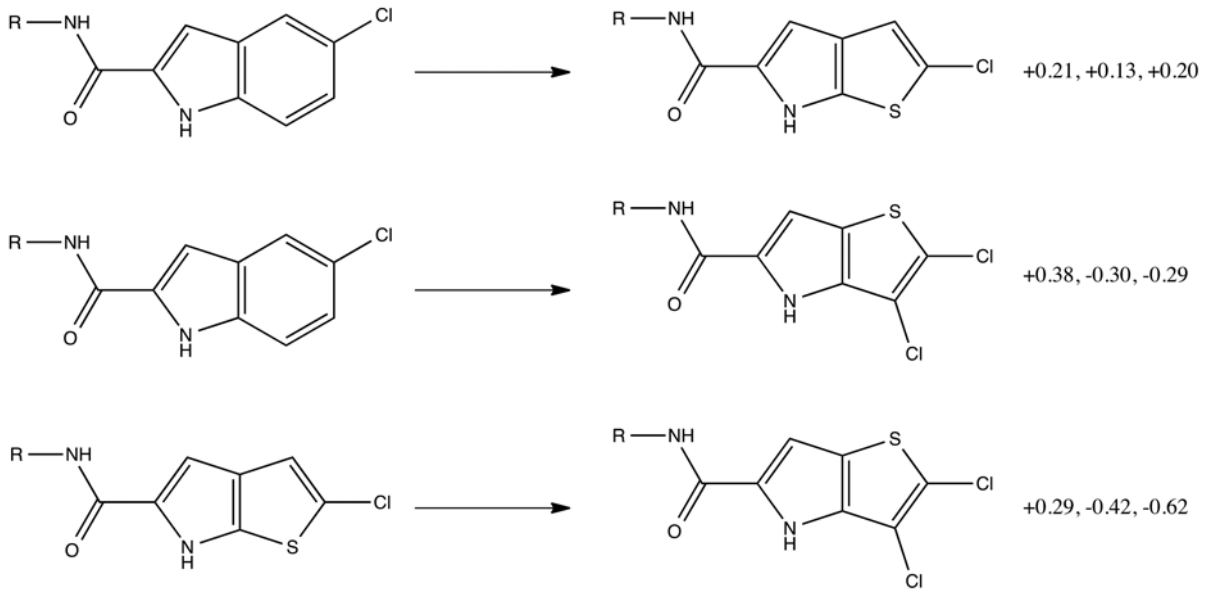

Fig. 9 Matched molecular pair analysis of inhibitors of glycogen phosphorylase. The mean change in pIC_{50}, $\log(f_u)$ for plasma protein binding, and log(Solubility) is given alongside each.

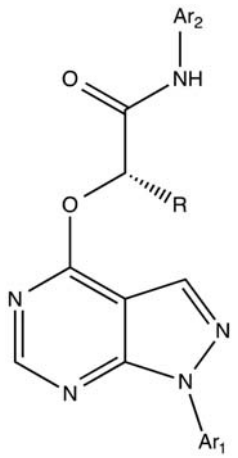

Fig. 10 In order to study the effect of different groups at R, Waring et al. set out to make sets of three representatives of each, in which Ar_1 and Ar_2 are varied.

block. The three representatives also permit them to rapidly build Free–Wilson type models in which representation is better, and therefore the models are more reliable.[6,69] It remains an open question whether three representatives are a large enough group to permit reliable predictions to be made. In a related piece of work, Tye and coworkers, when seeking to optimize dual inhibitors of the receptor tyrosine kinases IGF1R and InsR, emphasized the importance of making pairs of compounds varying only at one position.[17] They only made individual representatives so their analysis is less general and generalizable than that of Waring et al.

A significant effort to identify useful guidance concerning primary potency using MMPA is available as the SwissBioisostere database, described by Wirth et al. and is provided as a Web service.[54] This group has analyzed the ChEMBL database, using all values that have been annotated by the curators as confidence levels 8 and 9. Compounds with molecular weight above 1000 were excluded in order to keep run times down. They used Hussain and Rea's fragment and index method but modified the SMARTS definition for the bonds that are cut in order to prevent the cleavage of amide and similar bonds. The changing part was limited to 12 atoms or less, and context was encoded in a limited way according to whether the attachment point is an aromatic ring, an aliphatic ring, or an aliphatic chain. One of the starkest findings is that 47% of all the pairs that are found fall into sets with only one member. Only 13% of all pair sets have five or more pairs in them. Each pair was annotated according to the change in logP, tPSA, and molecular weight. The chemical diversity within each set is assessed by reporting the number of targets that have been studied, the number of target classes, and the number of Murcko scaffolds that contribute to the set.

Users can query the SwissBioisostere database in two ways: identifying all interesting changes for one substituent and investigating the effect of one specific transformation. In the first, a query substituent is drawn in. The database is then searched for all matched pairs in which that group has been replaced by others, and the changes reported as the number in which potency increased by more than 0.5 log units, the number in which the potency decreased by more than 0.5 log units, and the number where it stays the same (the magnitude of any change is less than 0.5 log units). These numbers are transposed into a score that ranks most highly those substituents likely to improve the activity and that are well exemplified. The changes in calculated physical properties are also provided in order to help the user select which groups to transform their query substituent into. The data can be downloaded as a CSV file. By way of example, the database was searched for replacements for the *t*-butyl group, and sets of pairs with at least five members were selected. The proportion of times that transforming t-butyl into a different group has caused an increase in potency is plotted against the mean change in logP for that transformation. This reveals that a wide variety of outcomes have been observed when replacing *t*-butyl, as is shown in **Fig. 11**. As discussed in the following section, the point in the top left corner of the plot in **Fig. 11** (at −2.8, 100) is for changing R-*t*-butyl to R-N(Me)Ac.

Users can also search for specific transformations in the SwissBioisostere database or drill down into the full set of pairs. The compound pairs can shed light on the applicability of any given change. For instance, the point in **Fig. 11** for R-*t*-butyl becoming R-N(Me)Ac is a set of nine compound pairs that are all histone deacetylase inhibitors. The user can therefore draw their own conclusion about whether this observation is likely to be relevant and effective in their own series. The data can also be searched back to the entries in ChEMBL allowing a very detailed level of scrutiny.

In 2008, Hajduk and Sauer from Abbott attempted to study the effect of adding certain substituents upon a host of different biological targets.[26] They computed the average effect upon potency of a set of 828 substituents. They discovered that for most of these, the mean change is close to 0 but that the widths of the distributions vary considerably. They highlighted a set of substituents that are worth trying in order to undertake an exploration of diversity and a set for when there is a need to increase potency; these groups all have a greater propensity to increase potency than the others (**Table 1**). This was one of the first general attempts to address the challenge that we have styled the "potency problem." When analyzing many properties with MMPA, the various positions around the molecule are not always strongly differentiated, but when considering the interaction with a specific target protein, each position is unique and is expected to have particular preferences. Capturing such effects in MMPA is exceptionally challenging. Recent attempts to use three-dimensional approaches go some way to address this.[47,49]

Dimova et al. also sought to address the "potency problem" by analyzing the ChEMBL database (limited to K_is) with MMPA in order to identify structural changes that reliably increase potency.[44] They found 31 such structural changes in which there were at least 21 examples, all of which change potency in the same direction. These are almost all GPCR modulators, and the structural changes showed mixed effects on logP, PSA, MW, and the number of rotatable bonds suggesting that this is a powerful set of ideas that could be tried during a drug discovery program.

In a study aimed at understanding the popularity of the *para*-chloro substituent on aromatic rings, Brown and coworkers studied matched pairs (among other things).[70] They discovered that *p*-Cl is reported about three times more commonly than *m*-Cl or *o*-Cl in IBEX, ChEMBL, the internal AstraZeneca compound collection, and the protein database of known drugs. Despite this, when they examined assays in ChEMBL to find matched pairs that differed by moving chlorine around a ring, they found that potency is not consistently better for any of these regioisomers, although there were discernible preferences for other properties.

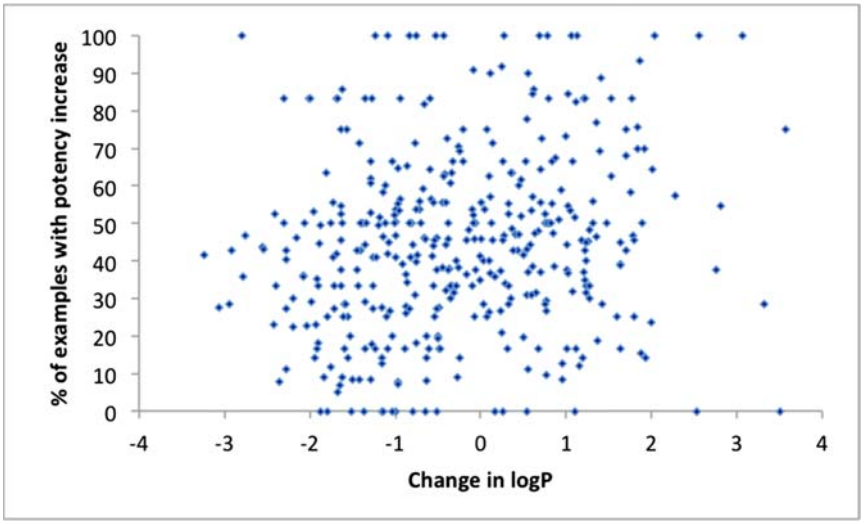

Fig. 11 The proportion of examples in which potency has increased is plotted against the calculated change in logP for a number of structural transformations in which *t*-butyl is replaced. The data are extracted from the SwissBioisostere database.

Table 1 A set of substituents recommended when seeking to sample diversity or to increase potency

Diversity set	*Potency set*
F	Br
Cl	CC(C)C
Br	C(F)(F)F
CC	C=C
C(F)(F)F	CC=C
OC	OC(C)C
N(C)C	OC(F)(F)F
CN(C)C	SC
CC(=O)OCC	CCN(C)C
C=O	S(=O)(=O)C
S(=O)(=O)C	S(=O)(=O)N
S(=O)(=O)N(C)C	c1ccccc1
c1ccncc1	c1cccnc1
c1ccco1	c1ccncc1
c1cccs1	c1ccco1
c1ccsc1	c1cccs1
C(=O)Nc1ccccc1	Cc1ccccc1
Cc1ccccn1	CCc1ccccc1
N1CCCC1	C(=O)Nc1ccccc1
N1CCOCC1	S(=O)(=O)c1ccccc1
N1CCN(C)CC1	C1CC1
CN1CCCC1	C1CCCC1
CN1CCOCC1	c1c(Cl)c(Cl)ccc1
c1c(C)c(C)ccc1	c1c(Cl)cc(Cl)cc1

Note: Groups are represented as their SMILES strings.

A significant set of contributions to understanding how potency might be improved using insights from matched molecular pairs has come from the extension of the concept to matched molecular series, which are described in the following section.[50,52,53]

3.10.3.2.2 In vivo pharmacokinetics

The ultimate measure of the pharmacokinetics of a compound during the discovery phase is in vivo studies in animals. These observations are complex and with a high degree of variability between them. The parameters derived are dependent upon a very large set of processes including the subtleties of absorption, distribution, metabolism, and excretion. As such, analyses of in vivo data often cannot reveal significant effects. This was exemplified by Leach et al., who contrasted the effects observed on solubility and plasma protein binding with much less distinct effects for the area under the plasma concentration–time curve (AUC) in rats. A significant difference between enantiomers was detected in in vivo pharmacokinetic parameters, despite the experimental variation inherent in such experiments.[3]

3.10.3.2.3 Metabolism

Achieving an appropriate level of metabolism is a requirement across all drug discovery programs. As such, it is unsurprising that it has received a great deal of attention in the MMPA field. It represents an interesting challenge from which certain general insights might be gleaned. Metabolism involves the action of a suite of enzymes (such as the cytochromes P450 and glutathione transferases), which are often viewed as tolerant to a diversity of substrates. In MMPA, the effect of structural changes upon interactions with one specific enzyme is considered challenging to analyze, whereas the effect of structural changes upon systems dependent upon a structurally tolerant enzyme or a large set of enzymes might be more likely to be amenable. Thus, metabolism may well represent the interesting intersection point in which certain specific effects are not captured by the analysis but in which general trends can be ascertained.

One of the most important contributions to understanding metabolism has been provided by a series of papers from Dossetter and coworkers at AstraZeneca. In these papers, the effects of changing the structure of moieties often associated with metabolic liabilities were investigated: aromatic rings and methylene carbons. In this case, metabolism was by human liver microsomes measured as the intrinsic clearance (Cl_{int}) for each compound. These values were transformed to $\log(Cl_{int})$ in order to place them on a linear scale. In the first of the series, the influence of substitution patterns in a set of phenyl rings was investigated.[23] In total, 73 combinations of substituents around the phenyl ring (as well as a small number of heteroaromatic replacements) were investigated. From the observed variations in Cl_{int}, Dossetter is able to produce a recommended sequence of substitution patterns that should be considered when attempting to optimize metabolism. These are compared to the decision tree-type recommendations of Topliss who suggested substituents to consider in order to proceed logically when trying to optimize the substitution

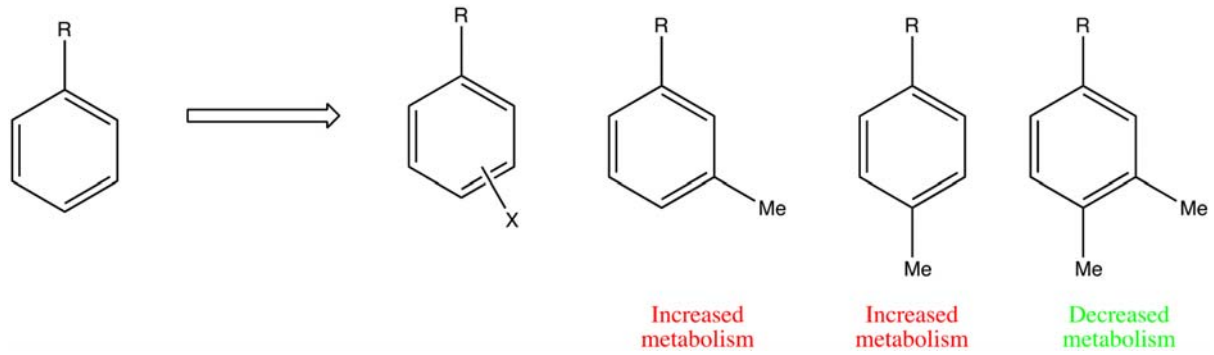

Fig. 12 Dossetter has applied MMPA to understand the effect upon metabolism by human liver microsomes (HLM) of changing phenyl to substituted phenyl. Surprising examples of adding methyl groups are shown.

pattern around phenyl rings. On average, the changes were found to center around zero, and less than 5% of all pairs showed an average change in Cl_{int} of more than an order of magnitude (in either direction). Most substituents were more likely to reduce metabolism at the 4-position than at the 2- or 3-position. Methyl is an exception to this rule and is better at the 2-position. Some interesting interactions were identified, such as that exemplified in Fig. 12 where adding a methyl at the 3-position was found, on average, to increase metabolism, as was adding a methyl at the 4-position. By contrast, adding two methyl groups, at both the 3- and the 4-positions, was found, on average, to reduce metabolism. This example may be one of those that exemplify the dilemma with metabolism discussed earlier. There is a general effect of adding the substituents, which changes the physical properties of the molecules. This increases the general metabolic liability. This is counteracted by a specific effect whereby one methyl group can sterically crowd another and reduce its liability to be metabolized.

It is emphasized that interpreting these observations is challenging because not only can the site of metabolism vary among the different structures, but also the isoform involved in the metabolism can change. Dossetter ultimately recommends using a combination of the Topliss approach (which is based on the electronic and lipophilic properties of substituents) and the metabolism-related approach in order to proceed logically to optimize a series with a minimal number of compounds being required.

The logical extension of the investigation of substitution patterns around phenyl rings was to heteroaromatic replacements. In particular, Dossetter and coworkers looked at disubstituted phenyl rings that were transformed into heteroaromatic alternatives.[13-] When undertaking these studies, several sets were found to be close to having enough pairs to be sufficiently diverse. In these cases, extra compounds were tested in order to expand the coverage with minimal extra testing. By obtaining data in the same run of the same assay, they were able to add pairs in which the data were as directly comparable as possible.[38] They discovered that changes to heteroaromatic rings from phenyl are more likely to lead to increases in metabolic stability than for any of the substitution patterns on a phenyl ring (see earlier) or changes to methylene carbons (see in the succeeding text). They were not able to identify any clear role for lipophilicity in determining the outcome. The various heteroaromatic ring alternatives are summarized in Fig. 13 in which the most stable alternative is on the left and the least stable on the right.

The final structural change considered by Dossetter was replacements for methylene carbons (Fig. 14).[22] Methylene carbons, particularly those next to aromatic rings, are often considered to be particularly liable to metabolism, likely due to the propensity for the C—H bonds on these carbons to undergo homolytic cleavage. MMPA investigated the change in $\log(Cl_{int})$ when CH_2 was transformed into a range of alternatives. These were divided into pairs in which the CH_2 was benzylic or alkyl. In general, and despite some suggestions in the literature, adding a methyl group at a benzyl position was not found to decrease metabolism. The exception to this may be the doubly benzyl substructure $ArCH_2Ar$. Transforming CH_2 to CF_2 was found to be approximately neutral with regard to metabolism for benzyl CH_2 groups but beneficial for alkyl CH_2 groups. Replacing CH_2 with O, NMe or SO_2 is beneficial in $AlkCH_2Alk$, and O and S are beneficial for $ArCH_2Ar$. Some of the observations were found to go in the opposite direction to that that might be expected based on lipophilicity considerations (which should see Cl_{int} increase as logD increases). There was only a weak correlation found when the change in $\log(Cl_{int})$ was plotted against the change in logD.

In a study of a range of properties by scientists at Pfizer, experimental data from studies using human liver microsomes were investigated.[39] They classified the observed changes in several properties, with one interesting class being on or off switches; these are groups that when added always either completely eliminate a property or universally introduce it. It was found that for human liver microsomes, such transformations were relatively common, corresponding to 4.3% of all transformations investigated. They ascribe this to the important role of specific molecular recognition patterns. They showed that changing 2-pyridyl to 1-imidazole decreased metabolism.

Lewis and Cucurull-Sanchez categorized changes in Cl_{int} measured with human liver microsomes according to whether they were greater than a twofold increase, less than a twofold decrease, or somewhere in between.[25] Like Dossetter, they investigated the transformation of phenyl to substituted phenyls. They found that there is a general correspondence with lipophilicity, as illustrated in Fig. 15. They suggest that 4-Me and 4-OMe are worse than might have been expected because they introduce a group that is specifically metabolized more rapidly than might have been caused by the change in physical properties. They also highlight that *p*–

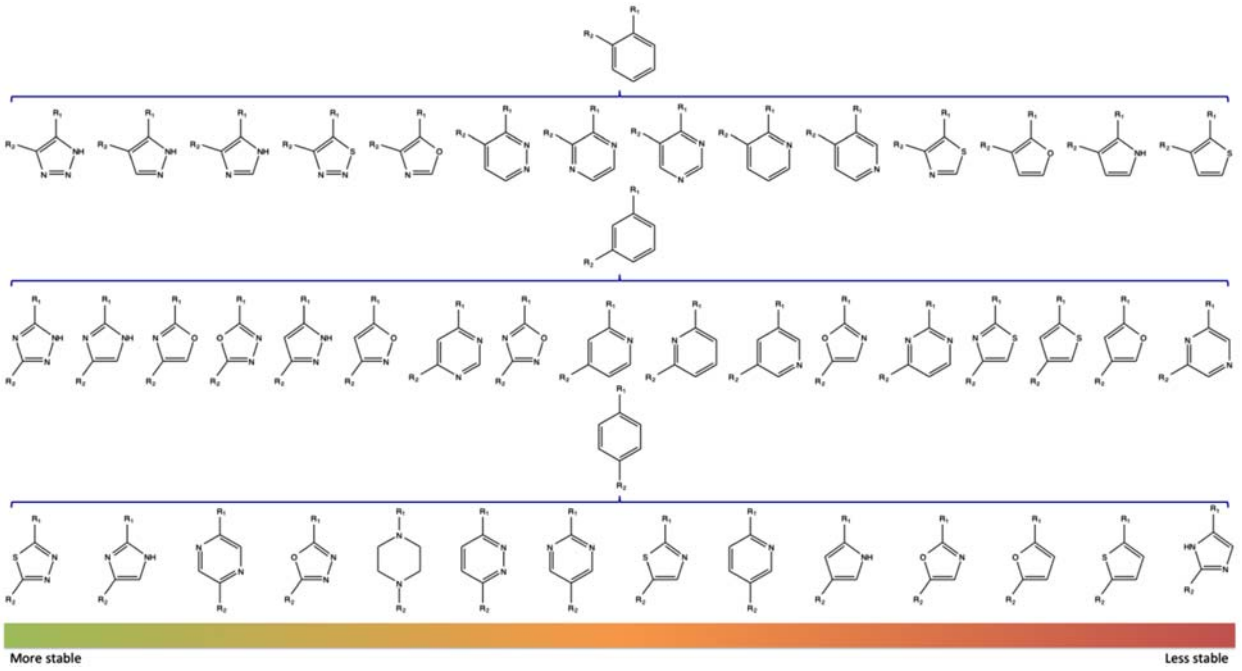

Fig. 13 The heteroaromatic alternatives to disubstituted phenyl rings studied by Dossetter et al. The top set are alternatives to 1,2-disubstituted phenyl, the middle set to 1,3-disubstituted phenyl, and the bottom set to 1,4-disubstituted phenyl. The most metabolically stable alternative is on the left and the least stable (most rapidly metabolized) on the right.

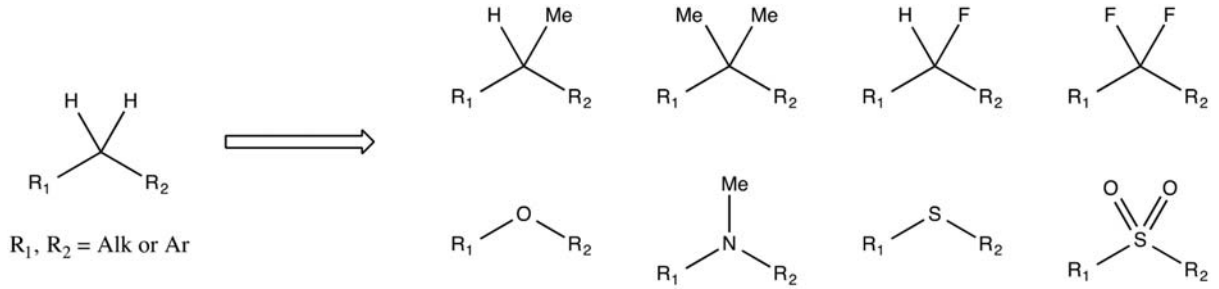

Fig. 14 Transformations of methylene carbons considered by Dossetter in his study of their effects upon metabolism by human liver microsomes.

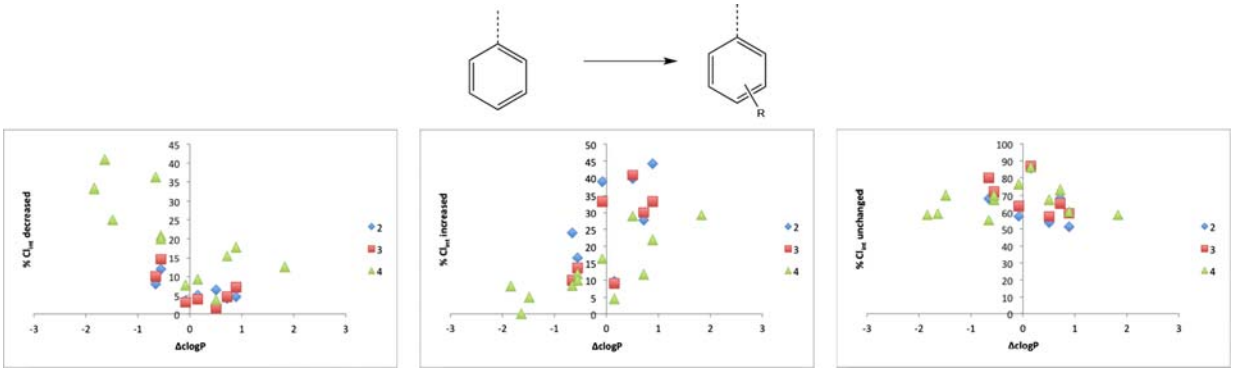

Fig. 15 Lewis and Cucurull-Sanchez investigated the effect of changing phenyl to substituted phenyl upon Cl_{int} measured in human liver microsomes. On the left, the percentage of cases in which Cl_{int} decreased is plotted against the corresponding change in clogP; in the middle, the percentage of case in which Cl_{int} increases is plotted; and on the right, the percentage of cases in which Cl_{int} is unaffected (within twofold) is plotted.

F performs more or less as expected according to lipophilicity, despite its reputation as a group for blocking metabolism. They found (as is apparent in the plots in Fig. 15) that groups at the 4-position tend to decrease metabolism more effectively than the same group at the other positions around the ring. A small number of disubstitutions were also investigated, and a Topliss-like decision tree for metabolism was proposed, much like that proposed by Dossetter.[23]

The effect of inverting chirality upon a number of properties was investigated by Leach et al. and by Bagdanoff et al.[3,4] In both cases, the measurements of metabolism were found to support significant differences between enantiomers. Similarly, Boström and coworkers found that 1,2,4-oxadiazoles tend to have higher rates of metabolism than the corresponding 1,3,4-oxadiazole.[27]

In further studies, scientists from Pfizer investigated the effect that changes to cyclic ethers have upon metabolism as measured by Cl_{int} in human liver microsome assays.[28] They had observed some interesting trends in one particular drug discovery project and wished to investigate whether this was specific to those compounds or a more general phenomenon. They identified matched pairs in which the ring size is changed and in which the oxygen atom is moved around the ring (Fig. 16). They found that reducing ring size always decreases the Cl_{int}, and they rationalize this as primarily driven by reductions in lipophilicity. They also found that 3- and 4-linked rings are generally more stable than the 2-linked equivalents. These changes are often in contradistinction to the small changes expected if lipophilicity were dominant. Given recent interest in the progress of the epoxide-containing molecule beloranib as an obesity therapy, it is a shame that these studies were not extended to epoxides.[71]

Reaction with glutathione (GSH), either chemically or biochemically (catalyzed by glutathione transferases), is also an important component of metabolism. In a study of the chemical reaction with GSH, Morley and coworkers investigated the effect of adding NH_2 to the position para to a reactive nitrile group (Fig. 17).[20] They were specifically interested in tempering the reactivity of covalent inhibitors, but this is nonetheless relevant to metabolism. They discovered that in this case, the reactivity is diminished and the half-life increases by a factor of more than 4.

3.10.3.2.4 Permeability and efflux

Absorption is a property of concern to all programs that seek orally dosed medications that require systemic exposure. Other routes of delivery may also need to pass through layers of cells that form sealed interfaces. The most common assay for measuring the permeability of compounds through such layers is the Caco2 assay in which a layer of cells (deriving from a colon carcinoma) is formed into barriers and the movement of compounds from the apical side of the layer to the basolateral and vice versa is studied. The Madin–Darby canine kidney (MDCK) assay is also used, particularly its variant in which the transporter Pgp is overexpressed. The PAMPA assay replaces the cells with an artificial membrane, usually infiltrated with long-chain hydrocarbons. In their studies

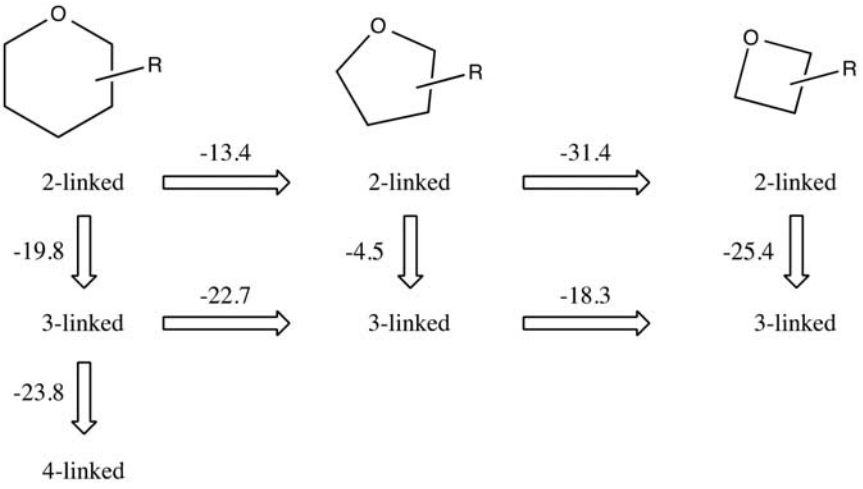

Fig. 16 The mean change in Cl_{int} for changes in the ring size and connectivity of some cyclic-ether-containing compounds.

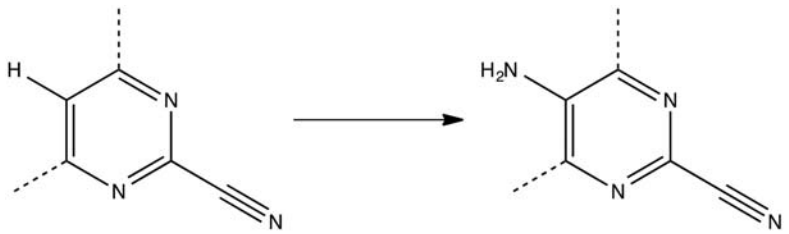

Fig. 17 The structural transformation investigated by Morley et al. for its effect on reaction with glutathione.

investigating the effect of inverting stereochemistry, scientists at AstraZeneca and independently at Novartis discovered that inverting chirality does not have a measurable effect upon absorption in either Caco2 or MDCK assays, even when active transport involving recognition by proteins is involved.[3,4] By contrast, Keefer et al. investigated the effect of structural changes upon Pgp-mediated efflux and found that this is the system in which so-called on switches or off switches were most common; 6.7% of all pair sets had one member of the pair not subject to efflux and the other member of the pair is.[39] This suggests that certain chemical groups can be responsible for the whole molecule property and their presence or absence is the determinant of their susceptibility to efflux. By contrast, such switches were rather uncommon for permeability. They also found that the change 2-pyridyl to 1-imidazole increased efflux. Gleeson and coworkers used MMPA to study permeability measured in PAMPA, which involves only passive processes.[24] They found that whereas many pharmaceutical properties get worse as clogP increases, permeability sees the opposite trend.

3.10.3.2.5 Toxicity

Toxicity is a multiheaded hydra, with many causes that can be linked to the structure of molecules in all manner of ways: direct interaction with specific targets, chemical reactivity (either specific or general), the same for metabolites of compounds, physical disruption of biological systems, or many other causes. The ultimate arbiter of toxicity during drug discovery is typically long-term studies in animals or indeed in humans during clinical trials. Typically, only very small numbers of compounds can be studied in such trials for ethical and economic reasons. As such, very few pairs of compounds that might be considered matched pairs have been studied.

Sushko et al. used MMPA to analyze the differences between measured values relevant to mutagenicity and aquatic toxicity. They also incorporated the differences between values predicted by QSAR models.[36]

During the course of the last few decades, a few targets have been linked with toxic or undesirable outcomes. A few of these have therefore been studied in more detail and with enough compounds to make them suitable for MMPA. Indeed, block of the hERG potassium ion channel may be one of the targets that have been studied most often in MMPA.

3.10.3.2.5.1 hERG

The hERG encodes a cardiac potassium ion channel. Blocking this channel can prolong the QT interval and lead to torsades de pointes.[72] This serious toxicological liability can now be screened for, and consequently, large datasets now exist, which are ripe for MMPA. In their studies of enantiomeric pairs, Leach et al. and Bagdanoff et al. discovered that hERG block has a small but significant dependency upon chirality, suggesting that molecular recognition can be important.[3,4] In what may be a related observation, Kramer and coworkers discovered that certain sets of matched pairs show a broader distribution (a larger standard deviation) than others.[38] They ascribe this to these sets having representatives in which the structural context is important, which is often the signature of effects that depend upon specific recognition at a receptor. By contrast, Gleeson suggests that changes to hERG inhibition are broadly in line with physical property changes.[24]

In their important contribution describing the influence that structural context can have upon properties, Papadatos et al. use hERG block to exemplify some interesting cases. For instance, they find that when a methoxy substituent is added (in place of H), across all molecular contexts, there is an approximately equal likelihood of hERG potency increasing or decreasing. When the same change is limited to adding to alkyl carbon atoms, the change is more likely to be beneficial, just as it is when added ortho to an aza nitrogen (**Fig. 18**). When methyl is transformed to fluorine, on average, it is equally likely to increase or decrease hERG binding. However, when the same change is made ortho to a benzylamine, it is most likely to be beneficial.

Boström et al., in their study of oxadiazoles, find that 1,2,4-oxadiazoles have higher hERG affinity than the corresponding 1,3,4-oxadiazoles, which is in line with their higher logD (**Fig. 19**).[27] They note that the changes in pK_a that are caused by this structural change do not influence hERG potency. A further study revealed that para-Cl is (on average) worse, from a hERG perspective, than the ortho or meta equivalents (**Fig. 19**).

In an example taken from a real drug discovery project, Waring et al. highlight an example in which MMPA was able to suggest changes that would retain potency while reducing hERG block (**Fig. 20**).[15] In a study from some of the same authors, sets of three compounds at a time were made in order to facilitate MMPA and Free–Wilson analysis (**Fig. 21**).[14] A number of effects upon hERG caused by structural changes at two positions around a specific scaffold of interest in a glucokinase program were discussed. These reveal effects that are broadly in line with lipophilicity although the cyanopyridine is an interesting exception to this where hERG potency increases despite a reduced lipophilicity.

In another example from a drug discovery project, Tye and coworkers discovered that for a series of IGF1R/InsR tyrosine kinase inhibitors, changes in hERG potency generally track with logD, with a slope of $\sim$0.4 for the line of best fit.

3.10.3.2.5.2 Inhibition of the cytochromes P450

One well-known liability that can cause dangerous drug–drug interactions is the inhibition of the enzymes involved in drug metabolism of which the cytochromes P450 are the most important group. As a consequence, the inhibition of these enzymes has been measured for a great many compounds, which makes this property amenable to MMPA. Examples of studies of cytochrome P450 inhibition include that by Sushko in which MMPA and QSAR were used.[36] They found that the performance of MMPA was similar when analyzing changes in experimentally derived data or data derived from a QSAR model for the 3A4 isoform. Gleeson examined the differences in inhibition for the isoforms 1A2, 2C9, 2C19, 2D6, and 3A4 and found SAR broadly in line with the known preferences and structures of these isoforms.[24] As with most of the properties he studied, inhibition of the cytochromes P450 tended to

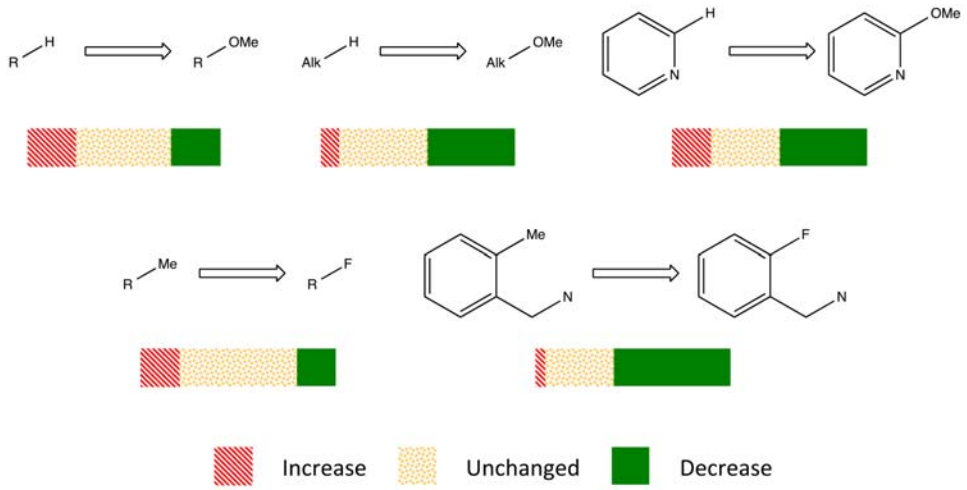

Fig. 18 The influence of structural context upon the effect on hERG block of some structural changes. The colored bar represents all of the examples (100%) and is divided into sections that correspond to the proportion of examples in which making the structural change causes hERG block to increase, decrease, or remain unchanged.

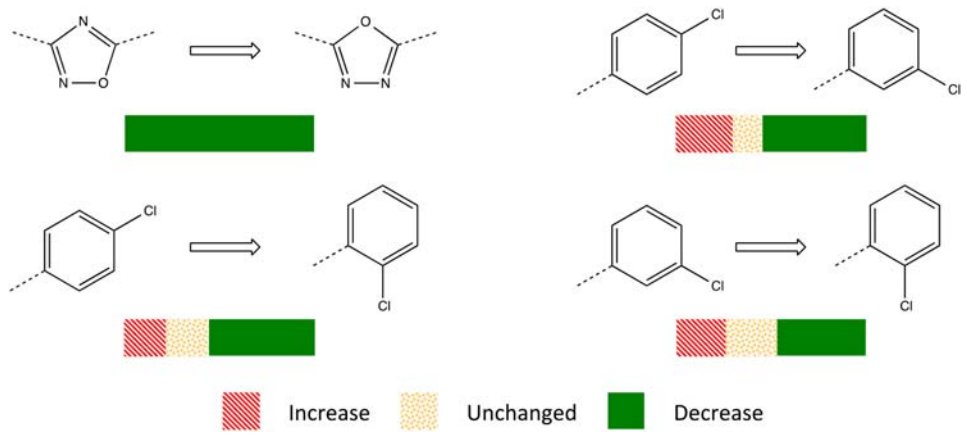

Fig. 19 Influence on hERG of some structural changes. The colored bar represents all of the examples (100%) and is divided into sections that correspond to the proportion of examples in which making the structural change causes hERG block to increase, decrease, or remain unchanged.

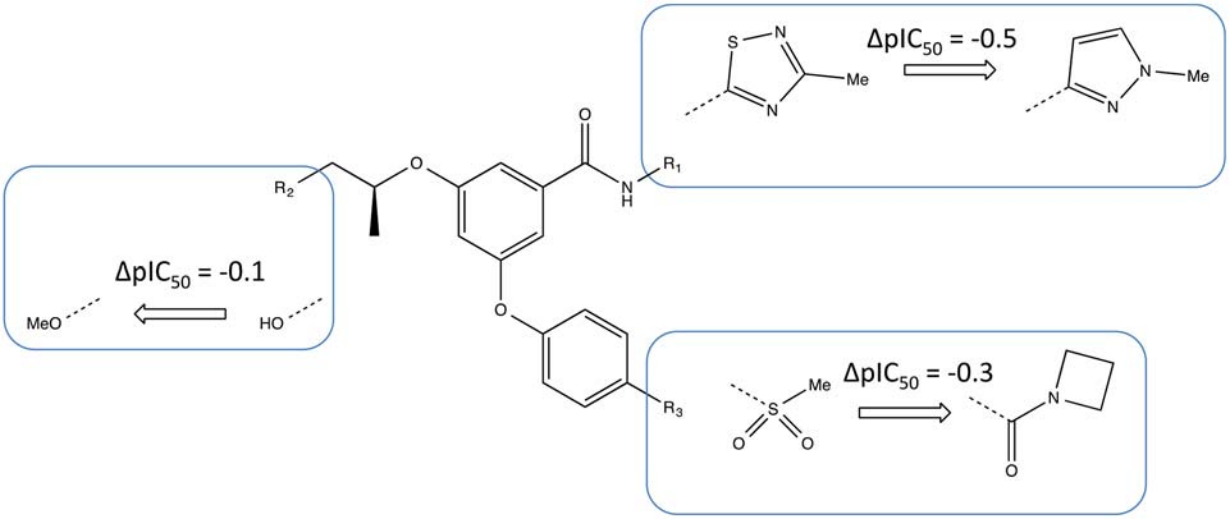

Fig. 20 Influence on hERG potency of changes around a glucokinase inhibitor core.

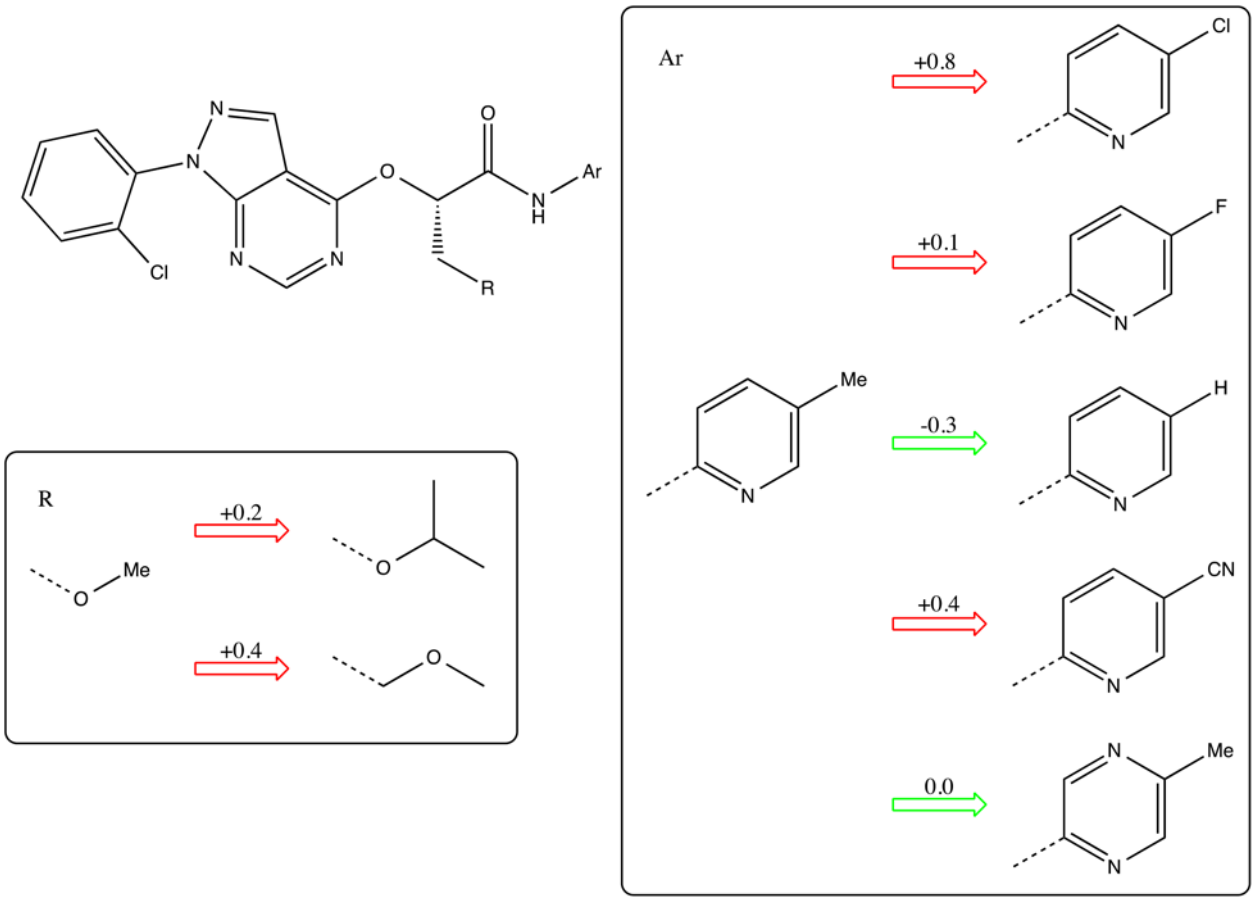

Fig. 21 Average changes in hERG pIC50 for sets of matched pairs with three representatives in each for specific structural changes in a glucokinase discovery project.

increase with changes that increase lipophilicity. In their studies of the effect of inverting stereochemistry, Leach et al. found a contradictory large difference between enantiomers for several isoforms despite the identical physical properties.[3] The isoforms studied, when placed in order of the difference between enantiomers (largest to smallest), are 2D6, 2C19, 1A2, 2C9, and 3A4. The fact that 3A4 was found to have only a small difference was in concurrence with the findings of Bagdanoff et al. who were unable to detect a difference between enantiomers for 3A4.[4] In studies comparing 1,2,4-oxadiazoles and the equivalent 1,3,4-oxadiazoles, Boström et al. found the former to be slightly stronger inhibitors of the cytochromes P450 than the latter. Geppert and Beck used cytochrome P450 data (from the 2C19, 2C9, 2D6, and 3A4 isoforms) in their studies using fuzzy matched pairs.[45]

3.10.3.2.6 Solubility

The first publication in which the term MMPA was coined included an analysis of the effect upon solubility of adding a small number of substituents to aromatic rings.[5] These are shown in Fig. 22. This analysis was extended by Leach et al. to a wider selection of substituents, and the mean change in log(Solubility) found by them is also shown in Fig. 22. A number of outliers in the distributions were highlighted, and (as discussed in "Context Dependence; Set Size Versus Specificity" section) these were generally assigned to different conformational preferences. The final column, describing the effect of adding methylsulfone, was revisited in a subsequent publication in which it was reported that since the first publication, many more pairs of molecules differing by this structural change had been made, presumably inspired by the attractive positive mean change found. However, these later pairs had been less successful, and the mean had become negative.[73] When the standard error in the mean (shown in the table at the bottom of Fig. 22) was considered, it was found that all the data for methyl sulfone addition are consistent with a mean that is positive but rather smaller than that originally found. The surprisingly weak solubility improvement caused by methyl sulfone addition, despite large decreases in logD, was investigated in a series of GPR119 agonists using small-molecule crystal structures that highlighted the geometric and electrostatic complementarity between the oxygen and CH bonds of these groups and that these form extended interaction networks in the solid state.[74] Haubertin and Bruneau also reported on the effect of substituents upon solubility but were less strict in defining the positions to which those substituents were attached.[31]

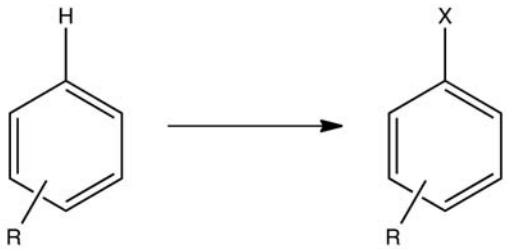

Substituent	Br	Cl	F	OMe	Me	CN	CF_3	OH	SO_2Me
Mean change in log(Sol) in Kenny and Sadowski	-1.2	-0.8	-0.2	-0.1	-0.2				
Mean change in log(Sol) in Leach et al. [S.E.M.]	-1.10 [0.10]	-0.67 [0.04]	-0.22 [0.03]	-0.11 [0.04]	-0.21 [0.06]	-0.26 [0.09]	-0.81 [0.09]	+0.07 [0.18]	+0.26 [0.12]

Fig. 22 Mean changes in log(Solubility) for the addition of a set of substituents to aromatic rings.

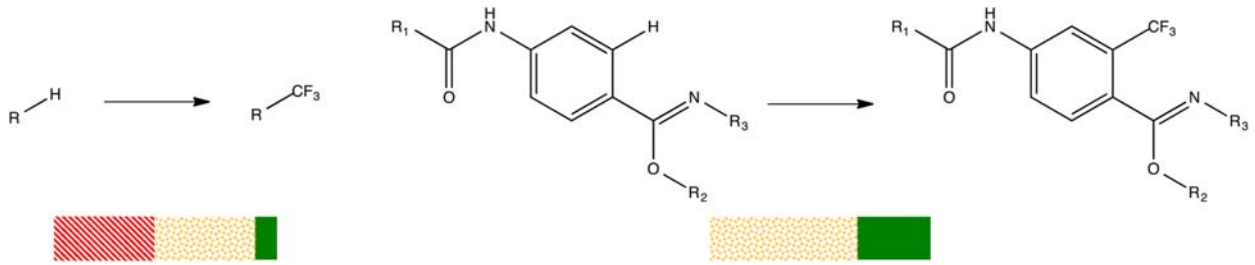

Fig. 23 Context specificity of the effect of adding CF_3 upon solubility. The colored bar represents all of the examples (100%) and is divided into sections that correspond to the proportion of examples in which making the structural change causes hERG block to increase, decrease, or remain unchanged.

This context specificity was explored further by Papadatos et al. who included solubility in their study of how chemical context can influence the outcome to be expected for matched pairs. They note that in general, adding CF_3 groups is very unlikely to increase solubility but identify a subset in a rather specific chemical context where there is a significant chance that solubility will increase and for which they found no examples in which solubility decreases (Fig. 23).

The effect of adding methyl groups to a number of heteroatom types has also been studied by a number of groups. The first publication in the MMPA area to investigate this was by Leach et al. but had been inspired by the work of Birch et al., which was not published until later.[1,21] Birch et al. reported that methylating the amides present in a series of indan-based glycogen phosphorylase inhibitors led to a surprising increase in solubility. They described some of the conformational and hydrogen-bonding effects that might contribute to this. Leach et al. extended this work to looking at the methylation of a number of heteroatom types, which are reported in Fig. 24.

Ritchie et al. also examined the effect of methylating some oxygen and nitrogen atom types.[43] They examined primary and secondary amides and sulfonamides, ureas, carbamates, amines, anilines, aromatic nitrogen atoms, carboxylic acids, phenols, and alkyl alcohols (Table 2). They ensured chemical diversity within each set of pairs by requiring each to contain at least 10 clusters when clustered using fingerprints, with the exception of a small number of sets that had less than 10 members in total. These studies used solubility as measured from a dimethylsulfoxide (DMSO) stock solution and therefore might not be expected to detect the important solid-state effects highlighted by Leach et al. or Zhang et al.[1,41] It is therefore interesting that methylation of secondary amides is still found to increase solubility. By contrast, methylating sulfonamides universally decreases solubility, in line with an increase in lipophilicity. Methylation of ureas is also found to increase solubility, but the sets of pairs are too small to be confident; they find a hint that the effect of methylation of ureas may depend upon the lipophilicity of the urea in question. Methylation of carbamates has little effect upon solubility. All the methylations of oxygen atoms that were investigated (alcohols and carboxylic acids) suggest that solubility decreases, on average, for each structural type.

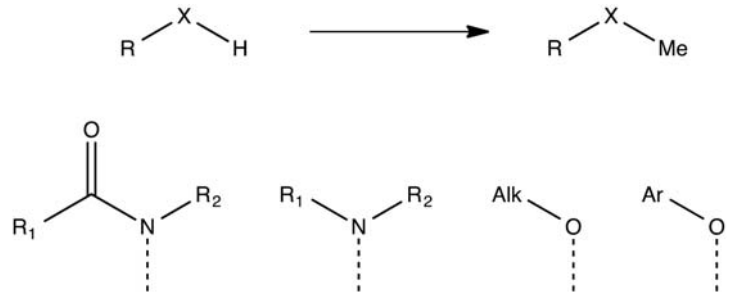

Substituent	Amide	Amine	Alkyl alcohol	Phenol
Mean change in log(Sol) [S.E.M.]	+0.64 [0.06]	-0.32 [0.07]	-0.01 [0.05]	-0.22 [0.20]

Fig. 24 The effect on log(Solubility) of methylating certain heteroatom types.

Table 2 The influence of methylation upon log(Solubility) and logD

Heteroatom type	*Subtype*	*Mean change in log(Sol) (SEM)*	*Mean change in logD (SEM)*
Amide	$AlkCONH_2$	+0.11 (0.04)	+0.35 (0.03)
	$ArCONH_2$	+0.07 (0.03)	+0.45 (0.02)
	AlkCONHAlk	+0.06 (0.02)	+0.54 (0.03)
	AlkCONHAr	+0.11 (0.03)	+0.45 (0.03)
	ArCONHAlk	+0.25 (0.03)	+0.14 (0.03)
	ArCONHAr	+0.39 (0.08)	−0.42 (0.13)
Sulfonamide	$AlkSO_2NH_2$	−0.09 (0.12)	+0.28 (0.20)
	$ArSO_2NH_2$	−0.10 (0.07)	+0.67 (0.02)
	$AlkSO_2NHAlk$	−0.33 (0.09)	+0.68 (0.06)
	$AlkSO_2NHAr$	−0.22 (0.08)	+0.83 (0.14)
	$ArSO_2NHAlk$	−0.23 (0.04)	+0.79 (0.03)
	$ArSO_2NHAr$	−0.42 (0.08)	+1.11 (0.08)
Ureas	AlkNHCONHAlk	+0.36 (0.11)	+0.62 (0.08)
	AlkNRCONHAlk	−0.02 (0.06)	+0.69 (0.04)
	ArNHCONHAr	+0.61 (0.14)	+0.01 (0.10)
	ArNRCONHAr	+0.94 (0.44)	−0.47 (0.25)
Carbamates	ROCONHR	−0.09 (0.06)	+0.58 (0.08)
Amines	AlkNHAlk	−0.01 (0.01)	+0.83 (0.02)
	AlkNHAr	−0.04 (0.02)	+0.78 (0.03)
	ArNHAr	+0.14 (0.04)	+0.54 (0.04)
	Aromatic NH	+0.04 (0.02)	+0.60 (0.02)
Alcohols	AlkOH	−0.19 (0.02)	+1.14 (0.03)
	ArOH	−0.21 (0.02)	+1.13 (0.03)
Carboxylic acids	AlkCOOH	−0.65 (0.04)	+3.02 (0.06)
	ArCOOH	−0.94 (0.04)	+3.36 (0.04)

The same authors also investigated the effect of exchanging an amide for a sulfonamide. They found that for R_1CONHR_2 becoming $R_1SO_2NHR_2$, the effect upon solubility is small, with a mean change of +0.12. However, when the nitrogen has been methylated, the effect of transforming $R_1CON(Me)R_2$ into $R_1SO_2N(Me)R_2$ corresponds to a large decrease in solubility, with a mean difference of −0.52 in log(solubility) measurements.

An interesting impact of chemical context was investigated by Ritchie et al.[43] They reported that when adding methyl to heteroatoms, it is important to consider the possibility that the hydrogen that is being replaced might be involved in an intramolecular hydrogen bond. When this is the case, they find that the outcome can often be very different to that that would otherwise be expected. For instance, methylating an amide in any of the contexts shown in Fig. 25 leads to large increases in solubility and decreases in logD because the hydrogen-bonding partners form better interactions with water in the absence of the intramolecular interaction.

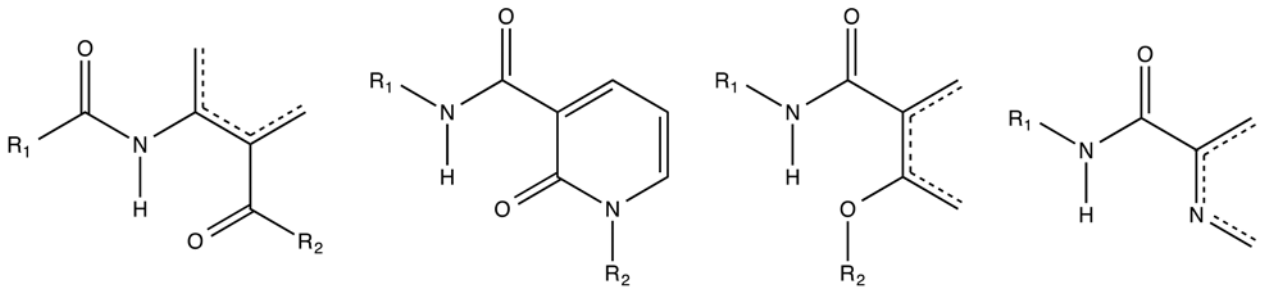

Fig. 25 Chemical contexts in which methylation disrupts an intramolecular hydrogen bond.

It is to be expected that in their survey of enantiomeric pairs, both Leach et al. and Bagdanoff et al. found that there is no difference between enantiomers in terms of their solubility.[1,4] Boström et al. found that 1,2,4-oxadiazoles tend to have lower solubility than the equivalent 1,3,4-oxadiazole, in line with their higher logD.

Zhang et al. used MMPA to study solubility data composed of 720 measurements from the literature and approximately 2000 internal data from Pfizer.[41] They focused upon the effects caused by group addition and by group exchange in sets of pairs that had at least 20 in the set. They compute the median value of the change in solubility and the percentage in which solubility increases or decreases. They highlight the general tendency of halides, pseudohalides (e.g., CF_3), and longer alkyl chains to decrease solubility. Certain polar groups were also found to reduce solubility more often than they increase it. These include primary amides, secondary amides, and reversed amides. Even the addition of a carboxylic acid was found to decrease the solubility in 55% of the matched pairs they studied. They ascribe this to a solid-state effect, with these polar groups forming crystal-packing motifs that stabilize the lattice to a greater degree than they enhance interactions with water in the liquid state. They contrast these findings, which are from an assay that uses solid samples, with an MMPA of kinetic solubility data in which the samples start in DMSO. In this other assay, they see the opposite effect with the polar groups causing an increase in solubility; for instance, almost all additions of carboxylate correspond to an increase in solubility in the kinetic solubility assay. They plot the changes in solubility in the assay from solids against pi values, and this highlights the three amide-containing groups already mentioned and SO_2NH_2 and SO_2Me. All of these groups contain donors and acceptors, which are able to form interactions with one another in the solid, apart from SO_2Me, but other studies found that these groups can form nonclassical hydrogen bonds in which the CH bonds adjacent to the sulfur can act as hydrogen-bond donors.[74] Zhang et al. also examined the effect of exchanging substituents and plotted their findings as heat maps, which provide useful guidance about which transformations might be considered when an increase in solubility is desired.

3.10.3.2.7 Melting point

An alternative means of investigating solid-state effects, such as those that so clearly influence solubility, is to perform MMPA on compounds with measured melting points. Such a study was undertaken by Schultes et al.[42] In order to ensure that, as far as it is possible, their studies related to the most stable polymorph, they used the highest melting point (T_m) that was reported for each compound in an in-house database and in the publicly available MDPI dataset. Each compound was classified according to a number of descriptors: the number of hydrogen-bond acceptors and donors, the number of halogen atoms, clogP, and the number of rotatable bonds. Pairs were identified using the fragment and index approach. In order to generalize their results, pairs were grouped such that all of the calculated descriptors stay the same except for one. This allowed them to deduce that increasing the number of hydrogen-bond acceptors tends to increase the melting point, increasing the number of hydrogen-bond donors increases T_m to a greater degree, and increasing the number of donors while decreasing the number of acceptors tends to still lead to increases in T_m. Increasing the number of rotatable bonds tends to increase T_m, while clogP does not have an influence that is significant once the change in the number of halogens is taken into account. They mention some examples, which illustrate the interplay of melting point and solubility; adding an OH not only increases solubility but also increases T_m suggesting that the enhanced affinity for water overrides the increased lattice energy. They highlight the five changes in each of the two datasets that they have studied, which cause the largest change in melting point, and for which, there are at least five examples. These are shown in **Fig. 26**.

3.10.3.2.8 Plasma protein binding

There are a number of proteins present in plasma at high concentration, which play an important role in transporting molecules including drugs. These proteins include albumin and α-acid glycoprotein. A few reports have been published describing the findings of MMPA applied to the binding affinity observed to these proteins. Leach et al. studied the same structural changes as they had for solubility (described earlier) and found the mean changes reported in **Table 3**.[1] These are broadly in line with the effect of the structural changes on lipophilicity.

Haubertin and Bruneau also investigated the effect of a range of common substituents upon plasma protein binding and also found changes broadly in line with lipophilicity.[31] Birch et al. investigated the effect of the common bioisosteric replacement of a carboxylic acid with a tetrazole and found that the fraction unbound would change by a factor of 0.3 on average suggesting

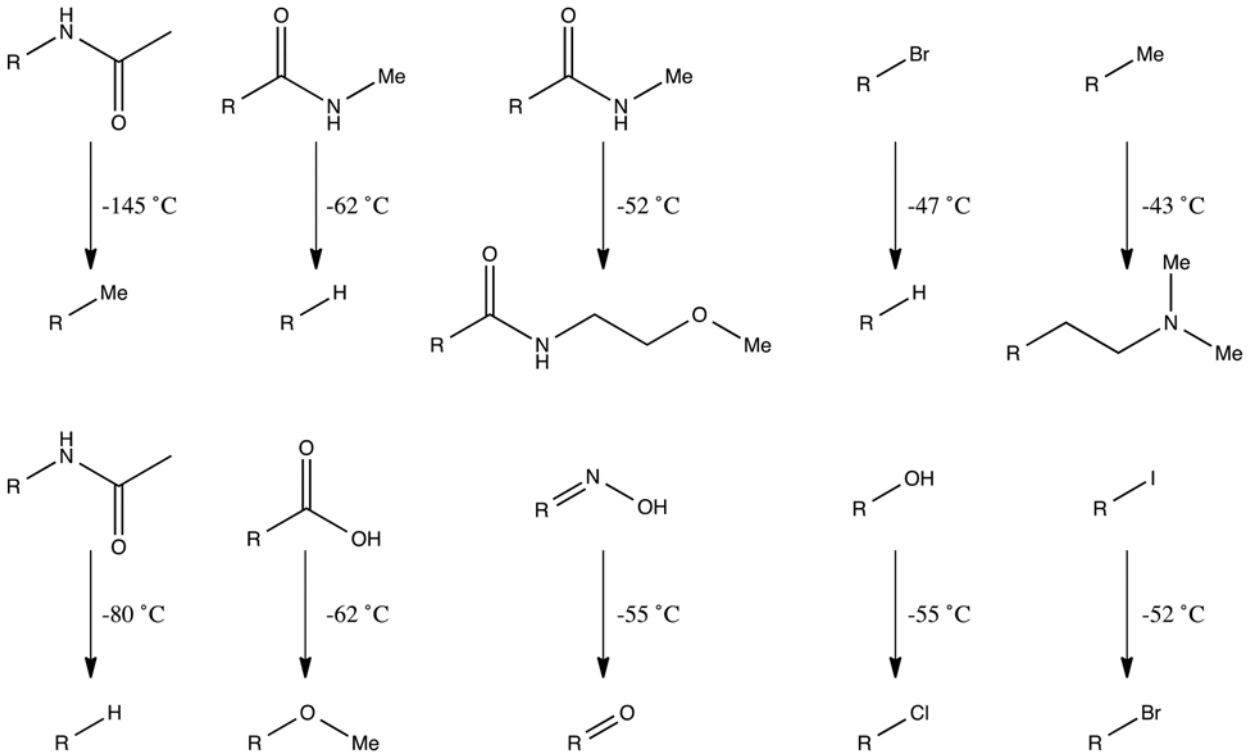

Fig. 26 The largest changes in melting point found for sets of at least five matched pairs.

Table 3 The influence of the structural changes shown in **Figs. 22** and **24** upon plasma protein binding

Substituent	*Br*	*Cl*	*F*	*OMe*	*Me*	*CN*	*CF_3*	*OH*	*SO_2Me*
Mean change in log(K_1) in Leach et al. (SEM)	+0.78 (0.07)	+0.54 (0.02)	+0.15 (0.01)	+0.02 (0.03)	+0.22 (0.03)	−0.06 (0.04)	+0.60 (0.07)	−0.24 (0.06)	−0.55 (0.08)

Substituent	*Amide*	*Amine*	*Alkyl alcohol*	*Phenol*
Mean change in log(K_1) (SEM)	−0.23 (0.03)	+0.17 (0.03)	+0.14 (0.02)	+0.09 (0.11)

that a significant increase in plasma protein binding should be expected for this change. In their investigation of the effect of inverting stereochemistry, Leach et al. discovered a measurable change in the extent of plasma protein binding between enantiomers.[3]

3.10.3.2.9 Lipophilicity (logD)

Changes in measured logD values are often used to support interpretation of other MMPA studies. The change in logD for a structural change permits its effect to be understood and rationalized and, more importantly, allows surprising results to be identified. Investigators who have studied experimentally measured logD by MMPA include Keefer et al. from Pfizer,[39] Haubertin and Bruneau,[31] Waring et al.,[14,15] Boström et al.,[27] Ritchie et al.,[43] and Dossetter and coworkers.[13,22]

Papadatos et al., in their investigation of the importance of chemical context, highlight the importance of certain electronic effects in overriding the usual expectations for the effect of a structural change on logD. For example, a nitrile group added ortho to an aromatic nitrogen atom generally increases logD, whereas addition to most other positions decreases logD. Leach et al. used logD as a benchmark for their studies of the influence of stereochemistry and found that it did not change between enantiomers, as was expected.[3]

3.10.3.3 Sharing Data Among Pharmaceutical Companies

Pharmaceutical companies rely upon keeping their databases of structures and measured properties secret in order to gain a competitive advantage and to protect their intellectual property. These databases contain a great deal of useful knowledge, and many

scientists have long lamented the unwillingness of the companies to share these data. As has been pointed out, MMPA transforms structures into changes in structure and measured property data into changes in property.[38,45] These differences rather than original values contain a great deal of useful information to drug designers but crucially do not disclose any original structures or measured values. As a consequence, they can be shared among companies. The company MedChemica has been facilitating data sharing between companies using exactly this principle. One of the more interesting consequences is that there is the potential when sets of pairs are brought together for the result to be more than the sum of the parts. Sets of pairs that are found to have a significant effect upon a property are referred to as rules.

In an investigation of this cooperativity of datasets, Kramer et al., in their analysis of hERG datasets from ChEMBL and Novartis, compare the derived mean changes in pIC_{50} using ChEMBL data to the mean changes for analogous sets of pairs found in their in-house data and find good agreement. There are some pairs that fall outside the expected range, but when they include a correct treatment of the expected variation by including the experimental variation in their considerations, these outliers are no longer found to be significant. All 69 sets of pairs found to be significant within both sources of data are found to correspond to the same direction of change. Adding ChEMBL homogeneous sets to the Novartis sets (which are all homogeneous) provides a significant enhancement in the dataset. There are 286 sets from Novartis, which become 393 after merging. It is interesting to note that when they are merged, 132 sets that were not significant become significant, but 25 that were lose significance. They do not report the outcome when considered from the other direction of how many pairs become significant or lose significance from the starting point of the ChEMBL set of pairs. There were 227 sets of pairs that were significant but not common to the Novartis set. Their analysis suggests that there has been an increase in the number of significant sets of pairs of between 37% and 116% overall.

When MedChemica arranged the sharing of physicochemical and in vitro pharmacokinetic data between three pharmaceutical companies, they found that there was generally a very substantial cooperativity between datasets. This means that each contributing partner gains on several fronts: if they did not have MMPA on their own data, this is generated giving them all the rules from their own data; they then get all of the rules from the other contributing companies; finally, they get the rules that did not exist until the data were shared. The latter category is often found to be the largest suggesting that the sharing process has generated an inherent benefit.

3.10.3.4 Elucidating Relationships in 3-D

One of the most exciting recent trends in MMPA has been to take the analysis into three dimensions. A number of reports have described tactics for translating the information extracted from MMPA into the three-dimensional context of a binding site or else into the optimal positions for pharmacophoric features.

One of these approaches, styling itself VAMMPIRE, relates changes in ligand structure to their protein context.[59] This work, by Weber et al., extracts data from the PDBbind database and ChEMBL.[75,76] The PDBbind database limits the sets of targets to those with high-quality crystal structure data available. The targets that are present in PDBbind were then located in ChEMBL, and the relevant information for ligand binding was extracted. The set excluded covalent binders, and where there was more than one value reported for a compound, the median was taken unless the values spanned a range of more than an order of magnitude in which case the compound was discounted from the analysis. Matched molecular pairs were identified within the resulting dataset using the MCSS approach, with the changing part constrained to have less than half the number of heavy atoms as the fixed part.

The key assumption of the VAMMPIRE approach is that matched molecular pairs will share a retained binding mode. The binding mode for each is found by overlaying the shared fixed part with a ligand that is present in the PDBbind set. In this way, the calculation of the MCSS serves a dual purpose; it identifies pairs and then permits their binding mode to be predicted. Having positioned the fixed part of each ligand by comparison to a structure with known binding mode, the changing part of each ligand is then constructed using the MOE pose refinement protocol.[77] Once positioned, the environment for this changing part is defined by identifying the three nearest amino acids (that are within 5 Å); any nonnatural amino acids are excluded. This protocol, as originally described in 2013, yielded 8972 matched pairs split across 142 targets. Unfortunately, most sets of pairs had only one pair, so that the usual statistical power of MMPA does not apply. However, by encoding the environment, they are able to use this to make links to pairs in other targets. This is an important attempt to tackle one of the great outstanding challenges of MMPA—identifying structural changes that will retain or enhance potency. They exemplify the method with an example from inhibitors of cyclooxygenase-2 in which SAR from factor Xa and thrombin was transposed to make suggestions about beneficial changes to make to the celecoxib series.

The same authors have subsequently expanded and updated the VAMMPIRE approach.[60] By allowing a conservative set of structures to be generated by docking and crystallography, the set has been expanded to 17,602 pairs. These are subdivided into the following:

Type I: both molecules in the pair are available in crystal structures of the appropriate protein–ligand complex. These account for 10% of the pairs.

Type II: one molecule in the pair is available as a crystal structure, and the second is inferred from a docking pose that places the fixed part (when evaluated as a matched pair with the crystal structure by MCSS) in such a way that the RMSD between the two is less than or equal to 1 Å. These account for 20% of the pairs.

Type III: both binding geometries are generated by docking but where one of the molecules in the pair is also a member of a type II pair. The second molecule's position is then treated analogously to the crystal structure in a type II pair. These account for 70% of the pairs.

As in the original VAMMPIRE paper but in a more specific way, the substituents and their environments are encoded. The user can specify a compound, a receptor, and a substituent of interest. The database is then searched for the same substituent in similar environments, and the SAR from those positions is presumed to have a high likelihood of transferring to the query molecule. A small-scale validation was performed to show that the more similar the substituent environment pairs are (as encoded in a new fingerprint introduced by the researchers), the more likely it is that correct SAR trends will be predicted. In a test using cyclooxygenase-2, 25 substituents were predicted to increase pIC_{50} by at least 0.5; 18 of these predictions were correct and seven incorrect. This protocol is made available as a Web server under the name VAMMPIRE-LORD.[63]

An alternative approach to a similar aim was taken by Posy et al.,[49] who assumed that any compound that has a binding mode revealed by crystallography in any kinase will adopt the same binding mode in any other kinase; their work was focused particularly on studying inhibitors of p38α. Some detailed studies were undertaken in order to investigate this assumption. They used the set of protein–ligand crystal structures in which the same ligand is bound to different targets and concluded that in 88% of cases, exactly the same binding mode is adopted and in 97% of cases, the binding modes are similar enough to be usefully classed as identical. The binding positions were compared using a method that computes the difference in shape and "color" where color is an assessment of the positioning of atom types of different pharmacophoric types. These comparisons provided a cutoff above which the binding mode can be considered the same. This same protocol could then be used to identify ligands that can adopt the same binding mode. Large sets of conformations were generated, and the best shape + color overlay with the most similar ligand that has a crystal structure available was selected as the likely binding mode. Only those ligands that achieve a required level of overlay were retained. This permits the SAR that has been found to be translated into three dimensions. A three-dimensional version of the fragment and index approach to matched-pair finding was adopted. Pairs are encoded according to the position of the attachment point, and attachment points that are within 1 Å of one another are clustered together; no constraints are placed on whether the substituent protrudes in the same direction or not. A large number of compounds can be incorporated into this approach, compared with other three-dimensional methods. The method has analogies to the BREED approach to processing crystal structures.[78] To exploit the set of structures, the user can select the structure of any compound and select a substituent. The system then recalls all substituents that have an attachment point within 1 Å and assumes that the structure–activity relationship from the corresponding compounds can be translated to the query molecule. They exemplified the approach with an i-Pr to c-Pr amide switch that gave a sevenfold improvement in potency against p38α. The results came from a set of pairs in which the c-Pr had replaced any other substituent, but in 79% of these cases, the potency had increased. The technique could also be used in the inverse fashion to identify cases where changing one substituent to another has the same effect on different cores, thereby identifying series with SAR transfer. The approach generates a three-dimensional map of the binding site with annotations indicating the regions in which change is tolerated and those where it is not.

A third approach to translating MMPA into three dimensions was described by Bradley et al. who studied inhibitors of the kinase CDK2 and of SAM methyl transferase.[47] They devised a method that will be applicable when a great many protein–ligand crystal structures are available. All matched pairs are identified in which one member of the pair is a crystallographically studied ligand. The pairs are identified by a fragment and index method. The fixed part is assumed to bind in identical locations for the two members of the pair. A set of 100 conformations for the changing part of the noncrystallographic compound is generated. The conformation with the highest shape overlay with the crystallographic ligand is selected. The structure is annotated by pharmacophoric features and whether potency increases or decreases. A three-dimensional visualizer presents the array of pharmacophoric points around a query molecule annotated according to the feature type and whether they correspond to increased or to decreased potency. These can come from any series and need not be due to molecules that are similar to the query. Indeed, the query may have no matched pairs available. The user is therefore presented with clear trends for which pharmacophoric features are favored in each part of the binding site. For example, the visualization might highlight that hydrogen-bond acceptors in one part of the site are associated with a loss of potency. The user will then know to avoid placing acceptors at that point or to remove any that are already present. The method is illustrated with some convincing examples in which consistent SAR within two different binding sites is clearly mapped. Unlike with two-dimensional SAR, statistical power is not directly available, but an array of similarly encoded points in three dimensions in close proximity is a useful three-dimensional analog.

3.10.3.5 Elucidating Pharmacophores

One means by which sets of pairs can be grouped together in order to make useful connections is to make the structural encodings more "fuzzy." One mechanism by which this can be achieved is by encoding the pharmacophoric elements of a molecule into a reduced graph, as illustrated in **Fig. 27**. By comparing these reduced graphs rather than full structures, MMPA can make connections between molecules, which it otherwise would not. Geppert and Beck explored a number of means by which this might be achieved.[45] They analyzed the ChEMBL data for inhibition of four isoforms of the cytochromes P450: 2C19, 2C9, 2D6, and 3A4. Compounds were classified as active or inactive. Lipinski's SMARTS patterns were used to encode the pharmacophoric elements in each molecule. Matched pairs were identified using the Hussain and Rea fragment and index approach. The changes in inhibition between molecules in a pair were processed in several ways that all entail a degree of "fuzziness."

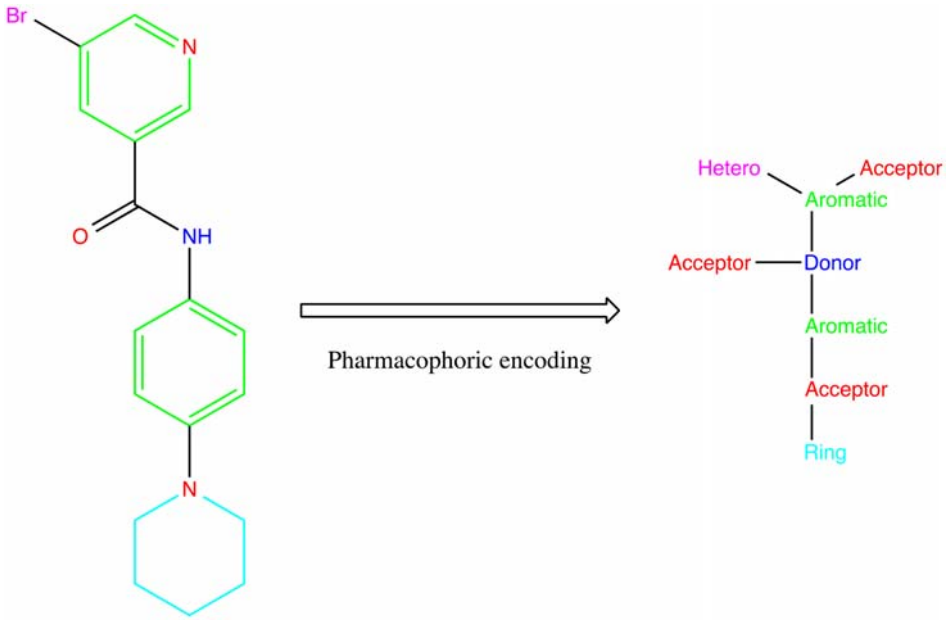

Fig. 27 The encoding of a molecular structure as a reduced graph of pharmacophore features.

The first type of grouping by pharmacophores saw Geppert and Beck define the context for the matched pair by the pharmacophoric encoding of just the attachment point. This is an abstraction of the context definition suggested by Papadatos et al.[40] The next level of abstraction was styled "value fuzzy matched pairs" in which the changing part is examined and pairs are grouped if the change in pharmacophore encoding is the same. This permits many sets of pairs to be grouped together and provides statistical advantages that are set against a reduction in chemical fidelity. Finally, full "fuzzy matched pairs" use the pharmacophoric encoding as shown in Fig. 27 as an input to pair finding, and thus, many more connections are made between compounds with different cores and substituents. This has a double advantage: it not only enhances the statistical strength of many observations but also naturally identifies the pharmacophoric requirements that certain properties have.

An alternative method for identifying the pharmacophoric requirements of certain properties is provided by the work of Bradley et al. who studied molecules in three dimensions and who use MMPA to generate maps of a binding site in which the preference for certain pharmacophoric elements is shown.[47] This method is described in the "**Elucidating Relationships in 3D**" section concerning three-dimensional approaches.

3.10.3.6 Matched Series

When identifying matched molecular pairs, it is quite possible to find that there are many compounds that have a shared fixed part. In MMPA, this information is not capitalized upon, but O'Boyle et al. have highlighted that there is a great deal of value that can be gained by setting each pair within the context of a broader series. For instance, there are (at least) two ways to study the effect of exchanging X_1, X_2, X_3, and X_4 as shown in Fig. 28. The matched-pair way would be to individually study X_1 being transformed into X_2 and then study X_2 being transformed in X_3 and separately X_1 being transformed in X_3. In each set of matched pairs, there might be a different number of pairs in the set. An alternative would be to identify sets with the same fixed part (R in Fig. 28) and thus generate a matched series in which all members are represented by the same number of compounds. This reduces the number of compounds under consideration and hence diminishes the statistical power for each pair, but this is set against an enhanced insight that is provided by placing the pair within a series.

The approach introduced by O'Boyle is styled Matsy and is applied to studying the reported ordering of particular substituent types according to which is the most potent.[52] Matched series are identified using Hussain and Rea's fragment and index method. They highlight some very useful insights that can be gleaned from matched series that address the biggest gap in MMPA—determining which changes are likely to increase potency. The set of substituents H, F, and Cl could correspond to compounds whose potency is ordered in one of six ways: F > Cl > H, F > H > Cl, Cl > F > H, Cl > H > F, H > F > Cl, or H > Cl > F. Some of these orderings are

Fig. 28 An example of a matched series.

observed much more frequently than others; H > F > Cl is the most common in this case. Moreover, this variable frequency allows predictions to be made about whether bromine is likely to be worth making. For instance, when the ordering H > F > Cl has been observed, Br has only been more potent in 7% of cases. Such series naturally provides guidance about what to make next (in terms of potency). The authors also describe the observed frequencies of ordering for small alkyl groups methyl, ethyl, *n*-propyl, and *n*-butyl. They highlight the interesting case of ethyl > *n*-propyl > methyl and suggest that if such an ordering has been observed, the best substituents to make next include *t*-butyl and cyclopentyl.

This work is a natural complement to the decision tree proposed by Topliss, which was based upon the lipophilic and electronic properties of various substituents.[7] O'Boyle et al. find that in many cases, their suggestions of what to make next agree with those proffered by Topliss but that there are some deviations. In more general terms, they suggest that the longer the matched series used to make deductions is, the more likely it is that correct predictions will be made. In a remarkable finding, they investigated the link between series ordering and physical properties and found that there is little link. Indeed, they find in their survey that lipophilic ordering more often gives the reverse ordering than it does exactly the correct ordering.

3.10.4 Related Approaches

3.10.4.1 Activity Cliffs

One interesting subset of matched molecular pairs is those in which the change in property is surprisingly large. A number of researchers, most prominently the Bajorath group in Bonn, have reported the insight that these pairs, which they call activity cliffs, can bring. Notable recent contributions include using Hussain and Rea's fragment and index method to identify matched series within all the high-confidence ChEMBL K_I data relating to activity against human targets. These reveal that coordinated activity cliffs can be identified in which the same structural change causes the same large change in property across several chemical series.[50] A similar method can be used to explore activity within large sets of screening hits.[51] Activity cliffs are analogous to the switches highlighted by Keefer et al. in their analysis of in-house data from Pfizer, which is discussed earlier.[39] Similarly, in their analysis in which they searched for similar compounds that had different kinase inhibition profiles, Milletti et al. and Chen et al. were locating activity cliffs considering multiple-target data rather than a single property.[79,80]

3.10.4.2 Bioisosteres

Bioisosteres have a long history in medicinal chemistry and have been identified as critical to the success of many drug discovery efforts.[81,82] MMPA has provided an approach to both evaluate and discover bioisosteres. For instance, Birch et al. were able to evaluate the effect of the common bioisosteric change of carboxylic acid with tetrazole and discovered that a significant increase in plasma protein binding is generally associated with this change.[21] One of the scientists who have contributed most to the science of bioisosteres in recent years, Brown, has highlighted the value of MMPA for identifying bioisosteres, and this was also discussed in a perspective article by Griffen et al.[73,83] In essence, when investigating the effect that changes in structure have upon properties, the focus is most often on those structural changes that can be determined to change the property, but there is also value in those properties that positively do not change a property. These changes though are more challenging to detect; a change in property can be found not significant because it genuinely does not change the property or because there are not yet enough data to detect that change. These two causes are difficult to disentangle and remain a work in progress for many in the MMPA field. One of the applications of the SwissBioisostere database is to identify sets of pairs in which a particular substituent has been changed many times and the potency has only changed by less than 0.5 log units in any direction. This is the origin of its name and is one of the applications to which the tool can be put. Some of the earliest efforts to consider the comparisons between molecules as a guide to discover bioisosteres were by Sheridan and Ertl who were investigating the prevalence of particular group types and transformations in medicinal chemistry.[33,84]

3.10.4.3 QSAR

One of the connections that have been made most often with MMPA is with QSAR. Both techniques can be used to make quantitative predictions about the properties of a particular molecule. This was compared by Griffen et al., who highlighted the reduced challenge involved in predicting differences in property rather than whole molecule properties.[73] Warner et al. also compared MMPA and QSAR in their study of how to predict potency against two ion channels, hKCNQ1 and hKCNE1. They found that QSAR using a random forest approach was less well able to predict the properties, giving a larger RMSE than MMPA. By contrast, oral reports of work undertaken at Pfizer have suggested that sometimes QSAR can outperform MMPA because it utilizes much more of the data than MMPA that only uses the small amount of data that are appropriate to each structural change.[85] As with much of the discussion earlier, the challenge is to find the optimum trade-off between data quantity and chemical specificity. A recent trend has been to incorporate QSAR more directly into MMPA. For instance, Sushko et al. used property values generated by QSAR for MMPA modeling.[36] An alternative method to permit QSAR to extend the scope of MMPA was shown by Beck and Springer who devised a means to encode structural changes and then built QSAR models for the mean values for the change in property.[86] In this way, they are able to predict the mean change for any structural change, whether it is exemplified or not.

3.10.5 Summary and Outlook

MMPA is about a decade old and as such is relatively young. New developments and directions are being proposed and investigated all of the time. Particular recent highlights include the translation of MMPA into three dimensions and the introduction of structural abstraction, which permits data to be grouped in new ways that remain relevant to medicinal chemistry. We are particularly excited to have demonstrated that MMPA can provide a vehicle for pharmaceutical companies to share data among themselves and to the benefit of others.

We look forward to improvements on many levels. At the algorithmic level, there remain issues about the scalability of pair finding and the storage of the resulting information (what form permits the most efficient exploitation by users). Advances in hardware and software will address some of these, but algorithmic innovations are likely to help too. There remain challenges about how matched pairs are encoded; while each organization has their own method, there remains a language barrier between them, and we feel certain that some standardization here would help. It is clear that a number of ideas for expanding matched pairs into three dimensions have been explored but that these require some refinement and integration in order to obtain the best insights for users. Similar efforts are likely required for the related area of pharmacophores and other structural abstractions. In general, the next decade is likely to see many of the techniques, which are described earlier in their pioneering forms become routine. We believe that MMPA is a necessity for any pharmaceutical company with large sets of data. These can be worth much more when useful knowledge is extracted via MMPA.

See also: 1.07. Beyond Bioisosterism: New Concepts in Drug Discovery.

References

1. Leach, A. G.; Jones, H. D.; Cosgrove, D. A.; Kenny, P. W.; Ruston, L.; Macfaul, P.; Wood, J. M.; Colclough, N.; Law, B. Matched Molecular Pairs as a Guide in the Optimization of Pharmaceutical Properties: A Study of Aqueous Solubility, Plasma Protein Binding and Oral Exposure. *J. Med. Chem.* **2006,** *49,* 6672–6682.
2. Hussain, J.; Rea, C. Computationally Efficient Algorithm to Identify Matched Molecular Pairs (MMPs) in Large Data Sets. *J. Chem. Inf. Model.* **2010,** *50,* 339–348.
3. Leach, A. G.; Pilling, E. A.; Rabow, A. A.; Tomasi, S.; Asaad, N.; Buurma, N. J.; Ballard, A.; Narduolo, S. Enantiomeric Pairs Reveal That Key Medicinal Chemistry Parameters Vary More Than Simple Physical Property Based Models Can Explain. *Med. Chem. Commun.* **2012,** *3,* 528–540.
4. Bagdanoff, J. T.; Xu, Y.; Dollinger, G.; Martin, E. Effect of Chirality on Common In Vitro Experiments: An Enantiomeric Pair Analysis. *J. Med. Chem.* **2015,** *58,* 5781–5788.
5. Kenny, P. W.; Sadowski, J. Structure Modification in Chemical Databases. *Methods Princ. Med. Chem.* **2005,** *23,* 271–285.
6. Free, S. M.; Wilson, J. W. A Mathematical Contribution to Structure-Activity Studies. *J. Med. Chem.* **1964,** *7,* 395–399.
7. Topliss, J. G. Utilization of Operational Schemes for Analog Synthesis in Drug Design. *J. Med. Chem.* **1972,** *15,* 1006–1011.
8. Fujita, T. Similarities in Bioanalogous Structural Transformation Patterns. *Am. Chem. Soc.* **2000,** *774,* 166–179.
9. Zachariae, U.; Giordanetto, F.; Leach, A. G. Side Chain Flexibilities in the Human Ether-a-go-go Related Gene Potassium Channel (hERG) Together With Matched-Pair Binding Studies Suggest a New Binding Mode for Channel Blockers. *J. Med. Chem.* **2009,** *52,* 4266–4276.
10. Dossetter, A. G.; Griffen, E. J.; Leach, A. G. Matched Molecular Pair Analysis in Drug Discovery. *Drug Discov. Today* **2013,** *18,* 724–731.
11. Kramer, C.; Kalliokoski, T.; Gedeck, P.; Vulpetti, A. The Experimental Uncertainty of Heterogeneous Public Ki Data. *J. Med. Chem.* **2012,** *55,* 5165–5173.
12. Kanetaka, H.; Koseki, Y.; Taira, J.; Umei, T.; Komatsu, H.; Sakamoto, H.; Gulten, G.; Sacchettini, J. C.; Kitamura, M.; Aoki, S. Discovery of InhA Inhibitors With Anti-Mycobacterial Activity Through a Matched Molecular Pair Approach. *Eur. J. Med. Chem.* **2015,** *94,* 378–385.
13. Dossetter, A. G.; Douglas, A.; O'Donnell, C. A. Matched Molecular Pair Analysis of In Vitro Human Microsomal Metabolic Stability Measurements for Heterocyclic Replacements of Di-substituted Benzene Containing Compounds–Identification of Those Isosteres More Likely to Have Beneficial Effects. *Med. Chem. Commun.* **2012,** *3,* 1164–1169.
14. Waring, M. J.; Bennett, S. N.; Boyd, S.; Campbell, L.; Davies, R. D.; Gerhardt, S.; Hargreaves, D.; Martin, N. G.; Robb, G. R.; Wilkinson, G. Matched Triplicate Design Sets in the Optimisation of Glucokinase Activators–Maximising Medicinal Chemistry Information Content. *Med. Chem. Commun.* **2013,** *4,* 657–662.
15. Waring, M. J.; Johnstone, C.; Mckerrecher, D.; Pike, K. G.; Robb, G. Matrix-Based Multiparameter Optimisation of Glucokinase Activators: The Discovery of AZD1092. *Med. Chem. Commun.* **2011,** *2,* 775–779.
16. Mccoull, W.; Barton, P.; Broo, A.; Brown, A. J. H.; Clarke, D. S.; Coope, G.; Davies, R. D. M.; Dossetter, A. G.; Kelly, E. E.; Knerr, L.; Macfaul, P.; Holmes, J. L.; Martin, N.; Moore, J. E.; Morgan, D.; Newton, C.; Osterlund, K.; Robb, G. R.; Rosevere, E.; Selmi, N.; Stokes, S.; Svensson, T. S.; Ullah, V. B. K.; Williams, E. J. Identification of Pyrazolo-pyrimidinones as GHS-R1a Antagonists and Inverse Agonists for the Treatment of Obesity. *Med. Chem. Commun.* **2013,** *4,* 456–462.
17. Tye, H.; Zahn, S.; Hofmann, M.; Sanderson, M.; Schaff, O.; Troy, M.; Mayer, M.; Rast, G.; Pal, S.; Guertler, U. Discovery of Novel Amino-Pyrimidine Inhibitors of the Insulin-Like Growth Factor 1 (IGF1R) and Insulin Receptor (INSR) Kinases; Parallel Optimization of Cell Potency and hERG Inhibition. *Med. Chem. Commun.* **2015,** *6,* 1244–1251.
18. http://www.daylight.com/dayhtml/doc/theory/.
19. Kenny, P. W.; Montanari, C. A.; Prokopczyk, I. M.; Sala, F. A.; Sartori, G. R. Automated Molecule Editing in Molecular Design. *J. Comput. Aided Mol. Des.* **2013,** *27,* 655–664.
20. Morley, A. D.; Kenny, P. W.; Burton, B.; Heald, R. A.; Macfaul, P. A.; Mullett, J.; Page, K.; Porres, S. S.; Ribeiro, L. R.; Smith, P.; Ward, S.; Wilkinson, T. J. 5-Aminopyrimidin-2-ylnitriles as Cathepsin K Inhibitors. *Bioorg. Med. Chem. Lett.* **2009,** *19,* 1658–1661.
21. Birch, A. M.; Kenny, P. W.; Simpson, I.; Whittamore, P. R. Matched Molecular Pair Analysis of Activity and Properties of Glycogen Phosphorylase Inhibitors. *Bioorg. Med. Chem. Lett.* **2009,** *19,* 850–853.
22. Dossetter, A. G. A. Matched Molecular Pair Analysis of In Vitro Human Microsomal Metabolic Stability Measurements for Methylene Substitution or Replacements–Identification of Those Transforms More Likely to Have Beneficial Effects. *Med. Chem. Commun.* **2012,** *3,* 1518–1525.
23. Dossetter, A. G. A. Statistical Analysis of In Vitro Human Microsomal Metabolic Stability of Small Phenyl Group Substituents, Leading to Improved Design Sets for Parallel SAR Exploration of a Chemical Series. *Bioorg. Med. Chem.* **2010,** *18,* 4405–4414.
24. Gleeson, P.; Bravi, G.; Modi, S.; Lowe, D. ADMET Rules of Thumb II: A Comparison of the Effects of Common Substituents on a Range of ADMET Parameters. *Bioorg. Med. Chem.* **2009,** *17,* 5906–5919.
25. Lewis, M. L.; Cucurull-Sanchez, L. Structural Pairwise Comparisons of HLM Stability of Phenyl Derivatives: Introduction of the Pfizer Metabolism Index (PMI) and Metabolism-Lipophilicity Efficiency (MLE). *J. Comput. Aided Mol. Des.* **2009,** *23,* 97–103.
26. Hajduk, P. J.; Sauer, D. R. Statistical Analysis of the Effects of Common Chemical Substituents on Ligand Potency. *J. Med. Chem.* **2008,** *51,* 553–564.
27. Boström, J.; Hogner, A.; Llinàs, A.; Wellner, E.; Plowright, A. T. Oxadiazoles in Medicinal Chemistry. *J. Med. Chem.* **2012,** *55,* 1817–1830.

28. Stepan, A. F.; Kauffman, G. W.; Keefer, C. E.; Verhoest, P. R.; Edwards, M. Evaluating the Differences in Cycloalkyl Ether Metabolism Using the Design Parameter "Lipophilic Metabolism Efficiency" (LipMetE) and a Matched Molecular Pairs Analysis. *J. Med. Chem.* **2013,** *56,* 6985–6990.
29. Sheridan, R. P.; Hunt, P.; Culberson, J. C. Molecular Transformations as a Way of Finding and Exploiting Consistent Local QSAR. *J. Chem. Inf. Model.* **2006,** *46,* 180–192.
30. Stewart, K. D.; Shiroda, M.; James, C. A. Drug Guru: A Computer Software Program for Drug Design Using Medicinal Chemistry Rules. *Bioorg. Med. Chem.* **2006,** *14,* 7011–7022.
31. Haubertin, D. Y.; Bruneau, P. A Database of Historically-Observed Chemical Replacements. *J. Chem. Inf. Model.* **2007,** *47,* 1294–1302.
32. Lewell, X. Q.; Judd, D. B.; Watson, S. P.; Hann, M. M. RECAP Retrosynthetic Combinatorial Analysis Procedure: A Powerful New Technique for Identifying Privileged Molecular Fragments With Useful Applications in Combinatorial Chemistry. *J. Chem. Inf. Comput. Sci.* **1998,** *38,* 511–522.
33. Ertl, P. Cheminformatics Analysis of Organic Substituents: Identification of the Most Common Substituents, Calculation of Substituent Properties, and Automatic Identification of Drug-Like Bioisosteric Groups. *J. Chem. Inf. Comput. Sci.* **2003,** *43,* 374–380.
34. Bemis, G. W.; Murcko, M. A. Properties of Known Drugs. 2. Side Chains. *J. Med. Chem.* **1999,** *42,* 5095–5099.
35. http://www.rdkit.org/docs/Overview.html.
36. Sushko, Y.; Novotarskyi, S.; Körner, R.; Vogt, J.; Abdelaziz, A.; Tetko, I. V. Prediction-Driven Matched Molecular Pairs to Interpret QSARs and Aid the Molecular Optimization Process. *J. Cheminf.* **2014,** *6,* 1–18.
37. MCpairs, Medchemica Ltd, Alderley Park, Macclesfield, SK10 4TG, UK.
38. Kramer, C.; Fuchs, J. E.; Whitebread, S.; Gedeck, P.; Liedl, K. R. Matched Molecular Pair Analysis: Significance and the Impact of Experimental Uncertainty. *J. Med. Chem.* **2014,** *57,* 3786–3802.
39. Keefer, C. E.; Chang, G.; Kauffman, G. W. Extraction of Tacit Knowledge From Large ADME Data Sets via Pairwise Analysis. *Bioorg. Med. Chem.* **2011,** *19,* 3739–3749.
40. Papadatos, G.; Alkarouri, M.; Gillet, V. J.; Willett, P.; Kadirkamanathan, V.; Luscombe, C. N.; Bravi, G.; Richmond, N. J.; Pickett, S. D.; Hussain, J.; Pritchard, J. M.; Cooper, A. W. J.; MacDonald, S. J. F. Lead Optimization Using Matched Molecular Pairs: Inclusion of Contextual Information for Enhanced Prediction of hERG Inhibition, Solubility, and Lipophilicity. *J. Chem. Inf. Model.* **2010,** *50,* 1872–1886.
41. Zhang, L.; Zhu, H.; Mathiowetz, A.; Gao, H. Deep Understanding of Structure–Solubility Relationship for a Diverse Set of Organic Compounds Using Matched Molecular Pairs. *Bioorg. Med. Chem.* **2011,** *19,* 5763–5770.
42. Schultes, S.; De Graaf, C.; Berger, H.; Mayer, M.; Steffen, A.; Haaksma, E. E.; De Esch, I. J.; Leurs, R.; Krämer, O. A. Medicinal Chemistry Perspective on Melting Point: Matched Molecular Pair Analysis of the Effects of Simple Descriptors on the Melting Point of Drug-Like Compounds. *Med. Chem. Commun.* **2012,** *3,* 584–591.
43. Ritchie, T. J.; MacDonald, S.; Pickett, S. Insights into the Impact of N-and O-Methylation on Aqueous Solubility and Lipophilicity Using Matched Molecular Pair Analysis. *Med. Chem. Commun.* **2015,** *6,* 1787–1797.
44. Dimova, D.; Stumpfe, D.; Bajorath, J. Specific Chemical Changes Leading to Consistent Potency Increases in Structurally Diverse Active Compounds. *Med. Chem. Commun.* **2014,** *5,* 742–749.
45. Geppert, T.; Beck, B. Fuzzy Matched Pairs: A Means to Determine the Pharmacophore Impact on Molecular Interaction. *J. Chem. Inf. Model.* **2014,** *54,* 1093–1102.
46. de la Vega de León, A.; Bajorath, J. Prediction of Compound Potency Changes in Matched Molecular Pairs Using Support Vector Regression. *J. Chem. Inf. Model.* **2014,** *54,* 2654–2663.
47. Bradley, A. R.; Wall, I. D.; Green, D. V.; Deane, C. M.; Marsden, B. D. OOMMPPAA: A Tool to Aid Directed Synthesis by the Combined Analysis of Activity and Structural Data. *J. Chem. Inf. Model.* **2014,** *54,* 2636–2646.
48. Gupta-Ostermann, D.; Bajorath, J. The 'SAR Matrix' Method and Its Extensions for Applications in Medicinal Chemistry and Chemogenomics. *F1000Res.* **2014,** *3,* 113.
49. Posy, S. L.; Claus, B. L.; Pokross, M. E.; Johnson, S. R. 3D Matched Pairs: Integrating Ligand-and Structure-Based Knowledge for Ligand Design and Receptor Annotation. *J. Chem. Inf. Model.* **2013,** *53,* 1576–1588.
50. Dimova, D.; Bajorath, J. Extraction of SAR Information From Activity Cliff Clusters via Matching Molecular Series. *Eur. J. Med. Chem.* **2014,** *87,* 454–460.
51. de la Vega de León, A.; Hu, Y.; Bajorath, J. Systematic Identification of Matching Molecular Series and Mapping of Screening Hits. *Mol. Inf.* **2014,** *33,* 257–263.
52. O'Boyle, N. M.; Boström, J.; Sayle, R. A.; Gill, A. Using Matched Molecular Series as a Predictive Tool to Optimize Biological Activity. *J. Med. Chem.* **2014,** *57,* 2704–2713.
53. Zhang, B.; Wassermann, A. M.; Vogt, M.; Bajorath, J. Systematic Assessment of Compound Series With SAR Transfer Potential. *J. Chem. Inf. Model.* **2012,** *52,* 3138–3143.
54. Wirth, M.; Zoete, V.; Michielin, O.; Sauer, W. H. SwissBioisostere: A Database of Molecular Replacements for Ligand Design. *Nucleic Acids Res.* **2013,** *41,* D1137–D1143.
55. Raymond, J. W.; Willett, P. Maximum Common Subgraph Isomorphism Algorithms for the Matching of Chemical Structures. *J. Comput. Aided Mol. Des.* **2002,** *16,* 521–533.
56. Warner, D. J.; Griffen, E. J.; St-Gallay, S. A. WizePairZ: A Novel Algorithm to Identify, Encode, and Exploit Matched Molecular Pairs With Unspecified Cores in Medicinal Chemistry. *J. Chem. Inf. Model.* **2010,** *50,* 1350–1357.
57. Openeye Scientific Software, Santa Fe, New Mexico, USA.
58. Warner, D. J.; Bridgland-Taylor, M. H.; Sefton, C. E.; Wood, D. J. Prospective Prediction of Antitarget Activity by Matched Molecular Pairs Analysis. *Mol. Inf.* **2012,** *31,* 365–368.
59. Weber, J.; Achenbach, J.; Moser, D.; Proschak, E. VAMMPIRE: A Matched Molecular Pairs Database for Structure-Based Drug Design and Optimization. *J. Med. Chem.* **2013,** *56* (12), 5203–5207.
60. Weber, J.; Achenbach, J.; Moser, D.; Proschak, E. VAMMPIRE-LORD: A Web Server for Straightforward Lead Optimization Using Matched Molecular Pairs. *J. Chem. Inf. Model.* **2015,** *55,* 207–213.
61. Ehrlich, H.; Rarey, M. Maximum Common Subgraph Isomorphism Algorithms and Their Applications in Molecular Science: A Review. *Wiley Interdiscip. Rev.: Comput. Mol. Sci.* **2011,** *1,* 68–79.
62. https://www.knime.org.
63. http://vammpire.pharmchem.uni-frankfurt.de.
64. Gobbi, A.; Lee, M. Handling of Tautomerism and Stereochemistry in Compound Registration. *J. Chem. Inf. Model.* **2011,** *52,* 285–292.
65. Guasch, L.; Sitzmann, M.; Nicklaus, M. C. Enumeration of Ring–Chain Tautomers Based on SMIRKS Rules. *J. Chem. Inf. Model.* **2014,** *54,* 2423–2432.
66. Fourches, D.; Muratov, E.; Tropsha, A. Trust, But Verify: on the Importance of Chemical Structure Curation in Cheminformatics and QSAR Modeling Research. *J. Chem. Inf. Model.* **2010,** *50,* 1189–1204.
67. Müller, K. The Power of MMPA and a Teaching Lesson in Medicinal Chemistry. *J. Med. Chem.* **2012,** *55,* 1815–1816.
68. Goldberg, K.; Groombridge, S.; Hudson, J.; Leach, A. G.; Macfaul, P. A.; Pickup, A.; Poultney, R.; Scott, J. S.; Svensson, P. H.; Sweeney, J. Oxadiazole Isomers: All Bioisosteres Are Not Created Equal. *Med. Chem. Commun.* **2012,** *3,* 600–604.
69. Patel, Y.; Gillet, V. J.; Howe, T.; Pastor, J.; Oyarzabal, J.; Willett, P. Assessment of Additive/Nonadditive Effects in Structure–Activity Relationships: Implications for Iterative Drug Design. *J. Med. Chem.* **2008,** *51,* 7552–7562.
70. Brown, D. G.; Gagnon, M. M.; Boström, J. Understanding Our Love Affair With p-Chlorophenyl: Present Day Implications From Historical Biases of Reagent Selection. *J. Med. Chem.* **2015,** *58,* 2390–2405.
71. Kim, D.; Krishnarajah, J.; Lillioja, S.; De Looze, F.; Marjason, J.; Proietto, J.; Shakib, S.; Stuckey, B.; Vath, J.; Hughes, T. Efficacy and Safety of Beloranib for Weight Loss in Obese Adults: A Randomized Controlled Trial. *Diabetes Obes. Metab.* **2015,** *17,* 566–572.
72. Sanguinetti, M. C.; Tristani-Firouzi, M. hERG Potassium Channels and Cardiac Arrhythmia. *Nature (London)* **2006,** *440,* 463–469.
73. Griffen, E.; Leach, A. G.; Robb, G. R.; Warner, D. J. Matched Molecular Pairs as a Medicinal Chemistry Tool. *J. Med. Chem.* **2011,** *54,* 7739–7750.

74. Scott, J. S.; Birch, A. M.; Brocklehurst, K. J.; Broo, A.; Brown, H. S.; Butlin, R. J.; Clarke, D. S.; Davidsson, O.; Ertan, A.; Goldberg, K.; Groombridge, S. D.; Hudson, J. A.; Laber, D.; Leach, A. G.; Macfaul, P. A.; Mckerrecher, D.; Pickup, A.; Schofield, P.; Svensson, P. H.; Sorme, P.; Teague, J. Use of Small-Molecule Crystal Structures to Address Solubility in a Novel Series of G Protein Coupled Receptor 119 Agonists: Optimization of a Lead and in vivo Evaluation. *J. Med. Chem.* **2012,** *55,* 5361–5379.
75. Wang, R.; Fang, X.; Lu, Y.; Yang, C.; Wang, S. The PDBbind Database: Methodologies and Updates. *J. Med. Chem.* **2005,** *48,* 4111–4119.
76. Wang, R.; Fang, X.; Lu, Y.; Wang, S. The PDBbind Database: Collection of Binding Affinities for Protein-Ligand Complexes With Known Three-Dimensional Structures. *J. Med. Chem.* **2004,** *47,* 2977–2980.
77. Molecular Operating Environment (MOE), 2013.08; Chemical Computing Group Inc., 1010 Sherbooke St. West, Suite #910, Montreal, QC, Canada, H3A 2R7, 2016.
78. Pierce, A. C.; Rao, G.; Bemis, G. W. BREED: Generating Novel Inhibitors Through Hybridization of Known Ligands. Application to CDK2, p38, and HIV Protease. *J. Med. Chem.* **2004,** *47,* 2768–2775.
79. Milletti, F.; Hermann, J. C. Targeted Kinase Selectivity From Kinase Profiling Data. *ACS Med. Chem. Lett.* **2012,** *3,* 383–386.
80. Chen, H.; Chan, B. K.; Drummond, J.; Estrada, A. A.; Gunzner-Toste, J.; Liu, X.; Liu, Y.; Moffat, J.; Shore, D.; Sweeney, Z. K. Discovery of Selective LRRK2 Inhibitors Guided by Computational Analysis and Molecular Modeling. *J. Med. Chem.* **2012,** *55,* 5536–5545.
81. Mannhold, R.; Kubinyi, H.; Folkers, G.; Brown, N. *Bioisosteres in Medicinal Chemistry*; **54**; John Wiley & Sons: Hoboken, NJ, 2012.
82. Meanwell, N. A. Synopsis of Some Recent Tactical Application of Bioisosteres in Drug Design. *J. Med. Chem.* **2011,** *54,* 2529–2591.
83. Brown, N. Bioisosteres and Scaffold Hopping in Medicinal Chemistry. *Mol. Inf.* **2014,** *33,* 458–462.
84. Sheridan, R. P. The Most Common Chemical Replacements in Drug-Like Compounds. *J. Chem. Inf. Comput. Sci.* **2002,** *42,* 103–108.
85. http://www.ukqsar.org/slides/Gardner.pdf.
86. Beck, J. M.; Springer, C. Quantitative Structure–Activity Relationship Models of Chemical Transformations From Matched Pairs Analyses. *J. Chem. Inf. Model.* **2014,** *54,* 1226–1234.

Relevant Websites

http://www.swissbioisostere.ch provides the ability to search the ChEMBL database for matched molecular pairs insights.
http://vammpire.pharmchem.uni-frankfurt.de provides access to the VAMMPIRE suite of tools for considering matched molecular pairs in their 3D context.
http://www.rdkit.org provides an open-source matched molecular pairs finder (F + I method).
https://www.knime.org an alternative open-source matched molecular pairs finder (F + I method) is available in the knime environment.
https://ochem.eu/home/show.do provides a web-tool for MMPA.

3.11 Lessons and Successes in the Use of Molecular Fields

P Tosco and M Mackey, Cresset, Litlington, United Kingdom

© 2017 Elsevier Ltd. All rights reserved.

3.11.1	**Introduction**	254
3.11.2	**Ligand-Based Applications**	254
3.11.2.1	Assessment of Ligand Similarity	254
3.11.2.1.1	COSMO*sim3D*	255
3.11.2.1.2	GRID/FLAP	257
3.11.2.1.3	XED/FieldAlign	258
3.11.2.2	Bioactive Pose Prediction	260
3.11.2.2.1	FieldTemplater	261
3.11.2.2.2	FLAPpharm	263
3.11.2.3	Virtual Screening	264
3.11.2.3.1	FieldScreen/Blaze	264
3.11.2.3.2	FLAP	264
3.11.2.4	Scaffold Hopping	266
3.11.2.4.1	SHOP	267
3.11.2.4.2	Spark	268
3.11.2.5	3D Clustering of Molecule Libraries	270
3.11.2.6	3D-QSAR	270
3.11.2.6.1	CoMFA	271
3.11.2.6.2	CoMSIA	273
3.11.2.6.3	Topomer CoMFA	273
3.11.2.6.4	Template CoMFA	274
3.11.2.6.5	COSMO*sar3D*	274
3.11.2.6.6	FieldQSAR	276
3.11.2.6.7	GRID/GOLPE/FLAP	277
3.11.2.6.8	GRIND	277
3.11.2.7	3D Activity Cliff Analysis	277
3.11.2.7.1	Activity Miner/Activity Atlas	278
3.11.2.8	ADME Prediction	281
3.11.2.8.1	VolSurf	282
3.11.2.8.2	MoKa	282
3.11.2.8.3	MetaSite	283
3.11.3	**Structure-Based Applications**	286
3.11.3.1	Binding Site Identification	286
3.11.3.1.1	Q-SiteFinder	286
3.11.3.1.2	SiteHound	286
3.11.3.1.3	FLAPsite	287
3.11.3.2	Binding Site Similarity Assessment	287
3.11.3.2.1	GRID/FLAP	287
3.11.3.2.2	IsoMIF	288
3.11.3.3	Docking	289
3.11.3.3.1	AFMoC	289
3.11.3.3.2	AutoDock	290
3.11.3.3.3	FLAPdock	291
3.11.3.3.4	Glide	291
3.11.3.3.5	GOLD	291
3.11.3.4	Determination of Water Positions	291
3.11.3.4.1	WaterFLAP	291
3.11.4	**Conclusions**	292
References		292

3.11.1 Introduction

Biological activity of drug-like molecules is determined by their interaction with biological targets. In turn, ligand recognition by a biological target depends on a number of factors, both enthalpic and entropic in nature. Enthalpic contributions are represented by van der Waals, electrostatic, and hydrogen bonding interactions, while the main entropic contribution is the hydrophobic effect arising from the desolvation step which precedes the formation of a ligand–target complex. While desolvation of highly structured water networks in contact with nonpolar surfaces gives a favorable contribution to binding, desolvation of polar surface segments is unfavorable, and is often only partially compensated by electrostatic and hydrogen bonding interactions established upon complex formation. The currently accepted view is that the hydrophobic effect is the term which contributes most to the free energy of binding, while electrostatic interactions and hydrogen bonds provide specificity.[1]

Molecular interaction fields (MIFs) are a useful tool for characterizing the ability of molecules to interact with other molecules.[2] Their usage in computational and medicinal chemistry has been introduced in the late 1970s by Cramer and Milne,[3] and developed by Cramer and Goodford over the following decade.[4,5] MIFs provide a very convenient way to focus on the enthalpic side of binding interactions as determined by the three-dimensional structure, while at the same time abstracting from the latter; in the following paragraphs, this statement will be expanded and made clearer.

An MIF is a collection of energy descriptors associated with 3D coordinates. The standard way to generate MIFs is to compute the interaction energy between a probe and a target, which may be a ligand or a biological macromolecule, at different positions in space. The nature (hydrogen bonding, electrostatic, van der Waals, hydrophobic, etc.) of an MIF depends on two main factors: (1) the chemical nature of each atom in the probe and in the target (typically defined through atom type/partial charge for force-field-based calculations, or just the element and the total formal charge for MIFs derived from quantum mechanics (QM)) and (2) the potential function used to compute the interaction energy.

The coordinates of each atom in the target and the coordinates at which energy values are sampled influence both the magnitude and the distribution of energy values in 3D space. While both the chemical nature and the 3D arrangement of the atoms involved in the calculation determine the properties of an MIF, collections of atoms which differ in chemical nature and 3D coordinates may give rise to similar MIFs. This explains how MIFs can abstract from the underlying chemical structure of molecules to capture the interaction properties which drive molecular recognition. Most importantly, MIFs inherently encode the concept of bioisosterism, and enable its application both on the ligand side (3D similarity, scaffold hopping, biological activity prediction), and on the target side (binding pocket characterization, cross-target structural homology identification).

MIFs address only the enthalpic contribution to the free energy of binding. Attempts have been made at modeling the desolvation term indirectly through the choice of appropriate probes, designed to detect hydrophobic regions and apply desolvation energy bonuses/penalties depending on their degree of hydrophobicity.[6] Fortunately, the realm of application of MIFs makes the lack of explicit support for the entropic component much less of a limitation than it might appear. An accurate estimation of entropy is crucial to the prediction of absolute binding free energies, but that is not among the goals for which MIFs were designed. To a large extent, molecules which share a significant similarity in their 3D Coulombic and van der Waals potentials implicitly share a similar desolvation behavior.

The wide range of interaction properties which may be computed through different probes/potential functions and the capacity to abstract from the chemical structure of the underlying molecule are among the main reasons for the continuing success of MIFs in drug discovery.[7] In the following, the main applications of MIFs will be reviewed, under separate sections depending on whether they involve mostly small molecules (ligand-based, LB) or biological macromolecules (structure-based, SB). We are aware that there is some degree of overlap between the two fields; nonetheless, we believe that the SB/LB distinction is both helpful and particularly relevant for the pure LB methodologies, which are the only option when the structure of the target is not available. Applications are presented in alphabetical order, along with relevant case studies and success stories. We realize that our list cannot be exhaustive within the scope of this article; we will therefore focus on those methods which have gained more widespread recognition within industrial and academic environments. In describing methods, we deliberately refrain from reporting the mathematical equations, which can be retrieved by the interested readers from the original literature references.

3.11.2 Ligand-Based Applications

All of the MIF-based methodologies cited in this section can be applied in the absence of any structural information about the target and hence can be regarded as purely LB applications. Nevertheless, some of them may usefully incorporate information from the target, if the latter is available; this possibility will be mentioned where appropriate.

3.11.2.1 Assessment of Ligand Similarity

Methods described in this paragraph present a theoretical framework, either based on QM or on molecular mechanics (MM), to assess MIF-based pairwise 3D similarities between small molecules. The first step of these calculations consists in maximizing the overlap between the MIFs of the two molecules through appropriate geometric transformations. As a consequence of these transformations, the underlying molecular structures are aligned based on their field properties. The first attempts to move from an atomistic description of a molecule to a structure-agnostic description founded on steric and electrostatic overlap were made

in 1990 by Kearsley and Smith[8] and by Cramer.[9] In the approach pursued by Kearsley and Smith in the SEAL program, electrostatic and volume descriptors were still connected to individual atoms, while Cramer introduced the concept of using grid-encoded MIFs to superimpose molecules in his Field Fit procedure, as a preliminary step to a comparative molecular field analysis (CoMFA).[9,10]

Over the 25 years which followed these groundbreaking intuitions, a large number of variations on the original methods have been published. The earlier approaches are covered by other reviews, one of the most comprehensive being the one by Lemmen and Lengauer,[11] so only the main points which are either distinctive or common to these methodologies will be summarized here.

The most significant differences involve the theoretical framework used for electrostatics (QM, MM with atom-centered charges (ACCs), MM with more sophisticated charge distributions) and the formalism chosen to describe potentials (numerical evaluation on a discrete number of points versus analytical calculation of atom-centered Gaussian functions). Elegant and computationally efficient, the analytical, Gaussian-based description formalized by Grant and Pickup[12] has become the standard method to assess and compare molecular shape. However, the early attempts by Good et al.[13] and Mestres et al.[14] to apply Gaussians to electrostatic potentials have largely been superseded by numerical descriptions based on discrete sampling, either on the nodes of a regular grid lattice or on a solvent-accessible surface. The reason is that analytical Gaussians describe very effectively fields which can be approximated by overlapping spheres, such as atomic van der Waals volumes, but are less suited to probe-based MIFs.

The common goal of MIF-based methods is to convey the degree of field similarity into a normalized score, ranging from 0 (no similarity) to 1 (identity) through a distance metric appropriate to the functional form used to compute and sample MIF potentials (e.g., Carbó, Tanimoto, Dice[15]). Summarizing the similarity in a single number enables straightforward computation of pairwise similarity matrices, which are the starting point for several clustering algorithms and chemometric data analysis techniques. However, since similarity is assessed in 3D taking into account the whole molecule MIFs, there is actually much more information about the nature and the distribution of local similarities than can be captured in a single number. This information can be conveniently visualized by plotting field isocontours, or color-coding molecular surfaces based on the field nature/value.

The following subsections will briefly describe three recent MIF-based methods to assess molecular similarity, representative of varying degrees of theoretical rigor in the description of molecular interactions and different computational approaches to similarity calculation and optimization.

3.11.2.1.1 *COSMO*sim3D

The COSMO*sim3D* method stems from COSMO-RS,[16,17] a widely used implicit solvation theory which allows the prediction of fluid phase thermodynamic properties of molecules based on QM calculations in a simulated conductor. Following a COSMO-enabled QM calculation, each molecule is characterized through a distribution of surface polarization charge density (σ). The molecular surface is tessellated into several hundred segments, each having defined coordinates, area and average σ charge density. The statistical distribution of the σ charge density across the 3D surface can be captured into a σ profile, a one-dimensional σ charge histogram, usually with a σ bin width of 0.1 e nm^{-2}. The area of each surface segment is assigned to the various bins of the histogram through a smooth and charge-conserving weighting scheme, such that the integral of the σ profile yields the total surface of the molecule, while the σ-weighted integral sums up to the total σ charge of the molecule. The σ profile provides a quantitative description of the amount of surface area of given polarity within a molecule (**Fig. 1**).

σ profiles have proved very valuable to quantify the ability of a molecule to give different types of interactions in the condensed phase. Furthermore, fast molecular similarity assessment through comparison of the 1D σ profiles is enabled by the COSMO*sim* methodology.[18] However, by design no information is included in the σ profiles regarding the localization of the patches with given polarity on the 3D surface. To overcome this limitation, the COSMO*sim3D* method[19] was introduced, which augments the description of the σ charge distribution for a molecule from a single 1D profile to a 3D grid of local σ profiles, one per each node of the grid (**Fig. 2**). The procedure through which σ surface segments are assigned to the grid nodes follows a weighting scheme similar to the one used to generate 1D σ profiles, just extended to three dimensions; the weighting ensures smooth linear interpolation and robustness against changes in the positioning of the 3D grid relative to the molecule. The COSMO*sim3D* procedure effectively yields a 4D description of a molecule, which may be regarded as an array of 3D MIFs, each MIF corresponding to one of the σ bins into which the local σ profiles are partitioned, and describing the 3D distribution of field intensity within the σ bin range.

As detailed in section "Assessment of Ligand Similarity", the 3D grid of local σ profiles enables pairwise 3D similarity calculations by maximizing the overlap between the grids to be compared. This is a global optimization problem, which has been tackled in COSMO*sim3D* by a Monte Carlo approach: *N* different starting configurations are optimized by a local line search along the direction of each of the three unit translations and rotations until a similarity maximum is reached; the highest similarity across the *N* samples is taken as the global similarity optimum. The superimposition of the 3D σ profile grids causes the underlying molecules to become aligned to a single or multiple references (**Fig. 2**).

The generation of a σ surface requires a single-point density functional theory (DFT) QM calculation, which can be carried out at different levels of theory, the more computationally expensive giving more accurate results. While the absence of adjusted parameters apart from the atomic COSMO radii warrants applicability to virtually any kind of chemistry, imparting a significant advantage over MM methods, the time requirements can be significant for larger datasets and/or flexible molecules which require multiple conformations to be considered. The COSMO*frag* procedure was developed to speed the procedure by quickly reconstituting a σ surface from precomputed fragments. While this causes a slight degradation of the surface quality due to imperfect match of the surface fragments, the actual impact on the similarity assessment was shown to be negligible.[19] In case fragments for the

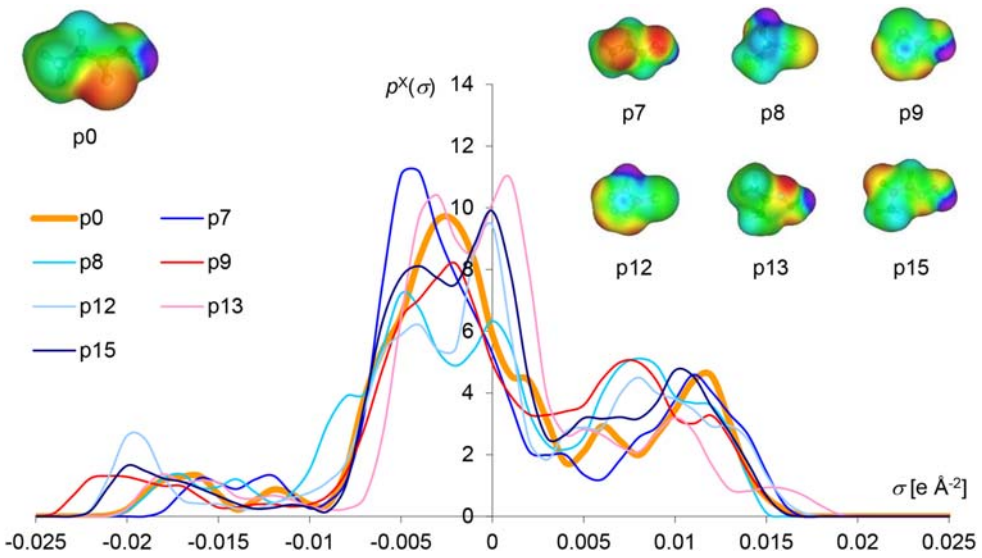

Fig. 1 The σ profile of propionic acid (p0) is compared to the σ profile of six other small molecules (p7, p8, p9, p12, p13, and p15). COSMO surfaces of the seven molecules are depicted, color-coded based on the distribution of their surface properties: strongly negative (*red*), strongly positive (*blue*), or nonpolar (*green*). The chart reports the amount of COSMO surface within a given interval of σ polarization charge density for each molecule (Adapted courtesy of A. Klamt, personal communication).

chemistry of interest are not available in the precomputed fragment database, the database can be extended or the procedure may fall back to the full DFT calculation on the whole molecule.

COSMO*sim3D* was validated in two exercises.[19] Firstly, its ability to separate true bioisosteric pairs from decoys was assessed on the BioSter database,[20] finding that 95% of the decoy pairs had similarities <0.2, whereas the true bioisosteres scored significantly higher. Setting a cut-off value at 0.2 similarity would retrieve only 5% false positives from the decoy set, and miss about 30% true positives in the true-bioisostere set (**Fig. 3A**). Secondly, the ability to identify ligands sharing at least one activity class based on their similarity was evaluated. Approximately 215 K structures were extracted from the MDDR database[21] and used to compute a pairwise similarity matrix by comparing their 1D σ profiles by the COSMO*sim* method. All pairs with a COSMO*sim* score >0.9 were subjected to a conformation/tautomer enumeration and then underwent a COSMO*frag*/COSMO*sim3D* similarity calculation. For COSMO*sim3D* scores <0.1, the probability for the molecule pair to share at least one activity class was in the 7–10% range, very close to the value obtained for random pairs drawn out of the MDDR database. Instead, the same probability increased to 50% for a similarity of 0.3, and to 80% for COSMO*sim3D* similarities of 0.45 (**Fig. 3B**).

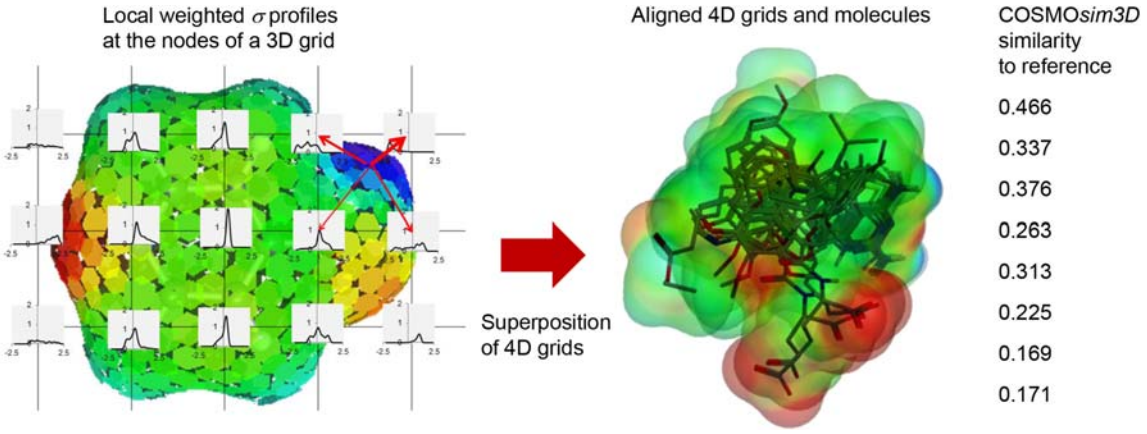

Fig. 2 For each molecule in a dataset, local σ profiles are computed at each node of a 3D grid (a 2D section is shown for clarity). This procedure yields a four-dimensional description of each molecule; superimposition of the grids causes the underlying molecules to be aligned against one or multiple reference(s) and yields a similarity score for each alignment. (Adapted courtesy of A. Klamt, personal communication).

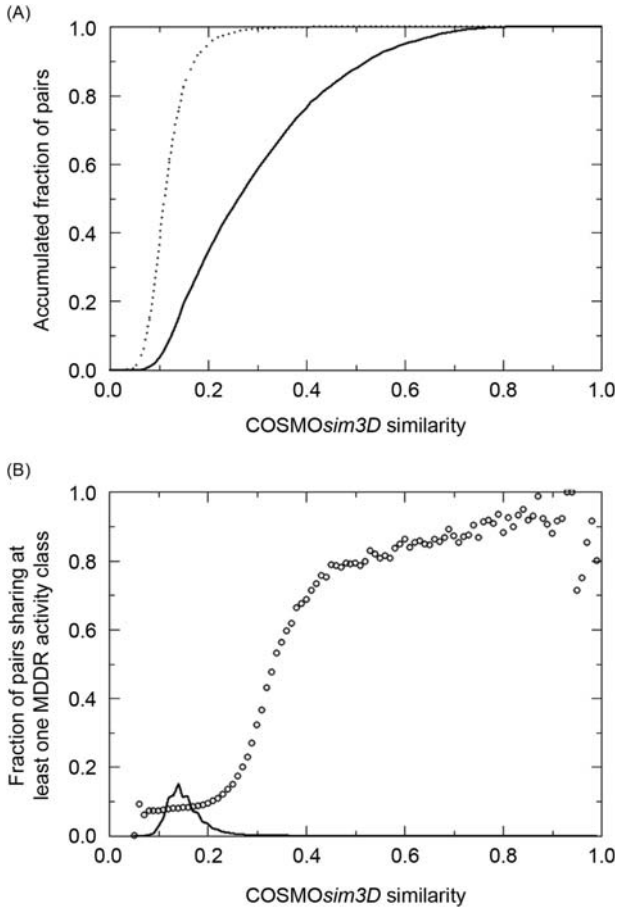

Fig. 3 (A) COSMO*sim3D* ability to separate true bioisosteric pairs (*solid line*) from decoys (*dotted line*) as assessed on the BioSter database. Setting a cut-off value at 0.2 similarity would retrieve only 5% false positives from the decoy set, and miss about 30% true positives in the true-bioisoster set. (B) COSMO*sim3D* ability to identify ligands sharing at least one activity class. When COSMO*sim3D* similarity is <0.1, the probability for the molecule pair to share at least one activity class is $<10\%$, while increasing to 50% for a similarity of 0.3, and to 80% for a similarity of 0.45. The solid line shows the distribution of COSMO*sim3D* similarity values within all tested pairs. Adapted from Figures 2 and 3 in Thormann, M.; Klamt, A.; Wichmann, K., COSMOsim3D: 3D-similarity and alignment based on COSMO polarization charge densities. *J. Chem. Inf. Model.* **2012**, *52*, 2149–2156. ACS Publication.

3.11.2.1.2 GRID/FLAP

The GRID program by Goodford[5] was the first to introduce the idea of generating an MIF using a probe which is not a simple neutral atom, but rather a more sophisticated and parametrized entity. In some cases, probes can be multiatomic with a predefined geometry, relevant for directional interactions such as hydrogen bonds. The original application for which the GRID force-field was developed was mapping protein-binding sites (see section "GRID/FLAP"), but the methodology has since been widely applied on small molecules. The molecular system under study is embedded in a 3D grid, a probe is placed at each node, and its interaction energy with the system is evaluated (**Fig. 4**). The range of available GRID probes covers the properties of functional groups commonly found in drug-like and biological molecules, and is meant to reproduce their interactions. GRID probe parameters are determined by the GRID force-field atom type of the constituting atoms; the atom type encodes hybridization, ACC, van der Waals and, when appropriate, hydrogen bond parameters. The GRID energy function uses a 12-6 Lennard–Jones potential for van der Waals interactions and a Coulombic potential for electrostatics; probes which can act as hydrogen bond donors and/or acceptors also feature an explicit hydrogen bonding term. In the latter case, a rotational scan is performed to optimize hydrogen bonding interactions with suitable partners around the probe. When parts of the target are treated as flexible, and therefore the loss of degrees of freedom upon binding needs to be accounted for, or hydrophobic/desolvation effects are to be captured, the energy function is augmented with an entropic term. This is particularly the case for the DRY probe which is tailored toward hydrophobic interactions. In this probe, the electrostatic term is replaced by an entropic term, while the hydrogen bonding potential is inverted to penalize interactions with polar surfaces.[5,6]

GRID MIFs have been used to compute pairwise 3D molecular similarity within the FLAP program.[22,23] The molecules are embedded in a 0.75 Å step grid box aligned to the principal axes of the molecule to avoid dependency from starting 3D Cartesian coordinates. MIFs are computed with a range of GRID probes, which normally include H (small, analyzes shape with good

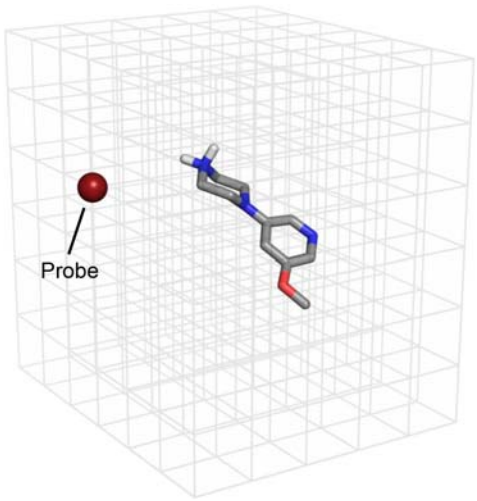

Fig. 4 Grid-based evaluation of the interaction energy between a molecular system and a probe placed at a grid node.

resolution), O (carbonyl oxygen, hydrogen bond acceptor), N1 (amide NH, hydrogen bond donor), and DRY (hydrophobic). The MIFs are then condensed into discrete points corresponding to the locations of energy minima, that is, the most favorable interactions, while providing adequate 3D space coverage across the molecule. These points are combined in four-tuples (quadruplets) according to all possible permutations, giving a set of MIF-based quadruplets. Another set of atom-based quadruplets is obtained out of GRID pseudoMIFs, which consist of electron-density-like fields associated to each atom. Each quadruplet identifies a tetrahedron with four vertices and six edges, whose volume and chirality can be computed (Fig. 5). The information contained in the quadruplet is stored in a fingerprint (FP), which consists of 11 fields encoding the 6 edge lengths (discretized as integer multiples of a small base length, such as 0.2 Å), followed by the indices of the four vertices (which allow accessing volume and chirality data), and finally by a value proportional to the sum of the energies of the four points. FP arrays are stored ordered by the first six fields (i.e., distances between minimum energy points) to enable fast searches. All possible quadruplet pairs are compared between the two molecules through their FPs; the FP pairs which match within a 1 Å distance tolerance and satisfy chirality constraints are used to overlay the molecules. The similarity between the molecules is assessed as the sum or the product of Tanimoto similarities of the individual MIFs, and the highest similarity value is retained as the 3D similarity score for the pair of molecules.[23,24] This methodology is fast enough to allow for similarity evaluations taking into account multiple conformations for each molecule.

3.11.2.1.3 XED/FieldAlign

The FieldAlign methodology[25] is based on the XED force-field.[26] In traditional force-fields, such as AMBER, CHARMM, MM2/MM3, MMFF94 and OPLS, the electrostatic term is modeled as a Coulombic potential generated by a collection of ACCs. ACCs are usually fitted to reproduce a QM-derived electrostatic potential, with the inclusion of appropriate constraints to evenly share charge on

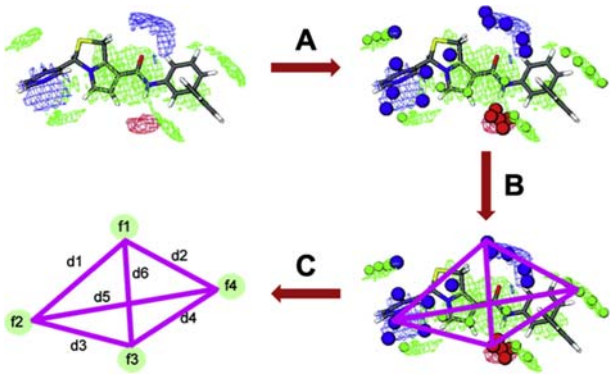

Fig. 5 GRID molecular interaction fields computed around the molecule are condensed into discrete points (A), which are then exhaustively combined into MIF-based quadruplets (B), identified by four vertices (*f1–4*) and six edges (*d1–6*) (C). Adapted from Figure 1 in Cross, S.; Baroni, M.; Carosati, E.; Benedetti, P.; Clementi, S. FLAP: GRID molecular interaction fields in virtual screening. Validation using the DUD data set. *J. Chem. Inf. Model.* **2010**, *50*, 1442–1450. ACS publication.

symmetric groups, such as in the RESP scheme.[27] However, the ACC model is rather crude, and fails to account for the properties of electronically anisotropic functional groups such as carbonyl. Also the interaction properties of aromatics cannot be correctly reproduced by ACC force-fields, with van der Waals stacking interactions dominating over the edge-to-face interactions experimentally observed in crystallographic complexes.[28]

To address these shortcomings, Hunter and Sanders introduced an innovative electrostatic treatment for aromatics, which models the σ-framework separately from the π electron clouds.[29] This paradigm is loosely reminiscent of the distributed monopole analysis (DMA),[30] and models the σ-framework through positive ACCs, while the π electrons are described by negative off-center charges. This model could successfully predict the geometry of intermolecular interactions in crystal structures of aromatic molecules, without the cost involved in computing a QM wavefunction. The seminal concepts proposed by Hunter and Sanders were implemented by Vinter in the XED force-field,[26] where the combination of traditional ACCs and off-center charges, termed XEDs (eXtended electron distributions), provides a computationally affordable way to describe electron anisotropy (**Fig. 6A**). The locations of the XEDs associated to each atom react to the local electrostatic potential, thus modeling molecular polarizability. A maximum of six XEDs is associated with each atom, the exact number depending on its type and hybridization. XED distances and charges were tuned on a number of complexes for which extensive experimental data was available, such as the acetone–water complex. Parameters derived on these specific test cases turned out to be generalizable, reinforcing the theoretical soundness of the XED model. Compared to ACCs, XEDs consistently led to better geometries and interaction energies, as the description of electrostatics is more coherent with the actual electron distributions and orbital shapes. In particular, remarkable successes were obtained in reproducing the experimental behavior of aromatic complexes (**Fig. 6B**).[28]

After undergoing extensive testing in the XEDRAW, XEDOCK, and XEDAST molecular modeling packages,[26] the XED force-field in its mature form was implemented in two programs, XedeX and XedMin, which are respectively a conformational search engine and a geometry optimizer. XedeX uses Monte Carlo randomization of torsions and library-based sampling for rings, falling back to molecular dynamics for rings not represented within the library.

The XED force-field provides the foundations upon which the FieldAlign methodology is grounded. Molecules are characterized through four MIFs, covering the different kinds of intermolecular interactions: (1) van der Waals (neutral probe, Morse potential);

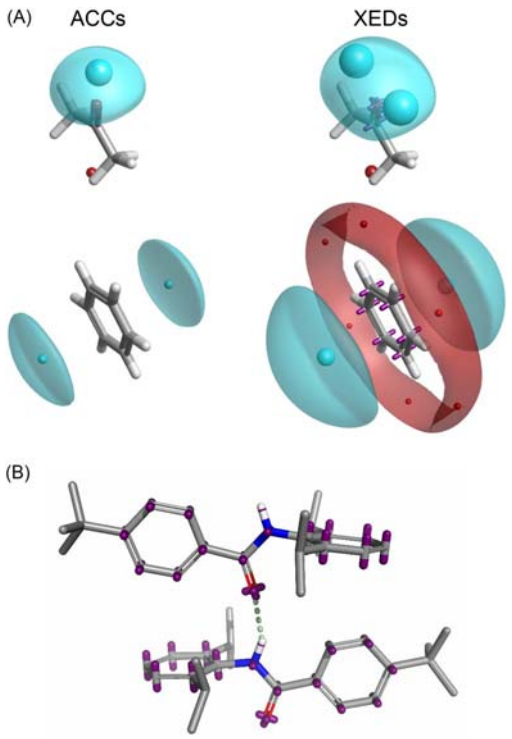

Fig. 6 (A) Comparison between electrostatic potential surfaces using ACCs (*left*) versus XED charges (*right*) for electronically anisotropic molecules such as acetone (*above*) and benzene (*below*). The XED model provides a more realistic description of the electrostatic potential distribution. XEDs are represented as purple dummy atoms; for atoms bearing XEDs, the partial charge is distributed across the atom itself and the XEDs. The XED coordinates can move independently from the respective atom in order to model molecular polarizability (see text). (B) Crystallographic complex of conformationally restricted benzamides which shows edge-to-face interactions between aromatic rings; hydrogens are hidden for clarity, while the hydrogen bond between amide groups is depicted as a *dotted green line*. Interaction enthalpies computed with the XED force-field have an excellent correlation with experimentally determined $\Delta\Delta G$ values ($r^2 = 0.95$), whereas the best ACC force-field, MM2, only achieves an r^2 of 0.69 (see Ref.[28] for details).

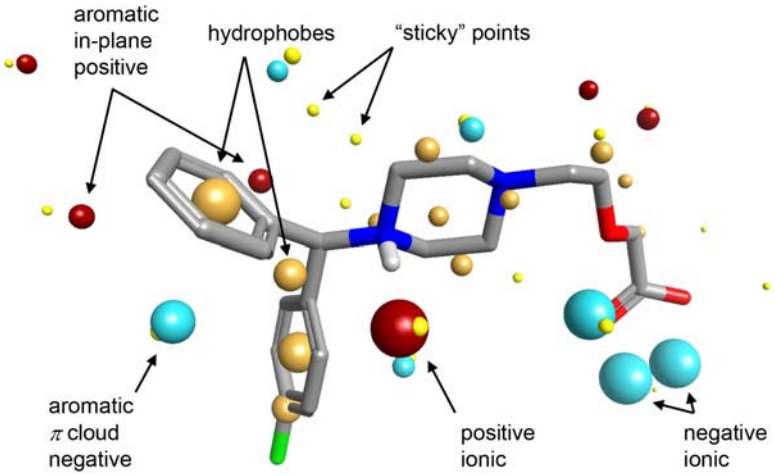

Fig. 7 Field points are shown for a drug-like molecule, cetirizine. While electrostatic and van der Waals field points are located in vicinity of the molecular surface, hydrophobic points are buried in the most hydrophobic regions. The extended charge distribution which characterizes the XED force-field allows a description of the interaction pattern of aromatic rings in good agreement with experimental and QM data.

(2) electrostatic (negative and positive probe, respectively, combined Coulombic and van der Waals potential, dielectric constant = 4); and (3) hydrophobic (neutral probe, attractive potential negatively weighted on atoms more electronegative than carbon and 0.5-weighted on hydrogens). In an attempt to condense the information contained in an MIF to a more succinct and computationally manageable form, the concept of field points was introduced. These four MIFs constitute collections of scalar interaction energies between a probe and the field generated by a molecule; such energies are sampled placing a probe at 120 points located at regular intervals over a slightly reduced solvent-accessible surface of each atom. At each point, the position of the probe relative to the molecule is optimized through a simplex to maximize the interaction energy. Many sampling points coalesce to common extrema, and after filtering out points with low interaction energy values a small set of "field points" is retained (usually comparable in number to the number of heavy atoms), which provides a 3D fingerprint of each molecule. Field points are visually represented as spheres whose color depends on the field type (*red*: electrophilic centers; *blue*: nucleophilic centers; *yellow*: van der Waals, or "sticky", points; *orange*: hydrophobic points), and whose radius is proportional to the MIF value at the field point position. While electrostatic and van der Waals field points tend to be located close to the molecular surface, the lack of the repulsive term allows hydrophobic points to penetrate the molecule and be buried inside the most hydrophobic regions of the molecule, such as ring centers or branched aliphatic substituents (Fig. 7).

Field points capture the concept of bioisosterism, since structurally diverse molecules may give rise to similar field point patterns. Contrary to classic pharmacophoric features, which are perceived in isolation from each other, field points encode interaction properties derived taking into account the whole molecule. Field point ensembles can be used for similarity assessment. As outlined in previous paragraphs, similarity assessment requires molecular superimposition as a preliminary step. To tackle the global optimization issue (see sections "COSMO*sim3D*" and "GRID/FLAP"), a two-step procedure is adopted. Firstly, colored cliques are generated out of those field points which are separated by similar distances across the reference and target molecule. Each clique is scored based on the number of matching points and their respective sizes; the top-ranked cliques are then used in a least-squares fitting procedure to generate aligned molecule pairs (Fig. 8A). In the second step, the clique-derived alignments are rescored by sampling the MIF of each molecule at the positions where the field points of the other molecule lie; all field points are used for the sampling, not only those constituting the clique (Fig. 8B). This MIF-based score is normally complemented by a shape-based score using the standard algorithm by Grant and Pickup (Fig. 8C);[12] the combined score is normally the average of the two, but the weights of the individual scores may be adjusted. Finally, the combined score is normalized through the Dice metric to a similarity value ranging from 0 to 1. The similarity value may then be maximized by a simplex optimizer through small roto-translations of one molecule relative to the other (Fig. 8D). Optionally, the alignment can be biased through user-defined constraints of variable magnitude on selected field points, in order to increase their weight in the molecule overlay algorithm.

3.11.2.2 Bioactive Pose Prediction

Whenever an X-ray structure of a ligand cocrystallized with its protein target is not available, its bioactive pose has to be predicted with computational methods. The general approach consists in looking for a common bioactive conformation across a series of ligands known to bind at a certain target, in the assumption that all of them adopt the same binding mode at the active site. All ligands in the series, when bound in that conformation, should share a reasonable overlap in their MIF patterns. Methods may differ in the size of the series used to derive the common binding mode and in the way the information extracted from this exercise is summarized and used in subsequent steps. In the following, we will describe two of the MIF-based methods most commonly used for this task.

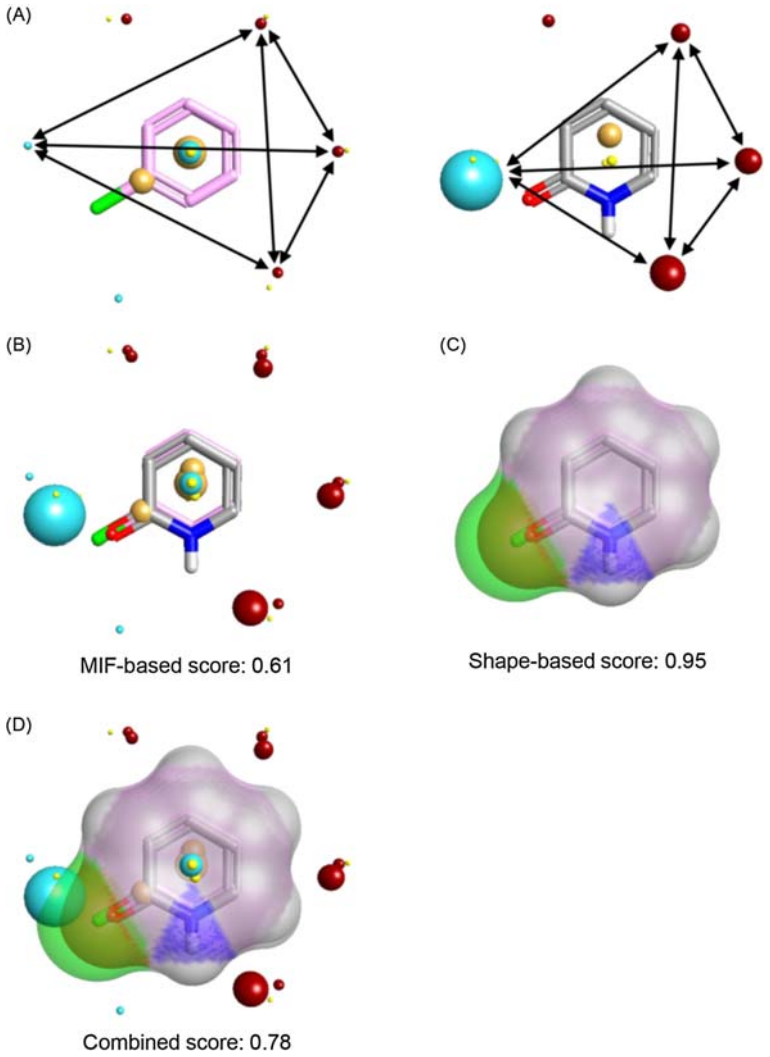

Fig. 8 (A) Generation of colored cliques and scoring based on the number of matching points and their sizes. (B) The best clique-derived alignments are rescored using the whole molecule MIFs. (C) The MIF-based alignment is used to compute a shape-based score. (D) The combined similarity score is maximized by a simplex optimizer.

3.11.2.2.1 FieldTemplater

FieldTemplater attempts to provide binding mode hypotheses for a small number of diverse ligands known to bind a certain target; the underlying assumption is that they bind at the same active site, and that to establish similar interactions with the latter they need to share significant similarity in their MIF patterns. Contrary to the FieldAlign method, FieldTemplater requires no a priori bioactive conformation hypothesis or target structure; instead, it attempts to identify the binding mode of the input structures by searching for common field patterns across their conformations. If multiple, independent, and structurally diverse active molecules can assume conformations characterized by a similar field pattern, then those conformations are likely candidates to represent the bioactive one. The binding mode hypothesis should ideally be unique; in case there are multiple and distinct common field patterns across the input molecules, hypotheses are scored and ranked. Each hypothesis ("template") is therefore constituted by a set of putative bioactive conformations, one per input molecule. Molecules in the template share the same 3D coordinate space, and are aligned relative to each other according to how they are supposed to interact with the surrounding binding pocket, whose structure may be unknown. The FieldTemplater workflow is summarized in Fig. 9.

A conformer pool is generated from each of the *N* input molecules using the conformational search engine XedeX (see section "XED/FieldAlign"). The *N* input molecules are then combined into all possible pairs, and the similarity of each pair is assessed with the two-stage algorithm described in section "XED/FieldAlign", taking into account all possible permutations of their conformations. If a pair of conformations yields a high similarity duo, the corresponding alignment is stored: with the standard settings, the best 100 duos are kept for each molecule pair. In case there are only two input molecules, the algorithm stops here, presenting a list of the best-aligned duos ranked by their combined field/shape similarity. If there were more than two input molecules, duos

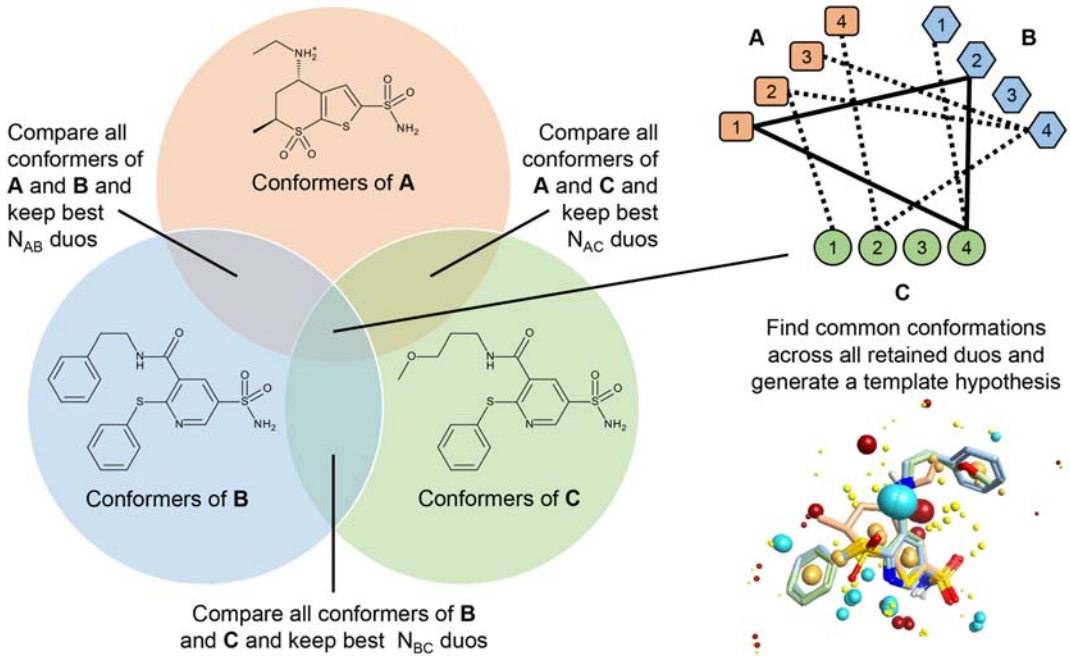

Fig. 9 Summary of the FieldTemplater workflow to generate a template hypothesis (i.e., a putative common binding mode) for three carbonic anhydrase inhibitors. A conformational search is run on each ligand, then pairwise comparisons are carried out among all conformers of each pair to retain the most promising duos. Finally, common conformations across all retained duos are sought and aligned to generate a template hypothesis.

are searched for common conformations: if molecule A, conformation 1 aligns with high similarity to molecule B, conformation 2, and molecule C, conformation 3 aligns with high similarity to the same conformations of molecules A and B, then a trio is formed, featuring a mutual alignment across the three molecules. The number of links required among N molecules is $N(N-1)/2$, so it becomes increasingly hard to satisfy all of them with increasing N; hence, the algorithm can be instructed to generate a template even if only a fraction of the links is found. The templating algorithm can also be biased by defining a set of distance constraints of user-defined magnitude between atoms on different molecules which need to be satisfied by the generated hypotheses.

Once the conformations to be combined have been identified, the template can be generated. The first step consists in combining pairwise alignments in order to minimize the RMS angular and translational deviations between their orientations in the original pair and those in the final template. The generation of a consensus alignment from a combination of pairwise alignments has usually been done in a piecewise fashion, introducing an order dependence, but the FieldTemplater algorithm does this analytically.

After generating a geometric mutual alignment, the template is further optimized in field space yielding the final overlay of conformations and then scored by field/shape similarity. All conformation tuples which satisfy the user-defined fraction of links undergo the same process, to generate a ranked list of templates for the input molecule set. The templates can be used to align a series of molecules against, or as a search query in a virtual screening (VS) exercise, just as would be expected from a more traditional pharmacophore.

To maximize the chances to obtain a small number of high-quality templates, three to five input molecules are required, which should be highly active, with comparable molecular weight (MW) and characterized by high structural diversity. Using only two input molecules most likely leads to a large number of conformation pairs being similar by mere chance, thus leaving a large degree of uncertainty about the common binding mode. Conversely, increasing the number of input molecules makes it more likely that at least one molecule does not have a binding mode in common with the others. It is important to avoid cases where the structures share a common torsion once aligned, as this leads to degeneracy in the solution. Since all molecules in the template could accommodate the same range of possible dihedral angles at that torsion, there would be no way to discriminate among them. For a similar reason, large differences in MW can lead to multiple under-defined templates, since moieties in the larger molecule(s) may not have any counterpart in the smaller one(s), thus making their unequivocal orientation impossible.

FieldTemplater was validated on a series of CCK_2 antagonists for which no structural information was available.[31] The highest scoring template obtained running the FieldTemplater algorithm on three input molecules was used to align the other molecules in the series, yielding a similarity value for each compound. The linear correlation between the experimental affinities (pK_B) and the similarity values had $r^2 = 0.75$ ($p < 10^{-6}$), while the r^2 constrained through origin of the linear regression between the recalculated pK_B values and the experimental ones was 0.67.

3.11.2.2.2 FLAPpharm

GRID MIF-based binding mode prediction has been implemented in FLAP within the FLAPpharm procedure.[32] A stochastic conformational search is carried out on the input molecule using the MM3 force-field, retaining only the most diverse conformations. For each conformation, MIFs are computed and FPs extracted as described in section "GRID/FLAP". Pairwise comparisons are carried out across all possible FP combinations such that for each molecule only the *N* conformations having the highest FP similarity are retained, with *N* being 5 or 10 depending on the desired tradeoff between speed and accuracy. Finally, the common binding mode is sought by taking each conformer of each molecule in turn as the starter molecule; subsequently, for the remaining molecules, the conformer which best fits those which have already been aligned is chosen. The resulting model is scored based on the average pairwise similarities between each molecule and the templates used to align it. The scoring function is a weighted sum of the individual MIF similarities; the shape MIF is down-weighted at 50% because the shape of the binding site is not known a priori, but rather inferred while the model is being built. The five top-ranked models are generally retained for subsequent analysis. For each of the four types of MIF overlaid in the model, a pharmacophoric interaction field (PIF) is derived as the average of the MIFs of individual molecules at each grid node. The PIF retains roughly the same intensity of the original MIFs at those positions where all fields had comparable energies, while it features a fraction of the original intensity at the positions which are not common to the majority of molecules. In addition to MIFs, for each molecule a corresponding set of pseudoMIFs is also generated (see section "GRID/FLAP"), from which a set of common pseudoPIFs can be derived with the same procedure used to extract PIFs. Finally, the centroids of pseudoPIFs are also included as further pharmacophoric points (**Fig. 10**). The pharmacophoric pseudomolecule identified by the collection of PIFs and pseudoPIFs can be used as a template for VS (see section "FLAP") or docked into a macromolecular target (see section "FLAPdock").

To assess the ability of the method to find the correct binding mode, an objective benchmarking suite was assembled (PharmBench[33]). This comprised 960 ligands from 81 different targets having high resolution X-ray structures in the Protein Data Bank (PDB).[34] For each target, the available complexes were manually curated with regards to protonation and tautomerism, and then superimposed using the protein alpha carbons. After the proteins were removed, the ligands were left in a binding site-aligned configuration, thus providing an objective benchmark to assess the ability of a binding mode prediction method to recover the experimental pose. The 3D structures of the cocrystallized ligands were generated de novo starting from their 2D counterparts and their conformations were populated; the FLAPpharm procedure was then applied twice on each target to obtain a pharmacophoric model, firstly using only the X-ray bioactive conformations as input, and secondly using those regenerated from the 2D layout, which are completely independent from the experimental ones. Four different metrics were adopted to evaluate the performance: (1) the ability of the conformational engine to generate the experimental pose within a 2.0 Å RMSD; the success rate was 91%; (2) the ability of the method to retrieve the correct bioactive conformation for each ligand, expressed as % of ligands having a RMSD < 2.0 Å once individually realigned to their experimental counterpart; the success rate was 65%; (3) the ability of the method to reconstitute the original binding mode for each target,[35] expressing results as % of datasets where at least half of the ligands had a RMSD < 2.0 Å from the X-ray pose; the success rate was 93% when starting from the X-ray conformations, and

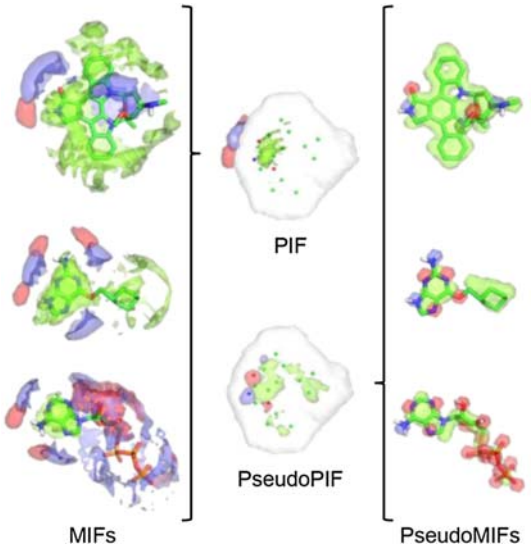

Fig. 10 For each of the top-ranked binding mode hypotheses, FLAPpharm generates a pharmacophoric interaction field (PIF; *top middle picture*) as the intersection of the MIFs of individual molecules (*left*). A pseudoPIF (*bottom middle picture*) is also similarly generated out of the ligands' pseudoMIFs (*right*). The ensemble of PIFs and pseudoPIFs gives rise to a pharmacophoric pseudomolecule which can be used as a template for virtual screening or docked into a macromolecular target. Adapted from Figure 1 in Cross, S.; Baroni, M.; Goracci, L.; Cruciani, G. GRID-based three-dimensional pharmacophores I: FLAPpharm, a novel approach for pharmacophore elucidation. *J. Chem. Inf. Model.* **2012**, *52*, 2587–2598. ACS publication.

67% when using the conformations generated from an unbiased 2D layout; (4) the similarity of the unbiased, regenerated pharmacophoric models to those built out of the experimental ligand coordinates; the average similarity was 0.72 when the X-ray conformations were used, and 0.53 when conformations were rebuilt from 2D coordinates.

3.11.2.3 Virtual Screening

MIF-based methods are very well suited for VS. Once the interaction properties of a molecule have been summarized into a more concise, field point-based or pharmacophore-like description, it is possible to use the latter to query a database of molecules (each represented by a population of conformers) for similar patterns. Since the MIFs are not directly related to the underlying chemical structure, the VS exercise has a chance to retrieve different chemotypes with comparable field properties, rather than just trivial structural analogs. This feature makes MIF-based VS particularly valuable compared to traditional methods based on 2D fingerprints. In the following, applications based on the XED and GRID force-fields will be reviewed.

3.11.2.3.1 FieldScreen/Blaze

One of the first applications of MIFs based on the XED force-field[26] (see section "XED/FieldAlign") was the FieldScreen LB VS methodology,[36] currently available within the Blaze web application. A ligand endowed with high activity is usually chosen as query; since FieldScreen is a 3D method, the bioactive conformation should ideally be used (if known) to maximize the likelihood of retrieving true actives, in the assumption that they bind with a similar conformation. MIFs are computed for the query and condensed into a field point pattern, which is then used to search a database of molecules prepopulated with conformations by the XedeX engine (see section "XED/FieldAlign"). For each conformation, field points corresponding to field extrema are identified and stored as previously described (see section "XED/FieldAlign"). A distance matrix is computed across field points and converted to a fingerprint, which may optionally be used as a coarse prefilter to remove from further consideration conformations with large deviations from the query. Subsequently, pairwise similarity scores between query and database entries are generated with the two-stage process outlined in section "XED/FieldAlign" (colored clique matching/simplex score optimization). The similarity assessment can optionally be biased through user-defined constraints of variable magnitude on selected field points, in order to force certain field features to be matched. If the structure of the macromolecular target is available, it is possible to penalize alignments which clash with the ligand-binding site, such that their similarity score is reduced. The 3D similarity value assigned to each retrieved molecule is the maximum similarity across its conformer pool. Search results are ranked by decreasing similarity; the optimal 3D overlay of the best-fitting conformation onto the search query is associated with each result.

FieldScreen was validated on the DUD dataset,[37] which was initially conceived as a benchmarking suite for docking methods. One of the strengths of DUD is that decoys were chosen to resemble actives not only in terms of MW but also of physical properties, while differing in topology. To extend its use to LB similarity methods, starting from DUD version two each set of actives is filtered for lead-likeness ($A\log P < 4.5$, MW < 450) and associated to a target-specific set of decoys, in order to make the discrimination more challenging for a LB VS application and avoid retrieving overly optimistic enrichment factors. Another well-known limitation of datasets for retrospective VS analysis is the fact that they usually contain many structural analogs; hence, a VS method able to retrieve a certain chemotype will easily retrieve all structures which share it. To correct this shortcoming, Good clustered active structures based on their reduced graph,[38,39] so that enrichment factors may be corrected by down-weighting each retrieved hit by the population of its cluster,[40,41] in order to put more emphasis on the ability of a method to retrieve different chemotypes rather than just trivial analogs. For this reason, FieldScreen validation was restricted to a subset of 13 of the 37 DUD datasets which contain ≥ 15 clusters, and only the dataset-specific decoys were taken into consideration. To enable direct comparison with DOCK,[42] the same ligand used for the active site definition was used as a search query. The conformation of the query was taken from the X-ray complex with the respective protein, except for *pdgfrb* (unavailable) and *vegfr2* (an apo structure), where a homology model and a complex with a different target protein were used. Two metrics were chosen to assess VS performance, namely the area under curve (AUC) of the receiver operating characteristic (ROC) curve, and the ROC enrichment (ROCE). While the ROC AUC measures the VS performance across the whole ranked database, ROCE is an indicator of early recovery, and evaluates the ability of the method to retrieve actives in the top fraction of the database. The latter is particularly desirable, given that in general only a very limited amount of the ranked database generated by VS can actually undergo wet lab screens. ROCE values were reported at 0.5%, 1.0%, 2.0%, and 5.0% of the true decoys having been screened. To account for the fact that actives are clustered by chemotype, both the ROC AUC and ROCE metrics were adjusted for clustering as explained earlier, yielding respectively awROC AUC and awROCE. Results are reported in Fig. 11. As far as the AUC metric is concerned, FieldScreen did not do significantly better than DOCK on average, but awROCE was significantly superior for all four percent thresholds (Wilcoxon signed-rank test, $p = 0.05$). Furthermore, FieldScreen consistently retrieved hits with a lower MW than DOCK, to the advantage of their likelihood to progress to the hit-to-lead development stage. Using the protein target structural information as excluded volume did not have a statistically significant impact on the quality of results.

3.11.2.3.2 FLAP

FLAP enables VS according to different paradigms: (1) LB: database ligands are compared against a query ligand in its putative bioactive conformation based on their quadruplets, as described in section "GRID/FLAP", and ranked based on their combined MIF Tanimoto similarity; (2) receptor-based (RB): the query is a receptor rather than a ligand and hence fields are computed placing a grid in the active site, yielding a series of quadruplets as for the previous case (see section "GRID/FLAP" for a detailed description);

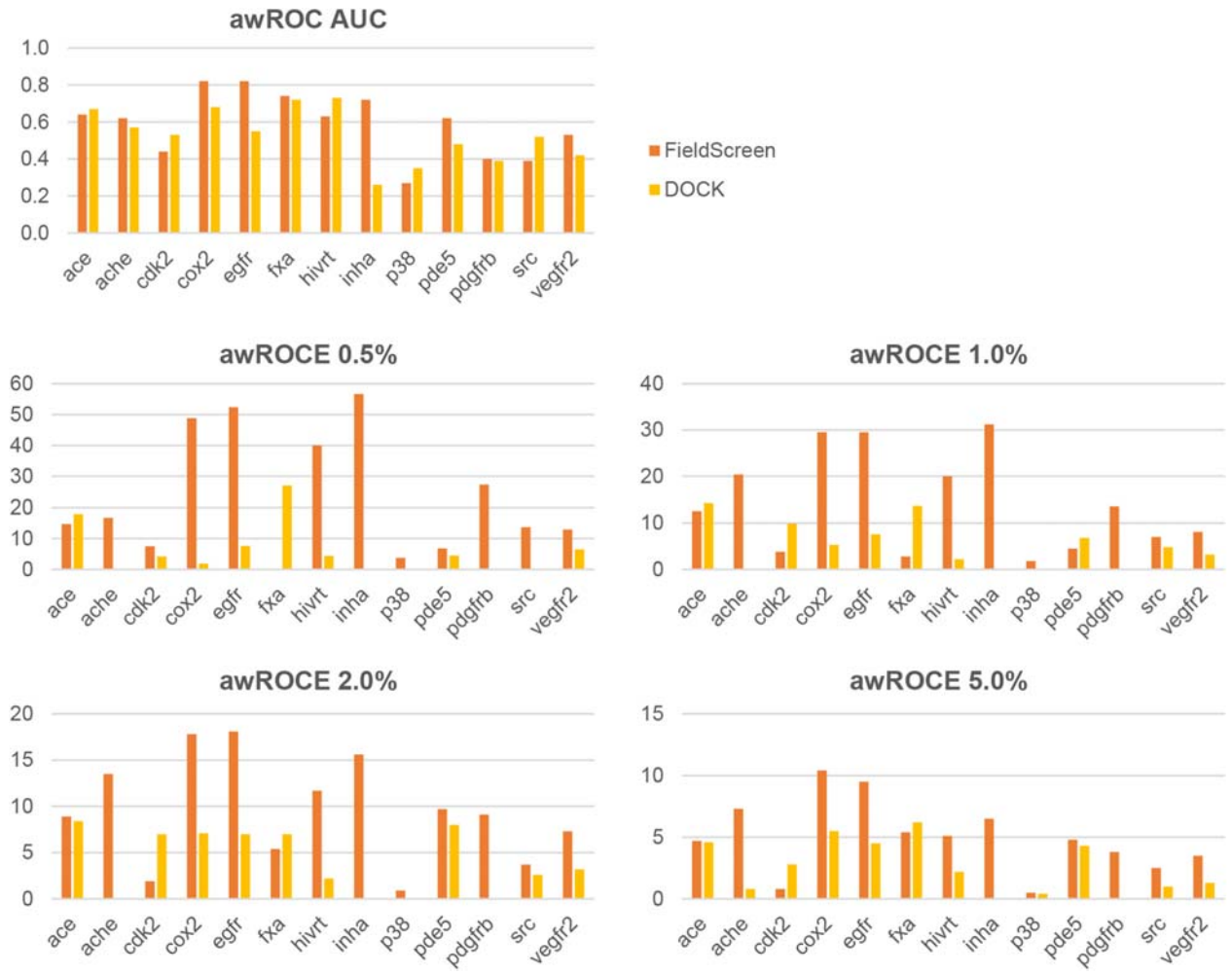

Fig. 11 Results from the VS exercise on 13 DUD datasets described in Ref.[37]. While FieldScreen on average does not perform significantly better than DOCK as far as the AUC metric is concerned, awROCE is significantly superior for all four percent thresholds (Wilcoxon signed-rank test, $p = 0.05$).

similarity is computed comparing such receptor quadruplets with pseudoMIFs (see section "GRID/FLAP" for a definition) centered on heavy atoms of the database ligands; (3) hybrid RB/LB (RBLB): the LB procedure is followed, using shape and features of the protein active site as a constraint in the database search. An early assessment of the RB performance of FLAP was carried out on two series of ligands against Factor Xa and thymidine kinase, respectively; databases were assembled from 10–20 actives and ~1000 decoys with comparable MW taken from the MDDR database. Screening against a crystal structure for each of the two targets gave better enrichment factors than a number of docking engines, and was an order of magnitude faster. LB enrichment performance was better than Catalyst's when tested on an internal Pfizer dataset and on a set of estrogen receptor alpha (ER-alpha) antagonists.[22] At a later stage, a more thorough and robust retrospective validation of the methodology was carried out on the same 13 datasets from the DUD benchmark suite previously used in the validation of FieldScreen,[36] and the results were compared to those obtained with FieldScreen[36] and DOCK.[42] The performances of the RB and the LB methods were substantially equivalent, while RBLB was slightly superior. When comparing the average arithmetic-weighted AUC across all 13 targets, there was no statistically significant difference among FLAP, DOCK, and FieldScreen (Wilcoxon signed-rank test, $p = 0.05$). With regards to early enrichment awROCE metrics, FLAP proved consistently superior to DOCK, as did FieldScreen. While differences in performance could be observed on individual datasets between FLAP and FieldScreen or among the different FLAP methods, on average no statistically significant difference could be detected across the 13 targets (Wilcoxon signed-rank test, $p = 0.05$) (**Fig. 12**). The authors reported other metrics obtained combining results from using multiple active compounds as search queries; however, these metrics cannot be taken into consideration for comparison purposes since they were not applied to the other methods.

With the introduction of FLAPpharm, FLAP can use also pharmacophore-like search queries in addition to individual molecules, simply replacing MIFs and pseudoMIFs with PIFs and pseudoPIFs (see section "FLAPpharm" for definitions).[22,23]

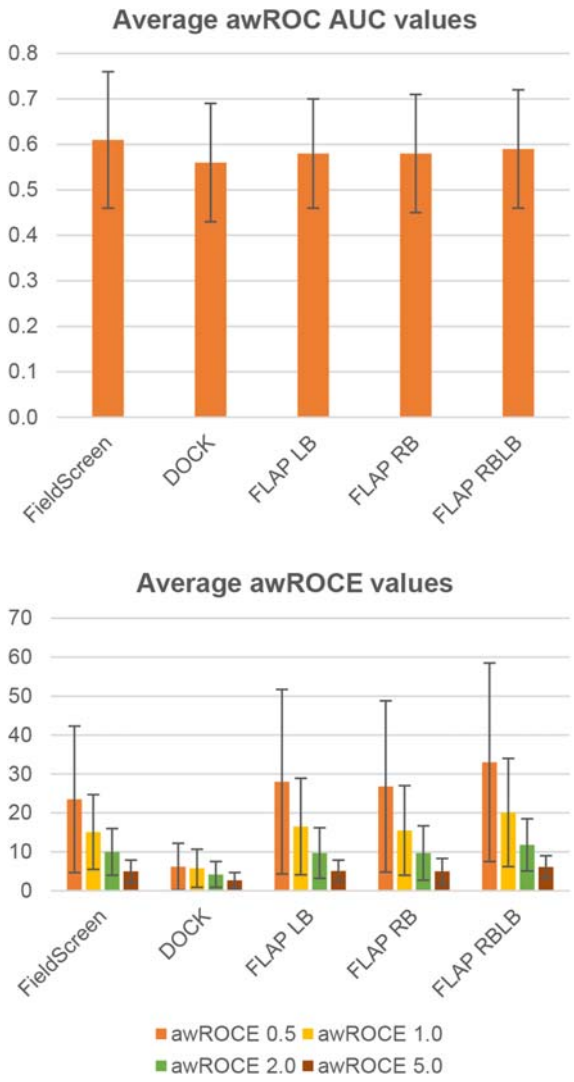

Fig. 12 Comparison of the average performance on 13 DUD datasets across different VS methodologies (FieldScreen, DOCK, and three FLAP methods), as described in Ref.[23]. With respect to the awROC AUC metric, all methodologies were roughly equivalent. FieldScreen and FLAP both proved to be superior to DOCK according to all awROCE metrics, while no statistically significant difference could be detected between FieldScreen and FLAP (Wilcoxon signed-rank test, $p = 0.05$).

3.11.2.4 Scaffold Hopping

Scaffold hopping, defined by Schneider as "identification of isofunctional molecular structures with significantly different molecular backbones"[43] is highly amenable to being implemented through MIFs. One of the virtues of MIFs is the ability to describe the general interaction properties rather than the specific chemical structures, exactly what is required in scaffold hopping. In contrast to VS, the goal of scaffold hopping is not finding novel structures as a whole, but rather replacing part(s) of a structure known to be active or to have favorable interaction properties at a certain target. The most common application is the replacement of a core structure, often a heterocyclic ring system, with a different chemotype, while keeping the decoration substantially intact (Fig. 13). From a medicinal chemistry standpoint, such an operation aims at improving pharmacodynamic/pharmacokinetic properties, selectivity, toxicity profile, or escaping intellectual property (IP) issues connected with patent coverage.

In general, MIF-based scaffold hopping methods provide a description of the moiety to be substituted in terms of geometric and field requirements; this description is used as a query to search conformationally populated fragment databases for possible matching replacements. The synthetic accessibility of the retrieved scaffolds is not guaranteed; however, assembling fragment databases out of available compound collections increases the likelihood of finding synthetically feasible options. While core scaffold replacement can be a purely LB exercise, structural information from the target can sometimes be used if available. In the following, a couple of applications of MIFs to scaffold hopping will be reviewed.

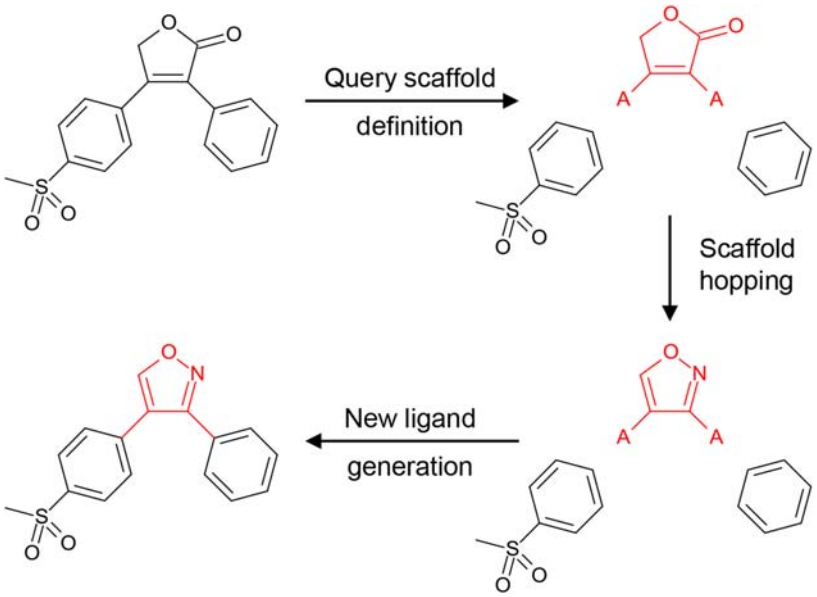

Fig. 13 Scaffold hopping exercise on rofecoxib. The five-membered lactone scaffold is identified as a candidate for replacement, detached from the side chains, and capped with dummy atoms as attachment points. A search is carried out in a database for bioisosteric replacements, and the retrieved scaffold is reconnected to the side chains to generate a new ligand.

3.11.2.4.1 SHOP

SHOP is a method based on GRID MIFs which enables scaffold hopping based on both ligand[44] and receptor structures.[45,46] The core to be replaced is identified through anchor points, namely dummy atoms which replace the side chain atoms originally attached to the core (Fig. 13). There may be a single anchor point or multiple ones; anchor points are converted into hydrogen atoms before the search is started. To enable retrieval of alternative structures from a fragment database, two geometric descriptors are computed for each scaffold: (1) a distance matrix across all anchor points and (2) a set of dihedral angles identified by the bonds from the anchor point to the scaffold atom connected to it (Fig. 14).

In the LB methodology, the geometric descriptors are complemented by a set of interaction energies between the scaffold and five different GRID probes: hydrophobic (DRY), hydrogen bond donor (N1), hydrogen bond acceptor (O), positively charged (N1+), and negatively charged (O−). Energies are sampled at the nodes of a regular 0.5 Å grid which embeds the scaffold to be replaced, excluding nodes which lie beyond a cut-off distance from any scaffold atom, and those lying within 3 Å from any anchor point. Energy values are then assigned to bins according to their distance from the anchor points; each bin is 0.4 Å wide. This procedure, reminiscent of the one used to generate GRIND descriptors (see section "GRIND"), gives rise to a correlogram, which records the most favorable energy value for each distance bin. The positive energy values of the N1 grid are used to evaluate shape, which in a similar fashion to the field energy values is converted into a correlogram, consisting of the binned frequency distribution of distances between anchor points and grid nodes. Distances are described by Gaussian functions to allow some overlap between neighboring bins (Fig. 14). The ensemble of geometric, field, and shape descriptors is used as a query to retrieve potential replacements from a fragment database previously populated with conformations. Fragments are ranked based on their similarity to the query, as assessed by the Carbó index. Each fragment is characterized by eight similarity values (two from geometric descriptors, one from shape, and five from GRID MIFs); the total similarity is a weighted sum of the eight individual values. Weights can be modified based on the features which are thought to be more important for a certain scaffold. The maximum similarity value across alignments obtained by all possible permutations of anchor points is taken as the score for each fragment.

The LB SHOP method was validated on a number of X-ray complexes chosen from three protein families (thrombin, HIV protease, and influenza virus neuraminidase). For each family, complexes were chosen such that the ligands had comparable binding mode and interactions with the target, and that scaffold replacement could be carried out using a variable number of anchor points (2–4).[44] A training set database was assembled from 471 scaffolds extracted from previously published combinatorial libraries, manually introducing anchor points as dummy atoms. For each scaffold, 3D conformations were generated. This database was then spiked with biologically active scaffolds in their X-ray bioactive conformation; unlike the decoys, the spike scaffolds were not subjected to a conformational search. Firstly, the weights for each of the eight similarity values mentioned earlier were optimized in order to maximize the recovery rate of actives for each protein family. The tailored set of parameters for each family was then used to recover scaffolds from a larger test set database, constructed with 2500 scaffolds extracted from the same literature sources as the training set. For each protein family, the 10 top-ranked scaffolds retrieved by SHOP were linked to the side chains originally chopped off the query scaffolds, and the complete ligands thus obtained were redocked in the X-ray complexes from which the query scaffold had been extracted. Binding modes, interactions, and docking scores were largely comparable to those

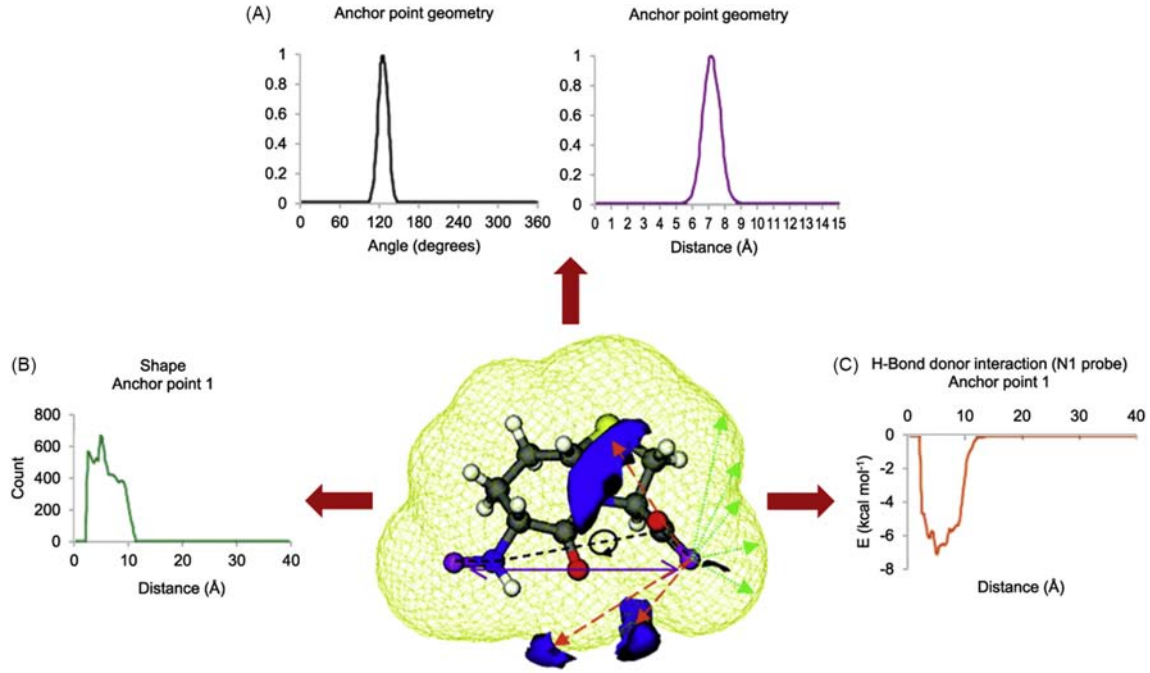

Fig. 14 SHOP descriptors computed for a scaffold with two anchor points (the corresponding dummy atoms are shown in *purple*). (A) Anchor point geometric features, namely distance (*purple full line*) and dihedral angle (*dashed black line*) between anchor points are described by Gaussian functions. (B) Scaffold shape is described by positive energy values of the N1 grid. Distances from anchor points to grid nodes (*green arrows*) are recorded in a correlogram. (C) The most favorable probe-scaffold interaction energies for each distance bin (*orange arrows*) are also recorded in a correlogram. Adapted from Figure 1 in Bergmann, R.; Linusson, A.; Zamora, I. SHOP: Scaffold HOPping by GRID-based similarity searches. *J. Med. Chem.* **2007**, *50*, 2708–2717.

of the original X-ray complexes. A set of default parameters with general good recovery performance was devised, but their performance outside the three protein families used to derive the parameters themselves was not determined.

The RB methodology requires a target–ligand complex as the starting point, from which the scaffold to be replaced is extracted. The procedure is similar to the LB one, the main difference being the fact that the MIF evaluation is carried out on the target binding site from which the query scaffold is extracted rather than on the query scaffold itself. Once the query scaffold has been removed from the complex, the binding site around it is characterized through the five aforementioned GRID probes, and probe interaction energies are binned in 0.4-Å increments based on their distance from anchor points, as for the LB method. An additional set of fingerprint-like descriptors is computed on the database fragments by characterizing each atom as hydrophobic, hydrogen bond donor/acceptor, positively/negatively charged, thus matching the nature of GRID probes used to compute MIFs. Next, anchor point-atom distances are binned in 0.4-Å increments for each atom type, and their presence/absence is recorded in a frequency vector.[45] The similarity between query and database scaffolds with matching numbers of anchor points is assessed by a Pearson similarity index, which takes into account both geometry and field descriptors. For field descriptors, query fingerprints are compared against database MIFs, and vice versa. As with the LB method, the maximum similarity across all possible anchor point alignments is taken. Optionally, a volume constraint can be applied to force database scaffolds to match the query ligand volume. Finally, the ranked scaffolds are linked to the side chains chopped off the original X-ray complex, and the complete ligand undergoes geometry optimization inside the binding site.[46]

The RB SHOP method was probed for its ability to return known scaffolds from a decoy pool, and the chemotype novelty of the results was evaluated. A total of 164 fragments with 1–3 anchor points belonging to 11 different targets were selected from the SHOP database generated from the PDBbind database,[47] and used as queries to search the same database for potential replacements. More than 40% of fragments with a single anchor point were recovered among the top five ranked results; the percentage raised to 90% for fragments with 2–3 anchor points, as they are better characterized from a geometric point of view. The retrieved scaffolds range from close analogs to more structurally unrelated motifs, which are probably the most interesting from a medicinal chemistry perspective, especially those which are able to establish new interactions with the target compared to the original query.

3.11.2.4.2 Spark

Spark is a tool which enables bioisosteric replacement and scaffold hopping based on the XED/FieldAlign technology (see section "XED/FieldAlign"). As with the SHOP methodology described in the previous paragraph, scaffold queries can be used to mine 3D conformational databases of fragments for analogs in property space. However, Spark has several distinctive differences. While in

SHOP the 3D grid description of MIFs is collapsed to a 1D histogram of distance frequencies of atoms or MIF-energy sampling points from anchor points, Spark retains a larger amount of 3D information in the search for potential scaffold replacements. Furthermore, SHOP scores scaffolds retrieved from the fragment database in isolation; the final geometry optimization stage inside the active site does not affect the scoring. Instead, Spark scores the final molecule rather than just the retrieved fragment, that is, it links the original side chains to the anchor points before the scoring step. This allows any electronic or conformational effects of the new scaffold on the rest of the molecule to be evaluated as part of the scoring process.

The Spark algorithm takes as input the 3D coordinates of the molecule which requires bioisosteric replacement (the "starter molecule"), and computes its field point pattern based on the XED force-field as described in section "XED/FieldAlign". The region of the starter molecule selected for replacement can have from one to four connections to the rest of the ligand, flagged by as many anchor points (Fig. 13). Distances between anchor points and angles between bonds connecting anchor points to the main scaffold are taken as geometric constraints in the search for similar moieties in the conformationally populated fragment databases. Further constraints can be set on the kind of scaffolds to be retrieved (alicyclic, aromatic, and acyclic), on the element/hybridization state allowed to be bound to anchor points, or on specific field points which should be matched with a greater weight than others. If available, a protein structure can be used as an excluded volume to rule out fragments that, once merged into the starter molecule, would clash with the binding site.

The search for compatible fragments happens in three stages. In the first stage, fragment conformations are compared to the query according to all possible permutations of the anchor points. If the geometric requirements at each anchor point are fulfilled within a threshold the fragment is carried on to the next stage. When the fragment has a single attachment point, or two collinear attachment points, an underdetermined rotational degree of freedom arises; in this case, a set of alternative rotamers is generated and carried on for subsequent evaluation. In the second stage, the field points of the fragment are merged with the field points of the side chains of the starter molecule in the orientation(s) determined during stage 1; the approximate field pattern thus generated is scored against the whole query. After the second stage is completed, the best-ranked results are carried on to the final stage, where fields are recomputed ex novo and used for the definitive scoring (Fig. 15). The latter includes a simplex optimization of the

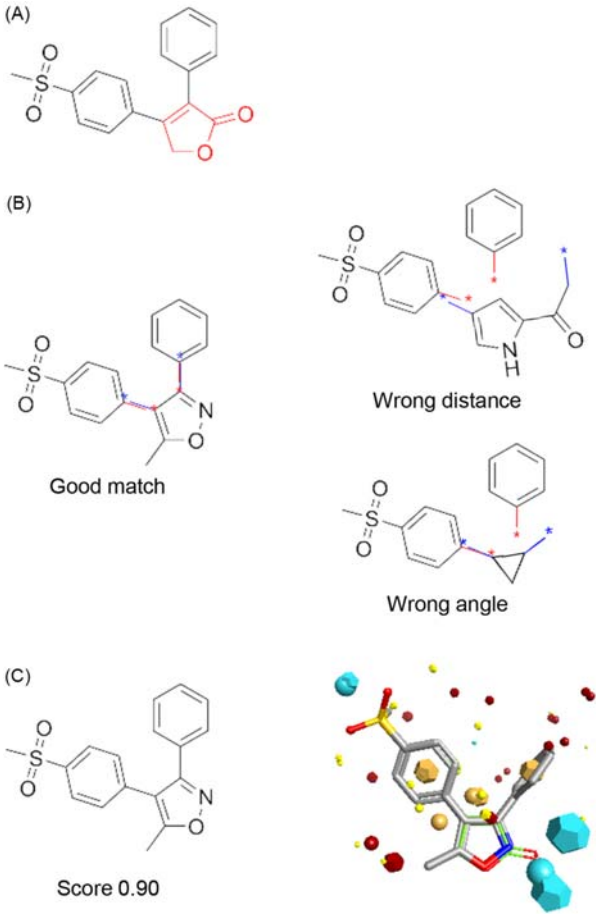

Fig. 15 Scheme describing Spark's workflow. (A) The scaffold to be replaced (*in red*) is identified. (B) During stage 1, a fragment database is searched for geometrically compatible fragments; fragments characterized by wrong distances and/or angles are discarded. (C) In stage 2, retrieved scaffolds are merged with side chains, including their field points; the approximate structures thus generated are scored and the best-ranked results are progressed to stage 3. In stage 3, fields are computed ex novo on the complete structures, and the latter are rescored and ranked.

similarity function through small rigid-body rotations and translations of the fragment relative to the query. Since fragments are scored after replacing the starter molecule's scaffold, it is possible to score the product of the bioisosteric replacement against reference(s) distinct from the starter molecule. This allows merging structural features across ligand series, replacing a core structure in molecule A to make it similar to molecule B, or to a weighted combination of A and B. Spark has been successfully used in prospective scaffold hopping studies to find novel HIV-1 entry inhibitors. Cocklin and coworkers identified through Blaze VS (see section "FieldScreen/Blaze") five hits active against HIV-1 in the high micromolar range, all of which shared a piperazine core with a known class of potent HIV-1 inhibitors developed by Bristol–Myers Squibb. After successfully replacing the piperazine scaffold with a dipyrrolidine core, inspired by an anti-HIV-1 lead developed by Pfizer, Spark was used to explore alternative decorations at the dipyrrolidine system. For this purpose, an ad hoc fragment database was generated out of 453 PubChem compounds which shared 2D similarity to one of the Bristol–Myers Squibb leads, and used to search for bioisosteric substituents. This chemotype merging strategy led to a low micromolar compound, which was further optimized to achieve a nanomolar lead.[48] A further round of Spark scaffold replacement enabled finding five novel alternatives to the dipyrrolidine core, all which were active, two of them in the nanomolar range.[49] Spark has been the subject of a couple of recent reviews.[50]

3.11.2.5 3D Clustering of Molecule Libraries

The assessment of 3D molecular similarity through the XED/FieldAlign methodology (see section "XED/FieldAlign") has been applied to the clustering of a large library of building blocks (~800 K) characterized by a wide variety of heterocyclic scaffolds with a high fraction of sp^3-hybridized carbons (Fsp^3).[51] The structures in the library were relatively rigid, with an average of ~4 conformations each, and featured a methyl handle to represent synthetic conjugation to a parent structure. The goal of the project was to cluster the library on 3D similarity into 25 K clusters, from which a subset of about 2000 compounds would be cherry-picked for synthesis. Analysis of the 2D topology and the 3D cluster network around each of the synthesized building blocks gives access to a number of analogs characterized by (1) similar core, different substitution pattern and vice versa; (2) being super/substructures of the parent; and (3) different 2D structure but comparable 3D interaction properties. If a molecule featuring one of the building blocks elicits promising activity in a high-throughput screening (HTS) assay, this network enables straightforward exploration of the surrounding chemical space.

The CLARANS *k*-medoids algorithm[52] allows clustering a large dataset around the chosen number of centroids, and it requires an upper triangular similarity matrix as input. Computing such a matrix across ~800 K molecules with a 3D method is too demanding even for a large cloud infrastructure. Instead, the cluster centroids were identified on a diverse subset of ~150 K structures, while the remaining ~650 K structures were assigned to the centroids identified in the first step. The presence of the methyl handle allowed the global optimization problem inherent in each pairwise similarity assessment to be addressed through the following workflow: (1) fragments were aligned by their methyl handle and the four XED MIFs were computed (see section "XED/FieldAlign"); (2) one fragment was systematically rotated relative to the other in 30-degree increments, and their 3D similarity was assessed; (3) the two highest similarities across the 12 samples were used as the starting point for a linear search in 5-degree increments to find the rotation giving the global similarity maximum; and (4) the similarity for each compound pair was taken as the maximum similarity across all pairs of conformations. Each pairwise comparison took 40 ms. The computation of the similarity matrix was split in square blocks of 100 molecules each and distributed over a 2048-CPU cloud computing facility, so that the ~14-CPU-year job could be completed in 4 days (**Fig. 16**).

A comparison of 3D similarity values against traditional 2D similarities based on ECFP4 fingerprints showed almost no correlation. The distribution of 2D similarity values was skewed toward significantly lower values, reflecting the sensitivity of 2D methods to small structural changes which may have little impact on 3D interaction properties relevant to biological recognition. In particular, the lack of stereochemistry awareness in fingerprints causes diastereomers with significantly different distribution of features in 3D space to be considered identical. Visual examination showed that the clusters obtained from 3D similarity metrics featured a much higher degree of internal consistency and appeared better classified from a medicinal chemistry standpoint than those from a 2D clustering.

3.11.2.6 3D-QSAR

Quantitative structure–activity relationships (QSAR) involve the application of statistical and data analysis methods to the prediction of biological activities from descriptors of structural properties. The ambition of QSAR approaches is to convey the similarity principle on which the practice of medicinal chemistry is founded (compounds with similar structures are expected to elicit similar biological activities) into quantitative mathematical equations.[53] Descriptors can be monodimensional (global molecular properties, e.g., MW, log P), two-dimensional (molecular topology-related, e.g., connectivity indices), or three-dimensional (related to 3D conformation, e.g., coordinate-dependent MIF energies); the latter are the focus of this section. One of the most appealing features of 3D-QSAR is its ability to yield a visually interpretable model, which provides information about the determinants of activity and gives hints about the structural modifications which can potentially improve ligand potency. This contrasts with 1D- and 2D-QSAR models which may sometimes provide "black-box" activity predictions which cannot be easily related to the original descriptor space.

A prominent criticism of 3D-QSAR methodologies is that they are not very amenable to being used in a prospective fashion, since they require a fairly large congeneric series upfront to provide meaningful predictions.[54] A recent review reports only a few

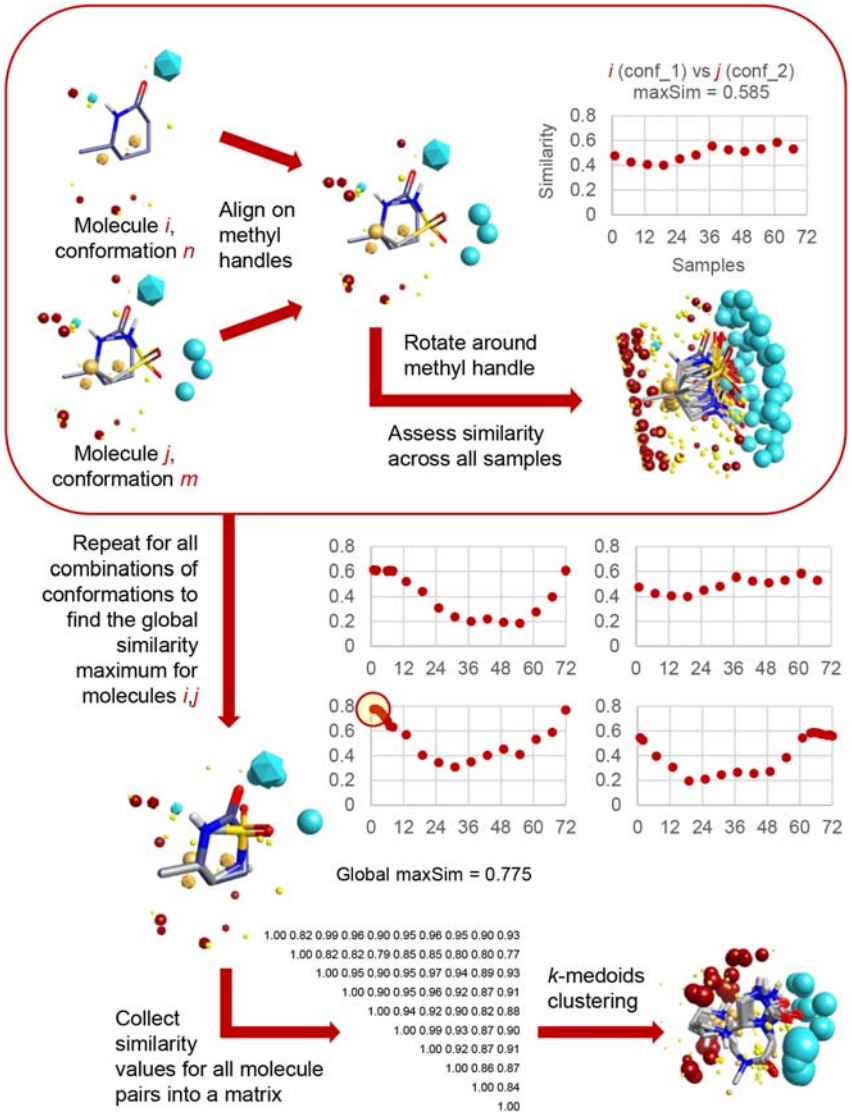

Fig. 16 The workflow depicted above allows clustering a large library of compounds bearing a methyl handle based on their 3D interaction properties as perceived using the XED/FieldAlign technology (see text for details).

cases where these techniques were used prospectively.[55] The majority of 3D-QSAR techniques require ligand 3D conformations to be mutually aligned, and in the absence of a relatively rigid crystallographic template the alignment step can be rather uncertain. The widespread practice of iteratively tweaking the alignment of individual substituents until the leave-one-out (LOO) cross-validated r^2 (q^2) reaches a maximum introduces a large user bias, and increases the likelihood of chance correlations[54,56]; such a procedure is clearly not viable for compounds whose activity is to be predicted.[57] The presence of close congeners in the dataset may partly invalidate the usefulness of LOO cross-validation, as their activity can be rather trivially predicted: more robust leave-many-out (LMO) cross-validation is thus usually recommended. Best practice also calls for the use of large, truly independent external test sets for model validation, and for the routine application of dependent variable scrambling to detect chance correlations.[54]

A full review of 3D-QSAR methodologies, including pros, cons, and pitfalls, is beyond the scope of this article but is covered in dedicated reviews.[58] In the following paragraphs, the most important 3D-QSAR methods which are currently implemented in available commercial or open-source software will be briefly reviewed.

3.11.2.6.1 CoMFA

CoMFA, invented in the late 1980s by Cramer[4] as a development of the earlier DYLOMMS method,[59] is the ancestor of all 3D-QSAR techniques. A set of molecules which share the same binding mode and site are aligned in their putative bioactive conformation; ideally, a crystallographic template should be available to guide the alignment. The set is then typically partitioned into a training set and a test set, and a grid box large enough to extend beyond the largest molecule by 5 Å in all directions is placed around the

compounds. The grid step size is normally in the 1–2 Å range. An sp^3-hybridized carbon probe bearing a +1 charge is placed at each grid node, and its steric and electrostatic interaction energies with each molecule are computed and stored in a matrix. The rows of the matrix hold the different molecules, while columns hold the energy values at each grid node. Columns which are characterized by a low standard deviation across the dataset are removed from further consideration. The matrix of energy descriptors is then regressed against biological activities to find a QSAR equation. Classic multilinear regression is not appropriate for such an underdetermined system, where thousands of independent variables need to be correlated with a number of dependent variables which is usually two orders of magnitude smaller. DYLOMMS attempted to address the problem using principal component analysis (PCA), with only limited success. A more appropriate regression tool, partial least-squares (PLS), proved critical to the acceptance of this method.[60,61] The number of principal components to be extracted is usually chosen as the one which yields the first local maximum of the LOO cross-validated r^2 coefficient (LOO q^2). The external test set is then used to provide more robust external validation to the model (Fig. 17).

CoMFA models are graphically interpretable, since PLS coefficients can be back-projected into the original descriptor space as pseudo-coefficients, optionally multiplied by the standard deviation of the corresponding energy variable across the dataset to amplify the importance of data points with larger variance. Therefore, each of the grid nodes is associated with a field-specific signed coefficient which tells, for instance, if steric bulk in a certain 3D region is beneficial to biological activity or if positive electrostatic potential is detrimental. This information may help to rationally guide medicinal chemistry optimization efforts (Fig. 17).

While CoMFA has enjoyed a vast success, as reflected in several thousand publications, it has some drawbacks. The first, and probably the most important, is common to all 3D-QSAR methods and is related to the initial requirement for aligned dataset structures (see section "3D-QSAR"). CoMFA-specific issues are connected with the grid-based evaluation of the energy function. Discontinuities arise close to atomic nuclei, which have been tempered by introducing steric energy cut-offs and excluding evaluation of the electrostatic potential at grid nodes which exceed the steric cut-off. Connected to the previous point, small translations of the grid relative to the molecules can have a dramatic influence on the energy values at grid nodes in vicinity of atom nuclei, which may acquire a large weight in the PLS analysis and trigger largely spurious correlations. Applying Laplacian smoothing to the grid helps to attenuate these artifacts.[62]

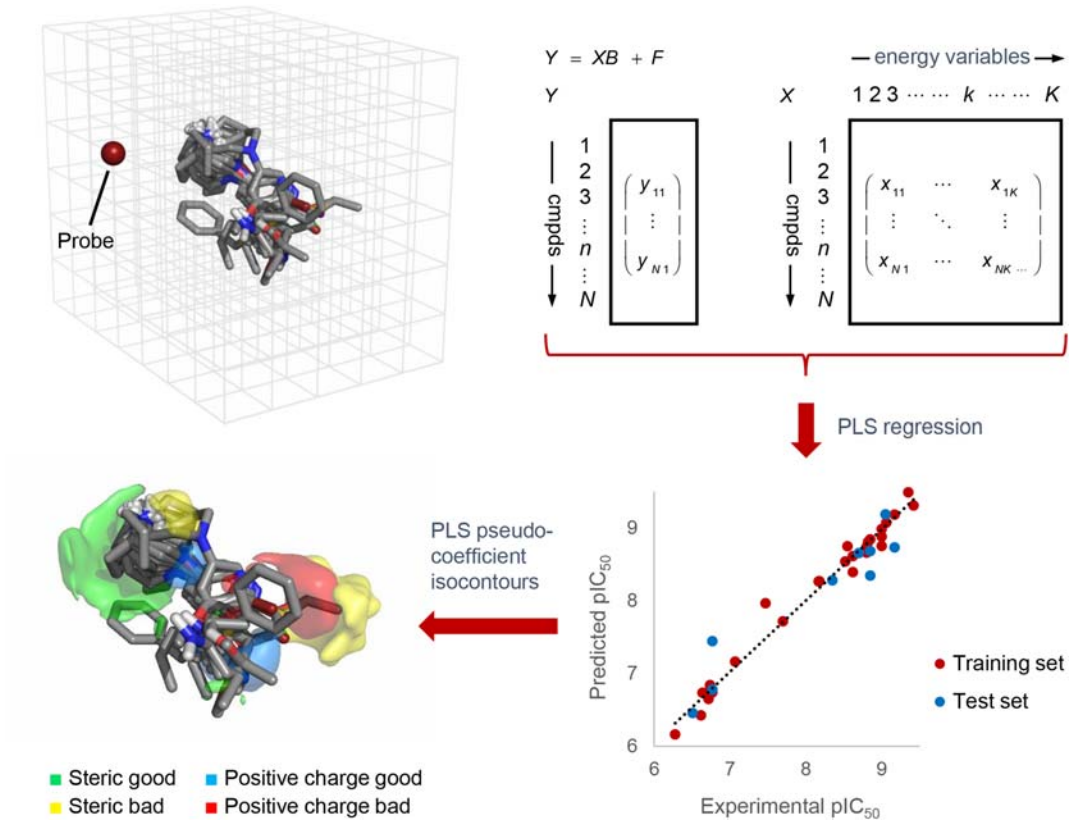

Fig. 17 An sp^3-hybridized carbon probe bearing a +1 charge is placed at each node of an evenly spaced grid surrounding an aligned set of molecules, split between a training and a test set. Steric and electrostatic interaction energies between the probe and each molecule are computed and stored in an *X* matrix, which is then regressed by PLS statistics against the *Y* vector of training set pIC_{50}s (or other logarithmic biological activity metric). The PLS model is used to predict test set pIC_{50}s; furthermore, PLS pseudo-coefficients enable a visual interpretation in 3D space of the impact of steric and electrostatic properties on the biological activity.

3.11.2.6.2 CoMSIA

In 1994, Klebe introduced the comparative molecular similarity indices analysis (CoMSIA), a variant of the CoMFA methodology aimed at improving some of the shortcomings of the latter.[63] In CoMSIA, the Lennard–Jones and Coulombic potentials used in CoMFA to compute the steric and electrostatic grids are replaced by an exponential functional form derived from the SEAL alignment algorithm.[8] In CoMSIA, the distance-dependent similarity of a probe to the atoms constituting the molecules of the dataset is evaluated at each grid node, but unlike CoMFA, grid nodes falling within the molecular volume are also taken into consideration. The exponential dependence from distance avoids singularities which characterize CoMFA potential maps in the vicinity of atomic nuclei, and eliminates the need for setting arbitrary energy cut-offs. Due to the difference in slope of the Lennard–Jones and Coulombic potentials, in CoMFA cut-offs intervene at varying distances from nuclei depending on the nature of the field; this requires block-weighting fields to give them comparable importance in the PLS matrix, which may in turn reduce the information content.

The first CoMSIA formulation consisted of three field maps: steric, electrostatic, and hydrophobic, the latter having the purpose of modeling the enthalpic component of desolvation.[63] Two further fields, encoding the hydrogen bond donor/acceptor character, were added at a later stage.[64] While CoMSIA has comparable predictive power to CoMFA and shares with the latter the requirement for aligned structures, the absence of cut-offs, the fact that all grid nodes are used to compute field maps, and the smoother distance dependence of the CoMSIA functional forms yield more continuous isocontour maps, to the advantage of their interpretability. This feature, together with the wider spectrum of the molecular properties covered by CoMSIA field maps, helps prospective usage of 3D-QSAR to guide further development of a ligand series.

3.11.2.6.3 Topomer CoMFA

Topomer CoMFA was introduced with the purpose of automating as much as possible the generation of a CoMFA model. Automation pursued a dual goal: (1) to remove the most inconvenient, error-prone, and user-biased stage: the choice of a ligand conformation and its alignment to a common template[65] and (2) to make CoMFA a viable scoring step in a VS workflow.[57] The topomer concept had been introduced several years before as a possible alternative to 2D fingerprints to retrieve R-group structures from a virtual database, having in mind the design of combinatorial chemistry libraries where a central core is decorated with variable fragments. A topomer is defined as "an invariant 3D representation of a molecular fragment, generated from its 2D topology by deterministic rules that produce absolute coordinates for each of its constituent atoms."[66] While in general 3D methods aim at providing the most informative and physicochemically sound description of a molecule possible, at the price of increased complexity, the topomer technology goes in the opposite direction. Having acknowledged the daunting difficulty of taking into account multiple tautomeric, protonation, and conformational states for each ligand due to combinatorial explosion of possible permutations, its authors decided to rather adopt a radically simplified approach, trading consistency, standardization, and computational expediency for physicochemical accuracy.[67]

The procedure to convert a ligand into topomers has evolved over time to become almost completely automated.[68] The only step which requires user intervention is ligand fragmentation into R-groups.[62] The procedure for generating a topomer from a monovalent molecular fragment is briefly outlined in the following: (1) cap the open valence of the monovalent fragment with a suitable group (e.g., a methyl) and generate a single 3D conformation out of the 2D topology, considering all ionizable groups as being in their uncharged form; (2) translate and rotate the model to overlay the bond joining the fragment to the cap onto a vector fixed in Cartesian space; (3) adjust acyclic torsions, invert stereocenters, and standardize ring puckering as required to obtain consistent topomer geometries as determined by a set of rules; and (4) remove the cap. Regarding chirality inversion, while the original stereochemistry is stored within the fragment metadata, the stereochemistry in 3D geometry is actually rule-based and independent from the original one, according to the aforementioned trade-off between consistency and accuracy; even eventual internal steric clashes are ignored.[68]

Once invariant topomers are obtained for each of the fragments constituting the molecule of interest, a separate CoMFA is computed for each topomer, after embedding the latter into a 2 Å, 1000-node fixed size grid. Compared to standard CoMFA, two main differences characterize the protocol. Firstly, an attenuation factor is applied to atomic field contributions depending on the number of acyclic single bonds intervening between the atom and the topomer's open valence; the rationale behind this modification is to reduce the impact of groups located on flexible linkers, as they are expected to undergo a larger degree of induced fit upon interaction with the target. Secondly, field values at each grid node are discretized in 2 kcal mol^{-1} increments, in order to simplify QSAR equations by removing many variables with low variance while preserving 90% of the overall variance.

Retrospective validation of the Topomer CoMFA methodology on 15 literature datasets showed that there is a decrease in predictive power compared to standard, whole-ligand CoMFA, quantified in an average $\sim$0.1 reduction in q^2. However, Topomer CoMFA training sets were aligned in a completely automated fashion, whereas the original investigations were most likely carefully tweaked to maximize q^2 (see section "3D-QSAR"). Interestingly, Topomer CoMFA models were on average characterized by a lower number of components, and the external test set SDEP values were comparable to standard CoMFA, which suggests that cross-validated q^2 values in the original publications were most likely inflated by their intentional maximization through individual conformation adjustments.[65]

One of the most appealing features of Topomer CoMFA is that topomers can be used as queries for fast similarity searches in virtual databases, whose topomers are already prealigned according to the same rules. Topomer similarity is evaluated as a combination of shape (as evaluated by the CoMFA steric field) and pharmacophoric features (aromatic, positive/negative charge, hydrogen bond acceptor/donor).[69] The effectiveness of topomer similarity was validated in two separate contexts, prospective

and retrospective. In the first, 308 compounds out of a pool of about 80K candidates having high topomeric similarity to 14 query structures were biologically tested for 13 different kinds of activity. Hit rates by topomeric similarity were 20% higher compared to a random selection. Interestingly, these hits shared a 2D fingerprint-based Tanimoto similarity to the original queries comparable to random compounds, thus indicating that hits had markedly different scaffolds compared to the query. In the second context, the differential ability of topomeric similarity and 2D Tanimoto distances to concentrate structures sharing the same World Drug Index activity class was assessed. Topomeric similarity appeared to be superior to 2D fingerprints by about 30%, again displaying greater propensity toward the correct classification of 2D-dissimilar scaffolds as members of the same activity class.[67]

Furthermore, the activity prediction generated by the model can be partitioned over topomers to yield a per-topomer activity contribution. This enables topomers found through the similarity search to be immediately scored through the CoMFA model to predict the activity contribution they would bring about if included in the ligand. The correctness of these predictions was assessed with a dual criterion: (1) absolute, evaluating the discrepancy between experimental and predicted activity and (2) relative, by evaluating the capacity to correctly rank-order ligands by their potency. Regarding absolute potency prediction, the average predictive r^2 was 0.495. The rank-ordering performance as determined by ROC curves was more encouraging, showing that there is a ~70% probability that the predicted ranking of a compound is confirmed experimentally (Kendall's tau ~0.4). The most prominent concerns about Topomer CoMFA are represented by the loss of information connected with collapsing a 3D R-group to a conformer-, protomer-, and stereoisomer-agnostic representation, by the difficulty in transferring context-ignorant topomer-based CoMFA contours to the full ligand in the context of its receptor, and by the assumption that individual fragments can make independent and additive contributions to pIC_{50}.[57]

3.11.2.6.4 Template CoMFA

Template CoMFA is an attempt to combine the best of standard CoMFA and Topomer CoMFA. While removing the most unattractive feature of standard CoMFA (the necessity to align ligands before the analysis), Topomer CoMFA also removed the possibility to include information about the ligand-binding mode when available (e.g., from an X-ray crystallographic complex between a ligand and its protein target). In fact, Topomer CoMFA operates on disconnected R-groups in isolation, making isocontour plots unable to be easily transferred to the protein context for interpretation. Furthermore, the protocol which generates topomers neglects intramolecular steric clashes, and may give rise to inconsistencies with certain side chain substitution patterns within homologous ligand series, both of which detract trustworthiness from the resulting model.[70]

In Template CoMFA, as in Topomer CoMFA, the alignment procedure is by default completely automatic. However, in Template CoMFA one or more templates must be supplied by the user. In Topomer CoMFA, for each candidate ligand the atom of the R-group topomer which bears an open valence is arbitrarily centered on the origin, and the bond which departs from the open valence is aligned along the *X* axis. In Template CoMFA, the fragmentation bond becomes an anchor bond; the bond which best matches the anchor bond is identified across all templates based on bond type, ring network, types of the atoms at the bond ends, and heavy atom count of their neighbors. Once a potential pairing has been found between the anchor bond in the candidate and a bond in the template, the connectivity graph starting from the anchor bond is compared between candidate and template. The anchor bond which yields the best mapping between candidate and template atoms is chosen among all potential bond pairings. It is worth pointing out that the algorithm used to map atoms between candidate and template is different from classical approaches based on maximal common subgraph (MCS) matching: Template CoMFA uses a two-stage mapping, where the first stage requires an exact match of atom and bond types, while the second relaxes the requirements to further extend the mapping. The atom mapping is carried out in a breadth-first fashion, reflecting the fact that in Template CoMFA, just like in Topomer CoMFA, the farther from the topomer's open valence, the lower is the weight of the atomic steric field descriptors (see section "Topomer CoMFA"), and therefore the less critical is the matching.[70,71]

Once the best atom mapping has been found, 3D coordinates of matching atoms are directly copied from the template to the candidate, while the topomer protocol is applied to atoms for which a match could not be found. In practice, Template CoMFA aims at prioritizing consistency to a template wherever possible, falling back to consistency *tout court* only when no template is available. This avoids unnecessary discrepancies between available data about the bioactive conformation and the rule-based conformation generated by the purely topomeric protocol.[70]

Template CoMFA was reapplied to the 15 datasets originally used to validate Topomer CoMFA without any significant change in the statistical quality of the models, in spite of the markedly different alignment protocol. While this may be interpreted as a greater importance of self-consistency over physicochemical realism,[70] it certainly removes any residual confidence that the statistical quality of the model may corroborate the underlying alignment hypothesis. This means that in the absence of a binding mode hypothesis supported by robust experimental evidence, the interpretation of CoMFA contours can be misleading.[72]

Further large-scale application of the Template CoMFA methodology to datasets extracted from BindingDB[73] and ChEMBL[72] adopting many different and contrasting alignment templates reinforced the absence of dependency of the model statistics on the 3D alignment. Template CoMFA activity predictions were about 50% less uncertain than the null model which predicts an unknown compound to have the average activity of the training set. 2D fingerprint-based Tanimoto distances yielded a similar performance, halving the frequency of false positives compared to Template CoMFA; however, Template CoMFA has a higher propensity for scaffold hopping, identifying actives missed by 2D metrics.[72]

3.11.2.6.5 COSMOsar3D

COSMO*sar3D*[74] is based on the QM-derived COSMO-RS theoretical framework already introduced in section "COSMO*sim3D*" when describing the COSMO*sim3D* method. Compared to traditional 3D-QSAR methods based on steric, electrostatic, hydrogen bonding, or hydrophobic potentials, where a linear relationship is assumed between experimental binding affinities and energy

descriptors, COSMO*sar3D* presents a more rigorous theoretical rationale to back up the expectation of such a linear relationship. In COSMO-RS, molecular interactions are quantified as local contact interactions of surface polarization charge densities within a conductor. This charge density distribution can be computed through a QM calculation at the DFT level, or be approximated by a collection of precomputed surface fragments (see section "COSMO*sim3D*").

The COSMO-RS method has initially been applied mainly to the prediction of the free energy of a molecule in a homogeneous liquid phase, computed as the surface integral of a solvent-specific, homogeneous σ-potential over the σ-surface of a molecule. The σ-potential expresses the affinity of a solvent for a molecular surface characterized by a certain σ-polarity. Subsequently, extensions to inhomogeneous phases such as micelles and biomembranes were presented, based on inhomogeneous σ-potentials.[75] Taking these extensions one step further, Klamt and coworkers conceived a receptor as a pseudo-liquid matrix with a locally varying affinity for a molecular surface characterized by a certain σ-polarity. Within such a model, the free energy of a ligand within a receptor would then be accessible as the surface integral of a receptor-specific, inhomogeneous σ-potential over the σ-surface of the ligand. As the surface integral can be conveniently approximated by a summation over a 3D grid, the free energy of a ligand in a receptor can be expressed as a linear function of the local σ profiles used by the COSMO*sim3D* method to assess molecular similarities.

Once the linear relationship between free energy of binding and local σ profiles has been established, the coefficients of such a relationship can be regressed using PLS against experimental free energies of binding as encoded in binding constants. The local σ-profiles used by COSMO*sim3D* have a resolution of 0.1 $e\,\mathrm{nm}^{-1}$ in σ space, which leads to partitioning the range of σ surface polarity into 61 bins. For the purpose of 3D-QSAR analysis such a degree of accuracy is not necessary, and the number of σ bins can be reduced to 11. The latter can be regarded as 11 MIFs, each describing intermolecular interactions within a defined polarity range. As in CoMSIA, but unlike CoMFA and CoMFA-like fields such as those implemented in Open3DQSAR,[76] COSMO*sar3D* fields are smooth and continuous, thus removing the need for arbitrary cut-offs and conferring significant robustness to translation of the grid relative to the molecules, variation of grid step size, and moderate ligand misalignment (Fig. 18A–C). As σ charges are

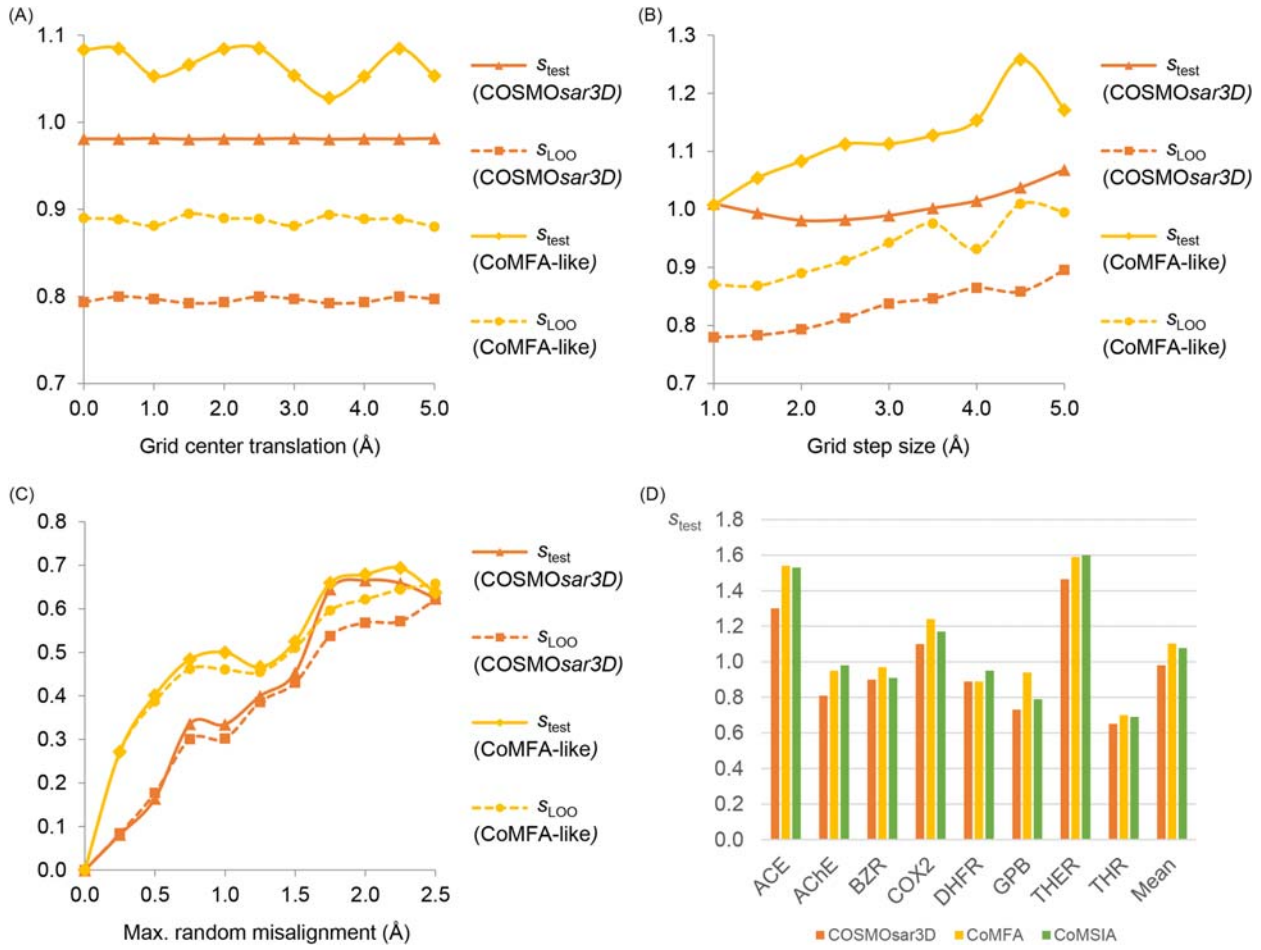

Fig. 18 Charts A–C show the effect on the standard error of external test set predictions (s_{test}) and of LOO predictions (s_{LOO}), as obtained through COSMO*sar3D* descriptors and through the CoMFA-like descriptors implemented in Open3DQSAR, of the following operations: (A) translating the grid center with respect to the aligned molecules by increasing amounts along the three Cartesian axes; (B) increasing the grid step size; and (C) applying random translational misalignments to individual compounds from 0.0 to 2.5 Å along the three Cartesian axes. In all cases, COSMO*sar3D* shows greater robustness against grid-related artifacts. Chart D shows that on the eight datasets of the Sutherland benchmark suite, COSMO*sar3D* consistently delivers a better performance (lower s_{test}) on external predictions compared to CoMFA and CoMSIA.

only defined on the molecular surface, there is also no need to extend the grid beyond the surface as in traditional 3D-QSAR techniques.

When its predictive performance was assessed on the Sutherland benchmark suite for QSAR methods,[77] COSMO*sar3D* outperformed both CoMFA and CoMSIA: the average standard error on external predictions was 0.1 logarithmic units lower(Fig. 18D). The performance loss moving from the computationally expensive QM surfaces to the inexpensive, fragment-derived ones was negligible.[74]

3.11.2.6.6 FieldQSAR

The XED/FieldAlign technology (see section "XED/FieldAlign") enables 3D-QSAR modeling through a somewhat different paradigm compared to the almost ubiquitous grid-based methods. Molecules in the training set are used to derive a common set of sampling points, based on the coordinates of the field points belonging to individual molecules. It has to be noted that since molecules have been aligned using their field points, the latter are likely to be located in close vicinity to each other. Therefore, a sphere-exclusion clustering algorithm[78] is used to reduce redundancy and retain only the largest field points, while keeping the same space coverage as the original set. Finally, for each molecule the value of the electrostatic potential is evaluated at each sampling point and stored in a vector. To avoid issues connected with the steep variations that the steric potential shows near the molecular surface (see sections "CoMFA" and "CoMSIA"), the steric field uses a binary indicator variable which takes the value 0 when the sampling position falls within the van der Waals volume of a molecule, and 1 elsewhere. Sampling positions for the steric potential are pruned with the same methodology described for the electrostatic potential, starting from heavy atom coordinates rather than from field points, and binary descriptors are stored in a vector.

Electrostatic and steric field vectors are mean-centered and block-scaled based on the overall variance of the respective field, in order to give the same weight to each descriptor block. Finally, the data matrix whose columns are constituted by the scaled vectors and the rows by training set molecules is fed to a PLS engine to seek a correlation with the dependent variable (usually some flavor of biological activity). The resulting models can be used to predict the activity of an external test set. Additionally, as in CoMFA, the product of PLS pseudo-coefficients and the standard deviation of the descriptors for each field can be plotted in order to visually grasp how field potentials influence biological activities. Alternatively, the field contributions to the predicted activity can be visualized on a per-molecule basis, such that the regions of the molecule which contribute most to defining SAR can be identified at a glance. To partially overcome a well-known limitation of 3D-QSAR methodologies, their inability to give any indications about the impact of a molecular feature when the latter is ubiquitous across the dataset, descriptor variance can also be plotted. This allows the modeler to attribute zero coefficients in a certain area of the molecule to an actual lack of correlation with biological activity (if the variance is high), or rather to highly consistent field properties across the training set (if the variance is low), as exemplified in Fig. 19.

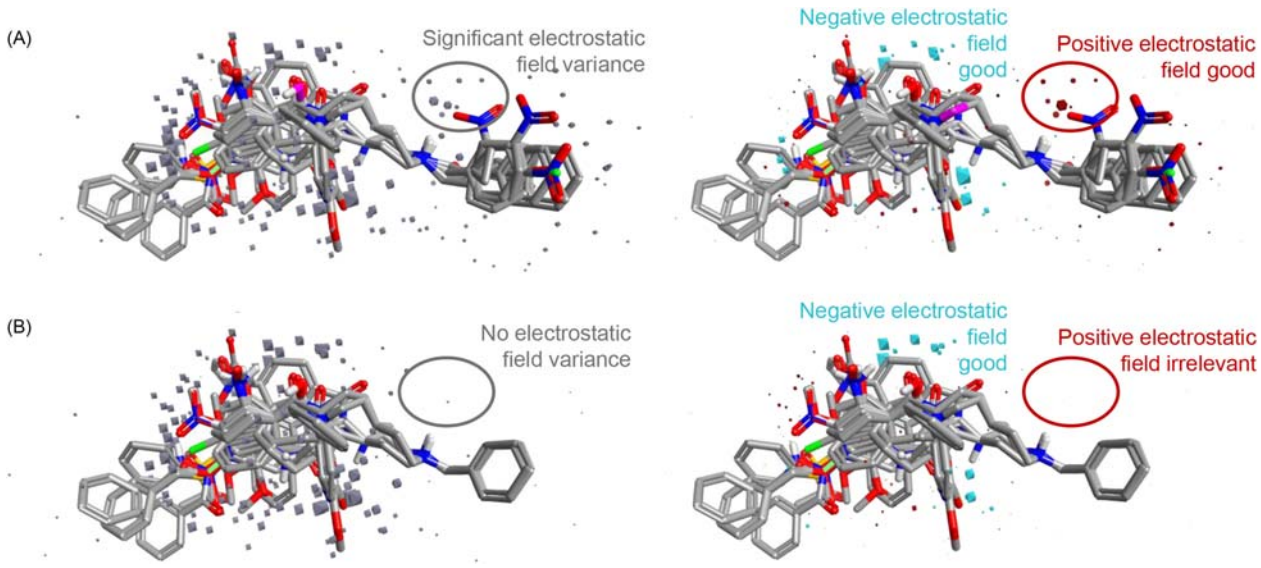

Fig. 19 Effect of descriptor variance on 3D-QSAR models as exemplified by a FieldQSAR model built using the Sutherland AChE dataset. (A) The whole set of 111 AChE inhibitors displays significant electrostatic descriptor variance in vicinity of the piperidine nitrogen (*left*), because in some of the ligands the latter is part of an amide group, hence not basic at all, while in phenylalkyl-substituted ligands its basicity depends on the ring substitution pattern. The PLS pseudo-coefficient plot (*right*) shows that biological activity is positively correlated with increasing positive electrostatic potential, that is, increasing basicity. (B) A reduced set of the 84 inhibitors featuring benzyl-substituted piperazines has no electrostatic descriptor variance in vicinity of the piperidine nitrogen (*left*), and hence the PLS pseudo-coefficient plot (*right*) shows no influence of electrostatic potential on biological activity in this region.

3.11.2.6.7 GRID/GOLPE/FLAP

CoMFA-like 3D-QSAR models based on MIFs evaluated with GRID probes can be built within the GOLPE chemometric tool,[79] as well as in FLAP. In general, there is not much to add from a methodological point of view compared to what has been described in section "CoMFA". The wide palette of available GRID probes expands the accessible range of 3D interaction properties relevant to biological activity beyond the pure steric and electrostatic potentials as in traditional CoMFA; the usual caveats associated with grid-based evaluation of potentials apply.

3.11.2.6.8 GRIND

As already mentioned during the description of Topomer and Template CoMFA approaches, the alignment prerequisite is one of the main drawbacks of 3D-QSAR, which reduces its amenability to high-throughput and unsupervised applications. GRid-INdependent Descriptors (GRIND) were developed by Pastor and coworkers[80] in an attempt to overcome this limitation. The GRIND method uses MIFs from a ligand-centric, alignment-agnostic perspective. The generation of GRIND involves two stages: (1) extraction of a small subset of highly relevant grid nodes from MIFs (usually computed through the hydrogen bond donor probe N1, the hydrogen bond acceptor probe O, and the hydrophobic probe DRY) and (2) computation of correlograms among those nodes.

Finding an efficient algorithm to identify the most relevant grid nodes is not trivial. In the original implementation within the ALMOND program, a fixed number of nodes (100–150) was extracted by iterative simultaneous optimization of two parameters, field intensity at each node (only favorable, negative energies are considered), and internode distances; the relative weights of these parameters could be user-adjusted. While this method guaranteed good coverage in terms of 3D space, it had two major shortcomings. The first was the computational cost, due to the iterative nature of the optimization algorithm which involves the computation of a distance matrix at each step. The second problem was that a fixed number of nodes was extracted, which might be insufficient for larger molecules or overkill for molecules devoid of many significant MIF-energy minima (e.g., a lipophilic molecule analyzed with a hydrogen bond donor/acceptor probe). The original algorithm was superseded by AMANDA,[2] which allows for extraction of a variable number of nodes depending on molecule size and MIF complexity. AMANDA starts by prefiltering MIF nodes based on a cut-off and tagging them by the atom which contributes most to the field energy. Then, for each atom a nonlinear fraction of the total nodes is extracted (one at the very least), prioritizing nodes with low energies initially, and gradually giving more weight to their distance from those already extracted. The ability of AMANDA to extract relevant ligand hotspots was validated with objective metrics on a set of ~800 complexes taken from the PDBbind database,[47] showing a satisfactory ability to identify the interaction partners in the protein just based on hotspot extraction from ligand MIFs.[2]

The subsequent step involves the computation of auto- (within the same MIF) and cross- (across different MIFs) correlograms between hotspot pairs. For each pair the product of MIF energies is computed and binned based on the discretized distance between the nodes (Fig. 20). While in classic autocorrelation analysis all pairs belonging to a bin are summed together, in GRIND only the highest product is retained for each bin, such that it is possible to trace back the descriptor to the nodes which originated it. A similar approach has also been exploited in SHOP (see section "SHOP"). Correlogram descriptor vectors are collected into a matrix, one ligand per row, which is then fed to a PLS engine to find correlations with biological activities. PLS pseudo-coefficients can be associated to a specific pair of nodes, thus making the model interpretable.

GRIND-2 descriptors (the evolution of GRIND obtained via the AMANDA method) demonstrated some promising potential in VS applications,[81] but still have some drawbacks. Even though GRIND descriptors are alignment-independent, they still are sensitive to ligand conformations, as they are based on intramolecular distances between hotspots. While the procedure used to generate GRIND descriptors allows the original hotpots associated with PLS pseudo-coefficients to be traced back, it has to be observed that each descriptor is associated with a pair of nodes separated by a certain distance range. Therefore, it can be not readily apparent which pair of nodes it refers to for a certain ligand, as ligands are not mutually aligned and there may be multiple node pairs whose distance falls within the same bin.[80] In an attempt to address this shortcoming, the Anchor-GRIND evolution of the methodology was proposed, where distances are computed not only between node pairs as in standard GRIND, but also between nodes and an anchor point common to all ligands.[82] While this makes less likely that variables can be confounded with interactions taking place at similar distances but involving different atoms, it can only be applied to homologous series and does not remove the conformational dependence.

3.11.2.7 3D Activity Cliff Analysis

As already mentioned in the introduction to this article, many modeling techniques are based on the assumption that compounds classified as similar by some metric will display similar biological activities; as a consequence, small changes to a molecule should cause only small changes in activity. However, there are cases where the similarity hypothesis breaks down.[83] These cases often turn out to be the most useful parts of the activity landscape for a compound series in terms of gaining a full understanding of interactions with the target protein. Pairs of similar compounds characterized by marked differences in biological activity form the so-called activity cliffs.[84] A quantitative definition of an activity cliff was proposed by Guha and coworkers through the Structure-Activity Landscape Index (SALI),[85] which is defined as the ratio between the difference in potency and the dissimilarity of the compounds. The larger the activity difference and the higher the similarity, the higher the SALI index.

Very relevant to this definition is the criterion used to assess similarity. When 2D similarity metrics such as Tanimoto distances between fingerprint vectors are used, a compound pair is generally only considered as a potential activity cliff if the similarity is above a threshold (0.55 for ECFP4 fingerprints and 0.85 for MACCS structural keys have been suggested). Moreover, an additional

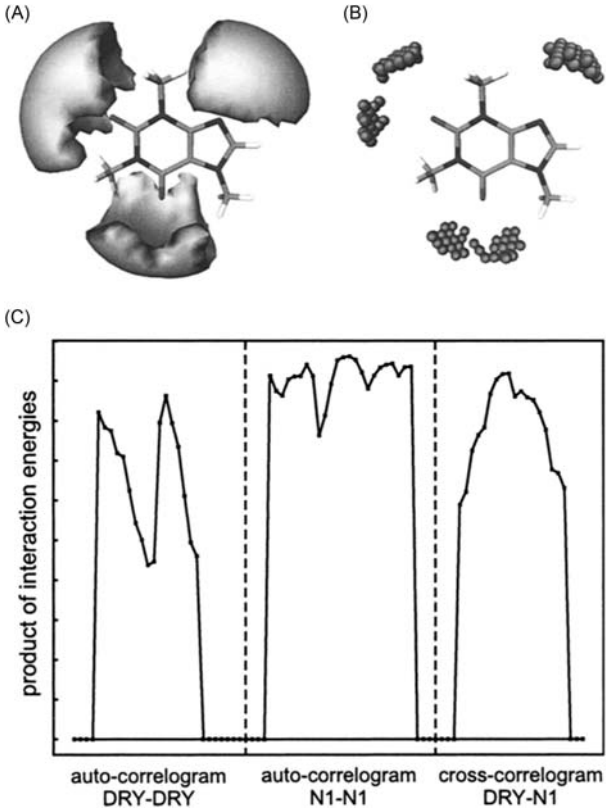

Fig. 20 Workflow to generate GRIND correlograms out of GRID MIFs: (A) A GRID MIF is computed with the N1 probe around caffeine; (B) the most relevant 100 nodes are extracted from the full GRID MIF; and (C) auto- and cross-correlogram profiles are generated with different probe combinations; the abscissa represents the discretized distance between the nodes. Adapted from Figures 1 and 2 in Pastor, M.; Cruciani, G.; McLay, I.; Pickett, S.; Clementi, S. GRid-INdependent descriptors (GRIND): a novel class of alignment-independent three-dimensional molecular descriptors. *J. Med. Chem.* **2000**, *43*, 3233–3243. ACS publication.

constraint is often put on activity, which should be in the nanomolar range.[84] Even though the majority of literature on activity cliffs is based on 2D similarity metrics, some comparisons with 3D metrics have been carried out.[86,87] Interestingly, these reports indicate that the classification of activity cliffs has a strong dependence on the similarity metric employed. In particular, only 40% of 3D activity cliffs were found to be conserved when moving to 2D metrics.[87] This is not surprising, as one of the main strengths of MIF-based approaches is to capture similarities in 3D property space which hide behind different 2D chemical structures. Activity cliffs which are missed by 2D methods can be highlighted by 3D metrics (**Fig. 21**), making their combined use highly advisable whenever possible to enrich the description of the activity landscape for a ligand series.[86,87]

3.11.2.7.1 Activity Miner/Activity Atlas

As described in the previous paragraph, navigation through activity landscapes taking advantage of both 3D and 2D similarity metrics is highly desirable from a medicinal chemist's standpoint. To facilitate this task, a methodology called Activity Miner has been developed,[88] based on the XED/FieldAlign technology (see section "XED/FieldAlign"). 3D Similarity metrics are stereochemistry- and conformation-dependent; therefore, as in 3D-QSAR, all of the structures need to be prealigned. The alignment requires one or more reference structures to act as templates, in the hypothesis that all molecules within the series bind at the same active site and share some common MIF features. Ideally, the bioactive conformation for a representative structure of each chemotype would be known, for example, from X-ray crystallography. If this is not the case, a 3D binding mode hypothesis could be generated with the FieldTemplater methodology (see section "FieldTemplater"), or a suitable low-energy conformer chosen. The alignment procedure is based on maximization of the combined field/shape score between each dataset molecule and the reference(s). As molecules exist as multiple conformations, all conformations are aligned to the reference(s) and the highest similarity value is taken as the similarity for that molecule. When there are multiple references, the final score can be either the average or the maximum across all references. If more emphasis is desired on common structural motifs (e.g., a common scaffold) between reference(s) and dataset molecules, it is possible to copy the coordinates of the maximum common substructure from the reference to each dataset molecule, and carry out the conformational search only on the molecular portions which are not part of the common scaffold. These portions are then aligned according to the standard shape/field paradigm. A similar constrained conformation search protocol has recently been published by Cappel et al.[89]

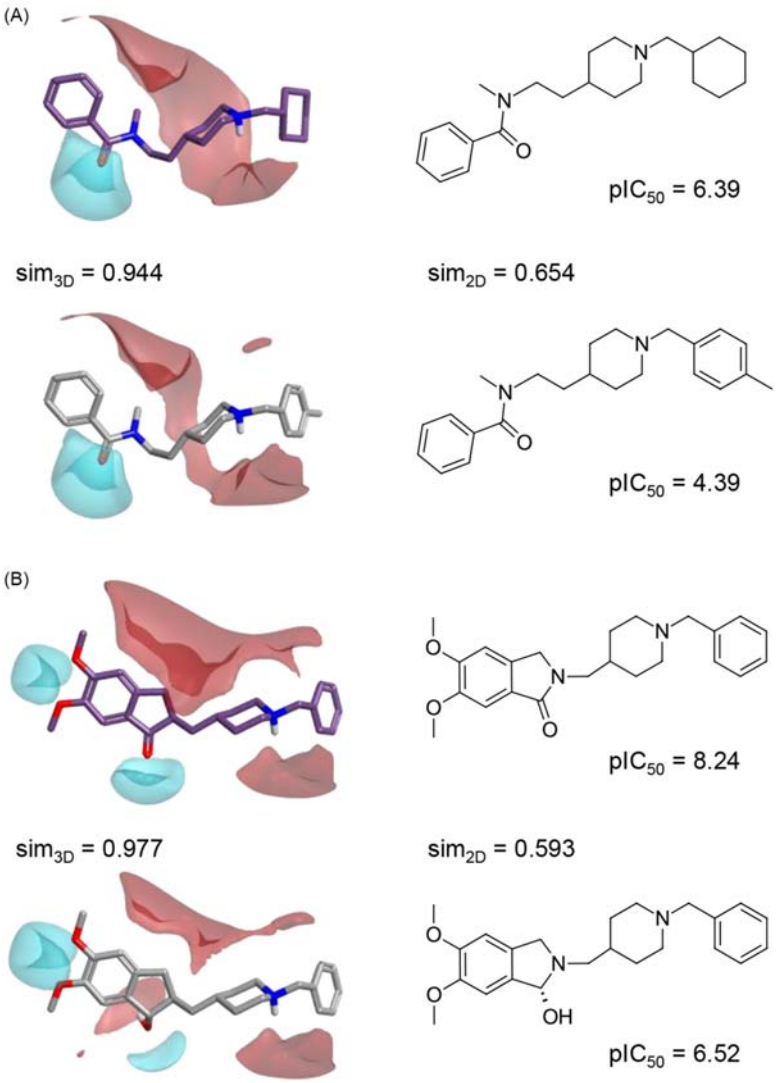

Fig. 21 Examples of AChE inhibitor pairs where the activity cliff missed by 2D fingerprints is captured by 3D metrics. (A) The 2D similarity between a cyclohexyl and a *p*-tolyl substituent is relatively low (0.654), while the 3D shape and electrostatic similarity is quite high (0.944). Although the tolyl group has more electrostatic character than the cyclohexyl, this is relatively weak, while the shape and hydrophobicity match between the two is very high. Conversely, the 2D similarity metric treats aromatic carbons as being totally dissimilar to aliphatic ones, and hence it misses this activity cliff. (B) The reduction of the carbonyl group to an alcohol causes a drop in activity of 1.7 log units. As this structural change occurs near the center of the molecule and involves a change in hybridization, the ECFP4 similarity is only 0.593, and no activity cliff is detected. However, the –OH group and the carbonyl oxygen are both electronegative and H-bond acceptors. The difference in the MIFs of the two molecules is quite modest, and a 3D activity cliff is detected.

Once molecules are aligned, pairwise 3D similarities across the dataset are displayed in a matrix whose cells are color-coded based on the value of the disparity characterizing each compound pair. The disparity is a quantitative measure of the degree to which two molecules constitute an activity cliff. It is defined as a slightly modified version of the above-mentioned SALI index: the maximum similarity of molecules is clipped to 0.95 to avoid discontinuities or overly large disparity values, and the standard error affecting biological activities is accounted for, in order to neglect differences in activity which are not significant. Pairs of compounds which constitute activity cliffs can be examined in 2D and in 3D to determine which differences in their topologies and in their 3D MIFs might be causally connected to the observed discontinuity in the activity landscape. Additionally, the most similar N molecules can be visualized for each member of the dataset, along with their disparity value and 3D structure/fields, enabling a similarity and activity-driven navigation through the dataset (Fig. 22). At any time, the 3D similarity matrix can be replaced by a traditional, fingerprint-based 2D similarity matrix, while keeping the 3D view on the dataset owing to the initial alignment operation. This allows combining most effectively the 3D and 2D classification of activity cliffs to amplify the insight on SAR for a ligand series.

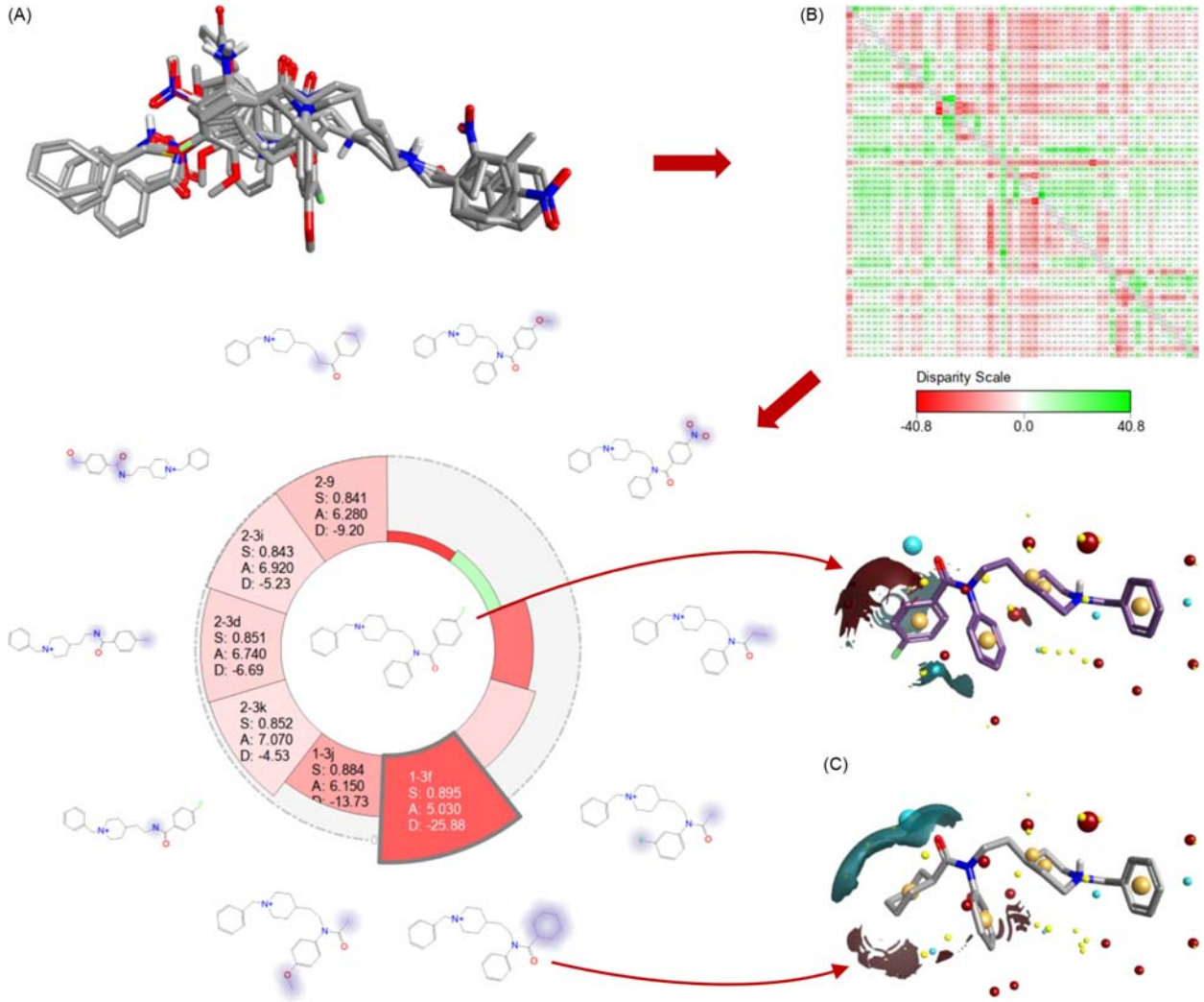

Fig. 22 Summary of the Activity Miner methodology. (A) A 3D-aligned set of 55 AChE inhibitors taken from the Sutherland benchmark suite undergoes exhaustive pairwise similarity assessment to generate a similarity matrix (A), which is colored by disparity: the most intense *red/green* shades respectively indicate the largest losses/gains in activity as a consequence of small structural changes. The similarity matrix is used to navigate the activity landscape of the dataset (B), in order to analyze the changes which give rise to the highest activity cliffs and compare the MIF differences underlying the latter (C).

While 3D activity cliffs do highlight the most informative local portions of the activity landscape (those where small 3D property modifications bring about large changes in the biological response), they are confined to individual compound pairs. In a large dataset, especially when multiple chemotypes are involved, it can be difficult to combine the information from many contrasting activity cliffs in a global picture which may guide further lead development efforts. 3D-QSAR techniques can summarize the SAR content of a dataset in a single picture through visualization of PLS pseudo-coefficient isocontours (see section "3D-QSAR"). However, most 3D-QSAR methods are much more suited for dealing with smooth, continuous regions of the activity landscape, rather than with the abrupt variations that characterize datasets with many activity cliffs. To enable a global view of the most rugged areas of the activity landscape, Activity Miner has been augmented by the Activity Atlas method.[90]

Activity Atlas uses a Bayesian approach to analyze activity and alignment data: each activity cliff provides evidence that a certain change in 3D properties causes a significant change in biological activity, the evidence being stronger for larger disparities. Furthermore, the 3D similarity of each aligned molecule to the alignment template provides an estimate of the chance that the alignment itself is correct: the higher the similarity, the more likely the molecule is to adopt the same binding mode. Based on these assumptions, the aligned molecules are embedded in a 3D grid. At each grid node, and for each pair of compounds, the product of three factors is computed: (1) the disparity value; (2) the field difference between the molecules constituting the pair; and (3) a weight determined by the likelihood that the alignment of the molecules constituting the pair is correct. The grid values are summed across all molecule pairs in the dataset, and the procedure is repeated for each of the MIFs used by the XED/FieldAlign technology (see section "XED/FieldAlign"). Finally, the grids thus obtained are contoured at the desired isolevel to identify the

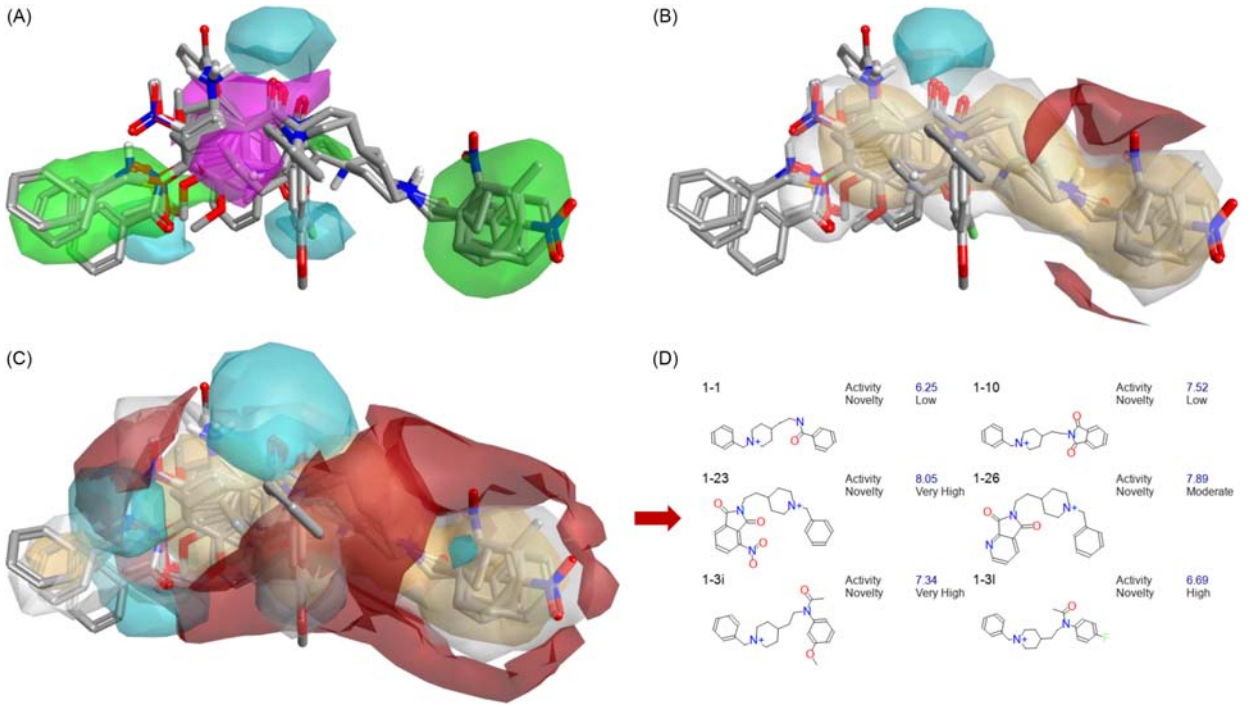

Fig. 23 The three pictorial SAR summaries provided by the Activity Atlas methodology are shown. (A) Cyan isocontours indicate regions where, based on the analysis of activity cliffs across the dataset, more negative electrostatic potential is linked to an increase in biological activity, while *green* and *purple* isocontours highlight regions where greater hydrophobicity is respectively favorable or unfavorable. (B) *Red/cyan* isocontours respectively show regions where positive/negative electrostatic potential consistently leads to highly active compounds, while ochre and white isocontours depict the average hydrophobicity and shape features of actives. (C) *Red* and *cyan* isocontours highlight regions where positive and negative electrostatics respectively have been thoroughly explored within the dataset, while *ochre* and *white* isocontours refer to hydrophobicity and shape. This qualitative map also enables a semiquantitative scoring of the degree of novelty of newly designed candidates (D).

regions where higher intensity in a certain field is linked to a change in activity (Fig. 23A). Contrary to 3D-QSAR models, Activity Atlas models are only qualitative, in that they do not yield an activity prediction, but they can be applied to smaller datasets characterized by a discontinuous activity landscape, which are outside the domain of applicability of the former.

The global summary of the influence of the various fields on biological activity derived from analysis of all compound pairs is complemented by two additional grid maps, one detailing where in 3D space the presence of certain field properties consistently leads to highly active molecules (Fig. 23B), and the other describing the 3D regions where different molecular properties have been thoroughly explored within a series (Fig. 23C). The latter map enables a medicinal chemist to score the degree of novelty of a design idea on a semiquantitative scale. Therefore, compounds which increase the further elucidation of SAR can be prioritized with respect to trivial analogs which do not contribute major novel insight to the already available knowledge about a target (Fig. 23D).[90]

3.11.2.8 ADME Prediction

During the 1980s and early 1990s, the pharmaceutical industry experienced high attrition rates at the clinical trial stage due to unfavorable drug metabolism and pharmacokinetic (DMPK) profiles. The large financial losses connected with such advanced stage failures prompted a search for fast and effective methods to assess the DMPK profile during the lead optimization stage. The widespread diffusion of preclinical absorption, distribution, metabolism, and excretion (ADME) profiling reduced the overall attrition rate in phase I clinical trials due to unfavorable DMPK properties to 16%,[91] whereas in 1991 it used to be ~40%.[92] In particular, during the 1990s in silico methods to predict ADME properties emerged as important techniques to complement medium and high-throughput LC/MS/MS, cell-line and microsomal wet lab assays. Computational methods can be applied earlier in the development pipeline than in vitro assays, even prior to synthesizing the compounds or buying them from an external supplier.[93] The earlier in silico ADME predictions are carried out, the larger the number of molecules that need to be predicted, which in turn limits the acceptable computational expense of the methods. For this reason, starting from the late 1990s technologies based on GRID MIFs became very popular. In the following paragraphs three such applications will be reviewed.

3.11.2.8.1 VolSurf

Bioavailability is related to a number of processes, including membrane permeation, transport, and biotransformation. In particular, the interaction of molecules with biological membranes is mediated by surface properties (steric, electrostatic, hydrogen bonding, and hydrophobic), which can be captured into MIFs through appropriate GRID probes. Subsequently, the large amount of information contained in GRID MIFs can be condensed to a smaller number of descriptors (72 in the original formulation, currently over 120) relevant to the prediction of pharmacokinetic properties, called the VolSurf descriptors.[94]

Two grid probes were originally used to compute MIFs, namely OH2 (water) to simulate solvation–desolvation processes, and DRY (hydrophobic) to simulate interactions between the polar headgroups and the hydrophobic core of biological membranes; subsequently the O (carbonyl oxygen) probe was added to account for hydrogen bonding interactions. Each node of the MIF grids encodes an interaction energy between the probe and the molecule under analysis. As previously mentioned, contouring the grid nodes at a certain isolevel identifies grid voxels (the minimum grid volume unit, depending on the grid step) whose energy value is greater or equal than the selected isolevel. Counting those voxels and multiplying by the voxel size provides a reliable estimate of the molecular, hydrophobic, and hydrophilic volumes and surface areas, provided that the resolution of the grid is at least 0.5 Å. Importantly, the energy level chosen for contouring voxels influences the size and shape of the volumes, hence in most cases multiple energy ranges for each MIF are explored.

VolSurf features five different categories of descriptors:[94,95,96]

(1) Shape and size descriptors: molecular volume and surface area are defined as the water-excluded volume and water-accessible surface as determined through a water probe contouring the molecule at a repulsive energy isolevel of 0.2 kcal mol^{-1}. Additional information about shape and size is provided by the rugosity (ratio between volume and surface), globularity (ratio between the molecular surface and the surface of a sphere of equivalent volume), elongation (maximum extension a molecule can assume), and EEFR (ratio of the elongation and the extension of the molecule's fixed scaffold) descriptors.
(2) Hydrophilic region descriptors: the hydrophilic descriptors describe the regions of the molecule which are accessible to water molecules and have negative interaction energies with the latter. The extents of the water-accessible volume depend on the contouring isolevel; the energy range from -0.2 to -1.0 kcal mol^{-1} covers polarizability and dispersion forces, while the -1.0 to -6.0 kcal mol^{-1} range accounts for polar and hydrogen bonding interactions. Additionally, the three most favorable interactions established by water molecules are recorded as "best volumes", contoured respectively at -1.0 and -3.0 kcal mol^{-1} (six descriptors overall). The last descriptor group is constituted by capacity factors, which represent the hydrophilic fraction of the molecular surface. These are computed at eight different energy isolevels, the same used to compute the hydrophilic descriptors.
(3) Hydrophobic region descriptors: similarly to their hydrophilic counterparts, they define the regions of the molecule which establish attractive hydrophobic interactions in the -0.2 to -1.6 kcal mol^{-1} range; "best volumes" for hydrophobic interactions are determined as well at -0.6 and -1.0 kcal mol^{-1}.
(4) Interaction energy moment descriptors: they capture the imbalance between the center of mass of a molecule and the centroid of its hydrophilic and hydrophobic regions. The larger the interaction energy moments, the less evenly spread hydrophilic and hydrophobic features are across the molecular surface.
(5) Mixed descriptors: they include various kinds of energy minima and distances among the latter, hydrophilic–lipophilic region ratios at different isolevels, the amphiphilic moment (a vector pointing from the centroid of the hydrophobic regions to the centroid of the hydrophilic ones, whose magnitude affects the ability of a compound to permeate biomembranes), critical packing (involves again hydrophilic/hydrophobic balance, but focused on molecular packing as involved, e.g., in micelle formation and solubility), hydrogen bonding and other non-MIF-based descriptors. Log P is also computed through a quantitative structure–property relationship (QSPR) approach by regressing VolSurf descriptors against experimental n-octanol/water partition coefficients.

VolSurf descriptors have been successfully used as independent variables in QSPR models to regress physicochemical properties (e.g., free energy of hydration, water solubility,[94] log P[95]) and pharmacokinetic parameters (e.g., skin and biomembrane permeation, protein binding,[94] volume of distribution,[95] blood–brain barrier penetration (Fig. 24),[96] drug absorption[96,97]) through PLS statistics.

3.11.2.8.2 MoKa

Prediction of dissociation constants (pK_a) is of key importance in medicinal chemistry, as both pharmacokinetic (solubility and lipophilicity) and pharmacodynamic (interaction with charged residues in target macromolecules) properties of drugs are influenced by their protonation state. Milletti and Cruciani have taken an MIF-based approach at pK_a prediction in their MoKa tool.[98] The application of MIFs for this purpose was not unprecedented at the time of their original publication (2007), but until then had been based on standard CoMFA techniques and so was limited to small homologous prealigned ligand series.[99] MoKa is itself a QSPR methodology, but it is based on the 2D topologies of ligands rather than on their 3D structures, which makes it computationally very fast. Contrary to other 2D methods, it is not based on linear free energy relationships derived from Hammett–Taft equations,[100] but rather on three-dimensional GRID MIF-derived descriptors precomputed on a large set of fragments.

MoKa generates its pK_a predictions based on the molecular environment in the vicinity of an ionizable center, using an algorithm reminiscent of the one used to compute circular fingerprints.[101] For each ionizable center in the molecule, the atoms lying within

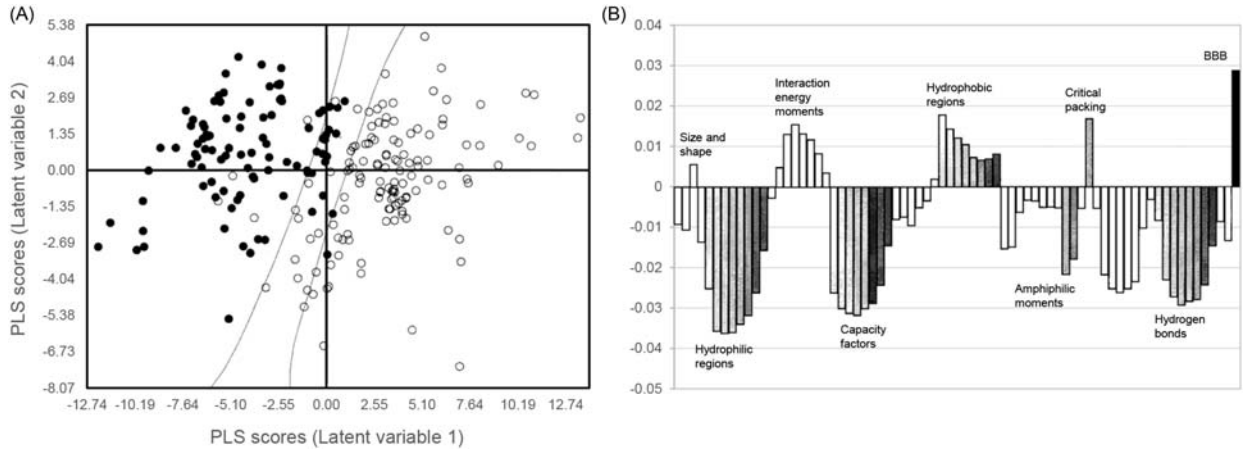

Fig. 24 (A) The discriminant plot between the PLS scores associated to the first two latent variables, as extracted by the PLS analysis carried out on a matrix of VolSurf descriptors, allows a good discrimination between the compounds which cross the BBB (•) and those which do not cross it (○), being able to assign a correct BBB profile to >90% of the compounds. A confidence interval is built in the space where BBB prediction can be doubtful. (B) PLS coefficient plot for the correlation of VolSurf descriptors with BBB permeation. The length of the bars is related to the contribution of individual descriptors, while shading refers to the different energy levels used (see text and Ref.[96] for more details). Adapted from Figures 4 and 5 in Crivori, P.; Cruciani, G.; Carrupt, P. A.; Testa, B. Predicting blood-brain barrier permeation from three-dimensional molecular structure. *J. Med. Chem.* **2000**, *43*, 2204–2216. ACS publication.

a certain topological radius are considered as part of the environment. The extent to which the neighboring topology is explored depends on the aromatic or aliphatic nature of system, which in turn influences the propagation range of electronic effects. GRID MIFs are precomputed using 10 different GRID probes (three positively charged, three negatively charged, and four neutral) on 466 small and semirigid molecular fragments, each represented by a single conformer. In each fragment a single atom, or a small group, is labeled as the center of interest, and associated with an MIF-energy minimum for each GRID probe. Energy minima are discretized and assigned to 25 bins; the energy range of each bin is chosen such that the population is roughly homogenous across bins.

To compute the ionization constant(s) for a molecule, each atom is considered individually: the fragment database is searched for the fragment whose center of interest has the best match to the atom and its environment. The energy minima associated with the center of interest of the chosen fragment, one for each of the 10 GRID probes, are then associated to the atom. Complications arise for charged fragments in polyprotic systems, as under some circumstances the same dissociation product may originate from different precursors (e.g., the fully dissociated anion of *m*-aminobenzoic acid may arise either from loss of the $^{+}$NH proton from the zwitterion or from loss of the OH proton from the carboxyl group in the neutral form); when available, dissociation microconstants are used to determine the most likely dissociation pathway in such situations. Once all atoms in the molecule whose dissociation profile is to be computed have been assigned a binned energy minimum taken from the fragment database, all energy minima having the same topological distance from the ionizable center are summed together, and for each probe and each topological level a vector of binned energies is obtained (**Fig. 25**). At the end of this procedure, each ionizable center is characterized by a number of descriptors given by the product of the number of GRID probes, the number of energy bins, and the number of topological levels.

MoKa was trained on ~19 K mono- and polyprotic molecules, associated with ~25 K pK_a values. Ionizable centers were classified into 33 categories, and for each category a separate pK_a prediction model was built by regressing the autoscaled matrix of descriptors against experimental pK_a values via PLS; as in CoMFA, the optimal number of principal components was chosen as the one which yields the first local maximum in LOO q^2. MoKa was validated on an external test set constituted by 28 different chemotypes chosen in order to include a nonionizable moiety not represented in any training set molecule at a constant distance from the ionizable center; good agreement was found with experimental pK_as (0.90 RMSE, as compared to 1.36 obtained with another 2D method based on Hammett–Taft constants).[98] MoKa has been recently augmented with a tautomer enumerator which uses computed pK_a values to estimate relative tautomer stabilities.[98]

3.11.2.8.3 MetaSite

Zamora and Cruciani have designed MetaSite, a training set-independent methodology based on GRID MIFs (see section "GRID/FLAP") which uses the 3D structures of both the xenobiotic substrate and the protein to predict the sites of metabolism (SoM).[103,104] Even if it uses protein structure information, we include MetaSite in this section because protein-derived parameters are built into the program, while the only required user input is the ligand 2D structure. Knowledge of the possible biotransformation pathways a compound may undergo at an early stage of development, possibly even before it has been synthesized, is of key importance. Labile molecules can either be removed from the pipeline, or alternatively strategies can be implemented to reduce the

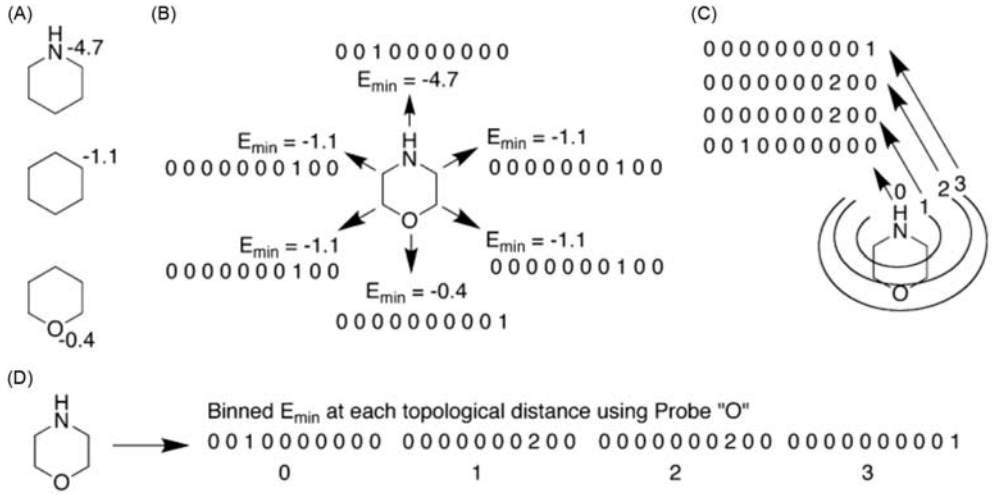

Fig. 25 Example of the workflow used to generate the MoKa descriptors for morpholine: (A) relevant fragments are chosen from the fragment database and used to compute the energy minima (kcal mol^{-1}) for reference atoms (in this example, via the O probe); (B) energy minima are discretized and assigned to 25 energy bins; (C) all energy minima having the same topological distance from the ionizable center are summed together; and (D) finally, each ionizable center is described by a vector of binned energies. Adapted from Figure 1 in Milletti, F.; Storchi, L.; Sforna, G.; Cruciani, G. New and original pKa prediction method using grid molecular interaction fields. *J. Chem. Inf. Model.* **2007**, *47*, 2172–2181. ACS publication.

metabolic lability, such as steric shielding of SoM or chemical protection of labile moieties. Finally, characterizing sites and routes of biotransformation is crucial in prodrug design and pharmacokinetic profile optimization.

While initially MetaSite was limited to the 2C9 isoform of human cytochrome P450 (CYP),[103] it was subsequently extended to four more CYP isoforms (1A2, 2C19, 2D6, and 3A4) and, most recently, also to the FMO3 isoform of flavin monooxygenase.[105] Homology models were used when X-ray structures of the human isoform were not available.[104] CYPs mainly carry out substrate oxidation through electrophilic reactions, which may also involve carbon centers. Instead, FMOs oxidize molecules catalyzing nucleophilic additions to substrate heteroatoms, and are responsible for 6% of phase I metabolic reactions of pharmaceutical interest.[106] MetaSite models two independent mechanisms: (1) recognition of the substrate by the enzyme via comparison of their respective GRID MIFs and (2) mechanism-based reactivity by a combination of ab initio and semiempirical calculations. The workflow, which is summarized in **Fig. 26**, will be briefly described in the following paragraphs.

The protein structure is mapped using three GRID probes: hydrophobic (DRY), hydrogen bond donor (N1), and hydrogen bond acceptor (O). MIFs are computed treating the protein backbone as rigid, while side chains may adapt their conformation to optimize their interactions with the GRID probe. In the original formulation of the method, the 3D GRID MIFs were compressed to 1D fingerprints,[103,104] then interatomic distances were computed between the probe and the catalytic center of the enzyme (i.e., the reactive oxene atom part of the heme-bound oxygen molecule) as in Anchor-GRIND (see section "GRIND"), yielding a 1D correlogram for each probe type. Subsequently, the 1D correlogram was replaced by the more sophisticated 3D algorithms implemented in FLAP. Currently, the shape of the enzyme active site is perceived with a 3D method, and enzyme MIFs (which take into account protein flexibility) are condensed to four-tuples (quadruplets, see section "GRID/FLAP") and stored.[107]

Substrates are modeled as conformational ensembles, and each substrate atom is assigned to one of the GRID probes depending on its characteristics (hydrophobic, hydrogen bond donor/acceptor). In the first incarnation of MetaSite, for each GRID probe type interatomic distances were discretized and binned, then converted to a 1D fingerprint vector as in the case of the enzyme. Comparison of protein and substrate fingerprints would then yield the degree of exposure (E_i) of each substrate atom i to the heme-bound reactive oxygen, as well as the influence of other molecular moieties to individual E_i values.[103,104] As part of the evolution of the method, the treatment of the substrate has undergone major development; currently, each conformer of the substrate is docked into the protein, whose active site is itself treated as being flexible. The docking procedure attempts to find the substrate conformer whose atom-centered quadruplets best match the enzyme's quadruplets. The docking score is not based on the thermodynamics of the interaction between enzyme and substrate, but rather on the complementarity of their respective GRID MIFs. The increased 3D character of the algorithm enables a more accurate estimation of atomic exposures E_i. Similarly, group contributions of the remainder of the structure to individual atomic exposures are computed with greater accuracy.[107]

Besides accessibility, for each substrate atom a reactivity score R_i is computed using QM calculations. R_i represents the activation energy required to generate the reactive intermediate, and it depends on the reaction mechanism, the 3D structure of the substrate, and its protonation state. To avoid the expense of running QM calculations on each substrate, a precomputed database of fragment-based QM descriptors is supplied with MetaSite and a semiempirical QM calculation is only needed for fragments which are not represented in the database. In reconstructing the original molecule from fragments, the R_i value for each atom is corrected taking into account inductive and/or mesomeric effects from neighboring groups. The substrate ionization state, which may be influenced

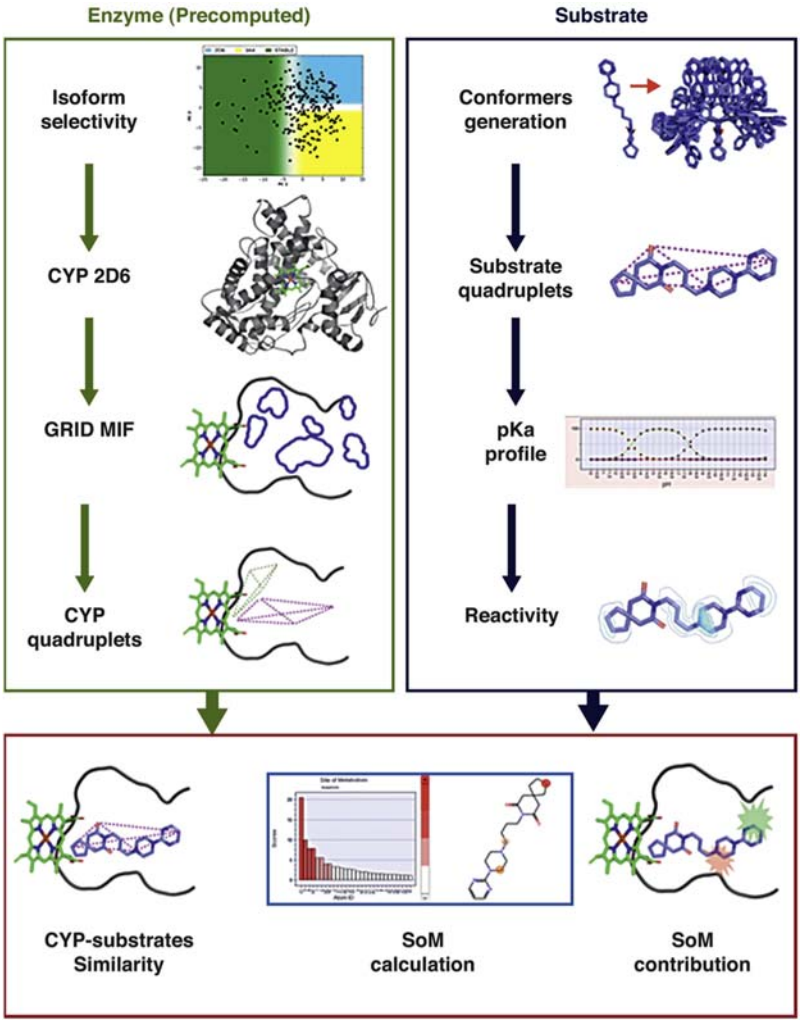

Fig. 26 Scheme summarizing the MetaSite4 algorithm. Once the CYP isoform has been selected, precomputed GRID MIFs and relative interaction hotspot quadruplets, mapped out of multiple enzyme structures to account for protein flexibility, are available for computation. GRID MIFs and ligand atom quadruplets are computed for each ligand conformation; pK_a profiling allows the consideration of multiple protomers/tautomers if required. Based on the complementarity between ligand and enzyme quadruplets an exposure score is computed, which is complemented by a QM-derived reactivity score. The combination of these two scores allows predicting the possible sites of metabolism (SoM), metabolite structures, and their relative ranking. Adapted from Figure 1 in Cruciani, G.; Baroni, M.; Benedetti, P.; Goracci, L.; Fortuna, C.G. Exposition and reactivity optimization to predict sites of metabolism in chemicals. Drug Discov Today Technol. **2013**, *10*, e155–e165. Elsevier publication.

by the environment provided by the enzyme active site, is adjusted using the MoKa methodology (see section "MoKa"), in order to pick the fragments with the appropriate protonation state. Multiple protonation states are considered where needed, and the final metabolism predictions are weighted on the relative abundance of each protomer.

The probability that an atom i may undergo metabolism via a certain mechanism is the product of the exposure E_i and the reactivity R_i according to that mechanism; this probability can be regarded as an approximation of the free energy of the metabolic transformation reaction. While in the original version of the MetaSite algorithm E_i and R_i used to have the same weight, later it was realized that their relative contributions depend on the substrate and enzyme features. For instance, low MW substrates can interact with enzyme cavities in multiple orientations, thus reducing the importance of the recognition factor in favor of reactivity. Conversely, when the volume of the substrate is comparable to the volume of the active site, recognition becomes very important as the substrate can establish several attractive interactions with the cavity, and the role of the reactivity parameter becomes secondary. Therefore, in the recent versions of MetaSite weights are automatically adjusted based on the relative sizes of substrate and enzyme cavity.

MetaSite metabolism predictions used to be only qualitative in nature; the top three solutions were returned and the algorithm could not provide a ranking of those three. In an attempt to provide semiquantitative predictions, a database of all metabolites for which experimental data on the relative abundances were available was compiled. Also an improved scoring scheme was implemented, in order to account for the varying degrees of difficulty in predicting the experimental SoM depending on the number

of possible alternatives, and to provide a consistent foundation to benchmark different procedures. Taking advantage of the experimental references and of the new scoring paradigm, MetaSite proved able to predict the correct metabolite structure and ranking in more than 80% of the cases for CYP 2D6 and 2C9, and in 75% for 3A4.[107]

A recent extension of MetaSite, Mass-MetaSite, provides an interface between experimental determination of metabolites through various mass spectrometry techniques and computational prediction of SoM.[108,109] The purpose of Mass-MetaSite is to automate as much as possible the structural identification of metabolites from experimental data. MIF-based SoM prediction complements the information based on fragmentation rules whenever fragments with identical mass can be resolved to several degenerate structures (e.g., metabolites bearing hydroxyl substituents on aromatic rings). Mass-MetaSite was shown to provide a 77% success rate in the structural elucidation of metabolites using mass spectrometry data from different sources.[109]

3.11.3 Structure-Based Applications

MIF maps of macromolecular targets have been used to identify binding sites and analyze their structural similarities, dock ligands, and determine the most favorable positions for water molecules when the X-ray resolution of the experimentally determined complexes does not allow their localization. The next paragraphs will describe these SB applications of MIFs.

3.11.3.1 Binding Site Identification

Identification of potential binding sites is the preliminary step to druggability analysis and protein function elucidation; some MIF-based approaches are presented here.

3.11.3.1.1 Q-SiteFinder

Q-SiteFinder detects druggable pockets on proteins upon analysis of their MIFs.[110] The methodology computes van der Waals interaction energies between a methyl probe, whose parameters are taken from the GRID force-field,[5] and the protein. The probe is placed at the nodes of a 0.9 Å step size grid embedding the whole protein. Only grid nodes corresponding to favorable interactions are retained, clustered depending on their spatial proximity, and ranked by decreasing total interaction energy.

The performance of the algorithm was assessed on a set of 134 protein–ligand complexes extracted from the PDB,[34] from which ligands, solvent, and ions were stripped before the analysis. Two success criteria were used. Firstly, the accuracy in the match between the predicted binding site and the actual ligand coordinates was determined as the percentage of selected grid nodes lying within a distance threshold from any ligand atom. A percentage higher than 25% was classified as a success, in consideration of the fact that a pocket may be only partially filled by the cocrystallized ligand. Secondly, if a ligand is successfully predicted in multiple sites, it is counted as a success only when the highest ranking site matches the experimental binding pocket. The maximum success rate was obtained setting -1.4 kcal mol^{-1} as the van der Waals energy threshold for a probe interaction to be considered as favorable. Seventy-one percent of the complexes fulfilled both success criteria, and the average accuracy in binding site perception was 68%; for 90% of the proteins, there was a successful prediction among the three top-ranked ones. The performance of Q-SiteFinder was significantly superior compared to Pocket-Finder, an in-house implementation of the purely volume-based algorithm LIGSITE[111] (48% success rate and 29% average accuracy, with 65% of the proteins featuring a successful prediction among the three top-ranked ones).

Since a typical use case for pocket detection algorithms is to identify binding sites on apo structures, a further benchmark was carried out on 35 apo proteins, comparing results with those obtained on 35 homologous ligand–protein complexes. The success rate for the first ranked site was much lower for the apo protein (51%) than for the complexes (80%), while there was a smaller difference in accuracy for the successful predictions (71% vs. 74%). The authors identified the different, more open shape of the main binding site in apo structures as the main reason behind the performance loss, causing other cavities to rank higher; indeed, the success rates considering the top three-ranked solutions were much closer (86% vs. 97%).

One of the greatest strengths of Q-SiteFinder is the good agreement between the average volume of the top-ranked binding site and the average ligand volume, and its weak dependence on the protein volume compared to other methods. Identifying a pocket with the correct size is especially important if the latter is to be used for ligand docking or binding site similarity analysis.

Morita and coworkers reported a significant improvement in the perception of binding sites on apo structures compared to Q-SiteFinder (77% vs. 51%) using a modification of the original algorithm.[112] Apart from the usage of van der Waals parameters from the AMBER force-field[113] rather than from GRID[5] and the adoption of a two-step clustering strategy, the most likely reason for the increased performance seems to be linked to the different selection of sampling points, which were generated in proximity of the surface via the double cubic lattice method[114] rather than across the whole protein.

3.11.3.1.2 SiteHound

SiteHound[115] is largely reminiscent of Q-SiteFinder, the main difference being that MIFs are computed combining steric and electrostatic potentials in a single map; various probes can be selected among the atom types defined in the GROMOS force-field.[116]

3.11.3.1.3 FLAPsite

The FLAPsite algorithm was designed as an augmentation of the purely geometric PocketPicker algorithm[117] with energy-based clustering as in Q-SiteFinder. As in PocketPicker, points in proximity of the protein surface are selected, and characterized through their DRY GRID probe energy rather than using a buriedness index as in the original methodology. Neighboring grid nodes whose energies are favorable according to a predefined threshold are clustered, and then refined through a shrinking/regrowth cycle limited by the protein surface. FLAPsite was reported to return the experimental ligand-binding pocket as the top-ranked one for 94% of 1300 protein–ligand complexes taken from the PDBbind database;[47] a detailed description of the algorithm has not been published.[118]

3.11.3.2 Binding Site Similarity Assessment

The most common approach to protein similarity assessment is the one based on primary sequence homology.[119] This approach has proven effective to group proteins into phylogenetic families as well as to identify common functionality. However, the advent of large-scale structural genomics initiatives has led to the structural determination of a large number of proteins whose function is unknown, because the attempts to match them to functionally characterized proteins via sequence homology failed.[120] At the same time, it has been shown that proteins may share significant local structural similarity in spite of a low global sequence identity.[121] Similarity search strategies comparable to those previously reviewed for small molecules may provide an alternative route to functional role elucidation,[122] in addition to giving hints at drug cross-reactivity, polypharmacology,[123] and repurposing.[124] In this framework, MIF-based methodologies are particularly fit to the purpose of finding similarities in binding site interactions independently of chemical similarity. A few applications of MIFs to binding site similarity assessment are reviewed here.

3.11.3.2.1 GRID/FLAP

The GRID force-field and the relative MIF maps were originally developed with the aim of predicting favorable ligand-binding spots on biological macromolecules.[5] Initially, most of the analysis on proteins was carried out visually, while quantitative 3D-QSAR approaches were mostly LB, and limited to modeling binding affinity. While some success has been reported in modeling selectivity through LB 3D-QSAR models,[125] the increasing availability of protein structural information prompted the search for tools able to extract valuable quantitative information from differences in protein-binding sites, and exploit it to improve ligand selectivity and predict off-target effects. Early approaches were based on the PCA analysis of binding site GRID MIF maps, using pairs (GRID/PCA[126]) or a series (GRID/CPCA[127]) of homologous targets. In particular, the consensus PCA (CPCA) evolution enabled a better discrimination of the differences among binding sites, as captured by different GRID probes, through block scaling of the relative descriptors. Even though some interesting results were reported,[128] the main limitation of both methodologies is their requirement, as in LB 3D-QSAR, for protein structures to be aligned. Since the alignment step is critical to the success of these analyses,[126] their scope is largely limited to proteins sharing a fair degree of structural conservation in the binding site area, such as isoforms or members of the same phylogenetic family.

An important advancement in applying GRID MIFs to the analysis of protein-binding pockets was introduced by the FLAP technology,[22,23] whose application to LB drug design has already been described in section "GRID/FLAP". The application of FLAP to proteins is thoroughly described in a paper by Sciabola et al.,[129] and consists of four steps: (1) binding site detection; (2) binding site characterization through GRID MIFs; (3) fingerprint generation; and (4) data analysis. At the time the paper was published, pocket detection was carried out through CAVGEN, an in-house modification of the purely geometric SURFNET algorithm;[130] recent versions of FLAP adopt the dedicated FLAPsite algorithm (see section "FLAPsite"), which incorporates energetic criteria. MIF and fingerprint generation stages are largely analogous to the procedures described in section "GRID/FLAP" for the ligands: the binding pocket is embedded in a grid and GRID MIFs are computed with four different probes (six at the time of the publication; the charged ones were dropped in later versions). MIFs are then condensed into a small number of MINI points, which consist of grid nodes whose 26 neighboring nodes must all have larger energies; this requirement prevents such points from being located on the outer surface of the grid, due to the lack of neighbors. All MINI points which fall outside the volume identified by the pocket detection algorithms are filtered out. The survivors represent the locations where a ligand atom of the same kind as the probe would establish favorable interactions with the residues lining the binding cavity. These points are exhaustively combined in all possible quadruplet permutations, and each quadruplet is stored as a fingerprint (**Fig. 27**). An array of several million FPs describes a protein-binding site, and can be used in multiple ways: (1) to retrieve analogs from a database of FPs derived from other protein-binding pockets; (2) to build a similarity matrix among FPs describing different binding sites, then identify common patterns through chemometric techniques such as PCA and clustering[129,131]; and (3) to find matches against an array of ligand-derived FPs in a docking-like approach, as described in sections "MetaSite" and "FLAPdock".

Regarding the first use case, the work by Sciabola[129] presents an example where two isoforms of chorismate mutase sharing a sequence identity below 20% were extracted from the PDB[34] and their FPs computed. One of the FPs was used as a query, while the other was added to a database of 990 decoy FPs obtained from random protein-binding sites; the FP from the chorismate mutase isoform was retrieved as the top-ranked hit. Concerning the second application, the ability of the FLAP methodology to correctly cluster protein active sites into families was assessed on a set of 23 kinases, selected from 6 different families (CDK2, GSK3β, P38α, PDK1, Pim1, and LCK), for which a high resolution X-ray structure was available. When two sets of quadruplets are compared between binding sites belonging to different proteins, the number of common quadruplets can be further reduced using a shape filtering criterion, that is, taking into account only the quadruplets which fall within the active site boundaries for both proteins. The FP comparison yields a normalized similarity score ranging from 0 to 1, which is stored in a similarity matrix

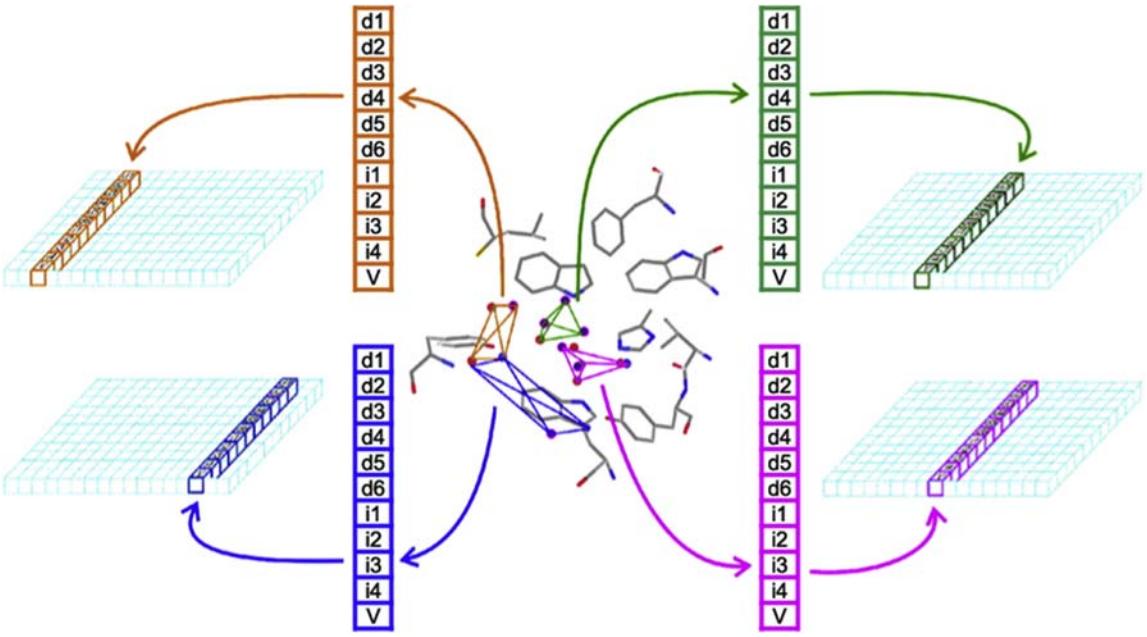

Fig. 27 FLAP encodes quadruplets of receptor MINI points as fingerprints (FPs) containing 11 integer values, corresponding to discretized distances between vertex pairs (*d1–d6*), vertex indices (*i1–i4*), and finally a value proportional to the sum of the energies of the four points (*V*). A protein-binding site is described by an array of several million FPs. Adapted from Figure 2 in Sciabola, S.; Stanton, R.V.; Mills, J.E.; Flocco, M.M.; Baroni, M.; Cruciani, G.; Perruccio, F.; Mason, J.S. High-throughput virtual screening of proteins using GRID molecular interaction fields. *J. Chem. Inf. Model.* **2010**, *50*, 155–169. ACS publication.

for each pairwise comparison. Once the kinase similarity matrix was analyzed by PCA, three main clusters could be identified by the first two components, the first containing Pim1, the second P38α and LCK, and the third CDK2, GSK3β, and PDK1. The fact that Pim1 was classified as a singleton is not surprising, as it features a unique hinge region lacking a hydrogen bond donor; on the contrary, it suggests the possibility to develop selective inhibitors. Interestingly, the analysis of the second and the third principal components enabled further classification into subfamilies of the kinases belonging to the other two clusters.

Finally, two separate SB VS exercises were carried out.[129] In the first, 4 different datasets were assembled, each consisting of 990 randomly selected decoy binding sites seeded with 10 proteins belonging to the same family, respectively HIV protease, L-arabinose binding protein, adipocyte lipid binding protein (ALBP), and ER-alpha. Each database was ranked by similarity against a query of the respective family; for ALBP and L-arabinose binding protein, all spikes were found within the first 4% of the database screened, seven HIV-proteases were retrieved within the first 5% and six ER-alpha were found within the first seven top-scoring hits. The second VS exercise aimed at assessing FLAP's ability to retrieve proteins with low sequence identity known to bind the same ligand as the query. For this purpose, 4 databases were assembled by seeding 990 random decoys with 10 proteins known to bind the same ligand (citrate, maltose, ATP and retinoic acid, respectively). All proteins were retrieved within the top 10% of database screened, except for those binding retinoic acid; however, the top-30 proteins retrieved in this latter case were bound to ligands with a high degree of structural similarity to retinoic acid, which explains the lower performance. Across all four targets, the enrichment was consistently superior to a BLAST[119] search based on primary sequence similarity.

3.11.3.2.2 IsoMIF

IsoMIF[132] is another technique aimed at computing pairwise MIF similarities between protein-binding sites. IsoMIF uses six different chemical probes, whose nature is largely reminiscent of the six used in the original formulation of the FLAP algorithm, with an aromatic probe in lieu of the hydrogen probe. However, the force-field used by IsoMIF is far less sophisticated than GRID, relying on a coarse-grained distance-dependent exponential function. Binding cavities are detected by GetCleft,[133] a reimplementation of the geometric algorithm SURFNET,[130] and embedded into a 0.5 Å step grid. Each of the six probes is placed in turn at the grid node locations, and its interaction energy with the protein is determined through the aforementioned exponential function by summation over all protein atoms. However, the weight of the contribution by individual protein atoms varies depending on the nature of the atom and the probe and on the geometric relationship between the two, which is particularly important for directional interactions such as hydrogen bonds. On each node, probes undergo a binary classification as 1 or 0, depending on whether the sum of weighted energies for that probe reaches a probe-specific minimum energy threshold.

Once the six-probe binary vectors have been defined on each node, an attempt is made to generate an association graph between the binding sites. To become part of the association graph, grid nodes need to share at least one nonzero binary value across the six-probe vectors; neighboring vertices in the association graph are joined by an edge if the distance between the corresponding

nodes in the respective MIF grids is within 3 Å. This threshold is significantly higher than in FLAP, where it is set to 1 Å, in order to allow for flexibility in the protein structure. A search for the largest clique is then carried out using the Bron–Kerbosch algorithm,[134] which tends to find the largest cliques first. Taking advantage of this, and in consideration of the fact that a complete maximal clique search is an NP-complete problem, the search is abandoned after the first 100 cliques have been found. After pruning cliques which do not satisfy chirality constraints (i.e., the respective nodes cannot be superimposed across the two MIF grids), the largest clique is scored through a Tanimoto metric taking into account the number of common probes and the number of those having energetically significant values. Interestingly, while the maximal clique detection does not require protein alignment at any stage, the grid nodes sharing nonzero binary values in their six-probe vectors can be used as superimposition points for a standard RMS fitting procedure, deriving a rotation/translation matrix which can be applied to the protein and the cocrystallized ligand 3D coordinates in order to visualize MIF similarities between binding sites (Fig. 28).

IsoMIF was benchmarked on six datasets, four of which were previously used for other methods. Its ability to retrieve proteins with varying degrees of sequence identity binding the same ligand (true positives) rather than decoy proteins (false positives) was assessed through the ROC AUC. IsoMIF featured the highest average AUC across four different methods. Unfortunately, FLAP (section "GRID/FLAP"), which is the closest methodology from an algorithmic point of view but features quite a different functional form for MIF potentials, was not included among the benchmarked methods.

3.11.3.3 Docking

MIF maps have been extensively used in ligand–target docking. A thorough description of docking algorithms, scoring functions, and their comparative evaluation is provided in other chapters of this book as well as in several dedicated reviews;[135,136] here we will focus on describing the role of MIFs in some commonly used docking methods.

3.11.3.3.1 AFMoC

Gohlke and Klebe made an interesting attempt to complement the knowledge-based DrugScore scoring function[137] with CoMFA-like regression analysis of MIFs, in order to take advantage of known ligand affinities where available to improve binding affinity predictions against a particular protein target.[138] Standard DrugScore exploits the structural information about ligand–protein atomic contact preferences as derived from crystallographically determined PDB complexes indexed in ReLiBase.[139] Docked poses are scored based on a combination of distance-dependent pair potentials (calculated from the frequency with which ligand–protein contacts between a specific pair of atom types have been experimentally observed at the specified distance) and a solvent-accessible surface-dependent potential. DrugScore was able to correctly rank binding modes and predict binding affinities, as well as to predict which ligand atom would bind more favorably at a certain binding site location.[140]

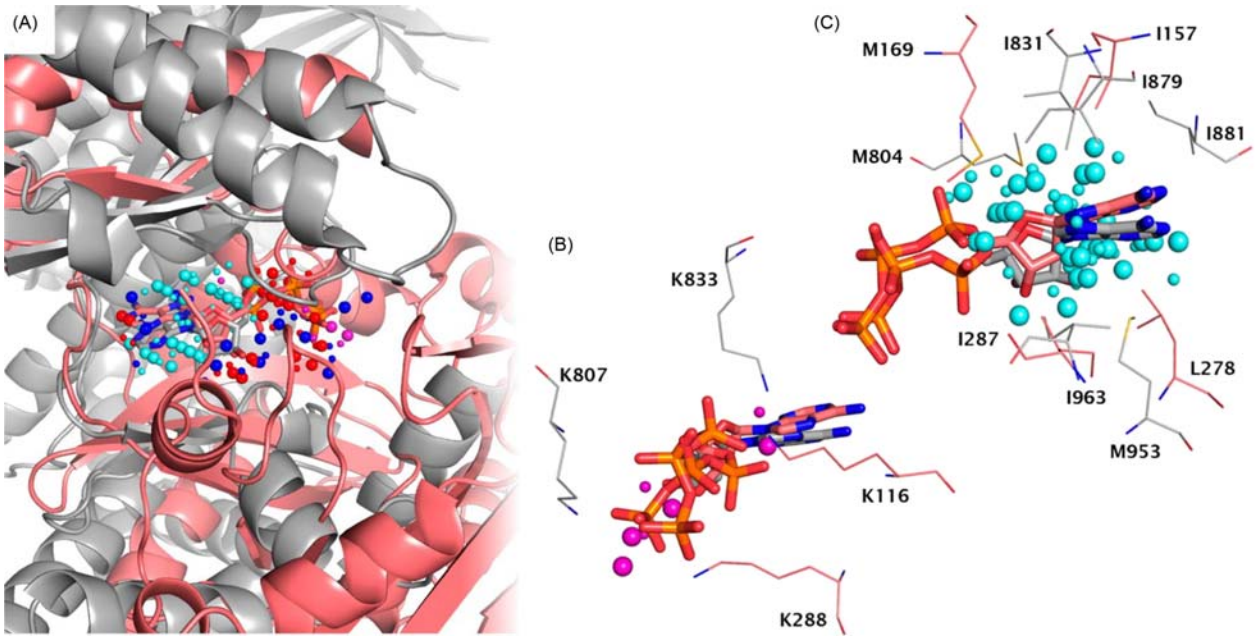

Fig. 28 MIF similarities found between 1E8X (*gray*) and 1DV2 (*light red*). (A) MIF similarities between proteins (*colored spheres*) are used to derive a rotation/translation matrix which is applied to the second protein–ligand complex. (B) Close-up on the bound ATP molecules (RMSD 1.87 Å) showing two lysine pairs (K807–K288 and K833–K116) with terminal amino groups in vicinity of phosphate groups yielding similar negatively charged probes (*magenta spheres*). (C) The adenine region is surrounded by hydrophobic similarities (*cyan spheres*) caused by the presence of methionine, isoleucine, and leucine residues in both binding sites. Adapted from Figure 6 in Chartier, M.; Najmanovich, R. Detection of binding site molecular interaction field similarities. *J. Chem. Inf. Model.* **2015**, *55*, 1600–1615. ACS publication.

With AFMoC, it becomes possible to tailor the scoring function against a specific target depending on the amount of available information about the affinity of existing ligands. The scoring function becomes a linear combination of the original DrugScore and the tailor-made function: the more experimental affinity information is available, the larger weight can be given to the regression-based scoring as compared to the knowledge-based one. The "AFMoC" name comes from the fact that MIFs rely on protein-binding site information, whereas in CoMFA MIFs are computed on ligands. Another difference to CoMFA is that MIFs are computed using atom types rather than simple steric and electrostatic probes.

In the AFMoC method, a grid is placed in the binding site, and distance-dependent pair potentials are mapped on the grid nodes. When an experimentally derived pair potential is not available because the grid node is too close to one of the protein atoms, an artificial repulsion term is used instead. For each training set ligand atom type, a Gaussian distance-dependent contribution is obtained, and multiplied by the potentials of the grid nodes within 6 Å of ligand atoms, which prevents solvent-exposed ligand atoms from having an influence on the binding score. The atom type-specific MIFs thus obtained are then correlated to known binding affinities via PLS regression as in CoMFA, resulting in individual weighting factors for each MIF value. Since some atom types present in the docked ligands might be insufficiently represented in the training set, binding affinities are factorized into contributions from each atom type using the standard DrugScore pair potentials; the contributions from the atom types which are not well represented in the training set are then removed before building the PLS model. The balance between the knowledge-based and regression-based pair potentials can be adjusted depending on the size and range of affinity covered by the training set, and on the degree of atom type similarity with the docked ligands. In principle, the linear combination of the two scoring schemes allows for a progressive increase of the regression-based scoring weight during the development of a drug discovery project, as more experimental affinity values become available.

AFMoC was initially tested on two difficult datasets of thermolysin and glycogen phosphorylase *b* inhibitors, for which standard DrugScore could find no correlation with experimental binding affinities, and it was found to provide a significant improvement.[138] Later, a further case study on a relatively small series of DOXP-reductoisomerase inhibitors was presented, in which AFMoC was able to generate a predictive model whereas classic LB CoMFA and CoMSIA had failed.[141] More recently, an extension of the AFMoC methodology which accounts for multiple ligand and receptor conformations has been developed.[142]

3.11.3.3.2 AutoDock

In AutoDock,[143] a grid box with a default step size of 0.375 Å (corresponding to roughly one quarter of a carbon-carbon single bond length) is centered on the active site where the ligand is to be docked. For each of the atom types present in the ligand, an MIF map is generated by the AutoGrid program by computing the interaction energy between a probe, having the parameters of the corresponding atom type, and the protein atoms located within a distance cut-off. Van der Waals interactions are computed by means of a smoothed 12-6 Lennard Jones potential; hydrogen bonding interactions are evaluated by a 12-10 function which incorporates a directionality term, that is, interactions which deviate from ideal hydrogen bonding geometries are progressively down-weighted. Additionally, a desolvation and a Coulombic map are computed, the latter using a probe with unit positive charge and no distance cut-off, given the long-range nature of electrostatic interactions. MIF isocontours can be mapped onto the protein active site to visualize interaction hotspots for each probe (**Fig. 29**). Since MIF maps do not depend on the ligand coordinates but only on its atom types and protein active site coordinates, a single set of MIF maps can be precomputed for each protein covering all atom types represented in the dataset of ligands to be docked, thus limiting to the conformational search the computational effort for each ligand. The interaction energy of each pose can then be obtained by trilinear interpolation of its atomic coordinates on the relevant potential grid depending on the atom type; electrostatic energies can be obtained multiplying the Coulombic potential by the atomic partial charge.[143]

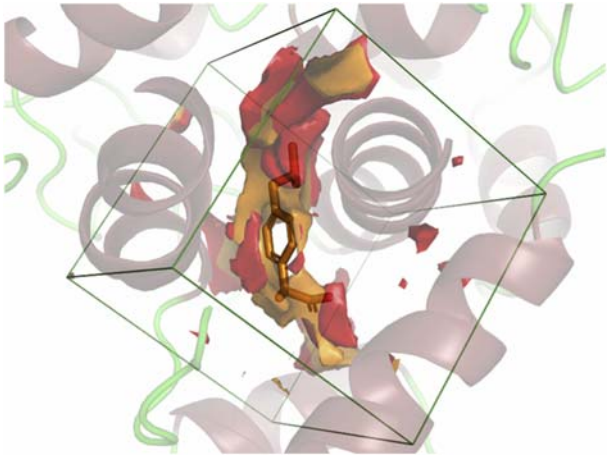

Fig. 29 3D view of the active site of the complex between COX-2 and ibuprofen (PDB ID 4PH9). The cocrystallized ligand is included as a reference and depicted with *orange* sticks. The boundaries of the cubic grid box where AutoGrid computed MIFs are highlighted with thin *green* lines; *orange* contours represent areas which are most favorable for binding of carbon atoms, while *red* contours flag areas that favor oxygen atoms.

3.11.3.3.3 FLAPdock

The FLAP fingerprint technology has already been described quite extensively in section "GRID/FLAP", and can be used to dock ligands into a binding site (e.g., as part of the MetaSite methodology, see section "MetaSite"). All members of a precomputed conformer population are fitted against quadruplets of energy minima derived from active site GRID MIF maps; potential matches are pruned based on their degree of geometric match against protein quadruplets and adherence to shape cavity constraints. The poses which pass these filters are then subjected to an in situ torsional and translational optimization of the ligand–target interaction energy, as assessed through the GRID force-field.[144,7,22] Milletti and Vulpetti[145] reported examples of the usage of FLAPdock in a VS setting and compared its performance against Glide[146] and GOLD,[147] while Ruiu and coworkers used FLAPdock along with Glide[146] and AutoDock[143] to elucidate the binding mode of a series of methoxyflavones at the μ-opioid receptor.[148]

3.11.3.3.4 Glide

Glide,[146] like AutoDock, uses precomputed grids of smoothed van der Waals and electrostatic potentials. Ligand–protein interaction energies and gradients (for minimizations) are obtained by trilinear interpolation on such grids. A peculiarity of Glide is that it uses increasing grid densities (up to 0.4 Å step size) the closer the grid box gets to the protein surface, thus allowing for a much higher resolution only where needed, in order to cut down computational costs and memory usage.

3.11.3.3.5 GOLD

GOLD[147] evaluates the van der Waals interaction energy between a carbon atom and the protein atoms over a fine grid; nodes whose interaction energy is below 2.5 kcal mol^{-1} are flagged as hydrophobic fitting points and used to place hydrophobic ligand atoms in the most favorable binding site locations during the pose generation stage. Fitting points can optionally also be identified using probes constituted by halogen and nonpolar sulfur atoms.

3.11.3.4 Determination of Water Positions

The determination of water positions within protein active sites and the estimate of their degree of "happiness" have been a primary focus over the last decade and have been addressed by many different techniques, among which the most prominent are WaterMap,[149] 3D-RISM,[150] SZMAP,[151] and WaterFLAP.[152] We will briefly describe WaterFLAP as, to the best of our knowledge, it is currently the only MIF-based approach in this arena.

3.11.3.4.1 WaterFLAP

WaterFLAP[152] generates and scores water networks in both apo proteins and ligand–target complexes. A water network is iteratively generated by placing water molecules in the most favorable positions as assessed by the GRID OH2 probe; after each molecule is added, water hotspots are redetermined before the next iteration. Only water molecules below an energy cut-off are considered for addition, and the cut-off is increased at each iteration. The initial network is then relaxed by means of a short molecular dynamics simulation, keeping protein and ligand heavy atoms restrained to their original positions. Finally, water molecules are rescored for their "happiness" using both the OH2 and CRY probes (Fig. 30); the CRY probe combines the C1= and DRY (which includes an

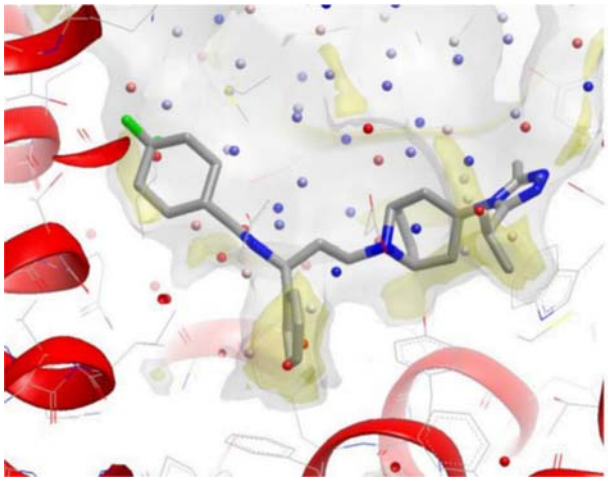

Fig. 30 Water network generated by WaterFLAP for the inactive conformation of the C–C chemokine receptor type 5 (CCR5) in complex with maraviroc (PDB ID 4MBS). Water molecules are scored for their "happiness" using both the OH2 and CRY probes, then color-coded accordingly from *red* (most "unhappy") to *blue* (most "happy"). Adapted from Figure 3 in Mason, J.S.; Bortolato, A.; Weiss, D.R.; Deflorian, F.; Tehan, B.; Marshall, F.H. High end GPCR design: crafted ligand design and druggability analysis using protein structure, lipophilic hotspots and explicit water networks. *In Silico Pharmacol.* **2013**, *1*, 23. Springer publication.

entropy term) probes to provide a more informative mapping of lipophilic, hydrophilic, and π-stacking hotspots in the binding site.[153] Although WaterFLAP is still under active development, it has already been used in production along with other water network characterization methods.[152,153,154]

3.11.4 Conclusions

In this article, we have presented a number of applications of MIFs, ranging from LB to SB drug design. The forefathers of field-based methods, CoMFA and GRID, were introduced roughly 30 years ago. CoMFA boasts thousands of citations; its ease of use coupled with the visually interpretable 3D models, in an era dominated by cryptic 1D and 2D QSAR descriptors, made it extremely popular in its first decade. The GRID-based discovery of zanamivir, subsequently marketed as Relenza, is one of the most well-known success stories in rational drug design.[155] While CoMFA and GRID are still used for the applications they were originally developed for, respectively 3D-QSAR modeling and protein active site mapping, their longevity is mostly due to the reincarnation of the seminal concepts in tools aimed at completely different purposes, in line with the evolution of drug discovery processes. The need for fast similarity-based screening of large virtual databases prompted the evolution of CoMFA into Topomer CoMFA. Likewise, most of the current interest in GRID depends on its application to in silico metabolism prediction, which has become of critical importance from the early stages of lead optimization to reduce the costs of clinical phase drug attrition, and constitutes a field of very active research.[93,156]

Thanks to the progresses in computer hardware, and in particular to the introduction of inexpensive, massively parallel graphic processing units (GPUs), 3D field-based VS has attracted renewed interest, as it can be routinely applied to large corporate collections. VS of a four-million molecule database with Blaze (see section "FieldScreen/Blaze") has recently led to the discovery of tioxazafen, a new broad-spectrum nematicide for agrochemical use.[157] Blaze VS has also been applied to the open innovation drug discovery (OIDD) program fostered by Lilly.[158] The aim of the OIDD initiative is to broaden the exploration of drug-like chemical space by encouraging independent academic and industrial researchers to submit compounds for evaluation on a panel of in-house biological assays, under a framework which protects their IP. The compounds in the OIDD database are available for in silico screening with Blaze; as the similarity assessment is based on comparison of field properties, the screening can be performed even if the chemical structures are blinded, thus safeguarding the IP.[159]

Gazing in the crystal ball, one can foresee a further development of the field-based algorithms to assess protein active site similarity, with applications in repurposing existing drugs, as well as predicting adverse drug reactions. The advances in massively parallel processors will open the way to field-based VS of unprecedentedly large collections. Eventually, the growth in computing power might enable the replacement of force-fields with QM, to the advantage of the accuracy of electrostatic and solvation models. Field-based ADMET prediction will gain further momentum from an even tighter integration with automated wet lab technologies (mass spectrometry, liquid chromatography, tissue cultures). As all good performers, 30 years after their debut molecular fields are still on stage.

References

1. Brooijmans, N.; Kuntz, I. D. Molecular Recognition and Docking Algorithms. *Annu. Rev. Biophys. Biomol.* **2003,** *32,* 335–373.
2. Durán, A.; Martínez, G. C.; Pastor, M. Development and Validation of AMANDA, a New Algorithm for Selecting Highly Relevant Regions in Molecular Interaction Fields. *J. Chem. Inf. Model.* **2008,** *48,* 1813–1823.
3. Cramer, R. D., III; Milne, M. *Am. Chem. Soc. Meeting, Honolulu,* 1979. Computer Chemistry Section, Abstract No. 44.
4. Cramer, R. D., III; Patterson, D. E.; Bunce, J. D. Comparative Molecular Field Analysis (CoMFA). 1. Effect of Shape on Binding of Steroids to Carrier Proteins. *J. Am. Chem. Soc.* **1988,** *110,* 5959–5967.
5. Goodford, P. J. A Computational Procedure for Determining Energetically Favorable Binding Sites on Biologically Important Macromolecules. *J. Med. Chem.* **1985,** *28,* 849–857.
6. Cruciani, G.; Carosati, E.; Wade, R. C.; Baroni, M. Characterization of Protein-Binding Sites and Ligands Using Molecular Interaction Fields. In *Comprehensive Medicinal Chemistry II, Vol. 4, Section 11;* Taylor, J. B., Triggle, D. J., Eds.; Elsevier: Oxford, 2007; pp 237–253.
7. Artese, A.; Cross, S.; Costa, G.; Distinto, S.; Parrotta, L.; Alcaro, S.; Ortuso, F.; Cruciani, G. Molecular Interaction Fields in Drug Discovery: Recent Advances and Future Perspectives. *WIREs Comput. Mol. Sci.* **2013,** 1–20.
8. Kearsley, S. K.; Smith, G. M. An Alternative Method for the Alignment of Molecular Structures: Maximizing Electrostatic and Steric Overlap. *Tetrahedron Comput. Methodol.* **1990,** *3,* 615–633.
9. Clark, M.; Cramer, R. D., III; Dumont, M. J.; Patterson, D. E.; Simeroth, P. E. Comparative Molecular Field Analysis (CoMFA). 2. Toward Its Use With 3D-Structural Databases. *Tetrahedron Comput. Methodol.* **1990,** *3,* 47–59.
10. Cramer, R. D., III; Clark, M.; Simeroth, P.; Patterson, D. E. Recent Developments in Comparative Molecular Field Analysis (CoMFA). In *QSAR: Rational Approaches to the Design of Bioactive Compounds;* Silipo, C., Vittoria, A., Eds.; Elsevier Science: Amsterdam, 1991; pp 239–242.
11. Lemmen, C.; Lengauer, T. Computational Methods for the Structural Alignment of Molecules. *J. Comput. Aided Mol. Des.* **2000,** *14,* 215–232.
12. (a) Grant, J. A.; Pickup, B. T. A Gaussian Description of Molecular Shape. *J. Phys. Chem.* **1995,** *99,* 3503–3510; (b) Grant, J. A.; Gallardo, M. A.; Pickup, B. T. A Fast Method of Molecular Shape Comparison: A Simple Application of a Gaussian Description of Molecular Shape. *J. Comput. Chem.* **1996,** *17,* 1653–1666.
13. Good, A. C.; Hodgkin, E. E.; Richards, W. G. Utilization of Gaussian Functions for the Rapid Evaluation of Molecular Similarity. *J. Chem. Inf. Comput. Sci.* **1992,** *32,* 188–191.
14. Mestres, J.; Rohrer, D. C.; Maggiora, G. M. MIMIC: A Molecular-Field Matching Program. Exploiting Applicability of Molecular Similarity Approaches. *J. Comput. Chem.* **1997,** *18,* 934–954.
15. Leach, A. R.; Gillet, V. J. *Similarity Methods. An Introduction to Chemoinformatics;* Springer: Netherlands, 2007; pp 99–117.
16. Klamt, A. *COSMO-RS: From Quantum Chemistry to Fluid Phase Thermodynamics and Drug Design;* Elsevier: Amsterdam, 2005.

17. Klamt, A. Conductor-Like Screening Model for Real Solvents: A New Approach to the Quantitative Calculation of Solvation Phenomena. *J. Phys. Chem.* **1995,** *99,* 2224–2235.
18. Thormann, M.; Klamt, A.; Hornig, M.; Almstetter, M. COSMOsim: Bioisosteric Similarity Based on COSMO-RS σ-Profiles. *J. Chem. Inf. Model.* **2006,** *64,* 1040–1053.
19. Thormann, M.; Klamt, A.; Wichmann, K. COSMO*sim3D*: 3D-Similarity and Alignment Based on COSMO Polarization Charge Densities. *J. Chem. Inf. Model.* **2012,** *52,* 2149–2156.
20. Ujváry, I.; Hayward, J. Bioster: A Database of Bioisosteres and Bioanalogues. In *Bioisosteres in Medicinal Chemistry;* Brown, N., Ed.; Wiley-VCH Verlag GmbH & Co. KGaA: Weinheim, 2012; pp 53–74.
21. The MDL Drug Data Report (MDDR). http://accelrys.com/products/collaborative-science/databases/bioactivity-databases/mddr.html (accessed 20.09.16).
22. Baroni, M.; Cruciani, G.; Sciabola, S.; Perruccio, F.; Mason, J. S. A Common Reference Framework for Analyzing/Comparing Proteins and Ligands. Fingerprints for Ligands and Proteins (FLAP): Theory and Application. *J. Chem. Inf. Model.* **2007,** *47,* 279–294.
23. Cross, S.; Baroni, M.; Carosati, E.; Benedetti, P.; Clementi, S. FLAP: GRID Molecular Interaction Fields in Virtual Screening. Validation Using the DUD Data Set. *J. Chem. Inf. Model.* **2010,** *50,* 1442–1450.
24. Sirci, F.; Goracci, L.; Rodríguez, D.; van Muijlwijk-Koezen, J.; Gutiérrez-de-Terán, H.; Mannhold, R. Ligand-, Structure- and Pharmacophore-Based Molecular Fingerprints: A Case Study on Adenosine A_1, A_{2A}, A_{2B}, and A_3 Receptor Antagonists. *J. Comput. Aided Mol. Des.* **2012,** *26,* 1247–1266.
25. Cheeseright, T.; Mackey, M.; Rose, S.; Vinter, A. Molecular Field Extrema as Descriptors of Biological Activity: Definition and Validation. *J. Chem. Inf. Model.* **2006,** *46,* 665–676.
26. (a) Vinter, J. G. Extended Electron Distributions Applied to the Molecular Mechanics of Intermolecular Interactions. II Organic Complexes. *J. Comput. Aided Mol. Des.* **1996,** *10,* 417–426; (b) Vinter, J. G. Extended Electron Distributions Applied to the Molecular Mechanics of Some Intermolecular Interactions. *J. Comput. Aided Mol. Des.* **1994,** *8,* 653–668.
27. Bayly, C. I.; Cieplak, P.; Cornell, W. D.; Kollman, P. A. A Well-Behaved Electrostatic Potential Based Method Using Charge Restraints for Deriving Atomic Charges: The RESP Model. *J. Phys. Chem.* **1993,** *97,* 10269–10280.
28. Chessari, G.; Hunter, C. A.; Low, C. M. R.; Packer, M. J.; Vinter, J. G.; Zonta, C. An Evaluation of Force-Field Treatments of Aromatic Interactions. *Chem. Eur. J.* **2002,** *8,* 2860–2867.
29. Hunter, C. A.; Sanders, J. K. M. The Nature of π–π Interactions. *J. Am. Chem. Soc.* **1990,** *112,* 5525–5534.
30. Stone, A. J.; Alderton, M. Distributed Multipole Analysis. Methods and Applications. *Mol. Phys.* **1985,** *56,* 1047–1064.
31. Low, C. M. R.; Vinter, J. G. Rationalizing the Activities of Diverse Cholecystokinin 2 Receptor Antagonists Using Molecular Field Points. *J. Med. Chem.* **2008,** *51,* 565–573.
32. Cross, S.; Baroni, M.; Goracci, L.; Cruciani, G. GRID-Based Three-Dimensional Pharmacophores I: FLAPpharm, a Novel Approach for Pharmacophore Elucidation. *J. Chem. Inf. Model.* **2012,** *52,* 2587–2598.
33. Cross, S.; Ortuso, F.; Baroni, M.; Costa, G.; Distinto, S.; Moraca, F.; Alcaro, S.; Cruciani, G. GRID-Based Three-Dimensional Pharmacophores II: PharmBench, a Benchmark Data Set for Evaluating Pharmacophore Elucidation Methods. *J. Chem. Inf. Model.* **2012,** *52,* 2599–2608.
34. Berman, H. M.; Westbrook, J.; Feng, Z.; Gilliland, G.; Bhat, T. N.; Weissig, H.; Shindyalov, I. N.; Bourne, P. E. The Protein Data Bank. *Nucleic Acids Res.* **2000,** *28,* 235–242. http://www.rcsb.org.
35. Jones, G. GAPE: An Improved Genetic Algorithm for Pharmacophore Elucidation. *J. Chem. Inf. Model.* **2010,** *50,* 2001–2018.
36. Cheeseright, T.; Mackey, M. D.; Melville, J. L.; Vinter, J. G. FieldScreen: Virtual Screening Using Molecular Fields. Application to the DUD Data Set. *J. Chem. Inf. Model.* **2008,** *48,* 2108–2117.
37. Huang, N.; Shoichet, B. K.; Irwin, J. J. Benchmarking Sets for Molecular Docking. *J. Med. Chem.* **2006,** *49,* 6789–6801.
38. Barker, E. J.; Gardiner, E. J.; Gillet, V. J.; Kitts, P.; Morris, J. Further Development of Reduced Graphs for Identifying Bioactive Compounds. *J. Chem. Inf. Comput. Sci.* **2003,** *43,* 346–356.
39. Good, A. C.; Oprea, T. I. Optimization of CAMD Techniques 3. Virtual Screening Enrichment Studies: A Help or Hindrance in Tool Selection? *J. Comput. Aided Mol. Des.* **2008,** *22,* 169–178.
40. Clark, R. D.; Webster-Clark, D. J. Managing Bias in ROC Curves. *J. Comput. Aided Mol. Des.* **2008,** *22,* 141–146.
41. Mackey, M. D.; Melville, J. L. Better Than Random? The Chemotype Enrichment Problem. *J. Chem. Inf. Model.* **2009,** *49,* 1154–1162.
42. Moustakas, D. T.; Lang, P. T.; Pegg, S.; Pettersen, E.; Kuntz, I. D.; Brooijmans, N.; Rizzo, R. C. Development and Validation of a Modular, Extensible Docking Program: DOCK 5. *J. Comput. Aided Mol. Des.* **2006,** *20,* 601–619.
43. Schneider, G.; Neidhart, W.; Giller, T.; Schmid, G. "Scaffold-Hopping" by Topological Pharmacophore Search: A Contribution to Virtual Screening. *Angew. Chem. Int. Ed.* **1999,** *38,* 2894–2896.
44. Bergmann, R.; Linusson, A.; Zamora, I. SHOP: Scaffold HOPping by GRID-Based Similarity Searches. *J. Med. Chem.* **2007,** *50,* 2708–2717.
45. Bergmann, R.; Liljefors, T.; Sørensen, M. D.; Zamora, I. SHOP: Receptor-Based Scaffold HOPping by GRID-Based Similarity Searches. *J. Chem. Inf. Model.* **2009,** *49,* 658–669.
46. Fontaine, F.; Cross, S.; Plasencia, G.; Pastor, M.; Zamora, I. SHOP: A Method for Structure-Based Fragment and Scaffold Hopping. *ChemMedChem* **2009,** *4,* 427–439.
47. Wang, R.; Fang, X.; Lu, Y.; Wang, S. The PDBbind Database: Collection of Binding Affinities for Protein–Ligand Complexes With Known Three-Dimensional Structures. *J. Med. Chem.* **2004,** *47,* 2977–2980.
48. Tuyishime, M.; Danish, M.; Princiotto, A.; Mankowski, M. K.; Lawrence, R.; Lombart, H.-G.; Esikov, K.; Berniac, J.; Liang, K.; Jingjing, J.; Ptak, R. G.; Madani, N.; Cocklin, S. Discovery and Optimization of Novel Small-Molecule HIV-1 Entry Inhibitors Using Field-Based Virtual Screening and Bioisosteric Replacement. *Bioorg. Med. Chem. Lett.* **2014,** *24,* 5439–5445.
49. Tuyishime, M.; Lawrence, R.; Cocklin, S. Core Chemotype Diversification in the HIV-1 Entry Inhibitor Class Using Field-Based Bioisosteric Replacement. *Bioorg. Med. Chem. Lett.* **2015,** *26,* 228–234.
50. (a) Slater, M.; Vinter, A. XED Force Field and Spark. In *Scaffold Hopping in Medicinal Chemistry, Vol. 58;* Brown, N., Ed.; Wiley-VCH: Weinheim, 2013; pp 195–213; (b) Gane, P. J.; Chan, A. W. E. Molecular Fields in Ligand Discovery. In *Protein–Ligand Interactions. Methods and Applications, Vol. 1008;* Williams, M. A., Daviter, T., Eds.; Humana Press: Clifton, NJ, 2013; pp 479–499.
51. Mackey, M.; Cheeseright, T.; Tosco, P.; Wade, W.; Meyer, T. *Examining the Diversity of Large Collections of Building Blocks in 3D. 250th ACS National Meeting & Exposition, 16–20 August 2015, Boston, MA,* 2015. COMP 67.
52. Ng, R. T.; Han, J. CLARANS: A Method for Clustering Objects for Spatial Data Mining. *IEEE Trans. Knowl. Data Eng.* **2002,** *14,* 1003–1016.
53. Tropsha, A. Best Practices for QSAR Model Development, Validation, and Exploitation. *Mol. Inf.* **2010,** *29,* 476–488.
54. Doweyko, A. M. 3D-QSAR Illusions. *J. Comput. Aided Mol. Des.* **2004,** *18,* 587–596.
55. Clark, R. D. Prospective Ligand- and Target-Based 3D QSAR: State of the Art 2008. *Curr. Top. Med. Chem.* **2009,** *9,* 791–810.
56. Cramer, R. D. Rethinking 3D QSAR. *J. Comput. Aided Mol. Des.* **2011,** *25,* 197–201.
57. Cramer, R. D.; Cruz, P.; Stahl, G.; Curtiss, W. C.; Campbell, B.; Masek, B. B.; Soltanshahi, F. Virtual Screening for R-Groups, Including Predicted pIC50 Contributions, Within Large Structural Databases, Using Topomer CoMFA. *J. Chem. Inf. Model.* **2008,** *48,* 2180–2195.
58. Verma, J.; Khedkar, V. M.; Coutinho, E. C. 3D QSAR in Drug Design—A Review. *Curr. Top. Med. Chem.* **2010,** *10,* 95–115.
59. Wise, M.; Cramer, R. D.; Smith, D.; Exman, I. Progress in Three-Dimensional Drug Design: The Use of Real Time Colour Graphics and Computer Postulation of Bioactive Molecules in DYLOMMS. In *Quantitative Approaches to Drug Design (Proceedings of the 4th European Symposium on Chemical Structure–Biological Activity: Quantitative Approaches);* Dearden, J., Ed.; Elsevier: Amsterdam, 1983; pp 145–146.

60. Cramer, R. D.; Bunce, J. D. The DYLOMMS Method: Initial Results From a Comparative Study of Approaches to 3D QSAR. In *QSAR in Drug Design and Toxicology;* Hadzi, D., Jerman-Blazic, B., Eds.; Elsevier: Amsterdam, 1987; pp 3–12.
61. Wold, S.; Ruhe, A.; Wold, H.; Dunn, W. J., III The Collinearity Problem in Linear Regression. The Partial Least Squares (PLS) Approach to Generalized Inverses. *SIAM J. Sci. Stat. Comput.* **1984,** *5,* 735–743.
62. Melville, J. L.; Hirst, J. D. On the Stability of CoMFA Models. *J. Chem. Inf. Comput. Sci.* **2004,** *44,* 1294–1300.
63. Klebe, G.; Abraham, U.; Mietzner, T. Molecular Similarity Indices in a Comparative Analysis (CoMSIA) of Drug Molecules to Correlate and Predict Their Biological Activity. *J. Med. Chem.* **1994,** *37,* 4130–4146.
64. Klebe, G.; Abraham, U. Comparative Molecular Similarity Index Analysis (CoMSIA) to Study Hydrogen-Bonding Properties and to Score Combinatorial Libraries. *J. Comput. Aided Mol. Des.* **1999,** *13,* 1–10.
65. Cramer, R. D. Topomer CoMFA: A Design Methodology for Rapid Lead Optimization. *J. Med. Chem.* **2003,** *46,* 374–388.
66. Cramer, R. D.; Clark, R. D.; Patterson, D. E.; Ferguson, A. M. Bioisosterism as a Molecular Diversity Descriptor: Steric Fields of Single "Topomeric" Conformers. *J. Med. Chem.* **1996,** *39,* 3060–3069.
67. Cramer, R. D.; Jilek, R. J.; Guessregen, S.; Clark, S. J.; Wendt, B.; Clark, R. D. "Lead Hopping". Validation of Topomer Similarity as a Superior Predictor of Similar Biological Activities. *J. Med. Chem.* **2004,** *47,* 6777–6791.
68. Cramer, R. D.; Jilek, R. J. Topomers: A Validated Protocol for Their Self-Consistent Generation. *J. Chem. Inf. Comput. Sci.* **2004,** *44,* 1221–1227.
69. Cramer, R. D.; Jilek, R. J.; Andrew, K. M. *Dbtop*: Topomer Similarity Searching of Conventional Structure Databases. *J. Mol. Graph. Model.* **2002,** *20,* 447–462.
70. Cramer, R. D. R-Group Template CoMFA Combines Benefits of "Ad Hoc" and Topomer Alignments Using 3D-QSAR for Lead Optimization. *J. Comput. Aided Mol. Des.* **2012,** *26,* 805–819.
71. Cramer, R. D.; Wendt, B. Template CoMFA: The 3D-QSAR Grail? *J. Chem. Inf. Model.* **2014,** *54,* 660–671.
72. Cramer, R. D. Template CoMFA Generates Single 3D-QSAR Models That, for Twelve of Twelve Biological Targets, Predict all ChEMBL-Tabulated Affinities. *PLoS ONE* **2015,** *10,* e0129307.
73. Cramer, R. D. Template CoMFA Applied to 116 Biological Targets. *J. Chem. Inf. Model.* **2014,** *54,* 2147–2156.
74. Klamt, A.; Thormann, M.; Wichmann, K.; Tosco, P. COSMOsar3D: Molecular Field Analysis Based on Local COSMO σ Profiles. *J. Chem. Inf. Model.* **2012,** *52,* 2157–2164.
75. Klamt, A.; Huniar, U.; Spycher, S.; Keldenich, J. COSMOmic: A Mechanistic Approach to the Calculation of Membrane-Water Partition Coefficients and Internal Distributions Within Membranes and Micelles. *J. Phys. Chem. B* **2008,** *112,* 12148–12157.
76. Tosco, P.; Balle, T. Open3DQSAR: A new Open-Source Software Aimed at High-Throughput Chemometric Analysis of Molecular Interaction Fields. *J. Mol. Model.* **2011,** *17,* 201–208.
77. Sutherland, J. J.; O'Brien, L. A.; Weaver, D. F. A Comparison of Methods for Modeling Quantitative Structure–Activity Relationships. *J. Med. Chem.* **2004,** *47,* 5541–5554.
78. Hudson, B. D.; Hyde, R. M.; Rahr, E.; Wood, J.; Osman, J. Parameter Based Methods for Compound Selection From Chemical Databases. *Quant. Struct. Act. Relat.* **1996,** *15,* 285–289.
79. Baroni, M.; Costantino, G.; Cruciani, G.; Riganelli, D.; Valigi, R.; Clementi, S. Generating Optimal Linear PLS Estimations (GOLPE): An Advanced Chemometric Tool for Handling 3D-QSAR Problems. *Quant. Struct. Act. Relat.* **1993,** *12,* 9–20.
80. Pastor, M.; Cruciani, G.; McLay, I.; Pickett, S.; Clementi, S. GRid-INdependent Descriptors (GRIND): A Novel Class of Alignment-Independent Three-Dimensional Molecular Descriptors. *J. Med. Chem.* **2000,** *43,* 3233–3243.
81. Durán, A.; Zamora, I.; Pastor, M. Suitability of GRIND-Based Principal Properties for the Description of Molecular Similarity and Ligand-Based Virtual Screening. *J. Chem. Inf. Model.* **2009,** *49,* 2129–2138.
82. Fontaine, F.; Pastor, M.; Zamora, I.; Sanz, F. Anchor-GRIND: Filling the Gap Between Standard 3D QSAR and the GRid-INdependent Descriptors. *J. Med. Chem.* **2005,** *48,* 2687–2694.
83. Martin, Y. C.; Kofron, J. L.; Traphagen, L. M. Do Structurally Similar Molecules Have Similar Biological Activity? *J. Med. Chem.* **2002,** *45,* 4350–4358.
84. Stumpfe, D.; Bajorath, J. Exploring Activity Cliffs in Medicinal Chemistry. *J. Med. Chem.* **2012,** *55,* 2932–2942.
85. Guha, R.; Van Drie, J. H. Structure–Activity Landscape Index: Identifying and Quantifying Activity Cliffs. *J. Chem. Inf. Model.* **2008,** *48,* 646–658.
86. Medina-Franco, J. L.; Martínez-Mayorga, K.; Bender, A.; Marín, R. M.; Giulianotti, M. A.; Pinilla, C.; Houghten, R. A. Characterization of Activity Landscapes Using 2D and 3D Similarity Methods: Consensus Activity Cliffs. *J. Chem. Inf. Model.* **2009,** *49,* 477–491.
87. Hu, Y.; Bajorath, J. Exploration of 3D Activity Cliffs on the Basis of Compound Binding Modes and Comparison of 2D and 3D Cliffs. *J. Chem. Inf. Model.* **2012,** *52,* 670–677.
88. Cheeseright, T.; Lawrence, R.; Mackey, M.; Slater, M. *Finding and Using Activity Cliffs in 3D: Gaining More SAR Information During Lead Optimization. 246th ACS National Meeting & Exposition, 8–12 September, Indianapolis, IN,* 2013. COMP 346.
89. Cappel, D.; Dixon, S. L.; Sherman, W.; Jianxin, D. Exploring Conformational Search Protocols for Ligand-Based Virtual Screening and 3-D QSAR Modeling. *J. Comput. Aided Mol. Des.* **2014,** *29,* 165–182.
90. Mackey, M. *Is it Worth Making? Assessing the Information Content of New Structures. 250th ACS National Meeting & Exposition, 16–20 August 2015, Boston, MA,* 2015. COMP 431.
91. Waring, M. J.; Arrowsmith, J.; Leach, A. R.; Leeson, P. D.; Mandrell, S.; Owen, R. M.; Pairaudeau, G.; Pennie, W. D.; Pickett, S. D.; Wang, J.; Wallace, O.; Weir, A. An Analysis of the Attrition of Drug Candidates From Four Major Pharmaceutical Companies. *Nat. Rev. Drug. Discov.* **2015,** *14,* 475–486.
92. Kola, I.; Landis, J. Can the Pharmaceutical Industry Reduce Attrition Rates? *Nat. Rev. Drug Discov.* **2004,** *3,* 711–716.
93. Summerfield, S.; Jeffrey, P. Discovery DMPK: Changing Paradigms in the Eighties, Nineties and Noughties. *Expert Opin. Drug Discov.* **2009,** *4,* 207–218.
94. Cruciani, G.; Crivori, P.; Carrupt, P.-A.; Testa, B. Molecular Fields in Quantitative Structure–Permeation Relationships: The VolSurf Approach. *J. Mol. Struct. Theochem.* **2000,** *503,* 17–30.
95. Mannhold, R.; Berellini, G.; Carosati, E.; Benedetti, P. Use of MIF-Based VolSurf Descriptors in Physicochemical and Pharmacokinetic Studies. In *Molecular Interaction Fields,* vol. 27, Cruciani, G., Ed.; Wiley-VCH Verlag GmbH & Co. KGaA: Weinheim, 2013; pp 173–196.
96. Crivori, P.; Cruciani, G.; Carrupt, P.-A.; Testa, B. Predicting Blood–Brain Barrier Permeation From Three-Dimensional Molecular Structure. *J. Med. Chem.* **2000,** *43,* 2204–2216.
97. Cruciani, G.; Pastor, M.; Guba, W. VolSurf: A New Tool for the Pharmacokinetic Optimization of Lead Compounds. *Eur. J. Pharm. Sci.* **2000,** *11,* S29–S39.
98. Milletti, F.; Storchi, L.; Sforna, G.; Cruciani, G. New and Original pK_a Prediction Method Using Grid Molecular Interaction Fields. *J. Chem. Inf. Model.* **2007,** *47,* 2172–2181.
99. Gargallo, R.; Sotriffer, C. A.; Liedl, K. R.; Rode, B. M. Application of Multivariate Data Analysis Methods to Comparative Molecular Field Analysis (CoMFA) Data: Proton Affinities and pK_a Prediction for Nucleic Acids Components. *J. Comput. Aided Mol. Des.* **1999,** *13,* 611–623.
100. Perrin, D. D.; Dempsey, B.; Serjeant, E. P.; *pK_a Prediction for Organic Acids and Bases,* vol. 1; Chapman and Hall: London, New York, 1981.
101. Glen, R. C.; Bender, A.; Arnby, C. H.; Carlsson, L.; Boyer, S.; Smith, J. Circular Fingerprints: Flexible Molecular Descriptors With Applications from Physical Chemistry to ADME. *IDrugs* **2006,** *9,* 199–204.
102. Milletti, F.; Storchi, L.; Sforna, G.; Cross, S.; Cruciani, G. Tautomer Enumeration and Stability Prediction for Virtual Screening on Large Chemical Databases. *J. Chem. Inf. Model.* **2009,** *49,* 68–75.
103. Zamora, I.; Afzelius, L.; Cruciani, G. Predicting Drug Metabolism: A Site of Metabolism Prediction Tool Applied to the Cytochrome P450 2C9. *J. Med. Chem.* **2003,** *46,* 2313–2324.
104. Cruciani, G.; Carosati, E.; De Boeck, B.; Ethirajulu, K.; Mackie, C.; Howe, T.; Vianello, R. MetaSite: Understanding Metabolism in Human Cytochromes From the Perspective of the Chemist. *J. Med. Chem.* **2005,** *48,* 6970–6979.

105. Cruciani, G.; Valeri, A.; Goracci, L.; Pellegrino, R. M.; Buonerba, F.; Baroni, M. Flavin Monooxygenase Metabolism: Why Medicinal Chemists Should Matter. *J. Med. Chem.* **2014,** *57,* 6183–6196.
106. Testa, B.; Pedretti, A.; Vistoli, G. Reactions and Enzymes in the Metabolism of Drugs and Other Xenobiotics. *Drug Disccov. Today* **2012,** *17,* 549–560.
107. Cruciani, G.; Baroni, M.; Benedetti, P.; Goracci, L.; Fortuna, C. G. Exposition and Reactivity Optimization to Predict Sites of Metabolism in Chemicals. *Drug Discov. Today Technol.* **2013,** *10,* e155–e165.
108. Bonn, B.; Leandersson, C.; Fontaine, F.; Zamora, I. Enhanced Metabolite Identification With MSE and a Semiautomated Software for Structural Elucidation. *Rapid Commun. Mass Spectrom.* **2010,** *24,* 3127–3138.
109. Zamora, I.; Fontaine, F.; Serra, B.; Plasencia, G. High-Throughput, Computer Assisted, Specific MetID. A Revolution for Drug Discovery. *Drug Discov. Today Technol.* **2013,** *10,* e199–e205.
110. Laurie, A. T. R.; Jackson, R. M. Q-SiteFinder: An Energy-Based Method for the Prediction of Protein–Ligand Binding Sites. *Bioinformatics* **2005,** *21,* 1908–1916.
111. Hendlich, M.; Rippmann, F.; Barnickel, G. LIGSITE: Automatic and Efficient Detection of Potential Small Molecule-Binding Sites in Proteins. *J. Mol. Graph. Model.* **1997,** *15,* 359–363.
112. Morita, M.; Nakamura, S.; Shimizu, K. Highly Accurate Method for Ligand-Binding Site Prediction in Unbound State (apo) Protein Structures. *Proteins* **2008,** *73,* 468–479.
113. Cornell, W. D.; Cieplak, P.; Bayly, C. I.; Gould, I. R.; Merz, K. M.; Ferguson, D. M.; Spellmeyer, D. C.; Fox, T.; Caldwell, J. W.; Kollman, P. A. A Second Generation Force Field for the Simulation of Proteins, Nucleic Acids, and Organic Molecules. *J. Am. Chem. Soc.* **1995,** *117,* 5179–5197.
114. Eisenhaber, F.; Lijnzaad, P.; Argos, P.; Sander, C.; Scharf, M. The Double Cubic Lattice Method: Efficient Approaches to Numerical Integration of Surface Area and Volume and to Dot Surface Contouring of Molecular Assemblies. *J. Comput. Chem.* **1995,** *16,* 273–284.
115. Ghersi, D.; Sanchez, R. EASYMIFS and SITEHOUND: A Toolkit for the Identification of Ligand-Binding Sites in Protein Structures. *Bioinformatics* **2009,** *25,* 3185–3186.
116. Schmid, N.; Eichenberger, A.; Choutko, A.; Riniker, S.; Winger, M.; Mark, A.; van Gunsteren, W. Definition and Testing of the GROMOS Force-Field Versions 54A7 and 54B7. *Eur. Biophys. J.* **2011,** *40,* 843–856.
117. Weisel, M.; Proschak, E.; Schneider, G. PocketPicker: Analysis of Ligand Binding-Sites With Shape Descriptors. *Chem. Cent. J.* **2007,** *1,* 7.
118. Henrich, S.; Salo-Ahen, O. M. H.; Huang, B.; Rippmann, F.; Cruciani, G.; Wade, R. C. Computational Approaches to Identifying and Characterizing Protein Binding Sites for Ligand Design. *J. Mol. Recognit.* **2010,** *23,* 209–221.
119. Altschul, S. F.; Gish, W.; Miller, W.; Meyers, E. W.; Lipman, D. J. Basic Local Alignment Search Tool. *J. Mol. Biol.* **1990,** *215,* 403–410.
120. Laskowski, R. A.; Watson, J. D.; Thornton, J. M. ProFunc: A Server for Predicting Protein Function From 3D Structure. *Nucleic Acids Res.* **2005,** *33,* W89–W93.
121. Rosen, M.; Lin, S. L.; Wolfson, H.; Nussinov, R. Molecular Shape Comparisons in Searches for Active Sites and Functional Similarity. *Protein Eng.* **1998,** *11,* 263–277.
122. Kinoshita, K.; Nakamura, H. Identification of Protein Biochemical Functions by Similarity Search Using the Molecular Surface Database eF-Site. *Protein Sci.* **2003,** *12,* 1589–1595.
123. Milletti, F.; Vulpetti, A. Predicting Polypharmacology by Binding Site Similarity: From Kinases to the Protein Universe. *J. Chem. Inf. Model.* **2010,** *50,* 1418–1431.
124. Weber, A.; Casini, A.; Heine, A.; Kuhn, D.; Supuran, C. T.; Scozzafava, A.; Klebe, G. Unexpected Nanomolar Inhibition of Carbonic Anhydrase by COX-2-Selective Celecoxib: New Pharmacological Opportunities Due to Related Binding Site Recognition. *J. Med. Chem.* **2004,** *47,* 550–557.
125. Weber, A.; Böhm, M.; Supuran, C. T.; Scozzafava, A.; Sotriffer, C. A.; Klebe, G. 3D QSAR Selectivity Analyses of Carbonic Anhydrase Inhibitors: Insights for the Design of Isozyme Selective Inhibitors. *J. Chem. Inf. Model.* **2006,** *46,* 2737–2760.
126. Pastor, M.; Cruciani, G. A Novel Strategy for Improving Ligand Selectivity in Receptor-Based Drug Design. *J. Med. Chem.* **1995,** *38,* 4637–4647.
127. Kastenholz, M. A.; Pastor, M.; Cruciani, G.; Haaksma, E. E. J.; Fox, T. GRID/CPCA: A New Computational Tool to Design Selective Ligands. *J. Med. Chem.* **2000,** *43,* 3033–3044.
128. (a) Naumann, T.; Matter, H. Structural Classification of Protein Kinases Using 3D Molecular Interaction Field Analysis of Their Ligand Binding Sites: Target Family Landscapes. *J. Med. Chem.* **2002,** *45,* 2366–2378; (b) Terp, G. E.; Cruciani, G.; Christensen, I. T.; Jørgensen, F. S. Structural Differences of Matrix Metalloproteinases With Potential Implications for Inhibitor Selectivity Examined by the GRID/CPCA Approach. *J. Med. Chem.* **2002,** *45,* 2675–2684.
129. Sciabola, S.; Stanton, R. V.; Mills, J. E.; Flocco, M. M.; Baroni, M.; Cruciani, G.; Perruccio, F.; Mason, J. S. High-Throughput Virtual Screening of Proteins Using GRID Molecular Interaction Fields. *J. Chem. Inf. Model.* **2010,** *50,* 155–169.
130. Laskowski, R. A. SURFNET: A Program for Visualizing Molecular Surfaces, Cavities, and Intermolecular Interactions. *J. Mol. Graph.* **1995,** *13,* 323–330.
131. Ferrario, V.; Siragusa, L.; Ebert, C.; Baroni, M.; Foscato, M.; Cruciani, G.; Gardossi, L. BioGPS Descriptors for Rational Engineering of Enzyme Promiscuity and Structure Based Bioinformatic Analysis. *PLoS ONE* **2014,** *9,* e109354.
132. Chartier, M.; Najmanovich, R. Detection of Binding Site Molecular Interaction Field Similarities. *J. Chem. Inf. Model.* **2015,** *55,* 1600–1615.
133. Gaudreault, F.; Morency, L.-P.; Najmanovich, R. J. NRGsuite: A PyMOL Plugin to Perform Docking Simulations in Real-Time Using FlexAID. *Bioinformatics* **2015,** *31,* 3856–3858.
134. Bron, C.; Kerbosch, J. Algorithm 457: Finding all Cliques of an Undirected Graph. *Commun. ACM* **1973,** *16,* 575–577.
135. Kitchen, D. B.; Decornez, H.; Furr, J. R.; Bajorath, J. Docking and Scoring in Virtual Screening for Drug Discovery: Methods and Applications. *Nat. Rev. Drug Discov.* **2004,** *3,* 935–949.
136. (a) Warren, G. L.; Andrews, C. W.; Capelli, A. M.; Clarke, B.; LaLonde, J.; Lambert, M. H.; Lindvall, M.; Nevins, N.; Semus, S. F.; Senger, S.; Tedesco, G. A Critical Assessment of Docking Programs and Scoring Functions. *J. Med. Chem.* **2006,** *49,* 5912–5931; (b) Plewczynski, D.; Łaźniewski, M.; Augustyniak, R.; Ginalski, K. Can we Trust Docking Results? Evaluation of Seven Commonly Used Programs on PDBbind Database. *J. Comput. Chem.* **2011,** *32,* 742–755.
137. Gohlke, H.; Hendlich, M.; Klebe, G. Knowledge-Based Scoring Function to Predict Protein–Ligand Interactions. *J. Mol. Biol.* **2000,** *295,* 337–356.
138. Gohlke, H.; Klebe, G. DrugScore Meets CoMFA: Adaptation of Fields for Molecular Comparison (AFMoC) or how to Tailor Knowledge-Based Pair-Potentials to a Particular Protein. *J. Med. Chem.* **2002,** *45,* 4153–4170.
139. Hendlich, M. Databases for Protein–Ligand Complexes. *Acta Crystallogr. Sect. D* **1998,** *54,* 1178–1182.
140. Gohlke, H.; Hendlich, M.; Klebe, G. Predicting Binding Modes, Binding Affinities and 'Hot Spots' for Protein–Ligand Complexes Using a Knowledge-Based Scoring Function. *Perspect. Drug Discov.* **2000,** *20,* 115–144.
141. Silber, K.; Heidler, P.; Kurz, T.; Klebe, G. AFMoC Enhances Predictivity of 3D QSAR: A Case Study With DOXP-Reductoisomerase. *J. Med. Chem.* **2005,** *48,* 3547–3563.
142. Breu, B.; Silber, K.; Gohlke, H. Consensus Adaptation of Fields for Molecular Comparison (AFMoC) Models Incorporate Ligand and Receptor Conformational Variability into Tailor-Made Scoring Functions. *J. Chem. Inf. Model.* **2007,** *47,* 2383–2400.
143. (a) Morris, G. M.; Huey, R.; Lindstrom, W.; Sanner, M. F.; Belew, R. K.; Goodsell, D. S.; Olson, A. J. AutoDock4 and AutoDockTools4: Automated Docking With Selective Receptor Flexibility. *J. Comput. Chem.* **2009,** *16,* 2785–2791; (b) Morris, G. M.; Goodsell, D. S.; Halliday, R. S.; Huey, R.; Hart, W. E.; Belew, R. K.; Olson, A. J. Automated Docking Using a Lamarckian Genetic Algorithm and an Empirical Binding Free Energy Function. *J. Comput. Chem.* **1998,** *19,* 1639–1662.
144. Perruccio, F.; Mason, J. S.; Sciabola, S.; Baroni, M. FLAP: 4-Point Pharmacophore Fingerprints From GRID. In *Molecular Interaction Fields,* vol. 27, Cruciani, G., Ed.; Wiley-VCH Verlag GmbH & Co. KGaA: Weinheim, 2013; pp 83–102.
145. Milletti, F.; Vulpetti, A. Tautomer Preference in PDB Complexes and Its Impact on Structure-Based Drug Discovery. *J. Chem. Inf. Model.* **2010,** *50,* 1062–1074.
146. Friesner, R. A.; Banks, J. L.; Murphy, R. B.; Halgren, T. A.; Klicic, J. J.; Mainz, D. T.; Repasky, M. P.; Knoll, E. H.; Shelley, M.; Perry, J. K.; Shaw, D. E. Glide: A new Approach for Rapid, Accurate Docking and Scoring. 1. Method and Assessment of Docking Accuracy. *J. Med. Chem.* **2004,** *47,* 1739–1749.
147. Jones, G.; Willett, P.; Glen, R. C.; Leach, A. R.; Taylor, R. Development and Validation of a Genetic Algorithm for Flexible Docking. *J. Mol. Biol.* **1997,** *267,* 727–748.
148. Ruiu, S.; Anzani, N.; Orrù, A.; Floris, C.; Caboni, P.; Alcaro, S.; Maccioni, E.; Distinto, S.; Cottiglia, F. Methoxyflavones from *Stachys Glutinosa* With Binding Affinity to Opioid Receptors: In Silico, In Vitro, and In Vivo Studies. *J. Nat. Prod.* **2015,** *78,* 69–76.

149. (a) Abel, R.; Young, T.; Farid, R.; Berne, B. J.; Friesner, R. A. Role of the Active-Site Solvent in the Thermodynamics of Factor Xa Ligand Binding. *J. Am. Chem. Soc.* **2008,** *130,* 2817–2831; (b) Young, T.; Abel, R.; Kim, B.; Berne, B. J.; Friesner, R. A. Motifs for Molecular Recognition Exploiting Hydrophobic Enclosure in Protein–Ligand Binding. *Proc. Natl. Acad. Sci. U. S. A.* **2007,** *104,* 808–813.
150. Kovalenko, A. Three-Dimensional RISM Theory for Molecular Liquids and Solid–Liquid Interfaces. In *Molecular Theory of Solvation (Understanding Chemical Reactivity),* vol. 24, Hirata, F., Ed.; Kluwer Academic Publishers: Dordrecht, 2003; pp 169–275.
151. SZMAP 1.2.1.4, OpenEye Scientific Software, Santa Fe, NM. http://www.eyesopen.com, 2015.
152. Mason, J. S.; Bortolato, A.; Weiss, D. R.; Deflorian, F.; Tehan, B.; Marshall, F. H. High end GPCR Design: Crafted Ligand Design and Druggability Analysis Using Protein Structure, Lipophilic Hotspots and Explicit Water Networks. *In Silico Pharmacol.* **2013,** *1,* 23.
153. Bortolato, A.; Tehan, B. G.; Bodnarchuk, M. S.; Essex, J. W.; Mason, J. S. Water Network Perturbation in Ligand Binding: Adenosine A_{2A} Antagonists as a Case Study. *J. Chem. Inf. Model.* **2013,** *53,* 1700–1713.
154. Harpsøe, K.; Isberg, V.; Tehan, B. G.; Weiss, D.; Arsova, A.; Marshall, F. H.; Bräuner-Osborne, H.; Gloriam, D. E. Selective Negative Allosteric Modulation of Metabotropic Glutamate Receptors—A Structural Perspective of Ligands and Mutants. *Sci. Rep.* **2015,** *5,* 13869.
155. Von Itzstein, M.; Wu, W. Y.; Kok, G. B.; Pegg, M. S.; Dyason, J. C.; Jin, B.; Van Phan, T.; Smythe, M. L.; White, H. F.; Oliver, S. W.; Colman, P. M. Rational Design of Potent Sialidase-Based Inhibitors of Influenza Virus Replication. *Nature* **1993,** *363,* 418–423.
156. Cross, S.; Cruciani, G. Molecular Fields in Drug Discovery: Getting Old or Reaching Maturity? *Drug Discov. Today* **2010,** *15,* 23–32.
157. Slomczynska, U.; South, M. S.; Bunkers, G. J.; Edgecomb, D.; Wyse-Pester, D.; Selness, S.; Ding, Y.; Christiansen, J.; Ediger, K.; Miller, W.; Charumilind, P.; Hartmann, G.; Williams, J.; Dimmic, M.; Shortt, B.; Haakenson, W.; Wideman, A.; Crawford, M.; Hresko, M.; McCarter, J. Tioxazafen: A New Broad-Spectrum Seed Treatment Nematicide. In *Discovery and Synthesis of Crop Protection Products, Chapter 10, ACS Symposium Series, Vol. 1204;* Maienfisch, P., Stevenson, T. M., Eds.; Oxford University Press Inc.: New York, 2015; pp 129–147.
158. Alvim-Gaston, M.; Grese, T.; Mahoui, A.; Palkowitz, A. D.; Pineiro-Nunez, M.; Watson, I. Open Innovation Drug Discovery (OIDD): A Potential Path to Novel Therapeutic Chemical Space. *Curr. Top. Med. Chem.* **2014,** *14,* 294–303.
159. Virtual Screening With Blaze. https://openinnovation.lilly.com/dd/includes/pdf/Virtual-Screening-with-Blaze-FINAL.pdf (accessed 20.09.16).

3.12 Molecular Docking—A Solved Problem?

J Cole, Cambridge Crystallographic Data Centre, Cambridge, United Kingdom
E Davis, The Cambridge Crystallographic Data Centre Inc, Piscataway, NJ, United States
G Jones and CR Sage, Arena Pharmaceuticals, San Diego, CA, United States

© 2017 Elsevier Ltd. All rights reserved.

3.12.1 Introduction 297
3.12.2 When is Docking Useful? 298
3.12.3 Defining Docking: A Solved Problem? 298
3.12.4 Pose Prediction in Docking 299
3.12.4.1 Sampling Algorithms: A Solved Problem 299
3.12.4.2 Tackling Ligand Flexibility: A Solved Problem 300
3.12.4.3 Tackling Binding Site Flexibility: An Unsolved Problem 302
3.12.4.4 Treating Solvent During Docking: An Unsolved Problem 303
3.12.5 Affinity Prediction in Docking: An Unsolved Problem 304
3.12.5.1 The Affinity Prediction Problem 304
3.12.5.2 Scoring Poses in Docking 306
3.12.5.3 Validation of Docking Programs and Their Associated Scores 306
3.12.5.4 Overall Conclusions on Affinity Prediction and Scoring 309
3.12.6 Other Unsolved Docking Problems 310
3.12.7 Democratization of Docking: An Unsolved Problem 310
3.12.8 Help! I am a Medicinal Chemist … What Do I Do Now???? 310
3.12.8.1 When Should I Use Docking? 310
3.12.8.2 How Should I Use Docking? 311
3.12.8.3 Learn How to Love the Software 311
3.12.8.4 Invest Time in Your Input Protein Structure! 311
3.12.8.5 Incorporate What You Know 312
3.12.8.6 Consider the Features That Are More Important to Your System, for Your Software 312
3.12.8.7 Do Not Over-Interpret Scores 313
3.12.8.8 Help! I am a Software Developer, How Do I Make My Users Love My Software? 313
3.12.8.9 Make the Results Less Susceptible to the Input Provided 313
3.12.8.10 Make it Easy for Your End-Users to Become Experts 314
3.12.8.11 Make Your Docking Software Self-Critical 314
3.12.9 Concluding Remarks 314
Acknowledgments 314
References 314

3.12.1 Introduction

The question "is docking a solved problem?" is a challenging and somewhat contentious one, and needs definition. Firstly, "what is docking?" Secondly, "what do we mean by a solved problem?"

If docking is merely the prediction of a binding pose of a ligand, of known protonation state, in a well-defined system, then one might be tempted to believe the problem solved. However, such a narrow definition is of little utility in the discipline of drug discovery. Here, we ideally would like to predict ligand activity yet do not know the exact ligand electronic configuration on binding. Additionally, accommodating the variation in the active site that frequently occurs upon ligand binding is important.

Consider the impact of docking on drug discovery if this truly was a "solved problem." Not only could docking techniques make a huge contribution to lead identification and activity prediction, but docking could also inform what is arguably the more challenging aspect of drug design: transforming an active hit compound to a viable lead pharmaceutical. Drug bioavailability is often compromised by off-target binding. Aside from proteins in other pathways, this can include various blood plasma proteins such as albumin and glycoprotein. A drug may be metabolized and cleared from the body by a cytochrome P450 enzyme, or alternatively it may inhibit such an enzyme preventing the clearance of other drugs (one of the primary sources of drug-drug interactions). A major safety concern of new medicines is inhibition of the hERG ion channel which mediates cardiac activity. Each of these interactions could be modeled successfully by a perfect docking program.

The end user of a perfect docking program would be able to sit down and use it without a deep understanding of the targets of interest: for example, they would not think "I need to dock into a model of the hERG receptor and interpret the results," rather they

would ask the question "will my lead show adverse cardiac activity?" and the software would understand how to answer the question and generate a reliable answer.

If we can only say "docking is a solved problem" when we have such a perfect docking program, then current user experience gives a short answer: "It's not." That said, for the lesser question "is docking useful?" the short answer is a resounding "yes."

Addressing whether docking is a solved problem requires extensive thought and elaboration, and inevitably leads to subdivision into a larger set of questions. In this article we try to identify those questions by evaluating aspects of docking, reviewing the literature in the various areas, and analyzing which parts of the problem are solved and which are unsolved.

We have attempted to break down the problem of docking into a number of subsections. The subsections are "When is docking useful?" which showcases some examples where docking has been impactful in medicinal chemistry programs, "defining docking," which tackles the input required for docking programs, "sampling algorithms," which tackles the underlying global search algorithms that are used to facilitate docking in a tractable time. The next three subsections, namely "Treating ligand flexibility," "Treating binding site flexibility," and "Treating solvent in docking" tackle the specific parts of a docking algorithm that require special treatment. We then consider the area of affinity prediction in docking.

Finally, we scrutinize the current state of the art, recommend general approaches for getting the best out of docking programs, and suggest how current or future programs could be improved to create the perfect docking program.

3.12.2 When is Docking Useful?

While it is unclear if docking is a solved problem, we can with certainty state that docking is a useful tool in the medicinal chemist's armory. Docking and structure-based drug design (SBDD) has become a critical tool in the medicinal chemist's armory. Aliskiren, Zanamivir, Lopinavir, and Ritonavir have all been highlighted as cases of marketed drugs that have been discovered by SBDD.[1] Captopril is believed to have been the first drug where SBDD played a major role in its discovery.[2]

There are many published examples of successful programs which have been aided and abetted by docking studies. A recent review[3] highlighted many examples where docking studies significantly contributed to a project's outcome through virtual screening.

There are also many examples in the literature which highlight medicinal chemistry programs in which docking plays a part in a structural optimization program. Indeed, when docking studies are performed they now rarely get more than a cursory line within a publication to note that the method was used and the consequences of their use (e.g., for a recent example, see Ref.[4]). In this study, the authors made a key synthetic choice to increase the affinity of their compound after docking showed that their proposed changes would lead to acceptable interactions with the binding site.

As is usually the case in such publications now, the docking studies are not significantly described. Such studies are regarded as a routine part of a medicinal chemistry program rather than anything particularly unusual. This reflects the success of docking as an approach for medicinal chemistry.

3.12.3 Defining Docking: A Solved Problem?

It is instructive to consider what expectations we may have of a docking program. In general, the docking problem may be defined thus: given an input protein structure and a ligand, the docking program will generate a predicted binding pose and associated score which may be used as surrogates for a crystal structure and activity data. This definition is sufficiently vague so that it is not clear what the exact inputs to the program are: is the assignment of protein and ligand protonation and charge states the responsibility of the user or the software? Likewise, who defines the role of water and the active site location and extent? These spheres of responsibility affect the complexity and difficulty of the docking problem. If a particular program requires input ligands to be correctly protonated for binding, then that is an easier scenario than if the charge state must be elucidated. Such a program may perform well on similar docking studies, but may not perform so well when, for example, docking novel ligands to metalloenzymes.

To an untutored user the expectation may be that a docking program simply requires a protein and a 2D representation of a ligand and the algorithm will return a putative binding mode. In practice both ligand and protein need careful preparation and many of the challenges for successful docking occur prior to the invocation of the docking algorithm. Here we consider the steps that may be required to prepare the protein and the ligand. Other decisions may be required from the user, such as force field or algorithm parameterizations, but most algorithms typically provide a user with reasonable default parameters for these settings.

Preparation of the protein for docking normally requires specification of the location and extent of the active site into which the ligand is placed. The location of the binding site in a given protein is usually specified by user input in most well-used docking programs. However, there are numerous algorithms that automatically identify binding pockets with reasonable accuracy, with success rates up to 75%. For example, Cavity Search,[5] Fpocket,[6] MDpocket,[7] Roll,[8] and KVFinder.[9]

Once a user has identified the active site, additional preparation of the active site may be required. Most programs require that hydrogens be present and, given that crystal structures are not normally sufficiently accurate to resolve proton positions, these have to be added. In most cases, assignment of protonation state is simple enough: at physiological pH it can be assumed that aspartate and glutamate residues are negatively charged and lysine and arginine residues are positively charged. There are, however, exceptions to these apparently straightforward rules: in the active site of aspartic proteases two aspartate residues bind a conserved water

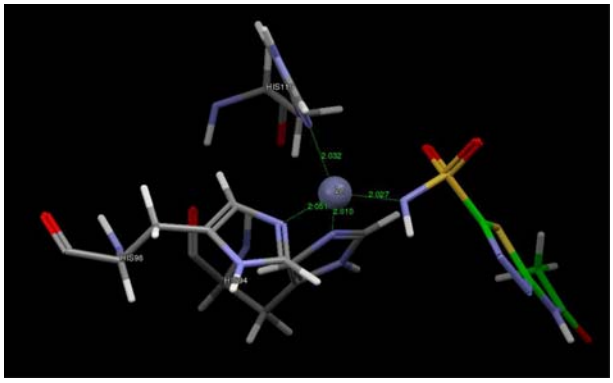

Fig. 1 Zinc ion coordination in 1JD0.

molecule, only one of which is charged. Histidine residues present unusual challenges as there are three protonation states available at pH 7: either or both of the imidazole side chain nitrogens may be protonated. A best guess of the protonation state is normally inferred from the residue environment by the user, but, ideally this is a task best suited to the docking algorithm.

Protonation state is only part of the challenge: one also needs to infer the position of the hydrogen atom. While often straightforward due to the chemical nature of the protein, there is ambiguity for certain residues due to flexibility.

The crystallographically derived protein structure also carries many caveats. It is important to remember that these are complex structures to solve. The model presented is a best fit to a data set of observations. In order to fit the data, crystallographers have to use extensive constraints and restraints in refinement as the volume of observed data is insufficient alone to provide a reliable least squares fit. There may be geometric errors, or imprecise placement of residues in these otherwise very flexible structures. Consequently, relaxation of the protein in a force field may be appropriate after preparation, though such minimizations also need care.

Lastly, decisions need to be made about whether or not to include water in the active site. Some docking programs offer the additional option of incorporation of waters into the search protocol (see below).

The most important decisions regarding preparation of the ligands likewise involve consideration of charge state. For the most part these are straightforward: basic amine nitrogens and groups such as aminopyridines or amidines will be protonated, whereas tetrazole groups or carboxylate oxygen atoms will be negatively charged. However, there are many instances where unusual protonation states are observed on ligand binding, for example, on binding to metalloenzymes. Consider the situation in **Fig. 1**, for the PDB entry 1JD0, where a zinc ion coordinates with three histidine residues and a deprotonated sulfonamide nitrogen in the ligand.[10] As this nitrogen would normally be neutral at physiological pH, it is unlikely that any automated ligand preparation tool would remove this proton. In cases like this, it would be preferable for the docking software to evaluate the protonation state of the ligand dynamically upon binding. Unfortunately, this is not automatically considered by current algorithms and so has to be addressed manually: If a ligand can adopt varying tautomeric states, the user will have to select one, or dock the different tautomers separately.

Some programs, such as GOLD,[11] require a high quality 3D ligand structure as the program does not manipulate bond lengths or angles. Other docking programs such as FRED[12] (assuming it is used, as intended, in conjunction with the OMEGA[13] conformer generator) or GLIDE[14] require only 2D structures as input.

In general, the specification of the docking program and the specification of the protein and ligand can be considered solved (with the exception of those ligands which bind with unusual protonation states). However, this process is often onerous for the end user and software designers could certainly do better in developing new tools and integrating existing tools to further automate this step.

3.12.4 Pose Prediction in Docking

3.12.4.1 Sampling Algorithms: A Solved Problem

As with all complex multivariate optimization problems, the search space for docking is potentially enormous. Even with a rigid receptor and ignoring explicit solvent, a reasonably complex ligand with 10 rotatable bonds gives rise to 36^{10} possible configurations (if we discretize each rotatable bond into 36 10 degree steps). Sampling such a space exhaustively is challenging, even with relatively rapid scoring evaluation, so most docking programs will use global sampling methods to try to find a quicker path to the global minimum.

A wide variety of sampling methods have been used in docking; publications on new methods are common in the academic literature. Algorithms vary from systematic searches across coarse-grained variable grids coupled with local optimization, to using well-established global search methods or metaheuristics such as Monte Carlo sampling (e.g., ICM[15]), Genetic Algorithms (GOLD,[11] AutoDock[16]), Ant Colony optimization (PLANTS[17]), Particle Swarm optimization (SODOCKER[18]), and Tabu searching

(ProLeads[19]). Other software uses algorithms that are not metaheuristic and are more directly related to the problem such as incremental construction (FlexX[20]) or sphere placement (DOCK[21]). GLIDE uses a somewhat original approach.[14,22] Starting from an initial set of ligand conformations, these conformations are placed on likely "site-points" within the active site. A series of filters followed by force-field minimization is used to identify the likely active pose. FRED leverages OpenEye's shape matching expertise to perform a systematic and non-stochastic examination of all possible protein-ligand poses, with shape complementarity and chemical feature alignment filtering.[12]

In order to perform a docking, an algorithm will need to sample the conformational space of the ligand and also the possible binding modes of each conformation. (This is the simpler docking case where the protein is rigid and explicit waters are ignored.) For all but the simplest ligands it is not possible to perform exhaustive search and the optimization procedure will invariably perform selective sampling. Optimization algorithms or metaheuristics such as the genetic algorithm and simulated annealing address this issue by using stochastic sampling to bias the search to areas where binding poses score well. Metaheuristic algorithms typically employ an encoding to navigate the problem space. For example, a naive encoding for docking might comprise a number of real numbers to encode angles of rotation about ligand rotatable bonds so as to generate a ligand conformation, together with six real numbers representing three translations and three rigid body rotations to position the pose in the active site. Improved performance may be achieved by further restricting the search space by constraining the encoding so as not to exhaustively cover all possible poses, but rather to focus the search on likely binding motifs. Such a heuristic strategy is employed by the GOLD program where the encoding used by the genetic algorithm matches features in the ligands to complementary features in the protein. So donor hydrogens in the ligand are matched to solvent accessible acceptors in the protein and vice versa. When this representation is decoded, during stochastic search, a least-squared fitting procedure attempts to form these associations. This encoding ensures that it is unlikely that GOLD explores possible poses that form no interactions with the protein.

In practice, the choice of search algorithm or metaheuristic is rare where the main search benefit is achieved. Well-designed heuristics such as those described above, used in tandem with the search algorithm, will usually have a strong positive influence on the overall performance by guiding the search algorithm to the global minimum. While we know of no known published analyses of such effects in protein-ligand docking, the phenomenon has been observed in the time-tabling problem where five different metaheuristics were tested and none was found to be clearly superior.[23]

We conclude, given the size of the computational problem, the increases in hardware speed and the power of the heuristics used, that sampling in docking is essentially a solved problem for the most common scenarios where typical scoring functions are used.

That said, there is enormous potential for new software in docking to take advantage of new computational architectures, such as GPU systems, cloud computing, or massively parallel computing grids. GPU-accelerated systems for docking have already been developed.[24] The impact of new technologies has been reviewed recently[25]: as is apparent, there are many opportunities for developers to take advantage of the latest hardware developments, though perhaps such technologies would have the most impact on scoring, rather than sampling.

3.12.4.2 Tackling Ligand Flexibility: A Solved Problem

As mentioned above, sampling is essentially a solved problem, due to heuristics in the docking program. One key area where such heuristics are applied is in tackling ligand flexibility. The earliest docking software (DOCK) grew out of the need for graphical visualization of binding in proteins on systems with very limited computational resources. To reduce complexity in this pioneering work, ligands and proteins were treated as rigid entities. With more available resources in computing the opportunity to treat ligand molecules as flexible became more tractable, and consequently tackling ligand flexibility became a component of docking software.

Various approaches to ligand flexibility have been used. Docking packages such as FlexX use incremental construction to sample ligand flexibility. In such an approach, a ligand is fragmented into rigid components which are separated by flexible torsion angles. A rigid part of a ligand is placed in the binding site interacting with the protein, and then the adjacent rigid part is placed such that the torsion angle between the two parts in a region of high likelihood and the binding to the protein is favorable. This is repeated for all fragments until the entire ligand has been placed. Often, the placed structure will then be locally optimized. Such an approach has the advantage that it linearizes the problem of selecting torsion angle values. The disadvantage, however, is that the code has to choose which fragment to place first. Consequently such algorithms are often accompanied by rules to optimize this selection process, or will be run multiple times for a given ligand with different start points to give a diverse range of results. Furthermore, the greedy nature of the incremental construction algorithm may prevent the discovery of global minima.

Some docking programs, such as FRED, avoid the complexity of dynamic ligand flexibility altogether by pregenerating conformational ensembles and then docking each pose in turn, followed by shape and chemical feature alignment-based filtering.

QXP-FLO takes this principle further: Multiple ligand conformations are treated synchronously by using an overlaid ensemble and are all effectively docked at once.[26] The advantage of such an approach is that the scoring of individual atoms can be reduced, as atoms can be shared between ligand poses within the ensemble.

Many stochastic metaheuristics (such as Genetic Algorithms, Ant Colony Optimization, or Particle Swarm Optimization to name but a few) will use a population of individuals in the search. The molecular conformation will be encoded in the representation of each individual. Operations within the search algorithm will in turn allow said values to vary, leading to a diverse set of sampled conformations.

Other stochastic algorithms, such as Monte Carlo simulation or Tabu searching, will instead explore a single conformation at a time, but allow the search algorithm to drive the conformation to favored regions.

All such approaches benefit from search space reduction. Distributions of torsion angles can be derived from the Cambridge Structural Database and can be highly effective in reducing ligand search space. The relevance of torsion distributions to drug-like conformations in binding sites has been studied extensively. We refer readers to work by Brameld and coworkers[27] for an excellent medicinal chemistry perspective on this subject.

By way of a very simple example, the distribution of torsion angles around an aromatic ester fragment is shown in Fig. 2: Such esters show a strong preference for forming a flat "trans" conformation; therefore there is a strong case for only sampling such torsion angles within this region of torsional space.

The ICM docking program uses rotamer distributions to bias the Monte Carlo sampling as an effective heuristic to speed up searching. FlexX and GOLD both use distributions of torsion angles for common substructures to set the ranges of allowed torsion angles in sampling.

Many docking programs essentially treat ligand flexibility by using force field-based terms, so in effect the motion of the structure in the binding site is controlled by the score in conjunction with the sampling algorithm.

The flexibility of ring residues is a challenge for docking programs, and indeed any molecular modeling system that has to allow for molecular flexibility. The most common approach is to treat a ring as essentially a sequence of acyclic fragments, but with the addition of constraints or restraints to reconnect the ring. Such an approach is used in the AutoDock docking program. Other approaches include switching between ring templates or corner flipping. All these approaches have significant drawbacks; choosing fully flexible rings significantly increases the search space for larger rings or multiple ring systems; ring templates are limited by the templates available, while ring flipping is only applicable to unfused ring systems. Ring sampling is an often overlooked area where improvements could be made to docking programs.

Another challenge facing docking packages is the handling of covalently bound linkages within binding sites. Most modern docking packages have systems to allow for specification of covalent linkages between the protein and a putative ligand. The implementations, however, face certain challenges; scoring functions have to be adapted appropriately to account for the nature of the covalent linkage and the reactive warhead in the ligand needs to be identified. CovalentDock, built on top of AutoDock, addresses some of these issues with automatic identification of the likely site of the covalent linkage in the ligand and an additional energy term for linkage formation.[28] An alternative approach describes an automated procedure for identifying reactive electrophilic ligand groups and preparing them for covalent docking using GOLD.[29] Another interesting challenge is the induced motion of the protein in the region of the covalent linkage, which needs to be considered. The Schrodinger protocol CovDock combines the GLIDE docking program with the protein structure modeling package Prime[30]: the reactive protein residue is mutated to Alanine and GLIDE used to perform non-covalent docking; the protein is restored and the binding poses are examined to identify those that can form covalent linkages; Prime is used to refine the complex; finally the ligand is scored using the mean of the GLIDE scores for the non-covalent form of the ligand and for the covalently bound ligand.[31]

Overall, however, with the caveats expressed above, we can say that the sampling of ligand flexibility within a binding site is a solved problem. There are viable and well-described methods that can be used to allow sampling of ligand geometry efficiently and effectively.

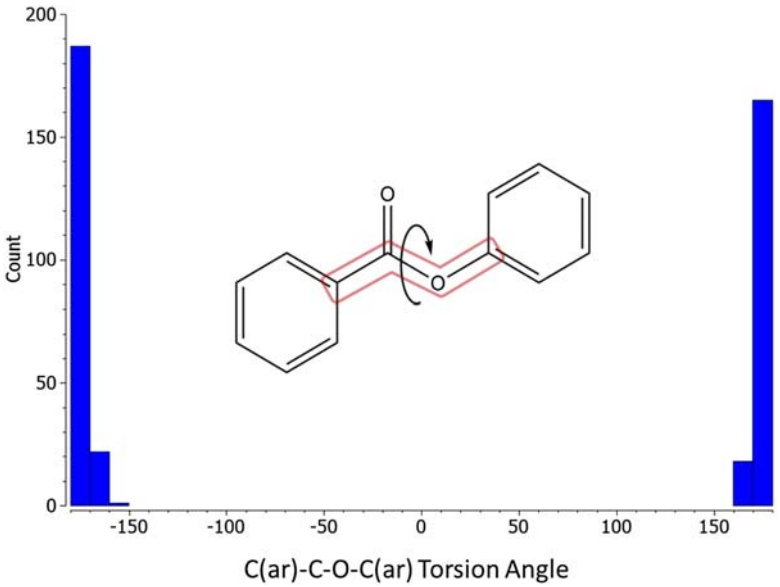

Fig. 2 The distribution of observed torsion angles around an aromatic ester in the Cambridge Structural Database. The distribution was generated with CSD Version 5.37. The search was limited to organic structures with a crystallographic *R*-factor $<5\%$.

3.12.4.3 Tackling Binding Site Flexibility: An Unsolved Problem

The majority of protein binding sites have some degree of flexibility, either by the motions of specific side chains or possibly by larger motions of protein backbones. Often motions are induced, or selected, by the binding of a given ligand, the well-known principle of induced fit.[32]

Historically, docking programs have generally treated binding sites as primarily rigid.

Early efforts attempted to tackle flexibility implicitly in the nature of the scoring function. Scoring functions were "softened" to allow a larger degree of clash against a rigid binding site. Such methods had the advantage that they did not increase computational complexity of the problem but had the disadvantage of only accounting for isotropic expansion of a binding site on binding rather than explicit motions of restricted parts of a given binding site. Furthermore, by allowing softer potentials, the docked results are harder to present and interpret, as typically one observes physically unrealistic contacts in the binding site.

Computational power has increased radically since these early attempts so more recent approaches incorporate some degree of protein flexibility into the docking process explicitly, typically using methods that are analogous to the approaches used for ligand flexibility. For example, an end user can decide to allow individual amino acid side chains to flex in a binding site, or to occupy specific conformational states.

Larger scale motions are handled via "ensemble"-based methods which sample multiple complete conformations of the protein. Any rigid docking program can be made flexible using a naive ensemble-based approach; an end user can dock each ligand multiple times against each different ensemble member and then use the best score attained for each ligand.

Knegtel and coworkers[33] presented the ensemble docking approach with experimental structures. They attempted to solve the problem of relative scoring of ensemble members by using weighted scores for each ligand derived from dockings into all ensemble members.

While the naive approach to ensemble docking is an effective approach, investing time in sequential docking for larger ensembles is computationally challenging. Consequently, developers have invested time and effort into docking approaches that try to remove the need for sequential docking.

FlexE[34] accounts for side chain motions as part of the incremental building algorithm, by treating the majority of the common core as a single protein. Side chains can then occupy variable locations as dictated by observations in the superimposed ensemble. The incremental nature of the algorithm means that the problem is reduced as ligand binding in turn drives the selection of given rotamer positions.

The ensemble approach implemented in GOLD[35] uses superposition of protein structures to inform the docking procedure of conserved regions in the binding site. The fitting points used by GOLD in its underlying mapping algorithm are then pruned to reduce the underlying size of the search space. Further, different ensemble members are distributed across "islands" in the underlying genetic algorithm with migration allowing for movement between members. FITTED[36] also uses a genetic algorithm with genetic operations reflecting switches between different conformations of proteins or different side chain configurations.

An interesting approach has been proposed by Bottegoni and coworkers,[37] who have developed so-called Four-dimensional docking. They try to treat conformational flexibility as a fourth discrete variable in sampling by using the root mean square deviation of the position of critical functional groups in a structural ensemble as a metric to order the structures in the ensemble. The consequence of such an approach is that the steps in the search algorithm from one ensemble member to the next will cause smaller perturbations to the protein model than by sampling ensemble members at random.

Recently, OpenEye have proposed extensions to their docking protocols to HYBRID and POSIT that attempt to incorporate ligand information into docking over ensembles.[38,39] In their approach, bound poses of known ligands in place are used to guide docking of unknown structures.

Ensemble docking methods rely on the availability of structural information to create the docking ensemble. Since the turn of the millennium the volume of experimental information about protein flexibility has increased hugely due to the growth of protein crystallography, which leads to the opportunity for using experimental observation to inform algorithms as to the nature of protein flexibility; in practice, most use of ensemble docking relies on such data sets.

An alternative approach to using experimental structures is to use computational methods to generate ensembles. Typically, a user would use molecular dynamics (MD) to generate snapshots of a structure and use these snapshots as the basis for ensemble docking. It is worth noting, however, that there are significant challenges in using such methods. MD tends to generate many snapshots; many more than would typically be used in an ensemble docking run and so the end user is still faced with having to select a subset of snapshots from the set generated. While it is possible to show that MD can generate a set of ensemble structures that improve docking performance, selecting the best subset to use a priori is very challenging.[40]

It is important to note what the net benefit of using ensembles in virtual screening actually is. The use of ensembles with GOLD has been studied extensively.[35] Interestingly, the authors observe that using an ensemble when undertaking virtual screening rarely improves the performance over a virtual screen using the best performing single structure in the ensemble, but generally gives better than average performance. One can then regard ensemble docking as a means to minimizing risk in virtual screening rather than a panacea.

Another alternative approach to tackling binding site flexibility uses protocols that use a modified binding site model for docking to circumvent flexibility, or treat side chains as partially flexible.

GLIDE's Induced Fit Docking protocol is an example of such a protocol where initially flexible residues are mutated to Alanine in the binding site: the modified representation is then used for initial pose prediction followed by a back mutation to the original site

and re-optimization. The approach still uses an ensemble to identify the flexible regions, but avoids the initial need for sampling into a large number of sites.

Other induced fit protocols tend to dock into a rigid structure and then post-process using relaxation of the binding site. More recently, docking programs such as DOLINA,[41] GalaxyDock,[42] and CDOCKER[43] attempt to handle flexibility without the need for a specific ensemble. BP-Dock attempts to model backbone flexibility as part of the search space.[44] Fleksy combines these methods by first docking into an ensemble and then relaxing the generated binding sites.[45]

Finally, Grebner and coworkers have used Protein Energy Landscape Exploration to explore docking of ligands with a fully flexible target structure.[46] Their method, computationally, lies between quick docking methods and full-blown MD simulations.

Handling binding site flexibility is still a very active area in the field of docking. Many other methods, (too numerous to describe) have been proposed for dealing with conformational ensembles.[47] While programs are improving in this area, we conclude that this is an area where development is still needed, though more effective methods are now becoming available and tractable. That said, we note that the current validation focus is primarily on reproducing observed binding modes. This is undoubtedly a highly desirable property of any docking program, but for us to regard the problem as "solved" the program has to achieve several further predictive criteria, namely the program must rank the correct binding mode highly against alternate binding modes of the same ligand; it must rank the correct binding mode of an active ligand higher than binding modes of alternative molecules of lower affinity; and it must select the correct receptor pose for the observed binding mode.

3.12.4.4 Treating Solvent During Docking: An Unsolved Problem

An additional degree of complexity in docking is presented by the presence or absence of water molecules in the binding site. The importance of accounting for water when docking has been recognized by many groups. For example, in a recent study,[48] the inclusion of water molecules was shown to be able to recover 56% of observed docking failures. In another study,[49] the authors note that it is important to include only key waters. Not all water molecules are beneficial to docking; some indeed can have an adverse effect on docking performance.

Most docking software can allow for the incorporation of water into a binding site as a rigid entity. In such situations, a given water molecule is treated as a part of the binding site into which a ligand is docked. In practice, however, experience with protein structure shows that certain water molecules are labile with respect to binding. It is therefore desirable to be able to treat water as a degree of flexibility within docking.

Again, any docking program can use a naive approach to handle docking by using sequential docking with a binding site containing a given water molecule, and then with a binding site with the water absent, but such an approach quickly becomes intractable when there are multiple water molecules that can be present or absent in a binding site.

A classic example from the literature is the protein OppA. Structures of OppA contain several bound waters (see **Fig. 3**) that contribute to different binding modes of ligands,[50] and can be either included or displaced depending on the nature of the bound ligand. Handling each configuration of the protein with static waters in such a system is impractical due to the combinatorial explosion of possible configurations. Consequently, it is desirable to allow water molecules to vary during docking.

Early work on including water explicitly in docking was carried out by Rarey and coworkers,[51] using the incremental construction algorithm implemented in the docking program FlexX. In their method, the solvent molecules are included as part of the

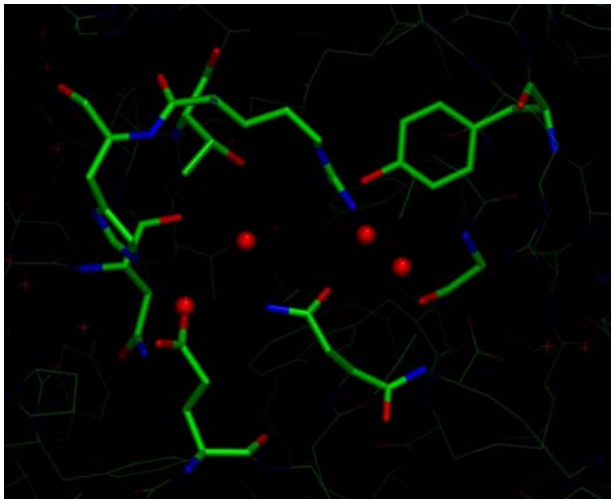

Fig. 3 Water molecules in the binding site of OppA with their interacting side chain residues (Taken from PDB entry 1b5i). The four water molecules can be displaced or retained on binding dependent binding ligand.

incremental construction algorithm used within FlexX: essentially water becomes a single particle that can optionally be switched on or off as a variable in incremental construction.

In the GOLD docking program, water molecules are included in the binding site explicitly at their start positions. Each water molecule is allowed to be switched on or off, controlled by a single discrete variable in each chromosome representation of the ligand. If switched on, additional variables are sampled that express the local rotation of the water and a constrained transformation such that the water remains within a user-specified distance of the original start position. Using this method can significantly improve the quality of docking performance for systems where water molecules form key mediating interactions between the protein and the ligand.[52]

Many other approaches have also been proposed. For example, one approach treats waters as being pre-attached to a ligand but then allowed to switch on or off during docking[53] rather than treating them as a static component of the protein. Such an approach has the advantage that the end user does not need to selectively include waters in the binding site.

It is worth noting that all these approaches introduce new challenges. Removal or inclusion of a solvent molecule in the binding site introduces an entropy change which is tricky to score. Typically, scoring methods either ignore this or treat the change as a constant factor. A recent paper attempts to tackle the scoring issue using a new model for scoring inclusion or exclusion of water molecules.[54] Further, choices as to which solvent molecules to include and to vary as part of the search protocol provide challenges.

Predicting such solvation sites has been an active area of research with tools of varying computational complexity being applied to the task.[55–58] A recent development[59] has seen the application of informatics in this area to provide a relatively rapid means for assessing the likelihood of solvation sites.

The problem of treating solvent during docking has solutions available which can be effective. There is, however, still work to be done: In particular, reliable a priori prediction of solvent inclusion or displacement is still a very active area of research, though recent developments do seem to show promise.

3.12.5 Affinity Prediction in Docking: An Unsolved Problem

3.12.5.1 The Affinity Prediction Problem

Affinity prediction remains a largely unsolved problem in computational chemistry. The reasons for this are rooted in the theory of statistical physics, which describes the energetics of binding. A primer is provided here for the reader, and full details may be found in any statistical physics[60] or physical chemistry[61] textbook. A more exact description of the theoretical principles for computing binding affinities is given in a review by Gilson et al.[62] Ligand binding typically occurs in an aqueous solvent. Upon binding a solvated ligand and protein form a bound complex within the solvent. More specifically, protein binding will occur if the change in free energy upon binding is negative. In other words, the free energy of the complex in solution should be less than the free energy of the separated ligand and protein in solution. For the purpose of this article we define binding affinity as the Gibb's free energy change (ΔG). Note that $\Delta G = -RT\ln K$, where R is the ideal gas constant, T is the temperature, and K is the equilibrium constant for binding. K is the concentration ratio between bound and free ligand and may be determined experimentally for many systems.

Consider a molecular state of the bound protein and ligand. This may be defined by the atomic coordinates of the system (though many methods also require momenta to be assigned to each atom). It is clear that a complex system such as a bound ligand can exist in a large number of differing states with varying energy levels. Statistical physics describes the probability, p_r, of each available state, r, with energy E_r via the Boltzmann distribution such that

$$p_r = \frac{e^{-(E_r/k_B T)}}{Q}$$

The normalization term

$$Q = \sum_r e^{-(E_r/k_B T)}$$

is known as the partition function (where k_B is the Boltzmann constant, equal to R divided by Avogadro's number). Any molecular system, such as ligand bound to a protein, should be visualized as an ensemble of available states where the Boltzmann distribution may be used to determine the relative likelihood of each state using only the energy of that state and the temperature of the system.

As an alternative to the Gibbs free energy, the Helmholtz free energy, A, may be used to predict binding as, under conditions of constant pressure and volume, $\Delta G = \Delta A$. Since $A = -k_B T \ln Q$, the partition function can be used to easily determine the Helmholtz free energy. It should be noted that reliable determination of the partition function requires the identification of many of the higher energy states and thus may be intractable for many systems.

The fact that many states have to be sampled in order to determine free energy reflects the role of entropy in driving ligand binding such that the change in free energy $\Delta G = \Delta H - T\Delta S$, where ΔH is the enthalpy change and ΔS is the entropy change. Entropy may be viewed as a measure of the amount of disorder in the system. For an ensemble system the entropy is

$$S = -k_B \sum_r p_r \ln p_r$$

where p_r is the Boltzmann probability described above for each state. The affinity of a ligand to a protein may be driven more by entropy than enthalpy. For example, the basis of the hydrophobic effect during ligand binding is the displacement of ordered water from within the protein active site and around the ligand to bulk solvent where it is free to adopt a less ordered state. Typically, docking scoring functions are better at capturing internal energies or enthalpies, rather than ensemble properties such as entropy.

Accurate determination of binding energies thus requires sampling of the Boltzmann distribution so as to identify the partition function for the initial system with the ligand and protein separately in the solvent, and for the final system which comprises the solvated complex. Not only will such a calculation require sampling of a large number of states, but also an accurate energy calculation will need to be performed for each state. Reliable affinity prediction is thus a Sisyphean task and remains a major challenge in the field of computational chemistry. Sampling of multiple states to determine binding affinities in this way is invariably too computationally demanding for docking algorithms which focus on the rapid prediction of a single binding pose. Nevertheless, an understanding of the theoretical basis for the calculation of binding energies is important in order to explain the failings of docking scoring functions.

In computational chemistry a standard technique to generate the ensemble of states to be included in a partition function would be to run an MD simulation, sampling from the trajectory once the system attained equilibrium.[63,64] Given this complexity much effort has been made to simplify the calculation of free energies in ligand binding.[65] While most of these techniques are not currently appropriate for docking methods (because of their compute-intensive nature), many may be used to rescore docking predictions,[66] and it is reasonable to imagine that we will see incorporation of free energy calculations into docking algorithms with improvements in computer hardware.[25]

The role of water is a major source of complexity in such calculations. If molecular systems are modeled using explicit waters the number of available states is much larger than the equivalent system in a vacuum, especially for areas of disordered bulk solvent. For this reason there is considerable focus on methods for calculating free energies in solution.[67] In particular, determination of the free energies of solvated systems can be greatly simplified if a polarizable continuum solvent model is used to approximate the free energy of explicit water molecules in the bulk solvent. The continuum potential may be expressed as extra terms in a molecular mechanics potential. Two continuum models in common usage include Generalized Born Surface Area (GBSA)[68] and Poisson Boltzmann Surface Area (PBSA).[69] Not only does the solvent model simplify the calculation of state energy, but the removal of the degrees of freedom required by explicit waters also significantly reduces the number of states in the system. The use of continuum models in docking has historically been restricted to rescoring,[70] though recently it has been included in the WScore scoring function.[54]

Additional techniques exist to further facilitate the calculation of free energy differences such as Free Energy Perturbation (FEP)[71] and Potentials of Mean Force (PMF).[72] During FEP, an ensemble of states created for one system is used for a second system. The free energy difference is readily calculated from the differences in energy between the two systems over each of the shared configurations. For example, an ensemble of states, each containing a set of coordinates and momenta, may have been generated for a ligand containing a Cl atom. Using those same states of coordinates and momenta the energy ensemble for second ligand with Br substituted for the Cl atom can be calculated together with the free energy difference for the substitution. Clearly, this approach works best for very similar systems, though the use of intermediate states allows the comparison of systems that do not share phase space[73] (where phase space comprises the positions and momenta of all atoms in the system). In the example above, where a Br is substituted for a Cl, phase space may be shared; this is not the case if the atom counts of the two systems differ. While FEP calculations are too intensive to be used in docking experiments, they may be used to rescore docking poses.[74]

Thermodynamic cycles make use of the fact that free energy, as a state function, is conserved around a cycle.[64] The use of nonphysical, but nevertheless valid, state changes enables the determination of binding energies while avoiding complex simulations of real-world processes. Consider, the thermodynamic cycle illustrated in **Fig. 4**. The binding energy in solution is

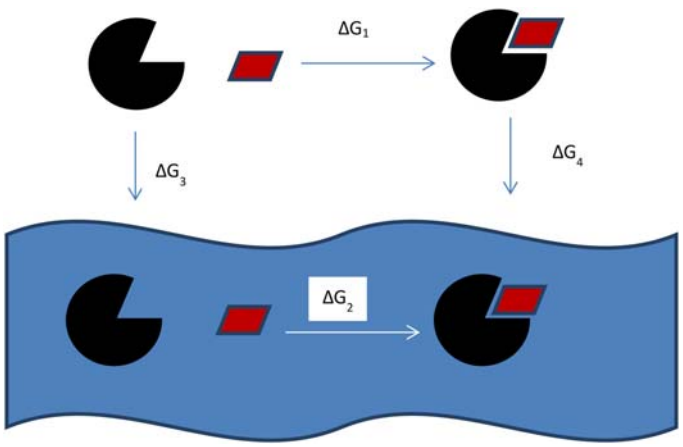

Fig. 4 Thermodynamic cycle as used by Autodock.

$\Delta G_2 = \Delta G_1 + \Delta G_4 - \Delta G_3$, where ΔG_1 is the free energy of binding in a vacuum, ΔG_3 is the free energy change on solvation of the separate molecules, and ΔG_4 is the free energy change on solvation of the bound complex. Docking results may be used to determine the structure of the complex and an estimate of ΔG_1 and the use of a continuum solvent model can facilitate the estimation of energies of solvation (ΔG_3 and ΔG_4).

The Autodock algorithm uses the free energy cycle described above to predict binding affinities in its scoring function.[16] Autodock does not attempt to identify the partition function but rather uses known complexes with associated inhibition data to parameterize docking and solvation potentials.

PMF calculations follow from the observation that, for atom pairs, the partition function is equivalent to the radial distribution between atoms. The radial distribution is normally defined by the distance between atom pairs. Using crystallographic databases the distribution of distances between atom pairs of interest (e.g., between a donor and acceptor or two hydrophobic atoms) may be used to determine the free energy contribution at as particular distance. This technique has been used to determine free energies of atom pairs within proteins[75] and has been adapted to score protein-ligand interactions.[76]

3.12.5.2 Scoring Poses in Docking

As implied above, affinity prediction in docking is a challenging task, but despite this, many research groups have attempted to tackle the problem at varying degrees of approximation. In this section we will review what can be predicted from docking results, given the scores available, how higher levels of theory can be incorporated into docking algorithms and how docking poses may be used to assist advanced calculations.

The scores used directly in docking programs are generally designed to be fast enough to allow them to be evaluated many times a second. This facilitates sufficient sampling in the global search algorithms that accompany docking. This means, however, that by necessity they have to compromise on accuracy in certain areas.

Traditionally, scoring functions are seen to be split into three different categories, namely molecular-mechanics like scoring functions such as the scores PLPScore,[77] Goldscore,[78] GlideScore,[14] and Emodel[14] which try to model the binding interaction energy based on approximations from chemical theory, empirical scoring functions such as ChemScore,[19] ChemPLP,[77] FlexX,[51] Fresno,[79] which are essentially trained for affinity prediction against sets of empirical data on binding, and knowledge-based functions such as PMF,[80] ASP,[81] and DrugScore[82] which are based around statistical potentials derived from databases of observations of interactions in chemical databases such as the Protein Data Bank[83] or the Cambridge Structural Database.[84]

It is worth noting that some scoring functions are specifically designed for rescoring rather than docking. For example, the HYDE docking function attempts to specifically model de-solvation of hydrogen bonding.[85] This score alone is an insufficient description of all the processes of binding, and so is used in tandem with a different score for the purpose of pose prediction: the HYDE score is then used alone to assess the quality of binding of the generated pose rather than to drive a docking exercise.

Rescoring can be a successful strategy in tandem with docking, as it facilitates the use of computationally more expensive methods for the rescoring.[66] Some notable examples where such methods have been applied include MM-PBSA for post-optimization,[86] and using the AMBER force field in rerefining fragment dockings.[87]

3.12.5.3 Validation of Docking Programs and Their Associated Scores

Self-validating docking studies, where a ligand is extracted from a crystallographic macromolecular complex and a docking algorithm is used to dock the ligand back into the protein, are the primary method of validation for docking algorithms. Normally, the docking program optimizes ligand position and geometry using molecular mechanics-like potentials; these typically reproduce observed binding modes by maximizing hydrophobic contact and reproducing hydrogen-bonding motifs.

Results published by algorithm developers are often impressive in this regard: for example, the original GOLD algorithm showed a 71% success rate (using subjective criteria) in self-docking[78] of 100 complexes; GLIDE was successful in two-thirds of 282 complexes, using a 2 Å RMSD cutoff.[14]

Studies by third parties, who are algorithm users rather than developers, show methods to be less effective; this is unsurprising given the sensitivity of these methods to input conditions such as protonation states and active site definitions and the common practice of refining algorithm performance against the validation test set. Third party studies may be broadly categorized as to the metrics evaluated: pose prediction, virtual screening enrichment, affinity prediction, and activity ranking. Here we review many of the third-party evaluations done to date. In view of the large number of algorithm evaluations and proof-of-concept studies we restrict our summary to comparative studies of multiple methods that are either performed by third parties or comprise blinded data. For these reasons we do not include participants' papers from the Docking challenge special issues in the Journal of Computer-Aided Molecular Design.[88] An exception is made for the Comparative Assessment of Scoring Functions (CASFs) papers,[89,90] authored by the developers of *X*-Score,[91] in light of the large number of other scoring functions evaluated therein.

In one of the first reviews of its kind, in 2000, Bissantz et al. evaluated the performance of Dock, FlexX, and Gold in combination with seven scoring functions against thymidine kinase and the estrogen receptor and found that the docking programs were capable of discriminating active from inactive compounds up to 70% of the time if consensus score methods were used.[92] Unfortunately, no clear relationship was observed between docking scores and activity ranking, and predicting binding free energy was not possible.

In a number of later papers, researchers confirmed the utility of docking algorithms for pose prediction (by showing close RMSD to the crystallographically observed binding mode) and virtual screening (by showing improved enrichment of hits over random), but did not evaluate affinity prediction. For example, a paper in 2001 from Stahl and Rarey tested FlexX in combination with four scoring functions (FlexX, PLP, DrugScore, and PMF) across seven systems for virtual screening.[93] A combination of FlexX and PLP scoring functions was found to have broad-based applicability for selecting actives during virtual screening. A similar paper from 2003 described the utility of several docking programs for virtual screening (in this case simply recovering the crystallographic ligand from a set of decoys) and pose prediction on 11 systems.[94]

In an interesting study from 2003, Autodock was employed to create an exhaustive set of bound conformers.[95] Eleven scoring functions were evaluated as to their ability to identify the experimentally observed binding mode, and six were shown to have success rates or 66% or greater (using a 2 Å RMSD criteria). Unusually, considerable success was observed in prediction of binding affinities with *X*-Score, PLP (as implemented in Cerius), DrugScore, and GOLD (as implemented in Tripos' CScore) scoring functions all giving correlation coefficients of over 0.5. This may be more to do with discrimination of active and inactive compounds as the datasets included millimolar compounds, rather than the relationships that would be required for SAR projects. In a later 2004 study by the same group using 14 scoring functions, on a set of 800 complexes from the newly released PDBbind[96] database of protein crystal structures and binding affinities, similar results were obtained in terms of correlation.[97] This later study also looked at the ability of scoring functions to classify ligands into categories of high, medium, and low activity where all methods showed modest ability to classify ligands into the high and low activity categories. The relationship between experimental activity and docking score was further studied using three test systems (HIV-1 protease, trypsin, and carbonic anhydrase II), this time on a per target basis. Reasonable performance was observed for many scoring functions in the trypsin and carbonic anhydrase II dataset though only one scoring function was effective for HIV-1 protease.

In 2004 a further number of papers again showed that docking algorithms were able to both predict binding poses and perform well in virtual screening enrichment studies. One study of FlexX and five scoring functions (FlexX, DOCK, GOLD, ChemScore, and PMF) showed significant enrichment during virtual screening.[98] A study of three docking algorithms (Glide, GOLD, and ICM) in three systems found Glide to be the best method for identifying the binding pose and enrichment performance to be scoring function dependent.[99] A comparison of 8 programs (DOCK, FlexX, Fred, Glide, GOLD, Slide, Surflex, and QXP) against 100 known ligands showed that the best tools for pose prediction (Glide, GOLD, and Surflex) were also the best for virtual screening ranking.[100] Another study focused only on the ability of common docking algorithms to predict ligand binding poses.[101] Interestingly, one study from 2004 using GOLD, FlexX, DOCK, and AutoDock on zinc metalloproteinases showed not only pose prediction but also strong activity correlations using DrugScore ($R^2 = 0.58$) and *X*-Score,[102] though this may reflect the composition of the PDB entries used to parameterize these knowledge-based functions.

One paper from 2004 compares traditional docking scoring functions with the charm force field augmented by continuum solvation models.[103] Nine scoring functions were evaluated across 189 complexes, with 5 scoring functions achieving binding pose prediction rates of over 80%. Surprisingly, despite the inclusion of implicit solvent only the knowledge-based ChemScore scoring function was able to show a reasonable correlation with activity. Another study from the same year used a dataset of known activities of 205 protein-ligand complexes.[104] Binding prediction experiments using four scoring functions failed to show any real correlation between docking scoring functions and activity, though useful correlations were observed in some subsets.

Further enrichment studies performed in 2005 continued to confirm the capability of docking in virtual screening via enrichment studies. Pose prediction and enrichment performance was assessed for three algorithms (FlexX, Glide, and DOCK) together with six scoring functions and the authors' finding was, unsurprisingly, that false positive prediction was lessened when bioactive poses were available.[105] Another study using DOCK, DockVision, FlexX, Glide, and GOLD into five protein test systems found reasonable rankings in virtual screening experiments even when docking programs failed to identify active poses.[106]

In 2006 a virtual screening study from AstraZeneca, FlexX, GOLD, GLIDE, and ICM was evaluated for virtual screening and pose prediction over 12 protein targets. Glide and ICM were shown to be superior in pose prediction and virtual screening enrichment.[107] Interestingly, the author compared the docking programs with 2D (ISIS fingerprint similarity) and 3D (ROCS). For the proteins investigated ROCS outperformed all algorithms except ICM in terms of enrichment and the simple 2D method did better than either GOLD or FlexX.

Also in 2006 a review from GlaxoSmithKline of the performance of 10 docking programs across 8 proteins and 1300 ligands showed that pose prediction success was at best 35%, using a 2 Å RMSD criteria.[108] Although, observing some success in pose prediction, this extensive study failed to show any statistically significant relationship between docking scores and affinity for any program, though a positive correlation was shown for a single compound series (but not for all compounds) against a kinase target. Other positive correlations were from discriminating between active and inactive compounds rather than rank ordering of active compounds. Where possible, the authors repeated this experiment using only dockings for which the pose had been correctly identified. With the exception of GOLD and PPARδ, where a significant relationship was observed, no improvement was observed.

An investigation from 2007 into the performance of GLIDE, GOLD, and DOCK over 21 systems showed that GLIDE outperformed GOLD and DOCK and, while 15 systems comprised the GLIDE training set, GLIDE created the highest enrichments in 5 of the remaining 6 systems.[109]

In 2009 a study by Wyeth also suggested the superiority of GLIDE which, together with ICM and Surflex, proved more effective in pose prediction than DOCK, FlexX, and PhDOCK over 68 protein ligand complexes (where ICM had a median RMSD of 0.98 Å against the observed binding mode).[110] The same study also researched the effectiveness of the docking methods for virtual

screening in 40 targets from the Directory of Useful Decoys database,[111] where GLIDE yielded the highest mean ROC AUC value of 0.72, though all methods had mean AUCs of better than random.

Also in 2009 the first comprehensive CASF was published.[89] Using a curated subset of PDBbind of 195 complexes, comprising 65 different proteins each bound to a high, medium, and low affinity ligand, this study performed an extensive evaluation of the ability of 16 scoring functions to perform pose prediction and to predict binding affinities. Pose prediction was tested by determining if the scoring function could discriminate the active pose from 100 decoy poses. Many functions did exceptionally well here, with the best performing scoring function (ASP) identifying either the active pose or a decoy pose within 1 Å RMSD from the active pose about 70% of the time (and 80% if the cutoff were 2 Å). Affinity prediction was evaluated in terms of correlation between activity and the score of the observed pose in its cognate active site over the entire test suite. Some scoring functions performed surprisingly well here with the best method, *X*-Score (HMScore), showing linear correlation of 0.65 with affinity. It should be noted that this test scenario is not representative of docking in practice: the active poses are known and scored directly and only three activities over a wide range are present for each target. Even with this optimistic system, five of the scoring functions were outperformed by simply using the ligand heavy atom count as a scoring function. The ability of scoring functions to rank order the three ligands by affinity for each of the 65 test proteins was investigated. The best method, again *X*-Score (HSSScore) was able to do this successfully only 60% of the time, confirming the conclusions of earlier studies that compounds of high activity cannot be consistently ranked over those with low activity. The paper also includes further ranking experiments on additional datasets, which show scoring function performance to be system dependent. The authors rightly conclude that the best scoring functions are competent at predicting binding poses, but affinity prediction requires improvement.

In 2011 the extensive CSAR (Community Structure-Activity Resource) benchmark exercise of 2010 was published.[112] This collaborative work of 16 groups evaluated 19 different methods over 343 high quality structures. R^2 correlations with experimental pK_i values ranged between 0.58 and 0.12, indicating that scoring functions were neither able to predict binding affinity nor rank relative activities. Although the results for individual scoring functions were blinded, all types of scoring functions were included and no type, force field, empirical, or knowledge-based, demonstrated any inherent superiority. A detailed analysis was performed to identify the differences between those systems that were amenable to affinity prediction and those complexes which scored poorly. Further illustrating the difficulty in scoring entropic contributions, it was found that, in cases of failure, scoring functions tended to overestimate the contribution of hydrogen bonds and underestimate hydrophobic interactions. Additionally, torsional strain was much lower in underscored ligands.

The results of a second CSAR benchmark exercise were disclosed in 2013.[113] This exercise was based around blinded experimental data for four proteins, 122 compounds with measured activity (or confirmed inactivity) and 30 crystal structures.[114] The compounds comprised of a number of congeneric series. The study metrics were binding pose identification, enrichment, and activity ranking. Twenty-one groups using 18 docking programs submitted predictions. The organizers of the challenge did not identify the particular groups or methods but provided scoring and sampling function categories (e.g., knowledge, empirical, or force field based). In terms of pose prediction the results were poorer than those typically observed-with only 34% of the highest scoring pose predictions being within 2 Å of the experimentally observed binding mode. An analysis of close ligand-protein contacts suggested that the scoring functions were underweighting contacts. Some of the poor results for pose prediction may have resulted from movements in the protein and reflected the challenges of cross docking. No clear winner was identified in terms of the best scoring function category, though there did appear to be an improvement when empirical scoring functions were used. In an interesting insight to the issues around docking inputs the authors provided the groups with a methodology questionnaire and ascertained that pose prediction was more likely to be successful if the active site had been minimized, if histidine residues were assigned correct tautomeric states, if a ligand conformer library were used, and if the method were trained on the native ligand. The results for binding affinity prediction were poor with only two methods averaging a correlation (per protein) of over 0.5 and no group being able to perform any meaningful predictions on one protein (Chk1). The ranking predictions were likewise poor, and the enrichment studies were equally uninspiring. Enrichment was only tested for two proteins, as one protein had no actives and another had an insufficient number of compounds. It was found that most methods were no better or worse than random, three methods were better than random, and three were worse. It should be noted that this enrichment study was somewhat unusual and certainly not representative of virtual screening as there were only a limited number of inactive compounds, which were presumably very similar to active ligands.

2014 saw the publication of the second CASF study.[90] In a design similar to the previous work 20 scoring functions were evaluated against a newly curated subset of PDBbind (the PDBbind core subset, version 2013[115]). In addition to evaluating scoring functions for binding pose prediction, affinity prediction, and activity ranking, a test for virtual screening enrichment was added. As in the previous study, the test set comprised 65 distinct proteins, each complexed with a high, medium, and low activity ligand, for a total of 195 systems. As before, in order to decouple scoring function evaluation from the problem of conformational search, decoy poses were generated using common docking programs, clustered and seeded with the bioactive pose. Further, to evaluate scoring in virtual screening, for each of the 65 proteins the 192 ligands that were active against the other proteins were used as negatives. Using the procedure for generating decoy poses, binding poses were created for over 12,000 protein-ligand negative pairs. The results were not dissimilar to the previous study, with the most impressive performance observed in the pose prediction tests, where the best scoring functions, such as ChemPLP (as implemented in GOLD), predicted the observed binding mode over 80% of the time. Likewise, the new virtual screening test confirmed that docking algorithms are able to discriminate between active and negative compounds, with enrichment rates for the Glide-SP scoring function being almost 20 times over random. As expected, the performance in activity ranking and prediction was much more disappointing. While *X*-Score (HMScore) performed best with

an apparently reasonable correlation of 0.6 to activity, a simplistic scoring function based on the change of solvent accessible surface area was runner-up with almost identical correlation. This naive function also outperformed almost half the scoring functions in the activity ranking test. Again *X*-Score (HMScore) was the best scoring function in this test, successfully ranking each of the three ligands 58% of the time. It should be noted that this is a simple ranking problem (discriminating between weak, medium, and good ligand) and is not indicative of the challenges experienced in SAR programs. Additional analyses of subsets of the test systems indicated that prediction of the binding modes of flexible or hydrophobic ligands remained a challenge. While polar interactions appeared to help scoring functions identify binding modes they fare poorly in activity prediction, suggesting issues in accounting for the desolvation of polar groups.

Another CSAR exercise, conducted in 2013 and published in 2015, contained not only a protein design challenge but also a pose prediction and an affinity prediction challenge.[116] The docking pose test contained two designed proteins that bound digoxigenin (an extremely rigid steroid), together with a set of poses (the binding pose and 199 decoys such that no decoy was within 2 Å RMSD of the binding pose). Fourteen groups submitted 25 methods for analysis with 17 and 18 methods identifying the binding mode for each of the two proteins, respectively. Notably, a submission using MM/GBSA proved unable to identify the binding mode for either protein. A relatively narrow binding pocket and a somewhat rigid ligand may have made this an easy task. For the final test the binding affinities of 10 small molecules (near-rigid analogs of digoxigenin) to one of the designed proteins were determined by the organizers. In this phase, the 14 groups submitted 27 methods and 12 methods showed correlations of over 0.7 between scores and activity, though only seven methods demonstrated similar correlations between ranks. Given the narrow range of activities, between 0.22 and 80 μM, and the similarities of the ligands, rank ordering proved a difficult task. It is also possible that, given the tightness of the activity values, because of error the benchmark experimental rankings were not correct. While anonymity was preserved and the performance of methods remains blinded, the method used were identified and were representative of common scoring and docking algorithms. Interestingly, despite using the same methods, different groups did not submit the same predictions, highlighting the role of input structure preparation and method parameterization in program outcomes.

In the most recently published study CSAR 2014 participants were invited to perform docking studies on three targets using blinded data provided by GlaxoSmithKline.[117] As in the CASF studies an attempt was made to separate scoring from docking and the first phase of the challenge involved selecting an active pose from 200 decoys, where 32 of 52 methods had excellent performance. A second phase involved prediction of binding affinities with few methods being able to rank actives with any statistical significance.

3.12.5.4 Overall Conclusions on Affinity Prediction and Scoring

In summary, an almost unanimous picture of docking capabilities emerges. Most methods are able to perform pose prediction with some accuracy. In virtual screening, most methods also perform well, achieving enrichments well in excess of random, though we should not regard random as the comparative baseline; if a docking study only performs as well as simple 2D properties, such as molecular weight, donor or acceptor counts, or simple measures of molecular flexibility, one can hardly regard that docking study as a success.

Comparative studies indicate that docking methods do not provide greater enrichment than either 2D or 3D ligand-based methods,[118] while the ligand-based methods are clearly easier to set up and computationally more tractable. It is, however, in affinity prediction that docking methods and scoring functions require the most improvements. In general, scoring functions correlate poorly with activity and are unable to rank order compounds by affinity. In fact the CASF studies indicate that current scoring functions are unable to reliably discriminate between compounds of low and high activity. This negates one of the potential gains of structure-based design; namely, that by inclusion of the protein structure, activity cliffs may be identified.

Despite the failure to predict affinity or rank order activity many of the studies showed that docking did result in significant enrichment in virtual screening, indicating that the scoring functions were at least able to distinguish between active and inactive compounds. This would appear to be a direct contradiction of the previous observation from the CASF studies. We suggest that the difference is that in the CASF studies the ligands are more likely to be from congeneric series, where compounds in virtual screening experiments are much more diverse. In fact, a recent extensive review of docking screens confirms this observation and found for many screens that, in terms of hit rate, docking studies for many enzymes were two to three orders of magnitude better than the comparable HTS screen.[3] This would suggest that active compounds may be identified simply by their ability to crudely fit into the active site. Given the simplistic nature of docking scoring functions this is not surprising and it may be that pose prediction requires only a simple geometric recognition. That is, recognition of hydrogen bonding motifs and hydrophobic surface area contact is sufficient to predict a binding pose (though, obviously, this would be insufficient to predict a free energy of binding).

Validations of docking programs are, of course, dependent on the quality of the systems that they can test their programs on and the way in which the user makes use of the program. It is worth noting that the test systems used for development and validation are far from perfect.[119] For example, a common validation method used is to compare relative performance of virtual screening against the results of high throughput screening, but experience shows that the high throughput screening results themselves can contain noisy information. Consequently, the validator must moderate their expectations of the docking program to account for the nature of the experimental data they are validating against.

3.12.6 Other Unsolved Docking Problems

We note that there are yet more areas where docking could have impact but where the solutions offered as yet are somewhat limited. Some software features the ability to perform covalent docking, for example, but the methods used could be significantly enhanced. Further, we are currently unaware of solutions that try to tackle significant conformational change on covalent binding to the protein in a structure agnostic way. Typically, the end user has to inform a program of the nature of the covalent linkage prior to docking and set up the docking appropriately rather than allowing the software to make choices regarding the nature of any covalent bond, or recognizing that the actual chemical reaction occurs.

Another area of interest would be the automatic recognition of dynamic changes in tautomeric state and protonation state of ligands that might occur on binding. Currently, tautomerism and protonation states are usually considered on input creation, and so rely on user choices to yield good results.

A longer term challenge lies in using docking to identify small molecules that could cause disruption of protein-protein interfaces. This growing area of interest has its own community, and has been subject to its own CASP-like collaborative effort (CAPRI[120]) in assessment of methods to aid the development of new and existing approaches. Finally, protein-protein docking itself is a very active area of research in its own right which is becoming of more interest with the development of biologic therapeutics.

While the focus here is medicinal chemistry, it is worth noting that docking can be applied to a wide variety of other problems. For example, docking of substrates into metallo-organic frameworks or zeolites,[121] or clefts into surface cavities of small molecule crystals could be useful in a variety of broader chemical applications, such as the understanding of the behavior of crystal growth inhibitors. (For an example of such an approach, see Coveney et al.[122])

Such problems present their own challenges: in particular, a broader range of atom types require parameterization, solvation effects are less predictable, due to the wider choice of solvents used in crystallization, and the nature of the problems in question mean that researchers have to consider behavior at non-ambient temperatures and pressures. These are potentially rich unexploited areas of research for a future generation of docking developers.

3.12.7 Democratization of Docking: An Unsolved Problem

The final area of contention in the area of docking, as with any software, is in "democratization." The definition of "Democratize" from Merriam-Webster's Dictionary says: "verb: to make (something) available to all people: to make it possible for all people to understand (something)." While commercial docking programs may not be freely available to all people, they should be easily understood by all users.

How is the idea of democratization translated into docking? For a docking package to be democratized, any user should be able to prepare the necessary inputs (a small molecule or set of small molecules, and a protein structure or PDB code) and return the same list of compounds as any other user inputting the same data.

From an end user's perspective, democratization is far off. There are dozens and dozens of programs that will take these inputs and return a ranked list. There are companies that argue that each has the "best" product. The problem starts way before the inputs (themselves often representing a large degree of uncertainty) are chosen and thrown against the virtual wall to see what sticks.

Let us just list the choices one has as one descends down the rabbit hole. There are many docking programs (we estimate at least 70) available to the community, some commercial, some academic.

Most of the stand-alone tools also make the user choose from a set of charge state models, force fields, conformational sampling approaches, water utilities, scoring functions, rescoring functions, and speed.

If we just assume that we have 70 programs, each with 10 features and there are 3 choices for each feature, we get a bewildering (70×3^{10}), that is, 4 million options for docking molecule collection A into protein B. Even if we only took a carefully curated crystal structure data set for validation, such as Iridium[123] (which has 728 structures), we would still have to somehow try to measure the performance of more than 4 billion dockings.

On the flip side, every single docking program available will return a ranked list of compounds that will help the user reduce the search space "worthy" of a closer look. Given the bewildering set of choices available then, what is the user of docking software to do?

Furthermore, the end user also has to consider not just how to do docking but also whether or not to use docking in the first place for the task at hand.

3.12.8 Help! I am a Medicinal Chemist … What Do I Do Now????

3.12.8.1 When Should I Use Docking?

The answer to this question will depend on the ethos of the organization in which an end user works, and the task that the end user is addressing. We note that all we can express here is opinion borne out of experience. Docking is typically applied in virtual screening and in lead optimization. Each use case is subtly different. In an excellent review, Irwin and Shoichet[3] recently analyze the impact of docking and other screening techniques on medicinal chemistry programs, and suggest good strategies and approaches that can lead to success. They show validated examples where docking is successful at identifying leads. Their choice

of examples was predicated against whether they could say with confidence that the discovered hits had led to new biology: that is, they were interested in cases where the resultant hits were validated against an organism. They conclude that while care is required, useful hit rates of 10% can be achieved if docking is applied with due care and attention in very high throughput virtual screening, both in the application of software and in the interpretation of results.

One notable element of this review is the need for attention to detail in the processes undertaken. A key issue to consider with any software is the age-old principle of "garbage in, garbage out": in effect the end user has to have a high degree of confidence in the inputs to the program to get good insights from the results.

Some organizations will have a large array of high quality protein structural data available to them which provides a bedrock for docking studies; other organizations may be relying on alternative models, such as homology models which, while valuable, are generally at a lower degree of accuracy than a high resolution crystal structure. One may not then expect such models to generate reliable docking results. In the context of virtual screening, it is possible that alternative approaches may yield comparable results in a shorter time frame.

We would recommend using docking prospectively when you have carefully validated protein crystal structures with a resolution better than 2.5 Å. Where possible, we would recommend testing the docking program by confirming the program can reproduce the poses of known bound actives against non-cognate protein structures; however, we accept that this may not be feasible in many early-stage projects.

Docking can, however, also be useful in protein structure validation. Protein crystal structures will typically only have ligands resolved in one binding mode. Docking can sometimes suggest alternate modes that might fit the electron density equally well. Using the docking program to cross-validate the refined pose can suggest alternative structural interpretations of the protein structure that may not have been originally considered.

3.12.8.2 How Should I Use Docking?

As illustrated in the introduction to this section, the choices available to an end user are bewildering. Some of this, however, can be ameliorated.

3.12.8.3 Learn How to Love the Software

Working with docking software is a labor of love; understanding the complexities and quirks will provide the best results. How can a user really get to understand the complexities and quirks? Firstly, stick to the best practices advised, at least initially. Use the approaches that are used in the detailed recipes, examples and tutorials that the software provider gives you and stick with that until you have an understanding of the ramifications of straying from it. Get to know its good points and bad points and gain an understanding of the likely outcomes of using it. This is, of course, easier said than done, but the investment of time is worthwhile: be annoying to your local experts, make use of your vendor's training materials, courses, and support options, and try to gain a level of expertise that allows you to make informed choices. When starting a new project, use the newest version of the software and ask for support from your software provider if necessary.

These recommendations may be surprising to some, in that it may seem obvious, but anecdotally, vendors have experience through support queries that indicate that not all end users gain a full understanding of the software they are using. For example, the CCDC has experienced a number of support queries where the end user has not understood that the docking program expects a three-dimensional representation of a chemical structure as its start point, and has tried to dock input files that contain two-dimensional structural representations only. Other problems seen include cases where the protein structure model being used had not had any explicit hydrogen atoms added or where cognate ligands were left in the binding site thus making it impossible for the docking program to place ligands there.

It may be that a reasonable expectation of the software is that it would attempt to automatically resolve these issues, and indeed many vendors provide preparation tools that aid the end user when using their software. The support queries mentioned above indeed sparked development at CCDC to improve the end user experience when setting up docking, but it is unrealistic to expect software to be able to resolve every possible mistake that could be made in user input.

It may not be possible for every end user to gain the requisite level of expertise: in such cases knowledge sharing is highly desirable. Where resources are available, it is better for end users to use software in a controlled environment. Many organizations will provide simplified (possibly web-based) interfaces to docking that provide access to specific target protocols. Such interfaces can allow an expert user to create predefined protocols that are best suited to a given target, which have been shown to be effective in practice.

Such interfaces also have a huge advantage of streamlining work. Rather than many users setting up their own protocols, one expert can take project responsibility for docking setup, meaning all end users are using the tools in the best way.

3.12.8.4 Invest Time in Your Input Protein Structure!

Docking relies on the input protein structure to generate reasonable results, and results can be influenced significantly by the way the initial protein structure is configured. Crystallographers place significant effort into getting a good structural model that fits the data they have collected, but end users need to understand the caveats associated with crystal structure determination. In particular:

1. Bear in mind that a crystal structure is an atomic model that fits experimental data; the quality of the model is dependent on both the experimental data quality (usually expressed via its resolution) and the modeling effort made. For example, it is quite easy for a crystallographer inadvertently to assign element types incorrectly; the effect on the fit to the model is quite small. For example, glutamine residues contain a carbonyl oxygen and a primary amine: The electron count of these two groups differs by just one electron and so they can be easily exchanged in a protein structure. Indeed, it may be impossible to decide which is which without additional evidence such as the interaction patterns the group forms. Similarly, water molecules can be erroneous; it is always worth understanding whether a water molecule is forming sensible interactions to the protein. For example, there have been cases in published structures where metallic ions such as sodium have been misinterpreted in binding sites as water molecules.
2. Unlike small molecule crystal structures, hydrogens are not generally resolved in protein crystal structures and are so placed at geometrically likely locations. This can lead to issues with tautomeric forms of side chains in protein residues that need careful resolution.
3. Side chains may be more labile than would be apparent from the input structure: the structural model will contain information such as occupancy factors and thermal parameters to inform the end user where this is the case, however such information can sometimes be lost to the end user: referring back to the original information is always worthwhile. In addition, note that there may be side chains in disordered states.
4. If possible, try to refer to the original crystallographic model files: they contain a lot of information, such as atomic occupancies, thermal parameters, or remarks regarding the approach taken to modeling structural data, that may not be apparent in your favorite modeling environment.
5. Remember that a crystal structure is not a model of an isolated protein, or even a whole protein. On occasion, neighboring crystallographically related molecules can interfere with the binding site and so can influence ligand binding, so it is worth ensuring that the structural model you are using is free from such issues. By that same token, it can often be difficult to crystallize a whole protein, so subunits are often crystallized individually. While these subunits are excellent guides for docking, do bear in mind that the structure can be impacted.

3.12.8.5 Incorporate What You Know

End users are often experts in a given target, or have access to experts on a given target, particularly in lead optimization. End users operating in pharmaceutical companies may have access to experimental information about a target from other sources beyond crystal structures. An example might be mutagenesis studies that inform the end user of the critical residues for substrate binding. Such information could be invaluable as it can inform the end user of key interacting residues within the binding site.

Most docking programs allow end users to incorporate prior information. Examples of such information might be to force a docking to form a particular interaction with the protein (e.g., a specific hydrogen bond) or forcing occupation of a particular part of the binding pocket. Some docking programs or protocols[38,124,125] can take advantage of known bound poses of ligands to bias docking toward related binding poses; in the case of lead optimization, such a docking approach can be useful in assessing the feasibility of functional change to a ligand as it forces docking to maintain the known binding mode of all ligands trialed, making the scores that result from docking more discriminating. On the downside this approach can bias against the identification of similar ligands that exhibit different binding modes.

3.12.8.6 Consider the Features That Are More Important to Your System, for Your Software

As we have explored above, docking software can vary substantially in its approach and strengths. Consider the biological system you are exploring, and prioritize docking features that are important to you. Below is a list of common features that could play important roles depending on your system.

Preparation
- Automatic assessment of ligand or receptor structure quality and indication of potential errors
- Automatic and intelligent protonation of protein and ligand
- 1D or 2D ligand conversion to 3D ligand

Docking
- Ability to treat ligand as flexible (via conformational database or creating conformers on the fly are popular routes). And do these mechanisms cover full conformational space?
- Receptor flexibility—popular mechanisms are via side-chain rotamer libraries, ensemble docking, and soft docking potentials
- Solvent handling—accounting for solvent displacement or water-mediated hydrogen bonding
- Ability to handle metal coordination
- Ensemble docking—often how protein flexibility is handled, also very useful for consensus crystal structures.
- Covalent docking
- Shape matching
- Pose refinement

- Ability to use crystallographic data as a docking guide
- Geometric or pharmacophore constraints
- Multiple scoring functions.

3.12.8.7 Do Not Over-Interpret Scores

All docking programs will generate a score for a given pose. An end user should regard their absolute values with caution, and avoid the tendency to rank values very close to each other in a strict hierarchy. This is particularly true when comparing scores between two different molecules which may have different molecular weights; each atom that is added to a structure increases the maximum theoretical score that a molecule could achieve. Indeed this effect is, to a certain extent, related to the ligand efficiency metric[126] which is used frequently in medicinal chemistry programs.

Given the observation that a relatively small change of interaction energy (1.4 kcal mol^{-1}) can lead to a 10-fold change in activity, one might expect relatively small score changes to be useful for predicting significant activity changes.

In practice though, for scoring functions, the above observation is a curse. Firstly, scores are built of compromises which make the score generated an approximation to either enthalpy or free energy. Secondly, the scores rarely account for uncertainty in the positions of atoms in the protein that remain fixed. Thirdly, it is possible that the docking program will find a local minimum close to the global minimum: while such a pose provides the end user with a lot of useful information and indeed may be a perfectly valid representation of the binding mode that a given ligand will adopt, it is eminently possible that its score will differ by a few score units from the true global minimum, which taken at face value would indicate a large change in binding affinity, but in practice is within the bounds of precision of the underlying algorithm.

An interesting question then is, "what should I use my result for in lead optimization?" Docking's main strength is in exploration of binding poses, and thus allows the end user to explore ligand structure-function, asking important questions beyond docking scores, which are all relative. For example:

- "What binding hypotheses are there for new ligand X?"
- "If I make chemical change 'X,' will I cause a significant change in the likely binding mode?"
- "If I make chemical change 'X,' will the new ligand occupy additional regions of my binding site?"
- "Can I improve the geometry of a specific interaction I observe by making a chemical change?"
- "Can I extend my ligand to form additional strong interactions to the binding site?"
- "How does the binding of my ligand differ between protein A and protein B?"
- "What is the preferred length of side chain Y in my series of analogs, based on predictive binding?"
- "Are there areas of potential positive interaction could be utilized by adding functionality to my ligand?"
- "Given the preferred binding motifs of my ligands, can I make structural changes to conformationally restrict them into preferred geometries?"

If one uses scores for direct affinity prediction, one needs to be fully aware of the level of approximation that is inherent in the score. These scores are, at best, relative to scores from the same run, under the same conditions, with the same system. The end user then should act accordingly and cautiously to avoid disappointment. However, as noted in examples above, the docking pose may be an acceptable starting point for rescoring using a higher level of theory. Similarly, if using a given method, understand its limitations (e.g., as earlier noted, ensemble docking minimizes the worst case outcome of docking rather than guaranteeing best possible performance).

3.12.8.8 Help! I am a Software Developer, How Do I Make My Users Love My Software?

Software developers want to see their programs used and loved. There are several things that the development community can do to achieve this goal. In considering software improvements one should discriminate between scientific improvements and the incorporation of existing technologies to improve usability. Obviously, new scientific breakthroughs, such as accurate affinity calculation or better treatment of protein flexibility, will increase the appeal of a developer's product. Fortunately, there are also plenty of available improvements that can leverage existing technology.

3.12.8.9 Make the Results Less Susceptible to the Input Provided

One constant frustration for end users is that results obtained with docking software can be adversely affected depending on the way in which inputs to the program are configured. For example, some sensitivity on the input provided has been shown in docking.[127] In another study, both GOLD and GLIDE were shown to have some dependence on input setup using different modeling environments.[128] Paradoxically, it appeared that GLIDE's performance was better with a setup protocol that used MOE, rather than the preparation tools provided with GLIDE. GOLD's scoring was shown to be improvable by using the score normalization factors in the docking to account for variations in molecular size. The authors of GLIDE have further studied the impact of preparation on their docking program and note the sorts of issues that can occur.[129]

In practical terms, users do not want to have to worry about such nuances, so ideally providers of software should try to improve the preparation and analysis tools to achieve optimal performance out of the box. For example, in most cases it would be simple to automate the preparation of the protonation states of ligand structures.

3.12.8.10 Make it Easy for Your End-Users to Become Experts

Software providers usually include tutorials, use case examples and documentation as part of a given docking package. Often this is accompanied by reference to published examples. Unfortunately this is hard for an end user to disentangle into principles of best practice.

Providers could improve the situation by providing more practical use case examples that reflect best practice and that highlight the pitfalls and issues that the end user needs to avoid in live use. In practice, the tutorials provided tend to "just work" and consequently become an exercise in handle turning, rather than truly educational.

Making the software easy to use is another way in which providers can improve an end user's lot. In development, fundamental "User eXperience (UX)" approaches should be adopted: the software should tackle the most common use cases easily and intuitively and avoid flooding the naive user with large numbers of options and settings (though these more advanced options should be easy to find, and intuitive when used.). Docking program developers are often scientists first, and software developers second. As scientists it is very easy to forget or down weigh the impact of these principles, as the fundamental science is the thing that a scientist finds most interesting, but in practice UX principles such as this can be the difference between great science being used or not.

3.12.8.11 Make Your Docking Software Self-Critical

A docking program generates one or more results for a given ligand. It is rare for the program to also generate a measure of confidence in its prediction. By way of example, a rule of thumb with the GOLD docking algorithm suggests that if the program repeatedly predicts the same pose, the pose is more likely to be similar to the truly observed pose. If GOLD predicts a wide range of poses with similar scores one has less confidence in the top ranked pose.

Such information could (and should) be more transparent to an end user. Ideally, a given docking would be accompanied by a confidence metric that would help the end user in result interpretation. Some effort is being made in this area. We note, for example, that the implementation of the HYDE score provided by BioSolveIT attempts to reduce the need for interpretation of scores by using visualization and color scales to present results in a more interpretable way.

3.12.9 Concluding Remarks

In being asked to review whether docking is a solved problem, we were presented with a challenge. The plethora of docking programs, approaches, and publications is, in a way, testament to the fact that the community clearly does not feel that docking is a solved problem, as this is an area of active research.

By reviewing the current state of the art, the deficiencies in current performance become very apparent. It may be a challenge too far to hope that any scoring method can achieve a level of predictive accuracy that would allow us to regard docking as solved, but we can at least see an active area of research and development and exciting changes which are leading to better systems year on year.

Acknowledgments

Colin Groom is thanked for careful reading of this manuscript.

References

1. Corey, E. J.; Czakó, B.; Kürti, L. *Molecules and Medicine;* John Wiley & Sons: Hoboken, NY, 2012.
2. Hardy, L. W.; Malikayil, A. The Impact of Structure-Guided Drug Design on Clinical Agents. *Curr. Drug Discov.* **2003,** *3,* 15–20.
3. Irwin, J. J.; Shoichet, B. K. Docking Screens for Novel Ligands Conferring New Biology. *J. Med. Chem.* **2016;** http://dx.doi.org/10.1021/acs.jmedchem.5b02008.
4. Davies, T. G.; Wixted, W. E.; Coyle, J. E.; Griffiths-Jones, C.; Hearn, K.; McMenamin, R.; Norton, D.; Rich, S. J.; Richardson, C.; Saxty, G.; Willems, H. M. G.; Woolford, A. J.-A.; Cottom, J. E.; Kou, J.-P.; Yonchuk, J. G.; Feldser, H. G.; Sanchez, Y.; Foley, J. P.; Bolognese, B. J.; Logan, G.; Podolin, P. L.; Yan, H.; Callahan, J. F.; Heightman, T. D.; Kerns, J. K. Monoacidic Inhibitors of the Kelch-Like ECH-Associated Protein 1: Nuclear Factor Erythroid 2-Related Factor 2 (KEAP1:NRF2) Protein–Protein Interaction With High Cell Potency Identified by Fragment-Based Discovery. *J. Med. Chem.* **2016,** *59,* 3991–4006. http://dx.doi.org/10.1021/acs.jmedchem.6b00228.
5. Ho, C. M. W.; Marshall, G. R. Cavity Search: An Algorithm for the Isolation and Display of Cavity-Like Binding Regions. *J. Comput. Aided Mol. Des.* **1990,** *4,* 337–354. http://dx.doi.org/10.1007/BF00117400.
6. Le Guilloux, V.; Schmidtke, P.; Tuffery, P. Fpocket: An Open Source Platform for Ligand Pocket Detection. *BMC Bioinformatics* **2009,** *10,* 168. http://dx.doi.org/10.1186/1471-2105-10-168.
7. Schmidtke, P.; Bidon-Chanal, A.; Luque, F. J.; Barril, X. MDpocket: Open-Source Cavity Detection and Characterization on Molecular Dynamics Trajectories. *Bioinformatics* **2011,** *27,* 3276–3285. http://dx.doi.org/10.1093/bioinformatics/btr550.

8. Yu, J.; Zhou, Y.; Tanaka, I.; Yao, M. Roll: A New Algorithm for the Detection of Protein Pockets and Cavities With a Rolling Probe Sphere. *Bioinformatics* **2010,** *26,* 46–52. http://dx.doi.org/10.1093/bioinformatics/btp599.
9. Oliveira, S. H.; Ferraz, F. A.; Honorato, R. V.; Xavier-Neto, J.; Sobreira, T. J.; de Oliveira, P. S. KVFinder: Steered Identification of Protein Cavities As a PyMOL Plugin. *BMC Bioinformatics* **2014,** *15,* 197. http://dx.doi.org/10.1186/1471-2105-15-197.
10. Whittington, D. A.; Waheed, A.; Ulmasov, B.; Shah, G. N.; Grubb, J. H.; Sly, W. S.; Christianson, D. W. Crystal Structure of the Dimeric Extracellular Domain of Human Carbonic Anhydrase XII, a Bitopic Membrane Protein Overexpressed in Certain Cancer Tumor Cells. *Proc. Natl. Acad. Sci.* **2001,** *98,* 9545–9550. http://dx.doi.org/10.1073/pnas.161301298.
11. Jones, G.; Willett, P.; Glen, R. C.; Leach, A. R.; Taylor, R. Development and Validation of a Genetic Algorithm for Flexible Docking. *J. Mol. Biol.* **1997,** *267,* 727–748. http://dx.doi.org/10.1006/jmbi.1996.0897.
12. McGann, M. FRED Pose Prediction and Virtual Screening Accuracy. *J. Chem. Inf. Model.* **2011,** *51,* 578–596. http://dx.doi.org/10.1021/ci100436p.
13. Hawkins, P. C. D.; Skillman, A. G.; Warren, G. L.; Ellingson, B. A.; Stahl, M. T. Conformer Generation With OMEGA: Algorithm and Validation Using High Quality Structures From the Protein Databank and Cambridge Structural Database. *J. Chem. Inf. Model.* **2010,** *50,* 572–584. http://dx.doi.org/10.1021/ci100031x.
14. Friesner, R. A.; Banks, J. L.; Murphy, R. B.; Halgren, T. A.; Klicic, J. J.; Mainz, D. T.; Repasky, M. P.; Knoll, E. H.; Shelley, M.; Perry, J. K.; Shaw, D. E.; Francis, P.; Shenkin, P. S. Glide: A New Approach for Rapid, Accurate Docking and Scoring. 1. Method and Assessment of Docking Accuracy. *J. Med. Chem.* **2004,** *47,* 1739–1749. http://dx.doi.org/10.1021/jm0306430.
15. Abagyan, R.; Totrov, M.; Kuznetsov, D. ICM—A New Method for Protein Modeling and Design: Applications to Docking and Structure Prediction From the Distorted Native Conformation. *J. Comput. Chem.* **1994,** *15,* 488–506. http://dx.doi.org/10.1002/jcc.540150503.
16. Morris, G. M.; Goodsell, D. S.; Halliday, R. S.; Huey, R.; Hart, W. E.; Belew, R. K.; Olson, A. J. Automated Docking Using a Lamarckian Genetic Algorithm and an Empirical Binding Free Energy Function. *J. Comput. Chem.* **1998,** *19,* 1639–1662. http://dx.doi.org/10.1002/(SICI)1096-987X(19981115)19:14<1639::AID-JCC10>3.0.CO;2-B.
17. Korb, O.; Stützle, T.; Exner, T. E. PLANTS: Application of Ant Colony Optimization to Structure-Based Drug Design. In *Ant Colony Optimization and Swarm Intelligence;* Dorigo, M., Gambardella, L. M., Birattari, M., Martinoli, A., Poli, R., Stützle, T., Eds.; Springer: Berlin, Heidelberg, 2006; pp 247–258 (accessed 12 April 2015).
18. Chen, H.-M.; Liu, B.-F.; Huang, H.-L.; Hwang, S.-F.; Ho, S.-Y. SODOCK: Swarm Optimization for Highly Flexible Protein–Ligand Docking. *J. Comput. Chem.* **2007,** *28,* 612–623. http://dx.doi.org/10.1002/jcc.20542.
19. Baxter, C. A.; Murray, C. W.; Clark, D. E.; Westhead, D. R.; Eldridge, M. D. Flexible Docking Using Tabu Search and an Empirical Estimate of Binding Affinity. *Proteins Struct. Funct. Bioinformatics* **1998,** *33,* 367–382. http://dx.doi.org/10.1002/(SICI)1097-0134(19981115)33:3<367::AID-PROT6>3.0.CO;2-W.
20. Rarey, M.; Kramer, B.; Lengauer, T.; Klebe, G. A Fast Flexible Docking Method Using an Incremental Construction Algorithm. *J. Mol. Biol.* **1996,** *261,* 470–489. http://dx.doi.org/10.1006/jmbi.1996.0477.
21. Ewing, T. J. A.; Kuntz, I. D. Critical Evaluation of Search Algorithms for Automated Molecular Docking and Database Screening. *J. Comput. Chem.* **1997,** *18,* 1175–1189. http://dx.doi.org/10.1002/(SICI)1096-987X(19970715)18:9<1175::AID-JCC6>3.0.CO;2-O.
22. Halgren, T. A.; Murphy, R. B.; Friesner, R. A.; Beard, H. S.; Frye, L. L.; Pollard, W. T.; Banks, J. L. Glide: A New Approach for Rapid, Accurate Docking and Scoring. 2. Enrichment Factors in Database Screening. *J. Med. Chem.* **2004,** *47,* 1750–1759. http://dx.doi.org/10.1021/jm030644s.
23. Rossi-Doria, O.; Sampels, M.; Birattari, M.; Chiarandini, M.; Dorigo, M.; Gambardella, L. M.; Knowles, J.; Manfrin, M.; Mastrolilli, M.; Paechter, B.; Paquete, L.; Stützle, T. A Comparison of the Performance of Different Metaheuristics on the Timetabling Problem. In *Practice and Theory of Automated Timetabling IV;* Burke, E., Causmaecker, P. D., Eds.; Springer: Berlin, Heidelberg, 2002; pp 329–351 (accessed 25 June 2016).
24. Korb, O.; Stützle, T.; Exner, T. E. Accelerating Molecular Docking Calculations Using Graphics Processing Units. *J. Chem. Inf. Model.* **2011,** *51,* 865–876. http://dx.doi.org/10.1021/ci100459b.
25. Korb, O.; Finn, P. W.; Jones, G. The Cloud and Other New Computational Methods to Improve Molecular Modelling. *Expert Opin. Drug Discov.* **2014,** *9,* 1121–1131. http://dx.doi.org/10.1517/17460441.2014.941800.
26. Mcmartin, C.; Bohacek, R. S. QXP: Powerful, Rapid Computer Algorithms for Structure-Based Drug Design. *J. Comput. Aided Mol. Des.* **1997,** *11,* 333–344. http://dx.doi.org/10.1023/A:1007907728892.
27. Brameld, K. A.; Kuhn, B.; Reuter, D. C.; Stahl, M. Small Molecule Conformational Preferences Derived From Crystal Structure Data. A Medicinal Chemistry Focused Analysis. *J. Chem. Inf. Model* **2008,** *48,* 1–24. http://dx.doi.org/10.1021/ci7002494.
28. Ouyang, X.; Zhou, S.; Su, C. T. T.; Ge, Z.; Li, R.; Kwoh, C. K. CovalentDock: Automated Covalent Docking With Parameterized Covalent Linkage Energy Estimation and Molecular Geometry Constraints. *J. Comput. Chem.* **2013,** *34,* 326–336. http://dx.doi.org/10.1002/jcc.23136.
29. Schröder, J.; Klinger, A.; Oellien, F.; Marhöfer, R. J.; Duszenko, M.; Selzer, P. M. Docking-Based Virtual Screening of Covalently Binding Ligands: An Orthogonal Lead Discovery Approach. *J. Med. Chem.* **2013,** *56,* 1478–1490. http://dx.doi.org/10.1021/jm3013932.
30. Jacobson, M. P.; Pincus, D. L.; Rapp, C. S.; Day, T. J. F.; Honig, B.; Shaw, D. E.; Friesner, R. A. A Hierarchical Approach to All-Atom Protein Loop Prediction. *Proteins Struct. Funct. Bioinformatics* **2004,** *55,* 351–367. http://dx.doi.org/10.1002/prot.10613.
31. Zhu, K.; Borrelli, K. W.; Greenwood, J. R.; Day, T.; Abel, R.; Farid, R. S.; Harder, E. Docking Covalent Inhibitors: A Parameter Free Approach to Pose Prediction and Scoring. *J. Chem. Inf. Model.* **2014,** *54,* 1932–1940. http://dx.doi.org/10.1021/ci500118s.
32. Koshland, D. Application of a Theory of Enzyme Specificity to Protein Synthesis. *Proc. Natl. Acad. Sci.* **1958,** *44,* 98–104.
33. Knegtel, R. M. A.; Kuntz, I. D.; Oshiro, C. M. Molecular Docking to Ensembles of Protein Structures. *J. Mol. Biol.* **1997,** *266,* 424–440. http://dx.doi.org/10.1006/jmbi.1996.0776.
34. Claußen, H.; Buning, C.; Rarey, M.; Lengauer, T. FlexE: Efficient Molecular Docking Considering Protein Structure Variations. *J. Mol. Biol.* **2001,** *308,* 377–395. http://dx.doi.org/10.1006/jmbi.2001.4551.
35. Korb, O.; Olsson, T. S. G.; Bowden, S. J.; Hall, R. J.; Verdonk, M. L.; Liebeschuetz, J. W.; Cole, J. C. Potential and Limitations of Ensemble Docking. *J. Chem. Inf. Model.* **2012,** *52,* 1262–1274. http://dx.doi.org/10.1021/ci2005934.
36. Corbeil, C. R.; Englebienne, P.; Moitessier, N. Docking Ligands Into Flexible and Solvated Macromolecules. 1. Development and Validation of FITTED 1.0. *J. Chem. Inf. Model.* **2007,** *47,* 435–449. http://dx.doi.org/10.1021/ci6002637.
37. Bottegoni, G.; Kufareva, I.; Totrov, M.; Abagyan, R. Four-Dimensional Docking: A Fast and Accurate Account of Discrete Receptor Flexibility in Ligand Docking. *J. Med. Chem.* **2009,** *52,* 397–406. http://dx.doi.org/10.1021/jm8009958.
38. Kelley, B. P.; Brown, S. P.; Warren, G. L.; Muchmore, S. W. POSIT: Flexible Shape-Guided Docking for Pose Prediction. *J. Chem. Inf. Model.* **2015,** *55,* 1771–1780. http://dx.doi.org/10.1021/acs.jcim.5b00142.
39. McGann, M. FRED and HYBRID Docking Performance on Standardized Datasets. *J. Comput. Aided Mol. Des.* **2012,** *26,* 897–906. http://dx.doi.org/10.1007/s10822-012-9584-8.
40. Sanders, B.; Korb, O.; Cole, J. C.; Essex, J. W. How to Pick a Winning Team: Assessment of Computationally Derived Protein Ensembles in Protein-Ligand Docking. *Abstr. Pap. Am. Chem. Soc.* **2012,** *244* (133-Comp).
41. Smieško, M. DOLINA—Docking Based on a Local Induced-Fit Algorithm: Application Toward Small-Molecule Binding to Nuclear Receptors. *J. Chem. Inf. Model.* **2013,** *53,* 1415–1423. http://dx.doi.org/10.1021/ci400098y.
42. Shin, W.-H.; Seok, C. GalaxyDock: Protein–Ligand Docking With Flexible Protein Side-Chains. *J. Chem. Inf. Model.* **2012,** *52,* 3225–3232. http://dx.doi.org/10.1021/ci300342z.
43. Gagnon, J. K.; Law, S. M.; Brooks, C. L. Flexible CDOCKER: Development and Application of a Pseudo-Explicit Structure-Based Docking Method Within CHARMM. *J. Comput. Chem.* **2015;** http://dx.doi.org/10.1002/jcc.24259. n/a-n/a.

44. Bolia, A.; Ozkan, S. B. Adaptive BP-Dock: An Induced Fit Docking Approach for Full Receptor Flexibility. *J. Chem. Inf. Model.* **2016;** http://dx.doi.org/10.1021/acs.jcim.5b00587.
45. Wagener, M.; Nabuurs, S.; de Vlieg, J. Fleksy: A Flexible Approach to Induced Fit Docking. *J. Cheminformatics* **2010,** *2,* O24. http://dx.doi.org/10.1186/1758-2946-2-S1-O24.
46. Cossins, B. P.; Hosseini, A.; Guallar, V. Exploration of Protein Conformational Change With PELE and Meta-Dynamics. *J. Chem. Theory Comput.* **2012,** *8,* 959–965. http://dx.doi.org/10.1021/ct200675g.
47. Yuriev, E.; Holien, J.; Ramsland, P. A. Improvements, Trends, and New Ideas in Molecular Docking: 2012–2013 in Review. *J. Mol. Recognit.* **2015,** *28,* 581–604. http://dx.doi.org/10.1002/jmr.2471.
48. Lemmon, G.; Meiler, J. Towards Ligand Docking Including Explicit Interface Water Molecules. *PLoS One* **2013,** *8,* e67536. http://dx.doi.org/10.1371/journal.pone.0067536.
49. Kumar, A.; Zhang, K. Y. J. Investigation on the Effect of Key Water Molecules on Docking Performance in CSARdock Exercise. *J. Chem. Inf. Model.* **2013,** *53,* 1880–1892. http://dx.doi.org/10.1021/ci400052w.
50. Sleigh, S. H.; Seavers, P. R.; Wilkinson, A. J.; Ladbury, J. E.; Tame, J. R. H. Crystallographic and Calorimetric Analysis of Peptide Binding to OppA Protein. *J. Mol. Biol.* **1999,** *291,* 393–415. http://dx.doi.org/10.1006/jmbi.1999.2929.
51. Rarey, M.; Kramer, B.; Lengauer, T. The Particle Concept: Placing Discrete Water Molecules During Protein-Ligand Docking Predictions. *Proteins Struct. Funct. Bioinformatics* **1999,** *34,* 17–28. http://dx.doi.org/10.1002/(SICI)1097-0134(19990101)34:1<17::AID-PROT3>3.0.CO;2-1.
52. Verdonk, M. L.; Chessari, G.; Cole, J. C.; Hartshorn, M. J.; Murray, C. W.; Nissink, J. W. M.; Taylor, R. D.; Taylor, R. Modeling Water Molecules in Protein – Ligand Docking Using GOLD. *J. Med. Chem.* **2005,** *48,* 6504–6515. http://dx.doi.org/10.1021/jm050543p.
53. Lie, M. A.; Thomsen, R.; Pedersen, C. N. S.; Schiøtt, B.; Christensen, M. H. Molecular Docking With Ligand Attached Water Molecules. *J. Chem. Inf. Model.* **2011,** *51,* 909–917. http://dx.doi.org/10.1021/ci100510m.
54. Murphy, R. B.; Repasky, M. P.; Greenwood, J. R.; Tubert-Brohman, I.; Jerome, S.; Annabhimoju, R.; Boyles, N. A.; Schmitz, C. D.; Abel, R.; Farid, R.; Friesner, R. A. WScore: A Flexible and Accurate Treatment of Explicit Water Molecules in Ligand-Receptor Docking. *J. Med. Chem.* **2016;** http://dx.doi.org/10.1021/acs.jmedchem.6b00131.
55. Young, T.; Abel, R.; Kim, B.; Berne, B. J.; Friesner, R. A. Motifs for Molecular Recognition Exploiting Hydrophobic Enclosure in Protein–Ligand Binding. *Proc. Natl. Acad. Sci.* **2007,** *104,* 808–813. http://dx.doi.org/10.1073/pnas.0610202104.
56. SZMAP, OpenEye Scientific Software, Santa Fe, NM., n.d. http://www.eyesopen.com (accessed 5 May 2017).
57. Bodnarchuk, M. S.; Viner, R.; Michel, J.; Essex, J. W. Strategies to Calculate Water Binding Free Energies in Protein–Ligand Complexes. *J. Chem. Inf. Model.* **2014;** http://dx.doi.org/10.1021/ci400674k.
58. Nikolić, D.; Blinov, N.; Wishart, D.; Kovalenko, A. 3D-RISM-Dock: A New Fragment-Based Drug Design Protocol. *J. Chem. Theory Comput.* **2012,** *8,* 3356–3372. http://dx.doi.org/10.1021/ct300257v.
59. Radoux, C. J.; Olsson, T. S. G.; Pitt, W. R.; Groom, C. R.; Blundell, T. L. Identifying Interactions That Determine Fragment Binding at Protein Hotspots. *J. Med. Chem.* **2016;** http://dx.doi.org/10.1021/acs.jmedchem.5b01980.
60. Mandl, F. *Statistical Physics;* John Wiley & Sons: New York, NY, 2013.
61. Atkins, P.; de Paula, J. *Atkins' Physical Chemistry;* OUP: Oxford, 2014.
62. Gilson, M. K.; Given, J. A.; Bush, B. L.; McCammon, J. A. The Statistical-Thermodynamic Basis for Computation of Binding Affinities: A Critical Review. *Biophys. J.* **1997,** *72,* 1047–1069.
63. Beveridge, D. L.; DiCapua, F. M. Free Energy Via Molecular Simulation: Applications to Chemical and Biomolecular Systems. *Annu. Rev. Biophys. Biophys. Chem.* **1989,** *18,* 431–492. http://dx.doi.org/10.1146/annurev.bb.18.060189.002243.
64. Leach, A. R. *Molecular Modelling: Principles and Applications;* Prentice Hall: Upper Saddle River, NI, 2001.
65. Ajay, M. A. Murcko, Computational Methods to Predict Binding Free Energy in Ligand-Receptor Complexes. *J. Med. Chem.* **1995,** *38,* 4953–4967. http://dx.doi.org/10.1021/jm00026a001.
66. Zhong, S.; Zhang, Y.; Xiu, Z. Rescoring Ligand Docking Poses. *Curr. Opin. Drug Discov. Devel.* **2010,** *13,* 326–334.
67. Skyner, R. E.; McDonagh, J. L.; Groom, C. R.; van Mourik, T.; Mitchell, J. B. O. A Review of Methods for the Calculation of Solution Free Energies and the Modelling of Systems in Solution. *Phys. Chem. Chem. Phys.* **2015,** *17,* 6174–6191. http://dx.doi.org/10.1039/C5CP00288E.
68. Still, W. C.; Tempczyk, A.; Hawley, R. C.; Hendrickson, T. Semianalytical Treatment of Solvation for Molecular Mechanics and Dynamics. *J. Am. Chem. Soc.* **1990,** *112,* 6127–6129. http://dx.doi.org/10.1021/ja00172a038.
69. Honig, B.; Nicholls, A. Classical Electrostatics in Biology and Chemistry. *Science* **1995,** *268,* 1144–1149.
70. Greenidge, P. A.; Kramer, C.; Mozziconacci, J.-C.; Sherman, W. Improving Docking Results via Reranking of Ensembles of Ligand Poses in Multiple X-ray Protein Conformations With MM-GBSA. *J. Chem. Inf. Model.* **2014,** *54,* 2697–2717. http://dx.doi.org/10.1021/ci5003735.
71. Zwanzig, R. W. High-Temperature Equation of State by a Perturbation Method. I. Nonpolar Gases. *J. Chem. Phys.* **1954,** *22,* 1420–1426. http://dx.doi.org/10.1063/1.1740409.
72. Kirkwood, J. G. Statistical Mechanics of Fluid Mixtures. *J. Chem. Phys.* **1935,** *3,* 300–313. http://dx.doi.org/10.1063/1.1749657.
73. Lu, N.; Kofke, D. A.; Woolf, T. B. Improving the Efficiency and Reliability of Free Energy Perturbation Calculations Using Overlap Sampling Methods. *J. Comput. Chem.* **2004,** *25,* 28–40. http://dx.doi.org/10.1002/jcc.10369.
74. Binkowski, T. A.; Jiang, W.; Roux, B.; Anderson, W. F.; Joachimiak, A. Virtual High-Throughput Ligand Screening. *Methods Mol. Biol. Clifton NJ* **2014,** *1140,* 251–261. http://dx.doi.org/10.1007/978-1-4939-0354-2_19.
75. Sippl, M. J.; Ortner, M.; Jaritz, M.; Lackner, P.; Flöckner, H. Helmholtz Free Energies of Atom Pair Interactions in Proteins. *Fold. Des.* **1996,** *1,* 289–298. http://dx.doi.org/10.1016/S1359-0278(96)00042-9.
76. Muegge, I. A Knowledge-Based Scoring Function for Protein-Ligand Interactions: Probing the Reference State. In *Virtual Screening: An Alternative or Complement. To High Throughput Screening;* Klebe, G., Ed.; Springer: Netherlands, 2000; pp 99–114 (accessed 12 April 2015).
77. Korb, O.; Stützle, T.; Exner, T. E. Empirical Scoring Functions for Advanced Protein – Ligand Docking With PLANTS. *J. Chem. Inf. Model.* **2009,** *49,* 84–96. http://dx.doi.org/10.1021/ci800298z.
78. Jones, G.; Willett, P.; Glen, R. C.; Leach, A. R.; Taylor, R. Development and Validation of a Genetic Algorithm for Flexible Docking. *J. Mol. Biol.* **1997,** *267,* 727–748. http://dx.doi.org/10.1006/jmbi.1996.0897.
79. Rognan, D.; Lauemøller, S. L.; Holm, A.; Buus, S.; Tschinke, V. Predicting Binding Affinities of Protein Ligands From Three-Dimensional Models: Application to Peptide Binding to Class I Major Histocompatibility Proteins. *J. Med. Chem.* **1999,** *42,* 4650–4658. http://dx.doi.org/10.1021/jm9910775.
80. Muegge, I.; Martin, Y. C. A General and Fast Scoring Function for Protein – Ligand Interactions: A Simplified Potential Approach. *J. Med. Chem.* **1999,** *42,* 791–804. http://dx.doi.org/10.1021/jm980536j.
81. Mooij, W. T. M.; Verdonk, M. L. General and Targeted Statistical Potentials for Protein–Ligand Interactions. *Proteins Struct. Funct. Bioinformatics* **2005,** *61,* 272–287. http://dx.doi.org/10.1002/prot.20588.
82. Gohlke, H.; Hendlich, M.; Klebe, G. Knowledge-Based Scoring Function to Predict Protein-Ligand Interactions. *J. Mol. Biol.* **2000,** *295,* 337–356. http://dx.doi.org/10.1006/jmbi.1999.3371.
83. Berman, H. M.; Westbrook, J.; Feng, Z.; Gilliland, G.; Bhat, T. N.; Weissig, H.; Shindyalov, I. N.; Bourne, P. E. The Protein Data Bank. *Nucleic Acids Res.* **2000,** *28,* 235–242.
84. Groom, C. R.; Bruno, I. J.; Lightfoot, M. P.; Ward, S. C. The Cambridge Structural Database. *Acta Crystallogr. Sect. B: Struct. Sci. Cryst. Eng. Mater.* **2016,** *72,* 171–179. http://dx.doi.org/10.1107/S2052520616003954.

85. Schneider, N.; Lange, G.; Hindle, S.; Klein, R.; Rarey, M. A Consistent Description of HYdrogen Bond and DEhydration Energies in Protein–Ligand Complexes: Methods Behind the HYDE Scoring Function. *J. Comput. Aided Mol. Des.* **2012,** *27,* 15–29. http://dx.doi.org/10.1007/s10822-012-9626-2.
86. Sun, H.; Li, Y.; Shen, M.; Tian, S.; Xu, L.; Pan, P.; Guan, Y.; Hou, T. Assessing the Performance of MM/PBSA and MM/GBSA Methods. 5. Improved Docking Performance Using High Solute Dielectric Constant MM/GBSA and MM/PBSA Rescoring. *Phys. Chem. Chem. Phys.* **2014,** *16,* 22035–22045. http://dx.doi.org/10.1039/C4CP03179B.
87. Graves, A. P.; Shivakumar, D. M.; Boyce, S. E.; Jacobson, M. P.; Case, D. A.; Shoichet, B. K. Rescoring Docking Hit Lists for Model Cavity Sites: Predictions and Experimental Testing. *J. Mol. Biol.* **2008,** *377,* 914–934. http://dx.doi.org/10.1016/j.jmb.2008.01.049.
88. Warren, G. L. Special Issue: A Snapshot in Time: Docking Challenge. *J. Comput. Aided Mol. Des.* **2012,** *26,* 675–799.
89. Cheng, T.; Li, X.; Li, Y.; Liu, Z.; Wang, R. Comparative Assessment of Scoring Functions on a Diverse Test Set. *J. Chem. Inf. Model.* **2009,** *49,* 1079–1093. http://dx.doi.org/10.1021/ci9000053.
90. Li, Y.; Han, L.; Liu, Z.; Wang, R. Comparative Assessment of Scoring Functions on an Updated Benchmark: 2. Evaluation Methods and General Results. *J. Chem. Inf. Model.* **2014,** *54,* 1717–1736. http://dx.doi.org/10.1021/ci500081m.
91. Wang, R.; Lai, L.; Wang, S. Further Development and Validation of Empirical Scoring Functions for Structure-Based Binding Affinity Prediction. *J. Comput. Aided Mol. Des.* **2002,** *16,* 11–26.
92. Bissantz, C.; Folkers, G.; Rognan, D. Protein-Based Virtual Screening of Chemical Databases. 1. Evaluation of Different Docking/Scoring Combinations. *J. Med. Chem.* **2000,** *43,* 4759–4767. http://dx.doi.org/10.1021/jm001044l.
93. Stahl, M.; Rarey, M. Detailed Analysis of Scoring Functions for Virtual Screening. *J. Med. Chem.* **2001,** *44,* 1035–1042. http://dx.doi.org/10.1021/jm0003992.
94. Bursulaya, B. D.; Totrov, M.; Abagyan, R.; Brooks, C. L. Comparative Study of Several Algorithms for Flexible Ligand Docking. *J. Comput. Aided Mol. Des.* **2003,** *17,* 755–763.
95. Wang, R.; Lu, Y.; Wang, S. Comparative Evaluation of 11 Scoring Functions for Molecular Docking. *J. Med. Chem.* **2003,** *46,* 2287–2303. http://dx.doi.org/10.1021/jm0203783.
96. Wang, R.; Fang, X.; Lu, Y.; Wang, S. The PDBbind Database: Collection of Binding Affinities for Protein − Ligand Complexes With Known Three-Dimensional Structures. *J. Med. Chem.* **2004,** *47,* 2977–2980. http://dx.doi.org/10.1021/jm030580l.
97. Wang, R.; Lu, Y.; Fang, X.; Wang, S. An Extensive Test of 14 Scoring Functions Using the PDBbind Refined Set of 800 Protein − Ligand Complexes. *J. Chem. Inf. Comput. Sci.* **2004,** *44,* 2114–2125. http://dx.doi.org/10.1021/ci049733j.
98. Xing, L.; Hodgkin, E.; Liu, Q.; Sedlock, D. Evaluation and Application of Multiple Scoring Functions for a Virtual Screening Experiment. *J. Comput. Aided Mol. Des.* **2004,** *18,* 333–344. http://dx.doi.org/10.1023/B:JCAM.0000047812.39758.ab.
99. Perola, E.; Walters, W. P.; Charifson, P. S. A Detailed Comparison of Current Docking and Scoring Methods on Systems of Pharmaceutical Relevance. *Proteins Struct. Funct. Bioinformatics* **2004,** *56,* 235–249. http://dx.doi.org/10.1002/prot.20088.
100. Kellenberger, E.; Rodrigo, J.; Muller, P.; Rognan, D. Comparative Evaluation of Eight Docking Tools for Docking and Virtual Screening Accuracy. *Proteins Struct. Funct. Bioinformatics* **2004,** *57,* 225–242. http://dx.doi.org/10.1002/prot.20149.
101. Kontoyianni, M.; McClellan, L. M.; Sokol, G. S. Evaluation of Docking Performance: Comparative Data on Docking Algorithms. *J. Med. Chem.* **2004,** *47,* 558–565. http://dx.doi.org/10.1021/jm0302997.
102. Hu, X.; Balaz, S.; Shelver, W. H. A Practical Approach to Docking of Zinc Metalloproteinase Inhibitors. *J. Mol. Graph. Model.* **2004,** *22,* 293–307. http://dx.doi.org/10.1016/j.jmgm.2003.11.002.
103. Ferrara, P.; Gohlke, H.; Price, D. J.; Klebe, G.; Brooks, C. L. Assessing Scoring Functions for Protein − Ligand Interactions. *J. Med. Chem.* **2004,** *47,* 3032–3047. http://dx.doi.org/10.1021/jm030489h.
104. Marsden, P. M.; Puvanendrampillai, D.; Mitchell, J. B. O.; Glen, R. C. Predicting Protein–Ligand Binding Affinities: A Low Scoring Game? *Org. Biomol. Chem.* **2004,** *2,* 3267–3273 http://dx.doi.org/10.1039/B409570G.
105. Kontoyianni, M.; Sokol, G. S.; MCclellan, L. M. Evaluation of Library Ranking Efficacy in Virtual Screening. *J. Comput. Chem.* **2005,** *26,* 11–22. http://dx.doi.org/10.1002/jcc.20141.
106. Cummings, M. D.; DesJarlais, R. L.; Gibbs, A. C.; Mohan, V.; Jaeger, E. P. Comparison of Automated Docking Programs As Virtual Screening Tools. *J. Med. Chem.* **2005,** *48,* 962–976. http://dx.doi.org/10.1021/jm049798d.
107. Chen, H.; Lyne, P. D.; Giordanetto, F.; Lovell, T.; Li, J. On Evaluating Molecular-Docking Methods for Pose Prediction and Enrichment Factors. *J. Chem. Inf. Model.* **2006,** *46,* 401–415. http://dx.doi.org/10.1021/ci0503255.
108. Warren, G. L.; Andrews, C. W.; Capelli, A.-M.; Clarke, B.; LaLonde, J.; Lambert, M. H.; Lindvall, M.; Nevins, N.; Semus, S. F.; Senger, S.; Tedesco, G.; Wall, I. D.; Woolven, J. M.; Peishoff, C. E.; Head, M. S. A Critical Assessment of Docking Programs and Scoring Functions. *J. Med. Chem.* **2006,** *49,* 5912–5931. http://dx.doi.org/10.1021/jm050362n.
109. Zhou, Z.; Felts, A. K.; Friesner, R. A.; Levy, R. M. Comparative Performance of Several Flexible Docking Programs and Scoring Functions: Enrichment Studies for a Diverse Set of Pharmaceutically Relevant Targets. *J. Chem. Inf. Model.* **2007,** *47,* 1599–1608. http://dx.doi.org/10.1021/ci7000346.
110. Cross, J. B.; Thompson, D. C.; Rai, B. K.; Baber, J. C.; Fan, K. Y.; Hu, Y.; Humblet, C. Comparison of Several Molecular Docking Programs: Pose Prediction and Virtual Screening Accuracy. *J. Chem. Inf. Model.* **2009,** *49,* 1455–1474. http://dx.doi.org/10.1021/ci900056c.
111. Huang, N.; Shoichet, B. K.; Irwin, J. J. Benchmarking Sets for Molecular Docking. *J. Med. Chem.* **2006,** *49,* 6789–6801. http://dx.doi.org/10.1021/jm0608356.
112. Smith, R. D.; Dunbar, J. B.; Ung, P. M.-U.; Esposito, E. X.; Yang, C.-Y.; Wang, S.; Carlson, H. A. CSAR Benchmark Exercise of 2010: Combined Evaluation Across All Submitted Scoring Functions. *J. Chem. Inf. Model.* **2011,** *51,* 2115–2131. http://dx.doi.org/10.1021/ci200269q.
113. Damm-Ganamet, K. L.; Smith, R. D.; Dunbar, J. B.; Stuckey, J. A.; Carlson, H. A. CSAR Benchmark Exercise 2011–2012: Evaluation of Results From Docking and Relative Ranking of Blinded Congeneric Series. *J. Chem. Inf. Model.* **2013,** *53,* 1853–1870. http://dx.doi.org/10.1021/ci400025f.
114. Dunbar, J. B.; Smith, R. D.; Damm-Ganamet, K. L.; Ahmed, A.; Esposito, E. X.; Delproposto, J.; Chinnaswamy, K.; Kang, Y.-N.; Kubish, G.; Gestwicki, J. E.; Stuckey, J. A.; Carlson, H. A. CSAR Data Set Release 2012: Ligands, Affinities, Complexes, and Docking Decoys. *J. Chem. Inf. Model.* **2013,** *53,* 1842–1852. http://dx.doi.org/10.1021/ci4000486.
115. Li, Y.; Liu, Z.; Li, J.; Han, L.; Liu, J.; Zhao, Z.; Wang, R. Comparative Assessment of Scoring Functions on an Updated Benchmark: 1. Compilation of the Test Set. *J. Chem. Inf. Model.* **2014,** *54,* 1700–1716. http://dx.doi.org/10.1021/ci500080q.
116. Smith, R. D.; Damm-Ganamet, K. L.; Dunbar, J. B.; Ahmed, A.; Chinnaswamy, K.; Delproposto, J. E.; Kubish, G. M.; Tinberg, C. E.; Khare, S. D.; Dou, J.; Doyle, L.; Stuckey, J. A.; Baker, D.; Carlson, H. A. CSAR Benchmark Exercise 2013: Evaluation of Results From a Combined Computational Protein Design, Docking, and Scoring/Ranking Challenge. *J. Chem. Inf. Model.* **2015;** http://dx.doi.org/10.1021/acs.jcim.5b00387.
117. Carlson, H. A.; Smith, R. D.; Damm-Ganamet, K. L.; Stuckey, J. A.; Ahmed, A.; Convery, M. A.; Somers, D. O.; Kranz, M.; Elkins, P. A.; Cui, G.; Peishoff, C. E.; Lambert, M. H.; Dunbar, J. B. CSAR 2014: A Benchmark Exercise Using Unpublished Data From Pharma. *J. Chem. Inf. Model.* **2016;** http://dx.doi.org/10.1021/acs.jcim.5b00523.
118. McGaughey, G. B.; Sheridan, R. P.; Bayly, C. I.; Culberson, J. C.; Kreatsoulas, C.; Lindsley, S.; Maiorov, V.; Truchon, J.-F.; Cornell, W. D. Comparison of Topological, Shape, and Docking Methods in Virtual Screening. *J. Chem. Inf. Model.* **2007,** *47,* 1504–1519. http://dx.doi.org/10.1021/ci700052x.
119. Cole, J. C.; Murray, C. W.; Nissink, J. W. M.; Taylor, R. D.; Taylor, R. Comparing Protein–Ligand Docking Programs Is Difficult. *Proteins Struct. Funct. Bioinformatics* **2005,** *60,* 325–332. http://dx.doi.org/10.1002/prot.20497.
120. Fernández-Recio, J.; Sternberg, M. J. E. The 4th Meeting on the Critical Assessment of Predicted Interaction (CAPRI) Held at the Mare Nostrum, Barcelona. *Proteins Struct. Funct. Bioinformatics* **2010,** *78,* 3065–3066. http://dx.doi.org/10.1002/prot.22801.

121. Korb, O.; Wood, P. A. Prediction of Framework–Guest Systems Using Molecular Docking. *Chem. Commun.* **2010,** *46,* 3318–3320. http://dx.doi.org/10.1039/C003080E.
122. Coveney, P. V.; Davey, R.; Griffin, J. L. W.; He, Y.; Hamlin, J. D.; Stackhouse, S.; Whiting, A. A New Design Strategy for Molecular Recognition in Heterogeneous Systems: A Universal Crystal-Face Growth Inhibitor for Barium Sulfate. *J. Am. Chem. Soc.* **2000,** *122,* 11557–11558. http://dx.doi.org/10.1021/ja990885i.
123. Warren, G. L.; Do, T. D.; Kelley, B. P.; Nicholls, A.; Warren, S. D. Essential Considerations for Using Protein–Ligand Structures in Drug Discovery. *Drug Discov. Today* **2012,** *17,* 1270–1281. http://dx.doi.org/10.1016/j.drudis.2012.06.011.
124. Fradera, X.; Knegtel, R. M. A.; Mestres, J. Similarity-Driven Flexible Ligand Docking. *Proteins Struct. Funct. Bioinformatics* **2000,** *40,* 623–636. http://dx.doi.org/10.1002/1097-0134(20000901)40:4<623::AID-PROT70>3.0.CO;2-I.
125. Cole, J. C. Onward Development of GOLD—Selective Dockings Using Known Protein Properties. In *EuroQSAR 2002: Designing Drugs and Crop Protectants: Processes, Problems and Solutions;* Ford, M. G., Livingstone, D., Dearden, J., Van de Waterbeemd, H., Eds.; Blackwell Science Inc: Bournemouth, UK, 2003.
126. Hopkins, A. L.; Groom, C. R.; Alex, A. Ligand Efficiency: A Useful Metric for Lead Selection. *Drug Discov. Today* **2004,** *9,* 430–431. http://dx.doi.org/10.1016/S1359-6446(04)03069-7.
127. Feher, M.; Williams, C. I. Numerical Errors and Chaotic Behavior in Docking Simulations. *J. Chem. Inf. Model.* **2012,** *52,* 724–738. http://dx.doi.org/10.1021/ci200598m.
128. Ibrahim, T. M.; Bauer, M. R.; Boeckler, F. M. Applying DEKOIS 2.0 in Structure-Based Virtual Screening to Probe the Impact of Preparation Procedures and Score Normalization. *J. Cheminformatics* **2015,** *7.* http://dx.doi.org/10.1186/s13321-015-0074-6.
129. Sastry, G. M.; Adzhigirey, M.; Day, T.; Annabhimoju, R.; Sherman, W. Protein and Ligand Preparation: Parameters, Protocols, and Influence on Virtual Screening Enrichments. *J. Comput. Aided Mol. Des.* **2013,** *27,* 221–234. http://dx.doi.org/10.1007/s10822-013-9644-8.

3.13 Modeling Protein Flexibility in Molecular Docking

C Yan and X Zou, University of Missouri, Columbia, MO, United States

© 2017 Elsevier Ltd. All rights reserved.

3.13.1	**Introduction**	319
3.13.2	**Models for the Mechanisms of Protein Binding**	319
3.13.3	**Computational Modeling of Protein–Ligand Interactions and Protein–Protein Interactions**	321
3.13.4	**Modeling Protein Flexibility in Molecular Docking**	321
3.13.4.1	Soft Docking	322
3.13.4.2	Induced-fit Docking	322
3.13.4.3	Ensemble Docking	322
3.13.4.3.1	Preparing the protein structural ensemble	322
3.13.4.3.2	Molecular docking against a structural ensemble	323
3.13.5	**Modeling Protein Flexibility in the Postdocking Stage**	324
3.13.6	**Modeling Peptide Flexibility in Protein–Peptide Docking**	325
3.13.7	**Conclusion**	326
Acknowledgment		326
References		327

3.13.1 Introduction

Proteins are flexible entities, which often undergo conformational changes when associating with other molecules such as small compounds or macromolecules. The flexibility of a protein is highly related to its intrinsic dynamics, i.e., the thermal fluctuation of a protein structure in cellular environment, which occurs on a broad range of time scales (*ps* to *s*) with varying amplitudes, including simple side chain motions, backbone motions, major domain rearrangements, partial refolding or unfolding, and even disorder-to-order transition (see **Fig. 1**).[1] Experiments such as NMR spectroscopy and biological small-angle scattering illustrate that a protein should be considered by a dynamic ensemble rather than a static entity, with a unique structure.[2–5] The nonstatic nature of protein plays an essential role in carrying out its functions.[6–8] Because of its dynamic characteristics, a protein is able to adapt its conformation to respond to the presence of other molecules and the environmental changes, which is crucial for many cellular processes such as signal transduction, immune response, and enzyme catalysis. For example, allosteric regulation is often a result of the protein conformational change caused by the effector's binding at a site (allosteric site), other than the enzyme's active site.[9] Modern theories of molecular recognition consider the protein binding as a process which couples the conformational-selection and induced-fit rather than a shape complementarity-based lock-and-key recognition process, which will be described in detail in the next section.[10]

3.13.2 Models for the Mechanisms of Protein Binding

The lock-and-key model is the earliest and also the simplest model to explain molecular recognition in enzyme actions. It was first proposed by Fischer in 1894.[11] The lock-and-key model assumes that the enzyme (lock) recognizes the substrate (key) through the shape complementarity between the enzyme's active site and the substrate. This model is insightful, but too simple to reflect the reality. In general, both the enzyme (i.e., a protein) and the substrate (e.g., a small compound or a protein) are dynamic entities as revealed by many experiments.[12] The comparison between the structures of a protein in complexes (i.e., holo structures) and unbound protein structures (i.e., apo structures) demonstrates that the protein often undergoes certain conformational changes when forming the complex structure with its binding partner.[13] The induced-fit model was first proposed by Koshland in 1958 to explain the protein conformational changes in the binding process.[14] This model suggests that an enzyme, when binding with its substrate, optimizes the interface through physical interactions to form the final complex structure. The induced-fit model is supported by the fact that many ligands are buried in the protein binding sites in the protein–ligand complex structures in the Protein Data Bank (PDB),[15] which suggests that these ligands may very probably be wrapped around by the binding-site residues after the initial binding event.[16] However, conformational changes such as backbone collective motions, domain rearrangements, and disorder-to-order transition for highly flexible proteins cannot be fully explained by this model.[9] In the late 1990s, the conformational-selection (population shift) model was proposed by several researchers.[17–19] The conformational-selection model suggests that the unbound protein receptor fluctuates among multiple conformational states, with their occupancy probabilities being determined by their relative free energies according to the Boltzmann distribution. Only a subset of these states allows the binding of its partner. The encounter with its binding partner shifts the distribution toward these states to form the final complex structure. The main difference between the induced-fit model and the conformational-selection model is whether the holo structure preexists before forming the complex. A schematic illustration of the three binding models is provided in **Fig. 2**.

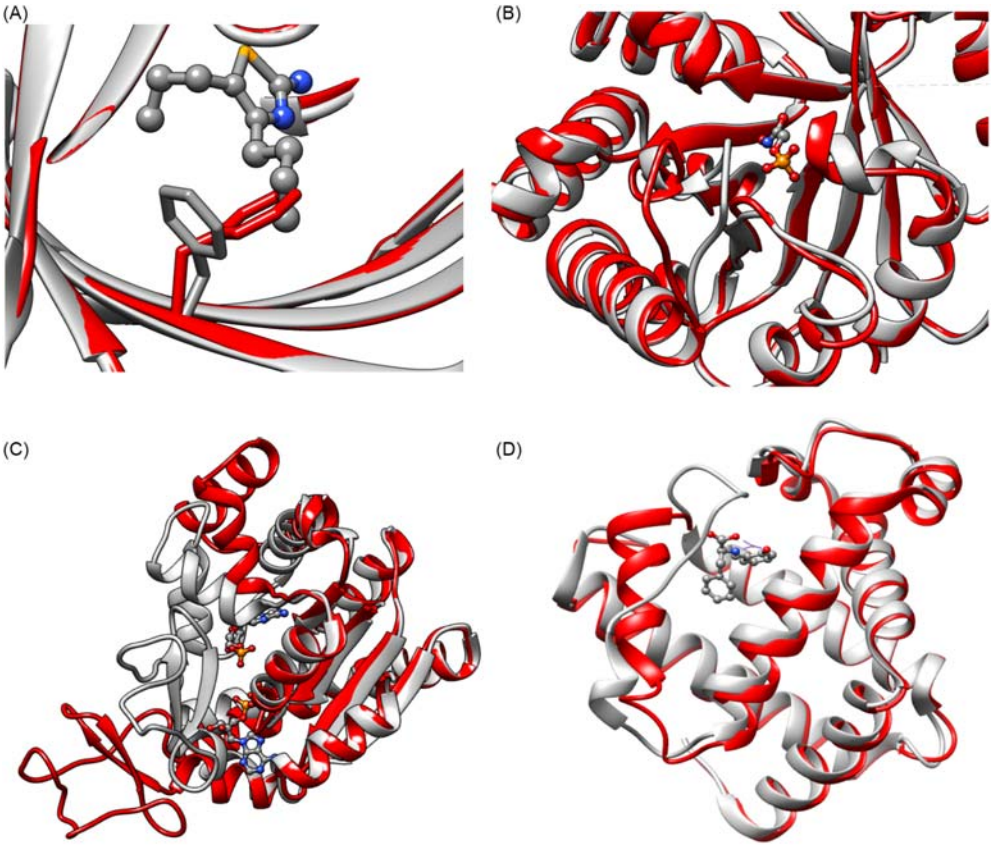

Fig. 1 Four examples of protein conformational changes in ligand binding, which represent four typical protein structural motions, respectively. (A) Protein side chain motions, (B) protein backbone motions, (C) protein domain motions, and (D) protein partial unfolding. For each case, the unbound protein structure is colored *red*, the bound protein structure in the complex is colored gray, and the ligand structure in the complex is colored by atom types. The unbound protein structure is superimposed on the bound protein structure.

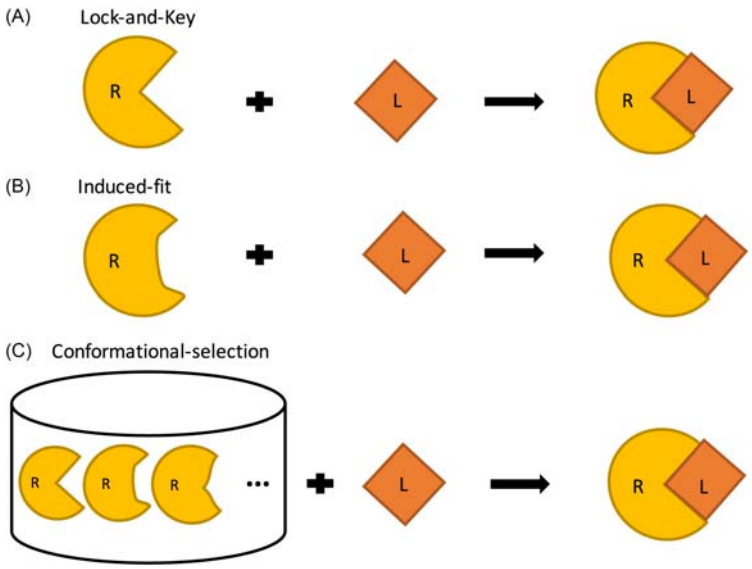

Fig. 2 Schematic diagrams for the three binding models. (A) The lock-and-key model, (B) induced-fit model, and (C) conformational-selection model.

Recent studies suggest that induced-fit and conformational-selection may co-exist in many cases.[20,21] Efforts were devoted to reconciling these two models into a unified model by coupling the induced-fit and the conformational-selection in a "serial" or "parallel" way.[1,22–25] In the serial coupling scenario, multiple protein conformations preexist in the unbound state, and the ligand recognizes a subset of these conformations to first reach a loose complex state, which is followed by the induced optimization to form the final complex structure. The parallel coupling provides a different scenario, for which the induced-fit pathway and the conformational-selection pathway co-exist and compete with each other. The fluxes of the two pathways determine the relative importance of the two mechanisms, which is often influenced by the concentration of the binding partner.

3.13.3 Computational Modeling of Protein–Ligand Interactions and Protein–Protein Interactions

Computational modeling of protein–ligand interactions and protein–protein interactions has great applications for mechanistic investigation of binding processes and also for the development of therapeutical interventions. Molecular dynamics (MD) simulation and molecular docking are two major computational methods to model bindings between molecules. MD simulation simulates the binding process using a physically based force field with explicit solvent models or implicit solvent models through integrating the equations of motion.[26–28] MD simulation simultaneously considers protein flexibility, ligand flexibility, solvent effect, and other environmental factors. The binding dynamics can also be obtained from MD trajectories. However, MD simulation is computationally demanding, which hinders large-scale applications, and simulating the whole binding process from scratch is only limited to several special cases.[29–31] In fact, MD simulation is often used for protein flexibility analysis before molecular docking, or it is used for refining the promising binding modes from molecular docking.

Molecular docking aims to predict the binding mode and binding affinity by employing efficient sampling algorithms and simplified scoring functions.[32–39] Molecular docking is much more efficient than MD simulation. However, the binding dynamics cannot be obtained from the results of molecular docking. A typical molecular docking method generally consists of two major stages, the sampling stage and the scoring stage. In the sampling stage, putative binding modes are generated using efficient searching algorithms. In the scoring stage, the sampled binding modes are scored with scoring functions; the binding modes associated with the lowest energy scores are predicted to be the binding modes, and the corresponding energy scores are used to evaluate the binding tightnesses.

There are two classes of molecular docking techniques depending on the molecular types: protein–ligand docking and protein–protein docking. Protein–ligand docking aims to model the interaction between a protein and a small compound, but protein–protein docking is developed for predicting interactions between two proteins. In protein–ligand docking, generally the ligand conformational space is exhaustively explored, but the protein structure is fixed or largely restricted. In protein–protein docking, both protein partners are fixed or largely restricted, and the shape complementarity between the interacting proteins plays the dominant role in the binding pose generation. Moreover, small compounds often bind to a pocket on the protein surface (often the largest pocket), and thus sampling during protein–ligand docking is often restricted to a specific binding pocket, whereas protein–protein docking often requires global sampling. After decades of development, molecular docking methods have achieved great successes and have played an important role in structure-based drug design (SBDD). For example, protein–ligand docking is widely used for initial-stage screening of huge chemical libraries for drug candidates, and protein–protein docking is often integrated with experiments for protein–protein interaction prediction and protein interface design.[40,41]

Despite numerous successes, incorrect predictions are often produced by molecular docking. One of the greatest challenges that limits the performance of molecular docking is the modeling of protein flexibility. Because the holo structure of a protein bound with a specific binding partner is generally unavailable, often the apo structure, the protein structure from a different complex or even the computational modeled protein structure, which often shows certain structural variations in comparison with the holo structure, is used in molecular docking. These structural variations, particularly the structural variations in the binding site, often exclude the generation of correct binding modes in the sampling stage of molecular docking. Properly modeling the protein flexibility is of great importance for improving the docking accuracy. In the next section, we review the methods to model protein flexibility in molecular docking.

3.13.4 Modeling Protein Flexibility in Molecular Docking

Although protein–ligand docking and protein–protein docking are quite different in the sampling stage, the methods to model protein flexibility in both protein–protein docking and protein–ligand docking can be classified into three groups: soft docking, induced-fit docking, and ensemble docking.[42–45] In soft docking, the protein flexibility is implicitly considered by allowing minor overlaps between atoms through the employment of soft molecular surface representation or soft interaction potentials. In induced-fit docking, the protein structural motions are sampled on the fly in the sampling stage of molecular docking. In ensemble docking, the protein structural motions are represented by a structural ensemble, which contains multiple protein conformations. The optimal protein conformation is automatically selected in the molecular docking (except for the united structure-based ensemble docking). To some extent, induced-fit docking can be considered as a class of methods inspired by the induced-fit model, and ensemble docking can be considered as a class of methods inspired by the conformational-selection model. Many docking programs integrated two or even all the three methods.

3.13.4.1 Soft Docking

Instead of explicitly modeling the protein conformational change in molecular docking, soft docking methods account for the protein flexibility through tolerating minor atomic clashes between the interacting molecules. Jiang and Fan developed the first soft docking algorithm for protein–ligand docking, in which both the protein surface and the ligand surface are represented by molecular surface cubes, and the binding poses are produced through matching the surface structures of the protein and of the ligand on the basis of their surface complementarity, allowing minor surface overlaps.[46] Because it is not convenient to explore the ligand conformational space with the surface representation, soft surface-based docking methods are more often used in the rigid-body protein–protein docking, in which certain amount of interface penetration is allowed.[47–49] In fact, in protein–ligand docking, the soft potential-based docking methods are more often used, in which both the protein and the ligand are represented with atomic models, and minor atomic overlaps are allowed by using scoring functions with attenuate repulsive terms in molecular docking. For example, the 12–6 Lennard-Jones potentials for calculating the van der Walls interactions were replaced with 9–6 potentials in many studies.[50–52] Soft docking is computationally as efficient as rigid docking, however, it can account for only minor protein side chain motions in the binding process.

3.13.4.2 Induced-fit Docking

Induced-fit docking represents a class of docking methods in which the protein conformational space is explored on the fly in the sampling stage of molecular docking. It is impractical to consider full protein flexibility because of the extremely high dimensions, thus many docking programs based on induced-fit docking only focus on the side chain motions. The side chain conformation can be sampled by exploring its discrete rotameric states or by continuously exploring its torsional angle space. Gray et al. developed RosettaDock, a protein–protein docking software.[53] RosettaDock starts the docking with a low-resolution search followed by a high-resolution refinement stage, in which the protein side chains and the rigid body displacement are simultaneously optimized using a Monte Carlo minimization (MCM) protocol. In the early work, the side chains were optimized in the discrete rotamer space. Later, the side chain modeling protocol was improved by introducing a gradient-based minimization step during the rotamer packing to allow the sampling of off rotamer conformations.[54] Currently, RosettaDock also allows to consider the protein backbone flexibility by including the backbone perturbation and refinement in the MCM procedure; it also allows us to employ structural ensembles to model the protein flexibility, which will be described in detail in the *Ensemble Docking* section.[55,56] The RosettaDock approach was extended to protein–ligand docking, which was referred to as RosettaLigand.[57,58]

AutoDock Vina, another program for protein–ligand docking, allows the user to specify several residues, and the side chain conformations of these residues are explored and optimized in the torsional angle space during molecular docking together with the ligand binding configuration.[59] Although the protein backbone and most of the side chains are fixed in docking, AutoDock Vina is much more computational efficient than RosettaLigand, which makes Vina suitable for large scale virtual screening.

In comparison with soft docking, which is extremely limited in considering protein flexibility, induced-fit docking is able to model protein side chain flexibility and even backbone flexibility at additional computational cost. However, as the induced-fit model cannot explain protein motions such as large backbone collective motions in the binding process, generally, the induced-fit docking methods are unable to deal with the cases in which proteins undergo significant backbone conformational changes.

3.13.4.3 Ensemble Docking

Ensemble docking approaches model the protein flexibility using protein structural ensembles. Specifically, a protein structural ensemble consisting of multiple protein structures (MPSs) is used in molecular docking, in comparison with soft docking and induced-fit docking for which only a single protein structure is used. The inclusion of diverse protein conformations in the ensemble provides the possibility to model large conformational changes. A typical ensemble docking method includes two major stages: preparing the protein structural ensemble, and molecular docking against the ensemble.

3.13.4.3.1 Preparing the protein structural ensemble

The preparation of the protein structural ensemble is a very important stage of ensemble docking. Whether the holo structure-like protein conformations are included in the ensemble largely determines the docking performance. Either experimental protein structures or computational structures can be used to form the structural ensemble.

First, protein structures determined by NMR spectroscopy can be conveniently used for ensemble docking. NMR spectroscopy, unlike X-ray crystallography, is able to provide tens of structures (NMR ensemble) rather than a single static structure. The NMR ensemble reflects the protein dynamics in solution. Thus, if the conformational-selection mechanism dominates the molecular recognition process, the holo structure-like conformations are likely included in the NMR ensemble. Huang and Zou tested their ensemble docking algorithm on the NMR ensemble of the HIV-1 protease.[60] The ensemble docking result was compared with that of single protein docking, and yielded significant improvement in both the binding mode prediction and the enrichment of virtual screening. Second, the crystal structures of the same protein from different sources, such as apo protein structures solved in different conditions or holo structures bound with different ligands can also be collected and aligned to form the structural ensemble.

In the cases that there are a few high-quality experimental structures to form the structural ensemble, computational modeling, and simulation techniques can be used to produce models to complement the experimental structures. First, in the absence of experimental protein structures and homologous protein structures, *ab initio* protein structure prediction techniques can be used to generate structures for the protein. However, for many proteins, *ab initio* protein structure prediction techniques are unable to produce sufficiently accurate models for molecular docking. If the experimental structures of a protein are scarce but the experimental structures of homologous proteins are available, the homology modeling techniques can be used to build models to form the structural ensemble. Moreover, the protein structural ensemble can also be constructed through exploring the conformational space from a single protein structure. Computational methods like MD simulation and normal mode analysis (NMA) are two popular methods to explore the protein conformational space.

MD simulation explores the protein conformational space by integrating the equations of motion, thus a continuum of protein conformations can be extracted from the trajectories of MD simulation. Carlson and colleagues developed dynamic pharmacophore models for HIV integrase from protein conformations produced by MD simulation.[61] This method, later referred to as the MPS method, was successfully applied to find novel inhibitors for targets including human MDM2-p53 and HIV-1 protease.[62,63] McCammon and co-workers developed the relaxed complex scheme (RCS), in which the structural ensemble generated by MD was used for molecular docking with AUTODOCK.[64–66] Based on the RCS method, the inhibitors of HIVp, avian influenza neuraminidase, and other disease-associated protein targets were successfully identified.[67–70] However, MD trajectories are easily trapped in local minima, thus simulating large motions of the protein is time consuming and can be very difficult. Methods such as replica exchange, simulated annealing, coarse-grained MD simulation, and metadynamics are developed to enhance the conformational sampling of MD simulation or accelerating MD simulation.

On the other hand, NMA approximates the potential energy function in the vicinity of a minimized protein structure through harmonic approximation or employs simple elastic network models (ENMs). The vibrational normal modes of the protein can be computed through diagonalizing the Hessian matrix to obtain its eigenvectors (movement directions) and eigenvalues (vibrational frequencies). Because functional motions in proteins often correspond to low-frequency normal modes, multiple protein conformations can be generated by perturbing the protein structure along the directions of several low-frequency normal modes. Benchmarked on 14 targets, each with 2 holo structures bound with different ligands, Rueda et al. showed that cross docking using an equilibrium ensemble of the binding-site conformers derived from all heavy-atom ENMs predicted 20% more near-native binding modes in the top-scored modes than using a single protein conformation.[71] Because collective motions in proteins can be explored at much lower computational cost than MD simulation, NMA is more suitable than MD simulation to prepare structural ensemble for flexible proteins, which may undergo collective backbone motions in binding processes. However, localized protein conformational displacements, such as loop motions, often correspond to high-frequency modes, which cannot be well modeled using NMA. Therefore, for modeling high-frequency protein structural motions, MD-based methods are generally better choices.

Besides MD simulation and NMA, MC-based methods and flexibility analysis-based methods can also be used to generate a structural ensemble for ensemble docking. For example, RosettaDock allows one to employ the computational ensembles created by RosettaRelax[72] as inputs in its ensemble docking protocol. RosettaRelax is a multiscale MC-based structural refinement algorithm, which integrates small backbone torsional angle perturbations, side chain packing, and energy-gradient-based minimization in the torsion space to sample the local protein conformational space. Zavodszky et al. integrated FIRST (Floppy Inclusion and Rigid Substructure Topography), a graph-theoretical approach to identify rigid and flexible regions based on protein bond network, and ROCK (Rigidity Optimized Conformational Kinetics), a restricted random-walk sampling approach to search the protein conformational space, to prepare the protein's main chain ensemble for docking with SLIDE, in which the protein's side chain flexibility and the ligand flexibility were handled by SLIDE based on induced-fit docking.[73]

An important question in preparing the protein structural ensemble is how many protein structures need to be included in the ensemble. Unfortunately, there is no general answer to this question. Many factors need to be considered, such as the source of the structures, the level of protein flexibility, and the docking method to incorporate the structural ensemble. The size of the experimental structural ensemble is limited by the number of the experimental structures available, whereas the computational methods are able to produce as many conformations as possible. Generally speaking, small structural ensembles may increase the risk of under representing holo structure-like protein conformations, but large structural ensembles require long computational time for docking and may reduce the docking performance due to the increase of false positives produced by imperfect scoring functions. Methods were developed to reduce the size of the structural ensemble. For example, in the improved version of RCS, McCammon and co-workers used hierarchical clustering based on pairwise root mean squared deviation (RMSD) between the MD snapshots to reduce the number of protein conformations generated by MD simulation.[65] Bolstad and Anderson developed a method to prune the structural ensemble by selecting protein conformations that preserve the geometry of the protein active core.[74]

3.13.4.3.2 Molecular docking against a structural ensemble

For protein–ligand docking, several protocols have been developed to dock a ligand against a structural ensemble. The straightforward way is to dock a ligand into MPSs in the ensemble independently (referred to as sequential docking), such as the method used in the RCS.[64,66] The advantage of this protocol is that a whole spectrum of binding scores is obtained in the docking. The ligand can be ranked based on the properties of multiple docking scores (e.g., the ensemble average) rather than a single score to reduce the risk of obtaining false positive results. However, docking the ligand into MPSs independently is time consuming, particularly when the ensemble size is large.

The computational cost can be significantly reduced by docking the ligand to a united protein structure averaged from the structural ensemble. For example, in the early work by Knegtel et al., a composite grid (energy-weighted grid or geometry-weighted grid) calculated from MPSs through DOCK3.5 was employed to consider the protein conformational variability.[75] Benchmarked using HIVp, ras p21, retinol binding protein, and uteroglobin, the results showed that the experimentally determined binding orientations and computed binding energies from standard grids can be successfully reproduced. However, in the cases with variable protein structures in the ensemble, the artificial average structure loses the geometric accuracy of the structures and may even have an unphysical conformation. In such cases, docking a ligand to an average structure may often produce incorrect results.

Claussen and colleagues developed a different united-protein-based docking method, referred to as FlexE.[76] In this method, similar parts of the structures in the ensemble are merged to one structure, whereas varying parts are explicitly treated as separate alternative conformations. In ligand docking, these alternative conformations are combinatorially joined, thus novel valid protein structures that are not included in the original ensemble can be created. FlexE was tested on 10 protein ensembles, and was compared with sequential docking that was performed using the single docking tool, FlexX. The result showed that FlexE performed comparably with sequential docking on binding mode prediction with only a little more than half (0.57-fold) of the computational cost. Shoichet and colleagues developed a method which is similar to FlexE but with higher computational efficiency.[77] In this method, the flexible parts of the protein are allowed to move independently, and the conformation of each part that best fits a given pose of the ligand is identified separately. Then, the identified conformations are combined and joined with the rigid parts to form a single, composite representation of the protein for ligand docking. In this way, the protein conformational space is significantly reduced, and the computational time grows linearly rather than exponentially with the degrees of freedom of the protein.

In the MPS method developed by Carlson and colleagues, MPS pharmacophore models are derived from computational ensembles produced by MD simulation or experimental ensembles (NMR ensembles or collections of crystal structures).[61,78] The MPS pharmacophore models are then employed to screen the compound library to find compounds with good chemical complementarity, and have achieved much better performance in identifying active inhibitors than the single-structure (static) pharmacophore model. It is notable that the MPS method is one of the few ensemble-based methods that has been successfully used to find novel active inhibitors.

In the ensemble docking method developed by Huang and Zou, the protein conformational state is considered as an additional dimension.[60,79] The protein conformational index is simultaneously optimized with the ligand position and orientation in molecular docking. The computational efficiency is prominently improved by not wasting time on searching/docking into obviously irrelevant protein conformations. The computational time of this ensemble docking method is comparable to that of the single protein docking method. The ensemble docking method was extensively tested on diverse protein targets by using either NMR ensembles or structural ensembles collected from different co-bound crystal structures, and performed comparably to the sequential docking in binding mode predictions, binding energy score predictions, and enrichment tests of virtual screening. This ensemble docking method was implemented in the molecular docking software, MDock, from the Zou lab.[80] A similar method was also developed by Abagyan and colleagues later, which was referred to as the four-dimensional (4D) docking approach.[81]

Ensemble-based methods were also developed to model protein flexibility in protein–protein docking. In the early work of Nilges and colleagues, MPSs were derived from representative MD snapshots for unbound receptor and ligand structures of 17 protein–protein complex structures.[82] Rigid docking was performed for all combinations of the multiple receptor and ligand structures (ensemble cross docking). The docking result suggests that the ensemble cross-docking approach can increase the likelihood of finding near-native binding modes.

Bastard and colleagues developed an ensemble docking method to model the loop flexibility during protein–protein docking.[83] In this method, multiple copies of loop conformations are systematically sampled in advance. Then, the weight of each copy for docking is adjusted according to the Boltzmann criterion, which gives the loop conformation a higher weight if it is associated with a lower binding energy. The receptor protein and the remaining residues in the ligand protein that interact with the loop experience the mean field of the loop ensemble. This mean-field approach was later implemented in the ATTRACT[84] and was tested on eight protein–protein complexes, in which either one binding partner presents large conformational changes within the loop region between its unbound and bound forms or the unbound structure has a missing loop at its interacting residues.[85] The result showed that this method significantly improved the predictions in comparison with rigid protein–protein docking.

RosettaDock was also extended to allow users to use computational ensembles from Rosetta or NMR ensembles as inputs to model the protein backbone flexibility in protein–protein docking.[56] In the ensemble docking of RosettaDock, an extra step was added to the low-resolution docking following the rigid-body move step, and preceding the Metropolis evaluation step. In this step, the ensemble is superposed along the interface residues. For each protein conformation, the centroid mode binding energy is calculated to generate a partition function, followed by conformational selection based on the Boltzmann-weighted probability. The Metropolis criterion is then applied to the combined rigid-body/conformational selection move, followed by the high-resolution refinement of RosettaDock. The whole docking procedure integrates the ensemble docking and the induced-fit docking in a serial way, which can be considered as a method inspired by the coupling of the conformational selection model and the induced-fit model.

3.13.5 Modeling Protein Flexibility in the Postdocking Stage

Following the computationally efficient docking calculations, more accurate and time-consuming methods are often employed to refine and rescore the promising binding modes from molecular docking. Comparing with modeling protein flexibility in the

molecular docking, modeling the protein flexibility in the postdocking refinement stage has the advantage of modeling the induced-fit conformational changes, because the crude binding pose has already been determined and computational efforts can focus on the internal dimensions of the protein near the interface.

MD simulation is the most commonly used method for structural refinement of the docked protein–ligand complexes. Protein flexibility, ligand flexibility, and the solvent effects are simultaneously considered in the MD simulation-based refinement. Moreover, the binding free energy is calculated with a physics-based method such as free energy perturbation, thermodynamics integration, MM/PBSA, and MM/GBSA from the trajectories of MD simulation. In addition, the kinetic stability of binding can also be studied from the MD trajectories, which is helpful for binding mode selection, because incorrect binding modes are likely to produce unstable trajectories. For example, Park and colleagues integrated molecular docking and MD simulation to study differential inhibition of two cyclin-dependent kinases (CDKs), CDK2 and CDK4, through simulating the dynamics of the docked complexes with three different selective inhibitors.[86] It was found that the mobility of a disordered loop of CDK4 was significantly reduced in the presence of the inhibitors, but not with the loop of CDK2. The CDK2 complexes have more water molecules diffused into the active site than the CDK4 complexes, which resulted in greater exposure of the interfaces of the CDK2 complexes to bulk solvent. Thus, weaker hydrogen bonding interaction with the active-site residues and greater exposure to the solvent are possibly responsible for the less stable CDK2 complexes than the CDK4 complexes. Okimoto and colleagues combined molecular docking and MD simulation in *in vitro* screening.[87] In this study, the binding modes obtained from molecular docking were refined by MD simulation and were then rescored with MM/PBSA. Benchmarked by four target proteins (trypsin, HIV-1 protease (HIV-PR), acetylcholine esterase (AChE), and CDK2), the enrichment performance of the top 100 compounds was improved by 1.6–4.0 fold in comparison with the enrichment performance of molecular docking.

MD simulation was also used to refine protein–protein complex structures from protein–protein docking. For example, in HADDOCK,[88] a protein–protein docking program, the rigid docking stage is followed by two refinement stages: first, a semiflexible refinement is performed in the torsional angle space of the protein–protein interface, with both the backbone and side chain atoms are allowed to move. Second, a restricted simulated annealing MD simulation with explicit solvent is performed to refine the whole complex.

Besides MD simulation, NMA can also be used for the postdocking refinement of complex structures from protein–protein docking. Wolfson developed FiberDock,[89] a flexible backbone refinement method for docking refinement. In this method, NMA is performed for the flexible protein (receptor) using anisotropic network model (ANM) prior to the docking refinement, and the docking solution is then refined by iteratively minimizing the backbone of the receptor along the most relevant normal modes to model the induced-fit backbone conformational changes. The pose-dependent NMA-based method for protein–protein complex structure refinement was developed by Ritchie and colleagues recently.[90] Comparing with FiberDock, the NMA is applied to the docking pose rather than one of the flexible binding partners, thus the flexibility of both binding partners can be modeled in this method. This is important, for both the binding partners may undergo conformational changes in the binding process. This method was applied to 63 "rigid body" targets in the Protein Docking Benchmark 2.0. It was seen that both the sampling performance and the rescoring performance were modestly but consistently improved.

3.13.6 Modeling Peptide Flexibility in Protein–Peptide Docking

Besides protein–ligand interactions and protein–protein interactions, protein–peptide interactions are another class of prevalent protein-involved interactions and play an important role in many cellular processes including signal transduction, immune response, and transcriptional regulation.[91] Moreover, peptides have also become attractive drug candidates.[92] Thus, computational modeling of protein–peptide interactions is of great importance for mechanistically investigating these cellular processes and developing peptide therapeutics. Molecular docking methods for modeling protein–peptide interactions, referred to as protein–peptide docking, have been developed in recent years. Protein–peptide docking is challenging particularly due to the high flexibility of the peptide. In fact, many peptides are disordered in the unbound state, and the binding of the peptide with its protein partner stabilizes the peptide to form the final bound structure. In some cases, the association of the peptide with its protein partner is a process that couples binding and folding, and the peptide undergoes a disorder-to-order transition in this process. Because peptides often do not have well-defined unbound structures, the traditional shape complementarity-based protein–protein docking methods cannot be directly used for predicting protein–peptide complex structures. Neither can protein–ligand docking methods be directly used for protein–peptide docking, because peptides usually contain many more rotatable bonds than small compounds and thus the peptide conformational space is too large to explore exhaustively in molecular docking.

Starting with the sequence of the peptide and the crystal structure of the protein, the majority of the existing protein–peptide docking methods focus on the flexibility of the peptide, and fix or largely restrict the protein structure. To reduce the computational requirement, the sampling stage of protein–peptide docking often uses a coarse-grained structural model or/and restrictive flexible sampling. For example, Raveh et al. developed Rosetta FlexPepDock *ab initio*, which performs simultaneous docking and folding of the peptide from an extended conformation onto the protein receptor with an approximate specification of the peptide binding site.[93,94] This method integrates the induced-fit docking protocol and the fragment-based *ab initio* protein structure prediction protocol. In the low-resolution stage, the peptide backbone conformations and the rigid orientations are sampled simultaneously over the protein surface of the given peptide binding site through the assembly of Rosetta's fragment library with a coarse-grained representation of the peptide and the protein. The low-resolution sampling stage is followed by all-atom refinement, which includes

fine backbone modeling and full side chain packing for both the protein and the peptide. Validation on 26 bound docking cases (i.e., with bound protein structures) and 14 unbound docking cases (i.e., with unbound protein structures) showed that near-native binding models can be sampled for 96.0% of the bound docking cases and for 69% of the unbound docking cases. However, Rosetta FlexPepDock is computationally demanding. Generally, it takes 24 h on a cluster of 120 processes for a typical protein–peptide docking. Trellet et al. extended the protein–protein docking protocol, HADDOCK, for protein–peptide docking.[95] This protein–peptide docking approach is a unification of the conformational selection and induced-fit mechanisms. Specifically, three typical peptide conformations (extended, alpha-helix, and polyproline-II) are rigidly docked into the binding site of the receptor for conformational selection, then the favorable conformations selected in the rigid docking stage are flexibly refined to improve the protein–peptide interface through the flexible refinement protocol of HADDOCK (i.e., the semiflexible refinement of the protein–peptide interface in the torsional angle space followed by the MD simulation-based refinement) as inspired by the induced-fit mechanism. This method was tested on the peptiDB[96] database, and was able to generate near-native binding modes for 79.4% of the bound docking cases, and for 69.4% of the unbound docking cases. Based on the similar idea, Schindler et al. developed a fully blind protein–peptide docking method, referred to as pepATTRACT.[97] In pepATTRACT, three peptide conformations are docked onto the whole surface of a protein rather than a specified peptide binding site. Encouragingly, without knowing the peptide binding site, pepATTRACT shows comparable performance on sampling near-native peptide binding modes with the aforementioned HADDOCK-based method. Kurcinski et al. developed CABS-dock, another blind protein–peptide docking method.[98,99] CABS-dock employs the coarse-grained CABS model, in which each amino acid is represented by up to four interaction centers and statistical potential-based force fields are used. The simulation dynamics is controlled by the Metropolis MC. Starting from random peptide conformations and positions, CABS-dock explores the peptide binding configurations over the global protein surface, allowing for full flexibility of the peptide and small backbone fluctuations of the protein receptor through Replica Exchange Monte Carlo dynamics. CABS-dock was also validated on the peptiDB database, and encouragingly, CABS-dock successfully generated near-native binding modes for over 80% of both the bound docking cases and unbound docking cases.

Recently, MDockPeP, a fully blind docking method at the atomic level for predicting protein–peptide complex structures, was developed in our laboratory.[100] In this work, first, the fragments of monomeric proteins are used as templates to model peptide conformations, and then these modeled peptide conformations are employed for sampling the peptide binding modes via our integrated global/flexible sampling approach, in which the peptide conformation is restricted to be close to the modeled peptide conformation (with backbone $RMSD < 5.5$ Å). It is noted that MDockPeP uses the all-atom peptide model in the process of flexible sampling and that the integration of peptide modeling and restrictive flexible sampling significantly reduces the configuration space for docking, allowing effective sampling of the peptide binding modes over the global protein surface at the all-atom level. MDockPeP was also assessed on the peptiDB database. In the peptide modeling stage, at least one of our top three modeled peptide conformations showed a similar structure to the bound peptide (with backbone $RMSD < 4.0$ Å) for 95% of the cases. In the sampling stage, near-native peptide binding modes were generated for more than 90% of both the bound docking cases and unbound docking cases.

3.13.7 Conclusion

Protein flexibility plays an important role in the binding of a protein with other molecules underlying the protein function. However, computational modeling of protein flexibility is challenging because of the extremely high dimensions of the degrees of freedom. In this article, we have reviewed the existing methods for modeling protein flexibility in two classes of molecular docking techniques, protein–ligand docking and protein–protein docking. For both classes, the methods for protein flexibility modeling can be classified into three types, soft docking, induced-fit docking, and ensemble docking. Soft docking is basically rigid docking but implicitly considers very minor side chain motions. Induced-fit docking simultaneously optimizes the protein conformation and the ligand binding configuration in the sampling stage of molecular docking, however, due to the extremely high dimensions of the degrees of freedom in a protein, induced-fit docking methods can model only moderate protein conformational changes. Ensemble docking employs the protein structural ensemble in molecular docking, which has the advantage to model large protein conformational changes. However, the preparation of the structural ensemble and the employment of the ensemble in docking calculations are not trivial, as previously discussed in detail in this article. Moreover, the induced-fit conformational changes can also be modeled in the postdocking stage through MD simulation and NMA.

Being different from protein–ligand docking and protein–protein docking, protein–peptide docking is an emerging docking technique. Modeling peptide flexibility is a big challenge in protein–peptide docking, because the peptide often does not have a stable 3D structure before binding and because the peptide often has much larger conformational space than a small compound. To some extent, modeling the peptide flexibility can be considered as a preliminary effort to model the disorder-to-order transition in the binding process. In this article, we have also reviewed the recent progress in modeling peptide flexibility in protein–peptide docking.

Acknowledgment

This work is supported by the NSF CAREER Award DBI-0953839, NIH R01GM109980, and American Heart Association (Midwest Affiliate) 13GRNT16990076 (XZ).

References

1. Buonfiglio, R.; Recanatini, M.; Masetti, M. *ChemMedChem* **2015,** *10,* 1141–1148.
2. Baldwin, A. J.; Walsh, P.; Hansen, D. F.; Hilton, G. R.; Benesch, J. L.; Sharpe, S.; Kay, L. E. *J. Am. Chem. Soc.* **2012,** *134,* 15343–15350.
3. Baldwin, A. J.; Kay, L. E. *Nat. Chem. Biol.* **2009,** *5,* 808–814.
4. Kay, L. E. *Biochem. Cell Biol.* **1998,** *76,* 145–152.
5. Bernadó, P.; Mylonas, E.; Petoukhov, M. V.; Blackledge, M.; Svergun, D. I. *J. Am. Chem. Soc.* **2007,** *129,* 5656–5664.
6. Teilum, K.; Olsen, J. G.; Kragelund, B. B. *Biochim. Biophys. Acta* **2011,** *1814,* 969–976.
7. Teilum, K.; Olsen, J. G.; Kragelund, B. B. *Cell. Mol. Life Sci.* **2009,** *66,* 2231–2247.
8. Karplus, M.; Kuriyan, J. *Proc. Natl. Acad. Sci. U. S. A.* **2005,** *102,* 6679–6685.
9. Bahar, I.; Chennubhotla, C.; Tobi, D. *Curr. Opin. Struct. Biol.* **2007,** *17,* 633–640.
10. Csermely, P.; Palotai, R.; Nussinov, R. *Trends Biochem. Sci.* **2010,** *35,* 539–546.
11. Fischer, E. *Ber. Dtsch. Chem. Ges.* **1894,** *27,* 2985–2993.
12. Lippincott-Schwartz, J.; Snapp, E.; Kenworthy, A. *Nat. Rev. Mol. Cell Biol.* **2001,** *2,* 444–456.
13. Brylinski, M.; Skolnick, J. *Proteins* **2008,** *70,* 363–377.
14. Koshland, D. *Proc. Natl. Acad. Sci. U. S. A.* **1958,** *44,* 98–104.
15. Berman, H. M.; Westbrook, J.; Feng, Z.; Gilliland, G.; Bhat, T. N.; Weissig, H.; Shindyalov, I. N.; Bourne, P. E. *Nucleic Acids Res.* **2000,** *28,* 235–242.
16. Teague, S. J. *Nat. Rev. Drug Discov.* **2003,** *2,* 527–541.
17. Tsai, C.-J.; Kumar, S.; Ma, B.; Nussinov, R. *Protein Sci.* **1999,** *8,* 1181–1190.
18. Ma, B.; Kumar, S.; Tsai, C.-J.; Nussinov, R. *Protein Eng.* **1999,** *12,* 713–720.
19. Kumar, S.; Ma, B.; Tsai, C.-J.; Sinha, N.; Nussinov, R. *Protein Sci.* **2000,** *9,* 10–19.
20. Bucher, D.; Grant, B. J.; McCammon, J. A. *Biochemistry* **2011,** *50,* 10530–10539.
21. Silva, D.-A.; Bowman, G. R.; Sosa-Peinado, A.; Huang, X. *PLoS Comput. Biol.* **2011,** *7,* e1002054.
22. Wlodarski, T.; Zagrovic, B. *Proc. Natl. Acad. Sci. U. S. A.* **2009,** *106,* 19346–19351.
23. Hammes, G. G.; Chang, Y.-C.; Oas, T. G. *Proc. Natl. Acad. Sci. U. S. A.* **2009,** *106,* 13737–13741.
24. Zhou, H.-X. *Biophys. J.* **2010,** *98,* L15–L17.
25. Espinoza-Fonseca, L. M. *Biochem. Biophys. Res. Commun.* **2009,** *382,* 479–482.
26. Wang, W.; Donini, O.; Reyes, C. M.; Kollman, P. A. *Annu. Rev. Biophys. Biomol. Struct.* **2001,** *30,* 211–243.
27. Åqvist, J.; Luzhkov, V. B.; Brandsdal, B. O. *Acc. Chem. Res.* **2002,** *35,* 358–365.
28. Gohlke, H.; Kiel, C.; Case, D. A. *J. Mol. Biol.* **2003,** *330,* 891–913.
29. Dror, R. O.; Pan, A. C.; Arlow, D. H.; Borhani, D. W.; Maragakis, P.; Shan, Y.; Xu, H.; Shaw, D. E. *Proc. Natl. Acad. Sci. U. S. A.* **2011,** *108,* 13118–13123.
30. Shan, Y.; Kim, E. T.; Eastwood, M. P.; Dror, R. O.; Seeliger, M. A.; Shaw, D. E. *J. Am. Chem. Soc.* **2011,** *133,* 9181–9183.
31. Buch, I.; Giorgino, T.; De Fabritiis, G. *Proc. Natl. Acad. Sci. U. S. A.* **2011,** *108,* 10184–10189.
32. Sousa, S. F.; Fernandes, P. A.; Ramos, M. J. *Proteins* **2006,** *65,* 15–26.
33. Shoichet, B. K.; McGovern, S. L.; Wei, B.; Irwin, J. J. *Curr. Opin. Chem. Biol.* **2002,** *6,* 439–446.
34. Huang, S. Y.; Grinter, S. Z.; Zou, X. *Phys. Chem. Chem. Phys.* **2010,** *12,* 12899–12908.
35. Broojimans, N.; Kuntz, I. D. *Annu. Rev. Biophys. Biomol. Struct.* **2003,** *32,* 335–373.
36. Huang, S.-Y.; Zou, X. *Int. J. Mol. Sci.* **2010,** *11,* 3016–3034.
37. Ritchie, D. W. *Curr. Protein Pept. Sci.* **2008,** *9,* 1–15.
38. Vajda, S.; Kozakov, D. *Curr. Opin. Struct. Biol.* **2009,** *19,* 164–170.
39. Huang, S.-Y. *Drug Discov. Today* **2015,** *20,* 969–977.
40. Kitchen, D. B.; Decornez, H.; Furr, J. R.; Bajorath, J. *Nat. Rev. Drug Discov.* **2004,** *3,* 935–949.
41. Schreiber, G.; Fleishman, S. J. *Curr. Opin. Struct. Biol.* **2013,** *23,* 903–910.
42. Lexa, K. W.; Carlson, H. A. *Q. Rev. Biol.* **2012,** *45,* 301–343.
43. Chandrika, B.-R.; Subramanian, J.; Sharma, S. D. *Drug Discov. Today* **2009,** *14,* 394–400.
44. Bonvin, A. M. *Curr. Opin. Struct. Biol.* **2006,** *16,* 194–200.
45. Andrusier, N.; Mashiach, E.; Nussinov, R.; Wolfson, H. J. *Proteins* **2008,** *73,* 271–289.
46. Jiang, F.; Kim, S.-H. *J. Mol. Biol.* **1991,** *219,* 79–102.
47. Gabb, H. A.; Jackson, R. M.; Sternberg, M. J. *J. Mol. Biol.* **1997,** *272,* 106–120.
48. Chen, R.; Weng, Z. *Proteins* **2003,** *51,* 397–408.
49. Palma, P. N.; Krippahl, L.; Wampler, J. E.; Moura, J. J. *Proteins* **2000,** *39,* 372–384.
50. Venkatachalam, C. M.; Jiang, X.; Oldfield, T.; Waldman, M. *J. Mol. Graph. Model.* **2003,** *21,* 289–307.
51. Krammer, A.; Kirchhoff, P. D.; Jiang, X.; Venkatachalam, C.; Waldman, M. *J. Mol. Graph. Model.* **2005,** *23,* 395–407.
52. Ferrari, A. M.; Wei, B. Q.; Costantino, L.; Shoichet, B. K. *J. Med. Chem.* **2004,** *47,* 5076–5084.
53. Gray, J. J.; Moughon, S.; Wang, C.; Schueler-Furman, O.; Kuhlman, B.; Rohl, C. A.; Baker, D. *J. Mol. Biol.* **2003,** *331,* 281–299.
54. Wang, C.; Schueler-Furman, O.; Baker, D. *Protein Sci.* **2005,** *14,* 1328–1339.
55. Wang, C.; Bradley, P.; Baker, D. *J. Mol. Biol.* **2007,** *373,* 503–519.
56. Chaudhury, S.; Gray, J. J. *J. Mol. Biol.* **2008,** *381,* 1068–1087.
57. Meiler, J.; Baker, D. *Proteins* **2006,** *65,* 538–548.
58. Davis, I. W.; Baker, D. *J. Mol. Biol.* **2009,** *385,* 381–392.
59. Trott, O.; Olson, A. J. *J. Comput. Chem.* **2010,** *31,* 455–461.
60. Huang, S.-Y.; Zou, X. *Protein Sci.* **2007,** *16,* 43–51.
61. Carlson, H. A.; Masukawa, K. M.; Rubins, K.; Bushman, F. D.; Jorgensen, W. L.; Lins, R. D.; Briggs, J. M.; McCammon, J. A. *J. Med. Chem.* **2000,** *43,* 2100–2114.
62. Bowman, A. L.; Nikolovska-Coleska, Z.; Zhong, H.; Wang, S.; Carlson, H. A. *J. Am. Chem. Soc.* **2007,** *129,* 12809–12814.
63. Damm, K. L.; Ung, P. M.; Quintero, J. J.; Gestwicki, J. E.; Carlson, H. A. *Biopolymers* **2008,** *89,* 643–652.
64. Lin, J.-H.; Perryman, A. L.; Schames, J. R.; McCammon, J. A. *J. Am. Chem. Soc.* **2002,** *124,* 5632–5633.
65. Amaro, R. E.; Baron, R.; McCammon, J. A. *J. Comput. Aided Mol. Des.* **2008,** *22,* 693–705.
66. Lin, J.-H.; Perryman, A. L.; Schames, J. R.; McCammon, J. A. *Biopolymers* **2003,** *68,* 47–62.
67. Perryman, A. L.; Lin, J.-H.; McCammon, J. A. *Chem. Biol. Drug Des.* **2006,** *67,* 336–345.
68. Cheng, L. S.; Amaro, R. E.; Xu, D.; Li, W. W.; Arzberger, P. W.; McCammon, J. A. *J. Med. Chem.* **2008,** *51,* 3878–3894.
69. Barakat, K.; Mane, J.; Friesen, D.; Tuszynski, J. *J. Mol. Graph. Model.* **2010,** *28,* 555–568.
70. Barakat, K.; Tuszynski, J. *J. Mol. Graph. Model.* **2011,** *29,* 702–716.

71. Rueda, M.; Bottegoni, G.; Abagyan, R. *J. Chem. Inf. Model.* **2009,** *49,* 716–725.
72. Misura, K.; Baker, D. *Proteins* **2005,** *59,* 15–29.
73. Zavodszky, M. I.; Lei, M.; Thorpe, M.; Day, A. R.; Kuhn, L. A. *Proteins* **2004,** *57,* 243–261.
74. Bolstad, E. S.; Anderson, A. C. *Proteins* **2009,** *75,* 62–74.
75. Knegtel, R. M.; Kuntz, I. D.; Oshiro, C. *J. Mol. Biol.* **1997,** *266,* 424–440.
76. Claussen, H.; Buning, C.; Rarey, M.; Lengauer, T. *J. Mol. Biol.* **2001,** *308,* 377–395.
77. Wei, B. Q.; Weaver, L. H.; Ferrari, A. M.; Matthews, B. W.; Shoichet, B. K. *J. Mol. Biol.* **2004,** *337,* 1161–1182.
78. Damm, K. L.; Carlson, H. A. *J. Am. Chem. Soc.* **2007,** *129,* 8225–8235.
79. Huang, S.-Y.; Zou, X. *Proteins* **2007,** *66,* 399–421.
80. Yan, C.; Zou, X. *Methods Pharmacol. Toxicol.* **2015,** 153.
81. Bottegoni, G.; Kufareva, I.; Totrov, M.; Abagyan, R. *J. Med. Chem.* **2008,** *52,* 397–406.
82. Grünberg, R.; Leckner, J.; Nilges, M. *Structure* **2004,** *12,* 2125–2136.
83. Bastard, K.; Thureau, A.; Lavery, R.; Prevost, C. *J. Comput. Chem.* **2003,** *24,* 1910–1920.
84. Zacharias, M. *Proteins* **2005,** *60,* 252–256.
85. Bastard, K.; Prévost, C.; Zacharias, M. *Proteins* **2006,** *62,* 956–969.
86. Park, H.; Yeom, M. S.; Lee, S. *ChemBioChem* **2004,** *5,* 1662–1672.
87. Okimoto, N.; Futatsugi, N.; Fuji, H.; Suenaga, A.; Morimoto, G.; Yanai, R.; Ohno, Y.; Narumi, T.; Taiji, M. *PLoS Comput. Biol.* **2009,** *5*, e1000528.
88. Dominguez, C.; Boelens, R.; Bonvin, A. M. *J. Am. Chem. Soc.* **2003,** *125,* 1731–1737.
89. Mashiach, E.; Nussinov, R.; Wolfson, H. J. *Proteins* **2010,** *78,* 1503–1519.
90. Venkatraman, V.; Ritchie, D. W. *Proteins* **2012,** *80,* 2262–2274.
91. Petsalaki, E.; Russell, R. B. *Curr. Opin. Biotechnol.* **2008,** *19,* 344–350.
92. Fosgerau, K.; Hoffmann, T. *Drug Discov. Today* **2015,** *20,* 122–128.
93. Raveh, B.; London, N.; Schueler-Furman, O. *Proteins* **2010,** *78,* 2029–2040.
94. Raveh, B.; London, N.; Zimmerman, L.; Schueler-Furman, O. *PLoS One* **2011,** *6*, e18934.
95. Trellet, M.; Melquiond, A. S.; Bonvin, A. M. *PLoS One* **2013,** *8*, e58769.
96. London, N.; Movshovitz-Attias, D.; Schueler-Furman, O. *Structure* **2010,** *18,* 188–199.
97. Schindler, C. E.; de Vries, S. J.; Zacharias, M. *Structure* **2015,** *23,* 1507–1515.
98. Kurcinski, M.; Jamroz, M.; Blaszczyk, M.; Kolinski, A.; Kmiecik, S. *Nucleic Acids Res.* **2015,** *43,* W419–W424.
99. Blaszczyk, M.; Kurcinski, M.; Kouza, M.; Wieteska, L.; Debinski, A.; Kolinski, A.; Kmiecik, S. *Methods* **2016,** *93,* 72–83.
100. Yan, C.; Xu, X.; Zou, X. *Structure* **2016,** *24,* 1842–1853.

3.14 Chemical Data Formats, Fingerprints, and Other Molecular Descriptions for Database Analysis and Searching

D Bajusz, Research Institute for Natural Sciences, Hungarian Academy of Sciences, Budapest, Hungary
A Rácz, Research Institute for Natural Sciences, Hungarian Academy of Sciences, Budapest, Hungary; and Szent István University, Budapest, Hungary
K Héberger, Research Institute for Natural Sciences, Hungarian Academy of Sciences, Budapest, Hungary

© 2017 Elsevier Ltd. All rights reserved.

3.14.1 Introduction 330
3.14.2 Chemical File Formats and Data Structures 330
3.14.2.1 Line Notation Formats 331
3.14.2.2 Simplified Molecular-Input Line-Entry System 332
3.14.2.3 Smiles Arbitrary Target Specification 332
3.14.2.3.1 SMIRKS 333
3.14.2.4 Molecular Query Language 333
3.14.2.4.1 International Chemical Identifier 333
3.14.3 Other Line Notation Formats 334
3.14.3.1 Wiswesser Line Notation 334
3.14.3.2 Representation of Organic Structures Description Arranged Linearly 334
3.14.3.3 Sybyl Line Notation 335
3.14.3.4 Chemical Table Files 335
3.14.3.4.1 Connection table (Ctab)-based file types 335
3.14.3.4.2 Tripos mol2 format 336
3.14.3.4.3 Other formats 336
3.14.3.4.4 Protein Data Bank file format (pdb) 336
3.14.3.4.5 FASTA 338
3.14.3.4.6 Chemical Markup Language 338
3.14.3.4.7 Structure recognition tools 338
3.14.4 Molecular Fingerprints 339
3.14.4.1 Substructure Key-Based Fingerprints 340
3.14.4.2 Topological Fingerprints 341
3.14.4.3 Path-Based Fingerprints 342
3.14.4.4 Circular Fingerprints 342
3.14.4.4.1 Topological subsets 343
3.14.4.5 Pharmacophore Fingerprints 344
3.14.4.6 Hybrid Fingerprint 344
3.14.4.7 Other Fingerprint Types 344
3.14.4.7.1 Text-based 345
3.14.4.7.2 EDPrints 345
3.14.4.7.3 Affinity fingerprints 345
3.14.4.7.4 Interaction fingerprints 346
3.14.4.7.5 Fingerprints for Ligands and Proteins (FLAP) 346
3.14.4.7.6 Reaction fingerprints 346
3.14.5 Numerical Descriptors and Similar Representations 346
3.14.5.1 2D Descriptors 347
3.14.5.1.1 Whole-molecular descriptors 347
3.14.5.1.2 Topological descriptors 349
3.14.5.1.3 Other 2D descriptors 351
3.14.5.2 3D Descriptors 351
3.14.5.2.1 Electronic descriptors 351
3.14.5.2.2 Size descriptors 352
3.14.5.2.3 Volume descriptors 352
3.14.5.2.4 Shape descriptors 352
3.14.5.2.5 van de Waals parameters 353
3.14.5.2.6 Molecular Shape Analysis descriptors 353
3.14.5.2.7 Molecular Field Analysis descriptors 353
3.14.5.2.8 Receptor Surface Analysis descriptors 353
3.14.5.2.9 3D descriptor families 353

3.14.5.3	4D and Other Special Descriptors	354
3.14.5.3.1	4D descriptors	354
3.14.5.3.2	Other special descriptors and approaches (outlook)	355
3.14.6	**Similarity—Dissimilarity Measures, Distance Metrics**	355
3.14.6.1	Common Measures of Similarity and Dissimilarity (Distance)	356
3.14.6.2	Similarity Fusion, Fusion Rules, Consensus Scoring	361
3.14.6.3	Clustering Algorithms	362
3.14.6.4	Similarity Measures for Special Tasks	363
3.14.6.4.1	Symmetric field-based similarity indices	363
3.14.6.4.2	Similarities of 1D structures	363
3.14.6.4.3	Graph (tree)-based similarities	364
3.14.6.4.4	Semantic similarity measures	365
3.14.6.4.5	Supervised similarity measures	365
3.14.6.4.6	Chemometric/Spectral similarity	366
3.14.6.4.7	Fuzzy similarity measures	366
3.14.6.4.8	Other similarity measures	367
3.14.7	**Online Web Resources**	367
3.14.8	**Case Studies**	368
3.14.9	**Outlook**	370
References		370

3.14.1 Introduction

Molecules possess an abundance of properties. 3D structure, atom connectivity, shape, and physicochemical descriptors such as molecular weight or log*P* (logarithm of the *n*-octanol/water partition coefficient) are just a few of such properties that are usually of interest in the overlapping domains of cheminformatics, molecular modeling, and drug design. Many of these properties have a quite intricate nature: for example, 3D structure, which can rarely be characterized with a single conformation (but instead an ensemble of conformations), or even simple properties, such as molecular weight that depends on the isotope distribution of the composing atoms. The affinity of the molecule toward various types of environment (such as a physiological solution, a mixture of solvents, or a particular protein-binding pocket)—which is of particular interest in the mentioned fields—expands the property space of even a single compound beyond comprehension.

As such, it is currently impossible to give a perfectly accurate and complete computational representation of a molecule that accounts for its every possible aspect; however in most cases this is not necessary. Nonetheless, one should always be aware of the implied simplifications in the computational representation of molecules, especially when making predictions based on them. In other words, the main responsibility of the computational chemist (or drug designer or cheminformatician) is to know, which aspects of a molecule are important to be considered for the given application. If it is so, then one can utilize the predictive power of computational chemistry techniques to provide invaluable guidance for medicinal chemistry endeavors.

In the recent decades, medicinal chemistry has been armed with a growing number of large, highly featured, and annotated databases. These databases contain the ever growing public (and proprietary) knowledge that is being aggregated by medicinal chemistry research, and they provide an invaluable foundation for retrospective analyses and prospective/predictive work. Databases containing chemical information can be queried in a number of ways, each of which requires specific types of molecular representations. Substructure searches require an efficient chemical query language (e.g., SMARTS), while similarity searches need means to quantify the similarity of two molecules and appropriate structural representations that allow for such operations (e.g., molecular fingerprints). It is also common to query databases for specific values or ranges of quantifiable molecular properties such as molecular weight or log*P*.

In this chapter, we provide a comprehensive overview of molecular representations, including file formats, fingerprints, and molecular descriptors—with an emphasis on those that are widely applied in works involving large databases. We also dedicate a section to molecular similarity (and the diverse methodologies that have been developed to elaborate this sub-field), as a ubiquitously applied concept in cheminformatics and drug design. Last but not least, we provide a short overview of the most prominent online resources of molecular information that ultimately fuel most of the computational chemical research that involves a consideration of large compound sets.

3.14.2 Chemical File Formats and Data Structures

The means to store chemical information started to develop in parallel with the first computers (in fact, earlier than computers became standard work tools). Since that time, generations of file formats have been developed (and have occasionally become obsolete). Since each file format was developed with a specific purpose, each encodes different aspects of the structure and

properties of a molecule. Some of them are optimized for compactness, while others allow the storage of various properties or other information besides the 3D structure of the molecule.

A complete overview of the available chemical file formats would be a futile effort—and probably pointless, as there is little relevance (from a cheminformatics point of view) of covering file formats that are developed for, e.g., specific molecular dynamics or quantum chemistry programs. Instead, we will dedicate this section to introduce the reader to today's most widely used, cross-platform, human-readable chemical file formats, with an emphasis on their use in database searching and other subfields of chem-informatics. Throughout these subsections, we will occasionally refer to the structural representation of L-phenylalanine (see **Fig. 1**) in the various file formats as a common example.

Before proceeding with the description of specific file formats, we make note of a convenient means for the interconversion of various chemical file formats. While many modeling software suites are capable of handling multiple file formats (and consequently, to convert them), computer programs dedicated specifically for this tasks also exist. Probably the best-known example is Open Babel, an open source software for the interconversion of chemical structures between an abundance of file formats (over 110 for the current version).[1] Also, we offer a quick overview of the contents of this section in **Table 1**.

3.14.2.1 Line Notation Formats

The principle of line notation formats is to store chemical structures unambiguously, but as compactly as possible (usually on a single line). In fact, the IUPAC Recommendations on Organic and Biochemical Nomenclature can be thought of as a line notation system as well.[2] (Though ironically it is not necessarily more human-readable than, e.g., the simplified molecular-input line-entry system (SMILES) format, especially for large molecules.) In that "format," the representation of L-phenylalanine would be *(2S)-2-amino-3-phenylpropanoic acid* (or somewhat less intuitively, *(2S)-2-azaniumyl-3-phenylpropanoate* for the zwitterionic form). While IUPAC names can unambiguously describe arbitrarily complicated molecules, the names themselves are often very complicated as well. Also, a substructure can usually be specified in multiple ways (depending on other groups, the order of priority, etc.), which essentially removes text-based IUPAC name queries from the toolbox of substructure searching.

From the available tools for chemical identification and documentation, today's standard is the CAS (Chemical Abstracts Service) Registry number.[3,4] CAS maintains a constantly updated database (the CAS Registry) to store every reported chemical structure (c.111 million at the time these lines are written) with a uniquely assigned identifier, the CAS Registry number (e.g., for L-phenylalanine: *63-91-2*). In addition to the database itself, the CAS Registry powers the two major chemical information services of CAS: Scifinder (for querying chemical structures and reactions, primarily in the literature)[5] and STN (a search engine that provides access to patent content).[6] While CAS Registry numbers are quite compact linear notations, they do not provide direct, human-readable information on molecular structure, or relation/proximity to another substance (e.g., the CAS number for racemic phenylalanine is *150-30-1*).

Efforts to provide compact means of chemical structure representation using line notations date back to the late 1940s when the Wiswesser Line Notation (WLN) was introduced.[7] Nowadays, multiple line notation formats are available. While we will only briefly cover those that are mostly of historic interest (e.g., WLN and ROSDAL), we introduce today's standard tools such as SMILES and International Chemical Identifier (InChI) in more detail.

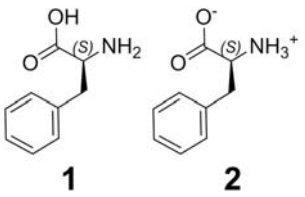

Fig. 1 Neural (1) and zwitterionic (2) forms of L-phenylalanine. The α-carbon is annotated with the absolute configuration of the stereogenic center.

Table 1 Chemical file formats presented in Section "**Chemical File Formats and Data Structures**"

Subsection	*Subsection*	*Comment*
Line notations	SMILES	The most widely used, human-readable line notation system and its extensions (e.g., SMARTS)
	InChI	A free, open-source and readily canonicalized line notation endorsed by IUPAC
	Other	Other, feature-rich or historically important line notation systems
Chemical tables	Ctab-based	The most widely used family of chemical table file formats, including *mol*, *sdf*, and *rxn* files
	Tripos *mol2*	A more flexible, free format file type, capable of storing various types of information
Other file types	PDB	A fixed format file type for macromolecules (introduced for the Protein Data Bank)
	FASTA	A compact format for storing DNA and protein sequence information
	CML	Chemical Markup Language, an XML-based free, open-source, portable, and versatile file format
	Structure recognition tools	Current solutions dedicated for the extraction of chemical structures from text and images

3.14.2.2 Simplified Molecular-Input Line-Entry System

SMILES was introduced by Weininger in 1987.[8] By that time, several line notation systems have already existed, and their flaws were also well known, which provided a need—but at the same time also a knowledge base—for the development of a mature, but easily understandable line notation language. SMILES provides a structure specification tool that is easily handled by both computers and humans, which is probably the main reason for its success in the past three decades. During this time, SMILES have become the de facto standard of molecular line notations, and a basis of inspiration for other line notation systems, such as SLN (see subsection "**Sybyl Line Notation**"). A concise overview of the format follows (a more complete documentation is available in the original SMILES paper[8] and on the website of Daylight[9]).

A SMILES string is a series of characters specifying primarily the heavy atoms (and optionally, hydrogens and bonds) of the molecule. Atoms are represented by their atomic symbols (first letter in upper case, second letter in lower case), and by default must be enclosed in square brackets: however, this is not required for elements in the "organic subset": *B*, *C*, *N*, *O*, *P*, *S*, *F*, *Cl*, *Br*, and *I* if the number of hydrogens conforms to the lowest normal valence minus those bonds that are explicitly given. Neighboring atoms are connected by bonds (single by default), and branches are enclosed in parentheses. Atoms in aromatic rings are denoted with lower case letters. Hydrogens must be explicitly specified by default, but they are implied in the absence of square brackets (which is most often the case). Single and aromatic bonds are implied, but they can be specified explicitly as well with "–" and ":", respectively (double and triple bonds are denoted by "=" and "#"). Attached hydrogens, charge, stereochemistry, and isotope numbers can be specified inside the square brackets of the given atom, e.g., *[15NH4+]* denotes an ammonium ion with a ^{15}N atom. As an example, SMILES strings of L-phenylalanine are provided in **Fig. 2**.

In the context of cheminformatics, canonicalization is a process through which a unique (*canonical*) representation of a molecule is achieved, which is essential for storing and identifying molecules in databases. Probably the greatest drawback of SMILES is the lack of an internal canonicalization approach: as seen on the above example, atoms can be mapped to the SMILES string in an arbitrary order. (In other words, while the conversion of SMILES to chemical structure is unambiguous, the inverse process is not, i.e., the relationship between SMILES and chemical structure is not *mutually unambiguous*.) While Weininger and colleagues have published a canonicalization algorithm shortly after the release of the SMILES format itself, their approach could not handle stereochemistry.[10] Moreover, this method was originally only included in the commercial software of Daylight,[11] resulting in many different variations of canonicalization being implemented in several cheminformatics toolkits. Recently, a universal SMILES representation based on the InChI canonicalization procedure was introduced by O'Boyle.[12] Schneider et al. have developed and published a robust, open-source, freely available SMILES canonicalization algorithm.[13] They conclude that their canonical labeling algorithm (which is also available in the open-source cheminformatics package RDKit[14]) "could be combined with the universal SMILES representation proposed by O'Boyle."

SMILES is also able to specify reactions. Notably, two available "grammars" for specifying reactions in SMILES are *reactant* ≫ *product* and *reactant* > *agent* > *product*. Disconnected molecules (e.g., two reactants) are separated by a dot (this is also available for single compounds that have, e.g., counterions). The functionality of SMILES has also been extended to support substructure querying and matching (SMARTS) and the description of generic reactions (SMIRKS). We will briefly cover these extensions in the following subsections.

3.14.2.3 Smiles Arbitrary Target Specification

Smiles Arbitrary Target Specification (SMARTS) is an extension of the SMILES language that was developed with the explicit intention to provide a query language for substructure searching.[15] As a result, any SMILES string is an acceptable SMARTS query by definition. To facilitate substructure searching, a number of additional features have been implemented for SMARTS, to allow for more general queries. These include atomic primitives (e.g., "**" denotes any atom, while *a* denotes any aromatic atom), bond primitives (e.g., "~" for any bond, "@" for any ring bond), and logical operators (e.g., "*!*" for *not*, "*&*" for *and*). Another interesting feature is recursive SMARTS, which enables to define an atomic environment starting with the atom of interest in the following form: *$(SMARTS)*. With these features, quite complex queries can be formulated, e.g., *C[$(aaO)&$(aaaN)]* would match any molecule that has a methyl carbon as a substituent of an aromatic ring with an oxygen in an *ortho* position and a nitrogen in a meta position. (For the reader's convenience, we refer to an easy-to-use, online SMARTS viewer.[16])

Like SMILES, SMARTS is able to handle, and in particular to query, reactions. A reaction query may consist of reactant, agent, and product parts (all optional), as introduced briefly above. The queries can be run against a set of "target" reactions (also specified in the SMILES format). Atom mapping is also supported in the query and the target, thus changes on a specific atom can be specified.

```
N[C@H](C(O)=O)Cc1ccccc1
[NH3+][C@@H](Cc1ccccc1)C([O-])=O
```

Fig. 2 SMILES strings of the neutral (*above*) and zwitterionic (*below*) form of L-phenylalanine. Breaking points of the phenyl ring are labeled as number 1. Attached hydrogens, charges, and stereochemical information are provided inside the square brackets. Note that the order of the substituents of the α-carbon is interchangeable but affects the specified stereochemistry of the α-carbon: looking from the nitrogen toward the α-carbon, the three following substituents (in sequential order) can appear counter-clockwise (@) or clockwise (@@).

For example, while C═O ≫ C−O would match any reaction that has a molecule with a C═O group on the reactant side and a molecule with a C−O moiety on the product side, [C:1]═O ≫ [C:1]−O is specific to the same carbon atom with a doubly bonded oxygen on the reactant side and a singly bonded oxygen on the product side. However, this would still match, e.g., a carboxyl group that is unchanged during the reaction as the oxygen was not specified to be the same atom on the reactant and product sides. Transformation of the double bond to a single bond is thus specified with the [C:1]═[O:2] ≫ [C:1]−[O:2] query. (However, to produce any matches, the atoms must be mapped in the target reactions as well!) A complete documentation of SMARTS is available on the website of Daylight Inc.[15]

3.14.2.3.1 SMIRKS

SMIRKS is a hybrid of SMILES and SMARTS, developed to provide a means to specify generic reactions.[17] It is a restricted version of reaction SMARTS with a set of rules that act as constraints. For example, the transformation of the oxo group in the SMARTS example above (see previous subsection) can be specified with the following SMIRKS transform:

$$[^*:1][C:2](=[O:3])[^*:4] >> [^*:1][C:2]([O:3][^*])[^*:4]$$

In some sense, SMIRKS can be considered the opposite of reaction SMARTS. While the latter can be used for querying already defined reactions, the former can be applied to enumerate reactions based on a generic reaction. A recent example is a paper of Guasch et al., describing the enumeration of ring-chain tautomers.[18] A complete description of SMIRKS is available on the website of Daylight Inc.[17]

3.14.2.4 Molecular Query Language

The Molecular Query Language (MQL) was developed in 2007 with the intention to provide a way to define more complex, feature-rich substructure queries.[19] MQL is based on the SMILES language and a context-free grammar, implementing concepts from Unix-style regular expressions such as brackets for grouping, "(…)?" for optional singular occurrence, "(…)*" for optional occurrence zero or more times, etc. MQL is open-source and was developed to be compatible with external cheminformatics toolkits, such as the Chemistry Development Kit (CDK).[20,21]

3.14.2.4.1 International Chemical Identifier

While it is slightly less human-readable than SMILES (especially for complicated structures), InChI is a fully featured, flexible, and standardized line notation.[22,23] It was developed with the support of IUPAC (International Union of Pure and Applied Chemistry)[24] with principal contributions from NIST (U.S. National Institute of Standards and Technology)[25] and is maintained by InChI Trust, a nonprofit organization established for this purpose.[26] This signifies some of the main advantages of InChI, i.e., that it is free, open-source and is maintained by a single organization (meaning that there are no concurrent, parallel implementations).

Compared to SMILES, InChI employs a greatly different logic (see **Fig. 3** for the InChI of L-phenylalanine as an example). An InChI code is made up of several layers separated with forward slashes ("/"), each of which presents specific information on the molecular structure. While some layers are mandatory, other layers (providing more subtle structural features) are optional. Hence, InChI is capable of providing molecular information at different levels of detail. We summarize the most important InChI layers and their syntax in **Table 2**.

A great advantage of InChI codes is that they are readily canonicalized at the time of generation, thus the relationship between substance and InChI code is mutually unambiguous. (Canonical atom numbers are assigned to elements in the order they appear in the empirical formula, i.e., first to carbons, then nitrogens, etc.) Further standardization was achieved with the introduction of the Standard InChI, which was designed to enable interoperability between large databases and web resources and "distinguishes between chemical substances at the level of 'connectivity', 'stereochemistry', and 'isotopic composition'."[23]

3.14.2.4.1.1 InChIKey

A drawback of InChI strings is that they can be really long for big molecules, which makes them unfit for web search queries. To remedy this deficiency, InChIKey, a compact hashed code derived from InChI was developed.[23] InChIKey compresses the information content of an InChI string to a fixed length of 27 characters in the following format:

AAAAAAAAAAAAAA-BBBBBBBBFV-P

```
InChI=1S/C9H11NO2/c10-8(9(11)12)6-7-4-2-1-3-5-7/h1-5,8H,6,10H2,
(H,11,12)/t8-/m0/s1
```

Fig. 3 InChI string of L-phenylalanine composed of the following layers: prefix ("InChI = 1S/"), empirical formula, skeletal connections ("/c"), hydrogens ("/h"), and stereochemistry, composed of three sublayers: tetrahedral centers ("/t") and two indicator layers ("/m" and "/s"). The InChI string for the zwitterionic form is identical to the neutral form, as they are derived from the same core parent structure and have the same number of protons.

Table 2 InChI layers and sublayers (with L-phenylalanine as an example, where applicable).[23]

Layer	*Syntax example*	*Comment*
Prefix	InChI=1/InChI=1S/	Denotes the major version number (currently 1, or 1S for standard InChI)
Formula	C9H11NO2	Represented according to the Hill convention (carbons first, then hydrogens, then other elements in alphabetical order). Canonical numbers are assigned to heavy atoms in the order they appear in the formula
Skeletal connections	/c10-8(9(11)12)6-7-4-2-1-3-5-7	Connections between skeletal atoms specified with their canonical numbers. Branches are specified in parentheses
Hydrogens	/h1-5,8H,6,10H2,(H,11,12)	Comma-separated list of the positions of hydrogen atoms in three sublayers: (i) bridging hydrogens (if applicable), (ii) immobile hydrogens, and (iii) mobile hydrogens. For L-phenylalanine, no bridging hydrogens are present, heavy atoms 1 through 5 (phenyl ring) and 8 (α carbon) are bonded to one hydrogen atom, while 6 (methylene) and 10 (nitrogen) to two. One hydrogen is shared between atoms 11 and 12 (carboxyl oxygens)
Charge	/q+1	Charge sublayer: net charge of the core parent structure
	/p+1	Protonation sublayer: net number of protons removed from or added to the core parent structure
Stereochemistry	/b4-3+	Z/E configuration of double bonds
	/t8-	Configuration of stereogenic centers
	/m0	Indicator sublayer of "/t": specifies the stereo arrangement relative to the canonicalized core parent structure ("/m0" for identical, "/m1" for inverse. Only for "/s1")
	/s1	Indicator sublayer of "/t": specifies if absolute ("/s1") or relative ("/s2") stereochemistry is provided
Isotopic	/i12+1	Specifies nonnatural isotopes. In the example: atom 12 consists of the isotope with mass increased by unity with respect to the natural value. May have its own stereochemistry sublayer
FixedH	/f10H3	Lists the exact positions of tautomeric (mobile) hydrogens. May have its own formula, charge, and stereochemistry sublayers

The first 14 characters encode the core molecular constitution (formula, connectivity, hydrogens, and charge), while the first 8 characters of the second block encode advanced structural features (stereochemistry, isotopic substitution, exact position of mobile hydrogens, metal ligation data). F is a flag for Standard (*S*) or nonstandard (*N*) InChI, V denotes the version (currently *A*, meaning version 1), and P is a protonation flag (*N* for neutral and other letters for various protonation states). By definition, the first block is the same for substances sharing the same molecular skeleton. As an example, the InChIKey of L-phenylalanine is: *COLNVLDHVKWLRT-QMMMGPOBSA-N*.

A key consideration in the design of the InChIKey was the compatibility with search engines. Thus, InChIKeys only contain uppercase letters and are restricted to a fixed length. While InChIKey collisions (i.e., two structures having the same InChIKey) are theoretically possible, their likeliness has been shown to be practically nonexistent in theory and in practice as well.[27] A disadvantage of InChIKey is that the chemical structure cannot be restored algorithmically. However, publicly available InChI Resolvers provide a lookup service for this task.[28]

3.14.3 Other Line Notation Formats

3.14.3.1 Wiswesser Line Notation

Once a widespread tool in chemical database searching,[29] the WLN is now mostly of historic interest. It was the first computer-processable line notation system, introduced in 1949.[7] It uses alphanumerical characters and a set of special characters (to indicate rings and substitution positions).[30] It makes use of letters not only to encode individual atoms, but also—quite intuitively—to denote common structural features (e.g., the letters *X* and *Y* denote branched chains of X- and Y-shapes). This approach has enabled a high degree of compactness (e.g., the WLN code for phenylalanine would be "*VQYZ1R*"—only six characters!), and WLN was applied for indexing large chemical databases, such as the Chemical Structure Index (CSI) or the Index Chemicus Registry System (ICRS).[31] However, the notation was error-prone and difficult to code, and with the advent of connection table formats, it has gradually lost its importance.

3.14.3.2 Representation of Organic Structures Description Arranged Linearly

The Representation of Organic Structures Description Arranged Linearly (ROSDAL) notation was developed in 1985 in the Beilstein Institute and has powered the Beilstein DIALOG system (or Beilstein-Online).[31] It is quite intuitive, but not easily readable: each atom (other than hydrogens) is assigned a unique number and the connections between the atoms are listed sequentially, e.g., for

phenylalanine: "1O-2=3O,2-4-5N,4-6-7=-12-7". As seen, heteroatoms (but not carbons) are specified with their chemical symbols, while bonds are denoted with the special characters - (single), = (double), # (triple), and ? (for any connection), and alternating bonds can be simplified, e.g., the substring denoting the phenyl ring is "7=-12". A great drawback of this notation is that atoms are arbitrarily numbered, and there is no unique representation of a molecule. Despite being mostly obsolete, some chemical drawing packages (such as ChemDoodle) still support the ROSDAL notation.[32] A common deficiency of WLN and ROSDAL is the lack of support for important structural features such as ions and stereochemistry.

3.14.3.3 Sybyl Line Notation

The SLN was developed at Tripos (now a subsidiary of Certara), and it was published in 1997.[33] In many senses, SLN is very similar to the SMILES notation although they employ different concepts regarding the representation of certain features. For example, in SLN, aromaticity is a property of the bonds, not the atoms (in contrast to SMILES): aromatic bonds are always explicitly represented with a colon. Each atom with a ring closure is assigned an ID number in square brackets (e.g., "*[1]*"), and subsequent connections to a previously defined ring closure atom are specified with a commercial at symbol, e.g., "@1". In addition, square brackets are also used to specify properties of atoms and bonds in a [*property=value*] format, e.g., a double dative bond is encoded by the following substring: "=[type=dative]". As an example, SLN strings for L-phenylalanine are provided in **Fig. 4**.

In 2008, the functionality of the SLN language was substantially expanded: support for reactions, queries, and virtual combinatorial libraries was implemented.[34] While SLN is a fully featured and versatile line notation language, its use is less common nowadays, possibly due to the decreased popularity of the Sybyl modeling suite.

3.14.3.4 Chemical Table Files

Chemical table files are the standard formats for the 3D representation of small molecules, but they are widely used to store 2D structures as well. Though not as compact as line notations, they are capable of storing specific 3D conformations, partial charges, database fields (such as molecular properties), etc. We briefly review the two most prominent tabular formats in this subsection: the Ctab-based format family (MDL molfiles) and the Tripos *mol2* format.

3.14.3.4.1 Connection table (Ctab)-based file types

Several file formats have been developed at Molecular Design Limited (MDL) that are built around the common concept of connection table (Ctab) blocks.[35] These include most notably *mol* files for storing a single molecule, *sdf* files (or SDfiles) for storing multiple molecules and associated data, as well as *rxn* and *rdf* files (or RDfiles) for storing single and multiple reactions, respectively. While the Ctab format is quite rich in features and optional fields, some of its functionalities are now rarely used or obsolete. Here we will only review its most important features, while we refer to the work of Dalby et al. for a more detailed description.[35]

The connection table (Ctab) consists of various blocks in a fixed order: the counts line, the atom block, the bond block, two optional blocks (atom list and Stext), and the properties block. The counts line specifies the total number of atoms and bonds in the molecule (among others), the atom and bond blocks list the coordinates (and other properties) of the atoms and the specification of the bond, while the properties block contains additional information on charge, radicals, isotopes, etc., and is always terminated by "*M END*". (See **Fig. 5** for the Ctab of L-phenylalanine.)

The Ctab itself is preceded by three lines—which can contain the molecule title and information about the program used for the production of the file—and is followed by data fields in *sdf* files, specified in a two-line format, where the first line is the *data header*—starting with ">" and specifying either the field name or the field number in the associated database—and the second line contains the data value. In multiple molecule formats (such as *sdf*), entries are separated with a line containing four dollar signs ($$$$).

While Ctab formats are "the closest thing cheminformatics has to a universally adopted standard," some argue that they are out-of-date.[37] It is worth noting that the format has been updated several times to resolve known issues. In 1995, the next-generation V3000 format was introduced by MDL (Molecular Design Limited) to overcome known limitations of the V2000 format, such as the hard limit on the number of atoms and bonds (999 in V2000) or the handling of partially defined stereochemistry. However, the position of V2000 as the de facto default format has been more or less unchanged ever since. In 2011, Clark proposed further changes to enable the handling of zero-order bonds and explicitly specified count of attached hydrogens in a backward compatible manner, thus extending the scope of Ctab files to store nonorganic substances, such as metal complexes.[38] Nonetheless, the superfluous atom specification and the lack of extensibility (among other known issues) constitute a valid base to criticism of the MDL Ctab format and call for an alternative, 21st century *lingua franca* for chemical information management.[39]

```
NC[S=S]H(C(O)=O)CC[5]H:CH:CH:CH:CH:CH@5
N[+]H3C[S=S]H(C(O[-])=O)CC[5]:C:C:C:C:C:@5
```

Fig. 4 SLN strings for the neutral (*above*) and zwitterionic (*below*) forms of L-phenylalanine. Hydrogens may or may not be specified explicitly. Formal charges are implemented as atomic properties, as well as absolute configurations, here specified with the "[S=S]" substring.

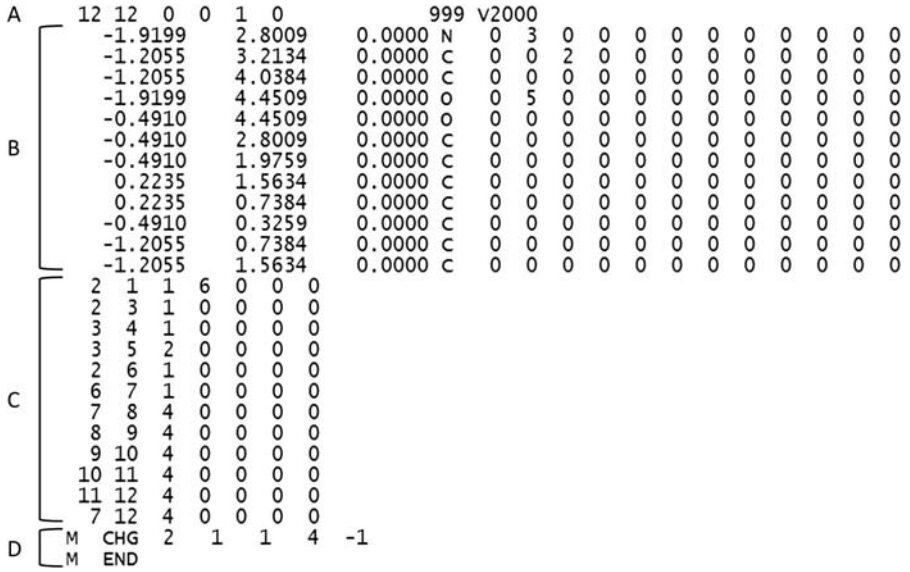

Fig. 5 Ctab block of the zwitterionic form of L-phenylalanine. (Written with Chemaxon Marvin.[36]) (A) The counts line contains the numbers of atoms and bonds (both 12), the chirality flag (1, as the molecule is chiral), the Ctab version (*V2000*), and some additional properties. (B) The atom block specifies the 3D coordinates, atom symbol, and various properties (such as mass difference, charge, hydrogen count) of each atom. In particular, the second column after the atom symbols contains formal charges (where 3 and 5 encode a charge of +1 and −1, respectively), and the third column specifies the atom stereo parity (see the work of Dalby et al. for a detailed specification).[35] (C) The bond block lists the bonds, specifying the numbers of the first and second atoms, the bond type (1 for single, 2 for double, etc.), the bond stereo specification, and a few additional properties. (D) The properties block can have a number of "*M XXX*" entries that specify additional properties and is always terminated by "*M END*". Here, the "*M CHG*" line specifies (from left to right) that there are two atoms with formal charges: atom number 1 with a formal charge of 1 and atom number 4 with a formal charge of −1.

3.14.3.4.2 Tripos mol2 format

Compared to Ctab files, the *mol2* format (developed at Tripos) offers a more flexible (and customizable) structure for chemical data storage.[40] One of the most important changes is that *mol2* files are "free format" files, meaning that the widths of the various data fields are not fixed. (Also, empty lines are ignored and comments can be specified on lines starting with #.) Additionally, a *mol2* file consists of so-called records (similar to the sub-blocks of the Ctab block) that may specify diverse types of information. Most of the records can be omitted, but the *MOLECULE*, *ATOM*, and *BOND* (and for some programs, the *SUBSTRUCTURE*) records are universally used. Other important features are the inclusion of partial charges by default and the concept of substructures, which effectively extends the usage of the *mol2* format to the domain of macromolecules (e.g., proteins). As a reference, the *mol2* entry of the zwitterionic L-phenylalanine is presented in Fig. 6.

Drawbacks of this file format include the lack of stereochemistry support in the absence of 3D coordinates, and the lack of a unified format specification: while *mol2* was originally developed for the Sybyl software suite of Tripos, now each program implements the *mol2* format with slight differences.

3.14.3.4.3 Other formats

The file formats covered so far are optimized for their usage in chemistry-related applications, mostly covering the domain of small molecules. The treatment of macromolecules (such as proteins and nucleotide chains) requires specific features, which led to the evolution of the specialized file formats of this domain. Of these, we will concisely cover the two that are probably most often encountered by computational medicinal chemists: pdb files and FASTA sequences. In addition, we briefly introduce the reader to novel chemical data management formats and tools, such as the Chemical Markup Language (CML) and structure recognition approaches.

3.14.3.4.4 Protein Data Bank file format (pdb)

The *pdb* format was introduced in 1992 as the official format specification of the Protein Data Bank (the standard global repository of experimentally solved macromolecular structures).[41] Since a great portion of medicinal chemistry-related modeling work deals with macromolecules, the use of *pdb* files is ubiquitous in this field.

Pdb files are fixed format, and they consist of single-line records (starting always with the record type). The diversity of record types allows for the specification of highly detailed information. Atom information is stored in *ATOM* and *HETATM* records (the latter is used for nonpolymer entries, such as waters or small molecules), while bond information is stored in *CONECT* records. Atom blocks (corresponding to polymer chains) are terminated with *TER* records. A more thorough overview of the different types

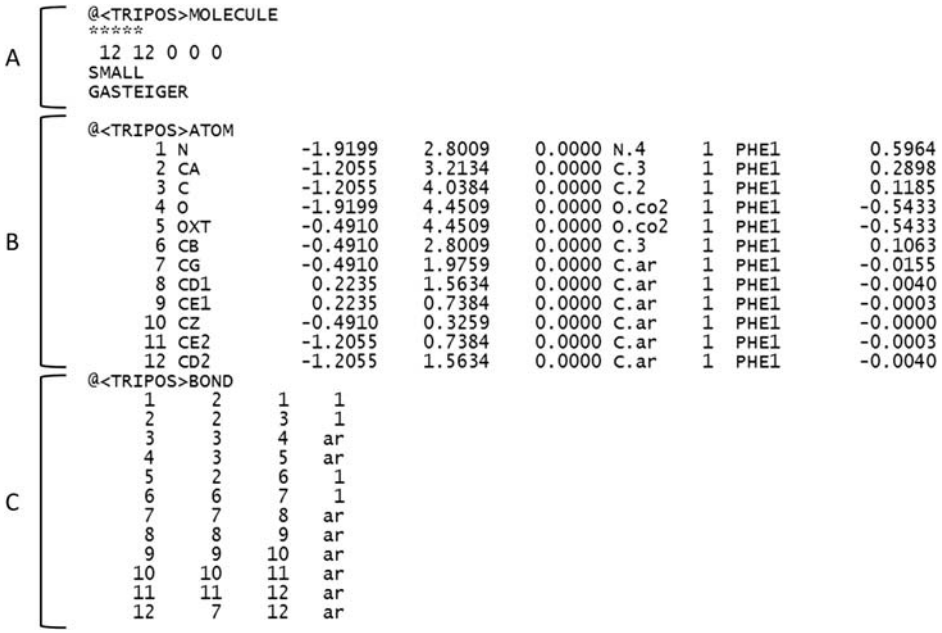

Fig. 6 Zwitterionic phenylalanine, *mol2* entry. (Written with Open Babel.[1]) (A) The *MOLECULE* record by default lists the molecule title (here, ***** denotes that it was not supplied), a line containing the numbers of atoms (12), bonds (12), substructures (0), features (0) and sets (0), the molecule type (*SMALL*), and the charge type (*GASTEIGER*). (B) The *ATOM* record lists the atoms in the following format: atom number, name, 3D coordinates, atom type, substructure ID, substructure name, and charge. (C) The *BOND* record lists the bonds in the following format: bond number, first and second atoms, and bond type (with *ar* for aromatic).

of records is provided in the official documentation of the PDB file format.[42] As an example, we provide the *ATOM* section of a phenylalanine residue from an actual PDB entry in **Fig. 7**.

A great advantage of the *pdb* format is the standard atom typing that was introduced for the common amino acids, nucleotides, cofactors, etc. These atom names are based on IUPAC rules,[43] and they are also listed in an appendix of the original *pdb* format documentation.[44] Their use eliminates the need to explicitly specify the bonds in the mentioned residue classes, saving a great amount of space in *pdb* files (however, they do have to be specified if nonstandard atom names are given).

Another widely used format for crystallographic data is the Crystallographic Information File (*cif*).[45,46] A merit of *cif* (in comparison with *pdb*) is that it is a free format—allowing for more flexibility (and removing any limitations on the number of atoms, residues, or chains). On the other hand, it is slightly less human-readable than *pdb*. By default, structures can be downloaded in both formats from the Protein Data Bank (in fact, the standard archive format of PDB is *PDBx/mmCIF*—a customized version of *cif*—since 2014).[47] In addition, an XML-based representation of the *pdb* format, PDBML (Protein Data Bank Markup

```
ATOM   4416  N   PHE A1116     108.052  79.091 -11.109  1.00 11.57           N
ATOM   4417  CA  PHE A1116     108.691  79.424  -9.827  1.00 11.89           C
ATOM   4418  C   PHE A1116     109.486  80.728  -9.898  1.00  9.97           C
ATOM   4419  O   PHE A1116     109.575  81.454  -8.905  1.00 10.78           O
ATOM   4420  CB  PHE A1116     109.613  78.293  -9.343  1.00 11.49           C
ATOM   4421  CG  PHE A1116     108.887  77.145  -8.708  1.00 14.69           C
ATOM   4422  CD1 PHE A1116     108.175  77.326  -7.518  1.00 12.55           C
ATOM   4423  CD2 PHE A1116     108.947  75.866  -9.275  1.00 13.15           C
ATOM   4424  CE1 PHE A1116     107.494  76.248  -6.919  1.00 14.21           C
ATOM   4425  CE2 PHE A1116     108.274  74.772  -8.673  1.00  8.56           C
ATOM   4426  CZ  PHE A1116     107.552  74.970  -7.505  1.00 10.32           C
ATOM   4427  H   PHE A1116     108.335  78.251 -11.595  1.00  0.00           H
ATOM   4428  HA  PHE A1116     107.933  79.481  -9.046  1.00  0.00           H
ATOM   4429  HB2 PHE A1116     110.172  77.891 -10.188  1.00  0.00           H
ATOM   4430  HB3 PHE A1116     110.309  78.683  -8.600  1.00  0.00           H
ATOM   4431  HD1 PHE A1116     108.143  78.299  -7.050  1.00  0.00           H
ATOM   4432  HD2 PHE A1116     109.511  75.703 -10.181  1.00  0.00           H
ATOM   4433  HE1 PHE A1116     106.929  76.404  -6.012  1.00  0.00           H
ATOM   4434  HE2 PHE A1116     108.325  73.792  -9.125  1.00  0.00           H
ATOM   4435  HZ  PHE A1116     107.034  74.142  -7.045  1.00  0.00           H
```

Fig. 7 *ATOM* section of a phenylalanine residue from a PDB entry. The record type (*ATOM*) is followed by the atom number, atom type, residue type, chain identifier, residue number, the 3D coordinates, the occupancy and temperature factor values, and element symbol (followed by the formal charge, where applicable). This example highlights a drawback of fixed format files: structures with more than 9999 residues would be problematic to represent, as only four character positions are specified for residue numbers (characters 23–26), and the format does not allow any overflow (character 22 is reserved for the chain identifier).

Language) has been developed and published, and is available in the Protein Data Bank.[48,49] While the XML implementation can provide better interoperability (see subsection "Chemical Markup Language"), this format currently lacks the compactness of *pdb* files.

3.14.3.4.5 FASTA

FASTA is a format that was introduced in a DNA and protein sequence alignment software of the same name, and it has been the de facto standard format for DNA and protein sequences ever since, owing to its simplicity.[50] It is essentially a sequence of one-letter amino acid (or nucleic acid) codes and special characters (*X* for any residue, – for gap, and * for sequence termination) with a single description line (the first line of the file, starting with ">").

Due to their compactness, *fasta* files (or more generally, one-letter amino acid sequences) are the ideal format for querying macromolecular databases on the basis of sequence identity/similarity. (This type of database querying is often needed in homology modeling and other domains of computational medicinal chemistry.) Such tasks can be decomposed to two (consecutive) questions: (i) how can I find the optimal alignment of two protein sequences, and (ii) how can I quantify the homology/similarity between the two aligned sequences?

While the basics of sequence alignments have been established as early as in the 1970 work of Needleman and Wunsch,[51] the BLAST (Basic Local Alignment Search Tool) algorithm (which is considered the standard tool for sequence-based similarity searches) was introduced in 1990 by Altschul et al.[52] In contrast to the approach of Needleman and Wunsch, which optimizes the overall alignment of the two sequences, BLAST is a local similarity algorithm, seeking only relatively conserved subsequences. BLAST (along with its numerous specialized versions) powers a web service of the same name, maintained by the National Center for Biotechnology Information (NCBI).[53]

For quantifying the similarity between two aligned sequences, scoring functions based on substitution matrices are usually applied. Substitution matrices contain additive score contributions for each possible exchange of amino acid A to amino acid B. After summing these score contributions, the alignment with a higher score is better. (The two most commonly used substitution matrix types are Point Accepted Mutation (PAM) matrices[54] and Blocks Substitution Matrices (BLOSUM).[55]) The introduction of gaps is usually allowed but penalized in the overall score. The BLAST web server also returns an Expect value (or E-value) for each alignment, which is the number of BLAST hits that are expected to result by chance with the observed score (or higher). While a low E-value alone does not prove that two sequences are homologous, it is a useful guideline to infer some sort of biological relationship.

3.14.3.4.6 Chemical Markup Language

The Chemical Markup Language (CML) is an application of XML (eXtensible Markup Language) for the management and integration of chemical data.[56] It was first introduced by Murray-Rust and Rzepa and has been extended numerous times in the following years.[57–64] The main goal of CML is to provide a portable data type that allows for the production of interoperable and reusable documents. In addition to chemical structure, it is capable of storing crystallographic, spectral,[63] and reaction[62] data and has been integrated with, e.g., RSS aggregators[61] and Microsoft Word.[65] It operates using various conventions, allowing for applicability by various subdomains of chemistry.[66] While CML provides interoperability with an explicit specification of properties via markup text, the *cml* format is still fairly compact in comparison with, e.g., the tabular file formats presented above. (The *cml* entry for L-phenylalanine is provided as an example in Fig. 8.) The Chemical Markup Language is entirely open-source and is developed on a voluntary basis. (In fact, it is considered as a project of the Blue Obelisk Movement, an Internet community dedicated to the development of open-source, interoperable cheminformatics software.[67]) Its flexibility, interoperability, and open-source implementation make CML (in the authors' opinion) a strong candidate for being the next-generation standard for chemical data storage and exchange.

Although it is independent of CML, we make note of a novel XML-based query language, the Chemical Subgraphs and Reactions Markup Language (CSRML).[68] CSRML was recently developed (together with the ChemoTyper software and the ToxPrint library) to support chemotypes as a novel approach in substructure querying. (Here, chemotypes are defined as a way of representing chemical entities with three objectives: they should be (i) publicly accessible, (ii) coded in a unique and reproducible manner, and (iii) capable of combining both connected and nonconnected chemical patterns as well as atom, bond, and molecule-based properties into a single query.) CSRML provides serious advancements over existing query languages in multiple respects, for example, it provides a way to produce canonical representations of queries (i.e., a query can be specified exactly one way). Also, complex queries can be formulated by defining chemotypes based on molecular properties (in addition to structural patterns). CSRML was developed based on the CML language, extending it with additional features.

3.14.3.4.7 Structure recognition tools

Besides the enormous amount of data that is publicly available in standard chemical information formats (such as those detailed above), chemical knowledge of similar (or even greater) multitude is gathered in "traditional" formats, such as text and images in scientific publications and patents. While the conversion of images and text to chemical data is manually cumbersome and time-demanding, recent advances in text mining and optical structure recognition (OSR) are already paving the way toward the seamless, automated processing of textual and pictorial chemical information. These applications provide researchers access to invaluable chemical information that can be utilized for many purposes, e.g., for supporting drug discovery and navigating in the intellectual property (IP) space. In this subsection, we present a brief overview of current sources and services dealing with chemical text mining

```
<?xml version="1.0" encoding="UTF-8"?>
<cml xmlns="http://www.xml-cml.org/schema" xmlns:convention="http://www.xml-cml.org/convention"
convention="convention:molecular" xmlns:marvin="http://www.chemaxon.com/marvin/marvinDictRef" version="ChemAxon file
format v16.02.15, generated by v16.4.25.0">
<molecule id="m1">
<atomArray>
    <atom id="a1" elementType="N" formalCharge="1" x2="-1.3336791218280317" y2="3.8500000000000054"></atom>
    <atom id="a2" elementType="C" x2="4.440892098500626E-15" y2="4.620000000000003"></atom>
    <atom id="a3" elementType="C" x2="7.105427357601002E-15" y2="6.160000000000004"></atom>
    <atom id="a4" elementType="O" formalCharge="-1" x2="-1.3336791218280273" y2="6.930000000000007"></atom>
    <atom id="a5" elementType="O" x2="1.3336791218280435" y2="6.930000000000003"></atom>
    <atom id="a6" elementType="C" x2="1.3336791218280039" y2="3.850000000000002"></atom>
    <atom id="a7" elementType="C" x2="1.3336791218280368" y2="2.310000000000002"></atom>
    <atom id="a8" elementType="C" x2="2.6673582436560745" y2="1.5399999999999978"></atom>
    <atom id="a9" elementType="C" x2="2.6673582436560714" y2="-2.220446049250313E-15"></atom>
    <atom id="a10" elementType="C" x2="1.3336791218280346" y2="-0.7700000000000000"></atom>
    <atom id="a11" elementType="C" x2="0.000000000000000" y2="1.9984014443252818E-15"></atom>
    <atom id="a12" elementType="C" x2="1.3322676295501878E-15" y2="1.5400000000000018"></atom>
</atomArray>
<bondArray>
    <bond id="b1" atomRefs2="a2 a1" order="1">
        <bondStereo>H</bondStereo>
    </bond>
    <bond id="b2" atomRefs2="a2 a3" order="1"></bond>
    <bond id="b3" atomRefs2="a3 a4" order="1"></bond>
    <bond id="b4" atomRefs2="a3 a5" order="2"></bond>
    <bond id="b5" atomRefs2="a2 a6" order="1"></bond>
    <bond id="b6" atomRefs2="a6 a7" order="1"></bond>
    <bond id="b7" atomRefs2="a7 a8" order="A"></bond>
    <bond id="b8" atomRefs2="a8 a9" order="A"></bond>
    <bond id="b9" atomRefs2="a9 a10" order="A"></bond>
    <bond id="b10" atomRefs2="a10 a11" order="A"></bond>
    <bond id="b11" atomRefs2="a11 a12" order="A"></bond>
    <bond id="b12" atomRefs2="a7 a12" order="A"></bond>
</bondArray>
</molecule>
</cml>
```

Fig. 8 CML entry for L-phenylalanine. (Written with Chemaxon Marvin.[36]) The <*cml*> element contains the CML specifications (such as the applied schema and convention), the <*molecule*> element summarizes all the sub-elements that belong to the given molecule (titled *m1* in this example). The <*atomArray*> and <*bondArray*> elements consist of <*atom*> and <*bond*> elements, respectively, with the relevant properties listed in a *name*="*value*" general format. It is worth noting that simultaneous storage of 2D and 3D representations is also possible with the *x2* and *y2* (2D structure), and the *x3*, *y3*, and *z3* (3D structure) attributes. (Here, only the 2D representation is stored.)

and image recognition. (Since a detailed review of the related techniques and methodologies would be out of the scope of this chapter, we only refer the reader to recent, well-written reviews in this respect.[69–71])

Currently the most complete set of chemical text mining tools is provided by ChemAxon in their commercial Chemistry Text Mining Suite.[72] The software package includes naming applications (such as Name to Structure), supports text mining from Asian languages (with Chinese Name to Structure and Japanese Name to Structure), and processes whole documents for extracting chemical data (Document to Structure) with the integration of current optical structure recognition software (see below). Most of these functionalities are also provided free of charge on the web server *chemicalize.org*.[73,74]

Current, freely available chemical text mining and named entity recognition (NER) tools include OSCAR (Open-Source Chemistry Analysis Routines),[75] CheNER (Chemical Named Entity Recognizer),[76] and OPSIN (Open Parser for Systematic IUPAC Nomenclature).[77] Although there are many challenges still unsolved in optical structure recognition—such as extracting chemical data from complex arrangements, such as SAR tables—this field is also quickly progressing. Several commercial and open source solutions are available as well, including CLiDE,[78] Imago,[79] OSRA,[80] and MLOCSR[81] (the latter two also operate as web services).

Since traditionally the analysis of the patent literature is a cumbersome task, possible applications in this sub-field provide great motivation for the development of text mining and structure recognition tools. In particular, Markush structures (i.e., generic representations of a compound class consisting of a core structure and multiple R-groups) are quite extensively used in patent documents.[82] Recent developments describe novel methods for the visualization of Markush structures,[83] as well as deconvoluting complex (nested) Markush structures,[84] mapping specific structures to Markush structures[85] or encoding and searching Markush structures.[86] Current research efforts also include the introduction of a unified Markush language for the two major Markush databases (CAS and Thomson Reuters "Derwent") with the potential to serve as a common, generalized description of Markush structures.[87] We anticipate that coupling these techniques with the text mining and OSR approaches mentioned above will effectively multiply the speed of patent analysis tasks, enabling the extraction of even more information from even more complex data structures than what state-of-the-art programs can currently handle.

3.14.4 Molecular Fingerprints

Fingerprints are an important and ubiquitous concept in the domain of cheminformatics. Their primary purpose is to provide numerical representations of the structure or certain features of molecules, thus enabling the quantification of the similarity of two molecules. While fingerprints are often represented as bit strings (streams of zeros and ones), in a general sense, any vector

of continuous, discrete, or categorical numerical values can be considered a fingerprint. Depending on the fingerprint, various similarity metrics can be used for similarity calculations between molecules. We will cover these options in detail in Section "Similarity—Dissimilarity Measures, Distance Metrics."

In general, molecular fingerprints are not applicable for chemical data storage, as they are generated with algorithms that, e.g., check for the presence of a predefined set of substructures or use hashing functions to set the values of certain bits in a bit string—thus converting fingerprints back to structures is not possible for most fingerprint types. This is not necessary however, as there are various options for the compact storage of 2D structures, as well as for more detailed representations including 3D structures and an arbitrary number of molecular properties, including even molecular fingerprints (see Section "Chemical file Formats and Data Structures").

On the other hand, various molecular fingerprints are used in ligand-based virtual screening approaches. In typical setups, novel bioactive molecules are sought based on their similarities to one or more reference compounds with known activity profiles. The greatest advantages of fingerprint-based virtual screening approaches are computational feasibility and minimal setup and configuration requirements.[88] On the other hand, fingerprint-based methods often fail to identify activity cliffs,[89] and their performance depends greatly on the particular fingerprint type.[90] (Although the latter issue can be addressed with data fusion techniques,[91] which we cover in more detail in Section "Similarity—Dissimilarity Measures, Distance Metrics.") Fingerprint similarity searching was compared to other virtual screening methods (such as shape similarity searching and ligand docking) in several works, with varying conclusions, but such comparisons are out of the focus of the present work.[92–94]

This section is dedicated to a thorough overview of current fingerprinting methods, an at-a-glance summary is provided in Table 3. Before moving on to an itemized description, however, we highlight some recent, well-written reviews of this field,[88,95] as well as some detailed, in-depth analyses of molecular fingerprints, dealing primarily with the similarities and differences among the fingerprinting methods themselves,[90] and the effects of various parameters (such as the addressable space, atom-typing schemes, and bit scaling rules) on fingerprints and their virtual screening performances (in particular on hashed fingerprints implemented in Schrödinger's Canvas).[96,97] In addition, a review by Heikamp and Bajorath summarizes fingerprint engineering strategies, i.e., methods for designing fingerprints with an optimized search performance.[98]

Addressing the need for standardized methods for the evaluation and comparison of fingerprints and their screening performances, Riniker and Landrum have assembled and published a standard benchmarking platform for fingerprints,[99] based on the open-source RDKit cheminformatics toolkit.[14] Earlier, the same authors have published *similarity maps*, a useful, open-source tool for the visualization of atomic contributions to the similarity between two molecules, which—depending on the fingerprint method—is not always straightforward to see.[100]

While a comprehensive collection of cheminformatics and molecular modeling applications have recently been published by Cereto-Massagué et al.[88] (and we also refer to them throughout this chapter), we make note of Cinfony, a Python-based common application programming interface (API) for integrating several cheminformatics toolkits, including Open Babel, RDKit, CDK, and others ("the toolkit of cheminformatics toolkits").[101,102] Another, recent addition to the set of publicly available fingerprint-related tools is ChemDes, an online platform capable of generating a rich selection of molecular fingerprints and descriptors, integrating the functionality of multiple popular cheminformatics packages.[103,104] While the former encompasses a larger scope of functionality, the latter offers a user-friendly graphical interface.

3.14.4.1 Substructure Key-Based Fingerprints

In key-based fingerprints, the bits are set according to the presence or absence of predefined substructures (*structural keys*), as shown in Fig. 9. The fingerprint length is determined by the number of structural keys, and each bit corresponds of a single, specific key. While key-based fingerprints are useful for molecules that are likely to be covered by the structural keys, the treatment of novel or

Table 3 Fingerprint types discussed in Section "Molecular Fingerprints"

Subsection	*Subsection*	*Comment*
Key-based		Fingerprints based on predefined substructure keys, such as MACCS
Topological	Path-based	Hashed fingerprints based on linear or branched fragments, e.g., Open Babel FP2 or OpenEye Tree fingerprints
	Circular	Hashed fingerprints based on circular atom environments, including the popular ECFP
	Topological subsets	Fingerprints based on other topological subsets, such as atom pairs or topological torsions
	Pharmacophore	Fingerprints based on a 2D or 3D representation of pharmacophore features
Hybrid		Fingerprints based on more than one concept, or optimized for a predefined goal
Other	Text-based	SMILES-based fingerprints employing text-processing algorithms
	EDPrints	Electron Density Fingerprins, based on chemical shifts and partial atomic charges
	Affinity	Fingerprints based on measured or predicted biological activities/affinities
	Interaction	Protein–ligand interaction fingerprints based on cocrystallized or docked complexes
	FLAP	Fingerprints for Ligands and Proteins: molecular interaction field (MIF)-based pharmacophore fingerprints
	Reaction	Extensions of molecular fingerprints to encode reactions

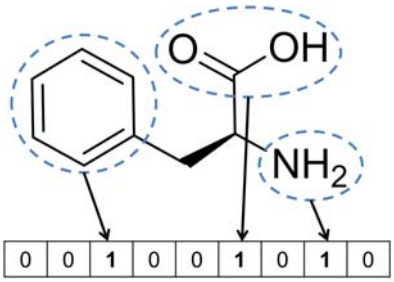

Fig. 9 In substructure key-based fingerprints, bits are set according to the substructures that are present in the molecule. (**1** or "on" if the given substructure is present and **0** or "off" if absent.) Thus, each bit position corresponds to a specific substructure.

less common substructural features is problematic. Nonetheless, several programs allow for customized keysets, thus the substructural keys can be easily updated, if needed.

Key-based fingerprints account for a set of specific structural features, which limits their ability to identify molecules that are similar to the query (on the level of, e.g., atom environments) but contain diverse fragments, rings, ring systems, etc. (In contrast, this is usually considered advantageous for several applications in drug discovery, such as hit expansion or scaffold hopping.) On the other hand, they are the tools of choice if the aim is to retrieve molecules that contain identical substructures with those found in the query molecule. As such, the use of key-based fingerprints with similarity metrics can be thought of as a transition between substructure searching and similarity searching. (In fact, structural keysets were historically used for substructure searching: in this case, molecules that did not have the same bits set as the query molecule were filtered out.[105])

MACCS (for Molecular Access System, a program developed by MDL) can be considered the prototype of key-based fingerprints—or at least it is the best-known. It was developed by MDL (Molecular Design Limited, now a subsidiary of BIOVIA[106]) and has two variants: one contains 166 keys, while the other contains 960 keys. While the former is almost universally implemented in cheminformatics applications (e.g., in RDKit[14] or Open Babel[1]), the latter is quite rare (it is available in BIOVIA's Discovery Studio, however[107]). The reason for the popularity of the 166-bit version is that while short, it covers most of the interesting features for drug discovery and virtual screening.[88] However, its application in virtual screening is somewhat ambiguous: while MACCS fingerprints show reasonably good retrieval rates in the work of Bender et al.,[90] they clearly perform weakly in the comparative study of Sastry and colleagues.[96] Nevertheless, Durant and colleagues have published useful guidelines for the reoptimization of MACCS keys, allowing for its optimization for specific scenarios.[108]

The PubChem fingerprint consists of 881 structural keys that encode quite diverse features.[109] It can be divided into seven sections, each corresponding to a given feature type (e.g., atom counts, bonded atom pairs, rings, etc.). It is implemented in the PubChem database for similarity searching, as well as some cheminformatics toolkits, such as CDK.[20,21] Further examples of key-based fingerprints include the modifiable BCI (Barnard Chemical Information Ltd., now Digital Chemistry) fingerprints,[110] two fingerprints of Open Babel (termed FP3 and FP4),[1] and two fingerprints implemented in CDK, based on the work of Klekota and Roth (a set of "privileged" substructures for biological activity),[111] and the electrotopological state formalism of Hall and Kier.[112]

A somewhat special substructure-based fingerprint is the set of MQNs (molecular quantum numbers) introduced by Nguyen et al.[113] MQNs are a set of 42 integer value descriptors of molecular structure, which count atoms, bonds, polar groups (such as H-bond donors and acceptors), and topological features (such as five-membered rings or acyclic tetravalent nodes). Consequently, they are not "traditional" key-based fingerprints in the sense that instead of encoding the presence or absence of substructures (either 0 or 1), they encode substructure counts. (On the other hand, feature counts are much more commonly applied in topological fingerprints, as detailed in the next subsection.) MQNs were primarily introduced as a tool to define, analyze, and visualize large chemical spaces (i.e., large databases), for which principal component analysis is proposed as a convenient dimension reduction method.[114]

3.14.4.2 Topological Fingerprints

Many molecular fingerprinting methods are inspired by more abstract concepts than substructure matching. In general, these methods perceive unique, nonpredefined (sub)structural features of molecules. Since there are no predefined substructures, no bit positions are assigned to specific features. Instead, mapping the features to a bit position (or more bit positions) is usually carried out with an appropriate *hashing function* (thus, topological fingerprints are often referred to as *hashed* fingerprints). Since the number of bit positions (the length of the fingerprint or *addressable space*) is finite, it can occur that two features are mapped to the same bit position: this phenomenon is called a *bit collision*. Bit collisions cause a loss of information and have been shown to deteriorate virtual screening performance in the work of Sastry et al.[96] (They can be avoided by increasing the addressable space although that results in a loss of speed as the individual fingerprints get larger.) Due to the possibility of bit collisions, hashed fingerprints would be—by default—inappropriate for substructure searching. However, with a large enough addressable space, the frequency of bit collisions becomes negligible: in this case, substructure searching can be carried out in the same way as mentioned in the previous subsection.

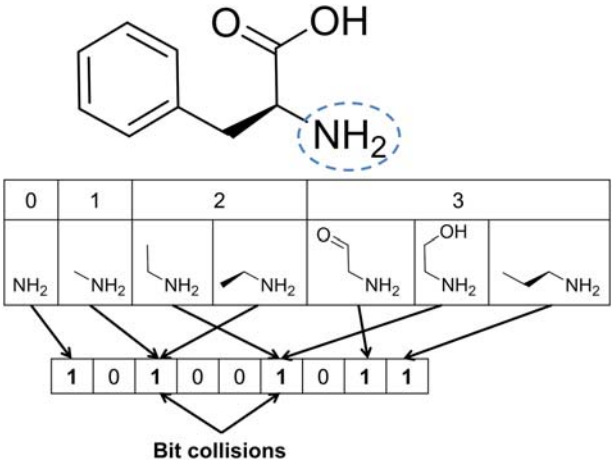

Fig. 10 In path-based fingerprints, linear (or in some cases, branched) paths up to a certain length (here three bonds) are enumerated and encoded. (In this example, the paths start from the nitrogen atom of L-phenylalanine, but in practice, the procedure is repeated for each heavy atom.) Note that depending on the applied fingerprint, the two paths (fragments) with 2 bonds of length can be treated as identical or different: this depends on the atom-typing scheme used (see main text).

3.14.4.3 Path-Based Fingerprints

Path-based topological fingerprints operate by enumerating all fragments of a molecule based on linear or branched paths up to a certain number of bonds and hashing them to the addressable space (see **Fig. 10** as an example). This removes the limitation of predefined substructures, i.e., any imaginable molecule produces a meaningful fingerprint.

An early example of path-based fingerprints is the Daylight fingerprint, consisting of 2048 bits and encoding all possible connectivity pathways of a molecule up to a predefined length.[115] (Interestingly, the original implementation employed a pseudorandom number generator as the hashing function that produces typically 4 or 5 bit positions per pattern.) The Daylight fingerprint and its variants are still popular: for example, Open Babel has implemented a similar fingerprint (FP2), which consists of 1024 bits and enumerates fragments with 1–7 atoms.[1]

For generating path-based fingerprints, a variety of atom-typing schemes are available. In Pipeline Pilot, functional classes (similar to pharmacophore features), A log*P* codes and *mol2* atom types can be used for this purpose (besides element types).[116] For example in **Fig. 10**, the two paths (fragments) with 2 bonds of length would be treated as identical (N-C-C) if element symbols are used for atom typing, but they are differentiated by mol2 atom types (N-CA-C vs. N-CA-CB, see **Fig. 6** for reference). Schrödinger's Canvas implements an even wider set of atom-typing schemes, ranging from "generic" (where all atoms and bonds are equivalent) to complex ones such as RTXHB (which takes into account ring size, aromaticity, H-bond acceptor/donor type, etc.).[117] Both programs implement the possibility to account for feature counts (rather than the mere presence or absence of the features), while Canvas also includes a variety of bit scaling rules to account for the fact that larger fragments (features) usually dominate the frequency distribution.[96]

Some path-based fingerprints employ an extended representation of molecular paths (or fragments) by involving branched fragments in the fingerprint generation. Notable examples are OpenEye's Tree fingerprints[118] and Schrödinger's Dendritic fingerprints.[117]

3.14.4.4 Circular Fingerprints

Instead of paths, circular fingerprints encode circular atom environments starting from the central atom and expanding to a given diameter. Circular fingerprints cannot be used for substructure searching (since a particular substructure in a different environment sets a different bit) but are ideal (and popular) choices for similarity searching. Two typical examples for circular fingerprints are Molprint2D and extended connectivity fingerprints.

Molprint2D was introduced in 2004 by Bender and colleagues.[119] This fingerprint encodes atom environments (for each heavy atom) within a distance of two bonds in the following way: the atom types found at distances of one and two bonds are listed and converted to the form *type-freq-distance*, where *freq* is the number of *type* atoms at the given *distance* from the central atom. These entries are sorted by distance and then by type, and hashed to a bit position. A 3D version called Molprint3D was also developed and published in the same year.[120] Molprint2D is available in many software packages, including Open Babel[1] and Canvas.[117]

Extended connectivity fingerprints (ECFP) can be considered as the de facto standard of circular fingerprints. They were first introduced in 2000 in Pipeline Pilot[116,121] but have since been implemented in various cheminformatics packages, including ChemAxon's JChem[122] and Schrödinger's Canvas.[117] A thorough description of extended connectivity fingerprints was published in 2010 by Rogers and Hahn.[123]

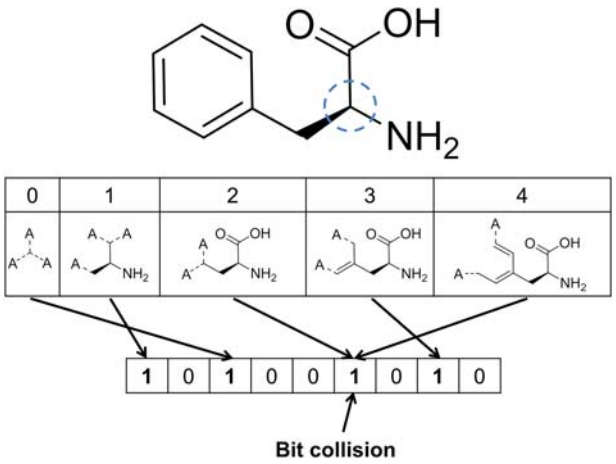

Fig. 11 Extended connectivity fingerprints encode full atom environments up to a predefined diameter (here, 4 bonds). For the terminal atoms, any other bonds (that are not part of the fragment) are also accounted for (here, the letter "A" denotes "any atom"). In this example, the central atom is the α-carbon, but in practice, the procedure is repeated for each heavy atom.

ECFPs are based on a modified version of the Morgan algorithm, which was originally introduced as a solution for the molecular isomorphism problem, i.e., to determine whether two molecules—with different atom numberings—are the same.[124] The ECFP generation process consists of three consecutive steps: (i) initial assignment, where each atom has an integer identifier assigned to it (based on atomic properties, such as atomic number, formal charge, etc.); (ii) iterative updating, where each atom identifier is updated to an array containing the atom identifiers of the central atom and the neighboring atoms (up to n bonds of distance, where n is the iteration number), which is hashed back into a new, single-integer identifier; and (iii) duplicate removal, where multiple occurrences of the same feature are removed (or counted, if feature counts are requested). The process is illustrated in Fig. 11.

ECFPs are highly customizable: in particular the diameter, the addressable space, the consideration of feature presence/absence vs. feature counts, and the atomic properties used for generating the atom identifiers are all influential parameters that affect the virtual screening performance either slightly or substantially. In Pipeline Pilot, there are a number of options for atom typing (similar to path-based fingerprints), such as *mol2* atom types, functional classes or Alog*P* codes and the diameter is variable as well. To distinguish between the various alternatives, a naming convention was introduced: *xyFz_n*, where *x* is the atom typing (*E* for atom type, *F* for functional class, *A* for Alog*P* code, and *S* for Sybyl *mol2* atom type), *y* is the fingerprint type (*C* for extended connectivity, *P* for path fingerprints), *z* indicates the presence/absence of a feature (*P*) or feature counts (*C*), and *n* is the diameter (e.g., ACFC_4 would be an extended connectivity fingerprint with Alog*P*-based atom types, a diameter of 4 and feature counts). Canvas includes some other options for configuration, such as bit scaling and bit filtering rules, while in JChem, the atomic properties used for identifier generation are highly customizable, and the whole configuration can be supplied in an *xml* file.

3.14.4.4.1 Topological subsets

Besides paths and circular atom environments, other topological subsets can also be used for fingerprint generation. Here, we briefly mention two examples whose theoretical basics have been laid down about 3 decades ago but are still implemented in current software packages.

Atom pairs have been introduced in 1985 by Carhart et al. as a topological descriptor for structure–activity studies.[125] Two years later the same laboratory published topological torsions for the same purpose.[126] The authors have also developed an atom-typing scheme for these descriptors, where an atom is characterized by its element type, the number of its heavy (i.e., nonhydrogen) neighbor atoms, and the number of its π electrons (e.g., the α-carbon of L-phenylalanine has three heavy neighbors and zero π electrons, so it could be represented as *C_3_0*). While alternative atom types (based on physicochemical properties) have been proposed by Kearsley et al., no general superiority is observed for any of these atom-typing schemes.[127]

Atom pairs are defined as two atom types and the topological distance (i.e., number of bonds in the shortest path) that separates them and are calculated for each pair of atoms in the molecule to produce the (hashed) atom pair fingerprint. For a molecule with n heavy atoms, the total number of atom pairs will be $n^*(n-1)/2$. On the other hand, a topological torsion is defined as four, consecutively bonded atom types and represent the topological analogue of the basic conformational element, the torsion angle. Similar to atom pairs, topological torsions are also enumerated for each quartet of consecutively bonded atoms of the molecule and hashed to a fingerprint.

The two descriptors capture different aspects of molecular topology. For example the original authors note that while atom pairs are generally sensitive to small changes (e.g., changing a single atom changes the $n-1$ atom pairs involving that atom), topological torsions provide local information and are hence less sensitive to such small local changes. In addition, atom pairs and topological torsions have provided a conceptual basis for the development of further, similar methods, such as geometric atom pairs (the 3D

analogue of atom pairs)[128] or fluorine environment fingerprints (a specialized implementation of topological torsions, focusing on fluorine atoms).[129] Meanwhile, the two core methods are implemented in a number of current software packages, including Canvas[117] and RDKit.[14]

APfp, a 2D atom pair fingerprint (not to be confused with the APFP_n fingerprints of Pipeline Pilot) published recently by Awale and Reymond is a simplified version of the atom pair fingerprints detailed above.[130] APfp is a set of 20 integer values, counting the total number of atom pairs in a molecule at distances of 1–20 bonds, while Xfp is a related 55-dimensional extended fingerprint that also encodes atomic properties: both have been shown to perceive molecular shape quite effectively. 3D analogues of these methods (based on through-space distances and atom pair Gaussian functions) have been published in 2015 by the same research group.[131]

3.14.4.5 Pharmacophore Fingerprints

While the category of pharmacophore fingerprints substantially overlaps with the fingerprints that were already covered (e.g., topological fingerprints with "functional class" or similar atom-typing schemes), we dedicate a separate subsection for pharmacophore fingerprints as a group of methods that are based on different considerations or design concepts. Pharmacophore fingerprints employ a similar concept to that of atom pair fingerprints (see previous subsection) in the sense that they provide a simplified representation of key interacting atoms/groups (i.e., pharmacophores), which are not necessarily bonded to each other—they can be separated by any number of bonds. On the other hand, in pharmacophore fingerprints, subsets consisting of more than two (typically three or four) features are often encoded: these subsets are called three[132,133] and four-point pharmacophores, respectively.[134] In addition to comparing and screening small molecules, pharmacophore fingerprints can also be used for protein-binding site similarity calculations.[135]

Among popular software packages, the Molecular Operating Environment (MOE) is particularly rich in pharmacophore fingerprints, with a total of seven choices, encompassing two-, three-, and four-point pharmacophores.[136] The two-point fingerprints TGD (Typed Graph Distances) and TAD (Typed Atom Distances) can be considered an implementation of atom pair and geometric atom pair fingerprints, respectively, with a different atom-typing scheme (H-bond donor, H-bond acceptor, cation, anion, hydrophobic, polar). Thus, TGD uses a 2D (graph-based) representation of the molecule, while TGT uses a 3D conformation. The three-point fingerprints TGT (Typed Graph Triangles) and TAT (Typed Atom Triangles) are extensions of TGD and TAD, using triplets of atoms instead of pairs. It was shown that the implementation of overlapping atom types, as well as feature counts, could improve the virtual screening performance of TGT fingerprints.[137] GpiDAPH3 and piDAPH3 are also three-point pharmacophore fingerprints, but they employ a different atom-typing scheme, in which atoms are differentiated based on three properties (in π system, is H-bond donor, is H-bond acceptor; a total of eight possible combinations). GpiDAPH3 is graph-based, while piDAPH3 is 3D conformation-based. The four-point fingerprint piDAPH4 is an extension of piDAPH3, which considers quartets of features instead of triangles. 2D (configurable) pharmacophore fingerprints are also available in JChem[122] and RDKit,[14] while 3D (three- and four-point) fingerprints are available in Canvas.[117]

3.14.4.6 Hybrid Fingerprint

In a general sense, the term "hybrid fingerprint" encompasses any method that utilizes more than one fingerprinting concept, but in a wider sense, we can also include in this definition single fingerprints that are optimized *post hoc* based on some known rationale or predefined goal.

An early example is the Unity 2D fingerprint of Tripos (now Certara), which is a 988-bit fingerprint that includes both structural keys and path fragments.[138] More recently, Xue and colleagues have introduced the concept of MFPs or "minifingerprints" (short binary fingerprints)[139] and designed various improved fingerprinting methods,[140] including MP-MFP, a hybrid fingerprint that contains 61 property-based and 110 structural key-based bits.[141] The more recent PDR-FP (Property Descriptor Range Fingerprint) employs solely property-based descriptors, selected systematically to correlate with activity-relevant molecular features.[142]

A common design concept behind these fingerprints is the selection of the most relevant pieces of information that will constitute the final fingerprint, which is often shorter than "traditional" fingerprints but retains their screening performance (or even improves upon it). In general, there are two (somewhat alternative) principles that underlie the design of such hybrid fingerprints: the recombination of bits (or features) from two or more different fingerprints[143,144] and the weighting (or scaling) of the bits (or features) of a single fingerprint, based on relative importance.[145,146] (The latter is not to be confused with the bit scaling rules implemented in Canvas, which is related to the feature counts of certain fingerprints.[96,117]) Due to their highly customized implementation, hybrid fingerprints can provide serious improvements over individual fingerprints even in tasks that are traditionally considered to be particularly difficult for 2D fingerprints—such as scaffold hopping.[144,147]

3.14.4.7 Other Fingerprint Types

All of the fingerprint methods presented so far are based (one way or another) on the topology or structural features of the molecules. In this subsection, we present several additional fingerprint types that are based on slightly or radically different ideas. (Nonetheless, these fingerprints are influenced by the molecular topologies as well, but this influence is more or less indirect.)

3.14.4.7.1 Text-based

SMILES strings (see subsection "Simplified molecular-input line-entry system") are very compact representations of molecular structure. Thus, it has been proposed that introducing a means to compare SMILES strings (and calculate their similarities) would speed up virtual screening, since the generation of molecular graphs or connection tables could be omitted. Here, we briefly include two, conceptually diverse SMILES-based fingerprints, LINGO and SMIfp. For a recent, detailed comparison of SMILES-based similarity methods, we refer to the work of Öztürk et al.[148]

LINGO is based on the fragmentation of the SMILES string into substrings.[149] In particular, "a q-LINGO is a q-character string, including letters, numbers, and symbols, such as *(,)*, *[,]*, #, etc. obtained by stepwise fragmentation of a canonical SMILES molecular representation." For producing these substrings, LINGO uses canonical SMILES strings. (Although multiple SMILES canonicalization approaches exist—see subsection "Simplified molecular-input line-entry system," the use of alternative canonicalization schemes provides very similar or identical results for property or similarity calculations, as long as the same canonicalization scheme is used consistently for the whole process.) For a SMILES string of length n, $(n-q+1)$ substrings of length q are extracted, and their occurrences are counted to provide the final LINGO profile. Such profiles can be thought of as fingerprints, and their similarities can be calculated with, e.g., the Tanimoto coefficient.

In contrast, SMIfp applies a fixed-size chemical space by counting the occurrences of 34 different symbols in the SMILES strings.[150] For SMIfp, the *city block* (or Manhattan) distance is proposed for similarity calculations. This combination has been shown to perform well in recovering several series of active molecules from multiple databases. SMIfp powers a series of SMIfp-browsers for searching popular chemical databases, available at the website of the authors.[151]

3.14.4.7.2 EDPrints

The recently developed EDPrints (Electron Density Fingerprints) approach of Kooistra et al. is based on a unique idea: chemical shifts (i.e., shifts in frequency of NMR spectroscopy signals), as well as partial atomic charges can represent the particular molecular environment of an atom (due to the asymmetric distribution of electrons in chemical bonds).[152] Therefore, both values are useful representations of the chemical and structural properties of molecules, thus they can be utilized in the construction of a fingerprint (as alternatives to the topology of the molecule). In EDPrints, ^{13}C and ^{1}H chemical shifts are calculated with the BatchNMRPredictor program,[153] and Merck molecular force field (MMFF94)-type nonpolarized partial atomic charges are calculated with Balloon.[154] These values are transformed into nonnegative integers and mapped to a bitstring, where each bit position reflects a particular descriptor value. The authors have found that EDPrints is able to achieve similar (and sometimes better) screening accuracies compared to other 2D ligand-based screening methods and exceeds their speed in terms of the time needed to compare a pair of molecules.

3.14.4.7.3 Affinity fingerprints

Instead of focusing on the molecular structure, affinity fingerprints encode the experimentally determined binding potencies of a compound against several target proteins. (Hence, an activity fingerprint is by default a vector of real numbers.) The concept was introduced in 1995 in the work of Kauvar et al., reporting the design of a small reference panel of eight proteins, which was used to define the affinity fingerprints of 122 structurally diverse compounds.[155] With the application of statistical methods (in particular, multivariate regression techniques), the authors were able to predict binding potencies quite effectively and concluded that affinity fingerprints can be useful tools in a number of applications, including chemical classification, compiling diversified chemical libraries, and guiding combinatorial chemistry efforts. Interestingly, a linear combination of the measured binding affinities can provide quite precise predictions for the binding affinities to proteins that are not included in the panel.[155,156] The methodology was further elaborated and compared with a structural fingerprint (MOLSKEYS) by Dixon and Villar.[157] Possibly the best-known and most extensively used public reference panel is the cancer cell line panel operated by the National Cancer Institute (NCI).[158] The panel consists of 60 human cancer cell lines, on which 50-percent growth-inhibitory concentrations (GI50) are determined for compounds submitted by research groups from around the world, and the results are published in NCI-operated databases.

The concept of affinity fingerprints was later expanded to *in silico* data with the introduction of "virtual affinity fingerprints," encoding interaction energies derived from docking (instead of experimentally determined affinities).[159] Since docking was not (and is still not) a reliable method for the prediction of ligand affinities, Bender and colleagues have introduced "Bayes Affinity Fingerprints" as an alternative of virtual affinity fingerprints.[160] In this approach, class-specific Bayes models are employed to predict a wide panel of bioactivities, and the resulting Bayes scores constitute the Bayes Affinity Fingerprint. Besides reporting consistently higher retrieval rates compared to ECFP_4 fingerprints, another valuable conclusion of the study is that information-optimal "bioactivity spaces" of low dimensionality can be utilized to answer complex questions about bioactivity profiles, e.g., "can I modulate off-target activity B independently of on-target activity A?". (A more general formulation of this question would be "can I predict possible targets for an arbitrary molecule?", which is the main question of an approach called target fishing that can be considered the inverse process of virtual screening.[161]) An alternative approach for the prediction of affinity fingerprints, called PASS (Prediction of Activity Spectra for Substances) was introduced in 2000[162] and was successfully applied in many subsequent works, including the discovery of novel cognition enhancers.[163] The further development of biological fingerprints—and chemogenomics (the study of systematic relationships between targets, based on their ligands) in general—was reviewed by Bender et al.[164]

3.14.4.7.4 Interaction fingerprints

As the name suggests, instead of chemical features, interaction fingerprints (IFP) encode information about the interactions between the molecule and its environment, usually a protein target. In this manner, protein–ligand complexes resolved with X-ray crystallography (or other experimental methods) or predicted with docking (or other computational methods) can be processed and compared. Consequently, interaction fingerprints can mostly be utilized in docking-based virtual screens or database analysis studies.

Interaction fingerprints consist of a fixed number of bits per residue, corresponding to a predefined set of general or specific interactions between the ligand and the residue. These interactions are checked based on standard cutoffs (in terms of, e.g., H-bond distance or angle), and the corresponding bits are set to either 1 (there is an interaction) or 0 (no interaction). The process is repeated for every residue of the protein, and the resulting substrings are concatenated in the sequential order of the residues to produce the final interaction fingerprint.

There are multiple reported methods for generating interaction fingerprints, the earliest of which to our knowledge is SIFt (Structural Interaction Fingerprints),[165,166] which implements seven different interaction types (including "any contact," "any backbone contact," and "any sidechain contact"). A somewhat modified version of SIFt is implemented in the Schrödinger Small-Molecule Drug Discovery Suite.[167]

Several similar (and similarly named) methodologies were introduced in the following years. The IFP implementation of Marcou and Rognan omits the most general interaction types of SIFt and enables the configuration of the fingerprinting algorithm, including the addition of weaker and scarcer interaction types such as cation-π interactions or metal complexation.[168] Mpamhanga et al. have designed interaction fingerprint based on an alternative concept: their IFPs are fixed-length bit strings that are as long as the number of heavy atoms in the binding site.[169] Pérez-Nueno and colleagues have introduced an atom-pair-based interaction fingerprint (APIF) that considers the relative positions of interacting atom pairs.[170] An implementation of interaction fingerprints (termed PLIF, or Protein–Ligand Interaction Fingerprints) is also included in the MOE.[136] A more recent approach is SPLIF (Structural Protein–Ligand Interaction Fingerprints), developed by Da and Kireev, in which "three-dimensional structures of interacting ligand and protein fragments are explicitly encoded" (as a result, the interactions themselves are encoded implicitly, in contrast to, e.g., SIFt).[171]

Trivially, interaction fingerprints can only be compared between the complexes of the same protein structure (as the length of the fingerprint varies according to the total number of residues). Alternatively, with a prior residue selection, such comparisons can be extended to multiple structures, or even multiple, similar proteins (in this case, a prior 3D alignment is needed to match the residues in the different proteins). These methodologies are utilized in recent works of the research group of de Graaf at the VU University of Amsterdam, where interaction fingerprints are employed to power class-specific protein–ligand structural databases such as KLIFS (for kinases)[172–174] or PDEstrian (for phosphodiesterases).[175,176]

3.14.4.7.5 Fingerprints for Ligands and Proteins (FLAP)

FLAP (Fingerprints for Ligands and Proteins) was developed in 2007 and is currently distributed by Molecular Discovery.[177,178] FLAP uses a unique approach for fingerprint generation and employs a wide range of important concepts from cheminformatics/molecular modeling, such as pharmacophores, molecular interaction fields and molecular shape. As such, it is quite distinct from the interaction fingerprints detailed in the previous subsection, even though it also encodes information about the interactions between the protein and the ligand.

FLAP uses molecular interaction fields (MIFs) based on the GRID force field to identify the active site of the protein. MIFs are then condensed into a few target-based pharmacophoric points (i.e., points where specific interactions with the protein would be favorable). To define FLAP fingerprints, one has to select (manually or automatically) a set of such pharmacophoric points. Then, all possible arrangements of four pharmacophoric points are generated and stored in a so-called protein fingerprint. Ligands are fitted to these pharmacophoric points to identify favorable interactions, and the resulting poses are filtered according to the complementarity of the shapes of the ligand and the binding site (to account for steric clashes).

3.14.4.7.6 Reaction fingerprints

Similar to line notations, the concept of fingerprints has also been extended to encode reactions (in addition to compounds). Reaction fingerprint generation has been a quite intuitive process since the earliest reported examples of such methods: molecular fingerprints or vectors (consisting of various descriptors) are generated for both the reactants and the products, from which a difference fingerprint (or vector) is calculated. The difference is calculated with a *bitwise OR* operation in the case of Daylight Structural Reaction Fingerprints,[115] and with a vector subtraction in the case of descriptor-based reaction vectors.[179] These methods have been successfully applied for a number of tasks, including metabolite prediction,[180] *de novo* molecular design,[181] and local QSAR analysis.[182] Most recently, Schneider and colleagues have developed a novel reaction fingerprint method based on atom-pair fingerprints of the products and reactants and a physicochemical property-based representation of the agents.[183] The method was successfully applied for building machine-learning models, assessing the similarities of reactions and classifying a large set of reactions based on reaction type.

3.14.5 Numerical Descriptors and Similar Representations

In the past few decades numerous books with hundreds of pages were published in the field of molecular descriptors. Although the topic is indeed huge, more and more novel molecular descriptors appear from year to year. In this section we would like to provide a general view of the world of molecular descriptors.

A basic definition of molecular descriptors (molecular representations) is that they are measured or computationally calculated properties of molecules. Another definition is stated in the popular and largely useful encyclopedia of Todeschini and Consonni[184]: "The molecular descriptor is the final result of a logical and mathematical procedure which transforms chemical information encoded within a symbolic representation of a molecule into a useful number or the result of some standardized experiment." These molecular representations can be used mostly for similarity searching, virtual screening, and QSAR (or related) models.

The molecular descriptors can be classified in several ways. There are binary, discreet, and continuous values, and we can also calculate other new descriptors from previously defined ones. Usually they are classified based on their dimensionality as 0, 1, 2, 3 … *n*D descriptors. We should mention the obvious confusion that while fingerprints can be calculated from the 2D or 3D representations or properties of the molecules, they are often termed 1D descriptors.[185] Another, truly 1D descriptor is reported in the work of Dixon and Merz, based on the projection of a 2D graph or a 3D conformation to a single dimension.[186] As for higher-dimensional descriptors, the term "2D descriptor" means that it is calculated from the 2D (graph) representation of the molecule, and in the same manner 3D descriptors are based on the 3D representation of the molecule. In the group of zero dimension descriptors are the molecular weight, the number of different atoms, etc. Thus, 0D descriptors are independent of the molecular structure and can be calculated from the molecular formula.

On the other hand, we can differentiate between physicochemical, structural, topological, electronic, geometric, and simple indicator parameters (based on their theoretical backgrounds). The term "whole-molecular descriptors" encompasses descriptors that can be calculated from the 2D representation of the molecule. Here we can distinguish between simple descriptors (number of H-bond donors and acceptors, number of ring systems and rotatable bonds, etc.) and physicochemical descriptors. When using molecular descriptors, one always has to decide between the computational demanding but precise, and the time-saving but less precise methods. Usually 2D descriptors are less time-demanding than 3D descriptors.

An overview of the most popular molecular descriptors, which are discussed in Section "**Numerical Descriptors and Similar Representations**" in details, can be seen in **Table 4**.

3.14.5.1 2D Descriptors

As it was mentioned above, 2D descriptors are always calculated from the 2D representation of molecules. 2D descriptors are also called graph invariants,[184] as their values do not depend on the numbering of the atoms in the molecule. Here the two main categories: whole-molecular and topological descriptors, as well as other smaller groups will be discussed.

3.14.5.1.1 Whole-molecular descriptors

Whole-molecular descriptors can be categorized into simple and the physicochemical descriptors. Simple 2D descriptors are the number of H-bonds acceptors, H-bond donors, the number of rings, or other countable parts of a molecule. They can be easily calculated.

Physicochemical descriptors are a larger and more diverse group. There are several parameters and several calculation types. The easiest ones (like molecular weight) are included in 0D descriptors, while we summarize the more complex ones here.

One of the most important physicochemical descriptors is the lipophilicity index, log*P*. Log*P* is part of Lipinski's rule of five to predict drug-likeness. Usually, log*P* means the logarithm of the *n*-octanol (organic)-water (aqueous) partition coefficient, but if

Table 4 The molecular descriptors discussed in Section "**Numerical Descriptors and Similar Representations**"

Subsection	*Subsection*	*Examples*
2D descriptors	Whole-molecular descriptors	Simple and physicochemical descriptors (log*P*, pK_a, solubility)
	Topological descriptors	Wiener index, Zagreb group index, Randic branching index, Balaban J-index, Kappa shape index, etc.
	Indicator variables	Free-Wilson descriptors, Fujita-Ban analysis, etc.
	Thermodynamic descriptors	Heat of formation, Bond dissociation energies
	Molecular identification numbers	BCUT descriptors
3D descriptors	Electronic descriptors	(Electric) Dipole moment, Highest occupied (HOMO) and lowest unoccupied (LUMO) molecular orbital energies, εLUMO, etc.
	Size descriptors	Radius of gyration
	Volume descriptors	McGowan's characteristic volume, Molecular volume index, Geometric volume, etc.
	Shape descriptors	Shadow indices
	Van de Waals parameters	Van de Waals molecular surface
	Molecular Shape Analysis descriptors	Receptor Surface Analysis descriptors
	Molecular Field Analysis descriptors	Steric field, electrostatic field
	Receptor Surface Analysis descriptors	Steric field, electrostatic field
	3D descriptor families	WHIM, GETAWAY, MEDV, EVA, VolSurf, etc.
4D and other descriptors	4–6D descriptors	Grid cell occupancy descriptors, etc.
	Other descriptors and approaches (outlook)	Shape-based approaches (ROCS), etc.

there are more lipophilicity indices at hand, it should be denoted as log $K_{o/w}$. It plays a role in drug absorption and distribution, thus this descriptor is one of the oldest and most important members of the descriptors applied in drug discovery. The log *P* and hydrophobicity descriptors are frequently used in quantitative structure–activity (and structure–property) relationships (QSAR, QSPR). Lipophilicity can be decomposed into two parts: hydrophobicity and polarity. While hydrophobicity and lipophilicity are often used interchangeably (the words themselves are synonyms in a grammatical sense), they denote slightly different concepts. Hydrophobicity entails the contribution of nonpolar interactions to lipophilicity, while lipophilicity itself is dominated by the entropic driving force of removing hydrophobic surface area from water. The equations relating the partition coefficient (log *P*) to the π substituent constant—which is a classical approach to quantify the lipophilicity of a chemical group—are the following:

$$\log P = \log K_{o/w} = \log \frac{[C]_{n-\text{octanol}}}{[C]_{\text{water}}} \tag{1}$$

where [*C*] is the concentration of the solute in different phases, and

$$\pi_X = \log P_X - \log P_H, \tag{2}$$

where the P_X and P_H values represent the substituted and the unsubstituted molecules' partition coefficients.

Several opportunities are developed for not just measuring, but also for calculating log*P* descriptors. Nowadays the use of *in silico* log*P* descriptors is also acceptable in the field of drug design. The work of Hansch and Fujita has pioneered the calculation of *in silico* log*P* descriptors.[187] Log*P* can be measured with the traditional shake flask method, with HPLC (high-performance liquid chromatography) or with TLC (thin layer chromatography) methods manually. It can be calculated *in silico* in several ways based on, for example, quantum chemical or semiempirical calculations. Two larger groups of *in silico* calculations are substructure-based and property-based methods. Some calculations—based on the summation of log*P* contributions of molecule fragments—were reviewed by Leo.[188] Typical *in silico* log*P* calculation methods are ALOGP, MLOGP, Clog*P*, XLOGP2, XLOGP3, etc. Nowadays there are several software packages that are freely accessible online. Due to the large number of choices, a careful evaluation of this descriptor is very important in every field of pharmaceutical science. In the past years some detailed comparisons of log*P* calculation methods were published.[189–192] They can help to decide and to answer questions like "what should be used" or "what is the best technique," etc. In the latter article the authors show that *in silico* calculations usually give more reliable results than TLC measurements.

Another highly important descriptor is the acidic dissociation constant and its negative logarithm (pK_a). It is connected not just to the pH value (and other descriptors like lipophilicity), but to many other ADME-related properties, such as membrane and blood–brain barrier permeability. The definition of the acidic dissociation constant is the following:

$$K_a = \frac{[A^-][H^+]}{[HA]} \tag{3}$$

where *HA* is the acidic form and A^- is the conjugate base.

There are several ways to measure pK_a values, for example, direct potentiometric titration and measurements based on chromatographic retention or UV absorption, etc.[193] One can also use *in silico* pK_a predictions, which have a serious advantage compared to experimental methods. Namely, the preparation of the molecules is not needed for the analysis. Most of the *in silico* pK_a prediction methods and commercial software are based on linear free energy relations (LFER) and the Hammett equation:[194,195]

$$pK_a = pK_a^u + \rho\Sigma\sigma \tag{4}$$

where pK_a^u is the dissociation constant of the unsubstitued molecule, ρ is the constant for an ionizable group, and σ is the constant of an exact substituent.

Other principles among *in silico* pK_a prediction software include fragment-based methods, QSAR models, and *ab initio* methods. Similar to *in silico* lipophilicity indices, comparisons between the pK_a predication methods and software have also been published.[196]

Last but not least the third crucially important physicochemical descriptor is the (aqueous) solubility (and its negative logarithm). In drug discovery the aqueous solubility of a drug candidate cannot be increased endlessly because strongly hydrophilic molecules cannot cross lipid membranes. Thus solubility has to be in an optimum range. There are many options for the *in silico* calculation of solubility, some of which are based on other physicochemical descriptors, such as the melting point or lipophilicity. The well-known Yalkowsky equation is a good example for this:[197]

$$log(S_0) = -0.01(\text{MP} - 25^\circ\text{C}) - logP + 0.50, \tag{5}$$

where S_0 is the water solubility, MP is the melting point, and log*P* is the lipophilicity index.

This equation has larger bias, due to the use of the melting point, which is hard to predict based on the molecular structure. The other opportunity for *in silico* solubility calculation is the use of different QSPR models. In this case we can use several chemometric tools for the prediction, such as partial least square regression (PLSR),[198] multiple linear regression (MLR),[199] random forest (RF),[200] and artificial neural network (ANN).[201] A comparison of the general solubility equation (GSE) and the above mentioned chemometric tools has also been published.[202]

One can find further physicochemical (molecular) descriptors, which are not discussed here in Todeschini's encyclopedia of descriptors.[184]

3.14.5.1.2 Topological descriptors

Topological descriptors (or topological indices) are numerical descriptors that can be calculated from the molecular structure. Topological descriptors are one of the most populated (and popular) members of the molecular descriptor (and 2D descriptor) family. Their importance is emphasized, as they can provide simple and useful information about the structures of the molecules. However, they do not contain any information about the stereochemistry and the 3D conformation. (With the words of Hugo Kubinyi: "The topology and topography of a molecule may be compared to the skeleton of a human being. How boring would life be if we recognize each other only by our skeletons and not by shape, behavior, and spirit!")[203] Thus, topological descriptors can be calculated without the optimization of molecular structure. With the combination of other molecular descriptors (such as physicochemical descriptors), they can be quite useful in QSAR and QSPR studies.

These descriptors are based on the 2D graph of a molecule. The calculation of the topological descriptors is closely connected to graph theory, where the molecular structures are built up from vertices (which symbolize the atoms) and edges (which denote covalent bonds). There are two types of these molecular graphs (or maps), the H-filled (contains the hydrogen atoms) and H-depleted (without hydrogen atoms). From these molecular graphs we can also create a graph theoretical matrix, where the relations between edges or vertices can be examined (defined). From another point of view we can distinguish between the adjacency matrices and the distance matrices (based on the original molecular graph). The former matrix contains the nonhydrogen adjacent atoms (for the H-depleted version) and assigns each pair of them as one (if they are adjacent) or zero (if not), while the latter one counts the number of edges between two vertices in the shortest path (topological distance). See **Fig. 12** for an example of a simple molecule's adjacency and distance matrices. Topological indices can be calculated from different molecular maps in an unequivocal way as they are based on the topological distances between the atoms of the molecule (through-bond indices). The topological indices can be topostructural (using only the atomic distances) or topochemical (using also atomic properties, like chemical identity or hybridization states).[204] The molecular graphs are also used for the creation of molecular signatures, which are also an appropriate way to calculate several topological indices.

In the following part the most popular and "good-to-know" examples from the huge pool of topological indices will be discussed in detail. Nowadays, it is a very hard task to select those ones, which are highly recommended to know from the enormous amount of literature in this field. In the work of Randic and Basak the question has already been posed: do we need more molecular descriptors?[205] (Naturally we do, because we want to have as diverse of a toolbox as possible and to cover the various possible descriptions of molecules as fully as possible. It is worth noting that this is true for other fields of science as well, in fact it is the essential part of making progress in science. Although there are some novel topological descriptors in the literature, most of the widely used ones were developed in the second part of the last century.

Wiener index: The most well-known first-generation topological index. First generation means that the integers are based on such graph properties like topological distances.[206] It is calculated by the half sum of all distance matrix entries. It was defined originally in 1947 by Wiener,[207] but there are several modified versions of it in the literature, for example, Hyper-Wiener or All-path Wiener indices, etc.[184] Basically we can conclude that in the past century the Wiener index has not just become popular, but it was used for the development of several other descriptors. The basic equation is the following:

$$W = \frac{1}{2}\sum_{i=1}^{N}\sum_{j=1}^{N}\delta_{ij}, \tag{6}$$

where N is the number of atoms and δ_{ij} is the distance matrix entry (shortest possible way between atoms i and j).

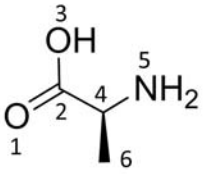

A	1	2	3	4	5	6
1	-	**1**	0	0	0	0
2	**1**	-	**1**	**1**	0	0
3	0	**1**	-	0	0	0
4	0	**1**	0	-	**1**	**1**
5	0	0	0	**1**	-	0
6	0	0	0	**1**	0	-

D	1	2	3	4	5	6
1	0	1	2	2	3	3
2	1	0	1	1	2	2
3	2	1	0	2	3	3
4	2	1	2	0	1	1
5	3	2	3	1	0	2
6	3	2	3	1	2	0

Fig. 12 Adjacency (A) and distance (D) matrices of L-alanine. In the adjacency matrix, an entry $a_{i,j}$ is **1** if atoms i and j are connected with a bond and 0 otherwise, while an entry $d_{i,j}$ in the distance matrix is the topological distance of atoms i and j. Both matrices are symmetric (i.e., their information content can be represented by either their upper or their lower triangular alone).

Zagreb group index: Another first-generation topological index, which is based on the vertex degrees of the atoms (denoted with δ and representing the number of σ bonds of the atom) in the molecule graph. The two types of this index were published in 1975.[208]

$$M_1 = \sum_a \delta_a^2 \text{and } M_2 = \sum_b \left(\delta_i \cdot \delta_j\right)_b, \tag{7}$$

where a runs over the A atoms of the molecule and b over all of the B bonds of the molecule. δ_i, δ_j are the vertex degrees of the atoms incident to the considered bond.

The first Zagreb index (M_1) is nowadays also called *Gutman index*, and the second Zagreb index (M_2) is also a part of the *Schultz molecular topological index*.

Balaban J-index: It was called "averaged distance sum connectivity" in the original article of Balaban.[204] The formula is connected to the Randic index (see below), but here the vertex degrees are changed to the averaged distance sums, thus the equation was modified.

$$J = \frac{1}{\mu + 1} \sum_b \left(\bar{\sigma}_i \bar{\sigma}_j\right)_b^{-0.5} = \frac{B}{\mu + 1} \sum_b \left(\sigma_i \sigma_j\right)_b^{-0.5} \tag{8}$$

where B is the number of edges (bonds), μ is the cyclomatic number (the number of bonds that needs to be deleted to break all rings—which in the majority of cases is equal to the number of rings), σ_i and σ_j are the distance sums of the vertices i and j (i.e., the sum of the distances in the ith and jth row of the molecule's distance matrix), and $\bar{\sigma}_i = \sigma_i / B$ is the averaged distance sum of i.

Kappa shape index: these are second-generation topological indices, based on the work of Kier.[209,210] Second-generation indices are real numbers based on integer graph properties. This group of indices has current applications in drug discovery.[206]

The first, second, and third ordered shape attributes can be calculated in the following ways:

$$^1\kappa = n(n-1)^2 / \left(^1_0P_i\right)^2 \tag{9}$$

$$^2\kappa = (n-1)(n-2)^2 / \left(^2P_i\right)^2 \tag{10}$$

$$^3\kappa = (n-1)(n-3)^2 / \left(^3P_i\right)^2, \text{ when } n \text{ is odd} \tag{11}$$

$$^3\kappa = (n-3)(n-2)^2 / \left(^3P_i\right)^2, \text{ when } n \text{ is even} \tag{12}$$

Where ^lP_i represents the number of paths of length l in molecule i, and n is the number of atoms. The maximum and minimum values of ^lP_i are:

$$^1P_{\max} = \frac{n(n-1)}{2} \tag{13}$$

$$^1P_{\min} = (n-1) \tag{14}$$

The kappa shape index was modified with a specific correction (α value), which can be calculated as:

$$\alpha_X = \left(\frac{r_X}{r_{Csp^3}}\right) - 1, \tag{15}$$

where α is the decrement or increment of n for a noncarbon element (X), r represents the covalent radius of atom X relative to sp^3 carbon atom. The modified kappa shape indices can be found in the work of Kier and Hall[211] or the article of Estrada et al.[206]

Randic branching index: also called connectivity index, it was the first connectivity index, developed by Randic[212] more than 40 years ago. He introduced it at first for alkanes, with the intention to produce a graph invariant topological index. The equation is the following:

$$\chi = \sum_{\text{all edges}} \left(\delta_i \delta_j\right)^{-0.5}, \tag{16}$$

where δ_i and δ_j are the number of nonhydrogen atoms bonded to atoms i and j and forming an edge (bond) ij.

In the past decades several modifications of connectivity indices were created, such as *mean Randic index*, *modified Randic index* and *edge connectivity index* (ε).[213] Regarding these, the reader is referred to the encyclopedia of Todeschini.[184]

Other important topological indices are the E-state index[214,215] or the valence molecular connectivity index.[216,217]

There is a third generation of topological indices as well, which are real numbers based on real-number local vertex invariants (LOVIs). Some third-generation types are based on information theory, which is applied to nonsymmetrical matrices or terms of distance sums. Balaban was the pioneer of this topic in the 90s.[218–220]

3.14.5.1.3 Other 2D descriptors

3.14.5.1.3.1 Indicator variables

Indicator variables are one of the simplest or easiest way to describe constituents of a molecule, thus they have been applied in QSAR and related analyses for many decades. They can take positive, negative, or zero values based on the state of a property (characteristic), for example, it can indicate the *cis*, *trans*, or no *cis*/*trans* isomer forms in the following way: -1 represents the *cis* isomers, $+1$ represents the trans isomers, and 0 means the characteristic is not applicable, i.e., no *cis*/*trans* isomers. Some well-known examples for indicator variables are the following: Free-Wilson descriptors (*de novo approach*),[221] Fujita-Ban analysis (modified version of Free-Wilson analysis),[222] Hansch or Hansch-Free-Wilson models.[223] In the latter cases the models or descriptors contain not just indicator variables but also their combinations with other parameters such as physicochemical descriptors.

Indicator variables are also called dummy or Boolean descriptors if they define the presence or lack of structural elements (1 or 0). They can indicate the presence of hydroxyl, carbonyl, etc., groups or even the different positions of substituents like *ortho*, *meta*, and *para*.[224] (Note that they are closely related to substructure key-based fingerprints, see subsection "**Substructure Key-Based**.") A typical example for Boolean descriptors can be found in the work of Devillers in which the descriptors indicate biodegradability.[225]

In a related example, the recent work of Borysov et al. introduces the concept of extreme descriptors as "those variables that have the same value for almost all compounds and only a few values that are different from the common median." Although it is a common practice in QSAR modeling to exclude such descriptors from model building, the authors have shown that they can be useful for activity prediction in a standard binary classification setting, and for the identification of mislabeled compounds.

3.14.5.1.3.2 Thermodynamic descriptors

Thermodynamic descriptors are a smaller segment of 2D descriptors, with some of them using 3D parameters of the molecules as well (at least optionally). A typical example is the *heat of formation* (ΔH_f) which can be calculated based on the method of Singh et al.[226]

3.14.5.1.3.3 Molecular identification numbers

In his 1989 work, Burden has introduced the concept of "molecular identification numbers," calculated from the matrix representation of the connection table of a molecule (without hydrogens).[227] It is useful for substructure searching and diversity/similarity searching tasks. This approach was refined and further developed, first by Rusinko and Lipkus and later by Pearlman and Smith to produce what is now known as the BCUT approach.[228] BCUT descriptors are calculated as the first few highest and lowest eigenvalues of such matrices, with several options for the property that defines the diagonal elements (including, e.g., partial charges, polarizabilities, and hydrogen-bonding properties).[229]

3.14.5.2 3D Descriptors

3D descriptors are calculated from the 3D representation of the molecule. Thus, 3D chemical structures (conformations) are needed, which in best case can be bioactive conformations of the molecules in the field of drug design. 3D descriptors are as useful and better known as their 2D siblings, but they were typically developed later than 2D descriptors, and their calculation is more time-consuming and computationally demanding. 3D descriptors (like 2D ones) are frequently applied for QSAR and similarity searching. Some of the descriptors are sensitive to the position and orientation of the molecular structure, but some of them are insensitive for these properties (in other words, they are *alignment-independent* or *alignment-free*). The alignment of molecules is often a time-consuming step of the procedure and not necessarily unambiguous. 3D descriptors can be classified in several ways, for example, based on the work of Kunal et al.[185] or Todeschini and Consonni.[184] Some of the typical and frequently used descriptor classes in the literature are the electronic, size, volume, shape, Molecular Shape Analysis (MSA), Molecular Field Analysis (MFA), and receptors surface analysis (RSA) descriptors. The family of 3D descriptors is too large to cover every aspect of it, thus in the following subsections the most popular ones will be discussed.

3.14.5.2.1 Electronic descriptors

Electronic descriptors can be defined in the group of 2D descriptors as well (see the Hammett equation and related descriptors). They can be local or global descriptors, i.e., they can define the electronic properties either of specific regions of the molecule or the whole molecule.[230] Electronic charges and electron densities play an important role in different chemical reactions and physicochemical parameters. Charged partial surface area descriptors are also built up from electronic descriptors with the combination of shape and steric descriptors. One important class of electronic descriptors are *charge descriptors*, which contain for example the *total absolute atomic charge (electronic charge index) descriptor*. Some typical examples for electronic descriptors are detailed below.

(Electric) Dipole moment: This is a quantum-chemical electronic descriptor (or also classified as electric polarization descriptor), based on the strength and orientation of the interaction of the examined molecule with an external electrostatic field. The magnitude of the dipole moment and its components μ_x, μ_y, and μ_z are usually calculated. The SI unit of dipole moment is *coulomb meter (Cm)*, but for practical reasons, *Debye* ($\approx 3.34 \times 10^{-30}$ Cm) is used more frequently. The components of μ are calculated in the following way:

$$\mu_x = \sum_i q_i \cdot x_i, \tag{17}$$

$$\mu_y = \sum_i q_i \cdot y_i, \tag{18}$$

$$\mu_z = \sum_i q_i \cdot z_i, \tag{19}$$

where x, y, and z are the coordinates and q is the charge of atom i.

Highest occupied (HOMO) and lowest unoccupied (LUMO) molecular orbital energies: They are also quantum-chemical descriptors. ε_{HOMO} is the energy of the highest energy orbital that contains electrons. A molecule with high HOMO energy values can donate electrons easily. The ionization potential (IP) is closely connected to this: IP = -ε_{HOMO}. Sometimes the energies of the second or third highest occupied orbitals are also used as descriptors. These descriptors are closely related to the nucleophilicity of a molecule.

ε_{LUMO} is the energy of the lowest energy molecular orbital that does not contain any electrons. A molecule with low LUMO energy values can accept electrons easily, thus this is connected to the definition of electronic affinity (EA): EA = -ε_{LUMO}. In other words, it measures the electrophilicity of a molecule.

3.14.5.2.2 Size descriptors

In addition to 3D descriptors, size descriptors can also be simple ones like molecular weight or the number of bonds and atoms. We can also find size descriptors in the group of topological indices, but several 3D size descriptors exist as well. Size, volume, and shape descriptors are often connected to each other, for example, steric descriptors account for the size and the shape of the molecule. On the other hand there are some volume descriptors, such as van der Waals volume, which can also be considered a size descriptor (see later). A popular 3D example is detailed below.

Radius of gyration: This descriptor characterizes the distribution of atomic masses in a molecule[231] and provides an absolute measure of molecular compactness.[232] It is defined as:

$$R_G = \sqrt{\frac{\sum_{i=1}^{A} m_i \cdot r_i^2}{MW}} \tag{20}$$

where r_i is the distance of ith atom from the center of mass of the molecule, m_i means the atomic mass, A is the number of atoms, and MW represents the molecular weight.

3.14.5.2.3 Volume descriptors

Volume descriptors are either steric or size descriptors (or both). There are both experimental and theoretical ways for determining the volume of the molecules. Some examples of volume descriptors are listed here (van der Waals volume is discussed later in detail).

McGowan's characteristic volume (V_x): As a steric descriptor it is calculated as the sum of the atomic volume parameters in the molecule. It can be used for example for cavity term measurements. The equation is the following:

$$V_x = \sum_{i=1}^{A} w_i - 6.56B, \tag{21}$$

where w_i means the McGowan volume parameter and B is the number of bonds. McGowan atomic parameters for the calculations can be found in his article from 1987.[233]

Molecular volume index (MVI): This volume descriptor is based on the summation of van der Waals volumes of each groups of the molecule.[234] With the double summation, each pair of nonhydrogen atoms is involved. The equation is the following:

$$MVI = \sum_{i=1}^{A} \sum_{j=i+1}^{A} \frac{V_i^{vdw} \cdot V_j^{vdw}}{D_{ij}^2}, \tag{22}$$

where V^{vdw} represents the van der Waals volume of each group and D_{ij}^2 is the square of the topological distance of v_i and v_j.

Geometric volume: The atoms can be defined as point masses, which construct the solid geometric shape of the molecule. Thus the geometric volume is the volume of this solid geometric shape. In the concept of this volume, the atoms are interconnected and form some regular and irregular tetrahedrons. The volumes of these tetrahedrons are computable in analytical and numerical ways as well.[235]

3.14.5.2.4 Shape descriptors

Molecular shape descriptors are very useful in the modeling of physicochemical processes. This topic has a large scientific literature and in the past 30–40 years several novel shape descriptors were developed.[232,236] Some of the most popular ones are *shadow indices*, *WHIM shape descriptors*,[237] or *molecular shape analysis* descriptors (see below in details).

Shadow indices (Jurs shape indices): geometrical descriptors related to the size and shape of the molecule. The basic principle is the projection of the molecular surface onto three mutually perpendicular planes *XY*, *XZ*, and *YZ*.[230] The descriptors encode the conformation and also the orientation of the molecule. Rotational invariance is obtained by the previous alignment of the *X*, *Y*, and *Z* axes along the three axes of principal inertia.[238,239]

3.14.5.2.5 van de Waals parameters

Another interesting part is the *van der Waals molecular surface (or area)* (SA^{vdw}), which can be included in the aforementioned descriptor groups as well. It is also called *total molecular surface area* (TSA), and it is connected to the hard-sphere model. The total van der Waals surface is calculated as the sum of the atomic van der Waals surfaces. This is related to binding, solubility, etc.

The *van der Waals volume* (V^{vdw}) is the volume of the space inside the van der Waals molecular surface. The van der Waals volume is closely connected to the *van der Waals radius* (R^{vdw}). The van der Waals radius is the distance, where the attractive and repulsive forces between the two nonbonded atoms are equal. Its calculation was originally described by Bondi,[240] but less time-consuming calculations have been developed as well by Zhao et al.[241] There is a vast literature in this field between the 1980s and 1990s, for instance molecular mechanics based methods,[242] as well as other techniques.[243]

3.14.5.2.6 Molecular Shape Analysis descriptors

Molecular Shape Analysis (MSA) is a common technique in QSAR analysis, which combines the molecular shape similarity and commonality measures (with other descriptors) to determine the similarities between molecules and build appropriate QSAR models.[244] In this section we do not cover MSA QSAR in detail, only the commonly used molecular shape similarity descriptors (MSA descriptors). Molecular shape similarity is applied to the comparison of 3D molecular shapes, which are represented by atomic properties. On the other hand, molecular shape commonality is using conformational energy and molecular shape together to measure molecular similarity. The basic concept of MSA in QSAR analysis is that the shape of the molecule is related to the binding site cavity (or pocket), thus it is related to biological activity as well. Some popular molecular shape similarity descriptors are listed below:

Common Overlap Steric Volume (COSV): It represents the overlapping volume of two superimposed molecules.[245] Van der Waals volume of the molecules is used for the determination.

$$M_0(i,j) \equiv V_0(i,j) = V_i \cap V_j \tag{23}$$

Non (Common) Overlap Steric Volume (NCOSV or V_{non}): It is defined as the volume of molecule *i*, which does not overlap with the volume of the reference molecule *j*. (Thus, it can be related to steric misfit.) Basically V_{non} is the difference between the $V_{i,j}$ composite steric volume of two aligned molecules and V_j (reference molecule).[245]

3.14.5.2.7 Molecular Field Analysis descriptors

Molecular Field Analysis (MFA) is also a frequently used technique in QSAR. It is a grid-based QSAR technique, mostly applied in Comparative Molecular Field Analysis (CoMFA) based on the work of Cramer et al.[246] (Here, we only briefly mention CoMFA, as a detailed introduction would be out of the scope of this chapter.) The molecular field can be represented by a 3D rectangular grid. MFA analysis is based on the calculation of interaction energies (steric and electrostatic interactions in the case of CoMFA) between some probes (H^+ or CH_3) and the molecule, represented by a rectangular grid. Thus the field of molecules can be described by MFA grids, and the energies associated with MFA grid points may serve as inputs (descriptors) for the calculation of QSAR models.

3.14.5.2.8 Receptor Surface Analysis descriptors

Receptor Surface Analysis (RSA) is another modeling method, primarily for such cases when the 3D structure of a receptor is unknown.[247] A hypothetical model can be created with this predictive tool for the receptor site. On the other hand, RSA descriptors are also useful in QSAR model building when the receptor surface is known. The RSA approach clearly differs from pharmacophore approaches, as it captures information about the receptor instead of the ligands. From receptor surface models, one can derive descriptors, which provide 3D information about the (steric or electrostatic) interaction energies between each point of the receptor surface and the ligand. RSA descriptors can be combined with other 3D or 2D descriptors for QSAR analysis. Some typical examples for RSA descriptors are *IntraEnergy*, *InterEnergy*, *StrainEnergy*, *MinIntraEnergy*, etc.[185]

3.14.5.2.9 3D descriptor families

3.14.5.2.9.1 WHIM descriptors

Weighted Holistic Invariant Molecular (WHIM) descriptors are based on statistical indices calculated on the projections of atoms around the *x*, *y*, and *z* axes.[237] The algorithm involves a principal component analysis (PCA) of the centered molecular matrix (coordinates of the molecule). Depending on the six different weighting schemes (such as atomic mass, van der Waals volume, etc.), different covariance matrices (and principal components) can be built. Directional WHIM descriptors can also be calculated. Typical groups of them are size descriptors (constructed from the eigenvalues of the covariance matrix), shape descriptors, symmetry descriptors, density descriptors, etc. In summary, there are 66 directional WHIM descriptors (11 for each weighting scheme). Global WHIM descriptors are calculated as combinations of directional WHIM descriptors.

3.14.5.2.9.2 GETAWAY descriptors

GETAWAY (GEometry, Topology, and Atom-Weights AssemblY) descriptors are based on the molecular influence matrix (**H**), which is calculated in the following way:[248]

$$\mathbf{H} = \mathbf{M} \times \left(\mathbf{M}^{\mathbf{T}} \times \mathbf{M}\right)^{-1} \times \mathbf{M}^{\mathbf{T}}, \tag{24}$$

where **M** represents the molecular matrix (containing the centered Cartesian coordinates of the atoms of the molecule).

The diagonal elements of the **H** matrix are called leverages. The combination of the molecular influence matrix with geometry matrix (**G**) is called the influence/distance matrix (**R**). It is very important because a set of GETAWAY descriptors are calculated from both of them based on different concepts and matrix operators. The GETAWAY approach also employs different atom weighting schemes, similar to WHIM. Some examples are: geometric mean of the leverage magnitude (H_{GM}), total information content on the leverage equality (I_{TH}), standardized information content on the leverage equality (I_{SH}), mean information content on the leverage magnitude (HIC), average row sum of the influence/distance matrix (RARS), etc.

There is another group of GETAWAY descriptors (denoted as R-GETAWAY), which combines the information mentioned above with geometric interatomic distances in the molecule.

3.14.5.2.9.3 EVA descriptors

EVA or EigenVAlue descriptors are based on the extraction of chemical structures from mid- and near-infrared spectra. The basic concept was developed in 1997 by Ferguson et al.[249] The fundamental molecular properties can be characterized potential energy functions (vibrations). The normal coordinate eigenvalues (and eigenvectors) from vibrational frequencies or atomic displacements can be calculated with the use of quantum and molecular mechanical methods.

EVA descriptors are 3D descriptors providing information about molecular size, shape, and electronic properties. A modification of the original conception is EEVA (Electronic EigenVAlues), which defines a set of vectorial descriptors.[250,251] Here the eigenvalues of the Schrödinger equation are used instead of the vibrational frequencies.

3.14.5.2.9.4 MEDV (MEDV-13) descriptors

The Molecular Electronegativity Distance Vector (MEDV) is a vectorial descriptor, which includes 91 terms that contain information about the relative electronegativities.[252] The electronegativities are represented by the modified E-state indices and topological distances between each possible pair of 13 atom types. In the first step of the MEDV descriptor calculation, one has to assign each atom in the molecule to one of the aforementioned atom types. The atom types are based on the most frequently occurring atoms in organic molecules and also the number of bonded nonhydrogen atoms (vertex degree).[230] The single molecular descriptor can be calculated with this equation:

$$h(u,v) = \sum_{i\in u}\sum_{j\in v}\frac{S_i^* \cdot S_j^*}{d_{ij}^2}, \quad u,v = 1,\ 2,\ \ldots,\ 13, \tag{25}$$

where u and v are the atom types, S^* represents the modified E-state index, d_{ij} is the topological distance between v_i and v_j vertices.

There is also an extension of MEDV-13, called Molecular Holographic Distance Vector (MHDV).[253] It is developed to describe more specific molecular structures like peptide sequences, which contain heteroatoms and multiple bonds.

3.14.5.2.9.5 GRIND descriptors

Grid-Independent Descriptors (GRIND) are based on molecular interaction fields (MIF), which can be calculated with the GRID method and software[254] (or other programs).[255] The calculation of the descriptors involves two main steps. The first step is the computation of molecular interaction field (MIF). The second step involves a particular type of autocorrelation transform to create alignment-independent variables. On the other hand, we can also construct the steps in the following way: (a) computing the MIF, (b) filtering the MIF, and (c) encoding the virtual receptor site (VRS) into GRIND (GRIND encodes geometrical relationships between the VRS regions). The molecular descriptors can be used for the creation of "correlograms" and also for different types of chemometric analysis. The original MIF descriptors can be generated with appropriate software from the autocorrelation transform.

3.14.5.2.9.6 VolSurf descriptors

VolSurf descriptors have a quite similar basis to G-WHIM and GRIND descriptors. These descriptors also encode information about molecular interaction fields (MIF) with a GRID force field parametrization.[256] The final descriptors are alignment independent and are related to molecular size or shape, distribution of hydrophobic or hydrophilic parts of the molecule, etc. Different probes such as H_2O, DRY (hydrophobic), or O (carbonyl oxygen, represents hydrogen-bonding donor groups) are used for the calculation of interaction fields. Some typical descriptors are: water-excluded volume (V) with H_2O probe, accessible surface (traced also with H_2O probe) of the water interaction field, rugosity (R), polarizability (POL, traced with DRY probe), elongation (E), volume of the interactions with the probe O (Wp1–Wp8), Integy moments (INTEraction enerGY moments), etc.

3.14.5.3 4D and Other Special Descriptors

3.14.5.3.1 4D descriptors

4D descriptors are also grid-based descriptors (but they are not derived from molecular interaction fields.) The fourth dimension represents ensemble sampling or conformational flexibility, which is defined by the *conformational ensemble profile* (CEP). The CEP is calculated with molecular dynamics (MD) simulations. 4D descriptors help identify the active conformations of the flexible molecules, and they are also useful tools in alignment problems. The pioneering work of Hopfinger et al. in 1997[257] has introduced 4D

descriptors to QSAR analysis. Hence, 4D descriptors are among the youngest members of the family of (now thousands of) molecular descriptors. There are two forms of 4D QSAR: receptor dependent and receptor independent.[258]

4D descriptors can be assigned to the occupancy frequencies of the different atom types in the cubic grid cells during the molecular dynamics simulation.[259,260] The generation of the descriptors has some basic steps, which are discussed here in detail. First the molecular structures are generated with a conformational search, and the conformers with the minimum energies are kept as the initial structures. The cell grid (with a default grid spacing of 1.0 Å) is constructed based on the largest compound in the data set. In the next step the interaction pharmacophore elements (IPE) are introduced. Every atom of each molecule can be classified into one of the IPE classes: "any type" or generic, nonpolar (NP), polar-positive charge (P+), polar-negative charge (P−), hydrogen-bond acceptor (HA), hydrogen-bond donor (HB), and aromatic (Ar). These types are created based on the interactions between the active site and the pharmacophore groups. The third step of the process is the estimation of the conformational ensemble profiles (CEP) with MD simulations. After that, each conformation of the CEP for each molecule is implemented in a reference grid cell based on the trial alignment. Finally, the grid cell occupancy descriptors are calculated from CEPs. This is important because we use a conformational ensemble profile of each compound instead of using only one starting conformation (which is the essence of the fourth dimension).

3.14.5.3.2 Other special descriptors and approaches (outlook)

The list does not stop at 4D descriptors, as one can easily find interesting articles about the application of higher (such as five or six) dimensional descriptors.[258] These are connected more to QSAR and related topics, thus they are only briefly mentioned. Five dimensional QSAR descriptions are calculated with the Quasar technology (and software) and are an extension of the 4D siblings with the multiple representation of the topology of the quasiatomistic receptor surrogate.[261,262] Another dimension is introduced in 6D descriptors for QSAR modeling, enabling the simultaneous consideration of different solvation models. It can be achieved, for example, by mapping parts of the surface area with solvent properties.[263]

Another interesting field is the discrimination of molecular shapes. Gaussian approximations can be used to optimize the alignment of two molecules, but Gaussian functions can also provide very good and realistic representations of molecular shapes.[264] The rapid overlay of chemical structures (ROCS) program applies the atom-centered Gaussians for the discrimination and optimal alignment of molecules.[265,266] ROCS alignments can be applied not just for similarity searching and virtual screening, but also for 3D QSAR and SAR analyses. Further examples of shape-based approaches include the normalized PMI (principal moments of inertia) ratios introduced by Sauer and Schwarz,[267] and Ultrafast Shape Recognition (USR), which employs three statistical moments (average, standard deviation, and kurtosis) of atomic distances in four reference locations, providing a vector of 12 shape descriptors for each molecule.[268]

3.14.6 Similarity—Dissimilarity Measures, Distance Metrics

The old adage dates back to the ancient Roman-Greek period: "similis simili gaudet" [like rejoices in like] and corresponds to the observation that similar entities behave similarly.

In the scientific domain of (medicinal) chemistry, there are some common formulations of the similarity principle, for example:

(i) Structurally similar molecules are presumed to exhibit similar properties and similar biological activities.[269]
(ii) "Molecular similarity in descriptor space is often called the "neighborhood principle" or "neighborhood behavior axiom."[270]
(iii) Other scientists formulate the same principle as the "concept of similarity", where molecules may be grouped according to their biological effects or physicochemical properties.[271]
(iv) "Structure–property similarity principle": similar structures generally have similar properties.[272]

The similarity principle plays a ubiquitous role in rational drug design, lead discovery, synthesis design, molecular diversity analysis, and compound optimization (e.g., optimization of ADMET properties, that is, similar absorption, distribution, metabolism, excretion, and toxicity). Virtual screening is able to find similar molecules from large databases. Finding a "patentable" compound with a desired property value is an important aim to be pointed out.

Naturally there are many examples violating the similarity principle. A small change in the molecular structure (changing the configuration of a stereo center, introducing a small molecular weight substituent, etc.) can lead to a dramatic increase (or decrease) in biological activity (e.g., dramatic difference in the toxicity of dioxins, or the carcinogenicity of polycyclic aromatic hydrocarbons (PAHs), etc.). On the other hand, a lot of compound classes (steranes, amphetamines, sulphonamides, etc.) possess very similar biological activities. If there is insufficient information about a new compound, the scientific community should resort to similar compounds and make estimations from "similar" molecules.

Similarity analysis can be simplified according to the following: First a molecule should be represented with an appropriate computational construct, such as a fingerprint or a set of descriptors (see Sections "**Molecular Fingerprints**" and "**Numerical Descriptors and Similar Representations**"). Then, a similarity measure (metric) should be applied for quantifying the similarities between pairs of molecules, and finally an algorithm can be applied for, e.g., clustering the molecules according to their biological activity, properties, etc.

As the available computing power has dramatically increased in recent years, application of similarity methods to large databases became feasible even with moderate computing resources. The goal of such calculations is usually either the identification of

Table 5 Section "Similarity—Dissimilarity Measures, Distance Metrics" at-a-glance

Subsection	*Examples/comments*
Common Measures of Similarity	Tanimoto, Euclidean, Cosine, Tversky, etc.
Similarity Fusion	MAX, MIN, SUM, RRF fusion rules, etc.
Clustering Algorithms	*k*-nearest neighbors, *k*-medoids, etc.
Similarity Measures for Special Tasks	See below
Symmetric field-based	Quantum chemical similarities
1D similarity	Similarity measures for 1D objects
Graph-based	Graph and tree-based metrics, including business similarity measures
Semantic	Text-based similarity measures
Supervised	Implementations and applications related to bioactivity, e.g., SALI
Chemometric/Spectral	Similarities for high-dimensional data, e.g., (N)IR spectra
Fuzzy	Similarities between fuzzy sets
Other	Interesting examples/applications from diverse fields

molecules that are similar to one or more reference molecules, or the compilation of a subset of molecules that are as diverse as possible. (The latter application is particularly important in early hit discovery where diverse molecular databases are desired.) The reader is referred to some straightforward reviews about similarity and diversity in the cheminformatics field.[270,273–275] For the present section, we provide a brief overview in Table 5.

3.14.6.1 Common Measures of Similarity and Dissimilarity (Distance)

Similarity and dissimilarity (distance) are used more or less interchangeably, in spite of some important differences, e.g., their directions are reversed, their scales are different by definition, etc. It is also important to note that there is an inherent asymmetry in the distributions of these metrics.

Holiday et al. have used three different clustering approaches and distinguished three types of measures: distance metrics, association coefficients, and similarity (correlation) coefficients.[276]

A distance metric $D_{A,B}$ between objects (molecules) A and B should obey four rules:[277]

$$\text{Distance values } (D) \text{ must be positive for non} - \text{identical objects}: \; D_{A,B} > 0 \tag{26}$$

$$\text{The distance from an object to itself must be zero}: D_{A,A} = D_{B,B} = 0 \tag{27}$$

$$\text{A distance value must be symmetric}: D_{A,B} = D_{B,A} \tag{28}$$

$$\text{A distance metric must obey the } \textit{triangular inequality}: D_{A,B} \leq D_{A,C} + D_{C,B} \tag{29}$$

If a distance coefficient fails to obey either of these four rules, it cannot be called a metric.

Similarity measures (S) are reversely scaled (the higher the more similar) as opposed to dissimilarity or distance (the lower the more similar). A similarity measure has to obey three rules[278]:

$$\text{Similarity values for non-identical objects must be}: 0 < S_{A,B} < 1 \tag{30}$$

$$\text{The similarity of an object to itself must be unity}: S_{A,A} = S_{B,B} = 1 \tag{31}$$

$$\text{A similarity value must also be symmetric}: S_{A,B} = S_{B,A} \tag{32}$$

(It should be noted that Eq. (6) is erroneous in the original publication.)

Similarity and distance values are almost always nonnegative, but their scales differ greatly: $S \in [0; +1]$ (or $S \in [-1; +1]$ for some correlation-based similarity definitions) and $D \in [0; +\infty]$. In practice, an inherent asymmetry is present in similarity/dissimilarity calculations in terms of the resulting value ranges. It is relatively simple to convert from similarities to dissimilarities:

$$D_{A,B} = 1 - S_{A,B}, \text{such special distances will bear the constraint of } D \in [0; +1]. \tag{33}$$

However, conversion in the opposite direction is somewhat less straightforward, as similarity values should be recalculated between zero and one, while distances can be arbitrarily large. Thus, a suitable conversion rule is:

$$S_{A,B} = \frac{1}{1 + D_{A,B}} \tag{34}$$

It is easy to see that similarity values calculated with this equation will always have a value between 0 and 1 (with 1 corresponding to identical objects, where the distance is 0). It should be noted that the typical value ranges of different similarity metrics can be different,[279] even though they cannot fall outside of the predefined range (i.e., $0 \leq S \leq 1$).

As distances are measured on different scales, their comparison should be preceded by appropriate scaling. Four basic scaling methods are to be used: (i) range scaling (between 0 and 1), (ii) standardization (autoscaling, i.e., centered and scaled to unit standard deviation), (iii) rank transformation, and (iv) normalization (scaled to unit length).

Table 6 summarizes the most frequently used similarity and distance measures. The first 10 items in the table are distance measures, and the remaining ones are similarity coefficients. For more binary similarity measures, the reader is referred to the work of Todeschini et al.[280] Additionally, several graph-based similarity measures have been proposed in the literature for molecular similarity calculations.[281,282] Some more specific similarity measures are defined in part 5.5.

The Minkowski distance is a generalization of distances; if $p=q=1$, it equals the Manhattan distance, whereas $p=q=2$ equals the Euclidean distance. The Tversky coefficient can also be considered as a generalization of similarity coefficients. The α and β parameters are always nonnegative, but in medicinal chemistry applications, they are usually set within the unit interval [0, 1]. If $\alpha \neq \beta$, then the Tversky coefficient is asymmetric. The case $\alpha=\beta=1$ equals the Tanimoto similarity. Similarity indices are intrinsically symmetric in nature, but asymmetric indices have some advantages: asymmetric forms allow for measuring and modulating the similarity of one molecule in the context of another, i.e., they have the potential of alleviating the size dependency often observed in chemical similarity searching. Inspired by Tversky's work, Mestres and Maggiora have defined an entire family of field-based molecular similarity indices.[283]

Distance and similarity metrics have been the subject of several comparative studies focusing on their applications in several fields. Bender et al. have compared a vast selection of molecular fingerprints and visualized their similarities (i.e., the similarities between the methods themselves) with principal component analysis.[90] Additionally, they have included some of the fingerprints in combination with the Cosine similarity metric (replacing the Tanimoto coefficient). Sum of ranking differences (SRD)[284] corroborates the authors' original observation that the exchange of the similarity metric from Tanimoto to Cosine does not affect the ranking behavior of these fingerprints significantly (see **Fig. 13**). In addition, all of the examined fingerprint methods have ranked the datasets significantly differently than random ranking.

More recently, Bajusz et al. have established that the Tanimoto index, Dice index, Cosine coefficient, and Soergel distance were identified to be the best and in some sense equivalent measures for similarity calculations (in combination with the path-based Chemaxon Chemical Fingerprint), whereas the similarity metrics derived from the Euclidean and Manhattan distances are not recommended on their own, although their variability and diversity from other similarity metrics might be advantageous in certain cases. The behavior of these similarity coefficients was very similar for fragment-sized, lead-like, and drug-like compounds. Analysis of variance (ANOVA) showed that the choice of the data preprocessing method (such as interval scaling, standardization, and rank transformation) does not affect the results significantly.[279]

Haws et al. have described an easy way to unfold symmetric diagonal matrices into vectors (so that they can be compared with, e.g., the similarity metrics included in **Table 6**).[285] Their first figure uses the example of a dissimilarity map, but it can also be used for correlation matrices as well (see **Fig. 14**).

Schuffenhauer and Brown have approached the problem from the opposite direction[286]: "diversity selection can be … only of value if used with dissimilarity cut-offs in ranges where the similar property principle is at least partially valid." Mean pairwise intermolecular dissimilarity has been calculated for a rapid selection of external datasets.[287]

Sheridan and Kearsley put the various approaches to define similarity into the context of receptors and bioactivities: "There is clearly a lot of 'art' involved in defining similarity, and different definitions are useful for different purposes … Different methods select different subsets of actives for the same biological activity and the same method might work better on some activities than others in a way that is difficult to predict beforehand. In retrospect, this makes sense because receptors are diverse, and chemical groups that appear equivalent to one descriptor might not be equivalent to another."[288] Novel types of plots for the comparison of binary similarity coefficients have been elaborated by Salim et al. These plots clearly show the differences between coefficients in size, and the size bias of similarity coefficients is revealed.[289]

There is no doubt that the Tanimoto coefficient is the most frequently applied similarity measure for bit strings. It can be advantageously applied in many cases, but it is not the best (and can even be deficient) in other cases. Below we summarize some (contradictory) findings concerning the Tanimoto coefficient. If a compound has a Tanimoto similarity coefficient (based on "Unity" fingerprints) larger than 0.85 to an active compound, then the compound has an 80% chance of itself being active in the same assay.[290] Martin et al. have shown that similar biological activity might be expected from structurally similar compounds: "as the structural similarity is increased, so is the biological similarity." The enrichment in active compounds is higher than the same of docking to proteins of known 3D structures. If setting the limit for Tanimoto coefficients higher than 0.85 in the case of Daylight fingerprints only 30% of compounds proved to be active.[269] Cosine and Tanimoto coefficients were compared. If the Cosine coefficient is used for the calculation of the intermolecular (dis)similarities, a set of dissimilar molecules is selected faster than earlier algorithms. The algorithm is applicable to any type of representation that characterizes a molecule by a set of attribute values and to any procedure that involves calculating a sum of intermolecular similarities.[291] The Tanimoto coefficient is not a perfect similarity measure, it also has some limitations. The distribution of Tanimoto coefficients for a comparison of 54-bit strings is peculiar: it is a multimodal skewed distribution.[292] "The Jaccard coefficient, also known as the Tanimoto coefficient is the most widely used in practice." "There cannot be one similarity measure and one descriptor that correlates with every molecular property at the same time. In different 'similarities,' different features emerge as being important (and in our case, different

Table 6 Formulas for frequently used similarity and distance measures

Similarity/distance measure	*Definition/Formula for numerical variables*[a]	*Formula for dichotomous variables*[b]
Hamming (Manhattan) distance	$D_{A,B} = \sum_{j=1}^{n} \lvert x_{j,A} - x_{j,B} \rvert$	$D_{A,B} = a + b - 2c$
Euclidean distance	$D_{A,B} = \sqrt{\sum_{j=1}^{n} (x_{j,A} - x_{j,B})^2}$	$D_{A,B} = \sqrt{a + b - 2c}$
Soergel distance	$D_{A,B} = \frac{\sum_{j=1}^{n} \lvert x_{j,A} - x_{j,B} \rvert}{\sum_{j=1}^{n} max(x_{j,A}, x_{j,B})}$	$D_{A,B} = 1 - \frac{c}{a+b-c}$
Pearson correlation (r) distance (PCD)	$PCD_{A,B} = 1 - abs(r)$. For centered x variables r is identical with cosine coefficient, otherwise: $r = \frac{\sum_{j=1}^{n} (x_{j,A} - \bar{x}_j)(x_{j,B} - \bar{x}_j)}{\sqrt{\sum_{j=1}^{n} (x_{j,A} - \bar{x}_j)^2 \sum_{j=1}^{n} (x_{j,B} - \bar{x}_j)^2}}$	$PCD_{A,B} = 1 - \frac{c}{\sqrt{ab}}$
Spearman rank correlation (ρ) distance	$SRCSD_{A,B} = 1 - abs(\rho)$ $\rho = \frac{\sum_{j=1}^{n} R(x_{j,A}) R(x_{j,B}) - n\left(\frac{n+1}{2}\right)^2}{\sqrt{\left(\sum_{j=1}^{n} R(x_{j,A})^2 - n\left(\frac{n+1}{2}\right)^2\right)\left(\sum_{j=1}^{n} R(x_{j,B})^2 - n\left(\frac{n+1}{2}\right)^2\right)}}$	Not defined
Pearson correlation squared distance	$PCSD_{A,B} = 1 - r^2$	$PCSD_{A,B} = 1 - \frac{c^2}{ab}$
Spearman rank correlation squared distance	$SRCD_{A,B} = 1 - \rho^2$	Not defined
Minkowski distance	$D_{A,B} = \left(\sum_{j=1}^{n} \lvert x_{j,A} - x_{j,B} \rvert^p\right)^{1/q}$ Where p and $q > 0$ and generally $p = q$	Not defined
Chebishev distance	$D_{A,B} = \lim_{n \to \infty} \left(\sum_{j=1}^{n} \lvert x_{j,A} - x_{j,B} \rvert^p\right)^{1/q}$	Not defined
Correlation coefficient	Pearson: $r = \frac{\sum_{j=1}^{n} (x_{j,A} - \bar{x}_j)(x_{j,B} - \bar{x}_j)}{\sqrt{\sum_{j=1}^{n} (x_{j,A} - \bar{x}_j)^2 \sum_{j=1}^{n} (x_{j,B} - \bar{x}_j)^2}}$	Matthews: $S_{A,B} = \frac{cd - (a-c)(b-c)}{\sqrt{ab(a-c+d)(b-c+d)}}$
Ochiai/Cosine coefficient	$S_{A,B} = \frac{\sum_{j=1}^{n} x_{j,A} x_{j,B}}{\sqrt{\sum_{j=1}^{n} (x_{j,A})^2 \sum_{j=1}^{n} (x_{j,B})^2}}$	$S_{A,B} = \frac{c}{\sqrt{ab}}$
Dice coefficient	$S_{A,B} = 2\frac{\sum_{j=1}^{n} x_{j,A} x_{j,B}}{\sum_{j=1}^{n} (x_{j,A})^2 + \sum_{j=1}^{n} (x_{j,B})^2}$	$S_{A,B} = \frac{2c}{a+b}$
Tanimoto coefficient	$S_{A,B} = \left[\frac{\sum_{j=1}^{n} x_{j,A} x_{j,B}}{\sum_{j=1}^{n} (x_{j,A})^2 + \sum_{j=1}^{n} (x_{j,B})^2 - \sum_{j=1}^{n} x_{j,A} x_{j,B}}\right]$	$S_{A,B} = \frac{c}{a+b-c}$
Russell-Rao coefficient	Not defined	$S_{A,B} = \frac{c}{n}$
Forbes coefficient	Not defined	$S_{A,B} = \frac{cn}{(a+c)(b+c)}$
Simpson coefficient	Not defined	$S_{A,B} = \frac{c}{min(a,b)}$
Simple matching coefficient	Not defined	$S_{A,B} = \frac{c+d}{n}$
Tversky coefficient	Not defined	$S_{A,B} = \frac{c}{\alpha(a-c) + \beta(b-c) + c}$

[a]In the definitions for continuous variables (such as physicochemical properties or biological activities), $x_{j,A}$ and $x_{j,B}$ are the values of feature j for molecules A and B, respectively; $\bar{x}_j$ is the average value of feature j; $R(x_{j,A})$ is the rank number of feature j of molecule A; and n is the number of features.
[b]In the definitions for binary variables (such as fingerprints), a is the number of *on* bits in molecule A, b is number of *on* bits in molecule B, c is the number of bits that are *on* in both molecules, d is the number of common *off* bits, and n is the bit length (total number of bits) of the fingerprint: $n = a + b - c + d$.

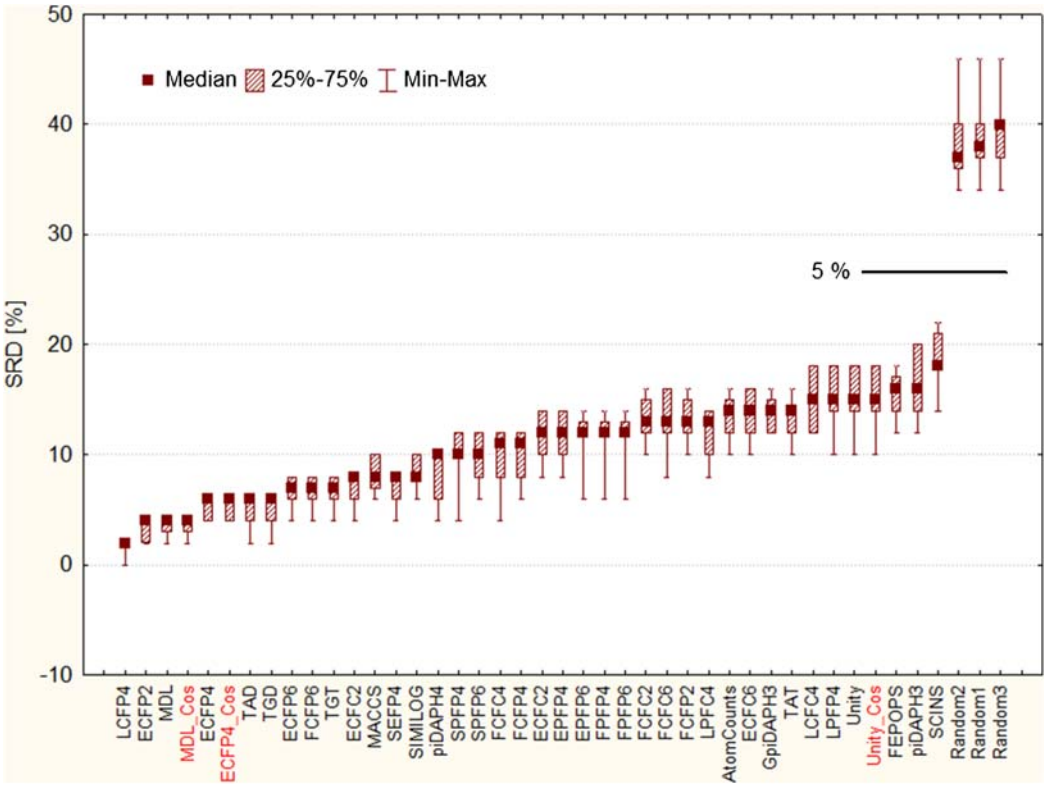

Fig. 13 Leave-one-out cross-validated SRD (sum of ranking differences) values for the fingerprint methods compared by Bender et al.[90] As SRD values measure a method's distance from the consensus (in terms of ranking the observations—here, molecules), the smaller SRD values are better. Here, LCFP4 proved to be the best (most consistent) fingerprint for these 11 activity classes. The ranking has passed the randomization test, 5% level of random ranking is shown in the figure. It can also be concluded that the similarity metrics (Tanimoto or Cosine, the latter is marked with red) do not affect the ranking behavior significantly.

bioactivities invariably require different descriptors)."[271] Even the efficiency of the well-known Tanimoto coefficient can be increased using a single, bioactive reference compound (or using several reference structures) with data fusion (see later) and machine-learning techniques.[293]

"It was also found that different coefficients perform better in certain ranges of molecular size (or bit density). The Russell–Rao coefficient was found to perform better in the case of large queries, while the Forbes coefficient performed better on small queries. The Tanimoto coefficient was outperformed in many cases, but not consistently. The good performance of Russell–Rao and the weak performance of Forbes were also observed in an application using the Dictionary of Natural Products database (DNP), where the Tanimoto coefficient was often outperformed by a factor of two."[294] "Certain coefficients whether single or in combination, appear repeatedly as best performers. One would definitely include the Russell/Rao, Forbes, and Simple Match in this pool and would probably add the Tanimoto, Cosine and others."[289] It was revealed that the size-bias and asymmetries that are inherent in most similarity coefficients lead to a bias in the selection of active compounds (altogether 14 coefficients were examined, including the Tanimoto coefficient).[295] Considering the large number of studies about the inconsistent and unsatisfactory behavior of the Tanimoto coefficient, it is somewhat surprising that it is still the "default" similarity metric. On the other hand, recent investigations show that Tanimoto index, Dice index, Cosine coefficient, and Soergel distance are the best ones, and they are in some sense equivalent metrics.[279]

Association coefficients may be more suitable for 2D fragment-based similarity searching than distance values. Atom sequences seem to perform best among the studied descriptors. Combination of atom sequences and the set theoretic Tanimoto coefficient is strongly recommended in similarity searching.[296] Fingerprint-based iterative similarity search with multiple active compounds as references performs better than 2D fingerprint similarity searching in a large-scale comparative analysis carried out on 208 well-defined compound activity classes.[297]

In the work of Reisen et al., six types of similarity measure were tested for their use in High-Content Screening (HCS)[298]: (i) distance measures (Euclidean, Manhattan, and Mahalanobis distances), (ii) linear correlation measures (Pearson correlation coefficient, Cosine similarity), (iii) nonlinear correlation measures on a ratio scale (Maximum information coefficient, Distance correlation), (iv) nonlinear correlation measures on an ordinal scale (Kendall's τ, Spearman's ρ), (v) comparison of up- and down-regulated features using a threshold (Tanimoto index, Dice coefficient), and (vi) CMAP-like similarity measures (see **Fig. 15**).

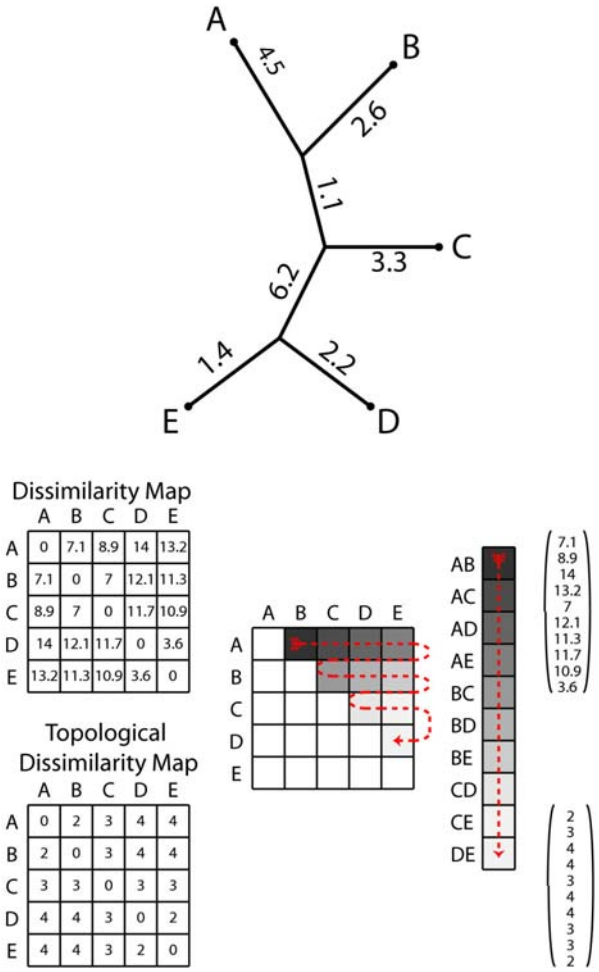

Fig. 14 A process to "unfold" diagonal dissimilarity maps into vectors according to Haws et al.[285] The dissimilarity map contains distances, whereas the topological dissimilarity map is calculated with path counts. While the original work revolves around phylogenetic trees, the concept presented can be easily translated to be applicable to distance, similarity, or correlation matrices, as well as topological distance matrices (as presented in subsection "**Topological descriptors**").

Receiver operating characteristic (ROC) curves are used to evaluate the performance of the similarity functions using the area under the curve (AUC). Data preprocessing greatly influences the results. The right choice of a similarity measure is a prerequisite for high-quality, high-content screening fingerprints. The nonlinear rank-based correlation methods (Kendall's τ and Spearman's ρ) seem to be suitable for identifying similarities and dissimilarities among the high-dimensional high-content screening readouts.

Scaffold hopping has played an increasing role in the last decade. Sufficient degree of diversity should be preserved not to overlook promising drug candidates or classes. A set of methods is presented that are designed to find compounds that are structurally different to a certain query compound while retaining its bioactivity properties (scaffold hops). These methods utilize various indirect ways of measuring the similarity between the query and a compound that take into account additional information beyond their structure-based similarities.[299] Stiefl et al. have defined scaffold hops based on whether the Extended reduced Graph approach (ErG) is able to switch among different chemotypes (and if yes, to what extent).[300] Group fusion is suitable for scaffold-hopping applications as well. Scaffold similarity searches were introduced by Ertl.[301] Classical similarity search and scaffold keys similarity search were compared, and the superiority of the latter has been proven. He also stated that the successful Tanimoto similarity measure unfortunately did not work well for scaffolds.

Structural unit analysis identifies the molecular substructures or fragments that distinguish compounds with high activity from those with average activity. The method is suitable to scaffold hopping, as well. A set of techniques were elaborated using the nearest-neighbor graph-based similarity.[302] Maggiora, in his editorial, discussed the reasons why QSAR modeling often fails and mentioned the idea of activity cliffs: "identifying and removing outliers may not necessarily always be a statistical problem as some outliers may only be *apparent* and may, in fact, arise from activity cliffs in the data."[303] Maggiora et al. outlined the various similarity concepts in an easily perceivable way.[304] Chemical, molecular, biological, global, and local similarity all have different meanings. They reformulated the definition of the Tanimoto coefficient in a more intuitive way to interpret it "as the ratio of the number of features shared by A and B molecules to the number of their unique features."

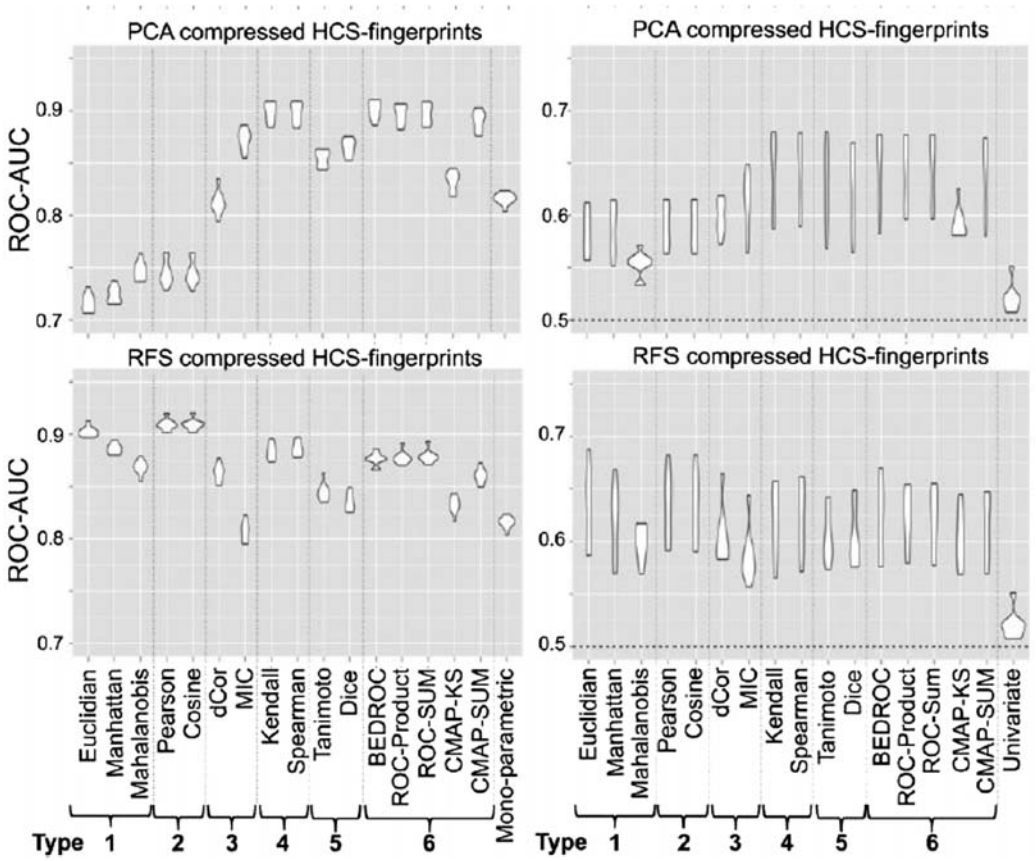

Fig. 15 Comparison of similarity metrics for high-content screening (HCS) fingerprints in the work of Reisen et al.[298] *Left* column: similarity analysis among replicates; *right* column: correlation between chemical and HCS fingerprints. Violin plots show the performance distribution over the 10 separate evaluation sets. © 2013 Society for Laboratory Automation and Screening.

Interestingly Muchmore et al. utilize a different terminology in their work, where they interpret fingerprints as similarity measures. A novel probabilistic framework was used for their interpretation. Tanimoto coefficients were calculated for 10 different similarity methods (MACCS keys, Daylight fingerprints, Maximum Common Subgraphs, Rapid Overlay of Chemical Structures (ROCS) shape similarity, and six connectivity-based fingerprints) combined with a database of more than 150,000 compounds and activity data against 23 protein targets. Different similarity measures were compared with Receiver Operating Characteristic curves (ROC) and the Boltzmann-Enhanced Discrimination of Receiver operating Characteristics (BEDROC). Decision theory helped in the data fusion, and the probability that any two molecules will exhibit similar biological activity is calculated.[305]

Density in chemical space is one of the limitations when using similarity methods. Insufficient density causes heavy computational time consumption and can lead to sometimes inaccurate results.[95] Todeschini et al. compared the largest pool of binary similarity coefficients.[280] Five pairs and a triplet of coefficients were found to yield identical similarity values, i.e., the same coefficients were rediscovered and bear different names. The similarity coefficients were grouped differently: symmetric, asymmetric, intermediate, and correlation-based binary coefficients (their shapes were plotted for the simulated data sets). Other partitioning options include metric–nonmetric, and—based on the shape behavior—increasing exponential, quasilinear, logarithmic, and sigmoidal. The best-ranked coefficient was CT4 (Consonni-Todeschini coefficient, fourth version),[306] which is basically the logarithmic transformation of the (shifted) Tanimoto index used for similarity analysis. Nonetheless, the Harris–Lahey, Tanimoto, Gower–Legendre, Sokal–Sneath and Jaccard (2012) coefficients are ranked similarly well on two real data sets (MDDR and WOMBAT).

3.14.6.2 Similarity Fusion, Fusion Rules, Consensus Scoring

In analytical chemistry data fusion usually means uniting data of vastly different origins and scales, for example, the fusion of NMR and mass spectrometry data[307] or the combination of "fluorescence with the biomarkers … and traditional metabolomics measurements in the form of ^{1}H NMR spectroscopy," as reported in the work of Bro et al.[308]

In chemoinformatics and medicinal chemistry, data fusion usually means "merging" different, eventually seriously conflicting rankings. The basic idea is far-reaching: multicriteria optimization, method comparison, feature ranking can all be considered as data fusion techniques.

Selection of structurally diverse subsets of chemical structures is a valuable aim. Several different algorithms have been compared, and all of them have been suggested for dissimilarity-based compound selection, provided that they are sufficiently rapid in execution for use with large files of compounds. MaxMin is the best algorithm currently available for nonfocused, dissimilarity-based compound selection based on a comparison of the number of activity classes identified using the MaxMin and other algorithms.[309]

Virtual screening based on fingerprints is rarely used as a standalone method. Methods such as group fusion, data fusion, or voting have been introduced to combine similarities calculated from multiple fingerprint methods.[95] Binary similarity coefficients (22) were compared using Unity fingerprints (2D fragment bit-strings), the coefficients were clustered, and a consensus scoring was calculated.[276] Two, three, and four binary similarity coefficients were merged in the work of Salim et al., who have established that the best fusions were better than the best single coefficients for 12 data sets out of 15. Consensus scoring has been shown to improve the hit rates in virtual library screening.[289] There are different possibilities to combine information from several scoring algorithms to provide a single prediction. Using several data sets, Ginn et al. used MIN, MAX, and SUM rules, defining the combined prediction by the lowest, highest, and average prediction of the individual methods. Both SUM and MAX are, overall, to be preferred to the individual results. The most effective for similarity fusion is generally the usage of the SUM rule with rank data. It was also found that consensus scoring performed better (and significant at $p < 0.05$) in 28 out of 30 runs if the SUM rule is used. In practice, one can use this information to determine how to deal with multiple known active structures: in particular it was shown that adding up individual scores of each pair of query and library compound improves the overall results.[310]

As so many similarity methods have been defined, it became a valid research goal to provide guidance on which similarity measure is the most suitable for solving a special task. Sheridan and Kearsley provided some justification to use a large number of molecular similarity methods.[288]

As some of the available similarity coefficients quantify different types of structural resemblance, it seems to be advantageous to use them in combination. Willett distinguishes between *similarity fusion* (combining the results of database searches that use a common reference structure but use different similarity coefficients) and *group fusion* (when several, structurally diverse reference structures are available, the reference molecule is allowed to vary and the similarity measure is kept constant).[91,311,312] *Consensus scoring* (combination of the results of different search algorithms and/or scoring functions) is a similar data fusion technique for structure-based approaches, such as docking.

Later, Willett extended the three accepted fusion rules (MIN, MAX, and SUM) to include the average, median, geometric and harmonic means, Euclidian norm, and some other rules concentrating on the top ranks only. Fusion rules are to be used for similarity scores or the ranks alike. Supervised fusion rules are also interpreted in the Bayesian framework when biological activity is also considered in the search.[312] Willett devoted a chapter to answer the question: why does data fusion work? He has established that "the SUM rule is likely to out-perform the MAX rule in similarity fusion; that the converse applies in group fusion; and that group fusion is generally far superior to similarity fusion." A further fusion rule is emphasized in Willett's work: the Reciprocal Rank Fusion (RRF) rule, which is applicable only to rank data and which derives from the fact that virtual screening often involves applying a cut-off on the similarity scores (such as the top-1%) so that only a small fraction of the database is considered further in a project.[91] Let p ($p \leq n$) be the number of times that an individual database structure dy occurs above the chosen cut-off. Then the RRF rule involves summing the reciprocal ranks for those p occurrences to give a fused score:

$$\sum_{x=1}^{p} \frac{1}{\mathrm{RANK}_x(dy)} \tag{35}$$

The reciprocal rank fusion rule outperformed all of the other rules that Chen et al. considered in their comparative study of 15 different fusion rules.[313] Group fusion is most effective when: (i) as many reference structures as possible are used, (ii) only a small proportion (1–5%) of each ranked similarity list is submitted to the final fusion rule, and (iii) when the reciprocal rank rule is used to combine the individual search outputs. The Pareto data fusion approach has been elaborated by Cross et al.[314] The Pareto approach counts for each molecule the number of times other molecules achieve a better rank in all of the lists, thus the best molecules will receive a Pareto score of 0. (The ties are managed by successive interactive ranking.)

Independently from virtual screening and similarity coefficients, data fusion is extensively used for method and model comparison.[284,315,316] Sum of Ranking Differences (SRD) are supported with theoretical considerations[317,318]: in particular, the average of ranks (or scores) is a better option than any of the individual ranks (or scores), as derived from the maximum likelihood principle. The SRD procedure involves two kinds of validation: a randomization test and a leave-one-out or leave-many-out cross-validation. Maximum for correct classification rates or minimum for error rates is the natural data fusion choice.[317]

The performance of ranking methods in the context of virtual screening cannot be evaluated without accepted, consensual metrics. Area under the Receiver Operating characteristic curve is not suitable to the "early recognition" problem. Performance indicators such as enrichment factors, robust initial enhancement, Boltzmann enhanced discrimination of receiver operating characteristic, area under the accumulation curve corresponding to an empirical cumulative density function, and their weighted variants were analyzed theoretically in detail.[319]

3.14.6.3 Clustering Algorithms

Clustering is the collective name for a group of methods, where the molecules (samples, objects, etc.) are arranged in groups (or "clusters") based on their distances from (in other words their similarities to) each other. Since clustering is not the main focus

of this chapter, we refer the reader to recent, well-written reviews on clustering methods and applications from the fields of chemometrics[278] and cheminformatics[320] and collect only a small set of diverse developments and applications in this subsection. (Also, it would be virtually impossible to enumerate all clustering algorithms that were provided by the machine-learning community.)

The following sentences are typical of the current literature and state: "Using various stopping rules the grouping of similarity coefficients resulted in three, 11 or 13 clusters."[289]

"The average clustering coefficient similarity threshold function can be characterized by the presence of a peak that covers a range of similarity threshold values. This peak is preceded by a steep decline in the number of edges of the similarity network. The maximum of this peak is well aligned with the best clustering outcome. If no reference set is available, choosing the similarity threshold associated with this peak would be a near-ideal setting for the subsequent network cluster analysis."[321]

"Despite the long tradition of pattern recognition research, there is no technique that yields the best classification in all scenarios. Therefore, as many techniques as possible should be considered in high accuracy applications. Typical related works either focus on the performance of a given algorithm or compare various classification methods." Amancio et al. compared the performance of nine well-known classifiers and found that the *k*-nearest-neighbor method frequently allowed the best accuracy.[322]

Large margin nearest-neighbors approach and its multimetric extensions have recently been elaborated by Kireeva et al.[323] Their algorithms cluster the compounds in the training set with the same property label together, while the compounds from different classes are separated by a large margin. In most of the cases the metric learning algorithm leads to better classification; the performance dependence from the data density has been discussed. The *k*-medoids clustering method was favored by Jaskowiak et al.[324] Saeh et al. generated robust models while combining 3D pharmacophore fingerprints and the support vector machine classification algorithm. Lead-hopping was also simulated: an entire class of compounds was excluded from the training set. Still, the model trained on the remaining compounds was able to recall 75% of the actives from the "new" lead series and correctly classifying >99% of the 5000 inactive compounds included in the validation set.[325]

The Generalized Metric Swarm Learning (GMSL) algorithm has been developed by Zhang and Zhang, where a sample pair is represented as a similarity vector *via* the well-learned metric swarm. The sample pairs are transformed into a vectorized similarity space (metric swarm space) *via* an established joint similarity function, whereas SVM-like classification can be easily implemented.[326] They have presented the efficiency of their approach on the example of face recognition, but it should have great potential in medicinal chemistry, as well. Gaussian Ensemble Screening (GES) was developed by Perez-Nueno et al.[327] "GES is a new and fast way to predict polypharmacological relationships between drug classes; it quantitatively provides an efficient way to measure the similarity between clusters of arbitrary numbers of members."

3.14.6.4 Similarity Measures for Special Tasks

3.14.6.4.1 Symmetric field-based similarity indices

The first quantum chemical similarity index was defined by the analogy of correlation coefficients in 1980:

$$r_{AB} = \frac{\int \rho_A \rho_B \mathrm{d}V}{\sqrt{\int \rho_A^2 \mathrm{d}V \sqrt{\int \rho_B^2 \mathrm{d}V}}} \tag{36}$$

where ρ_A and ρ_B are the first-order density functions for molecules A and B.[328] This is the most frequently used field-based similarity index. Similar ones are defined by Hodgkin and Richards[329] and Petke.[330] A comparative analysis of quantum chemical similarity and dissimilarity indices has been carried out not long ago.[331]

Standard Quantum-Based (SQB) similarity methods were compared with Tanimoto-based similarity, and it was established that "the use of a complex number format for molecular representation proved to be superior compared to real representation and benchmark Tanimoto method (TAN), where the complex SQB method outperformed TAN in nine cases."[332]

3.14.6.4.2 Similarities of 1D structures

Gene expression data analysis requires special similarity measures. The Jackknife correlation coefficient (successively removing the outlying features) provided the best results, showing better enrichments than other distance measures, whereas the second-ranked measure is the Kendall tau. Good results were also shown by Manhattan distance, popular distance measures in the gene expression clustering literature, namely, Euclidean distance, Spearman, and Pearson coefficients displayed inferior results to at least five other distances under evaluation.[324]

In another example, Dixon and Merz, Jr. have introduced a truly 1D representation of chemical structure. A 3D molecular model or a 2D chemical graph is projected onto a single coordinate of atomic positions. A novel measure of overall structural similarity has been defined after the alignment of 1D representations to match identical atom types:

$$\mathrm{Sim}_{A,B} = \frac{S_{A,B}^{\max}}{\sqrt{S_{A,A}^{\max} S_{B,B}^{\max}}} \tag{37}$$

1D similarity has been defined in such a way: molecule B is aligned at various offsets with respect to molecule A, and the total overlap area S_{AB} between rectangular regions of the same type is computed. The largest overlap area that can be achieved, $S_{A,B}^{\max}$, is

combined with normalization factors from aligning each molecule with itself. The constraint is valid: $0 < \mathrm{Sim}_{A,B} < +1$. These 1D similarities have been reported to consistently outperform both Daylight 2D fingerprints and Cerius2 pharmacophore fingerprints.[186]

Similarities of drug chemical structures, drug protein targets, and drug side-effect profiles (Tanimoto similarities and protein sequence similarities) were calculated and fused into an overall prediction score using the *k*-nearest-neighbor algorithm.[333]

A web-interfaced target identification program (called TargetHunter) with a built-in powerful data-mining algorithm (TAMOSIC) has been elaborated for predicting potential biological targets of query compounds. Its performance has been compared with the multiple-category models (MCM) for predicting protein targets and therapeutic activities.[334]

A revised algorithm based on Shannon's information theory, and the Neumann entropy characterizes each individual protein residue position with the number of significantly correlated pairs by computing the corresponding mutual information matrix.[335] Chemogenomics aspects were summarized by Bender et al. focusing on target prediction of small molecules with molecular descriptor-based models.[164] Semantic links between compounds and proteins, including *similarity neighboring links*, and interaction links were utilized to predict drug target interactions.[336] Features are structured according to prior knowledge into groups based on similarity in gene expression.[337] Pearson correlation similarity was calculated, and heatmaps were plotted.

3.14.6.4.3 Graph (tree)-based similarities

Direct similarity between two feature trees has been defined by Rarey and Dixon.[338] The similarity value of the feature trees is computed by a weighted average over the similarity values of the matches. The weight factor for each match is the sum of the subtree sizes size(m) of the match. The total weight is the sum of the sizes of the matched subtrees plus a scaling factor u times the total size of the unmatched subtrees:

$$S_M(A,B) = \frac{\sum_{x\in M} \mathrm{size}(m)\mathrm{sim}(m)}{u(\mathrm{size}(A)+\mathrm{size}(B)) + (1-u)\sum_{x\in M} \mathrm{size}(m)} \tag{38}$$

There is a notable research gap on comparing different approaches retrieving those models in the repository that most closely resemble a given process model or fragment thereof.[339] Business process graphs use various notations and customs. Three types of parameterized similarity metrics between business process models have been elaborated: (i) node matching similarity metrics based on properties of business process model elements (such as their labels and their other attributes), (ii) structural similarity metrics based on the relations between these elements, and (iii) behavior similarity metrics based on the intended behavior of process models.

A detailed, comprehensive survey on techniques to define and calculate business similarity measures has been carried out. Nine properties of distance measures were enumerated, and 21 business similarity measures have been compared in the work of Becker et al.[340] Sum of ranking differences using the average as reference provides the ordering presented in Fig. 16.

There is no doubt that similarity based on traces (Sbt) is the best, most consistent one according to the SRD methodology. Some similarity metrics (Edbrm, Lsged, Pcan, Lms, Fbas, Nlbs, Ged2, and Lsged2) are comparable with random ranking (the analysis was based on Table 26 in Ref. 340).

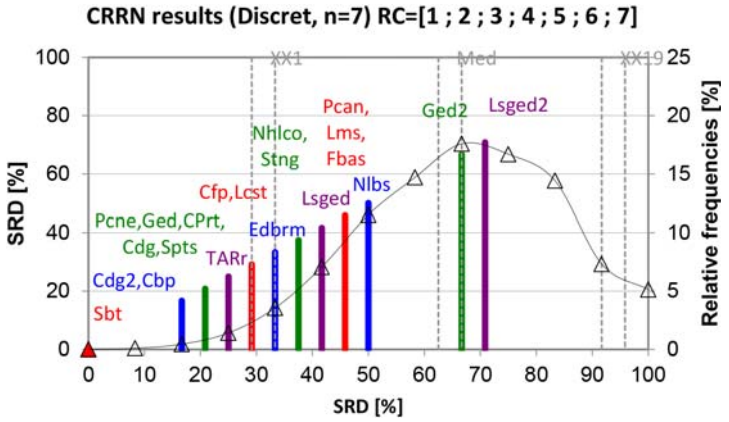

Fig. 16 Ordering of business similarity measures by sum of ranking differences (SRD). XX1 band corresponds to 5% first kind error, i.e., many of the similarity measures are indistinguishable from random ranking (black distorted Gaussian like curve and right *y* axis). Notations (in the order of appearance): Similarity based on traces (Sbt), Comparing dependency graphs (Cdg and Cdg2), Causal behavioral profiles (Cbp), Percentage of common nodes and edges (Pcne), Graph edit distance (Ged and Ged2), Comparing PMs represented as trees (CPrt), Similarity based on principal transition sequences (Spts), TAR-relationship (TARr), Causal foot prints (Cfp), Longest common subsequence of traces (Lcst), Edit distance between reduced models (Edbrm), Number of high-level change operations (Nhlco), Sets of traces as n-grams (Stng), Label similarity and graph edit distance (Lsged and Lsged2), Percentage of common activity names (Pcan), Label matching similarity (Lms), Feature-based activity similarity (Fbas), and Node- and link-based similarity (Nlbs).

In a ligand-based virtual screening experiment, the similarity between every library molecule and a query molecule is measured by some similarity function. An extension of the optimal assignment method for chemical graphs was produced that uses evolutionary algorithms to optimize edge weights. A variety of similarity functions can be improved by optimizing the edge weights.[341] The similarity between two chemical graphs can be evaluated by means of the Maximum Common Subgraph approach.[342] Ralaivola et al. reviewed graph kernels and developed new graph kernels (Tanimoto, MinMax, and Hybrid kernel) for molecules. These kernels measure the similarity between feature vectors, or molecular fingerprints, consisting of binary vectors or vectors of counts.[343]

3.14.6.4.4 Semantic similarity measures

Semantic similarity was defined by Resnik based on information content:[344]

$$\mathrm{sim}(c_1c_2) = \underset{c\in S(c_1c_2)}{max}\left[-\log p(c)\right] \tag{39}$$

where $\mathrm{sim}(c_1c_2)\in[0;+\infty]$ and $-\log p(c)$ is the negative log likelihood, or the *information content* of a concept c (not to be confused with the partition coefficient log*P*!).

A similar definition is given by Lin.[345] Lin defines the similarity between two terms as the ratio of the commonality of the terms, and the information needed to fully describe the two terms:

$$\mathrm{sim}(c_1c_2) = \underset{c\in S(c_1c_2)}{max}\left[\frac{2\log p(c)}{\log p(c_1)+\log p(c_2)}\right] \tag{40}$$

where $\mathrm{sim}(c_1c_2)\in[0;+\infty]$.

Schlicker et al. have combined Lin's and Resnik's similarities into relevance similarity:[346]

$$\mathrm{sim}(c_1c_2) = \underset{c\in S(c_1c_2)}{max}\left[\frac{2\log p(c)}{\log p(c_1)+\log p(c_2)}(1-p(c))\right] \tag{41}$$

Their approach enables the comparison of the underlying molecular biology of different taxonomic groups and provides a new comparative genomics tool identifying functionally related gene products.

A novel similarity measure for ligand-based virtual screening has been created from a text-processing similarity measure called Adapted Similarity Measure of Text Processing (ASMTP).[347] ASMTP was reported to outperform the Tanimoto coefficient-based virtual screening.

Kendall's τ has been the most widely used measure of similarity between two orderings, R^* and R^F; a novel similarity function is defined as:

$$\tau\left(R^*,R^F\right) = \frac{P}{P+Q} = \frac{Q}{\binom{|D|}{2}} \tag{42}$$

where P is the number of concordant pairs and Q is the number of discordant pairs on a data set D.[348] An optimal method has been derived based on rank support vector machine that selects the most ambiguous objects for ranking so that the ordering on the set maximizes the degree of learning.

In a linguistics application, Mandera et al. calculated the cosine distances between the cue word and all the other words in semantic spaces.[349] The similarity score for each associate was normalized by dividing it with the sum of all the similarity values for the cue. Next, an additive smoothing was applied to each distribution, and the relative entropy between probability distributions was computed. Finally, the relative entropies were averaged across all cue words, and the average relative entropy was used as the final score of a given semantic space. Semantic vectors for English and Dutch were provided for a range of models of psycholinguistic theories together with a convenient interface that can be used to extract a great number of semantic similarity measures.

3.14.6.4.5 Supervised similarity measures

Ligand similarity measures, such as shape similarity, are defined such a way: each atom of a molecule is mapped to a five-dimensional space, where the first three coordinates are determined by the 3D conformation of the molecule. The two remaining dimensions encode the atomic partial charges and the atomic lipophilicity (A log *P*).[350,351] Multiple logistic regression was applied to combine different similarity values.

One popular measure of the roughness of a structure–activity landscape is the structure–activity landscape index, SALI[352]:

$$\mathrm{SALI}_{A,B} = \frac{|A_A - A_B|}{1-\mathrm{Sim}_{A,B}}, \tag{43}$$

where A_A and A_B are the affinities/activities of compounds A and B, while $\mathrm{Sim}_{A,B}$ is their similarity. Basic characteristics of molecular similarity and dissimilarity *networks* are reviewed by Sukumar et al.[353] "The choice of descriptors affects the computed similarity—for instance, two molecules might be constructed from the same molecular scaffold and thus be very similar in size and shape, but have very different properties because of the different chemical natures of the functional groups or substituent atoms. Conversely, molecules with very different molecular scaffolds might look similar for binding to a protein."

Cuissart et al. have constituted two more similarity indices in the biodegradability context:[354]

$$\mathrm{Sim}_1(\mathrm{QS}, IS) = \frac{|\mathrm{MCS}|}{|\mathrm{QS}|} \tag{44}$$

and

$$\mathrm{Sim}_2(\mathrm{QS}, IS) = \frac{|\mathrm{MCS}|}{|\mathrm{QS}|} \times \frac{|\mathrm{MCS}|}{|\mathrm{IS}|} \tag{45}$$

where $|S|$ equals the number of nonhydrogen atoms within molecule S, and MCS is the maximum common substructure between two molecules. "IS" means "Instance Structure", whose biodegradability value is used to compute the prediction model, whereas QS means "Query Structure", whose biodegradability is predicted by this model. Both similarity indices are discriminant to a group of compounds of similar activity. The index Sim_2 operates more in conformity with the SAR principles than Sim_1.

Dropout training of artificial neural networks (ANNs) outperforms conventional ANNs when using two types of fingerprints and two similarity metrics (Tanimoto and Buser).[355] Dropout means randomly omitting a large portion of the nodes from an artificial neural network.

Naderi et al. have predicted drug-likeness for molecular synthesis. Each active compound in the DUD-E library was decomposed into fragments, and a molecular synthesis was simulated. A search space was constructed from small molecules, followed by the stochastic exploration of the chemical space by constructing multifragment molecules. Tanimoto coefficient was used to reveal the chemical similarity. Parent compounds are compared to those constructed with the eSynth computational package using molecular fingerprint matching.[356]

Sixteen different feature ranking methods were compared by Jankowski and Usowicz in combination of six weighting schemes, and the counts of winnings, defeats, and draws were presented.[357]

3.14.6.4.6 Chemometric/Spectral similarity

An adaptive similarity measure (sample similarity) was proposed to construct highly accurate locally weighted partial least squares (LW-PLS) calibration models. The method is based on the weighted Euclidean distance and was used for weighting in regression.[358]

Common mathematical methods to express similarity in NIR (near-infrared) spectroscopy are correlation coefficients and distances.[359] The authors of a recent work have successfully transformed differences in spectra into Bayesian hypothesis testing.[360] Logarithm values of the posterior odds ratios for the spectra are able to detect subtle differences, e.g., changes in the analytical process.

A novel spectral similarity measure was introduced by Bodis et al.[361] De Gelder and colleagues have shown that "various similarity and dissimilarity criteria previously described in literature can be written as special cases of a general expression." They have introduced a new similarity criterion, based on this generalized expression.[362]

The spectral-contrast-angle method introduced by Wan et al. is based on the vector representation of mass spectra and has been shown to perform better than the similarity index method for spectral comparison.[363] The spectral contrast angle is defined as the angle between two mass spectrum vectors.

The correlation and congruence coefficients (i.e., similarity values) of all total ion chromatograms relative to the reference chromatogram were calculated with median or averaged data. Principal component analysis and cluster analysis can successfully discriminate between mountain origins of green teas and therefore can be further applied to identify and authenticate Pu-Erh green teas.[364]

Three mass spectral similarity measures (NIST composite measure, the real part of Discrete Fourier Transform, and the detail of Discrete Wavelet Transform) were compared and integrated with retention indices. As a consequence compound identification was enhanced by 1.7–3.5%.[365]

Similarity of infrared spectra was characterized by: correlation coefficient of mean centered absorbance (i.e., cosine measure), mean of the absolute absorbance differences, mean of the squared absorbance differences, dot product of the absorbance vectors, each normalized to unit length, whereas Tanimoto index has provided the chemical structure similarity. The definitions were given in vector notations and scaled properly. The first hits corresponding to the most similar spectra yield the highest structural similarity with the query compound. Among the four investigated spectral similarity measures the correlation coefficient of mean-centered absorbances performed best.[366]

3.14.6.4.7 Fuzzy similarity measures

Enormous progress took place in the development of fuzzy similarity measures. Fuzzy sets are sets whose elements have degrees of membership. Thus, instead of 0 (not a member) and 1 (is a member), the membership of an element in a fuzzy set can be any real number between 0 and 1. Fuzzy similarity measures are defined for the comparison of such fuzzy sets. A small but characteristic selection can be found below.

Three new equations were suggested to calculate the distance between intuitionistic fuzzy sets (IFSs) on the basis of the Hausdorff distance. The proposed similarity measure is much simpler than the existing methods and is well suited to use with linguistic variables.[367]

Existing similarity measures can provide unreasonable results in some special cases. Therefore, several new similarity measures were proposed to differentiate different IFSs. The proposed similarity measures can deal with problems more effectively and reasonably than some of the existing methods.[368]

The degree of similarity between Intuitionistic Fuzzy Sets A and B (B^c is the complement of B) is defined as:

$$\dot{s}(A,B) = \sum_{j=1}^{n} \dot{s}(\alpha_j, \beta_j) = \frac{1}{n} \sum_{j=1}^{n} \frac{d\left(\alpha_j, \beta_j^c\right)}{d(\alpha_j, \beta_j) + d\left(\alpha_j, \beta_j^c\right)} \tag{46}$$

where α_j and β_j are the jth intuitionistic fuzzy values of A and B, respectively, and $d(\alpha_j, \beta_j)$ is the normalized Hamming distance. The analogous formula has been used for interval-valued Intuitionistic Fuzzy Sets, as well. Then, the developed similarity measure was applied for consensus analysis in group decision-making based on intuitionistic fuzzy preference relations, and it was extended to the interval-valued intuitionistic fuzzy sets.[369]

"Reasonable" measures to calculate the degree of similarity between Intuitionistic Fuzzy Sets were proposed based on the L_p metric.[370] A new similarity measure for IFSs was suggested and its usefulness in medical diagnostic reasoning was proven.[371]

An axiomatic definition of a similarity measure between dual hesitant fuzzy sets was proposed, and the shortcomings in existing similarity measures were enumerated.[372]

Some new distance measures between Intuitionistic Fuzzy Sets (IFSs) were suggested. Maximum degree of similarity between IFSs was applied for pattern recognition.[373]

Some similarity measures were introduced between two triangular fuzzy numbers based on the vector similarity measures in vector space (which can be used to aggregate the decision information). A methodology for multiple criteria group decision-making (MCGDM) problems with triangular fuzzy information is proposed; the criteria values take the form of linguistic values. The weighted similarity measures between each alternative and ideal alternative can be used to rank alternatives and select the most desirable alternative.[374]

Dual hesitant fuzzy sets include fuzzy sets, intuitionistic fuzzy sets, and hesitant fuzzy sets as its special cases. Some distance and similarity measures based on the Hamming distance, Euclidean distance, and Hausdorff distance were derived for usage in decision-making, pattern recognition, etc. Two examples illustrate these distance and similarity measures and their applications in pattern recognition.[375]

Novel discrete and continuous hesitant fuzzy distance measures and hesitant fuzzy-ordered distance measures between hesitant fuzzy sets were elaborated. A hesitant fuzzy clustering algorithm based on novel similarity measures was also created.[376]

3.14.6.4.8 Other similarity measures

The most detailed collection of dissimilarity measures and their comparison can be found in the work of Todeschini et al.[377] Methods of data preprocessing (transformation) and the next classification of dissimilarity measures can also be found there: distances for real-valued data, distances for ranked data, distances for frequency data, binary similarity measures, and mixed-type distances.

A novel asymmetric hybrid similarity function (metric) was recently introduced using Maximum Common Substructures (MCSs). The hybrid metric was designed molecules to detect structurally similar compounds of increasing size while using small reference compounds. This Tversky metric could detect similarity relationships between small and large compounds much better than other similarity measures.[378]

In other areas, an object is often described by sets of features instead of geometric points in a metric space. A new measure of remoteness between sets of nominal values is proposed instead of considering the distance between two sets: a new measure of perturbation type 1 of one set by another was introduced. The consideration is based on set-theoretic operations, and the proposed measure describes changes of the second set after adding the first set to it, or *vice versa*. The measure of the sets' perturbation returns a value in the range [0, 1], and this measure is not symmetric in general.[379]

According to a scientometric study by Hamers et al. the Cosine formula often yields a similarity measure in citation studies that is twice the number of that obtained by the Jaccard index.[380]

Most online shopping sites and many other applications now use collaborative recommender systems. The measurement of similarity plays a fundamental role in such systems. The accuracy of the most well-known similarity measures (Pearson's correlation coefficient, cosine similarity, and mean squared differences) decreases due to data sparsity. Therefore, a user–user potential matrix is calculated; potential similarities between users from this matrix are computed; the potential similarities are modified based on the users' preliminary neighborhoods; and k users with the highest modified similarity values are selected.[381] A novel similarity measure introduced by Cha can cope with the sparsity problem often encountered in the case of Pearson and cosine coefficients and mean squared differences. Cha enumerated and categorized a large variety of distance/similarity measures for comparing nominal type histograms. The grouping has concentrated upon three aspects: syntactic similarity, implementation caveats, and semantics.[382]

3.14.7 Online Web Resources

Since the pool of cheminformatics and molecular modeling software is quickly and constantly renewed, we refrain from providing a detailed overview of them: a current and prominent selection was presented recently by Cereto-Massagué et al.,[88] and we have

already referred to several of them throughout this chapter. However, online resources such as molecular databases are more permanent over time, thus we provide a short overview of top-level databases to provide some guidelines to anyone who wishes to apply them. These databases implement diverse ways of submitting search queries: besides recognizing chemical names and SMILES strings, many of them have an integrated sketching interface and support similarity searches (based on the entered queries). Most of these databases offer some possibilities for batch downloading and query automation as well, through a Graphical User Interface (GUI), an application programming interface (API), or other mechanisms.

- Chemical Abstracts Service (CAS) Registry: The CAS Registry (operated by the American Chemical Society) is the largest molecular database to date.[3,4] It is constantly updated and stores every reported chemical structure (c.111 million at the time these lines are written) with a uniquely assigned identifier, the CAS Registry number. In addition to the database itself, the CAS Registry powers the two major chemical information services of CAS: Scifinder (for querying chemical structures and reactions, primarily in the literature)[5] and STN (a search engine that provides access to patent content).[6] While these are paid services, a freely available website covering a subset of high interest of the CAS Registry entries—titled Common Chemistry—is also operated by CAS.[383]
- Pubchem: An open chemistry database operated by the National Center for Biotechnology Information.[109,384] The database covers a diverse set of information about the stored compounds, from chemical names, 2D and 3D structures, and line notations (InChI, InChIKey, SMILES) to calculated properties and even vendor and patent information. Pubchem operates separate (overlapping) databases for substances (i.e., depositor-supplied molecules) and compounds (i.e., unique chemical structures, including stereoisomers and even tautomers). In addition, the Pubchem Bioassay database is a rich source of deposited biochemical screening data.[385]
- ChemSpider: An open chemistry database operated by the Royal Society of Chemistry.[386] In addition to 2D and 3D representations and chemical names, ChemSpider also stores experimentally determined properties and NMR spectra, as well as links to literature articles and reference works.
- ChEMBL: Operated by the European Bioinformatics Institute (EMBL-EBI), ChEMBL is today's probably largest database of experimental bioactivity data.[387–389] In addition to bioactivity data, line notations, links to external databases and drug-related information (availability type, route of administration, etc.) are also stored. ChEMBL integrates bioactivity data from various sources, including full-matrix datasets such as DrugMatrix or the GSK Published Kinase Inhibitor Set, as well as screening results contributed by pharma companies. Lately, ChEMBL has integrated the full bioactivity content of PubChem BioAssays, which currently accounts for more than half of the data points in the ChEMBL database. EMBL-EBI also operates an open, searchable patent database called SureChEMBL.[390]
- Protein Data Bank (PDB): The Protein Data Bank is without question the largest and most commonly used repository for experimentally determined protein structures, hence it is one of the most important data sources for medicinal chemical and modeling work.[41] The database is thoroughly linked and annotated and offers a detailed and highly configurable "Advanced search" mechanism for exploring and analyzing not only the protein–ligand complexes but also the ligands themselves.
- ZINC (ZINC Is Not Commercial): Probably the largest molecular database focusing on commercially available compounds (storing approx. 35 million compounds the time these lines are written).[391,392] In addition to storing the molecules with calculated properties and links to vendor databases, ZINC also offers a plethora of subsets for downloading, categorized based on various attributes, such as physicochemical properties, targets, vendors, or availability. Thus, it is a flexible and customizable source of information for virtual screening. Other comprehensive vendor databases include eMolecules[393] and Mcule,[394] with the latter offering a wide set of online virtual screening tools as well.

  GDB databases: Besides commercially available compounds and experimentally determined data, databases of virtual compounds are also available, the most prominent of which are probably the GDB databases based on the work of the research group of Reymond.[151] GDB databases are generated with a systematic enumeration of all possible combinations of a predefined number of common heavy atoms (C, N, O, S, and halogens). For example, the latest database, GDB-17 enumerates molecules of up to 17 heavy atoms: a total of 166 billion molecules![395] Such approaches serve not only as a basis for analytical work but also define the future directions in synthetic medicinal chemistry by providing an abundance of ideas for new scaffolds. In addition to downloadable subsets, the same group has implemented online browsers based on various fingerprints, as well as molecular quantum numbers (MQN)[113] for the efficient exploration of the chemical universe.

3.14.8 Case Studies

In this section, we briefly summarize a few illustrative case studies that apply some of the methods discussed in this chapter: (i) fingerprints (Protein–Ligand Interaction Fingerprints, as well as hashed topological fingerprints), (ii) QSAR modeling using calculated molecular descriptors, and (iii) similarity measures in an application to support decision-making.

(i) As a case study for the use of fingerprints in drug discovery, we briefly summarize the work of de Graaf et al., who have applied docking in combination with Protein–Ligand Interaction Fingerprints for the virtual screening of fragment-like human histamine H_1 receptor (hH_1R) ligands.[396] The H_1 receptor is of key importance in allergic responses and the target of so-called antihistamines: a class of drugs used to relieve the symptoms of allergic rhinitis. The 2–3 years preceding the cited study[396] (2011) have seen several breakthroughs in GPCR crystallography, including the publication of the first crystal structure of the H_1

receptor, bound to a fragment-like ligand (doxepin). Based on this structure, the authors have developed a customized virtual screening protocol for the identification of novel H_1R fragments.

The protocol involved the use of PLANTS—a docking program based on ant colony optimization—and Interaction Fingerprints (IFPs, as defined by Marcou and Rognan[168]) as two orthogonal scoring methods for predicting ligand binding. (Quite literally, as the authors have compiled 2D plots of PLANTS and IFP scores to select a region retrospectively with a favorable enrichment of known H_1R ligands versus decoy molecules.) The IFPs contained seven bits per residue to encode hydrophobic, aromatic (face-to-face and edge-to-face), H-bond (donor and acceptor), and ionic (positive and negative) interactions, and IFP scores were defined as the Tanimoto similarities to the experimentally supported binding mode (IFP) of doxepin. The authors have confirmed that the use of the two orthogonal scoring methods greatly surpassed—in terms of the retrospective enrichment of known actives—the performance of PLANTS scores, as well as IFP scores, on their own. In addition to interaction fingerprints, ECFP_4 fingerprints were applied as a measure of ligand novelty: any ligand with a Tanimoto similarity of more than 0.4 to any known H_1R ligand was rejected. (Hence this work also exemplifies the popularity of the combination of ECFP_4 fingerprints and Tanimoto similarities to quantify molecular similarity.)

Prospectively, the screening protocol was applied to ultimately select 26 virtual hits from a set of 108,790 fragment-like compounds (282 before visual inspection). Upon experimental testing for their binding affinity to H_1R, 19 of them have been confirmed. Overall, the work of de Graaf et al. can be considered a proof-of-concept for crystal structure-based virtual screening for fragment-like GPCR ligands and has resulted in the identification of 19 diverse fragment-like H_1R ligands with a hit rate of 73%, which is exceptionally high in the area of drug discovery.

(ii) For a case study on the use of descriptors for QSAR model building, we refer to the work of Keserű on the prediction of hERG potassium channel affinities.[397] The hERG potassium ion channel is best-known for its regulatory role in the electrical activity of the heart that coordinates the heart's beating. Its inhibition can result in a potentially fatal disorder called long QT syndrome and create a risk of sudden death as a side effect. Thus, it is a very important off-target in drug discovery whose inhibition should always be avoided. The cited study employs traditional and hologram QSAR methods for the quick computational prediction of hERG affinities. Because of the multiple binding sites of hERG K^+ channels, a functional assays format is preferred for affinity evaluations. However, these techniques have limited capacity, thus a fast method for the *in silico* prediction of hERG affinity is needed.

The number of used compounds was 68, which was split into training and test sets: 55 compounds were applied for training and 13 for test set predictions. After the calculation of the 99 potentially relevant molecular descriptors, multiple linear regression was applied in stepwise mode for the training. In the next step, the model was validated with the 13 test set compounds and with an additional (external) test set of 82 compounds, as well. For the appropriate model building five descriptors were chosen, namely, Clog*P*, molar refractivity (CMR), Partial Negative Surface Area (PNSA1), and two VolSurf descriptors (W2—polarizability and D3—hydrophobicity). The created model had good quality parameters for the training ($R^2 = 0.97$) and test sets ($Q^2 = 0.75$) too.

Based on the chosen descriptors a concept of the interaction with the hERG channel was proposed: the compounds have to be larger, lipophilic and highly polarizable with a basic character. Because of the differences between the averages values of active and inactive molecules regarding the five used descriptors, discriminant analysis was also used for classification with correct classification rates of 83% for actives and 87% for inactives.

Since the generation of 3D VolSurf descriptors is time-consuming, hologram QSAR (HQSAR) was also applied. This methodology avoids the descriptor calculations, selection of conformers, and the structural alignment that makes the use of 3D QSAR nontrivial. The final model was also very good, and it was validated with the same dataset as in the previous case, but here a much lower correct classification rate was obtained for the inactive molecules (18 %). Thus, the work of Keserű also highlights the importance of the 3D aspects of QSAR modeling, in addition to providing a fine example of the use of molecular descriptors for affinity prediction for an important off-target.

(iii) An interesting example for a practical application of similarity measures can be found in Kwak et al.'s work on the detection of cancer in prostate tissue samples.[398] If a new tissue is evaluated, the closest matches and their clinical information are retrieved from a tissue database. Then, a pathologist makes a diagnosis and the database is updated, if necessary. Consistent and reliable diagnoses can be achieved via the automatic selection of similar tissues. Nine morphologic criteria were defined (they describe the architectural properties of a tissue): (1) Gland crowding, (2) Gland roundness, (3) Stromal reaction, (4) Nuclear grade, (5) Clefts, (6) Lumen/gland ratio, (7) Gland continuity, (8) Cell separation, and (9) Gleason score. Tissue morphologic similarity $\mathrm{TMS}(d_1, d_2)$ between two tissue samples d_1 and d_2 was defined as:

$$\mathrm{TMS}(d_1, d_2) = \sum_{i=1}^{9} \mathrm{TMS}^i(d_1, d_2) \tag{47}$$

where $\mathrm{TMS}^i(d_1, d_2)$ is the morphologic tissue similarity for ith criteria. It is calculated as follows:

$$\mathrm{TMS}^i(d_1, d_2) = 1 - \frac{\sum_{s=s^i_{d_1+1}}^{s=s^i_{d_2-1}} h^i(s) + \frac{1}{2}\left(h^i\left(s^i_{d_1}\right) + h^i\left(s^i_{d_2}\right)\right)}{Z} \tag{48}$$

where s_d^i is the ith morphologic criterion score of a tissue sample d, $h^i(s)$ is the number of samples having ith morphologic criterion score s, and Z is a normalization factor ensuring that as $1 \leq i \leq 9$, TMS(d_1,d_2) ranges between 0 and 9. TMS scores represent the true tissue similarity and served as the gold standard of tissue retrieval.

In summary, an efficient and effective tissue management and decision-support system was developed.[397]

3.14.9 Outlook

Cheminformatics—and by extension, computational medicinal chemistry—is a field that has the potential to change very quickly. Novel file formats and fingerprints, based on original ideas, continue to emerge, providing an always renewing toolbox for the researchers of these fields. However, applications seem to lag behind these technological advances. If we want to look for the reasons behind that, we might consider factors such as publication delays, customs, and personal preferences (i.e., if I have learned to apply one method that seems to work, I might not be open to learning a new one), or a sort of "canonization" (the process of a scholarly community accepting some works as the most important—not to be confused with canonicalization!) similar to that in literature. For example, if ECFP4 fingerprints are widely accepted for quantifying the 2D similarities of molecules, one might feel a motivation to prefer them over, e.g., topological torsion fingerprints, when the latter might be in fact more suited for the given application. Similarly, the MDL *mol* (and *sdf*) formats continue to be the most prevalent chemical file formats despite their flaws and limitations. Since we maintain that true progress requires the thorough and independent testing, validation, and application of the new computational tools, we expect a steady increase in the number of application-related works in this field. (Nonetheless, we hope to have provided useful guidance for that with this chapter.)

In terms of descriptors, the question is always open: "Do we need more and more molecular descriptors?" This question has been raised already in 2001 by Randic and Basak.[205] On the other hand, a distinguished publication of Cherkasov et al. paraphrases Mark Twain about QSAR (and thus molecular descriptors): "reports of [QSAR] death are an exaggeration."[399]

After carefully rereading many publications in the field of molecular descriptors, we can infer the following: although there are some novel descriptors in the recent literature, most of the widespread ones were developed in the second part of the last century. In the near future we expect more application-related articles and somewhat fewer works about the development of new descriptors and fingerprints. However, it is also clear based on the aforementioned works and our previous experience that we want to have as diverse of a toolbox as possible, to cover the various possible descriptions of molecules as fully as possible. (It is worth noting that this is true for other fields of science as well, in fact it is an essential part of making progress in science.)

Like molecular descriptors, similarity measures are abundantly developed recently. The machine-learning community provides a plethora of novel algorithms, whose limitations, usefulness, and applicability have been only scarcely studied as of yet. More and more specific applications are taken into account, e.g., the early recognition problem or the need for diverse data sets. Unfortunately, a lot of novel measures and algorithms require an elaborate computational and mathematical skill set and expertise from the user to understand and implement them. In addition, some factors (weighting, desirability) are too subjective to let the measures and algorithms spread widely and unambiguously.

Consensus modeling (the usage of the average for more similarity measures) becomes more and more popular, and multicriteria optimization seems to be unavoidable nowadays. Multicriteria Decision-Making (MCDM) and Multiresponse Optimization (MRO) intend to find compromising (optimal, consensus) solutions to unsolved problems. Recently the equivalency of MCDM with sum of ranking differences (SRD) has been proven.[400] SRD is a general, nonparametric procedure to compare alternative methods/models/etc. that provides optimal solutions without the above-mentioned subjectivity, and its propagation can be predicted without much risk. Like molecular representations, various similarity measures and algorithms can be used for solving different types of problems; a complex interplay of the mentioned methods should be considered and are expected as a future trend.

Novel similarity measures are to be expected from diverse disciplines (graph theoretical-, business similarity-, fuzzy measures, etc., are transferrable to pharmaceutical applications) with great probability. Such measures will be tested and filtered by the drug design community—possibly slowly but definitely.

While there are well-established methods and algorithms in cheminformatics, new problems and new approaches arise abundantly and the pharma industry needs economic and effective techniques. As the amount of the generated data increases, cheminformatics and rational drug design approach the domain of big data. Nevertheless, extensions of the current data analysis methodologies are already being developed and successfully applied in related fields. Machine-learning algorithms can operate with extremely complex models (e.g., neural networks with many thousands or even millions of nodes, ant colony, support vector machines, random forest, etc.) and may solve problems that scientists only dreamed of—even just several years ago. However, the validation practices are developing slowly and more emphasis should be placed on developing suitable validation techniques.

Finally, we refer to some recent reviews showing the present state of arts and some future trends in the cheminformatics field.[273–275]

References

1. O'Boyle, N. M.; Banck, M.; James, C. A.; Morley, C.; Vandermeersch, T.; Hutchison, G. R. Open Babel: An Open Chemical Toolbox. *J. Cheminform.* **2011,** *3* (1), 33.
2. IUPAC Nomenclature Home Page http://www.chem.qmul.ac.uk/iupac/ (accessed 27.04.16).
3. CAS Registry System. *J. Chem. Inf. Comput. Sci.* **1978,** *18* (1), 58.
4. Chemical Substances—CAS REGISTRY http://www.cas.org/content/chemical-substances (accessed 28.04.16).

5. Scifinder https://scifinder.cas.org (accessed 28.04.16).
6. STN—The Choice of Patent Experts http://www.cas.org/products/stn (accessed 28.04.16).
7. Wiswesser, W. J. How the WLN Began in 1949 and How It Might Be in 1999. *J. Chem. Inf. Comput. Sci.* **1982,** *22* (2), 88–93.
8. Weininger, D. SMILES, a Chemical Language and Information System. 1. Introduction to Methodology and Encoding Rules. *J. Chem. Inf. Model.* **1988,** *28* (1), 31–36.
9. SMILES—A Simplified Chemical Language http://www.daylight.com/dayhtml/doc/theory/theory.smiles.html (accessed 02.05.16).
10. Weininger, D.; Weininger, A.; Weininger, J. L. SMILES. 2. Algorithm for Generation of Unique SMILES Notation. *J. Chem. Inf. Model.* **1989,** *29* (2), 97–101.
11. Daylight Chemical Information Systems http://www.daylight.com/ (accessed 02.05.16).
12. O'Boyle, N. M. Towards a Universal SMILES Representation—A Standard Method to Generate Canonical SMILES Based on the InChI. *J. Chem. Theory Comput.* **2012,** *4* (1), 22.
13. Schneider, N.; Sayle, R. A.; Landrum, G. A. Get Your Atoms in Order—An Open-Source Implementation of a Novel and Robust Molecular Canonicalization Algorithm. *J. Chem. Inf. Model.* **2015,** *55* (10), 2111–2120.
14. RDKit: Open-Source Cheminformatics Software. http://rdkit.org/ (accessed 02.05.16).
15. SMARTS—A Language for Describing Molecular Patterns. http://www.daylight.com/dayhtml/doc/theory/theory.smarts.html (accessed 02.05.16).
16. Zentrum für Bioinformatik: Universität Hamburg—SMARTSviewer. http://smartsview.zbh.uni-hamburg.de/smartsview/view (accessed 22.08.16).
17. SMIRKS—A Reaction Transform Language. http://daylight.com/dayhtml/doc/theory/theory.smirks.html (accessed 02.05.16).
18. Guasch, L.; Sitzmann, M.; Nicklaus, M. C. Enumeration of Ring–Chain Tautomers Based on SMIRKS Rules. *J. Chem. Inf. Model.* **2014,** *54* (9), 2423–2432.
19. Proschak, E.; Wegner, J. K.; Schüller, A.; Schneider, G.; Fechner, U. Molecular Query Language (MQL)—A Context-Free Grammar for Substructure Matching. *J. Chem. Inf. Model.* **2007,** *47* (2), 295–301.
20. Steinbeck, C.; Han, Y.; Kuhn, S.; Horlacher, O.; Luttmann, E.; Willighagen, E. The Chemistry Development Kit (CDK): An Open-Source Java Library for Chemo- and Bioinformatics. *J. Chem. Inf. Comput. Sci.* **2003,** *43* (2), 493–500.
21. Steinbeck, C.; Hoppe, C.; Kuhn, S.; Floris, M.; Guha, R.; Willighagen, E. Recent Developments of the Chemistry Development Kit (CDK)—An Open-Source Java Library for Chemo- and Bioinformatics. *Curr. Pharm. Des.* **2006,** *12* (17), 2111–2120.
22. Heller, S.; McNaught, A.; Stein, S.; Tchekhovskoi, D.; Pletnev, I. InChI—The Worldwide Chemical Structure Identifier Standard. *J. Chem. Theory Comput.* **2013,** *5* (1), 7.
23. Heller, S. R.; McNaught, A.; Pletnev, I.; Stein, S.; Tchekhovskoi, D. InChI, the IUPAC International Chemical Identifier. *J. Chem. Theory Comput.* **2015,** *7,* 23.
24. IUPAC—International Union of Pure and Applied Chemistry: Home. http://www.iupac.org/ (accessed 28.04.16).
25. National Institute of Standards and Technology. http://www.nist.gov/ (accessed 28.04.16).
26. InChI Trust: Home. http://www.inchi-trust.org/ (accessed 28.04.16).
27. Pletnev, I.; Erin, A.; McNaught, A.; Blinov, K.; Tchekhovskoi, D.; Heller, S. InChIKey Collision Resistance: An Experimental Testing. *J. Chem. Theory Comput.* **2012,** *4* (1), 39.
28. Unichem. https://www.ebi.ac.uk/unichem/.
29. Fritts, L. E.; Schwind, M. M. Using the Wiswesser Line Notation (WLN) for Online, Interactive Searching of Chemical Structurest. *J. Chem. Inf. Comput. Sci.* **1982,** *22,* 106–109.
30. Vollmer, J. J. Wiswesser Line Notation: An Introduction. *J. Chem. Educ.* **1983,** *60* (3), 192.
31. Engel, T. Representation of Chemical Compounds. In *Chemoinformatics: A Textbook;* Gasteiger, J., Engel, T., Eds.; Wiley-VCH Verlag GmbH & Co. KGaA: Weinheim, Germany, 2003; pp 15–169.
32. ChemDoodle | Chemical Drawing Software. https://www.chemdoodle.com/ (accessed 27.04.16).
33. Ash, S.; Cline, M. A.; Homer, R. W.; Hurst, T.; Smith, G. B. SYBYL Line Notation (SLN): A Versatile Language for Chemical Structure Representation. *J. Chem. Inf. Comput. Sci.* **1997,** *37* (1), 71–79.
34. Homer, R. W.; Swanson, J.; Jilek, R. J.; Hurst, T.; Clark, R. D. SYBYL Line Notation (SLN): A Single Notation To Represent Chemical Structures, Queries, Reactions, and Virtual Libraries. *J. Chem. Inf. Model.* **2008,** *48* (12), 2294–2307.
35. Dalby, A.; Nourse, J. G.; Hounshell, W. D.; Gushurst, A. K. I.; Grier, D. L.; Leland, B. A.; Laufer, J. Description of Several Chemical Structure File Formats Used by Computer Programs Developed at Molecular Design Limited. *J. Chem. Inf. Model.* **1992,** *32* (3), 244–255.
36. Marvin 16.4.25. ChemAxon LLC, 2016 (http://www.chemaxon.com).
37. Apodaca, R. On the (F)utility of Extending the Molfile Format. http://depth-first.com/articles/2012/01/11/on-the-futility-of-extending-the-molfile-format/ (accessed 03.05.16).
38. Clark, A. M. Accurate Specification of Molecular Structures: The Case for Zero-Order Bonds and Explicit Hydrogen Counting. *J. Chem. Inf. Model.* **2011,** *51* (12), 3149–3157.
39. Clark, A. M. Why Not to Use MDL MOL/SDF. http://molmatinf.com/whynotmolsdf.html (accessed 03.05.16).
40. Tripos Mol2 File Format. http://www.tripos.com/data/support/mol2.pdf (accessed 17.05.16).
41. RCSB Protein Data Bank. http://www.rcsb.org/pdb/home/home.do (accessed 18.05.16).
42. wwPDB: File Format. http://www.wwpdb.org/documentation/file-format (accessed 18.05.16).
43. IUPAC-IUB Commission on Biochemical Nomenclature. Abbreviations and Symbols for the Description of the Conformation of Polypeptide Chains. Tentative Rules (1969). *J. Biol. Chem.* **1970,** *246* (24), 6489–6497.
44. PDB format 1992. http://www.wwpdb.org/docs/documentation/file-format/PDB_format_1992.pdf (accessed 18.05.16).
45. Hall, S. R.; Allen, F. H.; Brown, I. D. The Crystallographic Information File (CIF): A New Standard Archive File for Crystallography. *Acta Crystallogr. Sect. A: Found. Crystallogr.* **1991,** *47* (6), 655–685.
46. Brown, I. D.; McMahon, B. CIF: The Computer Language of Crystallography. *Acta Crystallogr. Sect. B: Struct. Sci.* **2002,** *58* (3), 317–324.
47. PDBx/mmCIF Dictionary Resources. http://mmcif.wwpdb.org/ (accessed 19.05.16).
48. Westbrook, J.; Ito, N.; Nakamura, H.; Henrick, K.; Berman, H. M. PDBML: The Representation of Archival Macromolecular Structure Data in XML. *Bioinformatics* **2005,** *21* (7), 988–99210.
49. PDBML Schema Resources. http://pdbml.pdb.org/ (accessed 19.05.16).
50. Lipman, D. J.; Pearson, W. R. Rapid and Sensitive Protein Similarity Searches. *Science* **1985,** *227* (4693), 1435–1441.
51. Needleman, S. B.; Wunsch, C. D. A General Method Applicable to the Search for Similarities in the Amino Acid Sequence of Two Proteins. *J. Mol. Biol.* **1970,** *48* (3), 443–453.
52. Altschul, S. F.; Gish, W.; Miller, W.; Myers, E. W.; Lipman, D. J. Basic Local Alignment Search Tool. *J. Mol. Biol.* **1990,** *215* (3), 403–410.
53. BLAST: Basic Local Alignment Search Tool. http://blast.ncbi.nlm.nih.gov/Blast.cgi (accessed 18.05.16).
54. Dayhoff, M. O.; Schwartz, R.; Orcutt, B. C. A Model of Evolutionary Change in Proteins. In *Atlas of Protein Sequence and Structure;* National Biomedical Research Foundation, 1978; pp 345–358.
55. Henikoff, S.; Henikoff, J. G. Amino Acid Substitution Matrices from Protein Blocks. *Biochemistry* **1992,** *89,* 10915–10919.
56. Chemical Markup Language | CML. http://www.xml-cml.org/ (accessed 18.05.16).
57. Murray-Rust, P.; Rzepa, H. S. Chemical Markup, XML, and the Worldwide Web. 1. Basic Principles. *J. Chem. Inf. Comput. Sci.* **1999,** *39* (6), 928–942.
58. Murray-Rust, P.; Rzepa, H. S. Chemical Markup, XML and the World-Wide Web. 2. Information Objects and the CMLDOM. *J. Chem. Inf. Comput. Sci.* **2001,** *41* (5), 1113–1123.
59. Gkoutos, G. V.; Murray-Rust, P.; Rzepa, H. S.; Wright, M. Chemical Markup, XML, and the World-Wide Web. 3. Toward a Signed Semantic Chemical Web of Trust. *J. Chem. Inf. Comput. Sci.* **2001,** *41* (5), 1124–1130.
60. Murray-Rust, P.; Rzepa, H. S. Chemical Markup, XML, and the World Wide Web. 4. CML Schema. *J. Chem. Inf. Comput. Sci.* **2003,** *43* (3), 757–772.

61. Murray-Rust, P.; Rzepa, H. S.; Williamson, M. J.; Willighagen, E. L. Chemical Markup, XML, and the World Wide Web. 5. Applications of Chemical Metadata in RSS Aggregators. *J. Chem. Inf. Comput. Sci.* **2004,** *44* (2), 462–469.
62. Holliday, G. L.; Murray-Rust, P.; Rzepa, H. S. Chemical Markup, XML, and the World Wide Web. 6. CMLReact, an XML Vocabulary for Chemical Reactions. *J. Chem. Inf. Model.* **2006,** *46* (1), 145–157.
63. Kuhn, S.; Helmus, T.; Lancashire, R. J.; Murray-Rust, P.; Rzepa, H. S.; Steinbeck, C.; Willighagen, E. L. Chemical Markup, XML, and the World Wide Web. 7. CMLSpect, an XML Vocabulary for Spectral Data. *J. Chem. Inf. Model.* **2007,** *47* (6), 2015–2034.
64. Adams, N.; Winter, J.; Murray-Rust, P.; Rzepa, H. S. Chemical Markup, XML and the World-Wide Web. 8. Polymer Markup Language. *J. Chem. Inf. Model.* **2008,** *48* (11), 2118–2128.
65. Chemistry Add-in for Word—Microsoft Research. http://research.microsoft.com/en-us/projects/chem4word/ (accessed 18.05.16).
66. Chemical Markup Language | Conventions. http://www.xml-cml.org/convention/ (accessed 18.05.16).
67. Guha, R.; Howard, M. T.; Hutchison, G. R.; Murray-Rust, P.; Rzepa, H.; Steinbeck, C.; Wegner, J.; Willighagen, E. L. The Blue Obelisk—Interoperability in Chemical Informatics. *J. Chem. Inf. Model.* **2006,** *46* (3), 991–998.
68. Yang, C.; Tarkhov, A.; Marusczyk, J.; Bienfait, B.; Gasteiger, J.; Kleinoeder, T.; Magdziarz, T.; Sacher, O.; Schwab, C. H.; Schwoebel, J.; et al. New Publicly Available Chemical Query Language, CSRML, To Support Chemotype Representations for Application to Data Mining and Modeling. *J. Chem. Inf. Model.* **2015,** *55* (3), 510–528.
69. Vazquez, M.; Krallinger, M.; Leitner, F.; Valencia, A. Text Mining for Drugs and Chemical Compounds: Methods, Tools and Applications. *Mol. Inform.* **2011,** *30* (6-7), 506–519.
70. Gurulingappa, H.; Mudi, A.; Toldo, L.; Hofmann-Apitius, M.; Bhate, J. Challenges in Mining the Literature for Chemical Information. *RSC Adv.* **2013,** *3* (37), 16194.
71. Eltyeb, S.; Salim, N. Chemical Named Entities Recognition: A Review on Approaches and Applications. *J. Chem. Theory Comput.* **2014,** *6* (1), 17.
72. Chemistry Text Mining Suite ChemAxon. https://www.chemaxon.com/products/chemistry-text-mining-suite/ (accessed 19.05.16).
73. chemicalize.org. http://www.chemicalize.org/ (accessed 19.05.16).
74. Southan, C.; Stracz, A. Extracting and Connecting Chemical Structures from Text Sources Using Chemicalize.org. *J. Cheminform.* **2013,** *5* (1), 20.
75. Jessop, D. M.; Adams, S. E.; Willighagen, E. L.; Hawizy, L.; Murray-Rust, P. OSCAR4: A Flexible Architecture for Chemical Text-Mining. *J. Chem. Theory Comput.* **2011,** *3* (1), 41.
76. Usié, A.; Alves, R.; Solsona, F.; Vázquez, M.; Valencia, A. CheNER: Chemical Named Entity Recognizer. *Bioinformatics* **2014,** *30* (7), 1039–1040.
77. Lowe, D. M.; Corbett, P. T.; Murray-Rust, P.; Glen, R. C. Chemical Name to Structure: OPSIN, an Open Source Solution. *J. Chem. Inf. Model.* **2011,** *51* (3), 739–753.
78. Valko, A. T.; Johnson, A. P. CLiDE Pro: The Latest Generation of CLiDE, a Tool for Optical Chemical Structure Recognition. *J. Chem. Inf. Model.* **2009,** *49* (4), 780–787.
79. Imago OCR—Life Sciences 0.3.0 documentation. http://lifescience.opensource.epam.com/imago/ (accessed 20.05.16).
80. Filippov, I. V.; Nicklaus, M. C. Optical Structure Recognition Software To Recover Chemical Information: OSRA, An Open Source Solution. *J. Chem. Inf. Model.* **2009,** *49* (3), 740–743.
81. Frasconi, P.; Gabbrielli, F.; Lippi, M.; Marinai, S. Markov Logic Networks for Optical Chemical Structure Recognition. *J. Chem. Inf. Model.* **2014,** *54* (8), 2380–2390.
82. Cosgrove, D. A. Markush Structures and Chemical Patents. In *Scaffold Hopping in Medicinal Chemistry;* Brown, N., Ed.; Wiley-VCH Verlag GmbH & Co. KGaA: Weinheim, Germany, 2013.
83. Deng, W.; Berthel, S. J.; So, W. V. Intuitive Patent Markush Structure Visualization Tool for Medicinal Chemists. *J. Chem. Inf. Model.* **2011,** *51* (3), 511–520.
84. Deng, W.; Scott, E.; Berthel, S. J.; So, W. V. Deconvoluting Complex Patent Markush Structures: A Novel R-Group Numbering System. *World Pat. Inf.* **2012,** *34* (2), 128–133.
85. Deng, W.; Schneider, G.; So, W. V. Mapping Chemical Structures to Markush Structures Using SMIRKS. *Mol. Inform.* **2011,** *30,* 665–671.
86. Cosgrove, D. A.; Green, K. M.; Leach, A. G.; Poirrette, A.; Winter, J. A System for Encoding and Searching Markush Structures. *J. Chem. Inf. Model.* **2012,** *52* (8), 1936–1947.
87. Barth, A.; Stengel, T.; Litterst, E.; Kraut, H.; Matuszczyk, H.; Ailer, F.; Hajkowski, S. A Novel Concept for the Search and Retrieval of the Derwent Markush Resource Database. *J. Chem. Inf. Model.* **2016,** *56* (5), 821–829.
88. Cereto-Massagué, A.; Ojeda, M. J.; Valls, C.; Mulero, M.; Garcia-Vallvé, S.; Pujadas, G. Molecular Fingerprint Similarity Search in Virtual Screening. *Methods* **2015,** *71,* 58–63.
89. Cruz-Monteagudo, M.; Medina-Franco, J. L.; Pérez-Castillo, Y.; Nicolotti, O.; Cordeiro, M. N. D. S.; Borges, F. Activity Cliffs in Drug Discovery: Dr Jekyll or Mr Hyde? *Drug Discov. Today* **2014,** *19* (8), 1069–1080.
90. Bender, A.; Jenkins, J. L.; Scheiber, J.; Sukuru, S. C. K.; Glick, M.; Davies, J. W. How Similar Are Similarity Searching Methods?: A Principal Component Analysis of Molecular Descriptor Space. *J. Chem. Inf. Model.* **2009,** *49* (1), 108–119.
91. Willett, P. Fusing Similarity Rankings in Ligand-Based Virtual Screening. *Comput. Struct. Biotechnol. J.* **2013,** *5*, e201302002.
92. McGaughey, G. B.; Sheridan, R. P.; Bayly, C. I.; Culberson, J. C.; Kreatsoulas, C.; Lindsley, S.; Maiorov, V.; Truchon, J.-F.; Cornell, W. D. Comparison of Topological, Shape, and Docking Methods in Virtual Screening. *J. Chem. Inf. Model.* **2007,** *47* (4), 1504–1519.
93. Tresadern, G.; Bemporad, D.; Howe, T. A Comparison of Ligand Based Virtual Screening Methods and Application to Corticotropin Releasing Factor 1 Receptor. *J. Mol. Graph. Model.* **2009,** *27* (8), 860–870.
94. Venkatraman, V.; Pérez-Nueno, V. I.; Mavridis, L.; Ritchie, D. W. Comprehensive Comparison of Ligand-Based Virtual Screening Tools Against the DUD Data Set Reveals Limitations of Current 3D Methods. *J. Chem. Inf. Model.* **2010,** *50* (12), 2079–2093.
95. Muegge, I.; Mukherjee, P. An Overview of Molecular Fingerprint Similarity Search in Virtual Screening. *Expert Opin. Drug Discov.* **2016,** *11* (2), 137–148.
96. Sastry, M.; Lowrie, J. F.; Dixon, S. L.; Sherman, W. Large-Scale Systematic Analysis of 2D Fingerprint Methods and Parameters to Improve Virtual Screening Enrichments. *J. Chem. Inf. Model.* **2010,** *50* (5), 771–784.
97. Duan, J.; Dixon, S. L.; Lowrie, J. F.; Sherman, W. Analysis and Comparison of 2D Fingerprints: Insights into Database Screening Performance Using Eight Fingerprint Methods. *J. Mol. Graph. Model.* **2010,** *29* (2), 157–170.
98. Heikamp, K.; Bajorath, J. Fingerprint Design and Engineering Strategies: Rationalizing and Improving Similarity Search Performance. *Future Med. Chem.* **2012,** *4* (15), 1945–1959.
99. Riniker, S.; Landrum, G. A. Open-Source Platform to Benchmark Fingerprints for Ligand-Based Virtual Screening. *J. Chem. Theory Comput.* **2013,** *5* (1), 26.
100. Riniker, S.; Landrum, G. A. Similarity Maps—A Visualization Strategy for Molecular Fingerprints and Machine-Learning Methods. *J. Chem. Theory Comput.* **2013,** *5* (1), 43.
101. O'Boyle, N. M.; Hutchison, G. R. Cinfony—Combining Open Source Cheminformatics Toolkits behind a Common Interface. *Chem. Cent. J.* **2008,** *2* (1), 24.
102. Cinfony—Cinfony 1.2 documentation. http://cinfony.github.io/ (accessed 03.06.16).
103. Dong, J.; Cao, D.-S.; Miao, H.-Y.; Liu, S.; Deng, B.-C.; Yun, Y.-H.; Wang, N.-N.; Lu, A.-P.; Zeng, W.-B.; Chen, A. F. ChemDes: An Integrated Web-Based Platform for Molecular Descriptor and Fingerprint Computation. *J. Chem. Theory Comput.* **2015,** *7* (1), 60.
104. ChemDes—An integrated web-based platform for molecular descriptor and fingerprint computation. http://www.scbdd.com/chemdes/ (accessed 30.05.16).
105. Christie, B. D.; Leland, B. A.; Nourse, J. G. Structure Searching in Chemical Databases by Direct Lookup Methods. *J. Chem. Inf. Model.* **1993,** *33* (4), 545–547.
106. BIOVIA—Scientific Enterprise Software for Chemical Research, Material Science R&D. http://accelrys.com/ (accessed 03.06.16).
107. Dassault Systèmes BIOVIA, Discovery Studio Modeling Environment, Release 2017, San Diego: Dassault Systèmes, 2016.
108. Durant, J. L.; Leland, B. A.; Henry, D. R.; Nourse, J. G. Reoptimization of MDL Keys for Use in Drug Discovery. *J. Chem. Inf. Comput. Sci.* **2002,** *42* (6), 1273–1280.
109. Bolton, E. E.; Wang, Y.; Thiessen, P. A.; Bryant, S. H. Chapter 12—PubChem: Integrated Platform of Small Molecules and Biological Activities. *Annu. Rep. Comput. Chem.* **2008,** *4,* 217–241.
110. Barnard, J. M.; Downs, G. M. Chemical Fragment Generation and Clustering Software [§]. *J. Chem. Inf. Comput. Sci.* **1997,** *37* (1), 141–142.

111. Klekota, J.; Roth, F. P. Chemical Substructures That Enrich for Biological Activity. *Bioinformatics* **2008,** *24* (21), 2518–2525.
112. Hall, L. H.; Kier, L. B. Electrotopological State Indices for Atom Types: A Novel Combination of Electronic, Topological, and Valence State Information. *J. Chem. Inf. Model.* **1995,** *35* (6), 1039–1045.
113. Nguyen, K. T.; Blum, L. C.; van Deursen, R.; Reymond, J.-L. Classification of Organic Molecules by Molecular Quantum Numbers. *ChemMedChem* **2009,** *4* (11), 1803–1805.
114. van Deursen, R.; Blum, L. C.; Reymond, J.-L. A Searchable Map of PubChem. *J. Chem. Inf. Model.* **2010,** *50* (11), 1924–1934.
115. Fingerprints—Screening and Similarity. http://www.daylight.com/dayhtml/doc/theory/theory.finger.html (accessed 23.05.16).
116. Dassault Systèmes BIOVIA, Pipeline Pilot, Version 9.5, San Diego: Dassault Systèmes, 2016.
117. Schrödinger Release 2016-2: Canvas, Version 2.8. Schrödinger, LLC: New York, NY, USA, 2016.
118. Cheminformatics and Molecular Modeling | OpenEye Scientific Software. http://eyesopen.com/ (accessed 09.06.16).
119. Bender, A.; Mussa, H. Y.; Glen, R. C.; Reiling, S. Similarity Searching of Chemical Databases Using Atom Environment Descriptors (MOLPRINT 2D): Evaluation of Performance. *J. Chem. Inf. Comput. Sci.* **2004,** *44* (5), 1708–1718.
120. Bender, A.; Mussa, H. Y.; Gill, G. S.; Glen, R. C. Molecular Surface Point Environments for Virtual Screening and the Elucidation of Binding Patterns (MOLPRINT 3D). *J. Med. Chem.* **2004,** *47* (26), 6569–6583.
121. Hassan, M.; Brown, R. D.; Varma-O'Brien, S.; Rogers, D. Cheminformatics Analysis and Learning in a Data Pipelining Environment. *Mol. Divers.* **2006,** *10* (3), 283–299.
122. JChem 15.7.27 (http://www.chemaxon.com). ChemAxon LLC, 2016.
123. Rogers, D.; Hahn, M. Extended-Connectivity Fingerprints. *J. Chem. Inf. Model.* **2010,** *50* (5), 742–754.
124. Morgan, H. L. The Generation of a Unique Machine Description for Chemical Structures-A Technique Developed at Chemical Abstracts Service. *J. Chem. Doc.* **1965,** *5* (2), 107–113.
125. Carhart, R. E.; Smith, D. H.; Venkataraghavan, R. Atom Pairs as Molecular Features in Structure-Activity Studies: Definition and Applications. *J. Chem. Inf. Model.* **1985,** *25* (2), 64–73.
126. Nilakantan, R.; Bauman, N.; Dixon, J. S.; Venkataraghavan, R. Topological Torsion: A New Molecular Descriptor for SAR Applications. Comparison with Other Descriptors. *J. Chem. Inf. Model.* **1987,** *27* (2), 82–85.
127. Kearsley, S. K.; Sallamack, S.; Fluder, E. M.; Andose, J. D.; Mosley, R. T.; Sheridan, R. P. Chemical Similarity Using Physiochemical Property Descriptors. *J. Chem. Inf. Comput. Sci.* **1996,** *36* (1), 118–127.
128. Sheridan, R. P.; Miller, M. D.; Underwood, D. J.; Kearsley, S. K. Chemical Similarity Using Geometric Atom Pair Descriptors. *J. Chem. Inf. Comput. Sci.* **1996,** *36* (1), 128–136.
129. Vulpetti, A.; Hommel, U.; Landrum, G.; Lewis, R.; Dalvit, C. Design and NMR-Based Screening of LEF, a Library of Chemical Fragments with Different Local Environment of Fluorine. *J. Am. Chem. Soc.* **2009,** *131* (36), 12949–12959.
130. Awale, M.; Reymond, J.-L. Atom Pair 2D-Fingerprints Perceive 3D-Molecular Shape and Pharmacophores for Very Fast Virtual Screening of ZINC and GDB-17. *J. Chem. Inf. Model.* **2014,** *54* (7), 1892–1907.
131. Awale, M.; Jin, X.; Reymond, J.-L. Stereoselective Virtual Screening of the ZINC Database Using Atom Pair 3D-Fingerprints. *J. Chem. Theory Comput.* **2015,** *7* (1), 3.
132. McGregor, M. J.; Muskal, S. M. Pharmacophore Fingerprinting. 1. Application to QSAR and Focused Library Design. *J. Chem. Inf. Comput. Sci.* **1999,** *39* (3), 569–574.
133. McGregor, M. J.; Muskal, S. M. Pharmacophore Fingerprinting. 2. Application to Primary Library Design. *J. Chem. Inf. Comput. Sci.* **2000,** *40* (1), 117–125.
134. Mason, J. S.; Morize, I.; Menard, P. R.; Cheney, D. L.; Hulme, C.; Labaudiniere, R. F. New 4-Point Pharmacophore Method for Molecular Similarity and Diversity Applications: Overview of the Method and Applications, Including a Novel Approach to the Design of Combinatorial Libraries Containing Privileged Substructures. *J. Med. Chem.* **1999,** *42* (17), 3251–3264.
135. Wood, D. J.; de Vlieg, J.; Wagener, M.; Ritschel, T. Pharmacophore Fingerprint-Based Approach to Binding Site Subpocket Similarity and Its Application to Bioisostere Replacement. *J. Chem. Inf. Model.* **2012,** *52* (8), 2031–2043.
136. Molecular Operating Environment (MOE), 2013.08. Chemical Computing Group Inc.: Montreal, QC, Canada, 2016.
137. Ewing, T.; Baber, J. C.; Feher, M. Novel 2D Fingerprints for Ligand-Based Virtual Screening. *J. Chem. Inf. Model.* **2006,** *46* (6), 2423–2431.
138. Certara. http://www.certara.com/ (accessed 14.06.16).
139. Xue, L.; Godden, J. W.; Bajorath, J. Database Searching for Compounds with Similar Biological Activity Using Short Binary Bit String Representations of Molecules. *J. Chem. Inf. Comput. Sci.* **1999,** *39* (5), 881–886.
140. Xue, L.; Godden, J. W.; Bajorath, J. Mini-Fingerprints for Virtual Screening: Design Principles and Generation of Novel Prototypes Based on Information Theory. *SAR QSAR Environ. Res.* **2003,** *14* (1), 27–40.
141. Xue, L.; Godden, J. W.; Stahura, F. L.; Bajorath, J. Design and Evaluation of a Molecular Fingerprint Involving the Transformation of Property Descriptor Values into a Binary Classification Scheme. *J. Chem. Inf. Model.* **2003,** *43* (4), 1151–1157.
142. Eckert, H.; Bajorath, J. Design and Evaluation of a Novel Class-Directed 2D Fingerprint to Search for Structurally Diverse Active Compounds. *J. Chem. Inf. Model.* **2006,** *46* (6), 2515–2526.
143. Nisius, B.; Bajorath, J. Molecular Fingerprint Recombination: Generating Hybrid Fingerprints for Similarity Searching from Different Fingerprint Types. *ChemMedChem* **2009,** *4* (11), 1859–1863.
144. Nisius, B.; Bajorath, J. Reduction and Recombination of Fingerprints of Different Design Increase Compound Recall and the Structural Diversity of Hits. *Chem. Biol. Drug Des.* **2010,** *75* (2), 152–160.
145. Xue, L.; Stahura, F. L.; Godden, J. W.; Bajorath, J. Fingerprint Scaling Increases the Probability of Identifying Molecules with Similar Activity in Virtual Screening Calculations. *J. Chem. Inf. Comput. Sci.* **2001,** *41* (3), 746–753.
146. Arif, S. M.; Holliday, J. D.; Willett, P. The Use of Weighted 2D Fingerprints in Similarity-Based Virtual Screening. In *Advances in Mathematical Chemistry and Applications;* Basak, S. C., Restrepo, G., Villaveces, J. L., Eds.; Bentham Science Publishers, 2014; pp 92–112.
147. Vogt, M.; Stumpfe, D.; Geppert, H.; Bajorath, J. Scaffold Hopping Using Two-Dimensional Fingerprints: True Potential, Black Magic, or a Hopeless Endeavor? Guidelines for Virtual Screening. *J. Med. Chem.* **2010,** *53* (15), 5707–5715.
148. Öztürk, H.; Ozkirimli, E.; Özgür, A. A Comparative Study of SMILES-Based Compound Similarity Functions for Drug-Target Interaction Prediction. *BMC Bioinformatics* **2016,** *17* (1), 128.
149. Vidal, D.; Thormann, M.; Pons, M. LINGO, an Efficient Holographic Text Based Method To Calculate Biophysical Properties and Intermolecular Similarities. *J. Chem. Inf. Model.* **2005,** *45* (2), 386–393.
150. Schwartz, J.; Awale, M.; Reymond, J.-L. SMIfp (SMILES Fingerprint) Chemical Space for Virtual Screening and Visualization of Large Databases of Organic Molecules. *J. Chem. Inf. Model.* **2013,** *53* (8), 1979–1989.
151. Research Group of Prof. Reymond. http://www.gdb.unibe.ch/ (accessed 31.05.16).
152. Kooistra, A. J.; Binsl, T. W.; van Beek, J. H. G. M.; de Graaf, C.; Heringa, J. Electron Density Fingerprints (EDprints): Virtual Screening Using Assembled Information of Electron Density. *J. Chem. Inf. Model.* **2010,** *50* (10), 1772–1780.
153. BatchNMRPredictor, Version 1.1a. Porta Nova Software GmbH: Zürich, Switzerland, 2010.
154. Vainio, M. J.; Johnson, M. S. Generating Conformer Ensembles Using a Multiobjective Genetic Algorithm. *J. Chem. Inf. Model.* **2007,** *47* (6), 2462–2474.
155. Kauvar, L. M.; Higgins, D. L.; Villar, H. O.; Sportsman, J. R.; Engqvist-Goldstein, Å.; Bukar, R.; Bauer, K. E.; Dilley, H.; Rocke, D. M. Predicting Ligand Binding to Proteins by Affinity Fingerprinting. *Chem. Biol.* **1995,** *2* (2), 107–118.
156. Beroza, P.; Villar, H. O.; Wick, M. M.; Martin, G. R. Chemoproteomics as a Basis for Post-Genomic Drug Discovery. *Drug Discov. Today* **2002,** *7* (15), 807–814.

157. Dixon, S. L.; Villar, H. O. Bioactive Diversity and Screening Library Selection via Affinity Fingerprinting. *J. Chem. Inf. Model.* **1998,** *38* (6), 1192–1203.
158. Weinstein, J. N.; Myers, T. G.; O'Connor, P. M.; Friend, S. H.; Fornace, A. J.; Kohn, K. W.; Fojo, T.; Bates, S. E.; Rubinstein, L. V.; Anderson, N. L.; et al. An Information-Intensive Approach to the Molecular Pharmacology of Cancer. *Science* **1997,** *275* (5298), 343–349.
159. Briem, H.; Lessel, U. F. In Vitro and in Silico Affinity Fingerprints: Finding Similarities beyond Structural Classes. *Perspect. Drug Discov. Des.* **2000,** *20* (1), 231–244.
160. Bender, A.; Jenkins, J. L.; Glick, M.; Deng, Z.; Nettles, J. H.; Davies, J. W. "Bayes Affinity Fingerprints" Improve Retrieval Rates in Virtual Screening and Define Orthogonal Bioactivity Space: When Are Multitarget Drugs a Feasible Concept? *J. Chem. Inf. Model.* **2006,** *46* (6), 2445–2456.
161. Jenkins, J. L.; Bender, A.; Davies, J. W. In Silico Target Fishing: Predicting Biological Targets From Chemical Structure. *Drug Discov. Today Technol.* **2006,** *3* (4), 413–421.
162. Lagunin, A.; Stepanchikova, A.; Filimonov, D.; Poroikov, V. PASS: Prediction of Activity Spectra for Biologically Active Substances. *Bioinformatics* **2000,** *16* (8), 747–748.
163. Geronikaki, A. A.; Dearden, J. C.; Filimonov, D.; Galaeva, I.; Garibova, T. L.; Gloriozova, T.; Krajneva, V.; Lagunin, A.; Macaev, F. Z.; Molodavkin, G.; et al. Design of New Cognition Enhancers: From Computer Prediction to Synthesis and Biological Evaluation. *J. Med. Chem.* **2004,** *47* (11), 2870–2876.
164. Bender, A.; Young, D. W.; Jenkins, J. L.; Serrano, M.; Mikhailov, D.; Clemons, P. A.; Davies, J. W. Chemogenomic Data Analysis: Prediction of Small-Molecule Targets and the Advent of Biological Fingerprints. *Comb. Chem. High Throughput Screen.* **2007,** *10* (8), 719–731.
165. Deng, Z.; Chuaqui, C.; Singh, J. Structural Interaction Fingerprint (SIFt): A Novel Method for Analyzing Three-Dimensional Protein-Ligand Binding Interactions. *J. Med. Chem.* **2004,** *47* (2), 337–344.
166. Singh, J.; Deng, Z.; Narale, G.; Chuaqui, C. Structural Interaction Fingerprints: A New Approach to Organizing, Mining, Analyzing, and Designing Protein-Small Molecule Complexes. *Chem. Biol. Drug Des.* **2006,** *67* (1), 5–12.
167. Small-Molecule Drug Discovery Suite 2016-1. Schrödinger, LLC: New York, NY, USA, 2016.
168. Marcou, G.; Rognan, D. Optimizing Fragment and Scaffold Docking by Use of Molecular Interaction Fingerprints. *J. Chem. Inf. Model.* **2007,** *47* (1), 195–207.
169. Mpamhanga, C. P.; Chen, B.; McLay, I. M.; Willett, P. Knowledge-Based Interaction Fingerprint Scoring: A Simple Method for Improving the Effectiveness of Fast Scoring Functions. *J. Chem. Inf. Model.* **2006,** *46* (2), 686–698.
170. Pérez-Nueno, V. I.; Rabal, O.; Borrell, J. I. Teixidó, J. APIF: A New Interaction Fingerprint Based on Atom Pairs and Its Application to Virtual Screening. *J. Chem. Inf. Model.* **2009,** *49* (5), 1245–1260.
171. Da, C.; Kireev, D. Structural Protein–Ligand Interaction Fingerprints (SPLIF) for Structure-Based Virtual Screening: Method and Benchmark Study. *J. Chem. Inf. Model.* **2014,** *54,* 2555–2561.
172. Kinase-Ligand Interaction Fingerprints and Structures database (KLIFS). http://klifs.vu-compmedchem.nl/ (accessed 26.05.16).
173. van Linden, O. P. J.; Kooistra, A. J.; Leurs, R.; de Esch, I. J. P.; de Graaf, C. KLIFS: A Knowledge-Based Structural Database to Navigate Kinase-Ligand Interaction Space. *J. Med. Chem.* **2014,** *57* (2), 249–277.
174. Kooistra, A. J.; Kanev, G. K.; van Linden, O. P. J.; Leurs, R.; de Esch, I. J. P.; de Graaf, C. KLIFS: A Structural Kinase-Ligand Interaction Database. *Nucleic Acids Res.* **2015,** *44* (D1), D365–D371.
175. PhosphoDiEsterase Structure and ligand Interaction Annotated database (PDEStrIAn). http://pdestrian.vu-compmedchem.nl/ (accessed 26.05.16).
176. Jansen, C.; Kooistra, A. J.; Kanev, G. K.; Leurs, R.; de Esch, I. J. P.; de Graaf, C. PDEStrIAn: A Phosphodiesterase Structure and Ligand Interaction Annotated Database As a Tool for Structure-Based Drug Design. *J. Med. Chem.* **2016,** *59,* 7029–7065. http://dx.doi.org/10.1021/acs.jmedchem.5b01813.
177. Baroni, M.; Cruciani, G.; Sciabola, S.; Perruccio, F.; Mason, J. S. A Common Reference Framework for Analyzing/Comparing Proteins and Ligands. Fingerprints for Ligands And Proteins (FLAP): Theory and Application. *J. Chem. Inf. Model.* **2007,** *47* (2), 279–294.
178. FLAP (Fingerprints for Ligands and Proteins). http://www.moldiscovery.com/software/flap/(accessed 31.05.16).
179. Broughton, H.; Hunt, P.; Mackey, M. Methods for Classifying and Searching Chemical Reactions. US 20030182094 A1, 2003.
180. Ridder, L.; Wagener, M. SyGMa: Combining Expert Knowledge and Empirical Scoring in the Prediction of Metabolites. *ChemMedChem* **2008,** *3* (5), 821–832.
181. Patel, H.; Bodkin, M. J.; Chen, B.; Gillet, V. J. Knowledge-Based Approach to *De Novo* Design Using Reaction Vectors. *J. Chem. Inf. Model.* **2009,** *49* (5), 1163–1184.
182. Sheridan, R. P.; Hunt, P.; Culberson, J. C. Molecular Transformations as a Way of Finding and Exploiting Consistent Local QSAR. *J. Chem. Inf. Model.* **2006,** *46* (1), 180–192.
183. Schneider, N.; Lowe, D. M.; Sayle, R. A.; Landrum, G. A. Development of a Novel Fingerprint for Chemical Reactions and Its Application to Large-Scale Reaction Classification and Similarity. *J. Chem. Inf. Model.* **2015,** *55* (1), 39–53.
184. Todeschini, R.; Consonni, V. *Handbook of Molecular Descriptors;* Wiley–VCH: Weinheim, Germany, 2000.
185. Roy, K.; Kar, S.; Das, R. N. *A Primer on QSAR/QSPR Modeling—Fundamental Concepts;* Springer, 2015.
186. Dixon, S. L.; Merz, K. M. One-Dimensional Molecular Representations and Similarity Calculations: Methodology and Validation. *J. Med. Chem.* **2001,** *44* (23), 3795–3809.
187. Hansch, C.; Fujita, T. A Method for the Correlation of Biological Activity and Chemical Structure. *J. Am. Chem. Soc.* **1964,** *86,* 1616–1626.
188. Leo, A. J. Calculating logPoct from Structures. *Chem. Rev.* **1993,** *93* (4), 1282–1306.
189. Mannhold, R.; Poda, G. I.; Ostermann, C.; Tetko, I. V. Calculation of Molecular Lipophilicity: State-of-the-Art and Comparison of Log P Methods on More than 96,000 Compounds. *J. Pharm. Sci.* **2009,** *98* (3), 861–893.
190. Andrić, F.; Bajusz, D.; Rácz, A.; Šegan, S.; Héberger, K. Multivariate Assessment of Lipophilicity Scales—Computational and Reversed Phase Thin-Layer Chromatographic Indices. *J. Pharm. Biomed. Anal.* **2016,** *127,* 81–93.
191. Andrić, F.; Héberger, K. Chromatographic and Computational Assessment of Lipophilicity Using Sum of Ranking Differences and Generalized Pair-Correlation. *J. Chromatogr. A* **2015,** *1380,* 130–138.
192. Andrić, F.; Héberger, K. Towards Better Understanding of Lipophilicity: Assessment of in Silico and Chromatographic logP Measures for Pharmaceutically Important Compounds by Nonparametric Rankings. *J. Pharm. Biomed. Anal.* **2015,** *115,* 183–191.
193. Doğan Daldal, Y.; Çakõr, C.; Yõlmaz, H.; Demiralay, E.Ç.; Özkan, S. A.; Alsancak, G. Liquid Chromatographic, Spectrophotometric and Potentiometric Pka Determination of Ranitidine and Famotidine. *Curr. Drug Ther.* **2015,** *9* (4), 277–284.
194. Hammett, L. P. Some Relations between Reaction Rates and Equilibrium Constants. *Chem. Rev.* **1935,** *17,* 125–136.
195. Hammett, L. P. The Effect of Structure upon the Reactions of Organic Compounds. Benzene Derivatives. *J. Am. Chem. Soc.* **1937,** *59,* 96–103.
196. Liao, C.; Nicklaus, M. C. Comparison of Nine Programs Predicting pKa Values of Pharmaceutical Substances. *J. Chem. Inf. Model.* **2009,** *49* (9), 2801–2812.
197. Sanghvi, T.; Jain, N.; Yang, G.; Yalkowsky, S. H. Estimation of Aqueous Solubility by the General Solubility Equation (GSE) the Easy Way. *QSAR Comb. Sci.* **2003,** *22* (2), 258–262.
198. Puzyn, T.; Mostrag, A.; Falandysz, J.; Kholod, Y.; Leszczynski, J. Predicting Water Solubility of Congeners: Chloronaphthalenes-A Case Study. *J. Hazard. Mater.* **2009,** *170,* 1014–1022.
199. Ghasemi, J.; Saaidpour, S. QSPR Prediction of Aqueous Solubility of Drug-like Organic Compounds. *Chem. Pharm. Bull. (Tokyo).* **2007,** *55* (4), 669–674.
200. Palmer, D. S.; O'Boyle, N. M.; Glen, R. C.; Mutchell, J. B. O. Random Forest Models to Predict Aqueous Solubility. *J. Chem. Inf. Model.* **2007,** *47,* 150–158.
201. Huuskonen, J.; Salo, M.; Taskinen, J. Aqueous Solubility Prediction of Drugs Based on Molecular Topology and Neural Network Modeling. *J. Chem. Inf. Comput. Sci.* **1998,** *38* (3), 450–456.
202. Ran, Y.; Jain, N.; Yalkowsky, S. H. Prediction of Aqueous Solubility of Organic Compounds by the General Solubility Equation (GSE). *J. Chem. Inf. Model.* **2001,** *41* (5), 1208–1217.
203. Kubinyi, H. A General View on Similarity and QSAR Studies. In *Computer-Assisted Lead Finding and Optimization;* van de Waterbeemd, H., Testa, B., Folkers, G., Eds.; Wiley-VHC, 1997; pp 9–28.
204. Balaban, A. T. Highly Discriminating Distance-Based Topological Index. *Chem. Phys. Lett.* **1982,** *89,* 399–404.
205. Randic, M.; Basak, S. C. A New Descriptor for Structure-Property and Structure-Activity Correlations. *J. Chem. Inf. Comput. Sci.* **2001,** *41,* 650–656.

206. Estradal, E.; Patlewicz, G.; Uriarte, E. From Molecular Graphs to Drugs.A Review on the Use of Topological Indices in Drug Design and Discovery. *Indian J. Chem.* **2003,** *42,* 1315–1329.
207. Wiener, H. Structural Determination of Paraffin Boiling Points. *J. Am. Chem. Soc.* **1947,** *69* (1), 17–20.
208. Gutman, I.; Ruščić, B.; Trinajstić, N.; Wilcox, C. F. Graph Theory and Molecular Orbitals. Xll. Acyclic Polyenes. *J. Chem. Phys.* **1975,** *62* (9), 3399–3405.
209. Kier, L. B. A Shape Index from Molecular Graphs. *Quant. Struct. Act. Relat.* **1985,** *4* (3), 109–116.
210. Kier, L. B. Distinguishing Atom Differences in A Molecular Graph Shape Index. *Quant. Struct. Act. Relat.* **1986,** *5* (1), 7–12.
211. Kier, L. B.; Hall, L. H. The Kappa Indices for Modeling Molecular Shape and Felxibility. In *Topological Indices and Related Descriptors in QSAR and QSPR;* Devillers, J., Balaban, A. T., Eds.; Gordon & Breach: Amsterdam, 1999; pp 455–489.
212. Randić, M. On Characterization of Molecular Branching. *J. Am. Chem. Soc.* **1975,** *97,* 6609–6615.
213. Estrada, E. Edge Adjacency Relationships and a Novel Topological Index Related to Molecular Volume. *J. Chem. Inf. Comput. Sci.* **1995,** *35* (1), 31–33.
214. Kier, L. B.; Hall, L. H. An Electrotopological-State Index for Atoms in Molecules. *Pharm. Res.* **1990,** *7,* 801–807.
215. Hall, L. H.; Mohney, B.; Kier, L. B. The Electrotopological State: Structure Information at the Atomic Level for Molecular Graphs. *J. Chem. Inf. Model.* **1991,** *31* (1), 76–82.
216. Kier, L. B.; Hall, L. H. *Molecular Connectivity in Chemistry and Drug Research;* Academic Press: New York, 1976.
217. Kier, L.; Hall, L. Intermolecular Accessibility: The Meaning of Molecular Connectivity. *J. Chem. Inf. Comput. Sci.* **2000,** *40* (3), 792–795.
218. Balaban, A. T.; Balaban, T.-S. New Vertex Invariants and Topological Indices of Chemical Graphs Based on Information on Distances. *J. Math. Chem.* **1991,** *8* (1), 383–397.
219. Balaban, A. T. Using Real Numbers as Vertex Invariants for Third-Generation Topological Indexes. *J. Chem. Inf. Comput. Sci.* **1992,** *32,* 23–28.
220. Balaban, A. T. Local versus Global (Le. Atomic versus Molecular) Numerical Modeling of Molecular Graphs. *J. Chem. Inf. Comput. Sci.* **1994,** *34,* 398–402.
221. Free, S. M.; Wilson, J. W. A Mathematical Contribution to Structure-Activity Studies. *J. Chem. Inf. Model.* **1964,** *7* (4), 395–399.
222. Fujita, T.; Ban, T. Structure-Activity Study of Phenethylamines as Substrates of Biosynthetic Enzymes of Sympathetic Transmitters. *J. Med. Chem.* **1971,** *14* (4), 148–152.
223. Kubinyi, H. Quantitative Structure-Activity Relationships. 2. A Mixed Approach, Based on Hansch and Free-Wilson Analysis. *J. Med. Chem.* **1976,** *19* (5), 587–600.
224. Devillers, J. No-Free-Lunch Molecular Descriptors in QSAR and QSPR. In *Topological Indices and Related Descriptors in QSAR and QSPR;* Devillers, J., Balaban, A. T., Eds.; Gordon & Breach: Amsterdam, 2000; pp 1–21.
225. Cambon, B.; Devillers, J. New Trends in Structure-Biodegradability Relationships. *Quant. Struct. Act. Relat.* **1993,** *12,* 49–56.
226. Singh, V. K.; Tewari, V. P.; Gupta, D. K.; Srivastava, A. K. Calculation of Heat of Formation: Molecular Connectivity and lOC-ω Technique, a Comparative Study. *Tetrahedron* **1984,** *40* (15), 2859–2863.
227. Burden, F. R. Molecular Identification Number for Substructure Searches. *J. Chem. Inf. Model.* **1989,** *29* (3), 225–227.
228. Pearlman, R. S.; Smith, K. M. Novel Software Tools for Chemical Diversity. *Perspect. Drug Discov. Des.* **1998,** *9,* 339–353.
229. ChemAxon. Fingerprint and descriptor generation—GenerateMD.
230. Todeschini, R.; Consonni, V. In *Molecular Descriptors for Chemoinformatics, Volumes I & II;* Mannhold, R., Kubinyi, H., Folkers, G., Eds., 2nd ed.; Wiley-VHC, 2009.
231. Tanford, C. *Physical Chemistry of Macromolecule;* Wiley: New York, 1961.
232. Arteca, G. A. Molecular Shape Descriptors. In *Reviews in Computational Chemistry*; vol. 9; VHC Publishers: New York, 1996, ; pp 191–253.
233. Abraham, M. H.; McGowan, J. C. The Use of Characteristic Volumes to Measure Cavity Terms in Reversed Phase Liquid Chromatography. *Chromatographia* **1987,** *23* (4), 243–246.
234. Cheng, Y. Y.; Yuan, H. Quantitative Study of Electrostatic and Steric Effects on Physicochemical Property and Biological Activity. *J. Mol. Graph. Model.* **2006,** *24* (4), 219–226.
235. Bhattacharjee, S.; Basak, A. C.; Dasgupta, P. Molecular Property Correlation in Haloethanes with Geometric Volume. *Comput. Chem.* **1992,** *16* (3), 223–228.
236. Zyrianov, Y. Distribution-Based Descriptors of the Molecular Shape. *J. Chem. Inf. Model.* **2005,** *45* (3), 657–672.
237. Todeschini, R.; Lasagni, M.; Marengo, E. New Molecular Descriptors for 2D and 3D Structures. Theory. *J. Chemom.* **1994,** *8* (4), 263–272.
238. Rohrbaugh, R. H.; Jurs, P. C. Descriptions of Molecular Shape Applied in Studies of Structure/activity and Structure/property Relationships. *Anal. Chim. Acta* **1987,** *199,* 99–109.
239. Rohrbaugh, R. H.; Jurs, P. C. Molecular Shape and the Prediction of High-Performance Liquid Chromatographic Retention Indexes of Polycyclic Aromatic Hydrocarbons. *Anal. Chem.* **1987,** *59,* 1046–1054.
240. Van Der Bondi, A. Waals Volumes and Radii. *J. Phys. Chem.* **1964,** *68,* 441–451.
241. Zhao, Y. H.; Abraham, M. H.; Zissimos, A. M. Fast Calculation of van Der Waals Volume as a Sum of Atomic and Bond Contributions and Its Application to Drug Compounds. *J. Org. Chem.* **2003,** *68* (19), 7368–7373.
242. Meyer, A. Y. Molecular Mechanics and Molecular Shape. Part 1. van Der Waals Descriptors of Simple Molecules. *J. Chem. Soc. Perkin Trans.* **1985,** *2* (8), 1161–1169.
243. Stouch, T. R.; Jurs, P. C. A Simple Method for the Representation, Quantification, and Comparison of the Volumes and Shapes of Chemical Compounds. *J. Chem. Inf. Comput. Sci.* **1986,** *26,* 4–12.
244. Hopfinger, A. J. A QSAR Investigation of Dihydrofolate Reductase Inhibition by Baker Triazines Based upon Molecular Shape Analysis. *J. Am. Chem. Soc.* **1980,** *102* (24), 7196–7206.
245. Tokarski, J. S.; Hopfinger, A. J. Three-Dimensional Molecular Shape Analysis-Quantitative Structure-Activity Relationship of a Series of Cholecystokinin-A Receptor Antagonists. *J. Med. Chem.* **1994,** *37* (21), 3639–3654.
246. Cramer, R. D.; Patterson, D. E.; Bunce, J. D. Comparative Molecular Field Analysis (CoMFA). 1. Effect of Shape on Binding of Steroids to Carrier Proteins. *J. Am. Chem. Soc.* **1988,** *110* (12), 5959–5967.
247. Hahn, M. Receptor Surface Models. 1. Definition and Construction. *J. Med. Chem.* **1995,** *38,* 2080–2090.
248. Consonni, V.; Todeschini, R.; Pavan, M. Structure/Response Correlations and Similarity/Diversity Analysis by GETAWAY Descriptors. 1. Theory of the Novel 3D Molecular Descriptors. *J. Chem. Inf. Comput. Sci.* **2002,** *42,* 682–692.
249. Ferguson, A. M.; Heritage, T.; Jonathon, P.; Pack, S. E.; Phillips, L.; Rogan, J.; Snaith, P. J. EVA: A New Theoretically Based Molecular Descriptor for Use in QSAR/QSPR Analysis. *J. Comput. Aided Mol. Des.* **1997,** *11,* 143–152.
250. Tuppurainen, K. EEVA (Electronic Eigenvalue): A New QSAR/QSPR Descriptor for Electronic Substituent Effects Based on Molecular Orbital Energies. *SAR QSAR Environ. Res.* **1999,** *10,* 39–46.
251. Tuppurainen, K.; Viisas, M.; Laatikainen, R.; Peräkylä, M. Evaluation of a Novel Electronic Eigenvalue (EEVA) Molecular Descriptor for QSAR/QSPR Studies: Validation Using a Benchmark Steroid Data Set. *J. Chem. Inf. Comput. Sci.* **2002,** *42* (3), 607–613.
252. Liu, S.; Cai, S.; Cao, C.; Li, Z. Molecular Electronegative Distance Vector (MEDV) Related to 15 Properties of Alkanes. *J. Chem. Inf. Comput. Sci.* **2000,** *40* (6), 1337–1348.
253. Liu, S. S.; Yin, C. S.; Cai, S. X.; Li, Z. L. A Novel MHDV Descriptor for Dipeptide QSAR Studies. *J. Chin. Chem. Soc.* **2001,** *48* (2), 253–260.
254. Kastenholz, M. A.; Pastor, M.; Cruciani, G.; Haaksma, E. E. J.; Fox, T. GRID/CPCA: A New Computational Tool to Design Selective Ligands. *J. Med. Chem.* **2000,** *43* (16), 3033–3044.
255. Pastor, M.; Cruciani, G.; McLay, I.; Pickett, S.; Clementi, S. GRid-INdependent Descriptors (GRIND): A Novel Class of Alignment-Independent Three-Dimensional Molecular Descriptors. *J. Med. Chem.* **2000,** *43* (17), 3233–3243.
256. Cruciani, G.; Crivori, P.; Carrupt, P. A.; Testa, B. Molecular Fields in Quantitative Structure-Permeation Relationships: The VolSurf Approach. *J. Mol. Struct. THEOCHEM* **2000,** *503* (1–2), 17–30.
257. Hopfinger, A. J.; Wang, S.; Tokarski, J. S.; Jin, B.; Albuquerque, M.; Madhav, P. J.; Duraiswami, C. Construction of 3D-QSAR Models Using the 4D-QSAR Analysis Formalism. *J. Am. Chem. Soc.* **1997,** *119* (43), 10509–10524.

258. Damale, M.; Harke, S.; Kalam Khan, F.; Shinde, D.; Sangshetti, J. Recent Advances in Multidimensional QSAR (4D-6D): A Critical Review. *Mini Rev. Med. Chem.* **2014,** *14* (1), 35–55.
259. Andrade, C. H.; Pasqualoto, K. F. M.; Ferreira, E. I.; Hopfinger, A. J. 4D-QSAR: Perspectives in Drug Design. *Molecules* **2010,** *15* (5), 3281–3294.
260. De Melo, E. B.; Ferreira, M. M. C. Four-Dimensional Structure-Activity Relationship Model to Predict HIV-1 Integrase Strand Transfer Inhibition Using LQTA-QSAR Methodology. *J. Chem. Inf. Model.* **2012,** *52* (7), 1722–1732.
261. Vedani, A.; Dobler, M. 5D-QSAR: The Key for Simulating Induced Fit? *J. Med. Chem.* **2002,** *45* (11), 2139–2149.
262. Vedani, A.; Dobler, M. MultiDimensional QSAR: Moving From 3 to 5 Dimensional Concepts. *Quant. Struct. Act. Relat.* **2002,** *21,* 382–390.
263. Vedani, A.; Dobler, M.; Lill, M. A. Combining Protein Modeling and 6D-QSAR. Simulating the Binding of Structurally Diverse Ligands to the Estrogen Receptor. *J. Med. Chem.* **2005,** *48* (11), 3700–3703.
264. Grant, J. A.; Gallardo, M. A.; Pickup, B. T. A Fast Method of Molecular Shape Comparison: A Simple Application of a Gaussian Description of Molecular Shape. *J. Comput. Chem.* **1996,** *17* (14), 1653–1666.
265. Hawkins, P. C. D.; Skillman, A. G.; Nicholls, A. Comparison of Shape-Matching and Docking as Virtual Screening Tools. *J. Med. Chem.* **2007,** *50* (1), 74–82.
266. Rush, T. S.; Grant, J. A.; Mosyak, L.; Nicholls, A. A Shape-Based 3-D Scaffold Hopping Method and Its Application to a Bacterial Protein-Protein Interaction. *J. Med. Chem.* **2005,** *48* (5), 1489–1495.
267. Sauer, W. H. B.; Schwarz, M. K. Molecular Shape Diversity of Combinatorial Libraries: A Prerequisite for Broad Bioactivity. *J. Chem. Inf. Comput. Sci.* **2003,** *43* (3), 987–1003.
268. Ballester, P. J.; Richards, W. G. Ultrafast Shape Recognition to Search Compound Databases for Similar Molecular Shapes. *J. Comput. Chem.* **2007,** *28* (10), 1711–1723.
269. Martin, Y. C.; Kofron, J. L.; Traphagen, L. M. Do Structurally Similar Molecules Have Similar Biological Activity? *J. Med. Chem.* **2002,** *45* (19), 4350–4358.
270. Nikolova, N.; Jaworska, J. Approaches to Measure Chemical Similarity—A Review. *QSAR Comb. Sci.* **2003,** *22* (910), 1006–1026.
271. Bender, A.; Glen, R. C. Molecular Similarity: A Key Technique in Molecular Informatics. *Org. Biomol. Chem.* **2004,** *2* (22), 3204–3218.
272. Wilkins, C. L.; Randić, M. A Graph Theoretical Approach to Structure-Property and Structure-Activity Correlations. *Theor. Chim. Acta* **1980,** *58* (1), 45–68.
273. Maldonado, A. G.; Doucet, J. P.; Petitjean, M.; Fan, B.-T. Molecular Similarity and Diversity in Chemoinformatics: From Theory to Applications. *Mol. Divers.* **2006,** *10* (1), 39–79.
274. Mathea, M.; Klingspohn, W.; Baumann, K. Chemoinformatic Classification Methods and Their Applicability Domain. *Mol. Inform.* **2016,** *35* (5), 160–180.
275. Vogt, M.; Bajorath, J. Chemoinformatics: A View of the Field and Current Trends in Method Development. *Bioorg. Med. Chem.* **2012,** *20* (18), 5317–5323.
276. Holliday, J. D.; Hu, C.-Y.; Willett, P. Grouping of Coefficients for the Calculation of Inter-Molecular Similarity and Dissimilarity Using 2D Fragment Bit-Strings. *Comb. Chem. High Throughput Screen.* **2002,** *5* (2), 155–166.
277. Willett, P.; Barnard, J. M.; Downs, G. M. Chemical Similarity Searching. *J. Chem. Inf. Comput. Sci.* **1998,** *38* (6), 983–996.
278. Drab, K.; Daszykowski, M. Clustering in Analytical Chemistry. *J. AOAC Int.* **2014,** *97* (1), 29–38.
279. Bajusz, D.; Rácz, A.; Héberger, K. Why Is Tanimoto Index an Appropriate Choice for Fingerprint-Based Similarity Calculations? *J. Chem. Theory Comput.* **2015,** *7,* 20.
280. Todeschini, R.; Consonni, V.; Xiang, H.; Holliday, J.; Buscema, M.; Willett, P. Similarity Coefficients for Binary Chemoinformatics Data: Overview and Extended Comparison Using Simulated and Real Data Sets. *J. Chem. Inf. Model.* **2012,** *52,* 2884–2901.
281. Yan, X.; Yu, P.; Han, J. Substructure Similarity Search in Graph Databases. In *Proceedings of the 2005 ACM SIGMOD International Conference on Management of Data;* Illinois, U. O., Ed.; ACM Press, 2005; pp 766–777.
282. Klinger, S.; Austin, J. Weighted Superstructures for Chemical Similarity Searching. Proceedings of the 9th Joint Conference on Information Sciences.
283. Mestres, J.; Maggiora, G. M. Putting Molecular Similarity into Context: Asymmetric Indices for Field-Based Similarity Measures. *J. Math. Chem.* **2006,** *39* (1), 107–118.
284. Héberger, K. Sum of Ranking Differences Compares Methods or Models Fairly. *TrAC Trends Anal. Chem.* **2010,** *29* (1), 101–109.
285. Haws, D. C.; Huggins, P.; O'Neill, E. M.; Weisrock, D. W.; Yoshida, R. A Support Vector Machine Based Test for Incongruence Between Sets of Trees in Tree Space. *BMC Bioinformatics* **2012,** *13* (1), 210.
286. Schuffenhauer, A.; Brown, N. Chemical Diversity and Biological Activity. *Drug Discov. Today Technol.* **2006,** *3* (4), 387–395.
287. Turner, D. B.; Tyrrell, S. M.; Willett, P. Rapid Quantification of Molecular Diversity for Selective Database Acquisition. *J. Chem. Inf. Comput. Sci.* **1997,** *37* (1), 18–22.
288. Sheridan, R. P.; Kearsley, S. K. Why Do We Need so Many Chemical Similarity Search Methods? *Drug Discov. Today* **2002,** *7* (17), 903–911.
289. Salim, N.; Holliday, J.; Willett, P. Combination of Fingerprint-Based Similarity Coefficients Using Data Fusion. *J. Chem. Inf. Comput. Sci.* **2003,** *43* (2), 435–442.
290. Brown, R. D.; Martin, Y. C. An Evaluation of Structural Descriptors and Clustering Methods for Use in Diversity Selection. *SAR QSAR Environ. Res.* **1998,** *8* (1–2), 23–39.
291. Holliday, J. D.; Ranade, S. S.; Willett, P. A Fast Algorithm For Selecting Sets Of Dissimilar Molecules From Large Chemical Databases. *Quant. Struct. Act. Relat.* **1995,** *14* (6), 501–506.
292. Godden, J. W.; Xue, L.; Bajorath, J. Combinatorial Preferences Affect Molecular Similarity/Diversity Calculations Using Binary Fingerprints and Tanimoto Coefficients. *J. Chem. Inf. Comput. Sci.* **2000,** *40* (1), 163–166.
293. Hert, J.; Willett, P.; Wilton, D. J.; Acklin, P.; Azzaoui, K.; Jacoby, E.; Schuffenhauer, A. New Methods for Ligand-Based Virtual Screening: Use of Data Fusion and Machine Learning to Enhance the Effectiveness of Similarity Searching. *J. Chem. Inf. Model.* **2006,** *46* (2), 462–470.
294. Whittle, M.; Willett, P.; Klaffke, W.; van Noort, P. Evaluation of Similarity Measures for Searching the *Dictionary of Natural Products* Database. *J. Chem. Inf. Comput. Sci.* **2003,** *43* (2), 449–457.
295. Holliday, J. D.; Salim, N.; Whittle, M.; Willett, P. Analysis and Display of the Size Dependence of Chemical Similarity Coefficients. *J. Chem. Inf. Comput. Sci.* **2003,** *43* (3), 819–828.
296. Chen, X.; Reynolds, C. H. Performance of Similarity Measures in 2D Fragment-Based Similarity Searching: Comparison of Structural Descriptors and Similarity Coefficients. *J. Chem. Inf. Comput. Sci.* **2002,** *42* (6), 1407–1414.
297. Yu, X.; Geer, L. Y.; Han, L.; Bryant, S. H. Target Enhanced 2D Similarity Search by Using Explicit Biological Activity Annotations and Profiles. *J. Chem. Theory Comput.* **2015,** *7,* 55.
298. Reisen, F.; Zhang, X.; Gabriel, D.; Selzer, P. Benchmarking of Multivariate Similarity Measures for High-Content Screening Fingerprints in Phenotypic Drug Discovery. *J. Biomol. Screen.* **2013,** *18* (10), 1284–1297.
299. Wale, N.; Watson, I. A.; Karypis, G. Indirect Similarity Based Methods for Effective Scaffold-Hopping in Chemical Compounds. *J. Chem. Inf. Model.* **2008,** *48* (4), 730–741.
300. Stiefl, N.; Watson, I. A.; Baumann, K.; Zaliani, A. ErG: 2D Pharmacophore Descriptions for Scaffold Hopping. *J. Chem. Inf. Model.* **2006,** *46* (1), 208–220.
301. Ertl, P. Intuitive Ordering of Scaffolds and Scaffold Similarity Searching Using Scaffold Keys. *J. Chem. Inf. Model.* **2014,** *54* (6), 1617–1622.
302. Wolohan, P. R. N.; Akella, L. B.; Dorfman, R. J.; Nell, P. G.; Mundt, S. M.; Clark, R. D. Structural Unit Analysis Identifies Lead Series and Facilitates Scaffold Hopping in Combinatorial Chemistry. *J. Chem. Inf. Model.* **2006,** *46* (3), 1188–1193.
303. Maggiora, G. M. On Outliers and Activity Cliffs—Why QSAR Often Disappoints. *J. Chem. Inf. Model.* **2006,** *46* (4), 1535.
304. Maggiora, G.; Vogt, M.; Stumpfe, D.; Bajorath, J. Molecular Similarity in Medicinal Chemistry. *J. Med. Chem.* **2014,** *57* (8), 3186–3204.
305. Muchmore, S. W.; Debe, D. A.; Metz, J. T.; Brown, S. P.; Martin, Y. C.; Hajduk, P. J. Application of Belief Theory to Similarity Data Fusion for Use in Analog Searching and Lead Hopping. *J. Chem. Inf. Model.* **2008,** *48* (5), 941–948.
306. Consonni, V.; Todeschini, R. New Similarity Coefficients for Binary Data. *MATCH Commun. Math. Comput. Chem.* **2012,** *68,* 581–592.
307. Spiteri, M.; Dubin, E.; Cotton, J.; Poirel, M.; Corman, B.; Jamin, E.; Lees, M.; Rutledge, D. Data Fusion between High Resolution (1)H-NMR and Mass Spectrometry: A Synergetic Approach to Honey Botanical Origin Characterization. *Anal. Bioanal. Chem.* **2016,** *408* (16), 4389–4401.
308. Bro, R.; Nielsen, H. J.; Savorani, F.; Kjeldahl, K.; Christensen, I. J.; Brünner, N.; Lawaetz, A. J. Data Fusion in Metabolomic Cancer Diagnostics. *Metabolomics* **2013,** *9* (1), 3–8.

309. Snarey, M.; Terrett, N. K.; Willett, P.; Wilton, D. J. Comparison of Algorithms for Dissimilarity-Based Compound Selection. *J. Mol. Graph. Model.* **1997,** *15* (6), 372–385.
310. Ginn, C. M. R.; Willett, P.; Bradshaw, J. Combination of Molecular Similarity Measures Using Data Fusion. In *Virtual Screening: An Alternative or Complement to High Throughput Screening?* Kluwer Academic Publishers: Dordrecht, 2000; pp 1–16.
311. Willett, P. Similarity-Based Virtual Screening Using 2D Fingerprints. *Drug Discov. Today* **2006,** *11* (23–24), 1046–1053.
312. Willett, P. Combination of Similarity Rankings Using Data Fusion. *J. Chem. Inf. Model.* **2013,** *53* (1), 1–10.
313. Chen, B.; Mueller, C.; Willett, P. Combination Rules for Group Fusion in Similarity-Based Virtual Screening. *Mol. Inform.* **2010,** *29* (6–7), 533–541.
314. Cross, S.; Baroni, M.; Carosati, E.; Benedetti, P.; Clementi, S. FLAP: GRID Molecular Interaction Fields in Virtual Screening. Validation Using the DUD Data Set. *J. Chem. Inf. Model.* **2010,** *50* (8), 1442–1450.
315. Kalivas, J. H.; Héberger, K.; Andries, E. Sum of Ranking Differences (SRD) to Ensemble Multivariate Calibration Model Merits for Tuning Parameter Selection and Comparing Calibration Methods. *Anal. Chim. Acta* **2015,** *869,* 21–33.
316. Tencate, A. J.; Kalivas, J. H.; White, A. J. Fusion Strategies for Selecting Multiple Tuning Parameters for Multivariate Calibration and Other Penalty Based Processes: A Model Updating Application for Pharmaceutical Analysis. *Anal. Chim. Acta* **2016,** *921,* 28–37.
317. Héberger, K.; Kollár-Hunek, K. Sum of Ranking Differences for Method Discrimination and Its Validation: Comparison of Ranks with Random Numbers. *J. Chemom.* **2011,** *25* (4), 151–158.
318. Kollár-Hunek, K.; Héberger, K. Method and Model Comparison by Sum of Ranking Differences in Cases of Repeated Observations (Ties). *Chemom. Intell. Lab. Syst.* **2013,** *127,* 139–146.
319. Truchon, J.-F.; Bayly, C. I. Evaluating Virtual Screening Methods: Good and Bad Metrics for the "Early Recognition" Problem. *J. Chem. Inf. Model.* **2007,** *47* (2), 488–508.
320. MacCuish, J. D.; MacCuish, N. E. Chemoinformatics Applications of Cluster Analysis. *Wiley Interdiscip. Rev. Comput. Mol. Sci.* **2014,** *4* (1), 34–48.
321. Zahoránszky-Kőhalmi, G.; Bologa, C. G.; Oprea, T. I. Impact of Similarity Threshold on the Topology of Molecular Similarity Networks and Clustering Outcomes. *J. Chem. Theory Comput.* **2016,** *8* (1), 16.
322. Amancio, D. R.; Comin, C. H.; Casanova, D.; Travieso, G.; Bruno, O. M.; Rodrigues, F. A.; da Fontoura Costa, L. A Systematic Comparison of Supervised Classifiers. *PLoS One* **2014,** *9* (4), e94137.
323. Kireeva, N. V.; Ovchinnikova, S. I.; Kuznetsov, S. L.; Kazennov, A. M.; Tsivadze, A. Y. Impact of Distance-Based Metric Learning on Classification and Visualization Model Performance and Structure-Activity Landscapes. *J. Comput. Aided Mol. Des.* **2014,** *28* (2), 61–73.
324. Jaskowiak, P. A.; Campello, R. J. G. B.; Costa, I. G. On the Selection of Appropriate Distances for Gene Expression Data Clustering. *BMC Bioinformatics* **2014,** *15* (Suppl 2), S2.
325. Saeh, J. C.; Lyne, P. D.; Takasaki, B. K.; Cosgrove, D. A. Lead Hopping Using SVM and 3D Pharmacophore Fingerprints. *J. Chem. Inf. Model.* **2005,** *45* (4), 1122–1133.
326. Zhang, L.; Zhang, D. MetricFusion: Generalized Metric Swarm Learning for Similarity Measure. *Inf. Fusion* **2016,** *30,* 80–90.
327. Pérez-Nueno, V. I.; Venkatraman, V.; Mavridis, L.; Ritchie, D. W. Detecting Drug Promiscuity Using Gaussian Ensemble Screening. *J. Chem. Inf. Model.* **2012,** *52* (8), 1948–1961.
328. Carbó, R.; Leyda, L.; Arnau, M. How Similar Is a Molecule to Another? An Electron Density Measure of Similarity between Two Molecular Structures. *Int. J. Quantum Chem.* **1980,** *17* (6), 1185–1189.
329. Hodgkin, E. E.; Richards, W. G. Molecular Similarity Based on Electrostatic Potential and Electric Field. *Int. J. Quantum Chem.* **1987,** *32* (S14), 105–110.
330. Petke, J. D. Cumulative and Discrete Similarity Analysis of Electrostatic Potentials and Fields. *J. Comput. Chem.* **1993,** *14* (8), 928–933.
331. Miranda-Quintana, R.-A.; Cruz-Rodes, R.; Codorniu-Hernandez, E.; Batista-Leyva, A. J. Formal Theory of the Comparative Relations: Its Application to the Study of Quantum Similarity and Dissimilarity Measures and Indices. *J. Math. Chem.* **2010,** *47* (4), 1344–1365.
332. Al-Dabbagh, M.; Salim, N.; Himmat, M.; Ahmed, A.; Saeed, F. A Quantum-Based Similarity Method in Virtual Screening. *Molecules* **2015,** *20* (10), 18107–18127.
333. Zhang, P.; Agarwal, P.; Obradovic, Z. Computational Drug Repositioning by Ranking and Integrating Multiple Data Sources. In *Machine Learning and Knowledge Discovery in Databases;* Blockeel, H., Kersting, K., Nijssen, S., Železný, F., Eds.; Springer: Berlin, Heidelberg, 2013; pp 579–594.
334. Wang, L.; Ma, C.; Wipf, P.; Liu, H.; Su, W.; Xie, X.-Q. TargetHunter: An in Silico Target Identification Tool for Predicting Therapeutic Potential of Small Organic Molecules Based on Chemogenomic Database. *AAPS J.* **2013,** *15* (2), 395–406.
335. Janda, J.-O.; Popal, A.; Bauer, J.; Busch, M.; Klocke, M.; Spitzer, W.; Keller, J.; Merkl, R. H2rs: Deducing Evolutionary and Functionally Important Residue Positions by Means of an Entropy and Similarity Based Analysis of Multiple Sequence Alignments. *BMC Bioinformatics* **2014,** *15,* 118.
336. Fu, G.; Ding, Y.; Seal, A.; Chen, B.; Sun, Y.; Bolton, E. Predicting Drug Target Interactions Using Meta-Path-Based Semantic Network Analysis. *BMC Bioinformatics* **2016,** *17,* 160.
337. Ghalwash, M. F.; Cao, X. H.; Stojkovic, I.; Obradovic, Z. Structured Feature Selection Using Coordinate Descent Optimization. *BMC Bioinformatics* **2016,** *17,* 158.
338. Rarey, M.; Dixon, J. S. Feature Trees: A New Molecular Similarity Measure Based on Tree Matching. *J. Comput. Aided Mol. Des.* **1998,** *12* (5), 471–490.
339. Dijkman, R.; Dumas, M.; van Dongen, B.; Käärik, R.; Mendling, J. Similarity of Business Process Models: Metrics and Evaluation. *Inf. Syst.* **2011,** *36* (2), 498–516.
340. Becker, M.; Laue, R. A Comparative Survey of Business Process Similarity Measures. *Comput. Ind.* **2012,** *63* (2), 148–167.
341. Rosenbaum, L.; Jahn, A.; Dörr, A.; Zell, A. Optimization and Visualization of the Edge Weights in Optimal Assignment Methods for Virtual Screening. *BioData Min.* **2013,** *6* (1), 7.
342. Mohr, J.; Jain, B.; Sutter, A.; Laak, A. Ter; Steger-Hartmann, T.; Heinrich, N.; Obermayer, K. A Maximum Common Subgraph Kernel Method for Predicting the Chromosome Aberration Test. *J. Chem. Inf. Model.* **2010,** *50* (10), 1821–1838.
343. Ralaivola, L.; Swamidass, S. J.; Saigo, H.; Baldi, P. Graph Kernels for Chemical Informatics. *Neural Netw.* **2005,** *18* (8), 1093–1110.
344. Resnik, P. Using Information Content to Evaluate Semantic Similarity in a Taxonomy. In *Proceedings of the 14th International Joint Conference on Artificial Intelligence—Volume 1;* Morgan Kaufmann Publishers Inc, 1995; pp 448–453.
345. Lin, D. An Information-Theoretic Definition of Similarity. In *Proceedings of the Fifteenth International Conference on Machine Learning;* Morgan Kaufmann Publishers, 1998; pp 296–304.
346. Schlicker, A.; Domingues, F. S.; Rahnenführer, J.; Lengauer, T. A New Measure for Functional Similarity of Gene Products Based on Gene Ontology. *BMC Bioinformatics* **2006,** *7,* 302.
347. Himmat, M.; Salim, N.; Al-Dabbagh, M. M.; Saeed, F.; Ahmed, A. Adapting Document Similarity Measures for Ligand-Based Virtual Screening. *Molecules* **2016,** *21* (4), 476.
348. Yu, H. Selective Sampling Techniques for Feedback-Based Data Retrieval. *Data Min. Knowl. Discov.* **2011,** *22* (1-2), 1–30.
349. Mandera, P.; Keuleers, E.; Brysbaert, M. Explaining Human Performance in Psycholinguistic Tasks with Models of Semantic Similarity Based on Prediction and Counting: A Review and Empirical Validation. *J. Mem. Lang.* **2017,** *92,* 57–78.
350. Armstrong, M. S.; Finn, P. W.; Morris, G. M.; Richards, W. G. Improving the Accuracy of Ultrafast Ligand-Based Screening: Incorporating Lipophilicity into ElectroShape as an Extra Dimension. *J. Comput. Aided Mol. Des.* **2011,** *25* (8), 785–790.
351. Gfeller, D.; Michielin, O.; Zoete, V. Shaping the Interaction Landscape of Bioactive Molecules. *Bioinformatics* **2013,** *29* (23), 3073–3079.
352. Guha, R.; Van Drie, J. H. Structure-Activity Landscape Index: Identifying and Quantifying Activity Cliffs. *J. Chem. Inf. Model.* **2008,** *48* (3), 646–658.
353. Sukumar, N.; Krein, M. P.; Prabhu, G.; Bhattacharya, S.; Sen, S. Network Measures for Chemical Library Design. *Drug Dev. Res.* **2014,** *75* (6), 402–411.
354. Cuissart, B.; Touffet, F.; Crémilleux, B.; Bureau, R.; Rault, S. The Maximum Common Substructure as a Molecular Depiction in a Supervised Classification Context: Experiments in Quantitative Structure/biodegradability Relationships. *J. Chem. Inf. Comput. Sci.* **2002,** *42* (5), 1043–1052.
355. Mendenhall, J.; Meiler, J. Improving Quantitative Structure–activity Relationship Models Using Artificial Neural Networks Trained with Dropout. *J. Comput. Aided Mol. Des.* **2016,** *30* (2), 177–189.

356. Naderi, M.; Alvin, C.; Ding, Y.; Mukhopadhyay, S.; Brylinski, M. A Graph-Based Approach to Construct Target-Focused Libraries for Virtual Screening. *J. Chem. Theory Comput.* **2016,** *8,* 14.
357. Jankowski, N.; Usowicz, K. Analysis of Feature Weighting Methods Based on Feature Ranking Methods for Classification. In *Neural Information Processing;* Lu, B.-L., Zhang, L., Kwok, J., Eds.; Springer: Berlin, Heidelberg, 2011; pp 238–247.
358. Kim, S.; Okajima, R.; Kano, M.; Hasebe, S. Development of Soft-Sensor Using Locally Weighted PLS with Adaptive Similarity Measure. *Chemom. Intell. Lab. Syst.* **2013,** *124,* 43–49.
359. Roggo, Y.; Chalus, P.; Maurer, L.; Lema-Martinez, C.; Edmond, A.; Jent, N. A Review of near Infrared Spectroscopy and Chemometrics in Pharmaceutical Technologies. *J. Pharm. Biomed. Anal.* **2007,** *44* (3), 683–700.
360. Gan, F.; Hopke, P. K.; Wang, J. A Spectral Similarity Measure Using Bayesian Statistics. *Anal. Chim. Acta* **2009,** *635* (2), 157–161.
361. Bodis, L.; Ross, A.; Pretsch, E. A Novel Spectra Similarity Measure. *Chemom. Intell. Lab. Syst.* **2007,** *85* (1), 1–8.
362. de Gelder, R.; Wehrens, R.; Hageman, J. A. A Generalized Expression for the Similarity of Spectra: Application to Powder Diffraction Pattern Classification. *J. Comput. Chem.* **2001,** *22* (3), 273–289.
363. Wan, K. X.; Vidavsky, I.; Gross, M. L. Comparing Similar Spectra: From Similarity Index to Spectral Contrast Angle. *J. Am. Soc. Mass Spectrom.* **2002,** *13* (1), 85–88.
364. Wu, Y.; Lv, S.; Wang, C.; Gao, X.; Li, J.; Meng, Q. Comparative Analysis of Volatiles Difference of Yunnan Sun-Dried Pu-Erh Green Tea from Different Tea Mountains: Jingmai and Wuliang Mountain by Chemical Fingerprint Similarity Combined with Principal Component Analysis and Cluster Analysis. *Chem. Cent. J.* **2016,** *10,* 11.
365. Zhang, J.; Koo, I.; Wang, B.; Gao, Q.-W.; Zheng, C.-H.; Zhang, X. A Large Scale Test Dataset to Determine Optimal Retention Index Threshold Based on Three Mass Spectral Similarity Measures. *J. Chromatogr. A* **2012,** *1251,* 188–193.
366. Varmuza, K.; Karlovits, M.; Demuth, W. Spectral Similarity versus Structural Similarity: Infrared Spectroscopy. *Anal. Chim. Acta* **2003,** *490* (1), 313–324.
367. Hung, W.-L.; Yang, M.-S. Similarity Measures of Intuitionistic Fuzzy Sets Based on Hausdorff Distance. *Pattern Recog. Lett.* **2004,** *25* (14), 1603–1611.
368. Liang, Z.; Shi, P. Similarity Measures on Intuitionistic Fuzzy Sets. *Pattern Recog. Lett.* **2003,** *24* (15), 2687–2693.
369. Xu, Z.; Yager, R. R. Intuitionistic and Interval-Valued Intutionistic Fuzzy Preference Relations and Their Measures of Similarity for the Evaluation of Agreement within a Group. *Fuzzy Optim. Decis. Mak.* **2009,** *8* (2), 123–139.
370. Hung, W.-L.; Yang, M.-S. Similarity Measures of Intuitionistic Fuzzy Sets Based on Lp Metric. *Int. J. Approx. Reason.* **2007,** *46* (1), 120–136.
371. Szmidt, E.; Kacprzyk, J. A Similarity Measure for Intuitionistic Fuzzy Sets and Its Application in Supporting Medical Diagnostic Reasoning. In *Artificial Intelligence and Soft Computing—ICAISC 2004;* Rutkowski, L., Siekmann, J. H., Tadeusiewicz, R., Zadeh, L. A., Eds.; Springer: Berlin, Heidelberg, 2004; pp 388–393.
372. Singh, P. A New Method for Solving Dual Hesitant Fuzzy Assignment Problems with Restrictions Based on Similarity Measure. *Appl. Soft Comput.* **2014,** *24,* 559–571.
373. Wang, W.; Xin, X. Distance Measure between Intuitionistic Fuzzy Sets. *Pattern Recog. Lett.* **2005,** *26* (13), 2063–2069.
374. Zhang, L.; Xu, X.; Tao, L.; Zhang, L.; Xu, X.; Tao, L. Some Similarity Measures for Triangular Fuzzy Number and Their Applications in Multiple Criteria Group Decision-Making. *J. Appl. Math.* **2013,** *2013,* 538261.
375. Su, Z.; Xu, Z.; Liu, H.; Liu, S. Distance and Similarity Measures for Dual Hesitant Fuzzy Sets and Their Applications in Pattern Recognition. *J. Intell. Fuzzy Syst.* **2015,** *29* (2), 731–745.
376. Zhang, X.; Xu, Z. Novel Distance and Similarity Measures on Hesitant Fuzzy Sets with Applications to Clustering Analysis. *J. Intell. Fuzzy Syst.* **2015,** *28* (5), 2279–2296.
377. Todeschini, R.; Ballabio, D.; Consonni, V. Distances and Other Dissimilarity Measures in Chemometrics. In *Encyclopedia of Analytical Chemistry;* John Wiley & Sons Ltd, 2015; pp 1–34.
378. Kunimoto, R.; Vogt, M.; Bajorath, J. Maximum Common Substructure-Based Tversky Index: An Asymmetric Hybrid Similarity Measure. *J. Comput. Aided Mol. Des.* **2016,** *30* (7), 523–531.
379. Krawczak, M.; Szkatuła, G. On Asymmetric Matching Between Sets. *Inf. Sci. (NY)* **2015,** *312,* 89–103.
380. Hamers, L.; Hemeryck, Y.; Herweyers, G.; Janssen, M.; Keters, H.; Rousseau, R.; Vanhoutte, A. Similarity Measures in Scientometric Research: The Jaccard Index Versus Salton's Cosine Formula. *Inf. Process. Manag.* **1989,** *25* (3), 315–318.
381. Leng, Y.; Lu, Q.; Liang, C. A Collaborative Filtering Similarity Measure Based on Potential Field. *Kybernetes* **2016,** *45* (3), 434–445. http://dx.doi.org/10.1108/K-10-2014-0212.
382. Cha, S.-H. Comprehensive Survey on Distance/Similarity Measures Between Probability Density Functions. *Int. J. Math. Mod. Meth. Appl. Sci* **2007,** *1* (4), 300–307.
383. Common Chemistry. http://www.commonchemistry.org/ (accessed 05.07.16).
384. PubChem. https://pubchem.ncbi.nlm.nih.gov/ (accessed 05.07.16).
385. PubChem BioAssay—NCBI. http://www.ncbi.nlm.nih.gov/pcassay (accessed 27.01.16).
386. ChemSpider | Search and share chemistry. http://www.chemspider.com/ (accessed 05.07.16).
387. Gaulton, A.; Bellis, L. J.; Bento, A. P.; Chambers, J.; Davies, M.; Hersey, A.; Light, Y.; McGlinchey, S.; Michalovich, D.; Al-Lazikani, B.; et al. ChEMBL: A Large-Scale Bioactivity Database for Drug Discovery. *Nucleic Acids Res.* **2012,** *40* (Database issue), D1100–D1107.
388. Bento, A. P.; Gaulton, A.; Hersey, A.; Bellis, L. J.; Chambers, J.; Davies, M.; Krüger, F. A.; Light, Y.; Mak, L.; McGlinchey, S.; et al. The ChEMBL Bioactivity Database: An Update. *Nucleic Acids Res.* **2014,** *42* (Database issue), D1083–D1090.
389. ChEMBL database (release 21). https://www.ebi.ac.uk/chembl/ (accessed 15.07.16).
390. SureChEMBL. https://www.surechembl.org/search/ (accessed 06.07.16).
391. Irwin, J. J.; Shoichet, B. K. ZINC—A Free Database of Commercially Available Compounds for Virtual Screening. *J. Chem. Inf. Model.* **2005,** *45* (1), 177–182.
392. Irwin, J. J.; Sterling, T.; Mysinger, M. M.; Bolstad, E. S.; Coleman, R. G. ZINC: A Free Tool to Discover Chemistry for Biology. *J. Chem. Inf. Model.* **2012,** *52* (7), 1757–1768.
393. eMolecules. https://www.emolecules.com/ (accessed 06.07.16).
394. Kiss, R.; Sándor, M.; Szalai, F. A. http://Mcule.com: A Public Web Service for Drug Discovery. *J. Chem. Theory Comput.* **2012,** *4* (Suppl. 1), 17.
395. Ruddigkeit, L.; van Deursen, R.; Blum, L. C.; Reymond, J.-L. Enumeration of 166 Billion Organic Small Molecules in the Chemical Universe Database GDB-17. *J. Chem. Inf. Model.* **2012,** *52* (11), 2864–2875.
396. de Graaf, C.; Kooistra, A. J.; Vischer, H. F.; Katrich, V.; Kuijer, M.; Shiroishi, M.; Iwata, S.; Shimamura, T.; Stevens, R. C.; De Esch, I. J. P.; et al. Crystal Structure-Based Virtual Screening for Fragment-like Ligands of the Human Histamine H1 Receptor. *J. Med. Chem.* **2011,** *54* (23), 8195–8206.
397. Keserü, G. M. Prediction of hERG Potassium Channel Affinity by Traditional and Hologram qSAR Methods. *Bioorg. Med. Chem. Lett.* **2003,** *13,* 2773–2775.
398. Kwak, J. T.; Hewitt, S. M.; Kajdacsy-Balla, A. A.; Sinha, S.; Bhargava, R. Automated Prostate Tissue Referencing for Cancer Detection and Diagnosis. *BMC Bioinformatics* **2016,** *17* (1), 227.
399. Cherkasov, A.; Muratov, E. N.; Fourches, D.; Varnek, A.; Baskin, I. I.; Cronin, M.; Dearden, J.; Gramatica, P.; Martin, Y. C.; Todeschini, R.; et al. QSAR Modeling: Where Have You Been? Where Are You Going To? *J. Med. Chem.* **2014,** *57* (12), 4977–5010.
400. Rácz, A.; Bajusz, D.; Héberger, K. Consistency of QSAR Models: Correct Split of Training and Test Sets, Ranking of Models and Performance Parameters. *SAR QSAR Environ. Res.* **2015,** *26* (7–9), 683–700.

3.15 Quantitative Structure–Activity Relationships

AM Davis, AstraZeneca R&D Gothenburg, Mölndal, Sweden

© 2017 Elsevier Ltd. All rights reserved.

3.15.1	**Quantitative Structure–Activity Relationships in Drug Design SAR**	379
3.15.2	**History of QSAR**	379
3.15.3	**QSAR Today**	380
3.15.4	**QSAR Model Building**	381
3.15.4.1	Calculating Descriptors	382
3.15.4.2	Preparation of the Dataset	382
3.15.4.3	Generating a Training and Test Set	382
3.15.4.4	Exploring the Dataset	383
3.15.4.5	Appropriate Measures of Goodness-of-Fit—Model Diagnostics	384
3.15.4.6	A Defined Domain of Applicability	385
3.15.5	**Examples of Influential QSAR Models**	387
3.15.6	**The Future of QSAR**	388
3.15.7	**Using QSAR Models**	390
3.15.8	**Conclusions**	391
References		391

3.15.1 Quantitative Structure–Activity Relationships in Drug Design SAR

Quantitative Structure–Activity Relationships (QSARs) are statistical empirical models that relate a quantitative description of chemical structure features of a series of molecules to the responses those molecules show in an experimental system. QSARs are empirical models as they are based on observed trends and correlations between the chemical descriptors and response variables, rather than on an a priori physics-based model. Although empirical in nature, a robust QSAR model can be used to propose a physical hypothesis that underlies an observed relationship. Medicinal chemistry structure–activity relationships are based on serial pairwise comparisons of structural changes with activity changes. QSAR takes a complementary approach and tries to identify how structural changes across a series of molecules are related to their activity.

3.15.2 History of QSAR

The first QSAR model is reputed to have come from the work of Alexander Crum-Brown and Thomas Frazer, which was read before the Royal Society of Edinburgh on Jan. 6, 1868.[1] They were studying the muscle paralyzing activities of quaternized alkaloid "poisons" and focused on differences in activity and chemical structure. As the constitution of the substances was not known, they hypothesized "there is more hope of arriving at some definite conclusion by studying the changes produced in the action of physiologically active substances, by performing on them certain well defined chemical operations which introduce known changes to their composition": They treated natural alkaloids from strychnia, brucia, thebaia, codeia, morphia, and nicotia with methyl iodide and studied their effects in rabbits and dogs. In the paper, they expressed the relationship between structural changes (Δ and changes activity as a mathematical equation, Eq. (1)

$$\Delta(\text{physiological activity}) = f(\Delta\ \text{constitution}) \tag{1}$$

QSAR still follows this formalism, where chemical descriptors are used to numerically quantify chemical constitution, and the mathematical tool, sometimes called a machine-learning algorithm, is used to define the function "*f*" that relates structure to activity.

In 1869, Richardson[2] showed that the narcotic effects of primary alcohols were inversely related to their molecular weights. In 1893, Richet[3] showed that the toxicities of simple ethers, alcohols, and ketones were inversely related to their solubility in water. A major step was taken toward QSAR as we know it when in 1899, Hans Horst Meyer[4] first proposed and demonstrated that anesthetic potency was related to lipid solubility. Two years later, a similar proposal was made by Charles Overton.[5] They showed the narcotic effect on tadpoles was proportional to the partition coefficient of the compounds from water into olive oil, as a model for the partition of the narcotics into the biological membrane. Further, their correlation prompted them to hypothesize that it was the compounds partitioning into nerve cells that led to the narcosis. Today, we still use partition coefficients as a measure of a compound's hydrophobicity, although *n*-octanol has superseded olive oil as a hydrophobic receptor phase.

In the 1930s, quantitative structure-property relationships (QSPRs) defined the field of physical organic chemistry through the work of Hammett,[6] Brönsted, Pederson, and others.[7]

Hammett proposed that the effect of substituents attached to the benzene ring, *meta* or *para* to a reaction center, upon the reaction rate or position of a chemical equilibrium in which the reaction center participates, is a property of the electronic effect substituent alone. Different reactions may have different sensitivities to the effect of this substituent. Hammett defined an experimentally based descriptor σ, to quantify the electronic effect of a substituent. The σ scale used the ionization of benzoic acids as the calibrating reaction, and σ_m or σ_p represented the difference in pK_a between the different m- or p-substituted benzoic acids and benzoic acid itself. The sensitivity of a particular reaction to the electronic effect of a substituent was described by ρ, the slope of the correlation between the logarithm of the equilibrium (K) or rate constant (k) for that reaction and the sigma values, Eq. (2)

$$log k = \rho\sigma + \text{constant} \tag{2}$$

In Hammett's initial publication, he tabulated σ values for 31 substituents, and linear energy correlations for 39 reactions. While Hammett's observations were empirical, he recognized that they may indicate a common underlying physics-based explanation relating to electron attraction or repulsion by inductive and resonance effects.

In the 1950s, Taft extended Hammett's work to define a sigma scale for aliphatic systems.[8] Taft used the acid- and base-catalyzed hydrolysis of esters as the calibrating reaction. He proposed that as the acid- and base-catalyzed hydrolysis of esters proceed through a very similar tetrahedral transition state structure, and under identical conditions, both reactions would experience similar steric influences. As the base-catalyzed reaction went from a neutral ground state to a negatively charged transition state, it would be more sensitive to electronic effects of substituents than the acid-catalyzed hydrolysis reaction which moves from a positively charged ground state (rapid preprotonation of the ester carbonyl) to a similarly positively charged transition state. Therefore the acid-catalyzed hydrolysis of esters would be less sensitive to the electronic effect of substituents, while remaining sensitive to their size. On the other hand, base-catalyzed hydrolysis would be sensitive to both size and electronic effects. Taft was therefore able to also define a new steric substituent constant scale, termed Es. Taft gave the symbol σ^* to the electronic effect of the aliphatic substituent. The sensitivity of a particular reaction to the electronic and steric effects of a substituent was described by ρ^* and d, respectively, the regression coefficients from the correlation between the logarithm of the equilibrium (K) or rate constant (k) for a given reaction and the σ^* and Es values of the substituents, Eq. (3).

$$log(k - R/k - \text{Me}) = \rho^*\sigma^* + d \times \text{Es} + \text{constant} \tag{3}$$

Modern QSAR began with the work of Corwin Hansch and Toshio Fujita.[9,10] They were studying the effect of auxins as growth regulators. Their hypothesis was that auxin mode of action was more chemical in nature, covalently modifying their molecular target. But attempts to apply a Hammett equation to describe biological activity failed and led them to reevaluate their hypothesis. Their new hypothesis was that transport through biological membranes to the site of activity in fact may be the rate-determining step. To describe the partitioning step, they defined a new substituent scale π. The π parameter was defined as the difference in logarithm of the partition coefficient between *n*-octanol and water of the aromatic-substituted compound to the logarithm of the partition coefficient of the unsubstituted aromatic compound, in an analogous fashion to Hammett's sigma scale. They modified the Hammett equation to incorporate both the linear and nonlinear dependence upon this new substituent constant π, incorporating both the π and π^2 terms. They took a multivariate approach to describe biological activity and used multiple linear regression (MLR) to fit the relationship between a set of descriptors and biological activity: they were successful in building a model based on their new hypothesis and their new approach to QSAR modeling. The work was extended in a follow-up paper to show the general application in a number of other systems.[11]

Also during the 1960s, Free and Wilson developed their own QSAR formalism to optimize substituent selection in a design-make-test cycle. One can consider the Free and Wilson analysis[12] as a limiting case of QSAR analysis, which directly correlates biological activity with the presence or absence of a substituent at a particular position. The presence of absence of the substituent in the Free–Wilson method is represented as a numerical "indicator" descriptor, where 1 = presence of a substituent and 0 = absence of a particular substituent. The Free–Wilson analysis has inspired the recently introduced molecular-matched pair analysis.

3.15.3 QSAR Today

QSAR remains a popular technique, and is now a fully embedded tool within drug discovery. But QSAR model derivation and use is fraught with pitfalls and complexity. Many literature QSAR models with apparently appealing statistics can in reality encode no more than chance relationships.

The statistical algorithms applied are very powerful tools to find correlation patterns in datasets, and the model builder may not know if these are true underlying relationships or statistical flukes that fail to predict forward in time, that is in real life usage.[13,14] For example, in Stouch and colleagues' paper "In silico ADME/Tox: why models fail," the authors highlight Bristol-Myers Squibb's own experience in trying to validate vendor built QSAR models for hERG inhibition, Caco-2 permeability, cytochrome P450 2D6 inhibition, and an aqueous solublility.[13] The authors concluded that even in the best case models, builders and users may have different criteria for success, and a lack of appreciation of the model quality and scope. In the worst cases the models were of no value. For example in the hERG model, they identified using validation compounds measured in both assays, that the assay used for the training's set hERG data gave results quite unlike the same compounds tested in their internal hERG assay. In the Caco-2 model, which was not predictive, (**Fig. 1**) they identified that the internal test set compounds, were quite unlike the literature training set compounds (based on 2-dimensional similarity). Nils Bohr was certainly right, when he said, "Prediction is very

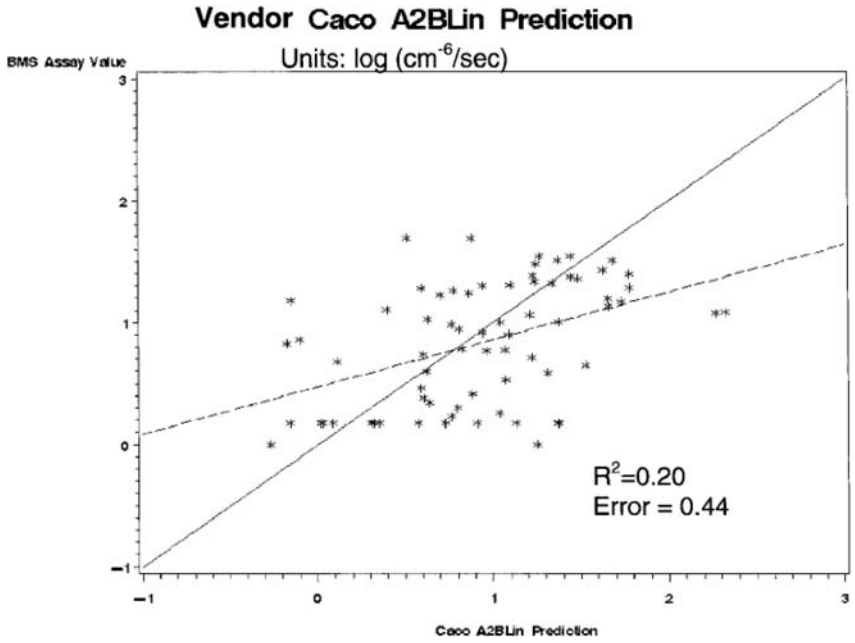

Fig. 1 Caco-2 A2B permeability predictions from a vendor QSAR model versus measured Caco-2 A2B permeability from Bristol-Myers Squibb validation. (Reproduced with permission from Stouch, T. R.; Kenyon, J. R.; Johnson, S. R.; Chen, X-Q.; Doweyko, A.; Li, Y. In Silico ADME/Tox: Why Models Fail. J. *Comput. Aided Mol. Des.* **2003**, *17* (2–4), 83–92.)

difficult, especially about the future". However, a carefully built and validated QSAR model can be a powerful tool to guide drug design. For example in AstraZeneca, hERG QSAR models[15] have contributed to the reduction in synthesized "red-flag" compounds (hERG potency <1 μM), from 25.8% of all compounds tested in 2003 to only 6% in 2010.

As an example of the impact of QSAR models, the European Community in its Registration Evaluation Authorisation and Restriction of Chemicals (REACH) now accept validated QSARs as part of the required complete dossier on the physicochemical, biological, and technological properties for every chemical circulating in Europe.[16] Because of this, and the complexity in building robust models, the Organisation for Economic Co-operation and Development (OECD) has defined good practice in the validation of QSAR models, with the aim of increasing regulatory body acceptance of QSAR models for toxicity and environmental assessment.[17] They have also published a "QSAR toolbox" for use by regulatory authorities and companies to allow look-up, near neighbor analysis, and robust prediction of toxicity and environmental properties of new compounds based on its database of structures and responses. The OECD guidelines, although focused on environmental toxicology, are recommended reading for any scientist involved in the derivation of QSAR models. The guidelines state that, to facilitate consideration of a QSAR model for regulatory purposes, the model should be associated with:

1. an unambiguous endpoint;
2. an unambiguous algorithm;
3. a defined domain of applicability;
4. appropriate measures of goodness-of-fit, robustness, and predictivity;
5. a mechanistic interpretation, if possible.

Peer-reviewed journals now require all data and molecular structures used to carry out a QSAR/QSPR study to be reported in the publication. This enables the reader to reproduce the analysis in the paper and to validate the quality of the published work.[18]

3.15.4 QSAR Model Building

Many tools for building QSAR models are freely available on the Internet. Integrated QSAR toolkits exist in commercial computational chemistry software packages and free integrated tools include Bioclipse[19] and KNIME.[20,21] Bioclipse can be freely downloaded, will run under Windows, Linux, and Macintosh operating systems, and contains a fully integrated QSAR toolkit that can be used for datasets of up to 2000 compounds.

Online systems are available for the automatic QSAR building, for example, OCHEM[22] and OECD QSAR toolbox.[23] Submitting datasets to online public QSAR engines may compromise an institution's requirements regarding confidentiality of structures, therefore local implementations are often preferable.

For computational chemists who prefer more flexibility, many machine-learning libraries exist for the R statistics suite,[24] and many descriptor calculators are available on the Internet.[25] Computational chemistry software suites contain useful QSAR implementations with descriptor calculation and machine-learning tools, but freely available integrated QSAR toolkits are less common.

The CDK toolkit is an open-source cheminformatics package, developed by more than 50 researchers worldwide, and widely used to provide chemical descriptors for QSAR modeling.[26] A number of other cheminformatics toolkits also exist, including RDkit and OpenBabel.[27] CINFONY is an open-source application program interface to a number of cheminformatics toolkits, including CDK, RDkit,[28] and OpenBabel. The previously mentioned BIOCLPSE system contains a choice of descriptor sets including Signature descriptors, which are a type of fingerprint descriptor, and which allows the results of the QSAR analysis to be mapped back onto the training set structure, highlighting areas of the molecule most significantly contributing to the response.

Where three-dimensional (3-D) structural information is known, whether from experimental X-ray structures, NMR, or computational models, descriptors can be calculated directly from the observed drug–receptor interactions (CoMFA,[29] GRID-GOLPE,[30,31] and VALIDATE[32]). Some of the scoring functions inside docking programs use methods based on QSAR equations to rank the affinity of molecules from the observed drug–receptor interactions (e.g., LUDI[33]).

3.15.4.1 Calculating Descriptors

How you describe changes in molecular structure across a series of molecules within a vector of numbers is one of the critical steps in setting up a QSAR model. Very many descriptors are available, representing molecular size, volume, lipophilicity, hydrogen bonding counts, shape, and electronic distribution. Representing 3-D shape within a single number vector is challenging, although many shape descriptors have been suggested. Some descriptors like H-bond donor counts are understandable by medicinal chemists. Other descriptors, in an attempt to encode complex properties such as shape, molecular connectivity, or charge distribution, although mathematically accurate, can be difficult for the medicinal chemist to deconvolute. There are whole books just devoted to descriptors for QSAR. The DRAGON descriptor suite contains 4885 molecular descriptors for use in QSAR.[34] Many of the mathematical tools used to define QSAR equations are very sensitive to the number of descriptors included in the analysis. Including more descriptors increases the probability of finding correlations just by chance, particularly when there are more descriptors than the number of molecules with biological activity being modeled. If this is the case, some regression tools such as partial least squares (PLS) analysis, which extract summary variables from a larger descriptor matrix, and uses "cross-validation" to assess the significant contribution of variables added to the model, are less sensitive to finding spurious correlations in what are called "over-square" matrices (more descriptor columns than compound rows).

Comparative molecular field analysis (CoMFA) and related 3-D QSAR methods attempt to describe both the 3-D shape and charge distribution of molecules by recording the interaction between the target molecules and a small probe molecule placed over a 3-D grid surrounding the molecules in the training set. The molecules have to be overlaid in 3-D space, so common molecular features occupy common volumes in space. The overlay can be thought of as a putative pharmacophore. The result of the QSAR analysis is the importance of the interactions the probe felt at each point in space to describing the response variable. These coefficients can be mapped back onto their respective points in 3-D space, to form a 3-D regression map. These can be interpreted by the medicinal chemist. For CoMFA, the probe is usually a positively charged methyl group, which perceives electrostatics and volume. The maps tell the medicinal chemists where in 3D space to place or remove charge and molecular volume to increase or decrease potency.[29]

As we have already mentioned a number of descriptor calculators are available on the Internet.[25] ACD physical property suite calculates log P, log $D_{7.4}$, and ionization constants. ACDLabs also makes available iLab, a pay for service web-based system for calculated physical properties.[35] The CDK toolkit, RDKit, OpenBabel, CINFONY BIOCLIPSE and KNIME are excellent sources of descriptors.

Whatever the dataset, descriptors being used, and machine-learning algorithm applied, the following steps are normally taken in deriving QSAR models.

3.15.4.2 Preparation of the Dataset

Some machine-learning methods are sensitive to the numerical range of the data in each descriptor. PLS regression is one example. Descriptors that have a larger range because of the units chosen can unduly influence the fitting of the descriptors to the y-response data using your chosen statistical learning method. Therefore the dataset is often "normalized," or "unit scaled" by subtracting the mean value of each descriptor vector from each descriptor value, and dividing by the standard deviation of the descriptor column. Hence each descriptor will have a mean of zero and standard deviation = 1.0. In those methods sensitive to scale, this process gives each descriptor an equal weight to contribute to the model.

3.15.4.3 Generating a Training and Test Set

Next the dataset is split into a training set and a test set. The training set is used to define the mathematical relationship, or correlation, between the y-response and x-descriptors, using the chosen machine-learning method. The test set is used to assess the quality of the QSAR model by its ability to predict a set of molecules that were not part of the training phase. Because many of the machine-learning methods used to define QSAR models are very good at fitting the x-descriptors to the y-response data, the

quality of the model is usually best assessed on how well it predicts an independent test set, rather than the fit to the training set compounds. Some methods require a training set, a tuning set, and a test set/validation set, where the tuning set is used for internal model validation and the test set for external validation. In this case, the tuning set is used to stop the model training phase, or to select between different models, while the validation set is an independent test of model performance. The disadvantage of this approach is that it limits the number of compounds available to train the machine-learning algorithm.

The test set/validation set can be selected from the original dataset in a number of ways, including random selection, by clustering and selecting representative examples from the original dataset, or in a way that would satisfy Nils Bohr, by selecting in time order, so the latest compounds make the test set. When the model is to be used in a design-make-test environment, a time-ordered test set most closely reflects how the model will be used, to predict future compounds. The size of the test set selected often depends on the amount of compounds on which you have activity data. The compounds selected for the test set limit the amount of information you make available to the machine-learning method to build a model from. A common approach is to select 20–30% of your dataset as a test set. If a QSAR has been used in a design-make-test environment, week on week, and confidence has been built in its predictivity, a much smaller test set could be used at later rebuilds, to maximize its ability to predict tomorrows compound.

3.15.4.4 Exploring the Dataset

A critical step in an QSAR analysis is getting to know your dataset. One can examine plots of response versus variables, as it may inform your choice of statistical tool, and it may allow you to refine your dataset. Projection methods such as principal component analysis may also help one identify clusters or outliers that may bias an analysis. This may affect how the training set for the model is selected. Often such visual explorations of the dataset are enough to understand important underlying QSAR relationships. There are a number of commercial tools for data exploration, and even powerful freely available tools such as DataWarrior.[36] A lot of information can be extracted by such a simple exploration, and this approach is very complementary to the traditional medicinal chemist pairwise approach to exploring SAR. During an analysis of the duration of action of dual acting β_2 adrenoceptor, dopamine D_2 receptor agonists, a simple visual analysis of such plots provided the catalyst for building a very predictive QSAR model.[37,38]

The next step is the choice of machine-learning algorithm. This can be informed by the data exploration step previously described, the descriptors to y-data point ratio, and by the modeler's experience and background. The choice can have a critical impact on the quality of the model derived. If the algorithm is very sensitive to parameterization, this again leads to a lack of confidence in the derived model. Investigations to automate QSAR model building have explored the effects of model and algorithm parameterization and found methods such as PLS and random forests are robust to changes in model parameterization.[39]

There are a number of statistical methods widely used in the QSAR analysis, and many that have been explored. They can be divided into two categories, unsupervised and supervised methods. Unsupervised methods are used to explore the distribution of the compounds through property space, and do not use the response variable to choose or weight variables. Supervised methods attempt to find correlations between the responses and descriptors. Here, we briefly describe four characteristic machine-learning tools, which have spawned many derivative methods. Still, other methods exist and are being explored and are not cited here. The reader is referred to SciFinder and we wish you good luck if you choose to work at the "bleeding edge" of the machine-learning space. The following methods are tried and tested.

Hansch used MLR, and this is still a common method today. It is limited to datasets where there are many more compounds than descriptors, as it is particularly sensitive to chance correlations where many descriptors are available. The principle on which MLR was built assumes all variables are relevant in the model. But MLR algorithms allow "forward and backward stepping," where descriptor variables are sequentially added or excluded from the models, facilitating QSAR scientists to pick and choose from a larger array of descriptors, those relevant to the model to find a good model. While this may be a useful data exploration method, it has a significant probability of leading to chance models. The statistics which govern the selection were not designed to allow such choice, and due to the combinatorial nature of selection a few relevant descriptors from a matrix of many more, MLR is particularly susceptible to chance correlations.[40] But MLR does produce simpler to interpret models, that is, if the descriptors are meaningful to a medicinal chemist.

MLR assumes all variables are uncorrelated with each other, but this is rarely the case. Where variables are correlated, then the coefficients of the regression equation become dependent upon each other, and so their size and even sign cannot be used independently of all the other descriptors in the model to deduce that variable's unique contribution.

PLS analysis, introduced by H Wold and his son S Wold, was developed in response to a request by the Swedish government for an objective method of handicapping state-run horse races,[41] it is a linear correlation method, that is less sensitive to chance correlations in datasets where there are more descriptors than compounds. It uses the intercorrelation structure of the descriptor set to form new underlying summary descriptors (components), as weighted linear combinations of the original variables. PLS forms these summary variables to maximize the correlation with the response variable. As the method uses the intercorrelation structure of the descriptor set, it makes it less sensitive to a chance correlation in any one variable. The method principal components analysis (PCA) is similar in that it forms summary variables as weighted linear combinations of the original variables. But in PCA, no response variable is defined to supervise the extraction of components. In PCA, each component is chosen in decreasing order of its ability to summarize the information on the x-descriptor set. Hence one can see that PLS is a development from PCA.

The influence of the original variables on the derivation of these new summary descriptors is described by the loadings or weightings of the variables on the new summary descriptor, and the summary descriptor's numerical values are the scores. Because all the

original variables contribute more or less to forming each summary variable, it is harder to interpret the underlying physical meaning of PLS and other multivariate models.

Neural networks as a group have a structure of a set of layered nodes interconnected to each other, which prompts the analogy to the structure of the human brain. They often consist of an input layer, one node per descriptor, one or more hidden layers, on which the input descriptor nodes are projected, and an output layer. There are nonlinear "transfer functions" that operate between the nodes of the input layer and the hidden layers, and mathematically transform the original data as it is combined onto the "hidden layer" which allows the neutral network to model nonlinear data. They usually run in an iterative fashion where either a random or a distribution (Bayesian approach) of weighting parameters are starting points for linking the input nodes to the hidden and output nodes. These weights are iteratively optimized, to drive a correlation between descriptors and response. The fitting routines together with the nonlinear transfer functions in neural networks are very powerful, and if unchecked, will fit both signal and noise in the training set. So neural networks often maintain a calibration set/tuning set, the prediction of which is used to stop the training phase. Neutral networks can generate a single QSAR equation, or in the case of Bayesian approaches, an ensemble of models.

Regression Trees and Random Forests are a form of classification method. In regression trees, the method attempts to classify the response into "bins" that represent ranges of activity. The method attempts to find critical values of x-variables which result in an improvement in the purity of y-bins with correctly classified compounds. Random Forests is an extension, where instead of one tree, an ensemble of trees are formed, with each tree built on a subset of the original dataset by sampling rows and columns. Each tree in the "forest" is a decision tree. When a prediction is made, all models participate in the prediction and the predicted value is an average from across the forest of trees. The dispersion of predictions from across the ensemble of models can give an indication of the confidence in the prediction. Like PLS, Random Forests appear less sensitive to the size of the descriptor matrix, as spurious models influence becomes averaged out across the ensemble of models. Because the prediction is made from across the forest of trees, it is more difficult to interpret which are the truly important underlying descriptors, although the method provides diagnostics to indicate important underlying variables.

3.15.4.5 Appropriate Measures of Goodness-of-Fit—Model Diagnostics

The coefficient of variation in fit to training set r^2, the fraction of the variation in response described by the model, and residual root mean square error (RMSE)—the variation in the response variable unexplained by the model is often reported. But the fit to the training set is not a good indication of a model's ability to generalize. Spurious models can have very appealing fit statistics, but with no ability to predict. Rather, most analyses focus on the performance of the model in prediction of a chosen test set. Similar quality of fit statistics to r^2 can be defined in this prediction mode, but to indicate that the assessment is based on prediction rather than fit, the r^2 diagnostic is replaced with Q^2 and RMSE with root mean square error in prediction (RMSE/RMSEP). Unlike r^2, which is bounded between 0 and 1, Q^2 can take values less than zero, meaning the model predicts the test set worse than if one had used the mean of the model as the prediction for every compound.

r^2 for the fitted model can be written as Eq. (4)

$$r^2 = 1 - \frac{\Sigma(y_{\text{obs}} - y_{\text{fitted}})^2}{\Sigma(y_{\text{obsd}} - y_{\text{mean}})^2} \tag{4}$$

Q^2, the r^2 in prediction, can be defined in a similar way, Eq. (5)

$$Q^2 = 1 - \frac{\Sigma(y_{\text{obs}} - y_{\text{predicted}})^2}{\Sigma(y_{\text{obsd}} - y_{\text{mean train set}})^2} \tag{5}$$

The root mean square error in prediction (RMSEP) value is particularly useful as it is in the same units as the experiment, and can be directly compared to the experimental error of the response variable. The RMSE of the test set gives the medicinal chemist an indication of the likely error associated with a prediction, Eq. (6).

$$\text{RMSE} = \frac{\Sigma(y_{\text{predicted}} - y_{\text{obs}})^2}{n - 1} \tag{6}$$

The average error in prediction tells you if there is any systematic bias in the predictions, Eq. (7).

$$\text{Mean absolute error/bias} = \frac{\Sigma_{i=1}^{n_{\text{ext}}}(y_{\text{obs}} - y_{\text{predicted}})}{n} \tag{7}$$

An external set of compounds may be predicted with a systematic bias, which would inflate RMSE, and decrease Q^2. A nonzero mean absolute error indicates that the predictions may not be accurate, but may still be useful in ranking compounds. It also may indicate a structural or substructural feature present in the test set but not encoded in the training set or its description.

Assessment of performance based on a test set only using Q^2 or even RMSE can still be problematic. An ambiguity occurs with the Q^2 statistic when the test set data is not evenly distributed over the range of the training set. As the variance of the external test set approaches the RMSE of the fitted model, the Q^2 measure would approach zero—even though it would appear the predictions are in accord with the model. Consonni defined a new Q^2 statistic that expresses the mean predicted error sum of squared deviations

between the observed and predicted values for the test set over the mean training set sum of squared deviations from the mean value, Eq. (8)

$$Q^2 = 1 - \frac{\left[\sum_{i=1}^{n_{ext}} (\hat{y}_i - y_i)^2\right]/n_{ext}}{\left[\sum_{i=1}^{n_{TR}} (y_i - \bar{y}_{TR})^2\right]/n_{TR}} = 1 - \frac{\mathrm{PRESS}/n_{ext}}{\mathrm{TSS}/n_{TR}} \tag{8}$$

where n_{ext} is the number of compounds in external set, $\hat{y}_i$ is the prediction estimate of y, y_i is the observed value, n_{TR} is the number of compound in the training set, $\bar{y}_{TR}$ is the mean of the training set observed values, PRESS is predicted error sum of squares deviations between the observed and measured y values, and TSS is the training set sum of squared deviations from the mean.

Consonni demonstrated this formulation of Q^2 is stable with test sets of different variances.[42]

The use of a test set in the model evaluation process protects you from using a spurious QSAR model, as it is less likely that a model that randomly fits the training set would also randomly predict a test set. The use of a test set in the model-building process excludes valuable chemical information from the model-building process, and so some methods attempt to utilize all the data, and perform an internal validation procedure known as cross-validation. In cross-validation, a number of cases from the training set are left out during the model fitting process and then predicted from the resulting model. Multiple models are built with a fraction of the compounds excluded at each build. Enough models are built so that each compound is predicted from a model from which it was excluded. The sub-models is then used to predict the excluded compounds. A prediction statistic can be defined as in Eq. 5. To differentiate this cross-validated measure of predictivity from a measure of predictivity calculated from an external test set, a lowercase q^2 symbol is often used to delineate a cross-validated statistic. A $q^2 > 0.3$ is often taken as a rule of thumb for a potentially useful model.

Leave-one-out cross-validation is the simplest and least challenging validation method, and has been widely criticized,[43] as being too easy a test of the model. Leaving out compounds in multiple groups is a tougher test for the model. The archetypal PLS program, SIMCA,[44] uses seven subsets as default, so at each rebuild 1/7th of the training set is left out at each model build.

Cross-validation can only give an unbiased estimate of future predictive ability if future compounds come from the same population as those in the cross-validation sample. This is not a safe assumption as the nature of drug design is that compounds evolve with time.

The assessment of the significance of the model can also be explored by performing a y-randomization experiment. The y-randomization procedure compares the performance of models built for a randomly shuffled y-response. When repeated multiple times, the distribution of r^2 values obtained is an assessment of the significance of the original model, without assuming the data follow a particular statistical distribution (nonparametric). Y-randomization has been referred to as probably the most powerful validation procedure,[45] although only if the full model generation procedure is repeated including variable selection, rather than just permuting the y-variables of the final model.[46]

Tropsha has recommended a set of criteria to be evaluated before one can claim a QSAR model is predictive.[47,48] Using the correlation coefficient R^2 between the predicted and observed activities; coefficients of determination (predicted vs. observed activities R_0^2 and observed vs. predicted activities R'^2_0); slopes k and k' of the regression lines through the origin, and considers a QSAR model predictive if the following conditions are satisfied:

$$q^2 > 0.5$$
$$R^2 > 0.6$$
$$\left(R^2 - R_0^2\right)/R^2 < 0.1 \quad \text{or} \quad \left(R^2 - R'^2_0\right)/R^2 < 0.1$$

$$0.85 \le 1.15 \quad \text{or} \quad 0.85 \le k' \le 1.15$$

Following the REACH recommendations, one of the most highly cited reviews on QSAR model validation was published by Gramatica.[49] In this review, Gramatica discussed whether Principle 4 of the OECD recommendations "appropriate measures of goodness-of-fit, robustness and predictivity" should have been split into two principles, reflecting internal validation and external validation. Originally they were separate principles, but were merged into the single Principal 4. Experts held different views, on the one hand splitting internal and external validation highlighted the importance of external validation, while having them merged was more appropriate to allow flexibility in regulatory acceptance. In the review, particular attention is paid to the differences between internal and external validation—strongly recommending that only models that have been validated externally, after their internal validation, can be considered reliable and applicable for external prediction and regulatory purposes. As an example, validation statistics for a 30 genetic algorithm population-models for mutagenic potential of 48 nitrated polycyclic aromatic hydrocarbon (PAH) compounds (31 in training and 17 in prediction set) was shown in fitting cross-validation (q^2_{LOO} and q^2_{boot}) and external validation (Q^2_{ext}).The example clearly shows that some models (in bold) appear stable and predictive by internal validation, but less predictive or indeed not predictive when applied to external compounds that were not presented to the genetic algorithm on model building (**Table 1**).

3.15.4.6 A Defined Domain of Applicability

The chemical space encompassed by the model is termed the domain of applicability. The hope is that molecules being predicted that are "near" the applicability domain of the training set compounds will be predicted with lower error and therefore with more confidence than compounds further away.

Table 1 Internal validation versus external validation shown on a set of 48 nitro-PAH compounds tested for mutagenic potential on TA100 cells

ID	*Model descriptors*		*Model descriptors*	R^2	Q^2_{LOO}	Q^2_{boot}	Q^2_{ext}
1	PW2	SIC1	PW2 SIC1	85.7	82.44	82.36	72.27
2	PW2	CIC1	PW2 CIC1	84.88	80.78	80.71	75.34
3	X1A	MATS1e	X1A MATS1e	82.42	79.32	79	85.75
4	Mv	MATS2e	Mv MATS2e	83.37	79.04	79.25	84.27
5	Mv	MATS1e	Mv MATS1e	81.76	78.47	78.42	74.86
6	Mv	GATS2m	Mv GATS2m	81.57	77.87	78.1	69.13
7	GATS1e	VED2	GATS1e VED2	81.07	77.64	77.68	88.06
8	Xt	nPyr	Xt nPyr	80.25	77.48	77.41	81.71
9	Mv	PW2	Mv PW2	80.95	77.39	77.97	71.85
10	**PW2**	**IC1**	**PW2 IC1**	**80.89**	**77.04**	**77.32**	**60.07**
11	JGI3	VED2	JGI3 VED2	80.27	76.76	76.91	66.67
12	Mp	LUMO	Mp LUMO	80.78	76.54	76.55	70.13
13	Mv	LUMO	Mv LUMO	80.26	76.15	76.11	63.74
14	**BELe8**	**HATS4u**	**BELe8 HATS4u**	**80.53**	**76.1**	**76.17**	**47.59**
15	IC1	VED2	IC1 VED2	80.17	76.09	76.55	80.94
16	Xt	MATS1e	Xt MATS1e	80.23	76.08	75.96	86.79
17	PW2	HIC	PW2 HIC	80.14	75.99	76.16	69.62
18	SIC1	VED2	SIC1 VED2	79.92	75.78	76.11	81.65
19	VED2	Hy	VED2 Hy	79.55	75.52	75.63	86.98
20	**VED2**	**R6u +**	**VED2 R6u +**	**79.27**	**75.52**	**75.5**	**27.18**
21	HATS3u	R3v	HATS3u R3v	**79.55**	**75.52**	**75.23**	**0**
22	Mv	MATS2m	Mv MATS2m	79.25	75.37	75.64	69.21
23	Xt	BELm2	Xt BELm2	79.89	75.35	75.4	69.54
24	GGI3	VED2	GGI3 VED2	79.1	75.34	75.58	63.5
25	**BELe8**	**R4u +**	**BELe8 R4u +**	**80.06**	**75.32**	**75.3**	**50.23**
26	**SIC2**	**BEHm8**	**SIC2 BEHm8**	**79.14**	**75.13**	**75.48**	**61.48**
27	VED2	RTe	VED2 RTe	78.65	75.13	75.32	69.76
28	CIC2	VED2	CIC2 VED2	79.49	75.06	75.08	77.75
29	**SIC2**	**BELv5**	**SIC2 BELv5**	**79.4**	**75.02**	**75.36**	**58.31**
30	X1A	LUMO	X1A LUMO	79.13	74.96	74.91	78.98

For a description of the QSAR model building, descriptor sets, and data, see the original reference 50.

Confidence in the model can be gained by examining the error in prediction of compounds in the test set most similar to your compounds.

Definition of domain of applicability of the QSAR model, and "distance" of a compound being predicted to the defined domain, is an intense area of research in QSAR. The OECD QSAR Guideline 3 states one should have a defined domain of applicability. The principles are easy to grasp, although the mathematics associated with some of the methods can be quite complex.

A suitable distance to model measure should show a dependence of the distance upon the error in prediction of the test set compounds. By knowing the distance of the compound being predicted to the model space, the confidence in the prediction can be inferred, based on the error in prediction of the test set compounds similarly distance from the model space. Unfortunately, many of the distance measures only produce a weak relationship to error in prediction, which limits the confidence that can be extracted from the statistic.

The relationship between of distance to model on prediction precision was clearly shown by Bruneau in an assessment of models built using a Bayesian neural network on an internal AstraZeneca (AZ) solubility dataset and on a public domain solubility data.[51] Bruneau found that when using the internal AZ model to predict internal AZ compounds, or the model built on the public domain data to predict the public domain test set, the models gave comparable prediction statistics, with similar root mean square errors in prediction. But when used to cross-predict each other's test set, the predictions were worse. Interestingly, while the solubility model built on external data did a worse job at predicting the AZ compound test set than its own test set, the predictions were not as bad as the AZ model predicting the public domain test set. When Bruneau examined how the prediction error depended on distance to model, the results became understandable. The AZ compounds were more distant from the public domain compounds than their own training set, which corresponded to an increase in the prediction error. But their error in prediction was similar to public domain compounds at a similar distance to the public domain training set compounds.

Different numerical approaches are taken to defining the domain of applicability, and the distance of compounds being predicted from it (distance to model). Euclidian distance (geometric distance) assumes that the model space is spherically distributed. Alternatively, one can use a Mahalanobis distance (probability distance) which takes note of the intercorrelation structure of the dataset and hence the shape of the model space to be nonspherical and more "ellipsoid." Distances can also be measured in structure space using molecular fingerprints, among many others.[52]

So far it appears there is no single measure that performs better than another across many datasets, although one should be used. A measure that correlates with error in prediction of the test set would be a useful and validated method for any particular dataset. Suffice to mention here that medicinal chemists should request information on the distance to the model space of the compound being predicted, and this distance can be calibrated based on the relationship of the error in prediction to distance to the model of the test set compounds.

While statistics can guide you, there are other ways a medicinal chemist can gain confidence in a QSAR model. Firstly work closely with your QSAR scientist when assessing the model's utility to your compounds. Medicinal chemists who do commit to synthesis based on the predictions from a model will get real-time feedback on the quality of the model, once their compounds are tested. Maybe this is a more useful confidence build for the practicing medicinal chemist than any QSAR diagnostic.

Interpretation of the QSAR model can also build confidence in the model itself. A predictive QSAR model must identify some of the underlying controlling physical features of the response variable being modeled, although in the case of multivariate models, it can be difficult to untangle the primary controlling properties when many variables contribute to the overall model. The case studies described so far led to mechanistic interpretations which guided further insights, from Overton and Meyer's theory of narcosis, Hammett's hypothesis for electronic induction and resonance, and Hansch's "random walk" of drugs to their receptors. The QSAR expert can work with the medicinal chemist in interpreting the model, to explore if it makes some kind of logical sense. If an interpretation can be made, then the model can be used to rationally design the next compound. Otherwise the QSAR model can only be used as a black box filter. Particularly with complex multivariate models, trying to interpret the controlling properties so new compounds can be rationally designed, the so-called inverse QSAR, can be challenging. So there has been a renewed interest in Free–Wilson type analyses. These methods do not use derived descriptors, but rather correlate the change in response to the structural change itself and this inspired the recently introduced method of matched molecular pairs

3.15.5 Examples of Influential QSAR Models

Many marketed drugs have depended, at least in part, on classical QSAR approaches in their discovery, including drugs as diverse as norfloxacin, lomerazine, flobufen,[53] and cimetidine, among many others.

QSAR has found a particular niche in predicting physicochemical and ADMET properties. This is because QSAR models attempt to find patterns across a series of molecules in a dataset, and ADMET endpoints are more bulk property-controlled than structurally dependent. Drug–receptor interactions inherent to primary potency endpoints are often fraught with "activity cliffs"—where activity falls away very rapidly with small structural variations. These are harder for QSAR models to identify without the knowledge of the nature of the drug–receptor interactions, as can be gained from X-ray crystallography and docking studies. This is the subject of a highly cited editorial by Maggiora. "On Outliers and Activity Cliffs—Why QSAR Often Disappoints."[54] The structure–activity relationships for activity landscapes as Maggiora describes them, tend to look more like "rugged landscapes of Utah's Bryce Canyon" than the "gently rolling hills of the Kansas Prairie." 3-D QSAR methods have found a particular niche here, but can still suffer from the steep SAR dependence of potency endpoints in prediction. The literature is replete with examples of QSAR models being applied in drug design. Nevertheless, QSAR models are often sought for primary potency endpoints, as they are easy to look for, and can at least help the medicinal chemist explore the SAR within a dataset, even if they are not refined enough to be used for accurate prediction.

The false negative prediction rate of potentially genotoxic impurities by in silico models was recently surveyed across eight companies. The methods for prediction were given and the approaches across the companies were very similar. The true negative prediction rate was found to be 94%, and when expert evaluation of the results was included in the decision this increased to 99%.[52] The results of this analysis are currently being written into an ICH guideline M7 on genotoxic impurities.

While the CLOG P algorithm from Pomona College was manually constructed as a fragmental-based system from a combination of first principles and empirical observations, a number of the most widely used clog P and clog D algorithms are QSAR based including Alog *P*,[55] Xlog *P*,[56] and Mlog *P*.[57] Many pharmaceutical companies have derived their own log *P* and log *D* calculators using QSAR approaches, which outperform the standard CLOG P method.[58] An implementation of Alog *P* has even been made available on a tablet computer within the RSC Medicinal Chemistry Toolkit IPAD app.[59]

The scoring functions used inside many structure-based design docking programs are QSAR derived. The archetypal scoring function in LUDI was derived from regression analysis of a set of predetermined physics-based descriptors calculated from the 82 protein-ligand X-ray crystal structures together with the reported ligand affinity.[60] The initial dataset defining scoring function SCORE1 of 45 complexes, Eq. (9) was extended to 82 complexes, and was named SCORE2, Eq. (10). The SCORE 2 function has a lower residual standard deviation of 8.8 kJ/mol (relative to 9.5 kJ/mol for SCORE1), suggesting SCORE2 fits the experimental data for $\Delta G_{binding}$ better than SCORE1. The prediction of an independent test set of 12 complexes showed a root mean square error in predicting RMSE = 8.8 kJ/mol, in good agreement with the unexplained error in fitting the training set data. It is interesting that the magnitude of some of the coefficient change significantly, which is probably due to the changing intercorrelation structure of the descriptors within the larger dataset. As mentioned earlier in the multiple linear regression section, the regression equation can be used to predict affinity, but the magnitude of the coefficients may not be quantitatively independently interpreted, as the intercorrelation of the descriptor set makes them dependent upon each other

$$\text{SCORE1}\ \Delta G\ \text{binding} = 5.4\,G_0 - 4.7\,G_{HB} - 8.3\,\text{Gionic} - 0.17\,\text{Gapolar} + 1.4\,\text{Grot kJ/mol}$$
$$N = 45, R = 0.835, s = 9.5 \quad (9)$$

$$\text{SCORE2}\ \Delta G\ \text{binding} = -1.4\,G_0 - 3.1\,G_{HB} - 6.6\,\text{Gionic} - 0.15\,\text{Gapolar} + 1.0\,\text{Grot kJ/mol}$$
$$N = 85, R = 0.841, s = 8.8 \quad (10)$$

LUDI scoring function has inspired many other docking scoring functions.

Large datasets are now available, not just for proprietary model building, but also for open-source initiatives, and research groups are eager to utilize them to learn from the past to guide the design of the future compounds. For example, GlaxoSmithKline have described simple interpretable QSAR models built on between 10,000 and 50,000 data-points across many assays.[61] Global initiatives from the likes of the NIH and EMBL have made available huge datasources to public model building such as PubChem and CHEMBL from which many QSAR models have grown.

3.15.6 The Future of QSAR

Subjectivity has been a big problem in the field of QSAR model building, from the subjective choice of training set and test set to the descriptor set choice of algorithm and its parameterization to the method of validation. QSAR models are empirical by nature and as such, as the prediction set gets further from the training set, the quality of predictions can become worse. For these reasons, a number of groups have explored the concept of auto-building and auto-updating QSAR models.[62–64] Where the choice of machine-learning method of descriptors is unclear, the use of consensus prediction has been adopted in a number of these systems.

Discovery Bus stakes the competition one step further, in that the choice of descriptor set is combined with a set of statistical methods to find the combination that predicts best at that point in time. The name Discovery Bus is derived from the "computer bus" which allows peripherals to be plugged or unplugged and be easily integrated into the signal flow. In the case of Discovery Bus, new machine-learning agents, datasets, or descriptors can be plugged in and be available for model building and model comparison within "a competitive workflow"—where Discovery Bus tries to find areas of data/descriptors/modeling methods where good models exist, and compare their performance to previous models built in older versions of the datasets. In this manner, good models can be found and kept up-to-date. The comparisons across models do increase the risk of chance correlations, due to the multiple testing, but the continuous feedback of measurements from predicted compounds builds confidence in the success of these approaches.

Rodgers and colleagues have explored the decay of a number of QSAR models in time-ordered datasets, where a model was build to predict increasingly later synthesized compounds.[65,66] They also explored the temporal dependence of a number of common QSAR machine-learning algorithms. They found that models built different machine-learning algorithms aged differently with time. PLS models appeared to be conservative and inferior to a Bayesian neural network model in predicting test sets near in time to the training set model, but maintained their predictivity better over the long term. In their study they also found that regression trees outperformed both methods. The "best" model may change depending on when you make your measure and how you use the model. The learnings were embodied into the AstraZeneca AutoQSAR system for building and maintaining a portfolio of QSAR models for projects. AutoQSAR includes comparison of chemical series versus project series versus global modeling—to find the best model for the next new compound.

Discovery Bus and AutoQSAR apply good modeling and validation practice, to maximize the robustness of models built and selected for use. Developments such as Discovery Bus and AutoQSAR help to minimize a number of major problems associated with QSAR modeling. They apply QSAR modeling in a consistent fashion using objective decision-making criteria. They allow for the updating of QSAR models with the most recent data, which, in active drug discovery programs, ensures the distance between the compound predicted and the domain of applicability of the QSAR model is minimised. Finally they apply the best model, whether it be a local chemical series model or the global cross-project model, based using temporal predictions to make the decision. A weakness in the competitive workflow approach is that, as multiple comparisons are being made, this increases the chance that a spurious model could be selected. AstraZeneca's experience shows that in practice, more accurate and precise predictions are made routinely across projects, so the benefit clearly outweighs the risk, and improved models are available to project teams.[67] In a 2-year temporal validation across 10 active projects, AstraZeneca demonstrated that the hierarchical and updating modeling method of AutoQSAR outperformed updating global models, which outperform static global models (**Fig. 2**, **Table 2**). Discovery Bus has inspired the machine-learning engine, Optiplex, one of the key technologies driving the drug discovery company, Molplex.[68]

The interest in auto-updating QSAR models is growing. The benefit of building local models over global models is a continuing debate. Sheridan compared local versus global mode building and concluded that local models may not have a benefit over global models, depending upon a descriptor set being able to discriminate between local series, and the machine-learning algorithm being able to utilize the descriptor distinction.[69] If such a descriptor exists, then the global model may predict just as well as any project or project series model. Carlsson and colleagues came to a similar conclusion using simulated data, that with suitable descriptors a local modeling strategy may be redundant.[70] They used simulated data to rigorously explore the benefit or deficit of local modeling over global modeling, as the underlying relationship could be better controlled than in real world data, where the underlying relationship is unknown. They defined local by clustering using Tanimoto distance-based DAYLIGHT fingerprints. They also validated their findings on an AMES dataset of 4253 examples, hERG dataset (6020), and a solubility dataset (1186 cases). They did

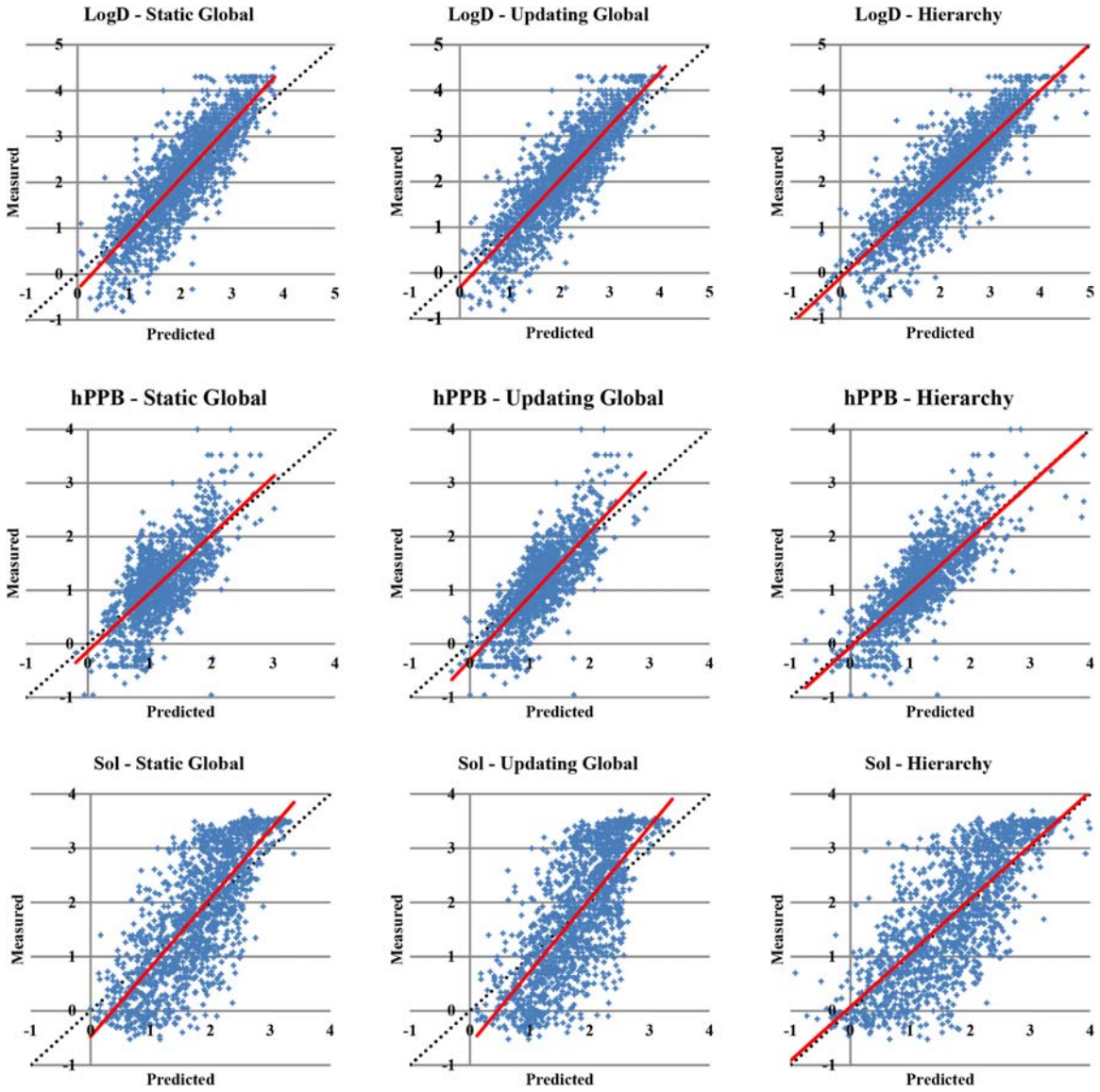

Fig. 2 Forward prediction time simulation of 10 active AZ Projects using the AutoQSAR method over 2 years—each month the AutoQSAR hierarchy selects the best model from chemical series, project or global updating model over the static global model, and uses the best model to predict next-month compounds. This hierarchy model is compared to using an updated global model (using data from all 10 projects each month), or a static global model. The accumulated next-month future predictions made on models from last month's data are shown here over the 2-year period. The figure shows predicted versus observed values for all "future" predictions from the three prediction strategies over the three endpoints. The *broken black line* shows the line of unity and the *solid red line* shows the fitted correlation between the observed and predicted values.

Table 2 Statistics on the full "future" prediction sets

Endpoint	*N*	*Mean*	*SD*	*Strategy*	*RMSE*	R^2	R_0^2
Log D7.4	1763	2.18	1.05	Static	0.58	0.73	0.69
				Updating	0.54	0.76	0.74
				Hierarchy	0.51	0.76	0.76
Human ppb	1291	1.13	0.73	Static	0.53	0.49	0.48
				Updating	0.47	0.62	0.60
Plasma protein binding				Hierarchy	0.43	0.65	0.65
Solubility	1401	1.77	1.13	Static	0.79	0.54	0.50
				Updating	0.73	0.61	0.58
pH 7.4 buffer				Hierarchy	0.72	0.60	0.60

N, the number of test compounds; *Mean*, the mean measured value of the test compounds; *SD*, the standard deviation of the measured values for the test compounds.

find some examples where local modeling gave an improvement over the global models, and these were where the local neighborhood could be well defined, but often this was not the case using the Tanimoto clustering, and then the global model was preferred. In the 10-project AZ case study described earlier, local was defined by project code (the manual definition of project membership recorded by the chemist at the time of first registration), a more robust definition of "local" then could be perceived by cheminformatic clustering. Overall the message is clear, updating QSAR models are better than static QSAR models, objective automated workflows can build predictive models and remove subjectivity from the QSAR model-building process and apply good practice. It seems updating global models can perform well, and with appropriate descriptors, may negate the need for extensive local modeling strategy, but if local can be well defined, then a local modeling strategy may be worth the extra computational effort. With automated workflows and easy availability of computational power, there is no reason why all levels of the hierarchy (global, project, and chemical series) cannot be continually evaluated.

When it comes to choice of machine-learning tool, is there a clear best method independent of dataset and parameterization? In a temporal test, a static QSAR model built with three machine-learning tools, predicting ever-growing temporal test set of compounds, Rodgers and colleagues found that random forests outperformed BNN and PLS methods.[66] Rodgers also found that random forest predictivity was quite stable to parameterization, and therefore a suitable tool for use in an AutoQSAR procedure. Norinder also found random forest to be an accurate method. But the dataset may dictate the most appropriate machine-learning tool, and many automated workflows, such as Discovery Bus and AstraZeneca's AutoQSAR, include choice of the machine-learning method within a competitive workflow.

GSK have described their QSAR Workbench, which provides a consistent set of routines for data preparation and chemical normalization that are also applied for predictions. The Workbench provides a large degree of automation with the ability to publish preconfigured model-building workflows for a variety of problem domains, while providing experienced users full access to the underlying parameterization if required. Methods are provided to allow for publication of selected models as web services, thus providing integration with the chemist's desktop. Green and coworkers demonstrated its utility on two large public datasets.[71] The QSAR workbench is now deployed within the Biovia's Discovery Studio.[72]

Recently Schrodinger has built an implementation of an auto-updating QSAR workflow, also called AutoQSAR, within the Schrodinger suite of software.[73]

3.15.7 Using QSAR Models

Many medicinal chemists will want to use QSAR models, rather than build their own. Many QSAR models for ADMET endpoints are available in the public domain, either as freeware or in commercial packages. These are based on literature datasets, and in the absence of any data from their own chemistry, or expertise to build their own QSAR models, these are the only models many medicinal chemists may have access to. How confident one can be in the predictions from such models requires careful thought. If the compounds you are predicting are unlike the compounds within the training set of the model, one may be concerned in the quality of the prediction. One should remember the OECD guidelines when assessing the utility of these models for your intended use. Before you use the model to prioritize your synthetic targets and commit valuable resources to synthesizing your chosen targets, consider the hints and tips given here as guidance.

For a medicinal chemist using a QSAR model, the following steps are recommended:

- Look at the distribution of compounds in the training set and test set over the range of responses. Are the data evenly distributed or is there a region of activity or property space that contains better coverage—indicating where better predictions are likely to be made?
- Examine the Q^2 and RMSE of the test set used to validate the model. Does the model have the resolution you require to solve your project problem. A high r^2 or q^2/Q^2 looks impressive, but if the range of the training set or test set is very large, the unexplained residual error in model can still be large. So examine the RMSE of the model. For example, if the RMSE of predictions of the test set is 0.7 log units and you only wish to move your property by 0.3 log units, it is likely you are within the noise of the model.
- Examine the error in prediction of compounds in the test set that are "closest" to the compound you are predicting (based on distance to model measures). You may find this gives you more or less confidence in the model. You may find that within the test set, compounds that are more similar to the training set are predicted better than the average across the test set. If these compounds are similar to your target compound, this will give you more confidence in the models ability to predict your compound.
- The QSAR model can be used as a filter for a virtual library, or interpreted to influence the compound design. Examine the controlling features of the QSAR model, this may give you an indication how you can rationally change your molecules to improve the property you are trying to optimize.
- Examine the QSAR model visually. Plot the important controlling variables against the response variable, this may allow you to see patterns in the dataset that can guide further design.
- Are the important variables similar as new compounds are added to the model, or if compounds are removed from the model, or if submodels are built during cross-validation? Instability in selected variables can point to a poor, spurious or unstable QSAR model.

- Are new compounds well predicted by your model? This is the ultimate test of any model.
- As new compounds are synthesized and measured in your assay, ask your computational chemist to update the QSAR model to minimize the distance the compounds are you will design will be from the domain of applicability of the QSAR model. Keep monitoring your predictions as compounds synthesized are subsequently measured in the assay your QSAR model is supposed to predict. This may give you increased confidence in the model, or highlight new features in your molecules not identified in the model (e.g., if it is surprisingly badly predicted where previous compounds had been well predicted). QSAR models may be automatically updated, ensuring your model always contains your latest compounds (AutoQSAR).

3.15.8 Conclusions

QSAR is a mature technique and a core part of the computational chemist's predictive armory. It is an empirical technique, identifying patterns from yesterday's compounds to predict tomorrow's. At worst, a QSAR model can be used like a black box, but if a model has true predictive power, it is highly likely it is identifying some of the underlying physics controlling the response variable being measured, whether that is activity, stability, or a physical property. The choices involved in the dataset, its partition and preparation, the choice of descriptors, and the machine-learning method, and validation can be subjective, leading to the risk of over fitted or even spurious models. The past 10 years have seen even this mature discipline taking its next steps, with the increasing need to mine ever-growing data sources to guide the design of tomorrow's compounds. Researchers have been increasingly focused on removing the subjectivity, and even automating QSAR model building to provide up-to-date and updating QSAR models. While the intellectual focus of the computational discipline has been on physics-based models over the past 10 years, these two powerful disciplines of physics and empirical modeling could become even closer together as we seek to choose which compound to make next.

See also: 2.03. Multiobjective Optimization of Biological and Physical Properties in Drug Discovery.

References

1. Crum-Brown, A.; Fraser, T. R. *J. Anat. Physiol.* **1868,** *2* (2), 224–242.
2. Richardson, B. J. *Medical Times and Gazette* **1869,** *2,* 703.
3. Richet, M. C. Note sur le Rapport Entre la Toxicite et les Proprire te s Physiques des Corps. *Compt. Rend. Soc. Biol. (Paris)* **1893,** *45,* 775–776.
4. Meyer, H. *Naunyn Schmiedebergs Arch. Exp. Path. Pharm.* **1899,** *42,* 109–118.
5. Overton, E. *Studien uber die Narkose, zugleich ein Beitragzur allgemeinen Pharmakologie* (*(Studies on Narcosis, Charles Ernest Overton)*). G. Fischer, Jena 1901; English translation by R. L. Lipnick,; Chapman and Hall: London, 1991.
6. Hammett, L. P. *J. Am. Chem. Soc.* **1937,** *59,* 96.
7. Bronsted, J. N.; Pedersen, K. *Z. Phys. Chem.* **1924,** *108,* 185.
8. Taft, R. W. *J. Am. Chem. Soc.* **1952,** *74,* 2729; Taft, R. W. *J. Am. Chem. Soc.* **1952,** *74,* 3120; Taft, R. W. *J. Am. Chem. Soc.* **1953,** *75,* 4538.
9. Hansch, C.; Maloney, P. P.; Fujita, T.; Muir, R. M. *Nature (London)* **1962,** *194,* 178–180.
10. For a more detailed description of the emergence of this very first QASR equation see Fujiita, T.. *J. Comput. Aided Mol. Des.* **2011,** *25,* 509–517.
11. Fujita, T.; Iwasa, J.; Hansch, C. A. New Substituent Constant π Derived From Partition Coefficients. *J. Amer. Chem. Soc.* **1964,** *86,* 5175–5180.
12. Free, S. M.; Wilson, J. W. A Mathematical Contribution to Structure–Activity Studies. *J. Amer. Chem. Soc.* **1964,** *7,* 395.
13. Stouch, T. R.; Kenyon, J. R.; Johnson, S. R.; Chen, X.-Q.; Doweyko, A.; Li, Y. In Silico ADME/Tox: Why Models Fail. *J. Comput. Aided Mol. Des.* **2003,** *17* (2–4), 83–92.
14. Davis, A. M. Assessing Quantitative Model Quality and Performance. In *RSC Drug Discovery Series,* 13, Davis, A. M., Livingstone, D. J., Eds.; RSC Publishing: London, 2012; pp 242–266 (Drug Design Strategies).
15. Gavaghan, C. L.; Arnby, C. H.; Blomberg, N.; Strandlund, G.; Boyer, S. Development, Interpretation and Temporal Evaluation of a Global QSAR of hERG Electrophysiology Screening Data. *J. Comput. Aided Mol. Des.* **2007,** *21* (4), 189–206.
16. Anon. *Regulatory Use of (Q)SARs Under REACH.* http://echa.europa.eu/doc/press/webinars/regulatory_use_of_qsars_under_reach_doris_hirmann_echa.pdf, 2009.
17. http://www.oecd.org/env/hazard/qsar.
18. See for instance the ACS guidelines on publication in Journal Medicinal Chemistry http://pubs.acs.org/paragonplus/submission/jmcmar/jmcmar_authguide.pdf.
19. Spjuth, O.; Carlsson, L.; Alvarsson, J.; Georgiev, V.; Willighagen, E.; Eklund, M. *Curr. Top. Med. Chem. (Sharjah, United Arab Emirates)* **2012,** *12* (18), 1980–1986.
20. http://www.knime.org.
21. Berthold, M. R.; Cebron, N.; Dill, F.; Gabriel, T. R.; Kötter, T.; Meinl, T.; Ohl, P.; Sieb, C.; Thiel, K.; Wiswedel, B. KNIME: The Konstanz Information Miner. In *Studies in Classification, Data Analysis, and Knowledge Organization;* GfKL, Springer: New York, 2007.
22. http://www.ochem.edu.
23. http://www.QSARtoolbox.org.
24. R Development Core Team. *R: A Language and Environment for Statistical Computing;* R Foundation for Statistical Computing: Vienna, ISBN 3-900051-07-0; 2008. http://www.R-project.org.
25. http://crdd.osdd.net/descriptors.php.
26. http://sourceforge.net/apps/mediawiki/cdk/index.php?title=Main_Page.
27. http://openbabel.org/wiki/Main_Page.
28. http://www.rdkit.org/.
29. Cramer, R. D., III; Patterson, D. E.; Bunce, J. D. *J. Am. Chem. Soc.* **1988,** *110* (18), 5959–5967.
30. Goodford, P. J. *J. Med. Chem.* **1985,** *28,* 849.
31. Nilsson, J.; Wikstrom, H.; Smilde, A.; Glase, S.; Pugsley, T.; Cruciani, G.; Pastor, M.; Clementi, S. *J. Med. Chem.* **1997,** *40* (6), 833–840.

32. Head, R.,. D.; Smythe, M. L.; Oprea, T. I.; Waller, C. L.; Green, S. M.; Marshall, G. R. *J. Am. Chem. Soc.* **1996,** *118* (16), 3959–3969.
33. Böhm, H.-J. Prediction of Binding Constants of Protein Ligands: A Fast Method for the Prioritisation of Hits Obtained From De Novo Design or 3D Database Search Programs. *J. Comput. Aided Mol. Des.* **1998,** *12,* 309.
34. Tetko, I. V.; Gasteiger, J.; Todeschini, R.; Mauri, A.; Livingstone, D.; Ertl, P.; Palyulin, V. A.; Radchenko, E. V.; Zefirov, N. S.; Makarenko, A. S.; Tanchuk, V. Y.; Prokopenko, V. V. Virtual Computational Chemistry Laboratory—Design and Description. *J. Comput. Aided Mol. Des.* **2005,** *19,* 453–463.
35. Advanced Chemistry Development, Toronto, ON, Canada, http://www.acdlabs.com, 2013.
36. http://www.openmolecules.org/.
37. Bonnert, R. V.; Brown, R. C.; Chapman, D.; Cheshire, D. R.; Dixon, J.; Ince, F.; Kinchin, E. C.; Lyons, A. J.; Davis, A. M.; Hallam, C.; Harper, S. T.; Unitt, J. F.; Dougall, I. G.; Jackson, D. M.; Mckechnie, K.; Young, A.; Simpson, W. T. Dual D_2-Receptor and β_2-Adrenoceptor Agonists for the Treatment of Airway Diseases. 1. Discovery and Biological Evaluation of Some 7-(2-Aminoethyl)-4-Hydroxybenzothiazol-2(3H)-one Analogs. *J. Med. Chem.* **1998,** *41,* 4915–4917.
38. Davis, A. M. Quantitative Structure Activity Relationships. In *Handbook of Medicinal Chemistry;* Davis, A. M., Ward, S., Eds.; RSC Publishing: London, 2014.
39. Rodgers, S. L.; Davis, A. M.; Tomkinson, N. P.; Van De Waterbeemd, H. *Mol. Inf.* **2011,** *30,* 256.
40. Livingston, D.; Salt, D. J.; Critchton, R.; Ajmani, S. *J. Chem. Inf. Model.* **2007,** *47,* 143.
41. Cramer, R. D., III Partial Least Squares (PLS): Its Strengths and Limitations. *Perspect. Drug Discov. Des.* **1993,** *1* (2), 269–278.
42. Consonni, V.; Ballabio, D.; Todeschini, R. *J. Chemom.* **2010,** *24* (3-4), 194–201.
43. Golbraikh, A.; Tropsha, A. Beware of q2!. *J. Mol. Graph. Model.* **2002,** *20* (4), 269–276.
44. SIMCA, Umetrics AB Box 7960 SE-907 19 Umeå Sweden.
45. Kubinyi, H. QSAR in Drug Design. In *Handbook of Chemoinformatics,* vol. 4, Gasteiger, J., Ed.; Wiley-VCH: Weinheim, 2003; pp 1532–1554.
46. Ruecker, C.; Ruecker, G.; Meringer, M. y—Randomization and Its Variants in QSPR/QSAR. *J. Chem. Inf. Model.* **2007,** *47* (6), 2345–2357.
47. Golbraikh, A.; Shen, M.; Xiao, Z.; Xiao, Y. D.; Lee, K. H.; Tropsha, A. *J. Comput. Aided Mol. Des.* **2003,** *17,* 241–253.
48. Golbraikh, A.; Tropsha, A. *J. Comput. Aided Mol. Des.* **2002,** *16,* 357–369.
49. Gramatica, P. Principles of QSAR Models Validation: Internal and External. *QSAR Comb. Sci.* **2007,** *26* (5), 694–701.
50. Gramatica, P.; Pilutti, P.; Papa, E. Approaches for externally validated QSAR modelling of Nitrated Polycyclic Aromatic Hydrocarbon mutagenicity. *SAR QSAR Environ. Res.* **2007,** *18,* 169–178.
51. Bruneau, P. *J. Chem. Inf. Comput. Sci.* **2001,** *41* (6), 1605–1616.
52. Weaver, S.; Gleeson, M. P. *J. Mol. Graph. Model.* **2008,** *26,* 1312.
53. Fujita, T. *Quant. Struct.-Act. Relat.* **1997,** *16,* 107.
54. Maggiora, G. M. On Outliers and Activity Cliffs—Why QSAR Often Disappoints. *J. Chem. Inf. Model.* **2006,** *46* (4), 1535.
55. Ghose, A. K.; Crippen, G. M. Atomic Physicochemical Parameters for Three-Dimensional Structure-Directed Quantitative Structure–Activity Relationships I. Partition Coefficients as a Measure of Hydrophobicity. *J. Comput. Chem.* **1986,** *7* (4), 565–577.
56. Ghose, A. K.; Viswanadhan, V. N.; Wendoloski, J. J. Prediction of Hydrophobic (Lipophilic) Properties of Small Organic Molecules Using Fragmental Methods: An Analysis of AlogP and ClogP Methods. *J. Phys. Chem. A* **1998,** *102* (21), 3762–3772.
57. Moriguchi, I.; Hirono, S.; Liu, Q.; Nakagome, I.; Matsushita, Y. Simple Method of Calculating Octanol/Water Partition Coefficient. *Chem. Pharm. Bull.* **1992,** *40* (1), 127–130.
58. Bruneau, P.; McElroy, N. R. *J. Chem. Inf. Model.* **2006,** *46* (3), 1379–1387.
59. https://itunes.apple.com/gb/app/medicinal-chemistry-toolkit/id910073742?mt=8.
60. Bohm, H. J. *J. Comput. Aided Mol. Des.* **1998,** *12,* 309.
61. Gleeson, M. P. Generation of a Set of Simple, Interpretable ADMET Rules of Thumb. *J. Med. Chem.* **2008,** *51* (4), 817–834.
62. Cartmell, J.; Krstajic, D.; Leahy, D. E. Competitive Workflow: Novel Software Architecture for Automating Drug Design. *Curr. Opin. Drug Discov. Dev.* **2007,** *10* (3), 347–352.
63. Cartmell, J.; Enoch, S.; Krstajic, D.; Leahy, D. E. Automated QSPR Through Competitive Workflow. *J. Comput. Aided Mol. Des.* **2005,** *19* (11), 821–833.
64. Wood, D. J.; Buttar, D.; Cumming, J. G.; Davis, A. M.; Norinder, U.; Rodgers, S. L. *Mol. Inf.* **2011,** *30* (11–12), 960–972.
65. Rodgers, S. L.; Davis, A. M.; Van De Waterbeemd, H. Time–Series QSAR Analysis of Human Plasma Protein Binding Data. *QSAR Comb. Sci.* **2007,** *26* (4), 511–521.
66. Rodgers, S. L.; Davis, A. M.; Tomkinson, N. P.; Van De Waterbeemd, H. Predictivity of Simulated ADME AutoQSAR Models Over Time. *Mol. Inf.* **2011,** *30* (2–3), 256–266.
67. Davis, A. M.; Wood, D. J. Quantitative Structure–Activity Relationship Models That Stand the Test of Time. *Mol. Pharm.* **2013,** *10* (4), 1183–1190.
68. http://www.molplex.com/#about.
69. Sheridan, R. P. Global Quantitative Structure–Activity Relationship Models vs Selected Local Models as Predictors of Off–Target Activities for Project Compounds. *J. Chem. Inf. Model.* **2014,** *54* (4), 1083–1092.
70. Helgee, E. A.; Carlsson, L.; Boyer, S.; Norinder, U. Evaluation of Quantitative Structure–Activity Relationship Modeling Strategies: Local and Global Models. *J. Chem. Inf. Model.* **2010,** *50* (4), 677–689.
71. Cox, R.; Green, D. V. S.; Luscombe, C. N.; Malcolm, N.; Pickett, S. D. QSAR Workbench: Automating QSAR Modeling to Drive Compound Design. *J. Comput. Aided Mol. Des.* **2013,** *27* (4), 321–336.
72. http://accelrys.com/products/collaborative-science/biovia-qsar-workbench/.
73. Dixon Steven, L.; Von Bargen Christopher, D.; Woody, S.; Jianxin, D.; Ethan, S.; Repasky Matthew, P. AutoQSAR: An Automated Machine Learning Tool for Best–Practice QSAR Modeling. *Future Med. Chem.* **2016,** *8* (15), 1825–1839.

3.16 Empirical and Physics-Based Calculations of Physical–Chemical Properties

EL Ratkova, Institute of Structural Biology, Neuherberg, Germany
YA Abramov, Pfizer Worldwide Research and Development, Groton, CT, United States
II Baskin, M.V. Lomonosov Moscow State University, Moscow, Russia
DJ Livingstone, ChemQuest, Isle of Wight, United Kingdom
MV Fedorov, Skolkovo Institute of Science and Technology, Moscow, Russia; and University of Strathclyde, Glasgow, United Kingdom
M Withnall, Institute of Structural Biology, Neuherberg, Germany
IV Tetko, Institute of Structural Biology, Neuherberg, Germany; and BIGCHEM GmbH, Neuherberg, Germany

© 2017 Elsevier Ltd. All rights reserved.

3.16.1 Introduction 394
3.16.1.1 Why We Need to Predict Physical–Chemical Properties? 394
3.16.1.2 Physical–Chemical Properties in Drug Design 394
3.16.1.3 A Brief Historical Overview 394
3.16.1.4 Main Questions in the Field 395
3.16.2 Background Information on Physical–Chemical Properties 396
3.16.2.1 Polymorphism 396
3.16.2.2 Melting (Fusion) of Crystals 397
3.16.2.3 From Condensed-Phase to Gaseous Phase 397
3.16.2.4 Dissolution and Solubility of Pharmaceuticals 397
3.16.2.4.1 Dissolution 397
3.16.2.4.2 Aqueous solubility 398
3.16.2.5 Drugs Properties in a Solution 399
3.16.2.5.1 Ionization constants 399
3.16.2.5.2 Solution stability 400
3.16.2.6 Passive Transport of Drugs 401
3.16.3 What Methods are Available for the Estimation of These Properties? 402
3.16.3.1 Physics-Based Methods 402
3.16.3.1.1 COSMO-RS 402
3.16.3.1.2 UNIFAC 404
3.16.3.1.3 SAFT 404
3.16.3.1.4 3D RISM 405
3.16.3.2 Statistical Methods 405
3.16.3.2.1 Linear methods 405
3.16.3.2.2 Nonlinear (machine learning) methods 406
3.16.4 Applications and Limitations of the Methods for Physical–Chemical Properties Prediction 406
3.16.4.1 Polymorphism 406
3.16.4.1.1 Physics-based models 407
3.16.4.1.2 Statistical methods 410
3.16.4.2 Melting Point 411
3.16.4.2.1 Physics-based methods 411
3.16.4.2.2 Statistical methods 412
3.16.4.3 Vapor Pressure 413
3.16.4.3.1 Physics-based models 413
3.16.4.3.2 Statistical methods 415
3.16.4.4 Aqueous and Nonaqueous Solubility 415
3.16.4.4.1 Physics-based models 415
3.16.4.4.2 Statistical methods 416
3.16.4.5 pK_a 417
3.16.4.5.1 Physics-based methods 417
3.16.4.5.2 Statistical methods 418
3.16.4.6 Chemical Stability/Degradation 419
3.16.4.6.1 Statistical methods 419

3.16.4.7	Partition Coefficients	419
3.16.4.7.1	Physics-based models	419
3.16.4.7.2	Statistical methods	420
3.16.5	**Conclusions**	421
References		421

3.16.1 Introduction

3.16.1.1 Why We Need to Predict Physical–Chemical Properties?

Attempts to predict physical–chemical properties began very shortly after the first few measurements were made. This happened for a variety of reasons. In some cases an estimate of the likely value of the property is a useful aid to measurement. Octanol/water partition coefficients determined by the shake-flask method are a good example of this since judicious selection of volumes is required in order to achieve an accurate measurement.[1,2] For other properties, the measurement may be expensive or difficult and thus prediction is desirable. When a property is being used to construct models aimed at the design of new and better materials, some method of prediction is essential. Examples of this most notably include "drug design" as discussed at length in the book, although of course this is equally well required in the development of other products such as agrochemicals, fragrances, paints, adhesives, and dyestuffs. Indeed, anywhere where a material involving one or more chemicals has some practical application.

Whatever the reason, different methods have evolved involving different levels of theoretical treatment ranging from purely empirical to totally theoretical. This article will examine the more important physical–chemical properties and their prediction showing how the techniques work, discussing the theoretical basis of the methods and highlighting their strengths and weaknesses including an examination of the likely errors.

3.16.1.2 Physical–Chemical Properties in Drug Design

To elicit its pharmacological and therapeutic effects, a drug has to cross various barriers (Fig. 1). Orally administrated drugs need to be dissolved at the site of absorption in the gastrointestinal tract (GIT), be chemically stable at the low pH of stomach media, be metabolized appropriately and traverse several membrane barriers before achieving high free concentrations at the target site. The behavior of a drug molecule in each of these environments is the direct result of the drug's physical–chemical properties that are determined by its chemical structure.

3.16.1.3 A Brief Historical Overview

Octanol/water partition coefficients ($\log P$) formed the basis of the first systematic application of a mathematical modeling approach to attempt to link the biological properties of molecules to their chemical structure, the so-called Hansch approach.[3] Hansch, being a chemist, applied the principles of physical organic chemistry to biological activity prediction using Hammett σ constants to describe electronic effects and his own chosen system of octanol/water to describe transport and/or hydrophobic effects in the biosystem. This was not the first application of partitioning in the explanation of biological properties as Meyer[4] and Overton[5] at the turn of the 19th century independently described the potency of local anesthetics in terms of olive oil/water partition

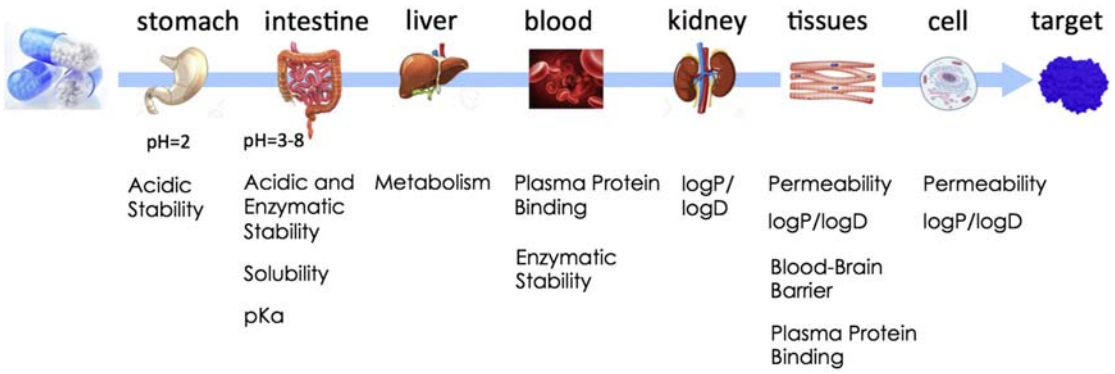

Fig. 1 Physiological and physical–chemical barriers affecting a drug bioavailability. Adapted from Kerns, E. H.; Di, L. Pharmaceutical Profiling in Drug Discovery. *Drug Discov. Today* **2003**, *8*, 316–323. Copyright (2003), with permission from Elsevier.

coefficients. Initially, Hansch employed a substituent constant approach, again in keeping with physical organic chemistry practice, and defined a substituent constant, π, thus:

$$\pi_x = \log P_x - \log P_H, \tag{1}$$

where the subscripts x and H refer to an x-substituted compound and the H-substituted (parent). Early measurements of $\log P$ showed that, broadly speaking, π values were additive but measurements became necessary for different parent systems such as phenols and anilines since there were systematic differences between them due principally to electronic effects.[6] The disadvantage of a substituent constant approach is that any models constructed using the constants are limited in terms of applicability to derivatives of the parent.

As a result of this, and because of the demonstrated importance of hydrophobic effects, focus began to be turned increasingly to the use of whole-molecule $\log P$ values. The use of whole molecule $\log P$ values prompted the development of predictive systems. The earliest of these, based on a statistical analysis of a large number of partition coefficient values, was reported in 1973.[7] This was a "reductionist" approach since it broke compounds down into a number of predefined structural fragments, which were combined with a single correction factor. Another system, based on an opposite "constructionist" approach, was published by Hansch and Leo toward the end of the 1970s[8] and this formed the basis of the first computer system for $\log P$ prediction and, indeed, one of the earliest physical–chemical property prediction programs. These early modeling approaches to drug discovery made use of measured physical–chemical properties and essentially empirical methods of prediction.

At about the same time as these studies reports began to emerge of the use of theoretical descriptors such as the correlation of antibacterial potency with superdelocalisability[9] and hallucinogenic activity with the energy of the highest occupied molecular orbital (E_{homo}).[10] The general scarcity of adequate computing resources, their low performance, and the lack of easily operated software combined to restrict the widespread use of theoretical descriptors until the 1980s.[11–13]

There was, however, one other form of theoretical descriptor, which saw widespread use from the middle of the 1970s and this was a topological descriptor known as the Randic index.[14] Topological descriptors are based solely on the standard 2D representation of a chemical structure and in their simplest form are calculated from the hydrogen-suppressed skeleton of the compound by the assignment of a degree of connectivity to each atom based on the number of atoms attached to it. The Randic index is computed by summation of the product of the degrees of connectivity of atoms over all edges of the hydrogen-suppressed molecular graph. Higher order indices may be generated by the consideration of longer paths in a molecule and other refinements have been considered, such as valence connectivity values, path, cluster, and chain connectivities.[15]

Although connectivity descriptors have been applied to compound design, they found most ready application in the area of environmental research. One of the principal reasons for this, at least in the early years of this type of research, is that the datasets tend to consist of quite diverse collections of molecules. Since topological descriptors just depend on the 2D structure with no reference to a parent, they were ideally suited for this purpose. A major problem with such parameters, though, is their physical and/or chemical interpretation and attempts were made to justify their significance.[16] This resulted in a dialog,[17,18] reminiscent of a debate, which took place between physical organic chemists over the F and R parameters (components of Hammett σ constants) of Swain and Lupton.[19] Whatever the truth or otherwise of these arguments, the debate was really about the wrong thing. If the models, which are being constructed with any type of descriptor, are intended for chemical understanding then it only makes sense to use parameters, which may be interpreted. If, on the other hand, models are being constructed solely from the point of view of prediction then the interpretability or otherwise of the descriptors used is unimportant. Since topological parameters are based on 2D structure they can be calculated very quickly, which is a great advantage when dealing with large collections of compounds such as libraries. They are also unambiguous, unlike properties derived from a 3D structure, since that structure must be generated in some way and there are debates about this and, indeed, which of the generated 3D structures is relevant. Topological descriptors have been shown to correlate with a number of different physical–chemical properties such as cavity surface area and molecular polarizability,[20] water solubility,[21] and partition coefficient[22], so there is little doubt that they do contain some chemical information. A principal component analysis of 108 molecular connectivity descriptors for a set of n-alkanes and polychlorinated biphenyls showed[23] that three principal components accounted for 98% of the variance in the dataset. These three principal components were associated with degree of branching, molecular size or bulk, and structural flexibility.

This has been a very brief and incomplete account of the development of computer-aided drug design intended to give the reader a flavor of how the field developed. A fairly comprehensive review of the description of molecules using physical–chemical properties was published at the turn of this century,[24] and to give some indication of the complexity of the field a handbook of descriptors lists over 3100 different parameters.[25]

3.16.1.4 Main Questions in the Field

An early reference work, which was subtitled "Environmental Behavior of Organic Compounds," was published by the American Chemical Society in 1990.[26] The origins of this handbook date to late 1978 when, to quote from the introduction to the book, "… with support from the US Army Medical Bioengineering Research and Development Laboratory (Fort Detrick, Frederick, MD) Arthur D. Little, Inc., undertook a preliminary problem definition study to answer the following questions:

(1) What are the important properties of organic chemicals with regard to their transport and fate in the environment?
(2) What methods are available for the estimation of these properties?

(3) What limitations and/or uncertainties are associated with these methods?
(4) Can a comprehensive user's manual incorporating the basic elements of these methods be prepared so they become not only easy to comprehend and use, but hard to misuse?"

These are excellent questions with a great deal of relevance today. The first one, despite more than 25 years of research, still remains to be answered completely although we do have many useful theories and models. The second one was partly answered in the referenced handbook and continues to be a topic of interest[27–29] including the subject of the present article. The third is important and often neglected when estimations are made, particularly when one or more estimated properties are used to calculate some further property from a model. Models, however, well developed, tested, and characterized are always dependent on the quality of the data subsequently used in them. The final question is an ongoing project with various attempts to provide this being made by different research groups.

3.16.2 Background Information on Physical–Chemical Properties

3.16.2.1 Polymorphism

A great majority of drug products marketed worldwide are formulated in oral solid dosage forms.[30] The pharmaceutical solid state may be characterized by a degree of a long-range order of molecular arrangement—in all three directions (crystalline), in one or two directions (liquid crystals), or only close-range order (amorphous). Typically, new drug candidates enter the pharmaceutical development process in molecular crystal forms, which makes it possible to ensure more desirable properties: superior stability, purity, and manufacturability relative to amorphous and liquid form formulations.

Different crystalline structures of one substance are named *polymorphs*.[31] Polymorphism, which exists as a result of different crystal packing of rigid molecules, is a *packing polymorphism*. *Conformational polymorphism* results from crystallization of different conformers of the same molecule(s), which is a more common phenomenon for typically flexible drug-like molecules. Based on an industrial solid form screening statistics, at least 50% of pharmaceutical molecules display a polymorphic behavior.[32] At any given set of environmental conditions (temperature, humidity, pressure, etc.) only one polymorph (and a corresponding solid form) is thermodynamically stable, having the lowest free energy and therefore the highest physical stability. All other forms are considered to be metastable.

Polymorphism can have impact on the performance of a drug in terms of solubility and bioavailability, chemical and physical stability, and mechanical properties.[33] Therefore, in the pharmaceutical industry, drug polymorphism can be a critical problem and is the subject of various regulatory considerations.[34,35] There are many reported cases when appearance of previously unknown more stable polymorphs significantly affected drug performance, typically causing a recall of the products from the market.[31] One of the most famous examples of polymorph-induced impact on drug performance is related to the marketed drug Norvir (ritonavir). Abbott Laboratories had to stop sales of Norvir in 1998 due to a failure in a dissolution test, which was caused by the precipitation of a more stable (and less soluble) form II of the compound.[36]

Therefore, in the pharmaceutical industry there is a strong interest in the prediction of crystalline solid-state structure and related properties of a molecule in question (ideally, with only the chemical structure known), allowing identification of potential polymorphic forms of a compound prior to synthesis in drug discovery. In addition, such calculations complement polymorph screening at early stages of drug development by facilitating an assessment of the likelihood of a missed stable form.[37]

The basic parameter to characterize a crystalline solid state and its polymorphic landscape is *lattice energy*. It corresponds to an internal energy of the crystal formation from infinitely separated molecules (in a vacuum). The lattice energy can be deduced from experimental sublimation enthalpy, $\triangle H_{sub}$,[38,39] according to the following relationship:[40]

$$E_{latt}(T) = -\Delta H_{sub}(T) + RT, \tag{2}$$

where T is the experimental temperature and R is the gas constant. The RT term is necessary to change enthalpy into an internal energy.

Since theoretical predictions of the lattice energies are typically performed at $T = 0$ K, an additional correction is needed to allow comparison with the experimental sublimation enthalpies. An approximate correction on the molecular motion contribution due to temperature differences leads to the following simple relationship:[40]

$$E_{latt}(0\,\mathrm{K}) = -\Delta H_{sub}(T) - 2RT \tag{3}$$

A significant limitation of the lattice energy property (as well as sublimation enthalpy) is that it lacks an entropic contribution and cannot accurately account for a phase transition phenomenon—such as crystal solubility or solid form conversion induced by a relative physical stability. Therefore, the most fundamental physical property of the crystalline state is a *lattice (crystal) free energy*, which is related to an experimental Gibbs (free) energy of sublimation, $\Delta G_{sub}(T)$.[41] Unfortunately, there is a very limited $\Delta G_{sub}(T)$ data available for the drug-like molecules.[38]

There are two contributions toward the lattice and sublimation energy properties—a long-range order and a short-range order, where the latter is the stronger one. Therefore, in some cases for computational considerations, a crystalline solid form may be approximated by an amorphous (or a supercooled liquid) state. In that case, energy ranking of the forms may be performed based on dominant contribution(s) into the short-range interactions. For drug-like molecules, such contribution is typically presented by intermolecular hydrogen bonding (H-bonding). The corresponding molecular property describes strength (or propensity) of the H-bonding.[42,43]

3.16.2.2 Melting (Fusion) of Crystals

The temperature at which a compound changes its state from solid to liquid at atmospheric pressure is called the *melting point* (MP). It is sensitive to the 3D structure of molecules and their packing in a crystal, which is determined by complex interactions including electrostatic, van der Waals, hydrogen bond formation (both internal and between molecules), and aromatic stacking as well as the flexibility and symmetry of molecules.[44] Therefore, MP is widely used as a criterion for compound purity and polymorph detection.

The recent increase in interest in MP prediction is connected with the development of ionic liquids (ILs).[45] By definition, ILs are a group of salts that have MP below 373.15 K, which clearly indicates that MP is a key parameter of this group of compounds. ILs have attracted great attention due to their green and tunable properties. Firstly, their negligible vapor pressures allow their use as an alternative to volatile organic solvents. Secondly, different cation/anion combinations permit fabrication of ILs with physical–chemical properties well fitted to a specific problem. Apart from the above factors influencing MP, ILs have a few specific problems: certain types of IL melt from eutectic mixtures of several crystalline polymorphs,[46] whose melting temperature is considerably lower than that of individual polymorphs. Moreover, ILs may form glasses instead of crystalline phases.[47] In this case, MP represents the glass transition temperature, which is rather different from MP of the corresponding crystalline state.

The MP can be also characterized by the free energy of fusion property, $\Delta G_{fus}(T)$ which can be presented as follows:

$$\Delta G_{fus} \approx \Delta H_{fus}\left(1 - \frac{T}{T_m}\right), \tag{4}$$

$$\Delta G_{fus} \approx \Delta H_{fus}(T_m - T)\frac{T}{T_m^2}, \tag{5}$$

$$\Delta G_{fus} \approx \Delta H_{fus}\frac{T}{T_m}\ln\frac{T_m}{T}, \tag{6}$$

where ΔG_{fus} and ΔH_{fus} are the free energy and enthalpy of fusion, respectively, T_m is the MP, and T is the temperature. Eqs. (4)–(6) are approximations based on various assumptions related to a difference in heat capacity between liquid and solid states of the compound. It was demonstrated that for drug-like molecules, approximation (5) (Hoffmann approximation) significantly outperforms approximation (4), while approximation (6) demonstrates an intermediate performance.[48]

3.16.2.3 From Condensed-Phase to Gaseous Phase

Volatility of compounds is described in terms of the *vapor pressure* (VP). It is reached when the condensed phase is in equilibrium with its own vapor (in the case of crystals, the rate of a solid's sublimation matches the rate of its vapor phase deposition).

Apart from pharmaceutical research, VP has widespread applications in environmental science since it is one of the key parameters determining the global fate of pollutants.[49] Thus, pesticides with high vapor pressures may become environmental problems because they can volatilize and disperse over a large area. Chemicals with a low vapor pressure do not move into atmosphere but they can accumulate into water, soil, and biota with respect to hydrophilic/hydrophobic properties. Volatility of pesticides is usually described with a flux (corresponding to the amount of chemical that flows from a unit of water/soil/biota surface into the atmosphere) or half-life (the time that is required for volatilization of half the chemical dose). In the case of the flux across air/water surfaces (Fig. 2) vapor pressure is required to calculate Henry's Law constant:

$$K_H = \lim_{x \to 0}\frac{p}{x} \tag{7}$$

where p is the vapor pressure of liquid and x is the molar fraction.

Due to the fact that drug-like compounds have extremely low vapor pressure, they are usually characterized in terms of sublimation thermodynamic parameters:

$$\Delta G^0_{sub} = -RT\ln\frac{p}{p^0}, \tag{8}$$

where ΔG^0_{sub} is the sublimation free energy (the free energy change that accompanies a molecule transfer from crystal to gaseous phase), p is the vapor pressure, p^0 is the atmospheric pressure (1 atm, 1.013×10^5 Pa), R is the ideal gas constant, and T is the temperature.

3.16.2.4 Dissolution and Solubility of Pharmaceuticals

3.16.2.4.1 Dissolution

Dissolution from the dosage form to the gastrointestinal (GI) fluids is the first property that has to be considered before any absorption (the movement of a drug into the bloodstream) can take place at all.[50] The Noyes–Whitney equation identifies key factors influencing the kinetics of drug dissolution:

$$DR = \frac{dm}{dt} = \frac{A \cdot D}{h}(C_s - C_b), \tag{9}$$

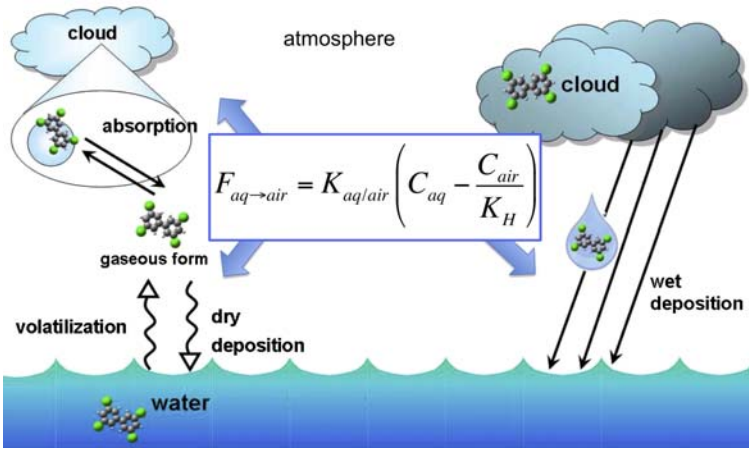

Fig. 2 Flux of a compound from aqueous media to atmosphere ($F_{aq \rightarrow air}$), where $K_{aq/air}$ is the kinetic parameter represented by the mass transfer coefficient on the molecule; C_{aq} and C_{air} are molecular concentrations of the compound in aqueous media and atmosphere, respectively. Adapted with permission from Ratkova, E. L.; Fedorov, M. V. Combination of RISM and Cheminformatics for Efficient Predictions of Hydration Free Energy of Polyfragment Molecules: Application to a Set of Organic Pollutants. *J. Chem. Theor. Comp.* **2011**, *7*(5), 1450–1457. Copyright (2011) American Chemical Society.

where *DR* is the dissolution rate, *m* is the mass of the dosage form, *t* is the time, *D* is the diffusion coefficient of the drug, *A* is the surface area of the solid wetted by the luminal fluids, *h* is the thickness of the boundary layer of the solvent at the surface, C_s and C_b are mass concentrations of the drug on the surface and in the bulk of the solvent, accordingly. The last parameter corresponds to the solubility of a drug in the GI contents, which is determined by such factors as crystalline form and pK_a.

Dissolution rate of immediate release (IR) solid oral dosage forms, such as tablets and capsules, depends on the specific formulation of the drug product (particle size, solid form, etc.). An IR product is considered rapidly dissolving when at least 85% of the labeled amount of the drug substance dissolves within 30 min using standard dissolution apparatus in the following media: 0.1 M HCl or simulated gastric fluid, pH 4.5 buffer and pH 6.8 buffer or simulated intestinal fluid.[51] An IR product is considered *very rapidly dissolving* when 85% or more of the labeled amount of the drug substance dissolves within 15 min using the abovementioned conditions. Rapid or very rapid in vitro dissolutions of IR solid oral dosage forms are required in combination with some other criteria (high solubility, etc.) to justify requests for biowaivers. http://www.fda.gov/downloads/Drugs/.../Guidances/ucm070246.pdf

3.16.2.4.2 Aqueous solubility

According to IUPAC,[52] aqueous solubility can be defined as the analytical composition of a saturated aqueous solution expressed in terms of the proportion of a solute in the solvent (concentration, molar fraction, molality, density, etc.). The definition is rather too general and may comprise different solubilities of the same compound. One can distinguish the following definitions of aqueous solubility:

Equilibrium aqueous solubility is the concentration of compound in a saturated solution when excess solid is present, and solution and solid are at equilibrium (two simultaneous opposite processes: dissolution and phase joining, e.g., precipitation of solids, proceed at constant rate). Under certain conditions equilibrium solubility may be exceeded to give metastable supersaturated solution, which will carry on precipitating until the system reaches equilibrium.

Intrinsic aqueous solubility (S_0) corresponds to the equilibrium solubility of neutral form of the compound (in the case of an ionizable compound this corresponds to the apparent aqueous solubility (see below) at pH where it is fully unionized).

Apparent aqueous solubility (S_{pH}) is defined for ionizable compounds in pH-buffered solutions. If the pK_a value of a drug is known, the apparent solubility can be calculated from the intrinsic solubility using the Henderson–Hasselbalch equation:

$$S_{pH} = S_0\left(1 + 10^{\pm(pH - pK_a)}\right), \tag{10}$$

A set of Eq. (10) should be considered for compounds with multiple ionizable centers.

Kinetic aqueous solubility is the solubility at the time when an induced precipitate first appears in a solution. It can be measured much faster than equilibrium solubility, but obtained values are often much higher. The kinetic aqueous solubility is employed for high-throughput screening (HTS) at early stage drug design. In this case, compounds are not isolated in the crystal form but stored as DMSO solutions.

Thermodynamic cycles: Solubility is a function not only of chemical structure but also of crystal form.[53] To estimate the significance of the solid state one can consider a thermodynamic cycle representing dissolution at equilibrium as a sum of two processes: sublimation/fusion, which allows estimation of the effect of crystal packing, and solvation/mixing—to analyze a molecular or liquid property (Fig. 3).

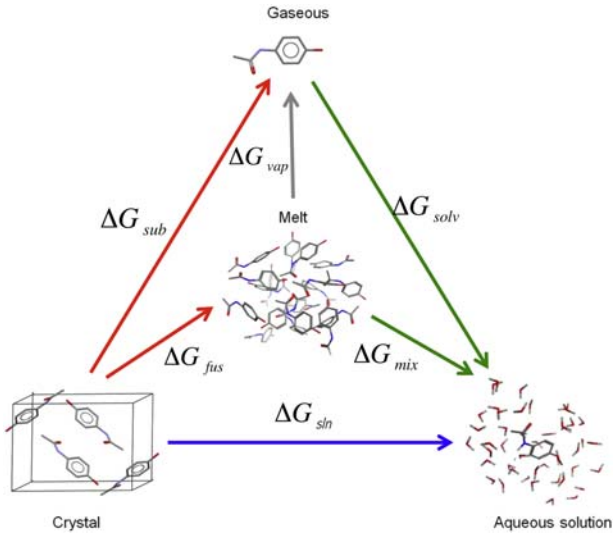

Fig. 3 Fusion and sublimation thermodynamic cycles describing aqueous solubility of crystalline compounds. Adapted with permission from Abramov, Y. A. Major Source of Error in QSPR Prediction of Intrinsic Thermodynamic Solubility of Drugs: Solid vs Nonsolid State Contributions? *Mol. Pharmacol.* **2015**, *12*(6), 2126–2141. Copyright (2015) American Chemical Society.

In this case, intrinsic aqueous solubility (referred to molar fractions) is connected to Gibbs free energy changes of the corresponding processes as follows:

$$\log S_0 = -\frac{\Delta G_{sub} + \Delta G_{solv}}{RT\ln(10)} = -\frac{\Delta G_{fus} + \Delta G_{mix}}{RT\ln(10)}. \tag{11}$$

BCS classification: Due to many cases of solubility-limited absorption, analysis of aqueous solubility is included in the early-stage drug design. Fig. 4 exhibits the minimal acceptable solubility that is required for compounds with low, medium, or high permeability values at a particular clinical dose.[54] With respect to their solubility and intestinal membrane permeability, drugs have been classified into four categories according to the Biopharmaceutics Classification System (BCS): class I, high solubility and high permeability; class II, low solubility and high permeability; class III, high solubility and low permeability; class IV, low solubility and low permeability.[55]

High aqueous solubility governs the possibility of oral administration of a drug, which is the most frequently used because of its convenience (high degree of drug stability and accurate dosage) and cost-effectiveness. However, oral drugs do not have such a high level of bioavailability (the proportion of a drug that reaches the systemic circulation) as that of drugs given parenterally. Therefore, in case absorption is not limited by intestinal permeability, the higher solubility an oral drug has, the higher bioavailability it should exhibit. Clearly, one of the key goals in pharmaceutics is solving the problem of poor drug aqueous solubility. Analysis of up-to-date databases of drug compounds shows that compounds with high biological activity (high affinity to the receptors) typically are poorly soluble in aqueous solutions.[56]

3.16.2.5 Drugs Properties in a Solution

3.16.2.5.1 Ionization constants

Many drug molecules are ionizable in aqueous media. Gaining and/or losing a proton they can form positively charged, negatively charged, or zwitterionic particles. The charge state of a drug molecule can be estimated from its ionization constant, pK_a, and pH of the medium in which the molecule is dissolved:

$$pK_a = pH - \log_{10}\left(\frac{[A^-]}{[HA]}\right), \tag{12}$$

where A^- is a conjugate base of the acid HA.

Eq. (12) corresponds to the Henderson–Hasselbalch approximation, which does not consider a proton transfer. Accounting for the process leads to the following expression:

$$pK_a = -\log_{10}\left(\frac{\left[A^-_{(aq)}\right]\left[H_3O^+_{(aq)}\right]}{\left[HA_{(aq)}\right]\left[H_2O_{(aq)}\right]}\right). \tag{13}$$

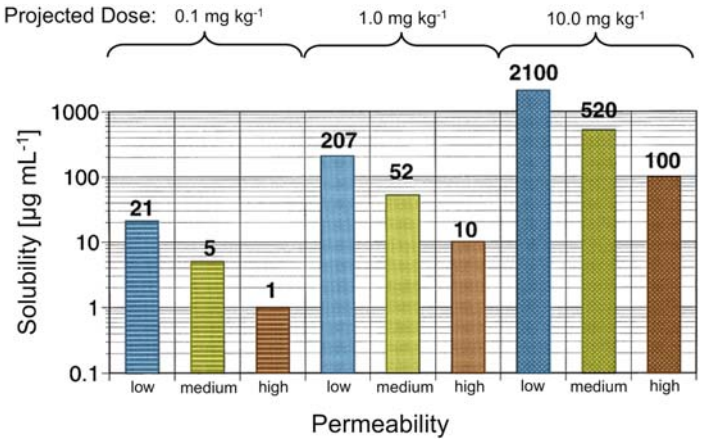

Fig. 4 Minimum thermodynamic aqueous solubility (at pH 6.5 or 7.0) that is required for low, medium, and high permeability values at a particular clinical dose. Reprinted from Lipinski, C. A. Drug-Like Properties and the Causes of Poor Solubility and Poor Permeability. *J. Pharmacol. Toxicol. Meth.* **2000**, *44*, 235–249. Copyright (2000), with permission from Elsevier.

pK_a plays a crucial role in pharmacokinetics of drugs since it significantly affects their ADME properties: absorption in GI tract, distribution in various organs, their metabolic transformation along the way, and, finally, excretion from the body (**Fig. 5**).[57]

Tautomerism: Some drug compounds can be represented by several structures (tautomers) that are related by an intramolecular movement of hydrogen from one atom to another, which is accompanied by changes of H-donor/acceptor properties of particular atoms, the rearrangement of double bonds, or ring opening/closing. Due to the fact that tautomers of a molecule have different structure, they usually have different pK_a values.[58] Therefore, even small changes in solvent environment can dramatically change the ratio of tautomers. If we consider a simplified case with two tautomers of the deprotonated state (A^-), total pK_a of the compound can be calculated as following:

$$\mathrm{p}K_a = \mathrm{p}K_a^{(1)} + \log\frac{[A_1^-]}{[A_1^-]+[A_2^-]} = \mathrm{p}K_a^{(2)} + \log\frac{[A_2^-]}{[A_1^-]+[A_2^-]}, \tag{14}$$

where $[A_i^-]$ is the equilibrium concentration of ith deprotonated tautomer of the molecule.

3.16.2.5.2 Solution stability

To reconcile slow solubility reactions to the HTS needs of drug discovery research, candidate compounds are not isolated in the crystalline form but are stored in DMSO solutions under various physical conditions.[57] The choice of the solvent is quite

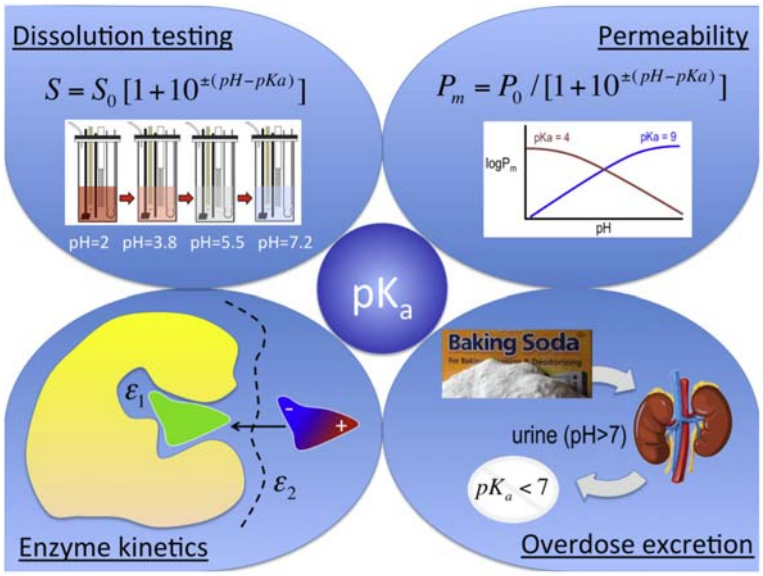

Fig. 5 Examples of pK_a application in pharmaceutical industry.

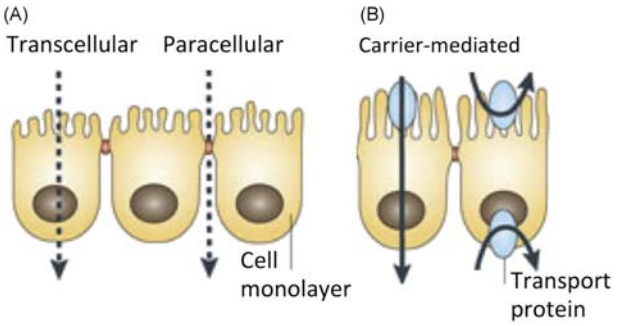

Fig. 6 Pathways of the intestinal barrier: (A) paracellular and transcellular passive diffusion, (B) influx/efflux transport by membrane proteins. Reprinted by permission from Macmillan Publishers Ltd. Sugano, K.; Kansy, M.; Artursson, P.; Avdeef, A.; Bendels, S.; Di, L.; Ecker, G. F.; Faller, B.; Fischer, H.; Gerebtzoff, G.; Lennernaes, H.; Senner, F. Coexistence of Passive and Carrier-Mediated Processes in Drug Transport. *Nat. Rev. Drug Discov.* **2010**, *9*, 597–614. Copyright (2010).

understandable; around 90% of the compounds that end up in a library will dissolve in DMSO (in chloroform or acetone, the figure is only 70%).[59] However, it is not an inert solvent. In addition to its mild reactivity, DMSO adsorbs a considerable amount of water. This causes the problem that part of that liquid stored can decompose over time (e.g., due to oxidation and hydrolysis). Degradation in stock solutions may occur also due to oxygen that gets absorbed from the air, light, heat, and trace materials (e.g., HCl, TFA, OH^-, and metals).[60] Degradation products of drugs in solution might have increased or decreased activity or toxicity than the parent compound, which can lead to either false positive or false negative conclusions in bioassays, and confuse structure–activity relationships.

3.16.2.6 Passive Transport of Drugs

Permeability is a measure of how fast a compound passes through a lipid membrane. Permeability of a drug through physiological barriers such as membranes of intestinal epithelium and blood–brain barrier is one of the key determinants of drug bioavailability. Generally, drugs can penetrate across a membrane passively or/and actively (Fig. 6).[61] In the case of macromolecules, compounds are very large and must be transported across membranes in vesicles (endocytosis/exocytosis).

Passive diffusion is considered as the primary route of membrane permeation for the majority of drugs in many cell types (e.g., in intestinal membrane permeation). The driving force of the process is the concentration gradient of a drug; a membrane does not actively participate in it. Passive diffusion can take place either through lipid structures of a membrane—*transcellular diffusion*, or through its aqueous pores and/or tight junctions—*paracellular transport*. In turn, active transport is assumed to coexist with passive diffusion for such cases as brain and liver distribution, and in renal excretion.[62]

It has being a long-term challenge to rationalize membrane permeability with physical–chemical properties.[63] Logarithm of *partition coefficient* ($\log P$) of a compound in equilibrium between two immiscible media (water and organic phases) is the most widely used parameter for this purpose:

$$\log P_{orq/wat} = \log \frac{[HA]_{org}}{[HA]_{wat}}, \tag{15}$$

where $[HA]_i$ is the equilibrium concentration of a compound in the compartment i. However, $\log P$ is applicable only for unionized drugs since it does not reflect the pH of media and acidity/basicity of a compound. The drawback can be overcome with the logarithm of distribution coefficient ($\log D$), which accounts for ionizable particles:

$$\log D_{org/wat} = \log \frac{[HA]_{org}}{[HA]_{wat} + [A^-]_{wat}}, \tag{16}$$

If $\log P$ and acid/base behavior of a drug are known, the $\log D$ can be calculated as following:

$$\log D_{org/wat} = \log P_{org/wat} - \log\left(1 + 10^{\pm(\mathrm{pH}-\mathrm{p}K_a)}\right), \tag{17}$$

It is a common practice to measure $\log D$ at pH 7.4, store these values in databases, and use them for QSAR/QSPR predictions. *n*-Octanol is the most widely used solvent to mimic cell membranes, despite the fact that it poorly reproduces the structure of the phospholipid bilayer. Different shapes of permeability—$\log D$ (water/octanol) relationship were reported: linear,[64] hyperbolic,[65] sigmoidal,[66] parabolic,[67] etc. In 1998, Camenisch et al.[68] suggested an aqueous pore model of diffusion, which brought some light to the problem (Fig. 7). The model was analyzed for compounds with various molecular weights (MWs). For low MW compounds they obtained sigmoidal shape of the relationship which corresponds to (i) diffusion through aqueous pores of hydrophilic compounds, and (ii) transcellular transport of lipophilic compounds, which became so rapid that convective diffusion through

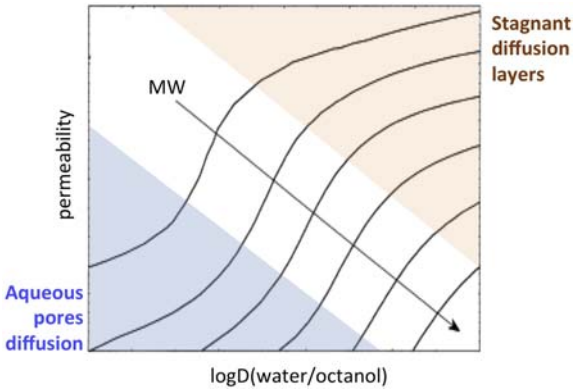

Fig. 7 Model correlation between permeability and log *P*(*oct*/*wat*). Simulation curves as a function of increasing MW. Reprinted with permission from Camenisch, G.; Folkers, G.; van de Waterbeemd, H. Shapes of Membrane Permeability-Lipophilicity Curves: Extension of Theoretical Models With an Aqueous Pore Pathway. *Eur. J. Pharm. Sci.* **1998**, *6*, 321–329. Copyright (1998), with permission from Elsevier.

the stagnant layers is rate limiting. In turn, for higher MW compounds the shape was found to be bilinear/hyperbolic, which can be described with a simple diffusional resistance model of van de Waterbeemd.[69]

Nevertheless, *n*-octanol does not always function as the universal standard for all types of membranes. For example, isopropyl myristate was found to be a better model for skin lipids permeability studies.[70] To cover the variation in biophysical characters of different membrane types, Taylor and coworkers[71] proposed a set of four solvents, the "critical quartet": *n*-octanol (amphitropic), alkane or 1,2-dichloroethane (inert), chloroform (proton donor), and propylene glycol dipelargonate (proton acceptor).

3.16.3 What Methods are Available for the Estimation of These Properties?

3.16.3.1 Physics-Based Methods

A comprehensive description of the main physics-based methods such as QM (quantum mechanics) and MD (molecular dynamics) are out of scope of this publication. Here, we give a short introduction to alternative approaches, which are of great value for physical–chemical properties prediction.

3.16.3.1.1 COSMO-RS

Conductor-like screening model for real solvents (COSMO-RS) is based on the statistical thermodynamics of interacting molecular surface segments. The polar and H-bond interactions are described by the surface screening charge densities, which result from a quantum-chemical continuum solvation calculation (COSMO solvation approach).[72–75] COSMOtherm is the first available and most advanced implementation of COSMO-RS theory.

(i) *COSMO*: Firstly, a gas-phase geometry optimization of a solute should be performed (Fig. 8A). Charge distribution of the solute is estimated. Secondly, a molecular shaped cavity is constructed around the solute molecule (Fig. 8B). The details of the cavity construction differ in various COSMO implementations. In most cases, it is constructed as an assembly of atom-centered spheres with radii approximately 20% larger than the van der Waals radius. For the actual calculation the cavity surface is approximated by a set of surface segments (e.g., hexagons). Thirdly, the solvent is treated as a dielectric continuum with a permittivity $\varepsilon = \infty$ (perfect conductor), surrounding the solute molecules outside of a molecular cavity. The dielectric polarization of the continuum is represented by a set of Coulomb charges $\underline{q}$ placed on the surface segments (Fig. 8C). They are calculated by a linear set of equations:

$$\underline{\underline{A}}\,\underline{q} + \underline{\underline{B}}\,\underline{Q} = 0, \tag{18}$$

where $\underline{Q}$ is the charge distribution of the solute, and $\underline{\underline{A}}$ and $\underline{\underline{B}}$ are linear operators dependent on the boundary conditions. Unlike other continuum solvation models, which employ the exact boundary conditions, COSMO uses scaled-conductor approximation:

$$\underline{\underline{A}} = \underline{\underline{V}} \quad \text{and} \quad \underline{\underline{B}} = \frac{\varepsilon - 1}{\varepsilon + x}\underline{\underline{V}}, \tag{19}$$

where $\underline{\underline{V}}$ is a matrix generating the electrostatic potential on each surface segment caused by polarization charges $\underline{q}$ (the potential is readily available in every QM program), and the value of x is set to 0.5 based on theoretical arguments. Then, the screening charges of surface segments (σ-surface) are resubstituted as external charges. This yields a modified electron density of the solute and requires repetition of the second step. Both sets of charges, $\underline{q}$ and $\underline{Q}$, are self-consistently optimized to find the minimum energy of the system. This can be achieved by different empirical, semi-empirical, or *ab initio* methods. In most cases, DFT methods are employed as these currently represent a good compromise between computational effort and reliability of the result. Finally, histograms of screening charge densities, the so-called σ-profiles, $p(\sigma)$, are constructed (Fig. 8D). They give the relative amount of

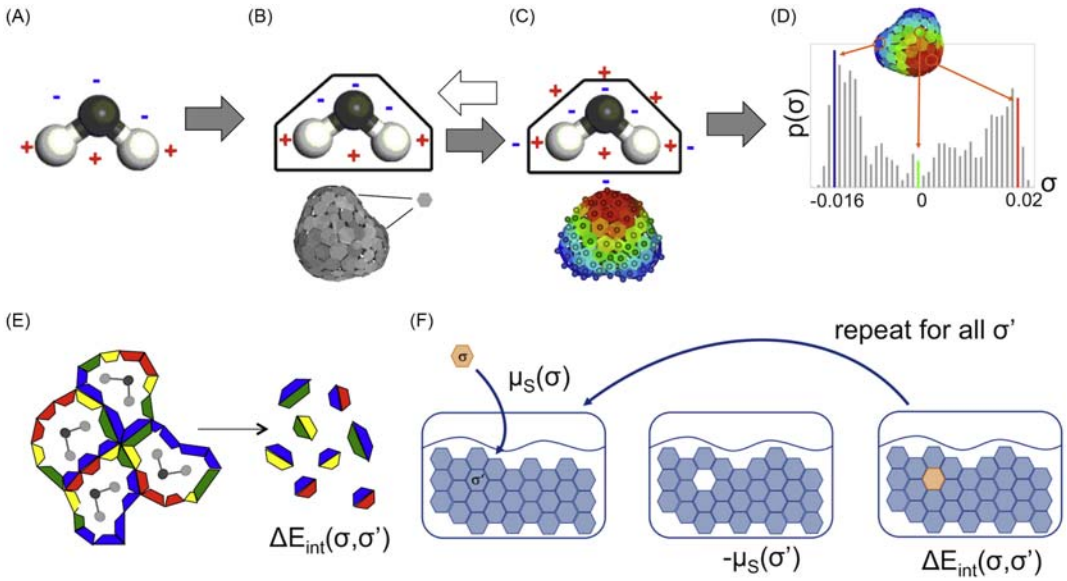

Fig. 8 COSMO (A–D) and COSMO-RS (E and F) steps of calculations. Subfigures (A–C) are adapted with permission from Mullins, E.; Liu, Y. A.; Ghaderi, A.; Fast, S. D. Sigma Profile Database for Predicting Solid Solubility in Pure and Mixed Solvent Mixtures for Organic Pharmacological Compounds with COSMO-Based Thermodynamic Methods. *Ind. Eng. Chem. Res.* **2008**, *47*(5), 1707–1725. Copyright (2008) American Chemical Society. Subfigure (E) is adapted from Klamt, A.; Eckert, F. COSMO-RS: A Novel and Efficient Method for the a Priori Prediction of Thermophysical Data of Liquids. *Fluid Phase Equilibr.* **2000**, *172*, 43–72, Copyright (2000) with permission from Elsevier. Subfigures (D and F) are adapted from http://www.cosmologic.de/files/downloads/theory/COSMO-RS-Theory-Basics.pdf (white papers).

surface with polarity σ for the solute molecule. In the case of flexible molecules or components with different tautomeric forms, the calculation needs to be repeated for different conformers and/or tautomers. The resulting geometries, energies, and σ-profiles are calculated only once and stored for later use in the so-called COSMO files.[76]

(ii) *COSMO-RS*: Methodology treats the solvent as an ensemble of pairwise interacting surface segments (**Fig. 8E**). The interaction energies of the surface pairs are defined in terms of screening charge densities σ and σ' of the respective surface segments:

$$\Delta E_{int}(\sigma,\sigma') = \Delta E_{misfit}(\sigma,\sigma') + \Delta E_{HB}(\sigma,\sigma'), \tag{20}$$

where ΔE_{misfit} is the electrostatic energy change corresponding to the difference in two polarities (in the case of perfect fit of the polarities $\sigma = -\sigma'$, e.g., in a perfect conductor, the term would be zero), ΔE_{HB} is an empirical term accounting for hydrogen bonding. In addition, there is van der Waals energy term, $E^X_{vdW}(A^X_\alpha)$, describing energy gain of a molecule X during the transfer from the gas phase to a solvent. Because this *vdW* term is independent of the neighborhood, it is not really an interaction energy, but it is considered as an additional contribution to the energy of the reference state in solution. $E^X_{vdW}(A^X_\alpha)$ is represented as a surface proportional term with element-specific coefficients. A^X_α is the COSMO surface on atom α. If we consider an ensemble of solvent molecules, its energy in comparison to the perfect conductor state can be expressed as the sum over all surface contacts k:

$$\Delta E^S_{tot} = \sum_k \Delta E_{int}\left(\sigma_k, \sigma'_k\right), \tag{21}$$

Instead of calculating all different mutual contacts of the three-dimensional representations of the molecules, a further approximation is introduced. A surface piece with polarity σ is added to the surface of a solvent molecule (**Fig. 8F**). The chemical potential of the process is calculated using the probability $p_S(\sigma')$ to find a certain polarity inside the solvent and the corresponding interaction energy:

$$\mu_S(\sigma) = -kT \ln \int p_S(\sigma') \exp\left\{-\frac{\Delta E_{int}(\sigma,\sigma')}{kT}\right\} d\sigma'. \tag{22}$$

Due to the fact that $\mu_S(\sigma)$ is present on both sides of Eq. (22), it needs to be solved iteratively with the first approximation of $\mu_S(\sigma') = 0$. The final step of COSMO-RS consists in the evaluation of the chemical potential of any solute molecule X in the solvent S as following:

$$\mu^X_S(\sigma) = \int p^X(\sigma)\mu_S(\sigma)d\sigma + kT\ln\left(x\gamma^X_{comb,S}\right). \tag{23}$$

The logarithmic term takes into account the dependence of the chemical potential of solute X on its mole fraction x, and a correction for the relative sizes of solute and solvent molecules.

3.16.3.1.2 UNIFAC

Universal quasichemical functional-group activity coefficients (UNIFAC) is based on combination of a group approach with an activity coefficients model UNIQUAC.[77] In principle, the statistical thermodynamic problem in UNIFAC is analogous to that in COSMO-RS; both approaches consider an ensemble of pairwise interacting species: surface segments in COSMO-RS (characterized by the screening charge density σ), and functional groups in UNIFAC (characterized by *vdW* volume and surface area). Instead of calculations of the corresponding interaction energy as a function of the interaction species parameters (as it was implemented in COSMO-RS), UNIFAC employs empirical pairwise interaction parameters, which are related to the interaction energy. In fact, UNIFAC is focused on the calculation of the activity coefficient of a molecule:

$$\ln \gamma_i = \ln \gamma_i^C + \ln \gamma_i^R, \tag{24}$$

where the combinatorial term (with superscript C) takes geometrical (entropic) effects into account, while the residual part (with superscript R) considers enthalpic interactions. The residual activity term, which is employed in vapor pressure calculations, can be estimated as the following (for a pure compound):

$$\ln \gamma^R = \sum_k \nu_k \ln \Gamma_k = \sum_k \nu_k Q_k \left(1 - \ln\left(\sum_m \Theta_m \Psi_{mk}\right) - \sum_m \frac{\Theta_m \Psi_{km}}{\sum_n \Theta_n \Psi_{nm}}\right), \tag{25}$$

where ν is the number of groups, Γ is the group residual activity coefficient, Q is the group van der Waals surface area, Θ is the surface area function, which is a function of x (the group mole fraction, Eq. (26)), Ψ is the group interaction parameter.

$$\Theta_m = \frac{Q_m x_m}{\sum_n Q_n x_n}. \tag{26}$$

3.16.3.1.3 SAFT

Statistical associating fluid theory (SAFT) is a method comprising theoretically based equations of state, originating in Wertheim's first-order perturbation theory.[78] In the SAFT approach, molecules are described as chains of bonded homonuclear monomer segments interacting via dispersion and associating forces (Fig. 9).

The Helmholtz energy of a fluid (a^{res}) is obtained by summing different contributions that account for (i) the monomer–monomer interactions (a^{seg}), including both reference system (e.g., hard-sphere) and dispersion terms, (ii) chain formation, and (iii) intermolecular association:

$$a^{res} = a^{seg} + a^{chain} + a^{assoc}. \tag{27}$$

If the Helmholtz free energy of a fluid is known, all other properties such as pressure, chemical potential, among others, can be calculated using basic thermodynamic equations.

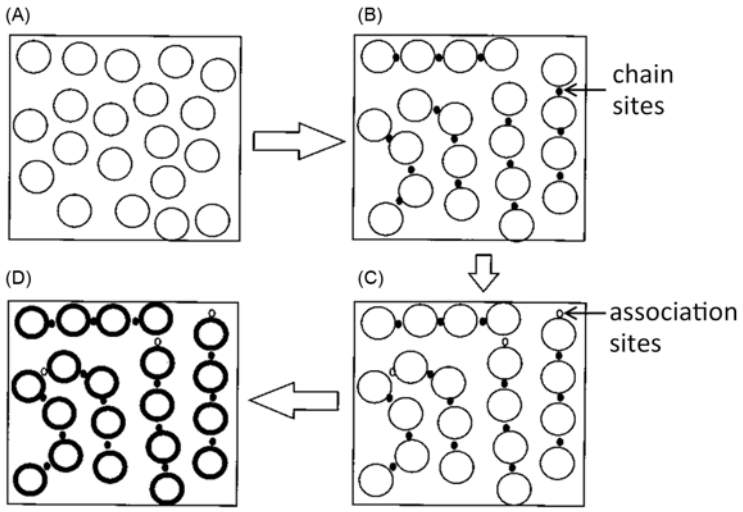

Fig. 9 Schematic representation of the physical basis of the SAFT model: (A) the reference fluid consists of hard spheres (repulsion forces only), (B) the reference fluid forms chains through covalent bonding (chain sites are added), (C) different chains form association complexes (oligomers) through hydrogen bonding between their terminal sites (association sites are added), (D) dispersive potential is added to account for attractive forces. Adapted with permission from Economou, I. G. Statistical Associating Fluid Theory: A Successful Model for the Calculation of Thermodynamic and Phase Equilibrium Properties of Complex Fluid Mixtures. *Ind. Eng. Chem. Res.* **2002**, *41*(5), 953–962. Copyright (2002) American Chemical Society.

During the past two decades, many versions of SAFT equations have been proposed, including original SAFT, Chen-Kreglewski SAFT (CK-SAFT), simplified SAFT, Lennard-Jones SAFT (LJ-SAFT), soft-SAFT, variable-range SAFT (SAFT-VR), perturbed-chain SAFT (PC-SAFT), and simplified PC-SAFT.[79] The principal differences among SAFT versions are in a^{seg} contribution, which requires the choice of reference system and description of repulsive and attractive interactions. Expressions for chain and association terms (a^{chain} and a^{accos}) correspond to Wertheim contributions, which stay unchanged in various versions of SAFT.

SAFT-type models contain a number of parameters for pure compounds. Typically, they contain 3–4 parameters for nonassociating compounds: the segment energy and diameter, the number of segments, polar term; and additionally two parameters: the association volume and energy, for associating compounds. The parameters are estimated from experimental data on vapor pressure and liquid density (optionally, monomer fractions and enthalpies of vaporization can be used).

However, the combination of SAFT equations with group-contribution type schemes (GC-SAFT) allows thermodynamic property (e.g., vapor pressure) predictions based solely on the chemical structure. As in the previous case, functional group parameters are determined by fitting the theory to experimental data but only for the smaller members of the chosen chemical families, whereas phase behavior of larger MW compounds (which were not included in the parameter estimation) is calculated using the obtained data without reparameterization.

3.16.3.1.4 3D RISM

3D reference interaction site model (3D RISM) is a statistical mechanical approach describing thermodynamic properties of molecular liquids.[80,81] It has a special place among implicit solvent methods, since it combines a reasonable level of molecular description of the solvent with low computational costs.[82] Within the approach a system is described in terms of intermolecular, $h_\alpha(\mathbf{r})$ and $c_\alpha(\mathbf{r})$, and intramolecular, $\omega_{\zeta\alpha}(r)$, correlation functions (Fig. 10). The functions are connected via a set of 3D Ornstein–Zernike equations and corresponding closure relations:

$$\begin{cases} h_\alpha(\mathbf{r}) = \sum\limits_{\zeta} \int c_\zeta(\mathbf{r}-\mathbf{r}')\chi_{\zeta\alpha}(|\mathbf{r}'|)d\mathbf{r}' \\ h_\alpha(\mathbf{r}) = \exp\{-\beta u_\alpha(\mathbf{r}) + h_\alpha(\mathbf{r}) - c_\alpha(\mathbf{r}) + B_\alpha(\mathbf{r})\} - 1 \end{cases} . \tag{28}$$

Here $u_\alpha(\mathbf{r})$ is the interaction potential, $B_\alpha(\mathbf{r})$ is the bridge functional, $\chi_{\zeta\alpha}(r)$ is the site–site bulk solvent susceptibility function, which is defined as following:

$$\chi_{\zeta\alpha}(r) = \omega_{\zeta\alpha}(r) + \rho h_{\zeta\alpha}(r). \tag{29}$$

Iterative solution of Eq. (28) yields intermolecular correlation functions of the system at thermodynamic equilibrium, which are further employed to calculate physical–chemical parameters of interest.

3.16.3.2 Statistical Methods

A large number of statistical and machine learning methods are used to predict physical–chemical properties of molecules. Traditionally methods can be separated into two large groups: linear and nonlinear methods. The use of both types of methods is strongly related to their assumptions as well as complexity of the analyzed problems and the used descriptors.

3.16.3.2.1 Linear methods

Linear methods, such as multiple linear regression analysis (MLRA), frequently assume an additivity of the investigated properties from the used descriptors. For some properties, for example, MW, which is calculated as a sum of contribution of individual atoms,

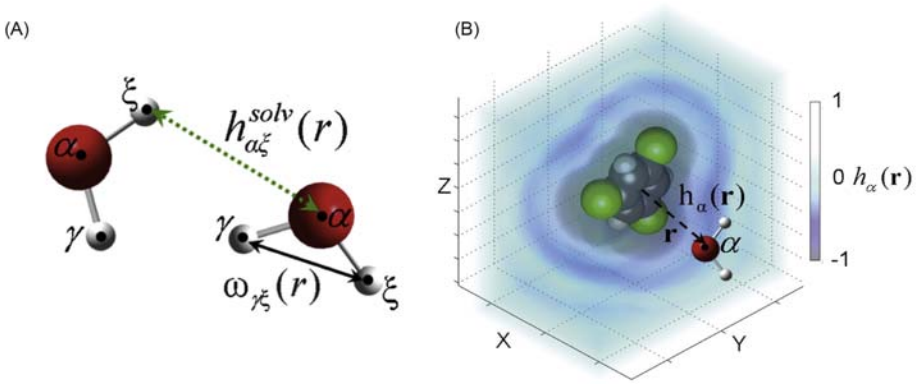

Fig. 10 3D-RISM correlation functions: (A) site–site intramolecular correlation functions ($\omega_{\gamma\xi}(r)$) and intermolecular correlation functions ($h_{\alpha\xi}(r)$) between sites of solvent molecules, (B) intermolecular site–molecule correlation function $h_\alpha(\mathbf{r})$ between α site of solvent and center of mass of solute. Reprinted with permission from Ratkova, E. L.; Palmer, D. S.; Fedorov, M. V. Solvation Thermodynamics of Organic Molecules by the Molecular Integral Equation Theory: Approaching Chemical Accuracy. *Chem. Rev.* **2015**, *115*(13), 6312–6356. Copyright (2015) American Chemical Society.

as well as for several other properties such as molecular refraction and parachor, such assumptions work very well. For more complex properties the additivity may not work and in order to account for deviations from linearity the equations start to include correction factors to account for nonlinear interactions. For example, the XLOGP program[83] includes four such factors, that is, number of hydrophobic atoms, indicator of amino acids, intramolecular hydrogen bonds, and halogen–halogen interactions.

In case additivity schemas based on atom contributions do not work very well, it is possible to use a more complex description of molecules, such as functional groups. They divide a molecule into chemically significant substructures, thus capturing interactions among its atoms and allowing the representation of the molecule at a higher level of description. The methods, which use the additivity principle to predict properties based on contribution of nonoverlapping groups, are also known as linear free energy relationships (LFER) methods. These methods actually assume that (for a congeneric series of compounds) an influence of a structural feature on the free energy change of a chemical process is constant. The properties, which depend on the free energy, thus can be approximated as a sum of a property of a basic structure (which can be also just one group) as well as a sum of properties of nonoverlapping predefined fragments. Frequently not only groups but also their interactions are used. For example, UNIFAC (see section "UNIQUAC functional-group activity coefficients") is widely used to predict nonelectrolyte activity in nonideal mixtures by using experimentally measured interaction parameters between the functional groups.

While functional groups in combination with linear methods are useful and easily interpretable, they may provide insufficient accuracy for modeling of some properties and their design can require considerable effort and chemical expertise. Such efforts are currently actively explored in an attempt to identify, for example, frequent hitters for high throughput screening (HTS) data analysis.[84,85] The functional groups, such as "toxicophores," are also used to identify molecules that are toxic, unstable, reactive, or frequent hitters.[86] One can also develop general purpose groups covering, for example, heterocyclic compounds, which could be useful for prediction of various properties.[87]

Instead of using predefined groups one can also generate all possible fragments of a predefined length, as is done in Isida fragmentor.[88] In addition to functional groups, the users can generate multiple descriptors using different software tools. For example, Dragon[25] currently includes 5270 descriptors separated in 30 different blocks. The analysis of such large descriptor sets can be also performed using linear regression methods. However, regression models derived using such sets are more difficult to analyze compared to LFER approach due to intercorrelations and dependencies amid the descriptors.

3.16.3.2.2 Nonlinear (machine learning) methods

Nonlinear methods, such as support vector machines (SVM),[89] neural networks (NN),[90] random forest (RF),[91] or metaheuristic algorithms, such as genetic algorithms (GA) and evolutionary programming (EP),[92] and many others were inspired either by the organization of the brain (NN), and/or natural evolution (GA and EP) or advances in statistical learning theory (SVM) and statistical properties of ensembles of models (RF). One of the most recent developments in this field includes deep learning NN,[93] which can find a lot of applications in the drug discovery field and is becoming an attractive method for the prediction of physical–chemical and biological properties of compounds.[94]

The machine learning methods usually provide better accuracy of predictions in comparison to linear methods, which justifies their application for prediction of different properties as shown in the respective articles below. At the same time models developed using these methods are more difficult to analyze compared to linear models. The interpretation of models using predicted matched molecular pairs (MMPs),[95] or based on descriptors used to generate models[96] represent important approaches to get deep insight into the models.

The model development includes several important steps: data preparation, descriptors selection, model development, and model validation.[97] The model validation performed as the last step is frequently based on prediction of test sets and/or on a cross-validation method. In the cross-validation method part of training set samples (e.g., 20% for fivefold-cross validation) are used as a test set and a new model is developed without them. The developed model is then used to predict the test set compounds. The exclusion of samples is repeated until all training samples are predicted. The predicted values for compounds in the test set are used to estimate the accuracy of models. Thus, this method reuses the whole training set as a test set. However, if validation of models is performed after optimization of parameters of models and, in particular, variable selection, it can be biased.[98] In order to avoid this problem all model development steps should be repeated.

Model development can be implemented manually or be executed on the web using integrated environments, such as the On-Line Chemical Database and Model Environment (OCHEM)[99] or CHEMBENCH.[100] The advantage of the use of the web platforms is that models published by them are publicly available to the research community and can be used by all interested partners on the web without a need to reimplement published models.

3.16.4 Applications and Limitations of the Methods for Physical–Chemical Properties Prediction

3.16.4.1 Polymorphism

There are two major applications of crystalline polymorphism prediction in the pharmaceutical industry. One is related to improving the solubility of crystalline compounds at early stages of drug discovery. This may be achieved by a better description of solid-state contribution to the solubility. Another application is related to an estimation of the likelihood of existence of a new stable form missed during initial experimental polymorph screening.[37]

3.16.4.1.1 Physics-based models

3.16.4.1.1.1 Crystal structure prediction

The most logical and at the same time the most complicated theoretical physical approach to study pharmaceutical crystalline solid form and polymorphism is based on the crystal structure prediction (CSP) approach. Milestones of the CSP method developments and compound complexity progress are reflected in the results of six blind tests,[277] and are covered in recent comprehensive reviews.[101–103] However, in spite of over 20 years of method development, it is only recently that a focus of CSP studies has shifted toward drug-like molecules. In addition, until recently the CSP studies were rarely verified by experimental polymorph screening. Examples of pharmaceutical molecules, for which combined computational and experimental solid form screenings were performed, are presented in **Fig. 11**.

Current CSP techniques describe the possible polymorphism of an organic molecule via lattice energy minimization. Minima of the lattice energy landscape within a certain energy range describe thermodynamically feasible polymorphs of the molecule at $T=0$ K. A schematic representation of CSP steps by global lattice energy minimization is presented in **Fig. 12**.

The resulting lattice energy values (and *in silico* polymorph stability ranking) reflect interplay between molecular (energy penalty relative to a free molecule in the gas phase) and intermolecular (interactions between the molecules in crystal) contributions:

$$E_{latt} = E_{intra} + E_{inter}. \tag{30}$$

The improvement of intrinsic solubility via the application of CSP is based on utilization of the sublimation thermodynamic cycle of solubility (**Fig. 3**). The thermodynamic cycle describes the intrinsic thermodynamic aqueous solubility as an interplay between crystal packing and molecular hydration contributions. There was recently presented a novel method, solid-state perturbation,[104–106] which perturbs both of these contributions by substitution of selected hydrogen atoms of a given molecule by a small group (such as, methyl, fluoro, or chlorine). The method is based on the assumption that the differences in free energy of sublimation within a drug compound series are dominated by enthalpic rather than entropic contributions, and one should expect a simple linear model between the intrinsic solubility and predicted CSP lattice and hydration energies:[104,105]

$$\log S_0 = \ln\left(\frac{p_0}{RT}\right) - \frac{\Delta H_{sub}}{RT} + \frac{\Delta S_{sub}}{R} - \frac{\Delta G_{hydr}}{RT} \approx k_1 + k_2\left(E_{latt} - \Delta G_{hydr}\right). \tag{31}$$

The solid-state perturbation method was validated on the benzodiazepines series (including nordiazepam),[104,105] GPR119 ligands,[106] and benzoylphenylurea (unpublished data of Yu. Abramov), in all studies correctly predicting the trend of the intrinsic solubility, allowing the most significant perturbations to be identified. As an example, the result of application of the solid-state perturbation method to benzodiazepines is presented in **Fig. 13**.

In application to the likelihood of a missed stable form, interpretation of different crystal energy landscape patterns depends on the energy separation of the predicted observed structure from all other real or potential polymorphic forms. An ideal scenario supporting a low likelihood of a missed stable form is described by a pattern in which the observed crystal form is a global minimum in lattice energy separated from all other structures by a considerable energy gap. The proposed energy gap is 6 kJ mol^{-1} or higher depending on the level of theory.[102] The oncology drug crizotinib (Xalcory)[37] and the antibacterial drug candidate sulopenem[107] (**Fig. 14**) are two reported pharmaceutical examples of a true monomorphic behavior in which the observed most stable forms are separated from all other simulated potential structures by an energy gap of ~8 and ~7 kJ mol^{-1}, respectively.

Strictly speaking, due to the limitations discussed below all other lattice energy landscape patterns cannot by themselves testify to a low likelihood of a missed stable form, and in certain cases may suggest that additional polymorph screening is required.

An interpretation of crystal energy landscapes should be performed bearing in mind *the limitations and challenges* of the CSP methodology:[37]

- *Potential energy*. The energy difference between possible structures is typically very small so that virtual polymorph ranking strongly depends on the way the lattice energy is calculated. Different methods may give significant differences, even in prediction of relative stabilities of observed polymorphs.[108,109] The density functional theory with dispersion energy corrections and a model with distributed multipole expansion of electrostatic interaction (DMA) appeared to be the most successful methods of the CSP.[110]
- *Temperature effect*. One of the most important limitations of polymorphism prediction by typical CSP techniques is related to the fact that the free energy landscape of possible crystal structures at ambient temperature is approximated by a static lattice energy landscape at $T=0$ K. It was recently demonstrated for 508 polymorphic organic molecules that though the distribution of vibrational energy differences between polymorphs is rarely exceeding 2 kJ mol^{-1}, these contributions are large enough to cause a reranking of polymorph stability below or at ambient temperature in 9% of the polymorph pairs.[111]
- *Kinetics effect*. Barriers of transformation between minima of the lattice energy landscape, which are important for polymorph kinetics, are typically not considered by the current CSP methods. It is reasonable to assume that kinetic effects may account for a lower number of observed polymorphs relative to the predicted ones.
- *System complexity*. The computational challenges of performing accurate CSP studies quickly increase with the system complexity (molecular size and flexibility, and number of molecules in an asymmetric unit cell).

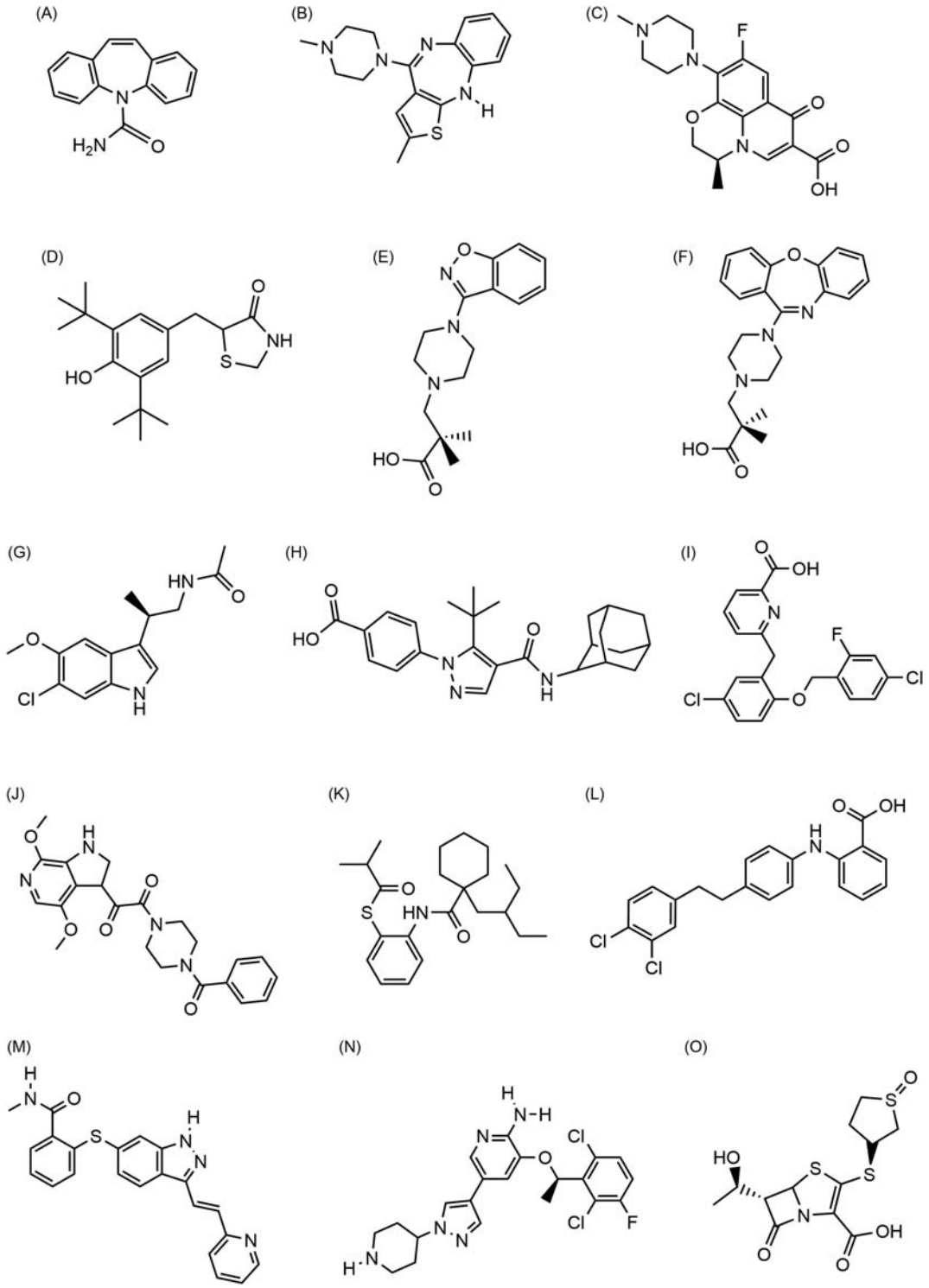

Fig. 11 Examples of pharmaceutical molecules for which both computational and experimental solid form screenings were performed: (A) carbamazepine,[278] (B) olanzapine,[279] (C) levofloxacin,[280] (D) tazofelone,[281] (E) LY2806920,[282] (F) LY2624803,[282] (G) LY156735,[283] (H) AZD8329,[284] (I) GSK269984B,[285] (J) BMS-488043,[286] (K) dalcetrapib,[287] (L) XXIII compound,[277] (M) axitinib,[37,101,288] (N) crizotinib,[37,101] and (O) sulopenem.[107]

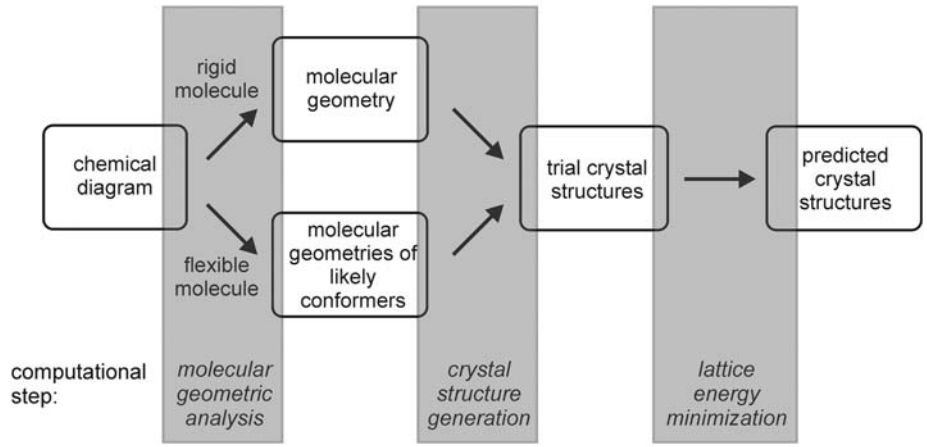

Fig. 12 Schematic representation of the steps of crystal structure prediction by global lattice energy minimization. Republished with permission of John Wiley and Sons, Inc. from Day, G. M. Advances in Crystal Structure Prediction and Applications to Pharmaceutical Materials. In *Computational Pharmaceutical Solid State Chemistry*; Abramov, Y. A., Ed.; John Wiley & Sons, Inc.: Hoboken, NJ, 2016; pp. 87–115.

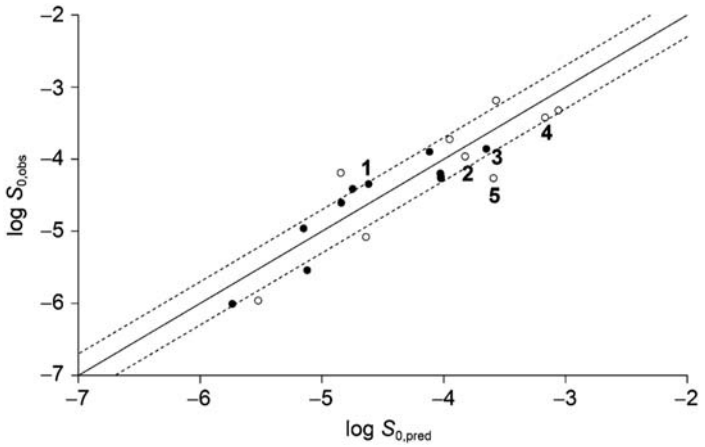

Fig. 13 Results for the training (●, RMSE = 0.264) and test set (○, RMSE = 0.424) of the benzodiazepines (all, RMSE = 0.349), based on the *in silico* perturbation strategy. The ±0.3 error lines are included as dotted lines. Reprinted with permission from Briggner, L. E.; Kloo, L.; Rosdahl, J.; Svensson, P. H. In Silico Solid State Perturbation for Solubility Improvement. *ChemMedChem* **2014**, *9*(4), 724–726. Copyright (2014) John Wiley and Sons, Inc.

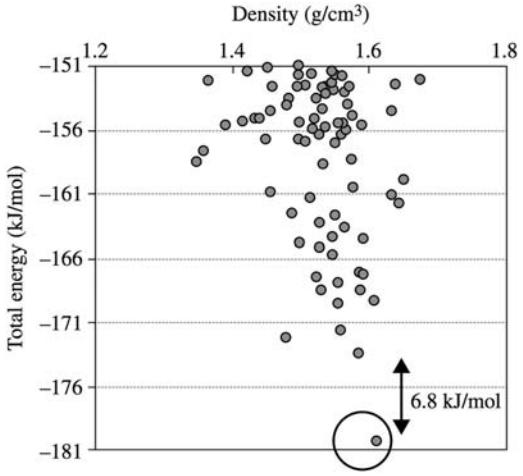

Fig. 14 Crystal structure prediction results for sulopenem. The circled structure matches the observed crystal structure. Republished with permission of John Wiley and Sons, Inc. from Krzyzaniak, J. F.; Meenan, P. A.; Doherty, C. L.; Pencheva, K.; Luthra, S.; Cruz-Cabeza, A. Integrating Computational Materials Science Tools in Form and Formulation Design. In *Computational Pharmaceutical Solid State Chemistry*; Abramov, Y. A., Ed.; John Wiley & Sons, Inc.: Hoboken, NJ, 2016; pp. 117–144.

3.16.4.1.1.2 Hydrogen bonding propensity approach

An alternative simplified approach to the classification of polymorph stability is based on selected dominant interaction analyses. Since H-bonds are the strongest and most specific (directional) interactions, they typically play a dominant role in the crystallization and stability of pharmaceutical solids. Therefore a probabilistic approach to analyses of organic crystal stabilities was recently developed[112] based on statistical analysis of hydrogen bonds in the Cambridge Crystal Structure Database (CSD).[113] This knowledge-based method analyzes potential H-bonding functional groups of a molecule of interest to predict statistically likely pairwise H-bonding interactions in the stable crystalline form. According to this approach, a crystal structure that adopts the highest propensity H-bonds displays a low likelihood of the existence of a more stable form indicating that the polymorph screening was likely to be complete. In contrast, the presence of only low propensity H-bonds indicates a high risk of existence of a more stable form and an additional study is likely to be required. Successful applications of the knowledge-based approach to multiple drug-like systems were reported in the literature for ritonavir,[114] N^2-(indol-3-ylacetyl)-L-asparagine,[112] lamotrigine,[115] crizotinib,[37] axitinib,[37] and sulopenem.[107]

An alternative and complementary approach to the knowledge-based one is based on theoretical prediction of H-bonding strength (propensities). From the diversity of the available theoretical methods of H-bonding analysis two approaches, COSMO-RS σ_{HB} charges and QTAIM (Quantum Theory of Atoms in Molecules), are the most popular in application to evaluation of stability of the crystalline solid form.[43]

There are several important limitations in stability ranking based on H-bonding propensity analysis in addition to the fact that H-bonding is not the only contribution to the stability of drug-like crystals. Similar to the CSP approach, the models based on the propensity of the H-bonding interaction generally cannot account for the temperature-dependent relationship between the polymorphic forms. In addition, an inherent limitation of the H-bonding propensity methods (the knowledge-based and the σ_{HB} charges analysis) is the inability to estimate the stability ranking of the polymorphs, which preserve similar H-bonding interactions.[37]

3.16.4.1.2 Statistical methods

Statistical approaches cannot replace physics-based methods (like CSP) in the prediction of molecule's polymorphic landscape. However difficulties in experimental determination of sublimation energy, along with significant computational complexity of CSP methods, make QSPR models an attractive alternative approach for calculation of representative values of lattice energies of drug-like molecules. Many studies have reported lattice or sublimation energy models of organic compounds based on QSPR/QSAR approaches. The reported QSPR models used a variety of statistical approaches (comparative molecular field analysis (CoMFA),[116] variations of MLR,[117–119] and NN[118,120] approaches, nearest neighbors,[38] RF,[127] and Cubist (https://www.rulequest.com/cubist-info.html)[126,127] and descriptor sets (VolSurf,[122] Dragon,[25] charged partial surface area (CPSA),[124] hydrogen bond thermodynamics (HYBOT),[125] fragment-based or group contribution (GC)). However many of the reported models were focused on a small dataset of homologous (and nondrug-like) series and are therefore of less interest to pharmaceutical applications.

A remarkably simple and relatively accurate ΔH_{sub} QSPR model was reported by Maryam Salahinejad et al.[118] In that study VolSurf and CPSA descriptors were utilized to build a four-parameter linear model based on a dataset of 1302 chemically diverse organic molecules:

$$\Delta H_{sub} = -(23.5 \pm 0.3) + (386.7 \pm 12.8)\mathrm{FPSA3} + (0.385 \pm 0.019)\mathrm{PSA} + (0.114 \pm 0.003)V + (0.0495 \pm 0.0027)W1. \quad (32)$$

Here, $W1$ is the volume of a molecular envelope at the selected energy level, which is accessible to and interacts favorably with water molecules. FPSA3 is the fractional CPSA, V is the water-excluded molecular volume, and PSA is the polar surface area. The model performance for a test set was reasonably good: $R^2_{test} = 0.95$, standard error of estimation (SPE) = 7.88 kJ mol^{-1}.

The same dataset was used for building a nonlinear recursive partition Cubist algorithm[122] utilizing VolSuf descriptor set.[126] The model performance for a test set of 260 compounds ($R^2_{test} = 0.97$, RMSE = 5.8 kJ mol^{-1}) appeared to be quite comparable with that of the MLR model. This observation supports the suggestion that the relationship between the molecular descriptors and the enthalpy of sublimation is predominately linear.[118]

The aforementioned Cubist ΔH_{sub} QSPR model was used to develop an approach describing compound solubility as interplay between molecular solvation features and packing properties.[126] The approach was based on a treatment of the crystal packing contribution to equilibrium solubility based on ΔH_{sub} QSPR calculations and a quantum mechanical treatment of solvation effect via free energy of mixing, ΔG_{mix}, of the supercooled liquid phase of the molecule of interest with water (**Fig. 15**). This model allows evaluating the source of poor solubility (crystal packing vs. molecular solvation) of a drug-like molecule. The model also allows prediction of likely solubility changes associated with molecular modification with no knowledge of the crystal solid state needed. Such an approach is attractive for lead optimization in pharmaceutical discovery where multiple compounds with limited structural experimental information are evaluated.

There are a limited number of studies reporting QSPR models of Gibbs energy of sublimation. Perlovich and Raevsky used 965 experimental observations to build a ΔG_{sub} QSPR model using a nearest neighbor approach based on HYBOT physicochemical descriptors.[38] The model performance for a test set of 279 compounds provided values of $R^2_{test} = 0.768$ and $\mathrm{RMSE}_{test} = 9.35$ kJ mol^{-1}.

Abramov used 1213 experimental observations of Gibbs energy of sublimation (a database provided by Dr. German Perlovich) for building a Cubist regression model based on a combination of Dragon, VolSurf, and SMARTS keys descriptors.[127] The model performance for a test set of 181 compounds provided values of $R^2_{test} = 0.88$ and $\mathrm{RMSE}_{test} = 7.0$ kJ mol^{-1}. An error propagation

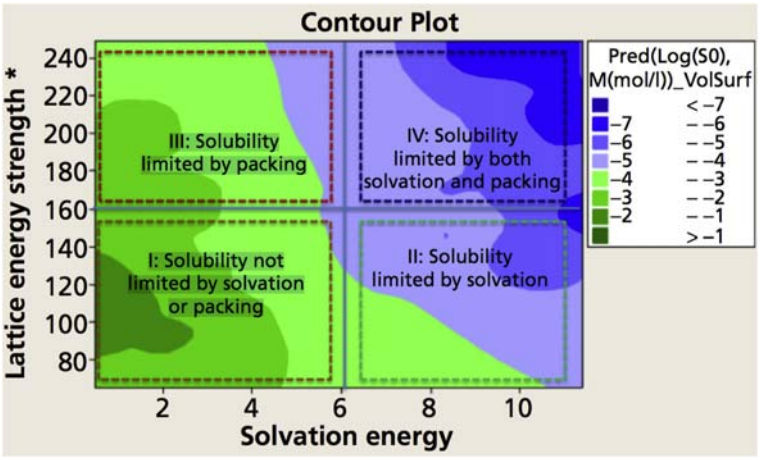

Fig. 15 Solvation packing grids based on free energy of mixing with water (kcal mol^{-1}) and lattice energy strength, as measured by QSPR estimated $\triangle H_{sub}$ energy (kJ mol^{-1}). The solvation energy is in kcal mol^{-1}. (I) Solubility not limited by solvation or packing; (II) solubility limited by solvation; (III) solubility limited by packing; (IV) solubility limited by both solvation and packing. Reprinted with permission from Docherty, R.; Pencheva, K.; Abramov, Y. A., Low Solubility in Drug Development: De-Convoluting the Relative Importance of Solvation and Crystal Packing. *J. Pharm. Pharmacol.* **2015**, *67*(6), 847–856. Copyright (2015) John Wiley and Sons, Inc.

consideration demonstrated that the resulting model accuracy was not good enough for a reasonably accurate (≤ 1 log unit) prediction of absolute values of solubility from a sublimation thermodynamic cycle. Indeed, assuming that sublimation and hydration free energies are independent from each other, one may approximate a standard error of log S prediction as (referred to molar fractions):

$$\sigma(\log S) = \frac{\sqrt{\sigma^2(\Delta G_{sub}) + \sigma^2(\Delta G_{hydr})}}{\ln(10)RT}. \tag{33}$$

Therefore, assuming that RMSEs can be interpreted as standard errors, even neglecting $\sigma^2(\Delta G_{hydr})$ contribution, RMSE(ΔG_{sub}) values should be below 5.7 kJ mol^{-1} in order to provide a standard error of log S prediction below 1 log value.

One of the important factors affecting QSPR/QSAR model building of sublimation and lattice energies is a limited amount of ΔG_{sub} and ΔH_{sub} observations available for the drug-like molecules. In addition, it was recently demonstrated[53] that a major limiting factor of accuracy of QSPR/QSAR models of crystalline state properties (such as solubility, fusion, and sublimation) is the lack of descriptor sets accounting for the long-range order (periodicity) phenomenon. There are also important entropic contributions, which are noticeably more pronounced in absolute value for the sublimation properties and should be appropriately considered for an accurate QSPR modeling of sublimation free energy, ΔG_{sub}.[127]

3.16.4.2 Melting Point

3.16.4.2.1 Physics-based methods

3.16.4.2.1.1 Molecular dynamics and Monte Carlo

The molecular simulation methods for MP prediction can be categorized into two groups: (i) "direct methods" such as the hysteresis method,[128] the voids method,[129] and solid–liquid interface methods[130]; and (ii) "free energy methods" including the single-occupancy cell method,[131] the Einstein crystal method,[132] and λ-integration methods.[133,134] The first group of approaches involve the direct simulation of the melting process in a dynamic manner. They are relatively easy to apply but their accuracy can be limited. In turn, the second group of approaches are more rigorous but are generally more complicated to apply. A comprehensive review of the methods can be found elsewhere.[135] The main problem is that all these methods require an experimental crystal structure as input, which means the calculation is not really predictive as the MP can be measured easily once the crystal structure is known. The first attempt to perform fully *in silico* prediction of MP was recently performed by Zhang and Maginn, where simulations were used to predict both a crystal structure and a MP for two rigid molecules (2-propenal and 4-cyanopyridine N-oxide).[136] The packages MOLPAK[137] and PMIN were employed for CSPs, while melting-point calculations were realized using the pseudosupercritical path[134] method of classical MD. The study was based on the assumption that accurate MP predictions can be made using predicted crystal structures with free energies that are close to that of the experimental structure. Indeed, despite the fact that CSPs failed to reproduce the experimental crystal structures of both molecules, MPs were estimated with an error of 15–25 K. The main problem, which Zhang and Maginn stressed in their work,[136] is inaccurate force fields, which lead to inaccurate MP predictions regardless of the methods applied.

3.16.4.2.2 Statistical methods

The MP has been a target of modeling for a long time. Already in 1881, Mills derived QSPR models for the hydrocarbon chain as following:[138]

$$\text{MP (K)} = \beta x/(1 + gx), \tag{34}$$

where β and g are constants for a given class to achieve accuracy of prediction less than 1 K and x is number of methyl groups. This result indicates that for some specific classes of chemicals a high accuracy of MP prediction can be achieved. Unfortunately, the high precision accuracy of Eq. (34) was a very particular case and, even after 140 years of research, such high precision models for diverse compounds do not exist and actually cannot be developed, as analyzed later.

During the second part of the last century there were a large number of articles devoted to analysis of other chemical series as nicely reviewed by Dearden.[44] Such studies frequently involved few tens and seldom few hundreds of compounds grouped by chemical class, for example, alkanes, hydrocarbons, PAHs (polycyclic aromatic hydrocarbon), alcohols, anilines, etc. The average errors for nonaromatic compounds were ~20 K and increased to ~30 K for aromatics, that is, indicating that prediction of the latter compounds was more difficult. The descriptors used for chemical series frequently included several topological indices or other descriptors (e.g., physical–chemical, quantum-chemical, and structural) while for larger diverse sets having more than a thousand compounds the GC, structural, and frequently correction factors were used too.

The GC methods assume additivity of the modeled property with respect to the groups. Since this assumption does not really hold for MP, the researchers frequently used correction factors to account for nonlinearity. For example, Simamora and Yalkowsky used correction factors accounting for hydrogen bond formation and disruption of planarity of biphenyl by the presence of substituent(s) at the 2,2′, 6, or 6′ positions to achieve STDE = 38 K for $n = 1690$ compounds. Such strategy and development of functional groups targeted for the MP allowed the authors to calculate much higher accuracy compared to the GC method of Joback and Reid,[121] STDE = 69 K. The latter method used the same groups for several properties.

Complex GC, which include three levels of description of molecules, were developed by Maerngo and Gani.[139] The first-order groups covered the whole molecule and did not overlap. The second- and third-order groups were overlapping and covered only specific parts of molecules, thus capturing interactions within larger molecular fragments to better cover complex polyfunctional molecules. De facto, such complex groups play a role of correction factors. This method allowed the authors to calculate STDE = 28 K for $n = 1547$ compounds.

There are only few studies published with large sets of MP data. Karthikeyan et al.[123] analyzed a diverse set with $n = 4173$ using NN and different sets of descriptors. The authors found that models developed with 2D descriptors provided better prediction accuracy (RMSE = 48–50 K) compared to those based on 3D indices (RMSE = 55–56 K). An attempt to improve the model by combination of both sets did not improve the results. The use of 3D descriptors also did not provide an advantage over 2D for analysis of MP of ILs of 717 bromides of nitrogen-containing organic cations.[140] In this study several methods, such as MLRA, partial least squares (PLS), k-nearest neighbors (kNN), NN, and SVM, were analyzed using fragment-based descriptors,[88] E-state indices,[141] and Dragon descriptors.[25] When analyzing the performance of the models for individual sets, the higher errors were calculated for more diverse ones. At the same time the results were dependent on the use of the machine learning methods: nonlinear methods such as NN and SVM provided consistently better prediction abilities.

When developing a model, it is important also to understand which molecular properties are responsible for a decrease/increase in MP. A comprehensive analysis using MMPs was performed for the public set of Karthikeyan as well as in-house data of $n = 746$ compounds by Schultes et al.[142] The authors identified four main factors influencing MP: number of hydrogen bond donors and acceptors as well as number of rotatable bonds and halogen atoms (I, Br, and Cl). In order to exclude intercorrelations, the analysis of MMPs was performed only for pairs of molecules when only one factor was changed. The number of hydrogen bonds had the highest impact, increasing MP for about 50 (30) K for in house (public) set, respectively. The increase in the number of hydrogen acceptors by one contributed an increase in MP by 22 (9) K, while the increase in the number of rotatable bonds leads to a decrease in MP by −17 (−10) K. It is also interesting that the effects were more pronounced for *in house* data, which shows their higher consistency. The addition of one Br atom increased MP by 47 (24) K. The significant increase of MP due to the addition of I (39) and Cl (7) was also observed for public set but no conclusion could be made for in-house data, due to limited number of MMPs.

The two largest models so far to predict MP were published by Tetko et al.[143,144] The first model was based on $n = 47{,}000$ compounds collected from the OCHEM database,[99] chemical compounds provided by Enamine, Bergstrom dataset of MP for drugs,[145] and the "Bradley" dataset[146] containing doubly curated data collected by Open Notebook science community members. The important result of this article was finding that the majority of MP data of pharmaceutical relevance, >90%, have MP in intervals of 50°C (323.15 K)–250°C (523.15 K) (drug-like MP range, **Fig. 16**). Thus, in principle, when developing and testing models to be used in pharma, one can concentrate on their performance for this temperature region. Like in study of Varnek et al.[140] it was demonstrated that MP is a nonlinear property: the use of Associative Neural Networks and SVM calculated significantly lower errors compared to the use of linear methods. This set was extended with $n = 225{,}000$ compounds mined from patents. These compounds also had about 90% of their data within drug-like MP region.

The error of the final consensus model for the patents data closely followed the estimated experimental error of the data. This error was 33 K for the drug-like MP range and perfectly matched STDE = 32 K calculated using experimental data. For MP < 50°C (323.15 K) the same model calculated RMSE = 47 K and RMSE = 28 K for data mined from patents and Bradley set, respectively. Again, the large difference in both errors is due to the higher accuracy of data in the latter set. This result showed that the used approach (consensus modeling) and descriptors were sufficient to predict MP up to the level of experimental data accuracy.

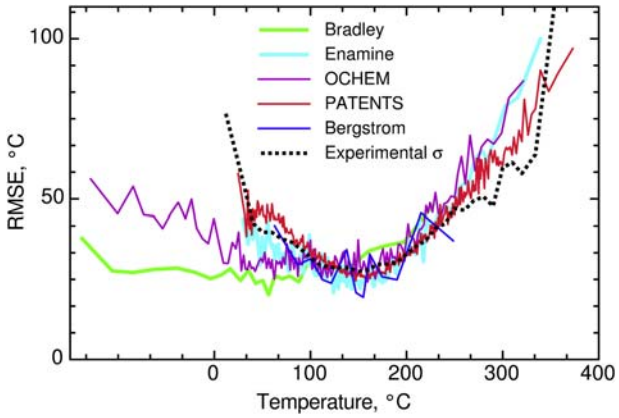

Fig. 16 The experimental and calculated errors of the consensus model as a function of the MP temperature for different subsets. The experimental accuracy line was built based on $N=18{,}058$ differences in the MP temperatures. Reproduced with permission from Tetko, I. V.; Lowe, D.; Williams, A. J. The Development of Models to Predict Melting and Pyrolysis Point Data Associated With Several Hundred Thousand Compounds Mined From PATENTS. *J. Cheminform.* **2016**, *8*, 2. Creative Commons Attribution 4.0 International License (http://creativecommons.org/licenses/by/4.0/).

Thus it is in contradiction to the conclusion of Hughes et al.,[147] who explained low accuracy of models to predict MP by deficiency of used descriptors.

The experimental error of 33 K looks very high. The majority of experimental measurements in patents were provided as intervals with standard deviation STDE = 3 K between both measurements, which can be used as an estimation of the reported experimental accuracy of measurements for single experiments. There are many more aspects contributing to the variation of MP measurements due to sample preparation of the same compound, which were nicely summarized by Preiss et al.[148] in their analysis of MP of organic salts. The author indicated that factors such as contamination, polymorphism, presence of liquid and plastic crystals, and decomposition could easily contribute variations in ten degrees. For example, the purity of compounds for HTS screening is usually about 85%–90%. The impact of contamination can be calculated as following:[148]

$$\Delta \mathrm{MP} = -\mathrm{MP}\frac{mR}{\Delta S_{fus}}, \tag{35}$$

where R is the Avogadro constant, m is the molar amount of contaminant, and ΔS_{fus} is the melting entropy of the target compound. The equation indicates that contamination has a higher effect not only on compounds with higher MP but also on compounds with higher molecular mass for the same mass% of contaminant. Considering that MP increases with MW of compounds, higher experimental errors (depression of MP) could be expected for high temperature MP values. Moreover, contaminants with lower mass will provide a stronger impact. In this respect the authors noticed that water, which is able to form strong hydrogen bonds and has low MW, could be the worst contaminant. In their example the authors considered the IL 1-*n*-hexyl-3-methylimidazolium bis(trifluoromethylsulfonyl)-imide which would have MP depression of 1 K for 1.85 mass% of moisture.

3.16.4.3 Vapor Pressure

3.16.4.3.1 Physics-based models

3.16.4.3.1.1 Molecular dynamics and Monte Carlo

Vapor pressure predictions with MD methods are based on the estimation of thermodynamic parameters of the corresponding process. First, one can calculate heat of vaporization using potential energies ($E^{potential}$) in the gaseous and liquid (pure compound) phases:

$$\Delta H_{vap}(T) = E_{gas}^{potential}(T) - E_{liquid}^{potential}(T) + RT + C, \tag{36}$$

where C is the correction term, which accounts for the difference in vibration energies calculated quantum mechanically and classically (it is usually neglected). Wang and Hou estimated heats of vaporization and the temperature dependence for a set of 71 small organic compounds covering diverse functional groups.[149] The best performing MD protocol predicted vapor pressure with RMSE = 1.2 kcal mol^{-1} (5.02 kJ mol^{-1}).

Secondly, one can estimate the free energy of vaporization, which can be performed using the free energy perturbation (FEP) method.[150] Unfortunately, FEP simulations for drug molecules in the MW range from 400 to 600 Da, typical of modern drugs, may be so time-consuming that they cannot be used routinely.[151] An alternative methodology was proposed by Lindfors and coworkers.[152] They suggested a relation between the free energy of solvation in the pure melt (opposite to the free energy of vaporization) on the one hand and more readily accessible quantities such as interaction energies and molar volumes on the other hand:

$$-\Delta G_{vap} \cong \Delta G_{cavity} + E_{LJ} + \frac{E_c}{2}, \tag{37}$$

where ΔG_{cavity} is the energy to create cavity in the melt, E_{LJ} is the Lennard-Jones energy, and E_C is the Coulomb energy. In general, the process can be considered as a sum of three following steps: (i) creating a cavity in a melt, (ii) insertion of a solute in the cavity, and (iii) turning on atomic partial charges. The two last steps can be performed with a coupling parameter λ using FEP simulations. The free energies of solvation of a drug in a pure melt were obtained at 400°C (673.15 K) for 46 drug molecules. Further cooling down of a system from 400°C (673.15 K) to 25°C (298.15 K) leads to vapor pressure predictions with accuracy close to that for FEP simulations.[153]

3.16.4.3.1.2 COSMO-RS

One of the widely used physics-based methods for vapor pressure prediction is COSMO-RS. As it was shown above it is a theory about molecules in the liquid phase. However, vapor pressure prediction requires chemical potential in the gas phase as well:

$$p_X^X = \exp\left\{-\frac{\mu_{gas}^X - \mu_X^X}{RT}\right\}. \tag{38}$$

The potential can be calculated using the difference between quantum-chemical total energies of the molecule X in the gas phase and the conductor (COSMO reference state):

$$\mu_{gas}^X = E_{gas}^X - E_{COSMO}^X - E_{vdW}^X + \omega n_{ring}^X + \eta_{gas}, \tag{39}$$

where E_{vdW}^X is the van der Waals energy of the solute (conductor reference state), ωn_{ring}^X is the correction for ring systems, and η_{gas} connects reference states in solution and in the gas phase. One should note that Eq. (39) does not take into account any gas-phase nonidealities such as dimerization of organic acids. They can be added externally starting from the ideal gas reference state. As it was reported by COSMO-RS developers,[154] the typical prediction accuracy of the approach for vapor pressure of neutral liquid compounds is better than 0.5 log units. The results were recently proved on a wide set of multi-functional oxygen-containing organic compounds, with an accuracy of prediction of about 0.5–1.0 log units, overestimating data for self-associating compounds (carboxylic acids and alcohols).[155] Liquid vapor pressure calculation for a set of polychlorinated aromatic compounds also showed a good match of the predicted data with experimental values (0.2–0.8 log units error).[156] Analysis of the method performance for more complicated systems, such as ILs,[154] showed that COSMO-RS underestimated the vapor pressure by roughly 0.5–4.0 log units depending on the composition of the IL.

COSMO-RS calculations are more complicated in the case of vapor pressure prediction for solid compounds since it requires chemical potential for crystalline phase. In general, solid–liquid equilibrium calculations with COSMO-RS employ an experimental estimation for the fusion free energy, which characterizes the melting of the crystal phase:

$$\Delta G_{fus}^X(T) = -\Delta H_{fus}^X\left(1 - \frac{T}{T_{melt}^X}\right) + \Delta Cp_{fus}^X\left(T_{melt}^X - T\right) - \Delta Cp_{fus}^X T \ln\frac{T_{melt}^X}{T}, \tag{40}$$

where T_{melt}^X is the MP, ΔH_{fus}^X is the heat of fusion, and ΔCp_{fus}^X is the heat capacity of fusion. However, experimental data are not always available, for example, for explosives.[157] Therefore, the following QSPR model was proposed for ΔG_{fus}^X estimation[157–159]:

$$\Delta G_{fus}^X(T) = a_1 V_{\mathrm{COSMO}}^X - a_2 N_{ring} + a_3 \mu_{water}^X + a_4 \mu_{gas}^X, \tag{41}$$

where V_{COSMO}^X is the cavity volume of the solute molecule and N_{ring} is the number of aromatic ring atoms. Several versions of the model differ in values of empirical coefficients a_i and presence of the last right-hand side term.

General limitations of the COSMO-RS method are its inapplicability for systems near or beyond the critical point, and low accuracy for systems with polar ions or tertiary amines.

3.16.4.3.1.3 UNIFAC

Among alternative physics-based approaches for vapor pressure predictions one can mention a GC method based on UNIFAC groups, which was developed by Fredenslund and Rasmussen in 1979.[160] The method is based on the Eq. (8), where Gibbs free energy of vaporization/sublimation is represented as following:

$$\Delta G_{vap/sub} = \sum_k v_k \Delta g_k + RT \sum_k v_k \ln \Gamma_k. \tag{42}$$

Here Δg_k is the difference between the molar free energy of group k in the pure state and in the gas at 1 atm (1.013×10^5 Pa), the second term is the UNIFAC "residual" term (Eq. (25)). Generally, UNIFAC is acknowledged to be an accurate predictive method for vapor pressure (deviation about 15% for hydrocarbons).[161] However, the method suffers from a number of inherent limitations:[162]

- Due to assumptions behind the theory, UNIFAC is accurate only for low or moderate pressures;
- It cannot be applied to systems containing ions, salts, polymers, or noncondensable gases;
- UNIFAC fails for mixtures of isomers because it does not account for the effect of surrounding groups on the particular fragment behavior;
- UNIFAC depends critically on the available experimental data and their quality. Existing interaction parameters are limited by 18 functional groups (covering aliphatic and aromatic hydrocarbons and oxygen-containing compounds).

3.16.4.3.1.4 SAFT

A GC approximation was also proposed for the SAFT method (GC-SAFT).[163–165] Elliott and coworkers[166] formulated its generalized methodology as follows: (i) pure component parameters were obtained by matching their boiling points, estimated solubility parameters, and estimated liquid density; (ii) GC were regressed for the shape factor (86 first-order functional groups were found to cover 19 different families of compounds). The method allows for vapor pressure predictions based solely on the chemical structure and very satisfactory results are reported (deviation around 30% of vapor pressure).

3.16.4.3.2 Statistical methods

There are two principal types of approaches to predict vapor pressure using statistical methods. The first one implies the use of other physical–chemical properties, along with additional descriptors that can be computed from chemical structures, to create predictive statistical (machine learning) models. In this way, Kühne et al.[167] have trained an ANN (artificial neural network) on a training set composed of 1200 compounds (hydrocarbons and halogenated hydrocarbons) represented by 23 descriptors computed from chemical structure, system temperature, and MP for solid compounds to create a model that can be used to predict vapor pressure for new compounds. The absolute average error of prediction of this model estimated using an external set of compounds is 0.13 log units. Similarly, Godavarthy et al.[168] have trained an ANN on a diverse dataset of 1100 compounds represented by several structural descriptors and the values of triple and critical points to obtain a model with relative average errors of less than 0.5%. The latter model can predict accurately the vapor pressure of organic chemicals over the entire saturation range from the triple point to the critical point. Nonetheless, in spite of an excellent prediction performance of such models, they are not capable of making predictions for compounds with unknown values of physical–chemical properties included in models. This can be considered a significant limitation of this approach.

The second type of approach is currently much more popular. In this case only descriptors computed from chemical structure are involved in building statistical models in the framework of a QSPR approach. Application of QSPR models to predicting vapor pressure is surveyed in Refs. 169–171. Here we consider several important examples. Chastrette et al.[172] built an MLR model with standard error of 0.1 log units for a set of 186 compounds (alkanes and alcohols) using the components of the autocorrelation vector calculated from Bondi's surface areas as descriptors. Basak et al.[173] used a hierarchical QSAR approach to build an MLR model with standard error 0.29 log units for a set of 476 diverse chemicals using topostructural, topochemical, and geometrical descriptors. Liang and Gallaher[174] developed an MLR model with standard error 0.53 log units for a diverse set of 479 compounds using polarizability and polar functional group count as descriptors. Katritzky et al.[175] built an MLR model with standard error 0.33 log units for a diverse set of 411 diverse compounds using an extensive set of constitutional, topological, electrostatic, geometrical, and quantum-chemical descriptors. Artemenko et al.[176,177] applied a combination of back-propagation neural network and fragmental descriptors to build models for a set of 352 organic compounds (linear, branched, and cyclic alkanes, alkenes, arenes, and halogen derivatives). The RMSE of prediction estimated using external cross-validation procedure of these model are 0.22 and 0.15 log units. The second model with enhanced predictive performance was obtained by the use of ensemble modeling. Cash[178] developed kNN models in a Euclidean space defined by electrotopological descriptors with errors 0.56 and 0.55 log units for a large dataset of 1676 compounds.

Vapor pressure is known to depend highly on temperature, and hence it is desirable to build temperature-dependent models. Chalk et al.[179] developed a temperature-dependent model based on a feed-forward neural net and quantum-chemical descriptors. A set of 7681 measurements at various temperatures performed on 2349 compounds was used for this study. The reported standard error of prediction for this model is 0.33 log units. Yaffe and Cohen[180] also developed a temperature-dependent neural network model using valence connectivity indexes based on a dataset of 274 hydrocarbons. An excellent average prediction error of 0.04 log units was demonstrated. Finally, Gharagheizi et al.[181] developed a temperature-dependent neural network model for an extremely large dataset of approximately 42,000 vapor pressure values belonging to about 1400 chemical compounds. The reported average absolute relative deviation of this model is 6%, while a squared correlation coefficient is 0.994.

In summary, the most popular statistical (machine learning) methods for building models to predict vapor pressure are multiple linear regression (mostly in earlier studies) and ANNs (in more recent studies), while descriptors are usually either fragmental[182] or quantum-chemical. The advantage of fragmental descriptors is the ease of their calculation and handling. The drawback of fragmental descriptors is the problem of "rare fragments," which sharply narrows applicability domain of model. Quantum-chemical descriptors are potentially capable of providing much larger applicability domain, but by the expense of the drastic loss of computational efficiency. Another general limitation of all statistical methods of predicting vapor pressure is related to the fact that this property may be measured only for volatile compounds, which usually have relatively low MW. This should be taken into account in the application of statistical models to predict the vapor pressure of new compounds.

3.16.4.4 Aqueous and Nonaqueous Solubility

3.16.4.4.1 Physics-based models

Physics-based modeling methods for predicting absolute solubility can be roughly classified into several main categories: (i) direct methods based on separate calculations of ΔG_{sub} and ΔG_{solv} terms, (ii) COSMO-RS model[159] and (iii) methods based on the GC approach that use UNIFAC and SAFT theories.[30] In this section we will briefly overview main principles of solubility prediction by the first approach.

The most straightforward approach to model solubility is to calculate it directly through the free energy of solution, ΔG_{sln} in the thermodynamic cycle (Fig. 3) using *ab initio* approaches for multibody molecular systems, like, for example, *ab initio* molecular dynamics[183] and use the fundamental relationship (referred to molar fractions):

$$\log S_0 = -\frac{\Delta G_{sln}}{RT\ln(10)}. \tag{43}$$

However, due to the number of molecules in the system, as well as the maximum simulation time being too small to properly sample the phase space of the system, there is an extremely large computational expense associated with such simulations, even with the use of modern high-performance computing (HPC) systems. Even less expensive molecular mechanics methods, that use classical force-fields, are still difficult to apply to direct modeling of dissolvation process due to the long timescales associated with the process and the overall complexity of the modeling setup due to the multiphase nature of the system (coexistence of the liquid and solid phases). Therefore, in practice, the most popular approaches are based on using the first part of the Eq. (11) and a consequent relationship: (referred to molar fractions)

$$\Delta G_{sln} = \Delta G_{sub} + \Delta G_{solv} \tag{44}$$

and calculating separately the ΔG_{sub} and ΔG_{solv} contributions into ΔG_{sln}. Such an approach has several advantages due to the flexibility of choices for ΔG_{sub} and ΔG_{solv} calculations. Thus, for ΔG_{sub} one can use different CSP methods[103,184] based on either QM of classical mechanics approaches. At the same time, for ΔG_{solv} calculations one can use suitable methods for simulations of liquid systems such as MD/MC,[151,185] molecular theories like 3D RISM,[186] or continuum solvation methods.[187] We would like to emphasize the role of recent series SAMPL blind challenges (http://www.eyesopen.com/sampl and https://drugdesigndata.org/about/sampl) that provoked a wave of interest in ΔG_{solv} predictions using different computational techniques. These works contain several benchmark datasets that can be used for verifying new models. The critical analyses of the performance of different methods in these challenges are insightful and provide interesting information.

However, the use of *different* methods in such an approach may lead to some problems due to the inherent inconsistencies between the theories involved at different steps of the overall modeling setup for calculating solubility as well as the input parameters for modeling ΔG_{sub} and ΔG_{solv}. Indeed, due to the accumulation of errors on different steps of the simulations, the overall accuracy of the predictions of ΔG_{sln} by direct simulation methods is in general within the range of 3–10 kJ mol^{-1}.[187,188] Such calculation errors in estimation of ΔG_{sln} lead to at least 10-fold error in the prediction of the solubility.[147] Overall, developing a consistent procedure for high-accuracy prediction of solubility of wide classes of pharmaceutical compounds based on direct simulation approach represents a challenge for the molecular modeling community.

3.16.4.4.2 Statistical methods

Statistical approaches to predicting aqueous and nonaqueous solubility of organic compounds in solid and liquid states are discussed in detail in the monograph of Yalkowski et al.[189] and several comprehensive review articles.[170,171]

According to Yalkowski and Banerjee,[189] there are three main categories of statistics-based solubility prediction methods: (i) using correlations with other experimentally measured properties such as partition coefficients and MP; (ii) using GC schemes; and (iii) using QSPR models based on descriptors computed only from molecular structure. Consider the most prominent examples for all of these categories.

In 1980 Yalkowski and Valvani[190] developed the general solubility equation for estimating the aqueous solubility of either liquid or crystalline organic nonelectrolytes, which uses three parameters, the octanol–water partition coefficient ($\log P_{oct/wat}$), melting point (MP, °C), and the entropy of fusion (ΔS_{fus}):

$$\log S_{aq} \approx -\log P_{oct/wat} - 1.11\frac{\Delta S_{fus}(\mathrm{MP}-25)}{1364} + 0.54 \tag{45}$$

Two terms in this equation, MP and ΔS_{fus}, reflect the role of crystal structure. Two terms, $\log P_{oct/wat}$ and ΔS_{fus}, could be estimated from chemical structure, while the value of MP should be either known or experimentally determined. For the case of rigid molecules, where the entropy of fusion of the solute could be taken as a constant, this equation takes a very simple form,[191] which depends only on two parameters, $\log P_{oct/wat}$ and MP:

$$\log S_{aq} \approx -0.01\mathrm{MP} - \log P_{oct/wat} + 1.05 \tag{46}$$

Later on Jain and Yalkowski[192] revised the general solubility equation and obtained a more accurate estimation of the aqueous solubility (the average absolute error was estimated as 0.54 log units).[192] This method was further expanded by Meylan et al.[193] to include MW. The main limitation of this category of solubility estimation methods is that they are based on experimental properties (at least, MP) and therefore they can be applied only to compounds for which the measured values of the required parameters are known and, hence, they are not suitable for compounds not yet synthesized.

Unlike the aforementioned methods, GC approaches do not require experimental measurements and therefore can be applied to new compounds. Several methods based on GC were developed to predict the aqueous solubility of organic compounds with rather good predictive performance.[194–196] For example, the average absolute calculation error of 0.5 log units was reported by Klopman.[196] The main limitation of all pure GC approaches is that they can be applied only to compounds composed of the groups well represented in the training set.

Most of the studies aimed at building statistical models for prediction of the solubility of organic compounds are based on the QSPR methodology and involve a large variety of different types of descriptors and machine learning methods. Several dozens of QSPR models built for this purpose are comprehensively surveyed in the review articles[170,171,197,198] covering literature up to 2010, while several recent models are listed by Winkler.[199] Kuhne and coworkers[200] compared the predictive performances of several previously developed GC and QSPR models using a reference set of 1826 compounds, and the standard prediction errors were reported to lie in the range from 0.86 to 1.69 log units. A similarity-based model selection method decreased the standard error to 0.71 log units.[200] In a recent study, Winkler et al.[199] have developed several QSPR models for aqueous solubility based on VolSurf[122] and CPSA[124] descriptors trained using several statistical and machine learning methods (standard multiple linear regression, robust multiple linear regression employing an expectation maximization algorithm, and Bayesian regularized ANN with Laplacian prior) using a dataset of 4558 chemically diverse compounds. The best statistical results with squared correlation coefficients of 0.90 and standard errors of 0.65–0.67 log units were reported.[199] Surprisingly, the inclusion of the descriptors capturing crystal lattice interactions appeared not to improve the models. Cheng et al.[201] have developed a binary classification model of aqueous solubility (showing whether a solute is soluble in water) built using SVM with descriptor selection on the largest known public dataset containing over 46,000 compounds.

Because aqueous solubility is a key physical–chemical property in drug development, much effort has been spent on the development of models with maximum predictive performance with respect to drug-like compounds.[197,202–205] A "solubility challenge" was conducted to assess the prediction accuracy of several aqueous solubility prediction models on a set of 32 drug-like compounds, using a set of 100 drug-like compounds with accurately measured solubility values as a training set.[206] The results of this "challenge" obtained for 99 different models are reported by Hopfinger et al.[207]

QSPR models for prediction of nonaqueous solubility of organic compounds have also been reported in several publications. Katritzky et al. have developed a series of models to predict free energies of solvation in various solvents.[208] A QSPR model for solubility of fullerene C60 in different organic solvents built using multiplicative SMILES-based optimal descriptors was reported by Toropov et al.[209] Kravtsov et al.[210] have developed a universal model for the estimation of solvation free energy of organic molecules in different solvents, which was built using NN and fragment descriptors for representing both solute and solvent structures.

So, various methods for predicting aqueous and nonaqueous solubility of organic compounds have been developed. Most of them are based on QSPR models. The most accurate prediction methods involve ANNs and physical–chemical molecular descriptors. They were built using large datasets of experimentally measured values of solubility. Since the solubility of chemical compound depends very strongly on the experimental conditions of the measurements, such as temperature and pH, there are considerable differences between solubility values measured in different laboratories for the same compound. As a result, the accuracy of the predictions based on statistical models is limited by the accuracy of experimental measurements.

3.16.4.5 pK_a

3.16.4.5.1 Physics-based methods

This group of methods is based on the relation between Gibbs free energy of the dissociation process and its constant:

$$\mathrm{p}K_\mathrm{a} = \Delta G^0_{(aq)} \frac{1}{RT\ln(10)}. \tag{47}$$

Historically, the methods rely on the fact that the Gibbs free energy is a state function. Therefore any convenient thermodynamic cycle that connects the initial reactants and final products provides a way to calculate acidity/basicity of a compound[211,212] (Fig. 17).

In this case, the main source of error in pK_a calculations is the uncertainty in the value of the solvation free energy of a bare proton H^+. At present, the best literature value is believed to be -265.6 ± 1 kcal mol^{-1} (-1111.27 kJ mol^{-1}) for a 1 M standard state.[213]

The gas-phase free energy calculation introduces the lowest source of error in pK_a calculations since quantum-chemical calculations can nowadays be good or even more accurate than experimental measurements of gas dissociation constants.[211] CCSD(T) (coupled cluster with all single and double substitutions along with a quasiperturbative treatment of connected triple excitations) is considered a gold standard method for the calculations.[214] It allows predictions with uncertainty of about 0.5 kcal mol^{-1} (2.0 kJ mol^{-1}) in comparison with experimental data from NIST database.[214] However, the problem here is producing accurate results with less computationally expensive levels of theory. Model chemistry methods (e.g., CBS-QB3, CBS-APNO, and W1) produce reliable predictions of $\Delta G^0_{(g)}$ with slightly lower accuracy, RMSE within 1.1–1.6 kcal mol^{-1} (4.60–6.69 kJ mol^{-1}) from experimental data.[214,215] In turn, DFT offers a more cost-effective approach. Various DFT functionals (PBE1PBE, P3P86, B3LYP, etc.) were tested against experimental data from NIST database and provided results with accuracy 1.6–2.7 kcal mol^{-1} (6.69–11.29 kJ mol^{-1}).[216] One should keep in mind that each particular DFT functional represents its own parameterization method and, therefore, requires benchmarking for the system of interest.

It was found that the detour through gas phase is counterproductive because any gain from improved accuracy in gas-phase calculations is outweighed by errors caused by liquid-phase pK_a calculations, which are much more complicated because of strong solvation effects.[217,218] Therefore, at computational levels that are routinely applicable today, it is preferable to calculate the free energy of the dissociation process directly in aqueous solution avoiding gas-phase calculations. Due to the very high cost of rigorous explicit solvent calculations (for a review, see Ref. 219) solvent effects are often approximated by implicit solvent models. Although

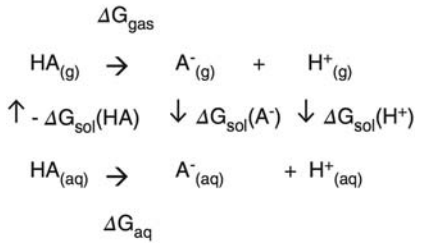

Fig. 17 Proton-based thermodynamic cycle. Reprinted with permission from Seybold, P. G.; Shields, G. C. Computational Estimation of p*K*(a) values. *Wiley Interdiscip. Rev. Comput. Mol. Sci.* **2015**, *5*(3), 290–297. Copyright (2015) John Wiley and Sons, Inc.

the models allow highly accurate solvation free energy predictions for neutral molecules, the corresponding predictions for ions still remain challenging.[211,220] Thus, the widely employed COSMO-RS method was quite successfully applied to the first principle prediction of aqueous acidity[218] and basicity,[221] but it still suffers from several systematic errors: (i) correlation between predicted free energies and experimental pK_a values has a slope that is lower than that expected from thermodynamic theory (Eq. (45)) and (ii) systematic deviations known from other continuum solvation models for aliphatic amine compounds remain for COSMO-RS predictions.[221]

It was found that including explicit water molecules within implicit solvation calculation ("cluster–continuum" or "implicit–explicit solvation" approach) improves overall pK_a predictions.[220,222,223] The discussion about how many explicit water molecules should be used still remains open,[223] although use of variation methods to determine the number of water molecules[223,224] and considering water molecules as clusters[224] were found to be promising.

3.16.4.5.2 Statistical methods

The first book on pK_a prediction using QSAR was published in 1981 by Perrin et al.[225] and covered mostly the use of classical approaches based on LFER, Hammett, and Taft equations. However, all these models can be applied only for very small congeneric series of organic compounds with simple structure and are impractical for large systems, especially for compounds of pharmaceutical interest. In the past 25 years, most of the methods for constructing statistical models for prediction of pK_a were based on QSAR/QSPR methodology.[171] In these studies, several types of descriptors were used to build models for predicting pK_a: quantum-chemical,[226] fragmental[182], etc. Most of the quantum-chemical descriptors used for this purpose describe local properties of atoms or bonds. For example, Citra[227] used partial atomic charges and bond orders as descriptors to predict the pK_a of phenols, carboxylic acids, and alcohols. Tehan et al.[228] used for this purpose semi-empirical quantum mechanical descriptors derived from frontier electron theory. Using these descriptors, the pK_a values of phenols, aromatic and aliphatic carboxyl acid, amines, anilines, oxygen-, and nitrogen-containing heterocyclic compounds were successfully modeled.[228] Chaudry and Popelier[229] applied descriptors from the "atoms in molecules" theory in the framework of the quantum topological molecular similarity approach. Correlations obtained were shown to outperform the use of Hammett and other traditional parameters to predict the pK_a values for simple carboxylic acids, anilines, and phenols. Various types of quantum-chemical descriptors were also used by Gross et al.,[230] Soriano et al.,[231] Habibi-Yangjeh et al.,[232] Baskin et al.[233] and other research groups to predict either the pK_a values or the Hammett constants closely related to them.

Ivanova et al.[234] developed models for predicting the pK_a values for phenols and carboxylic acids and closely related pK_b values for nitrogen-containing compounds using fragmental descriptors with labeled atoms,[235] local quantum-chemical indexes, and their combinations using multiple linear regression and ANNs. It was shown that combining both types of descriptors leads to QSPR models with more accurate prediction of pK_a as compared with models based either on quantum-chemical or fragmental descriptors. Different types of descriptors (constitutional, topological, geometrical, electrostatic, and quantum-chemical) were also mixed by Luan et al.[236] to obtain models for prediction for neutral and basic drugs.

A group of models for predicting pK_a were developed in the framework of 3D-QSAR approach. Gargallo et al.[237] applied the CoMFA to a set of nucleic acid components to obtain very strong correlation between pK_a and AM1 proton affinity values at grid nodes. Although a very small prediction error was reported (standard error 0.23 log units), the use of this method is efficient only for estimating the pK_a values within a congeneric set of compounds because of the necessity to perform spatial alignment of molecules. This imposes severe restrictions on the applicability of the CoMFA method, as well as other alignment-based 3D-QSAR approaches, for predicting the properties of wide heterogeneous sets of drug-like compounds. Milletti et al.[238] developed much more practical computational methods for pK_a prediction of organic compounds using descriptors based on molecular interaction fields precomputed on molecular fragments. External validation demonstrated good predictive performance (root mean square error 0.90 log units). For a validation set of 28 drug-like compounds, the method gave better results than the ACD/pK_a program (root mean square error 1.36 log units).

Several publications deal also with developing models for predicting the pK_a values for organic compounds in nonaqueous solvents. In this way, Jover et al. developed neural-network models to predict the pK_a values for phenols,[239] anilines,[240] carboxylic,[240] and benzoic[240] acids in arbitrary protic and aprotic solvents using a mixture of descriptors for solutes and solvents.

Because of the extreme importance of acidity constants, a number of commercial pK_a prediction tools are available: ACD pK_a/DB (Advanced Chemistry Development, Inc., www.acdlabs.com), ADMET Predictor (Simulations Plus, Inc., www.simulations-plus.com), Epik,[241] and Jaguar[242] (Schrödinger, Inc., www.schrodinger.com), Marvin pK_a (ChemAxon Ltd., www.chemaxon.com), Pallas pKalc (CompuDrug International, Inc., www.compudrug.com), Pipeline Pilot (SciTegic, Inc., accelrys.com), and SPARC[243] (University of Georgia, EPA). The programs ACD pK_a/DB, Epik, and Pallas pKalc are based on classical LFER; SPARC uses a combination of LFER with a perturbed molecular orbital method, whereas ADME Boxes, ADMET Predictor, Marvin, and Pipeline Pilot pK_a predictors are based on the use of QSPR models. Their prediction performances are compared in several publications.[244–247] In particular, the nine aforementioned commercial programs were compared in a benchmarking study[247] by applying them to 197 pharmaceutical substances with 261 carefully determined and highly reliable experimental pK_a values, and it was shown that ADME Boxes 4.9, ACD/pK_a DB 12.0, and SPARC 4.2 provide the most accurate predictions with mean absolute errors of 0.39, 0.48, and 0.65 log units, respectively. On the other hand, the latter LFER-based three programs failed to provide predictions for several sites.

The main limitation of all statistical methods of predicting pK_a values is related to the fact that most of the training compounds with experimentally measured values of pK_a contain a single acidic or basic center, and for this reason various combinations of such centers are poorly represented in training sets. However, organic compounds of pharmaceutical interest usually contain several such centers, and therefore it is necessary to take into account interactions between them. So, further development is needed in this direction.

3.16.4.6 Chemical Stability/Degradation

3.16.4.6.1 Statistical methods

The largest study of compound chemical stability was performed by SPECS.[248] The authors used $N = 12{,}700$ compounds provided by seven companies stored in pure DMSO and 20/80% DMSO/water solution. The study temperatures included 50, 25, 4, and −20°C (323.15, 298.15, 277.15, and 253.15 K), while the duration of experiment was up to 105 days. If a compound was not stable at a higher temperature, its stability was also investigated at a lower temperature until its purity was above 50%, which was used as a threshold to stop measurement for the investigated temperature. Since >60% of compounds were stable even after 105 days at $T = 50$°C (323.15 K), the dataset was biased with respect to stable compounds. Therefore, the authors limited the analysis using only data obtained at the following conditions: $T = 50$°C (323.15 K) and $\tau = 105$ days. The 80% purity was considered as a threshold for the stability of compounds.

The authors developed several local models assuming the reaction mechanism of instability, which were hydrolysis and oxidation. A use of local descriptors describing the reaction sites allowed the authors to model degradation of halides, esters, and amides, for which relatively large sets of compounds ($n \geq 25$) were found.

The accuracy of prediction using fivefold cross-validation was 80%–90% depending on the analyzed class. Unfortunately, due to a high diversity of data no large sets could be compiled for other chemical reactivity classes. An analysis of all data was done using molecular fragments based on Allen's schema, which was developed for prediction of heats of formation of molecules.[249] The use of different machine learning algorithms, such as kNN, RF, and PLS, calculated 10-fold cross-validation accuracy of about 70%–73%. The authors highlighted an importance of understanding of decomposition mechanisms, which can be achieved by analysis of decomposition products.

The same dataset was recently reanalyzed by Liu et al. to develop a naïve Bayesian model.[250] As in the case of previous study, only degradation data at 105 days and $T = 50$°C (323.15 K) were used. The authors used atom center fragments as descriptors. The use of new descriptors as well as a new machine learning method increased the accuracy of models in 10-fold cross-validation to 76% as compared to 73%. Unfortunately, it is not clear whether the improvements came from the use of different descriptors or machine learning method. The developed method uses Bayesian scores of fragments to interpret stability of molecules. The developed models are available as a web server (http://www.rcdd.org.cn/chemstable/) and can be used to predict the stability of new compounds.

The aforementioned studies indicate that prediction of stability of compounds is still in the initial stage of research and new approaches and, more importantly, properly generated data are strongly required to make a progress in this field.

3.16.4.7 Partition Coefficients

3.16.4.7.1 Physics-based models

The most straightforward approach for calculating the partition coefficient for a given compound with physics-based methods is to calculate the difference between the solvation free energies for the solute in the two different compartments as follows:

$$\log P_{oct/wat} = -\frac{\Delta G_{solv(oct)} - \Delta G_{hydr}}{RT\ln(10)}. \quad (48)$$

In the case of charged compounds, one has to estimate log D instead, which takes into account all relevant charged and neutral forms of the solute. If the log P and acid/base behavior of the compound are known, the log D can be calculated with Eq. (17).

Generally, the diverse sets of physics-based methods employed for hydration free energy calculations, including MD, QM, QM/MM, COSMO-RS, RISM, etc. (see section "Physics-based Methods"), can be applied to log *P*/log *D* predictions as well. A very recent SAMPL5 blind challenge[251] was focused on the prediction of cyclohexane–water distribution coefficients log $D_{cyclohex/wat}$ for 53 small molecules (log *D* replaces the previous focus on hydration free energy, see SAMPL0-4 (http://www.eyesopen.com/sampl and https://drugdesigndata.org/about/sampl), due to a lack of ongoing experimental work to generate new data). Organizers of the challenge performed an interesting analysis of the expected performance of computational methods for log *D* from the past hydration free energy calculations. In SAMPL4, the top performing submission achieved an RMSE around 1.5 kcal mol^{-1} (6.3 kJ mol^{-1}), which would correspond to a 1.54 log unit error in log $D_{cyclohex/wat}$ if both solvation free energies have comparable errors. However, in SAMPL5 only five submissions had a RMSE less than 2.5 log units.[251] The best performing submission (2.11 log units) was made by A. Klamt using COSMO-RS.[252] The main reasons for the much worse predictive ability of existing computational approaches are a more complex set of molecules (larger, more flexible, containing multiple functional groups per molecule), the complexity of tautomer enumeration, and the use of cyclohexane as a solvent, which appeared to be not completely immiscible with water. It was shown that the presence of water in the cyclohexane phase can dramatically affect the log *D* of the compound, depending on the affinity of the solute for water.[251]

3.16.4.7.2 Statistical methods

Numerous methods of calculating the log $P_{oct/wat}$ value are comprehensively reviewed in excellent publications.[170,171,253–258] So, we only give a very short overview of the most important approaches. All log $P_{oct/wat}$ prediction methods fall into two major categories: (i) the GC methods and (ii) the whole molecule methods. The GC methods can be either fragment-based or atom-based, in which the log $P_{oct/wat}$ value of a molecule is estimated by summation of the contributions from fragments (substructures) and atoms, respectively. The whole molecule methods are based on molecular properties, such as molecular surface area, electrostatic potential, molecular volume, or nonfragmental molecular descriptors.

The first method for prediction of log $P_{oct/wat}$ was developed in 1964 by Hansch and Fujita.[6] It was based on the summation of empirical π-constants of substituents and hence could be applied only within a congeneric series of compounds with the same framework. The limitations of this approach led Rekker[259] to develop the first fragment-based method, which was followed by the first atom-based method put forward by Broto.[260] The first computerized fragment-based method was developed by Leo and Hansch in 1982 and implemented in computer program CLogP.[255,261] The reported average deviation of this model is 0.31 log units. In 1994 Klopman et al.[262] developed KLogP method based on a multiple linear regression model with fragmental descriptors, which was built using a database of 1663 compounds. The reported average deviation of this model is 0.38 log units. In 1999 Wildman and Crippen[263] developed a purely atom-based model, ALogP, using a dataset of 9920 compounds and reported the average deviation to be 0.68 log units. In 2000 Viswanadhan[264] developed HLogP program based on a PLS regression model built on molecular holograms, a special type of fragmental descriptors. HLogP was shown to have better predictability for drug-like compounds as compared with the afore-mentioned CLogP and ALogP programs. Meylan and Howard[265] developed LOGKOW model based on 150 atoms and fragments with 250 correction factors. The model was derived from a training set of 2473 compounds and applied to an independent validation set of 10,589 compounds. Excellent prediction accuracy (standard deviation of 0.47 log units, and absolute mean error of 0.35 log units) was reported. Commercial program ACD/LogP (Advanced Chemistry Development Inc., www.acdlabs.com) is based on a model including 500 basic fragment descriptors and over 2000 correction factors.[266] In 1997 Wang et al.[83] built XLOGP model based on pure atomic contributions. Its version 2.0 includes 90 atom type descriptors with 10 correction factors, making rather good predictions with standard deviation of 0.35 log units on a dataset of 1853 compounds.[83] The commercial program Pallas ProLogP (CompuDrug International, Inc., www.compudrug.com) is also based on atomic contributions with additional correction terms.

There are also several whole-molecule approaches to predicting the log *P* values. Raevsky et al.[267] developed computer program SLIPPER-2001 based on the use of polarizability and hydrogen-bond descriptors in combination with structural similarity principle. The ALOGPS program developed by Tetko et al.[268,269] is based on a model built using associative neural network (ASNN) trained on 12,908 compounds from PHYSPROP database using 75 E-state indexes. For this model, the root mean square error of prediction is 0.35 log units and an absolute mean error is 0.26 log units. A dozen of other log *P* prediction models based on various physical–chemical, quantum-chemical, and topological descriptors are considered in a comprehensive review article by Katritzky et al.[171] At the same time a reliable prediction of this property remains a significant challenge as it was demonstrated by a benchmarking of commercial and academic algorithms for prediction of *in house* log *P* data.[270] The error of prediction >1 log unit of the best algorithms for $n=96$k compounds measured in Pfizer could be explained by differences in chemical diversity of *in house* and data used to develop the respective approaches. Thus, the majority of predictions were outside of the applicability domains[271] of the respective models, which contributed to their low accuracies of prediction. This conclusion was confirmed in the further study. The extension of the training set of the ALOGPS program[269] with new data allowed to reduce the error to 0.59 log unit for the same set.[272] Importantly, $>60\%$ of the most reliable predictions, as identified by the applicability domain,[271,272] had accuracy similar to that of experimental measurements.

Besides the *n*-octanol/water system, QSPR models for predicting partition coefficients in several other organic solvent–water systems have been developed. Leahy et al.[71,273] used physical–chemical Abraham's descriptors based on the linear solvation energy relationship to model log $P_{org/wat}$ for four solvents composing the "critical quartet": octanol, alkane, chloroform, and propylene glycol dipelargonate. It was argued that the set of solvents could be useful for modeling membrane binding and transport and therefore have particular reference to the rationalization of biological selectivity. Oliferenko et al.[274] used hydrogen bond basicity and

acidity scales to model partition coefficients in several systems: octanol–water, hexadecane–water, chloroform–water, gas–water, gas–octanol, gas–hexadecane, gas–chloroform.

To conclude, the majority of log $P_{oct/wat}$ prediction methods are based on atom- and fragment-based approaches. A serious limitation of these approaches is that reliable prediction can be made for only those compounds in which all atom and fragments types are also present and sufficiently abundant in the training set (the problem of "rare" fragments). Atom-based models can be applied for much larger sets of compounds than fragment-based models, but their predictions within the applicability domain of fragment-based models are less accurate. The problem of "rare" fragments can be partially solved using whole-molecule approaches based on physical–chemical properties or molecular descriptors. The main limitation of all log P prediction models, both atom/fragment-based and whole-molecule approaches, is they cannot be applied to compounds not similar to those in the training set.[98,271,272] One more limitation of almost all existing log P statistical prediction methods is they are not capable of taking into account sufficiently well 3D structures of molecules and the presence of intramolecular interactions.

3.16.5 Conclusions

Computational methods are important for the estimation of physical–chemical properties of chemical compounds for medicinal chemistry. Such methods are invaluable for the analysis and ranking of compounds from virtual libraries before such compounds are synthesized. During this century significant progress in prediction of physical–chemical properties was achieved for the prediction of pK_a. The current models are reported to achieve errors below 0.5 log units.[247] These models have made possible accurate prediction of log D and can also contribute better prediction of pH-dependent solubility. Still, a reliable prediction of properties such as intrinsic aqueous solubility,[207] or even partition coefficients[251,270] remains a significant challenge for complex compounds with many functional groups or those from *in house* libraries.

The development of text mining approaches has allowed automatic extraction of information from literature and, in particular, patents. This has made possible the collection of many MP data and the development of models to predict this property with errors of about 30 K for drug-like molecules.[144] Since the MP data measured in different laboratories have about the same accuracy, it is difficult to expect a further dramatic progress with prediction of this property. However, one may still develop more precise models for some particular classes of compounds, as it was reported in 150-year-old study of hydrocarbons.[138]

The estimation of the physical–chemical properties can be done using statistical or/and physics-based theoretical approaches, both groups of which were reviewed in this article. A limiting factor for the statistical methods is the availability of high-quality experimental data. The data also define the applicability domain of developed models and reliable predictions can be achieved only for similar molecules.[271,272] The further development of this group of methods can be expected with development of new HTS screening approaches allowing measurements of large datasets of experimental values; however, the HTS methods cannot be automatized for all properties. Moreover, costs of experimental measurements can significantly vary, which leads to different amount of data for various properties. In this respect the development of methods, which can explore intercorrelations between properties, for example, deep learning NN,[94], can further contribute to the advance of this field.

The development of physics-based approaches is related to the advance of theoretical methodologies and, actually, the development of HPC. The use of more physically relevant simulations, for example, explicit solvent or explicit–implicit solvent calculations, can result in a more accurate prediction of different physical–chemical properties of compounds. Despite the fact that the cost of rigorous explicit solvent calculations is still high,[219] the fast development of HPC should make the widespread use of such methods possible during the next decade.

Last but not least, the progress in the field strongly depends on public availability and user-friendliness of methods and models. The methods which are available on-line as free[275] or commercial software tools allow benchmarking of different approaches and, thus, significantly contribute to the development of computational and medicinal chemistry.[276]

References

1. Hersey, A.; Hill, A. P.; Hyde, R. M.; Livingstone, D. J. Principles of Method Selection in Partition Studies. *Quant. Struct. Act. Relat.* **1989,** *8,* 288–296.
2. Dearden, J. C.; Bresnen, G. M. The Measurement of Partition Coefficients. *Quant. Struct.-Act. Relat.* **1988,** *7,* 133–144.
3. Hansch, C.; Maloney, P. P.; Fujita, T.; Muir, R. M. Correlation of Biological Activity of Phenoxyacetic Acids With Hammett Substituent Constants and Partition Coefficients. *Nature* **1962,** *194,* 178–180.
4. Meyer, H. Zur Theorie der Alkoholnarkose. *Arch. Exp. Pathol. Pharmakol.* **1899,** *42,* 109–118.
5. Overton, E. Über die Osmotischen Eigenschaften der Zelle in Ihrer Bedeutung für die Toxikologie und Pharmakologie. *Z. Phys. Chem.* **1897,** *22,* 189–209.
6. Fujita, T.; Iwasa, J.; Hansch, C. A New Substituent Constant, π, Derived From Partition Coefficients. *J. Am. Chem. Soc.* **1964,** *86,* 5175–5180.
7. Nys, G. G.; Rekker, R. F. Statistical Analysis of a Series of Partition Coefficients With Special Reference to the Predictability of Folding of Drug Molecules. Introduction of Hydrophobic Fragmental Constants (f-Values). *Chim. Therap.* **1973,** *8,* 521–535.
8. Leo, A.; Jow, P. Y. C.; Silipo, C.; Hansch, C. Calculation of Hydrophobic Constant (log P) From pi and f Constants. *J. Med. Chem.* **1975,** *18,* 865–868.
9. Yoneda, F.; Nitta, Y. Electronic Structure and Antibacterial Activity of Nitrofuran Derivatives. *Chem. Pharm. Bull.* **1964,** *12,* 1264–1268.
10. Snyder, S. H.; Merril, C. R. A Relationship Between the Hallucinogenic Activity of Drugs and Their Electronic Configuration. *Proc. Natl. Acad. Sci. U. S. A.* **1965,** *54,* 258–266.
11. Kikuchi, O. Systematic QSAR Procedures With Quantum Chemical Descriptors. *Quant. Struct.-Act. Relat.* **1987,** *6,* 179–184.
12. Hyde, R. M.; Livingstone, D. J. Perspectives in QSAR: Computer Chemistry and Pattern Recognition. *J. Comput. Aided Mol. Des.* **1988,** *2,* 145–155.

13. Saunders, M. R.; Livingstone, D. J. Electronic Structure Calculations in Quantitative Structure Property Relationships. In *Advances in Quantitative Structure Property Relationship;* Charton, M., Ed.; Vol. 1; JAI Press: Greenwich, London, 1996; pp 53–79.
14. Randic, M. Characterization of Molecular Branching. *J. Am. Chem. Soc.* **1975,** *97,* 6609–6615.
15. Kier, L. B.; Hall, L. H. Molecular Connectivity in Structure–Activity Analysis. In John Wiley & Sons, Inc.: Hoboken, NJ, 1986; p 280.
16. Saxena, A. K. Physicochemical Significance of Topological Parameters, Connectivity Indices and Information Content. Part 1: Correlation Studies in the Sets With Aromatic and Aliphatic Substituents. *Quant. Struct.-Act. Relat.* **1995,** *14,* 31–38.
17. Kubinyi, H. The Physicochemical Significance of Topological Parameters. A Rebuttal. *Quant. Struct.-Act. Relat.* **1995,** *14,* 149–150.
18. Saxena, A. K. Reply to H. Kubinyi's Rebuttal. *Quant. Struct.-Act. Relat.* **1995,** *14,* 150.
19. Swain, C. G.; Lupton, E. C. Field and Resonance Components of Substituent Effects. *J. Am. Chem. Soc.* **1968,** *90,* 4328–4337.
20. Kier, L. B.; Hall, L. H.; Murray, W. J.; Randi, M. Molecular Connectivity I: Relationship to Nonspecific Local Anesthesia. *J. Pharm. Sci.* **1975,** *64,* 1971–1974.
21. Murray, W. J.; Hall, L. H.; Kier, L. B. Molecular Connectivity II: Relationship to Water Solubility and Boiling Point. *J. Pharm. Sci.* **1975,** *64,* 1974–1977.
22. Murray, W. J.; Hall, L. H.; Kier, L. B. Molecular Connectivity III: Relationship to Partition Coefficients. *J. Pharm. Sci.* **1975,** *64,* 1978–1981.
23. Burkhard, L. P.; Andren, A. W.; Armstrong, D. E. Structure Activity Relationships Using Molecular Connectivity Indices With Principal Component Analysis. *Chemosphere* **1983,** *12,* 935–943.
24. Livingstone, D. J. The Characterization of Chemical Structures Using Molecular Properties. A Survey. *J. Chem. Inf. Comput. Sci.* **2000,** *40,* 195–209.
25. Todeschini, R.; Consonni, V. Handbook of Molecular Descriptors. In Wiley-VCH Verlag: Weinheim, 2000; p 667.
26. Lyman, W. J.; Reehl, W. F.; Rosenblatt, D. H. Handbook of Chemical Property Estimation Methods: Environmental Behavior of Organic Compounds. In American Chemical Society: Washington, DC, 1990; p 960.
27. Baum, E. J. Chemical Property Estimation Theory and Application. In Lewis: Boca Raton, FL, 1998; p 386.
28. Jørgensen, S. E.; Halling-Sørensen, B.; Mahler, H. Handbook of Estimation Methods in Ecotoxicology and Environmental Chemistry. In Lewis Publishers: Boca Raton, FL, 1998; p 229.
29. Cronin, M. T. D.; Livingstone, D. Predicting Chemical Toxicity and Fate. In CRC Press: Boca Raton, FL, 2004; p 445.
30. Abramov, Y. A. Computational Pharmaceutical Solid State Chemistry. In John Wiley & Sons, Inc: Hoboken, NJ, 2016; p 424.
31. Lee, A. Y.; Erdemir, D.; Myerson, A. S. Crystal Polymorphism in Chemical Process Development. *Annu. Rev. Chem. Biomol. Eng.* **2011,** *2,* 259–280.
32. Cruz-Cabeza, A. J.; Reutzel-Edens, S. M.; Bernstein, J. Facts and Fictions About Polymorphism. *Chem. Soc. Rev.* **2015,** *44,* 8619–8635.
33. Huang, L. F.; Tong, W. Q. Impact of Solid State Properties on Developability Assessment of Drug Candidates. *Adv. Drug Deliv. Rev.* **2004,** *56,* 321–334.
34. Byrn, S.; Pfeiffer, R.; Ganey, M.; Hoiberg, C.; Poochikian, G. Pharmaceutical Solids: A Strategic Approach to Regulatory Considerations. *Pharm. Res.* **1995,** *12,* 945–954.
35. Yu, L. X.; Furness, M. S.; Raw, A.; Outlaw, K. P.; Nashed, N. E.; Ramos, E.; Miller, S. P.; Adams, R. C.; Fang, F.; Patel, R. M.; Holcombe, F. O., Jr.; Chiu, Y. Y.; Hussain, A. S. Scientific Considerations of Pharmaceutical Solid Polymorphism in Abbreviated New Drug Applications. *Pharm. Res.* **2003,** *20,* 531–536.
36. Bauer, J.; Spanton, S.; Henry, R.; Quick, J.; Dziki, W.; Porter, W.; Morris, J. Ritonavir: An Extraordinary Example of Conformational Polymorphism. *Pharm. Res.* **2001,** *18,* 859–866.
37. Abramov, Y. A. Current Computational Approaches to Support Pharmaceutical Solid Form Selection. *Org. Process. Res. Dev.* **2013,** *17,* 472–485.
38. Perlovich, G. L.; Raevsky, O. A. Sublimation of Molecular Crystals: Prediction of Sublimation Functions on the Basis of HYBOT Physicochemical Descriptors and Structural Clusterization. *Cryst. Growth Des.* **2010,** *10,* 2707–2712.
39. Chickos, J. S.; Acree, W. E. Enthalpies of Sublimation of Organic and Organometallic Compounds. 1910–2001. *J. Phys. Chem. Ref. Data* **2002,** *31,* 537–698.
40. Gavezzotti, A.; Filippini, G. Energetic Aspects of Crystal Packing: Experiment and Computer Simulations. In *Theoretical Aspects and Computer Modeling of the Molecular Solid State;* Gavezzotti, A., Ed.; John Wiley & Sons, Inc: Chichester, 1997; pp 61–99.
41. Perlovich, G. L. Thermodynamic Approaches to the Challenges of Solubility in Drug Discovery and Development. *Mol. Pharm.* **2014,** *11,* 1–11.
42. Galek, P. T. A.; Pidcock, E.; Wood, P. A.; Feeder, N.; Allen, F. H. Navigating the Solid Form Landscape With Structural Informatics. In *Computational Pharmaceutical Solid State Chemistry;* Abramov, Y. A., Ed.; John Wiley & Sons, Inc: Hoboken, NJ, 2016; pp 15–35.
43. Abramov, Y. A. Theoretical Hydrogen-Bonding Analysis for Assessment of Physical Stability of Pharmaceutical Solid Forms. In *Computational Pharmaceutical Solid State Chemistry;* Abramov, Y. A., Ed.; John Wiley & Sons, Inc: Hoboken, NJ, 2016; pp 37–56.
44. Dearden, J. C. Quantitative Structure–Property Relationships for Prediction of Boiling Point, Vapor Pressure, and Melting Point. *Environ. Toxicol. Chem.* **2003,** *22,* 1696–1709.
45. Wasserscheid, P.; Welton, T. Ionic Liquids in Synthesis. In Wiley-VCH Verlag: Weinheim, 2003; p 364.
46. Stolarska, O.; Rodriguez, H.; Smiglak, M. Eutectic Mixtures of Pyrrolidinium-Based Ionic Liquids. *Fluid Phase Equilib.* **2016,** *408,* 1–9.
47. Xu, W.; Cooper, E. I.; Angell, C. A. Ionic Liquids: Ion Mobilities, Glass Temperatures, and Fragilities. *J. Phys. Chem. B* **2003,** *107,* 6170–6178.
48. Abramov, Y. A.; Pencheva, K. Thermodynamics and Relative Solubility Prediction of Polymorphic Systems. In *Chemical Engineering in the Pharmaceutical Industry;* am Ende, D. J., Ed.; John Wiley & Sons, Inc: Hoboken, NJ, 2010; pp 477–490.
49. Valsaraj, K. T.; Thibodeaux, L. J. On the Physicochemical Aspects of the Global Fate and Long-Range Atmospheric Transport of Persistent Organic Pollutants. *J. Phys. Chem. Lett.* **2010,** *1,* 1694–1700.
50. Smith, D. A.; Allerton, C.; Kalgutkar, A. S.; van de Waterbeemd, H. Pharmacokinetics and Metabolism in Drug Design. In 3rd ed.;**51**; Wiley-VCH Verlag: Weinheim, 2012; p 268.
51. Yu, L. X.; Amidon, G. L.; Polli, J. E.; Zhao, H.; Mehta, M. U.; Conner, D. P.; Shah, V. P.; Lesko, L. J.; Chen, M. L.; Lee, V. H. L.; Hussain, A. S. Biopharmaceutics Classification System: The Scientific Basis for Biowaiver Extensions. *Pharm. Res.* **2002,** *19,* 921–925.
52. Calvert, J. G. Glossary of Atmospheric Chemistry Terms (Recommendations 1990). *Pure Appl. Chem.* **1990,** *62,* 2167–2219.
53. Abramov, Y. A. Major Source of Error in QSPR Prediction of Intrinsic Thermodynamic Solubility of Drugs: Solid vs Nonsolid State Contributions? *Mol. Pharm.* **2015,** *12,* 2126–2141.
54. Lipinski, C. A. Drug-Like Properties and the Causes of Poor Solubility and Poor Permeability. *J. Pharmacol. Toxicol. Methods* **2000,** *44,* 235–249.
55. Dahan, A.; Miller, J. M.; Amidon, G. L. Prediction of Solubility and Permeability Class Membership: Provisional BCS Classification of the World's Top Oral Drugs. *AAPS J.* **2009,** *11,* 740–746.
56. Stegemann, S.; Leveiller, F.; Franchi, D.; de Jong, H.; Linden, H. When Poor Solubility Becomes an Issue: From Early Stage to Proof of Concept. *Eur. J. Pharm. Sci.* **2007,** *31,* 249–261.
57. Avdeef, A. Absorption and Drug Development: Solubility, Permeability, and Charge State. In 2nd ed.; John Wiley & Sons, Inc: Hoboken, NJ, 2012; p 698.
58. Jang, Y. H.; Goddard, W. A., 3rd; Noyes, K. T.; Sowers, L. C.; Hwang, S.; Chung, D. S. First Principles Calculations of the Tautomers and p*K*(a) Values of 8-Oxoguanine: Implications for Mutagenicity and Repair. *Chem. Res. Toxicol.* **2002,** *15,* 1023–1035.
59. Wife, R. L.; Tijhuis, J. Library Quality Metrics. In *Drug Discovery and Development;* Chorghade, M. S., Ed.; 2; John Wiley & Sons, Inc: Hoboken, NJ, 2007; pp 265–277.
60. Kerns, E. H.; Di, L. Pharmaceutical Profiling in Drug Discovery. *Drug Discov. Today* **2003,** *8,* 316–323.
61. Brandl, M.; Eide Flaten, G.; Bauer-Brandl, A.; Begley, T. P. Passive Diffusion Across Membranes. In *Wiley Encyclopedia of Chemical Biology;* Hoboke, Ed.; Vol. 3; John Wiley & Sons, Inc: Hoboken, NJ, 2009; pp 541–550.
62. Sugano, K.; Kansy, M.; Artursson, P.; Avdeef, A.; Bendels, S.; Di, L.; Ecker, G. F.; Faller, B.; Fischer, H.; Gerebtzoff, G.; Lennernaes, H.; Senner, F. Coexistence of Passive and Carrier-Mediated Processes in Drug Transport. *Nat. Rev. Drug Discov.* **2010,** *9,* 597–614.
63. Chan, O. H.; Stewart, B. H. Physicochemical and Drug-Delivery Considerations for Oral Drug Bioavailability. *Drug Discov. Today* **1996,** *1,* 461–473.

64. Kakemi, K.; Arita, T.; Hori, R.; Konishi, R. Absorption and Excretion of Drugs. XXX. Absorption of Barbituric Acid Derivatives From Rat Stomach. *Chem. Pharm. Bull.* **1967,** *15,* 1534–1539.
65. Wagner, J. G.; Sedman, A. J. Quantitation of Rate of Gastrointestinal and Buccal Absorption of Acidic and Basic Drugs Based on Extraction Theory. *J. Pharmacokinet. Pharmacodyn.* **1973,** *1,* 23–50.
66. Camenisch, G.; Alsenz, J.; van de Waterbeemd, H.; Folkers, G. Estimation of Permeability by Passive Diffusion Through Caco-2 Cell Monolayers Using the Drugs' Lipophilicity and Molecular Weight. *Eur. J. Pharm. Sci.* **1998,** *6,* 313–319.
67. Hansch, C. Quantitative Approach to Biochemical Structure–Activity Relationships. *Acc. Chem. Res.* **1969,** *2,* 232–239.
68. Camenisch, G.; Folkers, G.; van de Waterbeemd, H. Shapes of Membrane Permeability-Lipophilicity Curves: Extension of Theoretical Models With an Aqueous Pore Pathway. *Eur. J. Pharm. Sci.* **1998,** *6,* 325–329.
69. van de Waterbeemd, J. T. M.; Jansen, A. C. A. Transport in QSAR V. *Pharm. Weekbl. Sci.* **1981,** *3,* 587–594.
70. Suh, H.; Jun, H. W. Effectiveness and Mode of Action of Isopropyl Myristate as a Permeation Enhancer for Naproxen Through Shed Snake Skin. *J. Pharm. Pharmacol.* **1996,** *48,* 812–816.
71. Leahy, D. E.; Taylor, P. J.; Wait, A. R. Model Solvent Systems for QSAR Part I. Propylene Glycol Dipelargonate (PGDP). A New Standard Solvent for Use in Partition Coefficient Determination. *Quant. Struct.-Act. Relat.* **1989,** *8,* 17–31.
72. Klamt, A. Conductor-Like Screening Model for Real Solvents: A New Approach to the Quantitative Calculation of Solvation Phenomena. *J. Phys. Chem.* **1995,** *99,* 2224–2235.
73. Klamt, A.; Eckert, F. COSMO-RS: A Novel and Efficient Method for the a Priori Prediction of Thermophysical Data of Liquids. *Fluid Phase Equilib.* **2000,** *172,* 43–72.
74. Klamt, A.; Eckert, F.; Arlt, W. COSMO-RS: An Alternative to Simulation for Calculating Thermodynamic Properties of Liquid Mixtures. *Annu. Rev. Chem. Biomol. Eng.* **2010,** *1,* 101–122.
75. Klamt, A. The COSMO and COSMO-RS Solvation Models. *Wiley Interdiscip. Rev. Comput. Mol. Sci.* **2011,** *1,* 699–709.
76. Mullins, E.; Liu, Y. A.; Ghaderi, A.; Fast, S. D. Sigma Profile Database for Predicting Solid Solubility in Pure and Mixed Solvent Mixtures for Organic Pharmacological Compounds With COSMO-Based Thermodynamic Methods. *Ind. Eng. Chem. Res.* **2008,** *47,* 1707–1725.
77. Abrams, D. S.; Prausnitz, J. M. Statistical Thermodynamics of Liquid Mixtures: A New Expression for the Excess Gibbs Energy of Partly or Completely Miscible Systems. *AIChE J.* **1975,** *21,* 116–128.
78. Wertheim, M. S. Fluids With Highly Directional Attractive Forces. I. Statistical Thermodynamics. *J. Stat. Phys.* **1984,** *35,* 19–34.
79. Kontogeorgis, G. M.; Folas, G. K. The Statistical Associating Fluid Theory (SAFT). In *Thermodynamic Models for Industrial Applications;* Kontogeorgis, G. M., Folas, G. K., Eds.; John Wiley & Sons, Inc: Hoboken, NJ, 2010; pp 221–259.
80. Chandler, D.; Andersen, H. C. Optimized Cluster Expansions for Classical Fluids. II. Theory of Molecular Liquids. *J. Chem. Phys.* **1972,** *57,* 1930–1937.
81. Beglov, D.; Roux, B. An Integral Equation to Describe the Solvation of Polar Molecules in Liquid Water. *J. Phys. Chem. B* **1997,** *101,* 7821–7826.
82. Ratkova, E. L.; Palmer, D. S.; Fedorov, M. V. Solvation Thermodynamics of Organic Molecules by the Molecular Integral Equation Theory: Approaching Chemical Accuracy. *Chem. Rev.* **2015,** *115,* 6312–6356.
83. Wang, R.; Fu, Y.; Lai, L. A New Atom-Additive Method for Calculating Partition Coefficients. *J. Chem. Inf. Comput. Sci.* **1997,** *37,* 615–621.
84. Brenke, J. K.; Salmina, E. S.; Ringelstetter, L.; Dornauer, S.; Kuzikov, M.; Rothenaigner, I.; Schorpp, K.; Giehler, F.; Gopalakrishnan, J.; Kieser, A.; Gul, S.; Tetko, I. V.; Hadian, K. Identification of Small-Molecule Frequent Hitters of Glutathione S-Transferase-Glutathione Interaction. *J. Biomol. Screen.* **2016,** *21,* 596–607.
85. Schorpp, K.; Rothenaigner, I.; Salmina, E.; Reinshagen, J.; Low, T.; Brenke, J. K.; Gopalakrishnan, J.; Tetko, I. V.; Gul, S.; Hadian, K. Identification of Small-Molecule Frequent Hitters From AlphaScreen High-Throughput Screens. *J. Biomol. Screen.* **2014,** *19,* 715–726.
86. Sushko, I.; Salmina, E.; Potemkin, V. A.; Poda, G.; Tetko, I. V. ToxAlerts: A Web Server of Structural Alerts for Toxic Chemicals and Compounds With Potential Adverse Reactions. *J. Chem. Inf. Model.* **2012,** *52,* 2310–2316.
87. Salmina, E. S.; Haider, N.; Tetko, I. V. Extended Functional Groups (EFG): An Efficient Set for Chemical Characterization and Structure–Activity Relationship Studies of Chemical Compounds. *Molecules* **2016,** *21,* 1.
88. Varnek, A.; Fourches, D.; Horvath, D.; Klimchuk, O.; Gaudin, C.; Vayer, P.; Solov'ev, V.; Hoonakker, F.; Tetko, I. V.; Marcou, G. ISIDA – Platform for Virtual Screening Based on Fragment and Pharmacophoric Descriptors. *Curr. Comput. Aided Drug Des.* **2008,** *4,* 191–198.
89. Vapnik, V. N. Statistical Leaning Theory. In John Wiley & Sons, Inc: New York, 1998; p 768.
90. Rumelhart, D. E.; Hinton, G. E.; Williams, R. J. Learning Representations by Back-Propagating Errors. *Nature* **1986,** *323,* 533–536.
91. Breiman, L. Random Forests. *Mach. Learn.* **2001,** *45,* 5–32.
92. Hingston, P. F.; Barone, L. C.; Michalewicz, Z. Design by Evolution: Advances in Evolutionary Design. In Springer: Berlin/London, 2008; p 350.
93. Schmidhuber, J. Deep Learning in Neural Networks: An Overview. *Neural Netw.* **2015,** *61,* 85–117.
94. Baskin, I. I.; Winkler, D.; Tetko, I. V. A Renaissance of Neural Networks in Drug Discovery. *Expert Opin. Drug Discov.* **2016,** *11,* 785–795.
95. Sushko, Y.; Novotarskyi, S.; Korner, R.; Vogt, J.; Abdelaziz, A.; Tetko, I. V. Prediction-Driven Matched Molecular Pairs to Interpret QSARs and Aid the Molecular Optimization Process. *J. Cheminform.* **2014,** *6,* 48.
96. Polishchuk, P. G.; Kuz'min, V. E.; Artemenko, A. G.; Muratov, E. N. Universal Approach for Structural Interpretation of QSAR/QSPR Models. *Mol. Inform.* **2013,** *32,* 843–853.
97. Tropsha, A. Best Practices for QSAR Model Development, Validation, and Exploitation. *Mol. Inform.* **2010,** *29,* 476–488.
98. Tetko, I. V.; Sushko, I.; Pandey, A. K.; Zhu, H.; Tropsha, A.; Papa, E.; Oberg, T.; Todeschini, R.; Fourches, D.; Varnek, A. Critical Assessment of QSAR Models of Environmental Toxicity Against Tetrahymena Pyriformis: Focusing on Applicability Domain and Overfitting by Variable Selection. *J. Chem. Inf. Model.* **2008,** *48,* 1733–1746.
99. Sushko, I.; Novotarskyi, S.; Korner, R.; Pandey, A. K.; Rupp, M.; Teetz, W.; Brandmaier, S.; Abdelaziz, A.; Prokopenko, V. V.; Tanchuk, V. Y.; Todeschini, R.; Varnek, A.; Marcou, G.; Ertl, P.; Potemkin, V.; Grishina, M.; Gasteiger, J.; Schwab, C.; Baskin, I. I.; Palyulin, V. A.; Radchenko, E. V.; Welsh, W. J.; Kholodovych, V.; Chekmarev, D.; Cherkasov, A.; Aires-de-Sousa, J.; Zhang, Q. Y.; Bender, A.; Nigsch, F.; Patiny, L.; Williams, A.; Tkachenko, V.; Tetko, I. V. Online Chemical Modeling Environment (OCHEM): Web Platform for Data Storage, Model Development and Publishing of Chemical Information. *J. Comput. Aided Mol. Des.* **2011,** *25,* 533–554.
100. Walker, T.; Grulke, C. M.; Pozefsky, D.; Tropsha, A. Chembench: A Cheminformatics Workbench. *Bioinformatics* **2010,** *26,* 3000–3001.
101. Price, S. L.; Braun, D. E.; Reutzel-Edens, S. M. Can Computed Crystal Energy Landscapes Help Understand Pharmaceutical Solids? *Chem. Commun.* **2016,** *52,* 7065–7077.
102. Price, S. L. Predicting Crystal Structures of Organic Compounds. *Chem. Soc. Rev.* **2014,** *43,* 2098–2111.
103. Day, G. M. Advances in Crystal Structure Prediction and Applications to Pharmaceutical Materials. In *Computational Pharmaceutical Solid State Chemistry;* Abramov, Y. A., Ed.; John Wiley & Sons, Inc: Hoboken, NJ, 2016; pp 87–115.
104. Briggner, L. E.; Hendrickx, R.; Kloo, L.; Rosdahl, J.; Svensson, P. H. Solid-State Perturbation for Solubility Improvement: A Proof of Concept. *ChemMedChem* **2011,** *6,* 60–62.
105. Briggner, L. E.; Kloo, L.; Rosdahl, J.; Svensson, P. H. In Silico Solid State Perturbation for Solubility Improvement. *ChemMedChem* **2014,** *9,* 724–726.
106. Lill, S. O. N.; Schantz, S.; Broo, V.; Broo, A. Current Computational Approaches at Astrazeneca for Solid-State and Property Predictions. In *Computational Pharmaceutical Solid State Chemistry;* Abramov, Y. A., Ed.; John Wiley & Sons, Inc: Hoboken, NJ, 2016; pp 145–173.
107. Krzyzaniak, J. F.; Meenan, P. A.; Doherty, C. L.; Pencheva, K.; Luthra, S.; Cruz-Cabeza, A. Integrating Computational Materials Science Tools in Form and Formulation Design. In *Computational Pharmaceutical Solid State Chemistry;* Abramov, Y. A., Ed.; John Wiley & Sons, Inc: Hoboken, NJ, 2016; pp 117–144.
108. Abramov, Y. A. QTAIM Application in Drug Development: Prediction of Relative Stability of Drug Polymorphs From Experimental Crystal Structures. *J. Phys. Chem. A* **2011,** *115,* 12809–12817.
109. Gelbrich, T.; Braun, D. E.; Ellern, A.; Griesser, U. J. Four Polymorphs of Methyl Paraben: Structural Relationships and Relative Energy Differences. *Cryst. Growth Des.* **2013,** *13,* 1206–1217.

110. Nyman, J.; Pundyke, O. S.; Day, G. M. Accurate Force Fields and Methods for Modelling Organic Molecular Crystals at Finite Temperatures. *Phys. Chem. Chem. Phys.* **2016,** *18,* 15828–15837.
111. Nyman, J.; Day, G. M. Static and Lattice Vibrational Energy Differences Between Polymorphs. *CrystEngComm* **2015,** *17,* 5154–5165.
112. Galek, P. T. A.; Fabian, L.; Motherwell, W. D. S.; Allen, F. H.; Feeder, N. Knowledge-Based Model of Hydrogen-Bonding Propensity in Organic Crystals. *Acta Crystallogr. Sect. B Struct. Sci.* **2007,** *63,* 768–782.
113. Groom, C. R.; Allen, F. H. The Cambridge Structural Database in Retrospect and Prospect. *Angew. Chem. Int. Ed. Engl.* **2014,** *53,* 662–671.
114. Galek, P. T. A.; Allen, F. H.; Fabian, L.; Feeder, N. Knowledge-Based H-Bond Prediction to Aid Experimental Polymorph Screening. *CrystEngComm* **2009,** *11,* 2634–2639.
115. Galek, P. T. A.; Pidcock, E.; Wood, P. A.; Bruno, I. J.; Groom, C. R. One in Half a Million: A Solid Form Informatics Study of a Pharmaceutical Crystal Structure. *CrystEngComm* **2012,** *14,* 2391–2403.
116. Puri, S.; Chickos, J. S.; Welsh, W. J. Three-Dimensional Quantitative Structure–Property Relationship (3D-QSPR) Models for Prediction of Thermodynamic Properties of Polychlorinated Biphenyls (PCBs): Enthalpy of Sublimation. *J. Chem. Inf. Comput. Sci.* **2002,** *42,* 109–116.
117. Gharagheizi, F. A new Molecular-Based Model for Prediction of Enthalpy of Sublimation of Pure Components. *Thermochim. Acta* **2008,** *469,* 8–11.
118. Salahinejad, M.; Le, T. C.; Winkler, D. A. Capturing the Crystal: Prediction of Enthalpy of Sublimation, Crystal Lattice Energy, and Melting Points of Organic Compounds. *J. Chem. Inf. Model.* **2013,** *53,* 223–229.
119. Ouvrard, C.; Mitchell, J. B. O. Can We Predict Lattice Energy From Molecular Structure? *Acta Crystallogr. Sect. B Struct. Sci.* **2003,** *59,* 676–685.
120. Gharagheizi, F.; Sattari, M.; Tirandazi, B. Prediction of Crystal Lattice Energy Using Enthalpy of Sublimation: A Group Contribution-Based Model. *Ind. Eng. Chem. Res.* **2011,** *50,* 2482–2486.
121. Joback, K. G.; Reid, R. C. Estimation of Pure-Component Properties From Group Contributions. *Chem. Eng. Commun.* **1987,** *57,* 233–243.
122. Cruciani, G.; Pastor, M.; Guba, W. VolSurf: A New Tool for the Pharmacokinetic Optimization of Lead Compounds. *Eur. J. Pharm. Sci.* **2000,** *11,* S29–S39.
123. Karthikeyan, M.; Glen, R. C.; Bender, A. General Melting Point Prediction Based on a Diverse Compound Data Set and Artificial Neural Networks. *J. Chem. Inf. Model.* **2005,** *45,* 581–590.
124. Stanton, D. T.; Dimitrov, S.; Grancharov, V.; Mekenyan, O. G. Charged Partial Surface Area (CPSA) Descriptors QSAR Applications. *SAR QSAR Environ. Res.* **2002,** *13,* 341–351.
125. Raevsky, O. A.; Skvortsov, V. S. 3D Hydrogen Bond Thermodynamics (HYBOT) Potentials in Molecular Modelling. *J. Comput. Aided Mol. Des.* **2002,** *16,* 1–10.
126. Docherty, R.; Pencheva, K.; Abramov, Y. A. Low Solubility in Drug Development: De-convoluting the Relative Importance of Solvation and Crystal Packing. *J. Pharm. Pharmacol.* **2015,** *67,* 847–856.
127. Abramov, Y. A. QSPR Modeling of Chemical and Physical Stability of Pharmaceuticals. 20th EuroQSAR, St. Petersburg, Russia.
128. Luo, S. N.; Ahrens, T. J.; Cagin, T.; Strachan, A.; Goddard, W. A.; Swift, D. C. Maximum Superheating and Undercooling: Systematics, Molecular Dynamics Simulations, and Dynamic Experiments. *Phys. Rev. B* **2003,** *68,* 134206.
129. Phillpot, S. R.; Lutsko, J. F.; Wolf, D.; Yip, S. Molecular-Dynamics Study of Lattice-Defect-Nucleated Melting in Silicon. *Phys. Rev. B* **1989,** *40,* 2831–2840.
130. Morris, J. R.; Wang, C. Z.; Ho, K. M.; Chan, C. T. Melting Line of Aluminum From Simulations of Coexisting Phases. *Phys. Rev. B* **1994,** *49,* 3109–3115.
131. Hoover, W. G.; Ree, F. H. Use of Computer Experiments to Locate the Melting Transition and Calculate the Entropy in the Solid Phase. *J. Chem. Phys.* **1967,** *47,* 4873–4878.
132. Frenkel, D.; Ladd, A. J. C. New Monte Carlo Method to Compute the Free Energy of Arbitrary Solids. Application to the fcc and hcp Phases of Hard Spheres. *J. Chem. Phys.* **1984,** *81,* 3188–3193.
133. Grochola, G. Constrained Fluid Lambda-Integration: Constructing a Reversible Thermodynamic Path Between the Solid and Liquid State. *J. Chem. Phys.* **2004,** *120,* 2122–2126.
134. Eike, D. M.; Brennecke, J. F.; Maginn, E. J. Toward a Robust and General Molecular Simulation Method for Computing Solid–Liquid Coexistence. *J. Chem. Phys.* **2005,** *122,* 14115.
135. Zhang, Y.; Maginn, E. J. A Comparison of Methods for Melting Point Calculation Using Molecular Dynamics Simulations. *J. Chem. Phys.* **2012,** *136,* 144116.
136. Zhang, Y.; Maginn, E. J. Toward Fully in Silico Melting Point Prediction Using Molecular Simulations. *J. Chem. Theory Comput.* **2013,** *9,* 1592–1599.
137. Holden, J. R.; Du, Z.; Ammon, H. L. Prediction of Possible Crystal Structures for C-, H-, N-, O-, and F-Containing Organic Compounds. *J. Comput. Chem.* **1993,** *14,* 422–437.
138. Mills, E. J. On Melting Point and Boiling Point as Related to Composition. *Philos. Mag.* **1884,** *17,* 173–187.
139. Marrero, J.; Gani, R. Group-Contribution Based Estimation of Pure Component Properties. *Fluid Phase Equilib.* **2001,** *183–184,* 183–208.
140. Varnek, A.; Kireeva, N.; Tetko, I. V.; Baskin, I. I.; Solov'ev, V. P. Exhaustive QSPR Studies of a Large Diverse Set of Ionic Liquids: How Accurately Can We Predict Melting Points? *J. Chem. Inf. Model.* **2007,** *47,* 1111–1122.
141. Hall, L. H.; Kier, L. B. Electrotopological State Indexes for Atom Types – A Novel Combination of Electronic, Topological, and Valence State Information. *J. Chem. Inf. Comput. Sci.* **1995,** *35,* 1039–1045.
142. Schultes, S.; de Graaf, C.; Berger, H.; Mayer, M.; Steffen, A.; Haaksma, E. E. J.; de Esch, I. J. P.; Leurs, R.; Kramer, O. A Medicinal Chemistry Perspective on Melting Point: Matched Molecular Pair Analysis of the Effects of Simple Descriptors on the Melting Point of Drug-Like Compounds. *Med. Chem. Commun.* **2012,** *3,* 584–591.
143. Tetko, I. V.; Sushko, Y.; Novotarskyi, S.; Patiny, L.; Kondratov, I.; Petrenko, A. E.; Charochkina, L.; Asiri, A. M. How Accurately Can We Predict the Melting Points of Drug-Like Compounds? *J. Chem. Inf. Model.* **2014,** *54,* 3320–3329.
144. Tetko, I. V.; Lowe, D.; Williams, A. J. The Development of Models to Predict Melting and Pyrolysis Point Data Associated With Several Hundred Thousand Compounds Mined From PATENTS. *J. Cheminform.* **2016,** *8,* 2.
145. Bergstrom, C. A.; Norinder, U.; Luthman, K.; Artursson, P. Molecular Descriptors Influencing Melting Point and Their Role in Classification of Solid Drugs. *J. Chem. Inf. Comput. Sci.* **2003,** *43,* 1177–1185.
146. Bradley, J.-C.; Lang, A.; Williams, A. *Jean-Claude Bradley Double Plus Good (Highly Curated and Validated) Melting Point Dataset,* 2014. http://figshare.com/articles/Jean_Claude_Bradley_Double_Plus_Good_Highly_Curated_and_Validated_Melting_Point_Dataset/1031638 (Accessed 20 May 2014).
147. Hughes, L. D.; Palmer, D. S.; Nigsch, F.; Mitchell, J. B. Why are Some Properties More Difficult to Predict Than Others? A Study of QSPR Models of Solubility, Melting Point, and Log P. *J. Chem. Inf. Model.* **2008,** *48,* 220–232.
148. Preiss, U. P.; Beichel, W.; Erle, A. M.; Paulechka, Y. U.; Krossing, I. Is Universal, Simple Melting Point Prediction Possible? *ChemPhysChem* **2011,** *12,* 2959–2972.
149. Wang, J.; Tingjun, H. Application of Molecular Dynamics Simulations in Molecular Property Prediction I: Density and Heat of Vaporization. *J. Chem. Theory Comput.* **2011,** *7,* 2151–2165.
150. Kuwajima, S.; Kikuchi, H.; Fukuda, M. Molecular-Dynamics Evaluation of Fluid-Phase Equilibrium Properties by a Novel Free-Energy Perturbation Approach: Application to Gas Solubility and Vapor Pressure of Liquid Hexane. *J. Chem. Phys.* **2006,** *124,* 124111.
151. Westergren, J.; Lindfors, L.; Höglund, T.; Lüder, K.; Nordholm, S.; Kjellander, R. In Silico Prediction of Drug Solubility: 1. Free Energy of Hydration. *J. Phys. Chem. B* **2007,** *111,* 1872–1882.
152. Lüder, K.; Lindfors, L.; Westergren, J.; Nordholm, S.; Kjellander, R. In Silico Prediction of Drug Solubility: 2. Free Energy of Solvation in Pure Melts. *J. Phys. Chem. B* **2007,** *111,* 1883–1892.
153. Lüder, K.; Lindfors, L.; Westergren, J.; Nordholm, S.; Kjellander, R. In Silico Prediction of Drug Solubility. 3. Free Energy of Solvation in Pure Amorphous Matter. *J. Phys. Chem. B* **2007,** *111,* 7303–7311.
154. Diedenhofen, M.; Klamt, A.; Marsh, K.; Schafer, A. Prediction of the Vapor Pressure and Vaporization Enthalpy of 1-*n*-Alkyl-3-methylimidazolium-bis-(trifluoromethanesulfonyl) Amide Ionic Liquids. *Phys. Chem. Chem. Phys.* **2007,** *9,* 4653–4656.

155. Schroder, B.; Fulem, M.; Martins, M. A. R. Vapor Pressure Predictions of Multi-Functional Oxygen-Containing Organic Compounds With COSMO-RS. *Atmos. Environ.* **2016,** *133,* 135–144.
156. Nakajoh, K.; Grabda, M.; Oleszek-Kudlak, S.; Shibata, E.; Eckert, F.; Nakamura, T. Prediction of Vapour Pressures of Chlorobenzenes and Selected Polychlorinated Biphenyls Using the COSMO-RS Model. *J. Mol. Struct.* **2009,** *895,* 9–17.
157. Alnemrat, S.; Hooper, J. P. Predicting Temperature-Dependent Solid Vapor Pressures of Explosives and Related Compounds Using a Quantum Mechanical Continuum Solvation Model. *J. Phys. Chem. A* **2013,** *117,* 2035–2043.
158. Kholod, Y. A.; Muratov, E. N.; Gorb, L. G.; Hill, F. C.; Artemenko, A. G.; Kuz'min, V. E.; Qasim, M.; Leszczynski, J. Application of Quantum Chemical Approximations to Environmental Problems: Prediction of Water Solubility for Nitro Compounds. *Environ. Sci. Technol.* **2009,** *43,* 9208–9215.
159. Klamt, A.; Eckert, F.; Hornig, M.; Beck, M. E.; Burger, T. Prediction of Aqueous Solubility of Drugs and Pesticides With COSMO-RS. *J. Comput. Chem.* **2002,** *23,* 275–281.
160. Fredenslund, A.; Rasmussen, P. Correlation of Pure Component Gibbs Energy. Using UNIFAC Group Contribution. *AIChE J.* **1979,** *25,* 203–205.
161. Rezakazemi, M.; Marjani, A.; Shirazian, S. Development of a Group Contribution Method Based on UNIFAC Groups for the Estimation of Vapor Pressures of Pure Hydrocarbon Compounds. *Chem. Eng. Technol.* **2013,** *36,* 483–491.
162. Papaioannou, V.; Adjiman, C. S.; Jackson, G.; Galindo, A. Group Contribution Methodologies for the Prediction of Thermodynamic Properties and Phase Behavior in Mixtures. In *Process Systems Engineering;* Pistikopoulos, E. N., Georgiadis, M. C., Dua, V., Adjiman, C. S., Galindo, A., Eds.; Vol. 6; Wiley-VCH Verlag: Weinheim, 2010; pp 135–172.
163. Tamouza, S.; Passarello, J. P.; Tobaly, P.; de Hemptinne, J. C. Group Contribution Method With SAFT EOS Applied to Vapor Liquid Equilibria of Various Hydrocarbon Series. *Fluid Phase Equilib.* **2004,** *222,* 67–76.
164. Tihic, A.; Kontogeorgis, G. M.; von Solms, N.; Michelsen, M. L.; Constantinou, L. A Predictive Group-Contribution Simplified PC-SAFT Equation of State: Application to Polymer Systems. *Ind. Eng. Chem. Res.* **2008,** *47,* 5092–5101.
165. Lymperiadis, A.; Adjiman, C. S.; Galindo, A.; Jackson, G. A Group Contribution Method for Associating Chain Molecules Based on the Statistical Associating Fluid Theory (SAFT-Gamma). *J. Chem. Phys.* **2007,** *127,* 234903.
166. Emami, F. S.; Vahid, A.; Elliott, J. R.; Feyzi, F. Group Contribution Prediction of Vapor Pressure With Statistical Associating Fluid Theory, Perturbed-Chain Statistical Associating Fluid Theory, and Elliott-Suresh-Donohue Equations of State. *Ind. Eng. Chem. Res.* **2008,** *47,* 8401–8411.
167. Kuhne, R.; Ebert, R. U.; Schuurmann, G. Estimation of Vapour Pressures for Hydrocarbons and Halogenated Hydrocarbons From Chemical Structure by a Neural Network. *Chemosphere* **1997,** *34,* 671–686.
168. Godavarthy, S. S.; Robinson, R. L.; Gasem, K. A. M. SVRC-QSPR Model for Predicting Saturated Vapor Pressures of Pure Fluids. *Fluid Phase Equilib.* **2006,** *246,* 39–51.
169. Chastrette, M.; Cretin, D. Estimation of Physical Properties of Organic Compounds. A Comparison of Methods in the Case of Vapor Pressure Estimation. In *Thermodynamic Modeling and Materials Data Engineering;* Springer: Berlin Heidelberg, 1998; pp 85–94.
170. Katritzky, A. R.; Maran, U.; Lobanov, V. S.; Karelson, M. Structurally Diverse Quantitative Structure–Property Relationship Correlations of Technologically Relevant Physical Properties. *J. Chem. Inf. Comput. Sci.* **2000,** *40,* 1–18.
171. Katritzky, A. R.; Kuanar, M.; Slavov, S.; Hall, C. D.; Karelson, M.; Kahn, I.; Dobchev, D. A. Quantitative Correlation of Physical and Chemical Properties With Chemical Structure: Utility for Prediction. *Chem. Rev.* **2010,** *110,* 5714–5789.
172. Chastrette, M.; Cretin, D.; Tiyal, F. Structure–Property Relationships-Determination of the Vapor-Pressure of Alkanes and Alcohols Using Multifunctional Autocorrelation Method (MAM). *C. R. Acad. Sci.* **1994,** *318,* 1059–1065.
173. Basak, S. C.; Gute, B. D.; Grunwald, G. D. Use of Topostructural, Topochemical, and Geometric Parameters in the Prediction of Vapor Pressure: A Hierarchical QSAR Approach. *J. Chem. Inf. Comput. Sci.* **1997,** *37,* 651–655.
174. Liang, C.; Gallagher, D. A. QSPR Prediction of Vapor Pressure From Solely Theoretically-Derived Descriptors. *J. Chem. Inf. Comput. Sci.* **1998,** *38,* 321–324.
175. Katritzky, A. R.; Wang, Y.; Sild, S.; Tamm, T.; Karelson, M. QSPR Studies on Vapor Pressure, Aqueous Solubility, and the Prediction of Water–Air Partition Coefficients. *J. Chem. Inf. Comput. Sci.* **1998,** *38,* 720–725.
176. Artemenko, N. V.; Baskin, I. I.; Palyulin, V. A.; Zefirov, N. S. Prediction of Physical Properties of Organic Compounds Using Artificial Neural Networks Within the Substructure Approach. *Dokl. Chem.* **2001,** *381,* 317–320.
177. Artemenko, N. V.; Baskin, I. I.; Palyulin, V. A.; Zefirov, N. S. Artificial Neural Network and Fragmental Approach in Prediction of Physicochemical Properties of Organic Compounds. *Russ. Chem. Bull.* **2003,** *52,* 20–29.
178. Cash, G. G. Prediction of Physicochemical Properties From Euclidean Distance Methods Based on Electrotopological State Indices. *Chemosphere* **1999,** *39,* 2583–2591.
179. Chalk, A. J.; Beck, B.; Clark, T. A Temperature-Dependent Quantum Mechanical/Neural Net Model for Vapor Pressure. *J. Chem. Inf. Comput. Sci.* **2001,** *41,* 1053–1059.
180. Yaffe, D.; Cohen, Y. Neural Network Based Temperature-Dependent Quantitative Structure Property Relations (QSPRs) for Predicting Vapor Pressure of Hydrocarbons. *J. Chem. Inf. Comput. Sci.* **2001,** *41,* 463–477.
181. Gharagheizi, F.; Eslamimanesh, A.; Ilani-Kashkouli, P.; Mohammadi, A. H.; Richon, D. Determination of Vapor Pressure of Chemical Compounds: A Group Contribution Model for an Extremely Large Database. *Ind. Eng. Chem. Res.* **2012,** *51,* 7119–7125.
182. Baskin, I.; Varnek, A. Fragment Descriptors in SAR/QSAR/QSPR Studies, Molecular Similarity Analysis and in Virtual Screening. In *Chemoinformatics Approaches to Virtual Screening;* Varnek, A., Tropsha, A., Eds.; RSC Publisher: Cambridge, 2008; pp 1–43.
183. Vuilleumier, R. Ab Initio Molecular Approach to Solvation and Chemical Reactions. In *Computational Trends in Solvation and Transport in Liquids;* Sutmann, G., Grotendorst, J., Gompper, G., Marx, D., Eds.; Vol. 28; Jülich: Jülich, 2015; pp 25–54.
184. Lupyan, D.; Abramov, Y. A.; Sherman, W. Improving Force Field Parameters for Small-Molecule Conformation Generation. In *Computational Pharmaceutical Solid State Chemistry;* Abramov, Y. A., Ed.; John Wiley & Sons, Inc: Hoboken, NJ, 2016; pp 57–86.
185. Shivakumar, D.; Harder, E.; Damm, W.; Friesner, R. A.; Sherman, W. Improving the Prediction of Absolute Solvation Free Energies Using the Next Generation OPLS Force Field. *J. Chem Theory Comput.* **2012,** *8,* 2553–2558.
186. Palmer, D. S.; McDonagh, J. L.; Mitchell, J. B.; van Mourik, T.; Fedorov, M. V. First-Principles Calculation of the Intrinsic Aqueous Solubility of Crystalline Druglike Molecules. *J. Chem. Theory Comput.* **2012,** *8,* 3322–3337.
187. Thompson, J. D.; Cramer, C. J.; Truhlar, D. G. Predicting Aqueous Solubilities From Aqueous Free Energies of Solvation and Experimental or Calculated Vapor Pressures of Pure Substances. *J. Chem. Phys.* **2003,** *119,* 1661–1670.
188. Palmer, D. S.; Fedorov, M. V. Molecular Simulation Methods to Compute Intrinsic Aqueous Solubility of Crystalline Drug-Like Molecules. In *Computational Pharmaceutical Solid State Chemistry;* Abramov, Y. A., Ed.; John Wiley & Sons, Inc: Hoboken, NJ, 2016; pp 263–286.
189. Yalkowsky, S. H.; Banerjee, S. Aqueous Solubility: Methods of Estimation for Organic Compounds. In Marcel Dekker: New York, 1992; p 264.
190. Yalkowsky, S. H.; Valvani, S. C. Solubility and Partitioning. 1. Solubility of Non-electrolytes in Water. *J. Pharm. Sci.* **1980,** *69,* 912–922.
191. Yalkowsky, S. H.; Valvani, S. C.; Roseman, T. J. Solubility and Partitioning. 6. Octanol Solubility and Octanol–Water Partition-Coefficients. *J. Pharm. Sci.* **1983,** *72,* 866–870.
192. Ran, Y. Q.; Jain, N.; Yalkowsky, S. H. Prediction of Aqueous Solubility of Organic Compounds by the General Solubility Equation (GSE). *J. Chem. Inf. Comput. Sci.* **2001,** *41,* 1208–1217.
193. Meylan, W. M.; Howard, P. H.; Boethling, R. S. Improved Method for Estimating Water Solubility From Octanol Water Partition Coefficient. *Environ. Toxicol. Chem.* **1996,** *15,* 100–106.
194. Wakita, K.; Yoshimoto, M.; Miyamoto, S.; Watanabe, H. A Method for Calculation of the Aqueous Solubility of Organic Compounds by Using New Fragment Solubility Constants. *Chem. Pharm. Bull.* **1986,** *34,* 4663–4681.
195. Suzuki, T. Development of an Automatic Estimation System for Both the Partition-Coefficient and Aqueous Solubility. *J. Comput. Aided Mol. Des.* **1991,** *5,* 149–166.
196. Klopman, G.; Zhu, H. Estimation of the Aqueous Solubility of Organic Molecules by the Group Contribution Approach. *J. Chem. Inf. Comput. Sci.* **2001,** *41,* 439–445.

197. Faller, B.; Ertl, P. Computational Approaches to Determine Drug Solubility. *Adv. Drug Deliv. Rev.* **2007,** *59,* 533–545.
198. Delaney, J. S. Predicting Aqueous Solubility From Structure. *Drug Discov. Today* **2005,** *10,* 289–295.
199. Salahinejad, M.; Le, T. C.; Winkler, D. A. Aqueous Solubility Prediction: Do Crystal Lattice Interactions Help? *Mol. Pharm.* **2013,** *10,* 2757–2766.
200. Kühne, R.; Ebert, R.-U.; Schüürmann, G. Model Selection Based on Structural Similarity-Method Description and Application to Water Solubility Prediction. *J. Chem. Inf. Model.* **2006,** *46,* 636–641.
201. Cheng, T.; Li, Q.; Wang, Y.; Bryant, S. H. Binary Classification of Aqueous Solubility Using Support Vector Machines With Reduction and Recombination Feature Selection. *J. Chem. Inf. Model.* **2011,** *51,* 229–236.
202. Duchowicz, P. R.; Talevi, A.; Bruno-Blanch, L. E.; Castro, E. A. New QSPR Study for the Prediction of Aqueous Solubility of Drug-Like Compounds. *Bioorg. Med. Chem.* **2008,** *16,* 7944–7955.
203. Kim, J.; Jung, D. H.; Rhee, H.; Choi, S. H.; Sung, M. J.; Choi, W. S. Aqueous Solubility of Poorly Water-Soluble Drugs: Prediction Using Similarity and Quantitative Structure–Property Relationship Models. *Korean J. Chem. Eng.* **2008,** *25,* 865–873.
204. Huuskonen, J.; Livingstone, D. J.; Manallack, D. T. Prediction of Drug Solubility From Molecular Structure Using a Drug-Like Training Set. *SAR QSAR Environ. Res.* **2008,** *19,* 191–212.
205. Du-Cuny, L.; Huwyler, J.; Wiese, M.; Kansy, M. Computational Aqueous Solubility Prediction for Drug-Like Compounds in Congeneric Series. *Eur. J. Med. Chem.* **2008,** *43,* 501–512.
206. Llinas, A.; Glen, R. C.; Goodman, J. M. Solubility Challenge: Can You Predict Solubilities of 32 Molecules Using a Database of 100 Reliable Measurements? *J. Chem. Inf. Model.* **2008,** *48,* 1289–1303.
207. Hopfinger, A. J.; Esposito, E. X.; Llinas, A.; Glen, R. C.; Goodman, J. M. Findings of the Challenge To Predict Aqueous Solubility. *J. Chem. Inf. Model.* **2009,** *49,* 1–5.
208. Katritzky, A. R.; Oliferenko, A. A.; Oliferenko, P. V.; Petrukhin, R.; Tatham, D. B.; Maran, U.; Lomaka, A.; Acree, W. E., Jr. A General Treatment of Solubility. 2. QSPR Prediction of Free Energies of Solvation of Specified Solutes in Ranges of Solvents. *J. Chem. Inf. Comput. Sci.* **2003,** *43,* 1806–1814.
209. Toropov, A. A.; Rasulev, B. F.; Leszczynska, D.; Leszczynski, J. Multiplicative SMILES-Based Optimal Descriptors: QSPR Modeling of Fullerene C(60) Solubility in Organic Solvents. *Chem. Phys. Lett.* **2008,** *457,* 332–336.
210. Kravtsov, A. A.; Karpov, P. V.; Baskin, I. I.; Palyulin, V. A.; Zefirov, N. S. "Bimolecular" QSPR: Estimation of the Solvation Free Energy of Organic Molecules in Different Solvents. *Dokl. Chem.* **2007,** *414,* 128–131.
211. Alongi, K. S.; Shields, G. C. Chapter 8 – Theoretical Calculations of Acid Dissociation Constants: A Review Article. In *Annual Reports in Computational Chemistry;* Ralph, A. W., Ed.; Vol. 6; Elsevier Science: Amsterdam, 2010; pp 113–138.
212. Seybold, P. G.; Shields, G. C. Computational Estimation of p*K*(a) Values. *Wiley Interdiscip. Rev. Comput. Mol. Sci.* **2015,** *5,* 290–297.
213. Zhan, C. G.; Dixon, D. A. Absolute Hydration Free Energy of the Proton From First-Principles Electronic Structure Calculations. *J. Phys. Chem. A* **2001,** *105,* 11534–11540.
214. Pickard, F. C.; Griffith, D. R.; Ferrara, S. J.; Liptak, M. D.; Kirschner, K. N.; Shields, G. C. CCSD(T), W1, and Other Model Chemistry Predictions for Gas-Phase Deprotonation Reactions. *Int. J. Quantum Chem.* **2006,** *106,* 3122–3128.
215. Pokon, E. K.; Liptak, M. D.; Feldgus, S.; Shields, G. C. Comparison of CBS-QB3, CBS-APNO, and G3 Predictions of Gas Phase Deprotonation Data. *J. Phys. Chem. A* **2001,** *105,* 10483–10487.
216. Liptak, M. D.; Shields, G. C. Comparison of Density Functional Theory Predictions of Gas-Phase Deprotonation Data. *Int. J. Quantum Chem.* **2005,** *105,* 580–587.
217. Zhang, S. M.; Baker, J.; Pulay, P. A Reliable and Efficient First Principles-Based Method for Predicting p*K*(a) Values. 1. Methodology. *J. Phys. Chem. A* **2010,** *114,* 425–431.
218. Klamt, A.; Eckert, F.; Diedenhofen, M.; Beck, M. E. First Principles Calculations of Aqueous p*K*(a) Values for Organic and Inorganic Acids Using COSMO-RS Reveal an Inconsistency in the Slope of the p*K*(a) Scale. *J. Phys. Chem. A* **2003,** *107,* 9380–9386.
219. Alexov, E.; Mehler, E. L.; Baker, N.; Baptista, A. M.; Huang, Y.; Milletti, F.; Nielsen, J. E.; Farrell, D.; Carstensen, T.; Olsson, M. H. M.; Shen, J. K.; Warwicker, J.; Williams, S.; Word, J. M. Progress in the Prediction of p*K*(a) Values in Proteins. *Proteins Struct. Funct. Bioinf.* **2011,** *79,* 3260–3275.
220. Kelly, C. P.; Cramer, C. J.; Truhlar, D. G. Adding Explicit Solvent Molecules to Continuum Solvent Calculations for the Calculation of Aqueous Acid Dissociation Constants. *J. Phys. Chem. A* **2006,** *110,* 2493–2499.
221. Eckert, F.; Klamt, A. Accurate Prediction of Basicity in Aqueous Solution With COSMO-RS. *J. Comput. Chem.* **2006,** *27,* 11–19.
222. Pliego, J. R.; Riveros, J. M. Theoretical Calculation of p*K*(a) Using the Cluster-Continuum Model. *J. Phys. Chem. A* **2002,** *106,* 7434–7439.
223. Eckert, F.; Diedenhofen, M.; Klamt, A. Towards a First Principles Prediction of p*K*(a): COSMO-RS and the Cluster-Continuum Approach. *Mol. Phys.* **2010,** *108,* 229–241.
224. Bryantsev, V. S.; Diallo, M. S.; Goddard, W. A. Calculation of Solvation Free Energies of Charged Solutes Using Mixed Cluster/Continuum Models. *J. Phys. Chem. B* **2008,** *112,* 9709–9719.
225. Perrin, D. D.; Dempsey, B.; Serjeant, E. P. pK_a Prediction for Organic Acids and Bases. In Vol. 1; Springer: Berlin Heidelberg, 1981; p 146.
226. Karelson, M.; Lobanov, V. S.; Katritzky, A. R. Quantum-Chemical Descriptors in QSAR/QSPR Studies. *Chem. Rev.* **1996,** *96,* 1027–1044.
227. Citra, M. J. Estimating the pK_a of Phenols, Carboxylic Acids and Alcohols From Semi-Empirical Quantum Chemical Methods. *Chemosphere* **1999,** *38,* 191–206.
228. Tehan, B. G.; Lloyd, E. J.; Wong, M. G.; Pitt, W. R.; Gancia, E.; Manallack, D. T. Estimation of pK_a Using Semiempirical Molecular Orbital Methods. Part 2: Application to Amines, Anilines and Various Nitrogen Containing Heterocyclic Compounds. *Quant. Struct.-Act. Relat.* **2002,** *21,* 473–485.
229. Chaudry, U. A.; Popelier, P. L. A. Estimation of p*K*(a) Using Quantum Topological Molecular Similarity Descriptors: Application to Carboxylic Acids, Anilines and Phenols. *J. Org. Chem.* **2004,** *69,* 233–241.
230. Gross, K. C.; Seybold, P. G.; Peralta-Inga, Z.; Murray, J. S.; Politzer, P. Comparison of Quantum Chemical Parameters and Hammett Constants in Correlating p*K*(a) Values of Substituted Anilines. *J. Org. Chem.* **2001,** *66,* 6919–6925.
231. Soriano, E.; Cerdan, S.; Ballesteros, P. Computational Determination of p*K*(a) Values. A Comparison of Different Theoretical Approaches and a Novel Procedure. *J. Mol. Struct.* **2004,** *684,* 121–128.
232. Habibi-Yangjeh, A.; Danandeh-Jenagharad, M.; Nooshyar, M. Application of Artificial Neural Networks for Predicting the Aqueous Acidity of Various Phenols Using QSAR. *J. Mol. Model.* **2006,** *12,* 338–347.
233. Baskin, I. I.; Keshtova, S. V.; Palyulin, V. A.; Zefirov, N. S. Combining Molecular Modelling With the Use of Artificial Neural Networks as an Approach to Predict Substituent Constants and Bioactivity. In *Molecular Modeling and Prediction of Bioactivity;* Gundertofte, K., Jorgensen, F. S., Eds.; Kluwer Academic/Plenum Publishers: New York/Boston/Dordrecht/London/Moscow, 2000; pp 468–469.
234. Ivanova, A. A.; Baskin, I. I.; Palyulin, V. A.; Zefirov, N. S. Estimation of Ionization Constants for Different Classes of Organic Compounds With the Use of the Fragmental Approach to the Search of Structure–Property Relationships. *Dokl. Chem.* **2007,** *413,* 90–94.
235. Zhokhova, N. I.; Baskin, I. I.; Palyulin, V. A.; Zefirov, A. N.; Zefirov, N. S. Fragmental Descriptors With Labeled Atoms and Their Application in QSAR/QSPR Studies. *Dokl. Chem.* **2007,** *417,* 282–284.
236. Luan, F.; Ma, W. P.; Zhang, H. X.; Zhang, X. Y.; Liu, M. C.; Hu, Z. D.; Fan, B. T. Prediction of p*K*(a) for Neutral and Basic Drugs Based on Radial Basis Function Neural Networks and the Heuristic Method. *Pharm. Res.* **2005,** *22,* 1454–1460.
237. Gargallo, R.; Sotriffer, C. A.; Liedl, K. R.; Rode, B. M. Application of Multivariate Data Analysis Methods to Comparative Molecular Field Analysis (CoMFA) Data: Proton Affinities and pK_a Prediction for Nucleic Acids Components. *J. Comput. Aided Mol. Des.* **1999,** *13,* 611–623.
238. Milletti, F.; Storchi, L.; Sforna, G.; Cruciani, G. New and Original pK_a Prediction Method Using Grid Molecular Interaction Fields. *J. Chem. Inf. Model.* **2007,** *47,* 2172–2181.
239. Jover, J.; Bosque, R.; Sales, J. Neural Network Based QSPR Study for Predicting p*K*(a) of Phenols in Different Solvents. *QSAR Comb. Sci.* **2007,** *26,* 385–397.
240. Jover, J.; Bosque, R.; Sales, J. QSPR Prediction of p*K*(a) for Benzoic Acids in Different Solvents. *QSAR Comb. Sci.* **2008,** *27,* 563–581.

241. Shelley, J. C.; Cholleti, A.; Frye, L. L.; Greenwood, J. R.; Timlin, M. R.; Uchimaya, M. Epik: A Software Program for pK_a Prediction and Protonation State Generation for Drug-Like Molecules. *J. Comput. Aided Mol. Des.* **2007,** *21,* 681–691.
242. Klicic, J. J.; Friesner, R. A.; Liu, S.-Y.; Guida, W. C. Accurate Prediction of Acidity Constants in Aqueous Solution via Density Functional Theory and Self-Consistent Reaction Field Methods. *J. Phys. Chem. A* **2002,** *106,* 1327–1335.
243. Lee, P. H.; Ayyampalayam, S. N.; Carreira, L. A.; Shalaeva, M.; Bhattachar, S.; Coselmon, R.; Poole, S.; Gifford, E.; Lombardo, F. In Silico Prediction of Ionization Constants of Drugs. *Mol. Pharm.* **2007,** *4,* 498–512.
244. Meloun, M.; Bordovska, S. Benchmarking and Validating Algorithms That Estimate pK_a Values of Drugs Based on Their Molecular Structures. *Anal. Bioanal. Chem.* **2007,** *389,* 1267–1281.
245. Balogh, G. T.; Gyarmati, B.; Nagy, B.; Molnar, L.; Keseru, G. M. Comparative Evaluation of In Silico pK_a Prediction Tools on the Gold Standard Dataset. *QSAR Comb. Sci.* **2009,** *28,* 1148–1155.
246. Settimo, L.; Bellman, K.; Knegtel, R. M. A. Comparison of the Accuracy of Experimental and Predicted pK_a Values of Basic and Acidic Compounds. *Pharm. Res.* **2014,** *31,* 1082–1095.
247. Liao, C.; Nicklaus, M. C. Comparison of Nine Programs Predicting pK_a Values of Pharmaceutical Substances. *J. Chem. Inf. Model.* **2009,** *49,* 2801–2812.
248. Zitha-Bovens, E.; Maas, P.; Wife, D.; Tijhuis, J.; Hu, Q. N.; Kleinoder, T.; Gasteiger, J. COMDECOM: Predicting the Lifetime of Screening Compounds in DMSO Solution. *J. Biomol. Screen.* **2009,** *14,* 557–565.
249. Allen, T. L. Bond Energies and the Interactions Between Next-Nearest Neighbors. I. Saturated Hydrocarbons, Diamond, Sulfanes, S8, and Organic Sulfur Compounds. *J. Chem. Phys.* **1959,** *31,* 1039–1049.
250. Liu, Z.; Zheng, M.; Yan, X.; Gu, Q.; Gasteiger, J.; Tijhuis, J.; Maas, P.; Li, J.; Xu, J. ChemStable: A Web Server for Rule-Embedded Naive Bayesian Learning Approach to Predict Compound Stability. *J. Comput. Aided Mol. Des.* **2014,** *28,* 941–950.
251. Bannan, C. C.; Burley, K. H.; Chiu, M.; Shirts, M. R.; Gilson, M. K.; Mobley, D. L. Blind Prediction of Cyclohexane-Water Distribution Coefficients From the SAMPL5 Challenge. *J. Comput. Aided Mol. Des.* **2016**. http://dx.doi.org/10.1007/s10822-016-9954-8.
252. Klamt, A.; Eckert, F.; Reinisch, J.; Wichmann, K. Prediction of Cyclohexane–Water Distribution Coefficients With COSMO-RS on the SAMPL5 Data Set. *J. Comput. Aided Mol. Des.* **2016**. http://dx.doi.org/10.1007/s10822-016-9927-y.
253. Leo, A.; Hansch, C.; Elkins, D. Partition Coefficients and Their Uses. *Chem. Rev.* **1971,** *71,* 525–616.
254. Sangster, J. Octanol–Water Partition Coefficients: Fundamentals and Physical Chemistry. In John Wiley & Sons, Inc: Hoboken, NJ, 1997; p 178.
255. Leo, A. J. Calculating Log Poct From Structures. *Chem. Rev.* **1993,** *93,* 1281–1306.
256. Mannhold, R.; Rekker, R. F.; Dross, K.; Bijloo, G.; de Vries, G. The Lipophilic Behaviour of Organic Compounds: 1. An Updating of the Hydrophobic Fragmental Constant Approach. *Quant. Struct.-Act. Relat.* **1998,** *17,* 517–536.
257. Buchwald, P.; Bodor, N. Octanol–Water Partition: Searching for Predictive Models. *Curr. Med. Chem.* **1998,** *5,* 353–380.
258. Leo, A. Octanol/Water Partition Coefficients. In *Handbook of Property Estimation Methods for Chemicals: Environmental and Health Sciences;* Mackay, D., Boethling, R. S., Eds.; CRC Press: Boca Raton, FL, 2000; pp 89–114.
259. Rekker, R. F. The Hydrophobic Fragmental Constant: Its Derivation and Application With a Means of Characterizing Membrane Systems. In Elsevier: Amsterdam, 1977; p 390.
260. Broto, P.; Moreau, G.; Vandycke, C. Molecular-Structures – Perception, Auto-Correlation Descriptor and SAR Studies – System of Atomic Contribution for the Calculation of the Normal-Octanol Water Partition-Coefficients. *Eur. J. Med. Chem.* **1984,** *19,* 71–78.
261. Leo, A. J.; Hoekman, D. Calculating Log *P*(oct) With no Missing Fragments; The Problem of Estimating New Interaction Parameters. *Perspect. Drug Discov. Des.* **2000,** *18,* 19–38.
262. Klopman, G.; Li, J.-Y.; Wang, S.; Dimayuga, M. Computer Automated Log *P* Calculations Based on an Extended Group Contribution Approach. *J. Chem. Inf. Comput. Sci.* **1994,** *34,* 752–781.
263. Wildman, S. A.; Crippen, G. M. Prediction of Physicochemical Parameters by Atomic Contributions. *J. Chem. Inf. Comput. Sci.* **1999,** *39,* 868–873.
264. Viswanadhan, V. N.; Ghose, A. K.; Wendoloski, J. J. Estimating Aqueous Solvation and Lipophilicity of Small Organic Molecules: A Comparative Overview of Atom/Group Contribution Methods. *Perspect. Drug Discov. Des.* **2000,** *19,* 85–98.
265. Meylan, W. M.; Howard, P. H. Estimating Log *P* With Atom/Fragments and Water Solubility With Log *P*. *Perspect. Drug Discov. Des.* **2000,** *19,* 67–84.
266. Petrauskas, A. A.; Kolovanov, E. A. ACD/Log *P* Method Description. *Perspect. Drug Discov. Des.* **2000,** *19,* 99–116.
267. Raevsky, O. A.; Trepalin, S. V.; Trepalina, H. P.; Gerasimenko, V. A.; Raevskaja, O. E. SLIPPER-2001 – Software for Predicting Molecular Properties on the Basis of Physicochemical Descriptors and Structural Similarity. *J. Chem. Inf. Comput. Sci.* **2002,** *42,* 540–549.
268. Tetko, I. V.; Tanchuk, V. Y.; Villa, A. E. P. Prediction of *n*-Octanol/Water Partition Coefficients From PHYSPROP Database Using Artificial Neural Networks and E-State Indices. *J. Chem. Inf. Comput. Sci.* **2001,** *41,* 1407–1421.
269. Tetko, I. V.; Tanchuk, V. Y. Application of Associative Neural Networks for Prediction of Lipophilicity in ALOGPS 2.1 Program. *J. Chem. Inf. Comput. Sci.* **2002,** *42,* 1136–1145.
270. Mannhold, R.; Poda, G. I.; Ostermann, C.; Tetko, I. V. Calculation of Molecular Lipophilicity: State-of-the-art and Comparison of Log *P* Methods on More Than 96,000 Compounds. *J. Pharm. Sci.* **2009,** *98,* 861–893.
271. Tetko, I. V.; Bruneau, P.; Mewes, H. W.; Rohrer, D. C.; Poda, G. I. Can We Estimate the Accuracy of ADME-Tox Predictions? *Drug Discov. Today* **2006,** *11,* 700–707.
272. Tetko, I. V.; Poda, G. I.; Ostermann, C.; Mannhold, R. Large-Scale Evaluation of Log *P* Predictors: Local Corrections May Compensate Insufficient Accuracy and Need of Experimentally Testing Every Other Compound. *Chem. Biodivers.* **2009,** *6,* 1837–1844.
273. Leahy, D. E.; Morris, J. J.; Taylor, P. J.; Wait, A. R. Model Solvent Systems for QSAR.2. Fragment Values (F-Values) for the Critical Quartet. *J. Chem. Soc., Perkin Trans. 2* **1992,** *4,* 723–731.
274. Oliferenko, A. A.; Oliferenko, P. V.; Huddleston, J. G.; Rogers, R. D.; Palyulin, V. A.; Zefirov, N. S.; Katritzky, A. R. Theoretical Scales of Hydrogen Bond Acidity and Basicity for Application in QSAR/QSPR Studies and Drug Design. Partitioning of Aliphatic Compounds. *J. Chem. Inf. Comput. Sci.* **2004,** *44,* 1042–1055.
275. Tetko, I. V.; Maran, U.; Tropsha, A. Public (Q)SAR Services, Integrated Modeling Environments and Model Repositories on the Web: State of the Art and Perspectives for Future Development. *Mol. Inform.* **2016**. http://dx.doi.org/10.1002/minf.201600082.
276. Tetko, I. V. The Perspectives of Computational Chemistry Modeling. *J. Comput. Aided Mol. Des.* **2012,** *26,* 135–136.
277. Reilly, A. M.; Cooper, R. I.; Adjiman, C. S.; Bhattacharya, S.; Boese, A. D.; Brandenburg, J. G.; Bygrave, P. J.; Bylsma, R.; Campbell, J. E.; Car, R.; Case, D. H.; Chadha, R.; Cole, J. C.; Cosburn, K.; Cuppen, H. M.; Curtis, F.; Day, G. M.; DiStasio, R. A., Jr.; Dzyabchenko, A.; van Eijck, B. P.; Elking, D. M.; van den Ende, J. A.; Facelli, J. C.; Ferraro, M. B.; Fusti-Molnar, L.; Gatsiou, C.-A.; Gee, T. S.; de Gelder, R.; Ghiringhelli, L. M.; Goto, H.; Grimme, S.; Guo, R.; Hofmann, D. W. M.; Hoja, J.; Hylton, R. K.; Iuzzolino, L.; Jankiewicz, W.; de Jong, D. T.; Kendrick, J.; de Klerk, N. J. J.; Ko, H.-Y.; Kuleshova, L. N.; Li, X.; Lohani, S.; Leusen, F. J. J.; Lund, A. M.; Lv, J.; Ma, Y.; Marom, N.; Masunov, A. E.; McCabe, P.; McMahon, D. P.; Meekes, H.; Metz, M. P.; Misquitta, A. J.; Mohamed, S.; Monserrat, B.; Needs, R. J.; Neumann, M. A.; Nyman, J.; Obata, S.; Oberhofer, H.; Oganov, A. R.; Orendt, A. M.; Pagola, G. I.; Pantelides, C. C.; Pickard, C. J.; Podeszwa, R.; Price, L. S.; Price, S. L.; Pulido, A.; Read, M. G.; Reuter, K.; Schneider, E.; Schober, C.; Shields, G. P.; Singh, P.; Sugden, I. J.; Szalewicz, K.; Taylor, C. R.; Tkatchenko, A.; Tuckerman, M. E.; Vacarro, F.; Vasileiadis, M.; Vazquez-Mayagoitia, A.; Vogt, L.; Wang, Y.; Watson, R. E.; de Wijs, G. A.; Yang, J. Z.; Zhu, Q.; Groom, C. R. Report on the sixth blind test of organic crystal structure prediction methods. *Acta Crystallogr. Sect. B: Struct. Sci.* **2016,** *72,* 439–459.
278. Arlin, J. B.; Price, L. S.; Price, S. L.; Florence, A. J. A Strategy for Producing Predicted Polymorphs: Catemeric Carbamazepine Form V. *Chem. Commun.* **2011,** *47,* 7074–7076.

279. Bhardwaj, R. M.; Price, L. S.; Price, S. L.; Reutzel-Edens, S. M.; Miller, G. J.; Oswald, I. D. H.; Johnston, B. F.; Florence, A. J. Exploring the Experimental and Computed Crystal Energy Landscape of Olanzapine. *Cryst. Growth Des* **2013,** *13* (4), 1602–1617.
280. Singh, S. S.; Thakur, T. S. New Crystalline Salt Forms of Levofloxacin: Conformational Analysis and Attempts Towards the Crystal Structure Prediction of the Anhydrous Form. *CrystEngComm* **2014,** *16* (20), 4215–4230.
281. Price, L. S.; McMahon, J. A.; Lingireddy, S. R.; Lau, S. F.; Diseroad, B. A.; Price, S. L.; Reutzel-Edens, S. M. A Molecular Picture of the Problems in Ensuring Structural Purity of Tazofelone. *J. Mol. Struct* **2014,** *1078,* 26–42.
282. Braun, D. E.; McMahon, J. A.; Koztecki, L. H.; Price, S. L.; Reutzel-Edens, S. M. Contrasting Polymorphism of Related Small Molecule Drugs Correlated and Guided by the Computed Crystal Energy Landscape. *Cryst. Growth Des* **2014,** *14* (4), 2056–2072.
283. Kendrick, J.; Stephenson, G. A.; Neumann, M. A.; Leusen, F. J. J. Crystal Structure Prediction of a Flexible Molecule of Pharmaceutical Interest with Unusual Polymorphic Behavior. *Cryst. Growth Des* **2013,** *13* (2), 581–589.
284. Baias, M.; Dumez, J. N.; Svensson, P. H.; Schantz, S.; Day, G. M.; Emsley, L. De Novo Determination of the Crystal Structure of a Large Drug Molecule by Crystal Structure Prediction-Based Powder NMR Crystallography. *J. Am. Chem. Soc.* **2013,** *135* (46), 17501–17507.
285. Ismail, S. Z.; Anderton, C. L.; Copley, R. C. B.; Price, L. S.; Price, S. L. Evaluating a Crystal Energy Landscape in the Context of Industrial Polymorph Screening. *Cryst Growth Des* **2013,** *13* (6), 2396–2406.
286. Fakes, M. G.; Vakkalagadda, B. J.; Qian, F.; Desikan, S.; Gandhi, R. B.; Lai, C. J.; Hsieh, A.; Franchini, M. K.; Toale, H.; Brown, J. Enhancement of Oral Bioavailability of an HIV-Attachment Inhibitor by Nanosizing and Amorphous Formulation Approaches. *Int. J. Pharmaceut* **2009,** *370* (1-2), 167–174.
287. Neumann, M. A.; de Streek, J. V.; Fabbiani, F. P. A.; Hidber, P.; Grassmann, O. Combined Crystal Structure Prediction and High-Pressure Crystallization in Rational Pharmaceutical Polymorph Screening. *Nat. Commun* **2015,** *6*.
288. Lupyan, D.; Abramov, Y. A.; Sherman, W. Close Intramolecular Sulfur–Oxygen Contacts: Modified Force Field Parameters for Improved Conformation Generation. *J. Comput. Aided Mol. Des.* **2012**, *26*, 1195–1205; Manolis Vasileiadis, Constantinos C. Pantelides, Claire S. Adjiman. Prediction of the Crystal Structures of Axitinib, a Polymorphic Pharmaceutical Molecule. *Chem. Eng. Sci.* **2015,** *121,* 60–76.

3.17 Predicting Target and Chemical Druggability

TI Oprea, University of New Mexico School of Medicine, Albuquerque, NM, United States
C Hasselgren, PureInfo Discovery, Albuquerque, NM, United States

© 2017 Elsevier Ltd. All rights reserved.

3.17.1	Introduction	429
3.17.2	Where Do Drug Targets Come From? Can We Compute Target Druggability?	429
3.17.3	Can We Compute Drug-Likeness?	431
3.17.4	Can We Use *In Silico* Methods to Evaluate Leads?	431
3.17.5	Are Computational Drug Discovery Criteria Useful?	433
3.17.6	Can *In Silico* Technologies Help Medicinal Chemists?	436
Acknowledgments		438
References		438

3.17.1 Introduction

Drug discovery, particularly from an industrial perspective, has been analyzed from many angles. Since the 1980s, R&D innovation and productivity have been stated to be in decline.[1,2] To some extent, fascination with animal models, rather than the study of man, has been considered the culprit,[3] although high-throughput technologies, from chemical synthesis to biological screening,[4] and intellectual property concerns[5] have also been associated with the decline. Diagnoses[6] and solutions[7] have been proposed.

In this article, we discuss the process of drug discovery from an informatics perspective and focus on some of the *in silico* aspects that are pertinent to the practice of medicinal chemistry. In doing so, we address five questions, outlined in the succeeding text, with focus on discrepancies and issues of general concern to the practice of medicinal chemistry.

1. Where do drug targets come from? Can we compute target druggability?
2. Can we compute drug-likeness?
3. Can we use *in silico* methods to evaluate leads?
4. Are computational drug discovery criteria useful?
5. Can *in silico* technologies help medicinal chemists?

3.17.2 Where Do Drug Targets Come From? Can We Compute Target Druggability?

In the most general sense, drug targets are entities with molecular mass that are present in living systems, which can be perturbed upon interacting with therapeutic agents. Here, "living systems" refers to not only humans (or animals, if veterinary medicines are discussed) but also foreign organisms such as viruses, bacteria, and parasites that may be present in the human body. Therapeutic agents ("drugs") are, in the widest sense, substances that are administered to influence the outcome of the disease, whether to cure it, to reduce, or to eliminate some of its symptoms, or simply to improve the quality of life for the patient in question. It is important to recall that the interaction between a drug and its target results in an observable clinical outcome. For drug targets, "mode of action" (MoA), more precisely referred to as "mechanism of action," refers to the manner in which drugs exert their action at the molecular (target) level, resulting in the desired or intended therapeutic outcome, that is, the indication(s) stated on the drug package insert ("drug label"). However, some targets interacting with medicines may be responsible for what are commonly referred to as "side effects," which are often neither related to nor compatible with the indication.

Historically, drugs have been discovered through phenotypic observations,[8] and the exact identification of targets associated with drug mechanisms of action remains an arduous process.[9] Only by means of modern molecular and cellular biology, specifically technologies related to genetic engineering, can we establish a causality relationship between drug–target interactions at the molecular level and phenotypic and clinical outcomes. *To answer the first part of the first question, drug targets emerge from causal inferences that relate molecular events and phenotypic observations.*

Establishing causal inferences, however, requires significant effort. A survey of 67 internal projects at Bayer Healthcare concluded that only 25% of the data published elsewhere were confirmed in-house,[10] whereas two-thirds of the projects were not reproducible. The Hematology–Oncology group at Amgen noted[11] that reproducibility from "landmark studies" over a 10-year period was as low as 11%. As the role of the scientific community is to detect and correct such errors, leading National Institutes of Health (NIH) scientists have announced NIH initiatives to improve reproducibility in preclinical research.[12] Ioannidis concludes that most biomedical research findings are false,[13] and the issue of scientific reproducibility has a dedicated Wikipedia entry.[14] Furthermore, the lack of dissemination of negative clinical trial data is likely to keep competitors and academics focused on targets that may have already

been proved to be inadequate.[15] Some of the corollaries stated by Ioannidis[13] can be applied verbatim to target selection for drug discovery: *"The greater the financial […] interests and prejudices in a scientific field, the less likely the research findings are to be true"* and *"The hotter a scientific field (with more scientific teams involved), the less likely the research findings are to be true."* Since "more scientific teams" may include pharmaceutical companies, one needs to contemplate no further the risks concerning target selection.

Target "druggability" is defined as the ability of a target to be therapeutically modulated by medicines, and by definition, the "druggable genome" is comprised of genes that encode proteins that can be modulated by drugs for therapeutic purposes.[16] Hopkins and Groom restricted their "druggable genome" analysis[16] to those targets that can be modulated by orally formulated drugs, as estimated by the "rule of five" (Ro5, *vide infra*)[17] and concluded that the intersection between disease-modifying genes and the "druggable genome" results in a set of 600–1500 drug targets. Although Kubinyi responded that in vivo, single proteins may combine in ways that could in fact lead to many more drug–target combinations across multiple pathways, that is, a "druggable proteome" (or "targetome"), thus questioning the single-gene view,[18] the concept of "druggable genome" has become quite popular.

To understand target druggability, we need to know how many drug targets exist. A 1997 estimate of 483 targets[19] was revised in 2006 to 218 [20] and 324,[21] respectively. DrugBank,[22] an online resource that indexes 8203 drug entries, including 2198 FDA-approved small-molecule drugs and biologics, linked to 4333 nonredundant proteins.[23] Small-molecule drugs are associated to 1682 unique targets, whereas biologics target 234 proteins.[23]

We conducted our own extensive, independent curation at the European Bioinformatics Institute (EMBL-EBI), at the Institute of Cancer Research (ICR), UK and at the University of New Mexico (UNM). We identified 893 human and pathogenic biomolecules that we annotate, at the molecular level as MoA drug targets for 1578 FDA-approved drugs, and a small number of drugs approved elsewhere in Europe and Japan.[9] The 601 human proteins of the MoA drug targets subset are referred to as *"Tclin,"* in other words, protein targets through which a therapeutic agent is known to bind with potency that is appropriate for leading to the desired therapeutic outcome via the intended mechanism of action.

The discrepancies between the number of drug targets in the *Tclin* subset, comparing DrugBank target statistics, the analyses reported in 1997 and 2006, respectively, and our own study, can only in part be attributed to an increasing amount of evidence regarding the way in which drugs act. Even more relevant is the assignment of a drug target to a certain drug, particularly when linking drug–target interactions to desired therapeutic response, to side effects, to off-label effects (i.e., desired for a different indication), and last but not least, when linking the drug effect to different types of patients (e.g., responders and nonresponders. Serious challenges were encountered when assigning MoA targets for anti-infectives, since pathogens themselves, not molecular targets, are the primary object of study in microbiology.

Predicting target druggability is not trivial. Structural biology, computational chemistry, and medicinal chemistry aim to predict and test whether a protein can bind small, drug-like compounds[24] with high affinity and specificity, with structural biologists and computational scientists focused on *in silico* techniques to assess these interactions.[25] Many in-house programs, both in industry and academia, rely on this type of computational druggability assessment, using, for example, automated detection of protein-binding sites, pocket-feature computations related to their size, shape, and hydrophobicity, in order to rapidly detect "druggable" proteins.[26]

Hopkins and Groom instead focused[16] on specific protein domains from the InterPro database[27] and assign protein "druggability" based on the presence within a protein primary sequence, of specific protein domains known to interact with small-molecule drugs. By manually examining InterPro domains and including genes from the Consensus Chemical Database Service,[28] Russ and Lampel concluded that there may be 2200 druggable genes.[29] Others have expanded the druggable genome either by evaluating side-effect similarity for known drugs[30] or by performing combined chemical and target similarity queries,[31] followed by experimental confirmation of novel drug targets derived from clinical observation[30] or computation.[31] *To answer the second part of the first question, there are many conceptually distinct methods to predict target druggability. However, none of them can perform a rigorous de novo evaluation for proteins for which little knowledge exists.*

The emergence of new knowledge was the focus of a recent bibliometric evaluation, which examined how many of the newly sequenced proteins, for several target families, are the subject of new studies, 10 years after the sequencing of the human genome was completed.[32] This analysis concluded that the process of druggable target selection is conservative and that limited progress has been observed with respect to understanding newly discovered proteins. Choosing the appropriate proteins as drug targets remains a complex process, where scientific elements need to be balanced against commercial ones, for example, company investors and medical insurance companies, societal ones, for example, physicians and patients, and legal aspects, for example, regulators.[33]

To assist with target prioritization and selection, two precompetitive initiatives have emerged. Hosted by EMBL-EBI since 2015, the Open Targets Consortium[34] is developing the Target Validation Platform,[35] which provides robust and comprehensive data integration linking genes and proteins with human disease. At NIH, the "Illuminating the Druggable Genome" (IDG) program was launched in 2014, with the aim to catalyze research around understudied targets.[36] The IDG categorizes proteins based on available data, information, and knowledge from more than 100 sources. Quantification of available data and knowledge from IDG confirms the presence of a bias toward well-described proteins, particularly drug targets, or *Tclin*, bias that is confirmed not only with respect to patents and publications but also with respect to experimental data and molecular probe availability (e.g., antibodies and chemicals). About 37.5% of the human proteome is comprised of understudied proteins (*"Tdark"*). Given the current level of knowledge, *Tdark* proteins are poorly understood, and a knowledge deficit exists concerning experimental data, availability of patents, and scientific literature. Perhaps, scientists engaged in target druggability prediction, and target selection should focus to a higher extent on *Tdark*, where novel research and commercial opportunities in drug discovery may exist.[74]

3.17.3 Can We Compute Drug-Likeness?

Target druggability remains a challenging task, yet an equally important task is prediction of compound druggability. At the outset, we note that "drug" is not an intrinsic quality of chemicals.[37] There is a growing body of scientific literature concerning the computation of drug-likeness, some of which we comparatively discussed previously.[37] Yet, the "drug" attribute is an authorization issued by a regulatory body such as the US Food and Drug Administration to the sponsor, to market that therapeutic agent. In other words, a "drug" is deemed safe based on scientific evidence available at the time of the New Drug Application (NDA). NDAs must be obtained in each country, where committees weigh in all evidence, compare the submission with existing therapies and drugs, and decide to approve, or sometimes withdraw, the "drug" attribute from the therapeutic agent on the basis of efficacy, safety, and cost-benefit. Therefore, "drug" is not an attribute one could compute from molecular structure and is not a natural property of chemicals. At best, compound druggability is time-dependent and remains a heuristic process that is likely to require frequent revisions, as our body of knowledge concerning drugs develops.

Although the property of "drug" remains a societal issue, there remains a stringent need to assess compound quality, particularly given the large numbers of chemicals available. The iResearch Library from ChemNavigator currently has over 60 million unique chemicals from more than 200 chemical vendors.[38] Another chemical procurement service, eMolecules, tracks over 7 million screening compounds.[39] Therefore, there is a critical need to develop abilities to evaluate compounds for purchasing or further downstream after high-throughput screening (HTS) campaigns. Therefore, drug-likeness (or chemical druggability) prediction is not a direct answer to the question "could this molecule be a drug?" but rather an *in silico* estimate of the molecule's probability for becoming a drug. Given the large number of chemicals in need of evaluation, this is regarded as a machine (not human) learning problem, since the ability to distinguish between "drugs" and "nondrugs" is likely to remain limited to those few scientists that are successful "drug hunters."

We reviewed 18 reports on successful "drug-likeness" models elsewhere.[37] The first two models were disclosed[40,41] shortly after the Ro5 publication.[17] Briefly stated, machine learning models start with (at least) two sets of molecules, namely, "drugs" (though given the small sample space of approved drugs, this is often a larger set of chemicals of pharmaceutical interest) and "nondrugs" (typically reagents or compounds available for procurement), for which a set of molecular descriptors, perhaps physicochemical properties, are computed. From these datasets, machine learning models that successfully discriminate (on average, at the 80–90% rate) "drugs" from "nondrugs" are developed. Of the 18 models reported, 9 used "Available Chemicals Directory" (ACD) as the "nondrug" reference set. ACD is a very ill-defined reference set for "nondrugs," since nearly 40% of ACD (after removing all chemical structures of drugs from the ACD catalog) are chemicals with a high content of drug-like fragments, that is, these molecules are likely to be chemically similar to drugs.[42] To make matters more complex, the set of "nondrugs" has been constantly evolving. *In silico* efforts to model drug-likeness use sets of chemicals offered for purchase from a variety of vendors, including Sigma and ACD. Yet, computational chemists are actively working within the chemical vendor companies to match selection criteria imposed by the customers (academic groups and primarily pharmaceutical companies). The net effect of this adaptive process is that, over time, the "nondrugs" reference set is shifting more and more toward "drugs," since chemical vendors are making deliberate efforts to improve their offerings and maintain a competitive offering.

To conclude, machine learning remains the preferred method when analyzing large sets of molecules, such as chemical libraries, and when prioritizing chemicals for procurement and HTS. Thus, the development of models for drug-likeness can provide tangible benefits by saving time and resources allocated to preclinical drug discovery. However, as stated from the outset, the effort to predict "compound druggability" from molecular structure is a poorly defined problem, since "drug" is an attribute decided by regulators. Moreover, the "nondrugs" reference set is increasingly becoming more similar to "drugs." Without proper filters in place, machine learning models are likely to be derived from ill-defined (noisy) data, which in turn leads to overfitting, and diminished performance on external (blind prediction) sets. *To answer the second question, many models have been developed to predict chemical drug-likeness. Their use should be restricted to large chemical libraries. Experienced scientists (experts in "human learning") should be the deciding factor concerning in-depth profiling of individual chemicals.*

3.17.4 Can We Use *In Silico* Methods to Evaluate Leads?

To discuss lead-likeness, we need to examine Ro5 criteria more closely. This was the first study[17] to alert the pharmaceutical industry to the importance of restricting small-molecule synthesis in the property space defined by molecular weight (MW), the calculated octanol/water partition coefficient (ClogP), number of hydrogen-bond donors (HDO), and the sum of nitrogen and oxygen atoms in a molecule, as a surrogate for the number of hydrogen-bond acceptors (N + O). Lipinski et al. started with the analysis of the early (1994) results of HTS and combinatorial chemistry at Pfizer, where most of the hits were large (high MW) and hydrophobic (high ClogP), which in turn increased the difficulty of optimizing them toward oral drugs. Their analysis,[17] based on 2245 compounds from the World Drug Index that had reached phase II clinical trials or higher, looked at the 90th percentile for the distribution of $MW \leq 500$, $CLogP \leq 5$, $HDO \leq 5$, and $N + O \leq 10$. Natural products and actively transported molecules were excluded from this analysis. The authors concluded that if any two of the aforementioned conditions are violated, the molecule is unlikely to be an orally active drug.

We compared oral drugs approved up to 1997 (the year of the Ro5 publication) with those approved in 1998 and later and noted[43] that two or more Ro5 violations were present in 15.7% of the newer drugs (191 small molecules), compared with 5.6%

in the prior set ($N=661$). This indicates that the 90th percentile cutoff values are already shifting, a trend already noted a decade earlier.[44] Leeson and Davis noted that the median values for MW, CLogP, and N + O, as well as other parameters, went up when comparing sets of drugs approved before 1983 and during the 1983–2002 period.[44] Although the discussion focused on median values, we believe that looking at 90th percentile, which was effectively used to define Ro5, makes it more amenable for direct comparisons.

Table 1 shows an extension of the analysis reported earlier, as we examine temporal trends for Ro5 criteria.[43] Here, we extracted all orally formulated drugs approved by the FDA from DrugCentral,[45] a total of 1491 drugs. Of these, 11 lack precisely defined chemical structures (e.g., benzonatate is a mixture of three aliphatic esters) and were thus excluded from the analysis. The remaining set was queried for approval date. A set of 479 drugs lack approval information and were excluded from the comparison; $N=671$ drugs were approved in 1997 or earlier, whereas $N=330$ drugs were approved in 1998 or later. By examining the 10th, the 50th (median), and the 90th percentile, we confirm the trend observed earlier. Oral drugs shown an increase in MW for the newly approved drugs (e.g., MW = 586.39 at 90%), compared with those approved pre-1998 (MW = 469.66 at 90%). The same can be said for CLogP, which shifts from 5.06 to 6.28 at the 90th percentile, and for the hydrogen-bond acceptors (N + O), which shift from 9 to 12. Of equal interest is the number of drugs that are fully compliant with Ro5 criteria: Within the "older" drugs set, 81.7% drugs have Ro5 = 0, 12.46% have Ro5 = 1, and 5.85% have Ro5 ≥ 2. For the "newer" set, 69% drugs have Ro5 = 0, 15.9% have Ro5 = 1, and 15.1% have Ro5 ≥ 2. Confirming what Leeson and Davis noted in 2004, the number of Ro5 compliant drugs is decreasing over time.

The Ro5 cutoff values should not have been a multiple of five after all: After a careful reevaluation[46] of the same set of World Drug Index compounds, the 90th percentile cutoff values for Ro5 parameters were as follows: MW ≤ 427.5, CLogP ≤ 5.3, HDO ≤ 3, and N + O ≤ 8. Differences between these values and those reported in the original Ro5 study were attributed to differences in salt handling, duplicate structure removal, and other details in data processing. The reader will also note discrepancies between these values and those obtained from orally formulated approved drugs shown in **Table 1**.

Highly influential and groundbreaking, the Ro5 work remains one of the most cited papers in medicinal chemistry. This work raised the awareness of the medicinal chemistry community regarding the existence of a property space for oral drugs, forced us to examine the design of combinatorial libraries,[47] what the properties of drugs are,[48] the origin of leads,[49] and sparked interest in lead discovery. Many library design programs, based on combinatorial chemistry or compound acquisition, subsequently included the default Ro5 filters. However, as shown earlier, *Ro5 cutoff values are not likely to stand the test of time*, but are likely to shift toward higher values.

The ability to develop machine learning models that discriminate between "drugs" and "nondrugs" based on chemical fingerprints caused some confusion, as it was by default assumed that Ro5 criteria are also "drug-like." We showed that this was not the case during a comprehensive survey[48] of "drugs" versus "nondrugs." The outcome of many HTS campaigns[47] is usually *micromolar hits*, which when filtered according to the drug-based Ro5, are not easily amenable to medicinal chemistry optimization. We also pointed out[49] that the aim of HTS and combinatorial library design programs is to identify *leads*, not drugs. Therefore, the use of Ro5 filters for lead discovery is not warranted, at least not with respect to small organic compounds.

As we discussed in part 1, from a chemical standpoint, it is not clear what a drug is. By the same extension, a chemical lead, or drug prototype,[50] cannot be discussed in strict chemical terms. *"Lead" is not an intrinsic property of chemicals*, just as "drug" is not. Although the process of approving a drug follows very strict protocols, a significant process involving multidisciplinary evaluations and due diligence is observed when nominating a lead for further optimization.[51] What is a lead? Though a high number of compounds may be HTS hits or potent bioactive chemicals, not all of these are leads. Leads are compounds that are part of a series of analogs with validated biological activity, both in primary and secondary screens, against known targets. Whereas specific criteria for nominating a lead are project-dependent, lead compounds must also allow favorable intellectual property positioning and display good solubility and permeability and overall a promising pharmacokinetics and toxicology profile.

Although there is a general consensus that lead discovery is an essential goal that precludes drug discovery, the only way to analyze the nature of the "lead-like" space has been to examine chemical structures that, historically, were leads. We had to face the question[49] whether these chemical structures could provide an objective link between the chemical space of leads and the chemical space of drugs. Our preliminary survey of 18 lead–drug pairs prompted us to suggest[47] that lead-like libraries should be designed with lower MW(≤300) and lower CLogP (≤3.0) cutoffs, which constituted a significant departure from Ro5 criteria. An extension to 96 lead–drug pairs allowed us to note[49] differences between the median property value of drugs and leads, as

Table 1 Property distributions of the four Ro5 parameters for FDA-approved oral drugs

	All oral drugs				*Oral drugs approved pre-1998*				*Oral drugs approved after 1997*			
Category	*N*	*10%*	*50%*	*90%*	*N*	*10%*	*50%*	*90%*	*N*	*10%*	*50%*	*90%*
MW	1480	187.2	324.4	513.5	671	170.2	311.4	469.7	330	240.9	397.5	586.4
CLogP	1412	−0.50	2.49	5.38	643	−0.77	2.33	5.06	320	0.04	3.03	6.28
O + N	1418	2	5	9	645	2	5	9	321	3	6	12
HDO	1418	0	1	4	645	0	1	4	321	0	1	4
Ro5 score	1412	0	0	1	643	0	0	1	320	0	0	2

Table 2 Property distribution for several parameters, for leads and FDA-approved oral drugs. Values shown at 90% for LogSw correspond to the 10th percentile

	Leads (from data reported earlier[54])			*Oral drugs approved pre-1998 (see also Table 1)*			*Oral drugs approved after 1997*		
Category	*N*	*50%*	*90%*	*N*	*50%*	*90%*	*N*	*50%*	*90%*
MW	385	287.4	436.9	671	311.4	469.7	330	397.5	586.4
CLogP	385	2.3	5.08	643	2.33	5.06	320	3.03	6.28
O + N	385	5	11	645	5	9	321	6	12
HDO	385	1	4	645	1	4	321	1	4
RTB	385	4	10	645	4	9	330	5	12
RNG	385	3	4	669	3	5	321	3	5
LogSw	385	−3.25	−5.24	643	−3.47	−5.31	320	−4.17	−5.53

follows: $\Delta MW = 69$, $\Delta N + O = 1$, and $\Delta CLogP = 0.43$ (among other properties). We concluded that lead structures exhibit, on the average, less molecular complexity (less MW and less number of rings and rotatable bonds) and are less hydrophobic (lower CLogP and LogD74) and less drug-like. An independent study reached similar conclusions,[52] starting with 470 lead–drug pairs extracted from Walter Sneader's monograph on drug prototypes.[50]

Criteria for lead-likeness have been subjected to several revisions. For example, a so-called "reduced complexity" lead-like set was assembled[53] at GSK using several computational criteria, for example, average values for $MW < 350$, $HDO \leq 3$, $N + O \leq 8$, $CLogP \leq 2.2$, and number of nonterminal rotatable bonds,[48] $RTB \leq 6$. The most extensive analysis was based on 385 documented leads, 1651 launched drugs, thousands of phase I, II, and III clinical trial drug candidates, and tens of thousands of literature-reported high-activity or inactive molecules.[54] The 90th percentile from the 385 leads were as follows: $MW \leq 436.9$, $CLogP \leq 5.08$, $HDO \leq 3$, $N + O \leq 11$, and $RTB \leq 10$. We also reported 90% values for calculated intrinsic aqueous solubility ($LogSw \geq -5.24$), computed with the ALOGPS software,[55] and for the number of rings ($RNG \leq 4$). For comparative purposes, these values, together with median values, are shown with properties of oral drugs in **Table 2**.

Whereas these data support the general notion that leads are, in fact, smaller compared to oral drugs, there is no definite conclusion regarding CLogP, RNG, and RTB (except for drugs post-1997 that are more hydrophobic, may have more rings and more flexible bonds). A weak trend is observed for LogSw, which is that leads are on average slightly more soluble, but not markedly so. However, without experimental data, it is difficult to draw additional conclusions.

Although based on a smaller statistical sample (below 500) compared to "drugs," the concept of lead-likeness appears to continue to play an important role in drug discovery, perhaps as important as the concept of "drug-likeness." *The answer to the question, can we compute lead-likeness, has a case-dependent answer. Just like "drug," "lead" cannot be computed from molecular structure. Although several paradigms for lead discovery have been proposed, it would be prudent to avoid "one-size-fits-all" criteria for leads, since each project has specific needs, both from a chemical series and from a therapeutic perspective.* For example, leads for a urinary tract anti-infective project would require high solubility and the ability to pass through glomerular filtration; by contrast, leads for an anti-inflammatory project for topical (skin) applications would require lower solubility but high CLogP.

3.17.5 Are Computational Drug Discovery Criteria Useful?

Some of the extensions of the Ro5 concept[17] and the lead-like concept[47] are summarized in **Fig. 1** and discussed in this section. The first Ro5 extension was developed[56] at GSK from rat bioavailability data from a proprietary set of 1117 compounds: Their model stated that using $RTB \leq 10$ and $PSA \leq 140$ Å^2 as cutoff values would capture ~80% of the compounds with oral availability above 20%. Not reproduced on 434 Pharmacia compounds,[57] this model is also not supported by oral drugs, data shown in **Table 3**. While the 90% cutoffs for oral drugs pre-1998 for PSA (127.1 Å^2) and for RTB (9) are well within the range proposed by Veber et al.,[56] these values would capture less than 90% of oral drugs approved after 1997. The 90% distribution moments are 150.8 Å^2 for PSA and 12 for RTB (data in **Tables 2** and **3**). When applied simultaneously, these two criteria capture 259 out of 330 oral drugs; the same criteria for pre-1998-launched drugs capture 575 out of 671 compounds. From the entire dataset ($N = 1480$; see **Table 1**), only 1418 drugs have PSA and RTB calculations; of these, 1228 (or 86.6%) satisfy the Veber criteria. This is a reasonable success rate given that one parameter (RTB) is not represented by Ro5 criteria (note that PSA and hydrogen-bond donors/acceptors correlate), but we should recall that 190 oral drugs (of which, 71 were launched after 1997) are excluded by these criteria. As shown by the increase in 90th percentile values for "newer" drugs, the Veber criteria are not likely to stand the test of time.

Conceptual developments in the rapid evaluation of large chemical libraries, in particular for compound druggability and lead-likeness, paved[58] the way for fragment-based drug discovery,[59] particularly after "rule of three" (Ro3) was formulated.[60] Stated succinctly, Ro3 imposed the following cutoff values for fragments: $MW < 300$, $CLogP \leq 3$, $RTB \leq 3$, $HDO \leq 3$, and $N + O \leq 3$. An additional parameter, polar surface area ($PSA \leq 60$ Å^2) was also considered useful during fragment selection (see **Fig. 1**). Although

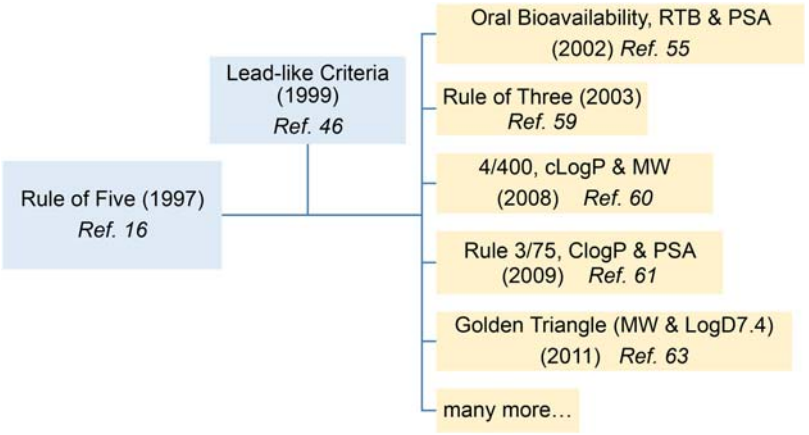

Fig. 1 The evolution of metrics in lead and drug discovery literature. Most of these metrics contain a measure of molecular size (typically MW), hydrophobicity (typically CLogP), and hydrogen-bonding capacity (e.g., PSA), which reflect the Ro5 criteria.

Table 3 Property distribution for additional parameters discussed throughout the text, for FDA-approved oral drugs. See text for details

	All oral drugs				*Oral drugs approved pre-1998*				*Oral drugs approved after 1997*			
Category	*N*	*10%*	*50%*	*90%*	*N*	*10%*	*50%*	*90%*	*N*	*10%*	*50%*	*90%*
PSA	1468	21.3	66.6	134	666	18.1	63.5	127.1	320	330	81.6	150.8
LogD74	1471	−2.18	1.31	3.97	669	−2.43	1.07	3.63	328	−1.14	1.97	5.03
FSP3	1450	0.13	0.40	0.76	656	0.12	0.40	0.78	327	0.13	0.36	0.69
Chiral#	1471	0	1	6	669	0	1	6	328	0	1	5

these parameters are designed for fragments, not drugs, it may be of interest to know how many oral drugs match Ro3 criteria: out of 1418 oral drugs in this set, 134 match the first 5 criteria, with only 119 matching the sixth one, PSA ≤ 60 Å^2. Of these, 21 drugs (16, including PSA) were approved in 1998 or later.

Looking at an information-rich set of ~30,000 internal GSK compounds, Gleeson chose to examine MW and CLogP, as two almost orthogonal dimensions derived from a set of 15 computational descriptors.[61] He then compared the influence of MW and CLogP on a number of pharmacokinetic properties, including solubility, permeability, bioavailability, and blood–brain-barrier penetration, metabolism via cytochrome P450 enzymes, efflux transport via P-glycoprotein, and inhibition of the K+ ion channel, hERG. Based on extensive analyses, he then identified two qualitative filters, namely, MW < 400 and CLogP < 4 (also known as the 4/400 rule), which are likely to lead to molecules having more desirable properties, compared with the molecules having one or both of these parameters above the cutoff values.

We applied the same filters on the 1412 oral drugs discussed throughout this work. Indeed, there appears to be an enrichment of drugs that match the 4/400 rule, as this parameter selects ~60% of the drugs (**Table 4**). However, nearly 40% of the drugs ($N = 577$) lie above this cutoff value, with CLogP having perhaps a slightly stronger influence than MW. We note that, while there are fewer (less than 10%) pre-1998 drugs in the high-MW/high-CLogP quadrant, there is a significant increase in the post-1997 (newer) drugs—more than 25% of the newer drugs have high MW/high CLogP. This is not surprising, as the data match similar trends concerning the Ro5 violations discussed in section "Can We Compute Drug-Likeness?" Although the 4/400 criteria appear to provide an overall enrichment for oral drugs, this filter appears to be less effective for newer drugs, as ~57% of these ($N = 183$) are not 4/400-rule compliant. Thus, the Gleeson criteria are unlikely to stand the test of time.

Table 4 Count of drugs using the 4/400 filters (MW and CLogP), for FDA-approved oral drugs. The second column (shaded) matches the Gleeson 4/400 criteria[61]

Oral drugs (N = 1412)	*MW < 400, CLogP > 4*	*MW < 400, CLogP ≤ 4*	*MW ≥ 400, CLogP ≤ 4*	*MW ≥ 400, CLogP > 4*	*Total*
Approved in 1997 or earlier	82	422	87	52	643
Approved in 1998 or later	25	137	71	87	320
Unknown launch date	73	276	56	44	449
Total	180	835	214	183	

Table 5 Count of drugs using the 3/75 filters (PSA and CLogP), for FDA-approved oral drugs. The first and third columns (shaded) match the Hughes et al. criteria[62] and the Hasselgren et al. criteria,[63] respectively

Oral drugs (N = 1412)	*PSA < 75 Å², CLogP > 3*	*PSA < 75 Å², CLogP ≤ 3*	*PSA ≥ 75 Å², CLogP ≤ 3*	*PSA ≥ 75 Å², CLogP > 3*	*Total*
Approved in 1997 or earlier	180	204	204	55	643
Approved in 1998 or later	78	59	100	83	320
Unknown launch date	157	127	134	31	449
Total	415	390	438	169	

By examining in vivo toxicology outcomes on 245 preclinical Pfizer compounds, Hughes et al. found an increased incidence of toxicity for low-polarity, high-lipophilicity compounds,[62] as defined by CLogP > 3 and PSA < 75 Å^2. The authors claimed that the promiscuity of highly lipophilic molecules may lead to an increased in vivo toxicity. This is currently referred to as the 3/75 rule. A dramatic illustration that dataset dependence can result in misleading conclusions is provided by Muthas et al., who examined toxicity observed before phase II studies of 150 AstraZeneca development compounds.[63] The exact opposite parameters, CLogP < 3 and PSA > 75 Å^2, provide enrichment for high-toxicity compounds on their internal dataset. They confirmed that this was also the case had they classified the dataset on toxicity observed in the preclinical in vivo studies and thus more closely resemble the Pfizer study.

Hughes et al. wrote[62] that *"high-CLogP/low-PSA compounds are approximately 2.5 times more likely to be toxic as to be clean, representing an odds ratio of greater than 6"* and that *"compounds with low CLogP/high PSA are approximately 2.5 times more likely to be clean as to be toxic."* If these parameters had any relevance for general clinical outcomes, we would have expected to see a skewed distribution of drug counts when examining the 1412 oral drugs discussed earlier. However, this effect is not present, regardless of the time point of the drug launch (**Table 5**), confirming a similar observation[63] made by Muthas et al. We note fewer approved drugs in the high-CLogP/high-PSA quadrant, probably due to the difficulty of making drugs that are highly lipophilic and water-soluble (as reflected by high PSA). Unless the in-house compound collection warrants this type of filtering, one should exercise care when applying the 3/75 rule.

Another proposal built on Ro5 criteria, the "Golden Triangle," is a visualization device that plots MW against LogD7.4, which is the octanol–buffer (pH 7.4) partition coefficient. The Golden Triangle is best explained by the authors: "*(1) As MW decreases, the lipophilicity range affording both permeable and stable compounds increases; (2) within a LogD bin, the relative number of permeable and stable compounds increases as MW declines; (3) Within a LogD range of 1.0–2.0, the opportunity for permeable and metabolically stable compounds increases; (4) all trends combined lead to the observation that the polarity and MW of in vitro permeable and low clearance compounds are concentrated within an area with a base-line from LogD = −2.0 to LogD = 5.0 at MW = 200 and an apex at LogD = 1.0–2.0 and MW = 450. These trends lead to a triangular shaped area known as the Golden Triangle and molecules within this area that are low clearance and permeable are said to obey the Golden Triangle Rule. While LogD positively correlates with permeability at a given molecular mass, LogD is negatively correlated with the in vitro clearance, giving rise to a balanced maximal effect near LogD 1.0–2.0. The strong influence of polarity and MW on permeability and in vitro metabolic stability give rise to the observed improvements in both clearance and absorption inside the Golden Triangle. In the center of the Golden Triangle (LogD = 1.5, MW = 350), 25% of the compounds pass permeability and clearance criteria, although percentages will vary according to limits imposed defining stable and permeable compounds. Compare this 25% "success" rate in the heart of the Golden Triangle with the 3% "success" rate at MW 450 at both LogD 0 and 3.0 and the odds of preparing an in vitro low clearance and permeable compound diminishes by roughly eightfold. Beyond a MW of 450, there is a precipitous lowering of likelihood that in vitro low clearance and permeable compounds exist."*[64] Furthermore, *"the Golden Triangle boundaries shift slightly from series to series."*[65]

It is quite challenging to compare data calculated from 1418 oral drugs with a set of parameters that is not precisely defined. Within this article (e.g., **Table 3**), we use calculated LogD7.4, using software from ChemAxon.[65] Data in **Table 3** shows that a LogD74 baseline between −2 and 5 covers most of the drugs ($N = 1228$ or 86.6%). We note that the calculated range goes from −14.42 (for paromomycin, an older aminoglycoside antibiotic) to +17.16 (for ubidecarenone, commonly known as coenzyme Q10, sold as a dietary supplement). Such extremes are clearly impossible to measure. After restricting our analysis to the range of LogD7.4 from −2 to +5, we were unable to detect a pattern reminiscing of a Golden Triangle, even after filtering MW to a range below 600. **Fig. 2** reproduces the visualization shown[65] in Figure 7. Based on an attempt to digitize an image and absent exact parameter cutoff values, we estimate that these filters remove approximately 500 drugs from the 1228 set. Recalling the 190 drugs eliminated because their LogD7.4 is outside the range from −2 to +5, we can conclude that the MW/LogD7.4 space defined by the Golden Triangle rule eliminates ~50% of the orally approved drugs.

We have shown, earlier, that most of these metrics have questionable values. Kenny and Montanari[66] highlighted that the importance, or strength, of many of the reported relationships, such as the Golden Triangle, is overstated because the approaches used to analyze and visually represent the data exaggerate trends in data. Another parameter covered in **Table 3** highlighted the apparently overlooked importance[67] of the fraction of sp3 carbons, FSP3. In that report,[67] binning FSP3 as a function of LogSw resulted in a high correlation ($r = 0.97$), which suggests a very strong relationship. Since these data were made available as supplementary material, Kenny and Montanari reanalyzed it without data binning, which inflate artificially the correlation for FSP3. They noted that the correlation coefficient between FSP3 and LogSw is only $r = 0.25$. We found no such relationship ($r = 0.06$) when computing the

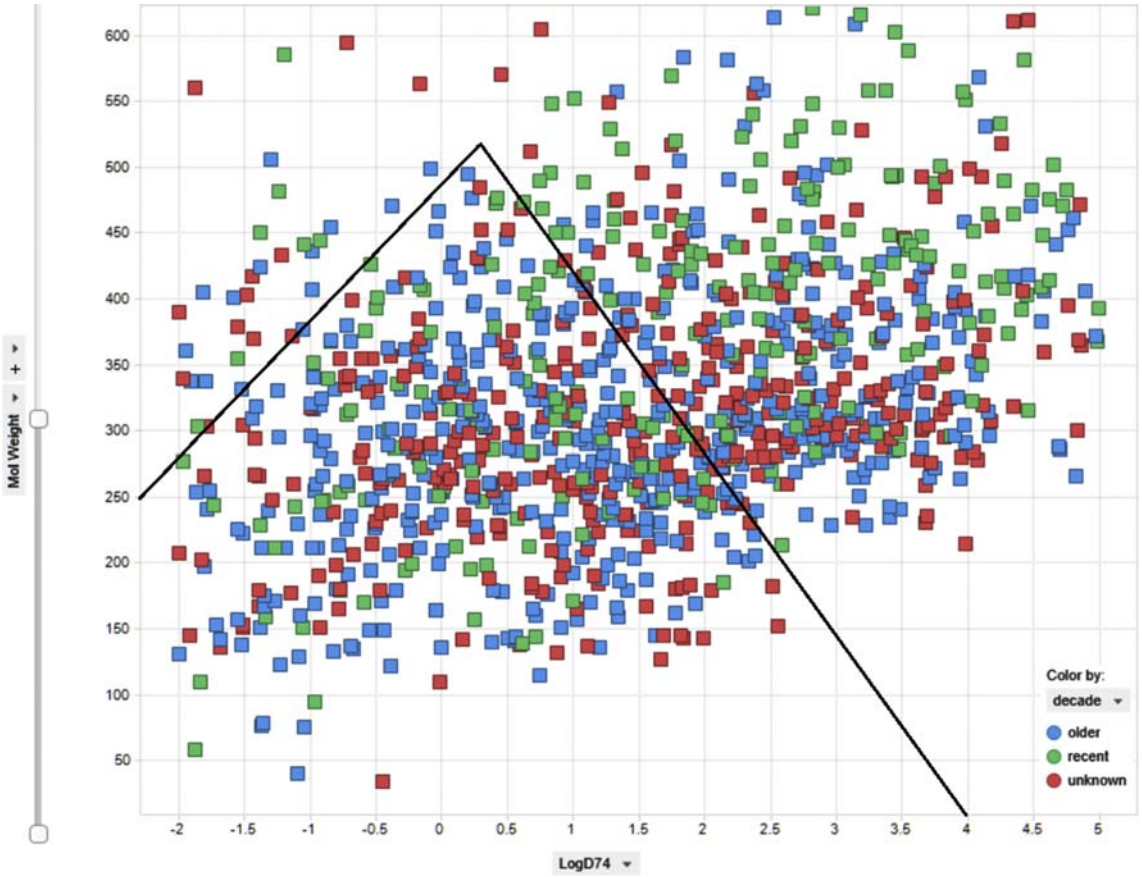

Fig. 2 Calculated LogD7.4 and MW values for oral drugs, using the Golden Triangle scheme. Older drugs refer to drugs approved pre-1998, whereas newer drugs refer to drugs approved post-1997.

relationship between FSP3 and LogSw for the $N = 1418$ drugs used in this article. However, Kenny and Montanari reported that the correlation between MW and LogSw for this study was actually much higher ($r = -0.62$) and questioned why Lovering et al. placed such an importance on FSP3, which only described 6% of the LogSw variance. We confirmed the MW/LogSw relationship ($r = -0.61$) for the 1418 drugs.

Lovering et al. stated[67] that *"as compounds are prepared in the drug discovery setting and transition from discovery through clinical trials to drugs, those that are more highly saturated are more likely to succeed in these transitions. Saturation also increased the likelihood of higher solubility and lower melting points. Compounds are much more likely to succeed as drugs if they have appropriate values for these properties. Another descriptor for complexity, the presence of stereo centers, also increases as we transition from discovery, through clinical trials, to drugs. This held true even after filtering compounds that failed any one of the Ro5, as well as had greater than 10 rotatable bonds."* As shown in **Table 3**, the median and the 90th percentile for FSP3 are slightly shifted, from 0.4 to 0.36 and from 0.78 to 0.69, when examining "older" versus "newer" drugs. Combined with the observation that the 90% number for chiral centers (chiral#) drops from 6 to 5 for the same period, we conclude that the opposite trend occurs. That is, newer drugs are less saturated and have lower complexity, whereas RTB, the number of rotatable bonds, is increasing (*vide supra*).

3.17.6 Can *In Silico* Technologies Help Medicinal Chemists?

> When a measure becomes a target, it ceases to be a good measure
>
> Charles Goodhart[68]

To properly address this question, we first note some of the systemic problems that exist in biomedical research, as they are pertinent to medicinal chemistry as well. The practice of Western (allopathic) medicine through the ages has introduced a separation of diseases by organs and by medical specialties. Whereas this separation is well suited for medical practice, it has translated into a conceptual fallacy with respect to biomedical research. Just as NIH institutes are separated by disease areas, so are medicinal

chemistry and drug discovery units separated by therapeutic areas. And yet, genomics, pharmacology, and molecular biology, to name a few sciences, have no such separation. The same molecular pathways, the same biology, are at work regardless of organ or cell. The consequences of this "mental divide" have yet to be examined, but we believe they hamper progress in the search for new cures.

Another systemic issue is the objectification of disease. As we stated elsewhere,[9] *"Medical care has two goals: to properly diagnose the disease and to select the appropriate therapeutic. As long as (drug-induced) phenotypic alterations are observed under appropriate conditions, it is possible to steer medical care and adjust the therapeutic management for a better outcome. Hence, the key to successful drug discovery and application resides in the seamless integration of pathological mechanisms of disease (that is, molecular and cellular level processes) with diagnoses (clinical embodiments of disease at the organ and/or organism level) and therapeutics (that is, modulating clinical manifestations at the molecular level via therapeutics)."* Somewhat related to overspecializing in a therapeutic area, this has practical implications for basic scientists, particularly in the pharmaceutical industry. It is quite common for clinician scientists, active at university hospitals, to interact with basic scientists on a daily basis. This provides a fertile, common ground, where clinical and fundamental scientific aspects are discussed. Unfortunately, clinicians are rarely accessible for industrial scientists, which may prove to be a detrimental practice, with respect to understanding physical manifestations of disease and practical approaches to therapeutics.

Throughout this article, we questioned most of the guidelines that are currently influencing the practice of medicinal chemistry. Analyses by Kenny and Montanari[66] and by Muthas et al.,[63] as well as our own analyses based on over 1400 oral drugs, highlight some of the issues associated with drug discovery "metrics." Many such metrics, not covered here, study the same space, of oral (or nonoral) drugs, chemical probes, leads and drug prototypes, and targets associated with drugs, while ignoring the basic tenet that "drug" is not a computable property, nor are "lead" or "drug target." To drill this point further, a MoA drug target would cease to be a Tclin target if the only approved drug that is known to act via that target is withdrawn. In other words, "Tclin" targets are a human-given attribute. Moreover, many of the "metric" studies are based on applied statistical analyses, but as Kenny and Montanari have shown,[66] several of these papers have questionable statistical and scientific validity—which reinforces the tenet by Ioannidis[13] even further.

One of the most popular metrics, ligand efficiency[69] (LE) and derivatives such as lipophilic ligand efficiency[70] (LLE) have been criticized at the fundamental level by Kenny et al.[71] They point out that the defining assumptions are made arbitrarily and take no account of the possibility that different activities might respond differently to a risk factor. This arbitrariness was highlighted by comparing LE and LLE. In the common formulation of LE, the scale taken for potency is free energy divided by the number of heavy atoms, whereas the ligand lipophilicity scale uses potency on a pIC50 scale and offset by lipophilicity. The thermodynamic standard states chosen for the metrics are not defined, and the choice has a large effect upon how these metrics perform. Whether logP is the most appropriate measure of hydrophobicity is seldom questioned, as the n-octanol–water scale is itself an arbitrary measure of hydrophobicity, and n-octanol partition "does not sense" hydrogen-bond donors to the same extent as it senses acceptors. As there are many methods to calculate LogP and some use LogD7.4 (also with multiple ways to compute it), the results are not likely to be comparable from one LE/LLE study to another. No consideration is given to the ionization state of the ligand as it binds to the receptor (which should be the most relevant state). Their recommendation is, that if the question is, do these compounds "beat the trend," then this trend should first be defined via a least-square regression to the risk factors. The residual of such a correlation would inform on the extent to which a compound forms the series "beats the trend." The variability of computer models and the dangers of generalization were also noted by Clark[72]: *"First, perhaps obviously to computational scientists, the precise values that are obtained for the number of rotatable bonds in a molecule and its polar surface area depend upon the software that is used to compute these quantities. So, unless it is certain that the software used is the same as in the work used to derive the "rule," then there is always the danger that a compound will be misclassified,"* and *"it is likely to be extremely difficult to obtain a simple and general rule to predict a complex physiological endpoint such as oral bioavailability; that great caution should be exercised when prospectively applying conclusions obtained from one set of data using one particular computational protocol to other data sets using different protocols."*

Some of these metrics cannot even be reproduced,[56,64,73] as we and others have illustrated. These metrics are becoming the target, as stated by Goodhart.[68] We fear that these metrics are invented to mask the lack of productivity and the inability to introduce new drugs in the market and that Ro5 derivative metrics are often used to justify productivity (or lack thereof). In other words, one of the reasons for this "soft science" of metrics is that it provides goals to be met and discussed during annual performance reviews. "How many Ro5 compliant compounds have you made/tested," a performance-review goal introduced at Pfizer in the late 1990s, has evolved into a plethora of rules, most of them derived only from one company's collection and not reproducible by others. In fact, the claim made by Ioannidis[13] that most published research findings are false is likely to apply to most (if not all) drug-space-derived metrics. Just like we are witnessing an increasing number of new drug approvals that are not Ro5 compliant, most of these rules will be rendered false by the emergence of new drugs within the next decade.

There is a growing division among medicinal chemists, those who believe that controlling fundamental properties is important in minimizing compound-related attrition through development and those who believe they are unimportant and/or these quality metrics are invalid. This later camp believes that these metrics unduly limit medicinal chemists, who should strive to break free from the "tyranny of Lipinski" and the Ro5 space. But there is a more nuanced third camp. It was Picasso who once said that it took him 4 years to paint like Raphael but his whole life to learn to paint like a child. Acceptance that certain property space limitations exist for some drug classes, because these properties reflect inherent pharmacokinetic or pharmacodynamic limitations (e.g., what drives low solubility or poor cell permeability) can stimulate creativity and more innovative ways to solve the problem at hand. For example, chemists who work with peptides, a drug class clearly outside the Ro5 space, are trying to work around physicochemical limitations by cyclization, N-methylation, or hydrogen-bond matching or making use of active uptake processes to get the peptides into cells or

via lipidation to increase peptide half-life for example. From this middle-ground perspective, metrics and *in silico* models can be used to adequately sample the chemical space and to limit the actual number of experiments, help interpret results, and guide future work.

Acknowledgments

This work was supported by NIH grants U54 CA189205, P30 CA118100, and UL1 TR001449 (TIO). We would like to thank Dr. Oleg Ursu (UNM) for preparing the DrugCentral database and Dr. John Overington (BenevolentAI), for countless conversations on the topic of druggability.

References

1. Steward, F.; Wibberly, G. Drug Innovation—What's Slowing It Down? *Nature* **1980,** *284,* 118–120.
2. Pammolli, F.; Magazzini, L.; Riccaboni, M. The Productivity Crisis in Pharmaceutical R & D. *Nat. Rev. Drug Discov.* **2011,** *10,* 428–438.
3. Horrobin, D. F. Modern Biomedical Research: An Internally Self-Consistent Universe With Little Contact With Medical Reality? *Nat. Rev. Drug Discov.* **2003,** *2,* 151–154.
4. Lahana, R. Who Wants to Be Irrational? *Drug Discov. Today* **2003,** *8,* 655–656.
5. Lipinski, C. A. The Anti-Intellectual Effects of Intellectual Property. *Curr. Opin. Chem. Biol.* **2006,** *10,* 380–383.
6. Scannell, J. W.; Blanckley, A.; Holdon, H.; Warrington, B. Diagnosing the Decline in Pharmaceutical R&D Efficiency. *Nat. Rev. Drug Discov.* **2012,** *11,* 191–200.
7. Paul, S. M.; Mytelka, D. S.; Dunwiddie, C. T.; Persinger, C. C.; Munos, B. H.; Lindborg, S. R.; Schacht, A. L. How to Improve R&D Productivity: The Pharmaceutical Industry's Grand Challenge. *Nat. Rev. Drug Discov.* **2010,** *9,* 203–214.
8. Swinney, D. C.; Anthony, J. How Were New Medicines Discovered? *Nat. Rev. Drug Discov.* **2011,** *10,* 507–519.
9. Santos, R.; Ursu, O.; Gaulton, A.; Bento, A. P.; Donadi, R. S.; Bologa, C.; Karlsson, A.; Al-Lazikani, B.; Hersey, A.; Oprea, T. I.; Overington, J. P. A Comprehensive Map of Molecular Drug Targets. *Nat. Rev. Drug Discov.* **2017,** *16,* 19–34. http://dx.doi.org/10.1038/nrd.2016.230.
10. Prinz, F.; Schlange, T.; Asadullah, K. Believe It or Not: How Much Can We Rely on Published Data on Potential Drug Targets? *Nat. Rev. Drug Discov.* **2011,** *10,* 712.
11. Begley, C. G.; Ellis, L. M. Drug Development: Raise Standards for Preclinical Cancer Research. *Nature* **2012,** *483,* 531–533.
12. Collins, F. S.; Tabak, L. A. NIH Plans to Enhance Reproducibility. *Nature* **2014,** *505,* 612–613.
13. Ioannidis, J. P. Why Most Published Research Findings Are False. *PLoS Med.* **2005,** *2,* e124.
14. https://en.wikipedia.org/wiki/Replication_crisis.
15. Hayes, A.; Hunter, J. Why Is Publication of Negative Clinical Trial Data Important? *Br. J. Pharmacol.* **2012,** *167,* 1395–1397.
16. Hopkins, A. L.; Groom, C. R. The Druggable Genome. *Nat. Rev. Drug Discov.* **2002,** *1,* 727–730.
17. Lipinski, C.; Lombardo, F.; Dominy, B.; Feeney, P. Experimental and Computational Approaches to Estimate Solubility and Permeability in Drug Discovery and Development Settings. *Adv. Drug Deliv. Rev.* **1997,** *23,* 3–25.
18. Kubinyi, H. Drug Research: Myths, Hype and Reality. *Nat. Rev. Drug Discov.* **2003,** *2,* 665–668.
19. Drews, J.; Ryser, S. The Role of Innovation in Drug Development. *Nat. Biotechnol.* **1997,** *15,* 1318–1319.
20. Imming, P.; Sinning, C.; Meyer, A. Drugs, Their Targets and the Nature and Number of Drug Targets. *Nat. Rev. Drug Discov.* **2006,** *5,* 821–834.
21. Overington, J.; Al-Lazikani, B.; Hopkins, A. L. How Many Drug Targets Are There? *Nat. Rev. Drug Discov.* **2006,** *5,* 993–996.
22. Wishart, D. S.; Knox, C.; Guo, A. C.; Shrivastava, S.; Hassanali, M.; Stothard, P.; Chang, Z.; Woolsey, J. DrugBank: A Comprehensive Resource for in Silico Drug Discovery and Exploration. *Nucleic Acids Res.* **2006,** *43,* D668–D672.
23. http://www.drugbank.ca/stats.
24. Hajduk, P. J.; Huth, J. R.; Tse, C. Predicting Protein Druggability. *Drug Discov. Today* **2005,** *10,* 1675–1682.
25. Cheng, A. C.; Coleman, R. G.; Smyth, K. T.; Cao, Q.; Soulard, P.; Caffrey, D. R.; Salzberg, A. C.; Huang, E. S. Structure-Based Maximal Affinity Model Predicts Small-Molecule Druggability. *Nat. Biotechnol.* **2007,** *25,* 71–75.
26. Fauman, E. B.; Rai, B. K.; Huang, E. S. Structure-Based Druggability Assessment—Identifying Suitable Targets for Small Molecule Therapeutics. *Curr. Opin. Chem. Biol.* **2011,** *15,* 463–468.
27. Hunter, S.; Jones, P.; Mitchell, A.; Apweiler, R.; Attwood, T. K.; Bateman, A.; Bernard, T.; Binns, D.; Bork, P.; Burge, S.; de Castro, E.; Coggill, P.; Corbett, M.; Das, U.; Daugherty, L.; Duquenne, L.; Finn, R. D.; Fraser, M.; Gough, J.; Haft, D.; Hulo, N.; Kahn, D.; Kelly, E.; Letunic, I.; Lonsdale, D.; Lopez, R.; Madera, M.; Maslen, J.; McAnulla, C.; McDowall, J.; McMenamin, C.; Mi, H.; Mutowo-Muellenet, P.; Mulder, N.; Natale, D.; Orengo, C.; Pesseat, S.; Punta, M.; Quinn, A. F.; Rivoire, C.; Sangrador-Vegas, A.; Selengut, J. D.; Sigrist, C. J.; Scheremetjew, M.; Tate, J.; Thimmajanarthanan, M.; Thomas, P. D.; Wu, C. H.; Yeats, C.; Yong, S. Y. InterPro in 2011: New Developments in the Family and Domain Prediction Database. *Nucleic Acids Res.* **2012,** *40,* D306–D312.
28. https://www.ncbi.nlm.nih.gov/projects/CCDS/CcdsBrowse.cgi.
29. Russ, A. P.; Lampel, S. The Druggable Genome: An Update. *Drug Discov. Today* **2005,** *10,* 1607–1610.
30. Campillos, M.; Kuhn, M.; Gavin, A. C.; Jensen, L. J.; Bork, P. Drug Target Identification Using Side-Effect Similarity. *Science* **2008,** *321,* 263–266.
31. Keiser, M. J.; Setola, V.; Irwin, J. J.; Laggner, C.; Abbas, A. I.; Hufeisen, S. J.; Jensen, N. H.; Kuijer, M. B.; Matos, R. C.; Tran, T. B.; Whaley, R. Predicting new Molecular Targets for Known Drugs. *Nature* **2009,** *462,* 175–181.
32. Edwards, A. M.; Isserlin, R.; Bader, G. D.; Frye, S. V.; Wilson, T. M.; Yu, F. H. Too Many Roads Not Taken. *Nature* **2011,** *470,* 163–165.
33. Knowles, J.; Gromo, G. Target Selection in Drug Discovery. *Nat. Rev. Drug Discov.* **2003,** *2,* 63–69.
34. Koscielny, G.; An, P.; Carvalho-Silva, D.; Cham, J. A.; Fumis, L.; Gasparyan, R.; Hasan, S.; Karamanis, N.; Maguire, M.; Papa, E.; Pierleoni, A.; Pignatelli, M.; Platt, T.; Rowland, F.; Wankar, P.; Bento, A. P.; Burdett, T.; Fabregat, A.; Forbes, S.; Gaulton, A.; Gonzalez, C. Y.; Hermjakob, H.; Hersey, A.; Jupe, S.; Kafkas, Ş; Keays, M.; Leroy, C.; Lopez, F. J.; Magarinos, M. P.; Malone, J.; McEntyre, J.; Munoz-Pomer Fuentes, A.; O'Donovan, C.; Papatheodorou, I.; Parkinson, H.; Palka, B.; Paschall, J.; Petryszak, R.; Pratanwanich, N.; Sarntivijal, S.; Saunders, G.; Sidiropoulos, K.; Smith, T.; Sondka, Z.; Stegle, O.; Tang, Y. A.; Turner, E.; Vaughan, B.; Vrousgou, O.; Watkins, X.; Martin, M. J.; Sanseau, P.; Vamathevan, J.; Birney, E.; Barrett, J.; Dunham, I. Open Targets: a platform for therapeutic target identification and validation. *Nucleic Acids Res.* **2017,** *45,* D985–D994. https://www.opentargets.org/.
35. https://www.targetvalidation.org/.
36. http://targetcentral.ws/.
37. Ursu, O.; Rayan, A.; Goldblum, A.; Oprea, T. I. Understanding Drug-Likeness. *Wiley Interdiscip. Rev. Comput. Mol. Sci.* **2011,** *1,* 760–781.
38. https://www.chemnavigator.com/cnc/products/iRL.asp.
39. https://www.emolecules.com/#?click=screening-compounds.
40. Ajay; Walters, W. P.; Murcko, M. A. Can We Learn to Distinguish Between "Drug-Like" and "Nondrug-Like" Molecules? *J. Med. Chem.* **1998,** *41,* 3314–3324.
41. Sadowski, J.; Kubinyi, H. A Scoring Scheme for Discriminating Between Drugs and Non-Drugs. *J. Med. Chem.* **1998,** *41,* 3325–3329.

42. Ursu, O.; Oprea, T. I. Model-Free Drug-Likeness From Fragments. *J. Chem. Inf. Model.* **2010,** *50,* 1387–1394.
43. Benet, L. Z.; Hosey, C. M.; Ursu, O.; Oprea, T. I. BDDCS, the Rule of 5 and Drugability. *Adv. Drug Deliv. Rev.* **2016,** *101,* 89–98.
44. Leeson, P. D.; Davis, A. M. Time-Related Differences in the Physical Property Profiles of Oral Drugs. *J. Med. Chem.* **2004,** *47* (2004), 6338–6348.
45. Ursu, O.; Holmes, J.; Knockel, J.; Bologa, C. G.; Yang, J. J.; Mathias, S. L.; Nelson, S. J.; Oprea, T. I. DrugCentral: online drug compendium. *Nucleic Acids Res.* **2017,** *45,* D932–D939. http://drugcentral.org/.
46. Vieth, M.; Siegel, M. G.; Higgs, R. E.; Watson, I. A.; Robertson, D. H.; Savin, K. A.; Durst, G. L.; Hipskind, P. A. Characteristic Physical Properties and Structural Fragments of Marketed Oral Drugs. *J. Med. Chem.* **2004,** *47,* 224–232.
47. Teague, S. J.; Davis, A. M.; Leeson, P. D.; Oprea, T. The Design of Leadlike Combinatorial Libraries. *Angew. Chem. Int. Ed.* **1999,** *38,* 3743–3748.
48. Oprea, T. I. Property Distribution of Drug-Related Chemical Databases. *J. Comput. Aided Mol. Des.* **2000,** *14,* 251–264.
49. Oprea, T. I.; Davis, A. M.; Teague, S. J.; Leeson, P. D. Is There a Difference Between Leads and Drugs? A Historical Perspective. *J. Chem. Inf. Comput. Sci.* **2001,** *41,* 1308–1315.
50. Sneader, W. *Drug Prototypes and Their Exploitation;* J. Wiley and sons: Chichester, 1996.
51. Bleicher, K. H.; Böhm, H. J.; Müller, K.; Alanine, A. I. Hit and Lead Generation: Beyond High-Throughput Screening. *Nat. Rev. Drug Discov.* **2003,** *2,* 369–378.
52. Hann, M. M.; Leach, A. R.; Harper, G. Molecular Complexity and Its Impact on the Probability of Finding Leads for Drug Discovery. *J. Chem. Inf. Comput. Sci.* **2001,** *41,* 856–864.
53. Hann, M. M.; Oprea, T. I. Pursuing the Leadlikeness Concept in Pharmaceutical Research. *Curr. Opin. Chem. Biol.* **2004,** *8* (3), 255–263.
54. Oprea, T. I.; Allu, T. K.; Fara, D. C.; Rad, R. F.; Ostopovici, L.; Bologa, C. G. Lead-Like, Drug-Like or "Pub-Like": How Different Are They? *J. Comput. Aided Mol. Des.* **2007,** *21,* 113–119.
55. Tetko, I. V.; Tanchuk, V. Y.; Kasheva, T. N.; Villa, A. E. Estimation of Aqueous Solubility of Chemical Compounds Using E-State Indices. *J. Chem. Inf. Comput. Sci.* **2001,** *41,* 1488–1493.
56. Veber, D. F.; Johnson, S. R.; Cheng, H. Y.; Smith, B. R.; Ward, K. W.; Kopple, K. D. Molecular Properties That Influence the Oral Bioavailability of Drug Candidates. *J. Med. Chem.* **2002,** *45,* 2615–2623.
57. Lu, J. J.; et al. Influence of Molecular Flexibility and Polar Surface Area Metrics on Oral Bioavailability in the Rat. *J. Med. Chem.* **2004,** *47,* 6104–6107.
58. Leeson, P. D.; Oprea, T. I. Drug-Like Physicochemical Properties. In *Drug Design Strategies: Quantitative Approaches;* Livingstone, D. J., Davis, A. M., Eds.; RSC: London, 2011; pp 35–59.
59. Erlanson, D. A.; McDowell, R. S.; O'Brien, T. Fragment-Based Drug Discovery. *J. Med. Chem.* **2004,** *47,* 3463–3482.
60. Congreve, M.; Carr, R.; Murray, C.; Jhoti, H. A 'Rule of Three' for Fragment-Based Lead Discovery. *Drug Discov. Today* **2003,** *8,* 876–877.
61. Gleeson, M. P. Generation of a set of Simple, Interpretable ADMET Rules of Thumb. *J. Med. Chem.* **2008,** *51,* 817–834.
62. Hughes, J. D.; Blagg, J.; Price, D. A.; Bailey, S.; DeCrescenzo, G. A.; Devraj, R. V.; Ellsworth, E.; Fobian, Y. M.; Gibbs, M. E.; Gilles, R. W.; Greene, N. Physiochemical Drug Properties Associated With In Vivo Toxicological Outcomes. *Bioorg. Med. Chem. Lett.* **2008,** *18,* 4872–4875.
63. Muthas, D.; Boyer, S.; Hasselgren, C. A Critical Assessment of Modeling Safety-Related Drug Attrition. *Med. Chem. Commun.* **2013,** *4,* 1058–1065.
64. Johnson, T. W.; Dress, K. R.; Edwards, M. Using the Golden Triangle to Optimize Clearance and Oral Absorption. *Bioorg. Med. Chem. Lett.* **2009,** *19,* 5560–5564.
65. https://www.chemaxon.com/.
66. Kenny, P. W.; Montanari, C. A. Inflation of Correlation in the Pursuit of Drug-Likeness. *J. Comput. Aided Mol. Des.* **2013,** *27,* 1–13.
67. Lovering, F.; Bikker, J.; Humblet, C. Escape from Flatland: Increasing Saturation as an Approach to Improving Clinical Success. *J. Med. Chem.* **2009,** *52,* 6752–6756.
68. https://en.wikipedia.org/wiki/Goodhart%27s_law.
69. Hopkins, A. L.; Groom, C. R.; Alex, A. Ligand Efficiency: A Useful Metric for Lead Selection. *Drug Discov. Today* **2004,** *9,* 430–431.
70. Hopkins, A. L.; Keserü, G. M.; Leeson, P. D.; Rees, D. C.; Reynolds, C. H. The Role of Ligand Efficiency Metrics in Drug Discovery. *Nat. Rev. Drug Discov.* **2014,** *13,* 105–121.
71. Kenny, P. W.; Leitao, A.; Montanari, C. A. Ligand Efficiency Metrics Considered Harmful. *J. Comput. Aided Mol. Des.* **2014,** *28,* 699–710.
72. Clark, D. Beware Generalizations!. *Drug Discov. Today* **2005,** *10,* 77.
73. Ritchie, T. J.; Macdonald, S. J.; Young, R. J.; Pickett, S. D. The Impact of Aromatic Ring Count on Compound Developability: Further Insights by Examining Carbo- and Hetero-Aromatic and -Aliphatic Ring Types. *Drug Discov. Today* **2011,** *16,* 164–171.
74. Oprea, T. I.; et al. Unexplored Opportunities in the Human Druggable Genome. *Nat. Rev. Drug Discov.* **2016**. Poster. Available at http://www.nature.com/nrd/posters/druggablegenome/index.html.

3.18 Data Analysis and Visualization Tools

CJ Swain, Cambridge MedChem Consulting, Cambridge, United Kingdom

© 2017 Elsevier Ltd. All rights reserved.

3.18.1	Introduction	440
3.18.2	Command Line/Programming Tools	440
3.18.3	Desktop Tools	448
3.18.4	Web-Based Tools	454
3.18.5	Mobile Applications	457
3.18.5.1	Mobile Apps Using a Client–Server Model	459
3.18.6	Big Data Analysis	460
3.18.7	Collaboration Tools	461
3.18.7.1	Workflow	461
3.18.8	Conclusion	463
References		463

3.18.1 Introduction

All scientists know that every experiment generates data, but collecting data is usually the easy part; indeed, experiments can often generate vast amounts of data ("big data"). The challenge has always been to turn the data into something useful. For this, we use a variety of different tools, and indeed, there is a vast array of tools from which to choose. These can range from open-source libraries or frameworks to sophisticated desktop applications costing many thousands of pounds. Some are command-line driven with a steep learning curve, while others offer a simple graphic user interface; others are components of computational chemistry or molecular modeling packages. The purpose of this article is not to try and detail every option available but to highlight selected tools that might be used in different environments bearing in mind that the audience will likely be scientists and most probably chemists. A number of molecular modeling packages also include data analysis tools, but they are not included in this article since data analysis is not the primary feature of the software. The first part of the article looks at command-line or programming languages, probably initially the preserve of specialists, but with the widespread adoption of Python as the lingua franca of scientific programming, many more scientists are using it for data analysis. The next section deals with desktop tools; this section could easily provide content for an entire book, and thus, this article focuses on those tools that provide cheminformatics support. The remainder of the article is intended to be rather more forward-looking, exploring the emergence of web-based or mobile apps and finally the possible implications of "big data."

3.18.2 Command Line/Programming Tools

R (http://www.r-project.org) is a programming language and statistical computing environment; it is open-source and cross platform, and precompiled versions are available for multiple platforms. In the 17th annual KDnuggets data miners poll in 2016 (http://www.kdnuggets.com/2016/06/r-python-top-analytics-data-mining-data-science-software.html), R was the most popular tool among data miners and scientists. While much of the source code for R is written in C, C++, and Fortran, many of R's main functions are written in R itself.

Perhaps the greatest strength of R is that it is highly extensible through user-submitted packages. Currently, there are 9715 packages listed (http://crantastic.org) (as of Jun. 2016). These packages provide access to a range of specialist statistical techniques; of note are caret (https://cran.r-project.org/package=caret) for machine learning and also randomForest (https://cran.r-project.org/web/packages/randomForest/index.html) and nnet (https://cran.r-project.org/web/packages/nnet/index.html). For plotting ggvis (https://cran.r-project.org/web/packages/ggvis/index.html) and ggplot2 (https://cran.r-project.org/package.ggplot2) support graphing, interactive plotting, and reporting tools.

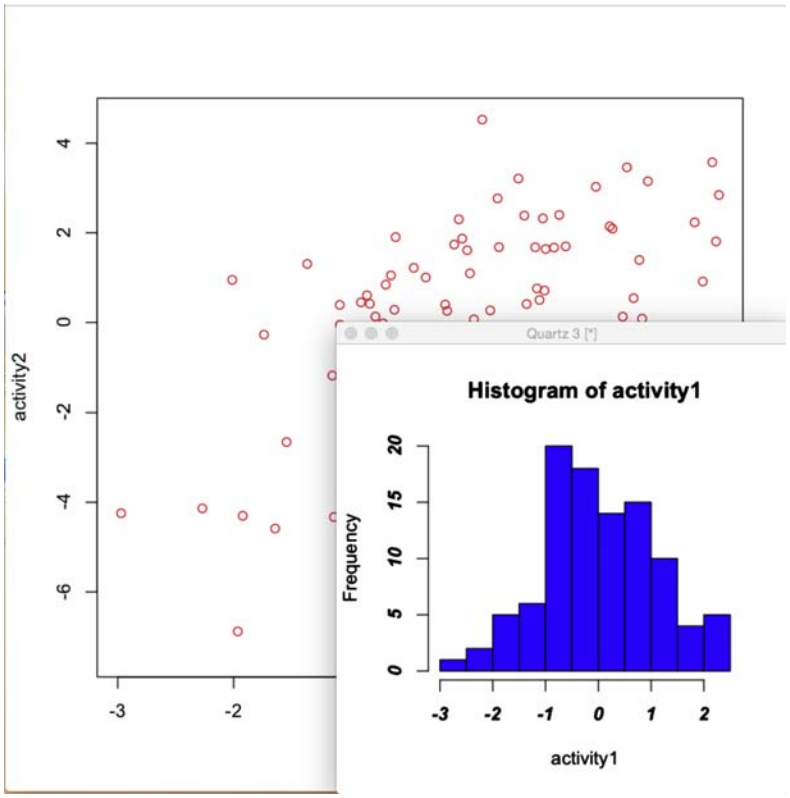

Example of plotting within R.

Bioconductor (http://www.bioconductor.org/about/) provides access to a fantastic range of statistical and graphic methods for the analysis of genomic data; however, the support for chemistry within R is limited.

ChemmineR (http://www.bioconductor.org/packages/devel/bioc/vignettes/ChemmineR/inst/doc/ChemmineR.html) is a cheminformatics package for analyzing drug-like small-molecule data in R. Its latest version contains functions for efficient processing of large numbers of small molecules, physicochemical/structural property predictions, structural similarity searching, classification, and clustering of compound libraries with a wide spectrum of algorithms. ChemmineOB provides access to some of the cheminformatics functionality available in Open Babel.

The rcdk[1] package provides R users access to CDK,[2] a cheminformatics framework written in Java. Rajarshi Guha has put together an excellent slide deck describing cheminformatics in R (http://www.slideshare.net/rguha/cheminformatics-in-r).

On importing molecules, it is often necessary to "wash" molecules to remove counterions, often done by simply selecting the largest component.

```
> m <- parse.smiles("c1ccccc1")
> is.connected(m)
[1] TRUE
>
> m <- parse.smiles("C1CC(N=C1)C(=O)[O-].[Na+]")
> is.connected(m)
[1] FALSE
>
> largest <- get.largest.component(m)
> length(get.atoms(largest))
[1] 8
```

Chemical structure-based queries are also possible using SMARTS (http://www.daylight.com/dayhtml/doc/theory/theory.smarts.html).

```
mols <- sapply(c("CC(C)(C)C",
                 "c1ccc(Cl)cc1C(=O)O",
                 "CCC(N)(N)CC"), parse.smiles)
query <- "[#6D2]"
hits <- matches(query, mols)

> print(hits)
CC(C)(C)C c1ccc(Cl)cc1C(=O)O CCC(N)(N)CC
FALSE TRUE TRUE
```

Julia (http://www.julialang.org) is a high-performance programming language designed to approach the performance of C while maintaining a code language format that would be readily accessible to scientists familiar with other mathematical languages. While most users probably use the command line, it is also possible to use the Jupyter Interactive Notebook environment (https://github.com/JuliaLang/IJulia.jl) originally developed for Python. This combination allows you to interact with the Julia language using Jupyter/IPython's graphic notebook, which allows the user to combine code, formatted text, math, and multimedia in a single document. In a similar manner to R, Julia can be extended by installing specific packages; currently, there are 624 packages (as Jul. 2015). It appears there are no packages supporting cheminformatics.

In the 17th annual KDnuggets data miners poll in 2016, Python (https://www.python.org) usage was highlighted as the fastest growing platform and likely to overtake R in 2 or 3 years. Python was also the most popular of the programming languages earning nearly three times the votes of Java, the next most popular.

Python is an open-source, cross platform scripting language; it has a relatively simple syntax and has a reputation for rapid prototyping. Similar to R, there is a very active community of users contributing libraries to support needs in very diverse fields. In addition, there is the IPython notebook, an interactive notebook environment,[3] which allows the user to combine code, formatted text, math, and multimedia in a single document.

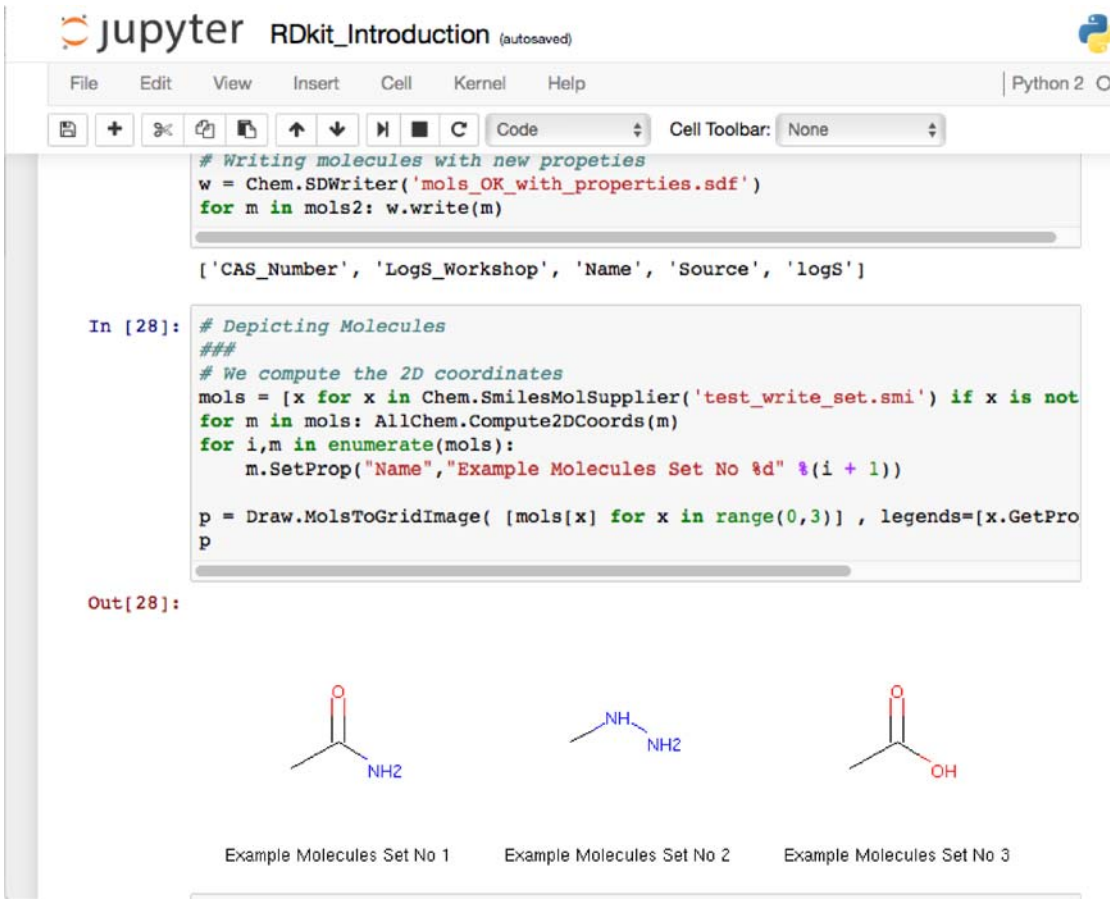

Originally developed by Fernando Pérez, a data scientist at the University of California, Berkeley, and computational physicist Brian Granger at California Polytechnic State University in San Luis Obispo, the IPython notebook concept is being expanded to incorporate other languages (http://jupyter.org). The IPython notebook provides an environment for scientists to write and test code but is also ideal for teaching, collaboration, and sharing (http://nbviewer.ipython.org).

The popularity of Python among scientists for data analysis is probably due to the strength of several core libraries matplotlib, NumPy, SciPy, pandas, and IPython notebook. Python is also excellent for acting as scripting language to integrate other programs into a workflow.

pandas (http://pandas.pydata.org) is a library providing a high-performance data framework within Python. NumPy (http://www.numpy.org) adds support for large, multidimensional arrays and matrices, together with a library of high-level mathematical functions. SciPy (http://www.scipy.org) provides modules for optimization, linear algebra, integration, statistics, and interpolation. scikit-learn (http://scikit-learn.org/stable/) is an open-source machine learning library giving access to classification, regression, and clustering algorithms including support vector machines, random forests, gradient boosting, *k*-means, and DBSCAN. matplotlib (http://matplotlib.org) provides publication-quality 2-D plotting and limited 3-D plotting. Rpy2 (http://rpy.sourceforge.net/index.html) provides both a low-level interface to R from Python and a high-level interface, including wrappers to graphic libraries and R-like structures and functions; the aim is to abstract some of the details and provide an intuitive interface to both Python and R programmers.

Cheminformatics is well supported under Python; cinfony[4] is a python library that provides access to a variety of cheminformatics toolkits via a common API, in particular Open Babel, RDKit, CDK, Indigo, JChem, OPSIN, and cheminformatics web services. Many of the toolkits also provide their own Python binding. The Cactvs toolkit is now accessible from Python,[5] and commercial cheminformatics packages such as ChemAxon (https://www.chemaxon.com/webservices/python/) and OpenEye (http://www.eyesopen.com/toolkits) provide python access.

There is a comprehensive listing of Python numeric and scientific here https://wiki.python.org/moin/NumericAndScientific.

George Papadatos, ChEMBL Group, and EMBL-EBI have kindly provided this example of IPython notebook for getting biological target predictions based on the current multicategory Naive Bayesian ChEMBL_20 models for a single-molecule input. The predictions are ranked by the output classifier probability or score (http://nbviewer.ipython.org/gist/madgpap/10457778).

First of all, get the models from the ChEMBL ftp site and import the necessary modules and set up plotting.

```
In [1]: !wget ftp://ftp.ebi.ac.uk/pub/databases/chembl/target_predictions/chembl_20_models.tar.gz

--2015-07-11 11:53:43--  ftp://ftp.ebi.ac.uk/pub/databases/chembl/target_predictions/chembl_20_
models.tar.gz
           => 'chembl_20_models.tar.gz.1'
Resolving ftp.ebi.ac.uk... 193.62.192.4
Connecting to ftp.ebi.ac.uk|193.62.192.4|:21... connected.
Logging in as anonymous ... Logged in!
==> SYST ... done.    ==> PWD ... done.
==> TYPE I ... done.  ==> CWD (1) /pub/databases/chembl/target_predictions ... done.
==> SIZE chembl_20_models.tar.gz ... 61511200
==> PASV ... done.    ==> RETR chembl_20_models.tar.gz ... done.
Length: 61511200 (59M) (unauthoritative)

chembl_20_models.ta 100%[====================>]  58.66M  4.43MB/s   in 13s

2015-07-11 11:53:58 (4.38 MB/s) - 'chembl_20_models.tar.gz.1' saved [61511200]

In [2]: !tar -zxf chembl_20_models.tar.gz

In [1]: from rdkit.Chem import AllChem as Chem
        from rdkit.Chem.Draw import IPythonConsole
        from rdkit.Chem import PandasTools
        from rdkit.Chem import Draw

        import pandas as pd
        from pandas import concat

        from collections import OrderedDict
        from pylab import rcParams

        import requests

In [2]: from sklearn.externals import joblib

In [34]: %matplotlib inline

In [35]: rcParams['figure.figsize'] = 10,10
```

Then, define a couple of utility functions and load one of the predictive models and then check the number of classes/targets.

```
In [5]: def calc_scores(classes):
            p = []
            for c in classes:
                p.append(pred_score(c))
            return p

In [6]:
        def pred_score(trgt):
            diff = morgan_nb.estimators_[classes.index(trgt)].feature_log_prob_[1] - morgan_nb.estimator
            return sum(diff*fp)

In [7]: morgan_nb = joblib.load('./models/1uM/mNB_1uM_all.pkl')

In [8]: classes = list(morgan_nb.classes_)

In [9]: morgan_nb.multilabel_
Out[9]: True

In [10]: len(classes)
Out[10]: 1114
```

Define the molecule to be used for the prediction (GS-5759) as a SMILES string; one of the nice things is you can then render the structure of the molecule within the notebook.

```
smiles = 'O[C@@H](CNCCCC#CC1=CC=C(C=C1)NC(=O)C=1C=C(C=CC1)S(=O)
(=O)C=1C=C2C(=C(C=NC2=C(C1)C)C(=O)N)NC1=CC(=CC=C1)OC)C1=C2C=CC(NC2=C(C=C1)O)=O' #GS-5759

In [13]: mol = Chem.MolFromSmiles(smiles)

In [14]: mol
Out[14]:
```

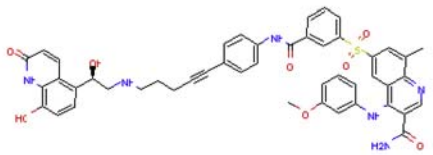

Convert to the Morgan fingerprint and save the bit dictionary for later and then get the predictions in a pandas frame and view the first few predictions.

```
In [36]: info={}
         fp = Chem.GetMorganFingerprintAsBitVect(mol,2,nBits=2048, bitInfo=info)

         predictions = pd.DataFrame(zip(classes, calc_scores(classes),list(morgan_nb.predict_proba(fp)
         [0])),columns=['id','score','proba'])

In [38]: predictions.head()
```

Out[38]:

	id	score	proba
0	CHEMBL1075051	-40.276028	6.546443e-22
1	CHEMBL1075104	-26.826197	2.590231e-15
2	CHEMBL1075115	-31.566940	2.468987e-18
3	CHEMBL1075138	-14.748362	1.086657e-09
4	CHEMBL1075140	-85.775527	3.434363e-41

Plot a histogram to show distribution of scores.

```
In [40]: predictions['score'].hist()
Out[40]: <matplotlib.axes._subplots.AxesSubplot at 0x10b27e950>
```

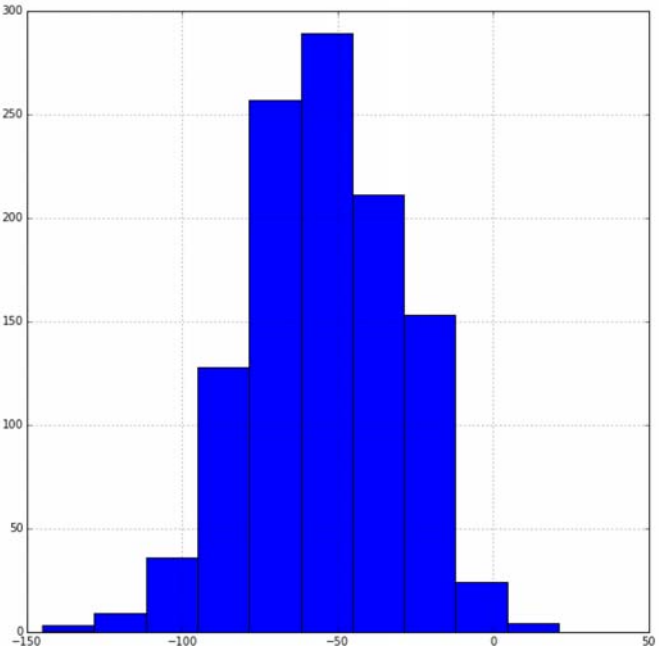

Sort by probability and display top 5.

```
In [41]: top_preds = predictions.sort(columns=['proba'],ascending=False).head(5)
In [42]: top_preds
Out[42]:
```

	id	score	proba
1020	CHEMBL5414	21.018563	0.999999
195	CHEMBL213	11.393305	0.996224
190	CHEMBL210	10.212841	0.989231
380	CHEMBL275	5.913751	0.465160
27	CHEMBL1293226	-5.304913	0.000007

Use ChEMBL web service to merge predictions with target information.

```
In [43]: def fetch_WS(trgt):
             re = requests.get('https://www.ebi.ac.uk/chemblws/targets/{0}.json'.format(trgt))
             return re.json()['target']

In [44]: plist = []
         for i,e in enumerate(top_preds['id']):
             p = pd.DataFrame(fetch_WS(e), index=(i,))
             plist.append(p)
         target_info = concat(plist)

In [45]: target_info.shape
Out[45]: (5, 10)

         target_info

In [26]: result = pd.merge(top_preds, target_info, left_on='id', right_on='chemblId')

In [27]: result
```

Out[27]:

	id	score	proba	bioactivityCount	chemblId	compoundCount	description	gen
0	CHEMBL5414	21.018563	0.999999	1283	CHEMBL5414	701	Beta-2 adrenergic receptor	Uns
1	CHEMBL213	11.393305	0.996224	4539	CHEMBL213	2843	Beta-1 adrenergic receptor	Uns
2	CHEMBL210	10.212841	0.989231	6994	CHEMBL210	4474	Beta-2 adrenergic receptor	Uns
3	CHEMBL275	5.913751	0.465160	1294	CHEMBL275	1139	Phosphodiesterase 4B	Uns
4	CHEMBL1293226	-5.304913	0.000007	40109	CHEMBL1293226	39484	Lysine-specific demethylase 4D-like	Uns

Which features of the active molecules in the training set were the most important? First, map the specific bits back to atomic environments and display the most important features, based on their enrichment in PDE4B actives in ChEMBL. The legend is the Bayesian score for each feature.

```
In [28]: bit_scores = (morgan_nb.estimators_[classes.index(result['id'][1])].feature_log_prob_[1] - morga

In [29]: frags = OrderedDict()
         for k in info.keys():
             if bit_scores[k] > 0.1:
                 atomId,radius = info[k][0]
                 env=Chem.FindAtomEnvironmentOfRadiusN(mol,radius,atomId)
                 ats = set([atomId])
                 for bidx in env:
                     bond = mol.GetBondWithIdx(bidx)
                     ats.add(bond.GetBeginAtomIdx())
                     ats.add(bond.GetEndAtomIdx())
                     frag = Chem.MolFragmentToSmiles(mol,atomsToUse=list(ats),bondsToUse=env,rootedAtAtor
                     legend = str(round(bit_scores[k],2))
                     frags[k] = (legend,frag)

In [30]: legends = [l[1][0] for l in sorted(frags.items(), key=lambda t: t[1][0], reverse=True)][:10]
         ffrags = [l[1][1] for l in sorted(frags.items(), key=lambda t: t[1][0], reverse=True)][:10]

In [31]: mol

Out[31]:
```

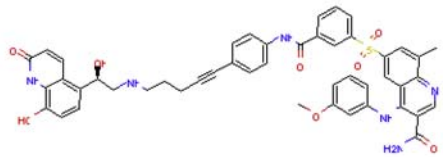

```
In [32]: fmols=[Chem.MolFromSmarts(s) for s in ffrags]

In [33]: Draw.MolsToGridImage(fmols, molsPerRow=5, legends=legends)

Out[33]:
```

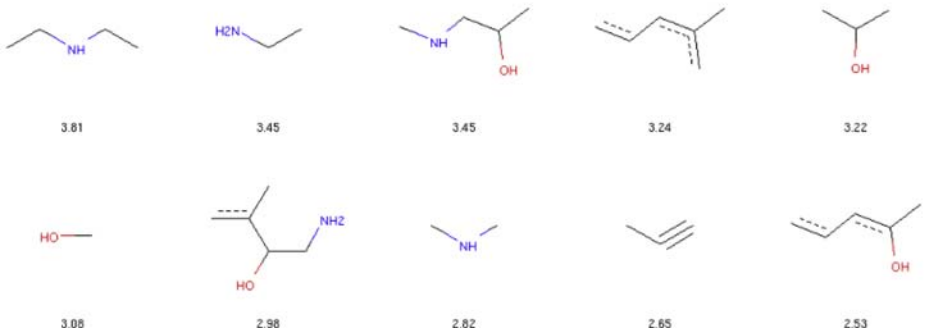

This IPython notebook nicely illustrates some of the features that make Python such a popular choice, in particular in-line display of plots and chemical structures, the easy integration of web services, and access to machine learning modules. In addition, the completed IPython notebook can act like an application; simply edit the path to an input file and then rerun.

In the recent poll (http://www.kdnuggets.com/2015/05/poll-r-rapidminer-python-big-data-spark.html#pro), Java was behind Python in popularity but still commands a significant number of users. Again, the popularity stems from open-source libraries; Java Data Mining Package (https://jdmp.org) is an open-source Java library for data analysis and machine learning. JDMP facilitates the access to data sources and machine learning algorithms (e.g., clustering, regression, classification, graphic models, and optimization); it also interfaces with Weka,[6] which is a collection of machine learning algorithms for data mining tasks. Weka contains tools for data preprocessing, classification, regression, clustering, association rules, and visualization. Cheminformatics support comes from CDK,[2] *JChem* (https://www.chemaxon.com/), or a wrapper for RDKit (http://www.rdkit.org/).

Bioclipse (http://bioclipse.net) is an open-source scientific workbench based on the popular Java Eclipse platform (http://eclipse.org). Cheminformatics support comes from CDK,[2] and data analysis is provided by integration of R (http://www.r-project.org). Bioclipse has its own scripting language based on Javascript.

MATLAB (http://uk.mathworks.com/products/matlab/) is a popular high-level language and interactive environment; it uses a proprietary programming language developed by MathWorks.

Mathematica (http://www.wolfram.com/mathematica/) is a very powerful software program used in many scientific, engineering, mathematical, and computing fields, based on symbolic mathematics.

GNU Octave (https://www.gnu.org/software/octave/) is a high-level interpreted language, primarily intended for numerical computations via a command-line interface. The Octave language is quite similar to MATLAB so that most programs are easily portable.

3.18.3 Desktop Tools

There is a vast array of desktop tools for data analysis, and it is impractical for this article to describe every package; instead, this article focuses on those tools that have support for chemistry.

Instant JChem (https://www.chemaxon.com/products/instant-jchem-suite/instant-jchem/) is a desktop client that provides database management functionality together with a variety of physicochemical property and molecular descriptor calculations. Instant *JChem* also supports graphic visualization of database content using a variety of plot formats. Any selection in one plot is instantly synchronized with other plots and the form view, allowing direct identification of chemical structures associated with the selected data point.

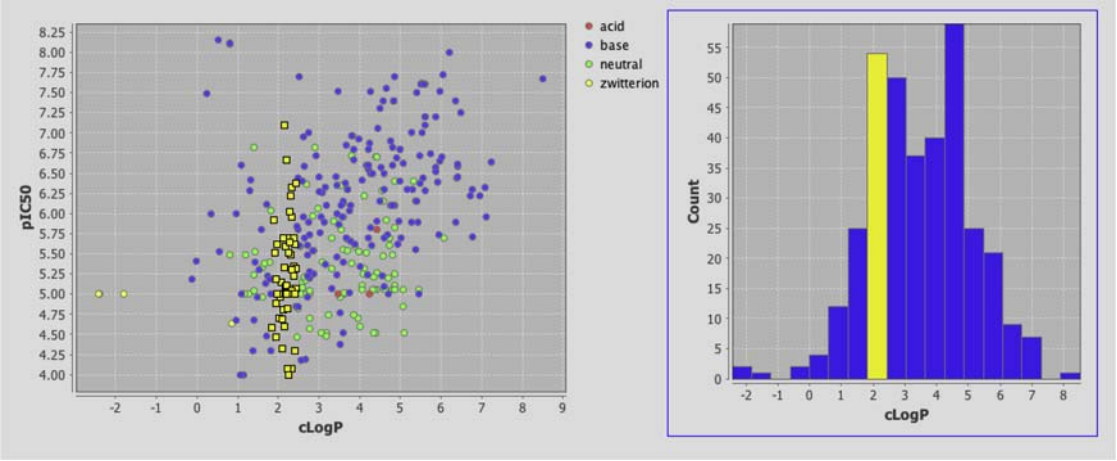

For more extensive data analysis, it can be integrated with KNIME or Spotfire.

DataWarrior (http://www.openmolecules.org/datawarrior/) is an open-source data analysis tool that understands chemistry; it provides an efficient way to search, sort, and analyze structure–activity data. DataWarrior was developed at Actelion; in 2014, it was decided to release DataWarrior as a stand-alone tool to the public available as compiled binaries and source code.

DataWarrior can import text-delimited files and chemical structure files in SDF format, a very widely accepted industry standard for exchanging chemical and associated alphanumeric data. After import, the data appear in the default view shown in the image in the succeeding text. Additional columns of calculated physicochemical properties can be added, and there is support for other calculated criteria such as "drug-like" and "ligand efficiency."

The table view supports data summarization tools such as pivot table and binning numerical data and allows calculating a new column from an expression using data within the table view. There is also support for principal component analysis (PCA), a widely used technique to convert a large number of highly correlated variables into a smaller number of uncorrelated variables.

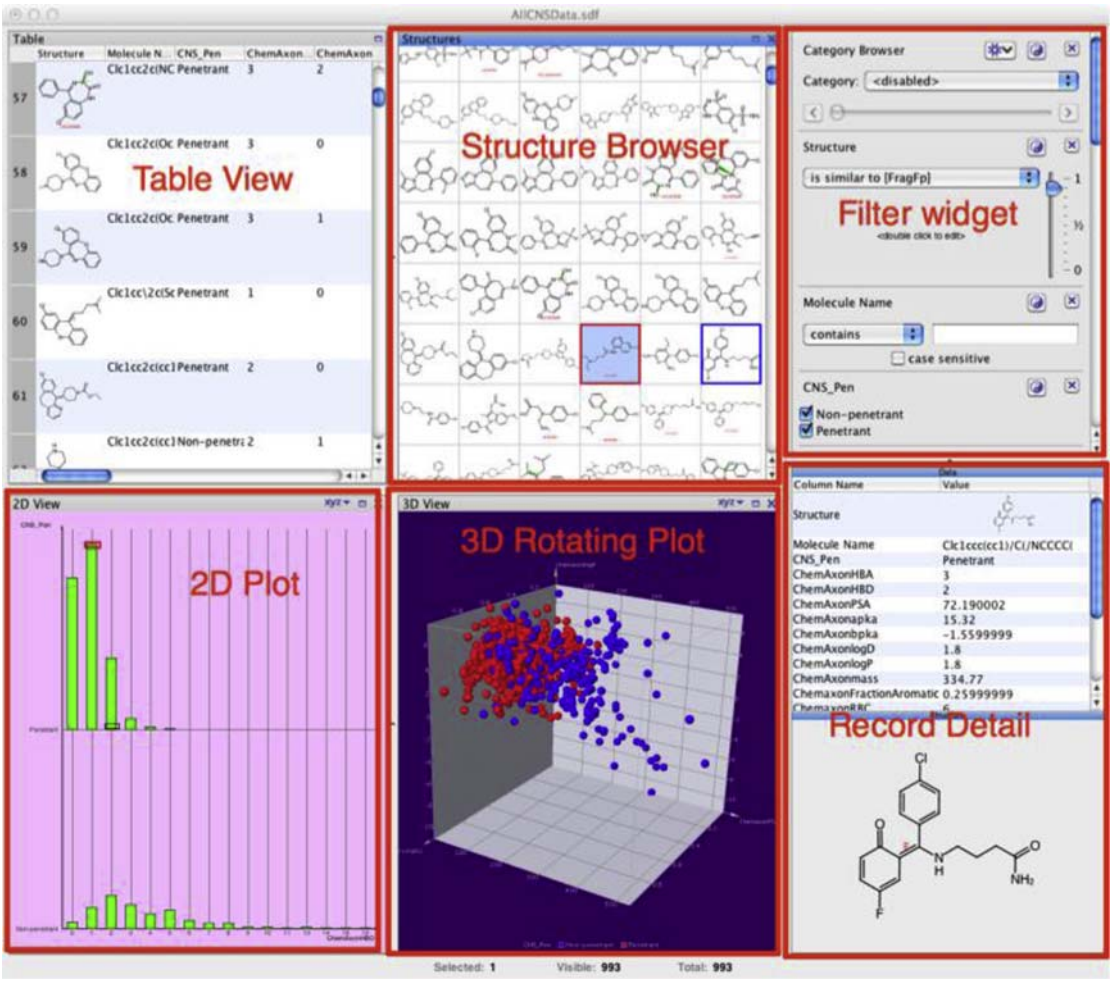

DataWarrior supports substructure and similarity searching, and there is limited support for compound clustering. There is also support for popular structure–activity analysis approaches including R-group analysis, Kohonen maps, and activity cliffs.

The graphic 2-D- and 3-D-views are potentially the most interesting for exploring data. The xyz button on the view's header area opens a drop-down menu for defining which property is to be assigned to each axis. Columns that do not contain numerical values, date values, category information, or chemical descriptors cannot be assigned to axes and, therefore, do not appear in the column menus. Columns with incomplete data, that is, with some empty cells, appear in red color indicating that some rows of the data may not be shown, if this column is selected. Nonnumerical category columns appear in blue color, while complete numerical or date columns are shown in black. Points selected in one plot are automatically highlighted in the other plots. You can change the chart type by simply right-clicking in the chart area. One nice feature is that if you right-click on a data point, there is the option to use the associated chemical structure as a filter.

DataWarrior can use macros to automatically follow a complicated or long series of tasks. These macros can be generated by recording a sequence of actions or by hand using the inbuilt macro editor.

Stardrop (http://www.optibrium.com/stardrop/) is a tool designed to aid data analysis and decision-making for scientists involved in drug discovery. Stardrop provides a wide variety of ways to view data from spreadsheets to scatterplots and histograms all interlinked such that selection of a data point in the scatterplot automatically highlights the relevant data in the other plots and the spreadsheet.

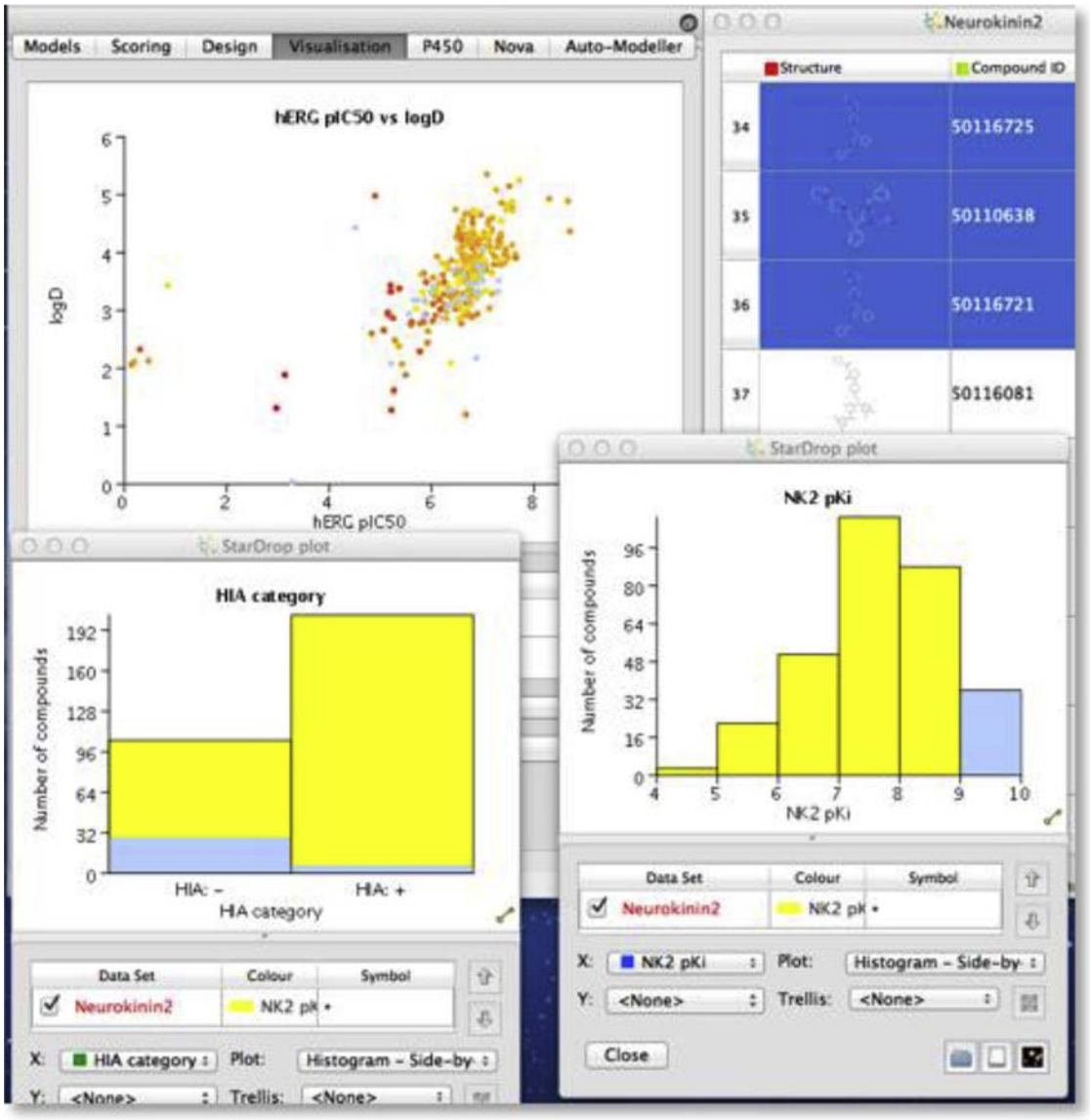

One very nice feature is the "glowing molecules" display; selecting a model results in the molecule display being rendered as a heat map to highlight the molecular features that are responsible for the activity in the model with red indicating structural features that have a positive effect in the model and the cooler blue a negative effect. Alternatively, there is a "card view" in which key data are displayed in a playing card format. These cards can be stacked and linked to aid analysis. This can be a useful way to view the results of clustering.

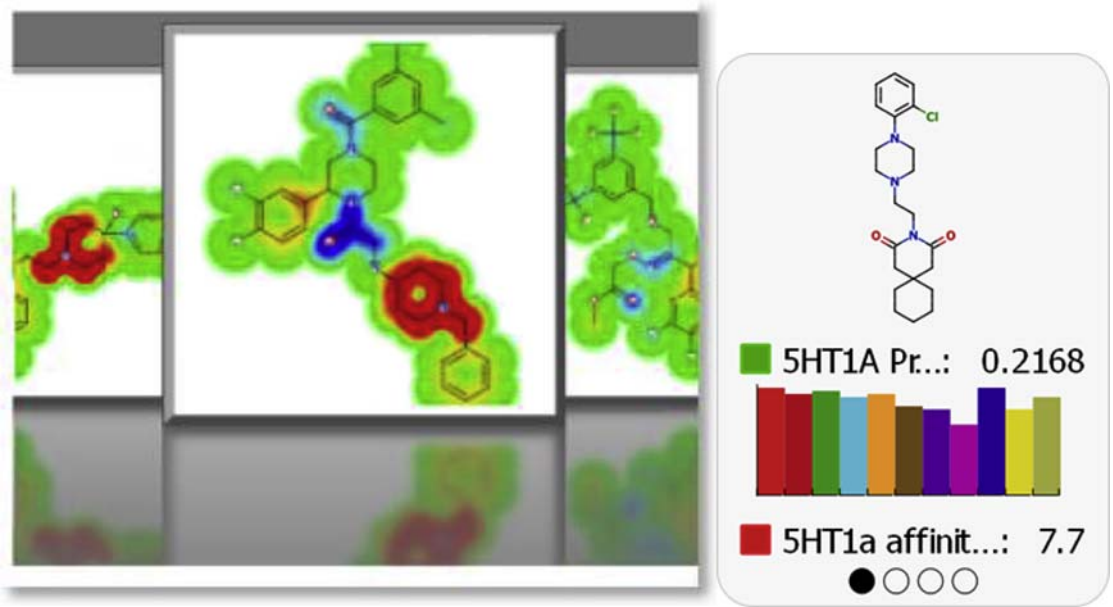

Stardrop has an interesting feature that allows you to set up a desired profile using all the experimental and calculated properties. You can set the desired value or range of values and the relative importance; this is then translated into a scoring profile and displayed in the molecular spreadsheet, together with a histogram of the property values (normalized from 0 to 1). For the low-scoring compounds, it is then very easy to see which properties need to be improved.

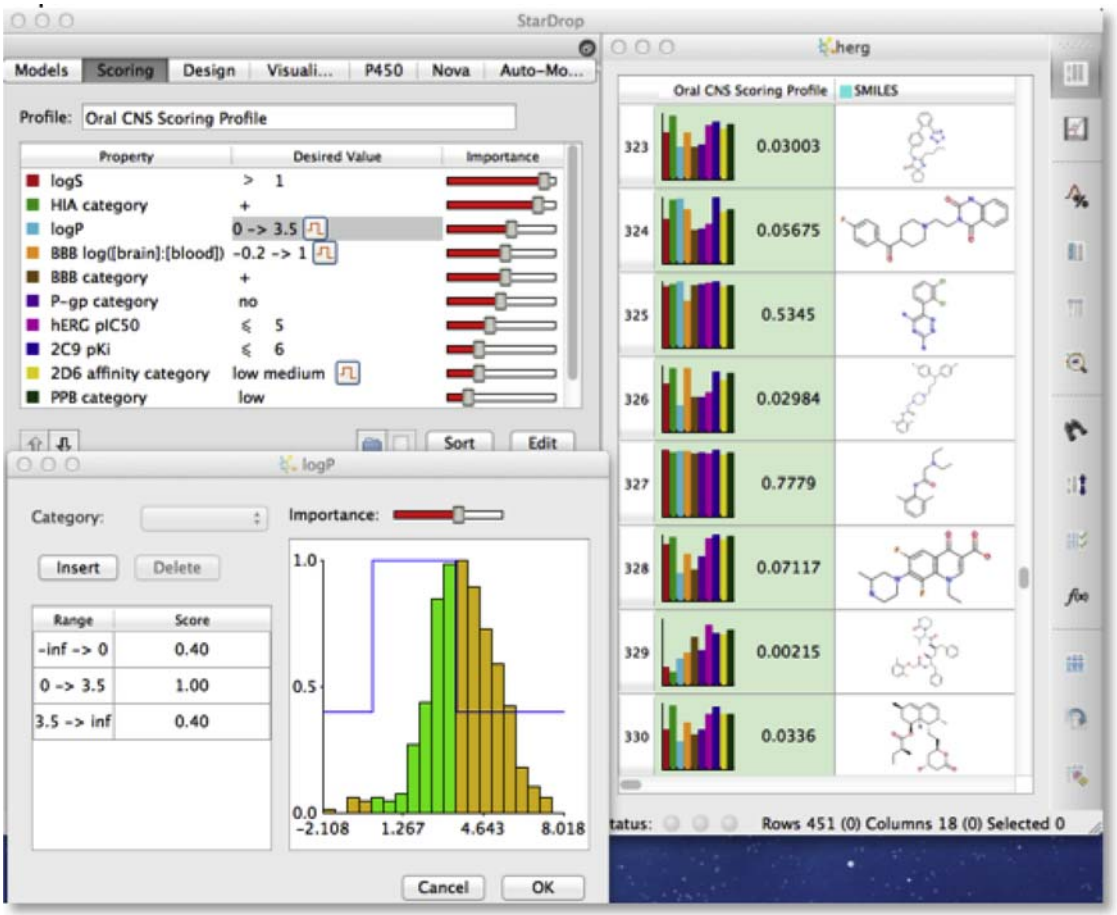

All that has been described earlier is part of the "desktop" portion of Stardrop; there is an equally important "server" side that is available on purchase of the appropriate plug-in modules. This includes predictive models and AutoModeller. AutoModeller, as the name suggests, allows expert and nonexpert users to build predictive QSAR models of data. The setup of calculations is controlled by a "wizard" that takes the user through the steps required, selecting the data set and activity, splitting into training, validating and testing sets, and choosing descriptors and type of model. A variety of modeling techniques are available, including Gaussian processes, random forests, radial basis functions, PLS, and decision trees.

Optional plug-ins provide access to a variety of predictive models covering key ADME and physicochemical properties, quantum mechanical simulation of drug metabolism, and knowledge-based toxicity prediction. There is also a module for the automatic generation and scoring of new compounds using bioisosteric replacements and virtual library enumeration.

Spotfire (http://spotfire.tibco.com) is a general-purpose data analytics platform; support for chemistry is provided by the PerkinElmer (http://www.perkinelmer.com) (better known as CambridgeSoft) tools. This includes ChemDraw for structure drawing and property calculations and fingerprints for searching/filtering/clustering. The API does provide access for other toolkits. Data can be imported as flat files or from an Oracle database.

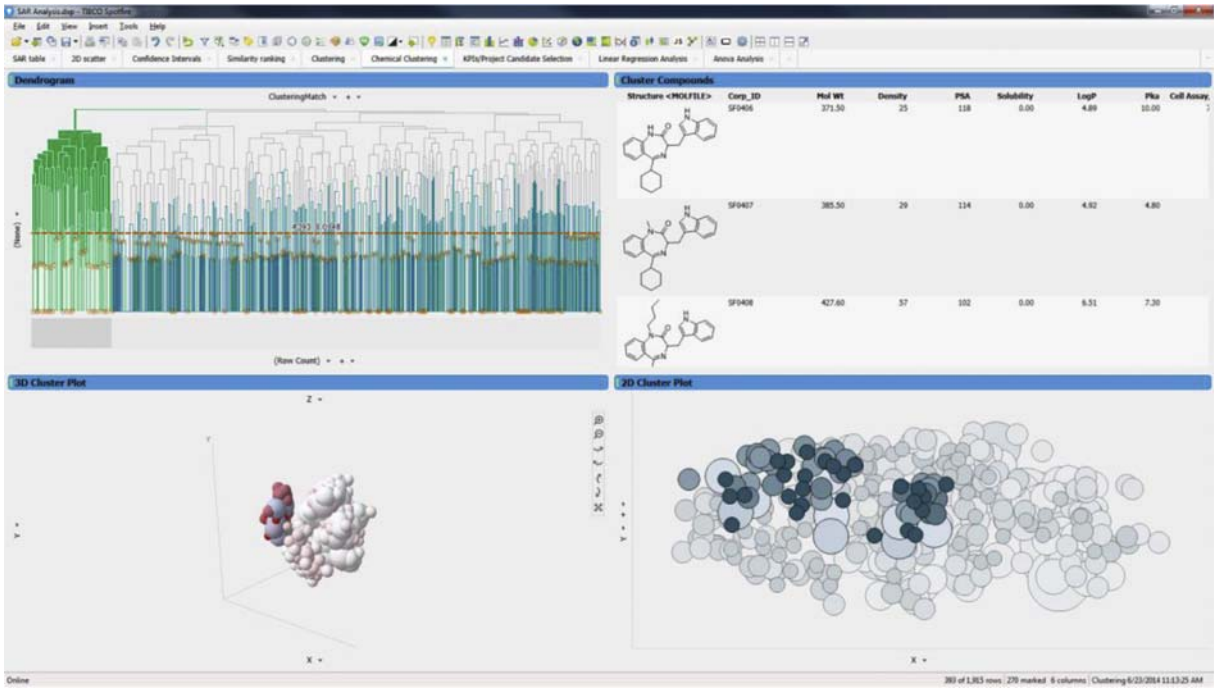

As the image earlier shows, a wide variety of plot types are supported, and selection of a data point in one plot highlights the corresponding point in other plots. The scatterplots can be coded by color, size, shape, or label allowing the display and exploration of multidimensional data, and sliders allow filtering of the data. It is also possible to provide connections between tables using an identifier such as molecule ID, allowing selections in one table to be flagged in another. The Spotfire server is also accessible via a mobile app.

Vortex (http://www.dotmatics.com/products/vortex/) is a high-performance data visualization platform suitable for many sciences. Vortex is available with full built-in chemical structure intelligence. Vortex can import files in a variety of formats and includes JDBC drivers to interface with Oracle, SQL Server, or MySQL databases. It provides chemical structure depiction and substructure or similarity-based searching, together with physicochemical property calculations tightly integrated with excellent charting and analysis tools.

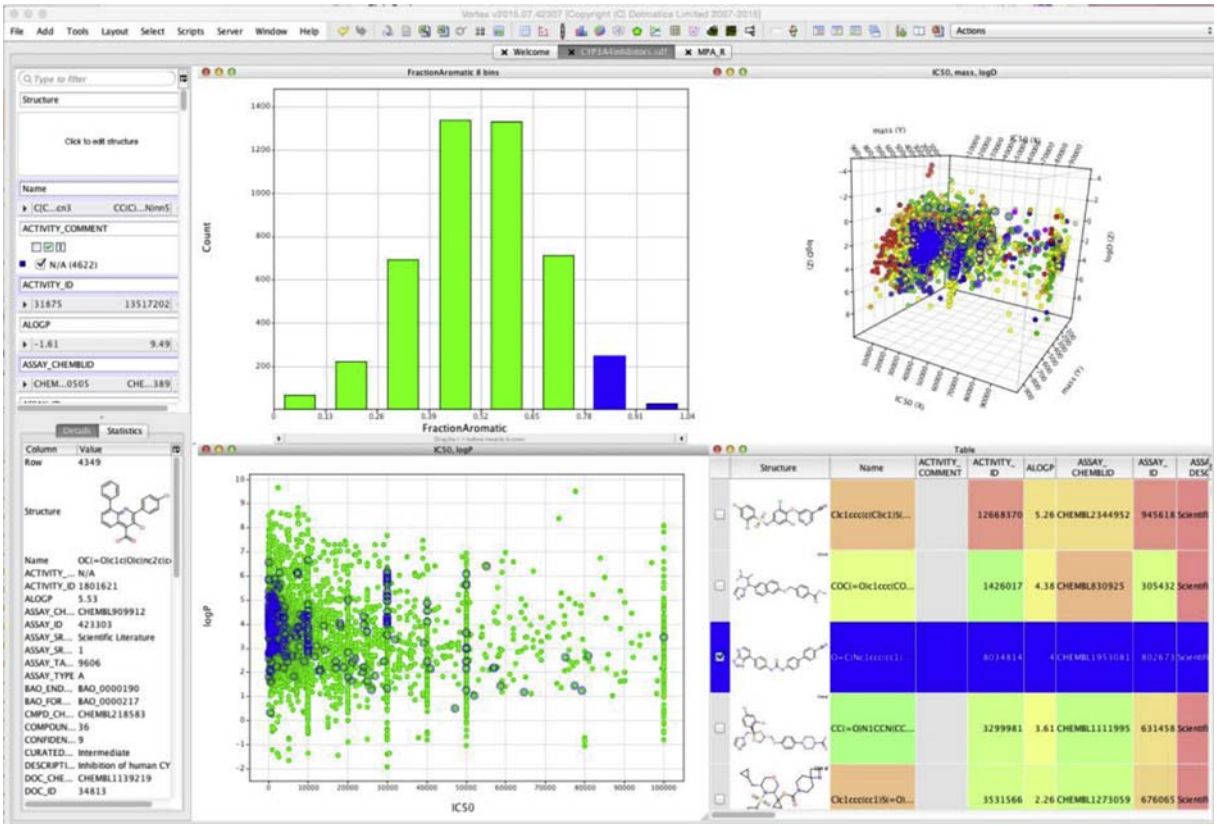

The image earlier contains 2-D and 3-D color-categorized scatterplots, a histogram, and a spreadsheet showing the molecular structure and all the alphanumeric data. The upper left hand panel contains a series of slider bars that allow the user to filter the details of the display, while the lower panel gives details of the highlighted molecule. The real beauty is that each of the displays is interlinked such that selection of a data point in the scatterplot automatically highlights the relevant data in the other plots and the spreadsheet. The spreadsheet also supports data summarization tools such as pivot table.

The tools menu allows the user to quickly add multiple scatterplots or to add extra columns of calculated physicochemical data such as molecular weight, various atom type counts, XlogP, and a variety of PSA measures. These take just a few seconds to calculate and are added to the end of the data table for use in plots, etc. You can rapidly look at the distribution of data within a column by selecting the bin option. The results can be displayed as either a bar chart or a pie chart. And of course if you select a bar, it highlights the corresponding points in the scatterplot. The ability to have multiple interactive plots of the data alongside grids of the highlighted structures is an enormous aid to understanding the data.

Vortex has a high-performance structure-searching engine capable of running at 2.36M matches per second on the PubChem 67 million structure data set (http://macinchem.org/reviews/vortex/tut24/scripting_vortex24.php).

While a useful selection of analysis tools is available including *k*-means clustering, matched-pair analysis, and R-group analysis, it is also possible to access other analytic tools via scripts.

Using Vortex to conduct a matched-pair analysis helps to identify small changes in chemical structure that have a significant influence activity. Using CYP3A4 inhibition data taken from ChEMBL, a matched-pair analysis was undertaken. In the image in the succeeding text, the scatterplot shows the activities of each of the matched pairs color-coded by the frequency in which a particular match occurs. By clicking on a point, we can see the details of the molecular change, the difference in activity, and the frequency with which the molecular change has occurred.

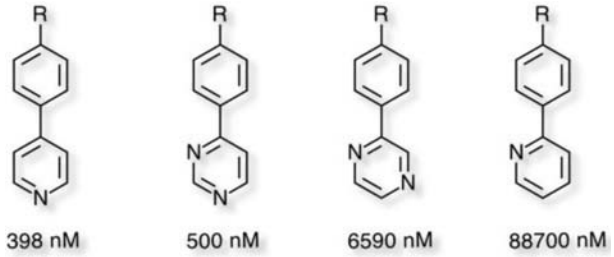

Matched-pair analysis 2D6 inhibition.

The points are also highlighted in the table, which means we can then filter the table by a molecular transformation to see other examples of the same transformation and see if it always has a similar effect on biological activity.

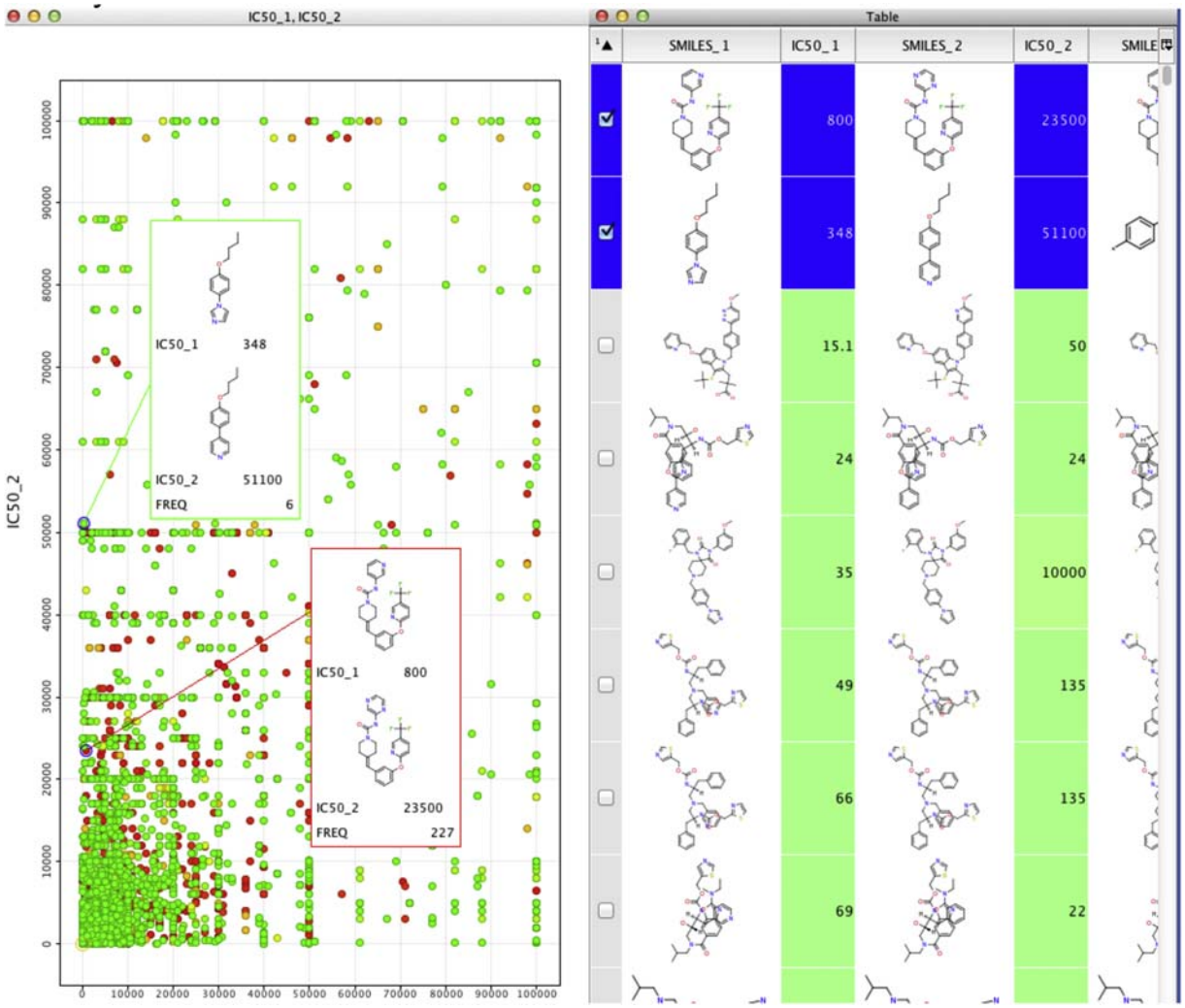

Vortex contains a powerful scripting facility built on Jython, a Java implementation of the Python programming language, and allows access to the key components of Vortex, Python, and Java. Scripting gives users the ability to extend Vortex to give access to web services such as ChEMBL and OCHEM, command-line applications such as Open Babel and SMARTCyp, Perl scripts, statistical packages like R, and linking via SOAP to computational chemistry packages. The increasing popularity of user group-generated scripts/libraries is a notable feature of many of the data analysis tools.

A number of computational chemistry and molecular modeling programs such as MOE (https://www.chemcomp.com/MOE-Molecular_Operating_Environment.htm), SPARTAN (https://www.wavefun.com/products/spartan.html), and SYBYL-X (http://tripos.com/index.php?family=modules,SimplePage&page=SYBYL-X) also combine data analysis tools but are not described in detail here since this is not the main purpose of these applications.

3.18.4 Web-Based Tools

Historically, web-based data analysis tools have relied on Java applets (https://en.wikipedia.org/wiki/Java_applet) or Flash (https://en.wikipedia.org/wiki/Adobe_Flash) to provide interactive content. More recently, with the increased security concerns, many web browsers no longer allow access to Java applets or Flash by default. This has been accentuated by the rapid increase in the use of mobile devices such as tablets and smartphones where neither Java nor Flash is supported. This has led to a movement toward the development of JavaScript-based data analysis tools that are accessible via the web browser on desktop or laptops, but, perhaps more importantly for the future, are also available on mobile devices.

Despite the name, JavaScript is unrelated to Java and is also known as ECMAScript. It is a lightweight scripting language capable of providing interactive content to web browsers without the need for a plug-in. Recent improvements to the compilers have resulted in execution speeds similar to native code.

Many of the web-based tools rely on jQuery (https://jquery.com), a JavaScript library designed to simplify access to document elements, load data, parsing, and handle events. There are many different JavaScript charting frameworks available (https://en.wikipedia.org/wiki/Comparison_of_JavaScript_charting_frameworks) that gives a comparison of 39 different frameworks, but there are many more available.

One of the most impressive demonstrations of the use of JavaScript that supports cheminformatics comes from work supporting http://www.cheminfo.org, first mentioned in a publication describing a web tool for exploring molecules in Wikipedia.[7] The structure-based searching in addition to the data and chemical structure visualization system is all written in JavaScript. The Wikipedia chemical structure explorer is accessible online at http://www.cheminfo.org/wikipedia.

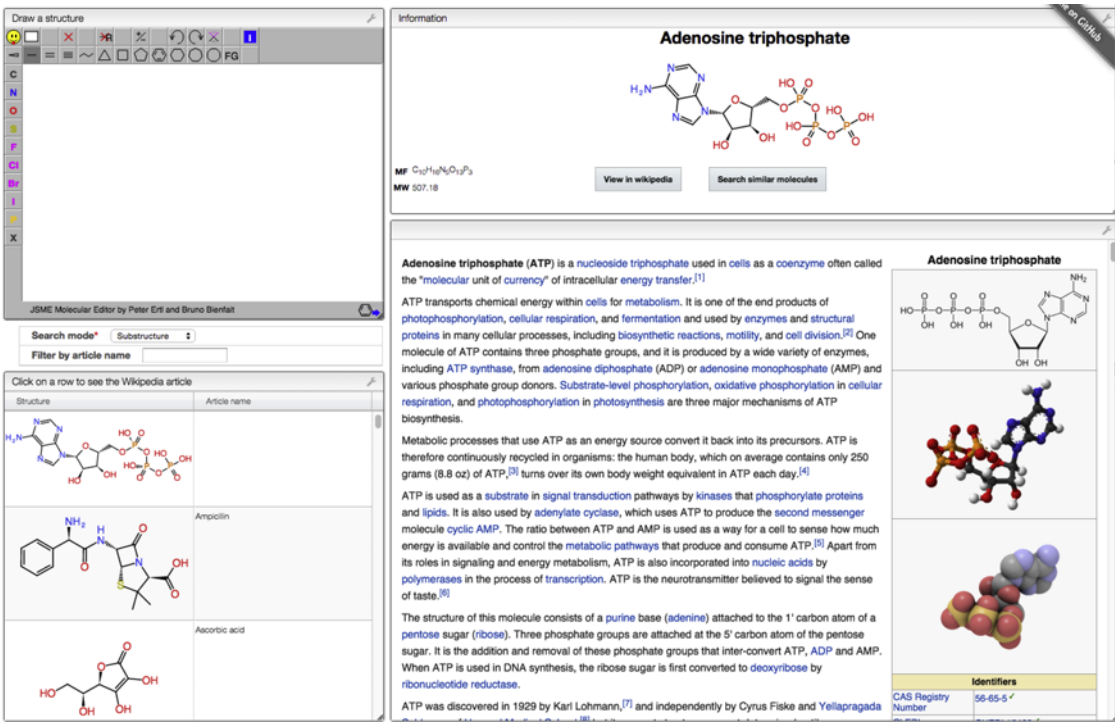

The display allows the user to add further modules; these include 2-D and 3-D scatterplots, pie or radar plot and more sophisticated plots such as self-organizing maps. As in the desktop applications described earlier, selecting a data point in one module highlights the corresponding data point in other modules.

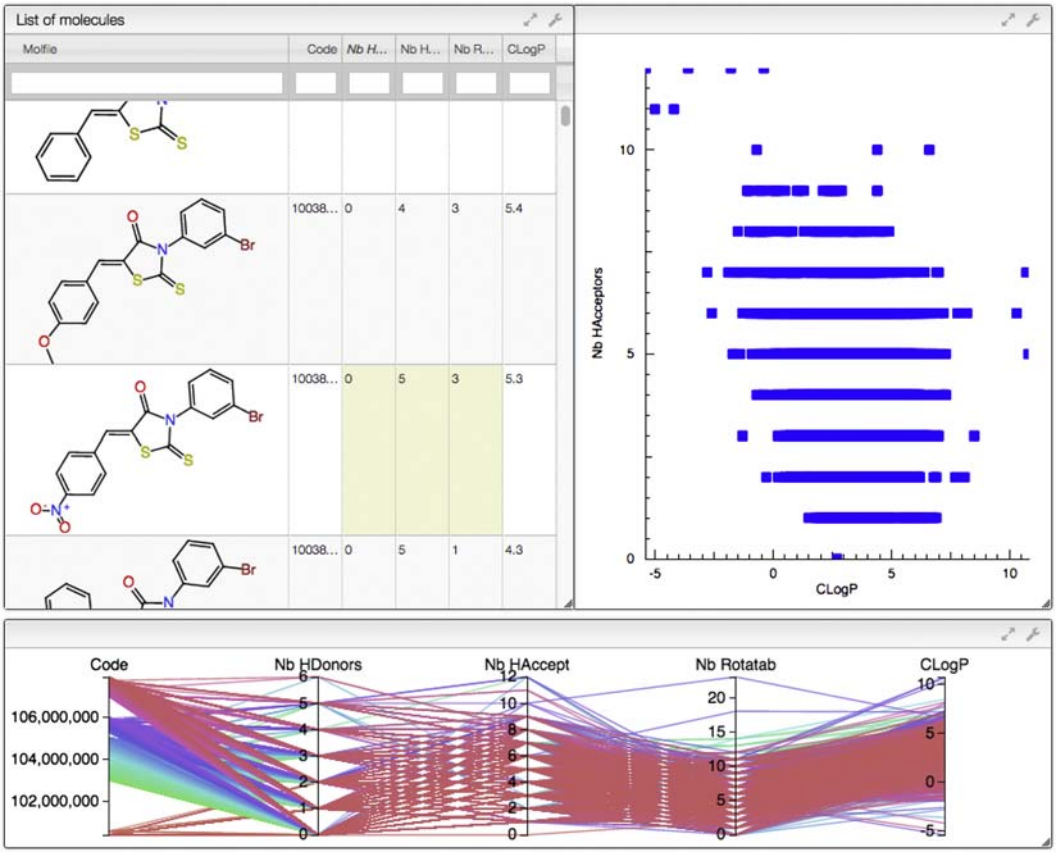

This sort of functionality allows the user to rapidly customize the display.

Flot (http://www.flotcharts.org) is a pure JavaScript plotting library for jQuery, in which it is simple to create attractive interactive plots. It supports all modern web browsers. Flot supports a variety of plot types even within the same plot, and it allows the user to interact with the plots, making selections or interacting with data points. It is also possible to update a chart periodically to get a real-time effect by using a timer to insert the new data in the plot and redraw it.

While many of the JavaScript libraries have little support for chemistry, it is possible to incorporate the ChemDoodle Web Components (http://web.chemdoodle.com), a JavaScript library designed to provide chemical graphics and cheminformatics support. In the plot shown in the succeeding text (http://macinchem.org/reviews/flot2.php), the scatterplot is implemented using the Flot JavaScript library, and the interactive mouseover pop-up displaying the chemical structure is rendered by ChemDoodle Web Components.

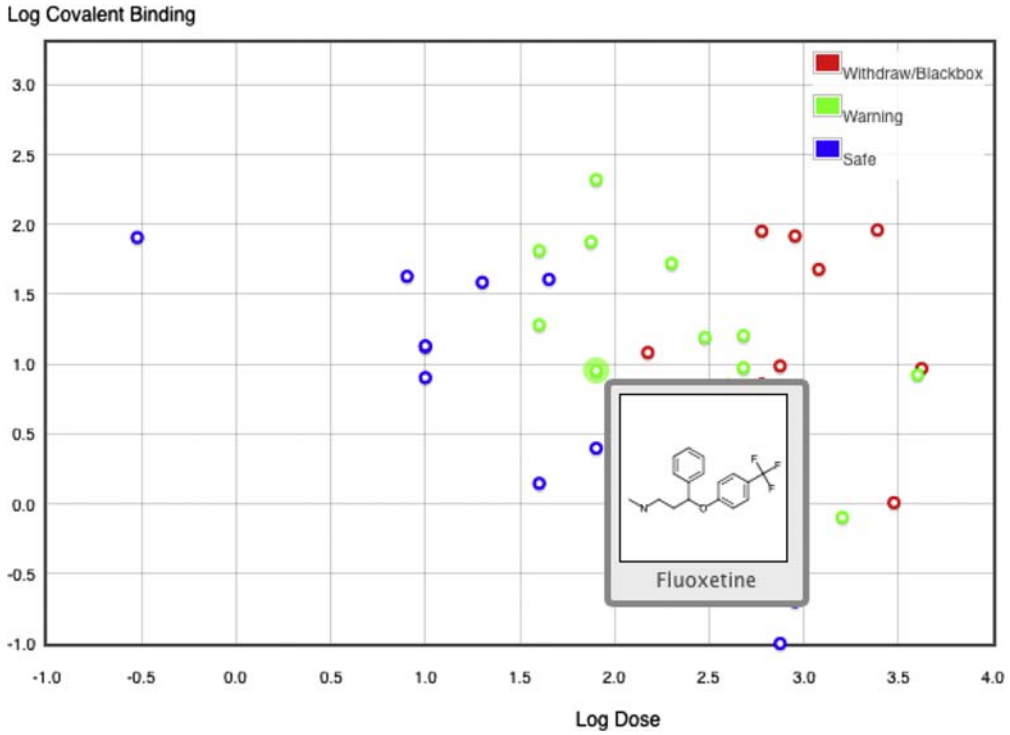

While Flot provides access to data visualization, it does not provide any statistical analysis. JStat (https://github.com/jstat/jstat) is a JavaScript statistical library intended for use in the browser. It optionally includes jQuery, jQuery UI, and Flot for creating plots. Science.js (https://github.com/jasondavies/science.js) is a JavaScript library for scientific and statistical computing that contains various implementations of statistical methods similar to those provided by R. Gauss, another JavaScript statistics, analytics library.

One of the most popular JavaScript libraries for data visualization is D3.js (http://d3js.org). This is in some ways similar to jQuery in that it allows the programmer to select specific document objects and manipulate them to create dynamic interactive plots. It handles multiple data formats including XML and CSV, as well as JSON.

While R is very well known for command-line desktop use, there is also a web application framework for R (http://shiny.rstudio.com) that enables users to access R from a simple web browser.

3.18.5 Mobile Applications

Slowly declining desktop/laptop computer growth and an enormous growth in mobile devices have led many to speculate that mobile devices would soon be the major computation platform. While they certainly dominate communication, it remains to be seen what their influence will be in science and data analysis. That being said, there are now a number of data analysis apps designed for mobile applications; in addition, there are now graphing/plotting libraries available for mobile platforms including iOS/chart (http://www.threedgraphics.com/tdg/products/tools/ioschart/) and Vivdget (http://www.vvidget.org/support/).

In addition to mobile client apps, there are a couple of examples where a client/server model has been used to provide analytics to mobile devices.

While there are simple spreadsheet applications such as Numbers (http://www.apple.com/support/ios/numbers/), Calc XLS (https://itunes.apple.com/us/app/calc-xls-free-spreadsheet/id468674805?mt=8), and Excel (https://itunes.apple.com/us/app/microsoft-excel/id586683407?mt=8) available for mobile devices, there are also a variety of other applications that might be of interest.

Chart Maker is a graphing tool for creating printable graphs from small sets of data (https://itunes.apple.com/us/app/chart-maker-lt/id489717377).

DataAnalysis (https://itunes.apple.com/us/app/dataanalysis/id375603883) is a general-purpose iPad app for the plotting and analysis of all types of data that can be formulated as x,y pairs.

Eigen (http://scical.net/eigen.html) is an app that performs PCA.

Graph (http://www.vvidget.org/graph/index.html) is the mobile version of a desktop application. It supports 1-D, 2-D, and 3-D graph types such as bar, column, pie, line, area, scatter, 3-D perspective scatter, trajectory and surface, volumetric, z-sliced cell, maps, linear, semilog, x-log, log–log, polar, and r-log. It also supports touch to allow the user to interact with the plots. Interestingly, full source code has now been made available (https://github.com/VVI). The idea is to provide scientists, engineers, and professional programmers the ability to import their own data and modeling algorithms and perhaps over time commit the work back to the GitHub repository.

StatsMate (http://www.statsmate.com) is a mobile app that comes with a variety of statistical tools including

- 17 Probability Distribution Calculators
- 10 Hypothesis Testing Calculators
- Four p-Value Calculators
- Two Confidence Interval Calculators
- A Basic Data Analysis Calculator with Histogram
- Two ANOVA Calculators
- A Linear Regression Calculator

TouchPlot (https://itunes.apple.com/app/touchplot/id286347960) is a graphing calculator.

Variables (http://variablesapp.com) is a data analysis tool designed specifically for touch devices, descriptive statistics, and supports:

Histograms
Kernel density estimates
Correlations and covariances
Scatterplots

All of the earlier methods are separated by categories of another variable:

Linear regression
Logistic regression
Poisson regression

Model summaries and per-predictor statistics are the following:

Actual versus fitted plots
Residuals versus fitted plots

Vernier Graphical Analysis (http://www.vernier.com/products/software/ga-app/) allows users to wirelessly collect, analyze, and share sensor data.

The Medicinal Chemistry Toolkit (https://itunes.apple.com/gb/app/medicinal-chemistry-toolkit/id910073742) illustrates an alternative approach; rather than provide analysis of raw data, it offers access to an increasing variety of predictive models.

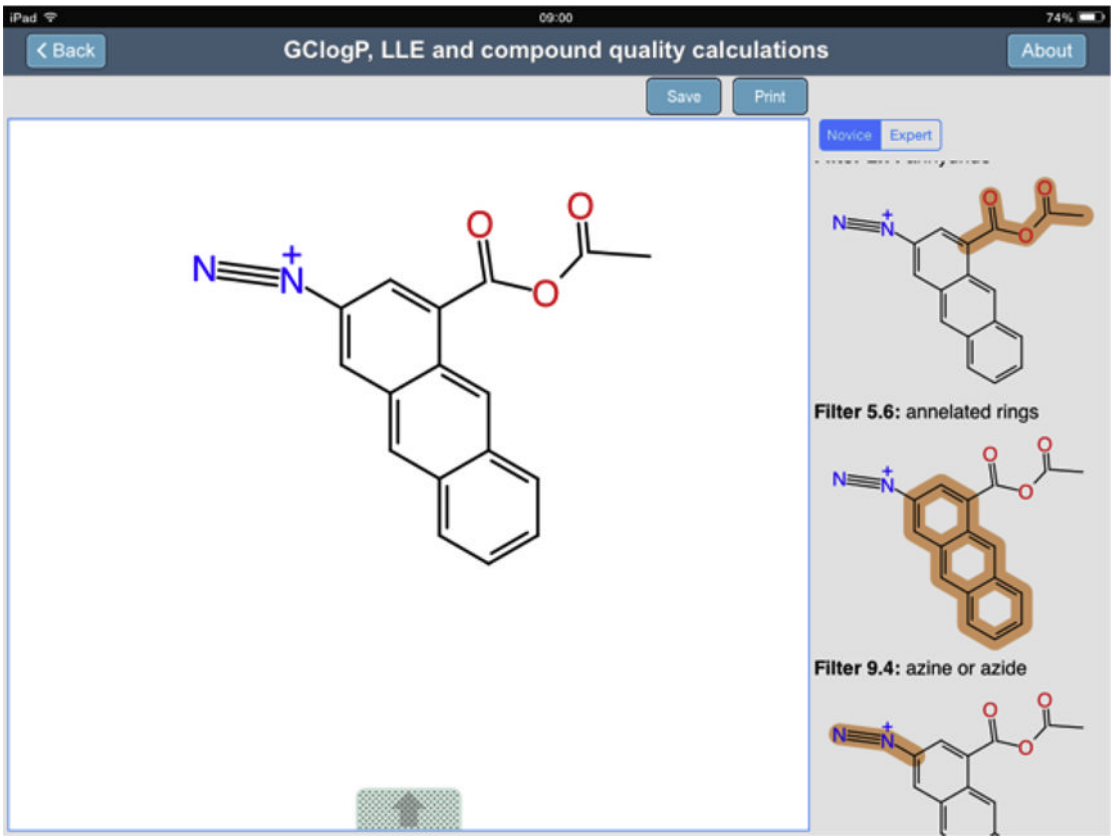

Properties are calculated on the device as you sketch in the molecule so you can actually see the contributions of functional groups as you add them. The currently available calculations are chemical formula, MWt, GCLogP, ligand efficiency, ligand lipophilic efficiency, AZfilters, Cheng–Prusoff, and plasma protein binding.

3.18.5.1 Mobile Apps Using a Client–Server Model

Asteris (http://www.asteris-app.com/support) is an iOS app that arose from a collaboration between Optibrium and Integrated Chemistry Design that allows medicinal chemists to design and analyze novel molecules on their iPad and then calculate a range of physiochemical and ADME properties. Once you have drawn the structure, you can calculate properties and use the "glowing molecule" display to highlight a particular property. All properties are calculated on the Asteris cloud server on Amazon Web Services; core properties include LogP/D, molecular weight, TPSA, and HBD/A. The StarDrop ADME properties include predictive models for hERG, PGP, 2C9, and 2D6 activities. In addition, any predictions derived by the user using StarDrop data analysis tool can also be accessed.

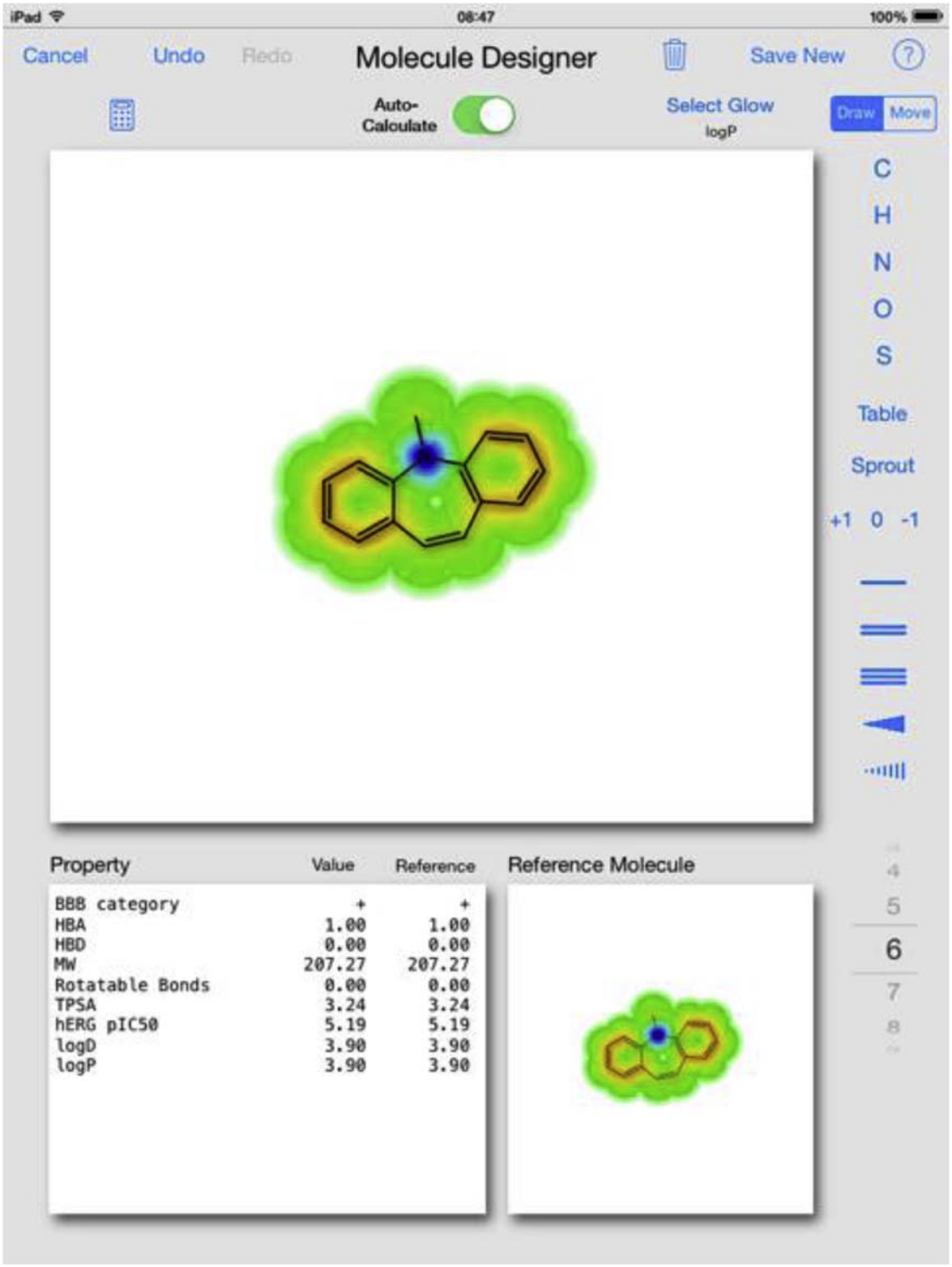

For regular StarDrop users, the results will be very familiar; you can select which calculated property is mapped onto the "glowing molecule"; this is very useful in determining which parts of the molecule contribute most to a particular calculated property or prediction.

Spotfire analytics (http://spotfire.tibco.com) for the iPad requires access to a TIBCO Spotfire Web Player Server to visualize, aggregate, filter, and drill into data sets of virtually any size. This offers the opportunity for institutions that use Spotfire to share data across multiple platforms.

3.18.6 Big Data Analysis

The definition of "big data" probably changes regularly as the improvements in hardware and software allow efficient handling of ever-greater data sets. At CERN, they generate more than 20 petabytes of data from CERN's Large Hadron Collider (LHC) every year. This has led to the construction of the Worldwide LHC Computing Grid (WLCG) (http://wlcg-public.web.cern.ch), a global computing infrastructure whose mission is to provide computing resources to store, distribute, and analyze the data generated by the LHC, making the data equally available to all partners, regardless of their physical location.

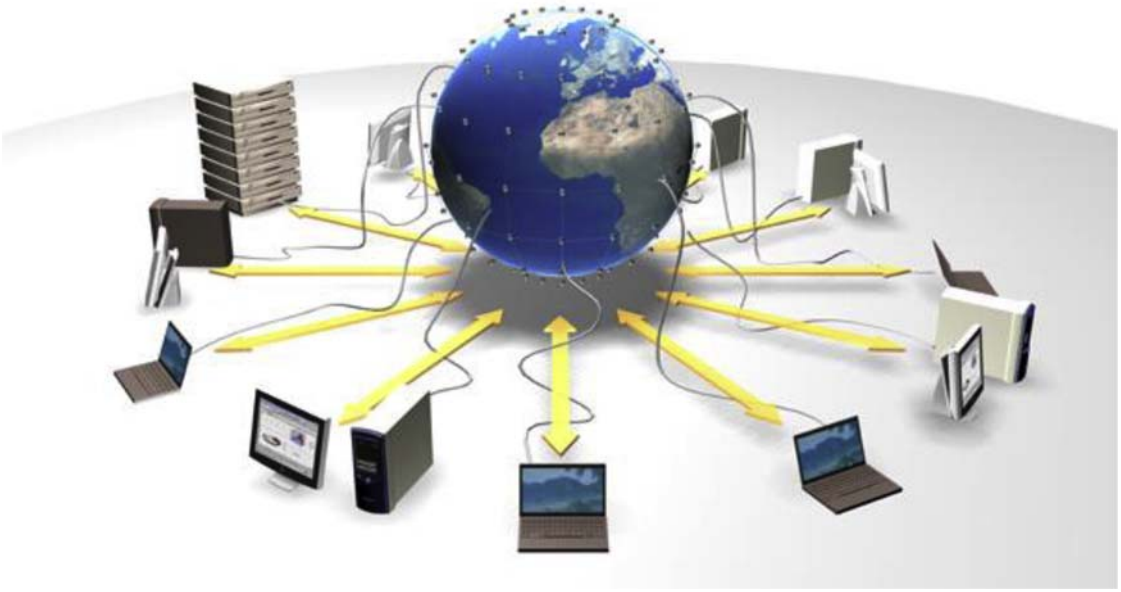

http://copyright.web.cern.ch.

The four main components of the WLCG are networking, hardware, middleware, and client software. Networking is via dedicated, private, high-bandwidth optical fiber links working at 10 gigabits per second, spanning oceans and continents. The grid centers and the 12 Tier-1 centers maintain disk and tape servers. Middleware is the software infrastructure that allows clients to access the vast distributed computing resource and the huge amount of data generated; full details of the middleware are available here (http://www.eu-emi.eu/middleware). The persistency framework is a project providing two software packages (CORAL and COOL) that address the data access requirements of the LHC experiments in several different areas.

At CERN, the workhorse for data analysis is ROOT (https://root.cern.ch/drupal/); the ROOT system provides a set of object-orientated frameworks with all the functionality needed to handle and analyze very large amounts of data quickly and efficiently. ROOT includes methods for creating 1-D, 2-D, and 3-D histograms, curve fitting, function evaluation, minimization, graphics, and visualization. It includes a built-in C++ interpreter so the command language; the scripting, or macro, language; and the programming language are all C++. While this helps performance, it results in a very steep learning curve. While this system is not designed for cheminformatics, it does give an indication of the hardware and software strategy that might be needed to handle increasingly larger data sets.

Within chemistry, the large data sources PubChem (68M structures), ChemSpider (34M structures), and ChEMBL (1.7M structures) probably do not count as "big data." These data sets would increase enormously if all the structures described by Markush structures (https://en.wikipedia.org/wiki/Markush_structure) in patents were exemplified or if multiple 3-D conformations were stored.

However, efforts to bring together chemical and physicochemical data, structural data (PDB) with pharmacological/biochemical/imaging, and genomic data such as Open PHACTS (https://www.openphacts.org) will result in large data sets with very complex interrelationships that traditional data processing applications will be inadequate to handle.

Distributed data storage is a critical component of big data analysis, and Hadoop (https://wiki.apache.org/hadoop/FrontPage) is an open-source software framework specifically written for distributed storage and distributed processing of very large data sets. In particular, it supports computer clusters built from commodity hardware rather than expensive custom hardware. It is designed to scale up from a single server to thousands of machines, with very high degree of fault tolerance. Rather than relying on high-end hardware, the resiliency of these clusters comes from the software's ability to detect and handle failures at the application layer. Yahoo has more than 100,000 CPUs in >40,000 computers running Hadoop (https://wiki.apache.org/hadoop/PoweredBy#Y). A key component is MapReduce (http://mapreduce.sandia.gov/index.html), a framework for handling parallelizable problems with huge data sets across large clusters.

An alternative to Hadoop is HPCC (http://hpccsystems.com). Perhaps the most significant difference is the implementation of Enterprise Control Language (ECL), the query and management language specifically designed to support large data sets.

While SQL databases lead the DB-Engine rankings (http://db-engines.com/en/ranking), NoSQL databases are increasingly used in big data applications, and MongoDB (https://www.mongodb.org) is by far the most extensively used. The popularity of MongoDB (and other NoSQL databases) is probably because the document-style data structure allows the capture of many different types of data within a document as key–value pairs. In addition, as the database outgrows a single machine, it can be distributed across multiple servers in a process called sharding (http://docs.mongodb.org/manual/sharding/). Chemistry support is very much in the early days, but several people are exploring chemical searching within MongoDB (http://chembl.blogspot.co.uk/2015/08/lsh-based-similarity-search-in-mongodb.html) and claim performance superior to the RDKit PostgreSQL cartridge (http://www.rdkit.org/docs/Cartridge.html). A recent paper ("Chemical data visualization and analysis with incremental generative topographic mapping: big data challenge") (http://doi.org/10.1021/ci500575y) describes the iGTM algorithm implemented in the ISIDA–GTM program being applied to a database of more than 2 million molecules, encoded either by MOE descriptors or by MACCS keys.

3.18.7 Collaboration Tools

3.18.7.1 Workflow

KNIME (https://www.knime.org) is an open-source data analytics and workflow platform that allows the user to perform sophisticated statistics and data mining on their data. The KNIME Analytics Platform incorporates hundreds of user-created custom processing nodes (https://tech.knime.org/community) for data I/O, preprocessing and data cleaning, modeling, analysis and data mining, and various interactive views, such as scatterplots, parallel coordinate, and histograms. One of the major strengths of KNIME is the ability to integrate best of breed data analysis, model building, and visualization tools and languages.

The screenshot in the succeeding text shows how code written in Python and R languages can be integrated in a KNIME analytics workflow. In this example, R is used to create a graphic, and Python is used for the model building.

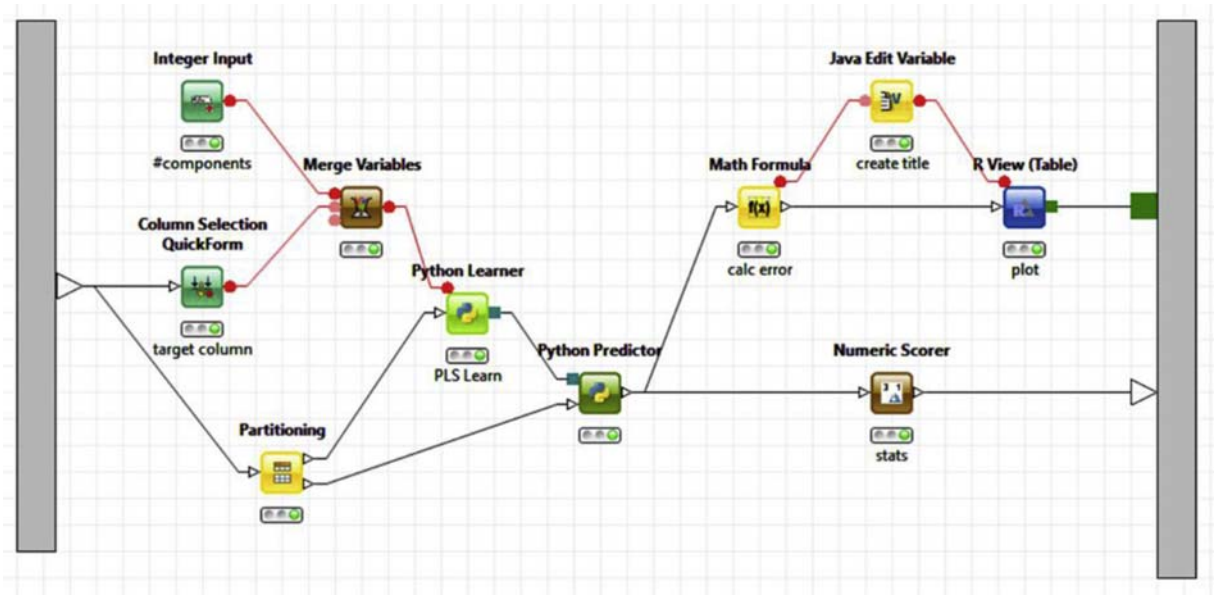

As mentioned previously, analysis of big data is likely to become more of a challenge, and KNIME Big Data Extension already has nodes giving access to Hadoop and Spark.

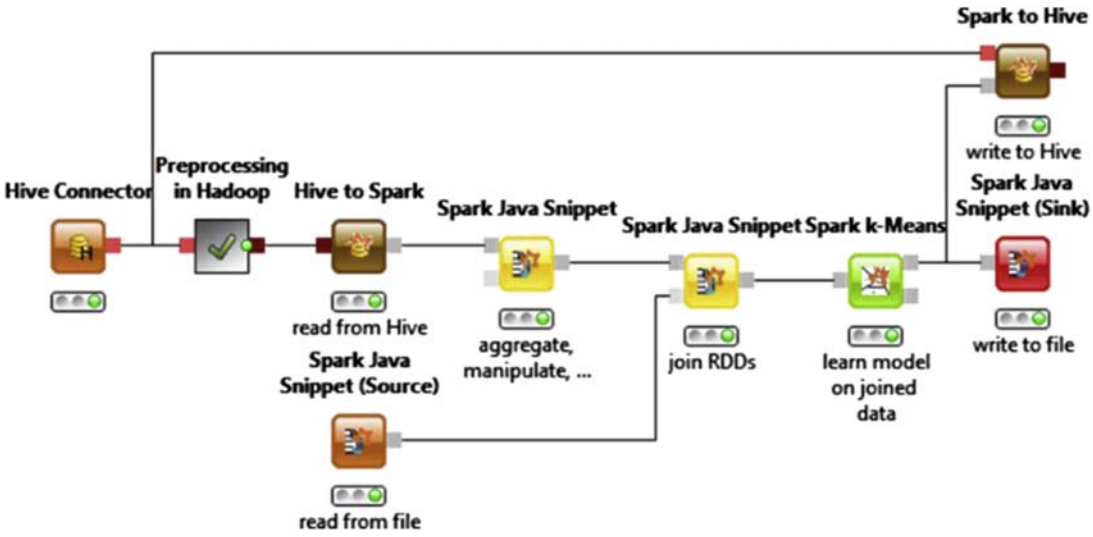

KNIME has recently also introduced a JavaScript node that quickly builds new visualizations and exposes them as KNIME nodes; the figure in the succeeding text shows an example of network graphics generated using the previously described D3 library, wrapped into a KNIME node.

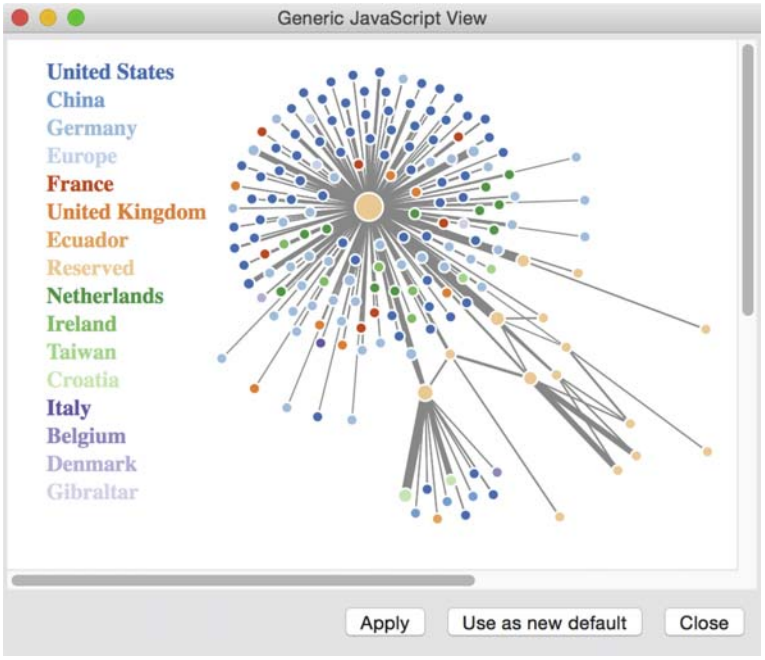

Example of the use of JavaScript plotting tool.

Access to many cheminformatics toolkits are available as KNIME nodes (https://tech.knime.org/cheminformatics-extensions) including OCHEM, RDKit, JChem, CDK, Open Babel, Dotmatics, BioSolveIT, Schrodinger, and MOE. In addition, database access for ChEMBL is available via a KNIME node as is ChemSpider and Open PHACTS. There are also contributions from pharma companies such as Vernalis (https://tech.knime.org/book/vernalis-cheminformatics-nodes).

Pipeline Pilot (http://accelrys.com/products/collaborative-science/biovia-pipeline-pilot/) is a graphic scientific workflow authoring application. It has been used in a wide variety of different areas of science. There are now many components that allow integration of many data types into automated workflows. A number of cheminformatics and computational chemistry software companies have developed Pipeline Pilot components to interface with their proprietary technologies such as ChemAxon (https://www.chemaxon.com/download/pipeline-pilot-components/) and BioSolveIT (http://www.biosolveit.de/PipelinePilot/). In addition, there are components that give access to visualization tools like Spotfire.

Taverna (http://www.taverna.org.uk) is an open-source scientific workflow system that provides modules for data access, for example, chemistry web services set (http://www.myexperiment.org/packs/135.html), management, analysis, and visualization tools including R, Bioconductor, and CDK.

3.18.8 Conclusion

In such a rapidly changing field, this article can only ever be an incomplete snapshot. New tools become available regularly, and support for others dwindles. Data analysis is one area of science where the open-source tools compete on an equal standing with commercial tools. Perhaps, the key difference is the level of guaranteed support provided by commercial versions. That said, community support for Python, R, etc. is outstanding and provides a model for successful open-source development. It does seem that the ones that have stood the test of time are perhaps those that offer a scripting interface allowing users to extend and/or integrate other toolkits.

Ever-increasing-size data sets suggest that "big data" will be of more interest in the future and will require a greater consideration of both hardware and software integration strategies.

Mobile devices are an interesting development, while server farms/cloud computing can offer vast compute resources; mobile devices offer the potential to connect to millions of human beings. The challenge is to phrase the data analysis problem in form that is accessible to millions of nonexperts. Perhaps "gamification" of problems offers a possible solution (https://vimeo.com/146537270).

See also: 1.14. Data Integration and Sharing Supporting Drug R&D. 1.15. Structural Chemogenomics Databases to Navigate Protein–Ligand Interaction Space.

References

1. Guha, R. *J. Stat. Softw.* **2007,** *18* (5), 1–16.
2. Steinbeck, C.; et al. *Curr. Pharm. Des.* **2006,** *12* (17), 2110–2120.
3. Pérez, F.; Granger, B. E. IPython: A System for Interactive Scientific Computing. *Comput. Sci. Eng.* **2007,** *9* (3), 21–29. http://dx.doi.org/10.1109/MCSE.2007.53. http://ipython.org.
4. O'Boyle, N. M.; Hutchison, G. R. *Chem. Cent. J.* **2008,** *2,* 24.
5. Ihlenfeldt, W. D. *J. Cheminform.* **2014,** *6* (Suppl. 1), 34.
6. Hall, M.; Frank, E.; Holmes, G.; Pfahringer, B.; Reutemann, P.; Witten, I. H. The WEKA Data Mining Software: An Update. *SIGKDD Explor.* **2009,** *11* (1). http://www.cs.waikato.ac.nz/ml/weka/.
7. Ertl, P.; Patiny, L.; Sander, T.; Rufener, C.; Zasso, M. *J. Cheminform.* **2015,** *7,* 10. http://dx.doi.org/10.1186/s13321-015-0061-y.

3.19 Examples of SAR-Centric Patent Mining Using Open Resources

C Southan, University of Edinburgh, Edinburgh, United Kingdom

© 2017 Elsevier Ltd. All rights reserved.

3.19.1	Introduction	464
3.19.2	Statistics of Extractable SAR	465
3.19.3	Statistics of Putative Patent SAR	467
3.19.4	Identifying Specific Patents	468
3.19.5	Chemistry Extraction	469
3.19.6	Patent SAR Retrieval From BindingDB	470
3.19.7	Patent Chemistry in SureChEMBL	471
3.19.8	Target Searching in SureChEMBL	476
3.19.9	Tools for Stand-Alone Extraction	478
3.19.10	Selecting for SAR	480
3.19.11	Connecting Between Patents and Papers via PubChem	482
3.19.12	Tracking Back to First-Filings	484
3.19.13	Conclusions and Prospects	485
3.19.13.1	*Note added in proof*	486
References		486
Relevant Websites		487

3.19.1 Introduction

This article will present examples of interrogating medicinal chemistry patent sources with the primary objective of digging out structure activity relationships (SAR). Since the details as described later will show this to be more difficult than for papers, it raises the question why bother? The main reasons are that patents not only contain more SAR but also that this published earlier than in the peer-reviewed literature. Statistics in support of both these advantages are difficult to obtain but will be partially addressed here. For discrete SAR values, a conservative estimate of at least twofold more data-mapped structures in patents can be made. If ranged values are included, the difference rises to at least fivefold. In support of this, it was reported in 2011 that Factor IXa (F10, P00742) had 5.8K assayed compounds mapped to it via extracted from papers by ChEMBL, but this had increased to 43K from combined literature and patent extractions by GVKBIO (i.e., papers:patents ~1:6).[1]

The time advantage is more difficult to support with data, but it is well known that pharmaceutical company drug discovery teams typically wait 2–3 years after a patent application before publishing in a journal. In some cases, high-quality project results will be exemplified as substantial SAR sets in patents but may never surface elsewhere.

As an important adjunct to SAR extraction per se, this article will also exemplify ways of exploring connectivity between papers and patents from the same teams. However, both aspects will be done using open databases and tools. Reasons for this restriction are outlined here:

- Commercial sources, even just major ones, now present too broad a spectrum of technical features to review (i.e., no author would have either the multiple licenses or capacity for detailed comparative evaluation).
- There has been a remarkable "big bang" in the availability of automated patent-extracted chemistry just in the last few years, culminating in the secondary deposition of ~19 million patent-derived entries in PubChem and primary extraction of ~17 million of these into SureChEMBL.[2]
- This has led to a democratization of patent mining that has now become more accessible for those without commercial databases or tools.
- Concomitantly, parallel interrogation of open resources has become essential for users of commercial databases anyway, since the inevitable divergence of coverage by different sources precludes any one-stop-shop.
- PubChem precomputes relationships between 2D and 3D chemical structures, patent documents, PubMed IDs (PMIDs), PDB entries, bioassay results, and annotation from many curated submitting sources.[3] This means that the combined PubChem and Entrez functionality now encompasses the majority of bioactive patent chemistry. This thus presents a scale of relationship navigation that closed commercial databases cannot match.

Although aspects of intellectual property (IP) focused searching and/or competitive intelligence analysis will briefly be touched upon, strategically they may be better addressed by commercial databases, depending on what value-added features they offer for these two domains. This may include enhancing the indexing depth and precision of public data in various ways, including manual annotation.

Additional caveats related to the coverage of this article need mentioning. The first is that the techniques exemplified here are small-scale, largely manual and thus more individual-orientated exercises rather than large-scale approaches. The second coverage

restriction is that illustrative examples can only be accompanied by short technical descriptions, although they will be referenced for users to access the details. The third is that the queries describe here we executed in Sep. 2016 and may thus give different results at later dates. The fourth is that, particularly in the patent domain, queries are rarely "clean" in terms of specificity or recall (some of the reasons for this will be discussed). The ones used here are presented in good faith with the expectation of some level of reproducibility. However, they can be disconcertingly noisy and inconsistent in practice. One reason is that patent offices and other sources often do not index document metadata in standardized ways (e.g., conflating applicants with inventors or multiple synonyms for the same applicant institutions). Another is that different interfaces to nominally the same document corpora can give different results (e.g., depending on the filtration options selected and the syntax used for complex queries). The fifth caveat is that while queries executed here have been designed to reflect real-world tasks they are also somewhat contrived for illustrative purposes and thus may not be the most efficient way to get to the explicit results. There are many choices of entry points, tools, query strategies, and technical tricks that may answer particular questions more quickly.

Five final points related to the usability of this article should be mentioned.

1. With the exception of a few novel structures not yet submitted to any public databases, specifically mentioned compounds will be specified either by a PubChem Compound Identifier or a Substance Identifier, or in some cases both.
2. Rather than necessitate the addition of many hyperlinks into the text, each of these can be accessed via two standard URLs. For example, atorvastatin, as CID 60823 can be linked out as https://pubchem.ncbi.nlm.nih.gov/compound/60823. The specific submission from SureChEMBL, SID 226395935, can be analogously linked as https://pubchem.ncbi.nlm.nih.gov/substance/226395935.
3. There are too many patents to be fully referenced so their numbers are specified in the text. These will usually retrieve links to the document in the upper ranks of a Google search result within seconds.
4. SAR retrievals will focus on beta-secretase 1 (BACE1, Swiss-Prot P56817) as an Alzheimer's disease protease.[4] The illustrative advantages of an intensively pursued drug target will become apparent as we track through over a decade of substantial SAR and explore patent-to-patent and patent-to-paper connections.
5. For reasons of space, a basic familiarity with querying databases and patents has to be assumed. In particular, this should include patent office websites (e.g., EPO Espacenet, USPTO, and WIPO), kind codes (A1, B2, etc.), patent classifications, the concept of patent family, and experience with searching in PubChem or other chemistry portals.

3.19.2 Statistics of Extractable SAR

The complex task of extracting chemical and biological entities from patents has been well studied. Some of the different approaches will be referred to here, but the complication is that SAR is defined by relationships between entities. For this reason, questions regarding SAR statistics both inside and outside patents are difficult to get precise answers to, but would be useful for making judgments on what is realistically achievable.

In this context it is useful to review our high-level assumptions. The first is that readers have an interest in bioactive chemistry in the wider sense, with the obvious proviso that very low or inactivity is crucial for SAR and control experiments, but data sets are biased toward activity and potent compounds. The second would be that, regardless of the dominance of medicinal chemistry, IP domains related to tropical diseases, antivirals, antibiotics herbicides, pesticides, toxicology, and chemical biology can be approached for SAR mining in broadly the same ways as described here for human target-centric drug discovery. It is also a reasonable assumption that medicinal chemists have at least some interest in extracted structures that were not designed to have biological effects per se (e.g., novel reactions, dyestuffs, photochemistry, etc.) but where the documented synthetic chemical space lies within the broad property envelope associated with potential bioactivity.

So what do we mean by SAR in the context of this article? The concept of a series of close structural analogs with a range of quantitative bioactivity data that can form the basis for different types of predictive modeling is well understood but also continually developing.[5] For in vitro data they need specific links between the entities of compounds, the protein bioentities whose activities they modulate, and the assays used to measure this. These can be classified as (data supported) compound-to-assay-to-protein relationships.[6] Typically, a document "D" describes a biochemical assay "A" with a quantitative result "R" (e.g., an IC_{50}) for compound "C" (with an explicit structure) defining it as an inhibitor of protein "P" (with a sequence and species-specific identifier). Useful shorthand for these relationships is thus "D–A–R–C–P" (note the substitution of "P" with target "T" can be used to indicate a black-box mechanism of action such as a tumor cell or a tropical disease parasite). This shorthand can be extended to describing a basic SAR series as a multiplexing of R and C, while a specificity cross-screen would be a multiplexing of A, R, and P. Separate patent filings of SAR interest often cover closely related but distinct chemical series. These can be linked as a set of "D" that have A–R–P in common (since they were from the same institution and reasonably close in time) but the different sets of "C" are varied.

Medicinal chemists have traditionally manually extracted the key entities from patents and papers of interest and organized the relationships locally, thereby converting unstructured data from document text, chemical images, result tables, and supplementary data into structured information (e.g., D–A–R–C–P in an Excel sheet). It should also be pointed out that, beyond a sketching tool, access to patent office portals along with a basic familiarity of enzymology, receptor pharmacology, and protein naming, a scientist can curate A–R–C–P sets from a patent on the day of publication within a few hours (i.e., in advance of any commercial extraction service). Notwithstanding, this presupposes that (a) the indexing of the title and abstract allowed the specific retrieval of patents of interest and (b) that these actually contained novel, useful, and extractable SAR.

While the ability to perform bespoke curation and annotation remains a core competence for medicinal chemists, they are increasingly likely to hand-off this activity for two main reasons. The first is that commercial or public databases, as well as internal support from Information Scientists, can provide project teams with partial or complete D–A–R–C–P extractions from various sources. For example, those with SciFinder access can collate the D–C records within days of publication but will still have to fill in A–R–C–P themselves (or from another resource). The second reason is that drug discovery enterprises (academic or commercial) usually have local systems for collating, mining, and modeling SAR originating from their own internal projects. These are now likely to include the use of electronic laboratory notebooks for primary chemical structure registration and data capture. These are then extracted to populate in-house databases that increasingly also integrate external bioactivity data sources. Pioneering examples of these include the AstraZeneca enterprise applications of Chemistry Connect[7] and SAR Connect.[8] What this means is that bespoke extractions are now expected to be format-compatible with internal systems and thus easily subsumed into them for intraorganization sharing rather than languishing in local directories.

An expanding range of curated compilations containing partial or complete D–A–R–C–(P or T) mappings are available as commercial products or deposited in public databases.[9] Depending on scale and update frequencies, these largely obviate the need for individuals to "do-it-yourself" extractions. However, a number of key points need to be made before reviewing some of these in the context of this article. Firstly, the facility with which a medicinal chemist can extract a document is reflected in the resource curation model (commercial or academic) where professional biocurators are hired or contracted for scaling-up essentially the same process. Secondly, D–A–R–C–P extraction with useable specificity has so far defied complete automation. While text mining combined with natural language processing (NLP) is making progress toward this goal, challenges remain. The principle one is the need to semantically link structures, assay descriptions, result tables, and protein identifiers extracted from different sections of a document. Experienced biocurators can cognitively discern these relationships in a matter of minutes, but they increasingly use automated tools for triage and to improve their efficiency of capture. Thirdly, while it actually violates the principle of patenting, some applicants in the medicinal chemistry domain deliberately introduce varying degrees of obfuscation into their documents (examples will be mentioned). In practice this can not only make the elucidation of SAR relationships more difficult but in some cases impossible.

The third point concerns patent coverage. As testimony to the difficulty of managing a patent curation pipeline, compared to processing papers, even now relatively few resources surface complete D–A–R–C–P sets from patents. Some commercial offerings may index a molecular mechanism of action (mmoa), but this is only a partial substitute for a standard protein identifier. The fourth point is that, in many cases, it is necessary to compare sources indexed for bioactivity as a surrogate for SAR per se. Consider for example, a published report on an orphan (i.e., with no analog structural neighbors) complex natural product that potently inhibits malaria in a mouse model. A record of this bioactivity is clearly valuable and worth finding but is not immediately useable for SAR exploration. In contrast, extended data sets either where "T" uses growth inhibition of the parasite in vitro with 100s of IC_{50} values for a designed synthetic library and/or recording K_i's for the identical chemical series against one or even multiple "P"s as purified *Plasmodium* enzyme targets. While filtering database entries between these different bioactivity levels can sometimes be done for papers, this is more difficult for patents.

The content statistics of three databases in **Table 1** are partitioned into D–A–R–C–P metrics. The reasons for selecting these in particular are not only that the relevant numbers are available from the teams concerned but also that, in combination, they sample the global "bioactivity space" and thus provide useful overviews of what could potentially be SAR-mined.

There are caveats associated with **Table 1**. These include that the individual data models give rise to differences in entity counts, redundancy reduction, and relationship definitions. Note also that GOSTAR is a merge of a suite of databases. Nonetheless, **Table 1** provides a useful quantitative overview. We can briefly go through them in sequence. As a commercial database, GOSTAR is the largest manually curated resource of chemical modulators of biological targets (mostly proteins) with associated activity data (mainly inhibition) extracted from papers and patents. Notwithstanding the fact it cannot serve as an example of open patent mining, it nonetheless provides data-supported upper limits of extractable SAR from public documents. A 2013 analysis indicated the journal:patent compound split was approximately 1:2.7 with a document number split of 82K:58K.[10] A recent update from Exelera (**Table 1**) records current counts as 2.2 million structures from the literature, 5.1 million from patents (i.e., a slight shift toward papers since 2013), and an overlap of 0.19 million (i.e., not much change). Other relevant figures from the 2013 publication included that manual extraction yielded, on average, 12 compounds from a paper and 45 from a patent.

The BindingDB figures are derived from an open database, not only in situ but also as a regular submitter to PubChem.[11] In addition, this resource supplies a set of D–A–R–C–P expert manual extractions of US patents (reviewed later). Since 2009 ChEMBL,

Table 1 Document, assay, result, compound, and protein target content counts for Excelra GOSTAR (commercial), BindingDB, and ChEMBL22 as recorded in Sep. 2016

Name	*D (pubs)*	*D (pats)*	*A*	*R*	*C*	*P*
GOSTAR	110,000	69,000	17 million	24 million	7.3 million	9,212
BindingDB	25,000	1,200	0.96 million	1.3 million	0.57 million	6,468
ChEMBL	65,000	1,200	0.9 million	5.6 million	1.2 million	6,888

Numbers for the latter were taken from the release notes except the protein target count was obtained from the UniProt cross-reference. Those from BindingDB were personally communicated by Michael Gilson and the Excelra figures by Anil Kumar and Sreeni Devidas.

also open and a PubChem submitter, is an open source of literature-extracted bioactivity and it also subsumes confirmatory PubChem BioAssays.[12] Full release statistics are available from which the headline numbers in Table 1 were obtained. Between BindingDB and ChEMBL there are similarities, differences, and complementarity in terms of SAR content. Firstly BindingDB subsumes protein-mapped ChEMBL content. Consequently, the former has 78% of compounds in common with the latter (although a proportion of these include identical structures collated by different routes). In addition, BindingDB has extracted 3000 PMIDs not in ChEMBL. The average of 18.5 extracted compounds per paper for ChEMBL22 is slightly higher than for BindingDB at16, but below the current GOSTAR average of 20. Thus, these three independent numbers indicate a reasonably consistent yield of manual compound extraction from the medicinal chemistry literature along with the linked A–R–P data.

So just how much total SAR is extractable from the journal corpus? This question provides context for comparisons with patents, but it is not easy to get a clean answer. On balance, the 2.2 million compounds from papers extracted into GOSTAR indicate a plausible lower boundary, since the spread of journals and curation backfill time span is larger than ChEMBL. However, quantifying how much of this is useful for SAR modeling (e.g., a series of analogs against the same protein as opposed to singletons with just one assay result) is less straightforward (but the distribution could probably be discerned from GOSTAR internal statistics). Upper boundaries remain uncertain but what we can record is that 92K PubMed entries are classified under the MeSH term "Chemistry, Pharmaceutical," and 713K under "Chemistry." While GOSTAR would not be expected to cover all bioactive chemical structures ever published, by their own selection criteria of SAR-density per paper, they have probably captured the major part. Given the PubMed figures earlier, we can thus estimate a conservative upper limit for ~3 million structures as being within the wider frame of SAR interest. Notwithstanding, as will be expanded on, ChEMBL constitutes the largest open resource of literature-extracted SAR against which patent sources and subsets can be intersected.

3.19.3 Statistics of Putative Patent SAR

As we have seen for the literature, precise comparative statistics for document corpora entity content are difficult to come by. Notwithstanding, useful calibrations from automated extractions with a 2015 time point have been provided by SureChEMBL and the Minesoft Chemical Explorer (commercial). The former declare 17 million compounds from 14 million patent documents, while the latter claim 12 million from 10 million. While the gap between these numbers and the 5.1 million selected for SAR linking from the same corpus for GOSTAR is wide, we can reconcile them to a certain extent via other methods of analysis and orthogonal queries to provide broadly plausible cuts. The first filter we need to consider is patent family redundancy. Using the World Intellectual Property Organization (WIPO) PATENTSCOPE database, we can establish that 58 million national documents collapse to 3 million international patent applications (PCTs or WO filings). This indicates an average family size of 19 that, for the purposes of mining, can be considered as having the same chemistry content (despite postexamination claim scope changes). The other advantage of selecting WO is that they are generally the first family members to publically surface (for the record thought, these are technically only published applications since granting is done by the national authorities). Their disadvantage for mining is that, compared to the XML format of USPTO applications from 2001 onward, WOs have poorer text and image quality from suppliers of the electronic transformations. This degrades chemistry extraction, sometimes severely (this topic is addressed later).

The second key filter is to identify relevant chemical content. As a first step toward the latter, we can use the Intentional Patent Classification (IPC, see website listing). This is a hierarchical system where C for "chemistry" accounts for 20% of the WO. However, the combination of C07 for "organic compounds" and A61K "preparations for medical purposes," while not 100% specific, is highly selective for small molecule drug discovery, medicinal chemistry, and therefore potential SAR content. (n.b. not all relevant national filings proceed to a PCT and some not captured in this intersect may be using submission tricks to "hide.") The individual numbers, via PATENTSCOPE, are 217K and 235K, respectively, with a C07/A61K intersect of 85K (for comparison A01N "herbicides and insecticides" has 29K WO with 7.4K of these intersecting with C07). The corresponding C07/A61K count for EPO publications is 371K which drops to 233K for USPTO. Despite the uncertainties on absolute document redundancy (e.g., further collapsing by Kind codes), we can make a plausible estimate that the medicinal chemistry relevant patent subset could be in the range of 100K to 200K. We can then use the average count of 257 unique IUPAC structures per patent from recent exhaustive extraction exercise to make a total chemistry estimate for the C07/A61K set of just over 25 million.

Compared to document counts in the high millions often highlighted by patent indexing and extraction resources, these numbers for the medicinal chemistry intersect seem lower than might be expected. However, it is comparable to the GOSTAR extracted patent count of ~70K in Table 1 which is SAR selective. The yearly WO published output corresponding to C07/A61K can be plotted (Fig. 1). The result clearly mirrors the published rise and fall in the concomitant GOSTAR chemistry extraction indication the amount of patent SAR has actually declined since ~2006.[10]

While commercial operations are triaging this output, it is difficult to get open statistics that could support SAR estimates. For example, the family redundancy between the WO, USPTO, and EPO is unclear (even though some measure might be obtainable from the INPADOC system). Note it is possible to select granted versus nongranted applications in USPTO as a nominal quality filter and redundancy reduction. However, not only does the time lag for examination run into years but also granting is by no means a guarantee of scientifically useful content. What we can attempt is to empirically divide C07/A61K into data-centric utility groups (i.e., not based on IP considerations) with respect to putative SAR content. These can be outlined as follows:

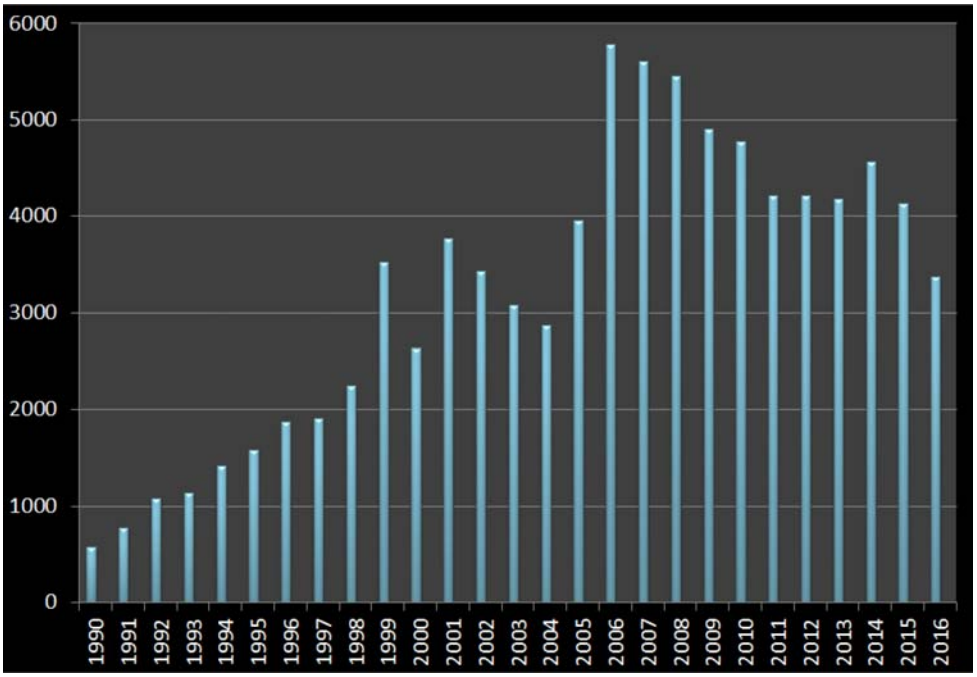

Fig. 1 A plot of the per-year WO patent counts for the intersect between the IPC codes C07 and A61K. The Sep. 2016 total was 85K.

1. An extended chemical series, including synthesis and analytical details with novel composition of matter, described as directed toward a specific target and a set of diseases, possibly including assay descriptions. However, beyond general statements, such as "found to be active," no data can be assigned to individual structures.
2. As above but with a proportion of the examples having aligned bioactivity data, although much less than the number of example structures and/or heavily gapped.
3. Assignments of activity to each exemplified structure but only as ranged values. This can be typically in the form "between 10 and 100 nM or 100 and 500 nM" or using a binning system of one to five stars, ABCDE or suchlike.
4. The document includes a complete set of discrete assay results, typically IC_{50} or K_i, displayed in a data table with anywhere between 5 and 500 rows. These can be aligned with the structures (novel at filing time) and their synthetic descriptions. By definition, this constitutes the most useful SAR patent (particularly if cross-screening data from two or more parologous proteins are included) but note the results may be generated with assay formats that do not use purified proteins (i.e., "T" not "P").
5. Documents similar to 3 and 4, ostensibly including an extensive set of results, but where the degree of obfuscation in the description or layout (e.g., activity and example numbering not being in register) is high enough to preclude unequivocal SAR mapping.
6. A category that encompasses what we can term secondary filings in the sense that structures have been filed previously are not novel and few in number. These can include crystallization or synthetic route descriptions by the erstwhile originators of the lead compounds as well as generic manufacturers jockeying for inventive claims on clinical candidates.
7. Outside the above there are many filings that defy any simple classification. They are still assigned the two codes we deem useful but for various reasons, difficult to discern SAR. Perhaps the most interesting are data-supported authentic new uses for previously claimed structures (i.e., repurposing). Others may cover mixture combinations, often with huge permutated listings. Some include various types of virtual enumeration where potential activities for structures are claimed that have neither been made nor tested.

The informal categories described earlier can be assigned by detailed inspection of patent documents. However, they expose the problem that there are no statistics as to how these are partitioned at scale. Consequently, there are no reliable methods of automated SAR detection. While 2, 3, and 4 are of primary interest, some of the other categories could be useful. For example, in category 1 there are fillings by drug discovery teams with an established reputation but whose project leaders or company management take the strategic decision to file a chemical series without disclosing any activity data. Notwithstanding, these are logically expected to include actives (i.e., a series with cryptic SAR) to justify the IP investment in the first place. They can certainly be used for modeling (e.g., building a pharmacophore) and some structures may be selected as a smaller SAR series and published later in a journal.

3.19.4 Identifying Specific Patents

Retrieval of patents with a view to significantly enriching for categories 2, 3, and 4 is a major subject that cannot be covered in depth here. However, examples will naturally emerge as we explore queries in different resources. In the interim, we can outline the general

challenges but even before this we need to clarify operational imperatives in the context of this article. In searching databases that include patent-extracted chemistry in the context of IP due-diligence, the consequences of false-negatives (e.g., overlooking relevant prior art) for any drug discovery organization can be dire in terms of economic cost and erosion of competitive position. However, the assumption is made here that if an individual happened to miss some patent SAR that was retrospectively found to be relevant, they would not be held to account too severely (although the same oversight from patent attorneys or Information Sciences teams might not be seen in such an equable light). Another real-world consideration is that researchers are likely to be more focused on the SAR of the present rather than the past. This is especially so since the latter is well covered by review articles (e.g., the journal "Expert Opinion on Therapeutic Patents"). This means researches are unlikely to want to pull back SAR from decades ago and are thus more likely to filter for more recent time spans (where the chemotypes, potencies, and properties should, at least implicitly, be improving). Thus, in regard to the strategic dilemma of specificity versus recall, examples used here will be high-specificity queries and recent time scales in order to reduce time spent triaging false-positives for rejection, rather than being overly concerned about missing false-negatives or older filings.

As we know patents can be identified by their metadata such as inventor names, affiliations, and patent classification codes (even though these can have noisy indexing). Filtering or ranking by publication date is of course useful but can be confounded by families, Kind codes, and priority equivalents which can surface identical documents across time spans of 5 years or more. However, examples here will concentrate on target-centric searching that, while certainly prone to false-negatives, has an acceptable specificity. In addition, target searching is the most common first-pass for literature searching so that grappling with protein naming issues becomes more familiar.

3.19.5 Chemistry Extraction

As mentioned, manual curation of SAR from a patent is intuitively obvious to medicinal chemists, many of whom have engaged in generating the data that goes into them and may even have had a hand in drafting applications. However, most sources that have pursued the large-scale manual extraction of chemical structures from patents (with or without A–R–C–P mapping) have been commercial. This means that technical details of their selection and triage are not usually disclosed. However, being proprietary about exactly how databases are populated always leaves users with uncertainties. In particular, it is important to know curation strategies and chemistry business rules that might directly affect how easily and how much SAR can be collated from any particular resource (as we will see in the section later). These include

- How are ambiguous partial stereo centers handled?
- Is the parent added as an extra structure where the document specifies a salt?
- Are obvious applicant-originated chemical errors fixed?
- What activity units do they normalize to?
- Which software do they use to output their sketched structures?
- What primary standardized chemical representations are captured from this output?
- Are activity figures rounded down?
- Do they number structures corresponding to their example numbers in the document (i.e., so the extracted structure can be unequivocally matched to the activity values even if it is exemplified multiple times)?
- Do they have capping rules for very large SAR tables?
- Are all examples extracted or only key structures selected by the curators?
- Do they add the structures of known drugs or clinical compounds even though these may only be specified by a semantic name?

Users who commit a lot of searching time to any particular curated resource may have to work these rules out "backwards" during the course of their analyses. They can also compare between sources (e.g., for the same patent number) but this does become time consuming.

By definition, the manual throughput of chemistry and other entity extractions (e.g., A–R–C–P) from documents factors linearly with the cost of biocurator time. For this reason, the technology with the greatest impact on open chemistry extraction in recent years (and provision of structures that can potentially be SAR-mapped) has been automated chemical named entity recognition (CNER). This approximately scales according to computing power and algorithmic efficiency. In essence, electronically formatted documents go into a pipeline and structures come out. As well as indexing the chemistry, outputs may be tagged with metadata, such as whether they were derived from text and/or images, recognized in the title, abstract, description, or claim sections. In practice, CNER extends beyond just text-to-structure (n2s) to encompass automated image-to-structure (i2s) as well as manually drawn ChemDraw files then automatically converted to molfiles structures. These are generated by the USPTO Complex Work Units (CWUs) process as part of their pipeline for complete electronic processing of patent applications. While researchers mining patents do not need to keep abreast of the details of CNER technology, it is important to understand the associated strength and weaknesses, particularly from the point of view of exploiting resources derived from it. A useful schematic describing SureChEMBL is shown in Fig. 2 (interrogation of this database will be described later).

The basic operations shown in Fig. 2 are n2s and i2s. The first is via conversion of IUPAC systematic names as text strings, but this also encompasses what we can call semantic n2s where names such as "atorvastatin" are converted into explicit structures via

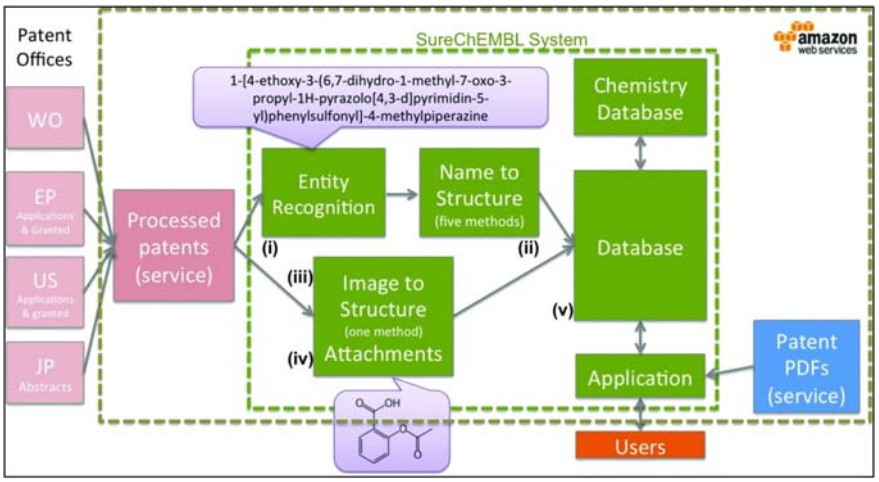

Fig. 2 A diagram of the SureChEMBL CNER pipeline. Adapted from Papadatos, G.; Davies, M; Dedman, N.; Chambers, J.; Gaulton, A.; Siddle, J.; et al. SureChEMBL: A Large-Scale, Chemically Annotated Patent Document Database. *Nucleic Acids Res.* **2016**, *44*, D1220–D1228. http://dx.doi.org/10.1093/nar/gkv1253.

a look-up dictionary. The second is via image processing for i2s that also includes the CWU-derived molfiles. We can now move on to see how the interplay between manual inspection and automated extraction can be exploited for SAR retrieval.

3.19.6 Patent SAR Retrieval From BindingDB

Before moving on to CNER resources, it is instructive to explore one of the few open resources that includes manual patent extraction of complete D–A–R–C–P sets. As of Sep. 2016 BindingDB had curated 1229 US patents with target-directed small molecule binding data. While a relatively small number (now mirrored in ChEMBL22) it has the advantage of being produced by the expert triage of recent USPTO publications selected via the inclusion of K_d, IC_{50}, K_i, or EC_{50} in the abstract. The triage also selects for CWU molfiles that provide complete sets of example structures, thereby enabling the expert manual curation to focus on target identification and activity mapping. There is a pointer to this section from the front page or lower down on the left-hand facets under citation sources. There is also an Advanced Search tools option for focused searches within just the patent data (or other sets). The top-10 patent extraction records by date added are shown in Fig. 3.

These BindingDB true-positives (i.e., most being from category 4) serve not only as a useful introduction of the principles of SAR mining but also to benchmark other resources. A disadvantage is that, as USPTO publications, these can lag some time behind the surfacing of WOs. For example, the most recent in the list, US9199947 published on Dec. 1, 2015, was first published as

Patent: (prefix with "US" like US6078908) Search

Patent	Data	Patent Title	Organization	Deposition
US9199947	140	Biaryl-propionic acid derivatives and their use as pharmaceuticals	Sanofi	09/20/16
US9199927	112	Guanidinobenzoic acid compound	Astellas Pharma Inc.	09/20/16
US9199944	155	N2,N4-bis(4-(piperazine-1-yl)phenyl)pirimidine-2,4-diamine derivative or pharmaceutically acceptable salt thereof, and composition containing same as active ingredient for preventing or treating cancer	KOREA RESEARCH INSTITUTE OF CHEMICAL TECHNOLOGY	09/20/16
US9199949	11	Selective glycosidase inhibitors and uses thereof	Alectos Therapeutics Inc.; Merck Sharp & Dohme Corp.	09/20/16
US9193689	18	3-aryl-5-substituted-isoquinolin-1-one compounds and their therapeutic use	INSTITUTE OF CANCER RESEARCH: ROYAL CANCER HOSPITAL (THE)	09/19/16
US9187487	46	Azaindole derivatives as tyrosine kinase inhibitors	PRINCIPIA BIOPHARMA, INC.	09/19/16
US9192603	67	Heterocyclic sulfone mGluR4 allosteric potentiators, compositions, and methods of treating neurological dysfunction	Vanderbilt University	09/19/16
US9193697	39	Oxazole derivatives useful as modulators of FAAH	MERCK SHARP & DOHME CORP.	09/19/16
US9193736	311	PDE 10a inhibitors for the treatment of type II diabetes	Janssen Pharmaceutica, NV	09/19/16
US9193762	57	Selective inhibitors of prolylcarboxypeptidase	UNIVERSITY OF MISSISSIPPI	09/19/16

Fig. 3 Entries from the BindingDB patent extraction page. The numbers under the "Data" column are measurement counts. Each of these has a PubChem CID derived either from a BindingDB submission (as an SID) or it matches a preexisting CID from another source. The majority are unique within this patent set, but there is some multiplexing for dual values (e.g., K_i and EC_{50}) or multiple target cross-screens.

WO2014154727 on Feb. 2, 2014. However, since it is the availability of the CWU structures that make this pipeline possible in the first place, WO documents cannot be used. As a first look at the set, we can plot the number of compounds per document to display the SAR distribution (Fig. 4).

The most common first-pass strategy is to search by target name. However, as we can see in the list, the use of unambiguous protein names by applicants is patchy and titles such as "Chemical compounds" (US9156831) immediately present the false-negative problem. Notwithstanding, in this case cell proliferative disorders are mentioned in the abstract, the description goes on to specify PI3K-α and PI3K-δ, and BindingDB curation has resolved the activities against PIK3CA, P42336. We can move on to the question "how many BACE1 patents can we find in this list?" Note that the BindingDB has already resolved the targets during their triage (i.e., there are 8030 records linked to BACE1, mostly from papers), but in this case we can use the text query to illustrate general principles of patent retrieval.

The results in Table 2 indicate some of the obstacles to target name resolution. An initial test with "BACE1" gave only four matches. A stemming variation "BACE" gave 17 matches but only to the 14 records in Table 2. It happens that BACE is both a synonym for BACE1 and a common stem for the paralogous pair of BACE1 and BACE2. Importantly for SAR aspects, these two are both targets for Alzheimer's disease and type 2 diabetes, respectively,[4] and are also sometimes used in reciprocal cross-screening (thus expanding the SAR). Hence "BACE" not only conveniently picks up all the BACE1 single-target filings but also US8754075 and US8748418 as "and/or" double-target filings.[14] We also find US8541427 that uses an incorrectly hyphenated BACE-1 as symbol. However, "BACE" misses two false-negatives that, from testing the common synonyms, we can retrieve with "beta-secretase" and "memapsin 1." The latter is a synonym for BACE2 which makes US9096541 nominally the only BACE2 single-target filing in this set, but the data also include BACE1 cross-screening results. With the proviso of needing a registration log-in, BindingDB facilitates the full download of SAR sets. An example is shown in Table 3.

Importantly, these can be related to their positions in the patent document and detailed connectivity information is available in the BindingDB entry (Figs. 5 and 6).

The utility of this "precooked" SAR is clear. However, if significant downstream effort is going to be invested in the data set (e.g., modeling and/or synthesis), it is prudent to cross-check extractions (from any source in fact) against the original document. In this case, US8748418 reveals 28 examples in the patent in Table 1, thus indicating the 53 BindingDB records have both BACE1 and BACE2 assay results as the SAR set. We can now compare this with a CNER source.

3.19.7 Patent Chemistry in SureChEMBL

In a relatively short space of time, SureChEMBL[13] has become the major public source of chemistry from patents since it had accumulated 17.25 million structures by the end of Aug. 2016 (as indexed in UniChem[15]).This not only offers advantages of scale but also speed because in situ (i.e., without the lag time associate with feeding-on to other databases such as UniChem or PubChem) chemistry from an individual patent document is downloadable within days of publication. The main limitation is that the primary relationship capture is only D–C. This means that users have to connect A–R–P data for the collation of SAR.

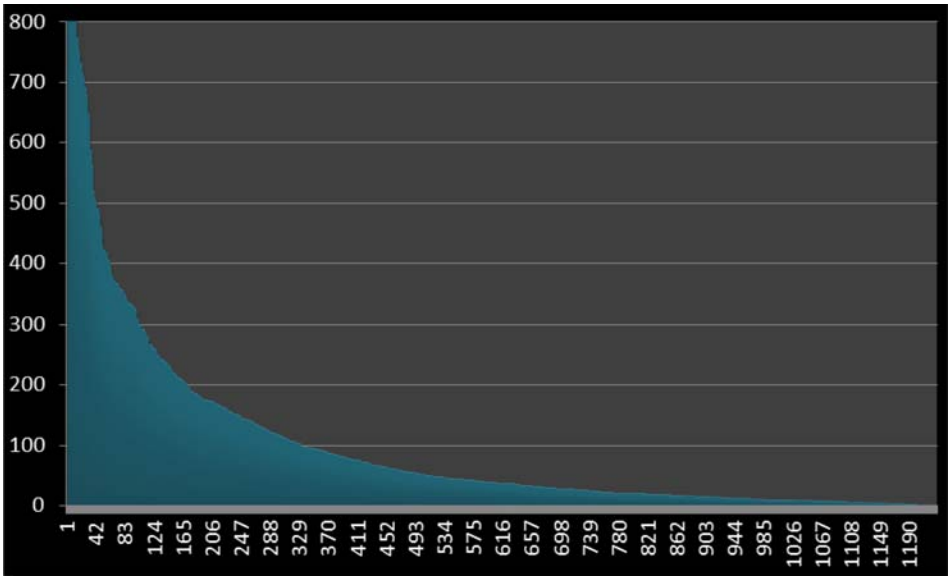

Fig. 4 1218 curated patent documents from BindingDB (horizontal axis) ranked by number of compounds × activities (the 14 with over 800 were truncated out of the vertical axis range). Over 80% have 20 or more SAR records and nearly 30% include at least 100. (Note: the average measurement record per patent of 98 is comparable to the GOSTAR nonredundant count of 65 structures per patent.)

Table 2 Entries from BindingDB patents that can be retrieved by related target names

Patent	*Data*	*Patent title*	*Organization*	*Deposition*
US9181236	290	2-Spiro-substituted iminothiazines and their mono-and dioxides as bace inhibitors, compositions, and their use	Merck Sharp & Dohme Corp.	08/29/2016
US8865911	180	Compounds and their use as BACE inhibitors	Astrazeneca AB	04/06/2015
US8754075	87	1,3-Oxazines as BACE1 and/or BACE2 inhibitors	Hoffmann-La Roche Inc.	11/11/2014
US8748418	53	1,4-Oxazepines as BACE1 and/or BACE2 inhibitors	Hoffmann-La Roche Inc.	11/11/2014
US8541427	45	Phenyl-substituted 2-imino-3-methyl pyrrolo pyrimidinone compounds as BACE-1 inhibitors, compositions, and their use	Merck, Sharp & Dohme, Corp.	11/26/2013
US9000182	41	2*H*-imidazol-4-amine compounds and their use as BACE inhibitors	AstraZeneca AB	10/19/2015
US9145426	38	Pyrrolidine-fused thiadiazine dioxide compounds as BACE inhibitors, compositions, and their use	Merck Sharp & Dohme Corp.	06/13/2016
US9000184	31	Cyclohexane-1,2′-naphthalene-1′,2″-imidazol compounds and their use as BACE inhibitors	AstraZeneca AB	10/19/2015
US9067924	24	1,4-Thiazepines/sulfones as BACE1 and/or BACE2 inhibitors	Hoffmann-La Roche Inc.	02/22/2016
US9000183	21	Cyclohexane-1,2′-indene-1′,2″-imidazol compounds and their use as BACE inhibitors	Astrazeneca AB	10/19/2015
US8940748	21	Iminothiadiazine dioxide compounds as BACE inhibitors, compositions, and their use	Merck Sharp & Dohme Corp.	06/16/2015
US9000185	18	Cycloalkyl ether compounds and their use as BACE inhibitors	AstraZeneca AB	10/19/2015
US8703785	9	2-Aminopyrimidin-4-one and 2-aminopyridine derivatives both having BACE1-inhibiting activity	Shionogi & Co., Ltd.	10/14/2014
US9029367	5	BACE inhibitors	Eli Lilly and Company	11/16/2015
Synonym matches				
US9096541	28	Inhibition of memapsin 1 cleavage in the treatment of diabetes	Oklahoma Medical Research Foundation; Purdue Research Foundation	03/28/2016
US8637504	37	Sulfur-containing heterocyclic derivative having beta-secretase inhibitory activity	Shionogi & Co., Ltd.	08/22/2014

The first 14 rows are matches for "BACE," ranked by compound count. The last two rows are matches to "memapsin" and "beta-secretase."

Table 3 Selected structure-to-activity records from US8748418

BindingDB MonomerID	*BindingDB Ligand Name*	*Target Name Assigned by Curator or DataSource*	*IC_{50} (nM)*	*PubChem CID*
123867	US8748418, 12	Beta-secretase 2 (BACE2)	5	68307545
123862	US8748418, 6	Beta-secretase 2 (BACE2)	11	60194542
123857	US8748418, 1	Beta-secretase 2 (BACE2)	24	66547140
123869	US8748418, 14	Beta-secretase 2 (BACE2)	28	66547488
123864	US8748418, 8	Beta-secretase 2 (BACE2)	30	66547317
123862	US8748418, 6	Beta-secretase 1	30	60194542
123858	US8748418, 2	Beta-secretase 2 (BACE2)	35	66547141
123858	US8748418, 2	Beta-secretase 1	40	66547141
123870	US8748418, 15	Beta-secretase 1	40	66547492
123870	US8748418, 15	Beta-secretase 2 (BACE2)	58	66547492
123857	US8748418, 1	Beta-secretase 1	70	66547140

The complete table of 53 rows and a detailed set of columns was edited down to just the columns and rows below and ranked by IC_{50}.

As an example we can compare what SureChEMBL extracted from US8748418 where we have just located the SAR series manually extracted by BindingDB. One of the many routes to query SureChEMBL is shown in **Fig. 7**.

We can download a table of the entire (i.e., unfiltered and redundant counts) chemistry records that SureChEMBL has extracted from US8748418 by a combination of n2s, i2s, and CWU molfiles. This gives 876 rows. Extending this to all the family members increases to 1581. We thus see the main advantage of CNER in presenting what is probably close to total chemistry extraction. The important proviso is that achieving this is dependent on preprocessed patent text and image quality. The problem is that a priori from the download we cannot directly establish which of these have any SAR (i.e., could correspond to the 28 examples that BindingDB has already identified). Notwithstanding, this can be done manually within SureChEMBL by scrolling though the automatic mark-up of **Table 1** in the document (i.e., each of the 28 images in this case). Insights into CNER output can be discerned in **Table 3**.

TABLE 1

IC_{50} values of selected examples

Ex.	Structure	BACE1 IC_{50} [μM]	BACE2 IC_{50} [μM]
1	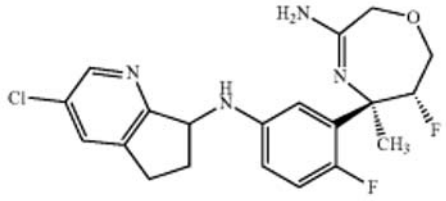	0.070	0.024
2	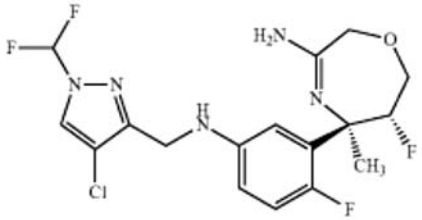	0.040	0.035

Fig. 5 Original SAR data from US8748418 aligned with the example images and IC_{50} data from page 32 of the PDF. Example 1 = BindingDB 123857 = US8748418, 1 = CID 66547140. For Example 2 = BindingDB 123858 = US8748418, 2 = CID 66547141.

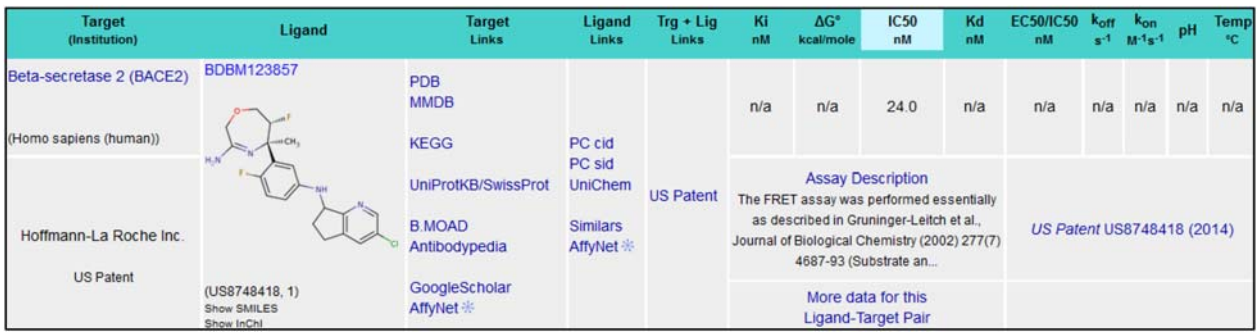

Fig. 6 The database entry for BindingDB 123857. The IC_{50} is specified along with a citation for the assay. In addition, many outlinks are presented such as the protein target in UniProt, the patent document (in Google and the USPTO portal), and the structure in PubChem (PC CID = CID 66547140).

The key points are:

- Multiple extractions of the same structure have been made from the four family members.
- The n2s and i2s are concordant (i.e., alternative extractions produce the same ID).
- For the US application (A1) and grant (B2), the intra-document count was eight, split between two different IUPACs and one image.
- The EP and WO missed one conversion (probably an image).
- The "corpus count" across all of SureChEMBL provides a reassuring inter-document consensus for this particular structure.
- Manual inspection of the documents confirms the statistics of the data download in that Roche have exemplified their active series eight times.
- This seems unusually high but we have no overall statistics to test this.

The useful aspect of this example is that, using foreknowledge of the BindingDB extraction (albeit done at a later date) we can explore multiple ways of discerning the correct SAR series. One of these is via the corpus count shown in Fig. 8.

The corpus count distribution of US8748418 shows the pros and cons of CNER pipelines in general. The problem is that most of the processing effort goes into the continual reextraction of frequently specified compounds (e.g., methanol occurs 7.2 million times across the SureChEMBL corpus and the name match finds 0.9 million documents). This is not to say that the statistics of common chemistry do not have utility for certain applications (e.g., surveying synthetic trends[16]), but these extractions can swamp

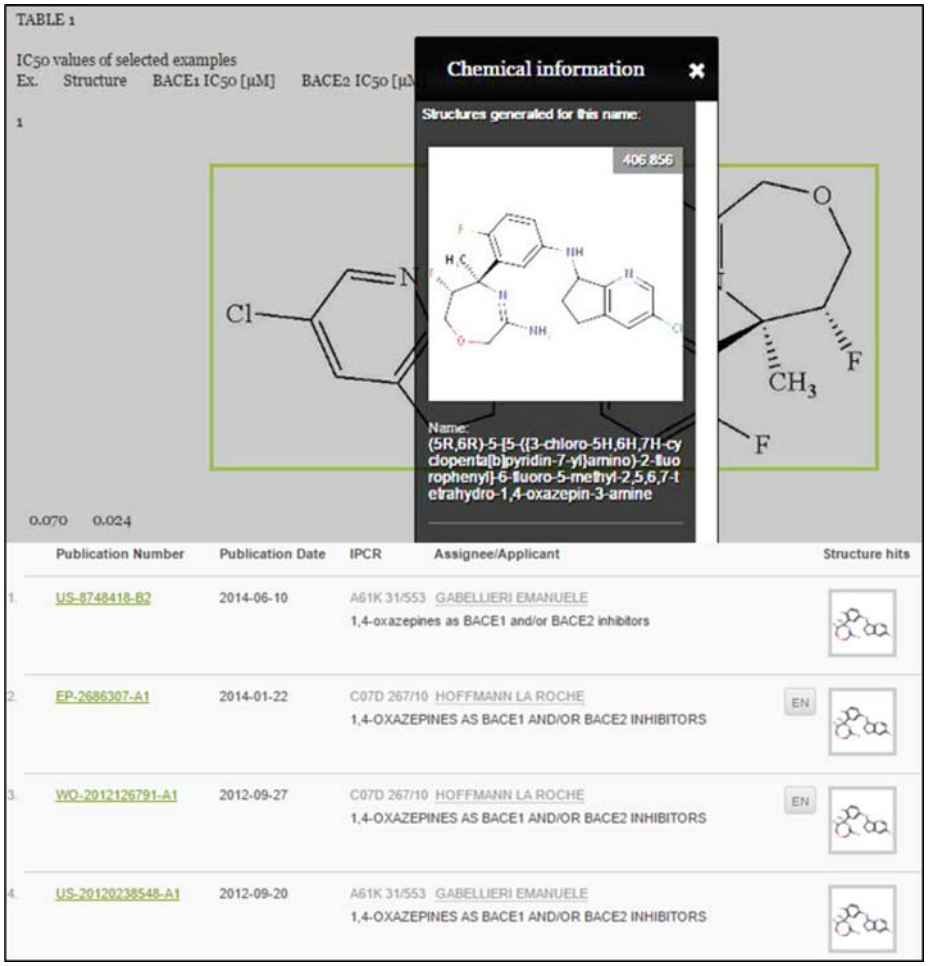

Fig. 7 SureChEMBL queries related to the BindingDB 123857 structure. The *upper panel* shows the result of an exact-match structure search. This gives nine intradocument matches, one of which an image-conversion (corresponding to **Fig. 5**) with the IC_{50} values in the lower left. The *lower panel* shows the interdocument matches across four family members.

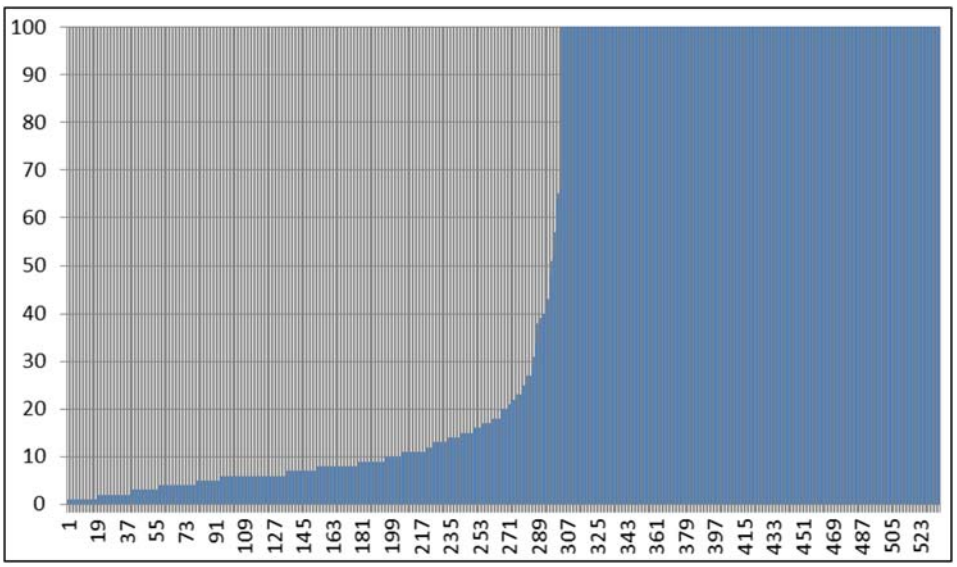

Fig. 8 A plot of the corpus count (the vertical axis, truncated at 100 occurrences) for the nonredundant SureChEMBL chemistry download for US8748418.

out the bioactives. However, the leftmost section of Fig. 8 indicates that lower corpus counts probably represent (a) novel structures and (b) encompass the SAR series. However, while from Table 3 we might expect 17 to be an SAR-specific cut-off, it turns out that the occurrences from 10 to 20 form a continuum of approximately 70 structures rather than a clean set. However, a key feature of SureChEMBL is the ability to filter downloads as shown in Fig. 9.

Toggling these settings can be complemented by further postdownload filtering (e.g., removing SureChEMBL ID duplicates and selecting occurrence ranges in the description section) to enrich for an SAR series. However, even with these options we are still left with 96 structures (i.e., within which should be the 28 we would like to identify). The caveat with Mw filtering is that it may encompass larger intermediates that are still novel structures but for which no bioactivity was reported. Corpus counting has the caveat that low frequencies of one or two (i.e., well below the document family count) may be chemically plausible structures but could represent artifactual extractions.

Regardless of the challenge of isolating an explicit SAR-linkable set, the facility to download patent chemistry extractions in SureChEMBL is powerful. There are, however, complementary ways to approach the isolation problem that can be revealed by manual inspection of context within the document. We have already seen this with the straightforward identification of the image structures and IC_{50} data in Table 1 of the patent. A second useful option is to simply browse the SureChEMBL mark-up and thereby spot sets of structures that look as though they could be matched to activity tables. An example of this is shown in Fig. 10 for US8748418.

The ability to identify such large sections in patent mark-up (either as a *blue*-highlighted IUPAC strings and/or a *green* border around the images) is useful for both assessing the quality of extraction and delineating examples. In this case, the series is not numbered so we cannot reliably link the structures to the data table rows in any automated way. However, example assignments (e.g., Examples 1, 2, 3, etc.) can be found further down in the synthesis descriptions and thus manually collated via the compound displays. This example thus shows both the generic problem for SAR-digging and the solution via manual collation. Additional ways of establishing these structure-to-data links will be shown later.

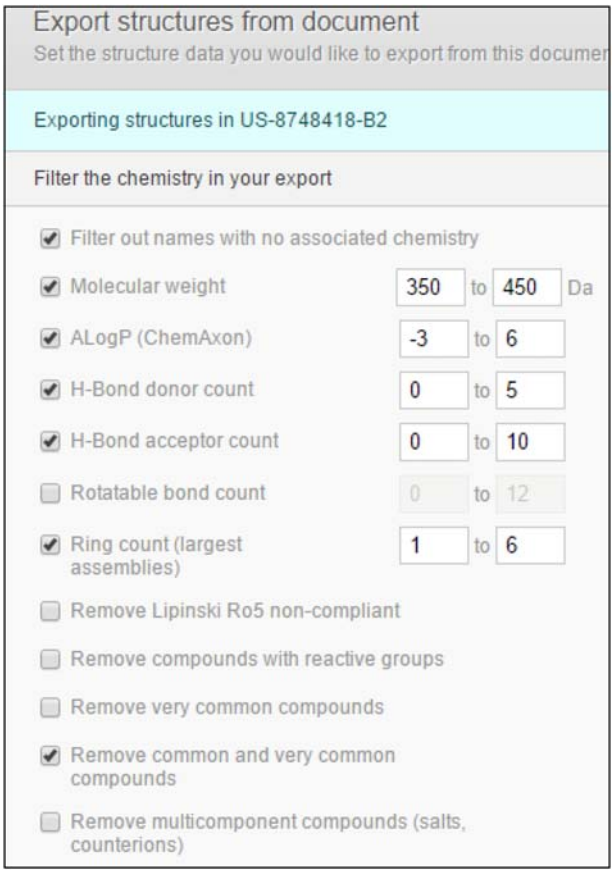

Fig. 9 SureChEMBL chemistry export filters for individual patent documents or whole family extractions. Note the default Mw window is 300–700, but this was narrowed down since we have established that SCHEMBL12273617 (CID 66547140) has an Mw of 407.

One embodiment of the invention is a compound of formula I, selected from the group consisting of

- [3-((5R,6R)-3-Amino-6-fluoro-5-methyl-2,5,6,7-tetrahydro-[1,4]oxazepin-5-yl)-4-fluoro-phenyl]-(3-chloro-6,7-dihydro-5H-[1]pyrindin-7-yl)-amine,
- (5R,6R)-5-{5-[(4-Chloro-1-difluoromethyl-1H-pyrazol-3-ylmethyl)-amino]-2-fluoro-phenyl}-6-fluoro-5-methyl-2,5,6,7-tetrahydro-[1,4]oxazepin-3-ylamine,
- (5R,6R)-6-Fluoro-5-[2-fluoro-5-(tetrahydro-furan-3-ylamino)-phenyl]-5-methyl-2,5,6,7-tetrahydro-[1,4]oxazepin-3-ylamine,
- (5R,6R)-6-Fluoro-5-[2-fluoro-5-(tetrahydro-pyran-3-ylamino)-phenyl]-5-methyl-2,5,6,7-tetrahydro-[1,4]oxazepin-3-ylamine,
- (5R,6R)-6-Fluoro-5-[2-fluoro-5-(tetrahydro-pyran-4-ylamino)-phenyl]-5-methyl-2,5,6,7-tetrahydro-[1,4]oxazepin-3-ylamine,
- (R)-5-[5-(6-Chloro-2,3-dihydro-benzofuran-3-ylamino)-2-fluoro-phenyl]-6,6-difluoro-5,7,7-trimethyl-2,5,6,7-tetrahydro-[1,4]oxazepin-3-ylamine,
- (R)-5-[5-(6-Chloro-pyridin-3-ylamino)-2-fluoro-phenyl]-6,6-difluoro-5,7,7-trimethyl-2,5,6,7-tetrahydro-[1,4]oxazepin-3-ylamine,
- (R)-5-{5-[(4-Chloro-1-difluoromethyl-1H-pyrazol-3-ylmethyl)-amino]-2-fluoro-phenyl}-6,6-difluoro-5-methyl-2,5,6,7-tetrahydro-[1,4]oxazepin-3-ylamine,
- (R)-5-{5-[(4-Chloro-1-difluoromethyl-1H-pyrazol-3-ylmethyl)-amino]-2-fluoro-phenyl}-5-ethyl-6,6-difluoro-2,5,6,7-tetrahydro-[1,4]oxazepin-3-ylamine,
- (R)-6,6-Difluoro-5-[2-fluoro-5-(1-methyl-1H-pyrazol-3-ylamino)-phenyl]-5,7,7-trimethyl-2,5,6,7-tetrahydro-[1,4]oxazepin-3-ylamine,
- (R)-6,6-Difluoro-5-[2-fluoro-5-(4-fluoro-phenylamino)-phenyl]-5,7,7-trimethyl-2,5,6,7-tetrahydro-[1,4]oxazepin-3-ylamine,
- (R)-6,6-Difluoro-5-[2-fluoro-5-(5-fluoro-pyridin-3-ylamino)-phenyl]-5,7,7-trimethyl-2,5,6,7-tetrahydro-[1,4]oxazepin-3-ylamine,
- (R)-6,6-Difluoro-5-[2-fluoro-5-(5-trifluoromethyl-pyridin-3-ylamino)-phenyl]-5,7,7-trimethyl-2,5,6,7-tetrahydro-[1,4]oxazepin-3-ylamine,
- (R)-6,6-Difluoro-5-[2-fluoro-5-(6-methoxy-pyridin-3-ylamino)-phenyl]-5,7,7-trimethyl-2,5,6,7-tetrahydro-[1,4]oxazepin-3-ylamine,
- (R)-6,6-Difluoro-5-[2-fluoro-5-(6-methyl-pyridin-3-ylamino)-phenyl]-5,7,7-trimethyl-2,5,6,7-tetrahydro-[1,4]oxazepin-3-ylamine,
- (R)-6,6-Difluoro-5-[2-fluoro-5-(pyridin-3-ylamino)-phenyl]-5,7,7-trimethyl-2,5,6,7-tetrahydro-[1,4]oxazepin-3-ylamine,
- (R)-7-[3-((R)-3-Amino-6,6-difluoro-5,7,7-trimethyl-2,5,6,7-tetrahydro-[1,4]oxazepin-5-yl)-4-fluoro-phenylamino]-6,7-dihydro-5H-[1]pyrindine-3-carbonitrile,
- (R)-7-[5-((R)-3-Amino-6,6-difluoro-5,7,7-trimethyl-2,5,6,7-tetrahydro-[1,4]oxazepin-5-yl)-2,4-difluoro-phenylamino]-6,7-dihydro-5H-[1]pyrindine-3-carbonitrile,
- (S)-7-[3-((R)-3-Amino-6,6-difluoro-5,7,7-trimethyl-2,5,6,7-tetrahydro-[1,4]oxazepin-5-yl)-4-fluoro-phenylamino]-6,7-dihydro-5H-[1]pyrindine-3-carbonitrile,
- [3-((R)-3-Amino-6,6-difluoro-5,7,7-trimethyl-2,5,6,7-tetrahydro-[1,4]oxazepin-5-yl)-4-fluoro-phenyl]-(3-chloro-6,7-dihydro-5H-[1]pyrindin-7-yl)-amine,
- [3-((R)-3-Amino-6,6-difluoro-5,7,7-trimethyl-2,5,6,7-tetrahydro-[1,4]oxazepin-5-yl)-4-fluoro-phenyl]-(6-chloro-2,3-dihydro-furo[3,2-b]pyridin-3-yl)-amine,
- [3-((R)-3-Amino-6,6-difluoro-5-methyl-2,5,6,7-tetrahydro-[1,4]oxazepin-5-yl)-4-fluoro-phenyl]-((S)-3-chloro-6,7-dihydro-5H-[1]pyrindin-7-yl)-amine,
- [3-((R)-3-Amino-6,6-difluoro-5-methyl-2,5,6,7-tetrahydro-[1,4]oxazepin-5-yl)-4-fluoro-phenyl]-((R)-3-chloro-6,7-dihydro-5H-[1]pyrindin-7-yl)-amine,
- 4-[3-((R)-3-Amino-6,6-difluoro-5-methyl-2,5,6,7-tetrahydro-[1,4]oxazepin-5-yl)-4-fluoro-phenylamino]-benzonitrile,
- 8-[3-((R)-3-Amino-6,6-difluoro-5,7,7-trimethyl-2,5,6,7-tetrahydro-[1,4]oxazepin-5-yl)-4-fluoro-phenylamino]-5,6,7,8-tetrahydro-quinoline-3-carbonitrile,
- (S)-7-[5-((R)-3-Amino-6,6-difluoro-5,7,7-trimethyl-2,5,6,7-tetrahydro-[1,4]oxazepin-5-yl)-2,4-difluoro-phenylamino]-6,7-dihydro-5H-[1]pyrindine-3-carbonitrile, and
- (R)-6,6-Difluoro-5-{2-fluoro-5-[6-(2,2,2-trifluoro-ethoxy)-pyridin-3-ylamino]-phenyl}-5,7,7-trimethyl-2,5,6,7-tetrahydro-[1,4]oxazepin-3-ylamine, or a pharmaceutical acceptable salt thereof.

Fig. 10 List of IUPAC names from page 11 of the US8748418 PDF. The unbroken *blue* highlighting means that SureChEMBL has made a successful IPUAC conversion to a structure in each of the 27 cases and they would thus be included in the download. In addition, each one has a link to information about the structure (as shown in **Fig. 7**).

3.19.8 Target Searching in SureChEMBL

Having looked at target-specific retrieval in BindingDB, we can compare this to searching the much larger patent set in SureChEMBL. It is also important to understand the major difference between these resources. The latter has indexed the full content of the documents, whereas BindingDB only indexes what has been expert selected (but this includes the target name, UniProt ID, quantitative affinity values, etc.). We can look at a configured query in the SureChEMBL interface (**Fig. 11**).

The filters in **Fig. 11** were selected primarily for specificity rather than recall (i.e., to give a good yield of true-positives). The first filter is the HGNC gene symbol and two common protein synonyms as described for the BindingDB search in **Table 2**. We have used C07D as the second select but we can skip A61K in this case since we are already selecting a biological target. The third select is to search only the title and abstract rather than the entire text that could include false-positives as incidental mentions of the target. The fourth select is for WO as already described. The retrieval results are shown in **Fig. 12**.

Useful circumstantial information on SAR-likelihood can be gleaned from inspecting the retrieved title list even before opening up the individual documents (although less obvious aspects need some experience to be discerned). For example, we can see all three synonyms have been used by applicants and the patent titles appear to be true-positives. (Note: We did not need this for the BindingDB search since they were preselected.) It is also clear that we might have used "inhibitor" as another filter, but this could have an associated false-negative risk. As we could already see from BindingDB, this larger result set confirms that BACE1 is a popular target since no less than five pharmaceutical companies are slugging it out even in just these 2016 publications. Another clue we can pick up is that Merck have a secondary filing as "crystalline forms" which, by implication, should connect the structure back to an earlier novel active series that might include SAR. As an additional context, we can also establish that both Merck and AstraZeneca

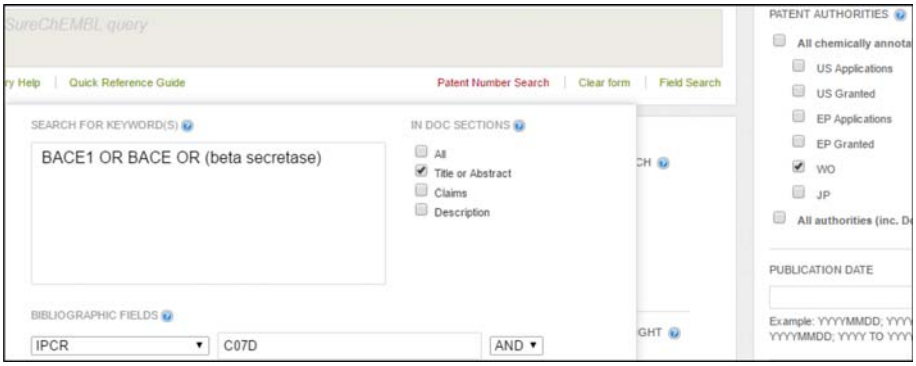

Fig. 11 A BACE1 target query in the SureChEMBL interface showing four filters, query string (main box) location (doc sections toggle) patent classification code (lower panel), and WO as patent authority (right hand panel).

	Publication Number	Publication Date	IPCR	Assignee/Applicant
1.	WO-2016096979-A1	2016-06-23	C07D 403/12	JANSSEN PHARMACEUTICA NV
			2,3,4,5-TETRAHYDROPYRIDIN-6-AMINE AND 3,4-DIHYDRO-2H-PYRROL-5-AMINE COMPOUND INHIBITORS OF BETA-SECRETASE	
2.	WO-2016075064-A1	2016-05-19	C07D 401/12	LUNDBECK & CO AS H
			2-AMINO-5,5-DIFLUORO-6-(FLUOROMETHYL)-6-PHENYL-3,4,5,6-TETRAHYDROPYRIDINES AS BACE1 INHIBITORS	
3.	WO-2016075063-A1	2016-05-19	C07D 401/12	LUNDBECK & CO AS H
			2-AMINO-6-(DIFLUOROMETHYL)- 5,5-DIFLUORO-6-PHENYL-3,4,5,6-TETRAHYDROPYRIDINES AS BACE1 INHIBITORS	
4.	WO-2016075062-A1	2016-05-19	C07D 401/12	LUNDBECK & CO AS H
			2-AMINO-3,5-DIFLUORO-3,6-DIMETHYL-6-PHENYL-3,4,5,6-TETRAHYDROPYRIDINES AS BACE1 INHIBITORS FOR TREATING ALZHEIMER'S DISEASE	
5.	WO-2016071211-A1	2016-05-12	C07D 513/04	HOFFMANN LA ROCHE
			BACE1 INHIBITORS	
6.	WO-2016055496-A1	2016-04-14	C07D 513/04	HOFFMANN LA ROCHE
			BACE1 INHIBITORS	
7.	WO-2016055858-A1	2016-04-14	C07D 263/52	ASTRAZENECA AB
			COMPOUNDS AND THEIR USE AS BACE INHIBITORS	
8.	WO-2016053767-A1	2016-04-07	A61P 25/28	MERCK SHARP & DOHME
			NOVEL CRYSTALLINE FORMS OF A BACE INHIBITOR, COMPOSITIONS, AND THEIR USE	
9.	WO-2016053828-A1	2016-04-07	C07D 513/14	MERCK SHARP & DOHME
			C5-C6-FUSED TRICYCLIC IMINOTHIADIAZINE DIOXIDE COMPOUNDS AS BACE INHIBITORS, COMPOSITIONS, AND THEIR USE	
10.	WO-2016044120-A1	2016-03-24	C07D 471/04	MERCK SHARP & DOHME
			DIAZINE-FUSED AMIDINE COMPOUNDS AS BACE INHIBITORS, COMPOSITIONS, AND THEIR USE	

Fig. 12 Results for a search in SureChEMBL with the selections specified in **Fig. 11**. Just the top-10 are shown from a total of 369 WO document hits.

have candidate BACE1 inhibitors still in clinical trials with Roche having had RG7129 in Phase 1 but terminated. We can thus infer that these recent filings from these three companies could include SAR from back-up and/or follow-on series for each of those clinical candidates. Roche have assigned identical titles to two different WO numbers that, by definition, should therefore include different chemistry claims (see IC_{50} search below).

Having assessed the titles we can focus on some of these documents to illustrate particular points. The trio of titles from Lundbeck seem worth investigating because, as mentioned in the introduction section, they could be a set of "D"s that have A–R–P in

common and where "C" is an extended series. This turns out to be the case, with the three filings including individual K_i data tables for 41, 14, and 19 structures. We can pick out the following aspects from this set:

- They present a complex set of patent families but further down in the hit list we can find a yet a forth SAR set of 48 structures with K_i results in WO2015124576 from a 2-amino-3,5,5-trifluoro-3,4,5,6-tetrahydropyridine series.
- SureChEMBL did a good job on all four sets. Notably, two had already appeared as US publications (e.g., WO2015124576 as US9353084 and WO2016075063 as US9346797) which, as expected, gave better extraction results.
- It turns out that WO2016075064 has unusual content. Firstly, there is a 3D crystal structure image of what was extracted as CID 121334268. This provides a configuration for the series but had no reported activity data. Secondly, examples 16 and 18 were deuterated. This confounds a standard CNER pipeline both because the i2s did not recognize "D-" and the text OCR missed the "-d3" (although the n2s would have converted it within an IUPAC string). To complete the SAR set, a chemical sketcher could be used to input the two deuterated compounds. (Note: It may also happen that when this filing eventually surfaces at the USPTO the deuterated images will be linked to the document as molfiles via CWU processing.)

3.19.9 Tools for Stand-Alone Extraction

There are several options to collate SAR from US9346797 but this needs the example numbers to be matched to the data table on page 30 of the PDF. Analogs to the conversions of the example list indicated in Fig. 10, the sets are visible in SureChEMBL but in this case the applicants have usefully numbered them to match the K_i values that the document processing has extracted as text. While the SureChEMBL document chemistry export (at default filter settings) produced 114 rows that reduced to 55 unique structures, there was no easy way to isolate the 14 examples in the correct sequence. However, we can exploit the ordering by converting them extrinsically using a stand-alone operation. The resource of choice here was the open ChemAxon chemicalize resource that allows users to run n2s on text from a variety of sources an input formats.[17] In this case, an external webpage was made for batch conversion with just the 14 IUPACs pasted across from the SureChEMBL text. (Note: This may seem redundant since they have already been converted to structures but note that isolating just the selected strings and maintaining the order is important in this case.) The results are shown in Fig. 13.

One of the features of chemicalize is that we can download an SD file from the webpage extractions in which the extraction order is maintained. This can then be easily transformed using commercial packages or open resources such as OpenBabel.[18] Thus,

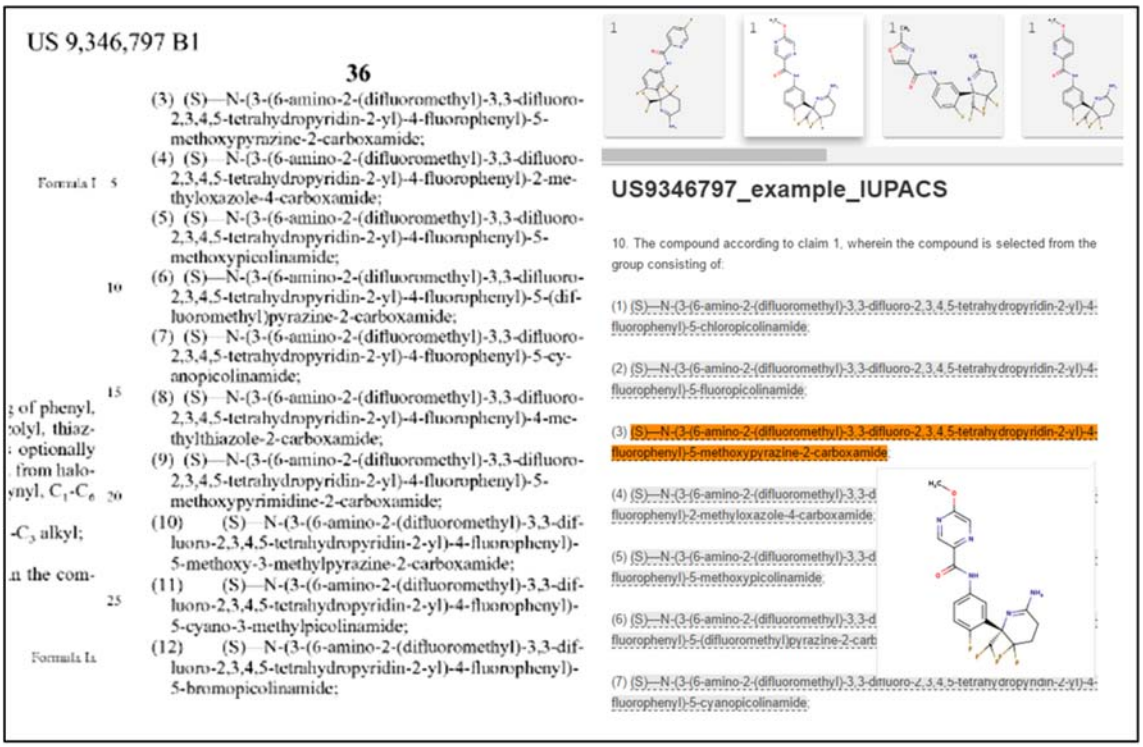

Fig. 13 The SAR series from US9346797 extracted using chemicalize. Page 36 from the patent PDF specifying the structure is shown on the left. On the right are the chemicalize webpage conversions of the same numbered examples pasted over in the same order. The IUPAC for example three is highlighted in *orange* which also displays the ChemAxon structure rendering on mouse-over.

a combination of using SureChEMBL, chemicalize.org together with some manual collation and cross-checking against the original PDFs to tie things together, we can generate a complete K_i SAR set for the 96 tetrahydropyridines.

Cases where SAR extraction presents more of challenge include the most recent in the Fig. 12 set, WO2016096979 from the Janssen team in Spain. We can quickly find SAR in the form of two different assays already log transformed to pIC_{50}s cross-referenced against 33 compound numbers. Here again the OCR does a sufficiently good job on the data table to be copied over to Excel with the rows staying in register and the greater than signs as we can see in Fig. 14 (even though the out-of-range results might be rejected for model building).

However, the failure of many of the ChEMBL chemistry conversions indicated that, compared to what we have looked at so far, it would not be straightforward to resolve compounds to match the numbers in the data table (Fig. 15).

Inspection of the SureChEMBL output establishes that text quality had confounded the n2s algorithms. The extraction problems in this document were compounded by the i2s introducing an artifactual iodine from converting the B7 image (unfortunately now permanently enshrined in CID 121433102). One option would be wait for the US patent to surface with improved conversions. However, we can see the original document contains the necessary information we need for SAR collation but arranged in a somewhat complex way (e.g., example numbers are nested intermediates for the compound numbers that are also depicted in Markush tables). Below is the SureChEMBL text associate with compound 19 from Fig. 16, where the obvious OCR errors are marked in *red*.

N-r3-r(26′,3i?)-5-amino-2-methyl-3-(trifluoromethyl)-3,4-dihvdropyrrol-2-yl1-4-fluoro-phenyl1-5-chloro-pyridine-2-carboxamide.

The tool we can use for stand-alone n2s is the open parser for systematic IUPAC nomenclature (OPSIN).[19] While the web interface is only suitable for small numbers of conversions, it has the advantage over chemicalize of presenting error notifications and also allowing trial-and-error iterative editing of the input text. By this means we can correct the compound 19 string from the incorrect one above to one that converts successfully.

With some editing it now becomes possible to generate compound 15 as the "flat" chloropicolinoamide as well as specifying the resolved enantiomers for 19 and 20 by editing the IUPAC S/R prefixes. To demonstrate another useful open tool set we can corroborate the i2s from the left-hand side of Fig. 15 by using the Optical Structure Recognition Application (OSRA) (Fig. 17).

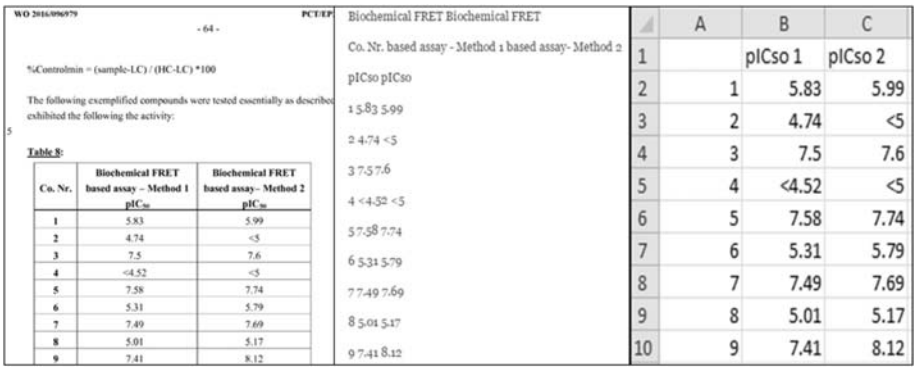

WO 2016/096979 PCT/EP

- 64 -

%Controlmin = (sample-LC) / (HC-LC) *100

The following exemplified compounds were tested essentially as describe exhibited the following the activity:

Table 8:

Co. Nr.	Biochemical FRET based assay – Method 1 pIC_{50}	Biochemical FRET based assay– Method 2 pIC_{50}
1	5.83	5.99
2	4.74	<5
3	7.5	7.6
4	<4.52	<5
5	7.58	7.74
6	5.31	5.79
7	7.49	7.69
8	5.01	5.17
9	7.41	8.12

Biochemical FRET Biochemical FRET

Co. Nr. based assay - Method 1 based assay- Method 2

pICso pICso

1 5.83 5.99

2 4.74 <5

3 7.5 7.6

4 <4.52 <5

5 7.58 7.74

6 5.31 5.79

7 7.49 7.69

8 5.01 5.17

9 7.41 8.12

	A	B	C
1		pICso 1	pICso 2
2	1	5.83	5.99
3	2	4.74	<5
4	3	7.5	7.6
5	4	<4.52	<5
6	5	7.58	7.74
7	6	5.31	5.79
8	7	7.49	7.69
9	8	5.01	5.17
10	9	7.41	8.12

Fig. 14 Three versions of the SAR table from WO2016096979. On the left is the original from page 64 of the PDF. In the center is the corresponding section of the SureChEMBL mark-up. The right hand panel is an Excel paste-across of the center section.

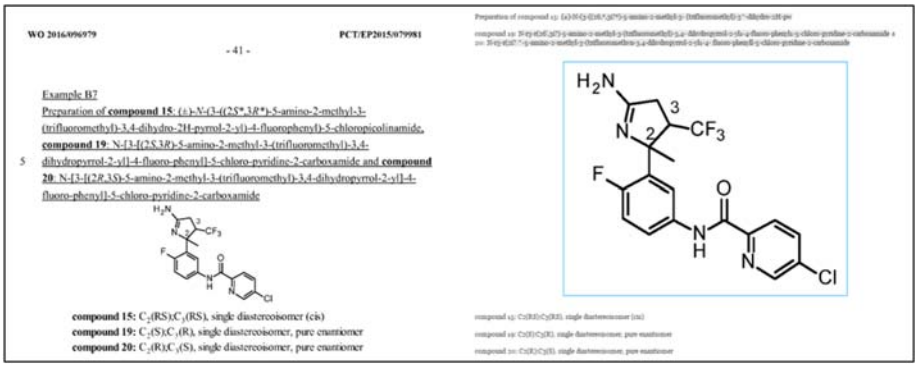

WO 2016/096979 PCT/EP2015/079981

- 41 -

Example B7

Preparation of **compound 15**: (±)-*N*-[3-[(2*S**,3*R**)-5-amino-2-methyl-3-(trifluoromethyl)-3,4-dihydro-2H-pyrrol-2-yl]-4-fluorophenyl]-5-chloropicolinamide, **compound 19**: *N*-[3-[(2*S*,3*R*)-5-amino-2-methyl-3-(trifluoromethyl)-3,4-dihydropyrrol-2-yl]-4-fluoro-phenyl]-5-chloro-pyridine-2-carboxamide and **compound 20**: *N*-[3-[(2*R*,3*S*)-5-amino-2-methyl-3-(trifluoromethyl)-3,4-dihydropyrrol-2-yl]-4-fluoro-phenyl]-5-chloro-pyridine-2-carboxamide

compound 15: $C_1(RS),C_1(RS)$, single diastereoisomer (cis)
compound 19: $C_1(S),C_1(R)$, single diastereoisomer, pure enantiomer
compound 20: $C_1(R),C_1(S)$, single diastereoisomer, pure enantiomer

Fig. 15 Chemistry for one example in WO2016096979. The compounds associated with example B7 in the original PDF are shown on the left with the corresponding SureChEMBL section on the left. Note the "Highlight additional recognized chemical terms" option was toggled on. The consequent appearance of the *gray* highlighting indicates where the n2s recognized a potential name (i.e., an IUPAC-like text string) but could not generate a structure (in which case the highlighting would have been *blue*).

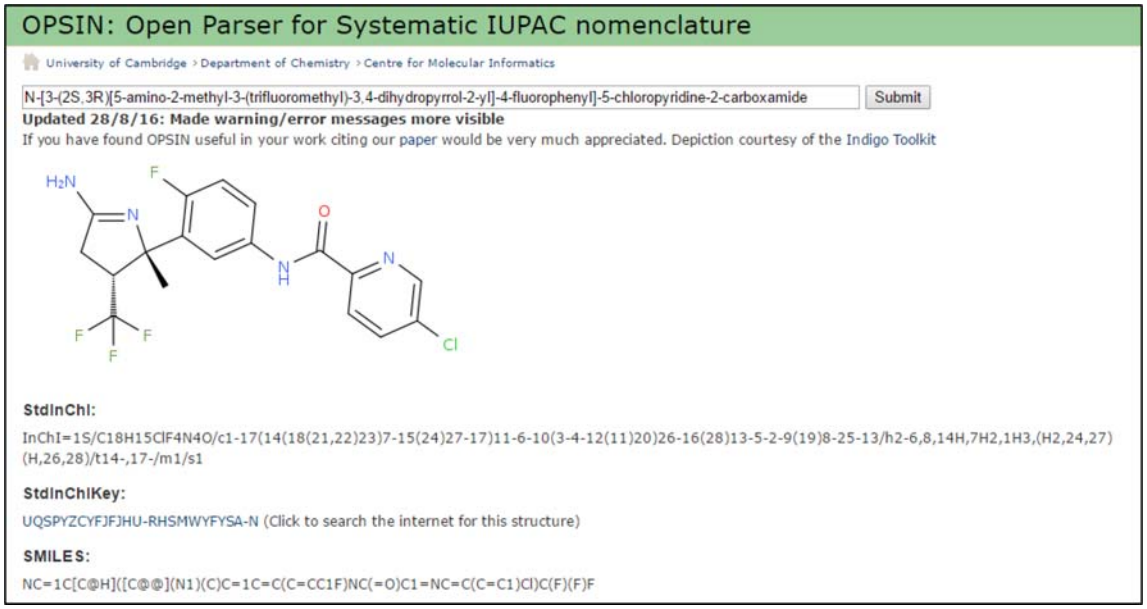

Fig. 16 Conversion of compound 19 from WO2016096979 using the OPSIN interface. The input (after editing corrections) was *N*-[3-(2*S*,3*R*)[5-amino-2-methyl-3-(trifluoromethyl)-3,4-dihydropyrrol-2-yl]-4-fluorophenyl]-5-chloropyridine-2-carboxamide.

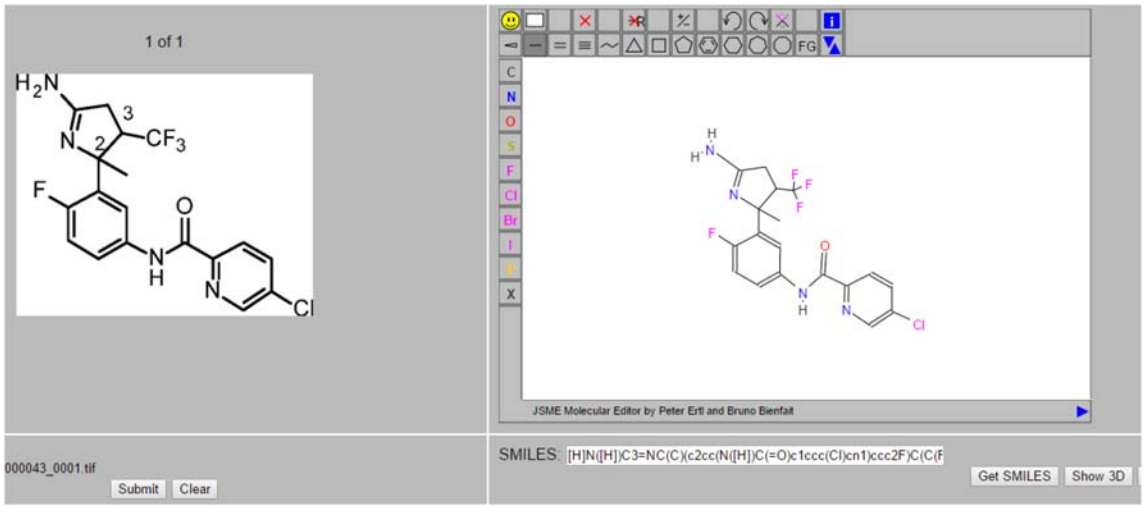

Fig. 17 The OSRA result for conversion of the downloaded image from **Fig. 15**. The SMILES output can be converted to the example 15 IUPAC of *N*-{3-[5-amino-2-methyl-3-(trifluoromethyl)-3,4-dihydro-2*H*-pyrrol-2-yl]-4-fluorophenyl}-5-chloropyridine-2-carboxamide.

This WO2016096979 example shows the synergies of working between the original document, the SureChEMBL output with the addition of the OPSIN and OSRA tools (chemicalize could also have utility here depending on individual preferences). While it has been said that collating the complete SAR set from these 33 examples, including the enantiomeric splits, would require some effort, the combined approach brings many other such "difficult" documents within practical reach of extractability. It is important to note that, due to partial failure of the SureChEMBL conversions, many of these examples will not be in PubChem.

3.19.10 Selecting for SAR

A particular advantage of full text indexing in resources such as SureChEMBL is that, regardless of the expected specificity issues, simple searches such as "IC_{50}" or "inhibitor" actually work (108,115 and 650,147 documents, respectively, with an AND union of 56,870). We can see a practical example in **Fig. 18**.

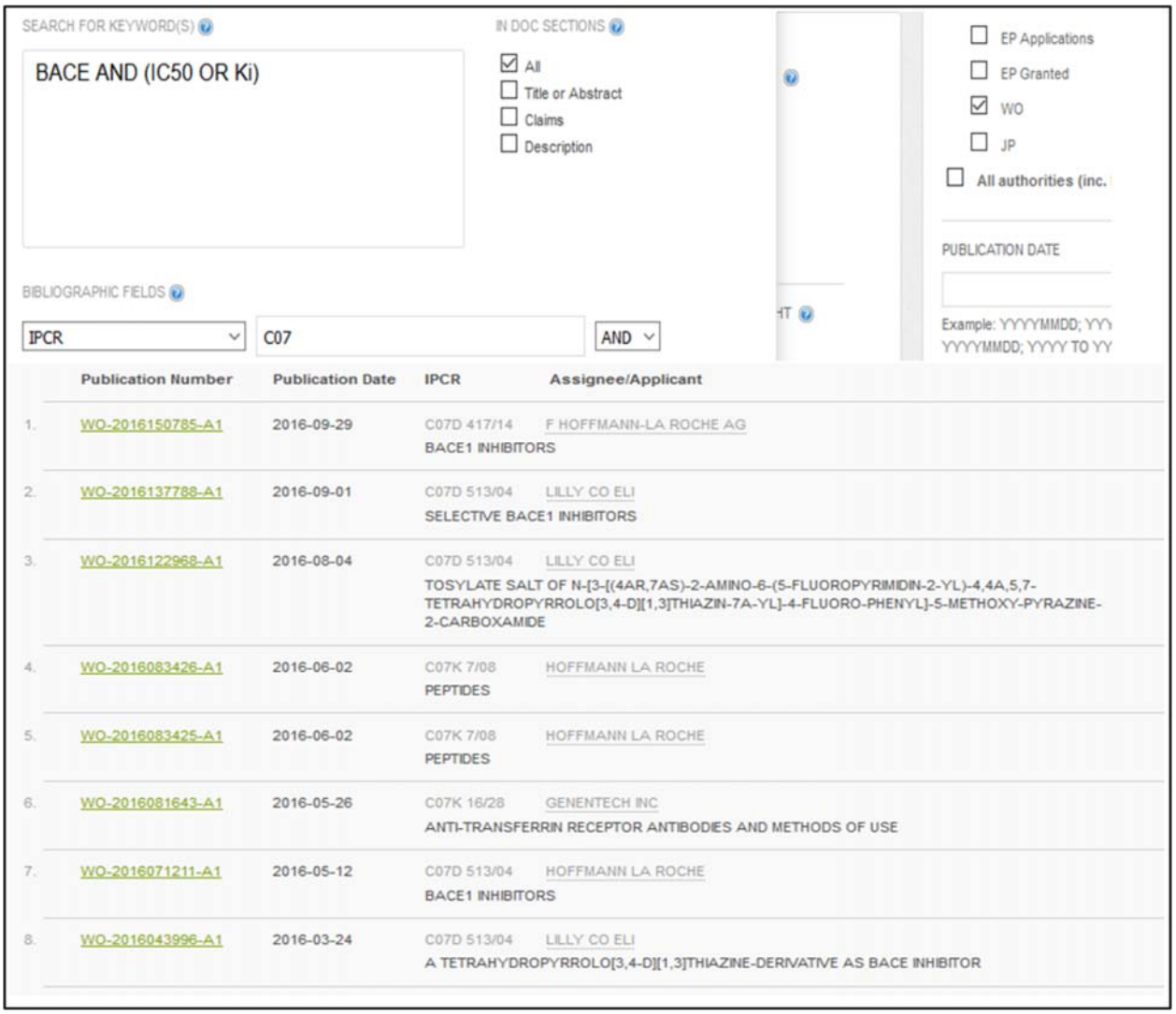

Fig. 18 The most recent matches (from 138 in total) SureChEMBL search with for matches to BACE1 and IC_{50} or K_i and C07 within WO documents.

We can see that Fig. 18 has matches in common with Fig. 12 and spot what seems a likely consecutive series from Roche as WO2016150785 and 4 months earlier WO2016071211 both titled "BACE1 inhibitors." Inspection reveals these to be true-positives with WO2016150785 having seven intradocument IC_{50} matches including "Table 1: IC_{50} values of selected examples." While there are only four intradocument matches in WO2016071211 and the result table is not numbered, we can pick out both tables. This Roche patent appears to be a true-positive for the IC_{50} trawl on the one hand, but may present borderline SAR value on the other. The first issue is data sparsity (compared with what we have seen so far) since in WO2016071211 only 12 of the 25 IC_{50} examples have data and in WO2016150785 its 38 from 44. We can also see signs of probable deliberate obfuscation in the use of confusing nested numbering systems. However, more serious issues we can immediately spot are difficulties for chemistry extraction, because the poor OCR has confounded most of the n2s (including extensive introduction of the notorious 1-to-l conversion errors). While the i2s has fared better in at least getting structures out, the multiple conversions from small images in the tables present a confusing picture. We can look at an example in Fig. 19.

We can follow these structures "back round" in the sense of mapping them back to their locations in the document (via PubChem or inside SureChEMBL). However, we see a peculiar pattern of stereo enumerations and "flat" structures that are matching multiple different example numbers (e.g., two and three are identical). The minimum parsimonious assumption is that these multiple mappings could be due to errors in the document. At the end of the day, this example can be seen as a cautionary tale. Thus, WO2016071211 would seem unreliable for SAR modeling and not worth spending time on with tools to try to sort things out. However, thanks to the SureChEMBL "efforts" we can at least see the series chemotype.

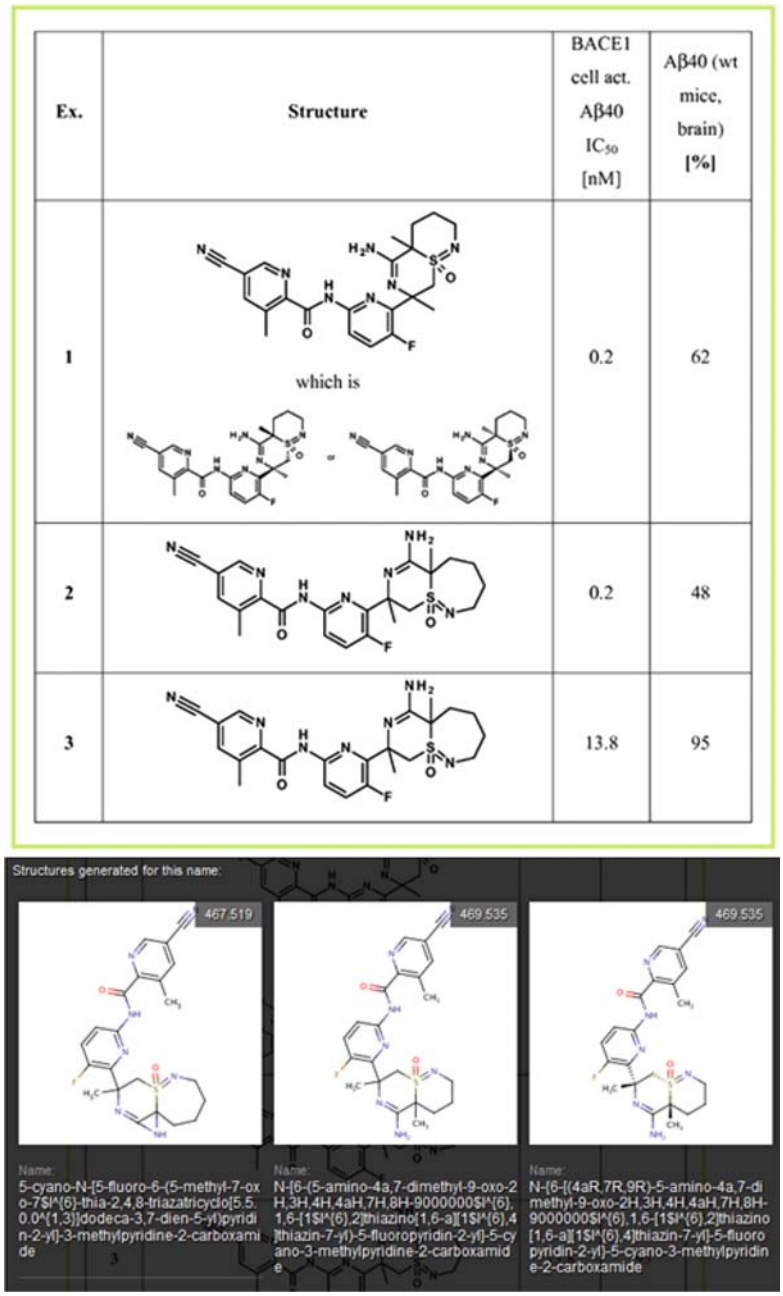

Fig. 19 The first three examples from **Table 1** in WO2016071211 are in the top panel. The SureChEMBL rendering is shown, with the *green* boarder signifying an intradocument search match. The image conversions from this section of the table have spawned the three structures in the lower panel (but not necessarily in order). From left to right in the panel these are in PubChem as CID 121329828, CID 121329766, and CID 121329765.

3.19.11 Connecting Between Patents and Papers via PubChem

Explorations of patent SAR naturally generate a range of questions with respect to the literature. The two basic ones are (Q1) "have any of the bioactive structures in this patent appeared in papers?" The converse question (Q2) is "have any of the bioactive structures in this paper (in particular the lead compound) appeared within a (possibly larger) SAR series in a patent?" These questions thus look forward or backward in time and can both be important. There are technically different ways to approach the questions and with different search stringencies (e.g., an exact match, a connectivity match, a similarity match, or multiple matches across a series). Before looking at some examples it is important to understand the time relationship of what surfaces where when, how much, and who cross-points to whom. Starting with patent chemistry in PubChem first we can establish that it contains 16.3 million substances

from SureChEMBL up to Aug. 6. We can also check that in situ the latest extractions were only 3 days behind the publication date. While the lag time in PubChem is thus about a month, this is more than acceptable for a free resource. There are four other sources of patent chemistry in PubChem that each have more than a million structures (see **Table 1** in ref. [2] for a 2015 snapshot) but three of these are static and are not likely to update. Selecting SureChEMBL, IBM, SCRIPDB, and NextMoveSoftware (all CNER sources) adds up to 19.7 million compounds with 82% coming from SureChEMBL.

PubChem is extensively connected to the literature via different types of CID-to-PubMed connectivity[20] one of which includes ChEMBL via the PubChem BioAssay database. However, there is an associated lag time for when PMIDs are connected to CIDs, because ChEMBL release times are well over 6 months. Nonetheless, there are multiple ways to answer Q1 and Q2. One of these is by following the reciprocal cross pointers between PubChem, SureChEMBL, ChEMBL, and UniChem. This means for any individual structure we can follow inter-database and paper-to-patent connectivity without doing any searches at all (this was already demonstrated for SureChEMBL-to-PubChem). Before we explore search examples we should examine the general question of what is the overall overlap between structures in papers and patents. The commercial GOSTAR figure is that 9% of compounds from papers are found in their patent extractions, indicating a slight rise from 6% in 2009.[6] By contrast 18% of ChEMBL has a SureChEMBL match. There are two possible reasons for the higher number. Firstly, ChEMBL subsumes ~0.5 million compounds from confirmed Molecular Libraries Screening Centers Network (MLSCN) assays so this substantial increase in structures would be expected to increase in turn the number of literature extraction matches. The second is that SureChEMBL extracts approximately three times the number of compounds GOSTAR does, which should also increase the percentage overlap with literature extraction.

We can approach the questions by looking at Q2. A simple PubMed search with "BACE1 inhibitor" brings up a relevant looking paper high in the result list (**Fig. 20**).

This very recent paper (not yet captured by ChEMBL) from Bristol–Myers (BMS) has the hallmarks of a drug discovery team pursuing an orally available, brain penetrant BACE1 inhibitor for which they already have activity in a mouse model. The bonus for our question answering is that they have deposited two PDB structures containing ligands from the paper. Because the NCBI

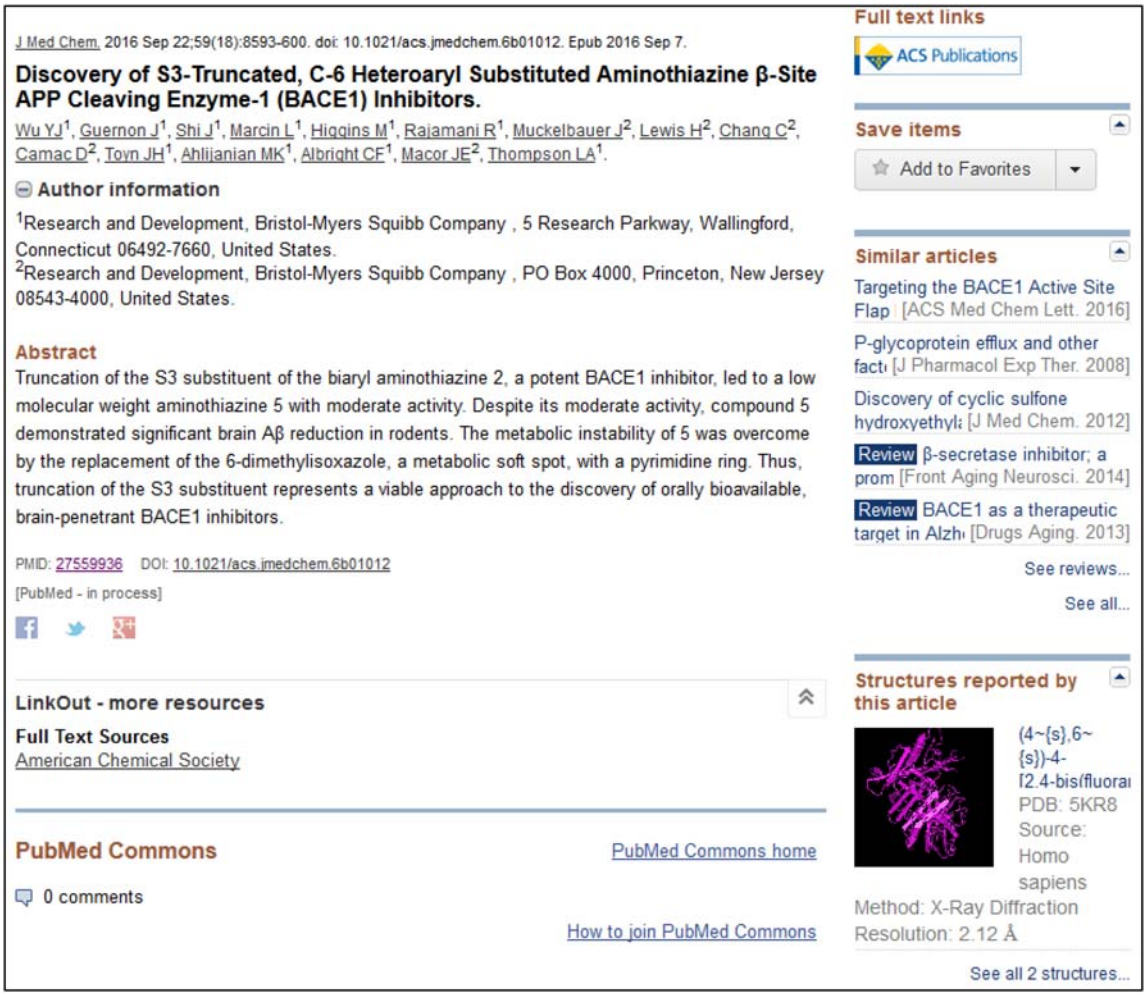

Fig. 20 The fourth ranking match in PubMed with the query "BACE1 inhibitor."

MMDB system assigns a CID-to-PDB ligands where possible, the resulting CID 90253397 connects us right through to the SureChEMBL patents (Fig. 21).

While the BMS paper has good SAR characterization for 18 structures in total,[21] the patent has cell-based IC_{50} data for a series of 62 compounds that, with some manual engagement, can all be identified from the SureChEMBL output. Note also that WO2014098831 was picked up in the Fig. 12 search but was a year further down the list. Of the possible approaches to Q1 perhaps the most effective is to download filtered patent chemistry from SureChEMBL and upload it to PubChem using the Indentifier Exchange Service. The next step is to intersect these CIDs with ChEMBL. Lead-like matches (i.e., not common chemistry) are likely to be from journal extractions at least 2 years or more after the patent date.

3.19.12 Tracking Back to First-Filings

This is a variation on the paper-to-patent Q2, but here the focus is searching backward for the early patents on clinical candidates or recently approved drugs. The special interest here is to possibly access patent SAR around a compound that has reached some level of success, even just in the preclinical stages. One resource that enables making the appropriate connections is the IUPHAR/BPS Guide to Pharmacology (GtoPdb).[22]Inspection of the BACE1 entry indicates the expert curation of 15 lead compound and clinical candidates as ligand entries. For some of these, patents have been curated into the reference where these were found to contain useful SAR. A section from this panel is shown in Fig. 22 and the SureChEMBL page shown in Fig. 23.

Given the verubecestat compound from Merck is now in Phase III, it is somewhat unusual in not having any journal publications. In this case, the curation of a patent link into GtoPdb is particularly useful. Although the discrete SAR in US8940748 is minimal there are BACE1 and BACE2 K_i values. Also somewhat unusually there are in the order of 200 analog structures fully described without inhibition data but many with permeability measurements. Using the approaches described earlier most lead compounds and drugs, using GtoPdb or other resources as entry points, can now be tracked back to their first-filings as novel structures, many of which include SAR.

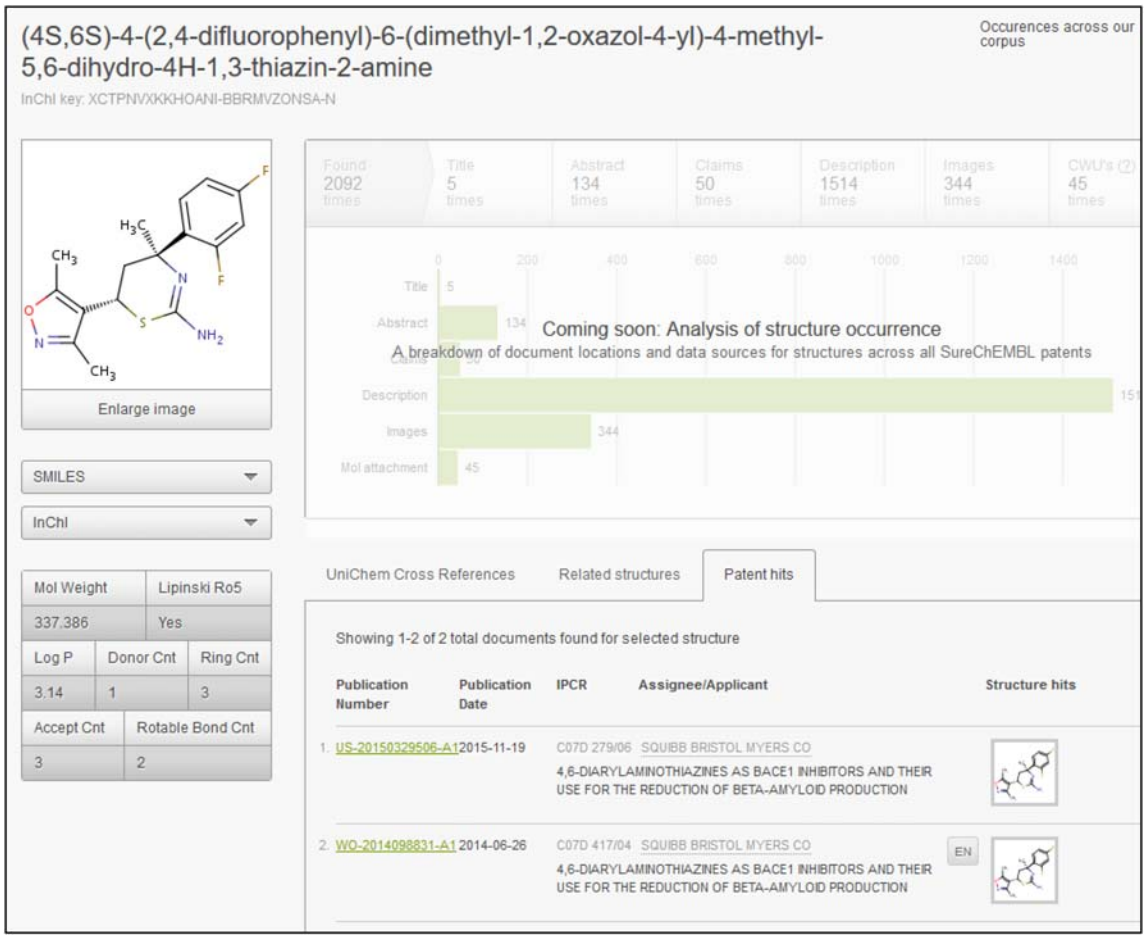

Fig. 21 The connection between the publication PMID 27559936, the PDB entry 5KR8, the CID 90253397, the SureChEMBL SID 240769892, and the two family BMS patents above.

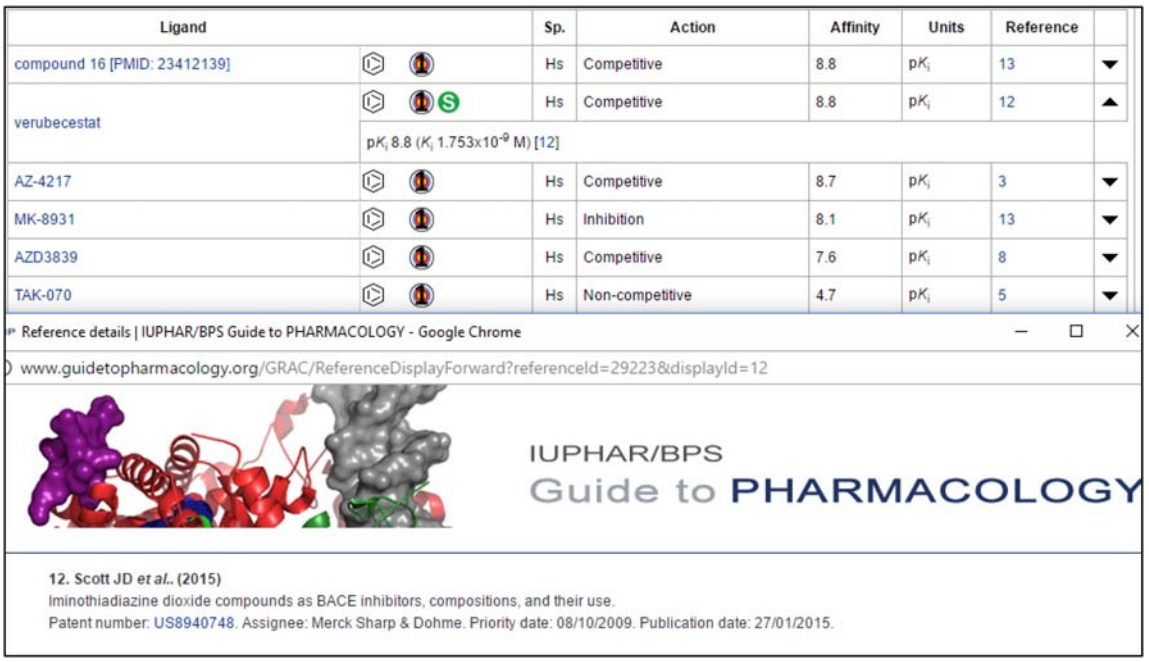

Fig. 22 Snapshot from the GtoPdb page for BACE1 ligands. The record for verubecestat is expanded to show the pK_i, the patent reference in the lower panel, a live link to the SureChEMBL patent document, and identification of the example number as 25.

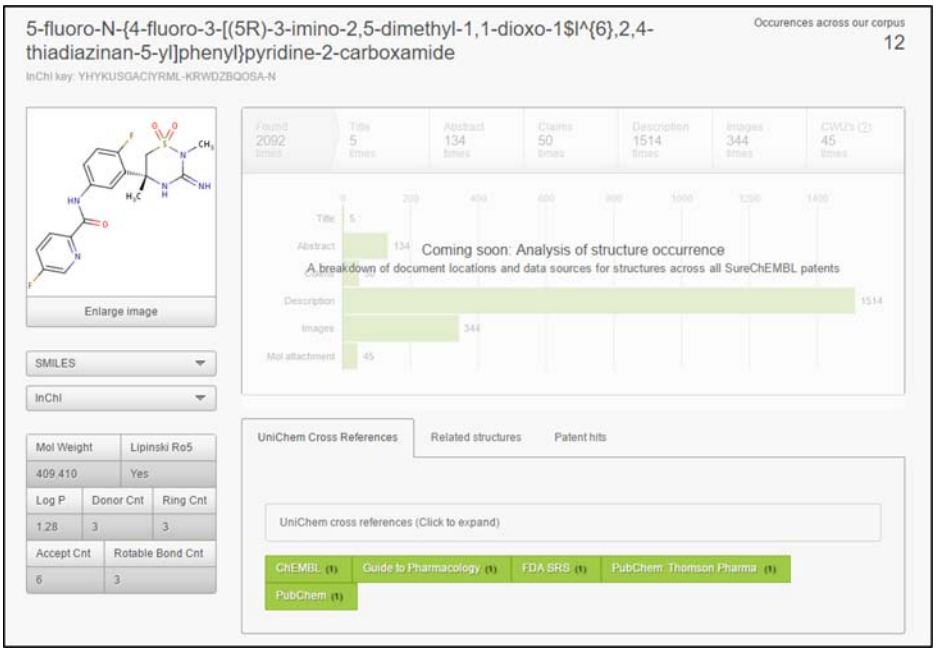

Fig. 23 The SureChEMBL page for verubecestat. The lower set of *green* panels show the cross pointers to other databases mediated via UniChem, including a GtoPdb link to **Fig. 22**. Note also if the 14 patent document hits are opened up we see Merck WO2016053767 for "Novel crystalline forms of a bace inhibitor, compositions, and their use" which was the secondary patent pointed out in **Fig. 12**.

3.19.13 Conclusions and Prospects

It is hoped that the approaches and examples presented here will not only encourage but also enable medicinal chemists to dig SAR out of patents. The recent "big bang" of patent chemistry flowing into public databases, alluded to above, now presents the best of both worlds situation in two senses. The first is that open patent data is becoming more synergistic with the features and content of

commercial resources. The second is that those without access to the latter are no longer constrained for SAR-digging even if it may take a bit more time and effort. So what of the future? It would be useful to see comparative modeling results that might illuminate similarities and differences between data sources (i.e., Could adding patent-only SAR improve models?).

Other developments will include significant optimization of the PubChem patent system in 2017 (Evan Bolton, personal communication). In addition, the development of patent information extraction systems continues (e.g., the 2015 BioCreative V challenge "Chemical and Drug Named Entity Recognition from patent text" CHEMDNER patents[23]). As an extension of these efforts, both the commercial and open sectors are pursuing the holy grail of fully automated D–A–R–C–P extraction using NLP and deep indexing approaches. In conjunction we may also see "big data" scale patent processing initiatives in the public domain. These can exploit Application Programming Interfaces (APIs) web services (WS) and Resource Description Frameworks (RDF). These are already becoming available for SureChEMBL as part of the OpenPHACTS initiative.[24] So might the major patent offices move toward fully electronic patent applications that would include XML full text, direct submission of chemical structures, use of bioassay ontologies, standardized data tables, and bioentity identifiers for C07/A61 applications?

3.19.13.1 *Note added in proof*

As an important new development, in October 2016 the WIPO PATENTSCOPE portal (see website below) released a chemical structure search feature for ~7 million compounds they have already indexed from WO patent documents.

See also: 1.20. Present and Future Challenges and Opportunities for Intellectual Property in an Open Landscape: Open Labs and the Internet.

References

1. Southan, C.; Boppana, K.; Jagarlapudi, S. A. A.; Muresan, S. Analysis of in vitro Bioactivity Data Extracted From Drug Discovery Literature and Patents: Ranking 1654 Human Protein Targets by Assayed Compounds and Molecular Scaffolds. *J. Cheminf.* **2011,** *3,* 14. http://dx.doi.org/10.1186/1758-2946-3-14.
2. Southan, C. Expanding Opportunities for Mining Bioactive Chemistry From Patents. *Drug Discov. Today Technol.* **2015,** *14,* 3–9. http://dx.doi.org/10.1016/j.ddtec.2014.12.001.
3. Kim, S.; Thiessen, P. A.; Bolton, E. E.; Chen, J.; Fu, G.; Gindulyte, A.; et al. PubChem Substance and Compound Databases. *Nucleic Acids Res.* **2016,** *44,* D1202–D1213. http://dx.doi.org/10.1093/nar/gkv951.
4. Southan, C.; Hancock, J. M. A Tale of Two Drug Targets: The Evolutionary History of BACE1 and BACE2. *Front. Genet.* **2013,** *4,* 293. http://dx.doi.org/10.3389/fgene.2013.00293.
5. Clark, A. M.; Dole, K.; Ekins, S. Open Source Bayesian Models. 3. Composite Models for Prediction of Binned Responses. *J. Chem. Inf. Model.* **2016,** *56,* 275–285. http://dx.doi.org/10.1021/acs.jcim.5b00555.
6. Southan, C.; Varkonyi, P.; Muresan, S. Quantitative Assessment of the Expanding Complementarity Between Public and Commercial Databases of Bioactive Compounds. *J. Cheminf.* **2009,** *1,* 10. http://dx.doi.org/10.1186/1758-2946-1-10.
7. Muresan, S.; Petrov, P.; Southan, C.; Kjellberg, M. J.; Kogej, T.; Tyrchan, C.; et al. Making Every SAR Point Count: The Development of Chemistry Connect for the Large-Scale Integration of Structure and Bioactivity Data. *Drug Discov. Today* **2011,** *16,* 1019–1030. http://dx.doi.org/10.1016/j.drudis.2011.10.005.
8. Eriksson, M.; Nilsson, I.; Kogej, T.; Southan, C.; Johansson, M.; Tyrchan, C.; et al. SARConnect: A Tool to Interrogate the Connectivity Between Proteins, Chemical Structures and Activity Data. *Mol. Inf.* **2012,** *31,* 555–568. http://dx.doi.org/10.1002/minf.201200030.
9. Ekins, S.; Clark, A. M.; Southan, C.; Bunin, B. A.; Williams, A. J. Small-Molecule Bioactivity Databases. In *High Throughput Screening Methods*: *Evolution and Refinement*; Ross, N.; Bittker, J.; Royal Society of Chemistry, in press, pp. 344–365.
10. Southan, C.; Varkonyi, P.; Boppana, K.; Jagarlapudi, S. A. R. P.; Muresan, S. Tracking 20 Years of Compound-to-Target Output From Literature and Patents. *PLoS One* **2013,** *8,* e77142. http://dx.doi.org/10.1371/journal.pone.0077142.
11. Gilson, M. K.; Liu, T.; Baitaluk, M.; Nicola, G.; Hwang, L.; Chong, J. BindingDB in 2015: A Public Database for Medicinal Chemistry, Computational Chemistry and Systems Pharmacology. *Nucleic Acids Res.* **2016,** *44,* D1045–D1053. http://dx.doi.org/10.1093/nar/gkv1072.
12. Bento, A. P.; Gaulton, A.; Hersey, A.; Bellis, L. J.; Chambers, J.; Davies, M.; et al. The ChEMBL Bioactivity Database: An Update. *Nucleic Acids Res.* **2014,** *42,* D1083–D1090. http://dx.doi.org/10.1093/nar/gkt1031.
13. Papadatos, G.; Davies, M.; Dedman, N.; Chambers, J.; Gaulton, A.; Siddle, J.; et al. SureChEMBL: A Large-Scale, Chemically Annotated Patent Document Database. *Nucleic Acids Res.* **2016,** *44,* D1220–D1228. http://dx.doi.org/10.1093/nar/gkv1253.
14. Southan, C. BACE2 as a New Diabetes Target: A Patent Review (2010–2012). *Expert Opin. Ther. Pat.* **2013,** *23,* 649–663. http://dx.doi.org/10.1517/13543776.2013.780032.
15. Chambers, J.; Davies, M.; Gaulton, A.; Papadatos, G.; Hersey, A.; Overington, J. P. UniChem: Extension of InChI-Based Compound Mapping to Salt, Connectivity and Stereochemistry Layers. *J. Cheminf.* **2014,** *6,* 43. http://dx.doi.org/10.1186/s13321-014-0043-5.
16. Schneider, N.; Lowe, D. M.; Sayle, R. A.; Tarselli, M. A.; Landrum, G. A. Big Data From Pharmaceutical Patents: A Computational Analysis of Medicinal Chemists' Bread and Butter. *J. Med. Chem.* **2016,** *59,* 4385–4402. http://dx.doi.org/10.1021/acs.jmedchem.6b00153.
17. Southan, C.; Stracz, A. Extracting and Connecting Chemical Structures From Text Sources Using Chemicalize.org. *J. Cheminf.* **2013,** *5,* 20. http://dx.doi.org/10.1186/1758-2946-5-20.
18. O'Boyle, N. M.; Banck, M.; James, C. A.; Morley, C.; Vandermeersch, T.; Hutchison, G. R. Open Babel: An Open Chemical Toolbox. *J. Cheminf.* **2011,** *3,* 33. http://dx.doi.org/10.1186/1758-2946-3-33.
19. Lowe, D. M.; Corbett, P. T.; Murray-Rust, P.; Glen, R. C. Chemical Name to Structure: OPSIN, an Open Source Solution. *J. Chem. Inf. Model.* **2011,** *51,* 739–753. http://dx.doi.org/10.1021/ci100384d.
20. Kim, S.; Thiessen, P. A.; Cheng, T.; Yu, B.; Shoemaker, B. A.; Wang, J.; et al. Literature Information in PubChem: Associations Between PubChem Records and Scientific Articles. *J. Cheminf.* **2016,** *8,* 32. http://dx.doi.org/10.1186/s13321-016-0142-6.
21. Wu, Y.-J.; Guernon, J.; Shi, J.; Marcin, L.; Higgins, M.; Rajamani, R.; et al. Discovery of S3-Truncated, C-6 Heteroaryl Substituted Aminothiazine β-Site APP Cleaving Enzyme-1 (BACE1) Inhibitors. *J. Med. Chem.* **2016,** *59,* 8593–8600. http://dx.doi.org/10.1021/acs.jmedchem.6b01012.

22. Southan, C.; Sharman, J. L.; Benson, H. E.; Faccenda, E.; Pawson, A. J.; Alexander, S. P. H.; et al. The IUPHAR/BPS Guide to PHARMACOLOGY in 2016: Towards Curated Quantitative Interactions Between 1300 Protein Targets and 6000 Ligands. *Nucleic Acids Res.* **2016,** *44,* D1054–D1068. http://dx.doi.org/10.1093/nar/gkv1037.
23. Akhondi, S. A.; Pons, E.; Afzal, Z.; van Haagen, H.; Becker, B. F. H.; Hettne, K. M.; et al. Chemical Entity Recognition in Patents by Combining Dictionary-Based and Statistical Approaches. *Database (Oxford)* **2016,** *2016.* http://dx.doi.org/10.1093/database/baw061.
24. Chichester, C.; Digles, D.; Siebes, R.; Loizou, A.; Groth, P.; Harland, L. Drug Discovery FAQs: Workflows for Answering Multidomain Drug Discovery Questions. *Drug Discov. Today* **2015,** *20,* 399–405. http://dx.doi.org/10.1016/j.drudis.2014.11.006.

Relevant Websites

http://bindingdb.org/bind/index.jsp—BindingDB (binding data for proteins and small molecules).
https://cactus.nci.nih.gov/osra/—OSRA: Optical Structure Recognition Application (i2s).
https://chemicalize.com/welcome—ChemAxon Chemicalize, text processing (n2s, with registration required).
https://www.ebi.ac.uk/chembl/—ChEMBL (large scale literature extraction).
https://www.ebi.ac.uk/unichem/—UniChem (cross-referencing of 137million structures including ChEMBL, SureChEMBL and PubChem).
http://www.excelra.com/gostar.php—GOSTAR (Excelra Knowledge Solutions).
http://www.guidetopharmacology.org/—IUPHAR/BPS Guide to PHARMACOLOGY (leads with patent connectivity).
https://pubchem.ncbi.nlm.nih.gov/—PubChem (92 million structures).
https://pubchem.ncbi.nlm.nih.gov/idexchange/idexchange.cgi—PubChem Identifier Exchange Service (mapping extrinsic chemistry into PubChem).
https://www.surechembl.org/search—SureChEMBL (large scale patent chemistry extraction).
https://www.uspto.gov/patents-application-process/search-patents—USPTOPatent Full-Text and Image Database.
http://www.wipo.int/classifications/ipc/en/—International Patent Classification (IPC).
http://www.wipo.int/patentscope/en/—WIPO PATENTSCOPE database of 58 million documents.
http://opsin.ch.cam.ac.uk/—OPSIN: Open Parser for Systematic IUPAC nomenclature (n2s).
https://worldwide.espacenet.com/—European Patent Office (EPO) Espacenet database of 90 million documents.

3.20 An Introduction to Systems Biology and Quantitative Systems Pharmacology

BC Gomes, Pharmacometrics Modeling and Simulation, Novartis, Cambridge, MA, United States

© 2017 Elsevier Ltd. All rights reserved.

3.20.1	**Introduction**	488
3.20.2	**Definitions**	490
3.20.2.1	Systems Biology	490
3.20.2.2	Simulation Versus Prediction	491
3.20.2.3	Multiscale Modeling	491
3.20.2.4	Metabolic Control Analysis	491
3.20.2.5	Pathway Modeling	491
3.20.2.6	Integrative Biology	491
3.20.2.7	Physiologically Based Pharmacokinetics	492
3.20.2.8	Quantitative Systems Pharmacology	492
3.20.3	**Mathematical Formalisms**	494
3.20.3.1	Boolean Modeling	494
3.20.3.2	Petri Nets	494
3.20.3.3	Agent-Based Modeling	495
3.20.3.4	Bayesian Network Models	496
3.20.3.5	ODE and PDE Models	496
3.20.4	**A Detailed Discussion of a Systems Biology and Quantitative Systems Model**	497
3.20.5	**Summary**	499
References		500
Relevant Websites		503

3.20.1 Introduction

At the heart of modern scientific progress is a reductionist belief that biology can be understood by close examination of the individual components of the whole. This idea was first suggested by Rene Descartes (1596–1650). "He formulated the notion that complex situations can be analyzed by reducing them to manageable pieces, examining each in turn, and reassembling the whole from the behavior of the pieces."[1] By contrast, systems biology seeks to comprehensively understand the time-dependent changes in a network of interactions in order to describe the integration of all the molecular or cellular components. As such, systems biology lies at the confluence point of three streams—biology, computer simulation, and high-throughput screening. As a tool of pharmaceutical drug discovery, the goal of systems biology is to find the most efficacious point(s) of intervention to change the pathophysiological state of the biological process (the system) in order to return it to a more healthy condition.

From a practical point of view, in academic and pharmaceutical industry labs, assays are usually created to test the effect of a single property at a time. For example, the concentration of a cytokine is varied and the amount of binding to its receptor is followed. After some calculation, this yields a binding affinity. A new candidate antagonist of that receptor can be tested to determine the strength of inhibition of that cytokine/receptor interaction, and hence provides a simple measure of the potency of a possible therapeutic. If a misguided investigator were to merely dose the same compound to an individual with a disease associated with this cytokine/receptor pair, and to ask whether the potential drug was effective in ameliorating the disease, he would find his questionable ethics and flawed experimental design justifiably criticized. We all "know" that successful drug discovery requires many steps (compound screening, chemical and/or biological refinement of candidates, animal models, safety assessment, dosing evaluation, etc.). And yet, in the modern pharmaceutical industry, at each step of this discovery and development process, different groups of individuals, with different focused skill sets, attempt to provide clear analysis by reducing the complexity of the system to a simple, human-comprehendible and variable-limited output. To be fair, this form of methodological reductionism[2] is usually the result of a sensible approach to the limitations of the human mind. Most people would not be able to understand assays that tested multiple parameters simultaneously. Perception and visualization of trends of multidimensional data can be difficult. However (properly programmed) computers have no difficulty processing high-dimensional data.

The availability of sufficient computing power and specialized modeling software is one of the influences that gave rise to systems biology. In fact, the notion of systems biology arose from the discipline of systems analysis and control theory, where self-monitoring circuits adapt outputs to varied inputs through amplification and feedback loops. The other major driver of the growth of systems biology was an increasing appreciation that a deeper comprehension of systems of metabolic pathways, genomic control, cellular signaling, etc., was available when biological processes were observed at larger scales than single, isolated reactions.

This is the result of the concept of "emergent properties." In the flocking of birds (or the schooling of fish, the coordinated migration of locust, and other complex systems), behavior of the flock is not the property of one leader, the master bird. Instead, all the birds move as if there is a linkage between individuals that supersedes an individual's actions. This linkage is an emergent property of the system. The demonstration that the sum is greater than the parts is the "holy grail" of systems biology. This same type of behavior is recapitulated at many levels in humans and other organisms. Each cell in a multicellular organism is constantly receiving myriad cues from neighboring cells within an organ and more distant organs through signaling molecules, direct contact with circulating sensor cells (e.g., T and B cells), or enervations from nerve cells. The cell processes this information and integrates it with its own current state, metabolic demands and specialized functions, and responds with alterations in transcriptional output and activation of regulatory networks within the cell and, in turn, communicates with the rest of the organism by initiating release of its own signaling molecules. No single cell is the "master switch" for any process in a human, and yet complex, emergent behaviors are observed in the regulation of metabolism, the growth or decline in subpopulations of cells, the maintenance of a beating heart, our immune response to invading infectious agents, and even truly astonishing supracellular things like thought. But the discovery of emergent properties goes beyond the purely observational when it can be practically applied, as it now is, in drug discovery. Understanding the origins of an emergent property, such as a feedback loop in a signaling pathway can lead to a drug that targets a pathway with greater precision than one directed at a single component enzyme.

Historically, one can always point to earlier and earlier harbingers and innovative people that led to the eventual creation of systems biology. It is the nature science to build on the work of others. Alan Hodgkin and Andrew Huxley are often cited as being instrumental in the founding of systems biology, though this discipline was not given that name at the time. Their success in creating a mathematical model of the generation and propagation of nerve impulses gave rise to other new attempts to apply mathematical principals to the description of fundamental physiological processes. By modeling the ion (K^+ and Na^+) conductances from a giant nerve fiber (see **Fig. 1**), they were able to construct a model that well mimicked the previously described, all-or-none action

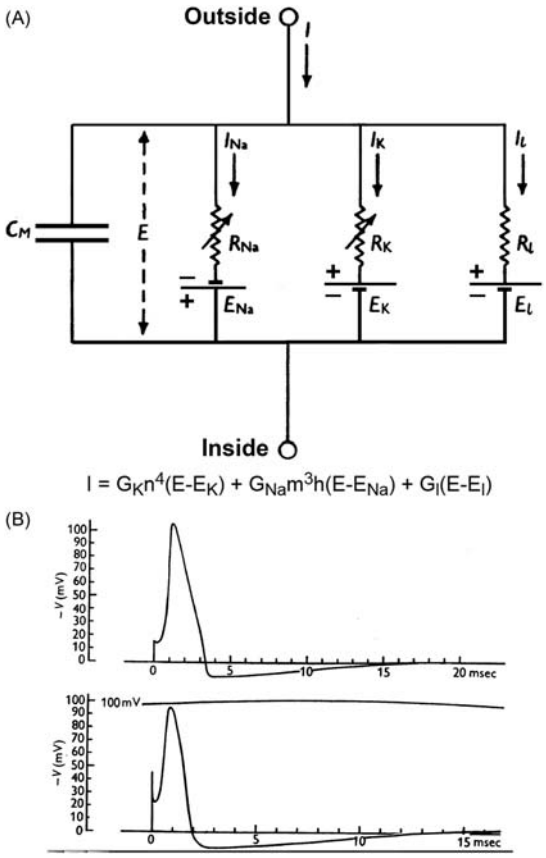

Fig. 1 (A) Hodgkin and Huxley represented the plasma membrane as a number of parallel circuits—one each for the movement of sodium, potassium, and other ions. In the equation shown, the G terms stand for conductances of the ions, E is the resting potential of the membrane, and ENa, EK, and El are the electrical potentials of each ionic circuit. The terms *n* and *m* represent the activation of potassium and sodium ion transport, respectively, while *h* stands for the inhibition of sodium transport. The standard methods of circuit analysis generated the equation shown. (B) The simple model of the conductances allowed for the comparison between the simulated (*upper curve*) and the measured biological response (*lower curve*). The model correctly predicted the magnitude and wave form of the propagation of an action potential, as well as the refractory period that occurs after the firing of the axon.

potential.[3] It should be noted that this mathematical model was formulated before the details of ion channel firing were fully envisioned. This highlights the idea that useful and innovative modeling does not require knowledge of every molecular and physical event in the process—only the important ones. Subsequently, Denis Noble built on the Hodgins–Huxley model to describe the action and pacemaker potential from the Purkinje fibers of the heart.[4] There has been a continuous building on these early works, culminating in the recent mathematical description of heart failure.[5] This paper describes how heart failure is a multiscale process that propagates from the modulation of sarcomere number, giving rise to alteration in muscle cell architecture. At the organ level, these changes then affect ventricular wall thickening and electrical properties of the heart.

Another formative force for systems biology was the rapid evolution of molecular biology. In the 1960s, molecular biology exploded with the basic understanding of the structure of genetic controls. The most thorough of these was the description of the *lac* operon.[6] It was realized, almost immediately, that these genetic processes were akin to the monitor-adapt-output cycles of mathematically approachable electronic circuitry. Labs began to construct reporter gene systems, genetic toggle switches, and simple memory, etc.[7] Hence, they had created biological analogues of many of the components of circuits, which are amenable to modeling.[8] By modularizing these control processes, they made it evident that biology is driven by recurring themes and, in turn, made in silico modeling of these processes tractable.

3.20.2 Definitions

Recently, systems biology has fragmented into many sub disciplines—systems immunology,[9,10] systems genetics,[11] systems oncology,[12,13] systems pharmacology,[14] etc. Even these more focused systems approaches vary widely in methodology. The following is a nonexhaustive explanation of some of the terms and forms of systems biology.

3.20.2.1 Systems Biology

Systems biology is somewhat difficult to define because different people use the term to mean different things. The term "systems biology" was first used in 1968 with a fairly strict mathematical and logic description,[15] but has evolved to encompass virtually any mathematical approach to elucidate biology. All these treatments share an in silico computational component and all are directed at some level of biology, but the methods and focus of this work varies greatly. Systems biology attempts to provide a quantitative and comprehensive view of some biological phenomenon by the use of a collection of connected equations. It has been used to describe biological topics as diverse as predator/prey population dynamics,[16] circadian rhythms,[17] cell cycle regulation,[18] the complement cascade,[19] DNA damage repair by surveillance driven by p53,[20] and many others. Systems biology seeks to find the underlying foundation for emergent properties in the biology under study. Mathematical formalisms will be discussed below, but all methods create a map—a topological organization of all the relevant components. Secondly, they have a linkage among elements that describes a time-dependent strength of interaction. In most cases, this means that rate constants are applied that determine the velocity of conversion of one species into another. Finally, the model ascribes initial concentrations for all species at the start of the simulation. The systems can be complex or simple, abstract or described in great detail, and often are nonlinear. They are dynamical (at each point in time there is a vector with a specified value for each species in the system). The concentration of the species and the relative contribution to the overall output of the model will mostly be changing throughout the simulation. To complete a molecular-level systems model, it is helpful to understand the full list of component parts (proteins, peptides, metabolites, etc.), as well as their concentrations. It is then a natural progression that systems biology has surged in usage with the completion of the human genome project (and the genome of species that are used in animal models) as well as advances in proteomics (e.g., mass spectrometric methods). Once all the pieces are elucidated, it becomes easier to create the network connections that make up a systems biology model. Thus, the definition of systems biology given by Leroy Hood, one of the leading voices in the human genome project as well as systems approaches, is most relevant—"Systems biology studies biological systems by systematically perturbing them (biologically, genetically, or chemically); monitoring the gene, protein, and informational pathway responses; integrating these data; and ultimately, formulating mathematical models that describe the structure of the system and its response to individual perturbations."[21] In the drug discovery area, it is a reasonable question to ask, "What does a pharmaceutical scientist gain by having a systems model of the healthy and diseased states that cannot be found by mass screening of drug candidates versus protein binding assays?" Firstly, it unlikely that binding or inhibition assays for all proteins that underlie the disease could be established in a timely manner (even if all the responsible proteins were known). Secondly, this kind of reductionism would discard all the interaction information in the crosstalk interrelationships of the network. The idea of "one disease–one target" is likely wrong for all but a few, enzyme deficiency disorders. Also, though it is an area of systems modeling that is in its infancy, systems biology does not necessarily uncover a single point of intervention, but often finds that synergistic effects are found by combinations of drugs.[22] A good example of the increased understanding of combination therapies provided by systems modeling is the work of Bown et al.[23] Using the previously described model of the PI3K/PTEN/AKT and RAF/MEK/ERK signaling pathways they simulated the development of drug-induced resistance to a first anticancer agent, followed by treatment with a second drug to correct for the resistance. Another example of modeling combination therapies is in the Nitric Oxide–cGMP pathway.[24] The authors investigated intervention at various points in the pathway as well as in combination. They give a conclusion that optimal therapy, when measured as maximizing cGMP accumulation, would be observed by intervention at three points in the pathway. This was confirmed by experimentation. A good mathematical discussion of how to evaluate synergy of combined treatment has been done.[25]

3.20.2.2 Simulation Versus Prediction

Some models seek to mimic the observed outputs (objective function) of known biology. The previously mentioned mathematical treatment by Hodgkin–Huxley simulates nerve conduction in an axon. All models start with this kind of approach because it allows the modeler to construct (most of) the critical components and links in a way that is verifiable from known data. However, particularly valuable models go beyond simulation to further predict undocumented behavior of the system. Experimental confirmation of nonobvious predictions builds the confidence in the model. These predictive models contribute to scientific progress by allowing the formation of new hypotheses for further understanding of the underlying biology. In the pharmaceutical setting, when models make strong, testable predictions, drug discovery is accelerated.

3.20.2.3 Multiscale Modeling

To some extent, most systems approaches use known information about component parts to find more holistic descriptions of biological processes. Thus, these models cross scales of structure or extend the scale of time predictions. For example, individual kinetic parameters and species concentrations are linked together to produce a simulation of a signaling network. The emergent properties of this linked system might give a picture of the dynamic relationships that occur at a cellular level in terms of signal and response. In turn, the summation of many specialized cells or organelles, for example, Islet cells in the pancreas,[26] mitochondria in the heart,[27] or endothelial cells in intestine[28] might exhibit an organism-level response of growth, correct cardiac rhythm, or ionic homeostasis in the blood. Does this understanding of multiscale processes lead to better drug discovery? To quote from a paper by Sanofi scientist, "… aiming for the discovery of novel targets increasing the glucose-dependent insulin secretion, we have established a mathematical model of the pancreatic beta cell. The 'virtual pancreatic beta-cell' has been generated by capturing all relevant processes in this cell type by combining three published models describing elements in the control of glucose-triggered insulin secretion in the beta-cell (GPCR/cAMP signaling, β-cell electrophysiology and calcium handling, insulin granule exocytosis)… The resulting model contains numerous enzymes, transporters and ion-channels involved in glucose stimulated insulin secretion… The 'virtual pancreatic β-cell' is currently used to predict the best drug targets or target combinations for increasing the glucose-dependent insulin secretion."[29]

3.20.2.4 Metabolic Control Analysis

This is an area of modeling that can see its direct antecedents in the mathematical analysis of single enzyme reactions. This area was pioneered by Westerhoff.[30] It is mostly used for looking at metabolic pathways. Earlier models had focused on synthesis and degradation pathways in which it was suggested that there was a single rate-limiting enzymatic conversion step, which was then studied in detail to understand regulation of the whole pathway. Metabolic Control Analysis seeks to understand the fluxes of metabolites through the whole collection of enzymes, in order to give a more refined view of the enzymatic ensemble. This technique is used for finding inhibitors that exploit metabolic differences as seen in disease-causing microorganisms or cancer cells.[31]

3.20.2.5 Pathway Modeling

One particularly well-worked area of systems biology is pathway modeling. This approach seeks to build mathematical models of cell-signaling networks.[32] The modeling requires setting the concentration and rates of each enzyme in the pathway, as well as the strength of any feedback and feedforward loops. This usually requires a certain amount of parameter optimization, that is, fitting of unknown (or poorly characterized) parameters. This is done by fitting a range of parameter values to a known, experimentally derived, output graph. For example, a fluorescent assay might measure the production of an intermediate of the pathway. The concentration or rate of an enzyme with unknown values is determined by varying the rate constant or protein concentration until a reasonable fit to the data is obtained. This value is then entered into the pathway. In this way, the MAPK[33,34] pathway and its connection to EGFR[35,36] signaling have been modeled extensively. The topology of the pathway had been previously determined and most of the phosphorylations and dephosphorylations had been parameterized and feedback loops had been mapped. This has led to insights about control of the pathway, which in turn, has led to better drug design[37] for this pathway, which is inappropriately regulated in breast cancer and other neoplasms. Many pathways have been modeled in this way, including the Wnt,[38] JAK/STAT,[39] PI3 kinase,[40] NF-κB,[41] Notch,[42] TGF-β,[43,44] and multiple others.

3.20.2.6 Integrative Biology

Integrative biology is every bit as difficult to define as systems biology. It stresses cross-discipline studies to unify a view of biological phenomenon into a cohesive whole.[45] Integrative biology emphasizes biology as information, thus bringing insights from genomic, physics, chemistry, etc., to provide a clearer view of the area of study. Many papers in integrative biology highlight taxonomy and comparative biology. Others stress a hybridization of bioinformatics and -omics that rely heavily on clustering of data and finding statistical means to understand informational content that underlies the organizational connectedness of interacting proteins, genes, etc. It has been suggested that systems biology is a subset of integrative biology since systems biology also gives priority to combining computational and biological disciplines.[46] Systems approaches face a challenge from "big data." The system under

study in a model, might be large, but does not contain influences from all other proteins and isoforms. Therefore, at some point integrative biology demarcates the most influential players in a system and allows systems modelers to draw operational boundaries for their studies. Quickly interrogating huge data files systematically, and incorporating the relevant pieces of them into a systems model has not been achieved (yet).

3.20.2.7 Physiologically Based Pharmacokinetics

PBPK is a specialized systems approach to drug distribution.[47] Each organ in the body is essentially treated as a compartment with physiology-based pharmacokinetics (PBPK) is a specialized systems approach to drug distribution specified input and output of flows, a volume and (sometimes) a measure of drug metabolism, and binding capacity.[48] These models can be quite useful to track the amount of a dosed drug that reaches the tissue in which the pathophysiology is located. They can also aid in understanding the half-life of a pharmaceutical and hence the required dosing regimen to be efficacious. Mostly, PBPK models have been used for molecules of low-molecular weight, though as more information becomes available on the physiological properties of different classes of macromolecules, they are also being studied in PBPK models.[49] In general, macromolecules are dosed intravenously, so absorption from the gut does not need to be addressed in the model. Absorption of orally delivered, small molecule drugs from the gut can be a very complex process,[50] and is idiosyncratic for each drug, but in combination with experimentally derived data, predictions of drug disposition can be helpful. While little information at the molecular level is usually present in these models, they can also have utility in informing more mechanistic models. An example of a physiologically informed simulation, with a significant degree of molecular detail is a model of calcium homeostasis and bone remodeling.[51] In this model, the authors mathematically explain the delicate balance of calcium intake from the gut, kidney reabsorption/excretion of phosphate and calcium mediated by multiple endocrine mechanisms, and the constant bone loss and growth driven by the osteoclasts and osteoblasts. This model allows hypothesis testing in an area of intense pharmaceutical industry interest, due to competition for safe and effective osteoporosis drugs.

3.20.2.8 Quantitative Systems Pharmacology

Quantitative systems pharmacology (QSP; also called systems pharmacology, systems clinical pharmacology, and mechanistic physiological modeling, pharmacologically-orientated systems biology) is an enhancement to the more standard PKPD (pharmacokinetics pharmacodynamics) simulation. PKPD modeling is the traditional modeling found in the pharmaceutical industry and academia. PKPD links the dose of a drug to an observed time-dependent appearance and clearance of the drug (PK) and correlates this with a desired physiological effect (PD) or the appearance of an undesirable side effect (toxicology).[52] While PKPD models are very valuable for aiding in dose prediction, cross species dose calculation, and drug safety assessment, they only rarely are based on understanding the basic biological phenomenon that they describe. To be fair, understanding basic biology is not the goal of PKPD models. Rather, they are mathematical constructs to give vital information that is necessary in registration of drugs with regulatory authorities. The models are descriptive and empirical. But to more firmly attach the PKPD framework to the physical characteristics of the pharmaceutical, it was a natural evolution that empirical PKPD models began to add some kinetic and mechanistic details to produce, what is known by the title, semimechanistic PKPD models. At early times in this migration to semi-mechanistic models, these simulations were standard PKPD models with details about drug/target binding added.[53] However, some of these models have become much more expansive (e.g., see references 54–57). To continue the evolution of this area, the idea of adding "some" mechanistic detail soon gave rise to adding sufficient information to build systems models.[58] However, systems models have now entered the regulatory arena.[59] The FDA advisory board recently used a QSP model to evaluate the dosage for a recombinant human parathyroid hormone, for the long-term treatment of hypoparathyroidism. The FDA committee suggested that, based on the model, dosing needed to be further refined to avoid the safety concern of hypocalciuria. This might be a harbinger of greater QSP modeling involvement in FDA oversight of pharmaceutical safety and efficacy. At this point, it would seem that systems biology and QSP are overlapping in goals and methodology. However, true to its name, QSP, remains focused on drug discovery, while systems biology describes a broader study of any biology, pharmaceutically related or not. Also QSP has found a niche in translational medicine,[60,61] the part of the drug discovery process that moves the new pharmaceutical agent from its research foundations in binding assays and early animal models of efficacy and preliminary toxicology onto the threshold of clinical trials, where human dose prediction and dosing regimen become paramount, that is, the "bench-to-bedside" bridge. One of the most ambitious and enlightening models was an immune response model[62] (**Fig. 2**). This model simulates the reaction to infection. It shows reactions at the protein level (e.g., cytokines) as well as at the cellular level. It predicts the kinetic changes in T and B cell subsets, macrophages, dendritic cells, and the clearance of antigens. This model, when fully validated, will allow for evaluation of drugs that alter the immune response.

Systems pharmacology is many times linked to pathways models. This is because many of the same signaling pathways are reoccurring themes in many disease states.[63] There is an underlying belief that models from one disease can be "recycled" for use in other pathology. The problem with this assumption is that the same pathway is used differently in different cells or that the concentration of reactants varies in different tissues. The network of crosstalk or influence from other pathways is different throughout the organism. This is a source of on target toxicology and is hard to predict.

Systems pharmacology has been suggested to be the future deliverer of personalized medicine.[64] In theory, a general model of a disease process could be parameterized with information from each patient. This hypothetical model would then choose a drug

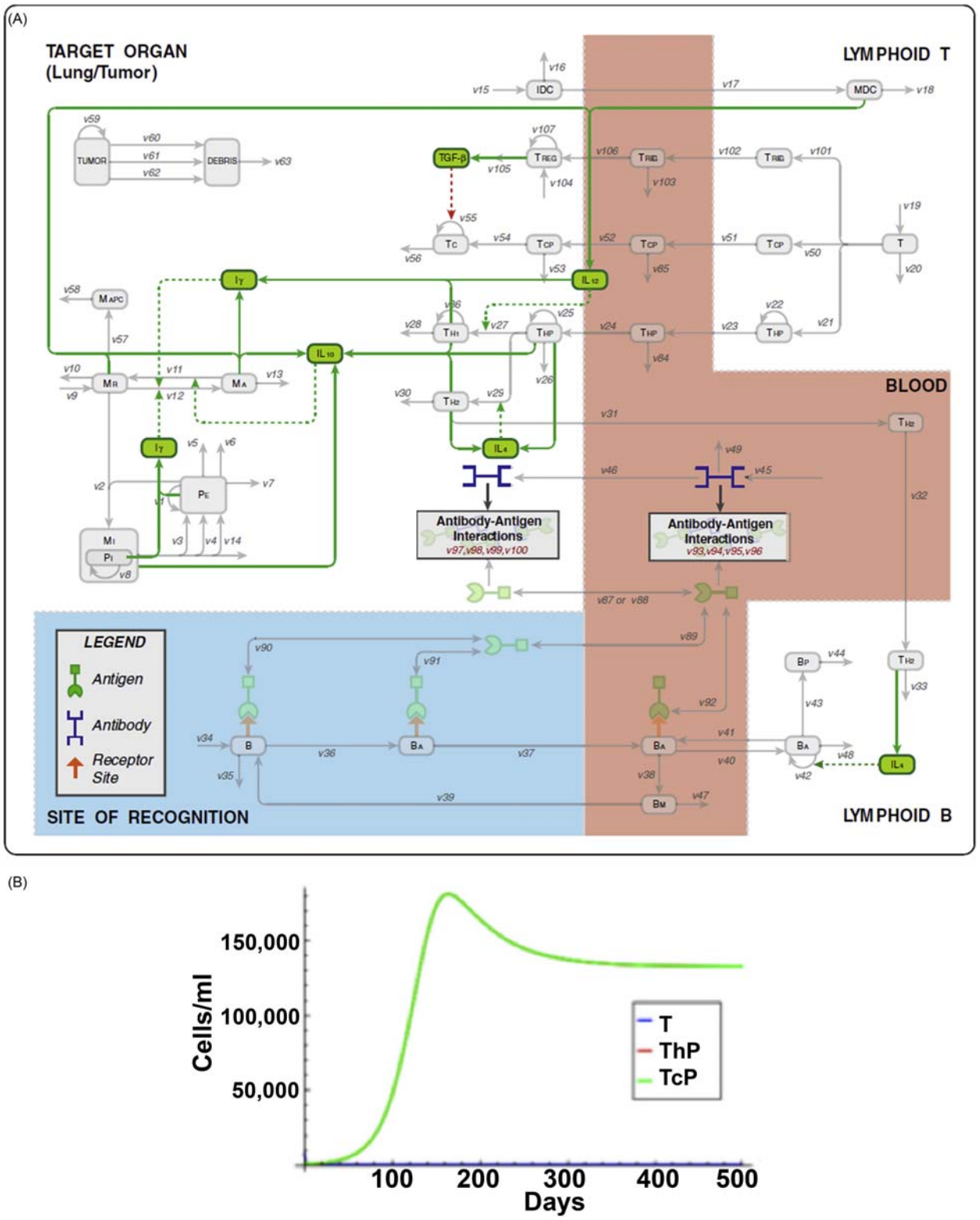

Fig. 2 A fully integrated immune response model. (Adapted from Palsson, S.; Hickling, T. P.; Bradshaw-Pierce, E. L.; Zager, M.; Jooss, K.; O'Brien, P. J.; Spilker, M. E.; Palsson, B. O.; Vicini, P. The Development of a Fully-Integrated Immune Response Model (FIRM) Simulator of the Immune Response Through Integration of Multiple Subset Models. *BMC Syst. Biol.* **2013**, *7*, 95.) The model seeks to show the immune response (in this case the effects on cellular reactions and cytokine production) to tumors, bacterial infections, etc. Abbreviations: *AB*, antibody; B, naïve B-cells; *BA*, activated B-cells; *BM*, memory B-cells; *BP*, plasma B-cells; *DEBRIS*, tumor cell debris; *IDC*, immature dendritic cells; *MA*, activated macrophages; *MAPC*, antigen-presenting macrophages; *MDC*, mature dendritic cells; *MI*, infected macrophages; *MR*, resting macrophages; *PE*, extracellular bacteria; *PI*, intracellular bacteria; *T*, naïve T-cells; *TC*, cytotoxic T-cells; *TCP*, cytotoxic precursor T-cells; *TH2*, T-helper 2 cells; *THP*, helper precursor T-calls; *TH1*, T-helper 1 cells; *Treg*, regulatory T-cells.; *TUMOR*, tumor mass. In panel A is part of the topology for the immune response in the lung/tumor. Panel B represents the model simulation of the time course of subsets of T cells after an intracellular bacterial infection. The model actually computes time courses for all the cells, cytokines, and antigens represented in the model.

(or mixture of drugs), dose, and dosing regimen for that person. But this is (at present) wishful thinking. QSP has considered the heterogeneity in drug action (epigenetic factors, environmental influences, proteomic variability, the individual's reaction to the physicochemical properties of the drug, etc.)[65] and it seems that without a massive computational approach, this will not be possible. However, this is a very complex system made of contributions from many disciplines. After all, even the prediction of an individual's toxicology is still not possible.[66] However, in science, today's impossible is tomorrow's attainable.

3.20.3 Mathematical Formalisms

As discussed above, systems biology seems dissectible into subdisciplines, based on the specific areas of biology addressed (systems toxicology, systems ecology, systems neuroscience, systems medicine, etc.). It can also be partitioned by the form of mathematics used to solve the complex network (rules-based modeling, process algebras, lattice-based cellular automata, Boolean analysis, ordinary differential equation-based models, etc.). The following is a brief description of some of the techniques used. The list is not exhaustive and the explanations are somewhat oversimplified. Additionally, many hybrid approaches exist. There is no single method of modeling that works under all conditions. Rather, the optimal choice of modeling algorithm is dependent on what questions need to be answered and what starting information is available. In the real world, modelers must also consider the audience for their work—some modeling methods are easier to visualize and explain to others with less modeling background. All modeling formalisms have limitations, strengths, and assumptions, and modelers must choose to balance these and other considerations.

3.20.3.1 Boolean Modeling

Boolean modeling[67,68] is, in some ways, the simplest modeling method that is applied to some of the most complex systems. It has been realized that the idea of discrete pathway models is an abstraction that does not match the cellular reality. For example, an MAP kinase pathway is easy to draw, with each enzyme having distinct, digitizable input and output kinetics, reactants, and products. But, at the next level of complexity, this pathway is modulated by signaling contact with other pathways (which are, in turn also regulated). Where do we draw the boundary between pathways in the network? Can this very complex system be parameterized? Many methods, simply practical or bounded by assumptions, try to address this conundrum. One approach is Boolean modeling,[69] which simplifies the problem by limiting the number of states that each component in the system can have. The modeling usually proceeds through two stages (see **Fig. 3A**). The first stage establishes the architecture of system. This is usually completed by information from the literature or pathway data banks. The second step is to train the system from data. Some connections are strengthened while others are eliminated due to low contribution to the measured output. Each molecular entity (DNA, RNA, enzyme, etc.) in the system is set to active or inactive (in some forms of Boolean modeling they have three states—high, medium, or low). It does this by determining the state of the components based on the sum of positive and negative (stimulatory and inhibitory) inputs at each node of the model, at a given time point. No intermediate states are allowed, only on or off. The model is then advanced one time unit and the states of nodes are reassessed. This leads to a time course for each node, for the length of the simulation. Because of the limited number of states for each node in the system, Boolean modeling is considered qualitative or semiquantitative. This type of reduced-complexity model is very useful for finding global steady states (called attractors) of the network, which can be, for instance, the homeostatic state or a disease state. It is obvious that ascribing only a binary status to each species does not mimic the observed behaviors of cells, tissues, or organisms. To address this limitation, a number of approaches have extended Boolean modeling, such as probabilistic approaches,[70] and the use of fuzzy logic.[71,72] Boolean modeling has found application in yeast budding,[73] oncogenic pathway regulation,[74,75] and T cell differentiation.[76] In this last publication, the authors were able to demonstrate that a minimal transcriptional control network composed of the proteins GATA-3, T-BET, Bcl6, FoxP3, and RORyt could explain the cell fate attainment and plasticity of $CD4^+$ T cells including Th0-, Th1-, Th2-, Th17-, Tfh-, Th9-, iTreg-, and Foxp3-independent T regulatory cells. The interconversion of some of these cell types and the lack of interconversion of others would be extraordinarily difficult to model with other types of mathematical formalisms.

3.20.3.2 Petri Nets

Petri nets[77] are graphical and computational representations of biological networks that, in their simplest form, represent species (formally called *places*) and reactions (formally called transitions) that can model multiple, concurrent processes (see **Fig. 3B**). Arcs (directed arrows) represent potential interactions and have specified weights.[78] This gives a visually intuitive picture that is akin to metabolic pathway maps, but with a time-dependent flow. Tokens, added to the model, represent molecules or concentrations. Thus, a given reaction (transition) fires if the concentration (number of tokens) reaches a threshold level and if there is sufficient capacity in the receiving specie. Also, molecule de novo synthesis (gain in token number) and decay (loss of token number) can be represented as transitions without input or output arcs, respectively.[79] Using petri nets, it is possible to get a dynamic picture of the system as it responds to stressors or modulators. This method has been used to model signal transduction induced by the proinflammatory cytokines, IL-1β and TNF-α[80] and the hypoxia response driven by HIF-1α.[81] In this last publication, the authors attempt to unravel the difficult hypoxia tolerance system that is activated in tumor. Petri nets were used to show the core regulatory net for this system. More importantly, they were able to identify the key node that allows for the switch-like behavior of the system.

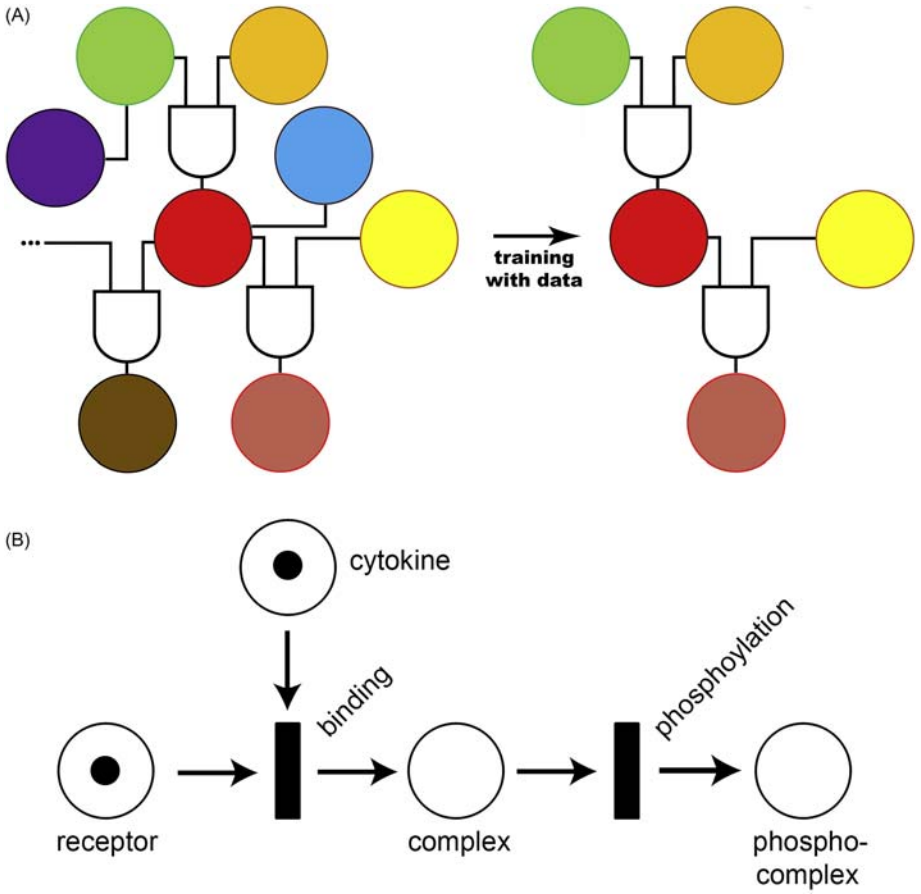

Fig. 3 (A) A simplified Boolean model. In the first step the model structure identifies entities, relationships, and connections. This structure is then trained with the biological data. For example, some stimulus is supplied to the system. The measured experimental time courses for the components (*circles*) are measured. Connections that allow the observed path outputs are given stronger weights and those that do not contribute are eliminated. (B) A simple Petri net for the binding of a cytokine and subsequent phosphorylation of the receptor. *Circles* represent species and boxes represent reactions. The *dark circle* within the circles represents tokens, which are interpreted as units of that species (number of molecules or concentrations).

3.20.3.3 Agent-Based Modeling[82]

In an agent-based model, a grid is created where each box (or cube in three-dimensional models) represents an independent entity. To make this easier to understand, let us assume that this entity is a cell. Within this cell a series of rules are established that create something like a decision tree. The rules can be complex or simple (in fact, in hybrid models the rules can be a mixture of discrete states and continuous variables). All the individual agent cells within the array are given a set of initial conditions and then apply their rules. The individual cell then "decides," based on a preordained, triggering threshold to either wait or create some output (e.g., growth or secretion of substance that is a proliferative stimulus). Within the lattice, each cell only interacts with a limited set of surrounding cells, that is, the output of a cell is not distributed to all agents in the grid, but rather only to those in the limited contact environment of the single cell. The neighboring semiautonomous cells respond to that "secreted stimuli" by applying their own set of (identical) rules. Each agent is integrating the response of their neighbors and reacting by making a state decision. Agent-based models are particularly appealing in oncology because tumor cells expand or undergo apoptosis as a response to cues from their microenvironments (oxygen levels, nutrient availability, proinflammatory cytokines, etc.) and their own internal rule set based on the somatic mutations that cause malignant aberrations (chromosomal rearrangements to place growth signals under the control of active promoters, loss of contact inhibition receptors, loss of apoptotic pathways, upregulation of secreted proteases to allow tissue infiltration, etc.). In this way, the overexpressed EGFR signaling pathway was used as a decision rule set to study neoplasm growth in nonsmall cell lung cancer[83] and brain glioblastoma.[84] Cell death, proliferation, and migration in cancer were modeled by an agent-based algorithm,[85] and the oncogenic cellular responses to DNA damaging compounds were also studied.[86] In this last publication, the authors attempt to understand the processes that underlie how tumor cells respond to chemotherapeutics and radiation therapy. At the level of single cells, the processes of repair of damaging agents are somewhat understood, and yet the tumor acts as if there are emergent properties that are not solely under the control of these mechanisms. Part of this finding is due to the cells of the tumor being asynchronous. This agent-based model used probabilistic methods to predict tumor cell survival curves due

to the population dynamics that result from the underlying DNA damage and repair processes. In other works, the study of cell cycle control in cancer, under the influence of checkpoint inhibitors, has benefited from agent-based models.[87] Agent-based models have also been used to model colonies of microorganisms, such as in the establishment of antibiotic resistant biofilms,[88] and to study Ebola virus epidemiology.[89]

3.20.3.4 Bayesian Network Models[90]

Like Petri Nets, Bayesian network analysis is a graph-based system. Unlike ordinary differential equation (ODE) modeling, which is deterministic, Bayesian network models are probabilistic. In other words, given the same set of initial conditions, ODE models will always give the same results. By contrast, given a data set, Bayesian models yield the likely probability of an ensemble of connections being found. Bayesian network models often start with large data sets, which are prone to noise. Bayesian network models look to uncover the statistical connections between a set of objects. In the case of signaling networks, the objects could be, for an example, phosphorylated proteins, activated enzymes, or genes.[91] The connections that are uncovered can be simple two object physical interactions, for example, protein A binds to protein B, or protein A and B are in a product/precursor relationship. Alternatively, the relationship could be a complex, functional, and previously unknown relationship between many objects (e.g., protein A leads to a downregulation of protein B via a transcriptional suppression mechanism). Bayesian network models not only tolerate large data sets but require sizable collections to detect subtle relationships. The model returns the conditional probability that a particular set of connections explains the data. Therefore, Bayesian network analysis allows the modeler to rank possible network topologies. Often in signaling networks, the connections are already drawn into convenient pathway structures of seemingly fixed architecture of nodes and edges (e.g., the Kyoto Encyclopedia of Genes and Genomes (KEGG) pathway maps[92]). Bayesian network analysis can test the likelihood of the connections that are drawn into this kind of map.[93] This kind of Bayesian network analysis was used to assess the relative strengths of several different regulatory mechanisms for IL-12 in $CD4^+$ T cells.[94] Biomarkers for oral squamous cell carcinoma were identified by use of this technique.[95] Also research based on microarrays was used in a Bayesian network to identify connections between ten receptor tyrosine kinases and two sites from Src kinase.[96]

3.20.3.5 ODE and PDE Models

Ordinary differential equation modeling is, by far, the most common mathematical methodology in systems biology and QSP because this approach is powerful and versatile. Ordinary differential modeling can supply a continuous and quantitative view of the dynamics of a system. In other words, the concentration of every species in the model is tracked over the time course of the simulation. If the topology and parameters are correctly specified, then the results of the model are accurate predictions. However, this is far from easy. To build ODE models, the initial concentrations of every species in the model and the rate constants of every reaction in the model must be known. For all but the simplest of models, the parameters are usually determined by experiments or derived from literature values. The values of literature-derived parameters are often difficult to use in a model. This is because the various parameters are inconsistent with respect to the choice of cells, tissues, animal species, and variations in experimental design. Later, we will discuss how modelers address some of these concerns. When a system shows spatial heterogeneity, that is, concentrations varies in both time and position, partial differential equation models are employed. For example, to model the growth and invasion of tumors, a partial differential equation model is desirable,[97,98] or to understand the contribution of diffusion in cell signaling, PDE modeling is essential.[99]

In the context of modeling, the ordinary differential equations are simply rate expressions that reflect the formation and consumption for each species in the system. Therefore, each species in the system has a differential equation that subtracts the sum of rates that consume the species from those that form it. For example, the equilibrium interconversion of A and B:

$$\mathrm{A} \underset{k_{\mathrm{reverse}}}{\overset{k_{\mathrm{forword}}}{\rightleftharpoons}} \mathrm{B}$$

This would yield two ODE equations (one for each species).

$$\frac{d\mathrm{A}}{dt} = k_{\mathrm{reverse}}\,\mathrm{B} - k_{\mathrm{forward}}\,\mathrm{A}$$

$$\frac{d\mathrm{B}}{dt} = k_{\mathrm{forward}}\,\mathrm{A} - k_{\mathrm{reverse}}\,\mathrm{B}$$

In the case of irreversible reactions, there may be no formation terms (e.g., the first-order decay of a species) or no consumption terms (e.g., the zeroth order synthesis of a species). These equations usually follow the conventions of mass action chemical reactions. However, more complex behavior such as Michaelis–Menten kinetics (hyperbolic reactions that exhibit saturation), Hill equation behavior (sigmoidal concentration dependencies and other more complex behaviors), and inhibition of the various kinds of kinetics, observed in standard enzyme assays can be simply reformulated into mass action formats,[100] though one must be careful that the assumptions of the original equation are understood (e.g., steady-state assumptions or the requirement that substrate concentration greatly exceeds levels of enzymes). Mass action is not the only kind of rate equations that can be incorporated

into models. Since ODE modeling is similar to chemical kinetics, any physical or chemical rate can be used in the model. For example, diffusion rates into tissues and tumors are routinely modeled using Fick's law of diffusion.

When the ODE formalism is applied to multistep reactions, the same methodology is employed that was shown above for a one step "system." The summation of formation and consumption terms for particular specie may grow quite large if that specie is used as a reactant, or produced as a product, in many steps in the network, however, the procedure remains the same. When the reaction scheme is simple, as for example, the binding of a ligand to a receptor or a straightforward enzyme-catalyzed reaction, the ODE equations can be solved analytically by simple (though often tedious) algebraic manipulations. However, for most signaling networks, pathway models, or multiscale models of proteins, tissues and cells, which usually exhibit nonlinear behaviors, this kind of exact solution is not practical or possible. Under these conditions, the numerical solution of the set of ODE or PDE equations is done by discretizing the time component (and space component for PDE models). In other words, initial values for the concentrations of all the species are used to simultaneously recalculate their values at a very small time step away from time zero. The results of that calculation are then used in the next small time interval to generate the next set of concentrations, and the process is repeated. In this manner, a seemingly continuous trajectory is produced for each system species. Many ODE solvers are available to do this type of calculation. MatLab has several ODE solvers available (ode15s, ode45, etc.) and open source solvers are available on the Internet at https://sourceforge.net.

As mentioned above, as the complexity of the ODE model increases, more care must be applied to parameterizing the model. Poor estimates of initial values can cascade through the model to produce spurious outputs. However, it is likely that some uncertainty will creep into most models that are large enough to have value. This uncertainty is further exacerbated if the model contains novel proteins, for which little information has been derived. One solution to the parameterization dilemma is "big data." In theory, the measurement of the concentration of "protein X" in a wide range of settings (e.g., measuring the same protein in the same cell type in many healthy people and the same protein in the same cell type in a disease state) could produce a relevant range of values to apply to the model. Unfortunately, most big data databases are not organized in this way or use RNA expression data, which does not correlate with protein levels under many conditions.[101] High-throughput proteomics by mass spectrometry is getting much closer to being able to deliver this kind of critical data. But even that approach can be hampered by biological heterogeneity (e.g., tumor cells exhibit great heterogeneity both between patients and within a single person[102–104]). Also, this approach only focuses on the concentration of reactants, not the rate constants. A second option is to do a sensitivity analysis on the model. All values are held constant except one, which is varied over a small range and the effect on the model is calculated. The same procedure is repeated for all parameters in the system. In this way, a modeler can determine which parameters in the model are uniquely sensitive to change, and whose exact values can cause large variation in modeling outputs. Those parameters with the most influence might need further experimental verification. This method also has flaws. If parameters synergize or are not mutually orthogonal, the "vary one at a time" method may not work. Also sensitivity analysis is notoriously sensitive to initial conditions, so being grossly incorrect about some important parameter in the model, might give erroneous sensitivity analysis results. There are global sensitivity analysis approaches that sample the huge parameter space and that bypass the problems of most single parameter methods.[105,106] Validated and easy to use global sensitivity analysis will be a boon to modelers but are not generally available. Often, when a sensitivity analysis is done, a particular parameter that was hard to uncover from the literature, proves to be not sensitive. The model output may not be sensitive to this parameter and hence the precision with which it is known (within a reasonable range) does not change the results of the model. The last method to address a truly unknown value within the model is use parameter optimization. This requires an experimentally verified objective function for the system. To choose a very simple example, assume that the system under examination is the same protein A to protein B interconversion that was used above. Assume the time courses of A conversion to B and B to A are independently known. Further assume the initial concentrations of A and B are available and the forward rate constant is known, but the reverse rate constant is uncertain. Given this highly simplified example, the computer modeling software can be asked to vary the unknown rate constant until the time courses are fit. In this way, the fit rate constant can then be used in the model. In more complicated (more realistic) cases, unknown or uncertain parameters can be established by this method, but if the number of these unknowns is too high, the reliability of the model is questionable. In practice, modelers often face the problem of unknown parameters and use parameters from closely related species or protein family members to get a rough approximation for the unknown values as a starting point for further refinement.

In addition to the pathway models mentioned in the "**Definitions**" section of this paper, ODE models have shown success in many systems. To name only a few, ODE models have been used to understand gene regulatory networks,[107,108] to explore the development of autoimmunity through regulation of T_{reg} cells,[109] to unravel the complex dynamics of the immune system's response to tumors,[110] and to investigate the progression of Type 1 diabetes during β cell death.[111]

3.20.4 A Detailed Discussion of a Systems Biology and Quantitative Systems Model

In this section, the goal is to look at an example of a computational model in more detail, in order to give the reader a better understanding of the capabilities and limitations of modeling. The example is an ODE-based antibody drug conjugate (ADC) model. An ADC is a combination of an antibody, a drug payload, and a chemical linker that attaches the two other parts and has unique properties to release the toxin only when inside a cell.[112–115] ADC molecules are, currently, highly effectively employed in cancer therapy.[116–118] However not all ADC molecules are successful.[119] To aid in the design of safe and effective ADC drugs, an ordinary differential equation model of the underlying biology of these drugs, was created.[120] Probably this model best fits under the heading

of a QSP model, as it was created to predict pharmacometric parameters. No model, no matter how detailed, can hope to get right all the details of any therapeutic. The human "system" is just too complex. However, from a practical standpoint, getting a validated model to correctly predict enough detail to design more successful drugs has been achieved with this model. To be an efficacious drug, an ADC must complete a series of rather stringent steps. ADC molecules are administered as an intravenous infusion into the blood. Therefore the potential drug must first traverse the capillary wall. With most reagents of the molecular weight and shape of an antibody, crossing the endothelial cell layer that makes up the blood vessels is tissue dependent. With some notable exceptions (such as brain and eye, for example), the concentration of an antibody-based drug in the tissue is about 5–15% of the blood concentration.[121] Tumors are thought to be somewhat more leaky than normal tissue due to tortuous capillary architecture in the neoplasms.[122] Hence tumor penetration by ADC drugs should be somewhat higher than normal tissue. Aberrant growth also produces lymphatic vessels that are not correctly connected. Hence there is little or no lymphatic drainage from tumors. This results in higher retention of ADC drugs, compared to that seen in normal tissues. The model must account for these differences. After leaving the blood vessels, the ADC is in the interstitial space of the tumor, where it encounters tumor cells, which express the target of the antibody moiety of the ADC. All tissues are arranged so that no cell is more than about three cells away from a blood vessel. This is due to the need for efficient transfer of nutrients and oxygen from the blood. Tumor cells can resist hypoxia due to the upregulation of the HIF-1α system, which results in some tumor cells being more distant from the capillary wall. This biology provides a radial symmetry to the cells of the tumor that allows the model to treat the capillary as if it is a long cylinder with cells projecting out from the center. This allowed simplification of the model, and is based on previous work.[123] It also means that cells proximal to the capillary see the highest concentration of ADC, while cells distal to the capillary see less drug (see below). The ADC then binds to the tumor cell. In some cases, the ADC might be designed as an agonist of the receptor target and then it internalizes relatively rapidly. However, even in the case where the ADC does not trigger internalization, receptors on the surface of cells spontaneously internalize with a slower rate. This internalization carries the ADC reagent (and the receptor target) into a lipid bilayer enclosed endosome. The endosome is acidified by proton pumps. Depending on the composition of the chemical linker, some payloads are released during this step. In other chemical linkers, the intact ADC moves to the lysosome. In the lysosome, a number of proteases release the payload by proteolytic degradation of the antibody and linker. The payload has one of three fates if it is a mitotic toxin. It can accumulate if the cell is not in mitosis, or it can move to the nuclear machinery if the cell is in mitosis, or it can leave the cell either by diffusion or through the action of drug pumps. If the cell is in mitosis the payload binds tubulin and prevents its polymerization, which halts the synthesis of the mitotic spindles that are necessary for transit through mitosis. Freezing the cell in mitosis causes the cell to initiate a program of cell death, apoptosis. All of the preceding steps are necessary to make an effective drug, and the model was created to give a picture of the best blend of properties to achieve this goal.

The model can be thought of as being divided into a number of modules (see **Fig. 3**). One component of the model computes the diffusion of the ADC reagent out of the capillary and across the tumor cells. It determines how much of the administered dose gets to the desired tissue (the tumor), and follows the fate of the payload (either delivery of the toxin to the tumor cells or the payload that is released from the tumor back into the interstitial space) (see **Fig. 4A**). This section also keeps track of how far the ADC must penetrate the tumor since different tumors are vascularized to different extents. Another section of equations explores the parameters for binding of the antibody moiety to its target receptor, the internalization kinetics of the ADC/receptor complex, rates of processing in the endosome or lysosome, and release of the payload by cleavage of the chemical linker (**Fig. 4B**). The third module of the model follows tumor dynamics (see **Fig. 2C**). Since the payload of the ADC (in the current state of the field) is usually a mitotic toxin. The payload will only act to kill the tumor if a neoplasm cell is in mitosis, and if the internal concentration of the payload exceeds a threshold level (the maximum tolerated dose, MTD). Thus the model must also track the proportion of cells that are in mitosis at any time point and decide if the internal cellular concentration is in excess of the MTD. The model then eliminates those cells that meet these criteria. Finally, this module of the model follows the tumor doubling rate, since the drug is only effective if the tumor is killed faster than it grows.

A number of the predictions of the model have been verified by experimental results. For example, the model predicts that, if the affinity of the antibody portion of the molecule for its target is too high, the drug will be trapped by the first cell of the tumor that is proximal to the tumor capillaries (especially if the tumor target is expressed at high levels), and will hence not diffuse effectively and will not markedly reduce the tumor mass. However, too weak of an interaction between ADC and target also limits utility. This has been verified by experiments.[124] Antibody moiety affinity is an important ADC consideration. Many ADC candidates are created by taking a preexisting antibody and coupling it to the payload. Preexisting antibodies are often those that have shown efficacy as drugs by themselves. These antibodies often exhibit high affinities. From the discussion above, it should be clear that high-affinity antibodies (especially those directed against high abundance targets) may not be optimal. The model predicts an optimal affinity for the antibody or suggests ways in which the drug can be adapted to compensate for binding that is too tight. The model shows that there is a delicate balance between several design properties of ADC reagents in addition to affinity. For example, molecular weight (and shape) of the reagent must be large enough to avoid rapid clearance by the kidneys, but not be so large that penetration of the capillary wall and tumor diffusion is unlikely. Antibody-based reagents have long half-lives because there is FcRn recycling, which is mediated by the Fc region of the immunoglobin. Molecules of less than about 50,000 Da molecular weight are cleared by the kidney (if they do not bind to larger molecules). Therefore, making hybrids of small and large molecules gives superior PK compared to small molecule drugs, but making ADC based on smaller parts of the IgG molecule can have some advantages.[125] There are further balances between tumor properties and ADC characteristics addressed by the model. Lower tumor intercapillary distances leads to rapid transport of the ADC, however, highly vascularized tumors (e.g., head and neck squamous cell carcinomas) tend to double at an accelerated rate versus tumors with poor vascularization (e.g., pancreatic ductal cancers). Another critical balance derives from

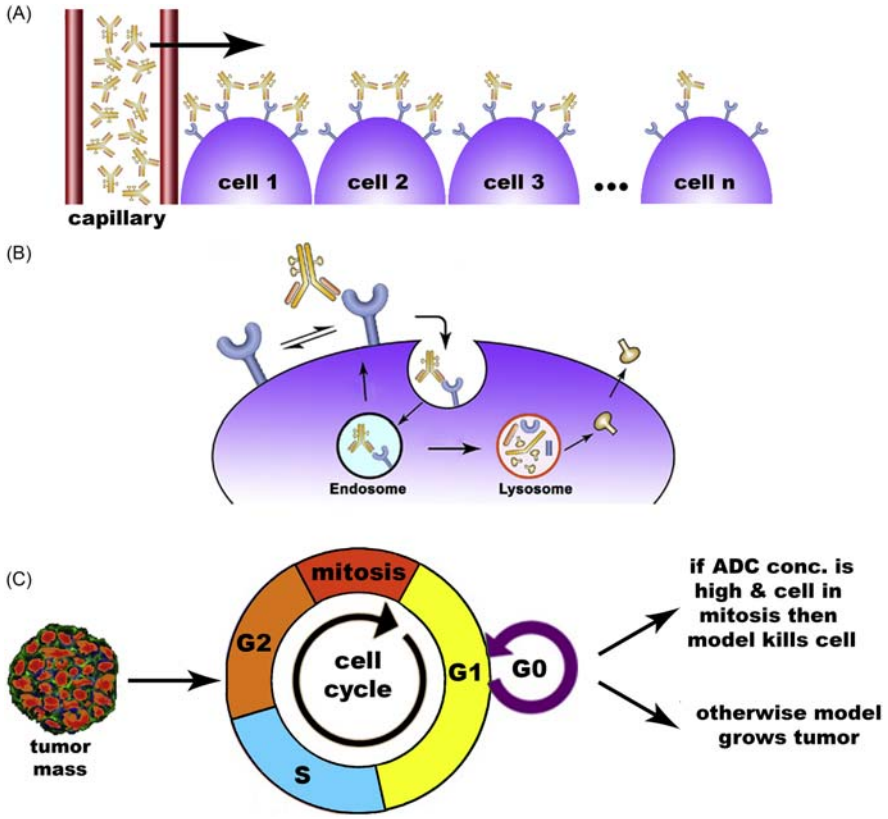

Fig. 4 A representation of the three conceptual modules in the antibody drug conjugate example. (A) The distribution of the ADC from the blood into the tumor. Because of the sink caused by the most capillary-proximal cells, a gradient of concentration is generated. (B) The kinetics of ADC binding, internalization, release of payload, and distribution of the toxin. (C) The module that keeps track of tumor dynamics, killing, and/or growth.

the loss of cleaved payload from the cell. On the one hand, this lowers the effective internal concentration of the drug, but it also promotes "bystander killing"[126] and increased tumor penetration. In theory, the model can be parameterized with tumor variables and, separately, with healthy tissue characteristics. This, in principle, allows for the generation of an in silico therapeutic index, though this avenue has not yet been extensively explored. Properly applied, this model allows the pharmaceutical drug designer a way to objectively choose ADC properties that best match with the tumor characteristics. The model can reduce the number of design/test/redesign cycles that are necessary to create an ADC candidate. Hopefully, this example demonstrates that ODE modeling can easily accommodate most kinds of problems that occur in deterministic models. Instead of only handling sequential steps associated with pathway modeling, this model allows the incorporation of the treatment of many biological processes—diffusion, cell cycle monitoring, and tumor dynamics, as well as binding and internalization kinetics.

3.20.5 Summary

This article has given the reader a beginner's guide to understanding systems approaches to biology and pharmaceutical discovery. Systems biology or QSP (or any of the other, myriad names this work is called) is at an important point in its development. The concomitant evolution of mass sequencing and even more massive biological data collection set out to give a complete components list of human biology, but has often left scientists to drown in vast information overload. Reductionism has been left behind for the very practical reason that there is just too much to study "one at a time." There seem to be more contradictions than grand unifiers of biological knowledge. This is where systems biology will play a crucial role. The need to quickly examine new hypotheses about the nature of biological processes and to suggest the most impactful experiments to test them is fertile ground for the growth of systems biology. The closely related field of QSP applies the same toolbox to finding new drugs and describing the optimal properties of those drugs to achieve the best chance for successful amelioration of disease. Systems biology or QSP are an amalgam of biology, chemistry, physics, and computer sciences. The English biochemist Fredrick Gowland Hopkins said "…where sciences meet, there growth occurs." The adoption of systems approaches in the pharmaceuticals industry is slow. Drug discoverers have been very successful without systems biology and systems pharmacology. Why change? The main driver of the growth in systems approaches

is the realization that biology is complex—patients vary in response to drugs; the same pathways giving rise to one output in one cell type gives a completely different outcome in another; arrangements of signaling networks are subverted by disease; and heterogeneity in toxicology is difficult to understand. Aristotle wrote, "The chief forms of beauty are order and symmetry and definiteness which the mathematical sciences demonstrate in a special degree." But maybe Aristotle was not a systems thinker because biology is messy and systems studies thrive on complexity.

See also: 2.18. Systems Biology: Methods and Applications. 2.19. Systems Chemical Biology: Integrating Medicinal Chemistry and Systems Biology for Drug Discovery.

References

1. Trewavas, A. A Brief History of Systems Biology. *Plant Cell* **2006,** *18,* 2420–2430.
2. Fang, F. C.; Casadevall, A. Reductionistic and Holistic Science. *Infect. Immun.* **2011,** *79* (4), 1401–1404.
3. Hodgkin, A. L.; Huxley, A. F. A Quantitative Description of Membrane Current and Its Application to Conduction and Excitation in Nerve. *J. Physiol.* **1952,** *117* (4), 500–544.
4. Noble, D. A Modification of the Hodgkin-Huxley Equations Applicable to the Purkinje Fiber Action and Pace-Maker Potentials. *J. Physiol.* **1962,** *160,* 317–352.
5. Genet, M.; Lee, L. C.; Baillargeon, B.; Guccione, J. M.; Kuhl, E. Modeling Pathologies of Diastolic and Systolic Heart Failure. *Ann. Biomed. Eng.* **2016,** *44* (1), 112–127.
6. Beckwith, J. R. Regulation of the Lac Operon. *Science* **1967,** *156* (3775), 597–604.
7. Kobayashi, H.; Kærn, M.; Araki, M.; Chung, K.; Gardner, T. S.; Cantor, C. R.; Collins, J. J. Programmable Cells: Interfacing Natural and Engineered Gene Networks. *Proc. Natl. Acad. Sci. U. S. A.* **2004,** *101* (22), 8414–8419.
8. Pintoa, M. C.; Fossa, L.; Mombachb, J. C. M.; Ribeiro, L. Modelling, Property Verification and Behavioural Equivalence of Lactose Operon Regulation. *Comput. Biol. Med.* **2007,** *37* (2), 134–148.
9. Chiche, L.; Jourde-Chiche, N.; Pascual, V.; Chaussabel, D. Disease Mechanisms in Rheumatology—Tools and Pathways: Current Perspectives on Systems Immunology Approaches to Rheumatic Diseases. *Arthritis Rheum.* **2013,** *65* (6), 1407–1417.
10. Narang, V.; Decraene, J.; Wong, S.-Y.; Aiswarya, B. S.; Wasem, A. R.; Leong, S. R.; Gouaillard, A. Systems Immunology: A Survey of Modeling Formalisms, Applications and Simulation Tools. *Immunol. Res.* **2012,** *53,* 251–326.
11. Li, H. Systems Genetics in "-Omics" Era: Current and Future Development. *Theory Biosci.* **2013,** *132* (1), 1–16.
12. Powathil, G. G.; Swat, M.; Chaplain, M. A. J. Systems Oncology: Towards Patient-Specific Treatment Regimes Informed by Multiscale Mathematical Modelling. *Semin. Cancer Biol.* **2015,** *30,* 13–20.
13. Masoudi-Nejad, A.; Bidkhori, G.; Ashtiani, S. H.; Najafi, A.; Bozorgmehr, J. H.; Wang, E. *Semin. Cancer Biol.* **2015,** *30,* 60–69.
14. Xie, L.; Ge, X.; Tan, H.; Xie, L.; Zhang, Y.; Hart, T.; Yang, X.; Bourne, P. E. Towards Structural Systems Pharmacology to Study Complex Diseases and Personalized Medicine. *PLoS Comput. Biol.* **2014,** *10* (5), 1–15.
15. Mesarović, M. *Systems Theory and Biology;* Springer: New York, 1968; pp. 59–87.
16. Lotka, A. J. Contribution to the Mathematical Theory of Capture: I Conditions for Capture. *Proc. Natl. Acad. Sci. U. S. A.* **1932,** *18* (2), 172–178.
17. Ukai, H.; Hiroki, R.; Ueda, H. R. Systems Biology of Mammalian Circadian Clocks. *Annu. Rev. Physiol.* **2010,** *72,* 579–603.
18. Csikász-Nagy, A. Computational Systems Biology of the Cell Cycle. *Brief. Bioinform.* **2009,** *10* (4), 424–434.
19. Liu, B.; Zhang, J.; Tan, P. Y.; Hsu, D.; Blom, A. M.; Leong, B.; Sethi, S.; Ho, B.; Ding, J. L.; Thiagarajan, P. S. A Computational and Experimental Study of the Regulatory Mechanisms of the Complement System. *PLoS Comput. Biol.* **2011,** *7* (1). e1001059.
20. Dolan, D. W. P.; Zupanic, A.; Nelson, G.; Hall, P.; Miwa, S.; Kirkwood, T. B. L.; Shanley, D. P. Integrated Stochastic Model of DNA Damage Repair by Non-Homologous End Joining and p53/p21-Mediated Early Senescence Signalling. *PLoS Comput. Biol.* **2015,** *11* (5). e1004246.
21. Ideker, T.; Galitski, T.; Hood, L. A New Approach to Decoding Life: Systems Biology. *Annu. Rev. Genomics Hum. Genet.* **2001,** *2,* 343–372.
22. Fitzgerald, J. B.; Schoeberl, B.; Nielsen, U. B.; Sorger, P. K. Systems Biology and Combination Therapy in the Quest for Clinical Efficacy. *Nat. Chem. Biol.* **2006,** *2,* 458–466.
23. Bown, J. L.; Shovman, M.; Robertson, P.; Boiko, A.; Goltsov, A.; Mullen, P.; Harrison, D. J. A signaling visualization toolkit to support rational design of combination therapies and biomarker discovery: SiViT. *Oncotarget* **2016** (epublication before print, PMID 27302920).
24. Garmaroudi, F. S.; Handy, D. E.; Liu, Y.-Y.; Loscalzo, J. Systems Pharmacology and Rational Polypharmacy: Nitric Oxide–Cyclic GMP Signaling Pathway as an Illustrative Example and Derivation of the General Case. *PLoS Comput. Biol.* **2016,** *12* (3). e1004822.
25. Gabrielsson, J.; Gibbons, F. D.; Peletier, L. A. Mixture Dynamics: Combination Therapy in Oncology. *Eur. J. Pharm. Sci.* **2016,** *88,* 132–146.
26. Felix-Mart, G. J.; Godõnez-Fernandez, J. R. Mathematical Models of Electrical Activity of the Pancreatic β-Cell: A Physiological Review. *Islets* **2014,** *6* (3). e949195.
27. Schmitz, J. P.; Vanlier, J.; van Riel, N. A.; Jeneson, J. A. Computational Modeling of Mitochondrial Energy Transduction. *Crit. Rev. Biomed. Eng.* **2011,** *39* (5), 363–377.
28. Larsen, E. H.; Sørensen, J. B.; Sørensen, J. N. Analysis of the Sodium Recirculation Theory of Solute-Coupled Water Transport in Small Intestine. *J. Physiol.* **2002,** *542* (Pt 1), 33–50.
29. Schneider, H.-C.; Klabunde, T. Understanding Drugs and Diseases by Systems Biology? *Bioorg. Med. Chem. Lett.* **2013,** *23* (5), 1168–1176.
30. Westerhoff, H. V.; Groen, A. K.; Wanders, R. J. Modern Theories of Metabolic Control and Their Applications. *Biosci. Rep.* **1984,** *4* (1), 1–22.
31. Moreno-Sanchez, R.; Saavedra, E.; Rodrõguez-Enrõquez, S.; Olõn-Sandoval, V. Metabolic Control Analysis: A Tool for Designing Strategies to Manipulate Metabolic Pathways. *J. Biomed. Biotechnol.* **2008,** *597913,* 1–30.
32. Aldridge, B. B.; Burke, J. M.; Lauffenburger, D. A.; Sorger, P. K. Physicochemical Modelling of Cell Signalling Pathways. *Nat. Cell Biol.* **2006,** *8,* 1195–1203.
33. MacNamara, A.; Henriques, D.; Saez-Rodriguez, J. Modeling Signaling Networks With Different Formalisms: A Preview. *Methods Mol. Biol.* **2013,** *1021,* 89–105.
34. Asthagiri, A. R.; Lauffenburger, D. A. A Computational Study of Feedback Effects on Signal Dynamics in a Mitogen-Activated Protein Kinase (MAPK) Pathway Model. *Biotechnol. Prog.* **2001,** *17* (2), 227–239.
35. Hendriks, B. S.; Orr, G.; Wells, A.; Wiley, H. S.; Lauffenburger, D. A. Parsing ERK Activation Reveals Quantitatively Equivalent Contributions From Epidermal Growth Factor Receptor and HER2 in Human Mammary Epithelial Cells. *J. Biol. Chem.* **2005,** *280* (7), 6157–6169.
36. Wiley, H. S.; Shvartsman, S. Y.; Lauffenburger, D. A. Computational Modeling of the EGF-Receptor System: A Paradigm for Systems Biology. *Trends Cell Biol.* **2003,** *13* (1), 43–50.
37. Kumar, N.; Hendriks, B. S.; Janes, K. A.; de Graaf, D.; Lauffenburger, D. A. Applying Computational Modeling to Drug Discovery and Development. *Drug Discov. Today* **2006,** *11* (17–18), 806–811.
38. Kogan, Y.; Halevi-Tobias, K. E.; Hochman, G.; Baczmanska, A. K.; Leyns, L.; Agur, Z. A New Validated Mathematical Model of the Wnt Signalling Pathway Predicts Effective Combinational Therapy by sFRP and Dkk. *Biochem. J.* **2012,** *444* (1), 115–125.
39. Yamadaa, S.; Shionoa, S.; Joob, A.; Yoshimurab, A. Control Mechanism of JAK/STAT Signal Transduction Pathway. *FEBS Lett.* **2003,** *534* (1–3), 190–196.
40. Heinrich, R.; Neel, B. G.; Tom, A.; Rapoport, T. A. Mathematical Models of Protein Kinase Signal Transduction. *Mol. Cell* **2002,** *9* (5), 957–970.

41. Lipniackia, T.; Paszek, P.; Brasierd, A. R.; Luxonc, B.; Kimmelb, M. Mathematical Model of NF-κB Regulatory Module. *J. Theor. Biol.* **2004,** *228* (2), 195–215.
42. Collier, J. R.; Monk, N. A. M.; Maini, P. K.; Lewis, J. H. Pattern Formation by Lateral Inhibition With Feedback: A Mathematical Model of Delta Notch Intercellular Signalling. *J. Theor. Biol.* **1996,** *183,* 429–446.
43. Zia, Z.; Chapnickb, D. A.; Liub, X. Dynamics of TGF-β/Smad Signaling. *FEBS Lett.* **2012,** *586* (14), 1921–1928.
44. Zi, Z.; Klipp, E. Constraint-Based Modeling and Kinetic Analysis of the Smad Dependent TGF-Beta Signaling Pathway. *PLoS ONE* **2007,** *2* (9), 1–21.
45. Wake, M. H. What Is "Integrative Biology"? *Integr. Comp. Biol.* **2003,** *43* (2), 239–241.
46. Wake, M. H. Integrative Biology: Science for the 21st Century. *Bioscience* **2008,** *58* (4), 349–353.
47. Kostewicza, E. S.; Aaronsb, L.; Bergstrandc, M.; Bolgerd, M. B.; Galetinb, A.; Hatleyb, O.; Jameie, M.; Lloydf, R.; Peping, X.; Rostami-Hodjeganb, A.; Sjögrenh, E.; Tannergreni, C.; Turnere, D. B.; Wagnera, C.; Weitschiesj, W.; Dressmana, J. PBPK Models for the Prediction of In Vivo Performance of Oral Dosage Forms. *Eur. J. Pharm. Sci.* **2014,** *57,* 300–321.
48. Rowland, M.; Peck, P.; Tucker, G. Physiologically-Based Pharmacokinetics in Drug Development and Regulatory Science. *Annu. Rev. Pharmacol. Toxicol.* **2011,** *51,* 45–73.
49. Thygesen, P.; Macheras, P.; Van Peer, A. Physiologically-Based PK/PD Modelling of Therapeutic Macromolecules. *Pharm. Res.* **2009,** *26* (12), 2543–2550.
50. Subramanian, G.; Kitchen, D. B. Computational Approaches for Modeling Human Intestinal Absorption and Permeability. *J. Mol. Model.* **2006,** *12* (5), 577–589.
51. Peterson, M. C.; Riggs, M. M. A Physiologically Based Mathematical Model of Integrated Calcium Homeostasis and Bone Remodeling. *Bone* **2010,** *46,* 49–63.
52. Meibohm, B.; Derendorf, H. Basic Concepts of Pharmacokinetic/Pharmacodynamic (PK/PD) Modelling. *Int. J. Clin. Pharmacol. Ther.* **1997,** *35* (10), 401–413.
53. Ploeger, B. A.; Van der Graaf, P. H.; Danhof, M. Incorporating Receptor Theory in Mechanism-Based Pharmacokinetic-Pharmacodynamic (PK-PD) Modeling. *Drug Metab. Pharmacokinet.* **2009,** *24* (1), 3–15.
54. Lu, D.; Jin, J. Y.; Girish, S.; Agarwal, P.; Li, D.; Prabhu, S.; Dere, R. C.; Saad, O. M.; Nazzal, D.; Koppada, N.; Ramanujan, S.; Ng, C. M. Semi-Mechanistic Multiple-Analyte Pharmacokinetic Model for an Antibody-Drug-Conjugate in Cynomolgus Monkeys. *Pharm. Res.* **2015,** *32* (6), 1907–1919.
55. Peng, J. Z.; Denney, W. S.; Musser, B. J.; Liu, R.; Tsai, K.; Fang, L.; Reitman, M. L.; Troyer, M. D.; Engel, S. S.; Xu, L.; Stoch, A.; Stone, J. A.; Kowalski, K. G. A Semi-Mechanistic Model for the Effects of a Novel Glucagon Receptor Antagonist on Glucagon and the Interaction Between Glucose, Glucagon, and Insulin Applied to Adaptive Phase II Design. *AAPS J.* **2014,** *16* (6), 1259–1270.
56. Yun, H. Y.; Kang, W.; Lee, B. Y.; Park, S.; Yoon, Y. R.; Yeul Ma, J.; Kwon, K. I. Semi-Mechanistic Modelling and Simulation of Inhibition of Platelet Aggregation by Antiplatelet Agents. *Basic Clin. Pharmacol. Toxicol.* **2014,** *115* (4), 352–359.
57. Gordi, T.; Xie, R.; Jusko, W. J. Semi-Mechanistic Pharmacokinetic/Pharmacodynamic Modelling of the Antimalarial Effect of Artemisinin. *Br. J. Clin. Pharmacol.* **2005,** *60* (6), 594–604.
58. Van der Graaf, P. H.; Benson, N. Systems Pharmacology: Bridging Systems Biology and Pharmacokinetics-Pharmacodynamics (PKPD) in Drug Discovery and Development. *Pharm. Res.* **2011,** *28,* 1460–1464.
59. Peterson, M. C.; Riggs, M. M. FDA Advisory Meeting Clinical Pharmacology Review Utilizes a Quantitative Systems Pharmacology (QSP) Model: A Watershed Moment? *CPT Pharmacometrics Syst. Pharmacol.* **2015,** *4* (3). e00020.
60. Sorger, P. K.; Allerheiligen, S. R. B.; Abernethy, D. R.; Altman, R. B.; Brouwer, K. L. R.; Califano, A.; D'Argenio, D. Z.; Iyengar, R.; Jusko, W. J.; Lalonde, R.; Lauffenburger, D. A.; Shoichet, B.; Stevens, J. L.; Subramaniam, S.; Van der Graaf, P.; Vicini, P.; Ward, R. Eds., Quantitative and Systems Pharmacology in the Post-genomic Era: New Approaches to Discovering Drugs and Understanding Therapeutic Mechanisms; NIH White Paper by the QSP Workshop Group, October, 2011.
61. Pérez-Nuenoa, V. I. Using Quantitative Systems Pharmacology for Novel Drug Discovery. *Expert Opin. Drug Discovery* **2015,** *10* (12), 1315–1331.
62. Palsson, S.; Hickling, T. P.; Bradshaw-Pierce, E. L.; Zager, M.; Jooss, K.; O'Brien, P. J.; Spilker, M. E.; Palsson, B. O.; Vicini, P. The Development of a Fully-Integrated Immune Response Model (FIRM) Simulator of the Immune Response Through Integration of Multiple Subset Models. *BMC Syst. Biol.* **2013,** *7* (95).
63. Wierling, C.; Kessler, T.; Ogilvie, L. A.; Lange, B. M. H.; Yaspo, M.-L.; Lehrach, H. Network and Systems Biology: Essential Steps in Virtualising Drug Discovery and Development. *Drug Discov. Today Technol.* **2015,** *15,* 34–40.
64. Wist, A. D.; Berger, S. I.; Iyengar, R. Systems Pharmacology and Genome Medicine: A Futher Perscective. *Genome Med.* **2009,** *1* (1), 1–11.
65. Turner, R. M.; Park, B. K.; Pirmohamed, M. Parsing Interindividual Drug Variability: An Emerging Role for Systems Pharmacology. *Wiley Interdiscip. Rev. Syst. Biol. Med.* **2015,** *7* (4), 221–241.
66. Bugrim, A.; Nikolskaya, T.; Nikolsky, Y. Early Prediction of Drug Metabolism and Toxicity: Systems Biology Approach and Modeling. *Drug Discov. Today* **2004,** *9* (3), 127–135.
67. Bornholdt, S. Boolean Network Models of Cellular Regulation: Prospects and Limitations. *J. R. Soc. Interface* **2008,** *5* (Suppl. 1), S85–S94.
68. Kauffman, S.; Peterson, C.; Samuelsson, B.; Troein, C. Random Boolean Network Models and the Yeast Transcriptional Network. *Proc. Natl. Acad. Sci. U. S. A.* **2003,** *100* (25), 14796–14799.
69. Huang, S. Genomics, Complexity and Drug Discovery: Insights From Boolean Network Models of Cellular Regulation. *Pharmacogenomics* **2001,** *2* (3), 203–222.
70. Trairatphisan, P.; Mizera, A.; Pang, J.; Tantar, A. A.; Schneider, J.; Sauter, T. Recent Development and Biomedical Applications of Probabilistic Boolean Networks. *Cell Commun. Signal.* **2013,** *11* (46), 1–25.
71. Morris, M. K.; Saez-Rodriguez, J.; Sorger, P. K.; Lauffenburger, D. A. Logic-Based Models for the Analysis of Cell Signaling Networks. *Biochemistry* **2010,** *49* (15), 3216–3224.
72. MacNamara, A.; Terfve, C.; Henriques, D.; Bernabé, B. P.; Saez-Rodriguez, J. State-Time Spectrum of Signal Transduction Logic Models. *Phys. Biol.* **2012,** *9* (4), 1–16.
73. Chen, H.; Wang, G.; Simha, R.; Du, C.; Zeng, C. Boolean Models of Biological Processes Explain Cascade-Like Behavior. *Sci. Rep.* **2016,** *7,* 20067.
74. Dahlhausa, M.; Burkovskib, A.; Hertwigd, F.; Musselb, C.; Vollandd, R.; Fischerd, M.; Debatina, K.-M.; Kestlerb, H. A.; Beltingera, C. Boolean Modeling Identifies Greatwall/MASTL as an Important Regulator in the AURKA Network of Neuroblastoma. *Cancer Lett.* **2016,** *37* (1), 179–189.
75. Zhang, R.; Shah, M. V.; Yang, J.; Nyland, S. B.; Liu, X.; Yun, J. K.; Albert, R.; Loughran, T. P., Jr. Network Model of Survival Signaling in Large Granular Lymphocyte Leukemia. *Proc. Natl. Acad. Sci. U. S. A.* **2008,** *105* (42), 16308–16313.
76. Martinez-Sanchez, M. E.; Mendoza, L.; Villarreal, C.; Alvarez-Buylla, E. R. A Minimal Regulatory Network of Extrinsic and Intrinsic Factors Recovers Observed Patterns of CD4+ T Cell Differentiation and Plasticity. *PLoS Comput. Biol.* **2015,** *11* (6). e1004324.
77. Pinney, J. W.; Westhead, D. R.; McConkey, G. A. Petri Net Representations in Systems Biology. *Biochem. Soc. Trans.* **2003,** *31* (6), 1513–1515.
78. Gilbert, D.; Fuβ, H.; Gu, X.; Orton, R.; Robinson, S.; Vyshemirsky, V.; Kurth, M. J.; Downes, C. S.; Dubitzky, W. Computational Methodologies for Modelling, Analysis and Simulation of Signalling Networks. *Brief. Bioinform.* **2006,** *7* (4), 339–353.
79. Moore, J. H.; Boczko, E. M.; Marshall, L.; Summar, M. L. Connecting the Dots Between Genes, Biochemistry, and Disease Susceptibility: Systems Biology Modeling in Human Genetics. *Mol. Genet. Metab.* **2005,** *84* (2), 104–111.
80. Lee, D. Y.; Zimmer, R.; Lee, S. Y.; Hanisch, D.; Park, S. Knowledge Representation Model for Systems-Level Analysis of Signal Transduction Network. *Genome Inform.* **2004,** *15* (2), 234–243.
81. Heiner, M.; Sriram, K. Structural Analysis to Determine the Core of Hypoxia Response Network. *PLoS ONE* **2010,** *5* (1). e8600.
82. Railsback, S. F.; Grimm, V. *Agent-Based and Individual-Based Modeling;* Princeton University Press: Princeton, NJ, 2012.
83. Wang, Z.; Zhang, L.; Sagotsky, J.; Deisboeck, T. S. Simulating Non-Small Cell Lung Cancer With a Multiscale Agent-Based Model. *Theor. Biol. Med. Model.* **2007,** *4* (50), 1–14.
84. Zhanga, L.; Athaleb, C. A.; Deisboecka, T. S. Development of a Three-Dimensional Multiscale Agent-Based Tumor Model: Simulating Gene-Protein Interaction Profiles, Cell Phenotypes and Multicellular Patterns in Brain Cancer. *J. Theor. Biol.* **2007,** *244* (1), 96–107.
85. Enderling, H.; Anderson, A. R. A.; Chaplain, M. A. J.; Beheshti, A.; Hlatky, L.; Hahnfeldt, P. Paradoxical Dependencies of Tumor Dormancy and Progression on Basic Cell Kinetics. *Cancer Res.* **2009,** *69,* 8814–8821.

86. Tomezaka, M.; Abbadieb, C.; Lartigauc, E.; Cleri, F. A Biophysical Model of Cell Evolution After Cytotoxic Treatments: Damage, Repair and Cell Response. *J. Theor. Biol.* **2016,** *389,* 146–158.
87. Kima, M.; Reedb, D.; Rejniak, K. A. The Formation of Tight Tumor Clusters Affects the Efficacy of Cell Cycle Inhibitors: A Hybrid Model Study. *J. Theor. Biol.* **2014,** *352,* 31–50.
88. Lardon, L. A.; Merkey, B. V.; Martins, S.; Dötsch, A.; Picioreanu, C.; Kreft, J. U.; Smets, B. F. iDynoMiCS: Next-Generation Individual-Based Modelling of Biofilms. *Environ. Microbiol.* **2011,** *13,* 2416–2434.
89. Siettos, C.; Anastassopoulou, C.; Russo, L.; Grigoras, C.; Mylonakis, E. Forecasting and Control Policy Assessment for the Ebola Virus Disease (EVD) Epidemic in Sierra Leone Using Small-World Networked Model Simulations. *BMJ Open* **2016,** *6* (1). e008649.
90. Pe'er, D. Bayesian Network Analysis of Signaling Networks: A Primer. *Sci. STKE* **2005,** *2005* (26), 1–14.
91. Sachs, K.; Gifford, D.; Jaakkola, T.; Sorger, P.; Lauffenburger, D. A. Bayesian Network Approach to Cell Signaling Pathway Modeling. *Sci. STKE* **2002,** *2002* (148), 1–6.
92. http://www.genome.jp/kegg/pathway.html
93. Klinke, D. J., 2nd. An Empirical Bayesian Approach for Model-Based Inference of Cellular Signaling Networks. *BMC Bioinf.* **2009,** *10* (371), 1–18.
94. Finley, S. D.; Gupta, D.; Cheng, N.; Klinke, D. J., 2nd Inferring Relevant Control Mechanisms for Interleukin-12 Signaling in Naïve CD4+ T Cells. *Immunol. Cell Biol.* **2011,** *89* (1), 100–110.
95. Kourou, K. A Bayesian Network-based approach for discovering oral cancer candidate biomarkers. Conference of the Proceedings of IEEE Engineering in Medicine and Biology Society; 2015; pp 7663–7666.
96. Ciaccio, M. F.; Wagner, J. P.; Chuu, C. P.; Lauffenburger, D. A.; Jones, R. B. Systems Analysis of EGF Receptor Signaling Dynamics With Microwestern Arrays. *Nat. Methods* **2010,** *7* (2), 148–155.
97. Hartung, N.; Mollard, S.; Barbolosi, D.; Benabdallah, A.; Chapuisat, G.; Henry, G.; Giacometti, S.; Iliadis, A.; Ciccolini, J.; Faivre, C.; Hubert, F. Mathematical Modeling of Tumor Growth and Metastatic Spreading: Validation in Tumor-Bearing Mice. *Cancer Res.* **2014,** *74,* 6397–6407.
98. Tao, Y.; Guo, Q.; Aihara, K. A Partial Differential Equation Model and Its Reduction to an Ordinary Differential Equation Model for Prostate Tumor Growth Under Intermittent Hormone Therapy. *J. Math. Biol.* **2014,** *69* (4), 817–838.
99. Friedmann, E. PDE/ODE Modeling and Simulation to Determine the Role of Diffusion in Long-Term and -Range Cellular Signaling. *BMC Biophys.* **2015,** *8* (10), 1–16.
100. Tyson, J. J.; Chen, K. C.; Novak, B. Sniffers, Buzzers, Toggles and Blinkers: Dynamics of Regulatory and Signaling Pathways in the Cell. *Curr. Opin. Cell Biol.* **2003,** *15,* 221–231.
101. Maier, T.; Güell, M.; Serrano, L. Correlation of mRNA and Protein in Complex Biological Samples. *FEBS Lett.* **2009,** *583* (24), 3966–3973.
102. Chéry, L.; Lam, H.-M.; Coleman, I.; Lakely, B.; Coleman, R.; Larson, S.; Aguirre-Ghiso, J. A.; Xia, J.; Gulati, R.; Nelson, P. S.; Montgomery, B.; Lange, P.; Snyder, L. A.; Vessella, R. L.; Morrissey, C. Characterization of Single Disseminated Prostate Cancer Cells Reveals Tumor Cell Heterogeneity and Identifies Dormancy Associated Pathways. *Oncotarget* **2014,** *5* (20), 9939–9951.
103. Sommer, L. Open Questions: Development of Tumor Cell Heterogeneity and Its Implications for Cancer Treatment. *BMC Biol.* **2014,** *12* (15), 1–2.
104. Chekhun, V. F.; Sherban, S. D.; Savtsova, Z. D. Tumor Cell Heterogeneity. *Exp. Oncol.* **2013,** *35* (3), 154–162.
105. Kiparissides, A.; Kucherenko, S. S.; Mantalaris, A.; Pistikopoulos, E. N. Global Sensitivity Analysis Challenges in Biological Systems Modeling. *Ind. Eng. Chem. Res.* **2009,** *48,* 7168–7180.
106. Sumner, T.; Shephard, E.; Bogle, I. D. L. A Methodology for Global-Sensitivity Analysis of Time-Dependent Outputs in Systems Biology Modelling. *J. R. Soc. Interface* **2012,** *9* (74), 2156–2166.
107. Wu, H.; Lu, T.; Xue, H.; Liang, H. Sparse Additive Ordinary Differential Equations for Dynamic Gene Regulatory Network Modeling. *J. Am. Stat. Assoc.* **2014,** *109* (506), 700–716.
108. Lu, T.; Liang, H.; Li, H.; Wu, H. High Dimensional ODEs Coupled With Mixed-Effects Modeling Techniques for Dynamic Gene Regulatory Network Identification. *J. Am. Stat. Assoc.* **2011,** *106* (496), 1242–1258.
109. Alexander, H. K.; Wahl, L. M. Self-Tolerance and Autoimmunity in a Regulatory T Cell Model. *Bull. Math. Biol.* **2011,** *73,* 33–71.
110. Nwabugwu, C. I.; Rakhra, K.; Felsher, D. W.; Paik, D. S. A Tumor-Immune Mathematical Model of CD4+ T Helper Cell Dependent Tumor Regression by Oncogene Inactivation. Conference of the Proceedings of IEEE Engineering in Medicine and Biology Society; **2013,** 4529–4532.
111. Marinković, T.; Sysi-Aho, M.; Orešič, M. Integrated Model of Metabolism and Autoimmune Response in β-Cell Death and Progression to Type 1 Diabetes. *PLoS ONE* **2012,** *7* (12). e51909.
112. Jerjian, T. V.; Glode, A. E.; Thompson, L. A.; O'Bryant, C. L. Antibody-Drug Conjugates: A Clinical Pharmacy Perspective on an Emerging Cancer Therapy. *Pharmacotherapy* **2016,** *36* (1), 99–116.
113. Peters, C.; Brown, S. Antibody–Drug Conjugates as Novel Anti-Cancer Chemotherapeutics. *Biosci. Rep.* **2015,** *35* (4). e00225.
114. Deonarain, M. P.; Yahioglu, G.; Stamati, I.; Marklew, J. Emerging Formats for Next-Generation Antibody Drug Conjugates. *Expert Opin. Drug Discovery* **2015,** *10* (5), 463–481.
115. Zolot, R. S.; Basu, S.; Million, R. P. Antibody-Drug Conjugates. *Nat. Rev. Drug Discov.* **2013,** *12* (4), 259–260.
116. Burris, H. A., 3rd; Rugo, H. S.; Vukelja, S. J.; Vogel, C. L.; Borson, R. A.; Limentani, S.; Tan-Chiu, E.; Krop, I. E.; Michaelson, R. A.; Girish, S.; Amler, L.; Zheng, M.; Chu, Y. W.; Klencke, B.; O'Shaughnessy, J. A. Phase II Study of the Antibody Drug Conjugate Trastuzumab-DM1 for the Treatment of Human Epidermal Growth Factor Receptor 2 (HER2)-Positive Breast Cancer After Prior HER2-Directed Therapy. *J. Clin. Oncol.* **2011,** *29* (4), 398–405.
117. Krop, I. E.; LoRusso, P.; Miller, K. D.; Modi, S.; Yardley, D.; Rodriguez, G.; Guardino, E.; Lu, M.; Zheng, M.; Girish, S.; Amler, L.; Winer, E. P.; Rugo, H. S. A Phase II Study of Trastuzumab Emtansine in Patients With Human Epidermal Growth Factor Receptor 2-Positive Metastatic Breast Cancer Who Were Previously Treated With Trastuzumab, Lapatinib, an Anthracycline, a Taxane, and Capecitabine. *J. Clin. Oncol.* **2012,** *30* (26), 3234–3241.
118. Younes, A.; Gopal, A. K.; Smith, S. E.; Ansell, S. M.; Rosenblatt, J. D.; Savage, K. J.; Ramchandren, R.; Bartlett, N. L.; Cheson, B. D.; de Vos, S.; Forero-Torres, A.; Moskowitz, C. H.; Connors, J. M.; Engert, A.; Larsen, E. K.; Kennedy, D. A.; Sievers, E. L.; Chen, R. Results of a Pivotal Phase II Study of Brentuximab Vedotin for Patients With Relapsed or Refractory Hodgkin's Lymphoma. *J. Clin. Oncol.* **2012,** *30* (18), 2183–2189.
119. Wadleigh, M.; Richardson, P. G.; Zahrieh, D.; Lee, S. J.; Cutler, C.; Ho, V.; Alyea, E. P.; Antin, J. H.; Stone, R. M.; Soiffer, R. J.; DeAngelo, D. Prior Gemtuzumab Ozogamicin Exposure Significantly Increases the Risk of Veno-Occlusive Disease in Patients Who Undergo Myeloablative Allogeneic Stem Cell Transplantation. *Blood* **2003,** *102* (5), 1578–1582.
120. Vasalou, C.; Helmlinger, G.; Gomes, B. A Mechanistic Tumor Penetration Model to Guide Antibody Drug Conjugate Design. *PLoS ONE* **2015,** *10* (3). e0118977.
121. Shah, D. K.; Betts, A. M. Antibody Biodistribution Coefficients: Inferring Tissue Concentrations of Monoclonal Antibodies Based on the Plasma Concentrations in Several Preclinical Species and Human. *MAbs* **2013,** *5* (2), 297–305.
122. McDonald, D. M.; Baluk, P. Significance of Blood Vessel Leakiness in Cancer. *Cancer Res.* **2002,** *62,* 5381–5385.
123. Thurber, G. M.; Weissleder, R. A Systems Approach for Tumor Pharmacokinetics. *PLoS ONE* **2011,** *6* (9). e24696.
124. Adams, G. P.; Schier, R.; McCall, A. M.; Simmons, H. H.; Horak, E. M.; Alpaugh, R. K.; Marks, J. D.; Weiner, L. M. High Affinity Restricts the Localization and Tumor Penetration of Single-Chain Fv Antibody Molecules. *Cancer Res.* **2001,** *61* (12), 4750–4755.
125. Martin-Killias, P.; Stefan, N.; Rothschild, S.; Plückthun, A.; Zangemeister-Wittke, U. A Novel Fusion Toxin Derived From an EpCAM-Specific Designed Ankyrin Repeat Protein Has Potent Antitumor Activity. *Clin. Cancer Res.* **2011,** *17* (1), 100–110.
126. Hong, E. E.; Erickson, H.; Lutz, R. J.; Whiteman, K. R.; Jones, G.; Kovtun, Y.; Blanc, V.; Lambert, J. M. Design of Coltuximab Ravtansine, a CD19-Targeting Antibody-Drug Conjugate (ADC) for the Treatment of B-Cell Malignancies: Structure-Activity Relationships and Preclinical Evaluation. *Mol. Pharm.* **2015,** *12* (6), 1703–1716.

Relevant Websites

[1]. https://www.systemsbiology.org—This the website of the Institute for Systems Biology.
[2]. http://www.systems-biology.org—This is the website is a great portal for tools, utilities, pointers to relevant journals, etc.
[3]. https://sysbio.med.harvard.edu—Harvard's Department of Systems Biology.
[4]. http://csbi.mit.edu/—MIT's program in computational and systems biology.
[5]. http://www.systemscenters.org—The National Institute for General Medical Sciences sponsored website for National Centers of Systems Biology—A collection of pointers to funded research in various branches of systems studies.
[6]. http://biomodels.caltech.edu—BioModels Database.

This page intentionally left blank

COMPREHENSIVE MEDICINAL CHEMISTRY III

This page intentionally left blank

COMPREHENSIVE MEDICINAL CHEMISTRY III

EDITORS-IN-CHIEF

Samuel Chackalamannil
Rutgers University, Piscataway, NJ, United States

David Rotella
Montclair State University, Montclair, NJ, United States

Simon E. Ward
University of Sussex, Brighton, United Kingdom

VOLUME 4

EXPERIMENTAL ADME AND TOXICOLOGY

VOLUME EDITOR

Alan G. E. Wilson
Lexicon Pharmaceuticals, The Woodlands, TX, United States

ELSEVIER

Elsevier
Radarweg 29, PO Box 211, 1000 AE Amsterdam, The Netherlands
The Boulevard, Langford Lane, Kidlington, Oxford OX5 1GB, United Kingdom
50 Hampshire Street, 5th Floor, Cambridge, MA 02139, United States

Copyright © 2017 Elsevier Ltd. All rights reserved

No part of this publication may be reproduced or transmitted in any form or by any means, electronic or mechanical, including photocopying, recording, or any information storage and retrieval system, without permission in writing from the publisher. Details on how to seek permission, further information about the Publisher's permissions policies and our arrangements with organizations such as the Copyright Clearance Center and the Copyright Licensing Agency, can be found at our website: www.elsevier.com/permissions.

This book and the individual contributions contained in it are protected under copyright by the Publisher (other than as may be noted herein).

Notices
Knowledge and best practice in this field are constantly changing. As new research and experience broaden our understanding, changes in research methods, professional practices, or medical treatment may become necessary.

Practitioners and researchers may always rely on their own experience and knowledge in evaluating and using any information, methods, compounds, or experiments described herein. In using such information or methods they should be mindful of their own safety and the safety of others, including parties for whom they have a professional responsibility.

To the fullest extent of the law, neither the Publisher nor the authors, contributors, or editors, assume any liability for any injury and/or damage to persons or property as a matter of products liability, negligence or otherwise, or from any use or operation of any methods, products, instructions, or ideas contained in the material herein.

Library of Congress Cataloging-in-Publication Data
A catalog record for this book is available from the Library of Congress

British Library Cataloguing-in-Publication Data
A catalogue record for this book is available from the British Library

ISBN 978-0-12-803200-8

For information on all publications visit our website at
http://store.elsevier.com

Working together
to grow libraries in
developing countries
www.elsevier.com • www.bookaid.org

Publisher: Oliver Walter
Acquisition Editor: Rachel Gerlis
Content Project Manager: Gemma Tomalin
Associate Content Project Manager: Marise Willis
Designer: Mark Rogers

Printed and bound in the United Kingdom

PREFACE

Previous editions of *Comprehensive Medicinal Chemistry*, published in 1990 and 2006, provided an integrated reference source that encompassed all major aspects of drug discovery research. The third edition follows this tradition and considerably expands its scope and content.

The trailblazing scientific discoveries of the 21st century have brought new opportunities for drug discovery research. The discipline of medicinal chemistry continues to evolve as it adapts to these new opportunities and strives to solve new challenges. Covered in the new edition are not only the breakthrough therapies of the past decade in cancer, hepatitis C, heart failure, dyslipidemia, cystic fibrosis, multiple sclerosis, HIV, etc., but also extensive discussion of new business models in drug discovery research, shifting industry demographics, emerging technologies, *in silico* drug discovery tools, experimental ADME and toxicology, and biologics medicine. The tone of this edition is prospective in which contributors identify outstanding issues and paths forward in their area of expertise. The aim is to provide drug discovery scientists in industry, government, academia, and research organizations with a contemporary global perspective on the field that includes a look ahead in selected areas.

The eight individual volumes fulfill these objectives and include extensive discussion of biomolecular therapeutics, drug targeting and delivery, development of chemical biology tools, data collection and analysis, *in silico* models as predictors for biological properties, identification/validation of new targets, approaches to quantify target engagement, new methods for synthesis of drug candidates such as green chemistry, development of novel scaffolds for drug discovery, and the role of regulatory agencies in drug discovery.

The individual volume editors have done an outstanding job to identify topics and contributors to meet these goals and we thank them for their hardwork and diligence. In volume 1, Ana Martinez and Carmen Gil recruited an international group of contributors who provide chapters on the emerging role of organizations other than traditional pharmaceutical companies in drug discovery, the evolving science of chemical biology, and new organic chemistry contributions to the discipline. In volume 2, Helmut Buschmann, Norbert Handler, and Andrea Wolkerstorfer have accomplished a seemingly impossible task and attracted world-leading experts across the wide field of drug discovery enabling technologies, covering contemporary thinking in a wide range of key disciplines that enable modern medicinal chemistry and drug discovery and development. The computational enabling technologies are the focus of volume 3, in which Andy Davis and Colin Edge have assembled chapters covering both ligand-based and protein structure–based advances as well as exciting new methodologies and case studies exploiting these. Alan Wilson identified experts in the fields of pharmacokinetics and toxicology who describe a wide range of contemporary advances in prediction and analysis of pharmaceutical properties and drug safety in volume 4. In volume 5, Ian Collins, Louis Lombardo, and Will Watkins have assembled leading experts to discuss high impact drug discovery accomplishments over the past decade in cancer chemotherapeutics, immunology and inflammation, and infectious diseases therapeutic areas. Ved Srivastava edited volume 6 on biologic medicines, a significant and rapidly evolving area where medicinal chemistry plays an important role. The chapters in this volume provide timely information on not only protein-based drugs, such as monoclonal antibodies and therapeutic proteins, but also peptides and nucleic acid–based therapeutics. Volume 7, edited by Adrian Hall, Santhosh Neelamkavil, and Rob Jones, presents a detailed account of the major advances in CNS, metabolic, and cardiovascular fields over the past decade and the promising new opportunities. Joerg Holenz edited volume 8 that presents case histories of successful drug discovery and strategic differentiation that have resulted in commercialized drugs and candidates in advanced clinical trials.

We are truly grateful to the publishing team at Elsevier that includes Gemma Tomalin, Rachel Gerlis, Marise Willis, and Sean Simms for their assistance and support throughout the process. With their expertise, this project became what we believe is a noteworthy and valuable resource for the discipline of medicinal chemistry. We look forward to the response and feedback of our colleagues who will use this information in their own work.

Samuel Chackalamannil, David P. Rotella, and Simon E. Ward

EDITORS-IN-CHIEF: BIOGRAPHIES

Dr. Samuel Chackalamannil

Dr. Chackalamannil obtained his PhD in chemistry from Yale University in 1984 and subsequently worked in drug discovery research at Schering-Plough Corporation and Merck Research Laboratories, where he was a distinguished fellow when he left in 2011. Since then, he has been teaching at Ernest Mario School of Pharmacy, Rutgers University, New Jersey.

Dr. Chackalamannil has significant accomplishments in the discovery of new medicines. He led the discovery of vorapaxar (Zontivity®), an FDA-approved antiplatelet drug for the prevention of heart attack and stroke. His group also discovered a PDE-5 inhibitor clinical candidate dasantafil and an adenosine A2a antagonist clinical candidate for the treatment of Parkinson's disease. Altogether, he was responsible for the discovery of nine development candidates in cardiovascular, central nervous system, and metabolic disease areas.

Dr. Chackalamannil is a coinventor of 62 allowed US patents and numerous patent applications worldwide. He has published 81 peer-reviewed articles and has coauthored a book. He has also given numerous lectures at international meetings and academic institutions.

Dr. Chackalamannil is a two-time recipient of the Thomas Alva Edison Award for Emerging Technology Patent and a two-time recipient of the Presidential Award for Discovery at Schering-Plough Research Institute. He has chaired several sessions at American Chemical Society national meetings and Gordon Research Conference on Medicinal Chemistry and was an organizer for Chemistry as a Life Science Symposium.

Dr. David Rotella

Dr. Rotella earned a PhD in medicinal chemistry from The Ohio State University and carried out postdoctoral research in organic chemistry at Penn State University. He joined the faculty at Montclair State University in July 2011 as the Margaret and Herman Sokol Professor of medicinal chemistry after a successful career in the pharmaceutical industry. He is an expert in the discovery and optimization of small molecule drug candidates for use in metabolic, cardiovascular, cancer, and central nervous system diseases. His current research is focused on discovering new lead compounds for use in parasitic and central nervous system diseases. He has coedited the seventh edition of *Burger's Medicinal Chemistry* and is a senior editor for the Royal Society of Chemistry's Drug Discovery book series. He has authored over 40 peer-reviewed articles, is an inventor on 8 issued US patents, and has contributed 10 book chapters.

Simon E. Ward

Simon Ward has an MA in natural sciences and PhD in synthetic organic chemistry from Cambridge University, UK. He has a wide-ranging experience of drug discovery in both large and small companies (GlaxoSmithKline, Knoll Pharmaceuticals, Vernalis, Chiroscience, BioCrea) and specialist experience of discovering and developing drugs for central nervous system indications. He has led multidisciplinary project teams and medicinal chemistry groups from target identification through to early clinical studies, delivering multiple clinical development candidates across indications. He is a fellow of the Royal Society of Chemistry. He is currently a professor of medicinal chemistry at the University of Sussex, UK, and the director of the Sussex Drug Discovery Centre, which he established within the University of Sussex in 2010.

This page intentionally left blank

CONTRIBUTORS TO VOLUME 4

J Adjaye
Institute for Stem Cell Research and Regenerative Medicine, Düsseldorf, Germany

C Alden
Mayflower Pharma, Lawrenceburg, IN, United States

K A Andrews
Simulations Plus, Inc., Buffalo, NY, United States

Sudheer Beedanagari
Alkermes Inc., Waltham, MA, United States

L D Beilke
Toxicology Solutions Inc, San Diego, CA, United States

L Z Benet
University of California, San Francisco, CA, United States

M B Bolger
Simulations Plus, Inc., Lancaster, CA, United States

R D Clark
Simulations Plus, Inc., Lancaster, CA, United States

J Commandeur
VU University Amsterdam, Amsterdam, The Netherlands

K P Cross
Leadsocpe, Inc, Columbus, Ohio, United States

A K Daly
Newcastle University, Newcastle upon Tyne, United Kingdom

L Faulkner
University of Liverpool, Liverpool, United Kingdom

N French
University of Liverpool, Liverpool, United Kingdom

C Goldring
University of Liverpool, Liverpool, United Kingdom

T H Grasela
Simulations Plus, Inc., Buffalo, NY, United States

K Grime
DMPK, Respiratory, Inflammation and Autoimmunity iMed, AstraZeneca, Gothenburg, Sweden

A Guillouzo
Université de Rennes 1, Rennes, France

J P Hanig
Center for Drug Evaluation and Research/FDA, Silver Spring, MD, United States

T Hartung
Johns Hopkins Bloomberg School of Public Health, Baltimore, MD, United States

C J Henderson
University of Dundee, Dundee, United Kingdom

C M Hosey
University of California, San Francisco, CA, United States

M Ingelman-Sundberg
Karolinska Institutet, Stockholm, Sweden

L Kamalian
University of Liverpool, Liverpool, United Kingdom

M-A Kawala
Institute for Stem Cell Research and Regenerative Medicine, Düsseldorf, Germany

B Kevin Park
University of Liverpool, Liverpool, United Kingdom

N Kitteringham
University of Liverpool, Liverpool, United Kingdom

U Klingmueller
German Cancer Research Center, Heidelberg, Germany

P Knolle
Technische Universität München, München, Germany

R Kovi
Experimental Pathology Laboratories, Inc., Durham, NC, United States

B Kramer
German Cancer Research Center, Heidelberg, Germany

V Lukacova
Simulations Plus, Inc., Lancaster, CA, United States

P Matz
Institute for Stem Cell Research and Regenerative Medicine, Düsseldorf, Germany

D F McGinnity
DMPK, Oncology iMed, AstraZeneca, Cambridge, United Kingdom

A Mercer
University of Liverpool, Liverpool, United Kingdom

D N Morris
Simulations Plus, Inc., Buffalo, NY, United States

G J Myatt
Leadsocpe, Inc, Columbus, OH, United States

D Naisbitt
University of Liverpool, Liverpool, United Kingdom

A Oppelt
German Cancer Research Center, Heidelberg, Germany

J Otte
Institute for Stem Cell Research and Regenerative Medicine, Düsseldorf, Germany

A Pandiri
Cellular and Molecular Pathology Branch, National Toxicology Program, Durham, NC, United States

K Sandy Pang
University of Toronto, Toronto, ON, Canada

R Pieters
Utrecht University, Utrecht, The Netherlands

C Pridgeon
University of Liverpool, Liverpool, United Kingdom

K Samuelsson
Independent Consultant, Åskloster, Sweden

N Scheer
CEVEC Pharmaceuticals GmbH, Cologne, Germany

J Sidaway
AstraZeneca R&D, Cheshire, United Kingdom

R Sills
Cellular and Molecular Pathology Branch, National Toxicology Program, Durham, NC, United States

R Sison-Young
University of Liverpool, Liverpool, United Kingdom

W Slikker
National Center for Toxicological Research/FDA, Jefferson, AR, United States

L-S Spitzhorn
Institute for Stem Cell Research and Regenerative Medicine, Düsseldorf, Germany

J Tarrant
Gilead Sciences Inc., Foster City, CA, United States

B Van der Water
Leiden University, Leiden, The Netherlands

R Weaver
Biologie Servier, Gidy, France

R E White
White Global Pharma Consultants, LLC, Cranbury, NJ, United States

I Wilson
Department of Surgery and Cancer, London, United Kingdom

J Woestmann
Institute for Stem Cell Research and Regenerative Medicine, Düsseldorf, Germany

C R Wolf
University of Dundee, Dundee, United Kingdom

W Wruck
Institute for Stem Cell Research and Regenerative Medicine, Düsseldorf, Germany

H Yamazaki
Showa Pharmaceutical University, Machida, Tokyo, Japan

Qi Joy Yang
University of Toronto, Toronto, ON, Canada

H Yigit
Institute for Stem Cell Research and Regenerative Medicine, Düsseldorf, Germany

CONTENTS OF VOLUME 4

Preface *v*

Editors-in-Chief: Biographies *vii*

Contributors to Volume 4 *ix*

Editorial Board *xiii*

4.01 Role of ADME/PK in Drug Discovery, Safety Assessment, and Clinical Development 1
R E White

4.02 ADME Optimization in Drug Discovery 34
D F McGinnity and K Grime

4.03 Drug-Metabolizing Enzyme Systems I 45
H Yamazaki

4.04 Human PK Prediction and Modeling 51
T H Grasela, V Lukacova, D N Morris, R D Clark, K A Andrews, and M B Bolger

4.05 PBPK Modeling to Estimate Metabolite Formation From First-Pass Organs: Intestine and Liver 83
Qi Joy Yang and K Sandy Pang

4.06 Drug Classification and Drug Disposition Prediction 102
C M Hosey and L Z Benet

4.07 Genetically Humanized Animal Models 130
K Samuelsson, N Scheer, I Wilson, C R Wolf, and C J Henderson

4.08 A Comprehensive Overview of the Current Status and Application of Predictive ADMET: Introduction and Overview 150
T Hartung

4.09 *In Silico* Tools and their Application 156
G J Myatt, L D Beilke, and K P Cross

4.10 Use of Stem Cells in Toxicology 177
P Matz, L-S Spitzhorn, J Otte, M-A Kawala, J Woestmann, H Yigit, W Wruck, and J Adjaye

4.11 Genetic Toxicology 195
Sudheer Beedanagari

4.12 Drug-Induced Liver Disease 204
A K Daly

4.13 Drug-Induced Liver Injury: Mechanism-Informed Prediction in Drug Development 217
C Goldring, R Weaver, B Kramer, U Klingmueller, A Oppelt, B Van der Water, J Commandeur, A Guillouzo, D Naisbitt, N French, N Kitteringham, C Pridgeon, P Knolle, J Sidaway, R Sison-Young, L Kamalian, A Mercer, L Faulkner, R Pieters, M Ingelman-Sundberg, and B Kevin Park

4.14 The Future of Carcinogenicity Testing 239
A Pandiri, R Kovi, C Alden, and R Sills

4.15 Emerging Translatable Safety Biomarkers 255
J Tarrant

4.16 Toxicity Prediction—Regulatory Perspective 285
J P Hanig and W Slikker

EDITORIAL BOARD

EDITORS-IN-CHIEF

Samuel Chackalamannil
Rutgers University, Piscataway, NJ, United States

David Rotella
Montclair State University, Montclair, NJ, United States

Simon E. Ward
University of Sussex, Brighton, United Kingdom

VOLUME 1
GENERAL PERSPECTIVE - THE FUTURE OF DRUG DISCOVERY

VOLUME EDITORS

Ana Martinez
Centro de Investigaciones Biologicas-CSIC, Madrid, Spain

Carmen Gil
Centro de Investigaciones Biologicas-CSIC, Madrid, Spain

VOLUME 2
DRUG DISCOVERY TECHNOLOGIES

VOLUME EDITORS

Helmut Buschmann
Savira Pharmaceuticals GmbH, Vienna, Austria

Norbert Handler
Savira Pharmaceuticals GmbH, Vienna, Austria

Andrea Wolkerstorfer
Baxalta Innovations GmbH — Now part of Shire, Vienna, Austria

VOLUME 3
IN SILICO DRUG DISCOVERY TOOLS

VOLUME EDITORS

Andrew M. Davis
AstraZeneca R&D Gothenburg, Gothenburg, Sweden

Colin Edge
GlaxoSmithKline Medicines Research Centre, Stevenage, United Kingdom

VOLUME 4
EXPERIMENTAL ADME AND TOXICOLOGY

VOLUME EDITOR

Alan G. E. Wilson
Lexicon Pharmaceuticals, The Woodlands, TX, United States

VOLUME 5
CANCER, IMMUNOLOGY AND INFLAMMATION, AND INFECTIOUS DISEASE

VOLUME EDITORS

Ian Collins
The Institute of Cancer Research, London, United Kingdom

William Watkins
Gilead Sciences, Foster City, CA, United States

Louis J. Lombardo
Bristol-Myers Squibb Research and Development, Princeton, NJ, United States

VOLUME 6
BIOLOGICS MEDICINE

VOLUME EDITOR

Ved Srivastava
Intarcia Therapeutics, Durham, NC, United States

VOLUME 7
CNS, PAIN, METABOLIC SYNDROME, CARDIOVASCULAR, TISSUE FIBROSIS AND URINARY INCONTINENCE

VOLUME EDITORS

Adrian Hall
UCB BioPharma SPRL, Brussels, Belgium

Santhosh Neelamkavil
Merck Research Laboratories, Kenilworth, NJ, United States

Rob Jones
BlackThorn Therapeutics, San Francisco, CA, United States

VOLUME 8
CASE HISTORIES IN RECENT DRUG DISCOVERY

VOLUME EDITOR

Joerg Holenz
R&D Neurosciences TAU, GSK, PA, United States

PERMISSION ACKNOWLEDGMENTS

The following material is reproduced with kind permission of Taylor & Francis

Scheme 2 Cellular Imaging in Drug Discovery: Biomolecular Imaging and Informatics (HCS, HCA, HCI)
Figure 2 Past Present Future
Figure 5 Past Present Future
Figure 6 Past Present Future
www.taylorandfrancisgroup.com

The following material is reproduced with kind permission of Oxford University press

Table 1 Targeting G-quadruplex Nucleic Acids for Cancer Therapy
Table 2 Targeting G-quadruplex Nucleic Acids for Cancer Therapy
Figure 1 Protein Structure Prediction and Homology Modelling
www.oup.com

The following material is reproduced with kind permission of American Association for the Advancement of Science

Figure 3b,c Cellular Imaging in Drug Discovery: Biomolecular Imaging and Informatics (HCS, HCA, HCI)
www.aaas.org

The following material is reproduced with kind permission of Nature Publishing Group

Table 4 Use of Stem Cells in Toxicology
Table 6 Use of Stem Cells in Toxicology
Figure 17 Strategy and Tactics for Designing Analogs; Biochemical Characterization of the Large Molecules
Figure 30 Strategy and Tactics for Designing Analogs; Biochemical Characterization of the Large Molecules
Figure 2 Cellular Imaging in Drug Discovery: Biomolecular Imaging and Informatics (HCS, HCA, HCI)
Figure 3a Cellular Imaging in Drug Discovery: Biomolecular Imaging and Informatics (HCS, HCA, HCI)
Figure 4 Cellular Imaging in Drug Discovery: Biomolecular Imaging and Informatics (HCS, HCA, HCI)
Figure 5a Cellular Imaging in Drug Discovery: Biomolecular Imaging and Informatics (HCS, HCA, HCI)
Figure 9a Cellular Imaging in Drug Discovery: Biomolecular Imaging and Informatics (HCS, HCA, HCI)
Figure 20 Epigenetics: Novel Therapeutics Targeting Epigenetics
Figure 1 UCB5857
Figure 6 Empirical and Physics Based Calculations of Physical Properties
Figure 4 Progress and Challenges in the Development if PET Ligands to Aid CNS Drug Discovery
http://www.nature.com

4.01 Role of ADME/PK in Drug Discovery, Safety Assessment, and Clinical Development

RE White, White Global Pharma Consultants, LLC, Cranbury, NJ, United States

© 2017 Elsevier Ltd. All rights reserved.

4.01.1	**Introduction**	1
4.01.1.1	The Meaning of ADME/PK	1
4.01.1.2	Bioavailability	2
4.01.1.3	Distribution	2
4.01.1.4	Persistence	2
4.01.1.5	Excretion	2
4.01.1.6	Safety Margin	3
4.01.1.7	The Goal of the Medicinal Chemist	3
4.01.2	**The Importance of ADME/PK in Drug Discovery**	3
4.01.2.1	The Continuing Need for ADME/PK During Drug Discovery	3
4.01.2.2	What Happens During Drug Discovery?	4
4.01.2.2.1	Biology	4
4.01.2.2.2	Chemistry	4
4.01.2.3	Major ADME/PK Characteristics to Optimize	5
4.01.2.3.1	"Right Box" analysis	5
4.01.2.3.2	Oral absorption and bioavailability	5
4.01.2.3.3	Distribution	12
4.01.2.3.4	Persistence	14
4.01.2.3.5	Excretion	16
4.01.2.3.6	Computational approaches to ADME/PK problems	17
4.01.2.3.7	Screening for DDI potential	17
4.01.2.3.8	Triage of ADME/PK screening assays	20
4.01.3	**The Importance of ADME/PK in Safety Assessment**	21
4.01.3.1	Early Toxicity Assessment	21
4.01.3.2	Reactive Metabolites	22
4.01.3.3	In Vivo Toxicology Assessment	22
4.01.3.4	Metabolites in Safety Testing	23
4.01.4	**The Importance of ADME/PK in Clinical Development**	23
4.01.4.1	IND-Enabling ADME/PK Studies	23
4.01.4.1.1	Purpose of IND-enabling ADME/PK studies	23
4.01.4.1.2	Animal PK and bioavailability	24
4.01.4.1.3	Major routes of clearance in animals	24
4.01.4.1.4	Active circulating metabolites in animals	24
4.01.4.1.5	Projection of human PK	25
4.01.4.1.6	Initial in vitro assessment of clinical DDI potential	25
4.01.4.2	Clinical ADME/PK Studies	25
4.01.4.2.1	Clinical pharmacokinetics	25
4.01.4.2.2	Definitive characterization of DDIs	26
4.01.4.2.3	Circulating human metabolites	27
4.01.4.2.4	Clinical ^{14}C-ADME study	28
4.01.5	**Summary**	29
References		29

4.01.1 Introduction

4.01.1.1 The Meaning of ADME/PK

It is well understood by now that for a clinical drug to produce the desired therapeutic benefit, the agent must be bioavailable by a suitable dosing route, distribute to the proper physiological compartment at concentrations sufficient to interact with the target receptor, maintain these concentrations long enough to modulate the target biological pathway, operate within an adequate safety margin, and be eliminated within a period short enough that unexpected adverse effects do not persist for a long time. Each of these

criteria is partially or fully controlled by the ADME/PK (absorption, distribution, metabolism, and excretion and pharmacokinetic) properties of the drug. To be sure, a successful drug must also have suitable properties of other sorts, such as solubility, chemical stability, receptor potency and selectivity, and synthetic accessibility. However, this article will focus on ADME/PK. Let us briefly elaborate the ways in which ADME/PK properties underlie these five aspects of the clinical performance of a drug candidate.

4.01.1.2 Bioavailability

This term refers to the efficiency of the intended dosing route (e.g., oral, intravenous, subcutaneous, and topical) to deliver into the body an external dose of the drug sufficient to have good clinical effect. It is typically measured as the ratio of the amount of drug reaching the systemic circulation to the administered amount, expressed as a percentage. Since the body presents various types of barriers to actively resist uptake of xenobiotic chemicals, especially by the oral route, bioavailability can range from 0% to 100%. Obviously, very low bioavailability will necessitate a very large, possibly unfeasible, administered dose to achieve an adequate absorbed dose. In addition, even if low bioavailability can be overcome by administration of a massive dose, one still has issues of large body burden of drug-related material (absorbed and unabsorbed parent drug and metabolites) and high cost of goods entailed by the requirement to administer an excessive dose in order to deliver only a small fraction of that dose. Thus, an important goal of a discovery and development program is to design a molecule that achieves acceptable bioavailability.

4.01.1.3 Distribution

Drugs enter the blood either by direct infusion by intravascular administration or by passive or active diffusion through membrane barriers, for instance, the membrane of the gut luminal wall, lung alveoli for an inhaled drug, or skin for a topical drug. Once in the blood, drug molecules circulate around the body and have the opportunity to diffuse from the blood into all organs. This is a good thing for the majority of drugs whose biological targets are outside of the blood compartment. However, distribution also allows the drug to enter compartments that are not relevant to the indicated disease condition, so that those tissues are exposed to the drug without the possibility of local therapeutic but with the possibility of off-target toxicity. Thus, it is desirable that a drug be preferentially distributed to target organs such as the brain for central nervous system (CNS) drugs and tumor for cancer drugs at concentrations sufficient to interact with the target receptor while distributed as little as possible to other compartments. In human subjects, extravascular distribution is only measurable by invasive techniques such as biopsy or, in some cases, by scanning techniques such as magnetic resonance imaging (MRI) and positron emission tomography (PET). Thus, most information about distribution of a drug is derived from animal studies.

4.01.1.4 Persistence

Just as mechanisms exist to limit the introduction of xenobiotics into the body, related mechanisms exist to eliminate those molecules that successfully enter. This elimination process is called clearance, and this term encompasses all mechanisms by which the drug can be eliminated from the blood, including metabolism and direct biliary and renal excretion. Therapeutic effect depends on concentrations in the local target compartment persisting long enough to modulate the target biological pathway. With most drugs, we strive to reach a PK steady state in which the local concentrations at the target receptor stay above the minimum therapeutic concentration for an entire dosing cycle but below the corresponding minimum toxic concentration. This steady state represents a balance between the rate at which molecules are cleared from the blood and the rate at which new molecules are introduced into the blood by successive doses. Up to a point, it is beneficial for a molecule to have low clearance (i.e., long persistence), so that dosing frequency can be made convenient, such as once per day. However, a drug whose clearance is too low may persist too long. A physician who encounters a patient exhibiting an adverse reaction to a drug desires to be able to stop dosing and expect the patient to improve in a day or so. Consequently, a desirable clinical characteristic in a drug is that once dosing stops, blood levels of the drug will drop significantly in a reasonable time. Thus, a good clinical drug has persistence that is not too short and not too long, although there are numerous exceptions to this rule depending on the nature of the therapeutic indication. Persistence is measured by serial sampling of blood followed by specific assay for the drug and reconstruction of the blood concentration–time curve. Persistence is usually quantified by the PK parameters' half-life and mean residence time (*MRT*).

4.01.1.5 Excretion

This term refers to the complete elimination of the mass of the drug and/or its metabolites from the body. It is distinguished from the term clearance, which specifically describes the process of elimination of the parent drug from tissues and blood. However, this clearance process may have merely converted the parent drug to a metabolite sharing many structural, pharmacological, and toxicological features with the parent. Only when the parent and the metabolites have been totally removed from the body has the possibility of continued pharmacological and/or toxicological effect been abolished. Excretion occurs when the drug mass (parent drug and metabolites) has been delivered to the urine and/or feces. The chemical form in which the mass is found in the excreta provides information about the clearance pathway. For instance, recovery of most of the dose as unchanged drug in urine (as happens with a number of antibiotics) informs us that renal elimination (by glomerular filtration and active transport from renal tubules) is the major route of clearance. Conversely, recovery of most of the mass of the dose as metabolites in excreta informs us

that one or more processes of metabolism of the parent drug were the major routes of clearance. Measurement of the rate of excretion may alert us that a long-lived metabolite is still in the body even though PK clearance of the parent drug from the blood is complete.

4.01.1.6 Safety Margin

Drug candidates invariably have some level of toxicity at a high enough dose, and their safety profile must be determined from a series of preclinical safety studies in animals followed by rising-dose safety and tolerance studies in humans. Although an occasional drug candidate has such a low level of toxicity that it is essentially not clinically relevant, the majority of drugs have a threshold for some type of adverse event that is at least *accessible* by clinically deliverable doses. Thus, in most cases, we can define an optimal range of blood concentrations that extend from the lowest concentration that gives clinically meaningful efficacy to the highest concentration that does not produce a dose-limiting toxicity. This concentration range would be considered the safety margin, which is usually expressed as the ratio of the corresponding administered doses (e.g., a 10-fold safety margin between the minimally effective dose and the lowest toxic dose). Most safety issues probably arise from the parent drug itself, but because the subject of this article is ADME/PK, we will only discuss issues resulting from toxic metabolites or metabolism-based drug–drug interactions (DDIs) resulting in magnified toxicity of either the drug candidate or a coadministered drug.

4.01.1.7 The Goal of the Medicinal Chemist

The medicinal chemist, in addition to designing molecules that strongly and selectively engage the target receptor, must also engineer a clinical candidate to have these ADME/PK and safety properties. How can the chemist determine that the effort has succeeded in the selected new drug candidate? This question encompasses the two main roles of ADME in drug discovery and development, and the organization of this article will separately examine each. Because the involvement of the medicinal chemist is mainly in the discovery phase of new drug candidates, the majority of attention in this article will be devoted to that phase. For the same reason, we will only discuss the ADME/PK properties of small-molecule drugs, although protein drugs have a corresponding set of ADME/PK properties to be studied.[1]

4.01.2 The Importance of ADME/PK in Drug Discovery

4.01.2.1 The Continuing Need for ADME/PK During Drug Discovery

Despite decades of intense effort, the attrition of drug candidates entering clinical trials remains high. The analyses of Kola and Landis,[2] Hay et al.[3] 10 years later, and Waring et al.[4] 11 years later show that the overall success rate of phase 1 entries to New Drug Application (NDA) approvals stubbornly remains at only about 1 in 10. The leading causes of failure are safety (51%, including both preclinical and clinical), efficacy (9%), and business reasons (21%).[4] In fairness to the industry, it must be noted that the bar for success has been steadily rising. Regulatory requirements continually increase, especially in the area of safety, and marketed drugs continually get better, making clinical trials based on superiority or even noninferiority of efficacy ever more difficult for next-generation candidates that must be compared with current "standard of care." Nonetheless, safety is clearly where the most progress is required.

On the other hand, the failure rate attributable to "bioavailability and pharmacokinetics" remains low at about 4–5%.[4] ADME/PK-related failures dropped from about 40% in 1991 to 10% by 2000,[2] reflective of the effort most drug discovery research institutions applied in the decade of the 1990s to detect and design out ADME/PK deficiencies. A further reduction from 10% to 5% occurred from 2000 to 2005, and the failure rate had plateaued at 4% by 2010,[4] a rate so low that further reduction of the rate of failure due to ADME/PK would probably not be meaningful.

Does the low rate of ADME/PK-related failure mean that the issue no longer requires the attention of the medicinal chemists in designing their drug candidates? No. The specter of poor ADME/PK has not gone away, and chemists who ignore ADME/PK will quickly find problems popping up again in this area. Chemists must continue to be vigilant in building in desirable characteristics from the beginning. However, the good news is that the continued success of efforts to produce clinical drug candidates with "drug-like" ADME/PK properties constitutes validation of the methods by which these properties are measured and extrapolated from preclinical in vitro and animal studies to humans. However, this statement does not mean that improvement of the process of ADME/PK support of discovery is impossible. One author has drawn attention to the need for better in vitro systems for testing drug candidates,[5] especially in the area of liver surrogates, a point where progress is already being made (see section "**Addressing high first-pass clearance**").

Another point worth noting is that just as with potency and efficacy, the average ADME/PK performance of new drugs continues to improve. The fact that drugs seldom fail for ADME/PK reasons merely means that the ADME/PK properties of new drug candidates are good enough not to be the cause of failure. Most new drug candidates have at least one, and often more than one, ADME/PK property that could be better. In fact, ADME/PK can be the source of major improvements in the clinical effectiveness of new drugs compared with predecessors that had "adequate" ADME/PK properties. One thinks of second-generation compounds with greater oral bioavailability so that lower doses are needed or with longer half-lives so that dosing frequency is reduced from three times a day (TID) to once a day (QD). But achieving these improvements requires more than

merely adhering to "rules" based on physical properties that describe "drug-like" compounds.[6] A fundamental understanding is necessary of the physiological processes with which drug candidates interact to exhibit their drug-like behavior. Imparting this understanding is a goal of this article.

4.01.2.2 What Happens During Drug Discovery?

To provide context for discussing the role of ADME/PK in drug discovery, let us consider the totality of what must be accomplished to nominate a new chemical entity for clinical development. A number of biological, chemical, and physical considerations are involved in the design, testing, and selection of clinical drug candidates.

4.01.2.2.1 Biology

4.01.2.2.1.1 Pharmacology

Innovations in therapy typically involve the discovery of new physiological targets, such as new enzymes or receptors, or the recognition of a regulatory relationship between biochemical pathways. The possibilities for modulation of these targets to affect a pathological condition are considered, and a specific molecular target is chosen for further investigation. Initial experiments often involve biological rather than chemical modulation, such as gene knockout or upregulation, to observe the effect in a disease model such as a cell line or a mouse. If the biological modulation gives positive results, then the decision is made to see if the target is "druggable" by finding a small-molecule ligand for the molecular target, often by high-throughput screening of libraries or collections of compounds. A chemical compound that shows a nontrivial level of binding to the receptor (e.g., $IC_{50} < 10\ \mu M$) would be considered a "hit" and would justify the dedication of medicinal chemistry resources to attempt to find novel synthetic analogs of the "hit" that show much tighter binding.

As the "hit-to-lead" phase of the discovery program proceeds, chemists will explore a variety of compound types corresponding to the most active of the "hits" that came out of screening, while pharmacologists will develop more holistic in vitro and in vivo disease models to enable the therapeutic concept to be tested with the "actives" coming out of the chemistry program. Eventually, a successful program will find compounds with binding activity sufficient to be classified as a "lead," and the program will focus on the most active of these to initiate a full exploration of the structure–activity relationship (SAR) for these chemotypes (i.e., "lead optimization"). Pharmacology has the task of creating even more sophisticated models to continue to investigate the biological events attending the modulation of the molecular target to understand whether the cell biology is actually responding in the way envisioned in the original pharmacological intervention concept.

4.01.2.2.1.2 Toxicology

The term "toxicology" will be used in a broad sense to indicate undesirable biological effects of the chemical compounds being tested as therapeutic agents, whether in the early-phase discovery period or full clinical development. In early discovery, candidates with levels of pharmacological activity exceeding a certain threshold will be tested in follow-up assays for binding to related enzymes or receptors, which often exist in multimembered families of closely related gene products. These are relatively easy to test with in vitro assays similar to those used for the target receptor. Ideally, the program will produce a compound that binds tightly to the exact target receptor and not at all to closely related receptors of the same family, which, however, control different physiological events.

At some point in the "lead optimization" process, the program will need to start investigating binding to receptors *not* closely related to the target receptor by submitting the most active candidate to a broad receptor-binding panel. This will reveal unanticipated "activities" that do not contribute to the desired therapeutic action but have the potential to produce adverse actions, if not outright toxicity. Ideally, no binding to unrelated receptors is discovered and the compound is "clean." More likely, however, some level of binding to an unrelated receptor is seen, and this binding must be monitored in subsequent analogs and possibly actively designed out. Another way to investigate "off-target" activities of a lead series is the use of in vitro cell-based toxicology screens, which have the advantage of looking at a living biological system without assumptions about which receptors may be engaged by the candidates. As with receptor-binding panels, detection of adverse activities with this approach requires monitoring and possibly active remediation.

4.01.2.2.2 Chemistry

4.01.2.2.2.1 Exploration of chemical space

During the hit-to-lead phase of discovery, chemists are often aware of the general ADME/PK properties of their early compounds, but these do not figure prominently in their design campaign. Once several chemical series are identified as leads, the lead optimization phase begins. The primary objective during lead optimization is to improve potency and receptor selectivity, but monitoring the ADME/PK profiles of the chemical series that they seek to optimize becomes a secondary goal. Although modeling strategies may be employed to guide the search for activity within the chemical space afforded by the chosen leads, the major approach is almost always the synthesis of many analogs of the lead series for direct assay of activity toward the target and off-target receptors.

Contemporary synthetic methods are so powerful that medicinal chemists seldom have to omit potential compounds from their list of design candidates simply because they are synthetically inaccessible. On the other hand, it is true that features such as short, convergent synthetic pathways; suitability to apply well-behaved, high-yield synthetic reactions; lack of complicating structural features such as stereoisomers; and probable ease of scalability from gram level to kilogram level to metric ton level enhance the

attractiveness of some compound series. But as a general rule during lead optimization, experienced medicinal chemists typically can freely pursue the exploration of whatever properties they seek to improve (e.g., activity, selectivity, solubility, and ADME/PK) without crippling synthetic limitations. In fact, we can say that this ready accessibility of a large number of active compounds *enables* the optimization of ADME/PK and pharmaceutical properties. As a practical matter, then, medicinal chemists are frequently able to define a certain core pharmacophore that can be modified in pharmacologically tolerant noncore parts of the molecular series to achieve a single molecule with an excellent balance of activity, selectivity, pharmaceutics, and ADME/PK.

4.01.2.2.2.2 Optimization of ADME/PK

ADME/PK depends almost completely on the chemical and physical properties of single molecules. This is because the biological systems with which drug molecules interact, such as drug-metabolizing cytochrome P450 (CYP) enzymes or membrane drug transporters, work on one molecule at a time. In fact, then, ADME/PK properties are often attributable to chemical features of the molecule that chemists intuitively understand. Of course, the interaction is not entirely a matter of the chemistry of the small molecule, since in almost all cases there is a large biological structure (i.e., a protein, polynucleotide, or membrane) that constitutes the second partner in the interaction. Thus, the interaction, while still chemical in nature, is complex and usually only approximately understood. Consequently, consideration of the chemical properties alone of the molecule (e.g., functional groups, chemical reactivities, and polarity) is insufficient to completely predict the interaction, and empirical methods are still necessary to assess these interactions. For example, one can look at the structure of a drug candidate and make note of the susceptibility of various portions of the molecule to biotransformation by oxidation, conjugation, or hydrolytic enzymes, but one cannot tell in a reliable way which pathway will be predominant or what absolute rate of metabolism will be observed. Thus, since the science is not yet advanced enough to provide fully dependable values of ADME/PK properties based on molecular properties alone, we still need to experimentally interrogate various in vitro and in vivo systems with the molecule of interest to get a trustworthy answer that can be used for selection decisions. Case histories have been published illustrating application of ADME/PK optimization to discovery and preclinical development.[7,8]

4.01.2.2.2.3 Optimization of pharmaceutics

In contrast to ADME/PK, pharmaceutics depends largely on bulk properties of the chemical compound. Examples of such biopharmaceutical properties are solubility, membrane permeability, wettability, rate of dissolution, hygroscopicity, storage stability, crystallinity, and crystal morphology. In practice, chemists don't worry too much about the pharmaceutics. With the exception of permeability, pharmaceutical properties tend not to be extremely critical to the ultimate success of a candidate molecule, and less-than-optimal characteristics can often be remedied with salt forms, amorphous preparations, and formulation excipients. Thus, for example, while chemists are aware of the desirability of good solubility, it is unusual to see an otherwise promising clinical candidate be discarded because solubility is poor. However, solubility can become a differentiating feature when multiple good compounds exist.

4.01.2.3 Major ADME/PK Characteristics to Optimize

4.01.2.3.1 "Right Box" analysis

Discovery lead optimization is the only chance that medicinal chemists have to build in desirable ADME/PK characteristics. During this phase, the structure is continually altered to optimize and balance activity, selectivity, toxicity, ADME/PK, and pharmaceutics. However, once a clinical candidate is nominated, all freedom of structural modification is frozen out. In particular, the ADME/PK properties are fixed. Therefore, it is important to be able to reasonably project the range into which each important PK parameter (e.g., oral bioavailability, half-life, and brain penetration) will fall in humans, well before there is any clinical experience with the compound, and only in vitro and animal in vivo data are available. It is usually not necessary to be able to predict the human value of each parameter exactly; it is only necessary to be able to say with confidence that the parameter will fall into the acceptable range. For instance, one can say that a successful oral drug should be at least 20% bioavailable. Therefore, it doesn't matter strongly if we predict 80% bioavailability, whereas the true value in the clinic turns out to be 40%. The drug would still be acceptable for oral use, although we obviously would prefer to have 80% compared with 40%. This tolerance of moderate error is true for essentially all ADME/PK properties and allows us to use "Right Box" analysis.[9] We have only to successfully project the compound's ADME/PK properties into the "right" box: poor, moderate, or good. With these considerations in mind, let us discuss the various ADME/PK properties that are necessary for a successful clinical drug and how we estimate them.

4.01.2.3.2 Oral absorption and bioavailability

4.01.2.3.2.1 In vivo determination of oral bioavailability

It is common practice at the beginning of a discovery program to characterize the pharmacokinetics of one or more of the "hit" compounds. This is merely to establish the general characteristics of the compound to help define the ADME/PK properties that present the biggest need for improvement. Mice or rats are used for a full intravascular (IV)/ per oral (PO) PK study, which reveals the fundamental PK parameters, such as oral bioavailability, systemic clearance, *MRT*, and terminal elimination half-life. Oral bioavailability (F) may be defined as the fraction of an orally administered dose that reaches the systemic blood circulation, where it becomes available (bioavailable) to the organs and tissues. Experimentally, oral bioavailability is determined from the ratio of the

area under curve (*AUC*) for the plasma concentration versus time curve for the PO and IV doses as shown in Eq. (1) (adjusted for the ratio of PO and IV doses):

$$F(\%) = \frac{AUC_{\text{PO}}}{AUC_{\text{IV}}} \times \frac{Dose_{\text{IV}}}{Dose_{\text{PO}}} \times 100\% \tag{1}$$

The discovered PK deficiencies, if any, define the types of in vitro ADME/PK assays that are incorporated into the screening funnel for the "hit-to-lead" process. When a certain predefined level of potency against the target receptor is achieved, the program identifies one or more lead series to advance to the "lead optimization" phase, and a full IV/PO study in mice or rats is conducted on each of these to establish again the PK baseline of each series. It is common for the screening funnel to change in lead optimization from the sequence of assays that were used in the hit-to-lead phase. At various points in the lead optimization process, full IV/PO PK is done yet again to provide unambiguous information about the in vivo performance of the compounds. And, as before, the PK deficiencies inform the team about which in vitro screens are to be retained or added in the screening funnel.

We occasionally need to conduct in vivo PK because in vitro assays have a level of uncertainty of interpretation and prediction that limits how precisely the assay results can be used to screen out bad compounds.[10,11] It is necessary to do some checking from time to time that apparent progress made in improving the in vitro PK parameters actually has translated to real in vivo performance. However, it is obvious that conventional full IV/PO PK studies take too long to be useful for screening compounds in a fast-moving lead optimization campaign. These studies take days to mount and carry out, because, among other reasons, one cannot determine that a drug candidate has a 12-h half-life in only an hour. In addition, a full IV/PO study requires a nontrivial amount of compound for dosing, an amount that typically exceeds the few milligrams that may have been prepared in the initial synthesis. The dilemma is that the in vitro assays give data on lots of compounds fast, but the data are not easy to interpret, while in vivo PK studies give full and easy-to-interpret data on a very few compounds, with significant compound and time requirements. For this reason, a number of discovery organizations have introduced various intermediate PK approaches to bridge the gap between purely in vitro surrogate PK assays and full in vivo PK.[11]

Cassette dosing (CD) involves dosing a number of compounds to a single animal to minimize the average time for results to be available and the number of animals to be used. Blood samples are taken at the appropriate times after PO or IV dosing and simultaneously analyzed for all dosed compounds, taking advantage of the capability of mass spectrometers to monitor the unique molecular weights (MWs) associated with each compound in a complex mixture. White and Manitpisitkul[9,12] provided a theoretical PK analysis of CD that prescribed the conditions under which the data would be relatively free of the inevitable DDIs that accompany dosing with multiple compounds at the same time. The rapid rat assay[13] was introduced as a compromise approach featuring single-compound dosing but other compensating accelerations to provide very rapid in vivo PK data, and rapid rat has been very successful.[14] A closely related method, snapshot PK, similarly provides a very quick but useful picture of the in vivo PK.[11] A third variation, the rapid PK approach, provides more PK information than rapid rat or snapshot PK, but results still come faster than with conventional full PK.[11] The combination of all these methods makes possible frequent "reality checks" on what the in vitro ADME/PK assays indicate, and most organizations use some combination of these in vitro and in vivo PK methods to drive the PK optimization in a time frame compatible with the rate of production of pharmacologically interesting analogs.

Once the PK deficiencies of the best lead compounds have been identified, chemists seek to improve these properties by making intelligent structural modifications to the chemotypes while maintaining (and even improving) the pharmacological properties of potency and selectivity according to the SAR, which has been discerned in the lead optimization process. First, let us examine the case in which in vivo testing has revealed that oral bioavailability is poor and needs to be brought at least into the acceptable range in order to nominate a clinical candidate. Let us consider how the chemist can approach the problem of low bioavailability in a systematic way. In subsequent sections, we will look at the corresponding problems of half-life and distribution.

4.01.2.3.2.2 Determinants of bioavailability

Good oral bioavailability depends on a compound being able to solubilize in the GI tract (or remain soluble if dosed as a solution), survive degradative enzymes in the intestinal lumen, diffuse through the intestinal wall, survive metabolism by enzymes in the intestinal wall, not be excreted into bile, and survive metabolism by hepatic enzymes during passage through the liver on its way to the systemic blood. We can summarize this concept symbolically with the simple equation in the succeeding text:

$$\text{Fraction of oral bioavailability } (F) = (1 - f_{\text{ld}}) \times f_{\text{a}} \times (1 - f_{\text{im}}) \times (1 - f_{\text{hm}}) \times (1 - f_{\text{eb}}) \tag{2}$$

where f_{ld} is the fraction degraded by the enzymes of the intestinal lumen, f_{a} is the fraction absorbed through the intestinal wall, f_{im} is the fraction metabolized by the drug-metabolizing enzymes of the intestinal wall, f_{hm} is the fraction metabolized by hepatic drug-metabolizing enzymes, and f_{eb} is the fraction excreted into the bile.

As with a multistep chemical synthetic sequence, even a 90% yield at each step still can produce a disappointing overall return. For example, a hypothetical drug that was 10% degraded by digestive enzymes during intestinal transit ($f_{\text{ld}} = 0.1$), 90% absorbed through the intestinal wall ($f_{\text{a}} = 0.9$), 10% metabolized by enzymes in the intestinal wall ($f_{\text{im}} = 0.1$), 10% metabolized by liver enzymes ($f_{\text{hm}} = 0.1$), and 10% excreted into the bile during the first pass ($f_{\text{eb}} = 0.1$) would have $F = 0.9 \times 0.9 \times 0.9 \times 0.9 \times 0.9 = 0.59\%$ or 59% oral bioavailability. Since each f factor can range from 0 to 1, one can easily see multiple ways that oral bioavailability could be severely limited, since if any of the f factors reached 0.9, bioavailability would be automatically reduced to 10% or less, no matter how good the other factors are. As an example, F is only 2% for the osteoporosis drug raloxifene, which is subject to extensive first-pass glucuronidation.[15] The chemist must get all five f factors into the good range.

It is easy to see why bioavailability is sometimes very low. In fact, it is somewhat surprising that high bioavailability, approaching 100%, is *ever* found, yet a number of drugs are nearly completely orally bioavailable (e.g., *F* for indomethacin is 98% and for rosiglitazone 99%).[15]

So what properties does the chemist have to build into the molecule during lead optimization to get good bioavailability? One approach to this question is to design molecules to have physicochemical properties in the range that favors good oral bioavailability. This approach requires the use of physicochemical descriptors that are readily calculable from the structure, and examples are MW, extent of ionization, lipophilicity, polar surface area, number of rotatable bonds, number of hydrogen bond donors and acceptors, and solubility.[16] However, another approach is to dissect the reasons that certain chemotypes fail to easily generate good bioavailability.

4.01.2.3.2.3 Absorption through the intestinal wall

Solubility and resistance to intestinal degradative enzymes such as proteases, esterases, amidases, and lipases are relatively easy for the chemist to circumvent. Although solubility is an intrinsic molecular property reflecting MW, degree of solvation, lipophilicity, and ionization state of the molecule at the pH of the biological medium, it can often be improved by the use of standard formulation excipients such as polyethylene glycol, surfactants, and cyclodextrins. The digestive enzymes usually (but not always) don't recognize nonbiological molecules well. Membrane permeability, on the other hand, is a more difficult property to build in, yet is essential for an orally deliverable drug, since it must diffuse through both the luminal and basolateral membranes of the gut wall to enter the blood. A few exceptions exist to the need for passive membrane permeability, for instance, the recognition of certain drugs by uptake transporters in the gut wall, such as the antiviral drug valacyclovir, which incorporates the amino acid L-valine as an ester of acyclovir, allowing it to be recognized by the intestinal peptide uptake transporter Pept1.[17,18] In most cases, however, the chemist must design the proper combination of solubility, membrane permeability, and lack of recognition by the intestinal efflux transporter P-glycoprotein (P-gp, also called MDR1).[19] The standard method for measurement of both intrinsic membrane permeability and P-gp recognition is measurement of bidirectional membrane transport across cell monolayers, such as Caco-2 or MDCK-MDR1 cells.[20] These systems have sufficient throughput that they can easily be placed into a screening paradigm for initial assessment of newly synthesized analogs during lead optimization. The result of these permeability assays is to characterize a compound into one of four categories: high permeability/non-P-gp substrate, high permeability/P-gp substrate, low permeability/non-P-gp substrate, and low permeability/P-gp substrate. This categorization can be used to screen out compounds likely to have poor intestinal absorption and is also helpful when seeking to diagnose poor bioavailability.

4.01.2.3.2.4 First-pass metabolism in the intestinal wall

As molecules pass through the luminal membrane into the interior of the enterocyte, the first of the barriers comprising the so-called first-pass elimination is encountered. Drug-metabolizing enzymes, especially CYP, sulfotransferase (SULT), and UDP-glucuronosyltransferase (UGT), are present in the enterocytes, with the role of providing a metabolic barrier to the entrance of nonnutritional molecules that were ingested from the diet or from therapeutic intervention (i.e., xenobiotics).[21] These enzymes are nonspecific as an important part of their function, ready to metabolize any small molecules that present themselves. In the case of molecules synthesized as part of lead optimization, this represents the first time in the history of Earth that these enzymes have encountered these molecules. The drug-metabolizing enzymes obviously did not evolve as specific catalysts for these particular drug molecules, yet the compounds nonetheless are often recognized and metabolized. Only the fact that the metabolism requires a finite time to occur prevents the metabolism from being complete, since the molecules are only transiently exposed to metabolism as they rapidly diffuse down the concentration gradient from the gut lumen to the bloodstream. Thus, some molecules with metabolic "hot spots" suffer a large fraction of gut metabolism and consequently have low bioavailability, while others that happen to be more resistant to metabolism can survive long enough to pass through the gauntlet.

4.01.2.3.2.5 First-pass metabolism in the liver

However, the danger is not over, for all the blood coming from the intestine is collected from the mesenteric circulation into a single vessel called the portal vein, which feeds directly into the liver. In cases of universal low bioavailability in a series, an in vivo diagnostic procedure such as portal vein cannulation[22] can help the discovery team decide if the principal first-pass barrier is the intestine or liver. The enzyme-rich liver acts as a second metabolic barrier, in which the same types of enzymes, and others such as aldo-keto reductase (AKR), alcohol dehydrogenase, glutathione *S*-transferase (GST), and carboxylesterase (CES),[23] have a chance to metabolize the drug candidate molecules. Only molecules with exceptional resistance to metabolism can survive the double metabolic barriers of the intestine and liver to finally reach the systemic bloodstream. Virtually, all drug candidate molecules contain functional groups or molecular features potentially susceptible to metabolism by at least one of these metabolic reactions. Given long enough exposure to hepatic enzymes, almost every possible small organic compound would be extensively metabolized. But, just as with the intestinal drug-metabolizing enzymes, time is the key. Different compounds display a wide range of kinetics for these metabolic reactions, so the challenge for the chemist that wants to improve bioavailability among a series of analogs that suffer a large first-pass metabolism effect is to slow down the rate of metabolism by making modifications that render the analogs less susceptible to metabolism. But how is that to be done?

4.01.2.3.2.6 Common metabolic reactions

To understand the problem better, we should first note that, by far, the most common metabolic reactions are those catalyzed by the CYP enzymes, with the UGTs being a distant second.[24] The reason that the CYPs dominate metabolism is simple: they catalyze a variety of oxidative reactions on groups, such as methyl, methylene, and aromatic rings, that are present in almost every drug candidate. All other drug-metabolizing enzymes carry out reactions that are specific to certain functional groups, such as hydroxyl groups, carboxylic acids, amides, esters, ketones, and alkyl halides, that are present only in some drugs. **Table 1** summarizes the frequency of various types of metabolic reactions and the enzymes that catalyze them. The typical reaction shown for CYP, methyl hydroxylation, is a specific example of the addition of an oxygen atom at many potentially oxidizable sites on drug molecules, including aliphatic and aromatic C–H bonds, double and triple bonds, and nitrogen and sulfur atoms. In contrast, other enzymes can only catalyze a specific reaction type on a specific functional group in the drug molecule, as shown.

Because of the central importance of the CYP enzymes in several ADME/PK phenomena, including metabolic clearance, drug interactions, and individual PK variability,[25] it is worthwhile to provide some additional helpful information to medicinal chemists about these enzymes. Although the human genome contains 57 CYP genes,[26] only about a dozen of these genes code for CYP enzymes that have a role in the metabolism of drugs (see **Table 2**). These enzymes are sometimes erroneously referred to as "isozymes," but the strict definition of that term refers to different proteins that catalyze the exact same reaction from the exact same substrate. **Table 2** clearly shows that although CYP enzymes catalyze similar oxidative reactions, the exact substrates and reactions vary widely among the different enzymes. Seven of the enzymes shown in **Table 2** (1A2, 2B6, 2C8, 2C9, 2C19, 2D6, and 3A4) are important in the metabolism of enough drugs to warrant the attention of regulatory agencies, especially in regard to drug interactions.[28,29]

The CYP enzymes are hemeproteins that, unlike the cytochromes of the mitochondrial respiratory chain or hemoglobin, contain a unique combination of thiolate ligand to the heme iron, a binding site for molecular oxygen on the iron, and a large open pocket above the plane of the heme that serves as a binding site for drug molecules. This arrangement allows for the simultaneous binding of molecular oxygen and an oxidizable drug molecule, allowing the characteristic CYP hydroxylation reaction:

$$R-H + O_2 + NADPH + H^+ \rightarrow R-OH + H_2O + NADP^+$$

The function of the cofactor NADPH is to provide reducing electrons to convert the iron-bound O_2 molecule to a highly reactive iron-oxo intermediate capable of oxidizing many different types of functional groups on drugs, including aliphatic C–H bonds, olefinic and aromatic double bonds, and the heteroatoms N, O, and S.[30] The oxidation reaction is a two-step process proceeding through a carbon radical intermediate, shown in simplified form in the succeeding text:

$$R-CH_2-H + Fe^{5+}=O \rightarrow R-CH_2^{\bullet} + Fe^{4+}-OH \rightarrow R-CH_2-OH + Fe^{3+}$$

As implied by the data in **Table 2**, the size, shape, and polarity of the binding site account for the selectivity of the various CYP enzymes for different types of drug substrates. The exact orientation and proximity of the drug molecule with respect to the iron-oxo unit determines which point on the drug molecule undergoes oxidation. The fact that so many drugs are metabolized by one or more CYP enzymes, then, is because most drug molecules will bind to at least one of the various CYP active sites. Once bound,

Table 1 Most important human drug-metabolizing enzymes

Enzyme[a]	*Subcellular localization*[b]	*Metabolic reaction*	*Percentage of all metabolism*[c]	*Diagnostic metabolite MW*[d]	*Example drug*
CYP	SER	R-CH_3 → R-CH_2-OH	40	*P*+16	Methyl hydroxylation of celecoxib
UGT	SER	ROH → RO-Gluc	14	*P*+176	Phenolic glucuronidation of ezetimibe
DH	CYT	R_2-CH-OH → R_2-C=O	8	*P*−2	Secondary alcohol dehydrogenation to ketone of ezetimibe
HYD	SER	RCOOR′ → RCOOH	7	*P*−R+1	Ethyl ester hydrolysis of prodrug enalapril
GST	CYT	R-X → R-SG	5	*P*+307-HX	Displacement of Cl on chlorambucil by glutathione
SULT	CYT	ROH → RO-SO_3H	5	*P*+80	Phenolic sulfonation of raloxifene
AKR	CYT	R_2C=O → R_2CH-OH	4	*P*+2	Reduction of keto group of warfarin
NAT	CYT	$ArNH_2$ → ArNH-$COCH_3$	2	*P*+42	*N*-Acetylation of sulfadiazine
Other	CYT, CYT, MIT, MIT, SER	Methylation, phosphorylation, monoamine oxidase, taurine conjugation, nitro reduction, etc.	15	*P*+14, *P*+80, *P*−1, *P*+107, *P*−30	

[a]*CYP*, cytochrome P450; *UGT*, UDP-glucuronosyltransferase; *DH*, dehydrogenase; *HYD*, hydrolase; *GST*, glutathione *S*-transferase; *SULT*, sulfotransferase; *AKR*, aldo-keto reductase; *NAT*, *N*-acetyl transferase.
[b]*CYT*, cytosol; *MIT*, mitochondria; *SER*, smooth endoplasmic reticulum (microsomes).
[c]Percentages as compiled by Testa et al.[24]
[d]MW is molecular weight of metabolite; *P* is molecular weight of parent drug.

Table 2 Properties of the most important human cytochrome P450 (CYP) enzymes involved in drug metabolism

CYP	*Active site volume*[a] ($Å^3$)	*Characteristic substrate drugs*	*Functional polymorphism*	*Inducible*	*Clinical inhibitor*
1A1	ND	Polycyclic aromatic hydrocarbons (benzo [*a*]pyrene)	No	Yes (cigarette smoke)	None
1A2	406	Heteroaromatic amines (theophylline, ondansetron)	No	Yes (heterocyclic amines; cigarette smoke)	Furafylline
1B1	398	Polycyclic aromatic hydrocarbons (benzo [*a*]pyrene)	Yes	Yes (cigarette smoke)	Resveratrol
2A6	230	Small lipophilic (nicotine, coumarin)	Yes	Yes (rifampicin)	Tranylcypromine
2B6	279	Small lipophilic (cyclophosphamide, bupropion)	No	Yes (barbiturates)	Orphenadrine
2C8	1536	Large lipophilic (paclitaxel, cerivastatin)	Yes	Yes (rifampicin)	None
2C9	1457	Large aromatic amides/esters (warfarin, tolbutamide)	Yes	Yes (rifampicin)	Sulfaphenazole
2C19	ND	Large lipophilic heteroaromatics (mephenytoin, diazepam)	Yes	Yes (rifampicin)	None
2D6	797	Lipophilic amines (dextromethorphan, fluoxetine)	Yes	No	Quinidine
2E1	190	Small hydrophilic (ethanol, acetaminophen)	No	Yes (ethanol)	Disulfiram
3A4	1508	Large lipophilic (midazolam, nifedipine)	No	Yes (rifampicin)	Ketoconazole, ritonavir

[a]Active site volume data taken from Dong et al.[27]

the molecule encounters a rich oxidative chemistry that can usually find an acceptable oxidative target somewhere on the drug molecule.

4.01.2.3.2.7 Addressing high first-pass clearance

If the in vitro membrane permeability assay (e.g., Caco-2) indicates that intestinal absorption is not the reason for low bioavailability, and we believe from the structure of the drug molecule that degradation by digestive enzymes in the stomach and intestinal lumen is unlikely (this can actually be tested, but usually simple inspection of the structure of the molecule is enough), then most likely, high first-pass clearance is the reason. First-pass clearance is the result of both first-pass metabolism and first-pass biliary excretion. The extent of biliary excretion of intact parent drug may be investigated in vivo with bile duct-cannulated (BDC) animals or in vitro with hepatocytes.[31] However, most commonly, the metabolic component of first-pass clearance is the greater of the two, so let us devote considerable discussion to this process.

We can investigate the rate of metabolism by in vitro methods, most notably liver *S*9 fraction, microsomes, and hepatocytes. One or another of these is commonly an in vitro assay in the screening funnel, so the information may be already at hand. Liver microsomes and *S*9 fractions are formed by homogenization of liver cells. Differential ultracentrifugation produces fractions containing various subcellular organelles and, therefore, various metabolic enzyme sources. Whole liver homogenate contains all components, including plasma membrane, smooth and rough endoplasmic reticulum (SER and RER), mitochondria, nuclei, and cytosol. Whole homogenate, which contains all metabolic enzymes and cofactors, is used when one is certain that the liver is a major metabolic organ, but the type of metabolism may be uncertain. To further distinguish the location of the metabolic process, subcellular fractions are isolated and tested for metabolic activity. Relatively slow-speed centrifugation at $9000 \times g$ precipitates the heavier components of unbroken cells, plasma membrane, RER, mitochondria, and nuclei, leaving behind the cytosol and the SER (combination referred to as *S*9, the supernatant from $9000 \times g$ centrifugation). Determining that the metabolic activity remains in *S*9 fraction demonstrates that the major metabolic process occurs in the SER or cytosol. If the activity is not found in *S*9, then the metabolic activity must have been associated with one of other subcellular organelles, such as the mitochondria. Assuming that activity is found in *S*9, then further ultracentrifugation of *S*9 at $105{,}000 \times g$ separates the microsomes (resulting from the SER being broken apart by homogenization and reforming as spherical bodies) and cytoplasm. Thus, testing metabolic stability (MetStab) in microsomes differentiates the enzyme type into membrane-bound enzymes, such as CYPs, and soluble enzymes, such as AKR (see **Table 1**). Because of the prominence of CYP enzymes in drug metabolism, *S*9 or microsomes are often used for MetStab screening. These two systems are easy to prepare, easy to use, and available from common laboratory species as well as humans. To have full metabolic competency, both systems must be supplemented with appropriate cofactors, such as NADPH for CYP-catalyzed oxidations, UDPGA for UGT-catalyzed glucuronidations, and glutathione for GST-catalyzed glutathionylations. Thus, results from these systems have to be interpreted carefully in terms of recognizing that the experimental question asked depends on which cofactors and in what ratios were supplied. Cytosolic and microsomal hydrolytic enzymes such as CES do not require a cofactor.

An alternative in vitro system for MetStab screening is hepatocytes. These have an advantage over *S*9 and microsomes in that they are a complete living system. All liver metabolic processes are present simultaneously in their normal in vivo proportions,

and hepatocytes do not require supplementation with cofactors. Thus, it is felt that hepatocytes provide a more complete and accurate assessment of metabolism of drug candidates without prior knowledge of the pertinent metabolic pathways. On the other hand, they are more difficult to prepare and require cell-culture methods to maintain, so they are correspondingly more expensive and difficult to use than *S*9 and microsomes. Since hepatocytes are a cell-based system, usually less protein can be applied in an assay, and absolute enzymatic rates are slower than for *S*9 and microsomes. However, the sensitivity of mass spectrometry (MS) as the analytic instrument of choice for ADME/PK work allows accurate measurements with even low concentrations of drug candidates.

Recent innovations in the preparation and use of hepatocytes have resulted in the availability of enhanced hepatocyte systems that will eventually replace the conventional systems that presently dominate ADME/PK work. Conventional hepatocytes only survive in an active metabolism experiment with an experimental drug for a few hours before dying. Because the absolute enzymatic rate in a typical hepatocyte experiment is already low, if the experimental drug is one with very low clearance, then the hepatocytes don't have enough catalytic capacity to appreciably metabolize the test article drug in the relatively short time before the cells die.

Admittedly, this sounds like an odd problem to discuss in the context of a discovery program seeking to slow down high clearance, but this problem actually has discovery-level ramifications as well. When we cannot detect a rate of metabolism of the parent drug because it is very low, then the most we can say is that the rate is less than a certain threshold number. Unfortunately, this low unmeasurable rate may not distinguish a rate corresponding to a 24-h clinical half-life (which might be very desirable) from a low unmeasurable rate corresponding to a 10-day clinical half-life (which we probably would not want to nominate as a clinical candidate). Thus, there is a need to magnify the rates below the threshold to measurable rates that can be used to distinguish compounds that would be problematic from those that would be acceptable.

The enhanced systems fall into three fundamentally different categories. First is the so-called relay method for extending the period over which a hepatocyte experiment can be run.[32] In the relay method, the culture medium, which contains the metabolizable drug substrate and the formed metabolites, is transferred to a fresh batch of cells every 4 h, allowing an unlimited period of time for a slow rate to be measured. Eventually, even a very slow rate will have depleted the drug enough that a useful estimate of the rate of metabolism could be derived. In practice, the total incubation times of 20 h were demonstrated to be feasible, greatly expanding the range of low rates that could be measured.

Other approaches use various biological approaches, including modifications to the hepatocytes themselves or the generation of hepatocyte-like cell lines, all of which survive much longer in culture during active metabolism experiments. One of these uses human pluripotent stem cell-derived hepatocytes as surrogates for conventional hepatocytes.[33] These cells seem to have all the function of true hepatocytes and last at least 2 weeks in culture. However, they have not yet been applied to MetStab assays. Another surrogate hepatocyte system is the human hepatoma cell line, HepaRG.[34,35]

Three long-lived true hepatocyte systems are available and in use. One is the HepatoPac micropatterned hepatocyte–fibroblast coculture system that can be used for continuous incubations of up to 7 days.[36–38] Validation experiments with a variety of low-clearance drugs established that these cells gave useful estimates of the absolute values of clearance, sufficient to serve as a screening assay. Another is the upcyte system of extended lifetime human hepatocytes.[39,40] The third is the HμREL hepatocyte coculture system,[41,42] which has been shown to maintain viability and fidelity of metabolism for at least 2 weeks. Each of these systems has advantages and disadvantages,[42] although the HμREL system is reported to show slightly superior overall assay performance.[41] Straightforward methods exist for converting these quantitative in vitro rate measurements into useful estimates of the in vivo first-pass clearance in order to judge the importance of metabolism in limiting bioavailability.[21,42–44]

In addition to their ability to measure low metabolic rates, these enhanced hepatocyte systems have applications to toxicity testing (see section Early Toxicity Assessment) and to determining routes of metabolism. All three uses reflect the facts that at least some of these systems retain fidelity to the metabolic processes existing in the liver of living human beings, as opposed to conventional hepatocytes, which have a tendency to lose their identity and dedifferentiate. One example illustrates this phenomenon. The marketed antihistamine desloratadine has long been known to be hydroxylated in the 3-position as the major human metabolic process,[45] although the enzyme responsible for the transformation could never be identified due to the inability of in vitro systems, including conventional hepatocytes, to produce the 3-hydroxy metabolite. But then, for the first time, the high-fidelity HμREL hepatocyte coculture system was applied to the problem and shown to produce this metabolite, even though in side-by-side experiments conventional hepatocytes did not.[46] Once it had been shown that an enhanced hepatocyte system could make the correct metabolite, Kazmi et al.[47] took a fresh look at the previous failures of conventional hepatocytes and discovered the unusual features of the metabolic process that had confounded prior attempts. The important lesson was that high-fidelity hepatocyte systems are likely to produce the correct answer the first time, without prior knowledge of what the correct answer is. This valuable characteristic will, in the opinion of this author, eventually result in broad use of such systems in pharmaceutical discovery and development and the requirement that they be used for hepatocyte-based assays submitted in regulatory filings.

It often happens that merely knowing that the rate of metabolism is high is enough to suggest to the medicinal chemist possible modifications to reduce the rate by chemical intuition and experience. Analogs with "fixes" to the proposed problems are easy to make and test in vitro. However, this cognitive approach is usually not enough and actual experimental data on sites of metabolism are needed, as elaborated in the succeeding text.

MS has seen tremendous improvement in the last few years, and new applications to the problem of metabolite detection and identification have emerged as a result. This applicability entirely rests on the capabilities of new high-resolution MS instruments, as well as inventive new algorithms, to detect metabolites in in vitro incubation mixtures and even ex vivo biofluids such as plasma, urine, and bile.[48–51] Several techniques are now widely available to afford rapid detection of metabolites without the use of

radiolabel. Furthermore, in almost all cases, partial structure identification is possible in the absence of authentic standards, with many instances of *full* identification possible.

First, let us discuss how metabolites can be reliably found without the use of radiolabel. The most intuitive and easily understood technique is baseline subtraction of control incubations or biofluid samples in which no metabolism occurred. Excellent concordance of the revealed metabolite peaks to those of corresponding incubations with radiolabeled drugs demonstrated the reliability of this enhanced baseline subtraction with noise-reduction algorithm to find metabolites without prior knowledge of their structures or presence in the sample.[52] One can also use the "list" technique in which one creates a table of common metabolic transformations of the parent compound, as illustrated in **Table 1**. The MS software marks peaks as likely metabolites when their nominal mass matches one in the list. Of course, unusual metabolites whose masses are not in the list would be missed, so that the list technique alone may not produce a complete answer. Another technique called isotope pattern filtering (IPF)[53] is applicable to drugs that contain a chlorine or bromine atom in the molecule, since all metabolites containing one of these halogens will show the characteristic isotope pattern (i.e., 35/37 in the ratio 3:1 for chlorine and 79/81 in the ratio 1:1 for bromine). The MS data-collection software is programmed to mark peaks with molecular ions showing a doublet in the proper proportions. Of course, this technique will not be applicable for nonhalogenated chemotypes, and furthermore, it assumes that the halogen has not been lost from the metabolite. But for chlorine/bromine-containing analogs, IPF is simple and unambiguous. Two additional techniques for finding metabolites rely on commonality of certain fragmentation patterns between parent and metabolite, namely, product ion filtering and neutral loss filtering.[48]

Finally, a technique called mass defect filtering (MDF) is much less intuitive than the others but very powerful with much less reliance on assumptions about the metabolites.[54] MDF is based on the fact that atomic weights are not exact integers. The difference between the nominal atomic weight and the actual atomic weight is called the mass deficit. Summing the deficits of the atoms composing the parent drug molecule allows one to define a characteristic molecular mass deficit. For example, the nominal molecular mass (MH^+ positive ion electrospray) of the antidepressant nefazodone ($C_{25}H_{32}ClN_5O_2$) is 470 (^{35}Cl isotope), but the actual measured MH^+ as determined in a high-resolution MS instrument is 470.2323.[48] Thus, the mass deficit for nefazodone is 0.2323 Da. Somewhat counterintuitively, the same mass deficit (within a window of ± 0.05 Da) is observed for metabolites of nefazodone that retain most of the full structure of the parent drug (e.g., the hydroxylated and deethylated metabolites). Extensive validation has established that the mass deficit of the parent carries through to the metabolites, so that the high-resolution MS software determines the mass deficit of each peak in the LC-MS chromatogram and marks those peaks whose deficit falls within the window established by the parent drug.

After application of some combination of the techniques in the preceding text, we can create with good confidence a set of discovered metabolites in the form of marked chromatographic peaks. But this information is almost useless by itself. We also need to quickly determine the chemical structure of each metabolite (metabolite identification (MetID)). The nominal mass of the molecular ion of the discovered metabolite encodes the nature of the metabolic modification. For example, as seen in **Table 1**, a metabolite with MW 16 Da higher than that of the parent drug (i.e., P + 16) is almost certainly a product of CYP oxidation of the parent drug. Similarly, a glucuronide will show an MW at P + 176. There are many such numerical combinations that automatically define the nature of the metabolic reaction, and often, this information alone is sufficient to exactly define the point of metabolism on the drug molecule. For example, a metabolite of MW at P-14 from a drug containing a dimethyl amine functional group must be the *N*-desmethyl metabolite, while a metabolite showing MW at P + 176 from a drug than contains a single hydroxyl group is surely the glucuronide attached through that hydroxyl, and a metabolite of an ethyl ester with MW of P-28 can confidently be identified as the corresponding carboxylic acid.

For a metabolite whose MW alone does not completely define the structure, fragmentation by standard MS/MS methodology provides very good information about the position of the metabolic modification. This is often important for hydroxylated metabolites, in which the parent drug usually contains multiple potentially oxidizable C–H bonds, and thus, the metabolites have many structures consistent with MW P + 16. The major fragmentation pathways are often similar between parent drug and metabolite, so that a change in the mass of one fragmentation daughter ion while other fragmentation daughters are constant signals the position of the hydroxylation. An MS-based method even exists now for distinguishing the position (e.g., *ortho*, *meta*, or *para*) of a metabolic modification on an aromatic ring, a useful additional MetID tool, since positional isomers can vary greatly in pharmacological and/or toxicological activity.[55] The techniques in the preceding text can be used singly or together in parallel to provide unambiguous detection of and structures for the major metabolites of drug candidates.[56] All major vendors of high-resolution mass spectrometers provide powerful auxiliary software to largely automate and facilitate the rapid discovery and structural elucidation of metabolites.

The advantage of this capability to chemists cannot be overstated. Before the advent of rapid MetID during lead optimization, the use of in vitro metabolic systems such as liver microsomes or hepatocytes was limited to measurement of the rate at which the in vitro system metabolized the drug analog. For example, a series of 10 analogs subjected to a MetStab screening assay might show that most of the analogs had very short in vitro half-lives and should be discarded. One or two, however, might have had half-lives approaching 1 h and would be retained as potentially good candidates. This would be a completely one-dimensional empirical process, with no fundamental chemical understanding of what was bad about the discarded compounds or good about the retained ones. However, as long as some good analogs *did* come out of the screening process, it didn't matter very much if the reason for success was fully understood by the chemists. But it is often the case that most, if not all, of the analogs have high rates of metabolism and few, if any, have suitable MetStab kinetics. The chemists don't want to keep throwing away compounds that had other desirable properties, especially potency and selectivity. Instead of relying on the empirical, trial-and-error approach, they want to rationally design out the metabolic liability.

Now imagine that the same in vitro incubates used for the rate determination were split, and the second sample was submitted for MetID. If the MetID data were available in the same time frame as the quantitative rate data, then an illuminating second dimension would be added to help the chemist fix the problem. With respect to timing of the availability of this valuable chemical information, it is enlightening to remember that liquid chromatography (LC)-MS/MS is almost invariably used for the quantitation of the rate of metabolism of the parent drug. The metabolites are present in the same samples as the parent drug and consequently also elute from the LC along with the parent drug (usually at an earlier retention time due to greater polarity). However, in the old one-dimensional approach, we only quantitate the parent drug, and the metabolites go straight through the mass spectrometer without detection, since we "close our eyes" as they elute. Such a waste!

The second dimension, being structurally based, is well understood by chemists and can be directly translated to structure evolution during lead optimization. In the past, chemists, who are typically not strong in pharmacokinetics, have been content to allow the pharmacokinetic scientists decide on what data to deliver. Conversely, the pharmacokineticists are typically not strong in chemistry and have not appreciated how valuable the MetID structural information would be to the medicinal chemists. The capability of obtaining at least partial structures of these metabolites currently exists in any bioanalytical group that supports MetStab, but chemists may have to insist on getting these structures, not just the rates. With a two-dimensional array of information about how and how fast analogs are metabolized, the problem of slowing down metabolism becomes a straightforward exercise in the SAR, something that medicinal chemists do as easily as breathing. And once the SAR is recognized, effective measures to slow down or even eliminate certain modes of metabolism are soon evident. It should be noted that these powerful MS metabolite recognition methods have already been in routine use for years in clinical phase 1 searches for circulating metabolites before the standard ^{14}C-ADME study has been accomplished (see section "**Circulating human metabolites**").

4.01.2.3.3 Distribution

4.01.2.3.3.1 Distribution to the target organ

Although we frequently measure the suitability of the PK of a drug candidate in terms of the blood concentrations achieved, the presence in the blood is not sufficient for most drug candidates to express their potential pharmacological activity. The compound must also distribute from the blood to the target organ (e.g., brain for CNS drugs, liver for hepatitis drugs, and tumor for cancer drugs). By the use of dosed animals, it is possible to determine drug levels in the target organ by excision of the organ, homogenization, organic solvent extraction, and LC-MS/MS assay for drug concentrations. Radiolabel is not required for this determination and in fact is potentially misleading if the method does not distinguish radiolabeled parent drug from radiolabeled metabolites. Tissue uptake is usually expressed as the tissue/plasma ratio to give the absolute concentration a context for interpretation.

The most common distribution issue encountered in drug discovery is restriction of net uptake of drug into the brain by the blood–brain barrier (BBB). The BBB is a set of three biological structures that inhibit diffusion of small organic molecules from the blood to brain tissue. The first is the plasma membrane of the cerebral vascular endothelial cells, which is poorly permeable by very polar or permanently ionic compounds (e.g., quaternary amines). The second barrier is the tight junctions between the cells, which prevent flow of drug molecules around the cells, bypassing the membranes. Third is the presence in the endothelial membrane of efflux transporters, such as P-gp[57] and BCRP,[58] which use ATP energy to actively pump some drugs from the interior of the brain back to the blood. There is nothing the medicinal chemist can do to defeat the tight junction barrier, but the other two barriers are surprisingly manageable.

The solution is found in the same membrane permeability assays that are used for assessing the intestinal absorption potential (i.e., bidirectional transport across monolayers of Caco-2 or MDCK-MDR1).[59] The bidirectional transport assay provides information about both the intrinsic permeability, as measured by the absolute rate that the compound can diffuse from one side to the other, and the substrate recognition by P-gp, as measured by the "efflux ratio" (ER) of transport in the basolateral-to-apical direction and the apical-to-basolateral direction.[59] Drugs that show a high ER (three or higher) are likely good substrates for P-gp, whereas those that show an ER about unity are not. Therefore, it is quite feasible to establish an SAR for BBB penetration based on measurable molecular properties that are modifiable by the chemist.

Measurement of BBB penetration is accomplished in lead optimization in mice and/or rats, often in concert with a full IV/PO PK study. This is considered sufficient to indicate whether human BBB penetration will be problematic, as this property is qualitatively, even if not exactly quantitatively, constant across species. CD (see section "**In vivo determination of oral bioavailability**") has also been used successfully to address problems of brain penetration, where the potential for error in PK determination due to DDIs is much less than in systemic PK studies.[60] One can also measure levels of drug in cerebrospinal fluid, although this is much more difficult and not applicable to rapid screening.[61] Although computational approaches to predicting BBB penetration have been used,[62] more recent recognition of the important role of efflux transporters in the process makes this more complicated than was originally believed. The astute medicinal chemist will notice that molecule features that give a molecule good intestinal absorption are the same as those that promote good BBB penetration, for the simple reason that both the BBB and the intestinal absorption barrier use the same biological exclusion strategy. Note that for non-CNS drugs, for which we may wish to *limit* brain exposure, the problem is turned on its head, but the properties that determine the susceptibility of a compound to be blocked by the BBB apply in both cases.[63]

4.01.2.3.3.2 Plasma protein binding

Blood plasma contains proteins that have binding sites for transporting small organic molecules such as fatty acids around the body. The principal binding protein, by mass, is serum albumin, but a number of other proteins are present as well, including α_1-acid

glycoprotein and various lipoproteins. Drug molecules bind to these proteins with various affinities, some poorly (such as amikacin, 4%[15]) and some extensively (such as diclofenac, >99.5%[15]). In addition to this binding being considered a type of distribution itself, it also tends to hold drugs in the plasma, thereby buffering their distribution into organs and tissues. This binding appears tight when expressed in the usual manner as "% bound drug in plasma." For instance, indomethacin is 90% plasma protein-bound,[15] which sounds as if only 10% of the drug is available to interact with target receptors. This, however, is misleading, and an excellent discussion on the misconceptions of applying in vitro estimations of the extent of plasma protein binding to in vivo pharmacology warns against the use of protein binding as a single-dimensional screening criterion.[64]

An important reason that a drug could be 90% bound is the pure mass action effect of the high concentration of protein in plasma. For instance, the normal concentration of human serum albumin is 42 mg mL^{-1} (~650 μM),[65] and each molecule has two or more drug binding sites.[66] However, the binding affinity itself is almost always rather loose. In the case of a typical drug 90% bound by albumin, one can back-calculate that the corresponding K_d for the protein–drug interaction is about 70 μM. This is very loose binding compared with the typical K_d for a target receptor of single-digit nanomolar. Obviously, then, molecules of a drug "only" 90% bound will easily be able to dissociate from albumin and bind to the thermodynamic sink represented by the receptor, and albumin binding will not effectively compete with receptor binding. However, even in the case of diclofenac binding of >99.5%, the usual dose is not high (50 mg), demonstrating that the drug is not seriously restricted from binding to its receptor, the COX-1/2 enzyme. On the other hand, drug binding to plasma proteins *can* be so tight that it actually *is* restrictive. The antiarrhythmic drug amiodarone has plasma protein binding of 99.98%,[15] corresponding to a K_d value of about 100 nM. In such a case, the assumption of no serious competition with receptor binding may not be true, and one would want to proceed with caution. Therefore, most discovery programs avoid compounds showing plasma protein binding higher than 99.9% if possible. But it is worth pointing out that some successful marketed drugs do display extremely high plasma protein binding, for instance, zamifenacin, which is 99.98% plasma protein-bound.[64]

Experimental measurement of plasma protein binding is accomplished by equilibrating drug with plasma in either a dialysis or ultrafiltration apparatus that segregates the unbound drug so that it's concentration can be independently measured, usually by LC-MS/MS. Simple arithmetic converts this unbound concentration into percent binding. This technique is too slow for high-throughput screening, but fast enough for a second-tier screen. Computational predictive approaches have been published,[67] but these have not had the accuracy to allow the chemists to compute their way out of unacceptable protein-binding problems.

4.01.2.3.3.3 Red blood cell uptake

Another type of distribution is uptake of the drug into blood cells. Although this can happen with any type of blood cell, only the red blood cells (RBCs) are numerous enough to actually sequester an appreciable fraction of the total drug contained in blood. Thus, one PK parameter that should be checked in a nomination candidate is the blood/plasma ratio. If this is higher than unity, then it means that the RBCs are sequestering the drug. This is not a problem per se, but it can lead to misinterpretation of PK results, particularly clearance values that are based on plasma concentrations (as they usually are). The result is that ultrahigh apparent clearance values may be calculated from the plasma PK measurements, leading the chemist to think that there is an issue, when in fact it is a distribution phenomenon. Thus, for instance, if calculated systemic clearance values were much higher than physiologically reasonable (e.g., three times hepatic blood flow), then one would want to measure the blood/plasma ratio as part of the diagnostic process. High RBC uptake can happen when a dibasic amine, such as some heteroaromatic compounds like chloroquine, get trapped in a low-pH compartment of cells, such as lysosomes. The trapping phenomenon is not limited to RBCs,[68] but its effect on the blood/plasma ratio makes it easily visible in RBCs.

4.01.2.3.3.4 Volume of distribution

Full IV/PO PK studies deliver as a derived parameter the so-called "apparent volume of distribution at steady state" (V_{ss}). This is an operationally defined parameter that can be applied to vaguely describe the physiological distribution of the drug candidate. The usual units of V_{ss} are liters per kg of body mass (i.e., L kg^{-1}), and it can be treated as the volume of blood (i.e., the sampled biological compartment) in which the drug *appears* to be dissolved. A more intuitive and useful way to think of V_{ss} is as the volume of total body water (TBW), reduced by factors such as plasma protein binding that tend to restrict it to plasma and increased by factors such as Log *P* and tissue binding that tend to pull it out of plasma. Let us now illustrate this intuitive approach.

A drug that is confined to the plasma compartment (perhaps by extremely strong plasma protein binding) would show a V_{ss} about 0.04 L kg^{-1}, because there is about 40 mL of plasma for every kg of body mass. One might think that such a low V_{ss} might be ideal for a drug whose target receptor is in the blood, since the entire dose of the drug would be in the blood, with essentially no distribution into other nontarget organs. However, a drug that has such strong plasma protein binding might not be able to effectively dissociate from plasma protein and bind to target receptors, even though they are in the blood (see section "**Plasma protein binding**"). Thus, a candidate with very high plasma levels due to very low V_{ss} may look promising, but one has to examine the magnitude of the pharmacological effect to avoid being misled.

A second value for V_{ss} that has an approximate physiological correlate is 0.21 L kg^{-1} (extracellular fluid). Amoxicillin, which is highly water-soluble, is poorly bound to plasma proteins, and does not permeate membranes well, has a V_{ss} of 0.21 L kg^{-1}. A third definable physiological compartment, TBW, has the value of 0.6 L kg^{-1} (i.e., our bodies are about 60% water). The water-soluble, poorly protein-bound, membrane-permeable drug theophylline has a V_{ss} of 0.5 L kg^{-1}, similar to TBW, and ethanol, which distributes uniformly everywhere in the body, has a V_{ss} of 0.7 L kg^{-1}.

A drug with V_{ss} significantly higher than 0.6 L kg^{-1} (of which there are many) *appears* to be dissolved in a volume higher than the total amount of water in the body. For instance, the calcium channel blocker diltiazem has a V_{ss} of 3.3 L kg^{-1}. Since this is a physiologically impossible volume, the only way for this to happen is that most of diltiazem is sequestered in some compartment such as the liver or adipose tissue. We often say that a drug with a high V_{ss} is well distributed into tissues, but this is misleading, because V_{ss} reflects the weighted average of distribution into all tissue compartments. There is no requirement that the distribution be uniform. Thus, we cannot say from the value of V_{ss} alone how much drug is distributed into what extravascular compartment, and it is possible, for example, that most of the drug is in one type of tissue such as adipose or liver, with very little in the brain.

4.01.2.3.4 Persistence

4.01.2.3.4.1 *Half-life and* MRT

Three of the ADME/PK characteristics that we have considered up to this point for optimization (i.e., plasma protein binding, RBC uptake, and V_{ss}) are important in determining the magnitude of dose to be administered and the target plasma concentration range. However, they seldom are the reason for a drug to fail in clinical trials, and the chemist operates with broad latitude in deciding that any of them are acceptable for a particular drug candidate. On the other hand, oral bioavailability must be above a threshold level of 10% for a drug to be considered a reasonable clinical candidate, at least for a drug intended for oral delivery. Just as important as bioavailability is the length of time that effective plasma levels are maintained by a drug candidate (i.e., its persistence). There are several ways that persistence is expressed, including terminal elimination half-life ($t_{1/2}$), accumulation half-life, operational multiple-dosing half-life,[69] *MRT*, and dosing interval. A variant is time above minimum inhibitory concentration (MIC), which is often used in the field of anti-infectives, but which we will not discuss further here.

The most common way to express persistence is $t_{1/2}$. This intuitive parameter nominally refers to the time for plasma levels to fall by half and is most often favored by chemists. Since an ideal drug follows simple first-order kinetics, then a $t_{1/2}$ value of 12 h means that from a given point, such as C_{max}, we can expect plasma concentrations to decline to 50% in the first 12 h and then 25% in the next 12-h period, 12.5% in the third period, etc. This simple relationship makes it easy to see that a drug with a clinical $t_{1/2}$ of 12 h would be easy to formulate as a once-a-day regimen, ideal for patient compliance. The plasma concentration–time curve is usually plotted as Log [drug] versus time (i.e., semilog plot), which for an ideal first-order drug will be a straight line. The value of $t_{1/2}$ is calculated from the slope of that line. However, the vast majority of drugs are not perfectly ideal, and consequently, the semilog plot is curved at early times. At some later time, the plot becomes a straight line, and this straight terminal phase is used for half-life calculation. The half-life is then called the terminal elimination half-life ($t_{1/2\beta}$).

A problem arises for the many drugs and drug candidates that show complex nonideal kinetics that do not break into a straight line in the semilog plot until the only last few percent of the concentration declines. In these cases, most of the molecules were apparently eliminated from plasma much faster than was indicated by $t_{1/2\beta}$. The question arises whether $t_{1/2\beta}$ is the "true" half-life and the earlier curved portion of the semilog plot merely reflected a slowly eq distribution process or is the half-life of only a small fraction of the drug contained in some slowly equilibrating compartment, such as adipose tissue or bone. In the latter case, $t_{1/2\beta}$ is unrealistic as an indicator of how long the plasma levels will stay in the effective range. One way to distinguish the two possibilities is to do multiple dosing to "steady state," operationally defined as a period in which the trough level between subsequent doses is constant. Without going into detail, one can calculate the average plasma that will be observed at steady state, assuming either that the early phase of the semilog plot is the true half-life or that $t_{1/2\beta}$ is the true half-life. Obviously, such an experiment takes a long time and a lot of the precious supply of drug candidate and is not suitable for a fast-moving lead optimization campaign.

Another measure of the realistic persistence of a drug candidate is *MRT*, and this is easily determined in the same single-dose experiment from which $t_{1/2\beta}$ derived. *MRT* is less familiar to most chemists than $t_{1/2\beta}$. It is a fundamental parameter of "noncompartmental kinetics," which uses the statistical theory of moments to treat the entire plasma concentration–time curve as a population of molecules that can be described by parameters that make no assumptions about the exact mechanisms of absorption, distribution, and clearance. As the name indicates, *MRT* is the average time that a molecule of the drug candidate stays in the plasma before elimination. For the ideal first-order drug we were considering in the preceding text, *MRT* has the value, derived from calculus, of $1.44 \times t_{1/2}$. To give *MRT* a clearer, more intuitive, meaning, we can simplistically estimate *MRT* in terms of half-life by a simple "back-of-the-envelope" calculation of the weighted average of the time that drug molecules stay in the plasma before being cleared. Half of the molecules last for one half-life, a quarter more last for two half-lives, an eighth last for three half-lives, etc. Thus,

$$MRT \approx 0.5 \times t_{1/2} + 0.25 \times 2\,t_{1/2} + 0.125 \times 3\,t_{1/2} + \cdots \approx 1.5 \times t_{1/2} \quad (3)$$

This equation should not be thought of as rigorously correct but as a way to estimate an "effective half-life" that applies to the entire ensemble of molecules, not just the final 1%.

MRT is valuable for a drug discovery program because it allows rapid diagnosis of whether $t_{1/2\beta}$ from an in vivo PK study of a drug candidate is realistic. If *MRT* is approximately the same or somewhat longer than $t_{1/2\beta}$, then $t_{1/2\beta}$ is representative of most of the molecules. On the other hand, if *MRT* is much shorter than $t_{1/2\beta}$, then $t_{1/2\beta}$ is misleading because it is representative of only a small fraction of the molecules. In the latter case, *MRT* would be a much better way than $t_{1/2\beta}$ to gauge the real persistence of the candidate. It is probably obvious that one can avoid the question of the relevance of the half-life by just always using *MRT* to

describe persistence, but the old practice of referring to half-life remains popular. For those who prefer to think in terms of half-life rather than *MRT*, then one can use Eq. (3) to calculate effective half-life from the value of *MRT* printed in the PK report.

Accordingly, to readily detect unrepresentative half-life values, chemists should always insist that the list of calculated PK parameters accompanying the preclinical PK study report includes *MRT*. One can even ask the question: why even bother with $t_{1/2\beta}$ when a more reliable parameter is easily available? Always use *MRT* when comparing drug candidates to make decisions about which ones to advance, since the terminal half-life may be inconsistently in error from compound to compound, whereas *MRT* is much more reliable and interpretable.

In addition to the reality check on the terminal elimination half-life, *MRT* provides a very useful insight into how fast the drug candidate is absorbed, because *MRT* is calculable for both the IV and PO doses. Making the very reasonable assumption that once a molecule has reached the bloodstream, its PK is the same regardless of the dosing route followed to get there, we can calculate the average time a molecule requires to be absorbed following oral dosing (mean absorption time (*MAT*)) by simple subtraction:

$$MAT = MRT_{PO} - MRT_{IV} \tag{4}$$

MAT is much easier to visualize and understand than the absorption rate constant (k_a), which is sometimes reported as a measure of the speed of absorption. Although T_{max} is most commonly used as a measure of speed of absorption, it can be very misleading, since it merely denotes the time when the rate of absorption happens to equal the rate of elimination, and therefore, plasma concentrations stop rising (i.e., C_{max}). T_{max} definitely does not indicate the end of the absorption process.

4.01.2.3.4.2 Clearance

While the PK parameter clearance (*CL*) is frequently used as a simple word for removal of drug from the plasma, it actually has a rigorous mathematical definition. *CL* is the volume of blood that is completely cleared of drug in unit time, and it is expressed in units of mL $min^{-1} kg^{-1}$ of body mass (or L $h^{-1} kg^{-1}$). While this definition is not very useful to a chemist as stated, it has great conceptual power when combined with volume of distribution. Returning to our consideration of an ideal first-order drug, an equation relating clearance and volume of distribution is

$$t_{1/2} = \frac{0.693 V_d}{CL} \tag{5}$$

Translating this equation into noncompartmental kinetic terms, we can write

$$MRT = \frac{V_{ss}}{CL} \tag{6}$$

Eq. (6) is normally used to calculate V_{ss}, but in this form, it is a very helpful way to think about clearance. We may consider Eq. (6) to state that a given clearance takes a characteristic amount of time to eliminate the drug from a given volume. For a given volume, the higher the clearance, the shorter the *MRT*, and the lower the clearance, the longer the *MRT*. Conversely, for a given value of clearance, the higher the V_{ss}, the longer the *MRT*, and the lower the V_{ss}, the shorter the *MRT*. This simple inverse relationship immediately explains why two drug candidates may have the same value of *CL*, determined either directly from an in vivo PK study or by calculation from in vitro MetStab data, yet much different in vivo half-lives. Because of the multifactorial origin of V_{ss}, it is difficult for chemists to try to target a certain range in designing their molecules. Therefore, we target a certain half-life range by adjusting *CL* and let V_{ss} fall where it may. Experimentally, clearance is calculated from another simple relationship between the easily measured quantity dose and *AUC* for the IV dose (Eq. 7). Eq. (7) shows us that for a given dose, high clearance gives low *AUC*, and vice versa:

$$CL = \frac{Dose}{AUC_{IV}} \tag{7}$$

What do we consider high clearance and low clearance? Because the liver is so often the principal clearing organ, we often express high and low clearance in terms of the fraction of liver blood flow (Q_H), remembering that *CL* and clearance and organ blood flow have the same units of mL $min^{-1} kg^{-1}$. For renally cleared drugs, we would compare *CL* and renal blood flow (Q_R). **Table 3** shows values of hepatic and renal blood flows for various laboratory species and humans. The value of *CL* reported in the table of PK parameters from a typical conventional IV/PO PK study can be directly compared with the values of blood flows for the species of interest to characterize the drug candidate as high or low clearance in that species. For instance, a measured clearance of

Table 3 Organ blood flows for common laboratory species and humans[a]

Blood flow (mL $min^{-1} kg^{-1}$)						
Organ	*Mouse*	*Rat*	*Rabbit*	*Dog*	*Monkey*	*Human*
Liver	90	55	71	31	44	21
Kidney	65	37	32	22	28	18

[a]Calculated from data published by Davies and Morris.[65]

5 mL $min^{-1}kg^{-1}$ for a drug candidate in rats would be considered low, while 50 mL $min^{-1}kg^{-1}$ would be high, because hepatic blood flow in rats is 55 mL $min^{-1}kg^{-1}$. In any species, clearance cannot exceed the value of blood flow for the clearing organ for the simple mass transport reason that an organ cannot clear a drug faster than the drug is delivered to the organ by blood flow. However, if clearance is not restricted to a particular clearance organ, for example, a drug that is subject to a high rate of metabolism in blood or that is cleared by both the liver and kidney, clearance can exceed liver blood flow.

Yet another useful way to think about clearance is in terms of the hepatic extraction ratio (E_H), the fraction of drug in the plasma that is removed by the liver during a single passage:

$$E_H = \frac{CL_H}{Q_H} \tag{8}$$

The fraction of drug escaping hepatic clearance on each passage is $1 - E_H$. We can similarly define a renal extraction ratio (E_R) for renally cleared drugs.

Suppose we have a drug whose clearance in an IV/PO PK study in rats is 52 mL $min^{-1}kg^{-1}$, and we believe that all clearance is due to metabolism in the liver (perhaps from in vitro data or experience with analogs). Substituting the values of rat hepatic blood flow from **Table 3** and measured clearance into Eq. (8), we estimate that oral bioavailability will be 5% or less, even if intestinal absorption was 100%. Since the PK study included both IV and PO doses, we have an experimental value of F to compare the estimate with, and if there is general agreement between the two, then we have learned something about the in vivo disposition of the drug. We can see that when chemists want to think about how long a drug candidate will stay in the body, they will apply Eq. (6), and for thinking about bioavailability, they will apply Eq. (8).

4.01.2.3.4.3 Mechanisms of clearance

A chemist facing short *MRT* values caused by high clearance in a series of compounds needs to do something to the series of molecules to reduce the clearance. There are three general mechanisms by which a compound is cleared from the body: metabolism, biliary excretion, and renal excretion. Transporters also have a role in clearance: uptake transporters expose a drug to metabolic clearance in the liver, and efflux transporters are fundamentally involved in biliary and urinary excretory clearance.

Metabolism was discussed in section "**Determinants of bioavailability**" in the context of oral bioavailability, and the same major clearance organ (liver) and metabolic enzymes are responsible for systemic clearance as well. A set of energy-linked active uptake transporters, including OATP1B1 and OCT1 to name but two of many, often supplement simple permeation of drug molecules from blood into liver cells, thereby increasing their rate of metabolism.[19,70–72] In addition to metabolism, some drug molecules are subject to excretion in bile and/or urine. Almost all excretion into bile is mediated by active transport from liver cells into bile by efflux transporters, including P-gp, breast cancer resistance protein (BCRP), and bile salt export pump (BSEP).[19] Similarly, many drugs require active transport from kidney cells into urine by efflux transporters, including but not limited to multidrug and toxic compound extrusion protein 1 (MATE1), multidrug resistance-associated protein 2 (MRP2), and P-gp,[19] although some soluble compounds with low plasma protein binding such as antibiotics can be excreted into urine by the glomerular filtration process.

Recognition by these metabolic enzymes and transporters of a drug candidate as a substrate is a principal determinant of the magnitude of clearance and, therefore, the macromolecular component of the SAR of clearance for drug candidates. Since these macromolecules can be studied in various in vitro systems, they represent an important way for chemists to adjust clearance in a data-driven fashion to solve problems of either too short or too long *MRT*. In other words, fast metabolism leading to short *MRT* can be studied in vitro with liver microsomes or hepatocytes to design metabolism-resistant analogs whose in vivo PK can then be tested in animals, perhaps first in one of the rapid PK methods described in section In vivo determination of oral bioavailability and then in full conventional PK studies for final confirmation that the metabolic "fix" has worked. However, so far, there is little use of in vitro transporter systems to design molecules that don't get transported into liver cells in the first place.

4.01.2.3.5 Excretion

Excretion is not a property that chemists seek to optimize when designing a drug candidate, except to the extent that it is reflective of clearance of the parent drug, as discussed in the preceding text. However, excretion is an important property of the clinical action of a drug, as this process prevents the accumulation of parent drug and metabolites in the body during the chronic dosing that is typical of most drugs. Consequently, during lead optimization, a drug discovery program does not monitor the excretion of drug-related materials during the ADME/PK testing of the list of potential drug candidates sequentially examined, except occasionally as part of a high-clearance problem-solving exercise. But as part of the final selection of a clinical candidate, the discovery team does want to eliminate the possibility that incomplete excretion will present an unwelcome surprise if discovered halfway through clinical development when the clinical ^{14}C-ADME studied is conducted (see section "**Clinical ^{14}C-ADME study**"). Thus, a BDC rat study is often part of the characterization package of a nominated drug candidate. The BDC rat study collects bile and urine quantitatively typically over a 12- or 24-h period to estimate the "mass balance" of the drug. Plasma samples are also collected at selected time points to validate against known concentrations of the drug from the IV/PO PK study, as well as investigate the presence of circulating metabolites. Sometimes, the BDC study is done with radiolabeled drug candidate, but with the powerful MS methods available today, mass balance can be determined with reasonable confidence without the use of radiolabeled drug.

4.01.2.3.6 Computational approaches to ADME/PK problems

In the context of modulating rates of metabolism, we note that an even more elegant approach than simply synthesizing and then testing metabolism-resistant analogs would be to use in silico methods to predict metabolism before any wet synthetic chemistry is ever done. The feat of qualitative and quantitative prediction of metabolism has been studied extensively for almost three decades, and there is no doubt that progress has been made.[73] Some approaches use knowledge-based algorithms, based on similarity to the metabolism of other compounds reported in the literature, and others rule-based. Some approaches are much more focused, such as prediction of sites of metabolism by specific enzymes such as CYP 2C9,[74] CYP 2D6,[75] CYP 3A4,[76] other CYPs,[77,78] and SULTs[67] with the use of computational molecular docking. A closely related activity is to predict which CYP will recognize a new drug candidate as a substrate.[27] Because direct inhibition of CYPs leading to DDIs is such a ubiquitous problem, much energy has been invested in developing software for docking CYPs[67] and computational approaches.[79] All three of these CYP-related processes are possible because considerable effort has been expended toward determination of the three-dimensional crystal structures of various CYP enzymes.[80,81]

However, both aspects of metabolism prediction, qualitative and quantitative, must be reasonably accurate to be useful to the chemist designing molecules. It is not sufficient to predict the approximate point of hydroxylation of a molecule, because the chemist needs to modulate the exact point of attack. Similarly, it is not acceptable to misidentify the major metabolic pathway that is to be slowed down. Yet the difference in rate might be only a small factor that is hard to predict by molecular docking methods. For instance, a difference in rate of only three would result in reducing the percent of total metabolism represented by a particular pathway from 100% to 30%, yet this rate difference amounts to less than a single kcal mol^{-1} of activation energy in the metabolic reaction. In other words, a small amount of error in estimating the difficulty of a chemical reaction is magnified in the absolute rate. This effect produces big uncertainty in predicting which of several potential qualitative pathways (e.g., *N*-demethylation vs. benzylic hydroxylation vs. aromatic hydroxylation) will *actually* be the one that need to be modified, and the prediction becomes useless to the synthetic chemist. As a practical matter, then, there is much skepticism among the community of chemists about the value of in silico prediction of sites and rates of metabolism, and, so far, there has been limited uptake of such methods as a driver of lead optimization. Still, in silico prediction *can* be useful in planning chemical scaffolds to be pursued in optimization of a selected lead series.

Cumming et al.[82] have provided a useful explanation of compound quality and overview of various modeling approaches to improving the absorption, distribution, metabolism, excretion and toxicity (ADMET) quality of clinical candidates. An interesting alternative way of using computational approaches to solving ADME issues is the graphic representation of physicochemical parameters and various desirable ADME properties, allowing the medicinal chemist to visually inspect a data set and see what properties need to be adjusted to achieve the goal.[83] The problem of knowing the mechanism of clearance as the first step in solving problems of high clearance has been addressed by a process designated as the Extended Clearance Classification System[84] in which the chemist can examine a variety of physicochemical and other features of drug candidates to determine the most likely means by which they are eliminated.

However, not all computational approaches to predicting ADME/PK properties work well. A quantitative structure–PK relationship was developed to predict the biliary clearance and percentage of dose eliminated in bile in humans based on simple physicochemical descriptors. However, extensive evaluation of compounds beyond the training set showed poor predictive capability except within a series of structurally related compounds,[85] a result that is not surprising given that biliary secretion depends mainly on transporter recognition, not simple physical processes such as membrane permeability and solubility. On the other hand, modulation of renal clearance can be reasonably successful for various chemotypes by recognition of the physicochemical determinants of the process, much as we do with processes such as absorption and first-pass metabolism. Not surprisingly, the most important determinants are MW, lipophilicity, polar surface area, number of rotatable bonds, and number of hydrogen bond donors and acceptors.[86]

4.01.2.3.7 Screening for DDI potential

4.01.2.3.7.1 Occurrence of DDIs

Virtually, every marketed drug will, at least with some patients, be coadministered with other xenobiotics, including prescription drugs, over-the-counter drugs, herbal medicines, and nutritional supplements. The prescribing physician often is not aware of everything else that a patient is taking. Anytime that two xenobiotics are in the body simultaneously, there is a potential for the two to interact with one another at the levels of therapeutic efficacy, toxicity, and PK phenomena. PK DDIs are particularly common because many of the physiological systems responsible for drug metabolism and disposition are nonspecific, leading to the probability of competition of the two xenobiotics for the same enzymes and transporters. These interactions can result in bioavailability of one or both of the drugs to be increased or reduced, plasma levels to be elevated or diminished, *MRT* to be increased or reduced, metabolic profiles to be altered, tissue distribution to be affected, etc. It is the responsibility of the medicinal chemist to design drug candidates that do not produce such interactions and are themselves insensitive to the presence of other drugs. There are two main strategies by which this is accomplished. First, the chemist wants to build drugs that are highly potent and specific for the target receptors, so that the drug candidate has a wide therapeutic margin between plasma levels that produce efficacy and those that produce adverse effects, in case PK DDIs do occur. Second, the chemist wants to build drugs that are unlikely to interfere with the disposition of other drugs (i.e., be a perpetrator drug) or have its own disposition strongly affected by other drugs (i.e., be a victim drug).

4.01.2.3.7.2 Screening assays for PK DDIs

Coadministered drugs may affect each other's pharmaceutical, pharmacological, toxicological, and dispositional behavior. For the purposes of this article, we will discuss only the last of these, the PK DDIs. The three most important ways that drugs interact at the PK level are the following:

- Inhibition of an important metabolic pathway, thereby slowing clearance and increasing bioavailability and/or *MRT*
- Induction of an important metabolic pathway, thereby increasing clearance and decreasing bioavailability and/or *MRT*
- Inhibition or induction of a transporter involved in direct excretion or exposure of the drug to metabolism

The first of these, inhibition of metabolic clearance, is the most common and potentially most serious and therefore receives the most attention. Furthermore, among the metabolic enzymes, the CYP family is definitely the most inhibition-prone, for which there are two reasons. First, the CYP enzymes are able to interact with almost every type of drug molecule (see section "**Common metabolic reactions**" and **Table 1**), resulting in a much greater statistical chance for two drugs to share an enzyme. Second, the CYP enzymes tend to have much lower enzymatic K_M values than other metabolic enzymes, often in the same single-digit micromolar range in which drug plasma levels occur. Thus, the resulting "$[I]/K_i$" ratio can easily be of sufficient magnitude to cause significant competitive inhibition.

The second main cause of PK DDIs (induction) occurs when the presence of one drug causes elevation of the net expressed levels of an enzyme capable of metabolizing other drugs. Most commonly, this induction occurs at the gene expression level through xenobiotic-sensing nuclear receptors,[87] although other mechanisms also exist. Obviously, if the levels of a particular drug-metabolizing enzyme are elevated, then clearance of drugs that are metabolized by that enzyme will increase, and plasma levels will decrease. Several members of the CYP family (e.g., 1A2, 2B6, and 3A4) are highly inducible and, for the same statistical reason as in the preceding text, commonly lead to DDIs.

The third type of DDI, involving transporters, is much less common and usually of smaller magnitude than the other two when it does occur. Consequently, when a discovery program has to make hard choices about where to put scarce screening resources, assaying for transporter inhibition/induction is seldom chosen. However, investigation of transporter inhibition, induction, and substrate recognition will be discussed in section "**Definitive characterization of DDIs**" covering ADME/PK as an objective of phase 1 clinical studies in which we have a single compound that must be thoroughly characterized.

From the earlier considerations, it is easy to see why discovery-level screening assays for DDIs almost exclusively focus on CYP enzymes. What types of assays are needed for this purpose? Let us first discuss assays for CYP inhibitors, which fall into two distinct categories: direct and time-dependent.

Direct inhibitors are those that bind to the substrate-binding site of one or more of the CYP family enzymes, usually in a simple competitive fashion, directly preventing metabolism of other drugs by that CYP enzyme. These type inhibitors exert their effect immediately, and, because the binding is reversible, the inhibition is lifted when the inhibitor is removed from the environment of the enzyme, as, for instance, by dialysis of an in vitro incubation mixture or by clearance of the inhibitor in vivo. Direct inhibition is the type most commonly encountered during lead optimization and also the easiest to detect. We measure the strength of the inhibition by the operational parameter IC_{50}[88] for each of several CYP enzymes that are most likely to metabolize drugs (typically 1A2, 2B6, 2C9, 2C19, 2D6, 2E1, and 3A4 or a subset of these).[89,90] The actual assay is an in vitro incubation of the test article with a metabolism-competent system such as cDNA-expressed single human CYP enzymes or human liver microsomes with enzyme-specific substrates. In most cases, assay of the metabolic reaction is accomplished with LC-MS/MS,[88] but systems using substrates that produce a fluorescent metabolite are also popular.[91]

For discovery lead optimization screening purposes, the assay is usually based on human liver microsomes, and CYP specificity is achieved by the use of a series of substrates that are metabolized by only one of the CYP enzymes. The degree of inhibition of the selected CYP is measured at several concentrations of the test article spanning the concentration range of interest for the plasma levels expected to be pharmacologically relevant in the clinic, for example, 0.03–30 μM. From the data so generated, the IC_{50} value may be calculated and the corresponding competitive inhibition constant (K_i) derived.[88] The chemist may use the K_i data in a cutoff fashion to screen out drug candidates that are likely to cause clinical CYP-based DDIs. For instance, a common paradigm is to designate ranges such as $K_i < 1$ μM (likely to cause drug interactions), K_i 1–10 μM (may cause drug interactions), and $K_i > 10$ μM (unlikely to cause drug interactions). Obviously, the ranges and interpretations given will depend on the expected clinically relevant plasma concentrations of the drug candidate.

DDIs resulting from competitive inhibition of a metabolic enzyme such as a CYP are governed by Eq. (9):

$$CL_{int} = \frac{V_{max}}{K_M\left(1 + \frac{[I]}{K_i}\right) + [S]} \tag{9}$$

where CL_{int} is the intrinsic clearance of that CYP enzyme to metabolize a victim drug, K_M is the Michaelis constant for the victim drug, $[I]$ is the concentration of the inhibitor drug, K_i is the competitive inhibition constant of the inhibitor drug for the CYP in question, and $[S]$ is the concentration of the victim drug. Related equations may be written for other types of enzyme inhibition, such as uncompetitive and noncompetitive. To make this equation a little simpler, further suppose that the victim drug, which is a substrate for CYP 3A4, is present at a concentration well below its K_M for CYP 3A4 (i.e., $[S] \ll K_M$), yielding Eq. (10):

$$CL_{int} = \frac{V_{max}}{K_M\left(1 + \frac{[I]}{K_i}\right)} \tag{10}$$

To illustrate the utility of this equation in the context of DDIs, suppose a drug candidate has a K_i of 1 μM for inhibition of CYP 3A4 and the expected clinical C_{max} is 10 μM. Note that in the following derivation, we are using the total plasma concentration as a surrogate for the intracellular concentration experienced by the drug-metabolizing enzymes. Although this assumption is not rigorously correct, it often gives a reasonable estimate of the net inhibitory effect of plasma drug concentrations on drug-metabolizing enzymes. In any event, this assumption is used in regulatory guidances for estimating the inhibitory potential for drug candidates[28,29] and is thus useful for discovery screening for eliminating candidates highly likely to cause DDIs. Turning our attention back to Eq. (10) and taking the ratio of the CL_{int} values in the presence and absence of the inhibitor drug, we can write the observed reduction of clearance of the victim drug as Eq. (11):

$$\frac{CL^*_{int}}{CL_{int}} = \frac{1}{1 + \frac{[I]}{K_i}} \tag{11}$$

where CL_{int}* is the reduced clearance of the victim drug in the presence of the inhibitor drug. In this example, clearance of the victim drug will be reduced to only 9% of its value in the absence of the inhibitor. One can readily see that the ratio $[I]/K_i$ is crucially important in determining the magnitude of a drug interaction caused by competition of two drugs for the same CYP enzyme. Simple inspection shows that even when the inhibitor drug is merely present at its K_i value, a reduction of clearance of the victim drug of 50% will occur. Thus, we see that if we expect the clinical C_{max} of a new drug candidate to be 10 μM, we will want its K_i value to be well above 10 μM to avoid clinically significant DDIs. Conversely, a drug candidate with expected C_{max} of 0.1 μM would be free of DDIs even with a K_i value of 1 μM.

Time-dependent inhibitors are those that do not exert their full inhibitory effect immediately, but may require minutes or even hours to reach maximal inhibition. The proximal inhibitory species is not the parent drug candidate per se, but rather a reactive intermediate formed by the action of the enzyme during the process of metabolism of the candidate. Typically, the reactive intermediate is an electrophile that reacts with a nucleophile from the enzyme resulting in covalent binding of a drug residue to the enzyme. With a large drug fragment covalently attached at or near the active site of the enzyme, additional drug molecules are sterically denied access to the active site, and that particular enzyme molecule has been permanently inactivated, even if the parent drug is subsequently cleared from the system. New drug-metabolizing activity is only restored by de novo protein synthesis of the enzyme molecule. The time dependency represents the amount of time required for the metabolic and subsequent covalent binding events to occur. Time-dependent inhibitors are often also called mechanism-based or metabolism-based inhibitors.

Detection of time-dependent inhibition is based on measuring enzyme inhibition as a function of time. For the purposes of rapid screening of a set of candidate compounds during lead optimization, the so-called shift assay is utilized. In this assay, the enzymatic assay toward a probe substrate for the enzyme of interest (e.g., midazolam for CYP 3A4) is tested after a preincubation period (usually 30 min) of the enzyme with several concentrations of the test article. From these data, an apparent K_i value for the test article is calculated. This apparent K_i is then compared with the K_i observed when the test article and probe substrate are added simultaneously. A significant difference in these two values of K_i (i.e., a shift) indicates that the inhibitory effect of the test article on the enzyme has changed over the period of 30 min. The K_i value can (1) decrease, indicating that the test article has apparently become more inhibitory with time, (2) be unaffected (within experimental error), or (3) increase, probably indicating that the concentration of the test article had been significantly depleted during the preincubation period by metabolism. In case (1), where a compound shows time-dependent inhibition, the compound may have been metabolized to a reactive electrophilic metabolite that inhibits the enzyme, as discussed in the preceding text. Note that it is theoretically possible that the compound was converted to a nonreactive metabolite that happens to be a much more potent direct inhibitor, but this is rarely observed.

Assuming that the time-dependent inhibition is due to covalent inactivation of the enzyme, then one must interpret the data in order to decide whether to eliminate the compound from further consideration as a candidate. This decision obviously has a measure of judgment involved in it, but a good rule of thumb is that if the K_i shift is 10× or more and the resulting shifted K_i is in a "danger" region for DDIs, then the compound probably should be eliminated. For example, a compound whose K_i shifted from 30 to 1 μM by a 30-min preincubation period is likely a true time-dependent inhibitor that will cause important clinical DDIs, and it should be discontinued in the lead optimization process. The usual procedure is to place the CYP inhibition "shift assay" in a second- or third-tier position in the screening paradigm (see section "**Triage of ADME/PK screening assays**") because it is more resource-intensive than the simple direct inhibition assay. Another question involves which CYP enzymes should be screened for time-dependent inhibition during lead optimization. Although it is possible to test all CYP enzymes that were tested for direct inhibition, as a practical matter, only two of the CYPs (1A2 and 3A4) have an appreciable likelihood of suffering time-dependent inhibition and represent a good use of discovery resources.

To illustrate time-dependent inhibition, we can consider bergamottin, a natural product found in grapefruit juice, that is a potent time-dependent inhibitor of CYP 3A4. Oxidation of bergamottin generates an arene oxide on the benzofuran group, which ring-opens to a γ-ketoenal Michael acceptor that reacts with the amide nitrogen of residue glutamine-273 in the 3A4 primary structure (a simplified representation of this process is shown in **Fig. 1**).[92] Covalent attachment of the bergamottin residue interferes with proper folding of the protein backbone and disrupts the structure of the active site, effectively quenching catalytic activity of the 3A4 enzyme. Another 3A4 time-dependent inhibitor, raloxifene, has been shown to be oxidized to an extended quinone structure that is captured by cysteine-239, blocking the substrate access channel.[93] Many other examples of time-dependent inhibition of CYPs are known, and a rich variety of electrophilic chemistries are displayed,[94,95] making the job of predicting these events by

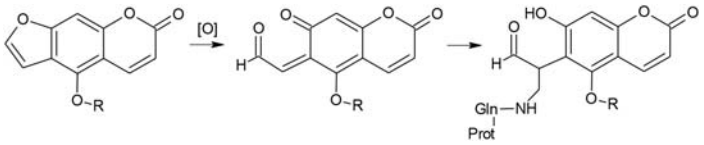
[O]
O
O
O

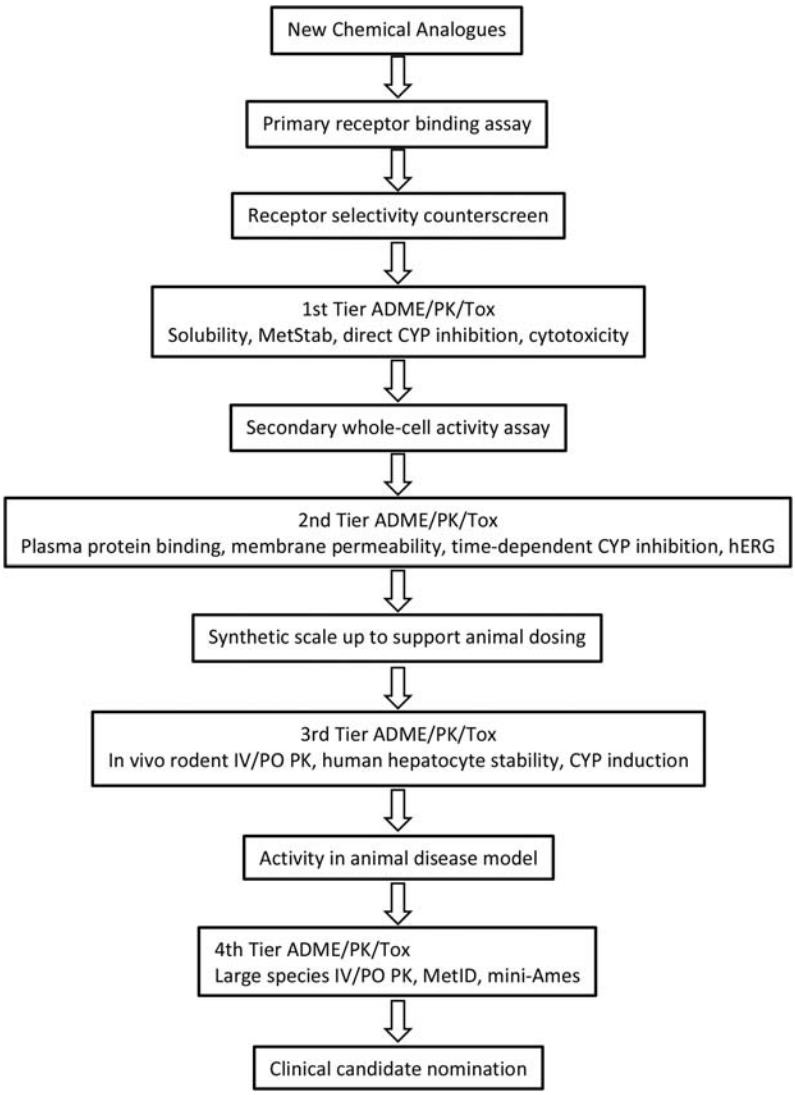

Fig. 2 Illustrative screening funnel for testing ADME/PK properties of analogs during lead optimization.

4.01.3 The Importance of ADME/PK in Safety Assessment

4.01.3.1 Early Toxicity Assessment

Often, the drug discovery program incorporates one or more assays to assess the toxicity potential of representative members of the most important chemotype series during lead optimization or perhaps as part of the final selection process between several possible nomination candidates. Most often, the assay is cell-based, investigating simple cytotoxicity or the more complicated hepatotoxicity.[99] As with ADME/PK, a number of computational approaches to predictive drug toxicity have been reported.[100,101] Hornberg et al. have proposed a comprehensive and integrated approach to early toxicity assessment that even includes exploratory in vivo rodent toxicity studies.[102,103] While these approaches should certainly be utilized to some extent during the drug discovery process, the medicinal chemist should not conclude that a series or an individual compound is "clean" based on favorable assay results, since in vitro and in silico are fundamentally limited in their abilities to predict toxicity (or lack thereof). However, a strongly positive indication of toxicity in an in vitro or in silico assay system should probably be taken at face value and that compound discontinued. If a structurally distinct analog from the same series shows similar toxicity, then the entire chemotype is brought into question. In vivo animal exploratory safety studies offer a much better chance of picking up toxicities and providing a level of comfort in their absence. However, the obvious limitations of compound mass requirement and time required to conduct the study mitigate against frequent use of this type of assay except for one or two compounds at the end of the discovery program.

4.01.3.2 Reactive Metabolites

Toxicities due to metabolites, not the parent drug, are well documented in the literature. For instance, efavirenz produces a nephrotoxic glutathione-adducted metabolite. Extensive cross-species comparison studies showed that this particular metabolite was produced only in rats, clearing a way to the clinic for this important HIV drug. Mechanistic work established that a reactive metabolite of the disubstituted acetylenic bond was the key step in production of the ultimate toxin.[104] This was an early example of what has become recognized as a frequent occurrence during drug metabolism, namely, the formation of reactive electrophiles that are capable of capturing various cellular nucleophiles, especially protein-derived nucleophiles such as lysine amino groups, cysteine thiols, and serine hydroxyls, leading to intracellular damage and possible cytotoxic and immunogenic effects.[105,106]

It is now common for drug discovery programs to incorporate various strategies for the detection of reactive metabolites and provide structural feedback to medicinal chemists on how to remediate the problematic functional group.[107] Many functional groups and molecular features have now been reported to be capable of electrophilic activation, most often by CYP-mediated oxidation. Because of the rich oxidative chemistry of the CYP iron-oxo intermediate (see section "**Common metabolic reactions**"), these events are often nonintuitive and difficult to anticipate, requiring an empirical approach to detect them.

In addition to the well-known example of furan-containing drugs generating reactive metabolites,[108] many other types of molecular configurations are also known to generate reactive metabolites, in not obvious ways, for instance, imidazothiazoles,[109] and vanilloid rings.[110] Lenz et al.[107] discovered that a homomorpholine ring, which most chemists would surely regard as innocuous, was metabolically activated to an unstable thiazolidine. The cannabinoid receptor antagonist rimonabant was oxidized to a cytotoxic iminium ion.[111] There are even cases when the CYP-mediated oxidative formation of a reactive intermediate produces the actual pharmacologically active molecular species. The tetrahydrothienopyridine antithrombotic drugs (ticlopidine, clopidogrel, and prasugrel) are metabolized to electrophilic thiolactone sulfoxides as precursors of the proximal antagonists of the platelet receptor P2Y12.[112]

There are also examples of reactive metabolites formed by non-CYP enzymes, such as SULTs, which can create an excellent sulfate leaving group on aliphatic hydroxyl groups as a precursor to an electrophilic intermediate.[113] Another example of non-CYP-produced electrophilic reactive metabolites is the acyl glucuronides, which are glucuronosyl esters of carboxylic acid drugs, that can react either by direct acylation of cellular nucleophiles or by rearrangement to form an aldehyde capable of reacting with amine groups of proteins to form covalent imine bonds.[114,115] Acyl glucuronides vary widely in their ability to covalently modify proteins, and it is possible to assess their potential of this potentially toxic reaction.[116]

The only chance in the development of a clinical candidate to avoid reactive metabolites is during discovery lead optimization and final candidate selection. Once the clinical candidate is chosen, one must live with whatever safety liabilities are carried by that molecule. Thus, it is important to assess the potentiality for reactive metabolites during discovery while there is still a chance to change the selection.[117–119]

4.01.3.3 In Vivo Toxicology Assessment

Having selected a single compound for clinical development, it is now necessary for a development sponsor to determine with definitive studies what ADME/PK profile has actually been achieved. A subset of these studies is conducted to enable the preclinical safety program. Because of the focus of this article on ADME/PK, we will only discuss safety of the parent drug itself to a limited extent, but will draw attention to the phenomenon of toxicity related to the production of various metabolites that may have safety profiles quite different from those of the parent drug. However, to understand the context in which metabolites are important in safety, it is necessary to briefly introduce the general outline of the preclinical safety program that is required to support the regulatory application for an investigative new drug.

The preclinical safety program investigates the limits of safe exposure of animal species to the clinical candidate that has been delivered from the discovery program. The core of the safety program is a series of increasingly long chronic dosing studies at several dose levels in at least one rodent and one large animal species (typically dog or monkey). During the "in-life" phase, blood samples are taken at appropriate intervals and analyzed for concentrations of the clinical candidate to estimate simple PK measures of exposure, such as C_{max}, C_{min}, and *AUC*. At the end of the in-life phase of an animal safety study, toxicologists and pathologists examine the animals in various ways for evidence of toxic effects of the clinical candidate. These examinations include clinical chemistries, morbidity, mortality, and dissection with both macroscopic examination of organs and microscopic inspection of many types of tissues.

The final report from a completed study will, ideally, identify the major toxicities and most affected organs (if any) of the candidate. From a comparison of the PK exposure data with the observed occurrences of toxicities, the report will also assess whether a "safe" exposure was observed, usually expressed as a dose labeled "no observed adverse effect level" (NOAEL). A related observation is the "maximum tolerated dose," which is the daily dose that the animals can tolerate for long intervals, though not necessarily without some minor degree of morbidity. And most importantly, the study should assess what dose constitutes an "effect level" and what specific toxicities are associated with that dose. This information establishes the limits of exposure to the candidate that may be accessed in phase 1 clinical trials. As a general rule, but with some exceptions, the phase 1 clinical PK exposures should not exceed the NOAEL established for the more sensitive one of the two preclinical safety species. The ratio of these two exposures (NOAEL/clinical dose) is called the "exposure multiple." Going forward, the preclinical safety program leads the clinical program, investigating longer exposures that allow longer studies in later stages of clinical

development. Thus, a goal of the discovery program is to produce a drug sufficiently potent that the efficacious clinical exposure is much less than that from the NOAEL.

One of the preliminary activities is a dose range-finding study to determine the low and high doses that will actually be used in the preclinical GLP safety studies. Part of dose range-finding is to determine the relation between administered dose and systemic exposure of the animal to parent drug. The highest dose used for dose range-finding will typically be one for which the plasma levels of drug as a function of dose either reach a maximum plateau or, conversely, tend to increase unpredictably. The first effect is due to saturation of absorption, while the second is due to saturation of clearance and excretion. This dose–exposure relationship usually has no fundamental importance for the clinical behavior of the drug because the toxicological doses are much higher than the clinical efficacious doses. Thus, these saturation phenomena serve merely as operational parameters relating to the feasibility of conducting a preclinical safety investigation beyond a certain top dose.[120]

4.01.3.4 Metabolites in Safety Testing

Both the US Food and Drug Administration (FDA) and the European Medicines Agency (EMA) require that safety assessment be conducted with major circulating plasma metabolites in addition to the parent drug.[121,122] The basic requirement is to establish that at the NOAEL dose in at least one of the preclinical safety species each major metabolite is present at an exposure level equal to or greater than its corresponding exposure in the pharmacologically relevant clinical dose. A major human metabolite is operationally defined as one that comprises more than 10% of the total exposure to drug-related material in the plasma. Exposure is measured as *AUC* at PK steady state. In most cases, the so-called "Metabolites in Safety Testing (MIST)" requirement is met by demonstrating that these metabolites were present at adequate levels in animal safety studies. Large-scale clinical trials, understood to refer to clinical phase 3, cannot proceed until safe exposures are delineated for major metabolites.

Therefore, to avoid a delay in the start of phase 3, a sponsor must identify major metabolites early in phase 1, so that there is adequate time to determine whether there is a problem and take remediation steps if necessary. The power of contemporary LC-MS methods to discover metabolites of the parent drug without resort to radiolabeling is of great utility in this regard (see section "**Addressing high first-pass clearance**"), allowing clinical plasma samples from phase 1 single- and multiple-ascending dose (SAD and MAD) studies to be directly scanned for the presence of metabolites. A problem of quantitation of metabolite concentrations in plasma results when, as is often the case, authentic standards of the major metabolites do not yet exist. However, clever methods have been published to use ratios of either metabolite/parent or metabolite/internal standard derived from animal and human plasma to estimate the relative exposure of the metabolite in animals and humans.[123–125] Useful examples of checking for "MIST" metabolites in early clinical development have been published.[126–128]

When exposures to a major metabolite in animals are substantially lower than the corresponding exposures in humans, then the safety of the metabolite has not been established by the standard animal safety study, and it must be considered that human beings are being exposed to a chemical compound of unknown toxic potential. In that case, a different approach must be used to assess safety of the metabolite in question. The two available methods are (1) identification of another animal species that *does* display adequate plasma levels of the metabolite and conduct a safety study of the clinical candidate in that species and (2) synthesis of the metabolite followed by direct study of its safety in one or more animal species. Option (1) is unattractive because it involves running additional unplanned safety studies, assuming that a suitable alternative species can even be found. Option (2) is also unattractive, since the metabolite must be prepared in kilogram quantities with GLP methods before a separate study of its safety can be conducted. Obviously, both options (1) and (2) will considerably add to the development timeline. Thus, it is advisable for the discovery program to compare the metabolites formed in human and animal hepatocytes as part of the ADME/PK characterization package during clinical candidate nomination. A clear absence in the animal hepatocytes of a major metabolic pathway in human hepatocytes should raise a caution flag. While in vitro metabolic profiles do not definitively predict in vivo metabolic profiles, they can at least somewhat derisk the clinical candidate. Ma and Chowdhury have provided an overview of the regulatory aspects of metabolites in drug development.[129]

4.01.4 The Importance of ADME/PK in Clinical Development

4.01.4.1 IND-Enabling ADME/PK Studies

4.01.4.1.1 Purpose of IND-enabling ADME/PK studies

As pointed out in section "Right-Box" analysis, once a single compound has been selected for clinical development, no additional chemical modifications can be made, and the role of the medicinal chemist ends, at least for that compound. Of course, process chemistry comes to the forefront, but that activity does not have an ADME/PK component and will not be discussed here. In this section, we will discuss the ADME/PK-related activities that occur in the IND-enabling period and the clinical development program. Because the main purpose of this article is to discuss the role of ADME/PK in the discovery and development of new drugs from the perspective of the medicinal chemist, the discussion of the ADME/PK activities will not be as detailed as those given for the discovery section. Mainly, we will focus on what is done and why it is important for the understanding and registration of a new chemical entity (NCE). This information will illuminate why it was important to optimize ADME/PK in discovery, when it was still possible to do so.

Having selected a single compound for clinical development, it is now necessary to determine with definitive studies what ADME/PK profile has actually been achieved. This profile includes the large and small species selected for GLP safety studies as well as other animal species that may be useful in characterizing the in vivo profile for purposes of understanding ADME/PK, pharmacology, off-target pharmacological effects, and adverse events. Most importantly, the sponsor will need to characterize the human in vivo ADME/PK profile, which up to this point relied on in vitro studies and extrapolation from animals for assessment.

As part of the Investigational New Drug (IND) application, we need to show regulatory authorities evidence that the drug candidate can likely be systemically delivered to clinical subjects, that it will likely persist in the body long enough to give a therapeutic benefit within a practical dosing regimen, that the potential for DDIs is at least partially understood, that significant active metabolites in the pharmacological model species have been detected and can be monitored in early clinical studies, and that preclinical safety studies likely exposed animals to the same major metabolites as humans. A sponsor is expected to make a good faith effort to provide a reasonable level of such prospective ADME/PK information before putting an NCE into human beings. However, in the real world, it is not feasible for an IND application to contain full information on all of these topics, and regulatory authorities recognize this reality. But an application that contained no information on any of these topics would be judged inadequate, and approval might well be delayed until basic ADME/PK information was provided.

4.01.4.1.2 Animal PK and bioavailability

The full IV/PO pharmacokinetics of the drug candidate should be presented in the IND application, providing a comprehensive determination of the PK parameters in several species. If this information is not already available from discovery, appropriate studies should be conducted in the IND-enabling period. The species studied should be both the rodent and large animal species used for pre-IND safety studies, plus one or two others, including the pharmacological animal model if applicable. This provides an evidential basis for the claim in the IND that the compound is expected to be orally bioavailable in humans. It also provides the PK parameters such as CL and V_{ss} that are used for human PK prediction. In addition, if PK in the pharmacological animal model was determined at a pharmacologically efficacious dose, the C_{max} and AUC data from that study are very useful in predicting the human efficacious dose. Eventually, a definitive GLP study of animal PK will be conducted as part of the animal ^{14}C-ADME study (see section "**Clinical ^{14}C-ADME study**"), but often, a scientifically valid non-GLP study conducted during candidate characterization in the last stage of discovery leading to nomination is adequate to be used for these purposes in the IND application.

4.01.4.1.3 Major routes of clearance in animals

As with animal pharmacokinetics, regulatory approval of a new drug requires full characterization of the routes of clearance and excretion of the drug and its metabolites in appropriate animal species, normally the rodent and large animal species used in animal safety studies. These studies are usually run in a GLP mode and are based on ^{14}C-radiolabeled drug. As such, there is no time to conduct two fully definitive animal ADME studies (or even one) during the IND-enabling period, and they are instead planned to begin after phase 1 SAD and MAD studies (see section "**Clinical pharmacokinetics**") have been completed, when it is more clear whether the NCE is a viable clinical candidate. To meet the requirement for animal ADME data in the IND application, then, it is desirable to collect animal metabolism and excretion data in non-GLP but scientifically valid studies during the discovery stage as part of clinical candidate nomination process.

Animal ADME studies have the triple goals of establishing the so-called mass balance, defining the mechanisms of clearance, and identifying plasma circulating metabolites (see section "**Active circulating metabolites in animals**"). "Mass balance" refers to quantitative excretion of the drug in a reasonable amount of time, either as unchanged parent drug or as metabolites. This is established by exhaustive collection of urine and feces and determining the total amount of drug-related material in these excreta, ideally with the use of ^{14}C-radiolabel as a means of detection. In some special cases, depending on the metabolic pathways present and the location of the ^{14}C-radiolabel in the molecule, expired $^{14}CO_2$ may need to be collected in special sealed environment chambers. The mechanisms of clearance are established by assessing the relative amounts of parent drug to metabolites in the excreta. Drugs that are cleared mainly by direct renal excretion of unchanged parent drug, for example, some antibiotics, will show almost the entire excreted dose in the urine. Conversely, a drug that shows little parent drug but almost entirely metabolites in either urine or bile must have been cleared mainly by initial metabolism of the parent drug. Identification of the chemical structures of the metabolites reveals which drug-metabolizing enzymes were involved. For example, if the predominant metabolite was formed by hydroxylation of an aromatic ring, then the CYP enzyme family was mainly responsible for clearance (see **Table 1**).

In recent years, some important leaders in the ADME/PK discipline have suggested that these animal ^{14}C-studies provide little benefit and should be discontinued,[130] but some others have felt uncomfortable about administering an NCE to a large number of humans without knowing as much as possible about its disposition in animals first.[131] Thus, at least until such time as regulatory authorities advise otherwise, sponsors continue to provide animal ADME data in the IND and NDA.

4.01.4.1.4 Active circulating metabolites in animals

As mentioned in the previous section, an important goal of animal ADME studies is to discover and identify metabolites circulating in the plasma. Since these metabolites are in the blood, they potentially can partition into all tissues, although some organs such as the brain have barriers between the tissue and plasma that may limit exposure. A special situation arises when one or more of these metabolites have significant pharmacological activity, since they may actually make a significant contribution to the expressed therapeutic benefit. Determination of whether circulating active metabolites are present is important in the interpretation of the expressed efficacy of the drug in the animal pharmacological model. Consequently, if circulating active metabolites are discovered

in animal plasma, the search for these metabolites in human plasma becomes a high priority in early clinical trials (this topic will be further discussed in section "Circulating human metabolites").

4.01.4.1.5 Projection of human PK

Planning for the conduct of clinical trials for a drug candidate requires some estimation of the range of human doses that will be explored, since we want to be sure that the corresponding exposures were covered in the GLP preclinical safety studies. Equally importantly, we need to estimate the number of milligrams of drug that will need to be combined with excipients in the solid dosage formulation to be used, and we have to plan a process chemistry campaign sufficient to provide the needed number of kilograms of active pharmaceutical ingredient (API) to support the planned clinical program. These needs require a preclinical method to estimate the efficacious dose, and the usual method is through allometric scaling.[132,133] In this procedure, the known PK parameters of three, or preferably four, animal species are used to project the corresponding parameters in humans. A parameter such as *CL* or V_{ss} is plotted against standard physiological parameters such as body mass and body surface area[65] in a double-log fashion to achieve a straight line. Extrapolation of the line to the corresponding physiological value for humans provides an estimate of the PK parameter in humans. Next, the *AUC* determined from an efficacious dose in the animal pharmacological model can be, with several assumptions, adjusted up or down based on the relative K_i values of the drug toward the target receptor to derive the *AUC* expected to be associated with efficacy in humans. With estimates of human *AUC* and *CL*, one can project the dose to be expected in humans by use of Eq. (7). Similarly, with estimates of *CL* and V_{ss}, the human *MRT* can be estimated by use of Eq. (6). These human projections are subject to several sources of uncertainty and error, so they must be conducted with experienced pharmacokineticists. Even so, the estimates of dose and *MRT* must be treated as only approximations useful for planning purposes. Thus, one can see the practical value of good animal PK studies prior to the initiation of phase 1 clinical trials.

4.01.4.1.6 Initial in vitro assessment of clinical DDI potential

In recent years, regulatory agencies have become more concerned about the safety of drugs due to DDIs. They are especially wary of DDIs in early clinical trials, when even the safety of the new drug candidate itself as a single agent is not yet fully understood. Consequently, a sponsor is expected to take measures to minimize the chance for DDIs by either investigating them in early clinical studies or severely limiting recruitment of subjects by imposing strict exclusion criteria based on comedications that the subjects may be taking. Since both of these options have the effect of slowing down early clinical development, regulatory agencies have provided a written guidance on how to test for DDIs with preclinical in vitro DDI studies.[28,29]

These documents provide a means for the sponsor to assess the potential for serious DDIs and in some cases avoid both the need to conduct some clinical DDI studies and the need to impose restrictive exclusion criteria. In vitro studies of the potential for the drug to inhibit, induce, or be a substrate for certain biochemical systems important in drug metabolism are delineated for the CYP and UGT families of enzymes, as well as a number of drug transporters. If the sponsor can show that the NCE interacts only insignificantly with any of these systems at expected clinical plasma concentration, then the sponsor may be able to proceed with phase 1/2 studies without having to first conduct clinical DDI studies with the drug-metabolizing systems that were "clean."

It is recognized that even doing in vitro studies rather than full clinical DDI studies is a substantial burden if they must all be accomplished prior to submission of the IND application. Therefore, the usual approach is for a sponsor to provide scientifically valid study results on the enzyme systems that most frequently cause clinical DDIs and then exclude a much smaller set of comedications that are of concern for a DDI. Thus, it is recommended that during the last stage of discovery and candidate nomination, a sponsor conduct (a) valid in vitro studies on inhibition and induction of CYP enzymes and (b) a study of substrate recognition by the efflux transporter P-gp. This subset of the guidance-required studies can be included in the IND application. The full list of recommended in vitro DDI studies can then be completed while phase 1 proceeds (this topic will be further discussed in section "Definitive characterization of DDIs").

4.01.4.2 Clinical ADME/PK Studies

4.01.4.2.1 Clinical pharmacokinetics

Up to this point in the discovery and development program, all information about human PK derived from use of in vitro human systems, such as hepatocytes, and extrapolations from animal in vivo studies. Now, in phase 1, the sponsor will determine in clinical dosing studies the true human ADME/PK properties of the drug candidate, including basic PK parameters, PK DDIs, presence and biological activities of circulating metabolites, relationship between plasma levels and therapeutic efficacy (pharmacokinetics/pharmacodynamics or PK/PD), and the interindividual variation of PK parameters in the patient population (population PK). Ideally, the results of the preclinical in vitro human and in vivo animal ADME/PK studies have been adequately predictive of the actual human ADME/PK profile of the candidate so that no big surprises are encountered. However, the science of in vitro-to-in vivo and animal-to-human extrapolation is not mature yet, and discrepancies between preclinical estimates and clinical reality are not uncommon.

Phase 1 clinical trials establish the safety, tolerability, and PK properties of a drug candidate in human beings. The subjects of phase 1 are normal healthy volunteers, although patients may be the subjects in cases where there is a known risk associated with the drug candidate, such as with cytotoxic cancer drugs. PK is determined in two foundational studies, the SAD and MAD studies. The route of dosing depends on the intended route of administration for the ultimate marketed product, typically oral, but possibly intravenous, intramuscular, or subcutaneous instead.

SAD involves giving each subject a single dose of the drug, with separate cohorts being singly dosed at escalating levels. MAD involves giving each subject several doses at a single dose level. Usually, doses are given once a day for 1 or 2 weeks. As with SAD, separate cohorts are dosed at escalating levels. Blood samples are collected from subjects at preselected time points based on the expected PK profile from animal studies and human PK prediction. Plasma concentrations are measured by LC-MS/MS in almost all cases of small-molecule drugs. The following PK parameters are then calculated: C_{max}, T_{max}, *AUC*, apparent volume of distribution (V_{ss}/F), apparent systemic clearance (CL/F), *MRT*, and terminal elimination half-life. An additional goal of the MAD study is to determine the time to reach PK steady state (usually defined as a state in which sequential predose trough levels of the drug are constant) and to define the average plasma level achieved at steady state. A plasma concentration versus time profile at steady state that deviates significantly from that predicted from simulations based on SAD data suggests that the PK of the drug changes with chronic dosing, possibly indicating a decrease in clearance due to a toxicity or an increase in clearance due to an autoinduction phenomenon. It is recommended for oral drugs that a separate single intravenous dose be given at an appropriate pharmacologically relevant dose level, allowing calculation of oral bioavailability (F) and the true values of V_{ss} and CL. Other PK-related phase 1 studies are usually conducted to determine the effects of food on oral bioavailability and of renal and liver impairment on clearance. Additionally, studies of PK as a function of age, gender, and pediatric applications may be required.

In phase 2, the subjects are patients with the disease or condition to be treated. These studies determine if the drug is actually therapeutically effective, and they tend to use one or two dose levels near the top of the tolerated dose range so that the drug candidate has the best possible chance to work. If the drug is intended for a new biological target, this may well be the first human in vivo test that modulation of the targeted receptor can actually provide a benefit, and so, phase 2 is sometimes called "proof of concept." PK is very important in phase 2 for two reasons. First, we must know if the PK is altered in patients compared with healthy volunteers. Second, if the drug failed to demonstrate POC, we can determine if the plasma levels expected to show efficacy were achieved and held long enough. Conversely, if POC was achieved, then we have the beginnings of a PK/PD relationship, which will be an expected part of the regulatory end-of-phase 2 (EOP2) meeting to justify the proposed doses for phase 3.

In phase 3, the need to collect PK information from the patients continues. Phase 3 is normally the first investigation of the drug in a large number of patients, unlike phases 1 and 2 in which much smaller numbers were examined. It therefore offers the opportunity to get statistically meaningful correlations of plasma levels and therapeutic effect, allowing the construction of the full PK/PD relationship. Regulatory authorities expect a sponsor to at least identify a nonefficacious dose, a minimally effective dose, a dose giving nearly full efficacy (perhaps 80%), and a dose that gives even higher efficacy, but at the cost of increasing adverse event issues, possibly to unacceptable levels. This understanding of the balance of safety and efficacy will be essential to select, in concert with regulatory authorities, the exact doses to be marketed. In addition, the large data set in phase 3 allows a population PK relationship to be created. In "Pop PK," statistical methods are used to create a generic PK profile for the drug that is then fine-tuned by identifying "covariates" drawn from readily obtainable demographic, physiological, or genetic characteristics such as age, gender, body weight, body mass index, race, ethnicity, and CYP genotype. The resulting Pop PK relationship can be useful in selecting the proper dose for a particular individual. The FDA encourages the sponsor to combine all of the available PK date to construct a physiologically based mathematical model of the PK of the new drug to demonstrate a complete understanding of its disposition in the human body.[134,135]

4.01.4.2.2 Definitive characterization of DDIs

Agency guidances (FDA and EMA) on clinically significant DDIs cover those resulting from competition between two drugs for metabolic enzymes (CYPs and UGTs), competition for clearance-related transporters, and induction of enzymes (CYPs) and transporters. The guidances encompass DDIs arising from the NCE as both a perpetrator and a victim. Thus, all NCEs must be investigated as both an inhibitor and inducer of CYPs, UGTs, and transporters (i.e., NCE is a perpetrator). In addition, if an NCE is a substrate of one of these systems, then a second drug has the potential to inhibit or induce its clearance (i.e., NCE is a victim). Thus, substrate phenotyping of the particular enzyme in the families of CYPs, UGTs, and/or transporters may also be required. Although these are the recommended systems to be studied because they are involved in the vast majority of known DDIs, in some cases, other enzyme systems not in these lists may still require investigation. In addition, major metabolites must be investigated for in vitro DDIs through the same guidance process, since there are a number of documented cases of major circulating metabolites being the cause of DDIs.[136–141] An extensive analysis of the situation of metabolites being CYP inhibitors has been provided by Callegari et al.[142] The process outlined in agency guidances for in vitro investigation of DDIs is structured as follows:

Metabolism-based DDIs
Drug candidate as a perpetrator of DDIs
 Inhibitor of DM enzymes
  CYP enzymes
   Direct inhibition (1A2, 2B6, 2C8, 2C9, 2C19, 2D6, 3A4)
   Time-dependent inhibition (1A2, 2B6, 2C8, 2C9, 2C19, 2D6, 3A4)
  UGT enzymes (1A1, 1A3, 1A4, 1A6, 1A9, 2B7, 2B15)
 Inducer of DM enzymes
  CYP enzymes (1A2, 2B6, 3A4)
  UGT enzymes (1A1, 1A4, 1A6, 1A9, 2B4 2B7)

(Continued)

Drug candidate as a victim of DDIs
Metabolic enzyme substrate phenotyping
CYP enzymes (1A1, 1A2, 1B1, 2A6, 2B6, 2C8, 2C9, 2C18, 2C19, 2D6, 2E1, 2F1, 2J2, 3A4, 3A5, 4F2)
UGT enzymes (1A1, 1A3, 1A4, 1A6, 1A9, 2B7, 2B15)
Transporter-based DDIs
Drug candidate as a perpetrator of DDIs
Inhibitor of drug transporters (P-gp, BCRP, OATP1B1, OATP1B3, OAT1, OAT3, OCT2)
Inducer of drug transporters (CAR and PXR nuclear receptors may induce transporters)
Drug candidate as a victim of DDIs
Transporter substrate phenotyping (P-gp, BCRP, OATP1B1, OATP1B3, OAT1, OAT3, OCT2)

The long experimental process entailed by the outline of regulatory DDI requirements in the preceding text means that typically only part of the work has been completed by the initiation of phase 1. It is generally understood that the agencies expect this work to be completed by the time of the EOP2 meeting. However, most sponsors lag behind this expectation and often have a comment by the agencies in their report of the EOP2 meeting that the remaining unfulfilled studies must be completed before phase 3 can proceed. In cases where only a discovery-level assessment of some of the in vitro DDI phenomena has occurred, the sponsor will be required to bring the quality of the studies up to full scientific rigor. For instance, if MBI was investigated previously with only the shift assay (see section Screening assays for pharmacokinetic drug-drug interactions), then the full MBI assay should be pursued in which the fundamental inhibition parameters K_i and k_{inact} are determined. These parameters can be used to provide much more accurate predictions of the risk of serious clinical DDIs due to MBI.[143] Similarly, if only the discovery-level assessment of induction based on activation of nuclear receptors was used for the IND, then a study with the "gold standard" human hepatocytes should be completed. Usually, there is little or no information on either the UGT enzymes or transporters[144–146] at the beginning of clinical phase 1, and these in vitro studies should be conducted during phase 1/2.

Finally, there is the question of substrate phenotyping for CYPs, UGTs, and transporters. Although it is possible to investigate all three of these with human in vitro systems, the information may not be relevant since in vitro metabolites are not guaranteed to be the important circulating in vivo metabolites. Therefore, the best procedure is to determine which metabolites are actually circulating in initial phase 1 studies (see section "**Circulating human metabolites**") and then conduct the phenotyping studies. The general procedure for enzyme phenotyping is to use an in vitro system such as human hepatocytes or microsomes that produces the metabolite seen in human plasma. This system is then challenged with known specific inhibitors of the various CYP and UGT enzymes to see which one knocks out the activity, thus revealing the identity of the enzyme responsible. Sometimes, more than one enzyme, for example, CYPs 2D6 and 3A4, produces the metabolite in question. Once the inhibition studies indicate the identity of the enzyme, then the results are confirmed by the use of single cDNA-expressed enzymes to provide a definitive conclusion. For transporters, the best procedure is to use a bank of single cDNA-expressed transporters to determine which, if any, are responsible for transport of the drug across membranes.

One can appreciate that these guidances represent a significant investment in time and resources for a sponsor, and for that reason, the process is triaged so that the most likely and most serious DDIs are evaluated first, preferably before the initiation of phase 1. For NCEs that show no significant interaction with these in vitro DM systems, the clinical DDI program may be dramatically simplified. However, any in vitro result that indicates a significant interaction will probably warrant a follow-up clinical DDI study between the NCE and a representative drug metabolized by the system giving the positive in vitro result. Agency guidances direct how these clinical DDI studies should be conducted.[28,29] The University of Washington has provided two useful tools that a sponsor may consult when interpreting clinical DDI data to evaluate such questions as how strong may a particular DDI be, which drugs are likely to interact with the NCE, and what is the DDI profile of related drugs in a therapeutic class.[147,148]

4.01.4.2.3 Circulating human metabolites

When one administers a small-molecule therapeutic agent, the patient is usually exposed to the biological activity of more than one chemical compound: the parent drug and any metabolites. We are particularly concerned with metabolites found in the plasma, as these circulate with the blood, and hence, all organ systems are exposed to their activity. It is the responsibility of the sponsor to find these metabolites, identify the chemical structures of the major ones, estimate their concentrations in plasma, and characterize their biological activities.

The four classifications of biological activity of metabolites are pharmacologically active, modulators of ADME systems, toxic, and innocuous. Pharmacologically active metabolites are not uncommon, and in some cases, they may account for a significant fraction, even the majority, of the expressed therapeutic effect. Obach has compiled an extensive list of such drugs.[149] A sponsor must be able to explain the observed PK/PD when conducting clinical trials, and sometimes, this means taking into account the activity contributed by the metabolite adding to that of the parent. For example, the angiotensin II antagonist losartan produces a long-lasting carboxylic acid metabolite that is responsible for approximately 14 times the activity of the parent drug.[149] Recognition of cases where an active metabolite is principally responsible for the in vivo pharmacology is important because DDIs or CYP polymorphisms that prevent the metabolism of the drug will also render it therapeutically ineffective. Note that we distinguish active metabolite-producing drugs from prodrugs, the difference being that a prodrug typically does not have activity itself and is only activated by metabolism.

As another example of biological activity, some metabolites are modulators (i.e., inhibitors and/or inducers) of drug-metabolizing enzymes or drug transporters. It is for this reason that regulatory agencies have included characterization of metabolites as an objective in the in vitro testing of drugs for DDIs in their guidances. Metabolites can also be toxic, which we can define as showing significant binding to off-target receptors. This could be manifest as a simple loss of selectivity compared with the parent drug among related receptors or binding to a completely different type of receptor with undesirable pharmacological effects. In a few cases, the metabolite may be frankly toxic, as, for instance, cyanide released during metabolism of the industrial chemicals acetonitrile and acrylonitrile[150,151] or the nephrotoxin thioformamide formed from thiabendazole.[152] A special case of circulating metabolites is the production of the opposite stereoisomer by chiral inversion, which has the effect of making a metabolite with similar dispositional properties to the parent drug but usually with loss of pharmacological activity but retention of toxicity.[153] Fortunately, despite the comments in the preceding text, most metabolites are innocuous, although perhaps this is not so surprising when one considers the chance that a random chemical modification to the structure of a drug molecule carefully crafted by the medicinal chemist to fit the binding pocket of a target receptor will result in retention of that fit.

It is worth noting that we are interested only in the major circulating metabolites, which are not necessarily inclusive of all the metabolites that are actually produced. The observed circulating concentration relative to the parent drug is the net result of the processes of formation, distribution, and clearance of the metabolites and is not reliably predictable from inspection of the structure alone.[154] Thus, we must rely on empirical means to become aware of them, and because of their potential clinical importance as outlined in the previous paragraph, it is necessary to initiate in vivo human exploration of the presence of circulating metabolites in phase 1. In this regard, we must depend on the new techniques of "cold" detection and structural identification of metabolites outlined in section "**Addressing high first-pass clearance**." However, once an apparent major circulating metabolite is found, it is almost always necessary to have a quantity of the metabolite synthesized, allowing it to be tested for pharmacological activity as well as providing a standard for LC-MS bioanalysis. However, it is often the case that a metabolite cannot be easily chemically synthesized. In such cases, the metabolite can usually be biosynthesized in quantities adequate for testing by using a human in vitro system such as liver microsomes or an enhanced hepatocyte system (see section "**Addressing high first-pass clearance**").[155,156]

4.01.4.2.4 Clinical ^{14}C-ADME study

The final part of the process of characterization of the human ADME/PK process is the clinical ^{14}C-ADME study. This study is commonly done with healthy volunteers and therefore classified as a phase 1 study, but it may not be started until phase 2 or even phase 3. Given that the sponsor has established the human circulating metabolite profile using "cold" methodology, there is not an urgent need to do the ^{14}C-ADME study until the results of phase 1/2 show that the new drug is safe and effective and likely to advance to phase 3. It is often called a "mass balance" study, but this is the least important of its objectives. The main objectives are to establish primary and secondary routes of clearance and excretion, provide definitive information on human circulating and excreted metabolites, and compare plasma PK of parent drug with PK of radioactivity.[157] Although FDA rules indicate that the PK and disposition of an NCE must be characterized in humans, they do not require these to be based on ^{14}C-radiolabeled drug.[158] However, a practical alternative methodology that avoids the use of radiolabel while maintaining the certainty of radiolabel is not yet available, although there is considerable interest in extending the capabilities of LC-MS to the human mass balance study in addition to its present utility to find and identify circulating metabolites.[52,53]

The study consists of administration of a single dose of a radiolabeled analog of the NCE with specific activity diluted down to a suitable level with nonradiolabeled drug to allow convenient administration of about 100 μCi of radiolabel at a total dose in the relevant pharmacological range. The use of a very low radioactive dose (~100 nCi) combined with quantitation by accelerator MS rather than conventional scintillation counting has also been demonstrated to be practical.[159] The radionuclide of choice for these studies is ^{14}C, which is generally easy to incorporate into the structure. Prior metabolism studies establish which positions in the molecule are likely to be stable toward release of small ^{14}C-containing fragments such as $^{14}CO_2$, which would be lost by expiration in the breath. Before humans can be exposed to a radiolabeled NCE, the sponsor must conduct a dosimetry study in rats to assess organ distribution and elimination kinetics of the radiolabel to determine the maximum exposure of various organs to ^{14}C-emitted beta radiation. These data establish the maximum dose of ^{14}C that can be dosed to humans. Achievement of mass balance requires total collection of urine and feces for typically 2 weeks after dosing, and thus, these studies are normally done in specialized "resident–subject" clinical sites. However, the collection period may need to be extended for long half-life drugs. The goal is to recover at least 90% of the radioactive dose.

The results of the mass balance study are important in several ways. Although the circulating metabolite profile was investigated by "cold" methodology in the SAD and MAD trials, those data are considered preliminary for registration purposes. The profile obtained from the ^{14}C-ADME study is the "gold standard," and only when we have the definitive human metabolite do we have a definitive assessment of the adequacy of the animal safety studies (i.e., MIST). It must be mentioned in the MIST context that the agency guidances stipulate that the human metabolite exposures that must be covered in the animal safety studies are to be measured at PK steady state to allow for possible accumulation of the metabolites after multiple dosing. But, of course, plasma metabolite concentrations in the ^{14}C-ADME study are measured after a single dose, since it is not feasible to multiply dose radiolabeled drug. However, Prakash et al. have demonstrated a method for meeting the MIST requirement by estimating the steady-state concentrations through standard PK simulations to steady state from single-dose data.[160] Another important objective of the mass balance study, central to the task of characterizing the ADME/PK of the new drug, is determining the main routes of clearance, since these are the determinants of clinically important phenomena such as susceptibility to DDIs, possibility of polymorphic PK, and changes in PK due to disease states. And let us not forget that, although the mass balance

component of the "mass balance" study is not the most important aspect, it is nonetheless necessary to establish the time required for a therapeutically relevant dose of the drug to be completely cleared from the body, including parent drug, metabolites, and possible strongly retained drug residues. A recent example of a well-executed mass balance study illustrates how much may be learned.[161] With the completion of the clinical ^{14}C-ADME study, one can consider that the human ADME/PK profile has been defined for the new drug candidate. In the absence of special metabolism issues, the ADME/PK package has been finished and is ready for inclusion in the NDA.

4.01.5 Summary

ADME/PK becomes a core activity of the drug discovery and development process very early. In fact, most discovery teams start to at least investigate ADME/PK properties shortly after the initiation of the hit-to-lead phase. During lead optimization, ADME/PK screening becomes as important as improving target receptor binding. Usually, the strategy is for the medicinal chemists to learn how to make potent and selective ligands to the target receptor, followed by optimization of ADME/PK while maintaining potency and selectivity. Many times, this is accomplished by modifications to the lead molecular series in pharmacologically tolerant portions of the molecule to adjust properties such as solubility, permeability, and polarity. On the other hand, for modulating metabolism, chemists must modify the molecule at the site where the metabolism occurs, whether or not the region is pharmacologically tolerant. But it is typically possible to build in MetStab while maintaining activity. The ADME/PK goals in discovery lead optimization are to design a molecule with acceptable bioavailability (for oral drugs), *MRT* consistent with once-a-day dosing, good target organ penetration, and little potential to cause DDIs.

Once a clinical candidate is nominated, all aspects of the molecular structure are locked in, with the exception of salt-form selection, and it is necessary to conduct a series of more rigorous in vitro tests with human systems and in vivo studies of ADME/PK in animals to define what profile has actually been achieved. Preclinical animal safety studies become the most important activity on the path to phase 1 clinical trials, but ADME/PK retains a role in defining exposures and metabolism/disposition of the clinical candidate in support of the safety program. In addition, in the preclinical period, projection of the ADME/PK profile in humans begins in order to help design the early clinical program. In vitro tests to investigate the potential for DDIs should also begin in the IND-enabling phase.

Finally, with the initiation of clinical phase 1, the sponsor at last has the opportunity to characterize the true human ADME/PK profile, including PK, drug interactions, metabolism, major routes of clearance, and excretion. These properties must be known to allow proper planning of phases 2 and 3. The ^{14}C-human ADME study becomes the final activity in definitive characterization of the human ADME/PK profile to accompany the new drug application. The three roles of ADME/PK are seen to be distinct but closely related and interlocking: discovery leads to safety assessment that leads to clinical development. And this is the reason that it is incumbent on the medicinal chemist to design the most ADME/PK-optimized structure possible.

References

1. Hall, M. P. Biotransformation and in vivo Stability of Protein Biotherapeutics: Impact on Candidate Selection and Pharmacokinetic Profiling. *Drug Metab. Dispos.* **2014,** *42,* 1873–1880.
2. Kola, I.; Landis, J. Can the Pharmaceutical Industry Reduce Attrition Rates? *Nat. Rev. Drug Discov.* **2004,** *3,* 711–715.
3. Hay, M.; Thomas, D. W.; Craighead, J. L.; Economides, C.; Rosenthal, J. Clinical Development Success Rates for Investigational Drugs. *Nat. Biotechnol.* **2014,** *32,* 40–51.
4. Waring, M. J.; Arrowsmith, J.; Leach, A. R.; Leeson, P. D.; Mandrell, S.; Owen, R. M.; Pairaudeau, G.; Pennie, W. D.; Pickett, S. D.; Wang, J.; Wallace, O.; Weir, A. An Analysis of the Attrition of Drug Candidates From Four Major Pharmaceutical Companies. *Nat. Rev. Drug Discov.* **2015,** *14,* 475–486.
5. Turner, M. J. The Current State of Drug Discovery and What It Might Take to Improve Drug Discovery Outcomes and Approval Successes. *Drug Discov. Today* **2015,** *9,* 917–919.
6. Yusof, I.; Segall, M. D. Considering the Impact Drug-Like Properties Have on the Chance of Success. *Drug Discov. Today* **2013,** *18,* 659–666.
7. Hsieh, Y.; Cheng, K.-C.; Wang, Y.; Chackalamannil, S.; Xia, Y.; Korfmacher, W. A.; White, R. E. The Role of Exploratory Drug Metabolism and Pharmacokinetics in New Drug Research: Case Study-Selection of a Thrombin Receptor Antagonist for Development. *Curr. Pharm. Des.* **2009,** *15,* 2262–2269.
8. Zhou, L.; Dockens, R. C.; Liu-Kreyche, P.; Grossman, S. J.; Iyer, R. A. In Vitro and in vivo Metabolism and Pharmacokinetics of BMS-562086, a Potent and Orally Bioavailable Corticotropin-Releasing Factor-1 Receptor Antagonist. *Drug Metab. Dispos.* **2012,** *40,* 1093–1103.
9. Manitpisitkul, P.; White, R. E. Whatever Happened to Cassette-Dosing Pharmacokinetics? *Drug Discov. Today* **2004,** *9,* 652–658.
10. Pelkonen, O.; Raunio, H. In Vitro Screening of Drug Metabolism During Drug Development: Can We Trust the Predictions? *Expert Opin. Drug Metab. Toxicol.* **2005,** *1,* 49–59.
11. Li, C.; Liu, B.; Chang, J.; Groessl, T.; Zimmerman, M.; He, Y.; Isbell, J.; Tuntland, T. A Modern in vivo Pharmacokinetic Paradigm: Combining Snapshot, Rapid and Full PK Approaches to Optimize and Expedite Early Drug Discovery. *Drug Discov. Today* **2013,** *18,* 71–78.
12. White, R. E.; Manitpisitkul, P. Pharmacokinetic Theory of Cassette Dosing in Drug Discovery Screening. *Drug Metab. Dispos.* **2001,** *29,* 957–966.
13. Korfmacher, W. A.; Cox, K. A.; Ng, K. J.; Veals, J.; Hsieh, Y.; Wainhaus, S.; Broske, L.; Prelusky, D.; Nomeir, A.; White, R. E. Cassette-Accelerated Rapid Rat Assay: A Systematic Procedure for the Dosing and Liquid Chromatography/Atmospheric Pressure Ionization Tandem Mass Spectrometric Analysis of New Chemical Entities as Part of New Drug Discovery. *Rapid Commun. Mass Spectrom.* **2001,** *15,* 335–340.
14. Mei, H.; Korfmacher, W.; Morrison, R. Rapid in vivo Oral Screening in Rats: Reliability, Acceptance Criteria, and Filtering Efficiency. *AAPS J.* **2006,** *8,* E493–E500.
15. Hardman, J. G., Limbird, L. H., Gilman, A. G., Eds. *Goodman and Gilman's The Pharmacological Basis of Therapeutics,* 10th ed.; McGraw-Hill: New York, 2001; pp 1924–2023.
16. Varma, M. V. S.; Obach, R. S.; Rotter, C.; Miller, H. R.; Chang, G.; Steyn, S. J.; El-Kattan, A.; Troutman, M. D. Physicochemical Space for Optimum Oral Bioavailability: Contribution of Human Intestinal Absorption and First-Pass Elimination. *J. Med. Chem.* **2010,** *53,* 1098–1108.

17. Huttunen, K. M.; Raunio, H.; Rautio, J. Prodrugs—From Serendipity to Rational Design. *Pharmacol. Rev.* **2011,** *63,* 750–771.
18. Poirier, A.; Belli, S.; Funk, C.; Otteneder, M. B.; Portmann, R.; Heinig, K.; Prinssen, E.; Lazic, S. E.; Rayner, C. R.; Hoffmann, G.; Singer, T.; Smith, D. E.; Schuler, F. Role of the Intestinal Peptide Transporter PEPT1 in Oseltamivir Absorption: in vitro and in vivo Studies. *Drug Metab. Dispos.* **2012,** *40,* 1556–1565.
19. Giacomini, K. M.; Huang, S.; Tweedie, D. J.; Benet, L. Z.; Brouwer, K. L. R.; Chu, X.; Dahlin, A.; Evers, R.; Fischer, V.; Hillgren, K. M.; Hoffmaster, K. A.; Ishikawa, T.; Keppler, D.; Kim, R. B.; Lee, C. A.; Niemi, M.; Polli, J. W.; Sugiyama, Y.; Swaan, P. W.; Ware, J. A.; Wright, S. H.; Yee, S. W.; Zamek-Gliszczynski, M. J.; Zhang, L. Membrane Transporters in Drug Development. *Nat. Rev. Drug Discov.* **2010,** *9,* 217–236.
20. Ballard, P.; Brassil, P.; Bui, K. H.; Dolgos, H.; Petersson, C.; Tunek, A.; Webborn, P. J. H. The Right Compound in the Right Assay at the Right Time: An Integrated Discovery DMPK Strategy. *Drug Metab. Rev.* **2012,** *3,* 224–252.
21. Karlsson, F. H.; Bouchene, S.; Hilgendorf, C.; Dolgos, H.; Peters, S. A. Utility of in vitro Systems and Preclinical Data for the Prediction of Human Intestinal First-Pass Metabolism During Drug Discovery and Preclinical Development. *Drug Metab. Dispos.* **2013,** *41,* 2033–2046.
22. Matsuda, Y.; Konno, Y.; Satsukawa, M.; Kobayashi, T.; Takimoto, Y.; Morisaki, K.; Yamashita, S. Assessment of Intestinal Availability of Various Drugs in the Oral Absorption Process Using Portal Vein-Cannulated Rats. *Drug Metab. Dispos.* **2012,** *40,* 2231–2238.
23. White, R. E. Review of Drug Metabolism in Drug Discovery and Development. In *Encyclopedia of Drug Metabolism and Interactions*; vol. 1; Wiley: Hoboken, NJ, 2012, ; pp 1–40.
24. Testa, B.; Pedretti, A.; Vistoli, G. Foundation Review: Reactions and Enzymes in the Metabolism of Drugs and Other Xenobiotics. *Drug Discov. Today* **2012,** *17,* 549–560.
25. Tracy, T. S.; Chaudhry, A. S.; Prasad, B.; Thummel, K. E.; Schuetz, E. G.; Zhong, X.; Tien, Y.; Jeong, H.; Pan, X.; Shireman, L. M.; Tay-Sontheimer, J.; Lin, Y. S. Interindividual Variability in Cytochrome P450-Mediated Drug Metabolism. *Drug Metab. Dispos.* **2016,** *44,* 343–351.
26. Guengerich, F. P. Human Cytochrome P450 Enzymes. In *Cytochrome P450. Structure, Mechanism, Biochemistry;* Ortiz de Montellano, P. R., Ed.; Kluwer Academic/Plenum Publishers: New York, 2005; pp 377–530.
27. Dong, D.; Wu, B.; Chow, D.; Hu, M. Substrate Selectivity of Drug-Metabolizing Cytochrome P450s Predicted From Crystal Structures and In Silico Modeling. *Drug Metab. Rev.* **2012,** *44,* 192–208.
28. European Medicines Agency. *Guideline on the Investigation of Drug Interactions*, 2013. Available at http://www.ema.europa.eu/docs/en_GB/document_library/Scientific_guideline/2012/07/WC500129606.pdf (accessed 26 April 2016).
29. United States Food and Drug Administration. *Guidance for Industry: Drug Interaction Studies—Study Design, Data Analysis, Implications for Dosing, and Labeling Recommendations;* Center for Drug Evaluation and Research: Rockville, MD, 2012. Available at http://www.fda.gov/downloads/Drugs/GuidanceComplianceRegulatoryInformation/Guidances/UCM292362.pdf (accessed 2016 April 26).
30. Krest, C. M.; Onderko, E. L.; Yosca, T. H.; Calixto, J. C.; Karp, R. F.; Livada, J.; Rittle, J.; Green, M. T. Reactive Intermediates in Cytochrome P450 Catalysis. *J. Biol. Chem.* **2013,** *288,* 17074–17081.
31. Lundquist, P.; Lööf, J.; Fagerholm, U.; Sjögren, I.; Johansson, J.; Briem, S.; Hoogstraate, J.; Afzelius, L.; Andersson, T. B. Prediction of in vivo Rat Biliary Drug Clearance From an in vitro Hepatocyte Efflux Model. *Drug Metab. Dispos.* **2014,** *42,* 459–468.
32. Di, L.; Atkinson, K.; Orozco, C. C.; Funk, C.; Zhang, H.; McDonald, T. S.; Tan, B.; Lin, J.; Chang, C.; Obach, R. S. In Vitro–In Vivo Correlation for Low-Clearance Compounds Using Hepatocyte Relay Method. *Drug Metab. Dispos.* **2013,** *41,* 2018–2023.
33. Holmgren, G.; Sjögren, A.; Barragan, I.; Sabirsh, A.; Sartipy, P.; Synnergren, J.; Björquist, P.; Ingleman-Sundberg, M.; Andersson, T. B.; Edsbagge, J. Long-Term Chronic Toxicity Testing Using Human Pluripotent Stem Cell-Derived Hepatocytes. *Drug Metab. Dispos.* **2014,** *42,* 1401–1406.
34. Andersson, T. B.; Kanebratt, K. P.; Kenna, J. G. The HepaRG Cell Line: A Unique in vitro Tool for Understanding Drug Metabolism and Toxicology in Humans. *Expert Opin. Drug Metab. Toxicol.* **2012,** *8,* 909–920.
35. Vermet, H.; Raoust, N.; Ngo, R.; Esserméant, L.; Klieber, S.; Fabre, G.; Boulenc, X. Evaluation of Normalization Methods to Predict CYP3A4 Induction in Six Fully Characterized Cryopreserved Human Hepatocyte Preparations and HepaRG Cells. *Drug Metab. Dispos.* **2016,** *44,* 50–60.
36. Chan, T. S.; Yu, H.; Moore, A.; Khetani, S. R.; Tweedie, D. Meeting the Challenge of Predicting Hepatic Clearance of Compounds Slowly Metabolized by Cytochrome P450 Using a Novel Hepatocyte Model, HepatoPac. *Drug Metab. Dispos.* **2013,** *41,* 2024–2032.
37. Lin, C.; Shi, J.; Moore, A.; Khetani, S. R. Prediction of Drug Clearance and Drug-Drug Interactions in Microscale Cultures of Human Hepatocytes. *Drug Metab. Dispos.* **2016,** *44,* 127–136.
38. Ballard, T. E.; Wang, S.; Cox, L. M.; Moen, M. A.; Krzyzewski, S.; Ukairo, O.; Obach, R. S. Application of a Micropatterned Cocultured Hepatocyte System to Predict Preclinical and Human-Specific Drug Metabolism. *Drug Metab. Dispos.* **2016,** *44,* 172–179.
39. Schaefer, M.; Schänzle, G.; Bischoff, D.; Süssmuth, R. D. Upcyte Human Hepatocytes: A Potent in vitro Tool for the Prediction of Hepatic Clearance of Metabolically Stable Compounds. *Drug Metab. Dispos.* **2016,** *44,* 435–444.
40. Ramachandran, S. D.; Vivarès, A.; Klieber, S.; Hewitt, N. J.; Muenst, B.; Heinz, S.; Walles, H.; Braspenning, J. Applicability of Second-Generation Upcyte® Human Hepatocytes for Use in CYP Inhibition and Induction Studies. *Pharmacol. Res. Perspect.* **2015,** *3* (5), e00161.
41. Bonn, B.; Svanberg, P.; Janefeldt, A.; Hultman, I.; Grime, K. Determination of Human Hepatocyte Intrinsic Clearance for Slowly Metabolized Compounds: Comparison of a Primary Hepatocyte/Stromal Cell Co-Culture With Plated Primary Hepatocytes and HepaRG. *Drug Metab. Dispos.* **2016,** *44,* 527–533.
42. Hutzler, J. M.; Ring, B. J.; Anderson, S. R. Low-Turnover Drug Molecules: A Current Challenge for Drug Metabolism Scientists. *Drug Metab. Dispos.* **2015,** *43,* 1917–1928.
43. Sohlenius-Sternbeck, A.-K.; Afzelius, L.; Prusis, P.; Neelissen, J.; Hoogstraate, J.; Johansson, J.; Floby, E.; Bengtsson, A.; Gissberg, O.; Sternbeck, J.; Petersson, C. Evaluation of the Human Prediction of Clearance From Hepatocyte and Microsome Intrinsic Clearance for 52 Drug Compounds. *Xenobiotica* **2010,** *40,* 637–649.
44. Di, L.; Feng, B.; Goosen, T. C.; Lai, Y.; Steyn, S. J.; Varma, M. V.; Obach, R. S. A Perspective on the Prediction of Drug Pharmacokinetics and Disposition in Drug Research and Development. *Drug Metab. Dispos.* **2013,** *41,* 1975–1993.
45. Ramanathan, R.; Reyderman, L.; Su, A. D.; Alvarez, N.; Chowdhury, S. K.; Alton, K. B.; Wirth, M. A.; Clement, R. P.; Statkevich, P.; Patrick, J. E. Disposition of Desloratadine in Healthy Volunteers. *Xenobiotica* **2007,** *37,* 770–787.
46. White, R. E. *The Importance of Full and Correct Prediction of Human Metabolites in Discovery and Preclinical Development, White Paper;* Hurel Corp.: Beverly Hills, CA, 2014. Available at http://hurelcorp.com/video/ (accessed 2016 April 26).
47. Kazmi, F.; Barbara, J. E.; Yerino, P.; Parkinson, A. A Long-Standing Mystery Solved: The Formation of 3-Hydroxydesloratadine is Catalyzed by CYP2C8 But Prior Glucuronidation of Desloratadine by UDP-Glucuronosyltransferase 2B10 Is an Obligatory Requirement. *Drug Metab. Dispos.* **2015,** *43,* 523–533.
48. Zhu, M.; Zhang, H.; Humphreys, W. G. Drug Metabolite Profiling and Identification by High-Resolution Mass Spectrometry. *J. Biol. Chem.* **2011,** *286,* 25419–25425.
49. Zamora, I.; Fontaine, F.; Serra, F.; Plasencia, G. High-Throughput, Computer Assisted, Specific MetID. A Revolution for Drug Discovery. *Drug Discov. Today Technol.* **2013,** *10,* e199–e205.
50. Wen, B.; Zhu, M. Applications of Mass Spectrometry in Drug Metabolism: 50 Years of Progress. *Drug Metab. Rev.* **2015,** *47,* 71–87.
51. Wright, P. Metabolite Identification by Mass Spectrometry: Forty Years of Evolution. *Xenobiotica* **2011,** *41,* 670–686.
52. Zhu, P.; Ding, W.; Tong, W.; Ghosal, A.; Alton, K.; Chowdhury, S. A Retention-Time-Shift-Tolerant Background Subtraction and Noise Reduction Algorithm (BgS-NoRA) for Extraction of Drug Metabolites in Liquid Chromatography/Mass Spectrometry Data From Biological Matrices. *Rapid Commun. Mass Spectrom.* **2009,** *23,* 1563–1572.
53. Zhu, P.; Tong, W.; Alton, K.; Chowdhury, S. An Accurate-Mass-Based Spectral-Averaging Isotope-Pattern-Filtering Algorithm for Extraction of Drug Metabolites Possessing a Distinct Isotope Pattern From LC-MS Data. *Anal. Chem.* **2009,** *81,* 5910–5917.
54. Zhang, H.; Zhang, D.; Ray, K.; Zhu, M. Mass Defect Filter Technique and Its Applications to Drug Metabolite Identification by High-Resolution Mass Spectrometry. *J. Mass Spectrom.* **2009,** *44,* 999–1016.
55. Shimizu, A.; Chiba, M. Ion Mobility Spectrometry–Mass Spectrometry Analysis for the Site of Aromatic Hydroxylation. *Drug Metab. Dispos.* **2013,** *41,* 1295–1299.

56. Xing, J.; Zang, M.; Zhang, H.; Zhu, M. The Application of High-Resolution Mass Spectrometry-Based Data-Mining Tools in Tandem to Metabolite Profiling of a Triple Drug Combination in Humans. *Anal. Chim. Acta* **2015,** *897,* 34–44.
57. Sugimoto, H.; Hirabayashi, H.; Amano, N.; Moriwaki, T. Retrospective Analysis of P-Glycoprotein-Mediated Drug-Drug Interactions at the Blood–Brain Barrier in Humans. *Drug Metab. Dispos.* **2013,** *41,* 683–688.
58. Li, L.; Agarwal, S.; Elmquist, W. F. Brain Efflux Index to Investigate the Influence of Active Efflux on Brain Distribution of Pemetrexed and Methotrexate. *Drug Metab. Dispos.* **2013,** *41,* 659–667.
59. Kikuchi, R.; de Morais, S. M.; Kalvass, J. C. In Vitro P-Glycoprotein Efflux Ratio Can Predict the in vivo Brain Penetration Regardless of Biopharmaceutics Drug Disposition Classification System Class. *Drug Metab. Dispos.* **2013,** *41,* 2012–2017.
60. Liu, X.; Ding, X.; Deshmukh, G.; Liederer, B. M.; Hop, C. E. C. A. Use of the Cassette-Dosing Approach to Assess Brain Penetration in Drug Discovery. *Drug Metab. Dispos.* **2012,** *40,* 963–969.
61. Yasuda, K.; Cline, C.; Vogel, P.; Onciu, M.; Fatima, S.; Sorrentino, B. P.; Thirumaran, R. K.; Ekins, S.; Urade, Y.; Fujimori, K.; Schuetz, E. G. Drug Transporters on Arachnoid Barrier Cells Contribute to the Blood–Cerebrospinal Fluid Barrier. *Drug Metab. Dispos.* **2013,** *41,* 923–931.
62. Ecker, G. F.; Noe, C. R. In Silico Prediction Models for Blood–Brain Barrier Permeation. *Curr. Med. Chem.* **2004,** *11,* 1617–1628.
63. Bagal, S. K.; Bungay, P. J. Minimizing Drug Exposure in the CNS While Maintaining Good Oral Absorption. *ACS Med. Chem. Lett.* **2012,** *3,* 948–950.
64. Smith, D. A.; Di, L.; Kerns, E. H. The Effect of Plasma Protein Binding on in vivo Efficacy: Misconceptions in Drug Discovery. *Nat. Rev. Drug Discov.* **2010,** *9,* 929–939.
65. Davies, B.; Morris, T. Physiological Parameters in Laboratory Animals and Humans. *Pharm. Res.* **1993,** *10,* 1093–1095.
66. Ghuman, J.; Zunszain, P. A.; Petitpas, I.; Bhattacharya, A. A.; Otagiri, M.; Curry, S. Structural Basis of the Drug-Binding Specificity of Human Serum Albumin. *J. Mol. Biol.* **2005,** *353,* 38–52.
67. Moroy, G.; Martiny, V. Y.; Vaye, P.; Villoutreix, B. O.; Miteva, M. A. Toward In Silico Structure-Based ADMET Prediction in Drug Discovery. *Drug Discov. Today* **2012,** *17,* 44–55.
68. Siebert, G. A.; Hung, D. Y.; Chang, P.; Roberts, M. S. Ion-Trapping, Microsomal Binding, and Unbound Drug Distribution in the Hepatic Retention of Basic Drugs. *J. Pharmacol. Exp. Ther.* **2004,** *308,* 228–235.
69. Sahin, S.; Benet, L. Z. The Operational Multiple Dosing Half-Life: A Key to Defining Drug Accumulation in Patients and to Designing Extended Release Dosage Forms. *Pharm. Res.* **2008,** *25,* 2869–2877.
70. Nigam, S. K. What Do Drug Transporters Really Do? *Nat. Rev. Drug Discov.* **2015,** *14,* 29–44.
71. Kell, D. B.; Dobson, P. D.; Bilsland, E.; Oliver, S. G. The Promiscuous Binding of Pharmaceutical Drugs and Their Transporter-Mediated Uptake Into Cells: What We (Need to) Know and How We Can Do So. *Drug Discov. Today* **2013,** *18,* 218–239.
72. Benet, L. Z. The Drug Transporter-Metabolism Alliance: Uncovering and Defining the Interplay. *Mol. Pharm.* **2009,** *6,* 1631–1643.
73. Kirchmair, J.; Göller, A. H.; Lang, D.; Kunze, J.; Testa, B.; Wilson, I. D.; Glen, R. C.; Schneider, G. Predicting Drug Metabolism: Experiment and/or Computation? *Nat. Rev. Drug Discov.* **2015,** *14,* 387–404.
74. Kingsley, L. J.; Wilson, G. L.; Essex, M. E.; Lill, M. A. Combining Structure and Ligand-Based Approaches to Improve Site of Metabolism Prediction in CYP2C9 Substrates. *Pharm. Res.* **2015,** *32,* 986–1001.
75. Forda, K. A.; Ryslikb, G.; Sodhic, J.; Halladayd, J.; Diaza, D.; Dambacha, D.; Masudaa, M. Computational Predictions of the Site of Metabolism of Cytochrome P450 2D6 Substrates: Comparative Analysis, Molecular Docking, Bioactivation and Toxicological Implications. *Drug Metab. Rev.* **2015,** *47,* 291–319.
76. Zaretzki, J.; Bergeron, C.; Rydberg, P.; Huang, T.; Bennett, K. P.; Breneman, C. M. RS-Predictor: A New Tool for Predicting Sites of Cytochrome P450-Mediated Metabolism Applied to CYP 3A4. *J. Chem. Inf. Model.* **2011,** *51,* 1667–1689.
77. Campagna-Slater, V.; Pottel, J.; Therrien, E.; Cantin, L.; Moitessier, N. Development of a Computational Tool to Rival Experts in the Prediction of Sites of Metabolism of Xenobiotics by P450s. *J. Chem. Inf. Model.* **2012,** *52,* 2471–2483.
78. Kirchmair, J.; Williamson, M. J.; Tyzack, J. D.; Tan, L.; Bond, P. J.; Bender, A.; Glen, R. C. Computational Prediction of Metabolism: Sites, Products, SAR, P450 Enzyme Dynamics, and Mechanisms. *J. Chem. Inf. Model.* **2012,** *52,* 617–648.
79. Rostkowski, M.; Spjuth, O.; Rydberg, P. WhichCyp: Prediction of Cytochromes P450 Inhibition. *Bioinformatics* **2013,** *29,* 2051–2052.
80. Johnson, E. F.; Stout, C. D. Structural Diversity of Human Xenobiotic-Metabolizing Cytochrome P450 Monooxygenases. *Biochem. Biophys. Res. Commun.* **2005,** *338,* 331–336.
81. Reynald, R. L.; Sansen, S.; Stout, C. D.; Johnson, E. F. Structural Characterization of Human Cytochrome P450 2C19. Active Site Differences Between P450s 2C8, 2C9, and 2C19. *J. Biol. Chem.* **2012,** *287,* 44581–44591.
82. Cumming, J. G.; Davis, A. M.; Muresan, S.; Haeberlein, M.; Chen, H. Chemical Predictive Modelling to Improve Compound Quality. *Nat. Rev. Drug Discov.* **2013,** *12,* 948–962.
83. Ritchie, T. J.; Ertl, P.; Lewis, R. The Graphical Representation of ADME-Related Molecule Properties for Medicinal Chemists. *Drug Discov. Today* **2011,** *16,* 65–72.
84. Varma, M. V.; Steyn, S. J.; Allerton, C.; El-Kattan, A. F. Predicting Clearance Mechanism in Drug Discovery: Extended Clearance Classification System (ECCS). *Pharm. Res.* **2015,** *32,* 3785–3802.
85. Gandhi, Y. A.; Morris, M. E. Reevaluation of a Quantitative Structure Pharmacokinetic Model for Biliary Excretion in Rats. *Drug Metab. Dispos.* **2012,** *40,* 1259–1262.
86. Varma, M. V. S.; Feng, B.; Obach, R. S.; Troutman, M. D.; Chupka, J.; Miller, H. R.; El-Kattan, A. Physicochemical Determinants of Human Renal Clearance. *J. Med. Chem.* **2009,** *52,* 4844–4852.
87. Wallace, B. D.; Redinbo, M. R. Xenobiotic-Sensing Nuclear Receptors Involved in Drug Metabolism: A Structural Perspective. *Drug Metab. Rev.* **2013,** *45* (1), 79–100.
88. Haupt, L. J.; Kazmi, F.; Ogilvie, B. W.; Buckley, D. B.; Smith, B. D.; Leatherman, S.; Paris, B.; Parkinson, O.; Parkinson, A. The Reliability of Estimating K_i Values for Direct, Reversible Inhibition of Cytochrome P450 Enzymes From Corresponding IC_{50} Values: A Retrospective Analysis of 343 Experiments. *Drug Metab. Dispos.* **2015,** *43,* 1744–1750.
89. Rendic, S.; Guengerich, F. P. Survey of Human Oxidoreductases and Cytochrome P450 Enzymes Involved in the Metabolism of Xenobiotic and Natural Chemicals. *Chem. Res. Toxicol.* **2015,** *28,* 38–42.
90. Brändén, G.; Sjögren, T.; Schnecke, V.; Xue, Y. Structure-Based Ligand Design to Overcome CYP Inhibition in Drug Discovery Projects. *Drug Discov. Today* **2014,** *19,* 905–911.
91. Bell, L.; Bickford, S.; Nguyen, P. H.; Wang, J.; He, T.; Zhang, B.; Friche, Y.; Zimmerlin, A.; Urban, L.; Bojanic, D. Evaluation of Fluorescence and Mass Spectrometry-Based CYP Inhibition Assays for Use in Drug Discovery. *J. Biomol. Screen.* **2008,** *13,* 343–353.
92. Lin, H.; Kenaan, C.; Hollenberg, P. F. Identification of the Residue in Human CYP3A4 That Is Covalently Modified by Bergamottin and the Reactive Intermediate That Contributes to the Grapefruit Juice Effect. *Drug Metab. Dispos.* **2012,** *40,* 998–1006.
93. Baer, B. R.; Wienkers, L. C.; Rock, D. A. Time-Dependent Inactivation of P450 3A4 by Raloxifene: Identification of Cys239 as the Site of Apoprotein Alkylation. *Chem. Res. Toxicol.* **2007,** *20,* 954–964.
94. D'Agostino, J.; Zhang, H.; Kenaan, C.; Hollenberg, P. F. Mechanism-Based Inactivation of Human Cytochrome P450 2B6 by Chlorpyrifos. *Chem. Res. Toxicol.* **2015,** *28,* 1484–1495.
95. Henne, K. R.; Tran, T. B.; VandenBrink, B. M.; Rock, D. A.; Aidasani, D. K.; Subramanian, R.; Mason, A. K.; Stresser, D. M.; Teffera, Y.; Wong, S. G.; Johnson, M. G.; Chen, X.; Tonn, G. R.; Wong, B. K. Sequential Metabolism of AMG 487, a Novel CXCR3 Antagonist, Results in Formation of Quinone Reactive Metabolites That Covalently Modify CYP3A4 Cys239 and Cause Time-Dependent Inhibition of the Enzyme. *Drug Metab. Dispos.* **2012,** *40,* 1429–1440.

96. Raucy, J.; Warfe, L.; Yueh, M. F.; Allen, S. W. A Cell-Based Reporter Gene Assay for Determining Induction of CYP3A4 in a High-Volume System. *J. Pharmacol. Exp. Ther.* **2002,** *303,* 412–423.
97. Shi, H.; Tian, H.; Li, Y.; Li, D.; Yu, H.; Zhen, X.; Hou, T. Absorption, Distribution, Metabolism, Excretion, and Toxicity Evaluation in Drug Discovery. 14. Prediction of Human Pregnane X Receptor Activators by Using Naive Bayesian Classification Technique. *Chem. Res. Toxicol.* **2015,** *28,* 116–125.
98. Stoll, F.; Goller, A. H.; Hillisch, A. Utility of Protein Structures in Overcoming ADME-Related Issues in Drug-Like Compounds. *Drug Discov. Today* **2011,** *16,* 530–538.
99. Atienzar, F. A.; Novik, E. I.; Gerets, H. H.; Parekh, A.; Delatour, C.; Cardenas, A.; MacDonald, J.; Yarmush, M. L.; Dhalluin, S. Predictivity of Dog Co-Culture Model, Primary Human Hepatocytes and HepG2 Cells for the Detection of Hepatotoxic Drugs in Humans. *Toxicol. Appl. Pharmacol.* **2014,** *275,* 44–61.
100. Garcia-Serna, R.; Vidal, D.; Remez, N.; Mestres, J. Large-Scale Predictive Drug Safety: From Structural Alerts to Biological Mechanisms. *Chem. Res. Toxicol.* **2015,** *28,* 1875–1887.
101. Merlot, C. Computational Toxicology—A Tool for Early Safety Evaluation. *Drug Discov. Today* **2010,** *15,* 16–22.
102. Hornberg, J. J.; Laursen, M.; Brenden, N.; Persson, M.; Thougaard, A. V.; Toft, D. B.; Mow, T. Exploratory Toxicology as an Integrated Part of Drug Discovery. Part I: Why and How. *Drug Discov. Today* **2014,** *19,* 1131–1136.
103. Hornberg, J. J.; Laursen, M.; Brenden, N.; Persson, M.; Thougaard, A. V.; Toft, D. B.; Mow, T. Exploratory Toxicology as an Integrated Part of Drug Discovery. Part II: Screening Strategies. *Drug Discov. Today* **2014,** *19,* 1137–1144.
104. Mutlib, A. E.; Gerson, R. J.; Meunier, P. C.; Haley, P. J.; Chen, H.; Gan, L. S.; Davies, M. H.; Gemzik, B.; Christ, D. D.; Krahn, D. F.; Markwalder, J. A.; Seitz, S. P.; Robertson, R. T.; Miwa, G. T. The Species-Dependent Metabolism of Efavirenz Produces a Nephrotoxic Glutathione Conjugate in Rats. *Toxicol. Appl. Pharmacol.* **2000,** *169,* 102–113.
105. Leung, L.; Kalgutkar, A. S.; Obach, R. S. Metabolic Activation in Drug-Induced Liver Injury. *Drug Metab. Rev.* **2012,** *44,* 18–33.
106. Stepan, A. F.; Walker, D. P.; Bauman, J.; Price, D. A.; Baillie, T. A.; Kalgutkar, A. S.; Aleo, M. D. Structural Alert/Reactive Metabolite Concept as Applied in Medicinal Chemistry to Mitigate the Risk of Idiosyncratic Drug Toxicity: A Perspective Based on the Critical Examination of Trends in the Top 200 Drugs Marketed in the United States. *Chem. Res. Toxicol.* **2011,** *24,* 1345–1410.
107. Lenz, E. M.; Martin, S.; Schmidt, R.; Morin, P.; Smith, R.; Weston, D. J.; Bayrakdarian, M. Reactive Metabolite Trapping Screens and Potential Pitfalls: Bioactivation of a Homomorpholine and Formation of an Unstable Thiazolidine Adduct. *Chem. Res. Toxicol.* **2014,** *27,* 968–980.
108. Peterson, L. A. Reactive Metabolites in the Biotransformation of Molecules Containing a Furan Ring. *Chem. Res. Toxicol.* **2013,** *26,* 6–25.
109. Kalgutkar, A. S.; Ryder, T. F.; Walker, G. S.; Orr, S. T. M.; Cabral, S.; Goosen, T. C.; Lapham, K.; Eng, H. Reactive Metabolite Trapping Studies on Imidazo- and 2-Methylimidazo[2,1-b]thiazole-Based Inverse Agonists of the Ghrelin Receptor. *Drug Metab. Dispos.* **2013,** *41,* 1375–1388.
110. Reilly, C. A.; Henion, F.; Bugni, T. S.; Ethirajan, M.; Stockmann, C.; Pramanik, K. C.; Srivastava, S. K.; Yost, G. S. Reactive Intermediates Produced From the Metabolism of the Vanilloid Ring of Capsaicinoids by P450 Enzymes. *Chem. Res. Toxicol.* **2013,** *26,* 55–66.
111. Foster, A. J.; Prime, L. H.; Gustafsson, F.; Temesi, D. G.; Isin, E. M.; Midlöv, J.; Castagnoli, N., Jr.; Kenna, J. G. Bioactivation of the Cannabinoid Receptor Antagonist Rimonabant to a Cytotoxic Iminium Ion Metabolite. *Chem. Res. Toxicol.* **2013,** *26,* 124–135.
112. Dansette, P. M.; Levent, D.; Hessani, A.; Bertho, G.; Mansuy, D. Thiolactone Sulfoxides as New Reactive Metabolites Acting as Bis-Electrophiles: Implication in Clopidogrel and Prasugrel Bioactivation. *Chem. Res. Toxicol.* **2013,** *26,* 794–802.
113. Bendadani, C.; Meinl, W.; Monien, B.; Dobbernack, G.; Florian, S.; Engst, W.; Nolden, T.; Himmelbauer, H.; Glatt, H. Determination of Sulfotransferase Forms Involved in the Metabolic Activation of the Genotoxicant 1-Hydroxymethylpyrene Using Bacterially Expressed Enzymes and Genetically Modified Mouse Models. *Chem. Res. Toxicol.* **2014,** *27,* 1060–1069.
114. Darnell, M.; Breitholtz, K.; Isin, E. M.; Jurva, U.; Weidolf, L. Significantly Different Covalent Binding of Oxidative Metabolites, Acyl Glucuronides, and S-Acyl CoA Conjugates Formed From Xenobiotic Carboxylic Acids in Human Liver Microsomes. *Chem. Res. Toxicol.* **2015,** *28,* 886–896.
115. Lassila, T.; Hokkanen, J.; Aatsinki, S.; Mattila, S.; Turpeinen, M.; Tolonen, A. Toxicity of Carboxylic Acid-Containing Drugs: The Role of Acyl Migration and CoA Conjugation Investigated. *Chem. Res. Toxicol.* **2015,** *28,* 2292–2303.
116. Zhong, S.; Jones, R.; Lu, W.; Schadt, S.; Ottaviani, G. A New Rapid in vitro Assay for Assessing Reactivity of Acyl Glucuronides. *Drug Metab. Dispos.* **2015,** *43,* 1711–1717.
117. Dalvie, D.; Kalgutkar, A. S.; Chen, W. Practical Approaches to Resolving Reactive Metabolite Liabilities in Early Discovery. *Drug Metab. Rev.* **2015,** *47,* 56–70.
118. Dahal, U. P.; Obach, R. S.; Gilbert, A. M. Benchmarking in vitro Covalent Binding Burden as a Tool to Assess Potential Toxicity Caused by Nonspecific Covalent Binding of Covalent Drugs. *Chem. Res. Toxicol.* **2013,** *26,* 1739–1745.
119. Gan, J.; Ruan, Q.; He, B.; Zhu, M.; Shyu, W. C.; Humphreys, W. G. In Vitro Screening of 50 Highly Prescribed Drugs for Thiol Adduct Formation—Comparison of Potential for Drug-Induced Toxicity and Extent of Adduct Formation. *Chem. Res. Toxicol.* **2009,** *22,* 690–698.
120. Higgins, J.; Cartwright, M. E.; Templeton, A. C. Foundation Review: Progressing Preclinical Drug Candidates: Strategies on Preclinical Safety Studies and the Quest for Adequate Exposure. *Drug Discov. Today* **2012,** *17,* 828–836.
121. United States Food and Drug Administration. *Guidance for Industry: Safety Testing of Drug Metabolites;* Center for Drug Evaluation and Research: Rockville, MD, 2008. Available at http://www.fda.gov/downloads/drugs/guidancecomplianceregulatoryinformation/guidances/ucm079266.pdf (accessed 2016 April 26).
122. *International Conference on Harmonisation of Technical Requirements for Registration of Pharmaceuticals for Human Use. Guidance on Nonclinical Safety Studies for the Conduct of Human Clinical Trials and Marketing Authorization for Pharmaceuticals*, M3(R2); Step 4 version, 11 June 2009. Available at http://www.ich.org/products/guidelines/multidisciplinary/article/multidisciplinary-guidelines.html (accessed 26 April 2016).
123. Gao, H.; Deng, S.; Obach, R. S. A Simple Liquid Chromatography-Tandem Mass Spectrometry Method to Determine Relative Plasma Exposures of Drug Metabolites Across Species for Metabolite Safety Assessments. *Drug Metab. Dispos.* **2010,** *38,* 2147–2156.
124. Haglund, J.; Halldin, M. M.; Brunnström, Å.; Eklund, G.; Kautiainen, A.; Sandholm, A.; Iverson, S. L. Pragmatic Approaches to Determine the Exposures of Drug Metabolites in Preclinical and Clinical Subjects in the MIST Evaluation of the Clinical Development Phase. *Chem. Res. Toxicol.* **2014,** *27,* 601–610.
125. Ma, S.; Li, Z.; Lee, K. J.; Chowdhury, S. K. Determination of Exposure Multiples of Human Metabolites for MIST Assessment in Preclinical Safety Species Without Using Reference Standards or Radiolabeled Compounds. *Chem. Res. Toxicol.* **2010,** *23,* 1871–1873.
126. Holmberg, A. A.; Ekdahl, A.; Weidolf, L. Systemic Exposure to the Metabolites of Lesogaberan in Humans and Animals: A Case Study of Metabolites in Safety Testing. *Drug Metab. Dispos.* **2014,** *42,* 1016–1021.
127. Sharma, R.; Litchfield, J.; Atkinson, K.; Eng, H.; Amin, N. B.; Denney, W. S.; Pettersen, J. C.; Goosen, T. C.; Di, L.; Lee, E.; Pfefferkorn, J. A.; Dalvie, D. K.; Kalgutkar, A. S. Metabolites in Safety Testing Assessment in Early Clinical Development: A Case Study With a Glucokinase Activator. *Drug Metab. Dispos.* **2014,** *42,* 1926–1939.
128. Li, Y.; Lai, W. G.; Whitcher-Johnstone, A.; Busacca, C. A.; Eriksson, M. C.; Lorenz, J. C.; Tweedie, D. J. Metabolic Switching of BILR 355 in the Presence of Ritonavir. I. Identifying an Unexpected Disproportionate Human Metabolite. *Drug Metab. Dispos.* **2012,** *40,* 1122–1129.
129. Ma, S.; Chowdhury, S. K. A Tiered Approach to Address Regulatory Drug Metabolite-Related Issues in Drug Development. *Bioanalysis* **2014,** *6,* 587–590.
130. Obach, R. S.; Nedderman, A. N.; Smith, D. A. Radiolabelled Mass-Balance Excretion and Metabolism Studies in Laboratory Animals: Are They Still Necessary? *Xenobiotica* **2012,** *42,* 46–56.
131. White, R. E.; Evans, D. C.; Hop, C. E. C. A.; Moore, D. J.; Prakash, C.; Surapaneni, S.; Tse, F. L. S. Radiolabeled Mass-Balance Excretion and Metabolism Studies in Laboratory Animals: A Commentary on Why They Are Still Necessary. *Xenobiotica* **2013,** *43,* 219–225.
132. Tang, H.; Mayersohn, M. Controversies in Allometric Scaling for Predicting Human Drug Clearance: an Historical Problem and Reflections on What Works and What Does Not. *Curr. Top. Med. Chem.* **2011,** *11,* 340–350.
133. Heimbach, T.; Lakshminarayana, S. B.; Hu, W.; He, H. Practical Anticipation of Human Efficacious Doses and Pharmacokinetics Using in vitro and Preclinical in vivo Data. *AAPS J.* **2009,** *11,* 602–614.

134. Sager, J. E.; Yu, J.; Ragueneau-Majlessi, I.; Isoherranen, N. Physiologically Based Pharmacokinetic (PBPK) Modeling and Simulation Approaches: A Systematic Review of Published Models, Applications, and Model Verification. *Drug Metab. Dispos.* **2015,** *43,* 1823–1837.
135. Shardlow, C. E.; Generaux, G. T.; Patel, A. H.; Tai, G.; Tran, T.; Bloomer, J. C. Impact of Physiologically Based Pharmacokinetic Modeling and Simulation in Drug Development. *Drug Metab. Dispos.* **2013,** *41,* 1994–2003.
136. Zamek-Gliszczynski, M. J.; Chu, X.; Polli, J. W.; Paine, M. F.; Galetin, A. Understanding the Transport Properties of Metabolites: Case Studies and Considerations for Drug Development. *Drug Metab. Dispos.* **2014,** *42,* 650–664.
137. Hu, Z.; Parker, R. B.; Laizure, S. C. In Vivo Information-Guided Prediction Approach for Assessing the Risks of Drug-Drug Interactions Associated With Circulating Inhibitory Metabolites. *Drug Metab. Dispos.* **2012,** *40,* 1487–1494.
138. Shirasaka, Y.; Sager, J. E.; Lutz, J. D.; Davis, C.; Isoherranen, N. Inhibition of CYP2C19 and CYP3A4 by Omeprazole Metabolites and Their Contribution to Drug-Drug Interactions. *Drug Metab. Dispos.* **2013,** *41,* 1414–1424.
139. Yu, H.; Tweedie, D. A Perspective on the Contribution of Metabolites to Drug-Drug Interaction Potential: The Need to Consider Both Circulating Levels and Inhibition Potency. *Drug Metab. Dispos.* **2013,** *41,* 536–540.
140. Yu, H.; Balani, S. K.; Chen, W.; Cui, D.; He, L.; Humphreys, W. G.; Mao, J.; Lai, W. G.; Lee, A. J.; Lim, H.; MacLauchlin, C.; Prakash, C.; Surapaneni, S.; Tse, S.; Upthagrove, A.; Walsky, R. L.; Wen, B.; Zeng, Z. Contribution of Metabolites to P450 Inhibition–Based Drug–Drug Interactions: Scholarship From the Drug Metabolism Leadership Group of the Innovation and Quality Consortium Metabolite Group. *Drug Metab. Dispos.* **2015,** *43,* 620–630.
141. Sane, R. S.; Ramsden, D.; Sabo, J. P.; Cooper, C.; Rowland, L.; Ting, N.; Whitcher-Johnstone, A.; Tweedie, D. J. Contribution of Major Metabolites Toward Complex Drug-Drug Interactions of Deleobuvir: in vitro Predictions and in vivo Outcomes. *Drug Metab. Dispos.* **2016,** *44,* 466–475.
142. Callegari, E.; Kalgutkar, A. S.; Leung, L.; Obach, R. S.; Plowchalk, D. R.; Tse, S. Drug Metabolites as Cytochrome P450 Inhibitors: A Retrospective Analysis and Proposed Algorithm for Evaluation of the Pharmacokinetic Interaction Potential of Metabolites in Drug Discovery and Development. *Drug Metab. Dispos.* **2013,** *41,* 2047–2055.
143. Fujioka, Y.; Kunze, K. L.; Isoherranen, N. Risk Assessment of Mechanism-Based Inactivation in Drug-Drug Interactions. *Drug Metab. Dispos.* **2012,** *40,* 1653–1657.
144. Döring, B.; Petzinger, E. Phase 0 and Phase III Transport in Various Organs: Combined Concept of Phases in Xenobiotic Transport and Metabolism. *Drug Metab. Rev.* **2014,** *46,* 261–282.
145. Zhang, L.; Zhang, Y.; Huang, S. M. Scientific and Regulatory Perspectives on Metabolizing Enzyme-Transporter Interplay and Its Role in Drug Interactions: Challenges in Predicting Drug Interactions. *Mol. Pharm.* **2009,** *6,* 1766–1774.
146. Zhang, D.; He, K.; Herbst, J. J.; Kolb, J.; Shou, W.; Wang, L.; Balimane, P. V.; Han, Y. H.; Gan, J.; Frost, C. E.; Humphreys, W. G. Characterization of Efflux Transporters Involved in Distribution and Disposition of Apixaban. *Drug Metab. Dispos.* **2013,** *41,* 827–835.
147. Hachad, H.; Ragueneau-Majlessi, I.; Levy, R. H. A Useful Tool for Drug Interaction Evaluation: The University of Washington Metabolism and Transport Drug Interaction Database. *Hum. Genomics* **2010,** *5,* 61–72.
148. Yu, J.; Ritchie, T. K.; Mulgaonkar, A.; Ragueneau-Majlessi, I. Drug Disposition and Drug-Drug Interaction Data in 2013 FDA New Drug Applications: A Systematic Review. *Drug Metab. Dispos.* **2014,** *42,* 1991–2001.
149. Obach, R. S. Pharmacologically Active Drug Metabolites: Impact on Drug Discovery and Pharmacotherapy. *Pharmacol. Rev.* **2013,** *65,* 578–640.
150. Grogan, J.; DeVito, S. C.; Pearlman, R. S.; Korzekwa, K. R. Modeling Cyanide Release From Nitriles: Prediction of Cytochrome P450 Mediated Acute Nitrile Toxicity? *Chem. Res. Toxicol.* **1992,** *5,* 548–552.
151. Wang, H.; Chanas, B.; Ghanayem, B. I. Cytochrome P450 2E1 (CYP2E1) is Essential for Acrylonitrile Metabolism to Cyanide: Comparative Studies Using CYP2E1-Null and Wild-Type Mice. *Drug Metab. Dispos.* **2002,** *30,* 911–917.
152. Thelingwani, R. S.; Zvada, S. P.; Dolgos, H.; Ungell, A.-L. B.; Masimirembwa, C. M. In Vitro and In Silico Identification and Characterization of Thiabendazole as a Mechanism-Based Inhibitor of CYP1A2 and Simulation of Possible Pharmacokinetic Drug-Drug Interactions. *Drug Metab. Dispos.* **2009,** *37,* 1286–1294.
153. Gong, J.; Gan, J.; Masson, E.; Syed, S.; Xia, Y. Q.; Williams, D.; Pursley, J.; Jemal, M.; Humphreys, W. G.; Iyer, R. A. Metabolic Chiral Inversion of Brivanib and Its Relevance to Safety and Pharmacology. *Drug Metab. Dispos.* **2012,** *40,* 2374–2380.
154. Loi, C.; Smith, D. A.; Dalvie, D. Which Metabolites Circulate? *Drug Metab. Dispos.* **2013,** *41,* 933–951.
155. Ballard, T. E.; Orozco, C. C.; Obach, R. S. Generation of Major Human Excretory and Circulating Drug Metabolites Using a Hepatocyte Relay Method. *Drug Metab. Dispos.* **2014,** *42,* 899–902.
156. Walker, G. S.; Bauman, J. N.; Ryder, T. F.; Smith, E. B.; Spracklin, D. K.; Obach, R. S. Biosynthesis of Drug Metabolites and Quantitation Using NMR Spectroscopy for Use in Pharmacologic and Drug Metabolism Studies. *Drug Metab. Dispos.* **2014,** *42,* 1627–1639.
157. Roffey, S. J.; Obach, R. S.; Gedge, J. I.; Smith, D. A. What Is the Objective of the Mass Balance Study? A Retrospective Analysis of Data in Animal and Human Excretion Studies Employing Radiolabeled Drugs. *Drug Metab. Rev.* **2007,** *39,* 17–43.
158. United States Code of Federal Regulations, Title 21, Part 314 Applications for FDA Approval to Market a New Drug, Section 314.50(d)(2)(iv).
159. Tse, S.; Leung, L.; Raje, S.; Seymour, M.; Shishikura, Y.; Obach, R. S. Disposition and Metabolic Profiling of [14C]Cerlapirdine Using Accelerator Mass Spectrometry. *Drug Metab. Dispos.* **2014,** *42,* 2023–2032.
160. Prakash, C.; Li, Z.; Orlandi, C.; Klunk, L. Assessment of Exposure of Metabolites in Preclinical Species and Humans at Steady State From the Single-Dose Radiolabeled Absorption, Distribution, Metabolism, and Excretion Studies: A Case Study. *Drug Metab. Dispos.* **2012,** *40,* 1308–1320.
161. Takahashi, R. H.; Choo, E. F.; Ma, S.; Wong, S.; Halladay, J.; Deng, Y.; Rooney, I.; Gates, M.; Hop, C. E. C. A.; Khojasteh, S. C.; Dresser, M. J.; Musib, L. Absorption, Metabolism, Excretion, and the Contribution of Intestinal Metabolism to the Oral Disposition of [14C]Cobimetinib, a MEK Inhibitor, in Humans. *Drug Metab. Dispos.* **2016,** *44,* 28–39.

4.02 ADME Optimization in Drug Discovery

DF McGinnity, DMPK, Oncology iMed, AstraZeneca, Cambridge, United Kingdom
K Grime, DMPK, Respiratory, Inflammation and Autoimmunity iMed, AstraZeneca, Gothenburg, Sweden

© 2017 Elsevier Ltd. All rights reserved.

4.02.1	**Introduction**	34
4.02.1.1	Absorption	34
4.02.1.2	Distribution	35
4.02.1.3	Metabolism	35
4.02.1.4	Excretion	35
4.02.2	**Optimization and Prediction of Key Human Pharmacokinetic Parameters in Drug Discovery**	36
4.02.2.1	Oral Absorption	36
4.02.2.2	Volume of Distribution	37
4.02.2.3	Human Clearance	39
4.02.3	**Summary**	42
References		43

4.02.1 Introduction

The application of pharmacokinetic (PK) principles in drug discovery and development is now widespread due to the recognition of the role of drug concentrations as a surrogate for measuring pharmacological effects. A basic tenet of pharmacology is that the magnitude of a pharmacological response is a function of the drug concentration at the site of action. Thus, the objective of therapy may be achieved by maintaining sufficient concentration of drug at the site of action for the necessary duration, yet not so high as to elicit a deleterious effect. The concentration of drug is typically measured in blood or plasma as direct measurement at the site of action is challenging.

PK is defined as the study of change of drug concentration over time and describes a systematic approach to relating dose to amount of drug in the body and is typically separated into the distinct physiological processes of absorption, distribution, metabolism, and excretion (ADME). The pharmaceutical industry is currently increasing the diversity of approaches to therapeutic intervention, including several different large molecule concepts. These are at various stages from hypothesis to clinical testing and pose interesting challenges to ADME scientists. However, this article restricts its focus on the more established ADME concepts for "traditional" small-molecule new chemical entities in drug discovery for oral therapies.

It is now recognized in the pharmaceutical industry that acceptable human PK parameters and minimized drug–drug interaction potential increase the probability of a promising candidate becoming a successful therapy. Moreover, the role of DMPK scientists in drug discovery is not to merely provide project teams with measurements and data from the plethora of DMPK related assays and models that have been developed and implemented in screening cascades over the past 10–20 years, but to develop a mechanistic understanding of the disposition of the candidate drugs toward the optimization and confident prediction of key properties associated with *human* drug absorption, clearance (CL), distribution, and elimination. This is achievable from a consideration of physicochemical properties and data from in vitro assays with human-derived material and from in vivo animal studies. This article is targeted at medicinal chemists and drug design teams and provides general definitions of fundamental PK parameters together with characterization, prediction, and optimization strategies employed at AstraZeneca.

4.02.1.1 Absorption

The route of administration for potential therapies is an important consideration in drug discovery. The oral route is most common and favored because of convenience and patient preference and is the focus of this article. Oral absorption can be defined as the irreversible transfer of a drug from the gut lumen across the mucosal membranes of the gastrointestinal tract. This is just one step in a multifaceted process, which transfers a drug from the site of administration (ie, mouth) to the systemic circulation. The active pharmaceutical ingredient (API), typically administered through the mouth using tablets or capsules, needs to get dissolved in the gastric fluids where prior to the absorptive step it may be degraded by the acidic pH of the gastric fluid and the enzymatic activity of the gut flora. The small intestine is the primary site of absorption due to its high surface area, drug permeability properties, and high blood flow. Additionally, drug movement through the gastrointestinal membranes is dependent on the physicochemical properties of the drug molecule. Drugs may be transported passively, via the transcellular route, that is, through the cell, passing through both apical and basolateral membranes, or the paracellular route, that is, between the cells. The majority of drugs are absorbed transcellularly since paracellular permeability through water-filled tight junctions between cells decreases significantly

with increasing molecular size (> 250 Mwt) and lipophilicity (logP > 0).[1] Absorption may also be facilitated or hindered by uptake and efflux transporter proteins.

It is important for the medicinal chemist to be able to differentiate the definitions of absorption versus oral bioavailability (F), which is the fraction of the dose of administered drug that reaches, in an unchanged form, the systemic circulation and is a measure of a compounds' ability to avoid all the processes that protect the body from exposure to xenobiotics. These processes include the physical barrier of the gut wall, active transport into the gut lumen, metabolism in the gut, metabolism in the liver, and biliary elimination. Thus, F is a product of the fraction of dose that is absorbed through the gut and the fraction of drug that escapes elimination by the intestinal tract and liver, the so-called "first-pass" elimination. High extraction drugs that are rapidly metabolized will have low systemic exposure following an oral dose and low F, whereas low extraction drugs that are relatively stable to metabolism, assuming they are absorbed across the gut wall, will have high systemic exposure following an oral dose and high F. Bioavailability is estimated from $F = AUC_{oral}/AUC_{IV}$, for an equivalent dose. Thus there exists interplay between the physiology of gastrointestinal tract and compounds' biopharmaceutical, physicochemical, and structure–activity properties with drug metabolizing enzymes (DMEs) and transporters, which are required to be understood to facilitate optimization of new chemical entities to enable acceptable oral absorption and bioavailability.

4.02.1.2 Distribution

Drug distribution describes the reversible transfer of drug from one location to another. For an orally administered drug, distribution occurs from the bloodstream into the interstitial and intercellular fluids. Volume of distribution (V_d) is the theoretical volume that would have been available for the drug to disperse everywhere in the body were it at the same concentration as in blood and can be derived following intravenous (IV) administration. A measured dose is administered and drug levels in plasma are determined over time. Early concentrations are back-extrapolated to estimate the concentration at $t = 0$, and simple mass balance considerations allow estimation of the volume that the dose would have to be distributed in to yield that concentration. This is the initial volume of distribution (with units of L or L kg^{-1}). If there is a mono exponential decline in plasma concentrations, this is the V_d. V_d is most usefully thought of as a measure of the relative affinity of the compound for tissues over the sampled blood or plasma, and hence the ratio of the total amount of drug in the body to the concentration in the blood. The volume term that most accurately describes this measure, for multiexponential profiles, is the volume of distribution at steady state (V_{ss}), since this is an estimate of drug distribution independent of elimination processes (steady state referring to the pseudo-equilibrium achieved between drug entering the tissues from the systemic blood and drug being eliminated from the body).

4.02.1.3 Metabolism

Xenobiotic metabolism can be defined as chemical transformation by a biological system usually via DMEs, which typically converts relatively lipophilic compounds into more readily excreted hydrophilic metabolites. Drug metabolites may be pharmacologically active, weakly active, inactive, or indeed reactive with endogenous macromolecules. The liver is the principal site of drug metabolism; moreover, hepatic metabolic CL is the predominant elimination route for oral marketed drugs.[2] The most important drug metabolism enzyme family is cytochrome P-450, a superfamily of membrane-bound isoenzymes that catalyses the oxidation of many drugs. In addition to oxidation, reduction and hydrolysis are common xenobiotic metabolism pathways and conjugation with endogenous polar substrates such as glucuronic acid and glutathione may occur directly to the parent molecule or subsequent to an initial transformation.

CL is the parameter that best describes the efficiency of the eliminating process. The area under the plasma concentration-time profile (AUC) for a given dose is a measure of how efficiently a compound is removed from the body. Compounds yielding low AUCs are eliminated by efficient processes. This ratio (Dose/AUC) is used to derive the CL of a compound and has units of flow (mL $min^{-1}kg^{-1}$). CL relates the rate of elimination (ng min^{-1}) to the substrate concentration (ng mL^{-1}), that is, CL = Rate of elimination/[Substrate]. CL has units of flow, and can be related to physiological parameters such as organ blood flows. A CL to hepatic blood flow ratio of 1:2 means 50% of drug is extracted in a passage through the liver.

4.02.1.4 Excretion

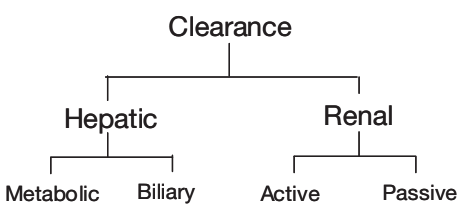

Metabolism together with renal and biliary excretion are the major drug elimination routes in humans and preclinical species. CLs are additive, if the processes are parallel. As human glomerular filtration rate (GFR) is only ~ 1.7 mL min^{-1} kg^{-1} and as the majority of drugs are, to various extents, bound to plasma proteins, CL via renal elimination is typically low whereas biliary excretion can be an important route of elimination and remains challenging to predict to man.

An important PK parameter obtained from a simple fit of IV data is the half-life ($T_{1/2}$). Of course multiexponential plasma drug concentration-time profiles have half-lives associated with each exponential phase of the decline (where the $T_{1/2}$ is ln(2)/exponential rate constant). The simplest case is often a profile that has an initial drug distribution phase (where the drug is subject to elimination but the major process is distribution from the central systemic circulation into the tissues) and an elimination phase (in which the majority of the drug in the body is eliminated). It is this latter phase that accounts for the largest proportion of the AUC (since the drug is being eliminated) and approximates to $\ln(2) \times V_{ss}/CL$. This is only the terminal $T_{1/2}$ if there is no later phase observed in the dose interval. Further phases of the plasma profile can occur beyond the elimination phase when, for example, the drug distributes into tissues or body compartments that release the drug with a rate lower than the elimination rate. This is typically true for lipophilic or basic drugs that have good distribution properties, but not for acidic drugs that do not distribute extensively beyond the plasma. The most important $T_{1/2}$ depends on the key phase of the profile for maintaining the drug concentration above the level required for efficacy. Generally the elimination $T_{1/2}$ is the most important, as it describes the decrease in plasma concentration associated with the largest proportion of the AUC and therefore largest drop in plasma (or blood) concentration of drug. This $T_{1/2}$ is consequently often the most influential in maintaining the drug concentration above the required minimum effective concentration. $T_{1/2}$ does not describe the efficiency of eliminating processes (this is CL) but is related to CL by the equation $T_{1/2} = \ln(2)V_d/CL$. As there is only one value for CL, each $T_{1/2}$ is associated with a different distribution volume (eg, initial, V_0; steady state, V_{ss}; terminal, V_z) and can be modulated accordingly by changing the V_d or CL.

After identification of a relevant druggable target, maximizing the likelihood of a chemical series yielding a candidate drug that subsequently becomes a marketed therapy can be achieved by optimizing potency and selectivity for the target protein together with a strategy that achieves an adequate PK profile in patients with minimal drug–drug interaction potential. A drug discovery approach of optimizing key properties in parallel while not guaranteeing, undoubtedly maximizes the probability of success. What can assist in this difficult, and at times seemingly insurmountable, challenge is that the key PK parameters of drugs are often strongly associated with their inherent physicochemical properties. Understanding these relationships is a key element of drug design. The most important physicochemical properties, in this context, are molecular size, hydrophobicity, aqueous solubility, and ionization state at physiological pH. These properties, to a greater or lesser extent, effect dissolution in the gastrointestinal tract and membrane permeability (and therefore oral absorption), susceptibility to DMEs and other elimination processes.

The sections below outline the authors' view of current best practice for optimizing and predicting the key ADME parameters in man. It is intended to be a practical guide directing both optimization strategies and mechanistic understanding for ADME properties in drug discovery and development. There are many literature sources that provide more fundamental information. The authors can strongly advocate *Metabolism, Pharmacokinetics and Toxicity of Functional Groups* edited by Dennis Smith[3] and for a comprehensive analysis of PKs and full derivation of equations the authoritative reference *Clinical Pharmacokinetics* by Rowland and Tozer[4] is recommended.

4.02.2 Optimization and Prediction of Key Human Pharmacokinetic Parameters in Drug Discovery

Both human PK and clinically efficacious dose may be estimated from in vitro experiments utilizing human-derived material and by in vivo animal studies. Prediction of clinical dose is a useful parameter in the optimization of compounds as a holistic measure of "quality" that relies on both human PK estimates and of the anticipated therapeutic concentration.[5] The prediction and refinement of therapeutic concentrations in relevant patient populations is vital. It is built on the foundation of a quantitative understanding between target engagement and relevant biomarkers, from an integrated assessment, in which the pharmacology and the role of the biological target in the pathophysiology of the disease are considered to establish an exposure profile most likely to deliver clinical efficacy. Thus pharmacokinetic–pharmacodynamic relationships should be derived from clinical precedents, preclinical PD, or disease models and mechanistic studies of the drug target interaction, and refined throughout the life of a project. The optimization and prediction of human PK and likely efficacious clinical dose are essential elements of drug discovery projects.[5]

In addition to potency and selectivity against the target, the focus for drug design teams with respect to PK optimization strategies should be on the influential parameters, F_{abs}, CL, and V_{ss}. Establishing a set of quantitative criteria for these parameters upfront in programs facilitates optimization toward, and discovery of, a promising candidate drug as rapidly and efficiently as possible. A PK property that remains challenging to determine is the free concentration of drug at the site of pharmacological action, which is dependent on the involvement of drug transporters, a rapidly developing yet still immature area of ADME science. The next sections outline the authors' experience and view of current best practice for predicting the key PK parameters for man.

4.02.2.1 Oral Absorption

Interpatient variability in drug exposure is inversely related to bioavailability,[6] and therefore absolute bioavailability in man of greater than 30% is an appropriate target for acceptable intersubject variability, and effect on dose size. As F is a product of the

fraction of absorbed drug, the fraction escaping intestinal metabolism and liver extraction as it passes from the portal vein to the systemic circulation ($F = F_{abs} \times F_g \times F_h$) targeting a human absorption of >50% is appropriate.

It is important to understand the relevance of the contribution of first-pass hepatic and intestinal metabolism, and of intestinal permeability and not just determine F in preclinical species. As animal in vivo PK may poorly predict human kinetics, good PK properties in animals per se are not necessarily a sign of quality in molecules, likewise a low animal bioavailability value and/or suboptimal PK profile is not necessarily an indicator of poor human PK. The real value of animal PK data is to validate, or otherwise, the approaches that are used to predict PK in man. Fundamentally, low bioavailability in animals may impact in limiting exposure in preclinical PD, efficacy, and safety testing.

An assessment of the role of intestinal drug extraction is a component of the human F prediction. Intestinal DMEs are well characterized with CYP3A, CYP2C9, and Uridine 5′-diphospho-glucuronosyltransferase (UGT) predominating.[7–12] Mathematical modeling can enable in vitro data to be used in the prediction of F_g[13] and extraction by the intestine can be similar to, or exceed, hepatic extraction, despite much less intestinal compared to hepatic cytochrome P450 (CYP).[13–17] Intestinal extraction is typically associated with metabolically unstable drugs. Efficient location of DMEs including CYP3A4 and p-glycoprotein efflux transporter (which also share substrate specificity), in the villus tip of enterocytes, facilitates cycling of drugs prolonging exposure and, therefore, intestinal metabolism.[13,14,18,19] Drug properties associated with limited permeability and being substrates for efflux transporters and DMEs are required to be efficiently extracted by the intestine. If optimization strategies early in the drug discovery process are efficient at mitigating these properties, intestinal metabolism should rarely be a significant issue for candidate drugs.

Optimizing toward compounds with appropriate physicochemical properties that ensure sufficient solubility of crystalline API and transmembrane permeability should maximize oral absorptive potential of candidate drugs. The apparent permeability measure (P_{app}) is typically obtained from assessment of drug flux across a monolayer of cells intended to mimic the intestinal barrier, most commonly determined using Madin–Darby canine kidney or Caco-2 cell lines.[13,20] P_{app} values are transformed into effective permeability (P_{eff}) values, describing intestinal permeability per unit surface area, as a prerequisite to develop relationships between in vitro permeability and human absorption.[13,21]

It is now widely accepted that efflux by p-glycoprotein or other intestinal drug transporters is unlikely in most cases to limit absorption of drugs with good permeability and solubility.[22,23] However, in vitro p-glycoprotein dependent efflux can be clinically relevant if the K_m between substrate-p-glycoprotein is high (>10s of μM) and/or the dose is low (<1 mg kg^{-1}).[24] The intestinal drug concentration range sufficient for interacting with p-glycoprotein may be estimated from the maximum dose taken per 250 mL (intestinal fluid volume) or alternatively, via an estimation of the maximum concentration in the enterocyte ($F_{abs} \times k_a \times \text{Dose}/Q_{ent}$) where Q_{ent} is enterocyte blood flow.[13,19]

In our laboratory, a solubility–permeability heat map has been generated and is used as a visual and simple tool, which demonstrates for a 1 mg kg^{-1} dose, a fraction absorbed in man of >50% requires a crystalline solubility of 100 μM and a Caco-2 P_{app} of 5×10^{-6} cm/s.[25] Especially for compounds that have borderline physicochemical properties, supplementary dynamic simulations incorporating measured in vitro permeability and dissolution rate measures, such as commercial software as Gastroplus® or SimCYP®, validated with known clinical data, are valuable at providing additional information for decision making.[24,26,27] Indeed more generally, physiologically based pharmacokinetic modeling approaches have great utility in the prediction and simulation of PK profiles, including the potential for assessing likely variability in man.

In oral drug discovery programs, an estimate of rat oral bioavailability is likely important for determining if safety or PD/efficacy studies can be adequately performed, yet poor oral absorption in the rat should not per se preclude progression of compounds. In our experience rat oral absorption is, generally, not a good predictor of human absorption.[5] This is most likely explained, at least in part, by the fact that once normalized for body surface area, the rat small intestine has a four-times lower surface area compared to human.[28] Predicting human absorption from preclinical in vivo data is more successful using dog as a model, since the dog to human absorption correlation appears strong for high molecular weight (>325) compounds, when absorption is not by the paracellular oral route (**Fig. 1**, adapted from McGinnity et al.[5]). In our experience, for drugs absorbed by the transcellular route, not only does dog PK data indicate a systematically greater absorption than in rat but also that dog absorption, using crystalline API and an appropriate formulation, is more akin to human. Good oral drug-like physicochemical properties providing sufficient aqueous solubility of the crystalline form and passive transcellular permeability can support a confident and acceptable human absorption prediction of >50%, which can be further strengthened by good in vivo absorption in the dog.

4.02.2.2 Volume of Distribution

V_d is a measure of the relative affinity of a drug for tissues and plasma, thus correlating with the relative affinity of compound for tissues. This is expressed by the equation $V_d = [fu_p/fu_T] \times V_T + V_P$, with units of L kg^{-1}, where fu_p is the unbound drug fraction in the plasma; fu_T is the unbound drug fraction in the tissue; V_T is the volume of the tissue (~1 L kg^{-1}); and V_P is the volume of the plasma (0.03 L kg^{-1}). As $V_T \gg V_P$, changes in fu_p will directly affect V_d.[4] Moreover, Oie and Tozer's approach defines the key driver of interspecies differences in V_d to be differences in ppb on the assumption that interspecies differences in tissue binding are minimal.[29] Using preclinical in vivo PK data and correcting for species ppb differences, V_d or V_{ss} as the most predictable of PK parameters: if unbound volumes are consistent across species, human volume can be predicted from animal data, by estimating V_u (**Fig. 2**). Based on our experience unbound V_{ss} is usually conserved within twofold across species.

In general bulk physicochemical properties rather than specific pharmacophores determine V_d values, albeit transporters can modulate distribution into and out of tissues. Typically, for drug-like molecules, acids have low (<1 L kg^{-1}), neutrals and

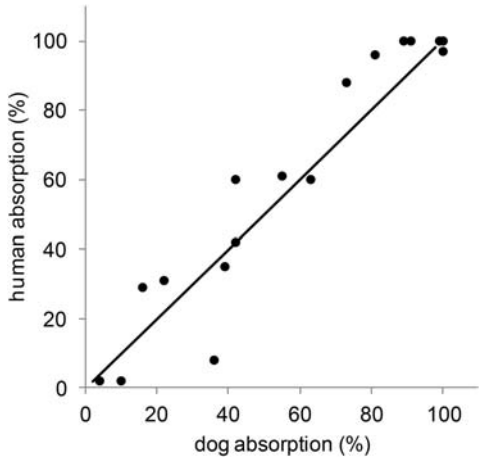

Fig. 1 Relationship showing correlation between human absorption and dog absorption for compounds with Mwt >325. Shown is the line of unity. Figure adapted with permission from McGinnity, D.F., Collington, J., Austin, R., Riley, R. Evaluation of Human Pharmacokinetics, Therapeutic Dose and Exposure Predictions Using Marketed Oral Drugs. *Curr. Drug Metab.* **2007**, *8*, 463.

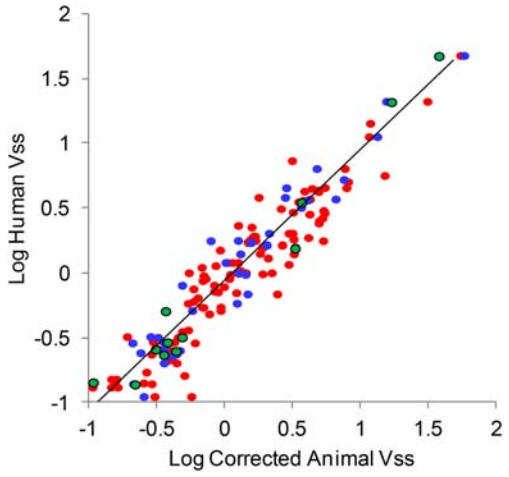

Fig. 2 Using preclinical species to predict human V_{ss}.[5] Relationship between human V_{ss} values and preclinical animal V_{ss} values corrected for human/animal differences in ppb as detailed in McGinnity et al., 2007.[5] The dataset includes both data generated in this laboratory and literature data from rat (red circles), dog (blue circles), and mouse (green circles) and compared to clinical V_{ss}. Line of regression shown with the equation $\log y = 1.\log x + 0.06$, $r^2 = 0.93$, $p = 4.6 \times 10^{-101}$, afe = 1.36. Thus human V_{ss} can be predicted from preclinical animals using Eq. (1). Figure adapted with permission from McGinnity, D.F., Collington, J., Austin, R., Riley, R. Evaluation of Human Pharmacokinetics, Therapeutic Dose and Exposure Predictions Using Marketed Oral Drugs. *Curr. Drug Metab.* **2007**, *8*, 463.

zwitterions moderate (1–3 L kg^{-1}), and bases high (>3 L kg^{-1}) steady state V_d values (Fig. 3). Basic drugs tend to have similar ppb to neutral drugs, in contrast to acids that show higher binding even for a given $\log D_{7.4}$.[30] The overriding influence on the distribution of acidic drugs is that of extensive binding to albumin in plasma. Apparent distribution volumes thus approach that of albumin, approximately 0.1 L kg^{-1} and do not typically exceed 0.3 L kg^{-1} unless active hepatic uptake or entero-hepatic recirculation is a factor. Recirculation of parent drug after elimination in bile (of parent or glucuronide that can be hydrolyzed to parent in the gastrointestinal tract) can lead to an extended PK profile and a larger apparent V_{ss}. Moreover, this can yield incorrect predictions if extrapolating to a species where recirculation does not occur to same extent. The V_d for neutral drugs is governed by hydrophobic interactions with plasma proteins and tissue membranes. Increasing lipophilicity raises tissue affinity but also has the counter effect of restricting tissue distribution due to an increase in ppb. Being positively charged at physiological pH, bases have favorable interactions with anionic phospholipid head groups leading to higher tissue affinity and therefore for the same ppb as a neutral compound, a base will tend to have a higher tissue distribution.[31] Ion trapping in lysosomes, subcellular acidic organelles abundant in liver and lung, also contribute.[32] V_d is not by itself a parameter that should be optimized in drug discovery, rather estimates of the boundaries of V_d for a given chemical series can be transformed into a strategy for obtaining the necessary human elimination $T_{1/2}$ via optimizing the elimination processes toward a target CL value.

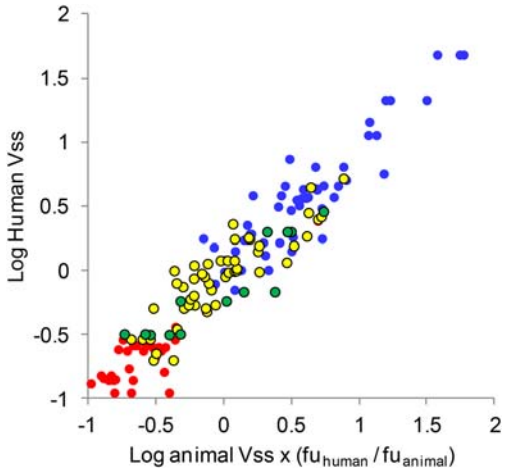

Fig. 3 Using preclinical species to predict human V_{ss} for compounds with a range of physicochemical properties. Relationship between human V_{ss} values and preclinical animal V_{ss} values corrected for human/animal differences in ppb. *Red circles* are acids, *green*–zwitterions, *yellow*–neutrals, and *blue*–bases. Same data included in **Fig. 2** and McGinnity et al., 2007.[5]

V_{ss} is reasonably predictable from physicochemical properties, in silico approaches[33,34] and in vitro data.[35–37] However the Oie and Tozer method from preclinical species PK appears superior for making human predictions, as demonstrated by several laboratories.[38–40] via Eq. (1). Also as determination of PK profiles is required for several reasons in at least two species before clinical candidate selection, this is the preferred predictive methodology in our laboratory for candidate drugs.

$$log\left(V_{ss_{human}}\right) = log\left(V_{ss_{animal}}\frac{fu_{human}}{fu_{animal}} + 0.1\left(1 - \frac{fu_{human}}{fu_{animal}}\right)\right) - 0.06 \quad (1)$$

4.02.2.3 Human Clearance

Identification of the elimination route and rate in preclinical species and optimization of human CL are major challenges and goals of most drug discovery projects. The major drug CL routes in humans and preclinical species are metabolic, biliary, and renal and as there is currently no reliable way to predict human elimination from purely in silico or in vitro methods, a combination of determining CL routes in preclinical species and use of in vitro human tools is required to predict human CL.

Liver is the major xenobiotic metabolizing organ and it is now widely accepted that in vitro–in vivo extrapolation (IVIVE) can be used to estimate hepatic metabolic CL in human and animals, via in vitro determination of rates of turnover and a mathematical liver model.[41–45] The model describes hepatic metabolic CL (CL_H), via terms for liver blood flow (Q_h), hepatic intrinsic clearance (CL_{int}), and blood binding (fu_b). Hepatocytes are the optimal in vitro system for predicting in vivo metabolic hepatic CL, as they contain the full complement of DMEs and transporters. However, data from subcellular liver fractions such as microsomes that define the oxidative metabolic component, and that have a larger dynamic range than hepatocytes, can add value by increasing the mechanistic understanding of the primary metabolic pathways for chemical series and key compounds. Both hepatic microsomes and hepatocytes are used routinely for this purpose in our laboratory. A panel of recombinant heterologously expressed CYPs can also be used to predict metabolic CL and to determine the individual CYPs responsible for the metabolism of key compounds. This information is important to understand likely variability of CL in the population associated with metabolism via polymorphic CYPs, potential intestinal CL contributions (eg, if via CYP3A and 2C9), and to determine the risk of drug–drug interactions as victims of coadministered inhibitors of the CYPs involved. There is less drug–drug interaction risk associated with compounds that are cleared via multiple CYPs and other elimination routes. For this latter reason alone, it is important to attempt to quantify all elimination pathways as far as possible.

Predicting in vivo hepatic metabolic CL involves initially building in vivo–in vitro CL_{int} models for each species using a training set of compounds with estimated in vivo hepatic metabolic CL values, via subtracting nonhepatic metabolic CL from total CL values. Hepatocyte CL_{int} is measured and fraction unbound in the incubation (fu_{inc}) incorporated to calculate unbound in vitro CL_{int}, which is scaled up to a whole liver unbound CL_{int}.[46] To establish prediction accuracy, the unbound in vivo CL_{int} of the test compound is calculated from in vivo hepatic metabolic CL adjusted for in vivo blood binding. The derived unbound in vitro and in vivo CL_{int} values form a line of correlation from which estimations of unbound in vivo CL_{int} values for test compounds can be made after determination of in vitro CL_{int}.[41,42,44,47] Evaluation of the predictive accuracy for the test compound is made against the linear relationship of unbound in vitro versus in vivo CL_{int}, not CL.

Fig. 4 and the regression equation in the legend demonstrate the approach, using all the in vitro measured terms on the X-axis and predicting in vivo CL_{int} from the Y-axis. This in vivo CL_{int} is put back through the Well Stirred Model equation ($CL_H = CL_{int} \cdot Q / CL_{int} + Q$) to predict human CL_H. As can be observed from **Fig. 4**, this approach yields a systematic under prediction of in vivo CL_{int}

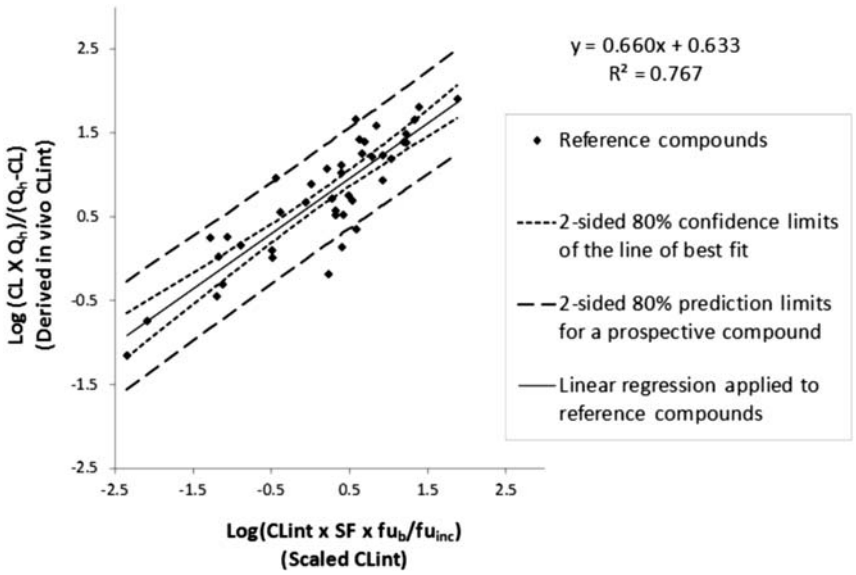

Fig. 4 Human hepatocyte regression line comparing in vitro CL_{int} with in vivo CL_{int} with all in vitro variables grouped together on *x*-axis. Figure adapted with permission from Sohlenius-Sternbeck, A.K., Jones, C., Ferguson, D., Middleton, B.J., Projean, D., Floby, E., Bylund, J., Afzelius, L. Practical Use of the Regression Offset Approach for the Prediction of in vivo Intrinsic Clearance From Hepatocytes. *Xenobiotica* **2012**, *42*, 841.

for reasons not yet mechanistically understood, although several rational explanations have been proposed. However, it is important to realize that this under prediction factor, corrected via use of the regression line, is associated with the assay not the compounds and is observed across several laboratories and species and using both hepatic microsomes and hepatocytes.

If the unbound in vivo CL_{int} has been accurately predicted in animals, typically rat and dog, the approach can be used in human with confidence that a similar relationship may apply. Moreover, if rat and dog hepatic metabolic in vivo CL_{int} cannot be predicted from in vitro data there should be little confidence that a similar approach will predict human CL_{int}. Importantly for candidate drugs, a quantitative mechanistic understanding of rates and routes of elimination pathways in human-derived in vitro milieu and preclinical species is critical to increase the likelihood of successful prediction of rates and routes in human.

In our laboratory the instances of "lack of scaling" of in vitro to in vivo CL_{int} in chemical series or key compounds are relatively frequent and require a systematic approach to investigate the possible causes of such disconnects. It is advisable that the first step should always be a close examination of existing in vitro CL_{int} and in vivo PK data as several experimental and/or biological phenomena may have led to an under or over estimation of in vitro or in vivo CL_{int}. An understanding of the known rates, and metabolic and excretion routes, from structurally related compounds may then provide mechanistic clues and a systematic in cerebro and experimental investigation of the key in vitro measured terms CL_{int}, *B*:*P*, ppb, and fu_{inc} can follow. Often discovering the cause of poor CL predictions adds to the mechanistic understanding of the compounds disposition, which may increase, or indeed decrease, the confidence in an accurate human CL prediction.

Consideration of significant extra-hepatic metabolic CL may include experimental identification of the enzymes responsible for metabolism. These may include amidases, esterases, amine oxidases, and transferases, for example, and experiments using hepatic and nonhepatic subcellular fractions and blood or plasma can be useful. Plasma hydrolysis of drugs can be scaled to whole body CL from in vitro data by multiplying the measured in vitro elimination rate constant ($\ln(2)/T_{1/2}$) by the volume of plasma. Unless the rate is rapid, hydrolysis solely in plasma is unlikely to be a major CL pathway but hydrolysis can occur at a number of sites throughout the body and the cumulative CL can thus be both high and challenging to estimate. Indeed for compounds cleared via DMEs other than the CYPs or UGTs on which the IVIVE approaches have been predominantly validated may require additional experimentation and refined methodologies can be applied as appropriate.

A common misconception is that high ppb is to be avoided or designed away from and decreasing ppb will result in a lower efficacious dose through the generation of higher circulating free drug concentrations available to the pharmacological target. However, this neglects the fact that decreasing ppb also results in higher CL. Thus for most drugs, decreasing ppb has no effect on the in vivo unbound drug concentration. The $T_{1/2}$ is, in most cases, also largely unaffected, since CL and V_d are impacted similarly by ppb changes. The only notable exception to this is when ppb is so high that drug distribution volume is restricted to that of plasma proteins. At this lower limiting value for V_d, increasing ppb further does indeed lower CL but with V_d unaffected, $T_{1/2}$ increases. These concepts are elegantly and comprehensively outlined in Smith DA et al.,[31] which provides guidance on the use of ppb in drug discovery. Therefore the focus should be on physiochemical parameters such as logP, pKa, and PSA or structural modifications based on knowledge of the metabolically liable functional groups to affect a change in CL, to optimize free drug concentration.

Renal excretion of untransformed compounds can be complex and may involve both passive and active components. The high pressure and relatively large pores in the glomerulus result in free drug in blood entering the proximal tubule. The filtration rate, as a CL, is the product of the compound's fraction unbound in blood and GFR (approximately 1.7 mL $min^{-1} kg^{-1}$ in human), and thus can be readily estimated. As the majority of drugs are highly bound to blood proteins, passive renal CL is low in particular relative to hepatic CL. Furthermore, only compounds with negative $logD_{7.4}$ values are passively renally cleared to any extent as the kidney tubules passively reabsorbs molecules of sufficient lipophilicity back into the blood.[48] Uptake transporter proteins may recover compounds if sufficient structural similarities exist to their physiological endogenous substrates. Active renal secretion consists of uptake across the basolateral membrane of the proximal tubule then egress across the apical membrane via combinations of different transporters polarized to the apical or basolateral membrane. In man, the principal transporters in the basolateral membrane are organic anion transporters OAT1 and OAT3 and organic cation transporter OCT2 are whilst the apical transporters include P-glycoprotein, breast cancer resistance protein (BCRP), multidrug resistance protein (MRP2, MRP4), organic anion transporters OAT4 and URAT1, and organic cation transporters OCTN1, OCTN2, and MATE-1.[49] Intuitively, transporter dependent renal CL is likely to be less predictable across species than when flow dependent passive processes predominate. However, in our laboratory, a reasonable prediction using dog renal CL corrected for ppb and kidney blood flow species differences emerged for a diverse set of 36 actively secreted drugs, forming the basis of our approach to predicting renal CL in human for candidate drugs (**Fig. 5**).[50] Male rat renal CL correlated less well with human possibly due to poor species crossover for OAT substrates or sex differences for rat organic anion transporting polypeptide (oatp) substrates.[50–52] The continued development of human-derived in vitro models for the prediction of active human renal CL and kidney transporter mediated drug–drug interactions is an area of ongoing research in our laboratory and others.

Biliary excretion is an important elimination route but in part due to the lack of high quality definitive clinical data there remains no consensus on the best practice strategy to predict human biliary CL and human-derived in vitro models are still in active development.[43,53,54] As for renal elimination, biliary excretion of drugs can be a two-step process involving the hepatic uptake transporters OATP, OAT, and OCT and bile canalicular efflux transporters P-gp, BCRP, MRP1, and MRP2.[55–58] High biliary CL is most often observed with acids, likely due to synergy between OATP and MRP transporters. In the authors' laboratory, rat, dog, and human biliary CL data from drugs of different chemotypes and therapeutic classes were compared (**Fig. 6**).[59] For the majority of the compounds studied, rat unbound biliary CL values, when corrected for body weight and ppb differences, were >10-fold higher than the human value with some >100-fold. Interestingly, these compounds appeared to be substrates for hepatic uptake OATP transporters. This is in line with the observation that rat uptake transporters are typically more efficient than the human and dog counterparts.[60,61] Albeit based on relatively few compounds, dog biliary CL when corrected for body weight and ppb differences appears to be more comparable to human than rat. However, for drugs that seemingly have no significant active hepatic uptake component, rat, dog, and human biliary CL were similar.

In the literature, several interspecies allometric scaling methodologies for biliary CL have been evaluated,[54,62,63] but a consensus is not apparent, likely due to the relatively few compounds analyzed, the fact that some used total drug related material rather than parent and that allometry underpredicts human biliary CL for some compounds but not others.[64,65] Simple allometry using unbound CL and an exponent of 0.66 gave the best predictions of 18 drugs between rat and human.[66] Human predictions were within threefold of observed values for 12 of the compounds, yet for others human CL was overestimated by one to two orders

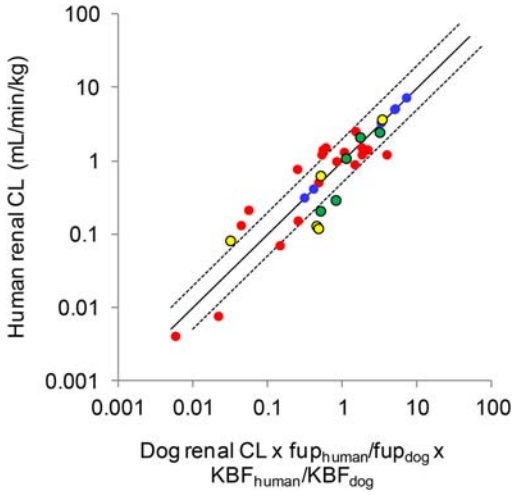

Fig. 5 Relationship between human renal clearance and dog renal clearance corrected for human/dog differences in ppb and kidney blood flow. *Red circles* are acids, *blue*–bases, *yellow*–neutrals, and *green*–zwitterions. Figure adapted with permission from Paine, S.W., Menochet, K., Denton, R., McGinnity, D.F., Riley, R.J. Prediction of human renal clearance from preclinical species for a diverse set of drugs that exhibit both active secretion and net reabsorption. *Drug Metab. Dispos.* **2011**, *39*, 1008.

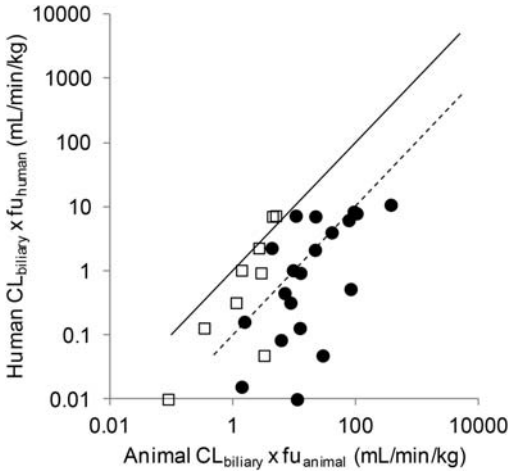

Fig. 6 Relationship between unbound human biliary clearance and unbound rat (*solid circles*) and unbound dog (*open squares*) biliary clearance. Figure adapted with permission from Grime, K., Paine, S.W., Species differences in biliary clearance and possible relevance of hepatic uptake and efflux transporters involvement. *Drug Metab Dispos.* **2013**, *41*(2), 372–378.

of magnitude. Compared to rat alone, multiple species allometry using biliary CL data corrected for ppb yielded improved predictions.[66]

Intuitively, because CL predictions require several input parameters (hepatocyte CL_{int}, extra-hepatic CL_{int}, renal and biliary CL, ppb, in vitro incubational binding, and B:P), human estimates are more uncertain than for oral absorption or V_{ss}. In summary, human CL can be predicted as follows: Human hepatic metabolic CL from human hepatocyte CL_{int}, human renal CL from dog renal CL, and human biliary CL tentatively estimated from the dog or rat biliary CL for non-OATP substrates. Both prediction of renal and biliary CL remain important challenges from human-derived in vitro tools. Publications from Pfizer, J&J, and GSK[67,68,40]confirm the authors' view that allometric scaling approaches offer fairly poor predictivity of human CL, in particular for metabolic CL where there may be clear species differences in metabolic rates and routes. However, for a key candidate drug an allometric prediction in agreement with the more mechanistic and validated approaches presented here may increase the confidence in that human CL prediction, thus adding value to decision making.

4.02.3 Summary

AstraZeneca drug project teams use a five-dimensional framework to maximize the probability of project success and pipeline quality, described as the five 'R's: the right target, right patient, right tissue and exposure, right safety, and right commercial potential.[69] Under this overarching framework, the focus of AstraZeneca drug design teams, with respect to clinical PK optimization, are on the key parameters that support PK profiles CL, V_{ss}, and F_{abs}, underpinned by an understanding of the candidate drug's exposure–effect relationship.[70] Other parameters such as those related to mitigating against drug–drug interactions are incorporated as necessary.

As outlined above, PK parameters have strong interdependencies with the physicochemical properties of compounds, and thus optimizing these fundamental properties may be a focus for project teams. However, a recent and extensive analysis of the relationship between physicochemical properties and drug attrition concluded further refinement of physicochemical properties within the oral drug-like space is unlikely to have a significant effect on attrition rates for small-molecule drug candidates.[71] Moreover, it is critical, in the authors' view, to develop as full a mechanistic understanding of the ADME disposition properties of key candidate drug(s) during drug discovery via detailed experimentation and thorough investigations to optimize toward a candidate drug with acceptable human PK profile and attain a sufficient degree of confidence in the predicted clinical PK parameters to make informed investment decisions. PK is complex and all predictions are fraught with uncertainty and somewhat paradoxically the establishment, in the last two decades, of a plethora of in silico methods, in vitro screens, and in vivo models could lead to a box-ticking checklist approach to drug discovery, generating in our opinion only a superficial understanding of the compounds disposition properties. Excellent ADME science contribution to drug design teams requires additional in cerebro and experimental application by experienced and expert scientists. Furthermore, the limitation of predictive accuracy should be appreciated. It is commonly and subjectively accepted within the DMPK community that a prediction within twofold of the measured value is a success. However, a successful prediction of individual parameters may not equate to a successful prediction of clinical dose and exposure due to the cumulative impact of twofold errors in CL and V_{ss} predictions on $T_{1/2}$, exposure, and dose.[5] This understanding of uncertainty and risk explains, for example, why for once daily dosing of a candidate drug, a human $T_{1/2}$ prediction of approximately 16 h is desirable, if drug effect is related to trough concentration, since being twofold out in

either direction elevates the dose and C_{max} by only twofold for a 8 h $T_{1/2}$ or results in only a fourfold accumulation from single dose to steady state for a 32 h $T_{1/2}$.

Based on a robust understanding of the interdependencies between physicochemical properties and key PK parameters and with targeted experimentation using well validated assays and models as a foundation, together with bespoke experiments designed to test specific hypotheses, an ADME optimization strategy toward clinical candidates with an acceptable clinical PK profile is achievable. DMPK scientists working in partnership with medicinal chemists and drug design teams can maximize the probability of success via building predictions, knowledge, and developing a thorough mechanistic understanding of the ADME disposition properties of the relevant chemical series and candidate drug.

References

1. Lennernäs, H. Does Fluid Flow Across the Intestinal Mucosa Affect Quantitative Oral Drug Absorption? Is It Time for a Reevaluation? *Pharm Res.* **1995,** *12* (11), 1573–1582.
2. Bertz, R. J.; Granneman, G. R. Use of in vitro and in vivo Data to Estimate the Likelihood of Metabolic Pharmacokinetic Interactions. *Clin. Pharmacokinet.* **1997,** *32* (3), 210–258.
3. Smith, D. A. Pharmacokinetics and Toxicity of Functional Groups. In *RSC Drug Discovery Series No 1*; Smith, D. A., Ed.; 2010.
4. Rowland, M.; Tozer, T. N. Clinical Pharmacokinetics—Concepts and Applications. In 3rd ed.; Williams and Wilkins, 1989. Philadelphia, PA.
5. McGinnity, D. F.; Collington, J.; Austin, R.; Riley, R. Evaluation of Human Pharmacokinetics, Therapeutic Dose and Exposure Predictions Using Marketed Oral Drugs. *Curr. Drug Metab.* **2007,** *8,* 463.
6. Hellriegel, E. T.; Bjornsson, T. D.; Hauck, W. W. Interpatient Variability in Bioavailability Is Related to the Extent of Absorption: Implications for Bioavailability and Bioequivalence Studies. *Clin. Pharmacol. Ther.* **1996,** *60,* 601.
7. Komura, H.; Iwaki, M. In Vitro and in vivo Small Intestinal Metabolism of CYP3A and UGT Substrates in Preclinical Animal Species and Humans: Species Differences. *Drug Metab. Rev.* **2011,** *43,* 476.
8. Galetin, A.; Gertz, M.; Houston, J. B. Contribution of Intestinal Cytochrome p450-Mediated Metabolism to Drug–Drug Inhibition and Induction Interactions. *Drug. Metab. Pharmacokinet.* **2010,** *25,* 28.
9. Thelen, K.; Dressman, J. B. Cytochrome P450-Mediated Metabolism in the Human Gut Wall. *J. Pharm. Pharmacol.* **2009,** *61,* 541.
10. Paine, M. F.; Hart, H. L.; Ludington, S. S.; Haining, R. L.; Rettie, A. E.; Zeldin, D. C. The Human Intestinal Cytochrome P450 "Pie". *Drug Metab. Dispos.* **2006,** *34,* 880.
11. Zhang, Q. Y.; Dunbar, D.; Ostrowska, A.; Zeisloft, S.; Yang, J.; Kaminsky, L. S. Characterization of Human Small Intestinal Cytochromes P-450. *Drug Metab. Dispos.* **1999,** *27,* 804.
12. Prueksaritanont, T.; Gorham, L. M.; Hochman, J. H.; Tran, L. O.; Vyas, K. P. Comparative Studies of Drug-Metabolizing Enzymes in Dog, Monkey, and Human Small Intestines, and in Caco-2 Cells. *Drug Metab. Dispos.* **1996,** *24,* 634.
13. Yang, J.; Jamei, M.; Yeo, K. R.; Tucker, G. T.; Rostami-Hodjegan, A. Prediction of Intestinal First-Pass Drug Metabolism. *Curr. Drug Metab.* **2007,** *8,* 676.
14. Doherty, M. M.; Charman, W. N. The Mucosa of the Small Intestine: How Clinically Relevant as an Organ of Drug Metabolism? *Clin. Pharmacokinet.* **2002,** *41,* 235.
15. Paine, M. F.; Khalighi, M.; Fisher, J. M.; Shen, D. D.; Kunze, K. L.; Marsh, C. L.; Perkins, J. D.; Thummel, K. E. Characterization of Interintestinal and Intraintestinal Variations in Human CYP3A-Dependent Metabolism. *J. Pharmacol. Exp. Ther.* **1997,** *283,* 1552.
16. Galetin, A.; Houston, J. B. Intestinal and Hepatic Metabolic Activity of Five Cytochrome P450 Enzymes: Impact on Prediction of First-Pass Metabolism. *J. Pharmacol. Exp. Ther.* **2006,** *318,* 1220.
17. Galetin, A. Intestinal First-Pass Metabolism: Bridging the Gap Between in vitro and In Vivo. *Curr. Drug Metab.* **2007,** *8,* 643.
18. Zhang, Y.; Benet, L. Z. The Gut as a Barrier to Drug Absorption: Combined Role of Cytochrome P450 3A and P-Glycoprotein. *Clin. Pharmacokinet.* **2001,** *40,* 159.
19. CDER. *Guidance for Industry Drug Interaction Studies—Study Design, Data Analysis, Implications for Dosing and Labeling Recommendations;* U.S. Department of Health and Human Services, Food and Drug Administration Center for Drug Evaluation and Research (CDER), 2012.
20. Hidalgo, I. J.; Raub, T. J.; Borchardt, R. T. Characterization of the Human Colon Carcinoma Cell Line (Caco-2) as a Model System for Intestinal Epithelial Permeability. *Gastroenterology* **1989,** *96,* 736.
21. Sun, D.; Lennernas, H.; Welage, L. S.; Barnett, J. L.; Landowski, C. P.; Foster, D.; Fleisher, D.; Lee, K. D.; Amidon, G. L. Comparison of Human Duodenum and Caco-2 Gene Expression Profiles for 12,000 Gene Sequences Tags and Correlation With Permeability of 26 Drugs. *Pharmacol. Res.* **2002,** *19,* 1400.
22. Lin, X.; Skolnik, S.; Chen, X.; Wang, J. Attenuation of Intestinal Absorption by Major Efflux Transporters: Quantitative Tools and Strategies Using a Caco-2 Model. *Drug Metab. Dispos.* **2011,** *39,* 265.
23. Murakami, T.; Takano, M. Intestinal Efflux Transporters and Drug Absorption. *Expert Opin. Drug Metab. Toxicol.* **2008,** *4,* 923.
24. Bolger, M. B.; Lukacova, V.; Woltosz, W. S. Simulations of the Nonlinear Dose Dependence for Substrates of Influx and Efflux Transporters in the Human Intestine. *AAPS J.* **2009,** *11,* 353.
25. Grime, K. H.; Barton, P.; McGinnity, D. F. Application of In Silico, in vitro and Preclinical Pharmacokinetic Data for the Effective and Efficient Prediction of Human Pharmacokinetics. *Mol. Pharm.* **2013,** *10,* 1191.
26. Jamei, M.; Marciniak, S.; Feng, K.; Barnett, A.; Tucker, G.; Rostami-Hodjegan, A. The Simcyp Population-Based ADME Simulator. *Expert Opin. Drug Metab. Toxicol.* **2009,** *5,* 211.
27. Sinha, V. K.; Snoeys, J.; Osselaer, N. V.; Peer, A. V.; Mackie, C.; Heald, D. From Preclinical to Human-Prediction of Oral Absorption and Drug–Drug Interaction Potential Using Physiologically Based Pharmacokinetic (PBPK) Modeling Approach in an Industrial Setting: A Workflow by Using Case Example. *Biopharm. Drug Dispos.* **2012,** *33,* 111.
28. DeSesso, J. M.; Jacobson, C. F. Anatomical and Physiological Parameters Affecting Gastrointestinal Absorption in Humans and Rats. *Food Chem. Toxicol.* **2001,** *39,* 209.
29. Øie, S.; Tozer, T. N. Effect of Altered Plasma Protein Binding on Apparent Volume of Distribution. *J. Pharm. Sci.* **1979,** *68,* 1203.
30. Riley, R. J.; Martin, I. J.; Cooper, A. E. The Influence of DMPK as an Integrated Partner in Modern Drug Discovery. *Curr. Drug Metab.* **2002,** *3,* 527.
31. Smith, D. A.; Di, L.; Kerns, E. H. The Effect of Plasma Protein Binding on in vivo Efficacy: Misconceptions in Drug Discovery. *Nat. Rev. Drug Discov.* **2010,** *9,* 929.
32. MacIntyre, A. C.; Cutler, D. J. The Potential Role of Lysosomes in Tissue Distribution of Weak Bases. *Biopharm. Drug Dispos.* **1988,** *9,* 513.
33. Berellini, G.; Springer, C.; Waters, N. J.; Lombardo, F. In Silico Prediction of Volume of Distribution in Human Using Linear and Nonlinear Models on a 669 Compound Data set. *Med. Chem.* **2009,** *52,* 4488.
34. Gleeson, M. P.; Waters, N. J.; Paine, S. W.; Davis, A. M. In Silico Human and Rat Vss Quantitative Structure–Activity Relationship Models. *J. Med. Chem.* **2006,** *49,* 1953.
35. Obach, R. S. Prediction of Human Volume of Distribution Using In Vivo, In Vitro, and In Silico Approaches. *Annu. Rep. Med. Chem.* **2007,** *42,* 469–488.
36. Berry, L. M.; Li, C.; Zhao, Z. Species Differences in Distribution and Prediction of Human V(ss) From Preclinical Data. *Drug Metab. Dispos.* **2011,** *39,* 2103–2116.
37. Berezhkovskiy, L. M. On the Accuracy of Determination of Unbound Drug Fraction in Tissue Using Diluted Tissue Homogenate. *J. Pharm. Sci.* **2012,** *101,* 1909–1916.
38. Zou, P.; Zheng, N.; Yang, Y.; Yu, L. X.; Sun, D. Prediction of Volume of Distribution at Steady State in Humans: Comparison of Different Approaches. *Expert Opin. Drug Metab. Toxicol.* **2012,** *8,* 855.

39. Jones, R. D.; Jones, H. M.; Rowland, M.; Gibson, C. R.; Yates, J. W.; Chien, J. Y.; Ring, B. J.; Adkison, K. K.; Ku, M. S.; He, H.; Vuppugalla, R.; Marathe, P.; Fischer, V.; Dutta, S.; Sinha, V. K.; Björnsson, T.; Lavé, T.; Poulin, P. PhRMA CPCDC Initiative on Predictive Models of Human Pharmacokinetics, Part 2: Comparative Assessment of Prediction Methods of Human Volume of Distribution. *J. Pharm. Sci.* **2011,** *100,* 4074.
40. Lombardo, F.; Waters, N. J.; Argikar, U. A.; Dennehy, M. K.; Zhan, J.; Gunduz, M.; Harriman, S. P.; Berellini, G.; Liric Rajlic, I.; Obach, R. S. Comprehensive Assessment of Human Pharmacokinetic Prediction Based on in vivo Animal Pharmacokinetic Data, Part 1: Volume of Distribution at Steady State. *J. Clin. Pharmacol.* **2013,** *53,* 178.
41. Grime, K.; Riley, R. J. The Impact of in vitro Binding on In Vitro–In Vivo Extrapolations, Projections of Metabolic Clearance and Clinical Drug-Drug Interactions. *Curr. Drug Metab.* **2006,** *7,* 251.
42. Sohlenius-Sternbeck, A.-K.; Jones, C.; Ferguson, D.; Middleton, B. J.; Projean, D.; Floby, E.; Bylund, J.; Afzelius, L. Practical Use of the Regression Offset Approach for the Prediction of in vivo Intrinsic Clearance From Hepatocytes. *Xenobiotica* **2012,** *42,* 841.
43. Lavé, T.; Chapman, K.; Goldsmith, P.; Rowland, M. Human Clearance Prediction: Shifting the Paradigm. *Expert Opin. Drug Metab. Toxicol.* **2009,** *9,* 1039.
44. Ito, K.; Houston, J. B. Prediction of Human Drug Clearance From in vitro and Preclinical Data Using Physiologically Based and Empirical Approaches. *Pharm. Res.* **2005,** *22,* 103.
45. Obach, R. S. Predicting Clearance in Humans From in vitro Data. *Curr. Top. Med. Chem.* **2011,** *11,* 334.
46. Houston, J. B. Utility of in vitro Drug Metabolism Data in Predicting in vivo Metabolic Clearance. *Biochem. Pharmacol.* **1994,** *47,* 1469.
47. Riley, R. J.; McGinnity, D. F.; Austin, R. P. A Unified Model for Predicting Human Hepatic, Metabolic Clearance From in vitro Intrinsic Clearance Data in Hepatocytes and Microsomes. *Drug Metab. Dispos.* **2005,** *33,* 1304.
48. Smith, D. A.; Jones, B. C.; Walker, D. K. Design of Drugs Involving the Concepts and Theories of Drug Metabolism and Pharmacokinetics. *Med. Res. Rev.* **1996,** *16,* 243.
49. Brown, C. D. A.; Sayer, R.; Windass, A. S.; Haslam, I. S.; De Broe, M. E.; D'Haese, P. C.; Verhulst, A. Characterisation of Human Tubular Cell Monolayers as a Model of Proximal Tubular Xenobiotic Handling. *Toxicol. Appl. Pharmacol.* **2008,** *233,* 428.
50. Paine, S. W.; Menochet, K.; Denton, R.; McGinnity, D. F.; Riley, R. J. Prediction of Human Renal Clearance From Preclinical Species for a Diverse Set of Drugs That Exhibit Both Active Secretion and Net Reabsorption. *Drug Metab. Dispos.* **2011,** *39,* 1008.
51. Tahara, H.; Shono, M.; Kusuhara, H.; Kinoshita, H.; Fuse, E.; Takadate, A.; Otagiri, M.; Sugiyama, Y. Molecular Cloning and Functional Analyses of OAT1 and OAT3 From Cynomolgus Monkey Kidney. *Pharm. Res.* **2005,** *22,* 647.
52. Kato, Y.; Kuge, K.; Kusuhara, H.; Meier, P. J.; Sugiyama, Y. Gender Difference in the Urinary Excretion of Organic Anions in Rats. *J. Pharmacol. Exp. Ther.* **2002,** *302,* 483.
53. Smith, D. A. Discovery and ADMET: Where Are We Now. *Curr. Top. Med. Chem.* **2011,** *11,* 467.
54. Shitara, Y.; Horie, T.; Sugiyama, Y. Transporters as a Determinant of Drug Clearance and Tissue Distribution. *Eur. J. Pharm. Sci.* **2006,** *27,* 425.
55. Ishikawa, T.; Akimaru, K.; Kuo, M. T.; Priebe, W.; Suzuki, M. How Does the MRP/GS-X Pump Export Doxorubicin? *J. Natl. Cancer Inst.* **1995,** *87,* 1639–1640.
56. Keppler, D.; Leier, I.; Jedlitschky, G. Transport of Glutathione Conjugates and Glucuronides by the Multidrug Resistance Proteins MRP1 and MRP2. *Biol. Chem.* **1997,** *378,* 787–791.
57. Müller, M.; Jansen, P. L. Molecular Aspects of Hepatobiliary Transport. *Am. J. Physiol.* **1997,** *272,* G1285–G1303.
58. Chandra, P.; Brouwer, K. L. The Complexities of Hepatic Drug Transport: Current Knowledge and Emerging Concepts. *Pharm. Res.* **2004,** *21,* 719–735.
59. Grime, K. H.; Paine, S. W. Species Differences in Biliary Clearance and Possible Relevance of Hepatic Uptake and Efflux Transporters Involvement. *Drug Metab. Dispos.* **2013,** *41,* 372.
60. Soars, M. G.; McGinnity, D. F.; Grime, K.; Riley, R. J. The Pivotal Role of Hepatocytes in Drug Discovery. *Chem. Biol. Interact.* **2007,** *168,* 2.
61. Gardiner, P.; Paine, S. W. The Impact of Hepatic Uptake on the Pharmacokinetics of Organic Anions. *Drug Metab. Dispos.* **2011,** *39,* 1930.
62. Mahmood, I. Interspecies Scaling of Biliary Excreted Drugs: A Comparison of Several Methods. *J. Pharm. Sci.* **2005,** *94,* 883.
63. Mahmood, I.; Sahajwalla, C. Interspecies Scaling of Biliary Excreted Drugs. *J. Pharm. Sci.* **2002,** *91,* 1908.
64. Scatina, J. A.; Hicks, D. R.; Kraml, M.; Cayen, M. N. Disposition of a New Tetrahydrocarbazole Analgesic Drug in Laboratory Animals and Man. *Xenobiotica* **1989,** *19,* 991.
65. Påhlman, I.; Edholm, M.; Kankaanranta, S.; Odell, M.-L. Pharmacokinetics of Susalimod, a Highly Biliary-Excreted Sulphasalazine Analogue, in Various Species. Nonpredictable Human Clearance by Allometric Scaling. *Pharm. Pharmacol. Commun.* **1998,** *4,* 493–498.
66. Morris, M.; Yang, Y.; Gandhi, Y. A.; Bhansalia, S. G.; Benincosa, L. J. Interspecies Scaling: Prediction of Human Biliary Clearance and Comparison With QSPKR. *Biopharm. Drug Dispos.* **2012,** *33,* 1.
67. Ward, K. W.; Smith, B. R. I. A Comprehensive Quantitative and Qualitative Evaluation of Extrapolation of Intravenous Pharmacokinetic Parameters From Rat, Dog, and Monkey to Humans. I. Clearance. *Drug Metab. Dispos.* **2004,** *32,* 603.
68. Caldwell, G. W.; Masucci, J. A.; Yan, Z.; Hageman, W. Allometric Scaling of Pharmacokinetic Parameters in Drug Discovery: Can Human CL, Vss and t1/2 be Predicted From In-Vivo Rat Data? *Eur. J. Drug Metab. Pharmacokinet.* **2004,** *29,* 133.
69. Cook, D.; Brown, D.; Alexander, R.; March, R.; Morgan, P.; Satterthwaite, G.; Pangalos, M. N. Lessons Learned From the Fate of AstraZeneca's Drug Pipeline: A Five-Dimensional Framework. *Nat. Rev. Drug Discov.* **2014,** *13,* 419–431.
70. Visser, S. A.; Aurell, M.; Jones, R. D.; Schuck, V. J.; Egnell, A. C.; Peters, S. A.; Brynne, L.; Yates, J. W.; Jansson-Löfmark, R.; Tan, B.; Cooke, M.; Barry, S. T.; Hughes, A.; Bredberg, U. Model-Based Drug Discovery: Implementation and Impact. *Drug Discov. Today* **2013,** *18,* 764–775.
71. Waring, M. J.; Arrowsmith, J.; Leach, A. R.; Leeson, P. D.; Mandrell, S.; Owen, R. M.; Pairaudeau, G.; Pennie, W. D.; Pickett, S. D.; Wang, J.; Wallace, O.; Weir, A. An Analysis of the Attrition of Drug Candidates From Four Major Pharmaceutical Companies. *Nat. Rev. Drug Discov.* **2015,** *14,* 475–486.

4.03 Drug-Metabolizing Enzyme Systems I

H Yamazaki, Showa Pharmaceutical University, Machida, Tokyo, Japan

© 2017 Elsevier Ltd. All rights reserved.

4.03.1	Introduction	45
4.03.2	In Vivo Pharmacokinetics of Human P450 Probes in Experimental Animals	45
4.03.3	Age-Related and Polymorphic Pharmacokinetic Changes of Human P450 Probes in Monkeys	47
4.03.4	Using Chimeric Mice With Humanized Liver to Investigate Drug-Induced Toxicity	48
4.03.5	Epilogue	48
Acknowledgments		49
References		49
Relevant Websites		50

4.03.1 Introduction

Accounting for species differences in drug metabolism and disposition between animals and humans is an important issue in the field of preclinical research. Before conducting a human microdosing study as the first-in-human administration of a potential new drug, a traditional distribution study of the radiolabeled compound in pigmented rats is often carried out to estimate the internal exposure in humans. To address the species differences, the levels of radioactivity per gram in animal organs need to be converted to the amount of injected activity in a whole organism, and this value is scaled up by the human body weight/animal body weight ratio.[1]

The human cytochrome *P450* gene superfamily is made up of 57 functional genes and 58 pseudogenes.[2] The corresponding P450 (P450 or CYP) enzymes are involved in the oxidative metabolism of a variety of drugs, toxic chemicals, and endogenous compounds. In the course of new drug development, rodents are often used as animal models, but it is well established that species differences exist in terms of drug metabolism mediated mainly by rodent P450 enzymes and human P450 isoforms. The relevance and limitations of all animal models used in nonclinical safety assessments of investigational products should be carefully considered.

Because of their genetic similarity to humans, nonhuman primates are often used in preclinical studies to predict the toxicity and pharmacokinetics of new drugs. Old World monkeys, such as cynomolgus monkeys (*Macaca fascicularis*), are most commonly used among the nonhuman primates. In addition, the common marmoset (*Callithrix jacchus*), a New World monkey, is beneficial in various research fields such as neuroscience, stem cell research, drug metabolism, toxicology, and immune and autoimmune diseases[3,4] because of their small size, availability, high reproductive efficiency, and early sexual maturity.[5] Although information on P450 enzymes in cynomolgus monkeys (hereafter, "monkey" means the cynomolgus monkey) is increasingly available, the characterization of marmoset P450 enzymes is currently limited. Chimeric mice with humanized liver or human *P450* genes are commonly used as animal models to investigate the human metabolites of new and known drug candidates.[6] In vivo models using chimeric mice with human hepatocytes also have potential for use in drug interaction studies and the investigation of human reactive metabolites.

Many drug-induced toxicity events are associated with immune-mediated hypersensitivity reactions, which are idiosyncratic in nature and therefore difficult to predict. In the United States, more than 50% of acute liver failure cases in adults are caused by drugs.[7] It is, therefore, not surprising that many drug regulatory authorities require evaluation of the potential for metabolic activation prior to market approval and during the post-marketing period. Both in vitro and in vivo studies play roles in the safe development and effective use of medicines. In this section, taking into account the aforementioned discussion, drug-metabolizing activities are compared among human, monkey, and marmoset P450 enzymes. The effects of age-related changes and genetic polymorphisms on P450 enzymes are seen in monkeys and in humans. Consequently, it is important to take into account species differences when evaluating the roles of human P450 enzymes in the metabolism of a variety of drugs.

4.03.2 In Vivo Pharmacokinetics of Human P450 Probes in Experimental Animals

Human cytochrome P450 enzymes have been well characterized with respect to drug metabolism. Research has also elucidated the P450 isoform contents in liver microsomes,[8] the relatively broad but selective P450 substrate specificities,[9,10] P450 induction and inhibition,[11] P450-mediated drug interactions,[12] and genetic polymorphisms of P450 enzymes. In addition, a nomenclature system for polymorphic human P450 alleles (http://www.cypalleles.ki.se/) has been established. Research has mainly focused on the P450s involved in the oxidation of compounds associated with pharmacological and/or toxicological actions.

A study of the pharmacokinetics in humans of caffeine (1,3,7-trimethylxanthine), *S*-warfarin, omeprazole, metoprolol, and midazolam in combination as probe substrates of P450 1A2, 2C9, 2C19, 2D6, and 3A, respectively, has been reported.[13] A different

human P450 probe cocktail using losartan and dextromethorphan with caffeine, omeprazole, and midazolam has also been reported.[14] In addition, studies have investigated the pharmacokinetics of the human P450 probes caffeine, warfarin, omeprazole, metoprolol, and midazolam in minipigs, marmosets, monkeys, and humans at doses of 1.0 mg kg^{-1} to clarify the similarities and occasional species differences.[15–17] Among these probe substrates, pharmacokinetic assessments of caffeine and metoprolol in dogs, minipigs, marmosets, monkeys,[15–17] and humans[13] are summarized in Fig. 1. The data show similar slowly decreasing plasma concentrations for caffeine in these animals; however, for metoprolol, the maximum concentration and the rate of decrease varied greatly among these animals. Plasma concentrations of metoprolol in orally treated minipigs and monkeys were at the level of the quantitative detection limits at doses of 1.0 mg kg^{-1} (Fig. 1). Metoprolol, a human P450 2D probe, was extensively metabolized by monkey P450 enzymes.[16] In addition, it has been reported that the typical human P450 3A4/5 probe midazolam is cleared more rapidly in monkeys than in humans.[18]

Caffeine is a standard phenotyping substrate for human P450 1A2. Although the caffeine disappearance rates were similar for minipigs, marmosets, monkeys, and humans (Fig. 1), the primary oxidative metabolites of caffeine were different among these species. The predominant reaction in caffeine metabolism in humans is reportedly the 3-demethylation of caffeine to generate 1,7-dimethylxanthine.[19–21] In humans, the 3-*N*-demethylation of caffeine is the major metabolic pathway (81% of total dimethylxanthines); in monkeys, however, 7-*N*-demethylation to form pharmacologically active theophylline is reportedly predominant (89%).[22] Interspecies differences regarding caffeine oxidation exist, but the predominant 8-hydroxylations of caffeine in mice, rabbits, and rats have been shown to be broadly similar.[22] In an analytic approach to investigate species differences in P450 activities, rat P450 1A2 (75% homologous with human 1A2) was aligned with the crystal structure of human P450 1A2 (PDB 2HI4) to model the three-dimensional structure. A docking simulation was able to explain the typical species differences in caffeine metabolism by these two orthologous enzyme forms with possibly different substrate pockets. An additional example of such species differences is the predominant caffeine 7-demethylation mediated by monkey P450 2C9 in contrast to the predominant caffeine 3-demethylation mediated by human P450 1A2.[23]

The well-established and clinically important anticoagulant drug *S*-warfarin is a typical human P450 2C9 substrate.[24] Monkey P450 2C19 reportedly has high activity toward *R*-warfarin 7-hydroxylation,[25] whereas in humans, *R*-warfarin 7-hydroxylation is much slower than *S*-warfarin 7-hydroxylation. The activities of orthologous P450 enzymes from humans and monkeys (Table 1) are generally similar, but some differences were recently recognized, such as those for warfarin hydroxylation described earlier. Marmoset liver microsomes efficiently catalyzed the 7-hydroxylation of *S*-warfarin, but not of *R*-warfarin; this finding was similar to that of humans but not to that of monkeys.[28] Among marmoset P450 2C enzymes,[27] P450 2C19 efficiently catalyzes the 7-hydroxylation of *S*-warfarin, but not of *R*-warfarin, which is similar to the findings for human P450 2C9.[28] The similar stereoselectivity for warfarin 7-hydroxylation between marmosets and humans indicates that the drug-metabolizing properties of marmoset P450 2C19 are similar to those of P450 2C9 in humans. Additionally, plasma concentrations of *S*-warfarin in marmosets after intravenous administration of warfarin decreased faster than those of *R*-warfarin, suggesting that *S*-warfarin was stereoselectively metabolized in marmoset livers in a similar way to that in human livers.[17] However, the metabolic clearances of *S*-warfarin in marmosets exhibited larger interindividual variations than those of *R*-warfarin, suggesting the possible genetic polymorphism of marmoset P450 2C19.[28] Other reported examples of polymorphic enzymes involved in drug oxidations include monkey P450 2C and 2D enzymes.[29–31] Clinical impacts of neonatal opioid toxicity should be noted following maternal use of codeine associated with highly polymorphic human P450 2D6.[32]

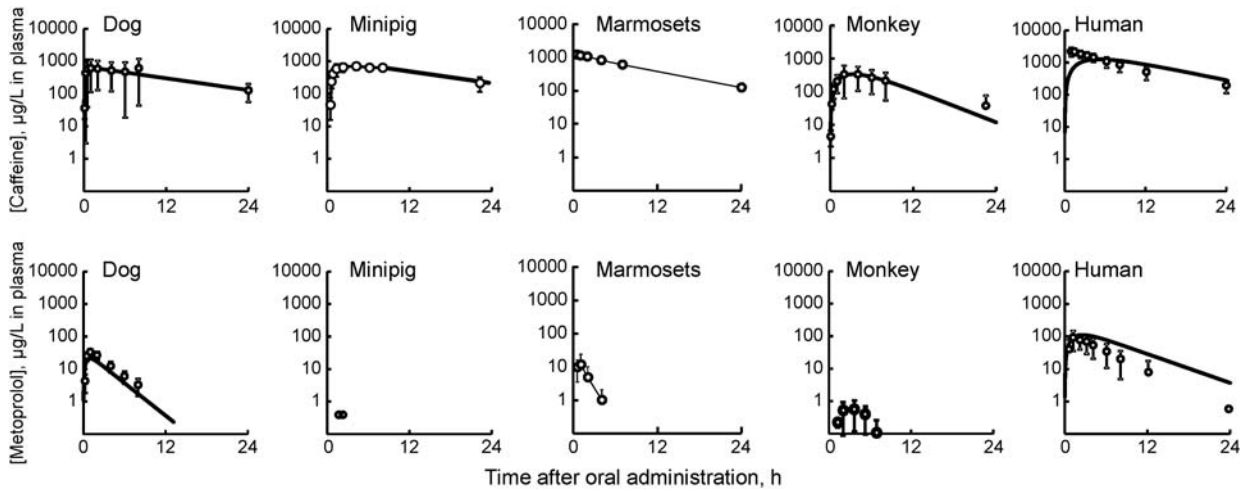

Fig. 1 Pharmacokinetic assessment of caffeine and metoprolol at doses of 1.0 mg kg^{-1} (oral administration) in dogs, minipigs, marmosets, monkeys, and humans. Data are means and standard deviations (SDs) (*circles and bars*, $n=4–6$). *Lines* represent results by PBPK simulations.

Table 1 Autologous P450 isoforms in humans, macaques, and marmosets

Human	*Monkey*	*Marmoset*
1A1	1A1	1A1
1A2	1A2	1A2
1B1	1B1	1B1
[1D1P]	1D1	
2A6	2A23	2A6
[2A7]	2A24	
2A13	2A26	
2B6	2B6	2B6
2C8	2C8(20)	2C8
[2C18]	2C18	2C18
2C9	2C9(43)	2C19
2C19	2C19(75)	2C58
	2C76	2C76
	2C93	
2D6	2D6(17)	2D6(19)
	2D8(44)	2D8
2E1	2E1	2E1
2G2P	2G2	
2J2	2J2	2J2
3A4	3A4(8)	3A4(21)
3A5	3A5	3A5
3A7		
3A43	3A43	3A90

Human P450s whose sequences are highly similar to P450s identified in monkeys or marmosets are listed. Rendic and Guengerich,[9,10] Uno et al.,[26] and Shimizu et al.[27] and updated. For P450s that have been renamed, the original names are indicated in parentheses. Human genes in brackets indicate nonactive ones.

4.03.3 Age-Related and Polymorphic Pharmacokinetic Changes of Human P450 Probes in Monkeys

Age-related changes in pharmacokinetics can alter drug responses (pharmacodynamics) and may cause adverse drug reactions. During drug development, it is important to predict how the pharmacokinetics of drug candidates will change in older patients to reduce such risks. There is currently more awareness of the need for modeling and simulation of special conditions as part of drug development. Early in vivo studies in a preclinical species such as the monkey or dog may be helpful. Monkey liver microsomal P450 contents were established in 2011 by immunochemical determinations.[33] Against this background, the pharmacokinetics of the human P450 probes caffeine, racemic warfarin, omeprazole, metoprolol, and midazolam in combination were recently investigated after single intravenous and oral administrations at doses of 0.20 and 1.0 mg kg^{-1}, respectively, to three young (3-year-old) and three aged (16-year-old) monkeys.[16] The mean maximum concentrations of *R*- and *S*-warfarin (4.6 and 3.7 μg mL^{-1}, respectively) in aged monkeys after oral administration were significantly higher than those in young monkeys (3.3 and 2.7 μg mL^{-1}).[16] The mean clearance value of midazolam in aged monkeys (9.5 mL $min^{-1}kg^{-1}$) was significantly lower than that in young monkeys (13 mL $min^{-1}kg^{-1}$).[16] These findings suggest that aged monkeys could be a good model for aging in humans, especially with particular characteristics of reduced clearances for some human P450 substrates in aged monkeys.[16]

In addition, hepatic blood flow rates, but not albumin concentrations, were found to decrease with age in monkeys and in humans.[34] The effects of aging on the pharmacokinetics of acetaminophen (a marker of gastric emptying), antipyrine (a marker of hepatic metabolic activity and total body water), diazepam (lipophilic and highly distributed), diphenhydramine (hepatic blood flow-limited and alpha-1 acid glycoprotein-bound), and ofloxacin (renally eliminated) have been found in monkeys; such changes likely resulted from increased concentrations of alpha-1 acid glycoprotein and total body fat and decreased hepatic blood flow, hepatic and renal clearance, and body water as a result of aging.[34] Consequently, intrinsic clearances, factors unbound in plasma fractions, and hepatic blood flow rates are important parameters for the determination of in vivo clearance values in models of aging.

Resequencing of the monkey *P450 2C19* gene identified three variants p.[(Phe100Asn; Ala103Val; Ile112Leu)] that showed substantially reduced activity compared with wild type *P450 2C19* in terms of *R*-/*S*-warfarin 7-hydroxylation.[30] Because such defective or impaired alleles of human *P450* genes must be considered in drug metabolism studies during drug development, the role of monkey *P450* genes, especially polymorphic monkey P450 2C19, was elucidated in vivo. It was found that interanimal variations of *R*-warfarin clearance in monkeys were associated with monkey *P450 2C19* genetic variants p.[(Phe100Asn; Ala103Val; Ile112-Leu)].[29] Because some interindividual variability of P450 2C-dependent drug metabolism in monkeys, as in humans, is accounted for by polymorphic *P450 2C19* variants, genotyping of drug metabolism enzymes should be considered before and after P450-dependent drug metabolism testing and evaluations in monkeys.

A widely used antiplatelet agent clopidogrel is a prodrug that is metabolized by two main metabolic pathways in humans:[35,36] an esterase-dependent pathway leading to hydrolysis into an inactive carboxylic acid derivative and a P450-dependent two-step oxidative process leading to its active metabolite.[36] Although contributions of human P450 1A2, 2B6, 2C19, and 3A4 on the activation pathway have been reported,[36] genetic polymorphisms of human *P450 2C19* could be one of the key clinical considerations in interindividual variability in clopidogrel pharmacokinetic and pharmacodynamic responsiveness[35,37] when clopidogrel treatment is initiated. It should be noted that recombinant monkey P450 2C9, 2C19, and 2C76 extensively metabolized clopidogrel to a similar extent in substrate deletion assays.[38–40]

4.03.4 Using Chimeric Mice With Humanized Liver to Investigate Drug-Induced Toxicity

Considerable discussion has centered on the importance of drug metabolites as potential determinants of drug safety.[41] This debate led to a guidance note for the drug development industry issued in 2008 by the US Food and Drug Administration, namely, "guidance for industry safety testing of drug metabolites," and ultimately culminated in recommendations from the International Conference on Harmonization M3(R2) in 2010. These guidance documents laid out criteria establishing when human metabolites need to be measured in laboratory animal species and defined the circumstances under which direct testing of a metabolite in animal toxicology studies is needed to provide a reliable risk assessment. Recent developments in bioanalytical methodology have yielded several strategies to provide robust data that can inform critical decisions related to metabolite quantification and monitoring in plasma.

The National Institutes of Health LiverTox database (http://livertox.nih.gov/) was developed by the Liver Disease Research Branch of the National Institute of Diabetes and Digestive and Kidney Diseases and the National Library of Medicine to promote basic and clinical research on drug-induced liver toxicity. This is a free online source of textual documents on liver injury caused by prescription and nonprescription drugs, herbal medicines, and dietary supplements collected from various databases, the scientific literature, and the interpretations of the curators.[42] Recently, systematic research into metabolic drug activation has become more comprehensive and more complex.[43] Drug-induced toxicity may be caused by active intermediates formed by human cytochrome P450 enzymes. To understand the roles of human P450 enzymes in drug metabolism, safety assessment of drug metabolites is proposed by potential application of engineered mouse models. Human drug-metabolizing P450 3A enzymes have been found to undergo thalidomide activation.[44] In in vivo models with chimeric mice with humanized liver, high midazolam clearance and a higher area under the plasma concentration–time curve of the metabolite 1′-hydroxymidazolam were obtained following coadministration of thalidomide, indicating that heterotropic cooperativity of human P450 3A4/5 by thalidomide occurs in vivo.[45] Thalidomide and its human disproportionate metabolite 5-hydroxythalidomide were oxidized by autoinduced human P450 3A enzymes[46] to reactive intermediates (with reactive sites on the aromatic ring) that were trapped as glutathione conjugates.[47,48]

As an example of species differences in metabolic drug activation, human liver P450 1A2 exhibited different functionality from rat P450 1A2 in bioactivation of the primary metabolite of 5-*n*-butyl-7-(3,4,5-trimethoxybenzoylamino)pyrazolo[1,5-*a*]pyrimidine (an amide moiety-bearing pyrazolopyrimidine derivative with potential analgesic effects).[49] A primary metabolite was metabolized by human P450 1A2 to form a proximate metabolite, which was conjugated with a peptide to form an adduct.[50] In rats, the same P450 1A2 enzyme formed some proximate metabolites but predominantly mediated the formation of another metabolite that exhibited no toxicity.[51] These metabolic differences highlight some of the perils of animal testing of drug candidates for metabolite toxicity. A zone analysis using electrophoresis with accelerator mass spectrometry revealed that in vivo bioactivated radiolabeled troglitazone and flutamide (both known to be hepatotoxic in humans) bound nonspecifically to a variety of microsomal and/or cytosolic proteins present in liver from chimeric mice with humanized liver.[52] In contrast with those of radiolabeled diazepam (rarely hepatotoxic) and 5-*n*-butyl-pyrazolo[1,5-*a*]pyrimidine (limited hepatotoxicity), some of the proteins binding troglitazone and flutamide were located high in a zone analysis of specific covalent binding contents and target protein concentrations.[52] Drug metabolism mediated by humanized livers in chimeric mice (leading to binding in vivo) may be a good tool for evaluating the relationship between nonspecific protein binding tendencies of medicines and their metabolites and potential hepatotoxicity in humans. These findings indicate the usefulness of using transplanted human liver cells in humanized mice to give accurate preclinical predictions of human drug metabolism.

Many results have also been reported on the in vitro–in vivo extrapolations of hepatic clearance, on the volume of distribution, and on the estimated unbound microsomal fraction for a wide variety of drugs.[53] Simplified human physiologically based pharmacokinetic (PBPK) models for acephate,[54] chlorpyrifos,[54] bisphenol A,[55] and di(2-ethylhexyl)phthalate[56] were recently developed based on the pharmacokinetics in humanized mice; these models successfully estimated the human pharmacokinetics. Glucuronide metabolites of bisphenol A[55] and mono(2-ethylhexyl)phthalate[56] were excreted in the urine of chimeric mice with humanized liver, in contrast with the results of experiments on rodents without humanized liver. Simplified PBPK models are able to estimate human plasma and urine concentrations of drugs after ingestion and are capable of both forward and reverse dosimetry. This simple system was also successful in estimating human plasma concentrations of various P450 probes based on monkey plasma data.[57]

4.03.5 Epilogue

The success of research into drug-metabolizing enzymes and its application in drug discovery and development has been remarkable. The combination of pharmacokinetic data with a simple PBPK model has great potential for assisting evaluations of the

pharmacological/toxicological potential of new drug substances and for estimating human radiation exposures from radiolabeled drugs when planning human studies.[58] The applications of P450 research continue to expand and develop. Interest should also focus on another monooxygenase, flavin-containing monooxygenase 3 (FMO3), because it is responsible for the *N*- or *S*-oxygenations of various drugs; moreover, genetic polymorphism in the human *FMO3* gene may result in changes of catalytic efficiency and lead to drug interactions.[59] Pharmacokinetics and safety assessments of drug metabolites should be done with marmosets/monkeys and mouse models with humanized liver to achieve a good understanding of the effects of drug-metabolizing enzymes on potential new drug candidates.

Acknowledgments

This work was partly supported by the MEXT-Supported Program for the Strategic Research Foundation at Private Universities (2013–2017).

References

1. Kirschner, A. S.; Ice, R. D.; Beierwaltes, W. H. Radiation Dosimetry of ^{131}I-19-Iodocholesterol: The Pitfalls of Using Tissue Concentration Data—Author's Reply. *J. Nucl. Med.* **1975,** *16,* 247–248.
2. Nelson, D. R.; Zeldin, D. C.; Hoffman, S. M. G.; Maltais, L. J.; Wain, H. M.; Nebert, D. W. Comparison of Cytochrome P450 (*CYP*) Genes From the Mouse and Human Genomes, Including Nomenclature Recommendations for Genes, Pseudogenes and Alternative-Splice Variants. *Pharmacogenetics* **2004,** *14,* 1–18.
3. Tokuno, H.; Watson, C.; Roberts, A.; Sasaki, E.; Okano, H. Marmoset Neuroscience. *Neurosci. Res.* **2015,** *93,* 1–2.
4. Cyranoski, D. Marmosets are Stars of Japan's Ambitious Brain Project. *Nature* **2014,** *514,* 151–152.
5. Sasaki, E. Prospects for Genetically Modified Non-Human Primate Models, Including the Common Marmoset. *Neurosci. Res.* **2015,** *93,* 110–115.
6. Yamazaki, H.; Suemizu, H.; Igaya, S.; Shimizu, M.; Shibata, M.; Nakamura, M.; Chowdhury, G.; Guengerich, F. P. In Vivo Formation of a Glutathione Conjugate Derived From Thalidomide in Humanized uPA-NOG Mice. *Chem. Res. Toxicol.* **2011,** *24,* 287–289.
7. Lee, W. M.; Squires, R. H., Jr.; Nyberg, S. L.; Doo, E.; Hoofnagle, J. H. Acute Liver Failure: Summary of a Workshop. *Hepatology* **2008,** *47,* 1401–1415.
8. Shimada, T.; Yamazaki, H.; Mimura, M.; Inui, Y.; Guengerich, F. P. Interindividual Variations in Human Liver Cytochrome P-450 Enzymes Involved in the Oxidation of Drugs, Carcinogens and Toxic Chemicals: Studies With Liver Microsomes of 30 Japanese and 30 Caucasians. *J. Pharmacol. Exp. Ther.* **1994,** *270,* 414–423.
9. Guengerich, F. P.; Rendic, S. Update Information on Drug Metabolism Systems—2009, Part I. *Curr. Drug Metab.* **2010,** *11,* 1–3.
10. Rendic, S.; Guengerich, F. P. Update Information on Drug Metabolism Systems—2009, Part II: Summary of Information on the Effects of Diseases and Environmental Factors on Human Cytochrome P450 (CYP) Enzymes and Transporters. *Curr. Drug Metab.* **2010,** *11,* 4–84.
11. Niwa, T.; Murayama, N.; Yamazaki, H. Stereoselectivity of Human Cytochrome p450 in Metabolic and Inhibitory Activities. *Curr. Drug Metab.* **2011,** *12,* 549–569.
12. Hisaka, A.; Ohno, Y.; Yamamoto, T.; Suzuki, H. Prediction of Pharmacokinetic Drug-Drug Interaction Caused by Changes in Cytochrome P450 Activity Using in vivo Information. *Pharmacol. Ther.* **2010,** *125,* 230–248.
13. Turpault, S.; Brian, W.; Van Horn, R.; Santoni, A.; Poitiers, F.; Donazzolo, Y.; Boulenc, X. Pharmacokinetic Assessment of a Five-Probe Cocktail for CYPs 1A2, 2C9, 2C19, 2D6 and 3A. *Br. J. Clin. Pharmacol.* **2009,** *68,* 928–935.
14. Ryu, J. Y.; Song, I. S.; Sunwoo, Y. E.; Shon, J. H.; Liu, K. H.; Cha, I. J.; Shin, J. G. Development of the "Inje Cocktail" for High-Throughput Evaluation of Five Human Cytochrome P450 Isoforms In Vivo. *Clin. Pharmacol. Ther.* **2007,** *82,* 531–540.
15. Sakai, C.; Iwano, S.; Yamazaki, Y.; Ando, Y.; Nakane, F.; Kouno, M.; Yamazaki, H.; Miyamoto, Y. Species Differences in the Pharmacokinetic Parameters of Cytochrome P450 Probe Substrates Between Experimental Animals, Such as Mice, Rats, Dogs, Monkeys, and Microminipigs, and Humans. *J. Drug Metab. Toxicol.* **2014,** *5,* 173.
16. Koyanagi, T.; Nakanishi, Y.; Murayama, N.; Yamaura, Y.; Ikeda, K.; Yano, K.; Uehara, S.; Utoh, M.; Kim, S.; Uno, Y.; Yamazaki, H. Age-Related Changes of Hepatic Clearances of Cytochrome P450 Probes Midazolam and *R*-/*S*-Warfarin in Combination With Caffeine, Omeprazole, and Metoprolol in Cynomolgus Monkeys Using In Vitro-In Vivo Correlation. *Xenobiotica* **2015,** *45,* 312–321.
17. Uehara, S.; Inoue, T.; Utoh, M.; Toda, A.; Shimizu, M.; Uno, Y.; Sasaki, E.; Yamazaki, H. Simultaneous Pharmacokinetics Evaluation of Human Cytochrome P450 Probes, Caffeine, Warfarin, Omeprazole, Metoprolol, and Midazolam, in Common Marmosets (*Callithrix jacchus*). *Xenobiotica* **2016,** *46,* 163–168.
18. Ohtsuka, T.; Yoshikawa, T.; Kozakai, K.; Tsuneto, Y.; Uno, Y.; Utoh, M.; Yamazaki, H.; Kume, T. Alprazolam as an in vivo Probe for Studying Induction of CYP3A in Cynomolgus Monkeys. *Drug Metab. Dispos.* **2010,** *38,* 1806–1813.
19. Berthou, F.; Flinois, J. P.; Ratanasavanh, D.; Beaune, P.; Riche, C. Evidence for the Involvement of Several Cytochromes P-450 in the First Steps of Caffeine Metabolism by Human Liver Microsomes. *Drug Metab. Dispos.* **1991,** *19,* 561–567.
20. Gu, L.; Gonzalez, F. J.; Kalow, W.; Tang, B. K. Biotransformation of Caffeine, Paraxanthine, Theobromine and Theophylline by cDNA-Expressed Human CYP1A2 and CYP2E1. *Pharmacogenetics* **1992,** *2,* 73–77.
21. Grant, D. M.; Campbell, M. E.; Tang, B. K.; Kalow, W. Biotransformation of Caffeine by Microsomes From Human Liver. Kinetics and Inhibition Studies. *Biochem. Pharmacol.* **1987,** *36,* 1251–1260.
22. Berthou, F.; Guillois, B.; Riche, C.; Dreano, Y.; Jacqz-Aigrain, E.; Beaune, P. H. Interspecies Variations in Caffeine Metabolism Related to Cytochrome P4501A Enzymes. *Xenobiotica* **1992,** *22,* 671–680.
23. Utoh, M.; Murayama, N.; Uno, Y.; Onose, Y.; Hosaka, S.; Fujino, H.; Shimizu, M.; Iwasaki, K.; Yamazaki, H. Monkey Liver Cytochrome P450 2C9 Is Involved in Caffeine 7-*N*-Demethylation to Form Theophylline. *Xenobiotica* **2013,** *43,* 1037–1042.
24. Yamazaki, H.; Shimada, T. Human Liver Cytochrome P450 Enzymes Involved in the 7-Hydroxylation of *R*- and *S*-Warfarin Enantiomers. *Biochem. Pharmacol.* **1997,** *54,* 1195–1203.
25. Hosoi, Y.; Uno, Y.; Murayama, N.; Fujino, H.; Shukuya, M.; Iwasaki, K.; Shimizu, M.; Utoh, M.; Yamazaki, H. Monkey Liver Cytochrome P450 2C19 Is Involved in *R*- and *S*-Warfarin 7-Hydroxylation. *Biochem. Pharmacol.* **2012,** *84,* 1691–1695.
26. Uno, Y.; Iwasaki, K.; Yamazaki, H.; Nelson, D. R. Macaque Cytochromes P450: Nomenclature, Transcript, Gene, Genomic Structure, and Function. *Drug Metab. Rev.* **2011,** *43,* 346–361.
27. Shimizu, M.; Iwano, S.; Uno, Y.; Uehara, S.; Inoue, T.; Murayama, N.; Onodera, J.; Sasaki, E.; Yamazaki, H. Qualitative De Novo Analysis of Full Length cDNA and Quantitative Analysis of Gene Expression for Common Marmoset (*Callithrix jacchus*) Transcriptomes Using Parallel Long-Read Technology and Short-Read Sequencing. *PLoS One* **2014,** *9,* e100936.
28. Uehara, S.; Uno, Y.; Inoue, S.; Kawano, M.; Shimizu, M.; Toda, A.; Utoh, M.; Sasaki, E.; Yamazaki, H. Novel Marmoset Cytochrome P450 2C19 in Livers Efficiently Metabolizes Human P450 2C9 and 2C19 Substrates, *S*-Warfarin, Tolbutamide, Flurbiprofen, and Omeprazole. *Drug Metab. Dispos.* **2015,** *43,* 1408–1416.
29. Utoh, M.; Yoshikawa, T.; Hayashi, Y.; Shimizu, M.; Iwasaki, K.; Uno, Y.; Yamazaki, H. Slow *R*-Warfarin 7-Hydroxylation Mediated by P450 2C19 Genetic Variants in Cynomolgus Monkeys In Vivo. *Biochem. Pharmacol.* **2015,** *95,* 110–114.

30. Uno, Y.; Matsushita, A.; Shukuya, M.; Matsumoto, Y.; Murayama, N.; Yamazaki, H. *CYP2C19* Polymorphisms Account for Inter-Individual Variability of Drug Metabolism in Cynomolgus Macaques. *Biochem. Pharmacol.* **2014,** *91,* 242–248.
31. Uno, Y.; Uehara, S.; Kohara, S.; Osada, N.; Murayama, N.; Yamazaki, H. *CYP2D44* Polymorphisms in Cynomolgus and Rhesus Macaques. *Mol. Biol. Rep.* **2015,** *42,* 1149–1155.
32. Madadi, P.; Ross, C. J.; Hayden, M. R.; Carleton, B. C.; Gaedigk, A.; Leeder, J. S.; Koren, G. Pharmacogenetics of Neonatal Opioid Toxicity Following Maternal Use of Codeine During Breastfeeding: A Case–Control Study. *Clin. Pharmacol. Ther.* **2009,** *85,* 31–35.
33. Uehara, S.; Murayama, N.; Nakanishi, Y.; Zeldin, D. C.; Yamazaki, H.; Uno, Y. Immunochemical Detection of Cytochrome P450 Enzymes in Liver Microsomes of 27 Cynomolgus Monkeys. *J. Pharmacol. Exp. Ther.* **2011,** *339,* 654–661.
34. Koyanagi, T.; Yamaura, K.; Yano, K.; Kim, S.; Yamazaki, H. Age-Related Pharmacokinetic Changes of Acetaminophen, Antipyrine, Diazepam, Diphenhydramine, and Ofloxacin in Male Cynomolgus Monkeys and Beagle Dogs. *Xenobiotica* **2014,** *44,* 893–901.
35. Djebli, N.; Fabre, D.; Boulenc, X.; Fabre, G.; Sultan, E.; Hurbin, F. Physiologically Based Pharmacokinetic Modeling for Sequential Metabolism: Effect of CYP2C19 Genetic Polymorphism on Clopidogrel and Clopidogrel Active Metabolite Pharmacokinetics. *Drug Metab. Dispos.* **2015,** *43,* 510–522.
36. Kazui, M.; Nishiya, Y.; Ishizuka, T.; Hagihara, K.; Farid, N. A.; Okazaki, O.; Ikeda, T.; Kurihara, A. Identification of the Human Cytochrome P450 Enzymes Involved in the Two Oxidative Steps in the Bioactivation of Clopidogrel to Its Pharmacologically Active Metabolite. *Drug Metab. Dispos.* **2010,** *38,* 92–99.
37. Hulot, J. S.; Bura, A.; Villard, E.; Azizi, M.; Remones, V.; Goyenvalle, C.; Aiach, M.; Lechat, P.; Gaussem, P. Cytochrome P450 2C19 Loss-of-Function Polymorphism Is a Major Determinant of Clopidogrel Responsiveness in Healthy Subjects. *Blood* **2006,** *108,* 2244–2247.
38. Hosaka, S.; Murayama, N.; Satsukawa, M.; Uehara, S.; Shimizu, M.; Iwasaki, K.; Iwano, S.; Uno, Y.; Yamazaki, H. Comprehensive Evaluation for Substrate Selectivity of Cynomolgus Monkey Cytochrome P450 2C9, a New Efavirenz Oxidase. *Drug Metab. Dispos.* **2015,** *43,* 1119–1122.
39. Hosaka, S.; Murayama, N.; Satsukawa, M.; Shimizu, M.; Uehara, S.; Fujino, H.; Iwasaki, K.; Iwano, S.; Uno, Y.; Yamazaki, H. Evaluation of 89 Compounds for Identification of Substrates for Cynomolgus Monkey Cytochrome P450 2C76, a New Bupropion/Nifedipine Oxidase. *Drug Metab. Dispos.* **2015,** *43,* 27–33.
40. Hosaka, S.; Murayama, N.; Satsukawa, M.; Uehara, S.; Shimizu, M.; Iwasaki, K.; Iwano, S.; Uno, Y.; Yamazaki, H. Similar Substrate Specificity of Cynomolgus Monkey Cytochrome P450 2C19 to Reported Human P450 2C Counterpart Enzymes by Evaluation of 89 Drug Clearances. *Biopharm. Drug Dispos.* **2015,** *36,* 636–643.
41. Gao, H.; Jacobs, A.; White, R. E.; Booth, B. P.; Obach, R. S. Meeting Report: Metabolites in Safety Testing (MIST) Symposium-Safety Assessment of Human Metabolites: What's Really Necessary to Ascertain Exposure Coverage in Safety Tests? *AAPS J.* **2013,** *15,* 970–973.
42. Hoofnagle, J. H.; Serrano, J.; Knoben, J. E.; Navarro, V. J. LiverTox: A Website on Drug-Induced Liver Injury. *Hepatology* **2013,** *57,* 873–874.
43. Yamazaki, H. Drug-Induced Liver Toxicity Studies: Research into Human Metabolites Clarifies Their Role in Drug Development. *Drug Metab. Pharmacokinet.* **2014,** *29,* 111.
44. Okada, Y.; Murayama, N.; Yanagida, C.; Shimizu, M.; Guengerich, F. P.; Yamazaki, H. Drug Interactions of Thalidomide With Midazolam and Cyclosporine A: Heterotropic Cooperativity of Human Cytochrome P450 3A5. *Drug Metab. Dispos.* **2009,** *37,* 18–23.
45. Yamazaki, H.; Suemizu, H.; Murayama, N.; Utoh, M.; Shibata, N.; Nakamura, M.; Guengerich, F. P. In Vivo Drug Interactions of the Teratogen Thalidomide With Midazolam: Heterotropic Cooperativity of Human Cytochrome P450 in Humanized TK-NOG Mice. *Chem. Res. Toxicol.* **2013,** *26,* 486–489.
46. Murayama, N.; van Beuningen, R.; Suemizu, H.; Guguen-Guillouzo, C.; Shibata, N.; Yajima, K.; Utoh, M.; Shimizu, M.; Chesne, C.; Nakamura, M.; Guengerich, F. P.; Houtman, R.; Yamazaki, H. Thalidomide Increases Human Hepatic Cytochrome P450 3A Enzymes by Direct Activation of Pregnane X Receptor. *Chem. Res. Toxicol.* **2014,** *27,* 304–308.
47. Chowdhury, G.; Murayama, N.; Okada, Y.; Uno, Y.; Shimizu, M.; Shibata, N.; Guengerich, F. P.; Yamazaki, H. Human Liver Microsomal Cytochrome P450 3A Enzymes Involved in Thalidomide 5-Hydroxylation and Formation of a Glutathione Conjugate. *Chem. Res. Toxicol.* **2010,** *23,* 1018–1024.
48. Yamazaki, H.; Suemizu, H.; Shimizu, M.; Igaya, S.; Shibata, N.; Nakamura, N.; Chowdhury, G.; Guengerich, F. P. In Vivo Formation of Dihydroxylated and Glutathione Conjugate Metabolites Derived From Thalidomide and 5-Hydroxythalidomide in Humanized TK-NOG Mice. *Chem. Res. Toxicol.* **2012,** *25,* 274–276.
49. Kuribayashi, S.; Goto, K.; Naito, S.; Kamataki, T.; Yamazaki, H. Human Cytochrome P450 1A2 Involvement in the Formation of Reactive Metabolites From a Species-Specific Hepatotoxic Pyrazolopyrimidine Derivative, 5-*n*-Butyl-7-(3,4,5-trimethoxybenzoylamino)pyrazolo[1,5-*a*]pyrimidine. *Chem. Res. Toxicol.* **2009,** *22,* 323–331.
50. Yamazaki, H.; Kuribayashi, S.; Inoue, T.; Tateno, C.; Nishikura, Y.; Oofusa, K.; Harada, D.; Naito, S.; Horie, T.; Ohta, S. Approach for in vivo Protein Bindings of 5-*n*-Butyl-pyrazolo[1,5-*a*]pyrimidine Bioactivated in Chimeric Mice With Humanized Liver by Two-Dimensional Electrophoresis With Accelerator Mass Spectrometry. *Chem. Res. Toxicol.* **2010,** *23,* 152–158.
51. Kuribayashi, S.; Uno, Y.; Naito, S.; Yamazaki, H. Different Metabolites of Human Hepatotoxic Pyrazolopyrimidine Derivative 5-*n*-Butyl-pyrazolo[1,5-*a*]pyrimidine Produced by Human, Rat, and Monkey Cytochrome P450 1A2 and Liver Microsomes. *Basic Clin. Pharmacol. Toxicol.* **2012,** *110,* 405–408.
52. Yamazaki, H.; Kuribayashi, S.; Inoue, T.; Honda, T.; Tateno, C.; Oofusa, K.; Ninomiya, S.; Ikeda, T.; Izumi, T.; Horie, T. Zone Analysis by Two-Dimensional Electrophoresis With Accelerator Mass Spectrometry of in vivo Protein Bindings of Idiosyncratic Hepatotoxicants Troglitazone and Flutamide Bioactivated in Chimeric Mice With Humanized Liver. *Toxicol. Res.* **2015,** *4,* 106–111.
53. Poulin, P.; Haddad, S. Hepatocyte Composition-Based Model as a Mechanistic Tool for Predicting the Cell Suspension: Aqueous Phase Partition Coefficient of Drugs in in vitro Metabolic Studies. *J. Pharm. Sci.* **2013,** *102,* 2806–2818.
54. Suemizu, H.; Sota, S.; Kuronuma, M.; Shimizu, M.; Yamazaki, H. Pharmacokinetics and Effects on Serum Cholinesterase Activities of Organophosphorus Pesticides Acephate and Chlorpyrifos in Chimeric Mice Transplanted With Human Hepatocytes. *Regul. Toxicol. Pharmacol.* **2014,** *70,* 468–473.
55. Miyaguchi, T.; Suemizu, H.; Shimizu, M.; Shida, S.; Nishiyama, S.; Takano, R.; Murayama, N.; Yamazaki, H. Human Urine and Plasma Concentrations of Bisphenol A Extrapolated From Pharmacokinetics Established in in vivo Experiments With Chimeric Mice With Humanized Liver and Semi-physiological Pharmacokinetic Modeling. *Regul. Toxicol. Pharmacol.* **2015,** *72,* 71–76.
56. Adachi, K.; Suemizu, H.; Murayama, N.; Shimizu, M.; Yamazaki, H. Human Biofluid Concentrations of Mono(2-ethylhexyl)phthalate Extrapolated From Pharmacokinetics in Chimeric Mice With Humanized Liver Administered With Di(2-ethylhexyl)phthalate and Physiologically Based Pharmacokinetic Modeling. *Environ. Toxicol. Pharmacol.* **2015,** *39,* 1067–1073.
57. Shida, S.; Utoh, M.; Murayama, N.; Shimizu, M.; Uno, Y.; Yamazaki, H. Human Plasma Concentrations of Cytochrome P450 Probes Extrapolated From Pharmacokinetics in Cynomolgus Monkeys Using Physiologically Based Pharmacokinetic Modeling. *Xenobiotica* **2015,** *45,* 881–886.
58. Yamazaki, H.; Kunikane, E.; Nishiyama, S.; Murayama, N.; Shimizu, M.; Sugiyama, Y.; Chiba, K.; Ikeda, T. Human Plasma Concentrations of Tolbutamide and Acetaminophen Extrapolated From in vivo Animal Pharmacokinetics Using in vitro Human Hepatic Clearances and Simple Physiologically Based Pharmacokinetic Modeling for Radio-Labeled Microdose Clinical Studies. *Radioisotopes* **2015,** *64,* 509–519.
59. Yamazaki, H.; Shimizu, M. Survey of Variants of Human Flavin-Containing Monooxygenase 3 (FMO3) and Their Drug Oxidation Activities. *Biochem. Pharmacol.* **2013,** *85,* 1588–1593.

Relevant Websites

http://www.cypalleles.ki.se/ – Polymorphic human P450 alleles.
http://livertox.nih.gov/ – LiverTox database.
http://www.pharmpk.com/PK_2002.html – PharmPK Discussion List Archive.

4.04 Human PK Prediction and Modeling

TH Grasela, Simulations Plus, Inc., Buffalo, NY, United States
V Lukacova, Simulations Plus, Inc., Lancaster, CA, United States
DN Morris, Simulations Plus, Inc., Buffalo, NY, United States
RD Clark, Simulations Plus, Inc., Lancaster, CA, United States
KA Andrews, Simulations Plus, Inc., Buffalo, NY, United States
MB Bolger, Simulations Plus, Inc., Lancaster, CA, United States

© 2017 Elsevier Ltd. All rights reserved.

4.04.1 Predicting Human Pharmacokinetics and the Future of In Silico-Based Research and Development 52
4.04.1.1 Prologue 52
4.04.1.2 Introduction 52
4.04.2 Overview of Pharmacokinetics and Pharmacodynamics 53
4.04.2.1 Pharmacokinetics 53
4.04.2.1.1 Clearance 53
4.04.2.1.2 Volume of distribution 54
4.04.2.1.3 Half-life 54
4.04.2.1.4 Absorption 54
4.04.2.2 Pharmacodynamics 55
4.04.3 The Relationship Between Physicochemical Properties and Pharmacokinetics 56
4.04.3.1 Molecular Size 56
4.04.3.2 Hydrophobicity 56
4.04.3.3 Solubility 57
4.04.3.4 pK_a 57
4.04.3.5 Hydrogen Bonding 57
4.04.3.6 Permeability 57
4.04.3.7 Implications of Physicochemical Properties 57
4.04.3.7.1 Biopharmaceutics Classification System 58
4.04.3.7.2 Lipinski Rule of 5 58
4.04.4 In Silico Predictions of Physicochemical Properties 58
4.04.4.1 Brief Descriptions of QSAR Methodologies 59
4.04.4.2 Case Study: Improving In Silico Predictions of pK_a 60
4.04.5 Physiologically Based Pharmacokinetic Modeling and Simulation Methodology 60
4.04.5.1 Brief Description of a Physiologically Based Pharmacokinetic Model 60
4.04.5.2 Representing a Physiologically Based Pharmacokinetic Model in GastroPlus 61
4.04.5.2.1 The absorption model 61
4.04.5.2.2 Tissue distribution model 63
4.04.5.3 Predicting In Vivo Pharmacokinetic Parameters 63
4.04.5.3.1 Predicting intestinal and hepatic clearance 64
4.04.5.3.2 Predicting volume of distribution 66
4.04.5.3.4 Predicting transporter effects 67
4.04.5.3.5 Predicting permeability 68
4.04.6 Applications of Physiologically Based Pharmacokinetic Methodology 68
4.04.6.1 Lessons Learned From the Early Applications of Physiologically Based Pharmacokinetic Modeling and Simulation 69
4.04.6.1.1 Reducing the use of animals in toxicology testing 69
4.04.6.1.2 Assessing the feasibility and performance of physiologically based pharmacokinetic predictions of human pharmacokinetics 69
4.04.6.1.3 First-in-human prediction and trial design 70
4.04.7 Generalized Approach to Building and Validating a Physiologically Based Pharmacokinetic Model 70
4.04.7.1 Model Building and Input Data 71
4.04.7.2 Model Optimization 71
4.04.7.3 Reporting 71
4.04.8 Case Studies 72
4.04.8.1 Predicting Bioavailability 72
4.04.8.2 Halofantrine Concentration-Related QTc Prolongation 73
4.04.9 Regulatory Implications 74
4.04.10 Future Directions 76

4.04.10.1 Scientific Challenges 76
4.04.10.2 Cultural Challenges 77
4.04.11 Epilogue 77
Acknowledgments 78
References 78

Biological systems are a complex mix of heterogeneous phases. Drug molecules usually traverse many of these phases to get from the site of administration to the eventual site of action. Along this random-walk process, they may perturb many other cellular components such as organelles, lipids, proteins, and so forth. These interactions are complex and vastly different from organic reactions in test tubes, even though the eventual interaction with a receptor is chemical or physicochemical in nature. Thus, depending on the biological system involved—isolated receptor, cell, or whole animal—one expects the response to be multifactorial and complex. The overall process, whether in vitro or in vivo, involves a mix of equilibrium and rate processes, a situation that defies easy separation and delineation.[1]

4.04.1 Predicting Human Pharmacokinetics and the Future of In Silico-Based Research and Development

4.04.1.1 Prologue

In his fascinating book, *The Vital Question. Why is life the way it is?*, Nick Lane puts forth his hypothesis on the origin of the electrochemical processes that led to the energy production essential for life on earth.[2] These early chemical processes from eons ago reverberate in the complex processes and supportive cellular structures resident in all eukaryotic cells today. Many of these processes have been extensively explored in cleverly designed experiments that led to theories that can explain many of the complex intricacies of drug absorption, distribution, metabolism, and excretion (ADME).

In silico tools are now available that encompass an amalgamation of reductionist-based theories and experimental results. The availability of software tools and complementary sources of input parameters, such as in silico predictions of drug properties from molecular structure and in vitro and in vivo experimentation, has led to an increasing use of physiologically based pharmacokinetic (PBPK) modeling and simulation in a wide variety of applications across the entire research and development (R&D) lifecycle.

PBPK modeling and simulation tools, such as GastroPlus™,[3] provide a framework for specifying species-specific physiological parameters and drug-specific physicochemical properties to predict and explain the pharmacokinetic (PK) behavior of drug molecules as they "traverse" the body.

The goal of this article is to explore some of the key concepts, theories, and practices involved in successfully using PBPK modeling and simulation to predict pharmacokinetics in preclinical and clinical settings. This includes the use of molecular–structure-based in silico predictions of physicochemical properties and the performance of in vitro to in vivo extrapolations (IVIVEs).

An overview of PBPK model development is provided, along with selected examples of applications of PBPK modeling and simulation. Future implications and applications of these approaches are also explored. The focus will be on small molecules, but it should be noted that PBPK modeling and simulations are being directed toward large molecules, such as proteins, antibodies, and antibody–drug conjugates.[4]

4.04.1.2 Introduction

Pharmaceutical R&D scientists continue to seek new knowledge and insights that can lead to innovative medicines. This search for safe and effective medicines is remarkably expensive and prone to failure. The productivity crisis engendered by past failures has led to a variety of new technologies and various attempts at innovation aimed at reducing the costs and improving the chances of successfully bringing new medicines to market.

Labor-intensive one-by-one synthesis has given way to combinatorial chemistry techniques that can quickly create unprecedentedly large libraries of new compounds. Tissue-culture-based, high-throughput phenotypic screening has replaced phenotypic screening in intact organisms as the preferred way to assess activity against selected targets that might lead to a clinically useful and commercially viable new medicine. This new generation of tools has produced notable successes and failures, albeit at an unsustainable expenditure in resources. One of the reasons for the productivity crisis is that compounds with limited potential are erroneously progressed through the R&D lifecycle. The costs of preclinical and clinical testing accumulate until further testing is made futile by unmistakably clear signs of a failure to meet minimal program objectives.[5] Every drug that fails was a failure as soon as the molecular structure was drawn for the first time, but determining that it was a failure in the traditional manner sometimes costs years of development time and hundreds of millions of dollars of wasted resources. Recognizing these failures as early as possible in discovery or very early development would save billions of dollars in pharmaceutical R&D expenses.

An analysis of failures in clinical development performed by Kola and Landis[6] demonstrated that the causes of attrition over a 10-year period from 1991 to 2000 changed substantially during that period of time. In 1991, adverse PK and bioavailability results were a significant cause of attrition, and accounted for approximately 40% of all attrition. By 2000, adverse PK and bioavailability

results had been dramatically reduced as a cause of attrition, but this was accompanied by a shift toward failures due to efficacy and safety issues, and overall attrition rates remain high to this day.[7] One explanation for the changing reasons for attrition was the recognition that most orally administered drugs are relatively small and moderately lipophilic molecules. Lipinski's Rule of 5 (Ro5)[8] was developed as a heuristic to predict whether a chemical was likely to be absorbed orally. The rule raised awareness of the importance of physicochemical properties, and not just in vitro potency, in predicting the likelihood of clinical success.[9]

The concern about attrition and the rising costs of R&D has inspired much debate among scientists and prompted a search for strategies to improve efficiencies and enhance the success rates for new medicines. The efforts to improve productivity have focused on ways to identify compounds likely to fail in later stages of development where failure is most expensive, or, alternatively, to find ways to optimize the R&D program for compounds with an acceptable level of promise in order to improve the chances for success.

The emergence of in silico tools, such as PBPK modeling, to predict human pharmacokinetics for new compounds now provides significant opportunities to anticipate the advantages and liabilities associated with compounds under consideration in discovery. Physiologically based PK modeling is being used in diverse applications including simulation of preclinical, Phase 1 healthy volunteer, and special population pharmacokinetics; modeling of absorption, impact of formulation differences, and food effects; and predicting the magnitude of drug–drug interactions (DDIs). These applications have had significant impact throughout the stages of drug discovery and development to increase efficiency, reduce the need for animal studies, and increase PK understanding in order to anticipate problems and optimize development programs.

The use of PBPK modeling and simulation methodology has increased considerably in the last few years, driven by a number of factors. First, there are now commercially available software tools, such as GastroPlus, that effectively deal with the complexity of the series of differential equations required to describe the transit of drug through the body. Second, enhancements in the design and utility of in vitro systems provide quantitative information on the relevant PK properties of a drug. Third, there have been enhancements to the in silico tools used to build models of quantitative structure–activity relationships (QSAR) that can accurately predict physiochemical properties from molecular structure. In combination, the in silico and in vitro systems enable a representation of in vivo processes that have proven to be valuable in the prediction of drug pharmacokinetics across a wide range of compounds and decision-making scenarios.[10] Lastly, regulatory agencies have been at the forefront of encouraging these applications of PBPK modeling and their inclusion in regulatory submissions. For example, the United States Food and Drug Administration (FDA),[11] the European Medicines Agency (EMA),[12,13] and the Ministry of Health, Labor, and Welfare (MHLW) of Japan[14] suggest the use of PBPK modeling in their latest guidance documents on DDI assessment and hepatic impairment studies.

Given the diversity of PBPK applications and the requirements for input data from multiple departments, there is a critical need for effective interdisciplinary collaboration in model development and interpretation. The knowledge and expertise of preclinical scientists, formulation scientists, pharmacometricians, clinical pharmacologists, clinicians, and statisticians are important for a number of reasons. First, the science and the theories behind in silico tools continue to advance and improve the accuracy of predictions. Second, scientists continue to find new and creative ways to apply in silico tools and the simulations are becoming central in decision-making at all levels of R&D. Third, science-based R&D enterprises, such as the pharmaceutical, biotechnology, and agrochemical industries, will continue to be shaped by emerging applications of in silico tools. The availability of in silico tools as a basis for decision-making will require new approaches to the management of the R&D enterprise in order to foster interdisciplinary collaboration and provide innovative training and career development strategies for scientists and managers alike.[15]

4.04.2 Overview of Pharmacokinetics and Pharmacodynamics

4.04.2.1 Pharmacokinetics

The term "pharmacokinetics" was first introduced in 1953 by F.H. Dost,[16] yet the concepts and ideology have been at the heart of medicine for over a century as outlined in Wagner's seminal article, "The History of Pharmacokinetics."[17] Pharmacokinetics is broadly known as the study of the time course of what the body does to the drug, characterized by the key ADME components.[18] The rate and extent of ADME mechanisms, particularly clearance, volume of distribution, and absorption, are of central importance in PBPK models and are described in the sections here.

4.04.2.1.1 Clearance

Organ clearance is defined as the volume of fluid presented to an eliminating organ that is completely cleared of drug per unit time. Clearance (CL) has units of volume per time, for example, L/h, and is mathematically described by Eq. (1).

$$\mathrm{CL} = Q \times E \tag{1}$$

where Q is the flow rate to the eliminating organ and E is the extraction ratio of the drug.

The total clearance of a drug represents the sum of all clearance mechanisms in all eliminating organs and tissues in the body including the gastrointestinal (GI) tract, liver, heart, lung, kidney, and so forth.[19] Clearance of a drug in the GI tract is important as it pertains to first-pass extraction of a drug before the drug even enters the systemic circulation. Once in the systemic circulation, the most important eliminating organs are generally the liver and the kidney.

Hepatic clearance is determined by hepatic blood flow, free fraction of unbound drug, and intrinsic clearance. Intrinsic clearance is the rate at which the liver is able to metabolize a drug when it has unrestricted access to it. Hepatic clearance of drugs is often classified according to the drug's hepatic extraction ratio. This ratio is the rate at which the liver clears drug divided by the rate

at which the liver is presented with the drug. For high extraction drugs, hepatic clearance is limited by blood flow, whereas for low extraction drugs, hepatic clearance is contingent upon fraction unbound and intrinsic clearance.[20]

Renal clearance is defined by the processes a drug is subjected to as it transits through the kidney. Renal filtration and renal secretion into the renal tubules positively contribute to renal clearance, whereas reabsorption from the renal tubules decreases renal clearance. Renal filtration is governed by molecular size and protein binding alone, while renal secretion is dependent on renal transporters—which can be inhibited or saturated—as well as on protein binding. Renal reabsorption can be active or passive, with passive resorption dependent on lipophilicity, the pH of the urine, the pK_a of the drug, and urine flow rate.

In addition to hepatic and renal clearance mechanisms described earlier, drugs can also be eliminated via biliary secretion and can undergo enterohepatic circulation. Enterohepatic circulation refers to the process whereby a drug or a metastable metabolite thereof in the liver is secreted into the bile, stored in the gall bladder, and subsequently released into the small intestine, where the drug can be reabsorbed back into circulation and subsequently returned to the liver. Enterohepatic circulation is clinically significant when the prolonged presence of the drug in the systemic circulation results in an increase in the duration or magnitude of the drug's pharmacologic effect.

4.04.2.1.2 Volume of distribution

The concentration of a drug in plasma after drug administration is a function of dose, the extent of distribution of drug into tissues, and the amount of drug eliminated during the distribution process.

There are two types of volume of distribution of interest. The apparent volume of distribution (V_d) is estimated during the terminal phase of elimination and is influenced by the relative speeds of distribution and elimination of the drug. The steady-state volume of distribution (V_{ss}) represents the volume required to explain the steady-state plasma concentration of a drug after all distribution-related phenomena have equilibrated. In either case, drugs distribute into various tissues and fluids of the body and binding to tissue components may be so great that the volume of distribution can exceed the physical volume of plasma in an individual.[20]

Drug concentrations are generally determined in plasma so that V_{ss} is the theoretical volume of plasma at a given drug concentration that would be required to account for the entire amount of drug in the body.

The volume of distribution of a specific drug is shaped by its unique characteristics, including the extent of binding in tissue and blood, mechanisms and rate of drug transport, physical volumes of distributing tissues, and rate and extent of metabolism and elimination. Volume of distribution is useful in estimating the dose required to achieve a given plasma concentration or, conversely, to estimate the amount of drug in the body when the plasma concentration is known.[20]

4.04.2.1.3 Half-life

The elimination half-life ($t½$) is the time it takes for the drug concentration to decrease by one-half. The half-life is a function of the V_d and the total CL of a drug as shown in Eq. (2).

$$t½ = (V_d \times log_e 2)/CL \tag{2}$$

This relationship is such that the larger the total clearance, the shorter the half-life and, conversely, the larger the V_d, the longer the half-life.[19,20]

Half-life is used to determine the optimal frequency of drug administration for chronically administered medicines. Often, drugs are administered every half-life in order to minimize the difference between peak and trough drug concentrations over the dosing interval.

"Steady state" is achieved when the rate of drug input is equal to the rate of drug output, and is generally recognized to be achieved after a drug has been repeatedly administered for approximately four to five "half-lives." Steady-state concentrations are considered therapeutically relevant, especially for chronically administered drugs, where these concentrations are associated with the desirable and undesirable clinical outcomes of drug therapy.

4.04.2.1.4 Absorption

An orally administered drug must clear several barriers in order to reach the systemic circulation. Accordingly, the overall systemic bioavailability, F, when a drug is administered orally, is computed by Eq. (3)

$$F = F_a \times F_g \times F_h \tag{3}$$

where F_a is the fraction of drug absorbed into enterocytes, F_g is the fraction of drug that escapes gut metabolism, and F_h is the fraction that escapes first-pass extraction by the liver. Bioavailability can be based on comparison of an intravenous dose with any extravascular (e.g., oral, dermal, nasal, pulmonary) dosage form (absolute bioavailability), or comparison of any two routes of extravascular administration (relative bioavailability).

PBPK modeling allows the scientist to mechanistically investigate the absorption of a compound and account for the various processes that can impact systemic bioavailability. Orally administered solid dosage forms must disintegrate and the drug molecules must enter into solution. In order to be absorbed systemically, drug in solution must then pass through the enterocytes lining the intestinal wall and enter into the portal vein, which then carries the drug molecules to the liver and into the systemic circulation. Moreover, some drug may not get absorbed and is lost in the feces or via decomposition in the lumen. All of these processes,

including incomplete disintegration or dissolution, slow penetration of the enterocyte membranes, decomposition in the gut lumen, and metabolism of the drug as it passes through the gut wall and the liver, can reduce the systemic availability of the drug.

The physicochemical properties of a drug play an important role in determining the rate and extent of absorption of a drug. The properties that can lead to poor absorption include low solubility and low permeability. The properties of a compound or a formulation might be altered or modulated to improve absorption; the solubility of a compound could be increased by physical, chemical, or other modifications. Formulation of a drug as a salt, for example, can favor ionization and dissolution in the GI tract thereby increasing absorption. Physical modifications including particle technologies, such as micronization, are used to increase surface area and allow an increased dissolution rate.[21] Alternatively, solubilizing agents can be added to the formulation.

Addition of an ionizable group that gets cleaved off after absorption—that is, generation of a prodrug—offers a unique way to address solubility or permeability problems. Such "promoieties" include a wide range of functional groups with well-established chemistry and safety. Besides being more soluble, such conjugates can act as substrates for influx transporters, all of which can improve absorption.[22]

4.04.2.2 Pharmacodynamics

Pharmacodynamics is the study of what the drug does to the body and describes the relationship between drug concentrations at its sites of action and the pharmacologic responses, either therapeutic or adverse. The time course and intensity of a drug's effect is a function of its concentration at receptor sites and is dependent on the pharmacokinetics of the drug. The target concentration range is the range of plasma drug concentrations defined by the minimum effective concentration and the maximum therapeutic concentration. Dosing regimens that deliver concentrations below the minimum effective concentration may not provide an adequate therapeutic response. Conversely, regimens that deliver concentrations above the maximum therapeutic concentration may result in adverse events.

The Hill equation shown in Eq. (4) defines the relationship between drug concentrations and pharmacologic effect.[23]

$$E = \frac{E_{max} \cdot C^{\gamma}}{EC_{50}{}^{\gamma} + C^{\gamma}} \tag{4}$$

where E_{max} is the maximum achievable effect, EC_{50} is the concentration eliciting half the maximal effect, and C represents the drug concentration at the site of action. The gamma superscript (γ)[24,25] is a coefficient used in the Hill equation as a mathematical adjustment which can account for a variety of pharmacologic processes, such as receptor cooperative binding, that cause deviation from a classic binding isotherm where $\gamma = 1$.

A variety of pharmacodynamic (PD) models that relate drug concentrations to pharmacologic effect have been introduced in the literature. These models include simple direct effects, biophase, indirect response, signal transduction, irreversible effects, and more complex models including tolerance, cell kill, receptor binding dynamics, and so forth.[23,26]

Fig. 1 shows an illustration of the drug concentration-time profile and the influence that drug dose and pharmacokinetic behavior can have on therapeutic response.

In the figure, the lag time of absorption is related to the time required for drug disintegration, dissolution, and passage to the systemic circulation. Time to peak effect is related to the rate of absorption, the volume of distribution, drug dose, and bioavailability. The duration of effect is related to the time the drug concentrations are within the therapeutic range, which in turn is related

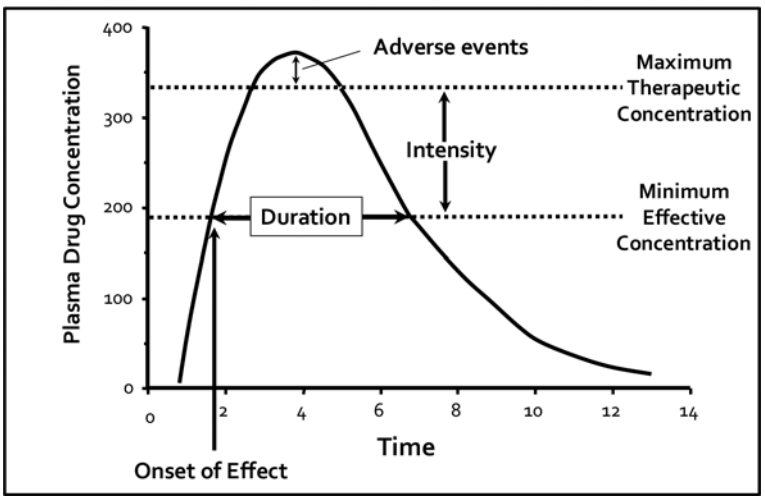

Fig. 1 The plasma concentration-time profile for a hypothetical drug after oral administration overlaid with the therapeutic range of the drug.

to the rate of absorption and the half-life of elimination. The magnitude of the dose and the frequency of administration are selected to achieve steady-state concentrations in the targeted therapeutic range which are correlated with the desired effects.

4.04.3 The Relationship Between Physicochemical Properties and Pharmacokinetics

The pharmacokinetic properties of a drug play an important role in determining the fate of drug molecules as they move through the body. These properties, in turn, reflect the drug's physicochemical characteristics. Much of the medicinal chemistry work done on a given series of compounds involves making relatively small modifications—that is, tweaking—the structure of a lead compound to address pharmacokinetic and/or toxicological issues discovered during lead optimization. Because it would be inefficient to assess every conceivable structural variation, the models employed by computational chemists are used to provide valuable guidance as to which part(s) of the problematic molecule to focus on when determining where to tweak the structure and what substitutions to try first. Indeed, much of the computational work performed in the early phases of drug development goes into collaborative brainstorming to determine which modifications or elaborations are most likely to address the issue(s) at hand without themselves creating new problems.

4.04.3.1 Molecular Size

The size of molecules that have a typical drug-like shape is commonly given as the molecular weight (MW), defined as the mass of one mole of a compound. MW is typically given in grams per mole or the more standard unit of daltons. MW of an active ingredient can have an impact on its ability to be effectively transported or to permeate cells. For example, drugs with a high MW often have poor bioavailability unless they are absorbed via a mechanism other than passive diffusion, such as active transport.

Historically, drugs with MWs below 600 Da were considered desirable due to the correlation between MW and absorption profile, that is, higher MW is associated with lower oral bioavailability. As a result, drugs with a low MW have been seen as more likely to make it through clinical trials.[27] The association between higher bioavailability and lower MW is not a result of MW per se, but MW may be a surrogate for other properties often associated with it.[28] Such correlated properties include molecular flexibility (rotatable bonds) and/or hydrophobicity, which may affect permeation or absorption across physiological membranes and therefore affect oral bioavailability in the absence of active transport.[28] The relationship between MW and properties such as hydrophobicity is complex in that up to certain values of hydrophobicity/lipophilicity, absorption may increase, and as the values continue to increase, compounds may have difficulty leaving biological membranes and may demonstrate reduced absorption. At the other end of the extreme, highly hydrophilic molecules will have trouble entering biological membranes in the first place.

4.04.3.2 Hydrophobicity

A *hydrophobic* molecule is "water fearing" in that it will prefer to be dissolved in a relatively nonpolar solvent over being dissolved in water. It is expressed in terms of the log of the partition coefficient P between 1-octanol and water,[29] which is a key physicochemical parameter for determining membrane permeability. The hydrophobicity of a molecule is often correlated with its absorption, distribution, and route of elimination.[29]

Biological membranes are comprised of a bilayer of phospholipids and other lipids as well as cholesterol. Each membrane is distinguished by a characteristic lipid composition as well as by a specific complement of embedded proteins. The lipids are amphiphilic, that is, each molecule has one hydrophobic end (typically derived from a fatty acid) and another *hydrophilic* ("water loving") end. The hydrophilic parts are localized at the inner and outer bilayer surfaces, whereas the hydrophobic portions make up the central region of the membrane. This composition makes it easy for nonpolar molecules to diffuse into the central region readily; however, a molecule which is too hydrophobic ($\log p > 5$) has trouble diffusing out into aqueous solution on the other side. This phenomenon underlies the use of the alternative term *lipophilic* ("lipid loving") to describe such molecules.

The inability of highly lipophilic molecules to traverse membranes leads to poor oral bioavailability. The absorption penalty for being too lipophilic is associated with high MW because it is relatively easy to synthesize large lipophilic compounds but relatively difficult to synthesize large hydrophilic ones. There are, however, many large commercial drug molecules, but they are generally derived from relatively hydrophilic natural products. To paraphrase Lipinski et al., there are large drugs and there are greasy drugs but large greasy drugs are a rarity in the therapeutic armamentarium.[9]

Highly lipophilic compounds also tend to bind to plasma proteins.[29] When drugs are bound to plasma proteins, there is less free drug in solution available to exert its effect at the sites of action. Lipophilic drugs can be filtered and excreted in the urine, or be reabsorbed and further metabolized. Passive reabsorption that occurs in the kidneys is governed by the molecule's lipophilicity, that is, the more lipophilic a molecule is, the more passive reabsorption occurs, and therefore the renal clearance of the molecule decreases. When a drug is reabsorbed, it might be subject to metabolism to a more polar metabolite and may then be filtered in the kidneys and renally excreted.

As described earlier, lipophilicity is often expressed as a partition coefficient (P), or $\log P$, and is defined in terms of the partitioning of neutral molecular species. Many drugs can ionize under physiological pH, however, and ions are much more hydrophilic than their neutral counterparts. A more appropriate measure of drug partitioning in the body is the distribution coefficient D at a specified pH (generally expressed as $\log D$).[29] In the experimental determination of $\log D$, an aqueous buffer at pH 7.4 is used to mimic blood, whereas an aqueous buffer at pH 6.5 is used to mimic intestinal conditions.

4.04.3.3 Solubility

Solubility of a drug in GI fluids is important and its determination is required by the FDA for new drug applications and bioequivalence testing. When a drug is orally administered in a solid dosage form, the first steps in the absorption process include the disintegration of the tablet or capsule followed by the dissolution of the active drug. Drug must be in solution before it can be absorbed; consequently, solubility and dissolution rate can limit absorption if they are low, as can premature precipitation. In general, compounds with low MW, low lipophilicity, and high polarity dissolve more readily. Conversely, compounds with high MW, high lipophilicity, and low polarity are less soluble. The solubility of a compound will be pH-dependent if it is ionized at the physiologic pH conditions encountered in the stomach and GI tract. A drug is considered highly soluble if the highest dose strength is soluble in ≤ 250 mL of water over the pH range of 1.0–7.5.[30] For drugs with low solubility, in vivo solubility can be enhanced by micellar solubilization due to bile salts.

4.04.3.4 pK_a

Most drugs are acidic or basic; many are both. In solution, they exist in equilibrium between unionized and ionized forms. The ratio of ionized and unionized forms is controlled by both the pH of the solution and the pK_a(s) of the drug according to the Henderson–Hasselbalch equation (Eqs. 5 and 6).

For acids that have a single ionizable center (i.e., monoprotic acids),

$$log_{10}(\text{ionized concentration}/\text{unionized concentration}) = \text{pH} - \text{p}K_a \tag{5}$$

and for monoprotic bases,

$$log_{10}(\text{unionized concentration}/\text{ionized concentration}) = \text{pH} - \text{p}K_a \tag{6}$$

Given that log10 (1) = 0, the pK_a of such compounds is the pH at which half of the molecules are ionized. If the pH of the environment is less than the pK_a of the molecule, then more molecules are protonated than are deprotonated: for bases this means the drug is mostly ionized and for acids this means the drug is mostly unionized.

The pH values observed in the body typically range from 1.0 to 7.5 in the GI tract and the renal tubule. For drugs that have a pK_a in the range of 3.0–7.5, the fraction unionized can change dramatically as the drug travels down the GI tract or is excreted in the urine. These changes in pH can have marked effects on permeability and diffusion across membranes. For instance, considering renally excreted drugs, ionized molecules are less likely to be passively reabsorbed and more likely to be eliminated in the urine. When the pH of the urine increases or decreases, the ionization and renal clearance of that drug can change. Therefore, renal excretion of a weak base is increased when the urine is acidified, whereas for a weak acid, increasing the pH of the urine increases renal excretion.

4.04.3.5 Hydrogen Bonding

The hydrogen-bonding capacity of a drug solute is an important determinant of permeability. In order to cross a membrane, a drug molecule needs to break hydrogen bonds with its aqueous environment. The more potential hydrogen bonds a molecule can make, the more energy this bond-breaking costs. Consequently, high hydrogen-bonding potential is an unfavorable property in that it reduces lipophilicity[31] and results in low permeability and poor absorption.

Hydrogen bonds are inherently important because too many hydrogen bond interactions with solvent and with the polar head groups of membrane lipids will impair membrane penetration. Water can serve as either a hydrogen bond donor or an acceptor, so having too many acceptors or donors on a drug molecule will usually reduce permeability. Hydrogen bond donors can be assessed by summing the number of hydrogens in NH and OH groups (i.e., NH_2 counts as two). Similarly, hydrogen bond acceptors in a drug molecule can be estimated by summing the number of nitrogen and oxygen atoms. This is not a precise measure, since it ignores the effects of protonation and deprotonation, but it works well as a rule of thumb when consistently applied.

4.04.3.6 Permeability

The permeability of a drug represents the cumulative effects of pK_a, lipophilicity, hydrogen bonding, and MW, which markedly affect the compound's ability to traverse the physiological barriers and reach the systemic circulation. Drugs that are lipophilic, have a low MW, and have significant unionized fraction at physiological pH generally exhibit good permeability. When a drug has poor permeability, it can lead to poor bioavailability, and alternative routes of administration, such as intravenous or intramuscular injection, may be required to achieve desired systemic concentrations.

4.04.3.7 Implications of Physicochemical Properties

Solubility and permeability are critical factors that affect the bioavailability of orally administered drugs. The importance of solubility and permeability emerged from research conducted in the 1990s by Amidon et al.[32] and separately by Lipinski[9] into the factors associated with good oral bioavailability. This research has had significant implications regarding management decisions

about advancing lead compounds during discovery, as well as regulatory decisions regarding the need for bioavailability and bioequivalence studies for immediate-release solid oral dosage forms.[30]

4.04.3.7.1 Biopharmaceutics Classification System

The Biopharmaceutics Classification System (BCS) is a scientific framework for classifying drug substances based on their aqueous solubility and intestinal permeability. A BCS was implemented by the FDA in 1995[33] after Amidon's seminal article established the influence of fundamental parameters of drug solubility and permeability on rate and extent of drug absorption.[32]

These parameters, combined with the dissolution rate of an oral formulation, address three major factors that govern the rate and extent of drug absorption from immediate-release solid dosage forms. The BCS approach to classifying compounds provided the FDA with a legally acceptable guideline for justifying waivers of in vivo bioavailability and/or bioequivalence studies for rapidly absorbed, immediate-release solid oral dosage forms of high solubility and high permeability (class 1) compounds.[30] The BCS also provides a basis for making inferences about the absorption rate behaviors of compounds in other classes. For example, class 2 compounds (low solubility–high permeability) are predicted to be well-absorbed, and the rate of absorption will be controlled by the dissolution rate of the formulation. Class 3 compounds (high solubility–low permeability) are predicted to have limited oral absorption. Lastly, class 4 compounds with low solubility and low permeability are likely to be poorly absorbed when administered orally.

4.04.3.7.2 Lipinski Rule of 5

Based on an analysis of the characteristics of orally administered drugs, Lipinski determined that, in general, a successful orally active drug has no more than one violation of the following criteria: no more than five hydrogen bond donors (N—H and O—H bonds), no more than 10 hydrogen bond acceptors (all nitrogen or oxygen atoms), a molecular mass less than 500 Da, and an octanol–water partition coefficient (log *P*) not greater than five. The Ro5 gained its name because its four criteria involve multiples of five.[9]

The Ro5 was proposed as a heuristic to guide the selection of small molecules that were likely to have favorable oral bioavailability during lead drug modification. The Ro5 was innovative and useful because, at the time it was introduced, there was not a guide to predict if a molecule produced from combinatorial chemistry would be likely to succeed.

Once it began to be applied, it became clear that much of the combinatorial chemistry then being done produced compounds that were unlikely to succeed as orally dosed drugs in vivo. Moreover, the hydrophobicity and size that limited their bioavailability tended to confer exaggerated potency in high-throughput in vitro screens. The collection of physicochemical properties included in the Ro5 gave interdisciplinary teams a basis, beyond just potency, for challenging the quality of compound candidates as put forth by discovery scientists.

The widespread application of the rule had a significant impact on the reasons for attrition and demonstrated that the R&D enterprise could be positively affected by what was essentially a simple model to predict absorption using data from molecular structure, including MW and polarity, and the computationally estimated (or, occasionally, measured) octanol–water partition coefficient (log *P*). The Ro5 demonstrated that physicochemical information was useful in moving toward a more productive drug discovery process.[34]

The success of the Ro5, its subsequent refinements,[28,35] and the implications of BCS have called attention to the importance of an early consideration of physicochemical properties in advancing compounds from discovery.

4.04.4 In Silico Predictions of Physicochemical Properties

The utility of PBPK modeling to support drug discovery and early development has previously been limited by the resource-intensive experiments required to generate the physiologically relevant ADME data used as input into the models. Large amounts of in vivo animal tissue concentration data were required[36,37] and PBPK models were mainly used to predict tissue exposure in toxicological, safety, and risk assessment studies.[38,39]

The large chemical libraries and capacity for high-throughput screening of biological activity has fed the need for early information on absorption, distribution, metabolism, excretion, and toxicity (ADMET) properties of compounds. Various in vitro ADMET screens are now in use, but many of these represent surrogate endpoints, that is, they are themselves models. There remains a need for tools capable of reliably estimating ADMET properties from a compound's structure alone at the earliest stages of discovery when only very small amounts of material are available or before a compound has even been synthesized.[40–42]

Oftentimes, direct measurements of drug-like properties, such as hydrophobicity, log *P*, and polarity, are not available in early discovery. This lack of information can delay a proper assessment of compound potential before the information about potency drives decision-making. This need for early information on physicochemical properties has led to interest in predicting physicochemical properties solely from compound structure. These predictions have proven useful in optimizing the screening and testing process by focusing on the most promising compounds with the goal of reducing the need for expensive in vitro and preclinical in vivo testing.[29]

4.04.4.1 Brief Descriptions of QSAR Methodologies

QSAR are based on the assumption that the geometric, steric, and electronic properties of a molecule are responsible for its physical, chemical, and biological properties and that these properties can be adequately represented by one or more numerical descriptors.[43] By developing QSAR models, many properties of a new or untested compound can be inferred from the molecular structure of compounds whose properties have already been determined.[44–48]

The model-building process makes use of three components, including: (1) a data set that provides experimental measures of activity or properties for a group of chemicals; (2) the molecular structure and/or descriptors for the chemicals, and (3) statistical tools for delineating the relationship between these two data sets.

The limiting factor in the development of predictive QSAR is typically the availability of high-quality experimental data. Ideally, the data set should address a well-defined endpoint and include enough molecules to provide adequate statistical representation of the chemical space of interest. For regression models, a wide range of response values is required, whereas an adequate number of representatives of each class are required for classification models. The response data must be accurate and precise and the corresponding compounds need to be sufficiently structurally diverse if the model built from them is going to be applicable to structures of future interest.

Data curation is an often underestimated task in helping to ensure the validity of models. The curation process includes correcting any errors in reported structures that can adversely affect the accuracy of the descriptors, addressing incomplete or inaccurate descriptors and verifying doubtful values, removal of duplicates, curation of tautomeric forms, removal of data that cannot be appropriately handled by conventional cheminformatics techniques such as inorganic and organometallic compounds, consideration of the removal of outliers if warranted, and so forth.[49]

In model-building efforts intended to provide a validated model for future predictive purposes, the curated data set is split into a training pool and a test set.

The training pool is used to generate several candidate models. Ideally, it has a high degree of molecular diversity and includes enough compounds to cover a large range of endpoint values or (classification models) to provide a reasonable balance between positive and negative examples.

The goal of the model-building process is to fit the information in the data but to avoid fitting the noise that is also inevitably present. This is done by splitting the training pool into a training set and a verification set; the former is used to build a candidate model and the latter is used to assess its performance. Performance on the verification set may be used to tune model parameters or to stop an iterative optimization process before it starts fitting the noise. This provides a measure of how well each model is likely to perform when applied to *new* compounds.

Using it to select among candidate models biases the validation set's performance statistics because doing so involves it in the overall model-building process. The following thought experiment may shed light on why this is so. Suppose two or more candidate models are equally predictive in terms of all possible compounds to which the model might be applied. Nonetheless, one model will perform better just by chance on this particular validation set and the corresponding statistics will look better than they would be for a different validation set. The effect gets worse as the data set gets more diverse.

The ("external") test set is not biased in that way, so the selected, final model's performance statistics when applied to *it* provide estimates for how well it is likely to perform in future applications. The data for the compounds in the external test set were not used to fit the models nor to select among them, so performance in predicting their endpoints is a reasonable surrogate for predicting endpoints for compounds altogether outside the data set.

The most straightforward way to split a data set into training, validation, and test subsets is by random selection. The training set is typically largest to provide as much information as possible into the model. The smaller the validation and test sets are, however, the more likely they are to not be representative of the whole. Unfortunately, the high-quality data sets available for many endpoints of interest are likely to be too small for random sampling to find a good trade-off. In such cases, some form of stratified sampling may be used.[50]

Guidelines assembled by the Organization for Economic Cooperation and Development provide a list of four things that a QSAR model should have if it is to be satisfactory from a regulatory standpoint. These characteristics include a defined endpoint; an unambiguous model-building algorithm; a defined domain of applicability; and appropriate measures of goodness-of-fit, robustness, and predictivity. Being mechanistically interpretable is desirable where possible but is not essential. Note that these are minimal criteria; satisfying them does not guarantee that a particular QSAR model is of practical use for a given endpoint. The model-building tools available today are powerful enough to extract signals from most data sets, so the usefulness of a model is now usually limited by the amount of *relevant* data available and how well that data has been curated.

A bewilderingly broad array of descriptors is available for building models. These include chemical descriptors such as log *P*; quantum chemical descriptors related to charge and energy values of individual atoms or the molecule as a whole; the presence or absence of characteristic substructures; and topological indices derived from graph theory as applied to the 2D structure. Other available descriptors include molecular volume; molecular properties based on electron distribution or spatial disposition of component atoms (conformation, geometry, shape, etc.); and physicochemical properties that quantify the hydrophobic, electronic, and steric attributes of a molecule.

Most QSAR models are constructed for the purpose of predicting endpoints for compounds which were not included in the data set used to build, select, and evaluate the performance of the model. In the context of drug development, the predictions that are of the greatest interest are those which are novel in terms of chemical structure or biological properties or both, which makes them

likely to fall "outside" the original data set to some degree. A QSAR model can only be claimed to be "predictive" if it successfully predicts the modeled endpoint for compounds in an external test set.

The applicability domain of a model describes the structure and property space covered by the compounds in the training set. It provides a basis for determining how similar a new compound structure must be to the compounds in the curated data set to be reasonably confident that the model's prediction for that compound will be reliable. Exactly how the domain should be defined is an active area of research, but the general goal is to avoid extrapolation. In some cases the degree of similarity is used, while in others the domain is defined by the range of values of the descriptors used in the model. Regardless, predictions for compounds falling outside the applicability domain are suspect. Such predictions may still be correct, but one cannot be confident that they are.

4.04.4.2 Case Study: Improving In Silico Predictions of pK_a

A drug candidate's predominant charge state at a given pH can be a major determinant of pharmacologic activity, aqueous solubility, permeability, plasma protein binding, metabolism, and so forth. The importance of pK_a is reflected in the commercial availability of automated instruments for high-throughput measurements of ionization constants and the use of in silico methods for predicting pK_a from molecular structure in virtual libraries. However, it is generally acknowledged that these in silico models do not perform very well when the data used for developing the models do not adequately cover the chemical space of interest to specific researchers.

Fraczkiewicz and his colleagues described a collaborative effort with Bayer to extend the pK_a model in Simulations Plus' ADMET Predictor™ program to include compounds from Bayer's chemical space.[51] The earlier version of the in silico model for pK_a had been trained on approximately 11,000 compounds collected from the scientific literature, herein referred to as the Public data set. Over the years this publically available data has been heavily curated at Simulations Plus to remove duplicates, correct erroneous chemical structures, verify doubtful values against original sources, and so forth. These data were supplemented by approximately 16,000 compounds from Bayer drug discovery programs with their experimentally determined pK_a values, herein referred to as the Industrial data set, and additional curation of the data was performed.

The model-building approach for both the Public data set and the combined Public and Industrial data was based on the use of artificial neural network ensembles (ANNE), microstates analysis, and the respective curated data. Model validation was performed with several test sets consisting of a total of approximately 31,000 new pK_a values measured at Bayer.

For the largest and most difficult test set with $>16{,}000$ pK_a values that were not used for training, the original model based on the Public data set achieved a mean absolute error (MAE) of 0.72, root-mean-square error (RMSE) of 0.94, and squared correlation coefficient (R^2) of 0.87. The new model based on the combined data achieved significantly improved prediction statistics, with MAE = 0.50, RMSE = 0.67, and $R^2 = 0.93$.

Interestingly, there were significant differences in the types of compounds included in publically available data versus the chemical space of current interest to Bayer drug discovery programs. In general, the Bayer compounds were significantly larger, more lipophilic, and possessed more basic ionizable groups than the compounds from the open literature. The distribution of pK_a values in the Public data set had a balanced bimodal distribution with peaks at $\sim$4 and $\sim$9, whereas the Bayer data pK_a values were significantly skewed toward 4. Taken together with the differential distribution of the number of basic groups, this clustering of pK_a values around 4 reflects the prevalence of weak bases (aromatic nitrogen) rather than carboxylic acids in this set.[51]

Note that many of the compounds in the Industrial data set violate the Ro5 criteria for MW and log *P*. A similar observation was made by Mannhold et al. when comparing the public literature's chemical space with that of Pfizer and Nycomed drug-like research compounds.[52] They cited this discrepancy as the main factor responsible for unsatisfactory performance of log *P* predictors trained on public data.

Taken together, these results suggest that the improvements in the predictive performance of the new model stem from a combination of factors, including the greater experimental consistency of the Bayer data than that seen for models built on data extracted from hundreds of published articles over the last few decades, the application of rigorous microstates analysis, the use of high-performance ANNE modeling tools, inclusion of the large amounts of data representing the chemical space of current interest to discovery scientists, and careful curation of the data.

The latest version of the in silico model for pK_a was included beginning in Version 7.2 of the ADMET Predictor™ software.[41]

4.04.5 Physiologically Based Pharmacokinetic Modeling and Simulation Methodology

4.04.5.1 Brief Description of a Physiologically Based Pharmacokinetic Model

Traditionally, PK data were analyzed using empirical compartmental models, as illustrated in Fig. 2. These models encompassed one or more mathematical compartments including a central compartment and peripheral compartments that served as reservoirs with different volumes and different rates of exchange of drug with the central compartment. The observed concentration-time profile data for a drug defined the number of compartments and the rates of exchange between the compartments rather than the physiology of the study subject. Consequently, compartmental models are used to describe the data rather than to provide mechanistic insights into the relationships between physiology, physiochemical properties, and the pharmacokinetics of the compound.

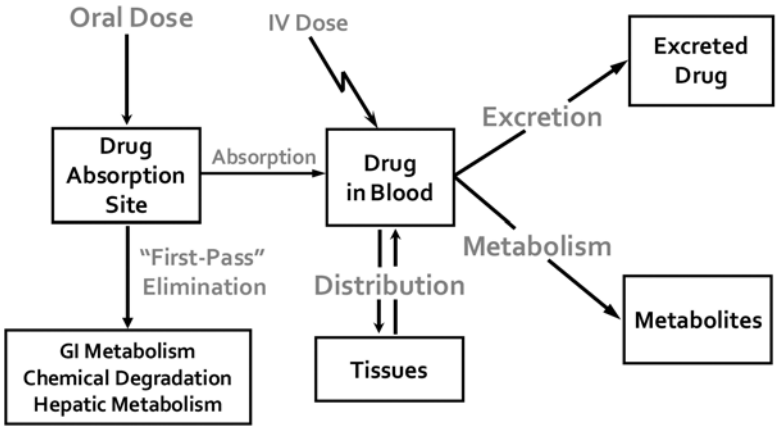

Fig. 2 Empirical compartmental model used to describe the concentration-time profile for a drug.

In contrast, PBPK models divide the body into anatomically and physiologically meaningful compartments. These compartments correspond to different tissues of the body, such as liver, kidney, and brain or tissue groups such as fat and muscle, all connected by the circulating blood system. Each tissue compartment is defined by a tissue volume or mass, a number of tissue-specific characteristic parameters (e.g., volume fraction of neutral lipids, volume fraction of phospholipids, volume fraction of water, and expression levels of enzymes and transporters), blood perfusion rate, and partition coefficients (K_p) dependent on the physicochemical properties of the drug and tissue composition.

Physiologically based PK models integrate system-specific properties together with drug-specific information in order to describe the ADME characteristics of a compound. A series of differential equations based upon mass balance considerations are constructed and solved numerically to simulate the plasma and tissue concentration versus time profiles of a compound in the animal or human system.[53–59] The goal is to predict the overall PK profile of a compound in the species of interest (e.g., rat, dog, or human), after various routes of administration (e.g., intravenous or oral administration). The concentration-time profile may be predicted for either plasma or site-specific tissue compartments.

4.04.5.2 Representing a Physiologically Based Pharmacokinetic Model in GastroPlus

Building a PBPK model requires the careful definition of the species-specific characteristics of a series of compartments. Each compartment represents a tissue, with a specified volume, a number of tissue-specific characteristic parameters, blood perfusion rate, and K_p supplied for each tissue. There are three types of compartments: blood, perfusion-limited tissue, and permeability-limited tissue. Tissues can have intrinsic clearance as a result of the presence of enzymes that may metabolize drug and can also harbor transporters that facilitate movement of drug into and/or out of the tissue.

Fig. 3 represents the GastroPlus schema for the compartments included in a typical PBPK model. Note each compartment is represented in an anatomically correct relationship, including species-specific tissue volumes, characteristic parameters, blood flows, and enzyme and transporter expression levels.

4.04.5.2.1 The absorption model

The rate and extent of absorption following oral administration is determined by the complex interaction of a variety of factors. Yu and Amidon[60] described a mechanistic absorption model that integrates all these factors. This model was further developed by Agoram et al.[61] into the Advanced Compartmental Absorption Transit™ (ACAT™) model and incorporated into the GastroPlus program. The model relies on a variety of in vitro and/or in silico input data such as solubility, permeability, particle size, lipophilicity, pK_a, interactions with intestinal transporters and enzymes, and dose to predict the kinetics associated with dissolution, precipitation, passive and carrier-mediated absorption, and intestinal first-pass elimination of a compound as it transits through the different segments of the GI tract.[56,62]

Fig. 4 illustrates the components of the ACAT model in GastroPlus.

Fig. 5 illustrates the various physical and physiological phenomena that must be represented to accurately describe drug movement from the lumen through the enterocytes lining the intestinal tract and on into the blood system. When formulated with long chain triglyceride lipids, a fraction of highly lipophilic compounds can be absorbed into the lymphatic system within the gut wall, bypassing the mesentery and portal vein delivery to the liver, thereby avoiding first-pass extraction in the liver.[63]

After a drug dissolves in the fluids of the GI tract, the molecules must traverse the enterocytes that line the GI tract and serve as a barrier to systemic entry. Entry can occur through several mechanisms. Paracellular and transcellular transfer are the routes by which a drug molecule can travel from the gut lumen to the blood.[64] Paracellular transport is dependent on the drug's physicochemical properties (molecular radius and geometry, pK_a, and diffusion coefficient) as well as physiological parameters (pore radius,

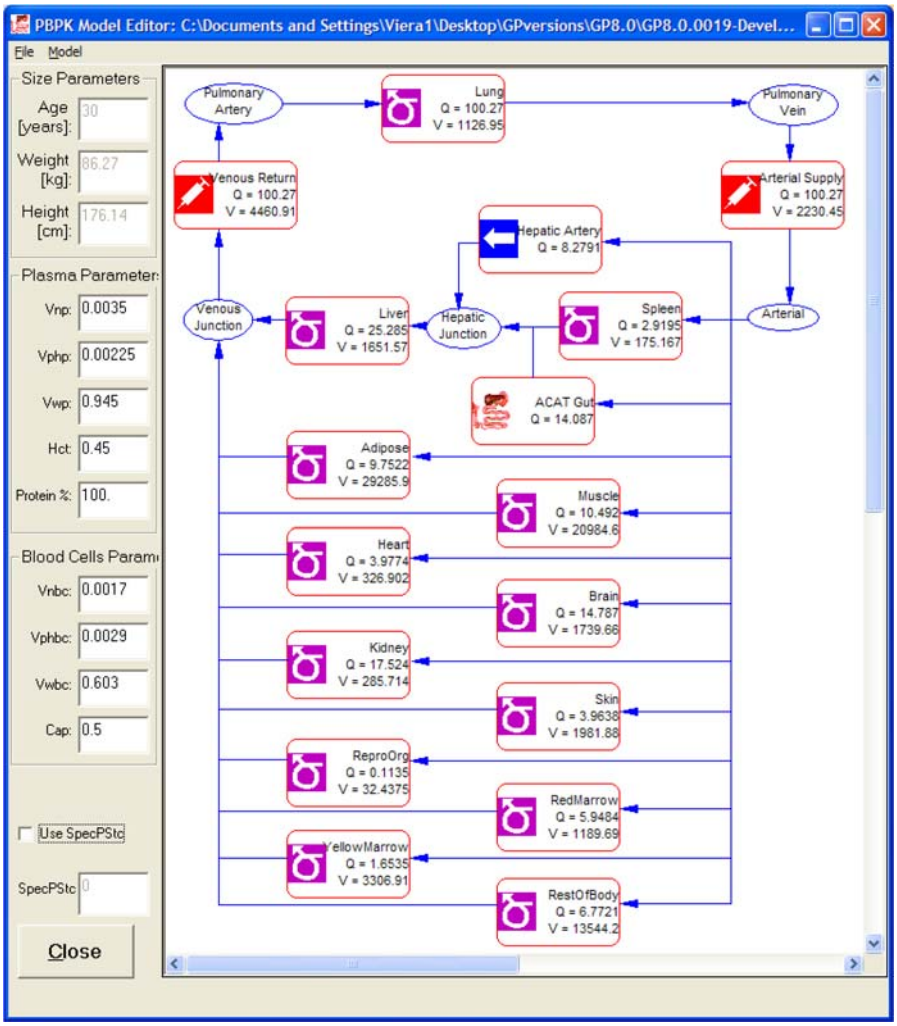

Fig. 3 Schematic from GastroPlus. Figure reproduced, with permission, from the GastroPlus™ product manual (Version 9.0).

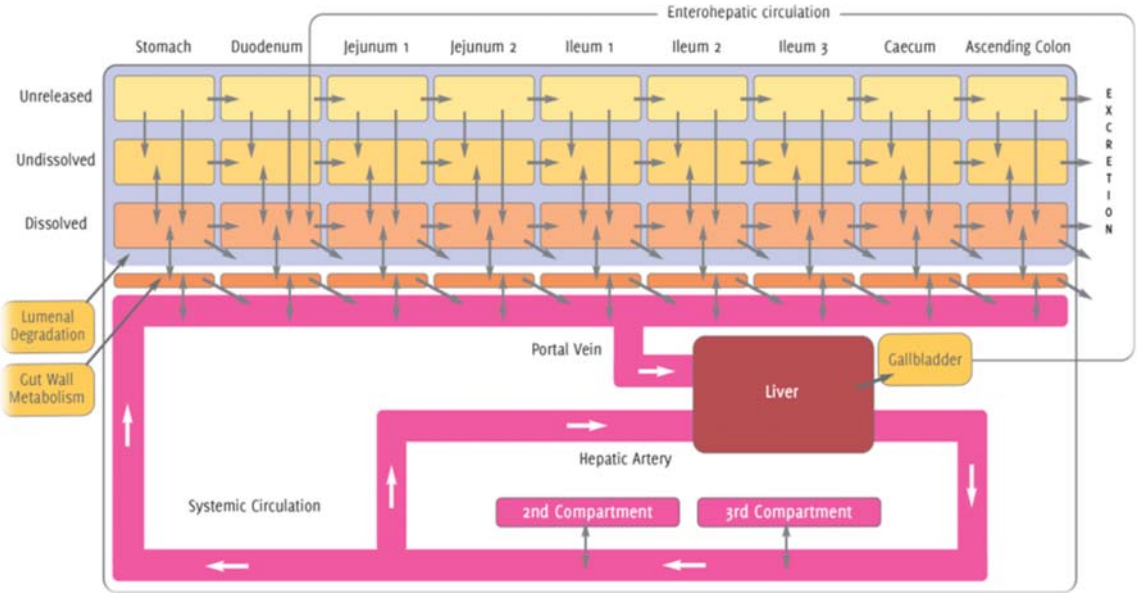

Fig. 4 Advanced compartmental absorption and transit model (ACAT™). Figure reproduced, with permission, from the GastroPlus™ product manual (Version 9.0).

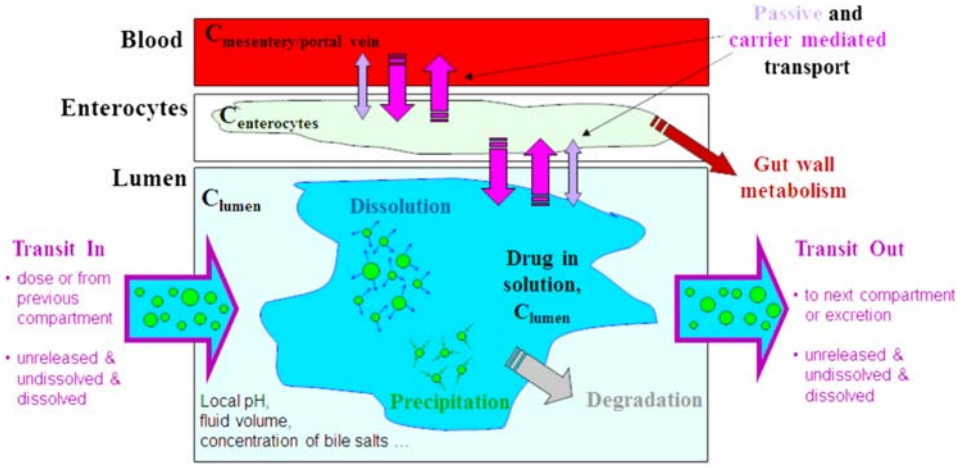

Fig. 5 A close-up view of processes involved in drug absorption through enterocytes. Figure reproduced, with permission, from the GastroPlus™ product manual (Version 9.0).

pore density, and electrical potential gradient across the GI tract). Interestingly, the paracellular permeability of a molecule is likely to change as it moves through the GI tract considering that the size and density of pores and the extent of ionization will change en route. There are also important differences in paracellular transport between species that reflect differences in the characteristics and distribution of pores along the respective animal's GI tract.

Transcellular absorption refers to transport through the cell, and includes passive diffusion as well as carrier-mediated influx and efflux due to transporters. Passive diffusion is not saturable and cannot be inhibited; this type of transport is dependent on lipophilicity and charge as the diffusion must occur without any energy expenditure. Carrier-mediated transport is saturable and inhibitable, and has structural specificity, stereospecificity, and cell specificity.

Paracellular transport occurs between the cells through the tight junctions that hold the cells together. It is important to account for paracellular in addition to transcellular absorption because, in the case of drugs that are substrates of intestinal enzymes or efflux transporters, paracellular absorption does not expose the drug to the enzymes or transporters, unlike transcellular mechanisms.

4.04.5.2.2 Tissue distribution model

Each tissue is described as either perfusion or permeability rate-limited. For perfusion-limited tissues, the rate of drug accumulation in the tissue is limited by the tissue blood flow rate (perfusion rate). Partitioning is assumed to be instantaneous and the tissue-specific partition coefficient, K_p, is used to calculate the drug partitioning between plasma and whole tissue at each time step. Consequently, the concentration of drug in the tissue is the product of the K_p for that tissue multiplied by the instantaneous concentration of drug in the plasma over the relevant time period. Perfusion-limited kinetics are generally observed for small lipophilic molecules where the blood flow to the tissue is the limiting process for drug transfer into the tissue. In some cases, a PBPK model can be developed using a mix of perfusion-limited and permeability-limited tissues to account for slower distribution into poorly perfused tissues like skin and bone marrow.[65]

For permeability-limited tissues, the rate of drug accumulation in the tissue is limited by the rate of drug transfer between extracellular and intracellular space. The tissue-specific K_p is used to calculate the drug partitioning between plasma and the extracellular space at each time step. The rate and direction of passive drug transfer between extracellular and intracellular space is calculated by the product of the permeability, the surface area of the tissue exposed to the plasma, and the gradient between the unbound drug concentrations in extracellular and intracellular space. If influx and/or efflux transporters are present, the intracellular tissue concentration will also be affected by carrier-mediated drug transfer across the cellular membrane.

4.04.5.3 Predicting In Vivo Pharmacokinetic Parameters

In the past, empirical methods, for example, allometric scaling, have been widely used to predict PK parameters in humans. The allometric approaches are descriptive only and provide little mechanistic information on the underlying processes of drug distribution, metabolism, and excretion. This approach uses in vivo data collected from preclinical animal experiments to obtain information about PK parameters, such as clearance and volume of distribution, and then scales the parameters by various measures of body size to account for differences with humans.

Allometric scaling is based on the principle that land mammals have similar physiology, biochemistry, and cellular structure, thus justifying an empirical relationship based on body size for interspecies scaling as illustrated for clearance in Eq. (7):

$$\mathrm{CL} = aW^b \tag{7}$$

where CL is the clearance of a drug, *a* and *b* are the coefficient (*a*) and exponent (*b*), respectively, for the equation. The value of the exponent for whole body metabolic rate is typically taken to be 0.75.[66] However, exponents in the range 0.6–0.8 have been reported for metabolic rate.[67] A value of 0.75 means that the whole body metabolic rate increases as body weight increases, but to a lesser extent than would be expected of a simple proportional relationship.[68]

This allometry equation has evolved from a simple transformation based upon body weight or surface area to more complex versions which can account for unbound clearance, renal and biliary excretion, or liver blood flow. The kidneys filter blood via the nephron, which scales reasonably well; however, when drugs are extensively actively secreted and require transporters, allometric predictions may not be accurate. Hepatic clearance can also be scaled by a simple ratio of hepatic blood flow between humans and animals. A more comprehensive review of different scaling methods can be found in a review paper by Zou et al.[69]

Attempts have been made to improve the prediction accuracy of these allometric scaling methods by applying corrections for protein binding, brain weight, maximum life span potential, and in vitro intrinsic metabolic clearance. These approaches have had varying degrees of success depending on compound properties.[70–74]

While allometric scaling of PK parameters is common, the literature is lacking for information on how to properly scale PD parameters. The Hill equation's parameters of capacity and sensitivity are unlikely to scale as well as biochemical or physiological variables using allometric principles.[75,76] Similar to allometric scaling of PK parameters, PD parameters also often require corrections based on physiological variations between species, such as the correction of half-maximal inhibitory concentration (IC_{50}) values for protein binding. Notably, allometric scaling has been combined with PBPK modeling in efforts to create more accurate predictions.[77]

Distinct from the purely descriptive allometric approaches, IVIVE methodologies generate inputs for PBPK modeling that are physiologically based and can provide mechanistic insights into the underlying processes responsible for the pharmacokinetic behavior of drugs. Using IVIVE, the results of in vitro experiments are scaled according to physiologically appropriate factors that effectively translate in vitro results into likely in vivo values. For example, liver microsomes, recombinantly expressed enzymes, and hepatocyte systems can be used to assess the intrinsic clearance and enzyme kinetic constants of a drug. These estimates can then be scaled with various correction factors, such as protein binding and hepatic blood flow, to obtain an estimate of in vivo hepatic clearance.[78]

Prior to the interest in PBPK modeling, data from in vivo and in vitro experimental systems were treated in a straightforward manner and static values of measurements of interest were reported. The input of these results into PBPK models has enabled the value of these data in providing dynamic, mechanistic insights into drug behavior to be realized.

Over time, a kind of symbiotic relationship has developed between experimental scientists and PBPK modelers. The in vivo and in vitro experimental protocols have undergone continued refinement and improvement as the data requirements of PBPK models were better appreciated. This has led to the design of more complex and informative experiments which allow the PBPK input parameters to be defined more precisely. This iterative relationship between the experimental models and the computational models has improved our understanding of the true complexity of experimental data and consequently improved the predictive performance of PBPK models and our understanding of the dynamic behavior of drug molecules in the body.[56]

4.04.5.3.1 Predicting intestinal and hepatic clearance

In vitro drug metabolism studies have traditionally focused on qualitative assessments of identifying metabolites, establishing the enzymes involved, and investigating the mechanism of reaction. This began to change in the 1990s as advances in in vitro methodologies along with improvements in the sensitivity of analytical chemistry techniques combined to permit the use of quantitative information from in vitro drug metabolism systems to predict in vivo drug behavior.[78] The marked species differences in the enzymology associated with common clearance processes necessitate the use of species-specific in vitro systems for the prediction of clearance in animals and man.[59]

The prediction of drug clearance from in vitro systems has been described in detail by Houston and Carlile.[78] The predictive performance of this approach has been evaluated in a variety of preclinical and clinical applications.[79–83]

When human in vitro and preclinical PK data suggest that a compound is eliminated via hepatic metabolic pathways, the in vivo prediction of hepatic clearance is based on IVIVE. The liver is arguably the most important organ for metabolism as it contains the highest number of drug metabolizing enzymes to which the drug is exposed prior to reaching the systemic circulation. However, even though intestinal epithelial cells have a much lower mass of cytochrome P450 enzyme (CYP) (10 to 100-fold less on a mg enzyme/whole tissue basis), each molecule that is absorbed by the transcellular pathway is exposed to those enzymes. Consequently, the magnitude of first-pass extraction for substrates of CYP3A4, 2C9, 2C19, and 2D6 can make a significant impact on bioavailability.[84] Notably, drugs which are inhibitors of enzymes located in the gut can, therefore, have a marked effect on resultant systemic concentrations of coadministered drugs which are substrates (e.g., furanocoumarins in grapefruit juice and their effect on simvastatin).

Even more significant is the potential for enzyme saturation in the gut by therapeutic doses of drugs due to the higher intraenterocyte concentrations compared to much lower free plasma concentrations. This saturation can result in nonlinear dose dependence as seen for substrates like midazolam and UK-343,664.[61,85]

Typically, a four-step process is required to perform IVIVE and predict in vivo drug behavior.[78] First, the metabolite formation of a particular drug is measured in vitro at relatively low concentrations across a range of microsomal protein concentrations or cell density and is used to obtain an estimate of intrinsic clearance (CL_{int}). Low concentrations are vital to ensure linear kinetics. The CL_{int} of a compound acts as a proportionality constant to describe the relationship between the rate of metabolism and low

concentrations of substrate. It is a measure of enzyme activity toward the drug that is independent of blood flow. The rate of metabolism at low concentration (v_0) is given by Eq. (8).

$$v_0 = \mathrm{CL_{int}} \times C_e \tag{8}$$

where C_e is the unbound concentration of drug within the metabolizing tissue, which is assumed to be the concentration available to the enzymes. The various CYP contributions to the overall $\mathrm{CL_{int}}$ are additive, so the overall value can be measured in human or murine microsomes. Typically, liver microsomes or hepatocytes are used, but the microsomes or cells from other tissues may be used to characterize the metabolism in other tissues. In many cases, the intrinsic clearance determined from liver microsomes can be used to parameterize the contribution of gut metabolism if the regional gut CYP distribution and level of expression compared to the liver is known.

The particular CYP isoforms responsible for metabolism can be identified by looking at the effects of isoform-specific inhibitors on microsomal or hepatocyte metabolism or by assaying recombinant CYPs (rCYPs) in microsomes from cell lines transfected with individual CYPs and cytochrome P450 reductase. Insect cell lines transformed with baculovirus are particularly useful for this purpose.[86]

The relationship between C_e and the rate of metabolism becomes nonlinear at higher substrate concentrations because CYPs, like most enzymes, are saturable—that is, their rate of catalysis approaches a limiting value (V_{max}) as substrate concentration increases. The susceptibility to saturation is different for each CYP/substrate combination, and the differences in affinity are not additive. As a result, kinetic parameters are best determined by fitting data from rCYP assays for contributing isoforms to:

$$v = V_{max} \times C_e/(K_m + C_e) \tag{9}$$

where v is the rate of metabolism at drug concentration C_e, and V_{max} is the maximal rate of metabolism. K_m is the Michaelis constant, which characterizes the affinity of the enzyme for its substrate. Note that when $C_e >> K_m$, the term $C_e/(K_m + C_e) \sim 1$, and $v \sim V_{max}$. Under linear conditions, when the free substrate concentration (C_e) is low relative to K_m, v approaches v_0 and Eq. (9) reduces to Eq. (8).

From which it is evident that:

$$\mathrm{CL_{int}} = \text{Rate of metabolism}/C_e = V_{max}/K_m$$

Several in vitro systems have been used to estimate intrinsic clearance. These systems range in structural integrity from liver slices, to freshly isolated hepatocytes, to subcellular fractions such as microsomes. The units used to report activity vary, but typically are $\mu L\ min^{-1}$ mg microsomal protein, $mL\ min^{-1}\ g^{-1}$ liver, or $mL\ h^{-1}\ kg^{-1}$ body weight. Hepatocyte $\mathrm{CL_{ints}}$ are reported in units of pL/min/10^6 cells.

Comparative experience with these systems suggests that hepatocyte preparations provide more accurate predictions of in vivo clearance estimates. Liver slices are poorly predictive, in part, because of delayed accessibility of substrate to cells with the core of the slice. Hepatic microsomes are the most inconsistent predictor of $\mathrm{CL_{int}}$. However, this system can provide acceptable predictions for many compounds and there is a need to fully define where its limitations occur. Hepatocytes have the virtue of incorporating transporter and Phase 2 metabolism effects such as glucuronidation and sulfation. This caveat is of particular relevance to the use of human tissue, as hepatic microsomes will continue to be the dominant system employed in vitro, while there is limited availability of suitable fresh human tissue for hepatocyte preparation.[78]

In the second step, the estimate of $\mathrm{CL_{int}}$ is scaled to quantify the full activity in the liver as measured in vitro. The choice of scaling factor relates to the type of in vitro system used for measuring $\mathrm{CL_{int}}$. For example, in the case of a hepatocyte preparation, the scaling factor is simply the number of hepatocytes found in an intact liver. The scaling factor for microsomal preparations is more complicated because the preparation of microsomes by differential centrifugation is incomplete and the scaling factor must represent this inefficiency.[87] In this case, the scaling factor is typically the microsomal protein ratio, which represents the amount of microsomal protein isolated per liver slice.[78] While recombinant enzyme systems provide useful information regarding enzyme kinetics, neither enzyme prevalence nor enzymatic activity is considered due to the innate simplicity and specificity of the preparation. Due to this lack of incorporation of the variable expression observed in human populations, different approaches exist to encompass these factors in an effort to create a more realistic metabolic clearance prediction. The relative activity factor and the relative abundance method are the two most commonly used approaches.[88] The details of how to apply these scaling procedures within PBPK models have been described elsewhere.[53]

In the third step, a model of liver metabolism is used to convert the estimated $\mathrm{CL_{int}}$ into the predicted hepatic clearance ($\mathrm{CL_h}$). The liver model uses information on species-specific hepatic blood flow and binding of drug in the blood to convert $\mathrm{CL_{int}}$ to an expression of hepatic clearance in terms of the circulating blood drug concentration rather than drug concentration within the liver. In the commonly used venous equilibration liver model, the distribution of drug within the liver is assumed to occur instantaneously with no concentration gradient. Consequently, the liver acts like a single, well-stirred compartment. This model enables hepatic clearance to be calculated as follows[78]:

$$\mathrm{CL_H} = \frac{Q_H \cdot \mathrm{CL_{int}} \cdot \mathrm{fub}}{Q_H + \mathrm{CL_{int}} \cdot \mathrm{fub}}$$

where Q_H is the hepatic blood flow and fub is the unbound concentration of drug in the blood for the species of interest. Other liver models, such as the parallel-tube model and dispersion model, may be utilized; it is important to consider the assumptions associated with the chosen model.

For compounds that are primarily metabolized by CYPs, detailed enzyme kinetic data based on metabolite formation are preferred over intrinsic clearance estimated from substrate depletion studies since the kinetic data capture the saturation effects that lead to dose-dependent metabolic clearance. Moreover, care must be taken to ensure that drug loss equates with enzyme-mediated metabolism and not some other process such as physical adsorption, incorporation into cellular components, or nonenzymatic degradation. As the time period for monitoring drug loss is likely to be substantial, the stability of the particular enzyme preparation becomes of prime concern.[78]

For cases in which Phase 2 conjugation or other non-CYP metabolism contributes significantly to the hepatic clearance, for example, based on the metabolite profile, the human hepatocyte intrinsic clearance is preferred over that from human liver microsomes.[79] This is due, in part, to the location of the majority of Phase 2 enzymes in the cytosol (those involved in methylation, acetylation, sulfation), which would not be detected in microsomal preparations. While some Phase 2 enzymes are microsomal, such as the glucuronosyl transferases, the lack of most enzymes and the need to add cofactors hinder the use of microsomal preparations. In contrast to the situation for CYP enzymes in the gut, where intrinsic clearance in the liver can be used to estimate gut first-pass extraction, many of the Phase 2 enzymes have very different expression in gut, liver, and kidney.[89]

Consequently, the application of IVIVE for Phase 2 enzymes is more complex.

Houston and Carlile[78] introduced criteria to determine whether a prediction of hepatic clearance is acceptable or not. They used the ratio of the predicted CL_{int} to the observed CL_{int} and an arbitrary precision limit of $\pm$ twofold of the in vivo prediction, that is, between a 50% underprediction and a 100% overprediction. The logarithm of the ratio is employed to achieve a symmetrical distribution. Hence, a twofold precision limit for this ratio corresponds to ± 0.3 log units. Perfect predictions would appear as zero values, underpredictions and overpredictions are represented as negative and positive values, respectively.

In the final step, nonhepatic routes of elimination, such as renal excretion of unchanged drug or extrahepatic metabolism, are incorporated into the prediction. The utility of IVIVE for hepatic metabolic clearance has been well established in the literature[90–92] and is developing to improve poor predictions by incorporating hepatic uptake and/or biliary excretion.[79,93,94]

4.04.5.3.2 Predicting volume of distribution

The use of PBPK models to simulate drug concentration-time profiles requires information on the distribution of drug into each organ and tissue compartment represented in the model. Previously, the determination of tissue-to-plasma partition coefficients (K_{ps}) required costly animal studies and limited the use of PBPK models in early drug research and development. The development of mechanistic tissue composition-based equations enabled the calculation of drug-specific K_{ps} in different tissues and organs based on physicochemical properties. These K_p values, in conjunction with tissue-specific volumes, are used to estimate the species-specific V_{ss} of a compound as the sum of the individual tissue (including blood) distribution volumes. These mechanism-based formulas have enabled the routine application of PBPK methods in early drug discovery by reducing the reliance on data from in vivo experiments.[79]

Experimental methods for determining V_{ss} require an intravenous drug administration followed by compartmental or statistical moment analysis of the resultant plasma concentration-time data. Since this information is generally not available in early discovery, the development of a PBPK model requires an alternative approach. Previously, the prediction of V_{ss} required a determination of drug affinities for various tissues and organs of the body along with measures of associated tissue and plasma volumes. The considerable time, resources, and costs associated with experimentally determining tissue affinities has lead to various attempts to predict V_{ss} based on information about the underlying distribution mechanisms, physiologic considerations, and physiochemical properties of the compound.

The mechanism-based equations to predict V_{ss} have evolved over time, and research has revealed more about the determinants of drug distribution into different tissues. Poulin and Theil were among the first to investigate these mechanistic approaches for drug molecules, and by expanding on the earlier work of Poulin and Krishan,[95] they demonstrated the ability to predict the affinity of small molecules for various tissues and organs.[96] In this method, homogeneous drug distribution into each tissue is assumed to occur by a process of passive diffusion. Tissue and plasma are assumed to be a combination of water, lipids, and proteins at pH = 7.4. The tissue composition method of calculating K_p derives from an assumption that drugs partition into tissues by virtue of nonspecific binding with neutral lipids and phospholipids in the tissues and these interactions may be further impeded or enhanced by specific binding to plasma or tissue proteins. Berezhkovskiy subsequently published a correction to the Poulin equation for calculating the tissue–plasma partition coefficients.[97]

In subsequent applications of these approaches, it was recognized that although the equations reliably predicted K_p values for neutral molecules, many drug substances that are cationic at physiologic pH were observed to have higher volumes of distribution compared to neutral and acidic molecules of similar lipophilicity. Consequently, adjustments were necessary to incorporate the extent of drug ionization in predicting tissue-to-plasma water partition coefficients (K_p).

Rodgers et al. developed equations to predict tissue distribution coefficients (K_p) for moderate to strong bases[98] and separately for acids, very weak bases, neutrals, and zwitterions.[99] These equations are based on the assumption that all drugs will dissolve in intra- and extracellular tissue water and partition into the neutral lipids and phospholipids located within tissue cells.[100] For compounds with at least one basic $pK_a \geq 7$, the corresponding equation accounted for electrostatic interactions with tissue acidic phospholipids. For compounds that bind with extracellular proteins, the affinity and extent of binding must also be considered. Acids and weakly basic compounds are assumed to bind primarily to albumin and neutral drugs to lipoproteins.

The major distributional processes that must be incorporated into these mechanistic equations to predict K_p include dissolution into tissue water, lipid partitioning, electrostatic interactions with acidic phospholipids, and extracellular protein binding.

The Rodgers et al. K_p calculations[98–100] are based on a distinction between strong bases and other compounds with an arbitrary cut-off at base $pK_a = 7$. This puts significant weight on an accurate measurement or prediction of base pK_a values, especially for those drugs with values around seven. Small errors in measurement or prediction of pK_a around seven can result in the selection of the wrong equation and subsequently significant errors in the estimated K_p values.

In order to address the dichotomy arising from the two Rodgers and Rowland equations, Lukacova and colleagues[101] derived a modified form that combines the two equations into one. This equation provides a continuous shift from neutrals and acids binding almost exclusively to albumin toward strong bases binding almost exclusively to acidic phospholipids. Moderate bases (base pK_a in the range of 6–8) will have neutral as well as cationic species present in plasma and in tissues at physiological pH values. It is assumed that these compounds could bind to both albumin (via their neutral forms) and acidic phospholipids (via their ionized cationic forms). As expected, in comparing the two approaches, the calculated K_{ps} will be similar to the original Rodgers approach for acids, neutrals, very weak bases, and very strong bases, where the fraction of molecules with positive charge will be either insignificant or nearly 100%. Differences in K_p values will be seen for moderate bases (with pK_as in the range of 6–8), where significant contributions from both types of binding can be expected.

Several situations arise that can result in over- or underpredictions of K_p and subsequently affect the accuracy of the predictions of V_{ss}. These situations arise when active transport processes, nonlinear pharmacokinetics, or binding to tissue constituents are not accounted for by the mechanistic equations. For example, doxorubicin extensively interacts with tissue DNA and the mechanistic equations result in significant underprediction of V_{ss}.[102,103] Another example is provided by chlorthalidone, a basic compound with a high affinity for human carbonic anhydrase, an enzyme primarily located in the cytosolic fraction of red blood cells.[104] This enzyme affinity results in a high blood-to-plasma concentration ratio and subsequent overprediction of V_{ss}.

It is important to recognize that uncertainty in parameters, for example, arising from the compilation of data from rats of different ages, strains, weights, and gender, can influence the accuracy of K_p predictions generated from these equations. Experimental difficulties can also be encountered for compounds that are extensively protein bound and/or highly lipophilic. Finally, the inherent variability in the measurements of the variables required for selected equations can also impact the accuracy of the predictions.[100]

4.04.5.3.3 Case study—impact of lysosomal trapping

Azithromycin (AZM) is a semisynthetic macrolide antibiotic with a broad range of activity against Gram-positive bacteria and some community-acquired Gram-negative pathogens. The drug has a large distribution volume of approximately 23 L kg^{-1} of body weight and a long half-life of 68–79 h.[105] These PK characteristics often allow for a convenient once-daily dosing regimen and a short overall duration of treatment, as brief as 3–5 days for some indications.[106]

Although the large distribution volume suggests extensive tissue distribution, the majority of the drug is confined to intracellular compartments and thus is unavailable for extracellular antimicrobial activity. This is due to the fact that AZM is a diprotic base (pK_a 1, 8.1; pK_a 2, 8.8).[107] Once it enters the acidic subcellular compartments, such as the lysosomes, the drug becomes protonated and is subsequently trapped there. This mechanism, known as lysosomal trapping, is responsible for the long elimination half-life and the retention of AZM within the tissue long after the administration of the last dose.[105,106,108]

In a clinical PK study, Matzneller et al.[106] determined the free concentrations of AZM in the interstitial fluid (ISF) of muscle and subcutaneous adipose tissue and total concentrations in polymorphonuclear leukocytes in six healthy male volunteers receiving 500 mg once-daily AZM for 3 days. This data was subsequently used by Zheng and colleagues[109] to develop a tissue distribution model for AZM that allowed the simultaneous characterization of free drug concentrations in the ISF of muscle and subcutaneous adipose tissue, taking into consideration the effects of protein binding and the differences in ionization state at physiological pH values in the different tissue sites.

This work demonstrated that AZM concentrations during and after treatment were the highest in white blood cells due to intracellular accumulation, whereas the total concentrations in plasma and the free concentrations in the ISF of muscle and subcutaneous adipose tissue were markedly lower. While the long terminal half-life of AZM helps to maintain drug concentrations above the minimum inhibitory concentration of the infecting pathogen in certain compartments, the persistent low drug concentrations in other tissue sites may potentially lead to an increased risk of the emergence of resistance.

4.04.5.3.4 Predicting transporter effects

Our understanding of the importance of endogenous influx and efflux transporters on drug absorption, distribution, and clearance has increased greatly since 2008. In fact, Kell and colleagues have suggested that carrier-mediated membrane transport greatly outweighs passive membrane permeability mechanisms.[110,111]

This view has not met with wide acceptance, but has invigorated strong debate and visibility of the importance of drug transporters.[112]

In many cases, nonlinear dose dependence for therapeutically relevant doses of drug molecules can be explained by saturation of intestinal influx and efflux transporters. Bolger and colleagues used transporter K_m values determined in vitro for substrates of intestinal influx transporters and in silico PBPK modeling to explain the nonlinear dose dependence for gabapentin, a substrate for organic cation transport-1 (OCTN1) and L-type amino acid transporter (LAT2), and for valacyclovir, a substrate for oligopeptide transporters (PepT1 and HPT1).[113]

In contrast to PBPK modeling for substrates of influx transporters, experimentally determined values of apparent K_m for efflux transporters do not reflect the intraenterocyte unbound concentration of drug molecules and must be corrected to accurately explain nonlinear dose dependence in vivo.[114,115]

These principles are reflected in PBPK modeling for the nonlinear dose dependence of talinolol, a substrate of P-glycoprotein (P-gp) and UK-343,664, a substrate for both CYP3A4 and P-gp.[85,113,116]

A general purpose cellular simulation program (MembranePlus™, Simulations Plus, Inc.) is available to facilitate the determination of intracellular unbound K_m values for substrates of efflux transporters by fitting in vitro permeability assay data. This program was used to estimate the K_m for interaction of digoxin with P-gp and GastroPlus was used for PBPK modeling of digoxin in vivo intravenous and oral Cp-versus-time data.[117]

Prior to the adoption of quantitative targeted absolute proteomics (QTAP) for the determination of absolute transporter expression in human tissues,[118] two approaches for performing IVIVE of transporter effects were published over the past few years.[119,120] The general consensus between these approaches is that the extrapolation requires an additional empirical scaling factor. Two types of scaling factors were proposed, system-specific and compound-specific. With system-specific scaling factors,[119] the same scaling factor would be used to extrapolate the transporter parameters from a specific in vitro assay setup to in vivo conditions for a wide range of compounds. With compound-specific scaling factors,[120] a compound-specific scaling factor is derived for extrapolation from in vitro assay to in vivo animal predictions and the same scaling factor is used for extrapolation from in vitro assay to in vivo human predictions. A common feature of the published approaches is the focus on low passive permeability and the importance of transporter effects in the gut, liver, and kidney. These approaches do not consider the effect of low passive permeability on the distribution of drug to other tissues with subsequent effects on plasma concentration.

Consideration of low passive permeability requires specification of the permeability-surface area product (PStc) value. Without knowledge of the total cell surface areas in different tissues, the model would typically require fitting the tissue-specific PStc values against in vivo data, which may be difficult with only available plasma concentration profiles. Lukacova et al.[121] suggested an alternative approach to obtaining the tissue-specific PStc values by introducing the "*Specific PStc*" parameter (*PStc* per mL of cell volume), which makes this extrapolation easy and straightforward. By accounting for low passive permeability in all tissues, more accurate IVIVE was obtained without the need for empirical scaling factors.

4.04.5.3.5 Predicting permeability

The permeability of a compound is a critical determinant of its potential to be absorbed from the GI tract and reach the systemic circulation. Consequently, in vitro assays to measure permeability have been developed to help predict a drug's permeability in humans.

Several experimental approaches to evaluate intestinal permeability are commonly used during drug development and the choice of assay is dependent upon the circumstance. The parallel artificial membrane permeability assay (PAMPA) measures passive transcellular transport and is good for high-throughput screening, having low cost compared to other methodologies. PAMPA is designed to mimic the lipid composition of enterocytes, but only assesses passive permeability in the intestine and does not account for transporter expression. More expensive assays which can provide additional information regarding transporter expression are also available, including human colorectal adenocarcinoma cells (Caco-2) as well as Madin–Darby canine kidney (MDCK) cells. These cells can be used in confluent monolayers as surrogates for the intestinal epithelium. They include the effects of some carrier-mediated transport, providing answers to questions regularly posed in transporter studies such as those listed by Brouwer and colleagues, investigating the influence of active uptake or apical efflux on intestinal absorption.[122]

Because these permeability assays are cell cultures, inherent variability exists between and even within laboratories as expression levels of transporters can differ. This is especially true for Caco-2, which come from a heterogeneous cell line. For this reason, MDCK cells transfected with specific transporters are often preferred. In both cases, varying expression of endogenous transporters should be considered while studying transport.[123] The results of these cellular studies can vary substantially even for drugs that are not substrates for transporters. This is because the results depend on many factors such as how long the cells were cultured, the pH on each side of the membrane, solvents used, amount of protein on receiver side, concentration of drug on donor side, nonspecific binding to plastic ware, among other variables. However, in vitro assays remain a reasonable foundation for predicting permeability of compounds.

4.04.6 Applications of Physiologically Based Pharmacokinetic Methodology

PBPK models are routinely applied in early discovery where limited in vivo data exists and in silico prediction of parameters or extrapolations from in vitro assay results are required to generate drug-related input parameters for model building. These applications have been bolstered of late by improved in silico and in vitro systems capable of acting as surrogates for in vivo absorption, distribution, metabolism, and excretion (ADME) processes and the advancement of strategies for the IVIVE of these data.[10]

The applications of PBPK in the preclinical space include predicting animal or human PK, and the use of PBPK models to inform the design and predict the outcomes of formulation, toxicokinetic, PK, and pharmacologic studies. These applications, which have aided in the reduction of animal use in research, play an important role in guiding R&D plans and focusing efforts on critical questions that can impact the future direction of development programs. In the preclinical setting, the questions focus on optimization

of the preclinical testing program and gaining an early understanding of critical factors that can affect the success of the clinical development program. These questions include,

- What is the expected PK profile in humans and what is our level of confidence in the PBPK model?
- Is there likely to be a food effect? Can we mitigate a food effect with an appropriate formulation strategy?
- Do we expect clinically relevant DDIs or pharmacogenetic effects in human populations? How should we best study these effects in clinical trials?

From the beginning of clinical development and into the post-approval period, PBPK models have been used to predict PK in various subpopulations, including pediatrics and patients with various disease states, in addition to oral absorption and DDI modeling. In this setting, the questions focus on improved understanding of the determinants of safety and efficacy outcomes, including:

- What is the expected plasma or tissue exposure in various subpopulations? How can we use this information to anticipate exposure-response relationships?
- What clinical dosing regimens are required to achieve therapeutically effective concentrations?
- How do we balance risk versus benefit? Would a modified release formulation improve the safety or efficacy profile and improve marketability of a compound?

A comprehensive listing of the various applications of PBPK modeling and simulation over the lifecycle of R&D is beyond the scope of this article. Publications are available that can shed additional light on the full scope of applications.[57,124]

4.04.6.1 Lessons Learned From the Early Applications of Physiologically Based Pharmacokinetic Modeling and Simulation

4.04.6.1.1 Reducing the use of animals in toxicology testing

Once a lead chemical series is identified, an early toxicology study (ETS) is typically performed in a rodent and nonrodent species prior to lead development to screen out toxic compounds. An ETS normally requires daily dosing over a 7- or 14-day period using a range of doses. To help set the dose, a preliminary single dose toxicokinetics study would be performed at three dose levels. In this scenario,[56] experience has shown that PBPK modeling can be used to reduce the need for the preliminary dose-setting study, thus reducing requirements for compound, improving process efficiency, and reducing animal usage. The same report showed that PBPK modeling can be used to predict saturation in absorption and formulation issues to ensure appropriate dose selection for toxicology studies. In a retrospective analysis using a cohort of 39 compounds to assess PK prediction accuracy, PBPK methods were shown to more accurately predict area under the curve (AUC) and C_{max} observed with high dose PK data than an approach assuming linearity from low dose studies.[56]

4.04.6.1.2 Assessing the feasibility and performance of physiologically based pharmacokinetic predictions of human pharmacokinetics

A series of publications in the early 2000s sought to evaluate the feasibility and performance of PBPK models for the prediction of human PK.[57–59,125–127]

Parrott et al. compared empirical and physiologically based approaches for the prediction of human pharmacokinetics using 19 diverse compounds taken from Roche clinical development projects.[59] Predicted values of PK parameters and plasma concentrations were compared to observed values in order to assess the accuracy of the prediction methods. Overall, the physiologically based approach gave more realistic predictions than the other methods with a greater proportion of the predicted parameters (e.g., C_{max}, AUC, $t½$) within twofold error of the observed values. For example, 76% versus 42% of compounds had a predicted AUC within twofold error of the observed value using physiologically based models versus an allometric approach, respectively.

Importantly, the authors recognized that poor predictions from the physiologically based models were often the result of processes that were not incorporated into the model due to uncertainty in the scaling between species (e.g., biliary clearance, enterohepatic recirculation). In this context, 70% of compounds were judged as being good candidates for a reliable extrapolation since such processes were not needed for good simulations in animals. Of these compounds, 92% had predicted AUC within twofold of the observed value.

De Buck and colleagues evaluated different PBPK modeling approaches for the prediction of human PK parameters.[125] GastroPlus was used to construct an absorption–disposition PBPK model and provided accurate predictions of area under the plasma concentration-time profile, oral apparent volume of distribution, and maximum plasma concentration after oral dosing, with 74%, 70%, and 65% of the predictions within a twofold error, respectively. However, the methods used to compute the model input parameters affected the results and better predictions were obtained when in silico predictions of V_{ss} were refined using rat experimental data and when binding was properly accounted for in computing estimates of clearance from in vitro measurements.

Jones and colleagues at Pfizer recognized that early predictions of human pharmacokinetics can reduce failures in clinic related to poor pharmacokinetics by enabling the early selection of the best candidates for development and rejection of those compounds with a low chance of success.[58] They compared the accuracy of a simple one-compartment approach using allometric scaling to obtain estimates of clearance and V_{ss} to a PBPK approach using tissue composition models to estimate K_p and, hence V_{ss}, and IVIVE methods to estimate clearance. The simulation results obtained from PBPK models were able to accurately predict

passive distribution and absorption processes and these predictions were superior to the one-compartment model previously employed for this purpose. Some issues and limitations were noted with respect to the prediction of clearance and active transport processes.

More recently, the Innovative Medicines Initiative (IMI) in the European Union funded a 5-year grant involving many academic and industrial collaborators in basic research to improve oral biopharmaceutical tools (OrBiTo). This collaboration will provide additional results for blinded prospective PBPK modeling of pharmaceutical active pharmaceutical ingredients that both failed and succeeded in regulatory approval.[128,129]

4.04.6.1.3 First-in-human prediction and trial design

Using a set of 19 compounds from F. Hoffmann la Roche, Jones et al.[57] proposed and validated a strategy for the use of PBPK for human PK simulations. Initially, the PBPK simulation is performed using animal PBPK models, animal in vitro data, and compound-specific physicochemical data. The animal simulation is compared with the in vivo data; if this simulation in animals is reasonable, then the human simulation is performed using a human PBPK model, human in vitro data, and compound-specific physicochemical data. If the simulation in animals is inaccurate, this would indicate a violation of one or more of the model assumptions; in this case, further experiments may be performed to understand the mismatch. For those compounds where good predictions of animal PK were achieved, 92%, 67%, and 100% of compounds had prediction accuracy within twofold in humans for AUC, C_{max}, and T_{max}, respectively. The prediction accuracy was reduced (76%, 47%, and 94% for AUC, C_{max}, and T_{max}, respectively) when the compounds that were judged as having poor predictions in animals were included in the human analysis, emphasizing the need for good understanding in animals prior to the simulation in human.

4.04.7 Generalized Approach to Building and Validating a Physiologically Based Pharmacokinetic Model

The development and validation of a PBPK model requires a step-wise approach to the assembly of the required system- and drug-specific information and its input into a well-constructed PBPK software product. The goal is to utilize all available in vitro and in vivo data as they become available during the R&D lifecycle to determine the most appropriate assumptions regarding model specification.[79] The completeness of a PBPK model can depend on the timing of model development with respect to the extant knowledge base for a drug. For example, early-stage PBPK models may utilize predicted physicochemical properties of the drugs of interest and simplifying assumptions about the nature of drug metabolism and elimination. These simplifying assumptions can then be updated as additional information becomes available about the compound.

It is important to note that the quality and certainty of predictions from the PBPK model can improve over time as in vitro data, preclinical in vivo data, and finally in vivo data in humans become available. A key aspect of this progression is that estimates from each stage can provide a valuable reality check for subsequent stages, for example, predictions sometimes disagree with experimental measurements because mistakes were made in carrying out the measurements.

Although the critical parameters for a specific compound will vary depending on the ADME properties of the compound, it is possible to define a generalized scheme for developing PBPK models and performing simulations.[130] The scheme outlined below illustrates the need to understand, as much as possible, the relevant properties of a drug (or related compounds) that might inform on likely characteristics and then to proceed in an iterative process of assessing the performance of the model against observed data. The importance of understanding the compound properties, the quality of data used as model inputs, and the nature of the interactions of the compound with human physiology are paramount in developing confidence in the model and accuracy of the predictions in humans.

Step 1: Identify the drug's ADME pathways and quantify the rate and extent of relevant parameters.
Step 2: Incorporate drug-specific parameters into the PBPK model.
Step 3: Compare the predicted concentration-time profiles with those obtained from available in vivo preclinical and/or human studies.
Step 4: Refine the model on the basis of the results from Step 3.
Step 5: Use the refined PBPK model for predicting PK profiles under various scenarios of interest that have not been studied experimentally.
Step 6: Incorporate information about the mean and upper/lower boundaries for relevant parameters in order to reflect interindividual variability or uncertainty in the parameter estimates in the simulations.[130]

In general, model building should begin as early as possible in the discovery stage in order to provide input for consideration in lead selection. Scientists must recognize that the database for use with the PBPK model will continue to evolve as the drug moves through different R&D stages and different issues are encountered. An interdisciplinary process for model building, evaluation, and adjudication should be established.

At each stage, the model must have a champion to manage the testing of model assumptions and performance. A system for alerting champions to changes in data or knowledge is critical to enabling the model to keep pace with changes in the knowledge base. It is important to keep good notes on model evolution so that subsequent champions can quickly pick up and continue model development. Given the complexity of interpretation of data and model assumptions, there is an important role for experienced

mentor(s) during model building in order to monitor the acceptability of model assumptions and data interpretations. It is important to establish a standard format for data retrieval and storage, along with a process for change control, naming conventions, and data archiving.

As experience with PBPK modeling and simulation has increased, so has an appreciation of the nuances involved in building PBPK models and the emergence of ideas for best practices in many aspects of the effort. Recent publications[10,131–137] have explored the various aspects of model building, parameter optimization, reporting, and model qualification with an eye toward improving the quality and confidence in relying on models to support corporate and regulatory decision-making. Aspects of PBPK modeling and simulation that warrant special consideration are described below.

4.04.7.1 Model Building and Input Data

The in vitro methodology used to determine input values for PBPK models, such as intrinsic clearance or permeability, can vary across companies and sometimes within companies as a compound moves through the R&D lifecycle. This can create sources of uncertainty that must be kept in mind as the knowledge base for a compound evolves over time.

Best practices in the use of in vitro and in vivo ADME data to provide drug-specific input parameters are emerging and the value of a quantitative mass balance diagram for a compound has been proposed.[132] When feasible, pharmacokinetic information obtained after both orally and intravenously administered dosing is valuable in the quantitative mechanistic understanding of drug disposition. Data to support this understanding should include answers to the following questions: (1) What are the clearance pathways and their quantitative contributions? (2) What is the extent of absorption of the drug and is parent drug in feces a result of lack of absorption (F_a) or biliary/intestinal excretion? (3) When oral bioavailability is low, what are the contributions of intestinal and hepatic first-pass loss? (4) What is the rate-limiting step in hepatic drug clearance (basolateral uptake, metabolism, or biliary secretion)?[132]

In building a PBPK model, tissue weights, tissue perfusion rates, tissue densities, and tissue-specific partition coefficients for the compound of interest are required. In GastroPlus, the initial estimates for these physiologic parameters are obtained from the Population Estimates for Age-Related Physiology™ (PEAR™ Physiology)[138–141] module within the software.

GastroPlus also has the ability to represent infant physiologies for infants less than 1 year of age who were born at term or up to 16 weeks premature.[142] Other sources of system-dependent parameters (e.g., tissue volume, blood flow) for human and preclinical species are available in the literature[139,143] and have recently been compiled.[144,145]

4.04.7.2 Model Optimization

The process of model optimization using sensitivity analysis and parameter optimization relative to observed data is integral to the development of robust PBPK models. The optimization process must explicitly recognize information gaps and the consequences with respect to specific applications of the model. The optimization process may lead to a more predictive model; however, the process should be transparent and consider available in vitro data, clinical DDI information, urinary excretion data, human mass balance data, and plasma PK data. The optimization process should be purpose-driven and the plausibility of the resultant model should be considered. For example, scaling factors used in IVIVE vary in plausibility; some being physiologically based, but others more empirical, and they may vary between analyses.

Sensitivity testing of model predictions to changes in model parameters is essential, and the range of sensitivity analyses performed should be defined depending on the physiochemical properties of the drug and/or the experimental systems under consideration. A reasonable range for sensitivity analysis should be provided and justified. Model parameters with known certainty can be prespecified, allowing more informed determination of candidate parameters for sensitivity analysis. Often optimization of several independent factors may lead to a model with superior predictive performance. When possible, the hypotheses that lead to the optimized parameters should be tested with experimental data.[131,132]

4.04.7.3 Reporting

There has been considerable discussion about the critical elements required for inclusion in PBPK reports submitted for regulatory consideration. Shepard et al.[132] pointed out that reports should clearly address the regulatory question, the clinical context, and whether the simulations will lead to changes in dose recommendations. The inclusion of background information, for example, clinical pharmacology, purpose of the modeling effort, history of PBPK model development, and so forth, is helpful and the level of detail should be adequate to support the desired application of the model. It is vital that the clinical pharmacology information be integrated across studies and that the adequacy of the model be assessed in conjunction with the known therapeutic index of the drug. Uncertainty, sensitivity analysis, and plausibility of the assumptions should always be presented and discussed. Reports of simulations used in support of a waiver of an in vivo study (such as a DDI study) require particular care to integrate the simulations with the rest of the clinical data, including a discussion of the implications for drug dosing.[132]

4.04.8 Case Studies

4.04.8.1 Predicting Bioavailability

Oral bioavailability (F) can determine the fate of a compound in clinical trials. Predicting F directly from the 2D structure of the molecule prior to first-in-human dosing is highly desirable. Lawless and colleagues[146] created a database of 62 drugs, primarily metabolized by CYP enzymes, that included the observed bioavailability (F) and the recommended dose. The reported %F values, defined as F times 100%, varied from 3% (fluphenazine) to 99% (diazepam, galantamine, glimepiride, indomethacin, and tamsulosin), with an average of 60%. For the 43 drugs with more than one reported value of %F, the average experimental CV% was 29%.

ANNE models based on 2D molecular structures were used to predict physicochemical properties and CYP pharmacokinetic parameters required as input into a PBPK model for each drug. These models were then used to predict the bioavailability solely from structure for each compound.[146]

The in silico predicted parameters included aqueous and biorelevant solubility, pK_a, log D, GI permeability, fraction unbound in human plasma, and blood-to-plasma concentration ratio. A hierarchical set of ANNE models was used to determine CYP metabolism. First, classification models predicted whether each compound was a substrate for each of five major CYP isoforms (1A2, 2C9, 2C19, 2D6, and 3A4). These predictions included confidence estimates that provide a measure of the confidence in the prediction that the compound is actually metabolized by a particular CYP isoform.[147] Next, sites of metabolism were predicted for those compounds that were projected to be substrates. Finally, K_m and V_{max} predictions were made for each predicted site of metabolism. These predictions were used as inputs for PBPK models implemented within GastroPlus. A 35-year-old American male physiology was used for all PBPK simulations.

Diltiazem provides a good example of how this sort of analysis is applied, in that it is metabolized by several CYP enzymes to yield several different metabolites in unequal amounts. The compound is predicted to be attacked by four of the major CYP isoforms, that is, 2C9, 2C19, 2D6, and 3A4 (Fig. 6).[146] The methoxy and dimethylamino groups are attacked by all four isoforms, whereas oxidation of the sulfur is only predicted for CYP isoforms 2D6 and 3A4. Examining the corresponding CL_{ints}, however, indicates that CYP3A4 will be responsible for the majority (86%) of the metabolism and that *N*-demethyldiltiazem will be the major (58%) metabolite.

Based on the modeling results, all of the drugs were predicted to be well-absorbed. All molecules were correctly predicted to be substrates of the CYPs associated with their major clearance pathways. Furthermore, these pathways had the highest predicted CYP intrinsic clearance in 42 of the 62 molecules. Overall, 58% of the molecules were predicted within 1.5-fold of their reported %F.

Fig. 7 shows the observed versus predicted %F for the 62 compounds in the database. The dashed line is the line of unity. The dotted lines represent 1.5-fold errors. On the right-hand graph, V_{max} was scaled by the confidence estimate from the CYP substrate model (i.e., multiplied $V_{max} \times$ Confidence%/100). This had the effect of reducing severe underpredictions of %F in order to avoid early rejection of good candidates.

Fig. 8 shows a graph of cumulative fraction and fold error. %F was predicted to be within 1.5-fold of the reported value for 58% of the compounds. For 46 compounds, the reported %F either spanned a range (e.g., 80–90%) or included a standard deviation (e.g., 80 + 15%). The area of the bubble is proportional to the expected measurement uncertainty. The %F of lovastatin is difficult to simulate due to opening and closing of the lactone ring. Tamsolusin has the highest fold error. Note that PBPK simulations using

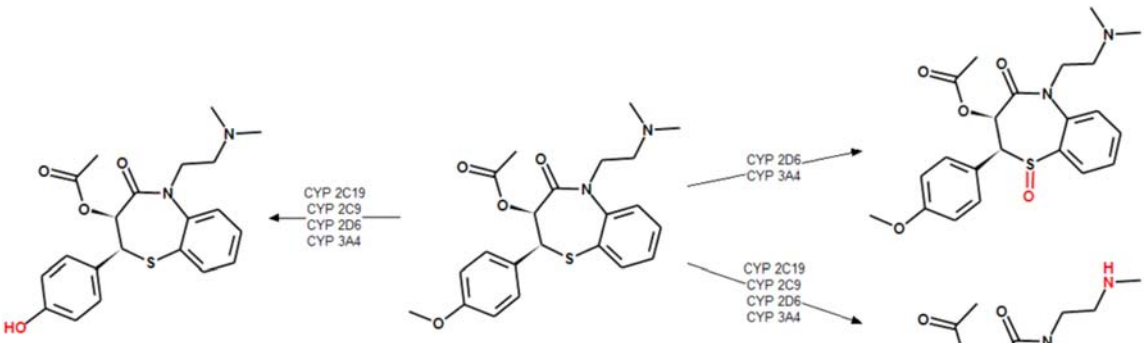

CYP Isoform	2C9 (54%)	2C19 (78%)	2D6 (81%)	3A4
Predicted CL_{int} [µl/min/mg MP]	1.2	4.6	3.1	54.3
fm%	2%	7%	5%	86%

Fig. 6 Metabolite predictions for diltiazem. Lawless M., DiBella J., Bolger M.B., Clark R.D., Huehn E., Waldman M., Zhang J., and Lukacova V. Poster Presented at International Society for the Study of Xenobiotics (ISSX): Prediction of Oral Bioavailability In Silico, 2015.

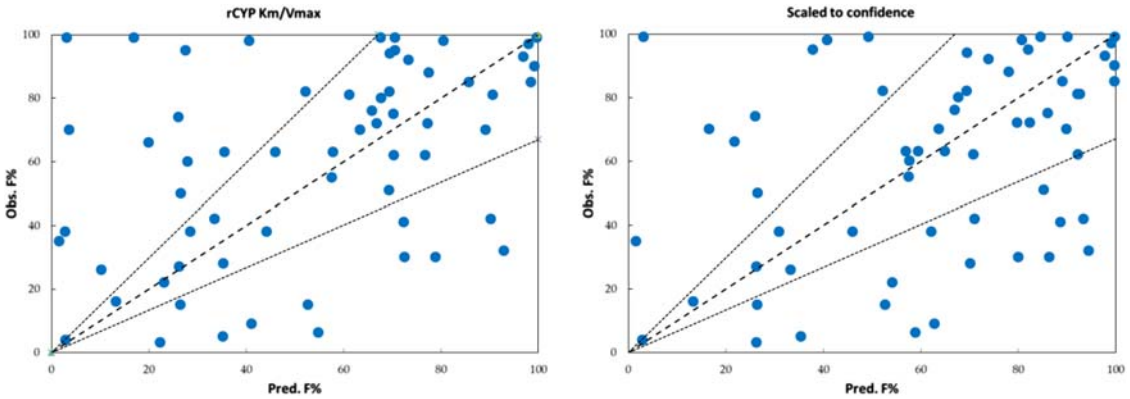

Fig. 7 Observed versus predicted %F for the 62 compounds in the database. Lawless M., DiBella J., Bolger M.B., Clark R.D., Huehn E., Waldman M., Zhang J., and Lukacova V. Poster Presented at International Society for the Study of Xenobiotics (ISSX): Prediction of Oral Bioavailability In Silico, 2015.

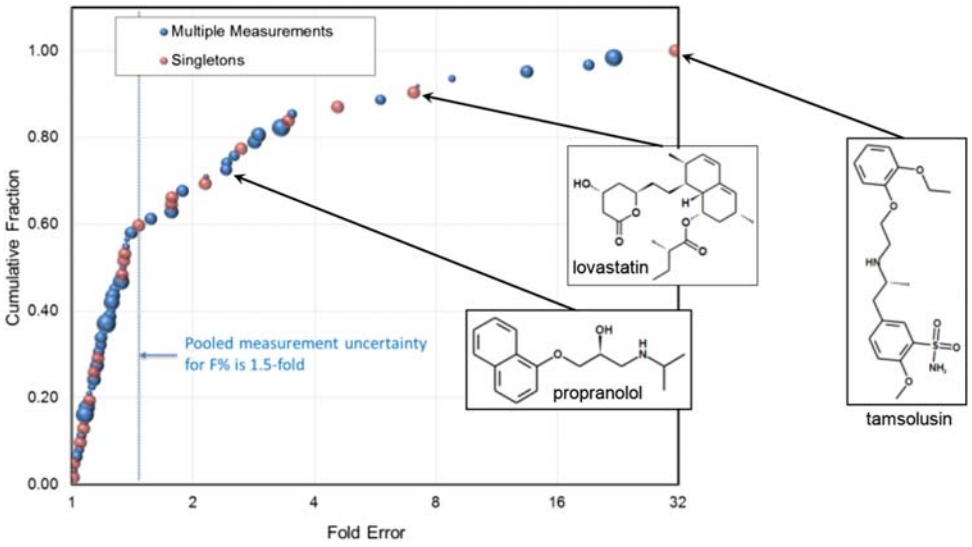

Fig. 8 Graph of cumulative fraction and fold error. Lawless M., DiBella J., Bolger M.B., Clark R.D., Huehn E., Waldman M., Zhang J., and Lukacova V. Poster Presented at International Society for the Study of Xenobiotics (ISSX): Prediction of Oral Bioavailability In Silico, 2015.

in vitro microsomal K_m and V_{max} values also resulted in large differences between reported and predicted %F. Propranolol was incorrectly predicted to be metabolized by 1A2; only including metabolism by 2D6 gives a correct %F prediction.

In silico tools predicting %F from 2D molecular structures can play an important role in anticipating challenges prior to initiating clinical development. Refining ANNE models based on the chemical space of interest is one strategy for improving prediction of %F. It is also important to note that PBPK simulations using in vitro microsomal K_m and V_{max} values also resulted in large differences between reported and predicted %F for some compounds. This reflects uncertainties in the bioavailability measurements themselves as well simplifying assumptions in the model details, for example, that the CYPs involved follow simple Michaelis–Menten kinetics across the entire concentration range, which is often not the case.[148]

4.04.8.2 Halofantrine Concentration-Related QTc Prolongation

Halofantrine hydrochloride is useful for the treatment of uncomplicated malaria and is effective when used against both chloroquine-sensitive and chloroquine-resistant *Plasmodium falciparum* infections. Halofantrine is orally administered as a racemic mixture and undergoes *N*-debutylation in the liver by CYP3A4 to its major metabolite *N*-desbutylhalofantrine. This metabolite is found in serum soon after administration of halofantrine, usually at lower concentrations. Both compounds are thought to contribute to the antimalarial activity.

Halofantrine is associated with lengthening of the QT interval and there have been reports of palpitations, syncope, and fatal or near-fatal arrhythmias in patients.[149–151] Electrophysiological studies on wild-type human ether-a-go-go gene (hERG)

demonstrated that both halofantrine and *N*-desbutylhalofantrine blocked hERG K^+ channels in a concentration-dependent manner with an IC_{50} of 21.6 and 71.7 nM, respectively.[152]

Proper interpretation of these results must take into consideration differences in the ADME characteristics of the parent and metabolite compounds. The reported elimination half-life of halofantrine is quite variable, ranging from 1.8 to 15.8 days. *N*-desbutylhalofantrine has been shown to have slower elimination kinetics and can achieve higher steady-state plasma concentrations than the parent compound.[153–155]

A PBPK model was developed for halofantrine and its metabolite using a combination of predicted and measured drug-related properties (see **Table 1**).

Fig. 9 shows the model-predicted plasma concentration-time profiles for halofantrine and *N*-desbutylhalofantrine and the respective observed concentrations for a 500-mg single oral dose given to a typical 28-year-old, 68 kg male subject. The considerably longer elimination half-life observed for *N*-desbutylhalofantrine results in considerable accumulation upon repeated dosing.

An important advantage of developing a whole body PBPK model and specifying the physiological characteristics of the various tissues in the body is the ability to predict tissue concentrations of drugs of interest. These tissue concentrations can be input into an appropriate PD model to obtain more clinically relevant predictions of drug effects beyond what can be obtained with plasma concentrations, particularly when the site of action of the drug resides outside the plasma compartment. In the example of halofantrine and *N*-desbutylhalofantrine, the PBPK model was used to predict tissue concentrations in the heart and these tissue concentrations were then input into an E_{max} model, similar to the one presented in Eq. (4) in the pharmacodynamic section.

The recommended dose for halofantrine in patients with no previous exposure or minimal exposure to malaria is 500 mg (2×250 mg tablets) of halofantrine hydrochloride every 6 hours for three doses. This course of therapy should be repeated 7 days after the first course. **Fig. 10** shows a population simulation for healthy adult males using the above dosing regimen, predicted tissue concentrations in the heart for halofantrine and *N*-desbutylhalofantrine, and the expected QTc interval (ms) impact for each moiety. This latter prediction is based on the observed IC_{50} for parent and metabolite in the hERG experiment.

Although *N*-desbutylhalofantrine has been suggested to be a safer antimalarial agent compared to halofantrine, these results suggest that the gain in safety margin for QT interval prolongation-related cardiotoxicity is minimal. In fact, with chronic dosing the higher concentrations of *N*-desbutylhalofantrine are likely to be associated with concentrations considerably higher than the IC_{50} for the hERG blockade. Consequently, the metabolite can play a substantial role in the cardiotoxicity of halofantrine.

4.04.9 Regulatory Implications

The cumulative academic, industry, and regulatory experience with PBPK modeling and simulation has led to the confidence in the value of PBPK predictions in various applications and an appreciation of the need for additional experience and validation efforts in

Table 1 Physicochemical, metabolism, and toxicity properties of halofantrine

Physicochemical properties	*Value*	*Reference*
Log *P* (octanol/water)[a]	7.58	ADMET Predictor[b]
Aqueous solubility at pH 5.5 ($\mu g\ mL^{-1}$)	1.3	Humberstone et al.[156]
FaSSIF ($\mu g\ mL^{-1}$)	2.1	
FeSSIF ($\mu g\ mL^{-1}$)	264	
pK_a base	9.2	ADMET Predictor[b]
Percent unbound in plasma (%)[c]—human	0.7	
Percent unbound in plasma (%)—rat	0.038	Brocks[157]
Blood/plasma concentration ratio	1.5	Klein et al.[158]
Metabolism		
In vitro CYP3A4 K_m halofantrine (μM)[d]	48	Baune et al.[159]
In vitro CYP3A4 V_{max} halofantrine (pmol $min^{-1}\ mg^{-1}$ protein)[d]	215	
In vitro CYP3A4 K_m *N*-desbutylhalofantrine (μM)	71.7	ADMET Predictor[b]
In vitro CYP3A4 V_{max} *N*-desbutylhalofantrine (pmol $min^{-1}\ mg^{-1}$ protein)	1410	ADMET Predictor[b]
Toxicity		
hERG IC_{50} halofantrine (nM)	21.6	Mbai et al.[152]
hERG IC_{50} *N*-desbutylhalofantrine (nM)	71.7	
Hill coefficient halofantrine	0.62	
Hill coefficient *N*-desbutylhalofantrine	1.36	

FaSSIF, fasted state simulated intestinal fluid; *FeSSIF*, fed-state simulated intestinal fluid; IC_{50}, concentration resulting in 50% of the maximum inhibition; K_m, concentration at 1/2 maximum metabolic velocity; Log *P*, octanol water partition coefficient; V_{max}, maximum metabolic velocity.

[a]Experimental log *P* not determined due to low aqueous solubility.

[b]ADMET Predictor. Version 7.2. Lancaster, CA: Simulations Plus, Inc.; 2015.

[c]Assumed fraction unbound in enterocytes to be 1% to account for lysosomal trapping.

[d]In vivo V_{max} and K_m calculated using the Halifax Fu calculation method and GastroPlus default values for CYP3A4 microsomal content and molecular weight.

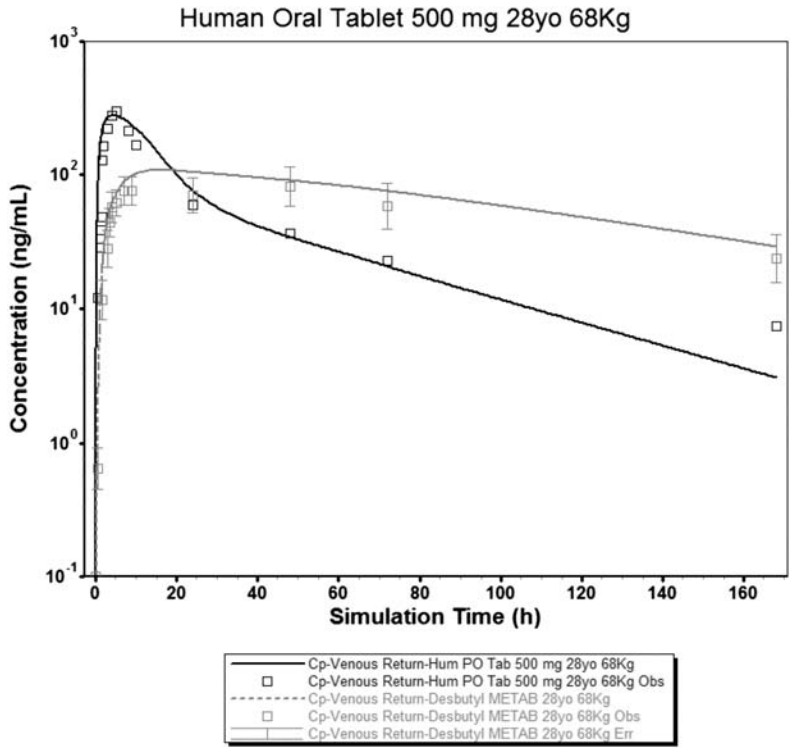

Fig. 9 Plasma concentration-time profiles for parent and metabolite following a 500-mg single oral dose. From GastroPlus.

others. In general, confidence is generally higher for BCS class 1 and 2 molecules that are also predominately eliminated by cytochrome P450 oxidation. Confidence is generally lower in cases where elimination is via non-CYP pathways or for interactions with transporters and enzymes. Similarly, there is a paucity of data and systematic experience in predicting the effects of disease states, such as hepatic and renal insufficiency.[10,131,132]

Regulatory agencies have recognized the value of PBPK modeling and simulations and have begun working to encourage their use in drug development. Workshops sponsored by the FDA and the EMA have been held to better define what constitutes a credible physiologically based simulation system and what evidentiary standards must be met to use such a system in various aspects of regulatory decision-making.[131,132]

In general, PBPK modeling is viewed as having great potential value to support benefit–risk assessments, providing a mechanistic basis for extrapolation beyond the clinical trial population, reducing uncertainty by understanding the sources of interindividual variability in the outcomes observed in clinical trials, enabling better labeling around DDIs, developing recommendations for dosing in specific populations (e.g., elderly, pediatric), and even predicting drug exposure in clinically untested treatment scenarios.[132]

Based on regulatory research and review experiences, predictive performance is considered well established for evaluating the DDI potential of an investigational drug as a substrate of metabolizing enzymes, specifically those metabolized by CYP3A isoforms and 2D6. In other areas of drug development, the predictive performances of PBPK are not as well established and there is an important need to establish methodological best practices and evidentiary standards.

A systematic understanding of the utility and validity of these model applications requires insight into the performance characteristics and properties of both the drug and the prediction tool. This understanding is a vital prerequisite for achieving reliable predictions and for developing general principles about the robustness, predictability, and reliability of the model, rather than looking at each case individually.

The FDA's views on the predictive performance of PBPK in different application areas have been summarized and considerations in demonstrating the validity and robustness of a PBPK model in various circumstances have been defined by Wagner:[131]

- Predictive performance should be reflected by the ability of a model to reasonably describe all available data.
- Biological plausibility of the model components should be demonstrated.
- Predictive performance of a system component should be demonstrated through modeling of multiple, relevant drugs.
- The predictability of a PBPK model should be seen in the context of its intended use and should not be over-interpreted, e.g., a PBPK model deemed adequate to predict drug interaction potential may not be sufficient to predict the effect of other patient factors such as organ impairment.

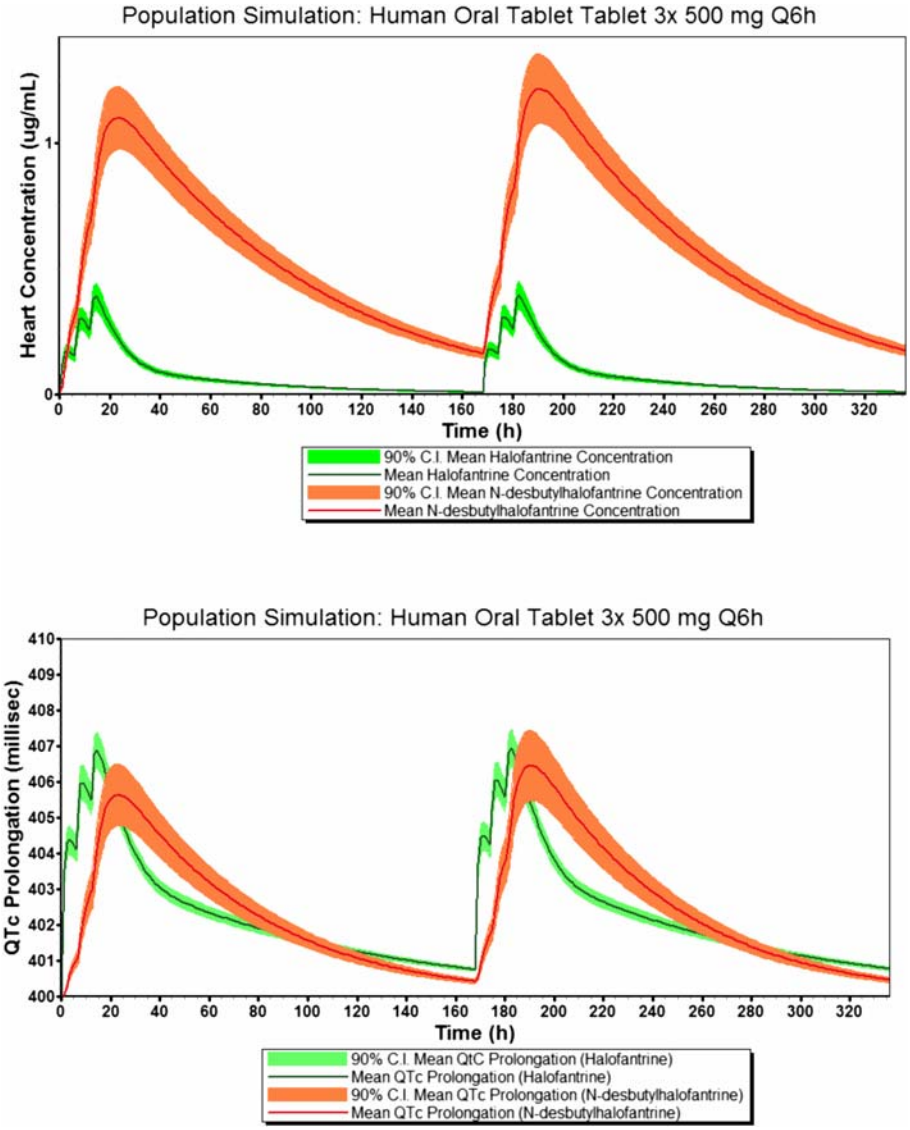

Fig. 10 Heart concentrations and effects on QTc interval from population simulation using recommended dosing regimen for treatment of malaria. From GastroPlus.

Regulatory agencies recognize the need for a full understanding and description of methodology to measure input parameters, preferably with adoption of common reference standards across companies, and a need for greater clarification and justification of empirical scaling factors.

4.04.10 Future Directions

4.04.10.1 Scientific Challenges

The mechanistic understanding of the myriad interactions between drug and system is the crucial factor enabling predictions for different scenarios in which in vivo or clinical studies have either not yet been performed or that are not technically or ethically feasible. As our knowledge of drug pharmacology and systems physiology continues to evolve, and we find innovative applications of PBPK that open new areas of research, we will continue to require additional information to address gaps in knowledge. For example, major challenges remain in the prediction of transporter effects and non-CYP related elimination; however, the introduction of QTAP for the determination of absolute transporter expression in human tissues[118] has opened the door for more accurate parameterization of IVIVE and PBPK modeling for substrates of influx and efflux transporters.[133–135]

As we move into predicting PK in the youngest pediatric patients, new information about the ontogeny of enzymes and transporter proteins are required.[136]

Further, understanding of the influence of disease on changes in enzyme or transporter abundance and distribution becomes necessary.

4.04.10.2 Cultural Challenges

Just as important as these scientific challenges are the cultural changes that loom large as modeling and simulation activities become more prominent in support of internal R&D and external regulatory decision-making. Applications of PBPK require input from many different disciplines over the lifecycle of R&D. This can create new challenges in terms of the collaborative environment required for success and the need to update drug- and system-specific input data as new knowledge emerges from preclinical and clinical studies. Given that PBPK modeling is an iterative learning process in which the PBPK model for a compound evolves with time, new strategies in terms of project and program management are required in order to ensure that the data required to achieve an acceptable level of confidence in the model are available when required for decision-making. This will require changes in scientist and management roles and responsibilities. Just as experimental models have evolved alongside the computational models in the PBPK software, so will management responsibilities change to improve the value and predictive performance of PBPK modeling and simulation.

The following questions are representative of the issues that will need to be addressed as PBPK models play a more prominent role in decision-making.

1. Goals for the modeling effort
   - What questions does the model need to address? What are the expectations of the model? What is the relationship between the available data and the required level of confidence to support decision-making in different phases of development?
2. Sources and completeness of input data
   - What data are required? Does some needed data already exist? Who has it? How do I identify inadequate or missing data? How do I to keep track of new or revised data? Are there data standards in place across projects that would enable the use of data from one program to be applied in other projects?
3. Interdisciplinary cooperation
   - What are considered reasonable parameter values or model assumptions from each discipline? What is the adjudication process when there is disagreement across disciplines? How much tolerance is there for model uncertainty? How do I best present the model and anticipate questions that will inspire confidence in the model from peers? Is the team willing to make the time commitment needed to understand the model and appropriately interpret the results?
4. Model refinement and validation
   - How do I use new information to make model refinements in order to create the best model for the next stage of drug development?
   - How robust are the predictions? Is the team asking good "what if" questions? What can I do to improve the quality of the predictions? Can I get different experiments performed to fill in the gaps?
5. Administrative aspects of in silico modeling and simulation
   - Who should have access to the model? What are appropriate change control procedures? Do I have adequate staff with appropriate training to develop and apply PBPK models?
6. Strategic application of modeling and simulation results
   - What evidentiary standards are acceptable for different risk levels of decision-making? How do I assess the value of alternative strategies to guide decision-making? How can this model-building process inform future drug development?

4.04.11 Epilogue

Sufficient experience in the use of in silico tools has accrued to clearly demonstrate the value that these tools provide to R&D decision-making. The emergence of in silico tools, such as PBPK modeling, to predict human pharmacokinetics for new compounds provides significant opportunities to anticipate the advantages and liabilities associated with compounds under consideration in discovery. Physiologically based PK modeling is being used in diverse applications and having a significant impact throughout the stages of drug discovery and development by providing mechanistic insights into drug PK and enabling scientists to anticipate problems and optimize development programs.

Given the diversity of PBPK applications and the requirements for input data from multiple departments, there is a critical need for effective interdisciplinary collaboration in model development and interpretation. The combined knowledge and expertise of preclinical scientists, formulation scientists, pharmacometricians, clinical pharmacologists, clinicians, and statisticians are critical to the successful application of PBPK modeling and simulation. We are just beginning to appreciate the need for new approaches to the management of the R&D enterprise in order to foster interdisciplinary collaboration and to provide innovative training and career development strategies for scientists and managers alike.[15]

The value of these interdisciplinary collaborations has been made apparent in the symbiotic relationships that have developed between experimental scientists and PBPK modelers. The in vivo and in vitro experimental protocols have undergone continued refinement and improvement as the data requirements of PBPK models are better appreciated. These improvements have led to the design of more informative experiments which allow the input parameters to be defined more precisely and to improvements in the software that allow for a more accurate representation of the phenomena of interest. This iterative relationship between the experimental models and the computational models has improved our understanding of the true complexity of experimental data and the predictive performance of PBPK models.[56]

It is important to note that the quality and certainty of predictions from the PBPK model can improve over time as in vitro data, preclinical in vivo data, and finally in vivo data in humans become available. A key aspect of this progression is that estimates from each stage can provide a valuable reality check for subsequent stages, for example, predictions sometimes disagree with experimental measurements because mistakes were made in carrying out the measurements. Metcalfe and Thomas have pointed out that much of the difficulty in predicting oral absorption, bioavailability, and clearance is in the experimental quantification of solubility, membrane permeability, plasma protein binding, metabolism, and active transport, rather than in the formulation of in silico models.[40]

As our knowledge of drug pharmacology and systems physiology continues to evolve, and we find innovative applications of PBPK that open new areas of research, we will continue to face new gaps in knowledge. The quote from Selassie[1] succinctly describes the challenges of PBPK modeling and simulation. During the early applications of PBPK modeling, the deficits in the knowledge base and in silico models were recognized and these deficits provided sources of inspiration for improvements. With each new application, the scientific community learns more about the interactions between physiology and pharmacology.

Although the job of learning and adapting to new knowledge will never end, we have amassed enough experience to know that PBPK modeling and simulation will continue to play an ever more vital role in science-based R&D.

Acknowledgments

The authors wish to acknowledge the valuable contributions of Sandra Cohen for her expert assistance in assembling the document and Jennifer Roberts for her careful editing of the content.

References

1. Selassie, C. D.; Abraham, D. J. History of Quantitative Structure–Activity Relationships. In *Burger's Medicinal Chemistry and Drug Discovery;* Abraham, D. J., Ed.; John Wiley & Sons, Inc: New Jersey, 2003; pp 1–48.
2. Lane, N. *The Vital Question: Why is Life the Way It Is?,* 1st ed.; Profile Books Ltd.: London, GB, 2015.
3. GastroPlus [computer program], Version 9.0, Lancaster, CA: Simulations Plus, Inc. 2015.
4. Thygesen, P.; Macheras, P.; Van Peer, A. Physiologically-Based PK/PD Modelling of Therapeutic Macromolecules. *Pharm. Res.* **2009,** *26,* 2543–2550.
5. Pammolli, F.; Magazzini, L.; Riccaboni, M. The Productivity Crisis in Pharmaceutical R&D. *Nat. Rev. Drug Discov.* **2011,** *10,* 428–438.
6. Kola, I.; Landis, J. Can the Pharmaceutical Industry Reduce Attrition Rates? *Nat. Rev. Drug Discov.* **2004,** *3,* 711–715.
7. Waring, M. J.; Arrowsmith, J.; Leach, A. R.; Leeson, P. D.; Mandrell, S.; Owen, R. M.; Pairaudeau, G.; Pennie, W. D.; Pickett, S. D.; Wang, J.; Wallace, O.; Weir, A. An Analysis of the Attrition of Drug Candidates from Four Major Pharmaceutical Companies. *Nat. Rev. Drug Discov.* **2015,** *14,* 475–486.
8. Lipinski, C.; Hopkins, A. Navigating Chemical Space for Biology and Medicine. *Nature* **2004,** *432,* 855–861.
9. Lipinski, C. A.; Lombardo, F.; Dominy, B. W.; Feeney, P. J. Experimental and Computational Approaches to Estimate Solubility and Permeability in Drug Discovery and Development Settings. *Adv. Drug Deliv. Rev.* **1997,** *23,* 3–25.
10. Jones, H. M.; Chen, Y.; Gibson, C.; Heimbach, T.; Parrott, N.; Peters, S. A.; Snoeys, J.; Upreti, V. V.; Zheng, M.; Hall, S. D. Physiologically Based Pharmacokinetic Modeling in Drug Discovery and Development: A Pharmaceutical Industry Perspective. *Clin. Pharmacol. Ther.* **2015,** *97,* 247–262.
11. Center for Drug Evaluation and Research. Draft Guidance for Industry: Drug Interaction Studies—Study Design, Data Analysis, Implications for Dosing and Labeling Recommendations, Food and Drug Administration February 2012.
12. Committee for Human Medicinal Products. Guideline on the Investigation of Ddrug Interactions, European Medicines Agency 21 June 2012.
13. Committee for Medicinal Products for Human Use. Guideline on the Evaluation of the Pharmacokinetics of Medicinal Products in Patients With Impaired Hepatic Function, European Medicines Agency 17 February 2005.
14. Japan Ministry of Health, Labor, and Welfare. Drug Interaction Guideline for Drug Development and Labeling Recommendations (Draft), 2014.
15. Grasela, T. H.; Slusser, R. The Paradox of Scientific Excellence and the Search for Productivity in Pharmaceutical Research and Development. *Clin. Pharmacol. Ther.* **2014,** *95,* 521–527.
16. Dost, F. H., [The clearance problem in children]. [Article in German], Kinderarztl Prax (1953) 227–232.
17. Wagner, J. G. History of Pharmacokinetics. *Pharmacol. Ther.* **1981,** *12,* 537–562.
18. Benet, L. Z.; Zia-Amirhosseini, P. Basic Principles of Pharmacokinetics. *Toxicol. Pathol.* **1995,** *23,* 115–123.
19. Gibaldi, M.; Perrier, D. *Pharmacokinetics,* 2nd ed.; Marcel Dekker, Inc.: New York, 1982.
20. Rowland, M.; Tozer, T. N. *Clinical Pharmacokinetics and Pharmacodynamics Concepts and Applications,* 4th ed.; Lippincott Williams & Wilkins: Philadelphia, PA, 2011.
21. Khadka, P.; Ro, J.; Kim, H.; Kim, I.; Kim, J. T.; Kim, H.; Cho, J. M.; Yun, G.; Lee, J. Pharmaceutical Particle Technologies: An Approach to Improve Drug Solubility, Dissolution and Bioavailability. *Asian J. Pharm. Sci.* **2014,** *9,* 304–316.
22. Rautio, J.; Kumpulainen, H.; Heimbach, T.; Oliyai, R.; Oh, D.; Jarvinen, T. Prodrugs: Design and Clinical Applications. *Nat. Rev. Drug Discov.* **2008,** *7,* 255–270.
23. Felmlee, M. A.; Morris, M. E.; Mager, D. E. Mechanism-Based Pharmacodynamic Modeling. *Methods Mol. Biol.* **2012,** *929,* 583–600.
24. Hoffman, A.; Goldberg, A. The Relationship Between Receptor-Effector Unit Heterogeneity and the Shape of the Concentration-Effect Profile: Pharmacodynamic Implications. *J. Pharmacokinet. Biopharm.* **1994,** *22,* 449–468.
25. Endrenyi, L.; Kwong, F. H. F.; Fajszi, C. Evaluation of Hill Slopes and Hill Coefficients When the Saturation Binding or Velocity is not Known. *FEBS J.* **1975,** *51,* 317–328.
26. Mager, D. E.; Wyska, E.; Jusko, W. J. Diversity of Mechanism-Based Pharmacodynamic Models. *Drug Metab. Dispos.* **2003,** *31,* 510–518.

27. Lajiness, M. S.; Vieth, M.; Erickson, J. Molecular Properties That Influence Oral Drug-Like Behavior. *Curr. Opin. Drug Discov. Devel.* **2004,** *7,* 470–477.
28. Veber, D. F.; Johnson, S. R.; Cheng, H. Y.; Smith, B. R.; Ward, K. W.; Kopple, K. D. Molecular Properties That Influence the Oral Bioavailability of Drug Candidates. *J. Med. Chem.* **2002,** *45,* 2615–2623.
29. van de Waterbeemd, H.; Gifford, E. ADMET In Silico Modelling: Towards Prediction Paradise? *Nat. Rev. Drug Discov.* **2003,** *2,* 192–204.
30. Center for Drug Evaluation and Research, Guidance for Industry: Waiver of In Vivo Bioavailability and Bioequivalence Studies for Immediate-Release Solid Oral Dosage Forms Based on a Biopharmaceutics Classification System, Food and Drug Administration, May 2015.
31. Fong, C. W. Permeability of the Blood–Brain Barrier: Molecular Mechanism of Transport of Drugs and Physiologically Important Compounds. *J. Membr. Biol.* **2015,** *24,* 651–669.
32. Amidon, G. L.; Lennernas, H.; Shah, V. P.; Crison, J. R. A Theoretical Basis for a Biopharmaceutic Drug Classification: The Correlation of In Vitro Drug Product Dissolution and In Vivo Bioavailability. *Pharm. Res.* **1995,** *12,* 413–420.
33. Center for Drug Evaluation and Research, Guidance for Industry: Immediate Release Solid Oral Dosage Forms: Scale-up and Postapproval Changes: Chemistry, Manufacturing, and Controls, In Vitro Dissolution Testing, and In Vivo Bioequivalence Documentation, Food and Drug Administration, November 1995.
34. Lipinski, C. A. Lead- and Drug-Like Compounds: The Rule-of-Five Revolution. *Drug Discov. Today* **2004,** *1,* 337–341.
35. Doak, B. C.; Zheng, J.; Dobritzsch, D.; Kihlberg, J. How Beyond Rule of 5 Drugs and Clinical Candidates Bind to Their Targets. *J. Med. Chem.* **2016,** *59,* 2312–2327.
36. Tanaka, C.; Kawai, R.; Rowland, M. Dose-Dependent Pharmacokinetics of Cyclosporin a in Rats: Events in Tissues. *Drug Metab. Dispos.* **2000,** *28,* 582–589.
37. Nestorov, I. Whole Body Pharmacokinetic Models. *Clin. Pharmacokinet.* **2003,** *42,* 883–908.
38. Krishnan, K. A.; Andersen, A. E. Physiologically Based Pharmacokinetic and Toxicokinetic Models. In *Principles and Methods of Toxicology;* Hayes, A. W., Ed.; CRC Press: Massachusetts, 1994; pp 231–292.
39. Andersen, M. E. Development of Physiologically Based Pharmacokinetic and Physiologically Based Pharmacodynamic Models for Applications in Toxicology and Risk Assessment. *Toxicol. Lett.* **1995,** *79,* 35–44.
40. Metcalfe, P. D.; Thomas, S. Challenges in the Prediction and Modeling of Oral Absorption and Bioavailability. *Curr. Opin. Drug Discov. Devel.* **2010,** *13,* 104–110.
41. ADMET Predictor [computer program], Version 7.2, Lancaster, CA: Simulations Plus, Inc. 2015, http://www.simulations-plus.com/Products.aspx?grplD = 1&clD = 11&plD = 13.
42. StarDrop [computer program], Cambridge, UK: Optibrium Ltd. http://www.optibrium.com/stardrop/stardrop-plugin-modules.php.
43. Tropsha, A. Best Practices for QSAR Model Development, Validation, and Exploitation. *Mol. Inf.* **2010,** *29,* 476–488.
44. Bolger, M. B.; Gilman, T. M.; Fraczkiewicz, R.; Steere, B.; Woltosz, W. S. Predicting Drug Absorption by Computational Methods. In *Cell Culture Models of Biological Barriers: In-Vitro Test Systems for Drug Absorption and Delivery;* Lehr, C.-M., Ed.; Taylor & Francis Inc.: New York, NY, 2002; pp 353–377.
45. Bolger, M. B.; Agoram, B.; Fraczkiewicz, R.; Steere, B. Simulation of Absorption, Metabolism, and Bioavailability. In *Drug Bioavailability: Estimation of Solubility, Permeability, Absorption and Bioavailability;* van de Waterbeemd, H., Lennernäs, H., Artursson, P., Eds.; WILEY-VCH Verlag GmbH & Co. KGaA: Weinheim, Germany, 2003; pp 420–443.
46. Bolger, M. B.; Fraczkiewicz, R.; Entzeroth, M.; Steere, B. Concepts for In Vitro Profiling: Drug Activity, Selectivity, and Liability. In *Exploiting Chemical Diversity for Drug Discovery;* Bartlett, P. A., Entzeroth, M., Eds.; Royal Society of Chemistry: London, 2006; pp 336–362.
47. Bolger, M. B.; Fraczkiewicz, R.; Steere, B. In Silico Surrogates for Vivo Properties: Profiling for ADME and Toxicological Behaviour. In *Exploiting Chemical Diversity for Drug Discovery;* Bartlett, P. A., Entzeroth, M., Eds.; Royal Society of Chemistry: London, 2006; pp 364–381.
48. Bolger, M. B.; Fraczkiewicz, R.; Lukacova, V. Simulation of Absorption, Metabolism, and Bioavailability. In *Drug Bioavailability: Estimation of Solubility, Permeability, Absorption and Bioavailability;* van de Waterbeemd, H., Testa, B., Eds., 2nd ed.; WILEY-VCH Verlag GmbH & Co. KGaA: Weinheim, Germany, 2009; pp 453–493.
49. Waldman, M.; Fraczkiewicz, R.; Clark, R. D. Tales From the War on Error: The Art and Science of Curating QSAR Data. *J. Comput. Aided Mol. Des.* **2015,** *29,* 897–910.
50. Clark, R. D. Boosted Leave-Many-Out Cross-Validation: The Effect of Training and Test Set Diversity on PLS Statistics. *J. Comput. Aided Mol. Des.* **2003,** *17,* 265–275.
51. Fraczkiewicz, R.; Lobell, M.; Göller, A. H.; Krenz, U.; Schoenneis, R.; Clark, R. D.; Hillisch, A. Best of Both Worlds: Combining Pharma Data and State of the Art Modeling Technology to Improve In Silico pK_a Prediction. *J. Chem. Inf. Model.* **2015,** *55,* 389–397.
52. Mannhold, R.; Poda, G. I.; Ostermann, C.; Tetko, I. V. Calculation of Molecular Lipophilicity: State-of-the-Art and Comparison of LogP Methods on More Than 96,000 Compounds. *J. Pharm. Sci.* **2009,** *98,* 861–893.
53. Jones, H. M.; Gardner, I. B.; Watson, K. J. Modelling and PBPK Simulation in Drug Discovery. *AAPS J.* **2009,** *11,* 155–166.
54. Lavé, T.; Parrott, N.; Grimm, H. P.; Fleury, A.; Reddy, M. Challenges and Opportunities With Modelling and Simulation in Drug Discovery and Drug Development. *Xenobiotica* **2007,** *37,* 1295–1310.
55. Rowland, M.; Peck, C.; Tucker, G. Physiologically-Based Pharmacokinetics in Drug Development and Regulatory Science. *Annu. Rev. Pharmacol. Toxicol.* **2011,** *51,* 45–73.
56. Jones, H. M.; Dickins, M.; Youdim, K.; Gosset, J. R.; Attkins, N. J.; Hay, T. L.; Gurrell, I. K.; Logan, Y. R.; Bungay, P. J.; Jones, B. C.; Gardner, I. B. Application of PBPK Modelling in Drug Discovery and Development at Pfizer. *Xenobiotica* **2012,** *42,* 94–106.
57. Jones, H. M.; Parrott, N.; Jorga, K.; Lave, T. A Novel Strategy for Physiologically Based Predictions of Human Pharmacokinetics. *Clin. Pharmacokinet.* **2006,** *45,* 511–542.
58. Jones, H. M.; Gardner, I. B.; Collard, W. T.; Stanley, P. J.; Oxley, P.; Hosea, N. A.; Plowchalk, D.; Gernhardt, S.; Lin, J.; Dickins, M.; Rahavendran, S. R.; Jones, B. C.; Watson, K. J.; Pertinez, H.; Kumar, V.; Cole, S. Simulation of Human Intravenous and Oral Pharmacokinetics of 21 Diverse Compounds Using Physiologically Based Pharmacokinetic Modelling. *Clin. Pharmacokinet.* **2011,** *50,* 331–347.
59. Parrott, N.; Jones, H.; Paquereau, N.; Lave, T. Application of Full Physiological Models for Pharmaceutical Drug Candidate Selection and Extrapolation of Pharmacokinetics to Man. *Basic Clin. Pharmacol. Toxicol.* **2005,** *96,* 193–199.
60. Yu, L. X.; Amidon, G. L. A Compartmental Absorption and Transit Model for Estimating Oral Drug Absorption. *Int. J. Pharm.* **1999,** *186,* 119–125.
61. Agoram, B.; Woltosz, W. S.; Bolger, M. B. Predicting the Impact of Physiological and Biochemical Processes on Oral Drug Bioavailability. *Adv. Drug Deliv. Rev.* **2001,** *50,* S41–67.
62. Woltosz, W. S.; Bolger, M. B.; Lukacova, V. Modeling of Absorption. *Methods Mol. Biol.* **2012,** *929,* 313–336.
63. Porter, C. J. H.; Trevaskis, N. L.; Charman, W. N. Lipids and Lipid-Based Formulations: Optimizing the Oral Delivery of Lipophilic Drugs. *Nat. Rev. Drug Discov.* **2007,** *6,* 231–248.
64. Komarova, Y.; Malik, A. B. Regulation of Endothelial Permeability via Paracellular and Transcellular Transport Pathways. *Annu. Rev. Physiol.* **2010,** *72,* 463–493.
65. Xia, B.; Heimbach, T.; Lin, T. H.; He, H.; Wang, Y.; Tan, E. Novel Physiologically Based Pharmacokinetic Modeling of Patupilone for Human Pharmacokinetic Predictions. *Cancer Chemother. Pharmacol.* **2012,** *69,* 1567–1582.
66. Schmidt-Nielsen, B. August and Marie Krogh and Respiratory Physiology. *J. Appl. Physiol. Respir. Environ. Exerc. Physiol.* **1984,** *57,* 293–303.
67. Agutter, P. S.; Wheatley, D. N. Metabolic Scaling: Consensus or Controversy? *Theor. Biol. Med. Model.* **2004,** *1,* 13.
68. West, G. B.; Brown, J. H.; Enquist, B. J. A General Model for the Origin of Allometric Scaling Laws in Biology. *Science* **1997,** *276,* 122–126.
69. Zou, P.; Yu, Y.; Zheng, N.; Yang, Y.; Paholak, H. J.; Yu, L. X.; Sun, D. Applications of Human Pharmacokinetic Prediction in First-in-Human Dose Estimation. *AAPS J.* **2012,** *14,* 262–281.
70. Boxenbaum, H. Interspecies Pharmacokinetic Scaling and the Evolutionary-Comparative Paradigm. *Drug Metab. Rev.* **1984,** *15,* 1071–1121.
71. Mahmood, I. Interspecies Scaling of Renally Secreted Drugs. *Life Sci.* **1998,** *63,* 2365–2371.
72. Lavé, T.; Coassolo, P.; Reigner, B. Prediction of Hepatic Metabolic Clearance Based on Interspecies Allometric Scaling Techniques and In Vitro-In Vivo Correlations. *Clin. Pharmacokinet.* **1999,** *36,* 211–231.
73. Zuegge, J.; Schneider, G.; Coassolo, P.; Lavé, T. Prediction of Hepatic Metabolic Clearance: Comparison and Assessment of Prediction Models. *Clin. Pharmacokinet.* **2001,** *40,* 553–563.

74. Hosea, N. A.; Collard, W. T.; Cole, S.; Maurer, T. S.; Fang, R. X.; Jones, H.; Kakar, S. M.; Nakai, Y.; Smith, B. J.; Webster, R.; Beaumont, K. Prediction of Human Pharmacokinetics From Preclinical Information: Comparative Accuracy of Quantitative Prediction Approaches. *J. Clin. Pharmacol.* **2009,** *49,* 513–533.
75. Lepist, E. I.; Jusko, W. J. Modeling and Allometric Scaling of s(+)-Ketoprofen Pharmacokinetics and Pharmacodynamics: A Retrospective Analysis. *J. Vet. Pharmacol. Ther.* **2004,** *27,* 211–218.
76. Woo, S.; Jusko, W. J. Interspecies Comparisons of Pharmacokinetics and Pharmacodynamics of Recombinant Human Erythropoietin. *Drug Metab. Dispos.* **2007,** *35,* 1672–1678.
77. Weber, O.; Willmann, S.; Bischoff, H.; Li, V.; Vakalopoulos, A.; Lustig, K.; Hafner, F. T.; Heinig, R.; Schmeck, C.; Buehner, K. Prediction of a Potentially Effective Dose in Humans for BAY 60–5521, a Potent Inhibitor of Cholesteryl Ester Transfer Protein (CETP) by Allometric Species Scaling and Combined Pharmacodynamic and Physiologically-Based Pharmacokinetic Modelling. *Br. J. Clin. Pharmacol.* **2012,** *73,* 219–231.
78. Houston, J. B.; Carlile, D. J. Prediction of Hepatic Clearance From Microsomes, Hepatocytes, and Liver Slices. *Drug Metab. Rev.* **1997,** *29,* 891–922.
79. Chen, Y.; Jin, J. Y.; Mukadam, S.; Malhi, V.; Kenny, J. R. Application of IVIVE and PBPK Modeling in Prospective Prediction of Clinical Pharmacokinetics: Strategy and Approach During the Drug Discovery Phase With Four Case Studies. *Biopharm. Drug Dispos.* **2012,** *33,* 85–98.
80. Iwatsubo, T.; Hirota, N.; Ooie, T.; Suzuki, H.; Shimada, N.; Chiba, K.; Ishizaki, T.; Green, C. E.; Tyson, C. A.; Sugiyama, Y. Prediction of In Vivo Drug Metabolism in the Human Liver From In Vitro Metabolism Data. *Pharmacol. Ther.* **1997,** *73,* 147–171.
81. Jones, H. M.; Houston, J. B. Substrate Depletion Approach for Determining In Vitro Metabolic Clearance: Time Dependencies in Hepatocyte and Microsomal Incubations. *Drug Metab. Dispos.* **2004,** *32,* 973–982.
82. Houston, J. B. Utility of In Vitro Drug Metabolism Data in Predicting In Vivo Metabolic Clearance. *Biochem. Pharmacol.* **1994,** *47,* 1469–1479.
83. Obach, R. S. Prediction of Human Clearance of Twenty-Nine Drugs From Hepatic Microsomal Intrinsic Clearance Data: An Examination of In Vitro Half-Life Approach and Nonspecific Binding to Microsomes. *Drug Metab. Dispos.* **1999,** *27,* 1350–1359.
84. Paine, M. F.; Hart, H. L.; Ludington, S. S.; Haining, R. L.; Rettie, A. E.; Zeldin, D. C. The Human Intestinal Cytochrome P450 "Pie". *Drug Metab. Dispos.* **2006,** *34,* 880–886.
85. Abuasal, B. S.; Bolger, M. B.; Walker, D. K.; Kaddoumi, A. In Silico Modeling for the Nonlinear Absorption Kinetics of UK-343,664: A P-gp and CYP3A4 Substrate. *Mol. Pharm.* **2012,** *9,* 492–504.
86. Galetin, A.; Brown, C.; Hallifax, D.; Ito, K.; Houston, J. B. Utility of Recombinant Enzyme Kinetics in Prediction of Human Clearance: Impact of Variability, CYP3A5, and CYP2C19 on CYP3A4 Probe Substrates. *Drug Metab. Dispos.* **2004,** *32,* 1411–1420.
87. Joly, J. G.; Doyon, C.; Pesant, Y. Cytochrome P-450 Measurement in Rat Liver Homogenate and Microsomes: Its Use for Correction of Microsomal Losses Incurred by Differential Centrifugation. *Drug Metab. Dispos.* **1975,** *3,* 577–586.
88. Proctor, N. J.; Tucker, G. T.; Rostami-Hodjegan, A. Predicting Drug Clearance From Recombinantly Expressed CYPs: Intersystem Extrapolation Factors. *Xenobiotica* **2004,** *34,* 151–178.
89. Ohno, S.; Nakajin, S. Determination of mRNA Expression of Human UDP-Glucuronosyltransferases and Application for Localization in Various Human Tissues by Real-Time Reverse Transcriptase-Polymerase Chain Reaction. *Drug Metab. Dispos.* **2009,** *37,* 32–40.
90. Riley, R. J.; McGinnity, D. F.; Austin, R. P. A Unified Model for Predicting Human Hepatic, Metabolic Clearance from In Vitro Intrinsic Clearance Data in Hepatocytes and Microsomes. *Drug Metab. Dispos.* **2005,** *33,* 1304–1311.
91. Houston, J. B.; Galetin, A. Methods for Predicting In Vivo Pharmacokinetics Using Data From In Vitro Assays. *Curr. Drug Metab.* **2008,** *9,* 940–951.
92. Obach, R. S. Predicting Clearance in Humans From In Vitro Data. *Curr. Top. Med. Chem.* **2011,** *11,* 334–339.
93. Chiba, M.; Ishii, Y.; Sugiyama, Y. Prediction of Hepatic Clearance in Human From In Vitro Data for Successful Drug Development. *AAPS J.* **2009,** *11,* 262–276.
94. Ghibellini, G.; Vasist, L. S.; Leslie, E. M.; Heizer, W. D.; Kowalsky, R. J.; Calvo, B. F.; Brouwer, K. L. In Vitro-In Vivo Correlation of Hepatobiliary Drug Clearance in Humans. *Clin. Pharmacol. Ther.* **2007,** *81,* 406–413.
95. Poulin, P.; Krishnan, K. A Tissue Composition-Based Algorithm for Predicting Tissue:Air Partition Coefficients of Organic Chemicals. *Toxicol. Appl. Pharmacol.* **1996,** *136,* 126–130.
96. Poulin, P.; Theil, F. P. A Priori Prediction of Tissue: Plasma Partition Coefficients of Drugs to Facilitate the Use of Physiologically-Based Pharmacokinetic Models in Drug Discovery. *J. Pharm. Sci.* **2000,** *89,* 16–35.
97. Berezhkovskiy, L. M. Determination of Volume of Distribution at Steady State With Complete Consideration of the Kinetics of Protein and Tissue Binding in Linear Pharmacokinetics. *J. Pharm. Sci.* **2004,** *93,* 364–374.
98. Rodgers, T.; Leahy, D.; Rowland, M. Physiologically Based Pharmacokinetic Modeling 1: Predicting the Tissue Distribution of Moderate-to-Strong Bases. *J. Pharm. Sci.* **2005,** *94,* 1259–1276.
99. Rodgers, T.; Rowland, M. Physiologically Based Pharmacokinetic Modelling 2: Predicting the Tissue Distribution of Acids, Very Weak Bases, Neutrals and Zwitterions. *J. Pharm. Sci.* **2006,** *95,* 1238–1257.
100. Rodgers, T.; Rowland, M. Mechanistic Approaches to Volume of Distribution Predictions: Understanding the Processes. *Pharm. Res.* **2007,** *24,* 918–933.
101. Lukacova, V.; Parrott, N.; Lavé, T.; Fraczkiewicz, G.; Bolger, M. B.; Woltosz, W. S. Poster Presented at AAPS Annual Meeting: General Approach to Calculation of Tissue:Plasma Partition Coefficients for Physiologically Based Pharmacokinetic (PBPK) Modeling.
102. Terasaki, T.; Iga, T.; Sugiyama, Y.; Hanano, M. Experimental Evidence of Characteristic Tissue Distribution of Adriamycin. Tissue DNA Concentration as a Determinant. *J. Pharm. Pharmacol.* **1982,** *34,* 597–600.
103. Terasaki, T.; Iga, T.; Sugiyama, Y.; Hanano, M. Pharmacokinetic Study on the Mechanism of Tissue Distribution of Doxorubicin: Interorgan and Interspecies Variation of Tissue-to-Plasma Partition Coefficients in Rats, Rabbits, and Guinea Pigs. *J. Pharm. Sci.* **1984,** *73,* 1359–1363.
104. Hinderling, P. H. Red Blood Cells: A Neglected Compartment in Pharmacokinetics and Pharmacodynamics. *Pharmacol. Rev.* **1997,** *49,* 279–295.
105. Amsden, G. W. Erythromycin, Clarithromycin, and Azithromycin: Are the Differences Real? *Clin. Ther.* **1996,** *18,* 56–72. discussion 55.
106. Matzneller, P.; Krasniqi, S.; Kinzig, M.; Sörgel, F.; Hüttner, S.; Lackner, E.; Müller, M.; Zeitlinger, M. Blood, Tissue, and Intracellular Concentrations of Azithromycin During and After End of Therapy. *Antimicrob. Agents Chemother.* **2013,** *57,* 1736–1742.
107. Lemaire, S.; Tulkens, P. M.; Van Bambeke, F. Cellular Pharmacokinetics of the Novel Biaryloxazolidinone Radezolid in Phagocytic Cells: Studies With Macrophages and Polymorphonuclear Neutrophils. *Antimicrob. Agents Chemother.* **2010,** *54,* 2540–2548.
108. Foulds, G.; Shepard, R. M.; Johnson, R. B. The Pharmacokinetics of Azithromycin in Human Serum and Tissues. *J. Antimicrob. Chemother.* **1990,** *25 Suppl A,* 73–82.
109. Zheng, S.; Matzneller, P.; Zeitlinger, M.; Schmidt, S. Development of a Population Pharmacokinetic Model Characterizing the Tissue Distribution of Azithromycin in Healthy Subjects. *Antimicrob. Agents Chemother.* **2014,** *58,* 6675–6684.
110. Kell, D. B.; Dobson, P. D.; Oliver, S. G. Pharmaceutical Drug Transport: The Issues and the Implications That It Is Essentially Carrier-Mediated Only. *Drug Discov. Today* **2011,** *16,* 704–714.
111. Dobson, P. D.; Kell, D. B. Carrier-Mediated Cellular Uptake of Pharmaceutical Drugs: An Exception or the Rule? *Nat. Rev. Drug Discov.* **2008,** *7,* 205–220.
112. Sugano, K.; Kansy, M.; Artursson, P.; Avdeef, A.; Bendels, S.; Di, L.; Ecker, G. F.; Faller, B.; Fischer, H.; Gerebtzoff, G.; Lennernaes, H.; Senner, F. Coexistence of Passive and Carrier-Mediated Processes in Drug Transport. *Nat. Rev. Drug Discov.* **2010,** *9,* 597–614.
113. Bolger, M. B.; Lukacova, V.; Woltosz, W. S. Simulations of the Nonlinear Dose Dependence for Substrates of Influx and Efflux Transporters in the Human Intestine. *AAPS J.* **2009,** *11,* 353–363.
114. Heikkinen, A. T.; Korjamo, T.; Lepikko, V.; Monkkonen, J. Effects of Experimental Setup on the Apparent Concentration Dependency of Active Efflux Transport in In Vitro Cell Permeation Experiments. *Mol. Pharm.* **2010,** *7,* 605–617.

115. Heikkinen, A. T.; Korjamo, T.; Monkkonen, J. Modelling of Drug Disposition Kinetics in In Vitro Intestinal Absorption Cell Models. *Basic Clin. Pharmacol. Toxicol.* **2010,** *106,* 180–188.
116. Tubic, M.; Wagner, D.; Spahn-Langguth, H.; Bolger, M. B.; Langguth, P. In Silico Modeling of Non-Linear Drug Absorption for the P-gp Substrate Talinolol and of Consequences for the Resulting Pharmacodynamic Effect. *Pharm. Res.* **2006,** *23,* 1712–1720.
117. Bolger, M. B.; Lukacova, V.; Mullin, J. M.; Szeto, K. Poster Presented at the AAPS Transporter Workshop: Simulation of In Vitro Caco-2 Papp From Molecular Structure Estimation of Intracellular Km for Efflux Transporters.
118. Ohtsuki, S.; Uchida, Y.; Kubo, Y.; Terasaki, T. Quantitative Targeted Absolute Proteomics-Based ADME Research as a New Path to Drug Discovery and Development: Methodology, Advantages, Strategy, and Prospects. *J. Pharm. Sci.* **2011,** *100,* 3547–3559.
119. Jones, H. M.; Barton, H. A.; Lai, Y.; Bi, Y. A.; Kimoto, E.; Kempshall, S.; Tate, S. C.; El-Kattan, A.; Houston, J. B.; Galetin, A.; Fenner, K. S. Mechanistic Pharmacokinetic Modeling for the Prediction of Transporter-Mediated Disposition in Humans From Sandwich Culture Human Hepatocyte Data. *Drug Metab. Dispos.* **2012,** *40,* 1007–1017.
120. Poirier, A.; Cascais, A. C.; Funk, C.; Lave, T. Prediction of Pharmacokinetic Profile of Valsartan in Human Based on In Vitro Uptake Transport Data. *J. Pharmacokinet. Pharmacodyn.* **2009,** *36,* 585–611.
121. Lukacova, V.; Bolger, M. B.; Woltosz, W. S.; Parrott, N. J.; Poirier, A.; Lavé, T. Poster Presented at 17th North American Regional ISSX Meeting: Transporter-Based In Vitro-In Vivo Extrapolation (IVIVE).
122. Brouwer, K. L.; Keppler, D.; Hoffmaster, K. A.; Bow, D. A.; Cheng, Y.; Lai, Y.; Palm, J. E.; Stieger, B.; Evers, R. In Vitro Methods to Support Transporter Evaluation in Drug Discovery and Development. *Clin. Pharmacol. Ther.* **2013,** *94,* 95–112.
123. Kuteykin-Teplyakov, K.; Luna-Tortos, C.; Ambroziak, K.; Loscher, W. Differences in the Expression of Endogenous Efflux Transporters in MDR1-Transfected Versus Wildtype Cell Lines Affect P-Glycoprotein Mediated Drug Transport. *Br. J. Pharmacol.* **2010,** *160,* 1453–1463.
124. Sager, J. E.; Yu, J.; Ragueneau-Majlessi, I.; Isoherranen, N. Physiologically Based Pharmacokinetic (PBPK) Modeling and Simulation Approaches: A Systematic Review of Published Models, Applications, and Model Verification. *Drug Metab. Dispos.* **2015,** *43,* 1823–1837.
125. De Buck, S. S.; Sinha, V. K.; Fenu, L. A.; Nijsen, M. J.; Mackie, C. E.; Gilissen, R. A. Prediction of Human Pharmacokinetics Using Physiologically Based Modeling: A Retrospective Analysis of 26 Clinically Tested Drugs. *Drug Metab. Dispos.* **2007,** *35,* 1766–1780.
126. Theil, F. P.; Guentert, T. W.; Haddad, S.; Poulin, P. Utility of Physiologically Based Pharmacokinetic Models to Drug Development and Rational Drug Discovery Candidate Selection. *Toxicol. Lett.* **2003,** *138,* 29–49.
127. Brightman, F. A.; Leahy, D. E.; Searle, G. E.; Thomas, S. Application of a Generic Physiologically Based Pharmacokinetic Model to the Estimation of Xenobiotic Levels in Human Plasma. *Drug Metab. Dispos.* **2006,** *34,* 94–101.
128. Sjogren, E.; Abrahamsson, B.; Augustijns, P.; Becker, D.; Bolger, M. B.; Brewster, M.; Brouwers, J.; Flanagan, T.; Harwood, M.; Heinen, C.; Holm, R.; Juretschke, H. P.; Kubbinga, M.; Lindahl, A.; Lukacova, V.; Munster, U.; Neuhoff, S.; Nguyen, M. A.; Peer, A.; Reppas, C.; Hodjegan, A. R.; Tannergren, C.; Weitschies, W.; Wilson, C.; Zane, P.; Lennernas, H.; Langguth, P. In Vivo Methods for Drug Absorption—Comparative Physiologies, Model Selection, Correlations With In Vitro Methods (IVIVC), and Applications for Formulation/API/Excipient Characterization Including Food Effects. *Eur. J. Pharm. Sci.* **2014,** *57,* 99–151.
129. Kostewicz, E. S.; Aarons, L.; Bergstrand, M.; Bolger, M. B.; Galetin, A.; Hatley, O.; Jamei, M.; Lloyd, R.; Pepin, X.; Rostami-Hodjegan, A.; Sjogren, E.; Tannergren, C.; Turner, D. B.; Wagner, C.; Weitschies, W.; Dressman, J. PBPK Models for the Prediction of In Vivo Performance of Oral Dosage Forms. *Eur. J. Pharm. Sci.* **2014,** *57,* 300–321.
130. Zhao, P.; Zhang, L.; Grillo, J. A.; Liu, Q.; Bullock, J. M.; Moon, Y. J.; Song, P.; Brar, S. S.; Madabushi, R.; Wu, T. C.; Booth, B. P.; Rahman, N. A.; Reynolds, K. S.; Gil, Berglund E.; Lesko, L. J.; Huang, S. M. Applications of Physiologically Based Pharmacokinetic (PBPK) Modeling and Simulation During Regulatory Review. *Clin. Pharmacol. Ther.* **2011,** *89,* 259–267.
131. Wagner, C.; Zhao, P.; Pan, Y.; Hsu, V.; Grillo, J.; Huang, S. M.; Sinha, V. Application of Physiologically Based Pharmacokinetic (PBPK) Modeling to Support Dose Selection: Report of an FDA Public Workshop on PBPK. *CPT Pharmacometrics Syst. Pharmacol.* **2015,** *4,* 226–230.
132. Shepard, T.; Scott, G.; Cole, S.; Nordmark, A.; Bouzom, F. Physiologically Based Models in Regulatory Submissions: Output From the ABPI/MHRA Forum on Physiologically Based Modeling and Simulation. *CPT Pharmacometrics Syst. Pharmacol.* **2015,** *4,* 221–225.
133. Harwood, M. D.; Achour, B.; Russell, M. R.; Carlson, G. L.; Warhurst, G.; Rostami-Hodjegan, A. Application of an LC-MS/MS Method for the Simultaneous Quantification of Human Intestinal Transporter Proteins Absolute Abundance Using a QconCAT Technique. *J. Pharm. Biomed. Anal.* **2015,** *110,* 27–33.
134. Kumar, V.; Prasad, B.; Patilea, G.; Gupta, A.; Salphati, L.; Evers, R.; Hop, C. E.; Unadkat, J. D. Quantitative Transporter Proteomics by Liquid Chromatography With Tandem Mass Spectrometry: Addressing Methodologic Issues of Plasma Membrane Isolation and Expression-Activity Relationship. *Drug Metab. Dispos.* **2015,** *43,* 284–288.
135. Prasad, B.; Evers, R.; Gupta, A.; Hop, C. E.; Salphati, L.; Shukla, S.; Ambudkar, S. V.; Unadkat, J. D. Interindividual Variability in Hepatic Organic Anion-Transporting Polypeptides and P-Glycoprotein (ABCB1) Protein Expression: Quantification by Liquid Chromatography Tandem Mass Spectroscopy and Influence of Genotype, Age, and Sex. *Drug Metab. Dispos.* **2014,** *42,* 78–88.
136. Brouwer, K. L.; Aleksunes, L. M.; Brandys, B.; Giacoia, G. P.; Knipp, G.; Lukacova, V.; Meibohm, B.; Nigam, S. K.; Rieder, M.; de Wildt, S. N.; Pediatric Transporter Working Group. Human Ontogeny of Drug Transporters: Review and Recommendations of the Pediatric Transporter Working Group. *Clin. Pharmacol. Ther.* **2015,** *98,* 266–287.
137. Zhao, P.; Rowland, M.; Huang, S. M. Best Practice in the Use of Physiologically Based Pharmacokinetic Modeling and Simulation to Address Clinical Pharmacology Regulatory Questions. *Clin. Pharmacol. Ther.* **2012,** *92,* 17–20.
138. National Center for Health Statistics, National Health And Nutrition Examination Survey, Centers for Disease Control and Prevention, February 2016, Hyattsville, MD, http://www.cdc.gov/nchs/nhanes.htm (Accessed April 28, 2016).
139. Davies, B.; Morris, T. Physiological Parameters in Laboratory Animals and Humans. *Pharm. Res.* **1993,** *10,* 1093–1095.
140. Brown, R. P.; Delp, M. D.; Lindstedt, S. L.; Rhomberg, L. R.; Beliles, R. P. Physiological Parameter Values for Physiologically Based Pharmacokinetic Models. *Toxicol. Ind. Health* **1997,** *13,* 407–484.
141. Ogiu, N.; Nakamura, Y.; Ijiri, I.; Hiraiwa, K.; Ogiu, T. A Statistical Analysis of the Internal Organ Weights of Normal Japanese People. *Health Phys.* **1997,** *72,* 368–383.
142. GastroPlus [User's Manual], Version 9.0, Lancaster, CA: Simulations Plus, Inc. 2015.
143. Bernareggi, A.; Rowland, M. Physiologic Modeling of Cyclosporin Kinetics in Rat and Man. *J. Pharmacokinet. Biopharm.* **1991,** *19,* 21–50.
144. Peters, S. A. Physiologically-Based Pharmacokinetic (PBPK) Modelling and Simulations. In *Principles, Methods and Applications in the Pharmaceutical Industry;* John Wiley & Sons, Inc: New Jersey, 2012.
145. Suenderhauf, C.; Parrott, N. A Physiologically Based Pharmacokinetic Model of the Minipig: Data Compilation and Model Implementation. *Pharm. Res.* **2013,** *30,* 1–15.
146. Lawless, M.; DiBella, J.; Bolger, M. B.; Clark, R. D.; Huehn, E.; Waldman, M.; Zhang, J.; Lukacova, V. Poster Presented at International Society for the Study of Xenobiotics (ISSX): Prediction of Oral Bioavailability In Silico.
147. Clark, R. D.; Liang, W.; Lee, A. C.; Lawless, M. S.; Fraczkiewicz, R.; Waldman, M. Using Beta Binomials to Estimate Classification Uncertainty for Ensemble Models. *J. Cheminf.* **2014,** *6,* 34.
148. Houston, J. B.; Kenworthy, K. E. In Vitro-In Vivo Scaling of CYP Kinetic Data not Consistent With the Classical Michaelis-Menten Model. *Drug Metab. Dispos.* **2000,** *28,* 246–254.
149. Gundersen, S. G.; Rostrup, M.; von der Lippe, E.; Platou, E. S.; Myrvang, B.; Edwards, G. Halofantrine-Associated Ventricular Fibrillation in a Young Woman With No Predisposing QTc Prolongation. *Scand. J. Infect. Dis.* **1997,** *29,* 207–208.
150. Milton, K. A.; Edwards, G.; Ward, S. A.; Orme, M. L.; Breckenridge, A. M. Pharmacokinetics of Halofantrine in Man: Effects of Food and Dose Size. *Br. J. Clin. Pharmacol.* **1989,** *28,* 71–77.
151. Akhtar, T.; Imran, M. Sudden Deaths While on Halofantrine Treatments—a Report of Two Cases From Peshawar. *J. Pak. Med. Assoc.* **1994,** *44,* 120–121.

152. Mbai, M.; Rajamani, S.; January, C. T. The Anti-Malarial Drug Halofantrine and Its Metabolite N-Desbutylhalofantrine Block HERG Potassium Channels. *Cardiovasc. Res.* **2002,** *55,* 799–805.
153. Abernethy, D. R.; Wesche, D. L.; Barbey, J. T.; Ohrt, C.; Mohanty, S.; Pezzullo, J. C.; Schuster, B. G. Stereoselective Halofantrine Disposition and Effect: Concentration-Related QTc Prolongation. *Br. J. Clin. Pharmacol.* **2001,** *51,* 231–237.
154. Karbwang, J.; Ward, S. A.; Milton, K. A.; Bangchang, K. N.; Edwards, G. Pharmacokinetics of Halofantrine in Healthy Thai Volunteers. *Br. J. Clin. Pharmacol.* **1991,** *32,* 639–640.
155. Watkins, W. M.; Winstanley, P. A.; Mberu, E. K.; Kokwaro, G.; Murphy, S. A.; Newton, C. J.; Mwangi, I.; Forster, D.; Marsh, K. Halofantrine Pharmacokinetics in Kenyan Children With Non-Severe and Severe Malaria. *Br. J. Clin. Pharmacol.* **1995,** *39,* 283–287.
156. Humberstone, A. J.; Cowman, A. F.; Horton, J.; Charman, W. N. Effect of Altered Serum Lipid Concentrations on the IC50 of Halofantrine Against Plasmodium Falciparum. *J. Pharm. Sci.* **1998,** *87,* 256–258.
157. Brocks, D. R. Stereoselective Halofantrine and Desbutylhalofantrine Disposition in the Rat: Cardiac and Plasma Concentrations and Plasma Protein Binding. *Biopharm. Drug Dispos.* **2002,** *23,* 9–15.
158. Klein, K.; Aarons, L.; Ter Kuile, F. O.; Nosten, F.; White, N. J.; Edstein, M. D.; Teja-Isavadharm, P. Population Pharmacokinetics of Halofantrine in Healthy Volunteers and Patients With Symptomatic Falciparum Malaria. *J. Pharm. Pharmacol.* **2012,** *64,* 1603–1613.
159. Baune, B.; Flinois, J. P.; Furlan, V.; Gimenez, F.; Taburet, A. M.; Becquemont, L.; Farinotti, R. Halofantrine Metabolism in Microsomes in Man: Major Role of CYP 3A4 and CYP 3A5. *J. Pharm. Pharmacol.* **1999,** *51,* 419–426.

4.05 PBPK Modeling to Estimate Metabolite Formation From First-Pass Organs: Intestine and Liver

Qi Joy Yang and K Sandy Pang, University of Toronto, Toronto, ON, Canada

© 2017 Elsevier Ltd. All rights reserved.

4.05.1	**Introduction**	83
4.05.2	**Parameters That Identify Metabolite Formation**	84
4.05.3	**PBPK Models to Study Metabolite Kinetics**	85
4.05.3.1	PBPK Modeling of the Intestine	85
4.05.3.2	PBPK Modeling of the Liver	87
4.05.3.3	PBPK Model of Whole Body	88
4.05.3.3.1	Intestine-liver: Modeling of first-pass metabolism	88
4.05.3.4	Case Studies, Showcasing the Usefulness of SFM-PBPK Modeling on First-Pass Removal	90
4.05.3.4.1	Case study 1: SFM to detect route-dependent intestinal glucuronidation of morphine	90
4.05.3.4.2	Case study 2: SFM to detect lack of codeine demethylation	94
4.05.4	**Other Considerations**	94
4.05.4.1	Intestine Segmental Heterogeneity	94
4.05.4.2	Liver Enzyme and Transporter Zonation	95
4.05.4.3	Futile Cycling Kinetics	97
4.05.4.4	Membrane Barrier for Metabolite	97
4.05.5	**Metabolite Data in Bioequivalence**	97
4.05.6	**Summary Remarks**	98
References		98

4.05.1 Introduction

Humans are capable of disposing foreign compounds, drugs, or xenobiotics, via a myriad of enzymes that reside predominantly in the liver, and in extrahepatic tissues such as the intestine, kidney, brain, lung, skin, and other tissues. Drug metabolism occurs via Phase I reactions by enzymes belonging to the cytochrome P450 family,[1–3] epoxide hydrolases[4], and Phase II enzymes including UDP-glucuronosyltransferases or UGTs, sulfotransferases or SULTs, and glutathione S-transferases or GSTs.[5,6] Phase I metabolites may be further metabolized by Phase II enzymes, which usually transforms metabolites to more polar and easily excretable forms for renal disposal.[7]

There is an increasing need to consider the importance of metabolites in drug development since metabolites exhibit pharmacological active or toxic properties, and may bind to therapeutic targets or interact with nontherapeutic targets to result in undesired side effects.[8–11] Due to our ability to assay extremely low quantities of metabolites, and there was a movement to consider Metabolite In Safety Testing.[12] In Feb. 2008, the US Food and Drug Administration issued guidance to industry that classified metabolites as major ones when the metabolite in the circulation exceeds 10% of drug exposure. Major metabolites can be defined by relative exposure (%exposure) or the area under the curve (AUC) of precursor and its formed metabolite. But typically, major metabolites are defined as those having %exposure exceeding 10% or 25% that of the precursor drug.[12,13] The modification in chemical structure will change the distribution volumes, lipophilicity, and pKa. It may not be meaningful, however, to consider the %AUC since the metabolite is usually of a smaller volume of distribution than for drug due to its higher polarity.[14] On the other hand, the monitoring of metabolites is especially important for metabolites that are unique and formed only in humans and whose levels are disproportionately greater ($>10\%$) when compared to other animal species.[15] It has been suggested that metabolites be synthesized and administered as preformed metabolites directly for testing in preclinical toxicity studies.[12,16–19] Often times, it may not be possible to administer the metabolite intravenously or give it to humans. Moreover, the %exposure might not be the only parameter to define whether metabolites are major or not, especially when the formed metabolite that is monitored in circulation has been formed and sequentially metabolized before reentering the systemic circulation.[20] Alternatively, the preformed metabolite may not be able to reach tissue sites due to the poor permeability, and exposure to the metabolite will differ from that of the formed metabolite. Others resort to defining parameters, for example, fraction of total or hepatic clearance or fraction of dose that forms the metabolite to describe metabolite formation.[21]

The need for a thorough understanding of kinetics of a formed metabolite from a precursor is paramount. Metabolites can undergo immediate removal within the formation organs, a phenomenon known as "sequential first-pass metabolism" of formed metabolites.[22] This aspect is often ignored and the removal extent of formed metabolites can differ from those for the preformed species.[14,23,24] The difference is particularly noticeable when the polar, preformed metabolite exhibits limited entry into the eliminating organ, contrasting the scenario for the formed metabolite, which is formed from a lipophilic precursor that is highly

permeable and enters the organ readily for formation within the organ.[25] Therefore, it is not guaranteed that preformed and formed metabolites behave similarly in vivo when the metabolite encounters a membrane barrier[23,26] or when enzyme zonation exists in the liver for metabolite formation and sequential removal.[27,28] Additionally, it is not easy to synthesize reactive, stable metabolites. Many of these aspects have been discussed.[14,18,24] What is the most proper way to administer preformed metabolites to best mimic the exposure of formed metabolite is uncertain.[20] For instance, direct administration of preformed metabolite could lead to formation of other metabolites which are not formed from parent.[20] Since metabolite kinetics is of great importance in pharmaceutical research and drug development due to toxicity issues, there have been rigorous efforts devoted toward the elucidation of how much of the dose or clearance forms the metabolite, and under which route of drug administration.

In this communication, we revisit descriptors used in metabolite formation and removal in specific organs or whole body.[21] We prefer use of physiologically based pharmacokinetic (PBPK) versus compartmental models, since the PBPK model can describe multiple tissues in metabolite formation, and the compartment model cannot.[22] The PBPK models are able to characterize the kinetics of preformed and formed metabolite simultaneously[14,24,29] in providing richer information for the understanding of metabolite disposition. An inherent advantage of PBPK models is the specification of the tissue (such as liver and intestine) for metabolite formation. The PBPK models can define intestinal removal of drugs given orally or intraluminally than when given intravenously. Moreover, here, we can accommodate the segregated flow model (SFM) that describes a lower, partial intestinal flow perfusing the enterocyte region where the majority of drug transporters and enzymes are located. The SFM distinguishes route-dependent intestinal metabolism,[30–34] that for drugs metabolized by the intestine, there will be a greater extent of intestinal metabolism for oral (PO) versus intravenous (IV) dosing. These methodologies will be useful in drug development in defining active or toxic metabolite formation and removal. PBPK models are readily scaled up from preclinical to clinical data.[35–37] In addition, the (SFM)PBPK model will consider drug/metabolite transporters, protein binding, sequential metabolism of parent and metabolites in metabolite formation, and removal and transmembrane barriers.

4.05.2 Parameters That Identify Metabolite Formation

One of the common terms that describes primary metabolite formation is the formation clearance of metabolite, mi, as a fraction of total body clearance, g_{mi}. This term, when multiplied to the IV dose, should yield the total amount of metabolite formed.[21] However, because the formed metabolite may be sequentially metabolized or excreted, only a fraction of the newly formed metabolite (denoted by $F^{mi,P}$) appears in systemic circulation.[22,38] Hence, the fraction of total body clearance of the precursor (g_{mi}) that forms the metabolite is given by:

$$g_{mi}F^{mi,P}\text{Dose}^{P,IV} = f_{mi}\text{Dose}^{P,IV} = \text{CL}^{mi,P}\text{AUC}^{P,IV}_{mi,P} \quad (1)$$

where $\text{CL}^{mi,P}$ and $\text{AUC}^{P,IV}_{mi,P}$ are the clearance of the metabolite and AUC of the formed metabolite after intravenous dosing ($\text{Dose}^{P,IV}$) of the precursor, *P*.[21] Note that the formation clearance could be expressed in terms of f_{mi}, the product of $g_{mi}F^{mi,P}$, or the fraction of drug clearance that *furnishes* mi to the circulation, after accounting for sequential elimination of the formed metabolite.[21] Alternatively, the metabolite may be expressed in terms of the hepatic clearance that forms mi, since $h_{mi} = (1 - f_e)g_{mi}$:

$$h_{mi}F^{mi,P}\text{Dose}^{P,IV} = (1 - f_e)g_{mi}F^{mi,P}\text{Dose}^{P,IV} = (1 - f_e)\text{CL}^{mi,P}\text{AUC}^{P,IV}_{mi,P} \quad (2)$$

The fraction of hepatic clearance (h_{mi}) that forms the metabolite is $g_{mi}(1 - f_e)$ where f_e is the fraction of the IV dose that is excreted. Detailed equations for g_{mi}, f_{mi}, and d_{mi} (fraction of intravenous dose that forms mi) were described in previous publications.[21,22,39,40] These parameters are useful descriptors for estimation of the fractional contribution of metabolite formation to total or hepatic clearances.[21]

Martin and colleagues and others[41–44] have described metabolite behavior and parameters. Early plots of the drug and metabolite show important parameters such as the total elimination rate constants of the precursor drug (k) and for the metabolite ($k\{mi\}$). Upon plotting the concentration–time profiles of drug and metabolite, two distinct patterns may be found. Both the elimination rate constants of drug and metabolite, k and $k\{mi\}$, are revealed as terminal slopes. Note that the metabolite formation rate constant, k_{mi}, does not appear in the slope but in the intercept. One shows that the decay profile of the metabolite is longer than that of the drug, with the metabolite formation rate constant (k_{mi}) being slower than its elimination rate constant ($k\{mi\}$) (**Fig. 1A**) and the second, with the decay rate constant for the metabolite ($k\{mi\}$) being parallel to that for drug (k), showing that metabolite elimination is formation rate-limited (**Fig. 1B**). Details surrounding the estimation of elimination rate constants of both drug and metabolites can be found.[44–46]

As more is learned about the handling of the metabolite, the compartmental approach described above may no longer be accurate or useful. First, metabolites formed within tissues are prone to sequential elimination and the available fraction ($F^{mi,P}$) differs. Second, metabolites are usually more polar and exhibit permeability barriers, and the fates of nascently formed metabolite and the metabolite that has returned to the circulation and exists in systemic blood can differ. Third, since both the intestine and liver are serially arranged metabolic organs, and it is very likely that intestinally formed metabolites would travel down to the liver and undergo further metabolism, especially if the metabolite is able to traverse the sinusoidal membrane. The notion that drug or metabolite exposure within eliminating organs or target tissues is additive and combined within the central or peripheral compartments as homogeneous compartments is not tenable. Generally, compartmental modeling fails to quantitatively distinguish the

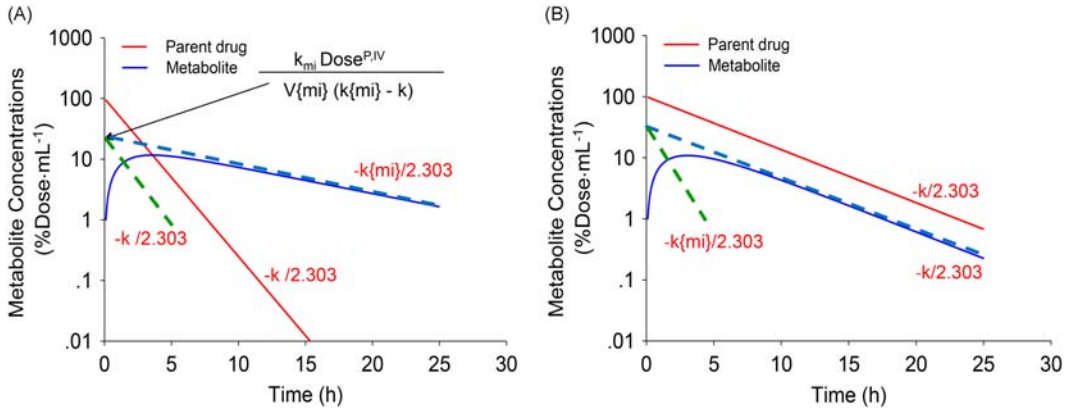

Fig. 1 Log concentrations versus time profiles of parent (*P*) and its formed metabolite (mi). The terminal slopes of parent and metabolite temporal profiles can either be nonparallel (A) or parallel (B), where *k* and *k*{mi} denote the elimination rate constants of *P* and mi, respectively; k_m is the metabolite formation rate; *V*{mi} is the volume of distribution of mi; Dose^{P,IV} is the intravenous dose of *P*. Simulations were performed with $k=0.5\ h^{-1}$, $k\{mi\}=0.1\ h^{-1}$ for (A) and $k=0.1\ h^{-1}$ and $k\{mi\}=0.5\ h^{-1}$ for (B). $k_m=0.1\ h^{-1}$, *V* and *V*{mi} = 1 L using ADAPT5 (BSMR, USC).

location (liver and intestine) of metabolite formation and secretion, characterize induction or inhibition of intestinal but not liver enzyme/transport.[47] For these reasons, compartmental modeling fails to reveal useful information on how much a metabolite is formed or excreted/metabolized in the intestine and liver.[47] Therefore, the PBPK modeling is evoked as the alternative approach to better address these deficiencies.

4.05.3 PBPK Models to Study Metabolite Kinetics

PBPK models provide a physiological approach to examine metabolite disposition when the organ/tissues are anatomically placed. In PBPK modeling of metabolites, it is important to know how many tissues form the metabolite in question from the precursor drug. Sequential metabolism within the same tissue or different tissues as the formation organ will reduce the net appearance of formed metabolite in the systemic circulation.[22] The approach interconnects tissues of discrete volumes by flow, and interrelates physical properties such as transmembrane transport, blood/plasma and tissue binding, and biochemical parameters, such as intrinsic clearances for influx and efflux, and metabolism and secretion in multiple tissues such as the intestine and liver.[47,48] Inherently, these PBPK models allow for consideration of both precursor and formed metabolite and sequential metabolism within the intestine and liver as first-pass organs. For drugs and metabolites of perfusion-limited distribution (no permeability barrier), the tissue-to-plasma/blood partitioning coefficients (K_Ps or K_Bs) that define the steady-state tissue-to-plasma/blood concentration ratio are chosen to simplify rate equations, since the outflow concentration (C) may be expressed as $\frac{C_{tissue}}{K_P \text{ or } K_B}$ when the K_P or $K_B = \frac{C_{tissue}}{C_P \text{ or } C_B}$. The K_P values can be estimated according to equations by Rodgers and Rowland,[49,50] and K_B is related to K_P as $\frac{K_P}{(C_B/C_P)}$. The K_P or K_B is useful to relate the effective volume of distribution of drug in tissue ($K_P \cdot V_{tissue}$, where V_{tissue} is tissue volume). In addition, these PBPK models are equipped to include, within the model, preformed metabolite data for modeling simultaneously.[51] Unlike compartmental models that are unable to separate metabolite formation from individual tissues, PBPK models can align discrete enzymes and transporters in different organ components and characterize the origin of metabolite formation within the organ and account for sequential metabolism.[22,52] The superiority of PBPK modeling over compartmental approach is supported by the fact that PBPK models can better predict human pharmacokinetics based on preclinical data and is more suitable for scale up to man.[35–37]

4.05.3.1 PBPK Modeling of the Intestine

Previously, a simple intestinal model, namely traditional model (TM), has been routinely used for the intestinal tissue where transport, binding, parallel, and sequential metabolism of both drug and metabolite are considered[30]; the intestinal tissue is homogeneous and receives 100% of the intestinal flow (Q_I) (Fig. 2A). In TM, first-order absorption rate constant (k_a), intestinal intrinsic influx ($CL_{in,I}$) and efflux ($CL_{ef,I}$) clearances through basolateral membrane, and intrinsic secretory clearance ($CL_{int,sec,I}$) are used to describe the transport of parent or metabolite through intestinal lumen, intestinal blood, and tissue regions. The intrinsic metabolite formation clearance ($CL_{int,met,I}$) includes formation of major metabolite ($CL_{int,met,I}^{P\rightarrow mi}$) and other metabolites ($CL_{int,met,I}^{P\rightarrow others}$).

However, much data have surfaced to show that the TM model fails to characterize the route-dependent nature of intestinal metabolite formation. This exists when a drug given orally shows extensive intestinal metabolite formation, but the drug produces only little or no intestinal metabolite when given systemically.[30–34] Examples of these that show route-dependent intestinal metabolism[32] include enalapril,[53] acetaminophen,[54] morphine (M),[31] erythromycin,[55] α(−)-6-aminocarbovir,[56] midazolam,[57,58], and

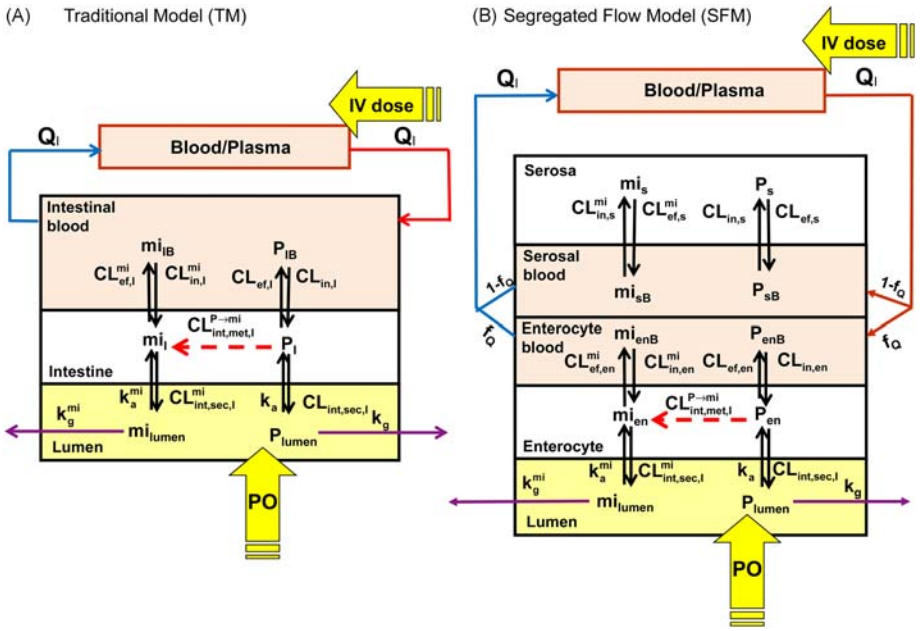

Fig. 2 Schematic representation of TM- (A) and SFM-PBPK (B) models for the intestine which consists of plasma/blood, intestinal blood (IB), and intestinal tissue (I) compartment. In the SFM-PBPK intestinal model (B), the intestinal compartment is subdivided into serosa (s) and enterocyte (en), where f_Q denotes the fraction of intestinal flow (Q) perfusing through enterocyte blood compartment. The intrinsic influx and efflux clearances of precursor (*P*) and formed metabolite (mi) through the intestinal membrane are denoted as $CL_{in,I}$ or $CL^{mi}_{in,I}$ and $CL_{ef,I}$ or $CL^{mi}_{ef,I}$, respectively. The intrinsic metabolite clearance is responsible for metabolite formation ($CL_{int,met,I}$) and intrinsic intestinal secretion for *P* ($CL_{int,sec,I}$) and mi ($CL^{mi}_{int,sec,I}$). The first-order absorption and degradation rate constants are denoted as k_a and k_g for *P*, and k^{mi}_a and k^{mi}_g for mi, respectively, where the fraction of oral dose absorbed, or $F_{abs} = k_a/(k_a + k_g)$. The intravenous (IV) dose is administered into blood/plasma compartment directly whereas oral (or PO) is given into intestinal lumen compartment.

bisphenol.[59] Such route-dependent intestinal metabolism is explained by the pattern that a smaller fraction (5%–30%) of intestinal blood flow perfuses the enzyme/excretory transporter-rich enterocyte region while the majority of blood flow perfuses the inactive, serosal region.[30,32] As the model defines a much lower percent of flow to the enterocyte region, the amount of parent drug in the circulation that enters the enterocyte for metabolism is also less following intravenous administration since most of the drug is shunted away to the serosal region. By contrast, during oral absorption, drug traverses the enterocyte region first before reaching systemic circulation, and all drug becomes available for intestinal metabolism.[32] Thus, there is no difference in intestinal metabolism between the TM and SFM for oral dosing and between IV and PO for TM, the extent of intestinal metabolism after IV dosing according to the SFM is much less than that for the TM. For this reason, a segregated flow intestinal model (SFM) is proposed[30] (**Fig. 2B**). In SFM, the enterocyte blood (enB) and the tissue (en) are perfused by the fractional (f_Q) intestinal blood flow (Q_I), whereas serosal blood (sB) and serosal (s) tissue are perfused by rest of intestinal flow $[(1-f_Q)\cdot Q_I]$. Previous studies have shown that the SFM better describes route-dependent intestinal glucuronidation of M in the rat intestine,[31,47] the kinetics of benzoic acid in perfused recirculating rat intestine[60], and apical excretion of digoxin by P-glycoprotein (P-gp), with and without induction from the pregnane X receptor ligand, pregnenolone-16α-carbonitrile.[61] Recently, PBPK modeling of 1α,25-dihydroxyl vitamin D_3 (an active ligand of vitamin D receptor), developed for consideration of feedback regulation of its synthesis and degradation enzymes, also favors the SFM. Inclusion of segregated, fractional intestinal flow ($f_Q = Q_{en}/Q_I = 10\%$) improves model fitting and prediction of the temporal drug plasma/tissue concentration profiles with escalating (2–120 pmol), repetitive intravenous doses.[62] The fitted value of f_Q is about 2.4%–20% (see **Table 1**).

Consideration of the SFM versus the TM only takes on addition of one extra compartment, namely, the intestine compartment, is not one but now two tissue subcompartments, one for the enterocyte and one for the serosa, with flows of $f_Q Q_I$ and $(1-f_Q)Q_I$, respectively. The impact is large since the SFM encompasses the idea of route-dependent intestinal metabolism and described the greater effects of inducers and inhibitors when given PO, together with the victim drug, also given PO, and less effect or virtually absence of effect when the victim drug is given IV. This was observed for the interaction between digoxin and rifampin in man.[65] Also, a greater inhibition of P-gp activities toward intravenously injected [^{3}H]digoxin by interferon-γ in liver and not intestine in the mouse was observed.[66]

Expression for the availability for the intestine (F_I) exists, and the same equation applies to the TM and SFM.[52] The only difference is in the value of f_Q, which, together with the flow term as $f_Q Q_I$, defines the effective flow to the enterocyte region. For SFM, $f_Q < 0.3$ and for TM, $f_Q = 1$. It is noted in the solution that the drug that is secreted into the gut lumen is subject to reabsorption, by the fraction F_{abs}.

Table 1 Summary of f_Q values for the SFM obtained from fitting

Compound	f_Q *values*	*Details on experiment*	*Intestinal removal*	*Reference*
Morphine	0.024	Recirculating perfused rat small intestine preparation	Morphine 3-glucuronide formed with intraduodenal (oral) but not intravenous dosing of M	30,31
Morphine	0.1	Rat in vivo following intravenous or intraduodenal dosing of M	M glucuronidation, greater with intraduodenal but not intravenous dosing of M; ratio of bile/urine of MG after PO is greater than that after iv	47
[^{3}H]Digoxin	0.2	Recirculating perfused rat small intestine preparation	Cyp3a and P-gp	61
[^{3}H]Digoxin	0.16	Mouse intestine in vivo	P-gp for excretion into gut lumen	63
1α,25-dihydroxyl vitamin D_3	0.11	Mouse in vivo with PBPK modeling	Cyp24a1 forming metabolite 1,24,25-trihydroxyl vitamin D_3	62
Benzoic acid	0.07	Recirculating perfused rat small intestine preparation	Better distribution; no metabolite data to substantiate SFM	60
Codeine	0.l6	Rat in vivo following intravenous or intraduodenal dosing of codeine	Minor intestinal contribution to overall first-pass metabolism	64

$$F_I = \frac{f_Q Q_I CL_{ef,I}}{f_Q Q_I CL_{ef,I} + \left(f_Q Q_I + f_B CL_{in,I}\right)\left[CL^{P\to mi}_{int,met,I} + CL^{P\to others}_{int,met,I} + CL_{int,sec,I}(1 - F_{abs})\right]} \tag{3}$$

where for the TM, $f_Q = 1$ and for SFM, $f_Q < 0.3$.

4.05.3.2 PBPK Modeling of the Liver

The liver is the most modeled tissue, mainly because it is the most important organ for drug metabolism and biliary excretion. A common strategy is to consider the liver as a "well-stirred" compartment where drug in the liver tissue is rapidly equilibrium with that in the emergent hepatic venous blood[67–70]; bulk blood flow exists, and the liver is viewed as a simple, well-mixed reactor.[71] Alternately, the liver may be considered as a series of parallel tubes that are surrounded with evenly distributed hepatic enzymes[72,73] for the "parallel tube" model.[68] Another flow model that considers plug (parallel tube model)[72,73] or dispersive flow (dispersion model)[74–77] is available for the modeling hepatic drug extractions. The properties of these models have been reviewed and differ primarily with the type, flow, and degree of mixing (characterized by the D_N number), which is infinite for the well-stirred model, nonexistent for the parallel tube model, and intermediate for the dispersion model.[77–79]

The "well-stirred" model is the most extensively used among the models to describe drug/metabolite kinetics in eliminating organs such as the liver, with or without diffusional barrier through sinusoidal membrane.[62,80] Generally speaking, the liver-PBPK model consists of plasma/blood and liver (tissue and liver blood) compartments that are interconnected by liver blood flow. The influx and efflux clearances through sinusoidal membrane for unbound precursor and formed metabolites are denoted by $CL^P_{in,L}$ and $CL^P_{ef,L}$ and $CL^{mi}_{in,L}$ and $CL^{mi}_{ef,L}$, respectively. The unbound precursor drug of concentration $f^P_L P_L$ (f^P_L is the unbound fraction of precursor in liver blood and P_L is concentration in liver) is metabolized to form the primary metabolite (mi) with intrinsic metabolite $CL^{P\to mi}_{int,met,L}$ (or $V^{P\to mi}_{max,L}/K^{P\to mi}_{m,L}$ for first-order condition), and mi can be also further metabolized to other secondary metabolites with intrinsic metabolic clearance $CL^{mi}_{int,met,L}$. Precursor and mi are secreted into bile with $CL^P_{int,sec,L}$ and $CL^{mi}_{int,sec,L}$, respectively). A representative model scheme is shown in **Fig. 3**. Binding of precursor and mi in blood (f^P_B and f^{mi}_B) and liver tissue (f^P_L and f^{mi}_L) is considered as well. The AUC for the precursor and metabolite, with the liver as the only eliminating organ for drug, have been solved,[52]

$$AUC^{P,IV}_P = \frac{Dose^{P,IV}}{CL} = \frac{Dose^{P,IV}\left[Q_L CL^P_{ef,L} + CL^P_{int,L}\left(Q_L + f^P_B CL^P_{in,L}\right)\right]}{Q_L f^P_B CL^P_{in,L} CL^P_{int,L}} \tag{4}$$

$$CL = \frac{Dose^{P,IV}}{AUC^{P,IV}_P} = Q_L \frac{f^P_B CL^P_{in,L} CL^P_{int,L}}{Q_L CL^P_{ef} + CL^P_{int,L}\left(Q_L + f^P_B CL^P_{in,L}\right)}$$

$$\text{where} \quad CL^P_{int,L} = CL^P_{int,met,L} + CL^P_{int,sec,L} \tag{5}$$

$$AUC^{P,IV}_{mi,P} = \frac{Dose^{P,IV} CL^{P\to mi}_{int,met,L} CL^{mi}_{ef,L}}{CL^P_{int,L} f^{mi}_B CL^{mi}_{in,L} CL^{mi}_{int,L}} \tag{6}$$

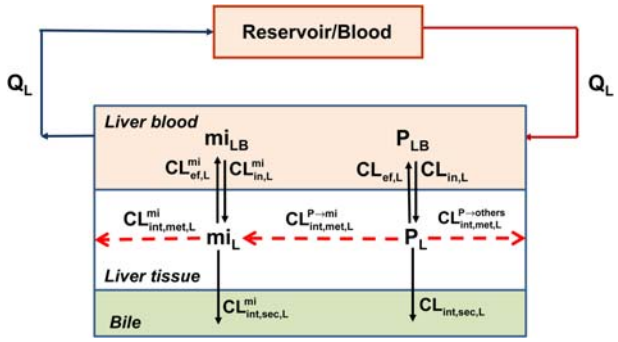

Fig. 3 Schematic representation of liver-PBPK model which consists of blood, liver blood (LB), and liver tissue (L) compartment. The influx and efflux clearances of precursor (*P*) and metabolite (mi) through the sinusoidal membrane are denoted as $CL_{in,L}$ or $CL^{mi}_{in,L}$ and $CL_{ef,L}$ or $CL^{mi}_{ef,L}$, respectively. The intrinsic metabolite clearance is responsible for metabolite formation ($CL_{int,met,L}$) and intrinsic biliary secretion for *P* ($CL_{int,sec,L}$) and mi E($CL^{mi}_{int,sec,L}$). Q_L denotes the hepatic plasma/blood flow.

These equations are applicable only when liver is the only eliminating organ[52] and total body clearance (CL) is hepatic clearance (CL_L). Hepatic availability (F_L) is

$$F_L = \frac{Q_L\left(CL_{ef,L} + CL_{int,sec,L} + CL_{int,met,L}\right)}{Q_L\left(CL_{ef,L} + CL_{int,sec,L} + CL_{int,met,L}\right) + f_B CL_{in,L}\left(CL_{int,sec,L} + CL_{int,met,L}\right)} \tag{7}$$

and may be determined by:

$$\frac{AUC_P^{P,PO}\Big/Dose_P^{P,PO}}{AUC_P^{P,IV}\Big/Dose_P^{P,IV}} \quad \text{or} \quad \frac{AUC_{mi,P}^{P,PO}\Big/Dose_P^{P,PO}}{AUC_{mi,P}^{P,IV}\Big/Dose_P^{P,IV}} \tag{8}$$

In the above relations, $AUC_P^{P,PO}$ and $AUC_P^{P,IV}$ are the AUC of parent drug after PO and IV administration, respectively; $AUC_{mi,P}^{P,PO}$ and $AUC_{mi,P}^{P,IV}$ are the AUC of the formed metabolite after PO and IV drug doses, respectively. Again, these equations are applicable only when the liver is the only eliminating organ.

Based on the above equations (especially, Eq. (5)), effects of the activities of enzyme (denoted by $CL_{int,met,L}$) and transporters (reflected by $CL_{ef,L}$, $CL_{in,L}$, and $CL_{int,sec,L}$) on hepatic availability (F_L) could be appraised with simulations based on increased/decreased values of the parameters of interest. The utility of Eq. (7) has been fully explored.[81] For example, an inhibition of the hepatic intrinsic metabolic pathway $\left(CL^{P\rightarrow mi}_{int,met,L}\right)$ will lead to increased $AUC_P^{P,IV}$ of parent drug and increased metabolic clearance of the alternative pathway but a decreased $AUC_{mi,P}^{P,IV}$ of the formed metabolite.[52] On the other hand, increased $CL_{int,sec,L}$ will increase biliary clearance and total hepatic clearance of parent drug but will decrease the metabolic clearance.[82] The observed transporter/enzyme interplay toward the competition of hepatic canalicular efflux transporter and metabolizing enzyme for the same intracellular substrate for hepatic elimination could be readily assessed.[52,81,83,84] Additionally, both lower $CL_{in,L}$ and higher $CL_{ef,L}$ allow high drug accumulation in systemic circulation (increased $AUC_P^{P,IV}$), and lower hepatic clearance of the drug, and vice and versa.[83,84]

4.05.3.3 PBPK Model of Whole Body

4.05.3.3.1 Intestine-liver: Modeling of first-pass metabolism

Because there are measureable intestinal enzymatic activities and because of the intestine being a gateway tissue to the liver for first-pass drug metabolism, it is paramount to assess the importance of the intestine versus the liver in first-pass removal. The model scheme, depicted in Fig. 4, shows that the intestine and liver are serially arranged tissues that are interconnected by blood flow through portal vein (Q_{PV} or Q_I or intestinal blood/plasma flow), a venous outflow that feeds into the liver as an input. In this circuit, it is crucial to investigate drug/metabolite kinetics in the whole-body setting, with consideration of appropriate physiological parameters for enzyme and transporter activities for drug as well as sequential metabolism. The systemic bioavailability (F_{sys}) is the product of hepatic availability (F_L), intestinal availability (F_I), and fraction absorbed [F_{abs} or $k_a/(k_a+k_g)$ where k_a and k_g are the absorption and luminal degradation rate constants, respectively]. The AUC and *F* of precursor drug and formed metabolite have be solved using matrix inversion based on rate equations derived from PBPK model,[20,52] under four different scenarios with different eliminating organ/metabolites.[52] F_L (Eq. (9)) and F_I (Eq. (10)) are solved[52,85]::

$$F_L = \frac{(Q_I + Q_{HA})\left(CL_{ef,L} + CL_{int,sec,L} + CL^{P\rightarrow mi}_{int,met,L} + CL^{P\rightarrow others}_{int,met,L}\right)}{(Q_I + Q_{HA})\left(CL_{ef,L} + CL_{int,sec,L} + CL^{P\rightarrow mi}_{int,met,L} + CL^{P\rightarrow others}_{int,met,L}\right) + f_B CL_{in,L}\left(CL_{int,sec,L} + CL^{P\rightarrow mi}_{int,met,L} + CL^{P\rightarrow others}_{int,met,L}\right)} \tag{9}$$

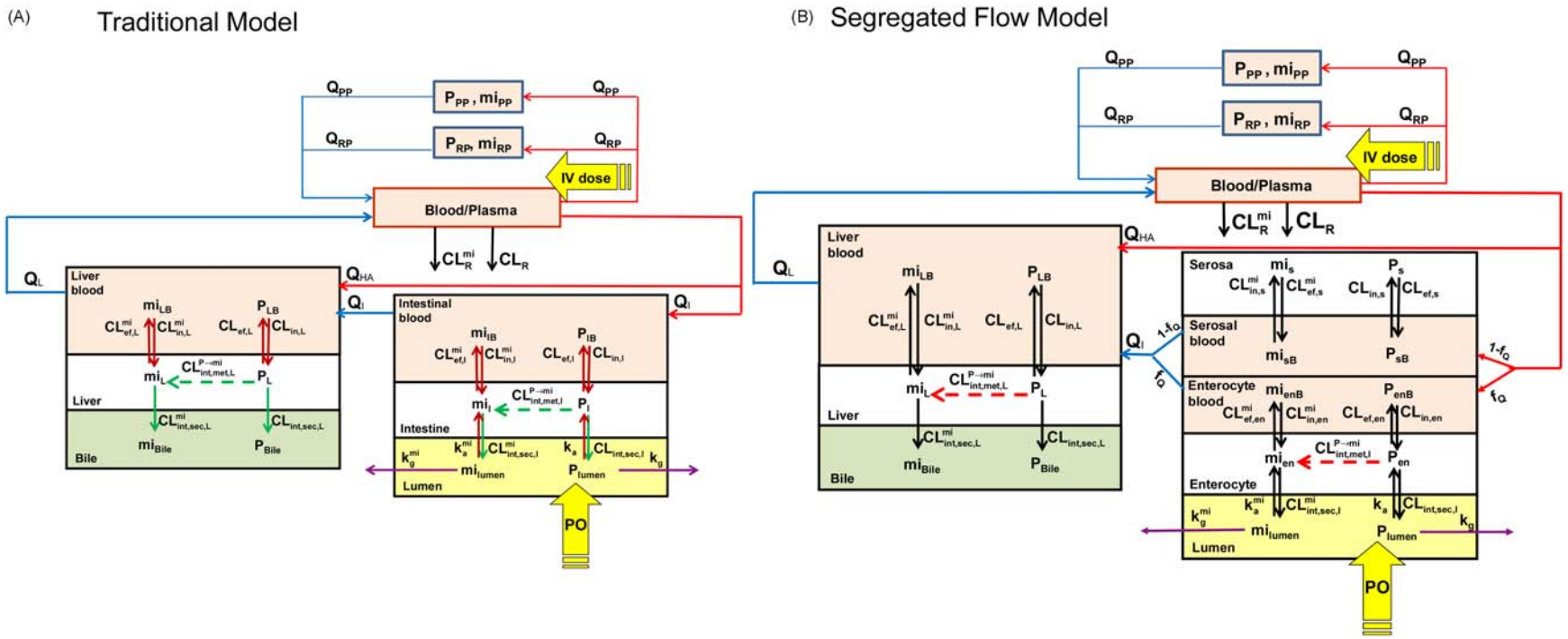

Fig. 4 Schematic representation of full TM- (A) and SFM-PBPK (B) model which consists of plasma/blood, liver (L), intestine (I), RP and PP compartments. The parameter descriptions are the same as those in **Figs. 2** and **3**. The renal clearances for *P* and mi are denoted as CL_R and CL_R^{mi} from blood/plasma compartment. The IV dose is administered into blood/plasma compartment directly whereas the PO dose is given directly into the intestinal lumen compartment.

$$F_I = F_{abs}\frac{f_Q Q_I CL_{ef,I}}{f_Q Q_I CL_{ef,I} + \left(f_Q Q_I + f_B CL_{in,I}\right)\left[CL_{int,met,I}^{P\rightarrow mi} + CL_{int,met,I}^{P\rightarrow others} + CL_{int,sec,I}(1 - F_{abs})\right]} \quad (10)$$

The systemic bioavailability (F_{sys}) is the product of fraction absorbed (F_{abs}), F_I and F_L, given by:

$$F_{sys} = F_{abs}F_I F_L = F_{abs}\frac{f_Q Q_I CL_{ef,I}}{f_Q Q_I CL_{ef,I} + \left(f_Q Q_I + f_B CL_{in,I}\right)\left[CL_{int,met,I}^{P\rightarrow mi} + CL_{int,met,I}^{P\rightarrow others} + CL_{int,sec,I}(1 - F_{abs})\right]} \times \frac{(Q_I + Q_{HA})\left(CL_{ef,L} + CL_{int,sec,L} + CL_{int,met,L}^{P\rightarrow mi} + CL_{int,met,L}^{P\rightarrow others}\right)}{(Q_I + Q_{HA})\left(CL_{ef,L} + CL_{int,sec,L} + CL_{int,met,L}^{P\rightarrow mi} + CL_{int,met,L}^{P\rightarrow others}\right) + f_B CL_{in,L}\left(CL_{int,sec,L} + CL_{int,met,L}^{P\rightarrow mi} + CL_{int,met,L}^{P\rightarrow others}\right)} \quad (11)$$

Note that for Eqs. (10) and (11), F_{abs} accounts for the influence of reabsorption of drug on the net apical secretion of drug; generally, a higher value of F_{abs} infers a lower net apical secretion.

As discussed before, PBPK model is useful in drug/metabolite kinetic testing as it integrates the pharmacokinetic data into a model with physiological, biochemical, and thermodynamic-relevant parameters.[86] However, the whole-body PBPK model has limited use due to its high complexity and dimensionality,[87–89] whereas lumping of organs/tissues with the same model specification and identical position in the system structure greatly simplifies these structural considerations.[86] The above TM- and SFM-PBPK models (Fig. 4) represent full PBPK models that define both intestine and liver as the first-pass metabolite formation organs, and lumped organ/tissue compartments into rapidly perfused (RP; such as heart, brain, lung, kidney) and poorly perfused (PP; such as muscle, fat, and skin) compartments. The primary metabolite (mi) is formed by liver and intestine with metabolite formation intrinsic clearance ($CL_{int,met}^{P\rightarrow mi}$), and the precursor also forms other metabolites ($CL_{int,met}^{P\rightarrow others}$). The formed metabolites can reenter the intestine and liver with influx clearances denoted as CL_{in}^{mi} and efflux back to systemic circulation with clearance that is denoted by CL_{ef}^{mi}. The same or different metabolites can be formed in liver ($CL_{int,met,L}^{P\rightarrow mi}$) and intestine ($CL_{int,met,I}^{P\rightarrow mi}$). Both precursor and metabolite can undergo biliary ($CL_{int,sec,L}^{P}$ and $CL_{int,sec,L}^{mi}$) and intestinal ($CL_{int,sec,I}^{P}$ and $CL_{int,sec,I}^{mi}$) secretion. The reabsorption (k_a^P and k_a^{mi}) and degradation (k_g^P and k_g^{mi}) of drug and metabolites in intestinal lumen are also considered. The renal clearances for precursor (CL_R^P) and metabolite (CL_R^{mi}) can be included, and, for the sake of simplicity, are assigned to the blood/plasma compartment. Similarly, the developed PBPK-SFM model can be used to appreciate the route-dependent pharmacokinetics.

4.05.3.4 Case Studies, Showcasing the Usefulness of SFM-PBPK Modeling on First-Pass Removal

4.05.3.4.1 Case study 1: SFM to detect route-dependent intestinal glucuronidation of morphine

The prevalence of intestinal first-pass metabolism has led to resurgence in PBPK modeling of the intestine and liver, with the newly developed SFM model being considered in parallel to that for the TM. M is avidly glucuronidated by the rat intestine[31] and liver.[90] M is a lipophilic substrate that can freely diffuse across membrane barrier, glucuronidated in liver and intestine,[91] and undergo renal and biliary secretion. Its polar, morphine 3β-glucuronide (MG) enters hepatocyte with a relatively low influx clearance (0.1 mL min^{-1} g^{-1} liver), due to the existence of a diffusional barrier at the sinusoidal membrane.[90] MG formed in liver is secreted via the multidrug resistance-associated protein 2 (Mrp2) into bile or is effluxed into the systemic circulation via the multidrug resistance-associated protein 3, Mrp3. Analogously, intestinally formed MG undergoes luminal secretion via Mrp2 or is effluxed out by Mrp3 back to the circulation[92] (Fig. 5).

The kinetics of MG excretion was studied in the rat in vivo for examination of the relative contributions of intestine and liver to MG formation following the intravenous or intraduodenal (or oral) dosing of M.[47] The extent of MG formed in liver and intestine is reflected by its appearance in urine or bile. As MG is poorly permeable, MG that is excreted into urine originates from both intestine and bile whereas MG secreted into bile is formed mostly from the liver. For this reason, the SFM will likely bring about large changes in the MG recovered in bile versus that in urine for IV versus PO dosing of M.

The substrate is uniquely suited for the discrimination between the SFM versus the TM. The SFM-PBPK model was found to fit the data better than the TM (Fig. 6). The rich data obtained from the perfused rat intestinal and liver preparations and background information from the literature were inputted into PBPK models comprising the intestine and liver in first-pass removal.[47] The SFM successfully describes the systemic delivery of M being shunted away from the enterocyte for metabolism whereas all M delivered intraduodenally/orally must enter the enterocyte first before reaching the recirculation. The MG species found in bile, originating mostly from liver metabolism of M, is higher with IV dosing of M, whereas urinary MG is higher with PO than IV dosing. Therefore SFM successfully predicts the urine/bile ratio of MG with PO dosing being higher than for IV dosing (2.6-fold). The observed ratio for urinary/bile excretion data of MG for PO is 2.6-fold that after IV dosing of M, as predicted by the SFM and not the TM or compartmental model. For the TM and compartmental models, a ratio of one is expected (Table 2).

The data fitting with the SFM-PBPK model is excellent (Fig. 6).[47] Model fitting further provided useful terms, expressed as products of the unbound tissue fraction and the efflux, secretory, or metabolic intrinsic clearances (Table 3). These estimates, expressed as ratios, could, in turn, provide estimates of the tissue distribution ratios ($K_{I,uu}$ and $K_{L,uu}$), intestinal availabilities of drug (F_I^P) and metabolite (F_I^{mi}), as well as those for the liver (F_L^P and F_L^{mi}).

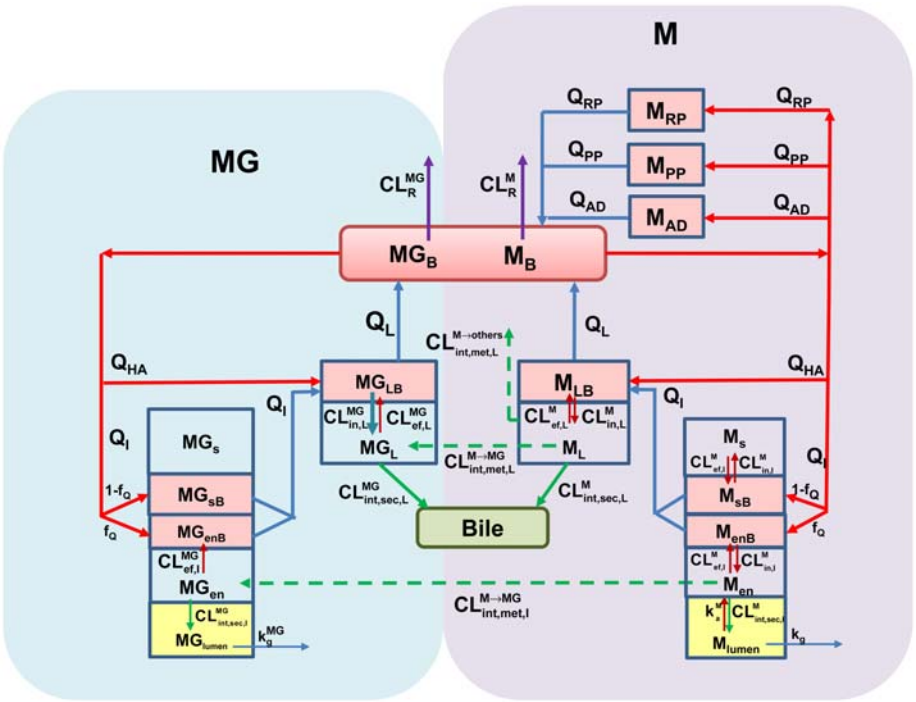

Fig. 5 Schematic representation of TM- (A) and SFM- PBPK (B) models has been used to describe the pharmacokinetics of M and its major metabolite, MG.[47] MG exhibits poor entry into tissues (including the intestine and liver) and is formed within the intestine and liver. The metabolite, mi (or MG) that appears in bile originates primarily from liver metabolism, since the MG in circulation experiences a permeability barrier to enter the liver tissue: $CL_{in,L}^{MG}$ is 1 mL min^{-1} according to Doherty et al.[90] The liver and intestine possess intrinsic metabolite clearances responsible for mi formation in liver $\left(CL_{int,met,L}^{P\rightarrow mi}\right)$ and in intestine $\left(CL_{int,met,I}^{P\rightarrow mi}\right)$, and for forming other metabolites $CL_{int,met,L}^{P\rightarrow others}$ and $CL_{int,met,I}^{P\rightarrow others}$.The intrinsic biliary and intestinal secretion for *P* ($CL_{int,sec,L}$ or $CL_{int,sec,I}$, respectively) and mi ($CL_{int,sec,L}^{mi}$ or $CL_{int,sec,I}^{mi}$, respectively). The first-order absorption and degradation rate constants are denoted as k_a and k_g for the precursor drug, and k_a^{mi} and k_g^{mi} for mi, respectively. The renal clearances for *P* and mi are denoted as CL_R and CL_R^{mi} and for the sake of simplicity, arise from the blood compartment. The IV dose is administered into blood/plasma compartment directly whereas intraduodenal (or PO) doses are injected into the intestinal luminal compartment. Obtained from Yang, Q. J.; Fan, J.; Chen, S.; Liu, L.; Sun, H. and Pang, K. S. Metabolite Kinetics: The Segregated Flow Model for Intestinal and Whole Body Physiologically Based Pharmacokinetic Modeling to Describe Intestinal and Hepatic Glucuronidation of Morphine in Rats In Vivo. *Drug Metab. Dispos.* **2016**, *44*, 1123–1138, with permission.

$$F_I^P = \frac{f_I^P CL_{ef,I}^P}{f_I^P CL_{ef,I}^P + f_I^P CL_{int,sec,I}^P + f_I^P CL_{int,met,I}^P} = \frac{CL_{ef,I}^P}{CL_{ef,I}^P + CL_{int,sec,I}^P + CL_{int,met,I}^P} \tag{12}$$

$$F_I^{mi} = \frac{f_I^{mi} CL_{ef,I}^{mi}}{f_I^{mi} CL_{ef,I}^{mi} + f_I^{mi} CL_{int,sec,I}^{mi} + f_I^{mi} CL_{int,met,I}^{mi}} = \frac{CL_{ef,I}^{mi}}{CL_{ef,I}^{mi} + CL_{int,sec,I}^{mi} + CL_{int,met,I}^{mi}} \tag{13}$$

$$F_L^P = \frac{f_L^P CL_{ef,L}^P}{f_L^P CL_{ef,L}^P + f_L^P CL_{int,sec,L}^P + f_I^P CL_{int,met,L}^P} = \frac{CL_{ef,L}^P}{CL_{ef,L}^P + CL_{int,sec,L}^P + CL_{int,met,L}^P} \tag{14}$$

$$F_L^{mi} = \frac{f_L^{mi} CL_{ef,L}^{mi}}{f_L^{mi} CL_{ef,L}^{mi} + f_L^{mi} CL_{int,sec,L}^{mi} + f_L^{mi} CL_{int,met,L}^{mi}} = \frac{CL_{ef,L}^{mi}}{CL_{ef,L}^{mi} + CL_{int,sec,L}^{mi} + CL_{int,met,L}^{mi}} \tag{15}$$

Another interesting comparison is the fractional contribution of intestine $\left(\frac{v_I}{v_I + v_L}\right)$ or liver $\left(\frac{v_L}{v_I + v_L}\right)$ to the overall intestinal–liver removal for a drug entering the first-pass organs via the circulation.[85] It must be noted that these equations estimate the % contribution of drug entering systemically (after IV dosing). The fractional contributions of intestine and liver to the overall intestinal–liver removal[85] are:

$$\frac{v_I}{v_I + v_L} = \frac{f_Q Q_I (1 - F_I)}{f_Q Q_I (1 - F_I) + E_L \langle Q_I [f_Q F_I + (1 - f_Q)] + Q_{HA} \rangle} \tag{16}$$

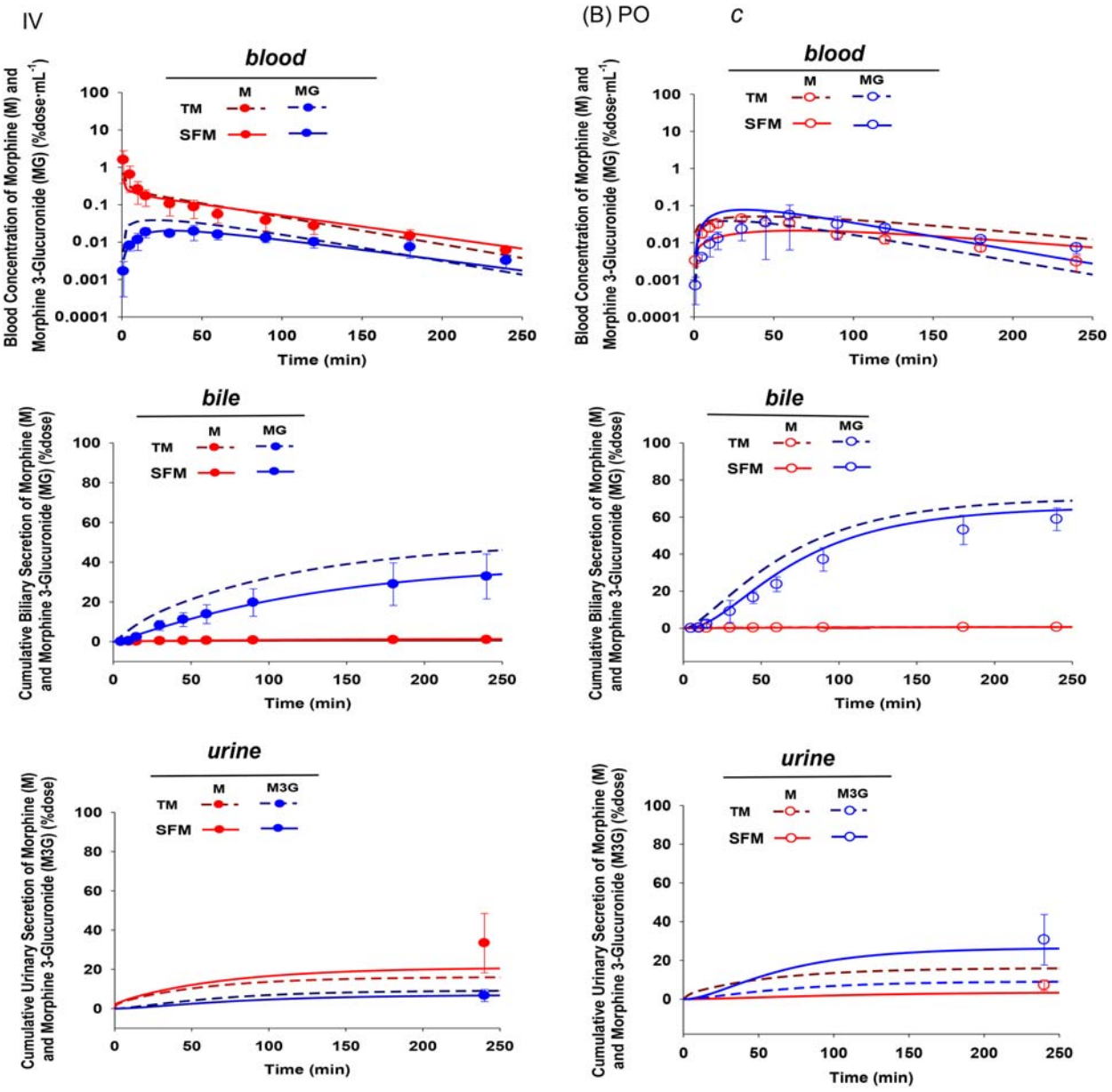

Fig. 6 Observed and fitted blood concentration–time profiles of M and MG as well as the cumulative amounts of M and MG in bile and urine after intravenous (A) intraduodenal or oral (B) administration of M (IV, *solid circles*, $n=4$; PO, *open circles*, $n=3$; M and MG are denoted as *red* and *blue symbols*, respectively). The fits of TM-PBPK are shown with dashed lines and SFM-PBPK is shown with solid lines. Data are presented as means ± SD. Obtained from Yang, Q. J.; Fan, J.; Chen, S.; Liu, L.; Sun, H. and Pang, K. S. Metabolite Kinetics: The Segregated Flow Model for Intestinal and Whole Body Physiologically Based Pharmacokinetic Modeling to Describe Intestinal and Hepatic Glucuronidation of Morphine in Rats In Vivo. *Drug Metab. Dispos.* **2016**, *44*, 1123–1138, with permission.

Table 2 Cumulative excretion of MG into urine/bile by 4 h or at infinity (predicted), after PO and IV administration of M

	Ratio of MG_{urine}/MG_{bile}					
	Intraduodenal (or PO) dosing		*Intravenous (IV) dosing*		*PO/IV dosing*	
	4 h	∞	4 h	∞	4 h	∞
Observed	0.541	–[a]	0.212	–[a]	2.55	–[a]
Compartmental model	0.485	0.485	0.485	0.485	1.0	1.0
TM-PBPK model	0.131	0.131	0.131	0.131	1.0	1.0
SFM-PBPK model	0.453	0.444	0.175	0.179	2.59	2.47

[a]Not measured.

Table 3 Estimates upon PBPK modeling of M in rat in vivo[47]

Parameter	*Definition*	*TM-PBPK*	*SFM-PBPK*
$\frac{f_B^M CL_{in,I}^M}{f_I^M CL_{ef,I}^M}$ or $K_{I,uu}$	Ratio of effective uptake/efflux clearance of M in intestine, or intestine to blood partitioning of unbound M	0.137	0.531
$\frac{f_B^M CL_{in,L}^M}{f_L^M CL_{ef,L}^M}$ or $K_{L,uu}$	Ratio of effective uptake/efflux clearance of M in liver, or liver to blood partitioning ratio of unbound M	1.42	2.46
F_I	Intestinal availability of M	0.654	0.457
	$\frac{CL_{ef,I}^M}{CL_{ef,I}^M + CL_{int,sec,I}^M(1-F_{abs}) + CL_{int,met,I}^{M\to MG}}$	0.629	0.282
	$\frac{f_Q Q_I CL_{ef,I}^M}{f_Q Q_I CL_{ef,I}^M + \left(f_Q Q_I + f_B^M CL_{in,I}^M\right)\left[CL_{int,met,I}^{M\to MG} + CL_{int,sec,I}^M(1-F_{abs})\right]}$ [a]		
F_L	Hepatic availability of M	0.574	0.574
	$\frac{CL_{ef,L}^M}{CL_{ef,L}^M + CL_{int,met,L}^{M\to MG} + CL_{int,met,L}^{M\to others} + CL_{int,sec,L}^M}$	0.710	0.717
	$\frac{(Q_I + Q_{HA})\left(CL_{ef,L}^M + CL_{int,sec,L}^M + CL_{int,met,L}^{M\to MG} + CL_{int,met,L}^{M\to others}\right)}{(Q_I+Q_{HA})\left(CL_{ef,L}^M + CL_{int,sec,L}^M + CL_{int,met,L}^{M\to MG} + CL_{int,met,L}^{M\to others}\right) + f_B^M CL_{in,L}^M\left(CL_{int,sec,L}^M + CL_{int,met,L}^{M\to MG} + CL_{int,met,L}^{M\to others}\right)}$ [a]		
$F_{sys} = F_{abs} \times F_I \times F_L$	Systemic bioavailability:	0.334	0.242
	$F_{abs} \times \frac{CL_{ef,I}^M}{CL_{ef,I}^M + CL_{int,sec,I}^M(1-F_{abs}) + CL_{int,met,I}^{M\to MG}} \times \frac{CL_{ef,L}^M}{CL_{ef,L}^M + CL_{int,met,L}^{M\to MG} + CL_{int,met,L}^{M\to others} + CL_{int,sec,L}^M}$	0.402	0.186
	$F_{abs}\frac{f_Q Q_I CL_{ef,I}^M}{f_Q Q_I CL_{ef,I}^M + \left(f_Q Q_I + f_B^M CL_{in,I}^M\right)\left[CL_{int,met,I}^{M\to MG} + CL_{int,sec,I}^M(1-F_{abs})\right]}$		
	$\times\frac{(Q_I + Q_{HA})\left(CL_{ef,L}^M + CL_{int,sec,L}^M + CL_{int,met,L}^{M\to MG} + CL_{int,met,L}^{M\to others}\right)}{(Q_I + Q_{HA})\left(CL_{ef,L}^M + CL_{int,sec,L}^M + CL_{int,met,L}^{M\to MG} + CL_{int,met,L}^{M\to others}\right) + f_B^M CL_{in,L}^M\left(CL_{int,sec,L}^M + CL_{int,met,L}^{M\to MG} + CL_{int,met,L}^{M\to others}\right)}$		
F_I^{mi}	Intestinal availability of MG	0.95	0.89
	$\frac{CL_{ef,I}^{MG}}{CL_{ef,I}^{MG} + CL_{int,sec,I}^{MG}}$		
F_L^{mi}	Hepatic availability of MG	0.11	0.22
	$\frac{CL_{ef,L}^{MG}}{CL_{ef,L}^{MG} + CL_{int,sec,L}^{MG}}$		
h_{mi}	Fraction of hepatic clearance of M forming MG	0.948	0.854
	$\frac{CL_{int,met,L}^{M\to MG}}{CL_{int,met,L}^{M\to MG} + CL_{int,met,L}^{M\to others} + CL_{int,sec,L}^M}$		
$g_{mi} = (1-f_e)h_{mi}$ [b]	Fraction of total body clearance of M forming MG ($f_e = 0.334$)	0.631	0.569
$\frac{v_I}{v_I+v_L}$ [c]	Fractional contribution of intestine to intestinal–liver removal	0.460	0.093
		0.570[e]	0.171[e]
$\frac{v_L}{v_I+v_L}$ [d]	Fractional contribution of liver to intestinal–liver removal	0.540	0.907
		0.430[e]	0.829[e]

[a] Equations from Sun and Pang.[52]
[b] Based on definition of Ref. 21.
[c] Calculated based on equations from Pang and Chow[85]: $\frac{v_I}{v_I+v_L} = \frac{f_Q Q_I(1-F_I)}{f_Q Q_I(1-F_I) + E_L\langle Q_I[f_Q F_I + (1-f_Q)] + Q_{HA}\rangle}$.

[d] Calculated based on equations from Pang and Chow[85]: $\frac{v_L}{v_I+v_L} = \frac{E_L\langle Q_I[f_Q F_I + (1-f_Q)] + Q_{HA}\rangle}{f_Q Q_I(1-F_I) + E_L\langle Q_I[f_Q F_I + (1-f_Q)] + Q_{HA}\rangle}$.

[e] F_I and F_L values, based on equations from Sun and Pang,[52] for method 2.

$$\frac{v_L}{v_I + v_L} = \frac{E_L\langle Q_I[f_Q F_I + (1 - f_Q)] + Q_{HA}\rangle}{f_Q Q_I(1 - F_I) + E_L\langle Q_I[f_Q F_I + (1 - f_Q)] + Q_{HA}\rangle} \quad (17)$$

Here, v_I and v_L define the rates of intestinal and liver secretion/metabolism, respectively, in forming the metabolites; Q_{HA} defines flow rate of hepatic artery; E_L or $(1-F_L)$ denotes the extraction ratio of the liver, where $f_Q = 0.1$ for the SFM and 1 for the TM.

With these equations, the first-pass effect by the intestine and liver could be estimated. For TM, the %contribution for the intestine and liver for PO and IV dosing are expected to be identical, and the %contribution for PO is the same for both TM and SFM, since the entire dose needs to traverse the enterocyte region. However, for SFM, the %intestinal contribution for IV dosing reflects the influence of shunting away from the enterocytes. This results in a greater %liver contribution. Consistent with this line of reasoning, fitted results for M show that 46% of the MG formed originates from the intestine and 53% of MG formed originates from the liver in first-pass metabolism with PO dosing for TM. The same ratio, 46%:53%, should apply for PO dosing of M according to the SFM. However, for IV dosing, the %contribution by the intestine and liver to M glucuronidation are 9.3% and 91%, respectively, according to the SFM.

4.05.3.4.2 Case study 2: SFM to detect lack of codeine demethylation

The above modeling strategy for analyzing intestinal versus liver metabolic activity was also applied to examine the demethylation activity toward codeine in the rat in vivo.[64] The blood, urine, and bile data of codeine (C), M, and MG after PO and IV dosing of codeine was examined under first-order conditions (Fig. 7). However, in this case, both the TM and SFM predicted the drug and metabolite data equally well (Fig. 8). There was little change in the ratio of urinary/bile ratio of M or MG after IV versus PO administration (Table 4). More importantly, the $\%\frac{v_I}{v_I + v_L}$ was low and F_I^C was high for both TM and SFM, and the values were virtually identical (Table 5). This suggests that there is little intestinal demethylation of codeine. By contrast, the $\%\frac{v_L}{v_I + v_L}$ was almost 100%. The ratio of the liver/intestinal intrinsic clearance was about 10-fold, and is consistent with literature data,[64] showing that liver activity greatly exceeds that of the intestine. PBPK modeling again provides detailed and meaningful information on first-pass drug metabolism of codeine.

4.05.4 Other Considerations

4.05.4.1 Intestine Segmental Heterogeneity

Further to the SFM, both the TM and SFM have been extended to describe segmental distributions of transporters and enzymes.[32,93] Much heterogeneity in transporter and enzyme among intestinal segments has been noted (see Refs. [23,34,94–97]). Inclusion of

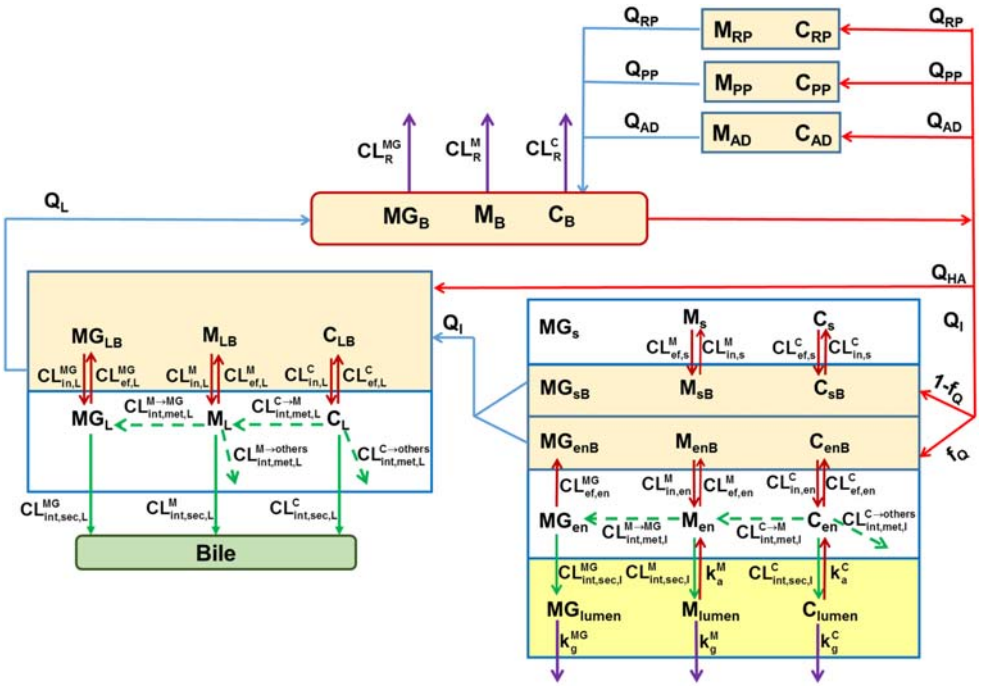

Fig. 7 The TM-nested PBPK (A) and SFM-nested PBPK (B) models were used to describe the pharmacokinetics of codeine (C), which is metabolized to M and MG in the rat (see Noh et al.[64]). The parameters are similar to Fig. 5. Obtained from Noh, K.; Chen, S.; Yang, Q. J. and Pang, K. S. Physiologically Based Pharmacokinetic Modeling Revealed Minimal Codeine Intestinal Metabolism in First-Pass Removal in Rats. *Biopharm. Drug. Dispos.* **2016**, 38(1), 50–74, with permission.

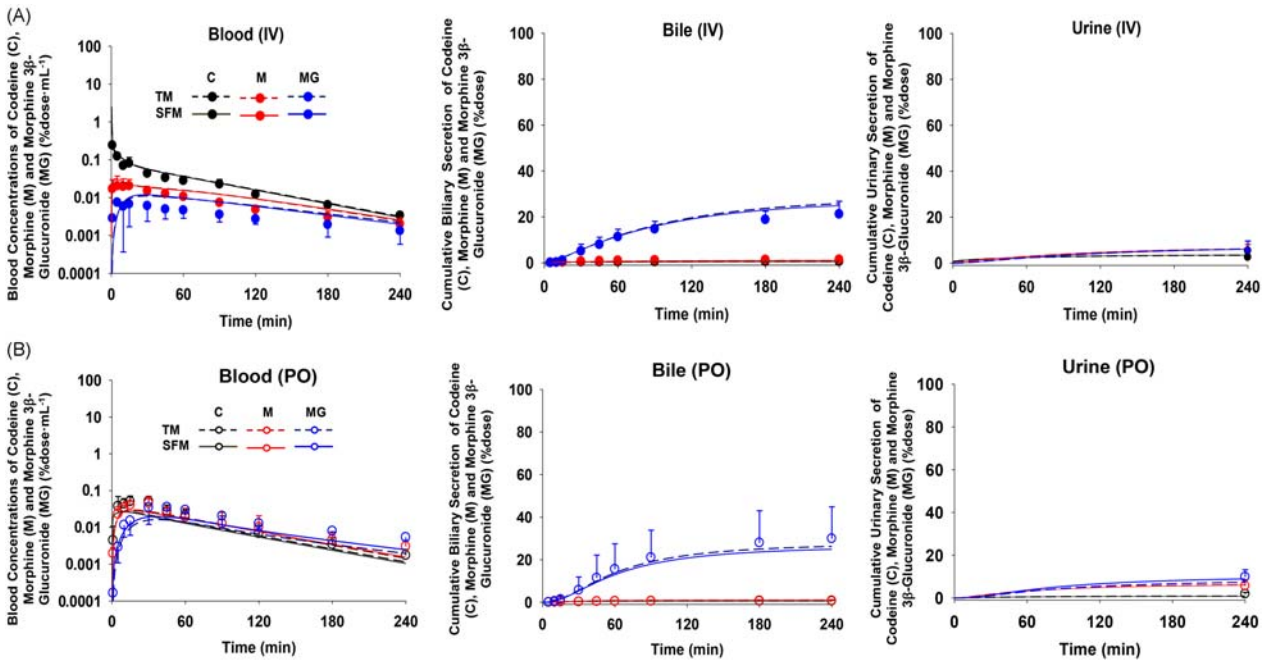

Fig. 8 Observed and fitted blood concentration–time profiles of codeine (C), M and MG and cumulative amounts of C, M, and MG in bile and urine following intravenous, IV (A) intraduodenal or oral (B) administration of C. The parameters are similar to **Fig. 5**. Obtained from Noh, K.; Chen, S.; Yang, Q. J. and Pang, K. S. Physiologically Based Pharmacokinetic Modeling Revealed Minimal Codeine Intestinal Metabolism in First-Pass Removal in Rats. *Biopharm. Drug. Dispos.* **2016**, 38(1), 50–74, with permission.

Table 4 Comparison of the predicted urine/bile ratio of M and MG after C dosing by TM-PBPK and SFM-PBPK models after intraduodenal (or PO) and IV administration of codeine[64]

	Ratio of M in urine/bile						*Ratio of MG in urine/bile*					
	PO dosing		*IV dosing*		*PO/IV*		*PO dosing*		*IV dosing*		*PO/IV*	
Model	*4 h*	∞	*4 h*	∞	*4 h*	∞	*4 h*	∞	*4 h*	∞	*4 h*	∞
Observed	9.9 ± 0.3[a]	–	4.1 ± 2.7[a]	–	2.4	–	0.4 ± 0.2[a]	–	0.3 ± 0.3[a]	–	1.3	–
TM-PBPK	6.13	6.24	6.05	6.23	1.0	1.0	0.28	0.30	0.24	0.26	1.2	1.2
SFM-PBPK	6.06	6.20	5.98	6.18	1.0	1.0	0.36	0.39	0.24	0.26	1.5	1.5

[a]Values are mean ± SD.

transporters and enzymes among different segments has been shown in recent modeling approaches.[98,99] The heterogeneous distribution of P450 (more proximal to duodenum) and P-gp (distal in ileum) was shown to reduce the intestinal availability of drugs,[100] and alter parent drug and metabolite profiles, especially when there is enterohepatic circulation, as shown for glucuronides.[101]

4.05.4.2 Liver Enzyme and Transporter Zonation

At least three zonal regions exist[102] and enzymes and transporters are not distributed evenly among the zones.[24,32] Enzyme metabolic zonation has long existed in terms of intermediary metabolism such as gluconeogenesis (periportal) and glycolysis (perivenous).[103] Zonal, metabolic zonation is the consequence of the gradients of oxygenation and hormone concentrations.[102] Liver metabolic zonation was revealed by techniques such as retrograde versus prograde perfusion in liver perfusion studies on P450 (Cyp1a2)[104,105] and UGT-mediated reactions (UGT1a toward *p*-nitrophenol[106]; or glucuronidation activity toward harmol[107] in the perivenous zone. Others showed the presence of enzyme heterogeneity with microlight guides for detection of loss of fluorescence of parent drug, or appearance of fluorescent metabolites, placed in periportal versus perivenous regions of the liver[108] or in microdissected tissue or zonally isolated hepatocytes.[105,109–111]

The same comment goes for the localization of transporters in the liver or intestine; some of the rat transporters such as Mrp3,[112] Oct1[113,] and Oatp4[114] are more enriched in perivenous region although many other transporters such as Oatp1a1, Oatp1a4, P-gp[115,116], and Mrp2[105] are found to be evenly distributed. Some laboratories, including our own, have examined the impact of

Table 5 Fitted estimates used for calculation of parameters for codeine[64]

Parameter	*Definition*	*TM-PBPK*	*SFM-PBPK*
$\frac{f_B^C CL_{in,I}^C}{f_I^C CL_{ef,I}^C}$ or $K_{I,uu}^C$	Ratio of effective uptake/efflux CL of C in intestine, or intestine to blood partitioning of unbound C	0.068 (62.8)[c]	0.040 (70.4)[c]
$\frac{f_B^C CL_{in,L}^C}{f_L^C CL_{ef,L}^C}$ or $K_{L,uu}^C$	Ratio of effective uptake/efflux CL of C in liver, or liver to blood partitioning of unbound C	1.79 (63.1)	1.68 (66.7)
$\frac{f_B^M CL_{in,I}^M}{f_I^M CL_{ef,I}^M}$ or $K_{I,uu}^M$	Ratio of effective uptake/efflux CL of M in intestine, or intestine to blood partitioning of unbound M	1.64 (43.2)	1.84 (31.8)
$\frac{f_B^M CL_{in,L}^M}{f_L^M CL_{ef,L}^M}$ or $K_{L,uu}^M$	Ratio of effective uptake/efflux CL of M in liver, or liver to blood partitioning of unbound M	16.9 (52.4)	18.4 (50.6)
$\frac{f_L^C CL_{int,met,L}^{C\to M}}{f_I^C CL_{int,met,I}^{C\to M}}$	Ratio of effective liver/intestine formation clearances of liver to intestine	9.2	13.3
F_I^C	Intestinal availability of C by methods 1 and 2	0.973 (1.4) 0.950 (3.5)	0.982 (1.1) 0.914 (4.8)
	$F_{I,\text{ Method 1}} = \frac{CL_{ef,I}^C}{CL_{ef,I}^C + CL_{int,sec,I}^C(1-F_{abs}) + CL_{int,met,I}^{C\to M} + CL_{int,met,I}^{C\to others}}$[a]		
	$F_{I,method2} = \frac{f_0 Q_I CL_{ef,I}^C}{f_0 Q_I CL_{ef,I}^C + \left(f_0 Q_I + f_B^C CL_{in,I}^C\right)\left[CL_{int,sec,I}^C(1-F_{abs}) + CL_{int,met,I}^{C\to M} + CL_{int,met,I}^{C\to others}\right]}$[b]		
F_L^C	Hepatic availability of C by methods 1 and 2	0.525 (11.7) 0.285 (37.9)	0.515 (11.0) 0.279 (41.2)
	$F_{H,method1} = \frac{CL_{ef,L}^C}{CL_{ef,L}^C + CL_{int,sec,L}^C + CL_{int,met,L}^{C\to M} + CL_{int,met,L}^{C\to others}}$[a]		
	$F_{H,method2} = \frac{(Q_I + Q_{HA})\left(CL_{ef,L}^C + CL_{int,sec,L}^C + CL_{int,met,L}^{C\to M} + CL_{int,met,L}^{C\to others}\right)}{(Q_I + Q_{HA})\left(CL_{ef,L}^C + CL_{int,sec,L}^C + CL_{int,met,L}^{C\to M} + CL_{int,met,L}^{C\to others}\right) + f_B^C CL_{in,L}^C\left(CL_{int,sec,L}^C + CL_{int,met,L}^{C\to M} + CL_{int,met,L}^{C\to others}\right)}$[b]		
F_{sys}	Systemic bioavailability by methods 1 and 2 $F_{abs} \cdot F_{I,method1} \cdot F_{H,method1}$ $F_{abs} \cdot F_{I,method2} \cdot F_{H,method2}$	0.496 (12.7) 0.263 (39.9)	0.494 (11.7) 0.249 (45.0)
$h_{mi}^{C\to M}$[d]	Fraction of hepatic CL of C forming M: $\frac{CL_{int,met,L}^{C\to M}}{CL_{int,met,L}^{C\to M} + CL_{int,met,L}^{C\to others} + CL_{int,sec,L}^C}$	0.852 (4.8)	0.899 (1.1)
g_{mi}^M[d]	Fraction of total body CL of C forming M : $\left(1 - f_e^C\right) h_{mi}^{C\to M}\ \left(f_e^C = 0.025\right)$	0.831 (4.8)	0.876 (1.1)
$\frac{v_I}{v_I + v_L}$[e]	Fractional contribution of intestine to intestinal–liver removal for Methods1 and 2	0.042 (43.4) 0.051 (58.0)[g]	0.004 (98.1) 0.014 (78.2)[g]
$\frac{v_L}{v_I + v_L}$[f]	Fractional contribution of liver to intestinal–liver removal for Methods 1 and 2	0.959 (1.9) 0.949 (3.1)[g]	0.996 (0.4) 0.986 (1.1)[g]

[a]Based on fitted estimates, as ratio of efflux intrinsic clearance/sum of all "out" intrinsic clearances.
[b]Based on equation from Sun and Pang.[52]
[c]Obtained estimates, with %coefficient of variation within brackets.
[d]Based on definition of Pang and Kwan.[21]
[e]Calculated based on equation from Pang and Chow[85]: $\frac{v_I}{v_I + v_L} = \frac{f_0 Q_I (1-F_I)}{f_0 Q_I (1-F_I) + E_L \langle Q_I [f_0 F_I + (1-f_0)] + Q_{HA} \rangle}$.

[f]Calculated based on equation from Pang and Chow[85]: $\frac{v_L}{v_I + v_L} = \frac{E_L \langle Q_I [f_0 F_I + (1-f_0)] + Q_{HA} \rangle}{f_0 Q_I (1-F_I) + E_L \langle Q_I [f_0 F_I + (1-f_0)] + Q_{HA} \rangle}$.

[g]F_I and F_L values, based on equations from Sun and Pang,[52] for method 2.

zonal distribution of enzymes and transporters on parent drug and metabolite removal.[104,107,116,117] We have identified that the coupling of formation and metabolic enzymes for the primary metabolite has led to the formation of gentisamide 5-glucuronide after formation of gentisamide from salicylamide, whereas gentisamide forms mainly the 5-sulfate conjugate, a more anterior distributed enzyme.[27,28]

4.05.4.3 Futile Cycling Kinetics

In addition to enzymes, transporters, flow, and binding, hepatic drug clearance is also influenced by futile cycling, namely the interconversion between drug and metabolite. The reaction is particularly prevalent for sulfate and glucuronide conjugates that can undergo deconjugation to form the parent drug again, notably, between estrone and estrone sulfate,[118] as well as estradiol-17β-glucuronide and estradiol-3-sulfate-17β-glucuronide[119] found in the rat liver. These reactions exist between prednisone/prednisolone and their methyl counterparts.[120–122] The presence of interconversion will increase the mean residence times of drug and metabolite in the organ,[120] and the species undergoing interconversion will display parallel decay profiles. However, the presence of uptake sinusoidal transporters or canalicular transporters will further modulate the profiles.[118,119]

In examining the interconversion between estradiol-17β-glucuronide and estradiol-3-sulfate-17β-glucuronide in the rat liver, Sun and colleagues[119] solved for the AUC for the precursor drug (P) and formed metabolite, mi, and have described terms to denote futile cycling. The effective coefficient for metabolite formation, ef''_m, considers the reformation intrinsic clearance of metabolite to the precursor drug, as well as the alternative metabolic and secretory intrinsic clearances of metabolite, $CL_{int,met,L}^{mi\rightarrow other}$ and $CL_{int,sec,L}^{mi}$, respectively.

$$ef''_m = \frac{CL_{int,sec,L}^{mi} + CL_{int,met,L}^{mi\rightarrow others}}{CL_{int,sec,L}^{mi} + CL_{int,met,L}^{mi\rightarrow P} + CL_{int,met,L}^{mi\rightarrow others}} \tag{18}$$

Conversely, the effective recycling coefficient, ef'_m, is

$$ef'_m = \frac{CL_{int,sec,L}^{P} + CL_{int,met,L}^{P\rightarrow others}}{CL_{int,sec,L}^{P} + CL_{int,met,L}^{P\rightarrow mi} + CL_{int,met,L}^{P\rightarrow others}} \tag{19}$$

The net metabolite formation intrinsic clearance of the precursor ef''_m will be reduced by the factor

$$\left(1 - ef''_m\right) \quad \text{or} \quad \frac{CL_{int,met,L}^{mi\rightarrow P}}{CL_{int,sec,L}^{mi} + CL_{int,met,L}^{mi\rightarrow P} + CL_{int,met,L}^{mi\rightarrow others}} \tag{20}$$

4.05.4.4 Membrane Barrier for Metabolite

Most formed metabolites are more polar than their precursors and therefore may have diffusional barrier when entering the organs. One of the drawbacks of compartmental modeling is the failure to consider transmembrane barriers that bar the entry of polar metabolites into the cell, but entrap the formed polar metabolite formed within the cell. For this reason, the extraction ratio and therefore the availability of the formed metabolite differ from that of the preformed species.[14,23,24] In this case, the extraction ratio of the formed metabolite is greater than that of the preformed metabolite, E^{pmi}, as the preformed metabolite cannot enter into the eliminating organ.[26,80,123,124] However, the validity of this assumption is rarely tested. Only when the metabolite is formed rapidly (high formation intrinsic clearance) and displays a high permeability, would the extraction ratio and availability of preformed and formed metabolite are equivalent.[14,125]

4.05.5 Metabolite Data in Bioequivalence

Our understanding of metabolite kinetics is key to drug development, not only for safety issues but also for drug regulation as to whether it is plausible to use metabolite data in bioequivalence study.[126–129] There are several reasons to use metabolite data for bioequivalence, such as (1) the precursor is inactive prodrug; (2) precursor concentrations are too low to be detected; (3) precursor is rapidly metabolized to form an active or toxic compound; (4) both precursor and its formed metabolite are pharmacologically active and metabolite is present in higher concentrations.[126] Previously, researchers investigated the role of metabolite in bioequivalence study by performing modeling and simulations with compartmental modeling,[128–130] and conducted sensitivity analysis of bioequivalence parameter (AUC, C_{max}) of parent and metabolites with two different formulations (test and reference).[131] Based on simulated results, both parent and metabolite were found equally useful when AUC was used as the bioequivalence measure, and, if the absorption phases of test and reference products are similar, metabolite data may further be used for the determination of bioequivalence.[131] However, we view that metabolite kinetics is highly dependent on the tissue location of the metabolite formed, and how it is sequentially metabolized. For this reason, we consider that the AUC of the formed metabolite ($AUC^{mi,P}$) is not useful to define bioavailability measurements. In the case of metabolites undergoing sequential first-pass metabolism, the measured metabolite concentrations from systemic circulation cannot represent the actual metabolite

concentrations since part of metabolites is immediately eliminated within the metabolite-forming organs.[22] If route-dependent intestinal metabolism occurs, as projected by the SFM, it is further inappropriate to compare metabolite concentrations resulted from oral dosing forms to those from intravenous administration. Additionally, multiple factors, including drug physiochemical properties, enzyme zonal distribution, and heterogeneity, are important but these are neglected when analyzing bioequivalence data arising from different formulations when based on compartmental modeling.

4.05.6 Summary Remarks

Metabolite testing is currently gaining more and more attention in drug development. In this communication, we have discussed the use of PBPK modeling as a useful tool for appraising parent drug and metabolite kinetics simultaneously. It is able to consider the physiochemical properties of precursor and metabolite as well as incorporate transporter-mediated process, sequential metabolism, drug binding, enzyme heterogeneity and segregated flow pattern on small intestine into one model. The SFM, in particular, is superior over the TM in description of route-dependent metabolism. Two case studies are given to appreciate the advantages of SFM over TM and compartmental modeling. Furthermore, PBPK model can integrate pharmacokinetic data with pharmacodynamic changes and toxicity data. Lastly, we highlighted several important considerations, such as enzyme/transporter interplay, enzyme zonal distribution, protein binding, and sequential first-pass metabolism in metabolite kinetics analysis. We also discussed that the use of metabolite in bioequivalence study is questionable, given the fact that the kinetics of formed metabolite is dependent on where and how it forms. Undoubtedly, PBPK modeling is an advanced and powerful approach that can be used to decipher metabolite kinetics in drug development.

References

1. Sheweita, S. A. Drug-Metabolizing Enzymes: Mechanisms and Functions. *Curr. Drug Metab.* **2000,** *1,* 107–132.
2. Anzenbacher, P.; Anzenbacherova, E. Cytochromes P450 and Metabolism of Xenobiotics. *Cell. Mol. Life Sci.* **2001,** *58,* 737–747.
3. Lampe, J.; Butschak, G. The Role of Cytochrome P-450 in the Toxicity of Xenobiotics. *Pharmazie* **1978,** *33,* 407–411.
4. de Waziers, I.; Cugnenc, P. H.; Yang, C. S.; Leroux, J. P.; Beaune, P. H. Cytochrome P 450 Isoenzymes, Epoxide Hydrolase and Glutathione Transferases in Rat and Human Hepatic and Extrahepatic Tissues. *J. Pharmacol. Exp. Ther.* **1990,** *253,* 387–394.
5. Ilett, K. F.; Tee, L. B.; Reeves, P. T.; Minchin, R. F. Metabolism of Drugs and Other Xenobiotics in the Gut Lumen and Wall. *Pharmacol. Ther.* **1990,** *46,* 67–93.
6. Remmer, H. The Role of the Liver in Drug Metabolism. *Am. J. Med.* **1970,** *49,* 617–629.
7. Jancova, P.; Anzenbacher, P.; Anzenbacherova, E. Phase II Drug Metabolizing Enzymes. *Biomed. Pap. Med. Fac. Univ. Palacky Olomouc Czech Repub.* **2010,** *154,* 103–116.
8. Drayer, D. E. Pharmacologically Active Drug Metabolites: Therapeutic and Toxic Activities, Plasma and Urine Data in Man, Accumulation in Renal Failure. *Clin. Pharmacokinet.* **1976,** *1,* 426–443.
9. Atkinson, A. J., Jr.; Strong, J. M. Effect of Active Drug Metabolites on Plasma Level-Response Correlations. *J. Pharmacokinet. Biopharm.* **1977,** *5,* 95–109.
10. Breimer, D. D. Pharmacokinetics and Metabolism of Various Benzodiazepines Used as Hypnotics. *Br. J. Clin. Pharmacol.* **1979,** *8,* 7S–13S.
11. Breimer, D. D.; Jochemsen, R.; von Albert, H. H. Pharmacokinetics of Benzodiazepines. Short-Acting Versus Long-Acting. *Arzneimittelforschung* **1980,** *30,* 875–881.
12. Baillie, T. A.; Cayen, M. N.; Fouda, H.; Gerson, R. J.; Green, J. D.; Grossman, S. J.; Klunk, L. J.; LeBlanc, B.; Perkins, D. G.; Shipley, L. A. Drug Metabolites in Safety Testing. *Toxicol. Appl. Pharmacol.* **2002,** *182,* 188–196.
13. Davis-Bruno, K. L.; Atrakchi, A. A Regulatory Perspective on Issues and Approaches in Characterizing Human Metabolites. *Chem. Res. Toxicol.* **2006,** *19,* 1561–1563.
14. Pang, K. S.; Morris, M. E.; Sun, H. Formed and Preformed Metabolites: Facts and Comparisons. *J. Pharm. Pharmacol.* **2008,** *60,* 1247–1275.
15. Naito, S.; Furuta, S.; Yoshida, T.; Kitada, M.; Fueki, O.; Unno, T.; Ohno, Y.; Onodera, H.; Kawamura, N.; Kurokawa, M.; Sagami, F.; Shinoda, K.; Nakazawa, T.; Yamazaki, T. Current Opinion: Safety Evaluation of Drug Metabolites in Development of Pharmaceuticals. *J. Toxicol. Sci.* **2007,** *32,* 329–341.
16. Hastings, K. L.; El-Hage, J.; Jacobs, A.; Leighton, J.; Morse, D.; Osterberg, R. E. Drug Metabolites in Safety Testing. *Toxicol. Appl. Pharmacol.* **2003,** *190,* 91–92. author reply 93–94.
17. Smith, D. A.; Obach, R. S. Metabolites and Safety: What Are the Concerns, and How Should We Address Them? *Chem. Res. Toxicol.* **2006,** *19,* 1570–1579.
18. Prueksaritanont, T.; Lin, J. H.; Baillie, T. A. Complicating Factors in Safety Testing of Drug Metabolites: Kinetic Differences Between Generated and Preformed Metabolites. *Toxicol. Appl. Pharmacol.* **2006,** *217,* 143–152.
19. Frederick, C. B.; Obach, R. S. Metabolites in Safety Testing: "MIST" for the Clinical Pharmacologist. *Clin. Pharmacol. Ther.* **2010,** *87,* 345–350.
20. Sun, H.; Pang, K. S. Disparity in Intestine Disposition Between Formed and Preformed Metabolites and Implications: A Theoretical Study. *Drug Metab. Dispos.* **2009,** *37,* 187–202.
21. Pang, K. S.; Kwan, K. C. A Commentary: Methods and Assumptions in the Kinetic Estimation of Metabolite Formation. *Drug Metab. Dispos.* **1983,** *11,* 79–84.
22. Pang, K. S.; Gillette, J. R. Sequential First-Pass Elimination of a Metabolite Derived From a Precursor. *J. Pharmacokinet. Biopharm.* **1979,** *7,* 275–290.
23. Pang, K. S.; Durk, M. R. Physiologically-Based Pharmacokinetic Modeling for Absorption, Transport, Metabolism and Excretion. *J. Pharmacokinet. Pharmacodyn.* **2010,** *37,* 591–615.
24. Pang, K. S. Safety Testing of Metabolites: Expectations and Outcomes. *Chem. Biol. Interact.* **2009,** *179,* 45–59.
25. Pang, K. S. A Review of Metabolite Kinetics. *J. Pharmacokinet. Biopharm.* **1985,** *13,* 633–662.
26. de Lannoy, I. A.; Pang, K. S. Effect of Diffusional Barriers on Drug and Metabolite Kinetics. *Drug Metab. Dispos.* **1987,** *15,* 51–58.
27. Xu, X.; Pang, K. S. Hepatic Modeling of Metabolite Kinetics in Sequential and Parallel Pathways: Salicylamide and Gentisamide Metabolism in Perfused Rat Liver. *J. Pharmacokinet. Biopharm.* **1989,** *17,* 645–671.
28. Xu, X.; Tang, B. K.; Pang, K. S. Sequential Metabolism of Salicylamide Exclusively to Gentisamide 5-Glucuronide and Not Gentisamide Sulfate Conjugates in Single-Pass In Situ Perfused Rat Liver. *J. Pharmacol. Exp. Ther.* **1990,** *253,* 965–973.
29. Yang, Q. J.; Si, L.; Tang, H.; Sveigaard, H. H.; Chow, E. C.; Pang, K. S. PBPK Modeling to Unravel Nonlinear Pharmacokinetics of Verapamil to Estimate the Fractional Clearance for Verapamil N-Demethylation in the Recirculating Rat Liver Preparation. *Drug Metab. Dispos.* **2015,** *43,* 631–645.
30. Cong, D.; Doherty, M.; Pang, K. S. A New Physiologically Based, Segregated-Flow Model to Explain Route-Dependent Intestinal Metabolism. *Drug Metab. Dispos.* **2000,** *28,* 224–235.
31. Doherty, M. M.; Pang, K. S. Route-Dependent Metabolism of Morphine in the Vascularly Perfused Rat Small Intestine Preparation. *Pharm. Res.* **2000,** *17,* 291–298.

32. Fan, J.; Chen, S.; Chow, E. C.; Pang, K. S. PBPK Modeling of Intestinal and Liver Enzymes and Transporters in Drug Absorption and Sequential Metabolism. *Curr. Drug Metab.* **2010,** *11,* 743–761.
33. Pang, K. S. Metabolic First-Pass Effects. *J. Clin. Pharmacol.* **1986,** *26,* 580–582.
34. Pang, K. S. Modeling of Intestinal Drug Absorption: Roles of Transporters and Metabolic Enzymes (for the Gillette Review Series). *Drug Metab. Dispos.* **2003,** *31,* 1507–1519.
35. De Buck, S. S.; Sinha, V. K.; Fenu, L. A.; Nijsen, M. J.; Mackie, C. E.; Gilissen, R. A. Prediction of Human Pharmacokinetics Using Physiologically Based Modeling: A Retrospective Analysis of 26 Clinically Tested Drugs. *Drug Metab. Dispos.* **2007,** *35,* 1766–1780.
36. Parrott, N.; Jones, H.; Paquereau, N.; Lave, T. Application of Full Physiological Models for Pharmaceutical Drug Candidate Selection and Extrapolation of Pharmacokinetics to Man. *Basic Clin. Pharmacol. Toxicol.* **2005,** *96,* 193–199.
37. Jones, H. M.; Parrott, N.; Jorga, K.; Lave, T. A Novel Strategy for Physiologically Based Predictions of Human Pharmacokinetics. *Clin. Pharmacokinet.* **2006,** *45,* 511–542.
38. Pang, K. S.; Gillette, J. R. Theoretical Relationships Between Area Under the Curve and Route of Administration of Drugs and Their Precursors for Evaluating Sites and Pathways of Metabolism. *J. Pharm. Sci.* **1978,** *67,* 703–704.
39. Hedaya, M. A. Metabolite Kinetics Basic Pharmacokinetics. In 2nd ed.; CRC Press: Boca Raton, FL, 2012.
40. Lutz, J. D.; Fujioka, Y.; Isoherranen, N. Rationalization and Prediction of In Vivo Metabolite Exposures: The Role of Metabolite Kinetics, Clearance Predictions and In Vitro Parameters. *Expert Opin. Drug Metab. Toxicol.* **2010,** *6,* 1095–1109.
41. Cummings, A. J.; Martin, B. K. Excretion and the Accrual of Drug Metabolites. *Nature* **1963,** *200,* 1296–1297.
42. Cummings, A. J.; King, M. L.; Martin, B. K. A Kinetic Study of Drug Elimination: The Excretion of Paracetamol and Its Metabolites in Man. *Br. J. Pharmacol. Chemother.* **1967,** *29,* 150–157.
43. Cummings, A. J.; Martin, B. K.; Park, G. S. Kinetic Considerations Relating to the Accrual and Elimination of Drug Metabolites. *Br. J. Pharmacol. Chemother.* **1967,** *29,* 136–149.
44. Rowland, M.; Riegelman, S. Pharmacokinetics of Acetylsalicylic Acid and Salicylic Acid After Intravenous Administration in Man. *J. Pharm. Sci.* **1968,** *57,* 1313–1319.
45. Pang, K. S.; Gillette, J. R. Kinetics of Metabolite Formation and Elimination in the Perfused Rat Liver Preparation: Differences Between the Elimination of Preformed Acetaminophen and Acetaminophen Formed From Phenacetin. *J. Pharmacol. Exp. Ther.* **1978,** *207,* 178–194.
46. Pang, K. S.; Gillette, J. R. Metabolite Pharmacokinetics: Methods for Simultaneous Estimates of Elimination Rate Constants of a Drug and Its Metabolite. A commentary. *Drug Metab. Dispos.* **1980,** *8,* 39–43.
47. Yang, Q. J.; Fan, J.; Chen, S.; Liu, L.; Sun, H.; Pang, K. S. Metabolite Kinetics: The Segregated Flow Model for Intestinal and Whole Body Physiologically Based Pharmacokinetic Modeling to Describe Intestinal and Hepatic Glucuronidation of Morphine in Rats In Vivo. *Drug Metab. Dispos.* **2016,** *44,* 1123–1138.
48. Pang, K. S.; Yang, Q. J.; Noh, K. Unequivocal Evidence Supporting the Segregated Flow Intestinal Model That Discriminates Intestine Versus Liver First-Pass Removal in PBPK Modeling. *Biopharm. Drug Dispos.* **2016** (manuscript under revision).
49. Rodgers, T.; Rowland, M. Physiologically Based Pharmacokinetic Modelling 2: Predicting the Tissue Distribution of Acids, Very Weak Bases, Neutrals and Zwitterions. *J. Pharm. Sci.* **2006,** *95,* 1238–1257.
50. Rodgers, T.; Rowland, M. Mechanistic Approaches to Volume of Distribution Predictions: Understanding the Processes. *Pharm. Res.* **2007,** *24,* 918–933.
51. Rowland, M.; Peck, C.; Tucker, G. Physiologically-Based Pharmacokinetics in Drug Development and Regulatory Science. *Annu. Rev. Pharmacol. Toxicol.* **2011,** *51,* 45–73.
52. Sun, H.; Pang, K. S. Physiological Modeling to Understand the Impact of Enzymes and Transporters on Drug and Metabolite Data and Bioavailability Estimates. *Pharm. Res.* **2010,** *27,* 1237–1254.
53. Pang, K. S.; Cherry, W. F.; Ulm, E. H. Disposition of Enalapril in the Perfused Rat Intestine-Liver Preparation: Absorption, Metabolism and First-Pass Effect. *J. Pharmacol. Exp. Ther.* **1985,** *233,* 788–795.
54. Pang, K. S.; Yuen, V.; Fayz, S.; te Koppele, J. M.; Mulder, G. J. Absorption and Metabolism of Acetaminophen by the In Situ Perfused Rat Small Intestine Preparation. *Drug Metab. Dispos.* **1986,** *14,* 102–111.
55. Lown, K. S.; Thummel, K. E.; Benedict, P. E.; Shen, D. D.; Turgeon, D. K.; Berent, S.; Watkins, P. B. The Erythromycin Breath Test Predicts the Clearance of Midazolam. *Clin. Pharmacol. Ther.* **1995,** *57,* 16–24.
56. Wen, Y.; Remmel, R. P.; Zimmerman, C. L. First-Pass Disposition of (−)-6-aminocarbovir in Rats. I. Prodrug Activation may be Limited by Access to Enzyme. *Drug Metab. Dispos.* **1999,** *27,* 113–121.
57. Paine, M. F.; Khalighi, M.; Fisher, J. M.; Shen, D. D.; Kunze, K. L.; Marsh, C. L.; Perkins, J. D.; Thummel, K. E. Characterization of Interintestinal and Intraintestinal Variations in Human CYP3A-Dependent Metabolism. *J. Pharmacol. Exp. Ther.* **1997,** *283,* 1552–1562.
58. Paine, M. F.; Shen, D. D.; Kunze, K. L.; Perkins, J. D.; Marsh, C. L.; McVicar, J. P.; Barr, D. M.; Gillies, B. S.; Thummel, K. E. First-Pass Metabolism of Midazolam by the Human Intestine. *Clin. Pharmacol. Ther.* **1996,** *60,* 14–24.
59. Pottenger, L. H.; Domoradzki, J. Y.; Markham, D. A.; Hansen, S. C.; Cagen, S. Z.; Waechter, J. M., Jr. The Relative Bioavailability and Metabolism of Bisphenol A in Rats is Dependent Upon the Route of Administration. *Toxicol. Sci.* **2000,** *54,* 3–18.
60. Cong, D.; Fong, A. K.; Lee, R.; Pang, K. S. Absorption of Benzoic Acid in Segmental Regions of the Vascularly Perfused Rat Small Intestine Preparation. *Drug Metab. Dispos.* **2001,** *29,* 1539–1547.
61. Liu, S.; Tam, D.; Chen, X.; Pang, K. S. P-Glycoprotein and an Unstirred Water Layer Barring Digoxin Absorption in the Vascularly Perfused rat Small Intestine Preparation: Induction Studies With Pregnenolone-16alpha-Carbonitrile. *Drug Metab. Dispos.* **2006,** *34,* 1468–1479.
62. Ramakrishnan, V.; Yang, Q. J.; Quach, H. P.; Cao, Y.; Chow, E. C.; Mager, D. E.; Pang, K. S. Physiologically-Based Pharmacokinetic-Pharmacodynamic Modeling of 1α,25-Dihydroxyvitamin D3 in Mice. *Drug Metab. Dispos.* **2016,** *44,* 189–208.
63. Chow, E. C.; Durk, M. R.; Cummins, C. L.; Pang, K. S. 1 α,25-Dihydroxyvitamin D_3 Up-Regulates P-Glycoprotein via the Vitamin D Receptor and Not Farnesoid X Receptor in Both fxr(−/−) and fxr(+/+) Mice and Increased Renal and Brain Efflux of Digoxin in Mice In Vivo. *J. Pharmacol. Exp. Ther.* **2011,** *337,* 846–859.
64. Noh, K.; Chen, S.; Yang, Q. J.; Pang, K. S. Physiologically Based Pharmacokinetic Modeling Revealed Minimal Codeine Intestinal Metabolism in First-Pass Removal in Rats. *Biopharm. Drug Dispos.* **2017,** *38* (1), 50–74.
65. Greiner, B.; Eichelbaum, M.; Fritz, P.; Kreichgauer, H. P.; von Richter, O.; Zundler, J.; Kroemer, H. K. The Role of Intestinal P-Glycoprotein in the Interaction of Digoxin and Rifampin. *J. Clin. Invest.* **1999,** *104,* 147–153.
66. Kawaguchi, H.; Matsui, Y.; Watanabe, Y.; Takakura, Y. Effect of Interferon-Gamma on the Pharmacokinetics of Digoxin, a P-Glycoprotein Substrate, Intravenously Injected Into the Mouse. *J. Pharmacol. Exp. Ther.* **2004,** *308,* 91–96.
67. Rowland, M.; Benet, L. Z.; Graham, G. G. Clearance Concepts in Pharmacokinetics. *J. Pharmacokinet. Biopharm.* **1973,** *1,* 123–136.
68. Pang, K. S.; Rowland, M. Hepatic Clearance of Drugs. I. Theoretical Considerations of a "Well-Stirred" Model and a "Parallel Tube" Model. Influence of Hepatic Blood Flow, Plasma and Blood Cell Binding, and the Hepatocellular Enzymatic Activity on Hepatic Drug Clearance. *J. Pharmacokinet. Biopharm.* **1977,** *5,* 625–653.
69. Pang, K. S.; Rowland, M. Hepatic Clearance of Drugs. II. Experimental Evidence for Acceptance of the "Well-Stirred" Model Over the "Parallel Tube" Model Using Lidocaine in the Perfused Rat Liver In Situ Preparation. *J. Pharmacokinet. Biopharm.* **1977,** *5,* 655–680.
70. Pang, K. S.; Rowland, M. Hepatic Clearance of Drugs. III. Additional Experimental Evidence Supporting the "Well-Stirred" Model, Using Metabolite (MEGX) Generated From Lidocaine Under Varying Hepatic Blood Flow Rates and Linear Conditions in the Perfused Rat Liver In Situ Preparation. *J. Pharmacokinet. Biopharm.* **1977,** *5,* 681–699.
71. Levenspiel, O. Chemical Reaction Engineering. In 2nd ed.; Wiley: New York, 1972.
72. Winkler, K.; Keiding, S.; Tygstrup, N. Clearance as a Quantitative Measure of Liver Function. In *The Liver: Quantitative Aspects of Structure and Functions;* Paumgartner, P., Presig, R., Eds.; Karger: Basel, 1973; pp 144–155.

73. Winkler, K.; Bass, L.; Keiding, S.; Tygstrup, N. The Effect of Hepatic Perfusion on Assessment of Kinetic Constants. In *Alfred Benson Symposium VI: Regulation of Hepatic Metabolism;* Lundquist, F., Tygstrup, N., Eds.; Munksgaard: Copenhagen, 1974; pp 797–807.
74. Roberts, M. S.; Rowland, M. A Dispersion Model of Hepatic Elimination: 3. Application to Metabolite Formation and Elimination Kinetics. *J. Pharmacokinet. Biopharm.* **1986,** *14,* 289–308.
75. Roberts, M. S.; Rowland, M. A Dispersion Model of Hepatic Elimination: 2. Steady-State Considerations—Influence of Hepatic Blood Flow, Binding Within Blood, and Hepatocellular Enzyme Activity. *J. Pharmacokinet. Biopharm.* **1986,** *14,* 261–288.
76. Roberts, M. S.; Rowland, M. A Dispersion Model of Hepatic Elimination: 1. Formulation of the Model and Bolus Considerations. *J. Pharmacokinet. Biopharm.* **1986,** *14,* 227–260.
77. Perl, W.; Chinard, F. P. A Convection-Diffusion Model of Indicator Transport Through an Organ. *Circ. Res.* **1968,** *22,* 273–298.
78. Roberts, M. S.; Rowland, M. Hepatic Elimination—Dispersion Model. *J. Pharm. Sci.* **1985,** *74,* 585–587.
79. Tirona, R. G.; Schwab, A. J.; Geng, W.; Pang, K. S. Hepatic Clearance Models: Comparison of the Dispersion and Goresky Models in Outflow Profiles From Multiple Indicator Dilution Rat Liver Studies. *Drug Metab. Dispos.* **1998,** *26,* 465–475.
80. de Lannoy, I. A.; Pang, K. S. Presence of a Diffusional Barrier on Metabolite Kinetics: Enalaprilat as a Generated Versus Preformed Metabolite. *Drug Metab. Dispos.* **1986,** *14,* 513–520.
81. Pang, K. S.; Maeng, H. J.; Fan, J. Interplay of Transporters and Enzymes in Drug and Metabolite Processing. *Mol. Pharm.* **2009,** *6,* 1734–1755.
82. Chow, E. C.; Pang, K. S. Why we Need Proper PBPK Models to Examine Intestine and Liver Oral Drug Absorption. *Curr. Drug Metab.* **2013,** *14,* 57–79.
83. Liu, L.; Pang, K. S. The Roles of Transporters and Enzymes in Hepatic Drug Processing. *Drug Metab. Dispos.* **2005,** *33,* 1–9.
84. Liu, L.; Pang, K. S. An Integrated Approach to Model Hepatic Drug Clearance. *Eur. J. Pharm. Sci.* **2006,** *29,* 215–230.
85. Pang, K. S.; Chow, E. C. Commentary: Theoretical Predictions of Flow Effects on Intestinal and Systemic Availability in Physiologically Based Pharmacokinetic Intestine Models: The Traditional Model, Segregated Flow Model, and QGut Model. *Drug Metab. Dispos.* **2012,** *40,* 1869–1877.
86. Nestorov, I. A.; Aarons, L. J.; Arundel, P. A.; Rowland, M. Lumping of Whole-Body Physiologically Based Pharmacokinetic Models. *J. Pharmacokinet. Biopharm.* **1998,** *26,* 21–46.
87. Charnick, S. B.; Kawai, R.; Nedelman, J. R.; Lemaire, M.; Niederberger, W.; Sato, H. Perspectives in Pharmacokinetics. Physiologically Based Pharmacokinetic Modeling as a Tool for Drug Development. *J. Pharmacokinet. Biopharm.* **1995,** *23,* 217–229.
88. Gerlowski, L. E.; Jain, R. K. Physiologically Based Pharmacokinetic Modeling: Principles and Applications. *J. Pharm. Sci.* **1983,** *72,* 1103–1127.
89. Andersen, M. E. Physiologically Based Pharmacokinetic (PB-PK) Models in the Study of the Disposition and Biological Effects of Xenobiotics and Drugs. *Toxicol. Lett.* **1995,** *82–83,* 341–348.
90. Doherty, M. M.; Poon, K.; Tsang, C.; Pang, K. S. Transport Is Not Rate-Limiting in Morphine Glucuronidation in the Single-Pass Perfused Rat Liver Preparation. *J. Pharmacol. Exp. Ther.* **2006,** *317,* 890–900.
91. Rane, A.; Gawronska-Szklarz, B.; Svensson, J. O. Natural (−)- and Unnatural (+)-Enantiomers of Morphine: Comparative Metabolism and Effect of Morphine and Phenobarbital Treatment. *J. Pharmacol. Exp. Ther.* **1985,** *234,* 761–765.
92. van Herwaarden, A. E.; Wagenaar, E.; van der Kruijssen, C. M.; van Waterschoot, R. A.; Smit, J. W.; Song, J. Y.; van der Valk, M. A.; van Tellingen, O.; van der Hoorn, J. W.; Rosing, H.; Beijnen, J. H.; Schinkel, A. H. Knockout of Cytochrome P450 3A Yields New Mouse Models for Understanding Xenobiotic Metabolism. *J. Clin. Invest.* **2007,** *117,* 3583–3592.
93. Tam, D.; Tirona, R. G.; Pang, K. S. Segmental Intestinal Transporters and Metabolic Enzymes on Intestinal Drug Absorption. *Drug Metab. Dispos.* **2003,** *31,* 373–383.
94. Haslam, I. S.; Wright, J. A.; O'Reilly, D. A.; Sherlock, D. J.; Coleman, T.; Simmons, N. L. Intestinal Ciprofloxacin Efflux: The Role of Breast Cancer Resistance Protein (ABCG2). *Drug Metab. Dispos.* **2011,** *39,* 2321–2328.
95. Englund, G.; Rorsman, F.; Ronnblom, A.; Karlbom, U.; Lazorova, L.; Grasjo, J.; Kindmark, A.; Artursson, P. Regional Levels of Drug Transporters Along the Human Intestinal Tract: Co-expression of ABC and SLC Transporters and Comparison With Caco-2 Cells. *Eur. J. Pharm. Sci.* **2006,** *29,* 269–277.
96. Meier, Y.; Eloranta, J. J.; Darimont, J.; Ismair, M. G.; Hiller, C.; Fried, M.; Kullak-Ublick, G. A.; Vavricka, S. R. Regional Distribution of Solute Carrier mRNA Expression Along the Human Intestinal Tract. *Drug Metab. Dispos.* **2007,** *35,* 590–594.
97. Mitschke, D.; Reichel, A.; Fricker, G.; Moenning, U. Characterization of Cytochrome P450 Protein Expression Along the Entire Length of the Intestine of Male and Female Rats. *Drug Metab. Dispos.* **2008,** *36,* 1039–1045.
98. Badhan, R.; Penny, J.; Galetin, A.; Houston, J. B. Methodology for Development of a Physiological Model Incorporating CYP3A and P-Glycoprotein for the Prediction of Intestinal Drug Absorption. *J. Pharm. Sci.* **2009,** *98,* 2180–2197.
99. Bruyere, A.; Decleves, X.; Bouzom, F.; Ball, K.; Marques, C.; Treton, X.; Pocard, M.; Valleur, P.; Bouhnik, Y.; Panis, Y.; Scherrmann, J. M.; Mouly, S. Effect of Variations in the Amounts of P-Glycoprotein (ABCB1), BCRP (ABCG2) and CYP3A4 Along the Human Small Intestine on PBPK Models for Predicting Intestinal First Pass. *Mol. Pharm.* **2010,** *7,* 1596–1607.
100. Tam, D.; Sun, H.; Pang, K. S. Influence of P-Glycoprotein, Transfer Clearances, and Drug Binding on Intestinal Metabolism in Caco-2 Cell Monolayers or Membrane Preparations: A Theoretical Analysis. *Drug Metab. Dispos.* **2003,** *31,* 1214–1226.
101. Wu, B. Use of Physiologically Based Pharmacokinetic Models to Evaluate the Impact of Intestinal Glucuronide Hydrolysis on the Pharmacokinetics of Aglycone. *J. Pharm. Sci.* **2012,** *101,* 1281–1301.
102. Rappaport, A. M. The Structural and Functional Unit in the Human Liver (Liver Acinus). *Anat. Rec.* **1958,** *130,* 673–689.
103. Jungermann, K. Functional Significance of Hepatocyte Heterogeneity for Glycolysis and Gluconeogenesis. *Pharmacol. Biochem. Behav.* **1983,** *18* (Suppl. 1), 409–414.
104. Pang, K. S.; Terrell, J. A. Retrograde Perfusion to Probe the Heterogeneous Distribution of Hepatic Drug Metabolizing Enzymes in Rats. *J. Pharmacol. Exp. Ther.* **1981,** *216,* 339–346.
105. Tirona, R. G.; Tan, E.; Meier, G.; Pang, K. S. Uptake and Glutathione Conjugation of Ethacrynic Acid and Efflux of the Glutathione Adduct by Periportal and Perivenous Rat Hepatocytes. *J. Pharmacol. Exp. Ther.* **1999,** *291,* 1210–1219.
106. Knapp, S. A.; Green, M. D.; Tephly, T. R.; Baron, J. Immunohistochemical Demonstration of Isozyme- and Strain-Specific Differences in the Intralobular Localizations and Distributions of UDP-Glucuronosyltransferases in Livers of Untreated Rats. *Mol. Pharmacol.* **1988,** *33,* 14–21.
107. Pang, K. S.; Koster, H.; Halsema, I. C.; Scholtens, E.; Mulder, G. J.; Stillwell, R. N. Normal and Retrograde Perfusion to Probe the Zonal Distribution of Sulfation and Glucuronidation Activities of Harmol in the Perfused Rat Liver Preparation. *J. Pharmacol. Exp. Ther.* **1983,** *224,* 647–653.
108. Conway, J. G.; Kauffman, F. C.; Tsukada, T.; Thurman, R. G. Glucuronidation of 7-Hydroxycoumarin in Periportal and Pericentral Regions of the Liver Lobule. *Mol. Pharmacol.* **1984,** *25,* 487–493.
109. el Mouelhi, M.; Kauffman, F. C. Sublobular Distribution of Transferases and Hydrolases Associated With Glucuronide, Sulfate and Glutathione Conjugation in Human Liver. *Hepatology* **1986,** *6,* 450–456.
110. Quistorff, B. Gluconeogenesis in Periportal and Perivenous Hepatocytes of Rat Liver, Isolated by a New High-Yield Digitonin/Collagenase Perfusion Technique. *Biochem. J.* **1985,** *229,* 221–226.
111. Tan, E.; Tirona, R. G.; Pang, K. S. Lack of Zonal Uptake of Estrone Sulfate in Enriched Periportal and Perivenous Isolated Rat Hepatocytes. *Drug Metab. Dispos.* **1999,** *27,* 336–341.
112. Donner, M. G.; Warskulat, U.; Saha, N.; Haussinger, D. Enhanced Expression of Basolateral Multidrug Resistance Protein Isoforms Mrp3 and Mrp5 in Rat Liver by LPS. *Biol. Chem.* **2004,** *385,* 331–339.

113. Meyer-Wentrup, F.; Karbach, U.; Gorboulev, V.; Arndt, P.; Koepsell, H. Membrane Localization of the Electrogenic Cation Transporter rOCT1 in Rat Liver. *Biochem. Biophys. Res. Commun.* **1998,** *248,* 673–678.
114. Cattori, V.; van Montfoort, J. E.; Stieger, B.; Landmann, L.; Meijer, D. K.; Winterhalter, K. H.; Meier, P. J.; Hagenbuch, B. Localization of Organic Anion Transporting Polypeptide 4 (Oatp4) in Rat Liver and Comparison of Its Substrate Specificity With Oatp1, Oatp2 and Oatp3. *Pflugers Arch.* **2001,** *443,* 188–195.
115. Abu-Zahra, T. N.; Wolkoff, A. W.; Kim, R. B.; Pang, K. S. Uptake of Enalapril and Expression of Organic Anion Transporting Polypeptide 1 in Zonal, Isolated Rat Hepatocytes. *Drug Metab. Dispos.* **2000,** *28,* 801–806.
116. Liu, L.; Mak, E.; Tirona, R. G.; Tan, E.; Novikoff, P. M.; Wang, P.; Wolkoff, A. W.; Pang, K. S. Vascular Binding, Blood Flow, Transporter, and Enzyme Interactions on the Processing of Digoxin in Rat Liver. *J. Pharmacol. Exp. Ther.* **2005,** *315,* 433–448.
117. Pang, K. S.; Stillwell, R. N. An Understanding of the Role of Enzyme Localization of the Liver on Metabolite Kinetics: A Computer Simulation. *J. Pharmacokinet. Biopharm.* **1983,** *11,* 451–468.
118. Tan, E.; Lu, T.; Pang, K. S. Futile Cycling of Estrone Sulfate and Estrone in the Recirculating Perfused Rat Liver Preparation. *J. Pharmacol. Exp. Ther.* **2001,** *297,* 423–436.
119. Sun, H.; Zeng, Y. Y.; Pang, K. S. Interplay of Phase II Enzymes and Transporters in Futile Cycling: Influence of Multidrug Resistance-Associated Protein 2-Mediated Excretion of Estradiol 17beta-D-Glucuronide and Its 3-Sulfate Metabolite on Net Sulfation in Perfused $TR^{(-)}$ and Wistar Rat Liver Preparations. *Drug Metab. Dispos.* **2010,** *38,* 769–780.
120. Huang, M. L.; Jusko, W. J. Nonlinear Pharmacokinetics and Interconversion of Prednisolone and Prednisone in Rats. *J. Pharmacokinet. Biopharm.* **1990,** *18,* 401–421.
121. Cheng, H.; Jusko, W. J. Mean Residence Time of Oral Drugs Undergoing First-Pass and Linear Reversible Metabolism. *Pharm. Res.* **1993,** *10,* 8–13.
122. Ebling, W. F.; Rich, S. A.; Szefler, S. J.; Jusko, W. J. Troleandomycin Effects on Methylprednisolone and Methylprednisone Interconversion and Disposition in the Rabbit. *Eur. J. Drug Metab. Pharmacokinet.* **1987,** *12,* 50–57.
123. de Lannoy, I. A.; Barker, F., 3rd; Pang, K. S. Formed and Preformed Metabolite Excretion Clearances in Liver, a Metabolite Formation Organ: Studies on Enalapril and Enalaprilat in the Single-Pass and Recirculating Perfused Rat Liver. *J. Pharmacokinet. Biopharm.* **1993,** *21,* 395–422.
124. de Lannoy, I. A.; Pang, K. S. Combined Recirculation of the Rat Liver and Kidney: Studies With Enalapril and Enalaprilat. *J. Pharmacokinet. Biopharm.* **1993,** *21,* 423–456.
125. Pang, K. S. The Effect of Intercellular Distribution of Drug-Metabolizing Enzymes on the Kinetics of Stable Metabolite Formation and Elimination by Liver: First-Pass Effects. *Drug Metab. Rev.* **1983,** *14,* 61–76.
126. Midha, K. K.; Rawson, M. J.; Hubbard, J. W. The Role of Metabolites in Bioequivalence. *Pharm. Res.* **2004,** *21,* 1331–1344.
127. Jackson, A. J.; Robbie, G.; Marroum, P. Metabolites and Bioequivalence: Past and Present. *Clin. Pharmacokinet.* **2004,** *43,* 655–672.
128. Jackson, A. J. The Role of Metabolites in Bioequivalency Assessment. III. Highly Variable Drugs With Linear Kinetics and First-Pass Effect. *Pharm. Res.* **2000,** *17,* 1432–1436.
129. Chen, M. L.; Jackson, A. J. The Role of Metabolites in Bioequivalency Assessment. II. Drugs With Linear Pharmacokinetics and First-Pass Effect. *Pharm. Res.* **1995,** *12,* 700–708.
130. Chen, M. L.; Jackson, A. J. The Role of Metabolites in Bioequivalency Assessment. I. Linear Pharmacokinetics Without First-Pass Effect. *Pharm. Res.* **1991,** *8,* 25–32.
131. Karalis, V.; Macheras, P. Examining the Role of Metabolites in Bioequivalence Assessment. *J. Pharm. Pharm. Sci.* **2010,** *13,* 198–217.

4.06 Drug Classification and Drug Disposition Prediction

CM Hosey and LZ Benet, University of California, San Francisco, CA, United States

© 2017 Elsevier Ltd. All rights reserved.

4.06.1	**Introduction**	103
4.06.2	**Current Issues and Challenges in Pharmacokinetics**	103
4.06.2.1	Predicting Oral Absorption and Availability	104
4.06.2.1.1	Physicochemical determinants of absorption	104
4.06.2.1.2	In vitro predictions	105
4.06.2.2	Predicting Distribution	105
4.06.2.2.1	Volume of distribution	105
4.06.2.3	Predicting Metabolism and Elimination	106
4.06.2.3.1	Characteristics of metabolism	106
4.06.2.3.2	In vitro predictions	107
4.06.2.3.3	In vivo predictions	108
4.06.2.3.4	In silico predictions	108
4.06.3	**Biopharmaceutics Classification System**	109
4.06.3.1	Biowaivers Granted by the US Food and Drug Administration	111
4.06.3.1.1	BCS class 1	111
4.06.3.1.2	BCS class 3	111
4.06.3.1.3	BCS class 2a	111
4.06.3.2	Determining Permeability	111
4.06.3.2.1	Determining permeability in humans	111
4.06.3.2.2	Determining permeability in vivo or in situ	112
4.06.3.2.3	Determining permeability in vitro	112
4.06.3.3	Approval of BCS Class 1 Classification	113
4.06.4	**Biopharmaceutics Drug Disposition Classification System**	113
4.06.4.1	Introduction to BDDCS and Comparison With BCS	113
4.06.4.1.1	Metabolism as a surrogate for absorption	113
4.06.4.1.2	Primary goals of the classification systems	113
4.06.4.1.3	Differences in defining permeability	113
4.06.4.1.4	Development of and dispositional predictions by BDDCS	113
4.06.4.1.5	Value and appropriate uses of BDDCS	114
4.06.4.1.6	How are interactions defined?	114
4.06.4.2	Role in Predicting Absorption	115
4.06.4.2.1	Processes affecting absorption	115
4.06.4.2.2	Requirements of absorption and predicting absorption	115
4.06.4.2.3	Transporter effects in the gut	115
4.06.4.2.4	Non-transport-mediated interactions affecting drug absorption	117
4.06.4.3	Role in Predicting Metabolism and Hepatic Elimination	117
4.06.4.3.1	Metabolism in the gut	117
4.06.4.3.2	Hepatic basolateral uptake	117
4.06.4.3.3	Hepatic apical efflux	118
4.06.4.3.4	Insights into metabolism from BDDCS	119
4.06.4.4	Predicting Bioavailability	119
4.06.4.4.1	Complex considerations: food effects	120
4.06.4.5	Role in Predicting Distribution	122
4.06.4.5.1	Distribution into the brain	122
4.06.4.5.2	Potential extensions to other membranes	124
4.06.4.6	Predicting BDDCS Class	125
4.06.4.6.1	In vitro	125
4.06.4.6.2	In silico	125
4.06.5	**Conclusions**	125
References		126

4.06.1 Introduction

For a drug to be effective, it must become available at the target site. However, target sites are often inaccessible and it is necessary to dose from a convenient location. The drug must therefore be absorbed from a dosing site, often from the gastrointestinal tract since many drugs are orally administered. Subsequently, the drug must distribute throughout the body until some drug reaches the target site. However, because drugs are xenobiotics, the body will attempt to protect itself by eliminating the drug, either by directly excreting it as the parent drug, usually in the urine or the bile, or by metabolizing it to something generally easier to excrete. The combination of these processes is given the acronym ADME and is regarded as drug disposition. Pharmaceutical scientists attempt to optimize each of these processes to ensure that drugs reach their targets safely and efficaciously, yet with few off-target effects, and can be dosed on a convenient schedule. This is affected by physiological factors and chemical properties of drugs. Pharmaceutical scientists have invested a lot of research into understanding these properties in order to predict disposition prior to developing a drug and testing it in humans.

ADME can be assessed with plasma concentrations over time. The area under this curve (AUC) represents drug exposure, which is generally correlated with therapeutic response. However, for some drugs, antibiotics, for example, the maximum concentration (C_{max}) may better predict therapeutic response. In other cases, a relatively immediate response is required, when using sleep-inducing hypnotics, for instance. Drugs of this nature must enter the systemic circulation and be able to access their target quickly, which means that the time to maximum concentration (t_{max}) must be short and that the drug must have properties that allow rapid distribution to the target tissue (e.g., the brain).

The primary goal of pharmacokinetics in therapeutics is to select an appropriate dose. AUC is the clinical output from which clearance, bioavailability, and volume of distribution, the primary pharmacokinetic parameters, can be calculated. Clearance and bioavailability contribute to dose and regimen selection. When conditions are nonnormal, pharmaceutical companies, physicians, or pharmacists must know how to adjust the dose. Changes in clearance and bioavailability are reflected in changes in AUC. By understanding how different factors can impact dispositional factors, we can deduce the mechanism of the observed exposure change and appropriately amend the treatment regimen.

Humans all have unique physiology, which is why some people can drink milk, eat wheat, or even smoke cigarettes for decades without a problem, while milk consumption can cause intestinal distress, wheat consumption can affect nutrient absorption, and cigarette smoke can lead to cancer in other people. Drugs also exhibit marked variability. Consider the chemotherapeutic drug cyclophosphamide, which is used to treat certain forms of leukemia: Some people experience extreme nausea, while others tolerate the treatment with no disturbance in their daily life. The dispositional profile of a drug also varies between people. The same dose can deliver poor systemic concentrations and lack of efficacy in some patients but overdose a second patient and leave them susceptible to toxicity. Pharmaceutical scientists and regulatory agencies recognize factors that increase this risk in variability and spend much time and money understanding the important contributing dispositional factors.

Much of the disposition is regulated by the active impact of metabolizing enzymes and drug transporters. Other factors such as blood flow, membrane permeability, pH, protein binding, and endogenous substances all play a significant role as well. There is marked variation in the expression and activity of metabolizing enzymes and drug transporters in healthy individuals. The impact of this variation is studied in a field called pharmacogenomics. In this article, we will discuss how pharmacists and physicians can garner this knowledge to predict how a drug will respond in an individual with a specific genetic profile. Even when a patient has a normal wild-type genetic variation of metabolizing enzymes and transporters, other drugs, supplements, and even food can alter the activity of metabolizing enzymes and transporters. Eating food also results in transient physiological changes that may impact how a drug is absorbed and disposed compared with when a drug is taken without food.

In renal disease, the ability to eliminate and clear drugs is directly impacted by decreased renal function. However, chronic kidney disease (CKD) can also impact drug disposition by affecting the concentrations of endogenous compounds, which can interact with drugs, or affecting physiological aspects like blood flow or protein binding. In celiac disease, structural and physiological changes and decreased CYP3A expression[1] in patients may potentially alter drug absorption.[2] Other diseases including, but certainly not limited to, diabetes, cystic fibrosis, cancer, and cardiac disease can significantly impact a drug's disposition.

Understanding how physiological systems change with disease and how interindividual differences, either biological or due to external factors such as copharmacy, will impact drug disposition helps pharmaceutical companies develop safer, more efficacious dosing regimens with a clearer understanding of necessary alterations in dosing. In fact, pharmacokinetics was once a leading cause of drug failure during development, but is no longer a significant concern due to our improved understanding of drug disposition.[3,4]

During development, it is advantageous to harness drug disposition predictions using preclinical models, including in silico, in vitro, or in vivo animal studies. Information can be gathered from predictive models more quickly and cheaply than from humans and mitigates unnecessary risk early in development. While evaluating some aspects of drug disposition, including the contribution of metabolizing enzymes or drug transporters, a negative result may obviate the need for additional studies in humans.

4.06.2 Current Issues and Challenges in Pharmacokinetics

Drugs can be administered through a myriad of routes. These include topical, optical, or oral administration or injections (including intramuscular, subcutaneous, or intravenous). Intravenously administered drugs are directly administered to the blood, and

therefore, the entire dose is available for distribution in the body. However, drugs administered by any other route must pass some barriers before entering the blood, in the process called absorption. Naturally, a percentage of the drug cannot pass through the barriers and is lost between the site of absorption and the blood. This loss depends on both the barrier that must be crossed and properties of the drug.

Some membranes are leakier than others, while some are perfused by higher blood flow. Other differences include higher or lower fat content, pH differences, and differences in the expression of transporters and metabolizing enzymes. This impacts how a drug can be administered. For instance, insulin is generally administered subcutaneously, but can also be inhaled because of the relatively high permeability of the alveolar epithelium.[5] Insulin, however, cannot be given orally due to degradation by proteolytic enzymes and an inability to be transported in and through the gastrointestinal tract.[6]

Metabolism dominated the understanding of drug disposition for a very long time. Eventually, scientists began to realize that drug transporters, initially called phase III metabolism, had an equally important role in drug absorption, distribution, and elimination. Hundreds of drug transporters have been identified in humans,[7] but currently, at least seven are considered clinically important in regulating drug disposition. The FDA 2012 guidance on drug interactions[8] recommends determining if a drug is a substrate, inhibitor, or inducer of P-gp and BCRP for all drugs, OATP1B1 and OATP1B3 if a drug is hepatically eliminated, and OAT1, OAT3, and OCT2 when a drug is renally eliminated. However, other transporters such as MATEs are considered clinically relevant by the International Transporter Consortium (ITC), who recommends prospectively studying MATE interactions. The ITC recommends that MRP2 and BSEP be evaluated in retrospective studies depending on clinical and preclinical observations. Other transporters such as OATP2B1, ENTs, and PEPTs are also considered clinically relevant.[7,9] Other drugs, high-fat food or components in food, endogenous substrates, disease, and genetics can alter the function of these and other transporters. Since transporters often highly regulate drug exposure in the systemic circulation and tissues as well as play a role in drug elimination, when their function is altered, the safety and efficacy of a drug can be compromised. We will discuss when transport is relevant to the clinical outcome of a drug, as well as many cases when it is not.

4.06.2.1 Predicting Oral Absorption and Availability

Most drugs are preferably administered by the oral route to increase patient compliance and facilitate delivery and packaging. Before a drug can enter the systemic circulation after oral dosing, it must (a) be absorbed in the gut, where it may be affected by apical uptake and efflux transporters, (b) pass through gut epithelial cells (enterocytes) where it may be metabolized, and then (c) escape from metabolism or biliary elimination in hepatocytes. The combination of these processes determines the bioavailability of the drug or the fraction of the dose that enters systemic circulation.

In humans, bioavailability (F) can be readily measured by comparing exposure from intravenous and oral dosage forms: $F = AUC_{oral}/AUC_{iv}$, correcting for dose if necessary. However, it is very difficult to predict the fraction of the bioavailability due to absorption (F_A) and thus the extent of absorption. Hepatic bioavailability (F_H) can be estimated when an intravenous dose is given and total and renal clearances are measured ($F_H = 1 - CL_H/Q_H$, where hepatic blood clearance (CL_H) equals total blood clearance (CL) minus renal blood clearance (CL_R) and Q_H is the estimate of hepatic blood flow rate). However, then, determining the fraction of the dose that is absorbed requires an estimate of the fraction of the dose that escapes gut metabolism since $F = F_A \times F_G \times F_H$. F_G, the gut bioavailability, requires invasive methods such as sampling from the portal vein. The rate and extent of absorption depend upon the physicochemical properties of the active component in a drug product, the formulation and release of the drug from the product, and physiological traits of the gastrointestinal system.

Additionally, microbiotic metabolism and luminal degradation of drugs can reduce the proportion of the parent drug that is available for absorption. Even after initial absorption, a drug can be effluxed by transporters in the enterocytes back into the gut lumen, effectively reducing absorption.

Drug absorption can be mediated through passive or active permeation across (primarily) enterocytes. Passively absorbed compounds can be transcellularly diffused (through the cell) or paracellularly diffused (between the cells). Active permeation requires the intercession of drug transporters, which can move a drug across either side of a polarized cell membrane. Active transporters are responsible for either bringing the drug into a cell or ejecting it from a cell.

4.06.2.1.1 Physicochemical determinants of absorption

It is generally presumed that lipophilicity correlates with cell permeability, within a reasonable boundary and when considering structurally similar compounds. (Lipophilicity is derived from the Greek "fat-loving." Highly lipophilic molecules are often nonpolar and prefer to partition into nonpolar versus polar phases.) In 1997, Lipinski et al.[10] developed a set of rules that aided in understanding the properties of drugs that are readily absorbed. Poor absorption is more likely when a drug has greater than 5 hydrogen bond donors (OH and NH), a molecular weight >500 Da, cLogPa >5, or greater than 10 hydrogen bond acceptors (oxygens and nitrogens). However, this rule does not apply when transporters mediate drug absorption.

4.06.2.1.1.1 Passive absorption

Passive absorption generally refers to permeation of compounds that have properties that allow them to cross through a cell (transcellular). Drugs can only pass transcellularly if they are small and relatively lipophilic. Compounds that instead pass between cells (paracellular permeation) may be small and hydrophilic.

4.06.2.1.1.2 Active absorption

Most compounds are known or presumed to be substrates of active transporters, even if they can also be passively absorbed. However, highly permeable, highly soluble compounds are not dependent upon active transporters for their absorption even if they are substrates and will not be impacted by disruptions to their function. This will be discussed in great detail in section "Biopharmaceutics Drug Disposition Classification System."

4.06.2.1.2 In vitro predictions

The Biopharmaceutics Classification System (BCS), as we will discuss later, opened the door to predicting absorption with surrogate in vitro systems, such as Caco-2 and Madin–Darby canine kidney (MDCK). The Biopharmaceutics Drug Disposition Classification System (BDDCS) allowed us to do the same with artificial membranes such as parallel artificial membrane permeability assay (PAMPA). Compounds with a high in vitro permeability rate are expected to be well absorbed.

Caco-2, an immortal cell line derived from colorectal adenocarcinoma cells, comes from human enterocytes. They confer the advantage of being human in nature with a microvillus surface. However, these cells take 2–3 weeks to culture and even then do not fully express transporters or metabolizing enzymes. Additionally, tight junctions predominate and resistance is high compared with in vivo morphology.[11] This can lead to significant underprediction of permeability rate and absorption. The in vitro lack of expression of highly expressed transporters in humans can greatly underpredict the extent of absorption.[12]

MDCK cells are immortal cells that come from the kidney of dogs. These cells have a shorter culture time than Caco-2 and have lower resistance than Caco-2 cells, a condition more similar to the human gut. However, these cells are not human in nature and, similar to Caco-2, they poorly express CYP3A.

PAMPA is an artificial membrane that does not express transporters and has no cells to create tight junctions or cellular pores. It is representative of passive permeability through a lipid bilayer.

All in vitro models lack the flow of gut contents and blood on either side of enterocytes. Portal blood flow constantly removes drugs from the basolateral membrane of enterocytes, resulting in "sink conditions," a downhill concentration gradient that facilitates drug absorption in vivo. The fluidity of gut contents means that drugs in the gut lumen will be exposed to the different morphologies and expressions in different segments of the gut in vivo that are not simulated in in vitro cell studies.

While highly permeable compounds are almost all extensively absorbed, in vitro permeability rate predictions often underpredict absorption. This is because many compounds are actively absorbed, but have low passive permeability. Predicting extent of absorption is improved by including active drug transport. Larregieu and Benet[12] showed that when transporter expression is decreased more than 10-fold in Caco-2 cells compared with humans, absorption of compounds that are substrates of highly expressed transporters such as PEPT1, amino acid transporters, and nucleoside transporters is poorly predicted.

Permeability rate as a surrogate for absorption will be extensively discussed in section "Biopharmaceutics Classification System."

4.06.2.2 Predicting Distribution

Drug distribution is determined by cardiac output, tissue blood flow and volume, and capillary permeability, as well as tissue permeability and drug transporters. Following drug dosing, well-perfused tissues such as the liver and kidney initially receive a high drug concentration. This initial distribution phase is apparent when considering the shape of a plasma concentration–time profile. A secondary distribution phase, characterized by slowly decreasing plasma concentrations, reflects drug distribution to the more poorly perfused tissues. Additionally, protein-bound drugs cannot traverse cellular membranes, and therefore, protein binding has an impact on drug distribution. In the plasma, drugs primarily bind to either albumin, if the drug is acidic, or α-1-acid glycoprotein, if the drug is basic. Protein binding can be modified by disease and drug–drug interactions. For instance, patients with cystic fibrosis often have hypoalbuminemia.[13] However, Benet and Hoener[14] have shown that changes in protein binding are only important for high-clearance, narrow therapeutic index drugs that are dosed intravenously, for example, lidocaine.

4.06.2.2.1 Volume of distribution

Distribution can be characterized by the theoretical pharmacokinetic term, the apparent volume of distribution. This term characterizes the apparent space in the body into which a drug distributes. That is, systemic concentration multiplied by the apparent volume of distribution is equal to the amount of drugs in the body. A large volume of distribution indicates that a compound is predominantly located outside of the systemic fluids flowing to the organs of elimination. Volume of distribution depends on the extent of drug binding to receptor sites, plasma proteins, and tissues, as well as the lipophilicity of a drug. Volume of distribution measures can be determined from plasma concentration–time curves. While the volume of distribution can be calculated a few ways, the volume at steady state or V_{ss} is the most useful measure of the apparent space available in the body into which drugs may distribute, since it is not affected by elimination. V_{ss} measures can be determined from plasma concentration–time curves using the following equation:

$$V_{ss} = \mathrm{CL} \times \frac{\mathrm{AUMC}}{\mathrm{AUC}}$$

Here, AUMC is the area under the moment curve or the area under the curve of the product of concentration and time versus time.

Additionally, physiologically based PK models such as GastroPlus™ and Simcyp provide estimates of V. Age, percent of body fat, sex, and disease can all affect the volume of distribution. Accurately predicting volume of distribution is vital in predicting C_{max} and can be important in defining clinically relevant half-life ($t_{1/2}$) measures. Volume of distribution is also predicted in animal models, which include physiological features like blood flow and organ topology. The volume of distribution can be estimated by collecting plasma concentrations over time and using allometric scaling approaches to predict the volume of distribution in humans.

4.06.2.3 Predicting Metabolism and Elimination

Most drugs are eliminated by metabolism, renal elimination of unchanged drug, or biliary elimination of unchanged drug. To ensure safety, pharmacokinetic studies are conducted with mass balance or collection of the entirety of a dose in eliminated equivalents (parent drug or metabolites). Ideally, the entirety of the dose is eliminated in either the urine or the bile. This provides evidence that the compound is not sequestered and accumulating in a peripheral tissue, potentially resulting in unanticipated toxicity, and lends support to the validity of the calculated pharmacokinetic parameters. Incomplete recovery sometimes indicates that a drug is eliminated by another organ (e.g., the lungs). However, mass balance may not be as simple as it sounds. Realistically, the entirety of the dose often cannot be collected. Some drugs have very long half-lives, which makes collections in a clinical setting unrealistically arduous.

Many metabolites and some parent drugs are eliminated in the bile, which is a difficult fluid to accurately obtain and analyze. The bile drains into the lumen of the intestine and its contents are eventually eliminated as part of the feces. Fecal samples could be collected to estimate the fraction of the dose that is eliminated in the bile. However, the feces also contain orally administered material that was never absorbed from the lumen of the intestine. For this reason, it is impossible to differentiate between parent drug that is unabsorbed from an oral administration and parent drug that is eliminated in the bile in fecal samples. This means that, unless a drug was administered non-orally so that all of the drug in the feces must therefore come from biliary excretion, direct bile collection approaches such as collection from T-tubes or nasobiliary tubes are necessary to account for the elimination of unchanged drug in the bile. However, such approaches are rarely conducted and when done are predominantly done during surgeries. The patients often have hepatobiliary disease, so the donor samples do not necessarily represent healthy conditions. Other methods such as the bile string or duodenal collection studies are slightly less invasive and can be conducted with healthy volunteers. Duodenal collection studies are difficult to conduct, however, and are still invasive.

It is much easier to determine the extent of urinary elimination of unchanged drug or the extent of metabolism. Urine samples are almost always collected during pharmacokinetic studies to account for mass balance, and the parent and metabolites can be readily quantified. Parent drug collected in the urine represents absorbed drug only since the drug can only reach the kidneys after entering the systemic circulation. Metabolites can be quantified in the urine and may also be collected in feces. If the drug was not degraded or metabolized by bacteria in the gut, we can assume that the drug was absorbed since most metabolism occurs postabsorption. Degradation and presystemic metabolism can be confirmed with stability studies to be described in section "**Determining permeability in humans**."

Prior to conducting trials in humans, pharmaceutical scientists try to predict what the major route of drug elimination will be. In silico, in vitro, and in vivo models of drug elimination have been developed to predict elimination routes and their potential liabilities. For instance, biliarily eliminated drugs may be subject to enterohepatic recycling, which exposes the drug to the intestine and liver multiple times and may result in several peaks. Metabolism may produce pharmacologically active or toxic metabolites that can alter pharmacodynamics or need to be evaluated for safety. A developer may want to avoid renal elimination if the drug is likely to be dosed to patients with failing kidneys. Alternatively, an eliminating organ may be the desired site of action and a developer may attempt to target that route.

Recently, there have been many efforts to associate the chemical properties of drugs with their major elimination routes. Certain trends have been noted for a long time, with properties such as lipophilicity, molecular weight, protein binding, and ionization state proposed as harbingers of elimination route. However, these relationships are sometimes considered too simple or were applied to small data sets of compounds that are often structurally similar. With the advent of "big-data" methodologies, more complicated and/or thorough analyses are possible.

4.06.2.3.1 Characteristics of metabolism

Most drugs are designed to be sufficiently lipophilic to cross biological membranes during absorption or distribution and to achieve biochemical potency by encouraging protein binding to a target site through hydrophobic interactions. Coincidentally, most drugs are metabolized, and indeed, lipophilicity is historically considered a prerequisite for drug metabolism.

There are at least a couple of reasons why lipophilicity and metabolism are associated with each other. The first is that relatively lipophilic drugs may be able to be passively reabsorbed across membrane barriers surrounding excretory fluids including the aqueous bile and urine.[15] Metabolic enzymes generally convert a lipophilic substance into a more hydrophilic substance, which aids in accumulation in and thus elimination from the aqueous bile or urine. Secondly, lipophilicity is correlated with protein binding[15] and may aid in binding to enzymatic proteins through hydrophobic interactions,[15] which will convert a drug to a more hydrophilic molecule.

Many very lipophilic molecules are indeed metabolized, and in fact, we are unaware of any marketed poorly metabolized drugs with a measured or calculated LogP > 5.[16] As always, it is important to note that these are trends and not rules. Despite the common assumption that metabolized compounds are lipophilic and vice versa, metabolized compounds cover a vast physicochemical

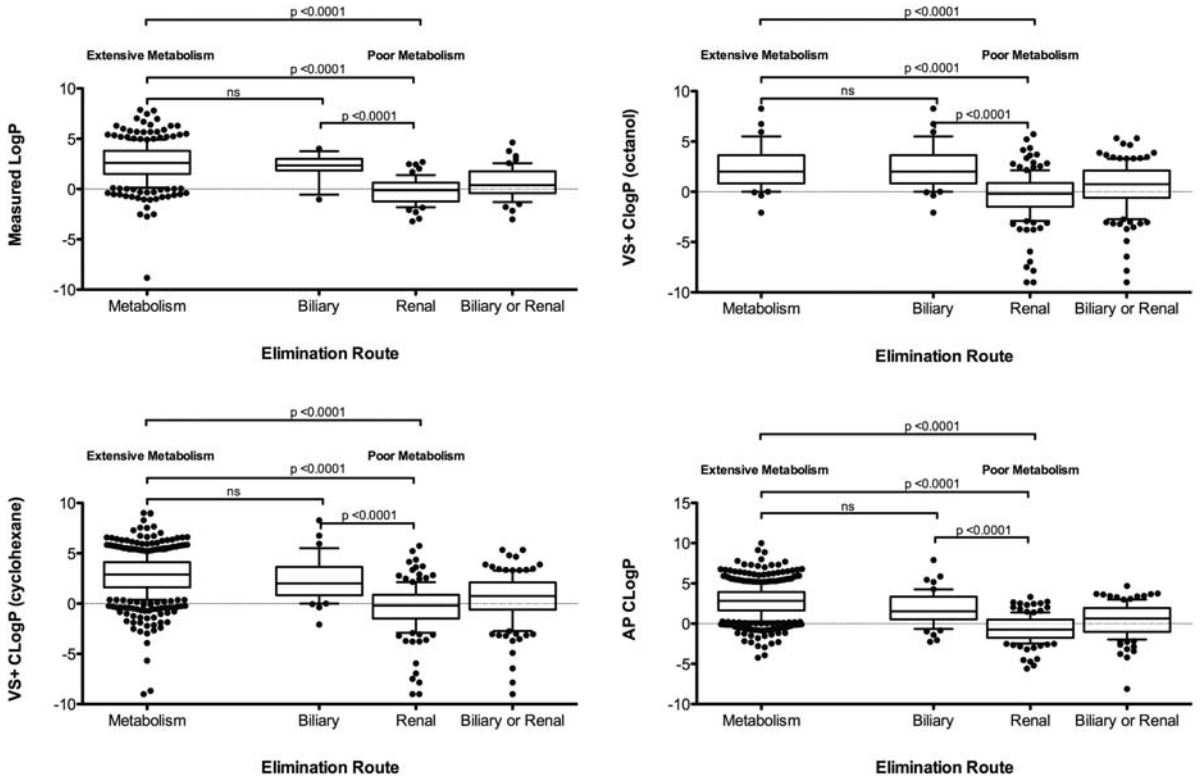

Fig. 1 Measured and calculated partition coefficients segregated by major route of elimination. Reprinted with permission from Hosey, C. M.; Benet, L. Z. Predicting the Extent of Metabolism Using In Vitro Permeability Rate Measurements and In Silico Permeability Rate Predictions. *Mol. Pharm.* **2015**, *12*, 1456–1466. Copyright (2015) American Chemical Society.

space, and not all lipophilic compounds are metabolized. In particular, drugs that are eliminated unchanged in the bile also exhibit relatively high LogP values, with no significant difference in this parameter from metabolized compounds as determined by the *t*-test (Fig. 1) and no rank-ordered differentiability as indicated by receiver operating characteristic curves. (The receiver operating characteristic is a plot that illustrates how well a continuous feature (e.g., LogP) classifies a binary outcome (e.g., biliary vs. metabolic elimination.) When the area under the ROC curve is greater than 0.8, the continuous feature is expected to differentiate between the classes well.) Furthermore, a large proportion of metabolized drugs have a low LogP. This may be because drugs eliminated unchanged in the bile require uptake and efflux transporters in the hepatocyte and therefore must be sufficiently lipophilic to bind to these transporters. Alternatively, almost all compounds eliminated as unchanged drug in the urine have a low LogP and are poorly bound to proteins.

However, given the somewhat ambiguous predictability of LogP, it is necessary to predict which compounds will be metabolized by other methods. Metabolism can be assessed using in vitro, in vivo, or in silico methodologies.

4.06.2.3.2 In vitro predictions

The extent, rate, and mechanisms of metabolism are often initially evaluated in vitro. Ideally, human hepatic and enterocytic tissues can be utilized to evaluate metabolism. However, these merely serve as predictive tools and are fraught with errors.

Microsomes are a subcellular fraction containing the contents of the endoplasmic reticulum including CYPs and UGTs. CYP metabolism accounts for about 70% of the metabolism of extensively metabolized drugs of the top 200 drugs,[17] while UGT metabolism accounts for about 14% of the metabolism of the top 200 drugs prescribed in the United States.[18]

In vitro microsomal experiments can determine the rate of microsomal metabolism, called the intrinsic clearance (CLint), representing the capacity of metabolizing enzymes to eliminate a compound in the absence of other factors like blood flow, membrane permeability, protein binding, and competing elimination mechanisms.

Intrinsic clearance can be expected to correlate with clinical clearance in humans, particularly for drugs that are primarily metabolized by CYP enzymes in the liver. Prior to the recognition of the contribution of transporters to drug disposition, human clearance was estimated from intrinsic clearance in microsomes generally using the well-stirred model. However, in the late 1990s, Miyauchi et al. proposed an extended clearance concept to include the effect of transporters on hepatic clearance.[19]

Microsomes can provide a reliable estimate of metabolic kinetics (clearance). However, microsomes have been used to predict the extent of metabolism by measuring the percent of dosed drug that is unmetabolized after a set period of time. This may be an unreliable predictor of the extent of metabolism[20–22] since presumably most drugs will be metabolized if they are left to incubate in

the presence of a variety of enzymes without interference. As we will discuss in detail later, in vitro permeability rate can predict the extent of metabolism in humans.

Supersomes, expressing only one enzyme, may be used to predict the metabolic intrinsic clearance by a single enzyme and to identify metabolites formed by a specific enzyme.

A major concern of predicting the extent and/or rate of metabolism in vitro, perhaps especially in microsomes, is that metabolism is assessed in isolation of competing processes. In vivo, transport-limited clearance into the bile or passive or transport-limited clearance into the urine may prevail. However, microsomal incubations cannot tell a researcher what is the major route of elimination, and metabolic clearance does not necessarily relate to extent of metabolism. Isolated or sandwich-cultured hepatocytes are more complex tools that incorporate transporters and may be used to predict metabolic or hepatic clearance.

4.06.2.3.3 In vivo predictions

In vivo approaches confer the advantage of including factors such as blood flow, sequestration due to transport, and membrane permeability. In vivo approaches include humanized animals and allometric predictions. Humanized animals, like supersomes, can help assess the impact of a single enzyme or transporter.

Allometry applies scaling factors based on body size to pharmacokinetics across species. Simple allometry from a single species is commonly used early in drug development, requiring only clearance data from preclinical species. Modifications of simple allometry have been proposed to improve the predictability of these models.[23]

These predictions require sampling plasma concentrations over time in preclinical animal models and may incorporate other physiological parameters such as plasma protein binding and the blood to plasma ratio. They can be supplemented with physicochemical drug properties such as molecular weight or LogP.

The most obvious disadvantage to using preclinical animal models is physiological differences. While allometry attempts to correct for differences in body weight, protein binding, blood flow, etc., animals often have different patterns of metabolizing enzyme and transporter expression and substrate specificity. While pharmacokinetics are frequently similar between species, marked differences can be seen in a variety of substrates. Consider, for instance, digoxin or zidovudine. Digoxin is extensively metabolized in rats,[24] but is primarily eliminated as unchanged drug in humans.[25] Zidovudine is extensively metabolized in humans,[26] but is primarily eliminated unchanged in rats.[27]

4.06.2.3.4 In silico predictions

Several in silico methods predict aspects of metabolism, including understanding the affinity for a particular enzyme[28] and the site of metabolism on the molecule,[28] predicting metabolic clearance,[29] identifying metabolites,[30] and predicting metabolic stability.[31] Unfortunately, many of the published methods rely on proprietary descriptors or are derived from small or structurally similar data sets.[32] Since many compounds are metabolized by several enzymes and/or are sequentially metabolized, it is crucial to integrate many predictive models. Several reviews discuss the challenges and applications of in silico predictions of drug metabolism in depth and discuss available predictive software.[28,30,32]

Second to metabolism, renal elimination of unchanged drug is responsible for the elimination of most drugs.

4.06.2.3.4.1 Renal elimination of parent drug

Renal elimination of drugs is dependent upon three renal processes: glomerular filtration, renal secretion, and renal reabsorption. Glomerular filtration is a passive process where free (unbound) small-molecule compounds are drained from the blood in the afferent arteriole and collected in the filtrate. Large molecules, including drugs bound to proteins, cannot sieve through the glomerulus and they remain in circulation. While glomerular filtration rate = 120 mL min^{-1}, urine is only formed at 1 mL min^{-1}, so 119 mL of water is reabsorbed from the kidney tubules every minute. For this reason, many compounds, especially metabolized compounds, are passively reabsorbed from the filtrate as water is actively retained in the body. Several compounds are actively secreted into the filtrate directly from the blood via drug transporters expressed on the proximal tubule.

Renal clearance tends to decrease with increasing lipophilicity.[33] This is intuitive, since highly lipophilic compounds are often susceptible to reabsorption. Additionally, lipophilic compounds are more likely to be protein-bound.[15] Unsurprisingly, compounds that are primarily eliminated as unchanged drug in the urine are expected to be small and polar, having low protein binding. However, Hosey et al. demonstrated that while this holds true for orally dosed compounds, many non-orally dosed (generally intravenously administered) compounds could be renally eliminated even if the molecular weight is high. Alternatively, protein binding of compounds primarily eliminated in the urine was low for both orally and non-orally administered medications.[22] This is likely because all small molecules ($<10{,}000$ Da)[34] can be filtered through the glomerulus, but compounds bound to proteins are not. Therefore, highly protein-bound drugs must be eliminated by other routes and protein binding is a determinant of renal elimination.

While charge does not determine if renal elimination is the primary route of elimination,[22] it does trend with renal clearance. Anions and cations are primarily secreted, whereas neutral compounds are primarily reabsorbed. Additionally, renal clearance tends to decrease with increasing compound lipophilicity, while renal secretion increases with polar descriptors.[33]

Table 1 Molecular weight distribution of orally and non-orally administered drugs by major elimination route[22]

	Molecular weight (Da)			
Major elimination route	*> 380*	*< 380*	*> 475*	*< 475*
Oral administration				
Biliary	22	5	13	14
Renal	13	65	0	78
Metabolism	153	345	53	445
Non-oral administration				
Biliary	11	1	7	5
Renal	42	21	21	42
Metabolism	42	50	29	63

4.06.2.3.4.2 Biliary elimination of parent drug

Biliary elimination of unchanged drug is the third major route of parent drug elimination. Biliary elimination is an active process requiring both uptake transporters on the hepatic basolateral membrane facing blood in the portal vein and efflux transporters on the hepatic apical membrane facing the bile canaliculi.

Historically, it was hypothesized that high-molecular-weight (>500 Da) anions would preferentially be eliminated in the bile and that biliary excretion was selective for these properties. This was likely derived by considering the weight and molecular species of the primary endogenous substrates: bile salts. Millburn et al.[35] suggested that drugs with a molecular weight $<500–600$ g mol^{-1} were less susceptible to biliary elimination. More recently, Yang et al.[36] predicted that when anions have molecular weights >475 Da, 10% or more of the dose is likely to be eliminated in the bile. Hosey et al. demonstrated that drugs whose major route of elimination is unchanged drug in the bile were poorly permeable and had a high polarizability, which is highly correlated with molecular weight, and a low predicted metabolic stability.[16,22] That study also points out that high molecular weight is descriptive of biliarily eliminated drugs, but that high molecular weight does not qualify biliary elimination. In other words, almost all drugs that are predominantly eliminated as unchanged drug in the bile are heavy, but the primary route of elimination is not biliary excretion for the majority of high-molecular-weight drugs (**Table 1**).

Other properties associated with biliary elimination have been less clearly defined and in some cases have contesting associations between studies. Greater hydrogen bond interactions have been associated with increased biliary excretion.[36,37] Some studies indicate that biliarily eliminated compounds are primarily anions,[36,37] while some indicate that cations are also eliminated in the bile,[38] and yet, others suggest that ionization is not an important characteristic.[22] Greater dipole moments,[36,38] the presence of a carboxylic acid group,[36,38,39] and more rotatable bonds[37,39] have also been associated with increased biliary excretion. Lipophilicity has varying indications between studies, with some indicating that biliarily eliminated drugs are hydrophilic,[37,38] some indicating they are lipophilic[16,40] and others discussing both lipophilic and polar regions, and some studies finding no relationship between lipophilicity and extent of biliary elimination.[36,41] While the bile is a hydrophilic medium, compounds likely require a degree of lipophilicity to bind to and be transported by drug transporters such as P-gp. This may be especially true as the most widely accepted mechanism of P-gp transport relies on an initial partition into the membrane.[42] These relationships likely depend on how "major" biliary elimination was defined and which drugs were included in the study.

As we mentioned earlier, biliary elimination data are difficult to gather and quantify in humans. However, in vitro, in vivo, and in silico approaches may provide a reasonable quantitative or qualitative understanding of biliary elimination.

Perhaps the most widely accepted in vitro approach to predict biliary clearance is the use of sandwich-cultured hepatocytes, isolated from humans or rats, which maintain the polarity of cell membranes, a crucial condition to determine canalicular efflux. These hepatocytes are plated on a collagen platform and maintained in the presence of calcium. After several days, transporter expression is optimized for vectorial transport. After introducing the test drug, the tight junctions are ruptured by removal of calcium, and differences in accumulated intracellular concentrations can be measured.[43]

In vivo, one of the most common approaches to estimate the contribution of biliary elimination is with bile duct cannulation in an isolated perfused rat liver. Unfortunately, rats have a higher bile flow (relative to body weight),[44] greater efflux transporter expression,[45] and increased rate of efflux[46] compared with humans, so more compounds are eliminated in the bile at greater concentrations and rats are not altogether reliable models.

Ghibellini et al.[47] have published a comprehensive review of methods of evaluating biliary excretion in humans.

4.06.3 Biopharmaceutics Classification System

Small changes in drug product composition may alter pharmacokinetics, potentially resulting in toxicity or lack of efficacy. For this reason, a drug must be evaluated for pharmacokinetic differences any time a company uses a new manufacturing site, new synthesis, or a new formulation. A drug product that demonstrates very similar pharmacokinetics to the original product is said to be bioequivalent. A bioequivalence study generally consists of a crossover study of a single dose of the highest dose strength of the

drug.[48] For a drug to be considered bioequivalent, the 90% confidence interval of C_{max}, $AUC_{0\rightarrow\infty}$, and $AUC_{0\rightarrow tlast}$ must be between 80% and 125% of the reference product.

While many non-orally administered compounds and compounds administered as oral solutions that meet certain requirements (minimally including dosage as an aqueous solution with the same concentration of active drug as the reference product and the same or similar excipients at comparable concentrations as the reference product) are exempt from bioequivalence testing,[48] the complexity of oral absorption requires bioequivalence testing for products administered orally outside of solutions. This is a large burden since the majority of compounds are administered orally and not in solution.

To determine bioequivalence in a clinical study, a drug is given to volunteers with 250 mL of water (about 8 oz.) on an empty stomach. Per the FDA, for a drug to be considered highly soluble, the highest dosage strength of the drug must be able to completely dissolve in this volume of water or less. The drug also needs to remain soluble over the entire pH range of the stomach and small intestine. The FDA recommends that solubility be tested at pH 1, pH 6.8, and a variety of pH in between, specifically at the pK_a of the compound and above and below the pK_a by one unit.[49] This pH range represents the range of pH from the stomach to the jejunum under fasting conditions.[50] Highly soluble drugs are defined by a dose number (D_o) ≤ 1, which can be calculated from the minimum solubility of a drug over the pH range 1–6.8, at body temperature, 37°C:

$$\text{Dose number} = \frac{\text{Highest dose strength (mg)}}{250\,\text{mL} \times \text{minimum solubility}\left(\text{mg mL}^{-1}\right)}$$

In 1995, Amidon et al. developed the BCS on the basis of a good correlation between human jejunal permeability in single-pass perfusion studies and the fraction of the dose absorbed across the gut wall.[51] They concluded that highly "permeable," highly soluble compounds were well absorbed and not susceptible to minor changes in the drug product.[51] If 85% or more of the drug is dissolved within 30 min, it is considered rapidly dissolved, and if 85% or more is dissolved in 15 min, it is very rapidly dissolved. The goal of this system is to use in vitro dissolution methodology to predict in vivo behavior.

The rate and extent of absorption for an immediate-release dosage form depend upon effective permeability, solubility, dissolution rate, and gastrointestinal transit time.[52] In order for a compound to be absorbed, it must be in solution. Therefore, the compound must be completely in solution prior to reaching the absorption site, most commonly the intestine. This is dictated by a dissolution rate. The compound must also remain in solution at the pH of the absorption site, which is ensured by measuring the minimum solubility throughout the pH range of the absorbable regions.

The BCS classifies drugs on the basis of solubility and permeability (Fig. 2). The BCS predicts that highly permeable, highly soluble class 1 drugs are well absorbed and rate-limited by gastric emptying if the compound dissolves rapidly. If the compound is contained in an immediate-release dosage form and rapidly dissolved, bioequivalence can be ensured. Class 2 drugs are well absorbed, but absorption is rate-limited by dissolution, and there may be variability in absorption due to the drug formulation or in vivo factors. Class 3 and 4 drugs are limited by permeability.

This system provides a major advantage to pharmaceutical companies because in vitro methodology may qualify drugs for a waiver of in vivo bioequivalence studies. The principles of the BCS were adopted by the FDA, EMA, and WHO in terms of biowaivers. Biowaivers grant regulatory approval based on dissolution studies to certain immediate-release drug products for drugs already on the market, but are being manufactured differently or by a different company (generics), or having formulation changes, without requiring clinical evaluation of bioequivalence. Prior to the development of this system, drug products undergoing any production changes (e.g., manufacturing location or equipment) required additional clinical bioequivalence trials to be proved

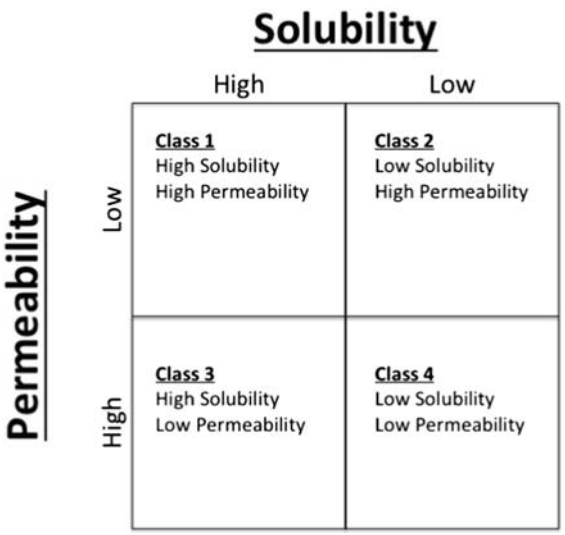

Fig. 2 Biopharmaceutics Classification System.

safe and efficacious. However, there are small differences in the regulations for biowaiver approval. As indicated in the 2015 draft guidance for biowaivers, the FDA now allows biowaivers for certain immediate-release, orally administered BCS class 1 and BCS class 3 drugs that have an acceptable therapeutic index, as well as some BDDCS class 1 drugs, which will be discussed in section "Biopharmaceutics Drug Disposition Classification System."[49] Biowaivers are not available to narrow therapeutic index drugs or drugs absorbed in the oral cavity.

The EMA now requires a stricter definition of solubility, using the highest dose administered in a single setting,[53,54] as opposed to the highest dose strength.[49] This impacts only a few drugs, but does shift the classification in some instances. For example, the highest formulated dosage strength of verapamil is 120 mg, but two tablets are often given in one setting, so the highest dose administered in a single setting is 240 mg. By the FDA definition, verapamil is considered a class 1 drug and is eligible for a biowaiver, but is ineligible for a biowaiver under the new EMA guidance.[55]

4.06.3.1 Biowaivers Granted by the US Food and Drug Administration

4.06.3.1.1 BCS class 1

These highly permeable, highly soluble compounds may be issued biowaivers if the compound is

- dosed as an immediate-release product,
- rapidly dissolved,
- an excipient in the formulation that does not interfere with the rate or extent of absorption,
- stable in the gastrointestinal tract.

Immediate-release products can be partially or completely dissolved in the stomach. These drugs are often rapidly absorbed, while extended-release products dissolve slowly in the small intestine by design. Using a highly soluble drug that is also rapidly dissolved ensures that solubility is not the rate-limiting step of absorption. Gastric emptying time is about 30 min to 1 h on a fasted stomach. Therefore, when 85% or more of a drug is dissolved within 30 min, the compound is likely to be dissolved prior to entering the intestine and is considered rapidly dissolving. In other words, the drug is ready to be absorbed once it reaches the small intestine. Additionally, the high permeability rate of class 1 drugs predicts little absorptive barrier. These BCS class 1 compounds do not have permeability barriers that would prevent the drug from being absorbed during the limited transit time through the gastrointestinal tract. Excipients that have been FDA-approved for immediate-release products will generally not interfere with drug absorption.[49]

4.06.3.1.2 BCS class 3

These highly soluble but poorly permeable compounds may be issued biowaivers if the compound is

- dosed as an immediate-release product,
- very rapidly dissolved,
- composed of the same ingredients, in similar quantities, as the reference compound.

Class 3 drugs have slightly stricter requirements than class 1 drugs, being limited by permeability rate. Additionally, since the absorption of class 3 drugs can be site-dependent, gastrointestinal transit time is a limiting factor in its absorption. Some excipients alter gastrointestinal transit time and membrane permeability[50]; therefore, there must be no alterations in the formulation including excipients. Class 3 drugs are required to be very rapidly dissolved (85% within 15 min).

4.06.3.1.3 BCS class 2a

In addition, the WHO also recommends that an additional category of BCS class 2 drugs,[56] "2a," be granted biowaivers. This subset is composed of weakly acidic class 2 drugs. They must be rapidly dissolving and highly soluble at pH 6.8. These drugs have a low solubility at the low pH in the stomach, but are well absorbed due to high solubility in the more basic intestine.

4.06.3.2 Determining Permeability

Per the FDA, compounds are considered highly permeable for the application of biowaivers when the extent of absorption is $\geq 85\%$ of the dose. The FDA permits a variety of methods of determining if a compound is highly permeable. Permeability can be assessed in humans, in vivo, or in vitro. When a pharmaceutical company intends to use a permeability-determining method for bioequivalence purposes, it should be validated by comparing permeability values generated in the assay with extents of absorption and confirming that they share a rank order.

4.06.3.2.1 Determining permeability in humans

Evaluating permeability rate by direct intestinal perfusion in humans is the most preferable method. However, acquiring such measurements is difficult and invasive. Alternative methods that are routinely assessed include evaluating the mass balance of a drug or evaluating its bioavailability.

- Mass balance: If 85% or more of the parent drug or its metabolites are eliminated in the urine, presumably, at least 85% of the drug must have been absorbed and is indicative of nearly complete absorption, and the compound meets the criteria for a high permeability compound. However, when the parent drug alone does not account for >85% of the dose, stability studies must be conducted to ensure that the metabolized compounds were not degradation products formed in the gut prior to absorption.

  Stability studies can be carried out in simulated fluids for the expected duration of drug contact with these fluids or about 1 h in simulated gastric fluid and about 3 h in simulated intestinal fluids. If <5% of the drug is degraded, it is likely stable in the stomach and intestinal lumen and the drug can be classified as extensively absorbed (BCS class 1 or 2).[49]
- Absolute bioavailability: If more than 85% of a compound is bioavailable, as compared with intravenous administration, at least 85% of the compound is absorbed and is therefore qualified as highly permeable.
- Intestinal perfusion (direct rate of mass transfer across the intestine): Drugs can be directly infused into jejunal segments of humans, and the mass that is lost between the two segments, which are sequestered by inflatable balloons, is assumed to be absorbed[57] if stability studies confirm that drugs were not metabolized or degraded in the lumen. Water absorption and secretion are corrected for with a nonabsorbable marker such as mannitol. Correlating intestinal perfusion studies to absorption extent in humans initially requires six drugs. After the protocol has been well established, the test drug must be compared with a high permeability and a low permeability standard. This study is not commonly used to quantify permeability due to its invasive nature.

If a compound is a passively diffused drug, pharmaceutical companies may employ in vitro or in vivo methodology to determine permeability. The FDA defines a passively permeable drug as one with an efflux ratio <2,[49] when linear pharmacokinetics exist between dose changes and bioavailability, and when in vivo or in vitro permeability does not depend upon the initial concentration. This specification exists because many animals or cell lines have low or nonexistent efflux compared with a well-expressed and active homolog in humans. An animal or cell line with negligible efflux can artificially boost permeability and overpredict human permeability. (An efflux ratio is defined as the basal to apical intestinal permeability divided by the apical to basal intestinal permeability).

4.06.3.2.2 Determining permeability in vivo or in situ

Animal models provide physiological conditions analogous, but not necessarily similar, to humans, including gastric and enteric dissolution, blood flow on the basolateral membrane of enterocytes, and the presence of endogenous components such as bile salts, which can impact drug solubility and absorption. Animal models may be advantageous because experiments in animals are less expensive and less time-consuming than clinical experiments in humans. In an acceptable animal model such as a rat, intestinal perfusion studies can be carried out to determine the rate and extent of drug absorption. Keep in mind, however, that while animal studies provide a physiological model, animal physiology significantly differs from humans.[44] Animal models have different expressions, activities, and substrate specificity of transporters and metabolizing enzymes as well as different blood flows, membrane permeabilities, and compositions of endogenous fluids (e.g., stomach acid and bile).

Single-pass intestinal perfusion studies examine the continuous perfusion of drug from the duodenum to the ileum of anesthetized animals, generally rats. Drugs containing fluid are introduced and removed from cannulas at either end. These models tend to correlate better with human effective permeability and human absorption than cell-based models like Caco-2.[58,59]

4.06.3.2.3 Determining permeability in vitro

Epithelial cell monolayers such as colorectal adenocarcinoma cells (Caco-2) or MDCK cells can be used to evaluate the permeability of the compound in question. The permeability of test drugs is assessed and compared with an acceptable standard compound to determine if the test compound has a relatively high or low permeability. As opposed to a quantitative value, a reference compound is an important control because permeability measurements are extremely variable between laboratories[60] and are very sensitive to experimental conditions.

Excised intestinal tissues can also be used. Excised intestinal segments from animals (most commonly rats) or humans can be mounted on an Ussing chamber, and effective permeability can be calculated. Rat tissues are more commonly used than human tissues because human tissues are scarce. This approach is beneficial because it incorporates flow as well as an intact membrane and maintains transport polarity.[61] The effective permeability rates calculated from rat tissues correlate very well with human jejunal permeability values.[52] It is, however, a laborious approach.

When the BCS was first introduced, cellular permeability of a test drug was compared with that of metoprolol.[62] As experiments progressed, however, it became readily apparent that metoprolol is an extremely permeable compound, and its usage resulted in many false negatives. The FDA now includes a list of potential model drugs representing high absorption, though pharmaceutical companies may select other drugs provided the mechanism of absorption is passive permeability and reliable human absorption data are available. To confirm the reliability of an in vitro permeability method, the sponsor should demonstrate a rank order between the permeability rate values determined via the method and human absorption values using high-, intermediate-, low-, and zero-permeability/absorption model drugs. A full list is provided in the FDA guidance.[49]

4.06.3.3 Approval of BCS Class 1 Classification

The FDA Center for Drug Evaluation and Research (CDER) has created a BCS committee that approves submissions for drugs to be officially given a class 1 assignment. Solubility criteria are well standardized, but permeability can be confirmed in a variety of manners, as listed in the preceding text. The most commonly submitted permeability evidence comes from mass balance studies, followed by Caco-2, absolute bioavailability, RLD label, and then rat intestinal perfusion.[63]

The BCS was developed and is successfully used to provide biowaivers for some highly soluble compounds. Since its development, similar classification systems have been created to predict aspects of drug disposition (BDDCS) and clearance (ECCS,[64] ECCCS,[65] and CPathPred[66]).

4.06.4 Biopharmaceutics Drug Disposition Classification System

The BDDCS was initially proposed when Wu and Benet[67] recognized that compounds with a high passive intestinal permeability rate in the BCS were extensively metabolized, while drugs eliminated in an unchanged form in the urine or bile were primarily poorly permeable in the BCS. In this seminal publication, they suggested that extent of metabolism might serve as an appropriate surrogate for absorption and/or intestinal permeability when those data are unavailable, since the extent of metabolism is easier to assess than intestinal permeability/absorption, thus expanding the number of class 1 drugs available for a biowaiver. Importantly, the modified system was also used to predict drug disposition, especially when predicting when transport or metabolizing enzymes are clinically relevant, for which it is most appreciated today.

4.06.4.1 Introduction to BDDCS and Comparison With BCS

4.06.4.1.1 Metabolism as a surrogate for absorption

The extent of drug metabolism is often quantified during phase I pharmacokinetic/mass balance studies.[68] Tabulating absorption, on the other hand, requires invasive intestinal perfusion studies in man or portal blood sampling. Absorption is a prerequisite to enzymatic metabolism, which occurs intracellularly in the endoplasmic reticulum or cytosol. Therefore, we can assume that enzymatically metabolized drugs are absorbed. Since metabolism is easier to quantify than absorption/intestinal permeability rate, Wu and Benet proposed that metabolism be used as an alternative measurement to predict absorption. The EMA and recently the FDA[49] have incorporated this suggestion into the guidance recommendations for granting biowaivers, and highly soluble compounds with $\geq$85% metabolism are eligible for biowaivers.

The BDDCS differs from the BCS in two major aspects: (1) the primary goals of the systems and (2) the definition, interpretation, and relationship of "highly permeable drugs."

4.06.4.1.2 Primary goals of the classification systems

The primary goal of the BCS is to grant biowaivers using in vitro methodology to predict drug absorption and its limiting steps. Alternatively, while the BDDCS provides the basis for recommending biowaiver extension to extensively metabolized compounds, the primary goal of the BDDCS is to predict drug disposition.

4.06.4.1.3 Differences in defining permeability

Via application of the BCS, biowaivers are granted based on extent of absorption, which may not always correlate well with intestinal permeability rate. A high permeability rate necessitates drug metabolism as we will discuss later. While high permeability rate also predicts a high extent of absorption, the opposite is not necessarily true. There are many examples of highly absorbed drugs that have a poor passive permeability rate, not reflecting their high absorption extent.[69,70] For example, sotalol, a BDDCS class 3 drug, is poorly permeable in Caco-2 cells, but has an absolute bioavailability of 98%, and thus is highly absorbed.[71–73] Its high absorption is likely mediated by transport[74] since it has a poor in vitro permeability rate, but is a substrate for the gut uptake transporter OATP1A2.[75] While some drugs are considered highly permeable in the BCS because of their high absorption, they are not, in fact, highly permeable in terms of rate measures. This is, in fact, the basis of a major difference between the BCS and BDDCS. Specifically, BCS class 1 and 2 compounds may be class 3 or 4 in the BDDCS, since drugs are classified by metabolism extent, and not absorptive extent. These differences are crucial in predicting drug disposition.

4.06.4.1.4 Development of and dispositional predictions by BDDCS

The BDDCS predicts when disposition is driven by metabolizing enzymes *versus* drug transport or when both are important, especially when transport regulates metabolism in transporter–enzyme interplay. When the BDDCS was initially developed, predictions were made for the gut and the liver. It has since been extended to transporter effects in noneliminating organs such as the brain.

Wu and Benet serendipitously recognized that high-permeability rate drugs were extensively metabolized, while low-permeability rate drugs were primarily eliminated as unchanged drug in the bile and the urine. They were simultaneously carrying out studies involving the transport of metabolized drugs and noticed that they did not recognize any clinically significant transporter interactions for BCS class 1 drugs. They therefore proposed that extent of metabolism and solubility might reflect other aspects of drug disposition, including the clinical relevance of drug transport. The BDDCS therefore classified drugs by their extent

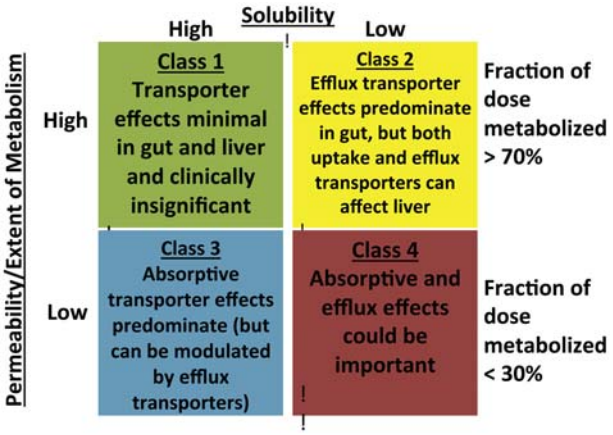

Fig. 3 Biopharmaceutics Drug Disposition Classification System and predicted transporter effects.

of metabolism and solubility (Fig. 3), where each class is associated with a series of predictions that will be thoroughly discussed. Initial applications included predicting when transporters, metabolizing enzymes, or the interplay between the two had clinically meaningful impacts on systemic concentrations and presystemic drug concentrations (after oral dosing), major routes of elimination and therefore drug–drug interactions, pharmacogenomics, and food effects in the intestine and liver.[67] Since then, the BDDCS has been expanded to understanding the effect of end-stage renal disease[76] on hepatic elimination and distribution across the blood–brain barrier. Hypotheses regarding toxicity, drug-induced liver injury (DILI), and clinical relevance in other tissues including the kidney will be discussed.

4.06.4.1.5 Value and appropriate uses of BDDCS

The BDDCS is invaluable during drug development because understanding the effect of transport and metabolizing enzymes is now essential for drug approval. Specifically, new drug applications must include the major routes of drug elimination, the quantitative contributions of enzymes and transporters, and drug–drug interaction studies.[8] The BDDCS can alert developers to which enzymes and transporters are likely important and may even justify negating some studies.

The BDDCS does not predict quantitative values of drug disposition. It can, however, provide qualitative information about the absorption of some compounds, the extent of metabolism, the extent of biliary or renal elimination of unchanged drugs, and distribution. More accurately, it predicts what processes, that is, transport at specific membranes and/or metabolism, will affect each aspect of disposition and the direction of the effect.

4.06.4.1.6 How are interactions defined?

Defining which enzymes and transporters are important in the disposition of a drug can be a cumbersome, though necessary, process. The FDA provides guidance to drug companies regarding appropriate methods to determine substrate, inhibitor, or inducer potential that may influence the safety of a drug prior to approval.[8] It initially consists of determining if a drug is a substrate, inhibitor, or inducer of a transporter or enzyme in vitro. For those drugs with positive identification in vitro, follow-up in vivo studies are conducted. Interactions are considered meaningful if they are "sufficiently large to necessitate a dosage adjustment …"[8] Full drug–drug interaction predictions are outside of the scope of this article.

4.06.4.1.6.1 Pillars of BDDCS

The BDDCS predicts when a transporter or a metabolizing enzyme can clinically regulate the disposition of a drug, whether or not the drug is a substrate. When the BDDCS predicts that drug transport at a membrane is not clinically relevant for a particular drug, it does not presume that the drug is not a substrate for a transporter. In fact, it is likely that almost all drugs are substrates for transporters. Instead, the BDDCS predicts if a transporter significantly contributes to the disposition of a drug compared with passive diffusion. These effects are perhaps most obvious in clinical studies examining the effect of transport inhibition on drug absorption, distribution, metabolism, and elimination. In cases where a transporter or metabolizing enzyme is important in a drug's disposition, affecting one, for example, by inhibiting transport, can cause clinically significant pharmacokinetic changes to elimination, bioavailability, or distribution, observed as changes in the plasma concentration versus time curve (AUC, C_{max}, t_{max}) and altering the parameters CL, V, and F that define dose. These changes may impact the safety or efficacy of the drug, resulting in a dose change. If inhibition of transport does not cause dispositional changes severe enough to necessitate a dosage change, the transporter is not considered clinically significant in the drug's disposition. The BDDCS predicts that extensively metabolized/highly soluble class 1 drugs are not *clinically relevant* substrates of drug transporters, even if in vitro evidence shows an affinity. In other words, while these drugs may have a biochemical affinity to transporters, the contribution of the active transporter to permeation across a membrane is minor compared with passive permeability, and any functional discrepancy of the transporter will not result in a significant change

that requires dose adjustment to achieve safety or efficacy. For class 1 drugs, in vitro studies will provide a false-positive predicting interaction, and studies in vivo or in humans are unlikely to replicate these results.[77] In vivo or clinical interaction studies are costly and time-restrictive. The FDA guidance recommends that P-gp and BCRP be evaluated as transporters for every drug, yet acknowledges that it may not be necessary for BCS class 1 drugs and sponsors may submit class 1 drugs without transporter data.[8] This would more appropriately be acknowledged for BDDCS class 1 drugs, since some BCS class 1 drugs (e.g., sotalol) may be subject to transporter interactions.

Furthermore, the BDDCS does not presume to predict that there *will* be an interaction for every drug in a class, but rather that an interaction *could* exist and should be tested during development. Finally, the BDDCS makes no predictions regarding inhibitor or inducer status.

4.06.4.1.6.2 Drugs as victims and perpetrators

Importantly, even if a transporter or metabolizing enzyme does not clinically affect the disposition of a drug, it does not mean that the drug cannot affect those transporters or metabolizing enzymes. In other words, the BDDCS predicts if a drug can be a victim of a drug interaction, but not whether or not it can be a perpetrator. Consider verapamil. Verapamil is a BDDCS class 1 drug and a P-gp substrate in vitro. As you will see throughout this article, inhibition of transport does not affect the disposition of class 1 drugs. Therefore, when P-gp is inhibited by quinidine, for example, the dispositional change is not severe enough to warrant a dosage change of verapamil. However, verapamil is a moderate inhibitor of P-gp. When verapamil is coadministered with digoxin, a BDDCS class 3 P-gp substrate, it inhibits P-gp, causing the plasma AUC of digoxin to spike into toxic concentrations. Digoxin then requires a lower dose.

4.06.4.2 Role in Predicting Absorption

4.06.4.2.1 Processes affecting absorption

The stomach and enterocytes are the body's initial security screening. The gastrointestinal environment is a harsh habitat. The pH in the stomach is so acidic that a mucosal layer protects the stomach lining. The stomach is responsible for initially grinding and dissolving oral tablets and regulating the release of its contents to the intestine. In the stomach and intestine, the acidic pH and an ecosystem of microorganisms contribute to the breakdown of foods, so that nutrients can be absorbed. Readers who are familiar with the concepts of probiotic diets will understand that bacteria significantly contribute to the breakdown and metabolism of foods. Bacteria are also capable of degrading or metabolizing drugs. To nourish the body, enterocytes must allow entry to many molecules. However, anything we eat may also contain substances toxic to our body. To reduce the harmful impact of xenobiotics, enterocytes are equipped with metabolizing enzymes, which can change a xenobiotic into a generally less toxic and easy to secrete substance, and transporters, which can help pump xenobiotics back into the gut. Transporters may also aid in absorption of nutrients and xenobiotics. One such example is PEPT1, which not only is responsible for bringing oligopeptides in but also helps to absorb compounds such as cefadroxil, a β-lactam antibiotic.[78] Food, other drugs, and endogenous substrates can affect the environment in which the drug is dissolved with their intrinsic chemical properties (e.g., percent fat, pH, and water content), as well as by stimulating physiological changes in the gut and stomach. They may also interact with transporters and metabolizing enzymes, which can regulate the rate and extent to which a drug is absorbed. Factors such as pharmacogenomics can likewise alter drug absorption.

4.06.4.2.2 Requirements of absorption and predicting absorption

For an orally administered drug to be effective at a peripheral location, the drug must obviously be well absorbed. This is, in fact, one of the major barriers during drug development, since oral administration is preferred due to compliance, convenience, and stability reasons. Predicting absorption is therefore very important when selecting drug candidates. As an addendum to the prediction that high passive permeability rate predicts extensive absorption, the BDDCS also predicts that extensively metabolized class 1 and 2 drugs are well absorbed.

As we have just discussed, high-permeability rate compounds are both extensively metabolized and well absorbed from the gastrointestinal tract. However, not all well-absorbed compounds are highly permeable. In other words, the BDDCS predicts that extensively metabolized class 1 and 2 drugs must be well absorbed, but offers no prediction of the extent of absorption of poorly metabolized, poorly permeable class 3 and 4 compounds, which can exhibit highly variable extents of absorption.

4.06.4.2.3 Transporter effects in the gut

4.06.4.2.3.1 Apical uptake

BDDCS class 1 and 2 drugs can so readily permeate enterocytes that gut apical uptake transporters have only a minor contribution to their absorption. Therefore, the BDDCS predicts no effect when uptake transporters are affected for highly permeable compounds since class 1 and 2 can enter enterocytes unaided by transporters.

Class 3 and 4 drugs are poorly permeable and require active uptake transporters to be absorbed, and therefore, alterations to their activity or expression will result in clinical differences in absorption and bioavailability. Specifically, decreased uptake transport functionality results in decreased absorption and increased function with increased absorption. Uptake transport in the gut must therefore be evaluated for BDDCS class 3 and 4 drugs.

4.06.4.2.3.2 Gut apical efflux and transporter–enzyme interplay

Apical efflux transporters counteract net xenobiotic absorption from the gut. Apical efflux transporters include P-gp, MRP2, and BCRP.[79] After a drug is absorbed into an enterocyte, substrates for apical efflux transporters are pumped back into the gut, reducing the effective absorption. Not only can efflux transporters affect parent drug absorption, but also they can regulate the extent of metabolism of some drugs:

- BDDCS class 1 drugs are clinically unaffected by changes in transporter expression or activity in the gut, even if they are substrates. These drugs will be affected only by changes in metabolism, and the degree of metabolism is unaffected by transporters.
- BDDCS class 2: Apical efflux transporters can have a clinical impact on the absorption of class 2 drugs. When efflux is inhibited, an increase in absorption may be observed. BDDCS class 2 drugs are in a unique position because efflux transporters in the gut can impact both their parent drug availabilities and their intestinal metabolism. Wacher and coworkers[80,81] discovered that inhibition of P-gp, even in the absence of CYP3A4 inhibition, decreases intestinal CYP3A4 metabolism, since CYP3A4 accounts for approximately 70% of CYP expression in the gut.[82,83] One might expect that inhibiting efflux in the gut would increase metabolism by forcing a drug to interact with metabolizing enzymes for longer. One might also expect that metabolism would not be affected, but that inhibiting efflux would increase absorption and therefore bioavailability. However, because CYP3A4 and P-gp are coregulated and share so many substrates,[84] P-gp substrates are also likely to be metabolized by CYP3A4. Metabolizing enzymes are located just below the microvillus border in enterocytes.[85] P-gp and CYP3A4 work in concert to eliminate the parent drug from the body. Efflux transporters recycle xenobiotics that have not yet been metabolized by CYP3A4, pumping them back into the gut lumen and allowing them to be absorbed multiple times, giving the drug not only multiple opportunities for drug exposure but also multiple opportunities for metabolism, a process called enzyme–transporter interplay. Therefore, when an enteric efflux transporter is inhibited, a class 2 drug may have decreased metabolism and increased bioavailability greater than would be expected by inhibiting absorption alone. This is specific to enterocytes, and inhibition of efflux transporters in hepatocytes leads to increased concentrations of parent drug and increased metabolism.
- BDDCS classes 3 and 4: Apical efflux transporters play a protective role against poorly permeable class 3 and 4 drugs by effectively limiting absorption of poorly permeable drugs that are substrates for an efflux transporter. Class 3 and 4 drugs that are substrates of apical efflux transporters may see an increase in drug absorption when these efflux transporters are inhibited.

4.06.4.2.3.3 Gut basolateral transporters

Little has been explored regarding basolateral transporters expressed on the enterocyte.[79] It is unlikely that basolateral efflux is extremely important since concentrations in the portal vein will be very low compared with the cell, encouraging passive diffusion. Apical uptake transporters may be necessary for more hydrophilic class 3 and 4 drugs to enter the cell, but leaving the cell requires passage through the hydrophilic portion of the membrane and is likely not a limiting factor.

4.06.4.2.3.4 Effects on absorption rate: flip-flop kinetics

When a drug is given as an extended-release formulation, absorption rate is often slower than elimination. Alternatively, the absorption of an immediate-release drug is generally a relatively quick process compared with elimination. For most immediate-release drugs, elimination is the rate-limiting step. However, a very small number of immediate-release drugs exhibit flip-flop kinetics, where the rate of absorption is the rate-limiting step in the disposition of a drug, instead of elimination. Flip-flop kinetics may be a developmental concern when a compound is poorly permeable/poorly metabolized and also has a relatively short $t_{1/2}$, specifically if it is shorter than gastrointestinal transit time. For drugs displaying flip-flop kinetics, the terminal slope of the systemic concentration–time curve actually reflects absorption processes because absorption rate is not limited for highly permeable/highly soluble drugs. We expect that only class 3 and 4 drugs would demonstrate flip-flop kinetics. Specifically, the absorption rate is probably limited by the affinity to and velocity of gut uptake transporters. Garrison et al. recently evaluated this hypothesis.[80] For 19 drugs exhibiting flip-flop kinetics, 16 were indeed class 3 or 4. While the absorption of class 2 drugs is unlikely limited by uptake transporters, their absorption may be slow as a result of poor dissolution, and very slowly dissolving class 2 drugs may display flip-flop kinetics, but very few examples of this phenomenon have been found.[80]

4.06.4.2.3.5 Pharmacogenomics affecting absorption

Genetics can directly impact a person's ability to absorb a drug. For instance, patients with inflammatory bowel disease have increased MRP1 expression in the intestine,[81] which can result in decreased absorption of class 2, 3, or 4 drugs. Genetic differences within healthy populations can also result in variation in absorption. The variant SLCO2B1*3, which codes for OATP2B1 and has decreased uptake activity, has an allele frequency of 30.9% in Japanese.[82,83] When fexofenadine, a BDDCS class 3 drug, was dosed to a Japanese population, those with the allele had a 37% lower AUC than those without the allele, indicating that genetic differences can impact drug absorption. Alternatively, there was no significant difference observed in AUC when midazolam, a class 1 drug, was dosed.[84] Genetic differences are sometimes highly related to race, highlighting the importance of selecting an appropriate population of healthy volunteers representing common genotypes for dosing in certain countries. Genetics, expression, and activity of metabolizing enzymes and transporters can directly impact absorption and other dispositional functions of a drug and increased or decreased functionality follow the predictions outlined for each class.

4.06.4.2.4 Non-transport-mediated interactions affecting drug absorption

Finally, concomitant food, drug, or supplement administration can potentially alter drug solubility. For instance, some tyrosine kinase inhibitors (TKIs), which are anticancer agents, or the malignancy itself, can cause gastric distress such as gastroesophageal reflux disease. To combat this unpleasant side effect, many patients take proton pump inhibitors, which increase gastric pH. Unfortunately, this can have the effect of decreasing the solubility of some of these weakly basic TKIs, thereby decreasing drug absorption.[85] Yago et al.[86] showed that absorption, presumably by improving drug solubility, could be improved in healthy volunteers with elevated gastric pH (hypochlorhydria) by predosing betaine hydrochloride, which acidified the stomach prior to dosing the TKI dasatinib. Solubility-based drug interactions are likely to affect poorly soluble BDDCS class 2 and 4 drugs only, since the solubility class is defined by the lowest solubility condition possible in the stomach and gut.

Food can have a significant impact on drug absorption by influencing drug solubility and active absorption. The complex interactions with food will be thoroughly covered in section "**Complex considerations: food effects**."

An orally administered drug must be able to bypass a significant degree of gut and hepatic metabolism to be systemically available. Additionally, metabolism is also very important in mediating drug elimination once the drug has entered systemic circulation for both orally and non-orally administered drugs.

4.06.4.3 Role in Predicting Metabolism and Hepatic Elimination

4.06.4.3.1 Metabolism in the gut

The majority of drug metabolism occurs after drug absorption. While metabolizing enzymes are expressed to a significantly smaller extent than in the liver, the gut wall contains relatively high concentrations of metabolizing enzymes compared with other organs. Gut metabolism (F_G) is a component responsible for decreasing a drug's bioavailability. Gut metabolizing enzymes are also frequently responsible for the bioactivation of prodrugs.

CYP3A is only expressed at 1.4% of the level found in hepatocytes,[87,88] but accounts for 70–80% of CYP expression in the gut,[87] and more than 50% of drugs eliminated by metabolism are substrates for CYP3A4[89] and may be presystemically metabolized. As a low-affinity, high-capacity enzyme, it may be particularly susceptible to drug concentration differences,[90] influenced by permeability, transport, or solubility.

The BDDCS predicts that highly permeable BDDCS class 1 and 2 drugs will be metabolized and thus may be subject to intestinal metabolism, which may contribute to a possible reduction in bioavailability. Alterations in gut metabolism may significantly change the bioavailability of these compounds. When metabolism is inhibited, these compounds are predicted to be significantly more available to the systemic circulation and may require a smaller dose. Poorly metabolized class 3 and 4 drugs are unlikely to be metabolized in the gut. Metabolism may not significantly contribute to reduced bioavailability of these compounds. Therefore, they may not experience significant pharmacokinetic changes when intestinal metabolism is inhibited or induced and will not require dose adjustments.

Genetic differences in expression or activity of a metabolizing enzyme or transporter can significantly impact the metabolism or elimination of drugs. For example, a significant percentage of people are poor CYP2C19 metabolizers. Therefore, when a CYP2C19 substrate is prescribed, we would expect increased exposure in these patients. In fact, poor metabolizers have greater acid suppression and ulcer healing than extensive metabolizers when they take proton pump inhibitors such as omeprazole as a result of their increased exposure.[91]

When the BDDCS was developed, a primary observation was that there was a very dichotomous extent of metabolism. Drugs tend toward a primary route of elimination. Specifically, metabolism tends to contribute $>70\%$ of total drug elimination for extensively metabolized drugs or $<30\%$ for drugs that are eliminated as unchanged drug. There are few examples of drugs being eliminated with an intermediate extent of metabolism.

4.06.4.3.2 Hepatic basolateral uptake

After oral absorption, the liver is the first organ to process drugs and so hepatic transport is important. Hepatic drug exposure is often regulated by hepatic basolateral uptake. While at least seven major transporters (OATP1B1, OATP1B3, OATP2B1, NTCP, OCT1, OCT3, and OAT2) and the bidirectional transporters ENT1, ENT2, OAT7, OCTN2, and OSTα-OSTβ facilitate hepatic distribution, the FDA considers OATP1B1 and OATP1B3 to be the most clinically relevant[8] and recommends evaluating hepatically eliminated drugs for their potential to interact with these transporters as substrates, inhibitors, or inducers.

As in the gut, the BDDCS predicts that uptake transport will be clinically irrelevant for class 1 drugs. The BDDCS predicts that hepatic basolateral uptake transporters may play a significant role in class 2 drugs, which differs from predictions for the gut, and are necessary for hepatic exposure of poorly permeable class 3 and 4 drugs. The gut has "leakier" membranes (composed of epithelial cells) than the liver, which is composed of endothelial cells. This may possibly explain the difference in observed uptake transporter effects for class 2 drugs.[68]

Metabolism in hepatocytes is the major eliminating mechanism of class 1 and 2 drugs. Since class 1 and 2 drugs are extensively metabolized and a substantial portion of metabolism occurs hepatically, it follows that hepatic transporters (for class 2 drugs) and/or metabolizing enzymes (for class 1 and 2 drugs) will be significant determinants in their disposition.

Class 1: Class 1 drugs do not depend on uptake for their hepatic access and transporters will have no impact on their disposition.

However, hepatic metabolizing enzymes mediate the majority of elimination of class 1 drugs and their function will affect the

disposition of class 1 drugs. If a hepatic metabolizing enzyme contributing to the clearance of a class 1 compound is inhibited, drug exposure (AUC) is expected to increase, and a lower dosage may be required to avoid toxicity. Alternatively, if the metabolizing enzyme is induced, clearance may be greater than expected, resulting in poor exposure and a potential for drug inefficacy.

Example: St. John's wort is an herbal supplement sometimes taken as an antidepressant. It also acts as an inducer of CYP3A4[92–94] and CYP1A2.[95] In numerous cases, drugs including the anticoagulant warfarin,[96] the immunosuppressant cyclosporine,[97–99] some oral contraceptives, and the HIV protease inhibitor indinavir[100] have seen decreased plasma concentrations or reduced drug-efficacy outcomes when a patient is also taking St. John's wort, presumably as a result of metabolizing enzyme induction. If a patient has a lower drug concentration than expected, it can lead to serious problems with drug efficacy. If, for instance, the efficacy of warfarin is compromised, INR levels can decrease, which indicates quick blood clotting and is potentially life-threatening. Inefficacy of immunosuppressants can instigate organ rejection, while inefficacy of HIV protease inhibitors could potentially see an increase in HIV viral load.

Class 2: The systemic and metabolic disposition of class 2 drugs can be affected by both transport and metabolism. For BDDCS class 2 drugs, the BDDCS predicts that decreased function of a hepatic basolateral uptake transporter may result in increased portal vein concentrations and decreased hepatocyte concentrations. Subsequently, when uptake is inhibited, metabolism in hepatocytes may be decreased, while induction may lead to increased metabolism. Obviously, when metabolism is inhibited, there may be increased plasma or hepatic concentrations of parent drug and decreased elimination.

Classes 3 and 4: Class 3 and 4 drugs are primarily eliminated by either renal or biliary elimination of unchanged drugs. We expect that the poorly permeable class 3 and 4 drugs require a transporter to enter hepatocytes, while biliarily eliminated drugs require active canalicular efflux into the highly concentrated bile. Thus, especially if a compound is biliarily eliminated, inhibition of uptake transporters in the liver may result in increased AUC and increased half-life as a result of decreased clearance. However, since inhibition of hepatic uptake transporters will usually also decrease volume of distribution for hepatically eliminated compounds,[101] the increase in half-life will not be as great as the decrease in clearance. A lower dose may be required for biliarily eliminated compounds whose hepatic uptake has been inhibited.

For instance, rosuvastatin and pravastatin are primarily eliminated as unchanged drug in the bile. They are clinically relevant substrates of OATP1B1, and polymorphisms in the gene encoding OATP1B1, SLCO1B1, or drugs inhibiting 1B1 have been shown to increase plasma concentrations and decrease hepatic concentrations of these drugs.[102,103] Not only does this decrease the efficacy of these statins,[104] whose mechanism of action is in the liver, but also it increases the risk of rhabdomyolysis, a severe muscle toxicity.[105]

4.06.4.3.3 Hepatic apical efflux

Apical efflux transporters regulate parent drug and metabolite entry into the bile. Apical efflux transporters in the liver can contribute to the disposition of some class 2, 3, and 4 drugs. Drugs that are eliminated as parent drug in the bile must be actively transported into the bile by canalicular efflux transporters and follow bile flow through the biliary tree until the biliary contents are dumped back into the duodenum. Some drugs, especially highly permeable class 1 or 2 drugs, may be reabsorbed through the gut. Sometimes, when this happens, the plasma concentration–time curve will show two or more peaks. This process is called enterohepatic recycling, which helps conserve bile salts and, in this case, drugs. Drugs that are not reabsorbed in the gut will be eliminated in the feces. Apical efflux can regulate biliary efflux as well as hepatic retention.

Class 2: When apical efflux is inhibited, concentrations in hepatocytes are increased. For class 2 drugs, this may result in increased metabolism. However, apical efflux inhibition in the gut results in the opposite effect: decreased metabolism. We hypothesize that this is because the drug is exposed to the apical transporter after metabolizing enzymes in the hepatocyte, while the drug interacts with efflux transporters prior to metabolizing enzymes in the gut.

Classes 3 and 4: It has been hypothesized that canalicular efflux does not contribute to the systemic clearance of poorly metabolized drugs.[64] If this is true, there will not be increased exposure of class 3 and 4 drugs. In this case, decreasing the dose may not be necessary to reduce toxic systemic exposure. However, accumulation within hepatocytes sometimes mediates hepatotoxicity, and a decreased dose may be required for this mechanism. There is a paucity of data regarding the effect of apical efflux inhibition on systemic concentrations.

Many parent drugs and metabolites may be (initially) eliminated in the bile. Upon inhibition of biliary efflux, class 2, 3, and 4 drugs may potentially accumulate in hepatocytes. Accumulation of drugs in hepatocytes sometimes leads to DILI. This injury is generally mediated by metabolites. Fortunately, compensatory mechanisms such as increased expression or activity of basolateral efflux transporters can pump some drugs back into the circulation to reduce the chance of injury. Additionally, while it has been generally presumed that unbound concentrations were equivalent throughout the body, we now understand that transporters alter the unbound concentrations of drugs inside a cell. Therefore, since class 1 drugs are not clinically relevant substrates of transporters, pharmaceutical companies presumably have a better understanding of class 1 drug concentrations inside the liver. We therefore expect that DILI may be less of a problem for class 1 drugs or for poorly metabolized class 3 or 4 drugs, but may be a greater problem for class 2 drugs. This hypothesis is currently being investigated. Analogously, the BDDCS may potentially predict as to which drugs may be problematic when dosed to people with dysfunctional efflux transporters, such as in disorders such as Dubin–Johnson syndrome, where MRP2 is poorly functional.

4.06.4.3.4 Insights into metabolism from BDDCS

The BDDCS was pivotal in observing that drugs with a high intestinal passive permeability rate were also extensively metabolized. The rationale behind this observation is that highly permeable drugs, when excreted into hydrophilic secretions, that is, urine and bile, are rapidly reabsorbed due to the high concentration gradients. This gives the drug multiple chances at metabolism, until eventually the compound is changed to a generally more hydrophilic substance that resides in fluidic secretions. Data sets examining reabsorbed compounds support this hypothesis. In a data set published by Dave and Morris,[106] 82% of drugs that were reabsorbed from the kidney tubule were extensively metabolized drugs. In a data set published from Pfizer,[33] slightly more than half of the extensively metabolized drugs were reabsorbed from the kidneys compared with $<20\%$ of class 3 and 4 drugs.[77] Renal reabsorption is primarily a passive process driven by high tubular concentrations compared with the blood, though reabsorptive transporters are functional and can play a role. Analyzing this data set and using permeability rate values generated from the same group, higher permeability rate compounds tended to be reabsorbed, while lower permeability rate compounds were either passively filtered or secreted (ROC AUC $= 0.80$).

Highly permeable drugs might also be reabsorbed directly from the biliary tract. When phenolphthalein glucuronide was dosed directly into the bile and prevented from undergoing enterohepatic recycling, it was recovered in hepatocytes, indicating that reabsorption from the bile is possible.[107] The BDDCS predicts that if highly permeable BDDCS class 1 and 2 drugs are initially secreted into the bile, they will be reabsorbed. This reabsorption process means that drugs will eventually be metabolized as a necessary elimination step. This is particularly important for some low-clearance compounds such as diazepam, which are too lipophilic to remain in secretions.

Passive permeability, not active transport or the extent of absorption, correlates with the extent of metabolism. In this way, extensive metabolism can be predicted with immortal cell lines such as Caco-2 and MDCK, which express low transport levels, or even artificial membranes such as PAMPA. Artificial membranes do not express transporters and accurately reflect passive permeability. This reduces the need for human tissue in evaluating metabolism with microsomes, supersomes, or hepatocytes. Permeability rate does not necessarily correlate with metabolic clearance, however.

Hosey and Benet showed that the extent of metabolism can be predicted with either in vitro or in silico tools.[16] Extreme variability in permeability rate values persists between labs,[60] and therefore, numerical permeability rate cutoffs are incapable of predicting the extent of metabolism or absorption. As a solution to this variability, metoprolol has generally been regarded as a standard to determine high permeability rate.[62] Compounds exhibiting a permeability rate greater than metoprolol were predicted to be extensively metabolized and highly absorbed. However, metoprolol's permeability rate is restrictively high when measured in MDCK or Caco-2,[12,16,108] mispredicting many extensively metabolized drugs because they had lower permeability rates than metoprolol, and the alternative standards labetalol and zidovudine were assigned for Caco-2 and MDCK, respectively,[16] and correctly predicted more compounds across several data sets. While metoprolol was far too conservative to be an effective standard compound in Caco-2 or MDCK, it performs well as a standard in PAMPA.[16] Theophylline was selected as an optimal standard when permeability rate studies are conducted in PAMPA and is also too conservative in MDCK or Caco-2. While the BDDCS predicts that drugs that are highly permeable in vitro will be extensively metabolized clinically, and therefore subject to changes in metabolizing enzymes, in vitro systems are not interchangeable and unique protocols must be established for each.

From 20 data sets, $97 \pm 5\%$ of compounds with a permeability rate greater than metoprolol were extensively metabolized.[16] While most compounds with a permeability rate greater than the selected standards labetalol, zidovudine, or theophylline are extensively metabolized, in many cases, 20–25% of the compounds with a permeability rate lower than these standards are also extensively metabolized. Therefore, while high-permeability rate compounds are almost always extensively metabolized, not all extensively metabolized compounds have a high permeability rate. For increased predictability, a very low-permeability rate marker, chlorothiazide, was established. Most compounds with a permeability rate less than chlorothiazide's are poorly metabolized. The predictability of compounds with a permeability rate between chlorothiazide and the reference standard is only around 50%, however, and these compounds should be investigated in humans.[16]

4.06.4.4 Predicting Bioavailability

Bioavailability depends upon the extent of absorption, the extent of metabolism in the gut and the liver, and drug loss due to first-pass biliary elimination. In addition to understanding the metabolic component of bioavailability, all of these processes can potentially be affected by drug transport.

High absorption does not necessarily predict high bioavailability, especially since many highly absorbed drugs are also extensively metabolized. As such, the BDDCS predicts that highly permeable class 1 and 2 drugs will have good absorption, but not necessarily good bioavailability. There is a caveat to this prediction, however. The BDDCS assumes that metabolized compounds are absorbed compounds. However, there may be some compounds that are not metabolized by phase I or phase II metabolism, but by bacteria in the gut lumen. When over 900 drugs were classified into the BDDCS, extensively metabolized drugs were categorized regardless of the mechanism. However, this is a nascent field and few drugs are currently known to be metabolized in this manner.

Class 1: The bioavailability of class 1 compounds can be affected by metabolizing enzymes and inhibition of metabolism will increase the bioavailability.

Table 2 Effects of gut apical transporters on pharmacokinetic parameters

	Decreased functionality of apical uptake					*Decreased functionality of apical efflux*				
	F	k_a	t_{max}	C_{max}	*AUC*	F	k_a	t_{max}	C_{max}	*AUC*
Class 1	⇔	⇔	⇔	⇔	⇔	⇔	⇔	⇔	⇔	⇔
Class 2	⇔	⇔	⇔	⇔	⇔	↑	↑	↓	↑	↑
Class 3	↓	↓	↑	↓	↓	↑	↑	↓	↑	↑
Class 4	↓	↓	↑	↓	↓	↑	↑	↓	↑	↑

Class 2: Class 2 compounds can be affected by both transporters and metabolizing enzymes. Inhibition of efflux transporters in the gut can lead to increased absorption, decreased metabolism, and increased bioavailability. Inhibition of hepatic basolateral uptake may lead to decreased metabolism and increased bioavailability, while inhibition of hepatic basolateral efflux may lead to increased metabolism and decreased bioavailability. Inhibition of metabolizing enzymes may increase bioavailability.

Classes 3 and 4: Metabolism is not a significant factor in the bioavailability of class 3 and 4 drugs. However, uptake and efflux transporters can potentially regulate bioavailability in both enterocytes and hepatocytes. One would expect decreased bioavailability if an enteric uptake transporter responsible for a drug's uptake was inhibited due to decreased absorption. Conversely, inhibition of enteric apical efflux would result in increased absorption and bioavailability. However, first-pass biliary excretion may play a role. Hepatic uptake is generally considered the rate-limiting step of biliary elimination. Therefore, inhibited hepatic uptake of class 3 and 4 drugs would likely result in a decrease in biliary elimination and an increase in bioavailability. It has been suggested that hepatic canalicular efflux does not regulate systemic clearance, and therefore, inhibition of hepatic canalicular efflux would not likely have an effect on bioavailability; however, given the lack of clinical studies on biliary elimination, there are little data to confirm or deny this hypothesis.

In **Table 2**, we tabulate pharmacokinetic changes that may be expected when the function of an enterocytic drug transporter is decreased for any number of reasons including chemical inhibition from other drugs, food, or endogenous substrates and genetic mutations.

4.06.4.4.1 Complex considerations: food effects

4.06.4.4.1.1 Predicting food effects

Eating a meal can have a substantial impact on pharmacokinetics. In fact, many drug labels advise that the drug be taken either with a meal or separate from a meal. The act of eating causes a cascade of physiological changes in the gastrointestinal system. These can greatly affect the solubility and the transit time of the drug. In turn, the transit time can affect the exposure to intestinal fluids and membranes, as well as the location of drug-membrane exposure, where different segments of the intestine have different properties including membrane tightness, transporter, and metabolizing enzyme expression. Additionally, food, drinks, and supplements can have a biochemical impact on the drug, where components of each can serve as inhibitors of transport or metabolism. Obviously, the effect of food on pharmacokinetics is a multifaceted problem, which makes predicting food effects a priori quite difficult. However, some general predictions have been proposed using BDDCS principles.

Because food effects are multifactorial, predicting them is a very difficult problem. For one, food chemistry is extremely complex. Even a single food can have multiple molecular components that inhibit uptake, efflux, metabolism, or any combination, forcing a complex interaction. For example, grapefruit juice, famous for its ability to inhibit CYP3A4, is composed of many compounds, including flavonoids and furanocoumarins. Because of the complexity of the composition of a food or drink such as grapefruit juice, the mechanism of inhibition has to be sifted from many compounds. While flavonoids were initially expected to be the perpetrators of this interaction, it was ascertained that certain furanocoumarins are the culprits.[109] When taken with antihistamines such as terfenadine and astemizole, grapefruit juice increased drug exposure to dangerous concentrations that caused cardiotoxicity and, in some cases, death. Both drugs were eventually removed from the market. Many drugs metabolized by CYP3A4 are now labeled with cautions against consuming grapefruit juice. Additionally, components in grapefruit juice have been shown to inhibit uptake transporters[110] and P-gp.[111] Meanwhile, human gastrointestinal physiology is incredibly variable, as are the contents of the gastrointestinal tract. Baseline gastric efflux on a fasted or fed stomach and pH can vary markedly between humans. The microbiome, which can break down drugs, having a direct effect, or influence food digestion, causing an indirect effect, is signature to each person. Despite this complexity and variability, the BDDCS is able to predict the effects of food for approximately 70% of drugs.[112]

4.06.4.4.1.2 Physiological responses to meals and their dispositional impact

After eating, some physiological changes occur that can result in dispositional changes to drugs. The predicted dispositional changes as a result of physiological response to food, and more specifically high-fat meals, are tabulated in **Table 3**.

4.06.4.4.1.3 Biochemical inhibition

Components in high-fat meals (a high-fat meal contains 800–1000 calories with 50–65% from fat and 25–30% from carbohydrates and 15–20% protein[125]) may inhibit intestinal transport. Lipids consumed, monoglycerides and fatty acids liberated during fat

Table 3 Dispositional impacts due to physiological changes after a meal

Physiological change	*Effect on absorptive component*	*Class 1*	*Class 2*	*Class 3*	*Class 4*
Gastric fluid increases from 300–500 to 800–900 mL, while intestinal fluid volume increases from 500 to 900–1000 mL[113–115]	Increase volume for drug dissolvation and solvent drag		F ↑		F ↑
Phospholipids and bile salts increase four- to fivefold[116,117]	• Bile salts increase breakdown of fats into monoglycerides • Bile salts inhibit P-gp • Bile salts inhibit uptake • Bile salts increase solubilization • Monoglycerides and lipids liberated by bile salts can inhibit uptake and efflux as well	F ⇔	F ↑	F ↑↓⇔ The majority of class 3 drugs will exhibit decreased F due to inhibition of uptake	F ↑↓⇔
pH decreases with some foods such as juices	Weakly acidic drugs have decreased solubility, while weakly basic drugs have increased solubility	F ⇔	F ↓ for acidic drugs F ↑ for basic drugs	F ⇔	F ↓ for acidic drugs F ↑ for basic drugs
pH generally increases with food	Decreases solubility for weakly basic drugs[115,118]		F ↓ for basic drugs F ↑ for acidic drugs		F ↓ for basic drugs F ↑ for acidic drugs
Splanchnic blood flow is increased	Improve bioavailability[115,119]	F ↑	F ↑	F ↑	F ↑
Gastric emptying is delayed	• Increases time before drug can be absorbed in the gut	t_{peak} ↑	t_{peak} ↑	t_{peak} ↑	
	• Increases interactions with gastric acid, which may contribute to drug decomposition[51,120]	F ↓	F ↓	F ↓	F ↓
Gastric secretions including bile are increased by up to fivefold[121]	• Increased bile volume allows for increased micellular solubilization and increased drug wetting of poorly soluble drugs • Increased bile concentrations • Break down fats into lipids • Bile salts and lipids can interfere with drug transport[122–124] • Aggregation into micelles that help with solubilization		F ↑		

digestion, and bile salts released to aid in digestion have all been shown to inhibit transport, especially that of P-gp[115,122–124,126] but also of uptake.[115]

Components in any food, whether or not it is part of a high-fat meal, have the potential to serve as biochemical inhibitors of transport or metabolism and, if consumed daily, inducers. Certain fruit juices, teas, beer, and wine can cause biochemical inhibition of transporters and/or metabolites. For instance, orange, grapefruit, and apple juice have been shown to inhibit OATPs and P-gp in the gut.[110,111,127]

The specific inhibitors in food can be quite difficult to identify since foods contain small concentrations of many compounds and compounds may have an additive effect.

4.06.4.4.1.4 Chemical solubility effect

Drug solubility depends on the pH of fluid, temperature, volume, and contents of fluid. The lipophilicity of a drug is also correlated with water solubility. The rate and extent of absorption can be altered by food.

Factors that increase the amount of drug solubilized are particularly important for BDDCS class 2 and 4 drugs, whose absorption is limited by their poor solubility. Foods can increase solubility by increasing the volume into which a drug can be solubilized, changing the pH of the fluid, and increasing concentrations of bile salts four- to fivefold.[116,117] After a meal, the volume of intestinal fluids increases two- to threefold, which can potentially increase the amount of drug that is solubilized, meaning more drugs may be available for absorption. Bile salts can improve the solubility of some drugs by acting as surfactants.[128] Changes in the pH of gastrointestinal fluids can alter the solubility of drugs. Acidic drugs will be more poorly soluble in acidic media, while basic drugs will lose solubility in basic media and vice versa.

4.06.4.4.1.5 Overall predicted food effects after consuming high-fat meals for each BDDCS class

Class 1: The overall extent of bioavailability is unlikely to change for BDDCS class 1 drugs since increasing solubility will have no effect and class 1 drugs are not subject to transporter inhibition. Since gastric emptying will be delayed after eating, however, these drugs may be more slowly absorbed, and t_{peak} may be later.

Class 2: When class 2 drugs are administered with a high-fat meal, the bioavailability will likely increase, while time to reach peak concentrations may shift in either direction.

High-fat meals may inhibit P-gp, resulting in increased bioavailability. As we discussed earlier, P-gp inhibition can also limit intestinal metabolism of BDDCS class 2 drugs. Therefore, by decreasing both efflux and metabolism, BDDCS class 2 drugs are likely to be more bioavailable when P-gp is inhibited. Additionally, fatty food and the release of bile acids can form micelles, promoting drug solubilization.

The time to reach a maximum concentration for a class 2 drug can be affected by a multitude of factors, and no single trend is predicted. By delaying gastric emptying, a high-fat meal can increase the amount of time it takes for the drug to be absorbed in the intestine, increasing t_{peak}. The time to reach a maximum concentration may also decrease due to the inhibition of efflux cycling by high-fat meals. Additionally, these processes may compete, causing no effective change in t_{peak}.

Class 3: High-fat meals, bile salts, and chemical components in food can inhibit intestinal uptake transporters, which class 3 drugs rely on to be absorbed. Patients taking a poorly permeable class 3 drug might experience decreased bioavailability and poor exposure when the drug is administered with a high-fat meal. Because their uptake is inhibited, the time to reach C_{max} may also increase. T_{peak} may also increase as a result of delayed gastric emptying after a high-fat meal.

Class 4: BDDCS class 4 drugs are very difficult to predict because of many interacting effects including increased solubility, increased gastric emptying time, and inhibited uptake. With so few class 4 drugs, it is difficult to predict a single trend.

4.06.4.5 Role in Predicting Distribution

Wu and Benet[67] observed that the volumes of distribution were somewhat higher in the highly permeable class 1 and 2 drugs compared with those for class 3 and 4 drugs.

Transporters can markedly affect the volume of distribution by concentrating drug in tissues. When certain major transporters in the liver or kidney are inhibited, Grover and Benet[101] noticed certain trends in distribution.

The liver has a primary effect on the volume of distribution. In peripheral tissues, altered transporter function may have a pharmacodynamic effect and the compound may be attenuated in tissues, but the calculated volume of distribution does not appear to change.

When hepatic uptake is inhibited, there is an increase in plasma concentration coupled with a decrease in hepatic distribution, leading to a decrease in volume of distribution. When hepatic efflux is inhibited, there is also a decrease in the volume of distribution (or is not predictable). Inhibition of hepatic basolateral efflux results in an increase in the volume of distribution.

However, when renal uptake is inhibited, there is generally no effect on the volume of distribution. When renal efflux is inhibited, the volume of distribution often increases. Grover and Benet hypothesize that the discrepancy between changes in volume of distribution due to inhibition of uptake in the liver versus the kidney is likely a result of the larger mass of the liver, coupled with increased capacity for transporter expression and drug sequestration.[101]

Finally, gut transporters will not have an effect on the volume of distribution because volume of distribution is a systemic parameter.

Since class 1 drugs have no clinically relevant transporter effects, we expect no changes in the volume of distribution of class 1 drugs when a transporter has increased or decreased function or expression. Alternatively, since uptake and efflux transporters can affect class 2, 3, and 4 drugs in the liver, we would expect changes to the volume of distribution as described in the preceding text.

4.06.4.5.1 Distribution into the brain

Distribution to various tissues can be predicted by the BDDCS. Specifically, we now understand the conditions necessary for central nervous system penetration. This is a particularly difficult problem during drug development of central nervous system

(CNS)-targeted drugs, as the brain is well protected from xenobiotics with tight junctions and high efflux transporter expression. Understanding and predicting brain penetration are also important to avoid central side effects for a peripherally acting drug. P-gp, BCRP, and various MRPs are expressed on the apical membrane of brain capillary endothelial cells, poised to extrude drugs that gain entry across its membrane. In development, substrate specificity for efflux transporters is a cue that the drug will be unable to successfully penetrate the brain. When the brain is the intended site of action, lipophilic compounds with a low polar surface area are expected to be available to the CNS.[129,130]

The brain is also a particularly concerning tissue for drug resistance. Some diseases, including some cancers and epilepsy, are resistant to drug penetration in the brain as a result of overexpressed P-gp or other efflux transporters. This overexpression is sometimes innate to the disease and sometimes acquired, potentially due to drug treatment. To overcome drug resistance, some scientists have proposed codosing with efflux inhibitors. Alternatively, dosing class 1 drugs may be a more thorough and facile approach when brain concentrations are desired.

Mahar Doan et al.[129] suggested that highly permeable, non-P-gp substrates were likely to cross the blood–brain barrier, while poorly permeable and P-gp substrates are less likely to cross the blood–brain barrier. While this holds true for a majority of compounds, an analysis by Wager et al. revealed that 20% of CNS drugs were both poorly permeable and P-gp substrates.[131] Broccatelli et al.[132] incorporated BDDCS classifications, correctly predicting the CNS distribution of >90% of their data set. Ninety-eight percent of class 1 drugs in their data set were able to cross the CNS, whether or not they were a substrate for P-gp. In fact, after correcting for a misclassified drug, all of the BDDCS class 1 P-gp substrates were able to distribute into the CNS.[77,132] Even when P-gp was able to partially efflux the drug, there was significant brain penetration. In contrast, 75% of P-gp substrates in classes 2, 3, and 4 were unable to traverse the blood–brain barrier. While presumably all of the class 1 drugs have CNS exposure, even if they are P-gp substrates, clearly, 25% of P-gp substrates in other classes were still able to access the brain, likely because they are good substrates for uptake transporters at the brain. While Broccatelli et al. only considered P-gp substrate specificity,[132] other efflux transporters such as BCRP are expressed at the blood–brain barrier and are responsible for extruding drugs. The same principles should apply to substrates of other efflux transporters. Based on these findings, each class is predicted to behave as follows:

Class 1: Transporter effects are minimal and drugs are expected to penetrate the CNS.
Class 2: Efflux transporters at the blood–brain barrier may affect class 2 drugs.
Class 3: Uptake transporters at the blood–brain barrier (OATP1A2 and OATP2B1) are required for brain penetration, while efflux transporters can extrude drugs from the brain.
Class 4: Uptake transporters at the blood–brain barrier are required for brain penetration, while efflux transporters can extrude drugs from the brain.

Therefore, when developing a drug with a CNS indication, a class 1 drug may be preferable for candidate selection, since it will penetrate, regardless of transporter affinity. Class 2 drugs may be developable as long as they are not substrates for efflux transporters. Class 3 and 4 drugs have more stringent requirements. For a class 3 or 4 drug to be effective as a CNS agent, it must be a substrate for an uptake transporter in the gut (if it is orally administered) and at the blood–brain barrier and should not be a substrate for efflux transporters at the blood–brain barrier.

Alternatively, when developing peripherally acting drugs, class 1 drugs may have potential CNS side effects, even if they are substrates for efflux transporters. Class 2 drugs may have central effects if they are not substrates of efflux transporters. To avoid central effects for class 3 and 4 drugs, it is best to avoid substrates of uptake transporters at the blood–brain barrier. Non-class 1 drugs will need to be evaluated as substrates of CNS-expressed transporters to predict brain penetration. In **Table 4**, we show the predicted effects of apical transporters on CNS exposure.

Table 4 Effect of apical transporters on central nervous system distribution

BDDCS class	*Apical uptake*	*Apical efflux*	*CNS exposure*
Class 1	No effect	No effect	Yes
Class 2	• May be necessary for some class 2 drugs to penetrate the brain • Inhibition may lead to decreased CNS exposure	• May decrease CNS exposure • Inhibition may lead to increased CNS exposure	If a nonsubstrate for efflux and may possibly require an uptake transporter
Class 3	• Required for CNS exposure • Inhibition will lead to decreased CNS exposure	• Will prevent exposure to the CNS • Inhibition may lead to increased CNS exposure	If a substrate for an uptake transporter and a nonsubstrate for an efflux transporter
Class 4	• Required for CNS exposure • Inhibition will lead to decreased CNS exposure	• Will prevent exposure to the CNS • Inhibition may lead to increased CNS exposure	If a substrate for an uptake transporter and a nonsubstrate for an efflux transporter

4.06.4.5.2 Potential extensions to other membranes

While distribution and transporters regulating distribution outside of the gut, liver, and brain have not been analyzed with respect to BDDCS dispositional predictions, we expect that most internal tissues (composed of tightly regulated endothelial cells) will behave in a similar manner to the liver and brain and not like the epithelial-based gut. Therefore, we expect that class 1 drugs will distribute to a tissue regardless of transporter function, while class 2 drugs may be affected by the function of uptake transporters regulating drug entry and may have less tissue penetration if they are a substrate of a relevant efflux transporter. Class 3 and 4 drugs will almost certainly require active transport into the tissue, and their distribution will be significantly impacted by efflux transporters expressed in the tissue. For class 1 drugs, there may be some concern about undesired distribution to off-target organs. Scientists can potentially use this information to aid in drug delivery to target tissues, including the heart and skeletal muscles. Distribution across the placenta could also potentially be predicted, which may be advantageous because its distribution cannot be studied for ethical reasons.

4.06.4.5.2.1 Distribution to the kidney

As discussed earlier, renal elimination is a combination of passive filtration processes, reabsorption, and active secretion. Reabsorption is primarily passive, and the vast majority of water and solutes are reabsorbed along the tubule, resulting in only 1 mL of urine production every minute. There are transporters responsible for active reabsorption expressed primarily in the proximal tubule, however. While a number of secretory transporters are expressed along the proximal tubule, OAT1, OAT3, and OCT2 are currently considered the most clinically significant, and the FDA recommends studying renally eliminated drugs for interactions with these transporters.[8] All drugs should be evaluated as substrates of P-gp, as well. However, the ITC lists a number of renal transporters that they consider important to evaluate during drug development, including the bidirectional transporters ENT2, expressed on the basolateral membrane, and ENT1, OCTN1, and OAT4, expressed on the apical membrane. Secretory transporters including OAT2 and OATP4C1, which are expressed on the basolateral membrane, and MATE1, MATE2-K, MATE2, MRP2, and MRP4, all of which are expressed on the apical membrane, are considered relevant by the ITC. They also include the absorptive transporter URAT1, which is expressed on the apical membrane.

Class 1 and 2 drugs are likely to be reabsorbed from the tubule, as we have discussed. We expect that class 2 drugs may interact with basolateral uptake and apical efflux transporters, similar to hepatic predictions. We expect that uptake and efflux transport will be required to contribute to net secretion of class 3 and 4 compounds. However, renal elimination can also be completely passive, and class 3 and 4 compounds are not necessarily substrates of renal transporters even if they are eliminated as unchanged drug in the urine.

4.06.4.5.2.2 Renal impairment

Chronic kidney disease (CKD) is a serious condition, affecting more than 10% of adults in the United States.[133] Since the kidney eliminates many drugs and metabolites, impaired renal function can also seriously decrease renal clearance of these drugs, mandating dose adjustments in patients. One may understandably, but mistakenly, conclude that renal dysfunction should only affect renally eliminated drugs. In fact, metabolism can be dangerously altered in CKD patients, particularly as disease progresses. When the kidneys begin to lose their function, endogenous compounds that are eliminated by the kidneys in healthy people can accumulate to toxic concentrations. These compounds are called uremic toxins. Initially, it was hypothesized that uremic toxins inhibited metabolizing enzymes. Investigations showed that uremic toxins inhibited some, but not all, CYP metabolizing enzymes.[134–139] As it became clear that drug transporters also played a role in controlling drug access to metabolizing enzymes, Reyes and Benet questioned if perhaps uremic toxins could also inhibit transporters, potentially reducing metabolic clearance in vivo.[76] They concluded that uremic toxins could inhibit uptake transporters in hepatocytes. Since the disposition of a class 1 drug is unlikely to be affected by drug transporters, they tested whether uremic toxins inhibited hepatic exposure of propranolol, a class 1 drug. While uremic toxins did not inhibit the uptake of propranolol, some uremic toxins did inhibit the uptake of losartan, a class 2 drug, and eprosartan, a class 4 drug.

In this study, uremic toxins were unable to inhibit phase I metabolism when human uremic serum was incubated with microsomes dosed with propranolol or losartan, both of which are extensively metabolized.[76]

Given previous evidence, it would be unwise to suggest that metabolizing enzymes are not inhibited by uremic toxins. Therefore, decreased metabolism may be observed for class 1 and 2 drugs taken by patients with CKD. Alternatively, uptake transporters are likely inhibited by uremic toxins, which may decrease the metabolism of class 2 drugs and decrease hepatic clearance of class 3 and 4 drugs. All drugs should be tested for increased parent drug exposure, though the mechanism of inhibition will differ between classes.

This is a critical prediction that may (a) increase the safety of drugs in end stage renal disease (ESRD) patients, many of whom require several drugs, and (b) ease the developmental burden. The FDA now recommends that most new molecular entities be evaluated in ESRD patients, excepting drugs predominantly cleared by the lungs, monoclonal antibodies, and drugs intended for single-dose administration.[140] However, generating these studies and recruiting patients are difficult, costly, and variable. Applying BDDCS concepts to pharmacokinetic studies in renal disease may help prioritize what studies are necessary and help understand if clinicians should be concerned about inhibition of transporters, metabolizing enzymes, or both in administering one or multiple drugs.

The BDDCS provides many valuable predictions that can be useful in guiding drug development decisions. It currently relies on the extent of metabolism, which cannot be assessed until phase I studies and solubility studies. It would be extremely useful to have accurate high-throughput methods to predict BDDCS class prior to phase I trials.

4.06.4.6 Predicting BDDCS Class

4.06.4.6.1 In vitro

Based on the recognition of the ability of membrane permeability rate to differentiate extensively versus poorly metabolized compounds in the development of the BDDCS, Varma et al.[141] have confirmed that BDDCS class can be predicted well using in vitro apparent permeability rate as measured in MDCK-LE (low efflux) cells at pH 6.5 for acids and pH 7.4 for bases and solubility measured at pH 1.2 in PBS for acidic compounds and in FaSSIF for all other compounds. They used an internally developed permeability rate cutoff of 5×10^{-6} cm s^{-1}, above which compounds were predicted to be extensively metabolized and below which compounds were predicted as poorly metabolized. Dose strength is generally determined during phase II and III clinical trials. This makes it difficult to accurately predict the dose number of a drug. This group proposed a solubility cutoff of 200 μg mL^{-1}, which corresponds to a 50 mg dose being entirely soluble in 250 mL of water. This approach correctly predicted 84% of the compounds in their data set, specifically 83%, 83%, 88%, and 67% of class 1, 2, 3, and 4 drugs, respectively. Additionally, over 90% of the drugs predicted as class 1 or class 2 actually belonged to those classes, and over 80% of the drugs predicted to be class 3 were actually class 3, while 40% of the drugs predicted to be class 4 actually were class 4. Due to the small number of drugs that actually are class 4 and that are predicted to be class 4, the poor class 4 results should not dissuade the reader from realizing how well this in vitro approach predicted BDDCS class.

4.06.4.6.2 In silico

To ease the time and cost of these predictions during development, an in silico approach is preferable. There have been at least two attempts to predict BDDCS class in silico. In 2007, Khandelwal et al.[142] developed models using machine learning methods including recursive partitioning, random forest, and support vector machines. They used molecular features to assign drugs to one of the four BDDCS classes, predicting 33.3% correctly overall. In 2012, using the extended data set published by Benet et al.,[71] Broccatelli et al.[143] used a binary approach to predict the solubility and the extent of metabolism of the drugs before making a class prediction. Solubility was predicted using naive Bayes, k-nearest neighbor, and support vector machine models, where the solubility class was assigned using a consensus model, which predicted the class based on how it was predicted in a majority of the models. This model was 77% accurate. The extent of metabolism was predicted from a consensus model of a naive Bayes and two support vector machine models. This model was 79% accurate. When combining the solubility and extent of metabolism models to predict BDDCS class, however, this approach was only 55% accurate.

There are currently other efforts ongoing to improve in silico BDDCS class predictions. However, at this time, in vitro approaches provide more accurate predictions.

4.06.5 Conclusions

Predicting drug disposition is often difficult since there are many variables at play, which we do not yet fully understand. While quantitative predictive approaches from in vitro and in vivo models serve a crucial role in drug development, qualitative classification approaches such as the Biopharmaceutics Classification System and the BDDCS can help predict when such in vitro and in vivo studies may provide useful and interpretable results. These systems can potentially reduce both time and cost of drug development, which is ideal for both developers and consumers.

The BCS has been successfully implemented to grant biowaivers to at least 41 drugs,[144] reducing time and costs, which can potentially be passed down to consumers.

The BDDCS makes a broad range of current and potential dispositional predictions. This system can be useful for drugs already on the market to predict potential transporter or metabolizing enzyme effects that were not tested during development, thereby ensuring that these drugs remain safe and efficacious. These predictions can also help guide the development of new drugs, where a complete understanding of transporters and enzymes is required. This system predicts when metabolizing enzymes and transporters will be important in the absorption, metabolism, and elimination of drugs and currently helps us understand where transporters are relevant in the distribution of drugs to the central nervous system, with potential applications to other organs such as the heart, kidneys, and placenta. In this way, important transporters and enzymes will certainly be evaluated during development, whereas transporters or enzymes that are predicted to be clinically irrelevant may be safely dismissed. This can help speed up the process of development and reduce unnecessary costs. The BDDCS has also been used to help understand disposition in special states, such as kidney failure, and is currently being investigated for its predictive utility in toxicology.

We know of no class 1 drugs for which a dose adjustment has been required due to a transporter alteration as a result of drug–drug interactions, food, endogenous substrates, or pharmacogenomics, among other possible alterations. Drug development is trending toward larger, more lipophilic, and less soluble drugs. Therefore, BDDCS class 2 drugs are rapidly becoming the most important class. While these drugs will likely have improved potency, we might also expect more dispositional issues since they

can be affected by both metabolizing enzymes and transporters. Finally, class 3 and 4 drugs are not significant substrates of metabolizing enzymes, but are substrates of many transporters and require transporter investigation.

References

1. Lang, C. C.; Brown, R. M.; Kinirons, M. T.; Deathridge, M.-A.; Guengerich, F. P.; Kelleher, D.; O'Briain, D. S.; Ghishan, F. K.; Wood, A. J. J. Decreased Intestinal CYP3A in Celiac Disease: Reversal After Successful Gluten-Free Diet: A Potential Source of Interindividual Variability in First-Pass Drug Metabolism. *Clin. Pharmacol. Ther.* **1996,** *59,* 41–46.
2. Tran, T. H.; Smith, C.; Mangione, R. A. Drug Absorption in Celiac Disease. *Am. J. Health Syst. Pharm.* **2013,** *70,* 2199–2206.
3. Kola, I.; Landis, J. Can the Pharmaceutical Industry Reduce Attrition Rates? *Nat. Rev. Drug Discov.* **2004,** *3,* 711–715.
4. Arrowsmith, J.; Miller, P. Trial Watch: Phase II and Phase III Attrition Rates 2011–2012. *Nat. Rev. Drug Discov.* **2013,** *12,* 569.
5. Choy, Y. B.; Prausnitz, M. R. The Rule of Five for Non-Oral Routes of Drug Delivery: Ophthalmic, Inhalation and Transdermal. *Pharm. Res.* **2011,** *28,* 943–948.
6. Fonte, P.; Araújo, F.; Reis, S.; Sarmento, B. Oral Insulin Delivery: How Far Are We? *J. Diabetes Sci. Technol.* **2013,** *7,* 520–531.
7. Giacomini, K. M.; Huang, S.-M. Transporters in Drug Development and Clinical Pharmacology. *Clin. Pharmacol. Ther.* **2013,** *94,* 3–9.
8. Food and Drug Administration Center for Drug Evaluation and Research, *Guidance for Industry: Drug Interaction Studies: Study Design, Data Analysis, and Implications for Dosing and Labeling*; 2012; pp 1–79.
9. Zamek-Gliszczynski, M. J.; Hoffmaster, K. A.; Tweedie, D. J.; Giacomini, K. M.; Hillgren, K. M. Highlights From the International Transporter Consortium Second Workshop. *Clin. Pharmacol. Ther.* **2012,** *92,* 553–556.
10. Lipinski, C. A.; Lombardo, F.; Dominy, B. W.; Feeney, P. J. Experimental and Computational Approaches to Estimate Solubility and Permeability in Drug Discovery and Development Settings. *Adv. Drug Deliv. Rev.* **2001,** *46,* 3–26.
11. Pelkonen, O.; Boobis, A. R.; Gundert-Remy, U. In Vitro Prediction of Gastrointestinal Absorption and Bioavailability: An Experts' Meeting Report. *Eur. J. Clin. Pharmacol.* **2014,** *57,* 621–629.
12. Larregieu, C. A.; Benet, L. Z. Distinguishing Between the Permeability Relationships With Absorption and Metabolism to Improve BCS and BDDCS Predictions in Early Drug Discovery. *Mol. Pharm.* **2014,** *11,* 1335–1344.
13. Strober, W.; Peter, G.; Schwartz, R. H. Albumin Metabolism in Cystic Fibrosis. *Pediatrics* **1969,** *43,* 416–426.
14. Benet, L. Z.; Hoener, B.-A. Changes in Plasma Protein Binding Have Little Clinical Relevance. *Clin. Pharmacol. Ther.* **2002,** *71,* 115–121.
15. Obach, R. S.; Lombardo, F.; Waters, N. J. Trend Analysis of a Database of Intravenous Pharmacokinetic Parameters in Humans for 670 Drug Compounds. *Drug Metab. Dispos.* **2008,** *36,* 1385–1405.
16. Hosey, C. M.; Benet, L. Z. Predicting the Extent of Metabolism Using In Vitro Permeability Rate Measurements and In Silico Permeability Rate Predictions. *Mol. Pharm.* **2015,** *12,* 1456–1466.
17. Wienkers, L. C.; Heath, T. G. Predicting In Vivo Drug Interactions From In Vitro Drug Discovery Data. *Nat. Rev. Drug Discov.* **2005,** *4,* 825–833.
18. Williams, J. A.; Hyland, R.; Jones, B. C.; Smith, D. A.; Hurst, S.; Goosen, T. C.; Peterkin, V.; Koup, J. R.; Ball, S. E. Drug-Drug Interactions for UDP-Glucuronosyltransferase Substrates: A Pharmacokinetic Explanation for Typically Observed Low Exposure (AUCi/AUC) Ratios. *Drug Metab. Dispos.* **2004,** *32,* 1201–1208.
19. Miyauchi, S.; Sugiyama, Y.; Sawada, Y.; Morita, K.; Iga, T.; Hanano, M. Kinetics of Hepatic Transport of 4-Methylumbelliferone in Rats. Analysis by Multiple Indicator Dilution Method. *J. Pharmacokinet. Biopharm.* **1987,** *15,* 25–38.
20. Masimirembwa, C. M.; Bredberg, U.; Andersson, T. B. Metabolic Stability for Drug Discovery and Development: Pharmacokinetic and Biochemical Challenges. *Clin. Pharmacokinet.* **2003,** *42,* 515–528.
21. Clarke, S. E.; Jeffrey, P. Utility of Metabolic Stability Screening: Comparison of In Vitro and In Vivo Clearance. *Xenobiotica* **2001,** *31,* 591–598.
22. Hosey, C. M.; Broccatelli, F.; Benet, L. Z. Predicting When Biliary Excretion of Parent Drug Is a Major Route of Elimination in Humans. *AAPS J.* **2014,** *16,* 1085–1096.
23. Ring, B. J.; Chien, J. Y.; Adkison, K. K.; Jones, H. M.; Rowland, M.; Jones, R. D.; Yates, J. W. T.; Ku, M. S.; Gibson, C. R.; He, H.; et al. PhRMA CPCDC Initiative on Predictive Models of Human Pharmacokinetics, Part 3: Comparative Assessment of Prediction Methods of Human Clearance. *J. Pharm. Sci.* **2011,** *100,* 4090–4110.
24. Harrison, L. I.; Gibaldi, M. Pharmacokinetics of Digoxin in the Rat. *Drug Metab. Dispos.* **1976,** *4,* 88–93.
25. Rodin, S. M.; Johnson, B. F. Pharmacokinetic Interactions With Digoxin. *Clin. Pharmacokinet.* **1988,** *15,* 227–244.
26. Veal, G. J.; Back, D. J. Metabolism of Zidovudine. *Gen. Pharmacol.* **1995,** *26,* 1469–1475.
27. Mays, D. C.; Dixon, K. F.; Balboa, A.; Pawluk, L. J.; Bauer, M. R.; Nawoot, S.; Gerber, N. A Nonprimate Animal Model Applicable to Zidovudine Pharmacokinetics in Humans: Inhibition of Glucuronidation and Renal Excretion of Zidovudine by Probenecid in Rats. *J. Pharmacol. Exp. Ther.* **1991,** *259,* 1261–1270.
28. Olsen, L.; Oostenbrink, C.; Jørgensen, F. S. Prediction of Cytochrome P450 Mediated Metabolism. *Adv. Drug Deliv. Rev.* **2015,** *86,* 61–71.
29. Simulations Plus, Inc. ADMET Predictor (Version6) {Software}. Available from. http://www.simulations-plus.com.
30. Kirchmair, J.; Göller, A. H.; Lang, D.; Kunze, J.; Testa, B.; Wilson, I. D.; Glen, R. C.; Schneider, G. Predicting Drug Metabolism: Experiment and/or Computation? *Nat. Rev. Drug Discov.* **2015,** *14,* 387–404.
31. Crivori, P.; Zamora, I.; Speed, B.; Orrenius, C.; Poggesi, I. Model Based on GRID-Derived Descriptors for Estimating CYP3A4 Enzyme Stability of Potential Drug Candidates. *J. Comput. Aided Mol. Des.* **2004,** *18,* 155–166.
32. Ekins, S. In Silico Approaches to Predicting Drug Metabolism, Toxicology and Beyond. *Biochem. Soc. Trans.* **2003,** *31,* 611–614.
33. Varma, M. V. S.; Feng, B.; Obach, R. S.; Troutman, M. D.; Chupka, J.; Miller, H. R.; El-Kattan, A. Physicochemical Determinants of Human Renal Clearance. *J. Med. Chem.* **2009,** *52,* 4844–4852.
34. Renkin, E. M.; Robinson, R. R. Glomerular Filtration. *N. Engl. J. Med.* **1974,** *290,* 785–792.
35. Millburn, P.; Smith, R. L.; Williams, R. T. Biliary Excretion of Foreign Compounds. Biphenyl, Stilboestrol and Phenolphthalein in the Rat: Molecular Weight, Polarity and Metabolism as Factors in Biliary Excretion. *Biochem. J.* **1967,** *105,* 1275–1281.
36. Yang, X.; Gandhi, Y. A.; Duignan, D. B.; Morris, M. E. Prediction of Biliary Excretion in Rats and Humans Using Molecular Weight and Quantitative Structure–Pharmacokinetic Relationships. *AAPS J.* **2009,** *11,* 511–525.
37. Varma, M. V. S.; Chang, G.; Lai, Y.; Feng, B.; El-Kattan, A. F.; Litchfield, J.; Goosen, T. C. Physicochemical Property Space of Hepatobiliary Transport and Computational Models for Predicting Rat Biliary Excretion. *Drug Metab. Dispos.* **2012,** *40,* 1527–1537.
38. Sharifi, M.; Ghafourian, T. Estimation of Biliary Excretion of Foreign Compounds Using Properties of Molecular Structure. *AAPS J.* **2013,** *16,* 65–78.
39. Luo, G.; Johnson, S.; Hsueh, M.-M.; Zheng, J.; Cai, H.; Xin, B.; Chong, S.; He, K.; Harper, T. W. In Silico Prediction of Biliary Excretion of Drugs in Rats Based on Physicochemical Properties. *Drug Metab. Dispos.* **2010,** *38,* 422–430.
40. Chen, Y.; Cameron, K.; Guzman-Perez, A.; Perry, D.; Li, D.; Gao, H. Structure-Pharmacokinetic Relationship of In Vivo Rat Biliary Excretion. *Biopharm. Drug Dispos.* **2010,** *31,* 82–90.
41. Proost, J. H.; Roggeveld, J.; Wierda, J. M.; Meijer, D. K. Relationship Between Chemical Structure and Physicochemical Properties of Series of Bulky Organic Cations and Their Hepatic Uptake and Biliary Excretion Rates. *J. Pharmacol. Exp. Ther.* **1997,** *282,* 715–726.
42. Al-Shawi, M. K.; Omote, H. The Remarkable Transport Mechanism of P-Glycoprotein: A Multidrug Transporter. *J. Bioenerg. Biomembr.* **2005,** *37,* 489–496.

43. Swift, B.; Pfeifer, N. D.; Brouwer, K. L. R. Sandwich-Cultured Hepatocytes: An In Vitro Model to Evaluate Hepatobiliary Transporter-Based Drug Interactions and Hepatotoxicity. *Drug Metab. Rev.* **2010,** *42,* 446–471.
44. Davies, B.; Morris, T. Physiological Parameters in Laboratory Animals and Humans. *Pharm. Res.* **1993,** *10,* 1093–1095.
45. Li, M.; Yuan, H.; Li, N.; Song, G.; Zheng, Y.; Baratta, M.; Hua, F.; Thurston, A.; Wang, J.; Lai, Y. Identification of Interspecies Difference in Efflux Transporters of Hepatocytes From Dog, Rat, Monkey and Human. *Eur. J. Pharm. Sci.* **2008,** *35,* 114–126.
46. Li, N.; Zhang, Y.; Hua, F.; Lai, Y. Absolute Difference of Hepatobiliary Transporter Multidrug Resistance-Associated Protein (MRP2/Mrp2) in Liver Tissues and Isolated Hepatocytes From Rat, Dog, Monkey, and Human. *Drug Metab. Dispos.* **2009,** *37,* 66–73.
47. Ghibellini, G.; Leslie, E. M.; Brouwer, K. L. R. Methods to Evaluate Biliary Excretion of Drugs in Humans: An Updated Review. *Mol. Pharm.* **2006,** *3,* 198–211.
48. Food and Drug Administration Center for Drug Evaluation and Research. *Guidance for Industry: Bioavailability and Bioequivalence Studies for Orally Administered Drug Products- General Considerations*; 2003; pp 1–26.
49. Food and Drug Administration Center for Drug Evaluation and Research. *Guidance for Industry: Waiver of In Vivo Bioavailability and Bioequivalence Studies for Immediate-Release Solid Oral Dosage Forms Based on a Biopharmaceutics Classification System*, 2015; pp 1–17.
50. Yu, L. X.; Amidon, G. L.; Polli, J. E.; Zhao, H.; Mehta, M. U.; Conner, D. P.; Shah, V. P.; Lesko, L. J.; Chen, M.-L.; Lee, V. H. L.; et al. Biopharmaceutics Classification System: The Scientific Basis for Biowaiver Extensions. *Pharm. Res.* **2002,** *19,* 921–925.
51. Amidon, G. L.; Lennernäs, H.; Shah, V. P.; Crison, J. R. A Theoretical Basis for a Biopharmaceutic Drug Classification: the Correlation of *In Vitro* Drug Product Dissolution and *In Vivo* Bioavailability. *Pharm. Res.* **1995,** *12,* 413–420.
52. Lennernäs, H. Animal Data: The Contributions of the Ussing Chamber and Perfusion Systems to Predicting Human Oral Drug Delivery In Vivo. *Adv. Drug Deliv. Rev.* **2007,** *59,* 1103–1120.
53. European Medicines Agency Committee for Medicinal Products for Human Use, *Guideline on the Investigation of Bioequivalence*, 2010; pp 1–27.
54. Daousani, C.; Macheras, P. Scientific Considerations Concerning the EMA Change in the Definition of "Dose" of the BCS-Based Biowaiver Guideline and Implications for Bioequivalence. *Int. J. Pharm. (Amsterdam, Neth.)* **2015,** *478,* 606–609.
55. Sediq, A.; Kubbinga, M.; Langguth, P.; Dressman, J. The Impact of the EMA Change in Definition of "Dose" on the BCS Dose-Solubility Ratio: A Review of the Biowaiver Monographs. *J. Pharm. Sci.* **2014,** *103,* 65–70.
56. World Health Organization (WHO). *Proposal to Waive In Vivo Bioequivalence Requirements for WHO Model List of Essential Medicines Immediate-Release, Solid Oral Dosage Forms*, 2006; pp 1–45.
57. Lennernäs, H.; Ahrenstedt, O.; Hällgren, R.; Knutson, L.; Ryde, M.; Paalzow, L. K. Regional Jejunal Perfusion, a New in vivo Approach to Study Oral Drug Absorption in Man. *Pharm. Res.* **1992,** *9,* 1243–1251.
58. Salphati, L.; Childers, K.; Pan, L.; Tsutsui, K.; Takahashi, L. Evaluation of a Single-Pass Intestinal-Perfusion Method in Rat for the Prediction of Absorption in Man. *J. Pharm. Pharmacol.* **2001,** *53,* 1007–1013.
59. Chiou, W. L.; Barve, A. Linear Correlation of the Fraction of Oral Dose Absorbed of 64 Drugs Between Humans and Rats. *Pharm. Res.* **1998,** *15,* 1792–1795.
60. Volpe, D. A. Variability in Caco-2 and MDCK Cell-Based Intestinal Permeability Assays. *J. Pharm. Sci.* **2007,** *97,* 712–725.
61. Li, H.; Jin, H.-E.; Shim, W.-S.; Shim, C.-K. An Improved Prediction of the Human In Vivo Intestinal Permeability and BCS Class of Drugs Using the In Vitro Permeability Ratio Obtained for Rat Intestine Using an Using Chamber System. *Drug Dev. Ind. Pharm.* **2013,** *39,* 1515–1522.
62. Dahan, A.; Lennernäs, H.; Amidon, G. L. The Fraction Dose Absorbed, in Humans, and High Jejunal Human Permeability Relationship. *Mol. Pharm.* **2012,** *9,* 1847–1851.
63. Mehta, M. Application of Biopharmaceutical Classification System (BCS) in Regulatory Submissions. *AAPS Webinar*, 2010; pp 1–66.
64. Varma, M. V.; Steyn, S. J.; Allerton, C.; El-Kattan, A. F. Predicting Clearance Mechanism in Drug Discovery: Extended Clearance Classification System (ECCS). *Pharm. Res.* **2015,** *32,* 3785–3802.
65. Kunze, A.; Poller, B.; Huwyler, J.; Camenisch, G. Application of the Extended Clearance Concept Classification System (ECCCS) to Predict the Victim Drug-Drug Interaction Potential of Statins. *Drug Metab. Pers. Ther.* **2015,** *30,* 175–188.
66. Kusama, M.; Toshimoto, K.; Maeda, K.; Hirai, Y.; Imai, S.; Chiba, K.; Akiyama, Y.; Sugiyama, Y. In Silico Classification of Major Clearance Pathways of Drugs With Their Physiochemical Parameters. *Drug Metab. Dispos.* **2010,** *38,* 1362–1370.
67. Wu, C.-Y.; Benet, L. Z. Predicting Drug Disposition via Application of BCS: Transport/Absorption/Elimination Interplay and Development of a Biopharmaceutics Drug Disposition Classification System. *Pharm. Res.* **2005,** *22,* 11–23.
68. Shugarts, S.; Benet, L. Z. The Role of Transporters in the Pharmacokinetics of Orally Administered Drugs. *Pharm. Res.* **2009,** *26,* 2039–2054.
69. Chen, M. L.; Yu, L. The Use of Drug Metabolism for Prediction of Intestinal Permeability. *Mol. Pharm.* **2009,** *6,* 74–81.
70. Benet, L. Z.; Larregieu, C. A. The FDA Should Eliminate the Ambiguities in the Current BCS Biowaiver Guidance and Make Public the Drugs for Which BCS Biowaivers Have Been Granted. *Clin. Pharmacol. Ther.* **2010,** *88,* 405–407.
71. Benet, L. Z.; Broccatelli, F.; Oprea, T. I. BDDCS Applied to Over 900 Drugs. *AAPS J.* **2011,** *13,* 519–547.
72. Chen, M.-L.; Amidon, G. L.; Benet, L. Z.; Lennernäs, H.; Yu, L. X. The BCS, BDDCS, and Regulatory Guidances. *Pharm. Res.* **2011,** *28,* 1774–1778.
73. Yang, Y.; Faustino, P. J.; Volpe, D. A.; Ellison, C. D.; Lyon, R. C.; Yu, L. X. Biopharmaceutics Classification of Selected Beta-Blockers: Solubility and Permeability Class Membership. *Mol. Pharm.* **2007,** *4,* 608–614.
74. Liu, W.; Okochi, H.; Benet, L. Z.; Zhai, S.-D. Sotalol Permeability in Cultured-Cell, Rat Intestine, and PAMPA System. *Pharm. Res.* **2012,** *29,* 1768–1774.
75. Kato, Y.; Miyazaki, T.; Kano, T.; Sugiura, T.; Kubo, Y.; Tsuji, A. Involvement of Influx and Efflux Transport Systems in Gastrointestinal Absorption of Celiprolol. *J. Pharm. Sci.* **2009,** *98,* 2529–2539.
76. Reyes, M.; Benet, L. Z. Effects of Uremic Toxins on Transport and Metabolism of Different Biopharmaceutics Drug Disposition Classification System Xenobiotics. *J. Pharm. Sci.* **2011,** *100,* 3831–3842.
77. Hosey, C. M.; Chan, R.; Benet, L. Z. BDDCS Predictions, Self-Correcting Aspects of BDDCS Assignments, BDDCS Assignment Corrections, and Classification for More Than 175 Additional Drugs. *AAPS J.* **2016,** *18,* 251–260.
78. Brandsch, M. Drug Transport via the Intestinal Peptide Transporter PepT1. *Curr. Opin. Pharmacol.* **2013,** *13,* 881–887.
79. Estudante, M.; Morais, J. G.; Soveral, G.; Benet, L. Z. Intestinal Drug Transporters: An Overview. *Adv. Drug Deliv. Rev.* **2013,** *65,* 1340–1356.
80. Garrison, K. L.; Sahin, S.; Benet, L. Z. Few Drugs Display Flip-Flop Pharmacokinetics and These Are Primarily Associated With Classes 3 and 4 of the BDDCS. *J. Pharm. Sci.* **2015,** *104,* 3229–3235.
81. Blokzijl, H.; van Steenpaal, A.; Vander Borght, S.; Bok, L. I. H.; Libbrecht, L.; Tamminga, M.; Geuken, M.; Roskams, T. A. D.; Dijkstra, G.; Moshage, H.; et al. Up-Regulation and Cytoprotective Role of Epithelial Multidrug Resistance-Associated Protein 1 in Inflammatory Bowel Disease. *J. Biol. Chem.* **2008,** *283,* 35630–35637.
82. Tamai, I. Oral Drug Delivery Utilizing Intestinal OATP Transporters. *Adv. Drug Deliv. Rev.* **2012,** *64,* 508–514.
83. Nozawa, T.; Nakajima, M.; Tamai, I.; Noda, K.; Nezu, J.-I.; Sai, Y.; Tsuji, A.; Yokoi, T. Genetic Polymorphisms of Human Organic Anion Transporters OATP-C (SLC21A6) and OATP-B (SLC21A9): Allele Frequencies in the Japanese Population and Functional Analysis. *J. Pharmacol. Exp. Ther.* **2002,** *302,* 804–813.
84. Imanaga, J.; Kotegawa, T.; Imai, H.; Tsutsumi, K.; Yoshizato, T.; Ohyama, T.; Shirasaka, Y.; Tamai, I.; Tateishi, T.; Ohashi, K. The Effects of the SLCO2B1 C.1457C > T Polymorphism and Apple Juice on the Pharmacokinetics of Fexofenadine and Midazolam in Humans. *Pharmacogenet. Genomics* **2011,** *21,* 84–93.
85. Budha, N. R.; Frymoyer, A.; Smelick, G. S.; Jin, J. Y.; Yago, M. R.; Dresser, M. J.; Holden, S. N.; Benet, L. Z.; Ware, J. A. Drug Absorption Interactions Between Oral Targeted Anticancer Agents and PPIs: Is pH-Dependent Solubility the Achilles Heel of Targeted Therapy? *Clin. Pharmacol. Ther.* **2012,** *92,* 203–213.
86. Yago, M. R.; Frymoyer, A.; Benet, L. Z.; Smelick, G. S.; Frassetto, L. A.; Ding, X.; Dean, B.; Salphati, L.; Budha, N.; Jin, J. Y.; et al. The Use of Betaine HCl to Enhance Dasatinib Absorption in Healthy Volunteers With Rabeprazole-Induced Hypochlorhydria. *AAPS J.* **2014,** *16,* 1358–1365.

87. Thelen, K.; Dressman, J. B. Cytochrome P450-Mediated Metabolism in the Human Gut Wall. *J. Pharm. Pharmacol.* **2009,** *61,* 541–558.
88. Paine, M. F.; Khalighi, M.; Fisher, J. M.; Shen, D. D.; Kunze, K. L.; Marsh, C. L.; Perkins, J. D.; Thummel, K. E. Characterization of Interintestinal and Intraintestinal Variations in Human CYP3A-Dependent Metabolism. *J. Pharmacol. Exp. Ther.* **1997,** *283,* 1552–1562.
89. Guengerich, F. P. Human Cytochrome P450 Enzymes. In *Cytochrome P450: Structure, Mechanism, and Biochemistry;* Ortiz de Montellano, P. R., Ed.; Springer: New York, 2005; pp 377–530.
90. Griffin, B.; O'Driscoll, C. Models of the Small Intestine. In *Drug Absorption Studies: In Situ, In Vitro, and In Silico Models;* Ehrhardt, C., Kim, K.-J., Eds.; Springer: New York, 2007; pp 34–76.
91. Desta, Z.; Zhao, X.; Shin, J.-G.; Flockhart, D. A. Clinical Significance of the Cytochrome P450 2C19 Genetic Polymorphism. *Clin. Pharmacokinet.* **2002,** *41,* 913–958.
92. Moore, L. B.; Goodwin, B.; Jones, S. A.; Wisely, G. B.; Serabjit-Singh, C. J.; Willson, T. M.; Collins, J. L.; Kliewer, S. A. St. John's Wort Induces Hepatic Drug Metabolism Through Activation of the Pregnane X Receptor. *Proc. Natl. Acad. Sci. U. S. A.* **2000,** *97,* 7500–7502.
93. Kerb, R.; Bauer, S.; Brockmöller, J.; Roots, I. Urinary 6 B-Hydroxycortisol Excretion Rate Is Affected by Treatment With Hypericum Extract. *Eur. J. Clin. Pharmacol.* **1997,** *52* (Suppl.), A186.
94. Roby, C. A.; Anderson, G. D.; Kantor, E.; Dryer, D. A.; Burstein, A. H. St John's Wort: Effect on CYP3A4 Activity. *Clin. Pharmacol. Ther.* **2000,** *67,* 451–457.
95. Nebel, A.; Schneider, B. J.; Baker, R. K.; Kroll, D. J. Potential Metabolic Interaction Between St. John's Wort and Theophylline. *Ann. Pharmacother.* **1999,** *33,* 502.
96. Maurer, A.; Johne, A.; Bauer, S.; Brockmöller, J.; Donath, F. Interaction of St. John's Wort Extract With Phenprocoumon. *Eur. J. Clin. Pharmacol.* **1999,** *55,* A22.
97. Ruschitzka, F.; Meier, P. J.; Turina, M.; Lüscher, T. F.; Noll, G. Acute Heart Transplant Rejection Due to Saint John's Wort. *Lancet* **2000,** *355,* 548–549.
98. Barone, G. W.; Gurley, B. J.; Ketel, B. L.; Lightfoot, M. L.; Abul-Ezz, S. R. Drug Interaction Between St. John's Wort and Cyclosporine. *Ann. Pharmacother.* **2000,** *34,* 1013–1016.
99. Mai, I.; Krüger, H.; Budde, K.; Johne, A.; Brockmöller, J.; Neumayer, H. H.; Roots, I. Hazardous Pharmacokinetic Interaction of Saint John's Wort (Hypericum Perforatum) With the Immunosuppressant Cyclosporin. *Int. J. Clin. Pharmacol. Ther.* **2000,** *38,* 500–502.
100. Piscitelli, S. C.; Burstein, A. H.; Chaitt, D.; Alfaro, R. M.; Falloon, J. Indinavir Concentrations and St John's Wort. *Lancet* **2000,** *355,* 547–548.
101. Grover, A.; Benet, L. Z. Effects of Drug Transporters on Volume of Distribution. *AAPS J.* **2009,** *11,* 250–261.
102. Niemi, M.; Schaeffeler, E.; Lang, T.; Fromm, M. F.; Neuvonen, M.; Kyrklund, C.; Backman, J. T.; Kerb, R.; Schwab, M.; Neuvonen, P. J.; et al. High Plasma Pravastatin Concentrations Are Associated With Single Nucleotide Polymorphisms and Haplotypes of Organic Anion Transporting Polypeptide-C (OATP-C, SLCO1B1). *Pharmacogenetics* **2004,** *14,* 429–440.
103. Lee, E.; Ryan, S.; Birmingham, B.; Zalikowski, J.; March, R.; Ambrose, H.; Moore, R.; Lee, C.; Chen, Y.; Schneck, D. Rosuvastatin Pharmacokinetics and Pharmacogenetics in White and Asian Subjects Residing in the Same Environment. *Clin. Pharmacol. Ther.* **2005,** *78,* 330–341.
104. Niemi, M.; Neuvonen, P. J.; Hofmann, U.; Backman, J. T.; Schwab, M.; Lütjohann, D.; von Bergmann, K.; Eichelbaum, M.; Kivistö, K. T. Acute Effects of Pravastatin on Cholesterol Synthesis Are Associated With SLCO1B1 (Encoding OATP1B1) Haplotype *17. *Pharmacogenet. Genomics* **2005,** *15,* 303–309.
105. Neuvonen, P. J.; Niemi, M.; Backman, J. T. Drug Interactions With Lipid-Lowering Drugs: Mechanisms and Clinical Relevance. *Clin. Pharmacol. Ther.* **2006,** *80,* 565–581.
106. Dave, R. A.; Morris, M. E. Quantitative Structure-Pharmacokinetic Relationships for the Prediction of Renal Clearance in Humans. *Drug Metab. Dispos.* **2015,** *43,* 73–81.
107. Gustafson, J. H.; Benet, L. Z. Biliary Excretion Kinetics of Phenolphthalein Glucuronide After Intravenous and Retrograde Biliary Administration. *J. Pharm. Pharmacol.* **1974,** *26,* 937–944.
108. Zur, M.; Gasparini, M.; Wolk, O.; Amidon, G. L.; Dahan, A. The Low/High BCS Permeability Class Boundary: Physicochemical Comparison of Metoprolol and Labetalol. *Mol. Pharm.* **2014,** *11,* 1707–1714.
109. He, K.; Iyer, K. R.; Hayes, R. N.; Sinz, M. W.; Woolf, T. F.; Hollenberg, P. F. Inactivation of Cytochrome P450 3A4 by Bergamottin, a Component of Grapefruit Juice. *Chem. Res. Toxicol.* **1998,** *11,* 252–259.
110. Dresser, G. K.; Bailey, D. G.; Leake, B. F.; Schwarz, U. I.; Dawson, P. A.; Freeman, D. J.; Kim, R. B. Fruit Juices Inhibit Organic Anion Transporting Polypeptide-Mediated Drug Uptake to Decrease the Oral Availability of Fexofenadine. *Clin. Pharmacol. Ther.* **2002,** *71,* 11–20.
111. Dresser, G. K.; Bailey, D. G. The Effects of Fruit Juices on Drug Disposition: A New Model for Drug Interactions. *Eur. J. Clin. Invest.* **2003,** *33* (Suppl. 2), 10–16.
112. Benet, L. Z. The Role of BCS (Biopharmaceutics Classification System) and BDDCS (Biopharmaceutics Drug Disposition Classification System) in Drug Development. *J. Pharm. Sci.* **2013,** *102,* 34–42.
113. Singh, B. N. Effects of Food on Clinical Pharmacokinetics. *Clin. Pharmacokinet.* **1999,** *37,* 213–255.
114. Brouwers, J.; Tack, J.; Augustijns, P. Parallel Monitoring of Plasma and Intraluminal Drug Concentrations in Man After Oral Administration of Fosamprenavir in the Fasted and Fed State. *Pharm. Res.* **2007,** *24,* 1862–1869.
115. Custodio, J. M.; Wu, C.-Y.; Benet, L. Z. Predicting Drug Disposition, Absorption/Elimination/Transporter Interplay and the Role of Food on Drug Absorption. *Adv. Drug Deliv. Rev.* **2008,** *60,* 717–733.
116. Galia, E.; Nicolaides, E.; Hörter, D.; Löbenberg, R.; Reppas, C.; Dressman, J. B. Evaluation of Various Dissolution Media for Predicting In Vivo Performance of Class I and II Drugs. *Pharm. Res.* **1998,** *15,* 698–705.
117. Dressman, J. B.; Reppas, C. In Vitro-In Vivo Correlations for Lipophilic, Poorly Water-Soluble Drugs. *Eur. J. Pharm. Sci.* **2000,** *11* (Suppl. 2), S73–S80.
118. Carver, P. L.; Fleisher, D.; Zhou, S. Y.; Kaul, D.; Kazanjian, P.; Li, C. Meal Composition Effects on the Oral Bioavailability of Indinavir in HIV-Infected Patients. *Pharm. Res.* **1999,** *16,* 718–724.
119. Liedholm, H.; Melander, A. Concomitant Food Intake Can Increase the Bioavailability of Propranolol by Transient Inhibition of Its Presystemic Primary Conjugation. *Clin. Pharmacol. Ther.* **1986,** *40,* 29–36.
120. Schmidt, L. E.; Dalhoff, K. Food-Drug Interactions. *Drugs* **2002,** *62,* 1481–1502.
121. Lui, C. Y.; Amidon, G. L.; Berardi, R. R.; Fleisher, D.; Youngberg, C.; Dressman, J. B. Comparison of Gastrointestinal pH in Dogs and Humans: Implications on the Use of the Beagle Dog as a Model for Oral Absorption in Humans. *J. Pharm. Sci.* **1986,** *75,* 271–274.
122. Konishi, T.; Satsu, H.; Hatsugai, Y.; Aizawa, K.; Inakuma, T.; Nagata, S.; Sakuda, S.-H.; Nagasawa, H.; Shimizu, M. A Bitter Melon Extract Inhibits the P-Glycoprotein Activity in Intestinal Caco-2 Cells: Monoglyceride as an Active Compound. *Biofactors* **2004,** *22,* 71–74.
123. Konishi, T.; Satsu, H.; Hatsugai, Y.; Aizawa, K.; Inakuma, T.; Nagata, S.; Sakuda, S.-H.; Nagasawa, H.; Shimizu, M. Inhibitory Effect of a Bitter Melon Extract on the P-Glycoprotein Activity in Intestinal Caco-2 Cells. *Br. J. Pharmacol.* **2004,** *143,* 379–387.
124. Balakrishnan, A.; Polli, J. E. Apical Sodium Dependent Bile Acid Transporter (ASBT, SLC10A2): A Potential Prodrug Target. *Mol. Pharm.* **2006,** *3,* 223–230.
125. Food and Drug Administration Center for Drug Evaluation and Research. *Guidance for Industry: Food-Effect Bioavailability and Fed Bioequivalence Studies*, 2002; pp 1–12.
126. Ingels, F.; Deferme, S.; Destexhe, E.; Oth, M.; Van den Mooter, G.; Augustijns, P. Simulated Intestinal Fluid as Transport Medium in the Caco-2 Cell Culture Model. *Int. J. Pharm. (Amsterdam, Neth.)* **2002,** *232,* 183–192.
127. Dresser, G. K.; Kim, R. B.; Bailey, D. G. Effect of Grapefruit Juice Volume on the Reduction of Fexofenadine Bioavailability: Possible Role of Organic Anion Transporting Polypeptides. *Clin. Pharmacol. Ther.* **2005,** *77,* 170–177.
128. Mithani, S. D.; Bakatselou, V.; TenHoor, C. N.; Dressman, J. B. Estimation of the Increase in Solubility of Drugs as a Function of Bile Salt Concentration. *Pharm. Res.* **1996,** *13,* 163–167.
129. Mahar Doan, K. M.; Humphreys, J. E.; Webster, L. O.; Wring, S. A.; Shampine, L. J.; Serabjit-Singh, C. J.; Adkison, K. K.; Polli, J. W. Passive Permeability and P-Glycoprotein-Mediated Efflux Differentiate Central Nervous System (CNS) and Non-CNS Marketed Drugs. *J. Pharmacol. Exp. Ther.* **2002,** *303,* 1029–1037.
130. van de Waterbeemd, H.; Camenisch, G.; Folkers, G.; Chretien, J. R.; Raevsky, O. A. Estimation of Blood–brain Barrier Crossing of Drugs Using Molecular Size and Shape, and H-Bonding Descriptors. *J. Drug Target.* **1998,** *6,* 151–165.

131. Wager, T. T.; Chandrasekaran, R. Y.; Hou, X.; Troutman, M. D.; Verhoest, P. R.; Villalobos, A.; Will, Y. Defining Desirable Central Nervous System Drug Space Through the Alignment of Molecular Properties, In Vitro ADME, and Safety Attributes. *ACS Chem. Neurosci.* **2010,** *1,* 420–434.
132. Broccatelli, F.; Larregieu, C. A.; Cruciani, G.; Oprea, T. I.; Benet, L. Z. Improving the Prediction of the Brain Disposition for Orally Administered Drugs Using BDDCS. *Adv. Drug Deliv. Rev.* **2012,** *64,* 95–109.
133. Centers for Disease Control and Prevention (CDC). *National Chronic Kidney Disease Fact Sheet: General Information and National Estimates on Chronic Kidney Disease in the United States, 2014;* US Department of Health and Human Services, Center for Disease Control and Prevention: Atlanta, GA, 2014.
134. Guévin, C.; Michaud, J.; Naud, J.; Leblond, F. A.; Pichette, V. Down-Regulation of Hepatic Cytochrome P450 in Chronic Renal Failure: Role of Uremic Mediators. *Br. J. Pharmacol.* **2002,** *137,* 1039–1046.
135. Nolin, T. D. Altered Nonrenal Drug Clearance in ESRD. *Curr. Opin. Nephrol. Hypertens.* **2008,** *17,* 555–559.
136. Pichette, V.; Leblond, F. A. Drug Metabolism in Chronic Renal Failure. *Curr. Drug Metab.* **2003,** *4,* 91–103.
137. Leblond, F.; Guévin, C.; Demers, C.; Pellerin, I.; Gascon-Barré, M.; Pichette, V. Downregulation of Hepatic Cytochrome P450 in Chronic Renal Failure. *J. Am. Soc. Nephrol.* **2001,** *12,* 326–332.
138. Dreisbach, A. W.; Lertora, J. J. L. The Effect of Chronic Renal Failure on Hepatic Drug Metabolism and Drug Disposition. *Semin. Dial.* **2003,** *16,* 45–50.
139. Michaud, J.; Nolin, T. D.; Naud, J.; Dani, M.; Lafrance, J.-P.; Leblond, F. A.; Himmelfarb, J.; Pichette, V. Effect of Hemodialysis on Hepatic Cytochrome P450 Functional Expression. *J. Pharmacol. Sci.* **2008,** *108,* 157–163.
140. Food and Drug Administration Center for Drug Evaluation and Research. *Guidance for Industry: Pharmacokinetics in Patients With Impaired Renal Function – Study Design, Data Analysis, and Impact on Dosing and Labeling*, 2010; pp 1–18.
141. Varma, M. V.; Gardner, I.; Steyn, S. J.; Nkansah, P.; Rotter, C. J.; Whitney-Pickett, C.; Zhang, H.; Di, L.; Cram, M.; Fenner, K. S.; et al. pH-Dependent Solubility and Permeability Criteria for Provisional Biopharmaceutics Classification (BCS and BDDCS) in Early Drug Discovery. *Mol. Pharm.* **2012,** *9,* 1199–1212.
142. Khandelwal, A.; Bahadduri, P. M.; Chang, C.; Polli, J. E.; Swaan, P. W.; Ekins, S. Computational Models to Assign Biopharmaceutics Drug Disposition Classification From Molecular Structure. *Pharm. Res.* **2007,** *24,* 2249–2262.
143. Broccatelli, F.; Cruciani, G.; Benet, L. Z.; Oprea, T. I. BDDCS Class Prediction for New Molecular Entities. *Mol. Pharm.* **2012,** *9,* 570–580.
144. Tampal, N.; Mandula, H.; Zhang, H.; Li, B. V.; Nguyen, H.; Conner, D. P. Biopharmaceutics Classification System-Based Biowaivers for Generic Oncology Drug Products: Case Studies. *AAPS PharmSciTech* **2015,** *16,* 5–9.

4.07 Genetically Humanized Animal Models

K Samuelsson, Independent Consultant, Åskloster, Sweden
N Scheer, CEVEC Pharmaceuticals GmbH, Cologne, Germany
I Wilson, Department of Surgery and Cancer, London, United Kingdom
CR Wolf and C J Henderson, University of Dundee, Dundee, United Kingdom

© 2017 Elsevier Ltd. All rights reserved.

4.07.1 Introduction 130
4.07.2 Genetically Humanized Mouse Models for Xenobiotic Receptors, Drug-Metabolizing Enzymes, and Transporters 132
4.07.2.1 Genetic Modifications of Xenobiotic Receptors 132
4.07.2.1.1 Examples of studies using receptor-humanized mice 133
4.07.2.2 Functionalization (Phase I) and Conjugative (Phase II) Drug-Metabolizing Enzymes 133
4.07.2.2.1 Functionalization by cytochrome P450 enzymes: species differences 134
4.07.2.2.2 Examples of studies using CYP P450-humanized mice 134
4.07.2.2.3 Conjugation enzymes: species differences 136
4.07.2.2.4 Examples of studies using UGT- and NAT-humanized mice 136
4.07.2.3 Drug Transporters 137
4.07.2.3.1 Transporter-humanized mice 137
4.07.2.3.2 Examples of studies using transporter-humanized mice 137
4.07.3 Chimeric Liver-Humanized Mice 138
4.07.3.1 Examples of Studies Using Chimeric Liver-Humanized Mice 138
4.07.3.1.1 Inhibition and induction studies 139
4.07.3.1.2 Biotransformation studies 139
4.07.4 Differences Between Genetically Humanized Mice and Chimeric Liver-Humanized Mouse Models 141
4.07.5 Additional Models 142
4.07.6 How to Choose a Humanized Mouse Model? 144
4.07.7 Humanized Mouse Models in the Future 145
References 146

4.07.1 Introduction

The discovery and development of any new drug is a long, complex, and expensive process with an uncertain outcome. Before reaching the market, drug candidates need to go through the conventional sequence of processes involved in drug discovery and development. This results in the identification of lead series of compounds and chemical optimization leading to candidate selection and then entry into development, including preclinical investigations to evaluate safety followed by clinical evaluations (usually considered in three phases I, II, and III). Currently, the typical development for investigational new drugs takes between 10 and 15 years and is associated with high costs and low rate of approval.[1,2] During discovery and development, the candidate drug has to pass through a series of stages (often referred to as tollgates), in terms of measurable objectives for efficacy and safety, which can enable decisions to be made on further investment, and once in development to gain approval from regulatory authorities such as the Food and Drug Administration (FDA) and European Agency for the Evaluation of Medicinal Products (EMEA), to move from one stage to another and finally gain marketing approval. It has been estimated that a compound entering clinical phase I testing has less than a 10% chance of reaching the market, and for some research areas, the limit can be even lower.[3] The rather low success rate may be due to a number of reasons including the lack of predictive preclinical models and sometimes inadequate and complex clinical trial designs. About 40% of compounds approved for entry into phase I trials do not progress further as a result of inappropriate pharmacokinetics (PK) of the test compound.[4–6] Other drug candidates fail in clinical testing because they do not behave pharmacologically as predicted from the preclinical animal studies used today or exhibit toxicity that was not anticipated based on the same preclinical safety studies.

It can then be summarized that a successful preclinical development program is of great importance when determining if the candidate drug is reasonably safe for initial testing in humans. The preclinical development program consists of a battery of in vitro and in vivo assays with the aim of accurately predicting PK, metabolism, efficacy, and safety in man. Of course, one can expect variability in drug PK and metabolism due to species differences, but good prediction of these properties represents vital factors in defining drug efficacy and side effects, and thus, there is an urgent need to obtain more informative experimental data predicting clinical outcomes. The use of traditional animal models is one of the key areas in the preclinical development of new drugs, and the companies developing drugs have relied on these "traditional" in vivo models for decades. These in vivo experiments are of great

importance and, in combination with, human in vitro data are used for predicting the PK and metabolic behavior of new compounds. The aim of the preclinical program is not only to ensure that a drug does not expose humans to unreasonable risks when used in limited, early-stage, clinical phase I studies but also to select a successful drug that does not fail in the later clinical phases.

The overall pathways of drug metabolism and disposition are highly conserved between species including xenobiotic receptors, biotransformation enzymes, and transporters. However, species differ with regard to isoform expression, catalytic activities, and mode of regulation of drug-metabolizing enzymes. The result is that the substrate specificity and amounts of the individual proteins mediating these processes can vary quite significantly between animals and man. Thus, the prediction of human drug metabolism and disposition by extrapolation from the results obtained using in vivo studies in traditional preclinical animal models is often limited and does not always faithfully predict or model what is observed in the clinic.[7–9] Investigators performing adsorption, distribution, metabolism, and excretion (ADME) studies have been aware of such species differences for almost as long as DMPK has been identified as a discipline and they have now been described for all the major components of the process of drug metabolism and disposition, that is, xenobiotic receptors,[10] oxidoreductases such as the cytochromes P450s,[8,11] conjugative enzymes,[12] and transporters.[13]

There are several approaches available to minimize the impact of the discrepancies between species, especially in the case of rodents, and the most frequently employed involves the use of the recently developed genetically modified humanized mouse models, which are now available on the market. One way to reduce the drug metabolism differences between mouse and human is to replace single or multiple mouse genes with their human counterparts. A great variety of such genetically humanized mouse models, expressing human instead of mouse receptors, drug-metabolizing enzymes, and transporters, have been described.[14,15] An alternative approach to overcome the boundaries associated with the traditional animal models is based on the central role of the liver as the major drug-metabolizing and detoxification organ for most drugs and xenobiotics. In this "chimeric" mouse model, the mouse liver is repopulated in vivo with human hepatocytes. Differently derived chimeric liver-humanized mouse models with human hepatocytes engrafted in their livers have been created.[16–19] Under optimal conditions, up to 95% of the hepatocytes in the mouse liver can be human. In the cases of both genetically humanized and chimeric liver-humanized mouse models, there are now numerous literature examples (see in the succeeding text) where their application has been shown to add value in drug/xenobiotic metabolism and toxicity studies.

The current literature describing both the genetically modified and the chimeric liver-humanized mouse models reveals that they are derived in two fundamentally different ways: In the genetically modified models, human genes are introduced into the mouse genome in order to generate genetically humanized mice, thereby expressing specific human genes on a mouse background. In the second "chimeric" model, human cells are transplanted into competent recipients resulting in tissue-humanized mouse models that may contain in excess of 95% human cells but with a residual unmodified mouse component amounting to 5% or more. While these two approaches are the focus of this article, two additional, nonhumanized models will be described that can aid in determining the role of cytochrome P450s in the gut and/or in the liver,[20,21] which provide additional powerful tools for the selection of the most appropriate humanized mouse model. These models both involve conditional deletion of P450 oxidoreductase (POR), either genetically in the liver through the expression of Cre recombinase driven by the albumin promoter hepatic reductase null (HRN) or chemically in the liver or liver and gut by induction of Cre expression driven by the Cyp1a1 promoter endogenous reductase locus (ERL).

As indicated earlier, the genetically humanized and chimeric liver-humanized mice have been used for a range of applications including components of the immune and hematopoietic system, as models for human aneuploidy and to reflect human diseases and for drug efficacy testing, for cancer research, and to enable infections with human pathogens.[22] In a similar manner, chimeric liver-humanized mice have been used to study human hematopoiesis, immune responses, autoimmunity, infectious diseases, cancer, and regenerative medicine.[23] Two disease areas where this second model has been particularly valuable are in studies on malaria and hepatitis B.[24,25] In addition, from being used as a model system in drug development, this model has also been used successfully in anti-doping research to define routes and rates by which different nutritional supplements are metabolized and excreted.[26–28]

Genetically humanized mice for proteins involved in drug metabolism and toxicity and mice engrafted with human hepatocytes provide powerful in vivo models for improving the prediction of PK, drug–drug interactions (DDI), and safety characteristics of compounds in humans. Certain of the models available at this time are not fully validated and accepted by the regulatory authorities as suitable for use on a regular basis; however, their potential to contribute to drug regulatory processes is being actively discussed. Although knockout models, where mouse genes have been deleted, are not humanized, they allow the murine enzymes involved in drug disposition to be defined. This is of central importance in the interpretation of data obtained using the humanized models. They also play an important role for gaining understanding of the different functions of certain proteins or functions of an organ, in relation to a dosed drug. As with all models, it is important to be aware that there are specific advantages and disadvantages inherent in each of these models and that these should be understood and taken into account in the interpretation of experimental data. In this article, similarities and differences between genetically modified and chimeric liver-humanized mouse models will be defined, and the most studied genetically modified varieties of these models will be described. How the most appropriate model can be selected for a particular pharmacological or toxicological question and the relative strengths and weaknesses of the two models systems will be described.

4.07.2 Genetically Humanized Mouse Models for Xenobiotic Receptors, Drug-Metabolizing Enzymes, and Transporters

In this section, the replacement of single or multiple mouse genes with their human counterparts is described as one way to reduce the differences in drug disposition between mouse and man. Such genetic modifications are transmitted through the germline and are present in all cells of the animal. This distinguishes these models from the chimeric mice discussed later in this article where the liver is the target organ for humanization.

The proteins involved in the different pathways of drug metabolism and disposition can be divided into three groups: receptors, drug-metabolizing enzymes, and transporters. These categories have also been targets for genetic modification in order to gain an increased understanding of the impact a certain protein has on the role in the metabolism, PK, and safety of drugs as an attempt to make the characterization of a drug more predictive for humans. The result of this is the generation of a large number of transgenic mice, grouped with respect to xenobiotic receptors and drug metabolism enzymes either responsible for the functionalization of drugs (the so-called phase I metabolism) or involved in conjugation reactions (the so-called phase II metabolism), transporter enzymes, and composite models of these (Fig. 1). The methods applied by the different research groups to generate these mice have varied significantly and included random insertions of human transgenes, freely segregating mouse or human artificial chromosomes (MACs or HACs) or targeted integrations at defined gene loci. These approaches have often been combined with deletions of the orthologous murine genes. The human transgenes have been expressed off heterologous promoters, the corresponding mouse promoters, or the human promoter of that gene.[14,22]

4.07.2.1 Genetic Modifications of Xenobiotic Receptors

As is well known, drugs and environmental chemicals may cause induction of both drug-metabolizing enzymes and transporters. Three nuclear receptors, pregnane X receptor (PXR), constitutive androstane receptor (CAR), and peroxisome proliferator-activated receptor alpha (PPARα), and the Per-Sim-ARNT domain receptor aryl hydrocarbon receptor (AHR) play a major role in this adaptive response.[29] Mice humanized for all of these receptors have been described.[14] These receptors interact with a vast array of drugs and xenobiotics to regulate the expression of some of the most important drug-metabolizing enzymes and transporters (Table 1). Receptor activation may accelerate not only the metabolism of the drug itself but also that of other drugs given concomitantly. This can result in adverse effects including DDI, loss of efficacy or increased toxicity. It is therefore essential to evaluate whether a drug has the capability to interact with these receptors at therapeutically relevant doses. Today, possible drug–receptor interactions are routinely tested using in vitro methodologies, which have merit in that they are cost-effective and partially scalable to high-throughput screening. However, in the end, there is generally need for the evaluation of these predictions of induction/DDI in vivo, while the in vitro models have made significant progress over the years, there remain some limitations.[30]

For example, a more informative in vitro CAR transactivation assay is required as, because of their high constitutive activity, indirect CAR activators such as phenobarbital do not work, and the potential role of CAR splice variants in CAR activation is not routinely determined. There is also a limitation in the extrapolation of in vitro assays to the more complex in vivo situation. Indeed, issues surrounding in vitro/in vivo correlation (IVIVC) have been the subject of much debate and arise from the fact that the complexities of tissue distribution, free drug fraction, etc. are not taken into account in the in vitro assays. The humanized

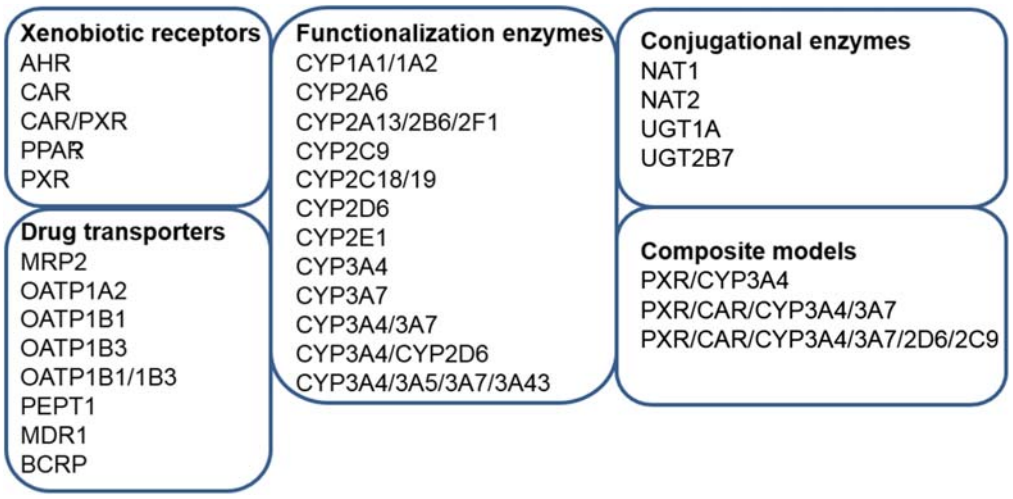

Fig. 1 Genetically humanized mouse models for proteins involved in drug metabolism and disposition. This figure is a modification of previous published work by Scheer, N.; Snaith, M.; Wolf, C. R.; and Seibler, J. Generation and utility of genetically humanized mouse models. *Drug Discov. Today* **2013** *18*(23/24), 1200–1211, with permission.

Table 1 Xenobiotic receptors regulating the gene expression of enzymes responsible for functionalization and conjugation (phase I and phase II) drug metabolism and transporters

Target genes	*PXR*	*CAR*	*PPAR*	*AHR*
Phase I	Cyp2b Cyp2c Cyp3a	Cyp2b Cyp2c Cyp3a	Cyp4a (Cyp3a)	Cyp1a Cyp1b1
Phase II	Ugts Gsts Sts	Ugts Gsts Sts	Ugts Gsts Sts	Ugts Gsts
Transporters	Mdr1 Mrp2 Mrp3	Mrp2 Mrp4	Mdr2 Cerp	Bcrp

Ugts, UDP-glucuronosyltransferases; *Gsts*, glutathione S-transferases; *Sts*, sulfotransferases; *MDR*, multidrug resistance; *MRP*, multidrug resistance protein; *Bcrp*, breast cancer resistance protein; *Cerp*, cholesterol efflux regulatory protein.
This table has been extracted from Scheer, N.; Wolf, C. R. Xenobiotic receptor humanized mice and their utility. *Drug Metab. Rev.* **2012**, *45*(1), 110–121, with permission.

receptor animal models, to a significant degree, bridge this gap. The DNA-binding domain of the receptors is usually highly conserved and the species differences in the activation of these receptors by drugs relate to sequence variability in the ligand-binding domains.[31] Applications of receptor-humanized mouse models and examples of their use are provided in Section "Examples of studies using receptor-humanized mice."

4.07.2.1.1 Examples of studies using receptor-humanized mice

The utility of the receptor-humanized mice has been demonstrated by a number of research groups by studying two potent mouse PXR activators (pregnenolone-16α-carbonitrile and dexamethasone) and rifampicin, which is a more selective human PXR activator. The first two compounds induce the expression of PXR-regulated downstream genes in wild-type (WT) mice but not in PXR-humanized mice, whereas the opposite was observed for rifampicin.[32–36] A number of compounds have been reported to activate CAR and its downstream genes in a species-specific manner. For example, the potent mouse CAR activator 1,4-bis[2-(3,5-dichloropyridyloxy)]benzene (TCPOBOP) showed profound induction of the downstream genes in WT animals but to a much lesser extent in humanized CAR mice.[35] The corresponding compound for activating human CAR, 6-(4-chlorophenyl)imidazo-[2,1-b][1,3]thiazole-5-carbaldehyde O-(3,4-dichlorobenzyl)oxime (CITCO), only showed elevated levels of CAR-activated genes in the humanized CAR mouse.[35] In contrast, phenobarbital induced a CAR signature in both WT- and CAR-humanized mice.[35]

Studies have also been performed using the AHR-humanized mouse model where induction of Cyp1a1 and Cyp1a2 genes by 2,3,7,8-tetrachlorodibenzop-dioxin (TCDD) and 3-methylcholanthrene was reported to be much more profound in WT controls compared with AHR-humanized mice.[37] This is in accordance with the fact that the mouse receptor has a higher binding affinity for these compounds than human AHR.[37] In addition, indirubin, a compound with higher affinity for the human receptor, was a more potent Cyp1a1 inducer in the AHR-humanized mouse hepatocytes than in WT samples.[38]

4.07.2.2 Functionalization (Phase I) and Conjugative (Phase II) Drug-Metabolizing Enzymes

Drug-metabolizing enzymes play a pivotal role in the bioavailability and clearance of a vast range of compounds and their metabolites consistent with their evolutionary role in detoxifying potentially harmful xenobiotics. It is widely accepted that the primary organ for metabolism is the liver, and this has led to the use of, for example, hepatocytes and hepatic microsomes as primary screens for metabolism in drug discovery and development. However, as discussed earlier, drug-metabolizing enzymes are also expressed in other organs such as the intestine, kidney, and lung.[39,40] These enzymes introduce new functional groups into xenobiotics via a range of oxidations, reduction or hydrolytic reactions, and the conjugation of suitable functional groups (preexisting or introduced) to endogenous molecules. The bulk of the oxidative reactions that introduce a functional group, such as a hydroxyl moiety onto the target molecule, are catalyzed by the super family of CYP enzymes. In addition to the CYP enzymes, which mediate approximately 75% of oxidative and reductive "functionalization" reactions in humans,[41,42] other enzymes such as the flavin-containing monooxygenases, monoamine oxidases, esterases, and amidases can also play a role in detoxification. Metabolites generated by these enzymes may either be eliminated directly from the body, undergo additional functionalization, or be subject to further biotransformation via conjugation to a range of polar endogenous substrates (most commonly, for example, sulfate and glucuronide but also including acetylation and conjugation to amino acids and glutathione). One major difference in the outcome of functionalization and conjugative metabolism is that the former can result in the production of active metabolites, while the second reaction produces metabolites that are (usually) less active than their substrates.[43] Conjugative metabolism, which can also occur directly on the parent drug itself if a suitable functional group is already present, in addition to providing a reduction in pharmacological/toxicological potency, also (usually) serves to increase the polarity of the xenobiotic/functionalized metabolite, which may aid elimination in urine or bile. Drug conjugation is catalyzed by a large

group of transferases, including the sulfotransferases (SULTs), UDP-glucuronosyltransferases (UGTs), glutathione S-transferases (GSTs), N-acetyltransferases (NATs), or amino acid transferases. It is important to note when looking at species differences in drug disposition that, following P450 reactions, glucuronidation by UGTs accounts for the largest proportion of drug metabolism in humans.[44] There are some major contributors to all UGT reactions with UGT2B7 being the most important (35%), followed by UGT1A4 (20%) and UGT1A1 (15%).[44]

4.07.2.2.1 Functionalization by cytochrome P450 enzymes: species differences

The CYP enzyme family is one of the most conserved across species and appears to have evolved from a single ancestral gene that originated more than 1 billion years ago.[7] Although there are highly conserved amino acid regions in P450s, there is great sequence and structural diversity between individual CYPs and between orthologous CYPs across species. These differences in amino acid sequences can give rise to profound differences in substrate specificity and catalytic activity. Furthermore, significant differences in the multiplicity and regulation of expression of CYPs also exist between species, and these differences are the major causes of the disparity in biotransformation between animals and human.[7] **Table 2** provides an overview of the similarities and differences in the number of major CYPs involved in drug metabolism in humans and the most commonly used preclinical animal species. However, even enzymes that are apparently conserved, according to this table, can show significant differences at a functional level. For example, while CYP1A1, CYP1A2, and CYP1B1 are present in human, mouse, rat, dog, and monkey with a $>80\%$ amino acid identity compared with human, the level and organ specificity of expression and the metabolic activity differ between species.[8,45,46] Thus, significant species differences in the interaction of compounds with drug-metabolizing enzymes sometimes limit the use of animal models to accurately predict human responses. Unforeseen DDIs can also result in adverse responses, life-threatening toxicity, or impaired efficacy. In order to overcome the limitation of traditional animal models in accurately predicting human responses, a large range of mouse models humanized for drug-metabolizing enzymes have been created (**Fig. 1**). Although such humanized mouse models have certain limitations (as further discussed later in this article), there is great potential for their use in basic research and in the testing and development of new medicines. As noted earlier, oxidative drug metabolism in humans mediated by cytochrome P450 enzymes is estimated to account for 75% of the total, and the bulk of this is performed by only 5 of the 57 human P450s (CYP1A2, CYP2C9, CYP2C19, CYP2D6, and CYP3A4).[41] The following section will highlight cases where mice expressing these human CYPs have been used.

4.07.2.2.2 Examples of studies using CYP P450-humanized mice

In recent years, a large number of CYP P450-humanized mice have been created. These models have application in studying the drug PK, DDI potential, and safety testing of compounds in drug discovery and development and for basic research into the function and QSAR of these enzymes. These models also have the potential to improve the prediction of PK/PD (pharmacodynamic) relationships and in the development of new in silico algorithms for extrapolation to human.

Most work using these models has been with CYP3A4-humanized mice. In the first reports of CYP3A4 transgenic models, the gene had been randomly introduced into the mouse genome without deletion of the mouse Cyp3a genes.[47] This resulted in intestinal, but not hepatic CYP3A4 expression in adult males. The CYP3A4 substrate, midazolam, when orally dosed to these mice and to WT mice was found to have significantly decreased Cmax, area under the curve (AUC) and bioavailability in the CYP3A4 transgenic mice. In addition, it was found that the PK profiles obtained for midazolam after intravenous administration were unchanged compared with the WT mice providing good evidence for the importance of the role of intestinal CYP3A4 in the first-pass metabolism of this compound.

Several other mouse models humanized for CYP3A4 have subsequently been developed; these include a model with liver-specific expression of CYP3A4 with or without deletion of the mouse Cyp3a gene cluster and a mouse line in which the Cyp3a gene cluster has been deleted and replaced with CYP3A4 and CYP3A7.[47–51] In a model where the mouse Cyp3a genes were not deleted, the AUCs of intravenously administered midazolam and cyclosporine A were significantly decreased compared with WT mice.[49,50] In addition, models with either selective gut CYP3A4 expression using an intestinal promoter or a combined model with both intestinal and hepatic CYP3A4 expression have also been generated.[50] The benefit of these models is that they allowed the relative contribution of hepatic and intestinal CYP3A4 to the pharmacokinetic profiles of the test compounds to be determined. In these studies, it was shown that intestinal rather than hepatic CYP3A4 expression decreased the circulating concentration of the chemotherapeutic agent docetaxel after oral administration, while hepatic expression largely accounted for the systemic clearance of intravenously administered drug.[50] This model has also been used to demonstrate that intestinal, but not hepatic, CYP3A4-related first-pass metabolism primarily determined the systemic exposure of triazolam or lopinavir following oral administration.[52,53] The model seems very promising in predicting a clinical outcome, based on the compounds studied; however, potential compensatory changes in murine cytochrome P450 expression need to be taken into account when using these mice.[54] For example, a significantly increased level of expression of mouse Cyp2c enzymes, which have midazolam hydroxylase activity, and compensatory effects in other genes involved in drug metabolism and disposition were identified in the Cyp3a knockout mice. These effects on the levels of CYPs in the knockout mouse were, however, reversed when human CYP3A4 was expressed in either the liver or intestine.[55] Thus, for some substrates, changes in PK may be masked in the knockout model by compensating changes in other metabolizing enzymes or transporters. For this reason, it is important to use the gene cluster KO models as a control in these experiments. Also, it should be noted that CYP3A4 expression in these models was driven off heterologous promoters. This can lead to unphysiologically high levels of expression, which could confound data interpretation.

Table 2 Major drug-metabolizing CYP families in human, rat, mouse, dog, and monkey[8]

Family	*Subfamily*	*Human*	*Mouse*	*Rat*	*Dog*	*Monkey*
CYP1	A	1A1, 1A2	1A1, 1A2	1A1, 1A2	1A1, 1A2	1A1, 1A2
	B	1B1	1B1	1B1	1B1	1B1
CYP2	A	2A6, 2A7, 2A13	2A6, 2A5, 2A12, 2A22	2A1, 2A2, 2A3	2A13, 2A25	2A23, 2A24
	B	2B6, 2B7	2B9, 2B10	2B1, 2B2, 2B3	2B11	2B17
	C	2C8, 2C9, 2C18, 2C19	2C29, 2C37, 2C38, 2C39, 2C40, 2C44, 2C50, 2C54, 2C55	2C6, 2C7, 2C11, 2C12, 2C13, 2C22, 2C23	2C21, 2C41	2C20, 2C43
	D	2D6, 2D7, 2D8	2D9, 2D10, 2D11, 2D12, 2D13, 2D22, 2D26, 2D34, 2D40	2D1, 2D2, 2D3, 2D4, 2D5, 2D18	2D15	2D17, 2D19, 2D29, 2D30
	E	2E1	2E1	2E1	2E1	2E1
CYP3	A	3A4, 3A5, 3A7, 3A43	3A11, 3A13, 3A16, 3A25, 3A41, 3A44	3A1/3A23, 3A2, 3A9, 3A18, 3A62	3A12, 3A26	3A8

This table is published with permission and originates from Martignoni, M.; Groothuis, G. M.; de Kanter, R. Species differences between mouse, rat, dog, monkey and human CYP-mediated drug metabolism, inhibition and induction. *Expert Opin Drug Metab Toxicol.* **2006**, *2*(6), 875–894.

Hasegawa et al.[56] used a humanized CYP3A4/3A7 model, lacking murine Cyp3a genes and also humanized for both CAR and PXR, to rank a range of PXR activators according to their potency to induce CYP3A4 expression in human liver, thus allowing a prediction of DDIs mediated by PXR/CYP3A4. Macleod et al.,[57] using the same model, investigated the role of the PXR/CYP3A4 axis in the disposition of the BRAF inhibitor vemurafenib. Vemurafenib activated PXR at clinically relevant concentrations, and while its disposition was more markedly affected through the regulation of efflux transporters than by CYP3A4 metabolism, there was a case for therapeutic monitoring in patients receiving concomitant medication, which might affect systemic drug levels and affect the outcome of vemurafenib therapy. The CAR/PXR/CYP3A4/3A7 model has also been used to study the role of the human enzyme in the disposition of the anticancer drugs.[58]

The PK of theophylline, predominantly metabolized by CYP1A2, has been investigated in a CYP1A1/1A2-humanized mouse model where the mouse Cyp1a2 gene had been knocked out. The systemic clearance of theophylline in the CYP1A1/1A2-humanized mouse was found to be significantly higher compared with the corresponding Cyp1a2 knockout line.[59] In contrast, oral administration of the polycyclic aromatic hydrocarbon benzo[*a*]pyrene resulted in high exposure in Cyp1a1 and Cyp1a1/1a2 knockout animals, but not in either WT, Cyp1a2 knockout, or CYP1A1/1A2-humanized mice lacking the mouse Cyp1a1/1a2 genes.[60] These results demonstrated the important role of human CYP1A2 in the metabolism of theophylline but not benzo[*a*]pyrene.

Validation of the CYP2A6-humanized mice was performed using the probe compound coumarin. The predicted role of CYP2A6 as the major coumarin hydroxylase in human liver was confirmed as clearance was significantly faster in the transgenic mice with hepatic expression of human CYP2A6 compared with WT controls.[61]

Tolbutamide is a CYP2C9 substrate, and its PK has been studied in WT, Cyp2c knockouts, and CYP2C9-humanized mice on a mouse Cyp2c cluster knockout background. The results showed lower plasma concentrations and AUCs in the WT and humanized mice relative to the knockout animals. These data correlated well with the in vitro results, which confirmed the in vivo contribution of the mouse Cyp2c enzymes and human CYP2C9 in the metabolism and disposition of this substrate.[62]

Debrisoquine is a well-known CYP2D6 probe substrate and has been used as a model compound for CYP-mediated biotransformation in humans and in investigations in both transgenic CYP2D6-humanized mice and chimeric liver-humanized mice (described later). Two different transgenic CYP2D6-humanized mouse models have been described. One carried the CYP2D6 transgene without deletion of the mouse Cyp2d gene cluster.[63] In the other model, the nine genes in the mouse Cyp2d gene cluster were replaced with the human CYP2D6 construct.[64] The systemic clearance of debrisoquine was significantly increased in both humanized models compared with WT controls.[63,64] This result demonstrated a clear species difference between the mouse Cyp2d enzymes and human CYP2D6 in the metabolism of debrisoquine. Evidence in support of this conclusion was the observation that there was no major difference in debrisoquine disposition between WT mice and a Cyp2d gene cluster knockout.[65] While these results confirmed the comparatively low catalytic activity of mouse Cyp2d enzymes toward debrisoquine, the clearance of bufuralol was found to be more rapid in WT compared with CYP2D6-humanized mice, an observation also seen in vitro.[65]

These published examples can be summarized as providing strong evidence that genetically humanized mouse models have significant potential in assessing the role of individual human CYPs in drug metabolism. It is important to note that in many of the humanized mouse lines, the human P450 genes are driven off their endogenous promoter and that they are also on a humanized CAR/PXR background. This allows studies to establish how variability in the expression of these genes affects drug PK and where there is an animal model available, drug efficacy. Also, mice have been made carrying humanizations involving multiple P450s and where the cognate mouse gene clusters have been deleted; for example, Scheer et al.[66] reported a multiple humanized mouse model in which 31 genes from the Cyp2c, Cyp2d, and Cyp3a gene clusters have been deleted and replaced with CYP2C9, CYP2D6, and CYP3A4/3A7, along with humanization for CAR and PXR.[66] These models simplify the interpretation of pharmacokinetic data and negate the need to use multiple individual humanized models if a drug is metabolized by multiple enzymes as is often the case.

4.07.2.2.3 Conjugation enzymes: species differences

Humanizations for the enzymes involved in drug conjugation have received much less attention relative to the P450s. Most of the focus has been on UGT-humanized mice due to the fact that glucuronidation accounts for the largest proportion of conjugation reactions in humans.[44] Within the UGT family, UGT2B7 is the major contributor to all glucuronidations (35%), followed by members of the UGT1A family, such as UGT1A4 (20%) and UGT1A1 (15%).[44] Even though a large number of drugs and their metabolites undergo glucuronidation and the fact that the UGT metabolism in the intestine has been reported to influence the PK of drugs, information concerning the differences in isoforms and their activities between species is limited.

The mRNA expression of 10 UGT isoforms in the intestine of humans and a number of preclinical animal models has been reported, and some of the UGT isoforms are selectively expressed by different species.[67–69] In the human intestine, UGT1A8 and UGT1A10 are selectively expressed,[68] whereas UGT1A2 and UGT1A7 were identified in rats[69] and UGT1A8 in monkeys.[70] However, different expression levels of these UGT isoforms among species may affect intestinal glucuronidation activity, and importantly, mRNA expression for UGTs might not reflect the actual levels of transcribed protein in the intestine and therefore its glucuronidation capacity.

4.07.2.2.4 Examples of studies using UGT- and NAT-humanized mice

The number of humanized mouse models where the UGTs have been humanized is few compared with the range of P450-humanized mice available (Fig. 1), and perhaps as a consequence, there are few reports of studies where UGT-humanized animal models have been utilized. Despite this, the role of UGTs and other conjugation systems remains an important area for

investigation. Caution may be needed when extrapolating PK data from laboratory animals to humans due to differences between isoforms and levels of enzymes expressed between different species. Even though the in vitro intrinsic clearance (CLint and UGT) in intestinal microsomes seems to provide a good correlation between humans and laboratory animals, values tended to be lower in humans than in preclinical animal models.[12] Selected studies where UGT-humanized animal models have been used are discussed in the succeeding text.

The role of UGT1A1 in clearance of 7-ethyl-10-hydroxy-camptothecin (SN-38) was investigated in a mouse model lacking the murine Ugt1 genes and expressing the human UGT1A1*28 allele. The humanized model showed minimal constitutive expression of hepatic UGT1A1 as expected, but even so, a significant increase in parent drug exposure in the humanized mice compared with WT controls following intravenous administration was observed.[71]

The clearance of naloxone and ezetimibe, considered to be substrates to UGT2B7 and UGT1A1, respectively, was also investigated in the same mouse model. However, only minor differences in the clearance between the WT and humanized mice were measured, suggesting no major contribution of UGT1A1 to the in vivo elimination of these compounds.[71]

Although most effort on conjugation reactions has been devoted to the UGTs, an NAT2-humanized mouse, with liver-selective expression on a mouse Nat1/2 null background, has been described. In this model, the AUC values of the human NAT2-selective substrate sulfamethazine were decreased by 97–98% compared with WT controls demonstrating the important role of this enzyme for clearance of this substrate.[72]

4.07.2.3 Drug Transporters

Drug transporters play an important role in the absorption, distribution, and elimination of drugs. This has resulted in a burgeoning literature and the issuing of guidance documents from FDA and EMA in the field.[73,74] In addition, the inhibition or induction of drug transporters can be a mechanism for pharmacokinetic-based DDIs and thus important from a safety perspective.[75] Predicting human PK and the selection of the starting dose in the clinic is challenging as data rely on several allometry-based approaches based on studies conducted in preclinical species such as rat, dog, and monkey. These methods generally perform poorly for transporter substrates due to species differences in substrate specificity for the transporters, differences in expression levels in various organs between species, and the lack of certain orthologues across species.[13]

4.07.2.3.1 Transporter-humanized mice

There are more than 400 human membrane transporters from the two major families, ATP-binding cassette (ABC) efflux pumps and uptake transporters from the solute carrier (SLC) group. In the regulatory guidance document, a relatively small number of transporters are thought to be of most important for drug development[73,74] and the following ABC transporters with most clinical relevance are P-glycoprotein (P-gp)/multidrug resistance (MDR) 1, MDR3, breast cancer-related protein (BCRP), bile salt export pump (BSEP), and the multidrug resistance proteins (MRP) 2, MRP3, and MRP4. The highlighted transporters in the SLC family are the organic anion-transporting polypeptide (OATP) 1B1, OATP1B3, OATP1A2, and OATP2B1; the organic anion transporter (OAT) 1 and OAT3; the organic cation transporter (OCT) 1 and OCT2; the peptide transporter (PEPT) 1 and PEPT2; and multidrug and toxin extrusion (MATE) 1 and MATE2-K.[76,77] Among these 20 transporters in focus, only a few humanized mouse models have been described to date including those for MRP2,[78] MDR1,[79] PEPT1,[80] BCRP,[81] OATP1A2, OATP1B1, and OAT1B3.[82–84]

4.07.2.3.2 Examples of studies using transporter-humanized mice

Two anticancer drugs methotrexate and paclitaxel have been used to investigate the role of transporters in drug bioavailability and disposition[84] and this study examined the influence of human OATP1 transporters on the PK of these drugs in OATP1B1-, OATP1B3-, and OATP1A2-humanized mice.

First, the roles of the mouse OATP1A and OATP1B proteins were illustrated. A significant decrease in liver uptake and an increase in plasma concentrations of both drugs were observed in mice where both transporter gene clusters of Oatp1a and Oatp1b had been knocked out. Human genes coding for OATP1B1, OATP1B3, or OATP1A2 were inserted in the knockout mouse line, and proteins were expressed selectively in the liver. In these studies, it was demonstrated that methotrexate showed significant, but relative to WT controls not completely restored, liver uptake in these three humanized transporter mice compared with the impaired liver uptake observed in the knockout model. The plasma concentrations of methotrexate were lower in the three humanized transporter mice than in the knockout model but not as low as observed in the WT mouse. Thus, methotrexate was found to be transported by all three human OATP1 proteins in vivo.

The reduced hepatic uptake observed in the knockout mouse dosed with paclitaxel was restored to WT levels in the OATP1B3 and in the OATP1A2 mice but not in the OATP1B1-humanized transporter mice. Thus, it was concluded that paclitaxel was transported only by OATP1B3 and OATP1A2, but not OATP1B1 in vivo. Less pronounced but similar effects of the plasma concentrations of the drug levels were observed at low doses of paclitaxel where a clearly reduced hepatic uptake seen in the Oatp1a/1b gene cluster knockout mouse was restored to WT levels in the OATP1B3 or OATP1A2, but not OATP1B1 transgenic mouse lines.

Cisplatin is commonly used for treatment of solid cancers even though the success of therapy is limited due to, for example, kidney injury by accumulation and toxicity of platinum. More than a third of the patients administered the drug develop signs of nephrotoxicity after receiving a single dose of cisplatin,[85] which will delay further treatment and limit the total number of chemotherapy cycles possible for an individual patient. The important role of the drug transporter MRP2 has been shown in

different in vitro assays to confer resistance to toxicity of cisplatin. Thus, Wen et al.[86] assessed the role of Mrp2 in mice in vivo. First, the Mrp2 knockout mice were compared with WT mice in which a twofold higher concentration of platinum was detected in the kidneys and livers of the knockout mice. Hence, the lack of an effective Mrp2 transporter seems to be linked to the in vivo toxicity of the drug. Cisplatin was also dosed to transporter-humanized MRP2 mice[86] in which the platinum concentrations and nephrotoxicity were similar to that of the WT mice and lower than seen for the knockouts. In summary, deficiency in Mrp2 lowers platinum excretion and increases susceptibility to kidney injury, which can be rescued by the human MRP2 orthologue.

These transporter models seem to be informative and helpful for gaining understanding of underlying mechanisms. However, it is important to remember that these mice still express murine transporters in addition to those that have been humanized and murine drug-metabolizing enzymes. Thus, in cases where there are multiple transporters and enzymes contributing to the elimination of drugs, it is still difficult to extrapolate the contribution of transporters to humans quantitatively based on humanized animal models alone.

4.07.3 Chimeric Liver-Humanized Mice

Taking together that drug-metabolizing enzymes and transporters differ between species, the use of a chimeric liver-humanized mouse, having most of its liver populated with human hepatocytes, provides an interesting complement to current preclinical species and genetically humanized mice. A number of different research groups have successfully generated chimeric liver-humanized mouse models, and the different strategies used to achieve the efficient repopulation of the mouse liver with human hepatocytes have led to several differently derived chimeric mouse models. Nevertheless, even though these chimeric mouse models are different, they do have some characteristics in common. First, to avoid rejection of the human transplanted cells, these mice need to carry deficiencies in certain components of the immune system. Secondly, the mouse hepatocytes need to be self-destructive to enable the liver to be "colonized" by the human hepatocytes, which can be achieved by genetic modifications resulting in toxicity within the murine liver cells. It is important to remember that even though the liver is humanized to a high degree, it is still in a mouse with metabolically active residual mouse hepatocytes. It is also important to know how well the human hepatocytes have repopulated the liver as it will have a direct impact on the results, and thus, the degree of humanization of the liver is determined by the replacement index (RI). The RI is the percentage of human hepatocytes in the liver of transplanted chimeric mice and is normally determined by measuring the concentrations of human serum albumin in the blood of the chimeric mice. RIs of up to 95% have been reported in almost all chimeric liver-humanized models. Here, the three most studied models are described: urokinase-type plasminogen activator (uPA)/severe combined immunodeficient (SCID) mice, FRG mice, and TK-NOG mice.

The uPA/SCID mouse, developed in the 1990s, was the first chimeric liver-humanized mouse to be described[87–89] and, as a result, is also the most published of the three models discussed here. This model is based on a SCID mouse, which is a mouse that lacks functional B and T cells, which are important cells in providing an immune response. The model has an albumin-promoted uPA gene inserted in the liver that results in expression of the liver toxic serine protease uPA, which destroys the native murine hepatocytes to allow donor-derived hepatocyte engraftment and proliferation.

The FRG mouse has three genes knocked out. The R stands for the recombination-activating gene 2 (Rag2) and G for the IL-2 receptor subunit g (IL2RG). By knocking out these two genes, an immunocompromised mouse, which lacks B and T cells and NK cells, respectively, is generated.[90] The F in FRG denotes the lack of fumarylacetoacetate hydrolase (FAH), which accounts for the liver failure associated with type 1 hereditary tyrosinemia (TH1) in humans. The lack of the FAH enzyme results in increased, and toxic, amounts of metabolites produced in the catabolic pathway of tyrosine, which is fatal. Both mice and humans survive the disease when treated with 2-(2-nitro-4-trifluoro-*O*-methylbenzoyl)-1,3-cyclohexanedione (NTBC), which inhibits the 4-hydroxyphenylpyruvate oxidase enzyme that generates the toxic metabolites. Thus, the FRG mice transplanted with human hepatocytes are "cycled" on NTBC to ensure that the animals survive with engraftment of human hepatocytes and destruction of the mouse hepatocytes occurring during the periods of NTBC withdrawal.

More recently, another chimeric liver-humanized mouse model TK-NOG, with inducible liver injury, was described.[91] Mouse hepatocyte ablation was achieved here through the liver-specific expression of the herpes simplex virus 1 thymidine kinase (HSVtk) in severely immunodeficient NOG mice. Ganciclovir (GCV) is normally nontoxic, but when administrated to these mice, it is converted by HSVtk into a toxic intermediate, which destroys the native hepatocytes.

4.07.3.1 Examples of Studies Using Chimeric Liver-Humanized Mice

In the preceding sections, selected examples of the use of genetically humanized mouse models were described, while in this section, a similar selection of representative examples for applications of chimeric liver-humanized mice is given.[11,92–99] The chimeric mouse livers have been shown to have expression levels and enzymatic activity of major human P450s and conjugation enzymes similar to that of the donor human hepatocytes.[100–102]These mice also demonstrate a humanlike susceptibility to inhibition and induction of the P450s,[100,103–105] which make these models interesting to study, while the concomitant presence of other human drug receptors and drug-metabolizing enzymes (for both functionalization and conjugation) and transporters provides a further level of sophistication.

4.07.3.1.1 Inhibition and induction studies

The inhibition of the metabolism of debrisoquine by quinidine was studied by Katoh et al.[106] Quinidine is a typical CYP2D6 inhibitor in human and a frequently prescribed antiarrhythmic drug. Debrisoquine is a well-known CYP2D6 substrate forming a human-selective 4-hydroxy metabolite excreted in urine when dosed to human. In rats and mice, there exist many isoforms of the CYP2D subfamily, and the large interspecies difference in the CYP2D6 substrate specificity is likely due to differences in levels of expression and the actual isoforms expressed.[107,108] In this study in chimeric uPA/SCID mice, the human-selective metabolite 4OH-debrisoquine was observed at significantly higher concentrations in the highly humanized chimeric mice (RI $>70\%$) compared with mice with a RI of less than 10%. The quantities of the metabolite decreased in the highly humanized mice when pretreated with quinidine, a selective CYP2D6 inhibitor, and the already small amounts of the metabolite in mice with a lower degree of humanization remained at the same level regardless of the quinidine pretreatment. The overall conclusion of the study was that the chimeric mice with a high RI exhibited a humanized profile of drug metabolism and the inhibition of P450 compared with the control and low RI chimeric mice.

Induction of CYP3A4 in chimeric liver-humanized mice was investigated using dexamethasone as a probe drug and rifampicin as a model drug to induce the enzyme.[103] The urinary excretion of 6β-hydroxydexamethasone and parent compound was measured before and after rifampicin treatment showing that the metabolic ratio (metabolite/parent) was significantly increased after rifampicin treatment. It was also shown by immunohistochemical staining that CYP3A4 was increased after rifampicin treatment. Hence, such chimeric liver-humanized mice could potentially be useful for detecting the induction of CYP3A4 using rifampicin[103] and similar compounds.

4.07.3.1.2 Biotransformation studies

Many research groups have now made studies on humanized chimeric liver mice to evaluate whether these mice can repeat the in vivo human metabolic profile of various xenobiotics. Representative examples of these applications include the CYP2D6-mediated metabolism of debrisoquine to 4-hydroxy debrisoquine[106] described earlier, the CYP2C9-catalyzed conversion of S-warfarin to 7-hydroxywarfarin,[109,110] the comparison with human metabolic profiles of three different GSK drug candidates[111] the metabolism of midazolam,[96] the prediction of human metabolism of FK3453 by aldehyde oxidase (AO),[98] the AO-catalyzed oxidation of zaleplon,[99] and the metabolism of ibuprofen and naproxen.[97] In addition to these studies, Bateman et al.[92] also evaluated the chimeric liver-humanized mouse model for prediction of human hepatobiliary drug metabolism and excretion using a series of compounds known to have a qualitatively distinct metabolic profile in humans relative to rodents. The compounds used in this study were lamotrigine, diclofenac, a Merck drug candidate (named MRK-A), and propafenone. Chimeric liver-humanized mouse models have also been used to study the nonspecific binding by reactive intermediates from idioscyncratic hepatotoxicants to human proteins[112,113] and to investigate the fate of troglitazone,[114,115] an idiosyncratic hepatotoxin in humans.

In human but not in mice, S-warfarin is predominantly metabolized to S-7-hydroxywarfarin, a reaction catalyzed by CYP2C9. As alluded to earlier, following warfarin administration, the concentration of S-7-hydroxywarfarin in the plasma of chimeric mice was approximately sevenfold higher than that in control mice. In addition to in vivo studies, the biotransformation was assessed in vitro using microsomes prepared from chimeric liver-humanized mice, and these showed a 10-fold higher 7-hydroxylase activity compared with those obtained from control mice. Furthermore, this reaction was markedly inhibited by sulfaphenazole in the chimeric liver microsomes, whereas the 7-hydroxylase activity of control mouse microsomes was unaffected.[109,110]

Three candidate drugs (**Fig. 2**) were selected by Serres et al.[111] because of qualitative and/or quantitative differences in routes of metabolism that were observed between humans and the preclinical species. For both the tetrahydroisoquinoline and benzophenone analogs, hepatic metabolic clearance was predominant in the preclinical species and humans. When investigated to assess the ability of chimeric liver-humanized mice to produce the human metabolites circulating systemically, the metabolism and disposition were found to be well represented for the benzophenone analog but less well in the case of tetrahydroisoquinoline. For the third test compound, a fluoropyrrolidine analog, the hepatic and extrahepatic metabolic clearance was used as a probe to see how well the chimeric mice would predict the urinary excretion of the metabolites seen in humans where the renal excretion of drug-related material was higher than found in mice. In the case of fluoropyrrolidine, the authors found that the chimeric mice were somewhat representative of the human situation, and they suggested that, while limitations for the prediction of human metabolism and disposition clearly exist, humanized chimeric mouse models can potentially provide informative new tools in drug discovery and development.[111]

Both ibuprofen and (S)-naproxen are nonsteroidal antiinflammatory drugs metabolized by P450 and UGT, SULT, and amino acid N-acyltransferase for taurine conjugation in the liver. A direct comparison of excretory metabolites in urine between chimeric liver-humanized mice and the published human data was made after administration of these two NSAIDs. Good agreement for the urinary excreted metabolites (percentage of dose) was observed between chimeric and human, providing further evidence that the chimeric liver-humanized mice should be helpful for predicting the quantitative metabolic profiles of drugs mediated by both P450 and conjugation routes in the liver.[97]

The aldehyde oxidase function of chimeric liver-humanized mice was investigated in two studies. In the first study of these species differences, the metabolism of the probe drug FK3453 was assessed using chimeric mice transplanted with either human or rat hepatocytes. Higher concentrations of the human-specific aldehyde oxidase-generated metabolite were present in the excreta for mice modified with human compared with rat hepatocytes, and a twofold higher clearance of the parent compound was observed in the former model. These results were in concordance with the known in vivo PK and metabolism of FK3453 determined

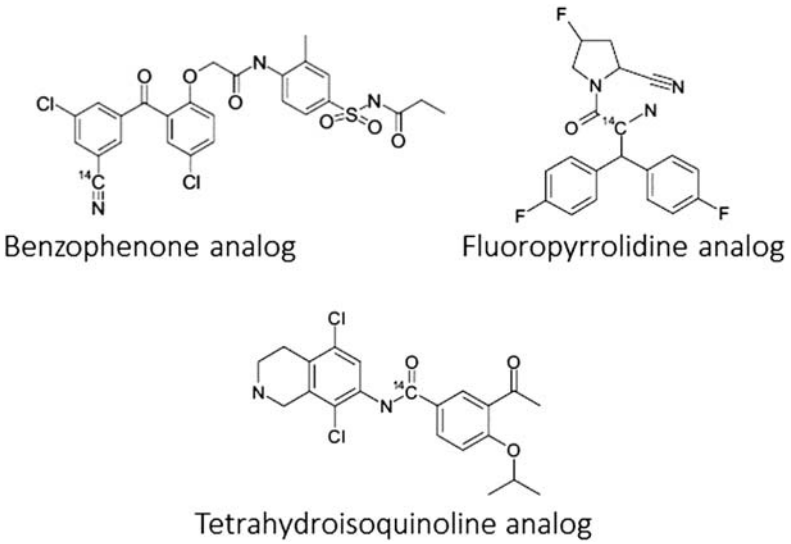

Fig. 2 Structures of benzophenone, fluoropyrrolidine, and tetrahydroisoquinoline. Reproduced from De Serres, M.; Bowers, G.; Boyle, G.; Beaumont, C.; Castellino, S.; Sigafoos, J.; Dave, M.; Roberts, A.; Shah, V.; Olson, K.; Patel, D.; Wagner, D.; Yeager, R.; Serabjit-Singh, C. Evaluation of a chimeric (uPA+/+)/SCID mouse model with a humanized liver for prediction of human. *Xenobiotica* **2011**, *41*(6), 464–475, with permission.

in human and rat.[98] In the second study using zaleplon , which is metabolized to 5-oxo-zaleplon by AO, the results showed that the in vivo concentrations of 5-oxo-zaleplon in the plasma of the chimeric liver-humanized mice were about sevenfold higher than that in control mice.[99]

Bateman et al.[92] investigated the use of chimeric liver-humanized mice using compounds metabolized via oxidation and glucuronidation. The four model drugs lamotrigine, diclofenac, MRK-A, and propafenone were known to exhibit human-specific metabolism. The results demonstrate that chimeric liver-humanized mice were able to reproduce the human-specific metabolite profile for lamotrigine, diclofenac, and MRK-A. However, in the case of propafenone, the metabolite profiles in native and humanized mice were similar and thought to be due to the presence of residual highly active propafenone-metabolizing mouse enzymes in chimeric mice.

The PK and metabolic fate of midazolam after the administration of doses of 0.1, 1, and 10 mg kg^{-1} PO to chimeric liver-humanized and control mice showed significant PK differences between the two with a higher Cmax in the humanized mice and a 14-fold greater exposure to 1′-hydroxymidazolam than to midazolam in the controls.[96] Overall metabolism of midazolam was faster in control versus humanized mice such that no PK profiles could be generated for midazolam in the former following dosing at 0.1 mg kg^{-1}. Both oxidative and conjugative metabolites were detected in the humanized mice with the major circulating metabolites observed in blood (1′-hydroxymidazolam, 4′-hydroxymidazolam, 1′,4′-dihydroxymidazolam, and 1′-hydroxymidazolam glucuronide, corresponding to those seen in humans). In contrast, two of these (4′-hydroxymidazolam and 1′-hydroxymidazolam glucuronide) were absent from samples of control mice, suggesting that the chimeric liver-humanized model might provide a suitable means of predicting circulating human metabolites. These differences are illustrated in the mass chromatograms obtained from pooled blood samples from these mice shown in **Fig. 3**.[96]

The PK, metabolism, and toxic effects of troglitazone were studied following PO administration at 300 and 600 mg kg^{-1}, for 7 days to chimeric liver-humanized and control mice.[115] PK profiles showed similar Tmax values for troglitazone in both groups but with three- to five- and two- to fivefold higher Cmaxs and AUCs, respectively, seen for the humanized animals. Both oxidative and conjugative metabolisms were observed with the primary oxidative pathways in humanized and control mice being mono- and dioxidations but no evidence of glutathione conjugation. With respect to conjugations, a sulfate was seen in greater amounts in humanized mice (4- to 13-fold higher in the liver and blood, respectively), where the major conjugate in control animals was instead a glucuronide. Several of the metabolites detected were unique to the humanized mice only, and the profiles generated in these animals were considered to be similar to those seen in humans. With respect to toxicity, standard clinical chemistry did not show any changes that could be linked to adverse effects on the livers of either mouse line; however, immunohistochemistry showed that human MRP2, but not mouse Mrp2, was downregulated as a result of exposure to troglitazone for 7 days. In a subsequent study[114] where troglitazone was dosed to the humanized mice for 14 or 23 days at 1000 mg kg^{-1} day^{-1} PO, it was seen that circulating ALT was increased by 2.1-fold at 14 days and 3.6-fold after 23 days administration. When coadministered with L-buthionine sulfoximine (BSO), this increase in ALT was not seen, suggesting that the production of reactive metabolites/glutathione depletion was not involved in the drug-related hepatotoxicity (a hypothesis supported by further measurements of hepatic GSH content, oxidative stress markers, and drug-metabolizing enzymes). The conclusion from both of these studies was that humanized mice may provide an animal model for studying the effects of idiosyncratic liver toxins such as troglitazone.

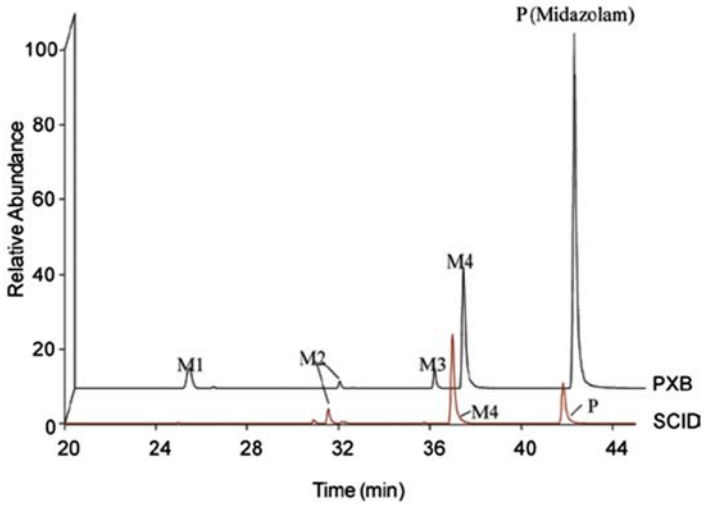

Fig. 3 Composite extracted mass chromatograms for midazolam (m/z 326, P), 1′-hydroxymidazolam glucuronide (m/z 518, M1), 1′,4′-dihydroxymidazolam (m/z 358, M2), 4′-hydroxymidazolam (m/z 342, M3), and 1′-hydroxymidazolam (m/z 342, M4) in chimeric liver-humanized mouse (PXB) and control mouse (SCID) blood samples. These traces are based on a pooled sample (samples from 0.083 to 3 h postdose) utilizing the AUC proportional manner.[96] Reproduced from Samuelsson, K.; Pickup, K.; Sarda, S.; Swales, J. G.; Morikawa, Y.; Schulz-Utermoehl, T.; Hutchison, M.; Wilson, I. D. Pharmacokinetics and Metabolism of Midazolam in Chimeric Mice With Humanised Livers. *Xenobiotica* **2012** *42* (11), 1128–1137, with permission.

Yamazaki et al.[112] studied the nonspecific binding of radiolabeled drugs to human proteins in chimeric liver-humanized mice. Hepatotoxic effects in humans were observed after treatment with a potential analgesic agent, 5-*n*-butyl-7-(3,4,5-trimethoxybenzoylamino)pyrazolo[1,5-a]pyrimidine, leading to its withdrawal from development. As the hepatotoxicity seen in humans was not predicted from regulatory animals or in vitro studies, an attempt was made to identify the underlying mechanism by dosing the structurally related model compound 5-*n*-butyl-pyrazolo[1,5-a]pyrimidine to chimeric liver-humanized mice and comparing these with mice transplanted with rat hepatocytes. The in vivo production of glutathione conjugates and concomitant covalent binding was studied following IV dosing to the mice with covalent binding to liver proteins detected over a period of 0.17–24 h postdose. Chimeric liver-humanized mice were seen to form a 3-hydroxy metabolite and its corresponding glutathione conjugate (detected in both the plasma and liver), while, in contrast, mice engrafted with rat hepatocytes formed a number of rat-specific metabolites. Bioactivation of 5-*n*-butyl-pyrazolo[1,5-a]pyrimidine was found to result in the radiolabel binding nonspecifically to a variety of cytosolic and microsomal proteins, including human P450 1A2, in the livers from chimeric humanized mice with hepatotoxicity perhaps the result.

There is now an extensive literature in the area of biotransformation utilizing chimeric humanized mice, and the results from these studies, including those discussed earlier, demonstrate that chimeric mice were able to reproduce the human-specific metabolite profiles for a many, but not all, of compounds investigated. One has to remember that apart from the liver, all the remaining parts and organs are still those of a mouse. Overall, for compounds where the major site of metabolism is in the liver, these data indicate that chimeric mice with humanized livers have the potential to be a useful tool for the prediction of human-specific metabolism of xenobiotics and warrant further investigation.

4.07.4 Differences Between Genetically Humanized Mice and Chimeric Liver-Humanized Mouse Models

Both genetically humanized and chimeric liver-humanized mouse models have advantages and disadvantages depending on their inherent differences.[116] One characteristic difference between the two models is that the genetically humanized mice are most likely to be modified throughout the whole body where the target gene is naturally present, while the humanization in chimeric liver-humanized mice is, self-evidently, restricted to the liver tissue. However, even though only this single organ is humanized, the human hepatocytes therein have all genes, proteins, and pathways of human origin, while in contrast, even in the most complex, genetically humanized mouse model, with multiple human genes present, they still represent only a minority on a mouse background. Another advantage of the chimeric liver-humanized mouse is that, for certain models, transplantation is possible using hepatocytes from donors with specific features, such as natural polymorphisms in drug-metabolizing enzymes or transporters or from diseased patients. In addition to primary hepatocyte transplantation, it is also possible to simultaneously insert human liver cancer cells to give a combined model. In one such study, Fujiwara et al.[117] divided mice into two groups, one of which was transplanted with human gastric cancer cells (GCCs) alone, while the second received both h-GCCs and human hepatocytes. In this second group, GCCs and hepatocytes repopulated the host liver with colonies of cancer cells forming around the human

hepatocytes to give "typical adenocarcinomatous glandular structures." Human hepatocyte-colonized mice also contained metastasized GCCs, which were not seen for those animals only colonized with the cancer cells alone. The authors concluded that this could be a useful humanized liver animal model for studying liver cancer metastasis in vivo, which would allow drug efficacy testing studies of these cells in a contextual and physiological environment, with human liver metabolism.[117]

A clear drawback of the chimeric liver-humanized mice is the presence of residual mouse liver, which may still represent a significant capacity for biotransformation, especially as livers in such chimeric animals are often 2–2.5 times larger than that of the WT mouse. The number of mouse cells in the chimeric liver is therefore still high. Thus, even in the case where the mouse has an RI of 90% and the remaining 10% may not, at first sight, seem to contribute greatly to the overall metabolic fate of a drug, their presence may complicate interpretation. This may have important consequences, particularly if a compound is efficiently metabolized by a particular drug-metabolizing enzyme present in the mouse but less well represented in humans, such that the rate of metabolism of this compound differs greatly between mouse and human hepatocytes.[92]

The genetically humanized mice, on the other hand, carry the risk of compensatory gene expression, which may change the PK and metabolism of a drug. That said, compared with knockout models, the expression of proteins involved in drug metabolism and disposition in genetically humanized mouse models indicates that this might not be of general concern. However, when knockout models are used as a control for a genetically humanized mouse model, it is recommended that the effect of potential changes in the expression of mouse pathways is taken into account, specifically if these pathways can contribute to the metabolism and disposition of the compound under investigation. Even so, the knockout controls should be seen as an advantage for using the genetically humanized mice. Thus, the availability of genetic knockout controls for a given human gene could be used as a complement to assess the relevance of the corresponding human gene product in the metabolism, disposition, or toxicity of a drug. Importantly, knockout control mice are available for most genetically humanized mice.

The organ responsible for metabolism does matter; however, since the liver is the predominant metabolizing organ in the body, one will be able to find metabolites of drugs derived from human liver enzymes in both chimeric and genetically humanized mice. On the other hand, in compounds known to be metabolized in organs other than the liver, when the liver does not represent the predominant metabolizing organ, no human-selective biotransformation is likely to be observed in chimeric liver-humanized mice. Hence, it is important to know if the compound intended to be dosed to a chimeric liver-humanized mouse predominantly is metabolized by the liver or not.

It is also important to remember that extrahepatic metabolism and transport can make major contributions to the fate of a drug in the human body even though the liver is the dominant organ of drug metabolism and disposition for many compounds.[118]

The chimeric liver-humanized mice make it feasible to use the same human hepatocytes for in vitro and in vivo applications. Primary human hepatocytes can be serially transplanted into the FRG model, and thus, it is possible to increase the number of human cells for in vitro applications.[90] A more accurate IVIVC could be established with this approach and also improve the extrapolation to the clinical situation.

Furthermore, there are other differences that may not be related to the outcome of DMPK investigations. A clear advantage of the genetically humanized compared with their chimeric counterparts is the ease of maintaining the models by simple breeding or cryopreservation of embryos or sperm. In the case for the chimeric liver-humanized mice, each individual mouse needs to be individually transplanted, and the humanization cannot be propagated to the next generation. The differences in how these two models are generated are evidently mirrored in cost of production and the variability between individual mice. The generation of chimeric liver-humanized mice is currently significantly more expensive compared with genetically humanized animals with a cost of a few thousand dollars for a chimeric liver-humanized animal compared with a few hundred dollars per genetically humanized mouse. The relatively high cost of chimeric liver mice is partly due to the fact that the RI in a group of mice will vary; thus, it is almost necessary to set a threshold for RI, for example, $>90\%$ for mice to be used in a study. Hence, a larger number of mice need to be transplanted compared with what will be used in the study, which of course will increase the costs of the mice.

Both types of humanized models are promising complements to traditional in vitro assays, but whether they will be suitable for the long-term (>1 month) toxicity studies required for drug registration has, however, yet to be established. Therefore, these models might help to understand the mechanism of toxicity of such compounds or to evaluate hepatotoxic potential before the first time in man (FTIM or FDIM if one chooses to use the term first dose in man).

4.07.5 Additional Models

The relative contribution of hepatic versus extrahepatic oxidative metabolism is an important factor for the bioavailability and thus also the therapeutic efficacy of a drug. Predicting the clearance of a drug in relation to the P450 metabolism of the drug is critical for new compounds and their progression in the preclinical phase of drug development.[119,120] Additionally, understanding the causes of poor oral bioavailability can also represent a challenge. In order to understand the factors that limit bioavailability and thereby optimize oral drug delivery, it is essential to characterize the contribution of first-pass metabolism in the gut and in the liver. A number of knockout models have been created that enable assessing the contribution of P450s to hepatic and gut/hepatic first-pass metabolism, and two such mouse models, the HRN mouse and the ERL mouse, are described in the succeeding text.

In the HRN mouse, the hepatic cytochrome P450 reductase (POR) is selectively "knocked out," which results in mice that are null only for the liver, but not in other tissues such as the gastrointestinal tract, kidney, and lung.[21] In the absence of a functional P450 reductase enzyme, the ability to reduce oxidized P450s via the transfer of an electron from NADPH via POR is no longer

possible, resulting in the loss of hepatic P450 activity. The HRN mouse provides obvious opportunities, especially in combination with studies using a WT strain, to investigate hepatic P450-related and also conjugative metabolism independently. Furthermore, the HRN mouse can potentially be used to determine whether P450-related metabolism or conjugation reactions are responsible for any covalent binding to cellular macromolecules in the liver, thus aiding the understanding of the relative contribution of such biotransformations to any hepatic effects observed in vivo. An example of the differences that can be seen between control and HRN mice is shown by studies on the metabolism of diclofenac[121] after a single 10 mg kg^{-1} PO dose to WT and HRN mice. In the case of the HRN animals, most of the [^{14}C]-diclofenac-related material was found in the urine/aqueous cage wash within 12 h of administration (~82%) with recovery from the control mice somewhat slower with ca52% found in urine and 15% in feces by 24 h postdose. Metabolism in the HRN mice was dominated by conjugation to either taurine or glucuronic acid to the carboxyl function, while the WT mice showed both oxidative and conjugative metabolisms. Covalent binding studies, however, showed no differences. The ^{14}C profiles obtained from urine for both HRN and WT mice are shown in Fig. 4, and the metabolic fate of diclofenac is illustrated in Fig. 5. The absence of large amount of oxidative metabolites attributable to P450-related metabolism in the HRN mice clearly indicates that the bulk of metabolism for the drug was hepatic. In contrast, when the metabolism of midazolam was studied in these mice while there was a significant increase in AUC compared with WT animals, a considerable amount of oxidative metabolism was still seen, clearly implicating extrahepatic metabolism of the drug and highlighting the utility of the model is detecting such effects.[122]

The benefit of the ERL mouse compared with HRN is that it allows direct comparison of hepatic and intestinal contributions of cytochrome P450 metabolism. In this mouse line, the Cre recombinase is driven off the endogenous Cyp1a1 gene promoter. This line was then crossed onto a floxed POR mouse to generate the ERL mouse.[20] In order to eliminate the expression of POR in both the liver and the small intestine, the mouse is dosed with a 40 mg kg^{-1} of the Cyp1a1 inducer 3-methylcholanthrene (3MC). To generate a mouse that holds the characteristics of an HRN mouse, with only elimination of the POR expression in the liver, the ERL mouse is dosed with 3MC at a 4 mg kg^{-1}. This enables the investigator to examine the effects of deleting both hepatic and intestinal

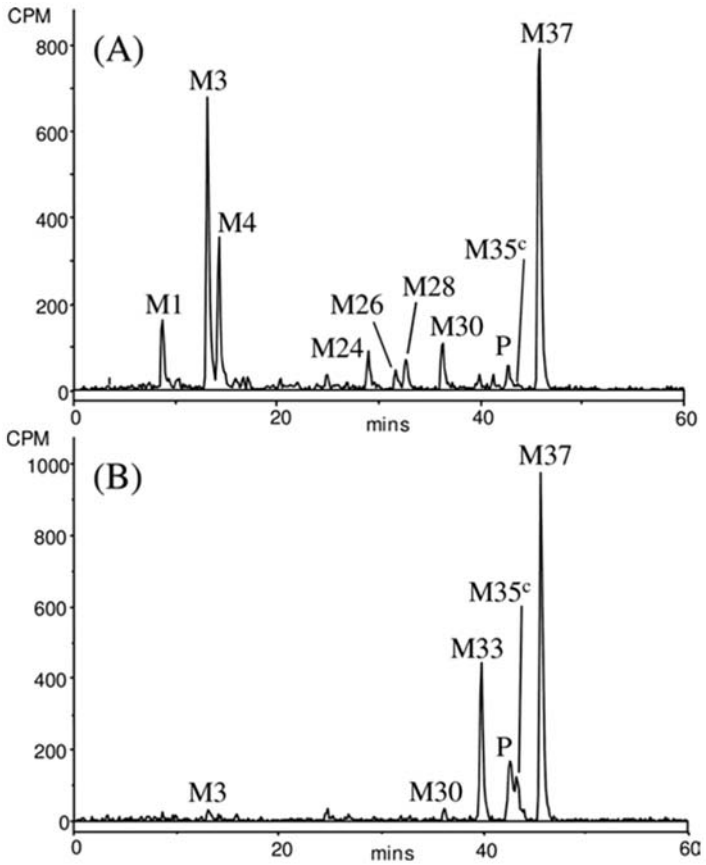

Fig. 4 Representative HPLC–RAD urinary profiles following a single oral dose of 10 mg kg^{-1} [14C]-diclofenac for the samples containing the highest proportion of the dose for each strain: (A) C57BL/6J (12–24 h) and (B) HRN mice (0–12 h). M35c represents a cluster of radio-peaks corresponding to 2,3,4-α/β transacylated acylglucuronide isomers.[121] Pickup, K.; Gavin, A.; Jones, H. B.; Karlsson, E.; Page, C.; Ratcliffe, K.; Sarda, S.; Schulz-Utermoehl, T.; Wilson, I. The Hepatic Reductase Null Mouse as a Model for Exploring Hepatic Conjugation of Xenobiotics: Application to the Metabolism of Diclofenac. *Xenobiotica* **2012**, *42* (2), 195–205, with permission.

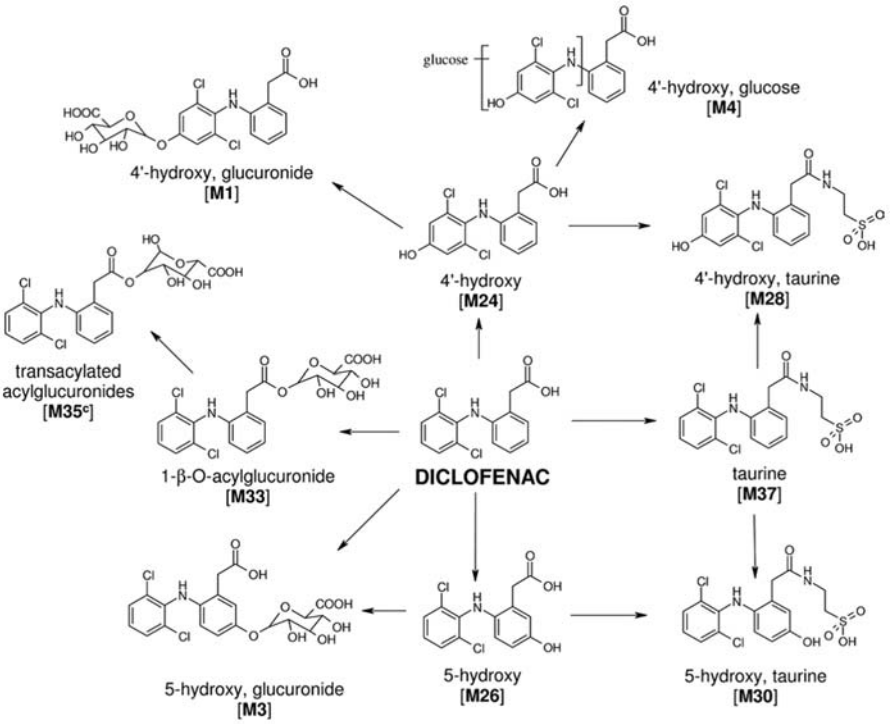

Fig. 5 The major metabolites of diclofenac seen in HRN and C57BL/6J mice as reported by Pickup et al.[121] Pickup, K.; Gavin, A.; Jones, H. B.; Karlsson, E.; Page, C.; Ratcliffe, K.; Sarda, S.; Schulz-Utermoehl, T.; Wilson, I. The Hepatic Reductase Null Mouse as a Model for Exploring Hepatic Conjugation of Xenobiotics: Application to the Metabolism of Diclofenac. *Xenobiotica* **2012**, *42* (2), 195–205, with permission.

P450-related metabolism at will to determine the relative importance of first-pass metabolism of these two important organs, as was demonstrated in studies on the PK of paroxetine, midazolam, and nelfinavir.[20]

These two models may also be of benefit to investigators by the fact that plasma concentrations of drugs with poor bioavailability due to presystemic metabolism by CYPs should be increased in their absence so that efficacy studies can be performed in mouse that would otherwise not be practicable. In addition, metabolism via conjugation of the parent molecule can be more clearly defined in drug disposition studies, as can non-P450-related metabolism. However, in addition, such studies may also act as a guide for the selection of the most appropriate humanized mouse model to choose, as discussed in the succeeding text.

4.07.6 How to Choose a Humanized Mouse Model?

Both the genetically humanized and chimeric liver-humanized mouse models can potentially mimic the human situation in terms of generation of human-selective metabolites and thus produce a humanlike metabolite profile. In addition to simply predicting the metabolic fate of the compound, they have been used to assess the PK and distribution of drug and metabolites and factors such as enzyme induction/inhibition and DDIs (see aforementioned text).

The choice of model (genetically humanized or chimeric) to use needs to be decided on a case-by-case basis as it depends on the question to be answered, which in turn will be defined by facts gathered from previous in vitro and preclinical in vivo assays. While these will be specific for each individual compound, it is still possible to provide some general guidance for the selection of the most appropriate strategy for using these models in problem solving/decision-making. So, in discovery, there may be good data on the metabolites produced from hepatic microsome/hepatocyte incubations, suggesting that there may be unique human metabolites or predicting a risk for unwanted DDIs. In addition, some of the individual P450s/transporters may have been identified as contributing to this potential risk. However, at this stage and in the absence of any IVIVC, it is difficult to recommend the application of any of these models. First, in vivo data may indicate or substantiate a potential risk, which might require further assessment. At this point, it might therefore become important to know the in vivo site of metabolism (hepatic, extrahepatic, and a mixture of both) in order to be able to decide on whether or not a liver only modified chimeric/humanized mouse represents a way forward or not. This information is important in order to avoid unnecessary efforts in dosing a drug to precious chimeric liver-humanized mice, if the problem is not targeted on hepatic uptake, metabolism, or efflux. The HRN and the ERL mouse models may be useful in enabling the site(s) of metabolism for the compound of interest to be determined.

In instances where extrahepatic metabolism via one or a few P450s (or transporters) is considered the most likely cause of the problem under investigation (e.g., a potential DDI or induction of a specific P450), then a chimeric liver-humanized mouse is not the optimum solution. In this situation, a genetically humanized mouse model, specifically modified to express the required human proteins, may represent a better means of investigating the problem, at lower cost.

If the role of individual, defined proteins in drug metabolism, disposition, or toxicity, is to be investigated, the genetically humanized mice are usually preferred, both on the basis of expense compared with chimeric humanized animals and the general availability of both knockout and WT controls, which enables the dissection of the function of a particular human P450 or transporter protein.

Where it seems clear that metabolism is hepatic but the route by which the metabolite is produced is not known or the desire is to predict a potentially complex human metabolite profile, detect/confirm unique human metabolites, etc., then the chimeric liver-humanized mice are the first choice. Essentially chimeric liver-humanized mice can be used to study the liver metabolism of all types of small molecules without any knowledge of the enzymes involved in their turnover. The chimeric liver-humanized mice, which of course have the whole panoply of human hepatic drug-metabolizing enzymes and transporters, may also represent the preferred model for hepatotoxicity testing, which provides the possibility to study the susceptibility of human hepatocytes to the toxicity of a compound and is probably more relevant to human than assessing an effect on mouse hepatocytes in a genetically humanized mouse model.[123,124] Perhaps of note in this respect is the observation by Schulz-Utermoehl et al.[115] that transporter effects caused by troglitazone administration were only observed in the human hepatocytes, but not the residual mouse hepatocytes in chimeric liver-humanized mice. On the other hand, the use of genetically humanized mouse models might add value in understanding the mechanism of action of a hepatotoxic drug when the enzymology has been properly defined. Apart from liver toxicity, genetically humanized mice offer the opportunity to study drug toxicity in extrahepatic tissues.

The same arguments apply to the choice of chimeric liver-humanized mouse or genetically humanized mouse in DDI studies. If the test compound is cleared via hepatic metabolism and in vitro studies indicate multiple enzymes to be involved in its turnover and the codrug inhibits or induces any of these enzymes, chimeric liver-humanized mice might be the preferred model. If it is a single enzyme that dominates the metabolism of the drug such as CYP3A4, any of the two types of models could be used. If oral administration is the preferred route of dosing and gut metabolism significantly contributes to first-pass metabolism of the drug, a genetically humanized mouse with intestinal expression of the desired drug-metabolizing enzyme or transporter would be a better choice than a chimeric mouse.

The selection of the appropriate model for its ability to accurately predict human drug clearance by employing genetically humanized or chimeric liver-humanized mouse models (either alone or in combination) is not trivial and greatly benefits from a proper understanding of the characteristics of both the compound itself and the earlier described advantages and limitations of the humanized models.

4.07.7 Humanized Mouse Models in the Future

Despite the potential utility of humanized mouse models to support various aspects of metabolism and toxicity testing, their limitations in terms of costs, the lack of historical background data, or fragility of immunocompromised animals will most likely restrict the use of these models to case-by-case problem solving rather than leading to generic applications, for the foreseeable future.

Genetically humanized and chimeric liver-humanized mouse models are still emerging, but the models discussed here are promising tools for improved prediction of the PK, disposition, metabolism, DDI, and safety characteristics of compounds in humans. However, these models are not yet fully accepted for ADME studies, and more work will be required to demonstrate their robustness and accuracy in predicting clinical outcomes and to gain wider acceptance. It can be expected that the increasing use of genetically humanized and chimeric liver-humanized mice by academia and industry and the growing number of publications will help to establish a solid database.

However, in our opinion, humanized mice of one sort or another, while unlikely to become "stand-alone" models for predicting human outcomes of all candidate drugs in a pipeline, will be increasingly used for problem solving and decision-making when difficulties arise in discovery and development for particular candidate drug. The results obtained from such studies will then be taken together with in silico predictions, in vitro data, and, if available, clinical results and used as part of the decisions on how to proceed through the discovery/development process. Hence, these in vivo models will be used as a complement to already-established technologies and not a replacement for them. Hopefully, the data obtained from the use of these models will help to de-risk the first single ascending dose and multiple ascending dose studies to human subjects (used to determine the starting doses for clinical studies) or to explain unexpected clinical findings.

A trend in the future is that more complex models, with mice multiply humanized for proteins involved in drug metabolism and disposition, will be generated to investigate interaction of compounds. In addition, there will be an increased number of transporter-humanized mouse models to satisfy the growing demand to consider the role of transporters in drug PK, DDI, and toxicity. Efficacy testing might be increasingly addressed in the future by combining the humanized models described here, with genetically engineered disease models or chemically induced disease phenotypes.

Further developments in the production of chimeric liver-humanized models may lead to an increased robustness in the generation of mice with high RI factors of 90% or more. There might be more liver-humanized mouse models with additional cellular humanizations, as exemplified by Wilson et al.[125] with a double humanization of both the liver and hematopoiesis in a FRG

mouse.[125] It may also be possible to generate chimeric liver-humanized mice using induced pluripotent stem cells (iPSCs) with high RI.

Furthermore, it is possible to predict that genetically humanized and chimeric liver-humanized rats will become available. Today, there are technologies to generate knockout rats,[126,127] and the first attempts to generate chimeric liver-humanized rats have been made,[128–130] but optimization will be required to achieve robust and efficient repopulation of human hepatocytes in the liver of a rat. The benefits of moving from mice to rats for Absorption, Distribution, Metabolism, and excretion - Toxicity (ADMET) studies are the much greater amount of background data available for the latter regarding toxicological readouts, which may help in understanding/interpreting the outcomes of studies performed in a chimeric humanized rat in the future.

Finally, neither genetically humanized or chimeric liver-humanized mice are officially accepted by regulatory authorities nor is their use for any particular application explicitly recommended. Hence, the use of these in vivo models is, at least for now, more for internal decision-making rather than for regulatory purposes. However, representatives from the FDA have taken an open-minded attitude toward the use of humanized mouse models to support regulatory submissions, if scientifically reasonable.[43]

In conclusion, these humanized models are still mostly mice, and studies need to be well thought-out and carefully executed. If undertaken with care studies, these genetically humanized and chimeric liver-humanized mice clearly do have a significant potential to increase the predictability of clinical drug PK, DDIs, and toxicity and to contribute to improving the success rates in drug development.

References

1. DiMasi, J. A.; Hansen, R. W.; Grabowski, H. G. The Price of Innovation: New Estimates of Drug Development Costs. *J. Health Econ.* **2003,** *22* (2), 151–185.
2. Marchetti, S.; Schellens, J. H. The Impact of FDA and EMEA Guidelines on Drug Development in Relation to Phase 0 Trials. *Br. J. Cancer* **2007,** *97* (5), 577–581.
3. Kola, I.; Landis, J. Can the Pharmaceutical Industry Reduce Attrition Rates? *Nat. Rev. Drug Discov.* **2004,** *3* (8), 711–715.
4. Dimasi, J. A. Risks in New Drug Development: Approval Success Rates for Investigational Drugs. *Clin. Pharmacol. Ther.* **2001,** *69* (5), 297–307.
5. DiMasi, J. A. The Value of Improving the Productivity of the Drug Development Process: Faster Times and Better Decisions. *Pharmacoeconomics* **2002,** *20* (Suppl 3), 1–10.
6. Wang, J. U. L. The Impact of Early ADME Profiling on Drug Discovery and Development. *Drug Discov. World* **2004,** 73–86.
7. Lin, J. H. Species Similarities and Differences in Pharmacokinetics. *Drug Metab. Dispos.* **1995,** *23* (10), 1008–1021.
8. Martignoni, M.; Groothuis, G. M.; de Kanter, R. Species Differences Between Mouse, Rat, Dog, Monkey and Human CYP-Mediated Drug Metabolism, Inhibition and Induction. *Expert Opin. Drug Metab. Toxicol.* **2006,** *2* (6), 875–894.
9. Owen, A.; Curley, P. Species Similarities and Differences in Pharmacokinetics and Distribution of Antiretroviral Drugs. In *Humanized Mice for HIV Research;* Springer Science and Business Media: New York, 2014; pp 339–360.
10. Stanley, L. A.; Horsburgh, B. C.; Ross, J.; Scheer, N.; Wolf, C. R. PXR and CAR: Nuclear Receptors Which Play a Pivotal Role in Drug Disposition and Chemical Toxicity. *Drug Metab. Rev.* **2006,** *38* (3), 515–597.
11. Nishimuta, H.; Nakagawa, T.; Nomura, N.; Yabuki, M. Species Differences in Hepatic and Intestinal Metabolic Activities for 43 Human Cytochrome P450 Substrates Between Humans and Rats or Dogs. *Xenobiotica* **2013,** *43* (11), 948–955.
12. Furukawa, T.; Naritomi, Y.; Tetsuka, K.; Nakamori, F.; Moriguchi, H.; Yamano, K.; Terashita, S.; Tabata, K.; Teramura, T. Species Differences in Intestinal Glucuronidation Activities Between Humans, Rats, Dogs and Monkeys. *Xenobiotica* **2014,** *44* (3), 205–216.
13. Chu, X.; Bleasby, K.; Evers, R. Species Differences in Drug Transporters and Implications for Translating Preclinical Findings to Humans. *Expert Opin. Drug Metab. Toxicol.* **2013,** *9* (3), 237–252.
14. Scheer, N.; Roland Wolf, C. Xenobiotic Receptor Humanized Mice and Their Utility. *Drug Metab. Rev.* **2013,** *45* (1), 110–121.
15. Scheer, N.; Wolf, C. R. Genetically Humanized Mouse Models of Drug Metabolizing Enzymes and Transporters and Their Applications. *Xenobiotica* **2014,** *44* (2), 96–108.
16. Bissig, K. D.; Grompe, M. Response to "Can 'Humanized' Mice Improve Drug Development in the 21st Century? *Trends Pharmacol. Sci.* **2013,** *34* (8), 425.
17. Peltz, G. Reply to Bissig and Grompe. *Trends Pharmacol. Sci.* **2013,** *34* (8), 426.
18. Peltz, G. Can 'Humanized' Mice Improve Drug Development in the 21st Century? *Trends Pharmacol. Sci.* **2013,** *34* (5), 255–260.
19. Strom, S. C.; Davila, J.; Grompe, M. Chimeric Mice With Humanized Liver: Tools for the Study of Drug Metabolism, Excretion, and Toxicity. *Methods Mol. Biol.* **2010,** *640,* 491–509.
20. Henderson, C. J.; McLaughlin, L. A.; Osuna-Cabello, M.; Taylor, M.; Gilbert, I.; McLaren, A. W.; Wolf, C. R. Application of a Novel Regulatable Cre Recombinase System to Define the Role of Liver and Gut Metabolism in Drug Oral Bioavailability. *Biochem. J.* **2015,** *465* (3), 479–488.
21. Henderson, C. J.; Otto, D. M.; Carrie, D.; Magnuson, M. A.; McLaren, A. W.; Rosewell, I.; Wolf, C. R. Inactivation of the Hepatic Cytochrome P450 System by Conditional Deletion of Hepatic Cytochrome P450 Reductase. *J. Biol. Chem.* **2003,** *278* (15), 13480–13486.
22. Scheer, N.; Snaith, M.; Wolf, C. R.; Seibler, J. Generation and Utility of Genetically Humanized Mouse Models. *Drug Discov. Today* **2013,** *18* (23–24), 1200–1211.
23. Shultz, L. D.; Ishikawa, F.; Greiner, D. L. Humanized Mice in Translational Biomedical Research. *Nat. Rev. Immunol.* **2007,** *7* (2), 118–130.
24. Iannacone, M.; Guidotti, L. G. Mouse Models of Hepatitis B Virus Pathogenesis. *Cold Spring Harb. Perspect. Med.* **2015,** *5* (11), 1–11.
25. Siu, E.; Ploss, A. Modeling Malaria in Humanized Mice: Opportunities and Challenges. *Ann. N. Y. Acad. Sci.* **2015,** *1342,* 29–36.
26. De Brabanter, N.; Esposito, S.; Tudela, E.; Lootens, L.; Meuleman, P.; Leroux-Roels, G.; Deventer, K.; Van Eenoo, P. In Vivo and in vitro Metabolism of the Synthetic Cannabinoid JWH-200. *Rapid Commun. Mass Spectrom.* **2013,** *27* (18), 2115–2126.
27. Geldof, L.; Lootens, L.; Polet, M.; Eichner, D.; Campbell, T.; Nair, V.; Botre, F.; Meuleman, P.; Leroux-Roels, G.; Deventer, K.; Eenoo, P. V. Metabolism of Methylstenbolone Studied With Human Liver Microsomes and the uPA(+)/(+)-SCID Chimeric Mouse Model. *Biomed. Chromatogr.* **2014,** *28* (7), 974–985.
28. Lootens, L.; Meuleman, P.; Leroux-Roels, G.; Van Eenoo, P. Metabolic Studies With Promagnon, Methylclostebol and Methasterone in the uPA+/+-SCID Chimeric Mice. *J. Steroid Biochem. Mol. Biol.* **2011,** *127* (3–5), 374–381.
29. Omiecinski, C. J.; Vanden Heuvel, J. P.; Perdew, G. H.; Peters, J. M. Xenobiotic Metabolism, Disposition, and Regulation by Receptors: From Biochemical Phenomenon to Predictors of Major Toxicities. *Toxicol. Sci.* **2011,** *120* (Suppl 1), S49–S75.
30. Kublbeck, J.; Laitinen, T.; Jyrkkarinne, J.; Rousu, T.; Tolonen, A.; Abel, T.; Kortelainen, T.; Uusitalo, J.; Korjamo, T.; Honkakoski, P.; Molnar, F. Use of Comprehensive Screening Methods to Detect Selective Human CAR Activators. *Biochem. Pharmacol.* **2011,** *82* (12), 1994–2007.
31. Kliewer, S. A.; Goodwin, B.; Willson, T. M. The Nuclear Pregnane X Receptor: A key Regulator of Xenobiotic Metabolism. *Endocr. Rev.* **2002,** *23* (5), 687–702.
32. Igarashi, K.; Kitajima, S.; Aisaki, K.; Tanemura, K.; Taquahashi, Y.; Moriyama, N.; Ikeno, E.; Matsuda, N.; Saga, Y.; Blumberg, B.; Kanno, J. Development of Humanized Steroid and Xenobiotic Receptor Mouse by Homologous Knock-In of the Human Steroid and Xenobiotic Receptor Ligand Binding Domain Sequence. *J. Toxicol. Sci.* **2012,** *37* (2), 373–380.

33. Ma, X.; Shah, Y.; Cheung, C.; Guo, G. L.; Feigenbaum, L.; Krausz, K. W.; Idle, J. R.; Gonzalez, F. J. The PREgnane X Receptor Gene-Humanized Mouse: A Model for Investigating Drug-Drug Interactions Mediated by Cytochromes P450 3A. *Drug Metab. Dispos.* **2007,** *35* (2), 194–200.
34. Scheer, N.; Ross, J.; Kapelyukh, Y.; Rode, A.; Wolf, C. R. In Vivo Responses of the Human and Murine Pregnane X Receptor to Dexamethasone in Mice. *Drug Metab. Dispos.* **2010,** *38* (7), 1046–1053.
35. Scheer, N.; Ross, J.; Rode, A.; Zevnik, B.; Niehaves, S.; Faust, N.; Wolf, C. R. A Novel Panel of Mouse Models to Evaluate the Role of Human Pregnane X Receptor and Constitutive Androstane Receptor in Drug Response. *J. Clin. Invest.* **2008,** *118* (9), 3228–3239.
36. Xie, W.; Barwick, J. L.; Downes, M.; Blumberg, B.; Simon, C. M.; Nelson, M. C.; Neuschwander-Tetri, B. A.; Brunt, E. M.; Guzelian, P. S.; Evans, R. M. Humanized Xenobiotic Response in Mice Expressing Nuclear Receptor SXR. *Nature* **2000,** *406* (6794), 435–439.
37. Moriguchi, T.; Motohashi, H.; Hosoya, T.; Nakajima, O.; Takahashi, S.; Ohsako, S.; Aoki, Y.; Nishimura, N.; Tohyama, C.; Fujii-Kuriyama, Y.; Yamamoto, M. Distinct Response to Dioxin in an Arylhydrocarbon Receptor (AHR)-Humanized Mouse. *Proc. Natl. Acad. Sci. U. S. A.* **2003,** *100* (10), 5652–5657.
38. Flaveny, C. A.; Murray, I. A.; Chiaro, C. R.; Perdew, G. H. Ligand Selectivity and Gene Regulation by the Human Aryl Hydrocarbon Receptor in Transgenic Mice. *Mol. Pharmacol.* **2009,** *75* (6), 1412–1420.
39. Paine, M. F.; Hart, H. L.; Ludington, S. S.; Haining, R. L.; Rettie, A. E.; Zeldin, D. C. The Human Intestinal Cytochrome P450 "Pie". *Drug Metab. Dispos.* **2006,** *34* (5), 880–886.
40. Sarikaya, D.; Bilgen, C.; Kamataki, T.; Topcu, Z. Comparative Cytochrome P450 -1A1, -2A6, -2B6, -2C, -2D6, -2E1, -3A5 and -4B1 Expressions in Human Larynx Tissue Analysed at mRNA Level. *Biopharm. Drug Dispos.* **2006,** *27* (8), 353–359.
41. Guengerich, F. P. Cytochrome p450 and Chemical Toxicology. *Chem. Res. Toxicol.* **2008,** *21* (1), 70–83.
42. Rendic, S.; Guengerich, F. P. Survey of Human Oxidoreductases and Cytochrome P450 Enzymes Involved in the Metabolism of Xenobiotic and Natural Chemicals. *Chem. Res. Toxicol.* **2015,** *28* (1), 38–42.
43. Robison, T. W.; Jacobs, A. Metabolites in Safety Testing. *Bioanalysis* **2009,** *1* (7), 1193–1200.
44. Williams, J. A.; Hyland, R.; Jones, B. C.; Smith, D. A.; Hurst, S.; Goosen, T. C.; Peterkin, V.; Koup, J. R.; Ball, S. E. Drug-Drug Interactions for UDP-Glucuronosyltransferase Substrates: A Pharmacokinetic Explanation for Typically Observed low Exposure (AUCi/AUC) Ratios. *Drug Metab. Dispos.* **2004,** *32* (11), 1201–1208.
45. Chen, C.; Meng, L.; Ma, X.; Krausz, K. W.; Pommier, Y.; Idle, J. R.; Gonzalez, F. J. Urinary Metabolite Profiling Reveals CYP1A2-Mediated Metabolism of NSC686288 (Aminoflavone). *J. Pharmacol. Exp. Ther.* **2006,** *318* (3), 1330–1342.
46. Cheung, C.; Loy, S.; Li, G. X.; Liu, A. B.; Yang, C. S. Rapid Induction of Colon Carcinogenesis in CYP1A-Humanized Mice by 2-Amino-1-Methyl-6-Phenylimidazo[4,5-b]Pyridine and Dextran Sodium Sulfate. *Carcinogenesis* **2011,** *32* (2), 233–239.
47. Granvil, C. P.; Yu, A. M.; Elizondo, G.; Akiyama, T. E.; Cheung, C.; Feigenbaum, L.; Krausz, K. W.; Gonzalez, F. J. Expression of the Human CYP3A4 Gene in the Small Intestine of Transgenic Mice: in vitro Metabolism and Pharmacokinetics of Midazolam. *Drug Metab. Dispos.* **2003,** *31* (5), 548–558.
48. Cheung, C.; Yu, A. M.; Chen, C. S.; Krausz, K. W.; Byrd, L. G.; Feigenbaum, L.; Edwards, R. J.; Waxman, D. J.; Gonzalez, F. J. Growth Hormone Determines Sexual Dimorphism of Hepatic Cytochrome P450 3A4 Expression in Transgenic Mice. *J. Pharmacol. Exp. Ther.* **2006,** *316* (3), 1328–1334.
49. van Herwaarden, A. E.; Smit, J. W.; Sparidans, R. W.; Wagenaar, E.; van der Kruijssen, C. M.; Schellens, J. H.; Beijnen, J. H.; Schinkel, A. H. Midazolam and Cyclosporin a Metabolism in Transgenic Mice With Liver-Specific Expression of Human CYP3A4. *Drug Metab. Dispos.* **2005,** *33* (7), 892–895.
50. van Herwaarden, A. E.; Wagenaar, E.; van der Kruijssen, C. M.; van Waterschoot, R. A.; Smit, J. W.; Song, J. Y.; van der Valk, M. A.; van Tellingen, O.; van der Hoorn, J. W.; Rosing, H.; Beijnen, J. H.; Schinkel, A. H. Knockout of Cytochrome P450 3A Yields New Mouse Models for Understanding Xenobiotic Metabolism. *J. Clin. Invest.* **2007,** *117* (11), 3583–3592.
51. Yu, A. M.; Fukamachi, K.; Krausz, K. W.; Cheung, C.; Gonzalez, F. J. Potential Role for Human Cytochrome P450 3A4 in Estradiol Homeostasis. *Endocrinology* **2005,** *146* (7), 2911–2919.
52. ter Heine, R.; Van Waterschoot, R. A.; Keizer, R. J.; Beijnen, J. H.; Schinkel, A. H.; Huitema, A. D. An Integrated Pharmacokinetic Model for the Influence of CYP3A4 Expression on the in vivo Disposition of Lopinavir and Its Modulation by Ritonavir. *J. Pharm. Sci.* **2011,** *100* (6), 2508–2515.
53. van Waterschoot, R. A.; Rooswinkel, R. W.; Sparidans, R. W.; van Herwaarden, A. E.; Beijnen, J. H.; Schinkel, A. H. Inhibition and Stimulation of Intestinal and Hepatic CYP3A Activity: Studies in Humanized CYP3A4 Transgenic Mice Using Triazolam. *Drug Metab. Dispos.* **2009,** *37* (12), 2305–2313.
54. van Waterschoot, R. A.; van Herwaarden, A. E.; Lagas, J. S.; Sparidans, R. W.; Wagenaar, E.; van der Kruijssen, C. M.; Goldstein, J. A.; Zeldin, D. C.; Beijnen, J. H.; Schinkel, A. H. Midazolam Metabolism in Cytochrome P450 3A Knockout Mice Can be Attributed to Up-Regulated CYP2C Enzymes. *Mol. Pharmacol.* **2008,** *73* (3), 1029–1036.
55. van Waterschoot, R. A.; Rooswinkel, R. W.; Wagenaar, E.; van der Kruijssen, C. M.; van Herwaarden, A. E.; Schinkel, A. H. Intestinal Cytochrome P450 3A Plays an Important Role in the Regulation of Detoxifying Systems in the Liver. *FASEB J.* **2009,** *23* (1), 224–231.
56. Hasegawa, M.; Kapelyukh, Y.; Tahara, H.; Seibler, J.; Rode, A.; Krueger, S.; Lee, D. N.; Wolf, C. R.; Scheer, N. Quantitative Prediction of Human Pregnane X Receptor and Cytochrome P450 3A4 Mediated Drug–Drug Interaction in a Novel Multiple Humanized Mouse Line. *Mol. Pharmacol.* **2011,** *80* (3), 518–528.
57. MacLeod, A. K.; McLaughlin, L. A.; Henderson, C. J.; Wolf, C. R. Activation Status of the Pregnane X Receptor Influences Vemurafenib Availability in Humanized Mouse Models. *Cancer Res.* **2015,** *75* (21), 4573–4581.
58. Choo, E. F.; Woolsey, S.; DeMent, K.; Ly, J.; Messick, K.; Qin, A.; Takahashi, R. Use of Transgenic Mouse Models to Understand the Oral Disposition and Drug–Drug Interaction Potential of Cobimetinib, a MEK Inhibitor. *Drug Metab. Dispos.* **2015,** *43* (6), 864–869.
59. Derkenne, S.; Curran, C. P.; Shertzer, H. G.; Dalton, T. P.; Dragin, N.; Nebert, D. W. Theophylline Pharmacokinetics: Comparison of Cyp1a1(-/-) and Cyp1a2(-/-) Knockout Mice, Humanized hCYP1A1_1A2 Knock-In Mice Lacking Either the Mouse Cyp1a1 or Cyp1a2 Gene, and Cyp1(+/+) Wild-Type Mice. *Pharmacogenet. Genomics* **2005,** *15* (7), 503–511.
60. Dragin, N.; Uno, S.; Wang, B.; Dalton, T. P.; Nebert, D. W. Generation of 'Humanized' hCYP1A1_1A2_Cyp1a1/1a2(-/-) Mouse Line. *Biochem. Biophys. Res. Commun.* **2007,** *359* (3), 635–642.
61. Zhang, R. R.; Zheng, Y. W.; Li, B.; Tsuchida, T.; Ueno, Y.; Nie, Y. Z.; Taniguchi, H. Human Hepatic Stem Cells Transplanted Into a Fulminant Hepatic Failure Alb-TRECK/SCID Mouse Model Exhibit Liver Reconstitution and Drug Metabolism Capabilities. *Stem Cell Res. Ther.* **2015,** *6,* 49.
62. Scheer, N.; Kapelyukh, Y.; Chatham, L.; Rode, A.; Buechel, S.; Wolf, C. R. Generation and Characterization of Novel Cytochrome P450 Cyp2c Gene Cluster Knockout and CYP2C9 Humanized Mouse Lines. *Mol. Pharmacol.* **2012,** *82* (6), 1022–1029.
63. Corchero, J.; Granvil, C. P.; Akiyama, T. E.; Hayhurst, G. P.; Pimprale, S.; Feigenbaum, L.; Idle, J. R.; Gonzalez, F. J. The CYP2D6 Humanized Mouse: Effect of the Human CYP2D6 Transgene and HNF4alpha on the Disposition of Debrisoquine in the Mouse. *Mol. Pharmacol.* **2001,** *60* (6), 1260–1267.
64. Scheer, N.; Kapelyukh, Y.; McEwan, J.; Beuger, V.; Stanley, L. A.; Rode, A.; Wolf, C. R. Modeling Human Cytochrome P450 2D6 Metabolism and Drug–Drug Interaction by a Novel Panel of Knockout and Humanized Mouse Lines. *Mol. Pharmacol.* **2012,** *81* (1), 63–72.
65. Henderson, C. J.; McLaughlin, L. A.; Scheer, N.; Stanley, L. A.; Wolf, C. R. Cytochrome b5 Is a Major Determinant of Human Cytochrome P450 CYP2D6 and CYP3A4 Activity In Vivo. *Mol. Pharmacol.* **2015,** *87* (4), 733–739.
66. Scheer, N.; Kapelyukh, Y.; Rode, A.; Oswald, S.; Busch, D.; McLaughlin, L. A.; Lin, D.; Henderson, C. J.; Wolf, C. R. Defining Human Pathways of Drug Metabolism in vivo Through the Development of a Multiple Humanized Mouse Model. *Drug Metab. Dispos.* **2015,** *43* (11), 1679–1690.
67. Komura, H.; Iwaki, M. In Vitro and in vivo Small Intestinal Metabolism of CYP3A and UGT Substrates in Preclinical Animals Species and Humans: Species Differences. *Drug Metab. Rev.* **2011,** *43* (4), 476–498.
68. Ohno, S.; Nakajin, S. Determination of mRNA Expression of Human UDP-Glucuronosyltransferases and Application for Localization in Various Human Tissues by Real-Time Reverse Transcriptase-Polymerase Chain Reaction. *Drug Metab. Dispos.* **2009,** *37* (1), 32–40.

69. Shelby, M. K.; Cherrington, N. J.; Vansell, N. R.; Klaassen, C. D. Tissue mRNA Expression of the Rat UDP-Glucuronosyltransferase Gene Family. *Drug Metab. Dispos.* **2003,** *31* (3), 326–333.
70. Nishimura, M.; Koeda, A.; Morikawa, H.; Satoh, T.; Narimatsu, S.; Naito, S. Tissue-Specific mRNA Expression Profiles of Drug-Metabolizing Enzymes and Transporters in the Cynomolgus Monkey. *Drug Metab. Pharmacokinet.* **2009,** *24* (2), 139–144.
71. Cai, H.; Nguyen, N.; Peterkin, V.; Yang, Y. S.; Hotz, K.; La Placa, D. B.; Chen, S.; Tukey, R. H.; Stevens, J. C. A Humanized UGT1 Mouse Model Expressing the UGT1A1*28 Allele for Assessing Drug Clearance by UGT1A1-Dependent Glucuronidation. *Drug Metab. Dispos.* **2010,** *38* (5), 879–886.
72. Sugamori, K. S.; Brenneman, D.; Grant, D. M. Liver-Selective Expression of Human Arylamine N-Acetyltransferase NAT2 in Transgenic Mice. *Drug Metab. Dispos.* **2011,** *39* (5), 882–890.
73. Services, U. S. D. o. H. a. H.; Administration, F. a. D.; (CDER), C. f. D. E. a. R., Guidance for industry: drug interaction studies-study design, data analysis, implications for dosing, and labeling recommendations (2012)
74. Agency, E. M.; 2**, C. E. R. C.; (CHMP), C. f. H. M. P., Guideline on the investigation of drug interactions. (2012).
75. Administration, F. a. D.; Services, U. S. D. o. H. a. H. Innovation or stagnation? Challenge and opportunity on the critical path to new medical products; 2004.
76. International Transporter, C.; Giacomini, K. M.; Huang, S. M.; Tweedie, D. J.; Benet, L. Z.; Brouwer, K. L.; Chu, X.; Dahlin, A.; Evers, R.; Fischer, V.; Hillgren, K. M.; Hoffmaster, K. A.; Ishikawa, T.; Keppler, D.; Kim, R. B.; Lee, C. A.; Niemi, M.; Polli, J. W.; Sugiyama, Y.; Swaan, P. W.; Ware, J. A.; Wright, S. H.; Yee, S. W.; Zamek-Gliszczynski, M. J.; Zhang, L. Membrane Transporters in Drug Development. *Nat. Rev. Drug Discov.* **2010,** *9* (3), 215–236.
77. Zamek-Gliszczynski, M. J.; Hoffmaster, K. A.; Tweedie, D. J.; Giacomini, K. M.; Hillgren, K. M. Highlights From the International Transporter Consortium Second Workshop. *Clin. Pharmacol. Ther.* **2012,** *92* (5), 553–556.
78. Scheer, N.; Balimane, P.; Hayward, M. D.; Buechel, S.; Kauselmann, G.; Wolf, C. R. Generation and Characterization of a Novel Multidrug Resistance Protein 2 Humanized Mouse Line. *Drug Metab. Dispos.* **2012,** *40* (11), 2212–2218.
79. Sadiq, M. W.; Uchida, Y.; Hoshi, Y.; Tachikawa, M.; Terasaki, T.; Hammarlund-Udenaes, M. Validation of a P-Glycoprotein (P-gp) Humanized Mouse Model by Integrating Selective Absolute Quantification of Human MDR1, Mouse Mdr1a and Mdr1b Protein Expressions With in vivo Functional Analysis for Blood-Brain Barrier Transport. *PLoS One* **2015,** *10* (5), e0118638.
80. Hu, Y.; Xie, Y.; Wang, Y.; Chen, X.; Smith, D. E. Development and Characterization of a Novel Mouse Line Humanized for the Intestinal Peptide Transporter PEPT1. *Mol. Pharm.* **2014,** *11* (10), 3737–3746.
81. Dallas, S.; Salphati, L.; Gomez-Zepeda, D.; Wanek, T.; Chen, L.; Chu, X.; Kunta, J.; Mezler, M.; Menet, M. C.; Chasseigneaux, S.; Decleves, X.; Langer, O.; Pierre, E.; DiLoreto, K.; Hoft, C.; Laplanche, L.; Pang, J.; Pereira, T.; Andonian, C.; Simic, D.; Rode, A.; Yabut, J.; Zhang, X.; Scheer, N. Generation and Characterization of a Breast Cancer Resistance Protein Humanized Mouse Model. *Mol. Pharmacol.* **2016,** *89* (5), 492–504.
82. van de Steeg, E.; Stranecky, V.; Hartmannova, H.; Noskova, L.; Hrebicek, M.; Wagenaar, E.; van Esch, A.; de Waart, D. R.; Oude Elferink, R. P.; Oude Elferink, R. P.; Kenworthy, K. E.; Sticova, E.; al-Edreesi, M.; Knisely, A. S.; Kmoch, S.; Jirsa, M.; Schinkel, A. H. Complete OATP1B1 and OATP1B3 Deficiency Causes Human Rotor Syndrome by Interrupting Conjugated Bilirubin Reuptake Into the Liver. *J. Clin. Invest.* **2012,** *122* (2), 519–528.
83. van de Steeg, E.; van der Kruijssen, C. M.; Wagenaar, E.; Burggraaff, J. E.; Mesman, E.; Kenworthy, K. E.; Schinkel, A. H. Methotrexate Pharmacokinetics in Transgenic Mice With Liver-Specific Expression of Human Organic Anion-Transporting Polypeptide 1B1 (SLCO1B1). *Drug Metab. Dispos.* **2009,** *37* (2), 277–281.
84. van de Steeg, E.; van Esch, A.; Wagenaar, E.; Kenworthy, K. E.; Schinkel, A. H. Influence of Human OATP1B1, OATP1B3, and OATP1A2 on the Pharmacokinetics of Methotrexate and Paclitaxel in Humanized Transgenic Mice. *Clin. Cancer Res.* **2013,** *19* (4), 821–832.
85. Shord, S. S.; Thompson, D. M.; Krempl, G. A.; Hanigan, M. H. Effect of Concurrent Medications on Cisplatin-Induced Nephrotoxicity in Patients With Head and Neck Cancer. *Anticancer Drugs* **2006,** *17* (2), 207–215.
86. Wen, X.; Buckley, B.; McCandlish, E.; Goedken, M. J.; Syed, S.; Pelis, R.; Manautou, J. E.; Aleksunes, L. M. Transgenic Expression of the Human MRP2 Transporter Reduces Cisplatin Accumulation and Nephrotoxicity in Mrp2-Null Mice. *Am. J. Pathol.* **2014,** *184* (5), 1299–1308.
87. Rhim, J. A.; Sandgren, E. P.; Degen, J. L.; Palmiter, R. D.; Brinster, R. L. Replacement of Diseased Mouse Liver by Hepatic Cell Transplantation. *Science* **1994,** *263* (5150), 1149–1152.
88. Rhim, J. A.; Sandgren, E. P.; Palmiter, R. D.; Brinster, R. L. Complete Reconstitution of Mouse Liver With Xenogeneic Hepatocytes. *Proc. Natl. Acad. Sci. U. S. A.* **1995,** *92* (11), 4942–4946.
89. Sandgren, E. P.; Palmiter, R. D.; Heckel, J. L.; Daugherty, C. C.; Brinster, R. L.; Degen, J. L. Complete Hepatic Regeneration After Somatic Deletion of an Albumin-Plasminogen Activator Transgene. *Cell* **1991,** *66* (2), 245–256.
90. Azuma, H.; Paulk, N.; Ranade, A.; Dorrell, C.; Al-Dhalimy, M.; Ellis, E.; Strom, S.; Kay, M. A.; Finegold, M.; Grompe, M. Robust Expansion of Human Hepatocytes in Fah-/-/Rag2-/-/Il2rg-/- Mice. *Nat. Biotechnol.* **2007,** *25* (8), 903–910.
91. Hasegawa, M.; Kawai, K.; Mitsui, T.; Taniguchi, K.; Monnai, M.; Wakui, M.; Ito, M.; Suematsu, M.; Peltz, G.; Nakamura, M.; Suemizu, H. The Reconstituted 'Humanized Liver' in TK-NOG Mice Is Mature and Functional. *Biochem. Biophys. Res. Commun.* **2011,** *405* (3), 405–410.
92. Bateman, T. J.; Reddy, V. G.; Kakuni, M.; Morikawa, Y.; Kumar, S. Application of Chimeric Mice With Humanized Liver for Study of Human-Specific Drug Metabolism. *Drug Metab. Dispos.* **2014,** *42* (6), 1055–1065.
93. Igawa, Y.; Fujitani, T.; Shah, B.; Oo, C.; Kanai, Y. In Vitro and in vivo Metabolism of a Novel Chymase Inhibitor, SUN13834, and the Predictability of Human Metabolism Using Mice With Humanized Liver. *Xenobiotica* **2014,** *44* (2), 154–163.
94. Kamimura, H.; Ito, S.; Nozawa, K.; Nakamura, S.; Chijiwa, H.; Nagatsuka, S.; Kuronuma, M.; Ohnishi, Y.; Suemizu, H.; Ninomiya, S. Formation of the Accumulative Human Metabolite and Human-Specific Glutathione Conjugate of Diclofenac in TK-NOG Chimeric Mice With Humanized Livers. *Drug Metab. Dispos.* **2015,** *43* (3), 309–316.
95. Samuelsson, K.; Pickup, K.; Sarda, S.; Foster, J. R.; Randall, K.; Abrahamsson, A.; Jacobsen, M.; Weidolf, L.; Wilson, I. Troglitazone Metabolism and Transporter Effects in Chimeric Mice: A Comparison Between Chimeric Humanized and Chimeric Murinized FRG Mice. *Xenobiotica* **2014,** *44* (2), 186–195.
96. Samuelsson, K.; Pickup, K.; Sarda, S.; Swales, J. G.; Morikawa, Y.; Schulz-Utermoehl, T.; Hutchison, M.; Wilson, I. D. Pharmacokinetics and Metabolism of Midazolam in Chimeric Mice With Humanised Livers. *Xenobiotica* **2012,** *42* (11), 1128–1137.
97. Sanoh, S.; Horiguchi, A.; Sugihara, K.; Kotake, Y.; Tayama, Y.; Uramaru, N.; Ohshita, H.; Tateno, C.; Horie, T.; Kitamura, S.; Ohta, S. Predictability of Metabolism of Ibuprofen and Naproxen Using Chimeric Mice With Human Hepatocytes. *Drug Metab. Dispos.* **2012,** *40* (12), 2267–2272.
98. Sanoh, S.; Nozaki, K.; Murai, H.; Terashita, S.; Teramura, T.; Ohta, S. Prediction of Human Metabolism of FK3453 by Aldehyde Oxidase Using Chimeric Mice Transplanted With Human or Rat Hepatocytes. *Drug Metab. Dispos.* **2012,** *40* (1), 76–82.
99. Tanoue, C.; Sugihara, K.; Uramaru, N.; Tayama, Y.; Watanabe, Y.; Horie, T.; Ohta, S.; Kitamura, S. Prediction of Human Metabolism of the Sedative-Hypnotic Zaleplon Using Chimeric Mice Transplanted With Human Hepatocytes. *Xenobiotica* **2013,** *43* (11), 956–962.
100. Katoh, M.; Matsui, T.; Nakajima, M.; Tateno, C.; Kataoka, M.; Soeno, Y.; Horie, T.; Iwasaki, K.; Yoshizato, K.; Yokoi, T. Expression of Human Cytochromes P450 in Chimeric Mice With Humanized Liver. *Drug Metab. Dispos.* **2004,** *32* (12), 1402–1410.
101. Katoh, M.; Matsui, T.; Okumura, H.; Nakajima, M.; Nishimura, M.; Naito, S.; Tateno, C.; Yoshizato, K.; Yokoi, T. Expression of Human Phase II Enzymes in Chimeric Mice With Humanized Liver. *Drug Metab. Dispos.* **2005,** *33* (9), 1333–1340.
102. Nishimura, M.; Yoshitsugu, H.; Yokoi, T.; Tateno, C.; Kataoka, M.; Horie, T.; Yoshizato, K.; Naito, S. Evaluation of mRNA Expression of Human Drug-Metabolizing Enzymes and Transporters in Chimeric Mouse With Humanized Liver. *Xenobiotica* **2005,** *35* (9), 877–890.
103. Emoto, C.; Yamato, Y.; Sato, Y.; Ohshita, H.; Katoh, M.; Tateno, C.; Yokoi, T.; Yoshizato, K.; Iwasaki, K. Non-Invasive Method to Detect Induction of CYP3A4 in Chimeric Mice With a Humanized Liver. *Xenobiotica* **2008,** *38* (3), 239–248.

104. Katoh, M.; Matsui, T.; Nakajima, M.; Tateno, C.; Soeno, Y.; Horie, T.; Iwasaki, K.; Yoshizato, K.; Yokoi, T. In Vivo Induction of Human Cytochrome P450 Enzymes Expressed in Chimeric Mice With Humanized Liver. *Drug Metab. Dispos.* **2005,** *33* (6), 754–763.
105. Katoh, M.; Watanabe, M.; Tabata, T.; Sato, Y.; Nakajima, M.; Nishimura, M.; Naito, S.; Tateno, C.; Iwasaki, K.; Yoshizato, K.; Yokoi, T. In Vivo Induction of Human Cytochrome P450 3A4 by Rifabutin in Chimeric Mice With Humanized Liver. *Xenobiotica* **2005,** *35* (9), 863–875.
106. Katoh, M.; Sawada, T.; Soeno, Y.; Nakajima, M.; Tateno, C.; Yoshizato, K.; Yokoi, T. In Vivo Drug Metabolism Model for Human Cytochrome P450 Enzyme Using Chimeric Mice With Humanized Liver. *J. Pharm. Sci.* **2007,** *96* (2), 428–437.
107. Hiroi, T.; Chow, T.; Imaoka, S.; Funae, Y. Catalytic Specificity of CYP2D Isoforms in Rat and Human. *Drug Metab. Dispos.* **2002,** *30* (9), 970–976.
108. Nelson, D. R.; Koymans, L.; Kamataki, T.; Stegeman, J. J.; Feyereisen, R.; Waxman, D. J.; Waterman, M. R.; Gotoh, O.; Coon, M. J.; Estabrook, R. W.; Gunsalus, I. C.; Nebert, D. W. P450 Superfamily: Update on New Sequences, Gene Mapping, Accession Numbers and Nomenclature. *Pharmacogenetics* **1996,** *6* (1), 1–42.
109. Inoue, T.; Nitta, K.; Sugihara, K.; Horie, T.; Kitamura, S.; Ohta, S. CYP2C9-Catalyzed Metabolism of S-Warfarin to 7-Hydroxywarfarin in vivo and in vitro in Chimeric Mice With Humanized Liver. *Drug Metab. Dispos.* **2008,** *36* (12), 2429–2433.
110. Inoue, T.; Sugihara, K.; Ohshita, H.; Horie, T.; Kitamura, S.; Ohta, S. Prediction of Human Disposition Toward S-3H-Warfarin Using Chimeric Mice With Humanized Liver. *Drug Metab. Pharmacokinet.* **2009,** *24* (2), 153–160.
111. De Serres, M.; Bowers, G.; Boyle, G.; Beaumont, C.; Castellino, S.; Sigafoos, J.; Dave, M.; Roberts, A.; Shah, V.; Olson, K.; Patel, D.; Wagner, D.; Yeager, R.; Serabjit-Singh, C. Evaluation of a Chimeric (uPA+/+)/SCID Mouse Model With a Humanized Liver for Prediction of Human Metabolism. *Xenobiotica* **2011,** *41* (6), 464–475.
112. Yamazaki, H.; Kuribayashi, S.; Inoue, T.; Tateno, C.; Nishikura, Y.; Oofusa, K.; Harada, D.; Naito, S.; Horie, T.; Ohta, S. Approach for in vivo Protein Binding of 5-n-Butyl-Pyrazolo[1,5-a]Pyrimidine Bioactivated in Chimeric Mice With Humanized Liver by Two-Dimensional Electrophoresis With Accelerator Mass Spectrometry. *Chem. Res. Toxicol.* **2010,** *23* (1), 152–158.
113. Yamazaki, H.; Kuribayashi, S.; Inoue, T.; Honda, T.; Tateno, C.; Oofusa, K.; Ninomiya, S.; Ikeda, T.; Izumid, T.; Horieh, T. Zone Analysis by Two-Dimensional Electrophoresis With Accelerator Mass Spectrometry of in vivo Protein Bindings of Idiosyncratic Hepatotoxicants Troglitazone and Flutamide Bioactivated in Chimeric Mice With Humanized Liver. *Toxicol. Res.* **2015,** *4* (1), 106–111.
114. Kakuni, M.; Morita, M.; Matsuo, K.; Katoh, Y.; Nakajima, M.; Tateno, C.; Yokoi, T. Chimeric Mice With a Humanized Liver as an Animal Model of Troglitazone-Induced Liver Injury. *Toxicol. Lett.* **2012,** *214* (1), 9–18.
115. Schulz-Utermoehl, T.; Sarda, S.; Foster, J. R.; Jacobsen, M.; Kenna, J. G.; Morikawa, Y.; Salmu, J.; Gross, G.; Wilson, I. D. Evaluation of the Pharmacokinetics, Biotransformation and Hepatic Transporter Effects of Troglitazone in Mice With Humanized Livers. *Xenobiotica* **2012,** *42* (6), 503–517.
116. Scheer, N.; Wilson, I. D. A Comparison Between Genetically Humanized and Chimeric Liver Humanized Mouse Models for Studies in Drug Metabolism and Toxicity. *Drug Discov. Today* **2016,** *21* (2), 250–263.
117. Fujiwara, S.; Fujioka, H.; Tateno, C.; Taniguchi, K.; Ito, M.; Ohishi, H.; Utoh, R.; Ishibashi, H.; Kanematsu, T.; Yoshizato, K. A Novel Animal Model for in vivo Study of Liver Cancer Metastasis. *World J. Gastroenterol.* **2012,** *18* (29), 3875–3882.
118. Krishna, D. R.; Klotz, U. Extrahepatic Metabolism of Drugs in Humans. *Clin. Pharmacokinet.* **1994,** *26* (2), 144–160.
119. Emoto, C.; Iwasaki, K. Approach to Predict the Contribution of Cytochrome P450 Enzymes to Drug Metabolism in the Early Drug-Discovery Stage: The Effect of the Expression of Cytochrome b(5) With Recombinant P450 Enzymes. *Xenobiotica* **2007,** *37* (9), 986–999.
120. Emoto, C.; Murayama, N.; Rostami-Hodjegan, A.; Yamazaki, H. Methodologies for Investigating Drug Metabolism at the Early Drug Discovery Stage: Prediction of Hepatic Drug Clearance and P450 Contribution. *Curr. Drug Metab.* **2010,** *11* (8), 678–685.
121. Pickup, K.; Gavin, A.; Jones, H. B.; Karlsson, E.; Page, C.; Ratcliffe, K.; Sarda, S.; Schulz-Utermoehl, T.; Wilson, I. The Hepatic Reductase Null Mouse as a Model for Exploring Hepatic Conjugation of Xenobiotics: Application to the Metabolism of Diclofenac. *Xenobiotica* **2012,** *42* (2), 195–205.
122. Grimsley, A.; Foster, A.; Gallagher, R.; Hutchison, M.; Lundqvist, A.; Pickup, K.; Wilson, I. D.; Samuelsson, K. A Comparison of the Metabolism of Midazolam in C57BL/6J and Hepatic Reductase Null (HRN) Mice. *Biochem. Pharmacol.* **2014,** *92* (4), 701–711.
123. Xu, D.; Nishimura, T.; Nishimura, S.; Zhang, H.; Zheng, M.; Guo, Y. Y.; Masek, M.; Michie, S. A.; Glenn, J.; Peltz, G. Fialuridine Induces Acute Liver Failure in Chimeric TK-NOG Mice: A Model for Detecting Hepatic Drug Toxicity Prior to Human Testing. *PLoS Med.* **2014,** *11* (4), e1001628.
124. Xu, D.; Wu, M.; Nishimura, S.; Nishimura, T.; Michie, S. A.; Zheng, M.; Yang, Z.; Yates, A. J.; Day, J. S.; Hillgren, K. M.; Takeda, S. T.; Guan, Y.; Guo, Y.; Peltz, G. Chimeric TK-NOG Mice: A Predictive Model for Cholestatic Human Liver Toxicity. *J. Pharmacol. Exp. Ther.* **2015,** *352* (2), 274–280.
125. Wilson, E. M.; Bial, J.; Tarlow, B.; Bial, G.; Jensen, B.; Greiner, D. L.; Brehm, M. A.; Grompe, M. Extensive Double Humanization of Both Liver and Hematopoiesis in FRGN Mice. *Stem Cell Res.* **2014,** *13* (3 Pt A), 404–412.
126. Li, D.; Qiu, Z.; Shao, Y.; Chen, Y.; Guan, Y.; Liu, M.; Li, Y.; Gao, N.; Wang, L.; Lu, X.; Zhao, Y.; Liu, M. Heritable Gene Targeting in the Mouse and rat Using a CRISPR-Cas System. *Nat. Biotechnol.* **2013,** *31* (8), 681–683.
127. Geurts, A. M.; Cost, G. J.; Freyvert, Y.; Zeitler, B.; Miller, J. C.; Choi, V. M.; Jenkins, S. S.; Wood, A.; Cui, X.; Meng, X.; Vincent, A.; Lam, S.; Michalkiewicz, M.; Schilling, R.; Foeckler, J.; Kalloway, S.; Weiler, H.; Menoret, S.; Anegon, I.; Davis, G. D.; Zhang, L.; Rebar, E. J.; Gregory, P. D.; Urnov, F. D.; Jacob, H. J.; Buelow, R. Knockout Rats via Embryo Microinjection of Zinc-Finger Nucleases. *Science* **2009,** *325* (5939), 433.
128. Igarashi, Y.; Tateno, C.; Tanaka, Y.; Tachibana, A.; Utoh, R.; Kataoka, M.; Ohdan, H.; Asahara, T.; Yoshizato, K. Engraftment of Human Hepatocytes in the Livers of Rats Bearing Bone Marrow Reconstructed With Immunodeficient Mouse Bone Marrow Cells. *Xenotransplantation* **2008,** *15* (4), 235–245.
129. Tachibana, A.; Tateno, C.; Yoshizato, K. Repopulation of the Immunosuppressed Retrorsine-Treated Infant Rat Liver With Human Hepatocytes. *Xenotransplantation* **2013,** *20* (4), 227–238.
130. Wu, C. H.; Ouyang, E. C.; Walton, C. M.; Wu, G. Y. Human Hepatocytes Transplanted Into Genetically Immunocompetent Rats Are Susceptible to Infection by Hepatitis B Virus In Situ. *J. Viral Hepat.* **2001,** *8* (2), 111–119.

4.08 A Comprehensive Overview of the Current Status and Application of Predictive ADMET: Introduction and Overview

T Hartung, Johns Hopkins Bloomberg School of Public Health, Baltimore, MD, United States

© 2017 Elsevier Ltd. All rights reserved.

4.08.1	**Introduction**	150
4.08.2	**The Critical Role of ADME in In Vivo and Human Toxicology—World's Apart**	150
4.08.3	**The Critical Role of ADME for the Future of In Vitro Toxicology**	151
4.08.3.1	Well-Established Uses of ADME in In Vitro Toxicology	151
4.08.3.1.1	Prediction of metabolites	151
4.08.3.1.2	Barrier models	151
4.08.3.1.3	Biokinetic modeling of the in vivo situation	151
4.08.3.2	The Emerging Role of ADME in In Vitro Toxicology	151
4.08.3.2.1	In vitro biokinetics	152
4.08.3.2.2	The lack of metabolism in vitro	152
4.08.3.2.3	Quantitative in vitro-to-in vivo extrapolation	152
4.08.3.2.4	ADME contributions to ITS	153
4.08.4	**The Advent of Systems Toxicology—Need for ADME**	153
4.08.5	**Conclusions**	153
References		154

4.08.1 Introduction

Paracelsus is hailed as the founding father of toxicology often summarized in the quote *All things are poison and nothing is without poison; only the dose makes a thing not a poison*. Almost 500 years later, we have refined this notion, that the portion of the dose, which interacts with the target in the body, the internal dose, is critical. This has revolutionized some parts of in vivo toxicology, especially in drug development. Other areas were left behind, such as the regulation of industrial chemicals or some food regulations based on hazard only.

Another area, which was left behind, is in vitro toxicology. Sure, in vitro models of metabolism and biological barriers exist, but still most in vitro toxicology neglects metabolism and we mostly do not care about the fate of substances in the culture dish, the in vitro biokinetics. However, similar to the impact on interpreting in vivo findings, kinetic phenomena impact on in vitro results and need to be considered for any prediction of the in vivo situation.

To some extent, in silico modeling of aspects of adsorption, distribution, metabolism, and excretion (ADME) has been possible and make especially their addition to integrated testing strategies (ITS) more feasible. While hazard is either a yes/no attribution of a property or ideally linked to some dose/response relationship, kinetics of a substance is a highly dynamic process. This prompts the need for dynamic modeling of toxicokinetics—today mainly used to explain phenomena but increasingly supporting predictive toxicology. The ultimate goal to make quantitative in vitro-to-in vivo extrapolations (QIVIVE)[1] or build a systems toxicology[2] approach clearly needs the integration of in silico and in vitro tools, which combine hazard assessments with ADME considerations.

In the context of developing a roadmap for animal-free systemic toxicity testing, an expert workgroup discussed the contribution of toxicokinetics,[3] which was then discussed in two stakeholder fora in Brussels and Washington.[4] Some key messages were:

- Kinetics is less a stand-alone test requirement but the necessary complement to in vitro approaches.
- Mainly in silico approaches are used that need to be further optimized.
- There is a need for more quality data collections and the incorporation of in vitro data (barrier models).
- Insufficient models exist for bioavailability and urinary excretion.
- All together, the required in vitro and in silico tools are with reasonable investment achievable.

This introduction aims to get the reader started with some food-for-thought before the dedicated chapters detail the state of the art of ADME in toxicology.

4.08.2 The Critical Role of ADME in In Vivo and Human Toxicology—World's Apart

The high attrition rate of drugs once entering human trials has concerned the pharmaceutical field for many years.[5] By 1997, it was reported[6] that poor ADME properties and toxicity accounted for 60% of failures of chemicals in the drug development process. It turned out that many failures could actually be attributed to differences in kinetics from the animal models to humans.[7–11]

Noteworthy, by tackling these issues, the number of failures due to ADME problems has fallen over the years.[12] In 1991, adverse pharmacokinetic and bioavailability results were the most significant cause of attrition (about 40%) dropping by 2000 to less than 10%. The availability of high-throughput and in silico techniques in drug metabolism and pharmacokinetics was critical here.[13–15]

While drug development has embraced the advantage of understanding ADME for predicting and analyzing substance effects,[16–18] other areas have not. For example, the largest regulatory industrial chemical program, the European REACH legislation, has no requirement for ADME data. Similarly, cosmetics are typically registered in Europe without such data,[19] though the ban on animal testing does name kinetics as an information requirement under the 2013 ban. In both cases, kinetics information is if at all used for weight of evidence evaluations and to adjust the impact of a hazard found for risk assessment. However, similar to exposure considerations, which are often similarly neglected, the "internal dose," that is, the kinetics of a given external dose in the organism, could help adapt information requirements and safety factors for risk assessments.

An area where kinetics makes most of the difference is nanotoxicology.[20] New hazards are rare, but we are only starting to understand the dramatically altered kinetics of nanomaterials and the biological consequences in vivo and in vitro.[21]

4.08.3 The Critical Role of ADME for the Future of In Vitro Toxicology

4.08.3.1 Well-Established Uses of ADME in In Vitro Toxicology

4.08.3.1.1 Prediction of metabolites

A broad variety of cellular and subcellular models of metabolism of xenobiotics is available.[22–27] Many focus on liver metabolism because of the enormous metabolic capacity of the organ, its central role in blood circulation, especially seeing first via the portal vein anything absorbed from the intestine, and as an important excretion organ via the bile. The latter is actually difficult to study in vitro and marked differences between rodents and humans also impair in vivo analysis. All together, there are still enormous challenges to predict the in vivo metabolism from in vitro data.[28] More recent developments with regard to hepatic models include the emergence of stem-cell-derived liver cells (still not fully matured though),[29] the more broad access to human primary cells via commercial vendors, and cell lines with some metabolic capacity, such as HepRG cells.[30] Increasingly, the in vitro data can support the prediction of in vivo metabolism of xenobiotics.[31]

4.08.3.1.2 Barrier models

The recent advances in barrier models have been covered in one of our recent workshops.[32] Models of the outer epithelia of the human body—namely the skin, the intestine, and the lung—have found valid applications in both research and industrial settings as attractive alternatives to animal testing. A variety of approaches to model these barriers are currently employed in such fields, ranging from the utilization of ex vivo tissue to reconstructed in vitro models, and further to chip-based technologies, synthetic membrane systems, and, of increasing current interest, in silico modeling approaches. An international group of experts in the field of epithelial barriers was convened from academia, industry, and regulatory bodies to present both the current state of the art of nonanimal models of the skin, intestinal, and pulmonary barriers in their various fields of application, and to discuss research-based, industry-driven, and regulatory-relevant future directions for both the development of new models and the refinement of existing test methods. Issues of model relevance and preference, validation and standardization, acceptance, and the need for simplicity versus complexity were focal themes of the discussions. The reader is referred to this state-of-the-art report.[32]

4.08.3.1.3 Biokinetic modeling of the in vivo situation

Biokinetic models can be divided into two general groups: data-based (classical) models and physiology-based models.[33,34]

Physiology-based biokinetic (PBBK) models are especially useful for in vitro-to-in vivo, route-to-route, and animal-to-human extrapolations because they incorporate relevant anatomical structures that can be parameterized using independently derived parameters.[3,35–37] Our earlier ECVAM workshop[38] addressed the state of physiology-based pharmacokinetic (or toxicokinetic) modeling, highlighting needs and opportunities to meet the 3Rs agenda. The report was instrumental to set up the consortium for the EU consortium Predict-IV, which combined PBPK modeling with long-term exposures and omics technologies to address repeated dose toxicity. The results of the project have been summarized in a special issue of *Toxicology In Vitro* in Dec. 2015.[39]

In contrast to data-based models, PBBK modeling allows the description of the time course of a compound's amount/concentration at the site of its action. In addition, PBBK models incorporating QSAR- and in vitro-derived parameters, coupled with in vitro assays of tissue/organ toxicity, have the potential to replace in vivo animal studies for quantitative assessment of the biological activity of xenobiotics.[40–43] Increasingly, information from barrier models and those of metabolite formation are included into PBPK models, often improving over mere in silico predictions.[44,45] PBPK models are seeing increasing use in risk assessment.[46–49] They offer promise especially for interspecies extrapolations.[50]

4.08.3.2 The Emerging Role of ADME in In Vitro Toxicology

The in vitro toxicology field is increasingly developing methods satisfying the information needs for regulatory toxicology as summarized on behalf of the European Commission[51] and confirmed by independent expert review.[52] Going a step further, a roadmap was developed by expert consensus how to achieve animal-free systemic toxicity testing including toxicokinetics,[3,4] see later.

4.08.3.2.1 In vitro biokinetics

It should be self-evident that the same gain in understanding is provided by kinetics in vivo and in vitro. However, in vitro behavior of an added substance is usually neglected and we use the nominal concentrations. Left aside that the purity claimed by vendors is often not met in reality and already therefore nominal concentrations are often not exact; many other factors affect the effective amount of substance in vitro (Fig. 1):

- solubility of the substance in the solvent and after addition to the culture;
- binding of the substance to culture plastics and medium constituents, such as albumin of fetal calf serum;
- oxidation and other conversions by the environmental conditions;
- metabolism by the cell of interest or cocultured cells;
- evaporation;
- particle sizes (distribution and agglomeration) in case of nanomaterials;
- other substances coapplied in mixtures and formulations.

All this will change the concentration of free substance, which is typically considered effective on a cellular target. However, we should keep in mind that it is not necessarily the concentration (as peak concentration or area under the curve) that matters, but that especially some lipophilic substances can accumulate in the biological systems, therefore making the absolute amount (and thus the proportion of cell culture media vs. cell mass) a determinant of substance's effects.

Another aspect often overlooked is that kinetics in vitro differ completely from those in vivo: While in vivo, especially for oral absorption, some type of Bateman function (slowly starting increase to a peak and the decrease due to redistribution, metabolism, and excretion, more precisely: a one compartment body model as a function of time with first-order invasion and first-order elimination[53]) is observed for blood and with some delay and distortion in the tissue; in vitro the substance is added typically in an instance and remains as we lack most elimination routes. It is not clear, what consequences this has, for example, the slowly increasing concentrations might induce defense mechanisms, which make the cell more resilient.[54]

4.08.3.2.2 The lack of metabolism in vitro

Awareness is high, that in vitro models mostly lack metabolic capacities.[55] However, the question might be raised, whether it is better to have no metabolism than the wrong metabolism (as most animal models represent), since substance metabolism is usually protective? How often might protective metabolism by animal species give false assurance of safety? At the same time, lack of defense mechanisms might be as important as lack of activation by metabolism to bias in vitro effects and thus model predictivity.[54]

4.08.3.2.3 Quantitative in vitro-to-in vivo extrapolation

It is obvious that in vitro toxicology ultimately wants to predict the effects on an organism level, which requires extrapolation (QIVIVE). Bas Blaauboer and colleagues long ago spearheaded a discussion on integrated testing of in vitro, in silico, and ADME information.[1,56–58] Over the years, a number of successful examples have been developed by them and others including neurotoxicity,[57,58] acute oral toxicity and repeated dose toxicity,[59] developmental toxicity,[60,61] and genotoxicity.[62] Within the framework of the European integrated Predict-IV[39], the work was devoted to pharmacokinetic modeling of in vitro experiments, physiology-based pharmacokinetic (PBPK) modeling, mechanistic models of toxicity for the kidney and brain, large-scale dose–response analysis methods, and biomarker discovery tools.[63]

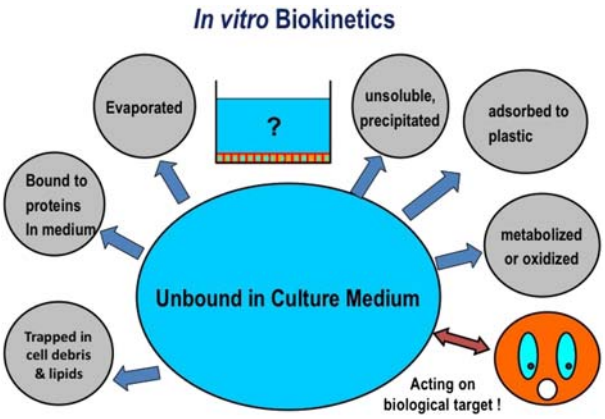

Fig. 1 Aspects of in vitro biokinetics impacting on the unbound portion of substance effecting the target cell.

4.08.3.2.4 ADME contributions to ITS

Increasingly, we acknowledge that our information needs as to the safety of substances cannot be satisfied by single assays. At the same time, a simple battery of tests bears the risk of accumulating false positive results. A more intelligent "integrated" combination of different tests (and in silico tools) promises to optimize resources and predictivity. This has been termed ITS or more recently by OECD Integrated Approaches to Testing and Assessment (IATA).[5,64,65] It is clear that an ideal ITS includes information on ADME to improve the prediction of in vivo results.

4.08.4 The Advent of Systems Toxicology—Need for ADME

The components of the body disturbed by the toxicant represent a network. Systems biology uses the relationships between all elements rather than approaching them separately, and attempts to unite biological fields.[66] Systems biology is defined as[67,68]

> Systems biology: Study of the mechanisms underlying complex biological processes as integrated systems of many diverse, interacting components. It involves (1) collection of large sets of experimental data (by high-throughput technologies and/or by mining the literature of reductionist molecular biology and biochemistry); (2) proposal of mathematical models that might account for at least some significant aspects of this data set; (3) accurate computer solution of the mathematical equations to obtain numerical predictions; and (4) assessment of the quality of the model by comparing numerical simulations with the experimental data.

It is very attractive to apply this concept to toxicology, creating a systems toxicology[69]: The move toward systems toxicology and massively parallel techniques opens new opportunities but, at the same time, raises problems in deriving meaningful information out of the wealth of generated data.[2] Such data is increasingly represented as networks, in which the vertices (e.g., transcripts, proteins, or metabolites) are linked by edges (correlations, interactions, or reactions, respectively). Networks can vary in their functionalities. Some are undirected graphs that enable only the study of structure; others, like the biochemical network, are characterized by interactions of varying strengths, strongly nonlinear dynamics, and saturating response to inputs.[70]

Network analysis has evolved into a very active and interdisciplinary area of research encompassing biology, computer science, social, and information sciences. Many studies are highly theoretical, but they may eventually help in identifying signatures (SoT) and pathways of toxicity (PoT).[71] The network research has three primary goals. First, it aims to understand statistical properties that characterize the network structure in order to suggest appropriate ways to measure these properties. This is very relevant to SoT identification. Second, it aims to create models of networks that can help us understand the meaning of these properties and how they interact with one another. Third, it aims to predict what the behavior of networked systems will be on the basis of measured structural properties. This direction can be very useful in elucidating PoT. Here, the relationship of ADME and systems toxicology is of special interest. Simply said, the ADME aspects are moving hazard data to a systems level. At the same time, the combination of PBPK and QIVIVE in systems biology has improved the prediction of ADME.[72]

Ultimately, systems toxicology aims at modeling the effects of toxicants in metabolic networks.[73,74] Integrating cellular metabolism into a multiscale whole-body model has been attempted[75] and drug effects on these networks (more systems pharmacology) have been proposed.[76] This depends critically on combining dynamic and kinetic information. Thus the avenues toward systems toxicology require the development components for ADME prediction.

4.08.5 Conclusions

Pharmaco- and toxicokinetics, that is, the assessment of adsorption, distribution, metabolism, and excretion of xenobiotics, have transformed our understanding of in vivo pharmacology and toxicology. Astonishingly, some areas of regulatory toxicology still do not request such information, which can boost our understanding of the human relevance of our findings. The respective models of substance kinetics, such as physiology-based pharmacokinetic models, are increasingly refined by the input from in vitro models, for example, for epithelial barrier function or metabolism of test agents. In vitro, kinetic phenomena play a similar role, that is, how the test agent is ultimately available to the cells as similar redistributions and transformations occur, but this is regularly neglected in our interpretations of results. Reverse biokinetics, that is, a quantitative in vitro-to-in vivo extrapolation, is critically important to predict in vivo exposures corresponding to active concentrations on a cell and tissue level, thus making predictive use of in vitro findings. This information represents the complement to hazard identification and characterization by cellular models in order to develop a systems toxicology approach.

The critical role of ADME for interpreting in vivo findings has been shown impressively by improving attrition of drugs in human trials due to such problems. The combination of in vivo, in vitro, and in silico tools is more common here than in many other fields of toxicology. There are enormous needs to move to more use of in vitro tools in toxicology, to improve human predictivity, and spare animal lives. To make ultimately sense of in vitro data, the case is made here that we need to address both the kinetics of substances in the in vitro models and the modeling to extrapolate to the in vivo situation. PBPK methods lend themselves for such reverse kinetics, but examples of their use for QIVIVE are rare and not yet generalizable. The expectation is though that the input from in vitro barrier and metabolism models can improve on the pure in silico models.

References

1. Blaauboer, B. J. Biokinetic Modeling and In Vitro–In Vivo Extrapolations. *J. Toxicol. Environ. Health B Crit. Rev.* **2010,** *13,* 242–252.
2. Hartung, T.; van Vliet, E.; Jaworska, J.; Bonilla, L.; Skinner, N.; Thomas, R. Systems Toxicology. *ALTEX* **2012,** *29,* 119–128.
3. Basketter, D. A.; Clewell, H.; Kimber, I.; Rossi, A.; Blaauboer, B.; Burrier, R.; Daneshian, M.; Eskes, C.; Goldberg, A.; Hasiwa, N.; Hoffmann, S.; Jaworska, J.; Knudsen, T. B.; Landsiedel, R.; Leist, M.; Locke, P.; Maxwell, G.; McKim, J.; McVey, E. A.; Ouédraogo, G.; Patlewicz, G.; Pelkonen, O.; Roggen, E.; Rovida, C.; Ruhdel, I.; Schwarz, M.; Schepky, A.; Schoeters, G.; Skinner, N.; Trentz, K.; Turner, M.; Vanparys, P.; Yager, J.; Zurlo, J.; Hartung, T. A Roadmap for the Development of Alternative (Non-animal) Methods for Systemic Toxicity Testing. *ALTEX* **2012,** *29,* 3–89.
4. Leist, M.; Hasiwa, N.; Rovida, C.; Daneshian, M.; Basketter, D.; Kimber, I.; Clewell, H.; Gocht, T.; Goldberg, A.; Busquet, F.; Rossi, A.-M.; Schwarz, M.; Stephens, M.; Taalman, R.; Knudsen, T. B.; McKim, J.; Harris, G.; Pamies, D.; Hartung, T. Consensus Report on the Future of Animal-Free Systemic Toxicity Testing. *ALTEX* **2014,** *31,* 341–356.
5. Hartung, T.; Luechtefeld, T.; Maertens, A.; Kleensang, A. Integrated Testing Strategies for Safety Assessments. *ALTEX* **2013,** *30,* 3–18.
6. Kennedy, T. Managing the Drug Discovery/Development Interface. *Drug Discov. Today* **1997,** *2,* 436–444.
7. Grass, G. M.; Sinko, P. J. Physiologically-Based Pharmacokinetic Simulation Modelling. *Adv. Drug Deliv. Rev.* **2002,** *54* (3), 433–451.
8. Lin, J. H. Species Similarities and Differences in Pharmacokinetics. *Drug Metab. Dispos.* **1995,** *23* (10), 1008–1021.
9. Martignoni, M.; Groothuis, G. M.; de Kanter, R. Species Differences Between Mouse, Rat, Dog, Monkey and Human CYP-Mediated Drug Metabolism, Inhibition and Induction. *Expert Opin. Drug Metab. Toxicol.* **2006,** *2* (6), 875–894.
10. Musther, H.; Olivares-Morales, A.; Hatley, O. J. D.; Liu, B.; Rostami-Hodjegan, A. Animal Versus Human Oral Drug Bioavailability: Do They Correlate? *Eur. J. Pharm. Sci.* **2014,** *57,* 280–291.
11. Shanks, N.; Greek, R.; Greek, J. Are Animal Models Predictive for Humans? *Philos. Ethics Humanit. Med.* **2009,** *4* (1), 2 http://dx.doi.org/10.1186/1747-5341-4-2.
12. Kola, I.; Landis, J. Can the Pharmaceutical Industry Reduce Attrition Rates? *Nat. Rev. Drug Discov.* **2004,** *3* (8), 711–715.
13. Dearden, J. C. In Silico Prediction of ADMET Properties: How Far Have We Come? *Expert Opin. Drug Metab. Toxicol.* **2007,** *3* (5), 635–639.
14. van de Waterbeemd, H. High-Throughput and In Silico Techniques in Drug Metabolism and Pharmacokinetics. *Curr. Opin. Drug Discov. Devel.* **2002,** *5* (1), 33–43.
15. van de Waterbeemd, H.; Gifford, E. ADMET In Silico Modelling: Towards Prediction Paradise? *Nat. Rev. Drug Discov.* **2003,** *2* (3), 192–204.
16. Singh, S. S. Preclinical Pharmacokinetics: An Approach Towards Safer and Efficacious Drugs. *Curr. Drug Metab.* **2006,** *7* (2), 165–182.
17. Tsaioun, K.; Jacewicz, M. De-risking Drug Discovery With ADDME—Avoiding Drug Development Mistakes Early. *Altern. Lab. Anim.* **2009,** *37* (Suppl 1), 47–55.
18. Zhang, D.; Luo, G.; Ding, X.; Lu, C. Preclinical Experimental Models of Drug Metabolism and Disposition in Drug Discovery and Development. *Acta Pharm. Sin. B* **2012,** *2* (6), 549–561.
19. Hartung, T. Food for Thought … on Alternative Methods for Cosmetics Safety Testing. *ALTEX* **2008,** *25,* 147–162.
20. Hartung, T. Food for Thought … on Alternative Methods for Nanoparticle Safety Testing. *ALTEX* **2010,** *27,* 87–95.
21. Hartung, T.; Sabbioni, E. Alternative In Vitro Assays in Nanomaterial Toxicology. *WIREs Nanomed. Nanobiotechnol.* **2011,** *3,* 545–573.
22. Costa, A.; Sarmento, B.; Seabra, V. An Evaluation of the Latest In Vitro Tools for Drug Metabolism Studies. *Expert Opin. Drug Metab. Toxicol.* **2014,** *10* (1), 103–119.
23. Donato, M. T.; Lahoz, A.; Castell, J. V.; Gomez-Lechon, M. J. Cell Lines: A Tool for In Vitro Drug Metabolism Studies. *Curr. Drug Metab.* **2008,** *9,* 1–11.
24. Gomez-Lechon, M. J.; Donato, T.; Ponsoda, X.; Castell, J. V. Human Hepatic Cell Cultures: In Vitro and In Vivo Drug Metabolism. *Altern. Lab. Anim.* **2003,** *31,* 257–265.
25. Godoy, P.; Hewitt, N. J.; Albrecht, U.; Andersen, M. E.; Ansari, N.; Bhattacharya, S.; et al. Recent Advances in 2D and 3D In Vitro Systems Using Primary Hepatocytes, Alternative Hepatocyte Sources and Non-parenchymal Liver Cells and Their Use in Investigating Mechanisms of Hepatotoxicity, Cell Signaling and ADME. *Arch. Toxicol.* **2013,** *87* (8), 1315–1530.
26. Vermeir, M.; Annaert, P.; Mamidi, R. N. V. S.; Roymans, D.; Meuldermans, W.; Mannens, G. Cell-Based Models to Study Hepatic Drug Metabolism and Enzyme Induction in Humans. *Expert Opin. Drug Metab. Toxicol.* **2005,** *1* (1), 75–90.
27. Williams, D. P. Modeling Hepatic Drug Metabolism and Toxicity: Where Are We Heading? *Future Med. Chem.* **2014,** *6* (7), 725–727.
28. Anderson, S.; Luffer-Atlas, D.; Knadler, M. P. Predicting Circulating Human Metabolites: How Good Are We? *Chem. Res. Toxicol.* **2009,** *22* (2), 243–256.
29. Guillouzo, A.; Corlu, A.; Aninat, C.; Glaise, D.; Morel, F.; Guguen-Guillouzo, C. The Human Hepatoma HepaRG Cells: A Highly Differentiated Model for Studies of Liver Metabolism and Toxicity of Xenobiotics. *Chem. Biol. Interact.* **2007,** *168* (1), 66–73.
30. Andersson, T. B.; Kanebratt, K. P.; Kenna, J. G. The HepaRG Cell Line: A Unique In Vitro Tool for Understanding Drug Metabolism and Toxicology in Human. *Expert Opin. Drug Metab. Toxicol.* **2012,** *8* (7), 909–920.
31. Rostami-Hodjegan, A.; Tucker, G. T. Simulation and Prediction of In Vivo Drug Metabolism in Human Populations From In Vitro Data. *Nat. Rev. Drug Discov.* **2007,** *6* (2), 140–148.
32. Gordon, S.; Daneshian, M.; Bouwstra, J.; Caloni, F.; Constant, S.; Davies, D. E.; Dandekar, G.; Guzman, C. A.; Fabian, E.; Haltner, E.; Hartung, T.; Hasiwa, N.; Hayden, P.; Kandarova, H.; Khare, S.; Krug, H. F.; Kneuer, C.; Leist, M.; Lian, G.; Marx, U.; Metzger, M.; Ott, K.; Prieto, P.; Roberts, M. S.; Roggen, E. L.; Tralau, T.; van den Braak, C.; Walles, H.; Lehr, C.-M. Non-animal Models of Epithelial Barriers (Skin, Intestine and Lung) in Research, Industrial Applications and Regulatory Toxicology. *ALTEX* **2015,** *32,* 327–378.
33. Andersen, M. E. Physiological Modelling of Organic Compounds. *Ann. Occup. Hyg.* **1991,** *35,* 309–321.
34. Filser, J. G.; Csanady, G. A.; Kreuzer, P. E.; et al. Toxicokinetic Models for Volatile Industrial Chemicals and Reactive Metabolites. *Toxicol. Lett.* **1995,** *82–83,* 357–366.
35. Clewell, R. A.; Clewell, H. J., 3rd. Development and Specification of Physiologically Based Pharmacokinetic Models for Use in Risk Assessment. *Regul. Toxicol. Pharmacol.* **2008,** *50,* 129–143.
36. Espié, P.; Tytgat, D.; Sargentini-Maier, M.-L.; Poggesi, I.; Watelet, J.-B. Physiologically Based Pharmacokinetics (PBPK). *Drug Metab. Rev.* **2009,** *41* (3), 391–407.
37. Rietjens, I. M. C. M.; Louisse, J.; Punt, A. Tutorial on Physiologically Based Kinetic Modeling in Molecular Nutrition and Food Research. *Mol. Nutr. Food Res.* **2011,** *55,* 941–956.
38. Bouvier d'Yvoire, M.; Prieto, P.; Blaauboer, B. J.; Bois, F. Y.; Boobis, A.; Brochot, C.; Coecke, S.; Freidig, A.; Gundert-Remy, U.; Hartung, T.; Jacobs, M. N.; Lavé, T.; Leahy, D. E.; Lennernäs, H.; Loizou, G. D.; Meek, B.; Pease, C.; Rowland, M.; Spendiff, M.; Yang, J.; Zeilmaker, M. Physiologically-Based Kinetic Modelling (PBK Modelling): Meeting the 3Rs Agenda. The Report and Recommendations of ECVAM Workshop 63. *ATLA: Altern. Lab. Anim.* **2007,** *35,* 661–671.
39. Pfaller, W.; Prieto, P.; Dekant, W.; Jennings, P.; Blaauboer, B. J. The Predict-IV Project: Towards Predictive Toxicology Using In Vitro Techniques. *Toxicol. In Vitro* **2015,** *30* (Part A), 1–3.
40. Blaauboer, B. J. Toxicodynamic Modelling and the Interpretation of In Vitro Toxicity Data. *Toxicol. Lett.* **2001,** *120,* 111–123.
41. Blaauboer, B. J. The Necessity of Biokinetic Information in the Interpretation of In Vitro Toxicity Data. *Altern. Lab. Anim.* **2002,** *30* (Suppl 2), 85–91.
42. Blaauboer, B. J. The Integration of Data on Physico-chemical Properties, In Vitro-Derived Toxicity Data and Physiologically Based Kinetic and Dynamic as Modelling a Tool in Hazard and Risk Assessment. A Commentary. *Toxicol. Lett.* **2003,** *138,* 161–171.
43. Punt, A.; Schiffelers, M.-J. W. A.; Jean Horbach, G.; van de Sandt, J. J. M.; Groothuis, G. M. M.; Rietjens, I. M. C. M.; Blaauboer, B. J. Evaluation of Research Activities and Research Needs to Increase the Impact and Applicability of Alternative Testing Strategies in Risk Assessment Practice. *Regul. Toxicol. Pharmacol.* **2011,** *61* (1), 105–114.
44. Rusyn, I.; Sedykh, A.; Low, Y.; Guyton, K. Z.; Tropsha, A. Predictive Modeling of Chemical Hazard by Integrating Numerical Descriptors of Chemical Structures and Short-Term Toxicity Assay Data. *Toxicol. Sci.* **2012,** *127* (1), 1–9.

45. Sung, J. H.; Esch, M. B.; Shuler, M. L. Integration of In Silico and In Vitro Platforms for Pharmacokinetic-Pharmacodynamic Modeling. *Expert Opin. Drug Metab. Toxicol.* **2010,** *6* (9), 1063–1081.
46. Chiu, W. A.; Barton, H. A.; DeWoskin, R. S.; Schlosser, P.; Thompson, C. M.; Sonawane, B.; et al. Evaluation of Physiologically Based Pharmacokinetic Models for Use in Risk Assessment. *J. Appl. Toxicol.* **2007,** *27* (3), 218–237.
47. Huynh, L.; Masereeuw, R.; Friedberg, T.; Ingelman-Sundberg, M.; Manivet, P. In Silico Platform for Xenobiotics ADME-T Pharmacological Properties Modeling and Prediction. Part I: Beyond the Reduction of Animal Model Use. *Drug Discov. Today* **2009,** *14* (7–8), 401–405.
48. McLanahan, E. D.; El-Masri, H. A.; Sweeney, L. M.; Kopylev, L. Y.; Clewell, H. J.; Wambaugh, J. F.; Schlosser, P. M. Physiologically Based Pharmacokinetic Model Use in Risk Assessment—Why Being Published Is Not Enough. *Toxicol. Sci.* **2012,** *126* (1), 5–15.
49. Thompson, C. M.; Sonawane, B.; Barton, H. A.; DeWoskin, R. S.; Lipscomb, J. C.; Schlosser, P.; et al. Approaches for Applications of Physiologically Based Pharmacokinetic Models in Risk Assessment. *J. Toxicol. Environ. Health B Crit. Rev.* **2008,** *11* (7), 519–547.
50. Thiel, C.; Schneckener, S.; Krauss, M.; Ghallab, A.; Hofmann, U.; Kanacher, T.; et al. A Systematic Evaluation of the Use of Physiologically Based Pharmacokinetic Modeling for Cross-Species Extrapolation. *J. Pharm. Sci.* **2014,** *104* (1), 191–206.
51. Adler, S.; Basketter, D.; Creton, S.; Pelkonen, O.; Benthem, J.; Zuang, V.; et al. Alternative (Non-animal) Methods for Cosmetics Testing: Current Status and Future Prospects—2010. *Arch. Toxicol.* **2011,** *85* (5), 367–485.
52. Hartung, T.; Blaauboer, G. J.; Bosgra, S.; Carney, E.; Coenen, J.; Conolly, R. B.; Corsini, E.; Green, S.; Faustman, E. M.; Gaspari, A.; Hayashi, M.; Hayes, A. W.; Hengstler, J. G.; Knudsen, L. E.; Knudsen, T. B.; McKim, J. M.; Pfaller, W.; Roggen, E. L. An Expert Consortium Review of the EC-Commissioned Report "Alternative (Non-Animal) Methods for Cosmetics Testing: Current Status and Future Prospects—2010". *ALTEX* **2011,** *28,* 183–209.
53. Garrett, E. R. The Bateman Function Revisited: A Critical Reevaluation of the Quantitative Expressions to Characterize Concentrations in the One Compartment Body Model as a Function of Time With First-Order Invasion and First-Order Elimination. *J. Pharmacokinet. Biopharm.* **1994,** *22* (2), 103–128.
54. Smirnova, L.; Harris, G.; Leist, M.; Hartung, T. Cellular Resilience. *ALTEX* **2015,** *32,* 247–260.
55. Coecke, S.; Ahr, H.; Blaauboer, B. J.; Bremer, S.; Casati, S.; Castell, J.; Combes, R.; Corvi, R.; Crespi, C. L.; Cunningham, M. L.; Elaut, G.; Eletti, B.; Freidig, A.; Gennari, A.; Ghersi-Egea, J.-F.; Guillouzo, A.; Hartung, T.; Hoet, P.; Ingelman-Sundberg, M.; Munn, S.; Janssens, W.; Ladstetter, B.; Leahy, D.; Long, A.; Meneguz, A.; Monshouwer, M.; Morath, S.; Nagelkerke, F.; Pelkonen, O.; Ponti, J.; Prieto, P.; Richert, L.; Sabbioni, E.; Schaack, B.; Steiling, W.; Testai, E.; Vericat, J.-A.; Worth, A. Metabolism: A Bottleneck in In Vitro Toxicological Test Development. *ATLA: Altern. Lab. Anim.* **2006,** *34,* 49–84.
56. Blaauboer, B.; Barratt, M. The Integrated Use of Alternative Methods in Toxicological Risk Evaluation. *Altern. Lab. Anim.* **1999,** *27,* 229–237.
57. DeJongh, J.; Nordin-Andersson, M.; Ploeger, B. A.; Forsby, A. Estimation of Systemic Toxicity of Acrylamide by Integration of In Vitro Toxicity Data With Kinetic Simulations. *Toxicol. Appl. Pharmacol.* **1999,** *158,* 261–268.
58. Forsby, A.; Blaauboer, B. J. Integration of In Vitro Neurotoxicity Data With Biokinetic Modelling for the Estimation of In Vivo Neurotoxicity. *Hum. Exp. Toxicol.* **2007,** *26,* 333–338.
59. Gubbels-van Hal, W. M.; Blaauboer, B. J.; Barentsen, H. M.; Hoitink, M. A.; Meerts, I. A.; van der Hoeven, J. C. An Alternative Approach for the Safety Evaluation of New and Existing Chemicals, an Exercise in Integrated Testing. *Regul. Toxicol. Pharmacol.* **2005,** *42,* 284–295.
60. Louisse, J.; de Jong, E.; van de Sandt, J. J.; Blaauboer, B. J.; Woutersen, R. A.; Piersma, A. H.; Rietjens, I. M. C. M.; Verwei, M. The Use of In Vitro Toxicity Data and Physiologically Based Kinetic Modeling to Predict Dose–Response Curves for In Vivo Developmental Toxicity of Glycol Ethers in Rat and Man. *Toxicol. Sci.* **2010,** *118,* 470–484.
61. Verwei, M.; van Burgsteden, J. A.; Krul, C. A.; van de Sandt, J. J.; Freidig, A. P. Prediction of In Vivo Embryotoxic Effect Levels With a Combination of in vitro Studies and PBPK Modelling. *Toxicol. Lett.* **2006,** *165,* 79–87.
62. Paini, A.; Punt, A.; Viton, F.; Scholz, G.; Delatour, T.; Marin-Kuan, M.; Schilter, B.; van Bladeren, P. J.; Rietjens, I. M. C. M. A Physiologically Based Biodynamic (PBBD) Model for Estragole DNA Binding in Rat Liver Based on In Vitro Kinetic Data and Estragole DNA Adduct Formation in Primary Hepatocytes. *Toxicol. Appl. Pharmacol.* **2010,** *245,* 57–66.
63. Hamon, J.; Renner, M.; Jamei, M.; Lukas, A.; Kopp-Schneider, A.; Bois, F. Y. Quantitative In Vitro to In Vivo Extrapolation of Tissues Toxicity. *Toxicol. In Vitro* **2015,** *30,* 203–216.
64. Rovida, C.; Alépée, N.; Api, A. M.; Basketter, D. A.; Bois, F. Y.; Caloni, F.; Corsini, E.; Daneshian, M.; Eskes, C.; Ezendam, J.; Fuchs, H.; Hayden, P.; Hegele-Hartung, C.; Hoffmann, S.; Hubesch, B.; Jacobs, M. N.; Jaworska, J.; Kleensang, A.; Kleinstreuer, N.; Lalko, J.; Landsiedel, R.; Lebreux, F.; Luechtefeld, T.; Locatelli, M.; Mehling, A.; Natsch, A.; Pitchford, J. W.; Prater, D.; Prieto, P.; Schepky, A.; Schuurmann, G.; Smirnova, L.; Toole, C.; van Vliet, E.; Weisensee, D.; Hartung, T. Integrated Testing Strategies (ITS) for Safety Assessment. *ALTEX* **2015,** *32,* 171–181.
65. Tollefsen, K. E.; Scholz, S.; Cronin, M. T.; Edwards, S. W.; de Knecht, J.; Crofton, K.; Garcia-Reyero, N.; Hartung, T.; Worth, A.; Patlewicz, G. Applying Adverse Outcome Pathways (AOPs) to Support Integrated Approaches to Testing and Assessment (IATA). *Regul. Toxicol. Pharmacol.* **2014,** *70,* 629–640.
66. Hood, L.; Galas, D. The Digital Code of DNA. *Nature* **2003,** *421* (6921), 444–448.
67. Duffus, J. H.; Nordberg, M.; Templeton, D. M. Glossary of Terms Used in Toxicology, 2nd Edition. *Pure Appl. Chem.* **2007,** *79,* 1153–1344.
68. Ferrario, D.; Hartung, T. Glossary of Reference Terms for Alternative Test Methods and Their Validation. *ALTEX* **2014,** *31,* 319–335.
69. Ekins, S.; Nikolsky, Y.; Nikolskaya, T. Techniques: Application of Systems Biology to Absorption, Distribution, Metabolism, Excretion and Toxicity. *Trends Pharmacol. Sci.* **2005,** *26* (4), 202–209.
70. Wagner, A. Does Evolutionary Plasticity Evolve? *Evolution* **1996,** *50,* 1008–1023.
71. Kleensang, A.; Maertens, A.; Rosenberg, M.; Fitzpatrick, S.; Lamb, J.; Auerbach, S.; Brennan, R.; Crofton, K. M.; Gordon, B.; Fornace, A. J., Jr.; Gaido, K.; Gerhold, D.; Haw, R.; Henney, A.; Ma'ayan, A.; McBride, M.; Monti, S.; Ochs, M. F.; Pandey, A.; Sharan, R.; Stierum, R.; Tugendreich, S.; Willett, C.; Wittwehr, C.; Xia, J.; Patton, G. W.; Arvidson, K.; Bouhifd, M.; Hogberg, H. T.; Luechtefeld, T.; Smirnova, L.; Zhao, L.; Adeleye, Y.; Kanehisa, M.; Carmichael, P.; Andersen, E. M.; Hartung, T. Pathways of Toxicity. *ALTEX* **2014,** *31,* 53–61.
72. Rostami-Hodjegan, A. Physiologically Based Pharmacokinetics Joined With In Vitro–In Vivo Extrapolation of ADME: A Marriage Under the Arch of Systems Pharmacology. *Clin. Pharmacol. Ther.* **2012,** *92* (1), 50–61.
73. Bugrim, A.; Nikolskaya, T.; Nikolsky, Y. Early Prediction of Drug Metabolism and Toxicity: Systems Biology Approach and Modeling. *Drug Discov. Today* **2004,** *9* (3), 127–135.
74. Tamaddoni-Nezhad, A.; Chaleil, R.; Kakas, A. C.; Sternberg, M.; Nicholson, J.; Muggleton, S. Modeling the Effects of Toxins in Metabolic Networks. *IEEE Eng. Med. Biol. Mag.* **2007,** *26* (2), 37–46.
75. Krauss, M.; Schaller, S.; Borchers, S.; Findeisen, R.; Lippert, J.; Kuepfer, L. Integrating Cellular Metabolism Into a Multiscale Whole-Body Model. *PLoS Comput. Biol.* **2012,** *8* (10), e1002750.
76. Li, C.; Shang, D.; Wang, Y.; Li, J.; Han, J.; Wang, S.; et al. Characterizing the Network of Drugs and Their Affected Metabolic Subpathways. *PLoS One* **2012,** *7* (10), e47326.

4.09 *In Silico* Tools and their Application

GJ Myatt, Leadsocpe, Inc, Columbus, OH, United States
LD Beilke, Toxicology Solutions Inc, San Diego, CA, United States
KP Cross, Leadsocpe, Inc, Columbus, Ohio, United States

© 2017 Elsevier Ltd. All rights reserved.

4.09.1	**Introduction to *In Silico* Tools and Applications**	156
4.09.2	**Statistical-Based Methodology**	158
4.09.2.1	Overview	158
4.09.2.2	Building Statistical-Based Models	159
4.09.2.3	Assessing Quality and Overfitting	160
4.09.2.4	Using Statistical-Based Methodologies	161
4.09.2.5	Available Models	162
4.09.2.5.1	Leadscope model applier	162
4.09.2.5.2	Sarah Nexus	163
4.09.2.5.3	TEST	164
4.09.2.5.4	CaseUltra	164
4.09.3	**Expert Rule-Based Methodology**	165
4.09.3.1	Overview	165
4.09.3.2	Building an Expert Alerts System	165
4.09.3.3	Using Expert Alerts	166
4.09.3.4	Available Systems	167
4.09.3.4.1	Leadscope expert alerts	167
4.09.3.4.2	DEREK	167
4.09.3.4.3	Toxtree	168
4.09.4	**Read-Across Methodology**	168
4.09.5	**Case Study: Using Statistical-Based (QSAR), Expert Rule-Based (Alerts), and Read-Across to Predict Mutagenicity**	171
4.09.6	**Conclusions**	174
References		174

4.09.1 Introduction to *In Silico* Tools and Applications

The goal of medicinal chemistry is to discover new pharmaceutical products through the design and synthesis of new compounds. This process simultaneously optimizes desirable biological effects including potency, metabolic stability and so on, at the same time as avoiding adverse effects. Toxicity is a significant adverse effect and one of the main reasons drugs fail in clinical trials or when drugs reach the market.[1] This attrition rate is a major impediment to bringing new drugs to the market and a significant contributor to the high cost of drug development.[2] Traditional approaches to testing compounds for toxicity rely on exposing groups of animals to a chemical or product, observing the pharmacokinetics and pharmacodynamics, gross and histological pathology, and signs of any adverse events. Animal studies are expensive and time-consuming, taking months or years, and costing hundreds of thousands or millions of dollars. In the early phases of drug discovery it is not possible to perform these types of tests because of both the cost as well as the throughput needed to rapidly profile the tens of thousands of compounds typically evaluated in the early phases of drug discovery. *In vitro* and *in silico* approaches are the only viable approaches for assessing toxicity as part of lead identification and optimization.

The use of *in silico* toxicology supports medicinal chemistry by identifying compounds with potential toxicity. The earlier in the drug discovery process a chemical or chemical series can be eliminated from consideration because of toxicity, the greater the impact on the overall productivity (i.e., the "fail early, fail fast" paradigm). Results from *in silico* methodologies can be generated quickly and cheaply based on the chemical structure alone. These methods also provide additional information to support future research directions, such as what areas of the molecule may need to be modified based on any predicted toxicity.

There are a number of areas where *in silico* toxicology is used in pharmaceutical R&D, including:

- *Prioritizing lead series*: It is possible to analyze the core scaffolds or lead series to understand whether they contain any structural elements associated with toxicity. *In silico* toxicology can help prioritize which chemical series to pursue or potentially modify to mitigate any projected toxicity.
- *Lead optimization*: *In silico* toxicology can support the design of analogs as part of lead optimization by helping to determine whether any structural modifications increase or decrease potential toxicity risk.

- *Supporting design of synthetic processes*: *In silico* toxicology can be used to assess the mutagenic potential of synthetic reagents, catalysts and intermediates to identify and reduce the possibility of having DNA-reactive impurities being present in a final drug product.
- *Prioritizing testing*: *In silico* toxicology can also be useful is selecting the order of toxicity testing in preclinical development. It is possible to use the predictions to initially focus on selecting those tests that would de-risk any potential toxicity identified (i.e., target organs). This again supports the "fail early, fail fast" paradigm. Often, low cost *in vitro* tests (such as the mini or modified Ames test or screening hERG assay) are conducted prior to the preclinical safety assessment phase.
- *Supporting regulatory submissions*: *In silico* toxicity predictions can be used to directly support submissions for drug impurities.[3] A computational assessment using *in silico* methodologies to predict the potential mutagenicity of impurities, degradants, intermediates, etc. can be performed.
- *Classification and labeling*: *In silico* approaches can be used to support classification and labeling where a complete battery of toxicity tests has not been performed. Once the potential mutagenicity has been determined using *in silico* approaches, compounds can be classified for control strategies (Muller et al., 2006).[4]

In the last several years, the use of *in silico* tools to predict toxicity has increased significantly as a result of improvements in the performance of the models, improvements in their ease-of-use and their acceptance as part of product development and some regulatory submissions. There are also an increasing number of guidelines to support the interpretation of results, an essential component to gain acceptance.[3,5] *In silico* software programs to predict toxicity combine biology and chemistry with modeling and computational science in order to increase the predictive power in the field of toxicology. *In silico* tools are inexpensive to run (once the model has been built), provide a level of confidence in the prediction and routinely provide an indication of the structural basis for any positive result. These approaches often provide an indication of the biological mechanism of the predicted toxicity. These criteria are useful for medicinal chemists since it is important to understand the basis of the predictions so that decisions can be made about future research directions.

The three most widely used *in silico* toxicity prediction methodologies used today are:

- *Statistical-based*: Statistical-based models, often referred to as Quantitative Structure-Activity Relationship (QSAR) models, are used to predict various toxicity endpoints based on the chemical structure.[6,7] These models are constructed from historical laboratory data (training set) where chemical substructures and molecular properties (descriptors) are generated from the list of chemicals. Statistically-based mathematical models are built using these descriptors to predict the target toxicological effect.
- *Expert rule-based*: Expert rule-based methodology (often referred to as alerts) is an approach to predict toxicity based upon the presence of structural rules.[6,8] Expert knowledge based on toxicity data and mechanisms is used to create rules on the likelihood of toxicity in a structure, with information from all applicable rules used to make an overall prediction. Rules usually are encoded as one or more substructures that are matched against the test chemical. A prediction is made when a predictive alert matches. These rules often indicate a mechanistic basis for any positive prediction.
- *Read-across*: Read-across is a semi-manual approach to making predictions from historical data.[9–12] It relies on the identification of appropriate analogs, based upon a mechanistic-based structural category or some other criteria. Data from these analogs are then used to make the prediction.

Other approaches include 3D modeling (e.g., CoMFA approaches)[13] and quantum chemistry (e.g., whole molecule reactivity descriptors such as E_{HOMO} and E_{LUMO} differences) are also used to a lesser degree.[14,15] Approaches that do not identify the structural basis for a prediction are limited in their applicability to medicinal chemistry.

Table 1 lists the some commonly used systems, the methodology used and the supplier.

All *in silico* approaches have strengths and weaknesses and **Table 2** summarizes them for the three methodologies described. One strength of all three methodologies is that they do not require compounds to be synthesized, and all are limited by the availability of relevant toxicity data. In practice, all three methods are often used together and an expert review based on the weight of the evidence is generated from (1) the prediction results and confidence scores, (2) the underlying basis for the predictions, as well as (3) expert

Table 1 List of common systems and suppliers of *in silico* software

System	*Supplier*	*Methodology*
Leadscope Model Applier Statistical QSAR suites	Leadscope (Columbus, OH)	Statistical-based
Sarah Nexus	Lhasa Limited (Leeds, UK)	
T.E.S.T.	U.S. EPA	
CaseUltra	MultiCASE (Beachwood, OH)	
Leadscope Model Applier Expert Alerts	Leadscope (Columbus, OH)	Expert rule-based
DEREK Nexus	Lhasa Limited (Leeds, UK)	
Toxtree	Ideaconsult Ltd (Sofia, Bulgaria)	

Table 2 Strengths and weaknesses of different *in silico* approaches

Method	*Strengths*	*Weaknesses*
Statistical-based	- Assesses all areas of the molecule, including whole molecular properties - Can often explain the structural basis for the prediction - Quick to generate a model - Fast to compute a prediction	- No direct mechanism provided, but may be elucidated as part of the QSAR explanation - Difficult to model complex *in vivo* outcomes
Expert rule-based	- Capable of precisely identifying reactive groups or pharmacophores that are linked to a mechanism - Includes reasons for activation and deactivation - Fast to compute a prediction	- Usually localized to the presence of a substructure and often does not take into account the whole molecule - Difficult to make supported negative predictions
Read-across	- Easy to understand and interpret - Has potential applicability in predicting complex *in vivo* outcomes where there is data on suitable analogs	- Manual methodology that may result in inconsistent results that are difficult to repeat - Time consuming to generate and fully document the results - Difficult to show that a chemical lacks toxicity

knowledge. This expert review has been shown to improve the accuracy of the overall prediction at the same time as providing an assessment of the overall confidence in the prediction.[16–19]

The Organization for Economic Co-operation and Development (OECD) has published a series of validation principles to help in understanding the applicability of these models for regulatory purposes: "1. *a defined endpoint*; 2. *an unambiguous algorithm*; 3. *a defined domain of applicability*; 4. *appropriate measures of goodness-of-fit, robustness and predictivity*; 5. *a mechanistic interpretation, if possible*".[20] These principles are important to use in assessing any model to use in predicting toxicity. The five validation principles are discussed in detail in this chapter; however, it is important to assess whether the model is fit-for-purpose. For example, a model that does not adhere to the principles may be acceptable for use in prioritizing candidates earlier in the process but not acceptable for regulatory submissions.

In silico models have been built to predict a wide range of endpoints important to assessing toxicity. These include *in vitro* and *in vivo* test results alongside information derived from human adverse events that are reported during clinical trials or post-approval drug monitoring.[21–25] The endpoints include: genotoxicity (*in vitro* and *in vivo*),[26] *in vivo* acute toxicity (oral, inhalation, dermal),[27] skin or eye irritation/corrosion,[28] skin sensitization,[28] repeated dose toxicity,[27] reproductive and developmental toxicity,[29] carcinogenicity,[26] specific organ toxicity and other areas of concern such as phospholipidosis.[30] Certain models identify the presence or absence of a specific hazard, whereas others provide an estimate of a safe dose and can be used to assess risk.

Models are often built from public domain data sources by commercial companies and academic laboratories which provide an off-the-shelf solution. These models are often updated when new data is made available; however, they invariably reflect the chemical space found in public domain compounds. They can be applied to proprietary test chemicals; however, if there is limited overlap in the chemical space they may be unable to make predictions for the types of chemical being assessed. Model and alerts that are built from proprietary data sources may provide suitable coverage of chemistry; however, there is a high cost associated with building such models and keeping them up-to-date. As a hybrid approach, many commercial organizations will work with pharmaceutical companies to ensure the public model correctly reflects proprietary chemical space. This reduces the burden of building such models for the pharmaceutical company and ensures more robust models are available and applicable to their chemistry.

The following chapter outlines the three commonly used *in silico* toxicology methodologies: statistical-based (QSAR) models, expert rule-based, and read-across. A description is provided illustrating how these models are built and how they make predictions. This will help to explain the strengths and limitations of the different methodologies since they may otherwise appear as a "black box". Examples are provided of commercial and academic systems used to make predictions. A case study will be presented to illustrate how all three methodologies can be used to support the prediction of mutagenicity. Finally, the chapter concludes with a discussion of these *in silico* methodologies alongside some future directions.

4.09.2 Statistical-Based Methodology

4.09.2.1 Overview

A statistical-based methodology or QSAR uses a mathematical model that, for a given chemical structure, will estimate a value for a biological effect such as a specific type of toxicity.[6,7] These models are referred to as "statistical-based methodologies" in regulatory guidelines.[3] The only input to the model is the chemical structure, which is an electronic record of the compounds' atoms, bonds and connectivity. These models are built using training sets containing a set of chemicals with a consistently measured toxicity response endpoint, such as positive/negative bacterial mutagenicity data or No Observed Adverse Effect Level (NOAEL) data.

Once a training set has been created, the model building process begins by calculating molecular descriptors directly from the chemical structures in the training set. A data table is generated and prepared containing the molecular descriptors as well as the toxicity response for all the training set compounds. A mathematical model is then built by selecting a subset of molecular descriptors as independent variables (x-variables) to predict the toxic response (y-variable). Once a model has been built and validated, it can be used to predict the toxic effect of test chemicals not present in the QSAR model training set. At this point it is important to be able to interrogate the QSAR model results and examine the underlying reasons for the prediction, especially any structural features of the test chemical that are responsible for a positive prediction.

In addition to the OECD validation principles discussed earlier, there are three important guiding principles when developing QSARs to support the prediction of toxicity:

(1). Keep the models simple with as few and simple descriptors as possible to avoid overtraining, support interpretation and ensure the model's domain is as broad as possible
(2). Generate models that provide a high level of prediction transparency, both the structural basis for the prediction, descriptor weighting, and an indication of the biological significance
(3). Provide information to support a hazard or risk assessment, that is, either classification of specific toxicity or the dosage required for toxic effects to appear

The following sections outline the general process of building, using and explaining QSAR models as well as examples of commercial and other types of QSAR models available today.

4.09.2.2 Building Statistical-Based Models

Constructing a suitable training set is the most important part of building the statistical-based (QSAR) model and often the most time consuming. Information on historical studies is generally publicly available through on-line websites (e.g., the National Toxicology Program (NTP) website[31]), toxicity study reports or in the public literature. Studies may have been generated across different organizations and according to different experimental protocols. When collating an electronic record of this information, it is important to record as much detail as possible about the source, the experimental design and other factors to assess how the study was performed (e.g., GLP status, dose levels, etc.). Criteria should be established as to what type of studies (based on the study protocols, design, quality, and source) to include in the training set. An overall study call (e.g., LD_{50} values or positive/negative mutagenicity) is usually provided alongside individual study findings and observations, such as whether as part of a reproductive study, cleft palates were observed and at what dose. The overall study call generated by the study director may be the biological response to be predicted; however, there will be situations where a different call might be calculated as the purpose for the original call is rarely for QSAR model development. For example, a training set may be based on the presence or dose at which an individual finding was reported (e.g., a cleft palette identified in a reproductive study). This process is important to satisfy OECD validation principle #1 "a defined endpoint." As discussed earlier, it is important to keep models simple, and modeling a specific effect is usually less complex than modeling an overall *in vivo* study (e.g., LD_{50} for an entire reproductive toxicity study covering all types of findings). Models created around specific phenotypes or mechanisms will generally be less complex and be easier to explain.

When combining the data from different sources it is important to ensure the data is recorded consistently. This includes simple checks such as if the data is recorded using the same units and how the chemical structures are recorded. A connection table (electronic record of the atoms, bonds, and connectivity) should be used for each chemical. Commonly used formats for storing chemical structures are an SD file, a list of MOL files or a list of SMILES strings.[6] It is important to determine if or when the same chemical has been tested more than once. This may result when the same chemical is: (1) tested in more than one laboratory, (2) tested in different salt forms and mixtures, (3) reported with different structural representations (e.g., the nitro group is drawn with different formatting conventions) or (4) reported with different stereo-chemical forms (i.e., known-stereo versus partial stereo or non-stereo forms). Different sources may have conflicting study calls resulting from different study protocols and reporting. It is important to establish consistent rules to handle these situations and determine an overall call for each chemical that may be derived from multiple study results.

Once the training set has been harvested, cleaned and processed, the next step is to determine the types of chemicals present in the training set and the frequency distribution of the toxicity data being modeled. Grouping the chemical structures based upon structural similarity will identify the chemical classes in the training set and hence the type of chemicals that the model will be able to ultimately predict. The absence of certain chemical classes may lead to further data harvesting efforts called "gap filling". The distribution of the toxic effect data should be examined and mathematical transformations considered. For example a continuous toxicity response may have an exponential frequency distribution, and to facilitate modeling efforts, it should be transformed using a log transformation.

The next step is to generate molecular descriptors from the chemical structures in the training set. There are many types of molecular descriptors used in statistical QSAR models and several approaches for generation of these descriptors have been developed.[14] One approach is to use a list of pre-defined substructures and match them against the training set.[32,33] Alternatively, different substructures can be generated algorithmically by either tracing paths through the compounds or combining smaller building blocks together into larger scaffold-like substructures.[34] Creation of these substructures may be guided using the toxicity response data to select discriminating substructures associated with predominantly positive or negative compounds in the training set (or compounds with predominantly high or low values). Molecular properties calculated from the whole molecule such as molecular

weight, logP, polar surface area, and so on can also be generated to ensure the model addresses more than just portions of the test compound. These molecular descriptors will also be used to explain the results; hence if it is important to explain the model results using structural features, then structural features need to be included as descriptors.

The different molecular descriptors calculated are added to a data table. The molecular descriptors that encode the presence or absence of structural features can be encoded as a binary property where "1" indicates the presence and "0" indicates the absence of a specific feature. Other properties, such as molecular weight, can be encoded directly after normalization. Further processing of this table is necessary prior to modeling. Again, to satisfy the "as simple as possible" rule, the list of possible descriptors should be reduced. Correlated descriptors should be identified and pruned and non-discriminating descriptors (i.e., those whose presence or absences results in predominantly the same value) should be removed. The toxic effect is also included in this table and can be used to filter these descriptors by magnitude of effect; for example, those descriptors highly correlated with the toxic response variable might be prioritized while descriptors with low correlation might be removed. Knowledge of the problem being modeled can be beneficial in the selection of descriptors. Additional normalization transformations are carried out, such as auto-scaling, to ensure all descriptors are considered equally in the modeling process based upon their population and distribution of values.

The next step is to build and optimize a statistical model that encodes the relationships between the molecular features and the biological response. Selection of the modeling approach should balance the need to keep the models as simple as possible, yet robust enough to model the complexities of the structure-activity relationship data and support prediction of the desired chemical classes. For simple data sets, such as those focused around a specific class of compounds, modeling techniques such as linear regression, logistic regression, and decision trees may be used; whereas more complex and structurally diverse datasets will require the use of modeling approaches such as Partial Least Squares, Partial Logistic Regression, Random Forests, Support Vector Machines, and Artificial Neural Networks.[35–40] All models mathematically encode the relationships between the individual descriptors and the toxic response by calculating one or more weights per descriptor, etc. and optimizing modeling parameters. The use of a specific modeling approach and optimization procedure is described as OECD validation principle #2 "an unambiguous algorithm." Fig. 1 summarizes this process of harvesting the data, generation of molecular descriptors, processing and preparation of a table and creation of a mathematical model relating toxicological response data to the selected descriptors.

4.09.2.3 Assessing Quality and Overfitting

A validation set is used to characterize statistical-based (QSAR) model performance. An external validation set is a list of chemicals not used in building the model (i.e., are not in the model's training set) which has the same toxicity response endpoint. The model predicts the values for this validation set and the performance is quantified by comparing the predictions against the actual values. The best validation set contains enough compounds to test all the chemical classes and toxicophores being modeled and has a distribution of data values similar to that in the training set.

Another approach, referred to as cross-validation, can be used to estimate the performance of the model without the burden of finding external data. It splits the training set into a series of training/test set pairs to predict all the training set compounds using a series of "reduced" models. For example, a 10% cross-validation will split the original training set into 10 different pairs. For each pair 10% is set aside for testing and the remaining 90% is used as a training set to build a reduced QSAR model used to predict the 10% in the test set. A total of ten models are built to predict all the training set compounds ensuring that no test set chemical is part

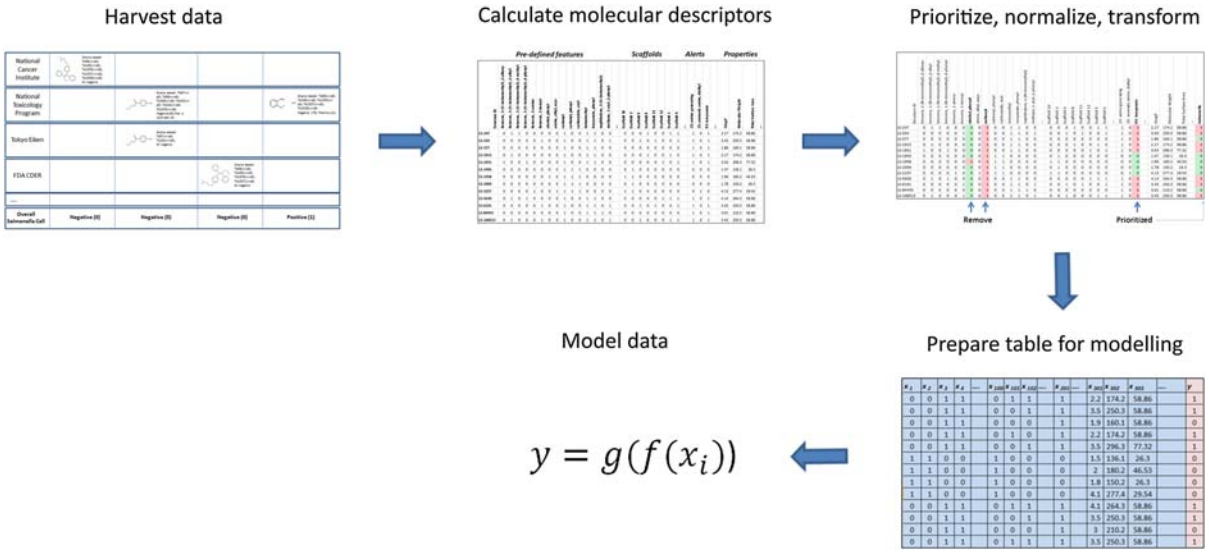

Fig. 1 Process of building a QSAR model from data.

of the model training set used to predict it. Cross-validation predicts every compound in the training set and is useful in estimating the predictive performance of the model in the absence of external data. However, the individual predictions are not representative of individual compound predictivity performance or that of chemical classes as they were not predicted by a complete QSAR model constructed using the entire training set.

The predictive performance of the QSAR model is calculated by comparing the actual and predicted values. When the toxicity response variable is binary (that is, it only contains positive or negative outcomes), the first step in assessing the performance of the model is to calculate a table (Table 3) that summarizes the number of true positive and true negative predictions, as well as the false positives and false negative predictions. These values support calculation of a series of "Cooper statistics",[41] which assess the overall performance of the model (Table 4). For QSAR models where the toxic response data is continuous, it is useful to use scatterplots to visualize the performance of the predicted versus actual data to illustrate regression performance and distribution of the residual values (as shown in Fig. 2). A well performing model has values close to the diagonal on the regression plot, while the residual plot has values randomly distributed about zero with no clear trends or bias. In addition, a number of different common statistics (Table 5) can also be used to assess the overall performance of the QSAR model. The formulas use y_i to represent the individual values of the response data, $\widehat{y}_i$ to indicate the value of the corresponding prediction, and $\bar{y}$ to indicate the mean response value.

4.09.2.4 Using Statistical-Based Methodologies

Any model adhering to OECD principles should initially consider whether each of the test chemicals is within the applicability domain of the QSAR model. This check often examines the model descriptors (e.g., the structural features present in the test chemical) used to make the prediction and whether the test compound is similar enough to the training set compounds to ensure its chemical subclass may be adequately predicted by the QSAR model.

All the QSAR model molecular descriptors are then calculated for the test compound(s). Once calculated, the values of these "x-variables" are used with the model weights (and other terms) to calculate a prediction. This value may be the actual toxic response estimate; however, with certain modeling approaches, this value may represent the probability of the positive outcome. In this case, this probability is usually converted to a classification where values above a threshold (e.g., 0.6) are assigned positive, values below a threshold (e.g., 0.4) are negative while those between these two values (e.g., 0.4 – 0.6) are considered indeterminate or to have equivocal results (since there is a lack of strong evidence and/or conflicting positive and negative evidence).

Once an estimate has been generated, it is important to understand how a model generated the prediction by understanding the structural basis for the prediction and potentially a mechanistic rationale. For simple models (such as a linear regression) inspecting the descriptors along with the model parameters may be sufficient to understand how the model generated the results. For more complex modeling approaches (such as non-linear approaches), it is not as easy to inspect the model parameters and descriptors

Table 3 Computation of the number of true/false positives and negatives

		Predicted		
		Positive	Negative	Total
Observed	Positive	TP	FN	TP+FN
	Negative	FP	TN	FP+TN
	Total	TP+FP	FN+TN	TP+FN+FP+TN

Table 4 Computation of statistics to assess QSAR models for binary endpoints

Statistic	*Formula*	*Description*
Concordance	(TP+TN)/(TP+FN+FP+TN)	Shows the overall accuracy of the model or the proportion of correctly predicted examples
Sensitivity	TP/(TP+FN)	Proportion of correctly assigned positive predictions out of all positive chemicals
Specificity	TN/(TN+FP)	Proportion of correctly assigned negative predictions out of all negative chemicals
Positive Predictivity	TP/(TP+FP)	Proportion of correctly assigned positive predictions out of all positive predictions
Negative Predictivity	TN/(TN+FN)	Proportion of correctly assigned negative predictions out of all negative predictions
False positive rate	FP/(FP+TN)	Proportion of negative chemicals that are incorrectly classified as positive
False negative rate	FN/(FN+TP)	Proportion of positive chemicals that are incorrectly classified as negative
Coverage		Proportion of chemicals in the test set that have been predicted

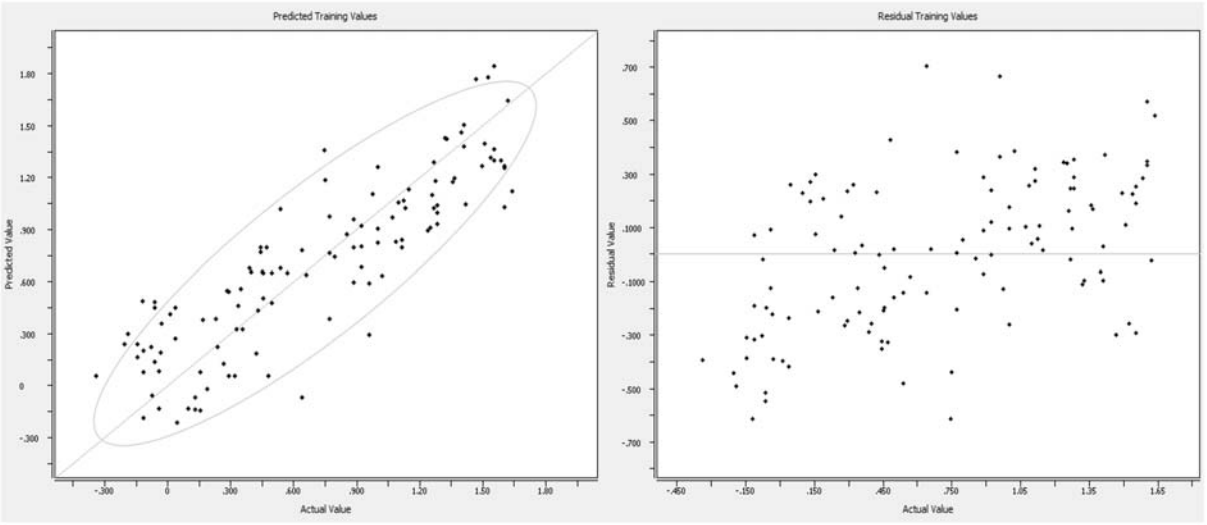

Fig. 2 Comparing predicted with actual values alongside a residual plot.

Table 5 Assessing the performance of QSAR models where the response is continuous

Statistic	*Definition*	*Formula*
MSE	Mean Square Error	$\sum_1^n (y_i - \hat{y}_i)^2 / n$
PRESS	Predictive Residual Sum of Square	$\sum_1^n (y_i - \hat{y}_i)^2$
Q2	Explained variance in the prediction	$\sum_1^n (y_i - \hat{y}_i)^2 / (y_i - \bar{y})^2$

directly. These approaches are usually accompanied by an "explanation" functionality that is capable of identifying the structural basis for the prediction. This structural basis may in turn help elucidate a mechanistic basis for the prediction.

4.09.2.5 Available Models

4.09.2.5.1 Leadscope model applier

The Leadscope® Model Applier is an application in which a series of QSAR models and expert alerts are distributed to support prediction of the potential toxicities of chemicals. All the QSAR models were constructed in collaboration with the U.S. Food and Drug Administration (FDA) by the Division of Applied Regulatory Science (DARS) staff (previously known as the Division of Drug Safety Research). The models were built under a Research Collaboration Agreement (RCA) using the Leadscope Predictive Data Miner software.[21–25,42–46] Complete documentation of the weight of evidence methodology used for the preparation of the model training sets and the sources of the data has been published by the DARS group. The RCA QSAR models were built from public information and include the training set structures and calls as part of the model description. The RCA models are implemented with molecular descriptors that include structural features and up to eight calculated properties. The structural features include Leadscope® default hierarchy features plus the predictive scaffolds constructed specifically for each model. The eight calculated properties include parent molecular weight, parent atom count, LogP, polar surface area, hydrogen bond acceptors, hydrogen bond donors, number of rotational bonds and, Lipinski score (rule violation).

There are currently eight suites containing RCA QSAR models with over 80 biological endpoints. The suites can be divided into two major groups of endpoint models: 1) human clinical endpoints; and 2) non-human toxicity endpoints, as shown in **Table 6**. The majority of the QSAR models are specifically designed to provide decision support for toxicological and clinical endpoints that are considered important in the safety analyses of substances. However, the Model Applier also includes a subset of models that have proven useful for research on toxicological properties of chemicals.

The prediction results for each model are presented as the "prediction" and the "positive prediction probability". The prediction can be "positive", "negative", "indeterminate", and "not-in-domain". The positive prediction probability is given as the likelihood value between 0 (non-toxic) and 1 (toxic). The higher the probability is, the greater chance there is of the test chemical being toxic for a particular endpoint. The model domain is defined for a test compound within the Leadscope application using two criteria: 1) containing structural model features in addition to property descriptors; 2) being within a group of similar structures in the training set.

Table 6 Summary of QSAR models available from Leadscope

Model suite	*Individual models*
Carcinogenicity	Carcinogenicity Male Mouse, Carcinogenicity Female Mouse, Carcinogenicity Male Rat, Carcinogenicity Female Rat, *In vitro* Cell transformation, SHE, BALB/c-3 T3, C3H10T1/2
Genetic Toxicity	*In vitro* Salmonella, In vitro E Coli - Sal 102 A-T Mut, *In vitro* CHO, HGPRT, Mouse Lymphoma, Micronucleus *in vivo* mouse, Chromosome Aberrations in vivo, Chromosome Aberrations In vivo rat, Chromosome Aberrations *in vivo* other rodent, *In vitro* chrom. ab. CHL, *In vitro* chrom. ab. CHO, SCE *in vitro*, SCE *in vitro* CHO, SCE *in vitro* other cells
Reproductive Toxicity	Repro Rat Male, Repro Mouse Male, Repro Rat Female, Repro Mouse Female, Sperm Rat, Sperm Mouse
Developmental Toxicity	Structural Dysmorphogenesis (rodent, rat, mouse, rabbit), Visceral Dysmorphogenesis (rodent, rat, mouse), Fetal Growth Retardation (rodent, rat, mouse, rabbit), Fetal Weight Decrease (rodent, rat, mouse, rabbit), Fetal Death (rodent, rat, mouse, rabbit), Post Implantation Loss (rodent, rat, mouse, rabbit), Pre Implantation Loss (rodent, rat, mouse, rabbit)
Neurotoxicity	Behavioral Toxicity Newborn Rodent, Behavioral Toxicity Newborn Rat, Behavioral Toxicity Newborn Mouse
Human Adverse Cardiological Effects	Conduction Disorders, Coronary Artery Disorders, Electrocardiogram Disorders, Heart Failure Disorders, Arrhythmia Disorders, Bradycardia Disorders, QT prolongation, Tachycardia Disorders, Torsades, Myocardial Infarct Disorders, Myocardial Disorders, Palpitations, Rate Rhythm Disorders
Human Adverse Hepatobiliary Effects	Bile Duct Disorders, Cholestasis, Liver Acute Damage, Liver Enzyme Release Disorders
Human Adverse Urinary Tract Effects	Bladder Disorders, Blood in Urine Disorders, Renal Disorders, Kidney Function Tests, Nephropathy Disorders, Urolithiasis Disorders

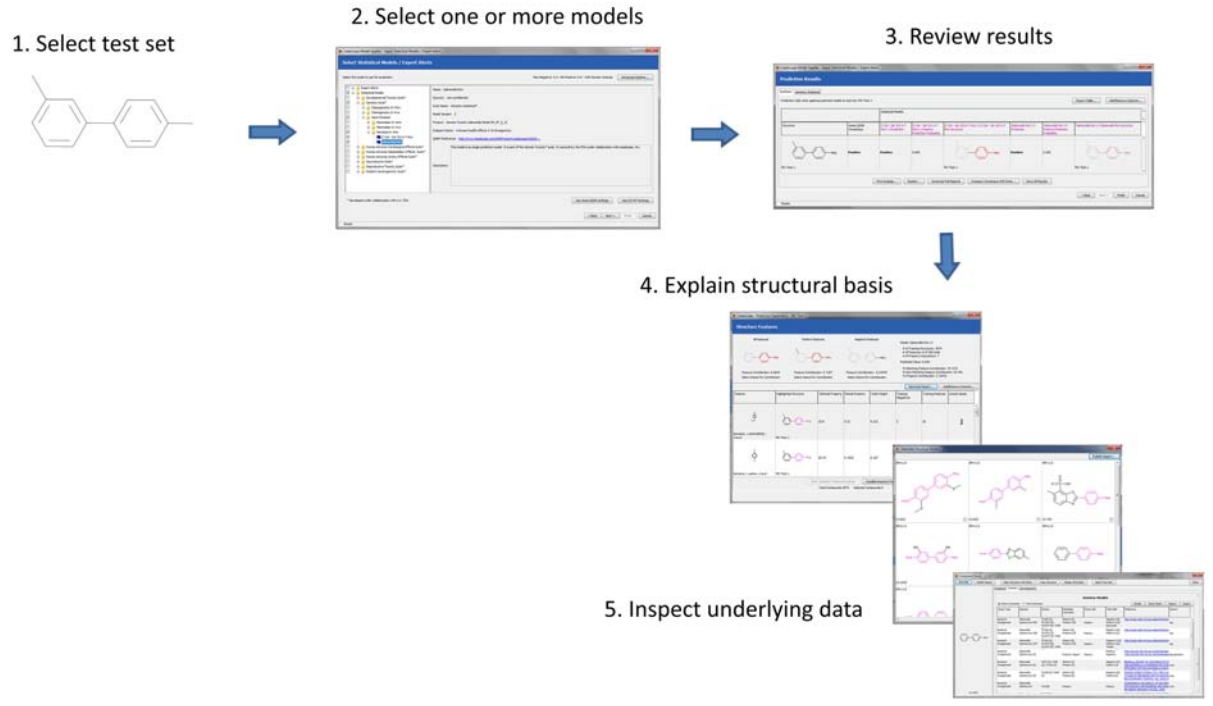

Fig. 3 Using the Leadscope Model Applier to make predictions using QSAR models.

Fig. 3 illustrates how QSAR models for one or more endpoint predict one or more test chemicals and how the information is explained, including the structural basis for the prediction and the underlying data.

4.09.2.5.2 Sarah Nexus

Sarah Nexus (Sarah) is a statistical-based software program that was created to provide mutagenicity predictions from analysis of 2-D chemical structures. The software is based on a hierarchal list of models that combines both global and local features, and will select the most appropriate model for the prediction. While a global model provides broad coverage it may not be as sensitive to local variations, whereas local models are more accurate for fragments within their chemical space, but they are narrower in their scope. The

software retrieves fragments of various sizes matched from the test structure, and includes fragments that overlap to ensure greater accuracy in predictions. Relevant fragments are arranged into local and global networks and information from each fragment is evaluated and a recursive learning method is used to assess each fragment's negative or positive contribution. The confidence associated with each relevant fragment then contributes to an overall prediction. The structural features considered meaningful in the prediction are highlighted in the test structure. A confidence score is provided and is intended to correlate with the accuracy of the prediction.

4.09.2.5.3 TEST

The Toxicity Estimation Software Tool (TEST) has been developed by the U.S. Environmental Protection Agency to allow users to easily estimate toxicity using a variety of QSAR methodologies. TEST provides multiple prediction methodologies (hierarchal, single model, group contribution, Contrera 2003 method, nearest neighbor and consensus). The Hierarchal method uses a variation of Ward's Method[47] to generate a series of individual models based upon clusters (chemicals from entire set which have similar properties) from the training set. Once the clustering process is complete, the clusters are analyzed for QSAR, and if acceptable, a genetic algorithm is used to determine an optimal descriptor set to characterize the toxicity values of chemicals within the cluster. Once the model has been optimized and validated, the test compound is checked to determine if it falls within the domain of applicability for the model before a prediction is determined. The Single Model approach uses a multiple linear regression model fit to the entire training set. The Group Contribution approach is based on methods by,[48] where fragment counts from at least three chemicals in the training set are used to fit a linear regression model to the entire data set. The method based on work from[49] is referred to here as the "Contrera 2003 method" and "FDA" in the documentation provided by EPA.[50] Predictions are made using a unique cluster that contains structurally similar chemicals selected from the overall training set. For the toxicity prediction to be valid, the value must be within the range of experimental values for the chemicals that were used to build the model. The Nearest Neighbor method uses the average toxicity of the three most similar analogous chemicals in the training set. The predicted toxicity from the Consensus method represents the average of the predicted toxicities from all the different QSAR methods incorporated into the TEST software, and this method achieved the best prediction accuracy (concordance) and prediction coverage for the Ames assay. The final dataset of 5743 chemicals were based upon the dataset compiled by Hansen et al., 2009.[51] A summary of the advantages and disadvantages of the different methods are presented in **Table 7**. In TEST, predicted values ≥ 0.50 are considered positive. Several endpoints are available for evaluation, as shown in **Table 8**.

4.09.2.5.4 CaseUltra

CASE Ultra (CU) is a fragment-based QSAR system that employs machine learning techniques from training set data.[52–54] As a QSAR model that evaluates the relationship between a structure and its biological activity, CU was specifically designed to work with "non-congeneric" databases, that is, databases consisting of structurally unrelated molecules. Based on a hypothesis

Table 7 TEST Analysis Methodologies

Method	*Advantages*	*Disadvantages*
Hierarchical	● Produces predictions from multiple models	● May generate predictions from a model based on only a few compounds
Single Model	● Single transparent model can be easily viewed/exported ● The model does not need to rely on clustering the chemicals correctly	● Since the model is fit to the entire dataset it may incorrectly predict the trends in toxicity for certain chemical classes ● Cannot provide external estimates of toxicity for compounds in the training set
Group Contribution	● Single transparent model can be easily viewed/exported ● Estimates of toxicity can be made without using a computer program	● Model doesn't correct for interactions of adjacent fragments ● Since the model is fit to the entire dataset, it may incorrectly predict the trends in toxicity for certain chemical classes ● Cannot provide external estimates of toxicity for compounds in the training set
Contrera 2003 method	● Can generate a new model based the closest analogs to the test compound ● Always provides an external prediction of toxicity	● Close analogs may not exist. The QSAR model must be regenerated and validated for each prediction
Nearest Neighbor	● Provides a quick estimate of toxicity ● Allows one to determine structural analogs for a given test compound ● Always provide an external prediction of toxicity	● Does not use a QSAR model to correlate the differences between the test compound and the nearest neighbors ● Was shown to achieve the worst prediction results during external validation
Consensus	● Was shown to achieve the best prediction results during external validation	● Cannot provide external estimates of toxicity for compounds in the training set

User's Guide for TEST (version 4.1), US EPA, 2012.[51]

Table 8 TEST Toxicity Endpoints

Toxicity Endpoints
96-Hr Fathead Minnow LC_{50}
48 hour Daphnia magna LC_{50}
48 hour *Tetrahymena pyriformis* IGC_{50}
Rat Oral LD_{50}
Bioaccumulation factor
Developmental toxicity
Ames mutagenicity

that a relationship does exist between chemical structure and activity, the program works to create a dictionary of molecular descriptors, identify fragments (or substructural units) and then differentiates activating features from deactivating features of the fragments. In CU, activating descriptors are termed 'biophore' and deactivating descriptors as 'biophobe'. The program also considers several other factors, such as molecular weight, octanol/water LogP, water solubility, Lipinski's rule of 5 and intestinal absorption. All of the alert contributions are considered and a scaled feature weight and regression coefficient are used in the final overall probability calculation. Unknown positive (activating) and deactivating features are highlighted in the program, and an overall positive probability is also provided. Case Ultra modules include mutagenicity, carcinogenicity, cardiotoxicity, hepatotoxicity, skin and eye toxicity and several others. Many of the modules were developed in collaboration with the CDER office of the US FDA under a RCA agreement with MultiCASE Inc.

4.09.3 Expert Rule-Based Methodology

4.09.3.1 Overview

Expert rule-based systems (also referred to as expert alerts or structural alert) are a widely used and easy-to-interpret approach to predicting toxicity. These approaches encode intellectually-derived structural rules as "structural alerts" that describe a portion of a chemical that is associated with a specific toxic effect or mechanism. When a test chemical contains any structural alert, it is flagged as potentially toxic. The following sections outline the process of building this type of knowledge base, describe how these alerts are used to make predictions and summarize a number of commonly used commercial and non-commercial systems.

4.09.3.2 Building an Expert Alerts System

In contrast to a statistical-based model (QSAR) which uses a training set to automatically extract knowledge from the data, an expert rule-based system (alerts) uses a reference data set to assess the predictive performance of any alert encoded intellectually or from the literature and support the assessment of applicability domain. This reference set can help refine the definition of the alerts and even identify new alerts. The same principles outlined in the development of a statistical-based model training set should be applied including capturing underlying information on the study protocol, study design and results, processing the chemical structures into a unique set, and preparing the toxicity response data that will be predicted using the expert alerts.

Alerts are often reported in the public literature where individual publications may identify one or more structural alerts, provide a mechanistic justification for the structural features, as well as examples. The information needs to be carefully reviewed before encoding this knowledge into any expert alert system. The same alert may have been described in multiple papers. It is important to understand how each paper described the alert as they may describe the same alert differently. Consolidating alerts from different references is an important part of the process. For example, **Fig. 4** shows different ways aziridines are defined in different publications.[55–58]

A complementary approach to extracting expert alerts from the literature is to analyze structure-activity data in a reference data set or other data sources. This approach helps in refining the definition of the alert and in understanding the limitations of its definition through empirical observation. These restrictions are encoded as structural features or other criteria required to either activate or deactivate the alert. Data analysis may also identify new alerts, by focusing on a chemical series containing positive examples but where no literature alerts exist.

Proprietary data is especially helpful in supporting the development of an expert alerts system. Since this information is not in the public domain, it is necessary to develop methodologies to support the extraction of knowledge while at the same time ensuring proprietary information on chemical structures and test results is not made public. This can be achieved by sharing the data under confidentiality restrictions, analyzing this data to refine existing alerts or identify new alerts and then adding this knowledge into the expert alerts knowledge base. Another approach is to use a SAR Fingerprint to refine specific alert classes.[94] A SAR Fingerprint uses a series of very specific substructures to explore structure-activity relationship (SAR) around a particular class of compounds. The substructures are searched against public and proprietary databases and the frequency of positive and negative compounds matching each substructure are pooled across all data collections. The results help to refine the alert definitions and support an understanding what additional features may activate or deactivate the alert.

The reference set is an essential resource for qualifying the expert alerts. All alerts should demonstrate a positive association with the toxicity response data. To help understand this association, the average toxicity response for compounds containing the alert can

"aromatic and aliphatic aziridinyl derivates" [Ashby 1988]	
"aziridine" [Kazius 2005]	SMARTS: C1NC1
"oriranes and azirdines" [Bailey 2005]	3-membered O- and N-containing rings
"AS_7: epoxides and aziridines" [Benigni 2008, 2011]	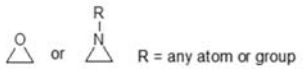

Fig. 4 Example of alerts definitions from different papers.

be compared to the average response for the entire set. A significantly higher than expected mean value for the subset containing the alert compared to the background mean indicates a positive association. This response can be statistically quantified and used to qualify the predictivity of the alert (e.g., as inactive, indeterminate, or high).

In many cases, compound structures possess more than one alert. It is helpful to analyze alert performance when no other alert is present to ensure that the response is attributable to the alert in question, and not another alert(s) that are coincidentally present. Proprietary data can also be used to verify alert predictivity and qualify alerts where no public data is available. Discrepancies between the public and private data are not uncommon and indicate that further restrictions on the alert are needed. For example, if an alert is generating too many false positives when applied to proprietary chemical space, that alert definition needs further refinement. Finally, understanding the biological mechanism(s) for the alert further supports it being active. There will invariably be alerts which lack enough evidence to mark them as active or inactive. These alerts are assigned to another category, such as indeterminate. Table 9 presents some examples of how alerts (developed to predict bacterial mutagenicity) were qualified using data from the reference set.

Once an alert has been identified, refined and qualified, it needs to be encoded into the system's knowledge base. The alert should include its precise structural definition as well as where and how the alert was identified. Supporting information on all plausible mechanisms should be recorded alongside other supporting information including examples. Any alert system can be used to predict the toxicity of a specific toxic response. Usually the presence of a qualified alert in any test compounds is used to generate a positive prediction and the absence of any alert (as long as the chemicals is within the applicability domain described in the next section) is used to support a negative classification. As such, the performance of any expert alert systems may be assessed using a validation set and the same "Cooper statistics" as described in Table 4.

4.09.3.3 Using Expert Alerts

For expert alert systems to adhere to OECD validation principal number 4, there must be an assessment of the applicability domain. This process usually involves an analysis of the chemical space covered by a reference set to define the chemical classes containing toxic chemical features which are adequately predicted by the alert set. Domain analysis may also consider the similarity of the entire test compound to the reference compounds. This qualifies the appropriateness of using alerts in predicting the entire

Table 9 Qualification of alerts using a reference dataset

Alert name	*Alert source*	*Frequency in reference set*	*Mean: Bacterial Mutation*	*Number of positives*	*Number of negatives*	*Status*
All compounds in reference set		10,295	0.49	5048	5247	
allylic alkoxides	Bailey 2005	83	0.46	38	45	Inactive - mean value is lower than background
benzene, 1-amino(NH2)-, 4-aryl-	Galloway 2013; Shamovsky 2011	58	0.91	53	5	Active – mean value is significantly higher than background; primary aromatic amine alert activator
benzene, 1-amino(NH2), - 4(aminosulfonyl)-	Analysis of reference set	18	0.11	2	16	Active – mean value is significantly lower than background; primary aromatic amine alert deactivator

compound beyond just identifying portions of the test compound that contain (or do not contain) active substructural features. This approach is particularly useful in supporting a negative prediction where a test compound has no matching alerts.

For chemicals within the applicability domain of the alert system, a prediction is made where an alert matches the test chemical. In performing the matching, an analysis of the activating and deactivating rules of the alert is also performed. For example, if the primary alert rule matches but a corresponding deactivating alert rule also matches, then no match is made. Wherever a match is present, the structural basis for the alert prediction can be highlighted and supporting information presented to explain the prediction. This includes information on the definition of the alert, the source of the alert, the structural rules for mitigation, the biological mechanism (OECD validation principle number 5), how the alert was qualified, and examples. Examples of how alerts are applied to the chemicals are presented in Fig. 5.

4.09.3.4 Available Systems

4.09.3.4.1 Leadscope expert alerts

The Leadscope expert alerts currently focus on predicting mutagenicity (based on the Ames test results) and is often used to support the ICH M7 guidelines on pharmaceutical impurities.[3] The system is based on a dictionary of structural alerts extracted from the public literature and qualified using a large and diverse database of bacterial mutagenicity data containing 10,295 chemicals (reference set). Activating alerts are encoded as separate rules for each primary alert. Deactivating features are also encoded alongside the primary alert whose mutagenicity they mitigate. A prediction is made when the test chemical is within the applicability domain based upon its structural similarity to reference set compounds. If an alert is present and there are no deactivating features also present in the test chemical, then a positive classification is made; whereas the absence of any alert or the presence of a deactivating fragment will result in the test chemical being predicted as negative. A precision score is also calculated based on data matching the alert from the reference set. The system captures information on the biological mechanisms reported in the literature, the source for the alert (e.g., a literature citation or data analysis), and examples. The alerts were qualified by their performance against a reference data set and against proprietary corporate databases. The performance of specific chemical classes has been improved using the SAR fingerprint methodology previously described. For example, a SAR fingerprint was used to improve the performance of primary aromatic amines by modifying the rules that activate or deactivate their mutagenicity. This resulted in a 39% increase in the specificity of this alert. The alert system is available through the Leadscope Model Applier and an example is shown in Fig. 6.

4.09.3.4.2 DEREK

DEREK Nexus (DEREK) was developed by Lhasa Limited, an organization that specializes in the development of expert computer systems for toxicity and metabolism predictions.[8] DEREK is a knowledge and rule based predictive toxicology software program that makes qualitative estimations of endpoint risk, and Nexus is the interface used to support the program. The qualitative estimations of risk are categorized, in descending order of probability, as 'certain', 'probable', 'plausible', 'equivocal', 'doubted', 'improbable' or 'impossible'. The most recent version of the software contains a new functionality to provide negative ('inactive') predictions for bacterial *in vitro* mutagenicity. When no alert is found for a structure, it is evaluated for unclassified and misclassified features. Unclassified features are those not found in the Lhasa reference set, and misclassified features are those derived from non-alerting mutagens in the Lhasa reference set. If all features in a structure are found and accurately classified in the reference set, a negative prediction (inactive) is displayed. Predictions for structures with misclassified or unclassified features are also called negative (inactive), and these features are highlighted such that they can be further evaluated by the user to de-risk the structure. For misclassified features, the program also displays the most similar compounds from the reference set along with a nearest neighbor similarity score. Negative predictivity has been reported to be 86–94.3% for structures without misclassified features and is more variable with misclassified features, ranging from approximately 83–89%. The Lhasa Ames reference set was composed of six data sets (Vitic NTP, Hansen, FDA CFSAN, ISSSTY, CGX and marketed pharmaceuticals) and is comprised of 10,243 compounds (Lhasa Knowledge Suite, Nexus 1.7 Release Notes). Several endpoints can be evaluated with DEREK, including carcinogenicity, mutagenicity, genotoxicity, skin sensitization, teratogenicity, irritation, respiratory sensitization and reproductive toxicity.

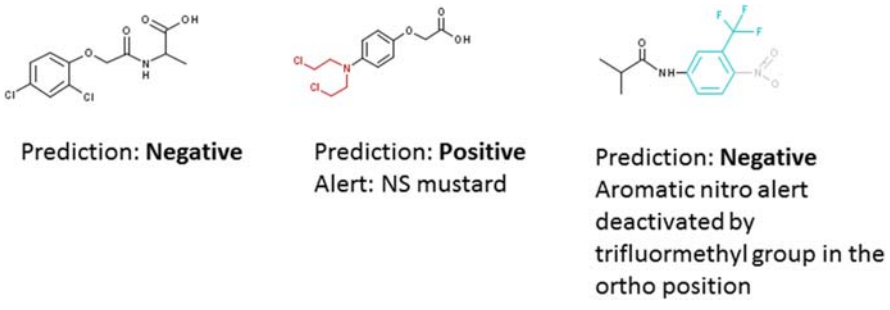

Fig. 5 Examples of expert alert predictions for bacterial mutagenicity.

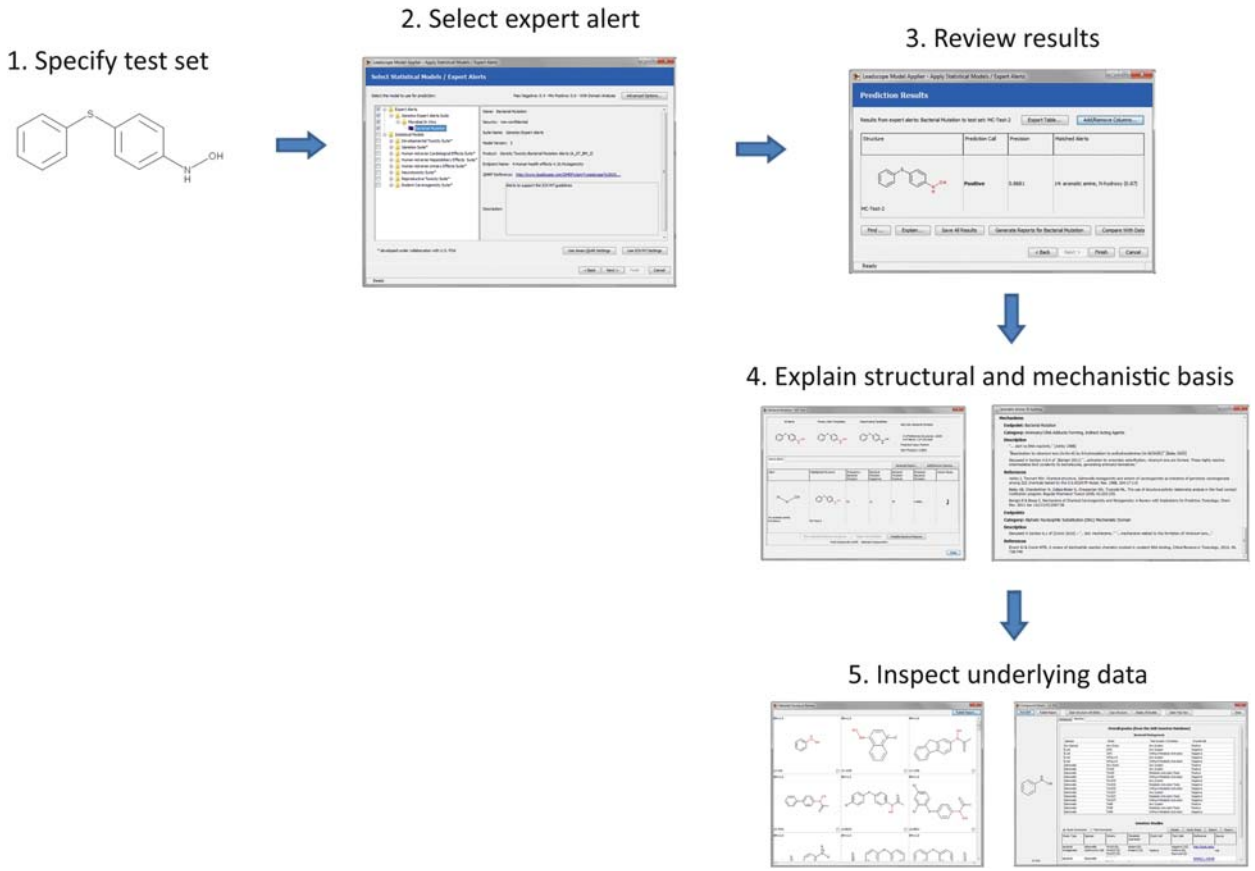

Fig. 6 Using the Leadscope model applier to predict bacterial mutagenicity using expert alerts.

4.09.3.4.3 Toxtree

Toxtree is an open-source, rule-based platform which is able to estimate toxic hazard by applying decision tree approaches, including those listed in (Table 10). The software was developed by Ideaconsult Ltd (Sofia, Bulgaria) and is freely available as a resource to the scientific community. It includes three rule-bases relevant to the Toxicological Threshold of Concern (TTC) assessment, including 1) the Cramer decision tree[59]; 2) the Cramer rule base with extensions; and 3) the TTC decision tree.[60] A more complete description of the software and its use of the Cramer classification scheme can be found Lapenna and Worth, 2011[61] and Patlewicz et al., 2008.[62]

4.09.4 Read-Across Methodology

Read-across is an approach to predicting toxicity which uses experimental data from one or more chemical analogs to generate a prediction of toxicity for a chemical with no data (referred to as the *target* chemical).[9–12] One common use of the read-across method is for evaluation of drug substance impurities, where information on the parent structure is used to predict potential toxicity of the impurity, providing there is enough structural similarity to compare the structures. High quality toxicity databases are an

Table 10 Toxtree Decision Tree Approaches

Cramer classification scheme
Kroes TTC decision tree
Verhaar scheme for predicting toxicity modes of action
The Skin Irritation Corrosion Rules Estimation Tool (SICRET)
Benigni-Bossa rule base for carcinogenicity and mutagenicity
START rule base for biodegradation and persistence
ToxMic rule base for *in vivo* micronucleus assay in rodents
Extended Cramer scheme for compound classification
Alerts for identification of Michael Acceptors

Table 11 Summary of toxicity databases to use as sources for identifying analogs

Database	*Description*	*References*
Leadscope	Contains over 600,000 studies reported for approximately 190,000 chemicals including (1) reproductive and developmental studies, (2) acute, chronic and subchronic studies, (3) carcinogenicity and genetic toxicity studies from the US FDA CDER (Center for Drug Evaluation and Research) approval packages, US FDA CFSAN (Center for Food Safety and Applied Nutrition) reviews along with data integrated from RTECS, NTP, CCRIS, DSSTox, and other sources.	[63]
RTECS	Registry of Toxic Effects of Chemical Substances, including 26,558 reproductive studies for 6,851 compounds; 279,237 acute studies for 154,702 chemicals; 52,730 multiple dose toxicity studies for 13,953 chemicals; 10,517 tumorigenic studies for 3,724 chemicals and 46,385 genetic toxicity studies for 13,343 chemicals.	[64,65]
ECHA	European Chemicals Agency database for REACH	[66]
ToxRefDB	Toxicity Reference Database containing *in vivo* animal toxicity studies on hundreds of chemicals	[67,68]
HSDB	Hazardous Substances Data Bank	[84]
DART	Developmental and Reproductive Toxicology and Environmental Teratology Information	[69,85]
DSSTox	Distributed Structure-Searchable Toxicity (DSSTox) Database Network	[70]
Mario Negri	Mario Negri Institute for Pharmacological Research developmental and reproductive toxicity database and repeated dose toxicity databases	[71]
VITIC	Commercial data from published and unpublished sources from Lhasa Limited.	[72]
RepDose	Repeated dose toxicity database	[86]
HESS	Hazard Evaluation Support System	[74]
CPDB	Carcinogenicity Potency Database	[75]
IARC	International Agency for Research on Cancer and Carcinogenicity classification	[94]
ISSCAN	Chemical carcinogens: structures and experimental data from Istituto Superiore di Sanita	[91]
CCRIS	Chemical carcinogens: structures and experimental data	[76,92]
NTP	National Toxicology Program database	[77,78]
GENETOX	Mutagenicity test data from the EPA	[93]
IRIS	Data from the EPA in support of human health risk assessment, focusing on hazard identification and dose-response assessment	[79]
IPS INCHEM	International Program on Chemical Safety	[80]
JECDB	Japanese Existing Chemical Data Base	[81]
Pharma Pendium	Toxicity data from FDA and EMA approval documents	[88]
DrugMatrix	Reference database containing studies of the effects of these compounds at multiple time points and in multiple target organs. These studies included pharmacology, clinical chemistry, hematology, histology, body and organ weights, and clinical observations.	[83]

essential resource for identification of these analogs (sometimes referred to as source chemical(s)). Table 11 highlights a number of important databases used to support read-across, as well as expert review of the prediction.

The first step in performing a read-across is to identify analogs similar enough to the target compound such that the toxicity data from these analogs can "read-across" onto the target compound with confidence. The analog selection process first attempts to identify analogs with similar structural features, which would presumably have similar pharmacokinetics and pharmacodynamics properties to the target chemical. A biological justification for any similarity should be generated and evidence gathered to support (or refute) the hypothesis of similar analogs. General structural similarity is often used as a starting point for finding analogs. A structural alert may also be used to generate a preliminary list for the chemical category, as long as the mechanism associated with the alert is relevant to the toxicity endpoint being predicted. Data on the analogs (and possibly the target chemical) such as physico-chemical properties, bioavailability, relevant *in vitro* or *in vivo* data, and so on can be used to filter the list of analogs to those most relevant for prediction. Any information on the projected biological pathway(s) common to both the target and the analogs can strengthen the justification for using the analogs, such as any projected similar metabolic pathways or reactivity, as well as links to common Molecular Initiating Events (MIEs). This process results in the construction of a high-quality "chemical category" of analogs which has knowledge (i.e., structure-activity relationships, properties and mechanisms) specific enough to support justification of a toxicology endpoint value for the category and general enough to extrapolate to a similar test compound.

The following example illustrates a number of concepts in performing a read-across to predict male rat carcinogenicity TD_{50}. Fig. 7 shows the target compound alongside a series of analogs with carcinogenicity data. In this example, the target compound contains an alert – an aliphatic nucleophilic substitution domain (SN1) alert (pyrrolizine alkaloids)[89] – which is highlighted in magenta. This alert was used to form the chemical category by identifying the analogs from a toxicity database containing that alert. Pyrrolizine alkaloids are DNA reactive after a metabolic conversion to a carbenium ion and a subsequent SN1 reaction, which makes this category appropriate for prediction of carcinogenicity.[89]

A data table containing both the target compound and the analogs should be generated to assess the suitability of the selected analogs, as shown in Table 12. Information on all available physico-chemical properties alongside the toxicity data provides input

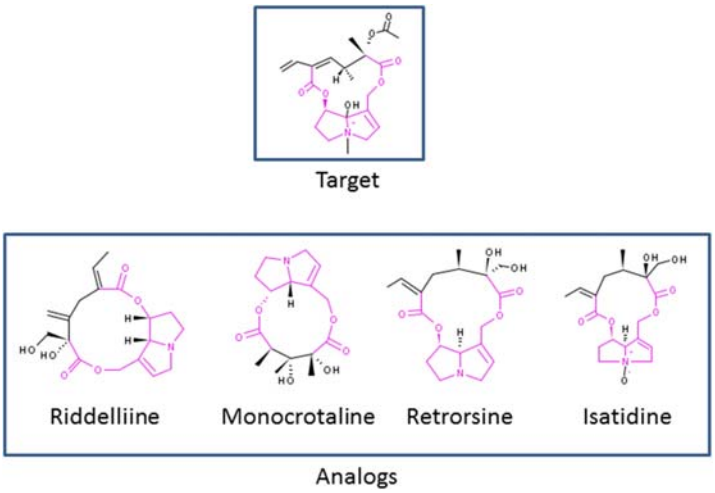

Fig. 7 Identification of analogs to support a read-across.

Table 12 Data table on analogs to support category formation and read-across

Status	*Chemical name*	*Melting point (deg C)*	*Solubility*	*Study Type*	*Species*	*Sex*	*TD_{50}*	*Sites*	*Reference*
Target	Clivorine	149-150	Soluble in chloroform	carcinogenicity	Rat	Male	?		
Analogs	Riddelliine	198	Soluble in chloroform; slightly soluble in water and ethanol	carcinogenicity	Rat	Male	0.119 mg kg^{-1}	System: Hematopoietic Liver System: Cardiovascular	http://toxnet.nlm.nih.gov/cpdb/chempages/RIDDELLIINE.html
Analogs	Isatidine	138	Soluble in water and ethanol	carcinogenicity	Rat	Male	0.716 mg kg^{-1}	Liver	http://toxnet.nlm.nih.gov/cpdb/chempages/ISATIDINE.html
Analogs	Retrorsine	212	Soluble in chloroform; slightly soluble in water and ethanol	carcinogenicity	Rat	Male	0.862 mg kg^{-1}	Liver	http://toxnet.nlm.nih.gov/cpdb/chempages/RETRORSINE.html
Analogs	Monocrotaline	202-203	Soluble in ethanol and chloroform	carcinogenicity	Rat	Male	0.94 mg kg^{-1}	Liver	http://toxnet.nlm.nih.gov/cpdb/chempages/MONOCROTALINE.html

into the weight of evidence to assess the suitability of the analogs for prediction. There should be a degree of consistency in the results to ensure the examples are acting in a similar manner. For example, the TD_{50} values for the selected analogs are within a narrow range and the all analogs indicate that liver is a major target organ. Here the chemical category was formed using a known alert (pyrrolidine alkaloids) that is associated with a known and relevant biological mechanism, which provides additional evidence to consider in assessing the quality of the chemical category.

If the analogs are found suitable for making a prediction, then the analogs' study results can be used to predict the target compound's toxicity. In this example, TD_{50} values from the analogs can be used to predict the TD_{50} value for the target compound. A conservative approach would be to take the minimum value of the analogs to use as the read-across value (0.119 mg kg^{-1}); however, a mean, medium or other approach for estimating the read-across value may be used if it can be justified.

Read-across is a time-consuming and predominantly manual approach to predicting toxicity more akin to an expert review than an automated prediction. The process of selecting analogs needs to be fully documented alongside the justification and an assessment of confidence based on the weight of the evidence.[95] Similarly, the number of studies and the quality of the study data used in the read-across should be assessed and a confidence level established to help support how this information will be used.

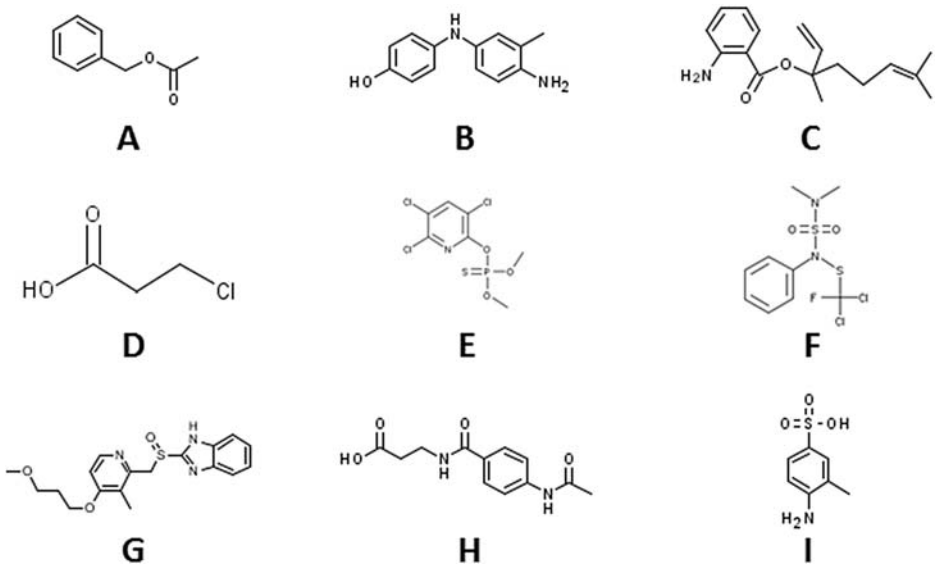

Fig. 8 Nine compounds to be predicted as mutagenic or not mutagenic.

4.09.5 Case Study: Using Statistical-Based (QSAR), Expert Rule-Based (Alerts), and Read-Across to Predict Mutagenicity

This case study illustrates the use of two different *in silico* methodologies (available through the Leadscope Model Applier) to predict whether a series of compounds shown in Fig. 8 are mutagenic or non-mutagenic (based on the results of the bacterial reverse mutation assay or Ames test). The ICH M7 guideline has documented the methodologies and criteria necessary to qualify and control DNA reactive impurities. In this example we will use the same approach to assess these compounds. The ICH M7 guideline recommends the use of the two complementary methodologies: "*expert rule-based*" (i.e., alerts) and "*statistical-based*" (i.e., QSAR). Using two methodologies ensures there will be fewer false negatives, but with a subsequent increase of false positives. The guideline also states that these methodologies "… … *should follow the general validation principles set forth by the Organisation for Economic Co-operation and Development* (*OECD*)." The results from both methodologies are used to predict the compound as either mutagenic or non-mutagenic; however, an expert review may be warranted especially where the results are marginal or conflicting. A read-across assessment of structural analogs is also an important component of such an expert review. Although the Leadscope Model Applier was used in this case study, other methodologies adhering to the requirements of the ICH M7 guideline may be used.

To generate prediction results based on the recommended methodologies, two statistical-based QSAR models were used (Leadscope Salmonella statistical-based QSAR model v3 and Leadscope E.coli/Sal TA102 statistical-based QSAR model v1, run within the Leadscope Model Applier v2.0.1) and a single expert rule-based model (Leadscope Genetox Expert Alerts v2 run within the Leadscope Model Applier v2.0.1), as shown in Fig. 9. The domain assessment was turned on for both methodologies and the QSAR models assigned a positive outcome when the probability was above 0.6, a negative outcome when the probability was below 0.4 and an indeterminate outcome between 0.4 and 0.6. The Figure shows the QSAR model results on the left and includes whether the compound was predicted as mutagenic (positive) or non-mutagenic (negative) as well as the probability of a positive outcome. The QSAR model results also highlight on the chemical structure where model features map onto the chemical structure. Areas of the compound that are not covered by a model feature are shown in black. Model features associated with mutagenic examples are shown in red, while model features associated with a lack of mutagenic examples are shown in green/blue and those lacking any association are shown in gray. Similarly, results from the expert rule-based methodology are shown in the right columns and indicate whether the examples are predicted to be mutagenic (positive) or predicted non-mutagenic (negative). A precision score indicates the proportion of historical compounds matching the alert that were positive. Where no alert matches, this precision score indicates the proportion of compounds in the alert reference set that did not match any alert (i.e., 0.1616 or 16.16%). Where an alert matches a compound, it is highlighted in red, and where an alert is deactivated because of the chemical environment it is highlighted in green/blue. The QSAR models include a probability of a positive outcome and the expert alerts contain a precision score. These values help assess the confidence in the prediction with high values (close to 1) representing higher confidence in a positive outcome and lower values (close to 0) representing higher confidence in a negative outcome.

Fig. 9 provides a summary of the results along with sufficient supporting information to start to assess the results. It shows the classification (positive or negative), the prediction confidence scores and the structural basis for the prediction. It is helpful to use this information to identify compounds that are clearly positive or clearly negative or cases where the results are either marginal, inconclusive or that would require further investigation as part of an expert review. For these example compounds, a simple review

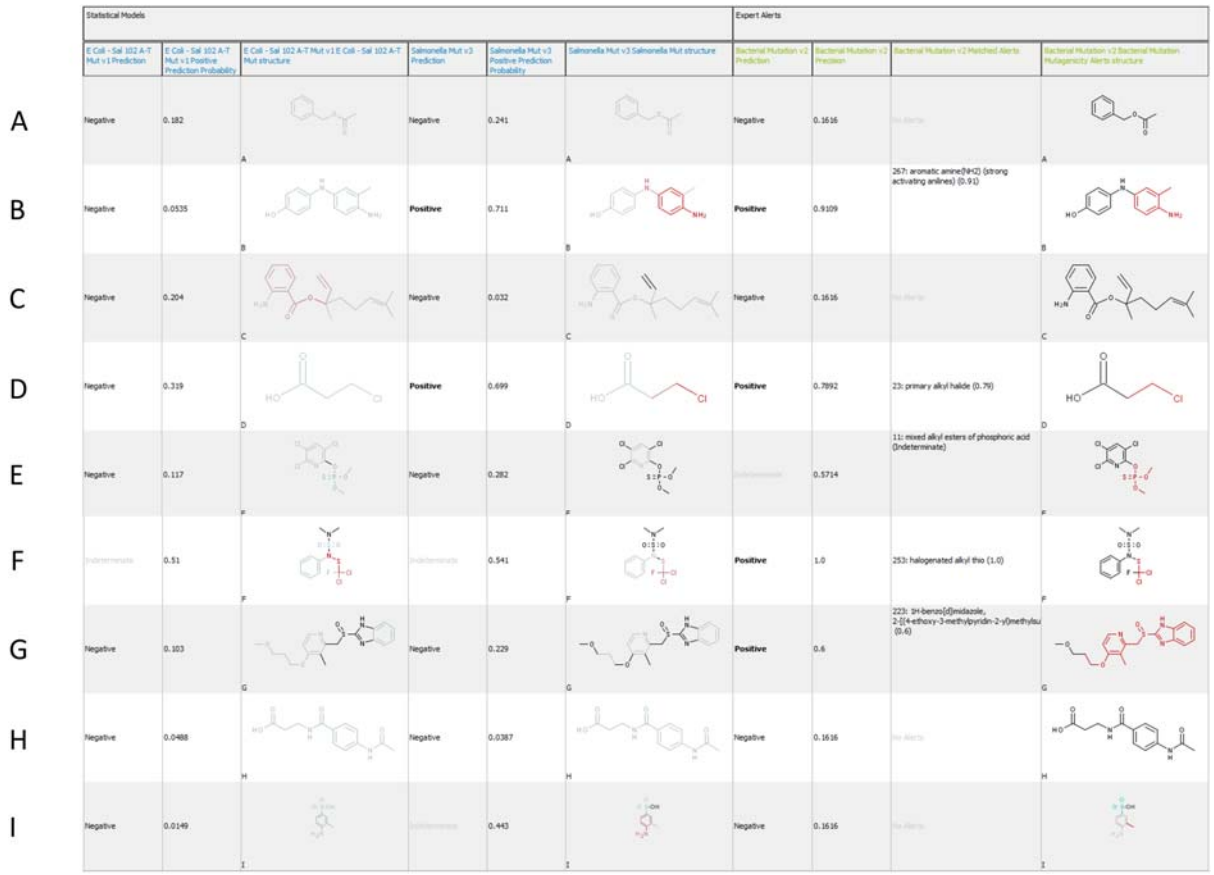

Fig. 9 Prediction of mutagenicity using statistical-based (QSAR) and expert rule-based (alerts).

of the *in silico* data has been used to provide an overall positive or negative prediction. A more in depth evaluation, using expert review, has not been provided here. An expert review may conclude the prediction should be accepted or even refuted; however, this sort of assessment is outside the scope of this chapter.[96]

From a preliminary inspection, compounds A and H were predicted as non-mutagenic in all models. The two statistical-based models considered all areas of the compounds (there are no black atoms or bonds in the QSAR model results) and the confidence scores indicate a high confidence in a negative prediction. The expert rule-based model also showed a high degree of negative predictivity and no alerts fired. These compounds would be predicted as non-mutagenic based on this initial visual inspection of the results.

Compound B was predicted positive in both the expert alerts and the Salmonella statistical-based methodology. This compound contained a strong activating primary aromatic amine structural alert with no identified feature that would deactivate the aromatic amine mutagenicity. This would be an example of a clear positive assignment.

Even though compound C contained a primary aromatic amine (an alert for mutagenicity), it was predicted negative in all models and the confidence scores reflected a high degree of confidence in the negative predictions. Compound C contained no additional feature that would activate the aromatic amine mutagenicity and thus would be considered overall negative.

Compound D is positive in both the expert rule-based and the Salmonella statistical-based methodologies, as it contains a well-known mutagenicity structural alert (alkyl halide[55,57]), which is also highlighted in the Salmonella QSAR model as being primarily responsible for the positive prediction. The positive predictions were marginally positive (<0.8) and while a simple evaluation would dictate a positive mutagenicity prediction, a better approach would include an expert review of the data, analogous structures, etc. to use a weight of evidence approach for an overall prediction.

In examples E, F, and G there are some conflicting results across the different models. In compound E, the Salmonella and E.coli/Sal TA102 statistical-based methodology was negative and the expert rule-based methodology was indeterminate, indicating conflicting Ames data or other information. A read-across inspection of chemical analogs (shown in **Fig. 10**) shows negative examples. Hence, this would support a negative prediction; however, this is another example where expert review would be beneficial.

Compound F was predicted positive in the expert rule-based methodology based on the halogenated alkyl thio group, and no prediction was made in either statistical-based model because of conflicting information. The halogenated alkyl thio group was also highlighted as a positively associated structural feature in the QSAR models. An inspection of the underlying data (although structurally dissimilar) indicated that all examples were positive (see **Fig. 11**). As compound F has no deactivating features (such as steric hindrance near the alkyl thio group) and several analogous structures were positive, this compound would be predicted as positive.

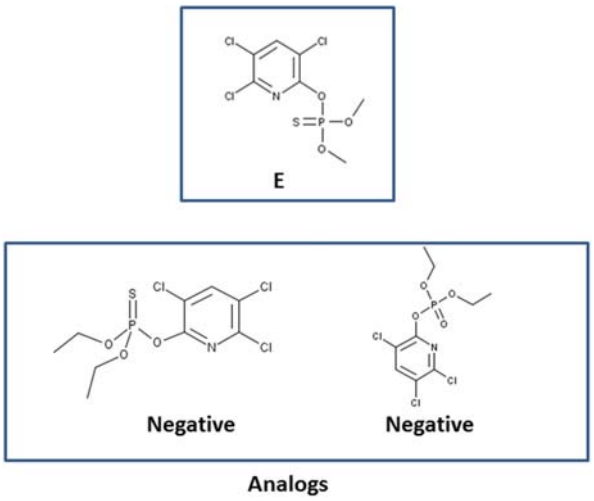

Fig. 10 Analogs of compound E.

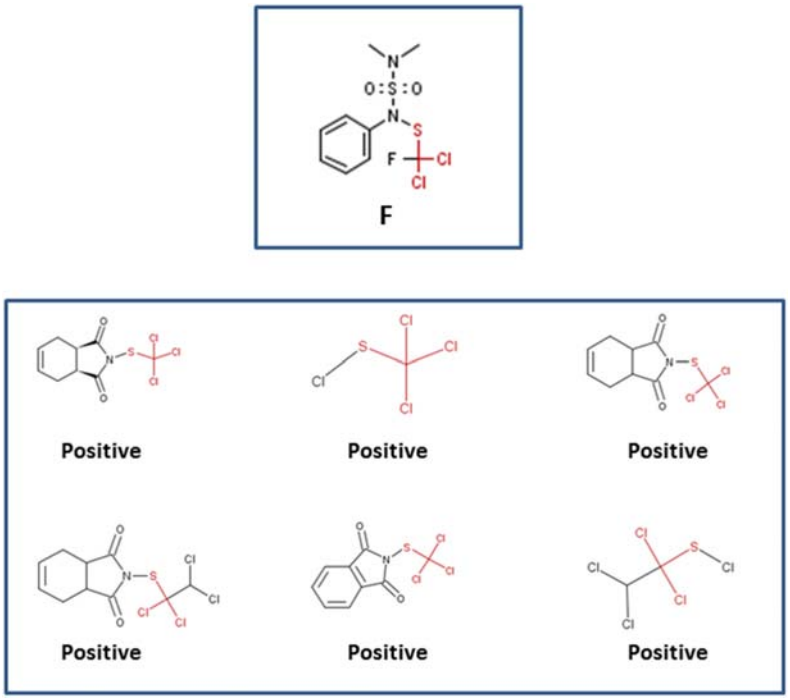

Fig. 11 Compounds matching the halogenated alkyl thio alert.

Compound G also showed conflicting results with the expert alerts predicting positive and the QSAR models predicting negative. When using the *in silico* data only, and one of the methodologies predicts the compound to be positive without any other activating or deactivating features, the overall prediction would be considered positive. This is another example where expert review would be beneficial. Note that expert review is not solely used to review positive predictions, but can also be used to verify negative predictions.

Compound I was predicted negative in the expert alert methodology; however, the Salmonella QSAR model did not generate a prediction and highlighted the primary aromatic amine functional group in red. The alerts system contains rules for activation and deactivation of primary aromatic amines. Compound I did contain a feature to activate the aromatic amine mutagenicity (the methyl group ortho to the amine) but the sulfonic acid in the para position was flagged as deactivating the mutagenicity. The presence of both an activating alert and a deactivating alert resulted in the indeterminate prediction in the Salmonella model. The deactivation of the alert in the Salmonella model along with the two negative predictions (with good negative predictivity scores) in the other models would result in a negative overall prediction for Compound I.

4.09.6 Conclusions

This chapter has summarized three different approaches for predicting toxicity: statistical-based (QSAR) models, expert rule-based (alerts), and read-across. These *in silico* approaches represent the state-of-the-art in toxicity prediction and are used for product design and regulatory decisions as part of pharmaceutical discovery and development. These approaches all have strengths and weaknesses and are often combined within an expert review using a weight of evidence approach. *In silico* approaches provide a great deal of promise in supporting the early detection and circumvention of toxicity as part of the medicinal chemistry process, that might otherwise delay, generate a warning on the drug label or result in withdrawal of a product in clinical trials or even after it reaches the market. *In silico* methods offer a rapid screen for candidate prioritization and often provide an indication of the structural basis (and sometimes a mechanistic basis) for any positive predictions. This information is critical to support decisions on research directions related to the design and/or prioritization of chemical classes, pursuit of individual chemicals, and identification of specific tests necessary to de-risk any predicted toxicity.

The field of *in silico* toxicology is today focusing on several important areas concerning the practical implementation of these methodologies. Despite its on-going expense, the development of toxicity databases, including both the harvesting of additional studies as well as the recording of new endpoints, supports the development of training and reference sets. This in turn leads to new and improved models for prediction and further support for read-across. Additional models and read-across approaches are needed to effectively estimate safe dose levels (with associated confidence intervals) to support an analysis of risk. Models to support an understanding of the margin of safety between the dose required for the drug to be effective and that producing adverse effects are important. These models need to be able to estimate this gap and its associated uncertainty. The development of guidelines, protocols, and workflow tools for application of these methodologies, as well as subsequent expert reviews, is important to ensure results are consistently generated, transparent, fully documented, and defendable. These guidelines can also support how these models are used in the wider context, such as in identifying follow-up tests to use in verifying any positive predictions from these *in silico* models. These guidelines also outline when to include an expert review that either accepts or refutes the prediction as well as the scope of such a review.

References

1. Schuster, D.; Laggner, C.; Langer, T. Why drugs fail–a study on side effects in new chemical entities. *Curr Pharm Des.* **2005,** *11* (27), 3545–3559.
2. Kramer, J. A. Designing safe drugs: What to consider? *Expert Opin Drug Discov.* **2008,** *3* (7), 707–713.
3. ICH, 2014. ICH M7 – assessment and control of DNA reactive (mutagenic) impurities in pharmaceuticals to limit potential carcinogenic risk. http://www.ich.org/fileadmin/Public_Web_Site/ICH_Products/Guidelines/Multidisciplinary/M7/M7_Step_4.pdf. http://www.ich.org/fileadmin/Public_Web_Site/ICH_Products/Guidelines/Multidisciplinary/M7/M7_Addendum_Step_2.pdf
4. Müller, L.; Mauthe, R.; Riley, C.; et al. A rationale for determining, testing, and controlling 724 specific impurities in pharmaceuticals that possess potential for genotoxicity. *Regul Toxicol Pharmacol.* **2006,** *44,* 198–211.
5. Guidance document for using the OECD (q)SAR application toolbox to develop chemical categories according to the OECD guidance on grouping chemicals, OECD Series on testing and assessment Number 102.
6. Myatt, G. J.; Cross, K. P. In silico Solutions for Predicting Efficacy and Toxicity. In *Human-based Systems for Translation Research;* Coleman, R., Ed.; Royal Society of Chemistry: London, UK, 2015; pp 190–214.
7. Benfenati, E., E-Book: Theory, guidance and applications on QSAR and REACH, (2012) ISBN 978-88-902405-4-6; Orchestra
8. Dearden, J. C.; Barratt, M. D.; et al. The development and validation of expert systems for predicting toxicity. *Alternatives to Laboratory Animals* **1997,** *25,* 223–252.
9. Dimitrov, S.; Mekenyan, O. An introduction to read-across for the prediction of effects of chemicals. In *In Silico Toxicology: Principles and Applications;* Cronin, M. T. D, Madden, J. C., Eds.; The Royal Society of Chemistry: Cambridge, 2010; pp 372–384.
10. van Leeuwen, K.; Schultz, T.; et al. Using chemical categories to fill data gaps in hazard assessment. *SAR QSAR Environ. Res.* **2009,** *20,* 207–220.
11. Cronin, M. T. D. An introduction to chemical grouping, categories and read across to predict toxicity. In *Chemical Toxicity Prediction: Category Formation and Read-Across Applications;* Cronin, M. T. D, Madden, J. C., Enoch, S. J., Roberts, D. W., Eds.; The Royal Society of Chemistry: Cambridge, 2013; pp 1–29.
12. Cronin, M. T. D. Evaluation of categories and read-across for toxicity prediction allowing for regulatory acceptance. In *Chemical Toxicity Prediction: Category Formation and Read-Across Applications;* Cronin, M. T. D, Madden, J. C., Enoch, S. J., Roberts, D. W., Eds.; The Royal Society of Chemistry: Cambridge, 2013; pp 155–167.
13. Kubinyi, H., Folkers, G., Martin, Y. C., Eds.; *3D QSAR in drug design, Ligand-protein interactions and molecular similarity*; Kluwer Academic Publishers: Dordrecht, 1998.
14. Todeschini, R.; Consonni, V. Molecular Descriptors for Chemoinformatics. In Mannhold, R., Kubinyi, H., Folkers, G., Eds.; Wiley-VCH: Weinheim, Germany, 2009.
15. Schuurman, G.; Schuurman, G. Quantum chemical descriptors in structure-activity relationships – calculation, interpretation, and comparison of methods. In *Predicting Chemical Toxicity and Fate;* Cronin, M. T. D, Ed.; CRC Press LLC: Boca Raton, FL, 2004; pp 85–149.
16. Dobo, K. L.; Greene, N.; Fred, C.; Glowienke, S.; Harvey, J. S.; Hasselgren, C.; Jolly, R.; Kenyon, M. O.; Munzner, J. B.; Muster, W.; Neft, R.; Reddy, M. V.; White, A. T.; Weiner, S. In silico methods combined with expert knowledge rule out mutagenic potential of pharmaceutical impurities: An industry survey. *Regul. Toxicol. Pharmacol.* **2012,** *62,* 449–455.
17. Kruhlak, N. L.; Benz, R. D.; Zhou, H.; Colatsky, T. J. (Q)SAR modeling and safety assessment in regulatory review. *Clin. Pharmacol. Ther.* **2012,** *91,* 529–534.
18. Naven, R. T.; Greene, N.; Williams, R. V. Latest advances in computational genotoxicity prediction. *Expert Opin. Drug Metab. Toxicol.* **2012,** *8,* 1579–1587.
19. Powley, M. W. (Q)SAR assessments of potentially mutagenic impurities: A regulatory perspective on the utility of expert knowledge and data submission. *Regul Toxicol Pharmacol* **2015,** *71,* 295–300.
20. OECD (2007). Guidance document on the validation of (Quantitative) structure activity relationships [(Q)SAR] models.(http://ihcp.jrc.ec.europa.eu/our_labs/predictive_toxicology/background/oecd-principles)
21. Ursem, C. J.; Kruhlak, N. L.; Contrera, J. F.; MacLaughlin, P. M.; Benz, R. D.; Matthews, E. J. Identification of structure-activity relationships for adverse effects of pharmaceuticals in humans. Part A: Use of FDA post-market reports to create a database of hepatobiliary and urinary tract toxicities. *Regul Toxicol Pharmacol.* **2009,** *54* (1), 1–22.
22. Matthews, E. J.; Ursem, C. J.; Kruhlak, N. L.; Benz, R. D.; Sabaté, D. A.; Yang, C.; Klopman, G.; Contrera, J. F. Identification of structure-activity relationships for adverse effects of pharmaceuticals in humans: Part B. Use of (Q)SAR systems for early detection of drug-induced hepatobiliary and urinary tract toxicities. *Regul Toxicol Pharmacol* **2009,** *54* (1), 23–42.

23. Matthews, E. J.; Kruhlak, N. L.; Benz, R. D.; Sabaté, D. A.; Marchant, C. A.; Contrera, J. F. Identification of structure-activity relationships for adverse effects of pharmaceuticals in humans: Part C: use of QSAR and an expert system for the estimation of the mechanism of action of drug-induced hepatobiliary and urinary tract toxicities. *Regul Toxicol Pharmacol.* **2009,** *54* (1), 43–65.
24. Matthews, E. J.; Frid, A. A. Prediction of drug-related cardiac adverse effects in humans–A: creation of a database of effects and identification of factors affecting their occurrence. *Regul Toxicol Pharmacol.* **2010,** *56* (3), 247–275.
25. Frid, A. A.; Matthews, E. J. Prediction of drug-related cardiac adverse effects in humans–B: Use of QSAR programs for early detection of drug-induced cardiac toxicities. *Regul Toxicol Pharmacol* **2010,** *56* (3), 276–289.
26. Serafimova, R.; Fuart-Gatnik, M.; Worth A. Review of QSAR Models and Software Tools for Predicting Genotoxicity and Carcinogenicity, EUR 24427 EN - 2010.
27. Lapenna, S., Fuart-Gatnik, M.; Worth A. Review of QSAR Models and Software Tools for predicting Acute and Chronic Systemic Toxicity, EUR 24639 EN – 2010
28. Saliner, A.G.; Patlewicz, G.; Worth A.P. Review of Literature-Based Models for Skin and Eye Irritation and Corrosion, 2006 EUR 22320 EN.
29. Piparo, E.L.; Worth A. Review of QSAR Models and Software Tools for predicting Developmental and Reproductive Toxicity, EUR 24522 EN – 2010
30. Kruhlak, N. L.; Choi, S. S.; Contrera, J. F.; Weaver, J. L.; Willard, J. M.; Hastings, K. L.; Sancilio, L. F. Development of a phospholipidosis database and predictive quantitative structure-activity relationship (QSAR) models. *Toxicol Mech Methods* **2008,** *18* (2–3), 217–227.
31. http://ntp.niehs.nih.gov/results/dbsearch/index.html.
32. Roberts, G.; Myatt, G. J.; Johnson, W. P.; Cross, K. P.; Blower, P. E., Jr. LeadScope: Software for exploring large sets of screening data. *J Chem Inf Comput Sci* **2000,** *40* (6), 1302–1314.
33. Johnson, D. E.; Blower, P. E.; Myatt, G. J.; Wolfgang, G. Chem-tox informatics: Data mining using a medicinal chemistry building block approach. *Current Opin. Drug Disc. Develop.* **2001,** *4* (1), 92–101.
34. Cross, K. P.; Myatt, G.; Yang, C.; Fligner, M. A.; Verducci, J. S.; Blower, P. E., Jr. Finding discriminating structural features by reassembling common building blocks. *J Med Chem* **2003,** *46* (22), 4770–4775.
35. Yee, L. C.; Wei, Y. C.; Yee, L. C.; Wei, Y. C. Current modeling methods used in QSAR/QSPR. In Dehmer, M., Varmuza, K., Bonchev, D., Eds; Statistical Modelling of Molecular Descriptors in QSAR/QSPREmmert-Streib, F., Ed.; Wiley-Blackwell: Hoboken, NJ, 2012.
36. Luco, J. M.; Ferretti, F. H. QSAR Based on Multiple Linear Regression and PLS Methods for the Anti-HIV Activity of a Large Group of HEPT Derivatives. *J. Chem. Inf. Comput. Sci.* **1997,** *37* (2), 392–401.
37. Nguyen, D. V.; Rocke, D. M. Tumor classification by partial least squares using microarray gene expression data. *Bioinformatics* **2002,** *18,* 39–50.
38. Geladi, P.; Kowalski, B. Partial least squares regression: A tutorial. *Anal. Chim. Acta* **1986,** *185,* 1–17.
39. Tong, W.; Hong, H.; Fang, H.; Xie, Q.; Perkins, R. Decision forest: Combining the predictions of multiple independent decision tree models. *J. Chem. Inf. Comput. Sci.* **2003,** *43* (2), 525–531.
40. Fausett, L. *Fundamentals of Neural Networks: Architecture, Algorithms, and Applications;* Pearson: USA, 1993.
41. Cooper, J. A.; Saracci, R.; Cole, P. Describing the validity of carcinogen screening tests. *British Journal of Cancer* **1979,** *39,* 87–89.
42. Matthews, E. J.; Kruhlak, N. L.; Cimino, M. C.; Benz, R. D.; Contrera, J. F. An analysis of genetic toxicity, reproductive and developmental toxicity, and carcinogenicity data: I. Identification of carcinogens using surrogate endpoints. *Regul Toxicol Pharmacol.* **2006,** *44,* 83–96.
43. Matthews, E. J.; Kruhlak, N. L.; Cimino, M. C.; Benz, R. D.; Contrera, J. F. An analysis of genetic toxicity, reproductive and developmental toxicity, and carcinogenicity data: Ii. identification of genotoxicants, reprotoxicants, and carcinogens using in silico methods. *Regul Toxicol Pharmacol* **2006,** *44,* 97–110.
44. Stavitskaya, L.; et al. Development of improved *salmonella* mutagenicity qsar models using structural fingerprints of known toxicophores. FDA Center for Drug Evaluation and Research, Soc. of Tox.
45. Stavitskaya, L.; et al. Development of Improved QSAR Models for Predicting A-T Base Pair Mutations. Genetic Toxicity Association Poster Presentation.
46. Matthews, E. J.; Kruhlak, N. L.; Weaver, J. L.; Benz, R. D.; Contrera, J. F. Assessment of the health effects of chemicals in humans: II. Construction of an adverse effects database for QSAR modeling. *Curr. Drug Discov. Technol.* **2004,** *1,* 243–254.
47. Romesburg, H. C. *Cluster Analysis for Researchers;* Lifetime Learning Publications: Belmont, CA, 1984.
48. Martin, T. M.; Young, D. M. Prediction of the acute toxicity (96-h LC50) of organic compounds to the Fathead Minnow (pimephales promelas) using a group contribution method. *Chem. Res. Toxicol.* **2001,** *14,* 1378–1385.
49. Contrera, J. F.; Matthews, E. J.; Benz, R. D. Predicting the carcinogenic potential of pharmaceuticals in rodents using molecular structural similarity and e-state indices. *Regul Toxicol Pharmacol* **2003,** *38,* 243–259.
50. U.S. EPA (2012). User's guide for T.E.S.T. (version 4.1): A program to estimate toxicity from molecular structure.
51. Hansen, K.; Mika, S.; Schroeter, T.; Sutter, A.; ter Laak, A.; Steger-Hartmann, T.; Heinrich, N.; Müller, K. R. Benchmark data set for in silico prediction of Ames mutagenicity. *J. Chem. Inf. Model.* **2009,** *49* (9), 2077–2081.
52. Kim, M. T.; Sedykh, A.; Chakravarti, S. K.; Saiakhov, R. D.; Zhu, H. Critical evaluation of human oral bioavailability for pharmaceutical drugs by using various cheminformatics approaches. *Pharm Res.* **2014,** *31* (4), 1002–1014.
53. Saiakhov, R. D.; Chakravarti, S. K.; Klopman, G. Effectiveness of CASE ultra expert system in evaluating adverse effects of drugs. *Mol. Inf.* **2012,** *32,* 87–97.
54. Chakravarti, S. K.; Saiakhov, R. D.; Klopman, G. Optimizing predictive performance of CASE Ultra expert system models using the applicability domains of individual toxicity alerts. *J. Chem. Inf. Model.* **2012,** *52,* 2609–2618.
55. Ashby, J.; Tennant, R. W. Chemical structure, Salmonella mutagenicity and extent of carcinogenicity as indicators of genotoxic carcinogenesis among 222 chemicals tested by the U.S.NCI/NTP. *Mutat. Res.* **1988,** *204,* 17–115.
56. Bailey, A. B.; Chanderbhan, N.; Collazo-Braier, N.; Cheeseman, M. A.; Twaroski, M. L. The use of structure-activity relationship analysis in the food contact notification program. *Regulat Pharmacol Toxicol* **2005,** *42,* 225–235.
57. Benigni, R.; Bossa, C.; Jeliazkova, N.; Worth, A. The Benigni/Bossa Rulebase for Mutagenicity and Carcinogenicity - A Module of Toxtree - EUR 23241 EN 2008.
58. Kazius, J.; McGuire, R.; Bursi, R. Derivation and validation of toxicophores for mutagenicity prediction. *J. Med. Chem.* **2005,** *48,* 312–320.
59. Cramer, G. M.; Ford, R. A.; Hall, R. L. Estimation of toxic hazard - a decision tree approach. *Food Cosmet. Toxicol.* **1978,** *16,* 255–276.
60. Kroes, R.; Kleiner, J.; Renwick, A. The threshold of toxicological concern concept in risk assessment. *Toxicol. Sci.* **2005,** *86* (2), 226–230.
61. Lapenna, S.; Worth, A. Analysis of the Cramer classification scheme for oral systemic toxicity - implications for its implementation in Toxtree, EUR 24898 EN – 2011
62. Patlewicz, G.; Jeliazkova, N.; Safford, R. J.; Worth, A. P.; Aleksiev, B. An evaluation of the implementation of the Cramer classification scheme in the Toxtree software. *SAR QSAR Environ. Res.* **2008,** *19* (5), 495–524.
63. http://www.leadscope.com/toxicity_databases/.
64. http://www.cdc.gov/niosh/rtecs/default.html.
65. Sweet, D. V.; Anderson, V. P.; Fang, J. C. F. An overview of the registry of toxic effects of chemical substances (RTECS): Critical information on chemical hazards. *Chem. Health Saf.* **1999,** *6* (6), 12–16.
66. http://echa.europa.eu.
67. http://www.epa.gov/NCCT/toxrefdb/.
68. Dix, D. J.; Houck, K. A.; Martin, M. T.; Richard, A. M.; Setzer, R. W.; Kavlock, R. J. The ToxCast Program for Prioritizing Toxicity Testing of Environmental Chemicals. *Toxicol. Sci.* **2007,** *95* (1), 5–12.
69. Ji, J. Z.; Han, L. Y.; Yap, C. W.; Sun, L. Z.; Chen, X.; Chen, Y. Z. Drug adverse reaction target database (DART): Proteins related to adverse drug reactions. *Drug Saf.* **2003,** *26* (10), 685–690.

70. http://www.epa.gov/ncct/dsstox/sdf_nctrer.html.
71. https://services.toxbank.net/.
72. http://www.lhaslimited.org/vitic-nexus.hlm.
73. Dix, D. J.; Houck, K. A.; Martin, M. T.; Richard, A. M.; Setzer, R. W.; Kavlock, R. J. The ToxCast program for prioritizing toxicity testing of environmental chemicals. *Toxicol. Sci* **2007,** *95* (1), 5–12.
74. Sakuratani, Y.; Zhang, H. Q.; Nishikawa, S.; Yamazaki, K.; Yamada, T.; Yamada, J.; Gerova, K.; Chankov, G.; Mekenyan, O.; Hayashi, M. Hazard Evaluation Support System (HESS) for predicting repeated dose toxicity using toxicological categories. *SAR QSAR Environ Res.* **2013,** *24* (5), 351–363.
75. http://toxnet.nlm.nih.gov.
76. http://toxnet.nlm.nih.gov/newtoxnet/ccris.htm.
77. http://www.niehs.nih.gov/research/resources/databases/cebs/index.cfm.
78. Tennant, R. W. The genetic toxicity database of the National Toxicology Program: evaluation of the relationships between genetic toxicity and carcinogenicity. *Environ Health Perspect* **1991,** *96,* 47–51.
79. http://www.epa.gov/ncct/dsstox/.
80. http://www.inchem.org.
81. http://Dra4.nihs.go.jp/mhlw_data/jsp/SearchPagesEND.jsp.
82. http://www.lhaslimited.org/vitic-nexus.hlm.
83. https://ntp.niehs.nih.gov/drugmatrix/index.html.
84. http://toxnet.nlm.nih.gov/newtoxnet/hsdb.htm.
85. http://toxnet.nlm.nih.gov/newtoxnet/dart.htm.
86. http://fraunhofer-repdose.de/.
87. http://www.epa.gov/NCCT/toxrefdb/.
8x8. http://www.pharmapendium.com.
89. Enoch, S. J.; Cronin, M. T. D. A review of electrophilic reaction chemistry involved in covalent DNA binding. *Crit Rev Toxicol* **2010,** *40,* 728–748.
90. Benigni, R.; Bossa, C.; Richard, A. M.; Yang, C. A novel approach: Chemical relational databases, and the role of the ISSCAN database on assessing chemical carcinogenicity. *Ann Ist Super Sanita.* **2008,** *44* (1), 48–56.
91. Young, R. R. Genetic toxicology: Web resources. *Toxicology* **2002,** *173* (1–2), 103–121.
92. Wexler, P. TOXNET. An evolving web resource for toxicology and environmental health information. *Toxicology* **2001,** *157* (1–2), 3–10.
93. http://monographs.iarc.fr/ENG/Classification/index.php.
94. Ahlberg, E.; Amberg, A.; Beilke, L. D.; Bower, D.; Cross, K. P.; Custer, L.; Ford, K. A.; Van Gompel, J.; Harvey, J.; Honma, M.; Jolly, R.; Joossens, E.; Kemper, R.; Kenyon, M.; Kruhlak, N.; Kuhnke, L.; Leavitt, P.; Neilan, C.; Quigley, D. P.; Shuey, D.; Spirkl, H. P.; Stavitskaya, L.; Teasdale, A.; White, A.; Wichard, J.; Zwickl, C.; Myatt, G. J. Ensuring regulatory acceptable (Q)SAR models reflect proprietary chemical space for aromatic amine mutagenicity. *Regulatory Toxicology and Pharmacology* **2016,** *77,* 1–12.
95. Blackburn, K.; Stuard, S. B. A framework to facilitate consistent characterization of read across uncertainty. *Regul Toxicol Pharmacol.* **2014,** *68*, 353–362.
96. Amberg, A.; Beilke, L.; Bercu, J.; Bower, D.; Brigo, A.; Cross, K. P.; Custer, L.; Dobo, K.; Dowdy, E.; Ford, K. A.; Glowienke, S.; Gompel, J. V.; Harvey, J.; Hasselgren, C.; Honma, M.; Jolly, R.; Kemper, R.; Kenyon, M.; Kruhlak, N.; Leavitt, P.; Miller, S.; Muster, W.; Nicolette, J.; Plaper, A.; Powley, M.; Quigley, D. P.; Reddy, M. V.; Spirkl, H. P.; Stavitskaya, L.; Teasdale, A.; Weiner, S.; Welch, D. S.; White, A.; Wichard, J.; Myatt, G. J. Principles and procedures for implementation of ICH M7 recommended (Q)SAR analyses. *Regulatory Toxicology and Pharmacology* **2016,** *77,* 13–24.

4.10 Use of Stem Cells in Toxicology

P Matz, L-S Spitzhorn, J Otte, M-A Kawala, J Woestmann, H Yigit, W Wruck, and J Adjaye, Institute for Stem Cell Research and Regenerative Medicine, Düsseldorf, Germany

© 2017 Elsevier Ltd. All rights reserved.

4.10.1	**Introduction**	178
4.10.2	**Pluripotent Stem Cells**	178
4.10.3	**Induced Pluripotent Stem Cell-Derived Hepatocytes**	180
4.10.4	**Induced Pluripotent Stem Cell-Derived Neuronal Cells**	182
4.10.5	**Induced Pluripotent Stem Cell-Derived Cardiomyocytes**	183
4.10.6	**Induced Pluripotent Stem Cell-Derived Organoids**	183
4.10.6.1	Liver Organoids	186
4.10.6.2	Brain Organoids	186
4.10.6.3	Heart Organoids	187
4.10.7	**Use of Induced Pluripotent Stem Cells for Toxicogenomics**	187
4.10.8	**The 3Rs**	189
References		189

Abbreviations

ABC Adenosine triphosphate-binding cassette
AD Alzheimer's disease
ADME Absorption, distribution, metabolism, and excretion
AFP α-Fetoprotein
ALK Transforming growth factor beta receptor (TGFBR)
ALS Amyotrophic lateral sclerosis
AP Action potential
aspirin Acetylsalicylic acid
ATP Adenosine triphosphate
bFGF Basic fibroblast growth factor
BMP4 Bone morphogenetic protein 4
CAS9 CRISPR- Associated endonuclease 9
CAT Catalase
CBR Carbonyl reductase
CDA Cytidine deaminase
CHST Carbohydrate sulfotransferase
CRISPR Clustered regularly interspaced short palindromic repeats
CYP Cytochromes
CYP2D6 Cytochrome P450 family 2 subfamily D member 6
CYP3A4 Cytochrome P450 family 3 subfamily A member 4
DEX Dexamethasone
DHRS Dehydrogenase/reductase
DILI Drug-induced liver injury
DMSO Dimethyl sulfoxide
DNA Deoxyribonucleic acid
DNMT DNA (cytosine-5)-methyltransferase
3-D Three-dimensional
EBs Embryoid bodies
EBNA-1 Epstein–Barr nuclear antigen 1
ECM Extracellular matrix
EGF Epidermal growth factor
ESCs Embryonic stem cells
EURL-ECVAM The European Union Reference Laboratory for alternatives to animal testing
FBS Fetal bovine serum
GSK-3ß Glycogen synthase kinase 3 beta
GST Glutathione S-transferase
HDAC Histone deacetylase
hESCs Human embryonic stem cells
HGF Hepatocyte growth factor
HIF Hypoxia inducible factor
HIF PHD1 Hypoxia-inducible factor PHD1
HLA Human leukocyte antigen
HLCs Hepatocyte-like cells
ICM Inner cell mass
iHeps Induced hepatocyte cells
iPSCs Induced pluripotent stem cells
iPSC-CM Induced pluripotent stem cell-derived cardiomyocytes
JLNS Jervell and Lange-Nielsen syndrome
KCNH2 Potassium voltage-gated channel subfamily H member 2
KLF4 Krueppel-like factor 4
LIN28 Lin-28 homologue A (*C. elegans*)
LQT2 Long QT syndrome
LSD1 Zinc finger protein
MEA Microelectrode array
MEF Mouse embryonic fibroblast
c-Myc Myelocytomatosis viral oncogene homologue
mRNA Messenger ribonucleic acid
miRNA Micro-ribonucleic acid
MRP Multidrug resistance-associated protein
NANOG Nanog homeobox

NAT N-acetyltransferase
NES Nestin
NPCs Neural progenitor cells
OCT4 Octamer-binding protein 4/POU class 5 homeobox 1
OECD Organisation for Economic Co-operation and Development
oriP Origin of plasmid replication
OSM Oncostatin M
PBTK Physiologically based toxicokinetic
PDK1 Pyruvate dehydrogenase kinase 1
PHH Primary human hepatocytes
PPARD Peroxisome proliferator-activated receptor delta
PPARG Peroxisome proliferator-activated receptor gamma
p53 Tumor protein p53
QSAR Quantitative structure–activity relationship
REACH Registration, Evaluation, Authorisation and Restriction of Chemicals
ROS Reactive oxygen species
RXRA Retinoid X receptor alpha
SERPINA7 Serpin family A member 7
SLC Solute carrier
α-SMA α-Smooth muscle actin
SNP Single nucleotide polymorphism
SOD Superoxide dismutase
SOX2 Sex-determining region Y (SRY)-box 2
SOX17 Sex-determining region Y (SRY)-box 17
SSEA-4 Stage-specific antigene 4
SULT Sulfotransferase
SVM Support vector machine
SV40LT Simian virus 40 large T antigen
TALEN Transcription activator-like effector nuclease
TdP Torsades de pointes
TG-GATE Toxicogenomics database
TGFß Transforming growth factor ß
TGP Japanese Toxicogenomics Project consortium
TK Toxicokinetic
TRA-1-60 Tumor-related antigen-1–60
TRA-1-81 Tumor-related antigen-1–81
TRA-2-49 Tumor-related antigen-2–49, alkaline phosphatase
TUJ1 Neuron-specific class III β-tubulin, β-tubulin III
UDP Uridine diphosphate
UGT Uridine diphosphate glucuronosyltransferase
WNT3a Wingless-type MMTV integration site family, member 3a

4.10.1 Introduction

Within the context of animal experimentation, the 3Rs are acronyms for replace, reduce, and refine meaning that animal tests—ordered by priority—should be replaced, be reduced, or at least take place under the best possible conditions for the animals (refine). To date, toxicology screens necessitate the use of significant numbers of animals, for example, the EU program REACH Registration, Evaluation, Authorisation and Restriction of Chemicals (REACH) shall assess the hazard risk of 30,000 chemicals involving estimated up to 54 million additional animals. Alternative testing strategies in the spirit of the 3Rs can achieve a reduction to below 10 million animals. Such an approach is based on human induced pluripotent stem cell (iPSC)-derived cell types for toxicity testing and drug development. iPSCs have the unique capacity to self-renew in the undifferentiated state in vitro while maintaining their ability to differentiate into a broad number of cell types. In addition, iPSCs can be generated from somatic cells of existing individuals with known genetic characteristics. These iPSC-derived hepatocytes, cardiomyocytes, or neuronal cells can model in vitro the patient's genetic disease or metabolic capability, thereby adding a further dimension to the current toxicity testing platforms. An iPSC–HLC-based strategy thus allows large-scale studies impossible to perform in mice, on human primary cell cultures, or from biopsies and also enables studies on hepatocytes genetically susceptible to drug-induced liver injury as in vitro models with genotypic relevance for toxicology screening. By employing patient-specific iPSC-derived hepatocytes, neurons, or cardiomyocytes and systems biology models, we can find strategies to reduce or—where possible—to replace animal tests. Systems biology modeling can provide whole-body human toxicokinetic data by in silico and in vitro methods assessing absorption, distribution, metabolism, and excretion (ADME) processes. These human-specific models can partly circumvent drawbacks of animal models, which cannot fully reflect the human condition.

4.10.2 Pluripotent Stem Cells

The focus of this article will be on the application of human pluripotent stem cells, which encompass both embryonic and induced pluripotent stem cells.

Human embryonic stem cells (hESCs) are derived from the inner cell mass (ICM) of blastocyst-stage embryos. hESCs can be differentiated into all cell types present in the three embryonic germ layers, endoderm (e.g., cells of the gastrointestinal tract), ectoderm (e.g., cells of the nervous system), mesoderm (e.g., cells of the bone and muscle), and also germ cells.

Currently, there are over 400 human embryonic stem cell (hESC) lines established but only a few of these are well characterized (lines H1 and H9) and used by most laboratories worldwide.[1,2]

To bypass ethical and moral concerns, scientists searched for alternative ways to derive embryonic stem cell-like cells. Takahashi and Yamanaka were the first to successfully derive induced pluripotent cells (iPSCs) from mouse fibroblasts. In 2006, they published the reprogramming of mouse fibroblasts to iPSCs employing retroviral transduction and coerced expression of transcription factors, which are normally only expressed in embryonic stem cells.[3] Shortly after that, two groups managed the reprogramming of human adult fibroblasts with viral transfection and overexpression of four transcription factors OCT4, SOX2, KLF4, and c-MYC [4] or OCT4, SOX2, NANOG, and LIN28.[5]

To generate iPSCs, transformation is attained by the use of *KLF4* and *c-MYC*. c-MYC affects p53-dependent apoptosis in fibroblasts, which is in all probability repressed by KLF4. KLF4 activates *p21* and affects proliferation. For this reason, the balance between c-MYC and KLF4 during the reprogramming process is critical. Furthermore, c-MYC enhances the expression of embryonic stem cell-specific genes by activating histone acetylase complexes. The enforced expression of c-MYC and KLF4 can lead to the formation of tumors. Probably OCT4 channels the cell from tumor to induced pluripotent cells. OCT4 and SOX2 synergistically activate target pluripotency-associated genes during the reprogramming process.[6,7]

The requirement of specified amounts of each transcription factor needed for the reprogramming process is realized in a small number of transfected cells. This could also be an explanation for the low efficiency of iPSC generation (>1%). Each cell type needs maybe another combination of factors and different amounts of each factor to achieve higher efficiencies of reprogramming.[3]

Induced pluripotent stem cells have the same properties as human embryonic stem cells, which are pluripotency, self-renewal, and the expression of surface markers such as SSEA-4, TRA-1-60, TRA-1-81, and TRA-2-49 (alkaline phosphatase) and transcription factors, for example, OCT4, NANOG, and SOX2.[4,5,8] Pluripotency is assayed both in vivo by the formation of teratomas when they are injected into immunodeficient mice and also in vitro by the formation of embryoid bodies (EBs). These EBs have the innate capacity to differentiate into endodermal lineages (expressing the marker genes SOX17 and AFP), mesodermal lineages (expressing the marker genes α-SMA and brachyury), and ectodermal lineages (expressing the maker genes TUJ1 and Nestin).[4] A typical assay to demonstrate pluripotency in vitro is shown in **Fig. 1**.

The efficiency of reprogramming human fibroblasts to iPSCs by using retroviruses to transduce OCT4, SOX2, KLF4, and c-MYC is approximately 0.02%.[9] The reprogramming of human fibroblasts to iPSCs through transduction of lentiviral constructs carrying OCT4, SOX2, NANOG, and LIN28 had an efficiency of 0.02–0.0095%.[5] Both methods are robust due to the fact that numerous groups have been able to reproduce the protocols. In addition, there are still unresolved problems, such as the random integration of proviruses into the genome of the reprogrammed cells and the fact that KLF4 and c-MYC are oncogenes that could be reactivated. These conditions cause a high probability of genomic instability and mutagenesis in iPSCs.[10] To enable regenerative medicine applications in the future, safer reprogramming by using fewer factors with OCT4, SOX2, and KLF4 but omitting c-MYC has been suggested.[11] To increase the efficiency of the viral reprogramming method, additional factors have been used such as the viral oncogene SV40LT, which enhances the efficiency of iPSC generation from fibroblasts by inhibition of p53. It has been demonstrated that the inhibition of p53 enhances the iPSC generation from human fibroblasts up to 100-fold.[12] Furthermore, Wang and Adjaye demonstrated that transient inhibition of p53 can increase the efficiency of reprogramming human dermal fibroblasts by approximately sevenfold.[13]

Over the years, a large number of somatic cell types have been reprogrammed, for example, fibroblasts, keratinocytes, amniotic fluid cells, and chorionic villi cells.[5,14–17] The integration of proviruses into genome of viral-derived iPSCs is a risk factor for clinical applications in the future.[18] To avoid this, nonviral integration protocols have been established.[19] Additionally, mRNA, miRNA, and protein-based reprogramming have been established as reviewed in Tavernier et al.[20]

Nonintegration reprogramming methods are established and standardized. Reagents and kits of various methods are also available on the market. One can select from the following methods: Sendai viral, episomal, and mRNA transfection. Sendai virus particles are used to infect the donor cells with RNA, which encode the reprogramming factors *OCT4*, *SOX2*, *c-MYC*, and *KLF4* without integration into the host genome.[21] The episomal vectors are derived from the Epstein–Barr virus without the viral packaging. These oriP/EBNA1 vectors contain DNA of the reprogramming factors OCT4, SOX2, NANOG, LIN28A, c-MYC, and KLF4 and express these independently.[22,23] In vitro transcribed mRNAs of *OCT4*, *SOX2*, LIN28A, c-MYC, and KLF4 have been transfected using the mRNA reprogramming method.[24] The mRNA method is the most inefficient and cumbersome protocol for reprogramming and is not applicable to all cell types. Due to the very short half-life of the mRNAs, daily, up to 7 days transfections are necessary to induce pluripotent stem cells. However, the main advantage of using mRNA to derive iPSCs is the absence of any exogenous viral or plasmid DNA in the host genome.[25]

Recently, numerous studies have been published in demonstrating reprogramming somatic cells with supplementation with small molecules, in addition to the Yamanaka factors.[26,27] Small molecules such as the cyclic AMP analog 8-Br-cAMP, valproic acid (a histone deacetylase inhibitor), and thiazovivin enhance reprogramming efficiency of human somatic cells.[10,13,26] Additionally, there exists a list of small-molecule compounds with the potential for replacing the Yamanaka factors. However, most compounds to date function more in reprogramming mouse cells.[28] **Table 1** lists a selection of small molecules, which increase the efficiency of reprogramming human somatic cells (modified from Lin and Wu 2015).[28]

In summary, iPSCs are promising in vitro tools for the application in tissue replacement therapies, for the generation of disease models, and for drug screening and toxicology studies.

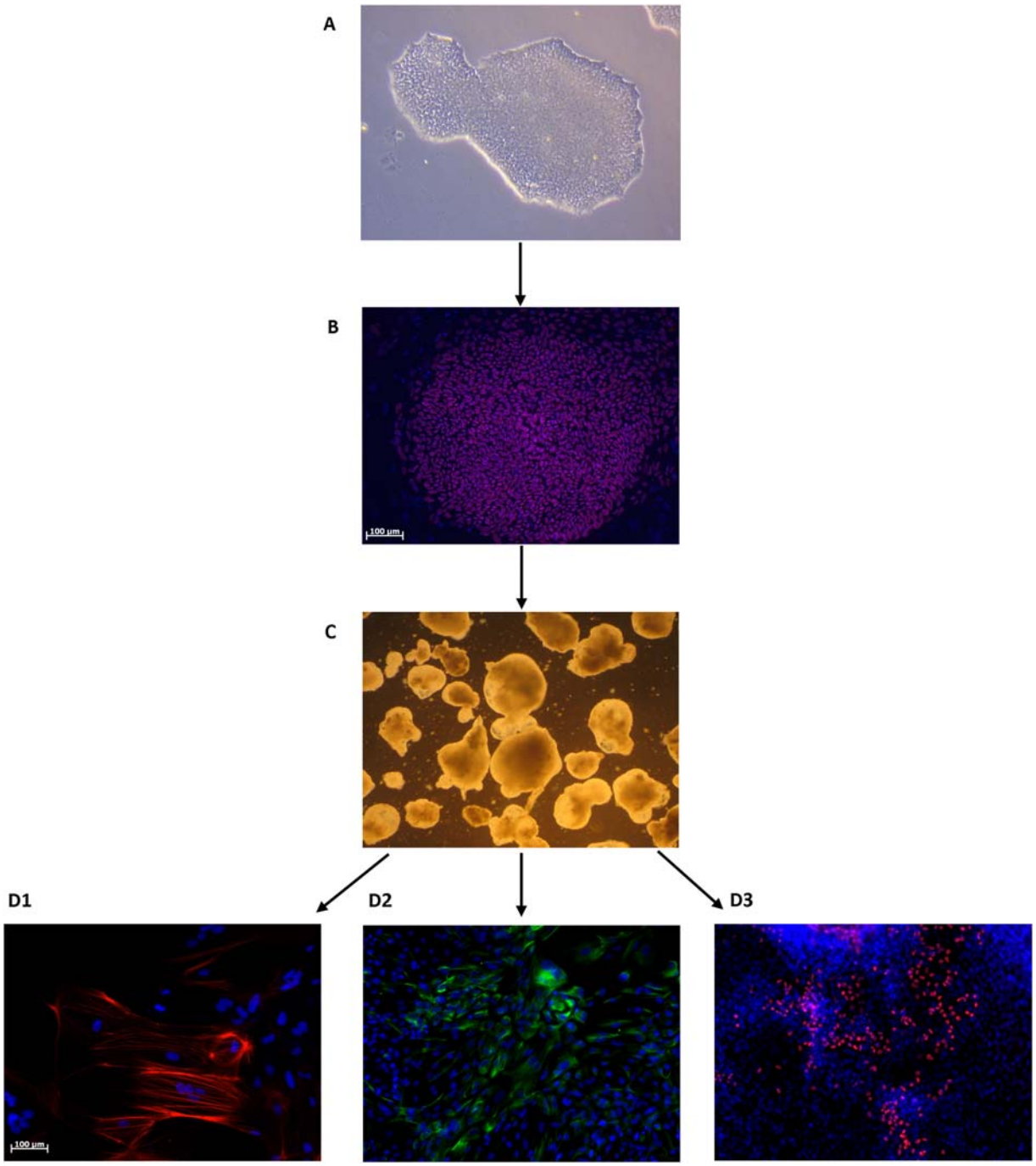

Fig. 1 iPS cells used in embryoid body-based differentiation into the three embryonic germ layers. Induced pluripotent stem cell (*iPSC*) colonies (A) express pluripotency-associated transcription factors such as OCT4 (B) and can be differentiated via embryoid bodies (*EBs*) (C) into cell types representative of the three germ layers (D). Immunofluorescence-based detection of expression of alpha-smooth muscle actin (α-*SMA*) identifies the mesoderm germ layer (D1), Nestin (*NES*) ectoderm (D2), and SOX17 endoderm (D3).

4.10.3 Induced Pluripotent Stem Cell-Derived Hepatocytes

The liver is the largest internal organ and is responsible for several key bodily functions such as metabolizing glucose and fatty acids and degradation of exogenous and endogenous toxins. There are several liver-associated diseases such as fatty liver, steatosis, and hepatitis. A broad range of mechanisms are associated with xenobiotic hepatotoxicity, for example, reactive metabolites, formation of reactive oxygen species (ROS) and impaired transporter, and cytochrome activities.[35,36]

Table 1 Small molecules used for increasing the efficiency of reprogramming human somatic cells into iPSCs

Signaling pathway or target	*Name of compound*	*Efficiency*	*Ref*
ALK4, ALK5, ALK7 inhibitors	SB431542	~200-fold	26
cAMP-dependent protein kinase activator	8-Br-cAMP	6.5-fold	29
DNMT inhibitor, histone deacetylase inhibitor	RSC133	Threefold	30
GSK-3β inhibitor, LSD1 inhibitor	LiCL	>10-fold	29
HDAC inhibitor	Sodium butyrate	100-fold	31
HDAC inhibitor	VPA	>100-fold	32
HIF PHD1 and PHD2 inhibitors	*N*-Oxalylglycine	3.5-fold	33
PDK1 activator	5-(4-Chloro-phenyl)-3-phenyl-pent-2-enoic acid (PS48)	15-fold	33
Phosphofructokinase 1 activator	Fructose-2,6-bisphosphate	Twofold	33
Rho-associated protein kinase inhibitor	Thiazovivin	~200-fold	26
Rho-associated protein kinase inhibitor	Y27632	Improved generation	34
Selective MEK/ERK inhibitor	PD0325901	~200-fold	26
TGF-β inhibitor	A83-01	Sevenfold	33

Modified from Lin, T.; Wu, S., Reprogramming With Small Molecules Instead of Exogenous Transcription Factors. *Stem Cells Int.* **2015,** *2015*, 794632.

Numerous studies have shown that findings in animals cannot be directly extrapolated to human because of species–species differences.[37] Current available in vitro models such as liver cancer cell lines and primary human hepatocytes (PHH) have been established to circumvent animal studies.[38] Advantages of PHHs are the functional cellular architecture, but unfortunately, these cells cannot be kept in culture for long periods.[39] Primary hepatocytes of course are ideal for appropriate drug and toxicity screens due to their high metabolic and functional properties.[40] However, there are several shortfalls associated with the use of primary hepatocytes, among these are variability between donors, low number of donors, and rapid decrease of cell-specific function in vitro.[35] The lack of healthy liver sample donors and the high variability between the samples are shortfalls associated with the use of primary liver cell. Due to this and the poor expandability, these cells are of limitation for high-throughput drug screening and toxicological studies. The current available human liver cell models are somehow limited, and thus, it is of prime importance to find alternatives.[41] Generation of hepatocyte-like cells (HLCs) from induced pluripotent stem cells (iPSCs) could circumvent these drawbacks.[42,43]

Protocols for generating HLCs are based on stepwise differentiation protocols resembling the developmental process in vivo. Most of these so far developed protocols are dependent on cytokines and growth factors, which try to mirror the partial differentiation stages cells go through to become hepatocytes. The first differentiation stage is the definitive endoderm, which is accomplished by supplementation with activin A and in some protocols WNT3a, bFGF, and BMP4. The second stage is the differentiation into hepatic endoderm, which resembles the bipotential hepatoblast stage in vivo. To attain a certain level of maturity, HGF, OSM, DEX, and insulin are used to advance from the hepatic endoderm to HLC stage. Several protocols for deriving HLCs in vitro have been published (**Table 2**).[42,45,46,50–52] Besides the improvement of supplements for derivation of hepatocytes from iPSC, there are several engineering approaches such as micropatterning, microfluidics, and synthetic biomaterials to improve hepatocyte culture for longer periods.[38] Another improvement of iPSC-derived hepatocytes with respect to maturity is culturing in three-dimensional (3-D) spheroids in contrast to the standard 2-D culture.[52] The leading reason why drugs are withdrawn from the market is the induction of drug-induced liver injury (DILI). HLCs could be powerful in predicting such reactions. Numerous groups have shown the functional ability of HLCs to metabolize drugs, which makes it possible to use these cells for toxicology studies.[54] HLCs can also be used to study host and virus interaction during an infection process like hepatitis C.[55] The use of iPSC-derived hepatocytes can also enlighten risk potentials of drugs for pregnant women and the fetus. Furthermore, it has been demonstrated that these cells are functional by metabolizing specific drugs although they do not reach the same level of metabolic activity like primary human hepatocytes, which was also shown on gene expression level.[42,56–59] iPSC-derived hepatocytes are used for drug screening and toxicity tests. Using this approach, it is possible to investigate the influence of the genetics of the outcome of different compounds.[43] For example, it has been shown that HLCs with an SNP in CYP2D6 have a higher persistence to tamoxifen, which is metabolized by CYP2D6 into toxic products. In parallel, these cells had a higher sensitivity to desipramine, which is detoxified by this enzyme. Derivation of a panel of HLCs bearing distinct genetic variations and polymorphisms would be a great tool for the evaluation of specific drug dosages for the particular individual.[52] Furthermore, such a panel of HLCs bearing distinct SNPS and HLA types would be a great tool for high-throughput drug screening and assays on drug metabolism.[43] Recently established methods allow gene editing by CRISPR/Cas9 and TALENs, which could be used for the creation of a pool of genetically distinct iPSC-derived hepatocytes.[43,60] Although transcriptome analysis showed that HLCs share more genes with fetal liver than with adult liver (underlining the lack of maturity in those cells), in vitro HLC differentiation can be used to study the molecular pathways involved in the liver development.

For the future, it will be important to mimic human physiological liver environment in vitro as close as possible to improve the maturity and function of HLCs and thus ensure a better prediction potential for drug screening and toxicology studies.[43] The number of studies using iPSC-derived hepatocytes is increasing with more improved protocols and approaches that try to mimic the liver environment. Future research will provide many possibilities for personalized medicine such as specific drug screenings

Table 2 Overview of protocols used to sequentially differentiate iPSCs into HLCs

Surface	*Endoderm*	*Hepatic ectoderm*	*Hepatic maturation*	*References*
MEF	Activin A, albumin fraction V (1 day) Activin A, albumin fraction V, ITS (2 days)	FGF4, BMP2 (5 days)	HGF (5 days) OSM, DEX (5 days)	44
MEF	Activin A (5 days)	FGF4, HGF (6 days)	FGF4, HGF, OSM, DEX (9 days)	45
Matrigel	Activin A (5 days)	2BME, DMSO (7 days)	Hydrocortisone 21-hemisuccinate, insulin, HGF, OSM (5 days)	46
MEF	Activin A, albumin fraction V (1 day) Activin A, albumin fraction V, ITS (2 days)	FGF2, BMP2 (4 days)	HGF, KGF (6 days) OSM, DEX, (5 days) OSM, DEX 2BME (3 days)	47
Fibronectin	Activin A, FGF2, BMP4, LY294002 (3 days)	FGF10 (3 days) FGF10, RA, SB43452 (2 days)	FGF4, HGF, EGF (10 days)	48
Matrigel	Activin A (5 days)	BMP4, FGF2 (5 days)	HGF (5 days) OSM (5 days)	49
Gelatine	Activin A, bFGF, LY (3 days) Activin A, bFGF (1 day) Activin A (3 days)	BMP4, FGF10 (4 days)	HGF, OSM (19 days)	50
Fibronectin/Matrigel	Activin A, CHIR, PI-103 (1 day) Activin A, DM3189 (2 days)	DM3189 IWP2, PD0325901, RA (1 day) BMP4, A-83-01, IWP2, RA (3 days)	BMP4 (2 days) DEX, OSM (10 days)	51
Matrigel	L-Wnt3A-expressing cells (ATCC, CRL2647), activin A (4 days)	BMP4, FGF4 (5 days) ITS, nicotinamide, NaHCO3, HGF, EGF (6 days)	HGF (5 days) OSM (11 days)	52
Matrigel/laminin-521/laminin-111	Activin A, Wnt3a (3 days)	DMSO (1 day)	HGF, OSM, hydrocortisone (11 days)	53

to identify the impact of specific genetic alterations for liver function; generation of HLCs from iPSCs from distinct genotypes makes it possible to evaluate new drugs.[61,62]

4.10.4 Induced Pluripotent Stem Cell-Derived Neuronal Cells

Worldwide, approximately one billion people are currently affected by a brain disorder.[63] Neurodegenerative- or neurodevelopmental-diseased persons suffer from the loss of cognitive function, movement, or muscle strength. Intellectual abilities such as communication and behavior are often impaired. Although neurological diseases are widespread, little is known about the underlying molecular mechanisms and hence the lack of effective therapies. Studies into neurological diseases are mostly carried out in animal models and transformed cell lines and tissues from aborted fetuses or poor-quality brain biopsies.[64,65] Experimental data obtained from animals and transformed cells are not representative of human neurological function due to the greater complexity of the human brain and interspecies physiological differences. Furthermore, neurons from different species behave differently with respect to electrophysiology.[66] For example, thalidomide and 13-*cis*-retinoic acid are well-known human teratogens but are harmless in murine models.[67, 68] The sensitivity of the human brain, chemical compounds, environmental changes, and naturally occurring substances has to be addressed in future studies.

Human induced pluripotent stem cell (iPSC)-derived neurons are more representative of human neural physiology than other model systems. They can recapitulate the in vivo conditions of neurodegenerative disorders in vitro and provide a promising tool for drug screening and neurotoxicological tests. In recent years, several neuronal disease models based on patient-specific iPSCs have been established and described.[69–71]

One of the pioneering examples was the establishment of in vitro models of amyotrophic lateral sclerosis (ALS) by differentiation of human embryonic stem cells and iPSCs into motor neurons.[68, 69] Currently, in vitro drug treatment has shown restoration of normal distribution of affected protein(s) for several neuronal diseases such as spinal muscular atrophy, Parkinson's disease, Rett syndrome, mucopolysaccharidosis type IIIB, schizophrenia, and Alzheimer's disease.[70–75] Utilizing iPSC-derived neuronal cells enables characterization of the effect of potential drugs and toxins on distinct cell types present in the human brain. Therefore, neuronal differentiation protocols, which are stepwise and produce distinct cell types of the brain (e.g., neural progenitor cells (NPCs)), represent a tool for neurotoxicity screening assay due to the highly sensitive response to neurotoxins as compared with other neural lineages.[76] So far, neurospheres developed from NPCs have been used to analyze migration, proliferation, viability, and differentiation of neural cells in the presence of different chemicals. Methylmercury chloride was identified as neurotoxic, which negatively impacts differentiation into neural cell types and inhibits the migration.[77]

More effort is needed to realize the promise of human iPSC-derived neurons in enhanced and cost-effective drug discovery and toxicology test for clinical use. A major obstacle is the low homogeneity and immature phenotype of the iPSC-derived neurons. To

develop reliable model system for drug discovery, the derivation of homogenous and more mature cell types is necessary in addition to establishing standardized and optimized protocols.

4.10.5 Induced Pluripotent Stem Cell-Derived Cardiomyocytes

Cardiotoxicity is a major problem not only for drugs targeting heart diseases but also for other compounds that act by systemic administration. Despite extensive testing with a variety of in vitro and animal models, nearly 40% of all drugs in clinical trials have to be withdrawn due to unanticipated cardiotoxic effects.[61,78] A reliable cardiotoxicity screening identifying adverse side effects on the cardiovascular system early in the drug discovering process is needed to reduce time and cost in the development of new compounds.

The action potential of a cardiomyocyte and thereby the overall electric activity of the myocardium originate from the complex interplay of multiple ionic currents. Every second case of cardiotoxicity-related drug withdrawal is caused by a risk of arrhythmia,[79] namely, an extension of the repolarization of the cell membrane detectable with an electrocardiogram as a prolongation of the QT interval. This delayed repolarization might cause a life-threatening ventricular arrhythmia termed *torsades de pointes* (TdP). In this very aspect of membrane repolarization, animal cardiac physiology relies on different currents making rat, mouse, or guinea pig an inappropriate model for human drug testing.[80] Not only in addressing safety concerns animal models lack important qualities but also today's advanced medicine uses monoclonal antibodies specifically designed against human drug targets.[81]

Cardiac physiology is difficult to mimic in vitro; there are high interspecies variation in cardiovascular physiology, which inhibits efficient preclinical testing. The main disadvantage of human adult cardiomyocytes is the limited proliferation rate, and therefore, this postmitotic cell type cannot be cultured for the durations needed for drug screenings.[81] New hopes for better drug screenings, diagnostics, and therapeutic options have been raised by induced pluripotent stem cell-derived cardiomyocytes (iPSC-CM). Theoretically, they provide an endless source of cardiomyocytes that can be kept in culture also for long-term experiments. Grown as a monolayer, iPSC-CM fit into two-dimensional assays and embryoid bodies (EBs), which constitute a three-dimensional assay system. The differentiation of cardiomyocytes from iPSCs is a complicated and multifactorial process. Since the first derivation of iPSC-CM from mouse iPSCs in 2008 [81,82] and from human in 2009,[83] many improved protocols have been established (**Table 2**).[84] Besides recent advantages in the differentiation process, today's iPSC-CM is still immature and resembles more a fetal-like phenotype of a cardiomyocyte than a fully mature adult cell type. This immaturity is, among other features, characterized by an altered current channel density manifesting in the spontaneous release of action potentials due to the less-negative resting potential of fetal cardiomyocytes.[80] Furthermore, the derived population of cardiomyocytes is heterogeneous as it usually consists of the three major subtypes of an atrial-, ventricular-, or nodal-like phenotype. Differences of these phenotypes manifest in different morphologies of the action potential and its response to drugs.[81,85] However, functional assays such as the treatment with cardioactive drugs (e.g., adrenaline, isoproterenol, and verapamil) can be conducted as iPSC-derived cardiomyocytes show a synchronized response in terms of changes in the contractility and the beating rate.[86] Additionally, at the single-cell level, the intracellular transmembrane potential can be measured with a detailed characterization of electrophysiological effects.[80] Even a higher resolution can be provided by the long-established patch clamp technique allowing the recording of current changes of single ion channels. On a larger scale, the extracellular field potential is often measured by a microelectrode array (MEA).[87] The MEA technique has been validated for iPSC-CM models showing a reliable detection of drug-induced arrhythmias and changes in the electric properties.[87,88] In addition to electrophysiological effects on cardiomyocytes caused by drug treatment, a contractile and structural cardiotoxicity (also termed as biochemical cardiotoxicity) is sometimes caused by chemotherapeutics as anthracyclines or kinase-targeted cancer drugs like trastuzumab.[89] Cardiotoxic side effects of noncardiac drugs are often not detected in preclinical or stage I trials. They only become significant during long-term treatment. Furthermore, the aged heart of older cancer patients might be more susceptible to an adverse reaction.

It has been shown in recent studies that long-term culture of iPSC-CM is possible and this results in increased maturity. A vascular coculture and newly designed biometrics also applying mechanical and electric forces have generated cardiomyocytes of higher maturation.[84,90] IPSC lines from patient-derived somatic cells have already been established (**Table 3**).[100,102] Critical mutations, like a missense mutation in the KCNH2 gene that causes one type of the long QT syndrome (LQT2), have been analyzed in functional assays for their response to corresponding drugs. Using MEA analysis, it has been shown that blocking calcium channels in LQT2 patients with nifedipine lead to a shortening of the AP duration and reduce arrhythmic activity.[81,103]

Recent breakthroughs in technological possibilities of genome editing using CRISPR/Cas9 and TALEN further allow the specific insertion or correction of critical mutations.[100] This will lead to a deeper understanding of cardiac disease and drug–target interactions and hold great promise for preclinical safety testing.

4.10.6 Induced Pluripotent Stem Cell-Derived Organoids

Cellular models based on using distinct cell lines, explanted tissues, or animal models all exhibit several limitations.[104–106] Established cell lines are usually immortalized or possess a malignant specimen origin.[107] Due to their long-term cultivation, they acquire several mutations or contaminations, and these probably limit their true biological relevance.[108,109] Furthermore, cell lines that are cultured in a two-dimensional system are not able to mimic human tissue since cells behave differently due to the lack of cell–cell

Table 3 Overview of protocols used to sequentially differentiate iPSCs into cardiomyocytes

Differentiation condition	*Cardiogenic factors*	*Small molecules*	*References*
EB formation	FBS		83
EB—suspension culture	FGF2, activin A, DKK1, BMP4	L-ascorbic acid, SB431542	91
Increased EB formation, forced aggregation	FBS/HSA, FGF2, BMP4	Polyvinyl alcohol, L-ascorbic acid	84
EB—suspension culture	FBS	L-ascorbic acid	92
Monolayer on gelatin		KY02111	93
Monolayer on Matrigel/Synthemax		IWP2/IWP4, CHIR99021, SB431542, DMH1	94
Monolayer on Matrigel		Purmorphamine, CHIR99021, IWR-1 endo, SB431542	95
Monolayer on Matrigel/Synthemax		L-ascorbic acid, CHIR99021, WNT-C59	96
EB—suspension culture	Activin A, BMP4	L-ascorbic acid, IWR-1, blebbistatin	97
Rotated Erlenmeyer flasks		CHIR99021, IWP2/IWP4	98
Spinner flask		SB431542, purmorphamine, CHIR99021, IWR-1	99
Increased EB formation, forced aggregation	FGF2, activin A, BMP4	CHIR99021, IWP2, WNT-C59	100
Patient-derived (JLNS)/genetic engineered-derived, Monolayer on Matrigel/EB formation	Activin A, BMP4, (FGF2)	CHIR99021, XAV939, (IWP-2)	101
Patient-derived (LQT3), EB formation	FGF2, activin A, BMP4	Polyvinyl alcohol, L-ascorbic acid, IWP-2	102

JLNS, Jervell and Lange-Nielsen syndrome.

and cell–matrix interactions.[104,106] Explanted tissues are particularly limited by their availability and their short-term nature.[110] Additionally, primary cell populations can lose their phenotype when they are cultured in two-dimensional systems.[106] In animal models, the performance of drug tests and modeling of diseases can demonstrate the effect on a complete organism. However, certain human diseases have been extremely difficult to model in animals due to their anatomical and physiological divergence.[111] In view of these limitations, attempts are being made to generate more relevant in vitro biological model systems.

In the 1960s, small aggregates of dissociated embryonic cells were shown to reconstitute tissues with an architecture resembling that of the original tissue.[112] Recently, this knowledge was applied into several studies, and in 2009, Sato et al. were able to create an organotypic culture system.[113] These gave rise to an epithelium-only organoid based on a single intestinal cell, which was isolated from murine intestinal crypts. They used Matrigel as an extracellular matrix (ECM) substitute and supplemented the culture medium with key growth factors of the intestinal stem cell niche, such as WNT, Noggin, R-spondin, and EGF. This culture system, referred to as the R-spondin method, appeared to be a major technological advance to the stem cell field. These organoids exhibited near-physiological and self-renewing capabilities and showed similar architecture to the native organ.[113] Observing these principles, organoids resembling tissues such as the eye, gut, breast, pancreas, prostate, liver, kidney, lung, or stomach have been generated by imitating the specific stem cell niche.[104] However, most organoids still lack several key cell types, for example, mesenchymal and endothelial.[105] In addition, they only mimic the very early developmental stages of the organ under investigation.[104] Consequently, these organoids are still limited for scientific research with respect to the physiology of the whole organism. Nevertheless, organoids provide an important bridge between traditional in vitro and in vivo models.

Historically, the term organoid was used for all three-dimensional organotypic cultures.[114,115] Recently, the definition of an organoid has changed. Organoids have to contain more than one cell type, organized similarly to the modeled tissue, and exhibit some functions that are specific to the native organ.[116] In their review, Lancaster and Knoblich defined organoids as cell clusters that "containing several cell types that develop from stem cells or organ progenitors and self-organize through cell sorting and spatially restricted lineage commitment, similar to the process in vivo."[116] Consequently, organoids represent a methodical evolution of an in vitro system called embryoid body (EB). EBs are three-dimensional aggregates of pluripotent stem cells that undergo initial developmental specification as almost identical to the pregastrulating embryo and can further differentiate to form various organized tissues. Nevertheless, not all three-dimensional organoid culture systems make use of an initial EB formation.[117] The term spheroid refers to another traditional three-dimensional culture system. However, spheroids lack the presence of relevant stem or progenitor cell populations performing self-renewal to sustain the three-dimensional cluster.[106]

Self-organization can be realized in organoids due to a growing movement away from the two-dimensional culture, which particularly relies on an artificial ECM. Here, Matrigel is a common and important component that provides a scaffold and additional supplementation of signaling cues.[118] Laminin, fibronectin, and collagen build a physical framework of tissues and influence cell behavior.[119] Due to the fact that Matrigel is not well defined, it disregards special ECM cues, which are required by different tissue types.[106] Current developed biotechnologies allow the incorporation of essential signals from native ECMs into synthetic matrices and produce designer ECMs. These synthetic scaffolds can be constructed from natural macromolecules and synthetic polymers.[119] Here, mechanical signaling can be mimicked by a hydrogel that contains technologies like light-mediated patterning. When exposed to light, photolabile cross-links can undergo local degradation and thereby soften the gel, whereas photoinitiators will cause local stiffness due to additional cross-linking.[120] Moreover, three-dimensional bioprinting is a new technique. The ink comprises a biomaterial with living cells that is precisely positioned in an additive layer-by-layer approach in order to create

Table 4 Advantages and limitations of three-dimensional organoid culture

Advantages	*Limitations*
Near-physiological model system	The lack of native microenvironment
High purity with minimal contributions from other cell types	The absence of several key cell types (e.g., mesenchymal, stromal, immune, neuronal cells)
Can be propagated for a long time without genomic alterations	Currently depend on mouse sarcoma-derived Matrigel (precludes transplantation into human)
Amenable to variety of established experimental techniques for 2-D culture systems	Inability to mimic in vivo growth factor/signaling gradients in Matrigel matrix
Can be derived from multiple sources (ESCs, iPSCs, primary cells/tissue)	Organoids in the same culture are heterogeneous in terms of viability, size, and shape
Limited amounts of starting material can be expanded	Inability to address questions regarding the whole organism
Human diseases that are difficult to model in animals can be studied with patient-derived organoids	Some tissues still remain resistant to 3-D organoid culture

Modified from Fatehullah, A.; Tan, S. H.; Barker, N., Organoids as an in vitro model of human development and disease. *Nat. Cell Biol.* **2016**, *18* (3), 246–254.

three-dimensional biological structures that mimic the structure and function of native tissues and organs.[121] By using this method, researchers were recently able to create a beating heart organoid.[106]

During organoid formation, several factors such as growth factors and small-molecule-based pathway activators or repressors are used to assist self-organization by controlling self-renewal and differentiation of stem cells. This is possible by mimicking the specific stem cell niche that contains ECM and cell–cell interactions and biophysical and biochemical signals.[106] However, cell–cell and cell–matrix interactions are difficult to control. Microfluidic devices, microbeads, and degradable vehicles in the culture matrices can deliver soluble growth factors and ligands by forming a gradient through manipulations.[106, 122] Furthermore, an important consideration in developing functional organoids is permitting sufficient nutrient and oxygen supply. Most attempts to create in vitro vascularization have been a combination of neoangiogenesis and synthetic scaffolds that are used to create micro-engineered three-dimensional structures.[123,124] An essential function is the cellular memory that enables the storage of otherwise transient responses. In this regard, sophisticated memory devices have been a key development to mimic cellular memory via genomic integrated circuits. Many synthetic circuits have been designed by using digital logic gates, relying on transcriptional control using activators, repressors, and other novel mechanisms.[125]

However, there are still tissues that remain to be resolved in three-dimensional organoid culture; among these is the heterogeneous nature of cultured organoids in terms of viability, size, and shape.[105] Regardless, the three-dimensional culture systems of organoids have advantages over the two-dimensional culture systems but still with some limitations (Table 4).[105]

The field of three-dimensional (3-D) organoids derived from human pluripotent stem cells is evolving rapidly, and there are many possibilities for potential applications (Table 5). The organoids have the potential to model adult homeostasis, and disease modeling will probably be a primary focus of future organoid-based studies.[116] The testing of efficacy and toxicity of drug components will be an important aspect, too. This could be applied to organoids that represent models for degenerative conditions. In particular, the development of, for example, human liver organoids would be of enormous relevance, because the liver often metabolizes drugs and animal-based toxicity tests often exhibit other metabolism-related pathways. Therefore, methods to screen

Table 5 Application of organoids[126]

Organoid	*Understanding of development*	*Understanding of diseases*	*Source of tissue transplantation/therapeutic cells*	*Identifying patient-tailored drugs*
Cerebral cortex	X	X		
Intestine				X
Optic cup			X	
Pituitary gland			X	
Kidney			X	X
Liver			X	X
Pancreas				X
Neural tube	X		X	
Stomach	X	X		
Prostate				X
Breast		X		
Heart	X			X
Lung	X	X		

Modified from Willyard et al. Rise of the Organoids. *Nature* **2015,** *523*, 520–522.

Table 6 Already established organoid in vitro models for human diseases

Organoids	*Types of human disease modeling*
Lingual	Lingual carcinoma
Taste bud	–
Salivary gland	Hyposalivation
Esophagus	Barrett's esophagus
Stomach	*H. pylori* infection, cancer
Intestine	Cancer, cystic fibrosis, infection model for viral and bacterial infection
Colon	IBD, cancer
Liver	Alagille syndrome, cystic fibrosis
Pancreas	Cancer
Prostate	Cancer
Lung	Cystic fibrosis
Retina	–
Inner ear	–
Brain	Autism, microcephaly
Kidney	–

Reproduced from Fatehullah, A.; Tan, S. H.; Barker, N. Organoids as an in vitro Model of Human Development and Disease. *Nat. Cell Biol.* **2016**, *18* (3), 246–254.

components in an in vitro 3-D human liver model are under investigation. This could be a great opportunity as an alternative in the drug discovery process.[127] So far, several organoid systems have been established, which are associated with human disease modeling (Table 6).[105]

4.10.6.1 Liver Organoids

Primary and adult liver cells are difficult to cultivate, and for decades, laboratory studies have failed to generate vascularized, functional, and complex organotypic cell cultures that resemble native liver.[128] Previous reported three-dimensional hepatic cell clusters were entirely composed of epithelial structures and lacked complex structures such as blood vessels.[129]

The embryonal gastrointestinal tract consists of foregut, midgut, and hindgut.[129] Each of these regions gives rise to different tissues and organs. The foregut gives rise to the oral cavity, pharynx, esophagus, stomach, liver, pancreas, and proximal duodenum. The midgut and hindgut give rise to the distal duodenum, jejunum, ileum, colon, anal canal, urethra, and bladder.[129] During liver development, ductal epithelium and hepatocytes arise from liver progenitor cells, referred to as hepatoblasts.[130] In order to attain maturity, these cells rely on a complex symphony of signals from other nearby cells. This leads to the initiation of human liver-bud formation in the third or fourth week of gestation.[128] By recapitulating these principals, Takebe et al. were recently able to create in vitro liver buds via cocultivation of hepatoblasts with mesenchymal and endothelial cells.[112] They plated the different cell types in two-dimensional conditions, and these cells self-organized into macroscopically visible three-dimensional clusters after 2 days of culture. They detected that the lack of one cell type results in failure of three-dimensional organoid formation. The created organoids were mechanically stable, could be manipulated physically, and were cultivated for 2 months while exhibiting a higher albumin production rate compared with traditional two-dimensional cultures. Takebe et al. discovered that the transplantation of these liver buds into mice led to maturation of the organoids into vascularized and functional human liver. Transplanted liver buds were capable of rescuing drug-induced liver failure in mice.[112]

More advanced methods like 3-D architecture of HLC derivatives in vitro show improvements in experimental outcome. Liver functions such as urea synthesis and activity of distinct cytochromes were higher in the 3-D organoids than in the 2-D culture approaches. Furthermore, these 3-D iPSC-derived hepatocyte-like cells (HLCs) were more susceptible for most of the tested drugs in comparison with the monolayer culture.[52] Furthermore, liver-bud-like tissue generation by self-organization of genetically engineered iPSCs is possible. These organoids are able to perform several liver key functions.[131]

Based on these advances, it is evident that three-dimensional organoid culture systems may be suitable not only for disease modeling, drug test performance, and developmental research but also for cell replacement therapies in the near future.

4.10.6.2 Brain Organoids

The brain is a complex organ. It derives from the neural ectoderm,[132] which gives rise to the neural plate which folds and fuses to form the neural tube. The neural tube is an epithelium with apical–basal polarity that is organized around fluid-filled lumen that likely represents the brain ventricles. The axes are built through concentration gradients and because of these axes the epithelial tube can subdivide into four major brain regions: the forebrain, midbrain, hindbrain, and spinal cord.[116] In general, neural stem cells that are resident next to the ventricles differentiate into neurons.[133] The neural stem cells expand through symmetric proliferative

and asymmetric divisions that give rise to self-renewing progenitors and differentiated cell types which migrate to other zones to generate stratified structures.[116, 134]

In previous studies, in vitro-derived neural stem cells from pluripotent stem cells were used to better decipher the mechanisms of neural differentiation.[135] These homogenous neural stem cells were generated in classical two-dimensional culture systems and could neither show the characteristic apical–basal polarity nor recapitulate the complicated lineage of neural stem cells. To gain knowledge in this field, protocols for generating neurospheres have been developed.[136] Neurospheres are aggregates of neural stem cells and have a self-renewing capacity. Though, neurospheres are not well organized and are limited in their capacity to generate different aspects of brain development.[116] Furthermore, neural tubelike structures and the neural rosettes have also been established. Neural rosettes derive from isolated neuroepithelium or directed differentiation of pluripotent stem cells.[137,138] They have the ability to recapitulate apical–basal polarity and exhibit radial organization similar to that of the neural tube. They show a higher capacity to recapitulate many aspects of brain development including the production of intermediate progenitor cells and the timed production of layer identities similar to those in vivo.[139] However, the two-dimensional aspect of this method results in many limitations in modeling the organization of the developing brain; hence, three-dimensional (3-D) culture methods were established to help overcome some of these limitations.[116,128,140–144] These methods have the potential to recapitulate brain tissue formation. To obtain the 3-D cultures, first, embryoid bodies have to be generated from pluripotent stem cells. Second, after embedding them in Matrigel, which provides an environment that is similar to the extracellular matrix, the embryonic bodies exhibit an outgrowth of large buds of neuroepithelium. These buds have the ability to expand and develop into various brain regions. The cerebral organoids can reach the size of a few millimeters and can be further maintained for over a year by using a bioreactor that provides sufficient oxygen and nutrient supply.[116,145] Cerebral organoids are able to mimic the development and disease conditions.[143] Furthermore, they offer potential for drug testing and even future organ replacement strategies.[146] However, like all in vitro systems, the method does not contain all crucial factors necessary for proper brain development. The surrounding embryonic tissues that have great importance on the interplay of neural and nonneural tissue are missing.[145]

4.10.6.3 Heart Organoids

Heart organogenesis and morphogenesis are complex anatomical processes. In the adult heart, myocardial cells are generated from mesodermal precursors during the embryonic period of heart growth.[147] Distinct signaling pathways lead to the formation of the first and second heart fields and afterward to the four-chambered heart.[148–150] After the forming of the early heart shape, some mesodermal cells from the proepicardium build the epicardium, which is a single layer of cells that envelope the heart.[151] Then, epicardial cells become migratory mesenchymal cells and enter the underlying myocardium and differentiate.[147]

There are three main points to consider, that is, scaffold, cell sources, and signaling factors, when generating three-dimensional (3-D) cardiac tissue for use in cardiovascular therapy or toxicological testing.[147] The differentiation of pluripotent stem cells into cardiomyocytes follows a distinct developmental lineage after mesoderm induction. Generating organoids involve mimicking the 3-D setting of an evolving embryo using embryoid bodies as intermediates.[152] These aggregates of cells are exposed to various growth factors and hypoxic environment for initiating the developmental processes. Other scaffold-free constructs are used by a relatively new developed method: the cell sheet engineering technique. There, a temperature-responsive culture surface is used that detaches myocardial layers as a confluent sheet. This is achieved by lowering the temperature, which then results in the stacking of myocardial layers to produce a 3-D cardiac construct.[153] The monolayers can rapidly attach and form cell–cell connections. However, the thickness of the 3-D construct is limited to three layers.[154] In contrast to the use of embryonic bodies and the cell sheet engineering technique, a scaffold can be used to obtain organoids via other pathways. A scaffold represents the structural platform for a new cellular microenvironment and supports new tissue formation. It provides cell attachment, migration, differentiation, and organization.[155] Biometric scaffolds are made of natural or synthetic polymers or hybrid copolymer and are similar to the native components of the extracellular matrix.[156] In general, biometric scaffolds should not be immunogenic but mechanically stable. They should mimic cardiac tissue flexibility and allow physiological electric propagation and sufficient oxygen and nutrient delivery to the cells and a degradation rate that is appropriate to the rate of native extracellular matrix replacement.[115,157] The biometric scaffolds are used alone or in combination with cells.[158–161] To gain success, the selection of cell types and scaffold material and the incorporation of bioactive molecules and bioreactors should be noted.[147] Another method for generating a 3-D cardiac tissue is the decellularization. Therefore, the success of this depends on specific requirements of the application as high density, high pressure, and stiffness.[162,163] The commonly used methods are microwave radiation and chemical, enzymatic, mechanical, and physical separation. The combination of physical, chemical, and enzymatic methods leads to better results in the decellularization process in whole organ and small tissues in cardiac applications.[164,165] In order to decellularize and recellularize an organ to serve as a scaffold, detergent or an enzymatic solution is first used to remove cellular material and then the stem cell of choice is applied to repopulate the scaffold in the presence of an appropriate culture environment.[147]

4.10.7 Use of Induced Pluripotent Stem Cells for Toxicogenomics

Toxicogenomics—an interdisciplinary between toxicology and genomics—is concerned with identification of potential human and environmental toxicants and their putative mechanisms of action through the use of genomic resources.[166] Measurements on the proteome, genome, and transcriptome level target at the prediction of toxicity, the finding of biomarkers, and the detection of

genetic variants associated with higher predisposition to toxicity. A broader concept of toxicogenomics also includes metabolomics.[167] A plethora of studies have demonstrated the advantages of the toxicogenomic approach.[168] For instance, McBurney et al. proposed a systems toxicology approach to discover toxicogenomic biomarkers to detect a drug's potential for human idiosyncratic drug-induced liver injury and could show that the molecular analyses employed in the study were detecting substantial "off-target" markers.[169] Ellinger-Ziegelbauer et al. could distinguish genotoxic carcinogens from nongenotoxic carcinogens via a toxicogenomic approach employing gene expression profiles from treated rat liver.[170] Based on the gene expression profiles and a support vector machine (SVM), classifiers of the carcinogens were determined in what would have usually required a 2-year evaluation with rodent lifetime bioassays. Obviously, in toxicogenomics, the accessibility of a large amount of existing toxicological information plays an important role. Hence, there is a need for databases making this knowledge accessible to the community and integrating newly acquired knowledge. Here, as an example, the Japanese Toxicogenomics Project consortium (TGP) provides a large-scale toxicogenomics database (open TG-GATEs) consisting of data from 170 compounds (mostly drugs) with the aim of improving and enhancing drug safety assessment.[171] The database (http://toxico.nibio.go.jp/english/index.html) comprises data and metadata including gene expression profiles and pathology and is freely available.

Although toxicity can affect various tissues such as neurotoxicity or kidney toxicity, the liver as a key metabolic organ plays a major role for toxicity studies. Most drugs promote their own metabolism by upregulating the enzyme systems responsible for their activation (phase I) and conjugation (phase II) to biochemical forms that can be excreted in bile or urine. The majority of drugs that are metabolized by the liver through such detoxification pathways induce particular subsets of cytochromes (CYP) P450.[172] The most ubiquitous of these, CYP3A4, is responsible for metabolizing a large fraction of hepatotoxic drugs, and indeed, CYP3A4 induction can be used as an index of exposure to them. The Adjaye group demonstrated the expression of cytochrome P450 family members in induced pluripotent stem cells (iPSCs) and embryonic stem cell (ESC)-derived hepatocyte-like cells, and others have shown the prediction of interindividual differences in hepatic functions and drug sensitivity by using human iPSC-derived hepatocytes.[42,52,58,173] These studies among others have provided evidence that human iPSC-derived hepatocytes can be used as an in vitro hepatocyte model for use in pharmacology and toxicology. **Fig. 2** shows expression of the drug-metabolism-associated absorption, distribution, metabolism, and excretion (ADME) genes in iPSCs differentiated into hepatocytes, cardiomyocytes, and neurons.[41,42,71,100,174] The iPSC-based strategy is also exploited by companies by providing human iPSC-derived hepatocyte cells (iHeps) for use in toxicology screening and studies.[173] The ADME genes have been shown to be associated with drug metabolism and can be grouped into four distinct categories (http://www.pharmaadme.org/):[35]

1. Phase I metabolism enzymes: CYP, DHRS, and CBR
2. Phase II metabolism enzymes: GST, SULT, UGT, CHST, and NAT, which are responsible for the modification of functional groups and the conjugation with endogenous moieties
3. Transporters: SLC, ABC, and MRP, which are responsible for the uptake and excretion of drugs in and out of cells
4. Modifiers: CAT, CDA, RXRA, PPARG, PPARD, SOD, and SERPINA7, which can have dual functions, that is, regulate the expression of other ADME genes or modulate the biochemistry of ADME enzymes

ADME genes can be employed to derive parameters from in vitro models, which can be combined with toxicokinetic (TK) parameters from in vivo models, which increasingly can be derived from physiologically based toxicokinetic (PBTK) modeling.[175]

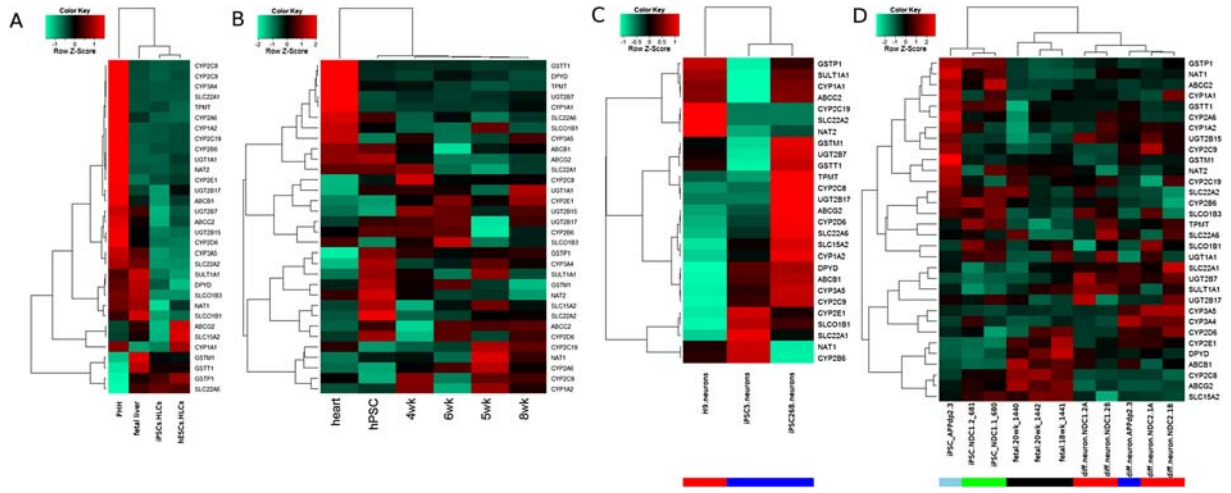

Fig. 2 Gene expression analysis of the ADME genes in iPSCs differentiated into cell types representative of endoderm, mesoderm, and ectoderm. The heatmaps represent genes encoding the core ADME enzymes based on the transcriptome data sets of iPSC- and ESC-derived HLCs (A),[42] cardiomyocytes (B),[100] and neurons for Alzheimer's disease models (C[174] and D).[71] The ADME genes have been shown to be associated with drug metabolism (http://pharmaadme.org/joomla/index.php?option=com_content&task=view&id=14&Itemid=29).[41] Color bars: *blue*, iPSC-derived neuron from AD; *red*, iPSC-derived neuron from healthy control; *light blue*, iPSC from AD; *green*, iPSCs from healthy control; black, fetal brain.

ADME-derived parameters depend on the tested chemicals and can be integrated with chemical-independent physiological and anatomical information in PBTK models to simulate TK profiles. Employing quantitative structure–activity relationship (QSAR) models and in vitro methods, ADME parameters can be determined. PBTK models are valuable tools for extrapolating in vitro results either interspecies or interindividuals and thus are gaining importance in toxicity testing.

4.10.8 The 3Rs

The 3Rs are first mentioned in a report by Russell and Burch originally published in 1959 and are acronyms for replace, reduce, and refine.[176] The first *R* means that as far as possible, animal tests should be replaced. If that is not possible, they should be reduced, and if that is also not possible, the experiments should at least take place under the best possible conditions for the animals (refine).

To date, toxicology screens necessitate the use of significant numbers of animals. In the EU program Registration, Evaluation, Authorisation and Restriction of Chemicals (REACH), the hazard risk of 30,000 chemicals shall be assessed, which had not been tested before. This testing of chemicals required under the REACH regulations has been variously estimated to require up to 54 million additional animals, therefore necessitating the development of alternative testing strategies (http://ec.europa.eu/enterprise/sectors/chemicals/reach/index_en.htm), which could achieve a reduction to below 10 million animals.[177]

3R approaches could tackle this problem by employing patient-specific iPSC-derived hepatocytes, neurons, or cardiomyocytes in order to reduce or—where possible—to replace animal tests. In a strategy paper, the European Union Reference Laboratory for alternatives to animal testing (EURL-ECVAM) outlines the possible use of physiologically based toxicokinetic (PBTK) models for toxicological tests with respect to the 3Rs.[175] These models have the potential to provide whole-body human toxicokinetic data by in silico and in vitro methods assessing ADME processes. Standardization and an infrastructure for these methods are important issues that when properly solved, could leverage their acceptance and use, thus leading to a more efficient use of available human and animal data. Höfer et al. mention the importance of databases and data management to ensure a more ubiquitous accessibility of existing data.[177] Adequate data management strategies are an issue for many scientific disciplines where large amounts of data are generated and, in particular for modern biology disciplines such as toxicogenomics and systems biology, where novel techniques produce data in high throughput.[178]

Predictions based on animals models not always reflect the human reactions but instead display sometimes qualitative and also quantitative differences in their physiology and metabolism; for example, animal test data for acetylsalicylic acid (aspirin) demonstrated that it could cause severe problems in rats but it is harmless to humans.[179–182] Would these animal experiments have been used to test the safety of aspirin, it may not have been permitted for clinical trials. Already in 1988, Lave et al. criticized the reliability and the cost-effectiveness of rodent models for carcinogenicity testing.[183] The report *Toxicity Testing in the 21st Century*: *A Vision and a Strategy* released by the US National Academy of Sciences envisioned toxicity testing firmly based on human biology and thus reducing animal testing.[184] Computational models would simulate dose–response behavior and extrapolate in vitro results to in vivo human blood and tissue concentrations. Thus, human relevance of test results would be increased.

However, a full replacement of animal tests at the moment is not feasible as the models still cannot fully reflect the in vivo reality. This is demonstrated by the demand for animal tests in most guidelines for toxicity testing, for example, the Organisation for Economic Co-operation and Development (OECD) guidelines for the testing of chemicals. In general, guideline methods such as OECD TGs 417 and 427 are based on animal tests.[175,185,186] Only OECD TG 428 for the in vitro method for skin absorption is an exception.[187] However, with the continuous improvement of the toxicological models, replacement can be envisioned as a long-term goal, and meanwhile, the two other *Rs*—reduction and refinement—should be followed as far as possible.

References

1. Jensen, J.; Hyllner, J.; Bjorquist, P. Human Embryonic Stem Cell Technologies and Drug Discovery. *J. Cell. Physiol.* **2009,** *219* (3), 513–519.
2. Lai, D.; Wang, Y.; Sun, J.; Chen, Y.; Li, T.; Wu, Y.; Guo, L.; Wei, C. Derivation and Characterization of Human Embryonic Stem Cells on Human Amnion Epithelial Cells. *Sci. Rep.* **2015,** *5,* 10014.
3. Takahashi, K.; Yamanaka, S. Induction of Pluripotent Stem Cells From Mouse Embryonic and Adult Fibroblast Cultures by Defined Factors. *Cell* **2006,** *126* (4), 663–676.
4. Takahashi, K.; Okita, K.; Nakagawa, M.; Yamanaka, S. Induction of Pluripotent Stem Cells From Fibroblast Cultures. *Nat. Protoc.* **2007,** *2* (12), 3081–3089.
5. Yu, J.; Vodyanik, M. A.; Smuga-Otto, K.; Antosiewicz-Bourget, J.; Frane, J. L.; Tian, S.; Nie, J.; Jonsdottir, G. A.; Ruotti, V.; Stewart, R.; Slukvin, I. I.; Thomson, J. A. Induced Pluripotent Stem Cell Lines Derived From Human Somatic Cells. *Science* **2007,** *318* (5858), 1917–1920.
6. Jung, M.; Peterson, H.; Chavez, L.; Kahlem, P.; Lehrach, H.; Vilo, J.; Adjaye, J. A Data Integration Approach to Mapping OCT4 Gene Regulatory Networks Operative in Embryonic Stem Cells and Embryonal Carcinoma Cells. *PLoS One* **2010,** *5* (5), e10709.
7. Goke, J.; Jung, M.; Behrens, S.; Chavez, L.; O'Keeffe, S.; Timmermann, B.; Lehrach, H.; Adjaye, J.; Vingron, M. Combinatorial Binding in Human and Mouse Embryonic Stem Cells Identifies Conserved Enhancers Active in Early Embryonic Development. *PLoS Comput. Biol.* **2011,** *7* (12), e1002304.
8. Thomson, J. A.; Itskovitz-Eldor, J.; Shapiro, S. S.; Waknitz, M. A.; Swiergiel, J. J.; Marshall, V. S.; Jones, J. M. Embryonic Stem Cell Lines Derived From Human Blastocysts. *Science* **1998,** *282* (5391), 1145–1147.
9. Yamanaka, S. Strategies and New Developments in the Generation of Patient-Specific Pluripotent Stem Cells. *Cell Stem Cell* **2007,** *1* (1), 39–49.
10. Wang, Y.; Mah, N.; Prigione, A.; Wolfrum, K.; Andrade-Navarro, M. A.; Adjaye, J. A Transcriptional Roadmap to the Induction of Pluripotency in Somatic Cells. *Stem Cell Rev.* **2010,** *6* (2), 282–296.
11. Masato Nakagawa, M. K.; Tanabe, K.; Takahashi, K.; Ichisaka, T.; Takashi Aoi, K. O.; Mochiduki, Y.; Takizawa, N.; Yamanaka, S. Generation of Induced Pluripotent Stem Cells Without Myc From Mouse and Human Fibroblasts. *Nat. Biotechnol.* **2008,** *26* (1), 101–106.

12. Zhao, Y.; Yin, X.; Qin, H.; Zhu, F.; Liu, H.; Yang, W.; Zhang, Q.; Xiang, C.; Hou, P.; Song, Z.; Liu, Y.; Yong, J.; Zhang, P.; Cai, J.; Liu, M.; Li, H.; Li, Y.; Qu, X.; Cui, K.; Zhang, W.; Xiang, T.; Wu, Y.; Zhao, Y.; Liu, C.; Yu, C.; Yuan, K.; Lou, J.; Ding, M.; Deng, H. Two Supporting Factors Greatly Improve the Efficiency of Human iPSC Generation. *Cell Stem Cell* **2008,** *3* (5), 475–479.
13. Wang, Y.; Adjaye, J. A Cyclic AMP Analog, 8-Br-cAMP, Enhances the Induction of Pluripotency in Human Fibroblast Cells. *Stem Cell Rev.* **2011,** *7* (2), 331–341.
14. Maherali, N.; Ahfeldt, T.; Rigamonti, A.; Utikal, J.; Cowan, C.; Hochedlinger, K. A High-Efficiency System for the Generation and Study of Human Induced Pluripotent Stem Cells. *Cell Stem Cell* **2008,** *3* (3), 340–345.
15. Prigione, A.; Fauler, B.; Lurz, R.; Lehrach, H.; Adjaye, J. The Senescence-Related Mitochondrial/Oxidative Stress Pathway Is Repressed in Human Induced Pluripotent Stem Cells. *Stem Cells* **2010,** *28* (4), 721–733.
16. Wolfrum, K.; Wang, Y.; Prigione, A.; Sperling, K.; Lehrach, H.; Adjaye, J. The Large Principle of Cellular Reprogramming: Lost, Acquired and Retained Gene Expression in Foreskin and Amniotic Fluid-Derived Human Ips Cells. *PLoS One* **2010,** *5* (10), e13703.
17. Lichtner, B.; Knaus, P.; Lehrach, H.; Adjaye, J. BMP10 as a Potent Inducer of Trophoblast Differentiation in Human Embryonic and Induced Pluripotent Stem Cells. *Biomaterials* **2013,** *34* (38), 9789–9802.
18. Chen, L.; Liu, L. Current Progress and Prospects of Induced Pluripotent Stem Cells. *Sci. Chin.* **2009,** *52* (7), 622–636.
19. Kiskinis, E.; Eggan, K. Progress Toward the Clinical Application of Patient-Specific Pluripotent Stem Cells. *J. Clin. Invest.* **2010,** *120* (1), 51–59.
20. Tavernier, G.; Wolfrum, K.; Demeester, J.; De Smedt, S. C.; Adjaye, J.; Rejman, J. Activation of Pluripotency-Associated Genes in Mouse Embryonic Fibroblasts by Non-Viral Transfection With In Vitro-Derived mRNAs Encoding Oct4, Sox2, Klf4 and cMyc. *Biomaterials* **2012,** *33* (2), 412–417.
21. Fusaki, N.; Ban, H.; Nishiyama, A.; Saeki, K.; Hasegawa, M. Efficient Induction of Transgene-Free Human Pluripotent Stem Cells Using a Vector Based on Sendai Virus, an RNA Virus That Does not Integrate Into the Host Genome. *Proc. Jpn. Acad. Ser. B Phys. Biol. Sci.* **2009,** *85* (8), 348–362.
22. Yu, J.; Hu, K.; Smuga-Otto, K.; Tian, S.; Stewart, R.; Slukvin, I. I.; Thomson, J. A. Human Induced Pluripotent Stem Cells Free of Vector and Transgene Sequences. *Science* **2009,** *324* (5928), 797–801.
23. Okita, K.; Matsumura, Y.; Sato, Y.; Okada, A.; Morizane, A.; Okamoto, S.; Hong, H.; Nakagawa, M.; Tanabe, K.; Tezuka, K.; Shibata, T.; Kunisada, T.; Takahashi, M.; Takahashi, J.; Saji, H.; Yamanaka, S. A More Efficient Method to Generate Integration-Free Human iPS Cells. *Nat. Methods* **2011,** *8* (5), 409–412.
24. Warren, L.; Manos, P. D.; Ahfeldt, T.; Loh, Y. H.; Li, H.; Lau, F.; Ebina, W.; Mandal, P. K.; Smith, Z. D.; Meissner, A.; Daley, G. Q.; Brack, A. S.; Collins, J. J.; Cowan, C.; Schlaeger, T. M.; Rossi, D. J. Highly Efficient Reprogramming to Pluripotency and Directed Differentiation of Human Cells With Synthetic Modified mRNA. *Cell Stem Cell* **2010,** *7* (5), 618–630.
25. Schlaeger, T. M.; Daheron, L.; Brickler, T. R.; Entwisle, S.; Chan, K.; Cianci, A.; DeVine, A.; Ettenger, A.; Fitzgerald, K.; Godfrey, M.; Gupta, D.; McPherson, J.; Malwadkar, P.; Gupta, M.; Bell, B.; Doi, A.; Jung, N.; Li, X.; Lynes, M. S.; Brookes, E.; Cherry, A. B.; Demirbas, D.; Tsankov, A. M.; Zon, L. I.; Rubin, L. L.; Feinberg, A. P.; Meissner, A.; Cowan, C. A.; Daley, G. Q. A Comparison of Non-Integrating Reprogramming Methods. *Nat. Biotechnol.* **2015,** *33* (1), 58–63.
26. Lin, T.; Ambasudhan, R.; Yuan, X.; Li, W.; Hilcove, S.; Abujarour, R.; Lin, X.; Hahm, H. S.; Hao, E.; Hayek, A.; Ding, S. A Chemical Platform for Improved Induction of Human iPSCs. *Nat. Methods* **2009,** *6* (11), 805–808.
27. Marson, A.; Foreman, R.; Chevalier, B.; Bilodeau, S.; Kahn, M.; Young, R. A.; Jaenisch, R. Wnt Signaling Promotes Reprogramming of Somatic Cells to Pluripotency. *Cell Stem Cell* **2008,** *3* (2), 132–135.
28. Lin, T.; Wu, S. Reprogramming With Small Molecules Instead of Exogenous Transcription Factors. *Stem Cells Int.* **2015,** *2015,* 794632.
29. Wang, Q.; Xu, X.; Li, J.; Liu, J.; Gu, H.; Zhang, R.; Chen, J.; Kuang, Y.; Fei, J.; Jiang, C.; Wang, P.; Pei, D.; Ding, S.; Xie, X. Lithium, an Anti-Psychotic Drug, Greatly Enhances the Generation of Induced Pluripotent Stem Cells. *Cell Res.* **2011,** *21* (10), 1424–1435.
30. Lee, J.; Xia, Y.; Son, M. Y.; Jin, G.; Seol, B.; Kim, M. J.; Son, M. J.; Do, M.; Lee, M.; Kim, D.; Lee, K.; Cho, Y. S. A Novel Small Molecule Facilitates the Reprogramming of Human Somatic Cells Into a Pluripotent State and Supports the Maintenance of an Undifferentiated State of Human Pluripotent Stem Cells. *Angew. Chem.* **2012,** *51* (50), 12509–12513.
31. Mali, P.; Chou, B. K.; Yen, J.; Ye, Z.; Zou, J.; Dowey, S.; Brodsky, R. A.; Ohm, J. E.; Yu, W.; Baylin, S. B.; Yusa, K.; Bradley, A.; Meyers, D. J.; Mukherjee, C.; Cole, P. A.; Cheng, L. Butyrate Greatly Enhances Derivation of Human Induced Pluripotent Stem Cells by Promoting Epigenetic Remodeling and the Expression of Pluripotency-Associated Genes. *Stem Cells* **2010,** *28* (4), 713–720.
32. Huangfu, D.; Maehr, R.; Guo, W.; Eijkelenboom, A.; Snitow, M.; Chen, A. E.; Melton, D. A. Induction of Pluripotent Stem Cells by Defined Factors Is Greatly Improved by Small-Molecule Compounds. *Nat. Biotechnol.* **2008,** *26* (7), 795–797.
33. Zhu, S.; Li, W.; Zhou, H.; Wei, W.; Ambasudhan, R.; Lin, T.; Kim, J.; Zhang, K.; Ding, S. Reprogramming of Human Primary Somatic Cells by OCT4 and Chemical Compounds. *Cell Stem Cell* **2010,** *7* (6), 651–655.
34. Claassen, D. A.; Desler, M. M.; Rizzino, A. ROCK Inhibition Enhances the Recovery and Growth of Cryopreserved Human Embryonic Stem Cells and Human Induced Pluripotent Stem Cells. *Mol. Reprod. Dev.* **2009,** *76* (8), 722–732.
35. Gomez-Lechon, M. J.; Donato, M. T.; Castell, J. V.; Jover, R. Human Hepatocytes as a Tool for Studying Toxicity and Drug Metabolism. *Curr. Drug Metab.* **2003,** *4* (4), 292–312.
36. Gunawan, B. K.; Kaplowitz, N. Mechanisms of Drug-Induced Liver Disease. *Clin. Liver Dis.* **2007,** *11* (3), 459–475. v.
37. Olson, H.; Betton, G.; Robinson, D.; Thomas, K.; Monro, A.; Kolaja, G.; Lilly, P.; Sanders, J.; Sipes, G.; Bracken, W.; Dorato, M.; Van Deun, K.; Smith, P.; Berger, B.; Heller, A. Concordance of the Toxicity of Pharmaceuticals in Humans and in Animals. *Regul. Toxicol. Pharmacol.* **2000,** *32* (1), 56–67.
38. Khetani, S. R.; Berger, D. R.; Ballinger, K. R.; Davidson, M. D.; Lin, C.; Ware, B. R. Microengineered Liver Tissues for Drug Testing. *J. Lab. Autom.* **2015,** *20* (3), 216–250.
39. LeCluyse, E. L.; Witek, R. P.; Andersen, M. E.; Powers, M. J. Organotypic Liver Culture Models: Meeting Current Challenges in Toxicity Testing. *Crit. Rev. Toxicol.* **2012,** *42* (6), 501–548.
40. Dambach, D. M.; Andrews, B. A.; Moulin, F. New Technologies and Screening Strategies for Hepatotoxicity: Use of in vitro Models. *Toxicol. Pathol.* **2005,** *33* (1), 17–26.
41. Graffmann, N.; Matz, P.; Wruck, W.; Adjaye, J. The Promise of Induced Pluripotent Stem Cells for Liver Disease, Toxicology and Drug Discovery. *Drug Target Rev.* **2015,** *2* (1), 8–11.
42. Jozefczuk, J.; Prigione, A.; Chavez, L.; Adjaye, J. Comparative Analysis of Human Embryonic Stem Cell and Induced Pluripotent Stem Cell-Derived Hepatocyte-Like Cells Reveals Current Drawbacks and Possible Strategies for Improved Differentiation. *Stem Cells Dev.* **2011,** *20* (7), 1259–1275.
43. Davidson, M. D.; Ware, B. R.; Khetani, S. R. Stem Cell-Derived Liver Cells for Drug Testing and Disease Modeling. *Discov. Med.* **2015,** *19* (106), 349–358.
44. Cai, J.; Zhao, Y.; Liu, Y.; Ye, F.; Song, Z.; Qin, H.; Meng, S.; Chen, Y.; Zhou, R.; Song, X.; Guo, Y.; Ding, M.; Deng, H. Directed Differentiation of Human Embryonic Stem Cells Into Functional Hepatic Cells. *Hepatology* **2007,** *45* (5), 1229–1239.
45. Agarwal, S.; Holton, K. L.; Lanza, R. Efficient Differentiation of Functional Hepatocytes From Human Embryonic Stem Cells. *Stem Cells* **2008,** *26* (5), 1117–1127.
46. Hay, D. C.; Zhao, D.; Fletcher, J.; Hewitt, Z. A.; McLean, D.; Urruticoechea-Uriguen, A.; Black, J. R.; Elcombe, C.; Ross, J. A.; Wolf, R.; Cui, W. Efficient Differentiation of Hepatocytes From Human Embryonic Stem Cells Exhibiting Markers Recapitulating Liver Development In Vivo. *Stem Cells* **2008,** *26* (4), 894–902.
47. Song, Z.; Cai, J.; Liu, Y.; Zhao, D.; Yong, J.; Duo, S.; Song, X.; Guo, Y.; Zhao, Y.; Qin, H.; Yin, X.; Wu, C.; Che, J.; Lu, S.; Ding, M.; Deng, H. Efficient Generation of Hepatocyte-Like Cells From Human Induced Pluripotent Stem Cells. *Cell Res.* **2009,** *19* (11), 1233–1242.
48. Touboul, T.; Hannan, N. R.; Corbineau, S.; Martinez, A.; Martinet, C.; Branchereau, S.; Mainot, S.; Strick-Marchand, H.; Pedersen, R.; Di Santo, J.; Weber, A.; Vallier, L. Generation of Functional Hepatocytes From Human Embryonic Stem Cells Under Chemically Defined Conditions That Recapitulate Liver Development. *Hepatology* **2010,** *51* (5), 1754–1765.
49. Si-Tayeb, K.; Noto, F. K.; Nagaoka, M.; Li, J.; Battle, M. A.; Duris, C.; North, P. E.; Dalton, S.; Duncan, S. A. Highly Efficient Generation of Human Hepatocyte-Like Cells From Induced Pluripotent Stem Cells. *Hepatology* **2010,** *51* (1), 297–305.

50. Hannan, N. R.; Segeritz, C. P.; Touboul, T.; Vallier, L. Production of Hepatocyte-Like Cells From Human Pluripotent Stem Cells. *Nat. Protoc.* **2013,** *8* (2), 430–437.
51. Loh, K. M.; Ang, L. T.; Zhang, J.; Kumar, V.; Ang, J.; Auyeong, J. Q.; Lee, K. L.; Choo, S. H.; Lim, C. Y.; Nichane, M.; Tan, J.; Noghabi, M. S.; Azzola, L.; Ng, E. S.; Durruthy-Durruthy, J.; Sebastiano, V.; Poellinger, L.; Elefanty, A. G.; Stanley, E. G.; Chen, Q.; Prabhakar, S.; Weissman, I. L.; Lim, B. Efficient Endoderm Induction From Human Pluripotent Stem Cells by Logically Directing Signals Controlling Lineage Bifurcations. *Cell Stem Cell* **2014,** *14* (2), 237–252.
52. Takayama, K.; Morisaki, Y.; Kuno, S.; Nagamoto, Y.; Harada, K.; Furukawa, N.; Ohtaka, M.; Nishimura, K.; Imagawa, K.; Sakurai, F.; Tachibana, M.; Sumazaki, R.; Noguchi, E.; Nakanishi, M.; Hirata, K.; Kawabata, K.; Mizuguchi, H. Prediction of Interindividual Differences in Hepatic Functions and Drug Sensitivity by Using Human iPS-Derived Hepatocytes. *Proc. Natl. Acad. Sci. U. S. A.* **2014,** *111* (47), 16772–16777.
53. Cameron, K.; Tan, R.; Schmidt-Heck, W.; Campos, G.; Lyall, M. J.; Wang, Y.; Lucendo-Villarin, B.; Szkolnicka, D.; Bates, N.; Kimber, S. J.; Hengstler, J. G.; Godoy, P.; Forbes, S. J.; Hay, D. C. Recombinant Laminins Drive the Differentiation and Self-Organization of HESC-Derived Hepatocytes. *Stem Cell Rep.* **2015,** *5* (6), 1250–1262.
54. Takayama, K.; Inamura, M.; Kawabata, K.; Katayama, K.; Higuchi, M.; Tashiro, K.; Nonaka, A.; Sakurai, F.; Hayakawa, T.; Furue, M. K.; Mizuguchi, H. Efficient Generation of Functional Hepatocytes From Human Embryonic Stem Cells and Induced Pluripotent Stem Cells by HNF4alpha Transduction. *Mol. Ther.* **2012,** *20* (1), 127–137.
55. Yoshida, T.; Takayama, K.; Kondoh, M.; Sakurai, F.; Tani, H.; Sakamoto, N.; Matsuura, Y.; Mizuguchi, H.; Yagi, K. Use of Human Hepatocyte-Like Cells Derived From Induced Pluripotent Stem Cells as a Model for Hepatocytes in Hepatitis C Virus Infection. *Biochem. Biophys. Res. Commun.* **2011,** *416* (1–2), 119–124.
56. Ulvestad, M.; Nordell, P.; Asplund, A.; Rehnstrom, M.; Jacobsson, S.; Holmgren, G.; Davidson, L.; Brolen, G.; Edsbagge, J.; Bjorquist, P.; Kuppers-Munther, B.; Andersson, T. B. Drug Metabolizing Enzyme and Transporter Protein Profiles of Hepatocytes Derived From Human Embryonic and Induced Pluripotent Stem Cells. *Biochem. Pharmacol.* **2013,** *86* (5), 691–702.
57. Medine, C. N.; Lucendo-Villarin, B.; Storck, C.; Wang, F.; Szkolnicka, D.; Khan, F.; Pernagallo, S.; Black, J. R.; Marriage, H. M.; Ross, J. A.; Bradley, M.; Iredale, J. P.; Flint, O.; Hay, D. C. Developing High-Fidelity Hepatotoxicity Models From Pluripotent Stem Cells. *Stem Cells Transl. Med.* **2013,** *2* (7), 505–509.
58. Holmgren, G.; Sjogren, A. K.; Barragan, I.; Sabirsh, A.; Sartipy, P.; Synnergren, J.; Bjorquist, P.; Ingelman-Sundberg, M.; Andersson, T. B.; Edsbagge, J. Long-Term Chronic Toxicity Testing Using Human Pluripotent Stem Cell-Derived Hepatocytes. *Drug Metab. Dispos.* **2014,** *42* (9), 1401–1406.
59. Sirenko, O.; Hesley, J.; Rusyn, I.; Cromwell, E. F. High-Content Assays for Hepatotoxicity Using Induced Pluripotent Stem Cell-Derived Cells. *Assay Drug Dev. Technol.* **2014,** *12* (1), 43–54.
60. Smith, C.; Abalde-Atristain, L.; He, C.; Brodsky, B. R.; Braunstein, E. M.; Chaudhari, P.; Jang, Y. Y.; Cheng, L.; Ye, Z. Efficient and Allele-Specific Genome Editing of Disease Loci in Human iPSCs. *Mol. Ther.* **2015,** *23* (3), 570–577.
61. Anson, B. D.; Kolaja, K. L.; Kamp, T. J. Opportunities for Use of Human iPS Cells in Predictive Toxicology. *Clin. Pharmacol. Ther.* **2011,** *89* (5), 754–758.
62. Dianat, N.; Steichen, C.; Vallier, L.; Weber, A.; Dubart-Kupperschmitt, A. Human Pluripotent Stem Cells for Modelling Human Liver Diseases and Cell Therapy. *Curr. Gene Ther.* **2013,** *13,* 120–132.
63. Aarli, J. A.; Janca, A.; Muscetta, A. *Neurological Disorders: Public Health Challenges;* World Health Organization: Geneva, 2006.
64. Breier, J. M.; Gassmann, K.; Kayser, R.; Stegeman, H.; De Groot, D.; Fritsche, E.; Shafer, T. J. Neural Progenitor Cells as Models for High-Throughput Screens of Developmental Neurotoxicity: State of the Science. *Neurotoxicol. Teratol.* **2010,** *32* (1), 4–15.
65. Yap, M. S.; Nathan, K. R.; Yeo, Y.; Lim, L. W.; Poh, C. L.; Richards, M.; Lim, W. L.; Othman, I.; Heng, B. C. Neural Differentiation of Human Pluripotent Stem Cells for Nontherapeutic Applications: Toxicology, Pharmacology, and in vitro Disease Modeling. *Stem Cells Int.* **2015,** *2015,* 105172.
66. Steffenhagen, C.; Kraus, S.; Dechant, F. X.; Kandasamy, M.; Lehner, B.; Poehler, A. M.; Furtner, T.; Siebzehnrubl, F. A.; Couillard-Despres, S.; Strauss, O.; Aigner, L.; Rivera, F. J. Identity, Fate and Potential of Cells Grown as Neurospheres: Species Matters. *Stem Cell Rev.* **2011,** *7* (4), 815–835.
67. NAU, H. Correlation of Transplacental and Maternal Pharmacokinetics of Retinoids During Organogenesis With Teratogenicity. *Methods Enzymol.* **1990,** *190,* 437–448.
68. Di Giorgio, F. P.; Carrasco, M. A.; Siao, M. C.; Maniatis, T.; Eggan, K. Non-Cell Autonomous Effect of Glia on Motor Neurons in an Embryonic Stem Cell-Based ALS Model. *Nat. Neurosci.* **2007,** *10* (5), 608–614.
69. Dimos, J. T.; Rodolfa, K. T.; Niakan, K. K.; Weisenthal, L. M.; Mitsumoto, H.; Chung, W.; Croft, G. F.; Saphier, G.; Leibel, R.; Goland, R.; Wichterle, H.; Henderson, C. E.; Eggan, K. Induced Pluripotent Stem Cells Generated From Patients With ALS Can Be Differentiated Into Motor Neurons. *Science* **2008,** *321,* 1218–1221.
70. Ebert, A. D.; Yu, J.; Rose, F. F., Jr.; Mattis, V. B.; Lorson, C. L.; Thomson, J. A.; Svendsen, C. N. Induced Pluripotent Stem Cells From a Spinal Muscular Atrophy Patient. *Nature* **2009,** *457* (7227), 277–280.
71. Israel, M. A.; Yuan, S. H.; Bardy, C.; Reyna, S. M.; Mu, Y.; Herrera, C.; Hefferan, M. P.; Van Gorp, S.; Nazor, K. L.; Boscolo, F. S.; Carson, C. T.; Laurent, L. C.; Marsala, M.; Gage, F. H.; Remes, A. M.; Koo, E. H.; Goldstein, L. S. Probing Sporadic and Familial Alzheimer's Disease Using Induced Pluripotent Stem Cells. *Nature* **2012,** *482* (7384), 216–220.
72. Hargus, G.; Cooper, O.; Deleidi, M.; Levy, A.; Lee, K.; Marlow, E.; Yow, A.; Soldner, F.; Hockemeyer, D.; Hallett, P. J.; Osborn, T.; Jaenisch, R.; Isacson, O. Differentiated Parkinson Patient-Derived Induced Pluripotent Stem Cells Grow in the Adult Rodent Brain and Reduce Motor Asymmetry in Parkinsonian Rats. *Proc. Natl. Acad. Sci. U. S. A.* **2010,** *107* (36), 15921–15926.
73. Hotta, A.; Cheung, A. Y.; Farra, N.; Vijayaragavan, K.; Seguin, C. A.; Draper, J. S.; Pasceri, P.; Maksakova, I. A.; Mager, D. L.; Rossant, J.; Bhatia, M.; Ellis, J. Isolation of Human iPS Cells Using EOS Lentiviral Vectors to Select for Pluripotency. *Nat. Methods* **2009,** *6* (5), 370–376.
74. Lemonnier, T.; Blanchard, S.; Toli, D.; Roy, E.; Bigou, S.; Froissart, R.; Rouvet, I.; Vitry, S.; Heard, J. M.; Bohl, D. Modeling Neuronal Defects Associated With a Lysosomal Disorder Using Patient-Derived Induced Pluripotent Stem Cells. *Hum. Mol. Genet.* **2011,** *20* (18), 3653–3666.
75. Brennand, K. J.; Simone, A.; Jou, J.; Gelboin-Burkhart, C.; Tran, N.; Sangar, S.; Li, Y.; Mu, Y.; Chen, G.; Yu, D.; McCarthy, S.; Sebat, J.; Gage, F. H. Modelling Schizophrenia Using Human Induced Pluripotent Stem Cells. *Nature* **2011,** *473* (7346), 221–225.
76. Llorens, J.; Li, A. A.; Ceccatelli, S.; Sunol, C. Strategies and Tools for Preventing Neurotoxicity: To Test, to Predict and How to Do It. *Neurotoxicology* **2012,** *33* (4), 796–804.
77. Moors, M.; Rockel, T. D.; Abel, J.; Cline, J. E.; Gassmann, K.; Schreiber, T.; Schuwald, J.; Weinmann, N.; Fritsche, E. Human Neurospheres as Three-Dimensional Cellular Systems for Developmental Neurotoxicity Testing. *Environ. Health Perspect.* **2009,** *117* (7), 1131–1138.
78. (a) Kola, I.; Landis, J. Can the Pharmaceutical Industry Reduce Attrition Rates? *Nat. Rev. Drug Discov.* **2004,** *3* (8), 711–716; (b) MacDonald, J. S.; Robertson, R. T. Toxicity Testing in the 21st Century: A View From the Pharmaceutical Industry. *Toxicol. Sci.* **2009,** *110* (1), 40–46.
79. Mandenius, C. F.; Steel, D.; Noor, F.; Meyer, T.; Heinzle, E.; Asp, J.; Arain, S.; Kraushaar, U.; Bremer, S.; Class, R.; Sartipy, P. Cardiotoxicity Testing Using Pluripotent Stem Cell-Derived Human Cardiomyocytes and State-of-the-Art Bioanalytics: A Review. *J. Appl. Toxicol.* **2011,** *31* (3), 191–205.
80. Gintant, G.; Sager, P. T.; Stockbridge, N. Evolution of Strategies to Improve Preclinical Cardiac Safety Testing. *Nat. Rev. Drug Discov.* **2016,** *15* (7), 457–471. http://dx.doi.org/10.1038/nrd.2015.34.
81. Khan, J. M.; Lyon, A. R.; Harding, S. E. The Case for Induced Pluripotent Stem Cell-Derived Cardiomyocytes in Pharmacological Screening. *Br. J. Pharmacol.* **2013,** *169* (2), 304–317.
82. (a) Mauritz, C.; Schwanke, K.; Reppel, M.; Neef, S.; Katsirntaki, K.; Maier, L. S.; Nguemo, F.; Menke, S.; Haustein, M.; Hescheler, J.; Hasenfuss, G.; Martin, U. Generation of Functional Murine Cardiac Myocytes From Induced Pluripotent Stem Cells. *Circulation* **2008,** *118* (5), 507–517; (b) Narazaki, G.; Uosaki, H.; Teranishi, M.; Okita, K.; Kim, B.; Matsuoka, S.; Yamanaka, S.; Yamashita, J. K. Directed and Systematic Differentiation of Cardiovascular Cells From Mouse Induced Pluripotent Stem Cells. *Circulation* **2008,** *118* (5), 498–506.
83. Zhang, J.; Wilson, G. F.; Soerens, A. G.; Koonce, C. H.; Yu, J.; Palecek, S. P.; Thomson, J. A.; Kamp, T. J. Functional Cardiomyocytes Derived From Human Induced Pluripotent Stem Cells. *Circ. Res.* **2009,** *104* (4), e30–e41.
84. Burridge, P. W.; Keller, G.; Gold, J. D.; Wu, J. C. Production of De Novo Cardiomyocytes: Human Pluripotent Stem Cell Differentiation and Direct Reprogramming. *Cell Stem Cell* **2012,** *10* (1), 16–28.
85. Birket, M. J.; Mummery, C. L. Pluripotent Stem Cell Derived Cardiovascular Progenitors—A Developmental Perspective. *Dev. Biol.* **2015,** *400* (2), 169–179.

86. Yokoo, N.; Baba, S.; Kaichi, S.; Niwa, A.; Mima, T.; Doi, H.; Yamanaka, S.; Nakahata, T.; Heike, T. The Effects of Cardioactive Drugs on Cardiomyocytes Derived From Human Induced Pluripotent Stem Cells. *Biochem. Biophys. Res. Commun.* **2009,** *387* (3), 482–488.
87. Bedada, F. B.; Wheelwright, M.; Metzger, J. M. Maturation Status of Sarcomere Structure and Function in Human iPSC-Derived Cardiac Myocytes. *Biochim. Biophys. Acta* **2015,** *1863,* 1829–1838.
88. Nakamura, Y.; Matsuo, J.; Miyamoto, N.; Ojima, A.; Ando, K.; Kanda, Y.; Sawada, K.; Sugiyama, A.; Sekino, Y. Assessment of Testing Methods for Drug-Induced Repolarization Delay and Arrhythmias in an iPS Cell-Derived Cardiomyocyte Sheet: Multi-Site Validation Study. *J. Pharmacol. Sci.* **2014,** *124* (4), 494–501.
89. (a) Wadhwa, D.; Fallah-Rad, N.; Grenier, D.; Krahn, M.; Fang, T.; Ahmadie, R.; Walker, J. R.; Lister, D.; Arora, R. C.; Barac, I.; Morris, A.; Jassal, D. S. Trastuzumab Mediated Cardiotoxicity in the Setting of Adjuvant Chemotherapy for Breast Cancer: A Retrospective Study. *Breast Cancer Res. Treat.* **2009,** *117* (2), 357–364; (b) Albini, A.; Pennesi, G.; Donatelli, F.; Cammarota, R.; De Flora, S.; Noonan, D. M. Cardiotoxicity of Anticancer Drugs: The Need for Cardio-Oncology and Cardio-Oncological Prevention. *J. Natl. Cancer Inst.* **2010,** *102* (1), 14–25.
90. 79 (a) Hirt, M. N.; Boeddinghaus, J.; Mitchell, A.; Schaaf, S.; Bornchen, C.; Muller, C.; Schulz, H.; Hubner, N.; Stenzig, J.; Stoehr, A.; Neuber, C.; Eder, A.; Luther, P. K.; Hansen, A.; Eschenhagen, T. Functional Improvement and Maturation of Rat and Human Engineered Heart Tissue by Chronic Electrical Stimulation. *J. Mol. Cell. Cardiol.* **2014,** *74,* 151–161; Vunjak Novakovic, G.; Eschenhagen, T.; Mummery, C. Myocardial Tissue Engineering: in vitro Models. *CSH Perspect Med J.* **2014,** *4* (3), a014076; (c) Tulloch, N. L.; Muskheli, V.; Razumova, M. V.; Korte, F. S.; Regnier, M.; Hauch, K. D.; Pabon, L.; Reinecke, H.; Murry, C. E. Growth of Engineered Human Myocardium With Mechanical Loading and Vascular Coculture. *Circ. Res.* **2011,** *109* (1), 47–59.
91. Kattman, S. J.; Witty, A. D.; Gagliardi, M.; Dubois, N. C.; Niapour, M.; Hotta, A.; Ellis, J.; Keller, G. Stage-Specific Optimization of Activin/Nodal and BMP Signaling Promotes Cardiac Differentiation of Mouse and Human Pluripotent Stem Cell Lines. *Cell Stem Cell* **2011,** *8* (2), 228–240.
92. Cao, N.; Liu, Z.; Chen, Z.; Wang, J.; Chen, T.; Zhao, X.; Ma, Y.; Qin, L.; Kang, J.; Wei, B.; Wang, L.; Jin, Y.; Yang, H. T. Ascorbic Acid Enhances the Cardiac Differentiation of Induced Pluripotent Stem Cells Through Promoting the Proliferation of Cardiac Progenitor Cells. *Cell Res.* **2012,** *22* (1), 219–236.
93. Minami, I.; Yamada, K.; Otsuji, T. G.; Yamamoto, T.; Shen, Y.; Otsuka, S.; Kadota, S.; Morone, N.; Barve, M.; Asai, Y.; Tenkova-Heuser, T.; Heuser, J. E.; Uesugi, M.; Aiba, K.; Nakatsuji, N. A Small Molecule That Promotes Cardiac Differentiation of Human Pluripotent Stem Cells Under Defined, Cytokine- and Xeno-Free Conditions. *Cell Rep.* **2012,** *2* (5), 1448–1460.
94. Xiaojun Lian, C. H.; Wilson, G.; Zhu, K.; Hazeltine, L. B.; Azarin, S. M.; Raval, K. K.; Zhang, J.; Kamp, T. J.; Palecek, S. P. Robust Cardiomyocyte Differentiation From Human Pluripotent Stem Cells via Temporal Modulation of Canonical Wnt Signaling. *Proc. Natl. Acad. Sci. U. S. A.* **2012,** *109* (27), E1848–E1857.
95. Gonzalez, R.; Lee, J. W.; Schultz, P. G. Stepwise Chemically Induced Cardiomyocyte Specification of Human Embryonic Stem Cells. *Angew. Chem. Int. Ed.* **2011,** *50* (47), 11181–11185.
96. Burridge, P. W.; Matsa, E.; Shukla, P.; Lin, Z. C.; Churko, J. M.; Ebert, A. D.; Lan, F.; Diecke, S.; Huber, B.; Mordwinkin, N. M.; Plews, J. R.; Abilez, O. J.; Cui, B.; Gold, J. D.; Wu, J. C. Chemically Defined Generation of Human Cardiomyocytes. *Nat. Methods* **2014,** *11* (8), 855–860.
97. Karakikes, I.; Senyei, G. D.; Hansen, J.; Kong, C. W.; Azeloglu, E. U.; Stillitano, F.; Lieu, D. K.; Wang, J.; Ren, L.; Hulot, J. S.; Iyengar, R.; Li, R. A.; Hajjar, R. J. Small Molecule-Mediated Directed Differentiation of Human Embryonic Stem Cells Toward Ventricular Cardiomyocytes. *Stem Cells Transl. Med.* **2014,** *3* (1), 18–31.
98. Kempf, H.; Olmer, R.; Kropp, C.; Ruckert, M.; Jara-Avaca, M.; Robles-Diaz, D.; Franke, A.; Elliott, D. A.; Wojciechowski, D.; Fischer, M.; Roa Lara, A.; Kensah, G.; Gruh, I.; Haverich, A.; Martin, U.; Zweigerdt, R. Controlling Expansion and Cardiomyogenic Differentiation of Human Pluripotent Stem Cells in Scalable Suspension Culture. *Stem Cell Rep.* **2014,** *3* (6), 1132–1146.
99. Fonoudi, H.; Ansari, H.; Abbasalizadeh, S.; Larijani, M. R.; Kiani, S.; Hashemizadeh, S.; Zarchi, A. S.; Bosman, A.; Blue, G. M.; Pahlavan, S.; Perry, M.; Orr, Y.; Mayorchak, Y.; Vandenberg, J.; Talkhabi, M.; Winlaw, D. S.; Harvey, R. P.; Aghdami, N.; Baharvand, H. A Universal and Robust Integrated Platform for the Scalable Production of Human Cardiomyocytes From Pluripotent Stem Cells. *Stem Cells Transl. Med.* **2015,** *4* (12), 1482–1494.
100. Zhang, M.; Schulte, J. S.; Heinick, A.; Piccini, I.; Rao, J.; Quaranta, R.; Zeuschner, D.; Malan, D.; Kim, K. P.; Ropke, A.; Sasse, P.; Arauzo-Bravo, M.; Seebohm, G.; Scholer, H.; Fabritz, L.; Kirchhof, P.; Muller, F. U.; Greber, B. Universal Cardiac Induction of Human Pluripotent Stem Cells in Two and Three-Dimensional Formats: Implications for in vitro Maturation. *Stem Cells* **2015,** *33* (5), 1456–1469.
101. Zhang, M.; D'Aniello, C.; Verkerk, A. O.; Wrobel, E.; Frank, S.; Ward-van Oostwaard, D.; Piccini, I.; Freund, C.; Rao, J.; Seebohm, G.; Atsma, D. E.; Schulze-Bahr, E.; Mummery, C. L.; Greber, B.; Bellin, M. Recessive Cardiac Phenotypes in Induced Pluripotent Stem Cell Models of Jervell and Lange-Nielsen Syndrome: Disease Mechanisms and Pharmacological Rescue. *Proc. Natl. Acad. Sci. U. S. A.* **2014,** *111* (50), E5383–E5392.
102. Malan, D.; Zhang, M.; Stallmeyer, B.; Muller, J.; Fleischmann, B. K.; Schulze-Bahr, E.; Sasse, P.; Greber, B. Human iPS Cell Model of Type 3 Long QT Syndrome Recapitulates Drug-Based Phenotype Correction. *Basic Res. Cardiol.* **2016,** *111* (2), 14.
103. Matsa, E.; Rajamohan, D.; Dick, E.; Young, L.; Mellor, I.; Staniforth, A.; Denning, C. Drug Evaluation in Cardiomyocytes Derived From Human Induced Pluripotent Stem Cells Carrying a Long QT Syndrome Type 2 Mutation. *Eur. Heart J.* **2011,** *32* (8), 952–962.
104. Willyard, C. The Boom in Mini Stomachs, Brains, Breasts, Kidneys and More. *Nature* **2015,** *523* (7562), 520–522.
105. Fatehullah, A.; Tan, S. H.; Barker, N. Organoids as an in vitro Model of Human Development and Disease. *Nat. Cell Biol.* **2016,** *18* (3), 246–254.
106. Yin, X.; Mead, B. E.; Safaee, H.; Langer, R.; Karp, J. M.; Levy, O. Engineering Stem Cell Organoids. *Cell Stem Cell* **2016,** *18* (1), 25–38.
107. Paul, E. C. A.; Hochman, J.; Quaroni, A. Conditionally Immortalized Intestinal Epithelial Cells: Novel Approach for Study of Differentiated Enterocytes. *Am. J. Physiol.* **1993,** 266–278.
108. Marx, V. Cell-Line Authentication Demystified. *Nat. Methods* **2014,** *11* (5), 483–488.
109. Masters, J. R.; Stacey, G. N. Changing Medium and Passaging Cell Lines. *Nat. Protoc.* **2007,** *2* (9), 2276–2284.
110. Randall, K. J.; Turton, J.; Foster, J. R. Explant Culture of Gastrointestinal Tissue: A Review of Methods and Applications. *Cell Biol. Toxicol.* **2011,** *27* (4), 267–284.
111. Shanks, N.; Greek, R.; Greek, J. Are Animal Models Predictive for Humans? *Philos. Ethics Humanit. Med.* **2009,** *4,* 2.
112. Takebe, T.; Enomura, M.; Yoshizawa, E.; Kimura, M.; Koike, H.; Ueno, Y.; Matsuzaki, T.; Yamazaki, T.; Toyohara, T.; Osafune, K.; Nakauchi, H.; Yoshikawa, H. Y.; Taniguchi, H. Vascularized and Complex Organ Buds From Diverse Tissues via Mesenchymal Cell-Driven Condensation. *Cell Stem Cell* **2015,** *16* (5), 556–565.
113. Sato, T.; Vries, R. G.; Snippert, H. J.; van de Wetering, M.; Barker, N.; Stange, D. E.; van Es, J. H.; Abo, A.; Kujala, P.; Peters, P. J.; Clevers, H. Single Lgr5 Stem Cells Build Crypt-Villus Structures in vitro Without a Mesenchymal Niche. *Nature* **2009,** *459* (7244), 262–265.
114. Hachitanda, Y.; Tsuneyoshi, M. Neuroblastoma With a Distinct Organoid Pattern. *Hum. Pathol.* **1994,** *25* (1), 67–72.
115. Zimmermann, W. H.; Melnychenko, I.; Eschenhagen, T. Engineered Heart Tissue for Regeneration of Diseased Hearts. *Biomaterials* **2004,** *25* (9), 1639–1647.
116. Lancaster, M. A.; Knoblich, J. A. Organogenesis in a Dish: Modeling Development and Disease Using Organoid Technologies. *Science* **2014,** *345* (6194), 1247125.
117. Weitzer, G. Embryonic Stem Cell-Derived Embryoid Bodies: An in vitro Model of Eutherian Pregastrulation Development and Early Gastrulation. *Handb. Exp. Pharmacol.* **2006,** *174,* 21–51.
118. Xu, C.; Inokuma, M. S.; Denham, J.; Golds, K.; Kundu, P.; Gold, J. D.; Carpenter, M. K. Feeder-Free Growth of Undifferentiated Human Embryonic Stem Cells. *Nat. Biotechnol.* **2001,** *19,* 971–974.
119. Vazin, T.; Schaffer, D. V. Engineering Strategies to Emulate the Stem Cell Niche. *Trends Biotechnol.* **2010,** *28* (3), 117–124.
120. Guvendiren, M.; Burdick, J. A. Stiffening Hydrogels to Probe Short- and Long-Term Cellular Responses to Dynamic Mechanics. *Nat. Commun.* **2012,** *3,* 792.
121. Atala, A.; Yoo, J. Bioprinting: 3D Printing Comes to Life. *Manuf. Eng.* **2015,** 63–66.
122. Stephan, M. T.; Irvine, D. J. Enhancing Cell Therapies From the Outside in: Cell Surface Engineering Using Synthetic Nanomaterials. *Nano Today* **2011,** *6* (3), 309–325.
123. Golden, A. P.; Tien, J. Fabrication of Microfluidic Hydrogels Using Molded Gelatin as a Sacrificial Element. *Lab Chip* **2007,** *7* (6), 720–725.

124. Visconti, R. P.; Kasyanov, V.; Gentile, C.; Zhang, J.; Markwald, R. R.; Mironov, V. Towards Organ Printing: Engineering an Intra-Organ Branched Vascular Tree. *Expert Opin. Biol. Ther.* **2010,** *10* (3), 409–420.
125. Purcell, O.; Lu, T. K. Synthetic Analog and Digital Circuits for Cellular Computation and Memory. *Curr. Opin. Biotechnol.* **2014,** *29,* 146–155.
126. Willyard, C. Rise of the Organoids. *Nature* **2015,** *523,* 520–522.
127. Luni, C.; Serena, E.; Elvassore, N. Human-on-Chip for Therapy Development and Fundamental Science. *Curr. Opin. Biotechnol.* **2014,** *25,* 45–50.
128. Takebe, T.; Sekine, K.; Enomura, M.; Koike, H.; Kimura, M.; Ogaeri, T.; Zhang, R. R.; Ueno, Y.; Zheng, Y. W.; Koike, N.; Aoyama, S.; Adachi, Y.; Taniguchi, H. Vascularized and Functional Human Liver From an iPSC-Derived Organ bud Transplant. *Nature* **2013,** *499* (7459), 481–484.
129. Dedhia, P. H.; Bertaux-Skeirik, N.; Zavros, Y.; Spence, J. R. Organoid Models of Human Gastrointestinal Development and Disease. *Gastroenterology* **2016,** *150,* 1098–1112.
130. Miyajima, A.; Tanaka, M.; Itoh, T. Stem/Progenitor Cells in Liver Development, Homeostasis, Regeneration, and Reprogramming. *Cell Stem Cell* **2014,** *14* (5), 561–574.
131. Sarada Devi Ramachandran, K. S.; Münst, B.; Heinz, S.; Ghafoory, S.; Wölfl, S.; Simon-Keller, K.; Marx, A.; Ionica Øie, C.; Ebert, M. P.; Walles, H.; Braspenning, J.; BreitkopfHeinlein, K. In Vitro Generation of Functional Liver Organoid-Like Structures Using Adult Human Cells. *PLoS One* **2015,** *10* (10), e0139345.
132. Gilbert, S. F. *Developmental Biology,* 6th ed.; Sinauer Associates: Sunderland, MA, 2000.
133. Lehtinen, M. K.; Walsh, C. A. Neurogenesis at the Brain-Cerebrospinal Fluid Interface. *Annu. Rev. Cell Dev. Biol.* **2011,** *27,* 653–679.
134. Lancaster, M. A.; Knoblich, J. A. Spindle Orientation in Mammalian Cerebral Cortical Development. *Curr. Opin. Neurobiol.* **2012,** *22* (5), 737–746.
135. Conti, L.; Cattaneo, E. Neural Stem Cell Systems: Physiological Players or in vitro Entities? *Nat. Rev. Neurosci.* **2010,** *11* (3), 176–187.
136. Reynolds, B. A.; Weiss, S. Generation of Neurons and Astrocytes From Isolated Cells of the Adult Mammalian Central Nervous System. *Science* **1992,** *255* (5052), 1707–1710.
137. Zhang, S. C.; Wernig, M.; Duncan, I. D.; Brustle, O.; Thomson, J. A. In Vitro Differentiation of Transplantable Neural Precursors From Human Embryonic Stem Cells. *Nat. Biotechnol.* **2001,** *19* (12), 1129–1133.
138. Elkabetz, Y.; Panagiotakos, G.; Al Shamy, G.; Socci, N. D.; Tabar, V.; Studer, L. Human ES Cell-Derived Neural Rosettes Reveal a Functionally Distinct Early Neural Stem Cell Stage. *Genes Dev.* **2008,** *22* (2), 152–165.
139. Gaspard, N.; Bouschet, T.; Hourez, R.; Dimidschstein, J.; Naeije, G.; van den Ameele, J.; Espuny-Camacho, I.; Herpoel, A.; Passante, L.; Schiffmann, S. N.; Gaillard, A.; Vanderhaeghen, P. An Intrinsic Mechanism of Corticogenesis From Embryonic Stem Cells. *Nature* **2008,** *455* (7211), 351–357.
140. Nakano, T.; Ando, S.; Takata, N.; Kawada, M.; Muguruma, K.; Sekiguchi, K.; Saito, K.; Yonemura, S.; Eiraku, M.; Sasai, Y. Self-Formation of Optic Cups and Storable Stratified Neural Retina From Human ESCs. *Cell Stem Cell* **2012,** *10* (6), 771–785.
141. Cyranoski, D. Tissue Engineering: The Brainmaker. *Nature* **2012,** *488* (7412), 444–446.
142. Spence, J. R.; Mayhew, C. N.; Rankin, S. A.; Kuhar, M. F.; Vallance, J. E.; Tolle, K.; Hoskins, E. E.; Kalinichenko, V. V.; Wells, S. I.; Zorn, A. M.; Shroyer, N. F.; Wells, J. M. Directed Differentiation of Human Pluripotent Stem Cells Into Intestinal Tissue In Vitro. *Nature* **2011,** *470* (7332), 105–109.
143. Lancaster, M. A.; Renner, M.; Martin, C. A.; Wenzel, D.; Bicknell, L. S.; Hurles, M. E.; Homfray, T.; Penninger, J. M.; Jackson, A. P.; Knoblich, J. A. Cerebral Organoids Model Human Brain Development and Microcephaly. *Nature* **2013,** *501* (7467), 373–379.
144. Humphreys, B. D. Kidney Structures Differentiated From Stem Cells. *Nat. Cell Biol.* **2014,** *16* (1), 19–21.
145. Lancaster, M. A.; Knoblich, J. A. Generation of Cerebral Organoids From Human Pluripotent Stem Cells. *Nat. Protoc.* **2014,** *9* (10), 2329–2340.
146. Belen, D. Cerebral Organoids Will Play an Essential Role in Understanding the Development of the Brain. *Turk. Neurosurg.* **2014,** *24* (5), 637–638.
147. Alrefai, M. T.; Murali, D.; Paul, A.; Ridwan, K. M.; Connell, J. M.; Shum-Tim, D. Cardiac Tissue Engineering and Regeneration Using Cell-Based Therapy. *Stem Cells Cloning* **2015,** *8,* 81–101.
148. Perez-Pomares, J. M.; de la Pompa, J. L. Signaling During Epicardium and Coronary Vessel Development. *Circ. Res.* **2011,** *109* (12), 1429–1442.
149. Tian, X.; Hu, T.; Zhang, H.; He, L.; Huang, X.; Liu, Q.; Yu, W.; Yang, Z.; Zhang, Z.; Zhong, T. P.; Yang, X.; Yan, Y.; Baldini, A.; Sun, Y.; Lu, J.; Schwartz, R. J.; Evans, S. M.; Gittenberger-de Groot, A. C.; Red-Horse, K.; Zhou, B. Subepicardial Endothelial Cells Invade the Embryonic Ventricle Wall to Form Coronary Arteries. *Cell Res.* **2013,** *23* (9), 1075–1090.
150. Cossette, S.; Misra, R. The Identification of Different Endothelial Cell Populations Within the Mouse Proepicardium. *Dev. Dyn.* **2011,** *240* (10), 2344–2353.
151. Tomanek, R. J. Formation of the Coronary Vasculature: A Brief Review. *Cardiovasc. Res.* **1996,** *31.* Spec No. E46-51.
152. Yang, L.; Soonpaa, M. H.; Adler, E. D.; Roepke, T. K.; Kattman, S. J.; Kennedy, M.; Henckaerts, E.; Bonham, K.; Abbott, G. W.; Linden, R. M.; Field, L. J.; Keller, G. M. Human Cardiovascular Progenitor Cells Develop From a KDR+ Embryonic-Stem-Cell-Derived Population. *Nature* **2008,** *453* (7194), 524–528.
153. Vunjak-Novakovic, G.; Tandon, N.; Godier, A.; Maidhof, R.; Marsano, A.; Martens, T. P.; Radisic, M. Challenges in Cardiac Tissue Engineering. *Tissue Eng. Part B Rev.* **2010,** *16* (2), 169–187.
154. Shimizu, T.; Sekine, H.; Yang, J.; Isoi, Y.; Yamato, M.; Kikuchi, A.; Kobayashi, E.; Okano, T. Polysurgery of Cell Sheet Grafts Overcomes Diffusion Limits to Produce Thick, Vascularized Myocardial Tissues. *Faseb J.* **2006,** *20* (6), 708–710.
155. Reddi, A. H.; Huggins, C. B. Influence of Geometry of Transplanted Tooth and Bone on Transformation of Fibroblasts. *Proc. Soc. Exp. Biol. Med.* **1973,** *143* (3), 634–637.
156. Lutolf, M. P.; Hubbell, J. A. Synthetic Biomaterials as Instructive Extracellular Microenvironments for Morphogenesis in Tissue Engineering. *Nat. Biotechnol.* **2005,** *23* (1), 47–55.
157. Leor, J.; Amsalem, Y.; Cohen, S. Cells, Scaffolds, and Molecules for Myocardial Tissue Engineering. *Pharmacol. Ther.* **2005,** *105* (2), 151–163.
158. Christman, K. L.; Lee, R. J. Biomaterials for the Treatment of Myocardial Infarction. *J. Am. Coll. Cardiol.* **2006,** *48* (5), 907–913.
159. Davis, M. E.; Hsieh, P. C.; Grodzinsky, A. J.; Lee, R. T. Custom Design of the Cardiac Microenvironment With Biomaterials. *Circ. Res.* **2005,** *97* (1), 8–15.
160. Huang, N. F.; Yu, J.; Sievers, R.; Li, S.; Lee, R. J. Injectable Biopolymers Enhance Angiogenesis After Myocardial Infarction. *Tissue Eng.* **2005,** *11* (11–12), 1860–1866.
161. Reffelmann, T.; Kloner, R. A. Cellular Cardiomyoplasty—Cardiomyocytes, Skeletal Myoblasts, or Stem Cells for Regenerating Myocardium and Treatment of Heart Failure? *Cardiovasc. Res.* **2003,** *58* (2), 358–368.
162. Henning, R. J.; Burgos, J. D.; Vasko, M.; Alvarado, F.; Sanberg, C. D.; Sanberg, P. R.; Morgan, M. B. Human Cord Blood Cells and Myocardial Infarction: Effect of Dose and Route of Administration on Infarct Size. *Cell Transplant.* **2007,** *16* (9), 907–917.
163. Fu, R. H.; Wang, Y. C.; Liu, S. P.; Shih, T. R.; Lin, H. L.; Chen, Y. M.; Sung, J. H.; Lu, C. H.; Wei, J. R.; Wang, Z. W.; Huang, S. J.; Tsai, C. H.; Shyu, W. C.; Lin, S. Z. Decellularization and Recellularization Technologies in Tissue Engineering. *Cell Transplant.* **2014,** *23* (4–5), 621–630.
164. Guyette, J. P.; Gilpin, S. E.; Charest, J. M.; Tapias, L. F.; Ren, X.; Ott, H. C. Perfusion Decellularization of Whole Organs. *Nat. Protoc.* **2014,** *9* (6), 1451–1468.
165. Venkatasubramanian, R. T.; Grassl, E. D.; Barocas, V. H.; Lafontaine, D.; Bischof, J. C. Effects of Freezing and Cryopreservation on the Mechanical Properties of Arteries. *Ann. Biomed. Eng.* **2006,** *34* (5), 823–832.
166. Nuwaysir, E. F.; Bittner, M.; Trent, J.; Barrett, J. C.; Afshari, C. A. Microarrays and Toxicology: The Advent of Toxicogenomics. *Mol. Carcinog.* **1999,** *24* (3), 153–159.
167. Afshari, C. A.; Hamadeh, H. K.; Bushel, P. R. The Evolution of Bioinformatics in Toxicology: Advancing Toxicogenomics. *Toxicol. Sci.* **2011,** *120* (Suppl 1), S225–S237.
168. Chen, M.; Zhang, M.; Borlak, J.; Tong, W. A Decade of Toxicogenomic Research and Its Contribution to Toxicological Science. *Toxicol. Sci.* **2012,** *130* (2), 217–228.
169. McBurney, R. N.; Hines, W. M.; VonTungeln, L. S.; Schnackenberg, L. K.; Beger, R. D.; Moland, C. L.; Han, T.; Fuscoe, J. C.; Chang, C. W.; Chen, J. J.; Su, Z.; Fan, X. H.; Tong, W.; Booth, S. A.; Balasubramanian, R.; Courchesne, P. L.; Campbell, J. M.; Graber, A.; Guo, Y.; Juhasz, P.; Li, T. Y.; Lynch, M. D.; Morel, N. M.; Plasterer, T. N.; Takach, E. J.; Zeng, C.; Beland, F. A. The Liver Toxicity Biomarker Study Phase I: Markers for the Effects of Tolcapone or Entacapone. *Toxicol. Pathol.* **2012,** *40* (6), 951–964.
170. Ellinger-Ziegelbauer, H.; Gmuender, H.; Bandenburg, A.; Ahr, H. J. Prediction of a Carcinogenic Potential of Rat Hepatocarcinogens Using Toxicogenomics Analysis of Short-Term in vivo Studies. *Mutat. Res.* **2008,** *637* (1–2), 23–39.
171. Igarashi, Y.; Nakatsu, N.; Yamashita, T.; Ono, A.; Ohno, Y.; Urushidani, T.; Yamada, H. Open TG-GATEs: A Large-Scale Toxicogenomics Database. *Nucleic Acids Res.* **2015,** *43* (Database issue), D921–D927.

172. Gerets, H. H.; Tilmant, K.; Gerin, B.; Chanteux, H.; Depelchin, B. O.; Dhalluin, S.; Atienzar, F. A. Characterization of Primary Human Hepatocytes, HepG2 Cells, and HepaRG Cells at the mRNA Level and CYP Activity in Response to Inducers and Their Predictivity for the Detection of Human Hepatotoxins. *Cell Biol. Toxicol.* **2012,** *28* (2), 69–87.
173. Berger, D. R.; Ware, B. R.; Davidson, M. D.; Allsup, S. R.; Khetani, S. R. Enhancing the Functional Maturity of Induced Pluripotent Stem Cell-Derived Human Hepatocytes by Controlled Presentation of Cell–Cell Interactions In Vitro. *Hepatology* **2015,** *61* (4), 1370–1381.
174. Hossini, A. M.; Megges, M.; Prigione, A.; Lichtner, B.; Toliat, M. R.; Wruck, W.; Schroter, F.; Nuernberg, P.; Kroll, H.; Makrantonaki, E.; Zouboulis, C. C.; Adjaye, J. Induced Pluripotent Stem Cell-Derived Neuronal Cells From a Sporadic Alzheimer's Disease Donor as a Model for Investigating AD-Associated Gene Regulatory Networks. *BMC Genomics* **2015,** *16,* 84.
175. Bessems, J.; Coeckey, S.; Gouliarmou, V.; Whelan, M.; Worth, A. *EURL ECVAM Strategy for Achieving 3Rs Impact in the Assessment of Toxicokinetics and Systemic Toxicity;* Publications Office: Luxembourg, 2015.
176. Russell, W. M. S.; Burch, R. L. *The Principles of Humane Experimental Technique;* Methuen: London, 1959. (Reprinted by UFAW, 1992: 8 Hamilton Close, South Mimms, Potters Bar, Herts EN6 3QD England.
177. Hofer, T.; Gerner, I.; Gundert-Remy, U.; Liebsch, M.; Schulte, A.; Spielmann, H.; Vogel, R.; Wettig, K. Animal Testing and Alternative Approaches for the Human Health Risk Assessment Under the Proposed new European Chemicals Regulation. *Arch. Toxicol.* **2004,** *78* (10), 549–564.
178. Wruck, W.; Peuker, M.; Regenbrecht, C. R. Data Management Strategies for Multinational Large-Scale Systems Biology Projects. *Brief. Bioinform.* **2014,** *15* (1), 65–78.
179. Pelkonen, O.; Tolonen, A.; Rousu, T.; Tursas, L.; Turpeinen, M.; Hokkanen, J.; Uusitalo, J.; Bouvier d'Yvoire, M.; Coecke, S. Comparison of Metabolic Stability and Metabolite Identification of 55 ECVAM/ICCVAM Validation Compounds Between Human and Rat Liver Homogenates and Microsomes—A Preliminary Analysis. *Altex* **2009,** *26* (3), 214–222.
180. Greek, R.; Menache, A. Systematic Reviews of Animal Models: Methodology Versus Epistemology. *Int. J. Med. Sci.* **2013,** *10* (3), 206–221.
181. Saker, B. M.; Kincaid-Smith, P. Papillary Necrosis in Experimental Analgesic Nephropathy. *Br. Med. J.* **1969,** *1* (5637), 161–162.
182. Gupta, U.; Cook, J. C.; Tassinari, M. S.; Hurtt, M. E. Comparison of Developmental Toxicology of Aspirin (Acetylsalicylic Acid) in Rats Using Selected Dosing Paradigms. *Birth Defects Res. B Dev. Reprod. Toxicol.* **2003,** *68* (1), 27–37.
183. Lave, L. B.; Rosenkranz, H. S.; Omenn, G. S. Information Value of the Rodent Bioassay. *Nature* **1988,** *336* (6200), 631–633.
184. Krewski, D.; Acosta, D., Jr.; Andersen, M.; Anderson, H.; Bailar, J. C., 3rd; Boekelheide, K.; Brent, R.; Charnley, G.; Cheung, V. G.; Green, S., Jr.; Kelsey, K. T.; Kerkvliet, N. I.; Li, A. A.; McCray, L.; Meyer, O.; Patterson, R. D.; Pennie, W.; Scala, R. A.; Solomon, G. M.; Stephens, M.; Yager, J.; Zeise, L. Toxicity Testing in the 21st Century: A Vision and a Strategy. *J. Toxicol. Environ. Health B Crit. Rev.* **2010,** *13* (2–4), 51–138.
185. Organisation for Economic Co-operation and Development. Test No. 427 skin absorption: in vivo method.
186. Organisation for Economic Co-operation and Development. Test no. 417: toxicokinetics.
187. Organisation for Economic Co-operation and Development. Skin absorption In vitro method.

4.11 Genetic Toxicology

Sudheer Beedanagari, Alkermes Inc., Waltham, MA, United States

© 2017 Elsevier Ltd. All rights reserved.
The views expressed in this article are those of the author's and does not necessarily reflect the views of author's work organization.

4.11.1	**Introduction**	195
4.11.2	**Genetic Damage (Genotoxicity) Detection Methods**	196
4.11.2.1	In Silico Approaches	196
4.11.2.2	In Vitro and In Vivo Assays for Genotoxicity Evaluation	197
4.11.2.2.1	Ames assay	197
4.11.2.2.2	Micronucleus assay	198
4.11.2.2.3	Chromosomal aberrations assay	199
4.11.2.2.4	Comet assay	199
4.11.2.2.5	Mouse lymphoma assay	201
4.11.2.2.6	Pig-a assay	201
4.11.2.2.7	Toxicogenomic signatures	201
4.11.3	**Genotoxicity Testing Paradigm in Pharmaceutical Industry**	202
4.11.4	**Concluding Remarks**	202
References		202
Further Reading		203

4.11.1 Introduction

Genetic toxicology is a subspecialty of toxicology that studies the effects of chemical and physical agents, on genetic material or deoxyribonucleic acid (DNA) causing alteration(s) in the structural integrity of the genome. Genetic damage is a natural phenomenon occurring endogenously in the cells as a result of oxidative respiration and metabolism, but this damage is continuously being repaired by a variety of DNA repair processes present in all cells. However, when the genetic damage becomes overwhelming for the cellular machinery to handle, it accumulates genetic lesions that could lead to a wide variety of adverse outcomes, including apoptosis or cell death, altered cell division or proliferation, DNA replication and mutagenesis which may result in carcinogenesis. Carcinogenesis is a multistep process but broadly defined as a three-step process, tumor initiation, promotion, and progression. DNA damage plays an important role in the initiation step of carcinogenesis, where a carcinogen or its activated metabolite covalently binds to DNA forming a DNA adduct, which may be repaired or following cell division may be fixed as a mutation leading to a heritable alteration in the DNA sequence. The field of genetic toxicology uses a wide array of in silico, in vitro, and in vivo assays to measure the DNA damage that can be caused by a wide range of endogenous and exogenous agents including but not limited to biological and chemical agents.

Genetic toxicology encompasses the study of a wide variety of DNA damage endpoints, including but not limited to mutagenicity, clastogenicity, and aneugenicity. Mutagenicity refers to the ability of an agent to alter the nucleotide sequence of DNA. Mutations are categorized as base-pair substitutions, frameshifts, additions, and deletions of nucleotide base(s) or chromosomes. Mutations are heritable and hence may pose a permanent or long lasting adverse effect on the health of an organism. Although, mutations naturally arise during evolution or DNA replication, most of them occur in areas of DNA that do not exert any harmful effects to organism and are referred to as silent mutations. However, if mutations occur in the coding regions (e.g., genes) or in the noncoding (e.g., regulatory regions of genes), then it may lead to adverse effects due to altered gene expression patterns, or formation of nonfunctional or altered proteins and enzymes, thus impacting the functional activities of the cells.

Clastogenicity and aneugenicity describe a type of DNA damage characterized by structural or numerical alterations to chromosomes. The DNA damage can be either chromosomal, affecting both sister chromatids of a chromosome, or of chromatid, involving only one of the two sister chromatids. Different types of DNA damages are accumulated due to clastogenicity, including insertions, deletions, translocations, inversions, and chromatid aberrations. Aneugenicity refers to the numerical changes to the number of chromosomes, resulting in polyploidy or monosomy or trisomy conditions. Aneugenicity occurs due to errors in chromosomal segregation, altered tubulin polymerization, and spindle apparatus instability. Aneugenic DNA damage is considered indirect DNA damage or secondary DNA damage, unlike clastogenicity which is considered direct DNA damage.

A wide variety of in silico, in vitro, and in vivo assays are used to predict the three common types of genotoxic damages, mutagenicity, clastogenicity, and aneugenicity. In vitro assays in general are designed to achieve high sensitivity in detecting DNA damage caused by chemicals or agents. High sensitivity of these in vitro assays often leads to decreased specificity in predicting the carcinogenic potential of chemicals. In vivo genotoxic assays on the other hand have high specificity but tend to exhibit low sensitivity in predicting the carcinogenic potential of chemicals. Therefore, to increase the specificity and sensitivity of detecting DNA damage,

Table 1 List of OECD guidelines for the genotoxicity assays discussed in this book article

OECD test number	*Genetic toxicology assay*
Test no. 471	Bacterial reverse mutation test
Test no. 487	In vitro mammalian cell micronucleus test
Test no. 474	Mammalian erythrocyte (in vivo) micronucleus test
Test no. 473	In vitro mammalian chromosome aberration test
Test no. 475	Mammalian bone marrow chromosome aberration test
Test no. 489	In vivo mammalian alkaline comet assay
Test no. 490	In vitro gene mutation assay using the TK locus

Table 2 Databases with genotoxicity and carcinogenicity information

Database name, information and link
ACToR (www.epa.gov/actor)
Aggregates toxicity data from 500 public sources on over 500,000 environmental chemicals
CPCD (Carcinogenicity Potency Database) (http://potency.berkely.edu/cpdb.html)
Contains information on carcinogenicity studies on 1547 chemicals
NTP (http://ntp.niehs.gov)
Contains data on subchronic, chronic, in vitro and in vivo genotoxicity assays, and carcinogenicity studies.
TOXNET (http://toxnet.nlm.nih.gov)
Contains mutagenicity, genotoxicity, carcinogenicity and tumor inhibition, and promotion tests results of over 9000 chemicals
ToxRefDB (http://www.epa.gov/ncct/toxrefdb)
Includes subchronic, chronic carcinogenicity, reproductive, and developmental studies
Tox Benchmark (http://ml.cs.tu-berlin.de/toxbenchmark/)
Ames mutagenicity dataset for 6500 chemicals
PharmaPendium (www.pharmapendium.com)
It offers searchable Food and Drug Administration (FDA) and European Medical Agency (EMA) approval packages with excerpted preclinical, clinical, and postmarketing safety data into a single longitudinal database
VITIC (www.lhasalimited.org/vitic_nexus)
Vitic (pronounced V-eye-tick) Nexus is a chemically intelligent database, emphasizing useful in (Quantitative) Structure-Activity Relationship (QSAR) modelling
SciFinder (www.cas.org/products/scifinder)

a combination of in vitro and in vivo genotoxicity assays is used, commonly referred to as "battery approach," for predicting the rodent bioassay outcomes, considered as a gold standard assay to predict human carcinogenicity potential of a test article. The use of a genotoxic battery approach has been proven to have high sensitivity and specificity (~85%–90%).[1]

The main emphasis of this article has been placed on providing a general overview of how genetic toxicology (genotoxicity) assessment is performed on chemical agents across diverse biological, chemical, and pharmaceutical industries. It is beyond the scope of this article to discuss in detail the guidelines on how to conduct the genotoxicity assays discussed as part of this article. Comprehensive details on the conduct of commonly used genetic toxicology assays can be reviewed by accessing the Organization for Economic Co-operation and Development (OECD) guidelines (www.oecd.org). OECD guidelines for the genetoxicity assays discussed in this book article are listed in **Table 1**. In addition, resources/websites where genotoxicity/carcinogenicity data can be found are listed in **Table 2**.

4.11.2 Genetic Damage (Genotoxicity) Detection Methods

4.11.2.1 In Silico Approaches

As indicated earlier and discussed next in this article, there are several in vitro and in vivo genotoxicity testing assays that are available to aid in identifying genotoxic damage. However, the global call for reduced animal usage with emphasis on 3Rs (Reduce, Refine, and Replace) and to phase out animal testing has led to the rapid expansion and evolution in a myriad of in vitro and in silico genetic toxicology screening assays. The objective of in silico screening techniques is to apply mathematical, statistical, chemical, and computational tools to the existing genetic toxicology data from the literature and to develop efficient and effective genotoxicity predictive models. These predictive models can be used to screen large numbers of untested new chemicals to predict their genotoxic potential. In silico genotoxicity screening methods offer a fast, reliable, and economical solution for preliminary screening of large numbers of chemicals. The crux of in silico models has its roots in structure activity relationship (SAR). The earliest examples of SAR were the Ashby–Tennant alerts, which associated certain chemical structures with mutation, based on the expert

knowledge and experience of these scientists. Others have continued to expand the list of structural alerts associated with DNA reactivity based on known chemical reactivity and expert knowledge. Later, an alternative approach was used based on quantifying structure activity relationships (QSARs) using statistical correlation and quantum chemical properties. QSAR models use linear free energy relationships to describe reaction rates and equilibrium. There are a wide variety of in silico tools that have been packaged into software programs capable of predicting a variety of genotoxic endpoints, but the best validated are models predicting bacterial mutagenicity endpoint. These in silico tools can be divided into three main categories: databases, virtual screening programs, and prediction systems.

The primary step in in silico assessment of a chemical is to perform a search in public databases to determine if any genotoxicity data exists for the chemical under investigation. The databases collect and store genotoxicity data obtained from multiple sources including published literature, public data sources, and proprietary in-house historical data from within a testing laboratory obtained over the years of conducting genotoxicity testing. The databases are either open to public use free of cost or available commercially, where the users pay service charges to access them. Examples of free databases are Toxicology Data Network (TOXNET), Aggregated Computational Toxicology Resource (ACToR) of EPA (http://www.epa.gov/actor/), National Toxicology Program (NTP), Carcinogenic Potency Database (CPDB), etc. (**Table 2**). Examples of commercial databases include Pharmapendium, SciFinder, STN, etc. There are some tools that serve the dual purpose of a database and prediction system. Examples include deductive estimation of risk from existing knowledge (DEREK), VITIC, Leadscope, etc.

Prediction systems are software programs that enable us to make prediction on species and assay-specific endpoints such as in vivo mouse micronucleus test, in vitro chromosome aberration test, mouse lymphoma assay, in vitro micronucleus in several species. These software programs use different types of algorithms to compute the propensity of a specific chemical to induce genotoxicity. The algorithms for these systems can be divided into three main categories—knowledge-based, statistical methods, and read-across systems. Knowledge-based predictive systems focus on organizing relevant experimental genotoxicity data as knowledge guidelines or rules in a computer program. The in silico software compares the structure of the chemical of interest/investigation with the chemicals in the knowledge library of the database. For example, one of the widely used commercial knowledge-based predictive systems is DEREK version 14 which comprises 82 rules or alerts for mutagenicity. The DEREK rules are written and maintained by experts from the nonprofit organization LHASA limited (www.lhasalimited.org).

A structural fragment statistically related to the biological activity is called as a biophore. Biophores of known genotoxic chemical(s) are compared in databases through biological activity or QSAR modeling. For example, the presence of the N−N═O (nitrosamine) fragment is strongly statistically correlated with mutagenicity of both aromatic and aliphatic chemicals. Biophores or structure moieties that are related to toxic or therapeutic endpoints are referred to as "toxicophore" and "pharmacophore," respectively. If a biophore is present, then the software predicts the chemical as active, and if no biophore is found the software predicts the chemical as inactive.[2,3] Based on the distribution of a biophore and its correlation to toxicity the statistical systems give a statistical value or predictive value of the biophore. For example, if the database contains 50 nitrosamines, and all of these are active, then the presence of the N−N═O biophore is a very strong predictor of toxicity. On the other hand, if only half of the nitrosamines in the ;database are active and half are inactive, then the confidence that chemicals containing N−N═O are active will be only 50%. The term "structural alert" has also been applied in computational toxicology, meaning a chemical moiety that serves as an indicator of toxic outcome.[2,3] The two widely used commercial statistically fragment based in silico systems are Leadscope (www.leadescope.com), whose QSAR models were developed by Informatics and Computational Safety Analysis Staff of Food and Drug Administration, and MultiCASE (www.multicase.com), whose QSAR models were based on proprietary statistical algorithms developed by Klopman.[4] There are also several free open source statistically fragment based in silico predicting software such as ToxTree (www.opentox.org/toxicity-prediction), Bioclipse-DS (www.bioclipse.net), etc. In read-across systems, the endpoint result of one chemical is used to predict the endpoint of a structurally similar chemical. The QSAR toolbox (www.oecd.org/toolbox) and AIM (Analog Identification Method) (www.epa.gov/oppt/sf/tools/aim.html) are examples of in silico tools that can be used to find structurally similar chemicals.

Although the in silico systems provide an economical, faster, and easy screening of large set of chemicals, they are far from replacement of in vitro and in vivo genetic toxicology screening assays, due to lack of strong correlation between the in silico prediction and experimental outcomes. However, currently, they serve as great tools for early genetic toxicology screening of chemicals, impurities, and degradants.

4.11.2.2 In Vitro and In Vivo Assays for Genotoxicity Evaluation

4.11.2.2.1 Ames assay

Ames assay is an in vitro bacterial assay, that measures bacterial revertant colony formation, named after Bruce Ames who first identified and reported the utility of this assay in detecting mutations in 1974.[5] In the Ames assay, auxotrophic bacteria that require the amino acid histidine for growth are treated with test chemical or vehicle or positive control on an agar plate consisting of growth media that lack histadine. Therefore, only bacteria that have reverted back to wild type histidine locus are now capable of growth and form colonies. Increased numbers of revertant colonies in test chemical treated plates compared to concurrent untreated or vehicle control plates are an indication of the mutagenic potential of the test chemical. A series of genetically modified *Salmonella typhimurium* and *Escherichia coli* bacterial strains were created to be used in Ames assay that are capable of detecting frameshift or base pair substitution mutations.

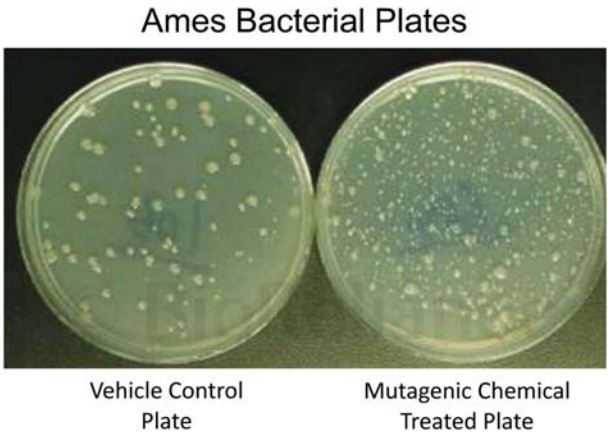

Fig. 1 Ames assay plates showing the increase revertant colony formation in mutagenic chemical treated plated relative to vehicle control plates. Images courtesy of James Wojciechowski and Andrew Henwood, Bristol Myers Squibb, NJ, USA.

It is a well known fact that mutations in the DNA sequence may trigger a cascade of reactions that may adversely impact cellular events such as replication, transcription, or translation and may eventually result in apoptosis (cell death). Mutations can be classified into two main types: inherited and acquired. Inherited mutations occur as a result of passage of the mutated DNA from the parent cell to the daughter cell. Acquired mutations occur as a result of DNA damage due to environmental agents such as nuclear radiation, UV exposure, chemical exposure (exogenous or endogenous), errors during the DNA replication or transcription process. Elegant repair mechanisms exist to revert DNA damage caused by various mutagens and to repair errors that occur during replication or transcription; however, these repair mechanisms have their limitations and are not able to sufficiently restore the damage that is caused by potent mutagens. During cell division, when an acquired mutation is passed on from the parent cell to the daughter cell, it becomes an inherited mutation. Gene mutation refers to changes that affect a single or multiple genes. These mutations may occur as a result of deletion of a nitrogenous base(s), insertion of nitrogenous base(s), or substitution of nitrogenous base(s).

Ames assay is the most commonly used assay to predict mutagenic potential of a test compound across several scientific disciplines and industries. The Ames assay is so widely used because, historically those chemicals shown to be positive in the Ames assay have also been shown to be positive in the in vivo rodent bioassay (~65% concordance), used to measure carcinogenic potential of a test chemical and is considered as a gold standard assay to predict human carcinogenic potential of a chemical by health regulatory authorities globally (Kirkland and Ardema, 2005). Ames assay is commonly carried out using several bacterial strains. The *S. typhimurium* strains detect base-pair substitution and frameshift mutations at GC base pairs, while *E. coli* strains damage at AT base pairs. These strains are genetically manipulated to increase their sensitivity to detect mutation frequency. A list of commonly used Ames bacterial strains and detailed assay guidelines can be obtained in OECD test 471 guideline (OECD 471, 1997).[6] Bacteria like several other rodent or human cell lines lack or have limited metabolic activation potential; thus Ames assay is almost always carried out with and without exogenous metabolic activation, usually in the presence of induced rat liver S9 fraction (Fig. 1)

4.11.2.2.2 Micronucleus assay

A micronucleus (MN) is often a broken chromosome fragment or rarely an entire chromosome that remains outside the nucleus after cell division. A MN may be formed following direct DNA damage (clastogenic mechanism) or following secondary interaction with DNA replication apparatus (indirect aneugenic mechanism). During anaphase stage of cell division process, acentric DNA fragments formed due to DNA damage may not be incorporated into the nucleus. Hence, chromosome fragments result in the formation of MN after telophase and cytokinesis stages of cell division. Micronuclei formed can be of various sizes but typically varies from 1/10th to 1/100th the size of original nucleus. Increased incidence of micronuclei formation serves as a good biomarker for genotoxic damage. MN assay can be performed either in vitro or in vivo. Micronuclei in peripheral human blood samples have been used to adjust doses of chemotherapy agents (Fig. 2).

The formation of MN can be readily measured in both in vitro in different cell types (in vitro MN assay) and in vivo samples (in vivo MN assay) including peripheral blood, bone marrow, and tissues of rodents and other species using MN assay. Although in principle the in vitro MN assay can be performed in any cell type (primary or immortalized cells), the most commonly used cell types are Chinese hamster ovary (CHO) strain -K1 and -WBL cells, Chinese hamster V79 lung epithelial cells, and L5178Y mouse lymphoma cells, TK6 human lymphoblastoid cells, and primary human lymphocytes. The in vitro MN assay is typically carried out with and without exogenous metabolic activation. For the in vivo MN assay, bone marrow or peripheral blood samples from rodents treated with multiple doses of test compound, vehicle, and appropriate positive control are analyzed for the formation of MN. Cell division (one mitosis) is required for the formation of micronuclei, and use of cytochalasin B (CytoB) blocks the cells in binucleated stage with micronuclei, hence this is called cytochalasin-blocked MN assay. Cells treated with CytoB undergo karyokinesis but not cytokinesis, resulting in binucleated cells, so by evaluating only binucleated cells only those cells which have

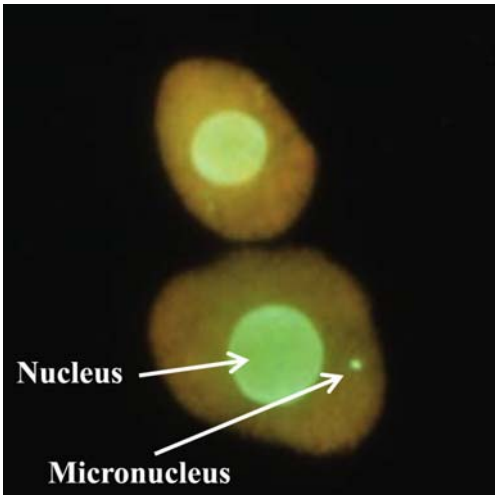

Fig. 2 Image showing the micronuclei formation in hepatocytes. Images courtesy of Rie Takashima, Mitsubishi Chemical Medience Corporation, Japan.

undergone one cell replication are evaluated. MN formation can be either due to a clastogenic and/or an aneugenic DNA damaging event. However, MN formed by clastogens lacks centromeres, while those micronuclei resulting from loss of an entire chromatid or chromosome (aneugenic event) contain a centromere. Hence, by centromere staining using various methods, such as fluorescence in situ hybridization (FISH) or other immunofluorescence methods, one can determine if micronuclei are a result of clastogenic or aneugenic events.[7–9] Although, yet debated, the size of MN can also serve as an indicator of an aneugenic or a clastogenic event, the size of MN formed due to aneugenic events is generally larger than those resulting from a clastogenic event.[10] Advanced and high-throughput MN detection technologies, such as flow cytometry and imaging-based technologies, make this a popular biomarker to measure genotoxic damage. More details on the conduct, analysis, and interpretation of in vitro and in vivo MN assays can be obtained in the OECD guidelines (OECD Test 474, 2012; OECD Test 487, 2010).[11–14]

4.11.2.2.3 Chromosomal aberrations assay

One of the traditional and direct cytogenetic methods to detect genotoxic damage is based on a direct observation of the changes in the chromosomes after exposure to a chemical insult in cell populations under a microscope. Chromosomal aberrations (CA) can be measured by the CA assay and are commonly used in both clinical and nonclinical settings. Different types of CA are accumulated due to genotoxic damage such as insertions, deletions, translocations, endoreduplication, poliploidy, chromatid aberrations, chromosomal gain, and chromosomal loss. Depending on the relative abundance of a particular type of CA in comparison with other types of aberrations occurred due to treatment with a chemical, it is possible to understand the mechanism of action of test chemical, for example abnormal number of chromosomes suggests aneuploidy, rather than clastogenicity. While numerical changes can be observed in the CA assay, the MN assay is far more sensitive to chemicals inducing this type of DNA damage. CA studies can be carried out in both in vitro and in vivo test models. In vitro CA studies may be conducted with primary or immortalized cells, but regardless of cell used all require addition of exogenous S9 liver metabolic fraction to enable detection of chemicals requiring metabolism to the ultimate genotoxicant. For in vivo CA studies bone marrow or peripheral blood samples from rodents are commonly used (**Fig. 3**).

CAs are usually studied in cell populations at metaphase stage of the cell division because chromosomes are condensed and damaged and can be easily visualized at this stage. The cell populations can be arrested in metaphase by treatment with chemicals such as colcemid. Similar to MN detection, in principle the CA assay can be performed in any cell type. However, CHO cells are most commonly used in the in vitro studies because of large size of chromosomes, fewer chromosomal numbers, stable and well-defined karyotype, and relatively shorter cell division interval. Although detection of CA assay is a direct subjective method of measuring genotoxicity levels, it is not amenable to automation and requires skilled cytogeneticists to analyze and score the CA. Invention of new technologies, such as FISH and chromosome painting, allows scientists to identify CA with relative ease and also to determine insertions and translocations more precisely which is not possible with traditional CA assay. More details on the conduct, analysis, and interpretation of the CA assay data can be inferred from Ref. 15.

4.11.2.2.4 Comet assay

Comet assay or single cell gel electrophoresis (SCGE) assay detects single or double strand breaks measured at the individual cell level. Unlike the other assays described above, the comet assay measures transient genetic damage that is not a permanent change or alteration to the DNA. The single or double strand breaks can be repaired by cellular machinery; hence, the comet assessments need

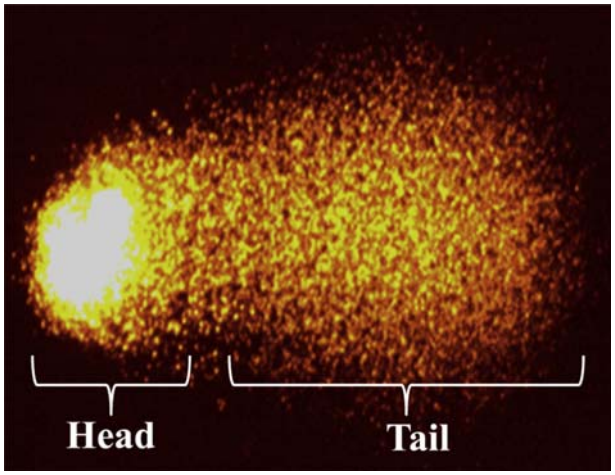

Fig. 3 Image showing the comet formation comprising of head (undamaged DNA) and tail (damaged DNA).

to be performed generally within 3–4 h after the exposure to a chemical agent. The comet assay can be conducted in vitro using single cells from immortalized cell lines or in vivo for any tissue that can be dispersed to a single cell suspension.

At the molecular level, the formation of comet in the DNA of cells upon genotoxic insult can be visualized through the method of gel electrophoresis and indicates DNA strand breaks, as the damaged DNA migrates at a different rate than nondamaged DNA during electrophoresis. In the comet assay, when damaged DNA containing single cell suspension embedded in low melting agarose is electrophoresed, the damaged DNA migrates away from undamaged DNA containing nucleoid body, resembling the structure of a "comet," hence the name comet assay. In the comet structure the undamaged DNA nucleoid part is referred to as "head" and the trailing damaged DNA streak is referred to as "tail." The percentage of DNA in the tail is directly proportional to the percentage of DNA damage that has occurred in a particular cell. Thus by counting a representative sample of ~100–300 cells per tissue it is possible to arrive at the average percentage of DNA damage accumulated in a particular tissue due to genotoxic stress. The comet assay is also referred to as SCGE assay. This assay was first developed by Ostling and Johansson in 1984, which was later revised by Singh et al. in 1988. With the advent of recent technological innovations such as fluorescent DNA stains and automated comet scoring for analysis, comet assay has emerged as a popular assay to detect DNA damage (Fig. 4).

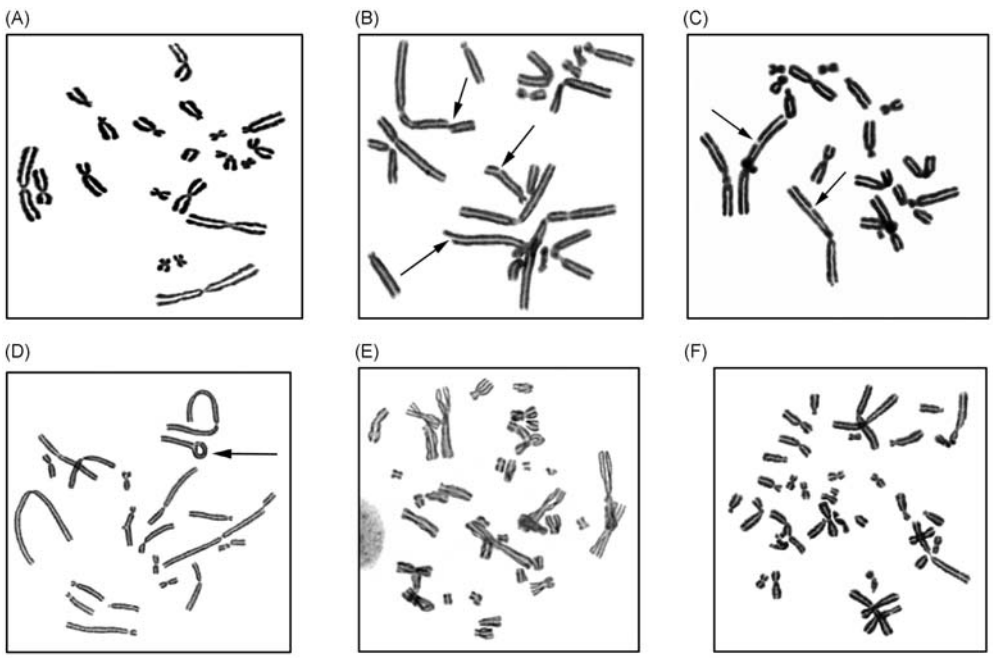

Fig. 4 Images showing different chromosomal aberrations in CHO cells normal (A), chromatid breaks (B), chromatid gaps (C), chromosome intra-change (D), endoreduplication (E), and polyploidy (F). Images courtesy of James Wojciechowski and Louis Nimzroff, Bristol Myers Squibb, NJ, USA.

The in vitro comet assay can be performed in any rodent, human cancer cell lines and human lymphocytes. It is typically carried out with and without exogenous metabolic activation, usually by supplementing with induced rat liver S9 fraction as indicated in other assays detailed earlier in this article. Although in principle any tissue can be used for in vivo comet assay analysis, high blood circulating organs such as liver, kidney, spleen are the target organ tissues that are analyzed. Also, if the route of administration is oral, then the site of contact or exposed tissue such as stomach mucosal cells is commonly used for comet analyses. More details on the conduct, analysis, and interpretation of the comet assay data can be inferred from Refs. 16–18.

4.11.2.2.5 Mouse lymphoma assay

The mouse lymphoma can be used to detect mutations and clastogenicity. The mouse lymphoma test utilizes a forward mutation assay in the heterozygous thyamidine kinase (tk+/−) locus in mammalian cell lines to determine the mutagenicity of chemicals. In this assay, L5178Y cells that acquire inactivating mutations of the wild type tk allele become resistant to triflurothymidine induced toxicity that are measured by determining cloning efficiency on soft agar. The increased mutant frequency from exposure to chemicals can be directly proportional to the mutagenic potential.

Cells in suspension or monolayer culture are exposed to the test substance, both with and without metabolic activation, for a suitable period of time and subcultured to determine cytotoxicity and to allow phenotypic expression prior to mutant selection. The treated cultures are maintained in growth medium for a sufficient period of time, characteristic of each selected locus and cell type, to allow near-optimal phenotypic expression of induced mutations. Mutant frequency is determined by seeding known numbers of cells in medium containing the selective agent to detect mutant cells, and in medium without selective agent to determine the cloning efficiency (viability). After a suitable incubation time, colonies are counted. The mutant frequency is derived from the number of mutant colonies in selective medium and the number of colonies in nonselective medium. This assay is able to detect mutagenicity (point and frameshift mutations evidenced by large colonies) and small deletions (small colonies) that involve the tk locus, either directly or through metabolic activation by S9 liver microsomes.

4.11.2.2.6 Pig-a assay

The Pig-a assay is a relatively new assay for measuring in vivo gene mutation in blood cells from humans, rats, mice, and monkeys. The *Pig-a* (phosphatidylinositol glycan, Class A) gene codes for a catalytic subunit of the *N*-acetylglucosamine transferase complex involved in an early step of glycosylphosphatidyl inositol (GPI) cell surface anchor synthesis. *Pig-a* is the only gene involved in GPI anchor synthesis that is on the X-chromosome, and research into the origins of an acquired genetic disease involving GPI anchor deficiency (paroxysmal nocturnal hemoglobinuria) indicates that cells lacking GPI anchors, or GPI-anchored cell surface proteins, almost always have mutations in the *Pig-a* gene.

This test detects mutations at the Pig-a gene that cause failure of "GPI anchors." Without these anchors, specific markers on the exterior of cells will not be present. This assay measures the frequency of cells without these surface markers, also known as "Pig-a mutant cells." Single-step forward mutations result in the loss of the GPI anchors and the surface marker phenotype, and these neutral mutations can be detected early in immature red blood cells (reticulocytes) by flow cytometry. Although the assay can be performed in vitro, it is commonly used as an in vivo follow up assay, to evaluate the positive mutagenicity findings from an in vitro bacterial Ames assay or similar assay. Although there exists no OECD guideline at this time for this assay there is sufficient literature available with well-defined principles and guidelines to conduct the assay in a scientifically sound manner. This assay can be used to support the approved regulatory assays to determine the mutagenicity potential of a chemical under investigation, based on weight-of-evidence approach.

4.11.2.2.7 Toxicogenomic signatures

Toxicogenomic studies in relation to genetic toxicology utilize the comprehensive gene expression data to identify gene expression signatures that strongly correlate with genetic toxicity. The use of these approaches has a long history and only in the past decade due to rapid development in gene expression technologies such as microarrays, real time PCR, RNA sequencing, and other bioinformatics tools the field of toxicogenomics has emerged as an area that may have immense potential for genotoxicity testing. In toxicogenomics studies, changes in gene expression patterns in response to genotoxic stress are most commonly studied but changes in protein expression or metabolite formation can also be investigated. In addition, toxicogenomics approaches have potential to overcome some of the limitations posed by traditional genotoxicity testing approaches such as use of limited number of animals especially when changes in a limited set of genes are being investigated. Also, toxicogenomics approaches are easily amenable for high-throughput and high-content screening than traditional methods, thus aiding in reducing the costs associated with genetic toxicity screening and risk assessment.

Several investigators to date have reported different toxicogenomic signatures both in vitro using rodent and human cancer cell lines and in vivo in rodent models, to predict carcinogenicity in rodents and/or in humans.[19–21] Although toxicogenomic signatures have been proposed to differentiate genotoxins versus nongenotoxins, aneugens versus clastogens, carcinogens versus noncarcinogens, genotoxic carcinogens versus nongenotoxic carcinogens, etc., there exists no general consensus on their usage in genetic toxicology testing. This is primarily because of diverse test models, gene expression analysis, and bioinformatics technologies used to arrive at these toxicogenomic signatures, independently by different groups. To address these challenges genetic toxicologists across industry, academia, and government are forming consortia (e.g., HESI Genomics Technical Committee, Safety Prediction Consortia) to identify and validate unique toxicogenomic signatures that can be utilized for identifying different classes of genotoxins, hazard identification, and risk assessment.

4.11.3 Genotoxicity Testing Paradigm in Pharmaceutical Industry

Genotoxicity testing in pharmaceutical industry follows ICH guidelines S2R1 that were revised in 2012 (www.fda.gov/downloads/Drugs/Guidances/ucm074931.pdf). The revised guideline provides two different options for genotoxicity evaluation of chemicals/drugs under investigation. These options follow a "battery" approach using multiple in vitro and in vivo tests capable of characterizing genotoxicity hazard of chemicals/drugs. The first option takes a tiered approach with a series of in vitro followed by in vivo genotoxicity evaluation assays. However, the second option takes a less tiered approach by using primarily in vivo genotoxicity evaluation assays in rodents, in addition to in vitro Ames mutagenicity test. The details of both options are listed below

Option 1

(a) A test for gene mutation in bacteria (Ames assay).
(b) A cytogenetic test for chromosomal damage (the in vitro metaphase chromosome aberration test or in vitro micronucleus test) or an in vitro mouse lymphoma tk gene mutation assay
(c) An in vivo test for genotoxicity, generally a test for chromosomal damage using rodent hematopoietic cells, either for micronuclei or for CAs in metaphase cells.

Option 2

(a) A test for gene mutation in bacteria (Ames assay).
(b) An in vivo assessment of genotoxicity with two different tissues, usually an assay for micronuclei using rodent hematopoietic cells and a second in vivo assay. Typically, this would be a DNA strand breakage assay in liver (Comet assay), unless otherwise justified.

Under both standard battery options, either acute or repeat-dose study designs in vivo can be used. In case of repeated administrations, attempts should be made to incorporate the genotoxicity endpoints into toxicity studies, if scientifically justified. When more than one endpoint is evaluated in vivo, it is preferable that they are incorporated into a single study. Often sufficient information on the likely suitability of the doses for the repeat-dose toxicology study is available before the study begins and can be used to determine whether an acute or an integrated test would be suitable.

For compounds that give negative results, the completion of either option of the standard test battery, performed and evaluated in accordance with current recommendations, will usually provide sufficient assurance of the absence of genotoxic activity and no additional tests are warranted. Compounds that give positive results in the standard test battery might, depending on their therapeutic use, need to be tested more extensively.

4.11.4 Concluding Remarks

Screening for genotoxic damage using a "battery" approach that includes in silico, in vitro, and in vivo screening assays is an important part of pharmaceuticals and chemical safety testing across wide range of industries. Existing genotoxic battery testing that investigates and monitors biomarkers of genotoxic damage, such as increased bacterial revertant colonies, MN formation, comet formation, and CAs, is of tremendous help in genotoxic hazard identification and risk assessment. However, currently there are no sensitive and specific short-term in vitro or in vivo assays to evaluate carcinogenicity of chemicals caused via nongenotoxic or epigenetic mechanisms. The 2-year in vivo rodent bioassay that is used currently to evaluate carcinogenicity of chemicals is extremely time-consuming and cost prohibitive for screening a plethora of potential genotoxic chemicals. In this regard, cutting edge technologies such as toxicogenomics, high-content imaging, FISH and high-throughput approaches, such as Next-Generation or NextGen Sequencing (NGS) technologies, would be valuable to gain insights into genotoxic, nongenotoxic, and epigenetic mechanisms that play an important role in carcinogenesis.

References

1. Kirkland, D.; Aardema, M.; Henderson, L.; Müller, L. Evaluation of the Ability of a Battery of Three In Vitro Genotoxicity Tests to Discriminate Rodent Carcinogens and Non-Carcinogens I. Sensitivity, Specificity and Relative Predictivity. *Mutat. Res.* **2005,** *584* (1–2), 1–256.
2. Klopman, G.; Frierson, M. R.; Rosenkranz, H. S. Computer Analysis of Toxicological Data Bases: Mutagenicity of Aromatic Amines in Salmonella Tester Strains. *Environ. Mutagen.* **1985,** *7* (5), 625–644.
3. Rosenkranz, H. S.; Klopman, G. Structural Basis of Carcinogenicity in Rodents of Genotoxicants and Non-Genotoxicants. *Mutat Res.* **1990,** *228* (2), 105–124.
4. Klopman, G.; Rosenkranz, H. S. Structural Requirements for the Mutagenicity of Environmental Nitroarenes. *Mutat. Res.* **1984,** *126* (3), 227–238.
5. Ames, B. N. A Combined Bacterial and Liver Test System for Detection and Classification of Carcinogens as Mutagens. *Genetics* **1974,** *78,* 91–95.
6. Mortelmans, K.; Zeiger, E. The Ames Salmonella/Microsome Mutagenicity Assay. *Mutat. Res.* **2000,** *455,* 29–60.
7. Degrassi, F.; Tanzarella, C. Immunofluorescent Staining of Kinetochores in Micronuclei: A New Assay for the Detection of Aneuploidy. *Mutat. Res.* **1988,** *203* (5), 339–345.
8. De Stoppelaar, J. M.; de Roos, B.; Mohn, G. R.; Hoebee, B. Analysis of DES-Induced Micronuclei in Binucleated Rat Fibroblasts: Comparison Between FISH With a Rat Satellite I Probe and Immunocytochemical Staining With CREST Serum. *Mutat. Res.* **1997,** *392,* 139–149.
9. Miller, B. M.; Adler, I. D. Application of Antikinetochore Antibody Staining (CREST Staining) to Micronuclei in Erythrocytes Induced In Vivo. *Mutagenesis* **1990,** *5,* 411–415.
10. Hashimoto, K.; Nakajima, Y.; Matsumura, S.; Chatani, F. An In Vitro Micronucleus Assay With Size-Classified Micronucleus Counting to Discriminate Aneugens from Clastogens. *Toxicol. In Vitro* **2010,** *24* (1), 208–216.

11. Hayashi, M.; MacGregor, J. T.; Gatehouse, D. G.; Adler, I. D.; Blakey, D. H.; Dertinger, S. D.; Krishna, G.; Morita, T.; Russo, A.; Sutou, S. In Vivo Rodent Erythrocyte Micronucleus Assay II. Some Aspects of Protocol Design Including Repeated Treatments, Integration With Toxicity Testing and Automated Scoring. *Environ. Mol. Mutagen.* **2000,** *35,* 234–252.
12. Kirsch-Volders, M.; Sofuni, T.; Aardema, M.; Albertini, S.; Eastmond, D.; Fenech, M.; Ishidate, M., Jr.; Kirchner, S.; Lorge, E.; Morita, T.; Norppa, H.; Surrallés, J.; Vanhauwaert, A.; Wakata, A. Report From the In Vitro Micronucleus Assay Working Group. *Mutat. Res.* **2003,** *540,* 153–163.
13. Krishna, M.; Hayashi, M. In Vivo Rodent Micronucleus Assay: Protocol, Conduct and Data Interpretation. *Mutat. Res.* **2000,** *455,* 155–166.
14. Lorge, E.; Thybaud, V.; Aardema, M.; Oliver, J.; Wakata, A.; Lorenzon, G.; Marzin, D. SFTG International Collaborative Study on In Vitro Micronucleus Test. I. General Conditions and Overall Conclusions of the Study. *Mutat. Res.* **2006,** *607,* 13–36.
15. Bignold, L. P. Mechanisms of Clastogen-Induced Chromosomal Aberrations: A Critical Review and Description of a Model Based on Failures of Tethering of DNA Strand Ends to Strand-Breaking Enzymes. *Mutat. Res. Rev. Mutat. Res.* **2009,** *681,* 271–298.
16. Azqueta, A.; Gutzkow, K. B.; Brunborg, G.; Collins, A. R. Towards a More Reliable Comet Assay: Optimising Agarose Concentration, Unwinding Time and Electrophoresis Conditions. *Mutat. Res.* **2011,** *724* (1–2), 41–45.
17. Burlinson, B. The In Vitro and In Vivo Comet Assays. *Methods Mol. Biol.* **2012,** *817,* 143–163.
18. Tice, R. R.; Agurell, E.; Anderson, D.; Burlinson, B.; Hartmann, A.; Kobayashi, H.; Miyamae, Y.; Rojas, E.; Ryu, J. C.; Sasaki, Y. F. Single Cell Gel/Comet Assay: Guidelines for In Vitro and In Vivo Genetic Toxicology Testing. *Environ. Mol. Mutagen.* **2000,** *35* (3), 206–221.
19. Ellinger-Ziegelbauer, H.; Fostel, J. M.; Aruga, C.; Bauer, D.; Boitier, E.; Deng, S.; Dickinson, D.; Le Fevre, A.; Fornace, A. J., Jr.; Grenet, O.; Gu, Y.; Hoflack, J.; Shiiyama, M.; Smith, R.; Snyder, R. D.; Spire, C.; Tanaka, G.; Aubrecht, J. Characterization and Interlaboratory Comparison of a Gene Expression Signature for Differentiating Genotoxic Mechanisms. *Toxicol. Sci.* **2009,** *110* (2), 341–352.
20. Fielden, M. R.; Adai, A.; Dunn, R. T.; Olaharski, A.; Searfoss, G.; Sina, J.; Aubrecht, J.; Boitier, E.; Nioi, P.; Auerbach, S.; Jacobson-Kram, D.; Raghavan, N.; Yang, Y.; Kincaid, A.; Sherlock, J.; Chen, S. J.; Car, B.; Predictive Safety Testing Consortium, Carcinogenicity Working Group. Development and Evaluation of a Genomic Signature for the Prediction and Mechanistic Assessment of Nongenotoxic Hepatocarcinogens in the Rat. *Toxicol. Sci.* **2011,** *124* (1), 54–74.
21. Thybaud, V.; Le Fevre, A. C.; Boiter, E. Application of Toxicogenomics to Genetic Toxicology Risk Assessment. *Environ. Mol. Mutagen.* **2007,** *48,* 369–379.

Further Reading

Miller, M. C.; Mohrenweiser, H. W.; Bell, D. A. Genetic Variability in Susceptibility and Response to Toxicants. *Toxicol. Lett.* **2001,** *120,* 269–280.
Weiseburger, J. H.; Williams, G. M. Carcinogen Testing: Current Problems and New Approaches. *Science* **1981,** *214,* 401–407.

4.12 Drug-Induced Liver Disease

AK Daly, Newcastle University, Newcastle upon Tyne, United Kingdom

© 2017 Elsevier Ltd. All rights reserved.

4.12.1	**Introduction**	204
4.12.2	**Clinical Aspects of DILI**	205
4.12.2.1	Structure and Function of the Liver	205
4.12.2.2	Phenotypes in DILI	205
4.12.3	**Detecting Hepatotoxicity During Drug Development**	205
4.12.3.1	Animal Models	205
4.12.3.2	Cell Culture	205
4.12.3.3	In Silico Approaches	206
4.12.4	**DILI in Patients Including Patient-Specific Risk Factors**	206
4.12.4.1	The Nature of DILI	206
4.12.4.1.1	Concentration-dependent DILI	206
4.12.4.1.2	Idiosyncratic DILI	207
4.12.4.1.3	Nongenetic Risk Factors for DILI	208
4.12.4.1.4	Age	208
4.12.4.1.5	Gender	208
4.12.4.1.6	Preexisting liver disease	208
4.12.4.1.7	Smoking and alcohol consumption	209
4.12.4.1.8	Infection	209
4.12.4.1.9	Drug–drug interactions	209
4.12.4.2	Genetic Factors Affecting DILI Due to Specific Drugs	210
4.12.4.2.1	Introduction	210
4.12.4.2.2	HLA associations	210
4.12.4.2.3	Non-HLA associations	211
4.12.5	**Conclusions**	213
References		214

4.12.1 Introduction

This article will provide an overview of drug-induced liver toxicity. Drug-induced liver injury (DILI) and drug hepatotoxicity generally are important issues both for those developing drugs and for those prescribing them. Following absorption, the liver is one of the first sites exposed to ingested xenobiotics and this may result in a variety of types of local damage. Because of the role of the liver in xenobiotic metabolism, toxicity may also result from metabolites, even if the parent compound is nontoxic.

Therapeutically valuable drugs are often toxic to the liver. During the drug development process, hepatotoxicity of a new compound may be detected at a number of different points. If the toxicity is detected in animal toxicology studies during preclinical development, this will usually lead to the development project being abandoned. Approximately 80% of project closures during the preclinical development stage are for safety reasons, including hepatotoxicity.[1] Sometimes, compounds showing hepatotoxicity at high doses in animals may still be taken forward if the risk–benefit ratio is considered favorable. If hepatotoxicity is detected either during preclinical studies or early in clinical development, it is likely to be a concentration-dependent event. A good example of such predictable toxicity is that seen in acetaminophen overdose which is discussed in more detail in Section "**Concentration-dependent DILI**." Unfortunately many drugs cause a different, more complex form of hepatotoxicity which is unlikely to be detected during phases 1 to 3 because it is rare and less concentration-dependent. This form of hepatotoxicity, which is usually referred to as idiosyncratic DILI, is much more difficult to detect during drug development. There are a number of recent examples of drugs withdrawn from the market due to causing idiosyncratic DILI such as troglitazone (Section "**Troglitazone**"). Though most patients who develop idiosyncratic DILI recover well following drug withdrawal, it is estimated that up to 10% of patients with drug-induced hepatitis, one form of idiosyncratic DILI (see Section "**Phenotypes in DILI**"), may develop potentially fatal acute liver failure (ALF).[2] Between 11% and 13% of all ALF cases in the United States and United Kingdom may be due to idiosyncratic DILI.[3] Despite some high profile market withdrawals in recent years, many drugs that occasionally cause idiosyncratic DILI remain on the market with appropriate warnings to the prescriber. Some specific drug examples will be discussed in Section "**Idiosyncratic DILI**."

Developing improved strategies to prevent idiosyncratic DILI by detecting drugs with a propensity to cause this toxicity early in development is an important priority. Understanding genetic risk factors so that individuals at risk of developing this toxicity can be identified prior to prescription is also a potentially useful approach, especially in preventing the removal of otherwise valuable drugs from the market. Both these issues will be discussed in more detail in this article.

4.12.2 Clinical Aspects of DILI

4.12.2.1 Structure and Function of the Liver

The liver has a large number of vital functions, including normal metabolism of dietary components, synthesis, and storage of vitamins, production of bile but also the metabolism of foreign compounds to promote their excretion. Many hepatic functions are carried out by the most abundant cell type, the hepatocyte, but a number of other cell types contribute to the various functions including endothelial cells which form specialized vessels transporting blood and bile, macrophage-like Kupfer cells which help protect the liver from pathogens, and stellate cells which store vitamin A and can differentiate to form fibroblasts. During drug metabolism, levels of the drug within the hepatocyte may be considerably higher than plasma levels, increasing the risk of local damage from hepatotoxic compounds.

4.12.2.2 Phenotypes in DILI

Hepatotoxic drugs can damage the liver via several different mechanisms. Generally there is a distinctive pattern of damage seen with individual drugs. As described in detail elsewhere,[4] typically the drug will cause one or more of the following: hepatocyte necrosis, hepatitis where inflammation occurs, cholestasis where the normal flow of bile through the bile duct is impaired, or steatosis where lipid accumulates. Idiosyncratic DILI generally involves hepatitis and/or cholestasis.[4] Necrosis is more common when the toxicity is directly concentration-dependent (e.g., in acetaminophen toxicity). Steatosis can also be induced by a number of relatively commonly prescribed drugs such as methotrexate and tamoxifen but is generally a more benign condition than drug-induced hepatitis or cholestasis. As mentioned in Section "**Introduction**," up to 13% of patients suffering from drug-induced hepatitis (also known as hepatocellular DILI) may progress to ALF. Drug-induced cholestasis is rarely fatal but may result occasionally in chronic liver disease.

Diagnosis of DILI is not straightforward but relies on a combination of measuring liver enzymes, physical symptoms, and drug history. The most important liver enzymes used as markers are the transaminases, especially alanine transaminase (ALT) but also aspartate transaminase. These enzymes are released into the circulatory system when hepatocellular damage (including necrosis) occurs. For cholestatic injury, increased plasma levels of the enzyme alkaline phosphatase indicate damage to the biliary tree rather than the hepatocyte. Elevated plasma bilirubin levels are also associated with cholestatic injury but also occur in hepatocellular injury, especially when this is severe. Liver biopsy provides valuable phenotypic data including, for example, the presence of inflammatory cells or damage to the biliary tree. For research studies and clinical trials, scoring systems to assess the probability that symptoms of liver disease are due to drug exposure have been developed. This is discussed in detail elsewhere.[5]

4.12.3 Detecting Hepatotoxicity During Drug Development

4.12.3.1 Animal Models

As discussed elsewhere,[6] preclinical animal toxicology studies normally involve administering the drug to at least two species (one rodent, one nonrodent) at a range of doses for multiple durations, including chronic administration for typically 6 months in rodents and 12 months in nonrodents. These studies do not always predict human hepatotoxicity, especially when it is immune-mediated.[6] If hepatotoxicity is seen at very high doses in animal models, this does not necessarily predict that the compound will be hepatotoxic in humans. However, further in vitro studies are likely to be required for the development to continue. Issues such as the intended patient population and planned dose in humans may determine suitability to proceed to clinical testing.

Increasingly, there is the possibility to use "humanized" animals for drug safety testing. Up to the present, most of the advances have involved development of human-chimeric mice including mice where human hepatocytes have replaced the normal mouse liver.[7] The development of such animals is very valuable for many aspects of drug development but for complete assessment of potential for hepatotoxicity, it seems likely that an immune system more similar to the human system will also be required.

4.12.3.2 Cell Culture

A variety of cell culture systems are in use to investigate the hepatotoxic potential of new drugs. The most widely used, at least up to recently, has been the human hepatoblastoma cell line HepG2. These cells are relatively easy to culture and have hepatocyte-like features. Some recent studies have evaluated the effect of a relatively large number of hepatotoxic drugs on a range of parameters such as cytotoxicity, mitochondrial function, and oxidative stress in HepG2 cells to evaluate the suitability of using these cells to screen for hepatotoxic potential of new drugs.[8] Most known hepatotoxic drugs appeared positive for several of the parameters evaluated, though a few well-established causes of hepatotoxicity did not. Overall these cells appear to show sensitivities and specificities for detection of hepatotoxicity of up to 90% providing a range of different screening tests are used. Cultured human hepatocytes are more difficult to source and have a limited lifespan. They are less suitable for high-throughput screening than HepG2 but have the advantage of retaining high levels of expression of cytochromes P450 and other drug-metabolizing enzymes. They also respond more strongly to enzyme inducers such as rifampicin and phenobarbital. Another more recently isolated human cell line, HepaRG, is being increasingly used to assess hepatotoxicity.[9] This cell line has a phenotype more comparable to that of

primary human hepatocytes than HepG2 but also has the ability to form cholangiocytes, the specialized cells lining the biliary tract. It may be possible to adapt the screening tests already developed for HepG2 cells for use in HepaRG cells and this could increase the overall sensitivity of cell-based systems in detected hepatotoxicity. There are also now improved methods for human hepatocyte culture available involving coculture with other cells (mainly fibroblasts) that may lead to improved sensitivity for detecting hepatotoxic compounds.[10] In general, none of the cell culture systems currently available to detect hepatotoxicity are completely specific, but intensive efforts are underway to improve this situation because of the importance of identifying drugs that cause DILI at an early stage in the development process.

4.12.3.3 In Silico Approaches

Using computer-based approaches to predict whether a newly developed drug will cause hepatotoxicity is attractive, especially in view of the limitations of both animal and in vitro screening discussed in Sections "**Animal Models**" and "**Cell Culture**." This approach often depends on establishing quantitative structure–activity relationships where a mathematical model to link a chemical structure with some aspect of a compounds biology is developed and is described in more detail elsewhere.[11] However, other in silico approaches may simply be based on data mining. Using any in silico approach to predict idiosyncratic hepatotoxicity remains challenging because the underlying mechanisms for the toxicity are still not completely clear, there is involvement of an immune response in many cases of DILI and though a relatively large number of compounds are now known to cause hepatotoxicity, data is still relatively scarce. The difficulties of developing an in silico model for DILI have been well summarized recently.[12] That article also mentions that interindividual variation due to genetic and environmental factors should be considered in any model. Current ability to do this is limited though there is increasing collection of both biological samples and clinical data which may facilitate this in the future.[13]

4.12.4 DILI in Patients Including Patient-Specific Risk Factors

4.12.4.1 The Nature of DILI

4.12.4.1.1 Concentration-dependent DILI

As mentioned previously, some forms of DILI are directly concentration-dependent. The classic example is DILI relating to acetaminophen overdose. This form of DILI may result in ALF; it is now well accepted that acetaminophen overdose is a common cause of ALF, representing approximately 45% of all ALF cases in the United States in several surveys, though DILI relating to other drugs may also sometimes progress to ALF and represents 11% of all ALF cases in a recent large study.[3b] The quantity of acetaminophen ingested for toxicity to occur in an adult is considered to be a minimum of 10–15 g[14] compared with the normal maximum recommended total daily dose of 4 g. The precise level of overdose which will lead to DILI may vary between patients, but a plasma acetaminophen level of 150 ug mL^{-1} 4 h after the overdose is generally considered the minimum level where treatment with *N*-acetylcysteine to replenish cellular glutathione and prevent DILI is initiated. Toxicity arises due to metabolism to the reactive imine *N*-acetyl-p-benzoquinone imine (NAPQI) by cytochromes P450 (**Fig. 1**). This compound binds to macromolecules including

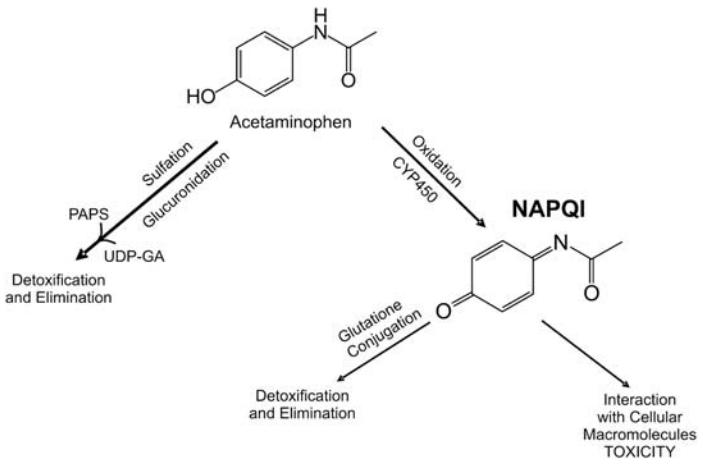

Fig. 1 Acetaminophen metabolism. Acetaminophen is metabolized by glucuronide, sulfate, and glutathione conjugation. Glucuronidation and sulfation produce nontoxic metabolites. *N*-acetyl-p-benzoquinoneimine (NAPQI) is a toxic intermediate produced by cytochrome P450-mediated oxidation. NAPQI can be conjugated by glutathione to form a nontoxic metabolite or may interact with cellular macromolecules triggering toxicity. From Moyer, A. M.; Fridley, B. L.; Jenkins, G. D.; Batzler, A. J.; Pelleymounter, L. L.; Kalari, K. R.; Ji, Y.; Chai, Y.; Nordgren, K. K.; Weinshilboum, R. M., Acetaminophen-NAPQI Hepatotoxicity: A Cell Line Model System Genome-Wide Association Study. *Toxicol. Sci.* **2011,** *120*(1), 33–41, Reproduced with permission from Oxford University Press.

protein, lipid, and DNA in hepatocytes. The formation of NAPQI adducts and cellular depletion of GSH trigger a still poorly understood sequence of events which result in cellular necrosis. Importantly, these events all occur very shortly after the overdose is taken with symptoms of liver injury including raised a large elevation in ALT evident between 24 and 72 h following drug ingestion. Though there is some limited evidence to suggest a role for genetic factors in susceptibility to acetaminophen-induced liver injury (see Section "**Acetaminophen**"), it is generally considered that all individuals are at high risk if sufficient drug is ingested. It is also generally accepted that DILI does not occur when acetaminophen is taken in accordance with dosing guidelines. However, approximately 40% of healthy adults receiving 4 g acetaminophen per day over a 14-day period were found to show moderately elevated ALT levels in excess of three times above upper limit of normal.[15] This rise was seen after 3 days of drug treatment, but ALT levels returned to normal in all participants within 14 days of the end of the 14-day treatment period. The elevated ALT observed here would normally be considered clinically important, especially during drug development. It was suggested that it may be an example of adaptation where the elevation resolves spontaneously even if drug treatment continues, but this has not yet been shown conclusively.[15]

4.12.4.1.2 Idiosyncratic DILI

Most cases of human DILI are of an idiosyncratic nature which is not predictable on the basis of plasma drug concentration. However, this does not mean that drug concentration is not relevant. It simply may be one of a number of factors that contribute to the development of DILI. There is data suggesting that when the normal dose of a drug is relatively high (>50–100 mg per day), the risk of DILI is higher.[16] For the purposes of this article, all forms of DILI with the exception of that induced by acetaminophen overdose are considered idiosyncratic. As summarized in **Table 1**, a large number of different prescribed drugs can give rise to DILI. The majority of drugs listed in **Table 1** are antimicrobial agents, but the basis for why DILI is relatively common with drugs of this class is still unclear. The fact that such a wide range of commonly prescribed drugs cause DILI and can still be prescribed may seem surprising, but this partly reflects the absence of a good nonhepatotoxic alternative to some of these drugs. The drug information sheets for these and other licensed hepatotoxic drugs normally provide clear warnings to prescribers about the possibility of liver toxicity.

The incidence of idiosyncratic DILI reactions tends to be low, but the precise frequency depends on the individual drug. A number of estimates of overall population frequency for idiosyncratic DILI generally are now available. A French study observed that while spontaneous adverse drug reaction reporting suggested an incidence of 0.9 cases of DILI per 100,000 per year, the rate from a rigorous, case-finding population study was higher at 13.9 per 100,000.[17] In the United Kingdom, the incidence of

Table 1 Common causes of idiosyncratic DILI

Drug	*Class*
Amoxicillin–clavulanate	Antimicrobial
Atorvastatin	Statin
Azathioprine	Thiopurine
Azithromycin	Antimicrobial
Ciprofloxacin	Antimicrobial
Diclofenac	Nonsteroidal antiinflammatory drug
Doxycycline	Antimicrobial
Flucloxacillin	Antimicrobial
Infliximab	Antitumor necrosis factor alpha
Isoniazid	Antimicrobial
Levofloxacin	Antimicrobial
Minocycline	Antimicrobial
Nitrofurantoin	Antimicrobial
Phenytoin	Anticonvulsant
Propylthiouracil	Thiourylene
Sulfamethoxazole–trimethoprim	Antimicrobial
Terbinafine	Antifungal
Valproic acid	Anticonvulsant

Based on data from the following sources Chalasani, N.; Bonkovsky, H. L.; Fontana, R.; Lee, W.; Stolz, A.; Talwalkar, J.; Reddy, K. R.; Watkins, P. B.; Navarro, V.; Barnhart, H.; Gu, J.; Serrano, J., Features and Outcomes of 899 Patients With Drug-Induced Liver Injury: The DILIN Prospective Study. *Gastroenterology* **2015,** *148*(7), 1340–1352.e7; Bjornsson, E. S.; Bergmann, O. M.; Bjornsson, H. K.; Kvaran, R. B.; Olafsson, S., Incidence, Presentation, and Outcomes in Patients With Drug-Induced Liver Injury in the General Population of Iceland. *Gastroenterology* **2013,** *144*(7), 1419–1425, 1425 e1-3; quiz e19-20; Suzuki, A.; Andrade, R. J.; Bjornsson, E.; Lucena, M. I.; Lee, W. M.; Yuen, N. A.; Hunt, C. M.; Freston, J. W., Drugs Associated With Hepatotoxicity and Their Reporting Frequency of Liver Adverse Events in VigiBase: Unified List Based on International Collaborative Work. *Drug Saf.* **2010,** *33*(6), 503–522; Shin, J.; Hunt, C. M.; Suzuki, A.; Papay, J. I.; Beach, K. J.; Cheetham, T. C., Characterizing Phenotypes and Outcomes of Drug-Associated Liver Injury Using Electronic Medical Record Data. *Pharmacoepidemiol. Drug Saf.* **2013,** *22*(2), 190–198.

hepatic adverse drug reactions reported to the government regulator is approximately 4 cases per 100,000 population per year,[18] but a more detailed epidemiological survey reported a higher incidence similar to the French study.[19]

The underlying mechanism for DILI is still not clear though some limited new insights have been obtained recently. As discussed in more detail in Section "**HLA associations**," human leukocyte antigen (HLA) genotype is an important determinant of susceptibility to a number of forms of DILI and it is now recognized that the immune system has a more important role in these reactions than originally thought. Up to recently, two main mechanisms for immune-mediated DILI reactions involving HLA associations and the adaptive immune system were postulated. One involved formation of a covalent complex between the drug or a metabolite and cellular proteins.[20] This complex could then be presented to T-cells by particular HLA molecules resulting in an inappropriate local T-cell response and damage to cells. An alternative mechanism proposed that drugs interact directly with HLA molecules resulting in a T-cell response without the need to form a covalent complex (p–I concept).[21] However, recent data on T-cell responses to the anti-HIV drug abacavir are more consistent with a third mechanism involving modification of the p–I concept. Abacavir does not cause DILI but instead a general hypersensitivity reaction in individuals positive for a particular HLA allele, *B*57:01*. Using several different approaches, it has been shown that abacavir binds to the *B*57:01* gene product and induces a conformational change in this protein. This results in incorrect recognition of self peptides as foreign by the immune system, triggering an inappropriate immune response.[22]

Not all DILI is HLA-associated though the innate immune system may still contribute to non-HLA-associated DILI by promoting local inflammatory responses following an initial cell damaging event. In some forms of DILI, the drug or a metabolite may have a direct toxic effect within the liver in a manner analogous to that known to occur during acetaminophen overdose.[2] Direct effects on a variety of organelles including mitochondria may occur resulting in cellular apoptosis or necrosis. A further mechanism for toxicity may involve accumulation of bile acids within hepatocytes at toxic levels due to inhibition of ABC transporters by the hepatotoxic drug. This may also result in apoptosis or necrosis.[23]

4.12.4.1.3 Nongenetic Risk Factors for DILI

The question of why so few patients develop DILI when treated with drugs that can cause this toxicity is an important ongoing question. Some answers have emerged recently, especially from genetic studies, but we are still some distance from being able to predict susceptibility. Risk factors can be subdivided into patient-related factors and environmental risk factors. This section will consider a range of nongenetic risk factors for DILI.

4.12.4.1.4 Age

Age is an extensively studied risk factor for DILI. The risk of developing DILI is generally higher in people aged 60 or more. Amoxicillin–clavulanate-related DILI and isoniazid-related DILI are two well-studied examples. For amoxicillin–clavulanate, a broad-spectrum antimicrobial agent, the incidence is 1.3 per 10,000 prescriptions in patients under 65 compared with 3.2 per 10,000 in those over this age.[24] For isoniazid, which is an important drug in the treatment of tuberculosis (TB), the overall DILI incidence is higher than that for amoxicillin–clavulanate with a rate of 5.6 per 1000 seen in a US study.[25] When this is examined across the age range, younger patients (<35 years) had a rate of 4.4 per 1000 compared with 20.83 for those ≥ 50 years. Despite these differences in incidence across age groups, there does not appear to be an age-related difference in overall outcomes following an occurrence of DILI.[26] The reason why older people are more susceptible to DILI is not completely clear but does not appear to relate simply to older people being prescribed the causative drugs more commonly than younger people. In the case of isoniazid, prescription of this drug is generally more common in a younger age group. Two possible explanations are that older people are more likely to be prescribed other drugs which could result in higher levels of the hepatotoxic agent in the liver if there is an interaction slowing its metabolism or overall clearance. In addition, blood flow to the liver is lower in the elderly[27] and this could also result in higher local drug concentrations.

4.12.4.1.5 Gender

Gender as a risk factor for DILI has also been well studied though the results obtained are less clear-cut than the effects seen for age. For some drugs where DILI has been suggested to be more common in women such as nitrofurantoin, minocycline, and flucloxacillin, prescription of these agents may also be more common in women because of the nature of the conditions they are used to treat. Similarly, amoxicillin–clavulanate-related DILI may be seen more commonly in men but could reflect use of this drug to treat conditions such as respiratory infections which may be more common in elderly males who smoke heavily. However, one interesting example of a drug-inducing DILI at a higher incidence in females than males is nevirapine. This anti-HIV drug is not prescribed more commonly in females than males but appears to cause DILI more commonly in women.[24] Pharmacokinetic data indicates a lower rate of clearance in females with both the parent drug and certain oxidative metabolites generated by cytochromes P450 present at higher plasma concentrations.[28] This could reflect differences in expression of certain cytochrome P450 isoforms between men and women which is now well established.[29]

4.12.4.1.6 Preexisting liver disease

It has been assumed that patients who have already suffered liver damage due to exposure to a toxic compound or infectious age will be more likely to develop DILI if exposed to a drug known to cause this adverse reaction. However, evidence to support this assumption strongly is still lacking. There are many instances where patients with a chronic liver disease may benefit from treatment with

drugs associated with idiosyncratic DILI. The best-studied examples relate to statin treatment of patients with nonalcoholic fatty liver disease (NAFLD) or hepatitis C infection and treatment of TB in patients with viral hepatitis or cirrhosis.

NAFLD is the most common liver disease in the developed world and a substantial proportion of patients are prescribed statins, mainly to protect against cardiovascular disease which is very common in NAFLD patients. There is also some evidence that statins may protect against the progression of the simple steatosis seen in most NAFLD cases to nonalcoholic steatohepatitis (NASH)[30] and may prevent symptoms such as insulin resistance in patients with chronic hepatitis C infection.[31] There is still controversy about whether statins can cause DILI, but it is increasingly accepted that statin-related DILI, though rare, does exist with serious consequences including some cases of liver failure.[32] One study of patients with raised ALT due to a variety of different liver diseases found no increase in statin-related DILI compared with a control population, suggesting the preexisting liver disease was not a risk factor.[33] In addition, in spite of the large numbers of NAFLD patients worldwide taking statins, no reports of substantial rises in DILI incidence have been reported.

Patients suffering from TB may also suffer from other infectious diseases, especially viral hepatitis and HIV. DILI is relatively common during treatment with anti-TB drugs and it has been suggested by the American Thoracic Society that avoiding treatment with isoniazid and, also in patients with very severe liver disease, pyrazinamide could be appropriate.[34] Alternative drug combinations avoiding these agents have been proposed.[34] Several studies have compared the incidence of DILI in TB patients with viral hepatitis or liver cirrhosis with TB patients without liver disease when standard drug treatment protocols involving isoniazid, rifampicin, pyrazinamide, and ethambutol are used. A Hong Kong-based study found hepatitis B carriers with TB were significantly more likely to develop DILI compared with noncarriers,[35] but this could not be confirmed in a similar study in Korea.[36] For hepatitis C infection, a US-based study suggested these patients were more likely to show elevated liver enzymes during anti-TB drug treatment but none of 68 patients with hepatitis C developed moderate to severe DILI, whereas there were 2 cases among 258 controls without hepatitis C.[37]

There is limited data on DILI due to other drugs in NAFLD patients, but one small study of NAFLD and hepatitis C cases followed up for 6 years suggests a small but significant increase in the incidence of DILI generally with most cases seen in patients with NASH.[38] A recent study of NASH patients investigated the pharmacokinetics of morphine and reported increased plasma levels of morphine glucuronide and altered plasma bile acids.[39] It seems possible that the findings for morphine, which is not generally hepatotoxic, can be extended to drugs known to cause DILI, especially since reactive acylglucuronide production is already known to contribute to risk for some types of DILI.[40] More studies of DILI in patients with NAFLD and NASH are needed, but the current data indicates there may be some increased risk but possibly this is drug-specific.

4.12.4.1.7 Smoking and alcohol consumption

Despite being an inducer of certain cytochrome P450 isoforms, there is little evidence that smoking has any significant effect on DILI susceptibility. However, ethanol, another P450 inducer, which can also itself cause liver toxicity has a more complex relationship with the risk of DILI. Though ethanol consumption combined with acetaminophen intake within recommended levels does not appear to increase risk of DILI, the situation is different in those consuming high levels of alcohol chronically who also take an acetaminophen overdose. Because ethanol is an inducer of CYP2E1, a key enzyme in NAPQI formation from acetaminophen, this may result in higher levels of this compound being generated if CYP2E1 is induced.[41] In addition, hepatic glutathione levels in alcoholics may be lower than normal.[42] It has been demonstrated that alcoholics were common among a large group of patients with ALF following acetaminophen overdose.[43] However, slightly paradoxically, consuming large quantities of alcohol concomitantly with acetaminophen overdose decreases the risk of ALF, probably due to competition for CYP2E1 binding between ethanol and acetaminophen.[44]

Some of the findings for acetaminophen toxicity such as the decreased levels of hepatic glutathione in alcoholics may also be relevant to risk of idiosyncratic DILI. It has been suggested that heavy alcohol consumption increases the risk of isoniazid-related DILI,[45] possibly because CYP2E1 which can produce reactive metabolites of isoniazid is induced. However, isoniazid is itself an inducer of CYP2E1 and not all studies suggest an increased incidence of DILI in those consuming high levels of alcohol.[46]

4.12.4.1.8 Infection

Many of the common causes of DILI are drugs used to treat infections or inflammatory conditions. As discussed in Section "**Idiosyncratic DILI**," there is increasing evidence for a role for the innate and adaptive immune systems in DILI so in many situations where potentially hepatotoxic drugs are prescribed, there is already an immune response triggered with high levels of inflammatory mediators. It is also well established that infection and inflammation are associated with downregulation of expression of cytochromes P450 and other drug-metabolizing enzymes and transporters.[47] Studies in animal models show that stimulation of release of inflammatory mediators and cells can affect severity of acetaminophen toxicity and also hepatotoxic responses to some drugs associated with idiosyncratic DILI in humans, most notably diclofenac and trovafloxacin.[48] It is therefore possible that a combination of decreased drug clearance with the presence of inflammatory cells and mediators results in an environment favorable to the onset of inappropriate immune responses to drug and local cellular damage leading to DILI.

4.12.4.1.9 Drug–drug interactions

The possibility that decreased cytochrome P450 levels could be important in DILI has been mentioned in Section "**Infection**." One of the most common causes of decreased cytochrome P450 activity is the inhibition of activity of particular isoforms in drug–drug interactions. Many of the predominantly elderly individuals who suffer idiosyncratic DILI will be taking a number of different

prescribed drugs. Very few systematic studies on the influence of multiple drug prescription on risk of DILI have been performed but one population study found a significant increased risk in individuals taking two or more drugs known to be hepatotoxic.[49] Though the US DILIN network has failed to confirm this finding in a prospective study,[50] this could reflect differences between the studies in design and power.

4.12.4.2 Genetic Factors Affecting DILI Due to Specific Drugs

4.12.4.2.1 Introduction

Evidence for a genetic component in susceptibility to idiosyncratic DILI continues to emerge. The first studies on DILI genetics date from the 1980s. There are studies dealing with both HLA genes and genes relevant to drug metabolism. These studies predated widespread human gene cloning and the human genome project and used a candidate approach where the frequency of a chosen phenotype was compared between cases (those with DILI) and population controls. Two examples of positive findings on DILI from the 1980s are an association between the HLA serotype DR2 and halothane-related DILI[51] and the finding that patients who were poor metabolizers of the drug debrisoquine were more likely to develop hepatitis when treated with the antianginal drug perhexiline.[52] Gene cloning and development of PCR-based genotyping methods have enabled more specific genetic associations to be investigated. Initially, this involved a candidate gene approach similar to the early studies on phenotype except that specific genes were being studied not just phenotypes. Candidate genes examined included HLA, genes encoding enzymes relevant to drug metabolism and transport, and genes encoding components of the innate immune response. The main limitation with genetic studies on DILI is that case finding is difficult so most studies have been small which limits the power to detect associations reliably. Replicating associations has also been difficult. The development of genome-wide association studies (GWAS) where the contribution of all genes in the human genome to disease susceptibility can be investigated[53] has been a useful development in understanding the genetics of DILI better but lack of large numbers of cases continues to be a limitation.

It is increasingly clear that when performing studies to identify genetic risk factors for DILI, it is essential to consider individual drug causes separately. As discussed in Section "**HLA associations**," there is some overlap in genetic risk factors for DILI due to different unrelated drugs but in general different risk factors have been detected for different drugs. This section will consider HLA gene associations with DILI caused by a number of drugs but will then consider other genetic associations on an individual drug basis. One of the key aims of these genetic studies is to develop strategies to enable patients at risk of DILI due to particular to be identified and prescribed alternative drugs. Unfortunately, the findings obtained so far are generally not sufficiently specific for this to be possible.

4.12.4.2.2 HLA associations

The proteins encoded by HLA genes are important in presenting foreign peptides, usually derived from invading pathogens, to T lymphocytes. A number of HLA genes are located in a large gene cluster on chromosome 6 in an area of the genome referred to as the major histocompatibility complex. More detailed descriptions of HLA genes and their biological roles are widely available.[54] HLA genes are divided into two types, classes I and II. The proteins encoded by these gene classes have overlapping but slightly different functions in the immune response. Class I genes tend to be expressed on most cells in the body and to have a role in presenting peptides to cytotoxic T-cells which may cause local damage. On the other hand, class II genes tend to be expressed mainly on immune system cells and to have a more important role in stimulating T-helper cells to produce proteins such as cytokines which may induce inflammation. HLA genes are subject to a large amount of genetic variation or polymorphism. This probably arose originally to help protect the body from pathogens but increasingly certain alternative forms of HLA genes (alleles) are considered to be risk factors for some types of autoimmune disease (e.g., multiple sclerosis or type I diabetes) and also for adverse drug reactions such as DILI. As discussed in Section "**Idiosyncratic DILI**," there is increasing evidence that some types of DILI involve an inappropriate immune response to a drug, possibly after a covalent link between the drug and a cellular protein has been formed. HLA proteins are likely to contribute by presenting the complex to T-cells.

Well-established and replicated HLA associations have been described for hypersensitivity reactions affecting various tissues, particularly the skin, and for DILI. Those carrying certain HLA alleles have an increased risk of these reactions. For DILI, some of the HLA-associated reactions do not show obvious features of a hypersensitivity reaction so findings of strong HLA associations have been slightly unexpected. For DILI, the first reports linking HLA with susceptibility to this type of reaction involved the general anesthetic halothane, which was used widely until the 1980s but was also an important cause of idiosyncratic DILI. This association, which was detected by an immunoassay and reported before the HLA genes, was well understood, concerned an increased risk of DILI in those with the HLA class II serotype DR2.[51] Other reports of associations between various HLA serotypes and DILI induced by particular drugs subsequently emerged though these usually involved very small numbers of patients and did not show statistical significance. More recently, HLA associations with DILI have been studied directly by genotyping rather than serotype determination and studies have been slightly larger than previously. The first HLA genotyping studies were candidate gene association studies on amoxicillin–clavulanate-related DILI. This form of DILI does not generally show classical immune-related features, but two independent candidate gene association studies reported an identical association with the *HLA-DRB1*15:01* allele, which corresponds to the DR2 serotype, which may be relevant to the original observation on halothane DILI.[51] Further studies have found additional HLA class I and II associations for DILI, including a second HLA association for amoxicillin–clavulanate-related toxicity (**Table 2**). Effect sizes vary depending on the drug with odds ratios for risk of DILI of between 2 and 80 reported. The strongest HLA association reported to date for DILI is for reactions due to the antimicrobial flucloxacillin, which is used in some countries to treat gram-

Table 2 HLA alleles associated with DILI

Compound	*No. of cases*	*HLA allele*	*Odds ratio (95% CI)*	*Reference*
Flucloxacillin	51	*B*57:01*	80.6 (22.8–284.9)	55
Amoxicillin–clavulanic acid	201	*A*02:01*	2.3 (1.8–2.9)	56
		*DRB1*15:01-DQB1*06:02*	2.8 (2.1–3.8)	
Lumiracoxib	41	*DRB1*15:01-DQB1*06:02*	5.0 (3.6–7.0)	57
Lapatinib	35	*DRB1*07:01-DQA1*02:01*	2.9 (1.3–6.6)	58
Ximelagatran	74	*DRB1*07:01-DQA1*02:01*	4.4 (2.2–8.9)	59
Ticlopidine	22	*A*33:03*	13.0 (4.4–38.6)	60

positive bacterial infections. This was detected in the first GWAS performed for any type of DILI. A very strong association (odds ratio 80) for development of flucloxacillin DILI was seen with the class I HLA allele *B*57:01*.[55] This allele had been shown previously to be a strong risk factor for hypersensitivity reactions to the drug abacavir but as mentioned in Section "**Idiosyncratic DILI**," these reactions generally do not involve the liver. Importantly, the underlying mechanism involved in the flucloxacillin DILI reaction appears to be different to the mechanism reported for abacavir.[61] No other DILI associations with *B*57:01* have been identified to date. However, other reported HLA associations may involve two different chemically unrelated drugs; for example, carrying the HLA class II allele *DRB1*15:01* is a risk factor for DILI related to both amoxicillin–clavulanate and lumiracoxib (**Table 2**) and could also be relevant to halothane-related DILI.

The observed HLA associations are interesting but even for flucloxacillin DILI, only 1 in every 500–1000 patients carrying the risk allele *B*57:01* develop the reaction when given the drug. This means additional risk factors contribute to risk and these may include the factors such as age and gender discussed earlier. Additional non-HLA genes may also contribute.

4.12.4.2.3 Non-HLA associations

After HLA genes, the best-studied genetic risk factors for DILI are polymorphisms relevant to drug disposition. Though recent GWAS studies have not found evidence that polymorphisms in these genes are significant contributors to DILI, candidate gene studies, mainly focusing on single genes only, have found limited evidence for some contribution. Most studies on this type have involved small numbers of cases and generally have not been replicated as yet, with the exception of an apparent association between *N*-acetyltransferase 2 (*NAT2*) and susceptibility to DILI relating to the anti-TB drug isoniazid. Isoniazid-related DILI is discussed in more detail further. Associations between DILI and particular cytochrome P450 genotypes have also been investigated but few positive findings have emerged, despite a key role for the cytochromes P450 in the formation of reactive metabolites. Phase 2 drug metabolism genes, genes encoding ABC transporters, genes relevant to the innate immune system, and oxidative stress have also been investigated. Some positive associations have been identified from these studies, as described here.

4.12.4.2.3.1 Isoniazid

Use of the drug isoniazid remains important in treatment of TB but approximately 1% of all patients treated with this drug develop moderate to severe DILI. A larger percentage (approximately 10%) develop elevation of transaminase enzymes soon after treatment, but the level of elevation may not be sufficient to require cessation of treatment and enzyme levels may revert to normal quite rapidly in an adaptation response. Even if treatment is stopped and then restarted after a few weeks, reintroduction of isoniazid may not result in a further transaminase elevation because of adaptation. Isoniazid is usually used in combination with rifampicin and there is considerable evidence that this combination is more hepatotoxic than either drug used alone. A third drug, pyrazinamide, which is used in the first 2 months of most treatment regimens is also hepatotoxic, even when used as a single agent. The complexity of TB treatment regimens has made genetic studies on DILI complicated, since it is not usually possible to assess the contribution of individual drugs separately. Despite these limitations, there is an extensive literature suggesting an association between the *NAT2* slow acetylator genotype and susceptibility to DILI in patients treated with isoniazid-containing treatment regimens. NAT2 has a key role in the metabolism of isoniazid and slow acetylators who essentially have no enzyme activity present have higher plasma levels of the parent drug but may also metabolize the drug via an alternative pathway probably involving a carboxyesterase enzyme to form hydrazine.[62] All studies showing an association between NAT2 genotype and susceptibility to isoniazid-related DILI have been candidate gene studies.[63] However, not all candidate gene studies confirm an association with *NAT2* and no significant association has been seen in a GWAS.[64] Importantly, however, the GWAS also failed to detect any HLA association for isoniazid-related DILI. There are some reports that the innate immune system is an important contributor to isoniazid toxicity[65] and this could occur independently of HLA genotype.

Both isoniazid itself and hydrazine can be converted to reactive metabolites by cytochromes P450, particularly CYP2E1. Genetic polymorphism in CYP2E1 is well studied though the functional effects of the various polymorphisms remain unclear.[66] A variant allele (*CYP2E1*5*) has a polymorphism in the upstream sequence close to a binding site for the transcription factor HNF-1 which results in higher transcriptional activity.[67] In one early study, patients homozygous for the normal "wild-type" *CYP2E1* allele had a significantly increased risk of developing isoniazid-induced DILI compared to those positive for *CYP2E1*5*.[68] This association has been confirmed recently in an independent study,[69] but other studies have failed to confirm any association. *CYP2E1* remains an

interesting candidate gene for isoniazid-induced DILI because of the role of the enzyme in isoniazid metabolism but its relevance as a risk factor can only be further investigated if larger numbers of cases can be collected.

Glutathione S-transferases (GST) contribute to the detoxication of a variety of drugs by glutathione conjugation and protect against reactive oxygen species (ROS). Two GST isoforms, GSTM1 and T1, are absent in significant numbers of individuals due to large gene deletions which are often referred to as null alleles. There is no specific role for either of these isoforms in the metabolism of isoniazid but the possibility that *GSTM1* and *T1* genotype influences the risk of isoniazid-related DILI related has been investigated. Two studies reported a higher frequency of *GSTM1* null genotypes among cases compared with controls but no difference with respect to *GSTT1*,[70] while a third reported no difference for *GSTM1* null genotype frequency in DILI cases compared to controls but a higher frequency of *GSTT1* null individuals among cases.[71] As discussed in Section "**Troglitazone**," GSTM1 and GSTT1 are also of relevance to DILI relating to troglitazone.

It seems likely that damage to cellular macromolecules by ROS leading to cellular damage may occur in at least some forms of DILI. A few studies on the mitochondrial manganese-dependent superoxide dismutase (MnSOD) as a risk factor for isoniazid-related DILI have been reported. A common polymorphism in the *SOD2* gene, which codes for MnSOD, was found to be a predictor of isoniazid-related DILI.[70b] The association between DILI and *SOD2* genotype was with an allele predicted result in high MnSOD activity, but it was suggested that this might be due to hydrogen peroxide generated by MnSOD also being toxic in addition to the superoxide substrate.[70b]

In summary, the *NAT2* genotype remains the most promising genetic factor for predicting risk of DILI due to isoniazid. A randomized clinical trial based in Japan involving differential dosing for the three different *NAT2* genotype groups has provided some encouraging data.[72] This study showed significant benefits with decreased incidence of DILI in a slow acetylator group. Patients predicted to show high NAT2 activity were given a higher than normal isoniazid dose in the genotype-guided arm and showed a lower rate of treatment failure. This encouraging study still needs replication.

4.12.4.2.3.2 Diclofenac

Diclofenac is a widely prescribed nonsteroidal antiinflammatory drug and, after flucloxacillin and amoxicillin–clavulanate, is among the most common drugs causing idiosyncratic DILI. It has been estimated that diclofenac-related DILI occurs in 4 in every 100,000 people prescribed this drug.[49] Susceptibility to diclofenac-related DILI does not appear to relate to HLA genotype.[64] Instead, it has been suggested that reactive metabolites may bind to hepatocyte proteins triggering local damage and inflammation. Diclofenac undergoes a relatively complex pattern of metabolism involving both cytochromes P450 and UDP-glucuronosyltransferases (UGT) (**Fig. 2**). Studies on polymorphisms relevant to diclofenac metabolism have indicated no role for CYP2C9 genotype,[73] a possible role for CYP2C8 genotype,[74] and a more likely role for UGT2B7 genotype[64,74] in susceptibility to diclofenac DILI. The underlying mechanism for the toxicity may involve the formation of a reactive acyl glucuronide by UGT2B7.

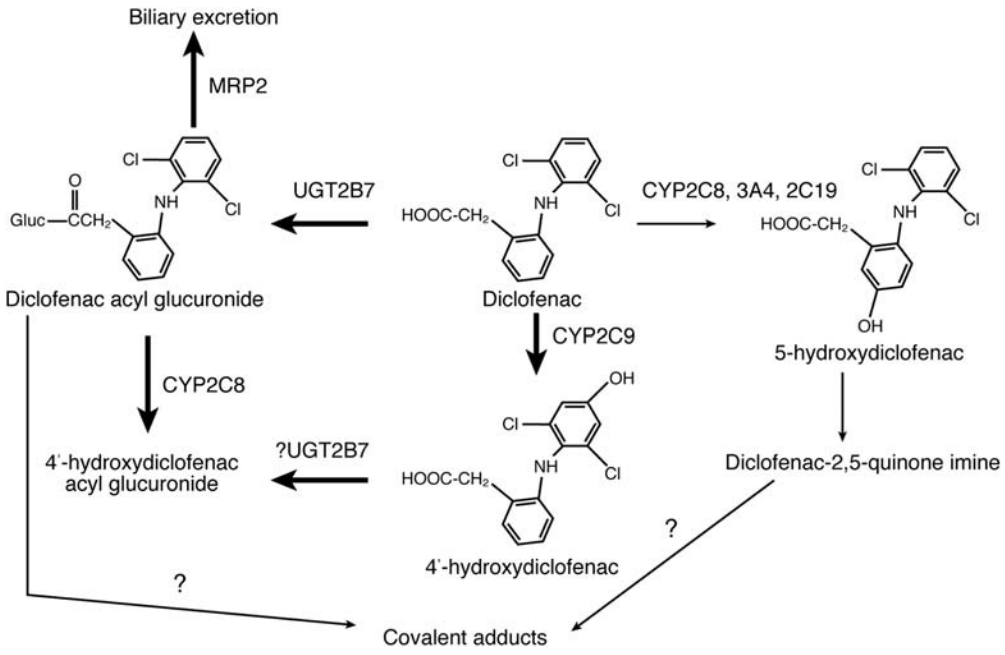

Fig. 2 Diclofenac metabolism. The main metabolic pathways for diclofenac and metabolites in the liver are indicated. Both the acyl glucuronide and the imine metabolite derived from 5-hydroxydiclofenac are believed to form protein adducts. From Daly, A. K.; Aithal, G. P.; Leathart, J. B.; Swainsbury, R. A.; Dang, T. S.; Day, C. P., Genetic Susceptibility to Diclofenac-Induced Hepatotoxicity: Contribution of UGT2B7, CYP2C8, and ABCC2 Genotypes. *Gastroenterology* **2007,** *132*(1), 272–281, © 2007 AGA Institute, Reproduced with permission from Elsevier.

Acyl glucuronides are well established to form adducts with proteins[75] and there is evidence that diclofenac acyl glucuronide is a reactive molecule based on low half-life in aqueous and protein solutions.[40,76] Drug glucuronide conjugates are often eliminated from hepatocytes by the canalicular drug transporter MRP2 which is coded for by *ABCC2*. There is also some evidence that carriage of a polymorphism in *ABCC2* which is associated with decreased levels of MRP2 expression and might therefore result in increased acyl glucuronide accumulation in the hepatocyte is a risk factor for diclofenac DILI.[74]

Formation of adducts between protein and a drug metabolite may not be sufficient to trigger DILI. It seems likely that in DILI patients, additional inflammatory responses occur within the liver once adduct formation has occurred. There is preliminary evidence that polymorphisms affecting cytokine expression may also be risk factors for diclofenac-related DILI.[77] Essentially therefore, it appears that both metabolic and inflammatory genotypes will affect the risk of this form of DILI.

4.12.4.2.3.3 Troglitazone

Troglitazone is a thiazolidinedione drug which is an agonist of the peroxisome proliferator receptor gamma and was approved by the FDA for treatment of type II diabetes in 1997. After a number of reports of serious hepatotoxicity, including at least 94 cases of liver failure in the United States,[78] the drug was withdrawn from the US market in 2000. The basis for this serious toxicity is still not entirely clear. No evidence for liver toxicity was seen during preclinical studies in animals and there was very limited collection of samples from those affected by DILI. However, there is a large body of in vitro data now available which provides some useful insights both in relation to troglitazone DILI specifically and to DILI more broadly. The major metabolite of troglitazone is troglitazone sulfate generated by the sulfotransferase enzyme ST1A3.[79] It has been demonstrated that both troglitazone and the sulfate metabolite inhibit the two ABC transporters BSEP and MRP4 (encoded by ABCC11 and ABCC4, respectively).[80] Both transporters have key roles in bile acid efflux from hepatocytes across both the canalicular and sinusoidal membranes. In the absence of biological material from those who suffered the toxicity, it has been possible recently, using a systems toxicology approach, to predict that the extent of inhibition of transporter activity by troglitazone and the sulfate metabolite would be sufficient to cause extensive bile acid accumulation in humans mainly in the form of the highly toxic lithocholic acid, whereas this is less likely to occur in the rat models used in toxicology studies.[80] The reason why toxicity was only seen in a relatively small number of exposed individuals is still unclear, but possibly low expression of the relevant bile acid transporters could be one factor. The only genetic study available on troglitazone toxicity indicates that individuals who showed significantly raised plasma transaminase levels during troglitazone treatment were likely to be positive for null genotypes for the GST *GSTM1* and *GSTT1*.[81] This finding seems quite consistent with glutathione conjugation being a route of metabolism for troglitazone, especially in the detoxication of a reactive and cytotoxic quinone metabolite, though this is mainly catalyzed by GSTM1 with no effect from GSTT1.[82]

4.12.4.2.3.4 Acetaminophen

Generally DILI due to acetaminophen is concentration-dependent with no risk of DILI at the normal recommended dose and a very high risk of developing DILI in overdose if treatment with *N*-acetylcysteine or a related compound is not administered within a specific timeframe after overdose. However, as discussed in Section "**Concentration-dependent DILI**," some individuals who take the recommended dose of acetaminophen over a prolonged period develop elevated transaminase enzymes but later appear to adapt.[15] In addition, there is some evidence that occasionally DILI develops in patients who unintentionally consume large quantities of acetaminophen, often over a more prolonged period than for the typical deliberate overdose.[43] A nonsynonymous polymorphism in the gene CD44, which codes for a protein that is involved in inflammation and cell communication, was shown to be more common in individuals showing transaminase elevation in response to acetaminophen treatment[83] and more recently in an unintentional overdose cohort.[84] In addition, polymorphisms in UGT1A and CYP3A5 also affected susceptibility in a cohort showing liver failure after acetaminophen overdose group in a biologically plausible manner.[84] Overall, the observed effects of the polymorphisms are not large, but an apparently genetic effect on susceptibility to overdose is novel and worth further investigation.

4.12.5 Conclusions

DILI continues to be an important issue in drug development. The absence of tests that can reliably identify hepatotoxic drugs at an early stage of development is a problem and developing such systems remains a priority for the pharmaceutical industry. The recent study on the mechanistic basis for troglitazone DILI using only in vitro data is an important advance.[80] Performing similar studies on newly developed molecules may be valuable. There is also increasing availability of genetically well-defined human hepatocyte-like cell lines derived from induced pluripotent stem cells. As the ability to generate hepatocytes in vitro improves, a range of such cell lines may prove useful as a screen for hepatotoxicity.[85] For example, cell lines could be isolated from individuals who had suffered idiosyncratic DILI previously but have now recovered. Such a cell line with a hepatocyte phenotype might have a general susceptibility to DILI, though there is still insufficient data from genetic studies on whether such a general susceptibility exists.

Considerable progress in identifying risk factors, especially genetic risk factors, for DILI has been made in the past 10 years. However, it is still not possible to provide a reliable prediction of individual susceptibility. This may become more feasible in the future as further genetic risk factors are identified by use of more sensitive techniques and larger number of cases. The contribution of other risk factors such as age and disease will also need to be considered and need to be understood better.

Diagnosis of DILI depends on phenotype and expert clinical judgment. Up to the present, marker enzymes such as ALT have been important in diagnosis and this is likely to continue. However, more sensitive biomarkers such as plasma microRNA (miRNA) levels are now available.[86] These appear to provide information about DILI earlier than ALT and other plasma enzyme levels and may be of particular value in the treatment of acetaminophen overdose where an antidote needs to be administered. Their relevance to diagnosis of idiosyncratic DILI is less clear since current approaches to diagnosis (Section "**Phenotypes in DILI**") appear adequate. However, it is possible that measurement of various miRNA molecules in plasma might provide novel insights into the underlying mechanisms for idiosyncratic DILI which remain poorly understood. Whether collection of suitable samples during the onset of DILI will be feasible remains unclear.

References

1. Cook, D.; Brown, D.; Alexander, R.; March, R.; Morgan, P.; Satterthwaite, G.; Pangalos, M. N. Lessons Learned From the Fate of AstraZeneca's Drug Pipeline: A Five-Dimensional Framework. *Nat. Rev. Drug Discov.* **2014,** *13* (6), 419–431.
2. Kaplowitz, N. Idiosyncratic Drug Hepatotoxicity. *Nat. Rev. Drug Discov.* **2005,** *4* (6), 489–499.
3. (a) Bell, L. N.; Chalasani, N. Epidemiology of Idiosyncratic Drug-Induced Liver Injury. *Semin. Liver Dis.* **2009,** *29* (4), 337–347; (b) Bernal, W.; Lee, W. M.; Wendon, J.; Larsen, F. S.; Williams, R. Acute Liver Failure: A Curable Disease by 2024? *J. Hepatol.* **2015,** *62* (1 Suppl), S112–S120.
4. Verma, S.; Kaplowitz, N. Diagnosis, Management and Prevention of Drug-Induced Liver Injury. *Gut* **2009,** *58* (11), 1555–1564.
5. Aithal, G. P.; Watkins, P. B.; Andrade, R. J.; Larrey, D.; Molokhia, M.; Takikawa, H.; Hunt, C. M.; Wilke, R. A.; Avigan, M.; Kaplowitz, N.; Bjornsson, E.; Daly, A. K. Case Definition and Phenotype Standardization in Drug-Induced Liver Injury. *Clin. Pharmacol. Ther.* **2011,** *89* (6), 806–815.
6. Peters, T. S. Do Preclinical Testing Strategies Help Predict Human Hepatotoxic Potentials? *Toxicol. Pathol.* **2005,** *33* (1), 146–154.
7. Kitamura, S.; Sugihara, K. Current Status of Prediction of Drug Disposition and Toxicity in Humans Using Chimeric Mice With Humanized Liver. *Xenobiotica* **2014,** *44* (2), 123–134.
8. (a) O'Brien, P. J.; Irwin, W.; Diaz, D.; Howard-Cofield, E.; Krejsa, C. M.; Slaughter, M. R.; Gao, B.; Kaludercic, N.; Angeline, A.; Bernardi, P.; Brain, P.; Hougham, C. High Concordance of Drug-Induced Human Hepatotoxicity With In Vitro Cytotoxicity Measured in a Novel Cell-Based Model Using High Content Screening. *Arch. Toxicol.* **2006,** *80* (9), 580–604; (b) Tolosa, L.; Pinto, S.; Donato, M. T.; Lahoz, A.; Castell, J. V.; O'Connor, J. E.; Gomez-Lechon, M. J. Development of a Multiparametric Cell-Based Protocol to Screen and Classify the Hepatotoxicity Potential of Drugs. *Toxicol. Sci.* **2012,** *127* (1), 187–198.
9. Andersson, T. B.; Kanebratt, K. P.; Kenna, J. G. The HepaRG Cell Line: A Unique In Vitro Tool for Understanding Drug Metabolism and Toxicology in Human. *Expert Opin. Drug Metab. Toxicol.* **2012,** *8* (7), 909–920.
10. Khetani, S. R.; Kanchagar, C.; Ukairo, O.; Krzyzewski, S.; Moore, A.; Shi, J.; Aoyama, S.; Aleo, M.; Will, Y. Use of Micropatterned Cocultures to Detect Compounds That Cause Drug-Induced Liver Injury in Humans. *Toxicol. Sci.* **2013,** *132* (1), 107–117.
11. Modi, S.; Hughes, M.; Garrow, A.; White, A. The Value of In Silico Chemistry in the Safety Assessment of Chemicals in the Consumer Goods and Pharmaceutical Industries. *Drug Discov. Today* **2012,** *17* (3–4), 135–142.
12. Przybylak, K. R.; Cronin, M. T. In Silico Models for Drug-Induced Liver Injury—Current Status. *Expert Opin. Drug Metab. Toxicol.* **2012,** *8* (2), 201–217.
13. Chalasani, N.; Bonkovsky, H. L.; Fontana, R.; Lee, W.; Stolz, A.; Talwalkar, J.; Reddy, K. R.; Watkins, P. B.; Navarro, V.; Barnhart, H.; Gu, J.; Serrano, J. Features and Outcomes of 899 Patients With Drug-Induced Liver Injury: The DILIN Prospective Study. *Gastroenterology* **2015,** *148* (7), 1340–1352. e7.
14. Prescott, L. F. Paracetamol Overdosage. Pharmacological Considerations and Clinical Management. *Drugs* **1983,** *25* (3), 290–314.
15. Watkins, P. B.; Kaplowitz, N.; Slattery, J. T.; Colonese, C. R.; Colucci, S. V.; Stewart, P. W.; Harris, S. C. Aminotransferase Elevations in Healthy Adults Receiving 4 Grams of Acetaminophen Daily: A Randomized Controlled Trial. *JAMA* **2006,** *296* (1), 87–93.
16. (a) Chen, M.; Borlak, J.; Tong, W. High Lipophilicity and High Daily Dose of Oral Medications Are Associated With Significant Risk for Drug-Induced Liver Injury. *Hepatology* **2013,** *58* (1), 388–396; (b) Lewis, J. H. The Art and Science of Diagnosing and Managing Drug-Induced Liver Injury in 2015 and Beyond. *Clin. Gastroenterol. Hepatol.* **2015,** *13* (12), 2173–2189.
17. Sgro, C.; Clinard, F.; Ouazir, K.; Chanay, H.; Allard, C.; Guilleminet, C.; Lenoir, C.; Lemoine, A.; Hillon, P. Incidence of Drug-Induced Hepatic Injuries: A French Population-Based Study. *Hepatology* **2002,** *36* (2), 451–455.
18. Aithal, P. G.; Day, C. P. The Natural History of Histologically Proved Drug Induced Liver Disease. *Gut* **1999,** *44* (5), 731–735.
19. Whitehead, M. W.; Hainsworth, I.; Kingham, J. G. C. The Causes of Obvious Jaundice in South West Wales: Perceptions Versus Reality. *Gut* **2001,** *48* (3), 409–413.
20. Uetrecht, J. Immunoallergic Drug-Induced Liver Injury in Humans. *Semin. Liver Dis.* **2009,** *29* (4), 383–392.
21. Adam, J.; Pichler, W. J.; Yerly, D. Delayed Drug Hypersensitivity: Models of T-Cell Stimulation. *Br. J. Clin. Pharmacol.* **2011,** *71* (5), 701–707.
22. Illing, P. T.; Vivian, J. P.; Dudek, N. L.; Kostenko, L.; Chen, Z.; Bharadwaj, M.; Miles, J. J.; Kjer-Nielsen, L.; Gras, S.; Williamson, N. A.; Burrows, S. R.; Purcell, A. W.; Rossjohn, J.; McCluskey, J. Immune Self-Reactivity Triggered by Drug-Modified HLA-Peptide Repertoire. *Nature* **2012,** *486* (7404), 554–558.
23. Woolbright, B. L.; Dorko, K.; Antoine, D. J.; Clarke, J. I.; Gholami, P.; Li, F.; Kumer, S. C.; Schmitt, T. M.; Forster, J.; Fan, F.; Jenkins, R. E.; Park, B. K.; Hagenbuch, B.; Olyaee, M.; Jaeschke, H. Bile Acid-Induced Necrosis in Primary Human Hepatocytes and in Patients With Obstructive Cholestasis. *Toxicol. Appl. Pharmacol.* **2015,** *283* (3), 168–177.
24. Lucena, M. I.; Andrade, R. J.; Fernandez, M. C.; Pachkoria, K.; Pelaez, G.; Duran, J. A.; Villar, M.; Rodrigo, L.; Romero-Gomez, M.; Planas, R.; Barriocanal, A.; Costa, J.; Guarner, C.; Blanco, S.; Navarro, J. M.; Pons, F.; Castiella, A.; Avila, S. Determinants of the Clinical Expression of Amoxicillin-Clavulanate Hepatotoxicity: A Prospective Series From Spain. *Hepatology* **2006,** *44* (4), 850–856.
25. Fountain, F. F.; Tolley, E.; Chrisman, C. R.; Self, T. H. Isoniazid Hepatotoxicity Associated With Treatment of Latent Tuberculosis Infection: A 7-Year Evaluation From a Public Health Tuberculosis Clinic. *Chest* **2005,** *128* (1), 116–123.
26. Lucena, M. I.; Andrade, R. J.; Kaplowitz, N.; Garcia-Cortes, M.; Fernandez, M. C.; Romero-Gomez, M.; Bruguera, M.; Hallal, H.; Robles-Diaz, M.; Rodriguez-Gonzalez, J. F.; Navarro, J. M.; Salmeron, J.; Martinez-Odriozola, P.; Perez-Alvarez, R.; Borraz, Y.; Hidalgo, R. Phenotypic Characterization of Idiosyncratic Drug-Induced Liver Injury: The Influence of Age and Sex. *Hepatology* **2009,** *49* (6), 2001–2009.
27. Wynne, H. A.; Cope, L. H.; Mutch, E.; Rawlins, M. D.; Woodhouse, K. W.; James, O. F. The Effect of Age Upon Liver Volume and Apparent Liver Blood Flow in Healthy Man. *Hepatology* **1989,** *9* (2), 297–301.
28. Marinho, A. T.; Rodrigues, P. M.; Caixas, U.; Antunes, A. M.; Branco, T.; Harjivan, S. G.; Marques, M. M.; Monteiro, E. C.; Pereira, S. A. Differences in Nevirapine Biotransformation as a Factor for Its Sex-Dependent Dimorphic Profile of Adverse Drug Reactions. *J. Antimicrob. Chemother.* **2014,** *69* (2), 476–482.
29. Zanger, U. M.; Schwab, M. Cytochrome P450 Enzymes in Drug Metabolism: Regulation of Gene Expression, Enzyme Activities, and Impact of Genetic Variation. *Pharmacol. Ther.* **2013,** *138* (1), 103–141.
30. Dongiovanni, P.; Petta, S.; Mannisto, V.; Mancina, R. M.; Pipitone, R.; Karja, V.; Maggioni, M.; Kakela, P.; Wiklund, O.; Mozzi, E.; Grimaudo, S.; Kaminska, D.; Rametta, R.; Craxi, A.; Fargion, S.; Nobili, V.; Romeo, S.; Pihlajamaki, J.; Valenti, L. Statin Use and Non-Alcoholic Steatohepatitis in at Risk Individuals. *J. Hepatol.* **2015,** *63* (3), 705–712.
31. Russo, M. W.; Scobey, M.; Bonkovsky, H. L. Drug-Induced Liver Injury Associated With Statins. *Semin. Liver Dis.* **2009,** *29* (4), 412–422.

32. Russo, M. W.; Hoofnagle, J. H.; Gu, J.; Fontana, R. J.; Barnhart, H.; Kleiner, D. E.; Chalasani, N.; Bonkovsky, H. L. Spectrum of Statin Hepatotoxicity: Experience of the Drug-Induced Liver Injury Network. *Hepatology* **2014,** *60* (2), 679–686.
33. Chalasani, N.; Aljadhey, H.; Kesterson, J.; Murray, M. D.; Hall, S. D. Patients With Elevated Liver Enzymes Are Not at Higher Risk for Statin Hepatotoxicity. *Gastroenterology* **2004,** *126* (5), 1287–1292.
34. Blumberg, H. M.; Burman, W. J.; Chaisson, R. E.; Daley, C. L.; Etkind, S. C.; Friedman, L. N.; Fujiwara, P.; Grzemska, M.; Hopewell, P. C.; Iseman, M. D.; Jasmer, R. M.; Koppaka, V.; Menzies, R. I.; O'Brien, R. J.; Reves, R. R.; Reichman, L. B.; Simone, P. M.; Starke, J. R.; Vernon, A. A. American Thoracic Society/Centers for Disease Control and Prevention/Infectious Diseases Society of America: Treatment of Tuberculosis. *Am. J. Respir. Crit. Care Med.* **2003,** *167* (4), 603–662.
35. Wong, W. M.; Wu, P. C.; Yuen, M. F.; Cheng, C. C.; Yew, W. W.; Wong, P. C.; Tam, C. M.; Leung, C. C.; Lai, C. L. Antituberculosis Drug-Related Liver Dysfunction in Chronic Hepatitis B Infection. *Hepatology* **2000,** *31* (1), 201–206.
36. Lee, B. H.; Koh, W. J.; Choi, M. S.; Suh, G. Y.; Chung, M. P.; Kim, H.; Kwon, O. J. Inactive Hepatitis B Surface Antigen Carrier State and Hepatotoxicity During Antituberculosis Chemotherapy. *Chest* **2005,** *127* (4), 1304–1311.
37. Lomtadze, N.; Kupreishvili, L.; Salakaia, A.; Vashakidze, S.; Sharvadze, L.; Kempker, R. R.; Magee, M. J.; del Rio, C.; Blumberg, H. M. Hepatitis C Virus co-Infection Increases the Risk of Anti-Tuberculosis Drug-Induced Hepatotoxicity Among Patients With Pulmonary Tuberculosis. *PLoS One* **2013,** *8* (12), e83892.
38. Tarantino, G.; Conca, P.; Basile, V.; Gentile, A.; Capone, D.; Polichetti, G.; Leo, E. A Prospective Study of Acute Drug-Induced Liver Injury in Patients Suffering From Non-Alcoholic Fatty Liver Disease. *Hepatol. Res.* **2007,** *37* (6), 410–415.
39. Ferslew, B. C.; Johnston, C. K.; Tsakalozou, E.; Bridges, A. S.; Paine, M. F.; Jia, W.; Stewart, P. W.; Barritt, A. S.; Brouwer, K. L. Altered Morphine Glucuronide and Bile Acid Disposition in Patients With Nonalcoholic Steatohepatitis. *Clin. Pharmacol. Ther.* **2015,** *97* (4), 419–427.
40. Zhong, S.; Jones, R.; Lu, W.; Schadt, S.; Ottaviani, G. A New Rapid In Vitro Assay for the Assessment of the Reactivity of Acyl Glucuronides. *Drug Metab. Dispos.* **2015,** *43* (11), 1711–1717.
41. Laine, J. E.; Auriola, S.; Pasanen, M.; Juvonen, R. O. Acetaminophen Bioactivation by Human Cytochrome P450 Enzymes and Animal Microsomes. *Xenobiotica* **2009,** *39* (1), 11–21.
42. Lauterburg, B. H.; Velez, M. E. Glutathione Deficiency in Alcoholics: Risk Factor for Paracetamol Hepatotoxicity. *Gut* **1988,** *29* (9), 1153–1157.
43. Larson, A. M.; Polson, J.; Fontana, R. J.; Davern, T. J.; Lalani, E.; Hynan, L. S.; Reisch, J. S.; Schiodt, F. V.; Ostapowicz, G.; Shakil, A. O.; Lee, W. M. Acetaminophen-Induced Acute Liver Failure: Results of a United States Multicenter, Prospective Study. *Hepatology* **2005,** *42* (6), 1364–1372.
44. Prescott, L. F. Paracetamol, Alcohol and the Liver. *Br. J. Clin. Pharmacol.* **2000,** *49* (4), 291–301.
45. Kopanoff, D. E.; Snider, D. E., Jr.; Caras, G. J. Isoniazid-Related Hepatitis: A U.S. Public Health Service Cooperative Surveillance Study. *Am. Rev. Respir. Dis.* **1978,** *117* (6), 991–1001.
46. Dossing, M.; Wilcke, J. T.; Askgaard, D. S.; Nybo, B. Liver Injury During Antituberculosis Treatment: An 11-Year Study. *Tuber. Lung Dis.* **1996,** *77* (4), 335–340.
47. Morgan, E. T. Impact of Infectious and Inflammatory Disease on Cytochrome P450-Mediated Drug Metabolism and Pharmacokinetics. *Clin. Pharmacol. Ther.* **2009,** *85* (4), 434–438.
48. Roth, R. A.; Ganey, P. E. Intrinsic Versus Idiosyncratic Drug-Induced Hepatotoxicity—Two Villains or One? *J. Pharmacol. Exp. Ther.* **2010,** *332* (3), 692–697.
49. de Abajo, F. J.; Montero, D.; Madurga, M.; Garcia Rodriguez, L. A. Acute and Clinically Relevant Drug-Induced Liver Injury: A Population Based Case–Control Study. *Br. J. Clin. Pharmacol.* **2004,** *58* (1), 71–80.
50. Chalasani, N.; Fontana, R. J.; Bonkovsky, H. L.; Watkins, P. B.; Davern, T.; Serrano, J.; Yang, H.; Rochon, J. Causes, Clinical Features, and Outcomes From a Prospective Study of Drug-Induced Liver Injury in the United States. *Gastroenterology* **2008,** *135* (6), 1924–1934, 1934 e1-4.
51. Otsuka, S.; Yamamoto, M.; Kasuya, S.; Ohtomo, H.; Yamamoto, Y.; Yoshida, T. O.; Akaza, T. HLA Antigens in Patients With Unexplained Hepatitis Following Halothane Anesthesia. *Acta Anaesthesiol. Scand.* **1985,** *29* (5), 497–501.
52. Morgan, M. Y.; Reshef, R.; Shah, R. R.; Oates, N. S.; Smith, R. L.; Sherlock, S. Impaired Oxidation of Debrisoquine in Patients With Perhexiline Liver Injury. *Gut* **1984,** *25* (10), 1057–1064.
53. Daly, A. K. Using Genome-Wide Association Studies to Identify Genes Important in Serious Adverse Drug Reactions. *Annu. Rev. Pharmacol. Toxicol.* **2012,** *52,* 21–35.
54. Mehta, N. K.e. *The Hla Complex in Biology and Medicine: A Resource Book,* 1st ed.; Jaypee Brothers Medical Publishers: New Delhi, India, 2010.
55. Daly, A. K.; Donaldson, P. T.; Bhatnagar, P.; Shen, Y.; Pe'er, I.; Floratos, A.; Daly, M. J.; Goldstein, D. B.; John, S.; Nelson, M. R.; Graham, J.; Park, B. K.; Dillon, J. F.; Bernal, W.; Cordell, H. J.; Pirmohamed, M.; Aithal, G. P.; Day, C. P. HLA-B*5701 Genotype is a Major Determinant of Drug-Induced Liver Injury Due to Flucloxacillin. *Nat. Genet.* **2009,** *41,* 816–819.
56. Lucena, M. I.; Molokhia, M.; Shen, Y.; Urban, T. J.; Aithal, G. P.; Andrade, R. J.; Day, C. P.; Ruiz-Cabello, F.; Donaldson, P. T.; Stephens, C.; Pirmohamed, M.; Romero-Gomez, M.; Navarro, J. M.; Fontana, R. J.; Miller, M.; Groome, M.; Bondon-Guitton, E.; Conforti, A.; Stricker, B. H.; Carvajal, A.; Ibanez, L.; Yue, Q. Y.; Eichelbaum, M.; Floratos, A.; Pe'er, I.; Daly, M. J.; Goldstein, D. B.; Dillon, J. F.; Nelson, M. R.; Watkins, P. B.; Daly, A. K. Susceptibility to Amoxicillin-Clavulanate-Induced Liver Injury Is Influenced by Multiple HLA Class I and II Alleles. *Gastroenterology* **2011,** *141* (1), 338–347.
57. Singer, J. B.; Lewitzky, S.; Leroy, E.; Yang, F.; Zhao, X.; Klickstein, L.; Wright, T. M.; Meyer, J.; Paulding, C. A. A Genome-Wide Study Identifies HLA Alleles Associated With Lumiracoxib-Related Liver Injury. *Nat. Genet.* **2010,** *42,* 711–714.
58. Spraggs, C. F.; Budde, L. R.; Briley, L. P.; Bing, N.; Cox, C. J.; King, K. S.; Whittaker, J. C.; Mooser, V. E.; Preston, A. J.; Stein, S. H.; Cardon, L. R. HLA-DQA1*02:01 Is a Major Risk Factor for Lapatinib-Induced Hepatotoxicity in Women With Advanced Breast Cancer. *J. Clin. Oncol.* **2011,** *29* (6), 667–673.
59. Kindmark, A.; Jawaid, A.; Harbron, C. G.; Barratt, B. J.; Bengtsson, O. F.; Andersson, T. B.; Carlsson, S.; Cederbrant, K. E.; Gibson, N. J.; Armstrong, M.; Lagerstrom-Fermer, M. E.; Dellsen, A.; Brown, E. M.; Thornton, M.; Dukes, C.; Jenkins, S. C.; Firth, M. A.; Harrod, G. O.; Pinel, T. H.; Billing-Clason, S. M.; Cardon, L. R.; March, R. E. Genome-Wide Pharmacogenetic Investigation of a Hepatic Adverse Event Without Clinical Signs of Immunopathology Suggests an Underlying Immune Pathogenesis. *Pharmacogenomics J.* **2008,** *8,* 186–195.
60. Hirata, K.; Takagi, H.; Yamamoto, M.; Matsumoto, T.; Nishiya, T.; Mori, K.; Shimizu, S.; Masumoto, H.; Okutani, Y. Ticlopidine-Induced Hepatotoxicity is Associated With Specific Human Leukocyte Antigen Genomic Subtypes in Japanese Patients: A Preliminary Case–Control Study. *Pharmacogenomics J.* **2008,** *8* (1), 29–33.
61. (a) Monshi, M. M.; Faulkner, L.; Gibson, A.; Jenkins, R. E.; Farrell, J.; Earnshaw, C. J.; Alfirevic, A.; Cederbrant, K.; Daly, A. K.; French, N.; Pirmohamed, M.; Park, B. K.; Naisbitt, D. J. Human Leukocyte Antigen (HLA)-B*57:01-Restricted Activation of Drug-Specific T Cells Provides the Immunological Basis for Flucloxacillin-Induced Liver Injury. *Hepatology* **2013,** *57* (2), 727–739; (b) Wuillemin, N.; Adam, J.; Fontana, S.; Krahenbuhl, S.; Pichler, W. J.; Yerly, D. HLA Haplotype Determines Hapten or p-i T Cell Reactivity to Flucloxacillin. *J. Immunol.* **2013,** *190* (10), 4956–4964.
62. Sarich, T. C.; Adams, S. P.; Petricca, G.; Wright, J. M. Inhibition of Isoniazid-Induced Hepatotoxicity in Rabbits by Pretreatment With an Amidase Inhibitor. *J. Pharmacol. Exp. Ther.* **1999,** *289* (2), 695–702.
63. Ng, C. S.; Hasnat, A.; Al Maruf, A.; Ahmed, M. U.; Pirmohamed, M.; Day, C. P.; Aithal, G. P.; Daly, A. K. N-Acetyltransferase 2 (NAT2) Genotype as a Risk Factor for Development of Drug-Induced Liver Injury Relating to Antituberculosis Drug Treatment in a Mixed-Ethnicity Patient Group. *Eur. J. Clin. Pharmacol.* **2014,** *70* (9), 1079–1086.
64. Urban, T. J.; Shen, Y.; Stolz, A.; Chalasani, N.; Fontana, R. J.; Rochon, J.; Ge, D.; Shianna, K. V.; Daly, A. K.; Lucena, M. I.; Nelson, M. R.; Molokhia, M.; Aithal, G. P.; Floratos, A.; Pe'er, I.; Serrano, J.; Bonkovsky, H.; Davern, T. J.; Lee, W. M.; Navarro, V. J.; Talwalkar, J. A.; Goldstein, D. B.; Watkins, P. B.; Drug-Induced Liver Injury Network, Diligen, Eudragene, Spanish DILI Registry, International Serious Adverse Events Consortium. Limited Contribution of Common Genetic Variants to Risk for Liver Injury Due to a Variety of Drugs. *Pharmacogenet. Genomics* **2012,** *22* (11), 784–795.
65. Metushi, I. G.; Zhu, X.; Chen, X.; Gardam, M. A.; Uetrecht, J. Mild Isoniazid-Induced Liver Injury in Humans is Associated With an Increase in Th17 Cells and T Cells Producing IL-10. *Chem. Res. Toxicol.* **2014,** *27* (4), 683–689.
66. Daly, A. K. Pharmacogenetics of the Cytochromes P450. *Curr. Top. Med. Chem.* **2004,** *4* (16), 1733–1744.

67. (a) Kato, S.; Shields, P. G.; Caporaso, N. E.; Hoover, R. N.; Trump, B. F.; Sugimura, H.; Weston, A.; Harris, C. C. Cytochrome P450IIE1 Genetic Polymorphisms, Racial Variation, and Lung Cancer Risk. *Cancer Res.* **1992,** *52,* 6712–6715; (b) Hayashi, S.; Watanabe, J.; Kawagiri, K. Genetic Polymorphisms in the 5'-Flanking Region Change Transcriptional Regulation of the Human Cytochrome P450IIE1 Gene. *J. Biochem.* **1991,** *110,* 559–565.
68. Huang, Y. S.; Chern, H. D.; Su, W. J.; Wu, J. C.; Chang, S. C.; Chiang, C. H.; Chang, F. Y.; Lee, S. D. Cytochrome p450 2E1 Genotype and the Susceptibility to Antituberculosis Drug-Induced Hepatitis. *Hepatology* **2003,** *37* (4), 924–930.
69. Lee, S. W.; Chung, L. S.; Huang, H. H.; Chuang, T. Y.; Liou, Y. H.; Wu, L. S. NAT2 and CYP2E1 Polymorphisms and Susceptibility to First-Line Anti-Tuberculosis Drug-Induced Hepatitis. *Int. J. Tuberc. Lung Dis.* **2010,** *14* (5), 622–626.
70. (a) Roy, B.; Chowdhury, A.; Kundu, S.; Santra, A.; Dey, B.; Chakraborty, M.; Majumder, P. P. Increased Risk of Antituberculosis Drug-Induced Hepatotoxicity in Individuals With Glutathione S-Transferase M1 'Null' Mutation. *J. Gastroenterol. Hepatol.* **2001,** *16* (9), 1033–1037; (b) Huang, Y. S.; Su, W. J.; Huang, Y. H.; Chen, C. Y.; Chang, F. Y.; Lin, H. C.; Lee, S. D. Genetic Polymorphisms of Manganese Superoxide Dismutase, NAD(P)H:Quinone Oxidoreductase, Glutathione S-Transferase M1 and T1, and the Susceptibility to Drug-Induced Liver Injury. *J. Hepatol.* **2007,** *47* (1), 128–134.
71. Leiro, V.; Fernandez-Villar, A.; Valverde, D.; Constenla, L.; Vazquez, R.; Pineiro, L.; Gonzalez-Quintela, A. Influence of Glutathione S-Transferase M1 and T1 Homozygous Null Mutations on the Risk of Antituberculosis Drug-Induced Hepatotoxicity in a Caucasian Population. *Liver Int.* **2008,** *28* (6), 835–839.
72. Azuma, J.; Ohno, M.; Kubota, R.; Yokota, S.; Nagai, T.; Tsuyuguchi, K.; Okuda, Y.; Takashima, T.; Kamimura, S.; Fujio, Y.; Kawase, I. NAT2 Genotype Guided Regimen Reduces Isoniazid-Induced Liver Injury and Early Treatment Failure in the 6-Month Four-Drug Standard Treatment of Tuberculosis: A Randomized Controlled Trial for Pharmacogenetics-Based Therapy. *Eur. J. Clin. Pharmacol.* **2013,** *69* (5), 1091–1101.
73. Aithal, G. P.; Day, C. P.; Leathart, J. B. S.; Daly, A. K. Relationship of Polymorphism in CYP2C9 to Genetic Susceptibility to Diclofenac-Induced Hepatitis. *Pharmacogenetics* **2000,** *10,* 511–518.
74. Daly, A. K.; Aithal, G. P.; Leathart, J. B.; Swainsbury, R. A.; Dang, T. S.; Day, C. P. Genetic Susceptibility to Diclofenac-Induced Hepatotoxicity: Contribution of UGT2B7, CYP2C8, and ABCC2 Genotypes. *Gastroenterology* **2007,** *132* (1), 272–281.
75. Bailey, M. J.; Dickinson, R. G. Acyl Glucuronide Reactivity in Perspective: Biological Consequences. *Chem. Biol. Interact.* **2003,** *145* (2), 117–137.
76. Sawamura, R.; Okudaira, N.; Watanabe, K.; Murai, T.; Kobayashi, Y.; Tachibana, M.; Ohnuki, T.; Masuda, K.; Honma, H.; Kurihara, A.; Okazaki, O. Predictability of Idiosyncratic Drug Toxicity Risk for Carboxylic Acid-Containing Drugs Based on the Chemical Stability of Acyl Glucuronide. *Drug Metab. Dispos.* **2010,** *38* (10), 1857–1864.
77. Aithal, G. P.; Ramsay, L.; Daly, A. K.; Sonchit, N.; Leathart, J. B.; Alexander, G.; Kenna, J. G.; Caldwell, J.; Day, C. P. Hepatic Adducts, Circulating Antibodies, and Cytokine Polymorphisms in Patients With Diclofenac Hepatotoxicity. *Hepatology* **2004,** *39* (5), 1430–1440.
78. Graham, D. J.; Green, L.; Senior, J. R.; Nourjah, P. Troglitazone-Induced Liver Failure: A Case Study. *Am. J. Med.* **2003,** *114* (4), 299–306.
79. Honma, W.; Shimada, M.; Sasano, H.; Ozawa, S.; Miyata, M.; Nagata, K.; Ikeda, T.; Yamazoe, Y. Phenol Sulfotransferase, ST1A3, as the Main Enzyme Catalyzing Sulfation of Troglitazone in Human Liver. *Drug Metab. Dispos.* **2002,** *30* (8), 944–949.
80. Yang, K.; Woodhead, J. L.; Watkins, P. B.; Howell, B. A.; Brouwer, K. L. Systems Pharmacology Modeling Predicts Delayed Presentation and Species Differences in Bile Acid-Mediated Troglitazone Hepatotoxicity. *Clin. Pharmacol. Ther.* **2014,** *96* (5), 589–598.
81. Watanabe, I.; Tomita, A.; Shimizu, M.; Sugawara, M.; Yasumo, H.; Koishi, R.; Takahashi, T.; Miyoshi, K.; Nakamura, K.; Izumi, T.; Matsushita, Y.; Furukawa, H.; Haruyama, H.; Koga, T. A Study to Survey Susceptible Genetic Factors Responsible for Troglitazone-Associated Hepatotoxicity in Japanese Patients With Type 2 Diabetes Mellitus. *Clin. Pharmacol. Ther.* **2003,** *73* (5), 435–455.
82. Okada, R.; Maeda, K.; Nishiyama, T.; Aoyama, S.; Tozuka, Z.; Hiratsuka, A.; Ikeda, T.; Kusuhara, H.; Sugiyama, Y. Involvement of Different Human Glutathione Transferase Isoforms in the Glutathione Conjugation of Reactive Metabolites of Troglitazone. *Drug Metab. Dispos.* **2011,** *39* (12), 2290–2297.
83. Harrill, A. H.; Watkins, P. B.; Su, S.; Ross, P. K.; Harbourt, D. E.; Stylianou, I. M.; Boorman, G. A.; Russo, M. W.; Sackler, R. S.; Harris, S. C.; Smith, P. C.; Tennant, R.; Bogue, M.; Paigen, K.; Harris, C.; Contractor, T.; Wiltshire, T.; Rusyn, I.; Threadgill, D. W. Mouse Population-Guided Resequencing Reveals That Variants in CD44 Contribute to Acetaminophen-Induced Liver Injury in Humans. *Genome Res.* **2009,** *19* (9), 1507–1515.
84. Court, M. H.; Peter, I.; Hazarika, S.; Vasiadi, M.; Greenblatt, D. J.; Lee, W. M. Candidate Gene Polymorphisms in Patients With Acetaminophen-Induced Acute Liver Failure. *Drug Metab. Dispos.* **2014,** *42* (1), 28–32.
85. Szkolnicka, D.; Farnworth, S. L.; Lucendo-Villarin, B.; Storck, C.; Zhou, W.; Iredale, J. P.; Flint, O.; Hay, D. C. Accurate Prediction of Drug-Induced Liver Injury Using Stem Cell-Derived Populations. *Stem Cells Transl. Med.* **2014,** *3* (2), 141–148.
86. Dear, J. W.; Antoine, D. J. Stratification of Paracetamol Overdose Patients Using New Toxicity Biomarkers: Current Candidates and Future Challenges. *Expert. Rev. Clin. Pharmacol.* **2014,** *7* (2), 181–189.

4.13 Drug-Induced Liver Injury: Mechanism-Informed Prediction in Drug Development

C Goldring, University of Liverpool, Liverpool, United Kingdom
R Weaver, Biologie Servier, Gidy, France
B Kramer, U Klingmueller, and A Oppelt, German Cancer Research Center, Heidelberg, Germany
B Van der Water, Leiden University, Leiden, The Netherlands
J Commandeur, VU University Amsterdam, Amsterdam, The Netherlands
A Guillouzo, Université de Rennes 1, Rennes, France
D Naisbitt, N French, N Kitteringham, and C Pridgeon, University of Liverpool, Liverpool, United Kingdom
P Knolle, Technische Universität München, München, Germany
J Sidaway, AstraZeneca R&D, Cheshire, United Kingdom
R Sison-Young, L Kamalian, A Mercer, and L Faulkner, University of Liverpool, Liverpool, United Kingdom
R Pieters, Utrecht University, Utrecht, The Netherlands
M Ingelman-Sundberg, Karolinska Institutet, Stockholm, Sweden
B Kevin Park, University of Liverpool, Liverpool, United Kingdom

© 2017 Elsevier Ltd. All rights reserved.

4.13.1	**Introduction**	218
4.13.2	**The Role of Reactive Drug Metabolites in DILI**	218
4.13.2.1	Introduction	218
4.13.2.2	Selectivity of Covalent Binding: Critical Versus Noncritical Covalent Binding?	219
4.13.2.3	Are Other Types of Reactive Intermediates More Important for the Onset of DILI?	220
4.13.2.4	Does an Imbalance in Activation and Inactivation of Drugs Determine Human Susceptibility to DILI?	220
4.13.2.5	Can We Link the Formation of Drug Reactive Metabolites to the Onset of DILI in Humans?	220
4.13.3	**Assessment and Prediction of Mitochondrial Dysfunction (In Vitro and In Vivo)**	221
4.13.3.1	Introduction	221
4.13.3.2	Mitochondrial Toxicity	221
4.13.3.3	Key Intracellular Signaling Pathways Implicated in Drug-Induced Mitochondrial Perturbation	221
4.13.3.3.1	JNK signaling	221
4.13.3.3.2	Inhibition of fatty acid oxidation and lipid transport	221
4.13.3.4	The Hepatic Specificity of Action for Drugs That Cause Mitochondrial Dysfunction	221
4.13.3.5	Structural Aspects of Drugs Eliciting Mitochondrial Damage	223
4.13.3.6	Mitochondrial Adaptation to Drugs	223
4.13.4	**Lysosomal Perturbation and DILI**	223
4.13.4.1	Introduction	223
4.13.4.2	Physicochemical Properties of Drugs and Lysosomes	223
4.13.4.3	Autophagy, Lysosomes, and DILI	224
4.13.4.4	Would Perturbation of Autophagy Trigger a Concern for DILI in Compound Assessment?	225
4.13.4.5	Lysosomal Perturbations and Cytotoxicity	225
4.13.5	**Assessment and Prediction of the Role of Transporters in Drug- and Bile Acid-Induced Liver Injury**	225
4.13.5.1	Introduction and Classification of Drug and Bile Acid Transporters	225
4.13.5.2	Bile Acid Uptake and Excretion	225
4.13.5.3	The Cellular and Hepatic Features of Cholestasis	226
4.13.5.4	Model Systems for Transport Evaluation	227
4.13.5.5	Bile Acid Toxicity	227
4.13.5.6	Transporters and Bile Acid Toxicity: Comments and Future Challenges	228
4.13.6	**Evidence for the Role of the Innate Immune System in DILI in Man**	228
4.13.6.1	Introduction	228
4.13.6.2	HLA Associations With DILI	228
4.13.6.3	Role of Cytokines and Chemokines	229
4.13.6.4	The Role of TNFα	229
4.13.6.5	Autoantibodies and DILI	229
4.13.6.6	The Role of the Innate Immune System in DILI	229
4.13.6.7	In Vitro Liver Models to Capture the Innate Immune System	230
4.13.7	**Evidence for a Role of the Adaptive Immune System in Humans**	230
4.13.7.1	Introduction	230
4.13.7.2	Evidence From Studies Using PBMC From Patients With DILI	230

4.13.8	**Signaling Pathways and Mathematical Models: Toward Prediction of DILI**	231
4.13.8.1	Introduction: What Experimental In Vitro and In Silico Models Are Available for the Detection of DILI?	231
4.13.8.2	How to Use In Silico Models to Detect Hepatocyte and NPC Perturbation?	232
4.13.8.3	What Can Be Learned From Modeling Signaling Pathways for Better Prediction?	232
4.13.8.4	How Can the Physiological Response and Toxicological Perturbation of Signaling Pathways for the Prediction of DILI Be Quantified?	233
4.13.8.5	How Mathematical Modeling Can Improve, for Example, the Human Relevance of Our In Vitro Models	233
4.13.8.6	Conclusions and Future Perspectives	233
References		234
Relevant Websites		238

4.13.1 Introduction

Adverse drug reactions (ADRs) are a major clinical problem in terms of patient morbidity and mortality, cost to healthcare systems, and failure of drugs in development. Of all the different forms of ADRs, the liver is among the most susceptible organs to drug toxicity. Drug-induced liver injury (DILI) is a particularly challenging for the pharmaceutical industry, while in the clinic, DILI accounts for more than 50% of acute liver failure cases.[1] Although many of these cases are attributable to intentional and unintentional acetaminophen overdose, a significant proportion is also due to idiosyncratic hepatotoxicity. DILI is a key cause for attrition of drugs in development and is the major reason for withdrawal of a drug post-marketing.[2,3,173] The main reason for this unsatisfactory situation is that current preclinical drug testing does not work to predict DILI in humans. A huge worldwide effort is therefore being applied to improve the assessment of potential hepatotoxic risk of new compounds.

A key truism concerning DILI is that it is a multidimensional and multifaceted disease. This means that it is inherently intractable to simple solutions, including some of the single-cell screening strategies used for many years in pharma, which with the benefit of hindsight seem overly simple. Some companies may screen for reactive metabolites and mitochondrial dysfunction, in sandwich cultures and micropatterned cocultures as well as in organelles to identify drugs causing DILI, but even these methods, which take us beyond a simple liver cancer cell line, that is, HepG2, in 2-D culture, and are good at identifying drugs that have no idiosyncratic DILI (90–95% predictability), perform less well for positive predictions (50–89%).[4–6]

At the heart of the efforts to improve the failing status quo, there is therefore the growing consensus that a much better understanding of the mechanisms underlying DILI is essential, particularly in the design and construction of the new improved predictive models that are likely to emerge. As part of this effort, the Innovative Medicines Initiative MIP-DILI Consortium here proposes current likely key mechanisms underlying DILI in all of its known guises, in order to ensure that these are properly addressed in the new and emerging models of DILI. While a number of reviews and perspective papers have been published over the last few years on the impact on drug development of idiosyncratic DILI,[7] chemically reactive metabolites,[8] genetic risk factors in ADRs,[9] and predictive models for DILI,[10] these have not covered in detail the likely individual mechanisms underlying DILI, from molecular reactivity, through intracellular organellar function, to the role of the immune system.

A graphic outline of the scope and scale of the mechanisms likely to underlie many of the different forms of DILI and that feature in this perspective is shown in **Fig. 1**. The overall thesis of this perspective is that only through a more comprehensive understanding of the mechanisms of human DILI will we be able to improve our efforts in the application of more meaningful models in the lab and thereby improve human prediction.

4.13.2 The Role of Reactive Drug Metabolites in DILI

4.13.2.1 Introduction

The work of many groups over many decades has clearly demonstrated that during the metabolic breakdown of chemicals, highly reactive metabolites are often produced. As early as the 1940s, the Millers demonstrated that the carcinogenicity and hepatotoxicity of aminoazo dyes result from their bioactivation to electrophilic species that bind covalently to DNA and proteins.[11,12] Since then, it has been demonstrated that a large number of pharmaceuticals known to cause DILI are also converted to electrophilic metabolites by drug-metabolizing enzymes, in particular by the cytochromes P450.[8,13–16] The chemical modification of biological macromolecules, which may lead to loss of function or which can trigger immune responses, is generally considered to play an important role in the onset of hepatotoxicity.[8,17] Therefore, a large number of analytic methodologies have been developed to detect and quantify the formation of reactive metabolites during drug development. Trapping of reactive metabolites by low-molecular-weight nucleophiles, such as GSH, GSH-analogs, cyanide, and model peptides, is now widely used to characterize the bioactivation of potentially toxic drugs. However, despite that fact that these qualitative studies have generated a large amount of knowledge about structural elements that are prone to bioactivation to reactive metabolites, that is, the so-called structural alerts, it is not yet possible to predict the toxic potential of drugs based on these types of covalent binding studies[18] (**Box 1**).

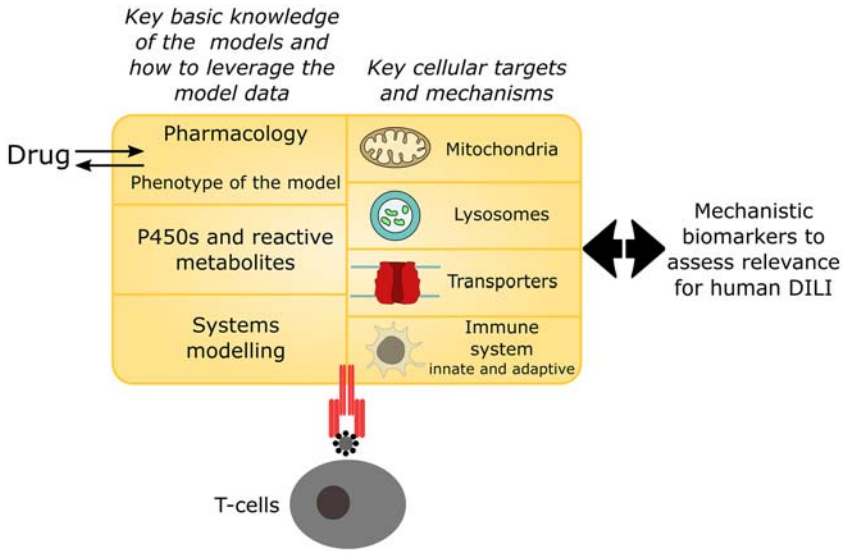

Fig. 1 Overview of the key likely DILI mechanisms that are covered in this review. While the field of mechanistic biomarkers is outside of the scope of this review, it is included in this scheme to illustrate how they should be used to "bridge back" from human clinical DILI to tell us whether our laboratory models are relevant.

Box 1

Linking protein modification with function: The holy grail of the reactive metabolite field?

Improvements in protein separation technology and detection of protein modification by mass spectrometry have enabled significant progress in the identification of specific target proteins that are chemically modified by reactive metabolites. For more than 48 chemicals, including APAP, diclofenac, flucloxacillin, and tienilic acid, several hundred target proteins have been identified and deposited in a web-accessible database (http://tpdb.medchem.ku.edu:8080/). Through bioinformatic approaches, efforts have been made to distinguish target proteins that might be critical for acute cytotoxicity. Initially, only a relatively small overlap of target proteins was observed when comparing different toxicants, which strongly suggests that this fairly laborious methodology may not be able to distinguish critical from noncritical targets. More recently, however, a new bioinformatic approach that assesses the disruption of protein–protein interactions resulted in the ranking of several target proteins that might play an important role in cell death.[19] Several target proteins, such as heat shock proteins, calreticulin, and glutathione *S*-transferase P1-1, were proposed as key target proteins, which upon chemical modification result in cytotoxicity. However, further studies will be required to confirm the critical causative role of modifications in these target proteins for cell death and their role in cell perturbation elicited by other hepatoxicants.

Assessment of the covalent binding of radiolabeled drugs or drug candidates to hepatic fractions is often considered as the gold standard to quantify the total amount of covalent binding of reactive metabolites in in vitro and in vivo model systems. In the perspective article by Evans et al. in 2004, a threshold of covalent binding of $\sim$1 nmol mg^{-1} microsomal protein was defined, which was considered as a high risk for hepatotoxicity, based on in vitro covalent binding studies of a range of hepatotoxic chemicals.[20] Subsequent studies, however, showed that many nontoxic drugs also produced relatively high levels of covalent binding when measured in a similar fashion as proposed by Evans et al.[20] Therefore, measuring covalent binding in vitro does not distinguish between toxic and nontoxic compounds. Consequently, several approaches have been developed to improve the capability to distinguish toxic from nontoxic compounds. The first approach was to combine in vitro covalent binding with total daily dose in order to estimate the body burden of covalent binding.[21] This approach significantly improved the correlation between covalent binding and hepatotoxicity of drugs and most likely explains why drugs that are dosed at less than 10 mg day^{-1} typically do not cause idiosyncratic drug reactions. However, many unresolved questions still remain regarding the factors that will determine whether or not a high-dose drug that is bioactivated to reactive metabolites will actually cause DILI, whether or not the reactive metabolites play a (crucial) role in the onset of DILI, and which individual is susceptible for DILI.

4.13.2.2 Selectivity of Covalent Binding: Critical Versus Noncritical Covalent Binding?

Although covalent binding is often considered as one of the mechanisms that can initiate the events leading to DILI, it has been observed that the total body burden of covalent binding as such is not predictive for hepatotoxicity. For example, both acetaminophen (APAP) and its structural analog 3-hydroxyacetanilide (AMAP) produce an equal amount of covalent binding to hepatic proteins after administration to mice; however, only APAP causes hepatotoxicity in mice. To account for this, it was proposed that the reactive metabolites of APAP and AMAP have different selectivities of covalent binding at the subcellular organelle level,

with APAP preferentially binding to mitochondrial proteins and AMAP preferentially binding to cytosolic targets.[22] Therefore, not only the total amount of covalent binding but also the selectivity of covalent binding seems to be critical for the toxic outcome.

For some drugs causing DILI, it has been shown that in patient serum, antibodies are found that are directed against the enzymes involved in their bioactivation.[23] For example, in the serum of patients suffering from tienilic acid-induced hepatitis, antibodies against CYP2C9 were detected.[24] Tienilic acid is a suicide substrate for CYP2C9, and an adduct of tienilic acid with CYP2C9 was identified by mass spectrometry in in vitro incubations.[25] By as yet unresolved mechanisms, the tienilic acid-CYP2C9 adducts appear to be processed by the immune system leading to an immune response.

4.13.2.3 Are Other Types of Reactive Intermediates More Important for the Onset of DILI?

The analytic methodologies to determine the role of bioactivation in drug toxicity are mainly focused on the covalent binding of electrophiles to proteins or trapping agents, since for covalent binding, many drug-specific radiochemical, mass spectroscopic, and immunochemical detection methods are available.[16,20] However, using these methods, the involvement of other types of toxicologically relevant reactive intermediates, such as oxidants, radicals, reactive oxygen species (ROS), and reactive nitrogen species, usually is not considered. It is well known that quinones are not only electrophiles that bind covalently to protein thiols but also oxidants that can oxidize GSH and protein thiols to (mixed) disulfides.[26] Because the hydroquinones formed can be reoxidized again to the quinones by cytochromes P450, redox cycling of the quinone/hydroquinone couple can cause a shift in the redox state of proteins to their oxidized state.[27] In contrast to covalent binding, where one electrophile molecule inactivates or haptenizes only a single protein, by redox cycling, multiple proteins can be oxidized per molecule of (hydro)quinone. Furthermore, quinones can redox cycle by one-electron reduction processes, by cellular reductases, or by interference with the mitochondrial respiration chain.[28,29] The concomitant production of massive amounts of superoxide anion radicals in turn can cause lipid peroxidation processes, which can instigate the formation of a large number of secondary electrophilic breakdown products (such as 4-hydroxynonenal), which might lead to much higher levels of covalent binding than the primary electrophilic drug metabolites.[30] As an example of this phenomenon, troglitazone is metabolized by CYP3A4 to a quinone metabolite, which is fully substituted and therefore cannot bind covalently to protein thiols.[31] The fact that troglitazone causes lipid peroxidation and cytotoxicity in CYP3A4-transfected cells, after downregulation of superoxide dismutase 2, shows that the redox-cycling properties, rather than the electrophilic properties of the quinone metabolite per se, plays an important role in cytotoxicity.[32]

Therefore, there is a need for additional analytic methodologies that can detect the types of reactive intermediates that are not covered by the covalent binding studies and that can quantify the body burden of exposure to potentially toxic oxidants, radicals, and ROS.

4.13.2.4 Does an Imbalance in Activation and Inactivation of Drugs Determine Human Susceptibility to DILI?

It is now well recognized that drugs which are administered at a relatively high daily dose and that undergo extensive metabolism are more likely to cause idiosyncratic drug reactions.[33,34] Nevertheless, it is still not completely understood why the large majority of patients treated with these high-dose drugs do not suffer from DILI. Therefore, patient-specific factors such as genetic polymorphisms at the level of adsorption, distribution, metabolism, and excretion (ADME)-related processes and/or human leukocyte antigen (HLA) also may determine the risk for DILI.[35–37] Although hepatocytes contain high levels of cytochromes P450 that can bioactivate drugs to reactive metabolites, they are also rich in GSH and protective enzymes such as glutathione *S*-transferases, epoxide hydrolases, and NADPH-quinone oxidoreductases (NQO) that inactivate reactive metabolites.[38] Also, the high activity of UDP-glucuronosyl transferases and sulfotransferase can divert metabolism of drugs away from the bioactivation pathway. In the case of APAP, at normal doses, metabolism is mainly by glucuronidation and sulfation; CYP-dependent bioactivation only occurs at high dose levels when cofactors of these protective pathways become depleted.[39] Therefore, it can be envisaged that for most individuals, the capacity of the protective enzyme systems is apparently high enough to deal with the burden of reactive metabolites. Furthermore, through the Nrf2-mediated stress response system, the levels of protective enzyme systems and antioxidants can be strongly upregulated, thereby further protecting against protein modifications.[40,41] It therefore can be hypothesized that the risk for DILI can be significantly increased in individuals in which the balance of activation and inactivation is disturbed by genetic factors or nongenetic factors. For example, several association studies suggest that genetically determined deficiencies in GSTM1-1 and GSTT1-1 increase the risk of idiosyncratic DILI.[31,42,43] However, because of the low number of cases in these association studies, the statistical power of these studies is relatively poor and requires confirmation by larger population studies or by mechanistic in vitro models.

4.13.2.5 Can We Link the Formation of Drug Reactive Metabolites to the Onset of DILI in Humans?

It remains a significant challenge to determine unequivocally whether or not reactive metabolites have any predictive value for the risk of DILI. It is also worth pointing out that while it is becoming clear that the majority of hepatotoxicities in humans involve the immune system (innate and/or adaptive), modeling the first chemical perturbation (through reactive metabolite formation or exposure to parent compound) of the likely initial target cell (hepatocyte) that will provide a danger signal will still be essential and is the only current feasible route for prediction (no in vitro recapitulation of the interaction of perturbed hepatocytes with components of the immune system is yet possible).[17]

4.13.3 Assessment and Prediction of Mitochondrial Dysfunction (In Vitro and In Vivo)

4.13.3.1 Introduction

More than 1000 recently developed drugs can induce liver injury, with various clinical consequences.[7,8] Of 300 drugs assessed, 50–60% of those that can elicit idiosyncratic toxicity cause mitochondrial perturbation, whereas among non-DILI drugs, this falls to $<5\%$.[44] Furthermore, there is also a positive correlation (89%) between exposure to idiosyncratic drugs and disruption of isolated mitochondria.[45]

Since 45% of idiosyncratic DILI cases have been shown to be caused by antimicrobials, a link can be suggested because of the bacterial ancestry of mitochondria.[46] Bacteria share many genetic and structural similarities with mitochondria; therefore, there is a strong argument to suggest that antibiotics may directly harm mitochondria to promote DILI. Many drugs showing idiosyncratic toxicity, such as amiodarone and valproic acid, directly disrupt mitochondria, thereby eliciting cellular stress in hepatocytes.

4.13.3.2 Mitochondrial Toxicity

Mitochondria harbor several key processes that are important for interactions with drugs causing mitochondrial toxicity and cell toxicity. The major ones are (i) the mitochondrial respiratory chain and oxidative phosphorylation, (ii) mitochondrial permeabilization, (iii) fatty acid oxidation, and (iv) mitochondrial DNA (mtDNA) synthesis. Inhibition of the first two pathways causes necrosis and/or apoptosis, whereas inhibition of fatty acid oxidation can induce microvesicular steatosis causing liver failure. The impairment of fatty acid oxidation indirectly inhibits the mitochondrial respiratory chain. These reactions can be triggered by inhibiting the respiratory chain or uncoupling of oxidative phosphorylation by the formation of drug cations in the acidic intermembrane space of the mitochondria. Inhibition of the respiratory chain causes increased formation of ROS and subsequent ROS-dependent toxicities. Since 13 proteins of the mitochondrial respiratory chain are encoded by mtDNA, drug-induced damage of the mtDNA or inhibition of mtDNA replication can impair oxidative phosphorylation.[47] Indeed, a recent review of drug-induced mitochondrial toxicity reveals that inhibition of mitochondrial respiration and inhibition of fatty acid oxidation are very common for about 50 different drugs.[48] Two of the mitochondrial processes likely to be sensitive to drug-induced perturbation, that is, mitochondrial respiration and/or β-oxidation, are shown in Fig. 2. Drugs that inhibit these processes are also shown in Table 1.

4.13.3.3 Key Intracellular Signaling Pathways Implicated in Drug-Induced Mitochondrial Perturbation

4.13.3.3.1 JNK signaling

c-Jun N-terminal kinase (JNK) is activated by ROS and cellular stress and after APAP toxicity when glutathione has been depleted by more than 90%. The early phase of JNK activation involves glycogen synthase kinase 3 beta (GSK-3β) and mixed lineage kinase 2 (MLK2).[45] GSK-3β can activate JNK through MEKK1- or MLK-dependent pathways. However, the late phase of JNK activation is believed to be mediated by apoptosis signal-regulating kinase 1 (ASK1) in the liver. Both ASK1 and JNK can be influenced by thioredoxin that binds to and inhibits ASK1 and by GST-Pi that binds to and inhibits JNK and phosphatases acting on JNK.

Upon activation by autophosphorylation, JNK translocates to the mitochondria where it binds to SH3-domain binding protein associating with Btk (Sab), a scaffold protein located on the outer membrane of the mitochondria. Silencing of Sab in knockout mice protects the liver from APAP toxicity.[49] The action of JNK in the mitochondria is believed to be through binding to Sab, which causes increased mitochondrial ROS formation and induction of mitochondrial permeability transition (MPT) in damaged mitochondria. The MPT involves increased permeability of the inner mitochondrial membrane resulting in mitochondrial swelling and death. Crucially, the action of JNK appears more prominent when the mitochondria have been primed for stress. Such stress can be achieved by the reactive metabolite of acetaminophen, NAPQI. However, the exact mechanism for JNK–Sab-mediated modulation of the electron transport chain and the increase in ROS and MPT are unknown.[46]

4.13.3.3.2 Inhibition of fatty acid oxidation and lipid transport

Drugs such as valproic acid, ibuprofen, tianeptine, amiodarone, and tamoxifen can directly inhibit fatty acid oxidases.[50–52] The action of valproic acid is likely to be exerted to a great extent by the D2,4-VPA-CoA reactive metabolite that irreversibly inactivates fatty acid oxidases. The ability of acetaminophen to induce steatosis in some individuals might also be caused by the ability of its major reactive metabolite, NAPQI, to cause similar inhibition. As well as the inhibition of the fatty acid synthases, the exact identity of which is not yet known, the inhibition of carnitine palmitoyltransferase-1 is a key point for the action of drugs such as amiodarone and tamoxifen. In addition, troglitazone is able to inhibit long-chain acyl-CoA synthase, thereby influencing the mitochondrial uptake of the long-chain fatty acids.[53]

4.13.3.4 The Hepatic Specificity of Action for Drugs That Cause Mitochondrial Dysfunction

Mitochondrial dysfunction has long been associated with a large variety of human disorders, such as cardiovascular and neurodegenerative diseases, cancer, migraine, infertility, kidney, and liver diseases.[54] It is evident, however, that the drugs that cause mitochondrial impairment and that are hepatotoxic largely exert their toxic effects specifically in the liver. The reasons for this are yet to be defined and would likely be inherent in two major tissue-specific processes, namely, (i) the capability of the liver to bioactivate

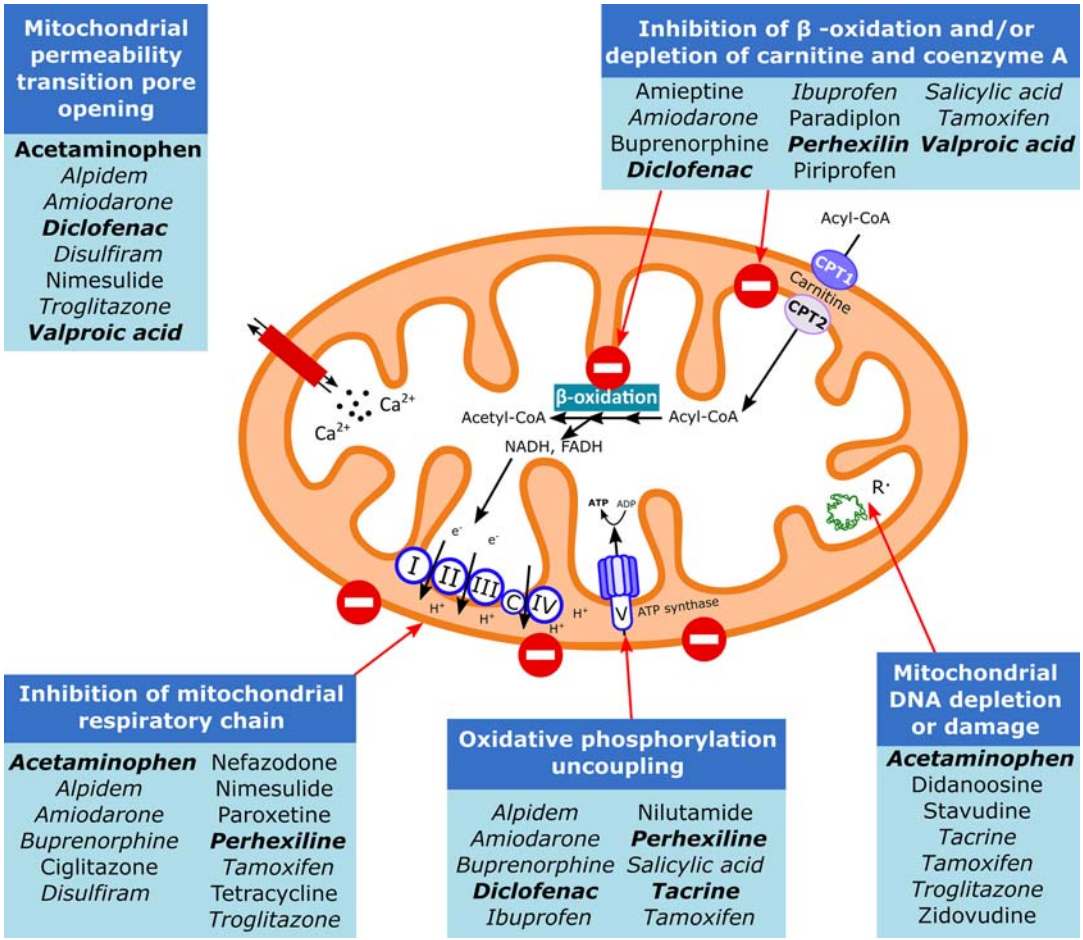

Fig. 2 Mechanisms of drug-induced mitochondrial perturbations. Examples are shown for selected drugs where the evidence for the mechanism of action is high. Drugs marked in bold require metabolic activation, and those in italics act on mitochondria at multiple sites.

Table 1 Drugs that inhibit mitochondrial respiration and/or β-oxidation

Drug	*Inhibition of respiration*	*Inhibition of β-oxidation*	*Drug*	*Inhibition of respiration*	*Inhibition of β-oxidation*
Amineptine	–	Yes	Ibuprofen	–	Yes
Amiodarone	–	Yes	Lovastatin	Yes	–
Aspirin/salicylic acid	Yes	Yes	Nefazodone	Yes	–
			Panadiplon	–	Yes
Benzarone	–	Yes	Paroxetine	Yes	–
Benzbromarone	Yes	Yes	Perhexiline	Yes	Yes
Buprenorphine	Yes	Yes	Phenformin	Yes	–
Carvedilol	Yes	–	Pirprofen	–	Yes
Cerivastatin	Yes	–	Pivampicillin	–	Yes
Chloroquine	Yes	–	Primaquine	Yes	–
Ciglitazone	Yes	–	Propofol	Yes	–
Darglitazone	Yes	–	Quinine	Yes	–
Diethylamino-ethoxyhexesterol	Yes	Yes	Simvastatin	Yes	–
			Tamoxifen	Yes	Yes
Efavirenz	Yes	–	Tetracyclines	–	Yes
Fenofibrate	Yes	–	Tianeptine	–	Yes
Flurbiprofen	–	Yes	Troglitazone	Yes	Yes
Glucocorticoids	–	Yes	Tiaprofenic acid	–	Yes
Hopantentate	–	Yes	Valproate	Yes	Yes

drugs into more toxic metabolites via the arsenal of drug-metabolizing enzymes which are highly expressed in the liver and (ii) that a major part of the mitochondrial impairment caused by different drugs is directly or indirectly linked to hepatic lipid metabolism. Thus, a majority of all drugs causing DILI do so through formation of reactive metabolites. Furthermore, direct or indirect inhibition of fatty acid oxidation or, in some cases, lipid transport causes steatohepatitis and decreased acetyl-CoA, inhibits gluconeogenesis and impaired glucose homeostasis, and also causes energy deficiency in extrahepatic tissues.[47] Also, the accumulation of drug cations (e.g. from amiodarone) in the intermembrane space causes the inhibition of mitochondrial respiration and subsequent inhibition of fatty acid oxidation. Eventually, these processes lead to secondary cellular impairment and cell death and result in the potentially catastrophic effect of uncoupling the mitochondrial respiratory chain.

4.13.3.5 Structural Aspects of Drugs Eliciting Mitochondrial Damage

Drug structure plays an important role in the propensity to cause mitochondrial dysfunction. Amphiphilic drugs such as amiodarone, perhexiline, buprenorphine, and tamoxifen harbor protonatable amine groups, thereby favoring their accumulation inside the mitochondrial matrix under the influence of the membrane potential.[8,47,55] Valproic acid (dipropylacetic acid) is activated by CoA and therefore reduces the intracellular levels of CoA.[47,56] Also the CYP2C9-mediated transformation of valproic acid to D4-valproic acid and subsequently to D2,4-VPA-CoA inactivates fatty acid oxidase enzymes. Furthermore, antiviral drugs inhibit mtDNA replication because they undergo phosphorylation to cognate endogenous nucleosides incorporated into mtDNA by DNA polymerase γ.[57] Apart from these examples, the structural aspects of drugs causing mitochondrial dysfunction are not well understood. In particular, there is a lack of identification of the fatty acid oxidases that are inhibited by these drugs, and such site identification will be necessary in order to improve predictive models that recapitulate drug-induced mitochondrial dysfunction.

4.13.3.6 Mitochondrial Adaptation to Drugs

DILI occurs when liver cells do not adapt to drug exposure. Adaptation may involve upregulation of defense systems such as Nrf2 and the unleashing of antioxidant defenses, upregulation of drug transport, development of immune tolerance through the adaptive immune system, and adaptation of the mitochondria to stress induced by drugs.[46] Mitochondrial adaptation to drugs include: activation of mitophagy, remodeling of the mitochondria to increase respiratory capacity, increased mitochondrial biogenesis, altered fusion–fission exchange of mtDNA, changes to respiratory chain complexes, and other constituents that alter mitochondrial morphology, for example, elongated mitochondria that are more resistant to mitophagy.[46,58] Examples of drugs known to cause mitochondrial pertubation leading to DILI include chloramphenicol and troglitazone which have been shown to cause the formation of megamitochondria[59,60] and trovafloxacin that alters mitochondrial gene expression, indicative of morphological changes.[61] However, as yet, a causative role for the increased size of the mitochondria and adaptation or failure to adapt to drug exposure has not been unequivocally proved.[46]

4.13.4 Lysosomal Perturbation and DILI

4.13.4.1 Introduction

There is clear evidence for a role of lysosomal perturbation in DILI. For example, DILI is clearly associated with the development of phospholipidosis, that is, the accumulation of lipids in the lysosomes as a consequence of disturbed phospholipid breakdown of lysosomes, for example, by phospholipases.[59] Phospholipidosis is related to the physicochemical characteristics of DILI compounds, in close association with the cellular function of lysosomes in critical liver functions during normal and adverse cell physiology.

The lysosomes are acidic organelles that play key roles in endolysosomal catabolism in (receptor-mediated) endocytosis, followed by fusion of late endosomes with lysosomes for degradation of their cargo. This degradation is mediated by around 50 hydrolases including proteases and phospholipases that are catalytically active at low pH. In addition, lysosomes are central to the macroautophagy program, which has been implicated in cellular stress responses triggered by drugs known to cause DILI.[60] Furthermore, lysosomal activity (and thereby correct cellular function) may be severely perturbed at the onset of hepatocyte death, through the release of proteolytic enzymes from injured lysosomes.[61] Each of these issues is discussed in more details in the succeeding text.

4.13.4.2 Physicochemical Properties of Drugs and Lysosomes

The physicochemical properties of a drug are a critical component in the development of phospholipidosis. In particular, compounds that are highly lipophilic ($\log P > 1$) or amphiphilic (cationic amphiphilic drugs) with ionizable amines ($pK_a > 6$) accumulate in the acidic lumen of lysosomes. Several chemoinformatics tools have been established that can predict relatively well the hazard for lysosomal accumulation.[62–64] Recently, such an in silico quantitative structure–activity relationship (QSAR) analysis of phospholipidosis showed around 80% concordance and $>80\%$ predictivity,[65] but discussions are ongoing what database is most

reliable for in silico modeling-based prediction of phospholipidosis.[66] In DILI, the dosing regimen is likely to be an important component for actual phospholipidosis development in vivo. Therefore, drugs that require high doses and fit the QSAR criteria for accumulation in the lysosomes are at risk of provoking drug-induced phospholipidosis, whereas patient-specific confounding factors may also be involved. In preclinical safety studies, phospholipidosis can easily be assessed in various cell types by the accumulation of phospholipid in the lysosomal compartment, using special fluorescently labeled lipids (i.e., LipidTOX Red or NBD-PE), followed by high-content imaging analysis of the lysosomal localization of these dyes and the comparison with electron microscopy techniques.[67–69] However, systematic comparisons between in silico QSAR approaches and cell-based assays for phospholipidosis prediction are still needed.

4.13.4.3 Autophagy, Lysosomes, and DILI

Lysosomal perturbations are related to different programs involved in the control of cell survival, namely, autophagy, apoptosis, and necrosis.[61] Autophagy is a rescue program that mediates intracellular degradation of injured macromolecules and organelles and can serve as an internal energy source during nutrient deprivation as well.[70] Autophagosomes are formed when macroautophagy is initiated, and this involves various ATG protein family members such as ATG5 and ATG7. These autophagosomes fuse the lysosomal compartment; this process is then followed by degradation of the lysosomal content. The onset of increased autophagy can be determined by the accumulation of LC3-phosphatidylethanolamine on the surface of these autophagosomes,[71] which is also easy to access in living cells using GFP-tagged LC3 (see Fig. 3). So far, there is little hard evidence of the effect of DILI-causing drugs on autophagy. Compounds that affect lysosomal acidification, such as chloroquine, readily induce the accumulation of autophagosomes in the cytosol, since these can no longer be engulfed by the lysosomes, which is represented by the accumulation of GFP-LC3 in the lysosomal compartment (see Fig. 3). The relationship between phospholipidosis and perturbations of autophagy remains unclear. Nevertheless, a perturbation of the lysosomes is likely to affect the autophagy flux; therefore, compounds that cause phospholipidosis are likely to disturb the endogenous autophagy process.

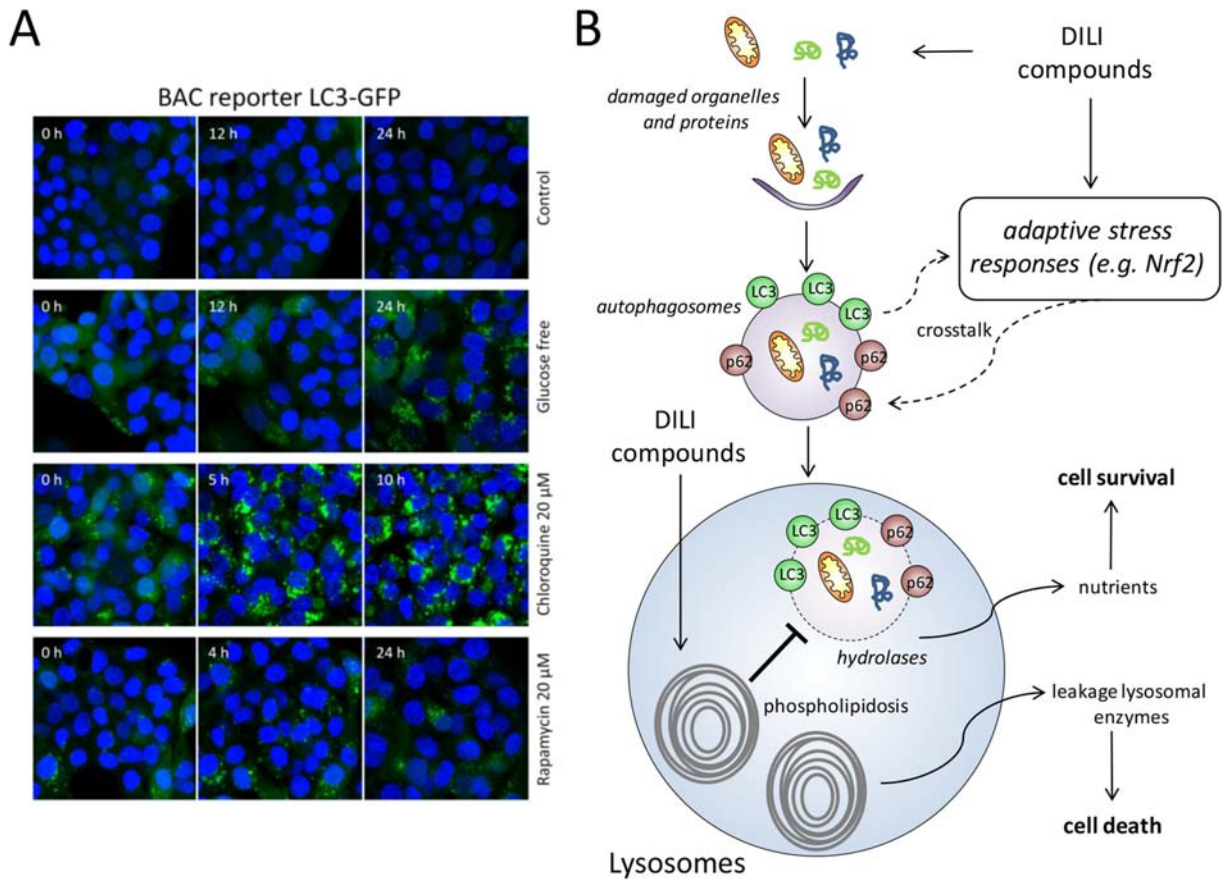

Fig. 3 Potential roles of autophagy and phospholipidosis in determining the sensitivity of the liver to drug exposure. (A) GFP-LC3 HepG2 reporter cell line for determining the effect of autophagy modulation, whereby rapamycin and glucose deprivation stimulate the rate of autophagy and whereby chloroquine prevents the turnover of autophagosomes. (B) Schematic overview how DILI compounds may affect the autophagy process and lysosomal function and likely consequences for cell survival.

4.13.4.4 Would Perturbation of Autophagy Trigger a Concern for DILI in Compound Assessment?

There is little published information on this topic. Intriguingly, carbamazepine, a well-established DILI compound, can induce an increase in autophagy.[72] Carbamazepine-induced autophagy can also protect against liver injury associated with fatty liver disease or fibrinogen storage disease.[73,74] Conversely, inhibition of autophagy by chloroquine exacerbated the liver injury caused by these diseases. Acetaminophen induces autophagy in vitro and in the liver in vivo, which seems to form part of a survival response. Thus, inhibition of autophagy, using ATG7 knockout mice, enhances the onset of acetaminophen-induced acute liver injury,[75] whereas stimulation of autophagy protects against APAP liver injury.[76] But, intriguingly, the ATG5 knockout is protective, and this appears to be linked to enhanced cytoprotection through the Nrf2 pathway.[77] Possibly, this is related to the induction of the expression of autophagy receptor p62/SQSTM1, which is involved in Nrf2 activation but is also a direct target of Nrf2.[78] Some putative roles of autophagy in DILI are illustrated in Fig. 3.

Clearly, autophagy plays a role in the cytoprotection of the liver. Hence, any drug that has the potential to interfere with the autophagy flux is likely to increase the susceptibility of liver injury. Such a perturbation of autophagy could also sensitize against the contribution of TNFα proapoptotic signalling in liver cells.[79] As yet, there is a limitation to a systematic analysis of the relationship between phospholipidosis, autophagy regulation, and susceptibility to liver cell injury. Simultaneous high-content imaging analysis of these processes, making use of the previously mentioned marker for phospholipidosis, and markers for autophagy such as GFP-LC3 could solve these issues.

4.13.4.5 Lysosomal Perturbations and Cytotoxicity

More than 50 hydrolases are present in the lumen of lysosomes; this creates a hazard for overall cellular maintenance: when these lysosomes break open, their content may evoke a serious problem in the cytosolic compartment. Cathepsins are proteases that can cleave critical target proteins and are released from the lysosomes and are involved in the onset of cytotoxicity.[61] Interestingly, cathepsins can directly target apoptotic machinery components that will sensitize cells to the onset of apoptosis. Thus, the proteolytic activation of Bid by cathepsins to truncated Bid may serve as a complementary trigger to speed up the onset of cell death.[80] In addition, the antiapoptotic Bcl2 protein is also cleaved. Cathepsins, in fact, play a critical role in liver injury in vivo.[81] An additional factor involved in cell death is both the presence and release of Fe(II) from lysosomes. Fe(II) accumulates in these organelles after the breakdown of iron-containing enzymes. Here, increased levels of Fe(II) may promote the onset of oxidative stress and the formation of hydroxyl radicals through the Fenton reaction,[82] causing membrane damage of lysosomes and further release of Fe(II) and the hydrolases into the cytosol. In cases where cells have an attenuated antioxidant potential, this may sensitize the cells toward lipid peroxidation and membrane damage and eventually cell death by necrosis. While these relationships have been demonstrated for individual cases of chemically induced cytotoxicity, it remains unclear if these programs are also relevant to DILI and to what extent sustained phospholipidosis actually contributes to DILI.

4.13.5 Assessment and Prediction of the Role of Transporters in Drug- and Bile Acid-Induced Liver Injury

4.13.5.1 Introduction and Classification of Drug and Bile Acid Transporters

Membrane transporters play an important part in drug absorption and disposition, therapeutic efficacy, and ADRs. They are grouped in two major families: ATP-binding cassette (ABC) and soluble carrier (SLC) proteins.[83] In the hepatocyte, transporters for drugs and endogenous substances are distributed among the basolateral (sinusoidal) and canalicular (apical) membranes, as illustrated in Fig. 4.

4.13.5.2 Bile Acid Uptake and Excretion

Synthesis of bile acids (BAs) and the biliary secretion of endogenous and exogenous substances, including drugs and metabolites, are the main functions of the liver. Vectorial transport of BA across hepatocytes is a major driving force for bile flow. Bile formation is a complex sequence of cellular events, which involves uptake of bile constituents and xenobiotics at the basolateral plasma membrane of hepatocytes and secretion of cholephilic compounds across the apical membrane. The transcellular transport of BA is mediated by transporter proteins located on the basolateral and canalicular membranes of hepatocytes. The sodium/taurocholate cotransporting peptide (NTCP) enables sodium-dependent uptake of BAs and some drugs from the space of Disse into hepatocytes (Box 2). Human NTCP accepts most physiological BAs and some organic anions. Sodium-independent uptake of BA is mediated by members of the OATP family. Although there are several carrier proteins capable of transporting BA, NTCP-mediated transport accounts for the bulk of BA uptake (about 90%).

Excretion of the individual bile constituents such as bile salts, phospholipids, and cholesterol mainly involves highly specialized canalicular proteins. BSEP is the major canalicular BA efflux system. However, the affinity and capacity of BSEP for individual BA conjugates differ between species. MRP2 mainly excretes bilirubin glucuronides and glutathione conjugates but also exports divalent sulfo-conjugated BAs into the bile. Other canalicular transporters include members of the family of P-glycoproteins such as MDR1 (ABCB1) and MDR3 (ABCB4) that mediate excretion of biliary phospholipids and cholesterol, respectively. Both MDR1 and BCRP have also been implicated in BA transport under cholestatic conditions. However, MDR1/P-glycoprotein is not thought

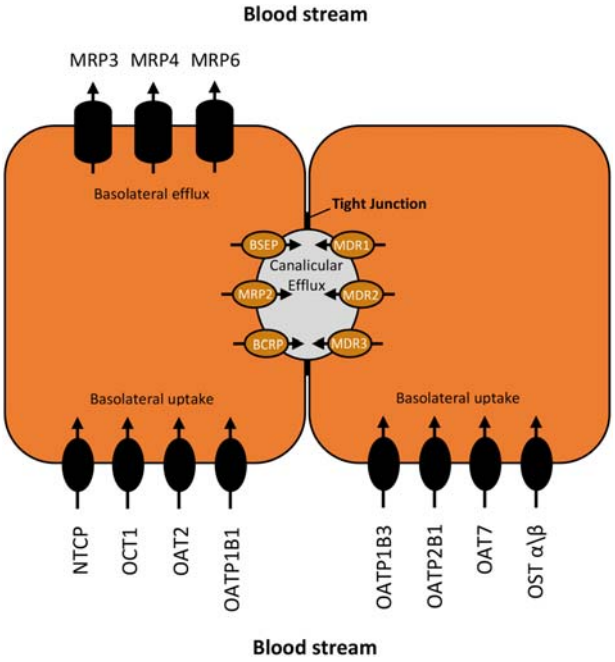

Fig. 4 Two major superfamilies of transporters exist in hepatocytes: ATP-binding cassette (ABC) and soluble carrier (SLC).

Box 2

Key basolateral transporter proteins include the sodium/taurocholate cotransporting peptide (NTCP; SLC10A1), three members of the organic anion transporting polypeptides (OATP) family (OATP1B1 (SLCO1B1), OATP1B3 (SLCO1B3), and OATP2B1 (SLCO2B1)), organic anion transporter 2 (OAT2; SLC22A7) and organic anion transporter 7 (OAT7; SLC22A9), and organic cation transporter 1 (OCT1). Efflux pumps include the multidrug resistance-associated proteins MRP3 (ABCC3), MRP4 (ABCC4), and MRP6 (ABCC6). Key canalicular (apical) efflux transporter proteins include P-glycoprotein (MDR1; ABCB1), bile-salt export pump (BSEP; ABCB11), multidrug resistance-associated protein 2 (MRP2; ABCC2), and breast cancer resistance protein (BCRP; ABCG2). In addition, the multidrug and toxin extrusion protein 1 (MATE1; SLC47A1) is also located in the apical membrane.

to have a primary role in the biliary excretion of drug conjugates, but it is one of the major determinants of cation excretion into bile. The basolateral membrane localizes members of the alternative basolateral BA efflux system, mainly, MRP3, MRP4, and the heterodimeric organic solute transporter OSTα/OSTβ. Any functional disturbance of the bile secretory process can lead to cholestatic liver disease, which is associated with intracellular accumulation of toxic bile constituents and consecutive cholestatic liver cell damage. Additionally, MATE1 has emerged as a transporter with an important role in the biliary excretion of cations.

4.13.5.3 The Cellular and Hepatic Features of Cholestasis

Since canalicular transporter proteins play a major role in hepatic drug clearance, changes in their expression or activity in acquired cholestasis have been reported to occur at the transcriptional, post-transcriptional, or post-translational levels within days, hours, or minutes/seconds, respectively. Cholestatic liver disorders are among the most severe clinical manifestations of DILI[84] and account for up to half of the cases of drug hepatotoxicity with high mortality rates.[85] They include a spectrum of acute or chronic hepatobiliary diseases of diverse etiologies that are characterized by impaired hepatocellular secretion of bile, resulting in accumulation of BAs, bilirubin, and cholesterol. Intrahepatic cholestasis represents a frequent manifestation of DILI in humans. In many cases, this results from changes in the hepatobiliary transporter system, in particular BSEP, which is the most physiologically important canalicular bile transporter. However, the mechanisms by which drugs induce cholestasis are diverse and remain poorly understood. Indeed, in addition to hepatobiliary transporter changes, other mechanisms, such as altered cell polarity, disruption of cell-to-cell junctions, and cytoskeletal modifications, can participate in cholestasis. A role for oxidative stress as a primary causal agent and/or as an aggravating factor has been shown in extrahepatic cholestasis induced by bile duct ligation, but it remains poorly documented in intrahepatic cholestasis. In addition, genetic mutations in genes encoding transporters may also result in the onset of cholestatic disorders and may increase the susceptibility to DILI. For instance, defects in BSEP, MDR3, and ATP8B1 cause progressive familial intrahepatic cholestasis. Defects in MRP2 cause the autosomal recessive liver disorder known as Dubin–Johnson syndrome, characterized by an elevated concentration of bilirubin glucuronides in blood.

Numerous drugs inhibit the biliary excretion of conjugated bile salts mediated by BSEP, which can result in DILI.[86] Noticeably, trafficking of hepatic efflux transporters is also an important concept: intracellular pools exist from which membrane transporters can be swiftly recruited and inserted into membranes as a result of xenobiotic treatment or physiological demand. Endocytic retrieval also occurs for BSEP and MRP2. As a result, substrates of efflux transporters are constantly accumulating within these vesicles.

Not all cholestatic drugs are BSEP inhibitors, and their detection can depend on the method and/or the model used. As examples, captopril and cimetidine caused cholestasis without interaction with BA transporters.[87] In a study using inverted membrane vesicles from cells overexpressing the human transporter and sandwich-cultured human hepatocytes, the BSEP-expressing inverted membrane vesicles were found to be suitable to evaluate the risk of DILI (according to FDA labeling) associated with BSEP inhibition. However, it resulted in many false positives. By contrast, the sandwich-cultured human hepatocytes allowed to separate BSEP inhibitors associated with severe DILI (e.g., cyclosporine, ritonavir, and troglitazone) from those with no or mild DILI (e.g., rifampicin).[88] In another study, 16 of the 42 drugs that were reported to cause cholestatic/mixed DILI (e.g., carbamazepine, dapsone, iproniazide, and ranitine) did not inhibit hBSEP using transfected inverted membrane vesicles.[89] Many BSEP inhibitors are also NTCP inhibitors, while some others, such as rifampicin, appear to be ineffective on NTCP activity.[90] Further investigations based on several methods and models could however be advisable.

As a result of BSEP inhibition or another mechanism, BAs can accumulate in the cytosol of the hepatocytes or in bile canaliculi and induce cellular damage. However, hepatocytes are able to counteract their intracellular accumulation; their uptake and synthesis decrease, while basolateral excretion and detoxification are enhanced.[91,92] Recent observations suggest that in vitro hepatocytes exhibit a rapid adaptive response to early cholestatic features induced by cholestatic drugs such as chlorpromazine (CPZ) and cyclosporine A, which are characterized by generation of an oxidative stress, inhibition of BSEP, and alteration of the pericanalicular cytoskeleton. This response is typified by rapid inhibition of NTCP activity, constriction of bile canaliculi with discharge of BAs, enhanced basolateral excretion, and downregulation of genes related to bile synthesis and detoxification.[93,94]

4.13.5.4 Model Systems for Transport Evaluation

Various in vivo and in vitro biological approaches are currently used for studying transporters. Whole tissues and whole animal models can be used in single-pass configuration and in a recirculating configuration. A number of knockout and mutant animal models have also been developed to analyze the role of transporters, but species differences and compensatory mechanisms can make interpretation of data from these models difficult. In vitro systems are mainly based on membrane and cell assays. Inverted vesicles derived from various nontransfected or transfected cell lines are used to analyze interactions between substrates and inhibitors with target transporters. A number of probe substrates and inhibitors are recommended for evaluation of human ATP-dependent transport into membrane vesicles.[95]

Polarized cell lines are standard models for evaluating drug transport. Primary hepatocytes should be the most appropriate cell model to mimic the hepatic uptake function. However, freshly isolated or cryopreserved hepatocytes are not polarized. In standard culture conditions, they rapidly lose their functional activities and functional bile canaliculi.[96] Rat hepatocyte couplets and primary rat and human hepatocytes in a sandwich configuration have been the most widely used in vitro cell models to analyze hepatic transport processes. In a sandwich configuration, hepatocytes recapitulate polarized architecture.[97] An alternative to sandwich-cultured primary hepatocytes is the human HepaRG cell line, a new liver cell line that expresses features of mature hepatocytes and exhibits typical functional bile canaliculi.[96] Recent studies have shown that cholestasis can be induced by CPZ and cyclosporine A in these cells.[93,94]

It is now recognized that compounds known to interfere with BSEP function are often not associated with significant liver cell injury in these preclinical models although they have been related to liver damage when administered in humans.[89,98] Moreover, since species-dependent differences have been reported, studies with human liver cells are preferable. For instance, taurocholic acid elimination through the basolateral membrane is much higher in rat hepatocytes than in their human counterparts.[99]

It is also important to note that in addition to biological models, computational modeling algorithms are used to evaluate drug–transporter interactions.

4.13.5.5 Bile Acid Toxicity

About 0.2–0.6 g of BAs are synthesized daily in humans, and serum (BA) concentrations of about 3–7 μM are considered physiological. However, in the μM range of supraphysiological BA concentrations, BA-induced apoptosis is believed to be the predominant mechanism. At higher concentrations, in the mM range, necrosis appears to be predominant.

Species differences in BA composition, synthesis, and regulation between humans and rodents exist.[100] The human liver synthesizes the two primary BAs cholic acid (CA) and chenodeoxycholic acid (CDCA), which are mostly conjugated to taurine and glycine. In the intestine, CA and CDCA conjugates are deconjugated and converted to the secondary BAs deoxycholic acid (DCA) and lithocholic acid (LCA), respectively. Sulfation is the major pathway for detoxification of extremely hydrophobic BA in humans such as LCA.[101] Conversely, in mice, the BA pool consists mostly of hydrophilic BA; it is predominantly composed of hydrophobic BAs. Only these latter are efficacious ligands of the nuclear receptors farnesoid X receptor (FXR), pregnane X receptor (PXR), and vitamin D receptor, which play a role not only in the regulation of BA synthesis and metabolism but also in the metabolism of chemicals and other endogenous compounds.[100] In humans, the five most important BAs present in plasma are glycochenodeoxycholic acid,

CDCA, glycodeoxycholic acid (GDCA), DCA, and glycocholic acid. The primary BAs CA and CDCA and the secondary BA DCA are present for 95% as conjugates of taurine and glycine. Sulfate and glucuronate forms are also present.

BA-mediated toxicity has been investigated in various in vitro systems, including isolated rat liver mitochondria, cell lines, isolated hepatocytes in suspension, and cryopreserved hepatocytes in conventional primary cultures. However, contrary to hepatocytes in a sandwich configuration and HepaRG cells, these in vitro systems do not reflect the polarity of hepatocytes.

The toxicity of BAs can be estimated by various assays of cell necrosis and apoptosis, oxidative stress (ROS generation), measurements of mRNA and activity levels of transporters, and other genes related to bile synthesis, detoxification, etc. It is important to note that the expression of BA-related genes is tightly controlled by nuclear receptors. Thus, the nuclear receptor FXR, activated by BAs, is a central player in the network while the nuclear receptors constitutive androstane receptor (CAR) and PXR facilitate adaptation to increased BA concentrations through the upregulation of alternative hepatic routes (MRP3 and MRP4) and induction of detoxifying enzymes (particularly CYP3A4).

Other endpoints of BA-induced toxicity are also used, that is, urea formation and the drug-induced cholestatic index (DICI):

$$\mathrm{DICI} = \frac{\text{Urea formation} - \text{test compound} + \text{BAs}}{\text{Urea formation} - \text{test compound alone}}$$

This reflects the residual urea formation by hepatocytes coincubated with the test drug and BAs.

4.13.5.6 Transporters and Bile Acid Toxicity: Comments and Future Challenges

The biology of liver transporters is a rapidly moving field. If major progress has been made in their knowledge, regulation, and interactions with drugs and substrates, further work is still required to better define their role in DILI, in particular in drug-induced cholestasis. Furthermore, BSEP inhibition alone is not sufficient to accurately predict drug-induced cholestasis for compounds exerting hepatotoxicity via multiple/or complex mechanisms.

New models such as humanized transporter animal models, hepatocytes derived from stem cells, and 3-D cultures of hepatocytes alone or with nonparenchymal cells (NPCs) could be useful to better understand drug-induced alterations of BA influx and efflux in the liver and related liver lesions and to evaluate which factors (inflammation, immune response, oxidative stress, viral infection, etc.) may contribute to aggravate such lesions. The use of new methodologies, for example, cell imaging to follow time-dependent cellular alterations, including induced by drugs and/or BAs, and sensitive methods to measure BAs, will also be of critical importance. Preliminary data have shown that by using HepaRG hepatocytes, two types of bile canaliculi alterations resulting in either constriction or dilatation associated with induction or inhibition of the Rho kinase pathway, respectively, could be observed with cholestatic drugs.[174]

In summary, more information is particularly needed on the following:

- BA profiles in liver cell models, the influence of culture time on these profiles, the capacity of the cell models to synthesize BAs from precursors, and their ability to form conjugates. Importantly, the composition of the culture medium must be considered; indeed, serum itself contains BAs.
- Early events induced by drugs and/or BAs and identification of the mechanisms involved should lead to the development of new predictive tests.
- Drug-induced alterations in BA profiles and the resulting toxicity, the mechanisms of short-term and long-term cell adaptation, and protection against intracellular accumulation of toxic BA. This should allow us to better understand DILI and hopefully even idiosyncratic DILI.

4.13.6 Evidence for the Role of the Innate Immune System in DILI in Man

4.13.6.1 Introduction

Involvement of the innate or the adaptive immune system in DILI in man is based on circumstantial evidence, and it remains to be established in man, whether immune alterations (inflamed tissue, changes in inflammatory cells (eosinophils or neutrophils)) found in DILI cases are causally related or if they are the consequence of inflammatory responses in the liver or elsewhere.

4.13.6.2 HLA Associations With DILI

A strong indication for a role of the adaptive immune system (i.e., T-cell sensitization) is based on genetic studies showing associations between DILI and certain HLA polymorphisms, but this is only reported for a limited number of drugs. HLA associations to DILI have been demonstrated for some drugs (HLA-A*33:03 for ticlopidine, HLA-B*57:01 for flucloxacillin, HLA-DQA1*02:01 for lapatinib, HLA-DRB1*15:01 for amoxicillin clavulanate, HLA-DRB1*15:01 for lumiracoxib, HLA-DRB1*07 for ximelagatran, and HLA-DRB1*01:01 for nevirapine (reviewed by Kaniwa and Saito,[102]) but not (yet) established for others (diclofenac are trovafloxacin). Associations between HLA and hypersensitivity syndromes have also been established for other drugs, for example, carbamazepine and abacavir.

The occurrence of HLA associations points to an important role of the adaptive immune system, in particular T-cell sensitization, which can only take place via HLA–TcR interactions combined with proper costimulatory help. In some cases (flucloxacillin),[103,104] drug-specific T cells have been found using IFNγ ELISpot, but again for most DILI-inducing drugs, this has not been tested.

4.13.6.3 Role of Cytokines and Chemokines

Cytokines are regulatory molecules serving as stimulators, regulators, or inhibitors of cells. Immune cells are among the most well known but certainly not unique cytokine-producing and cytokine-responding cells. For diclofenac-induced DILI, genetic associations have been found with IL4 and IL10, and for acetaminophen and other DILI associations, these have been found with blood (plasma or serum) levels of IL1a, IL6, IL8, IL10, IP-10, IL15, IL17, IL21, and monocyte chemoattractant protein 1 (MCP1) (reviewed in Laverty et al.[105] and Li et al.[106]) One of the key cytokines implicated here is TNFα, the role of which is outlined further in the succeeding text.

4.13.6.4 The Role of TNFα

It is evident that the hepatotoxicity of many drugs is dependent on activation of NPCs of the innate immune system, such as Kupffer cells, and consequent release of TNFα. TNFα binding to the hepatocyte will activate both a cytotoxic pathway involving JNK signaling and caspase 8 activation and a survival pathway involving NF-kB. ROS generation sensitizes hepatocytes to TNFα-induced apoptosis mainly through mitochondrial release of cytochrome *c*.[107,108] Many idiosyncratic drugs have been shown to induce redox perturbation and oxidative stress that may activate JNK and/or inhibit the NF-kB activity important in sensitization to TNFα. An example of this is shown by the action of the antipsychotic agent CPZ.[109]

4.13.6.5 Autoantibodies and DILI

Autoantibodies have been found in several cases,[106] that is, antinuclear antibodies (ANA) and anti-MPO in the case of diclofenac, including in a recent study in children, suffering from DILI.[110] In that study, ANA and anti-smooth muscle antibodies were found in 46% and 42% of the investigated population of children, respectively. Autoimmune responses may also point to an important role of the immune system, but one should be aware of the fact that autoimmune responses may occur due to mere adjuvant-mediated bystander activation (e.g., strong inflammatory responses) as well. It can by no means as yet be concluded that these autoimmune responses are causally related based on the occurrence of autoantibodies or autoreactive T cells. However, immune-mediated DILI may occur in patients with an autoimmune history. This was recently shown in a case report in which a patient with a history of systemic lupus erythematosus (SLE) was presented with autoimmune hepatitis to ibrandonates. The 61-year-old female patient showed elevated levels of IgG, and histology of liver biopsies showed the presence of portal and centrilobular hepatitis with lymphocytes, plasma cells, and eosinophils.[111]

4.13.6.6 The Role of the Innate Immune System in DILI

Despite the fact that the link with the immune system and DILI has not been formally proved in man, indications for at least part of the cases seem supportive. Studies in animals, showing liver injury with various drugs that are known to cause DILI in man, however clearly demonstrate that in particular the innate immune system is activated. The best studied drug in this case is trovafloxacin (TVX), at least in mice. Trovafloxacin but not the structurally related drug levofloxacin induced acute and profound liver pathology but only in combination with LPS, peptidoglycan-lipoteichoic acid (PGN-LTA), or TNFα.[112] The liver effects were accompanied by changes in various factors, including TNF-a, IL6, IL18, IL1b, MCP1, IFN-g, and MIP-2. In addition, liver effects were absent in $SOD^{-/-}$ mice, which is indicative of a role of mitochondrial stress, in neutrophil elastase-deficient mice[112] and in mice that lacked TNF-a receptor,[112] and in case CD18 was blocked. These findings together indicate a crucial role of the innate immune system in TVX-induced DILI, but the fast kinetics (effects occur within 4–24 h) also indicate that adaptive immune cells are not involved. Few other drugs (apart from APAP and TVX) have been demonstrated to induce liver pathology in mice, that is, CPZ, diclofenac (DF), and carbamazepine (CAR). CPZ-induced effects were also shown to be dependent on coexposure to LPS or LTA and in addition shown to be mediated by TIRAP-JNK-mediated cell death.

Diclofenac-induced liver effects (liver enzymes and pathology), at relatively high intraperitoneal dosing levels, and in addition a time-dependent increase in gene expression in the liver of STAT3, RORγT and of IL1b, TNF-a, MIP-2, FASL, MCP1, and IL17 have also been demonstrated.[113] Depletion of IL1b strongly reduced diclofenac-induced liver pathology, whereas depletion of IL17 had minor protective effects. Depletion of Kupffer cells with GdCl3 did not prevent liver damage.

CAR requires very high doses to induce a liver toxic effect in mice and also a high repeat dose.[114] In this situation, increases in similar innate immune system-related factors were observed, that is, IL6, IL17, IL13, MIP-2, and FASL. In addition, a role for oxidative stress and metabolism was demonstrated.

In summary, data that are available on DILI not only in mouse but also in rat suggest a triggering role of innate immune factors, but the effects are so rapid that one may conclude that adaptive immunity is not required to cause liver effects.

4.13.6.7 In Vitro Liver Models to Capture the Innate Immune System

Only a few in vitro studies have been performed with regard to the immune system in DILI. Mostly, they are done with hepatocyte cell lines and some with cocultures of hepatocytes and macrophages. In the latter combination, the role of interaction of both cell types can be evaluated, but macrophage activation by, for instance, LPS can also be mimicked by TNFα or other cytokines. This has, for instance, been done with CPZ.

4.13.7 Evidence for a Role of the Adaptive Immune System in Humans

4.13.7.1 Introduction

The adaptive immune system is often implicated in DILI. This is largely because a delayed onset is a common clinical characteristic. Many people develop reactions several months after drug exposure. For example, the median time to the onset of hepatic adverse events following exposure to the tyrosine kinase inhibitor lapatinib is 110 days.[115,116]This time course is very different to a classical drug hypersensitivity reaction (e.g., maculopapular eruption or SJS/TEN), which develops 1–4 weeks after initial drug exposure.[117] Thus, if the adaptive immune system is involved in DILI, additional yet to be elucidated factors trigger the immune response and subsequent tissue injury.

4.13.7.2 Evidence From Studies Using PBMC From Patients With DILI

A case report describing a patient with drug rash with eosinophilia and systemic symptoms has shown that a hypersensitivity reaction can develop into fulminant liver failure.[118] Histological investigations revealed infiltration of granzyme B-secreting CD3+ lymphocytes in close proximity to apoptotic hepatocytes suggesting that T-lymphocytes participate in the liver reaction. Isolation of drug-specific T-cells from DILI patients, but not drug-exposed controls, provides direct evidence that they participate in the disease pathogenesis. Early studies using the lymphocyte transformation test—a simple in vitro assay based on assessment of lymphocyte proliferative responses in drug-treated and vehicle control cultures—detected drug-specific lymphocyte responses in approximately 50% of patients with DILI.[119] Drugs to which T-cell reactivity was detected in more than one patient included co-trimoxazole, allopurinol, fentiazac, captopril, phenytoin, and carbamazepine. More recently, similar data has been reported in Chinese patients with DILI. The lymphocyte transformation test was reported to have a sensitivity (% of DILI patients with a positive lymphocyte transformation test) and specificity (% of control patients with a negative lymphocyte transformation test) of 47.5% and 95.9%, respectively.[120] The phenotype and function of the T-cells were not defined in either manuscript, and additional studies have not been forthcoming.

Liver dysfunction occurs in approximately 20% of patients exposed to isoniazid. As such, its ability to activate drug-specific T-lymphocytes has been studied in detail. Warrington reported that the lymphocyte transformation test was positive in 95% of DILI cases, whereas lymphocyte responses were not detected in patients receiving isoniazid without evidence of liver damage.[121] Interestingly, the patients T-lymphocytes were activated with the parent compound and/or an isonicotinic acid–human serum albumin conjugate. The predictive value of the lymphocyte transformation test in isoniazid-induced hepatitis was studied in a cohort of 61 patients receiving isoniazid for chemotherapy. Liver injury was detectable in not only 58% of the lymphocyte transformation test positive group but also 23% of the lymphocyte transformation test negative group.[122] Metushi et al.[123] have characterized a range of antidrug and autoantibodies in patients with isoniazid hepatotoxicity. Antibodies were not detected in tolerant patients. Although this study does not define the role antibodies play in the disease pathogenesis, the data provides strong evidence that isoniazid induces an immune response only in patients with DILI.

Most recently, the usefulness of the lymphocyte transformation test for diagnosing hepatic reactions to antituberculosis drugs has been studied.[124,125] The sensitivity of the lymphocyte transformation test for all four drugs studied was low (14% for isoniazid, 14% for rifampicin, 14% for ethambutol, and 0% for pyrazinamide[124]). We are conducting a similar study and finding similar data. The lymphocyte transformation test yields largely negative data. However, by cloning T-cells from DILI patients, it has been possible to isolate CD4+ T-cells that secrete an array of cytokines following isoniazid stimulation. Hence, the negative lymphocyte transformation test data likely relates to a low frequency of drug-specific T-cells in patient blood.

Therefore, it is clear that there is still much to learn regarding the role of T-lymphocytes in DILI. With this in mind, flucloxacillin-responsive T-cells have been isolated and fully characterized from patients with DILI. CD8+ clones expressing CCR4 and CCR9 migrated toward CCL17 and CCL25 and secreted IFN-γ, perforin, granzyme B, and FasL following drug stimulation.[104] These studies define the immune basis for flucloxacillin-induced liver injury; however, additional studies are needed to explore the drug-specific T-lymphocyte response in other forms of DILI.

For an increasing number of hepatotoxic drugs (e.g., flucloxacillin,[126] augmentin,[127] lumiracoxib,[128] lapatinib,[116] ximelagatran,[129] and isoniazid[130]), genome-wide association studies have identified specific HLA alleles as important susceptibility factors. These data suggest that a highly restricted drug-derived antigen interacts with the protein encoded by HLA risk allele to activate T-cells in susceptible patients. For flucloxacillin, the CD8+ T-lymphocyte response was shown to be HLA-B*57:01 restricted, which effectively links the genetic association to the tissue injury. Furthermore, naive CD45RA+CD8+ T-cells from volunteers expressing HLA-B*57:01 were activated with flucloxacillin when dendritic cells presented the drug antigen.[104] Similarly, Wuillemin et al. found that it was possible to isolate flucloxacillin-responsive T-cells directly from healthy donor blood lymphocytes using extended

3–8 week culture protocols that involved weekly stimulation with drug and autologous antigen-presenting cells.[131] One must emphasize that flucloxacillin is the only example to date where it has been possible to define the immunogenetic basis of the reaction.

One should also note the following:

- The majority of individuals who carry known HLA risk alleles do not develop clinically relevant reactions when exposed to the culprit drug.
- For most HLA-associated DILI drugs, many patients that develop DILI will not carry the risk allele.

Thus, with a small number of exceptions (e.g., abacavir hypersensitivity), HLA associations are not absolute indicators of risk. Therefore, there is an urgent need to characterize the immunologic parameters that are superimposed onto the HLA association and indeed HLA-restricted T-cell activation to determine why particular individuals develop DILI. One hypothesis that should be tested is that DILI drugs activate innate signaling and hence provide the wave of costimulatory signaling and a cytokine environment rich in inflammatory mediators, to drive the drug-specific T-lymphocyte response.

Finally, the hapten hypothesis states that a drug or a reactive metabolite must bind irreversibly to a protein to initiate an adaptive immune response. For reactions targeting liver, it is widely believed that drugs must modify hepatic protein. To activate T-cells through their T-cell receptor, peptides liberated from the modified proteins must associate with and be presented in the context of specific MHC molecules. In contrast, B-cells can be activated to produce antibodies through a direct interaction of the modified protein with the B-cell receptor. The majority of hepatotoxic drugs have been shown to form reactive metabolites in humans that subsequently modify protein.[8] However, as drugs modify multiple proteins and the drug protein binding interaction is incredibly heterogeneous, it is difficult to define which modifications are involved in the activation of the adaptive immune system.

4.13.8 Signaling Pathways and Mathematical Models: Toward Prediction of DILI

4.13.8.1 Introduction: What Experimental In Vitro and In Silico Models Are Available for the Detection of DILI?

This section should illustrate how the complexities of intracellular signaling pathways and intercellular communication can be addressed in a rational and mathematical approach in order to leverage the knowledge and data gained through mapping the mechanisms and processes.

DILI is a complex process resulting from intricate interactions at multiple levels that despite much effort is still poorly understood. In vitro assays and preclinical models are regularly updated, but increasingly in silico approaches are being considered in parallel with these efforts in order to assist the decision-making process during drug development and unravel underlying mechanisms.

To support selection of the most promising chemical structures at the earliest time point in the drug development, pipeline classification models, such as QSAR models, have been developed that link physicochemical properties of compounds to therapeutic categories like hepatotoxicity.[132–136] For example, Liu et al.[134] developed a drug-induced liver injury prediction system (DILIps) that is based on the identification of 13 types of hepatotoxic side effects. It utilizes information from clinical trials and postmarketing surveillance and the SIDER database[137] to relate drugs with associated side effects. To computationally screen compounds for each of the hepatotoxic side effects, a QSAR model was established. This showed that the combination of three hepatotoxic side effect models ("rule of three" criterion) was sufficient to identify compounds with a high potential of causing DILI.[134] The success of all these approaches depends on a reliable annotation of compounds that cause DILI.

Physiologically based pharmacokinetic (PBPK) modeling can be applied to appropriately simulate the distribution and action of pharmacologically active substances. This, in combination with other methods, will contribute to an improved understanding of DILI. PBPK are multicompartment models that consist of ordinary differential equations (ODEs) following the principles of mass transport, fluid dynamics, and biochemistry and attempt to predict ADME of compounds. ADME properties of a compound are estimated using the octanol-to-water partitioning coefficient and the acid dissociation constant, and from these values for oral absorption characteristics, metabolites binding to proteins (adduct formation), renal clearance, and organ partitioning are calculated. Key parameters related to drug metabolism are estimated using in vitro studies with primary hepatocytes or microsomes.[138] A prime example for the in silico representation of physiological processes involved in DILI is the DILIsym software that encompasses models that span from the organ to the cell and so far focuses on reactive metabolite-induced DILI.[139] The multiscale model is organized in multiple submodels that comprise compound distribution and metabolism, descriptions of glutathione depletion and recovery, mitochondrial dysfunction, hepatocyte life cycle with a focus on cell death, and clinically relevant endpoints such as alanine aminotransferase (ALT) levels. The submodels are integrated to simulate an organism level response. The model uses publicly available data and is highly simplified in several aspects but nevertheless has already supported the formulation of new hypotheses and the optimization of protocols.

Increasing effort is currently directed toward the development of improved in vitro assays, such as cell-based high-content screening[140] and expression profiling,[141] which will provide further insights into mechanisms contributing to hepatotoxicity and will help to significantly improve the accuracy of in silico approaches. So far, studies have primarily used endpoint measurements and focused on metabolic conversion of compounds in hepatocytes and correlating this with hepatotoxicity. However, hepatocyte damage also triggers regenerative processes in the liver, which are coordinated by multiple growth factors and cytokines that are secreted by hepatocytes and NPCs.

4.13.8.2 How to Use In Silico Models to Detect Hepatocyte and NPC Perturbation?

Usually, compounds are metabolized in hepatocytes and then conjugated with hydrophilic substances and excreted. However, during this process, reactive metabolites may be generated that result in protein adducts and stress responses that can lead to hepatocyte apoptosis and/or necrosis; this is considered to be an adverse outcome pathway (AOP).[142] The chemical reaction network of drug metabolism and clearance, for example, via GSH conjugation, has already been successfully modeled by ODEs[143] in an iterative way: clearance and production rates on a tissue level are estimated based on the kinetic rate laws of a PBPK model.

Based on these rates, a flux distribution of cellular exchange rates is computed by flux balance analysis based on stoichiometric models. Detailed mechanistic models of the intracellular events in hepatocytes will be required to specifically address the contribution of inflammatory signaling, reactive metabolite effects, and impaired transporters to hepatotoxicity of compounds. Apoptosis has been extensively investigated using mathematical models, mostly based on ODEs,[144,145] describing the dynamics of caspase 8, 9, and 3 activation. Additionally, apoptosis is highly regulated by feedback mechanisms, for example, via Bid/cytC or via IAP. A key aspect of apoptosis is its switch-like behavior that was theoretically approached by bifurcation analysis.[146] When apoptosis is initiated and ATP levels fall below the value needed for caspase activity, cells can switch to a necrotic state that has been shown to be regulated by signaling pathways.[147] To gain a more comprehensive understanding of the interlinked processes, it is necessary to couple the existing ODE models for redox signalling,[148,149] apoptosis pathways,[144] and drug metabolism.

Upon liver damage, inflammatory and proliferative ligands are excreted by NPCs, such as Kupffer cells, hepatic stellate cells, and liver sinusoidal endothelial cells. The impact of TNFα, primarily secreted by Kupffer cells, and transforming growth factor (TGF)β, secreted by hepatic stellate cells, on hepatocytes has been examined by ODE-based dynamic pathway models.[150,151] To capture the impact of NPC, realistic concentrations of these factors and cocultivation studies would be required to advance the existing models. Furthermore, examination of the impact of the NPC-secreted factors on cell death decisions and specific model adaptations would be important. Thereby, the systematic development of integrative in silico models, considering pro- and anti-inflammatory signaling pathways, offers a powerful tool to simulate and predict the occurrence of idiosyncratic liver injury.

4.13.8.3 What Can Be Learned From Modeling Signaling Pathways for Better Prediction?

DILI triggers regenerative processes comprising the secretion of inflammatory stimuli such as TNFα and TGFβ by NPCs. Infection of the liver elicits antiviral response that are initiated by interferon (IFN) secretion. These inflammatory stimuli activate multiple signaling pathways in hepatocytes and thereby can influence drug-induced hepatotoxicity. By integration of dynamic pathway models of the respective signaling pathways into the mathematical models of cell death, it is possible to simulate and integrate critical mechanisms of signaling effects on toxicity.

A prime example that shows the impact of inflammatory responses on the toxicity of compounds is the toxicity enhancing effect of TNFα on Diclofenac.[152] In general, upon liver injury or infection, Kupffer cells secrete TNFα, which either leads to an activation of NF-κB signaling, which promotes cell survival, or induces the TNFα death receptor complex formation leading to apoptosis. One of the key properties of this pathway is the oscillation of NF-κB translocation, as it shuttles between nucleus and cytoplasm upon TNFα stimulation.[153,154] Several mathematical NF-κB pathway models were designed in order to investigate and increase the understanding of the regulation and function of this oscillation.[150,153,155–157] In a computational analysis of the mathematical NF-κB model by Ashall et al.,[153] different TNFα levels in healthy individuals and patients with chronic inflammation are compared. Their model exhibits a bifurcation point, showing sustained NF-κB oscillations above a certain TNFα concentration and a dampened NF-κB oscillation below.[157] This is of interest for the prediction of DILI, especially in the context of known TNFα-induced compound-dependent hepatotoxicity.[158,159] By interfering with the oscillation, compounds could shift network outputs and thereby might increase the sensitivity to DILI. To unravel the underlying mechanisms, mathematical models need to be applied to predict the contribution to DILI.

During the late stages of liver regeneration, hepatic stellate cells secrete TGFβ, a member of a superfamily of proteins regulating cell proliferation, differentiation, and apoptosis. The formation of an activated ligand–receptor complex on the cell surface results in the activation of the Smad proteins, which translocate to the nucleus and regulate the transcription of target genes, for example, p53 or Bax.[160] Multiple dynamic pathway models of TGFβ signaling have been established.[160–163] The models focus on different aspects of the TGFβ signaling capturing receptor trafficking or nuclear-cytoplasmic shuttling of Smads. Since it was shown that TGFβ signaling is affected by other cytokines, for example, IFNγ,[164] and redox-sensitive reactions,[157] and that it is a key regulator of hepatic fibrosis, it is of particular interest in the context DILI.

In response to infection of the liver, IFN are secreted as important mediators of antiviral responses.[165] It was reported that the occurrence of DILI as an adverse effect of antiretroviral therapy in HIV/HCV coinfected patients was reduced by IFN therapy.[166] This suggests that IFN may affect different AOPs and thereby inhibit the onset of DILI. To date, several modeling approaches have been carried out to study perturbations in IFNα signaling. It was demonstrated that the positive feedback regulator IRF9 is crucial for the amplification of the early dynamics of IFNα-mediated signal transduction.[167–170] This suggests that if compounds or their metabolites affect IRF9, this could influence antiviral responses of an infected liver and consequently may have an impact on the threshold for hepatotoxic effects.

4.13.8.4 How Can the Physiological Response and Toxicological Perturbation of Signaling Pathways for the Prediction of DILI Be Quantified?

Measurements required for the calibration of a mathematical model depend on the modeling approach and the question that needs to be addressed. For example, classification models that link physicochemical properties of compounds to an effect are widely used, for example, the DILIps approach, which is based on databases of physicochemical properties of compounds, patient information, and side effects.[134]

Molecular-scale classification models predict the hepatotoxicity of a compound based on its chemical and physical features and in vitro endpoint measurements using, for example, high-content imaging.

PBPK models quantitatively describe the absorption, distribution, metabolism, and excretion of compounds and consist of compartmental representations of all relevant tissues and the vascular system. PBPK models use in vivo determinations such as measurements in biofluids (e.g., serum, plasma, and urine) and in vitro-derived physicochemical properties of compounds.

At the intracellular scale, stoichiometric models describe metabolic conversion of compounds. These models are constructed based on extensive biochemical knowledge on metabolic enzymes to establish the reaction network and use enzyme kinetics. The exchange rates determined by the stoichiometric models provide integration points into PBPK models, which quantitatively represent time–concentration profiles at higher scales.

Dynamic pathway models are calibrated using quantitative measurements of pathway activation. At the protein level, pathway activation is determined by quantitative immunoblotting, protein arrays mass spectrometry,[150] and various imaging techniques, whereas the dynamics of target gene expression is monitored by qRT-PCR.[171,172]

In conclusion, high-quality, quantitative, time-resolved data are required to establish reliable mathematical models that enable the understanding of mechanisms causing DILI and to facilitate quantitative predictions. Accurately calibrated models will allow the simulation of interindividual differences in enzyme kinetics and protein concentrations. From this, it may be possible to identify targets that positively or negatively affect compound toxicity and thresholds. Ultimately, it is clear that mathematical models capturing DILI mechanisms must be validated with patient-derived material.

4.13.8.5 How Mathematical Modeling Can Improve, for Example, the Human Relevance of Our In Vitro Models

As previously described, DILI results from the complex interplay of multiple biological processes. However, these underlying processes are likely to be clearly defined for every individual occurrence of DILI. Thus, one must identify which combination of inputs leads to detrimental reactions. This in turn allows the exact reproduction of these conditions in our in vitro systems. The difficulty here lies within the complexity of biological systems, making it extremely unlikely to identify and define each condition in which DILI or detrimental reactions occur experimentally. Given that the biological interactions are well defined, mathematical modeling provides the tools to simulate and assess all imaginable input combination and predicts the outcome that can then be validated in vitro.

Fig. 5 exemplifies the process how mathematical modeling is used to improve the predictability of DILI. In vitro data, such as from HepG2 and primary human hepatocytes, are used to define the possible interactions and the stoichiometry within the biological system. Then, PBPK modeling is applied to identify the conditions and concentration of active molecules at the cell surface. These are then used as input parameters for the dynamic pathway model, which in turn predicts the phenotype and reaction of cells, thereby providing crucial information as to whether DILI is likely to occur under these conditions.

4.13.8.6 Conclusions and Future Perspectives

From a general perspective, it is unlikely in the short-term that any single model system is able to incorporate physiologically relevant aspects of all of these mechanisms and thereby demonstrate predictivity for all types of human DILI. The uncracked nut is still the model of idiosyncratic DILI, in which there is real scientific progress being made, but we do not know how this understanding can help to develop predictive models in the laboratory. A particular case in point is our new understanding of the association of several forms of DILI with particular HLA variants. While this is certainly a step forward, it is unclear how this understanding can help us predict ab initio the DILI risk of new chemical entities.

Nevertheless, this review should provide sufficient knowledge to guide the field in its attempts to address the status quo through the development of models of improved physiological relevance. Currently used models that are unable to emulate all of the mechanisms described here but can address selected ones are likely to become part of a new testing paradigm, to be deployed at different points and on different scales, in the drug development process.

There are genuine signs that we are learning the lessons of past failures in safety assessment approaches. Beyond the new realization that prediction needs to be intelligent and mechanistically driven, as spelled out in this review, it is also important to note that several novel (bio)markers have recently been identified, which may be useful for early assessment of hepatotoxicity. For example, microRNAs (e.g., miR-122), HMGB1, and other intracellular proteins, which are passively or actively released by hepatocytes as they exist in the liver and in cell-based in vitro systems, may be helpful in our understanding of the physiological and mechanistic response to chemical stress and could provide an analytic bridge to help us assess the physiological relevance of in vitro models. In addition, high-content screening methods and cellular imaging techniques may provide important information on the physiological pathways that are perturbed by drugs causing DILI.

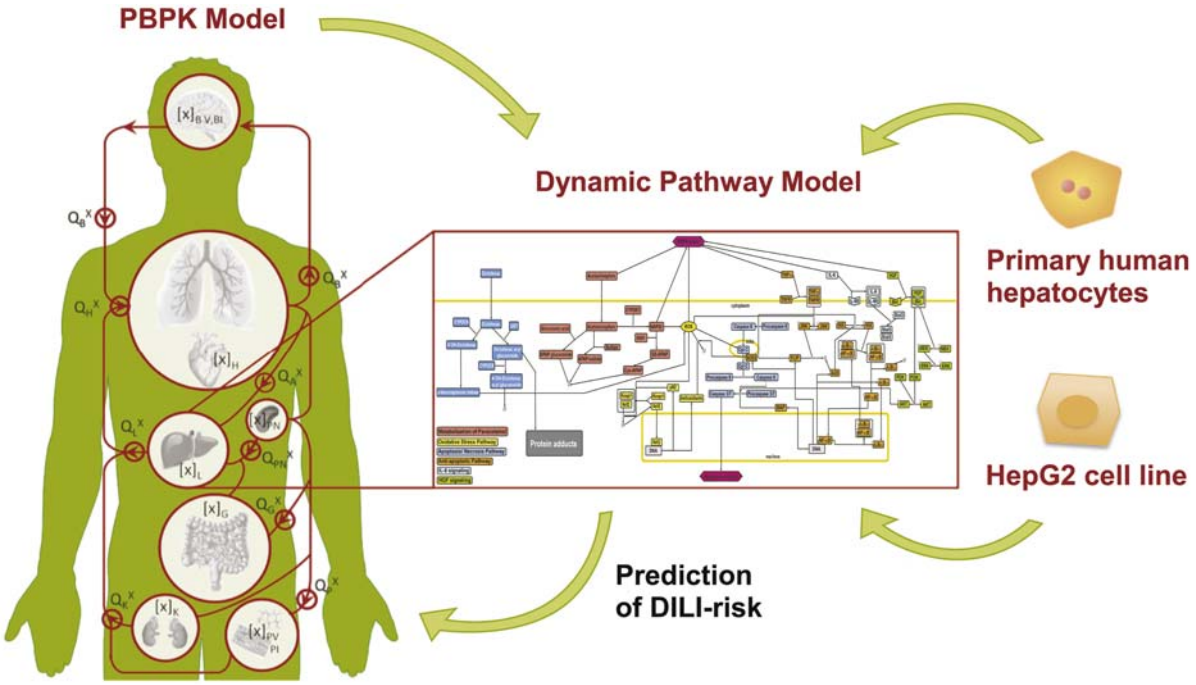

Fig. 5 Dynamics of signalling components from either primary human hepatocytes or the HepG2 cell line are integrated into dynamic pathway models. These models are then connected to the physiologically based pharmacokinetic (PBPK) model to improve the prediction of DILI. Information about compound absorption, distribution, metabolism, and excretion gained from the PBPK model is used for the refinement of dynamic pathway models.

References

1. Ostapowicz, G.; et al. Results of a Prospective Study of Acute Liver Failure at 17 Tertiary Care Centers in the United States. *Ann. Intern. Med.* **2002,** *137,* 947–954.
2. Fung, M.; et al. Evaluation of the Characteristics of Safety Withdrawal of Prescription Drugs from Worldwide Pharmaceutical Markets-1960 to 1999*. *Drug Inf. J.* **2001,** *35,* 293–317.
3. Chen, M.; et al. FDA-Approved Drug Labeling for the Study of Drug-Induced Liver Injury. *Drug Discov. Today* **2011,** *16,* 697–703.
4. Biour, M.; et al. Drug-Induced Liver Injury; Fourteenth Updated Edition of the Bibliographic Database of Liver Injuries and Related Drugs. *Gastroenterol. Clin. Biol.* **2004,** *28,* 720–759.
5. Larrey, D. Drug-Induced Liver Diseases. *J. Hepatol.* **2000,** *32,* 77–88.
6. Khetani, S. R.; et al. Use of Micropatterned Cocultures to Detect Compounds That Cause Drug-Induced Liver Injury in Humans. *Toxicol. Sci.* **2013,** *132,* 107–117.
7. Kaplowitz, N. Idiosyncratic Drug Hepatotoxicity. *Nat. Rev. Drug Discov.* **2005,** *4,* 489–499.
8. Park, B. K.; et al. Managing the Challenge of Chemically Reactive Metabolites in Drug Development. *Nat. Rev. Drug Discov.* **2011,** *10,* 292–306.
9. Wilke, R. A.; et al. Identifying Genetic Risk Factors for Serious Adverse Drug Reactions: Current Progress and Challenges. *Nat. Rev. Drug Discov.* **2007,** *6,* 904–916.
10. Chen, M.; et al. Toward Predictive Models for Drug-Induced Liver Injury in Humans: Are We There Yet? *Biomark. Med.* **2014,** *8,* 201–213.
11. Miller, E. C.; Miller, J. A. The Presence and Significance of Bound Aminoazo Dyes in the Livers of Rats Fed p-Dimethylaminoazobenzene. *Cancer Res.* **1947,** *7,* 468–480.
12. Miller, E. C.; Miller, J. A. *In Vivo* Combinations Between Carcinogens and Tissue Constituents and Their Possible Role in Carcinogenesis. *Cancer Res.* **1952,** *12,* 547–556.
13. Zhou, S.; Chan, E.; Duan, W.; Huang, M.; Chen, Y.-Z. Drug Bioactivation Covalent Binding to Target Proteins and Toxicity Relevance. *Drug Metab. Rev.* **2005,** *37,* 41–213.
14. Leung, L.; Kalgutkar, A. S.; Obach, R. S. Metabolic Activation in Drug-Induced Liver Injury. *Drug Metab. Rev.* **2012,** *44,* 18–33.
15. Park, B. K.; et al. Drug Bioactivation and Protein Adduct Formation in the Pathogenesis of Drug-Induced Toxicity. *Chem. Biol. Interact.* **2011,** *192,* 30–36.
16. Stachulski, A. V.; et al. The Generation, Detection, and Effects of Reactive Drug Metabolites. *Med. Res. Rev.* **2013,** *33,* 985–1080.
17. Naisbitt, D. J.; Gordon, S. F.; Pirmohamed, M.; Park, B. K. Immunological Principles of Adverse Drug Reactions: The Initiation and Propagation of Immune Responses Elicited by Drug Treatment. *Drug Saf.* **2000,** *23,* 483–507.
18. Kalgutkar, A. S.; Didiuk, M. T. Structural Alerts, Reactive Metabolites, and Protein Covalent Binding: How Reliable Are These Attributes as Predictors of Drug Toxicity? *Chem. Biodivers.* **2009,** *6,* 2115–2137.
19. Hanzlik, R. P.; Koen, Y. M.; Fang, J. Bioinformatic Analysis of 302 Reactive Metabolite Target Proteins. Which Ones are Important for Cell Death? *Toxicol Sci* **2013,** *135,* 390–401.
20. Evans, D. C.; Watt, A. P.; Nicoll-Griffith, D. A.; Baillie, T. A. Drug-Protein Adducts: An Industry Perspective on Minimizing the Potential for Drug Bioactivation in Drug Discovery and Development. *Chem. Res. Toxicol.* **2004,** *17,* 3–16.
21. Bauman, J. N.; et al. Can In Vitro Metabolism-Dependent Covalent Binding Data Distinguish Hepatotoxic From Nonhepatotoxic Drugs? An Analysis Using Human Hepatocytes and Liver S-9 Fraction. *Chem. Res. Toxicol.* **2009,** *22,* 332–340.
22. Tirmenstein, M. A.; Nelson, S. D. Subcellular Binding and Effects on Calcium Homeostasis Produced by Acetaminophen and a Nonhepatotoxic Regioisomer, 3′-Hydroxyacetanilide, in Mouse Liver. *J. Biol. Chem.* **1989,** *264,* 9814–9819.
23. Pessayre, D. Role of Reactive Metabolites in Drug-Induced Hepatitis. *J. Hepatol.* **1995,** *23* (Suppl. 1), 16–24.
24. Robin, M. A.; et al. Antigenic Targets in Tienilic Acid Hepatitis. Both Cytochrome P450 2C11 and 2C11-Tienilic Acid Adducts Are Transported to the Plasma Membrane of Rat Hepatocytes and Recognized by Human Sera. *J. Clin. Invest.* **1996,** *98,* 1471–1480.
25. Koenigs, L. L.; et al. Electrospray Ionization Mass Spectrometric Analysis of Intact Cytochrome P450: Identification of Tienilic Acid Adducts to P450 2C9. *Biochemistry* **1999,** *38,* 2312–2319.

26. Bolton, J. L.; Trush, M. A.; Penning, T. M.; Dryhurst, G.; Monks, T. J. Role of Quinones in Toxicology. *Chem. Res. Toxicol.* **2000,** *13,* 135–160.
27. Monks, T. J.; Jones, D. C. The Metabolism and Toxicity of Quinones, Quinonimines, Quinone Methides, and Quinone-Thioethers. *Curr. Drug Metab.* **2002,** *3,* 425–438.
28. Briere, J. J.; Schlemmer, D.; Chretien, D.; Rustin, P. Quinone Analogues Regulate Mitochondrial Substrate Competitive Oxidation. *Biochem. Biophys. Res. Commun.* **2004,** *316,* 1138–1142.
29. Genova, M. L.; et al. Mitochondrial Production of Oxygen Radical Species and the Role of Coenzyme Q as an Antioxidant. *Exp. Biol. Med. (Maywood)* **2003,** *228,* 506–513.
30. Codreanu, S. G.; Zhang, B.; Sobecki, S. M.; Billheimer, D. D.; Liebler, D. C. Global Analysis of Protein Damage by the Lipid Electrophile 4-Hydroxy-2-Nonenal. *Mol. Cell. Proteomics* **2009,** *8,* 670–680.
31. Ikeda, T. Drug-Induced Idiosyncratic Hepatotoxicity: Prevention Strategy Developed After the Troglitazone Case. *Drug Metab. Pharmacokinet.* **2011,** *26,* 60–70.
32. Yoshikawa, Y.; Hosomi, H.; Fukami, T.; Nakajima, M.; Yokoi, T. Establishment of Knockdown of Superoxide Dismutase 2 and Expression of CYP3A4 Cell System to Evaluate Drug-Induced Cytotoxicity. *Toxicol. In Vitro* **2009,** *23,* 1179–1187.
33. Lammert, C.; et al. Relationship Between Daily Dose of Oral Medications and Idiosyncratic Drug-Induced Liver Injury: Search for Signals. *Hepatology* **2008,** *47,* 2003–2009.
34. Lammert, C.; Bjornsson, E.; Niklasson, A.; Chalasani, N. Oral Medications With Significant Hepatic Metabolism at Higher Risk for Hepatic Adverse Events. *Hepatology* **2010,** *51,* 615–620.
35. Daly, A. Pharmacogenomics of Adverse Drug Reactions. *Genome Med.* **2013,** *5,* 5.
36. Urban, T. J.; Daly, A. K.; Aithal, G. P. Genetic Basis of Drug-Induced Liver Injury: Present and Future. *Semin. Liver Dis.* **2014,** *34,* 123–133.
37. Aithal, G. P.; et al. Hepatic Adducts, Circulating Antibodies, and Cytokine Polymorphisms in Patients With Diclofenac Hepatotoxicity. *Hepatology* **2004,** *39,* 1430–1440.
38. Rinaldi, R.; Eliasson, E.; Swedmark, S.; Morgenstern, R. Reactive Intermediates and the Dynamics of Glutathione Transferases. *Drug Metab. Dispos.* **2002,** *30,* 1053–1058.
39. Bessems, J. G.; Vermeulen, N. P. Paracetamol (Acetaminophen)-Induced Toxicity: Molecular and Biochemical Mechanisms, Analogues and Protective Approaches. *Crit. Rev. Toxicol.* **2001,** *31,* 55–138.
40. Hayes, J. D.; Dinkova-Kostova, A. T. The Nrf2 Regulatory Network Provides an Interface Between Redox and Intermediary Metabolism. *Trends Biochem. Sci.* **2014,** *39,* 199–218.
41. Klaassen, C. D.; Reisman, S. A. Nrf2 the Rescue: Effects of the Antioxidative/Electrophilic Response on the Liver. *Toxicol. Appl. Pharmacol.* **2010,** *244,* 57–65.
42. Watanabe, I.; et al. A Study to Survey Susceptible Genetic Factors Responsible for Troglitazone-Associated Hepatotoxicity in Japanese Patients With Type 2 Diabetes Mellitus. *Clin. Pharmacol. Ther.* **2003,** *73,* 435–455.
43. Lucena, M. I.; et al. Glutathione S-Transferase m1 and t1 Null Genotypes Increase Susceptibility to Idiosyncratic Drug-Induced Liver Injury. *Hepatology* **2008,** *48,* 588–596.
44. Begriche, K.; Massart, J.; Robin, M. A.; Borgne-Sanchez, A.; Fromenty, B. Drug-Induced Toxicity on Mitochondria and Lipid Metabolism: Mechanistic Diversity and Deleterious Consequences for the Liver. *J. Hepatol.* **2011,** *54,* 773–794.
45. Pessayre, D.; et al. Central Role of Mitochondria in Drug-Induced Liver Injury. *Drug Metab. Rev.* **2012,** *44,* 34–87.
46. Win, S.; Than, T. A.; Han, D.; Petrovic, L. M.; Kaplowitz, N. c-Jun N-Terminal Kinase (JNK)-Dependent Acute Liver Injury From Acetaminophen or Tumor Necrosis Factor (TNF) Requires Mitochondrial Sab Protein Expression in Mice. *J. Biol. Chem.* **2011,** *286,* 35071–35078.
47. Labbe, G.; Pessayre, D.; Fromenty, B. Drug-Induced Liver Injury Through Mitochondrial Dysfunction: Mechanisms and Detection During Preclinical Safety Studies. *Fundam. Clin. Pharmacol.* **2008,** *22,* 335–353.
48. Fromenty, B.; Pessayre, D. Inhibition of Mitochondrial Beta-Oxidation as a Mechanism of Hepatotoxicity. *Pharmacol. Ther.* **1995,** *67,* 101–154.
49. Larosche, I.; et al. Tamoxifen Inhibits Topoisomerases, Depletes Mitochondrial DNA, and Triggers Steatosis in Mouse Liver. *J. Pharmacol. Exp. Ther.* **2007,** *321,* 526–535.
50. Fulgencio, J. P.; Kohl, C.; Girard, J.; Pegorier, J. P. Troglitazone Inhibits Fatty Acid Oxidation and Esterification, and Gluconeogenesis in Isolated Hepatocytes From Starved Rats. *Diabetes* **1996,** *45,* 1556–1562.
51. Edeas, M.; Weissig, V. Targeting Mitochondria: Strategies, Innovations and Challenges: The Future of Medicine Will Come Through Mitochondria. *Mitochondrion* **2013,** *13,* 389–390.
52. Deschamps, D.; et al. Inhibition by Perhexiline of Oxidative Phosphorylation and the Beta-Oxidation of Fatty Acids: Possible Role in Pseudoalcoholic Liver Lesions. *Hepatology* **1994,** *19,* 948–961.
53. Silva, M. F.; et al. Synthesis and Intramitochondrial Levels of Valproyl-Coenzyme A Metabolites. *Anal. Biochem.* **2001,** *290,* 60–67.
54. Wu, Y.; et al. Mitochondrial DNA Base Excision Repair and Mitochondrial DNA Mutation in Human Hepatic HuH-7 Cells Exposed to Stavudine. *Mutat. Res.* **2009,** *664,* 28–38.
55. Gomes, L. C.; Di Benedetto, G.; Scorrano, L. During Autophagy Mitochondria Elongate, Are Spared From Degradation and Sustain Cell Viability. *Nat. Cell Biol.* **2011,** *13,* 589–598.
56. Karbowski, M.; et al. Free Radical-Induced Megamitochondria Formation and Apoptosis. *Free Radic. Biol. Med.* **1999,** *26,* 396–409.
57. Shishido, S.; et al. Hydrogen Peroxide Overproduction in Megamitochondria of Troglitazone-Treated Human Hepatocytes. *Hepatology* **2003,** *37,* 136–147.
58. Liguori, M. J.; et al. Microarray Analysis in Human Hepatocytes Suggests a Mechanism for Hepatotoxicity Induced by Trovafloxacin. *Hepatology* **2005,** *41,* 177–186.
59. Reasor, M. J.; Hastings, K. L.; Ulrich, R. G. Drug-Induced Phospholipidosis: Issues and Future Directions. *Expert Opin. Drug Saf.* **2006,** *5,* 567–583.
60. Schneider, J. L.; Cuervo, A. M. Liver Autophagy: Much More Than Just Taking Out the Trash. *Nat. Rev. Gastroenterol. Hepatol.* **2014,** *11,* 187–200.
61. Aits, S.; Jaattela, M. Lysosomal Cell Death at a Glance. *J. Cell Sci.* **2013,** *126,* 1905–1912.
62. Orogo, A. M.; Choi, S. S.; Minnier, B. L.; Kruhlak, N. L. Construction and Consensus Performance of (Q)SAR Models for Predicting Phospholipidosis Using a Dataset of 743 Compounds. *Mol. Inf.* **2012,** *31,* 725–739.
63. Pelletier, D. J.; Gehlhaar, D.; Tilloy-Ellul, A.; Johnson, T. O.; Greene, N. Evaluation of a Published in Silico Model and Construction of a Novel Bayesian Model for Predicting Phospholipidosis Inducing Potential. *J. Chem. Inf. Model.* **2007,** *47,* 1196–1205.
64. Vitovic, P.; Alakoskela, J. M.; Kinnunen, P. K. Assessment of Drug-Lipid Complex Formation by a High-Throughput Langmuir-Balance and Correlation to Phospholipidosis. *J. Med. Chem.* **2008,** *51,* 1842–1848.
65. Kruhlak, N. L.; et al. Development of a Phospholipidosis Database and Predictive Quantitative Structure-Activity Relationship (QSAR) Models. *Toxicol. Mech. Methods* **2008,** *18,* 217–227.
66. Goracci, L.; Ceccarelli, M.; Bonelli, D.; Cruciani, G. Modeling Phospholipidosis Induction: Reliability and Warnings. *J. Chem. Inf. Model.* **2013,** *53,* 1436–1446.
67. van de Water, F. M.; Havinga, J.; Ravesloot, W. T.; Horbach, G. J.; Schoonen, W. G. High Content Screening Analysis of Phospholipidosis: Validation of a 96-Well Assay With CHO-K1 and HepG2 Cells for the Prediction of *In Vivo* Based Phospholipidosis. *Toxicol. In Vitro* **2011,** *25,* 1870–1882.
68. Shahane, S. A.; et al. Detection of Phospholipidosis Induction: A Cell-Based Assay in High-Throughput and High-Content Format. *J. Biomol. Screen.* **2014,** *19,* 66–76.
69. Ferslew, B. C.; Brouwer, K. L. Identification of Hepatic Phospholipidosis Inducers in Sandwich-Cultured rat Hepatocytes, a Physiologically Relevant Model, Reveals Altered Basolateral Uptake and Biliary Excretion of Anionic Probe Substrates. *Toxicol. Sci.* **2014,** *139,* 99–107.
70. Marino, G.; Niso-Santano, M.; Baehrecke, E. H.; Kroemer, G. Self-Consumption: The Interplay of Autophagy and Apoptosis. *Nat. Rev. Mol. Cell Biol.* **2014,** *15,* 81–94.
71. Tanida, I.; Waguri, S. Measurement of Autophagy in Cells and Tissues. *Methods Mol. Biol.* **2010,** *648,* 193–214.
72. Hidvegi, T.; et al. An Autophagy-Enhancing Drug Promotes Degradation of Mutant alpha1-Antitrypsin Z and Reduces Hepatic Fibrosis. *Science* **2010,** *329,* 229–232.
73. Lin, C. W.; et al. Pharmacological Promotion of Autophagy Alleviates Steatosis and Injury in Alcoholic and Non-alcoholic Fatty Liver Conditions in Mice. *J. Hepatol.* **2013,** *58,* 993–999.
74. Puls, F.; et al. Autophagy-Enhancing Drug Carbamazepine Diminishes Hepatocellular Death in Fibrinogen Storage Disease. *J. Hepatol.* **2013,** *59,* 626–630.
75. Igusa, Y.; et al. Loss of Autophagy Promotes Murine Acetaminophen Hepatotoxicity. *J. Gastroenterol.* **2012,** *47,* 433–443.
76. Ni, H. M.; Bockus, A.; Boggess, N.; Jaeschke, H.; Ding, W. X. Activation of Autophagy Protects Against Acetaminophen-Induced Hepatotoxicity. *Hepatology* **2012,** *55,* 222–232.

77. Ni, H. M.; et al. Liver-Specific Loss of Atg5 Causes Persistent Activation of Nrf2 and Protects Against Acetaminophen-Induced Liver Injury. *Toxicol. Sci.* **2012,** *127,* 438–450.
78. Darvekar, S. R.; Elvenes, J.; Brenne, H. B.; Johansen, T.; Sjottem, E. SPBP Is a Sulforaphane Induced Transcriptional Coactivator of NRF2 Regulating Expression of the Autophagy Receptor p62/SQSTM1. *PLoS One* **2014,** *9,* e85262.
79. Amir, M.; et al. Inhibition of Hepatocyte Autophagy Increases Tumor Necrosis Factor-Dependent Liver Injury by Promoting Caspase-8 Activation. *Cell Death Differ.* **2013,** *20,* 878–887.
80. Droga-Mazovec, G.; et al. Cysteine Cathepsins Trigger Caspase-Dependent Cell Death Through Cleavage of Bid and Antiapoptotic Bcl-2 Homologues. *J. Biol. Chem.* **2008,** *283,* 19140–19150.
81. Canbay, A.; et al. Cathepsin B Inactivation Attenuates Hepatic Injury and Fibrosis During Cholestasis. *J. Clin. Invest.* **2003,** *112,* 152–159.
82. Terman, A.; Kurz, T. Lysosomal Iron, Iron Chelation, and Cell Death. *Antioxid. Redox Signal.* **2013,** *18,* 888–898.
83. Giacomini, K. M.; et al. Membrane Transporters in Drug Development. *Nat. Rev. Drug Discov.* **2010,** *9,* 215–236.
84. Padda, M. S.; Sanchez, M.; Akhtar, A. J.; Boyer, J. L. Drug-Induced Cholestasis. *Hepatology* **2011,** *53,* 1377–1387.
85. Bjornsson, E.; Olsson, R. Outcome and Prognostic Markers in Severe Drug-Induced Liver Disease. *Hepatology* **2005,** *42,* 481–489.
86. Sakurai, A.; Kurata, A.; Onishi, Y.; Hirano, H.; Ishikawa, T. Prediction of Drug-Induced Intrahepatic Cholestasis: In Vitro Screening and QSAR Analysis of Drugs Inhibiting the Human Bile Salt Export Pump. *Expert Opin. Drug Saf.* **2007,** *6,* 71–86.
87. Wang, E. J.; Casciano, C. N.; Clement, R. P.; Johnson, W. W. Fluorescent Substrates of Sister-P-Glycoprotein (BSEP) Evaluated as Markers of Active Transport and Inhibition: Evidence for Contingent Unequal Binding Sites. *Pharm. Res.* **2003,** *20,* 537–544.
88. Pedersen, J. M.; et al. Early Identification of Clinically Relevant Drug Interactions With the Human Bile Salt Export Pump (BSEP/ABCB11). *Toxicol. Sci.* **2013,** *136,* 328–343.
89. Dawson, S.; Stahl, S.; Paul, N.; Barber, J.; Kenna, J. G. In Vitro Inhibition of the Bile Salt Export Pump Correlates With Risk of Cholestatic Drug-Induced Liver Injury in Humans. *Drug Metab. Dispos.* **2012,** *40,* 130–138.
90. Mita, S.; et al. Inhibition of Bile Acid Transport across Na+/Taurocholate Cotransporting Polypeptide (SLC10A1) and Bile Salt Export Pump (ABCB 11)-Coexpressing LLC-PK1 Cells by Cholestasis-Inducing Drugs. *Drug Metab. Dispos.* **2006,** *34,* 1575–1581.
91. Weerachayaphorn, J.; Cai, S. Y.; Soroka, C. J.; Boyer, J. L. Nuclear Factor Erythroid 2-Related Factor 2 Is a Positive Regulator of Human Bile Salt Export Pump Expression. *Hepatology* **2009,** *50,* 1588–1596.
92. Wagner, M.; Zollner, G.; Trauner, M. New Molecular Insights Into the Mechanisms of Cholestasis. *J. Hepatol.* **2009,** *51,* 565–580.
93. Antherieu, S.; et al. Oxidative Stress Plays a Major Role in Chlorpromazine-Induced Cholestasis in Human HepaRG Cells. *Hepatology* **2013,** *57,* 1518–1529.
94. Sharanek, A.; et al. Different Dose-Dependent Mechanisms Are Involved in Early Cyclosporine A-Induced Cholestatic Effects in HepaRG Cells. *Toxicol. Sci.* **2014,** *141* (1), 244–253.
95. Brouwer, K. L.; et al. In Vitro Methods to Support Transporter Evaluation in Drug Discovery and Development. *Clin. Pharmacol. Ther.* **2013,** *94,* 95–112.
96. Guguen-Guillouzo, C.; Guillouzo, A. General Review on in vitro Hepatocyte Models and Their Applications. *Methods Mol. Biol.* **2010,** *640,* 1–40.
97. Swift, B.; Pfeifer, N. D.; Brouwer, K. L. Sandwich-Cultured Hepatocytes: An in vitro Model to Evaluate Hepatobiliary Transporter-Based Drug Interactions and Hepatotoxicity. *Drug Metab. Rev.* **2010,** *42,* 446–471.
98. Morgan, R. E.; et al. Interference With Bile Salt Export Pump Function Is a Susceptibility Factor for Human Liver Injury in Drug Development. *Toxicol. Sci.* **2010,** *118,* 485–500.
99. Jemnitz, K.; Veres, Z.; Vereczkey, L. Contribution of High Basolateral Bile Salt Efflux to the Lack of Hepatotoxicity in Rat in Response to Drugs Inducing Cholestasis in Human. *Toxicol. Sci.* **2010,** *115,* 80–88.
100. Chiang, J. Y. Bile Acids: Regulation of Synthesis. *J. Lipid Res.* **2009,** *50,* 1955–1966.
101. Hofmann, A. F. Detoxification of Lithocholic Acid, a Toxic Bile Acid: Relevance to Drug Hepatotoxicity. *Drug Metab. Rev.* **2004,** *36,* 703–722.
102. Kaniwa, N.; Saito, Y. Pharmacogenomics of Severe Cutaneous Adverse Reactions and Drug-Induced Liver Injury. *J. Hum. Genet.* **2013,** *58,* 317–326.
103. Jenkins, R. E.; et al. Characterisation of Flucloxacillin and 5-Hydroxymethyl Flucloxacillin Haptenated HSA *In Vitro* and *In Vivo*. *Proteomics Clin. Appl.* **2009,** *3,* 720–729.
104. Monshi, M. M.; et al. Human Leukocyte Antigen (HLA)-B*57:01-Restricted Activation of Drug-Specific T Cells Provides the Immunological Basis for Flucloxacillin-Induced Liver Injury. *Hepatology* **2013,** *57,* 727–739.
105. Laverty, H.; et al. The Potential of Cytokines as Safety Biomarkers for Drug-Induced Liver Injury. *Eur. J. Clin. Pharmacol.* **2010,** *66,* 961–976.
106. Li, J.; et al. Cytokine and Autoantibody Patterns in Acute Liver Failure. *J. Immunotoxicol.* **2010,** *7,* 157–164.
107. Han, D.; Hanawa, N.; Saberi, B.; Kaplowitz, N. Hydrogen Peroxide and Redox Modulation Sensitize Primary Mouse Hepatocytes to TNF-Induced Apoptosis. *Free Radic. Biol. Med.* **2006,** *41,* 627–639.
108. Lou, H.; Kaplowitz, N. Glutathione Depletion Down-Regulates Tumor Necrosis Factor α-Induced NF-kB Activity via IkB Kinase-Dependent and -Independent Mechanisms. *J. Biol. Chem.* **2007,** *282,* 29470–29481.
109. Gandhi, A.; Guo, T.; Ghose, R. Role of c-Jun N-Terminal Kinase (JNK) in Regulating Tumor Necrosis Factor-Alpha (TNF-Alpha) Mediated Increase of Acetaminophen (APAP) and Chlorpromazine (CPZ) Toxicity in Murine Hepatocytes. *J. Toxicol. Sci.* **2010,** *35,* 163–173.
110. Molleston, J. P.; et al. Characteristics of Idiosyncratic Drug-Induced Liver Injury in Children: Results From the DILIN Prospective Study. *J. Pediatr. Gastroenterol. Nutr.* **2011,** *53,* 182–189.
111. Goossens, N.; Spahr, L.; Rubbia-Brandt, L. Severe Immune-Mediated Drug-Induced Liver Injury Linked to Ibandronate: A Case Report. *J. Hepatol.* **2013,** *59,* 1139–1142.
112. Shaw, P. J.; et al. Trovafloxacin Enhances TNF-Induced Inflammatory Stress and Cell Death Signaling and Reduces TNF Clearance in a Murine Model of Idiosyncratic Hepatotoxicity. *Toxicol. Sci.* **2009,** *111,* 288–301.
113. Yano, A.; et al. Involvement of Immune-Related Factors in Diclofenac-Induced Acute Liver Injury in Mice. *Toxicology* **2012,** *293,* 107–114.
114. Higuchi, S.; et al. Metabolic Activation and Inflammation Reactions Involved in Carbamazepine-Induced Liver Injury. *Toxicol. Sci.* **2012,** *130,* 4–16.
115. Spraggs, C. F.; Parham, L. R.; Hunt, C. M.; Dollery, C. T. Lapatinib-Induced Liver Injury Characterized by Class II HLA and Gilbert's Syndrome Genotypes. *Clin. Pharmacol. Ther.* **2012,** *91,* 647–652.
116. Spraggs, C. F.; et al. HLA-DQA1*02:01 Is a Major Risk Factor for Lapatinib-Induced Hepatotoxicity in Women With Advanced Breast Cancer. *J. Clin. Oncol.* **2011,** *29,* 667–673.
117. Romano, A.; Torres, M. J.; Castells, M.; Sanz, M. L.; Blanca, M. Diagnosis and Management of Drug Hypersensitivity Reactions. *J. Allergy Clin. Immunol.* **2011,** *127,* S67–S73.
118. Mennicke, M.; et al. Fulminant Liver Failure After Vancomycin in a Sulfasalazine-Induced DRESS Syndrome: Fatal Recurrence After Liver Transplantation. *Am. J. Transplant.* **2009,** *9,* 2197–2202.
119. Maria, V. A.; Victorino, R. M. Diagnostic Value of Specific T Cell Reactivity to Drugs in 95 Cases of Drug Induced Liver Injury. *Gut* **1997,** *41,* 534–540.
120. Chen, G. Y.; et al. Set up Drug Lymphocyte Stimulation Test (3H-TdR) and Observe Its Application in Drug-Induced Liver Injury. *Zhonghua Gan Zang Bing Za Zhi* **2012,** *20,* 190–192.
121. Warrington, R. J.; Tse, K. S.; Gorski, B. A.; Schwenk, R.; Sehon, A. H. Evaluation of Isoniazid-Associated Hepatitis by Immunological Tests. *Clin. Exp. Immunol.* **1978,** *32,* 97–104.
122. Warrington, R. J.; McPhilips-Feener, S.; Rutherford, W. J. The Predictive Value of the Lymphocyte Transformation Test in Isoniazid-Associated Hepatitis. *Clin. Allergy* **1982,** *12,* 217–222.
123. Metushi, I. G.; Sanders, C.; Lee, W. M.; Uetrecht, J. Detection of Anti-Isoniazid and Anti-Cytochrome P450 Antibodies in Patients With Isoniazid-Induced Liver Failure. *Hepatology* **2014,** *59,* 1084–1093.
124. Suzuki, Y.; et al. Drug Lymphocyte Stimulation Test in the Diagnosis of Adverse Reactions to Antituberculosis Drugs. *Chest* **2008,** *134,* 1027–1032.

125. Schreiber, J.; Zissel, G.; Greinert, U.; Schlaak, M.; Muller-Quernheim, J. Lymphocyte Transformation Test for the Evaluation of Adverse Effects of Antituberculous Drugs. *Eur. J. Med. Res.* **1999,** *4,* 67–71.
126. Daly, A. K.; et al. HLA-B*5701 Genotype Is a Major Determinant of Drug-Induced Liver Injury Due to Flucloxacillin. *Nat. Genet.* **2009,** *41,* 816–819.
127. Donaldson, P. T.; et al. Human Leucocyte Antigen Class II Genotype in Susceptibility and Resistance to Co-Amoxiclav-Induced Liver Injury. *J. Hepatol.* **2010,** *53,* 1049–1053.
128. Singer, J. B.; et al. A Genome-Wide Study Identifies HLA Alleles Associated With Lumiracoxib-Related Liver Injury. *Nat. Genet.* **2010,** *42,* 711–714.
129. Kindmark, A.; et al. Genome-Wide Pharmacogenetic Investigation of a Hepatic Adverse Event Without Clinical Signs of Immunopathology Suggests an Underlying Immune Pathogenesis. *Pharmacogenomics J.* **2008,** *8,* 186–195.
130. Daly, A. K.; Day, C. P. Genetic Association Studies in Drug-Induced Liver Injury. *Drug Metab. Rev.* **2012,** *44,* 116–126.
131. Wuillemin, N.; et al. HLA Haplotype Determines Hapten or p-i T Cell Reactivity to Flucloxacillin. *J. Immunol.* **2013,** *190,* 4956–4964.
132. Chen, M.; et al. Quantitative Structure–Activity Relationship Models for Predicting Drug-Induced Liver Injury Based on FDA-Approved Drug Labeling Annotation and Using a Large Collection of Drugs. *Toxicol. Sci.* **2013,** *136,* 242–249.
133. Ekins, S.; Honeycutt, J. D.; Metz, J. T. Evolving Molecules Using Multi-Objective Optimization: Applying to ADME/Tox. *Drug Discov. Today* **2010,** *15,* 451–460.
134. Liu, Z.; et al. Translating Clinical Findings into Knowledge in Drug Safety Evaluation—Drug Induced Liver Injury Prediction System (DILIps). *PLoS Comput. Biol.* **2011,** *7,* e1002310.
135. Green, T. J.; et al. When Do the Aminotransferases Rise After Acute Acetaminophen Overdose? *Clin. Toxicol. (Phila.)* **2010,** *48,* 787–792.
136. Rodgers, A. D.; Zhu, H.; Fourches, D.; Rusyn, I.; Tropsha, A. Modeling Liver-Related Adverse Effects of Drugs Using Knearest Neighbor Quantitative Structure-Activity Relationship Method. *Chem. Res. Toxicol.* **2010,** *23,* 724–732.
137. Kuhn, M.; Campillos, M.; Letunic, I.; Jensen, L. J.; Bork, P. A Side Effect Resource to Capture Phenotypic Effects of Drugs. *Mol. Syst. Biol.* **2010,** *6,* 343.
138. Graham, E. E.; et al. Identification of the Thiophene Ring of Methapyrilene as a Novel Bioactivation-Dependent Hepatic Toxicophore. *J. Pharmacol. Exp. Ther.* **2008,** *326,* 657–671.
139. Howell, B. A.; et al. In Vitro to *In Vivo* Extrapolation and Species Response Comparisons for Drug-Induced Liver Injury (DILI) Using DILIsym: A Mechanistic, Mathematical Model of DILI. *J. Pharmacokinet. Pharmacodyn.* **2012,** *39,* 527–541.
140. O'Brien, P. J.; et al. High Concordance of Drug-Induced Human Hepatotoxicity With in vitro Cytotoxicity Measured in a Novel Cell-Based Model Using High Content Screening. *Arch. Toxicol.* **2006,** *80,* 580–604.
141. Hamadeh, H. K.; et al. Methapyrilene Toxicity: Anchorage of Pathologic Observations to Gene Expression Alterations. *Toxicol. Pathol.* **2002,** *30,* 470–482.
142. Godoy, P.; et al. Recent Advances in 2D and 3D in vitro Systems Using Primary Hepatocytes, Alternative Hepatocyte Sources and Non-parenchymal Liver Cells and Their Use in Investigating Mechanisms of Hepatotoxicity, Cell Signaling and ADME. *Arch. Toxicol.* **2013,** *87,* 1315–1530.
143. Ankley, G. T.; et al. Adverse Outcome Pathways: A Conceptual Framework to Support Ecotoxicology Research and Risk Assessment. *Environ. Toxicol. Chem.* **2010,** *29,* 730–741.
144. Krauss, M.; et al. Integrating Cellular Metabolism into a Multiscale Whole-Body Model. *PLoS Comput. Biol.* **2012,** *8,* e1002750.
145. Rehm, M.; Huber, H. J.; Dussmann, H.; Prehn, J. H. Systems Analysis of Effector Caspase Activation and Its Control by X-Linked Inhibitor of Apoptosis Protein. *EMBO J.* **2006,** *25,* 4338–4349.
146. Schleich, K.; Lavrik, I. N. Mathematical Modeling of Apoptosis. *Cell Commun. Signal* **2013,** *11,* 44.
147. Eissing, T.; et al. Bistability Analyses of a Caspase Activation Model for Receptor-Induced Apoptosis. *J. Biol. Chem.* **2004,** *279,* 36892–36897.
148. Saberi, B.; et al. Regulation of H(2)O(2)-Induced Necrosis by PKC and AMP-Activated Kinase Signaling in Primary Cultured Hepatocytes. *Am. J. Physiol. Cell Physiol.* **2008,** *295,* C50–C63.
149. Adimora, N. J.; Jones, D. P.; Kemp, M. L. A Model of Redox Kinetics Implicates the Thiol Proteome in Cellular Hydrogen Peroxide Responses. *Antioxid. Redox Signal.* **2010,** *13,* 731–743.
150. Kemp, M.; Go, Y. M.; Jones, D. P. Nonequilibrium Thermodynamics of Thiol/Disulfide Redox Systems: A Perspective on Redox Systems Biology. *Free Radic. Biol. Med.* **2008,** *44,* 921–937.
151. Pinna, F.; et al. A Systems Biology Study on NFkappaB Signaling in Primary Mouse Hepatocytes. *Front. Physiol.* **2012,** *3,* 466.
152. Wegner, K.; et al. Dynamics and Feedback Loops in the Transforming Growth Factor Beta Signaling Pathway. *Biophys. Chem.* **2012,** *162,* 22–34.
153. Ashall, L.; et al. Pulsatile Stimulation Determines Timing and Specificity of NF-kappaB-Dependent Transcription. *Science* **2009,** *324,* 242–246.
154. Cheong, R.; et al. Transient IkappaB Kinase Activity Mediates Temporal NF-kappaB Dynamics in Response to a Wide Range of Tumor Necrosis Factor-Alpha Doses. *J. Biol. Chem.* **2006,** *281,* 2945–2950.
155. Hoffmann, A.; Levchenko, A.; Scott, M. L.; Baltimore, D. The IkappaB-NF-kappaB Signaling Module: Temporal Control and Selective Gene Activation. *Science* **2002,** *298,* 1241–1245.
156. Wang, Y.; et al. A Systematic Survey of the Response of a Model NF-kappaB Signalling Pathway to TNFalpha Stimulation. *J. Theor. Biol.* **2012,** *297,* 137–147.
157. Nelson, D. E.; et al. Oscillations in NF-kappaB Signaling Control the Dynamics of Gene Expression. *Science* **2004,** *306,* 704–708.
158. Schwabe, R. F.; Brenner, D. A. Mechanisms of Liver Injury. I. TNF-Alpha-Induced Liver Injury: Role of IKK, JNK, and ROS Pathways. *Am. J. Physiol. Gastrointest. Liver Physiol.* **2006,** *290,* G583–G589.
159. Yin, M.; et al. Essential Role of Tumor Necrosis Factor Alpha in Alcohol-Induced Liver Injury in Mice. *Gastroenterology* **1999,** *117,* 942–952.
160. Clarke, D. C.; Betterton, M. D.; Liu, X. Systems Theory of Smad Signalling. *Syst. Biol. (Stevenage)* **2006,** *153,* 412–424.
161. Zi, Z.; Klipp, E. Constraint-Based Modeling and Kinetic Analysis of the Smad Dependent TGF-Beta Signaling Pathway. *PLoS One* **2007,** *2,* e936.
162. Melke, P.; Jonsson, H.; Pardali, E.; ten Dijke, P.; Peterson, C. A Rate Equation Approach to Elucidate the Kinetics and Robustness of the TGF-Beta Pathway. *Biophys. J.* **2006,** *91,* 4368–4380.
163. Vilar, J. M.; Jansen, R.; Sander, C. Signal Processing in the TGF-Beta Superfamily Ligand-Receptor Network. *PLoS Comput. Biol.* **2006,** *2,* e3.
164. Ulloa, L.; Doody, J.; Massague, J. Inhibition of Transforming Growth Factor-Beta/SMAD Signalling by the Interferon-Gamma/STAT Pathway. *Nature* **1999,** *397,* 710–713.
165. Borden, E. C.; et al. Interferons at Age 50: Past, Current and Future Impact on Biomedicine. *Nat. Rev. Drug Discov.* **2007,** *6,* 975–990.
166. McGovern, B. H.; et al. Managing Symptomatic Drug-Induced Liver Injury in HIV-Hepatitis C Virus-Coinfected Patients: A Role for Interferon. *Clin. Infect. Dis.* **2007,** *45,* 1386–1392.
167. Maiwald, T.; et al. Combining Theoretical Analysis and Experimental Data Generation Reveals IRF9 as a Crucial Factor for Accelerating Interferon Alpha-Induced Early Antiviral Signalling. *FEBS J.* **2010,** *277,* 4741–4754.
168. Smieja, J.; Jamaluddin, M.; Brasier, A. R.; Kimmel, M. Model-Based Analysis of Interferon-Beta Induced Signaling Pathway. *Bioinformatics* **2008,** *24,* 2363–2369.
169. Yamada, S.; Shiono, S.; Joo, A.; Yoshimura, A. Control Mechanism of JAK/STAT Signal Transduction Pathway. *FEBS Lett.* **2003,** *534,* 190–196.
170. Zi, Z.; et al. In Silico Identification of the Key Components and Steps in IFN-Gamma Induced JAK-STAT Signaling Pathway. *FEBS Lett.* **2005,** *579,* 1101–1108.
171. Bachmann, J.; et al. Division of Labor by Dual Feedback Regulators Controls JAK2/STAT5 Signaling Over Broad Ligand Range. *Mol. Syst. Biol.* **2011,** *7,* 516.
172. Steiert, B.; Raue, A.; Timmer, J.; Kreutz, C. Experimental Design for Parameter Estimation of Gene Regulatory Networks. *PLoS One* **2012,** *7,* e40052.
173. Onakpoya, I. J.; Heneghan, C. J.; Aronson, J. K. Post-marketing withdrawal of 462 medicinal products because of adverse drug reactions: a systematic review of the world literature. *BMC Med.* **2016,** *14,* 10. http://dx.doi.org/10.1186/s12916-016-0553-2.
174. Sharanek, A.; Burban, A.; Burbank, M.; et al. Rho-kinase/myosin light chain kinase pathway plays a key role in the impairment of bile canaliculi dynamics induced by cholestatic drugs. *Sci. Rep.* **2016,** *6,* 24709. http://dx.doi.org/10.1038/srep24709.

Relevant Websites

http://www.dilin.org—DILIN.
http://www.imi-safe-t.eu—Safe-T consortium.
http://livertox.nih.gov/intro.html—LiverTox Database.
http://www.mip-dili.eu—MIP-DILI Consortium.

4.14 The Future of Carcinogenicity Testing

A Pandiri, Cellular and Molecular Pathology Branch, National Toxicology Program, Durham, NC, United States
R Kovi, Experimental Pathology Laboratories, Inc., Durham, NC, United States
C Alden, Mayflower Pharma, Lawrenceburg, IN, United States
R Sills, Cellular and Molecular Pathology Branch, National Toxicology Program, Durham, NC, United States

© 2017 Elsevier Ltd. All rights reserved.

4.14.1	**Introduction**	239
4.14.2	**History of Carcinogenicity Testing**	239
4.14.3	**Current Approaches to Carcinogenicity Testing**	240
4.14.3.1	Experience With Transgenic Carcinogenicity Assays	243
4.14.4	**Future Approaches of Carcinogenicity Testing**	245
4.14.4.1	New Paradigms in Rodent Bioassays	246
4.14.4.2	Proposals for Pharmaceutical Carcinogenicity Studies	246
4.14.4.3	Future Paradigms for Environmental and Other Carcinogens	247
4.14.4.4	Toxicology Testing in the 21st Century (Tox21)	248
4.14.4.5	The Promise of -Omics Approaches	249
4.14.4.6	Adverse Outcome Pathway (AOP)/MOA Framework	250
4.14.5	**Conclusions**	251
References		252

4.14.1 Introduction

The advent of the modern age has provided several material comforts and luxuries. This may be directly correlated with the development of new chemicals, compounds, and materials. One of the main problems with several of these chemicals is the lack of complete safety data regarding their effects on human health as well as some deficiencies in the modern testing paradigm. There are several thousand (>75,000) legacy compounds in commerce that do not have definitive safety data regarding their potential to cause cancer in humans. Based on some estimates, 5–10% of these compounds might be reasonably anticipated to be carcinogenic to humans.[1] Unfortunately, in some instances we learn of the carcinogenicity hazard of compounds only after a cohort of the human population has been exposed to those chemicals and have suffered negative health effects. Due to obvious ethical reasons, humans should not serve as models for carcinogenicity testing, and hence a bioassay system that can confidently identify the carcinogenic hazards posed by these chemicals is needed. Bioassays using rodents have served as a surrogate for the human population and any chemical that is positive for carcinogenicity is deemed to be a human carcinogen unless mechanistic data suggest otherwise. However, continuous improvements are needed because of the recognized occurrences of false negatives and false positives in animal testing, though substantive improved understanding exists today as to the reasons for discrepancies.

Various national and international agencies have done a commendable job in identifying and classifying potential carcinogens using data from rodent carcinogenicity bioassays as well as human epidemiology. In addition, chemical and pharmaceutical companies also conduct rodent bioassays and provide other safety data for product registration and licensing. To date, the gold standard for identifying carcinogenicity hazard is the rodent chronic 2-year bioassay. There is no question regarding the pivotal role played by rodent bioassays in identifying chemicals that pose a carcinogenic hazard to people. Several chemical carcinogens were first identified by rodent bioassays before any epidemiological studies implicated them in causing cancer in the human population.[2] However, due to the substantive backlog of chemicals without safety data and the long time and high cost it takes to complete the rodent bioassays, alternative approaches that are fast and yet provide reliable data are urgently needed.[3] In addition, with increasing interest in the 3Rs (replace, reduce, refine) principal there is also a focus to reduce the number of rodents used in the bioassay while obtaining an answer in a shorter period of time at reduced expense. In order to gain an appreciation of this topic, the past, present, and future of carcinogenicity testing will be discussed. Discussions will be focused on small-molecule pharmaceuticals and environmental and occupational chemical exposures.

4.14.2 History of Carcinogenicity Testing

Before the advent of the rodent regulatory bioassays for cancer hazard identification in the late 1960s, the cancer hazards were usually identified from observational and epidemiological studies. Examples include breast cancer in nuns;[4] nasal cancer in tobacco snuff users;[5] scrotal and nasal cancers due to chimney soot;[6] skin cancer due to sunlight;[3] lung cancer in uranium miners;[7] bladder cancer in aniline dye workers;[8] skin and bladder cancers due to 2-napthylamine and benzidine in dye workers;[9] and lung cancers

due to chromium,[10] nickel,[11] asbestos, beryllium, and arsenicals.[12] Based on these epidemiological data, scientists established that certain chemicals and lifestyles cause cancers in people. In the early 20th century, scientists began experiments using animal models to study cancer hazards of novel chemicals that were being increasingly developed during and after both the world wars. Yamagiwa and Ichikawa[13] painted coal tar derivatives on rabbit ears and demonstrated skin cancer from those exposures. Subsequent studies purified several compounds from the coal tar mixture and demonstrated the carcinogenic hazard associated with the individual constituent compounds in rodents upon repeated exposures.[14]

The use of animals for testing the carcinogenic potential of agents continues to this day and will likely continue in the future. The major assumption of all these animal bioassays is that the changes observed in animals due to chemical exposures also would occur in humans unless proven otherwise. Though several long-term bioassays were conducted during the first half of the 20th century, the guidelines for the bioassays aimed to detect carcinogenic effects of chemicals were only first established in the FDA black book in 1949. Within the National Cancer Institute (NCI) in 1961, a Carcinogenesis Studies Branch was established under the leadership of Michael Shimkin for research on chemical carcinogenesis and also to monitor a contract program on the design and conduct of carcinogenicity studies.[15] One of the first studies included examination of 30 alkylating compounds in Strain A mice for a pulmonary carcinogenic response.[16] Following this study, 35 compounds plus 10 mixtures were examined for carcinogenicity in F344 rats. In 1962, Hans Falk,[17] the head of the bioassay section of the branch, set up a comparative study of 120 pesticides and industrial intermediates in two hybrid mice, including the B6C3F1 mouse, that became the standard National Toxicology Program (NTP) mouse model in later years. As newer environmental carcinogens were identified, more sensitive models such as infant mice and virgin female Sprague–Dawley rats (for mammary tumors) were explored. Due to the high background tumor incidence and the large size, the Sprague–Dawley rat was abandoned and the smaller, easy to maintain F344 that was sensitive to various chemical carcinogens became the preferred rat model in the NCI.[15] The guidelines for the cancer bioassay were published based on a workshop in 1973 and the study design remains essentially the same today.[18] By 1978, the carcinogenicity bioassay program expanded substantially and more than 400 chemicals comprising pharmaceuticals, pesticides, industrial chemicals, food, and tobacco ingredients were evaluated for carcinogenicity by rodent bioassays. In 1978, all the NCI carcinogenicity testing programs were merged with similar efforts at other agencies to form the NTP, housed at the National Institute of Environmental Health Sciences (NIEHS). The bioassay testing methods from the NCI after its various iterations were incorporated into the NTP bioassay.[19] Similar long-term carcinogenicity testing guidelines were published by the FDA,[20] the Environmental Protection Agency (EPA),[21] and the Organisation for Economic Co-operation and Development (OECD).[22] These standardized bioassay protocols increased the scientific validity and acceptance by various regulatory agencies worldwide.

For drug development, by the mid-1980s, carcinogenicity studies conducted by a drug sponsor for the FDA included 3 dose groups of at least 50 animals for rats and mice. In 1987, Center for Drug Evaluation and Research (CDER) was established within the FDA (from the Center for Drugs and Biologics), and soon after, the Carcinogenicity Assessment Committee (CAC) was created to review carcinogenicity protocols and results to promote consistency across the divisions. Although the quality assurance procedures for pathology assessment were outlined by the NTP, CDER/FDA relies on the sponsor for the pathology assessment, only occasionally requesting an external review.[23] Pharmaceutical cancer bioassays typically were conducted in the Sprague–Dawley or Wistar rat and the CD-1 mouse. The standards and system of quality control in the bioassay pathology process, developed at the NTP in the 1970s, are generally recognized and practiced by pharmaceutical companies and contractors conducting rodent cancer studies.

Several organizations have been established to identify and classify carcinogens. Among the data used by these agencies, relevant human epidemiological data followed by the animal (primarily rodent) carcinogenicity data carries the greatest weight in terms of evidence of human carcinogenic potential. Among these agencies, the International Agency for Research on Cancer (IARC), part of the World Health Organization, was established as an intergovernmental agency in 1965. Since 1971, IARC evaluated more than 900 agents, of which more than 400 have been identified as carcinogenic (Group 1), probably carcinogenic (Group 2A), or possibly carcinogenic (Group 2B) to humans, and this information is published in the monographs on the evaluation of carcinogenic risks to humans. In the United States, the National Institute for Occupational Safety and Health (NIOSH) and Occupational Safety and Health Administration (OSHA) were created in 1970 to ensure worker safety from occupational exposures by providing research, education, and training in occupational health and safety. In 1978, the Department of Health and Human Services established the NTP, an interagency initiative, to coordinate, test, and report on various carcinogenic hazards from environmental exposures. In addition, the NTP also publishes the Annual Report on Carcinogens (RoCs) by examining epidemiological, in vitro, and animal data associated with various exposures that a significant US population is exposed to and classifies these potential human carcinogens as known to be human carcinogen or reasonably anticipated to be human carcinogen in the advent of positive data. To date, the RoC has published 13 documents classifying more than 240 substances and exposures. Unlike the IARC, the RoC does not list agents that have been studied and found not to be carcinogens. Similar classifications of potential human carcinogens are provided by various other agencies such as the US Environmental Protection Agency (USEPA); (**Table 1**).

4.14.3 Current Approaches to Carcinogenicity Testing

The objective of the carcinogenicity bioassays for environmental and pharmaceutical chemicals as well as food additives and cosmetics is to examine the carcinogenic hazard associated with 2 years or lifetime exposure of the rodent to the agent in question. These bioassays will determine if there is an increase in the tumor incidence in exposed animals compared to the concurrent and historical controls, target organs of carcinogenicity, tumor latency, preneoplastic lesions, tumor progression, benign and malignant

Table 1 Classification of carcinogens by various agencies

Organization	*Classification*				
IARC (International Agency for Research on Cancer), World Health Organization	*Group 1*: Carcinogenic to humans (118 agents)	*Group 2A*: Probably carcinogenic to humans (79 agents)	*Group 2B*: Possibly carcinogenic to humans (290 agents)	*Group 3*: Not classifiable as to its carcinogenicity to humans (501 agents)	*Group 4*: Probably not carcinogenic to humans (1 agent)
RoC (Report on Carcinogens) National Toxicology Program	Known to be human carcinogen (56)	Reasonably anticipated to be a human carcinogen (187)			
EPA (Environmental Protection Agency)	*Group A*: Carcinogenic to humans	*Group B*: Likely to be carcinogenic to humans	*Group C*: Suggestive evidence of carcinogenic potential	*Group D*: Inadequate information to assess carcinogenic potential	*Group E*: Not likely to be carcinogenic to humans

tumors, tumor multiplicity, and tumor–dose response. This information will be used to determine the no-observed-adverse-effect level (NOAEL) or the benchmark dose (BMD) for establishing point of departure, extrapolation of carcinogenic effects to human exposure levels, and finally examination of potential mode of action (MOA) of carcinogenicity. The BMD is the dose at which a specific adverse response occurs compared to unexposed controls, and the lower 95% confidence limit is termed the benchmark dose level (BMDL). In addition to the lifetime animal bioassays, several in vitro and short-term in vivo tests have also been incorporated into carcinogenicity testing by various testing agencies and industry. These include testing for mutagenicity and clastogenicity using bacteria and other genotoxicity assays[24] (**Table 2**).

As discussed in the previous section, the current guidelines for carcinogenicity testing are the result of an iterative process over the past 65 years. These guidelines provide consistency to the cancer hazard identification process, as well as data for worldwide regulatory assessments and applications, while also optimizing the use of animals for these bioassays. The current guidance documents for carcinogenicity testing have been revised and published by various agencies.[20,25] Most of the details of the bioassay design are very similar across agencies and a brief summary of these guidelines are described here (**Table 3**).

The need for long-term testing of pharmaceutical chemicals and biologics is defined in the International Council for Harmonization (ICH) S1A and S6(R1) documents, respectively. In this article, the focus is only on the chemicals and not biologics. According to the ICH S1 guidelines, pharmaceuticals used clinically for 3 months or more generally require carcinogenicity studies, whereas, in Japan and Europe, carcinogenicity studies on pharmaceuticals are necessary if they are clinically administered continuously for at least 6 months or administered in an intermittent manner that equals 6 months of continuous administration in the clinic. Other pharmaceuticals that are used infrequently do not generally need carcinogenicity testing unless there is a cause for concern, such as radiolabeled imaging agents. Several other considerations for conducting a carcinogenicity bioassay include if there is a cause for concern of carcinogenicity of the pharmaceutical if the product class has carcinogenic potential, structural activity relationship alerts, preneoplastic lesions in repeated-dose toxicity studies, and long half-lives of the parent or its metabolites. In addition, the route of exposure, extent of systemic exposure, pharmacodynamics in animals and in humans (guidelines ICH S1C), genotoxicity of the compounds (guidelines ICH S2A and S2B), and finally the recommended indication and target patient populations are also considered (guidelines ICH S1A).

Table 2 Genotoxicity assays

Gene mutations
- Ames assay (*Salmonella typhimurium*, (*TA 98*, *100*, *1535*, *1537*, *97*, *97a*) *or E. coli* (WP2 *uvrA*)), with/without microsomes
- Tests in rodent somatic cells or transgenic animals
- *Drosophila* sex-linked recessive lethal assay

Chromosome aberrations
- Micronucleus assay in rodent bone marrow or peripheral blood
- Metaphase analysis in rodent bone marrow
- Human lymphocyte metaphase chromosome aberration assay
- Cytogenetic analysis of cultured Chinese hamster cells or human cells
- Mouse lymphoma L5178Y cell Tk (thymidine kinase) gene mutation assay

DNA damage
- Mitotic recombination assay in yeast or Drosophila
- Unscheduled DNA synthesis (UDS) test mostly in rodent hepatocytes
- Comet assay (single cell gel electrophoresis for DNA strand breakage)
- P^{32}-post labeling test (DNA adducts)

Table 3 Study parameters and general guidelines for rodent carcinogenicity studies[a]

Protocol parameter	*Guidelines*
Purpose of study	Identify oncogenic effects in a major proportion of rodents during a normal lifespan
Study design	
Study duration	24–30 months; in ERF bioassays, animals are allowed to live out their natural life spans after the 2 year repeat dose exposures
Animals	
Age at initiation	Male and female, rat and mouse; F344 rat, Sprague-Dawley, B6C3F1, or other strains
Sample size	$\leq$6–8 weeks old
No. of treatment groups	50/sex/group; 100–150/sex/group for "mega" experiment in ERF procedures
Dose selection	$\geq$3 dose groups; 1 concurrent control group/sex Maximum tolerated dose (MTD) is the highest dose based upon minimal toxic clinical and pathological effects in subchronic study; mid and lower doses are based on a variety of factors and purpose
Frequency of dosing	5–7 days/week for 24 months
In life	
Individual body weights	At initiation; 1 $\times$/week for 13 weeks and 4 week intervals to termination
Clinical pathology	Y—10 animals/sex all groups at 2 weeks, multiple time points during entire of study duration
Study termination	
Gross pathology (Y/N)	Y—Detailed necropsy and gross evaluation
Organ weights (Y/N)	Y—Variable number of organs included
Time to tumor (Y/N)	Y
Histopathology	
No. of tissues/organs	30–43
Pathology peer review (Y/N)	Y—Multistage review
GLP protocol (Y/N)	Y—Required by GLP
Statistical analysis of tumor incidence	Survival adjusted quantal-response by poly K testing

[a]These guidelines are compiled from OECD guidelines 451, FDA Redbook (Section IV.C.6 Rev. January 2006), US EPA (OPPTS Guideline 870.4200), National Toxicology Program (Bucher, 2002),[19] European Ramazzini Foundation (ERF) (Soffritti et al., 2002).[26b]

The guidelines on the need for long-term rodent carcinogenicity studies for environmental chemicals or agents (such as nonionizing radiation) are different since they can potentially affect all the human and animal populations in various environmental niches. For high production volume (HPV) chemicals ($>$1 million pounds in the United States or in the OECD $>$1000 tons) and compounds/agents for which widespread environmental exposures are suspected, the long-term rodent carcinogenicity bioassays are needed to assess the carcinogenic hazard associated with these exposures. Of course, not every HPV chemical is a carcinogen, so epidemiological studies, and exposure data (occupational and lifestyle) usually provide a justification for testing for carcinogenicity.

Guidelines on the selection of animal species in the long-term carcinogenicity bioassay suggesting use of the rat and mouse animal models are provided by the ICH S1B and OECD TG 451. The ICH guidelines suggest a number of criteria in selecting a species for long-term carcinogenicity studies. These include pharmacologic responsiveness, repeated-dose toxicologic response, comparative metabolic and toxicokinetic attributes, and intended route of administration. In the absence of clear evidence favoring one species, the rat is usually the recommended species. Additional in vivo tests for carcinogenicity that contributes to the weight of evidence (WOE) may involve short- or medium-term studies using transgenic mice or a long-term mouse study. The testing paradigm is different for the NTP bioassays where 2-year studies are required in both rat and mouse species. The carcinogenicity studies conducted by the European Foundation of Oncology and Environmental Sciences (Ramazzini foundation) consist of full natural lifespan studies in rats, where the repeat dose exposures are stopped at the 2-year time point and the rodents are allowed to live out their natural lifespan.[26] Though the goals of the bioassays conducted by the NTP and Ramazzini foundation are the same, the approaches are similar in some ways and different in others. For more details, please refer to the article by Bucher.[19]

Guidelines for dose selection are provided in ICH S1C, and OECD TG 451 documents, reports from the two International Life Sciences Institute (ILSI) workshops[27] and also other papers.[28] Please refer to these documents for detailed information. In brief, dose levels in the carcinogenicity bioassay are generally based on shorter-term repeated-dose range-finding studies (28-day or a 3-month repeat dose study). Ideally, the doses in the short-term repeat dose studies should be spaced in such a way that a NOAEL, the minimally toxic dose (MTD, also known as maximum tolerated dose), and the dose response curves may be generated. The animals are exposed by the most appropriate route of exposure (feed, drinking water, gavage, intravenous, inhalation, and dermal) that is relevant to the human exposure scenario. Effects specific to certain routes of exposures, such as gavage versus dietary or

drinking water exposures, should also be taken into consideration. The repeat dose exposure usually starts after weaning and continues until the end of the study. The study design should control for various confounding factors such as cage location, time of dose administration, and volume and frequency of handling or manipulation, feed, and litter effects. All the studies should be conducted according to the FDA's good laboratory practices.

Multiple dose groups (up to 5 treated for environmental molecules and 1 control) that capture the range of potential toxicities are included in the 3-month study and the group size is limited to 10 animals/sex/dose. For the 2-year study, groups of at least 50 male and female rats and mice are randomly assigned to 3 treated groups at high, medium, and low doses with 1 vehicle control group. The repeat dose exposure usually starts at weaning and continues till 2 years of age when the animals are euthanized, necropsied, sampled for a complete and systematic gross and microscopic evaluation. For any pharmaceutical compound requiring a cancer study, a 6-month rat chronic toxicity study is also conducted. On some occasions in NTP studies, interim sacrifices (at 6 months, 1 year) are scheduled to allow for tissue burden studies, toxicokinetics, and mechanistic studies. For some NTP studies where maternal exposure and transplacental exposure is suspected, exposure of pregnant rats begins in utero at 6 days of gestation and the resulting F1 pups are continuously exposed for 2 years as a regular chronic bioassay. Additional cohorts of animals are usually added to all dose groups to allow for toxicokinetic and metabolism studies to characterize quantitative dose–response relationships for any anticipated toxic effects.

The selection of the doses for the 2-year bioassay is one of the most critical decisions for the success of the bioassay, thus allowing for meaningful interpretation in terms of human health risk. If the doses are too low, the animals might not be challenged sufficiently resulting in a false negative response and if the doses are too high, it might lead to overwhelming of the metabolic or homeostatic mechanisms resulting in a false positive response. The lowest dose should also receive considerable attention since it should attempt to reflect environmental exposure levels or clinically relevant exposures and aid in the determination of NOAELs. Due to the inherent limitations of the statistical power of a bioassay that employs only 50 animals/dose group due to practical considerations, it is essential to maximize the sensitivity of the bioassay and make sure that the animals are challenged to the maximum extent without causing overt toxicity that impacts the natural lifespan of the animal on the study. It is also important that the animals be challenged at the MTD to give confidence in case of a negative study. This maximum challenge is accomplished by administering the chemicals at the MTD and is defined as a dose that causes no more than a 10% body weight decrement as compared with controls; and does not produce mortality, clinical signs of toxicity, or lesions that would be predicted to shorten the animal's natural lifespan.[18,28b] In addition, the MTD is also limited by physical criteria of the test agent such as solubility, suspendability, stability, aerosol generation limit, and also physiological limits of the animal such $\leq$5% in diet, 5 mL kg^{-1} (rats) and 10 mL kg^{-1} (mice) by gavage, 0.3 mL (rats) and 0.1 mL (mice) for dermal exposure; and lung burden (overload) levels.[29] Further information on the chemicals including the physicochemical characteristics, toxicokinetic data absorption, distribution, metabolism, and excretion (ADME), physiologically based toxicokinetic modeling, and any available literature on the proposed (MOA, especially for nongenotoxic carcinogens) should be taken into consideration during dose setting for the carcinogenicity bioassay. Comprehensive clinical examination and pathology data should capture qualitative and quantitative adverse and adaptive effects in subchronic studies. All this information will also aid in dose level spacing to allow for generation of meaningful dose response curves and determining NOAEL and BMDL as well as identifying threshold effects. Usually, it is very difficult to generate all this information (hazard identification/characterization and dose response data; NOAEL/BMDL-seeking threshold effects; safety assessment of human exposure levels) in one experiment but optimal study design approaches can assist in generation of the maximum relevant information for risk assessment purposes.

4.14.3.1 Experience With Transgenic Carcinogenicity Assays

Two-species rodent lifetime cancer bioassays have traditionally been the primary in vivo testing paradigm to identify cancer-causing agents for environmental agent cancer hazard identification.[30] However, it is not feasible to conduct the standard two-species/two-sex lifetime (2-year) carcinogenicity bioassays to assess the possible carcinogenicity of the many thousands of legacy chemicals in commerce. Also, it was determined that a second rodent cancer bioassay especially, the mouse does not add much value for pharmaceutical safety assessment when compared with alternative models.[31] With gain of significant insights into structure and nature of the human and rodent genomes and with recognition of the common alterations in cancer genes in many human and rodent tumors, genetically modified (GM) animals have been developed and utilized to provide insights into normal and disease-related processes.[32] GM mice have been proposed as adjuncts or replacements for the conventional mouse 2-year carcinogenicity bioassays.[33] Cancer bioassays involving genetically altered mice are shorter in time and less expensive than the traditional 2-year mouse cancer bioassay. Two major types of genetically altered mice have been developed; one type involves creation of GM animals by inserting one or more genes from the same or another species randomly into the host genome. The second type involves targeted insertion by homologous recombination in embryonic stem cells at the gene locus by either partial deletion or mutation at specific amino acid positions for loss or gain of function.[34]

Some of the desirable characteristics of GM animals include phenotypically normal physiology and health prior to chemical exposure, low level of spontaneous tumor incidence, intact genetic stability, increased sensitivity, decreased tumor latency, and expression of the genetic modification in a wide range of tissues to ensure assessment of nonneoplastic and neoplastic effects in all potential target organs.[35] Four mouse models, specifically the heterozygous *Trp53*$^{+/-}$ (B6.129-*Trp*^{tm1Brd}, Trp53$^{+/-}$, or *Trp53*^{def}),[36] FVB/N-Tg.AC (carrying the mouse mutant v-Ha-*Ras* oncogene under the control of the zeta-globin promoter),[37] *ras*H2 (carrying multiple copies of human *HRAS* proto-oncogene),[38] and the xeroderma pigmentosum group A (*Xpa*$^{-/-}$)[39] have been extensively

Table 4 Comparison of the NTP 2-year bioassay with the genetically altered mouse assays[a]

Assay characteristics	*2-year bioassay*	*Tg.AC*	Trpp53^{+-}	rasH2	Xpa$^{-/-}$
Mouse strain	B6C3F1	FCB/N-Tg.AC	B6.129-*Trp53*^{tm1brd*}	CB6F1-Tg-H*ras2*	B6.129-*Xpa*^{tm1Hvs}
Genetic background	C3HeN and C57B/6N	FVB/N	C57BL/6NTac	BALB/cByJJic and C57BL/6J	C57BL/6J
Zygosity/genotype	Heterozygous	Hemizygous for a mutant v-Hras1 transgene	Heterozygous	Hemizygous for human *HRAS* transgene	Homozygous
Recommended chemicals for testing	Wide range of agents	Genotoxic, nongenotoxic	Genotoxic	Genotoxic Nongenotoxic	Genotoxic Nongenotoxic
Age at start of the expt.	6–8 weeks	7–9 weeks	6–8 weeks	7–9 weeks	6–8 weeks
No. of mice/cage	10	1	5	5	1 (male), >1 (female)
Treatment duration	104 weeks	26 or 36 weeks	26 or 36 weeks	≤26 weeks	39 weeks
Route of exposure	Feed, gavage, inhalation, topical, drinking water, i.p.	Topical, feed, gavage	Topical, gavage	Gavage, feed, i.p., drinking water	Topical, gavage
No. of mice/dose	50	15–20	15–20	25	15
Basis for dose selection	MTD[b]	MTD from previous cancer bioassay	MTD from previous cancer bioassay or dose range finding	MTD from previous cancer bioassay	4-week dose range finding study with genetically modified mice
No. of tissues for necropsy and histopathology	>40 tissues	12 tissues	>40 (nongenotoxic) and 12 (genotoxic)	>40 tissues	>40 tissues
Common spontaneous tumor	Hepatocellular adenomas/ carcinomas Alveolar bronchiolar (A/B) carcinomas	Odontogenic tumors, forestomach and cutaneous papillomas, A/B adenomas	Lymphomas, osteosarcoma, hemangiosarcoma	Hemangiosarcoma, A/B carcinoma, cutaneous papilloma, Harderian gland carcinoma, lymphoma	Lymphoma, A/B adenoma, adrenal tumors

[a]Bucher (2002),[19] Huff (1999),[30] Donehower et al. (1992),[36] Leder et al. (1990),[37b] Spalding et al. (1993),[37] Saitoh et al. (1990),[38] van Kreijl et al. (2001),[39b] van Steeg et al. (2001), and Eastmond et al. (2013).[47b]
[b]MTD, maximally tolerated dose.
Adapted and modified from Eastmond, D. A.; Vulimiri, S. V.; French, J. E.; Sonawane, B. The Use of Genetically Modified Mice in Cancer Risk Assessment: Challenges and Limitations. *Crit. Rev. Toxicol.* **2013**, *43* (8), 611–631.

investigated by researchers as suitable models for accelerated cancer bioassays.[32,40] The characteristics of each of these models are summarized and compared to that of inbred mice used in the conventional 2-year bioassay, in **Table 4**. The *Trp53*$^{+/-}$ model has been reported to detect primarily genotoxic carcinogens, whereas the Tg.AC and the *ras*H2 models were able to include a broader range detecting both genotoxic and nongenotoxic carcinogens.[40c,41] The standard study design for a rasH2 mouse study includes 3 treatment groups and a vehicle control group composed of 25 animals/sex/group. A positive control group (usually N-Nitroso-N-methylurea (MNU) or urethane) composed of at least 10 animals/sex is required. Note that it is acceptable to only examine microscopically the thymus in the positive control (MNU-treated) group to conserve the pathology resources.[42]

There are several advantages of using GM mice in hazard identifications; use of fewer animals, a more rapid completion of the study (within 26 weeks), a significant reduction in the cost to test a chemical, a larger number of chemicals can be tested, and more translatability, relevant to humans (human cancer genes in the mouse). However, a number of potential problems and concerns have been recognized with the use of GM animals as a primary method to identify carcinogenic agents.[40a,b,43] There are significant genetic background differences, route and type of exposure, degree of organ specificity, between the animals used in conventional and short-term cancer assays. The mechanisms underlying the chemically induced cancers in the GM animals may differ fundamentally from those occurring in non-GM mice due to copy number variation in the transgene and altered global gene expression pattern as both *RAS* and *TP53* are master regulatory genes that control and/or influence many other genes and pathways within the cells.[44,45] Hence, there is a concern that the tumors in the genetically altered animals may arise from different mechanisms or be unique to specific genetic modifications that differ from those occurring in wild-type animal models. Further, the use of the current GM animal data in dose–response assessment (such as NOAEL or BMDL) and for quantitative risk estimation is more problematic due to small sample size typically used in the accelerated bioassay.

The predictivity of transgenic mouse models has been chronicled by workers in the NTP. The transgenic alternatives, specifically the combined predictivity data of *Tp53*$^{+/-}$ (for genotoxic molecules) and *ras*H2 (for nongenotoxic molecules), provide comparable

predictiveness for human response to known (Group 1) and probable (Group 2A) human carcinogens to the rat and mouse lifetime bioassays, alone or in combination. The Group 2A molecules tested in the NTP survey all tested positive using a combined Tg.AC, *Tp53*$^{+/-}$, and *ras*H2 test system. Similarly, of the 14 Group 1 carcinogens tested in this combined Tg.AC, *Tp53*$^{+/-}$, and *ras*H2 test system, 11 yielded positive responses, 1 yielded a negative response, and 2 were untested. In contrast, when applying the conventional 2-species lifetime rodent test system to this same list of 14 Group 1 carcinogens, 5 positive tests, and 1 negative test were reported, with most (8) untested. These data support the belief that the transgenic alternatives alone provide comparable ability to detect Group 1 and 2A carcinogens as the lifetime combined rat and mouse lifetime bioassays. Of course, the rat and mouse lifetime responses predict for rat and mouse carcinogenicity, thus predicting with precise accuracy for possible (Group 2B) human carcinogens, since all positive rodent responses are automatically classified as Group 2B by IARC, when there is inadequate evidence of carcinogenicity in humans. The *Tp53*$^{+/-}$ and *ras*H2 lifetime models do not predict as well for the rat and mouse lifetime bioassay outcomes; thus these two model systems reduce the generally recognized high false-positive rate, while not compromising the ability to identify known (Group 1) and probable (Group 2A) human carcinogens. That is, these models substantially improve the precision in the identification of human cancer risk for pharmaceutical agents. Numerous drugs that had rodent responses known to be nonpredictive are listed as IARC Group 2B agents, such as phenobarbital and benzoyl peroxide.[40b,46]

A direct evaluation of these models would be to compare the results of carcinogenicity assays conducted in the GM models with the tumor data seen in non-GM mouse bioassays even though the purpose of the bioassay is to predict for human response.[47] The degree of concordance for the bioassays conducted in *Trp53*$^{+/-}$, Tg.AC, and *ras*H2 bioassays with 2-year NTP mouse chronic bioassay was about 57% (17/30), 61% (20/33), and 82% (23/28) of the chemicals tested, respectively.[47b] There were 11 chemicals that induced tumors in the NTP mouse bioassays that were not detected as carcinogens by the bioassays conducted in GM models (tested in one or more but not all GM models). Four of the 11 chemicals were trans-species carcinogens with a positive response in both the rat and mouse NTP bioassays and the remaining 7 were carcinogenic in the NTP mouse only. In another comparison with chemicals independent of their genotoxicity and immunosuppressive ability but are identified as known human carcinogens or reasonably anticipated to be human carcinogens, the concordance was 86% (12/14), 67% (8/14), and 43% (6/14) in the *ras*H2, the Tg.AC, and the *Trp*53$^{+/-}$ model, respectively.[47b] On the other hand, the concordance with the NTP mouse (21/21) and rat (20/20) bioassays was 100%. This finding is a reflection of the ability of the traditional rodent studies to not miss true positives but they probably give rise to some false positives, as well. However, the traditional mouse or rat models have their limitations especially with false negatives when testing well-known human carcinogens such as cigarette smoke and certain immunosuppressive agents.

Even though the genetically altered mouse models have shown some value in identification of carcinogens and noncarcinogens, they cannot completely replace the traditional rodent models. These genetically altered mice seem to be more efficient in correctly identifying noncarcinogenic agents (thus reducing the false positives), but they tend to miss certain carcinogens, thus prone to some false negatives.[47b] Even combining multiple genetically altered mouse models will not likely detect all trans-species and human carcinogens. In summary, the overall accuracy in classifying carcinogens and noncarcinogens was good, but all GM strains failed to detect some chemicals known to be human carcinogens when used as stand-alone assays.[40b] However, when the GM models (especially the *ras*H2 mouse) were combined with a rat bioassay, the overall predictivity was better than the traditional rat and mouse cancer bioassays.[40b,48]

Further validation studies to optimize study designs and protocols can address some of the concerns associated with sample size, study duration, genetic instability, dose response curves, and reproducibility. The small sample size ($n=25$) of the GM mouse protocols compared to the traditional mouse protocol ($n=50$) may result in incongruent conclusions with respect to dose–response curves and detecting threshold effects for certain chemicals.[47b] In general, due to the small sample size and reduced study duration, no effect may be detected in the low dose group, falsely suggesting a threshold effect. This is especially apparent for chemicals such as phenolphthalein (lymphoma) and urethane (hemangiosarcoma, lung tumors).[47b] This is an important consideration for risk assessment purposes of environmental chemicals (probably not so much for pharmaceutical compounds) since the regulatory requirements of the EPA differ for chemicals with and without thresholds for carcinogenic response. Increasing the GM mouse sample size to 50 for studies aimed at detecting thresholds and comparing to the traditional mouse studies may be necessary for generating risk assessment data for environmental chemicals. Of course, there could be erroneous conclusions regarding thresholds even with a sample size of $n=50$ but with a smaller sample size, the error rate is probably high for certain chemicals. The issue of pathway-dependent effects and different mechanisms of chemical carcinogenesis, especially for nongenotoxic carcinogens, operating in these genetically altered models are a concern and further studies are needed to address the translatability of chemical carcinogenesis pathways in the genetically altered mice to humans. As we learn more about the mechanisms of chemical carcinogenesis, newer GM rodent models may be developed to advance the MOA and risk assessment studies. Genetically altered mouse models such as PPAR alpha knockout (KO), aryl hydrocarbon receptor (AhR) KO, CYP2E1 KO, and CYP1B1 KO mouse models have shown value in this regard.

4.14.4 Future Approaches of Carcinogenicity Testing

There has been a call to improve the carcinogenicity hazard identification process as well as to reduce, modify, or even abandon the 2-year bioassays over the past few decades. The often cited reasons are the cost of the 2-year studies, the use of large number of animals, the long duration of these bioassays, uncertainty of the outcomes in terms of equivocal evidence of carcinogenicity,

high background tumor response in the B6C3F1 mouse, and uncertainty in extrapolation of the rodent tumor response to human cancer risk.[49] On the other hand, the cancer bioassay (and other animal studies) has been evolving from a simple "cancer-no cancer" screening assay to one that provides more mechanistic information on toxicity and carcinogenicity over the past decades. In the following section, discussion will be focused on some of the current and future approaches to carcinogenicity testing.

4.14.4.1 New Paradigms in Rodent Bioassays

Most human carcinogens have proven to be rodent carcinogens when they were adequately tested. On the other hand, some of the rodent carcinogens do not necessarily pose a carcinogenic hazard to people due to species-specific mechanisms as well as laboratory testing artifacts, such as high dose exposures that greatly exceed human exposure values.[50] For genotoxic carcinogens, there is a high degree of correlation with tumor response across species. However, for nongenotoxic carcinogens, there are several examples of species-specific mechanisms that result in tumors in only certain species.[50] Historically, the rodent carcinogenicity data served a critical role for identifying carcinogenic hazards and due to historical knowledge and experience with this data, the risk assessors usually find comfort in having and using the rodent carcinogenicity data. When alternative approaches are proposed for replacing the traditional rodent carcinogenicity bioassays, the toxicology/pathology community becomes polarized between groups/individuals that believe that any positive response in rodents is relevant for humans regardless of the mechanism versus those that believe that the rodent lifetime bioassay no longer adds value, precluding toxicology/pathology community alignment for change. As a result, though imperfect, the rodent carcinogenicity bioassays continue to be central but modifications to those bioassays in terms of reduced animal numbers and alternate strategies based on WOE are increasingly being considered for hazard identification and risk assessment. In this next section, some of the current and future approaches that are being considered to optimize the rodent bioassays and in some cases, even obviate the need for the rodent carcinogenicity bioassays for cancer hazard identification are presented.

4.14.4.2 Proposals for Pharmaceutical Carcinogenicity Studies

The small-molecule carcinogenicity assessment guidelines of ICH suggest a 2-year rat bioassay and either a 2-year mouse or an alternative 6-month transgenic mouse carcinogenicity bioassay. There is increasing evidence that in certain cases, the 2-year rat bioassay may potentially be obviated in the absence of certain characteristics.[51] Monro[51a] has proposed that the few pharmaceuticals known to cause cancer in humans operate through at least one of four features: genotoxicity, immunosuppression, hormonal activity, and chronic toxicity. Reddy and colleagues[51b] demonstrated that the absence of histopathologic risk factors (cellular hypertrophy, hyperplasia, and atypical cellular foci) associated with neoplasia in *any* organ within the animal was highly predictive of a negative rat carcinogenicity bioassay. A consortium of pharmaceutical companies examined the various risk factors associated with rat carcinogenicity bioassay data from 182 pharmaceutical compounds and came up with a proposal termed NEGCARC (*N*egative for *E*ndocrine, *G*enotoxicity, and *C*hronic study *A*ssociated histopathologic *R*isk factors for *C*arcinogenicity).[51c] According to this proposal, little value is gained from a 2-year rat carcinogenicity bioassay for compounds that lack (1) treatment-related histopathologic risk factors (hypertrophy, hyperplasia, and atypical cellular foci) of rat neoplasia in *any* tissue within a 6- or 12-month chronic toxicity study, (2) positive response in any of the assays in the ICH S2 genotoxicity battery (bacterial mutation, in vitro mammalian cell mutation or clastogenicity, or in vivo clastogenicity), (3) perturbation of hormonal function by WOE approach, and (4) a positive response in a 6-month transgenic mouse carcinogenicity bioassay. Sistare et al. proposed that in the absence of these four NEGCARC criteria, the 2-year rat study may be waived and only the 6-month transgenic mouse study or a 2-year mouse study needs to be conducted, while in the presence of any one of the four NEGCARC criteria, then a 2-year rat study along with the corresponding mouse study need to be conducted. Their data suggests that the absence of any of these four risk factors is highly predictive of a negative rat carcinogenicity bioassay.[51c] Sistare and colleagues estimated that this decision paradigm has the potential to eliminate over 40% of the rat 2-year bioassays for new pharmaceutical compounds without compromising patient safety.

Based on this proposal, in 2013 the FDA considered a revision to the ICH S1 guidance on rodent carcinogenicity testing and issued a notice for public comments with the goal of introducing a more comprehensive and integrated approach to address the risk of human carcinogenicity associated with small-molecule pharmaceuticals (Federal register 78:52). The FDA applied the NEGCARC criteria on an independent set of 60 additional pharmaceutical compounds and achieved similar results as Sistare et al.(2011)[51c,52] In addition, the Japanese Pharmaceutical Manufacturer's Association (JPMA) also applied the NEGCARC criteria on a set of 64 compounds and attained similar results. The independent replication of the results by various agencies appears to give confidence for the application of NEGCARC criteria for current and future drug development.

There are, however, some reservations in following the NEGCARC criteria in its current form. Any one of three triggers based on histologic risk factors, hormonal perturbation, and genotoxicity can trigger a 2-year rat cancer bioassay. This rule has to be followed in its entirety and no exceptions should be made especially with arguments about the translational relevance of these respective triggers for tumor risk.[52] The NEGCARC proposal assumes that the endpoint of the bioassay is assessing tumor risk in rodent (rat) models and not necessarily of the tumor risk in humans, that is, the false negative cases (positive for 2-year rat carcinogenicity tumor response and negative for all the three risk factors) in their data set have no implications for human cancer risk. If there was positive rat carcinogenicity data, the sponsors and risk assessors would consider this during clinical trials. In the absence of this lifetime rat tumor data, the risk assessors and sponsors would be challenged if there was a tumor response during phase 3 clinical trials or during postmarketing.[52] Of course, demonstration of positive responses in humans in the presence of negative lifetime

mouse and rat studies plagues the current testing paradigm (e.g., cigarettes and tacrolimus), unfortunately there is no perfect testing strategy. While the NEGCARC proposal is reasonably sensitive (79%) in predicting rodent carcinogens based on just three risk factors, it does not consider equally important mechanistic data about the compound's pharmacology. In fact, when the compounds from various agencies (Pharmaceutical Research and Manufacturers of America (PhRMA), FDA, JPMA) were unblinded, the compound's known pharmacologic properties could easily predict the rodent tumor response of the false negatives (14%), where NEGCARC criteria failed to accurately predict rodent tumor response.[52] Immunosuppressive drugs represent a pharmacologic category that pose cancer risk in humans that is not detected in rodent bioassays, a category not included in the NEGCARC paradigm, but a risk factor that could possibly be identified in subchronic toxicology studies.

Based on the earlier observation and analysis of various datasets (by the PhRMA, FDA, JPMA, and European Union, EU), it was concluded that the NEGCARC criteria and the compound's pharmacology (WOE approach) could reasonably predict the outcome of the 2-year rat carcinogenicity bioassay at the two extremes of the spectrum, that is, negative predictions could be made when the predictive signals are absent and positive predictions could be made when the predictive signals are present. However, an in-between category of compounds exists where the outcomes of carcinogenicity outcomes cannot be predicted with certainty (Federal register 78:52). This WOE approach can potentially assess the need for conducting a 2-year rat carcinogenicity bioassay and subsequently classify the pharmaceutical compounds into three categories (1, 2, 3a, 3b): Category 1: product likely to be tumorigenic to humans and a 2-year rat study would not add value; Category 2: uncertain tumorigenic potential in humans and hence a 2-year rat study is likely to add value; Category 3a: likely to be tumorigenic in rats but not in humans based on prior-established and well-recognized carcinogenic mechanisms not relevant to humans and a 2-year rat study would not add value; Category 3b: likely not tumorigenic in either rats or humans and no 2-year rat study is needed. Based on these categories, as discussed earlier, it is easy to categorize compounds into Categories 1 and 3b. Classification of compounds into Category 3a may also be relatively easy provided the sponsor and the regulatory agency agree on the strength of the WOE. In the lack of sufficient or incomplete data for the WOE analysis, a number of compounds will be categorized into Category 2, where a 2-year rat study will provide value for risk assessment.

The ICH expert working group is currently conducting a prospective evaluation (exercise) where sponsors voluntarily submit carcinogenicity assessment documents or WOE assessments to the drug regulatory agencies prior to the initiation of the 2-year rat studies or before the results of the 2-year rat study are known. The sponsors also prospectively categorize (1, 2, 3a, or 3b) their compound regarding the need for a 2-year rat study. The ICH working group independently evaluates the data in a blinded manner and arrives at their own category for that data. The intention of this exercise is to check the predicted outcomes of their respective hypothesized categories against the actual tumor outcomes from the completed prospective 2-year rat studies. The information generated from this exercise will demonstrate the concordance or discrepancies between the WOE assessment by the sponsors and the FDA regulators. These experiences will provide an opportunity to generate more refined, uniform, unbiased approaches for the WOE assessment before it can be incorporated into ICH S1 guidelines.

As the learnings from this exercise result in changes in cancer hazard identification practices with the WOE approaches, it is clear that the rat 2-year studies will not be replaced completely in the near future. For EPA-regulated compounds, specifically the legacy compounds, the necessary subchronic data typically are not available, obviating utility in this circumstance, but this paradigm may have significance for compounds in development.

4.14.4.3 Future Paradigms for Environmental and Other Carcinogens

The paradigms of carcinogenicity testing of environmental chemicals appear to be similar to that of pharmaceuticals. However, there are significant differences between the two especially when it comes to the nature of the compounds. During pharmaceutical development, any compound exhibiting genotoxicity or indicating potential carcinogenicity are typically discarded early in development. The only exceptions are pharmaceutical compounds being developed for cancer (some of them are genotoxic compounds) or other life-threatening conditions or seriously debilitating disease such as lupus (immunosuppressive agents), where benefits may outweigh the risk of cancer. However, most of the environmental chemicals selected for carcinogenicity testing today are suspected carcinogens based on epidemiological data, or are likely widespread in the environment with no cancer hazard data, or are HPV chemicals with a high potential for occupational or environmental exposures. In addition, chemicals such as pesticides, feed additives, and packaging materials in contact with food also have the potential for widespread and indiscriminate exposure to humans and environment. The risk tolerance for environmental chemicals is very low compared to pharmaceutical compounds due to the widespread nature of environmental exposures compared to targeted exposures in patient populations, respectively. Even though false negatives and false positives are inherent in the current testing paradigm, it is very difficult if not impossible to eliminate a regulatory test although it is quite possible to add on new regulatory tests. Nonetheless, it behooves toxicologists/pathologists to periodically challenge the existing testing paradigms and work to improve the testing methods.

The NTP carcinogenicity bioassays are considered the gold standard, however, due to the time, expense (especially considering the large numbers of untested compounds in commerce), and the need to conserve animal resources through the 3Rs principle (*replace* rodents with lower order species or in vitro systems, *reduce* the number of animals, *refine* the endpoints to derive maximum information with minimal pain and improving animal welfare), NTP and other stakeholders are considering alternative approaches for determining toxicity and subsequently carcinogenicity hazard.[53] As discussed in the beginning of this article, there are several thousands of chemicals within the environment and in commerce and newer chemicals being produced every year, it is imperative to come up with newer resource efficient methods of identifying the cancer hazards associated with these chemicals. Of course, it

would be impractical to expect 2-year rodent bioassay data on all these legacy chemicals, though any new chemical must be tested using the contemporary paradigm prior to commercialization.

In developing the future carcinogenicity paradigms, the approaches taken by various investigators and programs fall into two broad categories: top down or bottom up, that is, the top-down approach is a traditional approach and typically starts with the chemical-induced adverse effect and the subsequent studies are focused in evaluating the MOA and mechanisms of action in animals with a focus on human relevance, while the bottom up is a predictive approach and typically consist of several high-throughput in vitro screening assays aimed at understanding the chemical-induced biological perturbations with a focus to elucidate the MOA and then apply quantitative in vitro to in vivo extrapolation (qIVIVE) and subsequently predict an adverse outcome (AO) in animals and humans.[54] None of these two approaches in isolation provide a solution for future carcinogenicity studies. However, the lessons learnt from these two approaches may provide unique approaches to carcinogenicity testing. Cancer is a chronic disease and a certain amount of time should elapse before the earliest cancer signature can be detected, that is, the process of carcinogenesis has initiated and progressed unequivocally (probably within 6–12 months in rodent cancer models). Biomarkers that can confidently detect these earliest cancer signatures will provide a path forward for future carcinogenicity testing. Hence, at least in some cases, the need for the traditional 2-year carcinogenicity studies may be obviated if these biomarkers can be identified. In the end, future cancer bioassays may probably be condensed to <2 years but since cancer is typically a chronic disease, a certain amount of time should elapse before the earliest signature of cancer can be detected.

In the following paragraphs, some of the alternative approaches that are being undertaken by various stakeholders in toxicity testing and regulation are discussed.

4.14.4.4 Toxicology Testing in the 21st Century (Tox21)

Tox21 is a federal collaboration among the EPA, FDA, and NIH (National Center for Advancing Translational Sciences (NCATS) and NTP) to test a collection of 10,000 environmental chemicals and approved drugs (Tox21 10K library) for their potential to disrupt biological pathways and cause toxicity by using several 100s of high-throughput screening (HTS) assays. EPA's Toxicity Forecaster (ToxCast) is a similar initiative that uses HTS screening methods (>700 in vitro assays) and computational toxicology approaches to rank and prioritize chemicals (>2000 chemicals) for further testing. The principal goals of the Tox21 program are to prioritize legacy chemicals for further in-depth toxicological evaluation, identify mechanisms of action for further investigations, and develop models that better predict chemical effects in biological systems.[53] One of the first objectives of the Tox21 program is to develop better methods to quickly and efficiently identify if a chemical has the potential to cause negative health effects in humans by identifying disruption of cellular processes. These data will be used to identify hazards associated with carcinogenicity, endocrine disruption, reproductive toxicity, immunotoxicity, neurotoxicity, genetic toxicity, and other potential toxic effects. These HTS assays together with bioinformatics and systems biology approaches examine the "hits" from the high-throughput assays and help understand the underlying cellular and molecular pathway alterations in biological systems. The chemicals identified in the initial screening assays will be prioritized for testing in more complex biological systems in the increasing order of biological complexity such as cells, organ cultures, *Caenorhabditis elegans*, zebrafish, and rodents. Since disruption of biological processes and toxicity plays a significant role in the process of neoplasia, identification of chemicals by these approaches can be a way to prioritize chemicals for further testing and also identify chemicals that are of not much concern, for regulatory purposes.

The HTS data that is being generated in the Tox21 initiative is providing multiple streams of data on biological perturbations induced by chemicals in various cell lines with and without metabolizing capability. While this information is important in understanding the alterations in molecular pathways, it still does not provide reliable information on the potential phenotypic alterations that could result from these molecular alterations, that is, there is still no convincing way to qualitatively measure the consequence of these molecular alterations on the phenotypic responses that could either result in adaptive or adverse responses in the whole organism. As discussed earlier, prioritizing and testing in higher order biological systems will provide more convincing information on the biological relevance of these molecular alterations. This paradigm of HTS testing and validation in more complex biological systems is an iterative process and a critical body of knowledge needs to be accumulated before these alternative toxicological methods become mainstream. For now, the regulatory agencies cannot rely exclusively on the HTS data to identify and regulate potential carcinogens. In the near term, these data could be operationally used to identify chemicals with few or no "hits," indicating that these legacy chemicals may be a low priority for carcinogenicity testing. These HTS data (and mechanistic data) can also be used to regulate chemicals with no safety data but that are within a class of chemicals with a well-defined MOA.

Some of the IARC Group 1 agents with less than sufficient evidence of carcinogenicity in humans were regulated based on the well-accepted relevant MOA that is conserved across species including humans. 2,3,7,8-Tetrachlorodibenzo-para-dioxin (2,3,7,8-TCDD) binds to AhR and causes similar downstream molecular alterations resulting in cell proliferation and inhibition of apoptosis, mechanisms that are conserved in humans and experimental animals. 2,3,7,8-TCDD was classified as Group I carcinogen based on the conserved MOA and even in the absence of sufficient epidemiological evidence of carcinogenicity. This classification was ratified in subsequent years by concordant human epidemiological data, supporting the cancer risk based on the conserved MOA.[55] Chemicals (such as 2,3,4,7,8 pentachlorodibenzofuran and 12 dioxin-like polychlorinated biphenyl (PCB) congeners) that activate the AhR nuclear receptors and cause subsequent downstream effects at very low concentrations and in a dose-dependent manner are classified in the same class as 2,3,7,8-TCDD (a known class I carcinogen) and can be categorized as IARC Group I carcinogens even without sufficient evidence of carcinogenicity in humans.

4.14.4.5 The Promise of -Omics Approaches

Genomic and epigenomic technologies (-omics) have the potential to alter the practice of traditional toxicology by providing data that describes genome-wide molecular alterations underlying toxicity and carcinogenicity in various organs and in vitro cell culture systems.

Toxicogenomics is the application of genomics (transcriptomics, RNA-Seq, DNA-seq), epigenomics (methylation and histone modifications, miRNA alterations), proteomics, and metabolomics to characterize tissue responses secondary to chemical exposures. Due to the substantial qualitative and quantitative dynamic range of protein alterations in toxicities, it is technically challenging to comprehensively capture these alterations by the currently available technologies.[56] On the other hand, the dynamic range of the transcriptomic responses is more amenable to capture by the oligonucleotide probesets (cDNA arrays) and have been adapted to such a wide extent in the field of toxicology that transcriptomic responses in toxicity are commonly referred to as toxicogenomics.

Toxicogenomics (transcriptomics) provide a genome-wide snapshot of the differential gene expression profiles and subsequently an insight into the molecular pathways associated with various toxicities and carcinogenicities.[57] This technology enables comparison of alterations in molecular pathways of various chemical-induced toxicities and carcinogenicity and thus promises to be a valuable tool for the identification of corresponding hazards related to chemical exposures. Initially and even currently, toxicogenomics are predominantly descriptive in nature, where the molecular pathways altered by various chemical exposures provide a clue to the MOA of a particular phenotype (toxicity or carcinogenicity).

The idea that transcriptomic data can be used for predictive toxicology was based on the demonstration that chemical-specific gene signatures may be derived from hepatic gene expression data from various chemical exposures.[58] Subsequent demonstration that gene signatures derived from training sets containing chemicals with known modes of action could be used to identify previously unknown or blinded chemicals with similar modes of action provided an impetus to use this approach to study carcinogens.[58b,59] With increasing knowledge based on chemically induced carcinogenic mechanisms, toxicogenomics is increasingly being leveraged for prediction of potential carcinogenic effects based on short exposures in which morphological evidence of neoplasia or preneoplasia are not typically present. The premise behind the use of toxicogenomics for the prediction of carcinogenicity using tissues from very early exposures (3 days to 3 months) is that repeat dose chemical exposure initiates unique chemical-specific molecular pathways in the cells early on that ultimately progress to neoplasia. Thus, predictive toxicogenomics aims to examine tissues from very early exposures for the alterations in these molecular pathways in tissues with or without morphologic evidence of preneoplasia or in some cases even without histologic lesions. This approach was successfully exploited in the areas of predictively toxicology and carcinogenicity, where a gene signature is generated based on the transcriptomic responses of known genotoxic and nongenotoxic carcinogens and this gene signature data is compared against unknown compounds for their genotoxic and nongenotoxic hepatocarcinogen phenotypes, respectively.[59b,60] The success of these prediction models depends heavily on the robustness and quality of the training set. In addition, the test tissue samples generated should have similar protocols as the training sets and any departures from the protocols of the training set result in poor signature performance.[60b,61] A metaanalysis of short-term rat studies on over 150 compounds from different laboratories suggested that gene signatures for nongenotoxic carcinogenicity were relatively robust and were deemed worthwhile in the early assessment of the chemicals for prioritizing for further validation studies but not yet for regulatory decision making.[62] An important limitation of these data is that most of the current toxicogenomic approaches are liver-centric and the predictive signatures probably may apply only to cancer hazards where liver is the target organ. In order to make these toxicogenomics approaches widely applicable for safety assessment, chemical-specific toxicogenomic signatures should also be developed for other target organ systems in the body.

These predictive toxicogenomics tools are not necessarily intended to replace the traditional chronic rodent bioassay for carcinogenicity but rather to guide compound prioritization, and provide mechanistic data to understand the MOA. It is generally accepted that the process of chemically induced toxicity or carcinogenicity consists of simultaneous alterations in numerous molecular pathways resulting in disruption of cellular homeostasis that eventually manifest as morphological phenotypes of cellular degeneration, necrosis, hyperplasia, and neoplasia. These changes occur over a period of time that range from hours to weeks to months to years. The time frames of predictive toxicogenomics studies usually range from 3 to 90 days and the odds of detecting an actual molecular alteration reflecting preneoplasia or neoplasia will probably increase with time. Another factor that is not typically considered in these predictive toxicogenomics studies especially for predicting carcinogenicity is the fact that any "gene signature" that is identified reflects a disruption of normal physiological homeostasis, but it does not take into account if that altered physiological state is an adaptive or adverse finding. However, with the generation of large databases with signatures for all known chemical carcinogens and noncarcinogens based on various time points and doses established in a single model system can potentially serve to predict carcinogens with greater accuracy. Until then, predictions that are based on limited training sets leave much to be desired for regulatory purposes.

Toxicogenomics may not accurately predict carcinogenicity from short-term studies but transcriptomic data from those studies could serve as valuable tools in dose response studies for calculating transcriptional BMDs and identifying points of departure (an estimated dose near the lower end of the observed range that serves as a reference point for human health risk assessment) for cancer and non-cancer endpoints.[63b] In the absence of a rodent cancer bioassay data or human epidemiological data, this approach is especially useful to arrive at a dose where there will be no transcriptional alterations and thereby no negative health effects would be expected at exposures below those doses. In a series of studies, Thomas et al.[63] used the BMD approach and has demonstrated a good concordance between the cancer or noncancer apical endpoints (any observable outcome such as a clinical sign, histological

change, or death) and transcriptional changes. These BMD values for the apical and transcriptional changes in the target organs (based on biological processes or signaling pathways) were comparable even with studies of varying duration ranging from 5 days to 13 weeks, suggesting this approach is robust for identifying doses at which there is minimal biological activity of the compounds in question.[63d] This approach could be expanded to other unknown chemicals by including a battery of eight tissues that represent the most common sites of rodent carcinogenicity and establish the lowest transcriptional BMD value across all analyzed tissues that would be used to estimate the point of departure. It should be emphasized here that this approach does not provide definitive evidence of carcinogenicity and cannot substitute a traditional rodent cancer bioassay but these values could serve as the starting point for risk assessment purposes especially for chemicals with limited toxicity or no carcinogenicity data.[64] However, one apparent limitation to this approach is that it may result in some false positives since alteration in transcriptional profiles does not necessarily mean an adverse response. For example, rodents exposed to chemicals such as theophylline or ginseng that were negative for carcinogenicity in rats and mice of both sexes could show transcriptional alterations and transcriptional BMDs could be calculated based on the dose responses. On the other hand, the issue of false negatives has not been sufficiently addressed by these approaches. Some chemicals may have limited transcriptomic alterations at early time points and there could be a latency in eliciting these significant transcriptomic changes and thus could potentially contribute to a false negative prediction. Further research is needed to fill this issue.

It has been demonstrated that cancers resulting from certain chemical exposures induce distinct mutation spectra and preferentially affect certain cancer genes.[65] Examples of chemical-specific mutation spectra in corresponding cancers include C:G>A:T in tobacco smoke induced lung cancers, T:A>A:T in aristolochic acid induced urothelial tumors, C:G>A:T in aflatoxin B1 induced hepatocellular carcinomas, and C:G>T:A in ultra violet (UV) light induced melanomas.[65a] Similarly examples of chemical-specific mutations in cancer genes include *KRAS* in tobacco smoke induced lung cancers, *EGFR* mutations in lung cancers in nonsmokers, *TP53* in aristolochic acid induced urothelial tumors, and *CTNNB1* in hepatocellular carcinomas. Demonstration of distinct genetic mutations in cancer genes and the corresponding mutation spectra in rodent tumors provides a translational context to human cancers.[66] As discussed earlier, the genetic events in the chemical carcinogenesis are initiated early on and their signatures may be identified by examining tissues from those animals at earlier time points before the cancer is presented clinically. Using in vitro approaches, it has been demonstrated that these mutation spectra and gene signatures may be identified in immortalized fibroblasts exposed to various chemicals such as aflatoxin B1, aristolochic acid, benzopyrene, and UV light.[67] These proof of concept studies provide an impetus for future approaches of understanding each of the unique chemical-induced mutation spectra using in vitro and shorter-term animal exposure studies.

Another area in toxicogenomics that could add value for future carcinogenicity testing is the field of epigenetics. Epigenetics comprises of any heritable change in the gene expression mediated by DNA methylation, histone modification (posttranslational modification of histone proteins by methylation, acetylation, phosphorylation, etc.), nucleosome positioning, and alterations in noncoding RNAs (miRNA, long ncRNA) that are not due to DNA sequence alteration. Alterations in global methylation of some cancer genomes is a well-known phenomenon and is responsible for the activation of the tumor promoting genes, loss of imprinting, and elevated mutation rates.[68] Data suggests that epigenetic alterations may be early events in the carcinogenic process and these alterations may be carcinogen specific and tissue specific, suggesting that epigenetic biomarkers could serve as surrogates for carcinogenicity prediction based on short-term animal studies.[69] In addition, just as in genetic mutations that may be either driver or passenger mutations, carcinogen induced epigenetic alterations may also be categorized into driver or passenger epigenetic changes. Monitoring for the driver epigenetic changes from shorter-term exposure studies may have value in carcinogenicity predictions. The volume 100 of the IARC monograph has highlighted the literature on the epigenetic mechanisms of carcinogenic chemicals such as diethylstilbestrol, chromium (IV), nickel chloride, tobacco, alcohol, and smoky coal emissions.[70] These examples demonstrate a promise of epigenetics in carcinogenicity assessment. However, the field of epigenetics in chemical carcinogenesis is still burgeoning and as more datagaps (normal epigenome in various tissues with and without chemical exposures and the corresponding phenotype anchoring) are filled, this information can be leveraged to study chemical carcinogenesis and risk assessment.

4.14.4.6 Adverse Outcome Pathway (AOP)/MOA Framework

The OECD launched the AOP approach to take the mechanistic data into consideration and link the exposures and its related consequences with the eventual phenotype (or AO).[71] The AOPs link the molecular initiating event (MIE) and one or more intervening key events (KEs) through key event relationships (KERs) to the eventual AO (apical endpoint such as toxicity or carcinogenicity).[72] An MIE is the first step in an AOP pathway and represents the initial interaction between a chemical and a protein within an organism that can be causally linked to the apical endpoint. A KE is a critical step(s) necessary for the progression of the MIE to the subsequent steps in the AOP. KER describes the causal relationships between KEs. These AOs may be at the cellular, tissue, organ, organism, or population level. Prior to the AOPs, the WHO/International Programme on Chemical Safety (IPCS) launched the MOA analytical framework for chemical carcinogenesis based on a series of KEs critical in carcinogenesis, identified using a weight-of-evidence approach based on the Bradford Hill criteria.[73] The MOA approaches are similar to the AOPs' but they are more chemical or chemical class specific, whereas the AOPs are pathway specific and not chemical specific. The advantage of these approaches is that when a key observation is made, the upstream or downstream events may be predicted based on the well-established AOPs or MOAs.

These frameworks are constantly being developed and refined for various apical endpoints. Once a comprehensive network of AOPs are developed and a critical toxicological knowledge base is built, in vitro approaches that can measure MIEs or KEs can be used for predicting and prioritizing chemicals for carcinogenicity. For example, detection of a MIE such as alkylating ability of a chemical could suggest an AO of a gene mutation. It is known that alkylation of DNA in male premeiotic germ cells leads to heritable mutations and alkylation of DNA in somatic cells leads to somatic mutations that may subsequently result in neoplastic transformation (initiation). DNA alkylation and adducts may be measured by high-performance liquid chromatography or immunological methods. The alkylation of DNA is the MIE; the failure to repair DNA sufficiently and subsequent mutation formation are KEs; and the inherited mutations in the off-spring or tumor formation are the AOs.[74] Thus, the AOPs may be able to predict AOs for various chemical exposures based on the large amounts of in vitro data generated from the HTS approaches on respective chemicals. This example is relatively linear and straightforward and very few disease processes have such elegantly defined pathways. In reality, disease processes are complex and could include multiple, interacting pathways (AOP networks) with shared KEs, feedback loops, thresholds, life stage, and sex and species specificity.[75] In addition, the quantitative information or magnitude of each of the MIEs and KEs are important variables in AOPs and are vital for differentiating adaptive from adverse effects in organs and organisms. Thus, at the moment, these AOPs and MOAs based on in vitro data may be useful for prioritization of compounds for further testing but do not replace the animal testing for carcinogenicity for the majority of the chemicals. A recent FutureTox II highlighted the need to accelerate the development and refinement of the AOPs in chemical carcinogenesis using short-term animal studies, computational models that integrate in vitro data with advanced literature data mining techniques.[76] Other highlighted future strategies include targeted development of cancer AOP-based assays and complex cell culture models that account for human genetic heterogeneity. Another approach is to conduct systematic literature mining that focus on key characteristics of carcinogens and hallmarks of cancer and develop assays that target these key features and hallmarks[76b,77] (**Table 5**). As implied earlier, it will take decades before a comprehensive database of AOPs are worked out for various chemical carcinogens and it is going to be an iterative refinement process until they can be confidently applied for risk assessment purposes.

4.14.5 Conclusions

The rodent cancer bioassay and genetic toxicity assays have served an important role in protecting public health from environmental and occupational carcinogens and also for developing safer pharmaceuticals. However, these approaches are low throughput, expensive, time consuming, and sometimes have debatable relevance for human health. In view of the lack of safety data for

Table 5 Key characteristics of chemical carcinogens

Characteristic	*Examples of relevant evidence*
1. Electrophilicity or can be metabolically activated	Parent compound or metabolite with an electrophilic structure (e.g., epoxide, quinone, etc.), formation of DNA and protein adducts
2. Genotoxicity	DNA damage (DNA strand breaks, DNA–protein cross-links, unscheduled DNA synthesis), intercalation, gene mutations, cytogenetic changes (e.g., chromosome aberrations, micronuclei)
3. Alters DNA repair or causes genomic instability	Alterations of DNA replication or repair (e.g., topoisomerase II, base-excision or double-strand break repair)
4. Induces epigenetic alterations	DNA methylation, histone modification, microRNA expression
5. Induces oxidative stress	Oxygen radicals, oxidative stress, oxidative damage to macromolecules (e.g., DNA, lipids)
6. Induces chronic inflammation	Elevated white blood cells, myeloperoxidase activity, altered cytokine and/or chemokine production
7. Immunosuppressive ability	Decreased immune-surveillance, immune system dysfunction
8. Modulates receptor-mediated effects	Receptor in/activation (e.g., ER, PPAR, AhR) or modulation of exogenous ligands (including hormones)
9. Causes immortalization	Inhibition of senescence, cell transformation
10. Alters cell proliferation, cell death, or nutrient supply	Increased proliferation, decreased apoptosis, changes in growth factors, energetics and signaling pathways related to cellular replication or cell cycle control, angiogenesis

Adapted from Smith, M. T.; Guyton, K. Z.; Gibbons, C. F.; Fritz, J. M.; Portier, C. J.; Rusyn, I.; DeMarini, D. M.; Caldwell, J. C.; Kavlock, R. J.; Lambert, P. F.; Hecht, S. S.; Bucher, J. R.; Stewart, B. W.; Baan, R. A.; Cogliano, V. J.; Straif, K. Key Characteristics of Carcinogens as a Basis for Organizing Data on Mechanisms of Carcinogenesis. *Environ. Health Perspect.* **2016**, *124* (6), 713–721.

1000s of legacy environmental chemicals, there is an urgent need to develop assays and methods targeted for cancer hazard identification that are inexpensive, high throughput, and have a short turnaround time. So far, no single alternative approach can satisfactorily replace the rodent cancer bioassay. However, these newer methods can arguably identify chemicals that may not pose a cancer hazard based on the absence of significant biological perturbations in the in vitro cell culture systems, assays in lower order organisms, qIVIVE models, and short-term animal studies coupled with toxicogenomics approaches. The recent NTP experience with the West Virginia Elk river chemical spill has taken these approaches (toxicogenomics, genotoxicity testing, in vitro approaches, testing in lower order organisms, short-term rodent studies) and provided safety information for risk assessment purposes without conducting a chronic rodent bioassay.[78] The pharmaceutical and chemical industry have been using these strategies for compound prioritization and dropping candidate compounds from the development pipeline for decades.

In the future, the rodent cancer bioassay will continue to provide value but may not be needed in some circumstances. Targeted in vitro assays, advanced literature mining tools, genotoxicity assays, quantitative structural activity relationship studies, cancer AOPs based on HTS data, short-term animal studies with mechanistic assessments (toxicogenomics, immunosuppression, hormonal perturbation, etc.), genetically altered animal models, and cancer biomarkers will inform on the potential carcinogenicity of a compound with sufficient confidence. In cases where these multiple streams of data do not confidently inform on the compound's carcinogenic ability, the traditional rodent bioassays will remain indispensable.

References

1. Fung, V. A.; Barrett, J. C.; Huff, J. The Carcinogenesis Bioassay in Perspective: Application in Identifying Human Cancer Hazards. *Environ. Health Perspect.* **1995,** *103* (7–8), 680–683.
2. Huff, J. Chemicals and Cancer in Humans: First Evidence in Experimental Animals. *Environ. Health Perspect.* **1993,** *100,* 201–210.
3. Thiersch, K. *Der Epithelialkrebs, Namentliehlder Ausseren Haut,* 1875.
4. Ramazzini, B. *De morbis artificum diatriba;* Mutinae: Typis Antonii Capponi, 1700.
5. (a) Redmond, D. E., Jr. Tobacco and Cancer: The First Clinical Report, 1761. *N. Engl. J. Med.* **1970,** *282* (1), 18–23; (b) Hill, J. *Cautions Against the Immoderate Use of Snuff: Founded on the Known Qualities of the Tobacco Plant: And the Effects it Must Produce When This Way Taken Into the Body: And Enforced by Instances of Persons Who Have Perished Miserably of Diseases, Occasioned, or Rendered Incurable by Its Use;* Printed for R. Baldwin in Paternoster Row and J. Jackson in St. James's Street: MDCCLXI: London, 1761.
6. Pott, P. *Chirurgical Observations: Relative to the Cataract, the Polypus of the Nose, the Cancer of the Scrotum, the Different Kinds of Ruptures, and the Mortification of the Toes and Feet;* Printed by T.J. Carnegy, for L. Hawes, W. Clarke, and R. Collins: London, 1775; pp 60–68.
7. Harting, F. H.; Hesse, W. Der lungenkrebs, die Bergkrankheit in den Schneeberger gruben. *Vjschr. Gerichtl. Med. Offentl. Gesundheitswesen* **1879,** *31,* 102–132, 313–337.
8. Rehn, L. Blasengeschwülste bei Fuchsin-arbeitern. *Arch. Klin. Chir.* **1895,** *50,* 588–600.
9. Hueper, W. C.; Wiley, F. H.; Wolfe, H. D. Experimental Production of Bladder Tumors in Dogs by Administration of Beta-Naphthylamine. *J. Ind. Hyg. Toxicol.* **1938,** *20,* 46–84.
10. Alwens, W.; Jonas, W. Chrome Lung Cancer. *Acta Unio Int. Contra Cancrum* **1938,** *3,* 1–114.
11. Stephens, G. A. An Important Factor in the Causation of Industrial Cancer. *Med. Press* **1933,** *36,* 194–200, 216–219.
12. Wood, W. B.; Gloyne, S. R. Pulmonary Asbestosis: A Review of One Hundred Cases. *Lancet* **1934,** *2,* 1383–1385.
13. Yamagiwa, K.; Ichikawa, K. Experimentelle Studie über die Pathogenese der Epithelialgeschwülste. *Mitt. Med. Fak. Kaiserl. Univ. Tokyo* **1915,** *15,* 295–344.
14. (a) Kennaway, E. L.; Hieger, I. Carcinogenic Substances and Their Fluorescence Spectra. *Br. Med. J.* **1930,** *1* (3622), 1044–1046; (b) Cook, J. W.; Hewett, C. L.; Hieger, I. The Isolation of a Cancer-Producing Hydrocarbon From Coal Tar. *J. Chem. Soc.* **1933,** *24,* 395–405.
15. Weisburger, E. K. History of the Bioassay Program of the National Cancer Institute. *Prog. Exp. Tumor Res.* **1983,** *26,* 187–201.
16. Shimkin, M. B.; Weisburger, J. H.; Weisburger, E. K.; Gubareff, N.; Suntzeff, V. Bioassay of 29 Alkylating Chemicals by Pulmonary-Tumor Response in strain A Mice. *J. Natl. Cancer Inst.* **1966,** *36* (5), 915–935.
17. Innes, J. R.; Ulland, B. M.; Valerio, M. G.; Petrucelli, L.; Fishbein, L.; Hart, E. R.; Pallotta, A. J.; Bates, R. R.; Falk, H. L.; Gart, J. J.; Klein, M.; Mitchell, I.; Peters, J. Bioassay of Pesticides and Industrial Chemicals for Tumorigenicity in Mice: A Preliminary Note. *J. Natl. Cancer Inst.* **1969,** *42* (6), 1101–1114.
18. Sontag, J. M.; Page, N. F.; Safiotti, U. Guidelines for Carcinogen Bioassay in Small Rodents. *Natl. Cancer Inst. Carcinog. Tech. Rep. Ser.* **1976,** *1,* 1–65.
19. Bucher, J. R. The National Toxicology Program Rodent Bioassay: Designs, Interpretations, and Scientific Contributions. *Ann. N. Y. Acad. Sci.* **2002,** *982,* 198–207.
20. Food and Drug Administration. Guidance for Industry and Other Stakeholders Toxicological Principles for the Safety Assessment of Food Ingredients. http://www.fda.gov/downloads/Food/GuidanceRegulation/UCM222779.pdf.
21. Environmental Protection Agency. The Risk Assessment Guidelines of 1986. http://nepis.epa.gov/Exe/ZyPURL.cgi?Dockey=30001GOF.txt.
22. Organization for Economic Co-operation and Development. *Decision of the Council Concerning the Mutual Acceptance of Data in the Assessment of Chemicals,* 1981.
23. Jacobs, A. C.; Hatfield, K. P. History of Chronic Toxicity and Animal Carcinogenicity Studies for Pharmaceuticals. *Vet. Pathol.* **2013,** *50* (2), 324–333.
24. Van Deun, K. K. J.; Vanparys, P. Carcinogenicity Testing Strategy: Past, Present, and Future. In *Encyclopedia of Pharmaceutical Science and Technology,* 4th ed.; CRC press: Taylor & Francis group, London, UK, 2013; pp 394–405.
25. (a) Organization for Economic Co-operation and Development. Guidance Document 116 on the Conduct and Design of Chronic Toxicity and Carcinogenicity Studies, Supporting Test Guidelines 451, 452, and 453, 2nd ed. http://www.oecd.org/officialdocuments/publicdisplaydocumentpdf/?cote=ENV/JM/MONO(2011)47&doclanguage=en;(b) Environmental Protection Agency. Health Effects Test Guidelines OPPTS 870.4300 Combined Chronic Toxicity/Carcinogenicity. https://www.regulations.gov/-!documentDetail;D=EPA-HQ-OPPT-2009-0156-0021;(c) International Conference on Harmonization. Guideline on the Need for Carcinogenicity Studies of Pharmaceuticals S1A, 1996;(d) International Conference on Harmonization. Testing for Carcinogenicity of Pharmaceuticals S1B. http://www.ich.org/fileadmin/Public_Web_Site/ICH_Products/Guidelines/Safety/S1B/Step4/S1B_Guideline.pdf;(e) International Conference on Harmonization. Guidance for Industry S1C (R2) Dose Selection for Carcinogenicity Studies of Pharmaceuticals. http://www.fda.gov/downloads/drugs/guidancecomplianceregulatoryinformation/guidances/ucm074919.pdf.
26. (a) Soffritti, M.; Belpoggi, F.; Minardi, F.; Bua, L.; Maltoni, C. Mega-Experiments to Identify and Assess Diffuse Carcinogenic Risks. *Ann. N. Y. Acad. Sci.* **1999,** *895,* 34–55; (b) Soffritti, M.; Belpoggi, F.; Minardi, F.; Maltoni, C. Ramazzini Foundation Cancer Program: History and Major Projects, Life-Span Carcinogenicity Bioassay Design, Chemicals Studied, and Results. *Ann. N. Y. Acad. Sci.* **2002,** *982,* 26–45.
27. (a) Foran, J. A. Principles for the Selection of Doses in Chronic Rodent Bioassays. ILSI Risk Science Working Group on Dose Selection. *Environ. Health Perspect.* **1997,** *105* (1), 18–20; (b) Rhomberg, L. R.; Baetcke, K.; Blancato, J.; Bus, J.; Cohen, S.; Conolly, R.; Dixit, R.; Doe, J.; Ekelman, K.; Fenner-Crisp, P.; Harvey, P.; Hattis, D.; Jacobs, A.; Jacobson-Kram, D.; Lewandowski, T.; Liteplo, R.; Pelkonen, O.; Rice, J.; Somers, D.; Turturro, A.; West, W.; Olin, S. Issues in the Design and Interpretation of Chronic Toxicity and Carcinogenicity Studies in Rodents: Approaches to Dose Selection. *Crit. Rev. Toxicol.* **2007,** *37* (9), 729–837.
28. (a) Haseman, J. K. Statistical Issues in the Design, Analysis and Interpretation of Animal Carcinogenicity Studies. *Environ. Health Perspect.* **1984,** *58,* 385–392; (b) Bucher, J. R. Doses in Rodent Cancer Studies: Sorting Fact From Fiction. *Drug Metab. Rev.* **2000,** *32* (2), 153–163.

29. Chhabra, R. S.; Huff, J. E.; Schwetz, B. S.; Selkirk, J. An Overview of Prechronic and Chronic Toxicity/Carcinogenicity Experimental Study Designs and Criteria Used by the National Toxicology Program. *Environ. Health Perspect.* **1990,** *86,* 313–321.
30. Huff, J. Value, Validity, and Historical Development of Carcinogenesis Studies for Predicting and Confirming Carcinogenic Risks to Humans. In *Carcinogenicity: Testing, Predicting, and Interpreting Chemical Effects;* Marcel Dekker: New York, NY, 1999; pp 21–123.
31. Alden, C. L.; Smith, P. F.; Piper, C. E.; Brej, L. A Critical Appraisal of the Value of the Mouse Cancer Bioassay in Safety Assessment. *Toxicol. Pathol.* **1996,** *24* (6), 722–725.
32. Gulezian, D.; Jacobson-Kram, D.; McCullough, C. B.; Olson, H.; Recio, L.; Robinson, D.; Storer, R.; Tennant, R.; Ward, J. M.; Neumann, D. A. Use of Transgenic Animals for Carcinogenicity Testing: Considerations and Implications for Risk Assessment. *Toxicol. Pathol.* **2000,** *28* (3), 482–499.
33. Alden, C.; Smith, P.; Morton, D. Application of Genetically Altered Models As Replacement for the Lifetime Mouse Bioassay in Pharmaceutical Development. *Toxicol. Pathol.* **2002,** *30* (1), 135–138.
34. Castrop, H. Genetically Modified Mice-Successes and Failures of a Widely Used Technology. *Pflugers Arch.* **2010,** *459* (4), 557–567.
35. Van Zeller, A.-M.; Combes, R. D. Transgenic Mouse Bioassays for Carcinogenicity Testing: A Step in the Right Direction? *ATLA* **1999,** *27,* 839–846.
36. Donehower, L. A.; Harvey, M.; Slagle, B. L.; McArthur, M. J.; Montgomery, C. A., Jr.; Butel, J. S.; Bradley, A. Mice Deficient for p53 Are Developmentally Normal but Susceptible to Spontaneous Tumours. *Nature* **1992,** *356* (6366), 215–221.
37. (a) Spalding, J. W.; Momma, J.; Elwell, M. R.; Tennant, R. W. Chemically Induced Skin Carcinogenesis in a Transgenic Mouse Line (TG.AC) Carrying a v-Ha-ras Gene. *Carcinogenesis* **1993,** *14* (7), 1335–1341; (b) Leder, A.; Kuo, A.; Cardiff, R. D.; Sinn, E.; Leder, P. v-Ha-ras Transgene Abrogates the Initiation Step in Mouse Skin Tumorigenesis: Effects of Phorbol Esters and Retinoic Acid. *Proc. Natl. Acad. Sci. U. S. A.* **1990,** *87* (23), 9178–9182.
38. Saitoh, A.; Kimura, M.; Takahashi, R.; Yokoyama, M.; Nomura, T.; Izawa, M.; Sekiya, T.; Nishimura, S.; Katsuki, M. Most Tumors in Transgenic Mice With Human c-Ha-ras Gene Contained Somatically Activated Transgenes. *Oncogene* **1990,** *5* (8), 1195–1200.
39. (a) van Steeg, H.; Klein, H.; Beems, R. B.; van Kreijl, C. F. Use of DNA Repair-Deficient XPA Transgenic Mice in Short-Term Carcinogenicity Testing. *Toxicol. Pathol.* **1998,** *26* (6), 742–749; (b) van Kreijl, C. F.; McAnulty, P. A.; Beems, R. B.; Vynckier, A.; van Steeg, H.; Fransson-Steen, R.; Alden, C. L.; Forster, R.; van der Laan, J. W.; Vandenberghe, J. Xpa and Xpa/p53 +/− Knockout Mice: Overview of Available Data. *Toxicol. Pathol.* **2001,** *29* (Suppl.), 117–127.
40. (a) Boverhof, D. R.; Chamberlain, M. P.; Elcombe, C. R.; Gonzalez, F. J.; Heflich, R. H.; Hernandez, L. G.; Jacobs, A. C.; Jacobson-Kram, D.; Luijten, M.; Maggi, A.; Manjanatha, M. G.; Benthem, J.; Gollapudi, B. B. Transgenic Animal Models in Toxicology: Historical Perspectives and Future Outlook. *Toxicol. Sci.* **2011,** *121* (2), 207–233; (b) Pritchard, J. B.; French, J. E.; Davis, B. J.; Haseman, J. K. The Role of Transgenic Mouse Models in Carcinogen Identification. *Environ. Health Perspect.* **2003,** *111* (4), 444–454; (c) Tennant, R. W.; Butterworth, B. E.; Preston, R. J. Genetically Engineered Cancer Models: Three Viewpoints on Issues From Testing to Risk Assessment. *CIIT Activities* **1999,** *19,* 1–7; (d) Tennant, R. W.; French, J. E.; Spalding, J. W. Identifying Chemical Carcinogens and Assessing Potential Risk in Short-Term Bioassays Using Transgenic Mouse Models. *Environ. Health Perspect.* **1995,** *103* (10), 942–950.
41. Yamamoto, S.; Urano, K.; Koizumi, H.; Wakana, S.; Hioki, K.; Mitsumori, K.; Kurokawa, Y.; Hayashi, Y.; Nomura, T. Validation of Transgenic Mice Carrying the Human Prototype C-Ha-Ras Gene As a Bioassay Model for Rapid Carcinogenicity Testing. *Environ. Health Perspect.* **1998,** *106* (Suppl. 1), 57–69.
42. Nambiar, P. R.; Turnquist, S. E.; Morton, D. Spontaneous Tumor Incidence in rasH2 Mice: Review of Internal Data and Published Literature. *Toxicol. Pathol.* **2012,** *40* (4), 614–623.
43. (a) French, J. E.; Leblanc, B.; Long, G. G.; Morton, D.; Storer, R.; Leighton, J.; Swenberg, J.; Tsuda, H. Panel Discussion: Alternative Mouse Models for Carcinogenicity Assessment. *Toxicol. Pathol.* **2010,** *38* (1), 72–75; (b) Lynch, D.; Svoboda, J.; Putta, S.; Hofland, H. E.; Chern, W. H.; Hansen, L. A. Mouse Skin Models for Carcinogenic Hazard Identification: Utilities and Challenges. *Toxicol. Pathol.* **2007,** *35* (7), 853–864.
44. Malumbres, M.; Barbacid, M. RAS Oncogenes: The First 30 Years. *Nat. Rev. Cancer* **2003,** *3* (6), 459–465.
45. (a) Menendez, D.; Inga, A.; Resnick, M. A. The Expanding Universe of p53 Targets. *Nat. Rev. Cancer* **2009,** *9* (10), 724–737; (b) Pylayeva-Gupta, Y.; Grabocka, E.; Bar-Sagi, D. RAS Oncogenes: Weaving a Tumorigenic Web. *Nat. Rev. Cancer* **2011,** *11,* 761–774.
46. Marselos, M.; Vainio, H. Carcinogenic Properties of Pharmaceutical Agents Evaluated in the IARC Monographs Programme. *Carcinogenesis* **1991,** *12* (10), 1751–1766.
47. (a) Bucher, J. R. Update on National Toxicology Program (NTP) Assays With Genetically Altered or "Transgenic" Mice. *Environ. Health Perspect.* **1998,** *106* (10), 619–621; (b) Eastmond, D. A.; Vulimiri, S. V.; French, J. E.; Sonawane, B. The Use of Genetically Modified Mice in Cancer Risk Assessment: Challenges and Limitations. *Crit. Rev. Toxicol.* **2013,** *43* (8), 611–631.
48. Storer, R. D.; Sistare, F. D.; Reddy, M. V.; DeGeorge, J. J. An Industry Perspective on the Utility of Short-Term Carcinogenicity Testing in Transgenic Mice in Pharmaceutical Development. *Toxicol. Pathol.* **2010,** *38* (1), 51–61.
49. Schwetz, B.; Gaylor, D. Alternative Tests: Carcinogenesis As an Example. *Environ. Health Perspect.* **1998,** *106* (Suppl. 2), 467–471.
50. (a) Alden, C. L. A Review of Unique Male Rat Hydrocarbon Nephropathy. *Toxicol. Pathol.* **1986,** *14* (1), 109–111; (b) Ellwein, L. B.; Cohen, S. M. The Health Risks of Saccharin Revisited. *Crit. Rev. Toxicol.* **1990,** *20* (5), 311–326.
51. (a) Monro, A. How Useful Are Chronic (Life-Span) Toxicology Studies in Rodents in Identifying Pharmaceuticals That Pose a Carcinogenic Risk to Humans? *Adverse Drug React. Toxicol. Rev.* **1993,** *12* (1), 5–34; (b) Reddy, M. V.; Sistare, F. D.; Christensen, J. S.; Deluca, J. G.; Wollenberg, G. K.; Degeorge, J. J. An Evaluation of Chronic 6- and 12-Month Rat Toxicology Studies As Predictors of 2-Year Tumor Outcome. *Vet. Pathol.* **2010,** *47* (4), 614–629; (c) Sistare, F. D.; Morton, D.; Alden, C.; Christensen, J.; Keller, D.; Jonghe, S. D.; Storer, R. D.; Reddy, M. V.; Kraynak, A.; Trela, B.; Bienvenu, J. G.; Bjurstrom, S.; Bosmans, V.; Brewster, D.; Colman, K.; Dominick, M.; Evans, J.; Hailey, J. R.; Kinter, L.; Liu, M.; Mahrt, C.; Marien, D.; Myer, J.; Perry, R.; Potenta, D.; Roth, A.; Sherratt, P.; Singer, T.; Slim, R.; Soper, K.; Fransson-Steen, R.; Stoltz, J.; Turner, O.; Turnquist, S.; van Heerden, M.; Woicke, J.; DeGeorge, J. J. An Analysis of Pharmaceutical Experience With Decades of Rat Carcinogenicity Testing: Support for a Proposal to Modify Current Regulatory Guidelines. *Toxicol. Pathol.* **2011,** *39* (4), 716–744; (d) Alden, C. L.; Lynn, A.; Bourdeau, A.; Morton, D.; Sistare, F. D.; Kadambi, V. J.; Silverman, L. A Critical Review of the Effectiveness of Rodent Pharmaceutical Carcinogenesis Testing in Predicting for Human Risk. *Vet. Pathol.* **2011,** *48* (3), 772–784.
52. Bourcier, T.; McGovern, T.; Stavitskaya, L.; Kruhlak, N.; Jacobson-Kram, D. Improving Prediction of Carcinogenicity to Reduce, Refine, and Replace the Use of Experimental Animals. *J. Am. Assoc. Lab. Anim. Sci.* **2015,** *54* (2), 163–169.
53. National Toxicology Program, 2004. http://ntp.niehs.nih.gov/ntp/main_pages/ntpvision.pdf.
54. Rouquie, D.; Heneweer, M.; Botham, J.; Ketelslegers, H.; Markell, L.; Pfister, T.; Steiling, W.; Strauss, V.; Hennes, C. Contribution of New Technologies to Characterization and Prediction of Adverse Effects. *Crit. Rev. Toxicol.* **2015,** *45* (2), 172–183.
55. Cogliano, V. J.; Baan, R.; Straif, K.; Grosse, Y.; Lauby-Secretan, B.; El Ghissassi, F.; Bouvard, V.; Benbrahim-Tallaa, L.; Guha, N.; Freeman, C.; Galichet, L.; Wild, C. P. Preventable Exposures Associated With Human Cancers. *J. Natl. Cancer Inst.* **2011,** *103* (24), 1827–1839.
56. (a) Corthals, G. L.; Wasinger, V. C.; Hochstrasser, D. F.; Sanchez, J. C. The Dynamic Range of Protein Expression: A Challenge for Proteomic Research. *Electrophoresis* **2000,** *21* (6), 1104–1115; (b) Zubarev, R. A. The Challenge of the Proteome Dynamic Range and Its Implications for In-Depth Proteomics. *Proteomics* **2013,** *13* (5), 723–726.
57. (a) Nuwaysir, E. F.; Bittner, M.; Trent, J.; Barrett, J. C.; Afshari, C. A. Microarrays and Toxicology: The Advent of Toxicogenomics. *Mol. Carcinog.* **1999,** *24* (3), 153–159; (b) Lovett, R. A. Toxicogenomics. Toxicologists Brace for Genomics Revolution. *Science* **2000,** *289* (5479), 536–537.
58. (a) Thomas, R. S.; Rank, D. R.; Penn, S. G.; Zastrow, G. M.; Hayes, K. R.; Pande, K.; Glover, E.; Silander, T.; Craven, M. W.; Reddy, J. K.; Jovanovich, S. B.; Bradfield, C. A. Identification of Toxicologically Predictive Gene Sets Using cDNA Microarrays. *Mol. Pharmacol.* **2001,** *60* (6), 1189–1194; (b) Hamadeh, H. K.; Bushel, P. R.; Jayadev, S.; DiSorbo, O.; Bennett, L.; Li, L.; Tennant, R.; Stoll, R.; Barrett, J. C.; Paules, R. S.; Blanchard, K.; Afshari, C. A. Prediction of Compound Signature Using High Density Gene Expression Profiling. *Toxicol. Sci.* **2002,** *67* (2), 232–240.
59. (a) Waring, J. F.; Jolly, R. A.; Ciurlionis, R.; Lum, P. Y.; Praestgaard, J. T.; Morfitt, D. C.; Buratto, B.; Roberts, C.; Schadt, E.; Ulrich, R. G. Clustering of Hepatotoxins Based on Mechanism of Toxicity Using Gene Expression Profiles. *Toxicol. Appl. Pharmacol.* **2001,** *175* (1), 28–42; (b) Ellinger-Ziegelbauer, H.; Stuart, B.; Wahle, B.; Bomann, W.; Ahr, H. J. Comparison of the Expression Profiles Induced by Genotoxic and Nongenotoxic Carcinogens in Rat Liver. *Mutat. Res.* **2005,** *575* (1–2), 61–84.

60. (a) Nie, A. Y.; McMillian, M.; Parker, J. B.; Leone, A.; Bryant, S.; Yieh, L.; Bittner, A.; Nelson, J.; Carmen, A.; Wan, J.; Lord, P. G. Predictive Toxicogenomics Approaches Reveal Underlying Molecular Mechanisms of Nongenotoxic Carcinogenicity. *Mol. Carcinog.* **2006,** *45* (12), 914–933; (b) Fielden, M. R.; Adai, A.; Dunn, R. T., II; Olaharski, A.; Searfoss, G.; Sina, J.; Aubrecht, J.; Boitier, E.; Nioi, P.; Auerbach, S.; Jacobson-Kram, D.; Raghavan, N.; Yang, Y.; Kincaid, A.; Sherlock, J.; Chen, S. J.; Car, B.; Predictive Safety Testing Consortium.; Carcinogenicity Working Group. Development and Evaluation of a Genomic Signature for the Prediction and Mechanistic Assessment of Non-genotoxic Hepatocarcinogens in the Rat. *Toxicol. Sci.* **2011,** *124* (1), 54–74.
61. Fielden, M. R.; Zacharewski, T. R. Challenges and Limitations of Gene Expression Profiling in Mechanistic and Predictive Toxicology. *Toxicol. Sci.* **2001,** *60* (1), 6–10.
62. Fielden, M. R.; Nie, A.; McMillian, M.; Elangbam, C. S.; Trela, B. A.; Yang, Y.; Dunn, R. T., II; Dragan, Y.; Fransson-Stehen, R.; Bogdanffy, M.; Adams, S. P.; Foster, W. R.; Chen, S. J.; Rossi, P.; Kasper, P.; Jacobson-Kram, D.; Tatsuoka, K. S.; Wier, P. J.; Gollub, J.; Halbert, D. N.; Roter, A.; Young, J. K.; Sina, J. F.; Marlowe, J.; Martus, H. J.; Aubrecht, J.; Olaharski, A. J.; Roome, N.; Nioi, P.; Pardo, I.; Snyder, R.; Perry, R.; Lord, P.; Mattes, W.; Car, B. D.; Predictive Safety Testing, Consortium; Carcinogenicity Working Group. Interlaboratory Evaluation of Genomic Signatures for Predicting Carcinogenicity in the Rat. *Toxicol. Sci.* **2008,** *103* (1), 28–34.
63. (a) Thomas, R. S.; Allen, B. C.; Nong, A.; Yang, L.; Bermudez, E.; Clewell, H. J., III; Andersen, M. E. A Method to Integrate Benchmark Dose Estimates With Genomic Data to Assess the Functional Effects of Chemical Exposure. *Toxicol. Sci.* **2007,** *98* (1), 240–248; (b) Thomas, R. S.; Clewell, H. J., III; Allen, B. C.; Wesselkamper, S. C.; Wang, N. C.; Lambert, J. C.; Hess-Wilson, J. K.; Zhao, Q. J.; Andersen, M. E. Application of Transcriptional Benchmark Dose Values in Quantitative Cancer and Noncancer Risk Assessment. *Toxicol. Sci.* **2011,** *120* (1), 194–205; (c) Thomas, R. S.; Clewell, H. J., III; Allen, B. C.; Yang, L.; Healy, E.; Andersen, M. E. Integrating Pathway-Based Transcriptomic Data Into Quantitative Chemical Risk Assessment: A Five Chemical Case Study. *Mutat. Res.* **2012,** *746* (2), 135–143; (d) Thomas, R. S.; Wesselkamper, S. C.; Wang, N. C.; Zhao, Q. J.; Petersen, D. D.; Lambert, J. C.; Cote, I.; Yang, L.; Healy, E.; Black, M. B.; Clewell, H. J., III; Allen, B. C.; Andersen, M. E. Temporal Concordance Between Apical and Transcriptional Points of Departure for Chemical Risk Assessment. *Toxicol. Sci.* **2013,** *134* (1), 180–194.
64. Thomas, R. S.; Philbert, M. A.; Auerbach, S. S.; Wetmore, B. A.; Devito, M. J.; Cote, I.; Rowlands, J. C.; Whelan, M. P.; Hays, S. M.; Andersen, M. E.; Meek, M. E.; Reiter, L. W.; Lambert, J. C.; Clewell, H. J., III; Stephens, M. L.; Zhao, Q. J.; Wesselkamper, S. C.; Flowers, L.; Carney, E. W.; Pastoor, T. P.; Petersen, D. D.; Yauk, C. L.; Nong, A. Incorporating New Technologies Into Toxicity Testing and Risk Assessment: Moving From 21st Century Vision to a Data-Driven Framework. *Toxicol. Sci.* **2013,** *136* (1), 4–18.
65. (a) Lee, W.; Ladanyi, M. Genomics Traces Carcinogen Fingerprints. *Sci. Transl. Med.* **2013,** *5* (197), 197fs31; (b) Alexandrov, L. B.; Nik-Zainal, S.; Wedge, D. C.; Aparicio, S. A.; Behjati, S.; Biankin, A. V.; Bignell, G. R.; Bolli, N.; Borg, A.; Borresen-Dale, A. L.; Boyault, S.; Burkhardt, B.; Butler, A. P.; Caldas, C.; Davies, H. R.; Desmedt, C.; Eils, R.; Eyfjord, J. E.; Foekens, J. A.; Greaves, M.; Hosoda, F.; Hutter, B.; Ilicic, T.; Imbeaud, S.; Imielinski, M.; Jager, N.; Jones, D. T.; Jones, D.; Knappskog, S.; Kool, M.; Lakhani, S. R.; Lopez-Otin, C.; Martin, S.; Munshi, N. C.; Nakamura, H.; Northcott, P. A.; Pajic, M.; Papaemmanuil, E.; Paradiso, A.; Pearson, J. V.; Puente, X. S.; Raine, K.; Ramakrishna, M.; Richardson, A. L.; Richter, J.; Rosenstiel, P.; Schlesner, M.; Schumacher, T. N.; Span, P. N.; Teague, J. W.; Totoki, Y.; Tutt, A. N.; Valdes-Mas, R.; van Buuren, M. M.; van't Veer, L.; Vincent-Salomon, A.; Waddell, N.; Yates, L. R.; ; Australian Pancreatic Cancer Genome.; ICGC Breast Cancer Consortium.; ICGC MMML-Seq Consortium.; ICGC PedBrain.; Zucman-Rossi, J.; Futreal, P. A.; McDermott, U.; Lichter, P.; Meyerson, M.; Grimmond, S. M.; Siebert, R.; Campo, E.; Shibata, T.; Pfister, S. M.; Campbell, P. J.; Stratton, M. R. Signatures of Mutational Processes in Human Cancer. *Nature* **2013,** *500* (7463), 415–421.
66. (a) Loeb, L. A.; Harris, C. C. Advances in Chemical Carcinogenesis: A Historical Review and Prospective. *Cancer Res.* **2008,** *68* (17), 6863–6872; (b) Balmain, A.; Harris, C. C. Carcinogenesis in Mouse and Human Cells: Parallels and Paradoxes. *Carcinogenesis* **2000,** *21* (3), 371–377.
67. (a) Nik-Zainal, S.; Kucab, J. E.; Morganella, S.; Glodzik, D.; Alexandrov, L. B.; Arlt, V. M.; Weninger, A.; Hollstein, M.; Stratton, M. R.; Phillips, D. H. The Genome As a Record of Environmental Exposure. *Mutagenesis* **2015,** *30* (6), 763–770; (b) Olivier, M.; Weninger, A.; Ardin, M.; Huskova, H.; Castells, X.; Vallee, M. P.; McKay, J.; Nedelko, T.; Muehlbauer, K. R.; Marusawa, H.; Alexander, J.; Hazelwood, L.; Byrnes, G.; Hollstein, M.; Zavadil, J. Modelling Mutational Landscapes of Human Cancers In Vitro. *Sci. Rep.* **2014,** *4,* 4482.
68. (a) Feinberg, A. P.; Tycko, B. The History of Cancer Epigenetics. *Nat. Rev. Cancer* **2004,** *4* (2), 143–153; (b) Ehrlich, M. DNA Hypomethylation in Cancer Cells. *Epigenomics* **2009,** *1* (2), 239–259; (c) Pogribny, I. P.; Rusyn, I. *Environmental Toxicants, Epigenetics, and Cancer;* Springer Science + Business Media: New York, NY, 2013; pp 215–232 (chapter 11).
69. Pogribny, I. P.; James, S. J.; Jernigan, S.; Pogribna, M. Genomic Hypomethylation Is Specific for Preneoplastic Liver in Folate/Methyl Deficient Rats and Does Not Occur in Non-Target Tissues. *Mutat. Res.* **2004,** *548* (1–2), 53–59.
70. Herceg, Z.; Lambert, M. P.; van Veldhoven, K.; Demetriou, C.; Vineis, P.; Smith, M. T.; Straif, K.; Wild, C. P. Towards Incorporating Epigenetic Mechanisms Into Carcinogen Identification and Evaluation. *Carcinogenesis* **2013,** *34* (9), 1955–1967.
71. OECD (2016), "Users' Handbook supplement to the Guidance Document for developing and assessing Adverse Outcome Pathways", OECD Series on Adverse Outcome Pathways, No. 1, OECD Publishing, Paris. http://dx.doi.org/10.1787/5jlv1m9d1g32-en.
72. Ankley, G. T.; Bennett, R. S.; Erickson, R. J.; Hoff, D. J.; Hornung, M. W.; Johnson, R. D.; Mount, D. R.; Nichols, J. W.; Russom, C. L.; Schmieder, P. K.; Serrrano, J. A.; Tietge, J. E.; Villeneuve, D. L. Adverse Outcome Pathways: A Conceptual Framework to Support Ecotoxicology Research and Risk Assessment. *Environ. Toxicol. Chem.* **2010,** *29* (3), 730–741.
73. Sonich-Mullin, C.; Fielder, R.; Wiltse, J.; Baetcke, K.; Dempsey, J.; Fenner-Crisp, P.; Grant, D.; Hartley, M.; Knaap, A.; Kroese, D.; Mangelsdorf, I.; Meek, E.; Rice, J. M.; Younes, M.; International Programme on Chemical Safety. IPCS Conceptual Framework for Evaluating a Mode of Action for Chemical Carcinogenesis. *Regul. Toxicol. Pharmacol.* **2001,** *34* (2), 146–152.
74. Yauk, C. L.; Lambert, I. B.; Meek, M. E.; Douglas, G. R.; Marchetti, F. Development of the Adverse Outcome Pathway "Alkylation of DNA in Male Premeiotic Germ Cells Leading to Heritable Mutations" Using the OECD's Users' Handbook Supplement. *Environ. Mol. Mutagen.* **2015,** *56* (9), 724–750.
75. Kleinstreuer, N. C.; Sullivan, K.; Allen, D.; Edwards, S.; Mendrick, D. L.; Embry, M.; Matheson, J.; Rowlands, J. C.; Munn, S.; Maull, E.; Casey, W. Adverse Outcome Pathways: From Research to Regulation Scientific Workshop Report. *Regul. Toxicol. Pharmacol.* **2016,** *76,* 39–50.
76. (a) Knudsen, T. B.; Keller, D. A.; Sander, M.; Carney, E. W.; Doerrer, N. G.; Eaton, D. L.; Fitzpatrick, S. C.; Hastings, K. L.; Mendrick, D. L.; Tice, R. R.; Watkins, P. B.; Whelan, M. FutureTox II: in vitro Data and In Silico Models for Predictive Toxicology. *Toxicol. Sci.* **2015,** *143* (2), 256–267; (b) Smith, M. T.; Guyton, K. Z.; Gibbons, C. F.; Fritz, J. M.; Portier, C. J.; Rusyn, I.; DeMarini, D. M.; Caldwell, J. C.; Kavlock, R. J.; Lambert, P. F.; Hecht, S. S.; Bucher, J. R.; Stewart, B. W.; Baan, R. A.; Cogliano, V. J.; Straif, K. Key Characteristics of Carcinogens As a Basis for Organizing Data on Mechanisms of Carcinogenesis. *Environ. Health Perspect.* **2016,** *124* (6), 713–721.
77. Hanahan, D.; Weinberg, R. A. Hallmarks of Cancer: The Next Generation. *Cell* **2011,** *144* (5), 646–674.
78. National Toxicology Program. West Virginia Chemical Spill: NTP Studies and Results, 2016. http://ntp.niehs.nih.gov/results/areas/wvspill/studies/index.html-results.

4.15 Emerging Translatable Safety Biomarkers

J Tarrant, Gilead Sciences Inc., Foster City, CA, United States

© 2017 Elsevier Ltd. All rights reserved.

4.15.1	**Introduction: Emerging Translatable Safety Biomarkers**	255
4.15.2	**Translational Safety Biomarkers**	256
4.15.3	**Methodology of Biomarker Qualification and Assay Validation**	256
4.15.3.1	Molecular Classes of Biomarkers	256
4.15.3.2	Biological Qualification	257
4.15.3.3	Statistical Approaches	258
4.15.3.4	Biomarker Evaluation	258
4.15.3.5	Normal Range and Threshold Setting	259
4.15.3.6	Assay Validation	260
4.15.3.7	Regulatory Qualification of New Toxicity Biomarkers	262
4.15.4	**Emerging Biomarkers of Drug-Induced Liver Injury**	263
4.15.4.1	General Characteristics of Emerging Liver Safety Biomarkers	264
4.15.4.2	Arginase-1	264
4.15.4.3	Alpha-Gluthathione-S-Transferase	265
4.15.4.4	Cytokeratin 18	266
4.15.4.5	Glutamate Dehydrogenase	266
4.15.4.6	HMGB1	267
4.15.4.7	miR-122	267
4.15.5	**Emerging Biomarkers of Acute Kidney Injury**	268
4.15.5.1	General Considerations for Preanalytical Factors, Assays, and Biomarker Biology	269
4.15.5.1.1	Preanalytical factors	269
4.15.5.1.2	Pathophysiologic factors	272
4.15.5.1.3	Assays	272
4.15.5.1.4	Postanalysis, interpretation	272
4.15.5.2	Beta-2-Microglobulin	273
4.15.5.3	Clusterin	273
4.15.5.4	Cystatin-C	273
4.15.5.5	KIM-1	274
4.15.5.6	*N*-Acetyl-β-D-Glucosaminidase	274
4.15.5.7	Neutrophil Gelatinase-Associated Lipocalin	274
4.15.5.8	Osteopontin	275
4.15.6	**Blood Cytokines as Safety Biomarkers**	275
4.15.6.1	Biology	275
4.15.6.2	Cytokine Biomarkers	276
4.15.7	**Bis(monoacylglycero)phosphate (BMP) a New Biomarker of Drug-induced Phospholipidosis**	277
4.15.7.1	Phospholipidosis	277
4.15.7.2	Bis(monoacylglycero)phosphate	278
4.15.8	**Future Prospects**	279
References		279
Relevant Websites		283

4.15.1 Introduction: Emerging Translatable Safety Biomarkers

Drug safety is an important cause of drug candidate attrition in the biopharmaceutical industry. Rates of attrition due to toxicity are highest in preclinical and Phase I clinical trials, with a failure rate estimated at 50% of drug candidates. Further attrition of drugs at regulatory filing (post a successful Phase III) and postmarketing highlight the need for improved prediction and assessment of safety in drug development.[1,2]

The FDA has recognized that innovation is needed to achieve more expeditious and accurate risk-benefit assessment in the drug development process. To this end, the critical path opportunities report and list of priorities was generated in 2004–06. An era of forward-looking regulatory science has emerged with new regulatory Guidances and instruments from multiple health authorities (FDA, EMA, and PMDA) that encourage the discovery, evaluation, and qualification on new safety biomarkers.[3]

This article will focus on several emerging biomarkers for toxicities that are considered by drug developers and health authorities to be poorly monitorable that is, when there are no existing biomarkers for detection or prediction of toxicity, or where specific performance attributes (i.e., sensitivity and/or specificity for the toxicity) could be improved. These emerging biomarkers denote an expanded toolkit of minimally invasive, stable, and tractable safety biomarkers for translational use that is, biomarker performance in preclinical drug testing is also applicable to clinical contexts of use. The value of these biomarkers lie in individual patient monitoring to detect or predict toxicity, or epidemiological evaluation of a population's risk status for developing drug-related toxicity. Although the emphasis here will be on biomarkers in body fluids, it is important to note that advances in bioimaging technology have resulted in innovative application of this modality in preclinical and clinical safety monitoring, particularly for cardiotoxicity, For toxicities where there are routine biomarkers (often clinical pathology tests) that provide a historic benchmark for safety monitoring, the intent of emerging biomarkers is to complement these existing markers by adding diagnostic accuracy and/or improving predictivity. A point of emphasis in this article, and germane to any new test, is that characterization and understanding of a biomarker is a lengthy and incremental process. Much still remains to be learnt of these emerging biomarkers, however their promise for improvement in drug development and patient care outweighs some information gaps that can be addressed by the greater scientific community generating and sharing new information on the biomarker.

4.15.2 Translational Safety Biomarkers

A toxicity biomarker is an objective measurement of a pathologic response to a therapeutic intervention resulting in a toxicologically important structural or functional change in a tissue or biological system. These biomarkers may signify tissue-specific toxicity that is; leakage of cytosolic enzymes such as ALT from the liver with liver injury, or a mechanistic process that is, elevated serum cytokine concentrations diagnostic of cytokine release syndrome (CRS). Translatable toxicity biomarkers are applicable to both animals and humans. The desired goal for new translatable safety biomarkers is to advance a minimally invasive tool that adds value or outperforms existing biomarkers in the detection or prediction of toxicity. These biomarkers are evaluated preclinically to identify relationships between drug exposure, drug activity, and toxicity to underpin safety assessment in clinical trials. In preclinical toxicity studies, the potential of a biomarker for noninvasive monitoring can be thoroughly evaluated in comparison to histopathology as the gold-standard safety endpoint. Response of the biomarker to the drug in preclinical safety studies can potentially predict biomarker changes in clinical trials.

In preclinical development, biomarkers can be used for internal decision-making to assist in lead drug optimization, candidate drug selection, evaluating the potential monitorability of the toxicity in patients, and to dose selection for first in human trials. Biomarkers in the preclinical setting should always be evaluated together with histopathology to provide an integrated assessment of toxicity and establish the utility and context of use (COU) for the biomarker for a specific drug-related toxicity.

Translatable safety biomarkers can be used to derisk uncertainty of the human translatability of suspected animal-specific drug toxicity. A sensitive and specific safety biomarker can ensure the safe conduct of clinical trials and proof of a hypothesis that toxicity seen in preclinical studies may not be relevant to patient populations under study. In clinical studies, safety biomarkers can predict future toxicity, risk stratify patients based on susceptibility to drug-related toxicity, and monitor for early safety signals. Safety biomarkers are used to profile the safety of a drug to assess the therapeutic index, which is the exposure margin between efficacious and toxic drug concentrations. Enhanced use of emerging safety biomarkers has the potential for improving patient safety by preventing unmanageable adverse drug reactions. In an era of tailored (or precision) medicine, defining the risk-benefit ratio in individual patients is an attractive prospect for improved patient outcomes.

4.15.3 Methodology of Biomarker Qualification and Assay Validation

4.15.3.1 Molecular Classes of Biomarkers

The majority of emerging safety biomarkers are proteins measured in easily accessible biofluids (i.e., blood, urine). Some of these markers are enzymes and are quantified with activity-based assays on clinical chemistry analyzers. Other proteins are quantified by mass with immunoassays, and less commonly, by mass spectrometry. For protein biomarkers, it is essential to characterize the molecular form (i.e., full length or fragment, monomer or higher order complex) of the biomarker that is qualified to diagnose toxicity. Particularly with immunoassays, antibody pairs may differ between assays and therefore various forms of the protein could be measured. Alternative forms of the protein may have widely different release kinetics into the circulation, half-life, and biological interactions. Various "omics approaches" for example, genomics, proteomics, metabolomics have surveyed vast numbers of molecules of a specific class (respectively, RNA, protein, metabolites) for biomarker discovery and are now maturing to evaluate individual or combinations of these candidates as biomarkers of toxicity. Subfields of these approaches have also been explored to search for unique molecules that may more sensitively and specifically relate to the toxicity under investigation, examples include lipid biomarkers and posttranslational modifications of proteins for example, glycomics (glycan modifications).

MicroRNA (miR) is an exciting new subfield of genomics that has emerged recently. MiRs are short noncoding RNA (19–23 nucleotides in length) that bind to complementary sequences within mRNA to destabilize the mRNA and/or repress protein translation. miRs are of interest as safety biomarkers due to the high species conservation and sequence homology for some molecules, stability, reagent availability (probes are easy to design and synthesize), and potential for tissue specificity.[4] There are 1881 annotated human

microRNA loci in the latest miR database (miRBase release 21). Extracellular forms of miRs are largely complexed to RNA-binding proteins such as Argonaute-2 and high density lipoprotein, or encased in exosomes, microparticles, or apoptotic bodies. The release mechanisms of miRs from cells into the circulation are still under active investigation, therefore it is not well understood what could influence the measured levels of a circulating miR species. Additionally, extracellular miRs may be transferred from cell to cell by exosomes. Consensus on optimized methodology for miR detection and assay validation criteria have yet to be established, owing to the novelty of this type of biomarker. There is currently no standardized approach for sample preparation, normalization, and quantification, which will hamper comparability and reproducibility between published reports[5]. The results of studies are best viewed independently, with relative differences (rather than absolute quantification) as a realistic measure for biomarker performance

4.15.3.2 Biological Qualification

The biological qualification of a biomarker is a process that provides adequate evidence that a biomarker quantifiably and accurately measures a toxic effect as compared to an accepted gold standard. In preclinical studies, the gold standard is often histopathological grading of tissue injury*. In clinical studies, less invasive measures, including preexisting monitoring tools, expert opinion of clinicopathologic findings, and ancillary testing may also be enlisted. The approach for biomarker qualification has a corollary with the diagnostic accuracy assessment of clinical laboratory tests for diagnosing disease. Formal regulatory qualification (outlined in the section below) includes specific claims on when and how the biomarker can be used to detect a specific toxicity.

Biomarker qualification is necessarily a step-wise approach that begins with discovery of candidate biomarkers (Fig. 1). The discovery stage may take the form of "omics experiments" where model toxicants are studied and genomics, proteomics, and

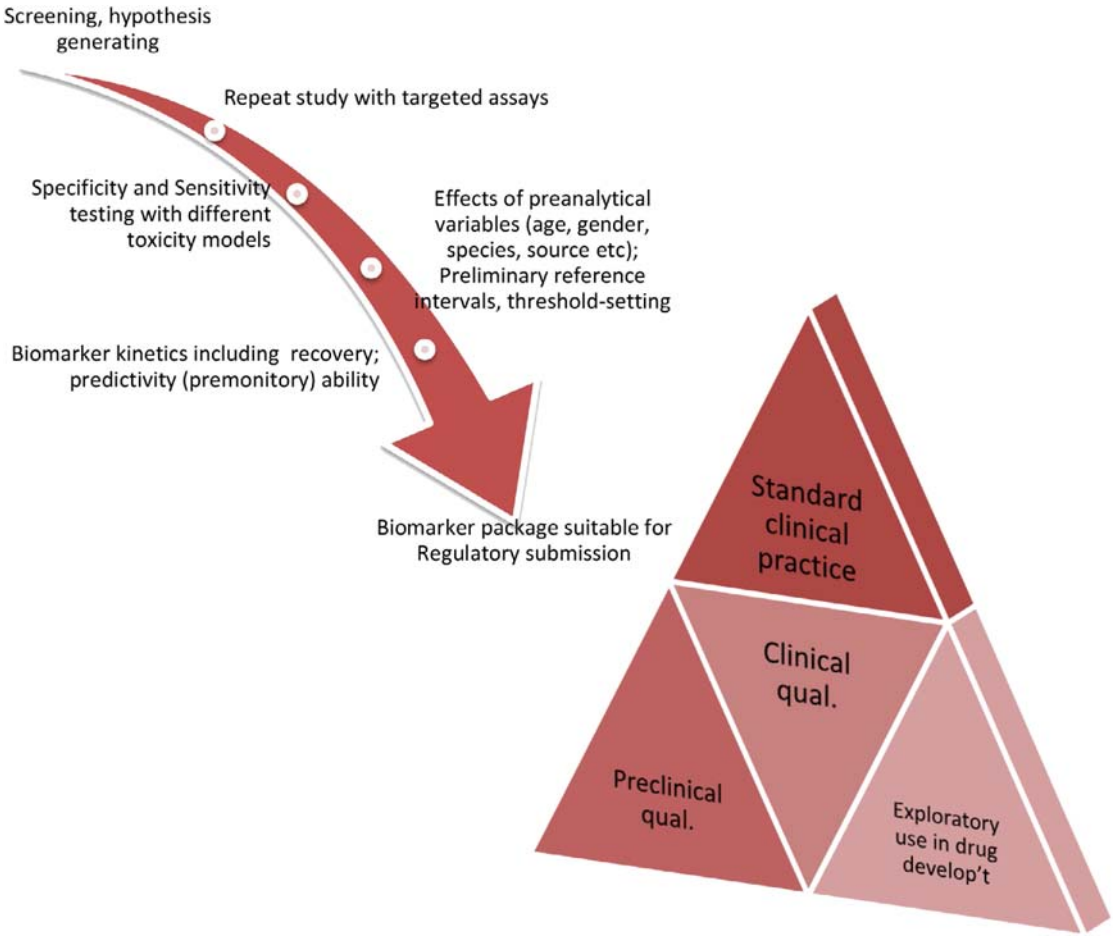

Fig. 1 The process of biomarker qualification from discovery to regulatory qualification. Biomarker discovery begins with studies that generate biomarker candidates that are correlated with a histologic and/or functional endpoint of toxicity. Biomarker candidates are interrogated with repeat studies using different models to determine if the relationship with toxicity is consistent across pharmacologic agents and toxicity mechanisms and to determine the kinetics and biologic behavior of the biomarker. Biomarker performance in preclinical models is followed-up with clinical qualification studies. Preanalytical aspects of sample handling, preliminary reference intervals and thresholds, together with analytical performance of targeted assays, are defined. These data are presented in a biomarker submission for regulatory qualification of the biomarker in defined contexts with an articulated approach to interpretation and application.

metabolomics (to name a few) analysis of biological samples profile the changes in a broad swath of these molecule classes associated with the toxicity. This can be conducted using clinical samples, but is more commonly done in animal studies using model toxicants. Animal models have considerable advantages by controlling multiple variables, adequate power, reduced selection bias (when selecting patients based on traditional/poor monitoring endpoints) and paired comparison to invasive measures of toxicity such as histopathology. In addition, multiple toxicants encompassing distinct mechanisms of toxicity can be evaluated for biomarker response with minimal resource (compared to clinical studies across multiple therapeutics). Results of screening studies must always be repeated in a follow-up study, preferably using targeted assays with higher performance specifications for sensitivity and quantification of the biomarkers of interest. Candidate biomarkers may also be selected based on the similarity of toxicity to spontaneous disease states and the hypothesis that clinical laboratory tests for the disease could potentially be relevant to toxicity monitoring.

The specificity of the biomarker for particular organ toxicity can initially be supported by the tissue expression profile of the biomarker and whether it is confined to a specific organ. The expression of some biomarkers is up- or downregulated with toxic insult and this dynamic expression adds to the understanding of the biomarker response. Tissue microarray experiments to document the expression pattern in multiple species are useful in determining the potential translatability of the biomarker across species, particularly from rodent to dog to human. Classic specificity studies for safety biomarkers test the performance of the biomarker for toxicity in a single organ in a model where multiple other organs are also affected. This will determine if there are other tissue sources for the biomarker and if a change in organ function associated with the drug will alter the clearance of the biomarker. These experiments are usually prioritized after proof that biomarkers have the required sensitivity.[6]

The biologic plausibility of the new biomarker helps substantiate its validity. Broadly, fluid-based biomarkers constitute (1) leakage markers liberated by the injured cell, (2) response markers to injury, and (3) measures of functional change. Determining the mechanism underlying the relationship of the biomarker to toxicity will allow greater understanding of the biomarker response and inference of its utility across different toxicities and drug classes.

The temporal kinetics of the biomarker response are important for ascertaining if the biomarker has suitable sensitivity and appearance (relative to dosing) to monitor early toxicity when tissue damage or functional change is nonadverse. Ideally the biomarker should also reverse with resolution of the toxicity. The onset, maxima, and reversal of the biomarker change should be characterized relative to a gold-standard measure of organ toxicity and in relation to drug exposure concentration. If blood volumes allow, modeling the exposure-biomarker-toxicity relationship can offer insight on the biomarker response and corroboration of the potential utility of the biomarker for the toxicity.

Due consideration must be given to preanalytical variables. These are factors that can influence the levels of the biomarker prior to variables introduced by technical analysis and later data handling and interpretation. Preanalytical variables include potential effects of biological variables of age, sex, strain, environment (to name a few) and impact of sample collection, handling, and storage. The final series of studies could include assessment of prognosis where there is sufficient range of toxicity to include reversible toxicity, adaptation, and persistence of toxicity without progression, progressive injury, and severe adverse injury.

Biomarker qualification is an iterative and progressive process. The current Regulatory strategy is used by private–public consortia to evaluate and qualify several new safety biomarkers with overlapping performance and contexts of use. Potentially these biomarkers may be used individually or as combinatorial measure. Qualification of a seemingly redundant set of biomarkers in the first instance is based on the logic that it is premature to "choose a winner" on what is essentially a limited dataset for emerging biomarkers. To fully understand the diagnostic performance of each biomarker over a multitude of drug classes in different species and different patient populations, they must be upheld and further explored by drug developers to characterize the ultimate utility in a variety of contexts.

4.15.3.3 Statistical Approaches

The statistical assessment of biomarker discovery and evaluation is itself a field of active investigation. Regulatory guidance for the statistical evaluation of clinical diagnostic tests exist,[7] however the statistical approaches to biomarker qualification are often the product of iterative consultation and advice discussion with health authorities. This can detract from the estimated performance of the new biomarker in the clinic. A brief description of common statistical approaches is provided to help familiarize the reader to this aspect of biomarker evaluation.

4.15.3.4 Biomarker Evaluation

Statistical approaches to biomarker selection and evaluation enlist classification, regression, and tree-based methods. The ability of a biomarker to classify or discriminate between the presence or absence of toxicity is most commonly assessed by the receiver operator characteristic curve (ROC). This graphical presentation compares the true positive rate (or sensitivity) on the *y*-axis, to the false positive rate (1-specificity) on the *x*-axis (Fig. 2). A curve is created relating the true positive rate to false positive rate at every biomarker cutpoint (or threshold value). The area under the ROC curve (AROC) provides a measure of accuracy, therefore perfect discrimination would be represented as a curve to the upper left of the graph, with an area of 1 (100% accuracy), and an area of 0.5 represents an equal rate of true positive and false positive detection, or 50% accuracy (curve A in Fig. 2). Desirable performance is considered to be ≥ 0.8 or 80% (curve B in Fig. 2). The 95% confidence intervals should be reported to indicate the precision of the estimate. The use of only one value to describe the whole curve results in a loss of information, therefore a partial AROC within a desirable range of false positive rates (i.e., focusing on the left portion of the curve) or a single measure of sensitivity at a cutpoint

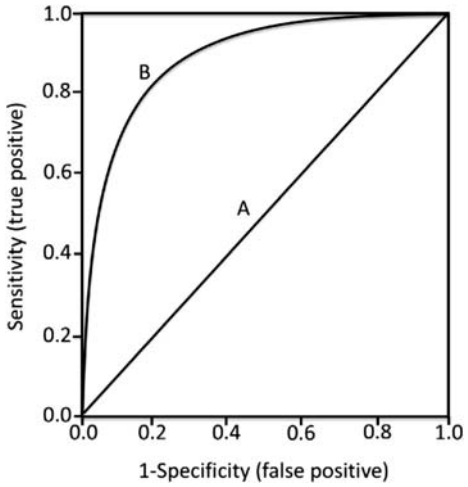

Fig. 2 The receiver operating characteristic (ROC) curve depicts the true-positive and false-positive rates at every cut-point threshold value of a biomarker or test. The area under the ROC curve (AROC) is a measure of the accuracy of a biomarker. As depicted by curve A, a biomarker that has an equal false-positive and false-negative rate (50% sensitivity, 50% specificity, 50% accuracy) has an AROC of 0.5 and is a poor test. A biomarker with good diagnostic performance would have a curve similar to B, with a diagnostic accuracy and AROC of at least 80% and 0.8, respectively.

of 90% specificity, can also be reported. The AROC is very useful during early evaluation of translational biomarkers, however in later stage assessment of clinical outcome testing, the metric lacks clinical meaning.[8]

Biomarker combinations (or panels) for diagnosing or predicting toxicity can be assessed using regression analysis and decision tree analysis. In the latter, various combinations of the biomarkers are evaluated for their ability to predict the outcome (i.e., toxicity) and are particularly useful for nonlinear relationships; random forest is one such method.[9]

To determine if novel biomarkers can improve diagnostic performance of the existing test or risk prediction model, several approaches are used. The delta of the AUC between the existing test with and without the new biomarker/s can be calculated to assess the improvement in discrimination. However, when the existing test performs reasonably well, it is harder to show significance. More importantly, this measure may produce incorrect estimates due to inherent bias when using highly correlated datasets.[8] New measures that describe net improvements in classifying both toxicity positive and toxicity negative states are becoming more popular and continue to be refined.[10] Two such measures are the net reclassification index (NRI) and the integrated discrimination improvement (IDI) index. The NRI evaluates the net proportion of subjects reassigned a diagnosis (i.e., toxicity vs. nontoxicity) or for clinical risk models, a risk categorization (e.g., low vs. high). Usually, the proportion of classifications that are improved or made worse for both toxicity cases and the controls are added to calculate a holistic index. The IDI is calculated by determining the average probability for toxicity minus the average probability for nontoxicity. An improved IDI assigns higher probability (or risk) to toxicity cases than to nontoxicity. There are strengths and limitations to these new measures of improved performance, which do not allow for a consensus approach at this stage.[8]

4.15.3.5 Normal Range and Threshold Setting

Understanding the biological variability of a biomarker is essential to interpreting changes in biomarker values. Characterization should include relevant species, strain, source (for preclinical testing), ethnicity (clinical testing), gender, and age stratification. Usually this data is first generated in healthy individuals, and with time may be expanded to different patient groups, and explore more detailed observations pertaining to circadian differences, diet, body mass index, and other variables. Understanding biological variability can help make rational use of reference intervals and for interpreting single measurements and serial analysis of a biomarker.

Reference intervals are usually constructed prior to clinical evaluation of a novel biomarker. These may be estimates in the first instance, simply to describe biological variability and 95% confidence intervals for a relatively small number of subjects.[11] In preclinical biomarker evaluation and toxicity studies, emphasis is most often placed on baseline data and/or the intervals (i.e., defining the upper and lower limit) determined from the control group within the study. This approach can better account for study variables (source, age, husbandry, dosing, vehicle formulation, blood collection, assay reagent changes, technical variables) than a "one size fits all" reference interval.

Between subject (or interindividual) and within subject (or intraindividual) variation can be derived by serial measurements in subjects representative of the population the biomarker will be used in. By determining these measures of biological variation, one can ascertain whether changes in a biomarker should be assessed compared to previous measurements in the individual or against a reference interval. Generally, if an individual has high variation in the biomarker in comparison to low variation between subjects, then evaluation is improved by use of a reference interval. On the other hand, low within individual compared to high between individual variation would support evaluating each individual based on previous measurements for that subject. The significance

of differences between serial measurements of a biomarker should also be interpreted with regard to expected biological variability. The concept of reference change value (RCV) defines the difference in value for serial measurements to be statistically likely to represent a change beyond that attributable to biologic variability alone at a defined probability (e.g., $p < 0.05$). The RCV can therefore be used to define a pharmacologic or toxicologic effect of a drug on the biomarker. These estimates of biological variability have been calculated for emerging kidney toxicity biomarkers in the rat.[12,13]

4.15.3.6 Assay Validation

Assay validation is the technical performance involving testing of biomarker assays evaluated against preset criteria (or specifications) for acceptance. This testing is designed to demonstrate that the assay is appropriate for its intended use. The analytical variables of the biomarker test are also identified in this stage and the contribution of technical error to the measured biomarker concentration can be estimated. There is an incremental approach to the rigor of assay validation and data quality that couples with the progressive stages of biomarker qualification from exploratory use to decision-making. Common terminology and basic principles related to assay validation are provided in (**Tables 1** and **2**, respectively) with a focus on immunoassays for protein

Table 1 Assay validation terminology

Parameter	*Definition*
Accuracy	Is a measure of the bias of a sample from the true or nominal/expected value. It is usually expressed as the percent of the expected value or percent recovery
Calibrator	A material that represents the biomarker. It may be purified native protein or a recombinant (synthesized) reagent. Also referred to as a standard
Calibration curve	The fitted concentration–response curve of a set of calibrators that define the quantification range of the assay. Also referred to as standard curve
Coefficient of variation	Calculated as the standard deviation of a set of repeated measures divided by the mean
Cross-site validation	Compares test results at different sites using the same assay and same sample aliquots
Dilutional linearity	Demonstration that samples with initial biomarker concentration above the upper limit of quantification can be diluted into the measuring range of the assay and meet acceptance criteria
Interference	Substances that result in physicochemical interference and artifact in the measured value of the biomarker (e.g., hemolysis, lipemia, icterus, pH)
Limit of detection	The limit of detection as defined by a signal greater than background. This is usually calculated as 2 or 3 standard deviations greater than the buffer (or blank matrix without biomarker)
Lower limit of quantification	The lowest measureable value that meets acceptance criteria for accuracy and precision
Minimal required dilution	Minimal dilution of biologic sample that removes matrix interference to meet criteria for accuracy and precision. Manufacturers of commercial kits will usually recommend dilution that optimizes assay performance
Multiplex	Multiple biomarkers tested together in one assay run
Parallelism	The biologic sample (sometimes spiked with a standard within the working range of the assay) is serially diluted with buffer to determine if there is a proportionate response relationship to that of the calibration curve thereby confirming the suitability of the calibration curve for biomarker quantification in the biologic sample
Precision	Precision is the random error assessment of repeated measures. It is calculated as the percent coefficient of variation = (standard deviation/mean) × 100%
Quality control sample	A set of sample pools, consisting of either native matrix with endogenous biomarker, native matrix spiked with calibrator, or calibrator-spiked buffer with a predetermined value that is used to verify the assay is performing to specified criteria. The QC samples should span the working range of the assay (i.e. high, medium, and low)
Recovery	Percent recovery of the measured compared to the nominal or expected value is a measure of accuracy. Recovery = measured value/expected value × 100%
Robustness	Ability of assay to withstand small variations in procedure to produce repeatable results
Selectivity	Detection of a specific protein biomarker in a complex biologic matrix without interference from endogenous substances of exogenous compounds (e.g., drug and metabolites)
Sensitivity	The lowest biomarker concentration measurable in the assay. This can refer to the limit of detection or the lower limit of quantification and should be defined
Singleplex	Single assay for an individual biomarker
Specificity	Ability of assay to detect the intended biomarker with negligible affinity for structurally similar molecules
Stability	The retention of *physicochemical* characteristics of the biomarker over storage conditions to maintain recovery of the biomarker within prespecified acceptable limits
Upper limit of quantification	The highest measureable value that meets acceptance criteria for accuracy and precision (often 20% CV, 80%–120% recovery)
Validation	Validation of an analytical method by assessing a series of performance measures against preset specifications
Working range	Measurement interval of the assay as defined by highest and lowest limit of quantification. Also known as dynamic range

Table 2 Assay validation principles

Assay performance measure	*Test (example)*	*Specification (example)*
Calibration curve	2–3 replicates of calibration curve (6 non-zerostandards) over 2–3 separate runs	CV $\leq$20% and recovery of 80%–120%; CV $\leq$25% and recovery of 75%–125% at LLOQ. 75% of calibrators (including LLOQ) should meet criteria for acceptance of curve
Accuracy	$\geq$3 samples (or QC) at low, medium, and high concentrations spanning the calibration curve range, $\geq$5 replicates of each sample. Calculate percent recovery of observed as a fraction of expected values	Recovery of 80%–120% and 75%–125% at LLOQ
Parallelism	$\geq$3 samples spiked with calibrator and serially diluted	Recovery of 80%–120% (compared to neat OR concentration at minimum recommended dilution)
Dilutional linearity	$\geq$3 samples spiked with calibrator to above the ULLOQ and serially diluted	Mean recovery of 80%–120%
Intraassay precision	$\geq$3 samples (or QC) at low, medium, and high concentrations spanning the calibration curve range, $\geq$5 replicates of each sample	CV $\leq$20% and 25% at LLOQ
Interassay precision	$\geq$3 samples at low, medium, and high concentrations spanning the calibration curve range, $\geq$3 replicates, $\geq$3 analytical runs	CV $\leq$20% and 25% at LLOQ
Lower limit of quantification	Lowest calibrator that meets criteria and verified with 5 biologic samples that surround the putative LLOQ	CV $\leq$25% and recovery of 75%–125% at LLOQ
Minimal recommended dilution	Dilution of sample that obtains best CV and accuracy for samples at different concentrations of biomarker spanning the analytical range	
Quality control	$\geq$3 samples at low, medium, and high concentrations spanning the calibration curve range, 2 replicates	$\leq$20% recovery met by at least 1 replicate at each QC concentration and 4 of 6 QC replicates in total for acceptance of run
Stability—short term	Hold sample at temperatures (i.e., room temp and 4C) and length of time expected for general running of the assay. Use 3 samples at different concentrations. Test 3 freeze–thaw cycles	Mean recovery 85%–115%
Stability—long term	Hold sample frozen at varying lengths of time. Use 3 samples at different concentrations	Mean recovery 85%–115%
Reference interval	At least 40 subjects per sex of a defined age range, strain, ethnicity, BMI/wieght	Estimate with nonparametric statistics (require 40 values/sex)
Upper limit of quantification	Highest calibrator that meets criteria	CV $\leq$20% and recovery of 80%–120%

biomarkers (i.e., ligand binding assays), which is the most common method used for the emerging safety biomarkers. However, these principles are generally applicable to other types of biomarkers using different techniques.

Regularly employed methodologies for analyzing protein biomarkers include immunoassay and mass spectrometry quantification of protein mass and enzyme activity assays. Immunoassays cover a variety of formats and detection methods with both singleplex and multiplex testing. Molecular biomarkers are generally quantified with PCR-based methods. As emerging biomarkers are in the early phase of commercialization and not widely implemented by industry, these assays are almost exclusively so-called "Research Use Only" (RUO) assays and are not approved by health authorities as an in vitro diagnostic assay for clinical diagnosis and patient management. Most often these are commercialized kits, with very few laboratory-developed assays. Reagent characterization and optimization of RUO assays can vary widely, requiring verification of the manufacturer's protocol and assay performance claims by each testing laboratory.

Assay validation for biomarkers is based on "fit for purpose" principles conceived by professional bodies in recognition that biomarkers used in drug development did not fit into published standards for diagnostic tests published by Clinical and Laboratory Standards Institute (CLSI), nor guidances for validation of bioanalytical assays for pharmacokinetic analysis.[14,15] This influential framework recommends that the parameters evaluated for performance testing of an assay fits (or matches) the intended use of the data. For example, if the objectives of the biomarker study are rudimentary, then a simple set of assay performance testing to verify that the assay reliably detects a biomarker, is satisfactory. The assay performance testing becomes more comprehensive, and acceptance criteria more stringent, as the biomarker advances from early stages of evaluation to later qualification. Biomarker measurement differs from the drug bioanalytical context due to the presence of endogenous levels of the biomarker in the biological matrix, lack of standardized reference material, and calibrators that are often synthetic and therefore only approximate the native form of the biomarker. The use of new technology (with limited independent technical characterization) is another difference.[16] The quantification of emerging biomarkers may consequently represent a relative quantification that provides an estimate of true accuracy. Moreover, without standardized reference material, there is often a lack of agreement in the measured value between different assays.

Currently there is no specific Health Authority Guidance for the analytical validation of safety biomarkers. Instead, expert groups and private–public partnerships have recommended approaches and criteria for biomarker assay validation in the spirit of best practice for bioanalaytical assays as recommended by major health authorities.[17–19] In the preclinical context, these assays are usually validated nonGLP but use the foundation of GLP principles.[16] Clinically, biomarker validation packages qualified through the Drug Development Tools mechanism (see section "Regulatory Qualification of New Toxicity Biomarkers") follow an approach consistent with that recommended by bodies such as the College of American Pathology but are generally not compliant with more rigorous CLSI criteria that is the standard for clinical diagnostic laboratories.

The fit for purpose, or progressive, approach to assay validation can be conceived broadly into two stages: assay feasibility and exploratory method validation stage, and then a more comprehensive validation stage incorporating key milestones.[14,16] Selection of assays for feasibility testing occurs at the beginning of the fit for purpose paradigm and constitutes a basic series of testing to demonstrate that the biomarker is quantifiable with the standard curve, and that the assay is selective for the biomarker and precise. Several approaches have been advocated.[19,20] To begin, the precision of the calibration curve and verification of the working range of the assay are conducted. Next, a parallelism study to characterize several key attributes of the assay including selectivity for the biomarker, suitability of the calibration curve to represent the biologic sample, and the minimal recommended dilution. Parallelism is an integral milestone of feasibility testing.[16] In this test, the sample (often spiked with a standard within the working range of the assay) is diluted with buffer to determine if the response in the diluted sample has a proportionate (i.e., linear) relationship to that of the calibration curve. Accordingly, these data evaluate the immunological similarity of the calibrators in buffer or matrix to the endogenous protein in sample matrix, hence the suitability of the calibration curve for biomarker quantification. The selectivity for the biomarker and relative accuracy is demonstrated by the percent recovery of the biomarker in this parallelism test. Basic repeatability of the assay is determined by intraassay precision of calibration curve and samples. The precision performance standards for these experiments are usually between 20% and 25% for the assay with marginally higher (an additional 5%) at the upper and lower limits of quantification. Short-term stability within the time frame of expected sample analysis in addition to freeze–thaw cycle comparisons complete this early assay feasibility evaluation.

When the biomarker is ready for biological qualification, an advanced assay validation is initiated which is more comprehensive. A sequence of key milestones begins with the generation of quality control material in biologic matrix for performance testing across multiple studies. Key performance measures include: intra and interassay precision, dilutional linearity, antibody specificity for the biomarker, interference testing, long-term freezer stability, and detailed evaluation of technical robustness by evaluating the effect of fine differences in assay protocol, lot–lot variability and cross-site validation.[16,20]

The seminal framework of fit for purpose assay validation is both appropriate and expedient for safety biomarker assays. The key performance measures of assay validation, precision, parallelism, selectivity, and stability are emphasized to ensure reliable and reproducible data. The framework rationalizes the time and resource commitment allocated to assay development and validation with the stage of biomarker qualification and COU.

4.15.3.7 Regulatory Qualification of New Toxicity Biomarkers

In order to meet the societal need for new therapies to treat unmet medical needs and to improve human health, there has been a push by regulators to improve assessment of drug benefit and risk. Innovative tools to enhance safety monitoring are an important element in achieving improved risk assessment.[21] A formal process has been instituted by Health Authorities to facilitate regulatory qualification of new drug development tools, which includes safety biomarkers (see referenced websites for the FDA and EMA). The FDA defines regulatory qualification as "a conclusion that within the stated COU, a biomarker can be relied upon to have a specific interpretation and application in drug development and regulatory review."[21] There are two major paths for qualification of safety biomarkers. Drug developers can seek approval for both a drug and a safety biomarker through the investigational new drug application for an individual therapeutic. Alternatively, a stand-alone qualification through the biomarker qualification process (BQP) is disclosed publically and allows broad application of the biomarker across multiple drugs, patient populations, and therapeutic indications (**Fig. 3**). The BQP has been enthusiastically embraced by private–public partnerships comprising pharmaceutical companies, diagnostic companies, academic groups and public organizations, and regulatory advisors to collaborate on the generation and voluntary submission of data packages that support the qualification of new safety biomarkers.

The BQP begins with an initiation stage where a sponsor submits a letter of intent (LOI) to the agency nominating novel safety biomarker/s, identifying the assays for biomarker measurement, and proposes a specific COU that frames the use and interpretation of the biomarker in regulatory decisions regarding the safety of a drug. If the LOI is approved, the agency forms a biomarker qualification review team (BQRT) and the process moves to a consultation and advice stage to help shape the qualification package for submission. The review stage follows submission of the qualification package and evaluation by the BQRT. If the biomarker is approved, draft guidance is issued by the FDA and posted for public comments.[21] A qualification can only set-out a base case for confidant application within a defined context, and therefore the use of emerging safety biomarkers is necessarily an iterative and progressive process that requires continuous review and dialog between the drug development community and Health Authorities. The initial qualification may be for a limited COU, which is later expanded in subsequent submissions (**Fig. 3**). A newer instrument, the letter of support (LOS), is a less rigorous process to bring greater public attention to promising new biomarkers with preliminary evaluation packages.[21] The LOS is a new mechanism provided by the EMA and FDA.

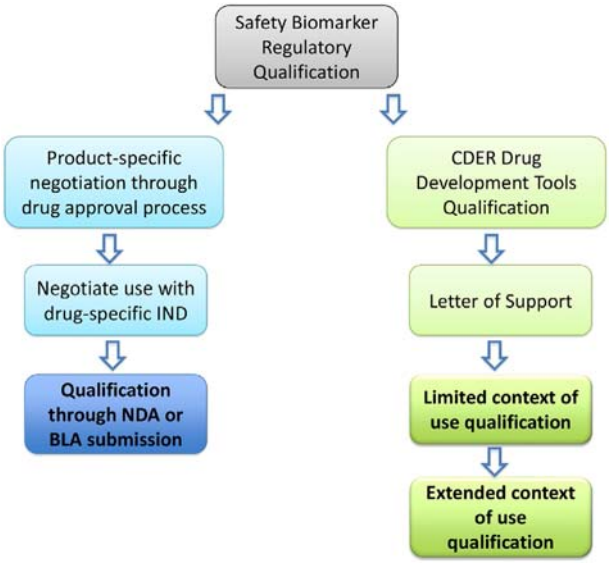

Fig. 3 An overview of the different regulatory paths to formal biomarker qualification for drug development use. The example here is representative of the process used by the U.S. Food and Drug Authority. The drug developer can qualify biomarkers for use with a specific drug through product-specific NDA or BLA submissions. The qualification data and biomarker performance may not be widely shared with the community in this path. Alternatively, sponsors of a biomarker can use a separate path to qualify the biomarker independent of a specific drug product. This is an incremental process, beginning with recognition of the potential of the biomarker by the agency (Letter of Support) and followed by a full qualification for specific contexts of use in various scenarios of drug development.

4.15.4 Emerging Biomarkers of Drug-Induced Liver Injury

Drug-induced liver injury (DILI) accounts for approximately half the cases of acute liver failure in the US and is a leading cause for regulatory actions post drug approval.[22–24] Together with cardiovascular toxicity, DILI (synonymous with hepatotoxicity) is the most common cause for safety-related attrition of drug development candidates from preclinical phases through clinical trials. The clinical epidemiology of DILI includes predictable DILI that is related to drug overdose, and idiosyncratic DILI, a rare category of toxicity. Idiosyncratic DILI is defined as an unpredictable, nondose-related, severe adverse event that can lead to liver failure and death and is the one of the most concerning and baffling risks to patient safety. Although it is recognized that predictive biomarkers for idiosyncratic DILI are a vital medical need, the rarity of idiosyncratic DILI continues to prove an out-sized challenge for biomarker discovery and evaluation. This article will focus on emerging biomarkers for predictable DILI.

The liver is particularly susceptible to drug toxicity as the major organ responsible for first-pass metabolism of orally administered drugs. The portal vein, which drains the gastrointestinal tract and spleen, supplies the liver with approximately 75% of its blood and exposes the liver to high concentrations of drugs absorbed directly from the gastrointestinal system. Portal blood is distributed in the liver via sinusoids, notable for having a discontinuous lining of endothelial cells without a basement membrane, maximizing contact of blood with hepatocytes. Hepatocytes are richly equipped with enzymes that metabolize drugs to active and inactive forms.

The diagnosis and monitoring of liver toxicity in drug development is based on a panel of serum clinical chemistry tests, including the enzyme activities of alanine aminotransferase (ALT), aspartate aminotransferase (AST), and alkaline phosphatase (ALP), and the concentration of total bilirubin. These enzymes are liberated from the parenchymal cells of the liver upon cell injury and reflect the cellular integrity of the organ. In contrast to the hepatic enzymes, total bilirubin is a marker of hepatocyte and biliary function. Additional (but insensitive) measures of hepatic function include serum levels of major hepatic biosynthetic products such as albumin, prealbumin (transthyretin), urea, glucose, and coagulation factors (indirectly measured as prothrombin time). These biomarkers are readily implemented and form part of the routine clinical pathology assessment of preclinical and clinical studies. Although this panel is remarkably broad, it fails to address some of the key needs for contemporary drug development and patient safety. Both ALT and AST are not liver specific and can increase with skeletal muscle and cardiac injury, and the functional markers are also nonspecific and notably insensitive.[25] Furthermore, the relatively long half-life of ALT and AST in humans (22 and 47 h, respectively) can impede close patient management of DILI for the in-patient setting. Major gaps in the current safety monitoring paradigm for DILI include a desire for biomarkers with improved specificity for liver injury and prediction of patients that will progress to liver failure versus adaptation to transient liver toxicity (i.e., manifest as transient increases in ALT despite continued drug exposure from drugs such as heparin) or nonprogressive DILI.[26] Additionally, mechanistic biomarkers would permit a more sophisticated characterization of DILI and could improve drug-causality assessment and potentially augment patient management and safety assessment. Biomarkers with shorter half-lives and faster appearance in the serum would also improve the ability to detect the onset and reversal of liver injury over current markers.

4.15.4.1 General Characteristics of Emerging Liver Safety Biomarkers

Assays for the emerging DILI biomarkers encompass a noteworthy variety of platforms, levels of standardization, diversity of biomarker type, and biomarker utility. Several promising biomarkers are laboratory-derived tests (acetylation status of high mobility group box 1 protein, HMGB1) and/or there is a lack of assay availability in preclinical species (measuring the different forms of cytokeratin 18, CK18) which has hindered investigation of these biomarkers. The enzyme leakage biomarkers, alpha-glutathione-S-transferase (alpha-GST), arginase-1, and glutamate dehydrogenase (GLDH), have been recognized as potential biomarkers of liver injury for decades. There could be several reasons as to why these liver enzyme leakage biomarkers may have been left on the shelf for so long. At first glance, these have a similar mechanism of release to ALT and may have been initially categorized as redundant. However, with the current desire to formalize and systematize the evaluation and use of emerging and nonroutine biomarkers, a specific COU for the added value of these biomarkers has been articulated, (1) monitoring liver injury with muscle comorbidity and (2) biomarkers with shorter half-life than standard markers (ALT, AST) that permit real-time monitoring and decision-making to improve patient care. Also, the potential for combinatorial biomarker panels to improve on individual biomarker performance is a valid path with new technology that multiplexes biomarkers. A summary of emerging DILI is provided in **Table 3**. A selection of these biomarkers is described in greater depth in this section.

Emerging liver safety biomarkers are intended for use with the standard liver panel (ALT, AST, ALP, total bilirubin) to add information and improve safety assessment and patient management. **Table 4** appraises the comparative performance of the more promising emerging liver safety biomarkers. GLDH, miR-122, arginase-1 have the potential for improved specificity over ALT. GLDH has particularly favorable technical and performance characteristics based on the availability of a standardized test on a clinical chemistry analyzer and data supporting equivalent sensitivity, with improved specificity, compared to ALT.[26] Alpha-GST has the advantage of fast kinetics, rising early with injury. However, the potential for high biological variability may ultimately challenge the performance of alpha-GST. miR-122 has equivalent sensitivity to ALT with the advantage of improved kinetics for close patient management, that is, earlier appearance, higher magnitude of change and faster reversal. CK18 and HMGB1 (and their modified forms) are mechanistic biomarkers, which could improve prediction of severity and outcome of DILI.

4.15.4.2 Arginase-1

Arginase-1 (EC 3.5.3.1) is a highly expressed liver cytosolic enzyme. Arginase-1 is confined to periportal and midzonal regions involved in the final step of the urea cycle converting L-arginine to L-ornithine and urea. The protein has also been demonstrated

Table 3 Emerging safety biomarkers of drug induced liver injury

Biomarker	*Description*	*Assay*	*Injury type*	*Biomarker utility*
Alpha-fetoprotein (AFP)	Protein in hepatocyte progenitors	Immunoassay	Hepatocellular regeneration	Prognosis
Arginase-1	Hepatocellular cytosolic enzyme	Immunoassay	Hepatocellular necrosis	Injury, specificity
Colony-stimulating factor-1 receptor (CSF1R; MCSFR1R)	Kupffer cell membrane receptor	Immunoassay	Inflammation	Mechanism, prognosis
Cytokeratin 18, full length (CK18, K18, M65)	Intermediate filament protein in hepatocytes	Immunoassay (human)	Hepatocellular necrosis	Injury, prognosis
Cytokeratin 18, caspase-cleaved fragments (ccCK18, ccK18, M30)	Caspase cleaved fragment of cytokeratin 18	Immunoassay (human)	Hepatocellular apoptosis	Injury, mechanism
Glutamate dehydrogenase (GLDH)	Hepatocellular mitochondrial enzyme	Clinical chemistry enzyme activity	Hepatocellular necrosis; mitochondrial dysfunction	Injury, specificity
Glutathione-*S*-transferase-alpha (GST-apha)	Hepatocellular enzyme	Immunoassay	Hepatocellular necrosis	Injury, specificity
High mobility group box 1 (HMGB-1), total	Hepatocellular and immune cell protein	Immunoassay	Hepatocellular necrosis	Injury, prognosis
High mobility group box 1 (HMGB-1), hyperacetylated	Activated immune cell protein	LCMS	Inflammation, immune cell activation	Injury, mechanism, prognosis
Leukocyte cell-derived chemotaxin2 (LECT2)	Hepatocellular cytosolic enzyme	Immunoassay	Hepatocellular regeneration	Injury, regeneration, prognosis
miR-122	22 nucleotide microRNA	qPCR	Leakage, hepatocellular injury	Specificity, clearance
Osteopontin	Kupffer cell secreted protein	Immunoassay	Inflammation and fibrosis	Injury, prognosis
Sorbitol dehydrogenase (SDH)	Hepatocellular cytosolic enzyme	Clinical chemistry enzyme activity	Hepatocellular necrosis	Injury, specificity

Table 4 Comparative performance of liver safety biomarkers[a]

	Standard biomarkers				*Emerging biomarkers*			
		Comparative performance				*Comparative performance*		
		Sensitivity	*Specificity*	*Mechanistic*		*Sensitivity*	*Specificity*	*Mechanistic*
Structural injury	ALT	+++	++	−	Arginase-1	+++	++	−
	AST	+++	+	−	CK-18 (full length and caspase cleaved)	++	++	++
	ALP	++	+	−	GLDH	+++	+++	−
	GGT	++	+++	−	GST-a	+++	++	−
					HMGB-1 (hypo and hyperacetylated)	++	−	++
					miR-122	+++	+++	−
					SDH	+++	+++	−
Functional injury	Total bilirubin (conjugated and unconjugated bilirubin)	++	++	+				
	Total bile acids	++	++	+				
	Albumin	+	+	−				
	Urea	+	+	−				
	Prothrombin time	+	++	−				

[a]This is a subjective, comparative performance of biomarkers based on available published data.

in lung (100-fold less than liver), with very low expression in the pancreas and kidney.[27,28] Arginase-1 is expressed in various blood cells including lymphocytes, tissue resident macrophages, and erythrocytes.

Arginase-1 is measured by immunoassay. Various preanalytical factors have been identified that could potentially influence the measured level of arginase-1, although these have not been rigorously assessed. Arginase-1 can be upregulated during Th2-type activation of kupffer cells (resident macrophages in the liver), although it is unknown if inflammatory liver injury would manifest in higher circulating levels of arginase-1. Erythrocytes show remarkable species differences in the level of arginase-1.[29] In rodents, rabbits, and dogs the levels are negligible, but are readily detectable in humans. Cynomolgus monkeys have polymorphisms that result in a range of arginase activity ranging from very low to higher than that of humans. Release of red cell arginase-1 during hemolysis in vivo or from poor sample handling could therefore result in increased arginase-1 measured in blood. There is also evidence in mice that this biomarker decreases with age and liver expression can be increased with dietary restriction.[30]

Serum arginase-1 in the blood has been shown to have good performance over many different hepatotoxicants in rats.[27,31,32] Interestingly, decreased levels of serum arginine have also demonstrated good correlation to ALT activity in rat DILI studies. The low serum arginine in these studies was likely a consequence of elevated arginase activity in the serum.[32] In a comprehensive characterization of biomarker performance using 31 different agents of acute hepatotoxicity in the rat, serum arginase-1 was more sensitive than ALT for detecting minor injury (single cell necrosis), improved specificity for toxicants causing muscle and/or gastrointestinal injury in the absence of liver injury. Additionally, it was shown to be specific for hepatocellular versus biliary toxicity.[27] The short half-life (approximately 20 min) and rapid release of arginase-1 in rat models may potentially provide advantages over ALT in clinical patient management where early detection of DILI is required, that is, following accidental overdose of drugs known to cause DILI.[31] To date, arginase-1 has not been well studied for DILI in patients.

4.15.4.3 Alpha-Gluthathione-S-Transferase

Alpha-GST (EC 2.5.1.18) is one of a family of Phase II metabolizing cytosolic enzymes that conjugate glutathione to substrates to augment water solubility and detoxify xenobiotics. There are eight classes of mammalian cytosolic GSTs and five alpha isoforms (or subunits). The alpha-GST class is the most abundant of liver GSTs and GSTs in general constitute approximately 2% of the liver's protein.[33] Alpha-GST is also abundant in the kidney tubules (equally in the rat, on protein mass/tissue weight), with low expression in the bladder, duodenum, femoral artery, spleen, testis, in addition to small intestine, pancreas, and adrenal in humans.[27,34,35]

GSTs are highly polymorphic in humans. An estimated 14% of the population is homozygous for the alpha-GST1 haplotype that results in lower levels of enzyme expression[36]. There are significant sex differences for the levels of alpha-GST in liver and plasma of human males and females, with higher levels in liver of females, and in contradistinction, higher plasma levels in males, which is also the case for rats.[33,37,38] Plasma levels in females (but not males) increase with age.[33,37] In rats, additional hormonal regulation has been demonstrated for growth hormone and testosterone on liver GST. GST can also be induced by consumption of cruciferous

vegetables (e.g., broccoli, cabbage, and Brussels sprouts), xenobiotics, and oxidative stress.[34,39,40] Alpha-GST may pose various challenges as a biomarker given this biological variability. A large interindividual variation has previously been demonstrated in plasma, with notable differences between genders.[33] Technical variations due to differences in antibody pairs and calibrators used in various immunoassays is another potential source of variation given the presence of multiple alpha-GST isoforms.

Studies in the rat have shown alpha-GST to be an early and sensitive marker in many models of DILI, outperforming ALT and AST including carbon tetrachloride, thioacetamide, bromobenzene, and ANIT.[41,27,35,42] The short half-life of the biomarker (~1 h) likely contributes to these attributes. Alpha-GST showed similar sensitivity to ALT in detecting liver necrosis over many rat hepatotoxicity models and showed additive performance to ALT for detecting hepatocellular vacuolation.[27] It was specific for hepatocellular versus biliary toxicity, however was increased with liver hypertrophy, a nonadverse toxicity.[27,35] A drawback of alpha-GST in these studies was the lower specificity than ALT with concurrent kidney, or gastrointestinal toxicity.[27]

In the clinical setting, alpha-GST outperformed AL/AST in patients with acetaminophen overdose,[43] and has been identified as a tool for monitoring hepatotoxicity with general anesthetics.[44]

4.15.4.4 Cytokeratin 18

CK18 is a cytoskeletal protein and the main intermediate filament family member expressed in the liver. The full-length form is liberated from necrotic cells, whereas a caspase-cleaved fragment is a product of the structural changes that occur during apoptosis. Soluble CK18 fragments can be detected in human serum with immunoassay.[45] The M65 assay detects total CK18 that is, full length and fragments of CK18 representing the necrotic and apoptotic biomarkers. The M30 assay detects a neopepitope created in the caspase-3 cleaved 30 kDa fragment (cc-CK18). CK18 fragments have been proposed as a promising biomarker for the diagnosis of nonalcoholic steatohepatitis by clinical gastroenterology organizations.[45]

Restricted availability of rodent reagents at the time of writing limits the preclinical assessment of these biomarkers. In a mouse acetaminophen model, both full length and cleaved CK18 (measured by immunoprecipitation-LC–MS assay) showed similar diagnostic performance to ALT. The pattern of change, with the apoptotic marker rising early and the necrosis marker progressively increasing with time conforming with morphologic and biochemical evidence of hepatocyte apoptosis and necrosis, indicated value as mechanistic biomarkers.[46]

In patients with suspected acetaminophen overdose, serum levels of CK18 total and cc-CK18 at hospital admission had good correlation with peak ALT and the liver functional marker, prothrombin time.[47,48] Furthermore, CK18 and cc-CK18 predicted patients that progressed to acute liver injury better than ALT in two important settings, when (1) ALT was still within normal range at admission and (2) patients presented to hospital within 8 h of overdose.[48] Conversely, in clinical settings of mild, nonprogressive and/or transient DILI, CK18 has shown concordance with mild changes. This was demonstrated at maximum therapeutic doses of APAP or patients treated with highly active antiretroviral therapy regimen (HAART) where CK18 had a comparable time to peak and magnitude fold change as ALT.[49] Also, generally mild-moderate increases in ALT associated cholestyramine treatment that caused mild DILI was associated with minor increases in CK18 (2.1-fold) and cc-CK18 (1.7-fold).[50] As a stand-alone marker CK18 (either form) has shown modest prognostic accuracy, with cc-CK18 apoptotic marker higher in patients that recovered from acute liver failure (of various etiologies including toxicity) compared to nonsurvivors.[51] However use of these markers in a panel-based approach may augment discrimination as demonstrated by improvement in the model for end-stage liver disease (MELD) score to predict survival in patients with acute liver failure.[52]

Specificity of CK18 for DILI has not been fully addressed in human populations. As cytokeratins are ubiquitously expressed in epithelial tissue, damage to nonhepatic tissues can contribute to increased circulating levels in addition to nondrug-related natural liver disease. Consequently, CK18 are increased in cancer, chronic kidney disease, and nonalcoholic steatohepatitis. A small cohort of humans subjected to exercise-induced muscle damage had no effect on circulating CK18 or cc-CK18.[49]

4.15.4.5 Glutamate Dehydrogenase

GLDH (E.C. 1.4.1.3) is a major liver enzyme. GLDH is predominately mitochondrial but low levels are also found in the endoplasmic reticulum.[53] Although expression in the liver is largely confined to centriblobular zone of the liver, there may be a dynamic aspect to subzonal expression that is influenced by diet, sex, and endocrine factors.[54] GLDH catalyzes the reversible conversion of glutamate to α-ketoglutarate and ammonia. Humans have 2 GLDH genes encoding 2 enzyme isoforms (hGDH1 and hGDH2), whereas preclinical species have only 1 gene (the homolog of GDH1). The major isoform (GDH1) is present in all mammals and is expressed largely in the liver. The human-specific homolog (hGDH2) is expressed in the brain and testis. The two human GLDH isoforms have different basal activity levels, enzyme properties, and are differentially regulated by GTP.[55] GLDH has a housekeeping role in cell metabolism, which explains its abundant levels in tissue. In mouse, tissue enzyme activity in the liver is approximately 5× activity levels of pancreas, small intestine, heart, and cerebellum, with trace activity in other tissues (including kidney). GLDH has been induced in cell culture systems by glucocorticoids and cytokines (TNFα, IL-1).[56,57] GLDH is measured by enzyme activity assay, an approved in vitro diagnostic assay in Europe, Canada, and China. Published reference ranges for GLDH in human populations are comparable as may be expected of a standardized clinical chemistry assays using highly precise testing platforms.

GLDH is released into the circulation following necrosis of the cell and/or mitochondrial injury and dysfunction. In theory, mitochondrial injury can be distinguished from frank cellular necrosis by the release of free GLDH in the former versus intact mitochondria as a consequence of hepatocellular necrosis.[58] Preclinically, GLDH has demonstrated similar or superior sensitivity to

ALT.[59] The half-life of GLDH in the rat is 8 h, similar to ALT and AST in that species. GLDH was highly correlated with ALT over a number of different drugs and liver injuries, with a higher magnitude of change and longer duration of increase in blood compared to ALT.[59] Circulating GLDH was increased with a hepatic mitogen (cyproterone) in the absence of necrosis, and also increased with corticosteroids[59,60] but did not show induction by phenobarbital.[42,59] Generally, GLDH has been demonstrated to be an early marker (3–24 h postdose) across models of acute hepatotoxicity comprising ANIT, acetaminophen,[42] thioacetamide, and bromobenzene.[35] GLDH had similar performance to ALT (but inferior to arginase-1) in acute allyl alcohol, lipopolysaccharide, and concanavalin A toxicity in the rat.[31]

GLDH was highly correlated with ALT over a variety of natural and drug related liver disease in patients and had equivalent diagnostic performance to ALT (AUROC 0.98 vs. 0.99).[26] GLDH measured at hospital admission in patients with normal ALT and/or within 8 h of overdose predicted patients that proceeded to have elevated ALT (>3 ULN).[48] Another group showed an increase in GLDH in lethal acetaminophen-induced acute liver failure compared to survivors however, due to the overlapping values between survivors and nonsurvivors, the sensitivity at 90% specificity for predicting lethality was 37%.[61] Perhaps the greatest advantage of GLDH is the liver specificity of the enzyme in contrast to ALT. In humans with exercise-induced muscle damage, there was no effect on serum GLDH confirming the liver specificity of this biomarker.[49]

4.15.4.6 HMGB1

HMGB1 is a nonhistone chromatin-associated protein that stabilizes the nucleosome and regulates transcription. HMGB1 is ubiquitously expressed, highly conserved (99% amino acid identity between rodents and humans), and abundant in the nucleus. There are six polymorphisms in the gene although it is undetermined whether this may impact the use of HMGB1 as a biomarker.[62] Hypoacetylated HMGB1 is loosely bound to nuclear chromatin and will leak out of necrotic cells. In activated monocytes, macrophages, and natural killer cells, and mature dendritic cells, HMGB1 can be hyperacetylated permitting translocation from the nucleus to the cytosol and active secretion as a cytokine.[63] Secreted HMGB1 binds to receptor for advanced glycation endproducts (RAGE) and Toll-like receptor 2 (TLR2) and 4 to act as a proinflammatory cytokine. In the extracellular environment, both forms of HMGB1 act as damage-associated molecular pattern molecules (DAMPs), orchestrating the immune activity and repair responses associated with tissue injury. HMGB1 was thought to be retained by apoptotic cells, although this notion has recently been challenged with evidence that chemotherapeutics and radiotherapy can release DAMPs such as HMGB1 during apoptosis.[64,65] Thus, circulating hyperacetylated HMGB1 represents an immune response marker and the hypoacetylated form is a marker of hepatocellular necrosis.

Total HMGB1 can be measured by immunoassay, however mass spectrometry is required to detect hyperacetylated forms, in addition to redox modifications. High titer autoantibodies to HMGB1 have been observed in healthy people and patients with autoimmune disease and are a potential interferent in the immunoassay.[66]

HMGB1 has only recently been investigated as a mechanistic biomarker for DILI. In a mouse model of acetaminophen toxicity, total HMGB1 was increased slightly earlier than ALT and showed similar diagnostic performance. The kinetics of the hypoacetylated (necrosis marker) and hyperacetylated HMGB1 (immune response) biomarkers were different and consistent with the pathogenesis of this toxicity. Hypoacetylated HMGB1 had a faster rise and reversal that corresponded to peak necrosis, whereas the hyperacetylated form had a later onset, lower magnitude of change, and sustained increase and was compatible with the phase of liver regeneration and systemic inflammation.[46]

In patients with suspected acetaminophen overdose, admission HMGB1 had good correlation with peak ALT and prothrombin time/international normalized ratio.[47,48] Elevated total HMGB1 on admission also had the best prediction and separation in values (little overlap) for patients with normal ALT and/or within 8 h of overdose that went on to have DILI with elevated ALT.[48] Total HMGB1 had a high positive predictive value and AROC for DILI in this patient population, outperforming other emerging hepatotoxicity biomarkers (CK18, ccCK18, GLDH) for prediction of DILI. Further support that HMGB1 may have prognostic capability was in a clinical study with cholestyramine treatment. This agent causes increased ALT without serious hepatotoxicity and only resulted in minor increases in HMGB1 (1.7-fold).[50]

4.15.4.7 miR-122

miR-122 is a liver-specific miR with expression orders of magnitude higher than any other tissue. miR is highly abundant in the liver, estimated to comprise 70% of hepatic miRs.[4]a,67,[4]b Several functional roles for miR-122 have been identified, such as the maintenance of a differentiated hepatocellular phenotype, tumor suppression, hepatic cholesterol, triglyceride, and iron metabolism. The intracellular half-life has been loosely determined to be longer than 24 h,[68] and the circulating half-life has not been reported.

Most reports on miR-122 to date have been in rodents and human studies, with limited reports in the dog.[69] Rat studies with different liver toxicants have shown a correlation with severity of liver lesions by histopathology.[42] In rodent acetaminophen models, this is an early marker, that is, at 1 h postdose in the mouse.[70] miR-122 was more sensitive than ALT for acetaminophen, CCl4, and CBrCl3 hepatotoxicity in rodents.[4]b,70 The rise in plasma miR-122 levels has been related to a corresponding loss in the liver tissue.[70]

The few clinical studies of miR-122 have revealed a comparable or improved performance to ALT. Investigation of miR-122 in patients with acetaminophen overdose correlated with ALT with an earlier rise and faster reversal to baseline in recovered patients.[49,71,48] The prognostic capability, that is, to predict outcome postadmission, of miR-122 in acetaminophen overdose is not clear from current investigations.[71,48] In states of benign elevations in ALT caused by cholestyramine treatment, miR-122

had similar increases relative to baseline.[50] Specificity studies are scarce for miR-122. Interestingly, miR-122 decreased postrace in a small study ($n=39$) examining effects of muscle injury from endurance exercise on liver biomarkers.[49]

4.15.5 Emerging Biomarkers of Acute Kidney Injury

Drug-induced kidney injury (DIKI) is a prominent cause of acute kidney injury (AKI), accounting for approximately 19–26% of cases over a number of large multicenter studies.[72] Tubular necrosis was the most common DIKI pathology.[72] Drugs frequently implicated in DIKI include aminoglycoside antibiotics (e.g., gentamicin and tobramycin), the immunosuppressive agents cyclosporine and tacrolimus, the antineoplastic drug cisplatin, NSAIDs, and contrast media. During drug development, DIKI is an important cause of safety-related attrition, responsible for termination of approximately 8% and 9% in preclinical and clinical candidates, respectively.[1,73]

Several aspects of kidney physiology influence susceptibility to DIKI. The kidney receives 25% of cardiac output, has the highest flow rate of any organ, and therefore renal clearance can influence small molecule drugs in circulation. Tubule cells are richly decorated with transporters that facilitate the uptake of drugs and contain multiple pathways for the biotransformation of drugs. These metabolic pathways generally detoxify the drug and facilitate excretion, but for some drugs the production of reactive metabolites may lead to renal toxicity.

The standard tests for nephrotoxicity, serum creatinine, and serum urea nitrogen concentration, are markers of kidney function. Creatinine is a byproduct of skeletal muscle metabolism. It is a low molecular weight (LMW) (113 Da) metabolite produced at a constant rate proportional to muscle mass and is freely filtered by the glomerulus. Blood urea nitrogen is also a metabolic waste product that is freely filtered by the glomerulus, therefore is a similar biomarker to creatinine, but less specific due to influences from diet, protein catabolism, and liver function. Both markers serve as indicators of glomerular filtration rate (GFR) and kidney function. Ancillary serum endpoints measured in routine monitoring, through nonspecific and insensitive markers also support detection of functional kidney injury and include serum protein, electrolytes, phosphorus, and calcium concentration. Additional tests for kidney toxicity are mentioned in the ICH S7A guideline for safety pharmacology, comprise urine tests for volume, specific gravity, osmolarity, pH, fluid/electrolyte balance, protein, and cytology.[74] Biomarkers of structural kidney injury were lacking in standard monitoring panels in preclinical and clinical drug development studies.

Standard functional markers for monitoring kidney toxicity are insensitive owing to the large functional reserve of the kidney. For example, serum BUN and creatinine only rise with loss of at least 50% of renal function. Also, serum creatinine has a parabolic response, with the magnitude of increase being low at the lower threshold for injury detection. Specificity of BUN and creatinine for renal injury is also compromised when transient prerenal factors such as reduced renal blood flow (i.e., states of dehydration). Therefore, there is a need for early markers of kidney injury with improved sensitivity and specificity for nephrotoxicity.

Emerging biomarkers for kidney injury conform to three major categories, which are not mutually exclusive. These comprise markers of structural injury that leak from cells, markers upregulated in states of damage and repair, and markers of tubular function (reabsorption and small molecule exchange). **Table 5** lists the emerging safety biomarkers of kidney injury. These markers are expressed in different locations of nephron and have the potential to localize injury and may assist in assigning drug causation to kidney effects in patients. Structural injury markers also offer the opportunity to detect subclinical kidney disease prior to functional impairment detected by standard markers. Furthermore, patients with subclinical kidney injury may be at higher risk for DIKI when exposed to nephrotoxicants.[75] The regional location of the emerging kidney safety biomarkers are depicted in **Fig. 4**.

The qualification of eight renal safety biomarkers by FDA, EMA, and PMDA in 2008–10 recognized that new urine biomarkers outperformed and/or added value to the measurement of serum creatinine and urea nitrogen, and represented an important advance in safety assessment.[76] The new biomarkers comprise: albumin, beta-2-microglobulin, clusterin, cystatin-C, kidney injury molecule-1 (KIM-1), renal papillary antigen 1 (RPA-1), trefoil factor 3 (TFF3), and total protein (**Table 5**). These urine biomarkers were qualified for use in rat studies and voluntary use on a case-by-case in clinical trials for the detection of tubular toxicity. Subsequently, osteopontin and neutrophil gelatinase-associated lipocalin (NGAL) have received a "Letter of Support" recognition from the FDA and EMA to encourage further evaluation of these biomarkers for their utility as kidney injury biomarkers.[77] The comparative performance of these new urine biomarkers is summarized in **Table 6**. The strategy used by the predictive safety testing consortia (PSTC) to qualify kidney biomarker qualification was to focus on renal tubular in the rat and use a thorough and standardized histomorphological assessment across a number of model toxicants with different mechanisms of toxicity as the gold standard for assessing biomarker performance. The translational value of these biomarkers would then be confirmed in human subjects with renal tubular DIKI within a limited COU. Subsequent qualifications for clinical use would be incremental, and extend the claims of biomarker performance in an expanded COU.[6] Glomerular toxicity biomarkers and contexts of use were to be undertaken at a later date by the PSTC.

Although information on the adoption of qualified renal safety biomarkers by drug developers is extremely limited, one survey of big pharma suggests they are used preclinically on a for-cause basis, with few sponsors measuring the entire panel of eight markers.[78] The most commonly evaluated new kidney biomarkers were reported to be total protein, albumin, and KIM-1.[78] In keeping with a phased and incremental approach to Regulatory qualification of biomarkers, consortia (PSTC) are actively investigating clusterin, cystatin-C, KIM-1, *N*-acetyl-beta-D-glucosaminidase (NAG), NGAL, and osteopontin for clinical use.

This section will focus on the new urine biomarkers qualified in the rat, and on the urine biomarkers under current evaluation for qualification in humans. As urine albumin and total protein have an extensive historical use with considerable evidence for their

Table 5 Emerging safety biomarkers of acute kidney injury

Biomarker	*Sample*	*Kidney association*	*Assay*	*Toxicity mechanism*	*Biomarker utility*
BUN	Serum	Filtered serum metabolite	Colorimetric assay	Reduced glomerular filtration	Function
Creatinine	Serum	Byproduct of muscle metabolism	Colorimetric dye-binding or enzymatic assay	Reduced glomerular filtration	Function
Albumin	Urine	Filtered serum protein	Immunoassay	PT transport; compromise of glomerular filtration barrier	Function: tubular and glomerular
alpha-1-microglobulin	Urine	Filtered serum protein	Immunoassay	PT transport; compromise of glomerular filtration barrier	Function: tubular and glomerular
beta-2-microglobulin	Urine	Filtered serum protein	Immunoassay	PT transport; compromise of glomerular filtration barrier	Function: tubular and glomerular
Calbindin D28	Urine	Tubular protein	Immunoassay	Injury, leakage	Distal tubule and collecting duct injury
Clusterin	Urine	Tubular protein, locally secreted protein	Immunoassay	Injury: upregulated, secreted	Proximal and distal tubular injury
Creatinine	Urine	Filtered serum protein and secreted by tubules	Colorimetric dye-binding or enzymatic assay	NA	Corrects biomarkers for dilution and urine flow rate
Cystatin-C	Urine	Filtered serum protein	Immunoassay	PT transport; compromise of glomerular filtration barrier	Function: tubular and glomerular
IL-18	Urine	Secreted tubular protein	Immunoassay	Injury: upregulated, secreted	Injury response
KIM-1	Urine	Transmembrane protein of proximal tubule	Immunoassay	Injury: upregulated and shed with injury	Proximal tubular injury
Liver fatty acid-binding protein	Urine	Proximal tubule cellular protein		Injury: upregulated, leakage	Proximal tubular injury
NAG	Urine	Lysosomal enzyme of proximal tubule	Colorimetric enzymatic activity	Injury, leakage	Proximal tubular injury
NGAL	Urine	Tubular cell and neutrophil protein	Immunoassay	Injury: upregulated, secreted	Tubular injury
Osteopontin	Urine	Secreted tubular protein	Immunoassay	Injury: upregulated, secreted	Proximal and distal tubular injury
Retinol-binding protein	Urine	Filtered serum protein	Immunoassay	PT transport; compromise of glomerular filtration barrier	Function: tubular and glomerular
Renal papillary antigen-1	Urine	Collecting duct cellular protein	Immunoassay	Injury, leakage	Collecting duct injury
Total protein	Urine	Filtered serum protein	Colorimetric binding assay	Compromise of glomerular filtration barrier	Function: glomerular
Trefoil factor 3	Urine	Secreted tubular protein	Immunoassay	Injury: downregulated	Proximal tubular injury (decreases)

diagnostic utility these will not be covered here. Both these biomarkers are readily implemented, particularly in clinical studies where diagnostic laboratories have access to standardized tests for automated platforms. Other new biomarkers not elaborated here due to a paucity of translational data in addition to reasons already stated, include alpha-GST, alpha-1-microglobulin, gamma glutamyltransferase, IL-18, liver fatty acid binding protein, RPA-1, and TFF3 (Table 5). The less attractive prospect of a marker that decreases with toxicity together with limited availability of assays have constrained further investigations of TFF3. Adding to the low appeal of TFF3, is the suggestion that it is a delayed marker of nephrotoxicity.[79] Circulating (i.e., serum) levels of some of these same biomarkers (e.g., osteopontin, albumin, NGAL, KIM-1) have also been evaluated as safety biomarkers for kidney injury, however information is sparse and these often have specificity concerns in the serum. The exception is serum cystatin-C, which has long been investigated as an alternative marker to serum creatinine for estimating GFR, a marker of kidney function. There continues to be conflicting evidence and opinion for the performance of serum cystatin-C compared to serum creatinine for estimating GFR.

4.15.5.1 General Considerations for Preanalytical Factors, Assays, and Biomarker Biology

4.15.5.1.1 Preanalytical factors

Urine presents one of the least invasive of body biofluids to sample with little impact on the health and discomfort of the subject. However, there is added complexity to the collection, analysis, and interpretation of urine biomarkers compared to those in the blood. Proteins may be degraded by bacterial action, the sample compromised by contaminants, and the biomarker bound to factors that interfere with the assay. Ideally, urine samples should be accompanied by a short description of the physical

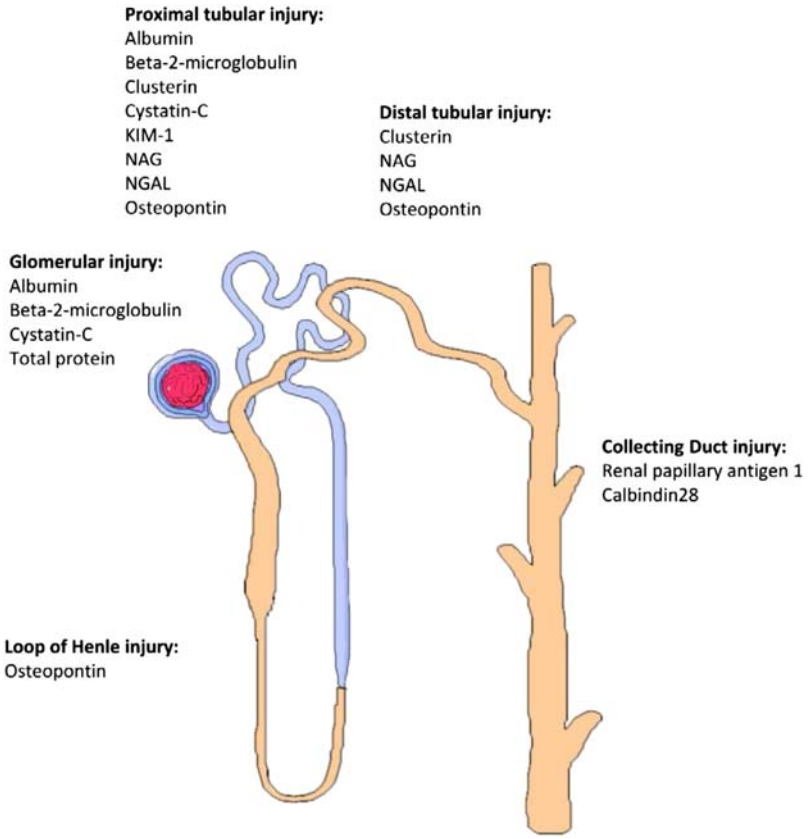

Fig. 4 Kidney toxicity biomarkers correspond to different anatomical regions of the nephron. Shown is a cartoon of the nephron, the structural and functional unit of the kidney. Injury to different segments of the nephron can result in increased excretion of specific biomarkers into the urine assisting in diagnosing the site of injury. Ferguson, M. A.1; Vaidya, V. S.; Bonventre, J. V. Biomarkers of Nephrotoxic Acute Kidney Injury. Toxicol. **2008**, *245*(3), 182–193. http://dx.doi.org/10.1016/j.tox.2007.12.024.

Table 6 Comparative performance of kidney safety biomarkers[a]

	Standard biomarkers			*Emerging biomarkers*		
		Comparative performance			*Comparative performance*	
		Sensitivity	*Specificity*		*Sensitivity*	*Specificity*
Structural injury	Serum protein and albumin	+	+	Urine clusterin	+++	+++
				Urine KIM-1	+++	+++
				Urine NAG	++	+++
				Urine NGAL	++	+++
Functional injury	Serum creatinine	+	++	Urine albumin	++	++
	Serum (blood) urea nitrogen	+	++	Urine beta-2-microglobulin	++	++
	Serum electrolytes (sodium, chloride, potassium)	+	++	Urine cystatin-C	++	+++
	Serum minerals (phosphorus, calcium)	+	+	Urine protein	++	++
	Urine electrolytes (sodium, chloride, potassium) and fractional excretion	+	++			
	Urine minerals (phosphorus, calcium) and fractional excretion	+	+			
	Urine osmolality	++	++			
	Urine specific gravity	++	++			
	Urine volume	+	+			

[a]This is a subjective, comparative performance of biomarkers based on available published data.

Table 7 Select preanalytical variables for urine analysis

	Factor/variable	*Effects*	*Recommendations*
Contamination	Gross external contamination	Interference with assay	Urine should be collected in clean environment and centrifuged postcollection
	Bacterial	Bacteria degrade biomarker; change pH of matrix and interfere with assay conditions	Keep urine at 4°C and minimize time at room temperature; centrifuge urine to remove gross debris and cells; acidivication of urine can be attempted (e.g., sodium azide) if proven not to interfere with biomarker analysis
	Endogenous not directly from the site of kidney injury	Circulating biomarker levels in blood add to measured concentration; blood interferes in assay; contribution of biomarkers in contaminating cells	Centrifuge, measure blood via dipstick, perform urine cytology to verify blood cells; check assays for interference; dilution of samples with visible hemolysis may reduce interference
Lower urinary tract inflammation	Inflammatory cells	Inflammatory cells contribute inflammatory biomarkers, e.g., NGAL	Determine if lower urinary tract information is present and relationship to drug; Inflammatory markers may be confounded if there is upper and lower UTI; spot samples with rapid processing may reduce effects on sample
Collection	Timed collection; spot (single sample collection); time of day for collection vs. random	Differences in biomarker concentration and excretion estimates	Timed collections may reduce variability and account for diurnal variations; suitability of spot collections should be established in relation to timed collections
	Temperature	Urine collected over longer periods at higher temperatures are susceptible to bacterial overgrowth	(see bacterial contamination above)
Processing and handling	Centrifugation	Potential for cellular contamination in whole urine (altering biomarker level; assay interference)	Standardized centrifugation protocols should be in place prior to sample collection
	Protease inhibitors	Potential degradation by endogenous proteases and reduced stability	Not usually of value
	Storage time/stability	Degradation of biomarkers or altered epitopes detected by immunoassay	Short-term, freeze–thaw effects, and long-term stability should be determined. Storage at −80°C is usually acceptable
Food effects		Alters biomarker concentration	Preliminary data indicates there are no food effects on major new kidney biomarkers (human)
Gender and age		Alters biomarker concentration	New biomarkers are likely to show differences between males and females (human)

characteristics (color, clarity) and routine dipstick analysis to provide a preliminary quality control check for the presence of blood contamination and inflammation, which may result in artefactual values when biomarkers are also present in blood. Beta-2-microglobulin has been reported to be unstable unless the pH is >6.5.[80] The long-term frozen stability at −80°C was poor for KIM-1, NAG, and NGAL and should be established for the assay and conditions to be used in a study.[81] **Table 7** provides a summary of major preanalytical factors that should be considered when measuring biomarkers in urine.

Timed collections over a period up to 24 h may be used to account for diurnal variations in biomarker release and can potentially reduce variability in the concentration of the analyte.[82] The convenience of spot samples (from a single collection) may trump timed collections if there is evidence of acceptable agreement to timed samples. Fresh urine has shown to be preferable to prolonged storage for several biomarkers (cystatin-C, KIM-1, NAG, NGAL). Alkalization (adjustment of urine pH to >8 with sodium hydroxide) or use of protease inhibitors did not improve frozen stability.[81,83] Urine biomarkers are generally normalized to creatinine to account for urine flow rate and variable dilution of the urine by water. Although most of the excreted creatinine is contributed by glomerular filtration, a portion is also derived from tubular secretion and this shows species and sex differences. For example, humans have a low proportion, 10–20%, of total urine creatinine that is secreted from the tubules, whereas in mice this may account for 35–50% of excreted creatinine.[84,85] With lower GFR and higher serum creatinine concentrations, the relative proportion of secreted vs filtered creatinine can also change.[84] This ratio may also be invalid when injury to tubules results in variations in the excretion of creatinine that may differ between individuals.[86] An alternate method to account for dilution and urine flow rate is by collecting a timed specimen and expressing values as total mass excreted over the time period that is, dilute urine will presumably have a higher

volume of urine and lower concentration and conversely, concentrated urine will have a lower volume and higher concentration of the analyte in healthy subjects. Despite these caveats, correcting to urine creatinine is usually favored, with studies in the rat demonstrating a stronger correlation between biomarker concentration and urine creatinine and less gender-related differences than urine volume.[12,13] The ratio to creatinine has been used in regulatory qualification of new urine biomarkers in rat and in human.

Biological variability of urine albumin, KIM-1, NAG, NGAL, osteopontin, RPA-1, and total protein has been evaluated in the rat.[12] These markers had intraindividual variation of $\leq$44% and interindividual variation $\leq$46%. Given these data, it is estimated that a twofold increase in any of these biomarkers (corrected for urine creatinine) is likely to indicate toxicity, with KIM-1 having the lowest threshold (at 1.4-fold baseline). Sex-related differences in rats have also been identified, with increased beta-2microglobulin, clusterin, cystatin-C excretion in male rats compared to females.[87,13] Although, still under active investigation, preliminary reference interval data in humans characterized NGAL, beta-2-microglobulin, clusterin, osteopontin as higher in females than males, with no gender effect for cystatin-C and KIM-1.[11,88] These qualification studies, and other studies in the last few years, have demonstrated no difference in biomarker performance in the major rat strains used in drug development (Sprague-Dawley, Han Wistar).[89]

4.15.5.1.2 Pathophysiologic factors

Several of the new biomarkers are freely filtered LMW proteins (beta-2-microglobulin, cystatin-C, L-FABP, NGAL, osteopontin) that are reabsorbed along with albumin by megalin–cubilin endocytic transporters present on the luminal border of proximal tubular epithelium. Consequently, increased excretion of these LMW biomarkers will reflect injury and/or dysfunction to the proximal tubule. However, additional mechanisms may affect these biomarkers. For example, competition for megalin–cubilin may lead to in saturation of active transport. This situation can occur in conditions that lead to increased albumin in the filtrate, as may occur in conditions with high serum protein load.[90] Glomerular injury and disease states accompanied by proteinuria (sepsis, chronic kidney disease) also resulted in increased LMW urine biomarkers. Additionally, a number of agents including nephrotxicants (puromycin), xenobiotics (e.g., the mTOR inhibitors sirolimus and everolimus) endotoxemia, and heavy metals (e.g., cadmium) may also downregulate megalin expression and increase LMW biomarker excretion.[91]

In a rat gentamycin model of nephrotoxicity, gender differences in biomarker response were explored for 16 candidate urinary biomarkers. Intriguingly, biomarker fold increases were generally higher in females equivalent microscopic severity grade of injury compared to males in Sprague-Dawley rats. Only for beta-2-microglobulin and TIMP-1 could that be clearly related to a lower baseline in females compared to males.[92]

4.15.5.1.3 Assays

The majority of these biomarkers are measured with immunoassays. Assays designed for detecting biomarkers in blood may not use buffers and reagents that adequately account for the different physicochemical properties of urine and performance evaluation of the assay in a urine matrix is a necessary feature of assay validation. Urine biomarkers are usually measured with multiplexed assays in the rat, but singleplex assays tend to be favored in human studies. The immunoassays are nonstandardized, and use different reagents (detection and capture antibodies, calibrators, diluent), therefore values for these biomarkers may differ across kits and labs. One study investigating assays for human urine biomarkers found a high correlation between singleplex and multiplex assays across vendors for most of these biomarkers, except for beta-2-microlobulin.[11] In the rat, different platforms have also shown reasonable correlation, similar direction of changes, but differences in the measured values.[13,93] On the other hand, a high level of agreement is expected across platforms and sites for those biomarkers that are measured on the automated clinical chemistry analyzer (urine creatinine, albumin, total protein) often with calibration to similar reference material. Although the enzyme activity of urine NAG is also measured simply and accurately with a colorimetric assay on an automated clinical chemistry analyzer, it did not show good cross-site correlation when evaluated by one group of investigators.[11]

Several assays are approved for measuring human urine NGAL in the European Union on automated clinical chemistry analyzers. These high throughput assays have shown good correlation with research-grade ELISA.[94] Development of new tests that can distinguish the monomeric form from the dimer released by neutrophils is expected to result in a gain of specificity and diagnostic performance.[94]

4.15.5.1.4 Postanalysis, interpretation

In preclinical qualification and published reports, the biomarkers have been evaluated as single biomarkers where the pattern of individual markers is related to toxicity. On the other hand, the clinical qualification strategy for the first stage limited COU is to propose a composite measure of the biomarker panel to detect deviation of human subjects from normal variability as a measure of potential toxicity. As more data is generated on the diagnostic performance of these biomarkers, both individually and in combination in patients exposed to drugs in different contexts, it will become evident how to optimally apply these biomarkers in clinical development.

The emerging kidney toxicity biomarkers have been qualified for nonclinical use in rats, with a submission planned for clinical qualification. These biomarkers have been demonstrated to at least add value to the diagnostic performance of serum BUN and creatinine standard endpoints (Table 6); therefore these biomarkers should be applied as adjunct tests that are interpreted together with changes in the serum markers. Consortia have focused the first round of qualification on acute tubular injury in a staged approach to manage the resource required to generate a data package for regulatory submission. Consequently, only a limited evaluation of these new biomarkers has been conducted by consortia or published by independent researchers in the context of glomerular injury.[95,96]

4.15.5.2 Beta-2-Microglobulin

Beta-2-microglobulin is a LMW (17 kDa) ubiquitously expressed protein and a component of the major histocompatibility class (MHC) I molecule family. It is produced at a constant rate and freely filtered by the kidney. Similar to other LMW proteins, beta 2-microglobulin is completely reabsorbed by megalin-mediated endocytosis on the proximal tubules and then completely catabolized within the tubular cell. The fractional urinary excretion of beta 2-microglobulin has been estimated at 0.03%.[97] Levels are increased in the urine if there is direct functional impairment of the proximal tubular epithelial cells or an indirect compromise to proximal tubular function from protein overload (e.g., states of glomerular injury) and saturation of tubular transporters.

In a gentamycin nephrotoxicity model of proximal tubular injury in the rat, beta-2-microglobuin increased prior to microscopic lesions after a single dose and was robustly increased in a multidose setting.[93,92] In part, this prodromal activity may be related to gentamycin-induced functional changes on transporter activity in the proximal tubules that impair LMW protein uptake. Beta-2-microglobulin outperformed serum BUN and creatinine in detecting glomerular injury in multidose acute studies using puromycin and doxorubicin in the rat.[95] However, in a single-dose puromycin model with low-grade glomerular injury this biomarker did not show a significant difference.[96] Beta-2-microglobulin was not an adequate immunohistochemistry (IHC) marker in kidney tissue for cistplatin nephrotoxicity in the rat.[79]

There is limited clinical data on DIKI with beta-2-microglobulin. Early studies with gentamycin did not reveal a close correlation with serum creatinine values, although stability in the urine was questionable in this study.[80] The diagnostic performance of this biomarker for detecting fumaric acid ester-induced nephrotoxicity was equivocal in one case series.[98]

4.15.5.3 Clusterin

Clusterin is ubiquitously expressed protein, with one isoform located in the nucleus and an 80 kDa secreted glycoprotein. Secreted clusterin is involved in lipid transport and is released in response to cell stress where it protects the cell by reducing oxidative stress and binding to misfolded proteins.[99,100] In mouse models of renal injury secreted clusterin is antifibrotic.[100] On the other hand, nuclear clusterin is upregulated by apoptosis and in-turn promote apoptosis through bax.[100] As a consequence of glomerular size exclusion, clusterin in urine should be locally derived from the urogenital tract. The secreted isoform is induced and released by the proximal and distal tubules, glomeruli, and collecting duct during drug-related kidney injury and is therefore considered a pan-nephron biomarker.[79,101] Clusterin secreted at or proximal to the proximal tubule is a ligand for megalin-facilitated endocytosis, therefore increased urine clusterin could also be influenced by effects on proximal tubular function. Of note, high concentrations are also found in seminal fluid[99] and could potentially contribute to urine samples in males of some species (e.g., rat, dog).

There is ample evidence in rat studies that urine clusterin is superior to serum BUN and creatinine for the detection tubular nephrotoxicity over a wide range of toxicants,[79,95,101,89,102] with limited reports in monkeys,[103] and dogs.[104] In a comprehensive multinephrotoxicant metaanalysis in the rat, clusterin was second only to KIM-1 as the best performing of the new urinary biomarkers of tubular injury.[102] Clusterin correlated with the microscopic severity of proximal tubular injury in the rat including lesions of minimal severity.[95] It also showed slow reversal with injury resolution in rat models, consistent with a role in the repair process.[105] In the monkey, upregulation of clusterin expression by quantitative PCR in kidney tissue correlated to gentamycin and everninomicin proximal tubular nephrotoxicity.[106] Consistent with the expression of clusterin throughout the nephron, a novel compound that selectively injured the distal tubule and/or collecting duct in the monkey was associated with increased urine clusterin.[103]

There are relatively few clinical studies evaluating urine clusterin in DIKI although investigators have begun to examine this biomarker in naturally occurring kidney disease. Clusterin did not perform well in liver transplant patients treated with the nephrotoxin Tacrolimus in one report.[107]

4.15.5.4 Cystatin-C

Urine cystatin-C is a 13 kDa, LMW protein, with similar characteristics to beta-2-microglobulin as a urinary biomarker of reduced proximal tubular function. The protein is ubiquitously expressed and is a cysteine protease inhibitor. Serum cystatin-C has long been evaluated as an endogenous marker of GFR. There is no clear advantage of using serum cystatin-C over estimates using serum creatinine.

Cystatin-C has shown mixed performance in rat models of nephrotoxicity. It did not change in single-dose cisplatin toxicity,[96] although at higher or multiple doses of cisplatin, cystatin-C was an early marker with urine elevations that preceded microscopic changes.[93,105] For other tubular toxicants in the rat, urine cystatin-C was an early marker for gentamycin[93] and correlated with the severity of renal histopathology for paraquat.[108] Cystatin-C outperformed serum BUN and creatinine in a glomerular injury in multidose acute studies using puromycin and doxorubicin in the rat, although not in a single-dose puromycin model.[96,95] In a metaanalysis of 12 rat nephrotoxicity models in cystatin-C did not perform as well as other new urinary biomarkers (KIM-1, clusterin, albumin, NGAL, ostopontin).[102] For gentamycin toxicity in the dog, it outperformed serum creatinine, urine NAG and NGAL, and significantly correlated with measured GFR ($r = -0.89$).[109]

There have been mixed results on the diagnostic and prognostic ability of urine cystatin-C for patients in intensive care units with AKI of various causes.[110,111] In contrast it showed good performance in diagnosis of patients with AKI from renal causes versus prerenal (circulatory) causes and was prognostic for in-hospital mortality.[112]

4.15.5.5 KIM-1

KIM-1 is a cell surface glycoprotein expressed on proximal tubular epithelial cells of the kidney and upregulated during injury. It is also known as T-cell immunoglobulin domain and mucin domain-1 or Hepatitis A virus cellular receptor 1 (HAVcr-1), and is expressed by innate and adaptive immune cells, including Th2 cells, activated B cells, B regulatory cells, dendritic cells, and invariant NKT cells.[113,114] The activity of this protein is highly cell and context-driven. In sum, the protein functions in antiinflammatory activities, scavenging, and self-tolerance.[114] KIM-1 is a receptor for phosphatidylserine (exposed on apoptotic cells), modified low density lipoprotein, and necrotic cell debris to impart the capacity of tubular epithelial cells to scavenge and remove apoptotic and necrotic debris in the lumen and participates in repair.[115]

KIM-1 has a cleavable ectodomain (90 kDa) that is shed into the tubular lumen by the action of metalloproteinases. KIM-1 is measured by immunoassay, however available reagents show limited species cross-reactivity.[116] There are reliable and accurate immunoassays for measuring KIM-1 in humans and rodents, which has allowed the evaluation and further investigation of KIM-1 biomarker in those species. Cross-reactivity and performance of KIM-1 assays for dogs and nonhuman primates have been questionable here-to-date, however new reagents and assays are in development and under validation by independent investigators.

In the rat, KIM-1 has repeatedly been shown to be an early and accurate marker of tubular injury in a variety of models, usually outperforming serum creatinine, and often outperforming other new biomarkers.[96,102,108,105,117–119] KIM-1 has good specificity for proximal tubule injury in the face of collecting duct necrosis and when there is nonkidney toxicity that is, liver.[117,119,105] KIM-1 also correlated with the histopathology severity grade in a rat model of cisplatin or paraquat nephrotoxicity[105,118,108] and showed excellent diagnostic performance across all severity grades (minimal to marked) of tubular injury using a variety of nephrotoxicants.[117] Further, KIM-1 IHC correlated to urinary biomarker levels in cisplatin nephrotoxicity in the rat.[79] KIM-1 reversed with injury resolution,[105,118] although with slow kinetics likely reflecting the activity of this protein in states of repair. In a monkey model of acute tubular injury due to polymyxin B, KIM-1 increased comparably to serum creatinine.[116]

KIM-1 is an early marker of clinical AKI, rising within 24 h of injury and moreover demonstrated good diagnostic performance in a variety of diseases in patients. KIM-1 was elevated in nondiabetic proteinuria and responded to therapy that improved proteinuria.[120] A study of AKI due to DIKI, contrast-nephropathy, and sepsis also showed a high diagnostic accuracy for KIM-1 in comparison to serum creatinine (AROC 0.9 l).[121] In patients with established acute renal failure, urine KIM-1 activity was associated with disease severity (according to standard clinical scoring systems) and had similar prognostic performance to serum creatinine.[122]

4.15.5.6 *N*-Acetyl-β-D-Glucosaminidase

NAG is a 140 kDa lysosomal enzyme that hydrolyzes glucosamine from oligosaccharides. NAG is largely located in the proximal tubule cells and is a leakage marker of epithelial injury.[123] It is a large protein and urine levels are believed to originate exclusively within the kidney. This marker has been noted as a marker of kidney disease for decades and more recently applied to nephrotoxicity.[124] NAG is also a marker of oxidative stress and increased levels have been shown to correlate to other markers of oxidation. There is a prominent sex difference in the dog for urinary NAG, due to contributions of NAG high in seminal fluid.[124]

NAG added value over a series of 17 rat studies using multiple nephrotoxicants.[117] NAG correlated to histopathological lesions in the proximal tubules in cisplatin rat model.[118] This marker has a lower appeal compared to other new urinary biomarkers in the rat owing to a lower fold change in addition to being less reliably increased in rat models of nephrotoxicity.[118,104,119,116] In contrast, NAG shows more value in dog and monkey DIKI. NAG has been evaluated in several models of proximal tubular toxicity in the dog and outperformed a standard renal panel.[124] It was significantly and closely correlated with measured GFR ($r = -0.82$) and showed an early increase that corresponded to lesion severity with a high AROC (0.948) that exceeded serum creatinine.[104,109,124] NAG has lower magnitude of change of NAG compared to other emerging biomarkers (e.g., urinary NGAL and clusterin) in the dog.[104] NAG performed usefully in monkey and dog models of acute tubular injury due to polymyxin B, increasing together with urine protein, and serum BUN.[116]

NAG activity in urine of patients with AKI has been shown by several groups to have prognostic utility for adverse outcomes. In patients with acute tubular necrosis, NAG could predict those who required renal replacement therapy however, the performance of cystatin-C was superior.[111] NAG also showed good performance with serum creatinine as the benchmark, in early detection of acute tubular necrosis in an intensive care unit setting.[125] Urine NAG activity was a prognostic marker for patients with AKI.[122] The specificity of urine NAG activity has been questioned with individual reports that NAG can be elevated in patients with rheumatoid arthritis, glucose intolerance, and hyperthyroidism in the absence of kidney injury.[126]

4.15.5.7 Neutrophil Gelatinase-Associated Lipocalin

NGAL, or lipocalin-2, is a protein covalently bound to gelatinases originally described in neutrophils, but also upregulated during disease in the parenchymal cells of many tissues including kidney, liver, and lung. Kidney NGAL is a 25 kDa monomer whereas neutrophils express the protein as a heterodimer. NGAL binds to siderophores (iron-containing complexes), and has multiple roles including controlling the exposure of the organism to iron, reducing oxidative stress, decreasing apoptosis, and participates in mesenchymal–epithelial transition during kidney development.[94] Epithelial cells upregulate NGAL in response to inflammation, infection, injury, or neoplasia[127] and are induced in the kidney during ischemia-reperfusion injury.[128] Serum NGAL is filtered freely

through the glomerulus and actively reabsorbed in the proximal tubule by megalin. Basal levels of NGAL in urine are thought to be released from epithelial cells of the thick ascending limb of the loop of Henle and the collecting duct.[129]

NGAL is significantly increased in rat models of glomerular injury caused by puromycin and tubular injury caused by cisplatin or gentamycin.[93,105,96] This biomarker showed reversal with recovery in rat nephrotoxicity models.[105] In a head–head study with new biomarkers, NGAL performed moderately well across many tubular toxicants (still improved upon the sensitivity of serum BUN and creatinine) but had issues with poorer specificity with muscle toxicants and endotoxemia related to LPS.[102] In contrast, this biomarker outperformed most of the emerging biomarkers with the exception of KIM-1 in rat studies proximal tubular injury caused by a number of polymyxin analogs.[116] In dog models of gentamycin toxicity, urine NGAL was an early and robust biomarker of toxicity, correlating with GFR and preceding microscopic evidence of toxicity.[104,109] The magnitude of NGAL increase corresponded with the severity grade assessed by histopathology.[130] NGAL performed equivalently to urine NAG and total protein and serum BUN in polymyxin B toxicity in the dog.[116]

A large metaanalysis of 58 studies in over 2000 patients at risk for AKI in the settings of critical care, postoperative cardiac surgery, and postkidney transplant revealed NGAL had good diagnostic accuracy (AUC of 0.79–0.87) and improved risk prediction for AKI compared to standard clinical models.[94] In similar clinical settings, increased urine NGAL in the absence of elevated serum creatinine detected patients with "subclinical AKI."[94] NGAL has also performed well as a diagnostic and predictive marker of DIKI for tacrolimus and contrast-induced nephropathy.[131,107]

4.15.5.8 Osteopontin

Osteopontin is a secreted glycoprotein. Osteopontin binds to integrins and CD44 family of cell–cell and cell–matrix receptors and has a variety of roles including cell adhesion, migration, cell signaling, and cell survival.[132] It is proinflammatory and protects against oxidation and ischemia.[133] Osteopontin is upregulated in the kidney during the processes of injury and repair in response to proinflammatory and profibrotic cytokines. Additionally, osteopontin is upregulated in response to parathyroid hormone (PTH), vitamin D_3, calcium, and phosphate.[132] Osteopontin is also involved in the pathogenesis of calcium-containing urine stone formation and an important organic component of the stone nucleus.[134]

The protein has wide expression in the body, predominately in the bone and epithelia, with lower levels in white blood cells, endothelium, and smooth muscle.[132] Osteopontin shows subtle species differences in the localization within the distal nephron. In the mouse kidney, it is primarily located in the thick ascending limbs of the loop of Henle and distal convoluted tubules, in rat, the descending thin limbs of the loop of Henle, and in human, the thick ascending limbs of the loop of Henle.[132] Osteopontin is readily measureable in the urine of healthy subjects.

Osteopontin correlated with the histopathologic grade of proximal tubular necrosis in a rat cisplatin model and reversed with injury resolution.[118] In this model tissue IHC of osteopontin expression also correlated closely with urinary biomarker measurements.[79] Other nephrotoxicity models have also demonstrated that osteopontin is a sensitive marker and can outperform traditional serum BUN and creatinine.[105,77] Moreover, urine osteopontin levels decreased with recovery in rat gentamycin and carbapenem A-models.[105] Osteopontin improved upon the sensitivity of serum BUN and creatinine for detecting nephrotoxicity over a number of different tubular toxicities, although compared to other new biomarkers, it was inferior to urine KIM-1 and clusterin and showed nonspecific rises in models of muscle toxicity and LPS-induced endotoxemia.[102] In monkey nephrotoxicity models using the tubular toxicants, gentamycin and everninomicin, osteopontin expression by quantitative PCR was increased in kidney tissue.[106]

Urine osteopontin is increased in various human kidney diseases including progressive idiopathic membranous nephropathy, cresentric glomerulonephritis, IgA nephritis, and diffuse proliferative lupus nephritis.[132] Little investigation has been done in DIKI. Osteopontin protein and RNA expression was upregulated in proximal tubules in biopsy samples of renal allografts prior to transplantation following cold ischemia and in patients with cyclosporine toxicity.[135] Osteopontin was not a good biomarker for tacrolimus-related nephrotoxicity.[107]

4.15.6 Blood Cytokines as Safety Biomarkers

4.15.6.1 Biology

Cytokines are small proteins produced by a variety of immune and nonimmune cells and act as messengers between cells. They are essential coordinators of inflammatory and immune responses. Cytokines also act as hematopoietic regulators and have roles in nervous, endocrine, and reproductive system function. These molecules generally have induced production, are short-lived, and act locally to deliver an effect. Cytokine profiles vary over time in response to an inflammatory event, displaying a cascade of cytokine synthesis and release. The cascade originates with production of proinflammatory cytokines TNFα and IL-1β, which then elicit downstream generation of other proinflammatory cytokines (e.g., IFN-γ and IL-6), chemokines, followed by the antiinflammatory cytokines, IL-1Ra and IL-10. The outcome of cytokine activity is contingent on the cell context and environment and reflects diverse receptor expression in different tissues and the potential for pleiotropic activity of cytokines that is, the same cytokine may have different actions depending on receptor and cell type.

4.15.6.2 Cytokine Biomarkers

The advent of multiplex assays for cytokine panels with improved sensitivity has fostered interest in the exploration of blood (serum or plasma) cytokines as general biomarkers for toxicity. Cytokines may provide a discriminating toxicity signal when sampled at time points proximal to the inflammatory event. In the context of monitoring specific organ toxicity that is, detection of lung toxicity that has an inflammatory mechanism, there are several caveats when considering the suitability of cytokines. Cytokines are general inflammatory biomarkers therefore are not specific for site/organ of toxicity, an important challenge for a translatable biomarker when used in a patient population with preexisting disease and multiple comorbidities, some of which may have an inflammatory basis. Circulating levels of biomarkers imply a systemic "spill-over" of cytokines that has overcome the local mechanisms for restricting cytokine diffusion such as proteases to release membrane-bound cytokines, competition with cell-associated receptors, binding by soluble inhibitors and receptors.[136] Local cytokine aberrations associated with organ toxicity may therefore not reach the magnitude or circumstances that permit measurable concentration in the circulation. Importantly, assays need to be sensitive enough to detect elevations that, using traditional cytokine assays (with high pg/mL lower limits of quantification), have a low to negligible baseline. New technologies are exploring the sub-pg/mL concentrations that may be necessary for blood cytokine levels to achieve acceptable diagnostic performance.*

It has been the emergence of immunotherapy, the reactivation of the immune system against cancer, which has bolstered the rationale for exploring systemic cytokine levels as biomarkers for safety assessment. In this case, cytokines may be used to demonstrate a pharmacodynamic effect of therapy-related immunostimulation and also to diagnose adverse immune events.[136] Given that many new molecules are still under development with few drugs licensed for use by health authorities, published biomarker data is also just emerging. Serious adverse systemic immune toxicities (i.e., potentially fatal) have been observed in patients administered both small molecule drugs and biotherapeutics. The exact pathogenesis is not often fully elucidated. Differences in severity may be in part related to the therapeutic agent, dose, duration, and patient factors including target density/distribution, concomitant medications, comorbidities and therefore difficult to predict a priori. Immune toxicities associated with cytokine biomarkers include: CRS, systemic inflammatory response syndrome (SIRS), macrophage activation syndrome (MAS, also referred to as hemophagocytic syndrome, secondary hematophagocytic lymphohistiocytosis), and vascular leak syndrome. A brief description of these toxicities follows, with diagnostic criteria provided in **Table 8**. For several of these conditions, notably, CRS and vascular leak, there is the diagnosis that is not harmonized and there exists an opportunity for evaluating new biomarkers for prognosis and safety monitoring. Cytokines that are currently recognized in association with these immune toxicities are listed in **Table 9**. CRS is the consequence of widespread immune cell stimulation and unregulated systemic release of cytokines. The syndrome can range from mild and transient to life-threatening. The major clinical symptoms include nausea, headache, tachycardia, hypotension, rash, and dyspnoea. It has been noted that agents targeting T or B lymphocytes, and NK cells, include superagonist anti-CD28 mAbs, alemtuzumab (anti-CD52), rituximab (anti-CD20) and muromonab-CD3 (OKT3), and CAR-T cells. SIRS is a state of uncontrolled systemic inflammation that affects multiple organs and may be the outcome of CRS. Ultimately SIRS can progress to multiple organ dysfunction, organ failure, and death.[137] Noninfectious SIRS related to drug administration is very uncommon, and less frequent than sepsis-related SIRS. MAS is characterized by excessive T-cell activation leading to dsyregulation of macrophage function, hemophagocytosis, cytopenias, hepatitis, and neurological symptoms. Vascular (or capillary) leak syndrome is caused by increased permeability of capillaries leading to movement of plasma out of the circulation. Clinicopathologic changes include edema of the face, trunk and extremities, hypotension, hemoconcentration, oliguria. The condition may progress to localized ischemia, renal failure, stroke, deep vein thrombosis, and cardio-pulmonary failure. This is a major dose-limiting toxicity associated with IL2 immunotherapy. It can be appreciated that overlap exists between the various symptoms related to adverse immunostimulation. Interestingly, one group claims that the cytokine profile of CRS associated with T-cell engaging therapies (i.e., chimeric antigen receptor-modified T-cells and bispecific antibodies) is interchangeable with MAS, also sharing common laboratory abnormalities (i.e., hyperferritinemia and hypofibrinogenemia).[138] The excessive IFN-γ produced by T-cell activation is hypothesized to result in pathological activation of the monocyte-macrophage system and MAS. The use of cytokine biomarkers for prediction and diagnosis is thus far not well studied.

Table 8 Select immunotoxicities associated with adverse drug-related immunostimulation

Immunotoxicity	*Diagnosis*
Cytokine release syndrome	Clinical symptoms including nausea, headache, tachycardia, hypotension, rash, and dyspnea. Severe events may have hypoxia and neurological symptoms (e.g., change in mental status, seizures). May have elevations of one or more of IL-2, IL-6, IFN-γ, TNF-α
Macrophage activation syndrome	Diagnosed with at least 5 of fever ($\geq$38.5°C), splenomegaly, cytopenia (2 or more lineages), hypertriglyceridemia and/or hypofibrinogenemia, hyperferritinemia, increased soluble CD25 (IL-2Ra), hemophagocytosis in bone marrow/spleen/lymph nodes, low NK cell activity
Systemic inflammatory response syndrome	Diagnosed with at least 2 of temperature change, ($<$36°C or $>$38°C), tachycardia ($>$90 bpm), tachypnea ($>$20 bpm), and leukocyte abnormality ($<$4.000, $>$12.000 mm^3)
Vascular leak syndrome	Clinical symptoms including edema of face, trunk and extremities, hypotension, hemoconcentration, oliguria, may progress to localized ischemia, renal failure, stroke, deep vein thrombosis, and cardio-pulmonary failure

Table 9 Cytokine biomarkers of drug-related adverse immunostimulation

Category	*Toxicity/response*	*Implicated circulating cytokines*	*Other key circulating biomarkers*
Toxicity	CRS	IL-2, IL-6, IFN-γ, TNF-α	
	Macrophage activation syndrome (also hemophagocytic syndrome, hemophagocytic lymphohistiocytosis)	IL-6, IL-10, IFN-γ, sIL2Ra	Ferritin
	Systemic inflammatory response syndrome	IL-1β, IL-6, IL-8, (IL-17), MCP-1, TNF-α	
	Vascular leak (capillary leak)	IL-2, IL-3, IL-6, CXCL8, G-CSF, GM-CSF, IFN-α, IFN-β, TNFα	
Mechanistic immune response	Acute phase response	IL-1β, IL-6, TNF-α	CRP, fibrinogen, α1-acid glycoprotein 1, α2-macroglobulin
	Innate immune response	IL-1β, IL-6, IL-8, MIP1a, MIP1b, MCPC-1, TNF-α	CRP
	Th1 response	IL-1, IL-2, IL-12, IFN-γ	
	Th2 response	IL-4, IL-5, IL-10, IL-13	

Cytokines are potentially translatable biomarkers; however there may be differences in the pattern of response (i.e., magnitude, cytokine type) observed in preclinical studies in animals compared to patients. There could be several factors underpinning differences between preclinical and clinical studies, most fundamentally species differences in biology and pharmacologic target expression, altered immune contexture in patients that have preexisting disease, altered populations of leukocyte subsets, and high baseline levels of cytokines that modify the cytokine profile.[136,139,140] Additionally, the cytokine response observed in young, healthy animals is not representative of patients with various diseases. Differences in assay performance such as specificity for the biomarker, sensitivity, and study-related factors including time points of assessment are also important factors that contribute to species disparities. Consequently, in vivo cytokine profiling in preclinical toxicity studies may in some cases (drug, therapeutic indications, intended patient populations, etc.) be more akin to hazard identification for toxicity, as proposed by professional groups for use and interpretation of in vitro cytokine release assays.[141] Despite these concerns, cytokines are potentially translatable biomarkers and fundamental in profiling the immune response, therefore investigation and ultimately, application, of these biomarkers for immunotoxicity assessment is warranted. It should be noted that measurement of blood cytokines is not covered by current regulatory guidances for general toxicity or immunotoxicity assessment in drug development, however the current ICH S8 Immunotoxicity Guidance predates the severe adverse CRS that occurred in the TGN1412 clinical trial in 2006.[142] Notably, CRS is included in the National Cancer Institute Common Terminology Criteria for Adverse Events (CTCAEs) Version 4.0 and routinely applied to clinical trials for cancer.[143]

4.15.7 Bis(monoacylglycero)phosphate (BMP) a New Biomarker of Drug-induced Phospholipidosis

4.15.7.1 Phospholipidosis

Drug-induced phospholipidosis is a toxicity characterized by an accumulation of intracellular phospholipids and drug within the lysosomes of cells. Microscopically, this appears as abnormal vacuolation within the cytoplasm of cells, often as so-called "foamy macrophages." The key ultrastructural finding is lamellar bodies within lysosomes. Phospholipidosis can be localized or generalized. The localized form affects parenchymal cells of specific tissues, notably the bile duct or kidney, likely due to higher exposure of the drug in those tissues.[144] The generalized form may be macrophage-associated with a primary effect on tissue resident macrophages (e.g., lung, liver, spleen, bone marrow, thymus) or alternatively, parenchymal-associated with effects on cells of the kidney tubules, bile ducts, liver, vascular endothelium, neurons of the CNS, and PNS. The key physicochemical characteristic of drugs that cause phospholipidosis is the presence of a cationic amphiphilic toxicophore comprising a basic amine side chain attached to a hydrophobic moiety. This toxicophore binds phospholipids and traps the drug within the acidic environment of the lysosome. The mechanism of phospholipid accumulation in the cell is often not well understood and can differ between compounds. Potential mechanisms include increased synthesis of phospholipids, dysfunction of lysosomal enzymes and membrane recycling, and altered endosomal trafficking. Drug-induced phospholipidosis is associated with multiple marketed drugs across many therapeutic classes. Classic examples include amiodarone, chloroquine, chlorpromazine, and gentamycin.[145]

Phospholipidosis occurs in animals and in humans, however in silico and in vitro systems do not necessarily predict toxicity in animals, which in turn do not always predict tissue pathology and toxicity in humans.[145,146] There is debate as to whether phospholipidosis is deleterious to cell function.[145] These potential associations, in addition to pathology findings that resemble inherited lysosomal storage disease, garner regulatory concern of the drug's safety. Phospholipidosis can therefore cause delay or attrition during drug development.

4.15.7.2 Bis(monoacylglycero)phosphate

Bis(monoacylglycero)phosphate is one of a family of phosphatidylglycerol-derived phospholipids that are located on the inner membrane of late endosomes and lysosomes and widely expressed in many tissues. BMP comprises less than 1% of total body phospholipids with the exception of the lung, which has higher concentrations as a product of the physiologic production of surfactant phospholipids that are crucial in alveolar function.[147] BMPs are involved in vesicle biogenesis within the late endosome, forming the multivesicular body structure (Fig. 5). Functional roles of BMP in the endolysosomal system include transport of lysosomal enzymes, recycling of membrane lipids, and intracellular cholesterol trafficking.[146,148] BMP is released from the intracellular environment into the circulation by exosomes.

Tissue levels of BMP were specifically enriched in the tissues of patients affected by inherited and drug-related phospholipidosis in the 1970s. Since that precedent, di-docosahexaenoyl (22:6) BMP (di-22:6-BMP) has been identified as the molecular species with highest induction in drug-induced phospholipidosis.[149] Similarly, this species is also highest in Nieman-Pick disease, the most analogous inherited lysosomal storage disorder to the toxic condition.[146]

BMP has been evaluated as a candidate biomarker for monitoring phospholipidosis in animals and humans. The biomarker is measured by mass spectrometry. BMP concentrations are approximately twofold higher in serum than plasma in healthy humans, with no reported sex differences, whereas males had slightly higher urine BMP (adjusted to urine creatinine) compared to females. Although reference intervals have not been published, species differences in BMP are apparent with serum levels in rodents higher than human, dog, and nonhuman primates. Rodent urine BMP concentration is an order of magnitude higher than other species. In rodent toxicity studies across many phospholipidosis-inducing agents (chloroquine, amiodarone, 4,4′-diethylaminoethoxyhexestrol dihydrochloride, gentamicin, azithromycin) di-22:6-BMP was demonstrated to monitor the onset, duration, and reversal of PL.[150,151,146,149] Urine di-22:6-BMP has been shown in several studies to have better diagnostic performance than serum, with the benefit of improved specificity in the context of concomitant (nonphospholipidosis) toxicity in the same target organ.[152,153] Urine di-22:6-BMP retained good diagnostic performance in the presence of nonphospholipidosis-related kidney toxicity.[130] Di-22:6-BMP has not been specifically evaluated in patients with drug-induced phospholipidosis, however it had high diagnostic accuracy (97% sensitivity and 100% specificity) for Nieman-pick disease.[146]

The role of di-22:6-BMP as a biomarker of lysoendosomal disorders has also been explored in genetic and pharmacologic models of leucine-rich repeat kinase 2 (LRRK2) depletion.[154] LRRK2 plays a role in endolysosomal trafficking and is a therapeutic target of intense interest for treatment of Parkinson's disease. However, a potential safety liability of reducing LRRK2 activity is the accumulation of lamellar bodies in type II pneumocytes of the lung, phenotypically resembling phospholipidosis. The mechanism of this cellular vacuolation is not clear and occurs in both knockout mice, and monkeys treated with several structurally variant inhibitors of

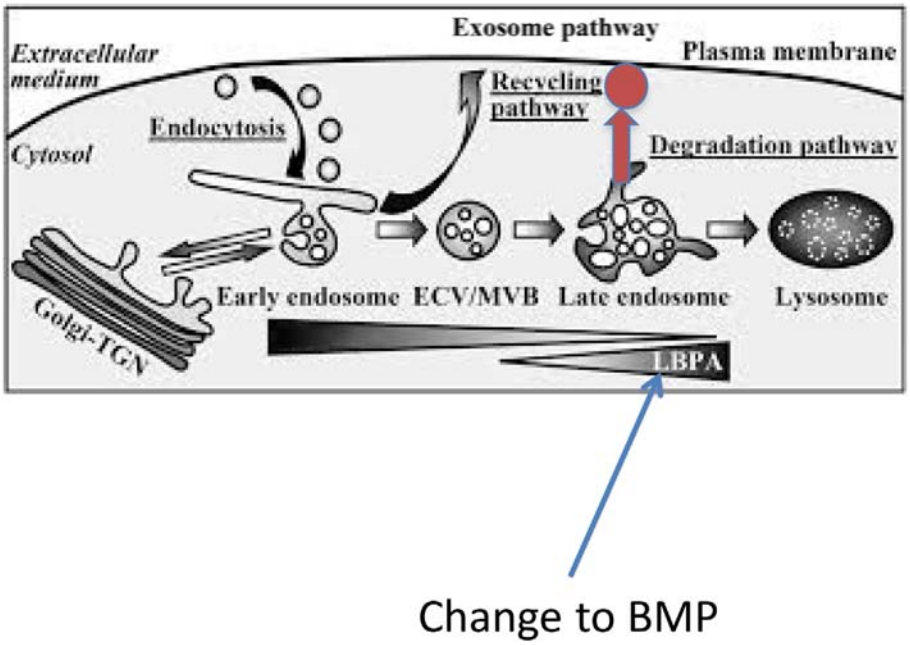

Fig. 5 Endosomal trafficking in the cell. Endosomal and exosomal movement facilitate the interchange of membrane proteins, receptors, macromolecules, and lysosomal enzymes. Early endosomes fuse to mature into larger endosomes. Mature endosomes undergo invagination of the outer membrane to form internal vesicles and form a multivesicular body or endosome. The phospholipid BMP is involved in the vesiculation process and is at high levels in these structures. Late endosomes can fuse with lysosomes or traffic to the cell membrane to be released as exosomes. Falguières, T.1; Luyet, P. P.; Gruenberg, J. Molecular assemblies and membrane domains in multivesicular endosome dynamics. *Exp Cell Res.* **2009**, *315*(9), 1567–1573.

LRRK2 kinase. Intriguingly, lamellar body accumulation in this model was related to clear decreases in urine di-22:6-BMP, indicating a more broad utility in monitoring aberrant endolysosomal trafficking.[154]

BMP shows great potential for monitoring of drug-induced phospholipidosis, however it is not specific for the tissue distribution. It is undetermined whether BMP is related to the severity of toxicity. This is an important marker in building the safety profile, and eventually a tool in population-based epidemiological studies to assist in determining the safety of drugs that induce phospholipidosis. The majority of current evidence for the diagnostic accuracy of di-22:6-BMP is derived from one laboratory-derived test. It is essential for this testing to become more widely available to allow further analytical validation and technical characterization in addition to greater data generation ensuing from improved accessibility. Only then can the potential of this promising biomarker be fully realized.

4.15.8 Future Prospects

These are still early days for the use of new safety biomarkers in regulated drug development. The value proposition of new safety biomarkers is to improve risk-benefit assessment at all stages of development. By employing new safety biomarkers where there are gaps in standard monitoring tools, drug developers are ensuring the safe conduct of clinical trials and permitting evaluation of innovative new therapies that may have previously been discontinued by unknown clinical translatability of preclinical toxicities and/or dose-escalation capped by perceived safety risk.

The exploratory use of emerging safety biomarkers is a break in the convention for safety assessment from reliance only on endpoints with a large historical database. There is still uncertainty in using emerging safety biomarkers, despite regulatory qualification and rigorous evaluation. To create a historic database and complete understanding of a new biomarker is a herculean task that has previously been undertaken by the entire medical community in the case of new clinical diagnostics for spontaneous disease. It is therefore unrealistic to believe this is also not required for safety biomarkers: it is incumbent on drug developers, regulators, and the medical community to generate this data by using the biomarkers across a broad range of scenarios. The "risk" of using emerging safety biomarkers is often defrayed by the concurrent use of routine tests or more sophisticated ancillary testing that are interpreted together to assess the presence or absence of toxicity. A necessary step in community-based qualification of new safety biomarkers is the ability to pool or aggregate data generated by drug developers to allow faster, more efficient, more nuanced, and ultimately more accurate evaluation of the utility and performance of safety biomarkers for improving risk assessment and drug development.

References

1. Cook, D.; Brown, D.; Alexander, R.; March, R.; Morgan, P.; Satterthwaite, G.; Pangalos, M. N. Lessons Learned From the Fate of AstraZeneca's Drug Pipeline: A Five-Dimensional Framework. *Nat. Rev. Drug Discov.* **2014,** *13* (6), 419–431.
2. Hay, M.; Thomas, D. W.; Craighead, J. L.; Economides, C.; Rosenthal, J. Clinical Development Success Rates for Investigational Drugs. *Nat. Biotechnol.* **2014,** *32* (1), 40–51.
3. Dennis, E. H.; Walker, E. G.; Baker, A. F.; Miller, R. T. Opportunities and Challenges of Safety Biomarker Qualification: Perspectives From the Predictive Safety Testing Consortium. *Drug Dev. Res.* **2013,** *74,* 112–126.
4. (a) Lagos-Quintana, M.; Rauhut, R.; Yalcin, A.; Meyer, J.; Lendeckel, W.; Tuschl, T. Identification of Tissue-Specific microRNAs From Mouse. *Curr. Biol.* **2002,** *12* (9), 735–739; (b) Laterza, O. F.; Lim, L.; Garrett-Engele, P. W.; Vlasakova, K.; Muniappa, N.; Tanaka, W. K.; Johnson, J. M.; Sina, J. F.; Fare, T. L.; Sistare, F. D.; Glaab, W. E. Plasma MicroRNAs as Sensitive and Specific Biomarkers of Tissue Injury. *Clin. Chem.* **2009,** *55* (11), 1977–1983.
5. Moldovan, L.; Batte, K. E.; Trgovcich, J.; Wisler, J.; Marsh, C. B.; Piper, M. Methodological Challenges in Utilizing miRNAs as Circulating Biomarkers. *J. Cell. Mol. Med.* **2014,** *18* (3), 371–390.
6. Sistare, F. D.; Dieterle, F.; Troth, S.; Holder, D. J.; Gerhold, D.; Andrews-Cleavenger, D.; Baer, W.; Betton, G.; Bounous, D.; Carl, K.; Collins, N.; Goering, P.; Goodsaid, F.; Gu, Y. Z.; Guilpin, V.; Harpur, E.; Hassan, A.; Jacobson-Kram, D.; Kasper, P.; Laurie, D.; Lima, B. S.; Maciulaitis, R.; Mattes, W.; Maurer, G.; Obert, L. A.; Ozer, J.; Papaluca-Amati, M.; Phillips, J. A.; Pinches, M.; Schipper, M. J.; Thompson, K. L.; Vamvakas, S.; Vidal, J. M.; Vonderscher, J.; Walker, E.; Webb, C.; Yu, Y. Towards Consensus Practices to Qualify Safety Biomarkers for Use in Early Drug Development. *Nat. Biotechnol.* **2010,** *28* (5), 446–454.
7. FDA Statistical Guidance on Reporting Results From Studies Evaluating Diagnostic Tests. http://www.fda.gov/RegulatoryInformation/Guidances/ucm071148.htm (accessed 01.09.15).
8. Parikh, C. R.; Thiessen-Philbrook, H. Key Concepts and Limitations of Statistical Methods for Evaluating Biomarkers of Kidney Disease. *J. Am. Soc. Nephrol.* **2014,** *25* (8), 1621–1629.
9. Tarrant, J. M.; Lewin-Koh, S. C.; Lewin-Koh, N. Development of a Safety Biomarker Signature to Detect Hepatic Sinusoidal Dilation Associated With an Anti-DLL4 Biotherapeutic. *Biomarkers* **2014,** *19* (5), 391–401.
10. Pencina, M. J.; D'Agostino, R. B.; Pencina, K. M.; Janssens, A. C.; Greenland, P. Interpreting Incremental Value of Markers Added to Risk Prediction Models. *Am. J. Epidemiol.* **2012,** *176* (6), 473–481.
11. Brott, D. A.; Adler, S. H.; Arani, R.; Lovick, S. C.; Pinches, M.; Furlong, S. T. Characterization of Renal Biomarkers for use in Clinical Trials: Biomarker Evaluation in Healthy Volunteers. *Drug Des. Dev. Ther.* **2014,** *8,* 227–237.
12. Pinches, M. D.; Betts, C. J.; Bickerton, S. J.; Beattie, L.; Burdett, L. D.; Thomas, H. T.; Derbyshire, N. A.; Moores, M.; Price, S. A. Evaluation of Novel Urinary Renal Biomarkers: Biological Variation and Reference Change Values. *Toxicol. Pathol.* **2012,** *40* (3), 541–549.
13. Gautier, J. C.; Gury, T.; Guffroy, M.; Khan-Malek, R.; Hoffman, D.; Pettit, S.; Harpur, E. Normal Ranges and Variability of Novel Urinary Renal Biomarkers in Sprague-Dawley Rats: Comparison of Constitutive Values Between Males and Females and Across Assay Platforms. *Toxicol. Pathol.* **2014,** *42* (7), 1092–1104.
14. Lee, J. W.; Devanarayan, V.; Barrett, Y. C.; Weiner, R.; Allinson, J.; Fountain, S.; Keller, S.; Weinryb, I.; Green, M.; Duan, L.; Rogers, J. A.; Millham, R.; O'Brien, P. J.; Sailstad, J.; Khan, M.; Ray, C.; Wagner, J. A. Fit-for-Purpose Method Development and Validation for Successful Biomarker Measurement. *Pharm. Res.* **2006,** *23* (2), 312–328.
15. Lee, J. W. Method Validation and Application of Protein Biomarkers: Basic Similarities and Differences From Biotherapeutics. *Bioanalysis* **2009,** *1* (8), 1461–1474.

16. Valentin, M. A.; Ma, S.; Zhao, A.; Legay, F.; Avrameas, A. Validation of Immunoassay for Protein Biomarkers: Bioanalytical Study Plan Implementation to Support Pre-Clinical and Clinical Studies. *J. Pharm. Biomed. Anal.* **2011,** *55* (5), 869–877.
17. ICH Harmonised Tripartite Guideline Q2(R1), Validation of Analytical Procedures: Text and Methodology, 2005.
18. E. M. A. (EMA), Guidance for Industry Bioanalytical Method Validation, 2011.
19. F. a. D. A. (FDA), Guidance for Industry: Bioanalytical Method Validation. http://www.fda.gov/downloads/drugs/guidancecomplianceregulatoryinformation/guidances/ucm368107.pdf.
20. Khan, M. U.; Bowsher, R. R.; Cameron, M.; Devanarayan, V.; Keller, S.; King, L.; Lee, J.; Morimoto, A.; Rhyne, P.; Stephen, L.; Wu, Y.; Wyant, T.; Lachno, D. R. Recommendations for Adaptation and Validation of Commercial Kits for Biomarker Quantification in Drug Development. *Bioanalysis* **2015,** *7* (2), 229–242.
21. Amur, S.; LaVange, L.; Zineh, I.; Buckman-Garner, S.; Woodcock, J. Biomarker Qualification: Toward a Multiple Stakeholder Framework for Biomarker Development, Regulatory Acceptance, and Utilization. *Clin. Pharmacol. Ther.* **2015,** *98* (1), 34–46.
22. Amar, P. J.; Schiff, E. R. Acetaminophen Safety and Hepatotoxicity—Where do we go From Here? *Expert Opin. Drug Saf.* **2007,** *6* (4), 341–355.
23. Reuben, A.; Koch, D. G.; Lee, W. M.; Acute Liver Failure Study Group. Drug-Induced Acute Liver Failure: Results of a U.S. Multicenter, Prospective Study. *Hepatology* **2010,** *52* (6), 2065–2076.
24. Lee, W. M. Drug-Induced Acute Liver Failure. *Clin. Liver Dis.* **2013,** *17* (4), 575–586.
25. Woreta, T. A.; Alqahtani, S. A. Evaluation of Abnormal Liver Tests. *Med. Clin. North Am.* **2014,** *98* (1), 1–16.
26. Schomaker, S.; Warner, R.; Bock, J.; Johnson, K.; Potter, D.; Van Winkle, J.; Aubrecht, J. Assessment of Emerging Biomarkers of Liver Injury in Human Subjects. *Toxicol. Sci.* **2013,** *132* (2), 276–283.
27. Bailey, W. J.; Holder, D.; Patel, H.; Devlin, P.; Gonzalez, R. J.; Hamilton, V.; Muniappa, N.; Hamlin, D. M.; Thomas, C. E.; Sistare, F. D.; Glaab, W. E. A Performance Evaluation of Three Drug-Induced Liver Injury Biomarkers in the Rat: Alpha-Glutathione S-Transferase, Arginase 1, and 4-Hydroxyphenyl-Pyruvate Dioxygenase. *Toxicol. Sci.* **2012,** *130* (2), 229–244.
28. Hochstedler, C. M.; Leidinger, M. R.; Maher-Sturm, M. T.; Gibson-Corley, K. N.; Meyerholz, D. K. Immunohistochemical Detection of Arginase-I Expression in Formalin-Fixed Lung and Other Tissues. *J. Histotechnol.* **2013,** *36* (4), 128–134.
29. Spector, E. B.; Rice, S. C.; Kern, R. M.; Hendrickson, R.; Cederbaum, S. D. Comparison of Arginase Activity in Red Blood Cells of Lower Mammals, Primates, and Man: Evolution to High Activity in Primates. *Am. J. Hum. Genet.* **1985,** *37* (6), 1138–1145.
30. Majaw, T.; Sharma, R. Arginase I Expression is Upregulated by Dietary Restriction in the Liver of Mice as a Function of Age. *Mol. Cell. Biochem.* **2015,** *407* (1–2), 1–7.
31. Murayama, H.; Ikemoto, M.; Fukuda, Y.; Nagata, A. Superiority of Serum Type-I Arginase and Ornithine Carbamyltransferase in the Detection of Toxicant-Induced Acute Hepatic Injury in Rats. *Clin. Chim. Acta* **2008,** *391* (1–2), 31–35.
32. Saitoh, W.; Yamauchi, S.; Watanabe, K.; Takasaki, W.; Mori, K. Metabolomic Analysis of Arginine Metabolism in Acute Hepatic Injury in Rats. *J. Toxicol. Sci.* **2014,** *39* (1), 41–50.
33. Mulder, T. P.; Court, D. A.; Peters, W. H. Variability of Glutathione S-Transferase Alpha in Human Liver and Plasma. *Clin. Chem.* **1999,** *45* (3), 355–359.
34. Sherratt, P. J.; Hayes, J. D. Glutathione S-Transferases. In *Enzyme Systems That Metabolise Drugs and Other Xenobiotics;* Ioannides, C., Ed.; John Wiley & Sons: Chichester, 2001; pp 319–352.
35. Giffen, P. S.; Pick, C. R.; Price, M. A.; Williams, A.; York, M. J. Alpha-Glutathione-S-Transferase in the Assessment of Hepatotoxicity—Its Diagnostic Utility in Comparison With Other Recognized Markers in the Wistar Han Rat. *Toxicol. Pathol.* **2002,** *30* (3), 365–372.
36. Coles, B. F.; Morel, F.; Rauch, C.; Huber, W. W.; Yang, M.; Teitel, C. H.; Green, B.; Lang, N. P.; Kadlubar, F. F. Effect of Polymorphism in the Human Glutathione S-Transferase A1 Promoter on Hepatic GSTA1 and GSTA2 Expression. *Pharmacogenetics* **2001,** *11* (8), 663–669.
37. Mulder, T. P.; Peters, W. H.; Court, D. A.; Jansen, J. B. Sandwich ELISA for Glutathione S-Transferase Alpha 1-1: Plasma Concentrations in Controls and in Patients With Gastrointestinal Disorders. *Clin. Chem.* **1996,** *42* (3), 416–419.
38. Staffas, L.; Ellis, E. M.; Hayes, J. D.; Lundgren, B.; Depierre, J. W.; Mankowitz, L. Growth Hormone- and Testosterone-Dependent Regulation of Glutathione Transferase Subunit A5 in Rat Liver. *Biochem. J.* **1998,** *332* (Pt 3), 763–768.
39. Cho, M. K.; Kim, S. G. Induction of Class Alpha Glutathione S-Transferases by 4-Methylthiazole in the Rat Liver: Role of Oxidative Stress. *Toxicol. Lett.* **2000,** *115* (2), 107–115.
40. Lampe, J. W.; Chen, C.; Li, S.; Prunty, J.; Grate, M. T.; Meehan, D. E.; Barale, K. V.; Dightman, D. A.; Feng, Z.; Potter, J. D. Modulation of Human Glutathione S-Transferases by Botanically Defined Vegetable Diets. *Cancer Epidemiol. Biomarkers Prev.* **2000,** *9* (8), 787–793.
41. Clarke, H.; Egan, D. A.; Heffernan, M.; Doyle, S.; Byrne, C.; Kilty, C.; Ryan, M. P. Alpha-Glutathione-S-Transferase (Alpha-GST) Release, an Early Indicator of Carbon Tetrachloride Hepatotoxicity in the Rat. *Hum. Exp. Toxicol.* **1997,** *16* (3), 154–157.
42. Starckx, S.; Batheja, A.; Verheyen, G. R.; Jonghe, S. D.; Steemans, K.; Dijck, B. V.; Singer, M.; Bogdan, N.; Snoeys, J.; Vinken, P.; Sasaki, J. C.; Gompel, J. V.; Guzzie-Peck, P.; Lampo, A.; Lammens, L. Evaluation of miR-122 and Other Biomarkers in Distinct Acute Liver Injury in Rats. *Toxicol. Pathol.* **2013,** *41* (5), 795–804.
43. Beckett, G. J.; Dyson, E. H.; Chapman, B. J.; Templeton, A. J.; Hayes, J. D. Plasma Glutathione S-Transferase Measurements by Radioimmunoassay: A Sensitive Index of Hepatocellular Damage in Man. *Clin. Chim. Acta* **1985,** *146* (1), 11–19.
44. Mikstacki, A.; Zakerska-Banaszak, O.; Skrzypczak-Zielinska, M.; Tamowicz, B.; Szalata, M.; Slomski, R. Glutathione S-Transferase as a Toxicity Indicator in General Anesthesia: Genetics and Biochemical Function. *J. Clin. Anesth.* **2015,** *27* (1), 73–79.
45. Chalasani, N.; Younossi, Z.; Lavine, J. E.; Diehl, A. M.; Brunt, E. M.; Cusi, K.; Charlton, M.; Sanyal, A. J. The Diagnosis and Management of non-Alcoholic Fatty Liver Disease: Practice Guideline by the American Association for the Study of Liver Diseases, American College of Gastroenterology, and the American Gastroenterological Association. *Hepatology* **2012,** *55* (6), 2005–2023.
46. Antoine, D. J.; Williams, D. P.; Kipar, A.; Jenkins, R. E.; Regan, S. L.; Sathish, J. G.; Kitteringham, N. R.; Park, B. K. High-Mobility Group box-1 Protein and Keratin-18, Circulating Serum Proteins Informative of Acetaminophen-Induced Necrosis and Apoptosis In Vivo. *Toxicol. Sci.* **2009,** *112* (2), 521–531.
47. Antoine, D. J.; Jenkins, R. E.; Dear, J. W.; Williams, D. P.; McGill, M. R.; Sharpe, M. R.; Craig, D. G.; Simpson, K. J.; Jaeschke, H.; Park, B. K. Molecular Forms of HMGB1 and Keratin-18 as Mechanistic Biomarkers for Mode of Cell Death and Prognosis During Clinical Acetaminophen Hepatotoxicity. *J. Hepatol.* **2012,** *56* (5), 1070–1079.
48. Antoine, D. J.; Dear, J. W.; Lewis, P. S.; Platt, V.; Coyle, J.; Masson, M.; Thanacoody, R. H.; Gray, A. J.; Webb, D. J.; Moggs, J. G.; Bateman, D. N.; Goldring, C. E.; Park, B. K. Mechanistic Biomarkers Provide Early and Sensitive Detection of Acetaminophen-Induced Acute Liver Injury at First Presentation to Hospital. *Hepatology* **2013,** *58* (2), 777–787.
49. Thulin, P.; Nordahl, G.; Gry, M.; Yimer, G.; Aklillu, E.; Makonnen, E.; Aderaye, G.; Lindquist, L.; Mattsson, C. M.; Ekblom, B.; Antoine, D. J.; Park, B. K.; Linder, S.; Harrill, A. H.; Watkins, P. B.; Glinghammar, B.; Schuppe-Koistinen, I. Keratin-18 and microRNA-122 Complement Alanine Aminotransferase as Novel Safety Biomarkers for Drug-Induced Liver Injury in Two Human Cohorts. *Liver Int.* **2014,** *34* (3), 367–378.
50. Singhal, R.; Harrill, A. H.; Menguy-Vacheron, F.; Jayyosi, Z.; Benzerdjeb, H.; Watkins, P. B. Benign Elevations in Serum Aminotransferases and Biomarkers of Hepatotoxicity in Healthy Volunteers Treated With Cholestyramine. *BMC Pharmacol. Toxicol.* **2014,** *15,* 42.
51. Volkmann, X.; Anstaett, M.; Hadem, J.; Stiefel, P.; Bahr, M. J.; Lehner, F.; Manns, M. P.; Schulze-Osthoff, K.; Bantel, H. Caspase Activation is Associated With Spontaneous Recovery From Acute Liver Failure. *Hepatology* **2008,** *47* (5), 1624–1633.
52. Bechmann, L. P.; Jochum, C.; Kocabayoglu, P.; Sowa, J. P.; Kassalik, M.; Gieseler, R. K.; Saner, F.; Paul, A.; Trautwein, C.; Gerken, G.; Canbay, A. Cytokeratin 18-Based Modification of the MELD Score Improves Prediction of Spontaneous Survival After Acute Liver Injury. *J. Hepatol.* **2010,** *53* (4), 639–647.
53. Mastorodemos, V.; Kotzamani, D.; Zaganas, I.; Arianoglou, G.; Latsoudis, H.; Plaitakis, A. Human GLUD1 and GLUD2 Glutamate Dehydrogenase Localize to Mitochondria and Endoplasmic Reticulum. *Biochem. Cell Biol.* **2009,** *87* (3), 505–516.

54. Botman, D.; Tigchelaar, W.; Van Noorden, C. J. Determination of Glutamate Dehydrogenase Activity and its Kinetics in Mouse Tissues Using Metabolic Mapping (Quantitative Enzyme Histochemistry). *J. Histochem. Cytochem.* **2014,** *62* (11), 802–812.
55. Zaganas, I. V.; Kanavouras, K.; Borompokas, N.; Arianoglou, G.; Dimovasili, C.; Latsoudis, H.; Vlassi, M.; Mastorodemos, V. The Odyssey of a Young Gene: Structure-Function Studies in Human Glutamate Dehydrogenases Reveal Evolutionary-Acquired Complex Allosteric Regulation Mechanisms. *Neurochem. Res.* **2014,** *39* (3), 471–486.
56. Hardin-Pouzet, H.; Giraudon, P.; Bernard, A.; Derrington, E.; Belin, M. F.; Didier-Bazes, M. Cytokines are Increased in the rat Hippocampus After Serotonergic Neuron Degeneration and Upregulate the Expression of GDH, an Enzyme Involved in Glutamate Detoxification. *J. Neuroimmunol.* **1996,** *69* (1–2), 117–122.
57. Timmerman, M.; Wilkening, R. B.; Regnault, T. R. Induction of Glutamate Dehydrogenase in the Ovine Fetal Liver by Dexamethasone Infusion During Late Gestation. *Exp. Biol. Med.* **2003,** *228* (1), 100–105.
58. McGill, M. R.; Sharpe, M. R.; Williams, C. D.; Taha, M.; Curry, S. C.; Jaeschke, H. The Mechanism Underlying Acetaminophen-Induced Hepatotoxicity in Humans and Mice Involves Mitochondrial Damage and Nuclear DNA Fragmentation. *J. Clin. Invest.* **2012,** *122* (4), 1574–1583.
59. O'Brien, P. J.; Slaughter, M. R.; Polley, S. R.; Kramer, K. Advantages of Glutamate Dehydrogenase as a Blood Biomarker of Acute Hepatic Injury in Rats. *Lab Anim.* **2002,** *36* (3), 313–321.
60. Jackson, E. R.; Kilroy, C.; Joslin, D. L.; Schomaker, S. J.; Pruimboom-Brees, I.; Amacher, D. E. The Early Effects of Short-Term Dexamethasone Administration on Hepatic and Serum Alanine Aminotransferase in the Rat. *Drug Chem. Toxicol.* **2008,** *31* (4), 427–445.
61. McGill, M. R.; Staggs, V. S.; Sharpe, M. R.; Lee, W. M.; Jaeschke, H.; Acute Liver Failure Study Group. Serum Mitochondrial Biomarkers and Damage-Associated Molecular Patterns are Higher in Acetaminophen Overdose Patients With Poor Outcome. *Hepatology* **2014,** *60* (4), 1336–1345.
62. Kornblit, B.; Munthe-Fog, L.; Petersen, S. L.; Madsen, H. O.; Vindelov, L.; Garred, P. The Genetic Variation of the Human HMGB1 Gene. *Tissue Antigens* **2007,** *70* (2), 151–156.
63. Lotze, M. T.; Tracey, K. J. High-Mobility Group box 1 Protein (HMGB1): Nuclear Weapon in the Immune Arsenal. *Nat. Rev. Immunol.* **2005,** *5* (4), 331–342.
64. Kazama, H.; Ricci, J. E.; Herndon, J. M.; Hoppe, G.; Green, D. R.; Ferguson, T. A. Induction of Immunological Tolerance by Apoptotic Cells Requires Caspase-Dependent Oxidation of High-Mobility Group box-1 Protein. *Immunity* **2008,** *29* (1), 21–32.
65. Brenner, C.; Galluzzi, L.; Kepp, O.; Kroemer, G. Decoding Cell Death Signals in Liver Inflammation. *J. Hepatol.* **2013,** *59* (3), 583–594.
66. Urbonaviciute, V.; Furnrohr, B. G.; Weber, C.; Haslbeck, M.; Wilhelm, S.; Herrmann, M.; Voll, R. E. Factors Masking HMGB1 in Human Serum and Plasma. *J. Leukoc. Biol.* **2007,** *81* (1), 67–74.
67. Landgraf, P.; Rusu, M.; Sheridan, R.; Sewer, A.; Iovino, N.; Aravin, A.; Pfeffer, S.; Rice, A.; Kamphorst, A. O.; Landthaler, M.; Lin, C.; Socci, N. D.; Hermida, L.; Fulci, V.; Chiaretti, S.; Foa, R.; Schliwka, J.; Fuchs, U.; Novosel, A.; Muller, R. U.; Schermer, B.; Bissels, U.; Inman, J.; Phan, Q.; Chien, M.; Weir, D. B.; Choksi, R.; De Vita, G.; Frezzetti, D.; Trompeter, H. I.; Hornung, V.; Teng, G.; Hartmann, G.; Palkovits, M.; Di Lauro, R.; Wernet, P.; Macino, G.; Rogler, C. E.; Nagle, J. W.; Ju, J.; Papavasiliou, F. N.; Benzing, T.; Lichter, P.; Tam, W.; Brownstein, M. J.; Bosio, A.; Borkhardt, A.; Russo, J. J.; Sander, C.; Zavolan, M.; Tuschl, T. A mammalian MicroRNA Expression Atlas Based on Small RNA Library Sequencing. *Cell* **2007,** *129* (7), 1401–1414.
68. Gatfield, D.; Le Martelot, G.; Vejnar, C. E.; Gerlach, D.; Schaad, O.; Fleury-Olela, F.; Ruskeepaa, A. L.; Oresic, M.; Esau, C. C.; Zdobnov, E. M.; Schibler, U. Integration of microRNA miR-122 in Hepatic Circadian Gene Expression. *Genes Dev.* **2009,** *23* (11), 1313–1326.
69. Harrill, A. H.; Eaddy, J. S.; Rose, K.; Cullen, J. M.; Ramanathan, L.; Wanaski, S.; Collins, S.; Ho, Y.; Watkins, P. B.; Lecluyse, E. L. Liver Biomarker and In Vitro Assessment Confirm the Hepatic Origin of Aminotransferase Elevations Lacking Histopathological Correlate in Beagle Dogs Treated With GABAA Receptor Antagonist NP260. *Toxicol. Appl. Pharmacol.* **2014,** *277* (2), 131–137.
70. Wang, K.; Zhang, S.; Marzolf, B.; Troisch, P.; Brightman, A.; Hu, Z.; Hood, L. E.; Galas, D. J. Circulating microRNAs, Potential Biomarkers for Drug-Induced Liver Injury. *Proc. Natl. Acad. Sci. U. S. A.* **2009,** *106* (11), 4402–4407.
71. Starkey Lewis, P. J.; Dear, J.; Platt, V.; Simpson, K. J.; Craig, D. G.; Antoine, D. J.; French, N. S.; Dhaun, N.; Webb, D. J.; Costello, E. M.; Neoptolemos, J. P.; Moggs, J.; Goldring, C. E.; Park, B. K. Circulating microRNAs as Potential Markers of Human Drug-Induced Liver Injury. *Hepatology* **2011,** *54* (5), 1767–1776.
72. Waikar, S. S.; Liu, K. D.; Chertow, G. M. Diagnosis, Epidemiology and Outcomes of Acute Kidney Injury. *Clin. J. Am. Soc. Nephrol.* **2008,** *3* (3), 844–861.
73. Redfern, W. S.; Ewart, L.; Hammond, T. G.; Bialecki, R.; Kinter, L.; Lindgren, S.; Pollard, C. E.; Roberts, R.; Rolf, M. G.; Valentin, J. P. Impact and Frequency of Different Toxicities Throughout the Pharmaceutical Life Cycle. *Toxicologist* **2010,** *114* (S1), 1081.
74. ICH ICHS7A: Safety Pharmacology Studies for Human Pharmaceuticals. http://www.ich.org/fileadmin/Public_Web_Site/ICH_Products/Guidelines/Safety/S7A/Step4/S7A_Guideline.pdf (accessed 01.09.15).
75. Porter, G. A. Risk Factors for Toxic Nephropathies. *Toxicol. Lett.* **1989,** *46* (1–3), 269–279.
76. Bonventre, J. V.; Vaidya, V. S.; Schmouder, R.; Feig, P.; Dieterle, F. Next-Generation Biomarkers for Detecting Kidney Toxicity. *Nat. Biotechnol.* **2010,** *28* (5), 436–440.
77. FDA Drug Development Approval Process Issued Letters of Support. http://www.fda.gov/Drugs/DevelopmentApprovalProcess/ucm434382.htm (accessed 01.09.15).
78. Benjamin, A.; Gallacher, D. J.; Greiter-Wilke, A.; Guillon, J. M.; Kasai, C.; Ledieu, D.; Levesque, P.; Prelle, K.; Ratcliffe, S.; Sannajust, F.; Valentin, J. P. Renal Studies in Safety Pharmacology and Toxicology: A Survey Conducted in the top 15 Pharmaceutical Companies. *J. Pharmacol. Toxicol. Methods* **2015**.
79. Wadey, R. M.; Pinches, M. G.; Jones, H. B.; Riccardi, D.; Price, S. A. Tissue Expression and Correlation of a Panel of Urinary Biomarkers Following Cisplatin-Induced Kidney Injury. *Toxicol. Pathol.* **2014,** *42* (3), 591–602.
80. Davey, P. G.; Cowley, D. M.; Geddes, A. M.; Terry, J. Clinical Evaluation of Beta 2-Microglobulin, Muramidase, and Alanine Aminopeptidase as Markers of Gentamicin Nephrotoxicity. *Contrib. Nephrol.* **1984,** *42,* 100–106.
81. Nauta, F. L.; Bakker, S. J.; Lambers Heerspink, H.; de Zeeuw, D.; van Oeveren, W.; Bilo, H.; de Jong, P. E.; Gansevoort, R. T. Effect of Frozen Storage on Urinary Concentration of Kidney Damage Markers. *Am. J. Kidney Dis.* **2012,** *59* (4), 586–589.
82. Thomas, C. E.; Sexton, W.; Benson, K.; Sutphen, R.; Koomen, J. Urine Collection and Processing for Protein Biomarker Discovery and Quantification. *Cancer Epidemiol. Biomarkers Prev.* **2010,** *19* (4), 953–959.
83. Havanapan, P. O.; Thongboonkerd, V. Are Protease Inhibitors Required for Gel-Based Proteomics of Kidney and Urine? *J. Proteome Res.* **2009,** *8* (6), 3109–3117.
84. Eisner, C.; Faulhaber-Walter, R.; Wang, Y.; Leelahavanichkul, A.; Yuen, P. S.; Mizel, D.; Star, R. A.; Briggs, J. P.; Levine, M.; Schnermann, J. Major Contribution of Tubular Secretion to Creatinine Clearance in Mice. *Kidney Int.* **2010,** *77* (6), 519–526.
85. Shemesh, O.; Golbetz, H.; Kriss, J. P.; Myers, B. D. Limitations of Creatinine as a Filtration Marker in Glomerulopathic Patients. *Kidney Int.* **1985,** *28* (5), 830–838.
86. Waikar, S. S.; Sabbisetti, V. S.; Bonventre, J. V. Normalization of Urinary Biomarkers to Creatinine During Changes in Glomerular Filtration Rate. *Kidney Int.* **2010,** *78* (5), 486–494.
87. Morel, G.; Payan, J. P.; de Ceaurriz, J. Assessment of Urinary Rat Beta 2-Microglobulin by Enzyme Immunoassay. *Toxicol. Lett.* **1990,** *52* (3), 301–309.
88. Pennemans, V.; Rigo, J. M.; Faes, C.; Reynders, C.; Penders, J.; Swennen, Q. Establishment of Reference Values for Novel Urinary Biomarkers for Renal Damage in the Healthy Population: Are Age and Gender an Issue? *Clin. Chem. Lab. Med.* **2013,** *51* (9), 1795–1802.
89. Gautier, J. C.; Riefke, B.; Walter, J.; Kurth, P.; Mylecraine, L.; Guilpin, V.; Barlow, N.; Gury, T.; Hoffman, D.; Ennulat, D.; Schuster, K.; Harpur, E.; Pettit, S. Evaluation of Novel Biomarkers of Nephrotoxicity in Two Strains of Rat Treated With Cisplatin. *Toxicol. Pathol.* **2010,** *38* (6), 943–956.
90. Nejat, M.; Hill, J. V.; Pickering, J. W.; Edelstein, C. L.; Devarajan, P.; Endre, Z. H. Albuminuria Increases Cystatin C Excretion: Implications for Urinary Biomarkers. *Nephrol. Dial. Transplant.* **2012,** *27* (Suppl. 3), iii96–iii103.

91. (a) Gena, P.; Calamita, G.; Guggino, W. B. Cadmium Impairs Albumin Reabsorption by Down-Regulating Megalin and ClC5 Channels in Renal Proximal Tubule Cells. *Environ. Health Perspect.* **2010,** *118* (11), 1551–1556; (b) Mahadevappa, R.; Nielsen, R.; Christensen, E. I.; Birn, H. Megalin in Acute Kidney Injury: Foe and Friend. *Am. J. Physiol. Renal Physiol.* **2014,** *306* (2), F147–F154; (c) Oroszlan, M.; Bieri, M.; Ligeti, N.; Farkas, A.; Meier, B.; Marti, H. P.; Mohacsi, P. Sirolimus and Everolimus Reduce Albumin Endocytosis in Proximal Tubule Cells via an Angiotensin II-Dependent Pathway. *Transpl. Immunol.* **2010,** *23* (3), 125–132; (d) Russo, L. M.; Sandoval, R. M.; McKee, M.; Osicka, T. M.; Collins, A. B.; Brown, D.; Molitoris, B. A.; Comper, W. D. The Normal Kidney Filters Nephrotic Levels of Albumin Retrieved by Proximal Tubule Cells: Retrieval is Disrupted in Nephrotic States. *Kidney Int.* **2007,** *71* (6), 504–513; (e) Schreiber, A.; Theilig, F.; Schweda, F.; Hocherl, K. Acute Endotoxemia in Mice Induces Downregulation of Megalin and Cubilin in the Kidney. *Kidney Int.* **2012,** *82* (1), 53–59.
92. Gautier, J. C.; Gury, T.; Guffroy, M.; Masson, R.; Khan-Malek, R.; Hoffman, D.; Pettit, S.; Harpur, E. Comparison Between Male and Female Sprague-Dawley Rats in the Response of Urinary Biomarkers to Injury Induced by Gentamicin. *Toxicol. Pathol.* **2014,** *42* (7), 1105–1116.
93. Sasaki, D.; Yamada, A.; Umeno, H.; Kurihara, H.; Nakatsuji, S.; Fujihira, S.; Tsubota, K.; Ono, M.; Moriguchi, A.; Watanabe, K.; Seki, J. Comparison of the Course of Biomarker Changes and Kidney Injury in a Rat Model of Drug-Induced Acute Kidney Injury. *Biomarkers* **2011,** *16* (7), 553–566.
94. Haase-Fielitz, A.; Haase, M.; Devarajan, P. Neutrophil Gelatinase-Associated Lipocalin as a Biomarker of Acute Kidney Injury: A Critical Evaluation of Current Status. *Ann. Clin. Biochem.* **2014,** *51* (Pt 3), 335–351.
95. Dieterle, F.; Perentes, E.; Cordier, A.; Roth, D. R.; Verdes, P.; Grenet, O.; Pantano, S.; Moulin, P.; Wahl, D.; Mahl, A.; End, P.; Staedtler, F.; Legay, F.; Carl, K.; Laurie, D.; Chibout, S. D.; Vonderscher, J.; Maurer, G. Urinary Clusterin, Cystatin C, beta2-Microglobulin and Total Protein as Markers to Detect Drug-Induced Kidney Injury. *Nat. Biotechnol.* **2010,** *28* (5), 463–469.
96. Tonomura, Y.; Tsuchiya, N.; Torii, M.; Uehara, T. Evaluation of the Usefulness of Urinary Biomarkers for Nephrotoxicity in Rats. *Toxicology* **2010,** *273* (1–3), 53–59.
97. Viau, C.; Bernard, A.; Lauwerys, R. Determination of rat Beta 2-Microglobulin in Urine and in Serum. I. Development of an Immunoassay Based on Latex Particles Agglutination. *J. Appl. Toxicol.* **1986,** *6* (3), 185–189.
98. Haring, N.; Mahr, H. S.; Mundle, M.; Strohal, R.; Lhotta, K. Early Detection of Renal Damage Caused by Fumaric Acid Ester Therapy by Determination of Urinary Beta2-Microglobulin. *Br. J. Dermatol.* **2011,** *164* (3), 648–651.
99. Rosenberg, M. E.; Silkensen, J. Clusterin: Physiologic and Pathophysiologic Considerations. *Int. J. Biochem. Cell Biol.* **1995,** *27* (7), 633–645.
100. Park, S.; Mathis, K. W.; Lee, I. K. The Physiological Roles of Apolipoprotein J/Clusterin in Metabolic and Cardiovascular Diseases. *Rev. Endocr. Metab. Disord.* **2014,** *15* (1), 45–53.
101. Correa-Rotter, R.; Ibarra-Rubio, M. E.; Schwochau, G.; Cruz, C.; Silkensen, J. R.; Pedraza-Chaverri, J.; Chmielewski, D.; Rosenberg, M. E. Induction of Clusterin in Tubules of Nephrotic Rats. *J. Am. Soc. Nephrol.* **1998,** *9* (1), 33–37.
102. Vlasakova, K.; Erdos, Z.; Troth, S. P.; McNulty, K.; Chapeau-Campredon, V.; Mokrzycki, N.; Muniappa, N.; Gu, Y. Z.; Holder, D.; Bailey, W. J.; Sistare, F. D.; Glaab, W. E. Evaluation of the Relative Performance of 12 Urinary Biomarkers for Renal Safety Across 22 rat Sensitivity and Specificity Studies. *Toxicol. Sci.* **2014,** *138* (1), 3–20.
103. Guha, M.; Heier, A.; Price, S.; Bielenstein, M.; Caccese, R. G.; Heathcote, D. I.; Simpson, T. R.; Stong, D. B.; Bodes, E. Assessment of Biomarkers of Drug-Induced Kidney Injury in Cynomolgus Monkeys Treated With a Triple Reuptake Inhibitor. *Toxicol. Sci.* **2011,** *120* (2), 269–283.
104. Zhou, X.; Ma, B.; Lin, Z.; Qu, Z.; Huo, Y.; Wang, J.; Li, B. Evaluation of the Usefulness of Novel Biomarkers for Drug-Induced Acute Kidney Injury in Beagle Dogs. *Toxicol. Appl. Pharmacol.* **2014,** *280* (1), 30–35.
105. Ozer, J. S.; Dieterle, F.; Troth, S.; Perentes, E.; Cordier, A.; Verdes, P.; Staedtler, F.; Mahl, A.; Grenet, O.; Roth, D. R.; Wahl, D.; Legay, F.; Holder, D.; Erdos, Z.; Vlasakova, K.; Jin, H.; Yu, Y.; Muniappa, N.; Forest, T.; Clouse, H. K.; Reynolds, S.; Bailey, W. J.; Thudium, D. T.; Topper, M. J.; Skopek, T. R.; Sina, J. F.; Glaab, W. E.; Vonderscher, J.; Maurer, G.; Chibout, S. D.; Sistare, F. D.; Gerhold, D. L. A Panel of Urinary Biomarkers to Monitor Reversibility of Renal Injury and a Serum Marker With Improved Potential to Assess Renal Function. *Nat. Biotechnol.* **2010,** *28* (5), 486–494.
106. Davis, J. W., 2nd; Goodsaid, F. M.; Bral, C. M.; Obert, L. A.; Mandakas, G.; Garner, C. E., 2nd; Collins, N. D.; Smith, R. J.; Rosenblum, I. Y. Quantitative Gene Expression Analysis in a Nonhuman Primate Model of Antibiotic-Induced Nephrotoxicity. *Toxicol. Appl. Pharmacol.* **2004,** *200* (1), 16–26.
107. Tsuchimoto, A.; Shinke, H.; Uesugi, M.; Kikuchi, M.; Hashimoto, E.; Sato, T.; Ogura, Y.; Hata, K.; Fujimoto, Y.; Kaido, T.; Kishimoto, J.; Yanagita, M.; Matsubara, K.; Uemoto, S.; Masuda, S. Urinary Neutrophil Gelatinase-Associated Lipocalin: A Useful Biomarker for Tacrolimus-Induced Acute Kidney Injury in Liver Transplant Patients. *PLoS ONE* **2014,** *9* (10), e110527.
108. Wunnapuk, K.; Liu, X.; Peake, P.; Gobe, G.; Endre, Z.; Grice, J. E.; Roberts, M. S.; Buckley, N. A. Renal Biomarkers Predict Nephrotoxicity After Paraquat. *Toxicol. Lett.* **2013,** *222* (3), 280–288.
109. Sasaki, A.; Sasaki, Y.; Iwama, R.; Shimamura, S.; Yabe, K.; Takasuna, K.; Ichijo, T.; Furuhama, K.; Satoh, H. Comparison of Renal Biomarkers With Glomerular Filtration Rate in Susceptibility to the Detection of Gentamicin-Induced Acute Kidney Injury in Dogs. *J. Comp. Pathol.* **2014,** *151* (2–3), 264–270.
110. Royakkers, A. A.; Korevaar, J. C.; van Suijlen, J. D.; Hofstra, L. S.; Kuiper, M. A.; Spronk, P. E.; Schultz, M. J.; Bouman, C. S. Serum and Urine Cystatin C are Poor Biomarkers for Acute Kidney Injury and Renal Replacement Therapy. *Intensive Care Med.* **2011,** *37* (3), 493–501.
111. Herget-Rosenthal, S.; Marggraf, G.; Husing, J.; Goring, F.; Pietruck, F.; Janssen, O.; Philipp, T.; Kribben, A. Early Detection of Acute Renal Failure by Serum Cystatin C. *Kidney Int.* **2004,** *66* (3), 1115–1122.
112. Park, M. Y.; Choi, S. J.; Kim, J. K.; Hwang, S. D.; Lee, Y. W. Urinary Cystatin C Levels as a Diagnostic and Prognostic Biomarker in Patients With Acute Kidney Injury. *Nephrology (Carlton)* **2013,** *18* (4), 256–262.
113. Rennert, P. D. Novel Roles for TIM-1 in Immunity and Infection. *Immunol. Lett.* **2011,** *141* (1), 28–35.
114. Yang, L.; Brooks, C. R.; Xiao, S.; Sabbisetti, V.; Yeung, M. Y.; Hsiao, L. L.; Ichimura, T.; Kuchroo, V.; Bonventre, J. V. KIM-1-Mediated Phagocytosis Reduces Acute Injury to the Kidney. *J. Clin. Invest.* **2015,** *125* (4), 1620–1636.
115. Ichimura, T.; Asseldonk, E. J.; Humphreys, B. D.; Gunaratnam, L.; Duffield, J. S.; Bonventre, J. V. Kidney Injury Molecule-1 is a Phosphatidylserine Receptor That Confers a Phagocytic Phenotype on Epithelial Cells. *J. Clin. Invest.* **2008,** *118* (5), 1657–1668.
116. Burt, D.; Crowell, S. J.; Ackley, D. C.; Magee, T. V.; Aubrecht, J. Application of Emerging Biomarkers of Acute Kidney Injury in Development of Kidney-Sparing Polypeptide-Based Antibiotics. *Drug Chem. Toxicol.* **2014,** *37* (2), 204–212.
117. Vaidya, V. S.; Ozer, J. S.; Dieterle, F.; Collings, F. B.; Ramirez, V.; Troth, S.; Muniappa, N.; Thudium, D.; Gerhold, D.; Holder, D. J.; Bobadilla, N. A.; Marrer, E.; Perentes, E.; Cordier, A.; Vonderscher, J.; Maurer, G.; Goering, P. L.; Sistare, F. D.; Bonventre, J. V. Kidney Injury Molecule-1 Outperforms Traditional Biomarkers of Kidney Injury in Preclinical Biomarker Qualification Studies. *Nat. Biotechnol.* **2010,** *28* (5), 478–485.
118. Pinches, M.; Betts, C.; Bickerton, S.; Burdett, L.; Thomas, H.; Derbyshire, N.; Jones, H. B.; Moores, M. Evaluation of Novel Renal Biomarkers With a Cisplatin Model of Kidney Injury: Gender and Dosage Differences. *Toxicol. Pathol.* **2012,** *40* (3), 522–533.
119. Zhou, Y.; Vaidya, V. S.; Brown, R. P.; Zhang, J.; Rosenzweig, B. A.; Thompson, K. L.; Miller, T. J.; Bonventre, J. V.; Goering, P. L. Comparison of Kidney Injury Molecule-1 and Other Nephrotoxicity Biomarkers in Urine and Kidney Following Acute Exposure to Gentamicin, Mercury, and Chromium. *Toxicol. Sci.* **2008,** *101* (1), 159–170.
120. Waanders, F.; Vaidya, V. S.; van Goor, H.; Leuvenink, H.; Damman, K.; Hamming, I.; Bonventre, J. V.; Vogt, L.; Navis, G. Effect of Renin-Angiotensin-Aldosterone System Inhibition, Dietary Sodium Restriction, and/or Diuretics on Urinary Kidney Injury Molecule 1 Excretion in Nondiabetic Proteinuric Kidney Disease: A Post Hoc Analysis of a Randomized Controlled Trial. *Am. J. Kidney Dis.* **2009,** *53* (1), 16–25.
121. Han, W. K.; Waikar, S. S.; Johnson, A.; Betensky, R. A.; Dent, C. L.; Devarajan, P.; Bonventre, J. V. Urinary Biomarkers in the Early Diagnosis of Acute Kidney Injury. *Kidney Int.* **2008,** *73* (7), 863–869.
122. Liangos, O.; Perianayagam, M. C.; Vaidya, V. S.; Han, W. K.; Wald, R.; Tighiouart, H.; MacKinnon, R. W.; Li, L.; Balakrishnan, V. S.; Pereira, B. J.; Bonventre, J. V.; Jaber, B. L. Urinary *N*-Acetyl-Beta-(D)-Glucosaminidase Activity and Kidney Injury Molecule-1 Level are Associated With Adverse Outcomes in Acute Renal Failure. *J. Am. Soc. Nephrol.* **2007,** *18* (3), 904–912.

123. Bourbouze, R.; Baumann, F. C.; Bonvalet, J. P.; Farman, N. Distribution of *N*-Acetyl-Beta-D-Glucosaminidase Isoenzymes Along the Rabbit Nephron. *Kidney Int.* **1984,** *25* (4), 636–642.
124. Clemo, F. A. Urinary Enzyme Evaluation of Nephrotoxicity in the Dog. *Toxicol. Pathol.* **1998,** *26* (1), 29–32.
125. Westhuyzen, J.; Endre, Z. H.; Reece, G.; Reith, D. M.; Saltissi, D.; Morgan, T. J. Measurement of Tubular Enzymuria Facilitates Early Detection of Acute Renal Impairment in the Intensive Care Unit. *Nephrol. Dial. Transplant.* **2003,** *18* (3), 543–551.
126. Vaidya, V. S.; Ferguson, M. A.; Bonventre, J. V. Biomarkers of Acute Kidney Injury. *Annu. Rev. Pharmacol. Toxicol.* **2008,** *48,* 463–493.
127. Nielsen, B. S.; Borregaard, N.; Bundgaard, J. R.; Timshel, S.; Sehested, M.; Kjeldsen, L. Induction of NGAL Synthesis in Epithelial Cells of Human Colorectal Neoplasia and Inflammatory Bowel Diseases. *Gut* **1996,** *38* (3), 414–420.
128. Supavekin, S.; Zhang, W.; Kucherlapati, R.; Kaskel, F. J.; Moore, L. C.; Devarajan, P. Differential Gene Expression Following Early Renal Ischemia/Reperfusion. *Kidney Int.* **2003,** *63* (5), 1714–1724.
129. Charlton, J. R.; Portilla, D.; Okusa, M. D. A Basic Science View of Acute Kidney Injury Biomarkers. *Nephrol. Dial. Transplant.* **2014,** *29* (7), 1301–1311.
130. Thompson, K. L.; Haskins, K.; Rosenzweig, B. A.; Stewart, S.; Zhang, J.; Peters, D.; Knapton, A.; Rouse, R.; Mans, D.; Colatsky, T. Comparison of the Diagnostic Accuracy of Di-22:6-bis(Monoacylglycerol)Phosphate and Other Urinary Phospholipids for Drug-Induced Phospholipidosis or Tissue Injury in the Rat. *Int. J. Toxicol.* **2012,** *31* (1), 14–24.
131. Ling, W.; Zhaohui, N.; Ben, H.; Leyi, G.; Jianping, L.; Huili, D.; Jiaqi, Q. Urinary IL-18 and NGAL as Early Predictive Biomarkers in Contrast-Induced Nephropathy After Coronary Angiography. *Nephron Clin. Pract.* **2008,** *108* (3), c176–c181.
132. Xie, Y.; Sakatsume, M.; Nishi, S.; Narita, I.; Arakawa, M.; Gejyo, F. Expression, Roles, Receptors, and Regulation of Osteopontin in the Kidney. *Kidney Int.* **2001,** *60* (5), 1645–1657.
133. Fuchs, T. C.; Hewitt, P. Biomarkers for Drug-Induced Renal Damage and Nephrotoxicity—An Overview for Applied Toxicology. *AAPS J.* **2011,** *13* (4), 615–631.
134. Kohri, K.; Yasui, T.; Okada, A.; Hirose, M.; Hamamoto, S.; Fujii, Y.; Niimi, K.; Taguchi, K. Biomolecular Mechanism of Urinary Stone Formation Involving Osteopontin. *Urol. Res.* **2012,** *40* (6), 623–637.
135. Hudkins, K. L.; Le, Q. C.; Segerer, S.; Johnson, R. J.; Davis, C. L.; Giachelli, C. M.; Alpers, C. E. Osteopontin Expression in Human Cyclosporine Toxicity. *Kidney Int.* **2001,** *60* (2), 635–640.
136. Tarrant, J. M. Blood Cytokines as Biomarkers of in vivo Toxicity in Preclinical Safety Assessment: Considerations for Their Use. *Toxicol. Sci.* **2010,** *117* (1), 4–16.
137. Prucha, M.; Bellingan, G.; Zazula, R. Sepsis Biomarkers. *Clin. Chim. Acta* **2015,** *440,* 97–103.
138. Maude, S. L.; Teachey, D. T.; Porter, D. L.; Grupp, S. A. CD19-Targeted Chimeric Antigen Receptor T-Cell Therapy for Acute Lymphoblastic Leukemia. *Blood* **2015,** *125* (26), 4017–4023.
139. Erickson, R. I.; Tarrant, J.; Cain, G.; Lewin-Koh, S. C.; Dybdal, N.; Wong, H.; Blackwood, E.; West, K.; Steigerwalt, R.; Mamounas, M.; Flygare, J. A.; Amemiya, K.; Dambach, D.; Fairbrother, W. J.; Diaz, D. Toxicity Profile of Small-Molecule IAP Antagonist GDC-0152 is Linked to TNF-Alpha Pharmacology. *Toxicol. Sci.* **2013,** *131* (1), 247–258.
140. Eastwood, D.; Findlay, L.; Poole, S.; Bird, C.; Wadhwa, M.; Moore, M.; Burns, C.; Thorpe, R.; Stebbings, R. Monoclonal Antibody TGN1412 Trial Failure Explained by Species Differences in CD28 Expression on CD4+ Effector Memory T-Cells. *Br. J. Pharmacol.* **2010,** *161* (3), 512–526.
141. Finco, D.; Grimaldi, C.; Fort, M.; Walker, M.; Kiessling, A.; Wolf, B.; Salcedo, T.; Faggioni, R.; Schneider, A.; Ibraghimov, A.; Scesney, S.; Serna, D.; Prell, R.; Stebbings, R.; Narayanan, P. K. Cytokine Release Assays: Current Practices and Future Directions. *Cytokine* **2014,** *66* (2), 143–155.
142. ICH Immunotoxicity Studies for Human Pharmaceuticals: S8. http://www.ich.org/fileadmin/Public_Web_Site/ICH_Products/Guidelines/Safety/S8/Step4/S8_Guideline.pdf (accessed 01.09.15).
143. NCI Common Terminology Criteria for Adverse Events: Version 4.0. http://evs.nci.nih.gov/ftp1/CTCAE/CTCAE_4.03_2010-06-14_QuickReference_5x7.pdf.
144. Nonoyama, T.; Fukuda, F. Drug-Induced Phospholipidosis—Pathological Aspects and Its Prediction. *J. Toxicol. Pathol.* **2008,** *21,* 9–24.
145. (a) Anderson, N.; Borlak, J. Drug-Induced Phospholipidosis. *FEBS Lett.* **2006,** *580* (23), 5533–5540; (b) Shayman, J. A.; Abe, A. Drug Induced Phospholipidosis: An Acquired Lysosomal Storage Disorder. *Biochim. Biophys. Acta* **2013,** *1831* (3), 602–611.
146. Liu, N.; Tengstrand, E. A.; Chourb, L.; Hsieh, F. Y. Di-22:6-bis(Monoacylglycerol)Phosphate: A Clinical Biomarker of Drug-Induced Phospholipidosis for Drug Development and Safety Assessment. *Toxicol. Appl. Pharmacol.* **2014,** *279* (3), 467–476.
147. Hullin-Matsuda, F.; Luquain-Costaz, C.; Bouvier, J.; Delton-Vandenbroucke, I. Bis(Monoacylglycero)Phosphate, a Peculiar Phospholipid to Control the Fate of Cholesterol: Implications in Pathology. *Prostaglandins Leukot. Essent. Fatty Acids* **2009,** *81* (5–6), 313–324.
148. Luquain-Costaz, C.; Lefai, E.; Arnal-Levron, M.; Markina, D.; Sakai, S.; Euthine, V.; Makino, A.; Guichardant, M.; Yamashita, S.; Kobayashi, T.; Lagarde, M.; Moulin, P.; Delton-Vandenbroucke, I. Bis(Monoacylglycero)Phosphate Accumulation in Macrophages Induces Intracellular Cholesterol Redistribution, Attenuates Liver-X Receptor/ATP-Binding Cassette Transporter A1/ATP-Binding Cassette Transporter G1 Pathway, and Impairs Cholesterol Efflux. *Arterioscler. Thromb. Vasc. Biol.* **2013,** *33* (8), 1803–1811.
149. Tengstrand, E. A.; Miwa, G. T.; Hsieh, F. Y. Bis(Monoacylglycerol)Phosphate as a Non-Invasive Biomarker to Monitor the Onset and Time-Course of Phospholipidosis With Drug-Induced Toxicities. *Expert Opin. Drug Metab. Toxicol.* **2010,** *6* (5), 555–570.
150. Mortuza, G. B.; Neville, W. A.; Delaney, J.; Waterfield, C. J.; Camilleri, P. Characterisation of a Potential Biomarker of Phospholipidosis From Amiodarone-Treated Rats. *Biochim. Biophys. Acta* **2003,** *1631* (2), 136–146.
151. Baronas, E. T.; Lee, J. W.; Alden, C.; Hsieh, F. Y. Biomarkers to Monitor Drug-Induced Phospholipidosis. *Toxicol. Appl. Pharmacol.* **2007,** *218* (1), 72–78.
152. Mesens, N.; Desmidt, M.; Verheyen, G. R.; Starckx, S.; Damsch, S.; De Vries, R.; Verhemeldonck, M.; Van Gompel, J.; Lampo, A.; Lammens, L. Phospholipidosis in Rats Treated With Amiodarone: Serum Biochemistry and Whole Genome Micro-Array Analysis Supporting the Lipid Traffic Jam Hypothesis and the Subsequent Rise of the Biomarker BMP. *Toxicol. Pathol.* **2012,** *40* (3), 491–503.
153. Thompson, K. L.; Zhang, J.; Stewart, S.; Rosenzweig, B. A.; Shea, K.; Mans, D.; Colatsky, T. Comparison of Urinary and Serum Levels of Di-22:6-bis(Monoacylglycerol) Phosphate as Noninvasive Biomarkers of Phospholipidosis in Rats. *Toxicol. Lett.* **2012,** *213* (2), 285–291.
154. Fuji, R. N.; Flagella, M.; Baca, M.; Baptista, M. A.; Brodbeck, J.; Chan, B. K.; Fiske, B. K.; Honigberg, L.; Jubb, A. M.; Katavolos, P.; Lee, D. W.; Lewin-Koh, S. C.; Lin, T.; Liu, X.; Liu, S.; Lyssikatos, J. P.; O'Mahony, J.; Reichelt, M.; Roose-Girma, M.; Sheng, Z.; Sherer, T.; Smith, A.; Solon, M.; Sweeney, Z. K.; Tarrant, J.; Urkowitz, A.; Warming, S.; Yaylaoglu, M.; Zhang, S.; Zhu, H.; Estrada, A. A.; Watts, R. J. Effect of Selective LRRK2 Kinase Inhibition on Nonhuman Primate Lung. *Sci. Transl. Med.* **2015,** *7* (273), 273ra15.

Relevant Websites

http://www.biomarkersconsortium.org—A Consortia for Advancing Promising Biomarkers to Expedite Development of Medicines and Therapies for Prevention, Early Detection, Diagnosis and Treatment of Disease. A Private–Public Consortia for Safety Biomarker Qualification. Founding Members include National Institutes of Health, Food and Drug Administration and the Pharmaceutical Research and Manufacturers of America With Partner Organizations, the Centers for Medicare & Medicaid Services and the Biotechnology Industry Organization.

http://www.ema.europa.eu/ema/index.jsp?curl=pages/special_topics/general/general_content_000349.jsp&mid=WC0b01ac05800baedb—European Medicines Agency Website Detailing Qualification Process for Novel Methodologies and Biomarkers and Endorsed Safety Biomarkers.

http://www.fda.gov/Drugs/DevelopmentApprovalProcess/DrugDevelopmentToolsQualificationProgram/default.htm—The Food and Drug Administration Website Detailing the Qualification Process For "Drug Development Tools" Including Safety Biomarkers. Qualified Biomarkers and Supporting Information are Posted in this Location.

http://www.mirbase.org—A Database of miRNA Sequences With Annotation.

http://c-path.org/programs/pstc/—A Private–Public Partnership With the Mission of Identifying New and Improved Safety Testing Methods for Submission to the FDA, EMA and PMDA for Regulatory Qualification.

http://www.imi-safe-t.eu—SAFE-T Consortium is a Private-Partnership of the European Pharmaceutical Industry, Academics and Small and Medium Enterprises to Qualify Translational Safety Biomarkers for Drug-Induced Kidney, Liver and Vascular Injury With Regulatory Agencies.

4.16 Toxicity Prediction—Regulatory Perspective

JP Hanig, Center for Drug Evaluation and Research/FDA, Silver Spring, MD, United States
W Slikker, National Center for Toxicological Research/FDA, Jefferson, AR, United States

© 2017 Elsevier Ltd. All rights reserved.

4.16.1	**Introduction**	285
4.16.2	**Historical Perspective**	286
4.16.3	**Important Documents and Programs Relating to Toxicology Prediction and Safety Issues**	287
4.16.3.1	Appraisal of the Safety of Chemicals in Foods, Drugs, and Cosmetics	287
4.16.3.2	Current Views on Safety Evaluation of Drugs	287
4.16.3.3	Redbook 2000; Revised Jul. 2007	287
4.16.3.4	Toxicology in the 21st Century (Tox21)—Tox21	288
4.16.3.4.1	Generating fit-for-purpose cellular models for secondary screening	288
4.16.3.4.2	Developing a high-throughput gene expression core facility	288
4.16.3.5	Toxicologic Testing Handbook	288
4.16.3.6	FDA Guidances on Safety Evaluation of Drugs	288
4.16.3.7	Tests Required for Safety Evaluation of New Drugs	288
4.16.3.8	Classical Methods for Toxicity Evaluation That Are No Longer Used	290
4.16.3.9	Current Methods for Toxicity Prediction and Safety Evaluation and Present Status	290
4.16.3.10	Life Cycle of Method Development, Validation, and Adoption	290
4.16.3.11	The Continuing Evolution of a Global Consensus on Regulatory Toxicology (ICH, etc.)	292
4.16.4	**Minimally- or Noninvasive Approaches to Assess Chemical and Drug Effects—Indicators of Efficacy and Toxicity**	293
4.16.4.1	Preclinical Imaging as a Translatable Biomarker	293
4.16.4.2	Emerging Imaging Biomarkers	294
4.16.4.3	Small Animal PET Imaging (Micro-PET)	294
4.16.4.3.1	[^{18}F]-Annexin V	295
4.16.4.3.2	[^{18}F]-DFNSH	295
4.16.4.3.3	[^{18}F]-FDG	295
4.16.4.3.4	[^{18}F]-FEPPA	295
4.16.4.3.5	[^{18}F]-FLT	295
4.16.4.4	MRI Applications	295
4.16.4.5	Blood-Borne Sampling: DNA Fragments and Micro-RNA	296
4.16.4.6	Three-Dimensional Cell Culture Models With an Emphasis on Neural Stem Cells	296
4.16.4.7	Microphysiological Models	296
4.16.4.8	Computational Toxicology	297
4.16.4.9	Global Trends, Initiatives, and Opportunities of Bioinformatics Approaches and Big Data	297
4.16.4.10	Application of Bioinformatics	298
4.16.5	**Lessons Learned and Challenges That Reflect and Focus on Contemporary Critical Issues**	298
4.16.6	**Horizons—A Vision of Future Directions for Toxicity Prediction and Safety Evaluation**	298
4.16.7	**Conclusions**	300
Acknowledgments		301
References		301

4.16.1 Introduction

This article on "Toxicology Prediction—Regulatory Perspective" is intended to describe and characterize the evolution of technological tools and regulatory instruments that facilitate and empower the contemporary approach to toxicology prediction, as well as current and future challenges and expectations. The section on historical perspective is a chronological encapsulation of the many events and issues that have influenced and molded the current approach to toxicology prediction, as well as the laws that allow for such implementation. Further, there is a compilation of significant documents, programs, guidances, and guidelines that have been used to describe various methods and tests performed to detect toxicity and insure the safety of products that are subject to federal regulation. This is followed by a discussion of the process involved in toxicology methods development as well as description of the key attributes that lead to validation and acceptance. A description of the tests required for safety evaluation of a new drug are followed by a table of accepted tests that have now been abandoned and a table that lists the current major tests and methods relative

to their status in 2005. A major section of this article is devoted to an extensive description of many of the latest new technologies that are being developed to detect toxicity and a table of each of the general subdiscipline areas as well as their current status compared to 2005. Finally, there is list of some of the more important critical issues in toxicology, their current status, as well as potential future directions of the technologies described and what conclusions can be drawn with respect to the overall field of toxicology prediction.

4.16.2 Historical Perspective

The historical record, going back to antiquity, has demonstrated the need for the regulation of food and much later drugs. Early English law dealt with the adulteration of food for economic gain. King John promulgated rules on contamination of flour, later referred to as the Assizes of Bread. In early America quack medicines, hidden ingredients and misbranding were typical. In 1848, Congress passed the Drugs and Medicines Act that represented the first recognition of the US Pharmacopeial Convention.

The Virus-Toxin Act of 1902 was passed in response to the production of a diphtheria vaccine that was contaminated with tetanus toxin resulting in the death of many children. This legislation was quite remarkable for its time because it provided for premarket clearance for safety and efficacy, factory inspection at every stage of manufacture, and individual batch certification of each lot of vaccine produced. This level of regulation was not achieved for drugs until another 60 years had passed and a significant number of catastrophic incidents had occurred.

The publication of "The Jungle" by Upton Sinclair in 1906,[1] as well as the rejection of US meat products by European countries lead to the passage of the Food and Drug Act of 1906, better known as the Wiley or Heyburn Act which was considered to be the first "modern" federal food and drug law which targeted adulteration and misbranding. It also established the US Pharmacopeia and National Formulary to establish and regulate reference standards. The Sherley Amendment of 1912 prohibited the use of fraudulent claims, but placed the burden of proof on the government. This resulted in weak or nonenforcement of the 1906 act due to the paucity of modern scientific techniques or tools needed to establish and prove the existence of evidence needed for prosecution. Many deaths occurred from "quack medicines" with hidden ingredients that were often extremely poisonous.[2] There was no animal testing to ensure safety until 1938.

The Federal Food, Drug, and Cosmetic Act (1938), also known as the Copeland Act was the response to a catastrophic event involving the addition of ethylene glycol as an excipient in elixir of sulfanilamide. This resulted in many deaths caused by the nephrotoxicity of the mixture. This legislation mandated, for the first time, that new drugs be tested in animals before human administration, thereby establishing premarket clearance for safety.

The next milestone piece of legislation that played a very significant role in the federal regulation of toxicity was the Federal Insecticide, Fungicide, and Rodenticide Act (FIFRA) of 1947. It defined the LD-50 concept, established classes of toxicity based on the order of magnitude of doses above and below the LD-50, and required a label to be written for pesticides as well as registration with USDA. This eventually led to the setting of tolerances and measurement of persistence in the environment by Food and Drug Administration (FDA) and ultimately, regulation by EPA[3] following its establishment in 1969.

Insulin and antibiotic certification amendments ('41, '43, '49, and '52) provided for batch certification of all master lots (insulin) and batches of finished product (insulin and antibiotics) to insure purity and potency, a very important process to insure safety and efficacy. These requirements were abolished in the late 1980s (antibiotics) and the late 1990s (insulin) when synthetic and recombinant products became available and the failure rate of tested products became miniscule.[4]

GRAS list (1958). GRAS or "generally recognized as safe" is a list of food additives that have been used since antiquity without any obvious adverse effects. Of course there are substances on the list such as NaCl which would never be approved today because of our current knowledge (e.g., the role of NaCl in hypertension). Since the original list was generated in 1958, any additions to the list must have their safety substantiated by published studies to that effect.[4]

The Durham-Humphrey Act of 1951 defined the modern practice of pharmacy as well as the relationship of the physician to the pharmacist (e.g., pharmacists were no longer allowed to practice medicine in lieu of a licensed physician). It established a separate class for narcotics and physician registration numbers for prescriptions and created "legend drugs" (e.g., Rx drugs or those that require a prescription).

The Kefauver-Harris Act of 1962 was precipitated by the thalidomide incident which resulted in phocomelia (flipper arms) in many children in Europe. This catastrophe was prevented from occurring in the United States by the caution of Dr. Francis Kelsey, an FDA medical officer at the time, who reviewed this submission. The resulting legislation, known as the Kefauver-Harris Act, mandated premarket clearance for both safety and efficacy and provided for various phases of investigation before drug approval. Its major provisions included initial preclinical studies in animals, followed by human studies in three phases (IND—first in human drug studies in normal subjects at low doses; Phase 2—small number of clinical trials; and Phase 3—large-scale clinical trials) prior to approval of a new drug application (NDA). It also called for postmarket surveillance of approved drugs including adverse effect reporting at defined intervals and immediately for severe occurrences.[3,4]

"The Toxic Substances Control Act (TSCA) of 1976 provides the EPA with authority to require reporting, record-keeping and testing requirements, and restrictions relating to chemical substances and/or mixtures. Certain substances are generally excluded from TSCA, including, among others, food, drugs, cosmetics and pesticides. It addresses the production, importation, use, and disposal of specific chemicals including polychlorinated biphenyls (PCBs), asbestos, radon and lead-based paint." There are many sections in the TSCA. Some of the more important of these include Section 5 that requires premanufacture notification

Table 1 Key features of the Lautenberg Act of 2016 versus TSCA[6]

Mandates safety reviews for chemicals in active commerce
Requires a safety finding before new chemicals are allowed on the market
Replaces TSCA's safety standard—which prevented the EPA even from banning asbestos—with a health-based, as opposed to cost-oriented, standard
Explicitly requires protection of vulnerable populations, such as children and pregnant women
Enhances the EPA's authority to require testing of both new and existing chemicals
Sets aggressive, judicially enforceable deadlines for EPA decisions and compliance with restrictions
Makes more information about chemicals available, by limiting companies' ability to claim information as confidential, and by giving states and health and environmental professionals' access to confidential information needed to perform their jobs
Requires the EPA to reduce animal testing where scientifically reliable alternatives exist that would generate equivalent or better information
Requires the EPA to prioritize chemicals that are persistent and bioaccumulative, and that are known human carcinogens and have high toxicity
Retains a significant role for states in assuring chemical safety, by grandfathering in past state actions, preserving states' ability to take many types of actions, and providing for states to get waivers to act both before and after the EPA takes final action on a chemical

Modified from Copyright © 2016 by The Bureau of National Affairs, Inc. (800-372-1033) http://www.bna.com; Daily Environment Report, Richard Denison, Ph.D. author, 111 DEN B-1, 6/9/16, 06/09/2016.

for new chemical substances before manufacture and Section 4 that requires testing of chemicals by manufacturers, importers, and processors where risks or exposures of concern are found. Section 8 requires the maintenance of the so-called TSCA inventory which contains more than 83,000 chemicals and new ones are being continually added. This section also requires extensive record keeping by manufacturers. There are also sections that cover compliance and enforcement.[5]

In May 2016, congress passed the Lautenberg Act by an overwhelming margin, which represents the first major update of the Toxic Substances Act of 1976 in 40 years. This landmark legislation of, which the EPA regulations have yet to be promulgated, has some important new provisions (see **Table 1**) that focus and strengthen the earlier TSCA Act, as well as compromises that were necessary to gain its passage. The new law is an enormous improvement over current law in every major respect.

4.16.3 Important Documents and Programs Relating to Toxicology Prediction and Safety Issues

4.16.3.1 Appraisal of the Safety of Chemicals in Foods, Drugs, and Cosmetics

This publication written by the staff of the Division of Pharmacology at the Food and Drug Administration (in various editions from 1955 to 1965) was the first modern compendium of tests, methods, and techniques for evaluating the safety of various chemicals in foods, drugs, and cosmetics. Often referred to as "Lehman's Bible," in 13 chapters it described the toxicological tests required to satisfy regulatory requirements demanded by the laws and regulations of the time. Areas covered included acute, subacute, chronic oral toxicity, and dermal toxicity, as well as the bioassay and evaluation of new drugs, safety evaluation of food additives, and carcinogenicity screening. It was the precursor of the FDA Redbook (see later) on food safety as well as the various guidance's on drug safety testing issued by the Bureau of Drugs later known as the Center for Drug Safety and Research.[7–10]

4.16.3.2 Current Views on Safety Evaluation of Drugs

A very comprehensive 1968 snapshot of the preclinical studies for toxicity prediction required for the initiation of various phases of clinical trials necessary for new drug evaluation and approval.[11] From an historical prospective, there are considerable contrasts between the 1968 requirements and those of the current 2016 FDA Guidances and ICH Guidelines. For instance in 1968, "prior to the beginning of a large scale clinical trial (Phase 3), we have insisted that studies of seven years duration in the dog and up to 10 years in the monkey be commenced."[11]

4.16.3.3 Redbook 2000; Revised Jul. 2007

Guidance for Industry and Other Stakeholders Containing Toxicological Principles for the Safety Assessment of Food Ingredients. This document includes an AGENCY REVIEW OF TOXICOLOGY INFORMATION submitted in support of the safety assessment of food ingredients; recommended toxicity studies; and guidelines for toxicity studies. The latter includes general guidelines for (a) conducting toxicity studies; (b) reporting results of those studies; (c) pathology considerations for those studies, and (d) statistical considerations. This is followed by guidelines for specific toxicity studies which are further broken out into short-term tests for genetic toxicity (bacterial reverse mutation test; *in vitro* mammalian chromosomal aberration test; *in vitro* mouse lymphoma TX; and *in vivo* mammalian erythrocyte micronucleus test). There are sections on Acute Oral Toxicity Tests; Short-Term, Subchronic and Chronic Toxicity Tests With Rodents and Non-Rodents; Carcinogenic and Combination Chronic Toxicity/Carcinogenic Studies in Rodents; Reproduction and Developmental Studies As Well As Neurotoxicity Studies. There is a section on additional studies that include Metabolism, Pharmacokinetics, and Immunotoxicity Studies and finally a section on human studies that includes clinical evaluation of food ingredients and epidemiology studies. This is a very comprehensive toxicological testing document generated and revised through the years by the FDA's Center for Food Safety and Applied Nutrition.[12–14]

4.16.3.4 Toxicology in the 21st Century (Tox21)—Tox21

A program introduced by the National Academy of Sciences to establish a comprehensive plan and strategy to broaden horizons for toxicity prediction in the 21st century.[15] "The goal of Tox21 is to develop more efficient and less time-consuming approaches to predict how chemicals may affect human health." Initially, the main focus of Tox21 is to help prioritize chemicals for more extensive testing using traditional methods. Tox21's ultimate aim is to develop strategies for agencies to use in regulating chemicals and reducing the current reliance on animal testing for toxicological evaluations. Some of the broad goals for the next 5 years include "Development and deployment of a suite of screening platforms for a Tox21 library; Addressing key technical limitations of *in vivo* chemical screening; Consolidation of chemical library management; Curation and characterization of legacy *in vivo* toxicology studies; Validation of high-throughput *in vitro* assays and integrated assays; Refinement and deployment of *in vitro* methods for characterizing biokinetics and pharmacokinetics"; and establishment of programs for outreach and training.[15] To achieve these goals, the objectives of the Tox21 program are to: "Identify environmental chemicals that lead to biological responses and determine their mechanisms of action on biological systems; Prioritize specific compounds for more extensive toxicological evaluation; Develop models that predict chemicals' negative health effects in humans; and Annotate all human biochemical pathways and design assays (tests) that can measure these pathways' responses to chemicals." Current screening efforts include two themes[15]:

4.16.3.4.1 Generating fit-for-purpose cellular models for secondary screening

Tox21 experts are developing a range of hepatocyte (liver), neuron, endothelial (skin), and cardiomyocyte (heart) cell models—including "disease-in-a-dish" models, 3-D culture methods, and multicellular coculture models, all derived from inducible pluripotent stem cells (iPSCs)—to further characterize hits from primary screening of 10,000 compounds (Tox21 10K library). These investigators working to advance Tox21 principles often use an iPSC-derived endothelial cell model from the National Heart, Lung, and Blood Institute to investigate tobacco lung toxicity through a grant from the FDA and NIH.

4.16.3.4.2 Developing a high-throughput gene expression core facility

Tox21 scientists have developed a high-throughput gene expression platform core facility with the goal of generating data from hundreds of thousands of samples across 1400 human genes each year. Although the team uses RNAseq technology to analyze all genes in a few samples, evaluating the effects of many compounds at multiple doses and times, each on several cell lines, requires higher throughput. To this end, the group is developing the RASL-Seq technology platform (link is external), which includes approximately 1400 human gene assays and a streamlined, automated procedure to serve both Tox21 collaborators and NCATS projects. The data analysis team is implementing a pipeline to enable data processing and statistical and systems analyses, which will be useful for RASL-Seq and RNAseq data.[15]

4.16.3.5 Toxicologic Testing Handbook[16]

A comprehensive monograph on principles, applications, and data interpretation was published by Jacobson-Kram and Keller in 2006[16] of many aspects of regulatory toxicology testing. It includes chapters on animal and *in vitro* models, acute and multidose general toxicology studies, toxicology of major organ systems, genetic and carcinogenicity studies, developmental, reproductive and juvenile studies, cancer risk assessment, nonclinical safety testing of pharmaceuticals, etc.

4.16.3.6 FDA Guidances on Safety Evaluation of Drugs

These are committee or cosensus generated documents that articulate the 'state of the art' as well as the status of scientific tools & tests for evaluation of drug safety.

4.16.3.7 Tests Required for Safety Evaluation of New Drugs

Ellis and Hastings (2006)[18] suggest in one of their chapter tables, the "Minimum nonclinical data required for most drug products before initial human exposure in the United States." These include safety pharmacology, limited pharmacokinetics, acute toxicity, local tolerance, cardiovascular, central nervous system (CNS) and respiratory system, C_{max}, AUC, studies in two mammalian species, use of the proposed route of administration, and tests for mutations and chromosomal damage. They go on to mention the need for studies involving reproduction toxicity, subacute and chronic toxicity, *in vivo* genetic studies, and a variety of specialty studies that include: abuse potential, ototoxicity, immunotoxicity, juvenile animal studies, and phototoxicity. These special studies are not always obligatory but may be required depending on the nature of the new drug being investigated or the outcome of the initial obligatory testing. Two-year carcinogenicity studies may be required if the drug yields positive findings in genetic tests or is intended for use longer than 6 months.

Many of these tests are continually being modified to reflect technological advances. The FDA does not require a specific test to be performed, but rather leaves the burden of proof on the innovator. Instead FDA publishes guidances intended for industry that reflect the agency's thoughts on what the current state of the art is in a particular area of safety testing. Examples of these finalized guidances, as well as ICH guidelines are listed in the tables below. (**Tables 2** and **3**).

Table 2 Selected FDA-finalized guidances for preclinical evaluation of drug safety

Category	*Title*	*Link*
Biologics	Immunogenicity Assessment for Therapeutic Protein Products (Aug. 2014)	http://www.fda.gov/downloads/Drugs/GuidanceComplianceRegulatoryInformation/Guidances/UCM338856.pdf
	S-6 Addendum to Preclinical Safety Evaluation of Biotechnology-Derived Pharmaceuticals; ICH-S-6(R1) (May 2012)	http://www.fda.gov/downloads/Drugs/GuidanceComplianceRegulatoryInformation/Guidances/UCM194490.pdf
	Preclinical Safety Evaluation of Biotechnology-Derived Pharmaceuticals; ICH-S-6 (Jul. 1997)	http://www.fda.gov/downloads/Drugs/GuidanceComplianceRegulatoryInformation/Guidances/ucm074957.pdf
Cardiovascular toxicity	Nonclinical Evaluation of the Potential for Delayed Ventricular Repolarization (QT Interval Prolongation by Human Pharmaceuticals; ICH S7B (Oct. 2005)	http://www.fda.gov/downloads/Drugs/GuidanceComplianceRegulatoryInformation/Guidances/ucm074963.pdf
Carcinogenicity	Testing for Carcinogenicity of Pharmaceuticals; ICH-SIB (Jul. 1997)	http://www.fda.gov/downloads/Drugs/GuidanceComplianceRegulatoryInformation/Guidances/ucm074916.pdf
	The Need for Long-Term Rodent Carcinogenicity Studies of Pharmaceuticals; ICH-S1A (Mar. 1996)	http://www.fda.gov/downloads/Drugs/GuidanceComplianceRegulatoryInformation/Guidances/ucm074911.pdf
Combinations (drugs or biologics)	Nonclinical Safety Evaluation of Drug or Biologic Combinations (Mar. 2006)	
Endocrine	Nonclinical Evaluation of Endocrine-Related Drugs (Sep. 2015)	http://www.fda.gov/downloads/Drugs/GuidanceComplianceRegulatoryInformation/Guidances/UCM369043.pdf
Genotoxicity	Genotoxicity Testing and Data Interpretation for Pharmaceutical Intended for Human Use; ICH-S2(R1) (Jun. 2012)	http://www.fda.gov/downloads/Drugs/GuidanceComplianceRegulatoryInformation/Guidances/UCM074931.pdf
Immunotoxicity	S8 Immunotoxicity Studies for Human Pharmaceutical; ICH-S-8 (Apr. 2006)	http://www.fda.gov/downloads/Drugs/GuidanceComplianceRegulatoryInformation/Guidances/ucm074965.pdf
	Immunotoxicology Evaluation of Investigational New Drugs (Oct. 2002)	http://www.fda.gov/downloads/Drugs/GuidanceComplianceRegulatoryInformation/Guidances/ucm079239.pdf
Juvenile animal studies	Nonclinical Safety Evaluation of Pediatric Drug Products (Feb. 2006)	http://www.fda.gov/downloads/Drugs/GuidanceComplianceRegulatoryInformation/Guidances/ucm079247.pdf
Metabolism/metabolites	Safety Testing of Drug Metabolites (Feb. 2008)	http://www.fda.gov/downloads/Drugs/GuidanceComplianceRegulatoryInformation/Guidances/ucm079266.pdf
Oncology	Nonclinical Evaluation for Anticancer Pharmaceuticals; ICH-S9 (Mar. 2010)	http://www.fda.gov/downloads/Drugs/GuidanceComplianceRegulatoryInformation/Guidances/ucm085389.pdf
Pharmacokinetics	Safety Testing of Drug Metabolites (Feb. 2008)	http://www.fda.gov/downloads/Drugs/GuidanceComplianceRegulatoryInformation/Guidances/ucm079266.pdf
Photosafety testing	S10 Photosafety Evaluation of Pharmaceuticals for Industry; ICH-S10 (Jan. 2015)	http://www.fda.gov/downloads/Drugs/GuidanceComplianceRegulatoryInformation/Guidances/UCM337572.pdf
Radiation	Nonclinical Evaluation of Late Radiation Toxicity of Therapeutic Radiopharmaceuticals (Nov. 2011)	
Reproductive and developmental toxicity	Detection of Toxicity to Reproduction for Medicinal Products; ICH-S5A (Sep. 1994)	http://www.fda.gov/downloads/Drugs/GuidanceComplianceRegulatoryInformation/Guidances/ucm074950.pdf
	Addendum on Male Fertility; ICH-S5B (Apr. 1996)	http://www.fda.gov/downloads/Drugs/GuidanceComplianceRegulatoryInformation/Guidances/ucm074954.pdf
	Toxicity to Male Fertility, an Addendum; ICH-S5(R2) (Nov. 1995; amended Nov. 2000)	

(Continued)

Table 2 Selected FDA-finalized guidances for preclinical evaluation of drug safety—cont'd

Category	*Title*	*Link*
Safety pharmacology	Safety Pharmacology Studies for Human Pharmaceuticals; ICHS7A (Jul. 2001)	http://www.fda.gov/downloads/Drugs/GuidanceComplianceRegulatoryInformation/Guidances/ucm074959.pdf
Toxicokinetics	The Assessment of Systemic Exposure in Toxicity Studies; ICH-S3A (Mar. 1995)	http://www.fda.gov/downloads/Drugs/GuidanceComplianceRegulatoryInformation/Guidances/ucm074937.pdf
Type, duration, and timing of nonclinical studies in support of clinical trials	Nonclinical Safety Studies for the Conduct of Human Clinical Trials and Marketing Authorization for Pharmaceuticals; ICH-M3(R2) (Jan. 2010; Revision 1)	http://www.fda.gov/downloads/Drugs/GuidanceComplianceRegulatoryInformation/Guidances/ucm073246.pdf

Table 3 ICH safety guidelines[17]

	Finalization date
S1A–S1C–carcinogenicity studies	
S2 genotoxicity studies	Nov. 2011
S3A S3B toxicokinetics and pharmacokinetics	Oct. 1994
S4 toxicity testing	Sep. 1998
S5 (R2) reproductive studies	Nov. 2000
S5 (R3) reproductive studies	–
S6 biotechnology products	Jun. 2011
S7A pharmacology studies (clinical)	Nov. 2009
S7B pharmacology studies (nonclinical)	May 2005
S8 immunotoxicology studies	Sep. 2005
S9 nonclinical evaluation for anticancer pharmaceuticals	Oct. 2009
S10 photosafety evaluation	Nov. 2013
S11 nonclinical safety testing	–
Cross-cutting topics	
M3 nonclinical safety studies	Jun. 2009
M6 gene therapy	–
M7 genotoxic impurities	Jun. 2014
Q3D elemental impurities	Sep. 2015

4.16.3.8 Classical Methods for Toxicity Evaluation That Are No Longer Used

There are a number of classical methods that were utilized for toxicity evaluation that are no longer used. Some of the problems or reasons for abandonment of those tests include: animal welfare issues that include pain production, other types of suffering, and/ or tissue damage and/or use of too many animals; method insensitivity or production of data artifacts; replacement by *in vitro* tests or chemical analysis; lack of universal validation; generation of false positives and negatives; and finally, inability to correlate test results with biological evidence of toxicity or lack of clinical translation or relevance. Examples of some of those tests are listed in Table 4.

4.16.3.9 Current Methods for Toxicity Prediction and Safety Evaluation and Present Status

Many of the current test methods that are used to generate drug safety data in the various toxicology subdisciplines are listed in Table 5 which describes the nature of the application, the stage of use and acceptance, and the level of incorporation into regulatory documents and publications.[19]

4.16.3.10 Life Cycle of Method Development, Validation, and Adoption

Method development is an evolutionary sequence that begins with the emergence and recognition of a need for a process and/or tool that will provide a metric(s) for evaluating a particular attribute of a specific entity that requires characterization and generally quantification. This process often begins in the laboratory involving a series of sequential experiments culminating in a successful configuration or process. This usually leads to the creation of a tool that yields the data necessary to achieve the required information. Once this step has been achieved there may be a series of internal efforts to validate the new method. This is often followed by the presentation of the new method at a scientific meeting. At that point, there are several choices. The method may be published in

Table 4 Accepted tests that are no longer routinely used

Name of the test	*Type of test*	*Problems or reasons for abandonment*
Esophageal corrosion	Application of acids and bases to whole animal potential irritants and corrosives	Issues of animal welfare (pain, suffering, and tissue damage)
Eye and skin irritation	Application of acids and bases to whole animal potential irritants and corrosives	Issues of animal welfare (pain, suffering, and tissue damage)
Chick embryo assay	Injection of drugs into fertile chicken eggs	A variety of artifacts caused by physical factors; pressure, sand, and water injection cause effects
Host-mediated assay	*In vivo* mouse genotoxicity	Use of S-9 allowed *in vitro* assay
Dominant—lethal test	Chromosome damage in reproductive cells	Insensitive test
Classical LD-50's	Three to five dose levels; 10 animals per group; 14-day observation period	Use of too many animals; animal welfare issues
Rabbit head drop	Curare assay	Replaced by HPLC
Hormone bioassays	*In vivo* tests of potency and toxicity	Replaced by *in vitro* assays or chemical analysis
Unscheduled DNA synthesis (UDS)	DNA repair assay	Detected limited set of chemical and damage; lack of universal validation
Sister chromatid exchange (SCE)	Chromatid rearrangements	Lots of false positives; no correlation with disease or biological end point
Comet assay	DNA strand break assay	Presently, unique utility not demonstrated
DNA adducts	Drug–DNA interactions	Cannot identify specific damage; no direct relationship with disease or biological end point
Rabbit pyrogen assay		Limulus amoebocyte assay is the *in vitro* substitute

Copyright 2006 from *Biological Concepts and Techniques in Toxicology: An Integrated Approach* edited by Jim E. Riviere. Reproduced by permission of Taylor and Francis Group, LLC, a division of Informa plc.

an appropriate journal for which peer review represents the first step of validation or prior to this, the method and appropriate samples are distributed to other investigators in the field as part of a collaborative study. The successful completion of this joint study can yield an initial element of validation that might be followed by publication whereas failure of the study might prompt the method to be modified or abandoned and discarded.

There are a number of important criteria that play a critical role in determining whether a regulatory method or test will gain acceptance and adoption. It should be translatable to relevant human end points. This means that the animal model, if one is utilized, has to be appropriate in terms of simulating human response. A notable example of a problem in this area has to do with pain measurement and the effectiveness of various analgesic drugs. The often used rodent tail flick or hot plate methods measure cord reflex pathways and do not represent pain perception that requires participation of higher centers in the brain. The latter require animal models that require Skinnerian paradigms.[20] Tests must also produce meaningful data that is easy to replicate (robust and reliable) in other laboratories. This means that there must be a paucity of false positives and false negatives and the results must be predictable in terms of human safety. The test should not only be considered useful, but also have a wide consensus of its utility. From a practical point of view, the test or methods should, where possible, be inexpensive or justifiable in terms of cost and time to complete. The ultimate challenge with respect to acceptance and adoption is whether the method generates data that is sufficient to convince FDA and other domestic and international regulatory bodies or agencies of its utility and value.

In the event that a method is published, there a very strong possibility that other groups will begin using it to generate data that may reinforce the applicability and the utility of the method. This is the beginning of the validation process that goes beyond the initial publication acceptance based on peer review. At this point, there is the possibility that many of the laboratories may generate false positives or false negatives that may lead to method abandonment. However, if this further peer review establishes the utility of the method, the following two processes may occur: (a) the method may begin to be widely used by academics to establish metrics for phenomenological and mechanistic studies with subsequent publication and (b) widespread publication may instill a perception that the method has potential for importance in regulatory decisions. This may be followed by drafting of a guidance that mentions or incorporates the method, which is then peer reviewed by the regulatory community. This step is the very beginning of the adoption process that is often followed by publication of the draft in the Federal Register calling for comments which represent additional peer review. Once this draft guidance has been finalized and published it may then be cited or incorporated into widely recognized monographs and other documents on safety toxicology methods. This further encourages wide use in laboratories of all sectors, especially those in the pharmaceutical industry. This ultimately leads to the method being widely endorsed by a variety of government agencies with regulatory functions related to safety toxicology. The final step in the adoption of a method is generally its acceptance by a wide body of international governments and agencies and its incorporation into documents such as regulatory guidances and guidelines. This action essentially completes the life cycle of a method from its conception to adoption and widespread utilization. It should be noted, however, that during the life cycle of a validated method there may be revisions and significant improvements prompted by technological advancements. These events often lead to the development of new methodologies and retirement of earlier ones, completing the life cycle as shown in Table 4. In summary, the vast majority of validated, adopted tests or methods for toxicity prediction are robust, reliable, easy to conduct and replicate in various laboratories, and

Table 5 Techniques, tests, and methods for drug approval: status and level of approval

Test, method, or technique	*Applications*	*Drug classes*[a]	*Early stages of use*	*FDA guidance*	*In a monograph*	*In ICH*
Ames test	Genetox	Many		X	X	X *S2(R1)*
Micronucleus	Genetox	Many	X *–X–*	X	X	X *S2(R1)*
In-vitro micronucleus	*Genetox*	*Many*				*S2(R1)*
Comet	*Genetox*	*Many*				*S2(R1)*
PET imaging	Efficacy Toxicity	Neurodrugs		X		
MRI	Imaging soft tissue injury			X		
High-throughput screening	Receptor binding, drug discovery	All types	X			
PET labeling		Anticancer		X		
Monoclonals	Autoimmune diseases	Immunotherapy	X	X		*S6(R1)*
Genomics	Gene expression	Drug toxicity	X *X*	X *For clinical*		
Proteomics	Protein expression		X			
Metabonomics	Metabolic products		X			
Photo cocarcinogenicity evaluation	Detect drug effect on UV-induced tumors	UV-absorbing chemicals [b]	As needed basis	X *—X—*		X *S10 no longer recommends it*
Biomarkers—troponins	Detect cardiac damage	Cardiac drugs	*Qualified biomarker*	X		
Biomarkers for drug-induced nephrotoxicity	*Detect kidney damage*		*Qualified biomarkers*			
QTC-IKR	Detect potential for arrhythmia	All types of drugs		X		X *S7B*
Combinatorial chemistry	SAR, new drug development	All drug classes	X		X	X *Q11*
In vitro substitutes	Cornea, skin, and cardiac cells	Various classes	X			*S10*
NIH 3T3 cell neutral red uptake	*Phototox assay*	*Various classes*				*S10*
Use of prodrugs	Active ingredient protection and delivery	Anticancer *Many*	X	X		
Nanotechnology	Drug formulations	Many drugs	X	*X*		
QSAR for mutagenicity	*Drug impurities*	*All*				*M7*
Transgenic mice	*Carcinogenicity*	*All*				*S1B*

Text in italics as of 2016 and others as of 2005.
[a]Not inclusive; abbreviations.
[b]UV blocking or skin modifying; abbreviations.
Modified from: Copyright 2006 from: *Biological Concepts and Techniques in Toxicology: An Integrated Approach* edited by Jim E. Riviere. Reproduced by permission of Taylor and Francis Group, LLC, a division of Informa plc.

justifiable in terms of cost and timeliness. They generate meaningful toxicity data, are translatable to humans, and address relevant regulatory safety issues (Fig. 1).[19,20]

4.16.3.11 The Continuing Evolution of a Global Consensus on Regulatory Toxicology (ICH, etc.)

There has been a continuing trend of international cooperation among regulatory agencies within the United States, Europe, and Japan to forge a consensus on requirements for safety testing. Some examples of international regulatory agencies and organizations that evaluate and/or validate methodology for drug safety approval include:

CPMP—Committee for Proprietary Medicinal Products
ECVAM—European Center for the Validation of Alternative Methods
EEC—European Economic Community
EMEA—European Agency for the Evaluation of Medicinal Products
EPA—Environmental Protection Agency
FDA-BVM—Bureau of Veterinary Medicine (now Center for Veterinary Medicine)

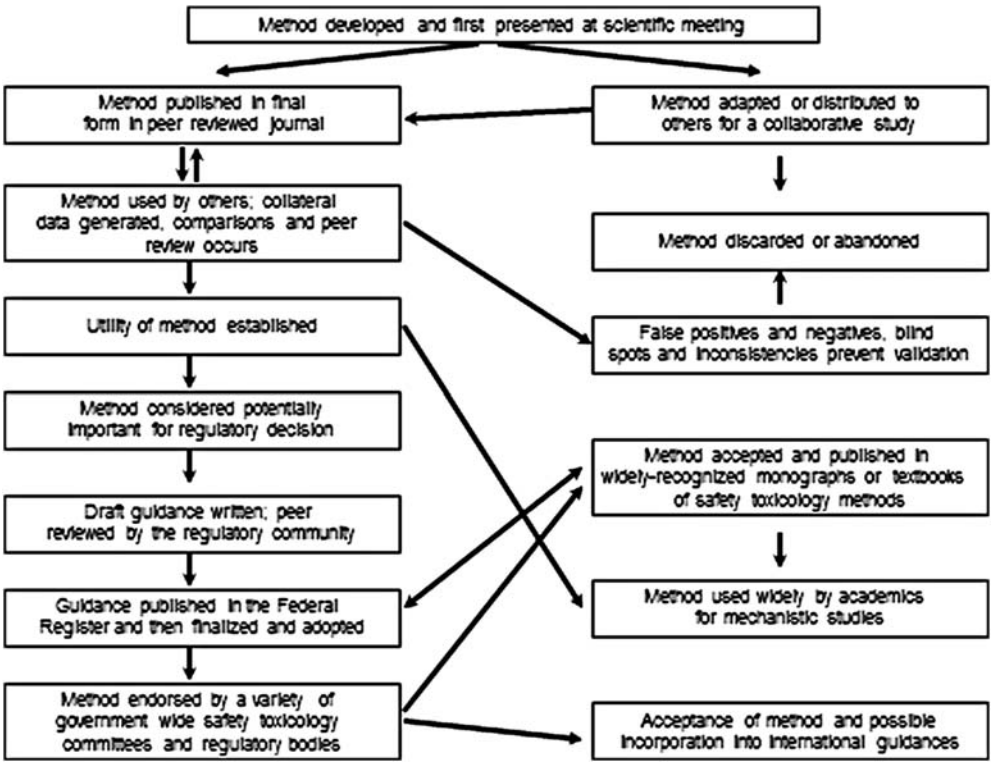

Fig. 1 Decision tree—acceptance of a safety toxicology method. Copyright 2006 from *Biological Concepts and Techniques in Toxicology: An Integrated Approach* edited by Jim E. Riviere. Reproduced by permission of Taylor and Francis Group, LLC, a division of Informa plc.

FDA-CFSAN—Center for Food Safety and Applied Nutrition
FDA-CBER—Center for Biologics Evaluation and Research
FDA-CDER—Center for Drug Evaluation and Research
FDA-CDRH—Center for Devices and Radiological Health
FDA-PTCC—Pharmacology/Toxicology Coordinating Committee (CDER)
HESI—Health and Environmental Sciences Institute
ICCVAM—Interagency Coordinating Committee on the Validation of Alternative Methods
ILSI—International Life Sciences Institute
ICH—International Conference on Harmonization of Technical Requirements for Registration of Pharmaceuticals for Human Use
JPMA—Japanese Pharmaceutical Manufacturers Association
MHLW—Ministry of Health, Labor, and Welfare (Japan)
OECD—Organization of Economic Cooperation and Development
USP—United States Pharmacopeia
Modified from: Copyright 2006 from *Biological Concepts and Techniques in Toxicology: An Integrated Approach* edited by Jim E. Riviere. Reproduced by permission of Taylor and Francis Group, LLC, a division of Informa plc.

Many of these groups meet on a regular basis to discuss safety issues, resolve differences, and arrive at a consensus that ultimately results in the issuance of guidances or guidelines (ICH) for regulatory studies.[17] These may serve as an example of best scientific practice or "state of the art" in terms of the design of preclinical studies that predict toxicity that is translatable to clinical trials. This tendency toward worldwide standardization of requirements for the generation of regulatory preclinical toxicity studies has in many ways been necessitated by the globalization of the pharmaceutical industry where mounting costs make it almost impossible to run multiple sets of safety studies to satisfy different geographical regulatory requirements.[21]

4.16.4 Minimally- or Noninvasive Approaches to Assess Chemical and Drug Effects—Indicators of Efficacy and Toxicity

4.16.4.1 Preclinical Imaging as a Translatable Biomarker

Minimally invasive imaging allows repeated observation of the structure and function of internal organs of laboratory animals under normal conditions and during toxicity or disease onset, progression, and recovery without significantly disturbing the subject.

Certain imaging signatures, or biomarkers, can serve as indicators of treatment efficacy and/or toxicity and can be readily replicated in clinical-imaging studies to ensure and enhance the effectiveness and safety of regulated products.[22]

Preclinical imaging can assist regulatory agencies to address newly developing technologies and the safety of new and existing medicines and other regulated products by (1) developing imaging biomarkers that increase the number of tools available for more thorough safety assessments of new chemicals, medical devices, drugs, and foods to help protect human health and well-being and (2) translating new preclinical methods and biomarkers into the clinical setting that allow scientists to enhance clinical practice, optimize clinical trials, and develop precision/personalized medicine treatments. Likewise, imaging approaches may identify toxicity following environmental chemical exposure.[23,24]

Real-time minimally invasive data collection over the lifetime of an animal model is now possible with the use of bioimaging. New technologies including magnetic resonance imaging (MRI), magnetic resonance spectroscopy, positron emission tomography (PET), optical Imaging, 3-D ultrasound, and computerized tomography are among the approaches available today which have demonstrated utility for safety assessment studies. Non- or minimally invasive imaging is the ideal medium for biomarker development because similar methods can be used in humans and laboratory animals, thus minimizing the assumptions in data interpretation and reducing uncertainty during product development or risk assessment. However, the routine use of imaging approaches for safety assessment studies has been slow to occur in part due to the lack of guidelines for application to traditional animal models and biomarker validation.

4.16.4.2 Emerging Imaging Biomarkers

Neuroimaging has tremendous advantages for identifying potential biomarkers of toxicity, primarily because it is less invasive than other procedures. Additionally, longitudinal studies can be completed and test animals can serve as their own controls. MRI and PET are two imaging techniques of potential utility for monitoring aspects of neurotoxicity (**Table 6**). MRI can provide *in vivo* information on cell toxicity by detecting changes in characteristics of the relevant tissue, such as cellular integrity, cell density, and water redistribution. There are several applicable MRI methods, but T2 relaxation is most useful in this context as it is simple, can result in evenly distributed time course scans, and can produce quantitative maps. Micro-PET imaging allows for functional imaging at the molecular level and thus, can provide valuable insights into biochemical, physiological, and pathological processes during the expression of toxicity *in vivo*.[22,25,26] PET imaging requires positron-emitting ligands which can be designed to track specific end points such as cellular membrane disruption thought to be associated with apoptosis or gliosis. The collection of data over multiple time points within the same subject is just one of the advantages of these imaging methods.

Molecular imaging technologies offer unique opportunities for conducting minimally invasive studies and PET is an imaging modality that is applicable at the molecular level and can provide valuable insights into biochemical, physiological, pathological, and pharmacological processes *in vivo*.[26–30] Dynamic imaging also has great potential to advance our understanding of chemical and drug-related toxicity processes, including those associated with neuronal plasticity, neurodegeneration, and neurotoxicity.[26]

4.16.4.3 Small Animal PET Imaging (Micro-PET)

PET technology was originally developed in the 1960s and the first human brain PET study was performed in 1975.[31,32] Recently, PET has become a relatively routine clinical imaging modality used in the diagnosis of cancer, cardiac disease, and neurological disorders. Similarly, micro-PET for rodents, nonhuman primates, and other animals has developed into an important research tool with increasing spatial resolution.[33–35] Micro-PET imaging provides an excellent bridging platform for extrapolating preclinical data to the human condition.[22]

Radioactive tracers are molecules labeled with short-lived positron-emitting radionuclides such as O-15, N-13, C-11, and F-18. After injection of a radiotracer, the labeled molecule can bind to highly specific targets in the laboratory animal and, thus, characterize the biodistribution of that specific tracer. The radiation emitted by the labeled tracer is then detected by the PET scanner allowing for the detection, localization, and quantification of signal intensity. By utilizing numerous radioactive tracers, multiple biological or pathological processes such as perfusion, metabolism, receptor binding, and protein expression can be qualitatively

Table 6 Different techniques of neuroimaging

Anatomy	*Physiology*	*Metabolism*	*Molecular*	*Functional*
X-Ray	USG	MRSI	PET	fPET
MRI	MRSI	PET	MRI	fMRI
CT	SPECT			OI
USG	PET			IR
	IR			

MRI, magnetic resonance imaging; *CT*, computed tomography; *USG*, ultrasonography; *MRSI*, magnetic resonance spectroscopic imaging; *PET*, positron emission tomography; *SPECT*, single photon emission computed tomography; *IR*, infrared; *fPET*, functional PET; *fMRI*, functional MRI; *OI*, optical imaging.[22]

and quantitatively assessed.[32,33,35] Several radiolabeled tracers have been developed to identify subcellular events associated with programmed cell death or apoptosis, glucose metabolism or microglial activation, and inflammation.[36,37]

4.16.4.3.1 [^{18}F]-Annexin V

In contrast to normal cells, phosphatidylserine (PS), one of the four major phospholipids that make up the cell membrane, externalizes from the intracellular to extracellular side of the plasma membrane in cells undergoing apoptosis.[38–41] The redistribution of PS to the exterior of the cell membrane in the early stages of apoptosis precedes most other apoptotic cascade hallmarks and serves as a signal to macrophages and adjacent normal cells to phagocytize and digest the components of the apoptotic cells.[42–44] Therefore, externalized PS is a target for the early *in vivo* detection of cells undergoing programmed cell death.[45]

4.16.4.3.2 [^{18}F]-DFNSH

[^{18}F]-5-(dimethylamino)-*N*′-(4-fluorobenzylidene) naphthalene-1-sulfonohydrazide ([^{18}F]-DFNSH) belongs to a newly developed group of small tracers that contain a fluorescent dansyl core. One of its advantages is that DFNSH can be synthesized with high yield and efficiency. Previous *in vivo* studies[46] have demonstrated that DFNSH is incorporated in the cytoplasm of different types of apoptotic cells. The mechanism underlying the intracellular uptake of DFNSH may relate, in part, to the complex membrane alterations that occur during apoptosis.[47]

4.16.4.3.3 [^{18}F]-FDG

[^{18}F]-FDG is the most widely used tracer for glucose metabolism assessment in the brain and other tissues and the uptake of [^{18}F]-FDG by neurons can be used to evaluate neuronal metabolic activation.[25,48,49]

4.16.4.3.4 [^{18}F]-FEPPA

CNS injury is often accompanied by an increase in activated microglia at the site. The peripheral benzodiazepine receptor (PBR) is expressed on the outer mitochondrial membrane of activated microglia and has been reported to be a sensitive biomarker for the detection of neuroinflammation. The PBR, also known as translocator protein (18 kDa) (TPSO), was first identified in 1977 and subsequently distinguished from the central benzodiazepine receptor structurally, functionally, physiologically, and pharmacologically.[50,51] In the CNS, PBRs are mainly located in glial cells, particularly microglia and astrocytes, with the highest densities found in the olfactory bulb, choroid plexus, and ependymal lining of the ventricles.[52,53] In the CNS, PBRs participate in multiple physiological functions including neurosteroid synthesis, nutritional support of neurons, and modulation of CNS immune reactions. PBR expression in the brain is significantly increased in response to a wide variety of CNS insults.[54,55]

Experimental results show that such increases in PBR are mainly due to activated glial cells. In response to intercellular signaling induced by neurotoxicant exposure, microglial activation is usually initiated several hours after exposure and can last for several days after injury onset.[56–58] In their activated state, microglia undergo morphological changes, accumulate and proliferate at the damage site, synthesize pro-inflammatory cytokines, and release toxic molecules and metabolites to eliminate damaged cells. Various studies have demonstrated that PBRs are involved in numerous nervous system disorders such as multiple sclerosis, cerebral ischemia and stroke, epilepsy, brain damage, and neurodegenerative diseases.[52,59–62] Following exposure to neurotoxicants or other forms of insult, PBR levels increase significantly in astrocytes and microglia in damaged brain areas in a time-dependent and region-specific fashion. After brain injury, immunolabeling of PBRs has been shown to increase in mitochondria and other cellular compartments.[26,52,63,64]

4.16.4.3.5 [^{18}F]-FLT

FLT, a thymidine analog, is incorporated into cells and phosphorylated by thymidine kinase (TK) 1, leading to its intracellular trapping. The phosphorylated FLT that is trapped within cells does not get incorporated into the cellular DNA because it lacks a 3′-hydroxyl group. TK 1 is a cytosolic isozyme of TK and its activity closely parallels that of cellular proliferation.[65] Therefore, the retention of [^{18}F]-FLT within the cells represents an *in vivo* marker of cell proliferation. [^{18}F]-FLT has been used in conjunction with PET imaging *in vivo* for the minimally invasive detection of endogenous neural stem cell proliferation in the normal and ischemic adult rat brain.[66,67]

4.16.4.4 MRI Applications

Preclinical MRI in laboratory animals can be utilized to target specific brain areas to be examined for classical neuropathology. This approach offers a dramatic improvement over the current practice of selecting three to five routine, but arbitrary brain sections for traditional analyses.[23] Those MRI-targeted areas can be assumed to include the neuropathology produced by exposure to an environmental agent, new or unknown compound, or drug. Because each subject can serve as its own control, longitudinal investigations can provide information on the onset of toxicity and its apex and regression. This advantage can decrease animal usage in routine preclinical toxicological studies and improve the statistical power of the resulting data. This approach also allows for the optimization of time of sacrifice and selection of an appropriate stain for definitive neuropathology. This is particularly important because a large number of neurodegenerative processes occur within a limited time after exposure and the evidence of such neurotoxicity can be scavenged away over time. Thus, use of an appropriate stain at the suboptimal time can result in false negative findings. Just as importantly, MRI images can inform the selection of appropriate stains. For example, if the MRI signal is concentrated in

white matter areas, myelin stains would be indicated. Finally, utilization of whole brain MRI to optimize target location for subsequent neuropathology accomplishes what would typically require more than 60 sections if only routine neuropathology techniques were employed. The impact of this approach on safety evaluation of new drug submissions could be considerable with respect to an enhanced ability to detect potential neurotoxicity by: (1) identifying precise location(s) and time course of drug-induced lesion development; (2) optimizing time of tissue sample collection; and (3) identifying an appropriate histological stain based on lesion location and tissue type (white matter vs. gray matter).

4.16.4.5 Blood-Borne Sampling: DNA Fragments and Micro-RNA

Liquid biopsies or sampling of blood-borne products have the potential to change medical oncology practice by providing a rapid and convenient method to interrogate DNA mutations present in the cell-free DNA fraction of blood via a routine blood draw. This allows for safer (i.e., nonsurgical) and more frequent monitoring as well as strategies to better screen for cancers enabling an earlier diagnosis. Cell-free circulating tumor DNA are small pieces of tumor in the blood (DNA shed products). For many years, researchers have sought to identify a cancer biomarker available with minimal invasion, namely, to find evidence in the blood (a specific molecule) that indicates the presence of disease, especially cancer and neurotoxicity.[68] Many cancers develop slowly and insidiously over a 10–20-year period and are lethal because they are diagnosed too late. Reducing cancer deaths through prevention and early detection, when such cancers are still potentially curable, are important public health strategies. Applications of liquid biopsies include: (1) early cancer detection, (2) assessment of molecular heterogeneity of overall disease, (3) monitoring of tumor dynamics, (4) identification of genetic determinants for targeted therapies, (5) evaluation of early response to therapy, (6) monitoring for minimal residual disease, and (7) assessment of the evolution of resistance to therapy in real time.

4.16.4.6 Three-Dimensional Cell Culture Models With an Emphasis on Neural Stem Cells

Use of stem cell models to explore issues relevant to toxicant-induced brain damage can advance our understanding of brain-related biological processes, including those critical for normal processes such as neural plasticity as well as those associated with the expression of toxicity.[69,70] Advances in the understanding of stem cell biology and neuroscience have opened new avenues of research for detecting early life stress-induced neurotoxicity and developing potential protection/prevention strategies against toxicant-induced neuronal injuries.[71,72] The classical definition of a stem cell requires that it has the capacity to self-renew and that it possesses potency. Self-renewal is defined as the ability of the stem cell to go through multiple cycles of cell division while maintaining its undifferentiated state. Potency refers to the ability of the stem cell to differentiate into specialized cell types.[73,74] Stem cell biology, when exploited with high-throughput molecular biological approaches including genomics, proteomics, and metabolomics, can be utilized to enhance the understanding of complex biological processes—such as apoptosis—that are associated with prolonged pediatric anesthetic exposure or other perinatal exposures. In addition, the study of stem cell biology can provide the building blocks necessary to construct relevant models of developing biological systems. As these models evolve and become integrated, they can provide the intermediate components necessary for informing a developmental biology/toxicology approach. The field of toxicant/drug-related toxicology has employed multiple scientific disciplines in attempts to identify the basic characteristics of chemicals or drugs that can result in harmful, acute, and/or chronic effects on the developing nervous system. Such characteristics continue to be defined at the molecular, biochemical, cellular, and physiological levels. The developing nervous system can vary dramatically in its susceptibility to neurotoxic insults depending on the developmental stage. Because of the complexity and temporal features underlying the expression of developmental neurotoxicity, this area of study may benefit greatly from the use of *in vitro* models including stem cell. Stem cell biology, in the context of toxicological problems, might provide an important focal area around which information can be arrayed in the form of a biological model. The goal of applying a stem cell biological approach to problems in developmental toxicology is to predict the functional outcomes of component-to-component relationships using integral *in vitro* models that allow for the directional and quantitative descriptions of responses at the cellular level. The stimuli that elicit such responses may be environmental alterations, exposures to drugs or other chemicals, or infectious agents.

The development of the CNS is initiated early in life by the induction of neural stem cells and neural progenitor cells; this stage in development is known as neural induction. The nervous system is one of the earliest organ systems to differentiate from the blastula-stage embryo. Neurogenesis is critical for nervous system development and maintenance. During neurogenesis, neural stem cells generate neural progenitors that mature into functional neurons. Pharmacological enhancement of neurogenesis represents a potential therapeutic approach for the treatment of the neuronal loss occurring in neurodegenerative diseases, such as stroke, brain damage, Parkinson's disease, and Alzheimer's disease.[71,72] Accordingly, there is great interest in using neural stem cells as tools for studying the adverse effects associated with exposure to drugs and other compounds.

4.16.4.7 Microphysiological Models

Recent advances in biomedical research have offered a broad range of approaches and tools that have enhanced our capability to practice evidence-based medicine and evidence-based regulation and thereby to improve human health. "Human-on-a-chip" and "human organ construct" microphysiological systems are new and emerging technologies that have the potential to correlate *in vivo* with *in vitro* and to simulate human organ systems. The human-on-a-chip technology uses *in vitro* human organ constructs in which the various cells communicate. Those chips and constructs are designed to reflect biological activity similar to the *in vivo* situation.

The organ on a chip can then be used to determine if drugs and chemicals can elicit *in vitro*, the physiological activity of a human organ observed *in vivo*. These microphysiological systems have the potential to be used to assess basic biology and physiology, as well as the pharmacology and toxicology of drugs and chemicals, to study organ–organ interactions, and/or to be used as a human disease model.[75]

The use of human cells is an enormous advantage because it eliminates the need to extrapolate across species, but even so, there may be the requirement that different cell types interact in a three-dimensional relationship in order to provide prediction of the intact human. The immediate environment of the cells in culture, including cell types (single or multiple origins), the need for specialized media to keep them in a differentiated state (e.g., presence of growth factors, cytokines, and other hormones), and the three-dimensional configuration can all affect outcome measures. Many animal stem cell studies have provided the principles and strategy for the use of human stem cells in 3-D and other organotypic *in vitro* models.

Another important consideration of simulating human outcomes is the quantification of chemical exposure. Absorption, distribution, metabolism, and elimination are features that must be quantified. The linking together of several organs on a chip to simulate an intact human on a chip is a possibility with well-constructed and well-tuned fluid dynamic systems. Microfluidic control of multiple organ systems is possible, and models envisioned by bioengineers have been developed. The challenges include the requirement for each organ type to have its own specialized media yet be connected so that the human circulatory system can be replicated.

4.16.4.8 Computational Toxicology

The applications of computational sciences, including bioinformatics and "big data," have great potential to improve the health and well-being of our communities through the development and use of chemicals, drugs treatments, and tools to manage the safety of foods and drugs. Examination of the "state of the art" in global trends, initiatives, and case studies reveals that data sets, analytical tools, skills, and expertise are rapidly developing, in many cases via large international collaborative consortia. However, significant research is still required to realize the potential regulatory applications of those technologies. While there is significant excitement in the possibilities offered by precision medicine to enhance treatments of serious and/or complex diseases, there is a clear need for further development of mechanisms to securely store, curate, and share data, integrate databases, and standardize quality control and data analysis procedures. Greater understanding of the biological significance of the data is also required to fully exploit vast data sets that are becoming available. The application of bioinformatics in the microbiological risk-analysis paradigm is delivering clear benefits both for the investigation of food-borne pathogens and for decision-making on clinically important treatments. While computational sciences and the advent of big data will have many beneficial applications, high-quality data, validated tools, and standardized processes will inform the regulatory science required to ensure the appropriate introduction of these applications.[76]

4.16.4.9 Global Trends, Initiatives, and Opportunities of Bioinformatics Approaches and Big Data

Emerging technologies are providing new opportunities to improve the health of our communities through the development and use of clinically important drugs treatments and tools to manage the safety of the food supply. Those technologies continue to rapidly generate and utilize large data sets for regulatory application. However, the use of such data sets also requires the development of policies, strategies, and approaches to appropriately curate, analyze, and interpret the data. This uniform understanding will strengthen the scientific evidence base and those advanced methodologies will produce tools to support regulatory decision-making, drug development, clinical application, and improved management of the food supply. Initiatives are underway globally aim to strengthen evidence-based application, thereby maximizing the opportunities made available by the emerging technologies.

Technologies such as next-generation sequencing (NGS) combined with bioinformatics analysis, have the potential to revolutionize food safety and the disease treatment. NGS enables human genomes to be sequenced rapidly and cost effectively, and tools are now available for analyzing the resulting large data sets, providing a mechanism for treating patients individually to enhance health outcomes as well as improving the success rate in the development of new therapeutic treatments. Individual treatment of patients or small groups of like patients (precision or personalized medicine) could take into account their genetic variation, environment, and lifestyle.[76]

To address these challenges, several countries/regions are implementing programs to support the application of precision medicine.[77] The United States is implementing the multifaceted Precision Medicine Initiative to develop high quality, curated databases, and interoperable standards and requirements that address privacy and enable secure exchange of data across systems. This initiative is focused on the determination of genomic drivers of diseases such as cardiovascular disease or cancer and identification of appropriate biomarkers. Those biomarkers can then be used to develop more effective treatments and improve understanding of the environmental, genetic, biochemical, and other factors predictive of disease risk, response to therapy, and disease outcomes.[78]

The current situation for NGS resembles the challenges faced about 10 years ago when microarray technologies were the principal tool for gene expression assessment. At that time, the realization generated a number of FDA efforts to utilize and evaluate those technologies with intercenter and cross-community collaborations. Examples include the FDA's Voluntary Exploratory Data Submission program to develop standards and bioinformatics solutions to receive and evaluate those new data in the review process[79] and the FDA-led community-wide microarray quality control consortium to address quality control and proper use of those new genomic methodologies.[80] Therefore, partnerships and cooperation among the regulatory agencies of different countries

are crucial for building consensus and best practices to expedite the translation from the exploratory nature of NGS to regulatory application.

Recent developments in the tools and applications of predictive toxicology are also significantly changing the way in which the risk of adverse events is assessed for chemicals used as drugs, and those added to foods or used for other purposes. One of the methodological approaches, quantitative structure-activity relationships (QSARs) is a well-established multidisciplinary methodology that integrates biological, chemical, and computational models to provide a new paradigm for chemical risk assessment.[81] Barriers to the acceptance of QSARs in regulatory settings range from scientific concerns (e.g., relevance, reliability, and interpretability) and practical considerations (e.g., availability and ease of use, portability/interoperability), to policy change that permit paradigm shifts that could incorporate QSARs into a modern toxicological framework with comprehensive assessment and credible outcomes. Those barriers have been addressed through the initiatives of regulatory agencies and multilateral bodies. Scientific concerns have been addressed for the use of QSARs through the development of globally accepted reporting formats for models and predictions and also guidance on how to interpret the prediction results. Guidance on use of QSARs for pesticides and other chemical categories has been established.[82] QSAR may also be used in concert with other strategies, thus positioning QSAR models as a part of integrated approaches to testing and assessment.

4.16.4.10 Application of Bioinformatics

Bioinformatics and novel approaches to using big data offer exciting possibilities for developing targeted medicine and therapeutics as well as postmarket monitoring of the safety of drugs. Personalized/precision medicine is the way of the future.[83] Significant resources are being devoted to realizing the potential of this approach that involves cross-sector collaborations and multidisciplinary approaches. A range of data sources and bioinformatics techniques are being exploited in the development of those approaches, such as electronic health records, patient data, genomic sequences, metadata, and predictive toxicology.

Many different types of big data exist and the power of analysis and data mining is generated from the analysts' ability to integrate many different layers of data sets for the synthesis of new information. Big data can include both structured and unstructured data sets and can be records with narratives and descriptors as well as databases of reports of adverse effects. In some cases, each database may require its own lexicons and rules. To support good regulatory decision-making, data sets must be of good quality, robust, verified, and have sufficient metadata. Big data poses new regulatory challenges and require new skill sets and new knowledge for successful interpretation.

4.16.5 Lessons Learned and Challenges That Reflect and Focus on Contemporary Critical Issues

1. Carcinogenicity testing of drugs need not be compulsory or obligatory, especially 2-year studies, if appropriate genetic and mutagenicity testing is negative.
2. Heavy funding cannot always buy technological advancement; time elapsed to allow the maturation of the technology as well as the development of collateral tools is often also required.
3. *In vitro* models have played a very important role in advancing the science of toxicity prediction, but there remain instances when the use of whole animal models is unavoidable and obligatory.
4. Toxicity prediction cannot rely solely on technological advances; insight into fundamental biological processes is not only necessary but critically needed to advance knowledge that is necessary to fully understand observed toxicological phenomenology.
5. Mechanistic toxicology studies cannot be conducted until the toxicological phenomenology is reliably and robustly reproduced in successful experiments that form the basis and foundation for mechanistic experiments.
6. The value of nonclinical studies relies heavily on the extent to which findings are translatable to clinical trials. A large percentage of animal models have been shown to translate poorly, particularly those involving sensory perception of pain by higher centers. For example, tail flick response in mice is a cord reflex and does not serve to measure pain originating in higher centers in the brain. Another modeling issue involves measurement of immunotoxicity, which is poorly characterized in rodents unless they are humanized.
7. Delivery of drugs to alveolar areas of the lungs is poorly understood since concentrations within that domain are rarely measured in contrast to aerosol concentrations and particle size distributions delivered to the nose and mouth that have been well characterized.
8. The period for chronic drug exposure has been progressively reduced from 7 years in dogs and 10 years in nonhuman primates, 40–50 years ago, to 6 months in rats despite the fact that certain approved drugs are given to older patients with chronic progressive diseases for the rest of their lives.
9. There is no formal testing of drugs for toxicity in geriatric animal models, although drugs are given to older patients for very long durations.

4.16.6 Horizons—A Vision of Future Directions for Toxicity Prediction and Safety Evaluation

Prediction of toxic responses has and will continue to benefit from the many technological breakthroughs described in this article (see **Table 7**). The capacity to image the brain in the living animal and in conscious humans opens up a whole new set of

Table 7 Critical issues and challenges for emerging technologies and methodologies

Genomics	Gene expression not necessarily always correlated with toxicity; comparison and validation of various platforms still in progress; informatics efforts to interpret data at an early stage; statistical models still being developed
	Refinement of initial statistical and interpretation models underway with exposure, agent metabolites, and stage of development issues under consideration
Proteomics	Labor intensive; correlation with toxicity in early stages
	Throughput still an issue, but new statistical approaches and chemical libraries are coming available
Metabolomics	Initial cost and resource outlay is quite extensive; relies more on pattern recognition than recognition of individual metabolites
	Powerful translational approach because of minimally invasive nature; analysis time shrinking based on faster software
Lipidomics	*A new and emerging technology that allows the analysis of 1100 or more lipids in a single sample. A very promising approach for characterizing CNS toxicity, particularly in brain samples*
PET imaging	Issues involving sensitivity and resolution
	Development of specific ligands has afforded unprecedented selectivity for identifying cancers and CNS metabolism
MRI	Very expensive initial outlay; limitations on acceptable or approved field strength for human studies impacts resolution; still extremely expensive and not widely used by preclinical researchers
	Although standards for preclinical assessments have not been universally accepted, cost-saving approaches for time and location of sample analysis has been developed
Biomarkers for toxicity	Issues of specificity; may be nonspecific, for example, generalized inflammation; not many validated for safety toxicity evaluation
	Guidelines for biomarker validation have been used to develop acceptable biomarkers for regulatory decision-making. Qualification of a biomarker for a specific context of use is now a commonly accepted practice
High-throughput screening	Very resource intensive; used only by very large well-endowed organizations; cross validation difficult
	Major data sets have been generated and data made available for many researchers to evaluate
Photo cocarcinogenesis	Expensive; chronic duration; uses many hairless mice
	New transgenic animals have reduced time to tumor and are undergoing assessment
Ames test	Does not detect the mutagenic effects of some antibiotics, metals, or proteins
	New more inclusive genetic tests have been developed that allow multiple species and tissue types to be evaluated
QTC–IKR	Does not directly correlate with Torsade de Points, but relates to the K^+ channels which is the first step in the production of arrhythmias
	In vitro approaches have been developed, but not fully accepted to assess cardiovascular toxicities
Combinatorial chemistry	Lack of sufficient information on novel chemical classes to make decisions; requires a large database; often requires large amount of proprietary information that must be protected and/or is not available to all
	New bioinformatics and NMR-based strategies have been developed and are undergoing validation
In vitro substitutes	Lack of immunocompetency; repair mechanisms absent; still need to use animals for tissue and cell harvesting
	Stem cells/3-D cell culture and microphysiological systems are under development
Nanotechnology	Methodology for safety evaluation in its infancy; toxicity of nanoparticles and nanoparticlized drugs relatively unexplored
	Several nanomedicines have been approved and standards for general assessments are under development

Statements in italics as of 2016 and others as of 2005.
Modified from: Copyright 2006 from *Biological Concepts and Techniques in Toxicology: An Integrated Approach* edited by Jim E. Riviere. Reproduced by permission of Taylor and Francis Group, LLC, a division of Informa plc.

opportunities to observe the ongoing physiology of this vital organ. The life cycle of a toxic agent can be observed in real time through its many stages which allows optimization of time of animal sacrifice, location of specific brain areas for sectioning as well as the choice of histological stains. This is necessary for precise visualization and characterization of the nature and extent brain lesions. The use of various imaging software algorithms can be utilized to quantify the extent of brain lesions, using precise cell counts, as a percentage of the overall section examined.[84]

The utilization of various imaging modalities will allow for the characterization of many aspects of thought processes (pathway sequences) that may be influenced by a variety of new psychotomimetic drugs intended for therapeutic purposes, but not without the potential for neurotoxicity. This is of particular importance when these agents are intended for use in children whose nervous systems are not yet mature and where normal future development may be inadvertently disrupted. Real-time imaging of the mechanism of action of drugs as they interact with diseased or damaged areas of the nervous system might allow the optimization of dosing regimens, as well as the prevention of drug-induced toxicity that might occur with overexposure or persistence in the brain.

Another exciting area that has begun to emerge is the use of humanized rodents (mice) for toxicity testing. This animal model is particularly useful for prediction of immunotoxicity in humans resulting from administration of large, high-molecular-weight therapeutic proteins. The humanized mouse has the potential to emulate these effects and allow characterization of their incidence and progression. This type of toxicity evaluation was previously unattainable because of species differences in immunomechanisms.[85]

Another area that has great potential for enlarging the scope of toxicity prediction is the characterization of the human microbiome with its potential for influencing the toxic outcome of a vast array of drugs that are administered orally.[86] Very little attention has been paid to the role of the gut flora in influencing drug action and toxicity. Characterization of the microbiome in patients that have a particular disease and humanizing the microbiome of the animal model for evaluating drug toxicity might, if translatable, vastly improve the prediction of toxicity of certain drugs in preclinical studies.

The use of microphysiological systems to simulate the dynamic functions of various organs is a big step forward beyond the routine use of varies types of cell culture systems. These may allow rapid *in vitro* screening of drugs with the additional advantage of incorporating physiological mechanisms that involve flow (microfluidics) and motion characteristics. An excellent example of this is the so-called "lung on a chip" which has an alveolar cell layer that has a "vascular" side with simulated blood flowing past it and an air or "lung" side. Mechanical distortion of this layer of cells simulating breathing allows lung function to be emulated. Bacteria introduced on the air side are quickly killed by the blood interface on the other side. This is a very valuable model for testing agents to counteract lung infection. The model is only really effective when respiration is simulated by the mechanical distortion of the alveolar cell layer.[87,88]

Nanotechnology has yielded a significant number of new nanoformulated drugs. At present, the FDA treats these new submissions as all others in terms of evaluation for safety and efficacy. This appears to be appropriate in the absence of any significant unique nanospecific adverse effects. There are, however, certain nanoformulation characteristics that have the potential to generate toxicity prediction issues in the future.[89] These include: (a) characterization of particle size distribution and standardization of individual particle size distribution, (b) stoichiometry (e.g., does a mole of nanoformulated drug have the same potency or toxicity as the same drug substance formulated using particles with standard size distributions or is potency and toxicity a function of particle area exposed to a tissue or receptor), (c) What is the distribution and disposition of dendrimers (nanoparticles) once they deliver drug to a target. Do they then accumulate in organs such as liver and spleen and are they toxic at these sites? What is the biological half-life of these "delivery shells" and what is the nature of their toxicity (vacuolation, etc.)?

The "omic" technologies have seen an explosion of new innovation that promises to generate a significant boost in the available capabilities for toxicity prediction. In the last 10 years, genomics has had the benefit of vastly improved and refined statistical and interpretation models. There are now libraries available to characterize genes that are significantly altered in their levels of expression by drug treatment. These tools are able to relate those alterations to physiological and pathological processes, some of which are reflective of significant toxicity. Proteomics is still quite labor intensive; however, there are data libraries and statistical approaches to identify vast arrays of peptides and characterize and utilize pattern recognition tools (principle component analysis, etc.) to identify global changes that have toxicological significance. The use of mass spectrometry and capillary electrophoresis has accelerated the analytical portion of the process. Metabolomics has made significant strides in terms of shortening analysis time with faster software that relates findings to significant treatment-related metabolic changes that are directly relatable to significant toxicologic effects.

Lipidomics offers the most recent exciting addition to the "omic" technologies and offers great promise in identifying treatment-induced toxic changes in the nervous system. This has been a largely ignored area for toxicity prediction, especially in light of the fact that the brain has the highest percentage of lipids, second only to adipose tissue itself. Analysis of changes in brain and spinal cord lipids may vastly alter our overall concept of toxicity patterns in the nervous system.[90,91]

The imaging technologies, discussed extensively earlier, offer significant opportunities for new types of toxicity prediction and detection, especially in the nervous system. The ability to do this in the living organism, in real time, (in the conscious state in humans) is a very exciting prospect, especially since cost is decreasing and MRI is rapidly becoming a biomarker for toxicity. PET imaging, which in the past has had sensitivity and resolution issues, is seeing the development of specific ligands for identifying cancers and providing a window on CNS metabolism that informs toxicity-predictive efforts.

Structure-activity relationships (SAR) and computer modeling offer many opportunities for expanding future capabilities for toxicity prediction. The development of reliable SAR modules for various classes of toxicity based on large chemical structure data sets gives both the researcher and the NDA reviewer a first glance at the potential for toxicity of new compounds. This process is based on algorithms that detect chemical signals embedded in the structure of new compounds under investigation and determine their similarity to the virtual toxicophore that is generated by the data set within the module for a given type of toxicity.[92] The sensitivity and selectivity of some of these modules is rather impressive (80–90%), particularly for carcinogenicity. This type of analysis represents the very first tier of toxicity evaluation that endeavors to predict what might be seen in subsequent tiers of investigation: *in vitro* → animal species → humans. SAR evaluation will play a larger role as a prelude to the use of ever improving *in vitro* models which precedes the use of animals in preclinical studies.[93]

The use of computer models has already begun to play a rather large role in toxicity prediction.[94] Target organ function, involving the physiological, pharmacological, and pathological responses are being modeled in silico, following the "virtual" administration of drugs and toxic agents. In other systems whole body physiological responses to virtual drug stimuli are being modeled and are generating responses that are referred to as those of a "virtual human." The latest frontier in the use of computer modeling involves the use of search engines that launch the so-called "spiders" that search the vast array of published information in millions of publications on the Internet using tools to read and interpret written language. They gather bits and pieces of information from a myriad of sources and compare and combine them to synthesize new information entities. These consist of answers to posed questions and various new conclusions based on the combination of information from different sources. This approach could be one of the ultimate tools used to advance toxicology prediction in the near and possibly distant future.[95]

4.16.7 Conclusions

The prediction of toxic responses is a constantly evolving science whose methodology is advanced by technological innovations that are often driven by regulatory imperatives stemming from adverse effects reports and, at times, occasional catastrophic incidents

that trigger legislative remediation. At times, legislation can indirectly or secondarily give birth to a whole new subdiscipline of toxicology such as alternatives to animal testing that resulted from the passage of the Animal Welfare Act, the formation of Institutional Animal Care and Use Committees (IACUCs), as well as the establishment of powerful animal welfare coalitions. The specter of being unable to work with animals on the same scale as in the past has given a tremendous boost to the development of very elegant *in vitro* systems, advances in tissue and organ culture, and the so-called organ or organism on a chip. The development and validation of a whole series of important biomarkers for toxicity has greatly streamlined the process and shortened the time involved in new drug development and approval. These biomarkers are qualified for a very specific context of use and have often detected significant toxicity of lead compounds in preclinical stages of testing rather than Phase 2 of clinical trials saving enormous amounts of money (often three orders of magnitude in dollars spent) and, more importantly, prevented adverse effects, suffering, and possible deaths in clinical trials. The advances made in toxicological methodology have made it possible to reduce drug lag and eventually enable the passage of prescription and ultimately generic drug user fee legislation (PDUFA and GDUFA) that has brought enormous amounts of funding to support the federal drug evaluation process and allowed the fulfillment of very tight evaluation deadlines. This has greatly accelerated the approval process without compromising safety or confirmation of efficacy. Finally, the astounding advances in various types of imaging (discussed earlier) have not only opened a brand new set of opportunities to evaluate toxicity, noninvasively in a multitude of organ systems in living organisms, but has given a brand new insight into fundamental aspects of human biology and physiology. The partnership between the science of predictive toxicology and legislative regulatory initiatives has contributed greatly to the advancement of each of these activities and this complementary relationship has contributed considerably to the enhancement of quality of life.

Acknowledgments

The authors wish to thank Drs. Paul Brown, John Lipscomb, and Sherry Ferguson for their excellent advice and suggestions concerning this article. Disclaimer: This document has been reviewed in accordance with United States Food and Drug Administration (FDA) policy and approved for publication. Approval does not signify that the contents necessarily reflect the position or opinions of the FDA. The findings and conclusions in this report are those of the authors and do not necessarily represent the views of the FDA.

References

1. Sinclair, U. *The Jungle;* Grosset and Dunlap: New York, 1906.
2. Lamb, R. D. *American Chamber of Horrors;* Grosset and Dunlap: New York, 1936.
3. Horton, L. R.; Hoog, T. C.; Stiff, M. J.; Levine, A. N. *Compilation of Food and Drug Laws;* The Food and Drug Law Institute: Washington, DC, 1993.
4. Milestones in U.S. Food and Drug Law History. http://www.fda.gov/aboutfda/whatwedo/history/milestones/ucm081229.htm.
5. The Toxic Substances Control Act of 1976. https://www.epa.gov/laws-regulations/summary-toxic-substances-control-act.
6. Daily Environment Report, 111 DEN B-1, 6/9/16, 06/09/2016. Copyright © 2016 by The Bureau of National Affairs, Inc. (800-372-1033) http://www.bna.com.
7. The Editorial Committee. *Appraisal of the Safety of Chemicals in Foods, Drugs and Cosmetics;* The Association of Food and Drug Officials of the United States: Topeka, 1959.
8. Appraisal of the Safety of Chemicals in Foods, Drugs, and Cosmetics, by the staff the Division of Pharmacology, Food and Drug Administration Department of Health, Education and, Welfare; Association of Food & Drug Officials of the United States: Austin, Tex., 1959.
9. Oser, B. L. Book Review. *J. Occup. Med.* **1960,** 105–106.
10. Division of Pharmacology, Food and Drug Administration, Department of Health, Education and Welfare. *Appraisal of the Safety of Chemicals in Foods, Drugs and Cosmetics;* The Association of Food and Drug Officials of the United States: Topeka, Kansas, 1965.
11. Goldenthal, E. L. Current Views on Safety Evaluation of Drugs; FDA Papers; Government Printing Office: Washington, DC, 1968; pp 2–8.
12. U.S. Food and Drug Administration, Bureau of Foods. *Toxicological Principles for the Safety Assessment of Direct Food Additives and Color Additives Used in Food (Redbook I);* National Technical Information Service: Springfield, VA, 1982.
13. *Redbook 2000—Guidance for Industry and Other Stakeholders. Toxicological Principles for the Safety Assessment of Food Ingredients.* U.S. Department of Health and Human Services Food and Drug Administration, Center for Food Safety and Applied Nutrition, July 2000; Updated July 2007.
14. Food, Drug and Cosmetic Act as amended in 2011. http://google2.fda.gov/search?client=FDAgov&proxystylesheet=FDAgov&output=xml_no_dtd&site=FDAgov&requiredfields=-archive:Yes&sort=date:D:L:d1&filter=1&ie=UTF-8&ulang=en&access=p&entqr=1&entqrm=0&wc=200&wc_mc=1&oe=UTF-8&ud=1&q=food+drug+and+cosmetic+act+amended+in+2011&&start=10.
15. Toxicology in the 21st Century (Tox21)–Tox21–NIH–National Center for Advancing Translational Sciences website: https://ncats.nih.gov/tox21/about/goals.
16. Jacobson-Kram, D.; Keller, K. A. *Toxicological Testing Handbook,* 2nd ed; Informa Healthcare, Inc.: New York, 2006.
17. ICH Guidelines on Safety Evaluation of Drugs: http://www.ich.org/products/guidelines/safety/article/safety-guidelines.html.
18. Ellis, A.; Hastings, K. L. Nonclinical Safety Testing of Pharmaceuticals. In *Toxicological Testing Handbook;* Jacobson-Kram, D., Keller, K. A., Eds.; Informa Healthcare: New York, 2004; pp 465–478, 2nd ed.
19. Hanig, J.; Osterberg, R. Drug Safety Toxicology. In *Biological Concepts and Techniques in Toxicology;* Reviere, J. E., Ed.; Informa, Taylor Francis Group: New York, 2006; pp 249–271.
20. ASPET 2016 Annual Meeting, Symposium: Beyond Traditional Assessments of Pain: Implications for Drug Discovery of Novel Pain Therapeutics, April 4, 2016, San Diego, CA.6*Reproduced with permission from Daily Environment Report, 111 DEN B-1, 6/9/16, 06/09/2016. Copyright © 2016 by The Bureau of National Affairs, Inc. (800-372-1033). http://www.bna.com.
21. Slikker, W., Jr.; Miller, M. A.; Lou Valdez, M.; Hamburg, M. A. Advancing Global Health Through Regulatory Science Research: Summary of the Global Summit on Regulatory Science Research and Innovation. *Regul. Toxicol. Pharmacol.* **2012,** *62* (3), 471–473.
22. Pogge, A.; Slikker, W., Jr. Neuroimaging: New Approaches for Neurotoxicology. *Neurotoxicology* **2004,** *25,* 525–531.
23. Hanig, J.; Paule, M. G.; Ramu, J.; Schmued, L.; Konak, T.; Chigurupati, S.; Slikker, W., Jr.; Sarkar, S.; Liachenko, S. The Use of MRI to Assist the Section Selections for Classical Pathology Assessment of Neurotoxicity. *Regul. Toxicol. Pharmacol.* **2014,** *70* (3), 641–647; Allen, R. T.; Hunter, W. J.; Agrawal, D. K. Morphological and Biochemical Characterization and Analysis of Apoptosis. *J. Pharmacol. Toxicol. Methods* **1997,** *37,* 215–228.

24. Liachenko, S.; Ramu, J.; Konak, T.; Paule, M. G.; Hanig, J. Quantitative Assessment of MRI T2 Response to Kainic Acid Neurotoxicity in Rats In Vivo. *Toxicol. Sci.* **2015,** *146* (1), 183–191; Bading, J. R.; Shields, A. F. Imaging of Cell Proliferation: Status and Prospects. *J. Nucl. Med.* **2008,** *49* (Suppl 2), 64S–80S.
25. Chen, Y. Y.; Shih, Y. Y.; Chien, C. N.; Chou, T. W.; Lee, T. W.; Jaw, F. S. MicroPET Study of Brain Neuronal Metabolism Under Electrical and Mechanical Stimulation of the Rat Tail. *Nucl. Med. Commun.* **2009,** *30,* 188–193.
26. Zhang, X.; Paule, M. G.; Wang, C.; Slikker, W., Jr. Application of microPET Imaging Approaches in the Study of Pediatric Anesthetic-Induced Neuronal Toxicity. *J. Appl. Toxicol.* **2013,** *33* (9), 861–868.
27. Phelps, M. E. Positron Emission Tomography Provides Molecular Imaging of Biological Processes. *Proc. Natl. Acad. Sci. U. S. A.* **2000,** *97,* 9226–9233.
28. Myers, R. The Biological Application of Small Animal PET Imaging. *Nucl. Med. Biol.* **2001,** *28,* 585–593.
29. Chatziioannou, A. F. Molecular Imaging of Small Animals With Dedicated PET Tomographs. *Eur. J. Nucl. Med. Mol. Imaging* **2002,** *29,* 98–114.
30. Luker, G. D.; Sharma, V.; Piwnica-Worms, D. Visualizing Protein–Protein Interactions in Living Animals. *Methods* **2003,** *29,* 110–122.
31. Hutchins, G. D.; Miller, M. A.; Soon, V. C.; Receveur, T. Small Animal PET Imaging. *ILAR J.* **2008,** *49,* 54–65.
32. Schnockel, U.; Hermann, S.; Stegger, L.; Law, M.; Kuhlmann, M.; Schober, O.; Schafers, K.; Schafers, M. Small-Animal PET: A Promising, Non-Invasive Tool in Pre-Clinical Research. *Eur. J. Pharm. Biopharm.* **2010,** *74,* 50–54.
33. Myers, R.; Hume, S. Small Animal PET. *Eur. Neuropsychopharmacol.* **2002,** *12,* 545–555.
34. Hume, S. P.; Myers, R. Dedicated Small Animal Scanners: A New Tool for Drug Development? *Curr. Pharm. Des.* **2002,** *8,* 1497–1511.
35. Lancelot, S.; Zimmer, L. Small-Animal Positron Emission Tomography as a Tool for Neuropharmacology. *Trends Pharmacol. Sci.* **2010,** *31,* 411–417.
36. Tait, J. F. Imaging of Apoptosis. *J. Nucl. Med.* **2008,** *49,* 1573–1576.
37. Berridge, M. S. A. S.; Hersh, J. M. Teflon Radiolysis as the Major Source of Carrier in Fluorine-18. *J. Labelled Compd Radiopharm.* **2009,** *52,* 543–548.
38. Allen, R. T.; Hunter, W. J.; Agrawal, D. K. Morphological and Biochemical Characterization and Analysis of Apoptosis. *J. Pharmacol. Toxicol. Methods* **1997,** *37,* 215–228.
39. Fadok, V. A.; Voelker, D. R.; Campbell, P. A.; Cohen, J. J.; Bratton, D. L.; Henson, P. M. Exposure of Phosphatidylserine on the Surface of Apoptotic Lymphocytes Triggers Recognition and Removal by Macrophages. *J. Immunol.* **1992,** *148,* 2207–2216.
40. Lahorte, C. M.; Vanderheyden, J. L.; Steinmetz, N.; Van de Wiele, C.; Dierckx, R. A.; Slegers, G. Apoptosis-Detecting Radioligands: Current State of the Art and Future Perspectives. *Eur. J. Nucl. Med. Mol. Imaging* **2004,** *31,* 887–919.
41. Saraste, A.; Pulkki, K. Morphologic and Biochemical Hallmarks of Apoptosis. *Cardiovasc. Res.* **2000,** *45,* 528–537.
42. Schlegel, R. A.; Williamson, P. Phosphatidylserine, a Death Knell. *Cell Death Differ.* **2001,** *8,* 551–563.
43. Strauss, H. W.; Blankenberg, F.; Vanderheyden, J. L.; Tait, J. Translational Imaging: Imaging of Apoptosis. *Handb. Exp. Pharmacol.* **2008,** *185,* 259–275.
44. Yagle, K. J.; Eary, J. F.; Tait, J. F.; Grierson, J. R.; Link, J. M.; Lewellen, B.; Gibson, D. F.; Krohn, K. A. Evaluation of 18F-Annexin V as a PET Imaging Agent in an Animal Model of Apoptosis. *J. Nucl. Med.* **2005,** *46,* 658–666.
45. Zhang, X.; Paule, M. G.; Newport, G. D.; Zou, X.; Sadovova, N.; Berridge, M. S.; Apana, S. M.; Hanig, J. P.; Slikker, W., Jr.; Wang, C. A Minimally Invasive, Translational Biomarker of Ketamine-Induced Neuronal Death in Rats: MicroPET Imaging Using 18F-Annexin V. *Toxicol. Sci.* **2009,** *111,* 355–361.
46. Zeng, W.; Yao, M. L.; Townsend, D.; Kabalka, G.; Wall, J.; Le Puil, M.; Biggerstaff, J.; Miao, W. Synthesis, Biological Evaluation and Radiochemical Labeling of a Dansyl-hydrazone Derivative as a Potential Imaging Agent for Apoptosis. *Bioorg. Med. Chem. Lett.* **2008,** *18,* 3573–3577.
47. Zhang, X.; Paule, M. G.; Newport, G. D.; Sadovova, N.; Berridge, M. S.; Apana, S. M.; Kabalka, G.; Miao, W.; Slikker, W., Jr.; Wang, C. MicroPET Imaging of Ketamine-Induced Neuronal Apoptosis With Radiolabeled DFNSH. *J. Neural Transm.* **2011,** *118,* 203–211.
48. Ohashi, K.; Ichikawa, K.; Chen, L.; Callahan, M.; Zasadny, K.; Kurebayashi, Y. MicroPET Detection of Regional Brain Activation Induced by Colonic Distention in a Rat Model of Visceral Hypersensitivity. *J. Vet. Med. Sci.* **2008,** *70,* 43–49.
49. Paul, A. K.; Lobarinas, E.; Simmons, R.; Wack, D.; Luisi, J. C.; Spernyak, J.; Mazurchuk, R.; Abdel-Nabi, H.; Salvi, R. Metabolic Imaging of Rat Brain During Pharmacologically-Induced Tinnitus. *Neuroimage* **2009,** *44,* 312–318.
50. Braestrup, C.; Albrechtsen, R.; Squires, R. F. High Densities of Benzodiazepine Receptors in Human Cortical Areas. *Nature* **1977,** *269,* 702–704.
51. Papadopoulos, V.; Baraldi, M.; Guilarte, T. R.; Knudsen, T. B.; Lacapere, J. J.; Lindemann, P.; Norenberg, M. D.; Nutt, D.; Weizman, A.; Zhang, M. R.; Gavish, M. Translocator Protein (18 kDa): New Nomenclature for the Peripheral-Type Benzodiazepine Receptor Based on Its Structure and Molecular Function. *Trends Pharmacol. Sci.* **2006,** *27,* 402–409.
52. Lang, S. The Role of Peripheral Benzodiazepine Receptors (PBRs) in CNS Pathophysiology. *Curr. Med. Chem.* **2002,** *9,* 1411–1415.
53. Imaizumi, M.; Briard, E.; Zoghbi, S. S.; Gourley, J. P.; Hong, J.; Fujimura, Y.; Pike, V. W.; Innis, R. B.; Fujita, M. Brain and Whole-Body Imaging in Nonhuman Primates of [11C] PBR28, a Promising PET Radioligand for Peripheral Benzodiazepine Receptors. *Neuroimage* **2008,** *39,* 1289–1298.
54. Zhang, X.; Paule, M. G.; Newport, G. D.; Liu, F.; Callicott, R.; Liu, S.; Berridge, M. S.; Apana, S. M.; Slikker, W., Jr.; Wang, C. MicroPET/CT Imaging of [18F]-FEPPA in the Nonhuman Primate: A Potential Biomarker of Pathogenic Processes Associated With Anesthetic-Induced Neurotoxicity. *ISRN Anesthesiol.* **2012,** *2012.* http://dx.doi.org/10.5402/2012/261640. Article ID 261640, 11 pp.
55. Tiwari, A. K.; Ji, B.; Yui, J.; Fujinaga, M.; Yamasaki, T.; Xie, L.; Luo, R.; Shimoda, Y.; Kumata, K.; Zhang, Y.; Hatori, A.; Maeda, J.; Higuchi, M.; Wang, F.; Zhang, M. R. [18F] FEBMP: Positron Emission Tomography Imaging of TSPO in a Model of Neuroinflammation in Rats, and in vitro Autoradiograms of the Human Brain. *Theranostics* **2015,** *26,* 961–969.
56. Takeuchi, A.; Isobe, K. I.; Miyaishi, O.; Sawada, M.; Fan, Z. H.; Nakashima, I.; Kiuchi, K. Microglial NO Induces Delayed Neuronal Death Following Acute Injury in the Striatum. *Eur. J. Neurosci.* **1998,** *10,* 1613–1620.
57. Banati, R. B. Neuropathological Imaging: in vivo Detection of Glial Activation as a Measure of Disease and Adaptive Change in the Brain. *Br. Med. Bull.* **2003,** *65,* 121–131.
58. Ito, F.; Toyama, H.; Kudo, G.; Suzuki, H.; Hatano, K.; Ichise, M.; Katada, K.; Ito, K.; Sawada, M. Two Activated Stages of Microglia and PET Imaging of Peripheral Benzodiazepine Receptors With [(11)C]PK11195 in Rats. *Ann. Nucl. Med.* **2010,** *24,* 163–169.
59. Benavides, J.; Fage, D.; Carter, C.; Scatton, B. Peripheral Type Benzodiazepine Binding Sites Are a Sensitive Indirect Index of Neuronal Damage. *Brain Res.* **1987,** *421,* 167–172.
60. Papadopoulos, V.; Lecanu, L.; Brown, R. C.; Han, Z.; Yao, Z. X. Peripheral-Type Benzodiazepine Receptor in Neurosteroid Biosynthesis, Neuropathology and Neurological Disorders. *Neuroscience* **2006,** *138,* 749–756.
61. Briard, E.; Zoghbi, S. S.; Imaizumi, M.; Gourley, J. P.; Shetty, H. U.; Hong, J.; Cropley, V.; Fujita, M.; Innis, R. B.; Pike, V. W. Synthesis and Evaluation in Monkey of Two Sensitive 11C-Labeled Aryloxyanilide Ligands for Imaging Brain Peripheral Benzodiazepine Receptors In Vivo. *J. Med. Chem.* **2008,** *51,* 17–30.
62. Oku, N.; Kashiwagi, T.; Hatazawa, J. Nuclear Neuroimaging in Acute and Subacute Ischemic Stroke. *Ann. Nucl. Med.* **2010,** *24,* 629–638.
63. Kuhlmann, A. C.; Guilarte, T. R. Regional and Temporal Expression of the Peripheral Benzodiazepine Receptor in MPTP Neurotoxicity. *Toxicol. Sci.* **1999,** *48,* 107–116.
64. Kuhlmann, A. C.; Guilarte, T. R. Cellular and Subcellular Localization of Peripheral Benzodiazepine Receptors After Trimethyltin Neurotoxicity. *J. Neurochem.* **2000,** *74,* 1694–1704.
65. Bading, J. R.; Shields, A. F. Imaging of Cell Proliferation: Status and Prospects. *J. Nucl. Med.* **2008,** *49* (Suppl 2), 64S–80S.
66. Jacobs, A. H.; Rueger, M. A.; Winkeler, A.; Li, H.; Vollmar, S.; Waerzeggers, Y.; Rueckriem, B.; Kummer, C.; Dittmar, C.; Klein, M.; Heneka, M. T.; Herrlinger, U.; Fraefel, C.; Graf, R.; Wienhard, K.; Heiss, W. D. Imaging-Guided Gene Therapy of Experimental Gliomas. *Cancer Res.* **2007,** *67,* 1706–1715.
67. Rueger, M. A.; Backes, H.; Walberer, M.; Neumaier, B.; Ullrich, R.; Simard, M. L.; Emig, B.; Fink, G. R.; Hoehn, M.; Graf, R.; Schroeter, M. Noninvasive Imaging of Endogenous Neural Stem Cell Mobilization in vivo Using Positron Emission Tomography. *J. Neurosci.* **2010,** *30,* 6454–6460.

68. Roberts, R. A.; Aschner, M.; Calligaro, D.; Guilarte, T. R.; Hanig, J. P.; Herr, D. W.; Hudzik, T. J.; Jeromin, A.; Kallman, M. J.; Liachenko, S.; Lynch, J. J., 3rd; Miller, D. B.; Moser, V. C.; O'Callaghan, J. P.; Slikker, W., Jr.; Paule, M. G. Translational Biomarkers of Neurotoxicity: A Health and Environmental Sciences Institute Perspective on the Way Forward. *Toxicol. Sci.* **2015,** *148* (2), 332–340.
69. Keirstead, H. S.; Nistor, G.; Bernal, G.; Totoiu, M.; Cloutier, F.; Sharp, K.; Steward, O. Human Embryonic Stem Cell-Derived Oligodendrocyte Progenitor Cell Transplants Remyelinate and Restore Locomotion After Spinal Cord Injury. *J. Neurosci.* **2005,** *25,* 4694–4705.
70. Kang, S. M.; Cho, M. S.; Seo, H.; Yoon, C. J.; Oh, S. K.; Choi, Y. M.; Kim, D. W. Efficient Induction of Oligodendrocytes From Human Embryonic Stem Cells. *Stem Cells* **2007,** *25,* 419–424.
71. Wang, C.; Rougon, G.; Kiss, J. Z. Requirement of Polysialic Acid for the Migration of the O-2A Glial Progenitor Cell From Neurohypophyseal Explants. *J. Neurosci.* **1994,** *14,* 4446–4457.
72. Trujillo, C. A.; Schwindt, T. T.; Martins, A. H.; Alves, J. M.; Mello, L. E.; Ulrich, H. Novel Perspectives of Neural Stem Cell Differentiation: From Neurotransmitters to Therapeutics. *Cytometry A* **2009,** *75,* 38–53.
73. Wilmut, I.; Schnieke, A. E.; McWhir, J.; Kind, A. J.; Campbell, K. H. Viable Offspring Derived From Fetal and Adult Mammalian Cells. *Nature* **1997,** *385,* 810–813.
74. Thomson, J. A.; Itskovitz-Eldor, J.; Shapiro, S. S.; Waknitz, M. A.; Swiergiel, J. J.; Marshall, V. S.; Jones, J. M. Embryonic Stem Cell Lines Derived From Human Blastocysts. *Science* **1998,** *282,* 1145–1147.
75. Slikker, W., Jr. Of Human-on-a-Chip and Humans: Considerations for Creating and Using Microphysiological Systems. *Exp. Biol. Med.* **2016;** http://dx.doi.org/10.1177/1535370214537754. Epub July 2014.
76. Tong, W.; Ostroff, S.; Blais, B.; Silva, P.; Dubuc, M.; Healy, M.; Slikker, W. Genomics in the Land of Regulatory Science. *Regul. Toxicol. Pharmacol.* **2015,** *72,* 102–106.
77. Winship, I. Precision Medicine: Are We There Yet? *Med. J. Aust.* **2015,** *203,* 132–133.
78. Collins, F. S.; Varmus, H. A New Initiative on Precision Medicine. *N. Engl. J. Med.* **2015,** *372,* 793–795.
79. Goodsaid, F. M.; Amur, S.; Aubrecht, J.; Burczynski, M. E.; Catalona, J.; Carl, K.; Charlab, R.; Cornu-Artis, C.; Essioux, L.; Fornace, A. J., Jr.; Hinman, L.; Hong, H.; Hunt, I.; Jacobson-Kram, D.; Jawaid, A.; Li, H. H.; Close, S.; Laurie, D.; Lesko, L.; Lindpainter, K.; Mayne, J.; Morrow, P.; Papaluca-Amati, M.; Robison, T. W.; Roth, J.; Schuppe-Koistinen, I.; Shi, L.; Spleiss, O.; Tong, W.; Truter, S. L.; Vonderscher, J.; Westelinck, A.; Zhang, L.; Zineh, I. Voluntary Exploratory Data Submissions to the US FDA and the EMA: Experience and Impact. *Nat. Rev. Drug Discov.* **2010,** *9,* 435–445.
80. SEQC/MAQC-III Consortium. A Comprehensive Assessment of RNA-seq Accuracy, Reproducibility and Information Content by the Sequence Quality Control Consortium. *Nat. Biotechnol.* **2014,** *32,* 903–914.
81. Sturla, S.; Boobis, J.; Alan, R.; FitzGerald, R.; Hoeng, E.; Julia, K.; Robert, J.; Schirmer, K.; Whelan, M.; Wilks, M. F.; Peitsch, M. C. Systems Toxicology: From Basic Research to Risk Assessment. *Chem. Res. Toxicol.* **2014,** *27,* 314–329.
82. OECD. *Guidance on Grouping of Chemicals*. OECD Environment, Health and Safety Publications Series on Testing and Assessment No. 194, 2nd ed., 2014.
83. Healy, M. J.; Tong, W.; Ostroff, S.; Eichler, H. G.; Patak, A.; Neuspiel, M.; Deluyker, H.; Slikker, W., Jr. *Regul. Toxicol. Pharmacol.* **2016;** http://dx.doi.org/10.1016/j.yrtph.2016.05.021. pii: S0273-2300(16)30134-9.
84. Negi, G.; Liachenko, S.; Paule, M.; Sarkar, S.; Hanig, J. Quantifying Drug-Induced Neurotoxicity in Brain, Using Image Analysis Algorithms to Evaluate Digitalized Histopathology Sections. ASPET 2016 Annual Meeting, April 4, San Diego, CA.
85. Howard, K. Humanized Mouse Models, Part Two. Progress Testing Biologics in Humanized Mice. PEGS Boston. Inaugural Immunogenicity Prediction and Modulation Meeting, Predictive Tools and Reassessment—How Far Have We Come? Humanized Models, April 2016.
86. Waldor, M. K.; Tyson, G.; Borenstein, E.; Ochman, H.; Moeller, A.; Finlay, B. B.; et al. Where Next for Microbiome Research? *PLoS Biol.* **2015,** *13* (1) http://dx.doi.org/10.1371/journal.pbio.1002050. e1002050.
87. Lung on a chip: http://wyss.harvard.edu/viewpage/240/.
88. Lung on a chip: http://news.harvard.edu/gazette/story/2010/06/living-breathing-human-lung-on-a-chip/.
89. Liu, Y.; Niu, T.; Zhang, L.; Yang, J. Review on Nano-Drugs. *Nat. Sci.* **2010,** *2,* 41–48. http://dx.doi.org/10.4236/ns.2010.21006.
90. Naudí, A.; Cabré, R.; Jové, M.; Ayala, V.; Gonzalo, H.; Portero-Otín, M.; Ferrer, I.; Pamplona, R. Lipidomics of Human Brain Aging and Alzheimer's Disease Pathology. *Int. Rev. Neurobiol.* **2015,** *122,* 133–189. http://dx.doi.org/10.1016/bs.irn.2015.05.008. Epub 2015 Jun 19.
91. Liu, F.; Rainosek, S. W.; Frisch-Daiello, J. L.; Patterson, T. P.; Paule, M. G.; Slikker, W., Jr.; Wang, C.; Han, X. Potential Adverse Effects of Prolonged Sevoflurane Exposure on Developing Monkey Brain: From Abnormal Lipid Metabolism to Neuronal Damage. *Toxicol. Sci.* **2015,** *147* (2), 562–572.
92. Slavov, S. H.; Wilkes, J. G.; Buzatu, D. A.; Kruhlak, N. L.; Willard, J. M.; Hanig, J. P.; Beger, R. D. Computational Identification of a Phospholipidosis Toxicophore Using C and N NMR-Distance Based Fingerprints. *Bioorg. Med. Chem.* **2014,** *22* (23), 6706–6714.
93. Kruhlak, N. L. Modeling and Simulation in Regulatory Review: A CDER Perspective. 2015 Science Writers Symposium, September.
94. Roncaglioni, A.; Toropov, A. A.; Toropova, A. P.; Benfenati, E. In Silico Methods to Predict Drug Toxicity. *Curr. Opin. Pharmacol.* **2013,** *13* (5), 802–806. http://dx.doi.org/10.1016/j.coph.2013.06.001. Epub 2013 Jun 21.
95. Computer modeling—use of 'spiders'. http://whatis.techtarget.com/definition/spider.

This page intentionally left blank

COMPREHENSIVE MEDICINAL CHEMISTRY III

This page intentionally left blank

COMPREHENSIVE MEDICINAL CHEMISTRY III

EDITORS-IN-CHIEF

Samuel Chackalamannil
Rutgers University, Piscataway, NJ, United States

David Rotella
Montclair State University, Montclair, NJ, United States

Simon E. Ward
University of Sussex, Brighton, United Kingdom

VOLUME 5

CANCER, IMMUNOLOGY AND INFLAMMATION, AND INFECTIOUS DISEASE

VOLUME EDITORS

Ian Collins
The Institute of Cancer Research, London, United Kingdom

William Watkins
Gilead Sciences, Foster City, CA, United States

Louis J. Lombardo
Bristol-Myers Squibb Research and Development, Princeton, NJ, United States

ELSEVIER

Elsevier
Radarweg 29, PO Box 211, 1000 AE Amsterdam, The Netherlands
The Boulevard, Langford Lane, Kidlington, Oxford OX5 1GB, United Kingdom
50 Hampshire Street, 5th Floor, Cambridge, MA 02139, United States

Copyright © 2017 Elsevier Ltd. All rights reserved

No part of this publication may be reproduced or transmitted in any form or by any means, electronic or mechanical, including photocopying, recording, or any information storage and retrieval system, without permission in writing from the publisher. Details on how to seek permission, further information about the Publisher's permissions policies and our arrangements with organizations such as the Copyright Clearance Center and the Copyright Licensing Agency, can be found at our website: www.elsevier.com/permissions.

This book and the individual contributions contained in it are protected under copyright by the Publisher (other than as may be noted herein).

Notices
Knowledge and best practice in this field are constantly changing. As new research and experience broaden our understanding, changes in research methods, professional practices, or medical treatment may become necessary.

Practitioners and researchers may always rely on their own experience and knowledge in evaluating and using any information, methods, compounds, or experiments described herein. In using such information or methods they should be mindful of their own safety and the safety of others, including parties for whom they have a professional responsibility.

To the fullest extent of the law, neither the Publisher nor the authors, contributors, or editors, assume any liability for any injury and/or damage to persons or property as a matter of products liability, negligence or otherwise, or from any use or operation of any methods, products, instructions, or ideas contained in the material herein.

Library of Congress Cataloging-in-Publication Data
A catalog record for this book is available from the Library of Congress

British Library Cataloguing-in-Publication Data
A catalogue record for this book is available from the British Library

ISBN 978-0-12-803200-8

For information on all publications visit our website at
http://store.elsevier.com

Working together
to grow libraries in
developing countries
www.elsevier.com • www.bookaid.org

Publisher: Oliver Walter
Acquisition Editor: Rachel Gerlis
Content Project Manager: Gemma Tomalin
Associate Content Project Manager: Marise Willis
Designer: Mark Rogers

Printed and bound in the United Kingdom

PREFACE

Previous editions of *Comprehensive Medicinal Chemistry*, published in 1990 and 2006, provided an integrated reference source that encompassed all major aspects of drug discovery research. The third edition follows this tradition and considerably expands its scope and content.

The trailblazing scientific discoveries of the 21st century have brought new opportunities for drug discovery research. The discipline of medicinal chemistry continues to evolve as it adapts to these new opportunities and strives to solve new challenges. Covered in the new edition are not only the breakthrough therapies of the past decade in cancer, hepatitis C, heart failure, dyslipidemia, cystic fibrosis, multiple sclerosis, HIV, etc., but also extensive discussion of new business models in drug discovery research, shifting industry demographics, emerging technologies, *in silico* drug discovery tools, experimental ADME and toxicology, and biologics medicine. The tone of this edition is prospective in which contributors identify outstanding issues and paths forward in their area of expertise. The aim is to provide drug discovery scientists in industry, government, academia, and research organizations with a contemporary global perspective on the field that includes a look ahead in selected areas.

The eight individual volumes fulfill these objectives and include extensive discussion of biomolecular therapeutics, drug targeting and delivery, development of chemical biology tools, data collection and analysis, *in silico* models as predictors for biological properties, identification/validation of new targets, approaches to quantify target engagement, new methods for synthesis of drug candidates such as green chemistry, development of novel scaffolds for drug discovery, and the role of regulatory agencies in drug discovery.

The individual volume editors have done an outstanding job to identify topics and contributors to meet these goals and we thank them for their hardwork and diligence. In volume 1, Ana Martinez and Carmen Gil recruited an international group of contributors who provide chapters on the emerging role of organizations other than traditional pharmaceutical companies in drug discovery, the evolving science of chemical biology, and new organic chemistry contributions to the discipline. In volume 2, Helmut Buschmann, Norbert Handler, and Andrea Wolkerstorfer have accomplished a seemingly impossible task and attracted world-leading experts across the wide field of drug discovery enabling technologies, covering contemporary thinking in a wide range of key disciplines that enable modern medicinal chemistry and drug discovery and development. The computational enabling technologies are the focus of volume 3, in which Andy Davis and Colin Edge have assembled chapters covering both ligand-based and protein structure–based advances as well as exciting new methodologies and case studies exploiting these. Alan Wilson identified experts in the fields of pharmacokinetics and toxicology who describe a wide range of contemporary advances in prediction and analysis of pharmaceutical properties and drug safety in volume 4. In volume 5, Ian Collins, Louis Lombardo, and Will Watkins have assembled leading experts to discuss high impact drug discovery accomplishments over the past decade in cancer chemotherapeutics, immunology and inflammation, and infectious diseases therapeutic areas. Ved Srivastava edited volume 6 on biologic medicines, a significant and rapidly evolving area where medicinal chemistry plays an important role. The chapters in this volume provide timely information on not only protein-based drugs, such as monoclonal antibodies and therapeutic proteins, but also peptides and nucleic acid–based therapeutics. Volume 7, edited by Adrian Hall, Santhosh Neelamkavil, and Rob Jones, presents a detailed account of the major advances in CNS, metabolic, and cardiovascular fields over the past decade and the promising new opportunities. Joerg Holenz edited volume 8 that presents case histories of successful drug discovery and strategic differentiation that have resulted in commercialized drugs and candidates in advanced clinical trials.

We are truly grateful to the publishing team at Elsevier that includes Gemma Tomalin, Rachel Gerlis, Marise Willis, and Sean Simms for their assistance and support throughout the process. With their expertise, this project became what we believe is a noteworthy and valuable resource for the discipline of medicinal chemistry. We look forward to the response and feedback of our colleagues who will use this information in their own work.

Samuel Chackalamannil, David P. Rotella, and Simon E. Ward

EDITORS-IN-CHIEF: BIOGRAPHIES

Dr. Samuel Chackalamannil

Dr. Chackalamannil obtained his PhD in chemistry from Yale University in 1984 and subsequently worked in drug discovery research at Schering-Plough Corporation and Merck Research Laboratories, where he was a distinguished fellow when he left in 2011. Since then, he has been teaching at Ernest Mario School of Pharmacy, Rutgers University, New Jersey.

Dr. Chackalamannil has significant accomplishments in the discovery of new medicines. He led the discovery of vorapaxar (Zontivity®), an FDA-approved antiplatelet drug for the prevention of heart attack and stroke. His group also discovered a PDE-5 inhibitor clinical candidate dasantafil and an adenosine A2a antagonist clinical candidate for the treatment of Parkinson's disease. Altogether, he was responsible for the discovery of nine development candidates in cardiovascular, central nervous system, and metabolic disease areas.

Dr. Chackalamannil is a coinventor of 62 allowed US patents and numerous patent applications worldwide. He has published 81 peer-reviewed articles and has coauthored a book. He has also given numerous lectures at international meetings and academic institutions.

Dr. Chackalamannil is a two-time recipient of the Thomas Alva Edison Award for Emerging Technology Patent and a two-time recipient of the Presidential Award for Discovery at Schering-Plough Research Institute. He has chaired several sessions at American Chemical Society national meetings and Gordon Research Conference on Medicinal Chemistry and was an organizer for Chemistry as a Life Science Symposium.

Dr. David Rotella

Dr. Rotella earned a PhD in medicinal chemistry from The Ohio State University and carried out postdoctoral research in organic chemistry at Penn State University. He joined the faculty at Montclair State University in July 2011 as the Margaret and Herman Sokol Professor of medicinal chemistry after a successful career in the pharmaceutical industry. He is an expert in the discovery and optimization of small molecule drug candidates for use in metabolic, cardiovascular, cancer, and central nervous system diseases. His current research is focused on discovering new lead compounds for use in parasitic and central nervous system diseases. He has coedited the seventh edition of *Burger's Medicinal Chemistry* and is a senior editor for the Royal Society of Chemistry's Drug Discovery book series. He has authored over 40 peer-reviewed articles, is an inventor on 8 issued US patents, and has contributed 10 book chapters.

Simon E. Ward

Simon Ward has an MA in natural sciences and PhD in synthetic organic chemistry from Cambridge University, UK. He has a wide-ranging experience of drug discovery in both large and small companies (GlaxoSmithKline, Knoll Pharmaceuticals, Vernalis, Chiroscience, BioCrea) and specialist experience of discovering and developing drugs for central nervous system indications. He has led multidisciplinary project teams and medicinal chemistry groups from target identification through to early clinical studies, delivering multiple clinical development candidates across indications. He is a fellow of the Royal Society of Chemistry. He is currently a professor of medicinal chemistry at the University of Sussex, UK, and the director of the Sussex Drug Discovery Centre, which he established within the University of Sussex in 2010.

This page intentionally left blank

CONTRIBUTORS TO VOLUME 5

Ganiy Opeyemi Abdulrahman
Newcastle University, Newcastle upon Tyne, United Kingdom

J L Adams
GlaxoSmithKline, Collegeville, PA, United States

M Birch
F2G Ltd, Manchester, United Kingdom

D G Brown
AstraZeneca Neurosciences, Innovative Medicines and Early Development Unit, Cambridge, United Kingdom

K Bush
Indiana University, Bloomington, IN, United States

C Callebaut
Gilead Sciences Inc., Foster City, CA, United States

C C Castillo
University College London, London, United Kingdom

A Cathcart
Gilead Sciences Inc., Foster City, CA, United States

M D Cheeseman
The Institute of Cancer Research, London, United Kingdom

A Cherkasov
University of British Columbia, Vancouver, BC, Canada

G S Cockerill
Durham University, Stockton on Tees, United Kingdom; and ReViral, Stevenage Bioscience Catalyst, Stevenage, United Kingdom

N J Curtin
Newcastle University, Newcastle upon Tyne, United Kingdom

T G Murali Dhar
Bristol-Myers Squibb, Research and Development, Princeton, NJ, United States

S D'Alonzo
PIQUR Therapeutics AG, Basel, Switzerland

K J Duffy
GlaxoSmithKline, Collegeville, PA, United States

A J Dyckman
Bristol-Myers Squibb, Research and Development, Princeton, NJ, United States

A Elisa Pasqua
The Institute of Cancer Research, London, United Kingdom

D Fabbro
PIQUR Therapeutics AG, Basel, Switzerland

L R Fitzpatrick
California Northstate University College of Pharmacy, Elk Grove, CA, United States

R Fleischmann
University of Texas, Southwestern Medical Center, Metroplex Clinical Research Center, Dallas, TX, United States

M Foley
Epizyme Inc., Cambridge, MA, United States

K M Foote
AstraZeneca, Cambridge, United Kingdom

F W Goldberg
AstraZeneca, Cambridge, United Kingdom

I R Hardcastle
Newcastle University, Newcastle Upon Tyne, United Kingdom

D Harvey
Epizyme Inc., Cambridge, MA, United States

P Hillmann
PIQUR Therapeutics AG, Basel, Switzerland

R T Jacobs
Anacor Pharmaceuticals, Palo Alto, CA, United States

K Jones
The Institute of Cancer Research, London, United Kingdom

J G Kettle
AstraZeneca, Cambridge, United Kingdom

L P Kotra
University of Toronto and University Health Network, Toronto, ON, Canada

V C Kyttaris
Beth Israel Deaconess Medical Center, Boston, MA, United States

S E Lazerwith
Gilead Sciences, Inc., Foster City, CA, United States

H Li
University of British Columbia, Vancouver, BC, Canada

Yan Lou
South San Francisco, CA, United States

R M McFadden
Gilead Sciences, Inc., Foster City, CA, United States

N A Meanwell
Bristol-Myers Squibb, 5 Research Parkway, Wallingford, CT, United States

J Mestan
PIQUR Therapeutics AG, Basel, Switzerland

M R Mish
Gilead Sciences, Inc., Foster City, CA, United States

M L Moore
GlaxoSmithKline, Collegeville, PA, United States

A A Mortlock
AstraZeneca, Cambridge, United Kingdom

S Neidle
University College London, London, United Kingdom

Timothy D Owens
South San Francisco, CA, United States

J Park
University of Toronto and University Health Network, Toronto, ON, Canada

A Paulo
University of Lisbon, Lisbon, Portugal

K L Powell
ReViral Ltd, Stevenage Bioscience Catalyst, Stevenage, United Kingdom

M J Pucci
Spero Therapeutics, Cambridge, MA, United States

P Rennie
University of British Columbia, Vancouver, BC, Canada

D Schmitz
PIQUR Therapeutics AG, Basel, Switzerland

G Sibley
F2G Ltd, Manchester, United Kingdom

D Siegel
Gilead Sciences, Inc., Foster City, CA, United States

S Stamm
University of Kentucky, Lexington, KY, United States

E Thomas
ReViral Ltd, Stevenage Bioscience Catalyst, Stevenage, United Kingdom

W C Tse
Gilead Sciences, Inc., Foster City, CA, United States

T R Webb
SRI International, Menlo Park, CA, United States

B Wilding
The Institute of Cancer Research, London, United Kingdom

D M Wilson
AstraZeneca, Cambridge, United Kingdom

T Woldemariam
California Northstate University College of Pharmacy, Elk Grove, CA, United States

J Yang
GlaxoSmithKline, Collegeville, PA, United States

CONTENTS OF VOLUME 5

Preface *v*

Editors-in-Chief: Biographies *vii*

Contributors to Volume 5 *ix*

Editorial Board *xiii*

5.01 Cancer Biology and the Principles of Targeted Cancer Drug Discovery 1
P Hillmann, D Schmitz, J Mestan, S D' Alonzo, and D Fabbro

5.02 Selective Kinase Inhibitors in Cancer 39
A A Mortlock, D M Wilson, J G Kettle, F W Goldberg, and K M Foote

5.03 Covalent Kinase Inhibitors for Cancer 76
Timothy D Owens and Yan Lou

5.04 Targeting DNA Damage Response Pathways in Cancer 104
Ganiy Opeyemi Abdulrahman, and N J Curtin

5.05 Targeting the Androgen Receptor Signaling Axis 134
H Li, P Rennie, and A Cherkasov

5.06 Protein–Protein Interaction Inhibitors in Cancer 154
I R Hardcastle

5.07 Targeting Protein Synthesis, Folding, and Degradation Pathways in Cancer 202
A Elisa Pasqua, B Wilding, M D Cheeseman, and K Jones

5.08 Inhibitors of Epigenetic Regulation in Cancer 281
D Harvey and M Foley

5.09 Targeting Promoter Quadruplex Nucleic Acids for Cancer Therapy 308
A Paulo, C C Castillo, and S Neidle

5.10 Targeting Pre-mRNA Processing in Cancer 341
T R Webb and S Stamm

5.11 Cancer Immunotherapy—An Emerging Field That Bridges Oncology and Immunology Research 357
J L Adams, K J Duffy, M L Moore, and J Yang

5.12 Evolution of Small-Molecule Immunology Research—Changes Since CMC II 395
T G Murali Dhar and A J Dyckman

5.13 Small Molecule Immunosuppressants in Inflammatory Disease 420
R Fleischmann

5.14 Therapeutic Approaches to MS and Other Neurodegenerative Diseases 439
L P Kotra and J Park

5.15 Lupus and Lupus Overlap Diseases: Emerging Therapies 474
V C Kyttaris

5.16 Small-Molecule Drugs for the Treatment of Inflammatory Bowel Disease 495
L R Fitzpatrick and T Woldemariam

5.17 Recent Epidemiological Changes in Infectious Diseases 511
M J Pucci, C Callebaut, A Cathcart, and K Bush

5.18 Direct-Acting Antiviral Agents for the Treatment of Hepatitis C Virus Infection 553
N A Meanwell

5.19 New Antiretrovirals for HIV and Antivirals for HBV 628
S E Lazerwith, D Siegel, R M McFadden, M R Mish, and W C Tse

5.20 Antiviral Drugs for Acute Infections 665
K L Powell, E Thomas, and G S Cockerill

5.21 New Drugs and Emerging Leads in Antibacterial Drug Discovery 682
D G Brown

5.22 Antifungal Chemistry Review 703
M Birch and G Sibley

5.23 Antiparasitic Agents 717
R T Jacobs

EDITORIAL BOARD

EDITORS-IN-CHIEF

Samuel Chackalamannil
Rutgers University, Piscataway, NJ, United States

David Rotella
Montclair State University, Montclair, NJ, United States

Simon E. Ward
University of Sussex, Brighton, United Kingdom

VOLUME 1
GENERAL PERSPECTIVE - THE FUTURE OF DRUG DISCOVERY

VOLUME EDITORS

Ana Martinez
Centro de Investigaciones Biologicas-CSIC, Madrid, Spain

Carmen Gil
Centro de Investigaciones Biologicas-CSIC, Madrid, Spain

VOLUME 2
DRUG DISCOVERY TECHNOLOGIES

VOLUME EDITORS

Helmut Buschmann
Savira Pharmaceuticals GmbH, Vienna, Austria

Norbert Handler
Savira Pharmaceuticals GmbH, Vienna, Austria

Andrea Wolkerstorfer
Baxalta Innovations GmbH — Now part of Shire, Vienna, Austria

VOLUME 3
IN SILICO DRUG DISCOVERY TOOLS

VOLUME EDITORS

Andrew M. Davis
AstraZeneca R&D Gothenburg, Gothenburg, Sweden

Colin Edge
GlaxoSmithKline Medicines Research Centre, Stevenage, United Kingdom

VOLUME 4
EXPERIMENTAL ADME AND TOXICOLOGY

VOLUME EDITOR

Alan G. E. Wilson
Lexicon Pharmaceuticals, The Woodlands, TX, United States

VOLUME 5
CANCER, IMMUNOLOGY AND INFLAMMATION, AND INFECTIOUS DISEASE

VOLUME EDITORS

Ian Collins
The Institute of Cancer Research, London, United Kingdom

William Watkins
Gilead Sciences, Foster City, CA, United States

Louis J. Lombardo
Bristol-Myers Squibb Research and Development, Princeton, NJ, United States

VOLUME 6
BIOLOGICS MEDICINE

VOLUME EDITOR

Ved Srivastava
Intarcia Therapeutics, Durham, NC, United States

VOLUME 7
CNS, PAIN, METABOLIC SYNDROME, CARDIOVASCULAR, TISSUE FIBROSIS AND URINARY INCONTINENCE

VOLUME EDITORS

Adrian Hall
UCB BioPharma SPRL, Brussels, Belgium

Santhosh Neelamkavil
Merck Research Laboratories, Kenilworth, NJ, United States

Rob Jones
BlackThorn Therapeutics, San Francisco, CA, United States

VOLUME 8
CASE HISTORIES IN RECENT DRUG DISCOVERY

VOLUME EDITOR

Joerg Holenz
R&D Neurosciences TAU, GSK, PA, United States

PERMISSION ACKNOWLEDGMENTS

The following material is reproduced with kind permission of Taylor & Francis

Scheme 2 Cellular Imaging in Drug Discovery: Biomolecular Imaging and Informatics (HCS, HCA, HCI)
Figure 2 Past Present Future
Figure 5 Past Present Future
Figure 6 Past Present Future
www.taylorandfrancisgroup.com

The following material is reproduced with kind permission of Oxford University press

Table 1 Targeting G-quadruplex Nucleic Acids for Cancer Therapy
Table 2 Targeting G-quadruplex Nucleic Acids for Cancer Therapy
Figure 1 Protein Structure Prediction and Homology Modelling
www.oup.com

The following material is reproduced with kind permission of American Association for the Advancement of Science

Figure 3b,c Cellular Imaging in Drug Discovery: Biomolecular Imaging and Informatics (HCS, HCA, HCI)
www.aaas.org

The following material is reproduced with kind permission of Nature Publishing Group

Table 4 Use of Stem Cells in Toxicology
Table 6 Use of Stem Cells in Toxicology
Figure 17 Strategy and Tactics for Designing Analogs; Biochemical Characterization of the Large Molecules
Figure 30 Strategy and Tactics for Designing Analogs; Biochemical Characterization of the Large Molecules
Figure 2 Cellular Imaging in Drug Discovery: Biomolecular Imaging and Informatics (HCS, HCA, HCI)
Figure 3a Cellular Imaging in Drug Discovery: Biomolecular Imaging and Informatics (HCS, HCA, HCI)
Figure 4 Cellular Imaging in Drug Discovery: Biomolecular Imaging and Informatics (HCS, HCA, HCI)
Figure 5a Cellular Imaging in Drug Discovery: Biomolecular Imaging and Informatics (HCS, HCA, HCI)
Figure 9a Cellular Imaging in Drug Discovery: Biomolecular Imaging and Informatics (HCS, HCA, HCI)
Figure 20 Epigenetics: Novel Therapeutics Targeting Epigenetics
Figure 1 UCB5857
Figure 6 Empirical and Physics Based Calculations of Physical Properties
Figure 4 Progress and Challenges in the Development if PET Ligands to Aid CNS Drug Discovery
http://www.nature.com

5.01 Cancer Biology and the Principles of Targeted Cancer Drug Discovery

P Hillmann, D Schmitz, J Mestan, S D'Alonzo, and D Fabbro, PIQUR Therapeutics AG, Basel, Switzerland

© 2017 Elsevier Ltd. All rights reserved.

5.01.1	**Introduction**	4
5.01.2	**Cancer Biology and Hallmarks of Cancer**	4
5.01.2.1	Sustaining Proliferative Signaling	4
5.01.2.2	Evading Growth Suppressors	4
5.01.2.3	Resisting Cell Death	5
5.01.2.4	Enabling Replicative Immortality	5
5.01.2.5	Inducing Angiogenesis	6
5.01.2.6	Activating Invasion and Metastasis	6
5.01.2.7	Genome Instability and Mutation	6
5.01.2.8	Tumor-Promoting Inflammation	6
5.01.2.9	Deregulating Cellular Energetics	6
5.01.2.10	Avoiding Immune Destruction	6
5.01.3	**TIDVAL: Target Identification and Validation**	6
5.01.3.1	Target Identification	7
5.01.3.2	Target Validation	8
5.01.4	**Stress Response and Cancer**	8
5.01.4.1	DNA Damage and Replication Stress	9
5.01.4.2	Mitotic Stress	9
5.01.4.3	Metabolic Stress	9
5.01.4.4	Oxidative Stress	10
5.01.4.5	Hypoxia and Nutrient Stress	10
5.01.4.6	Proteotoxic Stress	10
5.01.5	**Targets With Clinical Relevance**	11
5.01.5.1	Kinases and Inhibitors	11
5.01.5.1.1	Introduction	11
5.01.5.1.2	Kinase structure	11
5.01.5.1.3	Receptor tyrosine kinases (RTKs)	12
5.01.5.1.4	Kinase activation in cancer	12
5.01.5.1.5	Approved kinase inhibitors	13
5.01.5.1.6	Kinase inhibitor mode of action	13
5.01.5.1.7	Kinase mutations and resistance	13
5.01.5.1.8	Outlook	15
5.01.5.2	Targets in Induction of Apoptosis	15
5.01.5.3	Targets in Tumor Metabolism	17
5.01.5.3.1	Glucose metabolism	17
5.01.5.3.2	Amino acid metabolism	18
5.01.5.3.3	TCA cycle	18
5.01.5.4	Targets in Immuno-Oncology	18
5.01.5.4.1	Tumor-induced immunosuppression	18
5.01.5.4.2	Immuno-checkpoint inhibitors	19
5.01.5.4.3	Cytokine therapy	19
5.01.5.4.4	CARs	19
5.01.5.5	Targets in Protein Folding and Degradation	20
5.01.5.5.1	Intervention in protein folding	20
5.01.5.5.2	Inhibitors of protein degradation	20
5.01.5.6	Targets in Cancer Epigenetics	20
5.01.5.6.1	DNA methylation	21
5.01.5.6.2	Histone modifications	21
5.01.5.6.3	Histone acetylation readers	21
5.01.5.7	Targets in Genomic Stability	21
5.01.5.7.1	Telomerase inhibitors	21
5.01.5.7.2	PARP inhibitors	22
5.01.5.8	Targets in Neovascularization	23

5.01.6	**Biomarkers**	23
5.01.6.1	Definition	23
5.01.6.2	BMs in the Clinic	24
5.01.6.3	Challenges of BMs and Future Perspectives	25
5.01.7	**Challenges of Targeted Cancer Therapy**	25
5.01.7.1	Tumor Heterogeneity	25
5.01.7.2	Tumor Evolution and Development of Resistances	26
5.01.7.3	CSCs	26
5.01.7.4	Examples of Resistance and Approaches to Overcome Resistance	27
5.01.8	**Summary**	27
References		28
Relevant Websites		38

Abbreviations

α-KG α-Ketoglutarate
2HG 2-Hydroxyglutarate
4EBP eIF4E binding protein
ABL Abelson murine leukemia viral oncogene homologue 1
ADP Adenosine diphosphate
AKT Protein kinase B
ALK Anaplastic lymphoma kinase
A-loop Activation loop also called activation segment
AML Acute myeloid leukemia
AMPK 5′-Adenosine monophosphate-activated protein kinase
APC Antigen-presenting cell
ASM Aggressive systemic mastocytosis
ATM Ataxia telangiectasia mutated
ATP Adenosine triphosphate
ATR Ataxia telangiectasia and Rad3-related protein
BC Breast cancer
BCL B-cell lymphoma
BCR Breakpoint cluster region
BDNF Brain-derived neurotrophic factor
BET Bromodomain and extraterminal domain
BIR Baculovirus IAP repeat
BLA Biological license application
BM Biomarker
BRAF Murine sarcoma viral oncogene homologue B
BRCA1 Breast cancer gene
BTK Bruton's tyrosine kinase
BUB Mitotic checkpoint serine/threonine-protein kinase
CanSAR Cancer research and drug discovery knowledgebase
CAR Chimeric antigen receptor
Cas (In CRISPR-Cas): CRISPR-associated protein (nuclease or helicase)
CCLE Cancer Cell Line Encyclopedia
CDK Cyclin-dependent kinase
CGAP Cancer Genome Anatomy Project
Chk1 Checkpoint kinase 1
CIN Chromosome instability
CLL Chronic lymphocytic leukemia
CML Chronic myeloid leukemia
CMML Chronic monomyelocytic leukemia
COSMIC Catalogue of Somatic Mutations in Cancer
CRC Colorectal cancer
CRISPR Clustered regularly interspaced short palindromic repeat
CSC Cancer stem cell
CSF1R Colony-stimulating factor 1 receptor
CTLA4 Cytotoxic T lymphocyte-associated protein 4
DAG Diacylglycerol
DC Dendritic cell
DDR DNA damage response
DGF-motif Aspartate–glycine–phenylalanine or Asp-Gly-Phe
DIABLO IAP binding protein with low p*I*
DISC Death-inducing signaling complex
DNA Deoxyribonucleic acid
DNAPK DNA-dependent protein kinase
DNMT DNA methyltransferase
DSB Double-strand break
e.g. Exempli gratia (Latin) = for example
ECM Extracellular matrix
EGFR Epidermal growth factor receptor
ELK Eukaryotic-like kinase
EMT Epithelial–mesenchymal transition
ePK Eukaryotic protein kinase
ER Estrogen receptor
FACS Fluorescence-activated cell sorter
FASL Fas ligand
FDA Food and Drug Administration
FGFR Fibroblast growth factor receptor
FH Fumarate hydratase
FL Follicular lymphoma
FLT3 Fetal liver kinase-3
FOXO Forkhead box protein O3
GIST Gastrointestinal stromal tumor
G-loop Glycine-rich loop also known as P-loop Gly-loop catalytic loop: Y/HRD or Tyr/His-Arg-Asp
GLS Glutaminase
GPCR G protein-coupled receptor

GSK3β Glycogen synthase kinase 3 beta
HCC Hepatocellular carcinoma
HDAC Histone deacetylase
HER2 Human epidermal growth factor receptor 2
HES Hypereosinophilic syndrome
HGF Hepatocyte growth factor
HH Hedgehog
HIF Hypoxia-inducible factor
HK2 Hexokinase 2
HRR Homologous recombination repair
HSP90 Heat shock protein 90
IAP Inhibitor of apoptosis
ICGC International Cancer Genome Consortium
IDH Isocitrate dehydrogenase
IDO Indoleamine 2,3-dioxygenase
IL Interleukin
IMF Interstitial myelofibrosis
InsR Insulin receptor
IVD In vitro diagnostic
JAK2 Janus kinase 2
JH2 Jak homology domain 2
JUN JUN kinase
KAT Histone lysine acetyltransferase
KIT Mast/stem cell growth factor receptor
LDZ Laboratory development test
LKB1 Serine/threonine-protein kinase STK11
MAP2K Mitogen-activated protein kinase kinase, MEK
MAP3K Mitogen-activated protein kinase kinase kinase
MAP4K Mitogen-activated protein kinase kinase kinase kinase
MAPK Mitogen-activated protein kinase
MCL Mantle cell lymphoma
M-CSF Macrophage colony-stimulating factor
MDM2 Murine double minute 2 homologue
MET MET receptor, hepatocyte growth factor receptor (HGFR)
MHC Major histocompatibility complex
MPS1 Monopolar spindle 1 kinase
mRNR messenger RNA
MTC Medullary thyroid cancer
mTOR Mammalian target of rapamycin
MYC Myelocytomatosis viral oncogene homolog
NADPH Nicotinamide adenine dinucleotide phosphate
Nek NimA-related kinase
NFkB Nuclear factor "kappa-light-chain-enhancer" of activated B cell
NHL Non-Hodgkin's lymphoma
NRAS Neuroblastoma RAS Viral Oncogene Homolog
NSCLC Non-small cell lung cancer
PAH Pulmonary arterial hypertension
PAR Poly-ADP-ribose
PARP Poly-ADP-ribose polymerase
PD Programmed death
PD-1 Programmed cell death protein 1
PDGFR Platelet-derived growth factor receptor
PDK Pyruvate dehydrogenase kinase
PDK1 3-Phosphoinositide-dependent protein kinase-1
PD-L1 Programmed cell death protein ligand 1
PFKFB3 6-Phosphofructo-2-kinase/fructose-2,6-bisphosphatase 3
PFS Progression-free survival
Ph + − B-ALL Philadelphia chromosome-positive B-cell acute lymphoblastic leukemia
PI Phosphatidylinositol
PI3K Phosphatidylinositol 3-kinase
PI4K Phosphatidylinositol 4-kinase
PK Pyruvate kinase
PKL Protein kinase-like
PKR Protein kinase RNA-activated
PLK Polo-like kinase
PMA Premarket approval
PROTAC Proteolysis targeting chimeric molecule
pSer, pThr, pTyr Phosphoserine (pS), phosphothreonine (pT), phosphotyrosine (pY)
P-site Peptide site
PTEN Phosphatase and tensin homologue
RA Rheumatoid arthritis
Ras Rat sarcoma
RB Retinoblastoma
RCC Renal clear cell carcinoma
RET RTK Rearranged during transfection RTK
RHEB Ras homologue enriched in brain
RNA ribonucleic acid
Rock Rho-associated protein kinase
ROS Reactive oxygen species
RR Response rate
RSK Ribosomal S6 kinase
RTK Receptor tyrosine kinase
S6K Ribosomal protein S6 kinase
SAC Spindle assembly checkpoint
SDH Succinate dehydrogenase
SEGA Subependymal giant cell astrocytoma
shRNA Short hairpin RNA
siRNA Short interfering RNA
SLL Small lymphocytic leukemia
Smac Second mitochondria-derived activator caspase
SMAD Composite of names of non-human analogues MAD (Mothers Against Decapentaplegic Homolog 4, Drosophila melanogaster) and SMA (Samll body size, Caenorhabditis elegans)
SRC Proto-oncogene tyrosine-protein kinase Src
Src Proto-oncogene tyrosine-protein kinase Src
STAT Signal transducers and activators of transcription
STPK Serine- and threonine-specific protein kinase
STRAD1 STE20-related adaptor alpha
TALEN Transcription activator-like effector nuclease
TCA Tricarboxylic acid
TCGA The Cancer Genome Atlas

TERT Telomerase reverse transcriptase
TGF Transforming growth factor
TNFα Tumor necrosis factor α
TP53 Tumor protein
TPK Tyrosine-protein kinase
TRAIL Tumor necrosis factor-related apoptosis-inducing ligand
Treg Regulatory T cell
TrkB Tropomyosin receptor kinase B
TSC Tuberous sclerosis complex
VEGF Vascular endothelial growth factor
VEGFR Vascular endothelial growth factor receptor

5.01.1 Introduction

Cancer is one of the leading causes of death in the Western world. Still, 50% of patients diagnosed with cancer die from the disease or the treatment. Reasons for the development of cancer apart from age are multiple, complex, and often poorly explored. Tobacco smoke, dietary reasons, physical inactivity, alcohol, and obesity are among the main risk factors.[1] In the United States, the estimated number of cancer deaths for 2015 is 589,430. The likelihood of developing cancer in life is 43% for men and 38% for women (http://www.cancer.org/).

Despite the advances in targeted cancer therapies, current treatment options are still mainly based on surgery, radiation, and chemotherapy. However, numerous drugs that target special properties of a given malignancy (eg, gain of function of signaling pathways, overexpression of proteins, and changes in metabolism) are currently being developed or have entered routine clinical practice. These compounds aim to increase patient benefit, such as reduced side effects compared with chemotherapy and possibly even prolonged life span.

This article describes the basics of cancer biology as well as targets for clinical intervention, how to identify new targets, and the challenges we currently face in the development of novel, targeted small-molecule cancer therapeutics.

5.01.2 Cancer Biology and Hallmarks of Cancer

Cellular transformation and tumorigenesis arise from multiple processes. Induction of tumor formation can be based on mutations in three types of genes: oncogenes, tumor suppressor genes, and stability genes. Invasive cancer typically develops only when several genes are defective, which increases the complexity and heterogeneity of cancer.[2] The delineation of the pathways through which these genes act can be organized into biological capabilities necessary for tumor growth and progression. These core hallmarks of cancer as defined by Hanahan and Weinberg[3] include sustaining proliferative signaling, evading growth suppressors, resisting cell death, enabling replicative immortality, inducing angiogenesis, and activating invasion and metastasis. Further underlying and enabling these characteristics are emerging hallmark capabilities: genome instability, tumor-promoting inflammation, deregulating cellular energetics, and evading immune destruction (**Fig. 1**). Nonetheless, tumor pathogenesis is complex and requires, in addition to the hallmarks listed in the preceding text, a repertoire of seemingly normal cells forming tumor-associated stroma contributing to the development and expression of the hallmark capabilities. Therefore, only selective cotargeting of multiple cores and emerging hallmark capabilities as well as enabling characteristics in mechanism-guided combinations will result in more effective and durable therapies for human cancer.

5.01.2.1 Sustaining Proliferative Signaling

Whereas normal tissues carefully control the production and release of growth-promoting mitogenic signals, cancer cells, through deregulating these signals, become powerful entities with structure and function of their own kind that are able to proliferate without control. In fact, cancer cells acquire the capability of inducing and sustaining positively acting growth stimulatory signals by different ways:[4] (i) producing growth factor ligands themselves, (ii) sending signals to stimulate normal cells within the assisting tumor-associated stroma, (iii) deregulating receptor signaling by structural alterations in the receptor molecules, and (iv) elevating receptor protein levels displayed at the cancer cell surface (see sections "Kinases and Inhibitors," "Targets in Protein Folding and Degradation," and "Targets in Cancer Epigenetics").

5.01.2.2 Evading Growth Suppressors

Tumor suppressor genes negatively regulate cell proliferation. The two prototypical tumor suppressors encode the RB (retinoblastoma-associated) and TP53 proteins that operate as central control nodes within two key complementary cellular regulatory circuits that govern the decisions of cells to proliferate or, alternatively, activate senescence and apoptotic programs.[3] These two regulating tumor suppressors operate as part of a larger network that is wired for functional redundancy. In cancer cells, growth suppression is often circumvented due to inhibitory/loss of function mutation in tumor suppressors. Cell-to-cell contact inhibition is eliminated in various types of cancer leading to metastasis; the mechanism for the elimination of this cell-to-cell contact

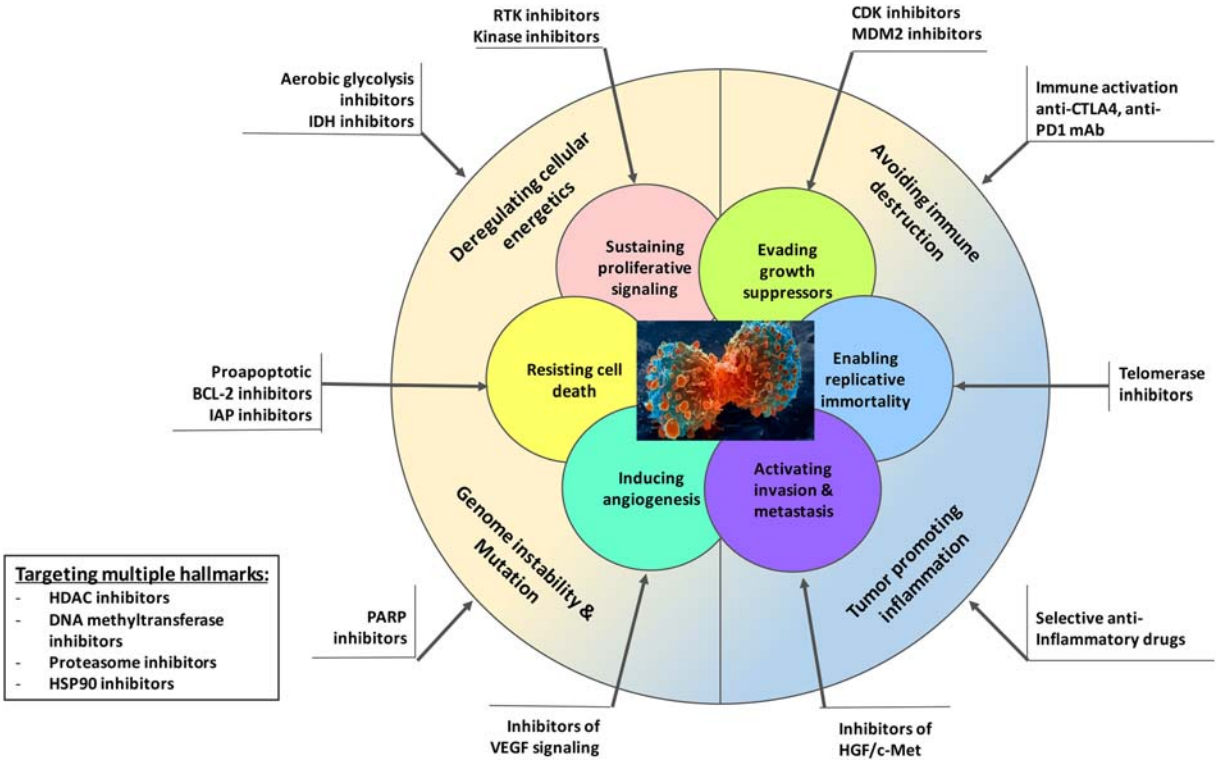

Fig. 1 Hallmarks of cancer and interfering treatments.

inhibition occurs by limiting the emission of mitogenic signals and counterbalancing inappropriate proliferation signals[3] (see sections "Kinases and Inhibitors," "Targets in Induction of Apoptosis," and "Targets in Protein Folding and Degradation").

5.01.2.3 Resisting Cell Death

Programmed cell death, apoptosis, is a process that results in suicide of malfunctional cells in order to maintain proper physiology of the whole body. Apoptosis serves as a natural barrier to cancer development; however, apoptosis is weakened in those tumors that succeed in progressing to states of high-grade malignancy and resistance to therapy.[5] The apoptotic program is compiled of both upstream regulators and downstream effector components that can be affected/mutated in cancer to resist apoptosis.

Autophagy represents an important cell physiological response for generation of nutrients as well as for degradation of malfunctional proteins that, like apoptosis, normally operate at low levels. However, autophagy can be induced in cellular stress situations, the most obvious of which is nutrient deficiency occurring during cancer growth.[6]

In contrast to apoptosis and autophagy, necrotic cell death releases pro-inflammatory signals into the surrounding tissue microenvironment. Although necrosis has historically been viewed much like organism death, cell death by necrosis is clearly under genetic control in some circumstances, rather than being a random and undirected process.[7] During tumor progression, necrosis-induced inflammation leads to growth stimulation (see sections "Stress Response and Cancer," "Kinases and Inhibitors," and "Targets in the Induction of Apoptosis").

5.01.2.4 Enabling Replicative Immortality

In contrast to normal cells, cancer cells require unlimited replicative potential. Most normal cell lineages in the body are able to pass through a limited number of successive cell growth and division cycles. There are two distinct barriers to proliferation: senescence, an irreversible entry into a nonproliferative but viable state, and crisis, which is a stage of extreme telomere dysfunction that is characterized by cell death. On rare occasions, cells emerge from a population in crisis and exhibit unlimited replicative potential; this transition has been termed immortalization. Telomeres, the protecting ends of chromosomes, are centrally involved in the hallmark of unlimited proliferation.[8] Thus, telomere maintenance has been confirmed as a condition critical to the neoplastic state (see section "Targets in Genomic Instability").

5.01.2.5 Inducing Angiogenesis

The tumor-associated neovasculature, generated by the process of angiogenesis, addresses the tumor's requirement of sustenance in the form of nutrients and oxygen as well as removing metabolic waste and carbon dioxide. In a healthy adult, angiogenesis is turned on only transiently. In contrast, during tumor progression, an "angiogenic switch" is almost always activated and remains on, causing normally dormant vasculature to continually sprout new vessels that help sustain expanding neoplastic growths.[9] The angiogenic switch is governed by angiogenic regulators such as vascular endothelial growth factor A (VEGF-A) and thrombospondin 1. Angiogenesis is induced early during the development of invasive cancers, and tumor neovasculature is characterized by precocious capillary sprouting, convoluted and excessive vessel branching, distorted and enlarged vessels, erratic blood flow, microhemorrhaging, leakiness, and abnormal levels of endothelial cell proliferation and apoptosis (see sections "Kinases and Inhibitors," "Targets in Protein Folding and Degradation," and "Targets in Neovascularization").

5.01.2.6 Activating Invasion and Metastasis

As carcinomas arising from epithelial tissues progress to higher pathological grades of malignancy, reflected in local invasion and distant metastasis, the associated cancer cells typically develop alterations in their shape as well as in their attachment to other cells and to the extracellular matrix. It has also become apparent that signaling between cancer cells and cells of the neoplastic stroma is involved in the acquired capability for invasive growth and metastasis.[10]

A developmental regulatory program, referred to as the "epithelial–mesenchymal transition" (EMT), has become prominently implicated as a means by which transformed epithelial cells can acquire the abilities to invade, to resist apoptosis, and to disseminate.[11] As for the plasticity in the invasive growth program, carcinoma cells that have undergone an EMT during initial invasion and metastatic dissemination may pass through the reverse process, termed the mesenchymal–epithelial transition (MET) (see section "Kinases and Inhibitors").

5.01.2.7 Genome Instability and Mutation

Genomic instability, and thus mutability, grants cancer cells genetic alterations that drive tumor progression. In tumorigenesis, cancer cells often increase the rates of mutation. This mutability is achieved through increased sensitivity to mutagenic agents. Indeed, the defects in genome maintenance and repair are selectively advantageous and therefore instrumental for tumor progression (see section "Targets in Genomic Instability").

5.01.2.8 Tumor-Promoting Inflammation

Every neoplastic lesion contains immune cells, but inflammation caused by innate immune cells designed to fight infections and heal wounds can instead result in their inadvertent support of multiple hallmark capabilities, thereby manifesting the tumor-promoting consequences of inflammatory responses (see section "Stress Response and Cancer").

5.01.2.9 Deregulating Cellular Energetics

Major reprogramming of cellular energy metabolism is needed in order to support continuous cell growth and proliferation. Tumor cells replace the oxidative metabolic program that operates in most normal tissues to provide cellular building blocks also under hypoxic conditions (see section "Targets in Tumor Metabolism").

5.01.2.10 Avoiding Immune Destruction

Highly immunogenic cancer cells may well evade immune destruction, in particular by T and B lymphocytes, macrophages, and natural killer cells, by disabling components of the immune system that have been dispatched to eliminate them (see section "Targets in Immuno-Oncology").

5.01.3 TIDVAL: Target Identification and Validation

In the early 20th century, the physician and Nobel laureate Paul Ehrlich (1854–1915) developed the concept of "magic bullets," meaning drugs chemically designed to very selectively hit the desired target (in his case, killing germs/bacteria) without affecting the normal tissue of the host.

The first "magic bullet" was the chemotherapeutic agent arsphenamine (trade name: Salvarsan), the first effective treatment for syphilis; it was introduced in 1910 and very successfully marketed until 1943, when it was replaced by penicillin.[12]

Today, targeted therapies are established (at least as component of therapy) for many kinds of diseases, for example, breast, colorectal, lung, and pancreatic cancers, lymphoma, leukemia, and multiple myeloma,[13] and are the focus of drug development efforts in many disease areas, especially in cancer research.

According to the "magic bullet" concept, the drugs developed for targeted cancer therapies are intended to selectively interact and interfere with the functions of defined cancer-specific biomolecules that are essential for deregulation of cell growth and proliferation, for cell transformation, and for tumor maintenance, progression, and metastasis. Small molecules that are able to pass the cell membrane are mostly developed for intracellular targets, for example, enzymes (signal transduction and metabolism), receptors, ion channels, or regulatory proteins. In contrast, large molecules, for example, antibodies, interact with tumor-specific cell surface proteins, for example, cytokine or growth factor receptors and tumor antigens, or with soluble plasma proteins, for example, receptor ligands, cytokines, and hormones involved in the regulation of tumor cell growth. The tumor cells can be affected either directly by action of small molecules or binding of antibodies or indirectly via recruitment and activation of humoral or cellular immunity (complement, killer cells, cytotoxic T cells, or macrophages). Antibodies are also used as carriers (Ab-drug conjugates) for cytotoxic molecules or specific inhibitors or activators to the designated target at the tumor site.[14]

Conventional chemotherapies using cytotoxic chemicals that unspecifically kill rapidly dividing cells are often associated with strong undesired side effects, since they also affect normal, noncancer cells throughout the body. In contrast, targeted therapies aim to reduce the collateral damage by specifically affecting only cancer cells.

5.01.3.1 Target Identification

Prerequisites for starting rational drug design and for developing a targeted drug (or for casting a magic bullet) are a thorough understanding of biological regulatory mechanisms and the identification of defined and valid targets (mostly proteins) that are altered only in the disease phenotype and are essential for the onset or the maintenance of the disease. Possible targets may be identified by examining (mining) general knowledge available in the literature and open-access databases and by intensive investigation of the disease pathobiology comparing characteristics of healthy and disease phenotypes. Generally, the evolution of malignant cells is a multistep process involving sequential acquisition and accumulation of different genetic alterations finally resulting in deregulation of the cellular signaling pathways and networks.[15] Therefore, the finding that one or two genes or proteins are modified or mutated may not be sufficient to understand or explain a malignant phenotype. In addition, manifold interactions, for example, positive or negative feedback loops, compensatory mechanisms, and redundancies, have also to be taken into consideration.[16] Modifications of genes or proteins, like overexpression or deletion, gain or loss of function by mutations, and deregulation of signaling pathways and functional networks detected in the disease context, are only the basis for identification and validation of potential drug targets. Only targets that are proved to be essential for the establishment or maintenance of the disease, and are druggable, are considered to be validated targets.[17]

There are several different approaches to the identification and validation of novel drug targets:

1. Comparative investigations of disease and normal phenotypes in tissues and cell lines aim to detect differentially modified genes or proteins (expression, activity, and regulation). Further characterization of these potential targets with biochemical or cell-based assays measuring their biological activities and the consequences for cell viability of their inhibition or activation may result in elucidation of their physiological roles and their relevance for the disease.
2. In phenotypic screening (also called "forward pharmacology" or "phenotypic drug discovery"), compound libraries are screened in cell-based assays or in animal models for selection of compounds that affect a certain phenotype by causing a desired physiological response, for example, growth inhibition of cancer cells or the reversal of a genetically induced defect.[18] Further investigation of active compounds in order to track down their mechanism of action by studying their influence on cellular regulatory pathways and their interactions with cellular molecular components may contribute to the discovery of unknown disease mechanisms and novel therapeutic targets.
3. Moreover, already established drugs can be investigated for their potential to interact with additional targets in different disease models. Identification of new targets for a marketed drug resulting in an extended full target profile may open up opportunities for novel therapeutic applications (drug repositioning) and expansion of the drug's life cycle.[19]

For new targets, pharmacological tools, either small-molecular-weight compounds or antibodies, are often not available or neither potent nor specific enough; therefore, impairment of target function by methodologies including meganucleases,[20] transcription activator-like effector nuclease (TALEN),[21] zinc finger nucleases,[22] clustered regularly interspaced short palindromic repeat-associated (CRISPR-Cas) proteins,[23,24] RNA interference (RNAi) with short interfering RNA (siRNA) or short hairpin RNA (shRNA),[25] and the PROTAC (proteolysis targeting chimeric molecule) approach[26] in combination with the concept of synthetic lethality is used to generate information on the interactions of cancer genes.[27]

TIDVAL needs a broad skill base and expertise in a large panel of biological and biochemical disciplines and requires effective and forthright transfer of knowledge and experience between academic and industrial researchers. A vital prerequisite for successful programs is the close collaboration of experts from different fields with experience in biochemistry, enzymology, crystallography, biochemical and biological assay design, molecular modeling, structural biochemistry, regulatory and signaling pathways, molecular pathology, toxicology, systems biology, and bioinformatics (analysis of "omics" and "big data"), as well as awareness of novel technologies and assay platforms.

Generally, the search for new targets starts with mining the publicly available information for differences between normal and disease phenotypes. During the last decades, major advances in biological methods and experimental technologies have led to a dramatic increase and accumulation of information that is collected in scientific publications and textbooks or is available on

websites of research institutes as well as of pharmaceutical and biotechnology companies. Enormous data sets can be generated from genomic and proteomic experiments and from biochemical and cell-based high-throughput and high-content assays.

Many of these websites are open-access portals to databases providing links and tools for searching and analyzing large data sets that are continuously collected and compiled from contributions of a network of a growing number of different scientific research and technology teams. The open access to the data should enable researchers to avoid duplication of efforts and to discover new and interesting interrelationships between disease-relevant modifications of genes, proteins, and signaling networks in different cancer types.

A few examples of open-access databases and the links to their home pages are presented here:

The Cancer Genome Atlas (TCGA)—http://cancergenome.nih.gov/
BioExpress® Oncology Suite (Ocimum Biosolutions)—http://www.ocimumbio.com/oncology-suite/
Network of Cancer Genes from King's College, London, the United Kingdom—http://ncg.kcl.ac.uk/
Catalogue of Somatic Mutations in Cancer (COSMIC) from the Wellcome Trust Sanger Institute, the United Kingdom—http://cancer.sanger.ac.uk/cosmic
Cancer Cell Line Encyclopedia (CCLE)—https://www.broadinstitute.org/software/cprg/?q=node/11
Cancer Genome Anatomy Project (CGAP) from the National Cancer Institute—http://cgap.nci.nih.gov
CanSAR from the Institute of Cancer Research and Cancer Research UK—https://cansar.icr.ac.uk/
The International Cancer Genome Consortium (ICGC)—https://icgc.org/[28]

A more comprehensive collection of databases is given in the recently published review article: Pavlopoulou et al., Human cancer databases.[28]

5.01.3.2 Target Validation

Validation of identified targets requires experiments proving their involvement and their relevance for the disease process, in which the target's role must be clearly defined. Depending on the nature of the target, modifying its biological activity by suppression or upregulation of its expression, or by inhibition or activation with tool compounds, should provoke a beneficial effect on the disease phenotype.

Expression levels may be modified by gene knockout resulting in loss of gene expression or gene knock-in resulting in expression of a modified/mutated protein.[29] Alternatively, gene expression can be regulated transiently or in an inducible manner at the RNA level (without changing the genetic code) by messenger RAN (mRNA) degradation with RNAi using shRNA or siRNA. This posttranscriptional reduction of gene expression is usually not complete resulting in downregulation, but not total elimination of the gene function (knockdown).[30]

Recent major advances in technologies allow for genome editing by targeted, permanent gene modifications using TALENs or CRISPR-Cas proteins.[23,24] Both methods work by cutting both DNA strands at a specifically targeted site, allowing for gene disruption or knockout, or, alternatively, gene modification (editing) by introduction of deletions, insertions, or specific point mutations. The more convenient and easier-to-use CRISPR-Cas technology has rapidly developed to a mainstream method, and the power of the system for easy and efficient alteration of genome sequences and gene expression simplifies the creation of cells and animals with designed properties and suitability as disease models.

One major challenge remaining after target identification and proving its relevance for the disease is druggability. Only targets that are druggable are valid targets for drug discovery. Approximately 15% (c. 3000) of all human genes are known disease genes, and 10–15% of all human genes are believed to be druggable based on sequence comparisons with those genes encoding proteins that are known targets of small molecules. There is only a 25% overlap of the disease genes with the group of the druggable genes implying a limited number of potential drug targets. However, expanded and diversified compound libraries based on new small-molecule scaffolds or natural products, and including larger, peptide-like molecules, may enable the modulation of large interaction interfaces (protein–protein interactions and DNA–protein interactions), thereby increasing the number of potential drug targets.[31]

Taken together, the process of TIDVAL underpins the development of targeted drugs and has evolved to a major effort needing the collaboration of experts from many different research and technology fields, which are constantly expanding and advancing. Access to public information and data collections and the availability of computational tools to mine, correlate, and interpret the vast amount of data that are accumulating continuously are essential for a successful targeted drug discovery program.

5.01.4 Stress Response and Cancer

Cancer is a complex collection of genetic and epigenetic disorders that can be integrated into common hallmarks.[3,32] In this respect, the stress phenotypes of cancer that include various stressors such as DNA damage and replication, oxidation, proteotoxicity, as well as mitotic, metabolic, and oxidative stress have recently emerged as important features of many tumor types.[32,33] As tumors display components of chronic inflammation, these stress phenotypes are not unique to cancer as they can be found in chronic inflammations or other immunologic disorders as well.

5.01.4.1 DNA Damage and Replication Stress

Cells are continuously faced with endogenous stress during replication and exogenous stress during exposure to ultraviolet (UV) radiation, which can ultimately lead to DNA damage. Following DNA damage, normal cells arrest proliferation, induce cellular senescence, or elicit apoptosis to preserve genomic integrity.[33,34] In contrast, cancer cells have learned to replicate in the presence of DNA damage thanks to the activation of the DNA damage response (DDR).[33–35] Increased DNA damage can occur due to shortening of telomeres leading to double-strand breaks (DSBs) at telomeric ends, which result in translocations and gene amplification events (see genomic stability).[36] Oncogene activation in precancerous lesions has been shown to increase DSBs and genomic instability.[37] Mutation of genes involved in either DNA repair programs (excision, cross-link, or mismatch repair) or the DDR pathways (such as ATM (ataxia telangiectasia mutated) and p53 signaling) can lead to increased DNA damage, inappropriate cell cycle progression, and genomic instability.[34,37] The DDR is a complex signal transduction pathway that has the ability to sense DNA damage and transduce this information to the cell to influence cellular responses to DNA damage.[34,37] Mutations in DDR genes result in a broad spectrum of disorders including disruption of homeostasis of the nervous, immune, and reproductive systems and can also lead to premature aging or cancer predisposition.[37] The notion that DDR pathways enhance sensitivity to agents that interfere with this stress response has been exploited by developing kinase inhibitors for ATM, ataxia telangiectasia and Rad3-related protein, DNA-dependent protein kinase, and checkpoint kinase 1, that indeed exhibit selective toxicity toward cancer cells and are being tested in the clinic.[38] Cancers defective in homologous recombination-mediated DNA repair due to loss of function of BRCA1 and BRCA2 (breast cancer gene) are particularly sensitive to cisplatin.[39] As these tumors also depend on other forms of DNA repair such as base excision repair, they are sensitive to inhibitors of enzymes that facilitate the repair of single-stranded DNA breaks like poly ADP ribose polymerase (PARP1).[40] While BRCA2 mutant cells are addicted to PARP1 function, the PARP1 inhibition is tolerated in normal cells because of functional compensation from homologous recombination-mediated repair.[40,41] As an extension of this principle, cancer cells with already elevated levels of DNA damage and replication stress cannot repair the additional damage and are therefore more vulnerable to the further extensive DNA damage resulting from radiation or chemotherapy that is lethal without a normal DDR pathway. This may explain how stress overload of the DDR pathway has been exploited therapeutically by radiation and chemotherapy.

5.01.4.2 Mitotic Stress

Chromosome missegregation often results in a shift in chromosome distribution and finally into the chromosome instability phenotype.[42] This phenotype is in part the result of defective pathways involved in the various checkpoints of chromosome segregation during anaphase where the spindle assembly checkpoint (SAC) plays a central role,[42] as well as the presence of extra centrosomes,[43] all of which stresses the mitotic apparatus.[42] Mitotic stress also occurs following activation of oncogenes like Ras or loss of function of tumor suppressors like p53 in the presence of an intact mitotic machinery.[42,44] Therefore, cancer cells with mutations that alter the fidelity of mitosis such as aneuploidy or weakened mitotic spindle regulatory machinery are likely to be more sensitive to catastrophic genomic instability caused by stress overload.[45] Thus, inhibiting the SAC may lead to lethality as a result of stress sensitization. Interfering with proper spindle–kinetochore attachment by the microtubule stabilizer taxol, an established anticancer agent, results in stress overload.[46] Inhibitors of mitotic kinases such as polo-like kinase, aurora kinases, monopolar spindle 1 kinase, NimA-related kinase, mitotic checkpoint serine/threonine-protein kinase, and Haspin and many others also promote stress overload, and some of them are currently undergoing clinical trials.[47]

5.01.4.3 Metabolic Stress

Multiple molecular mechanisms, both intrinsic and extrinsic, converge to alter cellular metabolism and provide support for rapid ATP (adenosine triphosphate) generation to maintain energy status, increased biosynthesis of macromolecules, and an appropriate cellular redox state in order to satisfy the energetic demands of rapidly dividing cancer cells (see tumor metabolism).[33,48] Most cancer cells have an increased glucose uptake and produce ATP by glycolysis, secreting a large amount of lactic acid, even under high oxygen conditions, while normal cells derive the bulk of their ATP through mitochondrial oxidative phosphorylation.[33,48] This glycolytic switch allows tumor cells to adapt to a low oxygen environment and promotes the acidification of the microenvironment, which in turn promotes tumor invasion and suppresses immune surveillance.[49] Thus, tumor cells activate biosynthetic pathways, reduce reactive oxygen species (ROS) by generation of NADPH (nicotinamide adenine dinucleotide phosphate), and adapt to the changes in oxygen availability in the tumor.[32,33,49] Therefore, inhibition of the glycolytic and biosynthetic pathways in a tumor cell will lead to stress overload due to incompatibility with the proliferative drive. Switching off pyruvate kinase (PK) can negatively impact the tumorigenic state, presumably by shunting pyruvate to the tricarboxylic acid (TCA) cycle and away from glycolysis.[50] The finding of an inherited mutation in protein kinase RNA activated (PKR), a tissue-specific isoform of PK, which causes the rare hematologic disorder known as PK deficiency,[51] triggered the discovery of AG-348 (Agios), a novel first-in-class activator of PKR that is being evaluated in the clinic.[52] Activating mutations in the NADP-dependent enzyme isocitrate dehydrogenase 1 (IDH1) and IDH2, which convert isocitrate to α-ketoglutarate (αKG) to produce NADPH, have been found in various tumors.[53] Mutated IDH1 and IDH2 are able to generate detectable levels of the oncometabolite αKG, which has been successfully used as response biomarker (BM) for AG-221 (Agios), an IDH2-specific inhibitor in advanced clinical trials for acute myeloid leukemia (AML) bearing the IDH2 mutation (https://clinicaltrials.gov/ct2/show/NCT02577406).

Glutamine is a known cell culture ingredient needed for robust cancer cell proliferation. In fact, many tumor cells are critically dependent on this amino acid.[33,54] The Myelocytomatosis Viral Oncogene Homolog (MYC) oncogene promotes not only proliferation but also the production of accompanying macromolecules and antioxidants that are required for growth.[54] Recent studies have shown that in MYC-dependent transformation, MYC stimulates and increases glutamine uptake by directly inducing the expression of the glutamine transporters slC5A1 and slC7A1,[33,54,55] which themselves are dependent on mTOR (mammalian target of rapamycin) activity.[56] In an amino acid-rich environment, mTOR not only is active and regulates protein translation but also inhibits autophagy. When extracellular amino acids are limiting, resulting in reduced mTOR activity, autophagy recycles intracellular constituents as a way to provide an alternative source of amino acids. Rapamycin, an inhibitor of the target of rapamycin (TOR), mimics the effect that amino acid starvation has on protein translation, cell cycle arrest, ribosome biogenesis, and autophagy.[56] Thus, glutamine flux regulates mTOR activity, translation, and autophagy to coordinate cell growth and proliferation.

In summary, targeting key metabolic enzymes in cancer cells may effectively attenuate tumor cell proliferation.

5.01.4.4 Oxidative Stress

Cancer cells typically generate more ROS than normal cells, a hallmark of oxidative stress response due to both, oncogenic signaling and downregulation of mitochondrial function.[57] Hypoxia in the tumor microenvironment leads to ROS production, which initiates mitochondrial damage and further ROS generation.[33,57] Oncogenes stimulate ROS production, facilitating oncogene-induced senescence causing oxidative damage to DNA, proteins, lipids, and other cellular components, and therefore pose a significant cellular stress.[57] Elevated ROS promotes activation of HIF-1 (hypoxia-inducible factor) by hypoxia, which itself promotes the glycolytic switch and angiogenesis observed in tumors.[57] To alleviate oxidative stress, cancer cells switch to glycolysis and downregulate mitochondrial function. Increasing ROS production is therefore expected to cause stress overload in cancer cells.[57] In support of this notion, it has been shown that inhibitors of pyruvate dehydrogenase kinase (PDK) stimulate mitochondrial oxidative phosphorylation and ROS production and selectively elicit apoptosis in cancer cells but not in normal cells.[58] Similarly, reducing the cellular ROS buffering capacity through the inhibition of glutamate–cysteine ligase can markedly increase the radiosensitivity of cancer cells.[32.a]

5.01.4.5 Hypoxia and Nutrient Stress

Tumor hypoxia, due to poor and abnormal tumor vasculature, is one of the best studied cell stress responses and is a poor prognostic factor in a number of malignancies.[57,59] Hypoxia alters transcription through the stabilization of HIF, which increases glycolytic capacity, decreases mitochondrial respiration, stimulates vessel sprouting via VEGF-A and angiopoietin-2, protects tumor cells from acidosis, and promotes the secretion of lactate (see section "Targets in Neovascularization").[57,59] Drugs targeting either HIF-1 or its effector pathways have been effective in various clinical settings by sensitizing tumor cells toward hypoxic stress.[60] If nutrients are not properly provided to tumor cells, they experience nutrient stress and resort to autophagy for survival, and, as hypoxia inhibits signaling via mTOR, this may facilitate the induction of autophagy.[56,61] Although impaired autophagy could contribute to oncogenesis by promoting genomic instability and cytokine release, autophagy is critical for the survival of apoptosis-resistant tumor cells during nutrient or growth factor restriction. It is therefore to date unclear which tumors may benefit from activation or inhibition of autophagy.[62]

5.01.4.6 Proteotoxic Stress

Aneuploidy and gene copy number changes alter the relative balance of growth and survival signals promoting tumorigenesis. The corresponding increases and decreases in transcript levels produce imbalances of the proteome.[33,63] Increased levels of unfolded protein aggregates in cancer cells burden the protein folding and degradation machineries resulting in a proteotoxic stress.[33,63,64] The heat shock response pathways with their heat shock proteins (HSPs) promote the proper folding and/or proteolytic degradation of proteins. The heat shock response is one of the countermeasures of this type of proteotoxic stress (see protein folding and degradation).[64,65] Pharmacological, genetic, and clinical evidence supports the notion that sensitizing tumor cells toward proteotoxic stress can strongly suppress tumorigenesis.[64–66] The chaperone activity of heat shock protein 90 (HSP90) requires its ATPase activity, which can be blocked by various HSP90 inhibitors and may display its antitumor effect either by destabilizing key HSP90 client proteins like cyclin-dependent kinase (CDK) 4 and human epidermal growth factor receptor 2 (HER2) or by sensitizing tumor cells to elevated general proteotoxic stress.[67] A convenient method of inducing protein unfolding is temperature elevation. Hyperthermia is being extensively investigated as a tumor treatment in combination with chemotherapy.[68] Unfolded proteins are generally turned over by the ubiquitin proteasome pathway.[69] Thus, a second key component of the proteotoxic stress response pathway is the proteasome.[69,70] Bortezomib (Velcade, Millennium Pharmaceuticals) was the first proteasome inhibitor showing clinical efficacy in multiple myeloma.[70] Proteasome inhibition leads to the stabilization of a particular subset of proteins that might be responsible for the antitumorigenic activity. More recently, the imbalance of proteins in cancer cells has also been addressed by targeting the ubiquitin-activating enzymes.[69,71] Moreover, using PROTACs, which are small molecules that inhibit the function of their target proteins by targeting them for degradation by the ubiquitin proteasome system, allows for rapid target identification and might be used as therapeutic strategy.[72]

5.01.5 Targets With Clinical Relevance

Many patients have profited from targeted cancer therapeutics over the last decade, and multiple novel compounds have started the development process. Besides classical kinases, targets in other areas relevant for cancer growth and tumorigenesis have been validated and are being utilized for the identification of innovative tumor therapies.

5.01.5.1 Kinases and Inhibitors

5.01.5.1.1 Introduction

Posttranslational modifications like phosphorylation, glycosylation, ubiquitination, nitrosylation, acylation, methylation, lipidation, and proteolysis, which are known to increase the diversity of the proteome, influence various aspects of normal and pathological physiology.[73] Aberrant phosphorylation in eukaryotes is associated with a variety of disorders ranging from cancer to inflammatory diseases, diabetes, infectious diseases, cardiovascular disorders, cell growth, and survival.[73,74] Kinases are enzymes that catalyze the transfer of phosphate groups from ATP (adenosine triphosphate) to proteins or lipids. A set of divergent kinases play essential roles for eukaryotic signaling. These include various protein kinases like murine sarcoma viral oncogene homologue B (BRAF), Abelson murine leukemia viral oncogene homologue 1 (ABL), ALK (anaplastic lymphoma kinase), and kinases that are able to phosphorylate phosphatidylinositol, such as PI3Ks (phosphatidylinositol 3-kinases) and phosphatidylinositol 4-kinases (Fig. 2).[75] Many human malignancies are associated with deregulated activation of protein or lipid kinases due to mutations, chromosomal rearrangements, and/or gene amplification.[32,74,76]

The human kinome, that consists of, all protein kinases in the genome, contains typical and atypical protein kinases as well as pseudokinases.[77] The latter make up 10% of the human protein kinases and are either inactive or only weakly active due to lack of at least one of three motifs in the catalytic domain that are essential for catalysis.[78] Despite lacking the ability to phosphorylate substrates, pseudokinases are still very important in regulating diverse cellular processes as indicated by the regulation of the serine/threonine-protein kinase STK11 by STE20-related adaptor alpha and the "activation" of JAK2 (Janus kinase) by mutation (C617F) of its JH2 pseudokinase domain.[78]

5.01.5.1.2 Kinase structure

The business end of protein kinases consists of a small, mostly β-structured N-lobe, connected by a short hinge fragment to a larger alpha-helical C-lobe. ATP binds in the cleft between the N- and C-terminal lobes of the kinase domain where the adenine group of ATP is sandwiched between hydrophobic residues and makes contact via hydrogen bonds to the hinge.[79] In most kinases just N-terminal of the hinge, deep in the ATP pocket is an important residue called the "gatekeeper," which is often mutated in kinase alleles resistant to inhibitors. This gatekeeper is not present in PI3K or mTOR. The gatekeeper controls the access to the hydrophobic

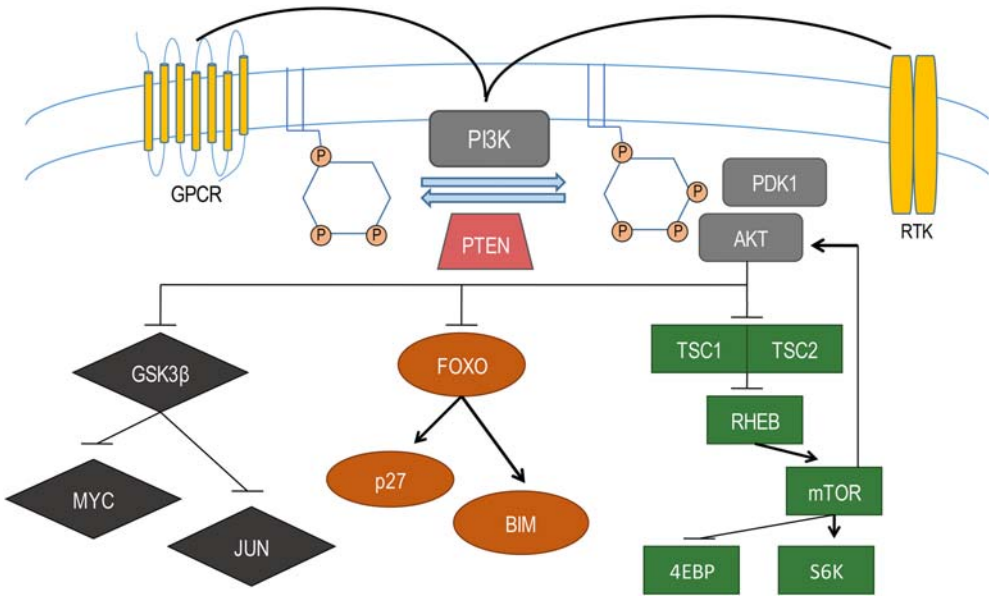

Fig. 2 The canonical PI3K signaling pathway. PI3K can be activated by G protein-coupled receptors (GPCRs) or receptor tyrosine kinases (RTKs) and then catalyzes the phosphorylation of phosphatidylinositol bisphosphate (PIP2) to PIP3. Subsequently, a cascade of kinases becomes activated leading to elevated translation, transcription, and growth. *PTEN*, phosphatase and tensin homologue; *PDK1*, 3-phosphoinositide-dependent protein kinase-1; *AKT*, protein kinase B; *GSK3β*, glycogen synthase kinase 3 beta; JUN, JUN kinase; FOXO, forkhead box protein O3; TSC, tuberous sclerosis complex; RHEB, Ras homologue enriched in brain; 4EBP, eIF4E binding protein; S6K, ribosomal protein S6 kinase.

"back pocket" of the kinase.[79,80] An outstanding structural element of the ATP binding sites is the activation loop (also called activation segment or A-loop) with its N-terminal Asp-Phe-Gly-motif (DFG-motif) whose orientation is pivotal for the access of the protein substrate sites.[79,81] Other elements required for catalysis are the C-helix, the catalytic loop, and finally the aforementioned DFG-motif[79,81,82] (see http://www0.nih.go.jp/mirror/Kinases/pkr/3D/xray/2cpk/2cpkwalk.html).

5.01.5.1.3 Receptor tyrosine kinases (RTKs)

RTKs are membrane-spanning receptors for growth factors, cytokines, and hormones. They consist of an extracellular region with the binding site for their ligand, a hydrophobic transmembrane domain, and an intracellular catalytic domain containing the kinase activity. Ligand binding stabilizes receptor dimerization and induces activation of intracellular phosphorylation processes that then induce activation of a signaling cascade such as PI3K and MAP kinase (mitogen-activated protein kinase) signaling. RTKs regulate many cellular processes and are key components in oncogenic transformation and tumor growth/development. Most relevant RTKs in cancer biology are EGFR (epidermal growth factor receptor), VEGFR (vascular epithelial growth factor receptor), KIT (mast/stem cell growth factor receptor), and HER2neu/ErbB2.[4]

5.01.5.1.4 Kinase activation in cancer

Kinase signaling pathways drive many of the hallmark phenotypes of tumor biology, including proliferation, survival, motility, metabolism, angiogenesis, and evasion of antitumor immune responses. Activation of kinase signaling derives from genetic and epigenetic events. Most frequently, somatic point mutations of kinases and RTKs, which induce gain of function, are present in tumor cells, for example, BRAF (V600), PI3K (E542, E545, and H1047), and KIT (D816). Many kinases that become independent of normal regulatory mechanisms due to constitutively activating mutations are oncogenic and transforming. Overexpression of kinases and deletion of negative regulators can also intrinsically activate cancer-stimulating signaling. Most frequent overexpression has been observed for RTKs, for example, EGFR and HER2, as well as CDK4 and CDK6.[83] Driver kinases are those with genetic alterations that contribute to the transformation of a normal cell to a proliferating cancerous cell. Several driver kinases have been identified and validated in human malignancies and disorders[32,76] by genome-wide screening for kinase amplifications, translocations, or mutations in conjunction with proteomic technologies (see section "TIDVAL: Target Identification and Validation"). These studies have revealed how the mutational status of kinases may be associated with various cancer conditions.[74,76,84]

5.01.5.1.4.1 Example: PI3K/mTOR inhibitors

The PI3K/mTOR signaling cascade serves many physiological and pathophysiological functions and is of major importance for cancer and inflammatory diseases.[75,85] Class I PI3K consists of four isoforms, PI3K α, β, γ, and δ, each with particular functions. The PI3K signaling pathway is frequently activated in human cancers inducing oncogenic transformation, growth, and survival. Pathway activation can be induced by gain of function mutations in PI3K or downstream effector proteins, loss of function mutations in the negative regulator of PI3K and PTEN (phosphatase and tensin homologue), or hyperactivation of an upstream receptor like HER (**Fig. 2**). mTOR is a major downstream target of PI3K signaling that is part of two complexes, mTORC1 and mTORC2 with distinct function.[75,83,86] Many drugs targeting the PI3K or the mTOR pathways are currently in clinical development for both adult and pediatric cancers.[85,87]

Rapamycin was the first mTOR inhibitor discovered. The marketed rapalogs Afinitor™ (everolimus, RAD001, Novartis) and Torisel™ (temsirolimus, CCI-779, Wyeth/Pfizer), which allosterically inhibit mTORC1, have been approved for various cancer[88] and noncancer indications.[89] These inhibitors have recently been joined by the PI3Kdelta inhibitor idelalisib (Zydelig, GS1101, CAL101, Gilead Sciences), which has been approved for various lymphoma indications.[90] Drug candidates inhibiting all the class I PI3Ks including mTORC1 and mTORC2 (dual PI3K/mTOR inhibitors) or all the class I PI3Ks without affecting mTOR (panPI3K inhibitors) or individual isoforms of the class I PI3K (isoform-selective PI3K inhibitors) or imTORC1/mTORC2 only (mTOR inhibitors)[85] have reached various stages of clinical development (http://clinicaltrials.gov/). In summary, there is a competitive landscape for PI3K/mTOR inhibitors, with multiple drugs in development having reached phase III clinical trials (ie, bursalisip (BKM120, Novartis), taselisib (GDC0032, Roche/Genentech), duvelisib (IPI-145, Infinity Pharmaceuticals), and alpelisib (BYL719, Novartis)). Duvelisib is being tested in lymphoma clinical trials. GDC0032 and BKM120 have recently entered phase III clinical trials in breast cancer in combination with the estrogen receptor (ER) degrader fulvestrant. Dual PI3K/mTOR inhibitors like PQR309 (Piqur Therapeutics) are following.

5.01.5.1.4.2 Example: CDKs and their inhibitors

CDKs and their associated cyclins regulate the cell cycle.[91] The human genome encodes 21 CDKs, although only 7 (CDK1, 2, 3, 4, 6, 10, and 11) have been shown to have a direct role in the cell cycle. According to the classical model, CDK4 or CDK6 regulate events in the early G1 phase of the cycle, CDK2 triggers the S phase, CDK2 and CDK1 regulate the completion of the S phase, and CDK1 is the master regulator of mitosis.[91] A second group of CDKs, which are not directly involved in the cell cycle regulation (CDK7, CDK8, CDK9, CDK10, and CDK11), regulates cellular transcription, especially of mRNA transcripts with rapid turnover.[91] Although CDKs and their respective cyclins are not commonly mutated in cancers, their respective inhibitor families, CDKN1 (INK2) and CDKN2 (INK4), show often loss of function due to mutations or epigenetic modulation.[91,92] CDK activity is needed for normal cell division, but in tumors, the CDK is hyperactivated. In particular, the cascade involving CDK4/CDK6-cyclinD, the endogenous protein inhibitor CDKN2A (INK4A or p16), the RB tumor suppressor RB, and the transcription factor E2F has been found to be altered in many cancers.[91,92] Although the importance of CDKs in normal cellular growth is undoubted, recent preclinical studies in which

researchers knocked out the various CDKs showed that CDK2, CDK4, and CDK6 are dispensable for the cell cycle of most normal cell types, while CDK1 is not.[92] As CDK1 appears to be essential for the division of normal cells, inhibiting CDK1 in cancer shows a much narrower therapeutic window with the same type of toxicities as traditional chemotherapy. In contrast, CDK4/CDK6 inhibitors may show a better therapeutic window as certain cancers may be addicted to CDK4/CDK6 activity and therefore will respond to these agents even though most normal cells may not require them for proliferation. Therefore, some of the early pan-CDK inhibitors have been discontinued.[91,93] At present, Pfizer (palbociclib), Lilly (abemaciclib), and Novartis (LEE011) are developing selective CDK4/CDK6 inhibitors that appear to be less toxic and have shown strong progression-free survival (PFS) in ER-positive breast cancer.[91,94]

5.01.5.1.5 Approved kinase inhibitors

Since the approval of fasudil in 1995, sirolimus in 1999, and imatinib in 2001, the number of approved kinase inhibitors has increased to 36 with many others still in preclinical development (**Table 1**). These inhibitors are mainly for oncological indications and are directed against only a handful of protein and lipid kinases, leaving 70% of the kinome untapped (**Table 1**). Despite these successes in kinase drug discovery, the development of kinase inhibitors with outstanding selectivity, the identification and validation of driver kinase(s) in diseases, and the emerging problem of resistance to the inhibition of key target kinases remain major challenges. Kinase inhibitors with outstanding selectivity are likely to become important not only for minimizing side effects and allowing chronic treatment of non-life-threatening diseases.[76,95]

Most of the approved kinase drugs are active against more than one type of cancer. Only few of them have been used for the treatment of non-oncological indications (tofacitinib for rheumatoid arthritis, nintedanib for idiopathic pulmonary fibrosis, everolimus for organ rejection of heart and kidney transplants, and fasudil for cerebral vasospasm; **Table 1**). On the other hand, there are multiple kinase drugs for one single indication. For example, imatinib, nilotinib, dasatinib, bosutinib, and ponatinib have all been approved for CML (chronic myeloid leukemia), while sorafenib, sunitinib, everolimus, temsirolimus, axitinib, and pazopanib are indicated for various stages of renal cell cancer. Ceritinib and crizotinib are indicated for non-small cell lung cancer (NSCLC) with ALK translocations, while gefitinib, erlotinib, afatinib, and osimertinib are indicated for NSCLC with activated EGFR. Finally, vemurafenib alone or the combination of dabrafenib with trametinib is indicated for metastatic melanoma with BRAF V600 mutations (**Table 1**).

5.01.5.1.6 Kinase inhibitor mode of action

With a few exceptions, such as the rapalogs (sirolimus, everolimus, and temsirolimus), trametinib, or cobimetinib, all of the small-molecular-weight kinase inhibitors are directed toward the ATP binding site (see **Table 1**). The conservation of the ATP binding in the human kinome causes these "ATP mimics" to often cross-react with many other different kinases resulting in compounds with promiscuous profiles, for example, dasatinib[96] and sunitinib.[97]

Kinase inhibitors show different modes of binding to kinases. In principle, one can divide kinase inhibitors into those that bind covalently or reversibly to the kinase.[83,95] ATP-competitive inhibitors bind to the hinge region of the kinase[79,81,95,98]; allosteric kinase inhibitors are non-ATP-competitive and do not have physical contact to the hinge. As they exploit binding sites and regulatory mechanisms that are unique to a particular kinase, they, therefore, show the highest degree of selectivity.[79,81,95,98] Similarly, agents targeting the extracellular domains of RTKs act outside the kinase domain. These include peptide mimetics, "peptoids" or antibodies,[99] or small molecules like SSR128129E (Sanofi), which targets the extracellular domains of the fibroblast growth factor receptor (FGFR).[100]

Targeting the allosteric sites of protein kinases may also lead to the identification of activators rather than inhibitors, which could be useful for therapeutic intervention or as pharmacological tools. There are a few protein kinases that require activation rather than inhibition to fulfill their therapeutic task as in the case of 5′-adenosine monophosphate-activated protein kinase (AMPK) and the insulin receptor for which activators have been identified.[101] Protein kinase C (PKC) activation by exogenous compounds acting at the diaclyglycerol binding site can have tumor-promoting or tumor-suppressive effects.[102] Another example of kinase activators includes a mimetic of the brain-derived neurotrophic factor that activates tropomyosin receptor kinase B or neurotrophin receptor kinase 2.[103] In some cases, kinase inhibitors can lead to unintended paradoxical activation either directly or via modulation of feedback loops. The most striking example is the paradoxical effect of BRAF inhibitors, which can activate the MAPK pathway in certain genetic backgrounds resulting in the promotion of hyperproliferative toxicities.[104] There is currently no general strategy for the identification of allosteric kinase inhibitors or activators as most of them have been discovered serendipitously by diverse approaches ranging from phenotypic screenings to highly sophisticated structure-based drug design.

5.01.5.1.7 Kinase mutations and resistance

Deregulation of protein kinase activity by gain of function mutations is essential to maintain the oncogenic state, and in many instances, these mutations can be linked to specific cancers.[84] Inhibitors are being and have been designed to specifically target kinase alleles with gain of functions.[74,105] Despite these successes, it should be emphasized that patients who benefit from these kinase inhibitors often relapse after an initial response (see section "Challenges of Targeted Cancer Therapy"). Multiple mechanisms of resistance have been and are being elucidated to improve the efficacy of these types of targeted therapies. Drug resistance to kinase inhibitors can occur either by compensatory mechanism or by mutations reducing the affinity of the kinase to its inhibitors.[76,106] Approaches to overcome resistances include the development of inhibitors that can tolerate mutations, that bind covalently to their target, or that bind to allosteric sites. Another option is targeting another protein in the same pathway or targeting alternate, activated pathways in combination with the first inhibitor used.[96,107]

Table 1 Approved kinase inhibitors as of Dec. 2015

Year	*Generic name (compound code, trade names)*	*Kinase target*	*Disease*	*Company (year, type)*
1995	Fasudil (HA-1077) [5181]	ROCK1/2	Cerebral vasospam, PAH	Asahi Kasei (1995, type 1)
1999	Sirolimus (Rapamune) [6031]	mTOR	Kidney transplants	Pfizer, Wyeth (1999, type 3)
2001	Imatinib (STI571, Glivec, Gleevec) [5687]	ABL, PDGFR, KIT	CML, Ph + B-ALL, CMML, HES, GIST	Novartis (2001, type 2)
2003	Gefitinib (ZD1839, Iressa) [4941]	EGFR	NSCLC	AZ (2003, type 1)
2004	Erlotinib (OSI-774, Tarceva) [4920]	EGFR	NSCLC, pancreatic cancer	Roche, OSI (2004, type 1)
2005	Sorafenib (BAY 43–9006, Nexavar) [5711]	VEGFR2, PDGFR, KIT, FLT3, BRAF	RCC, HCC	Bayer, Onyx (2005, type 2)
2006	Sunitinib (SU11248, Sutent) [5713]	VEGFR, KIT, PDGFR, RET, CSF1R, FLT3	RCC, imatinib-resistant GIST	Pfizer (2006, type 1)
2007	Lapatinib (GW2016, Tykerb) [5692]	EGFR, ERBB2	BC	GSK (2007, type 1.5)
2007	Dasatinib (BMS-354825, Sprycel) [5678]	ABL, PDGFR, KIT, SRC	CML	BMS (2007, type 1)
2007	Nilotinib (AMN107, Tasigna) [5697]	ABL, PDGFR, KIT	CML	Novartis (2007, type 2)
2009	Everolimus (Rad001, Certican, Zortress, Afinitor, Votubia) [5889]	mTOR	RCC, SEGA, transplantation	Novartis (2009, type 3)
2009	Temsirolimus (CCI-779, Torisel) [5892]	mTOR	RCC	Pfizer, Wyeth (2009, type 3)
2011	Crizotinib (PF-02341066, Xalkori) [4903]	MET and ALK	NSCLC with ALK translocations	Pfizer (2011, type 1)
2011	Vandetanib (ZD6474, Caprelsa) [5717]	RET, VEGFR1-2, FGFR, EGFR	MTC	AZ (2011, type 1)
2011	Ruxolitinib (INC424, Jakafi) [5688]	JAK2	IMF with JAK2V617F mutations	Novartis, Incyte (2011, type 1)
2011	Vemurafenib (PLX4032, RG7204, Zelboraf) [5893]	BRAF	Metastatic melanoma with BRAFV600E mutations	Roche, Plexxikon (2011, type 2)
2011	Axitinib (AG013736, Inlyta) [5659]	VEGFR, KIT, PDGFR, RET, CSF1R, FLT3	RCC	Pfizer (2012, type 1)
2012	Regorafenib (BAY 73-4506, Stivarga) [5891]	VEGFR2, Tie2	CRC, GIST	Bayer (2012, type 2)
2012	Pazopanib (GW-786034, Votrient) [5698]	VEGFR, PDGFR, KIT	RCC	GSK (2012, type 1)
2012	Tofacitinib (CP-690550, Xeljanz, tasocitinib) [5677]	JAK3	RA	Pfizer (2012, type 1)
2012	Cabozantinib (XL184, BMS-907351, Cometriq) [5887]	VEGFR2, PDGFR, KIT, FLT3	MTC	Exelexis (2012, type 1)
2012	Ponatinib (AP24534, Iclusig) [5890]	ABL	Imatinib-resistant CML with T315I mutations	Ariad (2012, type 1)
2012	Bosutinib (SKI-606, Bosulif) [5710]	ABL	CML resistant/intolerant to therapy	Pfizer (2012, type 1)
2013	Dabrafenib (Tafinlar) [6494]	BRAF	Metastatic melanoma with BRAFV600E mutations	GSK (2013, type 2)
2013	Trametinib (Mekinist) [6495]	MEK	Metastatic melanoma with BRAFV600E mutations	GSK (2013, type 3)
2013	Afatinib (Gilotrif, Tomtovok, Tovok) [5667]	EGFR	NSCLC with EGFR-activating mutations	BI (2013, covalent)
2013	Ibrutinib (PCI-32765, Imbruvica) [6912]	BTK	MCL, CLL	Janssen, Pharmacyclic (2013, covalent)
2014	Ceritinib (LDK378, Zykadia) [7397]	ALK	NSCLC with ALK translocations	Novartis (2014, type 1)
2014	Idelalisib (CAL101, GS1101, Zydelig) [6741]	PI3Kdelta	CLL, FL, and SLL	Gilead, Calistoga, ICOS (2014, type 1)
2014	Nintedanib (BIBF 1120, Vargatef, Intedanib) [5936]	VEGFR, PDGFR, FGFR	Idiopathic pulmonary fibrosis	BI (2014, type 1)
2014	Alectinib (AF802, Aliens) [7739]	ALK	ALK-rearranged NSCLC (brain mets)	Roche, Chugai (2014, type 1) appr. in Japan
2015	Palbociclib (PD-0332991, Ibrance) [7380]	CDK4/6	Advanced (metastatic) BC	Pfizer (2015, type 1)
2015	Lenvatinib (E7080, Lenvima) [7426]	VEGFRs multikinase	Thyroid cancer (DTC); kidney cancer	Eisai Co (2015, type 1)
2015	Cobimetinib (GDC-0973, XL-518, Cotellic)	MEK	Melanoma in combination with vemurafenib	Roche, Exelexis (2015, type 3)

Table 1 Approved kinase inhibitors as of Dec. 2015—cont'd

Year	Generic name (compound code, trade names)	Kinase target	Disease	Company (year, type)
2012	Radotinib (Supect)	BCR-ABL, PDGFR	CML	Ilyang, Daewoong Pharmaceutical (2015, type 2). Approved in South Korea only
2015	Osimertinib (mereletinib, AZD9291; Tagrisso)	EGFR (T790M)	NSCLC with EGFR-activating mutations or T790M	AZ (2015, covalent)

CML, chronic myeloid leukemia; *Ph+ − B-ALL*, Philadelphia chromosome-positive B-cell acute lymphoblastic leukemia; *CMML*, chronic monomyelocytic leukemia; *HES*, hypereosinophilic syndrome; *GIST*, gastrointestinal stromal tumor; *NSCLC*, non-small cell lung cancer; *RCC*, renal clear cell carcinoma; *HCC*, hepatocellular carcinoma; *BC*, breast cancer; *SEGA*, subependymal giant cell astrocytoma; *MTC*, medullary thyroid cancer; *IMF*, interstitial myelofibrosis; *CRC*, colorectal cancer; *RA*, rheumatoid arthritis; *MCL*, mantle cell lymphoma; *CLL*, chronic lymphocytic leukemia; *FL*, follicular lymphoma; *SLL*, small lymphocytic leukemia; *PAH*, pulmonary arterial hypertension; *Rock*, Rho-associated protein kinase; *RET RTK*, rearranged during transfection RTK; *CSF1R*, colony-stimulating factor 1 receptor; *JAK*, Janus kinase; *VEGFR*, vascular endothelial growth factor receptor; *mTOR*, mammalian target of rapamycin; *SRC*, proto-oncogene tyrosine-protein kinase Src; *BTK*, Bruton's tyrosine kinase; *ABL*, Abelson kinase; *BCR*, breakpoint cluster region; *PDGFR*, platelet-derived growth factor receptor; *FLT3*, fetal liver kinase 3; *ALK*, anaplastic lymphoma receptor tyrosine kinase; *MET*, MET receptor = hepatocyte growth factor receptor (HGFR); *MEK*, MAP2K, mitogen-activated protein kinase kinase; *FGFR*, fibroblast growth factor receptor.
The 36 kinase inhibitors approved to date are shown with generic name, compound code, trade name, primary indications, year of approval, company, and mode of binding. *GSK*, Glaxo Wellcome; *AZ*, AstraZeneca; *BI*, Boehringer Ingelheim. The chemical structures and biochemical profiles of the 36 approved kinase inhibitors can be viewed in the IUPHAR database (http://www.guidetopharmacology.org/GRAC/LigandListForward?type=Approved&database=all).

5.01.5.1.8 Outlook

The future of protein kinase-targeted therapeutics in cancer appears promising, despite the fact that several protein kinase inhibitors that have entered human clinical trials are not very specific and did not achieve the anticipated results. This situation may be improved by the upcoming second generation of kinase inhibitors with a better selectivity that will be applied to a genetically better defined patient population. The development of kinase inhibitors for non-life-threatening indications where chronic regimens are being used will require a priori a better target selectivity to minimize side effects. Identification of highly selective kinase inhibitors and activators should lead to an expansion of the chemical and biological kinase space as well as to an improved understanding of their therapeutic limitations and potentials.

Reversible, noncovalent kinase inhibitors can be classified as type 1, type 2, and type 3 reversible kinase inhibitors.[98] *Type 1 inhibitors* fulfill all the criteria of an ATP mimetic by binding to the hinge and targeting an active conformation of the kinase (often referred to as DFG-in). The type 1.5 inhibitor is a subtype of the type 1 inhibitor that binds to an inactive kinase conformation (DFG-in conformation, typical of an active kinase, but the C-helix is pushed out). *Type 2 inhibitors* bind to the inactive, so-called DFG-out conformation, maintaining contacts to the hinge region and usually displaying an ATP-competitive behavior similar to type 1 inhibitors. The transition of the active DFG-in to the inactive DFG-out conformation exposes an additional hydrophobic pocket adjacent to the ATP site that is used by type 2 inhibitors locking the kinase in the inactive conformation. *Type 3 inhibitors* are non-ATP-competitive (allosteric) kinase inhibitors that have no physical contact to the hinge. As they exploit binding sites and regulatory mechanisms that are unique to a particular kinase, they, therefore, show the highest degree of selectivity. Type 3 inhibitors can bind either to the kinase domain (close to or removed from the ATP site) or to sites that are located outside of the kinase domain (rapamycins).

5.01.5.2 Targets in Induction of Apoptosis

Programmed cell death, apoptosis, is a tightly regulated suicide program that plays a critical role in maintaining the survival/death balance. It is part of the machinery that eliminates cells with disturbed function. Impaired apoptosis can lead to the development of cancers or autoimmunity; increased apoptosis can induce degenerative disease.[108] DNA-damaged cells that do not undergo apoptosis can form cancerous lesions. Therefore, cancer cells frequently exhibit apoptotic defects resulting not only in oncogenicity but also in resistance to cytotoxic cancer treatments that induce apoptosis as a mode of action.[109] Affected cells survive beyond their intended life span and are protected from oxidative stress and hypoxia—both common features of solid tumors.

Apoptosis is initiated by different pathways. The so-called extrinsic (death receptor-dependent) or the intrinsic (mitochondrial) pathway is the most relevant in the cancer context. The intrinsic and extrinsic pathways activate upstream caspases, caspase 9 and caspase 8, respectively, and converge further downstream in the caspase activation cascade.[110] Caspases are intracellular proteases that cleave key cellular components and activate degrading enzymes (**Fig. 3**).[108,109,111]

Activation of the extrinsic pathway is triggered by cytokine ligands binding to death receptors of the tumor necrosis factor (TNF) family. An intracellular binding site recruits adaptor proteins like procaspases to form a death-inducing signaling complex that triggers caspase activation,[112] which initiates apoptosis. Tumor necrosis factor α (TNFα), Fas ligand (FASL), and tumor necrosis factor-related apoptosis-inducing ligand (TRAIL) are the most prominent death receptor ligands.

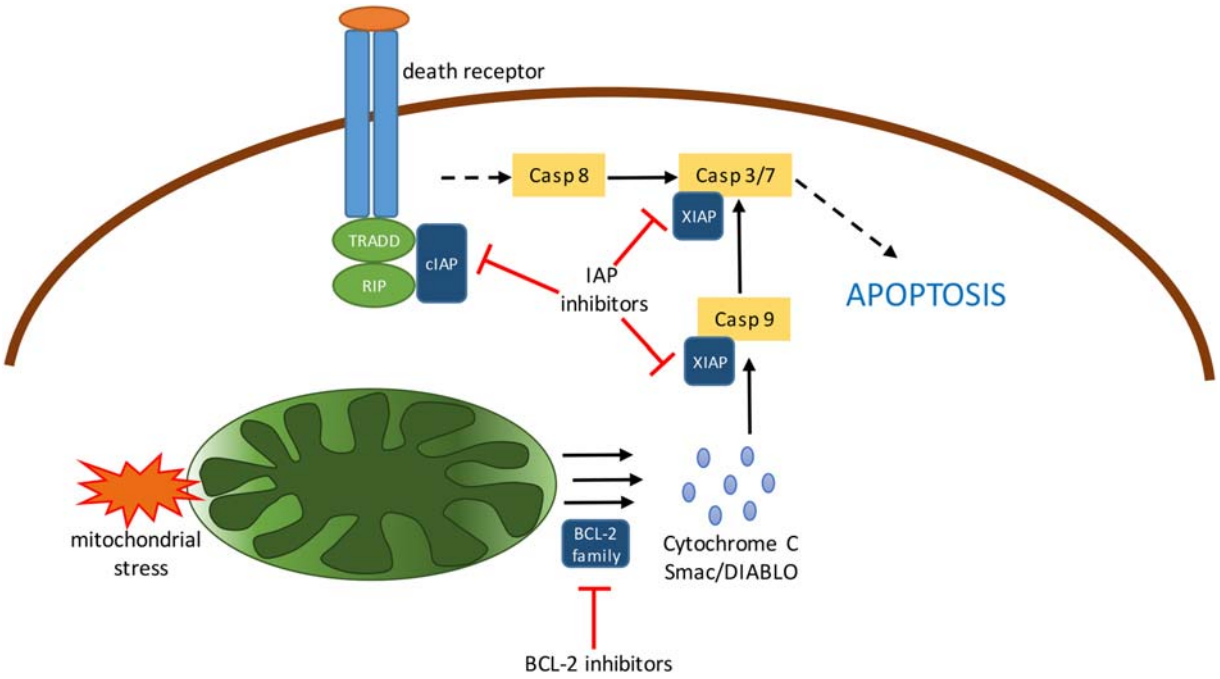

Fig. 3 Apoptosis is often inhibited in cancer. Induction of apoptosis can be achieved via the inhibition of apoptosis inhibitors of the IAP family or the BCL-2 family.

The intrinsic pathway can be activated by stress factors including DNA damage through radiation or UV as well as viruses or growth factor deprivation. In response to these stress factors, mitochondrial membrane permeabilization allows for mitochondrial proteins like cytochrome-c and Smac (second mitochondria-derived activator caspase, inhibitors of apoptosis (IAP) binding protein with low p*I*) to diffuse into the cytosol. IAPs are direct inhibitors of caspases (see succeeding text). Smac can activate caspases by neutralizing IAPs.[113] A complex called the apoptosome forms and starts the cascade of caspase activation resulting in apoptosis.[114] B-cell lymphoma 2 (BCL2) family members with antiapoptotic (BCL-2, BCL-XL, MCL1, BCL-W, A1, and BCL-B) and proapoptotic (eg, BAX, BAK, BIM, BCL-XL, BID, and BAD) functions regulate the permeabilization of the mitochondrial membrane.[5,115]

IAP proteins regulate apoptosis by binding to caspases and inhibiting their activity. All members of the IAP family (eg, XIAP, cIAP1/2, livin, and survivin) contain a Baculovirus IAP Repeat (BIR) domain that mediates the interaction with caspases and other proteins.[116] While XIAP is the strongest inhibitor of caspases, cIAP1/2 has additional roles in other signaling processes that induce apoptosis, particularly NFkB (nuclear factor "kappa-light-chain-enhancer" of activated B cell) signaling.[117] IAPs are overexpressed in most cancer cell lines and many cancers and correlate with poor prognosis and chemoresistance.[118]

Mechanisms that are used by tumor cells to evade apoptosis include imbalance of BCL-2 family proteins, impaired death receptor signaling, reduced caspase expression, and increased expression of IAPs. Particularly, overexpression of BCL-2 has been shown to protect many tumors, such as prostate cancer, glioblastoma, and lymphoma from apoptosis.[119] A central regulator of apoptosis genes is p53, a tumor suppressor that is mutated in about 50% of all cancers.[110,120]

Induction of apoptosis has been investigated in the clinic using two mechanisms: (1) IAP inhibition and (2) BCL-2 inhibition. IAP inhibitors target the BIR domains of IAP proteins and release caspases from IAP inhibition. IAP inhibitors with peptidomimetic and nonpeptidomimetic structures interrupt the protein–protein interaction between IAPs and caspases as well as the indirect apoptosis suppression of cIAP1/2 through cIAP proteasomal degradation and NFkB activation.[121] As single agents, IAP inhibitors induce apoptosis only in a small subset of cell lines but have a broader efficacy spectrum in vivo. Compounds seem to be particularly effective in combination with death receptor ligands like TRAIL.[121,122] Examples of IAP inhibitors in clinical phase I/II are birinapant (TL32711, TetraLogic), LCL161 (Novartis), and ASTX660 (Astex).

BCL-2 inhibitors target the BCL-2 family of antiapoptotic proteins that are commonly overexpressed in a wide range of solid and hematologic cancers. Besides efforts targeting the expression of BCL-2, direct small-molecule inhibitors are under clinical investigation. Preclinical data demonstrated synergistic cytotoxicity by combining induction of apoptosis with conventional therapy to overcome resistance.[123] ABT-263 (navitoclax, AbbVie) and the BCL-2 selective ABT-199 (venetoclax, AbbVie) are currently in clinical phase II trials in NSCLC (ABT-263 only), leukemia, and lymphoma and are showing positive results, particularly in hematologic malignancies with high BCL-2 overexpression and in combination.[124] Other clinical stage compounds are the pan-BCL-2 inhibitors obatoclax (GX15-070, Teva) and gossypol (AT-101, Ascenta) (www.clinicaltrials.gov).

5.01.5.3 Targets in Tumor Metabolism

Tumorigenesis is characterized by uncontrolled growth and proliferation. To maintain this process, tumor cells undergo major metabolic transformations. Alterations in nutrient metabolism can be induced by genetic mutations or epigenetic changes that might be targetable for therapy.[125] Oncogenes and tumor suppressors can regulate nutrient metabolism, and mutations in metabolic enzymes play a role in the development of cancer.[54]

5.01.5.3.1 Glucose metabolism

The so-called Warburg effect is part of metabolic reprogramming and has been known since the 1920s. Cancer cells use much more glucose than normal cells and transform glucose into lactate by aerobic glycolysis instead of metabolizing glucose by oxidative phosphorylation and shuttling the products of glycolysis into the TCA cycle.[126] These metabolic changes enable the generation of precursors for the formation of new biomass.[127] In many cases, metabolic events do not appear to be oncogenic drivers but can be induced by other events during oncogenesis. For example, activation of the PI3K pathway results in high rates of aerobic glycolysis through alterations of enzymes and glucose transporters.[125]

Targets that are involved in glycolytic changes have been suggested for the development of tumor therapeutics. 2-Deoxyglucose is an inhibitor of hexokinase 2 (HK2), an enzyme that is part of the glycolysis machinery and that, at the same time, binds to mitochondria. The HK2–mitochondria interaction facilitates immortalization of tumor cells. HK2 inhibition has shown some efficacy in patients with solid tumors at high concentration. Optimized inhibitors might give better clinical benefit.

Another targetable glycolytic enzyme is 6-phosphofructo-2-kinase/fructose-2,6-bisphosphatase 3 (PFKFB3). PFKFB3 is upregulated in low-pH, hypoxic tumors through Hif-1α as well as by the oncoprotein Ras and insulin signaling. The PFKFB3 inhibitor PFK158 (Advanced Cancer Therapeutics) has shown downregulation of glycolytic flux and inhibition of tumor growth in models and in a first clinical trial (Fig. 4).[128]

PK influences the fate of glycolytic products. PK catalyzes the final step of glycolysis from phosphoenolpyruvate to pyruvate, which is then either shuttled into the TCA cycle for ATP production or excreted as lactate (see Warburg effect). PKM2 is an isoform of PK that is specifically expressed in proliferating cells. Its activity is low and it acts as a sensor for amino acid generation. Due to slow metabolism of glucose mediated by PKM2 in cancer, upstream glycolytic intermediates become available for the formation of new cellular building blocks.[127] Furthermore, PKM2 exhibits activity as a transcriptional regulator and promoter of the Warburg

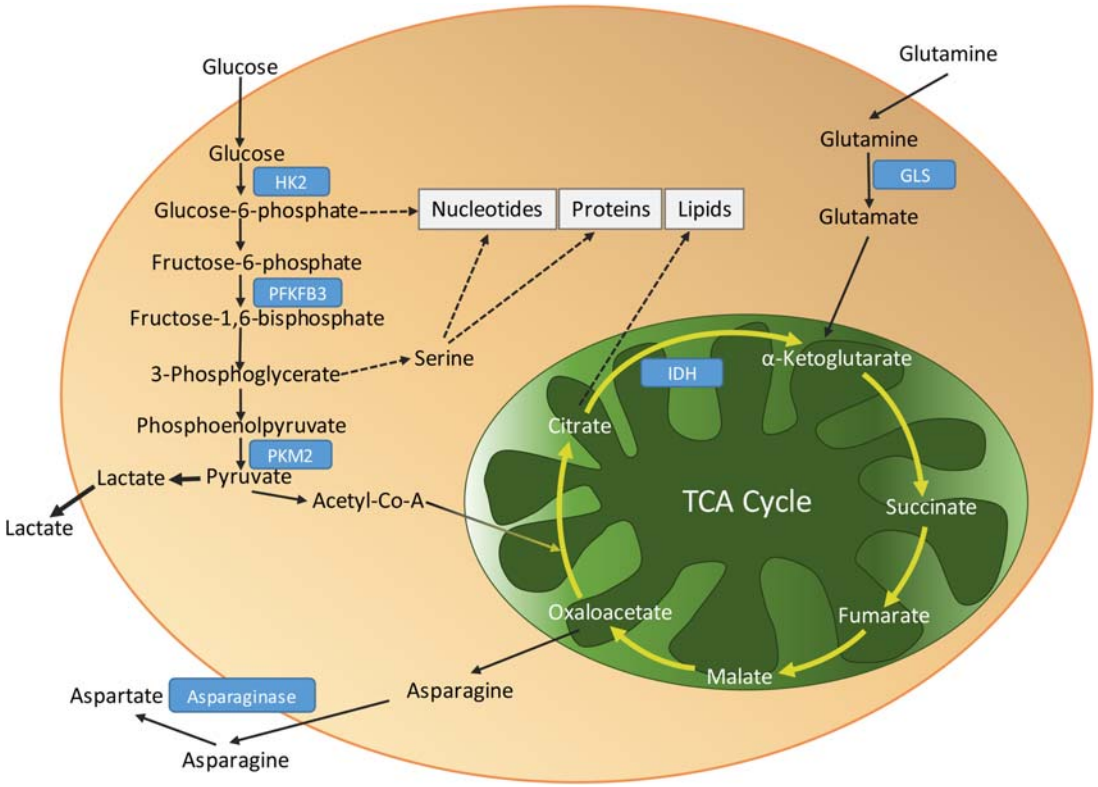

Fig. 4 Metabolic targets in tumor therapy. Metabolic reprogramming in cancer cells can be found in glucose and amino acid metabolism as well as during oxidative phosphorylation. Several targets that are particularly important for metabolic homeostasis of cancer cells can be targeted for therapy (*highlighted in blue*).

effect.[129] In vitro and in vivo studies indicate that activators of PKM2 might inhibit tumor growth, while PKM2 inhibitors give opposing results.

5.01.5.3.2 Amino acid metabolism

In cells with high proliferation rates, precursors for macromolecular synthesis are built from glycolytic intermediates and from products of the TCA cycle. Glutamine is a nonessential amino acid that plays an important role in anaplerotic mechanisms as it can be converted to αKG, a precursor of lipids, nucleotides, and other nonessential amino acids.[125] In cancer cells, glutamine demand is bigger than supply by the cell's own synthesis. Glutamine thus becomes conditionally essential (**Fig. 4**).[54] Furthermore, glutamine maintains redox homeostasis and ATP production in many cells. Glutaminase (GLS) is an enzyme involved in glutaminolysis that is upregulated in several cancers, for example, by overexpression of Myc. GLS is essential for Myc-driven tumors like neuroblastoma and renal cell carcinoma.[130] GLS inhibitors like CB-839 (Calithera) are under development and are being tested in clinical trials for solid and hematologic tumors[131] (www.clinicaltrials.gov).

In a subset of melanoma and hepatocellular carcinoma that lacks the ability to produce arginine, recombinant pegylated arginase can reduce tumor growth. The enzyme depletes arginine and cells that depend on an external supply die because of arginine starvation.[132] In certain leukemic cells, the same situation occurs due to their inability to produce asparagine. Asparaginase is approved for the treatment of acute lymphocytic leukemia in adults and children and is mostly used as combination agent. Clinical trials in other hematologic malignancies are ongoing (www.clinicaltrials.gov).[133]

5.01.5.3.3 TCA cycle

In some cancers, the TCA cycle does not work properly due to mutations in the metabolic enzymes fumarate hydratase (FH), succinate dehydrogenase (SDH), and IDH 1/2. FH and SDH are tumor suppressors and mutation leads to loss of function. IDH mutations change the function of the enzyme causing synthesis of a normally low concentration metabolite, (R)-2-hydroxyglutarate (2HG), and consumption of NADPH.[131,134] 2HG is a tumor marker for patients with IDH mutant tumors and has been suggested to inhibit enzymes that alter cellular epigenetics (**Fig. 4**).[135] Forty percent of adult gliomas and 50% of chondrosarcomas harbor mutations in IDH1 or IDH2.[136] Small-molecule inhibitors of IDH1/2 [eg, AG-120 and AG-221 (Agios)] are under clinical investigation in IDH-mutated tumors. Initial results indicate a good safety profile and signs of efficacy in phase I.[137]

5.01.5.4 Targets in Immuno-Oncology

The immune system is able to distinguish between the body's own and foreign cells. The changes that happen during oncogenic transformation result in expression of neoantigens that are sufficient to identify cancer cells as foreign. This ends in the eradication of subclinical tumors/cancer cells by the host immune cells.[138] Nevertheless, cancer cells frequently evade the immune system and proliferate to form a tumor.

During the noninhibited immune response to cancer cells, specific cancer cell antigens are released from the cells and presented on major histocompatibility complex class I and class II (MHCI or MHCII) of dendritic cells (DCs) or antigen-presenting cells (APCs), respectively. DCs and APCs travel to the lymph node where they present antigen to specific T lymphocytes. T cells are primed and activated by these antigens. Cancer cells can present peptides from tumor-specific antigens bound to MHCI. Previously activated T cells that infiltrate the tumor recognize cancer cells expressing their cognate antigen. They bind to this MHC complex via their T-cell receptor and kill their target cancer cell.[138]

T-cell activation is only partially understood. For full activation, additional costimulatory receptors need to form complexes with their counterparts on the respective APC or cancer cell besides the MHC recognition.[139] Additionally, T-cell activation is regulated by inhibitory cytokines [interleukin (IL) 10 and transforming growth factor (TGF) β] or activating cytokines (IL2 and IL12). Activation of PI3K/mTOR signaling inhibits T-cell activation (see section "Kinases and Inhibitors").

5.01.5.4.1 Tumor-induced immunosuppression

Tumors evolve to evade the immunologic response through different processes. Tumors and their microenvironment establish an immunosuppressive environment in which nearly every step of an effective antitumor response is inhibited:

1. Lack of "danger signals" from innate immune cells. Bacteria or viruses are recognized as "foreign" by DCs leading to their activation. Cancer cells can be well tolerated, and one reason is impaired DC maturation and poor DC recruitment. Mediators of DC maturation defects are vascular endothelial growth factor (VEGF), TGFβ, IL10, macrophage colony-stimulating factor, and IL6.[140] Another mechanism to evade DC and T-cell recognition is loss of MHC expression.[141]
2. Suppressed recruitment of T cells to the tumor site. T cells fail to invade the tumor at normal levels due to changes in cytokine production and barrier formation in the tumor vasculature.[142]
3. The tumor microenvironment produces an immunosuppressive milieu. Endothelial cells express mediators that suppress or kill effector cells, for example, indoleamine 2,3-dioxygenase (IDO), programmed cell death protein ligand 1 (PD-L1), and IL-10.[140,143] Hypoxia and low pH within solid tumors also negatively affect T lymphocytes.[144]
4. Resistance to T cell-mediated killing. T cells eliminate targets through the perforin/granzyme B pathway. Tumor cells express enzymes that inhibit granzyme B.[145]

5. Extrinsic suppression of CD8+ effector T cells by regulatory T cells (Tregs). Tregs are recruited to the tumor and undergo local expansion. Tregs mediate immunologic tolerance by secretion of immunosuppressive molecules that suppress T cell activity by direct killing of effector T cells and DCs, starvation of effector T cells leading to apoptosis, and inhibition of DC function.[146]
6. Tumor cell counterattack. Some tumors express the death receptor ligand FasL and TRAIL that can kill T cells directly.[145,147] Expression of IDO mediates suppressive effects on T cells and activates Tregs.[148]
7. Cancer cells take control over immune checkpoints. When antigen/MHC binding to the TCR is accompanied by engagement of costimulatory receptors, T cells will be primed/activated. Simultaneous engagement of coinhibitory receptors results in T-cell inhibition. Inadequate presentation of costimulatory ligands on tumor cells induces tolerance and insufficient priming and activation of immune cells toward their target antigens (see section "Immuno-checkpoint inhibitors").[28]

Cancer immunotherapy implements ways to promote the host's immune response against cancer cells and increase antitumor immunity. These methods include blockade of immune checkpoints and cytokine therapy. Lately, also treatment with modified, autologous T cells has been investigated (see section "CARs").

A major question is: Which immunosuppressive step is the best to be altered with therapy? One option is to distinguish between tumors with and without T-cell infiltration. For tumors with sufficient T-cell infiltration, the assumption that proper T-cell activation is the major issue can be made. In tumors without T-cell infiltration, most likely, the microenvironment forms a significant barrier. This information might serve as a decision support for choosing the most effective therapy. Combinations with other immune-stimulating drugs or different oncological therapeutics might be beneficial.

5.01.5.4.2 Immuno-checkpoint inhibitors

Immune checkpoints are coinhibitory receptors expressed on the cell surface of immune cells. These receptors inhibit the activation/priming of T cells or DCs when they are activated during MHC recognition. Normally, immune checkpoints are expressed on cells of the immune system in order to prevent overshooting immune reactions against self-antigens.[149] But cancer cells also express checkpoints to evade the host's immune response. Therefore, blocking the immunosuppressive effect of immune checkpoints can stimulate an immune response against cancer. Antibodies directed against two checkpoints have been approved by the FDA (US Food and Drug Administration): ipilimumab, an anti-CTLA4 (cytotoxic T-lymphocyte activation marker 4) antibody, and nivolumab and pembrolizumab, anti-PD-1 (programmed cell death protein 1) antibodies.

CTLA4 is an immune checkpoint receptor that is normally exclusively expressed on T cells. A variety of tumors overexpress CTLA4, which is associated with poor prognosis.[150] CTLA4 regulates early T-cell activation and counteracts the costimulatory receptor CD28. Depending on engagement of CTLA4 or CD28, T cells are activated or inhibited when the TCR interacts with antigen presentation on MHC. Ipilimumab prevents the inhibitory mechanisms of CTLA4 blockade and leads to uninhibited T-cell activation.[151]

PD-1 is another immunosuppressive coreceptor highly expressed on T lymphocytes. Upon activation, the receptor inhibits kinases that are involved in late, peripheral T-cell activation. The PD-1 ligands PD-L1 and PD-L2 are cell surface proteins that are overexpressed on some tumors like melanoma, glioblastoma, and lung cancer. They induce inactivation of T cells at the site of immunologic effect as well as T-cell apoptosis and downregulation of cytokine production. The PD-1 antibodies nivolumab and pembrolizumab block the interaction between PD-L1/2 and PD-1 inducing effector immune response.[151,152]

Anti-PD1 and anti-PDL1 monotherapy responses in patients range between 13% and 38%, and sometimes, even tumor eradication has been observed. Most cases of autoimmune side effects are treatable with steroids.[138] Nonresponders most likely have another (additional) form of tumor immunosuppression. Therefore, it would make sense to combine immunotherapy approaches, for example, chimeric antigen receptors (CARs) (see succeeding text) with PD-L1/PD-1 inhibitors. Combination of PD-1 with CTLA4 antibodies has shown a different immunologic profile and led to longer PFS than single-agent treatment in a particular group of melanoma patients.[153]

5.01.5.4.3 Cytokine therapy

ILs are cytokines that play an important role as immune modulatory proteins. They alter immune responses by binding specific receptors and influencing growth, differentiation, activation, and chemoattraction. ILs can induce pro- and anti-inflammatory responses.[154] For example, IL12 has immune stimulatory and antiangiogenic effects when delivered to the tumor in a targeted fashion or through gene therapy. Decrease in tumor burden has been observed in models of different cancer types like ovarian cancer and mesothelioma when treated with IL12.[155]

High-dose IL2 is approved to treat stage 4 solid cancers. First approval by the FDA was granted in 1992. IL2 therapy has a 15% response rate (RR) in metastatic renal cell carcinoma and a 21% RR in metastatic melanoma.[156] Five to ten percent of patients with metastatic renal cell carcinoma even experience complete remission. IL-2 stimulation improves T-cell proliferation and survival leading to unspecific immunologic effects on the tumor. Major side effects observed are autoimmunity directed against the kidneys and liver.[157]

5.01.5.4.4 CARs

Immunologic killing of cancer cells can also be induced by genetically modifying the patient's own immune cells. T cells are isolated from the patient's blood and expanded in culture. Then they are transfected with CARs comprising an antibody fragment directed against a tumor marker (usually CD19 or CD4) fused to T-cell receptor signaling domains. These CAR-expressing T cells are

infused back into the patient. Interaction between CARs and the target cell surface protein expressed on cancer cells induces physiological T-cell activation. T cells expressing CARs recognize the tumor cells and kill them.

The CAR approach has shown good signs of benefit in hematologic malignancies like lymphoma.[158] To increase the performance and persistence of engineered T cells, second- and third-generation CARs are under development. The approach is limited to antigens expressed on the cell surface and so far has not shown efficacy in solid tumors. The main toxicities observed with CAR treatment are the depletion of healthy B lymphocytes and the release of cytokines ranging from minor severity to lethal toxicity.[159]

5.01.5.5 Targets in Protein Folding and Degradation

Many signal transduction pathways that are altered in cancer are known, and direct inhibitors targeting proteins involved in these pathways are under development or have entered clinical practice. Another approach to target cancer signaling is the alteration of oncoprotein synthesis, folding, and degradation. These strategies have the potential to overcome resistances or to target so far undruggable proteins like Kirsten Rat Sarcoma Viral Oncogene Homolog (KRAS).[160]

5.01.5.5.1 Intervention in protein folding

Chaperones facilitate protein maturation, folding, and protection against heat stress. HSP90 is a chaperone protein that is critical for the homeostasis of over 600 client proteins. Cancer cells particularly depend on proteins that are under HSP90 control as several mutated and nonmutated oncoproteins like ALK, HER2, BRAF, EGFR, Met, JAK2, v-Src as well as androgen, ERs, HIF1α, VEGFR, breakpoint cluster region (BCR)-ABL, and AKT (protein kinase B) are affected by HSP90 activity.[161] Furthermore, HSP90 regulates apoptosis through interaction with NFkB.[162] Other clients like BCL-2, BRCA, and CDK1/4 are involved in resistance implying that HSP90 inhibitors might be good combination partners for therapies that evoke resistance. For example, the HSP90 inhibitor ganetespib is active in EGFR inhibitor-resistant tumors.[163] HSP90 buffers cellular stress induced by oncogenic transformation and tumor growth.[164] HSP90 is often overexpressed in cancers and associated with poor prognosis.[165] Inhibition of HSP90 leads to ubiquitin-mediated degradation of client proteins followed by inhibition of linked pathways. Finally, beneficial effects on several of the hallmarks of cancer can be observed.[67]

First-generation HSP90 inhibitors showed high levels of toxicity. Therefore, next-generation inhibitors from different chemotypes are under clinical development.[67] The most advanced compounds are ganetespib (Synta), which is under clinical investigation for NSCLC, as well as NVP-AUY922 (Novartis) and AT-13387 (Astex).[166]

5.01.5.5.2 Inhibitors of protein degradation

The balance between protein synthesis and degradation is tightly regulated. Most proteins are being degraded via the ubiquitin proteasome system. Ubiquitin-activating and ubiquitin-conjugating enzymes as well as ubiquitin ligases tag proteins with ubiquitin. Targets include a variety of enzymes and short-lived and non-properly folded proteins. Tagged proteins are recognized and degraded by the proteasome, a multiprotease complex. Blocking the proteasome leads to accumulation of defective proteins and can subsequently cause cell death. Increased proteasomal activity has been observed in malignant cells as these cells have a higher rate of protein synthesis. Furthermore, proteins that are degraded via the proteasome include molecules relevant for cell growth, cell cycle and proliferation, and other tumor relevant processes. Inhibition of the proteasome induces downregulation of angiogenesis, growth, and survival as well as induction of apoptosis. Cancer cells are more sensitive to proteasome inhibitors than normal cells.[167]

The first proteasome inhibitor, bortezomib (Velcade, Millennium Pharmaceuticals), is approved for patients with non-Hodgkin's lymphoma and multiple myeloma. Bortezomib binds to the 26S proteasome and inhibits the degradation of many cellular proteins. The mechanism of action is poorly understood as a vast number of proteins are affected by bortezomib. Treatment success is accompanied by severe side effects on neurons and blood cells,[168] and relapses often occur. Therefore, combination efforts have been investigated to gain a long lasting effect. Ixazomib (Ninlaro, Takeda) is the only orally bioavailable proteasome inhibitor that is approved by the FDA. Ixazomib targets the 20s proteasome and shows efficacy in multiple myeloma and has a better safety profile than bortezomib.[169] Carfilzomib (Kyprolis, Onyx) is an irreversible inhibitor that binds to the 20s proteasome and is approved for treatment of multiple myeloma.[170] Three other second-generation proteasome inhibitors are under clinical investigation not only in multiple myeloma but also in lymphomas, leukemias, and solid tumors: delanzomib, oprozomib, and marizomib.[167 a,b]

More specific inhibitors of protein degradation are in clinical development. E1, E2, and E3 ubiquitin-modifying enzymes are involved in targeting proteins for degradation. Distinct ubiquitin-modifying enzymes target a small family of cancer-relevant proteins and thus represent potentially more selective cancer targets. For example, the ubiquitin ligase MDM2 (murine double minute 2 homologue) is involved in the degradation of the tumor suppressor p53. Its inhibition keeps levels of p53 up. Inhibitors of the protein–protein interaction between p53 and MDM2 are under clinical investigation in leukemias, sarcomas, and other tumors.[171]

5.01.5.6 Targets in Cancer Epigenetics

Processes that modify chromatin—the macromolecular complex of DNA and histone proteins—and lead to alterations in the transcriptional potential of the cell are termed "epigenetics." There are different types of epigenetic modifications such as DNA methylation and histone acetylation or methylation that influence transcription and DNA repair (**Table 2**).[172] It is widely accepted

Table 2 Epigenetic modifications of DNA and histone proteins

DNA modifications	*Histone modifications*
Methylation, hydroxymethylation, formylation, carboxylation	Acetylation, methylation, phosphorylation, ubiquitylation, sumoylation, ADP ribosylation, deamination, proline isomerization, crotonylation, propionylation, butyration, formylation, hydroxylation, O-GlcNAcylation

that epigenetic modifications play a role in nearly every step of tumorigenesis. Genomic initiatives have found mutations in key enzymes that regulate epigenetic alterations. For example, histone methylase MLL2 and histone demethylase UTX are mutated in follicular lymphoma and acute lymphoblastic leukemia (ALL), respectively.[173]

5.01.5.6.1 DNA methylation

All tumors investigated so far show changes in their so-called epigenome. A well-described phenomenon in cancer cells is the hypermethylation of CpG island regions in promoters that leads to subsequent gene silencing.[174] Tumor suppressor genes are often targeted by these silencing effects, but also microRNAs with growth inhibitory functions and genes involved in cell cycle, DNA repair, apoptosis, and metabolism can be inhibited.[175] DNA methyltransferases 1, 2, and 3 are targets of the approved hypomethylating agents azacitidine (Vidaza, Celgene) and decitabine (Dacogen, Otsuka/Astex/Eisai/Janssen).

5.01.5.6.2 Histone modifications

Histone modification patterns are numerous and complex. In most cases, neither the mechanisms establishing these modifications nor the impact of modification patterns has been understood. Modifications can influence the electrostatic interaction between DNA and histone proteins leading to a more relaxed or condensed chromatin structure.[176] It is clear that histone modifications can substantially influence transcription and other DNA template processes.[172] Histone modifications are reversible and dynamically changing from activating to repressing patterns, and cross talk between modifications has been observed.[177]

Histone acetylation patterns are altered in cancer. Enzymes involved in histone acetylation/deacetylation are histone lysine acetyltransferases and histone deacetylases (HDACs).[178] So far, 18 HDAC proteins are known that target acetylated histone and nonhistone proteins. HDAC inhibitors restore a set of aberrantly silenced genes and induce growth arrest, differentiation, and apoptosis of tumor cells.[179] Three HDAC inhibitors have been approved for the treatment of T-cell lymphoma: belinostat (Beleodaq, Topotarget), romidepsin (Istodax, Celgene), and vorinostat (Zolinza, Merck). Other HDAC, partly specific, inhibitors are under development.[176]

5.01.5.6.3 Histone acetylation readers

Proteins that can bind to acetylated histones are able to "read" the epigenetic code. About 46 proteins that contain a bromodomain belong to this class. Bromodomain proteins translate the code of lysine acetylation into various phenotypes. Their functions include chromatin remodeling, histone modification, and transcriptional activation.[172,180] The Bromodomain and extraterminal domain (BET) family of proteins contains two bromodomains and an extra terminal domain. Members of this family are BRD2, BRD3, BRD4, and BRDT proteins. BET proteins regulate the expression of several oncogenes, like c-Myc and Bcl-2.[181] Inhibitors do not have the same effect on all cancers as the molecular context is an important factor determining the impact on regulatory mechanisms. Tissue-specific toxicities of inhibitors of certain bromodomain classes have been observed in rodents. Stem cell depletion, alopecia, and immunosuppression are among the observed side effects.[182] A large number of bromodomain inhibitors have been patented.[180] For example, OXT015 (OncoEthix) is currently being tested in different cancers. Other BET inhibitors like RVX000222 (Resverlogix) are under evaluation for oncological as well as non-oncological malignancies.[181]

5.01.5.7 Targets in Genomic Stability

Telomeres are protective caps of 5–10 kbp at the end of each chromosome. They prevent misrecognition of chromosomal ends as DNA breaks, which would lead to activation of DNA repair machinery and subsequently result in chromosomal instability. Telomeres cannot be replicated completely as DNA polymerase cannot replicate DNA toward its end. Therefore, during each cell division, part of the telomere is lost.[183] In normal cells, telomere shortening functions as a molecular clock and triggers senescence (irreversible cell cycle arrest) or apoptosis, preventing abnormal cell division and chromosomal instability.[184] With age, more and more cells experience telomere shortening, and for a few of those cells, senescence fails. Chromosomal instability then will be lethal to those cells as a second step of control.

5.01.5.7.1 Telomerase inhibitors

Cancer cells proliferate in an uncontrolled manner as they are able to overcome proliferative blocks induced by telomere shortening and chromosomal instability. One mechanism to maintain telomeres at stable length is activation of telomerase, a telomere-specific reverse transcriptase. Telomerase can add a six-nucleotide repeating sequence, 5′-TTAGGG, to the 3′ end of a chromosome.[185]

Telomerase activation has been observed in 90% of human cancers, while most normal cells have inactivated telomerase.[186] Tumor cells that do not have elevated telomerase activity use alternate pathways to maintain telomeres.[187] The expression of telomerase is regulated by tumor suppressors like p53 and oncogenes like Sp1 and Myc.[188] The deletion of telomerase inhibits the formation of tumors in vivo. For example, telomerase-deficient mice do not develop BCR-ABL-induced leukemia.[189] Stem cells in general and cancer stem cells (CSCs) in particular display elevated telomerase activity to maintain their prolonged proliferative activity.[190] Targeting telomerase appears to be a promising cancer therapy not only because most types of cancer depend on telomere maintenance but also because their stem cell population might be depleted by telomerase inhibitors.

Besides telomere extension, the catalytic component of telomerase, Telomerase Reverse Transcriptase (TERT), influences other signaling pathways involved in carcinogenesis including Wnt and PI3K. Through these pathways, telomerase regulates its own expression in a feedback system.[191]

Telomerase is a potential target for immunotherapy (see immuno-oncology). GRNVAC1 (VAC-1, Asterias Biotherapeutics) and GV1001 (Tertomtide, Kael-GemVax) are under clinical investigation as immune therapeutics and cancer vaccines. GRNVAC-1-treated AML patients showed a high rate of immune response and favorable outcome. Imetelstat (GRN163L, Johnson & Johnson) is a lipid-conjugated oligonucleotide that directly binds to the template region of telomerase RNA and is being evaluated for myelodysplastic syndrome and different neoplasms (www.clinicaltrials.gov).[192]

5.01.5.7.2 PARP inhibitors

DNA damage can occur through different processes: (1) exposure to UV light or chemicals, (2) spontaneous DNA-damaging events, and (3) failure in DNA processing. DNA damage repair (DDR) includes a variety of cellular responses to DNA damage including cell cycle arrest, regulation of DNA replication, and DNA repair as well as senescence and apoptosis. DNA repair is essential to maintain DNA integrity. While nucleotide excision repair fixes damage caused by UV, alkylating agents, or chemotherapeutics, base excision repair fixes damaged DNA bases. DNA mismatch repair is responsible for base/base mismatches and larger loop insertions or deletions, while Double strand break (DSB) repair mechanisms [homologous recombination repair (HRR) and nonhomologous end joining] join broken DNA ends. Depending on the cell cycle status, the DDR is different.[183,193] Targeting tumors that lack specific functions of the DDR with targeted DNA-damaging agents has a greater therapeutic window than using unspecific DNA-damaging chemotherapeutics as these cells are particularly sensitive.

Most cancers have lost one or more DDR pathways leading to uncontrolled growth and genomic instability on the one hand and a greater dependency on the other pathways on the other hand. If a cancer cell depends on a single DDR pathway for survival, targeting this pathway provides the potential for high cancer cell-killing activity while sparing normal cells of the body, a phenomenon termed synthetic lethality (**Fig. 5**).[193,194]

PARP is an essential component of the machinery that repairs single-strand DNA breaks. During this process, PARP binds to the DNA single-strand break, which activates its catalytic domain. PARP hydrolyzes NAD^+ and forms poly ADP ribose (PAR) chains that recruit DNA repair proteins which are required for relaxation of chromatin. PARylated PARP dissociates from the DNA and allows for completion of DNA repair. PARP inhibitors trap the inactivated protein at the damaged DNA and thus block cellular DNA replication and induce deleterious DSBs,[195] which would normally be repaired by homologous recombination repair (HRR). If this mechanism is defective, cells acquire an extent of DNA instability that leads to cancer cell death. A prominent example of HRR deficiency is a mutation in BRCA1 or BRCA2, typically found in breast and ovarian cancer. Therefore, cancers carrying a BRCA1/2 mutation are particularly responsive to PARP inhibitors.[196] This finding was verified in clinical trials of PARP inhibitors tested in BRCA-mutated breast cancer. For example, olaparib (Lynparza, AstraZeneca) showed an overall RR of 26% and a stable disease rate of 42% in a phase II study in patients with advanced cancers and a germ-line BRCA1/2 mutation.[193,197] Several trials are ongoing that investigate combinations of PARP inhibitors with DNA-damaging chemotherapy as well as with targeted

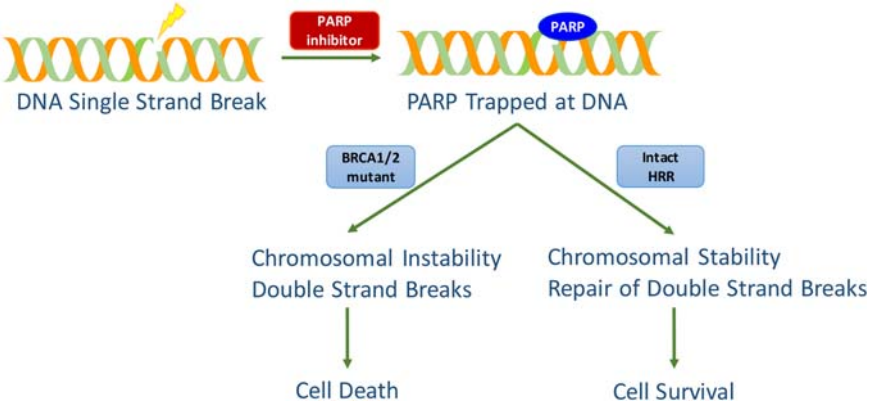

Fig. 5 Synthetic lethality. PARP inhibitors exhibit their potential in cells with BRACA1/2 mutation leading to irreparable chromosomal instability and cellular crisis that results in cancer cell death.

therapeutics. Olaparib is the first PARP inhibitor that has been approved for treatment of BRCA-mutated ovarian, breast, and prostate cancer.[197] Niraparib (Tesaro, MSD), rucaparib (Clovis Oncology), veliparib (Abbott), and talazoparib (Medivation) are currently undergoing clinical trials in BRCA-mutated cancers and in combination with radiation, chemotherapy, or targeted therapeutics (www.clinicaltrials.gov).

5.01.5.8 Targets in Neovascularization

The formation of new blood vessels from preexisting vessels is called angiogenesis. It has been shown that tumors stay dormant as long as they cannot form a new, internal vasculature. The neovasculature within a tumor provides oxygen and nutrients to cancer cells. Furthermore, cells of the newly formed vessels secrete growth factors (angiocrine signaling).[198] The main pathway driving neovascularization is constituted of the VEGF family and its receptors: VEGFR1, 2, and 3. VEGFRs are RTKs (see section "Kinases and Inhibitors") that form dimers in the cell membrane. VEGF signaling induces cell division, migration, vascular permeability, and chemotaxis of endothelial cell precursors.

Inhibitors of VEGF and VEGFR that have been approved or are at present under development target the main angiogenesis transmitting factors, VEGF-A and VEGFR2. Besides kinase inhibitors that target VEGFR [vatalanib (Bayer Schering), sunitinib (Pfizer), cediranib (AstraZeneca), and nintedanib (Boehringer Ingelheim)], the antibodies cetuximab (Merck, ImClone, Bristol-Myers Squibb), trastuzumab (Roche), and panitumumab (Amgen) also inhibit VEGF signaling at different nodes. Single-agent activity of VEGF signaling inhibitors has been observed in renal cell carcinoma, hepatocellular carcinoma, pancreatic neuroendocrine tumors, soft tissue sarcomas, and colorectal cancer. In other cancers, combination therapy has shown efficacy.[198,199] Overall, anti-VEGF treatment exhibits less therapeutic success than expected, although VEGF signaling is elevated in almost all solid tumors.

VEGF expression is upregulated by the hypoxia-inducible transcription factors HIF1α and HIF2α, which have been shown to be important in different models including renal cell carcinoma.[200] Other oncogenic factors that upregulate VEGF expression are p53 inactivation or Src, Ras, and EGFR activation as well as inflammatory cytokine stimulation.[198] As few cancers depend on VEGF, VEGF inhibition only leads to short periods of growth delay in the majority of cancers. A reason for this can be that metastatic tumors co-opt existing vessels for their energy supply and are therefore not affected by inhibition of angiogenesis.[201] VEGF therapy can induce the so-called vessel normalization observed in preclinical models and in clinical settings. Tumor vessels are immature; they exhibit higher permeability and elevated interstitial fluid pressure leading to hypoxia in the tumor tissue and an abnormal microenvironment. Vessel normalization induces improved perfusion and better oxygen coverage due to reformation of vessel architecture.[202] Consequently, the alterations of vasculature in cancers induced by VEGF pathway inhibition can positively influence uptake and potency of drugs given in combination. For example, bevacizumab potentiates the efficiency of immunotherapeutic treatment and sunitinib improves delivery of systematically administered chemotherapeutics. These data suggest a role of VEGF inhibitors as combination agents.[202,203] Resistance to VEGFR inhibition occurs due to upregulation of alternate proangiogenic pathways via HIF1α.[204]

In addition to VEGF, other pathways that influence neovascularization are angiopoietin (vessel maturation and angiogenesis) and Notch (tip and stalk formation). Angiopoietins, Ang-1, Ang-2, and Ang-3, are cytokines that regulate angiogenesis, inflammation, and vascular extravasation. They bind to and act via the vascular receptor kinase Tie2. Angiopoietins play a role in the initial step of neovascularization, the disruption of the two vessel layers: endothelial and perivascular cells. Ang-2 is upregulated at sites of tumor angiogenesis in cancers such as melanoma, malignant gliomas, and thyroid, renal, gastric, lung, neuroendocrine, and breast tumors. Moreover, Ang-2 is associated with poor survival in breast cancer and other malignancies.[205] Ang-1 contributes to the stabilization of newly produced vessels through activation of antiapoptotic pathways mediated by AKT. Inhibition of angiopoietin is currently being evaluated as single agent or in combination. For example, combining angiopoietin inhibitors with VEGF inhibitors might lead to synergism in inhibiting neovascularization. Trebananib (Amgen) is an Ang-1- and Ang-2-neutralizing peptibody that is currently in clinical trials as a single agent in patients with prostate cancer and in combination with the VEGFR inhibitor sunitinib in renal cell carcinoma.[206]

5.01.6 Biomarkers

5.01.6.1 Definition

Throughout the last two decades, the concept of the so-called BMs as a powerful tool driving rational drug development has entered all phases of targeted cancer therapy development. They are also a core component of the "personalized medicine" concept, which ultimately aspires to define the most efficient treatment for any given patient. While the term has been (mis-)used as a vague umbrella in certain cases, the Biomarkers Definitions Working Group has provided a comprehensive definition that is widely recognized, namely, "a characteristic that is objectively measured and evaluated as an indicator of normal biological processes, pathogenic processes or pharmacologic responses to a therapeutic intervention."[207]

To date, BMs are core components of targeted therapy development programs. As early as during the lead discovery phase, BMs contribute to evaluate target engagement and immediate impact on biological processes. In clinical development and beyond, "predictive BMs" help to identify patients who are likely to benefit from a given targeted agent. Importantly, predictive BMs can also define patient populations who will not benefit from a specific therapy or might even be at risk of developing severe drug-related toxicities. The so-called monitoring BMs contribute to monitoring safety, efficacy, and disease progression. In order to

respect the scope of this article, we will focus on examples of BMs that have been instrumental in developing targeted cancer therapies in the clinic. The majority of BMs currently applied in the clinic are genetic mutations, gene expression, and total protein levels (http://www.fda.gov/MedicalDevices/ProductsandMedicalProcedures/InVitroDiagnostics/ucm301431.htm). The advent of next-generation sequencing is providing large data sets for single patients at a reasonable cost. However, comprehensive and meaningful analyses of these data and translation into clinical benefit for the patient remain challenging. Other technologies such as noninvasive imaging techniques and mass spectrometry are also being explored in the context of BM development. Mass spectrometry-based assays are providing metabolite profiles and can detect posttranslational protein modifications that could reflect the active state of proteins more adequately than immunohistochemical approaches that mainly detect total protein levels and are largely of qualitative nature.

While the BM concept is widely applied in the preclinical setting, examples of BM translation into the clinical routine remain scarce. Reasons for this phenomenon are discussed later in the paragraph on challenges and perspectives.

5.01.6.2 BMs in the Clinic

The first targeted cancer therapy that formally integrated a BM to select patients that were likely to respond was Herceptin. Herceptin (generic name: trastuzumab, Roche/Genentech) is a monoclonal antibody that targets the HER2/Neu receptor, which is overexpressed in more aggressive types of breast cancer.[208] Breast cancer patients with normal expression of HER2/Neu—a significant fraction of the breast cancer patient population—do not respond to Herceptin. Therefore, HER2/Neu expression levels became a predictive BM for Herceptin response. Eighteen months prior to the biological license application (BLA) of herceptin to the FDA, Genentech initiated a partnership with the diagnostics company DAKO to develop a commercial test to identify patients who overexpress the HER2 gene (http://www.gene.com/media/product-information/herceptin-development-timeline). In May 1998, DAKO submitted a premarket approval application to the FDA for the diagnostic HercepTest® at the same time as Genentech submitted the BLA for Herceptin. Four months later, the FDA simultaneously approved Herceptin and HercepTest® to facilitate the identification of HER2/Neu-overexpressing patients. When used in this context, BMs are often referred to as "companion diagnostics." To date, 10 companion diagnostics for HER2/Neu expression have been approved or cleared by the FDA (http://www.fda.gov/MedicalDevices/ProductsandMedicalProcedures/InVitroDiagnostics/ucm301431.htm).

The next great breakthrough in the field of targeted cancer therapies was Glivec (United States: Gleevec; generic name: imatinib, Novartis), a small molecule inhibiting the ABL kinase approved for the treatment of CML by the FDA in 2001. Contrary to the varying levels of HER2/Neu expression in breast cancer patients, the vast majority of CML patients carry a chromosomal rearrangement, the so-called Philadelphia chromosome that results in high levels of the BCR-ABL fusion protein that drives the disease.[209] Therefore, a predictive BM to select patients was not needed in this setting. However, companion diagnostics were subsequently developed as the indication for Gleevec treatment was broadened to gastrointestinal stromal tumors (GISTs) and aggressive systemic mastocytosis (ASM). In both cases, the drug inhibits c-KIT, a close relative of the ABL kinase. While the companion diagnostic test for GIST patients detects protein levels of c-KIT by immunohistochemistry, the test applied to ASM patient samples detects the D816V mutation in the c-Kit receptor (http://www.fda.gov/MedicalDevices/ProductsandMedicalProcedures/InVitroDiagnostics/ucm301431.htm).

The EGFR receptor is overexpressed in 40–80% of NSCLC.[210] These findings prompted the development of gefitinib (trade name: Iressa, AstraZeneca), an EGFR inhibitor. Given the large fraction of NSCLC patients with EGFR overexpression, results from the initial clinical studies showing RRs of only 10–19% lagged behind expectations. Owing to the high unmet need for treatment options in relapsed NSCLC, gefitinib received accelerated approval nonetheless based on RR of only 10.6%. While the RR was low, the responding fraction of patients showed remarkable results.[211] It was also noted that responders were frequently female and nonsmokers. This prompted in-depth comparisons of responders with nonresponders, which eventually revealed that mutations in the EGFR gene were the decisive factor.[211,212] For yet unknown reasons, these mutations frequently occur in nonsmoking patients from East Asia (35% of NSCLC), compared with only 10% of NSCLC patients from the United States.[211,212] Given the clear correlation between EGFR mutation status and response to gefitinib, EGFR mutation status has become a powerful BM to determine which patients should be treated with EGFR inhibitors. Five companion diagnostic tests for EGFR mutation status have currently been approved by the FDA (http://www.fda.gov/MedicalDevices/ProductsandMedicalProcedures/InVitroDiagnostics/ucm301431.htm).

The BRAF kinase is an important component of the MAPK/ERK signaling pathway, which relays growth-promoting extracellular signals to the cell nucleus.[213] In 2002, Davies et al. reported that a large fraction of metastatic melanomas carried a particular mutation in the B-Raf gene, namely, V600E.[214] The mutation results in increased kinase activity, which is sufficient to transform NIH3T3 cells.[214] Subsequent studies revealed that mutated BRAF drives approximately half of all melanomas as well as several other cancers at lower frequencies.[215] In analogy to the BCR-ABL fusion in CML, this provided a strong rationale to target mutated BRAF in melanoma patients. Among other companies, Plexxikon was the most successful company in developing a targeting compound, vemurafenib (trade name: Zelboraf),[215] that received FDA approval in 2011 for treatment of metastatic melanoma. Importantly, selection of patients based on BRAF mutational status had resulted in an unprecedented unconfirmed overall RR of 81% in a phase I clinical trial.[216] Similar to the approach chosen for Herceptin, a diagnostic test detecting the V600E mutation was developed in parallel to clinical development of the targeting compound to enable patient selection.[215]

Several actively recruiting clinical studies in lung cancer [such as BATTLE-2 (NCT01248247) and Lung-MAP (NCT02154490)] are currently assigning patients to specific treatment arms based on their mutational status across a gene panel. Results are awaited to judge the predictive power of the respective BMs used for patient stratification.

5.01.6.3 Challenges of BMs and Future Perspectives

Although BM-based prospective patient selection has led to impressive overall RRs ranging from 50% to 80% in a few early-phase clinical trials,[217] the clinical success rates for investigational drugs in general remain low and are even declining if presented as a function of research and development expenditures, which have doubled over the past 10 years.[218] At present, only 1 in 10 drug indications that enter the clinic eventually receives FDA approval.[218] BMs have been perceived as one of the potential remedies to improve this sobering situation. While the potential use of BMs to predict and monitor patient responses to treatment has been widely recognized, the actual implementation remains challenging. Only a small subset of well-characterized BMs are currently serving as surrogates of clinical end points.[219] In order to serve as a surrogate for a clinical end point, both clinical relevance and validity of a given BM have to be established.[219] Importantly, the relationship between such surrogate end points and true clinical end points requires continuous reevaluation.[219] De Gramont and colleagues have summarized challenges and potential solutions for the evaluation of BMs for targeted cancer therapies in a recent review article.[220] They portray high levels of biological complexity and interpatient variability as particular challenges. Rather than relying on a single BM, the authors propose the use of BM panels, which are likely to be more robust and reflect complex biological processes more accurately.[220] From a technical perspective, the evolving nature of BM data leaves room for different interpretations.[220] Moreover, standardization of sample collection, processing, and robustness of BM assays remain areas that need improvement. These efforts should be supported by universal guidelines on specimen acquisition and standardized analytic methods.[220] Even to date, many FDA-recognized pharmacogenomic BMs are so-called laboratory developed tests (LDT). The LDT is a type of in vitro diagnostic (IVD) test that is designed, manufactured, and used within a single laboratory, sometimes even referred to as "home-brewed test" (http://www.fda.gov/MedicalDevices/ProductsandMedicalProcedures/InVitroDiagnostics/ucm407296.htm; "Regulation of Clinical Tests: in vitro Diagnostic (IVD) Devices, Laboratory Developed Tests (LDTs), and Genetic Tests"—https://www.fas.org/sgp/crs/misc/R43438.pdf), invoking potentially considerable variability in the test results. Given the growing impact of LDTs on health-care choices for a larger patient population, the FDA decided in 2014 to broadly regulate LDTs using a risk-based approach ("Regulation of Clinical Tests: in vitro Diagnostic (IVD) Devices, Laboratory Developed Tests (LDTs), and Genetic Tests"—https://www.fas.org/sgp/crs/misc/R43438.pdf).

If a BM is to be used as a decisive tool in clinical treatment decisions, a high degree of stringency has to be applied to its validation. Consequently, development and validation of a BM can be as difficult as bringing a drug to the market: only 1 in 10 BMs coupled to drug development actually reaches the clinic.[220] Given that both challenges and potential benefit of BMs are considerable, public–private partnerships are formed around the world to identify, validate, and apply new BMs.[221] While improvements in technologies and standardization will be important, a deeper understanding of basic and cancer biology will be at least equally valuable to transform BMs into valid end points for patient outcome.

5.01.7 Challenges of Targeted Cancer Therapy

Several therapeutics for targeted cancer therapy are currently being explored, are under development, or have already reached the clinic. Despite promising data that have fostered high hopes for better tolerable treatment options or even cure, the field faces tumor characteristics that make the development of therapeutics more challenging than initially expected. Tumors evade therapeutic agents due to their heterogeneity and due to formation of resistance by changing their driving features.

5.01.7.1 Tumor Heterogeneity

Tumors undergo an evolution as the disease progresses. Whole exome sequencing approaches show that mutational events and copy number alterations occur early in tumor evolution. Additional somatic events have been observed only in some of the tumor cells in later stages leading to distinct heterogenic cell populations within one tumor.[222] While the majority of mutations will not be beneficial for the tumor and result in cancer cell death, a distinct subset will help the tumor to adapt to its environment and necessities occurring during tumor growth or to evade therapy (see succeeding text). The formation of subclones within a tumor is independent and occurs at different locations and points in time and differs from tumor to tumor. Several studies have analyzed tumor heterogeneity by single-cell sequencing.[223] Up to 70% of all mutations in renal cell carcinoma cannot be detected in all regions of the tumor, while NSCLC tumors and metastases show a high degree of concordance.[224] Metastatic lesions can form from different cell populations within the primary tumor and then start their own evolutionary process. Each metastasis can have different genetic features and, therefore, different sensitivities to cancer drugs.

Tumor heterogeneity has been observed in several cancer types including renal cell carcinoma, lung cancer, breast cancer, leukemia, pancreatic cancer, and prostate cancer.[224,225] Designated clinical studies, such as TRACERx (NCT01888601) and DARWIN (NCT02183883), investigate whether formation of subclonal populations and changes in driver mutations are associated with PFS in patients with NSCLC.[226]

As mutations occur, oncogenic drivers may change. Targeted therapeutics do not necessarily hit all types of cells within one tumor. In order to be efficacious, personalized medicine approaches will have to consider the entire mutational landscape of each tumor and predict therapeutic combinations. In some cases, minority subclones drive the progression of the tumor mass, which makes prognostic and therapeutic predictions extremely difficult. Technical possibilities like high-throughput second- and third-generation sequencing of biopsies, single cells, cell-free tumor DNA, or circulating tumor cells provide an opportunity to analyze tumor/metastasis genetics in a more comprehensive manner. Another option is the use of patient-derived xenografts that carry the whole population of a tumor from a patient and might help to model the evolution of the tumor. However, at present, these techniques are too expensive to be covered by the public health systems, and we still have to learn how to best analyze the vast amount of data generated.

5.01.7.2 Tumor Evolution and Development of Resistances

One of the main challenges of almost any cancer therapy is the presence or development of resistances. Resistance to classical chemotherapy, and radiation, as well as to newer targeted approaches, can occur during the course of treatment leading to relapse. In many cases, novel therapeutics were even ineffective from the beginning in the clinical setting due to existing resistance mechanisms.[227] The decision to use a targeted therapy is often based on the presence of the target in the primary lesion. But, as mentioned in the preceding text, because of the heterogeneity of a tumor, the therapeutic response might not be the same within the cancer mass. Therefore, a tumor can evolve not only during adaptation to initiate growth and formation of metastasis but also under treatment.[227] Less sensitive cell populations become dominant and enable the tumor to (re-)grow under a specific therapy (Fig. 6).

Several resistance mechanisms have been defined: (1) mutations in the target protein, (2) acquisition of new mutations in the same pathway, (3) acquisition of driver mutations in a different pathway, (4) enhanced antiapoptotic protein expression, (5) high expression of drug efflux pumps, and (6) cross talk with the tumor microenvironment. On top of these cell intrinsic mechanisms, different types of cells can repopulate the tumor: smaller parts of the heterogenic tumor mass that are resistant to therapy, cells that were quiescent, and CSCs.[227]

5.01.7.3 CSCs

CSCs are the root of cancers and resist chemo- and radiotherapy. Therefore, these cells can repopulate a tumor and lead to relapse, even after years. CSCs comprise minorities in a cancer population. They are highly tumorigenic in vivo and display properties normally attributed to stem cells: self-renewal, pluripotency, and differentiation into more specialized cancer cell types.[228] CSCs are difficult to investigate in vitro as they are rare and quickly lost in tissue culture. They can be enriched by a fluorescence-activated cell sorter (FACS) using cell surface markers like CD133, exclusively expressed on stem cells. Leukemia CSCs exhibit a $CD34^{+}/CD38^{-}$ phenotype.[229] CSCs can be grown in tumor spheres in culture or *in vivo*. In animal models, they form tumors enriched in CSCs from a minimal amount of cells established by serial dilutions.[230]

CSCs are multidrug-resistant. They often have a higher threshold for induction of apoptosis due to upregulation of antiapoptotic proteins and have a high level of multifunctional efflux transporters that pump anticancer therapeutics out of the cell.[231] Active pathways that promote survival and self-renewal in CSCs are Wnt, Notch, and Hedgehog.[232] Therefore, agents targeting one of those three pathways or antiapoptic proteins like Bcl-2 and XIAP can eliminate or sensitize CSCs to standard therapy and might have the potential to reduce likelihood of relapse.[232] Other therapeutic options under investigation are antibodies targeting surface proteins expressed on CSCs. These antibodies either are coupled to cytotoxic agents or induce phagocytosis by the so-called eat-me signals. CSCs can be targeted to macrophage-mediated cell removal by inhibition of the cell surface protein CD47 and become eliminated by the immune system.[233] Attempts have been made to differentiate CSCs, for example, with recombinant IL15. The self-renewal capacities and tumorigenic properties of the CSC population were successfully blocked leading to increased sensitivity to chemotherapeutic agents.[234]

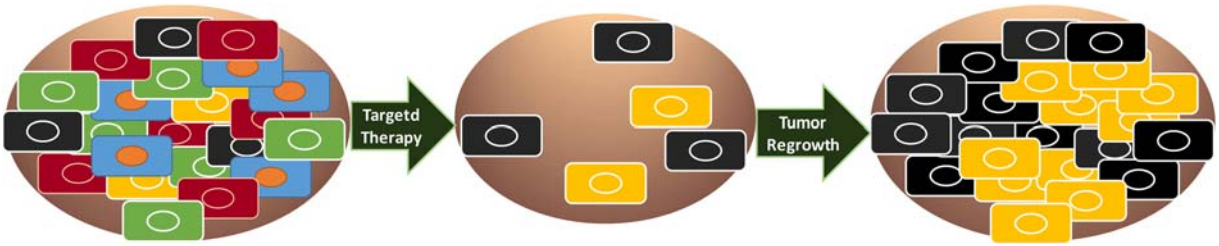

Fig. 6 Tumor heterogeneity. Upon treatment of a heterogenic cancer cell population with any targeted therapeutic, only sensitive cells will die. Resistant clones survive. The tumor progresses from these clones and forms new oncogenic dependencies.

5.01.7.4 Examples of Resistance and Approaches to Overcome Resistance

The most commonly found point mutation leading to resistance to kinase inhibitors that is concomitant with relapses affects the gatekeeper residue, whose size and shape regulate the properties of the hydrophobic pocket located at the back of the ATP binding site.[235] Mutations of the gatekeeper residue as well as other kinase domain mutations confer resistance to a wide spectrum of kinase inhibitors without affecting the kinase activity and may explain a fraction of cases of acquired resistance. The resistance mechanisms to kinase inhibitors in cancer treatment are multiple but result mostly in the restoration of activity of the original "cancer-addicting" pathway. This can occur either by conformational changes in the kinase domain or by reactivating the pathway downstream and/or parallel to the targeted kinase.[76,84,86,236] All of these mechanisms demonstrate the plasticity of cancer cells and the many ways by which a tumor can evade targeted therapies. The only way to approach these problems is to use rational combinations of drugs, a mainstay in cancer therapy.

The HER2 antibodies trastuzumab and lapatinib are part of the first-line therapy for HER2-positive breast cancers. Resistance is induced through downstream activation of the HER2 signaling pathway, for example, through activation of PI3K signaling (PTEN loss and PIK3CA mutation).[237]

One of the most prominent cases of acquired resistance is the often short-lived efficacy of the BRAF inhibitor vemurafenib in melanoma patients with the activating V600E BRAF mutation. Different mechanisms including upregulation of other parallel pathways like MAP kinase and Neuroblastoma RAS Viral Oncogene Homolog (NRAS) signaling have been suggested from patient samples, cell lines, and patient-derived xenografts.[238]

Colorectal cancers that acquire resistance to EGFR blockade are very likely to have a resistance mutation in the KRAS or NRAS gene. Gain of function mutations in KRAS reactivates MAP kinase signaling downstream of EGFR.[239]

Another form of resistance is the cell adhesion-mediated interaction with the tumor microenvironment described for multiple myeloma and leukemia.[240] Cell–cell contact of leukemia cells with bone marrow stromal cells leads to persistence of resistant clones.[241] Integrins mediate cell–cell contact and play a central role in this process. Furthermore, secretion of stromal proteins can activate growth pathways.[242]

To circumvent target-dependent drug resistance, "second-generation" kinase inhibitors have been developed. Inhibitors that bind covalently to the ATP binding site of EGFR have been developed for the emerging resistance to gefitinib and erlotinib.[243] Several of these covalent agents are in late-stage clinical trials.[73] As an example, the BTK inhibitor ibrutinib has been rationally designed to bind covalently to Cys481 of the kinase and was recently approved for B-cell malignancies.[244] Although ibrutinib has shown impressive clinical results, patients that progressed under treatment revealed a C481S mutation in their BTK that abrogates the covalent binding to ibrutinib.[245]

Additional approaches have attempted to develop noncovalent inhibitors that can tolerate amino acid exchanges at the gatekeeper position. Imatinib (Gleevec, Novartis) inhibits the tyrosine kinase BCR-ABL, which is present in the majority of CML patients. BCR-ABL mutations occur in high frequency in patients that develop imatinib resistance. These mutations prevent imatinib from binding to its target. Some patients even had multiple mutated clones.[246] Meanwhile, several ATP site-directed inhibitors active against the T315I ABL1 gatekeeper mutant, like nilotinib and dasatinib, that also target the mutated protein have been approved or are under investigation.[247]

In order to equally target kinases with gatekeeper mutations, these types of compounds display a rather low selectivity. Such so-called dirty inhibitors can have deleterious side effects that may lead to a withdrawal from the market for safety concerns.[248] A further approach is to target the kinase outside the ATP binding sites with the goal to combine ATP site-directed inhibitors with allosteric inhibitors[95] or to combine different kinase inhibitors targeting kinases in the same pathway, as in the case of vemurafenib where the emerging resistance is not due to mutations in BRAF (V600E) itself but rather in the downstream kinase MEK1.[249] Unfortunately, only a very limited number of non-ATP-competitive kinase inhibitors have thus far been identified, which could also be used to address the resistance caused by mutations in the ATP binding site.[95]

Understanding resistance mechanisms is an extremely important step to reduce the risk of relapse and to successfully treat a larger number of cancer patients. In order to make treatment regimens more efficient, it is necessary to use targeted therapies in logically chosen combinations. Knowledge about subclones within the tumor and likelihood of evolutionary development might give the chance to predict rationales for combination therapy that would tackle upcoming resistances.[222]

5.01.8 Summary

Targeted cancer therapy is directed against particular features of cancer cells or the tumor microenvironment. Currently, a broad spectrum of drugs interfering with the hallmarks of cancer, like sustaining proliferation, evading immune response, or genomic instability, is being developed or entering the market. At the same time, more basic research that characterizes cancer biology and reveals potential novel targets is nurtured by the availability of improved technology and big data sets. Many drugs resulting from those efforts would be most beneficial when used for personalized medicine, as single agent or in combination. In order to evaluate and predict treatment success and the best combination options, several obstacles like choice of BMs and knowledge about tumor evolution and development of resistances need to be overcome.

See also: 2.21. Companion Diagnostics: From Biomarkers to Diagnostics. 5.11. Cancer Immunotherapy—An Emerging Field That Bridges Oncology and Immunology Research.

References

1. Danaei, G.; Vander Hoorn, S.; Lopez, A. D.; Murray, C. J. L.; Ezzati, M. Causes of Cancer in the World: Comparative Risk Assessment of Nine Behavioural and Environmental Risk Factors. *Lancet* **2005,** *366* (9499), 1784–1793.
2. Vogelstein, B.; Kinzler, K. W. Cancer Genes and the Pathways They Control. *Nat. Med.* **2004,** *10* (8), 789–799.
3. Hanahan, D.; Weinberg, R. A. Hallmarks of Cancer: The Next Generation. *Cell* **2011,** *144* (5), 646–674.
4. (a) Lemmon, M. A.; Schlessinger, J. Cell Signaling by Receptor Tyrosine Kinases. *Cell* **2010,** *141* (7), 1117–1134; (b) Witsch, E.; Sela, M.; Yarden, Y. Roles for Growth Factors in Cancer Progression. *Physiology (Bethesda)* **2010,** *25* (2), 85–101.
5. Adams, J. M.; Cory, S. The Bcl-2 Apoptotic Switch in Cancer Development and Therapy. *Oncogene* **2007,** *26* (9), 1324–1337.
6. Levine, B.; Kroemer, G. Autophagy in the Pathogenesis of Disease. *Cell* **2008,** *132* (1), 27–42.
7. Galluzzi, L.; Kroemer, G. Necroptosis: A Specialized Pathway of Programmed Necrosis. *Cell* **2008,** *135* (7), 1161–1163.
8. (a) Blasco, M. A. Telomeres and Human Disease: Ageing, Cancer and Beyond. *Nat. Rev. Genet.* **2005,** *6* (8), 611–622; (b) Shay, J. W.; Wright, W. E. Hayflick, His Limit, and Cellular Ageing. *Nat. Rev. Mol. Cell Biol.* **2000,** *1* (1), 72–76.
9. Hanahan, D.; Folkman, J. Patterns and Emerging Mechanisms of the Angiogenic Switch During Tumorigenesis. *Cell* **1996,** *86* (3), 353–364.
10. (a) Egeblad, M.; Nakasone, E. S.; Werb, Z. Tumors as Organs: Complex Tissues That Interface With the Entire Organism. *Dev. Cell* **2010,** *18* (6), 884–901; (b) Qian, B. Z.; Pollard, J. W. Macrophage Diversity Enhances Tumor Progression and Metastasis. *Cell* **2010,** *141* (1), 39–51.
11. (a) Klymkowsky, M. W.; Savagner, P. Epithelial-Mesenchymal Transition: A Cancer Researcher's Conceptual Friend and Foe. *Am. J. Pathol.* **2009,** *174* (5), 1588–1593; (b) Polyak, K.; Weinberg, R. A. Transitions Between Epithelial and Mesenchymal States: Acquisition of Malignant and Stem Cell Traits. *Nat. Rev. Cancer* **2009,** *9* (4), 265–273.
12. Lloyd, N. C.; Morgan, H. W.; Nicholson, B. K.; Ronimus, R. S.; Riethmiller, S. Salvarsan the First Chemotherapeutic Compound. *Chem. N. Z.* **2005,** *69* (1), 24–27.
13. Gerber, D. E. Targeted Therapies: A New Generation of Cancer Treatments. *Am. Fam. Physician* **2008,** *77* (3), 311–319.
14. (a) Scott, A. M.; Wolchok, J. D.; Old, L. J. Antibody Therapy of Cancer. *Nat. Rev. Cancer* **2012,** *12* (4), 278–287; (b) Trail, P. Antibody Drug Conjugates as Cancer Therapeutics. *Antibodies* **2013,** *2* (1), 113.
15. (a) Vogelstein, B.; Kinzler, K. W. The Multistep Nature of Cancer. *Trends Genet.* **1993,** *9* (4), 138–141; (b) Hanahan, D.; Weinberg, R. A. Hallmarks of Cancer: The Next Generation. *Cell* **2011,** *144,* 646–674; (c) Rozhok, A. I.; DeGregori, J. Toward an Evolutionary Model of Cancer: Considering the Mechanisms That Govern the Fate of Somatic Mutations. *Proc. Natl. Acad. Sci. U. S. A.* **2015,** *112* (29), 8914–8921.
16. Tang, J.; Karhinen, L.; Xu, T.; Szwajda, A.; Yadav, B.; Wennerberg, K.; Aittokallio, T. Target Inhibition Networks: Predicting Selective Combinations of Druggable Targets to Block Cancer Survival Pathways. *PLoS Comput. Biol.* **2013,** *9* (9), e1003226.
17. Wyatt, P. G.; Gilbert, I. H.; Read, K. D.; Fairlamb, A. H. Target Validation: Linking Target and Chemical Properties to Desired Product Profile. *Curr. Top. Med. Chem.* **2011,** *11* (10), 1275–1283.
18. (a) Zheng, W.; Thorne, N.; McKew, J. C. Phenotypic Screens As a Renewed Approach for Drug Discovery. *Drug Discov. Today* **2013,** *18* (21–22), 1067–1073; (b) Vogt, A.; Lazo, J. S. Chemical Complementation: A Definitive Phenotypic Strategy for Identifying Small Molecule Inhibitors of Elusive Cellular Targets. *Pharmacol. Ther.* **2005,** *107* (2), 212–221.
19. Shim, J. S.; Liu, J. O. Recent Advances in Drug Repositioning for the Discovery of New Anticancer Drugs. *Int. J. Biol. Sci.* **2014,** *10* (7), 654–663.
20. (a) Silva, G.; Poirot, L.; Galetto, R.; Smith, J.; Montoya, G.; Duchateau, P.; Paques, F. Meganucleases and Other Tools for Targeted Genome Engineering: Perspectives and Challenges for Gene Therapy. *Curr. Gene Ther.* **2011,** *11* (1), 11–27; (b) Zaslavskiy, M.; Bertonati, C.; Duchateau, P.; Duclert, A.; Silva, G. H. Efficient Design of Mega-nucleases Using a Machine Learning Approach. *BMC Bioinformatics* **2014,** *15* (1), 1–11.
21. Carlson, D. F.; Tan, W.; Lillico, S. G.; Stverakova, D.; Proudfoot, C.; Christian, M.; Voytas, D. F.; Long, C. R.; Whitelaw, C. B. A.; Fahrenkrug, S. C. Efficient TALEN-Mediated Gene Knockout in Livestock. *Proc. Natl. Acad. Sci.* **2012,** *109* (43), 17382–17387.
22. (a) Carroll, D. Genome Engineering With Zinc-Finger Nucleases. *Genetics* **2011,** *188* (4), 773–782; (b) Kim, H. J.; Lee, H. J.; Kim, H.; Cho, S. W.; Kim, J.-S. Targeted Genome Editing in Human Cells With Zinc Finger Nucleases Constructed via Modular Assembly. *Genome Res.* **2009,** *19* (7), 1279–1288; (c) Santiago, Y.; Chan, E.; Liu, P.-Q.; Orlando, S.; Zhang, L.; Urnov, F. D.; Holmes, M. C.; Guschin, D.; Waite, A.; Miller, J. C.; Rebar, E. J.; Gregory, P. D.; Klug, A.; Collingwood, T. N. Targeted Gene Knockout in Mammalian Cells by Using Engineered Zinc-Finger Nucleases. *Proc. Natl. Acad. Sci.* **2008,** *105* (15), 5809–5814.
23. Sander, J. D.; Joung, J. K. CRISPR-Cas Systems for Editing, Regulating and Targeting Genomes. *Nat. Biotechnol.* **2014,** *32* (4), 347–355.
24. (a) Gaj, T.; Gersbach, C. A.; Barbas, C. F. ZFN, TALEN and CRISPR/Cas-Based Methods for Genome Engineering. *Trends Biotechnol.* **2013,** *31* (7), 397–405; (b) Mahfouz, M. M.; Piatek, A.; Stewart, C. N., Jr. Genome Engineering via TALENs and CRISPR/Cas9 Systems: Challenges and Perspectives. *Plant Biotechnol. J.* **2014,** *12* (8), 1006–1014.
25. (a) Leung, R. K.; Whittaker, P. A. RNA Interference: From Gene Silencing to Gene-Specific Therapeutics. *Pharmacol. Ther.* **2005,** *107* (2), 222–239; (b) Rao, D. D.; Vorhies, J. S.; Senzer, N.; Nemunaitis, J. siRNA vs. shRNA: Similarities and Differences. *Adv. Drug Deliv. Rev.* **2009,** *61* (9), 746–759; (c) Tilesi, F.; Fradiani, P.; Socci, V.; Willems, D.; Ascenzioni, F. Design and Validation of siRNAs and shRNAs. *Curr. Opin. Mol. Ther.* **2009,** *11* (2), 156–164.
26. a Bondeson, D. P.; Mares, A.; Smith, I. E. D.; Ko, E.; Campos, S.; Miah, A. H.; Mulholland, K. E.; Routly, N.; Buckley, D. L.; Gustafson, J. L.; Zinn, N.; Grandi, P.; Shimamura, S.; Bergamini, G.; Faelth-Savitski, M.; Bantscheff, M.; Cox, C.; Gordon, D. A.; Willard, R. R.; Flanagan, J. J.; Casillas, L. N.; Votta, B. J.; den Besten, W.; Famm, K.; Kruidenier, L.; Carter, P. S.; Harling, J. D.; Churcher, I.; Crews, C. M. Catalytic in vivo Protein Knockdown by Small-Molecule PROTACs. *Nat. Chem. Biol.* **2015,** *11* (8), 611–617; (b) Carmony, K. C.; Kim, K. B. PROTAC-Induced Proteolytic Targeting. *Methods Mol. Biol.* **2012,** *832,* 627–638.
27. (a) Kaelin, W. G. The Concept of Synthetic Lethality in the Context of Anticancer Therapy. *Nat. Rev. Cancer* **2005,** *5* (9), 689–698; (b) Lord, C. J.; Tutt, A. N. J.; Ashworth, A. Synthetic Lethality and Cancer Therapy: Lessons Learned From the Development of PARP Inhibitors. *Annu. Rev. Med.* **2015,** *66* (1), 455–470; (c) Nijman, S. M. Synthetic Lethality: General Principles, Utility and Detection Using Genetic Screens in Human Cells. *FEBS Lett.* **2011,** *585,* 1–6.
28. (a) La-Beck, N. M.; Jean, G. W.; Huynh, C.; Alzghari, S. K.; Lowe, D. B. Immune Checkpoint Inhibitors: New Insights and Current Place in Cancer Therapy. *Pharmacotherapy* **2015,** *35* (10), 963–976; (b) Tomczak, K.; Czerwinska, P.; Wiznerowicz, M. The Cancer Genome Atlas (TCGA): An Immeasurable Source of Knowledge. *Contemp. Oncol.* **2015,** *19* (1A), A68–A77; (c) An, O.; Dall'Olio, G. M.; Mourikis, T. P.; Ciccarelli, F. D. NCG 5.0: Updates of a Manually Curated Repository of Cancer Genes and Associated Properties From Cancer Mutational Screenings. *Nucleic Acids Res.* **2016,** *44* (D1), D992–D999; (d) Forbes, S. A.; Beare, D.; Gunasekaran, P.; Leung, K.; Bindal, N.; Boutselakis, H.; Ding, M.; Bamford, S.; Cole, C.; Ward, S.; Kok, C. Y.; Jia, M.; De, T.; Teague, J. W.; Stratton, M. R.; McDermott, U.; Campbell, P. J. COSMIC: Exploring the World's Knowledge of Somatic Mutations in Human Cancer. *Nucleic Acids Res.* **2015,** *43* (Database issue), D805–D811; (e) Barretina, J.; Caponigro, G.; Stransky, N.; Venkatesan, K.; Margolin, A. A.; Kim, S.; Wilson, C. J.; Lehar, J.; Kryukov, G. V.; Sonkin, D.; Reddy, A.; Liu, M.; Murray, L.; Berger, M. F.; Monahan, J. E.; Morais, P.; Meltzer, J.; Korejwa, A.; Jane-Valbuena, J.; Mapa, F. A.; Thibault, J.; Bric-Furlong, E.; Raman, P.; Shipway, A.; Engels, I. H.; Cheng, J.; Yu, G. K.; Yu, J.; Aspesi, P.; de Silva, M.; Jagtap, K.; Jones, M. D.; Wang, L.; Hatton, C.; Palescandolo, E.; Gupta, S.; Mahan, S.; Sougnez, C.; Onofrio, R. C.; Liefeld, T.; MacConaill, L.; Winckler, W.; Reich, M.; Li, N.; Mesirov, J. P.; Gabriel, S. B.; Getz, G.; Ardlie, K.; Chan, V.; Myer, V. E.; Weber, B. L.; Porter, J.; Warmuth, M.; Finan, P.; Harris, J. L.; Meyerson, M.; Golub, T. R.; Morrissey, M. P.; Sellers, W. R.; Schlegel, R.; Garraway, L. A. The Cancer Cell Line Encyclopedia Enables Predictive Modelling of Anticancer Drug Sensitivity. *Nature* **2012,** *483* (7391), 603–607; (f) Sonkin, D.; Hassan, M.; Murphy, D. J.; Tatarinova, T. V. Tumor Suppressors Status in Cancer Cell Line Encyclopedia. *Mol. Oncol.* **2013,** *7* (4), 791–798; (g) Strausberg, R. L. *Cancer Genome Anatomy Project;* John Wiley & Sons, Ltd, 2001. Chichester, West Sussex, UK; (h) Pavlopoulou, A.; Spandidos, D. A.; Michalopoulos, I. Human Cancer Databases (Review). *Oncol. Rep.* **2015,** *33* (1), 3–18.

29. (a) Manis, J. P. Knock Out, Knock In, Knock Down—Genetically Manipulated Mice and the Nobel Prize. *N. Engl. J. Med.* **2007,** *357* (24), 2426–2429; (b) Doyle, A.; McGarry, M. P.; Lee, N. A.; Lee, J. J. The Construction of Transgenic and Gene Knockout/Knockin Mouse Models of Human Disease. *Transgenic Res.* **2012,** *21* (2), 327–349; (c) Owens, J. B.; Mathews, J.; Davy, P.; Stoytchev, I.; Moisyadi, S.; Allsopp, R. Effective Targeted Gene Knockdown in Mammalian Cells Using the piggyBac Transposase-Based Delivery System. *Mol. Ther. Nucleic Acids* **2013,** *2,* e137.
30. (a) Sharma, S.; Rao, A. RNAi Screening: Tips and Techniques. *Nat. Immunol.* **2009,** *10* (8), 799–804; (b) Mansoori, B.; Sandoghchian Shotorbani, S.; Baradaran, B. RNA Interference and Its Role in Cancer Therapy. *Adv. Pharm. Bull.* **2014,** *4* (4), 313–321; (c) Vickers, T. A.; Koo, S.; Bennett, C. F.; Crooke, S. T.; Dean, N. M.; Baker, B. F. Efficient Reduction of Target RNAs by Small Interfering RNA and RNase H-Dependent Antisense Agents: A Comparative Analysis. *J. Biol. Chem.* **2003,** *278* (9), 7108–7118.
31. (a) Makley, L. N.; Gestwicki, J. E. Expanding the Number of 'Druggable' Targets: Non-Enzymes and Protein-Protein Interactions. *Chem. Biol. Drug Des.* **2013,** *81* (1), 22–32; (b) Dixon, S. J.; Stockwell, B. R. Identifying Druggable Disease-Modifying Gene Products. *Curr. Opin. Chem. Biol.* **2009,** *13* (5–6), 549–555.
32. (a) Luo, J.; Solimini, N. L.; Elledge, S. J. Principles of Cancer Therapy: Oncogene and Non-Oncogene Addiction. *Cell* **2009,** *136* (5), 823–837; (b) Hanahan, D.; Weinberg, R. A. The Hallmarks of Cancer. *Cell* **2000,** *100* (1), 57–70.
33. (a) Mazouzi, A.; Velimezi, G.; Loizou, J. I. DNA Replication Stress: Causes, Resolution and Disease. *Exp. Cell Res.* **2014,** *329* (1), 85–93; (b) Chircop, M.; Speidel, D. Cellular Stress Responses in Cancer and Cancer Therapy. *Front. Oncol.* **2014,** *4,* 304; (c) Herr, I.; Debatin, K. M. Cellular Stress Response and Apoptosis in Cancer Therapy. *Blood* **2001,** *98* (9), 2603–2614; (d) Polo, S. E.; Jackson, S. P. Dynamics of DNA Damage Response Proteins at DNA Breaks: A Focus on Protein Modifications. *Genes Dev.* **2011,** *25* (5), 409–433; (e) Morimoto, R. I. The Heat Shock Response: Systems Biology of Proteotoxic Stress in Aging and Disease. *Cold Spring Harb. Symp. Quant. Biol.* **2011,** *76,* 91–99; (f) Gaillard, H.; Garcia-Muse, T.; Aguilera, A. Replication Stress and Cancer. *Nat. Rev. Cancer* **2015,** *15* (5), 276–289; (g) Cairns, R. A.; Harris, I. S.; Mak, T. W. Regulation of Cancer Cell Metabolism. *Nat. Rev. Cancer* **2011,** *11* (2), 85–95.
34. (a) Ciccia, A.; Elledge, S. J. The DNA Damage Response: Making it Safe to Play With Knives. *Mol. Cell* **2014,** *40* (2), 179–204; (b) Pearl, L. H.; Schierz, A. C.; Ward, S. E.; Al-Lazikani, B.; Pearl, F. M. G. Therapeutic Opportunities Within the DNA Damage Response. *Nat. Rev. Cancer* **2015,** *15* (3), 166–180.
35. Marteijn, J. A.; Lans, H.; Vermeulen, W.; Hoeijmakers, J. H. J. Understanding Nucleotide Excision Repair and Its Roles in Cancer and Ageing. *Nat. Rev. Mol. Cell Biol.* **2014,** *15* (7), 465–481.
36. Longhese, M. P. DNA Damage Response at Functional and Dysfunctional Telomeres. *Genes Dev.* **2008,** *22* (2), 125–140.
37. (a) Gorgoulis, V. G.; Vassiliou, L.-V. F.; Karakaidos, P.; Zacharatos, P.; Kotsinas, A.; Liloglou, T.; Venere, M.; DiTullio, R. A.; Kastrinakis, N. G.; Levy, B.; Kletsas, D.; Yoneta, A.; Herlyn, M.; Kittas, C.; Halazonetis, T. D. Activation of the DNA Damage Checkpoint and Genomic Instability in Human Precancerous Lesions. *Nature* **2005,** *434* (7035), 907–913; (b) Da-Re, C.; Halazonetis, T. D. DNA Replication Stress As an Achilles' Heel of Cancer. *Oncotarget* **2015,** *6* (1), 1–2; (c) Macheret, M.; Halazonetis, T. D. DNA Replication Stress As a Hallmark of Cancer. *Annu. Rev. Pathol.* **2015,** *10,* 425–448.
38. Manic, G.; Obrist, F.; Sistigu, A.; Vitale, I. Trial Watch: Targeting ATM–CHK2 and ATR–CHK1 Pathways for Anticancer Therapy. *Mol. Cell. Oncol.* **2015,** *2* (4), e1012976.
39. Dhillon, K. K.; Swisher, E. M.; Taniguchi, T. Secondary Mutations of BRCA1/2 and Drug Resistance. *Cancer Sci.* **2011,** *102* (4), 663–669.
40. Sonnenblick, A.; de Azambuja, E.; Azim, H. A., Jr.; Piccart, M. An Update on PARP Inhibitors—Moving to the Adjuvant Setting. *Nat. Rev. Clin. Oncol.* **2015,** *12* (1), 27–41.
41. Garber, K. PARP Inhibitors Bounce Back. *Nat. Rev. Drug Discov.* **2013,** *12* (10), 725–727.
42. Knouse, K. A.; Amon, A. The Many Sides of CIN. *Nat. Rev. Mol. Cell Biol.* **2013,** *14* (10), 611.
43. (a) Conduit, P. T.; Wainman, A.; Raff, J. W. Centrosome Function and Assembly in Animal Cells. *Nat. Rev. Mol. Cell Biol.* **2015,** *16* (10), 611–624; (b) Gasic, I.; Nerurkar, P.; Meraldi, P. Centrosome Age Regulates Kinetochore–Microtubule Stability and Biases Chromosome Mis-Segregation. *eLife* **2015,** *4,* e07909.
44. Dikovskaya, D.; Cole, J. J.; Mason, S. M.; Nixon, C.; Karim, S. A.; McGarry, L.; Clark, W.; Hewitt, R. N.; Sammons, M. A.; Zhu, J.; Athineos, D.; Leach, J. D.; Marchesi, F.; van Tuyn, J.; Tait, S. W.; Brock, C.; Morton, J. P.; Wu, H.; Berger, S. L.; Blyth, K.; Adams, P. D. Mitotic Stress Is an Integral Part of the Oncogene-Induced Senescence Program That Promotes Multinucleation and Cell Cycle Arrest. *Cell Rep.* **2015,** *12* (9), 1483–1496.
45. Mc Gee, M. M. Targeting the Mitotic Catastrophe Signaling Pathway in Cancer. *Mediat. Inflamm.* **2015,** *2015,* 13.
46. Magidson, V.; He, J.; Ault, J. G.; O'Connell, C. B.; Yang, N.; Tikhonenko, I.; McEwen, B. F.; Sui, H.; Khodjakov, A. Unattached Kinetochores Rather Than Intrakinetochore Tension Arrest Mitosis in Taxol-Treated Cells. *J. Cell Biol.* **2016,** *212* (3), 307–319.
47. a Bayliss, R.; Fry, A.; Haq, T.; Yeoh, S. On the Molecular Mechanisms of Mitotic Kinase Activation. *Open Biol.* **2012,** *2* (11), 1–20; (b) Komlodi-Pasztor, E.; Sackett, D. L.; Fojo, A. T. Inhibitors Targeting Mitosis: Tales of How Great Drugs Against a Promising Target Were Brought Down by a Flawed Rationale. *Clin. Cancer Res.* **2012,** *18* (1), 51–63.
48. Jose, C.; Bellance, N.; Rossignol, R. Choosing Between Glycolysis and Oxidative Phosphorylation: A Tumor's Dilemma? *Biochim. Biophys. Acta* **2011,** *1807* (6), 552–561.
49. Bailey, K. M.; Wojtkowiak, J. W.; Hashim, A. I.; Gillies, R. J. Targeting the Metabolic Microenvironment of Tumors. *Adv. Pharmacol.* **2012,** *65,* 63–107.
50. Zhan, C.; Yan, L.; Wang, L.; Ma, J.; Jiang, W.; Zhang, Y.; Shi, Y.; Wang, Q. Isoform Switch of Pyruvate Kinase M1 Indeed Occurs but Not to Pyruvate Kinase M2 in Human Tumorigenesis. *PLoS One* **2015,** *10* (3), e0118663.
51. Zanella, A.; Fermo, E.; Bianchi, P.; Chiarelli, L. R.; Valentini, G. Pyruvate Kinase Deficiency: The Genotype-Phenotype Association. *Blood Rev.* **2007,** *21* (4), 217–231.
52. Barbier, A.; Silver, B.; Merica, E.; Cohen, M.; Kung, C.; Yang, H.; Grace, R. F.; Glader, B.; Agresta, S. DRIVE PK: A Phase 2 Trial of AG-348 in Patients With Pyruvate Kinase Deficiency. *Blood* **2015,** *126* (23), 4548.
53. (a) Figueroa, M. E.; Abdel-Wahab, O.; Lu, C.; Ward, P. S.; Patel, J.; Shih, A.; Li, Y.; Bhagwat, N.; Vasanthakumar, A.; Fernandez, H. F.; Tallman, M. S.; Sun, Z.; Wolniak, K.; Peeters, J. K.; Liu, W.; Choe, S. E.; Fantin, V. R.; Paietta, E.; Löwenberg, B.; Licht, J. D.; Godley, L. A.; Delwel, R.; Valk, P. J. M.; Thompson, C. B.; Levine, R. L.; Melnick, A. Leukemic IDH1 and IDH2 Mutations Result in a Hypermethylation Phenotype, Disrupt TET2 Function, and Impair Hematopoietic Differentiation. *Cancer Cell* **2010,** *18* (6), 553–567; (b) Yang, H.; Ye, D.; Guan, K.-L.; Xiong, Y. IDH1 and IDH2 Mutations in Tumorigenesis: Mechanistic Insights and Clinical Perspectives. *Clin. Cancer Res.* **2012,** *18* (20), 5562–5571.
54. Hensley, C. T.; Wasti, A. T.; DeBerardinis, R. J. Glutamine and Cancer: Cell Biology, Physiology, and Clinical Opportunities. *J. Clin. Invest.* **2013,** *123* (9), 3678–3684.
55. Wise, D. R.; DeBerardinis, R. J.; Mancuso, A.; Sayed, N.; Zhang, X.-Y.; Pfeiffer, H. K.; Nissim, I.; Daikhin, E.; Yudkoff, M.; McMahon, S. B.; Thompson, C. B. Myc Regulates a Transcriptional Program That Stimulates Mitochondrial Glutaminolysis and Leads to Glutamine Addiction. *Proc. Natl. Acad. Sci. U. S. A.* **2008,** *105* (48), 18782–18787.
56. Csibi, A.; Fendt, S.-M.; Li, C.; Poulogiannis, G.; Choo, A. Y.; Chapski, D. J.; Jeong, S. M.; Dempsey, J.; Parkhitko, A.; Morrison, T.; Henske, E.; Haigis, M.; Cantley, L. C.; Stephanopoulos, G.; Yu, J.; Blenis, J. The mTORC1 Pathway Stimulates Glutamine Metabolism and Cell Proliferation by Repressing SIRT4. *Cell* **2013,** *153* (4), 840–854.
57. (a) Filomeni, G.; De Zio, D.; Cecconi, F. Oxidative Stress and Autophagy: The Clash Between Damage and Metabolic Needs. *Cell Death Differ.* **2015,** *22* (3), 377–388; (b) Sabharwal, S. S.; Schumacker, P. T. Mitochondrial ROS in Cancer: Initiators, Amplifiers or an Achilles' Heel? *Nat. Rev. Cancer* **2014,** *14* (11), 709–721; (c) Görlach, A.; Dimova, E. Y.; Petry, A.; Martínez-Ruiz, A.; Hernansanz-Agustín, P.; Rolo, A. P.; Palmeira, C. M.; Kietzmann, T. Reactive Oxygen Species, Nutrition, Hypoxia and Diseases: Problems Solved? *Redox Biol.* **2015,** *6,* 372–385.
58. Sutendra, G.; Michelakis, E. D. Pyruvate Dehydrogenase Kinase As a Novel Therapeutic Target in Oncology. *Front. Oncol.* **2013,** *3,* 38.
59. Wilson, W. R.; Hay, M. P. Targeting Hypoxia in Cancer Therapy. *Nat. Rev. Cancer* **2011,** *11* (6), 393–410.
60. (a) Masoud, G. N.; Li, W. HIF-1α Pathway: Role, Regulation and Intervention for Cancer Therapy. *Acta Pharm. Sin. B* **2015,** *5* (5), 378–389; (b) Niu, G.; Chen, X. Vascular Endothelial Growth Factor as an Anti-Angiogenic Target for Cancer Therapy. *Curr. Drug Targets* **2010,** *11* (8), 1000–1017.
61. Jewell, J. L.; Guan, K.-L. Nutrient Signaling to mTOR and Cell Growth. *Trends Biochem. Sci.* **2013,** *38* (5), 233–242.
62. White, E. The Role for Autophagy in Cancer. *J. Clin. Invest.* **2015,** *125* (1), 42–46.
63. (a) Pavelka, N.; Rancati, G.; Zhu, J.; Bradford, W. D.; Saraf, A.; Florens, L. Aneuploidy Confers Quantitative Proteome Changes and Phenotypic Variation in Budding Yeast. *Nature* **2010,** *468,* 321–325; (b) Stingele, S.; Stoehr, G.; Peplowska, K.; Cox, J.; Mann, M.; Storchova, Z. Global Analysis of Genome, Transcriptome and Proteome Reveals the Response to Aneuploidy in Human Cells. *Mol. Syst. Biol.* **2012,** *8,* 608.
64. Dai, C.; Dai, S.; Cao, J. Proteotoxic Stress of Cancer: Implication of the Heat-Shock Response in Oncogenesis. *J. Cell. Physiol.* **2012,** *227* (8), 2982–2987.

65. Chen, G.; Bradford, W. D.; Seidel, C. W.; Li, R. Hsp90 Stress Potentiates Rapid Cellular Adaptation Through Induction of Aneuploidy. *Nature* **2012,** *482,* 246–250.
66. Dobbelstein, M.; Moll, U. Targeting Tumour-Supportive Cellular Machineries in Anticancer Drug Development. *Nat. Rev. Drug Discov.* **2014,** *13* (3), 179–196.
67. Neckers, L.; Workman, P. Hsp90 Molecular Chaperone Inhibitors: Are We There Yet? *Clin. Cancer Res.* **2012,** *18* (1), 64–76.
68. Wust, P.; Hildebrandt, B.; Sreenivasa, G.; Rau, B.; Gellermann, J.; Riess, H.; Felix, R.; Schlag, P. M. Hyperthermia in Combined Treatment of Cancer. *Lancet Oncol.* **2008,** *3* (8), 487–497.
69. Nalepa, G.; Rolfe, M.; Harper, J. W. Drug Discovery in the Ubiquitin-Proteasome System. *Nat. Rev. Drug Discov.* **2006,** *5* (7), 596–613.
70. Crawford, L. J.; Walker, B.; Irvine, A. E. Proteasome Inhibitors in Cancer Therapy. *J. Cell Commun. Signal.* **2011,** *5* (2), 101–110.
71. Liu, J.; Shaik, S.; Dai, X.; Wu, Q.; Zhou, X.; Wang, Z.; Wei, W. Targeting the Ubiquitin Pathway for Cancer Treatment. *Biochim. Biophys. Acta* **2015,** *1855* (1), 50–60.
72. Carmony, K. C.; Kim, K.-B. PROTAC-Induced Proteolytic Targeting. *Methods Mol. Biol.* **2012,** *832,* 627–638.
73. (a) Walsh, C. T.; Garneau-Tsodikova, S.; Gatto, G. J., Jr. Protein Posttranslational Modifications: The Chemistry of Proteome Diversifications. *Angew. Chem.* **2005,** *44* (45), 7342–7372; (b) Liu, Q.; Sabnis, Y.; Zhao, Z.; Zhang, T.; Buhrlage, S. J.; Jones, L. H.; Gray, N. S. Developing Irreversible Inhibitors of the Protein Kinase Cysteinome. *Chem. Biol.* **2013,** *20* (2), 146–159.
74. (a) Ubersax, J. A.; Ferrell, J. E., Jr. Mechanisms of Specificity in Protein Phosphorylation. *Nat. Rev. Mol. Cell Biol.* **2007,** *8* (7), 530–541; (b) Cohen, P. The Role of Protein Phosphorylation in Human Health and Disease. The Sir Hans Krebs Medal Lecture. *Eur. J. Biochem.* **2001,** *268* (19), 5001–5010; (c) Blume-Jensen, P.; Hunter, T. Oncogenic Kinase Signalling. *Nature* **2001,** *411* (6835), 355–365; (d) Lahiry, P.; Torkamani, A.; Schork, N. J.; Hegele, R. A. Kinase Mutations in Human Disease: Interpreting Genotype-Phenotype Relationships. *Nat. Rev. Genet.* **2010,** *11* (1), 60–74.
75. (a) Courtney, K. D.; Corcoran, R. B.; Engelman, J. A. The PI3K Pathway As Drug Target in Human Cancer. *J. Clin. Oncol.* **2010,** *28* (6), 1075–1083; (b) Engelman, J. A. Targeting PI3K Signalling in Cancer: Opportunities, Challenges and Limitations. *Nat. Rev. Cancer* **2009,** *9* (8), 550–562.
76. (a) Hunter, T. Signaling—2000 and Beyond. *Cell* **2000,** *100* (1), 113–127; (b) Weinstein, I. B. Cancer. Addiction to Oncogenes—The Achilles Heal of Cancer. *Science* **2002,** *297* (5578), 63–64; (c) Hahn, W. C.; Weinberg, R. A. Modelling the Molecular Circuitry of Cancer. *Nat. Rev. Cancer* **2002,** *2* (5), 331–341; (d) Bardelli, A.; Parsons, D. W.; Silliman, N.; Ptak, J.; Szabo, S.; Saha, S.; Markowitz, S.; Willson, J. K.; Parmigiani, G.; Kinzler, K. W.; Vogelstein, B.; Velculescu, V. E. Mutational Analysis of the Tyrosine Kinome in Colorectal Cancers. *Science* **2003,** *300* (5621), 949; (e) Cohen, P. Protein Kinases—The Major Drug Targets of the Twenty-First Century? *Nat. Rev. Drug Discov.* **2002,** *1* (4), 309–315; (f) Vieth, M.; Higgs, R. E.; Robertson, D. H.; Shapiro, M.; Gragg, E. A.; Hemmerle, H. Kinomics-Structural Biology and Chemogenomics of Kinase Inhibitors and Targets. *Biochim. Biophys. Acta* **2004,** *1697* (1–2), 243–257; (g) Vieth, M.; Sutherland, J. J.; Robertson, D. H.; Campbell, R. M. Kinomics: Characterizing the Therapeutically Validated Kinase Space. *Drug Discov. Today* **2005,** *10* (12), 839–846; (h) Levitzki, A. Protein Kinase Inhibitors As a Therapeutic Modality. *Acc. Chem. Res.* **2003,** *36* (6), 462–469; (i) Fedorov, O.; Muller, S.; Knapp, S. The (Un)Targeted Cancer Kinome. *Nat. Chem. Biol.* **2010,** *6* (3), 166–169; (j) Fabbro, D.; Cowan-Jacob, S. W.; Mobitz, H.; Martiny-Baron, G. Targeting Cancer With Small-Molecular-Weight Kinase Inhibitors. *Methods Mol. Biol.* **2011,** *795,* 1–34.
77. (a) http://kinase.com/kinbase, The human kinome online. http://kinase.com/kinbase 2014.
(b) Manning, G.; Whyte, D. B.; Martinez, R.; Hunter, T.; Sudarsanam, S. The Protein Kinase Complement of the Human Genome. *Science* **2002,** *298* (5600), 1912–1934.
78. (a) Boudeau, J.; Miranda-Saavedra, D.; Barton, G. J.; Alessi, D. R. Emerging Roles of Pseudokinases. *Trends Cell Biol.* **2006,** *16* (9), 443–452; (b) Kannan, N.; Taylor, S. S. Rethinking Pseudokinases. *Cell* **2008,** *133* (2), 204–205.
79. (a) Nolen, B.; Taylor, S.; Ghosh, G. Regulation of Protein Kinases; Controlling Activity Through Activation Segment Conformation. *Mol. Cell* **2004,** *15* (5), 661–675; (b) Taylor, S. S.; Kornev, A. P. Protein Kinases: Evolution of Dynamic Regulatory Proteins. *Trends Biochem. Sci.* **2011,** *36* (2), 65–77.
80. (a) Kornev, A. P.; Haste, N. M.; Taylor, S. S.; Eyck, L. F. Surface Comparison of Active and Inactive Protein Kinases Identifies a Conserved Activation Mechanism. *Proc. Natl. Acad. Sci. U. S. A.* **2006,** *103* (47), 17783–17788; (b) Moebitz, H.; Fabbro, D. Conformational Bias: A Key Concept for Protein Kinase Inhibition. *Eur. Pharm. Rev.* **2012,** *17,* 41–51; (c) Cowan-Jacob, S. W.; Moebitz, H.; Fabbro, D. Structural Biology Contributions to Tyrosine Kinase Drug Discovery. *Curr. Opin. Cell Biol.* **2009,** *21* (2), 280–287.
81. Cowan-Jacob, S. W. Structural Biology of Protein Tyrosine Kinases. *Cell. Mol. Life Sci.* **2006,** *63* (22), 2608–2625.
82. Hanks, S. K.; Hunter, T. Protein Kinases 6. The Eukaryotic Protein Kinase Superfamily: Kinase (Catalytic) Domain Structure and Classification. *FASEB J.* **1995,** *9* (8), 576–596.
83. (a) Gross, S.; Rahal, R.; Stransky, N.; Lengauer, C.; Hoeflich, K. P. Targeting Cancer With Kinase Inhibitors. *J. Clin. Invest.* **2015,** *125* (5), 1780–1789; (b) Liu, P.; Cheng, H.; Roberts, T. M.; Zhao, J. J. Targeting the Phosphoinositide 3-Kinase (PI3K) Pathway in Cancer. *Nat. Rev. Drug Discov.* **2009,** *8* (8), 627–644; (c) Zhang, J.; Yang, P. L.; Gray, N. S. Targeting Cancer With Small Molecule Kinase Inhibitors. *Nat. Rev. Cancer* **2009,** *9* (1), 28–39.
84. (a) Greenman, C.; Stephens, P.; Smith, R.; Dalgliesh, G. L.; Hunter, C.; Bignell, G.; Davies, H.; Teague, J.; Butler, A.; Stevens, C.; Edkins, S.; O'Meara, S.; Vastrik, I.; Schmidt, E. E.; Avis, T.; Barthorpe, S.; Bhamra, G.; Buck, G.; Choudhury, B.; Clements, J.; Cole, J.; Dicks, E.; Forbes, S.; Gray, K.; Halliday, K.; Harrison, R.; Hills, K.; Hinton, J.; Jenkinson, A.; Jones, D.; Menzies, A.; Mironenko, T.; Perry, J.; Raine, K.; Richardson, D.; Shepherd, R.; Small, A.; Tofts, C.; Varian, J.; Webb, T.; West, S.; Widaa, S.; Yates, A.; Cahill, D. P.; Louis, D. N.; Goldstraw, P.; Nicholson, A. G.; Brasseur, F.; Looijenga, L.; Weber, B. L.; Chiew, Y. E.; DeFazio, A.; Greaves, M. F.; Green, A. R.; Campbell, P.; Birney, E.; Easton, D. F.; Chenevix-Trench, G.; Tan, M. H.; Khoo, S. K.; Teh, B. T.; Yuen, S. T.; Leung, S. Y.; Wooster, R.; Futreal, P. A.; Stratton, M. R. Patterns of Somatic Mutation in Human Cancer Genomes. *Nature* **2007,** *446* (7132), 153–158; (b) Thomas, R. K.; Baker, A. C.; Debiasi, R. M.; Winckler, W.; Laframboise, T.; Lin, W. M.; Wang, M.; Feng, W.; Zander, T.; MacConaill, L.; Lee, J. C.; Nicoletti, R.; Hatton, C.; Goyette, M.; Girard, L.; Majmudar, K.; Ziaugra, L.; Wong, K. K.; Gabriel, S.; Beroukhim, R.; Peyton, M.; Barretina, J.; Dutt, A.; Emery, C.; Greulich, H.; Shah, K.; Sasaki, H.; Gazdar, A.; Minna, J.; Armstrong, S. A.; Mellinghoff, I. K.; Hodi, F. S.; Dranoff, G.; Mischel, P. S.; Cloughesy, T. F.; Nelson, S. F.; Liau, L. M.; Mertz, K.; Rubin, M. A.; Moch, H.; Loda, M.; Catalona, W.; Fletcher, J.; Signoretti, S.; Kaye, F.; Anderson, K. C.; Demetri, G. D.; Dummer, R.; Wagner, S.; Herlyn, M.; Sellers, W. R.; Meyerson, M.; Garraway, L. A. High-Throughput Oncogene Mutation Profiling in Human Cancer. *Nat. Genet.* **2007,** *39* (3), 347–351; (c) Sawyers, C. Targeted Cancer Therapy. *Nature* **2004,** *432* (7015), 294–297; (d) Wolf-Yadlin, A.; Kumar, N.; Zhang, Y.; Hautaniemi, S.; Zaman, M.; Kim, H. D.; Grantcharova, V.; Lauffenburger, D. A.; White, F. M. Effects of HER2 Overexpression on Cell Signaling Networks Governing Proliferation and Migration. *Mol. Syst. Biol.* **2006,** *2,* 54; (e) Ventura, J. J.; Nebreda, A. R. Protein Kinases and Phosphatases As Therapeutic Targets in Cancer. *Clin. Transl. Oncol.* **2006,** *8* (3), 153–160; (f) Engelman, J. A.; Zejnullahu, K.; Mitsudomi, T.; Song, Y.; Hyland, C.; Park, J. O.; Lindeman, N.; Gale, C. M.; Zhao, X.; Christensen, J.; Kosaka, T.; Holmes, A. J.; Rogers, A. M.; Cappuzzo, F.; Mok, T.; Lee, C.; Johnson, B. E.; Cantley, L. C.; Janne, P. A. MET Amplification Leads to Gefitinib Resistance in Lung Cancer by Activating ERBB3 Signaling. *Science* **2007,** *316* (5827), 1039–1043; (g) Takano, T.; Ohe, Y.; Sakamoto, H.; Tsuta, K.; Matsuno, Y.; Tateishi, U.; Yamamoto, S.; Nokihara, H.; Yamamoto, N.; Sekine, I.; Kunitoh, H.; Shibata, T.; Sakiyama, T.; Yoshida, T.; Tamura, T. Epidermal Growth Factor Receptor Gene Mutations and Increased Copy Numbers Predict Gefitinib Sensitivity in Patients With Recurrent Non-Small-Cell Lung Cancer. *J. Clin. Oncol.* **2005,** *23* (28), 6829–6837; (h) Ali, S.; Ali, S. Role of c-kit/SCF in Cause and Treatment of Gastrointestinal Stromal Tumors (GIST). *Gene* **2007,** *401* (1–2), 38–45.
85. (a) Yuan, T. L.; Cantley, L. C. PI3K Pathway Alterations in Cancer: Variations on a Theme. *Oncogene* **2008,** *27* (41), 5497–5510; (b) Banham-Hall, E.; Clatworthy, M. R.; Okkenhaug, K. The Therapeutic Potential for PI3K Inhibitors in Autoimmune Rheumatic Diseases. *Open Rheumatol. J.* **2012,** *6,* 245–258; (c) So, L.; Fruman, D. A. PI3K Signalling in B- and T-Lymphocytes: New Developments and Therapeutic Advances. *Biochem. J.* **2012,** *442* (3), 465–481; (d) So, L.; Yea, S. S.; Oak, J. S.; Lu, M.; Manmadhan, A.; Ke, Q. H.; Janes, M. R.; Kessler, L. V.; Kucharski, J. M.; Li, L. S.; Martin, M. B.; Ren, P.; Jessen, K. A.; Liu, Y.; Rommel, C.; Fruman, D. A. Selective Inhibition of Phosphoinositide 3-Kinase p110alpha Preserves Lymphocyte Function. *J. Biol. Chem.* **2013,** *288* (8), 5718–5731; (e) Brana, I.; Siu, L. L. Clinical Development of Phosphatidylinositol 3-Kinase Inhibitors for Cancer Treatment. *BMC Med.* **2012,** *10,* 161; (f) Rodon, J.; Dienstmann, R.; Serra, V.; Tabernero, J. Development of PI3K Inhibitors: Lessons Learned From Early Clinical Trials. *Nat. Rev. Clin. Oncol.* **2013,** *10* (3), 143–153.
86. Serra, V.; Scaltriti, M.; Prudkin, L.; Eichhorn, P. J. A.; Ibrahim, Y. H.; Chandarlapaty, S.; Markman, B.; Rodriguez, O.; Guzman, M.; Rodriguez, S.; Gili, M.; Russillo, M.; Parra, J. L.; Singh, S.; Arribas, J.; Rosen, N.; Baselga, J. PI3K Inhibition Results in Enhanced HER Signaling and Acquired ERK Dependency in HER2-Overexpressing Breast Cancer. *Oncogene* **2011,** *30* (22), 2547–2557.
87. Tasian, S. K.; Teachey, D. T.; Rheingold, S. R. Targeting the PI3K/mTOR Pathway in Pediatric Hematologic Malignancies. *Front. Oncol.* **2014,** *4,* 108.

88. (a) Bellmunt, J.; Szczylik, C.; Feingold, J.; Strahs, A.; Berkenblit, A. Temsirolimus Safety Profile and Management of Toxic Effects in Patients With Advanced Renal Cell Carcinoma and Poor Prognostic Features. *Ann. Oncol.* **2008,** *19* (8), 1387–1392; (b) Motzer, R. J.; Escudier, B.; Oudard, S.; Hutson, T. E.; Porta, C.; Bracarda, S.; Grunwald, V.; Thompson, J. A.; Figlin, R. A.; Hollaender, N.; Kay, A.; Ravaud, A. Phase 3 Trial of Everolimus for Metastatic Renal Cell Carcinoma: Final Results and Analysis of Prognostic Factors. *Cancer* **2010,** *116* (18), 4256–4265; (c) FDA, FDA Approves Afinitor for Advanced Breast Cancer 2012.(d) Nordqvist, C. Afinitor (Everolimus) Combo for Breast Cancer Approved by FDA. http://www.medicalnewstoday.com/articles/248144.php 2012.
89. (a) Novartis-Media-Releases-2011-09-08, Novartis Receives EU Approval for Votubia®, the First Medication to Treat Children and Adults With SEGA Associated With TSC. http://www.novartis.com/newsroom/media-releases/1544915.shtml.(b) Drugs, FDA Advisory Committee Recommends Additional Study Data to Support Approval of Certican in Heart Transplant Recipients. http://www.drugs.com/nda/certican_051116.html 2005.
90. (a) Furman, R. R.; Sharman, J. P.; Coutre, S. E.; Cheson, B. D.; Pagel, J. M.; Hillmen, P.; Barrientos, J. C.; Zelenetz, A. D.; Kipps, T. J.; Flinn, I.; Ghia, P.; Eradat, H.; Ervin, T.; Lamanna, N.; Coiffier, B.; Pettitt, A. R.; Ma, S.; Stilgenbauer, S.; Cramer, P.; Aiello, M.; Johnson, D. M.; Miller, L. L.; Li, D.; Jahn, T. M.; Dansey, R. D.; Hallek, M.; O'Brien, S. M. Idelalisib and Rituximab in Relapsed Chronic Lymphocytic Leukemia. *N. Engl. J. Med.* **2014,** *370* (11), 997–1007; (b) Gopal, A.; Kahl, B. S.; de Vos, S.; Wagner-Johnston, N. D.; Schuster, S. J.; Jurczak, W. J.; Flinn, I. W.; Flowers, C. R.; Martin, P.; Viardot, A.; Blum, K. A.; Goy, A. H.; Davies, A. J.; Zinzani, P. L.; Dreyling, M.; Johnson, D.; Miller, L. L.; Holes, L.; Li, D.; Dansey, R. D.; Godfrey, W. R.; Salles, G. A. PI3Kδ Inhibition by Idelalisib in Patients With Relapsed Indolent Lymphoma. *N. Engl. J. Med.* **2014,** *370* (11), 1008–1018.
91. (a) Asghar, U.; Witkiewicz, A. K.; Turner, N. C.; Knudsen, E. S. The History and Future of Targeting Cyclin-Dependent Kinases in Cancer Therapy. *Nat. Rev. Drug Discov.* **2015,** *14* (2), 130–146; (b) Peyressatre, M.; Prével, C.; Pellerano, M.; Morris, M. Targeting Cyclin-Dependent Kinases in Human Cancers: From Small Molecules to Peptide Inhibitors. *Cancers* **2015,** *7* (1), 179; (c) Malumbres, M. Cyclin-Dependent Kinases. *Genome Biol.* **2014,** *15* (6), 122.
92. Malumbres, M.; Barbacid, M. Cell Cycle, CDKs and Cancer: A Changing Paradigm. *Nat. Rev. Cancer* **2009,** *9* (3), 153–166.
93. Wang, Q.; Su, L.; Liu, N.; Zhang, L.; Xu, W.; Fang, H. Cyclin Dependent Kinase 1 Inhibitors: A Review of Recent Progress. *Curr. Med. Chem.* **2011,** *18* (13), 2025–2043.
94. Cicenas, J.; Kalyan, K.; Sorokinas, A.; Jatulyte, A.; Valiunas, D.; Kaupinis, A.; Valius, M. Highlights of the Latest Advances in Research on CDK Inhibitors. *Cancers* **2014,** *6* (4), 2224–2242.
95. (a) Noble, M. E.; Endicott, J. A.; Johnson, L. N. Protein Kinase Inhibitors: Insights Into Drug Design From Structure. *Science* **2004,** *303* (5665), 1800–1805; (b) Cowan-Jacob, S. W.; Jahnke, W.; Knapp, S. Novel Approaches for Targeting Kinases: Allosteric Inhibition, Allosteric Activation and Pseudokinases. *Future Med. Chem.* **2014,** *6* (5), 541–561.
96. Lombardo, L. J.; Lee, F. Y.; Chen, P.; Norris, D.; Barrish, J. C.; Behnia, K.; Castaneda, S.; Cornelius, L. A.; Das, J.; Doweyko, A. M.; Fairchild, C.; Hunt, J. T.; Inigo, I.; Johnston, K.; Kamath, A.; Kan, D.; Klei, H.; Marathe, P.; Pang, S.; Peterson, R.; Pitt, S.; Schieven, G. L.; Schmidt, R. J.; Tokarski, J.; Wen, M. L.; Wityak, J.; Borzilleri, R. M. Discovery of *N*-(2-Chloro-6-methyl-phenyl)-2-(6-(4-(2-hydroxyethyl)-piperazin-1-yl)-2-methylpyrimidin-4-ylamino)thiazole-5-carboxamide (BMS-354825), a Dual Src/Abl Kinase Inhibitor With Potent Antitumor Activity in Preclinical Assays. *J. Med. Chem.* **2004,** *47* (27), 6658–6661.
97. (a) Motzer, R. J.; Hoosen, S.; Bello, C. L.; Christensen, J. G. Sunitinib Malate for the Treatment of Solid Tumours: A Review of Current Clinical Data. *Expert Opin. Investig. Drugs* **2006,** *15* (5), 553–561; (b) Faivre, S.; Demetri, G.; Sargent, W.; Raymond, E. Molecular Basis for Sunitinib Efficacy and Future Clinical Development. *Nat. Rev. Drug Discov.* **2007,** *6* (9), 734–745.
98. Liu, Y.; Gray, N. S. Rational Design of Inhibitors That Bind to Inactive Kinase Conformations. *Nat. Chem. Biol.* **2006,** *2* (7), 358–364.
99. (a) Christopoulos, A.; Changeux, J. P.; Catterall, W. A.; Fabbro, D.; Burris, T. P.; Cidlowski, J. A.; Olsen, R. W.; Peters, J. A.; Neubig, R. R.; Pin, J. P.; Sexton, P. M.; Kenakin, T. P.; Ehlert, F. J.; Spedding, M.; Langmead, C. J. International Union of Basic and Clinical Pharmacology. XC. Multisite Pharmacology: Recommendations for the Nomenclature of Receptor Allosterism and Allosteric Ligands. *Pharmacol. Rev.* **2014,** *66* (4), 918–947; (b) Fleishman, S. J.; Schlessinger, J.; Ben-Tal, N. A Putative Molecular-Activation Switch in the Transmembrane Domain of erbB2. *Proc. Natl. Acad. Sci. U. S. A.* **2002,** *99* (25), 15937–15940; (c) Udugamasooriya, D. G.; Dineen, S. P.; Brekken, R. A.; Kodadek, T. A Peptoid "Antibody Surrogate" That Antagonizes VEGF Receptor 2 Activity. *J. Am. Chem. Soc.* **2008,** *130* (17), 5744–5752; (d) Jura, N.; Zhang, X.; Endres, N. F.; Seeliger, M. A.; Schindler, T.; Kuriyan, J. Catalytic Control in the EGF Receptor and Its Connection to General Kinase Regulatory Mechanisms. *Mol. Cell* **2011,** *42* (1), 9–22; (e) Cazorla, M.; Jouvenceau, A.; Rose, C.; Guilloux, J. P.; Pilon, C.; Dranovsky, A.; Premont, J. Cyclotraxin-B, the First Highly Potent and Selective TrkB Inhibitor, Has Anxiolytic Properties in Mice. *PLoS One* **2010,** *5* (3), e9777; (f) Cho, H. S.; Mason, K.; Ramyar, K. X.; Stanley, A. M.; Gabelli, S. B.; Denney, D. W., Jr.; Leahy, D. J. Structure of the Extracellular Region of HER2 Alone and in Complex With the Herceptin Fab. *Nature* **2003,** *421* (6924), 756–760; (g) Hynes, N. E.; Lane, H. A. ERBB Receptors and Cancer: The Complexity of Targeted Inhibitors. *Nat. Rev. Cancer* **2005,** *5* (5), 341–354; (h) Hsieh, A. C.; Moasser, M. M. Targeting HER Proteins in Cancer Therapy and the Role of the Non-Target HER3. *Br. J. Cancer* **2007,** *97* (4), 453–457.
100. (a) Bono, F.; De Smet, F.; Herbert, C.; De Bock, K.; Georgiadou, M.; Fons, P.; Tjwa, M.; Alcouffe, C.; Ny, A.; Bianciotto, M.; Jonckx, B.; Murakami, M.; Lanahan, A. A.; Michielsen, C.; Sibrac, D.; Dol-Gleizes, F.; Mazzone, M.; Zacchigna, S.; Herault, J. P.; Fischer, C.; Rigon, P.; Ruiz de Almodovar, C.; Claes, F.; Blanc, I.; Poesen, K.; Zhang, J.; Segura, I.; Gueguen, G.; Bordes, M. F.; Lambrechts, D.; Broussy, R.; van de Wouwer, M.; Michaux, C.; Shimada, T.; Jean, I.; Blacher, S.; Noel, A.; Motte, P.; Rom, E.; Rakic, J. M.; Katsuma, S.; Schaeffer, P.; Yayon, A.; Van Schepdael, A.; Schwalbe, H.; Gervasio, F. L.; Carmeliet, G.; Rozensky, J.; Dewerchin, M.; Simons, M.; Christopoulos, A.; Herbert, J. M.; Carmeliet, P. Inhibition of Tumor Angiogenesis and Growth by a Small-Molecule Multi-FGF Receptor Blocker With Allosteric Properties. *Cancer Cell* **2013,** *23* (4), 477–488; (b) Herbert, C.; Schieborr, U.; Saxena, K.; Juraszek, J.; De Smet, F.; Alcouffe, C.; Bianciotto, M.; Saladino, G.; Sibrac, D.; Kudlinzki, D.; Sreeramulu, S.; Brown, A.; Rigon, P.; Herault, J. P.; Lassalle, G.; Blundell, T. L.; Rousseau, F.; Gils, A.; Schymkowitz, J.; Tompa, P.; Herbert, J. M.; Carmeliet, P.; Gervasio, F. L.; Schwalbe, H.; Bono, F. Molecular Mechanism of SSR128129E, an Extracellularly Acting, Small-Molecule, Allosteric Inhibitor of FGF Receptor Signaling. *Cancer Cell* **2013,** *23* (4), 489–501.
101. (a) Sanders, M. J.; Ali, Z. S.; Hegarty, B. D.; Heath, R.; Snowden, M. A.; Carling, D. Defining the Mechanism of Activation of AMP-Activated Protein Kinase by the Small Molecule A-769662, a Member of the Thienopyridone Family. *J. Biol. Chem.* **2007,** *282* (45), 32539–32548; (b) Lee, K. H.; Hsu, E. C.; Guh, J. H.; Yang, H. C.; Wang, D.; Kulp, S. K.; Shapiro, C. L.; Chen, C. S. Targeting Energy Metabolic and Oncogenic Signaling Pathways in Triple-Negative Breast Cancer by a Novel Adenosine Monophosphate-Activated Protein Kinase (AMPK) Activator. *J. Biol. Chem.* **2011,** *286* (45), 39247–39258; (c) Salt, I. P.; Palmer, T. M. Exploiting the Anti-Inflammatory Effects of AMP-Activated Protein Kinase Activation. *Expert Opin. Investig. Drugs* **2012,** *21* (8), 1155–1167; (d) Li, M.; Youngren, J. F.; Manchem, V. P.; Kozlowski, M.; Zhang, B. B.; Maddux, B. A.; Goldfine, I. D. Small Molecule Insulin Receptor Activators Potentiate Insulin Action in Insulin-Resistant Cells. *Diabetes* **2001,** *50* (10), 2323–2328; (e) Pender, C.; Goldfine, I. D.; Manchem, V. P.; Evans, J. L.; Spevak, W. R.; Shi, S.; Rao, S.; Bajjalieh, S.; Maddux, B. A.; Youngren, J. F. Regulation of Insulin Receptor Function by a Small Molecule Insulin Receptor Activator. *J. Biol. Chem.* **2002,** *277* (46), 43565–43571.
102. Martiny-Baron, G.; Fabbro, D. Classical PKC Isoforms in Cancer. *Pharmacol. Res.* **2007,** *55* (6), 477–486.
103. Massa, S. M.; Yang, T.; Xie, Y.; Shi, J.; Bilgen, M.; Joyce, J. N.; Nehama, D.; Rajadas, J.; Longo, F. M. Small Molecule BDNF Mimetics Activate TrkB Signaling and Prevent Neuronal Degeneration in Rodents. *J. Clin. Invest.* **2010,** *120* (5), 1774–1785.
104. (a) Hall-Jackson, C. A.; Goedert, M.; Hedge, P.; Cohen, P. Effect of SB 203580 on the Activity of c-Raf in vitro and In Vivo. *Oncogene* **1999,** *18* (12), 2047–2054; (b) Su, F.; Viros, A.; Milagre, C.; Trunzer, K.; Bollag, G.; Spleiss, O.; Reis-Filho, J. S.; Kong, X.; Koya, R. C.; Flaherty, K. T.; Chapman, P. B.; Kim, M. J.; Hayward, R.; Martin, M.; Yang, H.; Wang, Q.; Hilton, H.; Hang, J. S.; Noe, J.; Lambros, M.; Geyer, F.; Dhomen, N.; Niculescu-Duvaz, I.; Zambon, A.; Niculescu-Duvaz, D.; Preece, N.; Robert, L.; Otte, N. J.; Mok, S.; Kee, D.; Ma, Y.; Zhang, C.; Habets, G.; Burton, E. A.; Wong, B.; Nguyen, H.; Kockx, M.; Andries, L.; Lestini, B.; Nolop, K. B.; Lee, R. J.; Joe, A. K.; Troy, J. L.; Gonzalez, R.; Hutson, T. E.; Puzanov, I.; Chmielowski, B.; Springer, C. J.; McArthur, G. A.; Sosman, J. A.; Lo, R. S.; Ribas, A.; Marais, R. RAS Mutations in Cutaneous Squamous-Cell Carcinomas in Patients Treated With BRAF Inhibitors. *N. Engl. J. Med.* **2012,** *366* (3), 207–215.
105. Fabbro, D.; Garcia-Echeverria, C. Targeting Protein Kinases in Cancer Therapy. *Curr. Opin. Drug Discov. Devel.* **2002,** *5* (5), 701–712.
106. Szakacs, G.; Paterson, J. K.; Ludwig, J. A.; Booth-Genthe, C.; Gottesman, M. M. Targeting Multidrug Resistance in Cancer. *Nat. Rev. Drug Discov.* **2006,** *5* (3), 219–234.

107. (a) Engelman, J. A.; Chen, L.; Tan, X.; Crosby, K.; Guimaraes, A. R.; Upadhyay, R.; Maira, M.; McNamara, K.; Perera, S. A.; Song, Y.; Chirieac, L. R.; Kaur, R.; Lightbown, A.; Simendinger, J.; Li, T.; Padera, R. F.; Garcia-Echeverria, C.; Weissleder, R.; Mahmood, U.; Cantley, L. C.; Wong, K. K. Effective Use of PI3K and MEK Inhibitors to Treat Mutant Kras G12D and PIK3CA H1047R Murine Lung Cancers. *Nat. Med.* **2008,** *14* (12), 1351–1356; (b) Weisberg, E.; Manley, P. W.; Breitenstein, W.; Bruggen, J.; Cowan-Jacob, S. W.; Ray, A.; Huntly, B.; Fabbro, D.; Fendrich, G.; Hall-Meyers, E.; Kung, A. L.; Mestan, J.; Daley, G. Q.; Callahan, L.; Catley, L.; Cavazza, C.; Azam, M.; Neuberg, D.; Wright, R. D.; Gilliland, D. G.; Griffin, J. D. Characterization of AMN107, a Selective Inhibitor of Native and Mutant Bcr-Abl. *Cancer Cell* **2005,** *7* (2), 129–141; (c) Quintas-Cardama, A.; Kantarjian, H.; Cortes, J. Flying Under the Radar: The New Wave of BCR-ABL Inhibitors. *Nat. Rev. Drug Discov.* **2007,** *6* (10), 834–848; (d) Adrian, F. J.; Ding, Q.; Sim, T.; Velentza, A.; Sloan, C.; Liu, Y.; Zhang, G.; Hur, W.; Ding, S.; Manley, P.; Mestan, J.; Fabbro, D.; Gray, N. S. Allosteric Inhibitors of Bcr-abl-Dependent Cell Proliferation. *Nat. Chem. Biol.* **2006,** *2* (2), 95–102.
108. Hassan, M.; Watari, H.; AbuAlmaaty, A.; Ohba, Y.; Sakuragi, N. Apoptosis and Molecular Targeting Therapy in Cancer. *Biomed. Res. Int.* **2014,** *2014,* 23.
109. Plati, J.; Bucur, O.; Khosravi-Far, R. Dysregulation of Apoptotic Signaling in Cancer: Molecular Mechanisms and Therapeutic Opportunities. *J. Cell. Biochem.* **2008,** *104* (4), 1124–1149.
110. Wong, R. S. Apoptosis in Cancer: From Pathogenesis to Treatment. *J. Exp. Clin. Cancer Res.* **2011,** *30* (1), 1–14.
111. Slee, E. A.; Harte, M. T.; Kluck, R. M.; Wolf, B. B.; Casiano, C. A.; Newmeyer, D. D.; Wang, H. G.; Reed, J. C.; Nicholson, D. W.; Alnemri, E. S.; Green, D. R.; Martin, S. J. Ordering the Cytochrome *c*-Initiated Caspase Cascade: Hierarchical Activation of Caspases-2, −3, −6, −7, −8, and −10 in a Caspase-9-Dependent Manner. *J. Cell Biol.* **1999,** *144* (2), 281–292.
112. Khosravi-Far, R.; Esposti, M. D. Death Receptor Signals to Mitochondria. *Cancer Biol. Ther.* **2004,** *3* (11), 1051–1057.
113. Wu, G.; Chai, J.; Suber, T. L.; Wu, J.-W.; Du, C.; Wang, X.; Shi, Y. Structural Basis of IAP Recognition by Smac/DIABLO. *Nature* **2000,** *408* (6815), 1008–1012.
114. (a) Li, P.; Nijhawan, D.; Budihardjo, I.; Srinivasula, S. M.; Ahmad, M.; Alnemri, E. S.; Wang, X. Cytochrome *c* and dATP-Dependent Formation of Apaf-1/Caspase-9 Complex Initiates an Apoptotic Protease Cascade. *Cell* **1997,** *91* (4), 479–489; (b) Zou, H.; Li, Y.; Liu, X.; Wang, X. An APAF-1·Cytochrome *c* Multimeric Complex Is a Functional Apoptosome That Activates Procaspase-9. *J. Biol. Chem.* **1999,** *274* (17), 11549–11556.
115. Kroemer, G.; Galluzzi, L.; Brenner, C. Mitochondrial Membrane Permeabilisation in Cell Death. *Physiol. Rev.* **2007,** *87,* 99–163.
116. Plati, J.; Bucur, O.; Khosravi-Far, R. Apoptotic Cell Signaling in Cancer Progression and Therapy. *Integr. Biol.* **2011,** *3* (4), 279–296.
117. (a) Chai, J.; Shiozaki, E.; Srinivasula, S. M.; Wu, Q.; Dataa, P.; Alnemri, E. S.; Shi, Y. Structural Basis of Caspase-7 Inhibition by XIAP. *Cell* **2001,** *104* (5), 769–780; (b) Eckelman, B. P.; Salvesen, G. S.; Scott, F. L. Human Inhibitor of Apoptosis Proteins: Why XIAP Is the Black Sheep of the Family. *EMBO Rep.* **2006,** *7* (10), 988–994.
118. (a) Fulda, S.; Vucic, D. Targeting IAP Proteins for Therapeutic Intervention in Cancer. *Nat. Rev. Drug Discov.* **2012,** *11* (2), 109–124; (b) Fong, W. G.; Liston, P.; Rajcan-Separovic, E.; St Jean, M.; Craig, C.; Korneluk, R. G. Expression and Genetic Analysis of XIAP-Associated Factor 1 (XAF1) in Cancer Cell Lines. *Genomics* **2000,** *70* (1), 113–122; (c) Augello, C.; Caruso, L.; Maggioni, M.; Donadon, M.; Montorsi, M.; Santambrogio, R.; Torzilli, G.; Vaira, V.; Pellegrini, C.; Roncalli, M.; Coggi, G.; Bosari, S. Inhibitors of Apoptosis Proteins (IAPs) Expression and Their Prognostic Significance in Hepatocellular Carcinoma. *BMC Cancer* **2009,** *9,* 125.
119. (a) Raffo, A. J.; Perlman, H.; Chen, M. W.; Day, M. L.; Streitman, J. S.; Buttyan, R. Overexpression of bcl-2 Protects Prostate Cancer Cells From Apoptosis in vitro and Confers Resistance to Androgen Depletion In Vivo. *Cancer Res.* **1995,** *55,* 4438–4445; (b) Karpel-Massler, G.; Shu, C.; Chau, L.; Banu, M.; Halatsch, M.-E.; Westhoff, M.-A.; Ramirez, Y.; Ross, A. H.; Bruce, J. N.; Canoll, P.; Siegelin, M. D. Combined Inhibition of Bcl-2/Bcl-xL and Usp9X/Bag3 Overcomes Apoptotic Resistance in Glioblastoma in vitro and In Vivo. *Oncotarget* **2015,** *6* (16), 14507–14521; (c) Hockenbery, D.; Nunez, G.; Milliman, C.; Schreiber, R. D.; Korsmeyer, S. J. Bcl-2 is an Inner Mitochondrial Membrane Protein That Blocks Programmed Cell Death. *Nature* **1990,** *348* (6299), 334–336.
120. Fridman, J. S.; Lowe, S. W. Control of Apoptosis by p53. *Oncogene* **2003,** *22* (56), 9030–9040.
121. Bai, L.; Zhu, W. G. p53: Structure, Function and Therapeutic Applications. *J. Cancer Mol.* **2006,** *2,* 141–153.
122. (a) Ndubaku, C.; Varfolomeev, E.; Wang, L.; Zobel, K.; Lau, K.; Elliott, L. O.; Maurer, B.; Fedorova, A. V.; Dynek, J. N.; Koehler, M.; Hymowitz, S. G.; Tsui, V.; Deshayes, K.; Fairbrother, W. J.; Flygare, J. A.; Vucic, D. Antagonism of c-IAP and XIAP Proteins Is Required for Efficient Induction of Cell Death by Small-Molecule IAP Antagonists. *ACS Chem. Biol.* **2009,** *4* (7), 557–566; (b) Varfolomeev, E.; Blankenship, J. W.; Wayson, S. M.; Fedorova, A. V.; Kayagaki, N.; Garg, P.; Zobel, K.; Dynek, J. N.; Elliott, L. O.; Wallweber, H. J.; Flygare, J. A.; Fairbrother, W. J.; Deshayes, K.; Dixit, V. M.; Vucic, D. IAP Antagonists Induce Autoubiquitination of c-IAPs, NF-kappaB Activation, and TNFalpha-Dependent Apoptosis. *Cell* **2007,** *131* (4), 669–681; (c) Zhuang, J.; Laing, N.; Oates, M.; Lin, K.; Johnson, G.; Pettitt, A. R. Selective IAP Inhibition Results in Sensitization of Unstimulated but Not CD40-Stimulated Chronic Lymphocytic Leukaemia Cells to TRAIL-Induced Apoptosis. *Pharmacol. Res. Perspect.* **2014,** *2* (6), e00081.
123. (a) Wang, C.; Huang, S.-B.; Yang, M.-C.; Lin, Y.-T.; Chu, I. H.; Shen, Y.-N.; Chiu, Y.-H.; Hung, S.-H.; Kang, L.; Hong, Y.-R.; Chen, C.-H. Combining Paclitaxel With ABT-263 Has a Synergistic Effect on Paclitaxel Resistant Prostate Cancer Cells. *PLoS One* **2015,** *10* (3), e0120913; (b) Kawashima-Goto, S.; Imamura, T.; Tomoyasu, C.; Yano, M.; Yoshida, H.; Fujiki, A.; Tamura, S.; Osone, S.; Ishida, H.; Morimoto, A.; Kuroda, H.; Hosoi, H. BCL2 Inhibitor (ABT-737): A Restorer of Prednisolone Sensitivity in Early T-Cell Precursor-Acute Lymphoblastic Leukemia With High MEF2C Expression? *PLoS One* **2015,** *10* (7), e0132926.
124. (a) Souers, A. J.; Leverson, J. D.; Boghaert, E. R.; Ackler, S. L.; Catron, N. D.; Chen, J.; Dayton, B. D.; Ding, H.; Enschede, S. H.; Fairbrother, W. J.; Huang, D. C. S.; Hymowitz, S. G.; Jin, S.; Khaw, S. L.; Kovar, P. J.; Lam, L. T.; Lee, J.; Maecker, H. L.; Marsh, K. C.; Mason, K. D.; Mitten, M. J.; Nimmer, P. M.; Oleksijew, A.; Park, C. H.; Park, C.-M.; Phillips, D. C.; Roberts, A. W.; Sampath, D.; Seymour, J. F.; Smith, M. L.; Sullivan, G. M.; Tahir, S. K.; Tse, C.; Wendt, M. D.; Xiao, Y.; Xue, J. C.; Zhang, H.; Humerickhouse, R. A.; Rosenberg, S. H.; Elmore, S. W. ABT-199, a Potent and Selective BCL-2 Inhibitor, Achieves Antitumor Activity While Sparing Platelets. *Nat. Med.* **2013,** *19* (2), 202–208; (b) Tse, C.; Shoemaker, A. R.; Adickes, J.; Anderson, M. G.; Chen, J.; Jin, S.; Johnson, E. F.; Marsh, K. C.; Mitten, M. J.; Nimmer, P.; Roberts, L.; Tahir, S. K.; Xiao, Y.; Yang, X.; Zhang, H.; Fesik, S.; Rosenberg, S. H.; Elmore, S. W. ABT-263: A Potent and Orally Bioavailable Bcl-2 Family Inhibitor. *Cancer Res.* **2008,** *68* (9), 3421–3428.
125. Hirschey, M. D.; DeBerardinis, R. J.; Diehl, A. M.; Drew, J. E.; Frezza, C.; Green, M. F.; Jones, L. W.; Ko, Y. H.; Le, A.; Lea, M. A.; Locasale, J. W.; Longo, V. D.; Lyssiotis, C. A.; McDonnell, E.; Mehrmohamadi, M.; Michelotti, G.; Muralidhar, V.; Murphy, M. P.; Pedersen, P. L.; Poore, B.; Raffaghello, L.; Rathmell, J. C.; Sivanand, S.; Vander Heiden, M. G.; Wellen, K. E.; Target Validation, T. Dysregulated Metabolism Contributes to Oncogenesis. *Semin. Cancer Biol.* **2015,** *35* (Suppl), S129–S150.
126. (a) Warburg, O.; Wind, F.; Negelein, E. The Metabolism of Tumors in the Body. *J. Gen. Physiol.* **1927,** *8* (6), 519–530; (b) Vaitheesvaran, B.; Xu, J.; Yee, J.; Q-Y, L.; Go, V. L.; Xiao, G. G.; Lee, W. N. The Warburg Effect: A Balance of Flux Analysis. *Metabolomics* **2015,** *11* (4), 787–796.
127. (a) Vander Heiden, M. G.; Cantley, L. C.; Thompson, C. B. Understanding the Warburg Effect: The Metabolic Requirements of Cell Proliferation. *Science* **2009,** *324* (5930), 1029–1033; (b) Chaneton, B.; Hillmann, P.; Zheng, L.; Martin, A. C.; Maddocks, O. D.; Chokkathukalam, A.; Coyle, J. E.; Jankevics, A.; Holding, F. P.; Vousden, K. H.; Frezza, C.; O'Reilly, M.; Gottlieb, E. Serine is a Natural Ligand and Allosteric Activator of Pyruvate Kinase M2. *Nature* **2012,** *491* (7424), 458–462.
128. (a) Clem, B. F.; O'Neal, J.; Klarer, A. C.; Telang, S.; Chesney, J. Clinical Development of Cancer Therapeutics That Target Metabolism. *QJM* **2015,** *109* (6), 367–372; (b) Trefely, S.; Khoo, P.-S.; Krycer, J. R.; Chaudhuri, R.; Fazakerley, D. J.; Parker, B. L.; Sultani, G.; Lee, J.; Stephan, J.-P.; Torres, E.; Jung, K.; Kuijl, C.; James, D. E.; Junutula, J. R.; Stöckli, J. Kinome Screen Identifies PFKFB3 and Glucose Metabolism as Important Regulators of the Insulin/Insulin-Like Growth Factor (IGF)-1 Signaling Pathway. *J. Biol. Chem.* **2015,** *290* (43), 25834–25846.
129. (a) Luo, W.; Hu, H.; Chang, R.; Zhong, J.; Knabel, M.; O'Meally, R.; Cole, R. N.; Pandey, A.; Semenza, G. L. Pyruvate Kinase M2 is a PHD3-Stimulated Coactivator for Hypoxia-Inducible Factor 1. *Cell* **2011,** *145* (5), 732–744; (b) Yang, W.; Xia, Y.; Hawke, D.; Li, X.; Liang, J.; Xing, D.; Aldape, K.; Hunter, T.; Alfred Yung, W. K.; Lu, Z. PKM2 Phosphorylates Histone H3 and Promotes Gene Transcription and Tumorigenesis. *Cell* **2012,** *150* (4), 685–696.
130. (a) Xiao, D.; Ren, P.; Su, H.; Yue, M.; Xiu, R.; Hu, Y.; Liu, H.; Qing, G. Myc Promotes Glutaminolysis in Human Neuroblastoma Through Direct Activation of Glutaminase 2. *Oncotarget* **2015,** *6* (38), 40655–40666; (b) Shroff, E. H.; Eberlin, L. S.; Dang, V. M.; Gouw, A. M.; Gabay, M.; Adam, S. J.; Bellovin, D. I.; Tran, P. T.; Philbrick, W. M.; Garcia-Ocana, A.; Casey, S. C.; Li, Y.; Dang, C. V.; Zare, R. N.; Felsher, D. W. MYC Oncogene Overexpression Drives Renal Cell Carcinoma in a Mouse Model Through Glutamine Metabolism. *Proc. Natl. Acad. Sci.* **2015,** *112* (21), 6539–6544.

131. Jacque, N.; Ronchetti, A. M.; Larrue, C.; Meunier, G.; Birsen, R.; Willems, L.; Saland, E.; Decroocq, J.; Thiago, T. T.; Lambert, M.; Poulain, L.; Hospital, M. A.; Sujobert, P.; Joseph, L.; Chapuis, N.; Lacombe, C.; Moura, I. C.; Demo, S.; Sarry, J. E.; Recher, C.; Mayeux, P.; Tamburini, J.; Bouscary, D. Targeting Glutaminolysis Has Antileukemic Activity in Acute Myeloid Leukemia and Synergizes With BCL-2 Inhibition. *Blood* **2015,** *126* (11), 1346–1356.
132. Kuo, M. T.; Savaraj, N.; Feun, L. G. Targeted Cellular Metabolism for Cancer Chemotherapy With Recombinant Arginine-Degrading Enzymes. *Oncotarget* **2010,** *1* (4), 246–251.
133. Kurtzberg, J.; Asselin, B.; Bernstein, M.; Buchanan, G. R.; Pollock, B. H.; Camitta, B. M. Polyethylene Glycol-Conjugated L-Asparaginase Versus Native L-Asparaginase in Combination With Standard Agents for Children With Acute Lymphoblastic Leukemia in Second Bone Marrow Relapse: A Children's Oncology Group Study (POG 8866). *J. Pediatr. Hematol. Oncol.* **2011,** *33* (8), 610–616.
134. Dang, L.; White, D. W.; Gross, S.; Bennett, B. D.; Bittinger, M. A.; Driggers, E. M.; Fantin, V. R.; Jang, H. G.; Jin, S.; Keenan, M. C.; Marks, K. M.; Prins, R. M.; Ward, P. S.; Yen, K. E.; Liau, L. M.; Rabinowitz, J. D.; Cantley, L. C.; Thompson, C. B.; Vander Heiden, M. G.; Su, S. M. Cancer-Associated IDH1 Mutations Produce 2-Hydroxyglutarate. *Nature* **2010,** *465* (7300), 966.
135. Losman, J. A.; Looper, R. E.; Koivunen, P.; Lee, S.; Schneider, R. K.; McMahon, C.; Cowley, G. S.; Root, D. E.; Ebert, B. L.; Kaelin, W. G., Jr. (R)-2-Hydroxyglutarate Is Sufficient to Promote Leukemogenesis and Its Effects Are Reversible. *Science* **2013,** *339* (6127), 1621–1625.
136. (a) Wang, X.-W.; Ciccarino, P.; Rossetto, M.; Boisselier, B.; Marie, Y.; Desestret, V.; Gleize, V.; Mokhtari, K.; Sanson, M.; Labussière, M. IDH Mutations: Genotype-Phenotype Correlation and Prognostic Impact. *Biomed Res. Int.* **2014,** *2014,* 540236; (b) Arai, M.; Nobusawa, S.; Ikota, H.; Takemura, S.; Nakazato, Y. Frequent IDH1/2 Mutations in Intracranial Chondrosarcoma: A Possible Diagnostic Clue for Its Differentiation From Chordoma. *Brain Tumor Pathol.* **2012,** *29* (4), 201–206.
137. No author. IDH1 Inhibitor Shows Promising Early Results. *Cancer Discov.* **2015,** *5* (1), 4.
138. (a) Chen, D. S.; Mellman, I. Oncology Meets Immunology: The Cancer-Immunity Cycle. *Immunity* **2013,** *39* (1), 1–10; (b) Harris, T. J.; Drake, C. G. Primer on Tumor Immunology and Cancer Immunotherapy. *J. Immunother. Cancer* **2013,** *1,* 12.
139. Azuma, M.; Cayabyab, M.; Buck, D.; Phillips, J. H.; Lanier, L. L. CD28 Interaction With B7 Costimulates Primary Allogeneic Proliferative Responses and Cytotoxicity Mediated by Small, Resting T Lymphocytes. *J. Exp. Med.* **1992,** *175* (2), 353–360.
140. (a) Motz, G. T.; Coukos, G. Deciphering and Reversing Tumor Immune Suppression. *Immunity* **2013,** *39* (1), 61–73; (b) Takahashi, A.; Kono, K.; Ichihara, F.; Sugai, H.; Fujii, H.; Matsumoto, Y. Vascular Endothelial Growth Factor Inhibits Maturation of Dendritic Cells Induced by Lipopolysaccharide, but Not by Proinflammatory Cytokines. *Cancer Immunol. Immunother.* **2004,** *53* (6), 543–550; (c) Corinti, S.; Albanesi, C.; la Sala, A.; Pastore, S.; Girolomoni, G. Regulatory Activity of Autocrine IL-10 on Dendritic Cell Functions. *J. Immunol.* **2001,** *166* (7), 4312–4318; (d) Geissmann, F.; Revy, P.; Regnault, A.; Lepelletier, Y.; Dy, M.; Brousse, N.; Amigorena, S.; Hermine, O.; Durandy, A. TGF-Beta 1 Prevents the Noncognate Maturation of Human Dendritic Langerhans Cells. *J. Immunol.* **1999,** *162* (8), 4567–4575; (e) García-Rocha, R.; Moreno-Lafont, M.; Mora-García, M. L.; Weiss-Steider, B.; Montesinos, J. J.; Piña-Sánchez, P.; Monroy-García, A. Mesenchymal Stromal Cells Derived From Cervical Cancer Tumors Induce TGF-β1 Expression and IL-10 Expression and Secretion in the Cervical Cancer Cells, Resulting in Protection From Cytotoxic T Cell Activity. *Cytokine* **2015,** *76* (2), 382–390.
141. (a) Garcia-Lora, A.; Martinez, M.; Algarra, I.; Gaforio, J. J.; Garrido, F. MHC Class I-Deficient Metastatic Tumor Variants Immunoselected by T Lymphocytes Originate From the Coordinated Downregulation of APM Components. *Int. J. Cancer* **2003,** *106* (4), 521–527; (b) Garrido, C.; Paco, L.; Romero, I.; Berruguilla, E.; Stefansky, J.; Collado, A.; Algarra, I.; Garrido, F.; Garcia-Lora, A. M. MHC Class I Molecules Act As Tumor Suppressor Genes Regulating the Cell Cycle Gene Expression, Invasion and Intrinsic Tumorigenicity of Melanoma Cells. *Carcinogenesis* **2012,** *33* (3), 687–693.
142. (a) Lund, A. W.; Duraes, F. V.; Hirosue, S.; Raghavan, V. R.; Nembrini, C.; Thomas, S. N.; Issa, A.; Hugues, S.; Swartz, M. A. VEGF-C Promotes Immune Tolerance in B16 Melanomas and Cross-Presentation of Tumor Antigen by Lymph Node Lymphatics. *Cell Rep.* **2012,** *1* (3), 191–199; (b) Shrimali, R. K.; Yu, Z.; Theoret, M. R.; Chinnasamy, D.; Restifo, N. P.; Rosenberg, S. A. Antiangiogenic Agents Can Increase Lymphocyte Infiltration Into Tumor and Enhance the Effectiveness of Adoptive Immunotherapy of Cancer. *Cancer Res.* **2010,** *70* (15), 6171–6180.
143. (a) Spranger, S.; Spaapen, R. M.; Zha, Y.; Williams, J.; Meng, Y.; Ha, T. T.; Gajewski, T. F. Up-Regulation of PD-L1, IDO, and Tregs in the Melanoma Tumor Microenvironment Is Driven by CD8+ T Cells. *Sci. Transl. Med.* **2013,** *5* (200), 200ra116; (b) Wilcox, R. A.; Feldman, A. L.; Wada, D. A.; Yang, Z.-Z.; Comfere, N. I.; Dong, H.; Kwon, E. D.; Novak, A. J.; Markovic, S. N.; Pittelkow, M. R.; Witzig, T. E.; Ansell, S. M. B7-H1 (PD-L1, CD274) Suppresses Host Immunity in T-Cell Lymphoproliferative Disorders. *Blood* **2009,** *114* (10), 2149–2158; (c) Mazanet, M. M.; Hughes, C. C. B7-H1 Is Expressed by Human Endothelial Cells and Suppresses T Cell Cytokine Synthesis. *J. Immunol.* **2002,** *169* (7), 3581–3588; (d) Yamada, Y.; Sugita, S.; Horie, S.; Yamagami, S.; Mochizuki, M. Mechanisms of Immune Suppression for CD8+ T Cells by Human Corneal Endothelial Cells via Membrane-Bound TGFβ. *Invest. Ophthalmol. Vis. Sci.* **2010,** *51* (5), 2548–2557; (e) Joyce, J. A.; Fearon, D. T. T Cell Exclusion, Immune Privilege, and the Tumor Microenvironment. *Science* **2015,** *348* (6230), 74–80.
144. Mendler, A. N.; Hu, B.; Prinz, P. U.; Kreutz, M.; Gottfried, E.; Noessner, E. Tumor Lactic Acidosis Suppresses CTL Function by Inhibition of p38 and JNK/c-Jun Activation. *Int. J. Cancer* **2012,** *131* (3), 633–640.
145. Töpfer, K.; Kempe, S.; Müller, N.; Schmitz, M.; Bachmann, M.; Cartellieri, M.; Schackert, G.; Temme, A. Tumor Evasion From T Cell Surveillance. *J. Biomed. Biotechnol.* **2011,** *2011,* 19.
146. (a) Sainz-Perez, A.; Lim, A.; Lemercier, B.; Leclerc, C. The T-Cell Receptor Repertoire of Tumor-Infiltrating Regulatory T Lymphocytes Is Skewed Toward Public Sequences. *Cancer Res.* **2012,** *72* (14), 3557–3569; (b) Facciabene, A.; Motz, G. T.; Coukos, G. T-Regulatory Cells: Key Players in Tumor Immune Escape and Angiogenesis. *Cancer Res.* **2012,** *72* (9), 2162–2171.
147. Hahne, M.; Rimoldi, D.; Schroter, M.; Romero, P.; Schreier, M.; French, L. E.; Schneider, P.; Bornand, T.; Fontana, A.; Lienard, D.; Cerottini, J.; Tschopp, J. Melanoma Cell Expression of Fas(Apo-1/CD95) Ligand: Implications for Tumor Immune Escape. *Science* **1996,** *274* (5291), 1363–1366.
148. Holmgaard, R. B.; Zamarin, D.; Munn, D. H.; Wolchok, J. D.; Allison, J. P. Indoleamine 2,3-Dioxygenase Is a Critical Resistance Mechanism in Antitumor T Cell Immunotherapy Targeting CTLA-4. *J. Exp. Med.* **2013,** *210* (7), 1389–1402.
149. Pardoll, D. M. The Blockade of Immune Checkpoints in Cancer Immunotherapy. *Nat. Rev. Cancer* **2012,** *12* (4), 252–264.
150. (a) Yu, H.; Yang, J.; Jiao, S.; Li, Y.; Zhang, W.; Wang, J. Cytotoxic T Lymphocyte Antigen 4 Expression in Human Breast Cancer: Implications for Prognosis. *Cancer Immunol. Immunother.* **2015,** *64* (7), 853–860; (b) Contardi, E.; Palmisano, G. L.; Tazzari, P. L.; Martelli, A. M.; Falà, F.; Fabbi, M.; Kato, T.; Lucarelli, E.; Donati, D.; Polito, L.; Bolognesi, A.; Ricci, F.; Salvi, S.; Gargaglione, V.; Mantero, S.; Alberghini, M.; Ferrara, G. B.; Pistillo, M. P. CTLA-4 is Constitutively Expressed on Tumor Cells and Can Trigger Apoptosis Upon Ligand Interaction. *Int. J. Cancer* **2005,** *117* (4), 538–550.
151. Lee, L.; Gupta, M.; Sahasranaman, S. Immune Checkpoint Inhibitors: An Introduction to the Next-Generation Cancer Immunotherapy. *J. Clin. Pharmacol.* **2016,** *56* (2), 157–169.
152. (a) D'Incecco, A.; Andreozzi, M.; Ludovini, V.; Rossi, E.; Capodanno, A.; Landi, L.; Tibaldi, C.; Minuti, G.; Salvini, J.; Coppi, E.; Chella, A.; Fontanini, G.; Filice, M. E.; Tornillo, L.; Incensati, R. M.; Sani, S.; Crino, L.; Terracciano, L.; Cappuzzo, F. PD-1 and PD-L1 Expression in Molecularly Selected Non-Small-Cell Lung Cancer Patients. *Br. J. Cancer* **2015,** *112* (1), 95–102; (b) Nduom, E. K.; Wei, J.; Yaghi, N. K.; Huang, N.; Kong, L.-Y.; Gabrusiewicz, K.; Ling, X.; Zhou, S.; Ivan, C.; Chen, J. Q.; Burks, J. K.; Fuller, G. N.; Calin, G. A.; Conrad, C. A.; Creasy, C.; Ritthipichai, K.; Radvanyi, L.; Heimberger, A. B. PD-L1 Expression and Prognostic Impact in Glioblastoma. *Neuro-Oncology* **2015,** *18* (2), 195–205; (c) Dong, H.; Strome, S. E.; Salomao, D. R.; Tamura, H.; Hirano, F.; Flies, D. B.; Roche, P. C.; Lu, J.; Zhu, G.; Tamada, K.; Lennon, V. A.; Celis, E.; Chen, L. Tumor-Associated B7-H1 Promotes T-Cell Apoptosis: A Potential Mechanism of Immune Evasion. *Nat. Med.* **2002,** *8* (8), 793–800.
153. (a) Das, R.; Verma, R.; Sznol, M.; Boddupalli, C. S.; Gettinger, S. N.; Kluger, H.; Callahan, M.; Wolchok, J. D.; Halaban, R.; Dhodapkar, M. V.; Dhodapkar, K. M. Combination Therapy With Anti–CTLA-4 and Anti–PD-1 Leads to Distinct Immunologic Changes In Vivo. *J. Immunol.* **2015,** *194* (3), 950–959; (b) Larkin, J.; Chiarion-Sileni, V.; Gonzalez, R.; Grob, J. J.; Cowey, C. L.; Lao, C. D.; Schadendorf, D.; Dummer, R.; Smylie, M.; Rutkowski, P.; Ferrucci, P. F.; Hill, A.; Wagstaff, J.; Carlino, M. S.; Haanen, J. B.; Maio, M.; Marquez-Rodas, I.; McArthur, G. A.; Ascierto, P. A.; Long, G. V.; Callahan, M. K.; Postow, M. A.; Grossmann, K.; Sznol, M.; Dreno, B.; Bastholt, L.; Yang, A.; Rollin, L. M.; Horak, C.; Hodi, F. S.; Wolchok, J. D. Combined Nivolumab and Ipilimumab or Monotherapy in Untreated Melanoma. *N. Engl. J. Med.* **2015,** *373* (1), 23–34.

154. Anestakis, D.; Petanidis, S.; Kalyvas, S.; Nday, C. M.; Tsave, O.; Kioseoglou, E.; Salifoglou, A. Mechanisms and Applications of Interleukins in Cancer Immunotherapy. *Int. J. Mol. Sci.* **2015,** *16* (1), 1691–1710.
155. (a) Cohen, C. A.; Shea, A. A.; Heffron, C. L.; Schmelz, E. M.; Roberts, P. C. Interleukin-12 Immunomodulation Delays the Onset of Lethal Peritoneal Disease of Ovarian Cancer. *J. Interferon Cytokine Res.* **2016,** *36* (1), 62–73; (b) Kim, H.; Gao, W.; Ho, M. Novel Immunocytokine IL12-SS1 (Fv) Inhibits Mesothelioma Tumor Growth in Nude Mice. *PLoS One* **2013,** *8* (11), e81919.
156. (a) Hanzly, M.; Aboumohamed, A.; Yarlagadda, N.; Creighton, T.; Digiorgio, L.; Fredrick, A.; Rao, G.; Mehedint, D.; George, S.; Attwood, K.; Kauffman, E.; Narashima, D.; Khushalani, N. I.; Pili, R.; Schwaab, T. High-Dose Interleukin-2 Therapy for Metastatic Renal Cell Carcinoma: A Contemporary Experience. *Urology* **2014,** *83* (5), 1129–1134; (b) Weinreich, D. M.; Rosenberg, S. A. Response Rates of Patients With Metastatic Melanoma to High-Dose Intravenous Interleukin-2 After Prior Exposure to Alpha-Interferon or Low-Dose Interleukin-2. *J. Immunother.* **2002,** *25* (2), 185–187.
157. Muhitch, J. B.; Schwaab, T. High-Dose IL-2 for Metastatic Renal Cell Carcinoma: Can the First Antitumor Immunotherapy Be Reinvented? *Immunotherapy* **2014,** *6* (9), 955–958.
158. (a) Kochenderfer, J. N.; Dudley, M. E.; Kassim, S. H.; Somerville, R. P.; Carpenter, R. O.; Stetler-Stevenson, M.; Yang, J. C.; Phan, G. Q.; Hughes, M. S.; Sherry, R. M.; Raffeld, M.; Feldman, S.; Lu, L.; Li, Y. F.; Ngo, L. T.; Goy, A.; Feldman, T.; Spaner, D. E.; Wang, M. L.; Chen, C. C.; Kranick, S. M.; Nath, A.; Nathan, D. A.; Morton, K. E.; Toomey, M. A.; Rosenberg, S. A. Chemotherapy-Refractory Diffuse Large B-Cell Lymphoma and Indolent B-Cell Malignancies Can Be Effectively Treated With Autologous T Cells Expressing an Anti-CD19 Chimeric Antigen Receptor. *J. Clin. Oncol.* **2015,** *33* (6), 540–549; (b) Pinz, K.; Liu, H.; Golightly, M.; Jares, A.; Lan, F.; Zieve, G. W.; Hagag, N.; Schuster, M.; Firor, A. E.; Jiang, X.; Ma, Y. Preclinical Targeting of Human T Cell Malignancies Using CD4-Specific Chimeric Antigen Receptor (CAR)-Engineered T Cells. *Leukemia* **2016,** *30* (3), 701–707.
159. Sangiolo, D. Redirected T Cells in Cancer Therapy. *Expert Opin. Biol. Ther.* **2015,** *15,* 1667–1670.
160. Ray, D.; Cuneo, K. C.; Rehemtulla, A.; Lawrence, T. S.; Nyati, M. K. Inducing Oncoprotein Degradation to Improve Targeted Cancer Therapy. *Neoplasia* **2015,** *17* (9), 697–703.
161. (a) Koga, F.; Kihara, K.; Neckers, L. Inhibition of Cancer Invasion and Metastasis by Targeting the Molecular Chaperone Heat-Shock Protein 90. *Anticancer Res.* **2009,** *29* (3), 797–807; (b) Koga, F.; Xu, W.; Karpova, T. S.; McNally, J. G.; Baron, R.; Neckers, L. Hsp90 Inhibition Transiently Activates Src Kinase and Promotes Src-Dependent Akt and Erk Activation. *Proc. Natl. Acad. Sci. U. S. A.* **2006,** *103* (30), 11318–11322.
162. Broemer, M.; Krappmann, D.; Scheidereit, C. Requirement of Hsp90 Activity for I[Kappa]B Kinase (IKK) Biosynthesis and for Constitutive and Inducible IKK and NF-[Kappa]B Activation. *Oncogene* **2004,** *23* (31), 5378–5386.
163. Shimamura, T.; Perera, S. A.; Foley, K. P.; Sang, J.; Rodig, S. J.; Inoue, T.; Chen, L.; Li, D.; Carretero, J.; Li, Y.-C.; Sinha, P.; Carey, C. D.; Borgman, C. L.; Jimenez, J.-P.; Meyerson, M.; Ying, W.; Barsoum, J.; Wong, K.-K.; Shapiro, G. I. Ganetespib (STA-9090), a Nongeldanamycin HSP90 Inhibitor, Has Potent Antitumor Activity in in vitro and in vivo Models of Non-Small Cell Lung Cancer. *Clin. Cancer Res.* **2012,** *18* (18), 4973–4985.
164. Workman, P.; Burrows, F.; Neckers, L.; Rosen, N. Drugging the Cancer Chaperone HSP90: Combinatorial Therapeutic Exploitation of Oncogene Addiction and Tumor Stress. *Ann. N. Y. Acad. Sci.* **2007,** *1113,* 202–216.
165. Pick, E.; Kluger, Y.; Giltnane, J. M.; Moeder, C.; Camp, R. L.; Rimm, D. L.; Kluger, H. M. High HSP90 Expression Is Associated With Decreased Survival in Breast Cancer. *Cancer Res.* **2007,** *67* (7), 2932–2937.
166. (a) Jhaveri, K.; Modi, S. Ganetespib: Research and Clinical Development. *Onco Targets Ther.* **2015,** *8,* 1849–1858; (b) Tatokoro, M.; Koga, F.; Yoshida, S.; Kihara, K. Heat Shock Protein 90 Targeting Therapy: State of the Art and Future Perspective. *EXCLI J.* **2015,** *14,* 48–58.
167. (a) Dou, Q. P.; Zonder, J. A. Overview of Proteasome Inhibitor-Based Anti-cancer Therapies: Perspective on Bortezomib and Second Generation Proteasome Inhibitors versus Future Generation Inhibitors of Ubiquitin-Proteasome System. *Curr. Cancer Drug Targets* **2014,** *14* (6), 517–536; (b) Potts, B. C.; Albitar, M. X.; Anderson, K. C.; Baritaki, S.; Berkers, C.; Bonavida, B.; Chandra, J.; Chauhan, D.; Cusack, J. C.; Fenical, W.; Ghobrial, I. M.; Groll, M.; Jensen, P. R.; Lam, K. S.; Lloyd, G. K.; McBride, W.; McConkey, D. J.; Miller, C. P.; Neuteboom, S. T. C.; Oki, Y.; Ovaa, H.; Pajonk, F.; Richardson, P. G.; Roccaro, A. M.; Sloss, C. M.; Spear, M. A.; Valashi, E.; Younes, A.; Palladino, M. A. Marizomib, a Proteasome Inhibitor for All Seasons: Preclinical Profile and a Framework for Clinical Trials. *Curr. Cancer Drug Targets* **2011,** *11* (3), 254–284; (c) Frankland-Searby, S.; Bhaumik, S. R. The 26S Proteasome Complex: An Attractive Target for Cancer Therapy. *Biochim. Biophys. Acta* **2012,** *1825* (1), 64–76.
168. Lub, S.; Maes, K.; Menu, E.; Bruyne, E.; Vanderkerken, K.; Valckenborgh, E. V. Novel Strategies to Target the Ubiquitin Proteasome System in Multiple Myeloma. *Oncotarget* **2016,** *7* (6), 6521–6537.
169. Kumar, S. K.; LaPlant, B.; Roy, V.; Reeder, C. B.; Lacy, M. Q.; Gertz, M. A.; Laumann, K.; Thompson, M. A.; Witzig, T. E.; Buadi, F. K.; Rivera, C. E.; Mikhael, J. R.; Bergsagel, P. L.; Kapoor, P.; Hwa, L.; Fonseca, R.; Stewart, A. K.; Chanan-Khan, A.; Rajkumar, S. V.; Dispenzieri, A. Phase 2 Trial of Ixazomib in Patients With Relapsed Multiple Myeloma Not Refractory to Bortezomib. *Blood Cancer J.* **2015,** *5* (8), e338.
170. Dimopoulos, M. A.; Sonneveld, P.; Siegel, D.; Palumbo, A.; San-Miguel, J. Carfilzomib and Pomalidomide in Patients With Relapsed and/or Refractory Multiple Myeloma With Baseline Risk Factors. *Ann. Oncol.* **2015,** *26* (11), 2247–2256.
171. (a) Bill, K. L.; Garnett, J.; Meaux, I.; Ma, X. Y.; Bolshakov, S.; Creighton, C. J.; Barriere, C.; Dubusche, L.; Lazar, A.; Prudner, B. C.; Casadei, L.; Braggio, D. A.; Lopez, G.; Zewdu, A.; Bid, H. K.; Lev, D.; Pollock, R. E. SAR405838: A Novel and Potent Inhibitor of the MDM2:p53 Axis for the Treatment of Dedifferentiated Liposarcoma. *Clin. Cancer Res.* **2015,** *22,* 1150–1160; (b) Zauli, G.; Celeghini, C.; Melloni, E.; Voltan, R.; Ongari, M.; Tiribelli, M.; di Iasio, M. G.; Lanza, F.; Secchiero, P. The Sorafenib Plus Nutlin-3 Combination Promotes Synergistic Cytotoxicity in Acute Myeloid Leukemic Cells Irrespectively of FLT3 and p53 Status. *Haematologica* **2012,** *97* (11), 1722–1730; (c) Biswas, S.; Killick, E.; Jochemsen, A. G.; Lunec, J. The Clinical Development of p53-Reactivating Drugs in Sarcomas—Charting Future Therapeutic Approaches and Understanding the Clinical Molecular Toxicology of Nutlins. *Expert Opin. Investig. Drugs* **2014,** *23* (5), 629–645.
172. Dawson, M. A.; Kouzarides, T. Cancer Epigenetics: From Mechanism to Therapy. *Cell* **2012,** *150* (1), 12–27.
173. (a) Okosun, J.; Bödör, C.; Wang, J.; Araf, S.; Yang, C.-Y.; Pan, C.; Boller, S.; Cittaro, D.; Bozek, M.; Iqbal, S.; Matthews, J.; Wrench, D.; Marzec, J.; Tawana, K.; Popov, N.; O'Riain, C.; O'Shea, D.; Carlotti, E.; Davies, A.; Lawrie, C. H.; Matolcsy, A.; Calaminici, M.; Norton, A.; Byers, R. J.; Mein, C.; Stupka, E.; Lister, T. A.; Lenz, G.; Montoto, S.; Gribben, J. G.; Fan, Y.; Grosschedl, R.; Chelala, C.; Fitzgibbon, J. Integrated Genomic Analysis Identifies Recurrent Mutations and Evolution Patterns Driving the Initiation and Progression of Follicular Lymphoma. *Nat. Genet.* **2014,** *46* (2), 176–181; (b) Van der Meulen, J.; Sanghvi, V.; Mavrakis, K.; Durinck, K.; Fang, F.; Matthijssens, F.; Rondou, P.; Rosen, M.; Pieters, T.; Vandenberghe, P.; Delabesse, E.; Lammens, T.; De Moerloose, B.; Menten, B.; Van Roy, N.; Verhasselt, B.; Poppe, B.; Benoit, Y.; Taghon, T.; Melnick, A. M.; Speleman, F.; Wendel, H.-G.; Van Vlierberghe, P. The H3K27me3 Demethylase UTX is a Gender-Specific Tumor Suppressor in T-Cell Acute Lymphoblastic Leukemia. *Blood* **2015,** *125* (1), 13–21.
174. Baylin, S. B. The Cancer Epigenome: Its Origins, Contributions to Tumorigenesis, and Translational Implications. *Proc. Am. Thorac. Soc.* **2012,** *9* (2), 64–65.
175. Esteller, M. Epigenetic Gene Silencing in Cancer: The DNA Hypermethylome. *Hum. Mol. Genet.* **2007,** *16* (R1), R50–R59.
176. Hamm, C. A.; Costa, F. F. Epigenomes as Therapeutic Targets. *Pharmacol. Ther.* **2015,** *151,* 72–86.
177. Ma, M. K.-W.; Heath, C.; Hair, A.; West, A. G. Histone Crosstalk Directed by H2B Ubiquitination Is Required for Chromatin Boundary Integrity. *PLoS Genet.* **2011,** *7* (7), e1002175.
178. Fraga, M. F.; Ballestar, E.; Villar-Garea, A.; Boix-Chornet, M.; Espada, J.; Schotta, G.; Bonaldi, T.; Haydon, C.; Ropero, S.; Petrie, K.; Iyer, N. G.; Perez-Rosado, A.; Calvo, E.; Lopez, J. A.; Cano, A.; Calasanz, M. J.; Colomer, D.; Piris, M. A.; Ahn, N.; Imhof, A.; Caldas, C.; Jenuwein, T.; Esteller, M. Loss of Acetylation at Lys16 and Trimethylation at Lys20 of Histone H4 is a Common Hallmark of Human Cancer. *Nat. Genet.* **2005,** *37* (4), 391–400.
179. Federico, M.; Bagella, L. Histone Deacetylase Inhibitors in the Treatment of Hematological Malignancies and Solid Tumors. *J. Biomed. Biotechnol.* **2011,** *2011,* 475641.
180. Filippakopoulos, P.; Knapp, S. Targeting Bromodomains: Epigenetic Readers of Lysine Acetylation. *Nat. Rev. Drug Discov.* **2014,** *13* (5), 337–356.
181. Wang, C.-Y.; Filippakopoulos, P. Beating the Odds: BETs in Disease. *Trends Biochem. Sci.* **2015,** *40* (8), 468–479.

182. Bolden, J. E.; Tasdemir, N.; Dow, L. E.; van Es, J. H.; Wilkinson, J. E.; Zhao, Z.; Clevers, H.; Lowe, S. W. Inducible in vivo Silencing of Brd4 Identifies Potential Toxicities of Sustained BET Protein Inhibition. *Cell Rep.* **2014,** *8* (6), 1919–1929.
183. (a) Ferguson, L. R.; Chen, H.; Collins, A. R.; Connell, M.; Damia, G.; Dasgupta, S.; Malhotra, M.; Meeker, A. K.; Amedei, A.; Amin, A.; Ashraf, S. S.; Aquilano, K.; Azmi, A. S.; Bhakta, D.; Bilsland, A.; Boosani, C. S.; Chen, S.; Ciriolo, M. R.; Fujii, H.; Guha, G.; Halicka, D.; Helferich, W. G.; Keith, W. N.; Mohammed, S. I.; Niccolai, E.; Yang, X.; Honoki, K.; Parslow, V. R.; Prakash, S.; Rezazadeh, S.; Shackelford, R. E.; Sidransky, D.; Tran, P. T.; Yang, E. S.; Maxwell, C. A. Genomic Instability in Human Cancer: Molecular Insights and Opportunities for Therapeutic Attack and Prevention Through Diet and Nutrition. *Semin. Cancer Biol.* **2015,** *35* (Suppl), S5–S24; (b) Harley, C. B.; Futcher, A. B.; Greider, C. W. Telomeres Shorten During Ageing of Human Fibroblasts. *Nature* **1990,** *345* (6274), 458–460.
184. Bodnar, A. G.; Ouellette, M.; Frolkis, M.; Holt, S. E.; Chiu, C. P.; Morin, G. B.; Harley, C. B.; Shay, J. W.; Lichtsteiner, S.; Wright, W. E. Extension of Life-Span by Introduction of Telomerase Into Normal Human Cells. *Science* **1998,** *279* (5349), 349–352.
185. Gavory, G.; Farrow, M.; Balasubramanian, S. Minimum Length Requirement of the Alignment Domain of Human Telomerase RNA to Sustain Catalytic Activity In Vitro. *Nucleic Acids Res.* **2002,** *30* (20), 4470–4480.
186. (a) Morin, G. B. The Human Telomere Terminal Transferase Enzyme Is a Ribonucleoprotein That Synthesizes TTAGGG Repeats. *Cell* **1989,** *59* (3), 521–529; (b) Artandi, S. E.; DePinho, R. A. Telomeres and Telomerase in Cancer. *Carcinogenesis* **2010,** *31* (1), 9–18.
187. Henson, J. D.; Neumann, A. A.; Yeager, T. R.; Reddel, R. R. Alternative Lengthening of Telomeres in Mammalian Cells. *Oncogene* **2002,** *21* (4), 598–610.
188. Takakura, M.; Kyo, S.; Kanaya, T.; Hirano, H.; Takeda, J.; Yutsudo, M.; Inoue, M. Cloning of Human Telomerase Catalytic Subunit (hTERT) Gene Promoter and Identification of Proximal Core Promoter Sequences Essential for Transcriptional Activation in Immortalized and Cancer Cells. *Cancer Res.* **1999,** *59* (3), 551–557.
189. Vicente-Dueñas, C.; Barajas-Diego, M.; Romero-Camarero, I.; Gonzalez-Herrero, I.; Flores, T.; Sanchez-Garcia, I. Essential Role for Telomerase in Chronic Myeloid Leukemia Induced by BCR-ABL in Mice. *Oncotarget* **2012,** *3* (3), 261–266.
190. Günes, C.; Rudolph, K. L. The Role of Telomeres in Stem Cells and Cancer. *Cell* **2013,** *152* (3), 390–393.
191. Wu, X.-Q.; Huang, C.; He, X.; Tian, Y.-Y.; Zhou, D.-X.; He, Y.; Liu, X.-H.; Li, J. Feedback Regulation of Telomerase Reverse Transcriptase: New Insight Into the Evolving Field of Telomerase in Cancer. *Cell. Signal.* **2013,** *25* (12), 2462–2468.
192. Ruden, M.; Puri, N. Novel Anticancer Therapeutics Targeting Telomerase. *Cancer Treat. Rev.* **2013,** *39* (5), 444–456.
193. O'Connor, M. J. Targeting the DNA Damage Response in Cancer. *Mol. Cell* **2015,** *60* (4), 547–560.
194. Ashworth, A. A Synthetic Lethal Therapeutic Approach: Poly(ADP) Ribose Polymerase Inhibitors for the Treatment of Cancers Deficient in DNA Double-Strand Break Repair. *J. Clin. Oncol.* **2008,** *26* (22), 3785–3790.
195. (a) Murai, J.; Huang, S. Y.; Das, B. B.; Renaud, A.; Zhang, Y.; Doroshow, J. H.; Ji, J.; Takeda, S.; Pommier, Y. Trapping of PARP1 and PARP2 by Clinical PARP Inhibitors. *Cancer Res.* **2012,** *72* (21), 5588–5599; (b) Ricks, T. K.; Chiu, H.-J.; Ison, G.; Kim, G.; McKee, A. E.; Kluetz, P.; Pazdur, R. Successes and Challenges of PARP Inhibitors in Cancer Therapy. *Front. Oncol.* **2015,** *5,* 222.
196. (a) Patel, A. G.; Sarkaria, J. N.; Kaufmann, S. H. Nonhomologous End Joining Drives Poly(ADP-Ribose) Polymerase (PARP) Inhibitor Lethality in Homologous Recombination-Deficient Cells. *Proc. Natl. Acad. Sci.* **2011,** *108* (8), 3406–3411; (b) Farmer, H.; McCabe, N.; Lord, C. J.; Tutt, A. N.; Johnson, D. A.; Richardson, T. B.; Santarosa, M.; Dillon, K. J.; Hickson, I.; Knights, C.; Martin, N. M.; Jackson, S. P.; Smith, G. C.; Ashworth, A. Targeting the DNA Repair Defect in BRCA Mutant Cells As a Therapeutic Strategy. *Nature* **2005,** *434* (7035), 917–921.
197. Kaufman, B.; Shapira-Frommer, R.; Schmutzler, R. K.; Audeh, M. W.; Friedlander, M.; Balmaña, J.; Mitchell, G.; Fried, G.; Stemmer, S. M.; Hubert, A.; Rosengarten, O.; Steiner, M.; Loman, N.; Bowen, K.; Fielding, A.; Domchek, S. M. Olaparib Monotherapy in Patients With Advanced Cancer and a Germline BRCA1/2 Mutation. *J. Clin. Oncol.* **2015,** *33* (3), 244–250.
198. (a) Jayson, G. C.; Kerbel, R.; Ellis, L. M.; Harris, A. L. Antiangiogenic Therapy in Oncology: Current Status and Future Directions. *Lancet* **2016,** *15,* S0140–S6736; (b) Butler, J. M.; Kobayashi, H.; Rafii, S. Instructive Role of the Vascular Niche in Promoting Tumour Growth and Tissue Repair by Angiocrine Factors. *Nat. Rev. Cancer* **2010,** *10* (2), 138–146.
199. Arjaans, M.; Schröder, C. P.; Oosting, S. F.; Dafni, U.; Kleibeuker, J. E.; de Vries, E. G. E. VEGF Pathway Targeting Agents, Vessel Normalization and Tumor Drug Uptake: From Bench to Bedside. *Oncotarget* **2016**.
200. (a) Mazure, N. M.; Chen, E. Y.; Yeh, P.; Laderoute, K. R.; Giaccia, A. J. Oncogenic Transformation and Hypoxia Synergistically Act to Modulate Vascular Endothelial Growth Factor Expression. *Cancer Res.* **1996,** *56* (15), 3436–3440; (b) Wiesener, M. S.; Münchenhagen, P. M.; Berger, I.; Morgan, N. V.; Roigas, J.; Schwiertz, A.; Jürgensen, J. S.; Gruber, G.; Maxwell, P. H.; Löning, S. A.; Frei, U.; Maher, E. R.; Gröne, H.-J.; Eckardt, K.-U. Constitutive Activation of Hypoxia-inducible Genes Related to Overexpression of Hypoxia-inducible Factor-1α in Clear Cell Renal Carcinomas. *Cancer Res.* **2001,** *61* (13), 5215–5222.
201. Pezzella, F.; Di Bacco, A.; Andreola, S.; Nicholson, A. G.; Pastorino, U.; Harris, A. L. Angiogenesis in Primary Lung Cancer and Lung Secondaries. *Eur. J. Cancer* **1996,** *32A* (14), 2494–2500.
202. (a) Jain, R. K. Normalizing Tumor Microenvironment to Treat Cancer: Bench to Bedside to Biomarkers. *J. Clin. Oncol.* **2013,** *31* (17), 2205–2218; (b) Goel, S.; Wong, A. H.-K.; Jain, R. K. Vascular Normalization as a Therapeutic Strategy for Malignant and Nonmalignant Disease. *Cold Spring Harb. Perspect. Med.* **2012,** *2* (3), a006486.
203. (a) Huang, Y.; Goel, S.; Duda, D. G.; Fukumura, D.; Jain, R. K. Vascular Normalization As an Emerging Strategy to Enhance Cancer Immunotherapy. *Cancer Res.* **2013,** *73* (10), 2943–2948; (b) Zhou, Q.; Guo, P.; Gallo, J. M. Impact of Angiogenesis Inhibition by Sunitinib on Tumor Distribution of Temozolomide. *Clin. Cancer Res.* **2008,** *14* (5), 1540–1549.
204. Rapisarda, A.; Hollingshead, M.; Uranchimeg, B.; Bonomi, C. A.; Borgel, S. D.; Carter, J. P.; Gehrs, B.; Raffeld, M.; Kinders, R. J.; Parchment, R.; Anver, M. R.; Shoemaker, R. H.; Melillo, G. Increased Antitumor Activity of Bevacizumab in Combination With Hypoxia Inducible Factor-1 Inhibition. *Mol. Cancer Ther.* **2009,** *8* (7), 1867–1877.
205. (a) Eroglu, Z.; Stein, C. A.; Pal, S. K. Targeting Angiopoietin-2 Signaling in Cancer Therapy. *Expert Opin. Investig. Drugs* **2013,** *22* (7), 813–825; (b) Sfiligoi, C.; de Luca, A.; Cascone, I.; Sorbello, V.; Fuso, L.; Ponzone, R.; Biglia, N.; Audero, E.; Arisio, R.; Bussolino, F.; Sismondi, P.; De Bortoli, M. Angiopoietin-2 Expression in Breast Cancer Correlates With Lymph Node Invasion and Short Survival. *Int. J. Cancer* **2003,** *103* (4), 466–474.
206. (a) Gadducci, A.; Lanfredini, N.; Sergiampietri, C. Antiangiogenic Agents in Gynecological Cancer: State of Art and Perspectives of Clinical Research. *Critical Rev. Oncol. Hematol.* **2015,** *96* (1), 113–128; (b) Atkins, M. B.; Gravis, G.; Drosik, K.; Demkow, T.; Tomczak, P.; Wong, S. S.; Michaelson, M. D.; Choueiri, T. K.; Wu, B.; Navale, L.; Warner, D.; Ravaud, A. Trebananib (AMG 386) in Combination With Sunitinib in Patients With Metastatic Renal Cell Cancer: An Open-Label, Multicenter, Phase II Study. *J. Clin. Oncol.* **2015,** *33* (30), 3431–3438.
207. Biomarkers Definitions Working Group. Biomarkers and Surrogate Endpoints: Preferred Definitions and Conceptual Framework. *Clin. Pharmacol. Ther.* **2001,** *69* (3), 89–95.
208. Slamon, D. J.; Clark, G. M.; Wong, S. G.; Levin, W. J.; Ullrich, A.; McGuire, W. L. Human Breast Cancer: Correlation of Relapse and Survival With Amplification of the HER-2/neu Oncogene. *Science* **1987,** *235* (4785), 177–182.
209. Druker, B. J.; Talpaz, M.; Resta, D. J.; Peng, B.; Buchdunger, E.; Ford, J. M.; Lydon, N. B.; Kantarjian, H.; Capdeville, R.; Ohno-Jones, S.; Sawyers, C. L. Efficacy and Safety of a Specific Inhibitor of the BCR-ABL Tyrosine Kinase in Chronic Myeloid Leukemia. *N. Engl. J. Med.* **2001,** *344* (14), 1031–1037.
210. Arteaga, C. L. ErbB-Targeted Therapeutic Approaches in Human Cancer. *Exp. Cell Res.* **2003,** *284* (1), 122–130.
211. Lynch, T. J.; Bell, D. W.; Sordella, R.; Gurubhagavatula, S.; Okimoto, R. A.; Brannigan, B. W.; Harris, P. L.; Haserlat, S. M.; Supko, J. G.; Haluska, F. G.; Louis, D. N.; Christiani, D. C.; Settleman, J.; Haber, D. A. Activating Mutations in the Epidermal Growth Factor Receptor Underlying Responsiveness of Non-Small-Cell Lung Cancer to Gefitinib. *N. Engl. J. Med.* **2004,** *350* (21), 2129–2139.

212. (a) Paez, J. G.; Janne, P. A.; Lee, J. C.; Tracy, S.; Greulich, H.; Gabriel, S.; Herman, P.; Kaye, F. J.; Lindeman, N.; Boggon, T. J.; Naoki, K.; Sasaki, H.; Fujii, Y.; Eck, M. J.; Sellers, W. R.; Johnson, B. E.; Meyerson, M. EGFR Mutations in Lung Cancer: Correlation With Clinical Response to Gefitinib Therapy. *Science* **2004,** *304* (5676), 1497–1500; (b) Pao, W.; Miller, V.; Zakowski, M.; Doherty, J.; Politi, K.; Sarkaria, I.; Singh, B.; Heelan, R.; Rusch, V.; Fulton, L.; Mardis, E.; Kupfer, D.; Wilson, R.; Kris, M.; Varmus, H. EGF Receptor Gene Mutations Are Common in Lung Cancers From "Never Smokers" and Are Associated With Sensitivity of Tumors to Gefitinib and Erlotinib. *Proc. Natl. Acad. Sci. U. S. A.* **2004,** *101* (36), 13306–13311.
213. Peyssonnaux, C.; Eychene, A. The Raf/MEK/ERK Pathway: New Concepts of Activation. *Biol Cell.* **2001,** *93* (1–2), 53–62.
214. Davies, H.; Bignell, G. R.; Cox, C.; Stephens, P.; Edkins, S.; Clegg, S.; Teague, J.; Woffendin, H.; Garnett, M. J.; Bottomley, W.; Davis, N.; Dicks, E.; Ewing, R.; Floyd, Y.; Gray, K.; Hall, S.; Hawes, R.; Hughes, J.; Kosmidou, V.; Menzies, A.; Mould, C.; Parker, A.; Stevens, C.; Watt, S.; Hooper, S.; Wilson, R.; Jayatilake, H.; Gusterson, B. A.; Cooper, C.; Shipley, J.; Hargrave, D.; Pritchard-Jones, K.; Maitland, N.; Chenevix-Trench, G.; Riggins, G. J.; Bigner, D. D.; Palmieri, G.; Cossu, A.; Flanagan, A.; Nicholson, A.; Ho, J. W.; Leung, S. Y.; Yuen, S. T.; Weber, B. L.; Seigler, H. F.; Darrow, T. L.; Paterson, H.; Marais, R.; Marshall, C. J.; Wooster, R.; Stratton, M. R.; Futreal, P. A. Mutations of the BRAF Gene in Human Cancer. *Nature* **2002,** *417* (6892), 949–954.
215. Bollag, G.; Tsai, J.; Zhang, J.; Zhang, C.; Ibrahim, P.; Nolop, K.; Hirth, P. Vemurafenib: The First Drug Approved for BRAF-Mutant Cancer. *Nat. Rev. Drug Discov.* **2012,** *11* (11), 873–886.
216. Flaherty, K. T.; Puzanov, I.; Kim, K. B.; Ribas, A.; McArthur, G. A.; Sosman, J. A.; O'Dwyer, P. J.; Lee, R. J.; Grippo, J. F.; Nolop, K.; Chapman, P. B. Inhibition of Mutated, Activated BRAF in Metastatic Melanoma. *N. Engl. J. Med.* **2010,** *363* (9), 809–819.
217. Yan, L.; Rosen, N.; Arteaga, C. Targeted Cancer Therapies. *Chin. J. Cancer* **2011,** *30* (1), 1–4.
218. Hay, M.; Thomas, D. W.; Craighead, J. L.; Economides, C.; Rosenthal, J. Clinical Development Success Rates for Investigational Drugs. *Nat. Biotechnol.* **2014,** *32* (1), 40–51.
219. Strimbu, K.; Tavel, J. A. What are Biomarkers? *Curr. Opin. HIV AIDS* **2010,** *5* (6), 463–466.
220. de Gramont, A.; Watson, S.; Ellis, L. M.; Rodon, J.; Tabernero, J.; de Gramont, A.; Hamilton, S. R. Pragmatic Issues in Biomarker Evaluation for Targeted Therapies in Cancer. *Nat. Rev. Clin. Oncol.* **2015,** *12* (4), 197–212.
221. Asadullah, K.; Busch, A.; Gottwald, M.; Reinke, P.; Landeck, L. Industry-Academia Collaborations for Biomarkers. *Nat. Rev. Drug Discov.* **2015,** *14* (12), 805–806.
222. Jamal-Hanjani, M.; Quezada, S. A.; Larkin, J.; Swanton, C. Translational Implications of Tumor Heterogeneity. *Clin. Cancer Res.* **2015,** *21* (6), 1258–1266.
223. Navin, N. E. Delineating Cancer Evolution With Single-Cell Sequencing. *Sci. Transl. Med.* **2015,** *7* (296), 296fs29.
224. (a) Gerlinger, M.; Rowan, A. J.; Horswell, S.; Larkin, J.; Endesfelder, D.; Gronroos, E.; Martinez, P.; Matthews, N.; Stewart, A.; Tarpey, P.; Varela, I.; Phillimore, B.; Begum, S.; McDonald, N. Q.; Butler, A.; Jones, D.; Raine, K.; Latimer, C.; Santos, C. R.; Nohadani, M.; Eklund, A. C.; Spencer-Dene, B.; Clark, G.; Pickering, L.; Stamp, G.; Gore, M.; Szallasi, Z.; Downward, J.; Futreal, P. A.; Swanton, C. Intratumor Heterogeneity and Branched Evolution Revealed by Multiregion Sequencing. *N. Engl. J. Med.* **2012,** *366* (10), 883–892; (b) Vignot, S.; Frampton, G. M.; Soria, J. C.; Yelensky, R.; Commo, F.; Brambilla, C.; Palmer, G.; Moro-Sibilot, D.; Ross, J. S.; Cronin, M. T.; Andre, F.; Stephens, P. J.; Lazar, V.; Miller, V. A.; Brambilla, E. Next-Generation Sequencing Reveals High Concordance of Recurrent Somatic Alterations Between Primary Tumor and Metastases From Patients With Non-Small-Cell Lung Cancer. *J. Clin. Oncol.* **2013,** *31* (17), 2167–2172.
225. (a) Nik-Zainal, S.; Van Loo, P.; Wedge, D. C.; Alexandrov, L. B.; Greenman, C. D.; Lau, K. W.; Raine, K.; Jones, D.; Marshall, J.; Ramakrishna, M.; Shlien, A.; Cooke, S. L.; Hinton, J.; Menzies, A.; Stebbings, L. A.; Leroy, C.; Jia, M.; Rance, R.; Mudie, L. J.; Gamble, S. J.; Stephens, P. J.; McLaren, S.; Tarpey, P. S.; Papaemmanuil, E.; Davies, H. R.; Varela, I.; McBride, D. J.; Bignell, G. R.; Leung, K.; Butler, A. P.; Teague, J. W.; Martin, S.; Jonsson, G.; Mariani, O.; Boyault, S.; Miron, P.; Fatima, A.; Langerod, A.; Aparicio, S. A.; Tutt, A.; Sieuwerts, A. M.; Borg, A.; Thomas, G.; Salomon, A. V.; Richardson, A. L.; Borresen-Dale, A. L.; Futreal, P. A.; Stratton, M. R.; Campbell, P. J.; Breast Cancer Working Group of the International Cancer Genome Consortium. The Life History of 21 Breast Cancers. *Cell* **2012,** *149* (5), 994–1007; (b) Walter, M. J.; Shen, D.; Ding, L.; Shao, J.; Koboldt, D. C.; Chen, K.; Larson, D. E.; McLellan, M. D.; Dooling, D.; Abbott, R.; Fulton, R.; Magrini, V.; Schmidt, H.; Kalicki-Veizer, J.; O'Laughlin, M.; Fan, X.; Grillot, M.; Witowski, S.; Heath, S.; Frater, J. L.; Eades, W.; Tomasson, M.; Westervelt, P.; DiPersio, J. F.; Link, D. C.; Mardis, E. R.; Ley, T. J.; Wilson, R. K.; Graubert, T. A. Clonal Architecture of Secondary Acute Myeloid Leukemia. *N. Engl. J. Med.* **2012,** *366* (12), 1090–1098; (c) Campbell, P. J.; Yachida, S.; Mudie, L. J.; Stephens, P. J.; Pleasance, E. D.; Stebbings, L. A.; Morsberger, L. A.; Latimer, C.; McLaren, S.; Lin, M. L.; McBride, D. J.; Varela, I.; Nik-Zainal, S. A.; Leroy, C.; Jia, M.; Menzies, A.; Butler, A. P.; Teague, J. W.; Griffin, C. A.; Burton, J.; Swerdlow, H.; Quail, M. A.; Stratton, M. R.; Iacobuzio-Donahue, C.; Futreal, P. A. The Patterns and Dynamics of Genomic Instability in Metastatic Pancreatic Cancer. *Nature* **2010,** *467* (7319), 1109–1113; (d) Cooper, C. S.; Eeles, R.; Wedge, D. C.; Van Loo, P.; Gundem, G.; Alexandrov, L. B.; Kremeyer, B.; Butler, A.; Lynch, A. G.; Camacho, N.; Massie, C. E.; Kay, J.; Luxton, H. J.; Edwards, S.; Kote-Jarai, Z.; Dennis, N.; Merson, S.; Leongamornlert, D.; Zamora, J.; Corbishley, C.; Thomas, S.; Nik-Zainal, S.; Ramakrishna, M.; O'Meara, S.; Matthews, L.; Clark, J.; Hurst, R.; Mithen, R.; Bristow, R. G.; Boutros, P. C.; Fraser, M.; Cooke, S.; Raine, K.; Jones, D.; Menzies, A.; Stebbings, L.; Hinton, J.; Teague, J.; McLaren, S.; Mudie, L.; Hardy, C.; Anderson, E.; Joseph, O.; Goody, V.; Robinson, B.; Maddison, M.; Gamble, S.; Greenman, C.; Berney, D.; Hazell, S.; Livni, N.; Group, I. P.; Fisher, C.; Ogden, C.; Kumar, P.; Thompson, A.; Woodhouse, C.; Nicol, D.; Mayer, E.; Dudderidge, T.; Shah, N. C.; Gnanapragasam, V.; Voet, T.; Campbell, P.; Futreal, A.; Easton, D.; Warren, A. Y.; Foster, C. S.; Stratton, M. R.; Whitaker, H. C.; McDermott, U.; Brewer, D. S.; Neal, D. E. Analysis of the Genetic Phylogeny of Multifocal Prostate Cancer Identifies Multiple Independent Clonal Expansions in Neoplastic and Morphologically Normal Prostate Tissue. *Nat. Genet.* **2015,** *47* (4), 367–372.
226. Jamal-Hanjani, M.; Hackshaw, A.; Ngai, Y.; Shaw, J.; Dive, C.; Quezada, S.; Middleton, G.; de Bruin, E.; Le Quesne, J.; Shafi, S.; Falzon, M.; Horswell, S.; Blackhall, F.; Khan, I.; Janes, S.; Nicolson, M.; Lawrence, D.; Forster, M.; Fennell, D.; Lee, S. M.; Lester, J.; Kerr, K.; Muller, S.; Iles, N.; Smith, S.; Murugaesu, N.; Mitter, R.; Salm, M.; Stuart, A.; Matthews, N.; Adams, H.; Ahmad, T.; Attanoos, R.; Bennett, J.; Birkbak, N. J.; Booton, R.; Brady, G.; Buchan, K.; Capitano, A.; Chetty, M.; Cobbold, M.; Crosbie, P.; Davies, H.; Denison, A.; Djearman, M.; Goldman, J.; Haswell, T.; Joseph, L.; Kornaszewska, M.; Krebs, M.; Langman, G.; MacKenzie, M.; Millar, J.; Morgan, B.; Naidu, B.; Nonaka, D.; Peggs, K.; Pritchard, C.; Remmen, H.; Rowan, A.; Shah, R.; Smith, E.; Summers, Y.; Taylor, M.; Veeriah, S.; Waller, D.; Wilcox, B.; Wilcox, M.; Woolhouse, I.; McGranahan, N.; Swanton, C. Tracking Genomic Cancer Evolution for Precision Medicine: The Lung TRACERx Study. *PLoS Biol.* **2014,** *12* (7), e1001906.
227. Ramos, P.; Bentires-Alj, M. Mechanism-Based Cancer Therapy: Resistance to Therapy, Therapy for Resistance. *Oncogene* **2015,** *34* (28), 3617–3626.
228. Colak, S.; Medema, J. P. Cancer Stem Cells—Important Players in Tumor Therapy Resistance. *FEBS J.* **2014,** *281* (21), 4779–4791.
229. Chen, K.; Huang, Y. H.; Chen, J. L. Understanding and Targeting Cancer Stem Cells: Therapeutic Implications and Challenges. *Acta Pharmacol. Sin.* **2013,** *34* (6), 732–740.
230. (a) Cheng, J.-X.; Liu, B.-L.; Zhang, X. How Powerful Is CD133 As a Cancer Stem Cell Marker in Brain Tumors? *Cancer Treat. Rev.* **2009,** *35* (5), 403–408; (b) Kim, S. S.; Pirollo, K. F.; Chang, E. H. Isolation and Culturing of Glioma Cancer Stem Cells. *Curr. Protoc. Cell Biol.* **2015,** *67,* 23.10.1-10.
231. (a) Konopleva, M.; Zhao, S.; Hu, W.; Jiang, S.; Snell, V.; Weidner, D.; Jackson, C. E.; Zhang, X.; Champlin, R.; Estey, E.; Reed, J. C.; Andreeff, M. The Anti-Apoptotic Genes Bcl-X(L) and Bcl-2 Are Over-Expressed and Contribute to Chemoresistance of Non-Proliferating Leukaemic CD34+ Cells. *Br. J. Haematol.* **2002,** *118* (2), 521–534; (b) Moitra, K.; Lou, H.; Dean, M. Multidrug Efflux Pumps and Cancer Stem Cells: Insights Into Multidrug Resistance and Therapeutic Development. *Clin. Pharmacol. Ther.* **2011,** *89* (4), 491–502.
232. (a) Gupta, P. B.; Onder, T. T.; Jiang, G.; Tao, K.; Kuperwasser, C.; Weinberg, R. A.; Lander, E. S. Identification of Selective Inhibitors of Cancer Stem Cells by High-Throughput Screening. *Cell* **2009,** *138* (4), 645–659; (b) Sikandar, S. S.; Pate, K. T.; Anderson, S.; Dizon, D.; Edwards, R. A.; Waterman, M. L.; Lipkin, S. M. NOTCH Signaling Is Required for Formation and Self-Renewal of Tumor-Initiating Cells and for Repression of Secretory Cell Differentiation in Colon Cancer. *Cancer Res.* **2010,** *70* (4), 1469–1478; (c) Liu, S.; Dontu, G.; Mantle, I. D.; Patel, S.; Ahn, N. S.; Jackson, K. W.; Suri, P.; Wicha, M. S. Hedgehog Signaling and Bmi-1 Regulate Self-Renewal of Normal and Malignant Human Mammary Stem Cells. *Cancer Res.* **2006,** *66* (12), 6063–6071.
233. (a) Feng, M.; Chen, J. Y.; Weissman-Tsukamoto, R.; Volkmer, J.-P.; Ho, P. Y.; McKenna, K. M.; Cheshier, S.; Zhang, M.; Guo, N.; Gip, P.; Mitra, S. S.; Weissman, I. L. Macrophages Eat Cancer Cells Using Their Own Calreticulin As a Guide: Roles of TLR and Btk. *Proc. Natl. Acad. Sci. U. S. A.* **2015,** *112* (7), 2145–2150; (b) Cioffi, M.; Trabulo, S.; Hidalgo, M.; Costello, E.; Greenhalf, W.; Erkan, M.; Kleeff, J.; Sainz, B.; Heeschen, C. Inhibition of CD47 Effectively Targets Pancreatic Cancer Stem Cells via Dual Mechanisms. *Clin. Cancer Res.* **2015,** *21* (10), 2325–2337.
234. Azzi, S.; Bruno, S.; Giron-Michel, J.; Clay, D.; Devocelle, A.; Croce, M.; Ferrini, S.; Chouaib, S.; Vazquez, A.; Charpentier, B.; Camussi, G.; Azzarone, B.; Eid, P. Differentiation Therapy: Targeting Human Renal Cancer Stem Cells With Interleukin 15. *J. Natl. Cancer Inst.* **2011,** *103* (24), 1884–1898.

235. (a) Blencke, S.; Zech, B.; Engkvist, O.; Greff, Z.; Orfi, L.; Horvath, Z.; Keri, G.; Ullrich, A.; Daub, H. Characterization of a Conserved Structural Determinant Controlling Protein Kinase Sensitivity to Selective Inhibitors. *Chem. Biol.* **2004,** *11* (5), 691–701; (b) Fabbro, D.; Fendrich, G.; Guez, V.; Meyer, T.; Furet, P.; Mestan, P.; Griffin, J. D.; Manley, P. W.; Cowan-Jacob, S. W. *Targeted Therapy With Imatinib: An Exception or a Rule?,. Handbook of Experimental Pharmacology, Inhibitors of Protein Kinases and Protein Phosphates* vol. 167; Springer: Berlin, Heidleberg, 2005, , 361–389.
236. (a) Gorre, M. E.; Mohammed, M.; Ellwood, K.; Hsu, N.; Paquette, R.; Rao, P. N.; Sawyers, C. L. Clinical Resistance to STI-571 Cancer Therapy Caused by BCR-ABL Gene Mutation or Amplification. *Science* **2001,** *293* (5531), 876–880; (b) Kobayashi, S.; Boggon, T. J.; Dayaram, T.; Janne, P. A.; Kocher, O.; Meyerson, M.; Johnson, B. E.; Eck, M. J.; Tenen, D. G.; Halmos, B. EGFR Mutation and Resistance of Non-Small-Cell Lung Cancer to Gefitinib. *N. Engl. J. Med.* **2005,** *352* (8), 786–792; (c) Chandarlapaty, S.; Sawai, A.; Scaltriti, M.; Rodrik-Outmezguine, V.; Grbovic-Huezo, O.; Serra, V.; Majumder, P. K.; Baselga, J.; Rosen, N. AKT Inhibition Relieves Feedback Suppression of Receptor Tyrosine Kinase Expression and Activity. *Cancer Cell* **2011,** *19* (1), 58–71; (d) Logue, J. S.; Morrison, D. K. Complexity in the Signaling Network: Insights From the Use of Targeted Inhibitors in Cancer Therapy. *Genes Dev.* **2012,** *26* (7), 641–650; (e) Trusolino, L.; Bertotti, A. Compensatory Pathways in Oncogenic Kinase Signaling and Resistance to Targeted Therapies: Six Degrees of Separation. *Cancer Discov.* **2012,** *2* (10), 876–880; (f) Workman, P.; Al-Lazikani, B.; Clarke, P. A. Genome-Based Cancer Therapeutics: Targets, Kinase Drug Resistance and Future Strategies for Precision Oncology. *Curr. Opin. Pharmacol.* **2013,** *13* (4), 486–496; (g) Rubin, B. P.; Duensing, A. Mechanisms of Resistance to Small Molecule Kinase Inhibition in the Treatment of Solid Tumors. *Lab. Invest.* **2006,** *86* (10), 981–986; (h) Fabbro, D.; Cowan-Jacob, S. W.; Mobitz, H.; Martiny-Baron, G. Targeting Cancer With Small-Molecular-Weight Kinase Inhibitors. *Methods Mol. Biol.* **2012,** *795,* 1–34; (i) Fabbro, D.; Cowan-Jacob, S. W.; Moebitz, H. Ten Things You Should Know About Protein Kinases: IUPHAR Review 14. *Br. J. Pharmacol.* **2015,** *172* (11), 2675–2700.
237. (a) Chandarlapaty, S.; Sakr, R. A.; Giri, D.; Patil, S.; Heguy, A.; Morrow, M.; Modi, S.; Norton, L.; Rosen, N.; Hudis, C.; King, T. A. Frequent Mutational Activation of the PI3K-AKT Pathway in Trastuzumab-Resistant Breast Cancer. *Clin. Cancer Res.* **2012,** *18* (24), 6784–6791; (b) Berns, K.; Horlings, H. M.; Hennessy, B. T.; Madiredjo, M.; Hijmans, E. M.; Beelen, K.; Linn, S. C.; Gonzalez-Angulo, A. M.; Stemke-Hale, K.; Hauptmann, M.; Beijersbergen, R. L.; Mills, G. B.; van de Vijver, M. J.; Bernards, R. A Functional Genetic Approach Identifies the PI3K Pathway As a Major Determinant of Trastuzumab Resistance in Breast Cancer. *Cancer Cell* **2007,** *12* (4), 395–402.
238. (a) Lidsky, M.; Antoun, G.; Speicher, P.; Adams, B.; Turley, R.; Augustine, C.; Tyler, D.; Ali-Osman, F. Mitogen-Activated Protein Kinase (MAPK) Hyperactivation and Enhanced NRAS Expression Drive Acquired Vemurafenib Resistance in V600E BRAF Melanoma Cells. *J. Biol. Chem.* **2014,** *289* (40), 27714–27726; (b) Monsma, D. J.; Cherba, D. M.; Eugster, E. E.; Dylewski, D. L.; Davidson, P. T.; Peterson, C. A.; Borgman, A. S.; Winn, M. E.; Dykema, K. J.; Webb, C. P.; MacKeigan, J. P.; Duesbery, N. S.; Nickoloff, B. J.; Monks, N. R. Melanoma Patient Derived Xenografts Acquire Distinct Vemurafenib Resistance Mechanisms. *Am. J. Cancer Res.* **2015,** *5* (4), 1507–1518.
239. (a) Bettegowda, C.; Sausen, M.; Leary, R. J.; Kinde, I.; Wang, Y.; Agrawal, N.; Bartlett, B. R.; Wang, H.; Luber, B.; Alani, R. M.; Antonarakis, E. S.; Azad, N. S.; Bardelli, A.; Brem, H.; Cameron, J. L.; Lee, C. C.; Fecher, L. A.; Gallia, G. L.; Gibbs, P.; Le, D.; Giuntoli, R. L.; Goggins, M.; Hogarty, M. D.; Holdhoff, M.; Hong, S. M.; Jiao, Y.; Juhl, H. H.; Kim, J. J.; Siravegna, G.; Laheru, D. A.; Lauricella, C.; Lim, M.; Lipson, E. J.; Marie, S. K.; Netto, G. J.; Oliner, K. S.; Olivi, A.; Olsson, L.; Riggins, G. J.; Sartore-Bianchi, A.; Schmidt, K.; Shih I, M.; Oba-Shinjo, S. M.; Siena, S.; Theodorescu, D.; Tie, J.; Harkins, T. T.; Veronese, S.; Wang, T. L.; Weingart, J. D.; Wolfgang, C. L.; Wood, L. D.; Xing, D.; Hruban, R. H.; Wu, J.; Allen, P. J.; Schmidt, C. M.; Choti, M. A.; Velculescu, V. E.; Kinzler, K. W.; Vogelstein, B.; Papadopoulos, N.; Diaz, L. A., Jr. Detection of Circulating Tumor DNA in Early- and Late-Stage Human Malignancies. *Sci. Transl. Med.* **2014,** *6* (224), 224ra24; (b) Heinemann, V.; Stintzing, S.; Kirchner, T.; Boeck, S.; Jung, A. Clinical Relevance of EGFR- and KRAS-Status in Colorectal Cancer Patients Treated With Monoclonal Antibodies Directed Against the EGFR. *Cancer Treat. Rev.* **2009,** *35* (3), 262–271.
240. Mori, Y.; Shimizu, N.; Dallas, M.; Niewolna, M.; Story, B.; Williams, P. J.; Mundy, G. R.; Yoneda, T. Anti-Alpha4 Integrin Antibody Suppresses the Development of Multiple Myeloma and Associated Osteoclastic Osteolysis. *Blood* **2004,** *104* (7), 2149–2154.
241. Shishido, S.; Bönig, H.; Kim, Y. M. Role of Integrin Alpha4 in Drug Resistance of Leukemia. *Front. Oncol.* **2014,** *4,* 99.
242. Straussman, R.; Morikawa, T.; Shee, K.; Barzily-Rokni, M.; Qian, Z. R.; Du, J.; Davis, A.; Mongare, M. M.; Gould, J.; Frederick, D. T.; Cooper, Z. A.; Chapman, P. B.; Solit, D. B.; Ribas, A.; Lo, R. S.; Flaherty, K. T.; Ogino, S.; Wargo, J. A.; Golub, T. R. Tumour Microenvironment Induces Innate RAF-Inhibitor Resistance Through HGF Secretion. *Nature* **2012,** *487* (7408), 500–504.
243. (a) Heymach, J. V.; Nilsson, M.; Blumenschein, G.; Papadimitrakopoulou, V.; Herbst, R. Epidermal Growth Factor Receptor Inhibitors in Development for the Treatment of Non-Small Cell Lung Cancer. *Clin. Cancer Res.* **2006,** *12* (14 Pt 2), 4441s–4445s; (b) Kwak, E. L.; Sordella, R.; Bell, D. W.; Godin-Heymann, N.; Okimoto, R. A.; Brannigan, B. W.; Harris, P. L.; Driscoll, D. R.; Fidias, P.; Lynch, T. J.; Rabindran, S. K.; McGinnis, J. P.; Wissner, A.; Sharma, S. V.; Isselbacher, K. J.; Settleman, J.; Haber, D. A. Irreversible Inhibitors of the EGF Receptor May Circumvent Acquired Resistance to Gefitinib. *Proc. Natl. Acad. Sci. U. S. A.* **2005,** *102* (21), 7665–7670; (c) Felip, E.; Santarpia, M.; Rosell, R. Emerging Drugs for Non-Small-Cell Lung Cancer. *Expert Opin. Emerg. Drugs* **2007,** *12* (3), 449–460; (d) Zhou, W.; Ercan, D.; Janne, P. A.; Gray, N. S. Discovery of Selective Irreversible Inhibitors for EGFR-T790M. *Bioorg. Med. Chem. Lett.* **2011,** *21* (2), 638–643.
244. (a) Wiestner, A. Targeting B-Cell Receptor Signaling for Anticancer Therapy: The Bruton's Tyrosine Kinase Inhibitor Ibrutinib Induces Impressive Responses in B-Cell Malignancies. *J. Clin. Oncol.* **2013,** *31* (1), 128–130; (b) Byrd, J. C.; Furman, R. R.; Coutre, S. E.; Flinn, I. W.; Burger, J. A.; Blum, K. A.; Grant, B.; Sharman, J. P.; Coleman, M.; Wierda, W. G.; Jones, J. A.; Zhao, W.; Heerema, N. A.; Johnson, A. J.; Sukbuntherng, J.; Chang, B. Y.; Clow, F.; Hedrick, E.; Buggy, J. J.; James, D. F.; O'Brien, S. Targeting BTK With Ibrutinib in Relapsed Chronic Lymphocytic Leukemia. *N. Engl. J. Med.* **2013,** *369* (1), 32–42; (c) Akinleye, A.; Furqan, M.; Adekunle, O. Ibrutinib and Indolent B-Cell Lymphomas. *Clin. Lymphoma Myeloma Leuk.* **2014,** *14* (4), 253–260.
245. Furman, R. R.; Cheng, S.; Lu, P.; Setty, M.; Perez, A. R.; Guo, A.; Racchumi, J.; Xu, G.; Wu, H.; Ma, J.; Steggerda, S. M.; Coleman, M.; Leslie, C.; Wang, Y. L. Ibrutinib Resistance in Chronic Lymphocytic Leukemia. *N. Engl. J. Med.* **2014,** *370* (24), 2352–2354.
246. Shah, N. P.; Nicoll, J. M.; Nagar, B.; Gorre, M. E.; Paquette, R. L.; Kuriyan, J.; Sawyers, C. L. Multiple BCR-ABL Kinase Domain Mutations Confer Polyclonal Resistance to the Tyrosine Kinase Inhibitor Imatinib (STI571) in Chronic Phase and Blast Crisis Chronic Myeloid Leukemia. *Cancer Cell* **2002,** *2* (2), 117–125.
247. (a) Gray, N. S.; Fabbro, D. Discovery of Allosteric Bcr–Abl Inhibitors From Phenotypic Screen to Clinical Candidate. *Methods Enzymol.* **2014,** *548,* 173–188. Elsevier, USA; (b) Hochhaus, A.; Rosti, G.; Cross, N. C. P.; Steegmann, J. L.; le Coutre, P.; Ossenkoppele, G.; Petrov, L.; Masszi, T.; Hellmann, A.; Griskevicius, L.; Wiktor-Jedrzejczak, W.; Rea, D.; Coriu, D.; Brummendorf, T. H.; Porkka, K.; Saglio, G.; Gastl, G.; Muller, M. C.; Schuld, P.; Di Matteo, P.; Pellegrino, A.; Dezzani, L.; Mahon, F. X.; Baccarani, M.; Giles, F. J. Frontline Nilotinib in Patients With Chronic Myeloid Leukemia in Chronic Phase: Results From the European ENEST1st Study. *Leukemia* **2015,** *30* (1), 57–64; (c) Jabbour, E.; Kantarjian, H. M.; Saglio, G.; Steegmann, J. L.; Shah, N. P.; Boqué, C.; Chuah, C.; Pavlovsky, C.; Mayer, J.; Cortes, J.; Baccarani, M.; Kim, D.-W.; Bradley-Garelik, M. B.; Mohamed, H.; Wildgust, M.; Hochhaus, A. Early Response With Dasatinib or Imatinib in Chronic Myeloid Leukemia: 3-Year Follow-Up From a Randomized Phase 3 Trial (DASISION). *Blood* **2014,** *123* (4), 494–500; (d) Ciarcia, R.; Damiano, S.; Puzio, M. V.; Montagnaro, S.; Pagnini, F.; Pacilio, C.; Caparrotti, G.; Bellan, C.; Garofano, T.; Polito, M. S.; Giordano, A.; Florio, S. Comparison of Dasatinib, Nilotinib, and Imatinib in the Treatment of Chronic Myeloid Leukemia. *J. Cell. Physiol.* **2016,** *231* (3), 680–687; (e) O'Hare, T.; Shakespeare, W. C.; Zhu, X.; Eide, C. A.; Rivera, V. M.; Wang, F.; Adrian, L. T.; Zhou, T.; Huang, W. S.; Xu, Q.; Metcalf, C. A., III; Tyner, J. W.; Loriaux, M. M.; Corbin, A. S.; Wardwell, S.; Ning, Y.; Keats, J. A.; Wang, Y.; Sundaramoorthi, R.; Thomas, M.; Zhou, D.; Snodgrass, J.; Commodore, L.; Sawyer, T. K.; Dalgarno, D. C.; Deininger, M. W.; Druker, B. J.; Clackson, T. AP24534, a Pan-BCR-ABL Inhibitor for Chronic Myeloid Leukemia, Potently Inhibits the T315I Mutant and Overcomes Mutation-Based Resistance. *Cancer Cell* **2009,** *16* (5), 401–412; (f) Hoy, S. M. Ponatinib: A Review of Its Use in Adults With Chronic Myeloid Leukaemia or Philadelphia Chromosome-Positive Acute Lymphoblastic Leukaemia. *Drugs* **2014,** *74* (7), 793–806.
248. (a) Cheng, H.; Force, T. Why Do Kinase Inhibitors Cause Cardiotoxicity and What Can Be Done About It? *Prog. Cardiovasc. Dis.* **2010,** *53* (2), 114–120; (b) Force, T.; Krause, D. S.; Van Etten, R. A. Molecular Mechanisms of Cardiotoxicity of Tyrosine Kinase Inhibition. *Nat. Rev. Cancer* **2007,** *7* (5), 332–344; (c) Dalzell, M. D. Ponatinib Pulled Off Market Over Safety Issues. *Manag. Care* **2013,** *22* (12), 42–43.
249. (a) Wagle, N.; Emery, C.; Berger, M. F.; Davis, M. J.; Sawyer, A.; Pochanard, P.; Kehoe, S. M.; Johannessen, C. M.; Macconaill, L. E.; Hahn, W. C.; Meyerson, M.; Garraway, L. A. Dissecting Therapeutic Resistance to RAF Inhibition in Melanoma by Tumor Genomic Profiling. *J. Clin. Oncol.* **2011,** *29* (22), 3085–3096; (b) Medina, T.; Amaria, M. N.; Jimeno, A. Dabrafenib in the Treatment of Advanced Melanoma. *Drugs Today* **2013,** *49* (6), 377–385.

Relevant Websites

http://www.cancer.org/—The American Cancer Society releases cancer facts and figures every year. Information include estimated incidence rate and cancer related deaths in the US.

http://cancergenome.nih.gov/—The Cancer Genome Atlas (TCGA), a collaboration between the National Cancer Institute (NCI) and National Human Genome Research Institute (NHGRI), aims to generate comprehensive, multi-dimensional maps of the key genomic changes in major types and subtypes of cancer. Provides e.g. gene-expression, copy numbers, mutations and miRNA expression data and a platform for searching and analyzing data sets.

https://icgc.org/—The International Cancer Genome Consortium (ICGC) obtains a comprehensive description of genomic, transcriptomic and epigenomic changes in 50 different tumor types. The data portal provides tools for visualizing and downloading available mutational data.

http://www.ocimumbio.com/oncology-suite/—BioExpress® Oncology Suite (Ocimum Biosolutions) provides gene expression data from primary, metastatic, and benign tumor samples, and normal samples, including matched adjacent controls or allows to compare gene expression profiles between normal and tumor tissues, differential gene expression between different tissue types and different stages of cancer and to discover tumor associated potential drug targets, biomarkers and common pathways leading to cancer.

http://ncg.kcl.ac.uk/—Network of Cancer Genes from Kings College, London, UKcompiles data for 1571 cancer genes from 175 studies, 188 mutational screenings, 13,315 cancer samples from 49 cancer types (duplicability, orthology, evolutionary origin, expression profile, function and interactions).

http://cancer.sanger.ac.uk/cosmic—Catalogue Of Somatic Mutations In Cancer (COSMIC) from Wellcome Trust Sanger Institute, UK provides expert manual curation data and systematic screen data compiled from literature exploring impact of somatic mutations in human cancer (e.g. coding point mutations, non-coding mutations, gene fusions, genome rearrangements, copy number abnormalities, abnormal expression variants).

https://www.broadinstitute.org/software/cprg/?q=node/11—Cancer Cell Line Encyclopedia (CCLE)provides detailed genetic characterization of more than 1000 cancer cell lines (DNA copy number, mRNA expression, mutation data and more) as well as links to several other data bases.

http://cgap.nci.nih.gov—Cancer Genome Anatomy Project (CGAP) from National Cancer Instituteprovides gene expression profiles of normal, pre-cancer and cancer cells, as well as bioinformatics analysis and data mining tools.

https://cansar.icr.ac.uk/—CanSAR from The Institute of Cancer Research and Cancer Research UK is an integrated knowledge-base that brings together multidisciplinary data including structural protein information, expression and mutation data as well as chemical and pharmacological tools.

https://clinicaltrials.gov/—ClinicalTrials.gov is a registry and results database for clinical studies in humans conducted around the world.

http://www.guidetopharmacology.org/—IUPHAR/BPS expert-driven guide to pharmacological targets and the substances that act on them.

http://www0.nih.go.jp/mirror/Kinases/—The Protein Kinase Resource (PKR) is a web accessible compendium of information on the protein kinase family of enzymes that includes structural and computational analyses.

www.gene.com/media/product-information/herceptin-development-timeline—This website is owned by Genentech and describes both independent key academic discoveries and milestones of the development of Herceptin.

www.fda.gov/MedicalDevices/ProductsandMedicalProcedures/InVitroDiagnostics/ucm301431.htm—This website is published by the FDA and lists all currently cleared or approved companion diagnostics. The accessed content was last updated on December 21st 2015.

http://www.fda.gov/MedicalDevices/ProductsandMedicalProcedures/InVitroDiagnostics/ucm407296.htm—This website is published by the FDA and provides definitions and descriptions for Laboratory Developed Tests (LTD). The accessed content was last updated on November 17th 2015.

https://www.fas.org/sgp/crs/misc/R43438.pdf—This document was issued by the Congressional Research Services. It describes the "Regulation of Clinical Tests: in vitro Diagnostic (IVD) Devices, Laboratory Developed Tests (LDTs), and Genetic Tests". The document is authored by Amanda K. Sarata (Specialist in Health Policy) and Judith A. Johnson (Specialist in Biomedical Policy) and dated December 17th 2014.

5.02 Selective Kinase Inhibitors in Cancer

AA Mortlock, DM Wilson, JG Kettle, FW Goldberg, and KM Foote, AstraZeneca, Cambridge, United Kingdom

© 2017 Elsevier Ltd. All rights reserved.

5.02.1	**Introduction: Kinase Inhibitors in Cancer**	40
5.02.2	**Kinases and Cancer**	40
5.02.2.1	Kinase Fusion Proteins	41
5.02.2.2	Activating Mutations	41
5.02.2.3	Upstream Pathway Activation	42
5.02.2.4	Protein Overexpression	43
5.02.2.5	Gene Amplification	43
5.02.3	**Clinical Lessons Learned From First-Generation Inhibitors**	43
5.02.3.1	Target Engagement	44
5.02.3.2	On-Target Selectivity	44
5.02.3.3	Targeting Resistance	45
5.02.3.4	Combinability	45
5.02.4	**Bcr-Abl Inhibitors**	45
5.02.4.1	Chronic Myeloid Leukemia and the Discovery of Imatinib	45
5.02.4.2	Mechanism of Resistance to Imatinib	46
5.02.4.3	Second-Generation Therapies	47
5.02.4.3.1	Nilotinib	47
5.02.4.3.2	Dasatinib	48
5.02.4.3.3	Bosutinib	48
5.02.4.4	Addressing the Gatekeeper T315I Mutation	48
5.02.4.4.1	Ponatinib: An ATP-competitive inhibitor of T315I	49
5.02.4.4.2	Allosteric Bcr-Abl inhibitors	49
5.02.5	**Optimizing Kinase Inhibitors for Selectivity and Acquired Resistance for Lung Cancer**	51
5.02.5.1	Introduction	51
5.02.5.2	Design of Mutant Selective EGFR Inhibitors	51
5.02.5.2.1	Early inhibitors of EGFR, targeting activating mutations	51
5.02.5.2.2	Design of T790M mutant selective EGFR inhibitors	52
5.02.5.2.3	Future outlook	55
5.02.5.3	Design of ALK Inhibitors With Potency Against Mutations	55
5.02.5.3.1	Design of crizotinib as an effective inhibitor of WT ALK	55
5.02.5.3.2	Design of ALK inhibitors that can target the L1196M gatekeeper mutation	56
5.02.5.3.3	Future outlook	57
5.02.5.4	Conclusion	58
5.02.6	**Kinases in the DDR**	59
5.02.6.1	Introduction	59
5.02.6.2	ATM	59
5.02.6.2.1	ATM inhibitors	60
5.02.6.3	ATR	61
5.02.6.3.1	ATR inhibitors	62
5.02.6.4	DNA-PK	64
5.02.6.4.1	DNA-PK inhibitors	64
5.02.6.5	WEE1 and CHK1	66
5.02.6.5.1	WEE1 inhibitors	66
5.02.6.5.2	CHK1 inhibitors	67
5.02.6.6	Summary and Outlook	69
References		69

Abbreviations

AKT Protein kinase B
ALK Anaplastic lymphoma kinase
ALL Acute lymphoblastic leukemias
AML Acute myeloid leukemia
ATM Ataxia-telangiectasia mutated
ATP Adenosine triphosphate
ATR Ataxia-telangiectasia and RAD3-related
BBB Blood–brain barrier

BID Twice daily dosing
CDK Cyclin-dependent kinase
CED Convection-enhanced delivery
CHK Checkpoint kinase
CLL Chronic lymphocytic leukemia
CML Chronic myelogeneous leukemia
CNS Central nervous system
DDR DNA-damage response
DLT Dose-limiting toxicity
DNA-PK DNA-dependent protein kinase
DSB Double-strand break
EGFR Epidermal growth factor receptor
EGFRm Epidermal growth factor receptor mutation
ER Estrogen receptor
FDA Food and Drug Administration
FGFR Fibroblast growth factor receptor
FISH Fluorescence in situ hybridization
GBM Glioblastoma multiforme
GIST Gastrointestinal stromal tumors
HR Homologous recombination
i.p. Intraperitoneal
i.v. Intravenous
IHC Immunohistochemistry
IMF Idiopathic myelofibrosis
IR Ionizing radiation
Jak Janus kinase
LLE Ligand lipophilicity efficiency (or LipE)
MAPK Mitogen-activated protein kinases
MCL Mantle cell lymphoma
MPL Thrombopoietin receptor
mTOR Mammalian target of rapamycin
NGS Next-generation sequencing
NHEJ Nonhomologous end joining
NSCLC Nonsmall cell lung cancer
PARP Poly ADP-ribose polymerase
PDGFR Platelet-derived growth factor receptor
Pgp P-glycoprotein (or MDR-1)
Ph Philadelphia
PI3K Phosphatidylinositol 3-kinase
PIKK Phosphatidylinositol 3-kinase-related kinase
PK Pharmacokinetics
PKC Protein kinase C
PTEN Phosphatase and tensin homolog
QD Once daily dosing
RSR Replication stress response
SAR Structure–activity relationship
SOC Standard-of-care
TGI Tumor growth inhibition
TNBC Triple negative breast cancer
VEGFR Vascular endothelial growth factor receptor
WT Wild type

5.02.1 Introduction: Kinase Inhibitors in Cancer

In the 15 years which have passed since the Food and Drug Administration (FDA) approval of imatinib in May 2001,[1] more than 25 small molecule kinase inhibitors have been approved by that agency for the treatment of various types of cancer.[2] As the single largest class of new cancer drugs developed in this period, kinase inhibitors have rapidly established themselves as widely used standards-of-care (SOC) and have transformed the treatment of many cancers, notably chronic myelogenous leukemia,[3] nonsmall cell lung cancer (NSCLC),[4] renal cell carcinoma,[5] and idiopathic myelofibrosis (IMF).[6] Along with antibodies targeting the extracellular binding domain of receptor tyrosine kinases (such as trastuzumab[7] and bevacizumab[8]) these new agents have been at the forefront of the development of personalized medicine[9] (also called stratified or precision medicine); exploiting molecular diagnoses to identify the most appropriate patient group for the drug, based on a detailed understanding of its molecular mode of action.

With such rapid progress the technical demands placed on new kinase inhibitors are typically much greater than those of the "first-generation" inhibitors. Clinical experience with the early compounds has often shown the limitations of suboptimal selectivity, modest pharmacokinetic properties, and, typically, an inability to suppress resistance mechanisms. Fortunately our understanding of how these and other issues can be addressed has developed dramatically over the past decade. Indeed, it has become clear that in a number of cases the precise biology which can be effected by the kinase inhibitor can be "tuned" by attention to detailed aspects of the inhibitor's binding mode and kinetics, meaning that novel inhibitors have the potential to open up research in kinase targets which were previously thought to be of limited interest. Using a range of published examples this article aims to highlight how medicinal chemistry is now delivering a new generation of highly selective kinase inhibitors which are already delivering a step-change in clinical benefit in many tumors. Clearly most focus is on areas such as Bcr-Abl, epidermal growth factor receptor (EGFR), and ALK inhibition where the field has had the greatest time to mature and where the limitations of current inhibitors are best understood. However, the lessons from the first-generation inhibitors can also be applied in the design of compounds against more novel targets, and this has been illustrated in the section on kinases which control the DNA-damage response (DDR).

5.02.2 Kinases and Cancer

The rationale for targeting kinases as a potential treatment for cancer has become increasingly sophisticated, as increasing amounts of genetic information has become available with the development of relatively low cost sequencing. When the first kinase

inhibitors entered clinical trials in the mid-1990s the decision as to which tumor type to target was made either on the basis of total protein expression in biopsies or based even more simplistically on the way the compounds behaved in preclinical xenograft models.[10] It is now recognized that achieving good clinical activity typically requires identification of the oncogenic driver which the tumor has become addicted to for growth and survival. In these cases the kinase acts as an oncogene, and those tumor cells which are oncogene addicted can be killed all the time the kinase being targeted remains a critical component of that oncogenic drive. Clearly there are also examples where kinase inhibition can be effective without the kinase being itself an oncogene although this would typically be in combination. A good example of this "nononcogene addicted" approach will be discussed later in the section describing kinases involved in the repair of DNA damage where kinase inhibitors prevent full repair of DNA damage which can lead to additional cancer cell death.

Although there are just over 500 kinases in the human genome, there are 5 main ways in which they can present as targets for cancer treatment.

5.02.2.1 Kinase Fusion Proteins

Imatinib, the first small-molecule kinase inhibitor to be approved for the treatment of cancer targets Bcr-Abl.[11] This form of Abl is a fusion protein formed from the gene fusion of part of the *Bcr* gene (chromosome 22) with the *Abl* gene (chromosome 9). Bcr-Abl is only formed through this gene translocation, and consequently the chimeric kinase only occurs in individuals with chronic myelogeneous leukemia (CML).[12] The discovery that all CML is due to Bcr-Abl and the fact that the underlying gene translocation can readily be identified through the characteristic shortened allele of chromosome 22 (the so-called Philadelphia chromosome[13]) led to a major breakthrough in kinase inhibitors as, for the first time, patients could be selected on the basis of underlying pathogenomic events.[14] Furthermore, the simplicity and robustness of the genetic assay required to identify patients ensured both rapid uptake of the drug by the medical community and the ability to treat early-stage patients with considerable success.[15] More recent attempts to achieve greater levels of Bcr-Abl inhibition by targeting alternative binding sites on the kinase will be covered in more detail.

Several other kinase fusion proteins are now known, but in general, despite their being constitutively active, and typically transforming, they are generally rare events and are consequently found in relatively small numbers of patients.[16] In some cases, such as the EML4–ALK fusion which is found in 3–4% of lung adenocarcinoma,[17] the number of patients involved is sufficiently large to support full drug development and crizotinib was approved in this indication in 2012.[18] That said, the provisional approval of crizotinib was achieved using single-arm studies using a response-based endpoint which was a very novel regulatory approach compared to typical approvals in lung cancer.[19] The supporting companion diagnostic test uses a break-apart fluorescence in situ hybridization (FISH) assay,[20] a technique which is potentially applicable to other kinase fusion proteins, although in the future the use of next-generation sequencing (NGS) may become more routine.[21]

Other kinase fusion proteins occur in such low frequency that it is debatable whether formal trials will be carried out or whether patients with these genetic aberrations may be treated with medicines in an "off-label" setting. Among the more notable examples are fibroblast growth factor receptor (FGFR) fusions (reported in glioblastoma[22] and extrahepatic biliary tract carcinoma[23]), Ret fusions (reported in lung cancer[24]), and platelet-derived growth factor receptor (PDGFR) fusions (reported in chronic myelomonocytic leukemia).[25] It is interesting to note that in contrast to Abl and ALK (which are both discussed later in this article), these fusion proteins have been found with a number of nonkinase fusion partners, suggesting that the fusion partner may be less important for constitutive activation, rather it is the loss of autoregulatory domains on the wild-type (WT) kinase which is transforming.[26] In terms of a challenge for development of novel inhibitors, targeting fusion proteins presents no specific issues to medicinal chemistry although preclinical assays need to be developed and selectivity over the full-length WT kinase can be difficult to achieve. The bigger issue is more often around the practicality of running clinical trials in populations who may be difficult to identify due to the rarity of the genetic event.[27]

5.02.2.2 Activating Mutations

The development of EGFR tyrosine kinase inhibitors has been fundamental to understanding how activating mutations can play a critical role.[28] When gefitinib[29] and erlotinib[30] were first trialed in lung cancer patients they were used without any further patient selection. Trials in combination with SOC chemotherapy showed no benefit of adding the EGFR inhibitor, while monotherapy results were modest and, in the case of gefitinib, did not lead to full FDA approval.[31] Within the gefitinib data however it was clear that certain patient groups did derive significant clinical benefit; thus women typically did better than men, nonsmokers did better than those with a history of smoking while more Asian patients seemed to have responses than those of Caucasian origin.[32] In 2004 a paper from Lynch et al. provided both an explanation for these data and, critically, a testable hypothesis by highlighting the role of a number of mutations in EGFR which were more common in those patient groups who responded to erlotinib or gefitinib treatment.[33] Two particular genetic events were highly prevalent in the responder groups, namely, a point mutation at position 858 (L858R) and also deletions in a region of exon 19.[34] The IPASS trial explored this hypothesis in an Asian patient population and in 2008 was able to demonstrate striking activity with gefitinib compared to a SOC chemotherapy regimen in a group of NSCLC patients who had been selected on the basis of genetic aberration.[35] This trial was the first lung cancer trial to demonstrate the value of prospective patient selection and led to both the approval of gefitinib (and a companion diagnostic test) and heralding a transformation in the treatment of lung adenocarcinoma.

While the use of first-generation EGFR tyrosine kinase inhibitors has rapidly become a SOC for these patients, the great majority of patients do relapse, most commonly through the acquisition of a secondary kinase mutation (although there are a number of other mechanisms of resistance which are documented).[36] Approaches to find the so-called third-generation EGFR inhibitors, which can target the acquired mutations alongside preserving activity against the original primary mutation, are described in more detail later. The success of these agents is further proof that constitutively active kinases, such as the various mutant forms of EGFR, can be highly oncogenic and tumors which carry them typically remain "addicted" to signaling through the primary oncogenic mechanism.[37] In terms of drug design, the ability to predict which acquired mutational forms of the kinase may be important has increased as our knowledge of the different resistance mechanisms has increased. In particular, mutation of the "gatekeeper" residue to introduce a more bulky amino acid (which typically sits above the entry to the selectivity pocket) is often observed as these gatekeeper mutations are often poorly inhibited by compounds targeting the active site of the WT kinase.[38] Preclinical evaluation of potential gatekeeper mutations has been described for certain kinases and inhibitors can now be designed to be active for these kinase forms even before they have been observed in clinical studies.[39]

With a clear link established using EGFR, a number of other mutated kinase variants have been either validated or proposed as promising anticancer targets. Mutated forms of the receptor tyrosine kinase c-Kit are known to drive gastrointestinal stromal tumors (GIST),[40] while mutations in FGFR3 are involved in certain bladder tumors.[41] Intracellular kinases can also be found with activating mutations such as B-Raf (melanoma),[42] AKT1 (breast and endometrial cancers),[43] and the lipid kinase PI3Kα (ER+ve breast cancer).[44] While many of these mutations are relatively uncommon, they are typically easy to detect if suitable biopsy material can be collected. The challenge of developing novel kinase inhibitors capable of targeting specific mutations with high selectivity is not to be underestimated and is highly dependent on the structures of the mutated forms of the kinase. However the availability of large (and validated) kinase screening libraries together with the ability to generate structural information which can guide development of pharmacophore models makes this a realistic aim for many kinases in a way which would not have been possible even a few years ago.

5.02.2.3 Upstream Pathway Activation

The majority of kinases are cytosolic or nuclear, that is they are not activated by extracellular ligands but rather by intracellular signal transduction, often phosphorylation by other kinases.[45] Consequently there are many kinases which are validated targets for cancer which have no reported activating mutations or where mutational load is only partially responsible for their oncogenic drive. The two best known examples in oncology are the mitogen-activated protein kinases (MAPK) and AKT signaling pathways both of which are widely disregulated in human cancer.[46,47] Thus MEK inhibitors have been demonstrated to show significant activity in B-Raf mutant malignant melanoma.[48] In this case the mutant B-Raf signals exclusively through MEK, so the link between activating mutation and kinase inhibitor is well established.[49] What makes this example particularly interesting is the possibility of targeting multiple points in the signaling cascade to achieve better responses. This approach was first demonstrated to have clinical utility through the successful use of a combination of B-Raf and MEK inhibitors in B-Raf mutant malignant melanoma.[50]

The other well-known example of pathway activation is the canonical PI3K/AKT/mTOR signaling pathway.[51] In this case, pathway activation is even more complicated and can be driven by a range of cell surface and cytosolic factors as well as by dynamic responses driven by the pathway itself in response to kinase inhibitors.[52] Pathway activation can be driven by mutations (in either the p85 subunits of the type I PI3 kinases or in AKT)[53] although functional loss of the phosphatase tumor suppressor Phosphatase and tensin homolog (PTEN) is likely a more significant intrapathway cause of pathway disregulation.[54] In parallel there are well-understood examples of the so-called cross-talk between the major intracellular signaling pathways such that blockade of MAPK signaling can lead to activation of PI3K/AKT/mTOR signaling.[55]

Another clinically important signaling pathway is that involving the Jak2 kinase which is central to the control of hematopoesis and which consequently plays a critical role in the development of myeloproliferative neoplasias such as IMF and polycythemia rubra vera (PRV).[56] The initial interest in Jak2 as a target came from the discovery by a number of groups in 2005 that a mutated form of Jak2 (V617F) was found in approximately 50% of patients with myelofibrosis and more than 85% of those with polycythemia.[57] When the first Jak2 inhibitors (including ruxolitinib which is now registered for this indication) were taken into clinical studies efforts were made to ensure that the drug could be tested in both V617 and Jak2 WT patients with the obvious concern that the latter might be significantly less responsive.[58] In reality the Jak2 mutation status was not found to be a significant predictor of response to Jak2 kinase inhibitors, and no genetic patient selection assay was required to support approval of ruxolitinib. In practice, all IMF patients have constitutively active Jak2 signaling; half the time this is caused by mutation in Jak2, but the other half is due to genetic disregulation of proteins higher up the signaling cascade, such as the thrombopoietin receptor (MPL).[59]

In terms of generating novel inhibitors to target cancers where there are a range of molecular aberrations which are driving signal transduction, the key issue is often around "combinability" and scheduling. That is to say, future treatment will require synergistic use of two or more kinase inhibitors, either to target parallel signaling pathways or to prevent upregulation of resistance pathways. The dynamics of the latter processes is often quite fast and consequently kinase inhibitors which can be dosed for relatively short periods and then withdrawn may be of particular interest and value. One example that will be discussed in more detail is when kinase agents are given to potentiate the tumor cell killing effects of either chemotherapy- or radiotherapy-induced DNA damage (see "**Kinases in the DDR**" section). While this may not seem to be a major change, it is interesting to note that only one of the kinase inhibitors currently approved by the FDA is routinely administered in combination with chemotherapy (lapatinib), and oral dosing on a continuous basis is the overwhelming choice of clinical schedule.[60]

5.02.2.4 Protein Overexpression

In some cases the cause of excessive kinase activity is not that the kinase has become activated (or become insensitive to growth inhibitory signals) but rather the intracellular levels of kinase protein have increased, leading directly to increased flux through the pathway. From a biochemical perspective the increase in protein levels will only lead to an increase in pathway output if the rate of the phosphorylation reaction which the kinase catalyzes is pseudo-first order with respect to kinase concentration, that is the reaction is not limited by availability of kinase substrate or cofactors. While this is often true, it is also important to recognize that in many cases the cancer cell will respond to any increase in pathway signaling through a range of adaptive mechanisms which will typically seek to suppress the pathway, dampening down the effect of the protein overexpression.

The underlying reason for the presence of unusually high protein levels can be due to excessive gene transcription, increase in mRNA message stability, or downregulation of pathways (such as ubiquitinylation) which in an untransformed cell would lead to protein degradation through the 26S proteosome.[61] Whatever the underlying cause, protein overexpression is usually relatively easy to detect in patient-derived tumor samples using immunohistochemistry (IHC) assays.[62] One interesting recent observation comes from patients who have a deletion in exon 14 of the c-Met oncogene.[63] This deletion has been shown to remove a region of the protein which is typically ubiquitinylated; consequently if the aberrant form of c-Met protein cannot be readily be ubiquitinylated and cleared by the proteosome, its levels will build up and consequently kinase activity will increase.[64]

The most important current example of treating cancer by inhibiting a kinase which is overexpressed is probably in HER2+ve breast cancer.[65] HER2+ve breast cancer accounts for ~20–25% of newly diagnosed cases of breast cancer with roughly half of these cases also showing estrogen receptor positive lineage markers (ER+ve).[66] Current treatments are dominated by trastuzumab,[67] which targets the extracellular domain of the HER2 (ErbB2) kinase although a number of small-molecule kinase inhibitors (including lapatinib[68] and neratinib[69]) have shown good clinical activity, suggesting that small-molecule kinase inhibitors have value in this setting and might have some benefit in patients with cranial metastases due to better drug penetration to the brain. Perhaps the most critical issue which has emerged in HER2+ve breast cancer is the most simple—who to treat? While the IHC assay used in support of trastuzumab has clear cut-offs which are relatively easy to use in clinical practice,[70] it is clear that many patients with lower levels of overexpression (HER2 ++ rather than +++) do get benefit with anti-HER2 treatments when they are used. For the development of novel inhibitors, it is critical to understand how protein overexpression is going to be evaluated clinically and the importance (or not) of the exact level of overexpression. This highlights that protein overexpression is a continuous variable which will require cut-offs to be established to guide clinical practice, in contrast to the detection of kinase fusions or mutations. These genetic events are by their very nature, either present or absent, although even here the enormous heterogeneity in most solid tumors is such that biopsies from distinct sites in the same tumor can often present very differently.[71]

5.02.2.5 Gene Amplification

The final major mechanism by which kinases can become inappropriately activated in cancer cells is through gene amplification.[72] While this is clearly linked with downstream protein expression the correlation is not absolute and critically the method of detection is DNA based rather than by quantification of protein levels.[73] In practical terms, selection of patients based on gene amplification has all the same issues of setting cut-offs as does IHC when scoring protein levels, and the same caveats about needing to understand who to include in the treatment population apply. In general terms, selecting patients by gene amplification (e.g., using a FISH assay[74]) tends to identify a smaller number of patients than if the same group were evaluated for protein levels. However, there are a number of important clinical examples where patient groups selected on the basis of high gene amplification have responded well, in contrast to use of an IHC-based test which may include excessive numbers of nonresponders, thereby compromising the response rate to the novel therapy.

Although the use of gene amplification as a routine method for selection patients for kinase-based therapy is not yet established, it is often used in combination with the IHC test for HER2 to select patients with gastric and breast cancer for trastuzumab.[75] Gene amplification assays are however being developed as the most promising methodology for patient selection linked with emerging use of c-Met and FGFR inhibitors.[76,77]

5.02.3 Clinical Lessons Learned From First-Generation Inhibitors

Without the information which has already been gleaned from the clinical development of first-generation kinase inhibitors such as gefitinib, we could not understand the parameters which need to be controlled in order to deliver compounds which can optimally treat a patient with a carcinoma that is, to a greater or lesser degree, "kinase addicted." And while the great majority of kinase inhibitors do not show the debilitating toxicities associated with chemotherapy (such as hair loss, sterility, gastrointestinal toxicity, and neutropenia) they still make significant demands of the patient. Only by understanding the limitations of these early compounds from the patients' perspective can we identify ways to replace these compounds with true "best-in-class" drugs and ensure that inhibitors of new kinase types are better suited to long-term clinical utility.

For the majority of cancer patients, their families, their friends, and their physicians the most worrying limitation of first-generation inhibitors is lack of efficacy. For those patients who see no clinical benefit the question immediately arises as to whether the diagnostic methodology used to match the kinase inhibitor to the underlying genetic aberration(s) is appropriate. As we have

seen above, there remains no simple answer to this problem although it is clear from analysis of "superresponders" by NGS that increased levels of deep sequencing will, in time, allow increasing numbers of patients to receive a "personalized treatment."[78] For those patients who are fortunate enough to achieve a partial response the issue quickly becomes how durable the clinical benefit will last before acquired resistance occurs. While limited durability is undoubtedly linked to suboptimal target engagement in some patients, the emergence of drug-resistant kinase variants is well documented for kinases such as EGFR,[79] ErbB2,[80] ALK,[81] Abl,[82] and c-Kit.[83]

Given what is now an extensive clinical experience with these first-generation inhibitors a number of clear lessons emerge which need to be considered as new compounds progress into clinical studies. This comes down to some very basic parameters which the compound needs to satisfy. Although there are many risks with the development of an inhibitor of a novel, nonvalidated kinase target, it surely makes sense before spending millions of dollars on a clinical development program to find a compound with the potential to be truly best-in-class. First, does the compound engage its molecular target hard enough, long enough, and is it able to access the target in potential sanctuary sites (such as the brain)? Second, does it have the appropriate selectivity to target only the physiologically relevant form of the target and avoid dose-limiting off-target toxicities? Third, does the inhibitor have the ability to inhibit the predicted resistant mechanisms and prolong therapeutic benefit? Finally, can the new drug combine successfully with established and/or novel treatments, avoiding unwanted drug–drug interactions and other liabilities?

5.02.3.1 Target Engagement

A number of first-generation inhibitors do not achieve optimal target engagement; that is, on the basis of basic pharmacology they do not inhibit the protein sufficiently to shut down its activity to the required level. In the majority of cases this is due to the fact that the compounds lack selectivity for the desired target compared and as dose levels increase the compound starts to inhibit other targets, causing unwanted pharmacology before the target kinase has been completely "shut down." Examination of the 25 FDA-approved kinase inhibitors shows that over half of them have dose-limiting toxicities (DLTs) which are most likely *not associated* with the primary mechanism of action. Put another way, if these compounds had been more selective could they have been dosed to higher levels and shown greater efficacy? There is emerging data with a number of new kinase inhibitors to demonstrate that achieving greater target engagement may lead to greater clinical efficacy, and the story of second-generation ALK inhibitors will be covered later (see "**Design of ALK Inhibitors With Potency Against Mutations**" section).

For those cancer types which are associated with the development of secondary metastatic tumors in the brain (e.g., epidermal growth factor receptor mutation (EGFRm) NSCLC,[84] HER2 + ve breast cancer,[85] or triple negative breast cancer (TNBC)[86]) there is a critical need to ensure that the inhibitor can access the brain. If the inhibitor lacks the physicochemical properties to cross the blood–brain barrier (BBB),[87] or is a substrate for one of the major efflux transporters,[88] drug levels in the brain and cerebrospinal fluid will be below those necessary to achieve effective kinase inhibition and the brain may become a "sanctuary site," where metastatic lesions can develop away from the drug.[89] Design of kinase inhibitors which cross the BBB is possible although the relative size and complexity of many kinase inhibitors means this can be nontrivial. That said, the properties of small-molecule inhibitors which can be expected to increase the level of brain penetration are well known in the literature around a range of central nervous system (CNS) targets, and these lessons can be applied to the design of novel kinase inhibitors.[90]

5.02.3.2 On-Target Selectivity

The early literature of kinase inhibitors is dominated by the simple question of whether high selectivity (with respect to other kinases) was a positive property or whether the polypharmacology of many first-generation inhibitors was actually intrinsic to their clinical activity.[91] Although the question remains unanswered in a number of cases the movement toward precision medicine means that the objective of most new drug discovery programs is high selectivity against one (or certainly no more than 2 or 3) target kinases. In many major indications (e.g., Bruton's tyrosine kinase (BTK) inhibitors in chronic lymphocytic leukemia (CLL),[92] ALK inhibitors in NSCLC,[93] or c-Met inhibitors in papillary renal cell carcinoma[94]) highly selective inhibitors are already providing data which suggests that greater on-target selectivity may well provide meaningful additional clinical benefit. However in a number of more niche indications, such as the use of Ret inhibitors in medullary thyroid cancer, it remains less clear whether compounds without vascular endothelial growth factor receptor (VEGFR) activity will be evaluated in the near future.[95,96]

Secondary kinase activity while undesirable may of course not limit therapeutic benefit if the DLT is driven by a different pharmacology, or if optimal target engagement can still be achieved. Inhibition of kinases such as VEGFR[97] and the cell cycle kinases (cyclin-dependent kinases (CDK)[98], aurora kinases,[99] and polo-like kinases[100]) can be dominant in many settings. A number of first-generation inhibitors have been successful while having poor selectivity, but it is clear that if our ambition is to treat patients with earlier, less advanced, disease the patient's willingness to tolerate side effects will be much reduced. This is not just about compounds having severe (Common Terminology Criteria for Adverse Events Grade 3) toxicities; it is a recognition that in earlier disease patients will be on treatment for much longer periods of time, potentially years. Over these longer timescales the ability to tolerate chronic low-level toxicities becomes much more important.[101]

With the increase in understanding of how to design selective small-molecule kinase inhibitors (driven by empirical structure–activity relationship (SAR) data-sets and protein structural information) it is becoming possible in many cases to design inhibitors to have selectivity for mutant (or fusion) proteins over the WT kinase.[102] This is an exciting development which has the opportunity to further increase therapeutic index in settings such as EGFR-mutant NSCLC where the first-generation of inhibitors is limited by

skin rash and gastrointestinal toxicity which are driven by WT EGFR.[103] New generation compounds which are "WT sparing" are currently being explored in the first-line setting where it may be possible to both increase the number and durability of clinical responses *and* at the same time reduce rash and diarrhea. If this approach is successful it is likely we will see a number of new (best-in-class) inhibitors able to selectively target kinases which become cancer targets as a consequence of genetic mutation.

5.02.3.3 Targeting Resistance

The selection applied by the blockade of a pathogenomic driver not only will kill cells which are reliant on that pathway for survival but also provides a survival advantage for any clones which can avoid total dependence on the molecular target being inhibited. This form of Darwinian survival advantage[104] was first observed in the classical chemotherapy of bacterial pathogens where drug-resistant clones can be generated (both clinically and in culture) if the drug exposure was maintained at a sublethal concentration.[105] This form of clonal selection is so well established that it has been considered a clear proof of mechanism demonstrating that the bacterium has been forced into an adaptive response.[106]

In oncology the development of resistance in response to a selective kinase inhibitor was first explored in those CML patients who relapsed on imatinib following an initial response.[107] Careful follow-up of these individuals highlighted a number of mechanisms including increased Abl protein expression[108] and the evolution of a range of single-point mutations in Abl.[109] Curiously the spectrum of resistant mutations was found to be highly dependent on the specific kinase inhibitor being used with very different resistant profiles being recorded with nilotinib[110] and dasatinib.[111] However, both these compounds were "defeated" by the T315I mutation, a protein where the threonine gatekeeper had been mutated to an isoleucine.[112] Although it has subsequently been possible to develop compounds capable of inhibiting the Abl gatekeeper mutant the observation that the mutations in the gatekeeper residue are peculiarly difficult to target has been seen with other kinases, notably EGFR and HER2.[113,38]

Given that there are a finite number of possible gatekeeper mutations (based on the possible single-nucleotide changes which can give mutant kinases retaining the ability to fold) it is now possible to explore activity against these mutants before a compound has even entered the clinic. This approach can either exploit structural chemistry approaches or can generate the actual kinases for screening. While such studies need confirmation from clinical data it is clear that compounds which include activity against gatekeeper and other relevant mutant forms of the kinase should enjoy major advantages in clinical practice.[114]

5.02.3.4 Combinability

Given the concerns described earlier, and the polyclonal nature of solid tumors, it is perhaps a surprise that the vast majority of first-generation kinase inhibitors are actually approved for use as monotherapy. Currently only lapatinib is prescribed in combination with chemotherapy[60] while the use of kinase/kinase combinations is currently restricted to the use of trametinib and dabrafenib for the treatment of B-Raf mutant malignant melanoma.[115] Given everything we have learned about the underlying causes of cancer and the nature of acquired resistance, the concept of "combinability" should be of paramount concern in the selection of any new kinase inhibitor. While it is certainly possible that two kinase inhibitors may not be easy to codose due to their having overlapping on-target toxicities, it is a very different matter if a combination cannot be dosed due to a liability (such as a PK interaction) which is fundamentally down to suboptimal inhibitor design. As kinase inhibitors will undoubtedly be used more and more in combination, the avoidance of off-target toxicities and drug–drug interactions will become increasingly critical in compound selection.

Of course, combination treatment does not necessarily mean concomitant dosing of both agents on continuous schedules at the same doses used when given as monotherapy treatment, although there are examples, such as the use of anti-VEGFR and anti-EGFR therapies where this has been very successful, such as in first-line EGFR-mutant NSCLC. Another good example is the combination of B-Raf inhibitors with MEK inhibitors where concomitant dosing is the current SOC.[116] However other kinase inhibitors may be better tolerated on episodic schedules, and consequently the kinetics of drug elimination become more important and compounds with shorter clinical half-life may have advantages over those which can achieve very flat pharmacokinetic profiles with low peak/trough ratios. Dinaciclib is a CDK9-selective inhibitor which has been demonstrated to be active given by i.v. infusion on a weekly schedule. Furthermore, by limiting the period of time where the kinase inhibitor is present at biologically effective concentrations, the off-target effects of inhibiting the cell cycle kinases CDK1 and CDK2 are dramatically reduced.[117]

In summary, despite the success of a number of first-generation inhibitors which do not match up to the four criteria described, it is clear that novel kinase inhibitors need to be much better designed if they are to realize the full benefits that may be achieved in a world of precision medicine with molecular diagnosis at the heart of the way in which cancer is treated. The next sections will highlight examples which show how various research groups are pushing the boundaries of our current understanding and, in doing so, are starting to generate clinical data which offers a step-change in the way kinase inhibitors are used for the treatment of cancer.

5.02.4 Bcr-Abl Inhibitors

5.02.4.1 Chronic Myeloid Leukemia and the Discovery of Imatinib

A reciprocal translocation between chromosome 9 and 22 leads to the short Philadelphia (Ph) chromosome[118,119] containing the oncogene Bcr-Abl (breakpoint cluster region–Abelson leukemia) which is the drive for initiation of CML.[120] The Bcr-Abl fusion

protein contains a truncated regulatory domain which leads to a constitutively activated Abl tyrosine kinase domain, which in turn drives the proliferation of stem cells in bone marrow and the progression of this aggressive hematological disorder. In 2001, <3 years after the start of Phase I studies, imatinib (Glivec, Gleevec) was approved for the treatment of CML, ultimately transforming how the disease is currently treated.[121] The discovery of imatinib also represents an industry landmark being the first kinase inhibitor to receive regulatory approval and at the same time heralding the era of targeted drug therapies in cancer. The recommended dose for imatinib is 400 mg QD, with a higher dose of 600 mg QD for accelerated/blast phases of the disease. Imatinib is a relatively selective kinase inhibitor, being shown to inhibit c-Kit and PDGFR in addition to Bcr-Abl. At the time this high selectivity was attributed to the observation that imatinib bound to and stabilized an inactive DFG-out conformation of the kinase (a type II mechanism) although more extensive characterization of other type II inhibitors discovered subsequently has shown that high selectivity does not necessarily follow from such a mechanism, and indeed, many inhibitors which exhibit a type I mechanism (binding to the active DFG-in kinase) can show high degrees of selectivity.[122]

The discovery of imatinib followed a high-throughput screen with compound **1** found as a promising if modestly potent inhibitor of c-Abl (Fig. 1) albeit the screen was in fact seeking to identify Protein kinase C (PKC)-α inhibitors.[123] SAR studies led to replacement of the imidazole in **1** with a benzamide moiety which boosted Bcr-Abl potency, and critically, addition of a methyl group onto the central ring resulted in abrogation of PKC-α and CDK1 activities. This "flag-methyl" is a feature of numerous subsequently characterized DFG-out kinase inhibitors. In order to overcome poor bioavailability, a solubilizing basic side chain was appended to the benzamide although in subsequent structures this basic group was additionally shown to make key hydrogen-bonding interactions with Ile360 and His361. The pyridine of imatinib forms the key hinge hydrogen bond to Met318. The anilino NH donates a key hydrogen bond to the gatekeeper Thr315 with the amide carbonyl bonding to Ala380. The benzamide ring occupies the pocket vacated by the shifted Phe in the DFG sequence.

Imatinib is able to reduce the number of Ph + stem cells in the bone marrow and normalizes peripheral white blood cell counts although it cannot completely deplete Ph + stem cells. It is thought that this is because stem cells in a quiescent state are not dependent on Bcr-Abl signaling, which is why patients invariably relapse on therapy.[124] However despite its enormous clinical impact, for some patients imatinib proved to be relatively ineffective against more advanced stages of the disease, including against other Ph + leukemias such as acute lymphoblastic leukemias (ALL), due to the emergence of significant acquired resistance. Rates of resistance vary according to the stage of the disease, with resistance much higher in later stages. In newly diagnosed cases resistance rates are low, in the region of 3–4% of patients, but in end stage blast phase, can be as high as 80%.

5.02.4.2 Mechanism of Resistance to Imatinib

A variety of mechanisms of resistance to imatinib have been reported in both clinical samples and through preclinical in vitro studies, but the major mechanism is via single-point mutations in the kinase domain which render imatinib unable to efficiently inhibit Abl kinase activity.[125] The transforming potential of these mutations varies significantly, with patients experiencing different prognostic outcomes depending on their mutational profile; a specific mutant may not always confer resistance to imatinib, and the presence of a mutant may not always explain drug resistance. As with EGFR inhibitor treatment, some mutations have been shown to preexist at low levels in newly diagnosed patients and may be selected for under the pressure of imatinib drug therapy. Other studies have shown that these point mutations more typically arise during treatment although this remains an area of significant debate.[125] To date over 100 single-point mutations have been detected in patients treated with imatinib. Lack of imatinib activity against the gatekeeper T315I mutation may be rationalized by the loss of the hydrogen bond between Thr315 and the aniline-NH of imatinib which is further compounded by a clash between the aniline ring and Ile315. Gatekeeper mutations have been observed as

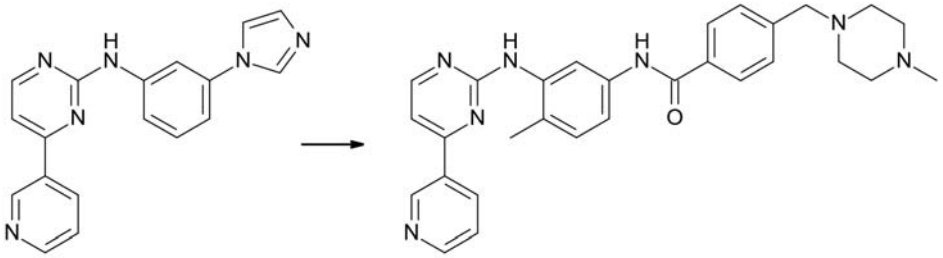

1
c-Abl IC_{50} = 3300 nM

Imatinib
c-Abl IC_{50} = 188 nM
Kit IC_{50} = 413 nM
PDGFRβ IC_{50} = 386 nM

Fig. 1 From screening hit to imatinib.

an escape mechanism in other targeted therapies such as in the use of gefitinib and erlotinib in EGFR mutation positive NSCLC, as will be discussed in "Optimizing Kinase Inhibitors for Selectivity and Acquired Resistance for Lung Cancer" section. Reduced activity against the L248V mutant has been postulated to be due to both a poorer topological fit with imatinib and also to a destabilization of the protein inactive conformation to which imatinib prefers to bind. Similarly, this destabilization of the inactive form of the kinase is thought also to be relevant with the gatekeeper T315I mutation leading to an activated kinase state. Resistance by M351T is thought to be due to an indirect consequence of an increase in protein entropy which disfavors inhibitor binding. All of these mutants are considered highly prevalent, and all are still able to efficiently bind adenosine triphosphate (ATP) and thus drive cellular signaling.

In some cases overexpression of Bcr-Abl has been linked to resistance,[125] and while increasing the dose of imatinib may be effective in some cases, the relative lack of potency of imatinib limits this approach. In addition, studies have implicated the overexpression of Src family kinases in CML disease progression, and this has provided a rationale for the testing and ultimate approval of dual Src/Abl tyrosine kinase inhibitors (the Src family kinases consist of Src, Fyn, Lck, Lyn, Hck, Yes, Blk, and Fgr). Bcr-Abl is known to directly phosphorylate Src kinase, and Lyn kinase is overexpressed in cells resistant to imatinib therapy. Patient samples taken before and after therapy with imatinib have also demonstrated activation of Lyn and Hck. Resistance to imatinib may also occur as a consequence of it being a substrate for the multidrug resistance-associated P-glycoprotein (PgP), where overexpression of PgP in tumor cells has been shown to limit uptake of imatinib.

5.02.4.3 Second-Generation Therapies

Following an understanding of the mutations that lead to imatinib resistance, second-generation inhibitors have been developed which are able to effectively inhibit most of these mutations although these agents are unable to inhibit the key gatekeeper T315I mutation (in which the usual threonine gatekeeper is replaced with a more bulky isoleucine). This mutation is seen in 15–20% of clinical samples and so represents a significant escape mechanism following imatinib treatment. Kinase inhibitors that have been launched to address the emergence of imatinib resistance are shown in Fig. 2. However, in a number of cases these inhibitors were not specifically designed to target imatinib-resistant populations, rather their broader Bcr-Abl mutant activity was discovered through serendipity.

5.02.4.3.1 Nilotinib

Nilotinib (Tasigna) is an analog of imatinib that demonstrates superior potency and a broader profile of activity against imatinib-resistant mutants. The compound was discovered through structure-based design efforts aimed at understanding why certain

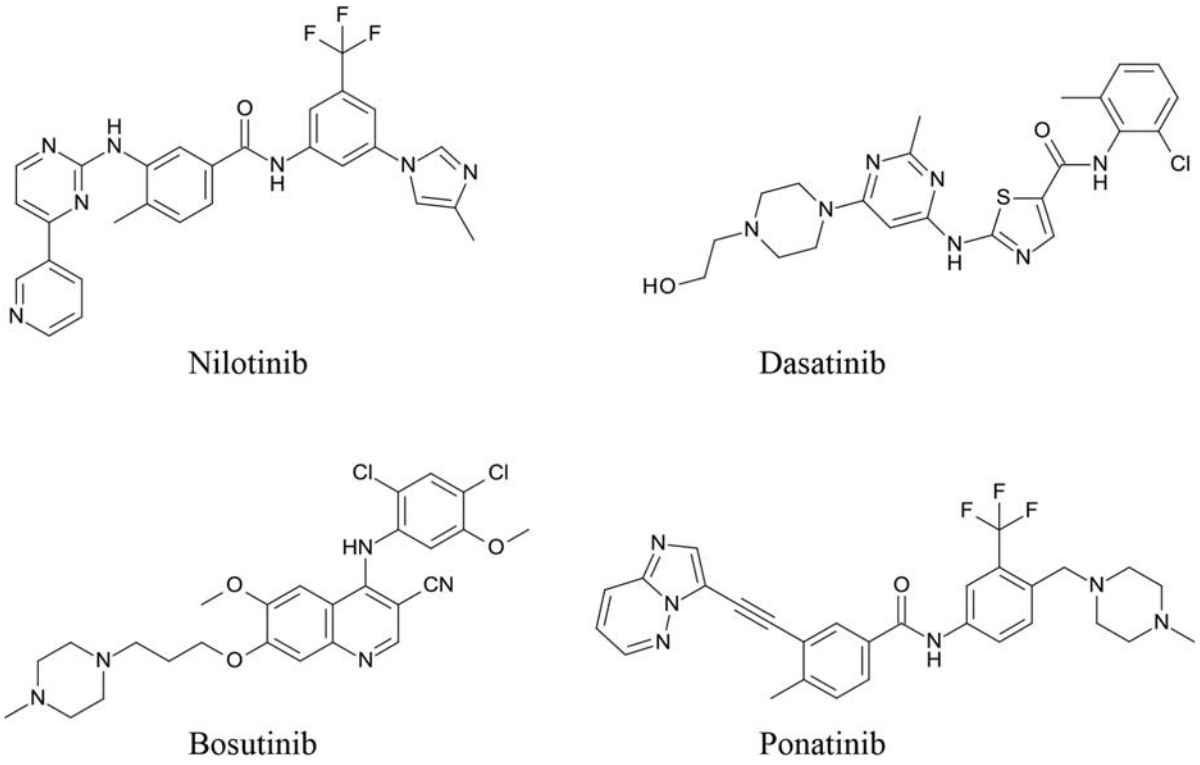

Fig. 2 Bcr-Abl inhibitors that address the emergence of resistance to imatinib therapy.

mutations confer imatinib resistance.[126] Nilotinib contains much of the same architecture of imatinib but differs in the nature of the group that occupies the DFG pocket. Not only is nilotinib much more potent than imatinib (about 30-fold more potent), it sustains activity against 32 out of 33 clinically relevant Bcr-Abl mutants. That nilotinib is active against most of the mutants that drive resistance to imatinib is thought to be due simply to its increased affinity for Abl, allowing it to overcome the shift in equilibrium toward the active state of the kinase which is typically seen with most of the mutants. The increased affinity of nilotinib is thought to be related in part to the observation that it is a better fit in the DFG pocket compared with imatinib. However, there is also a likely contribution from a weak electrostatic interaction between the trifluoromethyl substituent and the polarized C atom of the Ala380 carbonyl. It was approved as a first-line treatment for CML in 2010 with a recommended dose of 300 mg BID; although for patients resistant to or intolerant of imatinib, the dose is 400 mg BID in the chronic or accelerated phases of the disease. Interestingly, it has a distinctly different safety profile to imatinib and patients are generally not cross-intolerant to these agents. Significant fluid retention can be observed in imatinib-treated patients which has been attributed to the off-target inhibition of PDGFR. However, this assertion is questionable given that this is not a common side effect of nilotinib treatment despite it being a significantly more potent PDGFR kinase inhibitor.[127] As with imatinib, point mutations also occur on nilotinib therapy, ultimately leading to the emergence of clinical resistance. In a cell-based screen, point mutations in eight amino acids were observed following nilotinib treatment. However, all of the mutants proved to be sensitive to higher doses of nilotinib. Around 20 different mutations have been observed in Phase I trials for nilotinib affecting around 40% of patients although no differences in clinical outcome were observed based on the mutational status in this study, and patients with mutations continued to respond to treatment.[127]

5.02.4.3.2 Dasatinib

Dasatinib (Sprycel) was initially identified as a dual Lck/Src inhibitor.[128] Like many Src inhibitors it was subsequently shown to possess potent activity against all Src-family kinases, Bcr-Abl, and a wide range of imatinib-resistant Bcr-Abl mutants, including 21 out of 22 clinically observed forms of the kinase. There is a high degree of homology between Src and Abl in their active states and dasatinib, being a type I inhibitor, binds exclusively to the active form of Bcr-Abl. Interestingly, the reverse is not generally true, i.e., DFG-out Abl inhibitors do not typically possess potent Src activity. For example, imatinib and nilotinib do not inhibit Src kinases, thus it was presumed that Src is unable to adopt a DFG-out conformation. Dasatinib, like nilotinib, was approved in 2010 for first-line treatment with a recommended dose of 100 or 140 mg QD for accelerated/blast phases of disease, including in patients resistant or intolerant to imatinib. Cell-based mutational screens have demonstrated the emergence of some mutations that confer resistance to dasatinib that are also coincident with imatinib and nilotinib resistance. However, as with nilotinib, in the clinic many patients harboring mutations in the kinase domain continue to respond to treatment. The exception to this is the T315I gatekeeper mutation which typically leads to clinical failure. In 2011 the FDA identified that dasatinib may increase the risk of pulmonary arterial hypertension, a rare but serious adverse event associated with an increase in blood pressure in lung arteries.

5.02.4.3.3 Bosutinib

Bosutinib is another example of a therapy originally designed as a Src inhibitor that has demonstrated clinical activity against many of the imatinib resistance mutants by virtue of its potent Bcr-Abl activity.[129] Hits optimized from a Src-dependent yeast screen delivered bosutinib, and its activity against Bcr-Abl was deconvoluted after showing an antiproliferative phenotype in a panel of leukemic cell lines. Like dasatinib, bosutinib is a type I kinase inhibitor although unlike the other agents utilized in the treatment of CML, including dasatinib, it shows no appreciable activity against either c-Kit or PDGFR. Despite this, bosutinib is now known to inhibit a range of other seemingly unrelated kinases including Csk and Axl and is classed as a multitargeted kinase inhibitor in the manner of dasatinib. As with the other second-generation inhibitors, bosutinib inhibits all imatinib-resistant mutants with the exception of T315I. Bosutinib was approved in 2012 at a dose of 500 mg QD for the treatment of all phases of CML in patients who are resistant to or intolerant of prior Bcr-Abl therapies, a more limited indication than seen for other second-generation therapies.

5.02.4.4 Addressing the Gatekeeper T315I Mutation

The gatekeeper T315I mutation was identified very early in the clinical use of imatinib, and while subsequent agents have addressed a spectrum of the observed mutations that emerge upon imatinib treatment, the T315I mutation continues to represent a key unmet medical need. Conceptually, it could be envisaged that there are two orthogonal approaches to targeting the T315I gatekeeper mutant. The first approach, and the most widely explored, is to develop ATP-competitive inhibitors (type I or type II) that retain high affinity for the T315I gatekeeper mutant. The second and potentially complimentary approach to inhibiting the T315I gatekeeper mutant, as well as other clinically relevant Bcr-Abl mutants, is to seek to identify allosteric inhibitors that are non-ATP competitive and have a distinct mode of action. Allosteric inhibitors could also be combined with existing ATP-competitive agents to deliver additive activity with the potential to inhibit a wider spectrum of clinically relevant Bcr-Abl mutants. Conceptually, this would enable a "double-hit" strategy, whereby the kinase is simultaneously inhibited by two distinct inhibitors with nonoverlapping binding sites as well as possessing different modes of inhibition. In addition to offering the potential for synergism, a "double-hit" strategy may also reduce the emergence of resistance in the clinic.

5.02.4.4.1 Ponatinib: An ATP-competitive inhibitor of T315I

Ponatinib was originally developed as a multitargeted kinase inhibitor and is an example of a type II inhibitor with a relatively promiscuous profile.[130] In addition to Bcr-Abl mutants, it has potent activity against FLT3, FGFR, and VEGFR family kinases, together with c-Kit and PDGFR. Unusually for an agent with this mechanism it also retains potent Src inhibitory activity, and not only does it inhibit all imatinib-resistant Bcr-Abl mutants, but it is also able to suppress emergence of resistance mutations in cellular systems in vitro. While this compound shares some structural similarity to nilotinib in the region of the gatekeeper/DFG pocket, it is noteworthy that ponatinib is able to effectively inhibit the T315I mutation whereas nilotinib does not. Docking studies have highlighted a steric clash between the amino group on the pyrimidine ring of imatinib and the bulkier isoleucine residue which is not seen with ponatinib. Additionally, loss of the threonine removes a hydrogen bond between the hydroxyl of the amino acid and the amino group seen with imatinib. The same interaction is not relevant in the binding of ponatinib. Ponatinib was approved in 2012 for patients with T315I-positive CML or T315I-positive Ph + ALL for whom no other tyrosine kinase therapy is indicated. However, a series of patient safety events led to the temporary suspension of sales in Oct. 2013 due to the observation of life-threatening blood clots and severe narrowing of blood vessels. This suspension was lifted in Dec. 2013, with a new Black Box Warning applied, together with a risk evaluation and mitigation strategy (REMS).

5.02.4.4.2 Allosteric Bcr-Abl inhibitors

In 2006 researchers from Novartis and the Scripps Research Institute reported on the first successful effort to identify an allosteric inhibitor of Bcr-Abl.[131] Using an unbiased differential cytotoxicity screen, GNF-1 (Fig. 3) was identified as a moderately potent inhibitor with an IC_{50} of 400 nM in Bcr-Abl expressing cells versus an IC_{50} of 40 μM in cells that did not express Bcr-Abl. A follow-up medicinal chemistry optimization effort, starting from GNF-1, generated 350 related analogs and revealed a clear cellular SAR across the series. An early lead to emerge from this effort was GNF-2 which retained the 4-trifluoromethoxyaniline group appended off the pyrimidine core. GNF-2 had increased potency over GNF-1 with an IC_{50} in Bcr-Abl-dependent cells of 138 nM. In the same antiproliferative assay, the established Bcr-Abl inhibitor imatinib had a cellular IC_{50} of 190 nM. Upon further profiling, GNF-2 was confirmed to be specific for Bcr-Abl-transformed cell lines (K562 and SUP-B15) but did not block proliferation in cells transformed with other oncogenic kinases. Further characterization of GNF-2 highlighted that the compound was unable to block Abl kinase activity in vitro (unlike imatinib) but was able to block Bcr-Abl signaling in the cell which pointed to either a different mechanism of action or that potentially GNF-2 was inhibiting a different component of the Bcr-Abl signaling complex. However, evidence that the molecular target for GNF-2 was in fact Abl was provided initially through chemoproteomic studies. Using an affinity probe (GNF-2 immobilized onto Sepharose beads) it was shown that endogenous Bcr-Abl could be scavenged from cell lysates prepared from Bcr-Abl-dependent cells. Performing the same affinity chromatography screens in the presence of either ATP or imatinib failed to displace Bcr-Abl from the GNF-2 affinity beads. In contrast, competition experiments using

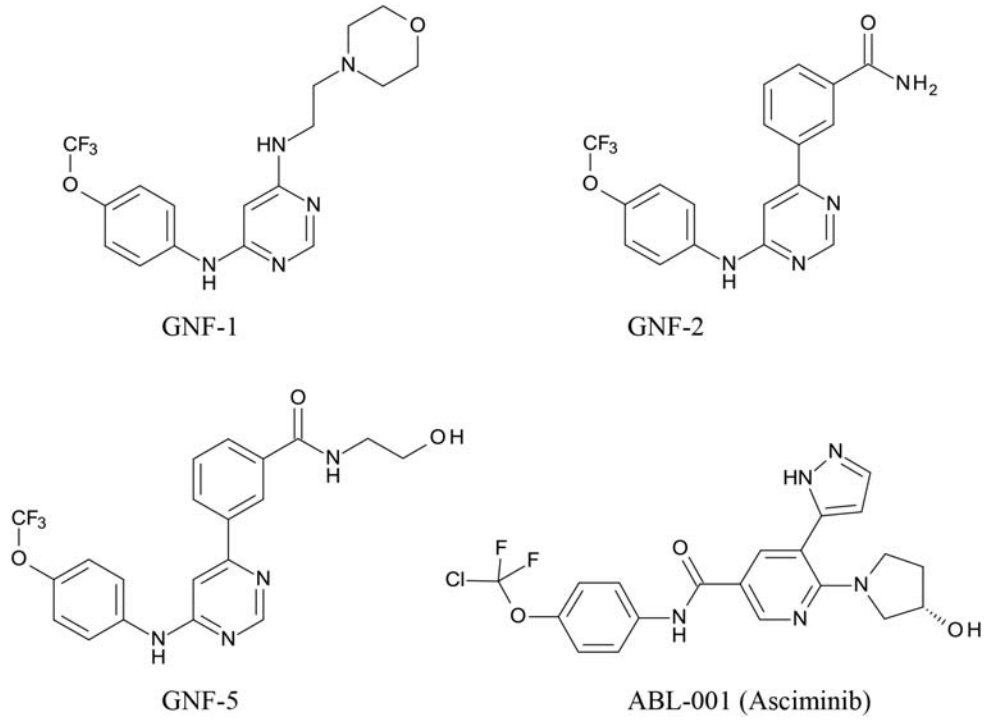

Fig. 3 Allosteric inhibitors of Bcr-Abl.

a truncated N-myristoylated peptide of Abl (residues 2–16) blocked the capture of Abl using the same GNF-2 affinity beads which suggested that the compound bound to the myristate-binding cleft of Abl. This hypothesis was further strengthened following the observation that single-point mutations introduced into the myristate-binding cleft (A337N and A344L) induced resistance to GNF-2 but did not significantly affect the activity of imatinib. Furthermore, combination experiments with imatinib and GNF-2 highlighted a moderate synergy which was also potentially consistent with the evidence that both compounds bound to Abl but targeted different regions of the protein. This hypothesis was subsequently validated through solution NMR studies in combination with X-ray crystallography which both confirmed that GNF-2 bound to the myristate-binding cleft in Abl and had a unique mode of action.[132] The binding mode was consistent with the observed SAR and explained the importance of the para-substituted trifluoromethoxy group and the need for the aniline NH which is required for a through water hydrogen bond with the backbone carbonyls of A433 and E462. Mechanism of action studies, including detailed enzyme kinetics, defined that GNF-2 and related analogs mimic the endogenous role of the N-terminal myristoyl group in Abl, in that they induce and stabilize a clamped catalytically inactive state, whereby the SH2 and SH3 domains of Abl bind into the kinase domain resulting in inhibition of kinase function.[133]

Combining two compounds that inhibit the same oncogenic kinase, but which have distinct modes of action including binding to different regions of the target protein (e.g., combining an ATP competitive with an allosteric inhibitor), could be envisaged conceptually as offering two potential advantages over established monotherapy approaches. First, there is the potential that the combination is synergistic such that greater target inhibition can be achieved from the same clinically tolerated dose of the respective single agents. Potentially this could enable resistant mutants that would otherwise be insensitive to the single agent alone at clinically tolerated drug exposures to be successfully inhibited though the use of a combination partner drug with a different mode of action targeting the same kinase. A second hypothetical advantage is the potential to delay the emergence of resistance in the clinic leading to a more resilient therapeutic strategy. In this regard, a carefully selected drug combination whereby there is a nonoverlapping mutant sensitivity would mean that under drug pressure the cancer cell would need to develop mutations that confer resistance to both drug molecules in order to remain "fit" and thus able to proliferate. In order to understand this potential further, the Novartis group performed combination experiments with imatinib (1 μM) and GNF-2 (5 μM) which led to a 90% reduction in the generation of resistant clones from Bcr-Abl-dependent cells compared with imatinib alone.[133] In addition, using a cellular barcode methodology (ClonTracer) to track cell lineage, clonal responses to imatinib, nilotinib (ATP competitive), and GNF-2 in KCL-22 cells (an acute myeloid leukemia (AML) cell line harboring the Bcr-Abl translocation) were determined.[134] In these experiments, resistance to the allosteric inhibitor emerged more rapidly than with the ATP-competitive inhibitors. Moreover, there were a greater number of GNF-2-resistant clones in each replicate compared to resistant populations of either imatinib or nilotinib. However, the pattern of resistance for the ATP-competitive inhibitors was largely distinct when compared to the GNF-2-resistant populations with only a small number of overlapping mutations conferring resistance to both mechanisms. For example, the gatekeeper mutation in Abl, T315I, was highly enriched in the imatinib- and nilotinib-resistant populations, whereas the A337V mutation, which is in the myristate-binding cleft, was highly prevalent in the GNF-2-resistant populations, consistent with its novel mode of action. Modeling the data from these cellular barcode experiments also suggested that most if not all of the resistant clones were preexisting which supports the concept of codosing both ATP competitive and allosteric Bcr-Abl inhibitors together in order to delay the emergence of resistance in the clinic.

Synergistic activity was also observed when combining allosteric and ATP-competitive inhibitors.[132] GNF-5 (**Fig. 3**), a close analog of GNF-2 with comparable cellular activity but with improved pharmacokinetic properties, was profiled in both in vitro and in vivo experiments to understand potential advantages of combining allosteric and ATP-competitive inhibitors. Against Bcr-Abl-dependent cells harboring the gatekeeper mutation (T315I), a combination of GNF-5 (at a concentration of 2 μM) and nilotinib showed potent inhibition of proliferation (IC_{50} for nilotinib of ~0.8 μM) which was moderately synergistic with a combination index of 0.6. Similar cooperativity was observed against WT Bcr-Abl-dependent cells. Against recombinant Abl kinase, a combination of GNF-5 and nilotinib exhibited synergistic activity against both WT and the T315I gatekeeper mutant with the IC_{50} of nilotinib increasing fivefold against the T315I mutant in the presence of GNF-5 at 10 μM. Evidence of cross-talk between the distal myristate-binding cleft and the ATP-binding site was confirmed using hydrogen-exchange mass spectrometry. Upon GNF-5 binding, changes in the peptides surrounding both the myristate-binding cleft as well as the ATP-binding site were observed in WT Abl. In contrast, no changes were observed with the E506K myristate site mutant thus providing clear evidence that GNF-5 binding directly affects the conformation of amino acid residues in the ATP-binding site, providing a basis for how the allosteric inhibitor is able to enhance binding of nilotinib to mutant and WT Abl.

In a human CML disease model driven by the T315I Bcr-Abl mutant, dosing with either GNF-5 or nilotinib alone failed to deliver any significant activity.[132] In contrast, combining the two inhibitors at the same respective doses delivered significant efficacy with the normalization of both blood counts and spleen weights being observed without any evidence of acute toxicity. In mice transplanted with transduced bone marrow harboring the T315I Bcr-Abl mutant, a combination of GNF-5 and nilotinib showed a significant survival benefit compared to mice treated with either inhibitor alone or vehicle. Median survival for animals treated with either GNF-5 or nilotinib alone was 28 or 32 days, respectively. In contrast, in the combination group all animals survived to day 50 which was the end of the dosing schedule. After a further 46 days of observation, 4 out of the 5 animals on study had survived with no observable disease.

The discovery and characterization of novel allosteric inhibitors to Bcr-Abl has for the first time validated a kinase "double-hit" strategy that has the potential to treat mutant T315I-positive CML/Ph + ALL. Through binding to the myristate site on Abl, the allosteric inhibitors GNF-2/5 are able to induce/stabilize an inactive state of the kinase that results in the inhibition of Bcr-Abl signaling in the cell. Moreover, the allosteric inhibitors synergize with existing ATP-competitive inhibitors to enable the in vitro/in vivo

targeting of the difficult to inhibit T315I Abl mutant. A potential further benefit of the "double-hit" approach is the opportunity to suppress the emergence of resistance. This was conceptually demonstrated in vitro through combining GNF-2 with imatinib and has the clear potential to be a relevant strategy in the clinic. However, GNF-5 has only modest potency which limits its potential as a clinical drug candidate. To resolve this deficiency, the Novartis group, through a fragment-based hit generation effort followed by a traditional medicinal chemistry lead optimization campaign, identified ABL-001 (Fig. 3) which possesses overall excellent developability properties and has increased potency as an allosteric inhibitor compared with GNF-5.[135] ABL-001 was progressed into clinical studies and is currently being investigated in a Phase I trial in leukemia patients, both as a single agent and in combination with ATP-competitive inhibitors such as imatinib and nilotinib.

A similar myristate-binding cleft is present in a small number of other kinases including Src family members; however it is not understood whether this pocket is generally amenable to identifying allosteric inhibitors. The concept of combining an allosteric inhibitor with a suitable ATP-competitive inhibitor to enable a "double-hit" approach appears to be a valid medicinal chemistry strategy that could be used more broadly to develop novel cancer treatments that may deliver both increased clinical efficacy and delaying the emergence of resistance.

5.02.5 Optimizing Kinase Inhibitors for Selectivity and Acquired Resistance for Lung Cancer

5.02.5.1 Introduction

In this section we will discuss a selection of drugs and clinical candidates that have been developed for NSCLC, a disease for which there has been significant progress in segmentation of patients according to genetic status,[136] focusing on inhibitors of EGFR ("Design of Mutant Selective EGFR Inhibitors" section) or anaplastic lymphoma kinase (ALK, "Design of ALK Inhibitors With Potency Against Mutations" section). These targets are being discussed together because there are a number of similarities between the drug discovery efforts that have addressed them in recent years. Success in the clinic against both targets initially depended on an understanding of how to select patients that would be sensitive to such agents, and further success has depended upon an understanding of resistance mechanisms and how to target specific mutations that are relevant to those resistance settings.

5.02.5.2 Design of Mutant Selective EGFR Inhibitors

EGFR was one of the early kinases to attract interest from the pharmaceutical industry, as an approach to treating cancer patients. The first patients on EGFR inhibitors (as part of a more general interest in the Her family) were filed in the 1990s, and yet this is still a highly active area of research which has seen recent breakthroughs, over 20 years later. Achieving success in the clinic has required an understanding of the mutation status of EGFR in patients, and consequently the medicinal chemistry strategies have had to adapt to target particular mutations and consider selectivity margins, in this case against the WT form of EGFR. In this section we will describe the early clinical candidates for EGFR ("Early inhibitors of EGFR, targeting activating mutations" section), go on to describe medicinal chemistry tactics to target the T790M mutation ("Design of T790M mutant selective EGFR inhibitors" section), and then provide a future outlook ("Future outlook" section).

5.02.5.2.1 Early inhibitors of EGFR, targeting activating mutations

Many of the early reported EGFR inhibitors used a quinazoline hinge binder (Fig. 4), linked off C4 with a lipophilic aniline moiety to access a lipophilic region of the ATP pocket (the so-called selectivity pocket)[137] although this was not the first reported series to inhibit EGFR.[138] The first marketed EGFR inhibitors used related templates, but with the addition of a solubilizing side chain to improve solubility and optimized anilines, such as gefitinib (Iressa, launched 2002)[139] and erlotinib (Tarceva, 2004).[140] These inhibitors (Fig. 4) were discovered by screening versus the WT form of EGFR and are potent inhibitors against the WT. Initially it was not understood that the mutation status of EGFR was correlated to response rate, neither was the mutation status assessed in the early clinical trials. However, it was observed that certain groups of patients had higher response rates in trials with these agents, specifically nonsmokers, people with Asian ethnicity and females, and subsequently the connection between response rate and EGFR mutation status was made.[141] Patients with mutated forms of EGFR (such as L858R and exon 19 deletion), which

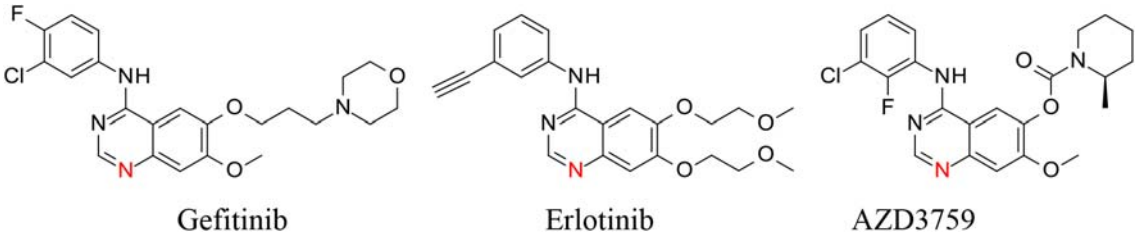

Fig. 4 Reversible quinazoline-based EGFR inhibitors. Throughout this section, structures are orientated with the assumed hinge-binding motif at the bottom (key donor/acceptor atoms in *red*), with the solvent channel[137] group to the right where this is known.

have reduced affinity for ATP and have been described as "activating mutations," respond well with gefitinib and erlotinib, and these agents are now marketed drugs for NSCLC patients with EGFR activating mutations.

5.02.5.2.2 Design of T790M mutant selective EGFR inhibitors

While the majority of NSCLC patients with EGFR activating mutations respond well to these agents, they generally relapse and become resistant to treatment. While a wide variety of acquired resistance mechanisms have been reported,[142,143] a common mechanism is by secondary mutations in EGFR itself, of which the most common is a mutation of the threonine gatekeeper of the kinase to methionine (T790M).[144] The inhibitors shown in Fig. 4 do not have significant activity against the double mutants, so developing inhibitors against the L858R/T790M and exon 19 deletion/T790M forms of EGFR became a priority. The challenge is that the T790M mutation increases the affinity for ATP,[145] and therefore developing inhibitors against these double mutants are more difficult, particularly in a cellular setting where high concentrations of ATP compete effectively with an inhibitor. An additional challenge is that the larger gatekeeper in T790M may make it harder to position a group into the selectivity pocket or reduce direct interactions with the gatekeeper for molecules that have been optimized against the Thr gatekeeper.

A particularly successful tactic to target the T790M mutation has been the addition of a covalent warhead at just the right position to bind irreversibly to one of the cysteines accessible in the EGFR-binding site. The resulting irreversible inhibitors overcome the difficulty with ATP competition in cells. Thus addition of an acrylamide to specific positions within the anilino quinazoline template led to a number of compounds that have progressed into the clinic, including those shown in Fig. 5. Canertinib was the first irreversible inhibitor to enter clinical trials and progressed as far as Phase II.[146] This compound, along with other irreversible inhibitors such as afatinib[147] (Gilotrif, approved 2013) and dacomitinib[148] (Phase III), employs the same selectivity pocket group as gefitinib, whereas neratinib[149] (Phase III) employs a larger group that is capable of pushing out the C-helix, in a similar manner to the reversible inhibitor lapatinib. Reversible binding of these quinazoline inhibitors into the ATP pocket places the acrylamide in close proximity to the cysteine (C797), which can then result in covalent bond formation and deactivation of the kinase, as shown in the published WT structure of afatinib.[150] These inhibitors still have activity against the WT and single (activating) mutant forms of EGFR but also have significant activity against the double mutant forms although they were not designed to target the T790M mutation. They should therefore in theory be effective compounds for patients who harbor both single (activating) mutations and double (activating + T790M) mutations of EGFR.

In practice, the limitation with these agents has been tolerability, which can limit the dose and therefore limit the efficacy. The toxicities that have been described, chiefly rash and diarrhea, have been attributed to the fact that these compounds inhibit WT EGFR more potently than T790M containing mutants. This clinical data suggested that inhibitors that target both single activating and double (T790M) mutants, but have selectivity over the WT form, would be desirable. A number of approaches that have resulted in such compounds have been described preclinically, and several compounds have subsequently progressed into the clinic. Fig. 6 shows some examples, where an acrylamide has been used as before to obtain potency against the mutant forms of the kinase in cells. However, these examples differ from those in Fig. 5, in that the acrylamide has been added to a scaffold that has some inherent degree of selectivity versus the WT form, and not the quinazoline template used previously. Scientists from the Dana-Farber institute reported one such approach in 2009,[151] which included a crystal structure of WZ4002

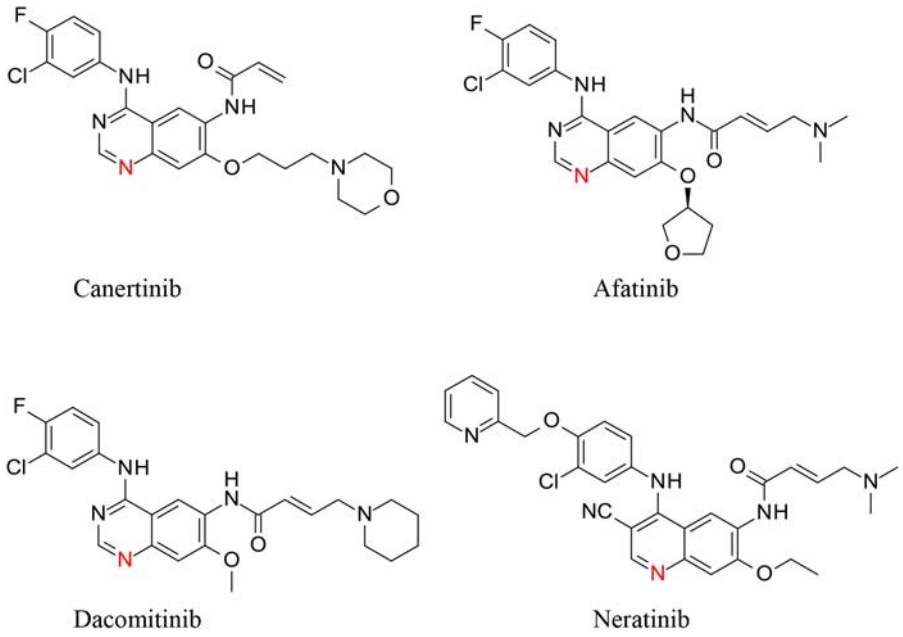

Fig. 5 Irreversible quinazoline-based inhibitors that target single and double mutants.

(Fig. 6, Gatekeeper pharmaceuticals) covalently bound to the active conformation of EGFR. The acrylamide group that covalently targets the Cys797 residue is attached to the phenolic group in the 4 position of the anilinopyrimidine hinge binder. The aniline contains a piperazine and a methoxy group ortho to the aniline that was reported to improve kinase selectivity. By switching templates from quinazoline to anilinopyrimidine, this compound now hits the single (activating) mutations and the double (T790M + activating) mutations, with a margin over WT; an attractive profile as this profile could achieve efficacy and tolerability. The chlorine substituent at the C5 position of the pyrimidine ring contacts the lipophilic gatekeeper residue (Met 790) and may contribute to its potency versus the T790M mutant.[151]

At this point no clinical trials have been initiated on the Gatekeeper compounds. However, both Clovis and AstraZeneca (and other companies, more recently) progressed compounds from their programs into the clinic. Rociletinib/CO-1686 (Fig. 6, Clovis) progressed as far as Phase III clinical trials, although Clovis had to modify the disclosed data on confirmed response rates as the efficacy data matured,[152] and has since terminated its clinical development. This compound uses a similar template to WZ-4002, in that it has an anilinopyrimidine hinge binder and targets Cys797 with an acrylamide attached to the aryl ring in the C4 position of the pyrimidine (now O linked). There are subtle differences in the solvent channel (acetyl vs methyl piperazine)

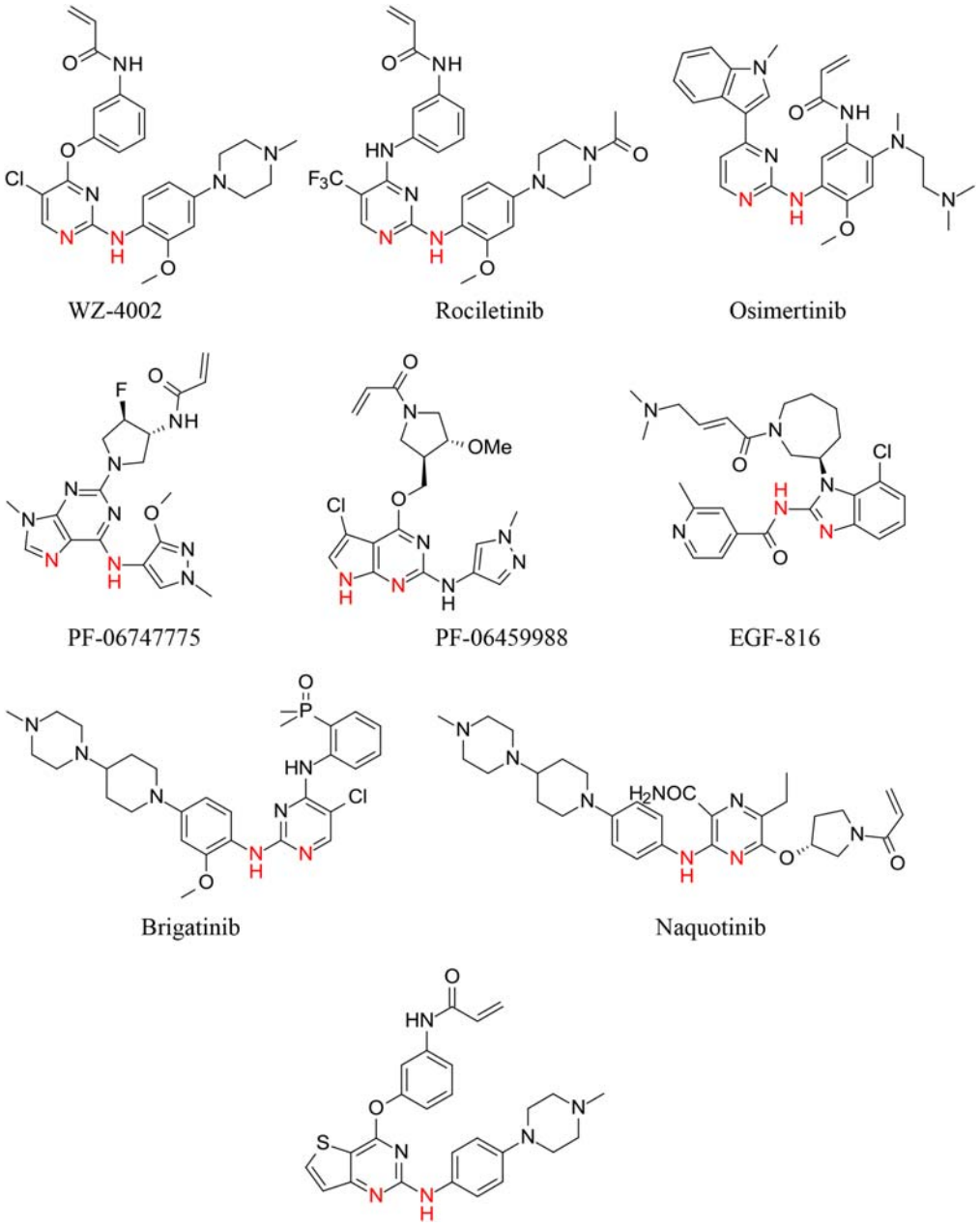

Fig. 6 EGFR covalent inhibitors that target single and double mutants, with selectivity versus wild type.

and the pyrimidine C5 substituent that points toward the gatekeeper (CF_3 vs Cl). This compound has a similar profile of greater activity against both single and double mutants versus WT. Clovis have published data on their compounds suggesting a greater L858R/T790M to WT margin than observed for WZ4002, when comparing mechanism of action (MoA) cell assays that measure pEGFR, although the margins look similar between rociletinib and WZ4002 when measuring relative GI_{50} values in antiproliferative assays.[153]

AstraZeneca has also progressed a mutant selective compound into the clinic and recently obtained FDA approval of osimertinib (AZD9291, Tagrisso **Fig. 6**) launched in 2015. The research program that ultimately led to the discovery of osimertinib initially involved work to find reversible inhibitors that showed a favorable level of selectivity between the double mutant and WT EGFR forms. Next, internally developed insight was applied to add an appropriately placed acrylamide onto the scaffold to achieve improved cell potency. Although this work was initiated prior to the Dana-Farber disclosure of WZ-4002,[154] a similarity can be seen in that the hinge-binding motif is an anilinopyrimidine in both cases. However, there are significant differences too. The AstraZeneca series used a bicyclic aromatic group directly linked to the C4 of the pyrimidine, and the acrylamide was positioned in a different place—added to the solvent channel aniline.[154] Further rounds of evolution of the chemical structure involved migrating the basic group from the acrylamide side chain onto the aniline ring, changing the bicyclic aromatic group and removing the chlorine at C5 of the pyrimidine to ultimately arrive at osimertinib.[155] This compound achieved the desired profile in vitro (potent double-mutant activity, potent single-mutant activity, and good WT selectivity against both mutant forms). It also showed promising xenograft activity and was subsequently nominated for clinical trials, where in recently disclosed data (European Cancer Congress 2015), it achieved an objective response rate of 66.1% in patients with EGFRm NSCLC and the T790M mutation. It is noteworthy that the clinical development phase of osimertinib through to regulatory agency approval was particularly fast, 2 years and 8 months from the start of clinical trials to US approval. Both osimertinib (Apr. 2014) and rociletinib (May 2014) received Breakthrough Therapy designation from the FDA, highlighting the significant unmet medical need for these potential therapies.

Another noteworthy example from a structural viewpoint is PF-06747775 (**Fig. 6**, Phase I). Although this compound uses a different chemical scaffold, it places the acrylamide in a similar position to target Cys797, as reported in both AACR and ACS presentations in 2015. Pfizer has also reported the optimization and discovery of a preclinical compound PF-06459988.[156] Although these last two Pfizer compounds look structurally related, the binding modes to the hinge are dissimilar (see **Fig. 6**, hinge-binding motif in red), and the substituents on the core are switched round to be consistent with that binding mode change. This publication is noteworthy in that it emphasizes the generation of estimated K_i/K_{inact} values quickly and in high throughput, to drive optimization of hit compounds.[156] Other noteworthy WT selective inhibitors that have progressed into the clinic include EGF-816 (**Fig. 6**, Novartis, Phase II),[157] olmutinib (Hanmi, launched in Korea in 2016), brigatinib (Ariad, Phase II), and naquotinib/ASP-8273 (Astellas, Phase III) although the medicinal chemistry efforts toward these compounds have not yet been reported.

These irreversible inhibitors of T790M containing mutants, with selectivity over the WT, represent an exciting new paradigm for treating NSCLC patients. They can also be viewed as a significant milestone for medicinal chemistry, as the design brief for the compounds arose from previous clinical understanding of the importance of activities against specific mutations and a selectivity requirement.

More recently, preclinical approaches have been disclosed that target the T790M active/WT sparing profile with noncovalent inhibitors. As previously discussed, this is a challenging approach as activity in cells is difficult to achieve against the sensitizing mutations due to high ATP affinity. However, there are reasons to persevere with this approach.[158] There are hypothetical risks with the covalent mechanism of time-dependent inhibition of WT, or from idiosyncratic toxicity from off-target activities. However these potential issues have not apparently manifested themselves in the clinical trials for agents such as rociletinib or osimertinib, as these compounds were well tolerated in an oncology setting. Another possible reason is to avoid resistance mechanisms that may occur in response to treatment with a covalent inhibitor. This latter point has some support from the literature. Mutations have been observed in vitro when cancer cells are challenged by the agents in **Figs. 5** and **6**, most notably the C797S mutation where the cysteine that is targeted by the covalent inhibitors is mutated to a nonreactive serine.[159,160] The C797S mutation has also been observed in some patients whose tumors have progressed on osimertinib in clinical trials.[161]

Collaborative efforts between Argenta and Genentech have been described to this end, with some example structures given in **Fig. 7**. The discovery of compound **10**[162] started from a Jak2/Tyk2 inhibitor, which was subsequently optimized to improve activity versus T790M-containing mutants such as T790M/L858R, with selectivity against WT and general kinase selectivity. The data (**Fig. 7**) suggest a successful optimization at the enzyme level, with modest but promising cell activity. In a subsequent publication,

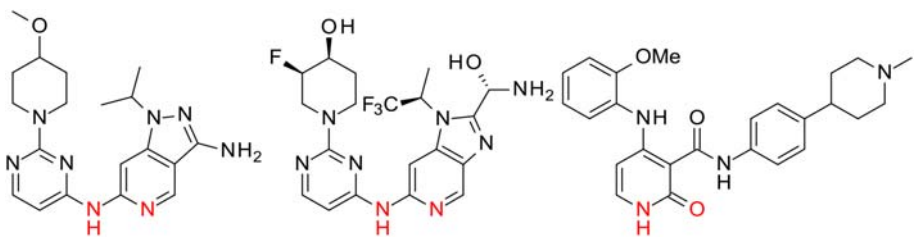

Fig. 7 EGFR reversible inhibitors that target single and double mutants, with selectivity versus wild type.

additional optimization of the same series was disclosed,[163] including an investigation into the effects of fluorination on the ring, leading to compound **42** (in the reference) which had improved H1975 pEGFR cell potency (0.26 μM) and showed PD activity in a H1975 xenograft model measuring pathway inhibition (pEGFR, pERK, and pAKT) at 300 mg kg^{-1}. In a separate publication,[164] authors from the same organizations have published efforts to optimize a series of pyridones. The original hit suffered from poor WT selectivity and general kinase selectivity but was successfully optimized to more selective lead compounds, such as compound shown (compound **29** in the reference).[164] Submicromolar cell potency in a T790M/L858R cell line (0.43 μM) and good cell selectivity (23 × versus WT cell line) were achieved for this compound. While further improvements in cell potency may be necessary for this noncovalent approach to be successful, these efforts show promise.

5.02.5.2.3 Future outlook

The drug discovery of EGFR inhibitors already has a long history, with early success in the identification of marketed drugs that treated the sensitizing mutations of EGFR, which can claim to be the first targeted therapies for lung cancer. Despite that long history, EGFR remains a highly active kinase target today. The design of covalent compounds that are efficacious against particular mutations, while sparing the WT, has yielded compounds that have given exciting efficacy in the clinic, including one recently approved marketed drug.

Further efforts are underway to treat other mutations, such as the C797S mutation which necessitates the development of noncovalent inhibitors, and there may still be further opportunities by defining additional patient populations and designing compounds with profiles to address that population. Another relevant primary mutation is the exon 20 insertion, which may not be well treated by all current therapies[165,166] although there are reports of in vitro exon 20 activity for both osimertinib[167] and EGF-816.[157] In addition, as EGFR inhibitors are increasingly considered as candidates for combination approaches (e.g., with other targeted agents, with chemotherapy, or with immunotherapy), additional challenges may arise in the design of future inhibitors to suit those combination approaches, or potentially to investigate alternative (e.g., allosteric) mechanisms. Indeed, an allosteric inhibitor was recently disclosed by Novartis (GTC, San Diego, Mar. 2016). This compound was efficacious against the L858R/T790M/C797S mutant when combined with cetuximab, but interestingly it was reported to have weak activity against the Ex19del/T790M mutant, which was rationalized structurally by the shorter loop to the C-helix preventing binding (publications are expected in due course).

An additional consideration for future drug discovery efforts may be to include brain penetration as a key part of the design brief, as the improved treatment of lung cancer patients may result in an increased rate of brain metastases, for which the prognosis is worse. Such an effort has already been reported toward a CNS-penetrant anilinoquinazoline compound AZD3759 (**Fig. 4**) that can target the sensitizing mutations of EGFR, which was designed to be brain penetrant (unbound brain:plasma drug concentration $K_{puu} = 1.3$ in rat, $K_{puu} = 0.5$ in cynomolgus monkey).[168] Similar efforts may be expected for other mutations. Osimertinib has also been shown to have good CNS penetration in mouse models, with resulting efficacy in a PC9 mouse brain metastases model, and has shown early clinical evidence of activity in patients with EGFRm advanced NSCLC and brain metastases.[169]

5.02.5.3 Design of ALK Inhibitors With Potency Against Mutations

While this story has emerged more recently than EGFR, the focus of medicinal chemistry efforts against anaplastic lymphoma kinase (generally shortened to ALK, not to be confused with the activin receptor-like kinases which are often denoted as ALK1-ALK7) has a number of similarities with EGFR. This target is of interest for the treatment of a wide variety of cancers, but for the purposes of this article we will focus on the implication of ALK fusions in lung cancer, as these prompted a renewed focus on this target and ultimately the development of crizotinib as an efficacious agent for ALK-positive NSCLC patients, covered in "**Design of crizotinib as an effective inhibitor of WT ALK**" section. However, it should be noted that ALK fusions are not as common as EGFR mutations are among NSCLC patients.[136,170] As for EGFR, medicinal chemistry programs have subsequently focussed on activity against a key gatekeeper mutation for ALK (L1196M) that is not well treated by crizotinib, and these efforts resulted in a number of clinical candidates and recent approvals and will be covered in "**Design of ALK inhibitors that can target the L1196M gatekeeper mutation**" section. Activity against a number of other mutated forms of the kinase has also been reported as relevant to NSCLC patients, and some recent medicinal chemistry publications that report data versus these mutants will be covered in "**Future outlook**" section.

5.02.5.3.1 Design of crizotinib as an effective inhibitor of WT ALK

Crizotinib was initially designed as a potent inhibitor of c-Met by scientists at Sugen (now Pfizer) and was the result of a series of optimization steps and scaffold hops from a structurally distinct indolin-2-one hit (**Fig. 8**),[171] where the hinge-binding donor–acceptor motif has been changed from the lactam in the indolin-2-one core to an aminopyridine. This scaffold was reported to be a more efficient way to link to the lipophilic poly-halogenated selectivity pocket group. A polar/basic side chain (piperidine-substituted pyrazole) was employed in the solvent channel, which achieved a dramatic improvement in ligand lipophilicity efficiency (LLE or LipE, in this case defined as enzyme pIC_{50}–$clogD_{7.4}$). Although this compound was designed for c-Met, entering Phase I trials in 2006, it was subsequently found to be a potent inhibitor of ALK. As the link between ALK fusions and NSCLC emerged in 2007, in particular the EML4–ALK fusion, this compound was repositioned for ALK-positive NSCLC patients and was ultimately approved for that indication in 2011, just 4 years after the discovery of the relevance of ALK fusions in this setting.

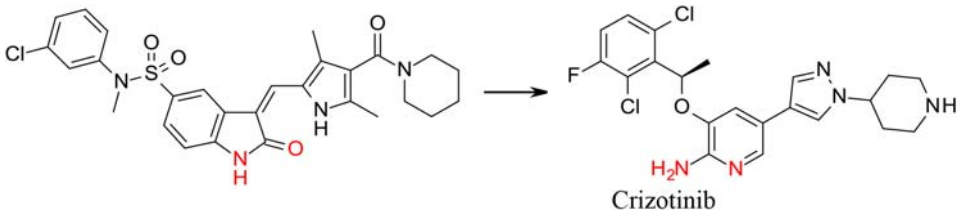

Fig. 8 Scaffold change from indolin-2-one to aminopyridine to give crizotinib, hinge binder in *red*.

5.02.5.3.2 Design of ALK inhibitors that can target the L1196M gatekeeper mutation

While crizotinib achieved Breakthrough Therapy designation and was the first agent to be approved in the ALK-positive NSCLC setting, resistance to crizotinib has been observed in a similar manner to the emergence of the double activating/gatekeeper mutations observed for EGFR. Thus, patients that relapsed on crizotinib have been observed to harbor a number of ALK mutations for which crizotinib has limited efficacy, of which the most frequent one is again a mutation of the gatekeeper residue to methionine (L1196M for ALK, cf. T790M for EGFR) although the frequency of L1196M for ALK is not as marked as T790M for EGFR, as the ALK mutations are more diverse.[170] This finding has led to a number of medicinal chemistry programs to identify a "2nd generation" of ALK inhibitors that can target L1196M although, unlike EGFR, selectivity over WT ALK is not required to manage tolerability.

Novartis has reported their optimization of a bis-anilino pyrimidine series, which ultimately led to ceritinib (FDA approved 2014).[172,173] The reported design of this compound started with TAE-684, a potent inhibitor of ALK. The base was optimized to avoid a reactive metabolite liability with their startpoint (Fig. 9), which can generate a 1,4-diiminoquinone intermediate, by changing it from a N-linked base to a C-linked base. In addition, the alkoxy group was optimized to maximize kinase selectivity, to give LDK-378/ceritinib. Ceritinib was reported to be a highly potent inhibitor of ALK at enzymatic level (0.2 nM), with good inhibitory activity against ALK (41 nM) and EML4–ALK fusion (2.2 nM) in Ba/F3 cells,[173] but the early medicinal chemistry papers did not report activity (or optimization) versus mutant forms of ALK that are important to the setting of crizotinib resistance.

Subsequently ceritinib has been reported[174] as being active against four of the mutations present in models of acquired resistance to crizotinib, including the gatekeeper mutation L1196M, but not active versus two others (G1202R and F1174C). Crystal structures of crizotinib (2XP2) and ceritinib (4MKC) have been compared to rationalize the activities versus the relevant mutant forms (Fig. 10).[174] The chlorine on the pyrimidine core is hypothesized to be important for L1196M activity (hydrophobic interaction with the more lipophilic gatekeeper), plus there is the potential for unfavorable interactions between the NH_2 and chiral methyl groups on crizotinib and Met1196. By contrast, neither crizotinib nor ceritinib have significant activity versus G1202R, a residue in the solvent channel. This is consistent with the fact that both drugs have large basic side chains in that region of the binding site, which may not be compatible with mutation of Gly to a large basic residue (Arg).

After a promising Phase I trial in NSCLC ALK+ patients who had progressed after treatment with crizotinib, ceritinib received a Breakthrough Therapy designation from the FDA in Mar. 2013 and was approved in 2014, once again demonstrating the impressive speed in development that targeted therapies with a clear patient selection hypothesis and beneficial profile can achieve.

Chugai has reported the optimization of a tetracyclic series of ALK inhibitors. Starting with a weak hit (Fig. 11) the core was changed to a pyrrole,[175] and then the side chains were optimized[175,176] for kinase selectivity, cellular activity, and metabolic stability to give alectinib, now licensed to Roche. The hinge binder (hydrogen bond acceptor) in this case is thought to be the ketone, with the basic group pointing along the solvent channel (Fig. 11). Alectinib is a potent inhibitor of WT ALK, as well as L1196M, F1174L, and R1275Q mutations. Similar to ceritinib, alectinib showed a promising objective response rate (59%) in a Phase I trial in NSCLC ALK+ patients who had progressed after treatment with crizotinib and was subsequently granted a Breakthrough Therapy designation by the FDA (Sep. 2013) and was approved by the FDA in 2015.

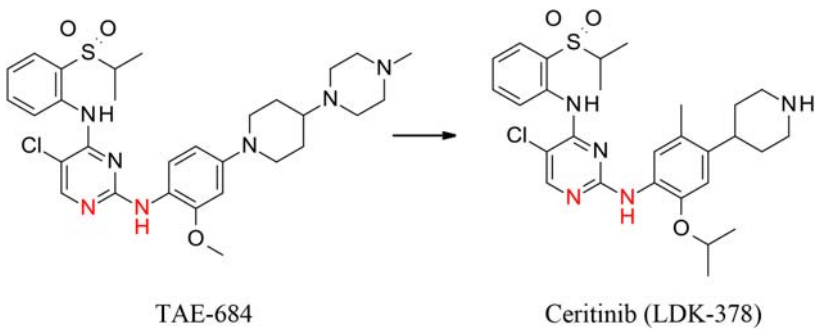

Fig. 9 Optimization of a bis-anilino pyrimidine series to give ceritinib.

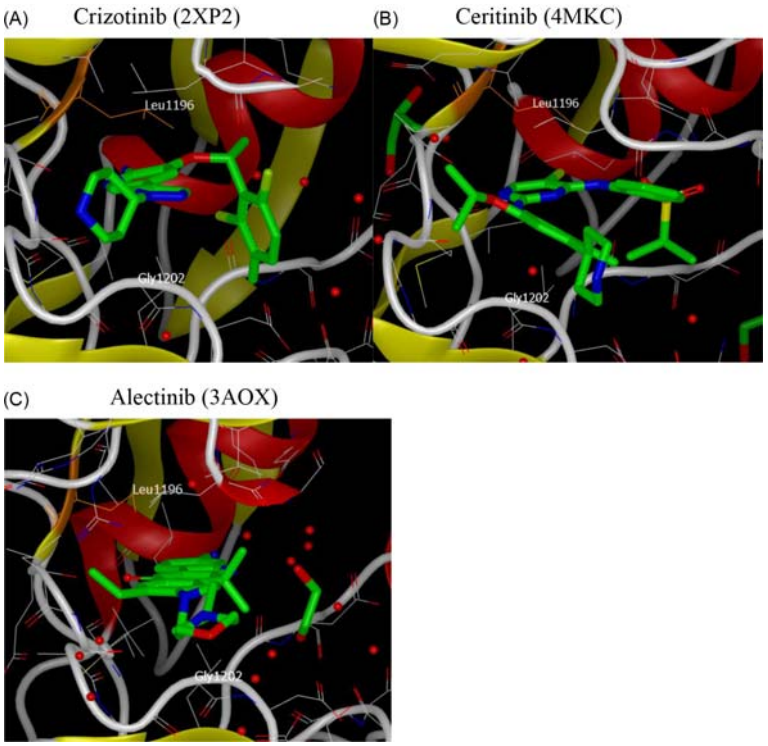

Fig. 10 Comparison of the binding modes of (A) crizotinib, (B) ceritinib, and (C) alectinib in ALK, showing relevant residues for the L1196M and G1202R mutations.

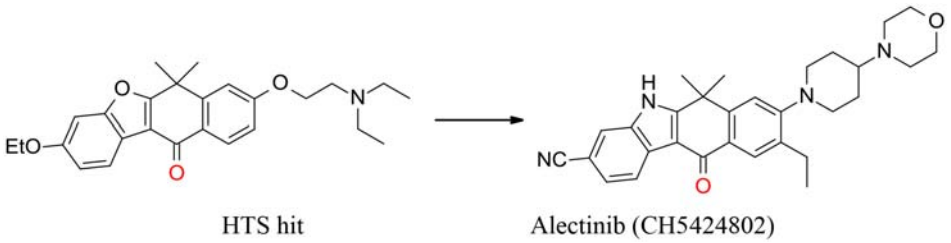

Fig. 11 Scaffold hop and optimization to give alectinib.

Pfizer has reported two approaches to modify the structure of crizotinib directly, to increase L1196M activity (Fig. 12). In one approach,[177] the pyrazole group and the substituents on the benzyloxy group were modified to increase potency, using both structure-based design and LLE-driven SAR approaches. This resulted in compound **8e** (in the reference) as shown in Fig. 9, which is still 10-fold more active against WT in cell assays, but as both WT and L1196M potencies have been increased it is now a suitable tool compound to target both in vivo. Another reported approach[178] used macrocyclic analogs of crizotinib to increase potency against both WT and L1196M. This approach led to the discovery of lorlatinib (PF-06463922, Fig. 12), currently in Phase II clinical trials for ALK- and ROS-positive NSCLC patients. Lorlatinib has been reported as being active against a number of clinically relevant ALK mutations, including the G1202R mutation.[179] Additionally, it is a modestly brain penetrant molecule, with a measured free brain to free plasma AUC ratio of 0.2 in rat,[178] so may offer the potential to treat patients with brain metastases.

5.02.5.3.3 Future outlook

The "2nd generation" of ALK inhibitors discussed in "**Design of ALK inhibitors that can target the L1196M gatekeeper mutation**" section succeed in having sufficient potency against the L1196M mutation but lack broad spectrum activity against all of the reported ALK mutations. Therefore there may be opportunities to develop further inhibitors that address these mutations, which may be efficacious with patients that relapse after treatment with crizotinib and/or ceritinib. Two recently published approaches approach this by subtle modifications of the known 2nd generation compounds. Thus one approach has been reported[180] where the structure of alectinib was modified to improve potency against a number of mutations, but especially against the G1202R mutation. The G1202R mutation has been reported to be the most frequent mutation present in patients that relapse after treatment with

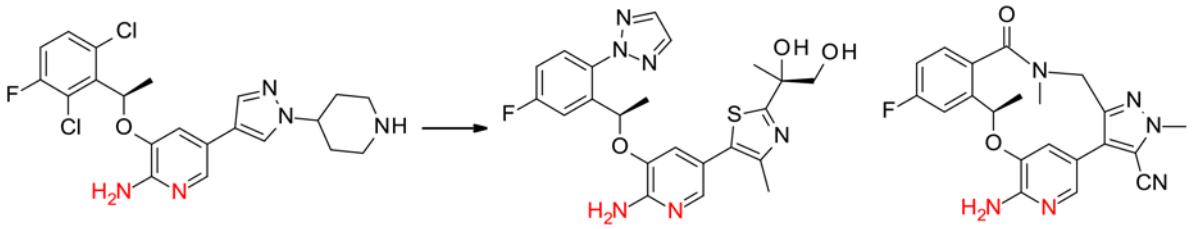

Crizotinib (Xalkori)	Compound 8e in reference[179]	Lorlatinib
WT: 80 nM	0.8 nM	1.3 nM
L1196M: 843 nM	6.6 nM	21 nM

Fig. 12 ALK cell IC_{50} data for analogs of crizotinib in WT and L1196M cell lines.

ceritinib. This optimization required modification of the basic side chain to a substituted pyrazole (**Fig. 13A**), as this group may avoid a steric clash with the larger arginine present in the mutated form. In another approach, the basic aniline of ceritinib was modified to a tetrahydroquinoline (THIQ) group although this change only gave a modest improvement to G1202R activity at the enzyme level, and the resulting inhibitor (**Fig. 13B**, compound **8** in Ref. 173) was a significantly more promiscuous inhibitor across the kinome.[181]

It seems likely that the remaining opportunities to target a diverse ALK mutation profile will continue to be addressed with medicinal chemistry efforts. These efforts may come from known ALK inhibitors although in principle screening for new chemical series that may be developable against this profile could also be an attractive approach. Aiming for broad activity against all clinically relevant ALK mutations is likely to bring in the additional challenge of maintaining general kinome selectivity, so careful optimization will be required, ideally with the support of X-ray crystallography.

5.02.5.4 Conclusion

A feature of the recent approved drugs that are discussed in this section for both targets is their speed through development. This has been facilitated, in many cases, by designation by the FDA as a Breakthough Therapy.[182] Examples of compounds in this section with that designation are osimertinib and rociletinib for EGFR, and crizotinib, ceritinib, alectinib, and brigatinib for ALK. This speed has been achieved by having a clear genetic hypothesis for patient selection, combined with high-quality compounds from a medicinal chemistry perspective. In this context, success may require a careful consideration of the required target profile, for example, achievement of activity versus clinically relevant fusions and mutations and (e.g., WT) selectivity, in addition to primary potency, pharmacokinetic properties, and more generic safety criteria. Medicinal chemists have played an important role in selecting and evolving compounds that meet such specific target profiles, and this has required significant expertise in kinase drug design

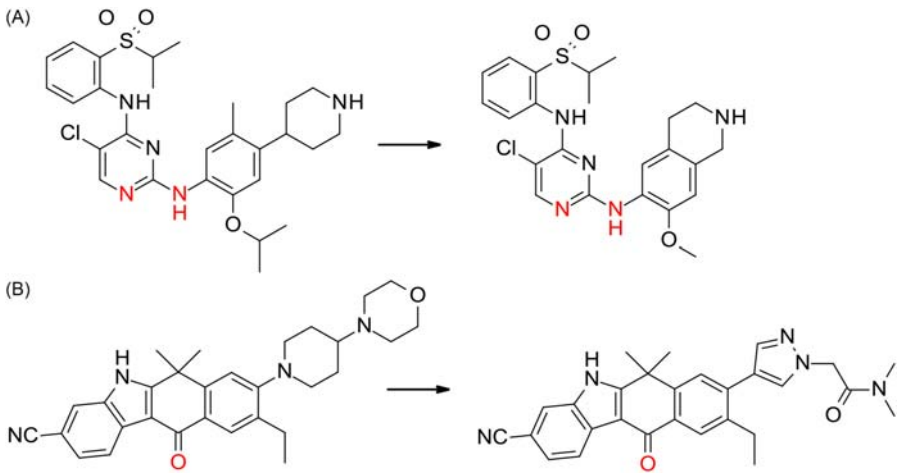

Fig. 13 (A) Optimization of alectinib to increase potency against the G1202R mutant[180] and (B) optimization of ceritinib.[181]

(including structural understanding) coupled with a suitable project cascade to demonstrate in vitro and in vivo activity against particular mutant forms of the kinase.

5.02.6 Kinases in the DDR

5.02.6.1 Introduction

Every one of our cells experiences tens of thousands of DNA-damage events per day through normal cell function, DNA processing, or environmental factors. The DDR is an integrated group of biological pathways evolved to recognize, signal, and promote the repair of damaged DNA in order to suppress genomic instability.[183–188] In human cells there are five major DDR pathways: homologous recombination (HR), nonhomologous end joining (NHEJ), mismatch repair (MMR), base excision repair (BER), and nucleotide excision repair (NER) as well as replication stress and cell cycle checkpoint pathways.[187] Cancers have high levels of genomic instability, an underlying hallmark of cancer,[189] associated with a greater propensity to accumulate DNA-damage through defects in the DNA-repair machinery and failure of one or more cell cycle checkpoints which serve to halt cell division so that DNA-damage may be repaired. The use of DNA-damaging chemotherapy and radiotherapy to kill cancer cells relies on this principle but is also associated with damage to normal tissue leading to significant toxicity. DNA-damage leads to cell death if sufficiently high and left unrepaired and is the concept behind DDR inhibition for cancer therapy.[183–188] DNA-repair processes are a potential mechanism of resistance to DNA-damaging agents, and therefore inhibition of DDR pathway targets has been actively investigated as chemo- and radiosensitizing agents. DDR defects are common in tumors which can become dependent on the remaining DNA-repair pathways. Targeted DDR therapies aim to improve outcome for patients by taking advantage of these specific tumor cell abnormalities, thereby limiting normal tissue toxicity.[187,188]

Kinases play a central role in the DDR. The phosphatidylinositol 3-kinase-related kinase (PIKK) family of proteins in particular has been an area of intense focus for drug hunters. ATM (ataxia telangiectasia mutated), ATR (ataxia telangiectasia and RAD3-related), and DNA-PK (DNA-dependent protein kinase) are three PIKK proteins with key roles in the DDR. Together with SMG-1 (suppressor of morphogenesis in genitalia-1), TRRAP (transformation/transcription-associated protein), and mTOR (mammalian target of rapamycin) they make up the PIKK family of proteins.[190–193] The PIKK protein family are sometimes referred to as Class IV PI3 kinases, but they are functionally distinct from the PI3K classes I–III and do not phosphorylate lipids.[194] While many inhibitors of PI3 kinases and mTOR have entered advanced clinical testing and some have been approved, identification of clinical quality inhibitors of ATM, ATR, and DNA-PK has proved more challenging.[195] The first compounds identified typically lacked the global properties to make good drugs, but some did possess high potency and selectivity for their primary target to clearly demonstrate in preclinical studies the therapeutic potential of DDR pathway modulation. Recent years have seen the advancement of DDR inhibitors optimized for potency and selectivity together with the required physicochemical, pharmacokinetic, and toxicology properties to support clinical investment (summarized in **Fig. 14**). While none have been approved, the first compounds are moving in sight of late-stage clinical testing where their full potential in the fight against cancer will become clear.

5.02.6.2 ATM

Ataxia-telangiectasia (A-T), the human autosomal recessive disorder, is caused by mutation of the *ATM* gene which codes for the serine/threonine protein kinase ATM.[196,197] A-T cells display hypersensitivity to ionizing radiation (IR) failing to repair DNA

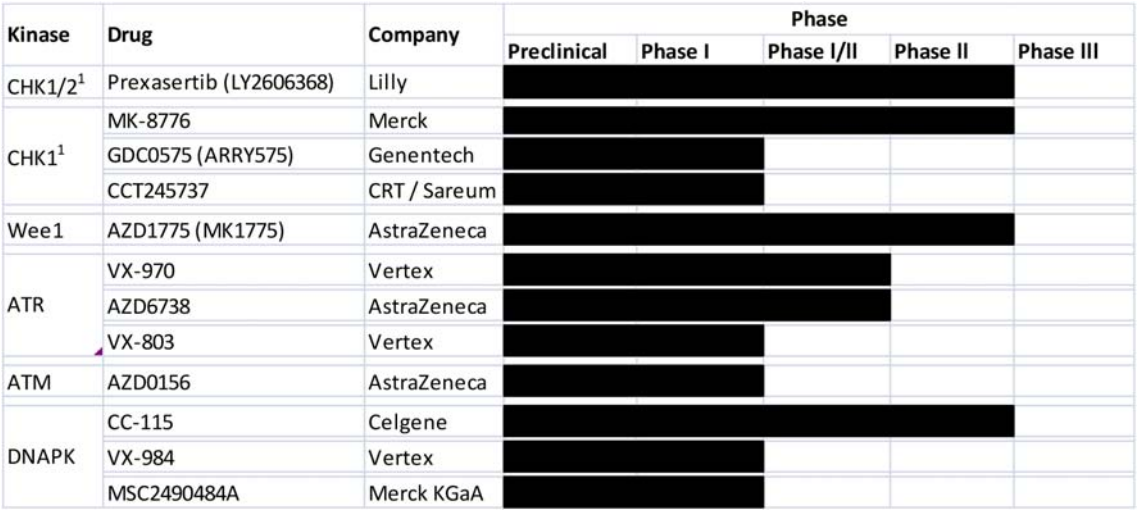

Fig. 14 Inhibitors of DDR kinases in the clinic.

double-strand breaks (DSBs) and to arrest the cell cycle following DNA-damage with an inability to mediate cell cycle checkpoints.[196,197] ATM plays a key role in many cell signaling pathways and is a key component of DNA DSB detection and NHEJ and HR repair pathways as well as regulation of cell cycle checkpoints.[198,199] A-T and other ATM-deficient cells are hypersensitive to agents where DNA DSBs is the primary driver of cytotoxicity.[197–199] ATM phosphorylates a wide range of proteins linked to DNA DSBs in response to DNA-damage including H2AX, KAP1, and 53BP1.[200] Phosphorylation of additional downstream targets such as p53, checkpoint kinase (CHK) 2, and BRCA1 indicate ATM's complex and multifaceted cellular function, linked to a range of other key cellular process/responses in various pathophysiological conditions involving DNA-damage and beyond.[201]

5.02.6.2.1 ATM inhibitors

KU-55933 (Fig. 15), one of the first potent and selective ATM inhibitors to be reported, was identified from an extensive SAR study exploring PIKK kinase (DNA-PK and ATM) activity of a series of 2-morpholino-pyran-4-ones and 2-morpholinothiopyran-4-ones.[202,203] Highly divergent SAR between DNA-PK and ATM is evident with only the thianthrene KU-55933, from a large number of analogs tested, showing potent inhibition of ATM kinase activity.[203] KU-55933 is a potent ATM enzyme inhibitor ($IC_{50} = 12$ nM) with impressive selectivity for ATM over DNA-PK, ATR, mTOR, and PI3 kinase.[202] In one of the first reports highlighting the importance of the morpholine group as a kinase hinge-binding motif, Hickson et al. replaced the oxygen atom of the morpholine in KU-55933 with a carbon, thus removing the ability to accept a key hydrogen bond resulting in loss of kinase activity.[202] The quinazoline CP-466722 was identified following a directed screen of 1500 compounds selected on the basis of known and predicted kinase pharmacophores. KU-55933 and CP-466722 have been shown to recapitulate the phenotype of A-T cells. KU-55933 rapidly inhibits IR-induced phosphorylation of p53 (ser-15) with an IC_{50} of ~0.3 μM and complete ablation at 10 μM. KU-55933 does not impact UV-induced phosphorylation of H2AX (ser-139) or CHK1 (ser-345), characteristic of ATR inhibition at a concentration of 10 μM. KU-55933 and CP-466722 inhibit IR-induced H2AX (ser-139) phosphorylation in ATM WT cells but not A-T cells, indicative of selective inhibition for ATM over related proteins such as DNA-PK.[202,204] KU-55933 alone was shown not to affect the clonogenic survival of HeLa cells at concentrations up to 10 μM but was shown to sensitize IR-induced cytotoxicity using a range of IR doses.[202] In addition, KU-55933 sensitizes HeLa cells to the topoisomerase I/II inhibitors etoposide, doxorubicin, and camptothecin.[202] While KU-55933 alone had no effect on cell cycle progression, the combination with IR and agents such as etoposide resulted in an increase in the G2M population indicating KU-55933 inhibits the ATM-dependent elements of cell cycle checkpoints.[202]

KU-55933 and CP-466722 do not possess the drug-like properties to be developed further, as they have low aqueous solubility and high lipophilicity. Introduction of hydrophilic groups on the tricyclic ring of compounds such as KU-55933 has been explored

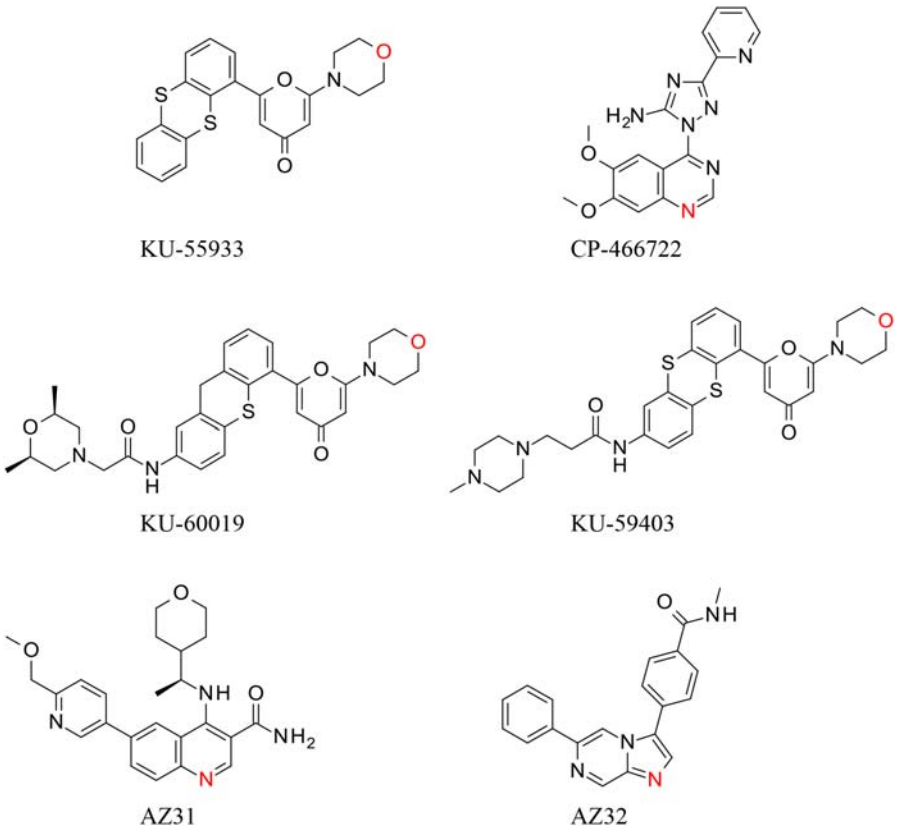

Fig. 15 ATM inhibitors (assumed hinge-binding atoms highlighted in *red*).

in an attempt to improve physicochemical properties.[205] With no ATM structure available medicinal chemistry design was directed through the use of homology modeling to guide positioning of the hydrophilic group.[205] The thioxanthene KU-60019[206] and thianthrene KU-59403[207] achieved some improvement in physicochemical properties and improved potency in enzyme assays (ATM $IC_{50} = 6.3$ and 3 nM, respectively) while retaining very high selectivity versus related PIKKs (ATR, DNA-PK, mTOR) and PI3Ks. A more profound improvement of cellular potency was seen with KU-60019 being an effective chemosensitizer at a concentration of 3 μM, while KU-59403 appears more potent still, effective at 1 μM.[206,207] These compounds show 10-fold greater potency blocking IR-induced phosphorylation of ATM targets compared with KU-55933 but are not significantly cytotoxic alone.[206,207] KU-59403 enhances the cytotoxicity of the DNA DSB-inducing agents camptothecin, etoposide, and doxorubicin.[207] No consistent enhancement of cytotoxicity with KU-59403 was observed in cell lines with mutant p53 compared with WT p53, with LoVo colorectal tumors (p53 WT) shown to be particularly susceptible to inhibitor-induced etoposide sensitization.[207] When KU-59403 is dosed at 50 mg kg^{-1} i.p., peak plasma concentration reached 5 μM at 4 h with concentration in tumor measured at 1.9 μM, in excess of the 1 μM concentration shown to be effective.[207] Dosed immediately prior to etoposide (12.5 and 25 mg kg^{-1} i.p. BID for 5 days), KU-59403 resulted in a dose-dependent increase in tumor growth delay, increasing etoposide efficacy by 190% at the highest dose. Sequencing of the agents is important to achieve efficacy, with ATM inhibition required concurrently with induction of DNA DSBs. The combination of KU-59403 with irinotecan in SW620 colorectal cancer xenografts was also effective using the same combination schedule. In both cases KU-59403 alone did not result in significant antitumor efficacy and the combinations did not lead to unacceptable toxicity as measured by reduced body weight.[207]

Glioblastoma multiforme (GBM) is the most common and aggressive primary brain tumor in adults. More effective treatments have been sought to improve on the existing standard treatment of surgical resection followed by temozolomide and radiation.[208] Around one-third of GBM have p53 mutations and ~80% harbor other cell cycle checkpoint defects leading to investigation of ATM inhibitors in this setting.[209] KU-60019 has been shown to reduce glioma cell migration and invasion and to potently radiosensitize p53-mutant human gliomas in vivo.[206,210,211] KU-60019 has low BBB penetration with very low concentrations of drug detected in the brain following systemic administration.[210] However, in two studies, KU-60019 was administered direct to the tumor to circumvent the BBB and achieve meaningful drug concentrations in the brain.[210,211] Biddlestone-Thorpe et al. demonstrated the combined effect of KU-60019, dosed through locally positioned mini-pumps, and radiation in mice bearing human orthotopic gliomas.[211] This combination led to effective ATM inhibition (measured by γH2AX and p-Ser824-KAP1) and to a significant increase in survival of mice compared with either KU-60019 or radiation given alone.[211] Delivery of KU-60019 has also been explored by convection-enhanced delivery (CED), a method of direct drug delivery to the brain through one or more catheters which are surgically placed into the tumor mass, around the tumor or into the resection cavity.[212] KU-60019 infused over 30 min led to fast and extensive diffusion followed by rapid draining and excretion from the brain by 24 h.[210] Mice infused with KU-60019 by CED, dosed three times to mimic clinical practice, immediately followed each time by 3 Gy radiation showed an increased survival and reduced tumor burden compared with KU-60019 or radiation alone.[211] Gliomas which were p53-mutant were shown to be more radiosensitive in combination with KU-60019 than genetically matched p53 WT lines. A trend to increased survival of mice treated with KU-60019 alone could link with the observed effect on glioma cell migration and invasion, potentially indicative of an additional benefit in controlling tumor growth between radiation fractions.[206,211] Importantly in these short-term mouse studies, KU-60019 did not appear to worsen the toxicity of radiotherapy in normal brain tissue.

Local delivery through CED is an established clinical technique for direct intracranial treatment of GBM and has the advantage of bypassing the BBB, thus improving efficacy with compounds unable to effectively penetrate the CNS. Local delivery may also reduce systemic toxicity, but the benefits of CED need to be balanced with the complexity and cost of the procedure. AstraZeneca has described two potent and specific ATM inhibitors with good oral bioavailability which differ in their ability to penetrate the BBB.[213] AZ31 and AZ32 are potent ATM enzyme ($IC_{50} < 0.0012$ and < 0.006 μM, respectively) and cell ($IC_{50} = 0.046$ and 0.31 μM, respectively) inhibitors with good selectivity over ATR (pCHK1 HT29 cell $IC_{50} > 30$ and > 23 μM, respectively).[213] AZ31 was shown to radiosensitize a panel of GBM cell lines, with p53-mutant lines among the most sensitive, and both compounds benefit from high free exposure in plasma following oral dosing.[213] AZ31 is highly effluxed in an MDR1 overexpressing MDCK line (efflux ratio = 10.7) and had limited (3 h) free exposure over the ATM cell IC_{50} in mouse brain following an oral dose of 100 mg kg^{-1}.[213] In contrast, while AZ32 is less potent, it is highly permeable with low efflux (efflux ratio = 0.4) and achieves free exposure for 22 h over the ATM cell IC_{50} in mouse brain. The difference in permeability/efflux is presumably a result of physicochemical properties such as lipophilicity, hydrogen bond donors, and polar surface area. AZ31 effectively radiosensitizes p53 mutant HT29 subcutaneous xenografts but does not significantly sensitize a syngeneic p53-defective intracranial mouse glioma model. In contrast the CNS-penetrant ATM inhibitor AZ32 results in significant improvement in survival in the intracranial model when given orally prior to fractionated whole brain radiation.[213]

The effective in vivo radiation- and chemotherapy-sensitization demonstrated by the compounds described above has provided impetus to identify ATM inhibitors for the treatment of human cancers. To date AZD0156 is the first and only ATM inhibitor to enter clinical development. AZD0156 is currently active in a Phase I trial in solid tumors in combination with the poly ADP-ribose polymerase (PARP)1/2 inhibitor olaparib (NCT02588105).

5.02.6.3 ATR

ATR is a serine/threonine protein kinase with a key role in the DNA replication stress response (RSR) activating DNA-damage checkpoints.[214,215] Replication stress is a hallmark of cancer and can be broadly defined as the slowing or stalling of replication fork

progression or DNA synthesis.[216,217] This can result from DNA-damage lesions or through lack of factors (e.g., sufficient nucleotide pools) which prevents replication proceeding in a coordinated fashion. One possible consequence of persistent replication stress is generation of stretches of replication protein A (RPA)-coated single-stranded DNA and activation of primarily ATR-dependent DDR pathway repair.[183,218] ATR inhibitors have shown promise for the treatment of cancer through exploiting tumor cell dependency on RSR for viability showing preferential cell killing in tumor cells where baseline replicative stress levels are high.[219] Therefore ATR inhibitors have potential for use in combination with replicative stress-inducing radiation or chemotherapy.[217,220] The loss of ATM in tumor cells also creates a synthetic lethality-like dependency leading to a greater reliance on ATR to maintain viability.[221] In ATM-deficient tumor cells, the activity of ATR inhibitors is enhanced in combination, and for some compounds single-agent efficacy has been demonstrated.[217,220]

5.02.6.3.1 ATR inhibitors

The earliest pharmacological tool ATR inhibitors were identified largely from known inhibitors of related targets. These compounds had weak potency, nonspecific ATR activity, and/or poor drug-like properties.[217] Subsequently inhibitors whose primary pharmacology is driven through selective ATR inhibition have been generated, combined with the properties required to enable detailed preclinical in vitro and in vivo target assessment. The clinical ATR inhibitors are derived from two distinct chemotypes: the aminopyrazines VX-970 and VE-821 from Vertex and the morpholinopyrimidine AZD6738 from AstraZeneca (**Fig. 16**).

VE-821 was the first selective aminopyrazine lead compound to be described arising from a 2-benzamido-3-amino-6-arylpyrazine screening hit.[221–223] The kinase-binding mode of this series has been extensively characterized with the N-4 pyrazine nitrogen together with the adjacent amino group forming a hydrogen bond acceptor–donor pair to the ATR hinge. Charrier et al. showed that addition of the 4-sulfonylmethyl group found in VE-821 led to an increase in potency, maintained selectivity versus PIKK family targets, and crucially improved cellular potency measured through inhibition of CHK1 (Ser-345) phosphorylation, a direct measure of ATR activation ($IC_{50} = 0.8\ \mu M$).[222] VE-821 was shown to potentiate multiple classes of chemotherapy and radiation particularly in tumor cells with mutant p53 or with loss of ATM.[221,223] Despite the utility of VE-821 as an in vitro tool compound, potency and physicochemical properties limited its further development. Exploration of SAR of the anilide moiety led to the discovery that the amide group could be productively replaced with a range of heterocyclic groups without loss of potency.[222] Surprisingly groups such as benzoxazole, which are unable to form the same hydrogen-bonding network to the protein observed with VE-821, have similar levels of ATR enzyme inhibitory potency. The SAR which led to the identification of VX-970 has not been described, but it is clear that the 4-(methylamino)methyl phenyl moiety linked through either isoxazole or oxadiazole to the aminopyrazine hinge binder is a key motif common to the majority of the compounds made.[217] VX-970 benefits from enhanced ATR enzyme ($IC_{50} < 0.0002\ \mu M$) and cellular potency ($IC_{50} = 0.019\ \mu M$) with high cellular selectivity over ATM and is also highly selective in a panel of kinase enzyme assays.[224] VX-970 shows potent tumor growth inhibition in vivo across multiple tumor types in combination with SOC chemotherapy agents but does not significantly inhibit tumor growth as monotherapy in the models and schedules published (up to 6 consecutive days of oral administration).[224–226] The apparent lack of monotherapy activity with VX-970 is interesting when compared with inhibitors from the morpholinopyrimidine series (vide infra). Exposure of VX-970 appears good with the concentration of VX-970 measured in tumor maintained in large excess of the ATR cellular IC_{50} for an extended duration (>24 h) following oral doses of VX-970 at 60 mg kg^{-1}.[225] At this dose, VX-970 alone shows a modest reduction in pCHK1 (Ser-345) and increased γH2AX consistent with the observed antitumor activity.[224–226] When VX-970 is given in combination with DNA-damaging chemotherapy and/or radiation, a far greater effect on tumor ATR and DDR biomarkers is observed together

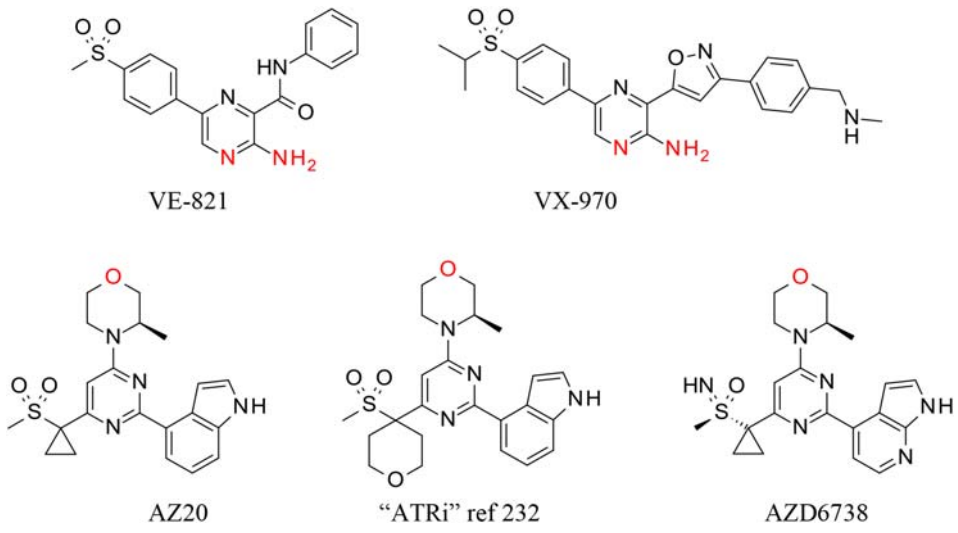

Fig. 16 ATR inhibitors (assumed hinge-binding atoms highlighted in *red*).

with marked increase in efficacy compared with chemotherapy or radiation alone.[224–226] VX-970 combines with different classes of DNA-damaging agents, with platinum agents such as cisplatin producing the most synergistic effects, and was shown to enhance the therapeutic efficacy of IR and gemcitabine in xenograft models of pancreatic cancer,[224] of irinotecan in colorectal xenograft models,[225] and of cisplatin in patient-derived lung tumor xenografts.[226] The enhancement of in vivo efficacy in combination in these mouse models is seemingly well tolerated; the combination of VX-970 with cisplatin resulted in some albeit not significant reduction in body weight, which was reversible with animal weight regained between cycles of treatment.[225]

AstraZeneca reported the discovery of AZ20 from a screening campaign identifying the high-quality sulfonylmorpholinopyrimidine series generated from an earlier mTOR program.[227] The 4-indole moiety was found to be critical for ATR potency with other isomers of indole losing potency and substitution for other heterocyles nonproductive. A medicinal chemistry campaign with the goal of maintaining the attractive physicochemical properties of this series while improving potency for ATR, e.g., by maximizing LLE was prosecuted.[227] Unsubstituted indole and sulfonyl groups were found to be preferred motifs, but improvements in both potency (for ATR) and selectivity (over PI3K) were obtained from cyclization adjacent to the sulfonylmethyl group and crucially by addition of a methyl group to the morpholine hinge binder motif.[227] Potency was found to be highly dependent on the stereochemistry of the morpholine 3-methyl group with the (*R*)-enantiomer possessing 100× higher potency than the corresponding (*S*)-enantiomer in cellular assays.[227] AZ20 has low aqueous solubility (10 μM at pH 7.4) driven by efficient packing in the solid state that is dominated by centrosymmetric methylsulfone to methylsulfone contacts leading to a high crystalline melting temperature (204°C).[227] AZ20 was also found to be a time-dependent inhibitor (TDI) of CYP3A4. Despite these shortcomings, AZ20 has been successfully utilized to explore the in vivo pharmacology of ATR inhibition by virtue of high target specificity and high free exposure in vivo, maintaining concentration over the target IC_{50} for 12 h in mouse following a single oral dose of 50 mg kg^{-1}.[227] LoVo tumors, which are MRE11A (ATM pathway) deficient and characterized by diffuse pan-nuclear γH2AX staining suggestive of high replication stress, have been shown to be sensitive to AZ20 ($GI_{50} = 0.20$ μM following 72 h continuous exposure).[227] In contrast to VX-970, AZ20 was shown to significantly increase tumor γH2AX levels as monotherapy in vivo. AZ20-treated mice bearing LoVo xenografts resulted in significant inhibition of tumor growth (TGI = 78%, $P < 0.0005$) following 21 days continuous dosing.[227,228] The reasons behind this key difference are not clear, but it should be noted that the described studies are likely to result in differences in free exposure versus potency and use quite different dosing schedules.

Menezes et al. usefully demonstrated the therapeutic potential of ATR inhibitors based on mutation or deletion of ATM with compound "ATRi" from the same family as AZ20 (**Fig. 16**).[229] Compound "ATRi" (ATR enzyme $IC_{50} = 0.00023$ μM; ATR cell $IC_{50} = 0.13$ μM) leads to regression in ATM-deficient Granta-519 mantle cell lymphoma (MCL) xenografts but has minimal impact on the growth of ATM-WT JVM-2 tumors using a dose and schedule shown to be selective for ATR inhibition.[229] The sulfoximine morpholinopyrimidine AZD6738 maintains excellent potency for ATR in enzyme ($IC_{50} = 0.002$ μM) and cell ($IC_{50} = 0.074$ μM) assays combined with high specificity in a large kinase panel, including all of the related PIKK targets, while overcoming the main liabilities of AZ20.[230–232] AZD6738 has much higher aqueous solubility (661 μM at pH 7.4) and is devoid of measurable CYP3A4 TDI activity while maintaining high bioavailability in preclinical species.[230] We can speculate that replacement of the indole ring in AZ20 with the more electron-deficient 7-azaindole moiety in AZD6738 reduces the propensity for ring oxidation and subsequent formation of reactive metabolites that could bind covalently to the CYP heme. The improvement in aqueous solubility is likely a combination of reduced lipophilicity ($LogD_{7.4} = 1.9$ for AZD6738 compared with 2.7 for AZ20), and disruption of the sulfone–sulfone contacts seen in AZ20 albeit the melting temperature remains high. Reduction in lipophilicity and introduction of a hydrogen bond donor has a slight impact on the permeability of AZD6738 in Caco-2 cells compared with AZ20, but permeability remains high for AZD6738 which has an excellent PK profile with high fraction absorbed, low clearance, and high bioavailability in preclinical species.[230] The sulfoximine group has subsequently been highlighted as a useful fragment for use in drug discovery[233,234] and is found in other molecules in clinical development such as the pan-CDK inhibitor BAY-1000394.[235]

Similar to the results demonstrated with AZ20, exposure of AZD6738 results in a durable increase in tumor γH2AX compared with normal tissue such as bone marrow and GI, suggestive of a positive therapeutic index.[231] Continuous oral dosing schedules with AZD6738 are well tolerated with body weight loss dose limiting,[232] and single-agent tumor growth inhibition has been demonstrated in LoVo xenografts with less effect in ATM-proficient models such as HT29.[231] Duration of drug exposure and persistence of γH2AX have been shown to correlate with the antitumor efficacy in vivo.[231] Durable tumor regression without unacceptable toxicity has also been shown with AZD6738 in combination with the PARP1/2 inhibitor olaparib.[236] In a primary explant model (HBCx-10) of TNBC with BRCA2 and TP53 gene mutations, antitumor efficacy of the combination was significantly greater than either olaparib or AZD6738 dosed alone.[236] In a further study, AZD6738 has been shown to inhibit the growth of NSCLC cells inducing a DDR.[232] AZD6738 treatment synergized with cisplatin in ATM-deficient NSCLC cells resulting in rapid cell death.[232] In vivo the same combination of AZD6738, 25 mg kg^{-1} administered orally daily over 14 consecutive days, with cisplatin, 3 mg kg^{-1} administered IP on days 1 and 8 of a 2 week cycle, was well tolerated and led to robust tumor regression of ATM-deficient H23 tumors.[232] The combination led to limited body weight loss similar in extent to cisplatin treatment alone, further demonstrating the tolerability of ATR inhibitors in preclinical mouse models.[232]

To date three compounds have entered human clinical trials: VX-970, AZD6738, and VX-803; the structure of VX-803 has not been disclosed. VX-970 and AZD6738 are currently being tested in Phase I/II clinical trials across multiple tumor types. In these trials VX-970 is administered as a short i.v. infusion with episodic dosing regimens despite showing preclinical utility as an oral agent. Multiple combinations are being explored with a range of DNA-damaging agents reflecting the preclinical activity demonstrated. In a Phase I study in refractory advanced solid tumors, VX-970 monotherapy and VX-970 + carboplatin combination therapy were explored.[237] Paired tumor biopsies taken 1 h before and after VX-970 administration following carboplatin separated

by 24 h showed a 73% reduction in pCHK1 biomarker at the recommended Phase II dose of 90 mg m^{-2}.[238] Encouragingly early signs of clinical efficacy were noted. A patient with metastatic colorectal cancer with complete ATM-loss treated with monotherapy VX-970 and a patient with platinum-refractory metastatic high-grade serous ovarian cancer with BRCA1 + TP53 mutations treated with VX-970 in combination with carboplatin were reported with clinical responses.[237] VX-970 exploration is ongoing in Phase I/II studies across tumor types with cytotoxic chemotherapies (NCT02157792) and the PARP1/2 inhibitor veliparib and cisplatin in patients with refractory solid tumors (NCT02723864). The second compound from Vertex, VX-803, looks to be orally dosed and is being explored in early trials as monotherapy and in combination with carboplatin in patients with solid tumors and lymphoma (NCT02278250). Phase I/II studies with AZD6738 are underway as monotherapy and in combination with radiation in head and neck cancer (NCT02223923), and with carboplatin, olaparib, or the anti-PD-L1 checkpoint inhibitor durvalumab in advanced solid tumors (NCT02264678). The reported combination trial with cancer immunotherapy indicates a potentially exciting new approach, whereby ATR inhibitors could be used to prime an immune response.

ATR drug discovery remains a highly active field with further compounds from additional series being reported. New patent applications describing novel ATR inhibitors are emerging such as from the Spanish National Cancer Research Centre (CNIO),[239] who have an ongoing collaboration with Merck Serono, and most recently from Bayer Pharma[240] and Atrin.[241] It is clear from the continuing interest in discovery of new ATR inhibitors that further compounds will be identified that are likely to enter clinical development in the near future.

5.02.6.4 DNA-PK

DNA-PK is a serine/threonine protein kinase from the same family as ATR and ATM.[190,191] DNA-PK, made up of a catalytic subunit (DNA-PKcs) and the Ku70/80 heterodimer, plays a key role in NHEJ the preeminent pathway for repair of DNA DSBs in mammalian cells.[242,243] DNA DSBs are considered the most cytotoxic of DNA lesions, and mammalian cells have evolved two major pathways to repair them in cells: HR and NHEJ.[244,245] The kinase activity of DNA-PKcs is essential for successful NHEJ; the Ku70/80 heterodimer senses and binds to the DNA DSB ends, and it is this DNA–Ku complex that binds DNA-PKcs to form DNA-PK resulting in activation of the catalytic activity of the enzyme.[242,243] Inhibition of NHEJ through inhibition of DNA-PK activity offers a unique approach to enhance the cancer cell toxicity of DSB-inducing IR and chemotherapeutic agents. Multiple substrates are known for DNA-PKcs involved in NHEJ and the DDR more widely, the best characterized of which is DNA-PKcs itself.[242,243] Autophosphorylation occurs on a number of sites and is associated with kinase inactivation and dissociation from the DNA–Ku70/80 complex. In addition to its central role in NHEJ, the role of DNA-PKcs in the regulation of mitosis and other cellular processes has been described.[242] DNA-PKcs has been shown to interact with PLK1 and to phosphorylate CHK2 during mitosis.[242,243] The activity of DNA-PKcs outside of NHEJ is quite likely different, with the observation that the catalytic activity of DNA-PKcs can be independent of Ku70/80.[242,243]

5.02.6.4.1 DNA-PK inhibitors

Wortmannin (Fig. 17) was described initially as a potent irreversible inhibitor of PI3 kinases but then was also shown to bind covalently forming ATP-site adducts with DNA-PK, ATM, and ATR.[246,247] For DNA-PK in particular, Wortmannin has good potency ($K_i \sim 120$ nM) and its mechanism of action in sensitizing cells to IR is recognized as most likely driven through inhibition of DNA-PK and inhibition of DNA DSB repair,[248] but the compound suffers from poor stability.

The importance of the arylmorpholine pharmacophore is nicely demonstrated by IC87361, a potent DNA-PK inhibitor ($IC_{50} = 0.034$ μM) with selectivity over PI3Kα ($IC_{50} = 3.8$ μM).[249] Treatment of cells with IC87361 alone did not induce cytotoxicity, but the combination with radiation in mouse tumor models resulted in a slowing of tumor growth compared with radiation alone with no apparent toxicity to normal tissues.[249] Willmore et al. identified the 2-(morpholin-4-yl)-benzo[h]chomen-4-one NU7026.[250] NU7026 is an ATP-competitive and highly selective inhibitor of DNA-PK, with a 60-fold greater potency for DNA-PK compared to PI3Ks, and is inactive against both ATM and ATR.[251] NU7026 demonstrated the ability of DNA-PK inhibitors to potentiate chemotherapeutic-induced DSBs from agents such as etoposide while having no effect as a single agent. Further SAR investigation from the same group led to the discovery of the 2-*N*-morpholino-8-dibenzothiophenyl-chromen-4-one NU7441 with further enhancement of potency ($IC_{50} = 14$ nM) and specificity for DNA-PK (at least 100-fold selectivity over PIKK family kinases).[252] Treatment of cells with NU7441 substantially retarded the repair of IR-induced and etoposide-induced DSBs and the clonogenic survival of both p53-mutant and p53-WT human colon cancer cell lines.[253] In vivo proof of concept with NU7441 has been demonstrated in mice bearing SW620 xenografts. The combination of NU7441 and etoposide increased etoposide-induced tumor growth delay twofold without exacerbating toxicity to unacceptable levels.[253] The high lipophilicity of these compounds results in low aqueous solubility (KU7441 pH 7.4 aqueous solubility < 0.3 μM) and high protein binding (hu free drug = 0.04%), properties that restrict full in vivo evaluation and further development. To address these limitations, the addition of water-solubilizing primary and secondary amine groups linked through a polar amide was investigated. Compounds such as KU60648 were developed that retain the high level of potency for DNA-PK ($IC_{50} = 5$ nM) described for NU7441.[254] KU60648 has much lower plasma protein binding and higher aqueous solubility, albeit variability between assays was observed.[254] KU60648 was unexpectedly found to also inhibit PI3Kα ($IC_{50} = 0.004$ μM), but it did retain selectivity over mTOR, ATM, and ATR.[254] The dual kinase activity profile is mirrored in cells; KU60648 potently inhibits the autophosphorylation of DNA-PK ($IC_{50} = 0.019$ μM in MCF7 cells) and PI3K-mediated AKT phosphorylation ($IC_{50} = 0.039$ μM in MCF7 cells).[254] KU60648 potentiated the cytotoxicity of anticancer agents and IR, and in contrast to the DNA-PK selective inhibitors described before, drug

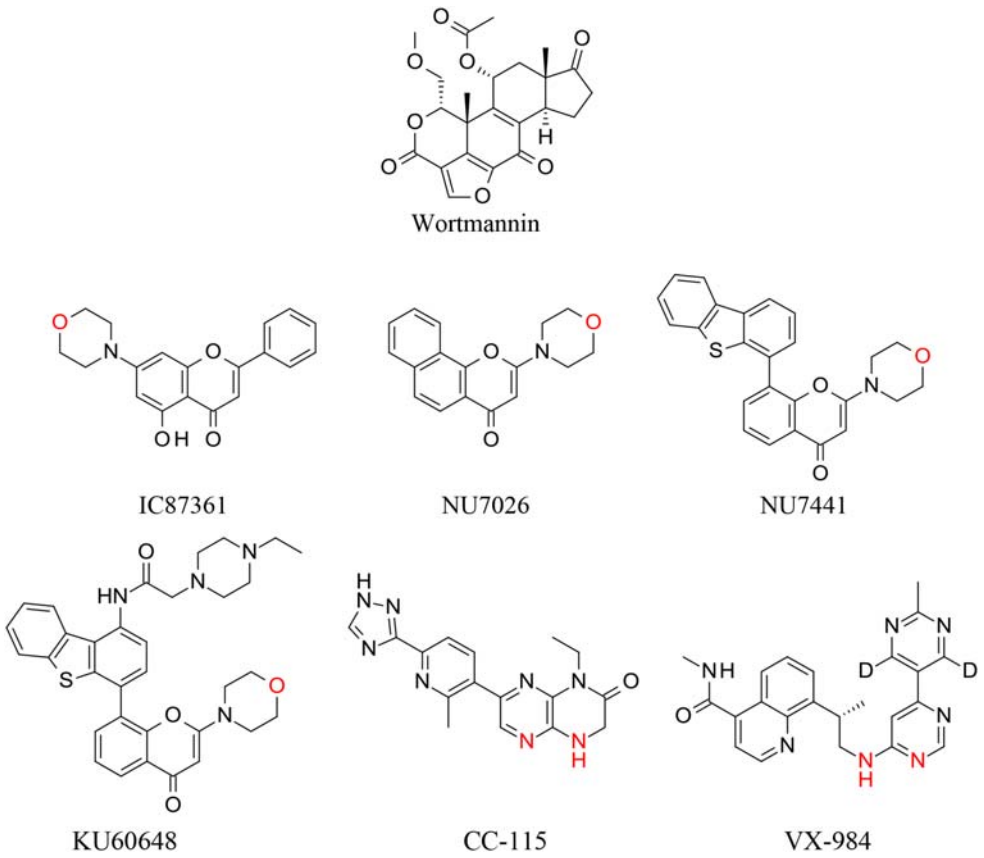

Fig. 17 DNA-PK inhibitors (assumed hinge-binding atoms highlighted in *red*).

treatment alone was found to inhibit cell proliferation.[254] Treatment with KU60648 alone delayed the growth of MCF7 xenografts and increased tumor growth delay in combination with etoposide in both SW620 and MCF7 xenograft models by up to 4.5-fold.[254] In rat toxicity studies however, KU60648 was not well tolerated perhaps linked to its nonspecific kinase activity profile. In addition, despite the addition of solubilizing groups, the biopharmaceutical properties of compounds such as KU60648 negated further development investment.[205]

Three DNA-PK inhibitors each from a chemotype not previously described have entered clinical development. CC-115 from Celgene is a dual mTOR, DNA-PK inhibitor derived from an earlier mTOR-selective compound series.[255] Screening CC-115 in a panel of kinase assays led to the discovery of DNA-PK as an equipotent target while it was shown to be selective against PI3Ks, ATR, and ATM.[255] It does not appear that the dual mTOR and DNA-PK inhibitory activity profile of CC-115 was a result of rational design and preclinical characterization of CC-115 detailing the benefit or otherwise of adding DNA-PK activity to mTOR has yet to be reported. However, the distinct activity profile may allow a differentiated clinical positioning. A Phase I study of CC-115 administered orally to patients with advanced solid tumors and hematologic malignancies is underway (NCT0135362). MSC2490484A from Merck Serono is also in a Phase I study in patients with advanced solid tumors with alterations in DNA-repair mechanisms (such as BRCA and ATM), or CLL in combination with radiotherapy (NCT02516813). The structure of MSC2490484A has not been released. A third compound, VX-984 from Vertex, is an ATP-site inhibitor of DNA-PKcs, deuterated to slow the rate of oxidative metabolism by aldehyde oxidase.[256] VX-984 is a highly potent and ATP-competitive inhibitor of DNA-PKcs enzyme ($K_i = 0.002$ μM) and in cells (autophosphorylation in A549 $IC_{50} = 0.088$ μM) with high selectivity over PIKKs.[256] VX-984 showed minimal effects on cell viability as a single agent but in combination with radiation decreased clonogenic survival of a range of human lung cancer cell lines.[256] In vivo, oral administration of VX-984 inhibited DNA-PKcs autophosphorylation in a dose-dependent manner and potentiated the antitumor efficacy of IR in an NSCLC PDX mouse model.[256] A first in human study of VX-984 is recruiting to evaluate safety and tolerability administered alone and in combination with i.v. dosed pegylated liposomal doxorubicin (PLD), in patients with advanced solid tumors or lymphomas (NCT02644278). PLD is a drug formulation where doxorubicin is delivered encapsulated in a bilayer sphere of lipids.[257] It has been reported that the size of the liposome particles results in a greater deposition of the encapsulated drug in the tumor compared with other tissues resulting in a differential toxicity profile through the enhanced permeability and retention (EPR) effect.[258] It may also be the case that a change in PK profile is equally important in any observed effect; the development of nanomedicines in oncology is of significant interest for classical cytotoxic and targeted agents.[259]

5.02.6.5 WEE1 and CHK1

WEE1, a dual-specificity protein tyrosine kinase,[260–263] and CHK1, a serine/threonine protein kinase,[264–266] are activated in response to DNA-damage and function as key regulators of the G2-M and S-phase checkpoints protecting the cell from apoptotic cell death until DNA-damage is repaired. CHK1 is activated through phosphorylation by ATR in response to replication stress or DNA-damage inducing radiotherapy or chemotherapy.[266] WEE1 and CHK1 inhibitors have potential as chemosensitizing drugs inducing G2/M checkpoint escape and releasing the tumor cell from cell cycle arrest, resulting in mitotic catastrophe.[267] A potential synthetic lethality occurs in tumors with mutated p53 which plays a key role in G1-S checkpoint regulation.[268] Abnormalities in the p53 pathway are common in the majority of human cancers.[269] Tumor cells lacking a functioning G1 checkpoint have greater dependency on the S and G2-M checkpoints, whereas loss of checkpoint regulation is thought to be compensated in normal tissue by functioning p53. Therefore a favorable therapeutic index is expected when WEE1 or CHK1 inhibition is combined with DNA-damaging agents in tumors lacking functioning p53. Inhibition of WEE1 kinase has been shown to be effective in p53 WT tumors. Regulation of G2-M arrest and DNA-repair pathways is highly complex, and the impact of WEE1 inhibition is likely determined through mechanisms of cell cycle regulation other than p53 or defective DNA-repair pathways independent of cell cycle regulation.[261] WEE1 signals through phosphorylation and inhibition of CDK1 and 2.[260] Knockdown or inhibition of WEE1 causes abnormally high CDK1/2 activity in S-phase cells that eventually results in an induction of DNA DSBs. Likewise, inhibition of CHK1 alone can result in replication fork collapse and formation of DNA DSBs. Therefore WEE1 and CHK1 inhibitors may also be anticipated to have antitumor activity in the absence of added chemotherapy.

5.02.6.5.1 WEE1 inhibitors

A single WEE1 inhibitor AZD1775 (MK-1775, Fig. 18), developed by Merck & Co. Inc. and licensed to AstraZeneca, is under clinical investigation, and a small number of additional compounds have been reported in the preclinical phase. AZD1775 was developed from a screening hit derived from a small chemical compound library aimed at identification of inhibitors of WEE1 enzymatic activity.[270,271]

The medicinal chemistry design of AZD1775 has not been reported. AZD1775 contains a recognizable anilino-pyrimidine kinase hinge-binding motif and is an ATP-competitive inhibitor of WEE1 ($IC_{50} = 5.2$ nM), is orally bioavailable, and has shown to be highly selective for WEE1 in a panel of 223 protein kinase assays.[270] Activity of AZD1775 for a single additional kinase, Yes ($IC_{50} = 14$ nM) was demonstrated within 10-fold of the WEE1 potency.[270] AZD1775 inhibited phosphorylation of CDC2 at Tyr15 in WiDr cells (human colorectal cancer cell line with mutated p53) pretreated with gemcitabine ($EC_{50} = 85$ nM) and potently induced pHH3, reflecting premature mitotic entry resulting from abrogation of DNA-damage checkpoints, in combination with gemcitabine and platinum agents.[270] AZD1775 was shown to selectively sensitize p53-deficient tumor cells to a range of DNA-damaging agents such as gemcitabine, platinum agents, and radiation, potentiating tumor growth inhibition without significant increased toxicity in mouse in vivo models across multiple tumor types.[270] Inhibition of CDC2 phosphorylation and induction of pHH3 phosphorylation was demonstrated in tumor and correlated with antitumor efficacy in vivo.[270] Single-agent efficacy of AZD1775 has been demonstrated in NSCLC (A427 and SK-MES-1) and colorectal (LoVo) xenograft models. Sensitivity has been linked to PKMYT1 expression providing a potential foundation for exploring the anticancer activity of AZD1775 independent of cytotoxic combinations.[271]

In early clinical trials as a single agent in refractory solid tumors, AZD1775 was administered orally twice daily over 2.5 days per week for up to 2 weeks in a 21-day cycle.[272] The MTD was established at 225 mg with common toxicities including myelosuppression and diarrhea. Proof-of-mechanism was demonstrated by target modulation and DDR in paired tumor biopsies with a reduction in pY15-CDK and increased γH2AX. Encouragingly, single-agent activity was shown with partial responses in two patients (one with head and neck cancer and one with ovarian cancer) both carrying *BRCA1* mutations.[272] AZD1775 is being evaluated in numerous Phase II clinical studies as monotherapy and as a potentiator of DNA damage in combination with SOC therapies in patients with NSCLC, head and neck, gastric, breast, and ovarian cancers. Multiple trials have investigated AZD1775 in ovarian cancer, and in 2012 AZD1775 received Orphan Drug designation in the European Union for this indication. Promising clinical efficacy was established in a Phase II study (NCT01164995) in combination with carboplatin in patients with chemotherapy-resistant p53-mutated ovarian cancer.[273] Dosing of AZD1775 followed the same schedule (225 mg BID for 2.5 days) with concomitant dosing of

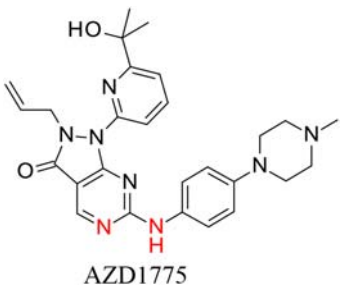

AZD1775

Fig. 18 WEE1 inhibitors (assumed hinge-binding atoms highlighted in *red*).

carboplatin AUC5 by short (30 min) i.v. infusion on day 1, following a 21-day cycle. This combination was tolerated albeit toxicity to bone marrow was common.[273] Out of 22 evaluable patients, 6 showed a confirmed partial response (PR), while 9 patients exhibited stable disease (SD).[273]

In addition to combinations with chemotherapy and radiation, the combination of WEE1 inhibitors with CHK1 or PARP1/2 inhibitors has been investigated in preclinical studies, and these novel–novel combinations have started to be investigated in the clinic. The key role played by CHK1 and CHK2 in cell cycle control and the link between BRCA1 and CHK1 modulation in the G2-M checkpoint control together with the marked sensitivity of BRCA1-mutated tumors to PARP1/2 inhibitors, provides a rationale for exploring inhibitor combinations of these targets. Simultaneous inhibition of CHK1 and WEE1 has been demonstrated to have a strong synergistic cytotoxic effect in MCL cells, associated with deregulation of the cell cycle and increased activity of CDK1 and 2.[274] The combination of AZD1775 with the CHK1 inhibitor PF-00477736 in JeKo-1 xenografts led to marked tumor regression at tolerated doses, providing a potential rationale for testing this combination in the clinic albeit no such studies have started.[274] The radiosensitizing efficacy of AZD1775 and the PARP1/2 inhibitor olaparib in pancreatic cancer has been demonstrated in MiaPaCa-2 xenografts, where radiosensitization from this combination was associated with G2 checkpoint abrogation and persistent DNA damage.[275] A Phase I multicenter, dose escalation study of AZD1775 combined with olaparib in refractory solid tumors is currently recruiting (NCT02511795). In addition, other novel agent–novel agent combinations underway include a Phase I study of AZD1775 in combination with the anti-PD-L1 inhibitor durvalumab (MEDI4736) in patients with advanced solid tumors (NCT02617277).

5.02.6.5.2 CHK1 inhibitors

The concept of modulating DNA-damage checkpoints to enhance the efficacy of DNA-damaging agents has been demonstrated in preclinical studies with small-molecule inhibitors of CHK with varying CHK1/2 selectivity. The compounds that remain active in human clinical trials are summarized in **Fig. 14**. Many CHK1 inhibitors have been developed and have entered clinical trials, demonstrating tolerability with DNA-damaging agents.[276] However, further progression has proven difficult, and development of many of these compounds has since been terminated for toxicity or business-related reasons.[277]

LY2603618 (rabusertib, **Fig. 19**) and MK-8776 (SCH-900776) were in clinical trials but have since been discontinued. The biaryl urea motif in LY2603618 is an atypical ATP-site binder identified following a HTS against catalytic CHK1 activity. X-ray crystallography revealed a strong conformational preference of the biaryl urea structure with intramolecular hydrogen bonds between the pyrazine N1 and the distal urea N−H with the oxygen of the alkoxy moiety further stabilizing the bioactive conformation.[278] In this conformation, the carbonyl and remaining urea N−H form a recognizable hydrogen bond donor/acceptor pair to the kinase hinge. Both pyrazine nitrogens are important for CHK1 activity with an observed interaction between the 2nd pyrazine nitrogen and a conserved water molecule in the active site. Appending amines, particularly conformationally constrained cyclic amine groups on the alkoxy, led to large increases in potency and provided a valuable way to modulate physicochemical and pharmacokinetic properties.[278] Cyclic amines with reduced basicity (e.g., morpholine) were found to be equipotent and benefitted from reduced hERG potency. LY2603618 is a potent CHK1 inhibitor ($IC_{50}=0.007$ μM) with selectivity over CHK2 ($IC_{50}=12$ μM) and >100-fold selectivity in a panel of protein kinases. LY2603618 is a potent inhibitor of CHK1 activity in cells inhibiting CHK1 autophosphorylation

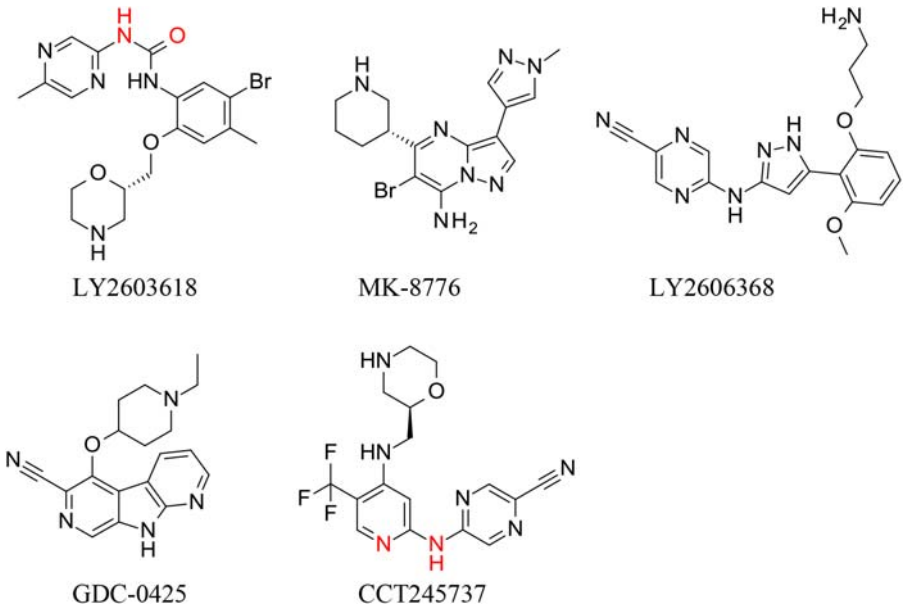

Fig. 19 CHK1/2 (assumed hinge-binding atoms highlighted in *red*).

(Ser-296) following treatment with doxorubicin in HeLa cells ($EC_{50} = 0.12$ μM following 24 h treatment with 100 nM doxorubicin). A concentration of 250 nM of LY2603618 is effective at potentiating the potency of gemcitabine in p53 mutant, but not in p53 WT cells. LY2603618 treatment led to an increase in the mitotic marker pHH3 (Ser10) in HeLa cells treated with doxorubicin indicating inactivation of the G2/M DNA-damage checkpoint. In p53-mutant Calu-6 xenografts CHK1 autophosphorylation is strongly inhibited by coadministration of 200 mg kg^{-1} LY2603618 with gemcitabine for at least 24 h. In efficacy studies, LY2603618 treatment alone has little effect on tumor growth but enhances the antitumor efficacy in combination with gemcitabine and with pemetrexed in pancreatic and NSCLC xenograft models, respectively.[279,280] Scheduling of the combination is key to efficacy with enhanced tumor growth inhibition obtained only when LY2603618 was given 24 h after the DNA-damaging agent.[279,280] In combination with gemcitabine, durable efficacy was also demonstrated in a p53-WT pancreatic patient explant model (PAXF1869) using the same offset dosing schedule; interestingly the PAXF 1869 model contains a mutation in the *CHK2* gene and CHK2 contributes to the p53-dependent G1-S checkpoint.[279] The results of three early clinical studies with LY2603618 have been published.[280–282] In these studies LY2603618 has been administered as a short (1 h) i.v. infusion in combination with pemetrexed, pemetrexed, and cisplatin and with gemcitabine. In each case scheduling of LY2603618 has followed the reported optimized preclinical 24-h gap schedule. In the absence of validated biomarkers to assess PD, the biological effective dose was established based on achieving exposure in excess of that shown preclinically to generate the maximal PD response and used as a surrogate to establish a dose for later-stage studies. Early signs of clinical responses were reported at doses considered tolerated, albeit with signs of hematological toxicity, but despite these reports the development of LY2603618 has now been discontinued.

MK-8776 (SCH900776) is a more potent inhibitor of CHK1 ($IC_{50} = 3$ nM) than CHK2 ($IC_{50} = 1500$ nM) and other cell cycle kinases such as CDK2 ($IC_{50} = 160$ nM) and leads to synergistic antitumor activity in combination with DNA-damaging agents which activate CHK1 such as gemcitabine and cytarabine.[283,284] In a Phase I trial, MK-8776 was administered as an i.v. infusion in combination with cytarabine to patients with relapsed refactory acute leukemias. Complete remissions occurred in 8 of 24 patients with DLTs including corrected QT interval prolongation.[285] The clinical combination of MK-8776 with gemcitabine has also been explored. In contrast to the 24 h gap schedule utilized for LY2603618, MK-8776 was administered with only a 30 min interval to gemcitabine. Despite this, the combination led to a PR in two patients and SD in 13 others.[286] The development of MK-8776 may have been discontinued although a Phase II trial in AML (NCT01870596) is recorded as ongoing.

A second-generation compound from Lilly LY2606368 (prexasertib) is active in Phase II studies. LY2606368 contains a cyanopyrazine group linked via an amine to a pyrazole core. LY2606368 is a potent ATP-competitive inhibitor of CHK1 ($K_i = 0.9$ nM; $IC_{50} < 1$ nM) and, in contrast to LY2603618, also potently inhibits CHK2 ($IC_{50} = 8$ nM).[287] Otherwise LY2606368 is highly selective in a panel of 224 protein kinases with an $IC_{50} < 100$ nM for 5 kinases.[287] In cells LY2606368 potently inhibits both CHK1 and CHK2 autophosphorylation ($EC_{50} < 1$ and < 31 nM, respectively) and potently abrogated the doxorubicin-activated G2-M checkpoint in p53-deficient HeLa cells ($EC_{50} = 9$ nM).[287] Interestingly LY2606368 is broadly and potently antiproliferative as a single agent with IC_{50} values typically < 50 nM in sensitive cell lines. Treatment with LY2606368 alone was shown to result in DNA DSBs together with dysregulation of DNA-damage checkpoints. LY2606368 was shown to reduce CHK1 autophosphorylation and increase DDR markers such as γH2AX in Calu6 xenografts in vivo and episodic dosing of LY2606368 led to tumor growth inhibition without excessive body weight loss.[287] LY2606368 is being assessed as both a single agent and in combination with cytotoxic agents in the clinic. Administration of LY2606368 as monotherapy by short i.v. infusion over 1 h using an episodic schedule of 1 or 3 consecutive doses per day every 2 weeks has been reported.[288] Drug exposure at the MTD was found to match the exposure in preclinical mouse xenografts that achieved antitumor activity. LY2606368 has shown early clinical activity; from 45 patients in the study, 2 had a PR and 15 others exhibited SD with DLTs all hematological related.[288] A Phase I study of GDC-0425,[289] an orally bioavailable compound dosed in combination with gemcitabine in solid tumors or lymphoma (NCT01359696), has completed, but there are no reports describing this molecule's preclinical characterization or clinical results.

CCT245737 is the newest CHK1 inhibitor to enter clinical development. CCT245737 was discovered following a multiparameter optimization campaign aimed at identifying compounds with high selectivity for CHK1 over CHK2 and other protein kinases such as CDK1, balancing lipophilicity, and basicity for potent CHK1 activity with effective cellular potency and favorable PK properties without detrimental activity such as inhibition of the hERG ion-channel.[290] An orally dosed drug was the goal to give maximum flexibility of dosing for use as a single agent and in combination with DNA-damaging agents. The CCT245737 series binds through the 2-aminopyridine moiety to the kinase hinge with nitrile and N-4 of the pyrazine interacting with an atypical conserved water leading to high kinase selectivity.[290] CCT245737 is an ATP-competitive and highly potent inhibitor of CHK1 ($IC_{50} = 1.4$ nM) with >1000-fold selectivity over CHK2 and CDK1. CCT245737 potently inhibits cellular CHK1 and CDK1 phosphorylation induced by gemcitabine at 0.5 μM and results in DNA DSBs and abrogates cell cycle checkpoints.[290,291] CCT245737 potentiates the cytotoxicity of gemcitabine across a range of human tumor cell lines and achieves high free exposure in mouse from oral doses.[291] The in vitro PD activity is recapitulated in vivo with the same 24 h gap schedule described for other CHK1 inhibitors in combination with gemcitabine. Single-agent CCT245737 at 150 mg kg^{-1} had marginal antitumor inhibition alone but the combination with gemcitabine led to significant increase in tumor growth delay over gemcitabine treatment alone in HT29 and SW620 xenografts without unacceptable body weight loss. Similar tolerated antitumor efficacy was demonstrated in combination with the topoisomerase 1 inhibitor irinotecan and as a single-agent activity in a MYC-driven model of B-cell lymphoma.[291] CCT245737 is recruiting in two Phase I studies, administered orally in patients with advanced cancer (NCT02797964) and in combination with either gemcitabine or gemcitabine plus cisplatin in patients with advanced cancer (NCT02797977). A PD marker of CHK1 activity, pS296 CHK1, will be explored clinically to define dose and schedule.[291]

5.02.6.6 Summary and Outlook

The collective DDR offers a rich source of anticancer drug targets. Kinases in particular provide validated and druggable new drug targets to exploit for a new generation of cancer therapies. The DDR is fundamental to genomic integrity in normal cells leading to a concern over the expected toxicity from targeting particular DDR proteins. However it is clear from the published preclinical studies in mouse models, using highly potent and specific small-molecule inhibitors, that pharmacological DDR kinase inhibition is not overtly toxic and a positive therapeutic index can be achieved. Moreover DDR inhibitors are now being successfully applied in the clinic. A number of key therapeutic concepts are utilized in targeting the DDR in cancer cells offering the potential for selective tumor cell killing. First, cancer cells have high DNA-damage load, exhibiting replication stress and a reliance on DDR for survival. Second, the loss of specific DDR capability through mutations is common and leads to an exploitable DDR dependency. Third, potentiation of the cytotoxicity of DNA-damaging chemotherapy and radiotherapy through combination with DDR inhibitors is an important therapeutic strategy particularly in the context of DDR dependency.

A major advance in recent years has been the progression of multiple compounds into human trials (Fig. 14). It is clear that DDR inhibitors with high specificity are preferred over compounds that inhibit multiple targets as they are most likely to achieve greater tolerability. In some cases different organizations have arrived at compounds targeting the same kinase with quite different properties, such as preferred route of administration. The impact of these differences on both efficacy and tolerability will become clear as the clinical data matures. It is interesting that AZD1775 is the only WEE1 kinase inhibitor reported in clinical development. As the clinical utility of AZD1775 becomes evident (and any limitations also) further compounds will no doubt be developed. The use of early compounds, even without properties suitable for development, has enabled detailed preclinical proof of principle studies to be completed encouraging the development of improved inhibitors for clinical use. These preclinical studies reveal the exciting therapeutic potential of DDR kinase inhibitors to enhance the efficacy of a range of established anticancer drugs across multiple tumor types. The detailed preclinical studies have been influential supporting clinical trial design, for example, identification of the optimal combination partner and schedule, responsive tumor type, and required biological effective dose. These results demonstrate wide ranging potential for clinical use and the ongoing trials reflect this diversity of opportunity. Combinations with DNA-damaging chemo, radiotherapy, or novel agents are being explored for all of the compounds described. Inhibitors of some DDR kinases (e.g., ATR, WEE1, and some CHK1 inhibitors) have demonstrated potent single-agent antitumor activity in appropriate tumor subsets (e.g., tumors lacking functional p53 or with loss of ATM). There is some overlap between sensitive tumor types and combination partners between DDR targets. However, the precise mechanisms of DNA-damage and repair are quite different and likely therefore to lead to complementary activity such as the responsive patient segments between targets.

Early clinical responses are encouraging, and some compounds are advancing into the later stages of development albeit none yet are being explored in trials which will lead directly to regulatory approval. The combination of DDR kinase inhibitors with DNA-damaging chemotherapy and/or radiotherapy has led to toxicity particularly where there are overlapping toxicities such as to the bone marrow. However, success has come from careful scheduling, selection of the appropriate agent based on a clear mechanistic rationale supported by preclinical evidence for a synergistic combination. Biomarkers to identify likely responders will be especially important to achieve a favorable therapeutic index. In particular circumstances, selective delivery to the tumor or judicious choice of route of administration may prove to be important. Novel agent–novel agent combinations such as with PARP1/2 inhibitors or the combination with immunotherapies are now being explored clinically, offering an exciting extension to combinations with classical cytotoxic agents that have been the focus to date.

DDR inhibition is a distinct therapeutic strategy that has received much interest from drug hunters, and targeted DDR kinase inhibitors are set to form a new wave of drugs for the treatment of cancer and potentially other diseases.

See also: 5.03. Covalent Kinase Inhibitors for Cancer. 5.04. Targeting DNA Damage Response Pathways in Cancer. 7.10. Inhibiting Kinases in the CNS. 8.02. Trametinib. 8.05. The Discovery of p97 Inhibitors. 8.06. Discovery of AMG 337: Using Structure Guided Scaffold Hybridization to Optimize Physicochemical Properties and Target Coverage of a MET Kinase Inhibitor. 8.07. Discovery of AZD0156: The First Potent and Selective Inhibitor of ATM Kinase for Clinical Evaluation. 8.08. Tepotinib. 8.16. Medicinal Chemistry Case History: Structure-Based Drug Design of Oral and Inhaled p38 MAP Kinase Inhibitors as Clinical Candidates.

References

1. Druker, B. J.; Tamura, S.; Buchdunger, E.; Ohno, S.; Segal, G. M.; Fanning, S.; Zimmermann, J.; Lydon, N. B. *Nat. Med.* **1996,** *2,* 561–566.
2. Wu, P.; Nielsen, T. E.; Clausen, M. H. *Drug Discov. Today* **2016,** *21,* 5–10.
3. Kujak, C.; Kolesar, J. M. *Am. J. Health Syst. Pharm.* **2016,** *73,* 113–120.
4. Saito, M.; Shiraishi, K.; Kunitoh, H.; Takenoshita, S.; Yokota, J.; Kohno, T. *Cancer Sci.* **2016,** *107,* 713–720.
5. Logan, J. E.; Rampersaud, E. N.; Sonn, G. A.; Chamie, K.; Belldegrun, A. S.; Pantuck, A. J.; Slamon, D. J.; Kabbinavar, F. F. *Rev. Urol.* **2012,** *14,* 65–78.
6. Saeidi, K. *Crit. Rev. Oncol. Hematol.* **2016,** *98,* 375–389.
7. Yoshikawa, S.; Kukimoto-Niino, M.; Parker, L.; Handa, N.; Terada, T.; Fujimoto, T.; Terazawa, Y.; Wakiyama, M.; Sato, M.; Sano, S.; Kobayashi, T.; Tanaka, T.; Chen, L.; Liu, Z. J.; Wang, B. C.; Shirouzu, M.; Kawa, S.; Semba, K.; Yamamoto, T.; Yokoyama, S. *Oncogene* **2013,** *32,* 27–38.
8. Braghiroli, M. I.; Sabbaga, J.; Hoff, P. M. *Expert. Rev. Anticancer. Ther.* **2012,** *12,* 567–580.
9. Jackson, S. E.; Chester, J. D. *Int. J. Cancer* **2015,** *137,* 262–266.
10. Morgan, R. A. *Mol. Ther.* **2012,** *20,* 882–884.

11. Buchdunger, E.; Matter, A.; Druker, B. J. *Biochim. Biophys. Acta* **2001,** *1551,* M11–M18.
12. Harvery, A. J.; Crompton, M. R. *Anti-Cancer Drugs* **2004,** *15,* 107–111.
13. Rengifo-Cam, W.; Konishi, A.; Morishita, N.; Matsuoka, H.; Yamori, T.; Nada, S.; Okada, M. *Oncogene* **2004,** *23,* 289–297.
14. Sawyers, C. L. *Semin. Hematol.* **2001,** *38,* 15–21.
15. Buchdunger, E.; Cioffi, C. L.; Law, N.; Stover, D.; Ohno-Jones, S.; Druker, B. J.; Lydon, N. B. J. *Pharmacol. Exp. Ther.* **2000,** *295,* 139–145.
16. Gunby, R. H.; Sala, E.; Tartari, C. J.; Puttini, M.; Gambacorti-Passerini, C.; Mologni, L. *Anticancer Agents Med. Chem.* **2007,** *7,* 594–611.
17. Lopes de Menezes, D. E.; Peng, J.; Garrett, E. N.; Louie, S. G.; Lee, S. H.; Wiesmann, M.; Tang, Y.; Shephard, L.; Goldbeck, C.; Oei, Y.; Ye, H.; Aukerman, S. L.; Heise, C. *Clin. Cancer Res.* **2005,** *11,* 5281–5291.
18. Bello, E.; Colella, G.; Scarlato, V.; Oliva, P.; Berndt, A.; Valbusa, G.; Serra, S. C.; D'Incalci, M.; Cavalletti, E.; Giavazzi, R.; Damia, G.; Camboni, G. *Cancer Res.* **2011,** *71,* 1396–1405.
19. Gandhi, L.; Jänne, P. A. *Clin. Cancer Res.* **2012,** *18,* 3737–3742.
20. Schildhaus, H. U.; Deml, K. F.; Schmitz, K.; Meiboom, M.; Binot, E.; Hauke, S.; Merkelbach-Bruse, S.; Büttner, R. *Mod. Pathol.* **2013,** *26,* 1468–1477.
21. Dong, L.; Wang, W.; Li, A.; Kansal, R.; Chen, Y.; Chen, H.; Li, X. *Curr. Genomics* **2015,** *16,* 253–263.
22. Singh, D.; Chan, J. M.; Zoppoli, P.; Niola, F.; Sullivan, R.; Castano, A.; Liu, E. M.; Reichel, J.; Porrati, P.; Pellegatta, S.; Qiu, K.; Gao, Z.; Ceccarelli, M.; Riccardi, R.; Brat, D. J.; Guha, A.; Aldape, K.; Golfinos, J. G.; Zagzag, D.; Mikkelsen, T.; Finocchiaro, G.; Lasorella, A.; Rabadan, R.; Iavarone, A. *Science* **2012,** *337,* 1231–1235.
23. Arai, Y.; Totoki, Y.; Hosoda, F.; Shirota, T.; Hama, N.; Nakamura, H.; Ojima, H.; Furuta, K.; Shimada, K.; Okusaka, T.; Kosuge, T.; Shibata, T. *Hepatology* **2014,** *59,* 1427–1434.
24. Song, M. *J. Med. Chem.* **2015,** *58,* 3672–3681.
25. Levitzki, A. *Cytokine Growth Factor Rev.* **2004,** *15,* 229–235.
26. Nakanishi, Y.; Akiyama, N.; Tsukaguchi, T.; Fujii, T.; Satoh, Y.; Ishii, N.; Aoki, M. *Mol. Cancer Ther.* **2015,** *14,* 704–712.
27. Biankin, A. V.; Piantadosi, S.; Hollingsworth, S. J. *Nature* **2015,** *526,* 361–370.
28. Kris, M. G.; Natale, R. B.; Herbst, R. S.; Lynch, T. J.; Prager, D.; Belini, C. P.; Schiller, J. H.; Kelly, K.; Spiridonidis, H.; Sandler, A.; Cella, D.; Wolf, M. K.; Averbuch, S. D.; Ochs, J. J.; Kay, A. C. *JAMA* **2003,** *290,* 2149–2158.
29. Reck, M. *Expert. Rev. Anticancer. Ther.* **2009,** *9,* 401–412.
30. Townsley, C. A.; Major, P.; Siu, L. L.; Dancey, J.; Chen, E.; Pond, G. R.; Nicklee, T.; Ho, J.; Hedley, D.; Tsao, M.; Moore, M. J.; Oza, A. M. *Br. J. Cancer* **2006,** *94,* 1136–1143.
31. Kazandjian, D.; Blumenthal, G. M.; Yuan, W.; He, K.; Keegan, P.; Pazdur, R. *Clin. Cancer Res.* **2016,** *22,* 1307–1312.
32. Akita, R. W.; Sliwkowski, M. X. *Semin. Oncol.* **2003,** *30* (Suppl. 7), 15–24.
33. Lynch, T. J.; Bell, D. W.; Sordella, R.; Gurubhagavatula, S.; Okimoto, R. A.; Brannigan, B. W.; Harris, P. L.; Haserlat, S. M.; Supko, G. J.; Haluska, F. G.; Louis, D. N.; Christiani, D. C.; Settleman, J.; Haber, D. A. *N. Engl. J. Med.* **2004,** *350,* 2129–2139.
34. Fukuoka, M.; Yano, S.; Giaccone, G.; Tamura, T.; Nakagawa, K.; Douillard, J.-Y.; Nishiwaki, Y.; Vansteenkiste, J.; Kudoh, S.; Rischin, D.; Eek, R.; Horai, T.; Noda, K.; Takata, I.; Smit, E.; Averbuch, S. D.; Macleod, A.; Feyereislova, A.; Dong, R.-P.; Baselga, J. *J. Clin. Oncol.* **2003,** *21,* 2237–2246.
35. Kris, M.; Ranson, M.; Ferry, D.; Hammond, L.; Averbush, S.; Ochs, J.; Rowinsky, J. *Clin. Cancer Res.* **1999,** *5,* 3749S.
36. Norkowski, E.; Ghigna, M. R.; Lacroix, L.; Le Chevalier, T.; Fadel, É.; Dartevelle, P.; Dorfmuller, P.; Dorfmuller, P.; Thomas de Montpréville, V. *J. Thorac. Oncol.* **2013,** *8,* 1265–1271.
37. Rothenberg, S. M.; Engelman, J. A.; Le, S.; Riese, D. J.; Haber, D. A.; Settleman, J. *Proc. Natl. Acad. Sci. U. S. A.* **2008,** *105,* 12480–12484.
38. Meng, X.; Li, Y.; Tang, H.; Mao, W.; Yang, H.; Wang, X.; Ding, X.; Xie, S. *Amino Acids* **2016,** *48,* 487–497.
39. Mondal, J.; Tiwary, P.; Berne, B. J. J. *Am. Chem. Soc.* **2016,** *138,* 4608–4615.
40. Kim, T. S.; Cavnar, M. J.; Cohen, N. A.; Sorenson, E. C.; Greer, J. B.; Seifert, A. M.; Crawley, M. H.; Green, B. L.; Popow, R.; Pillarsetty, N.; Veach, D. R.; Ku, A. T.; Rossi, F.; Besmer, P.; Antonescu, C. R.; Zeng, S.; Dematteo, R. P. *Clin. Cancer Res.* **2014,** *20,* 2350–2362.
41. Brierley, G. V.; Macaulay, S. L.; Forbes, B. E.; Wallace, J. C.; Cosgrove, L. J.; Macaulay, V. M. *Endocrinology* **2010,** *151,* 1418–1427.
42. Mandalà, M.; Voit, C. *Crit. Rev. Oncol. Hematol.* **2013,** *87,* 239–255.
43. Shoji, K.; Oda, K.; Nakagawa, S.; Hosokawa, S.; Nagae, G.; Uehara, Y.; Sone, K.; Miyamoto, Y.; Hiraike, H.; Hiraike-Wada, O.; Nei, T.; Kawana, K.; Kuramoto, H.; Aburatani, H.; Yano, T.; Taketani, Y. *Br. J. Cancer* **2009,** *101,* 145–148.
44. Liu, Y. R.; Jiang, Y. Z.; Zuo, W. J.; Yu, K. D.; Shao, Z. M. *Onco. Targets Ther.* **2014,** *7,* 543–552.
45. Yoon, S.; Seger, R. *Growth Factors* **2006,** *24,* 21–44.
46. Santarpia, L.; Lippman, S. M.; El-Naggar, A. K. *Expert Opin. Ther. Targets* **2012,** *16,* 103–119.
47. Mayer, I. A.; Arteaga, C. L. *Annu. Rev. Med.* **2016,** *67,* 11–28.
48. Grimaldi, A. M.; Simeone, E.; Festino, L.; Vanella, V.; Palla, M.; Ascierto, P. A. *Discov. Med.* **2015,** *19,* 455–461.
49. Dossett, L. A.; Kudchadkar, R. R.; Zager, J. S. *Expert Opin. Drug Saf.* **2015,** *14,* 559–570.
50. Flaherty, K. T.; Infante, J. R.; Daud, A.; Gonzalez, R.; Kefford, R. F.; Sosman, J.; Hamid, O.; Schuchter, L.; Cebon, J.; Ibrahim, N.; Kudchadkar, R.; Burris, H. A.; Falchook, G.; Algazi, A.; Lewis, K.; Long, G. V.; Puzanov, I.; Lebowitz, P.; Singh, A.; Little, S.; Sun, P.; Allred, A.; Ouellet, D.; Kim, K. B.; Patel, K.; Weber, J. *N. Eng. J. Med.* **2012,** *367,* 1694–1703.
51. Liu, P.; Cheng, H.; Roberts, T. M.; Zhao, J. J. *Nat. Rev. Drug Discov.* **2009,** *8,* 627–644.
52. Schwartz, S.; Wongvipat, J.; Trigwell, C. B.; Hancox, U.; Carver, B. S.; Rodrik-Outmezguine, V.; Will, M.; Yellen, P.; de Stanchina, E.; Baselga, J.; Scher, H. I.; Barry, S. T.; Sawyers, C. L.; Chandarlapaty, S.; Rosen, N. *Cancer Cell* **2015,** *27,* 109–122.
53. Kim, M. S.; Jeong, E. G.; Yoo, N. Y.; Lee, S. H. *Br. J. Cancer* **2008,** *98,* 1533–1535.
54. Dillon, L. M.; Miller, T. W. *Curr. Drug Targets* **2014,** *15,* 65–79.
55. Yuen, H. F.; Abramczyk, O.; Montgomery, G.; Chan, K. K.; Huang, Y. H.; Sasazuki, T.; Shirasawa, S.; Gopesh, S.; Chan, K. W.; Fennell, D.; Janne, P.; El-Tanani, M.; Murray, J. T. *Biosci. Rep.* **2012,** *32,* 413–422.
56. Vicente, C.; Vázquez, I.; Marcotegui, N.; Conchillo, A.; Carranza, C.; Rivell, G.; Bandrés, E.; Cristobal, I.; Lahortiga, I.; Calasanz, M. J.; Odero, M. D. *Leukemia* **2007,** *21,* 2386–2390.
57. Becker, H.; Engelhardt, M.; von Bubnoff, N.; Wäsch, R. *Recent Results Cancer Res.* **2014,** *201,* 249–257.
58. Langabeer, S. E.; Andrikovics, H.; Asp, J.; Bellosillo, B.; Carillo, S.; Haslam, K.; Kjaer, L.; Lippert, E.; Mansier, O.; Oppliger Leibundgut, E.; Percy, M. J.; Porret, N.; Palmqvist, L.; Schwarz, J.; McMullin, M. F.; Schnittger, S.; Pallisgaard, N.; Hermouet, S. *Eur. J. Haematol.* **2015,** *95,* 270–279.
59. Sangkhae, V.; Etheridge, S. L.; Kaushansky, K.; Hitchcock, I. S. *Blood* **2014,** *124,* 3956–3963.
60. Cameron, D.; Casey, M.; Press, M.; Lindquist, D.; Pienkowski, T.; Romieu, C. G.; Chan, S.; Jagiello-Gruszfeld, A.; Kaufman, B.; Crown, J.; Chan, A.; Campone, M.; Viens, P.; Davidson, N.; Gorbounova, V.; Raats, J. I.; Skarlos, D.; Newstat, B.; Roychowdhury, D.; Paoletti, P.; Oliva, C.; Rubin, S.; Stein, S.; Geyer, C. E. *Breast Cancer Res. Treat.* **2008,** *112,* 533–543.
61. Grigoreva, T. A.; Tribulovich, V. G.; Garabadzhiu, A. V.; Melino, G.; Barlev, N. A. *Oncotarget* **2015,** *6,* 24733–24749.
62. Matos, L. L.; Trufelli, D. C.; de Matos, M. G.; da Silva Pinhal, M. A. *Biomark. Insights* **2010,** *5,* 9–20.
63. Tong, J. H.; Yeung, S. F.; Chan, A. W.; Chung, L. Y.; Chau, S. L.; Lung, R. W.; Tong, C. Y.; Chow, C.; Tin, E. K.; Yu, Y. H.; Li, H.; Pan, Y.; Chak, W. P.; Ng, C. S.; Mok, T. S.; To, K. F. *Clin. Cancer Res.* **2016,** *22,* 3048–3056.

64. Heist, R. S.; Shim, H. S.; Gingipally, S.; Mino-Kenudson, M.; Le, L.; Gainor, J. F.; Zheng, Z.; Aryee, M.; Xia, J.; Jia, P.; Jin, H.; Zhao, Z.; Pao, W.; Engelman, J. A.; Iafrate, A. J. *Oncologist* **2016,** *21,* 481–486.
65. Thill, M.; Kraft, C.; Friedrich, M. *Oncol. Res. Treat.* **2016,** *39,* 295–302.
66. Dai, X.; Xiang, L.; Li, T.; Bai, Z. J. *Cancer* **2016,** *7,* 1281–1294.
67. Shepard, H. M.; Jin, P.; Slamon, D. J.; Pirot, Z.; Maneval, D. C. *Handb. Exp. Pharmacol.* **2008,** *181,* 183–219.
68. Nelson, M. H.; Dolder, C. R. *Ther. Clin. Risk Manag.* **2007,** *3,* 665–673.
69. López-Tarruella, S.; Jerez, Y.; Márquez-Rodas, I.; Martín, M. *Future Oncol.* **2012,** *8,* 671–681.
70. Gown, A. M. *Mod. Pathol.* **2008,** *21* (Suppl. 2), S8–S15.
71. Joung, J.-G.; Bae, J. S.; Kim, C. S.; Jung, H.; Park, W.-Y.; Song, S.-Y. *PLoS One* **2016,** *11* (3), e0152574.
72. Matsui, A.; Ihara, T.; Suda, H.; Mikami, H.; Semba, K. *Biomol. Concepts* **2013,** *4,* 567–582.
73. Bagci, O.; Kurtgöz, S. N. *Am. J. Med. Sci.* **2015,** *7,* 341–346.
74. Volpi, E. V.; Bridger, J. M. *Biotechniques* **2008,** *45,* 385–386.
75. Kurosumi, M. *Breast Cancer* **2009,** *16,* 284–287.
76. Lim, E. H.; Zhang, S. L.; Li, J. L.; Yap, W. S.; Howe, T. C.; Tan, B. P.; Lee, Y. S.; Wong, D.; Khoo, K. L.; Seto, K. Y.; Tan, L.; Agasthian, T.; Koong, H. N.; Tam, J.; Tan, C.; Caleb, M.; Chang, A.; Ng, A.; Tan, P. *J. Thorac. Oncol.* **2009,** *4,* 12–21.
77. Cihoric, N.; Savic, S.; Schneider, S.; Ackermann, I.; Bichsel-Naef, M.; Schmid, R. A.; Lardinois, D.; Gugger, M.; Bubendorf, L.; Zlobec, I.; Tapia, C. *Br. J. Cancer* **2014,** *110,* 2914–2922.
78. Strom, S. P. *Cancer Biol. Med.* **2016,** *13,* 3–11.
79. Maione, P.; Sacco, P. C.; Casaluce, F.; Sgambato, A.; Santabarbara, G.; Rossi, A.; Gridelli, C. *Rev. Recent Clin. Trials* **2016,** *11,* 99–105.
80. Rexer, B. N.; Arteaga, C. L. *Crit. Rev. Oncog.* **2012,** *17,* 1–16.
81. Ye, M.; Zhang, X.; Li, N.; Zhang, Y.; Jing, P.; Chang, N.; Wu, J.; Ren, X.; Zhang, J. *Oncotarget* **2016,** *7,* 12289–12304.
82. Wilson, F. H.; Johannesses, C. M.; Piccioni, F.; Tamayo, P.; Kim, J. W.; Van Allen, E. M.; Corsello, S. M.; Capelletti, M.; Calles, A.; Butaney, M.; Sharifnia, T.; Gabriel, S. B.; Mesirov, J. P.; Hahn, W. C.; Engelmann, J. A.; Meyerson, M.; Root, D. E.; Janne, P. A.; Garraway, L. A. *Cancer Cell* **2015,** *27,* 397–408.
83. DiNitto, J. P.; Wu, J. C. *Crit. Rev. Biochem. Mol. Biol.* **2011,** *46,* 295–309.
84. Dempke, W. C.; Edvardsen, K.; Lu, S.; Reinmuth, N.; Reck, M.; Inoue, A. *Anticancer Res.* **2015,** *35,* 5797–5806.
85. Mehta, A. I.; Brufsky, A. M.; Sampson, J. H. *Cancer Treat. Rev.* **2013,** *39,* 261–269.
86. Liu, M. C.; Cortés, J.; O'Shaughnessy, J. *Cancer Metastasis Rev.* **2016,** *35,* 323–332.
87. Aiken, R. *Semin. Oncol.* **2014,** *41,* 438–445.
88. Miller, D. S. *Adv. Cancer Res.* **2015,** *125,* 43–70.
89. Toyokawa, G.; Seto, T.; Takenoyama, M.; Ichinose, Y. *Cancer Metastasis Rev.* **2015,** *34,* 797–805.
90. Heffron, T. P.; Ndubaku, C. O.; Salphati, L.; Alicke, B.; Cheong, J.; Drobnick, J.; Edgar, K.; Gould, S. E.; Lee, L. B.; Lesnick, J. D.; Lewis, C.; Nonomiya, J.; Pang, J.; Plise, E. G.; Sideris, S.; Wallin, J.; Wang, L.; Zhang, X.; Olivero, A. G. *ACS Med. Chem. Lett.* **2016,** *7,* 351–356.
91. Aronov, A. M.; McClain, B.; Moody, C. S.; Murcko, M. A. J. *Med. Chem.* **2008,** *51,* 1214–1222.
92. Maddocks, K.; Jones, J. A. *Semin. Oncol.* **2016,** *43,* 251–259.
93. Iams, W. T.; Lovly, C. M. *Cancer J.* **2015,** *21,* 378–382.
94. Schuller, A. G.; Barry, E. R.; Jones, R. D.; Henry, R. E.; Frigault, M. M.; Beran, G.; Linsenmayer, D.; Hattersley, M.; Smith, A.; Wilson, J.; Cairo, S.; Déas, O.; Nicolle, D.; Adam, A.; Zinda, M.; Reimer, C.; Fawell, S. E.; Clark, E. A.; D'Cruz, C. M. *Clin. Cancer Res.* **2015,** *21,* 2811–2819.
95. Wells, S. A.; Gosnell, J. E.; Gagel, R. F.; Moley, J.; Pfister, D.; Sosa, J. A.; Skinner, M.; Krebs, A.; Vasselli, J.; Schlumberger, M. J. *Clin. Oncol.* **2010,** *28,* 767–772.
96. Krajewska, J.; Olczyk, T.; Jarzab, B. *Expert. Rev. Clin. Pharmacol.* **2016,** *9,* 69–79.
97. Chan, E.; Mulkerin, D.; Rothenberg, M.; Holen, K. D.; Lockhart, A. C.; Thomas, J.; Berlin, J. *Invest. New Drugs* **2008,** *26,* 241–247.
98. Canavese, M.; Santo, L.; Raje, N. *Cancer Biol. Ther.* **2012,** *13,* 451–457.
99. Mortlock, A. A.; Keen, N. J.; Jung, F. H.; Heron, N. M.; Foote, K. M.; Wilkinson, R. W.; Green, S. *Curr. Top. Med. Chem.* **2005,** *5,* 807–821.
100. Talati, C.; Griffiths, E. A.; Wetzler, M.; Wang, E. S. *Crit. Rev. Oncol. Hematol.* **2016,** *98,* 200–210.
101. Thanopoulou, E.; Judson, I. *Arch. Toxicol.* **2012,** *86,* 1–12.
102. Barlaam, B.; Cosulich, S.; Fitzek, M.; Green, S.; Harris, C. S.; Hudson, K.; Lambert-van der Brempt, C.; Ouvry, G.; Page, K.; Ruston, L.; Ward, L.; Delouvrié, B. *Bioorg. Med. Chem. Lett.* **2015,** *25,* 2679–2685.
103. Steffens, M.; Paul, T.; Hichert, V.; Scholl, C.; von Mallek, D.; Stelzer, C.; Sörgel, F.; Reiser, B.; Schumann, C.; Rüdiger, S.; Boeck, S.; Heinemann, V.; Kächele, V.; Seufferlein, T.; Stingl, J. *Eur. J. Cancer* **2016,** *55,* 131–139.
104. Vineis, P.; Berwick, M. *Int. J. Epidemiol.* **2006,** *35,* 1151–1159.
105. Hughes, D.; Andersson, D. I. *Nat. Rev. Genet.* **2015,** *16,* 459–471.
106. Ford, C. W.; Zurenko, G. E.; Barbachyn, M. R. *Curr. Drug Targets Infect. Disord.* **2001,** *1,* 181–199.
107. Gambacorti-Passerini, C.; le Coutre, P.; Mologni, L.; Fanelli, M.; Bertazzoli, C.; Marchesi, E.; Di Nicola, M.; Biondi, A.; Corneo, G. M.; Belotti, D.; Pogliani, E.; Lydon, N. B. *Blood Cell Mol. Dis.* **1997,** *23,* 380–394.
108. Wang, J. Y. J. *Oncogene* **2000,** *19,* 5643–5650.
109. Le Coutre, P.; Mologni, L.; Cleris, L.; Marchesi, E.; Buchdunger, E.; Giardini, R.; Formelli, F.; Gambacorti-Passerini, C. *J. Natl. Cancer Inst.* **1999,** *91,* 163–168.
110. Schindler, T.; Bornmann, W.; Pellicena, P.; Miller, W. T.; Clarkson, B.; Kuriyan, J. *Science* **2000,** *289,* 1938–1942.
111. Branford, S.; Rudzki, Z.; Walsh, S.; Grigg, A.; Arthur, C.; Taylor, K.; Herrmann, R.; Lynch, K. P.; Hughes, T. P. *Blood* **2002,** *99,* 3472–3475.
112. Travis, J. *Science* **2004,** *305,* 319–321.
113. Bell, D. W.; Gore, I.; Okimoto, R. A.; Godin-Heymann, N.; Sordella, R.; Mulloy, R.; Sharma, S. V.; Brannigan, B. W.; Mohapatra, G.; Settleman, J.; Haber, D. A. *Nat. Genet.* **2005,** *37,* 1315–1316.
114. Zuccotto, F.; Ardini, E.; Casale, E.; Angiolini, M. J. *Med. Chem.* **2010,** *53,* 2681–2694.
115. Galván-Banqueri, M.; Ubago-Pérez, R.; Molina-López, T. *J. Clin. Pharm. Ther.* **2016,** *41,* 285–289.
116. Lim, S. M.; Jeong, Y.; Hong, S. *Future Med. Chem.* **2016,** *8,* 853–878.
117. Mitri, Z.; Karakas, C.; Wei, C.; Briones, B.; Simmons, H.; Ibrahim, N.; Alvarez, R.; Murray, J. L.; Keyomarsi, K.; Moulder, S. *Invest. New Drugs* **2015,** *33,* 890–894.
118. Nowell, P. C.; Hungerford, D. A. *Science* **1960,** *132,* 1497.
119. Nowell, P. C. *J. Clin. Invest.* **2007,** *117,* 2033–2035.
120. Quintás-Cardama, A.; Cortes, J. *Blood* **2009,** *113,* 1619–1630.
121. Capdeville, R.; Buchdunger, E.; Zimmermann, J.; Matter, A. *Nat. Rev. Drug Discov.* **2002,** *1,* 493–502.
122. Zhao, Z.; Wu, H.; Wang, L.; Liu, Y.; Knapp, S.; Liu, Q.; Gray, N. S. *ACS Chem. Biol.* **2014,** *9,* 1230–1241.
123. Manley, P. W.; Cowan-Jacob, S. W.; Buchdunger, E.; Fabbro, D.; Fendrich, G.; Furet, P.; Meyer, T.; Zimmermann, J. *Eur. J. Cancer* **2002,** *38* (Suppl. 5), S19–S27.
124. Bhatia, R.; Holtz, M.; Niu, N.; Gray, R.; Snyder, D. S.; Sawyers, C. L.; Arber, D. A.; Slovak, M. L.; Forman, S. J. *Blood* **2003,** *101,* 4701–4707.
125. Apperley, J. F. *Lancet Oncol.* **2007,** *8,* 1018–1029.
126. Blay, J.-Y.; von Mehren, M. *Semin. Oncol.* **2011,** *38* (Suppl. 1), S3–S9.

127. Weisberg, E.; Manley, P. W.; Cowan-Jacob, S. W.; Hochhaus, A.; Griffin, J. D. *Nat. Rev. Cancer* **2007,** *7,* 345–356.
128. Das, J.; Chen, P.; Norris, D.; Padmanabha, R.; Lin, J.; Moquin, R. V.; Shen, Z.; Cook, L. S.; Doweyko, A. M.; Pitt, S.; Pang, S.; Shen, D. R.; Fang, Q.; de Fex, H. F.; McIntyre, K. W.; Shuster, D. J.; Gillooly, K. M.; Behnia, K.; Schieven, G. L.; Wityak, J.; Barrish, J. C. J. *Med. Chem.* **2006,** *49,* 6819–6832.
129. Golas, J. M.; Arndt, K.; Etienne, C.; Lucas, J.; Nardin, D.; Gibbons, J.; Frost, P.; Ye, F.; Boschelli, D. H.; Boschelli, F. *Cancer Res.* **2003,** *63,* 375–381.
130. Huang, W.-S.; Metcalf, C. A.; Sundaramoorthi, R.; Wang, Y.; Zou, D.; Thomas, R. M.; Zhu, X.; Cai, L.; Wen, D.; Liu, S.; Romero, J.; Qi, J.; Chen, I.; Banda, G.; Lentini, S. P.; Das, S.; Xu, Q.; Keats, J.; Wang, F.; Wardwell, S.; Ning, Y.; Snodgrass, J. T.; Broudy, M. I.; Russian, K.; Zhou, T.; Commodore, L.; Narasimhan, N. I.; Mohemmad, Q. K.; Iuliucci, J.; Rivera, V. M.; Dalgarno, D. C.; Sawyer, T. K.; Clackson, T.; Shakespeare, W. C. *J. Med. Chem.* **2010,** *53,* 4701–4719.
131. Adrian, F. J.; Ding, Q.; Sim, T.; Velentza, A.; Sloan, C.; Liu, Y.; Zhang, G.; Hur, W.; Ding, S.; Manley, P.; Mestan, J.; Fabbro, D.; Gray, N. S. *Nat. Chem. Biol.* **2006,** *2* (2), 95–102.
132. Zhang, J.; Adrian, F. J.; Jahnke, W.; Cowan-Jacob, S. W.; Li, A. G.; Iacob, R. E.; Sim, T.; Powers, J.; Dierks, C.; Sun, F.; Guo, G.; Ding, Q.; Okram, B.; Choi, Y.; Wojciechowski, A.; Deng, X.; Liu, G.; Fendrich, G.; Strauss, A.; Vajpai, N.; Grzesiek, S.; Tuntland, T.; Liu, Y.; Bursulaya, B.; Azam, M.; Manley, P. W.; Engen, J. R.; Daley, G. Q.; Warmuth, M.; Gray, N. S. *Nature* **2010,** *463* (28), 501–507.
133. Fabbro, D.; Manley, P. W.; Jahnke, W.; Liebetanz, J.; Szyttenholm, A.; Fendrich, G.; Strauss, A.; Zhang, J.; Gray, N. S.; Adrian, F.; Warmuth, M.; Pelle, X.; Grotzfeld, R.; Berst, F.; Marzinzik, A.; Cowan-Jacob, S. W.; Furet, P.; Mestan, J. *Biochim. Biophys. Acta* **2010,** *1804,* 454–462.
134. Bhang, H. C.; Ruddy, D. A.; Krishnamurthy Radhakrishna, V.; Caushi, J. X.; Zhao, R.; Hims, M. M.; Singh, A. P.; Kao, I.; Rakiec, D.; Shaw, P.; Balak, M.; Raza, A.; Ackley, E.; Keen, N.; Schlabach, M. R.; Palmer, M.; Leary, R. J.; Chiang, D. Y.; Sellers, W. R.; Michor, F.; Cooke, V. G.; Korn, J. M.; Stegmeier, F. *Nat. Med.* **2015,** *21* (5), 440–448.
135. Schoepfer, J.; Berellini, G.; Cai, H.; Caravatti, G.; Dodd, S.; Furet, P.; Gangal, G.; Grotzfeld, R. M.; Hassan, A. Q.; Hood, T.; Cowan-Jacob, S.; Jahnke, W.; Loo, A.; Manley, P.; Pelle, X.; Salem, B.; Sharma, S.; Zhu, W.; Marzinzik, A.; Gabriel, T.; Keen, N.; Petruzzelli, L.; Vanasse, G.; Sellers, W. R.; Wylie, A. 250th ACS National Meeting & Exposition, Boston, MA.
136. Gaughan, E. M.; Costa, D. B. *Ther. Adv. Med. Oncol.* **2011,** *3,* 113–125.
137. Ghose, A. K.; Herbertz, T.; Pippin, D. A.; Salvino, J. M.; Mallamo, J. P. J. *Med. Chem.* **2008,** *51,* 5149–5171.
138. Yaish, P.; Gazit, A.; Gilon, C.; Levitzki, A. *Science* **1988,** *242,* 933–935.
139. Barker, A. J.; Gibson, K. H.; Grundy, W.; Godfrey, A. A.; Barlow, J. J.; Healy, M. P.; Woodburn, J. R.; Ashton, S. E.; Curry, B. J.; Scarlett, L.; Henthorn, L.; Richards, L. *Bioorg. Med. Chem. Lett.* **2001,** *11,* 1911–1914.
140. Dowell, J.; Minna, J. D.; Kirkpatrick, P. *Nat. Rev. Drug Discov.* **2005,** *4,* 13–14.
141. Sharma, S. V.; Bell, D. W.; Settleman, J.; Haber, D. A. *Nat. Rev. Cancer* **2007,** *7,* 169–181.
142. Yu, H. A.; Riely, G. J.; Lovly, C. M. *Clin. Cancer Res.* **2014,** *20,* 5898–5907.
143. Jotte, R. M.; Spigel, D. R. *Cancer Med.* **2015,** *4,* 1621–1632.
144. Kobayashi, S.; Boggon, T. J.; Dayaram, T.; Jänne, P. A.; Kocher, O.; Meyerson, M.; Johnson, B. E.; Eck, M. J.; Tenen, D. G.; Halmos, B. *N. Engl. J. Med.* **2005,** *352,* 786–792.
145. Yun, C.; Mengwasser, K. E.; Toms, A. V.; Woo, M. S.; Greulich, H.; Wong, K.; Meyerson, M.; Eck, M. J. *Proc. Natl. Acad. Sci.* **2008,** *105,* 2070–2075.
146. Smaill, J. B.; Rewcastle, G. W.; Loo, J. A.; Greis, K. D.; Chan, O. H.; Reyner, E. L.; Lipka, E.; Showalter, H. D. H.; Vincent, P. W.; Elliott, W. L.; Denny, W. A. J. *Med. Chem.* **2000,** *43,* 1380–1397.
147. Minkovsky, M.; Berezov, A. *Curr. Opin. Investig. Drugs* **2008,** *9,* 1335–1346.
148. Gonzales, A. J.; Hook, K. E.; Althaus, I. W.; Ellis, P. A.; Trachet, E.; Delaney, A. M.; Harvey, P. J.; Ellis, T. A.; Amato, D. M.; Nelson, J. M.; Fry, D. W.; Zhu, T.; Loi, C.-M.; Fakhoury, S. A.; Schlosser, K. M.; Sexton, K. E.; Winters, R. T.; Reed, J. E.; Bridges, A. J.; Lettiere, D. J.; Baker, D. A.; Yang, J.; Lee, H. T.; Tecle, H.; Vincent, P. W. *Mol. Cancer Ther.* **2008,** *7,* 1880–1889.
149. Tsou, H.-R.; Overbeek-Klumpers, E. G.; Hallett, W. A.; Reich, M. F.; Floyd, M. B.; Johnson, B. D.; Michalak, R. S.; Nilakantan, R.; Discafani, C.; Golas, J.; Rabindran, S. K.; Shen, R.; Shi, X.; Wang, Y.-F.; Upeslacis, J.; Wissner, A. *J. Med. Chem.* **2005,** *48,* 1107–1131.
150. Solca, F.; Dahl, G.; Zoephel, A.; Bader, G.; Sanderson, M.; Klein, C.; Kraemer, O.; Himmelsbach, F.; Haaksma, E.; Adolf, G. R. *J. Pharmacol. Exp. Ther.* **2012,** *343,* 342–350.
151. Zhou, W.; Ercan, D.; Chen, L.; Yun, C.; Li, D.; Capelletti, M.; Cortot, A. B.; Chirieac, L.; Iacob, R. E.; Padera, R.; Engen, J. R.; Wong, K.; Eck, M. J.; Gray, N. S.; Janne, P. A. *Nature* **2009,** *462,* 1070–1074.
152. Dhingra, K. *Ann. Oncol.* **2016,** *27* (6), 1161–1164.
153. Tjin Tham Sjin, R.; Lee, K.; Walter, A. O.; Dubrovskiy, A.; Sheets, M.; Martin, T. S.; Labenski, M. T.; Zhu, Z.; Tester, R.; Karp, R.; Medikonda, A.; Chaturvedi, P.; Ren, Y.; Haringsma, H.; Etter, J.; Raponi, M.; Simmons, A. D.; Harding, T. C.; Niu, D.; Nacht, M.; Westlin, W. F.; Petter, R. C.; Allen, A.; Singh, J. *Mol. Cancer Ther.* **2014,** *13,* 1468–1479.
154. Ward, R. A.; Anderton, M. J.; Ashton, S.; Bethel, P. A.; Box, M.; Butterworth, S.; Colclough, N.; Chorley, C. G.; Chuaqui, C.; Cross, D. A. E.; Dakin, L. A.; Debreczeni, J. E.; Eberlein, C.; Finlay, M. R.; Hill, G. B.; Grist, M.; Klinowska, T. C. M.; Lane, C.; Martin, S.; Orme, J. P.; Smith, P.; Wang, F.; Waring, M. J. J. *Med. Chem.* **2013,** *56,* 7025–7048.
155. Finlay, M. R.; Anderton, M.; Ashton, S.; Ballard, P.; Bethel, P. A.; Box, M. R.; Bradbury, R. H.; Brown, S. J.; Butterworth, S.; Campbell, A.; Chorley, C.; Colclough, N.; Cross, D. A. E.; Currie, G. S.; Grist, M.; Hassall, L.; Hill, G. B.; James, D.; James, M.; Kemmitt, P.; Klinowska, T.; Lamont, G.; Lamont, S. G.; Martin, N.; McFarland, H. L.; Mellor, M. J.; Orme, J. P.; Perkins, D.; Perkins, P.; Richmond, G.; Smith, P.; Ward, R. A.; Waring, M. J.; Whittaker, D.; Wells, S.; Wrigley, G. L. *J. Med. Chem.* **2014,** *57,* 8249–8267.
156. Cheng, H.; Nair, S. K.; Murray, B. W.; Almaden, C.; Bailey, S.; Baxi, S.; Behenna, D.; Cho-Schultz, S.; Dalvie, D.; Dinh, D. M.; Edwards, M. P.; Feng, J. L.; Ferre, R. A.; Gajiwala, K. S.; Hemkens, M. D.; Jackson-Fisher, A.; Jalaie, M.; Johnson, T. O.; Kania, R. S.; Kephart, S.; Lafontaine, J.; Lunney, B.; Liu, K. K.; Liu, Z.; Matthews, J.; Nagata, A.; Niessen, S.; Ornelas, M. A.; Orr, S. T. M.; Pairish, M.; Planken, S.; Ren, S.; Richter, D.; Ryan, K.; Sach, N.; Shen, H.; Smeal, T.; Solowiej, J.; Sutton, S.; Tran, K.; Tseng, E.; Vernier, W.; Walls, M.; Wang, S.; Weinrich, S. L.; Xin, S.; Xu, H.; Yin, M.; Zientek, M.; Zhou, R.; Kath, J. C. *J. Med. Chem.* **2016,** *59* (5), 2005–2024.
157. Jia, Y.; Juarez, J.; Li, J.; Manuia, M.; Niederst, M. J.; Tompkins, C.; Timple, N.; Vaillancourt, M.; Culazzo Pferdekamper, A.; Lockerman, E. L.; Li, C.; Anderson, J.; Costa, C.; Liao, D.; Murphy, E.; DiDonato, M.; Bursulaya, B.; Lelais, G.; Barretina, J.; McNeill, M.; Epple, R.; Marsilje, T. H.; Pathan, N.; Engelman, J. A.; Michellys, P.; McNamara, P.; Harris, J.; Bender, S.; Kasibhatla, S. *Cancer Res.* **2016,** *76* (6), 1591–1602.
158. Engel, J.; Lategahn, J.; Rauh, D. *ACS Med. Chem. Lett.* **2016,** *7,* 2–5.
159. Ercan, D.; Choi, H. G.; Yun, C.; Capelletti, M.; Xie, T.; Eck, M. J.; Gray, N. S.; Jänne, P. A. *Clin. Cancer Res.* **2015,** *21,* 3913–3923.
160. Avizienyte, E.; Ward, R.; Garner, A. *Biochem. J.* **2008,** *415,* 197–206.
161. Thress, K. S.; Paweletz, C. P.; Felip, E.; Cho, B. C.; Stetson, D.; Dougherty, B.; Lai, Z.; Markovets, A.; Vivancos, A.; Kuang, Y.; Ercan, D.; Matthews, S. E.; Cantarini, M.; Barrett, J. C.; Janne, P. A.; Oxnard, G. R. *Nat. Med.* **2015,** *21,* 560–562.
162. Hanan, E. J.; Eigenbrot, C.; Bryan, M. C.; Burdick, D. J.; Chan, B. K.; Chen, Y.; Dotson, J.; Heald, R. A.; Jackson, P. S.; La, H.; Lainchbury, M. D.; Malek, S.; Purkey, H. E.; Schaefer, G.; Schmidt, S.; Seward, E. M.; Sideris, S.; Tam, C.; Wang, S.; Yeap, S. K.; Yen, I.; Yin, J.; Yu, C.; Zilberleyb, I.; Heffron, T. P. *J. Med. Chem.* **2014,** *57,* 10176–10191.
163. Heald, R.; Bowman, K. K.; Bryan, M. C.; Burdick, D.; Chan, B.; Chan, E.; Chen, Y.; Clausen, S.; Dominguez-Fernandez, B.; Eigenbrot, C.; Elliott, R.; Hanan, E. J.; Jackson, P.; Knight, J.; La, H.; Lainchbury, M.; Malek, S.; Mann, S.; Merchant, M.; Mortara, K.; Purkey, H.; Schaefer, G.; Schmidt, S.; Seward, E.; Sideris, S.; Shao, L.; Wang, S.; Yeap, K.; Yen, I.; Yu, C.; Heffron, T. P. *J. Med. Chem.* **2015,** *58,* 8877–8895.
164. Bryan, M. C.; Burdick, D. J.; Chan, B. K.; Chen, Y.; Clausen, S.; Dotson, J.; Eigenbrot, C.; Elliott, R.; Hanan, E. J.; Heald, R.; Jackson, P.; La, H.; Lainchbury, M.; Malek, S.; Mann, S. E.; Purkey, H. E.; Schaefer, G.; Schmidt, S.; Seward, E.; Sideris, S.; Wang, S.; Yen, I.; Yu, C.; Heffron, T. P. *ACS Med. Chem. Lett.* **2016,** *7,* 100–104.
165. Arcila, M. E.; Nafa, K.; Chaft, J. E.; Rekhtman, N.; Lau, C.; Reva, B. A.; Zakowski, M. F.; Kris, M. G.; Ladanyi, M. *Mol. Cancer Ther.* **2013,** *12,* 220–229.

166. Yasuda, H.; Park, E.; Yun, C.; Sng, N. J.; Lucena-Araujo, A.; Yeo, W.; Huberman, M. S.; Cohen, D. W.; Nakayama, S.; Ishioka, K.; Yamaguchi, N.; Hanna, M.; Oxnard, G. R.; Lathan, C. S.; Moran, T.; Sequist, L. V.; Chaft, J. E.; Riely, G. J.; Arcila, M. E.; Soo, R. A.; Meyerson, M.; Eck, M. J.; Kobayashi, S. S.; Costa, D. B. *Sci. Transl. Med.* **2013,** *5,* 216ra177.
167. Hirano, T.; Yasuda, H.; Tani, T.; Hamamoto, J.; Oashi, A.; Ishioka, K.; Arai, D.; Nukaga, S.; Miyawaki, M.; Kawada, I.; Naoki, K.; Costa, D. B.; Kobayashi, S. S.; Betsuyaku, T.; Soejima, K. *Oncotarget* **2015,** *6,* 38789–38803.
168. Zeng, Q.; Wang, J.; Cheng, Z.; Chen, K.; Johnstrom, P.; Varnas, K.; Li, D. Y.; Yang, Z. F.; Zhang, X. J. *Med. Chem.* **2015,** *58,* 8200–8215.
169. Ballard, P.; Yates, J. W.; Yang, Z.; Kim, D. W.; Yang, J. C.; Cantarini, M.; Pickup, K.; Jordan, A.; Hickey, M.; Grist, M.; Box, M.; Johnström, P.; Varnäs, K.; Malmquist, J.; Thress, K. S.; Janne, P. A.; Cross, D. *Clin. Cancer Res.* **2016,** *22* (20), 5130–5140. pii: clincanres.0399.2015 (Epub ahead of print).
170. Gainor, J. F.; Shaw, A. T. *J. Clin. Oncol.* **2013,** *31,* 3987–3996.
171. Cui, J. J.; Tran-Dube, M.; Shen, H.; Nambu, M.; Kung, P.; Pairish, M.; Jia, L.; Meng, J.; Funk, L.; Botrous, I.; McTigue, M.; Grodsky, N.; Ryan, K.; Padrique, E.; Alton, G.; Timofeevski, S.; Yamazaki, S.; Li, Q.; Zou, H.; Christensen, J.; Mroczkowski, B.; Bender, S.; Kania, R. S.; Edwards, M. P. *J. Med. Chem.* **2011,** *54,* 6342–6363.
172. Chen, J.; Jiang, C.; Wang, S. *J. Med. Chem.* **2013,** *56,* 5673–5674.
173. Marsilje, T. H.; Pei, W.; Chen, B.; Lu, W.; Uno, T.; Jin, Y.; Jiang, T.; Kim, S.; Li, N.; Warmuth, M.; Sarkisova, Y.; Sun, F.; Steffy, A.; Pferdekamper, A. C.; Li, A. G.; Joseph, S. B.; Kim, Y.; Liu, B.; Tuntland, T.; Cui, X.; Gray, N. S.; Steensma, R.; Wan, Y.; Jiang, J.; Chopiuk, G.; Li, J.; Gordon, W. P.; Richmond, W.; Johnson, K.; Chang, J.; Groessl, T.; He, Y.; Phimister, A.; Aycinena, A.; Lee, C. C.; Bursulaya, B.; Karanewsky, D. S.; Seidel, H. M.; Harris, J. L.; Michellys, P. *J. Med. Chem.* **2013,** *56,* 5675–5690.
174. Friboulet, L.; Li, N.; Katayama, R.; Lee, C. C.; Gainor, J. F.; Crystal, A. S.; Michellys, P.; Awad, M. M.; Yanagitani, N.; Kim, S.; Pferdekamper, A. C.; Li, J.; Kasibhatla, S.; Sun, F.; Sun, X.; Hua, S.; McNamara, P.; Mahmood, S.; Lockerman, E. L.; Fujita, N.; Nishio, M.; Harris, J. L.; Shaw, A. T.; Engelman, J. A. *Cancer Discov.* **2014,** *4,* 662–673.
175. Kinoshita, K.; Ono, Y.; Emura, T.; Asoh, K.; Furuichi, N.; Ito, T.; Kawada, H.; Tanaka, S.; Morikami, K.; Tsukaguchi, T.; Sakamoto, H.; Tsukuda, T.; Oikawa, N. *Bioorg. Med. Chem. Lett.* **2011,** *21,* 3788–3793.
176. Kinoshita, K.; Asoh, K.; Furuichi, N.; Ito, T.; Kawada, H.; Hara, S.; Ohwada, J.; Miyagi, T.; Kobayashi, T.; Takanashi, K.; Tsukaguchi, T.; Sakamoto, H.; Tsukuda, T.; Oikawa, N. *Bioorg. Med. Chem.* **2012,** *20,* 1271–1280.
177. Huang, Q.; Johnson, T. W.; Bailey, S.; Brooun, A.; Bunker, K. D.; Burke, B. J.; Collins, M. R.; Cook, A. S.; Cui, J. J.; Dack, K. N.; Deal, J. G.; Deng, Y.; Dinh, D.; Engstrom, L. D.; He, M.; Hoffman, J.; Hoffman, R. L.; Johnson, P. S.; Kania, R. S.; Lam, H.; Lam, J. L.; Le, P. T.; Li, Q.; Lingardo, L.; Liu, W.; Lu, M. W.; McTigue, M.; Palmer, C. L.; Richardson, P. F.; Sach, N. W.; Shen, H.; Smeal, T.; Smith, G. L.; Stewart, A. E.; Timofeevski, S.; Tsaparikos, K.; Wang, H.; Zhu, H.; Zhu, J.; Zou, H. Y.; Edwards, M. P. *J. Med. Chem.* **2014,** *57,* 1170–1187.
178. Johnson, T. W.; Richardson, P. F.; Bailey, S.; Brooun, A.; Burke, B. J.; Collins, M. R.; Cui, J. J.; Deal, J. G.; Deng, Y.; Dinh, D.; Engstrom, L. D.; He, M.; Hoffman, J.; Hoffman, R. L.; Huang, Q.; Kania, R. S.; Kath, J. C.; Lam, H.; Lam, J. L.; Le, P. T.; Lingardo, L.; Liu, W.; McTigue, M.; Palmer, C. L.; Sach, N. W.; Smeal, T.; Smith, G. L.; Stewart, A. E.; Timofeevski, S.; Zhu, H.; Zhu, J.; Zou, H. Y.; Edwards, M. P. *J. Med. Chem.* **2014,** *57,* 4720–4744.
179. Zou, H. Y.; Friboulet, L.; Kodack, D. P.; Engstrom, L. D.; Li, Q.; West, M.; Tang, R. W.; Wang, H.; Tsaparikos, K.; Wang, J.; Timofeevski, S.; Katayama, R.; Dinh, D. M.; Lam, H.; Lam, J. L.; Yamazaki, S.; Hu, W.; Patel, B.; Bezwada, D.; Frias, R. L.; Lifshits, E.; Mahmood, S.; Gainor, J. F.; Affolter, T.; Lappin, P. B.; Gukasyan, H.; Lee, N.; Deng, S.; Jain, R. K.; Johnson, T. W.; Shaw, A. T.; Fantin, V. R.; Smeal, T. *Cancer Cell* **2015,** *28,* 70–81.
180. Hatcher, J. M.; Bahcall, M.; Choi, H. G.; Gao, Y.; Sim, T.; George, R.; Janne, P. A.; Gray, N. S. *J. Med. Chem.* **2015,** *58,* 9296–9308.
181. Achary, R.; Yun, J. I.; Park, C. M.; Mathi, G. R.; Lee, J. Y.; Ha, J. D.; Chae, C. H.; Ahn, S.; Park, C. H.; Lee, C. O.; Hwang, J. Y.; Yun, C.; Jung, H. J.; Cho, S. Y.; Kim, H. R.; Kim, P. *Bioorg. Med. Chem.* **2016,** *24,* 207–219.
182. Chizkov, R. R.; Million, R. P. *Nat. Rev. Drug Discov.* **2015,** *14,* 597–598.
183. Sancar, A.; Lindsey-Boltz, L. A.; Unsal-Kacmaz, K.; et al. *Annu. Rev. Biochem.* **2004,** *73,* 39–85.
184. Jackson, S. P.; Bartek, J. *Nature* **2009,** *461,* 1071–1078.
185. Lord, C. J.; Ashworth, A. *Nature* **2012,** *481* (7381), 287–294.
186. Hosoya, N.; Miyagawa, K. *Cancer Sci.* **2014,** *105* (4), 370–388.
187. O'Connor, M. *J. Mol. Cell* **2015,** *60* (4), 547–560.
188. Jackson, S. P.; Helleday, T. *Science* **2016,** *352* (6290), 1178–1179.
189. Hanahan, D.; Weinberg, R. A. *Cell* **2011,** *144* (5), 646–674.
190. Hartley, K. O.; Gell, D.; Smith, G. C.; et al. *Cell* **1995,** *82,* 849–856.
191. Durocher, D.; Jackson, S. P. *Curr. Opin. Cell Biol.* **2001,** *13* (2), 225–231.
192. Shiloh, Y.; Ziv, Y. *Nat. Rev. Mol. Cell Biol.* **2013,** *14,* 197–210.
193. Hill, R.; Lee, P. W. K. *Cell Cycle* **2010,** *9,* 3460–3469.
194. Smith, G. C.; Jackson, S. P.; The PIKK family of protein kinases.; In Handbook of Cell Signaling; Elsevier Academic Press: New York, 2003; pp 557–561.
195. Mortlock, A.; Foote, K.; Kettle, J.; Aquila, B. *Elsevier Reference Module in Chemistry, Molecular Sciences and Chemical Engineering;* New York: Elsevier Academic Press, 2014. http://dx.doi.org/10.1016/B978-0-12-409547-2.11033-9.
196. Lavin, M. F.; Shiloh, Y. *Annu. Rev. Immunol.* **1997,** *15,* 177–202.
197. Rotman, G.; Shiloh, Y. *Hum. Mol. Genet.* **1998,** *7* (10), 1555–1563.
198. Lavin, M. F. *Nat. Rev. Mol. Cell Biol.* **2008,** *9* (10), 759–769.
199. Bensimon, A.; Aebersold, R.; Shiloh, Y. *FEBS Lett.* **2011,** *585* (11), 1625–1639.
200. Matsuoka, S.; Ballif, B. A.; Smogorzewska, A.; McDonald, E. R., 3rd; Hurov, K. E.; Luo, J.; Bakalarski, C. E.; Zhao, Z.; Solimini, N.; Lerenthal, Y.; Shiloh, Y.; Gygi, S. P.; Elledge, S. J. *Science* **2007,** *316* (5828), 1160–1166.
201. Guleria, A.; Chandna, S. *DNA Repair (Amst)* **2016,** *39,* 1–20.
202. Hickson, I.; Zhao, Y.; Richardson, C. J.; Green, S. J.; Martin, N. M.; Orr, A. I.; Reaper, P. M.; Jackson, S. P.; Curtin, N. J.; Smith, G. C. *Cancer Res.* **2004,** *64* (24), 9152–9159.
203. Hollick, J. J.; Rigoreau, L. J.; Cano-Soumillac, C.; Cockcroft, X.; Curtin, N. J.; Frigerio, M.; Golding, B. T.; Guiard, S.; Hardcastle, I. R.; Hickson, I.; Hummersone, M. G.; Menear, K. A.; Martin, N. M.; Matthews, I.; Newell, D. R.; Ord, R.; Richardson, C. J.; Smith, G. C.; Griffin, R. J. *J. Med. Chem.* **2007,** *50* (8), 1958–1972.
204. Rainey, M. D.; Charlton, M. E.; Stanton, R. V.; Kastan, M. B. *Cancer Res.* **2008,** *68* (18), 7466–7474.
205. Finlay, M. R.; Griffin, R. J. *Bioorg. Med. Chem. Lett.* **2012,** *22* (17), 5352–5359.
206. Golding, S. E.; Rosenberg, E.; Valerie, N.; Hussaini, I.; Frigerio, M.; Cockcroft, X. F.; Chong, W. Y.; Hummersone, M.; Rigoreau, L.; Menear, K. A.; O'Connor, M. J.; Povirk, L. F.; van Meter, T.; Valerie, K. *Mol. Cancer Ther.* **2009,** *8* (10), 2894–2902.
207. Batey, M. A.; Zhao, Y.; Kyle, S.; Richardson, C.; Slade, A.; Martin, N. M.; Lau, A.; Newell, D. R.; Curtin, N. *J. Mol. Cancer Ther.* **2013,** *12* (6), 959–967.
208. Stupp, R.; Hegi, M. E.; Mason, W. P.; van den Bent, M. J.; Taphoorn, M. J.; Janzer, R. C.; Ludwin, S. K.; Allgeier, A.; Fisher, B.; Belanger, K.; Hau, P.; Brandes, A. A.; Gijtenbeek, J.; Marosi, C.; Vecht, C. J.; Mokhtari, K.; Wesseling, P.; Villa, S.; Eisenhauer, E.; Gorlia, T.; Weller, M.; Lacombe, D.; Cairncross, J. G.; Mirimanoff, R. O. *Lancet Oncol.* **2009,** *10* (5), 459–466.
209. Cancer Genome Atlas Research Network *Nature* **2008,** *455* (7216), 1061–1068.
210. Vecchio, D.; Daga, A.; Carra, E.; Marubbi, D.; Raso, A.; Mascelli, S.; Nozza, P.; Garrè, M. L.; Pitto, F.; Ravetti, J. L.; Vagge, S.; Corvò, R.; Profumo, A.; Baio, G.; Marcello, D.; Frosina, G. *Int. J. Cancer* **2015,** *136* (6), 1445–1457.
211. Biddlestone-Thorpe, L.; Sajjad, M.; Rosenberg, E.; Beckta, J. M.; Valerie, N. C.; Tokarz, M.; Adams, B. R.; Wagner, A. F.; Khalil, A.; Gilfor, D.; Golding, S. E.; Deb, S.; Temesi, D. G.; Lau, A.; O'Connor, M. J.; Choe, K. S.; Parada, L. F.; Lim, S. K.; Mukhopadhyay, N. D.; Valerie, K. *Clin. Cancer Res.* **2013,** *19* (12), 3189–3200.

212. Debinski, W.; Tatter, S. B. *Expert Rev. Neurother.* **2009,** *9* (10), 1519–1527.
213. Karlin, J.; Allen, J.; Odedra, R.; Hughes, G.; Farrington, P.; Ducray, R.; Ouvry, G.; Degorce, S.; Wilson, J.; Smith, A.; Patel, B.; Thomason, A.; Vincent, J.; Colclough, N.; Ahmad, S. F.; Beckta, J. M.; Tokarz, M.; Mukhopadhyay, N. D.; Barlaam, B.; Pike, K.; Cadogan, E.; Pass, M.; Valerie, K.; Durant, S. AACR 2016; Abstract #3041.
214. Cimprich, K. A.; Cortez, D. *Nat. Rev. Mol. Cell Biol.* **2008,** *9,* 616–627.
215. Nyberg, K. A.; Michelson, R. J.; Putnam, C. W.; Weinert, T. A. *Annu. Rev. Genet.* **2002,** *36,* 617–656.
216. Macheret, M.; Halazonetis, T. D. *Annu. Rev. Pathol.* **2015,** *10,* 425–448.
217. Foote, K. M.; Lau, A.; Nissink, J. W. *Future Med. Chem.* **2015,** *7* (7), 873–891.
218. Nam, E. A.; Cortez, D. *Biochem. J.* **2011,** *436* (3), 527–536.
219. Fokas, E.; Prevo, R.; Hammond, E. M.; Brunner, T. B.; McKenna, G. W.; Muschel, R. J. *Cancer Treat. Rev.* **2014,** *40,* 109–117.
220. Weber, A. M.; Ryan, A. J. *Pharmacol. Ther.* **2015,** *149,* 124–138.
221. Reaper, P. M.; Griffiths, M. R.; Long, J. M.; Charrier, J. D.; Maccormick, S.; Charlton, P. A.; Golec, J. M.; Pollard, J. R. *Nat. Chem. Biol.* **2011,** *7* (7), 428–430.
222. Charrier, J. D.; Durrant, S. J.; Golec, J. M.; Kay, D. P.; Knegtel, R. M.; MacCormick, S.; Mortimore, M.; O'Donnell, M. E.; Pinder, J. L.; Reaper, P. M.; Rutherford, A. P.; Wang, P. S.; Young, S. C.; Pollard, J. R. J. *Med. Chem.* **2011,** *54* (7), 2320–2330.
223. Prevo, R.; Fokas, E.; Reaper, P. M.; Charlton, P. A.; Pollard, J. R.; McKenna, W. G.; Muschel, R. J.; Brunner, T. B. *Cancer Biol. Ther.* **2012,** *13* (11), 1072–1081.
224. Fokas, E.; Prevo, R.; Pollard, J. R.; Reaper, P. M.; Charlton, P. A.; Cornelissen, B.; Vallis, K. A.; Hammond, E. M.; Olcina, M. M.; Gillies McKenna, W.; Muschel, R. J.; Brunner, T. B. *Cell Death Dis.* **2012,** *3,* e441.
225. Hall, A. B.; Newsome, D.; Wang, Y.; Boucher, D. M.; Eustace, B.; Gu, Y.; Hare, B.; Johnson, M. A.; Milton, S.; Murphy, C. E.; Takemoto, D.; Tolman, C.; Wood, M.; Charlton, P.; Charrier, J. D.; Furey, B.; Golec, J.; Reaper, P. M.; Pollard, J. R. *Oncotarget* **2014,** *5* (14), 5674–5685.
226. Josse, R.; Martin, S. E.; Guha, R.; Ormanoglu, P.; Pfister, T. D.; Reaper, P. M.; Barnes, C. S.; Jones, J.; Charlton, P.; Pollard, J. R.; Morris, J.; Doroshow, J. H.; Pommier, Y. *Cancer Res.* **2014,** *74* (23), 6968–6979.
227. Foote, K. M.; Blades, K.; Cronin, A.; Fillery, S.; Guichard, S. S.; Hassall, L.; Hickson, I.; Jacq, X.; Jewsbury, P. J.; McGuire, T. M.; Nissink, J. W.; Odedra, R.; Page, K.; Perkins, P.; Suleman, A.; Tam, K.; Thommes, P.; Broadhurst, R.; Wood, C. J. *Med. Chem.* **2013,** *56* (5), 2125–2138.
228. Jacq, X.; Smith, L.; Brown, E.; et al. *Cancer Res.* **2012,** *72* (8 Suppl. 1.).
229. Menezes, D. L.; Holt, J.; Tang, Y.; Feng, J.; Barsanti, P.; Pan, Y.; Ghoddusi, M.; Zhang, W.; Thomas, G.; Holash, J.; Lees, E.; Taricani, L. *Mol. Cancer Res.* **2015,** *13* (1), 120–129.
230. Jones, C. D.; Blades, K.; Foote, K. M.; et al. *Cancer Res.* **2013,** *73* (8 Suppl. 1.).
231. Guichard, S. M.; Brown, E.; Odedra, R.; et al. *Cancer Res.* **2013,** *73* (8 Suppl. 1).
232. Vendetti, F. P.; Lau, A.; Schamus, S.; Conrads, T. P.; O'Connor, M. J.; Bakkenist, C. J. *Oncotarget* **2015,** *6* (42), 44289–44305.
233. Lücking, U. *Angew. Chem. Int. Ed. Engl.* **2013,** *52* (36), 9399–9408.
234. Goldberg, F. W.; Kettle, J. G.; Xiong, J.; Lin, D. *Tetrahedron* **2014,** *70* (37), 6613–6622.
235. Siemeister, G.; Lücking, U.; Wengner, A. M.; Lienau, P.; Steinke, W.; Schatz, C.; Mumberg, D.; Ziegelbauer, K. *Mol. Cancer Ther.* **2012,** *11* (10), 2265–2273.
236. Brown, E.; Odedra, R.; Sheridan, V.; Hughes, G.; Jones, D. R.; Xu, S.; Cui, A.; Gavine, P.; O'Connor, M.; Lau, A. *Mol. Cancer Ther.* **2015,** *14* (12 Suppl. 2). Abstract nr. C60.
237. Pollard, J.; Reaper, P.; Jones, J.; Barnes, C.; Gladwell, S.; Hughes, S.; Peak, A.; Djeha, H.; Hall, A.; Newsome, D.; Wang, Y.; Boucher, D.; Eustace, B.; Gu, Y.; Hare, B.; Johnson, M.; Milton, S.; Murphy, C.; Takemoto, D.; Tolman, C.; Wood, M.; Furey, B.; Penney, M.; Li, H.; Defranco, C.; Asmal, M.; Fields, S. *Cancer Res.* **2015,** *75* (15 Suppl.). Abstract nr. 1644.
238. Chen, T.; Middleton, F. K.; Falcon, S.; Reaper, P. M.; Pollard, J. R.; Curtin, N. J. *Mol. Oncol.* **2015,** *9* (2), 463–472.
239. Pastor Fernández, J.; Fernández-Capetillo Ruiz, O.; Martínez González, S.; Blanco Aparicio, C.; Rico Ferreira, M.; Toledo Lázaro, L.; Rodríguez Arísteguí, S.; Murga Costa, M.; Varela Busto, C.; Lopez Contreras, A.; Renner, O.; Nieto Soler, M.; Cebrián Muñoz, D. Chemical entities, WO2014/140644, 2014.
240. Wortmann, L.; Lücking, U.; Lefranc, J.; Briem, H.; Koppitz, M.; Eis, K.; Von Nussbaum, F.; Bader, B.; Wengner, A.; Siemeister, G.; Bone, W.; Lienau, P.; Grudzinska-Goebel, J.; Moosmayer, D.; Eberspächer, U.; Schick, H. 2-(Morpholin-4-yl)-l,7-naphthyridines, WO2016/020320, 2015.
241. Breslin, H.; Gilad, O. Ataxia Telengiectasia And Rad3-Related (ATR) Protein Kinase Inhibitors, US2016/0102104, 2015.
242. Jette, N.; Lees-Miller, S. P. *Prog. Biophys. Mol. Biol.* **2015,** *117,* 194–205.
243. Davis, A. J.; Chen, B. P.; Chen, D. J. *DNA Repair (Amst)* **2014,** *17,* 21–29.
244. Kanaar, R.; Hoeijmakers, J. H.; van Gent, D. C. *Trends Cell Biol.* **1998,** *8* (12), 483–489.
245. Jackson, S. P. *Carcinogenesis* **2002,** *23* (5), 687–696.
246. Wipf, P.; Halter, R. J. *Org. Biomol. Chem.* **2005,** *3,* 2053–2061.
247. Sarkaria, J. N.; Tibbetts, R. S.; Busby, E. C.; Kennedy, A. P.; Hill, D. E.; Abraham, R. T. *Cancer Res.* **1998,** *58* (19), 4375–4382.
248. Price, B. D.; Youmell, M. B. *Cancer Res.* **1996,** *56* (2), 246–250.
249. Shinohara, E. T.; Geng, L.; Tan, J.; Chen, H.; Shir, Y.; Edwards, E.; Halbrook, J.; Kesicki, E. A.; Kashishian, A.; Hallahan, D. E. *Cancer Res.* **2005,** *65* (12), 4987–4992.
250. Willmore, E.; de Caux, S.; Sunter, N. J.; Tilby, M. J.; Jackson, G. H.; Austin, C. A.; Durkacz, B. W. *Blood* **2004,** *103* (12), 4659–4665.
251. Veuger, S. J.; Curtin, N. J.; Richardson, C. J.; Smith, G. C.; Durkacz, B. W. *Cancer Res.* **2003,** *63* (18), 6008–6015.
252. Hardcastle, I. R.; Cockcroft, X.; Curtin, N. J.; El-Murr, M. D.; Leahy, J. J.; Stockley, M.; Golding, B. T.; Rigoreau, L.; Richardson, C.; Smith, G. C.; Griffin, R. J. *J. Med. Chem.* **2005,** *48* (24), 7829–7846.
253. Zhao, Y.; Thomas, H. D.; Batey, M. A.; Cowell, I. G.; Richardson, C. J.; Griffin, R. J.; Calvert, A. H.; Newell, D. R.; Smith, G. C.; Curtin, N. J. *Cancer Res.* **2006,** *66* (10), 5354–5362.
254. Munck, J. M.; Batey, M. A.; Zhao, Y.; Jenkins, H.; Richardson, C. J.; Cano, C.; Tavecchio, M.; Barbeau, J.; Bardos, J.; Cornell, L.; Griffin, R. J.; Menear, K.; Slade, A.; Thommes, P.; Martin, N. M.; Newell, D. R.; Smith, G. C.; Curtin, N. *J. Mol. Cancer Ther.* **2012,** *11* (8), 1789–1798.
255. Mortensen, D. S.; Perrin-Ninkovic, S. M.; Shevlin, G.; Elsner, J.; Zhao, J.; Whitefield, B.; Tehrani, L.; Sapienza, J.; Riggs, J. R.; Parnes, J. S.; Papa, P.; Packard, G.; Lee, B. G.; Harris, R.; Correa, M.; Bahmanyar, S.; Richardson, S. J.; Peng, S. X.; Leisten, J.; Khambatta, G.; Hickman, M.; Gamez, J. C.; Bisonette, R. R.; Apuy, J.; Cathers, B. E.; Canan, S. S.; Moghaddam, M. F.; Raymon, H. K.; Worland, P.; Narla, R. K.; Fultz, K. E.; Sankar, S. *J. Med. Chem.* **2015,** *58* (14), 5599–5608.
256. Boucher, D. M.; Hoover, R.; Wang, Y.; Gu, Y.; Newsome, D.; Ford, P.; Moody, C.; Damagnex, V.; Arimoto, R.; Hillier, S.; Wood, M.; Markland, W.; Eustace, B.; Cottrell, K.; Penney, M.; Furey, B.; Tanner, K.; Maxwell, J. P.; Charison, P. AACR Annual Meeting. Abstract#3716.
257. Gabizon, A. A. *Cancer Invest.* **2001,** *19* (4), 424–436.
258. Maeda, H. *Adv. Drug Deliv. Rev.* **2015,** *91,* 3–6.
259. Hare, J. I.; Lammers, T.; Ashford, M. B.; Puri, S.; Storm, G.; Barry, S. T. *Adv. Drug Deliv. Rev.* **2016 2016**, (April 29). pii: S0169-409X(16)30135-1.
260. Russell, P.; Nurse, P. *Cell* **1987,** *49* (4), 559–567.
261. Stathis, A.; Oza, A. *Drug News Perspect.* **2010,** *23* (7), 425–429.
262. Do, K.; Doroshow, J. H.; Kummar, S. *Cell Cycle* **2013,** *12* (19), 3159–3164.
263. Mueller, S.; Haas-Kogan, D. A. J. *Clin. Oncol.* **2015,** *33* (30), 3485–3487.
264. Dai, Y.; Grant, S. *Clin. Cancer Res.* **2010,** *16* (2), 376–383.
265. McNeely, S.; Beckmann, R.; Bence Lin, A. K. *Pharmacol. Ther.* **2014,** *142* (1), 1–10.
266. Zhang, Y.; Hunter, T. *Int. J. Cancer* **2014,** *134* (5), 1013–1023.
267. Castedo, M.; Perfettini, J. L.; Roumier, T.; Andreau, K.; Medema, R.; Kroemer, G. *Oncogene* **2004,** *23* (16), 2825–2837.

268. Levine, A. J. *Cell* **1997,** *88* (3), 323–331.
269. Olivier, M.; Hollstein, M.; Hainaut, P. *Cold Spring Harb. Perspect. Biol.* **2010,** *2* (1), a001008.
270. Hirai, H.; Iwasawa, Y.; Okada, M.; Arai, T.; Nishibata, T.; Kobayashi, M.; Kimura, T.; Kaneko, N.; Ohtani, J.; Yamanaka, K.; Itadani, H.; Takahashi-Suzuki, I.; Fukasawa, K.; Oki, H.; Nambu, T.; Jiang, J.; Sakai, T.; Arakawa, H.; Sakamoto, T.; Sagara, T.; Yoshizumi, T.; Mizuarai, S.; Kotani, H. *Mol. Cancer Ther.* **2009,** *8* (11), 2992–3000.
271. Guertin, A. D.; Li, J.; Liu, Y.; Hurd, M. S.; Schuller, A. G.; Long, B.; Hirsch, H. A.; Feldman, I.; Benita, Y.; Toniatti, C.; Zawel, L.; Fawell, S. E.; Gilliland, D. G.; Shumway, S. D. *Mol. Cancer Ther.* **2013,** *12* (8), 1442–1452.
272. Do, K.; Wilsker, D.; Ji, J.; Zlott, J.; Freshwater, T.; Kinders, R. J.; Collins, J.; Chen, A. P.; Doroshow, J. H.; Kummar, S. *J. Clin. Oncol.* **2015,** *33* (30), 3409–3415.
273. Leijen, S.; van Geel, R.; Sonke, G. S.; de Jong, D.; Rosenberg, E. H.; Marchetti, S.; Pluim, D.; van Werkhoven, E. D.; Rose, S.; Lee, M. A.; Beijnen, J. H.; Schellens, J. H. M. *J. Clin. Oncol.* **2015,** *33* (suppl; abstr 2507).
274. Chilà, R.; Basana, A.; Lupi, M.; Guffanti, F.; Gaudio, E.; Rinaldi, A.; Cascione, L.; Restelli, V.; Tarantelli, C.; Bertoni, F.; Damia, G.; Carrassa, L. *Oncotarget* **2015,** *6* (5), 3394–3408.
275. Karnak, D.; Engelke, C. G.; Parsels, L. A.; Kausar, T.; Wei, D.; Robertson, J. R.; Marsh, K. B.; Davis, M. A.; Zhao, L.; Maybaum, J.; Lawrence, T. S.; Morgan, M. A. *Clin. Cancer Res.* **2014,** *20* (19), 5085–5096.
276. Chen, T.; Stephens, P. A.; Middleton, F. K.; Curtin, N. J. *Drug Discov. Today* **2012,** *17* (5–6), 194–202.
277. Sakurikar, N.; Eastman, A. J. *Clin. Oncol.* **2015,** *33* (9), 1075–1077.
278. King, C.; Diaz, H.; Barnard, D.; Barda, D.; Clawson, D.; Blosser, W.; Cox, K.; Guo, S.; Marshall, M. *Invest. New Drugs* **2014,** *32* (2), 213–226.
279. Barnard, D.; Diaz, H. B.; Burke, T.; Donoho, G.; Beckmann, R.; Jones, B.; Barda, D.; King, C.; Marshall, M. *Invest. New Drugs* **2016,** *34* (1), 49–60.
280. Calvo, E.; Chen, V. J.; Marshall, M.; Ohnmacht, U.; Hynes, S. M.; Kumm, E.; Diaz, H. B.; Barnard, D.; Merzoug, F. F.; Huber, L.; Kays, L.; Iversen, P.; Calles, A.; Voss, B.; Lin, A. B.; Dickgreber, N.; Wehler, T.; Sebastian, M. *Invest. New Drugs* **2014,** *32* (5), 955–968.
281. Doi, T.; Yoshino, T.; Shitara, K.; Matsubara, N.; Fuse, N.; Naito, Y.; Uenaka, K.; Nakamura, T.; Hynes, S. M. *Anticancer Drugs* **2015,** *26* (10), 1043–1053.
282. Weiss, G. J.; Donehower, R. C.; Iyengar, T.; Ramanathan, R. K.; Lewandowski, K.; Westin, E.; Hurt, K.; Hynes, S. M.; Anthony, S. P.; McKane, S. *Invest. New Drugs* **2013,** *31* (1), 136–144.
283. Guzi, T. J.; Paruch, K.; Dwyer, M. P.; Labroli, M.; Shanahan, F.; Davis, N.; Taricani, L.; Wiswell, D.; Seghezzi, W.; Penaflor, E.; Bhagwat, B.; Wang, W.; Gu, D.; Hsieh, Y.; Lee, S.; Liu, M.; Parry, D. *Mol. Cancer Ther.* **2011,** *10,* 591–602.
284. Montano, R.; Chung, I.; Garner, K. M.; Parry, D.; Eastman, A. *Mol. Cancer Ther.* **2012,** *11,* 427–438.
285. Karp, J. E.; Thomas, B. M.; Greer, J. M.; Sorge, C.; Gore, S. D.; Pratz, K. W.; Smith, B. D.; Flatten, K. S.; Peterson, K.; Schneider, P.; Mackey, K.; Freshwater, T.; Levis, M. J.; McDevitt, M. A.; Carraway, H. E.; Gladstone, D. E.; Showel, M. M.; Loechner, S.; Parry, D. A.; Horowitz, J. A.; Isaacs, R.; Kaufmann, S. H. *Clin. Cancer Res.* **2012,** *18,* 6723–6731.
286. Daud, A. I.; Ashworth, M. T.; Strosberg, J.; Goldman, J. W.; Mendelson, D.; Springett, G.; Venook, A. P.; Loechner, S.; Rosen, L. S.; Shanahan, F.; Parry, D.; Shumway, S.; Grabowsky, J. A.; Freshwater, T.; Sorge, C.; Kang, S. P.; Isaacs, R.; Munster, P. N. *J. Clin. Oncol.* **2015,** *33* (9), 1060–1066.
287. King, C.; Diaz, H. B.; McNeely, S.; Barnard, D.; Dempsey, J.; Blosser, W.; Beckmann, R.; Barda, D.; Marshall, M. S. *Mol. Cancer Ther.* **2015,** *14* (9), 2004–2013.
288. Hong, D.; Infante, J.; Janku, F.; Jones, S.; Nguyen, L. M.; Burris, H.; Naing, A.; Bauer, T. M.; Piha-Paul, S.; Johnson, F. M.; Kurzrock, R.; Golden, L.; Hynes, S.; Lin, J.; Lin, A. B.; Bendell, J. *J. Clin. Oncol.* **2016,** *34* (15), 1764–1771.
289. Stumpf, A.; Cheng, Z. K.; Wong, B.; Reynolds, M.; Angelaud, R.; Girotti, J.; Deese, A.; Gu, C.; Gazzard, L. *Org. Process Res. Dev.* **2015,** *19,* 661–672.
290. Osborne, J. D.; Matthews, T. P.; McHardy, T.; Proisy, N.; Cheung, K. M.; Lainchbury, M.; Brown, N.; Walton, M. I.; Eve, P. D.; Boxall, K. J.; Hayes, A.; Henley, A. T.; Valenti, M. R.; De Haven Brandon, A. K.; Box, G.; Jamin, Y.; Robinson, S. P.; Westwood, I. M.; van Montfort, R. L.; Leonard, P. M.; Lamers, M. B.; Reader, J. C.; Aherne, G. W.; Raynaud, F. I.; Eccles, S. A.; Garrett, M. D.; Collins, I. *J. Med. Chem.* **2016,** *59* (11), 5221–5237.
291. Walton, M. I.; Eve, P. D.; Hayes, A.; Henley, A. T.; Valenti, M. R.; De Haven Brandon, A. K.; Box, G.; Boxall, K. J.; Tall, M.; Swales, K.; Matthews, T. P.; McHardy, T.; Lainchbury, M.; Osborne, J.; Hunter, J. E.; Perkins, N. D.; Aherne, G. W.; Reader, J. C.; Raynaud, F. I.; Eccles, S. A.; Collins, I.; Garrett, M. D. *Oncotarget* **2016,** *7* (3), 2329–2342.

5.03 Covalent Kinase Inhibitors for Cancer

Timothy D Owens and Yan Lou, South San Francisco, CA, USA

© 2017 Elsevier Ltd. All rights reserved.

5.03.1	**Introduction**	77
5.03.2	**The Advantages of Covalent Kinase Inhibitors in Cancer**	78
5.03.2.1	Achieving Highly Selective Kinase Inhibitors	78
5.03.2.2	The Benefits of Prolonged Residence Time via Covalency	78
5.03.3	**Assessment and Optimization of Covalent Kinase Inhibitors in Cancer**	78
5.03.3.1	On-Target In Vitro Activity	78
5.03.3.2	Structure and Reactivity of Covalent Electrophiles	80
5.03.3.3	Safety Concerns	80
5.03.3.4	Pharmacodynamics of Covalent Inhibitors	81
5.03.4	**BTK Inhibitors**	81
5.03.4.1	Introduction of Target Biology	81
5.03.4.2	Development of Clinical Covalent BTK Inhibitors	82
5.03.4.3	Covalent BTK Inhibitor Outlook	84
5.03.5	**Covalent Inhibitors of HER Family Kinases**	84
5.03.5.1	Introduction of Target Biology	84
5.03.5.2	Covalent HER Family Kinase Inhibitors	84
5.03.5.3	Second-Generation Irreversible HER Family Inhibitors	86
5.03.5.4	Third-Generation Irreversible Mutant-Selective EGFR Inhibitors	86
5.03.5.4.1	Development of rociletinib (19)	87
5.03.5.4.2	Osimertinib (20)	87
5.03.5.5	Acquired Resistance to Third-Generation Covalent EGFR Inhibitors	88
5.03.6	**Covalent Inhibitors of FGFR Family Kinases**	88
5.03.6.1	Introduction of Target Biology	88
5.03.6.2	Covalent FGFR Family Kinase Inhibitors	89
5.03.6.2.1	FIIN-1 (35)	90
5.03.6.2.2	FIIN-2 (36)/FIIN-3 (37)	90
5.03.6.2.3	TAS-120 (38)/PRN1371 (39)	90
5.03.6.2.4	BLU9931 (40)/BLU-554 (41)	90
5.03.7	**Other Kinase Targets for Covalent Inhibition**	91
5.03.7.1	Akt	91
5.03.7.2	BMX	92
5.03.7.3	CDK7	93
5.03.7.4	ERK1/2	93
5.03.7.5	ITK	94
5.03.7.6	JAK3	95
5.03.7.7	PI3Kα	96
5.03.7.8	Miscellaneous Kinases	97
5.03.8	**Emerging Strategies and Technologies**	98
5.03.8.1	Covalent Reversible Cysteine Inhibition of Kinases	98
5.03.8.2	Non-cysteine-Targeting Covalent Inhibitors	99
5.03.8.3	Screening Approaches to Discover Covalent Inhibitor Leads	100
5.03.8.4	Virtual Screening of Covalent Inhibitors	100
5.03.9	**Conclusions**	100
References		101

Ancillary Information

ABPP Activity-based protein profiling
Akt Protein kinase B
ATP Adenosine triphosphate
AUC Area under curve
Ba/F3 Murine interleukin-3-dependent pro-B cell line
BID *Bis in die*, Latin for "twice daily"
BLK B lymphocyte kinase
BMX Bone marrow kinase on chromosome X
BODIPY Boron-dipyrromethene
BTK Bruton's tyrosine kinase
CDK Cyclin-dependent kinase 7
CLL Chronic lymphocytic leukemia

 http://dx.doi.org/10.1016/B978-0-12-409547-2.12399-6

DDI Drug–drug interaction
EGFR Epidermal growth factor receptor
ELISA Enzyme-linked immunosorbent assay
EMT Epithelial–mesenchymal transition
ERK TGFbeta-activated kinase 1
FGFR Fibroblast growth factor receptor
GEM Genetically engineered model
HCC Hepatocellular carcinoma
HER Human epidermal growth factor receptor
HWB Human whole blood
IADR Idiosyncratic adverse drug reactions
ITK IL2-inducible T-cell kinase
JAK3 Janus kinase 3 (associated with family members JAK1 and JAK2)
JNK Jun N-terminal kinase
LCK Lymphocyte-specific protein tyrosine kinase
LYN Protein kinase encoded by the *LYN* gene
MCL Mantle cell lymphoma
mTOR Molecular target of rapamycin
NHL Non-Hodgkin's lymphoma
NSCLC Nonsmall-cell lung carcinoma
ORR Overall response rate
PBMC Peripheral blood mononuclear cell
PCa Prostate cancer
PD Pharmacodynamics
PFS Progression-free survival
PH Pleckstrin homology
PI3K Phosphoinositide 3-kinase
PK Pharmacokinetics
QTc QT interval
RTK Receptor tyrosine kinase
SDS-PAGE Sodium dodecyl sulfate-polyacrylamide gel electrophoresis
c-SRC Sarcoma kinase
TCR T-cell receptor
TAK1 TGFbeta-activated kinase 1
TEC Tyrosine kinase encoded by the *TEC* gene
TXK Tyrosine kinase encoded by the *TXK* gene
WM Waldenström's macroglobulinemia
WT Wild type
XLA X-linked agammaglobulinemia

5.03.1 Introduction

The fundamental signaling role of kinases in cell function and survival has long been recognized as a potentially critical point for pharmacological intervention. The medicinal chemistry of kinase inhibitors has grown in importance over the past several decades (see 50002, Selective kinase inhibitors for cancer), from the development and commercial success of early inhibitors such as Gleevec®, first approved by the FDA in 2001, to more than 28 FDA-approved kinase inhibitors as of January 2016.[1] These molecules have found use among a variety of different cancers and malignancies and have made a tremendous impact on patients' lives. While the number of approved entities has risen dramatically over the years, there exist two fundamental challenges to the development of new drugs that must be overcome. Key among these challenges is minimizing activity versus the other human kinases (which number >500), which share the common adenosine triphosphate (ATP)-binding pocket most often targeted. Even if this selectivity hurdle can be met, the compound must be further optimized to achieve sufficient systemic exposure for 24 h kinase inhibition with once- or twice-daily dosing. One means of overcoming these hurdles is to utilize designed covalent inhibitors of target kinases. When the amino acid residues targeted by covalent inhibitors (most often cysteine) are shared by only a small group of kinases, this approach provides an extremely successful way of imparting selectivity. Furthermore, covalent binding by its nature avoids the need for systemic exposure to provide target coverage, as the inhibition lasts until new protein can be resynthesized. This review will provide an overview of the key concepts to be considered before embarking on a medicinal chemistry campaign using a covalent approach.

We will begin with a review of key considerations that should be analyzed with respect to the protein of interest. Is a targetable cysteine present? What other proteins share this cysteine? What is the protein turnover of this protein? Under what context is this measured? What is the potential for mutation and subsequent loss of efficacy? What risks are being taken by utilizing inhibitors that covalently modify proteins and can these be mitigated? Most fundamentally, what are the best ways to assess and optimize on-target efficacy using this approach?

The next portion of the review will look in detail at published efforts to inhibit specific kinases by utilizing covalent inhibitors. The examples will be grouped by protein target of interest, with particular focus placed on those targets (BTK, EGFR/HER2, and FGFR) where the approach has resulted in evaluation of covalent inhibitors in a clinical setting. Pioneering work that helped drive understanding will be highlighted, and the evolution of design elements and drug optimization strategies will be discussed. In cases where efforts have led to actual drug approvals (most notably with HER2, EGFR, and BTK inhibitors), emerging second-generation approaches and potential therapies will also be highlighted.

Finally, emerging trends in the field will be considered. Given the large number of kinases potentially targetable by covalent inhibitors, the field is likely to remain a vibrant area of research and an important source of new treatments for patients.

5.03.2 The Advantages of Covalent Kinase Inhibitors in Cancer

5.03.2.1 Achieving Highly Selective Kinase Inhibitors

Protein kinases, through the posttranslational phosphorylation of a wide variety of proteins in the body, play a critical role in human physiology. Dysregulation of these kinases, via activating mutation or upregulation, is implicated with a variety of different cancers. Recognition of this has led to focused efforts from the medicinal chemistry community to yield marketed drugs. However, due to the conserved nature of the nucleotide-binding pocket in kinases, many of these drugs have minimal selectivity versus the other kinases expressed.[2] Selective inhibition of kinases has been achieved by targeting binding pockets exposed in alternative kinase conformations, such as imatinib, which binds to the "DFG-out" conformation of c-Abl,[3] and lapatinib, which binds to the "C-helix-out" conformation of EGFR and HER2. Targeting nonconserved cysteines provides an attractive approach to achieving selectivity as many of these noncatalytic cysteines are in accessible regions of the catalytic binding site and share sequence alignment with a small subset of the broader kinase family. A recent analysis revealed that over 200 kinases contain an accessible cysteine near the ATP-binding pocket. These were categorized broadly into four distinct groups based on the common location of the cysteine.[4] These are highlighted in **Fig. 1**, which depicts the location of kinases sharing homologous cysteines within the phylogenetic tree.[5] Examples of selective kinase inhibitors targeting kinases in each of these classes will be described in detail in Sections "**Assessment and Optimization of Covalent Kinase Inhibitors in Cancer**" to "**Covalent Inhibitors of HER Family Kinases.**" A more recent exercise evaluated accessible cysteines predicted to be accessible in kinases in the "C-helix-out" and "DFG-out" conformations further broadening the potential targets amenable to cysteine targeting.[6]

It should be noted that the cysteine residues are not necessarily conserved across kinase genetic families. For example, the well-studied group 3F kinases share a common cysteine and include multiple members of the Tec (BMX, BTK, ITK, RLK, and TEC) and ERBB/HER (EGFR, ERBB2, and ERBB4) families. Group 3F also includes MKK7 (STE7 family), BLK (Src family), and JAK3 (Tec family), which are unique within their families in harboring a cysteine in this position. Structural differences among family members and patterns of cellular distribution allow for further selectivity to be realized, even where a targeted cysteine is shared by multiple kinases.

5.03.2.2 The Benefits of Prolonged Residence Time via Covalency

Many recent reviews have highlighted the concept of drug–target residence time as a factor, which should be optimized and exploited by medicinal chemists.[7] Covalent irreversible inhibition pushes this concept to an extreme case, wherein the inhibitor remains bound to protein and pharmacologically active until new protein is synthesized. If protein turnover is sufficiently slow (see in the succeeding text), the effect of a covalent inhibitor manifests itself long after clearance of the molecule from systemic circulation. This allows the possibility of achieving prolonged inhibition with relatively short periods of systemic exposure, lowered overall pharmacokinetic area under the curve (AUC), and potentially lower overall total body burden of drug. A second advantage arises from the fact that irreversible inhibition fundamentally changes the equilibrium toward bound complex. In cells, inhibitors must compete with the native endogenous kinase ligand ATP, which is present at concentrations of roughly 5 mM. The reduced cellular potency of many kinase inhibitors relative to inhibition of isolated kinases (cellular shift) due to high Km (ATP) can be mitigated with covalent inhibitors.[8] When assessing the selectivity of a covalent inhibitor, it is important to consider these benefits rather than relying on standard kinase inhibition assays. Noncovalent off-target inhibition should be transient, and therefore, the functional selectivity in vivo is underestimated by simple binding or activity assays, particularly as the drug clears rapidly from systemic circulation. On the other extreme, it should be noted that inhibitors possessing electrophilic moieties with very high intrinsic reactivity are prone to react with endogenous cellular cysteines such as glutathione, thereby reducing on-target cellular potency and leading to additional safety issues.

5.03.3 Assessment and Optimization of Covalent Kinase Inhibitors in Cancer

5.03.3.1 On-Target In Vitro Activity

In many instances, standard assays utilized in noncovalent medicinal chemistry campaigns targeting kinases are useful when screening for or optimizing covalent inhibitors. However, there are several caveats that should be noted when assessing data from these assays. Equilibrium measurements, IC_{50}s, while often reported and used for rank ordering inhibitors are technically inappropriate for use with covalent inhibitors where the off rate is very slow. These are often used due to assay simplicity, but longer incubation times will lead to more complete inhibition, and therefore, conditions should be rigorously controlled when producing "IC_{50} apparent" values, and caution should be taken when data are compared from different sources. While more time consuming, determination of a k_{inact}/K_i value is a preferred method of assessing the reactivity of a covalent inhibitor. In a crude sense, this differentiates the contribution of reversible binding-driven noncovalent interactions (K_i) from the irreversible covalent bond formation kinetics (k_{inact}). However, assuming typical incubation times are used (0.5–2 h), an IC_{50} apparent is reflective of physiologically relevant exposure, and the term IC_{50} will be used in this article when literature data are reported.

Validation that covalent bonding to a cysteine of interest is of critical importance when initiating a lead optimization campaign. In many instances, simple structure–activity relationships (SAR) allow one to determine that covalent bonding is occurring at a protein site of interest. A sharp reduction in activity by replacement of the electrophilic moiety (e.g., reduction of an acrylamide to an ethyl amide) is a typical hallmark of covalent inhibitors. Other indirect methods of confirming cysteine engagement include single-point mutation of the putative reactive cysteine. This should coincide with the loss of activity. Additionally, with irreversible

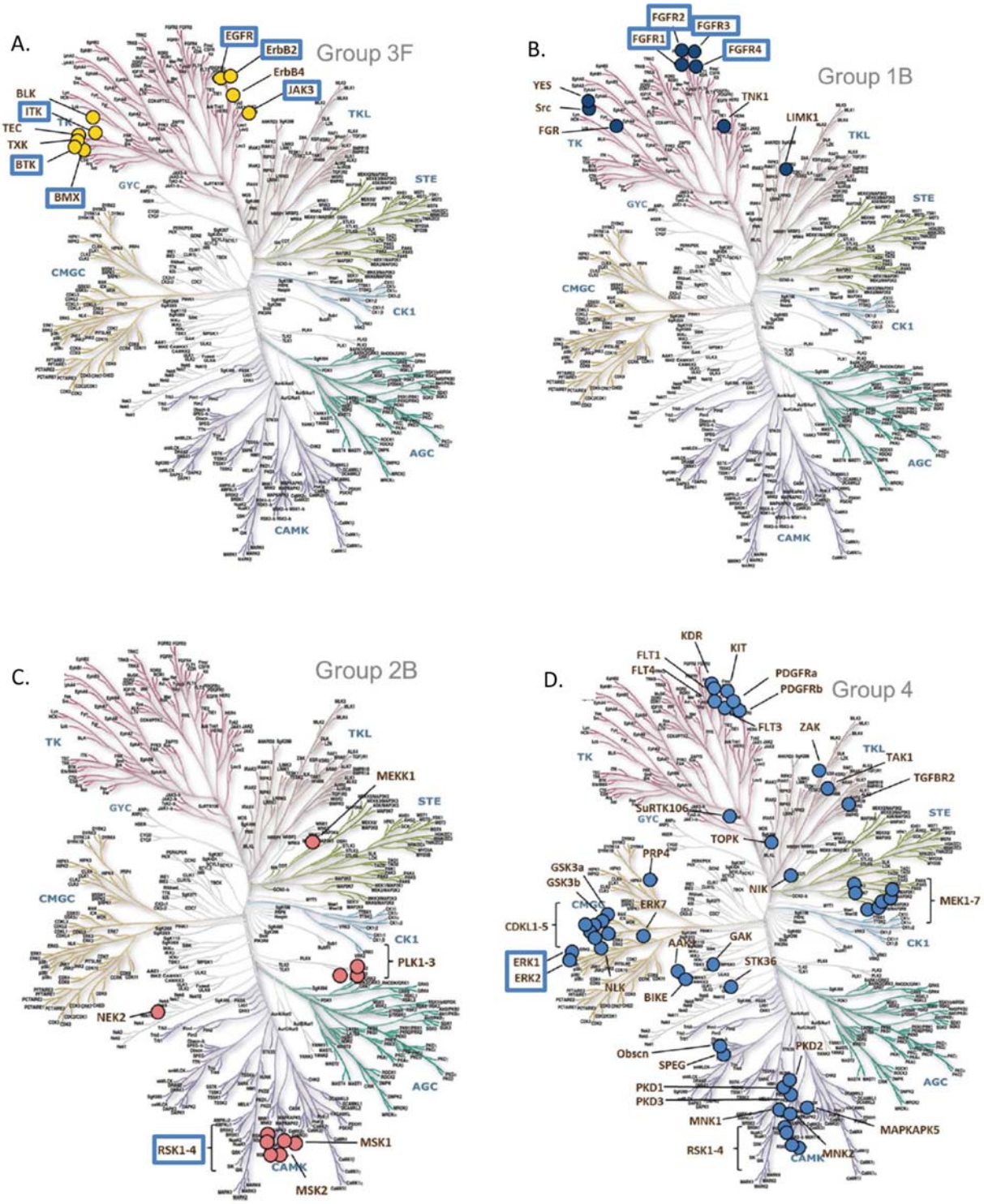

Fig. 1 The human kinome (adapted from Ref. 5 and courtesy of cellsignalling.com). Each phylogenetic tree highlights kinases containing shared targetable cysteines from a specific cysteine class. Kinases boxed in blue are proteins targeted covalently and discussed in this article. (A) group 1B, (B) group 2B, (C) group 3F, and (D) group 4 kinases.

covalent inhibitors, mass spectroscopy analysis allows unequivocal detection of the inhibitor bound to protein or peptide fragment from enzymatic digestion. Most informative for the medicinal chemist is confirmation of binding via x-ray diffraction as this confirms the covalent nature of the inhibition and also allows a snapshot of other critical binding (noncovalent) interactions and provides solid basis for structure-based optimization.

5.03.3.2 Structure and Reactivity of Covalent Electrophiles

Various electrophiles have been incorporated into covalent inhibitor designs and undoubtedly play a critical role in the success of this approach. The electrophile should be sufficiently reactive to engage the cysteine of interest after an initial binding event mediated by noncovalent interactions brings it into proximity. Preferably, the electrophile should not indiscriminately react with sulfhydryl groups present in off-target proteins or other endogenous thiols (such as glutathione). Among the more reactive groups (Fig. 2), the chloroacetamides, vinyl sulfonamides, and unsubstituted alkynyl amides have been incorporated into relatively selective inhibitors and found utility as chemical biology probes. Similarly, α,β-unsaturated esters and aldehydes are presumably too reactive to have found utility in kinase drug development. However, to date, kinase inhibitors utilizing these electrophiles have not been reported as clinical-stage drug candidates. As will be highlighted in individual examples later, the most prevalent electrophiles among approved drugs and clinical-stage inhibitors are the acrylamides, acrylamides substituted with pendant allylic amines, and butynamides. For Michael acceptors, substitution at the beta position greatly reduces the intrinsic reactivity. However, pendant allylic amines can serve to deprotonate nearby thiols and thereby assist the formation of the covalent adduct. Besides providing a linkage to the critical kinase hinge binding site, the substitution on the amide nitrogen is also critical to reactivity. Generally, acrylamides have been shown to be functionally inert with respect to common thiols such as glutathione, standing in contrast to more reactive electrophiles such as chloroacetamides.[9] The intrinsic reactivity can be modulated by steric and electronic factors, and a variety of attempts to experimentally determine reactivity have been undertaken. The rate of reaction with glutathione was assessed for a wide variety of chemical reactive groups (CRGs) incorporated into small fragment like molecules.[10] In addition to rank ordering functional groups for intrinsic reactivity, the data were compared with predicted reactivity from quantum chemical calculations to identify in silico methods with greatest prognostic value. The reactivity of aniline-based acrylamides with glutathione has also been assessed in the context of an EGFR inhibitor program.[11] The authors found that reactivity increased with electron-withdrawing groups and trended with EGFR IC_{50} measurements. A more recent study produced similar findings and also found a correlation between NMR chemical shifts of acrylamides and reactivity.[12] The reactivity of approved drugs can provide guidance and benchmarks when using these data. Generally, the intrinsic reactivity should be matched to the cysteine of interest, with selectivity driven by the proximity effect due to the concentration of inhibitor in its binding pocket. This should mitigate the possibility of unwanted side effects due to undesired modification of other thiols.

5.03.3.3 Safety Concerns

Despite the advantages discussed earlier and their immense promise as therapeutics, safety concerns have arisen over the development of drugs designed to permanently modify proteins, even to treat life-threatening conditions such as cancer. The risk is quite understandable, given the association between idiosyncratic adverse drug reactions (IADRs) and the potential of drugs to generate reactive metabolites, which can irreversibly bind proteins.[13] Besides permanently inhibiting a protein, covalent inhibitors remaining bound to proteins or protein fragments raise the risk of haptenization and potentially severe allergic responses. It should be noted that the reactivity of reactive metabolites associated with IADRs is typically much greater than that of the electrophiles described earlier. Of note, the overall daily dose of a drug has been shown to correlate well with the rate of IADRs and there are no examples of IADRs with drugs dosed below 20 mg/day.[14] Intriguingly, irreversible kinase inhibitors have great potential to meet this requirement due to the attributes described earlier (the lack of ATP competition and extended inhibition due to covalent mechanism of action). Nonetheless, efforts have been made to determine the propensity of a designed covalent inhibitor to react indiscriminately with cysteine-containing proteins.

Existing methods used in screening for reactive metabolites can be utilized for the purpose of assessing off-target activity, with the important caveat that these should be run without metabolic activation if one is to determine the intrinsic off-target liabilities of the parent drug. Typically, surrogates of native thiols such as glutathione are used to assess intrinsic reactivity of covalent kinase inhibitors.[15] Similarly, depletion of free drug after incubation in whole blood can be a sign of indiscriminate binding of a reactive inhibitor to proteins. In addition to being an operationally simple assay, it more closely mimics thiols in a native protein environment. More intricate methods have also been developed not only to look at reactivity but also to quantitate and identify proteins, which react with electrophilic inhibitors. Cravatt and coworkers have recently utilized activity-based protein profiling (ABPP) to demonstrate that at high concentrations in cells, a large number of kinases and nonkinase off-target proteins can react with

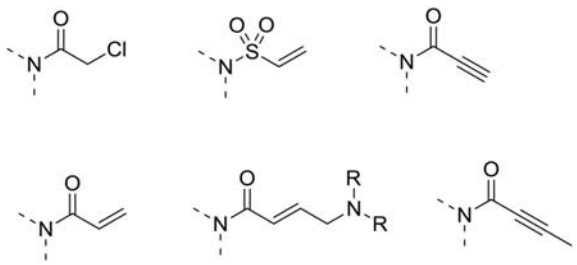

Fig. 2 Electrophilic moieties commonly used in covalent kinase inhibitors.

seemingly very selective acrylamide-based inhibitors.[16] In this study, structural analogs of ibrutinib (see 7.08.4) incorporated an alkyne to allow coupling to an azide-rhodanine tag via click chemistry. After incubation in cells or cell lysates at varying concentrations, incorporation of the tag allows one to visualize the proteins to which the probes bound via SDS-PAGE and in-gel fluorescence scanning. Using this method, Cravatt and coworkers uncovered multiple expected bands for the covalent binding of the probes to BTK and EGFR and unexpected bands, indicating the attachment to unrelated enzymes, which also contain reactive cysteine moieties. The use of covalent reversible inhibitors targeting RSK highlights a possible way to eliminate the risk of permanent modification of off-target proteins while benefiting from the long residence time and selectivity of irreversible inhibitors.[17] This concept has since been applied to BTK and FGFR,[18] as well as EGFR,[19] and is clearly an emerging area of the field. Regardless of reactivity, as with noncovalent drugs, standard safety assessments (time-dependent inhibition, genotoxicity, hERG, drug–drug interactions, etc.) must be taken into account with covalent inhibitors.

5.03.3.4 Pharmacodynamics of Covalent Inhibitors

The key advantages of covalent inhibitors rely on their ability to permanently modify and inhibit the protein of interest, thereby preventing signaling until new protein is produced. Protein turnover rate of a target of interest is therefore a critical element to understand when beginning a covalent inhibitor program. If protein synthesis takes place too quickly, unbound inhibitor must remain present to inhibit the newly formed protein. However, when protein synthesis is slow, prolonged inhibition with an irreversible inhibitor is expected even after the inhibitor has been cleared from systemic circulation. In this scenario, a disconnection exists between pharmacokinetics (PK) of the inhibitor and its pharmacodynamic (PD) effect.[20,21] For receptor tyrosine kinase EGFR, the rate of protein turnover is thought to be highly dependent on cell lines studied and the activation state of the receptor signaling pathway, with more rapid turnover when activated by EGF (1–4 h) and relatively slow turnover (7–28 h) under nonstimulated conditions.[22–24] Meanwhile, for the nonreceptor kinase BTK, a more consistent turnover rate has been estimated to be between 18 and 24 h.[18] With slower rates of protein turnover, high levels of target engagement and inhibition are expected for irreversible inhibitors long after clearance of the molecule. Methods to evaluate potential extended PD effects in preclinical and clinical studies are therefore fundamental to the development of covalent drugs given the challenges to predicting inhibition from PK exposure alone or simple cell-based turnover studies. Assessing in vivo target engagement during preclinical studies with model organisms or more critically in a clinical setting is crucial for development of drugs that cause a desired pharmacological effect while providing the greatest possible safety window possible. Noninvasive methods of determining target engagement can be challenging and include in vivo imaging techniques and ex vivo chemoproteomic analysis of human blood samples.[25] However, many targets are not amenable to these techniques or the readouts can be ambiguous if the effects measured are not directly proximal to the enzymatic activity (e.g., if multiple enzymes can perform the same function). Activity-based protein profiling (ABPP) methods, utilizing irreversible inhibitors that incorporate a reporter group, allow for ex vivo assessment of samples. For kinases inhibited by covalent inhibitors with prolonged target engagement, covalent inhibitor probe molecules can be designed for this purpose. If the probe molecule is cell-permeable, the probes can be used to monitor the level of target protein engagement ex vivo at different time points after administration of a drug. At certain time periods after dosing, blood or tissue samples can be harvested, and if the kinase of interest has been covalently modified, added probe molecule cannot bind, and the reporter signal is blocked. The amount of protein bound (percent occupancy) can then be estimated by comparison with control samples where no inhibitor is present. If full occupancy is achieved, probe molecules are able to bind only as new protein is produced and signal is restored, allowing an assessment of the role of protein turnover in an in vivo system. This ability to directly measure the occupancy of a drug on target allows preclinical and clinical assessment of target coverage requirements expected for efficacy. This has been used with great success in the development of BTK inhibitors (*vide infra*).[26]

5.03.4 BTK Inhibitors

5.03.4.1 Introduction of Target Biology

Bruton's tyrosine kinase (BTK) is a critical enzyme for the development and function of B cells, and genetic defects leading to X-linked agammaglobulinemia resulted in its discovery. It is believed to play an important role in a variety of hematologic malignancies and cancers and is implicated in a variety of autoimmune diseases and inflammatory conditions.[27] As such, great effort has been made by the medicinal chemistry community to identify potent and selective inhibitors of this enzyme. Along with 10 other kinases (including EGFR, HER2, JAK3, and ITK described in the succeeding text), BTK contains a cysteine (C481) that is accessible from the ATP-binding pocket with small-molecule inhibitors.[28] While noncovalent medicinal chemistry approaches have resulted in selective and potent inhibitors, to date, only covalent inhibitors have reached clinical efficacy studies. Ibrutinib (**1**) (**Fig. 3**), the first commercialized BTK inhibitor, is marketed as Imbruvica® and has now been approved for the treatment of a variety of cancers including chronic lymphocytic leukemia (CLL), mantle cell lymphoma (MCL), and Waldenström's macroglobulinemia.[29,30] Several groups have subsequently progressed covalent BTK inhibitors into the clinic. These compounds have been designed from various kinase inhibitor scaffolds and possess differentiated electrophilic warheads, with significant effects on intrinsic activity on BTK and inhibition selectivity within the 11 kinase "Cys family."

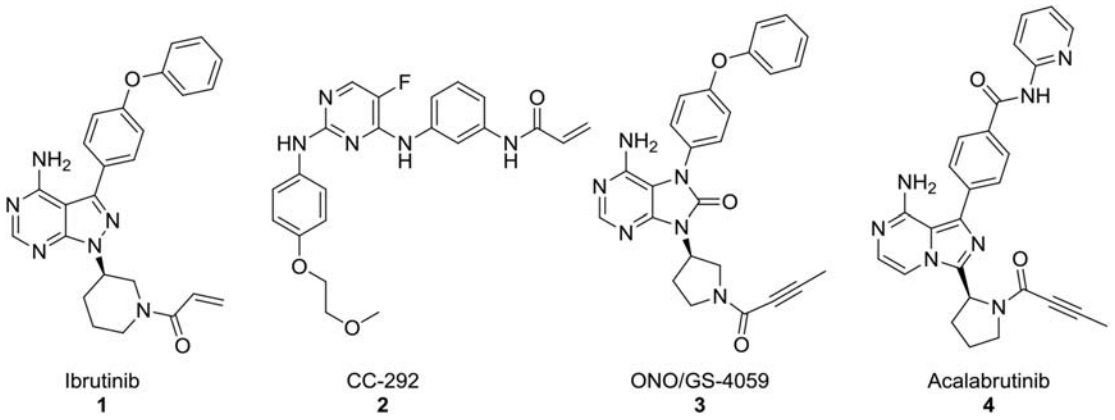

Fig. 3 Clinical-stage covalent BTK inhibitors.

5.03.4.2 Development of Clinical Covalent BTK Inhibitors

Using PCI-29732 (**5**) as a starting point, a variety of electrophiles and linker combinations were evaluated for their ability to engage C481 (Fig. 4).[31] While vinyl sulfonamides, chloromethyl amides, and alkynyl amides all exhibited excellent potency, the acrylamide using the (*R*)-piperidine linker was preferred. As expected by the covalent mechanism, compound **1** exhibited improved selectivity compared with **5**, which was reported to strongly inhibit both LCK and LYN. Furthermore, in preliminary arthritis models, efficacy was achieved with doses that did not require sustained exposure due to the irreversible inhibition of BTK. Subsequently, the utility of **1** for the treatment of B-cell malignancy was demonstrated by its effectiveness in treating naturally occurring canine B-cell non-Hodgkin lymphoma (NHL).[26] A partial response was seen in three of eight dogs at dosages between 2.5 and 20 mg/kg per day helping provide validation of the potential utility in clinic.

Critical to understanding mechanism and correlating level of BTK inhibition and effect, a prolonged inhibition of BTK was monitored by labeling peripheral blood mononuclear cells (PBMCs) with a fluorescently labeled analog of **1**. The BODIPY-FL fluorophore was attached via an aminoethyl piperizine linker to the electrophilic site of compound **1** to afford compound **6** (Fig. 5). Critically, probe **6** is cell-permeable and maintains activity against BTK. After treatment of B-cell lymphoma line DOHH2 cells with **6**, irreversibly bound proteins in cell lysates were resolved by electrophoresis and the predominant band identified as BTK. Binding of **6** could be completely blocked by prior treatment of cells with **1**, therefore providing a platform for preclinical and clinical measurement of BTK target occupancy via a competitive binding assay. This assay format was used successfully to confirm BTK occupancy in the canine lymphoma model earlier and subsequently with clinical PBMC samples. Similarly, modification of other clinical-stage BTK inhibitors described in the succeeding text resulted in cell-permeable probes utilized to assess occupancy in clinical studies. For example, CNX-500 (**7**) was developed as a probe and used for analysis of BTK occupancy in an ELISA-based format.

Clinically, **1** has shown excellent efficacy, with particularly high response rates in CLL and MCL,[32] resulting in breakthrough designations and subsequent approvals across a variety of hematologic cancers. In CLL, partial responses were seen in 89% of 85 patients.[29] Importantly, excellent activity has been seen in CLL patients with the difficult to treat del(17p) abnormality. Aside from excellent clinical activity, the side effects reported have been relatively mild with grade 1–2 diarrhea as the most frequently occurring event and diminished occurrence of grade 3 or greater events over prolonged treatment (3-year follow-up).[33]

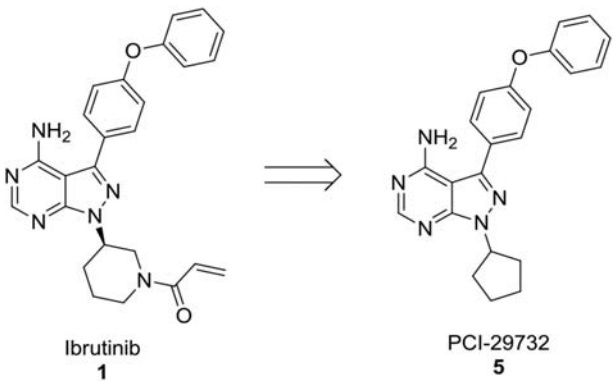

Fig. 4 Structural design evolution of ibrutinib.

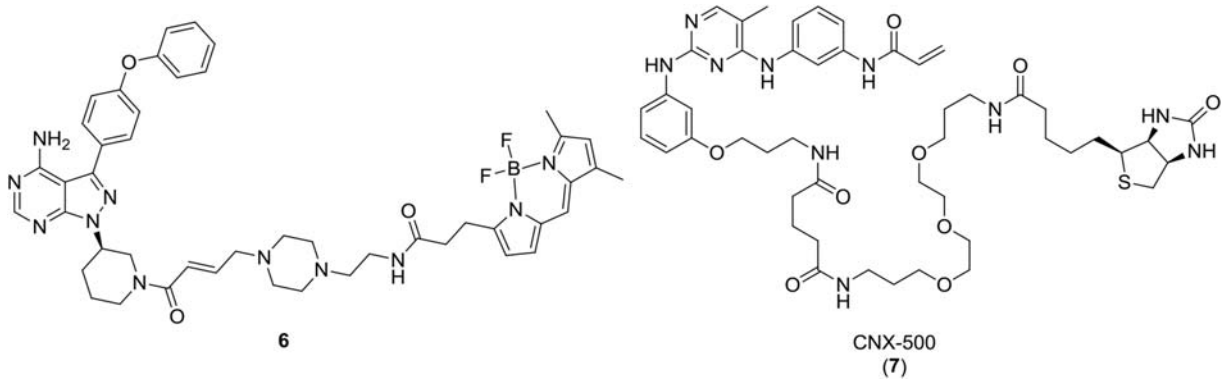

Fig. 5 Covalent BTK probe molecules.

From a pharmacokinetic standpoint, **1** is able to achieve excellent occupancy and inhibition of BTK long after clearance of the drug from systemic circulation. As described in the Section "The Benefits of Prolonged Residence Time via Covalency," this is a favorable attribute for an irreversible inhibitor as a lower AUC is required for efficacy. Interestingly, PK is highly dependent on whether **1** is dosed in a fed or fasted state, with a *c.* 40% reduction in exposure if dosed in the fasted state.[34] Furthermore, **1** is almost exclusively metabolized by CYP3A4, and there is therefore an associated risk for drug–drug interactions (DDI). Clinical trials in healthy volunteers found that administration of **1** after treatment with the CYP3A4 inhibitor ketoconazole greatly increased exposure, with the dose-normalized AUC increasing from 71.4 to 1599 ng·h/mL and dose-normalized C_{max} increasing c. 29-fold. This was associated with a reduction of the primary circulating metabolite PCI-4527 (the diol resulting from oxidation and hydrolysis of the acrylamide).

The selectivity of **1** in standard biochemical assays likely underrepresents the high selectivity within the kinome due to the disconnection between PK and PD. Even for kinases where the apparent IC_{50} is quite low, the concentration of drug is only transiently above this level, and the effects are therefore mitigated. Within the 10 kinases, which contain a homologous cysteine, however, the selectivity profile is significant. Among these 10, EGFR is known to be associated with side effects, such as often severe rashes on the face and upper body and indeed is inhibited by **1** ($IC_{50} = 5.6$ nM).[26] However, the inhibition of other kinases may possibly be of clinical benefit. For example, the inhibition of ITK ($IC_{50} = 2.2$ nM) is reported to be critical for the possible synergistic effect of **1** when coadministered with immune checkpoint inhibitors.[35]

Following the success of ibrutinib, multiple C481-targeting inhibitors have advanced into trials for treatment of hematologic malignancies. Avila and Celgene optimized an aminopyrimidine scaffold, attaching an acrylamide via an aniline linkage, culminating in CC-292 (**2**).[36] Compound **2** is a potent ($IC_{50} < 0.5$ nM and $K_{inact}/K_I = 7.69 \times 104\ M^{-1}\ s^{-1}$) and selective BTK inhibitor, which has no reported EGFR activity in cell-based assays. Clinically, **2** was tolerated at doses up to 1000 mg QD (once daily) and 500 mg BID (twice daily); however overall response rates did not achieve those of ibrutinib.

More recently, two BTK inhibitors containing a methyl alkynamide warhead have reached clinical studies. ONO/GS-4059 (**3**) utilizes a urea-based scaffold to display a phenoxy phenyl group in a similar position to that in **1**, with the electrophilic warhead attached via a pyrrolidine ring. Compound **3** is reported to have an $IC_{50} = 2.0$ nM and results of phase I studies have been published.[37] Treatment in patients with B-cell malignancies was well tolerated up to 600 mg QD and 300 mg BID in CLL with grade 3 or 4 adverse events occurring in 14% of patients in the CLL cohort. Initial efficacy looks promising with 66% of patients with CLL or MCL remaining on trial (median therapy duration of 21 months). From a pharmacokinetic standpoint, the drug is cleared rapidly with $T_{1/2}$ values between 6.5 and 8 h and shows dose linear increases in AUC. Using a twice-daily dosing regimen (240 mg or 300 mg), exposures did not change significantly from day 1 to day 28, highlighting a lack of drug accumulation.

Scientists from Acerta have advanced the imidazolopyrazine-based BTK inhibitor **4** into clinical trials, and it is reportedly advancing into phase III efficacy studies.[38] In addition to building from a different scaffold, inhibitor **4** also differs in that it displays the butynamide electrophile at the 2-position of the pyrrolidine ring relative to the scaffold versus the 3-position in compound **3**. Meanwhile, the phenoxyphenyl system common to **1** and **3** has been replaced with a pyridinyl benzamide group. A publication describing noncovalent BTK inhibitors with the same scaffold mentions that this substitution provides improved kinase selectivity.[39] The compound inhibits BTK slightly less potently (reported $IC_{50} = 5.1$ nM) but has a more selective inhibition profile compared with **1** with only BMX, TEC, TXK, and ERBB4 having $IC_{50} < 1$ μM among kinases containing the common cysteine. Based on reported phase I and II data, the drug is well tolerated with 53 of 61 patients remaining on treatment (median therapy duration of 14.3 months) with nausea (4 patients) being the most common grade 3 or 4 adverse event. Activity is encouraging, with an overall response rate of 95% across all cohorts. In contrast to **1**, the phase II expansion cohort was dosed twice daily (100 mg BID), presumably to maintain greater than 90% occupancy at BTK over 24 h. This may be critical for efficacy and possibly preventing progression to the more lethal Richter's transformation in this patient group.

5.03.4.3 Covalent BTK Inhibitor Outlook

With the approval of **1** for treatment of a variety of hematologic malignancies and multiple other covalent BTK inhibitors at various stages of clinical trials, a clearer vision of the safety and efficacy of this approach will emerge. Given the potential for BTK inhibitors as a component in combination therapies, their utility is likely to be tested in settings beyond blood cancers. One unique benefit of using covalent approaches will remain the ability to monitor the BTK occupancy of a clinical inhibitor ex *vivo*. This has been demonstrated with BODIPY-based probe **6** and with biotinylated probes such as **7** in an ELISA-based format. Regardless of approach, the ability to target-specific levels of occupancy throughout a dosing cycle is critical not only to maintain efficacy but also possibly to prevent or minimize protein mutation or transformation.

Intriguingly, the level of off-target (non-BTK) occupancy in theory can also be monitored. As an alternative to the direct readout probe approaches, a second option utilizes "two -step" bioorthogonal activity-based probes.[40] The cell-permeable and potent BTK inhibitor **8** (Fig. 6), incorporating a pendant alkyne to the phenoxyphenyl ring found in **1**, has been used as a surrogate to investigate the panproteome reactivity of compound **1**.[16] After incubating cells with **8** at varying concentrations, a reporter molecule containing an azide handle can be attached via "click" chemistry to allow visualization and identification of proteins that are likely irreversibly modified by **1**. Similarly, reactive terminal alkynes (**9**) or azides (**10**) have been attached to the electrophilic acrylamide center via a spacer similar to compound **6**.[41]

5.03.5 Covalent Inhibitors of HER Family Kinases

5.03.5.1 Introduction of Target Biology

The human epidermal growth factor receptor (HER) family of receptor tyrosine kinases (RTKs) is a well-established target for treating multiple types of solid tumors, most notably EGFR+ (positive) nonsmall-cell lung cancer (NSCLC) and Her+ breast cancer. The four members, epidermal growth factor receptor (EGFR; also known as HER1 (ErbB1), HER2 (ErbB2), HER3 (ErbB3), and HER4 (ErbB4)), play critical roles in various signaling pathways, leading to cell growth, proliferation, differentiation, and survival.

5.03.5.2 Covalent HER Family Kinase Inhibitors

Activating mutations in EGFR are responsible for a significant percentage of NSCLC malignancy (10–15% for European descent; c. 30% for patients of East Asian descent). First-generation, noncovalent EGFR inhibitors such as erlotinib (**10**) and gefitinib (**11**) (Fig. 7) showed dramatic clinical responses in patients with the most common EGFR mutations (L858R mutation in exon 21 and delE746-A750 in exon 19). Discovery of oncogenic drivers such as EGFR and specific targeting has been a major breakthrough in targeted cancer therapy and led to a paradigm shift in cancer treatment. However, patients often acquire drug resistances, often as a result of mutations that render drugs significantly less active.

In approximately 60% of patients that developed resistance to first-generation EGFR inhibitors, a point mutation occurred at the gatekeeper position of the EGFR kinase domain (T790M). There are two proposed mechanisms for the loss of clinical efficacy of first generation of EGFR inhibitors associated with the single amino acid mutation of threonine to methionine: (1) The mutated methionine residue possesses a bulkier side chain that can sterically impede the binding of the reversible inhibitors and disrupt the formation of a crucial water-mediated hydrogen bond between inhibitors and T790M EGFR;[42] (2) T790M EGFR was shown to have an increased affinity for ATP, resulting in reduced cellular potency for first-generation noncovalent ATP-competitive EGFR inhibitors.[43] It was found that the T790M-mutant EGFR remains sensitive to covalent irreversible EGFR inhibitors, such as EKB-569 (**12**, pelitinib) and HKI-272 (**13**, neratinib).[42] The activity toward mutant EGFR was attributed to the irreversible mechanism of action of covalent inhibitors, overcoming competitive binding of ATP. A number of these second-generation covalent EGFR inhibitors

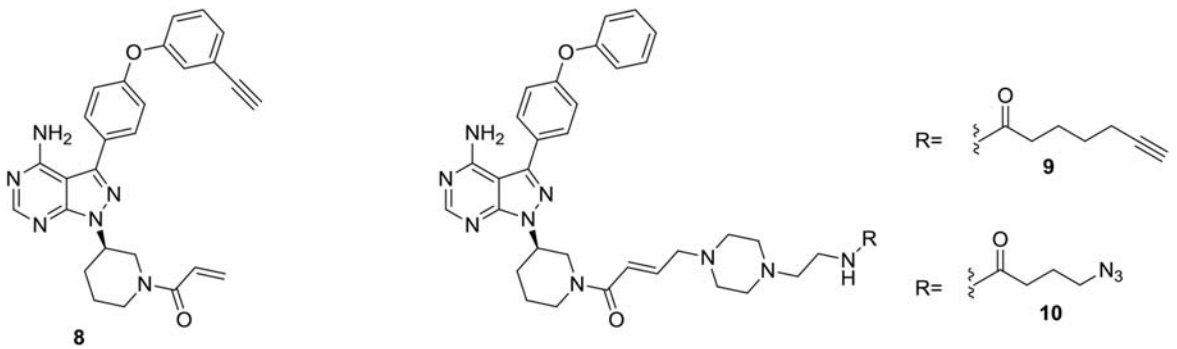

Fig. 6 Covalent BTK bioorthogonal probe molecules.

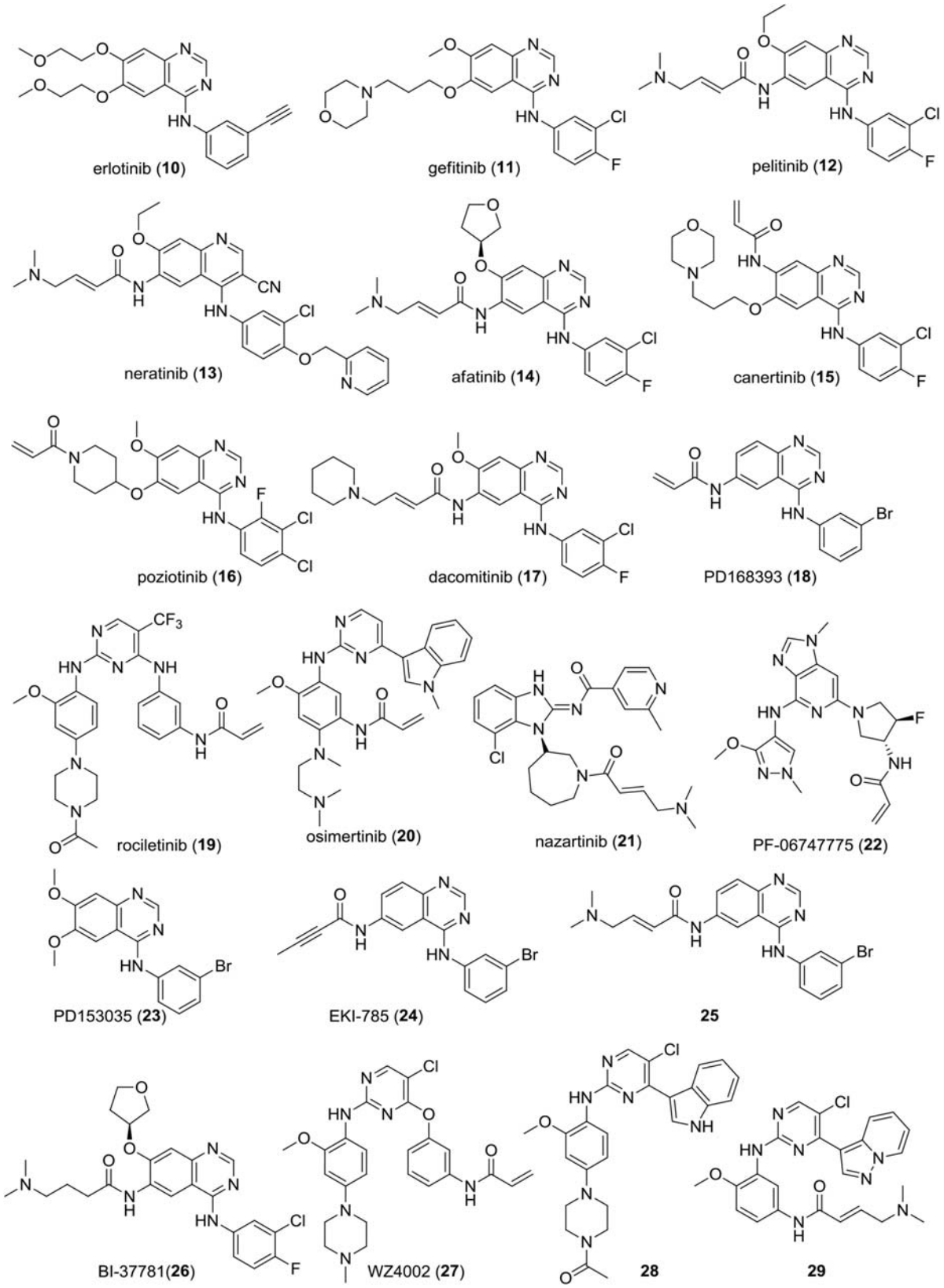

Fig. 7 Chemical structure of EGFR inhibitors.

were advanced into clinical trials, including **12**, **13**, afatinib (**14**, BIBW2992), canertinib (**15**, CI1033), poziotinib (**16**, HM781-36B), dacomitinib (**17**, PF299804), and PD168393 (**18**). Some of these drugs were developed as pan-HER inhibitors for HER+ breast cancer due to their concurrent activity against HER2, such as **13** and **18**.

Although second-generation irreversible HER family inhibitors are able to inhibit T790M-mutant EGFR in vitro, and thus progressed into clinic, these agents have not been shown to induce compelling responses in patients that have failed first-generation tyrosine kinase inhibitors (TKIs).[44] This is likely due to their potent inhibition of wild-type (WT) EGFR and consequent dose-limiting toxicities including diarrhea and skin rash, which prevented them from reaching exposures in the clinic required to inhibit T790M in tumor tissue. Therefore, third-generation, WT-sparing covalent EGFR inhibitors were developed, and multiple compounds have advanced into clinic trials, including rociletinib (**19**, also known as CO-1686/AVL-301/CNX-419), osimertinib (**20**, AZD9291), nazartinib (**21**, EGF816), and PF-06747775 (**22**).

5.03.5.3 Second-Generation Irreversible HER Family Inhibitors

The pioneering work by the Wyeth group in the area of covalent EGFR inhibitor discovery was partly driven by uncovering unique intellectual property derived from a quinazoline scaffold utilized in potent and reversible EGFR inhibitors[45] such as PD153035 (**23**) disclosed by Parke-Davis. Modeling efforts using the crystal structure of **10** bound to EGFR contributed to the design and evaluation of compounds with an acrylamide Michael acceptor group attached at diverse positions on the 4-anilinoquinazoline core including the 6- and 7-positions of the bicycle and various positions on the aniline group. This led to the discovery of PD168393 (**18**) with the acrylamide at the 6-position, exhibiting exceptional potency against EGFR (IC_{50} of 2 nM). Washout experiments provided substantial indirect evidence that **18** was indeed an irreversible inhibitor. Interestingly, Parke-Davis independently discovered compound **18** at almost same time and confirmed its irreversible inhibition of EGFR by mass spectral studies and identified C773 as the target residue.[19] The first preclinical candidate from the effort was EKI-785 (**24**), containing 6-butynamide as the electrophile. Despite good in vitro and in vivo activity, poor oral exposures due to poor aqueous solubility together with histological findings in the kidneys prevented its advancement into clinic. Though simple alkyl substitutions of the acrylamide olefin resulted in the loss of activity, it was found that incorporation of a basic water-solubilizing group in compound **25** maintained potent EGFR inhibition. By measuring the relative amounts of Michael addition products with glutathione, the order of reactivity was found to be **25** > **18** > **24**. The enhanced reactivity of **25** was hypothesized to be the result of the dialkylamino group functioning as an intramolecular general base catalyst for the Michael addition reaction. Further optimization effort led to the discovery of two clinical molecules, first **12** (EGFR IC_{50} of 8 nM and HER2 IC_{50} of 378 nM) and then **13** with more potent HER2 activity (pEGFR IC_{50} of 92 nM and pHER2 of 59 nM).[45] Phase I studies of **13** with once-daily doses in the range of 40–500 mg determined the maximum-tolerated dose to be 320 mg, with grade 3 diarrhea as a dose-limiting toxicity. In Phase II trial of patients with advanced NSCLC where disease had progressed following treatment with **10** or **11**, no meaningful clinical benefit was observed. Despite the preclinical data supporting **13** in overcoming T790M mutation, no patients with a known T790M mutation responded.[46] This could be due to insufficient drug exposure achieved in clinic; as in particular, the patients initially receiving 320 mg/day received a reduced dose of 240 mg/day due to dose delays and dose-limiting diarrhea. Because of its significant HER1/HER2/HER4 activity, **13** is currently undergoing multiple phase III clinical trials to evaluate its efficacy in HER2+ breast cancer patients as single agent or in combination.[47]

Structurally related **14** is currently the only marketed second-generation covalent EGFR inhibitor, approved for first-line treatment of patients with metastatic NSCLC with EGFR exon 19 deletions or exon 21 (L858R) mutations. Compound **14** potently inhibited wild-type EGFR (IC_{50} of 0.5 nM) and oncogenic mutants EGFRL858R (0.4 nM) and EGFRL858R/T790M (10 nM). Compound **14** also displayed nM activity-inhibiting proliferation of H1975 cells (EGFRL858R/T790M) with EC_{50} of 92 nM, whereas its corresponding noncovalent analog BI-37781 (**26**) was ineffective even at very high concentrations (>4 μM).[48] In two randomized, open-label, multinational phase III trials, progression-free survival (PFS) was significantly prolonged with **14** compared with pemetrexed plus cisplatin (LUX-Lung 3) or gemcitabine plus cisplatin (LUX-Lung 6) in treatment-naïve patients with advanced NSCLC with activating EGFR mutations.[49] Phase III trial (LUX-Lung 5) demonstrated clinical benefit in patients with NSCLC progressing after treatment with **10** or **11**. Despite no difference in overall survival, PFS and overall response rate (ORR) were significantly improved with **14** plus paclitaxel compared with paclitaxel alone (5.6 months and 32.1% vs. 2.8 months and 13.2%). The common side effects were in line with anticipated wild-type EGFR inhibition.[50] Given the marginal clinical benefits, if any, for nonmutant-selective irreversible EGFR inhibitors, it was clear that to better evaluate the potential of irreversible EGFR inhibition in treating acquired secondary mutation, new molecule was necessary. In particular, minimizing the dose-limiting toxicities of diarrhea and rash via improved selectivity against wild-type EGFR would be desirable to attain the maximum drug concentration in plasma and in tumors required to inhibit T790M EGFR.

5.03.5.4 Third-Generation Irreversible Mutant-Selective EGFR Inhibitors

Discovery of WZ4002 (**27**) marked a significant advance in discovering next-generation mutant-specific EGFR inhibitors that could overcome gatekeeper T790M mutation while sparing wild-type EGFR.[51] The pursuit started with synthesis of a focused library of common kinase inhibitor core scaffolds where one of the side chains was modified with an acrylamide group at a position that molecular modeling predicted to react with C797 of EGFR. Then, the library was screened for compounds that could inhibit the growth of PC9GR EGFRdel19/T790M and PC9 EGFRdel19 cell lines but was not toxic up to 10 μM against EGFR wild-type cells.

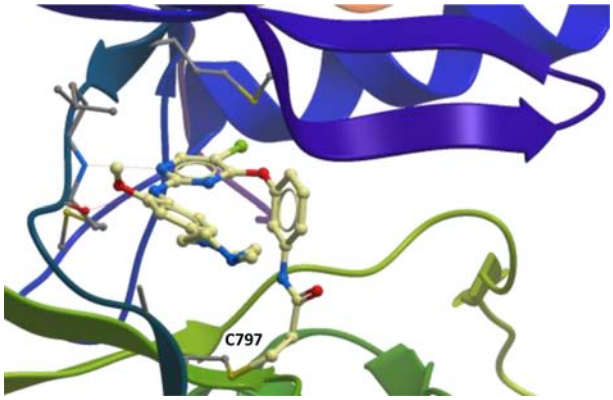

Fig. 8 WZ4002 (**27**) covalently bound to EGFR 696-1022 T790M mutant (PDB code, 3IKA; 2.9 Å).

27, with an aminopyrimidine core, was one of the three hits that possessed 300-fold lower EC_{50} (14 nM) against PC9GR EGFR-del19/T790M than **13** (>3.3 μM). It was more potent against EGFR double-mutant Ba/F3 cells (EC_{50} of 8 nM) than WT EGFR Ba/F3 cells (EC_{50} of 113 nM). Mass spectrometry studies confirmed a covalent mechanism of action and C797 as the site of modification. Crystallographic studies provided insight into why **27** was much more effective against L858R/T790M EGFR than **13**. In contrast to **13** that wrapped around the gatekeeper residue, **27** approached but did not surround the gatekeeper residue. While both compounds are irreversible inhibitors, the binding mode of **27**, together with the increased ATP affinity for the T790M mutant, accounts for its greater potency against T790M mutants versus better activity of **13** in WT EGFR. (Fig. 8).

5.03.5.4.1 Development of rociletinib (19)

Though **17** did not advance into clinical testing, structurally related **19** was discovered as the first mutant-selective inhibitor that progressed into clinical studies for patients with EGFR-mutant advanced NSCLC who have received prior EGFR therapies.[52–54] Compound **19** potently inhibited proliferation in the mutant-EGFR NSCLC cells with EC_{50} values ranging from 7 to 32 nM albeit with much weaker EC_{50} of 547 nM for WT EGFR A431 cells.[54] Cellular time-dependent inhibition and target occupancy studies were conducted in H1975 EGFRL858R/T790M cells, taking advantage of the lack of binding of L858R-specific EGFR antibody to ligand-bound protein.[53] H1975 cells were treated with 500 nM (c. 10-fold EC_{50}) of **19** for 1 h, followed by wash off of excess compound. Recovery of EGFR modulation and target occupancy by **19** was evaluated over time. Approximately 50% of activity was recovered at 16 h, which is consistent with reported mutant protein turnover rate under these conditions.[53] To determine time-dependent inhibition of EGFRL858R/T790M kinase, H1975 cells were treated with 500 nM **19** for 5–60 min and evaluated for EGFR modulation. Inhibition occurred rapidly with more than 50% EGFR signaling modulation achieved within 15 min of compound exposure and complete inhibition at 30 min. In line with in vitro observations, in vivo PK/PD experiments in H1975 xenograft model showed that maximum pharmacodynamic modulation (>90%) was observed at 6 h postfinal dose despite plasma exposure of **19** dropping fivefold at 100 mg/kg dose. Tumor regressions were observed in dose groups of either 100 mg/kg once daily (QD) or 50 mg/kg twice daily (BID), where BID schedule was statistically superior to QD schedule.[54] Immunohistochemical analysis of normal mouse skin from **26**-treated animals showed no inhibition of WT EGFR, confirming that compound **19** was wild-type sparing. Clinical evaluation of **19** supported significant benefit for NSCLC patients with the EGFR T790M mutation with no dose-related diarrhea or rash, clearly differentiated from previous EGFR inhibitors. Compound **19** won FDA breakthrough drug designation based on an overall tumor response rate that was reported early on at more than 50%. However, the final response rate reported for its 500 mg dose was lowered to 38%. The agency's review also noted serious adverse events in the studies of **19**, singling out hyperglycemia and QTc prolongation leading to torsades de pointes—a lethal irregular heart rhythm—which would require a "black box" warning if the drug is approved for marketing. Further clinical development of **19** was recently halted, which highlights the challenges and the need for optimization of covalent drug molecules.

5.03.5.4.2 Osimertinib (20)

Compound **20** is the first mutant-selective EGFR approved to treat T790M-positive NSCLC patients who progressed on or after EGFR inhibitor therapy. Its discovery started with testing a selected set of internal AstraZeneca compounds against the EGFR wild-type and double-mutant enzymes using biochemical assays to look for desirable hits suitable for medicinal chemistry optimization.[11] In the screen, a series of compounds were found to be active against double-mutant EGFR with selectivity over wild type, represented by **28** with a pyrimidine core containing an indole headgroup. It had an IC_{50} of 9 nM against the double mutant with 88-fold selectivity over wild-type EGFR, albeit with a large enzyme to cell drop-off of around 90-fold when it was tested in double-mutant cellular assays (IC_{50} 0.77 μM). The lead optimization effort focused on reducing lipophilicity, using $LogD_{7.4}$ measurement as a surrogate to improve upon in vivo clearance. Effort was also focused on modulating compound reactivity with glutathione (GSH) to find a "reactivity window" to achieve sufficient chemical reactivity toward the active-site residue while balancing against

unwanted target binding that could lead to high compound clearance and/or idiosyncratic toxicity. Using **14** as a reference compound with limited off-target effects, a half-life of 25 min (disappearance of electrophile on incubation) was adopted as the upper limit to the window of reactivity to work within. The optimization resulted in the identification of an in vivo tool compound **29**. Compound **29** potently inhibited H1975 EGFRL858R/T790M cells with EC_{50} of 96 nM and very weakly inhibited WT LoVo cells with EC_{50} of 23 μM. Its LogD7.4 and half-life against GSH were found to be 3.6 and 352 min, respectively. **29** had good bioavailability in rat (F = 45%) and showed 134% tumor growth inhibition (TGI) in the PC9-activating EGFR-mutant xenograft model versus modest 46% TGI in the WT EGFR-driven A431 xenograft model when dosed at 60 mg/kg/day. Assessment of kinome selectivity for this series of compounds revealed significant off-target inhibition of IGF1R (IC_{50} of 4 nM for **29**), which also bears a methionine gatekeeper residue. While IGF1R inhibitors have been employed in a clinical setting, they have been associated with dose-limiting toxicity of hyperglycemia, which was observed as a side effect for **19**. Further optimization effort led to the identification of **20** with improved rat PK (rat F = 45%) and improved IGF1R selectivity (IC_{50} of 2.9 μM) while maintaining good cellular activity for T790M EGFR (H1795 EC_{50} 24 nM) and selectivity against WT EGFR (LoVo EC_{50} 264 nM).[55] Daily dosing of 5 mg/kg of **20** induced profound and sustained regression in multiple mutant EGFR xenograft models and transgenic models. Although, in mice, the pharmacokinetic half-life of **20** is only approximately 3 h, phospho-EGFR staining remained significantly diminished even after the 30 h time point, consistent with its expected irreversible mode of action.[56] The development of **20** represented one of the fastest successful development programs—going from the start of clinical trials (2013) to approval (2015) in just over two and a half years and satisfying an unmet patient need. The FDA approval of **20** is based on data from the two AURA phase II studies (AURA extension and AURA2), which demonstrated efficacy in 411 EGFR T790M NSCLC patients that had progressed on or after prior EGFR TKI treatment. In those trials, overall objective response rate (ORR) as a measurement of tumor shrinkage was 59% (95% CI, 54–64%). In a separate part of the AURA study in 63 patients, ORR was 51%, and median duration of response was 12.4 months. It was worthy to note that common side effects of **20** include rash and diarrhea, commonly observed in patients treated with nonselective EGFR inhibitors. However, the severity of the side effects seems to be reduced, with, for example, 0.5% of grade 3–4 rash observed in patients treated with **20** versus 6% of grade 3–4 rash observed in patients treated with **10**.

5.03.5.5 Acquired Resistance to Third-Generation Covalent EGFR Inhibitors

The clinical success of third-generation mutant-selective covalent EGFR inhibitors for the treatment of T790M-positive patients was again met with new resistance within months.[57] In a reported study of **20**, 6 out of the 15 resistant patients (all positive for T790M mutation before treatment) developed a mutation that substitutes a less nucleophilic serine residue for the reactive cysteine residue (C797S), while four lost T790M mutation despite the presence of the underlying EGFR-activating mutation.[58] This point mutation of C797S compromises the irreversible bond formation as the nonactivated serine residue at this location no longer undergoes Michael addition at physiological conditions, leading to a substantial loss of potency. Furthermore, with the change in mechanism of action from covalent irreversible inhibition to noncovalent reversible inhibition, the benefits of sustained pharmacodynamics are lost. Particularly troublesome, the C797S mutation is refractory to all existing EGFR therapies.[58] Interestingly, resistance mechanisms for **19** include the loss of T790M mutation, EGFR amplification, and transformation to small-cell lung cancer, where 6 out of 12 patients lost T790M mutation.[59] It is interesting to note that the loss of T790M, not C797S mutation, is a common resistance mechanism identified for the two structurally differentiated inhibitors.[60] This may be due to the loss of favorable interactions both compounds make with the gatekeeper methionine residue of the T790M EGFR mutant. Therefore, it will be interesting to see the clinical performance of other wild-type-sparing covalent EGFR inhibitors, which maintain potent activity against both T790 wild type and T790M-activating EGFR mutants. One such compound in clinical evaluation is EGF816 (**21**).[61] Compound **21** had potent cellular activity for inhibition of proliferation of mutant EGFR cell lines: H3255L858R (EC_{50} 9 nM), HCC827del19 (EC_{50} 11 nM), and H1975L858R/T790M (EC_{50} 25 nM). Furthermore, **21** was selective against WT EGFR cell lines: HN1 (EC_{50} 5.8 μM) and MGH025 (ALK+, EC_{50} 29.7 μM). C797S mutation, MET amplification, and epithelial–mesenchymal transition (EMT) were found to be the major mechanisms of acquired resistance to **21** in preclinical models.[61] Phase I/II trials of **21** are ongoing for NSCLC patients harboring EGFR mutations (ClinicalTrials.gov identifier, NCT02108964). Clinical efficacy readouts and tracking the development of resistance mechanisms of **21** will further advance our understanding of the prospects and the potential concerns of emerging resistance with third-generation mutant-selective covalent EGFR inhibitors.

5.03.6 Covalent Inhibitors of FGFR Family Kinases

5.03.6.1 Introduction of Target Biology

The human fibroblast growth factor receptor (FGFR) family of receptor tyrosine kinases (RTKs) consists of four isomers FGFR1-4, which are sensors of a diverse family of eighteen FGF ligands. FGFRs are key regulators of fibrogenesis, embryogenesis, angiogenesis, metabolism, and many other processes of proliferation and differentiation.[62] Dysregulation of FGFR signaling through mutation, chromosomal translocation, gene amplification, or overexpression has been linked to numerous cancers and resistance to cancer therapies.[63] For example, FGFR1 amplification and translocation occur in various cancers including squamous nonsmall-cell lung carcinoma; FGFR2 amplification, mutation, and translocation are observed in gastric cancer and other cancers; FGFR3 is commonly amplified in bladder cancer; FGFR4 is amplified in multiple cancers, including hepatocellular carcinoma.[64]

5.03.6.2 Covalent FGFR Family Kinase Inhibitors

Supported by compelling genetic data implicating FGFRs in cancers, several small-molecule ATP-competitive inhibitors have been discovered and are being evaluated in clinical studies, which include the noncovalent selective pan-FGFR inhibitors NVP-BGJ398 (**30**),[65] AZD4547 (**31**),[66] LY2874455 (**32**),[67] and JNJ-42756493 (**33**)[68] (Fig. 9). While early-stage clinical results from selective pan-FGFR inhibitors show a clear signal of biological activity, preclinical in vitro studies have suggested the possibility of gatekeeper residue mutation as an emerging mechanism of resistance.[69]

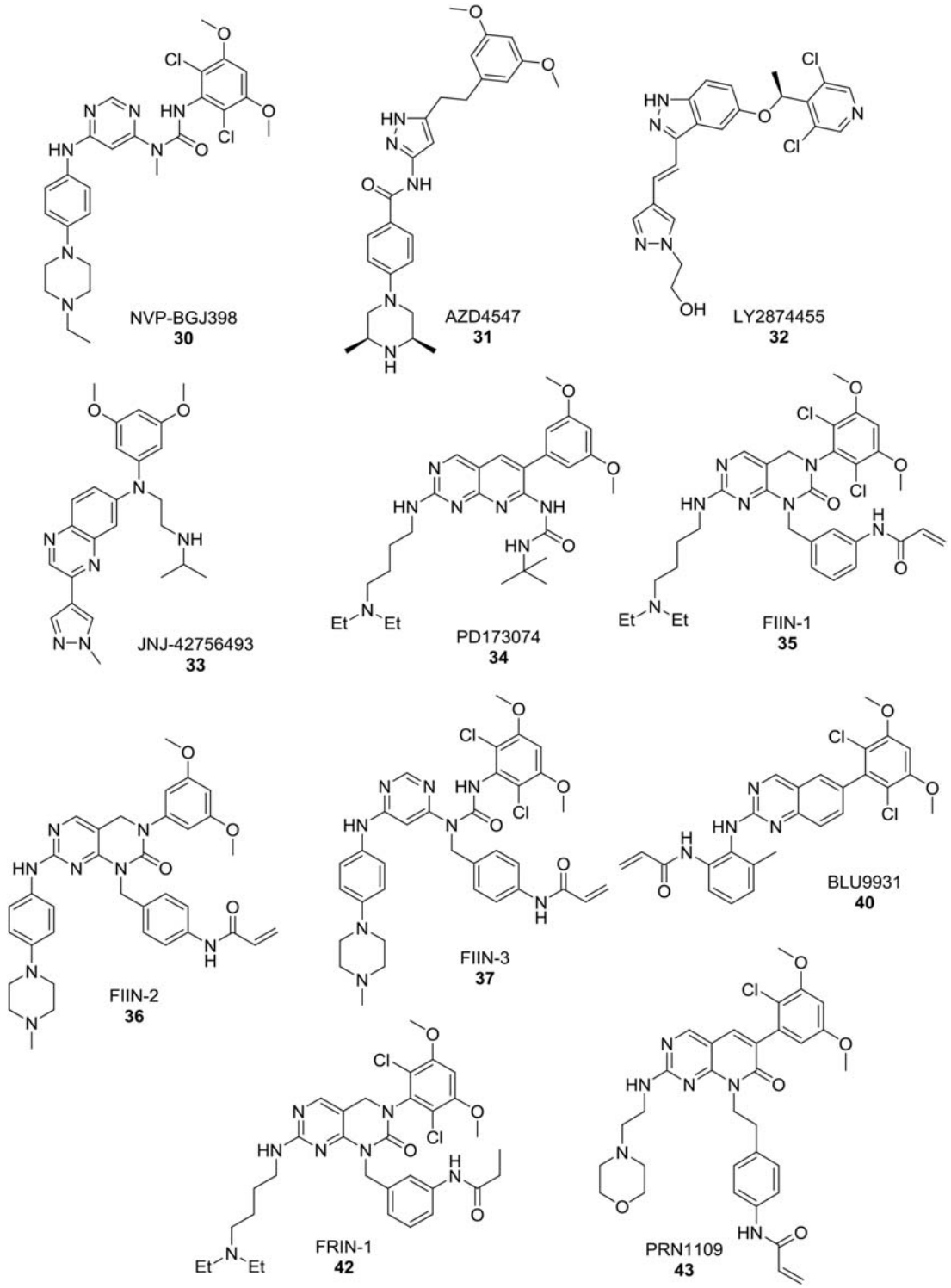

Fig. 9 Chemical structures of FGFR inhibitors.

All FGFR kinases have a valine residue at the kinase gatekeeper position, in contrast to other tyrosine kinases such as EGFR, which possesses a threonine gatekeeper whose mutation to a larger hydrophobic methionine residue in clinic leads to drug resistance.[42] Gatekeeper FGFR1 V561M mutation was reported to induce strong resistance to the noncovalent FGFR inhibitor PD173074 (**34**).[70] Similarly, FGFR3 V555M was found to be cross-resistant to **34** and **31**.[71] Somatic FGFR4 V550M mutation was reported in 9% of embryonal rhabdomyosarcoma tumors[72] and 13% of neuroendocrine breast carcinomas.[73]

Given the precedence of covalent EGFR inhibition overcoming gatekeeper EGFR T790M mutation in treating NSCLC, covalent FGFR inhibitors such as FIIN-1 (**35**),[70] FIIN-2 (**36**), and FIIN-3 (**37**)[69] were discovered and shown preclinically to maintain potent antiproliferative activity toward Ba/F3 cells expressing gatekeeper FGFR mutations.[69] Two covalent pan-FGFR inhibitors TAS120 (**38**, structure not disclosed)[74] and PRN1371 (**39**, structure not disclosed),[75] targeting the FGFR family conserved cysteine in the kinase P-loop, have been advanced into clinical trials. Isoform-selective irreversible FGFR4 inhibitors such as BLU9931 (**40**)[76] and BLU-554 (**41**, structure not disclosed), targeting the unique hinge C552, have also been discovered and developed to treat FGFR4-dependent cancers, with limited off-target activity against other FGFR family members.[76]

5.03.6.2.1 FIIN-1 (35)

The design of **35** was based on using the pyrimidopyridine **34** as the lead scaffold, given its selectivity for FGFR and available cocrystal structure with FGFR1.[70] Inspection of the crystal structure implicated that C486 in the P-loop of FGFR1, which was mutated to alanine, was approximately 10 Å away from the pyridine nitrogen of **34**. Switching to a bioisosteric pyrimido[4,5]pyrimidine core allowed attachment of a benzyl linker group, which provided a suitable vector to install an acrylamide warhead group to engage C486. The properly displayed acrylamide was combined in **35** with optimized back-pocket substituents for improved FGFR activity and selectivity. Compound **35** has potent binding affinity for FGFRs with K_d values of 2.8, 6.9, 5.4, and 120 nM for FGFR1/2/3/4, respectively, in agreement with corresponding biochemical IC_{50} values of 9.2, 6.2, 11.9, and 189 nM. Evaluation of selectivity against a panel of 402 kinases using Ambit KINOMEscan® technology at 10 μM concentration showed excellent selectivity, including kinases such as c-Src, TNK1, and YES that have a P-loop cysteine at the same positions as the FGFRs. The importance of the acrylamide function was confirmed by significant loss of activity for the isosteric propyl amide analog FRIN-1 (**42**). Compound **35** potently inhibited the proliferation of MCF10A cells with inducible FGFR1 with IC_{50} of 2.7 nM, as compared with the 10-fold activity loss for **42** in the same system (IC_{50} of 29 nM). In line with the importance of covalently targeting C486, **35** and **42** were found to be equally potent for the same cell line with C486S FGFR1 mutant. Compound **35** was active in a number of FGFR-dependent cancer cell lines versus EC_{50} of 14 nM and 30 nM for KATO III and SNU-16, two gastric cancer cell lines with FGFR2 amplification and activation. Compound **35** was also evaluated for its activity against the V561M gatekeeper mutant of FGFR1 in HEK293 cells transiently transfected with WT FGFR1 or V561M FGFR1. It was found that **35** could effectively block autophosphorylation of FGFR1 V561M at high concentration (10 μM) while the noncovalent inhibitor **42** was inactive. However, further optimization would be required to obtain an inhibitor with a useful level of potency against the V561M mutant.[70]

5.03.6.2.2 FIIN-2 (36)/FIIN-3 (37)

SAR work around side chains and core scaffolds of **35** led to two compounds **36** and **37** with improved activity for inhibiting the proliferation of Ba/F3 cells engineered to be dependent on WT FGFRs and V564M FGFR2.[69] The key new feature of **36** was the replacement of the aliphatic amine in **35** with a stronger hinge-binding group, 4-(4-methylpiperazine-yl) aniline. Compound **36** incorporated a pyrimidyl urea core that could form a *pseudo*-six-membered ring, a feature of **30**, which might provide greater rotatory flexibility for the substituted phenyl group binding in the back pocket. Additionally, both **36** and **37** display the acrylamide moiety at the *para*position of the benzyl linker, in contrast to the *meta*position in **35**. Both compounds inhibited WT FGFRs with EC_{50} values in the 1–93 nM range and maintained potent activity against V564M FGFR2 (58 nM for **36** and 64 nM for **37**), as compared with 1000 nM for **35** and 1500 nM for **30**. In line with this observation, **36** and **37** showed less than fivefold loss for FGFR1 V561M mutants in both H2077 and H1581 lung cancer cells, whereas the noncovalent inhibitor **30** had an over 50-fold activity loss.[69] The cocrystal structure of **36** with FGFR4 confirmed its covalent mechanism of action engaging the conserved cysteine (C477 for FGFR4) (Fig. 10).

5.03.6.2.3 TAS-120 (38)/PRN1371 (39)

At least two covalent pan-FGFR inhibitors, **38** (ClinicalTrials.gov identifier, NCT02052778) and **39** (ClinicalTrials.gov identifier, NCT02608125), have been advanced into clinical trials for patients with advanced solid tumors. PRN1371 (**39**) is structurally related to PRN1109 (**43**).[75] Both **39** and **43** are potent pan-FGFR inhibitors yet with very favorable kinome selectivity. Compound **39** also conveyed high potency against cell lines harboring FGFR amplifications, mutations, and translocations. For example, **39** inhibited SNU16 (FGFR2 amplification) gastric cancer cell proliferation with EC_{50} of <5 nM. Oral dosing of **39** induced rapid tumor regression at 15 mg/kg BID, and intermittent dosing at 20 mg/kg also resulted in prolonged tumor regression. It will be interesting to see whether **38** and **39** will outperform the noncovalent FGFR inhibitors being studied in clinic and whether cysteine mutation will emerge as a potential resistance mechanism, as observed in the cases of BTK and EGFR.

5.03.6.2.4 BLU9931 (40)/BLU-554 (41)

The high sequence homology between FGFRs presents significant challenges to develop isoform-selective FGFR inhibitors. However, a unique cysteine residue C552 in the hinge of FGFR4 (tyrosine for FGFR1–3) was exploited to discover selective FGFR4 inhibitors to treat hepatocellular carcinoma (HCC) with potentially fewer dose-limiting side effects associated with

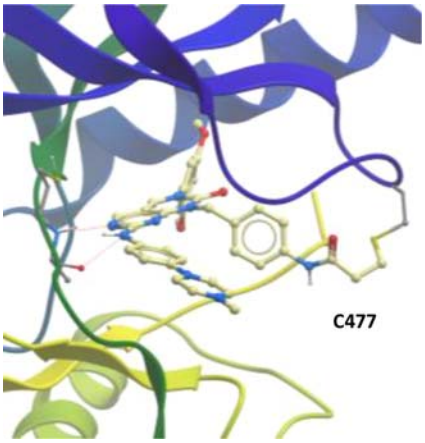

Fig. 10 Bound structure of FIIN-2 (**36**) to FGFR4 (PDB code, 4QQC; 2.4 Å).

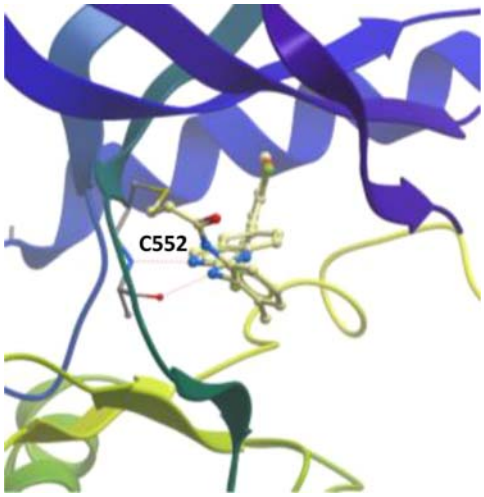

Fig. 11 Bound structure of BLU9931 (**40**) to FGFR4 (PDB code, 4XCU; 1.7 Å).

pan-FGFR inhibition. Only six other kinases possess a cysteine at the equivalent location but with low overall sequence similarity: MAPKAPK3, MAPKAPK2, p70S6Kb, TTK, PI4K, and ChaK1. Similar to **35**–**37**, the discovery of BLU9931 (**40**) was also based on the scaffold of **34**, whose dimethoxyphenyl substituent was important for its high potency and good kinome selectivity, occupying a hydrophobic pocket near the gatekeeper valine in all FGFR family members including FGFR4.[76] It was found that an acrylamide at the *ortho*position of the aniline of an anilinoquinazoline hinge-binding core, substituted with the dichlorodimethoxyphenyl group, was capable of forming a covalent bond with C552 of FGFR4 (Fig. 11). Further introduction of a 3-methyl substituent on the aniline ring led to the identification of **40** with optimal FGFR4 potency (IC_{50} of 3 nM) and selectivity over FGFR1–3 (IC_{50} values of 591, 493, and 150 nM, respectively). The methyl substituent forces the aniline ring to adopt a nonplanar dihedral rotation, better positioning it in proximity to covalently react with C552 sulfur, while introducing a significant steric clash with the tyrosine side chains of FGFR1–3. The nonreactive propylamide analog exhibited much less potent inhibition of FGFR4 enzyme activity (IC_{50} of 938 nM). Compound **40** also potently inhibited the proliferation of the HCC Hep3B cell line with EC_{50} of 70 nM. Moderate bioavailability of **40** (F% of 18 and $t_{1/2}$ of 2.5 h at 10 mg/kg dose in mice) enabled preclinical in vivo evaluation of FGF4 inhibition. With a 100 mg/kg twice-daily dose, **40** caused tumor regression in a Hep3B xenograft model, and at 300 mg/kg twice-daily dose, it caused tumor regression in LIXC012 (an HCC patient-derived cell line) tumor-bearing mice.[76] Further optimization of this chemical series resulted in the identification of BLU-554 (**41**), which is undergoing phase I clinical trials in patients with hepatocellular carcinoma and cholangiocarcinoma (ClinicalTrials.gov identifier, NCT02508467).

5.03.7 Other Kinase Targets for Covalent Inhibition

5.03.7.1 Akt

PI3K/Akt signaling pathway is an important mediator of cellular processes, and Akt dysregulation is directly associated with neoplastic transformation and malignant progression, as well as increased resistance to cancer therapies.[77] Akt features a regulatory pleckstrin

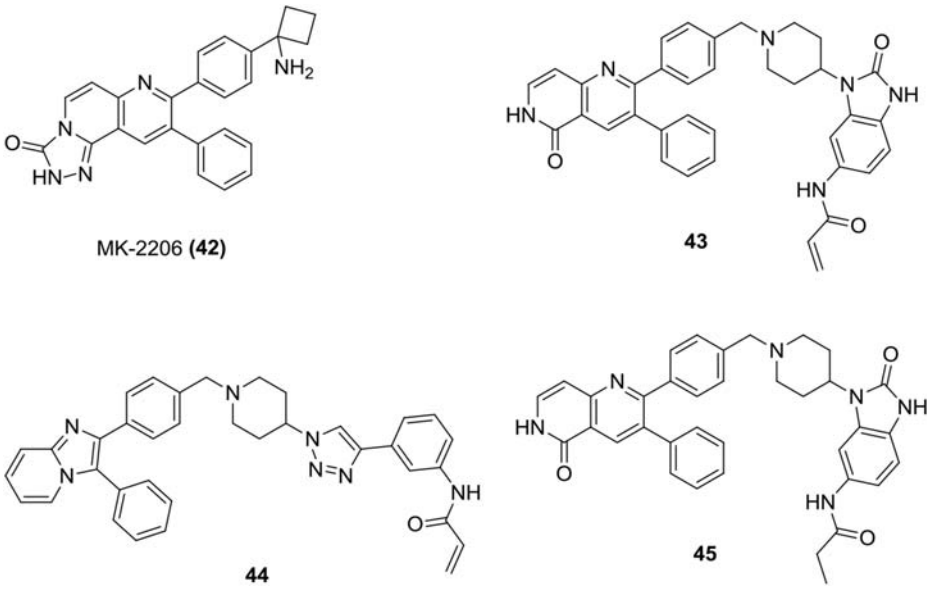

Fig. 12 Chemical structure of Akt inhibitors.

homology (PH) domain, along with the catalytic kinase domain, allowing for membrane attachment upon growth factor stimulation and activation. Allosteric PH domain-dependent Akt inhibitors (Fig. 12), such as MK-2206 (**42**), bind to a unique pocket at the interface of the regulatory PH and the kinase domain, stabilizing the inactive "PH-in" conformation.[78] Analysis of x-ray structures of full-length Akt in complex with allosteric inhibitors revealed the close proximity of a disulfide bridge between C296 and C310, which are known to be redox-sensitive, and therefore potentially amenable for targeted covalent inhibition. Based on two different chemical scaffolds, two probe compounds **43** and **44** featuring an acrylamide warhead group were prepared to target C296 and C310.[78]

While **44** had weak activity against Akt (IC_{50} of 372 nM), **43** exhibited a subnanomolar IC_{50} (0.2 nM) against Akt, significantly more potent than isosteric nonreactive propyl amide analog **45** with IC_{50} of 7.5 nM. Kinetic characterization of **43** further supported a covalent mode of action with K_{inact}/K_i of 3.29 $\mu M^{-1}\,s^{-1}$. Treatment of Akt1 with **43** resulted in mass increases corresponding (587 Da) to formation of a 1:1 adduct of Akt1 and **43**. Trypsin digestion of **43**-treated Akt1 and subsequent ESI-MS/MS analysis suggested mutually exclusive modification of either C296 or C310 with no preference, which was in line with the accessibility for either cysteine located on the flexible activation loop. **43** also exhibited excellent kinome selectivity. At 1 μM concentration, it was found to only inhibit significantly Akt1, Akt2, and Akt3 (98%, 96%, and 83%). No significant inhibition was observed for kinases with analogous cysteines such as PKCθ (35%), MAPKAPK2 (30%), MELK (30%), and 43 additional kinases harboring analogous cysteines (<30% inhibition). Furthermore, **43** induced dose-dependent decreases of pAkt1 in PC3 and BT474 cancer cell lines while demonstrating selectivity against c-KIT and Erk1/2 in GIST-T1 cells.[78]

5.03.7.2 BMX

Bone marrow kinase on chromosome X (BMX) is a member of the TEC family of nonreceptor cytosolic tyrosine kinases, which includes BTK, ITK, TEC, and TXK. BMX is expressed in hematopoietic cells of the myeloid lineage and potentially plays an essential role in various diseases of inflammation, cardiovascular disease, and cancer.[79] In particular, increased BMX activity and expression have been associated with prostate cancer (PCa) and castration-resistant prostate cancer (CRPC).[80] In order to determine the pharmacological consequences of inhibition of BMX kinase activity in PCa, Gray and coworkers sought to develop potent and selective covalent BMX inhibitors, targeting C496 at the lip of the ATP-binding site analogous to C797 of EGFR and C481 of BTK.[80] They performed a search for inhibitors with modest binding affinity and selectivity for BMX in their internal database of kinase inhibitor selectivity profiles generated from using the KINOMEscan approach for ATP-competitive pharmacophores. Subsequent modeling studies of the top hits in a published BMX crystal structure (PDB code, 3SXR) gave a probable binding conformation, which was used to design BMX-IN-1 (**46**) with a properly positioned electrophile-targeting C496 (Fig. 13).[80]

Compound **46** was found to be a potent and selective BMX inhibitor with IC_{50} of 8 nM and an S(10) selectivity score of 0.01 using the KinaseScan approach at 1 μM concentration against a panel of 442 kinases. The only significant off target was BTK with IC_{50} of 10.4 nM, which possesses an equivalently placed cysteine as BMX C496. Compound **46** was demonstrated to potently inhibit the proliferation of TEL-BMX-transformed Ba/F3 cells with an IC_{50} of 25 nM. The approximately isosteric analog BMX-IN-1R (**47**), in which the electrophile acrylamide is replaced with a nonreactive propyl amide, was inactive in TEL-BMX-transformed Ba/F3 proliferation assay. Furthermore, C496S TEL-BMX Ba/F3 cells were resistant to **46**. However, **46** only inhibited the proliferation of a panel of prostate cancer cell lines at single-digit micromolar concentration. Therefore, additional experiments are required to further assess whether BMX is a therapeutically useful target.[80]

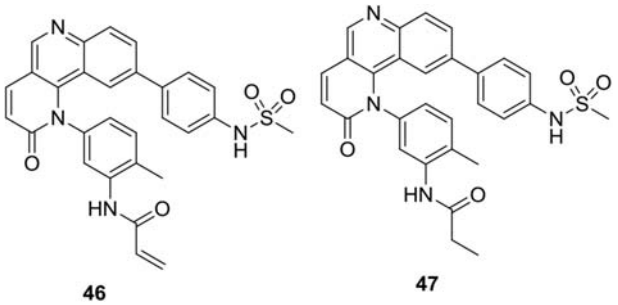

Fig. 13 Chemical structure of BMX inhibitors.

5.03.7.3 CDK7

The first covalent CDK7 inhibitor was discovered through cell-based screening and kinase selectivity profiling of a library of ATP-site-directed kinase inhibitors, in an effort to discover new kinase inhibitors that regulate gene transcription.[81] THZ1 (**48**, Fig. 14), an aminopyrimidine with an acrylamide warhead group, was identified as a low nanomolar inhibitor of cell proliferation (IC_{50} of 50 nM in Jurkat T-ALL cell line) and biochemical CDK7 activity (IC_{50} of 3.2 nM). Kinome-wide profiling and kinetics studies showed that CDK7 is the only target with time-dependent inhibition, suggestive of covalent binding. Corresponding noncysteine reactive analog **49** showed comparatively less activity on CDK7 (IC_{50} of 146 nM) and reduced antiproliferative potency (IC_{50} of 2008 nM in Jurkat T-ALL cell line).

Mass spectrometry identified the site of covalent modification by **48** as C312, a residue outside the kinase domain. Computational studies predicted that the reactive acrylamide of **48** would be positioned in close proximity to C312. Mutation to serine (C312S) prevented **48** from covalently binding to CDK7. Sequence alignment of the 20-member CDK family suggested the uniqueness of C312, providing a structural basis for the covalent selectivity of **48**.[81]

Cancer cell line profiling suggested broad cellular activity of CDK7 inhibition, and a subset of cancer cell lines, including T-ALL, were exceptionally sensitive to **48**. This correlated to transcriptional modulation of the RUNX1 super-enhancer. Pharmacological activity of **48** was confirmed in xenograft mouse models of multiple cancer types,[81–83] justifying continued investigation of clinical potential of CDK7 inhibition.

5.03.7.4 ERK1/2

The RAS/RAF/MEK/ERK pathway plays a central role in many cellular processes, and its deregulation has been associated with multiple human tumors. Direct ERK1/2 inhibition not only provides an option in tumors with mutational activation of RAS or Raf genes but also may overcome acquired resistance to RAF and MEK inhibitors where RAS/RAF/MEK/ERK pathway reactivation has occurred.[84]

In-house screening by AstraZeneca using an ERK2 biochemical assay and subsequent SAR identified a series of potent and reversible ERK inhibitors including **50** (Fig. 15) with ERK2 IC_{50} up to 44 nM and good kinase selectivity (>75% inhibition of only four kinases out of 125 kinase panel). Based on cocrystal structure information of **50** with ERK2 (Fig. 16), inversion of aniline amide allowed installation of an acrylamide warhead group to engage C166 and concurrent modification to a more potent aminopyridine core, resulting in **51** with ERK2 IC_{50} of 8.5 nM. It maintained good kinase selectivity with >75% inhibition of four kinases out of 125 kinase panel. Compound **51** inhibited A375 cell line with IC_{50} of 57 nM. Its reversible matched pair compound **52** had ERK2

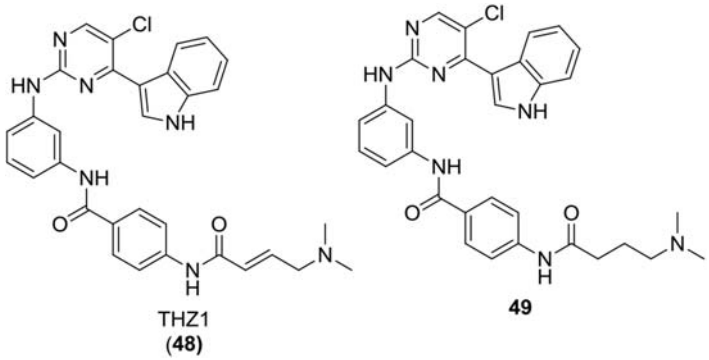

Fig. 14 Chemical structure of CDK7 inhibitors.

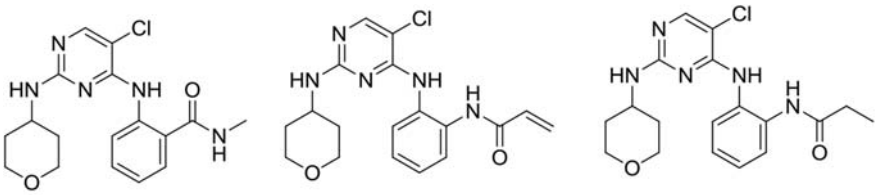

50 51 52

Fig. 15 Chemical structure of ERK1/2 inhibitors.

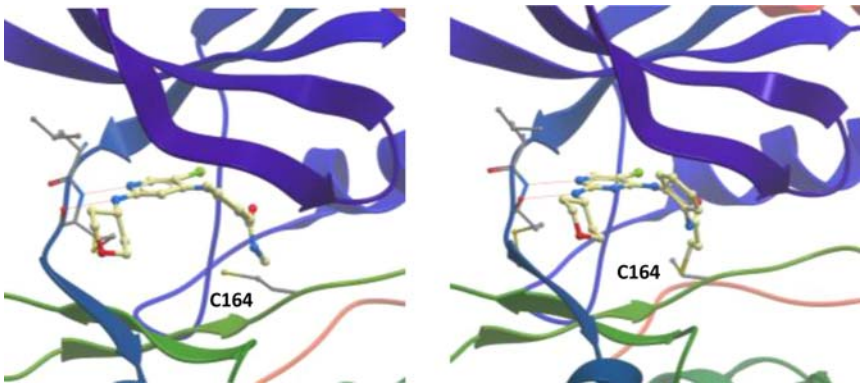

Fig. 16 (A) Left, bound structure of **50** to human ERK2 (PDB code, 4ZZN; 1.3 Å); (B) right, bound structure of **52** to human ERK2 (PDB code, 4ZZO; 1.6 Å).

IC_{50} showed significantly weaker activity across the assays. Mass spectrometry confirmed covalent binding of **51** to ERK2, which was not observed with **52** as expected. Further profiling in preclinical animal models would be needed to assess the efficacy and safety of covalent ERK inhibition, which could be used to guide potential clinical development.

5.03.7.5 ITK

The nonreceptor tyrosine kinase interleukin-2-inducible T-cell kinase (ITK) is a member of the TEC kinase family. It is expressed mainly in immune cells such as T cells, mast cells, NK cells, and NKT cells. ITK positively regulates T-cell receptor (TCR) signaling and plays a role in many T-cell responses; therefore, ITK inhibition has been pursued as potential treatment for a number of autoimmune, inflammatory, and malignant diseases that may involve normal or neoplastic T cells.[85,86]

Covalent ITK inhibition was reported for ibrutinib, which may have contributions to its clinical efficacy in B-cell malignancies.[29,87] This was not unexpected given that C442 of ITK is at an analogous position to C481 of BTK, which was targeted by **1** for covalent modification. In an effort to discover a more potent and specific covalent ITK inhibitor, screening of the Pfizer corporate compound repository yielded a potent hit (**53**) with an IC_{50} of 73 nM in the presence of 1 mM ATP (Fig. 17).[85] A solved x-ray crystal structure (Fig. 18) confirmed the engagement of C442 by **53** through a covalent bond between the β-carbon of the acrylamide group of **53** and the cysteine sulfhydryl (C-S distance 2.0 Å). Further optimization of the back-pocket group led to compound **54** with improved biological activity with a biochemical ITK IC_{50} of 2 nM and an IC_{50} of 48 nM in a human whole-blood assay. However, **54** retained significant BTK activity, and its fast in vivo clearance prevented further pharmacological studies.

To develop a more selective covalent ITK inhibitor, a different approach was undertaken by installation of warhead groups to engage C442 on existing selective noncovalent ITK scaffolds.[86] This led to the discovery of PRN694 (**55**) with biochemical IC_{50} of 0.3 nM for ITK. Profiling against potential off-target kinases with a cysteine analogous to C442 in ITK showed high potency against ITK and RLK with IC_{50} of 0.3 nM and 1.4 nM, as well as the other TEC family member BTK with IC_{50} of 17 nM. Kinetic analysis of **55** revealed time-dependent inhibition of ITK and RLK, whereas occupancy studies showed that the inhibition of BTK was reversible, with only 27% occupancy of BTK after 6 h. Furthermore, durable in vivo ITK inhibition was achieved for **55**, supported by its occupancy of ITK being 98%, 95%, and 54% at 1, 6, and 14 h, respectively, after a single 20 mg/kg intraperitoneal dose in mice.[86] Additional studies showed that **55** was a potent inhibitor of Th1 and Th17 cell differentiation and cytokine production, and in vivo administration of **55** markedly reduced disease progression in a T-cell-adoptive transfer model of colitis, providing further support for the therapeutic potential of ITK inhibition in certain inflammatory diseases.[88]

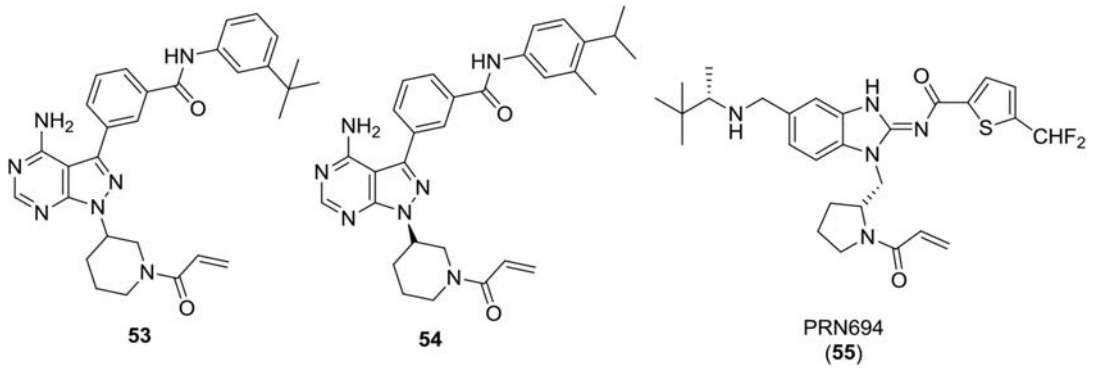

Fig. 17 Chemical structure of ITK inhibitors.

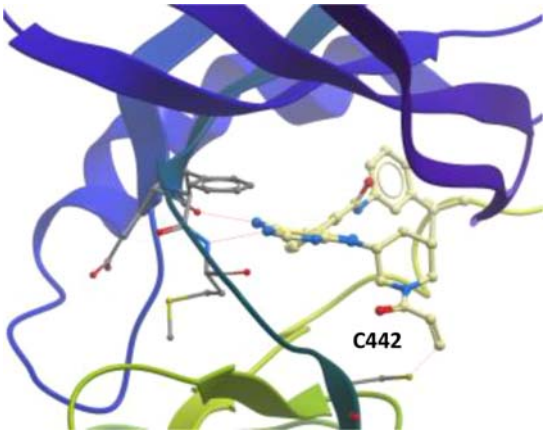

Fig. 18 Bound structure of **53** to human ITK (PDB code, 4HCT; 1.5 Å).

5.03.7.6 JAK3

The Janus kinase family, comprising of JAK1, JAK2, JAK3, and TYK2, and their downstream effectors play important roles in regulating multiple cytokine signaling pathways. Given the importance of the JAK family in autoimmune disease and cancer, many small-molecule ATP-competitive inhibitors (Fig. 19) with different isoform-selectivity profiles have been developed, including ruxolitinib (**56**, JAK1/2 inhibitor) approved for myelofibrosis and tofacitinib (**57**, pan-JAK inhibitor) approved for rheumatoid arthritis.[89] The high degree of structural homology, particularly in the active site of kinase domains, posed a significant challenge to the discovery of highly selective inhibitors to better understand pharmacological contributions of individual family member in diseases. JAK3 is expressed predominantly in immune cells and is a potential therapeutic target for autoimmune diseases. JAK3 mutations have also been associated with certain cancers such as natural killer/T-cell lymphoma.[90]

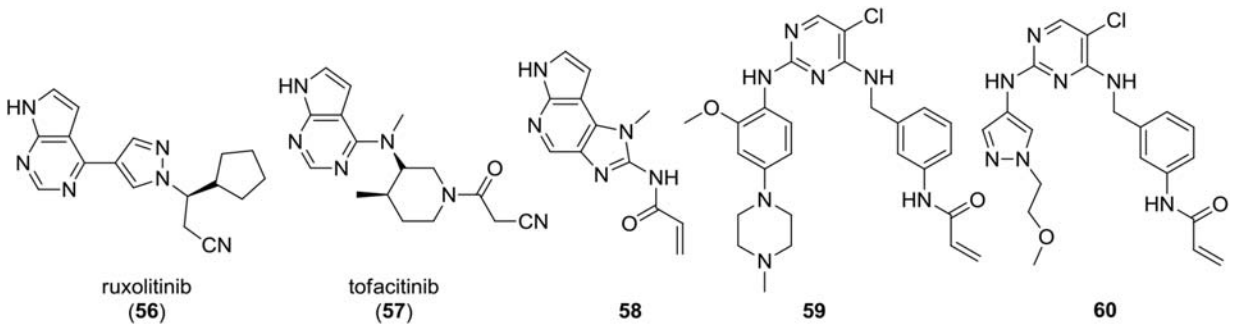

Fig. 19 Chemical structure of JAK3 inhibitors.

Despite > 80% homology in the active sites for JAK3 versus JAK1/JAK2/TYK2, there is a unique cysteine residue in JAK3 (C909) in the ATP-binding site, analogous to EGFR and BTK, thus presenting a great opportunity to achieve potency and selectivity through a covalent approach.[91] One approach undertaken was to use docking experiments in available crystal structures of JAK family kinase domains, which led to tricyclic JAK3 inhibitor **58**.[91] Compound **58** had potent JAK3 activity with $IC_{50} < 3$ nM, and kinetic studies and mass spectrometry profiling confirmed its irreversible covalent modification of C909. Compound **58** was selective against JAK family members (JAK1 $IC_{50} = 4$ μM; JAK2 $IC_{50} = 1.6$ μM; TYK2 $IC_{50} > 50$ μM) and ten other kinases with cysteine residues at analogous positions (ITK $IC_{50} = 0.83$ μM; BTK $IC_{50} = 14$ μM; EGFR $IC_{50} = 11$ μM). Compound **58** also showed potent inhibition of JAK3/IL-2 signaling pathway with IC_{50} of 19 nM in U4C epithelial cells while being inactive against JAK1- or JAK2-driven signaling pathways. Unfortunately, **58** was not suitable for in vivo studies to assess JAK3 pharmacology due to its unfavorable pharmacokinetics.[91]

A different approach was adopted to discover another potent and selective JAK3 inhibitor **59** by optimizing EGFR inhibitor **27** (Fig. 20), a T790M-mutant EGFR inhibitor with observed off-target JAK3 activity (K_d of 150 nM).[89] Syntheses and profiling of a small set of analogs led to **60**, where the ether linkage of **27** was replaced with an aminomethylene (-$NHCH_2$-) linkage, which had a greatly improved JAK3 activity (IC_{50} of 4.8 nM). In T-ALL-1 cells, IL-2-induced STAT5 phosphorylation was completely inhibited by **60** at 1 μM concentration. However, oral administration of **60** at 75 mg/kg QD for 8 days in genetically engineered models (GEM) of lung adenocarcinoma in mice did not show any effect on the tumor growth despite reasonable pharmacokinetic properties. More comprehensive investigations with these potent and selective JAK3 inhibitors are required to further elucidate the role of JAK3 in relevant disease models.

5.03.7.7 PI3Kα

The family of lipid phosphoinositide 3-kinases (PI3Ks) plays a key regulatory role in many cellular processes including proliferation and survival. There are three classes of PI3Ks, which includes the best studied class I PI3Ks consisting of a p110 catalytic subunit and a p85 regulatory unit. The PI3K class I family has four isoforms α, β, γ, and δ. PIK3CA, the gene that encodes the p110α subunit, is mutated in up to 30% of human cancers.[15] Multiple pan-PI3K inhibitors have been advanced into clinical development, but a selective PI3Kα inhibitor would have a more favorable safety profile by sparing toxicities due to inhibiting other isoforms.

Examination of the ATP-binding site and nearby residues of PI3Kα identified C862 as a unique cysteine residue (L or Q at the analogous position for other isoforms) that might be amenable to a covalent inhibition strategy to achieve selectivity. A series of design cycles exploring linker spacing and electrophiles based on x-ray structure of GDC-0941 (**61**, Fig. 21) bound to PI3Kα resulted in the discovery of CNX-1351 (**62**) as a potent and selective PI3Kα inhibitor with an uncommon dimethylenone warhead group.[15] Compound **62** had a PI3Kα biochemical IC_{50} of 6.8 nM, and its activity for β, γ, and δ was much weaker with IC_{50} values of 166 nM, 240 nM, and 3020 nM, respectively. Mass spectrometry experiments confirmed covalent binding of **62** to PI3Kα but not to the other class I isoforms. Trypsin digestion and subsequent peptide analysis further confirmed modification of C862. x-Ray crystallography of **62** with PI3Kα was obtained and supported the computational binding mode (Fig. 22). Broader profiling of **62** against a panel of 60 kinases, representing all branches of the kinome tree, showed excellent selectivity as no kinases were inhibited by greater than 40% using 1 μM concentration. Compound **62** also showed potent growth inhibition of SKOV3 ovarian cancer cells and MCF-7 breast cancer cells with PIK3CA-activating mutations (GI_{50} of 78 and 55 nM, respectively). Though prolonged PI3Kα occupancy and inhibition of p-Akt was achieved in vivo with **62** (100 mg/kg ip) despite poor pharmacokinetic properties, further optimization was needed to improve upon **62** to yield a more suitable selective and durable PI3Kα inhibitor for further studies and preclinical development.[15]

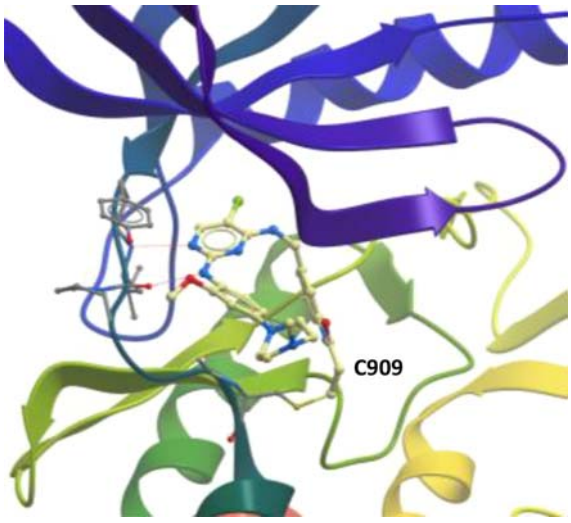

Fig. 20 Bound structure of **59** to human JAK3 (PDB code, 4Z16; 2.9 Å).

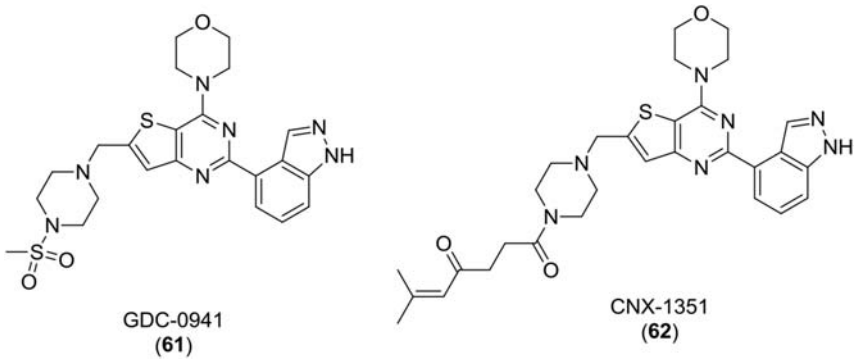

Fig. 21 Chemical structure of PI3Kα inhibitors.

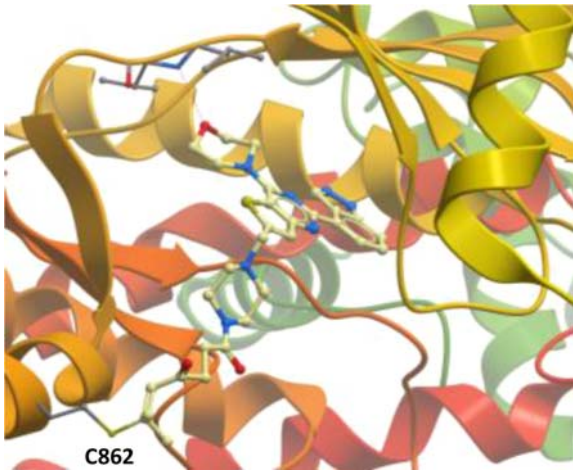

Fig. 22 Bound structure of **62** to human PI3Kα (PDB code, 3ZIM; 2.8 Å).

5.03.7.8 Miscellaneous Kinases

There have been reports of additional novel covalent kinase inhibitors, such as JNK-IN-8 (**63**) for JNK,[92] RMM-46 (**64**) for MSK/RSK,[93] (5*Z*)-7-oxozeaenol (**65**) for TAK1,[94] **66** for c-SRC,[95] and DHM25 (**67**) for mTOR (Fig. 23).[96] These new covalent inhibitor tools helped better understand the biology and pharmacology of functions of their respective kinase targets and potentially set good foundational research work for discovering novel cancer drugs modulating the activity of these kinases.

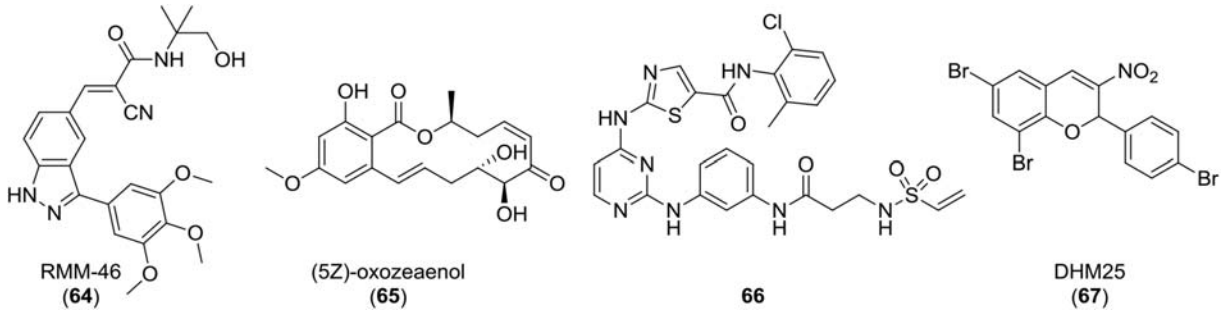

Fig. 23 Chemical structure of additional covalent kinase inhibitors.

5.03.8 Emerging Strategies and Technologies

5.03.8.1 Covalent Reversible Cysteine Inhibition of Kinases

The concept of covalent reversible inhibition has been exploited in drug discovery efforts of protease and proteasome inhibitors, leading to multiple approved drugs such as bortezomib[97] and boceprevir[98] that target reactive catalytic amino acid residues in the active site. However, covalent reversible targeting of noncatalytic cysteine was not reported until the recent discovery that cyanoacrylates and cyanoacrylamides react with cysteine thiols reversibly, as exemplified by inhibition of RSK2 with compound **68** (Figs. 24 and 25).[17] It was found that incorporation of a nitrile group converts irreversible acrylamide Michael acceptors into electrophiles with unanticipated facile yet reversible reactivity with cysteine thiols under physiological conditions. It was rationalized that the electron-withdrawing cyano substitution renders the β-carbon more susceptible to nucleophilic attack and also stabilizes the resulting carbanion, thereby accelerating the thiol addition reaction. On the other hand, the electron-withdrawing cyano substitution drastically increases the α-CH acidity of the thiol adducts, facilitating rapid elimination of thiol adducts when nonbonded interactions between inhibitor and protein are lost, particularly upon protein unfolding after trypsin digestion or denaturing.

Inhibitors that form a covalent reversible bond with a noncatalytic cysteine of the target may provide a broadly applicable platform that facilitates "residence time by design" and the ability to modulate and improve the duration of target engagement in vivo.[18] The application of this concept in medicinal chemistry was powerfully demonstrated in studies with inhibitors of two kinases with importance in oncology, BTK (Section "**Assessment and Optimization of Covalent Kinase Inhibitors in Cancer**") and FGFR (Section "**Covalent inhibitors of HER family kinases**"). Systematic studies of a series of reversible covalent BTK inhibitors with inverted cyanoacrylamide warhead groups identified potent and selective analogs that demonstrated residence times spanning from minutes to 7 days. An inverted cyanoacrylamide **69** with a branched-alkyl capping group remained bound to BTK for more than 18 h after clearance from the circulation. The research effort has resulted in the discovery of PRN1008 (**70**, structure not disclosed), which is currently in phase II clinical development to treat pemphigus vulgaris, a rare, potentially life-threatening autoimmune disease associated with painful chronic blistering of the skin and limited treatment options (ClinicalTrials.gov identifier, NCT02704429). Despite some potential limitations such as high steric demand for accommodating branched-alkyl capping groups, cysteine targeting with inverted cyanoacrylamides is likely to be broadly applicable for targets with solvent-exposed noncatalytic cysteines. Furthermore, additional covalent reversible chemistries have emerged, expanding the tool boxes available to successfully target cysteines of interest.[99]

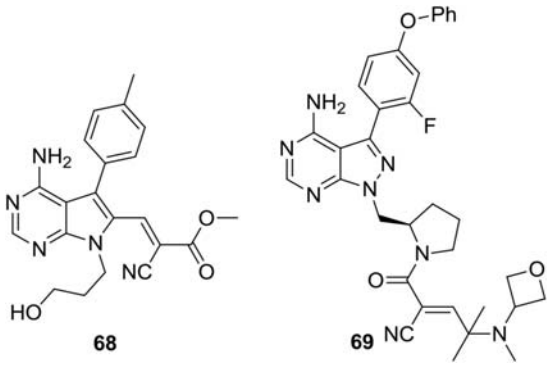

Fig. 24 Chemical structures of covalent reversible inhibitors.

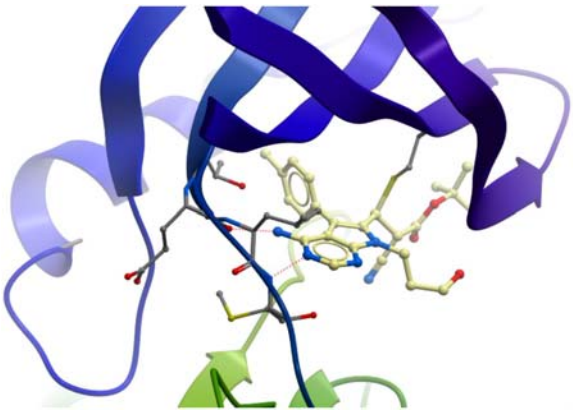

Fig. 25 Compound **68** bound to RSK2 (PDB code, rD9U; 2.4 Å).

The on-target activity of covalent reversible inhibitors with extended residence time is in theory functionally equivalent to that of covalent irreversible inhibitors. Therefore, they could achieve similar levels of target occupancy and thus efficacy in cancer treatment. Though the safety requirements for single agents in oncology indications are typically lower than for nonlife-threatening diseases, an improved safety profile could make covalent reversible inhibitors more amenable for combination therapies. In addition, the increased intrinsic reactivity of covalent reversible warhead groups could be advantageous for targeting cysteines that are less reactive toward classical covalent irreversible electrophiles.

5.03.8.2 Non-cysteine-Targeting Covalent Inhibitors

Cysteine's nucleophilic thiol group and its relatively low abundance in proteins make noncatalytic cysteine residues ideal for targeting with covalent drugs to achieve high levels of selectivity, potency, and durability. Targeting noncatalytic amino acid residues other than cysteine has been much more challenging, though there have been a number of reported covalent inhibitors targeting lysine residues.[5,96,100] Multiple nonselective inhibitors (Fig. 26) were found to covalently engage the conserved lysine involved in the kinase phosphate transfer reaction, including irreversible wortmannin (**71**),[101,102] FSBA (**72**),[103–106] and fluorosulfonylbenzoate (**73**).[107] Interestingly, members of a novel class of pyrrole aldehydes typified by **74** were found to be selective covalent inhibitors of IGFRK, targeting the same catalytic lysine residue.[108] Compound **74** inhibited IGFRK autophosphorylation with IC_{50} of 0.11 μM. Though only modestly selective against closely related IRK with IC_{50} of 0.6 μM, **74** was inactive against ten other kinases with $IC_{50} > 100$ μM. The key aldehyde functionality apparently formed a Schiff base with the IGFRK active-site residue K1003, and the covalent complex could be trapped by borohydride reduction and studied by mass spectroscopy after trypsin digestion. A crystal structure of **74** bound to IRK confirmed the covalent interaction with K1030, corresponding to K1003 in IGFRK that had been modified by reductive alkylation with aldehyde **74**.

Selective targeting of a nonconserved lysine was recently reported for covalent inhibition of CDK2 by NU6300 (**75**).[100] Inhibitor **75** was discovered serendipitously as an intermediate to synthesize a library of analogs of a known CDK2 inhibitor NU6102 (**76**). Kinetic studies and mass spectroscopy experiments suggested covalent inhibition of CDK2 with K_d of 1.31 μM and K_{inact} of $5.0 \times 10^{-3}\ M^{-1}\ s^{-1}$. The solution of a crystal structure of **75** bound to CDK2/cyclin A (Fig. 27) confirmed the covalent bond formation of the side-chain ε-amino group of K89 that lies just outside the CDK2 ATP-binding cleft with the vinyl sulfone group of **75**. Assessment of its selectivity against 131 protein kinases identified 13 kinases that exhibited less than 20% activity in the presence of 1 μM **75**, among which only Aurora A, Mst2, and GCK (MAP4K3) showed a > 50% additional loss of activity. It will be interesting to see whether further optimization can generate suitable lead molecules to study CDK2 pharmacology and validate the approach of covalently targeting noncatalytic lysines. Discovery of drug-like warhead groups for reaction with lysine certainly will play an important role.[109]

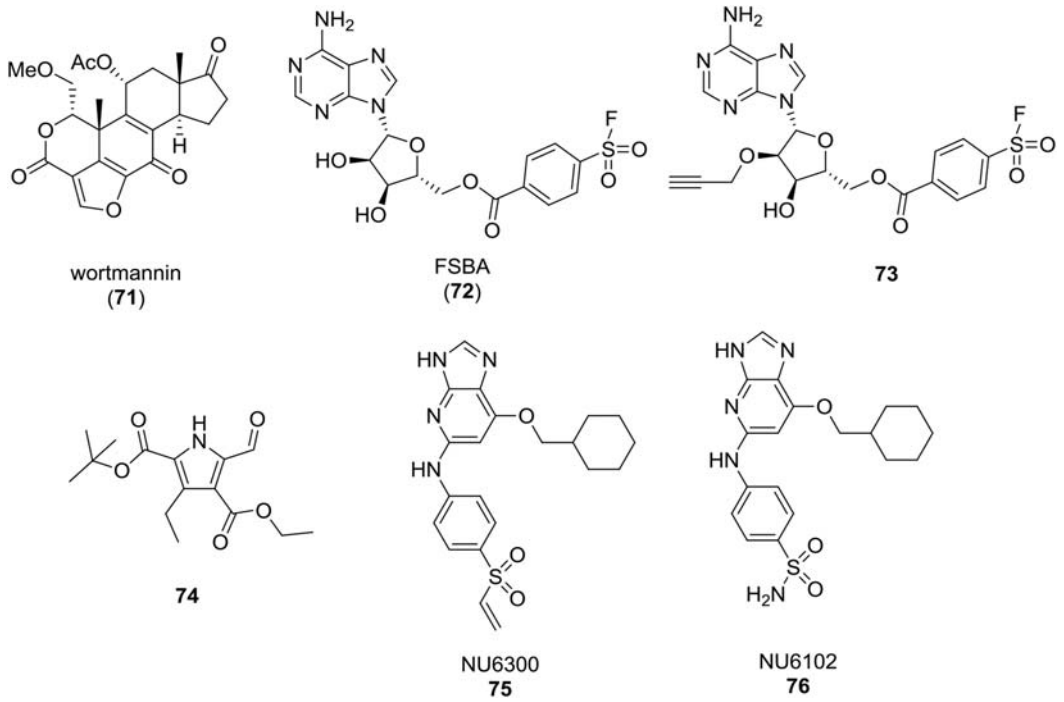

Fig. 26 Compounds with targeted covalent binding to lysines.

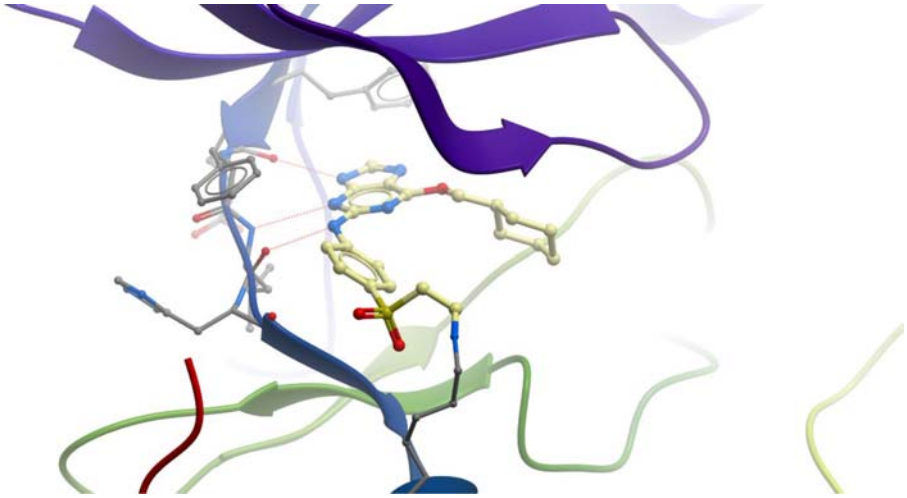

Fig. 27 Compound **75** bound to human CDK2 (PDB code, 5CYI; 2.0 Å).

5.03.8.3 Screening Approaches to Discover Covalent Inhibitor Leads

Installing covalent warhead groups to reversible inhibitor scaffolds has been a very successful approach, resulting in three approved covalent kinase drugs: ibrutinib, afatinib, and osimertinib. Despite the success, there are certain limitations to the approach, such as the necessity of existing lead molecules and a reasonable understanding of their binding mode to guide the installation of the warhead group, from either cocrystal structures or computational studies.

A complementary lead discovery approach is to identify compounds with a covalent mechanism of action by screening a library of compounds incorporating electrophiles that are capable of trapping the targeted amino acid residues of interest. There are a number of factors that one should consider for such an approach including: the nature of the warhead groups, the size of the library, the appropriate construct of the target protein, the screening method, and hit triage and confirmation studies. While incorporating highly reactive electrophiles might increase the hit rate, it could also generate increased numbers of promiscuous hits, which would pose greater challenges for subsequent hit elucidation and optimization. Given the proved utility of the acrylamide unit as a drug-like warhead group for cysteine, it is not surprising to see growing interest in studying the construction and screening of acrylamide- and cyanoacrylamide-containing libraries.[93,110–113] Mass spectroscopy has been a popular screening method given its high throughput and general applicability and simplicity to look for the desired mass of protein–ligand adducts.[93,113] As an example of hit confirmation, the loss of activity against the C436V RSK2 mutant was used to confirm the covalent mechanism of action for the fragment screening hits of a small library of cyanoacrylamides.[114] Improvement in mass spectroscopy studies and workflow has enabled the screening of approximately 1000 acrylamide-containing compounds.[113] It remains to be seen whether future effort in this area will deliver clinical molecules to help cancer patients.

5.03.8.4 Virtual Screening of Covalent Inhibitors

With the resurgence of covalent inhibitors, there has been growing interest in computational studies of covalent docking of ligands with an electrophile group targeting the amino acid residue of interest.[115,116] Some key obstacles to this approach include combining classical noncovalent scoring with covalent restraints and bond energies and developing compound libraries that are suited to covalent modification of the protein residue of interest. Recent progress in covalent docking has largely been restricted to retrospective recapitulation of covalent complexes or to screens of a few hundred compounds.[117–119] The potential benefit of prospective, large-scale covalent docking screens was recently demonstrated in finding new inhibitors against targets with previously unknown covalent ligands.[114] Much work and progress are still needed for virtual screening of covalent inhibitors to become a routine approach in covalent drug discovery.

5.03.9 Conclusions

Targeted covalent bond formation has evolved into a key component of the medicinal chemist's armamentarium when looking to discover drugs targeting kinases of importance in the oncology field. High-profile successes with clinically approved EGFR and BTK inhibitors attest to the importance of the approach, and treatment with these drugs has had profound benefits for those affected by cancer. Emerging targets such as FGFR hold promise for further successes in the near future. The efforts of numerous scientists and organizations referenced herein have also led to a greater understanding of the science underlying the development of covalent kinase inhibitors. This has resulted in a better understanding of which proteins might be targeted by this approach and how to best identify, optimize, and develop covalent inhibitors so that they can reach patients.

See also: 5.02. Selective Kinase Inhibitors in Cancer. 8.01. Medicinal Chemistry Case History: Osimertinib (AZD9291).

References

1. Wu, P.; Nielsen, T. E.; Clausen, M. H. *Drug Discov. Today* **2016,** *21,* 5.
2. Karaman, M. W.; Herrgard, S.; Treiber, D. K.; Gallant, P.; Atteridge, C. E.; Campbell, B. T.; Chan, K. W.; Ciceri, P.; Davis, M. I.; Edeen, P. T.; Faraoni, R.; Floyd, M.; Hunt, J. P.; Lockhart, D. J.; Milanov, Z. V.; Morrison, M. J.; Pallares, G.; Patel, H. K.; Pritchard, S.; Wodicka, L. M.; Zarrinkar, P. P. *Nat. Biotechnol.* **2008,** *26,* 127.
3. Nagar, B.; Hantschel, O.; Young, M. A.; Scheffzek, K.; Veach, D.; Bornmann, W.; Clarkson, B.; Superti-Furga, G.; Kuriyan, J. *Cell* **2003,** *112,* 859.
4. Zhang, J.; Yang, P. L.; Gray, N. S. *Nat. Rev. Cancer* **2009,** *9,* 28.
5. Barf, T.; Kaptein, A. *J. Med. Chem.* **2012,** *55,* 6243.
6. Leproult, E.; Barluenga, S.; Moras, D.; Wurtz, J.-M.; Winssinger, N. *J. Med. Chem.* **2011,** *54,* 1347.
7. Copeland, R. A. *Nat. Rev. Drug Discov.* **2016,** *15,* 87.
8. Singh, J.; Petter, R. C.; Kluge, A. F. *Curr. Opin. Chem. Biol.* **2010,** *14,* 475.
9. Jöst, C.; Nitsche, C.; Scholz, T.; Roux, L.; Klein, C. D. *J. Med. Chem.* **2014,** *57,* 7590.
10. Flanagan, M. E.; Abramite, J. A.; Anderson, D. P.; Aulabaugh, A.; Dahal, U. P.; Gilbert, A. M.; Li, C.; Montgomery, J.; Oppenheimer, S. R.; Ryder, T.; Schuff, B. P.; Uccello, D. P.; Walker, G. S.; Wu, Y.; Brown, M. F.; Chen, J. M.; Hayward, M. M.; Noe, M. C.; Obach, R. S.; Philippe, L.; Shanmugasundaram, V.; Shapiro, M. J.; Starr, J.; Stroh, J.; Che, Y. *J. Med. Chem.* **2014,** *57,* 10072.
11. Ward, R. A.; Anderton, M. J.; Ashton, S.; Bethel, P. A.; Box, M.; Butterworth, S.; Colclough, N.; Chorley, C. G.; Chuaqui, C.; Cross, D. A. E.; Dakin, L. A.; Debreczeni, J.É.; Eberlein, C.; Finlay, M. R. V.; Hill, G. B.; Grist, M.; Klinowska, T. C. M.; Lane, C.; Martin, S.; Orme, J. P.; Smith, P.; Wang, F.; Waring, M. *J. Med. Chem.* **2013,** *56,* 7025.
12. Cee, V. J.; Volak, L. P.; Chen, Y.; Bartberger, M. D.; Tegley, C.; Arvedson, T.; McCarter, J.; Tasker, A. S.; Fotsch, C. *J. Med. Chem.* **2015,** *58,* 9171.
13. Stepan, A. F.; Walker, D. P.; Bauman, J.; Price, D. A.; Baillie, T. A.; Kalgutkar, A. S.; Aleo, M. D. *Chem. Res. Toxicol.* **2011,** *24,* 1345.
14. Kalgutkar, A. S.; Dalvie, D. K. *Expert Opin. Drug Discovery* **2012,** *7,* 561.
15. Nacht, M.; Qiao, L.; Sheets, M. P.; St Martin, T.; Labenski, M.; Mazdiyasni, H.; Karp, R.; Zhu, Z.; Chaturvedi, P.; Bhavsar, D.; Niu, D.; Westlin, W.; Petter, R. C.; Medikonda, A. P.; Singh, J. *J. Med. Chem.* **2013,** *56,* 712.
16. Lanning, B. R.; Whitby, L. R.; Dix, M. M.; Douhan, J.; Gilbert, A. M.; Hett, E. C.; Johnson, T. O.; Joslyn, C.; Kath, J. C.; Niessen, S.; Roberts, L. R.; Schnute, M. E.; Wang, C.; Hulce, J. J.; Wei, B.; Whiteley, L. O.; Hayward, M. M.; Cravatt, B. F. *Nat. Chem. Biol.* **2014,** *10,* 760.
17. Serafimova, I. M.; Pufall, M. A.; Krishnan, S.; Duda, K.; Cohen, M. S.; Maglathlin, R. L.; McFarland, J. M.; Miller, R. M.; Frödin, M.; Taunton, J. *Nat. Chem. Biol.* **2012,** *8,* 471.
18. Bradshaw, J. M.; McFarland, J. M.; Paavilainen, V. O.; Bisconte, A.; Tam, D.; Phan, V. T.; Romanov, S.; Finkle, D.; Shu, J.; Patel, V.; Ton, T.; Li, X.; Loughhead, D. G.; Nunn, P. A.; Karr, D. E.; Gerritsen, M. E.; Funk, J. O.; Owens, T. D.; Verner, E.; Brameld, K. A.; Hill, R. J.; Goldstein, D. M.; Taunton, J. *Nat. Chem. Biol.* **2015**.
19. Basu, D.; Richters, A.; Rauh, D. *Bioorg. Med. Chem.* **2015,** *23,* 2767.
20. Copeland, R. A. *Expert Opin. Drug Discovery* **2010,** *5,* 305.
21. Walkup, G. K.; You, Z.; Ross, P. L.; Allen, E. K. H.; Daryaee, F.; Hale, M. R.; O'Donnell, J.; Ehmann, D. E.; Schuck, V. J. A.; Buurman, E. T.; Choy, A. L.; Hajec, L.; Murphy-Benenato, K.; Marone, V.; Patey, S. A.; Grosser, L. A.; Johnstone, M.; Walker, S. G.; Tonge, P. J.; Fisher, S. L. *Nat. Chem. Biol.* **2015,** *11,* 416.
22. Greig, M. J.; Niessen, S.; Weinrich, S. L.; Feng, J. L.; Shi, M.; Shi, M.; Johnson, T. O. *Int. J. Cell Biol.* **2015,** *2015,* 798936.
23. Burke, P. M.; Wiley, H. S. *J. Cell. Physiol.* **1999,** *180,* 448.
24. Wang, Y.; Roche, O.; Yan, M. S.; Finak, G.; Evans, A. J.; Metcalf, J. L.; Hast, B. E.; Hanna, S. C.; Wondergem, B.; Furge, K. A.; Irwin, M. S.; Kim, W. Y.; Teh, B. T.; Grinstein, S.; Park, M.; Marsden, P. A.; Ohh, M. *Nat. Med.* **2009,** *15,* 319.
25. Simon, G. M.; Niphakis, M. J.; Cravatt, B. F. *Nat. Chem. Biol.* **2013,** *9,* 200.
26. Honigberg, L. A.; Smith, A. M.; Sirisawad, M.; Verner, E.; Loury, D.; Chang, B.; Li, S.; Pan, Z.; Thamm, D. H.; Miller, R. A.; Buggy, J. *Proc. Natl. Acad. Sci. U. S. A.* **2010,** *107,* 13075.
27. Nisitani, S.; Satterthwaite, A. B.; Akashi, K.; Weissman, I. L.; Witte, O. N.; Wahl, M. I. *Proc. Natl. Acad. Sci. U. S. A.* **2000,** *97,* 2737.
28. Lou, Y.; Owens, T. D.; Kuglstatter, A.; Kondru, R. K.; Goldstein, D. M. *J. Med. Chem.* **2012,** *55,* 4539.
29. Byrd, J. C.; Furman, R. R.; Coutre, S. E.; Flinn, I. W.; Burger, J. A.; Blum, K. A.; Grant, B.; Sharman, J. P.; Coleman, M.; Wierda, W. G.; Jones, J. A.; Zhao, W.; Heerema, N. A.; Johnson, A. J.; Sukbuntherng, J.; Chang, B. Y.; Clow, F.; Hedrick, E.; Buggy, J. J.; James, D. F.; O'Brien, S. *N. Engl. J. Med.* **2013,** *369,* 32.
30. de Claro, R. A.; McGinn, K. M.; Verdun, N.; Lee, S.-L.; Chiu, H.-J.; Saber, H.; Brower, M. E.; Chang, C. J. G.; Pfuma, E.; Habtemariam, B.; Bullock, J.; Wang, Y.; Nie, L.; Chen, X.-H.; Lu, D.; Al-Hakim, A.; Kane, R. C.; Kaminskas, E.; Justice, R.; Farrell, A. T.; Pazdur, R. *Clin. Cancer Res.* **2015,** *21,* 3586.
31. Pan, Z.; Scheerens, H.; Li, S.-J.; Schultz, B. E.; Sprengeler, P. A.; Burrill, L. C.; Mendonca, R. V.; Sweeney, M. D.; Scott, K. C. K.; Grothaus, P. G.; Jeffery, D. A.; Spoerke, J. M.; Honigberg, L. A.; Young, P. R.; Dalrymple, S. A.; Palmer, J. T. *ChemMedChem* **2007,** *2,* 58.
32. Wang, Y.; Zhang, L.; Champlin, R.; Wang, M. *Clin. Pharmacol. Ther.* **2015,** *97,* 455.
33. Byrd, J. C.; Furman, R. R.; Coutre, S. E.; Burger, J. A.; Blum, K. A.; Coleman, M.; Wierda, W. G.; Jones, J. A.; Zhao, W.; Heerema, N. A.; Johnson, A. J.; Shaw, Y.; Bilotti, E.; Zhou, C.; James, D. F.; O'Brien, S. *Blood* **2015,** *125,* 2497.
34. Jong, J.; Sukbuntherng, J.; Skee, D.; Murphy, J.; O'Brien, S.; Byrd, J. C.; James, D.; Hellemans, P.; Loury, D. J.; Jiao, J.; Chauhan, V.; Mannaert, E. *Cancer Chemother. Pharmacol.* **2015,** *75,* 907.
35. Sagiv-Barfi, I.; Kohrt, H. E. K.; Czerwinski, D. K.; Ng, P. P.; Chang, B. Y.; Levy, R. Proc. Nat. Acad. Sci. U. S. A. **2015**, *112*, E966.
36. Evans, E. K.; Tester, R.; Aslanian, S.; Karp, R.; Sheets, M.; Labenski, M. T.; Witowski, S. R.; Lounsbury, H.; Chaturvedi, P.; Mazdiyasni, H.; Zhu, Z.; Nacht, M.; Freed, M. I.; Petter, R. C.; Dubrovskiy, A.; Singh, J.; Westlin, W. F. *J. Pharmacol. Exp. Ther.* **2013,** *346,* 219.
37. Walter, H. S.; Rule, S. A.; Dyer, M. J. S.; Karlin, L.; Jones, C.; Cazin, B.; Quittet, P.; Shah, N.; Hutchinson, C. V.; Honda, H.; Duffy, K.; Birkett, J.; Jamieson, V.; Courtenay-Luck, N.; Yoshizawa, T.; Sharpe, J.; Ohno, T.; Abe, S.; Nishimura, A.; Cartron, G.; Morschhauser, F.; Fegan, C.; Salles, G. *Blood* **2015**.
38. Byrd, J. C.; Harrington, B.; O'Brien, S.; Jones, J. A.; Schuh, A.; Devereux, S.; Chaves, J.; Wierda, W. G.; Awan, F. T.; Brown, J. R.; Hillmen, P.; Stephens, D. M.; Ghia, P.; Barrientos, J. C.; Pagel, J. M.; Woyach, J.; Johnson, D.; Huang, J.; Wang, X.; Kaptein, A.; Lannutti, B. J.; Covey, T.; Fardis, M.; McGreivy, J.; Hamdy, A.; Rothbaum, W.; Izumi, R.; Diacovo, T. G.; Johnson, A. J.; Furman, R. *N. Engl. J. Med.* **2015,** *374,* 323.
39. Liu, J.; Guiadeen, D.; Krikorian, A.; Gao, X.; Wang, J.; Boga, S. B.; Alhassan, A. B.; Yu, Y.; Vaccaro, H.; Liu, S.; Yang, C.; Wu, H.; Cooper, A.; de Man, J.; Kaptein, A.; Maloney, K.; Hornak, V.; Gao, Y. D.; Fischmann, T. O.; Raaijmakers, H.; Vu-Pham, D.; Presland, J.; Mansueto, M.; Xu, Z.; Leccese, E.; Zhang-Hoover, J.; Knemeyer, I.; Garlisi, C. G.; Bays, N.; Stivers, P.; Brandish, P. E.; Hicks, A.; Kim, R.; Kozlowski, J. A. *ACS Med. Chem. Lett.* **2016,** *7,* 198.
40. Weerapana, E.; Wang, C.; Simon, G. M.; Richter, F.; Khare, S.; Dillon, M. B. D.; Bachovchin, D. A.; Mowen, K.; Baker, D.; Cravatt, B. F. *Nature* **2010,** *468,* 790.
41. Liu, N.; Hoogendoorn, S.; van de Kar, B.; Kaptein, A.; Barf, T.; Driessen, C.; Filippov, D. V.; van der Marel, G. A.; van der Stelt, M.; Overkleeft, H. S. *Org. Biomol. Chem.* **2015,** *13,* 5147.
42. Michalczyk, A. *Bioorg. Med. Chem.* **2008,** *16,* 3482.
43. Cai-Hong Yun, K. E. M.; Toms, A. V.; Woo, M. I. S.; Greulich, H.; Wong, K.-K.; Meyerson, M.; Eck, M. J. *Proc. Natl. Acad. Sci. U. S. A.* **2008,** *105,* 2070.
44. Miller, V. A.; Cadranel, J.; Chen, Y. M.; Park, K.; Kim, S. W. *Lancet Oncol.* **2012,** *13,* 528.
45. Wissner, A.; Mansour, T. S. *Arch. Pharm. (Weinheim)* **2008,** *341,* 465.
46. Sequist, L. V.; Besse, B.; Lynch, T. J.; Miller, V. A.; Wong, K. K.; Gitlitz, B.; Eaton, K.; Zacharchuk, C.; Freyman, A.; Powell, C.; Ananthakrishnan, R.; Quinn, S.; Soria, J. C. *J. Clin. Oncol.* **2010,** *28,* 3076.
47. Chan, A.; Delaloge, S.; Holmes, F. A.; Moy, B.; Iwata, H.; Harvey, V. J.; Robert, N. J.; Silovski, T.; Gokmen, E.; von Minckwitz, G.; Ejlertsen, B.; Chia, S. K.; Mansi, J.; Barrios, C. H.; Gnant, M.; Buyse, M.; Gore, I.; Smith, J., 2nd.; Harker, G.; Masuda, N.; Petrakova, K.; Zotano, A. G.; Iannotti, N.; Rodriguez, G.; Tassone, P.; Wong, A.; Bryce, R.; Ye, Y.; Yao, B.; Martin, M.; ExteNET Study Group. *Lancet Oncol.* **2016,** *17,* 367.

48. Solca, F.; Dahl, G.; Zoephel, A.; Bader, G.; Sanderson, M.; Klein, C.; Kraemer, O.; Himmelsbach, F.; Haaksma, E.; Adolf, G. R. *J. Pharmacol. Exp. Ther.* **2012,** *343,* 342.
49. Keating, G. M. *Drugs* **2014,** *74,* 207.
50. Schuler, M.; Yang, J. C.; Park, K.; Kim, J. H.; Bennouna, J.; Chen, Y. M.; Chouaid, C.; De Marinis, F.; Feng, J. F.; Grossi, F.; Kim, D. W.; Liu, X.; Lu, S.; Strausz, J.; Vinnyk, Y.; Wiewrodt, R.; Zhou, C.; Wang, B.; Chand, V. K.; Planchard, D.; Investigators, L. U.-L. *Ann. Oncol.* **2016,** *27,* 417.
51. Zhou, W.; Ercan, D.; Chen, L.; Yun, C.-H.; Li, D.; Capelletti, M.; Cortot, A. B.; Chirieac, L.; Iacob, R. E.; Padera, R.; Engen, J. R.; Wong, K.-K.; Eck, M. J.; Gray, N. S.; Jänne, P. A. *Nature* **2009,** *462,* 1070.
52. Singh, J.; Evans, E.; Hagel, M.; Labinski, M.; Dubrovskiy, A.; Nacht, M.; Petter, R. C.; Prasad, A.; Sheets, M.; St Martin, T.; Tjin Tham Sjin, R.; Westlin, W.; Zhu, Z. *Med. Chem. Commun.* **2012,** *3,* 780.
53. Tjin Tham Sjin, R.; Lee, K.; Walter, A. O.; Dubrovskiy, A.; Sheets, M.; Martin, T. S.; Labenski, M. T.; Zhu, Z.; Tester, R.; Karp, R.; Medikonda, A.; Chaturvedi, P.; Ren, Y.; Haringsma, H.; Etter, J.; Raponi, M.; Simmons, A. D.; Harding, T. C.; Niu, D.; Nacht, M.; Westlin, W. F.; Petter, R. C.; Allen, A.; Singh, J. *Mol. Cancer Ther.* **2014,** *13,* 1468.
54. Walter, A. O.; Tjin Tham Sjin, R.; Haringsma, H. J.; Ohashi, K.; Sun, J.; Lee, K.; Dubrovsky, A.; Labenski, M.; Zhu, Z.; Wang, Z.; Sheets, M.; St Martin, K.; Karp, R.; van Kalken, D.; Chaturvedi, P.; Niu, D.; Nacht, M.; Petter, R. C.; Westlin, W.; Lin, K.; Jaw-Tsai, S.; Raponi, M.; Van Dyke, T.; Etter, J.; Weaver, Z.; Pao, W.; Singh, J.; Simmons, A. D.; Harding, T. C.; Allen, A. *Cancer Discov.* **2013,** *3,* 1404.
55. Finlay, M. R. V.; Anderton, M.; Ashton, S.; Ballard, P.; Bethel, P. A.; Box, M. R.; Bradbury, R. H.; Brown, S. J.; Butterworth, S.; Campbell, A.; Chorley, C.; Colclough, N.; Cross, D. A. E.; Currie, G. S.; Grist, M.; Hassall, L.; Hill, G. B.; James, D.; James, M.; Kemmitt, P.; Klinowska, T.; Lamont, G.; Lamont, S. G.; Martin, N.; McFarland, H. L.; Mellor, M. J.; Orme, J. P.; Perkins, D.; Perkins, P.; Richmond, G.; Smith, P.; Ward, R. A.; Waring, M. J.; Whitaker, D.; Wells, S.; Wrigley, G. L. *J. Med. Chem.* **2014,** *57,* 8249.
56. Cross, D. A.; Ashton, S. E.; Ghiorghiu, S.; Eberlein, C.; Nebhan, C. A.; Spitzler, P. J.; Orme, J. P.; Finlay, M. R.; Ward, R. A.; Mellor, M. J.; Hughes, G.; Rahi, A.; Jacobs, V. N.; Red Brewer, M.; Ichihara, E.; Sun, J.; Jin, H.; Ballard, P.; Al-Kadhimi, K.; Rowlinson, R.; Klinowska, T.; Richmond, G. H.; Cantarini, M.; Kim, D. W.; Ranson, M. R.; Pao, W. *Cancer Discov.* **2014,** *4,* 1046.
57. Engel, J.; Jonas, L.; Rauh, D. *ACS Med. Chem. Lett.* **2016,** *7,* 2.
58. Thress, K. S.; Paweletz, C. P.; Felip, E.; Cho, B. C.; Stetson, D.; Dougherty, B.; Lai, Z.; Markovets, A.; Vivancos, A.; Kuang, Y.; Ercan, D.; Matthews, S. E.; Cantarini, M.; Barrett, J. C.; Janne, P. A.; Oxnard, G. R. *Nat. Med.* **2015,** *21,* 560.
59. Piotrowska, Z.; Niederst, M. J.; Karlovich, C. A.; Wakelee, H. A.; Neal, J. W.; Mino-Kenudson, M.; Fulton, L.; Hata, A. N.; Lockerman, E. L.; Kalsy, A.; Digumarthy, S.; Muzikansky, A.; Raponi, M.; Garcia, A. R.; Mulvey, H. E.; Parks, M. K.; DiCecca, R. H.; Dias-Santagata, D.; Iafrate, A. J.; Shaw, A. T.; Allen, A. R.; Engelman, J. A.; Sequist, L. V. *Cancer Discov.* **2015,** *5,* 713.
60. Cheng, H. N.; Nair, S. K.; Murray, B. W.; Almaden, C.; Bailey, S.; Baxi, S.; Cho-Schultz, S.; Dalvie, D.; Dinh, D. M.; Edwards, M. P.; Feng, J. L.; Ferre, R. A.; Gajiwala, K. S.; Hemkens, M. D.; Jackson-Fisher, A.; Jalaie, M.; Johnson, T. O.; Kania, R. S.; Kephart, S.; Lafontaine, J.; Lunney, B.; Liu, K. K. C.; Liu, Z.; Matthews, J.; Nagata, A.; Niessen, S.; Ornelas, M. A.; Orr, S. T. M.; Pairish, M.; Planken, S.; Ren, S.; Richter, D.; Ryan, K.; Sach, N.; Shen, H.; Smeal, T.; Solowiej, J.; Sutton, S.; Tran, K.; Tseng, E.; Vernier, W.; Walls, M.; Wang, S.; Weinrich, S. L.; Xin, S.; Xu, H.; Yin, M.; Zhou, R.; Kath, J. C. *Bioorg. Med. Chem. Lett.* **2016,** *26,* 1861.
61. Jia, Y.; Juarez, J.; Li, J.; Manuia, M.; Niederst, M. J.; Tompkins, C.; Timple, N.; Vaillancourt, M. T.; Pferdekamper, A. C.; Lockerman, E. L.; Li, C.; Anderson, J.; Costa, C.; Liao, D.; Murphy, E.; DiDonato, M.; Bursulaya, B.; Lelais, G.; Barretina, J.; McNeill, M.; Epple, R.; Marsilje, T. H.; Pathan, N.; Engelman, J. A.; Michellys, P. Y.; McNamara, P.; Harris, J.; Bender, S.; Kasibhatla, S. *Cancer Res.* **2016,** *76,* 1591.
62. Tiong, K. H.; Mah, L. Y.; Leong, C. O. *Apoptosis* **2013,** *18,* 1447.
63. Dieci, M. V.; Arnedos, M.; Andre, F.; Soria, J. C. *Cancer Discov.* **2013,** *3,* 264.
64. Tan, L.; Wang, J.; Tanizaki, J.; Huang, Z.; Aref, A. R.; Rusan, M.; Zhu, S.-J.; Zhang, Y.; Ercan, D.; Liao, R. G.; Capelletti, M.; Zhou, W.; Hur, W.; Kim, N.; Sim, T.; Gaudet, S.; Barbie, D. A.; Yeh, J.-R. J.; Yun, C.-H.; Hammerman, P. S.; Mohammadi, M.; Janne, P. A.; Gray, N. *PNAS* **2014,** *111,* 4867.
65. Guagnano, V.; Furet, P.; Spanka, C.; Bordas, V.; Le Douget, M.; Stamm, C.; Brueggen, J.; Jensen, M. R.; Schnell, C.; Schmid, H.; Wartmann, M.; Berghausen, J.; Drueckes, P.; Zimmerlin, A.; Bussiere, D.; Murray, J.; Graus Porta, D. *J. Med. Chem.* **2011,** *54,* 7066.
66. Gavine, P. R.; Mooney, L.; Kilgour, E.; Thomas, A. P.; Al-Kadhimi, K.; Beck, S.; Rooney, C.; Coleman, T.; Baker, D.; Mellor, M. J.; Brooks, A. N.; Klinowska, T. *Cancer Res.* **2012,** *72,* 2045.
67. Zhao, G.; Li, W.-Y.; Chen, D.; Henry, J. R.; Li, H.-Y.; Chen, Z.; Zia-Ebrahimi, M.; Bloem, L.; Zhai, Y.; Huss, K.; Peng, S.-B.; McCann, D. *Mol. Cancer Ther.* **2011,** *10,* 2200.
68. Angibaud, P. R. Proceedings of the 105th Annual Meeting of the American Association for Cancer Research, 74, 19, Abstract nr 4748.
69. Tan, L.; Wang, J.; Tanizaki, J.; Huang, Z.; Aref, A. R.; Rusan, M.; Zhu, S.-J.; Zhang, Y.; Ercan, D.; Liao, R. G.; Capelletti, M.; Zhou, W.; Hur, W.; Kim, N.; Sim, T.; Gaudet, S.; Barbie, D. A.; Yeh, J.-R. J.; Yun, C.-H.; Hammerman, P. S.; Mohammadi, M.; Jänne, P. A.; Gray, N. S. *Proc. Natl. Acad. Sci. U. S. A.* **2014,** *111*, E4869.
70. Zhou, W.; Hur, W.; McDermott, U.; Dutt, A.; Xian, W.; Ficarro, S. B.; Zhang, J.; Sharma, S. V.; Brugge, J.; Meyerson, M.; Settleman, J.; Gray, N. S. *Chem. Biol.* **2010,** *17,* 285.
71. Chell, V.; Balmanno, K.; Little, A. S.; Wilson, M.; Andrews, S.; Blockley, L.; Hampson, M.; Gavine, P. R.; Cook, S. *J. Oncogene* **2013,** *32,* 3059.
72. Shukla, N.; Ameur, N.; Yilmaz, I.; Nafa, K.; Lau, C. Y.; Marchetti, A.; Borsu, L.; Barr, F. G.; Ladanyi, M. *Clin. Cancer Res.* **2012,** *18,* 748.
73. Ang, D.; Ballard, M.; Beadling, C.; Warrick, A.; Schilling, A.; O'Gara, R.; Pukay, M.; Neff, T. L.; West, R. B.; Corless, C. L.; Troxell, M. L. *Appl. Immunohistochem. Mol. Morphol.* **2015,** *23,* 97.
74. Ochiiwa, H.; et al. Proceedings of the AACR-NCI-EORTC international Conference: Molecular Targets and Cancer Therapeutics, 12 (11 Suppl), Abstract nr A270.
75. Phan, V. T.; Verner, E.; Gerritsen, M.; Bradshaw, J. M.; Goldstein, D. M.; Hill, R. J.; Karr, D.; LaStant, J.; Nunn, P.; Tam, D.; Shu, J.; Funk, J. O.; Brameld, K. *Eur. J. Cancer* **2014,** *50,* 157.
76. Hagel, M.; Miduturu, C.; Sheets, M.; Rubin, N.; Weng, W.; Stransky, N.; Bifulco, N.; Kim, J. L.; Hodous, B.; Brooijmans, N.; Shutes, A.; Winter, C.; Lengauer, C.; Kohl, N. E.; Guzi, T. *Cancer Discov* **2015**, *5*, 424.
77. Weisner, J.; Gontla, R.; van der Westhuizen, L.; Oeck, S.; Ketzer, J.; Janning, P.; Richters, A.; Mühlenberg, T.; Fang, Z.; Taher, A.; Jendrossek, V.; Pelly, S. C.; Bauer, S.; van Otterlo, W. A. L.; Rauh, D. *Angew. Chem. Int. Ed. Engl.* **2015,** *54,* 10313.
78. Barnett, S. F.; D.-J., D.; Fu, S.; Hancock, P. J.; Haskell, K. M.; Jones, R. E.; Kahana, J. A.; Kral, A. M.; Leander, K.; Lee, L. L.; Malinowski, J.; McAvoy, E. M.; Nahas, D. D.; Robinson, R. G.; Huber, H. E. *Biochem. J.* **2005,** *385,* 399.
79. Cenni, B.; Gutmann, S.; Gottar-Guillier, M. *Int. Rev. Immunol.* **2012,** *31,* 166.
80. Liu, F.; Zhang, X.; Weisberg, E.; Chen, S.; Hur, W.; Wu, H.; Zhao, Z.; Wang, W.; Mao, M.; Cai, C.; Simon, N. I.; Sanda, T.; Wang, J.; Look, A. T.; Griffin, J. D.; Balk, S. P.; Liu, Q.; Gray, N. S. *ACS Chem. Biol.* **2013,** *8,* 1423.
81. Christensen, C. L.; Kwiatkowski, N.; Abraham, B. J.; Carretero, J.; Al-Shahrour, F.; Zhang, T.; Chipumuro, E.; Herter-Sprie, G. S.; Akbay, E. A.; Altabef, A.; Zhang, J.; Shimamura, T.; Capelletti, M.; Reibel, J. B.; Cavanaugh, J. D.; Gao, P.; Liu, Y.; Michaelsen, S. R.; Poulsen, H. S.; Aref, A. R.; Barbie, D. A.; Bradner, J. E.; George, R. E.; Gray, N. S.; Young, R. A.; Wong, K.-K. *Cancer Cell* **2014,** *26,* 909.
82. Wang, Y.; Zhang, T.; Kwiatkowski, N.; Abraham, B. J.; Lee, T. I.; Xie, S.; Yuzugullu, H.; Von, T.; Li, H.; Lin, Z.; Stover, D. G.; Lim, E.; Wang, Z. C.; Iglehart, J. D.; Young, R. A.; Gray, N. S.; Zhao, J. J. *Cell* **2015,** *163,* 174.
83. Chipumuro, E.; Marco, E.; Christensen, C. L.; Kwiatkowski, N.; Zhang, T.; Hatheway, C. M.; Abraham, B. J.; Sharma, B.; Yeung, C.; Altabef, A.; Perez-Atayde, A.; Wong, K.-K.; Yuan, G.-C.; Gray, N. S.; Young, R. A.; George, R. E. *Cell* **2014,** *159,* 1126.
84. Ward, R. A.; Colclough, N.; Challinor, M.; Debreczeni, J. E.; Eckersley, K.; Fairley, G.; Feron, L.; Flemington, V.; Graham, M. A.; Greenwood, R.; Hopcroft, P.; Howard, T. D.; James, M.; Jones, C. D.; Jones, C. R.; Renshaw, J.; Roberts, K.; Snow, L.; Tonge, M.; Yeung, K. *J. Med. Chem.* **2015,** *58,* 4790.

85. Zapf, C. W.; Gerstenberger, B. S.; Xing, L.; Limburg, D. C.; Anderson, D. R.; Caspers, N.; Han, S.; Aulabaugh, A.; Kurumbail, R.; Shakya, S.; Li, X.; Spaulding, V.; Czerwinski, R. M.; Seth, N.; Medley, Q. G. *J. Med. Chem.* **2012,** *55,* 10047.
86. Zhong, Y.; Dong, S.; Strattan, E.; Ren, L.; Butchar, J. P.; Thornton, K.; Mishra, A.; Porcu, P.; Bradshaw, J. M.; Bisconte, A.; Owens, T. D.; Verner, E.; Brameld, K. A.; Funk, J. O.; Hill, R. J.; Johnson, A. J.; Dubovsky, J. A. *J. Biol. Chem.* **2015,** *290,* 5960.
87. Dubovsky, J. A.; Beckwith, K. A.; Natarajan, G.; Woyach, J. A.; Jaglowski, S.; Zhong, Y.; Hessler, J. D.; Liu, T.-M.; Chang, B. Y.; Larkin, K. M.; Stefanovski, M. R.; Chappell, D. L.; Frissora, F. W.; Smith, L. L.; Smucker, K. A.; Flynn, J. M.; Jones, J. A.; Andritsos, L. A.; Maddocks, K.; Lehman, A. M.; Furman, R.; Sharman, J.; Mishra, A.; Caligiuri, M. A.; Satoskar, A. R.; Buggy, J. J.; Muthusamy, N.; Johnson, A. J.; Byrd, J. C. *Blood* **2013,** *122,* 2539.
88. Cho, H.-S.; Shin, H. M.; Haberstock-Debic, H.; Xing, Y.; Owens, T. D.; Funk, J. O.; Hill, R. J.; Bradshaw, J. M.; Berg, L. J. *J. Immunol.* **2015**, *195,* 4822.
89. Tan, L.; Akahane, K.; McNally, R.; Reyskens, K. M. S. E.; Ficarro, S. B.; Liu, S.; Herter-Sprie, G. S.; Koyama, S.; Pattison, M. J.; Labella, K.; Johannessen, L.; Akbay, E. A.; Wong, K.-K.; Frank, D. A.; Marto, J. A.; Look, T. A.; Arthur, J. S. C.; Eck, M. J.; Gray, N. S. *J. Med. Chem.* **2015,** *58,* 6589.
90. Koo, G.; et al. *Cancer Discov.* **2012,** *2,* 591.
91. Goedken, E. R.; Argiriadi, M. A.; Banach, D. L.; Fiamengo, B. A.; Foley, S. E.; Frank, K. E.; George, J. S.; Harris, C. M.; Hobson, A. D.; Ihle, D. C.; Marcotte, D.; Merta, P. J.; Michalak, M. E.; Murdock, S. E.; Tomlinson, M. J.; Voss, J. W. *J. Biol. Chem.* **2015,** *290,* 4573.
92. Zhang, T.; Inesta-Vaquera, F.; Niepel, M.; Zhang, J.; Ficarro, S. B.; Machleidt, T.; Xie, T.; Marto, J. A.; Kim, N.; Sim, T.; Laughlin, J. D.; Park, H.; LoGrasso, P. V.; Patricelli, M.; Nomanbhoy, T. K.; Sorger, P. K.; Alessi, D. R.; Gray, N. S. *Chem. Biol.* **2012,** *19,* 140.
93. Miller, R. M.; Paavilainen, V. O.; Krishnan, S.; Serafimova, I. M.; Taunton, J. *J. Am. Chem. Soc.* **2013,** *135,* 5298.
94. Wu, J.; Powell, F.; Larsen, N. A.; Lai, Z.; Byth, K. F.; Read, J.; Gu, R.-F.; Roth, M.; Toader, D.; Saeh, J. C.; Chen, H. *ACS Chem. Biol.* **2013,** *8,* 643.
95. Kwarcinski, F. E.; Fox, C. C.; Steffey, M. E.; Soellner, M. B. *ACS Chem. Biol.* **2012,** *7,* 1910.
96. Fouque, A.; Delalande, O.; Jean, M.; Castellano, R.; Josselin, E.; Malleter, M.; Shoji, K. F.; Hung, M. D.; Rampanarivo, H.; Collette, Y.; van de Weghe, P.; Legembre, P. *J. Med. Chem.* **2015,** *58,* 6559.
97. Groll, M.; Berkers, C. R.; Ploegh, H. L.; Ovaa, H. *Structure* **2006,** *14,* 451.
98. Lin, C.; Kwong, A. D.; Perni, R. B. *Infect. Disord. Drug Targets* **2006,** *6,* 3.
99. Krishnan, S.; Miller, R. M.; Tian, B.; Mullins, R. D.; Jacobson, M. P.; Taunton, J. *J. Am. Chem. Soc.* **2014,** *136,* 12624.
100. Anscombe, E.; Meschini, E.; Mora-Vidal, R.; Martin, M. P.; Staunton, D.; Geitmann, M.; Danielson, U. H.; Stanley, W. A.; Wang, L. Z.; Reuillon, T.; Golding, B. T.; Cano, C.; Newell, D. R.; Noble, M. E.; Wedge, S. R.; Endicott, J. A.; Griffin, R. J. *Chem. Biol.* **2015,** *22,* 1159.
101. Wymann, M. P.; Bulgarelli-Leva, G.; Zvelebil, M. J.; Pirola, L.; Vanhaesebroeck, B.; Waterfield, M. D.; Panayotou, G. *Mol. Cell. Biol.* **1996,** *16,* 1722.
102. Liu, Y.; Jiang, N.; Wu, J.; Dai, W.; Rosenblum, J. S. *J. Biol. Chem.* **2007,** *282,* 2505.
103. Buhrow, S. A.; Cohen, S.; Staros, J. V. *J. Biol. Chem.* **1982,** *257,* 4019.
104. Fox, T.; Fitzgibbon, M. J.; Fleming, M. A.; Hsiao, H.-M.; Brummel, C. L.; Su, M. S. *FEBS Lett.* **1999,** *461,* 323.
105. Vereb, G.; Balla, A.; Gergely, P.; Wymann, M. P.; Gulkan, H.; Suer, S.; Heilmeyer, L. M., Jr. *Int. J. Biochem. Cell Biol.* **2001,** *33,* 249.
106. Narayanan, A.; Jones, L. H. *Chem. Sci.* **2015,** *6,* 2650.
107. Gushwa, N. N.; Kang, S.; Chen, J.; Taunton, J. *J. Am. Chem. Soc.* **2012,** *134,* 20214.
108. Bell, I. M.; Stirdivant, S. M.; Ahern, J.; Culberson, J. C.; Darke, P. L.; Dinsmore, C. J.; Drakas, R. A.; Gallicchio, S. N.; Graham, S. L.; Heimbrook, D. C.; Hall, D. L.; Hua, J.; Kett, N. R.; Kim, A. S.; Kornienko, M.; Kuo, L. C.; Munshi, S. K.; et al. *Biochemistry* **2005,** *44,* 9430.
109. Larraufie, M.-H.; Yang, W. S.; Jiang, E.; Thomas, A. G.; Slusher, B. S.; Stockwell, B. R. *Bioorg. Med. Chem. Lett.* **2015,** *25,* 4787.
110. Banerjee, R.; Pace, N. J.; Brown, D. R.; Weerapana, E. *J. Am. Chem. Soc.* **2013,** *135,* 2497.
111. Kathman, S. G.; Xu, Z.; Statsyuk, A. V. *J. Med. Chem.* **2014,** *57,* 4969.
112. Allen, C. E.; Curran, P. R.; Brearley, A. S.; Boissel, V.; Sviridenko, L.; Press, N. J.; Stonehouse, J. P.; Armstrong, A. *Org. Lett.* **2015,** *17,* 458.
113. Campuzano, I. D.; San Miguel, T.; Rowe, T.; Onea, D.; Cee, V. J.; Arvedson, T.; McCarter, J. D. *J. Biomol. Screen.* **2015,** *21,* 136.
114. London, N.; Miller, R. M.; Krishnan, S.; Uchida, K.; Irwin, J. J.; Eidam, O.; Gibold, L.; Cimermančič, P.; Bonnet, R.; Shoichet, B. K.; Taunton, J. *Nat. Chem. Biol.* **2014,** *10,* 1066.
115. Kumalo, H. M.; Bhakat, S.; Soliman, M. E. S. *Molecules* **2015,** *20,* 1984.
116. Adeniyi, A. A.; Muthusamy, R.; Soliman, M. E. S. *Expert Opin. Drug Discovery* **2016,** *11,* 79.
117. Ouyang, X.; Zhou, S.; Su, C. T. T.; Ge, Z.; Li, R.; Kwoh, C. K. *J. Comput. Chem.* **2013,** *34,* 326.
118. Schröder, J.; Klinger, A.; Oellien, F.; Marhöfer, R. J.; Duszenko, M.; Selzer, P. M. *J. Med. Chem.* **2013,** *56,* 1478.
119. Toledo Warshaviak, D.; Golan, G.; Borrelli, K. W.; Zhu, K.; Kalid, O. *J. Chem. Inf. Model.* **2014,** *54,* 1941.

5.04 Targeting DNA Damage Response Pathways in Cancer

Ganiy Opeyemi Abdulrahman and NJ Curtin, Newcastle University, Newcastle upon Tyne, United Kingdom

© 2017 Elsevier Ltd. All rights reserved.

5.04.1	**Introduction**	105
5.04.2	**Poly(ADP-Ribose) Polymerase (PARP)**	107
5.04.2.1	PARP Discovery and Function	107
5.04.2.2	PARP Inhibitors	107
5.04.2.2.1	Chemosensitization and radiosentitization	109
5.04.2.2.2	Vasoactivity of PARPi	109
5.04.2.2.3	Single-agent activity	110
5.04.2.2.4	Combinations with molecularly targeted agents	110
5.04.2.3	Clinical Development of PARP Inhibitors	111
5.04.2.3.1	Combination chemotherapy	111
5.04.2.3.2	Exploiting the synthetic lethality of PARPi in HRR-defective cancers	112
5.04.2.3.3	PARPi in combination with molecularly targeted agents	113
5.04.2.3.4	PARPi in combination with radiation	113
5.04.2.3.5	Biomarkers to detect HRR deficiency	114
5.04.2.4	**DNA-Dependent Protein Kinase**	115
5.04.2.4.1	DNA-PK Inhibitors	115
5.04.2.4.2	Clinical Development of DNA-PK Inhibitors	116
5.04.2.5	**ATM/CHK2 Signaling**	117
5.04.2.5.1	ATM Inhibitors	117
5.04.2.5.2	CHK2 Inhibitors	118
5.04.2.5.3	Clinical Development of CHK2 and ATM Inhibitors	119
5.04.2.6	**ATR/CH1 Signaling**	119
5.04.2.6.1	ATR Inhibitors	121
5.04.2.6.2	CHK1 Inhibitors	122
5.04.2.6.3	Clinical Development of CHK1 and ATR Inhibitors	123
5.04.2.6.3.1	CHK1 inhibitors	123
5.04.2.6.3.2	ATR inhibitors	124
5.04.2.7	**Summary, Conclusions, and Future Perspectives**	125
References		125
Relevant Websites		133

Abbreviations

A-T Ataxia-telangiectasia
ATM Ataxia telangiectasia mutated
ATR ATM and Rad3-related
BER/SSBR Base excision repair/single-strand break repair
BID or BD Twice daily
BROCA Panel of cancer risk genes (named after Paul Broca)
CDK Cyclin-dependent kinase
CHK1 Checkpoint kinase 1
CHK2 Checkpoint kinase 2
CLL Chronic lymphocytic leukemia
CPD Cyclobutane pyrimidine dimers
DDR DNA damage response
DNA-PK DNA-dependent protein kinase
dNTP Deoxynucleotide triphosphate
DSB Double-strand break
EGFR Epidermal growth factor receptor
HDAC Histone deacetylase
HRD Homologous recombination DNA repair defective
HRR Homologous recombination DNA repair
ICL Interstrand cross-link
IGFR Insulin-like growth factor receptor
IHC Immunohistochemistry
LOH Loss of heterozygosity
LST Large-scale state transition
MGMT Methylguanine DNA methyltransferase
MMR Mismatch repair
MTD Maximum tolerated dose
mTOR Mammalian target of rapamycin
NER Nucleotide excision repair
NHEJ Nonhomologous end-joining
NSCLC Nonsmall-cell lung cancer
OD Once daily
OS Overall survival
PARP Poly(ADP-ribose) polymerase
PARPi PARP inhibitors
PCNA Proliferating cell nuclear antigen
PFS Progression-free survival
PI-3K Phosphoinositol-3 kinase

 http://dx.doi.org/10.1016/B978-0-12-409547-2.12394-7

PIKK PI-3K-like kinase
PTEN Phosphatase and tensin homolog
ROS Reactive oxygen species
SAM *S*-Adenosylmethionine
SAR Structure–activity relationship
SSB Single-strand break
TIA Telomeric allelic imbalance
TMA Tissue microarray
TMZ Temozolomide
UV Ultraviolet

5.04.1 Introduction

The DNA damage response (DDR) consists of an elegantly orchestrated network of pathways signaling not only for repair of DNA lesions but also for activation of checkpoints that arrest the cell at key points in the cell cycle. When DNA was first discovered it was thought to be a very stable molecule because it is essential that it remains essentially unchanged from one generation to the next. However, thanks to the pioneering work of Thomas Lindahl, we now know DNA is continuously subject to an astonishing amount and spectrum of damage at an alarming rate, which would be incompatible with life if it were not dealt with at a similar rate. Lindahl, Modrich, and Sancar were awarded the Nobel Prize for Chemistry in 2015 for their ground-breaking work on DNA repair, underscoring the importance of the understanding of DNA repair.[1]

The most common lesions are base modification and DNA breaks caused by reactive oxygen species (ROS). ROS are generated at a high level due to normal metabolism, and this is increased during inflammation. It is estimated that these lesions occur at a rate of 10,000–100,000 events/cell/day. In general, they are repaired by the base excision repair/single-strand break repair (BER/SSBR pathway described by Lindahl.[2,3] Failure to repair these lesions before DNA replication leads to the collapse of replication forks and single-ended double-strand breaks (DSBs). Other common endogenously formed lesions can arise from errors of replication when the wrong nucleotide is incorporated by mistake (base mismatch), or one more or one less nucleotide is inserted (Indels, usually in a string of the same nucleotide)—leading to a loop. Although the polymerase DNA polα has a proof-reading function, it is not infallible, requiring the DNA mismatch repair (MMR) to repair the error, as first demonstrated by Modrich.[4] Natural exogenous sources also damage DNA, such as UV light, which causes cyclobutane pyrimidine dimers (CPD). These lesions kink the DNA and are repaired by nucleotide excision repair (NER) that Aziz Sancar described.[5] These are just three of the types of DNA damage and repair, but there are many sources and types of DNA damage. There are seven basic repair pathways to cope with them, the additional ones being: direct repair, nonhomologous end-joining (NHEJ), homologous recombination DNA repair (HRR), and interstrand cross-link (ICL) repair.

Direct repair is the simplest type of repair, and it involves the direct reversal of the lesion. Alkylations at the O^6-position of guanine from dietary nitrosamines or as a result of erroneous methylation by *S*-adenosylmethionine (SAM) are removed by methylguanine DNA methyltransferase (MGMT) leaving behind the natural base, guanine. Two highly cytotoxic lesions are DSBs and ICLs. DSBs arise from ROS-induced damage and background ionizing radiation (IR) and the prime natural source of ICLs are lipid peroxidation products, e.g., acrolein.[6] NHEJ is the simplest way of dealing with DNA DSB, and this process can occur at any phase of the cell cycle (although it is suppressed during S-phase). However, the fidelity of NHEJ is not completely accurate. When the sister chromatid is available, i.e., late S-phase and G2, it can be used as a copy for high-fidelity repair of DSB by the HRR pathway. The repair of ICLs is highly complex and involves elements of both NER and HRR, especially the Fanconi proteins.

Of course, it is no good having multiple repair pathways if the cell does not stop its proliferation long enough for repair to be completed. The cell proliferation cycle starts with G1, the period from the birth of the daughter cell to when DNA synthesis starts in S-phase, after S-phase the cell goes into G2 before progressing into mitosis or M-phase when the two identical daughter cells are born. For the cell to retain its genomic integrity, and hence vitality, any DNA damage occurring during G1 must be repaired before the cell enters S-phase and any occurring during G2 must be repaired before the cell divides. Damage occurring during S-phase must be repaired immediately or during G2. Failure to both arrest and repair will lead to mutations in the daughter cells, and most likely, cell death. To ensure cell survival the DDR is engaged. Two principal kinases, ataxia telangiectasia mutated (ATM) and ataxia telangiectasia and Rad3-related (ATR), are involved in transducing the signal from DNA damage to the different outcomes, which are cell-cycle arrest and DNA repair or, if the damage is too great, cell death. There is some overlap in their targets, but on the whole ATM signals via checkpoint kinase 2 (CHK2) and p53 to arrest the cell in G1 and ATR signals via checkpoint kinase 1 (CHK1) to S and G2/M arrest. An overview of the lesions and DDR pathways involved is given in **Fig. 1**.

These DDR pathways pose both challenges and opportunities for cancer therapy.[7] Inhibiting DNA repair or impairing DNA damage checkpoint signaling can sensitize cells to genotoxic anticancer agents (**Fig. 2A**). For example, IR (e.g., radiotherapy) causes base damage and single-strand breaks (SSBs) that depend on the BER/SSBR pathway for repair, and also DSBs that are repaired by NHEJ and HRR. Therefore inhibiting BER/SSBR, NHEJ, or HRR can increase the radiosensitivity of tumor cells. Similarly cisplatin and carboplatin cause both intra- and interstrand cross-links in the DNA. The former are repaired by NER and the latter by ICL repair, the NER intermediates, and the stalled replication forks, which arise due to the ICL, trigger ATR-dependent checkpoint signaling. Therefore inhibition of ATR will sensitize cells to cisplatin. This approach risks also increasing the sensitivity of normal cells. This means that the ratio of the dose that produces toxicity relative to the dose that is effective—termed the therapeutic index—may be unchanged, and the doses may just be lower. For example, the first studies to use inhibition of DNA repair as

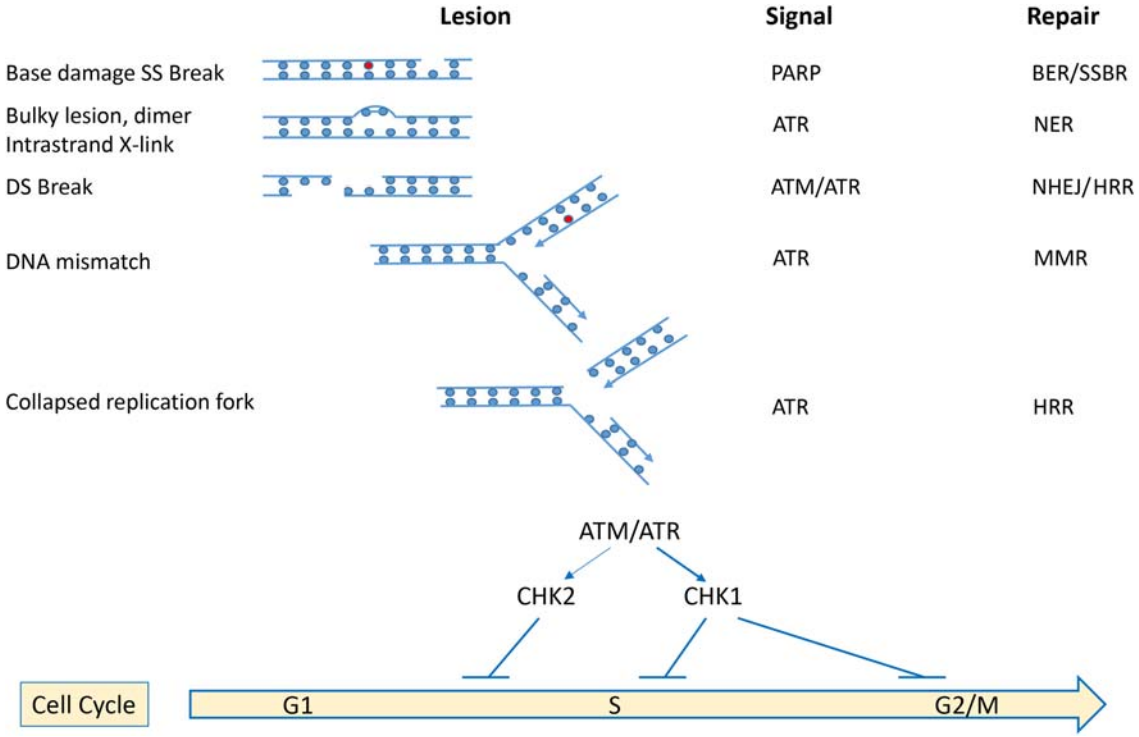

Fig. 1 DNA lesions and activation of the DNA damage response. Base damage and single-strand breaks are signaled via PARP for BER/SSBR, ATR is activated by various lesions to effect S/G2 arrest and DNA repair, and ATM activates cell-cycle arrest and repair of DSBs.

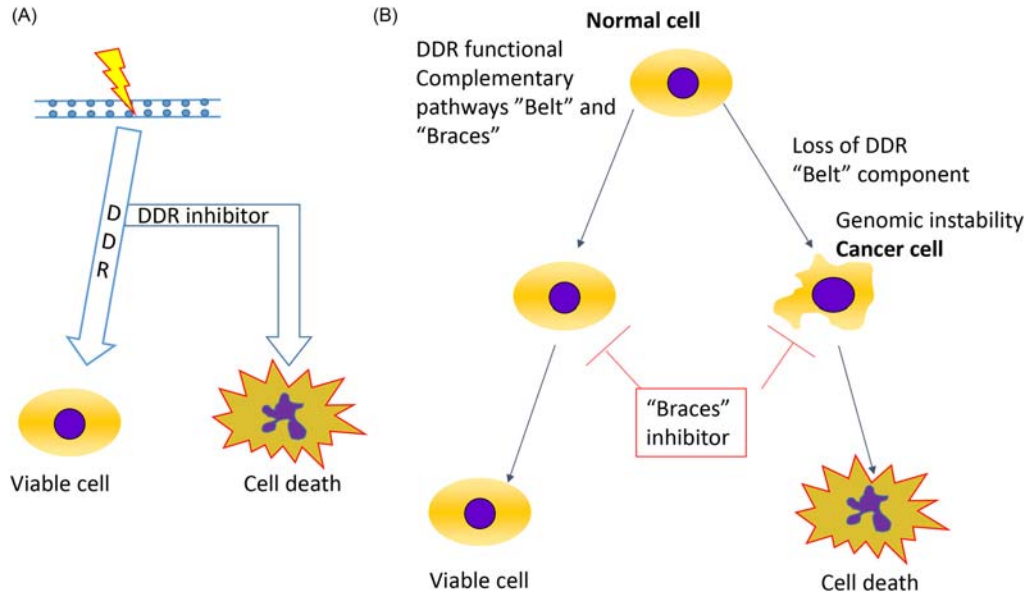

Fig. 2 The rationale for the use of DDR inhibitors in combination with DNA-damaging agents and as single agents for synthetic lethality. (A) Where a DDR pathway promotes survival following exposure to a DNA-damaging anticancer agent, inhibition of a key element of that pathway can increase the sensitivity or overcome resistance. (B) Cells frequently employ back-up pathways to counteract the lethal effects of common endogenous damage in a "belt and braces approach." Dysfunction in one DDR pathway, the "belt," leads to cancer development but also increased reliance on the back-up "braces" pathway such that inhibition of this "braces" pathway results in cell death by synthetic lethality.

a strategy to sensitize tumors to genotoxic agents employed inhibitors of methylguanine methyltransferase (MGMT). MGMT conducts the direct repair of O^6-alkylguanine—the most cytotoxic lesion caused by alkylating agents. Despite being a promising approach in preclinical studies these MGMT inhibitors have not shown clinical utility in combination with alkylating agents because of concomitantly increased toxicity.[8] However, because cancer cells generally have dysfunctional DDR they tend to be more sensitive to genotoxic stress, and so there will still be a therapeutic index, but how great that is will depend on the cancer phenotype.

One way of increasing the therapeutic index is to exploit the principle of "synthetic lethality." Synthetic lethality is when inactivation of two proteins, or pathways, results in cell death, but inactivation of either alone does not compromise viability. This principle is particularly applicable to the molecular derangements that occur in cancer.[9] One of the enabling characteristics of cancer is "genomic instability"[10] that is frequently caused by loss of an element of the DDR. Therefore targeting the DDR using the synthetic lethal approach is particularly applicable in cancer. Dysfunction of one element of the DDR creates genomic instability because either DNA damage will not be repaired efficiently or the cell will not arrest its proliferation cycle properly. This makes it more likely that the damage will be passed to the next generation and that mutations will accumulate. The accumulation of mutations can lead to cancer. Inhibiting one aspect of the DDR can have preferential cytotoxicity to a cell that already has a DDR dysfunction. It exploits the "belt and braces" approach that cells employ for critical functions such that if the "belt" is lost the "braces" can perform the same function, albeit in a different way. Cells that have lost the "belt" are exquisitely vulnerable to an attack on the "braces" (**Fig. 2B**).

The most common DDR defect is the loss of the G1 checkpoint by various means, most frequently, but not exclusively, by p53/pRb pathway disruption.[11] Both p53 and pRb are classic tumor suppressor genes and function primarily to trigger the G1 checkpoint. Many tumor suppressors are DDR proteins, e.g., BRCA1/2, the breast and ovarian cancer susceptibility genes, which play key roles in HRR.[12] Other DDR components may also be considered tumor suppressors, e.g., mutations in MMR genes are associated with Lynch syndrome that confers colon and ovarian cancer susceptibilities.[13] DDR dysfunction can also result in "non-oncogene addiction," whereby loss of one DDR component may be compensated for by upregulation of another DDR component on which the tumor cell depends to maintain sufficient integrity of its genome for survival. This imbalance of the DDR poses both challenges, e.g., if the upregulated component confers therapy resistance, and opportunities to exploit defects. Inhibitors of the DDR have been developed both to be used in combination with DNA-damaging agents to overcome resistance, and as single agents to exploit vulnerabilities caused by DDR dysfunction. For this approach to work, it is important to identify determinants of sensitivity and robust biomarkers are needed to identify whether a tumor has that determinant. Such biomarkers are necessary to be able to target tumors appropriately and spare patients unnecessary side effects if their tumor is likely to be unresponsive. Identification of the synthetic lethality of PARP inhibitors (PARPi) in BRCA mutant cells is the classic example as will be described in the next section.

5.04.2 Poly(ADP-Ribose) Polymerase (PARP)

5.04.2.1 PARP Discovery and Function

The enzyme we now call PARP1 was discovered in the 1960s by workers in Strasbourg and Tokyo.[14,15] The observation that led to its discovery was the rapid consumption of NAD^+ when cells were exposed to alkylating agents (the first chemicals used to treat cancer).[16] The ADP-ribose polymer product was found before the enzyme and originally thought to be a type of nucleic acid. PARP1 is activated by DNA breaks arising directly through, e.g., oxidative cleavage of the backbone, BER intermediates, and trapped topoisomerase I. PARP1 binds to the nick in DNA via its zinc fingers causing it to change to its active conformation. Active PARP1 consumes NAD^+ as a substrate to produce polymers of ADP-ribose attached to itself and nuclear proteins, especially histones. The powerful negative charge of the polymers helps both loosen chromatin to facilitate repair and also recruits XRCC1, the scaffold protein for the enzymes DNA polb and ligase III, which effect repair. The creation of the PARP1 knockout mouse led to the discovery of a second DNA damage-activated PARP, PARP2,[17–19] and subsequently, based on sequence homology, a family of 17 PARP-like enzymes were discovered.[20] Only six have the ability to polymerize ADP-ribose, and the others have mono-ADP ribosylation or unknown activity. PARP1 is the principal DNA damage-activated PARP, followed by PARP2. There is substantial functional redundancy between these two enzymes but not complete overlap. Genetic deletion of either PARP1 or PARP2 independently results in viable and fertile mice with only mild pathologies, but deletion of both enzymes is embryonically lethal[21] underscoring their important function. PARP1 and 2 both function in DNA SSBR and PARP1 also participates in DNA DSB repair, either through interaction with DNA-dependent protein kinase (DNA-PK) or via an alternative NHEJ pathway.[22,23] PARP3 may also cooperate with PARP1 in DSB repair although this enzyme may not have polymerization activity.[24]

5.04.2.2 PARP Inhibitors

PARPi were first developed to elucidate the function of PARP and were based on the PARP catalytic mechanism, that is, the cleavage of NAD into ADP-ribose (for polymer formation) and nicotinamide as a by-product. Nicotinamide exerts a weak feedback inhibition, and the early PARPi were simple analogues of nicotinamide, the benzamides. A pivotal moment in the development of PARPi was in 1980 when 3-aminobenzamide (3AB) (**Fig. 3**) was first shown to inhibit DNA repair and to enhance the cytotoxicity of a DNA-methylating agent, MMS.[25]

PARPi discovery and development has been undertaken by a number of academic groups since the 1980s, with a shift to the pharmaceutical industry with time. During the 1990s PARPi of increasing potency and specificity were discovered using various approaches. One approach, based on the notion that elaboration of nicotinamide/benzamide would identify novel inhibitors,

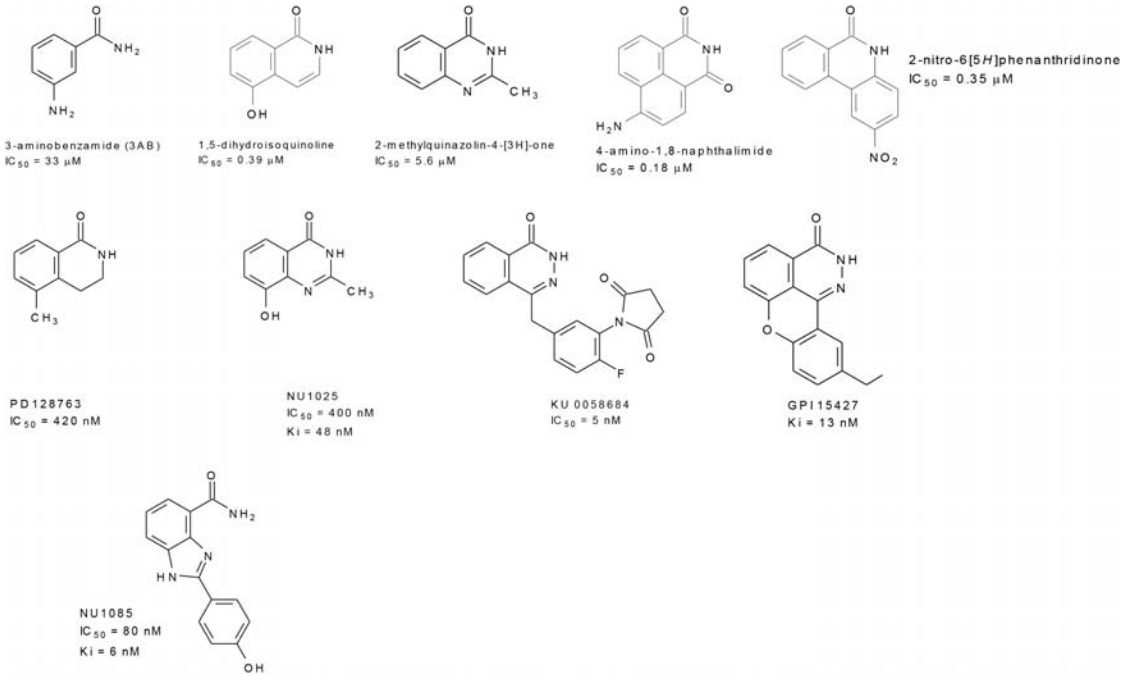

Fig. 3 First- and second-generation PARP inhibitors. 3-Aminobenzamide, the first PARPi, and the compounds identified by Banasik et al.[26] are shown on the top row, while those identified by synthetic chemistry or screening of compound libraries are shown below.

was to search for chemicals that contained this pharmacophore, the so-called analogue by catalog approach. Screening 170 commercially available compounds for their PARP inhibitory activity identified several potent compounds, making a major contribution to inhibitor design[26] (Fig. 3). Several of these compounds have been used as leads for subsequent drug development by various groups, including PJ-34 (Fig. 3) and subsequently INO-1001 (Fig. 4) that entered clinical trials.[27,28] Screening of the Maybridge compound library led to the identification of compounds with potent PARPi activity, e.g., KU0058684 (Fig. 3), similar to those identified by Banasik et al. that led ultimately to the development of olaparib[29] (Fig. 4). Using a conventional synthetic chemistry approach to develop structure–activity relationships (SARs) led to the identification of PARPi with increased potency,

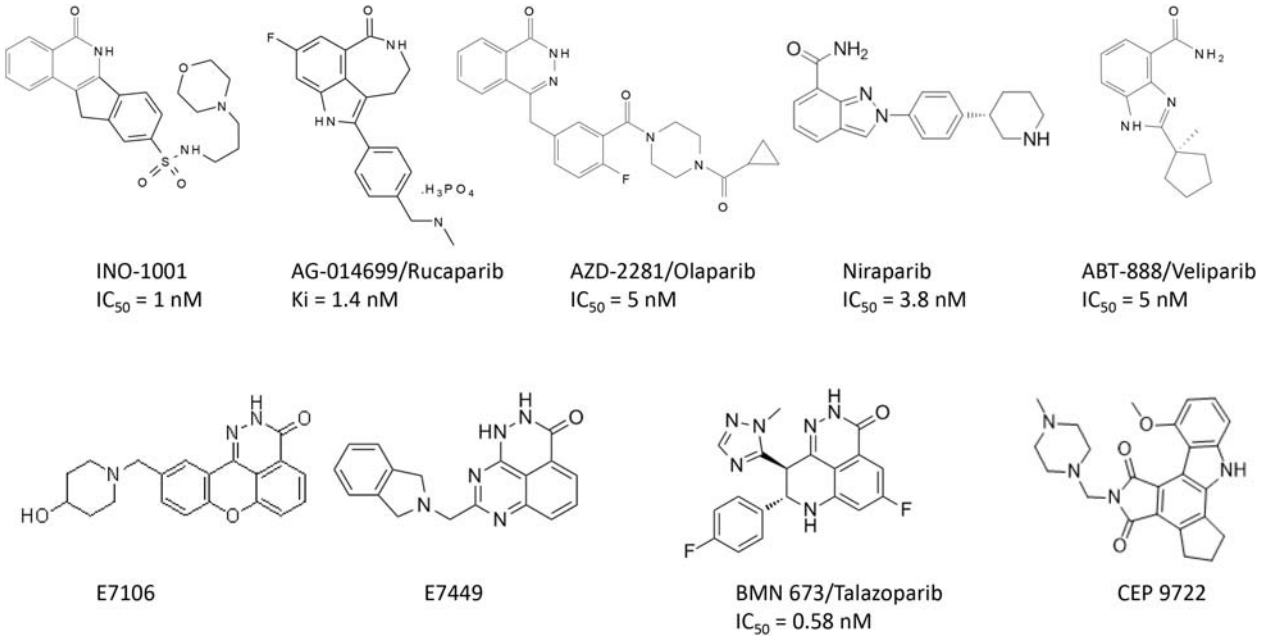

Fig. 4 PARP inhibitors that have entered clinical trial.

including PD128763 and the NU compounds including NU1025 and NU1085 (Fig. 3), ABT-888 (Veliparib), and MK-4827 (Niriparib)[28] (Fig. 4). The third approach was to use structure-based drug design by crystallization of inhibitors in the NAD^+-binding site of the PARP1 catalytic domain, and this demonstrated several key interactions that confirmed SAR and analogue by catalog data.[30,31] This structure-based drug design approach led to the development of AG014699 (rucaparib, Fig. 4) that was the first PARPi to enter clinical trial in cancer patients.[32,33]

5.04.2.2.1 Chemosensitization and radiosentitization

Consistent sensitization of DNA-methylating agents, IR, and topoisomerase I poisons has been observed across a wide spectrum of PARPi and validated by genetic knockdown in cells and mouse models.[34] Sensitization of other genotoxic agents by PARPi has also been reported, but the sporadic nature of the reports suggests that they may be peculiar to an individual PARPi, so possibly an off-target effect, or cell line dependent. For example, sensitization of cisplatin may be dependent on a defect in HRR since AZD2281 (olaparib) selectively sensitized BRCA2 defective cell lines, but not BRCA2-proficient cells to platinum therapy.[35]

Inhibition of PARP activity has a greater impact on repair than does loss of the enzyme. The mechanism that was originally proposed, on the basis of some elegant experiments in Lindahl's lab in the early 1990s, was that inhibition of PARP1 activity did not prevent DNA binding but did inhibit its dissociation from the DNA, driven by auto-poly(ADPribosylation). Therefore, PARP1 remained bound to DNA breaks obstructing repair. This was based on the observation that repair of SSB by nuclear extracts was unaffected by the depletion of PARP1 but abrogated by depletion of NAD^+ or the addition of 3AB in extracts containing PARP1.[36] This has been verified by chromatin immunoprecipitation experiments that showed an increase of the binding of PARP1 to DNA in the presence of an inhibitor.[37] Recently it was proposed that the ability of inhibitors to "trap" PARP1 on DNA was independent of catalytic inhibitory potency and via an allosteric mechanism,[38,39] but further investigations demonstrate that trapping is due to catalytic inhibition.[40]

Monofunctional DNA-methylating agents are the most potent activators of PARP, and prior to 2005 when the synthetic lethality of PARPi with BRCA mutations was identified, most of the initial drive to develop PARPi was as sensitizers of these agents. DNA-methylating agents currently used in anticancer therapy include dacarbazine (DTIC) and temozolomide (TMZ), currently largely used to treat brain tumors and melanoma. TMZ and DTIC methylate purines, and PARP is critical to the repair of this by BER/SSBR. Early studies showed that PD128763 and NU1025 (Fig. 3) were about 50× as potent as 3AB in increasing TMZ-induced DNA-strand breakage and cytotoxicity.[41] Various preclinical PARPi have been demonstrated to enhance TMZ in a variety of cell lines from different cancer types and, where studied, independently of p53 status.[42–44] Defects in MMR confer resistance to TMZ and studies of MMR-deficient and -proficient cells demonstrated that PARPi preferentially potentiated TMZ in the MMR-defective cells, overcoming resistance.[45–47] Since only tumors lack MMR, PARP inhibition, in combination with TMZ, represents a potentially selective therapeutic approach. Many of the PARPi that have entered clinical trials have been shown to potentiate TMZ in the preclinical setting. ABT-888 (veliparib) was shown to enhance TMZ cytotoxicity preferentially during S-phase, indicating that an accumulation of replication-associated DSBs was largely responsible for cell death.[48] The most potent PARPi, BMN 673 (Fig. 4) potentiated TMZ in a variety of breast and lung cancer cell lines, independently of BRCA status.[49] The cellular potentiation of TMZ by PARPi has been confirmed in xenograft studies in a huge variety of tumor types.[34] Since TMZ is largely used in the treatment of brain tumors the inhibitors that are able to cross the blood–brain barrier, ABT-888 (veliparib) and GPI-15427 (Fig. 3) and the closely related drugs E7016 and E7449 (Fig. 4), are particularly relevant. Both E7016 and ABT-888 (Fig. 4) have demonstrated enhancement of TMZ, or a combination of IR and TMZ, antitumor activity in in vivo models of glioblastoma.[50,51]

The limited application of TMZ and DTIC in cancer chemotherapy compared to the topoisomerase I poisons, which PARPi also sensitize cells to make the latter combination more attractive. Topoisomerase I poisons are used in the treatment of a variety of cancers; irinotecan is used to treat colorectal cancer, and topotecan is used in the treatment of small-cell lung cancer, and ovarian and cervical cancer. Topoisomerase I catalyzes the transient single-strand breakage, and reannealing of DNA to relieve torsional strain and the topoisomerase I poisons, such as the camptothecins, cause the accumulation of SSB by preventing reannealing. NU1025 was shown to increase camptothecin-induced DNA breaks and cytotoxicity in L1210 cells,[52,53] and later several studies confirmed potentiation with camptothecins (topotecan and irinotecan) and related drugs in a variety of models, independently of p53 status, in human cancer cell lines and xenografts.[34]

The most commonly administered genotoxic agent for cancer therapy is IR with radiotherapy being used at some stage in the treatment of around 50% of cancer patients. Early studies revealed that 3AB radiosensitized mammalian cells[54] and numerous studies have demonstrated the ability of PARPi in general to radiosensitize both cells and xenografts.[34] Where studied, radiosensitization appears to be greatest in S-phase cells, possibly because by inhibiting their repair, SSB accumulate, leading to the much more toxic collapsed replication forks. This hypothesis is supported by the increase in both γH2AX and RAD51 foci following exposure to radiation and PARPi.[55] On the other hand, PARP1 is proposed both to participate in DNA DSB repair either through cooperation with NHEJ or through a role in alt-NHEJ.[56,22,23]

5.04.2.2.2 Vasoactivity of PARPi

Another interesting feature that may lead to greater chemo- and radiosensitization in vivo than is observed in vitro is the observed vasoactivity of two clinically active PARPi (olaparib and rucaparib) as well as nicotinamide, which may indicate a class-effect. The vasoactive effects of AG14361 and AG014699 have been shown to lead to increased tumor perfusion with the implication that this improves drug delivery and oxygenation.[57,58] Using preconstricted rat arteries both inhibitors had a direct effect on the blood vessels' smooth muscle, and AG014699 was more potent than the common antihypertensive drug, hydralazine.[58] Similarly,

radiosensitization by olaparib in xenograft studies was found to be at least partly due to increased perfusion of the tumors, thereby reducing the hypoxic radio-resistant fraction.[59] Nicotinamide itself and simple analogues have long been known to cause vasodilation, improve oxygenation, and cause radiosensitization in preclinical studies,[60] and nicotinamide has been used as a radiosensitizer in clinical trials.[61,62]

5.04.2.2.3 Single-agent activity

The most exciting use of PARPi is as single agents, based on the paradigm-shifting studies demonstrating the synthetic lethality (Fig. 2B) of PARPi in tumors defective in HRR.[63,64] These initial studies demonstrated that concentrations of a panel of PARPi that were noncytotoxic to cells with functional HRR killed cells lacking BRCA2, XRCC2, XRCC3 or with silenced BRCA2.[63] Additionally, the PARPi KU0058948 and KU0058684 were particularly cytotoxic to BRCA1- and BRCA2-defective mouse embryonic stem cells.[64] The proposed mechanism is dependent on the high rate of endogenously ROS-induced SSBs; inhibition of PARP1 prevents their repair, so when they meet the advancing replication fork this results in collapsed replication forks that require HRR for repair. When HRR is defective these lesions prove lethal (Fig. 5). This is likely to be a tumor-specific therapy because HRR defects are relatively common in tumors but very rare in normal tissues.[65,66]

Defects in HRR in tumors are associated with more than just germline mutations in BRCA1 and 2, since mutations in these genes can arise in spontaneous cancers and BRCA1 can be silenced epigenetically, which also confers hypersensitivity to PARP inhibition.[67] HRR is a complex process involving several components including ATM, ATR, CHK1, MRN (MRE11/RAD50/NBS1), several FANC proteins, and RAD51 and its homologues. The loss of any one of these components can confer HRR dysfunction and cause PARPi sensitivity.[68] In addition, under hypoxic conditions, which are a common feature of cancer cells due to their deranged vasculature, HRR appears to be downregulated thereby conferring a "contextual synthetic lethality" with PARPi.[69]

Some interesting data are emerging regarding the interaction of PARP and the phosphoinositol-3 kinase (PI-3K)/mammalian target of rapamycin (mTOR) pathway. Phosphatase and tensin homolog (PTEN), a commonly mutated tumor suppressors in human cancer, is involved in the PI-3K pathway and has also been implicated in HRR. Some studies show that PTEN loss or disruption conferred sensitivity to PARPi.[70,71] However, subsequent data suggest that PTEN loss is not a universal indicator of PARPi sensitivity.[72,73]

5.04.2.2.4 Combinations with molecularly targeted agents

As PARPi have progressed in the clinic an increasing number of studies have assessed the potential of PARPi in combination with molecularly targeted agents, most commonly kinase inhibitors of various descriptions.

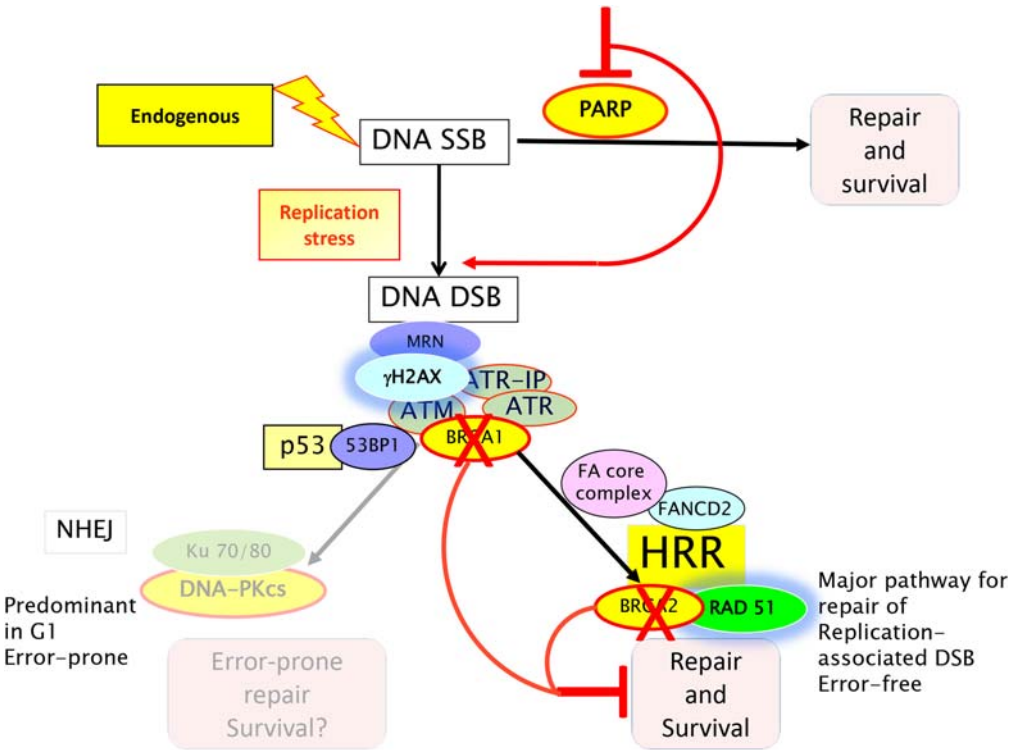

Fig. 5 The synthetic lethality of PARP inhibitors. Due to the high level of endogenously generated DNA single-strand breaks, inhibition of their repair by PARPi leads to replication stress that is repaired by HRR, of which BRCA1 and 2 are key components. When HRR is compromised, e.g., due to BRCA1/2 mutations the DNA cannot be repaired and the cells die.

Many studies have investigated PI-3K inhibitors. However, PI-3K-like kinases (PIKKs) include mTOR and those PIKKs involved in the DDR: ATM, ATR, and DNA-PKcs, so data on PI-3K and mTOR inhibition may deserve some cautious interpretation. It is possible that the effect of the inhibitors may be due to so-far unidentified interactions with the other DDR PIKKs. For example, the dual PI-3K/mTOR inhibitor, NVP-BEZ235 has been shown to inhibit ATM, ATR, and DNA-PKcs.[74,75] Studies indicate that PI-3K inhibition downregulated BRCA and reduced RAD51 focus formation, indicating a negative impact on HRR, and that PI-3K inhibitors increased the antitumor activity of PARPi in breast cancer models.[75-78] Recent studies indicate that PARP inhibition causes PI-3K/mTOR activation and that inhibition of PI-3K can be synergistic with the PARPi BMN 673 in small-cell lung cancer models.[79] Another PIKK, mTOR may also be implicated in HRR, and data indicate that mTOR inhibition suppresses HRR and sensitizes triple-negative breast cancer cells to PARPi in vitro and in vivo.[80–82] Because there are somewhat conflicting data regarding the targeting of the PI-3K/mTOR pathway for PARPi sensitization, further work is needed to determine if the effectiveness of these combinations is cell-type or drug-specific. Nevertheless the data so far present promising avenues to pursue. Receptor tyrosine kinases that act via PI-3K signaling may also be good targets for PARPi sensitization. EGFR and IGFR inhibitors have also been shown to suppress HRR function and increase the sensitivity of cells to PARPi.[83,84] Histone deacetylases (HDACs) may be necessary for HRR function, and HDAC inhibitors have been shown to reduce the expression of BRCA1 and RAD51, increase DNA damage, and sensitize cells to PARPi.[85,86]

Targeting cell-cycle control with CHK1 inhibitors sensitizes cells to PARPi as discussed later, for example, three different CHK1/2 inhibitors in combination with four different PARPi resulted in increased DNA damage and cell death.[87] Other studies showed that CDK1 regulates BRCA1 activity and that CDK1 inhibition increased the sensitivity of lung cancer cells, xenografts, and spontaneous lung cancers in mice to the PARPi, AG-014699 (rucaparib) without significant toxicity.[88] Subsequent studies showed that the CDK1 inhibitor, dinaciclib, inhibits HRR and sensitizes multiple myeloma cells to PARPi.[89]

Taken together, these data offer exciting possibilities for the combination of PARPi with other molecularly targeted agents.

5.04.2.3 Clinical Development of PARP Inhibitors

5.04.2.3.1 Combination chemotherapy

The first Phase I trial of PARPi in cancer patients was initiated in 2003. AG014699 (rucaparib) was given in combination with TMZ as the synthetic lethality of PARPi had not been revealed at this stage. In this study, of 33 patients with advanced solid tumors, PARP inhibition was seen at all doses.[33] The average tumor PARP inhibition was greater than 90% at 5 h (range 46–97%), and an increase in DNA SSB was seen in all patients treated with PARP-inhibitory dose. There was encouraging evidence of activity observed, and rucaparib alone was not associated with observed toxicity, but it increased the myelosuppression associated with TMZ, particularly at the maximum dose of rucaparib (18 mg/m^2), including thrombocytopenia and neutropenia. The safe dose for Phase II studies in combination with full-dose TMZ was determined to be 12 mg/m^2.

When rucaparib (at 12 mg/m^2) was combined with TMZ in a Phase II trial of patients with metastatic melanoma, there was a response rate of 17.4% among the 46 patients that were entered into the study with improved progression free survival (PFS).[90] However, just as observed in the Phase I trial, myelosuppression was seen in more than half of the patients, and the dose of TMZ had to be reduced by a quarter.

Other studies have investigated the combination of TMZ and PARPi. Following on the rucaparib study in melanoma patients a double-blinded Phase II study of veliparib in advanced metastatic melanoma (stage III or IV) revealed an increase in PFS of 2 months in the placebo-treated patients compared to 3.6 or 3.7 months in the veliparib (20 or 40 mg) arms. The patients having the best responses expressed low levels of ERCC1. Unfortunately, this did not translate to an increase in overall survival.[91] Similarly, the combination of olaparib with dacarbazine (DTIC, similar to TMZ) in patients with melanoma was well tolerated, but no objective response was demonstrated.[92]

TMZ and dacarbazine are used in the treatment of brain tumors, including glioblastoma multiforme (GBM) because they readily cross the blood–brain barrier. The most advanced PARPi that also penetrates the brain is veliparib, and this has been used in combination with these alkylating agents. In a Phase I/II trial of patients with glioblastoma, the combination of veliparib and TMZ was well tolerated, but there was no difference in PFS and overall survival when compared to TMZ alone.[93] However, these were unselected patients, and translational studies in patient-derived GBM xenografts reveal that those with hypermethylation of the 0^6-methylguanine-DNA-methyltransferase (MGMT) promoter responded better to the combination of TMZ + veliparib.[94] This has now formed the basis of an ongoing phase II/III trial of the combination of veliparib and TMZ in GBM patients with MGMT promoter hypermethylation (NCT02152982).

The combination of veliparib and TMZ has also been trialed in patients with hepatocellular cancer in a Phase II trial. Sixteen patients with hepatocellular cancer were administered with 40 mg OD of veliparib over 7 days and 150 mg/m^2 of TMZ over 5 days.[95] However, even though the combination regime was well tolerated in the patients, survival benefit was not observed and the study had to be discontinued.

Veliparib, in combination with TMZ, has also been evaluated in the pediatric population. In a Phase I trial, 29 children with recurrent brain tumors were given escalating doses of veliparib and TMZ as a fraction of established doses in the adult population.[96] The combination therapy was well tolerated in the children, and although objective response was not seen, a small fraction of the patients had stable disease for more than 6 months.[96] Having established the recommended phase II doses, a phase I/II clinical trial is now ongoing to evaluate the efficacy of the combination regime in children with brainstem gliomas.

PARPi have also been evaluated in combination with topoisomerase poisons. In the first published study, Kummar and colleagues evaluated the effect of the combination of 10 mg of oral veliparib in combination with varying doses and schedules of intravenous topotecan in 24 patients with refractory solid tumors and lymphomas.[97] PARP inhibition of greater than 75% was observed in three paired tumor biopsy samples and by >50% in peripheral blood mononuclear cells (PBMCs) from 19 of the 23 patients. The combination resulted in an increase in γH2AX in both circulating tumor cells and PBMCs suggesting that repair was inhibited. Some limited efficacy was observed: Stable disease in four out of six patients at dose-level 1 of topotecan (1.2 mg/m^2) but dose-limiting myelosuppression was observed in four/six patients, necessitating dose reductions and schedule changes.[97] A similar Phase I study with olaparib in combination with topotecan in patients with solid tumors also observed a dose-dependent increase in dose-limiting neutropenia as well as gastrointestinal toxicity and established an MTD of topotecan of 1 mg/m^2 × 3 days in combination with olaparib at 100 mg bid. This combination was not pursued due to lack of increased efficacy of the combination.[98] The tolerability and efficacy of PARPi and irinotecan were evaluated in a Phase I study of patients with advanced solid tumors who were administered with 100 mg/m^2 of irinotecan on days 1 and 8 of a 21-day cycle and escalating doses of veliparib.[99] Veliparib decreased ADP-ribose polymer levels at all doses, and there was evidence of increased DNA damage. Anti-tumor activity was observed at all doses with partial response in almost 20% of the 35 patients.[99] Olaparib has also been investigated further with irinotecan in patients with colorectal cancer: 11 patients who received continuous olaparib with irinotecan every 3 weeks had higher than expected toxicity, but a schedule of intermittent olaparib with irinotecan every 2 weeks was better tolerated. Toxicities were hematological and gastrointestinal, and the best response was stable disease for 4–13 months. The recommended schedule for Phase II was olaprarib 50 mg po BID days 1–5 and irinotecan 125 mg/m^2 every 2 weeks.[100]

Combinations with topoisomerase II poisons have also been evaluated. The safety profile of the triple combination of 100 mg dose of veliparib with cisplatin (75 mg/m^2 on day 1) and etoposide (100 mg/m^2 on days 1–3) in a 21-day cycle was evaluated in patients with small-cell lung cancer and was well tolerated with minimal adverse effects.[101]

The combination of PARPi with platinum-based chemotherapy has also been evaluated in a number of studies. This followed the confirmation of antitumor activity of this combination regime in preclinical studies.[39,102] Olaparib, in combination with cisplatin, was administered to patients with advanced solid tumors in a Phase I trial. The patients were given 50 mg BD of olaparib and 60 mg/m^2 of cisplatin, with a favorable objective response rate observed in more than 40% in patients with BRCA 1/2-mutated ovarian cancer and 71% among patients with BRCA1/2-mutated breast cancer.[103]

Not all combination studies have demonstrated clinical efficacy. In another Phase I study of the combination of olaparib with gemcitabine in patients with pancreatic cancer, escalating doses did not achieve desired clinical efficacy.[104] These findings suggest that while certain PARPi combination therapies offer exciting novel treatment strategy in some malignancies, they are not particularly effective in other cancers.

Lee and colleagues evaluated the safety profile of olaparib in combination with carboplatin in patients with BRCA-mutated breast or ovarian cancer and established 400 mg BD of olaparib as a tolerable dose.[105] In another study, olaparib was administered in combination with cisplatin and gemcitabine in patients with advanced solid tumors, but myelosuppression was observed even at relatively lower doses, which could limit the effectiveness of this combination therapy in further trials.[106] The long-term use of olaparib following combination therapy was evaluated in a study of 21 patients with breast, ovarian, and fallopian tube cancers who were initially administered with olaparib plus carboplatin and/or paclitaxel and then olaparib monotherapy.[107] In patients with initial response to the combination therapy, this response was maintained with long-term use of olaparib monotherapy and was well tolerated although adverse effects of myelosuppression, fatigue, and pain were observed in some patients.

It appears that there is an association between myelosuppression and PARPi. Establishing a therapeutic window of these combinations, which could be narrow in certain combinations, could reduce these adverse events and encourage progression from bench to bedside. Despite this shortcoming, the trial results from PARPi in combination with other chemotherapy agents are very encouraging indeed and could eventually be established in standard clinical care.

5.04.2.3.2 Exploiting the synthetic lethality of PARPi in HRR-defective cancers

The most exciting clinical use of PARPi is as a single agent to exploit HRR defects in tumors by synthetic lethality. The first Phase I trial of olaparib was as a single agent and as soon as the data regarding the synthetic lethality of PARPi in models of BRCA mutant cancer became known, the patient population was enriched for those with germline BRCA 1/2-mutations. In this pivotal study of 60 patients with or without BRCA-mutated cancers, objective antitumor response was observed only in the patients with BRCA mutation when they were administered with 200 mg of olaparib or more twice a day in 4-week cycles. Out of 19 pretreated breast, ovarian, or prostate cancers there were 12 responses (nine partial or complete, two stable disease, and one tumor marker decrease). Most of the responses in ovarian (8), the two breast and one prostate cancer responders were BRCA2 carriers. The side effects were mild, mostly nausea and fatigue with no significant increase in side effects among the mutation carriers.[108] PARP inhibition by more than 90% was observed in patients that received 60 mg or more of olaparib twice daily. When the dose was increased to 400 or 600 mg twice a day, toxicity was observed in three patients. These include mood change in a patient with advanced ovarian cancer, thrombocytopenia in a patient with mesothelioma, and somnolence in a patient with metastatic breast cancer. This publication provided a significant further stimulus to the clinical development of PARPi as single agents, with the most advanced being olaparib, niriparib, and rucaparib, and the highly potent talozaparib (BMN 673) more recently advancing rapidly in clinical trials. In another trial of olaparib in patients with BRCA-mutated advanced breast cancer, women were given either 400 mg BD oral olaparib or 100 mg BD of oral olaparib. The objective response rate was 41% in the cohort with the higher dose and 22% in the cohort with lower dose of olaparib.[109] Olaparib has also been evaluated in BRCA-mutated ovarian cancer in a Phase II trial where women

with either BRCA1 or BRCA2 mutations were administered with 400 mg BD ($n=33$) of olaparib and another cohort with 100 mg BD ($n=24$). The objective response rate was 33% in the first cohort that received 400 mg BD olaparib compared to 13% in the cohort that received the lesser regime.[110] This confirms that response is highly dependent on dosing, but this will have to be balanced with potential adverse effects.

Olaparib has demonstrated its greatest efficacy in ovarian cancer. In a Phase II trial where the efficacy of olaparib was evaluated in women with high-grade ovarian cancer and triple-negative breast cancer with and without BRCA mutation, 90 women received 400 mg BD of olaparib.[111] In the ovarian cancer cohort, the objective response rate was 41% among women with BRCA mutation and 24% in women without BRCA mutation. Surprisingly, there was no improvement in the response rate in the breast cancer group. The fact that there was response in women without BRCA mutation is probably because there are other defects that result in compromised HRR besides BRCA mutation.

The efficacy of another PARPi, rucaparib, was evaluated in a Phase II multicenter trial of patients with BRCA-mutated breast or ovarian cancer.[112] Escalating doses of rucaparib were administered and were well tolerated. Although the objective response rate was disappointing at 2%, more than 40% of the patients had stable disease for more than 3 months. More importantly however, it was observed that patients that were maintained on oral rucaparib following intravenous rucaparib had a higher response rate of 15%, suggesting that continuous therapy is needed for sustained response, although it will be important to monitor potential side effects in long-term use.

To evaluate the efficacy of veliparib as a single agent, 50 patients with BRCA-mutated recurrent ovarian cancer were given 400 mg BD oral veliparib.[113] The overall objective response rate was 26%, with a higher response rate of 35% observed in platinum-sensitive patients compared to 20% in platinum-refractory patients.

Niraparib has also been evaluated in patients with BRCA-mutated malignancies and sporadic cancer. Escalating doses of niraparib were administered to patients with BRCA-mutated ovarian and breast cancers as well as patients with sporadic ovarian cancer, prostate cancer, and nonsmall-cell lung malignancies.[114] The maximum tolerated dose of niraparib was 300 mg/day. Partial response was reported in 8 out of 20 patients with BRCA-mutated ovarian cancer, and antitumor activity was observed in patients with sporadic ovarian, prostate, and nonsmall-cell lung malignancies.[114] These findings suggest that while the antitumor activity of PARPi was previously mostly limited to BRCA-mutated cancers, PARPi could also be beneficial in sporadic cancers.

The promising results from these trials led to an international, randomized, double-blind, placebo-controlled trial of olaparib in women with platinum-sensitive serous ovarian cancer (Study 19). Patients were randomized to receive 400 mg olaparib BID (136) or placebo (129). The median PFS was 11.2 months in the olaparib group and 4.3 months in the placebo group in the patients with BRCA mutations, with similar findings in patients with wild-type BRCA (PFS = 7.4 months vs. 5.5 months).[115] Although Phase III trials on olaparib are still ongoing, the results from the Study 19 Phase II trial were compelling enough to convince the National Institute for Health and Care Excellence (NICE) in the United Kingdom to recommend Olaparib for the management BRCA-mutated ovarian, fallopian tube, or peritoneal cancers in women.[116]

5.04.2.3.3 PARPi in combination with molecularly targeted agents

The effects of PARPi in combination with molecularly targeted agents are currently being studied. There is an ongoing Phase I study of the effects of the combination of veliparib (ABT-888) and CDK inhibitor, dinaciclib (SCH727965), in advanced study tumors (NCT01434316). In another ongoing Phase I/II trial, EGFR inhibitor, gefitinib in combination with olaparib (AZD2281) is being trialed in patients with advanced nonsmall-cell lung cancer (NSCLC) (NCT01513174). Although many of the studies are ongoing, there have been some results published on the combination of PARPi with molecularly targeted agents. The combination of the VEGF inhibitor, bevacizumab, and olaparib showed no dose-limiting toxicities and was well tolerated in a Phase I trial in patients with advanced solid tumors.[117] To assess the efficacy of olaparib with the VEGFR inhibitor, cediranib, 28 patients with ovarian and breast cancer were administered with varying doses of olaparib and cediranib.[118] An overall response rate of 44% was observed in the patients with ovarian cancer with a clinical benefit of 61%, while no response rate was seen in the breast cancer patients.[118] Dose limiting toxicities were reached at 30 mg cediranib OD and 400 mg BD of olaparib, and a combination dose of cediranib 30 mg OD and olaparib 200 mg BD was therefore recommended for a Phase II trial. In the subsequent Phase II trial, 90 women received either the combination of olaparib 200 mg BD and cediranib 30 mg OD or olaparib monotherapy 400 mg BD. An improved PFS was observed in the combination group (17.7 months vs. 9.0 months).[119] A Phase III trial of this combination therapy is now ongoing (NCT02446600).

5.04.2.3.4 PARPi in combination with radiation

About 60% of all cancer patients receive radiotherapy at some part of their therapy, and while many show excellent responses some have high levels of intrinsic radioresistance. There is good preclinical evidence to suggest that combining PARP inhibition with radiotherapy should be clinically beneficial. To date, veliparib is the most studied PARPi in combination with radiotherapy in the clinical setting. In a Phase I study of 22 patients with peritoneal carcinomatosis, patients were administered with 80–320 mg OD of veliparib for three cycles and 60 cGy of fractionated whole abdominal radiation on days 1 and 5 for 4 weeks.[120] Although no objective responses were observed, prolonged disease stability was observed in patients with ovarian and fallopian cancer.

The combination of PARPi and radiation therapy has also been evaluated in patients with brain metastases from primary solid tumors. In a Phase I trial, 81 patients with brain metastases were administered with whole brain radiation therapy and increasing doses of veliparib. The combination was well tolerated with better median survival time than initially predicted.[121] Veliparib was also investigated in combination with capecitabine and radiotherapy in patients with rectal cancer.[122] The combination was well

tolerated, and 28% of the patients had complete responses. However, despite these promising results, there are fewer clinical trials involving PARPi and radiotherapy than combination chemotherapy, and progression to standard clinical therapy has been slower.

The current status of ongoing clinical trials with PARPi is given in Table 1.

5.04.2.3.5 Biomarkers to detect HRR deficiency

Since PARPi therapy has been proven to be effective in HRR-deficient tumors, which is caused by more than just BRCA mutations, having biomarkers to detect HRR deficiency will help identify patients that are likely to benefit from PARPi therapy. It is clear that mutational screening for germline BRCA1 and 2 defects will only identify a small subset of HRR-defective tumors and will not detect sporadic tumor-specific mutations or epigenetic silencing events such as methylation of the *BRCA1* gene, which is observed in up to 30% of sporadic ovarian cancers and breast cancers.[123] There are several studies carried out to establish ways of identifying tumors with HRR deficiency including BROCA screening which identifies loss of function mutations in a panel of genes, mostly involved in HRR that are associated with breast and ovarian cancer,[124] loss of heterozygosity (LOH), telomeric allelic imbalance (TAI), large-scale state transition (LST) scores, gene expression profiling,[125] immunohistochemical analysis of TMAs,[97] or ex vivo functional assays,[126–129] all of which have been reported with varying degrees of predictive power.

Table 1 PARP inhibitors in clinical trials

Compound	*Latest stage of development and trial details*	*Clinical trial identifier(s)*
Olaparib	Phase I in combination with radiotherapy (or radiotherapy plus chemotherapy) in various tumor types (oesophageal, head and neck, breast)	NCT01460888, NCT02229656, NCT02227082, NCT01758731
	Phase II as a monotherapy, maintenance monotherapy, and in combination with chemotherapy in various tumor types (prostate, nonsmall-cell lung)	NCT01682772, NCT02679963
	Phase III as monotherapy, maintenance monotherapy, and in combination with chemotherapy or cediranib in multiple tumor types (ovarian, breast, pancreatic, gastric)	NCT02502266, NCT02446600, NCT02032823, NCT02184195, NCT02000622, NCT02282020, NCT01874353, NCT02446600
	Phase IV as maintenance monotherapy in ovarian cancer	NCT02476968
Rucaparib	Phase II as a monotherapy in various tumor types (pancreatic, breast)	NCT02042378, NCT01074970
	Phase III as maintenance monotherapy in ovarian cancer	NCT01968213
Veliparib	Phase II in combination with temozolomide in small-cell lung cancer	NCT01638546
	Phase III in combination with chemotherapy in multiple tumor types	NCT02163694, NCT02106546, NCT02264990, NCT02152982, NCT02470585
Niraparib	Phase I in combination with temozolomide or irinotecan in Ewing Sarcoma	NCT02044120
	Phase III as maintenance monotherapy in ovarian cancer	NCT01847274
Talazoparib	Phase II as a monotherapy in BRCA1/2 mutation-associated ovarian cancer	NCT02326844
	Phase III as a monotherapy in metastatic breast cancer	NCT01945775
BGB-290	Phase I in combination with BGB-A317 in advanced solid tumors	NCT02660034
E7016	Phase I in combination with temozolomide in advanced solid tumors	NCT01127178
E7449	Phase I/II in combination with carboplatin and eribulin mesylate in BRCA-mutated cancers Terminated due to lack of funding	NCT02396433
	Phase I/II as a monotherapy and in combination with temozolomide (TMZ) or with carboplatin and paclitaxel in advanced solid tumors	NCT01618136
CEP-9722	Phase I in combination with gemcitabine and cisplatin in patients with advanced solid tumors or mantle cell lymphoma This study has been completed	NCT01345357
	Phase I as single-agent therapy and as combination therapy with temozolomide in patients with advanced solid tumors This study has been completed	NCT00920595

Currently, detecting HRR deficiency is not standard clinical practice, but there are ongoing studies to validate various methodologies. LOH score has been used to identify tumors deficient in BRCA1, BRCA2, and Rad51C.[130] LOH is strongly associated with BRCA 1/2 mutations,[130,131] and therefore it could potentially be used to identify patients that could benefit from PARPi. LOH has been used to identify BRCA-mutated ovarian, pancreatic, and breast cancers[130–132] with high sensitivity. Based on these findings Myriad developed the HRD assay, which has been used to support clinical trials with olaparib.[115,133] The presence of germline and somatic mutation in several key HRR genes has been shown to be associated with sensitivity to platinum therapy and improved survival.[134] This has formed the basis of many clinical studies of PARPi and other chemotherapy agents in the treatment of HRR-deficient tumors.[135–137]

Quantification of TAI has been shown to identify tumors that are sensitive to DNA-damaging agents.[136] Triple-negative breast cancers sensitive to cisplatin-based chemotherapy have been shown to have high levels of TAI.[136] It has been established that low expression of BRCA1 is associated with high levels of TAI with a corresponding positive response to cisplatin, therefore suggesting that TAI could identify tumors that are HRR deficient.[138]

As these scores have been shown to be individually capable of identifying tumors that are HRR deficient and sensitive to anticancer agents, there are some suggestions that combining the scores could offer further potential clinical benefit. In a study of 86 patients with triple-negative breast cancer who received cisplatin or carboplatin, the mean HRD-LOH/HRD-LST score was significantly higher in patients that responded than patients that did not in the subgroup of patients without BRCA1/2 mutations.[139] The combination of these scores is now known as "HRD scores," and if its use does progress to clinical setting, it could facilitate the identification of patients that are likely to benefit from certain anticancer agents, therefore optimizing their clinical management.

BROCA-type genomic profiling has been shown to identify defective HRR.[124,140] Using a combination of BROCA screening, SNP analysis, and LOH, a new diagnostic test was developed by Foundation Medicine, Inc., and this has been used to identify HRR-deficiency in a Phase II study of rucaparib in ovarian cancer (Ariel 2).[141] The overall response rate (Recist + CA-125) was 82% in patients identified as being carrier of BRCA mutation (median PFS = 9.4 months) and 45% in patients identified as HRR-deficient using the screen (PFS = 7.1 months), but only 21% in the biomarker-negative patients (PFS = 3.7 months). The commonest mutation in the biomarker-positive group that responded to rucaparib was RAD51C.

Assessing HRR function in viable tumor cells would be an alternative approach that could capture all previously identified and currently unknown defects. This has the advantage of identifying tumors in which HRR has been restored by secondary mutations in BRCA1 or 2 or through inactivation of 53BP1 or DNA-PK, but it relies on the availability of viable patient material that can be exposed to DNA damage ex vivo. RAD51 foci, together with BRCA1 and FANCD2 foci, have been successfully measured in fresh breast tumor biopsies, following ex vivo irradiation[128,142] in a study of AML primary cultures, ascites cells from patients with ovarian cancer, and pleural effusions from patients with both primary lung cancer and lung metastases from other primary cancers following exposure to PARPi.[126,127,143,144] NSCLC may be associated with HRR defects as one study found that RAD51 costaining with proliferating cell nuclear antigen (PCNA) in breast and NSCLC explants treated with cisplatin revealed that 3/13 NSCLC lacked the ability to form RAD51 foci,[143] and another study revealed that 3 out of 4 primary cultures of NSCLC cells were unable to form RAD51 foci after rucaparib exposure.[144] RAD51 foci may be measured in formalin-fixed tumor biopsies taken after chemotherapy, a low RAD51 score correlated with a favorable response to treatment.[145,146]

5.04.2.4 DNA-Dependent Protein Kinase

The repair of DNA DSBs is crucial to survival if left unrepaired DSBs will trigger cell death. Natural sources of DSBs are ROS, trapped topoisomerase II complexes, and environmental sources of irradiation. DSBs may be repaired by the rapid and efficient NHEJ pathway, in which DNA-PK is a key component. DNA-PK is a trimeric protein consisting of the DNA-binding components Ku70 and Ku80 and the catalytic subunit, DNA-PKcs. Because NHEJ rejoins broken DNA ends without reference to a second template it is responsible for not only DSB repair during G1 or G0 phase but also operational during other cell-cycle phases.[147] Cells lacking DNA-PKcs are very sensitive to IR and topoisomerase II poisons, such as doxorubicin and etoposide that are used clinically.[148] DNA-PK activity seems to be upregulated in several cancer types and is generally a predictor of poor prognosis.[149] Increased DNA-PK activity not only confers resistance to radiotherapy and some chemotherapies but also, somewhat antiintuitively, confers genomic instability (an enabling characteristic of cancer). NHEJ, the simple religation of broken DNA double-strand ends can lead to the loss of nucleotides and the introduction of errors, and DNA-PK may also compete with HRR, the high-fidelity DSB repair pathway.[150] DNA-PK may also negatively impact on genomic stability through interaction with Snail1 and decreased checkpoint signaling.[149] DNA-PKcs is therefore an attractive target for anticancer therapy for multiple reasons, not just the inhibition of DSB repair.

5.04.2.4.1 DNA-PK Inhibitors

The first identified inhibitor was wortmanin, (Fig. 6) a fungal metabolite that is a pan PI-3K inhibitor, which was shown to enhance the cytotoxicity of IR and etoposide.[151]

DNA-PKcs is a PIKK family member, and in the search for inhibitors most have targeted the ATP-binding domain with PI-3K inhibitors often being the starting point for drug development. Achieving selectivity of inhibitors for DNA-PKcs over other PIKKs, ATM, ATR, mTOR as well as the different PI-3K isoforms, has been a challenge. The PI-3K inhibitor LY294002 was found to have equivalent activity against DNA-PKcs and mTOR in in vitro assays[152] and was used as a "hit" compound for subsequent drug

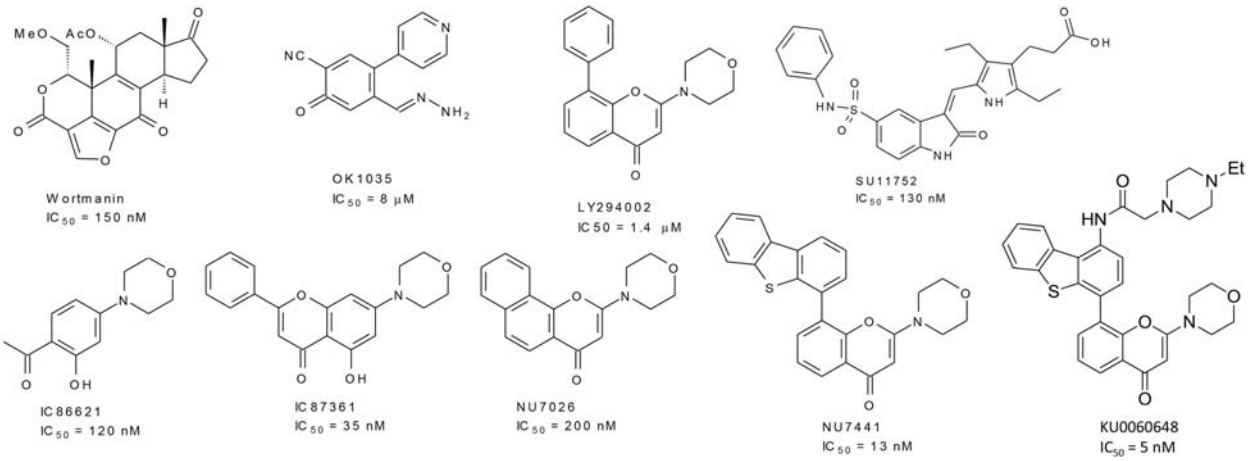

Fig. 6 DNA-PK inhibitors.

discovery that led to the identification of NU7026, NU7441, and KU-0060648 (Fig. 6) with improved selectivity and potency although the last compound was also found to be a PI-3K inhibitor.[153] These inhibitors increased DNA DSB induction/persistence and enhanced the cytotoxicity of IR and topoisomerase II poisons (doxorubicin and etoposide) in a variety of cell culture models of human cancers and with some limited in vivo efficacy data.[154–156] NU7441 has also been shown to potentiate mitoxantrone cytotoxicity in primary cultures of human chronic lymphocytic leukemia (CLL) cells.[157] Early inhibitors of DNA-PKcs include OK-1035 and SU11752 (Fig. 6) that inhibit DNA-PKcs in an ATP-competitive manner and inhibit repair of X-ray-induced DNA damage (OK-1035) and sensitize cells to radiation-induced cytotoxicity (SU11752) with increased specificity for DNA-PKcs.[158,159] Another series of PIKK inhibitors with selectivity for DNA-PKcs includes IC86621 (Fig. 6) that increase IR-induced DNA DSBs and enhance the cytotoxicity of IR and etoposide in cells with functional DNA-PKcs but not those lacking DNA-PKcs, and, in combination with fractionated irradiation, prolonged the survival of tumor bearing mice.[160] Further development of this series led to IC87361 (Fig. 6), which increased the radiosensitivity of endothelial cells in vitro and tumor vascular cells in vivo from wild-type mice but not those that from SCID mice that were deficient in DNA-PKcs.[161] The dual mTOR/DNA-PK inhibitor CC-155 was found to inhibit the growth of PC-3 prostate cancer xenografts as a single agent.[162]

5.04.2.4.2 Clinical Development of DNA-PK Inhibitors

There are a few ongoing clinical trials of DNA-PK inhibitors in various tumors, all at Phase I (Table 2). In the first-in-human Phase I trial of CC-155, which is a dual DNA-PK and TOR kinase inhibitor, 44 patients with various malignancies were administered with increasing dose of 0.5–40 mg. There was a complete tumor response in a patient with endometrial cancer, partial response in a patient with melanoma, and 18 (41%) of the patients exhibited stable disease.[163] When the established dose of 10 mg twice daily was administered to a further 62 patients, stable disease was observed in 64% of patients with prostate cancer, 53% of patients with head and neck squamous carcinoma, 21% of patients with GBM, and 22% of patients with Ewing's sarcoma. These findings offer promising prospects for DNA-PK inhibitors in future clinical setting.

MSC2490484A (chemical structure undisclosed) is another DNA-PK inhibitor that is currently in Phase I trial for CLL (NCT02316197). It is also being evaluated in combination with radiotherapy in advanced solid tumors (NCT02516813).

Table 2 DNA-PK inhibitors in clinical trial

Compound	*Latest stage of development and trial details*	*Clinical trial identifier(s)*
MSC2490484A	Phase I as a monotherapy in advanced solid tumors or chronic lymphocytic leukemia	NCT02316197
MSC2490484A	Phase I in combination with radiotherapy in advanced solid tumors	NCT02516813
CC-115	Phase I as a monotherapy in various advanced solid tumors and hematological malignancies	NCT01353625, NCT01421524
CC-122	Phase I as a monotherapy in advanced solid tumors, nonHodgkin's lymphoma, or multiple myeloma	NCT01421524

5.04.2.5 ATM/CHK2 Signaling

The signaling of DNA DSBs to cell-cycle checkpoints is equally important for survival. ATM is key PIKK that signals DSB to cell-cycle arrest. The Ataxia Telangiectasia Mutated (ATM) gene was discovered through the study of the autosomal recessive disorder, ataxia-telangiectasia (A-T). As well as having poor coordination (ataxia) and small dilated blood vessels (telangiectasia), growth and mental retardation, and immunodeficiency, individuals with A-T are extremely radiosensitive and are cancer prone.[164–167] The study of cells from people with A-T revealed that the reason for their radiosensitivity was most likely due to a failure to induce G1 arrest after irradiation and progress into S-phase with damaged DNA.[168–170] Subsequently, A-T cells were also found to have reduced DSB repair.[171] In the absence of DSBs ATM remains in inactive homodimers or multimers but is activated to undergo autophosphorylation at serine1981 and dissociate into monomers. There is some uncertainty about what activates ATM in response to DSB, whether it needs to locate somehow to the break to be activated by the MRN (MRE11-Rad50-Nbs1) or whether it can be activated while still distal to the break by DSB-induced conformational change of chromatin.[172] Further phosphorylations at serine367 and serine1893 do seem to be MRN dependent, and all three are needed for full activation, with serine1981 being the most critical. This is of course a simplified version of events; ATM sets off a cascade of phosphorylation events in response to DNA DSBs.[173] Activated ATM phosphorylates target proteins in the DDR pathway, some of which are themselves kinases, setting off a surge of activating and repressing phosphorylation events to effect cell-cycle arrest. Like DNA-PK, ATM phosphorylates histone H2AX contributing to the accumulation of γH2AX into foci at DSBs.

ATM activates G1 arrest by direct phosphorylation of p53 at serine 15 and activating phosphorylation of CHK2, which then also phosphorylates p53 at serine 20. These phosphorylations lead to the stabilization of p53 by preventing the binding of the E3 ubiquitin ligase, MDM2, and hence proteasomal degradation. The stabilization of p53 is also enhanced by the phosphorylation of MDM2 by ATM.[174] The accumulation of p53 results in G1 arrest by transactivation of p21, a repressor of CDK2-mediated G1/S transition. The extreme hypersensitivity of A-T cells to DSB-inducing agents and the persistence of DSBs in nonreplicating A-T cells suggested that ATM might also play a role in DSB repair. In response to IR, ATM is reported to phosphorylate BRCA1,[175] a key component of the HRR DNA DSB repair pathway. In addition, Artemis, a nuclease involved in the processing of complex DSBs prior to repair by NHEJ, has been identified as a target of ATM, and ATM has been shown to be an upstream component of the NHEJ pathway.[176]

Several publications have suggested a role for ATM in HRR, largely based on the observation that key HRR components, e.g., CtIP and BRCA1, are targets for ATM phosphorylation.[175,177–179] This proposal is supported by the slower recruitment of RAD51 to DSBs in A-T cells.[180] However, there are substantial phenotypic differences in ATM-deficient and HRR dysfunctional cells when it comes to the sensitivity to different types of DNA damage. A-T cells are highly radiosensitive but are not particularly sensitive to DNA cross-linking agents, such as cisplatin[181,182,164]; conversely HRR-defective BRCA1/2 or RAD51 mutant cells are very sensitive to DNA cross-linking agents but not particularly radiosensitive.[183–186] Studies in mice suggest that while BRCA1 is crucial for HRR, ATM is dispensible although ATM inhibition may interfere with HRR.[187] Other studies also show that inhibition of ATM appears to have more profound effects than does ATM deletion, which could reflect additional off-target effects of the inhibitors or that the inhibitors trap ATM at the DSB and block repair in the same way that PARPi are proposed to trap PARP.[188]

5.04.2.5.1 ATM Inhibitors

The radiosensitivity of individuals with A-T and cells derived from them suggested that targeting ATM might be a means to enhance the radio-responsiveness of tumor cells. The first inhibitors of ATM were the pan-PIKK inhibitors, caffeine and wortmanin (**Fig. 6**), but since they also inhibited DNA-PKcs and ATR it was not possible to attribute their radiosensitization purely to ATM.[189,190] The PI-3K inhibitor LY294002 (**Fig. 6**) that was found to also inhibit DNA-PKcs and ATM was used as the starting point for the development of ATM inhibitors as well as DNA-PK inhibitors. The first selective ATM inhibitor to be described was KU55933 (**Fig. 7**).[191] KU55933 was a potent radiosensitizer in two human colon cancer cell lines, with 10 μM concentration causing a 4- to 20-fold reduction in survival.

KU55933 also enhanced the cytotoxicity of the topoisomerase II poisons etoposide, amsacrine and doxorubicin, and the topoisomerase I poison, camptothecin. It profoundly decreased the G1- and S-phase fraction of etoposide-treated cells. Interestingly, KU55933 also sensitized cells lacking DNA-PKcs, suggesting that the checkpoint activation and DNA repair functions of ATM both contribute to its prosurvival activity. The cellular specificity of KU55933 for ATM was shown by its total lack of radiosensitization in A-T cells.[191] KU55933 was also able to induce cells that had become senescent following treatment with low-dose hydrogen peroxide, doxorubicin, or camptothecin to undergo apoptosis.[192] Although ATM signals to cell-cycle checkpoints via p53, chemosensitization and radiosensitization by KU55933 and a later more potent analogue, KU59403 (**Fig. 7**), was not p53-dependent. Equal sensitization by both drugs observed in matched pairs of p53 wild-type and mutant cells.[193]

Screening a compound library identified CP466722 (**Fig. 7**) as an ATM inhibitor,[194] exposure to CP466722 (6 μM) for 4 h did not affect HeLa survival but reduced survival of irradiated HeLa cells and resulted in reduced G1 and increased G2/M accumulation after irradiation.

Two more analogues of KU55933 with sufficient potency and suitable pharmacological properties to be used in tumor xenograft models have been reported: KU-60019 and KU-59403 (**Fig. 7**).[193,195,196] KU-60019 inhibited p53 and CHK2 phosphorylation and was also a potent radiosensitizer of glioma cells with ATM function but not A-T cells, confirming its specificity. It also inhibited cell migration and invasion and AKT phosphorylation, which was interpreted as ATM regulating an ATK phosphorylase.[196] However, it

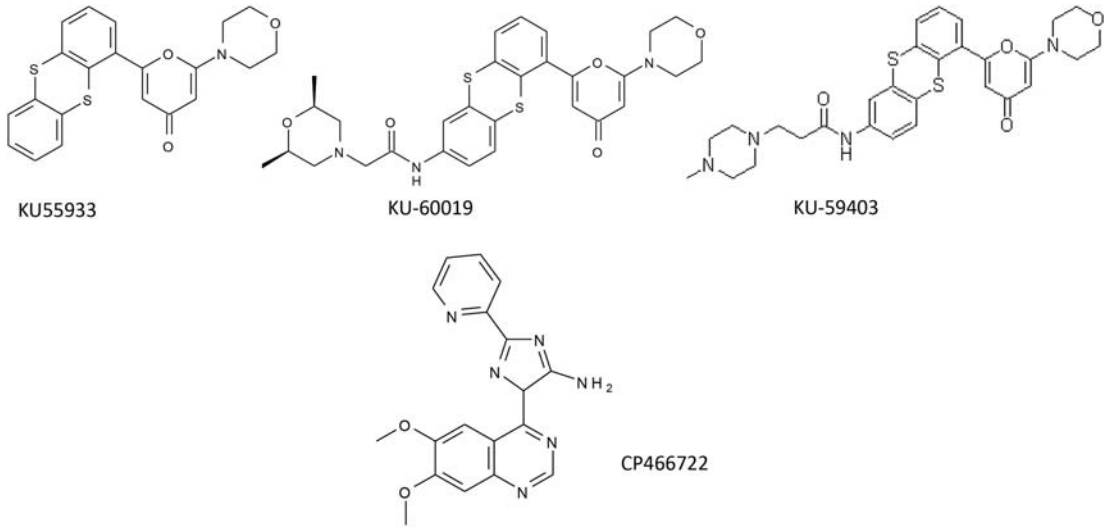

Fig. 7 ATM inhibitors.

is possible that it may affect PI-3K or mTOR in the cellular milieu despite the lack of in vitro activity. Subsequent studies by the same group showed that continuous exposure to KU-60019 at nanomolar concentrations potentiated radiation and radiation + TMZ sensitivity in the glioma model without affecting normal astrocytes.[197] In in vivo models of glioma (orthotopic xenografts) KU-60019 administered intracranially increased the survival of mice given cranial irradiation. In these studies both the intrinsic radiosensitivity and the radiopotentiation by KU-60019 were greater in the p53-mutant xenografts than the wild-type ones.[195] Similarly, for the radiosensitization of glioblastoma-initiating cells, in vitro and in an orthotopic model by intracranial administration, KU-60019 was more effective in cells expressing low levels of p53 but high levels of PI-3K (which may also suggest an activity of KU-60019 against the PI-3K pathway).[198] In contrast, chemo- and radiosensitization by KU-59403 as well as KU-55933 was not p53 dependent, and KU-59403 enhanced the cytotoxicity of topoisomerase I and II poisons and irradiation in a panel of cell lines, irrespective of p53 status. In in vivo studies sufficient concentrations of KU-59403 were achievable after intraperitoneal injection to increase the sensitivity of colon cancer xenografts to both etoposide and irinotecan.[193]

5.04.2.5.2 CHK2 Inhibitors

The downstream signaling of ATM is to a large part mediated by phosphorylation of CHK2 on Thr68 and other residues in the N-terminus, which triggers a conformational change and autophosphorylation that is necessary for full CHK2 activation. CHK2 blocks the cell cycle by stabilization of p53 and inactivating phosphorylations of the CDC25 family[199] and may promote DNA repair via phosphorylation of BRCA2[200] making it an attractive target for the sensitization of DNA-damaging anticancer agents.

NSC109555 was identified as a CHK2 inhibitor in a high-throughput screen of a 100,000-compound library using an immobilized metal ion affinity-based fluorescence polarization assay[201] (Fig. 8). This compound was found to increase the cytotoxicity of gemcitabine in a panel of pancreatic cell lines, which may have been mediated by increasing ROS levels.[202] PV1019 (Fig. 8) is

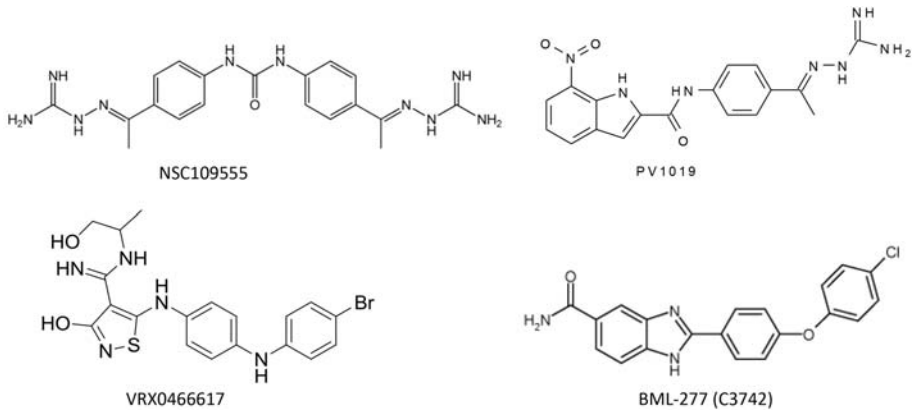

Fig. 8 CHK2 inhibitors.

a derivative of NSC109555 and was confirmed as a competitive inhibitor of CHK2 with respect to ATP. In cell-based studies PV1019 inhibited CHK2 autophosphorylation. It also potentiated the antiproliferative activity of topoisomerase I poisons and IR in a panel of human cancer lines. In cells expressing high levels of CHK2 PV1019 was growth inhibitory as a single agent.[203] Using a fragment-based approach supported by X-ray crystallography, identified CHK2-binding scaffolds and a hydrophobic area near the binding site that had the potential for exploitation in further design of CHK2 inhibitors to improve potency and selectivity.[204] However, so far these early hits have not led to CHK2 inhibitors suitable for cell-based studies. Other CHK2 inhibitors that have been reported include CCT241533 (**Fig. 8**), which potentiated the cytotoxicity of PARPi AG14447 (rucaparib) and olaparib although it did not increase the cytotoxicity of DNA-damaging agents (MMC, bleomycin, and irradiation) in a panel of human cancer cell lines.[205] Several reported CHK2 inhibitors, the aryl-benzimidazole BML277/C3742, a derivative of a marine sponge debromohymenialdisine and VRX0466617 (**Fig. 8**), protect p53 wild-type cells from radiation-induced cytotoxicity so may have a chemoprotective role against normal tissue radiotoxicity. However, the general lack of chemosensitization by the class as a whole somewhat limits their clinical potential.[206–209]

5.04.2.5.3 Clinical Development of CHK2 and ATM Inhibitors

Based on promising preclinical studies, a Phase II clinical trial of LY2606368 which is a CHK1/2 inhibitor is now ongoing (**Table 3**) with recruitment of participants with BRCA-mutated breast or ovarian cancer, and other cancers likely to be HRR-defective: high-grade serous ovarian cancer, triple-negative breast cancer, and metastatic prostate cancer (NCT02203513). AZD0156, which inhibits the kinase activity of ATM and ATM-mediated signaling, is currently in a Phase I trial as a monotherapy agent and in combination with a range of chemotherapy agents in different advanced cancers (NCT02588105).

5.04.2.6 ATR/CH1 Signaling

ATM and Rad3-related (ATR) is the third, and most versatile member of the PI-3K-like family of kinases (PIKKs), which include ATM and DNA-PKcs,[210] involved in DNA damage signaling and repair. ATR is a critical in the response to DNA replication stress and a variety of other DNA lesions. It plays a crucial role in the presence of these lesions by signaling to initiate cell-cycle arrest at the S and G2 checkpoints as well as initiation of DNA repair via HRR. Many of the phosphorylation substrates of ATR are also common to ATM, and there is cross talk between the two PIKKs. Between them, ATM and ATR phosphorylate >900 sites on >700 proteins in response to DNA damage with most of their targets being involved in DNA replication, recombination and repair, and cell-cycle regulation.[211]

The major target for ATR is CHK1, and both are crucial for genome maintenance even in the absence of exogenous sources of DNA damage. Homozygous deletion of either ATR or CHK1 leads to periimplantation embryonic lethality at E7[212] or between E3.5 and E7.5, respectively.[213] Blastocysts from ATR knockout mice had increased apoptosis and chromosomal fragmentation,[212] which is an indicator of mitotic catastrophe that results from cells entering mitosis prematurely before completing DNA synthesis.[214] This was one of the first indications that ATR is critical to cell-cycle arrest. Defective G2 checkpoint activation after DNA damage or replication stress results from inactivation of ATR,[215] and defective proliferation and subsequent cell death result from CHK1 deficiency in embryonic stem cells.[216] No living humans have been identified as completely lacking either ATR or CHK1 function, underscoring the essential roles of these kinases. However, Seckel syndrome, characterized by growth retardation and microcephaly, similar to other DNA repair and checkpoint syndromes is linked to a hypomorphic mutation in ATR.[217] Lymphoblasts from Seckel patients exhibited a three- to sevenfold increase in chromosomal fragmentation following inhibition of DNA synthesis,[218] which was similar to that seen in $ATR^{+/-}$ mice.[212] Interestingly, although $ATR^{+/-}$ mice have an increased incidence of tumor formation, Seckel syndrome patients do not have an increased prevalence of cancer.

Unlike ATM and DNA-PKcs, which are activated by DNA DSBs, ATR is activated by diverse DNA lesions that give rise to stretches of single-stranded DNA (**Fig. 9A**). These occur principally at stalled replication forks, resected DSBs, and NER intermediates. Replication stress results in stalled or collapsed replication forks, depending on the severity. This situation occurs when the replication machinery encounters a DNA lesion, when the dNTP pool is depleted, or when the number of origins of replication exceeds dNTP supply. The DNA lesions that can stall/collapse the advancing replication fork are SSBs, bulky adducts, and ICLs.[219] Resection of

Table 3 ATM/CHK2 inhibitors in clinical trial; LY2606368 is a CHK1/2 inhibitor

Compound	*Latest stage of development and trial details*	*Clinical trial identifier(s)*
Prexasertib (LY2606368)	Phase I in combination with chemotherapy in various tumor types (hematological, colorectal)	NCT02649764, NCT02124148
Prexasertib (LY2606368)	Phase I in combination with radiotherapy and chemotherapy in head and neck cancer	NCT02555644
Prexasertib (LY2606368)	Phase II as a monotherapy in breast, ovarian, and prostate cancers	NCT02203513

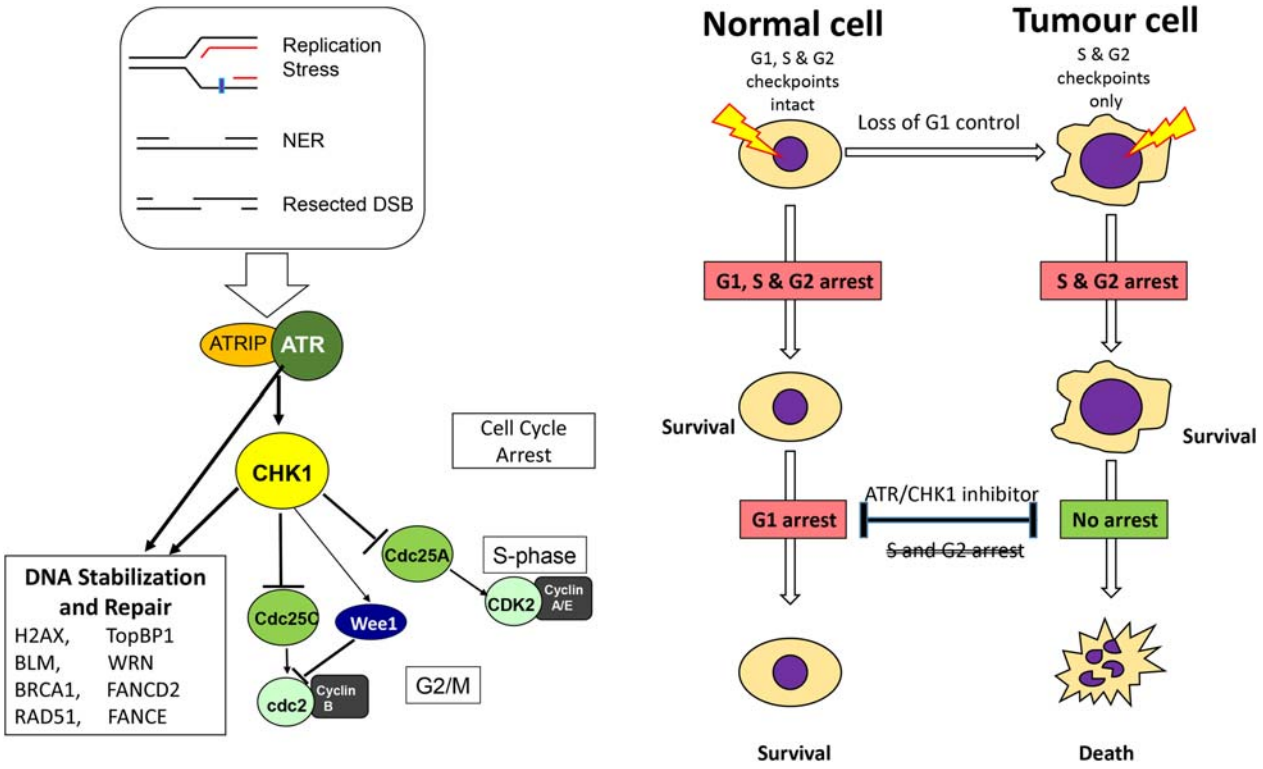

Fig. 9 ATR/CHK1 pathway and potential for cancer-specific chemo/radiosensitization. Left: The lesions that activate ATR and signaling via CHK1 to cell-cycle arrest and DNA repair. Right: Potential for specific antitumor effects of ATR/CHK1 inhibition: Cancer cells usually develop with dysfunctional G1 control making them reliant on S/G2 checkpoints such that when these are inhibited the tumor cell specifically is killed while the normal cell with a functional G1 checkpoint is not. With permission from Middleton, F. K.; Curtin, N. J. ATR as a therapeutic target. In *Advances in DNA repair in cancer therapy;* Panasci, L., Aloyz, R., Alaoui-Jamali, M., Eds.; Publisher Humana Press, Springer, New York, 2013. ISBN 978-1-4614-4740-5.

DSBs is a prerequisite step in HRR, and ATR activation by these lesions enhances the repair (see below). The NER pathway activates ATR, as in the process of removing bulky lesions on one strand of the DNA, such as UV-induced 6,4-photoproducts; it excises 20–30 nucleotides flanking the lesion and thereby exposes a region of single-stranded DNA on the nonresected strand.[220] Replication protein A coats the single-stranded DNA to prevent its degradation and is then replaced by the ATR-interacting protein (ATRIP), which is necessary for the recruitment of ATR to the lesion. Activation of ATR by DNA lesions has two functions: (i) to activate the S and G2 checkpoints via CHK1 kinase and the cdc25 family of phosphatases and (ii) to promote DNA repair.

ATR phosphorylates CHK1 on serine residues 317 and 345, which is essential for CHK1 kinase activation and often used as a marker of ATR activity.[221,222,216,223] Phosphorylation by ATR activates CHK1 triggering its autophosphorylation at serine 296.[223] CHK1 then activates cell-cycle arrest catalyzing the inactivating phosphorylation of the cell-cycle Cdc25 checkpoint phosphatase proteins.[224,225] S-phase entry is promoted by Cdc25A dephosphorylation of the CDK2/Cyclin A or E complex, and entry into mitosis follows Cdc25C-mediated activation of the Cdc2/Cyclin B complex by removing the Wee1-catalyzed inactivating phosphates on threonine 14 and tyrosine 15 of Cdc2 (Fig. 9A).[226,227] Thus, by inactivating the Cdc25 proteins the inactivating phosphorylations on CDK2/cyclinA and cdc2/cyclinB persist, thereby preventing cell-cycle transition. CHK1 also phosphorylates and stabilizes Wee1 further strengthening the prevention of the G2/M transition.

ATR also is key to the stabilization of replication forks, and activation of the ATR/CHK1 pathway promotes DNA repair. The principle repair pathway promoted is HRR, which is compromised in cells lacking ATR kinase function, and knockdown of CHK1 by siRNA also reduces RAD51 focus formation.[228,229] Key targets of ATR phosphorylation include those involved in DNA repair and the stabilization of stalled replication forks such as ATRIP, Rad17, Rad9, TopBP1, Claspin, H2AX, BRCA1, FANCD2, WRN, and BLM (some of which also feedback activate the ATR-CHK1 pathway) thus linking ATR to HRR and DNA cross-link repair.[230,231] CHK1 also targets RAD51, FANCD2, and FANCE regulating HRR and stabilizing stalled replication forks.[226] ATR may also interact with components of other DDR pathways; for instance, ATR phosphorylates DNA-PKcs, a key kinase in the NHEJ pathway.[232] The G2 arrest that accompanies MMR-mediated repair of 6-thioguanine lesions in DNA is ATR dependent,[233] and ATR may indirectly influence the BER pathway.[234]

There are two reasons why the ATR/CHK1 pathway is an attractive target for anticancer drug development: first, because of the variety of DNA lesions that activate the pathway, and second, because cancer cells are generally defective in their G1 checkpoint making them more vulnerable to inhibition of their S and G2 checkpoints (Fig. 9B).

Many of the conventional anticancer agents that are the mainstay of cancer therapy act by damaging the DNA. They may stall replication forks (i) by limiting dNTP supply or incorporation of fraudulent nucleosides; such agents are the antimetabolites that include nucleoside analogues such as gemcitabine, hydroxyurea, and the plethora of antifolates, (ii) by causing base damage DNA, e.g., by DNA-methylating agents such as TMZ or dacarbazine, or (iii) by the induction of SSBs, e.g., topoisomerase I poisons and irradiation. They may directly cause DNA DSBs, e.g., IR or topoisomerase II poisons (such as doxorubicin, mitoxantrone, or etoposide) or bulky adducts that are repaired by NER, e.g., cisplatin. The most difficult of all lesions to repair are ICLs, induced by cisplatin and the bifunctional alkylating agents. ATR is activated by all of these lesions to promote survival; therefore inhibition of ATR should promote cell killing.

The loss of G1 checkpoints in cancer cells suggests that inhibitors of the ATR/CHK1 pathway should specifically target cancer cells and not (or to a lesser extent) normal cells, which retain their G1 checkpoints (Fig. 9B). Classically loss of G1 checkpoints is attributed to defects in the tumor suppressors, p53 and pRb, which are to be found in more than 50% of all tumors, but G1 checkpoint function can have a variety of causes such as increases in the cyclins and CDKs that promote S-phase entry and loss of their suppressors.[11] Moreover, cancer cells are predicted to have a greater sensitivity to inhibitors of the ATR/CHK1 pathway in the absence of clinically induced DNA damage for the following reasons: because of activation of oncogenes that promote S-phase entry and loss of G1 control, cancer cells are more likely to enter S-phase when appropriate biomolecules (e.g., dNTPs) are limited and so have a high level of replicative stress; they have higher levels of ROS because of increased metabolic activity, mitochondrial dysfunction, various oxidases, and inflammation[235,236] resulting in approximately 100-fold higher levels of oxidative DNA lesions than in normal tissues.[237]

5.04.2.6.1 ATR Inhibitors

Inhibitors of ATR have somewhat lagged behind those of CHK1 (see below) and initial validation of the target was by genetic means. Two early independent studies using cells expressing dominant-negative kinase-dead ATR mutants showed that they were more sensitive to a variety of DNA-damaging chemotherapeutic agents, including antimetabolites, DNA cross-linking agents, and both UV and IR, and failed to engage in DNA damage-induced G2 arrest.[238,239] Caffeine (Fig. 10) was the first small molecule to be identified as inhibiting ATR, but it was weak ($IC_{50} = 1.1$ mM) and also inhibited ATM, DNA-PKcs, and mTOR making it difficult to attribute any pharmacological effect to activity against ATR. Nevertheless its UV sensitization, and possibly sensitization of TMZ + irradiation as well as its abrogation of G2 checkpoints may be attributable to ATR inhibition.[189,240] A natural product, Shisandrin B, (Fig. 10) has been identified as an ATR inhibitor. Shisandrin B abrogated UV-induced S and G2/M checkpoint induction and increased UV-induced cytotoxicity.[241] PI-3K inhibitors have also been shown to inhibit ATR, e.g., PI-103 and PI-124 (Fig. 10).[222] Indeed some of the supposedly specific PI-3K inhibitors have also been shown to inhibit ATR, such as

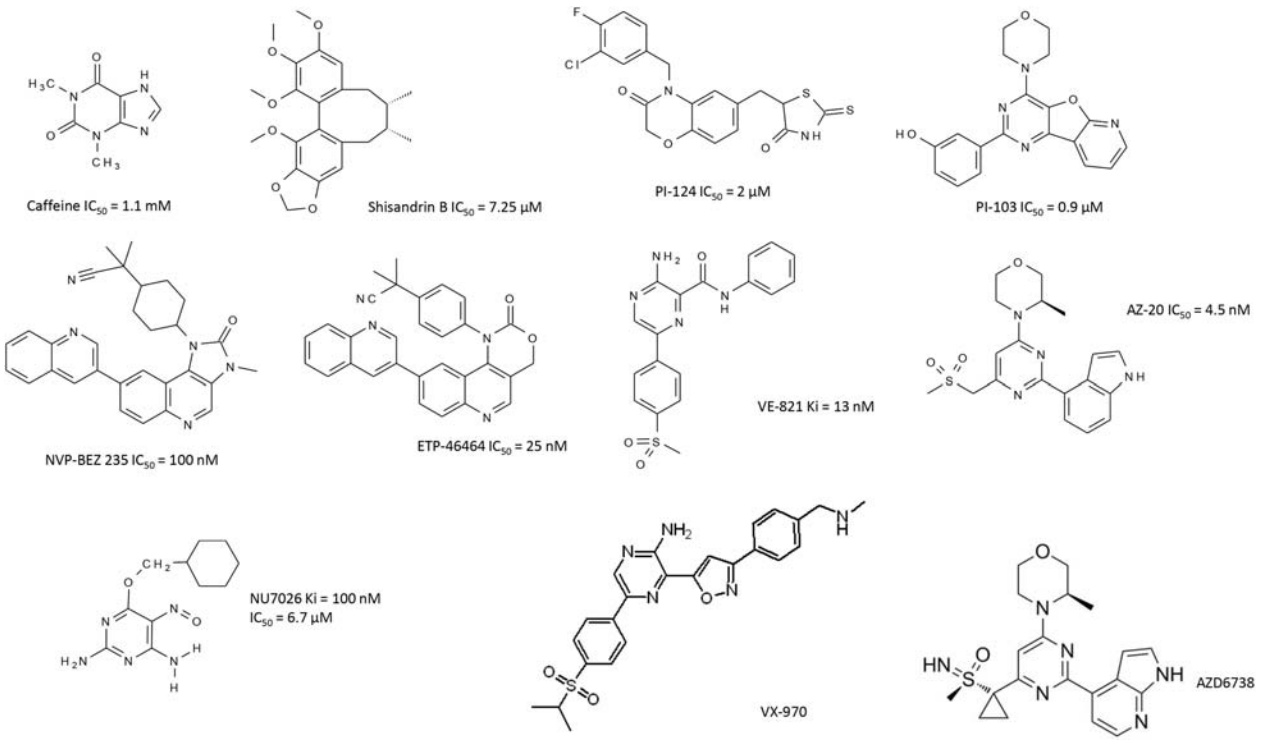

Fig. 10 ATR inhibitors.

NVP-BEZ235 (Fig. 10), which although it is claimed to be a dual PI-3K/mTOR inhibitor also inhibits ATRs (as well as ATM and DNA-PKcs).[75] Data attributing the effects of NVP-BEZ235to PI-3K or mTOR inhibition should therefore be viewed with some skepticism. This screen also identified a highly potent ATR inhibitor, ETP-46464 (Fig. 10) ($IC_{50} = 25$ nM) that inhibited the restart of stalled replication forks and abrogated S-phase arrest after HU exposure.

Unexpected potentiation of cisplatin by the CDK2 inhibitor, NU6027 (Fig. 10), led to the investigation of its potential as an ATR inhibitor. In cell-based studies, NU6027 was found to be a more potent inhibitor of $CHK1^{S345}$ phosphorylation (cellular $IC_{50} = 6.7$ μM) than it was of pRb (the CDK2 target) phosphorylation, and NU6027 increased the sensitivity of MCF7 cells to representatives of the major classes of DNA-damaging agents: the antimetabolite hydroxyurea, the DNA-methylating agent TMZ, the topoisomerase I poison camptothecin, the topoisomerase II poison doxorubicin, the DNA cross-linking agent, cisplatin, and irradiation, but not to the antitubulin agent, paclitaxel.[222] These effects could be attributed to ATR inhibition as they were not seen in cells expressing a dominant-negative kinase-dead ATR mutant. The potentiation of TMZ by NU6027 was greater in MMR-defective cells than in MMR-proficient cells, in agreement with previous suggestions that TMZ and 6-thioguanine potentiation by ATR inactivation required an intact MMR system.[222,233,242] In the studies with NU6027, mutations in p53 had different effects on the degree of sensitization depending on the DNA-damaging agent: TMZ sensitization was greatest in p53-mutant cells, but cisplatin sensitization was greater in cells with wild-type p53. The studies with NU6027 revealed that it reduced RAD51 focus formation and increased cell killing in cells exposed to the PARPi, rucaparib, and that cells defective in BER were more sensitive to single agent NU6027-induced cytotoxicity, indicating an element of synthetic lethality between ATR and the BER pathway, which has been confirmed in further studies with NU6027[243] and with other ATR inhibitors (see below).

VE-821 (Fig. 10) is a potent and selective ATR inhibitor ($K_i = 13$ nM)[244,245] that has been shown to increase the cytotoxicity of cisplatin, gemcitabine, camptothecin, etoposide, and IR, but not the antitubulin agent, docetaxel, in HCT116 colon cancer cells. VE-821 potentiated cisplatin to a much greater extent in a panel of human cancer cell lines than in normal human cell lines and was more active in cells lacking p53 or ATM. VE-821 has been investigated as a radiosensitizer in hypoxic cells. Hypoxic regions in tumors, resulting from deranged tumor vasculature, are radio- and chemoresistant and generally are associated with poor outcome. VE-821 increased the radiosensitivity in a panel of 12 human cancer cell lines, and to a greater extent in hypoxic cells. VE-821 also increased reoxygenation-induced DNA damage and decreased the survival of cells undergoing reoxygenation.[246] In a panel of pancreatic cell lines VE-821 increased gemcitabine as well as radiation-induced cytotoxicity under both normoxic and hypoxic conditions and led to the persistence of DNA damage through the inhibition of HRR (persistence of γH2AX and inhibition of RAD51 foci).[247]

Cancer cells have high levels of replication stress due to oncogene activation and hyperactive growth factor signaling making them particularly dependent on the ATR pathway for survival.[248] Knocking down ATR to 16% of normal levels was synthetically lethal in Ras-transformed cells.[249] Similarly, overexpression of cMYC has previously been shown to cause replicative stress and confer sensitivity to CHK1 inhibitors and ATR knockdown.[250,251] Cyclin E is commonly overexpressed in cancer and leads to replication stress and DNA damage by promoting S-phase entry. The ATR inhibitor, ETP-46464 was cytotoxic to cells with induced overexpression of cyclin E.[75] VE-821 alone also caused a concentration-dependent suppression of the growth and survival of two breast cancer cell lines, one with wild-type p53 and one with mutant.[252] Investigation of the single-agent activity of VE-821 in cell lines with defined DNA repair defects confirmed that loss of XRCC1 (BER) was a determinant of sensitivity to ATR inhibition and also demonstrated that deletion of BRCA2, XRCC3 (HRR), and ATM also conferred sensitivity to VE-821. Interestingly, cells lacking DNA-PKcs (but not Ku80) were resistant to VE-821, and those overexpressing DNA-PKcs were more sensitive.[253]

A more potent inhibitor with improved pharmacological properties, VE-822 (VX-970) (Fig. 10), was the first ATR inhibitor to be taken forward to clinical trial (NCT02157792). VE-822 inhibited checkpoint function and HRR and potentiated gemcitabine and irradiation in models of pancreatic cancer in vitro and in vivo. There was a substantial increase in tumor growth delay without a corresponding increase in normal tissue toxicity.[254,255] The effect of VX-970 on the sensitivity to cisplatin, gemcitabine, etoposide, oxaliplatin, and SN38 (the active metabolite of irinotecan) was determined in a panel of 35 lung cancer cell lines, with potentiation observed in most cases. Greater sensitization was seen when p53 was deleted, but by itself p53 mutation was not a significant determinant of potentiation across the panel of nonisogenic cell lines. Cisplatin sensitization was also seen in primary cultures of patients' lung tumor cells in vitro. ATR was inhibited, and impressive sensitization of the antitumor activity of cisplatin was observed in patient-derived xenografts.[255] A pharmacodynamic biomarker has been developed to evaluate the clinical activity of ATR inhibitors, using VE-821 and VX-970, based on $CHK1^{S345}$ phosphorylation after ex vivo activation of ATR with the UV-mimetic 4NQO in whole blood.[256]

Another series of ATR inhibitors was developed from an initial screening hit AZ-20 (Fig. 10), which itself showed in vitro and in vivo activity against Lovo cells and xenografts as a single agent.[257] AZD6738 (Fig.10) is a derivative of AZ-20 that entered clinical trials (NCT10955668). This inhibitor has been shown to be cytotoxic to p53 or ATM-defective patient-derived CLL cells that had been induced to proliferate ex vivo or xenotransplanted into immunocompromised mice.[258,259]

5.04.2.6.2 CHK1 Inhibitors

The first CHK1 inhibitor was a staurosporine derivative, UCN-01, (Fig. 11) that inhibits several kinases, including CHK1. Consistent with a role in CHK1 inhibition UCN-01 reduced radiation-induced degradation of Cdc25A, abrogated doxorubicin-induced G2/M arrest, and potentiated cisplatin and camptothecin cytotoxicity.[260] Further analogues of UCN-01 such as PD-321852 (Fig. 11) have been developed[261] as well as other structural types. Most are ATP competitive and, where investigated, found to bind in the hinge

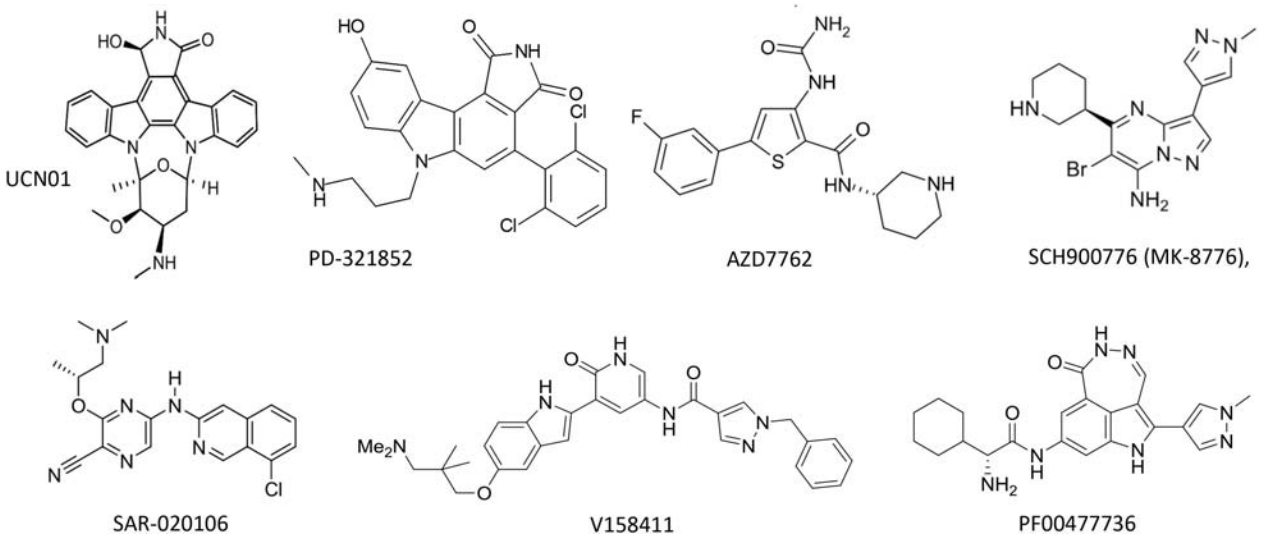

Fig. 11 CHK1 inhibitors.

region of CHK1. Some inhibit both CHK1 and CHK2, e.g., AZD7762 (Fig. 11) and XL9844 (structure not disclosed; K_i CHK2 = 2.2 nM, K_i CHK1 = 0.07 nM), and others are more selective for CHK1, e.g., SCH900776 (MK-8776), SAR-010106, and PF00477736 (Fig. 11) and CEP-3891 (structure not disclosed; IC_{50} = 4 nM). The earlier development of these inhibitors compared to the ATR inhibitors means that there are more studies of the CHK1 inhibitors in vivo and in clinical trials.

As described above, a major role of CHK1 is to transduce the signal from ATR to S and G2/M cell-cycle arrest. As expected, most CHK1 inhibitors do not affect cell-cycle progression in unperturbed cells but do block cell-cycle arrest and enhance the cytotoxicity in cells exposed to DNA-damaging agents. CHK1 inhibitors do not exactly phenocopy ATR inhibitors; even though CHK1 is thought to be the major target of ATR, key differences have been observed. For example the potentiation of cisplatin, carboplatin, and oxaliplatin cytotoxicity by ATR inhibition, seen in a variety of cell lines, was not replicated when CHK1 was inhibited. The CHK1 inhibitor, PF-00477736, unlike the ATR inhibitor NU6027, caused only modest sensitization of cisplatin and camptothecin but did enhance the cytotoxicity of paclitaxel in MCF7.[262,263] Although CHK1 inhibitors do not appear to synergize with cisplatin they do show high levels of sensitization of the antimetabolites and in particular gemcitabine, and topoisomerase I poisons such as camptothecin, which stall replication forks.[165,260,264,265] For example, PD-321852 inhibited gemcitabine-induced RAD51 focus formation and potentiated gemcitabine cytotoxicity in pancreatic cancer cell lines.[261] The dual CHK1/CHK2 inhibitor, V158411 (Fig. 11), potentiated gemcitabine, cisplatin, and the topoisomerase I poisons, camptothecin and SN38 in vitro in a p53-dependent manner and in vivo studies revealed enhancement of irinotecan anticancer activity without an increase in toxicity.[266] Some studies have investigated the radiosensitization potential of the CHK1 inhibitors: AZD7762 increased the radiation-induced cytotoxicity in a panel of human cancer cell lines.[267] There seem to be cell line-specific differences in the dependence on p53; radiosensitization by UCN-01 and CEP-3891 was dependent on p53 status in HCT116 cells, but independent in U2OS cells.[268]

Several studies have investigated the in vivo potential of CHK1 inhibitors, for example, PF-00477736 enhanced the antitumor activity of gemcitabine in mice bearing CoLo205 (human colon cancer) xenografts.[269] AZD7762 increased the antitumor activity of gemcitabine and irinotecan against human cancer xenografts in both mice and rats,[270] and XL-844 increased the efficacy of gemcitabine against PANC-1 xenografts.[271] AZD7762 has also been shown to be a radiosensitizer in lung cancer cell lines and xenograft models of lung cancer with brain metastasis resulting in prolonged survival.[272]

The cancer-specificity of the CHK1 inhibitors and the potential for synthetic lethality or synthetic sickness is postulated to be due to two key properties of cancer cells, loss of p53 and activation of oncogenes that cause replication stress. In some studies, there seems to be greater potentiation of p53 dysfunctional cells, but the differences may only be apparent in isogenically matched p53 functional and dysfunctional cells. Interestingly, CHK1 is upregulated in Myc overexpressing murine and human lymphomas, and its inactivation was cytotoxic in Myc amplified cells and prolonged the survival of Myc-lymphoma-bearing mice.[273,274] Also CCT245737 has recently been shown to have single-agent activity in MYC-driven mouse model of B-cell lymphoma.[275] In addition, recent studies in a panel of human breast and pancreatic cell lines revealed that the combination of CHK1 inhibitors (UCN-01, AZD7762) was synthetically lethal with various PARPi, including those in clinical trial (ABT-888 and AZD2281).[276]

5.04.2.6.3 Clinical Development of CHK1 and ATR Inhibitors

5.04.2.6.3.1 CHK1 inhibitors

UCN-01 has been evaluated in clinical trials in patients with melanoma, triple-negative breast cancer, and ovarian cancer.[277–279] However, the results of these Phase II trials have not been promising both as a single agent and in combination with other

chemotherapy agents mainly because of lack of efficacy. In a trial of 25 patients with triple-negative breast cancer who were administered with varying doses of UCN-01, the response rate was only 4%.[278] When UCN-01 was combined with topotecan in 29 patients with advanced recurrent ovarian cancer, only three patients achieved a partial response with no patient achieving a complete response.[279] SCH900776 has been evaluated in a Phase 1 trial, in combination with cytarabine, in patients with acute leukemia and was well tolerated.[280] It has therefore been taken into a Phase II trial in patients with acute myeloid leukemia, and the trial is currently still active but not recruiting (NCT01870596). In another Phase I trial of 43 patients with advanced solid tumor malignancies, intravenous infusion of SCH900776 was administered at dose levels ranging from 10 to 150 mg/m^2 as monotherapy followed by combination with gemcitabine 800 mg/m^2 in 26 patients or gemcitabine 1000 mg/m^2 in 17 patients.[281] SCH900776 was well tolerated as a monotherapy and in combination with gemcitabine, with 2 patients showing partial response and 13 patients demonstrating stable disease.

An initial Phase I trial of PF-00477736 in combination with gemcitabine in patients with advanced solid tumors was terminated due to business reasons (NCT00437203). However, in another Phase I trial, 36 patients were administered with 750 mg/m^2 of gemcitabine and increasing dose of PF-00477736. Partial responses were observed in three patients with squamous cell cancer of the skin, NSCLC and mesothelioma.[282] Although this combination therapy showed some clinical activity, it will be interesting to see if better response is observed in combination with other chemotherapy agents or with higher dose of gemcitabine.

AZD7762 was a promising CHK1/2 kinase inhibitor, but its development had to be halted due to safety concerns in Phase I trials. In a Phase I trial of patients with advanced solid tumors, AZD7762 was associated with cardiac toxicity.[283] LY2603618 is another CHK1 kinase inhibitor that was evaluated in a Phase I trial in combination with gemcitabine in patients with advanced solid tumors with acceptable safety profile.[284] Phase II trials of LY2603618 in NSCLC and pancreatic cancer have now been completed, and results are awaited (NCT00988858; NCT00839332). A phase I trial of GDC-0425 in combination with gemcitabine in lymphoma has been completed, and results are also awaited (NCT01359696). GDC-0575 is currently in a Phase I trial as monotherapy agents or in combination with other chemotherapy agents in solid tumors and lymphoma (NCT01564251). Despite initial setbacks, CHK1 inhibitors offer promising cancer therapy, and they could prove effective beyond hematological malignancies (Table 4).

5.04.2.6.3.2 ATR inhibitors

VE-822 (VX-970) was the first ATR inhibitor to be taken forward to clinical trial (Table 5). Following promising results in preclinical models, VX-970 is currently in Phase I/II trials in patients with small-cell lung cancer and NSCLC. There is a planned Phase II study of VX-970 in patients with ovarian, primary peritoneal, or fallopian tube cancers (NCT02595892). VX-970 has been evaluated as a monotherapy and in combination therapy. In a Phase I trial of patients with advanced malignancies receiving VX-970 monotherapy or combination therapy with carboplatin, both regimes were well tolerated and antitumor activity was observed.[285] VX-970 has also been evaluated in combination with gemcitabine in patients with advanced solid tumors—colorectal, pancreatic, breast, and NSCLC. In a Phase I study of this combination therapy, there was evidence of antitumor activity and two patients with papillary cancer and gastrointestinal stromal tumors, which are usually resistant to chemotherapy, had prolonged PFS.[286] An optimal combination dose of 210 mg/m^2 and gemtacitabine 1000 mg/m^2 was determined to be taken forward into Phase II trial. A Phase II trial of combination of VX-970 and topotecan in patients with small-cell lung cancer is currently recruiting patients.[287]

AZD6738 is another ATR inhibitor that is currently being evaluated in early phase clinical trials (Table 5). It is being investigated as a monotherapy and as a sensitizing agent to radiation therapy in patients with advanced solid malignancies in the PATRIOT trial.[288] AZD6738 is also being evaluated in combination with carboplatin, olaparib, and MEDI4736 in patients with advanced and metastatic tumors in a Phase I trial (NCT02264678). These trials offer exciting possibilities in the management of many terminal cancers, and it will be interesting to see if they progress to the bedside.

Table 4 CHK1 inhibitors in clinical trial

Compound	*Latest stage of development and trial details*	*Clinical trial identifier(s)*
PF-00477736	Phase I in combination with gemcitabine in advanced solid tumors Terminated due to business reasons	NCT00437203
AZD7762	Phase I in combination with gemcitabine in advanced solid tumors Terminated after assessment of risk-benefit profile	NCT00473616
SCH 900776	Phase II in combination with cytarabine in Acute Myeloid Leukemia	NCT01870596
GDC-0575	Phase I as a monotherapy and in combination with gemcitabine in solid tumors and lymphoma	NCT01564251
CCT245737	Phase I as a monotherapy and in combination with gemcitabine, and gemcitabine plus cisplatin, in solid tumors	NCT02797964, NCT02797977

Table 5 ATR inhibitors in clinical trial

Compound	*Latest stage of development and trial details*	*Clinical trial identifier(s)*
VX-970	Phase I in combination with PARP inhibitor and chemotherapy in solid tumors	NCT02723864
VX-970	Phase I in combination with chemotherapy in small-cell lung cancer	NCT02487095
AZD6738	Phase I as monotherapy and in combination with radiotherapy in solid tumors	NCT02223923

5.04.2.7 Summary, Conclusions, and Future Perspectives

There has been considerable progress in our understanding of the DDR, how it protects the living organism, and how its dysfunction can lead to the development of cancer. Moreover, as most conventional anticancer therapy acts by damaging DNA, we have learnt that the dysfunction of the DDR in cancer can lead it to be not only more sensitive to therapy (in the case where a critical pathway is lost or attenuated) but also more resistant (where the protective pathway is increased in activity). The initial rationale for inhibiting DDR pathway inhibitors was to increase response to DNA-damaging anticancer therapy by targeting survival mechanisms. However, this strategy can come at a cost in terms of exacerbating normal tissue toxicity and hence little or no improvement of the therapeutic index. The increase in host toxicity was responsible for the lack of progress of the early DDR inhibitors, those targeting MGMT to improve alkylating agent activity, beyond Phase II clinical trials. So far, combination of conventional DNA-damaging therapies with the next class of DDR inhibitors, PARPi, has also been associated with toxicities and not progressed beyond Phase II. It is possible that through careful titration of dose, both for the cytotoxic and the PARPi, and schedule adjustments that the therapeutic index may be improved. Alternatively, a subset of tumor types which are exceptionally vulnerable to this approach may be identified.

It is to be hoped that the CHK1 and ATR inhibitors, which exploit an almost universal feature of cancer cells, i.e., the dysfunction of the G1 checkpoint, to sensitize such cells to DNA-damaging therapy, turn out to be more tumor specific and less toxic in combination therapy. The trials with the early CHK1 inhibitors were associated with unacceptable toxicities, but, as these drugs lacked specificity for CHK1, it is likely that the more specific next-generation inhibitors will meet with greater success. Combinations with molecularly targeted agents, that may or may not also act by compromising DDR function, are also being investigated, but whether this will lead to an improvement in the therapeutic index remains to be seen. Combinations of DDR inhibitors with radiotherapy may be associated with fewer generalized toxicities, such as myelosuppression, but care will be needed to assess toxicities in normal tissues in the irradiation field, especially as many are late-presenting. Preclinically, DNA-PK inhibitors are the most potent radiosensitizers, but it is too early to tell if this will translate into radiosensitization with acceptable toxicity in the clinic.

A more exciting approach is to exploit defects in the DDR that are *tumor-specific* by targeting a complementary pathway and thereby selectively targeting the tumor and not the host tissues. This approach, although promising, had been paid little attention until the synthetic lethality of the PARPi in cells lacking HRR function was demonstrated. These initial laboratory findings translated rapidly into the clinic, where the progress and success has been so great that within 10 years of the publication of the preclinical data the first PARPi have been licensed for use in cancer patients. This single-agent approach does not cause unacceptable toxicity and has been remarkably effective in a subset of patients with BRCA mutations. Broadening the application to other tumors has necessitated the development of biomarkers of HRR defects. Several approaches to develop such biomarkers have been taken, and these are being used to select patients for PARPi therapy in clinical trials. However, responses in biomarker-positive tumors have not been as great as those with a BRCA mutation suggesting either that the biomarkers are not 100% reliable or that different components of the HRR pathway have greater or lesser impact on its overall function. Nevertheless, the biomarker-positive group generally responds better than the biomarker-negative one. This highlights the need for effective predictive biomarkers. Determinants of sensitivity identified in the laboratory setting need to be translated to reliable biomarkers that may be developed for routine clinical use if we are to treat those patients likely to benefit and spare those who are not from unnecessary toxicity.

See also: 5.02. Selective Kinase Inhibitors in Cancer. 8.07. Discovery of AZD0156: The First Potent and Selective Inhibitor of ATM Kinase for Clinical Evaluation.

References

1. Lindahl, T.; Modrich, P.; Sancar, A. The 2015 Nobel Prize in Chemistry the Discovery of Essential Mechanisms That Repair DNA Damage. *J. Assoc. Genet. Technol.* **2016,** *42* (1), 37–41.
2. Lindahl, T. Instability and Decay of the Primary Structure of DNA. *Nature* **1993,** *362* (6422), 709–715.
3. Lindahl, T. DNA Glycosylases, Endonucleases for Apurinic/Apyrimidinic Sites, and Base Excision-Repair. *Prog. Nucleic Acid Res. Mol. Biol.* **1979,** *22* (1), 35–92.

4. Modrich, P. DNA Mismatch Correction. *Annu. Rev. Biochem.* **1987,** *56,* 435–466.
5. Sancar, A.; Rupp, W. D. A novel Repair Enzyme: UVRABC Excision Nuclease of *Escherichia coli* Cuts a DNA Strand on Both Sides of the Damaged Region. *Cell* **1983,** *33* (1), 249–260.
6. Deans, A. J.; West, S. C. DNA Interstrand Crosslink Repair and Cancer. *Nat. Rev. Cancer* **2011,** *11* (7), 467–480.
7. Curtin, N. J. DNA Repair Dysregulation from Cancer Driver to Therapeutic Target. *Nat. Rev. Cancer* **2012,** *12* (12), 801–817.
8. Kaina, B.; Margison, G. P.; Christmann, M. Targeting O^6-Methylguanine–DNA Methyltransferase With Specific Inhibitors as a Strategy in Cancer Therapy. *Cell. Mol. Life Sci.* **2010,** *67* (21), 3663–3681.
9. Kaelin, W. G., Jr. The Concept of Synthetic Lethality in the Context of Anticancer Therapy. *Nat. Rev. Cancer* **2005,** *5* (9), 689–698.
10. Hanahan, D.; Weinberg, R. A. Hallmarks of Cancer: The Next Generation. *Cell* **2011,** *144* (5), 646–674.
11. Massagué, J. G1 Cell-Cycle Control and Cancer. *Nature* **2004,** *432* (7015), 298–306.
12. Jasin, M. Homologous Repair of DNA Damage and Tumorigenesis: The BRCA Connection. *Oncogene* **2002,** *21* (58), 8981–8993.
13. Plotz, G.; Zeuzem, S.; Raedle, J. DNA Mismatch Repair and Lynch Syndrome. *J. Mol. Histol.* **2006,** *37* (5-7), 271–283.
14. Champon, P.; Weill, J. D.; Mandel, P. Nicotinamide Mononucleotide Activation of new DNA-Dependent Polyadenylic Acid Synthesizing Nuclear Enzyme. *Biochem. Biophys. Res. Commun.* **1963,** *11,* 39–43.
15. Sugimura, T.; Fujimura, S.; Hasegawa, S.; Kawamura, Y. Polymerization of the Adenosine 5′-Diphosphate Ribose Moiety of NAD by Rat Liver Nuclear Enzyme. *Biochim. Biophys. Acta* **1967,** *138* (2), 438–441.
16. Roitt, I. M. The Inhibition of Carbohydrate Metabolism in Ascites-Tumour Cells by Ethyleneimines. *Biochem. J.* **1956,** *63* (2), 300–307.
17. Wang, Z. Q.; Stingl, L.; Morrison, C.; et al. PARP is Important for Genomic Stability but Dispensable in Apoptosis. *Genes Dev.* **1997,** *11* (18), 2347–2358.
18. Shieh, W. M.; Amé, J. C.; Wilson, M. V.; et al. Poly(ADP-Ribose) Polymerase Null Mouse Cells Synthesize ADP-Ribose Polymers. *J. Biol. Chem.* **1998,** *273* (46), 30069–30072.
19. Amé, J. C.; Rolli, V.; Schreiber, V.; et al. PARP-2, A Novel Mammalian DNA Damage-Dependent Poly(ADP-Ribose) Polymerase. *J. Biol. Chem.* **1999,** *274* (25), 17860–17868.
20. Schreiber, V.; Dantzer, F.; Ame, J. C.; de Murcia, G. Poly(ADP-Ribose): Novel Functions for an Old Molecule. *Nat. Rev. Mol. Cell Biol.* **2006,** *7* (7), 517–528.
21. Ménissier de Murcia, J.; Ricoul, M.; Tartier, L.; et al. Functional Interaction Between PARP-1 and PARP-2 in Chromosome Stability and Embryonic Development in Mouse. *EMBO J.* **2003,** *22* (9), 2255–2263.
22. Spagnolo, L.; Barbeau, J.; Curtin, N. J.; Morris, E. P.; Pearl, L. H. Visualization of a DNA-PK/PARP1 Complex. *Nucleic Acids Res.* **2012,** *40* (9), 4168–4177.
23. Iliakis, G. Backup Pathways of NHEJ in Cells of Higher Eukaryotes: Cell Cycle Dependence. *Radiother. Oncol.* **2009,** *92* (3), 310–315.
24. Beck, C.; Robert, I.; Reina-San-Martin, B.; Schreiber, V.; Dantzer, F. Poly(ADP-Ribose) Polymerases in Double-Strand Break Repair: Focus on PARP1, PARP2 and PARP3. *Exp. Cell Res.* **2014,** *329* (1), 18–25.
25. Durkacz, B. W.; Omidiji, O.; Gray, D. A.; Shall, S. (ADP-Ribose)n Participates in DNA Excision Repair. *Nature* **1980,** *283* (5747), 593–596.
26. Banasik, M.; Komura, H.; Shimoyama, M.; Ueda, K. Specific Inhibitors of Poly(ADP-Ribose) Synthetase and Mono(ADP-Ribosyl)Transferase. *J. Biol. Chem.* **1992,** *267* (3), 1569–1575.
27. Jagtap, P.; Szabó, C. Poly(ADP-Ribose) Polymerase and the Therapeutic Effects of its Inhibitors. *Nat. Rev. Drug Discov.* **2005,** *4* (5), 421–440.
28. Ferraris, D. V. Evolution of Poly(ADP-Ribose) Polymerase-1 (PARP-1) Inhibitors. From Concept to Clinic. *J. Med. Chem.* **2010,** *53* (12), 4561–4584.
29. Menear, K. A.; Adcock, C.; Boulter, R.; et al. 4-[3-(4-Cyclopropanecarbonylpiperazine-1-Carbonyl)-4-Fluorobenzyl]-2H-Phthalazin-1-one: A Novel Bioavailable Inhibitor of Poly(ADP-Ribose) Polymerase-1. *J. Med. Chem.* **2008,** *51* (20), 6581–6591.
30. Ruf, A.; de Murcia, G.; Schulz, G. E. Inhibitor and NAD + Binding to Poly(ADP-Ribose) Polymerase as Derived from Crystal Structures and Homology Modeling. *Biochemistry* **1998,** *37* (11), 3893–3900.
31. Ruf, A.; Menissier de Murcia, J.; de Murcia, G.; Schulz, G. E. Structure of the Catalytic Fragment of Poly(AD-Ribose) Polymerase From Chicken. *Proc. Natl. Acad. Sci. U. S. A.* **1996,** *93* (15), 7481–7485.
32. Thomas, H. D.; Calabrese, C. R.; Batey, M. A.; et al. Preclinical Selection of a Novel Poly(ADP-Ribose) Polymerase Inhibitor for Clinical Trial. *Mol. Cancer Ther.* **2007,** *6* (3), 945–956.
33. Plummer, R.; Jones, C.; Middleton, M.; et al. Phase I Study of the Poly(ADP-Ribose) Polymerase Inhibitor, AG014699, in Combination With Temozolomide in Patients With Advanced Solid Tumors. *Clin. Cancer Res.* **2008,** *14* (23), 7917–7923.
34. Curtin, N. J.; Szabo, C. Therapeutic Applications of PARP Inhibitors: Anticancer Therapy and Beyond. *Mol. Aspects Med.* **2013,** *34* (6), 1217–1256.
35. Evers, B.; Drost, R.; Schut, E.; et al. Selective Inhibition of BRCA2-Deficient Mammary Tumor Cell Growth by AZD2281 and Cisplatin. *Clin. Cancer Res.* **2008,** *14* (12), 3916–3925.
36. Satoh, M. S.; Lindahl, T. Role of Poly(ADP-Ribose) Formation in DNA Repair. *Nature* **1992,** *356* (6367), 356–358.
37. Kedar, P. S.; Stefanick, D. F.; Horton, J. K.; Wilson, S. H. Increased PARP-1 Association With DNA in Alkylation Damaged, PARP-Inhibited Mouse Fibroblasts. *Mol. Cancer Res.* **2012,** *10* (3), 360–368.
38. Murai, J.; Huang, S. Y.; Das, B. B.; et al. Trapping of PARP1 and PARP2 by Clinical PARP Inhibitors. *Cancer Res.* **2012,** *72* (21), 5588–5599.
39. Murai, J.; Zhang, Y.; Morris, J.; et al. Rationale for Poly(ADP-Ribose) Polymerase (PARP) Inhibitors in Combination Therapy With Camptothecins or Temozolomide Based on PARP Trapping Versus Catalytic Inhibition. *J. Pharmacol. Exp. Ther.* **2014,** *349* (3), 408–416.
40. Hopkins, T. A.; Shi, Y.; Rodriguez, L. E.; et al. Mechanistic Dissection of PARP1 Trapping and the Impact on *In Vivo* Tolerability and Efficacy of PARP Inhibitors. *Mol. Cancer Res.* **2015,** *13* (11), 1465–1477.
41. Boulton, S.; Pemberton, L. C.; Porteous, J. K.; et al. Potentiation of Temozolomide-Induced Cytotoxicity: A Comparative Study of the Biological Effects of Poly(ADP-Ribose) Polymerase Inhibitors. *Br. J. Cancer* **1995,** *72* (4), 849–856.
42. Delaney, C. A.; Wang, L. Z.; Kyle, S.; et al. Potentiation of Temozolomide and Topotecan Growth Inhibition and Cytotoxicity by Novel Poly(Adenosine Diphosphoribose) Polymerase Inhibitors in a Panel of Human Tumor Cell Lines. *Clin. Cancer Res.* **2000,** *6* (7), 2860–2867.
43. Tentori, L.; Leonetti, C.; Scarsella, M.; et al. Systemic Administration of GPI 15427, a Novel Poly(ADP-Ribose) Polymerase-1 Inhibitor, Increases the Antitumor Activity of Temozolomide Against Intracranial Melanoma, Glioma, Lymphoma. *Clin. Cancer Res.* **2003,** *9* (14), 5370–5379.
44. Miknyoczki, S. J.; Jones-Bolin, S.; Pritchard, S.; et al. Chemopotentiation of Temozolomide, Irinotecan, and Cisplatin Activity by CEP-6800, a Poly(ADP-Ribose) Polymerase Inhibitor. *Mol. Cancer Ther.* **2003,** *2* (4), 371–382.
45. Wedge, S. R.; Porteous, J. K.; Newlands, E. S. 3-Aminobenzamide and/or O^6-Benzylguanine Evaluated as an Adjuvant to Temozolomide or BCNU Treatment in Cell Lines of Variable Mismatch Repair Status and O^6-Alkylguanine-DNA Alkyltransferase Activity. *Br. J. Cancer* **1996,** *74* (7), 1030–1036.
46. Curtin, N. J.; Wang, L. Z.; Yiakouvaki, A.; et al. Novel Poly(ADP-Ribose) Polymerase-1 Inhibitor, AG14361, Restores Sensitivity to Temozolomide in Mismatch Repair-Deficient Cells. *Clin. Cancer Res.* **2004,** *10* (3), 881–889.
47. Horton, T. M.; Jenkins, G.; Pati, D.; et al. Poly(ADP-Ribose) Polymerase Inhibitor ABT-888 Potentiates the Cytotoxic Activity of Temozolomide in Leukemia Cells: Influence of Mismatch Repair Status and O^6-Methylguanine–DNA Methyltransferase Activity. *Mol. Cancer Ther.* **2009,** *8* (8), 2232–2242.
48. Liu, X.; Shi, Y.; Guan, R.; et al. Potentiation of Temozolomide Cytotoxicity by Poly(ADP)Ribose Polymerase Inhibitor ABT-888 Requires a Conversion of Single-Stranded DNA Damages to Double-Stranded DNA Breaks. *Mol. Cancer Res.* **2008,** *6* (10), 1621–1629.
49. Feng, Y.; Post, L.; Wang, B.; Shen, Y. Preclinical evaluation of BMN 673 in combination with temozolomide (TMZ) in various tumor types including small cell. *Lung Cancer* **2013,** *12* (11 Suppl.), B93.

50. Russo, A. L.; Kwon, H. C.; Burgan, W. E.; et al. *In Vitro* and *In Vivo* Radiosensitization of Glioblastoma Cells by the Poly (ADP-Ribose) Polymerase Inhibitor E7016. *Clin. Cancer Res.* **2009,** *15* (2), 607–612.
51. Lemasson, B.; Wang, H.; Galbán, S.; et al. Evaluation of Concurrent Radiation, Temozolomide and ABT-888 Treatment Followed by Maintenance Therapy With Temozolomide and ABT-888 in a Genetically Engineered Glioblastoma Mouse Model. *Neoplasia* **2016,** *18* (2), 82–89.
52. Bowman, K. J.; Newell, D. R.; Calvert, A. H.; Curtin, N. J. Differential Effects of the Poly (ADP-Ribose) Polymerase (PARP) Inhibitor NU1025 on Topoisomerase I and II Inhibitor Cytotoxicity in L1210 Cells *In Vitro*. *Br. J. Cancer* **2001,** *84* (1), 106–112.
53. Bowman, K. J.; White, A.; Golding, B. T.; Griffin, R. J.; Curtin, N. J. Potentiation of Anti-Cancer Agent Cytotoxicity by the Potent Poly(ADP-Ribose) Polymerase Inhibitors NU1025 and NU1064. *Br. J. Cancer* **1998,** *78* (10), 1269–1277.
54. Ben-Hur, E.; Utsumi, H.; Elkind, M. M. Inhibitors of Poly (ADP-Ribose) Synthesis Enhance Radiation Response by Differentially Affecting Repair of Potentially Lethal Versus Sublethal Damage. *Br. J. Cancer Suppl.* **1984,** *6,* 39–42.
55. Harper, J. V.; Anderson, J. A.; O'Neill, P. Radiation Induced DNA DSBs: Contribution from Stalled Replication Forks? *DNA Repair (Amst.)* **2010,** *9* (8), 907–913.
56. Mitchell, J.; Smith, G. C.; Curtin, N. J. Poly(ADP-Ribose) Polymerase-1 and DNA-Dependent Protein Kinase Have Equivalent Roles in Double Strand Break Repair Following Ionizing Radiation. *Int. J. Radiat. Oncol. Biol. Phys.* **2009,** *75* (5), 1520–1527.
57. Calabrese, C. R.; Almassy, R.; Barton, S.; et al. Anticancer Chemosensitization and Radiosensitization by the Novel Poly(ADP-Ribose) Polymerase-1 Inhibitor AG14361. *J. Natl. Cancer Inst.* **2004,** *96* (1), 56–67.
58. Ali, M.; Telfer, B. A.; McCrudden, C.; et al. Vasoactivity of AG014699, a Clinically Active Small Molecule Inhibitor of Poly(ADP-Ribose) Polymerase: A Contributory Factor to Chemopotentiation *In Vivo*? *Clin. Cancer Res.* **2009,** *15* (19), 6106–6112.
59. Senra, J. M.; Telfer, B. A.; Cherry, K. E.; et al. Inhibition of PARP-1 by Olaparib (AZD2281) Increases the Radiosensitivity of a Lung Tumor Xenograft. *Mol. Cancer Ther.* **2011,** *10* (10), 1949–1958.
60. Horsman, M. R. Nicotinamide and Other Benzamide Analogs as Agents for Overcoming Hypoxic Cell Radiation Resistance in Tumours. A review. *Acta Oncol.* **1995,** *34* (5), 571–587.
61. Janssens, G. O.; Rademakers, S. E.; Terhaard, C. H.; et al. Accelerated Radiotherapy With Carbogen and Nicotinamide for Laryngeal Cancer: Results of a Phase III Randomized Trial. *J. Clin. Oncol.* **2012,** *30* (15), 1777–1783.
62. Janssens, G. O.; Rademakers, S. E.; Terhaard, C. H.; et al. Improved Recurrence-Free Survival With ARCON for Anemic Patients With Laryngeal Cancer. *Clin. Cancer Res.* **2014,** *20* (5), 1345–1354.
63. Bryant, H. E.; Schultz, N.; Thomas, H. D.; et al. Specific Killing of BRCA2-Deficient Tumours With Inhibitors of Poly(ADP-Ribose) Polymerase. *Nature* **2005,** *434* (7035), 913–917.
64. Farmer, H.; McCabe, N.; Lord, C. J.; et al. Targeting the DNA Repair Defect in BRCA Mutant Cells as a Therapeutic Strategy. *Nature* **2005,** *434* (7035), 917–921.
65. Kennedy, R. D.; D'Andrea, A. D. DNA Repair Pathways in Clinical Practice: Lessons From Pediatric Cancer Susceptibility Syndromes. *J. Clin. Oncol.* **2006,** *24* (23), 3799–3808.
66. Cerbinskaite, A.; Mukhopadhyay, A.; Plummer, E. R.; Curtin, N. J.; Edmondson, R. J. Defective Homologous Recombination in Human Cancers. *Cancer Treat. Rev.* **2012,** *38* (2), 89–100.
67. Drew, Y.; Mulligan, E. A.; Vong, W. T.; et al. Therapeutic Potential of Poly(ADP-Ribose) Polymerase Inhibitor AG014699 in Human Cancers With Mutated or Methylated BRCA1 or BRCA2. *J. Natl. Cancer Inst.* **2011,** *103* (4), 334–346.
68. McCabe, N.; Turner, N. C.; Lord, C. J.; et al. Deficiency in the Repair of DNA Damage by Homologous Recombination and Sensitivity to Poly(ADP-Ribose) Polymerase Inhibition. *Cancer Res.* **2006,** *66* (16), 8109–8115.
69. Chan, N.; Pires, I. M.; Bencokova, Z.; et al. Contextual Synthetic Lethality of Cancer Cell Kill Based on the Tumor Microenvironment. *Cancer Res.* **2010,** *70* (20), 8045–8054.
70. Mendes-Pereira, A. M.; Martin, S. A.; Brough, R.; et al. Synthetic Lethal Targeting of PTEN Mutant Cells With PARP Inhibitors. *EMBO Mol. Med.* **2009,** *1* (6-7), 315–322.
71. McEllin, B.; Camacho, C. V.; Mukherjee, B.; et al. PTEN Loss Compromises Homologous Recombination Repair in Astrocytes: Implications for Glioblastoma Therapy With Temozolomide or Poly(ADP-Ribose) Polymerase Inhibitors. *Cancer Res.* **2010,** *70* (13), 5457–5464.
72. Hunt, C. R.; Gupta, A.; Horikoshi, N.; Pandita, T. K. Does PTEN Loss Impair DNA Double-Strand Break Repair by Homologous Recombination? *Clin. Cancer Res.* **2012,** *18* (4), 920–922.
73. Fraser, M.; Zhao, H.; Luoto, K. R.; et al. PTEN Deletion in Prostate Cancer Cells Does not Associate With Loss of RAD51 Function: Implications for Radiotherapy and Chemotherapy. *Clin. Cancer Res.* **2012,** *18* (4), 1015–1027.
74. Mukherjee, B.; Tomimatsu, N.; Amancherla, K.; Camacho, C. V.; Pichamoorthy, N.; Burma, S. The Dual PI-3K/mTOR Inhibitor NVP-BEZ235 is a Potent Inhibitor of ATM- and DNA-PKCs-Mediated DNA Damage Responses. *Neoplasia* **2012,** *14* (1), 34–43.
75. Toledo, L. I.; Murga, M.; Zur, R.; Soria, R.; et al. A Cell-Based Screen Identifies ATR Inhibitors With Synthetic Lethal Properties for Cancer-Associated Mutations. *Nat. Struct. Mol. Biol.* **2011,** *18* (6), 721–727.
76. Ibrahim, Y. H.; García-García, C.; Serra, V.; He, L.; et al. PI-3K Inhibition Impairs BRCA1/2 Expression and Sensitizes BRCA-Proficient Triple-Negative Breast Cancer to PARP Inhibition. *Cancer Discov.* **2012,** *2* (11), 1036–1047.
77. Juvekar, A.; Burga, L. N.; Hu, H.; Lunsford, E. P.; et al. Combining a PI-3K Inhibitor With a PARP Inhibitor Provides an Effective Therapy for BRCA1-Related Breast Cancer. *Cancer Discov.* **2012,** *2* (11), 1048–1063.
78. Jang, N. Y.; Kim, D. H.; Cho, B. J.; et al. Radiosensitization With Combined Use of Olaparib and PI-103 in Triple-Negative Breast Cancer. *BMC Cancer* **2015,** *15,* 89.
79. Cardnell, R. J.; Feng, Y.; Mukherjee, S.; et al. Activation of the PI-3K/mTOR Pathway Following PARP Inhibition in Small Cell Lung Cancer. *PLoS ONE* **2016,** *11* (4), e0152584.
80. Mo, W.; Liu, Q.; Lin, C. C.; et al. mTOR Inhibitors Suppress Homologous Recombination Repair and Synergize With PARP Inhibitors *via* Regulating SUV39H1 in BRCA-Proficient Triple-Negative Breast Cancer. *Clin. Cancer Res.* **2016,** *22* (7), 1699–1712.
81. De, P.; Sun, Y.; Carlson, J. H.; et al. Doubling Down on the PI-3K-AKT-mTOR Pathway Enhances the Antitumor Efficacy of PARP Inhibitor in Triple Negative Breast Cancer Model Beyond BRCA-Ness. *Neoplasia* **2014,** *16* (1), 43–72.
82. Wang, D.; Wang, M.; Jiang, N.; et al. Effective use of PI-3K Inhibitor BKM120 and PARP Inhibitor Olaparib to Treat PIK3CA Mutant Ovarian Cancer. *Oncotarget* **2016,** *7* (11), 13153–13166.
83. Sui, H.; Shi, C.; Yan, Z.; Li, H. Combination of Erlotinib and a PARP Inhibitor Inhibits Growth of A2780 Tumor Xenografts due to Increased Autophagy. *Drug Des. Dev. Ther.* **2015,** *9,* 3183–3190.
84. Amin, O.; Beauchamp, M. C.; Nader, P. A.; et al. Suppression of Homologous Recombination by Insulin-Like Growth Factor-1 Inhibition Sensitizes Cancer Cells to PARP Inhibitors. *BMC Cancer* **2015,** *15,* 817.
85. Min, A.; Im, S. A.; Kim, D. K.; et al. Histone Deacetylase Inhibitor, Suberoylanilide Hydroxamic Acid (SAHA), Enhances Anti-Tumor Effects of the Poly (ADP-Ribose) Polymerase (PARP) Inhibitor Olaparib in Triple-Negative Breast Cancer Cells. *Breast Cancer Res.* **2015,** *17,* 33.
86. Chao, O. S.; Goodman, O. B., Jr. Synergistic Loss of Prostate Cancer Cell Viability by Coinhibition of HDAC and PARP. *Mol. Cancer Res.* **2014,** *12* (12), 1755–1766.
87. Booth, L.; Cruickshanks, N.; Ridder, T.; Dai, Y.; Grant, S.; Dent, P. PARP and CHK Inhibitors Interact to Cause DNA Damage and Cell Death in Mammary Carcinoma Cells. *Cancer Biol. Ther.* **2013,** *14* (5), 458–465.
88. Johnson, N.; Li, Y. C.; Walton, Z. E.; et al. Compromised CDK1 Activity Sensitizes BRCA-Proficient Cancers to PARP Inhibition. *Nat. Med.* **2011,** *17* (7), 875–882.
89. Alagpulinsa, D. A.; Ayyadevara, S.; Yaccoby, S.; Shmookler Reis, R. J. A Cyclin-Dependent Kinase Inhibitor, Dinaciclib, Impairs Homologous Recombination and Sensitizes Multiple Myeloma Cells to PARP Inhibition. *Mol. Cancer Ther.* **2016,** *15* (2), 241–250.

90. Plummer, R.; Lorigan, P.; Steven, N.; et al. A Phase II Study of the Potent PARP Inhibitor, Rucaparib (PF-01367338, AG014699), With Temozolomide in Patients With Metastatic Melanoma Demonstrating Evidence of Chemopotentiation. *Cancer Chemother. Pharmacol.* **2013,** *71* (5), 1191–1199.
91. Middleton, M. R.; Friedlander, P.; Hamid, O.; et al. Randomized Phase II Study Evaluating Veliparib (ABT-888) With Temozolomide in Patients With Metastatic Melanoma. *Ann. Oncol.* **2015,** *26* (10), 2173–2179.
92. Khan, O. A.; Gore, M.; Lorigan, P.; et al. A Phase I Study of the Safety and Tolerability of Olaparib (AZD2281, KU0059436) and Dacarbazine in Patients With Advanced Solid Tumours. *Br. J. Cancer* **2011,** *104* (5), 750–755.
93. Robins, H. I.; Zhang, P.; Gilbert, M. R.; et al. A Randomized Phase I/II Study of ABT-888 in Combination With Temozolomide in Recurrent Temozolomide Resistant Glioblastoma: An NRG Oncology RTOG Group Study. *J. Neurooncol.* **2016,** *126* (2), 309–316.
94. Gupta, S. K.; Kizilbash, S. H.; Carlson, B. L.; et al. Delineation of MGMT Hypermethylation as a Biomarker for Veliparib-Mediated Temozolomide-Sensitizing Therapy of Glioblastoma. *J. Natl. Cancer Inst.* **2015,** *108* (5). pii: djv369.
95. Gabrielson, A.; Tesfaye, A. A.; Marshall, J. L.; et al. Phase II Study of Temozolomide and Veliparib Combination Therapy for Sorafenib-Refractory Advanced Hepatocellular Carcinoma. *Cancer Chemother. Pharmacol.* **2015,** *76* (5), 1073–1079.
96. Su, J. M.; Thompson, P.; Adesina, A.; et al. A Phase I Trial of Veliparib (ABT-888) and Temozolomide in Children With Recurrent CNS Tumors: A Pediatric Brain Tumor Consortium Report. *Neuro Oncol.* **2014,** *16* (12), 1661–1668.
97. Kummar, S.; Chen, A.; Ji, J.; et al. Phase I Study of PARP Inhibitor ABT-888 in Combination With Topotecan in Adults With Refractory Solid Tumors and Lymphomas. *Cancer Res.* **2011,** *71* (17), 5626–5634.
98. Samol, J.; Ranson, M.; Scott, E.; et al. Safety and Tolerability of the Poly(ADP-Ribose) Polymerase (PARP) Inhibitor, Olaparib (AZD2281) in Combination With Topotecan for the Treatment of Patients With Advanced Solid Tumors: A Phase I Study. *Invest. New Drugs* **2012,** *30* (4), 1493–1500.
99. LoRusso, P. M.; Li, J.; Burger, A.; et al. Phase I Safety, Pharmacokinetic, and Pharmacodynamic Study of the Poly(ADP-Ribose) Polymerase (PARP) Inhibitor Veliparib (ABT-888) in Combination With Irinotecan in Patients With Advanced Solid Tumors. *Clin. Cancer Res.* **2016,** *22* (13), 3227–3237.
100. Chen, E. X.; Jonker, D. J.; Siu, L. L.; et al. A Phase I Study of Olaparib and Irinotecan in Patients With Colorectal Cancer: Canadian Cancer Trials Group IND 187. *Invest. New Drugs* **2016,** *34* (4), 450–457.
101. Owonikoko, T. K.; Dahlberg, S. E.; Khan, S. A.; et al. A Phase 1 Safety Study of Veliparib Combined With Cisplatin and Etoposide in Extensive Stage Small Cell Lung Cancer: A Trial of the ECOG-ACRIN Cancer Research Group (E2511). *Lung Cancer* **2015,** *89* (1), 66–70.
102. Nguewa, P. A.; Fuertes, M. A.; Cepeda, V.; et al. Poly(ADP-Ribose) Polymerase-1 Inhibitor 3-Aminobenzamide Enhances Apoptosis Induction by Platinum Complexes in Cisplatin-Resistant Tumor Cells. *Med. Chem.* **2006,** *2* (1), 47–53.
103. Balmaña, J.; Tung, N. M.; Isakoff, S. J.; et al. Phase I Trial of Olaparib in Combination With Cisplatin for the Treatment of Patients With Advanced Breast, Ovarian and Other Solid Tumors. *Ann. Oncol.* **2014,** *25* (8), 1656–1663.
104. Bendell, J.; O'Reilly, E. M.; Middleton, M. R.; et al. Phase I Study of Olaparib Plus Gemcitabine in Patients With Advanced Solid Tumours and Comparison With Gemcitabine Alone in Patients With Locally Advanced/Metastatic Pancreatic Cancer. *Ann. Oncol.* **2015,** *26* (4), 804–811.
105. Lee, J. M.; Hays, J. L.; Annunziata, C. M.; et al. Phase I/Ib Study of Olaparib and Carboplatin in BRCA1 or BRCA2 Mutation-Associated Breast or Ovarian Cancer With Biomarker Analyses. *J. Natl. Cancer Inst.* **2014,** *106* (6). dju089.
106. Rajan, A.; Carter, C. A.; Kelly, R. J.; et al. A Phase I Combination Study of Olaparib With Cisplatin and Gemcitabine in Adults With Solid Tumors. *Clin. Cancer Res.* **2012,** *18* (8), 2344–2351.
107. van der Noll, R.; Marchetti, S.; Steeghs, N.; et al. Long-Term Safety and Anti-Tumour Activity of Olaparib Monotherapy After Combination With Carboplatin and Paclitaxel in Patients With Advanced Breast, Ovarian or Fallopian Tube Cancer. *Br. J. Cancer* **2015,** *113* (3), 396–402.
108. Fong, P. C.; Boss, D. S.; Yap, T. A.; et al. Inhibition of Poly(ADP-Ribose) Polymerase in Tumors From BRCA Mutation Carriers. *N. Engl. J. Med.* **2009,** *361* (2), 123–134.
109. Tutt, A.; Robson, M.; Garber, J. E.; et al. Oral Poly(ADP-Ribose) Polymerase Inhibitor Olaparib in Patients With BRCA1 or BRCA2 Mutations and Advanced Breast Cancer: A Proof-of-Concept Trial. *Lancet* **2010,** *376* (9737), 235–244.
110. Audeh, M. W.; Carmichael, J.; Penson, R. T.; et al. Oral Poly(ADP-Ribose) Polymerase Inhibitor Olaparib in Patients With BRCA1 or BRCA2 Mutations and Recurrent Ovarian Cancer: A Proof-of-Concept Trial. *Lancet* **2010,** *376* (9737), 245–251.
111. Gelmon, K. A.; Tischkowitz, M.; Mackay, H.; et al. Olaparib in Patients With Recurrent High-Grade Serous or Poorly Differentiated Ovarian Carcinoma or Triple-Negative Breast Cancer: A Phase 2, Multicentre, Open-Label, Non-Randomised Study. *Lancet Oncol.* **2011,** *12* (9), 852–861.
112. Drew, Y.; Ledermann, J.; Hall, G.; et al. Phase 2 Multicentre Trial Investigating Intermittent and Continuous Dosing Schedules of the Poly(ADP-Ribose) Polymerase Inhibitor Rucaparib in Germline BRCA Mutation Carriers With Advanced Ovarian and Breast Cancer. *Br. J. Cancer* **2016,** *114* (7), 723–730.
113. Coleman, R. L.; Sill, M. W.; Bell-McGuinn, K.; et al. A Phase II Evaluation of the Potent, Highly Selective PARP Inhibitor Veliparib in the Treatment of Persistent or Recurrent Epithelial Ovarian, Fallopian Tube, or Primary Peritoneal Cancer in Patients Who Carry a Germline BRCA1 or BRCA2 Mutation—An NRG Oncology/Gynecologic Oncology Group Study. *Gynecol. Oncol.* **2015,** *137* (3), 386–391.
114. Sandhu, S. K.; Schelman, W. R.; Wilding, G.; et al. The Poly(ADP-Ribose) Polymerase Inhibitor Niraparib (MK4827) in BRCA Mutation Carriers and Patients With Sporadic Cancer: A Phase 1 Dose-Escalation Trial. *Lancet Oncol.* **2013,** *14* (9), 882–892.
115. Ledermann, J.; Harter, P.; Gourley, C.; et al. Olaparib Maintenance Therapy in Patients With Platinum-Sensitive Relapsed Serous Ovarian Cancer: A Preplanned Retrospective Analysis of Outcomes by BRCA Status in a Randomised Phase 2 Trial. *Lancet Oncol.* **2014,** *15* (8), 852–861.
116. NICE Guideline. Olaparib for Maintenance Treatment of Relapsed, Platinum-Sensitive, BRCA Mutation-Positive Ovarian, Fallopian Tube and Peritoneal Cancer After Response to Second-Line or Subsequent Platinumbased Chemotherapy, 2016.
117. Dean, E.; Middleton, M. R.; Pwint, T.; et al. Phase I Study to Assess the Safety and Tolerability of Olaparib in Combination With Bevacizumab in Patients With Advanced Solid Tumours. *Br. J. Cancer* **2012,** *106* (3), 468–474.
118. Liu, J. F.; Tolaney, S. M.; Birrer, M.; et al. A Phase 1 Trial of the Poly(ADP-Ribose) Polymerase Inhibitor Olaparib (AZD2281) in Combination With the Anti-Angiogenic Cediranib (AZD2171) in Recurrent Epithelial Ovarian or Triple-Negative Breast Cancer. *Eur. J. Cancer* **2013,** *49* (14), 2972–2978.
119. Liu, J. F.; Barry, W. T.; Birrer, M.; et al. Combination Cediranib and Olaparib Versus Olaparib Alone for Women With Recurrent Platinum-Sensitive Ovarian Cancer: A Randomised Phase 2 Study. *Lancet Oncol.* **2014,** *15* (11), 1207–1214.
120. Reiss, K. A.; Herman, J. M.; Zahurak, M.; et al. A Phase I Study of Veliparib (ABT-888) in Combination With low-Dose Fractionated Whole Abdominal Radiation Therapy in Patients With Advanced Solid Malignancies and Peritoneal Carcinomatosis. *Clin. Cancer Res.* **2015,** *21* (1), 68–76.
121. Mehta, M. P.; Wang, D.; Wang, F.; et al. Veliparib in Combination With Whole Brain Radiation Therapy in Patients With Brain Metastases: Results of a Phase 1 Study. *J. Neurooncol.* **2015,** *122* (2), 409–417.
122. Michael, M.; Mulcahy, M. F.; Deming, D. A.; et al. Safety and Tolerability of Veliparib Combined With Capecitabine Plus Radiotherapy in Patients With Locally Advanced Rectal Cancer (LARC): Final Results of a Phase Ib Study. *J. Clin. Oncol.* **2015,** *33* (suppl.; abstr. 3517).
123. Esteller, M.; Silva, J. M.; Dominguez, G.; et al. Promoter Hypermethylation and BRCA1 Inactivation in Sporadic Breast and Ovarian Tumors. *J. Natl. Cancer Inst.* **2000,** *92* (7), 564–569.
124. Walsh, T.; Casadei, S.; Lee, M. K.; et al. Mutations in 12 Genes for Inherited Ovarian, Fallopian Tube, and Peritoneal Carcinoma Identified by Massively Parallel Sequencing. *Proc. Natl. Acad. Sci. U. S. A.* **2011,** *108* (44), 18032–18037.
125. Ahluwalia, A.; Hurteau, J. A.; Bigsby, R. M.; Nephew, K. P. DNA Methylation in Ovarian Cancer. II. Expression of DNA Methyltransferases in Ovarian Cancer Cell Lines and Normal Ovarian Epithelial Cells. *Gynecol. Oncol.* **2001,** *82* (2), 299–304.

126. Gaymes, T. J.; Shall, S.; Farzaneh, F.; Mufti, G. J. Chromosomal Instability Syndromes are Sensitive to Poly ADP-Ribose Polymerase Inhibitors. *Haematologica* **2008,** *93* (12), 1886–1889.
127. Mukhopadhyay, A.; Elattar, A.; Cerbinskaite, A.; et al. Development of a Functional Assay for Homologous Recombination Status in Primary Cultures of Epithelial Ovarian Tumor And Correlation With Sensitivity to Poly(ADP-Ribose) Polymerase Inhibitors. *Clin. Cancer Res.* **2010,** *16* (8), 2344–2351.
128. Willers, H.; Taghian, A. G.; Luo, C.-M.; Treszezamsky, A. D.; Sgroi, D.; Powell, S. N. Utility of DNA Repair Protein Foci for the Detection of Putative BRCA1-Pathway Defects in Breast Cancer Biopsies. *Mol. Cancer Res.* **2009,** *7,* 1304–1309.
129. Powell, S. N.; Kachnic, L. A. Therapeutic Exploitation of Tumor Cell Defects in Homologous Recombination. *Anticancer Agents Med. Chem.* **2008,** *8* (4), 448–460.
130. Abkevich, V.; Timms, K. M.; Hennessy, B. T.; et al. Patterns of Genomic Loss of Heterozygosity Predict Homologous Recombination Repair Defects in Epithelial Ovarian Cancer. *Br. J. Cancer* **2012,** *107* (10), 1776–1782.
131. Lucas, A. L.; Shakya, R.; Lipsyc, M. D.; et al. High Prevalence of BRCA1 and BRCA2 Germline Mutations With Loss of Heterozygosity in a Series of Resected Pancreatic Adenocarcinoma and Other Neoplastic Lesions. *Clin. Cancer Res.* **2013,** *19* (13), 3396–3403.
132. Hanby, A. M.; Kelsell, D. P.; Potts, H. W.; et al. Association Between Loss of Heterozygosity of BRCA1 and BRCA2 and Morphological Attributes of Sporadic Breast Cancer. *Int. J. Cancer* **2000,** *88* (2), 204–208.
133. Globe Newswire. *Myriad Receives FDA Approval of BRACAnalysis CDx(TM) as Companion Diagnostic for Lynparza(TM) (Olaparib) in Ovarian Cancer Patients;* Myriad Genetics, Inc.: Salt Lake City, UT, 2014. Available from: https://globenewswire.com/news-release/2014/12/19/693082/10113116/en/Myriad-Receives-FDA-Approval-of-BRACAnalysis-CDx-TM-as-Companion-Diagnostic-for-Lynparza-TM-olaparib-in-Ovarian-Cancer-Patients.html (accessed 13.08.16).
134. Pennington, K. P.; Walsh, T.; Harrell, M. I.; et al. Germline and Somatic Mutations in Homologous Recombination Genes Predict Platinum Response and Survival in Ovarian, Fallopian Tube, and Peritoneal Carcinomas. *Clin. Cancer Res.* **2014,** *20* (3), 764–775.
135. Yang, D.; Khan, S.; Sun, Y.; et al. Association of BRCA1 and BRCA2 Mutations With Survival, Chemotherapy Sensitivity, and Gene Mutator Phenotype in Patients With Ovarian Cancer. *JAMA* **2011,** *306* (14), 1557–1565.
136. Birkbak, N. J.; Kochupurakkal, B.; Izarzugaza, J. M.; et al. Tumor Mutation Burden Forecasts Outcome in Ovarian Cancer With BRCA1 or BRCA2 Mutations. *PLoS ONE* **2013,** *8* (11), e80023.
137. Dann, R. B.; DeLoia, J. A.; Timms, K. M.; et al. BRCA1/2 Mutations and Expression: Response to Platinum Chemotherapy in Patients With Advanced Stage Epithelial Ovarian Cancer. *Gynecol. Oncol.* **2012,** *125* (3), 677–682.
138. Birkbak, N. J.; Wang, Z. C.; Kim, J. Y.; et al. Telomeric Allelic Imbalance Indicates Defective DNA Repair and Sensitivity to DNA-Damaging Agents. *Cancer Discov.* **2012,** *2* (4), 366–375.
139. Isakoff, S. J.; Mayer, E. L.; He, L.; et al. TBCRC009: A Multicenter Phase II Clinical Trial of Platinum Monotherapy With Biomarker Assessment in Metastatic Triple-Negative Breast Cancer. *J. Clin. Oncol.* **2015,** *33,* 1902–1909.
140. Walsh, C. S. Two Decades Beyond BRCA1/2: Homologous Recombination, Hereditary Cancer Risk and a Target for Ovarian Cancer Therapy. *Gynecol. Oncol.* **2015,** *137* (2), 343–350.
141. Kristeleit, R.; Swisher, E.; Oza, A.; et al. 2700 Final Results of ARIEL2 (Part 1): A Phase 2 Trial to Prospectively Identify Ovarian Cancer (OC) Responders to Rucaparib Using Tumor Genetic Analysis. *Eur. J. Cancer* **2015,** *51* (3), S531.
142. Kachnic, L. A.; Fournier, L.; Gheorghiu, L.; Rosenberg, C.; Powell, S. N.; Willers, H. Utility of Chemotherapy-Induced Rad51 Foci for the Identification of Homologous Recombination Defects in Breast Cancer Cell Lines. *Proceedings of the 55th Annual Meeting of the Radiatation Research Society, Savannah, GA,* 2009; p 99.
143. Birkelbach, M.; Ferraiolo, N.; Gheorghiu, L.; et al. Detection of Impaired Homologous Recombination Repair in NSCLC Cells and Tissues. *J. Thorac. Oncol.* **2013,** *8,* 279–286.
144. Patterson, M. J.; Sutton, R. E.; Forrest, I.; et al. Assessing the Function of Homologous Recombination DNA Repair in Malignant Pleural Effusion (MPE) Samples. *Br. J. Cancer* **2014,** *111,* 94–100.
145. Asakawa, H.; Koizumi, H.; Koike, A.; et al. Prediction of Breast Cancer Sensitivity to Neoadjuvant Chemotherapy Based on Status of DNA Damage Repair Proteins. *Breast Cancer Res.* **2010,** *12* (2), R17.
146. Graeser, M.; McCarthy, A.; Lord, C. J.; et al. A Marker of Homologous Recombination Predicts Pathologic Complete Response to Neoadjuvant Chemotherapy in Primary Breast Cancer. *Clin. Cancer Res.* **2010,** *16* (24), 6159–6168.
147. Rothkamm, K.; Krüger, I.; Thompson, L. H.; Lobrich, M. Pathways of DNA Double-Strand Break Repair During the Mammalian Cell Cycle. *Mol. Cell Biol.* **2003,** *23,* 5706–5715.
148. Mahaney, B. L.; Meek, K.; Lees-Miller, S. P. Repair of Ionizing Radiation-Induced DNA Double-Strand Breaks by Non-Homologous End-Joining. *Biochem. J.* **2009,** *417* (3), 639–650.
149. Goodwin, J. F.; Knudsen, K. E. Beyond DNA Repair: DNA-PK Function in Cancer. *Cancer Discov.* **2014,** *4* (10), 1126–1139.
150. Neal, J. A.; Meek, K. Choosing the Right Path: Does DNA-PK Help Make the Decision? *Mutat. Res.* **2011,** *711,* 73–86.
151. Boulton, S.; Kyle, S.; Yalçintepe, L.; Durkacz, B. W. Wortmannin is a Potent Inhibitor of DNA Double Strand Break but not Single Strand Break Repair in Chinese Hamster Ovary Cells. *Carcinogenesis* **1996,** *17* (11), 2285–2290.
152. Hill, R.; Lee, P. W. K. The DNA-Dependent Protein Kinase (DNA-PK). *Cell Cycle* **2010,** *9,* 3460–3469.
153. Munck, J. M.; Batey, M. A.; Zhao, Y.; et al. Chemosensitization of Cancer Cells by KU-0060648, a Dual Inhibitor of DNA-PK and PI-3K. *Mol. Cancer Ther.* **2012,** *11* (8), 1789–1798.
154. Zhao, Y.; Thomas, H. D.; Batey, M.; et al. Preclinical Evaluation of a Potent Novel DNA-Dependent Protein Kinase Inhibitor NU7441. *Cancer Res.* **2006,** *66,* 5354.
155. Willmore, E.; de Caux, S.; Sunter, N. J.; Tilby, M. J.; Jackson, G. H.; Austin, C. A.; Durkacz, B. W. A Novel DNA-Dependent Protein Kinase Inhibitor, NU7026, Potentiates the Cytotoxicity of Topoisomerase II Poisons Used in the Treatment of Leukemia. *Blood* **2004,** *103* (12), 4659–4665.
156. Nutley, B. P.; Smith, N. F.; Hayes, A.; et al. Preclinical Pharmacokinetics and Metabolism of a Novel Prototype DNA-PK Inhibitor NU7026. *Br. J. Cancer* **2005,** *93* (9), 1011–1018.
157. Elliott, S. L.; Crawford, C.; Mulligan, E.; et al. Mitoxantrone in Combination With an Inhibitor of DNA-Dependent Protein Kinase: A Potential Therapy for High Risk B-Cell Chronic Lymphocytic Leukaemia. *Br. J. Haematol.* **2011,** *152* (1), 61–71.
158. Kruszewski, M.; Wojewódzka, M.; Iwaneńko, T.; Szumiel, I.; Okuyama, A. Differential Inhibitory Effect of OK-1035 on DNA Repair in L5178Y Murine Lymphoma Sublines With Functional or Defective Repair of Double Strand Breaks. *Mutat. Res.* **1998,** *409* (1), 31–36.
159. Ismail, I. H.; Mårtensson, S.; Moshinsky, D.; Rice, A.; Tang, C.; Howlett, A.; McMahon, G.; Hammarsten, O. SU11752 Inhibits the DNA-Dependent Protein Kinase and DNA Double-Strand Break Repair Resulting in Ionizing Radiation Sensitization. *Oncogene* **2004,** *23* (4), 873–882.
160. Kashishian, A.; Douangpanya, H.; Clark, D.; et al. DNA-Dependent Protein Kinase Inhibitors as Drug Candidates for the Treatment of Cancer. *Mol. Cancer Ther.* **2003,** *2* (12), 1257–1264.
161. Shinohara, E. T.; Geng, L.; Tan, J.; Chen, H.; et al. DNA-Dependent Protein Kinase is a Molecular Target for the Development of Noncytotoxic Radiation-Sensitizing Drugs. *Cancer Res.* **2005,** *65* (12), 4987–4992.
162. Mortensen, D. S.; Perrin-Ninkovic, S. M.; Shevlin, G.; et al. Optimization of a Series of Triazole Containing Mammalian Target of Rapamycin (mTOR) Kinase Inhibitors and the Discovery of CC-115. *J. Med. Chem.* **2015,** *58* (14), 5599–5608.
163. Munster, P. N.; Mahipal, A.; Nemunaitis, J. J.; et al. Phase I Trial of a Dual TOR Kinase and DNA-PK Inhibitor (CC-115) in Advanced Solid and Hematologic Cancers. *J. Clin. Oncol.* **2016,** *34* (15), S2505.
164. Taylor, A. M.; Harnden, D. G.; Arlett, C. F.; et al. Ataxia Telangiectasia: A Human Mutation With Abnormal Radiation Sensitivity. *Nature* **1975,** *258* (5534), 427–429.
165. Lavin, M. F. Ataxia-Telangiectasia: From a Rare Disorder to a Paradigm for Cell Signalling and Cancer. *Nat. Rev. Mol. Cell Biol.* **2008,** *9* (10), 759–769.

166. Lavin, M. F.; Shiloh, Y. The Genetic Defect in Ataxia-Telangiectasia. *Annu. Rev. Immunol.* **1997,** *15,* 177–202.
167. Rotman, G.; Shiloh, Y. ATM: From Gene to Function. *Hum. Mol. Genet.* **1998,** *7* (10), 1555–1563.
168. Houldsworth, J.; Lavin, M. F. Effect of Ionizing Radiation on DNA Synthesis in Ataxia Telangiectasia Cells. *Nucleic Acids Res.* **1980,** *8* (16), 3709–3720.
169. Painter, R. B.; Young, B. R. Radiosensitivity in Ataxia-Telangiectasia: A New Explanation. *Proc. Natl. Acad. Sci. U. S. A.* **1980,** *77* (12), 7315–7317.
170. Kastan, M. B.; Zhan, Q.; el-Deiry, W. S.; et al. A Mammalian Cell Cycle Checkpoint Pathway Utilizing p53 and GADD45 is Defective in Ataxia-Telangiectasia. *Cell* **1992,** *71* (4), 587–597.
171. Foray, N.; Priestley, A.; Alsbeih, G.; et al. Hypersensitivity of Ataxia Telangiectasia Fibroblasts to Ionizing Radiation is Associated With a Repair Deficiency of DNA Double-Strand Breaks. *Int. J. Radiat. Biol.* **1997,** *72* (3), 271–283.
172. Thompson, L. H. Recognition, Signaling, and Repair of DNA Double-Strand Breaks Produced by Ionizing Radiation in Mammalian Cells: The Molecular Choreography. *Mutat. Res.* **2012,** *751* (2), 158–246.
173. Shiloh, Y.; Ziv, Y. The ATM Protein Kinase: Regulating the Cellular Response to Genotoxic Stress, and More. *Nat. Rev. Mol. Cell Biol.* **2013,** *14* (4), 197–210.
174. Weber, A. M.; Ryan, A. J. ATM and ATR as Therapeutic Targets in Cancer. *Pharmacol. Ther.* **2015,** *149,* 124–138.
175. Cortez, D.; Wang, Y.; Qin, J.; Elledge, S. J. Requirement of ATM-Dependent Phosphorylation of brca1 in the DNA Damage Response to Double-Strand Breaks. *Science* **1999,** *286* (5442), 1162–1166.
176. Riballo, E.; Kühne, M.; Rief, N.; et al. A Pathway of Double-Strand Break Rejoining Dependent Upon ATM, Artemis, and Proteins Locating to Gamma-H2AX Foci. *Mol. Cell* **2004,** *16* (5), 715–724.
177. Wang, H.; Shi, L. Z.; Wong, C. C.; et al. The Interaction of CtIP and Nbs1 Connects CDK and ATM to Regulate HR-Mediated Double-Strand Break Repair. *PLoS Genet.* **2013,** *9* (2), e1003277.
178. Li, S.; Ting, N. S.; Zheng, L.; et al. Functional Link of BRCA1 and Ataxia Telangiectasia Gene Product in DNA Damage Response. *Nature* **2000,** *406* (6792), 210–215.
179. Gatei, M.; Zhou, B. B.; Hobson, K.; Scott, S.; Young, D.; Khanna, K. K. Ataxia Telangiectasia Mutated (ATM) Kinase and ATM and Rad3 Related Kinase Mediate Phosphorylation of Brca1 at Distinct and Overlapping Sites. *In Vivo* Assessment Using Phospho-Specific Antibodies. *J. Biol. Chem.* **2001,** *276* (20), 17276–17280.
180. Morrison, C.; Sonoda, E.; Takao, N.; Shinohara, A.; Yamamoto, K.; Takeda, S. The Controlling Role of ATM in Homologous Recombinational Repair of DNA Damage. *EMBO J.* **2000,** *19* (3), 463–471.
181. Fedier, A.; Schlamminger, M.; Schwarz, V. A.; Haller, U.; Howell, S. B.; Fink, D. Loss of atm Sensitises p53-Deficient Cells to Topoisomerase Poisons and Antimetabolites. *Ann. Oncol.* **2003,** *14* (6), 938–945.
182. Jaspers, N. G.; de Wit, J.; Regulski, M. R.; Bootsma, D. Abnormal Regulation of DNA Replication and Increased Lethality in Ataxia Telangiectasia Cells Exposed to Carcinogenic Agents. *Cancer Res.* **1982,** *42* (1), 335–341.
183. Helleday, T. Homologous Recombination in Cancer Development, Treatment and Development of Drug Resistance. *Carcinogenesis* **2010,** *31* (6), 955–960.
184. Yun, J.; Zhong, Q.; Kwak, J. Y.; Lee, W. H. Hypersensitivity of Brca1-Deficient MEF to the DNA Interstrand Crosslinking Agent Mitomycin C is Associated With Defect in Homologous Recombination Repair and Aberrant S-Phase Arrest. *Oncogene* **2005,** *24* (25), 4009–4016.
185. Moynahan, M. E.; Cui, T. Y.; Jasin, M. Homology-Directed dna Repair, Mitomycin-c Resistance, and Chromosome Stability is Restored With Correction of a Brca1 Mutation. *Cancer Res.* **2001,** *61* (12), 4842–4850.
186. Bhattacharyya, A.; Ear, U. S.; Koller, B. H.; Weichselbaum, R. R.; Bishop, D. K. The Breast Cancer Susceptibility Gene BRCA1 is Required for Subnuclear Assembly of Rad51 and Survival Following Treatment With the DNA Cross-Linking Agent Cisplatin. *J. Biol. Chem.* **2000,** *275* (31), 23899–23903.
187. Kass, E. M.; Helgadottir, H. R.; Chen, C. C.; et al. Double-Strand Break Repair by Homologous Recombination in Primary Mouse Somatic Cells Requires BRCA1 but not the ATM Kinase. *Proc. Natl. Acad. Sci. U. S. A.* **2013,** *110* (14), 5564–5569.
188. Choi, S.; Gamper, A. M.; White, J. S.; Bakkenist, C. J. Inhibition of ATM Kinase Activity Does not Phenocopy ATM Protein Disruption: Implications for the Clinical Utility of ATM Kinase Inhibitors. *Cell Cycle* **2010,** *9* (20), 4052–4057.
189. Sarkaria, J. N.; Tibbetts, R. S.; Busby, E. C.; Kennedy, A. P.; Hill, D. E.; Abraham, R. T. Inhibition of Phosphoinositide 3-Kinase Related Kinases by the Radiosensitizing Agent Wortmannin. *Cancer Res.* **1998,** *58* (19), 4375–4382.
190. Sarkaria, J. N.; Busby, E. C.; Tibbetts, R. S.; Roos, P.; Taya, Y.; Karnitz, L. M.; Abraham, R. T. Inhibition of ATM and ATR Kinase Activities by the Radiosensitizing Agent, Caffeine. *Cancer Res.* **1999,** *59* (17), 4375–4382.
191. Hickson, I.; Zhao, Y.; Richardson, C. J.; et al. Identification and Characterization of a Novel and Specific Inhibitor of the Ataxia-Telangiectasia Mutated Kinase ATM. *Cancer Res.* **2004,** *64* (24), 9152–9159.
192. Crescenzi, E.; Palumbo, G.; de Boer, J.; Brady, H. J. Ataxia Telangiectasia Mutated and p21CIP1 Modulate Cell Survival of Drug-Induced Senescent Tumor Cells: Implications for Chemotherapy. *Clin. Cancer Res.* **2008,** *14* (6), 1877–1887.
193. Batey, M. A.; Zhao, Y.; Kyle, S.; et al. Preclinical Evaluation of a Novel ATM Inhibitor, KU59403, *in Vitro* and *in Vivo* in p53 Functional and Dysfunctional Models of Human Cancer. *Mol. Cancer Ther.* **2013,** *12* (6), 959–967.
194. Rainey, M. D.; Charlton, M. E.; Stanton, R. V.; Kastan, M. B. Transient Inhibition of ATM Kinase is Sufficient to Enhance Cellular Sensitivity to Ionizing Radiation. *Cancer Res.* **2008,** *68* (18), 7466–7474.
195. Biddlestone-Thorpe, L.; Sajjad, M.; Rosenberg, E.; et al. ATM Kinase Inhibition Preferentially Sensitizes p53-Mutant Glioma to Ionizing Radiation. *Clin. Cancer Res.* **2013,** *19* (12), 3189–3200.
196. Golding, S. E.; Rosenberg, E.; Valerie, N.; et al. Improved ATM Kinase Inhibitor KU-60019 Radiosensitizes Glioma Cells, Compromises Insulin, AKT and ERK Prosurvival Signaling, and Inhibits Migration and Invasion. *Mol. Cancer Ther.* **2009,** *8* (10), 2894–2902.
197. Golding, S. E.; Rosenberg, E.; Adams, B. R.; et al. Dynamic Inhibition of ATM Kinase Provides a Strategy for Glioblastoma Multiforme Radiosensitization and Growth Control. *Cell Cycle* **2012,** *11* (6), 1167–1173.
198. Vecchio, D.; Daga, A.; Carra, E.; et al. Predictability, Efficacy and Safety of Radiosensitization of Glioblastoma-Initiating Cells by the ATM Inhibitor KU-60019. *Int. J. Cancer* **2014,** *135* (2), 479–491.
199. Blasina, A.; de Weyer, I. V.; Laus, M. C.; et al. A Human Homologue of the Checkpoint Kinase Cds1 Directly Inhibits Cdc25 Phosphatase. *Curr. Biol.* **1999,** *9* (1), 1–10.
200. Bahassi, E. M.; Ovesen, J. L.; Riesenberg, A. L.; Bernstein, W. Z.; Hasty, P. E.; Stambrook, P. J. The Checkpoint Kinases Chk1 and Chk2 Regulate the Functional Associations Between hBRCA2 and Rad51 in Response to DNA Damage. *Oncogene* **2008,** *27* (28), 3977–3985.
201. Jobson, A. G.; Cardellina, J. H., 2nd; Scudiero, D. Identification of a Bis-Guanylhydrazone [4,4′-Diacetyldiphenylurea-bis(Guanylhydrazone); NSC 109555] as a Novel Chemotype for Inhibition of Chk2 Kinase. *Mol. Pharmacol.* **2007,** *72* (4), 876–884.
202. Duong, H. Q.; Hong, Y. B.; Kim, J. S.; et al. Inhibition of Checkpoint Kinase 2 (CHK2) Enhances Sensitivity of Pancreatic Adenocarcinoma Cells to Gemcitabine. *J. Cell. Mol. Med.* **2013,** *17* (10), 1261–1270.
203. Jobson, A. G.; Lountos, G. T.; Lorenzi, P. L.; et al. Cellular Inhibition of Checkpoint Kinase 2 (Chk2) and Potentiation of Camptothecins and Radiation by the Novel Chk2 Inhibitor PV1019 [7-Nitro-1H-Indole-2-Carboxylic Acid {4-[1-(Guanidinohydrazone)-Ethyl]-Phenyl}-Amide]. *J. Pharmacol. Exp. Ther.* **2009,** *331* (3), 816–826.
204. Silva-Santisteban, M. C.; Westwood, I. M.; Boxall, K.; et al. Fragment-Based Screening Maps Inhibitor Interactions in the ATP-Binding Site of Checkpoint Kinase 2. *PLoS ONE* **2013,** *8* (6), e65689.
205. Anderson, V. E.; Walton, M. I.; Eve, P. D.; et al. CCT241533 is a Potent and Selective Inhibitor of CHK2 That Potentiates the Cytotoxicity of PARP Inhibitors. *Cancer Res.* **2011,** *71* (2), 463–472.
206. Arienti, K. L.; Brunmark, A.; Axe, F. U.; et al. Checkpoint Kinase Inhibitors: SAR and Radioprotective Properties of a Series of 2-Arylbenzimidazoles. *J. Med. Chem.* **2005,** *48* (6), 1873–1885.

207. Nguyen, T. N.; Saleem, R. S.; Luderer, M. J.; Hovde, S.; Henry, R. W.; Tepe, J. J. Radioprotection by Hymenialdisine-Derived Checkpoint Kinase 2 Inhibitors. *ACS Chem. Biol.* **2012,** *7* (1), 172–184.
208. Carlessi, L.; Buscemi, G.; Larson, G.; Hong, Z.; Wu, J. Z.; Delia, D. Biochemical and Cellular Characterization of VRX0466617, a Novel and Selective Inhibitor for the Checkpoint Kinase Chk2. *Mol. Cancer Ther.* **2007,** *6* (3), 935–944.
209. Matthews, T. P.; Jones, A. M.; Collins, I. Structure-Based Design, Discovery and Development of Checkpoint Kinase Inhibitors as Potential Anticancer Therapies. *Expert. Opin. Drug Discov.* **2013,** *8* (6), 621–640.
210. Durocher, D.; Jackson, S. P. DNA-PK, ATM and ATR as Sensors of DNA Damage: Variations on a Theme? *Curr. Opin. Cell Biol.* **2001,** *13* (2), 225–231.
211. Matsuoka, S.; Ballif, B. A.; Smogorzewska, A.; et al. ATM and ATR Substrate Analysis Reveals Extensive Protein Networks Responsive to DNA Damage. *Science* **2007,** *316* (5828), 1160–1166.
212. Brown, E. J.; Baltimore, D. ATR Disruption Leads to Chromosomal Fragmentation and Early Embryonic Lethality. *Genes Dev.* **2000,** *14* (4), 397–402.
213. Takai, H.; Tominaga, K.; Motoyama, N.; et al. Aberrant Cell Cycle Checkpoint Function and Early Embryonic Death in Chk1(−/−) Mice. *Genes Dev.* **2000,** *14* (12), 1439–1447.
214. Schlegel, R.; Pardee, A. B. Caffeine-Induced Uncoupling of Mitosis From the Completion of DNA Replication in Mammalian Cells. *Science* **1986,** *232* (4755), 1264–1266.
215. Smith, J.; Tho, L. M.; Xu, N.; Gillespie, D. A. The ATM-Chk2 and ATR-Chk1 Pathways in DNA Damage Signaling and Cancer. *Adv. Cancer Res.* **2010,** *108,* 73–112.
216. Liu, Q.; Guntuku, S.; Cui, X. S.; et al. Chk1 is an Essential Kinase That is Regulated by Atr and Required for the G(2)/M DNA Damage Checkpoint. *Genes Dev.* **2000,** *14* (12), 1448–1459.
217. O'Driscoll, M.; Ruiz-Perez, V. L.; Woods, C. G.; Jeggo, P. A.; Goodship, J. A. A Splicing Mutation Affecting Expression of Ataxia-Telangiectasia and Rad3-Related Protein (ATR) Results in Seckel Syndrome. *Nat. Genet.* **2003,** *33* (4), 497–501.
218. Casper, A. M.; Durkin, S. G.; Arlt, M. F.; Glover, T. W. Chromosomal Instability at Common Fragile Sites in Seckel Syndrome. *Am. J. Hum. Genet.* **2004,** *75* (4), 654–660.
219. Saleh-Gohari, N.; Bryant, H. E.; Schultz, N.; Parker, K. M.; Cassel, T. N.; Helleday, T. Spontaneous Homologous Recombination is Induced by Collapsed Replication Forks That are Caused by Endogenous DNA Single-Strand Breaks. *Mol. Cell. Biol.* **2005,** *25* (16), 7158–7169.
220. Hoeijmakers, J. H. Genome Maintenance Mechanisms for Preventing Cancer. *Nature* **2001,** *411* (6835), 366–374.
221. Walker, M.; Black, E. J.; Oehler, V.; Gillespie, D. A.; Scott, M. T. Chk1 C-Terminal Regulatory Phosphorylation Mediates Checkpoint Activation by De-Repression of Chk1 Catalytic Activity. *Oncogene* **2009,** *28* (24), 2314–2323.
222. Peasland, A.; Wang, L. Z.; Rowling, E.; et al. Identification and Evaluation of a Potent Novel ATR Inhibitor, NU6027, in Breast and Ovarian Cancer Cell Lines. *Br. J. Cancer* **2011,** *105* (3), 372–381.
223. Parsels, L. A.; Qian, Y.; Tanska, D. M.; et al. Assessment of chk1 Phosphorylation as a Pharmacodynamic Biomarker of chk1 Inhibition. *Clin. Cancer Res.* **2011,** *17* (11), 3706–3715.
224. Sørensen, C. S.; Syljuåsen, R. G. Safeguarding Genome Integrity: The Checkpoint Kinases ATR, CHK1 and WEE1 Restrain CDK Activity During Normal DNA Replication. *Nucleic Acids Res.* **2012,** *40* (2), 477–486.
225. Chen, M. S.; Ryan, C. E.; Piwnica-Worms, H. Chk1 Kinase Negatively Regulates Mitotic Function of Cdc25A Phosphatase Through 14-3-3 Binding. *Mol. Cell. Biol.* **2003,** *23* (21), 7488–7497.
226. Dai, Y.; Grant, S. New Insights Into Checkpoint Kinase 1 in the DNA Damage Response Signaling Network. *Clin. Cancer Res.* **2010,** *16* (2), 376–383.
227. Lee, J.; Kumagai, A.; Dunphy, W. G. Positive Regulation of Wee1 by Chk1 and 14-3-3 Proteins. *Mol. Biol. Cell* **2001,** *12* (3), 551–563.
228. Wang, H.; Wang, H.; Powell, S. N.; Iliakis, G.; Wang, Y. ATR Affecting Cell Radiosensitivity is Dependent on Homologous Recombination Repair but Independent of Nonhomologous End Joining. *Cancer Res.* **2004,** *64* (19), 7139–7143.
229. Sørensen, C. S.; Hansen, L. T.; Dziegielewski, J.; et al. The Cell-Cycle Checkpoint Kinase Chk1 is Required for Mammalian Homologous Recombination Repair. *Nat. Cell Biol.* **2005,** *7* (2), 195–201.
230. Tripathi, V.; Kaur, S.; Sengupta, S. Phosphorylation-Dependent Interactions of BLM and 53BP1 are Required for Their Anti-Recombinogenic Roles During Homologous Recombination. *Carcinogenesis* **2008,** *29* (1), 52–61.
231. Patro, B. S.; Frøhlich, R.; Bohr, V. A.; Stevnsner, T. WRN Helicase Regulates the ATR-CHK1-Induced S-Phase Checkpoint Pathway in Response to Topoisomerase-I-DNA Covalent Complexes. *J. Cell Sci.* **2011,** *124* (Pt 23), 3967–3979.
232. Yajima, H.; Lee, K. J.; Chen, B. P. ATR-Dependent Phosphorylation of DNA-Dependent Protein Kinase Catalytic Subunit in Response to UV-Induced Replication Stress. *Mol. Cell. Biol.* **2006,** *26* (20), 7520–7528.
233. Yamane, K.; Taylor, K.; Kinsella, T. J. Mismatch Repair-Mediated G2/M Arrest by 6-Thioguanine Involves the ATR-Chk1 Pathway. *Biochem. Biophys. Res. Commun.* **2004,** *318* (1), 297–302.
234. Stauffer, D.; Chang, B.; Huang, J.; Dunn, A.; Thayer, M. p300/CREB-Binding Protein Interacts With ATR and is Required for the DNA Replication Checkpoint. *J. Biol. Chem.* **2007,** *282* (13), 9678–9687.
235. Storz, P. Reactive Oxygen Species in Tumor Progression. *Front. Biosci.* **2005,** *10,* 1881–1896.
236. Berasain, C.; Castillo, J.; Perugorria, M. J.; Latasa, M. U.; Prieto, J.; Avila, M. A. Inflammation and Liver Cancer: New Molecular Links. *Ann. N. Y. Acad. Sci.* **2009,** *1155,* 206–221.
237. Wiseman, H.; Halliwell, B. Damage to DNA by Reactive Oxygen and Nitrogen Species: Role in Inflammatory Disease and Progression to Cancer. *Biochem. J.* **1996,** *313* (Pt 1), 17–29.
238. Cliby, W. A.; Roberts, C. J.; Cimprich, K. A.; et al. Overexpression of a Kinase-Inactive ATR Protein Causes Sensitivity to DNA-Damaging Agents and Defects in Cell Cycle Checkpoints. *EMBO J.* **1998,** *17* (1), 159–169.
239. Nghiem, P.; Park, P. K.; Kim, Y.; Vaziri, C.; Schreiber, S. L. ATR Inhibition Selectively Sensitizes G1 Checkpoint-Deficient Cells to Lethal Premature Chromatin Condensation. *Proc. Natl. Acad. Sci. U. S. A.* **2001,** *98* (16), 9092–9097.
240. Chalmers, A. J.; Ruff, E. M.; Martindale, C.; Lovegrove, N.; Short, S. C. Cytotoxic Effects of Temozolomide and Radiation are Additive- and Schedule-Dependent. *Int. J. Radiat. Oncol. Biol. Phys.* **2009,** *75* (5), 1511–1519.
241. Nishida, H.; Tatewaki, N.; Nakajima, Y.; et al. Inhibition of ATR Protein Kinase Activity by Schisandrin B in DNA Damage Response. *Nucleic Acids Res.* **2009,** *37* (17), 5678–5689.
242. Caporali, S.; Falcinelli, S.; Starace, G.; et al. DNA Damage Induced by Temozolomide Signals to Both ATM and ATR: Role of the Mismatch Repair System. *Mol. Pharmacol.* **2004,** *66* (3), 478–491.
243. Sultana, R.; Abdel-Fatah, T.; Perry, C.; et al. Ataxia Telangiectasia Mutated and Rad3 Related (ATR) Protein Kinase Inhibition is Synthetically Lethal in XRCC1 Deficient Ovarian Cancer Cells. *PLoS ONE* **2013,** *8* (2), e57098.
244. Charrier, J. D.; Durrant, S. J.; Golec, J. M.; et al. Discovery of Potent and Selective Inhibitors of Ataxia Telangiectasia Mutated and Rad3 Related (Atr) Protein Kinase as Potential Anticancer Agents. *J. Med. Chem.* **2011,** *54* (7), 2320–2330.
245. Reaper, P. M.; Griffiths, M. R.; Long, J. M.; et al. Selective Killing of ATM- or p53-Deficient Cancer Cells Through Inhibition of ATR. *Nat. Chem. Biol.* **2011,** *7* (7), 428–430.
246. Pires, I. M.; Olcina, M. M.; Anbalagan, S.; et al. Targeting Radiation-Resistant Hypoxic Tumour Cells Through ATR Inhibition. *Br. J. Cancer* **2012,** *107* (2), 291–299.
247. Prevo, R.; Fokas, E.; Reaper, P. M.; et al. The Novel ATR Inhibitor VE-821 Increases Sensitivity of Pancreatic Cancer Cells to Radiation and Chemotherapy. *Cancer Biol. Ther.* **2012,** *13* (11), 1072–1081.
248. Halazonetis, T. D.; Gorgoulis, V. G.; Bartek, J. An Oncogene-Induced DNA Damage Model for Cancer Development. *Science* **2008,** *319* (5868), 1352–1355.

249. Gilad, O.; Nabet, B. Y.; Ragland, R. L.; et al. Combining ATR Suppression With Oncogenic Ras Synergistically Increases Genomic Instability, Causing Synthetic Lethality or Tumorigenesis in a Dosage-Dependent Manner. *Cancer Res.* **2010,** *70* (23), 9693–9702.
250. Schoppy, D. W.; Ragland, R. L.; Gilad, O.; et al. Oncogenic Stress Sensitizes Murine Cancers to Hypomorphic Suppression of ATR. *J. Clin. Invest.* **2012,** *122* (1), 241–252.
251. Murga, M.; Campaner, S.; Lopez-Contreras, A. J.; et al. Exploiting Oncogene-Induced Replicative Stress for the Selective Killing of Myc-Driven Tumors. *Nat. Struct. Mol. Biol.* **2011,** *18* (12), 1331–1335.
252. Abdel-Fatah, T. M.; Middleton, F. K.; Arora, A.; et al. Untangling the ATR-CHEK1 Network for Prognostication, Prediction and Therapeutic Target Validation in Breast Cancer. *Mol. Oncol.* **2015,** *9* (3), 569–585.
253. Middleton, F. K.; Patterson, M. J.; Elstob, C. J.; et al. Common Cancer-Associated Imbalances in the DNA Damage Response Confer Sensitivity to Single Agent ATR Inhibition. *Oncotarget* **2015,** *6* (32), 32396–32409.
254. Fokas, E.; Prevo, R.; Pollard, J. R.; et al. Targeting ATR *In Vivo* Using the Novel Inhibitor VE-822 Results in Selective Sensitization of Pancreatic Tumors to Radiation. *Cell Death Dis.* **2012,** *3,* e441.
255. Hall, A. B.; Newsome, D.; Wang, Y.; et al. Potentiation of Tumor Responses to DNA Damaging Therapy by the Selective ATR Inhibitor VX-970. *Oncotarget* **2014,** *5* (14), 5674–5685.
256. Chen, T.; Middleton, F. K.; Falcon, S.; Reaper, P. M.; Pollard, J. R.; Curtin, N. J. Development of Pharmacodynamic Biomarkers for ATR Inhibitors. *Mol. Oncol.* **2015,** *9* (2), 463–472.
257. Foote, K. M.; Blades, K.; Cronin, A.; et al. Discovery of 4-{4-[(3R)-3-Methylmorpholin-4-yl]-6-[1-(Methylsulfonyl)Cyclopropyl]Pyrimidin-2-yl}-1H-Indole (AZ20): a Potent and Selective Inhibitor of ATR Protein Kinase With Monotherapy *In Vivo* Antitumor Activity. *J. Med. Chem.* **2013,** *56* (5), 2125–2138.
258. Kwok, M.; Davies, N.; Agathanggelou, A.; et al. ATR Inhibition Induces Synthetic Lethality and Overcomes Chemoresistance in TP53- or ATM-Defective Chronic Lymphocytic Leukemia Cells. *Blood* **2016,** *127* (5), 582–595.
259. Kwok, M.; Davies, N.; Agathanggelou, A.; et al. Synthetic Lethality in Chronic Lymphocytic Leukaemia With DNA Damage Response Defects by Targeting the ATR Pathway. *Lancet* **2015,** *385* (Suppl. 1), S58.
260. Chen, T.; Stephens, P. A.; Middleton, F. K.; Curtin, N. J. Targeting the S and G2 Checkpoint to Treat Cancer. Targeting the S and G2 Checkpoint to Treat Cancer. *Drug Discov. Today* **2012,** *17* (5–6), 194–202.
261. Parsels, L. A.; Morgan, M. A.; Tanska, D. M.; et al. Gemcitabine Sensitization by Checkpoint Kinase 1 Inhibition Correlates With Inhibition of a Rad51 DNA Damage Response in Pancreatic Cancer Cells. *Mol. Cancer Ther.* **2009,** *8* (1), 45–54.
262. Wagner, J. M.; Karnitz, L. M. Cisplatin-Induced DNA Damage Activates Replication Checkpoint Signaling Components That Differentially Affect Tumor Cell Survival. *Mol. Pharmacol.* **2009,** *76* (1), 208–214.
263. Zhang, C.; Yan, Z.; Painter, C. L.; et al. PF-00477736 Mediates Checkpoint Kinase 1 Signaling Pathway and Potentiates Docetaxel-Induced Efficacy in Xenografts. *Clin. Cancer Res.* **2009,** *15* (14), 4630–4640.
264. Ma, C. X.; Janetka, J. W.; Piwnica-Worms, H. Death by Releasing the Breaks: CHK1 Inhibitors as Cancer Therapeutics. *Trends Mol. Med.* **2011,** *17* (2), 88–96.
265. Garrett, M. D.; Collins, I. Anticancer Therapy With Checkpoint Inhibitors: What, Where and When? *Trends Pharmacol. Sci.* **2011,** *32* (5), 308–316.
266. Massey, A. J.; Stokes, S.; Browne, H.; et al. Identification of Novel, *In Vivo* Active Chk1 Inhibitors Utilizing Structure Guided Drug Design. *Oncotarget* **2015,** *6* (34), 35797–35812.
267. Mitchell, J. B.; Choudhuri, R.; Fabre, K.; et al. *In Vitro* and *In Vivo* Radiation Sensitization of Human Tumor Cells by a Novel Checkpoint Kinase Inhibitor, AZD7762. *Clin. Cancer Res.* **2010,** *16* (7), 2076–2084.
268. Petersen, L.; Hasvold, G.; Lukas, J.; Bartek, J.; Syljuåsen, R. G. p53-Dependent G(1) Arrest in 1st or 2nd Cell Cycle may Protect Human Cancer Cells from Cell Death After Treatment With Ionizing Radiation and Chk1 Inhibitors. *Cell Prolif.* **2010,** *43* (4), 365–371.
269. Blasina, A.; Hallin, J.; Chen, E.; et al. Breaching the DNA Damage Checkpoint *via* PF-00477736, a Novel Small-Molecule Inhibitor of Checkpoint Kinase 1. *Mol. Cancer Ther.* **2008,** *7* (8), 2394–2404.
270. Zabludoff, S. D.; Deng, C.; Grondine, M. R.; et al. AZD7762, a Novel Checkpoint Kinase Inhibitor, Drives Checkpoint Abrogation and Potentiates DNA-Targeted Therapies. *Mol. Cancer Ther.* **2008,** *7* (9), 2955–2966.
271. Matthews, D. J.; Yakes, F. M.; Chen, J.; et al. Pharmacological Abrogation of S-Phase Checkpoint Enhances the Anti-Tumor Activity of Gemcitabine *In Vivo*. *Cell Cycle* **2007,** *6* (1), 104–110.
272. Yang, H.; Yoon, S. J.; Jin, J.; et al. Inhibition of Checkpoint Kinase 1 Sensitizes Lung Cancer Brain Metastases to Radiotherapy. *Biochem. Biophys. Res. Commun.* **2011,** *406* (1), 53–58.
273. Höglund, A.; Nilsson, L. M.; Muralidharan, S. V.; et al. Therapeutic Implications for the Induced Levels of Chk1 in Myc-Expressing Cancer Cells. *Clin. Cancer Res.* **2011,** *17* (22), 7067–7079.
274. Ferrao, P. T.; Bukczynska, E. P.; Johnstone, R. W.; McArthur, G. A. Efficacy of CHK Inhibitors as Single Agents in MYC-Driven Lymphoma Cells. *Oncogene* **2012,** *31* (13), 1661–1672.
275. Walton, M. I.; Eve, P. D.; Hayes, A.; et al. The Clinical Development Candidate CCT245737 is an Orally Active CHK1 Inhibitor With Preclinical Activity in RAS Mutant NSCLC and Eμ-MYC Driven B-Cell Lymphoma. *Oncotarget* **2016,** *7* (3), 2329–2342.
276. Mitchell, C.; Park, M.; Eulitt, P.; Yang, C.; Yacoub, A.; Dent, P. Poly(ADP-Ribose) Polymerase 1 Modulates the Lethality of CHK1 Inhibitors in Carcinoma Cells. *Mol. Pharmacol.* **2010,** *78* (5), 909–917.
277. Li, T.; Christensen, S. D.; Frankel, P. H.; et al. A Phase II Study of Cell Cycle Inhibitor UCN-01 in Patients With Metastatic Melanoma: A California Cancer Consortium Trial. *Invest. New Drugs* **2012,** *30* (2), 741–748.
278. Ma, C. X.; Ellis, M. J.; Petroni, G. R.; et al. A Phase II Study of UCN-01 in Combination With Irinotecan in Patients With Metastatic Triple Negative Breast Cancer. *Breast Cancer Res. Treat.* **2013,** *137* (2), 483–492.
279. Welch, S.; Hirte, H. W.; Carey, M. S.; et al. UCN-01 in Combination With Topotecan in Patients With Advanced Recurrent Ovarian Cancer: A Study of the Princess Margaret Hospital Phase II Consortium. *Gynecol. Oncol.* **2007,** *106* (2), 305–310.
280. Karp, J. E.; Thomas, B. M.; Greer, J. M.; et al. Phase I and Pharmacologic Trial of Cytosine Arabinoside With the Selective Checkpoint 1 Inhibitor Sch 900776 in Refractory Acute Leukemias. *Clin. Cancer Res.* **2012,** *18* (24), 6723–6731.
281. Daud, A. I.; Ashworth, M. T.; Strosberg, J.; et al. Phase I Dose-Escalation Trial of Checkpoint Kinase 1 Inhibitor MK-8776 as Monotherapy and in Combination With Gemcitabine in Patients With Advanced Solid Tumors. *J. Clin. Oncol.* **2015,** *33* (9), 1060–1066.
282. Brega, N.; McArthur, G. A.; Britten, C.; et al. Phase I Clinical Trial of Gemcitabine (GEM) in Combination With PF-00477736 (PF-736), a Selective Inhibitor of CHK1 Kinase. *J. Clin. Oncol.* **2010,** *28,* 15s.
283. Sausville, E.; Lorusso, P.; Carducci, M.; et al. Phase I Dose-Escalation Study of AZD7762, a Checkpoint Kinase Inhibitor, in Combination With Gemcitabine in US Patients With Advanced Solid Tumors. *Cancer Chemother. Pharmacol.* **2014,** *73* (3), 539–549.
284. Doi, T.; Yoshino, T.; Shitara, K.; et al. Phase I Study of LY2603618, a CHK1 Inhibitor, in Combination With Gemcitabine in Japanese Patients With Solid Tumors. *Anticancer Drugs* **2015,** *26* (10), 1043–1053.
285. O'Carrigan, B.; de Miguel-Luken, M. J.; Papadatos-Pastos, D.; et al. Phase I Trial of a First-In-Class ATR Inhibitor VX-970 as Monotherapy (Mono) or in Combination (Combo) With Carboplatin (CP) Incorporating Pharmacodynamics (PD) Studies. *J. Clin. Oncol.* **2016,** *34* (suppl.; abstr. 2504).
286. Plummer, E. R.; Dean, E. J.; Evans, T. J.; et al. Phase I Trial of First-In-Class ATR Inhibitor VX-970 in Combination With Gemcitabine (Gem) in Advanced Solid Tumors (NCT02157792). *J. Clin. Oncol.* **2016,** *34* (suppl.; abstr. 2513).
287. Thomas, A.; Sciuto, L.; Padiernos, E.; Pommier, Y. Trial of Topotecan With VX970, an ATR Kinase Inhibitor, in Relapsed or Refractory Small Cell Lung Cancer (NCT02487095). *J. Clin. Oncol.* **2016,** *34* (suppl.; abstr. TPS8581).

288. Dillon, M.; Ellis, S.; Grove, L.; et al. PATRIOT: A Phase I Study to Assess the Tolerability, Safety and Biological Effects of a Specific Ataxia Telangiectasia and Rad3-Related (ATR) Inhibitor (AZD6738) as a Single Agent and in Combination With Palliative Radiation Therapy in Patients With Solid Tumours. *J. Clin. Oncol. (Meet. Abstr.)* **2016,** *34* (15) (suppl. TPS2603).

Relevant Websites

https://clinicaltrials.gov/—Details of all Current Clinical Trials Using Search Function.
http://www.ncbi.nlm.nih.gov/pubmed/—Searchable Publications Database.

5.05 Targeting the Androgen Receptor Signaling Axis

H Li, P Rennie, and A Cherkasov, University of British Columbia, Vancouver, BC, Canada

© 2017 Elsevier Ltd. All rights reserved.

5.05.1	**Introduction**	135
5.05.2	**The Androgen Signaling Pathway**	135
5.05.2.1	Androgens	135
5.05.2.2	The Androgen Receptor	136
5.05.2.3	Mechanism of AR Activation	138
5.05.3	**Conventional Antiandrogens Targeting the AR ABS**	138
5.05.3.1	The AR ABS	138
5.05.3.2	First-Generation Antiandrogens	140
5.05.3.3	Second- and Next-Generation AR Inhibitors	141
5.05.3.3.1	Enzalutamide and ARN509	141
5.05.3.3.2	ODM-201	142
5.05.3.3.3	Abiraterone	142
5.05.3.3.4	Galeterone	143
5.05.3.4	The Resistance Problem of Conventional Antiandrogens	144
5.05.4	**Novel AR Inhibitors Targeting Alternative Sites**	144
5.05.4.1	AR LBD Surface Site Inhibitors	144
5.05.4.2	AR NTD Inhibitors	146
5.05.4.3	AR DBD Inhibitors	147
5.05.4.4	Other Nonconventional Strategies of Targeting AR Signaling	148
5.05.5	**Summary**	148
References		149
Relevant Websites		153

Abbreviations

3D Three-dimensional
ABS Androgen binding site
ADT Androgen deprivation therapy
AF1 Activation function 1
AF2 Activation function 2
AKR1C3 Aldo-ketoreductase
AR Androgen receptor
ARE Androgen response element
ARVs Androgen receptor splice variants
BF3 Binding function 3
CRPC Castration-resistant prostate cancer
CTE Carboxyl-terminal extension
CYP11A1 Cholesterol side-chain cleavage enzyme
CYP17A1 17α-Hydroxylase/17, 20-lyase
DBD DNA-binding domain
DHEA Dehydroepiandrosterone
DHT 5α-Dihydrotestosterone
ER Estrogen receptor
FKBP5 FK506 binding protein 5
GABA ϒ-Aminobutyric acid
GR Glucocorticoid receptor
HSD3B 3β-Hydroxysteroid dehydrogenase
HSP90 Heat shock protein 90
LBD Ligand-binding domain
LH Luteinizing hormone
LHRH Luteinizing-hormone releasing hormone
MR Mineralocorticoid receptor
NLS Nuclear localization signal
NR Nuclear receptor
NTD N-terminal domain
PCa Prostate cancer
PI3K Phosphoinositide 3-kinase
PK Pharmacokinetics
PPARγ Peroxisome proliferator-activated receptor-gamma
PPI Protein–protein interaction
PR Progesterone receptor
PSA Prostate-specific antigen
SHR Steroidal hormone receptor
SRD5A 5α-Reductase
TMPRSS2 Transmembrane protease serine 2

5.05.1 Introduction

Nuclear receptors (NRs) function as transcription factors, and they are activated by cognate ligands (such as hormones, vitamins, and fatty acids among others) that bind to NR-response elements and regulate the transcription of genes encoding enzymes, transporters, and other proteins.[1] NRs play an important role in a myriad of human physiological processes, including development, reproduction, immune response, cardiovascular function, tumorigenesis, and metabolic homeostasis.[2] Importantly, NRs are also involved in a wide range of diseases such as cancers and metabolic syndromes (**70002. PPAR, REV-ERB & ROR Nuclear Receptors**).[3,4] NRs represent the second biggest family of drug targets, and over a third of NRs are targets of currently marketed drugs.[5] Thus, NR-directed compounds account for 13% of the Food and Drug Administration (FDA)-approved therapeutics; 20 of the top 200 most prescribed drugs target NRs.[6]

The human NR superfamily consists of 48 members, which all share a similar organization of constituent domains, including a highly variable N-terminal domain (NTD), a conserved DNA-binding domain (DBD), a similar ligand-binding domain (LBD), and a hinge region connecting the DBD and LBD (**Fig. 1**).[7–9] NRs are conventionally divided into three subgroups based on their native ligands: steroid hormone receptors (SHRs), nonsteroid receptors, and orphan receptors. The SHRs are activated by endogenous hormones and bind to hormone response elements via homodimerization, including the androgen receptor (AR), estrogen receptor (ER), progesterone receptor (PR), glucocorticoid receptor (GR), and mineralocorticoid receptor (MR). Due to the presence of the LBD and known native ligands, SHRs have received considerable attention as attractive drug targets for prostate and breast cancers among other diseases.[10,11] In particular, the human AR has been intensively studied for its critical role in the development and progression of prostate cancer (PCa), and a large number of synthetic AR inhibitors have been developed as potential therapeutics for PCa.[10]

PCa is the most commonly diagnosed malignancy in men, and the second leading cause of male cancer death in North America.[12] The majority of PCas that are diagnosed early is localized to the prostate gland, and the disease may be cured by local therapy such as prostatectomy and radiation. However, a portion of patients will have recurrence, and their diseases eventually progress to a lethal castration-resistant state (CRPC). CRPC has historically been thought to be androgen independent; however, accumulating evidence demonstrates that CRPC continues to depend on the AR transactivation, which resumes the PCa proliferation despite low levels of circulating androgens.[13]

For high-risk PCa and CRPC, androgen deprivation therapy (ADT) is the mainstay treatment that aims at reducing androgen level or blocking the AR function. ADT includes orchiectomy, estrogen, luteinizing-hormone releasing hormone (LHRH) agonists/antagonists, 17α-hydroxylase/17, 20-lyase (CYP17A1) inhibitors, and AR inhibitors/antiandrogens.[14,15] The persistent reactivation of the AR in CRPC has been indicated by clinical responses and overall survival benefits of CRPC patients from the latest ADT drugs enzalutamide and abiraterone.[16–18] This provides evidence to demonstrate that the human androgen signaling pathway continues to play a critical role in PCa and CRPC, where the AR still represents the master regulator and the most validated drug target. This article focuses on reviewing the existing and emerging AR signaling-targeted therapies, including androgen synthesis inhibitors, conventional antiandrogens, and AR inhibitors targeting alternative sites with novel mechanisms of action.

5.05.2 The Androgen Signaling Pathway

5.05.2.1 Androgens

Endogenous androgens (testosterone and 5α-dihydrotestosterone—DHT) are male sex hormones responsible for the development of the male phenotype during embryogenesis and male sexual maturation during puberty. In adult men, androgens remain critical for the development and maintenance of the reproductive system, and affect many other tissues such as muscle and bone.[19] The

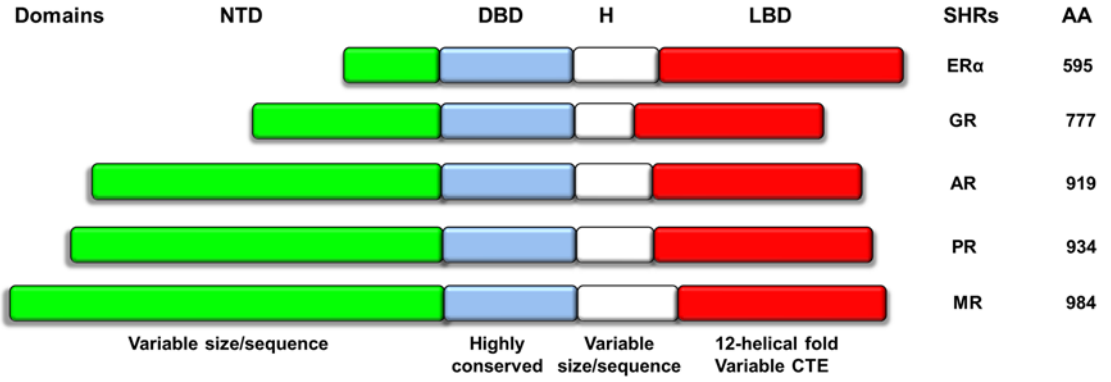

Fig. 1 Schematic diagram of organizational domains of steroidal hormone receptors (*SHRs*) of estrogen receptor-α (ERα), glucocorticoid receptor (*GR*), androgen receptor (*AR*), progesterone receptor (*PR*), and mineralocorticoid receptor (*MR*), including the *N*-terminal domain (*NTD*), the DNA-binding domain (*DBD*), the hinge (H), and the ligand-binding domain (*LBD*). The number of total amino acids (*AA*) is also annotated.

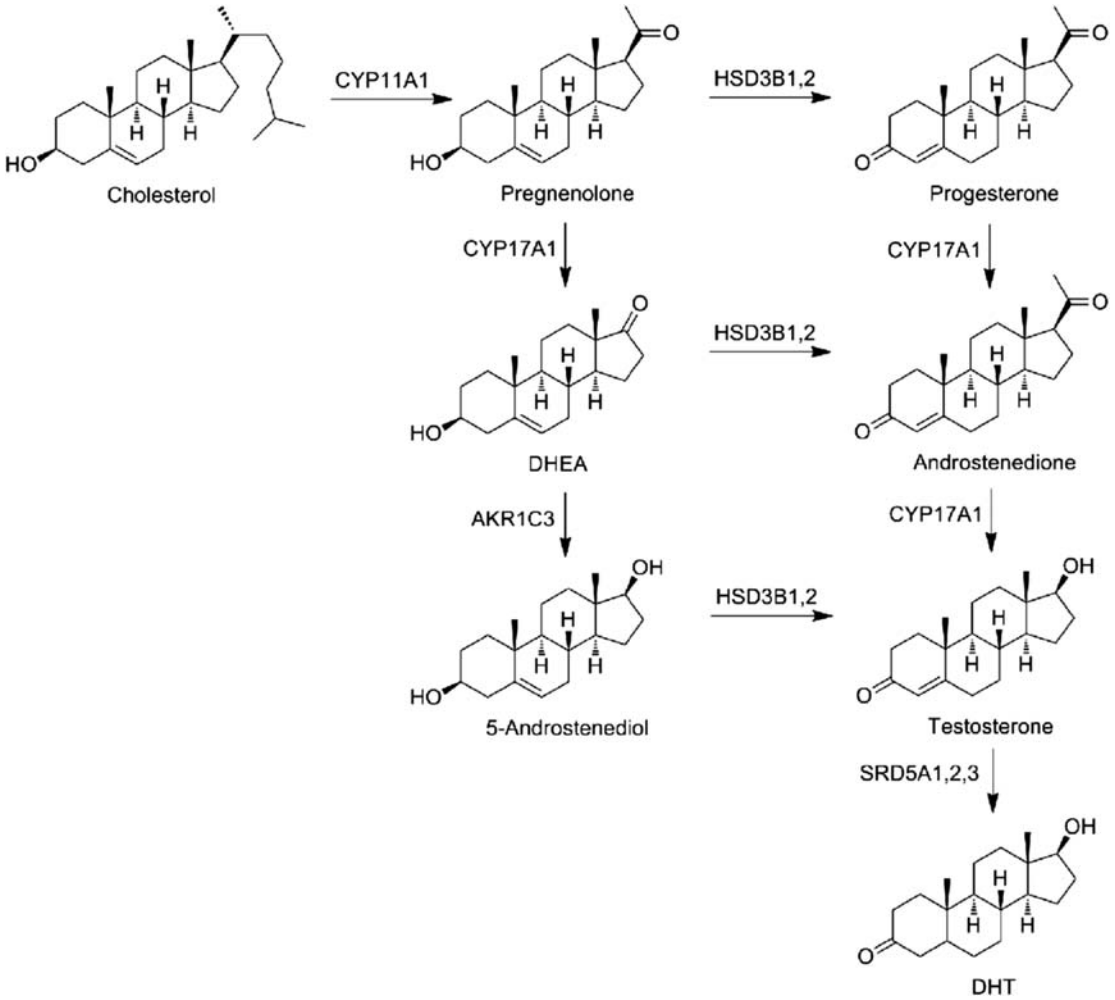

Fig. 2 The androgen biosynthesis pathway. *CYP11A1*, cholesterol side-chain cleavage enzyme; *HSD3B*, 3β-hydroxysteroid dehydrogenase; *CYP17A1*, 17α-hydroxylase/17, 20-lyase; *DHEA*, dehydroepiandrosterone; *AKR1C3*, aldo-ketoreductase; *SRD5A*, 5α-reductase.

action of androgens in reproductive tissues (prostate and testis) is known as the androgenic effect, while the effect in muscle and bone is known as the anabolic effect.[20]

Approximately 90–95% of testosterone is produced in the testes, and 5–10% of testosterone is synthesized in the adrenal gland. The synthesis of androgens is tightly regulated by the hypothalamus–pituitary–gonadal and hypothalamus–pituitary–adrenal axes.[21,22] The LHRH (also known as gonadotropin-releasing hormone) and corticotropic hormone (CTH), which are secreted by the hypothalamus, stimulate the release of luteinizing hormone (LH) and adrenocorticotropic hormone (ACTH) by the pituitary gland. The LH binds to LH receptors in the testis and initiates the production of testosterone; the ACTH binds to its receptors in the adrenal gland and triggers the synthesis of testosterone. The androgen biosynthesis pathway involves a number of steroidogenic enzymes, such as the CYP17A1, 3β-hydroxysteroid dehydrogenase (HSD3B1, HSD3B2), and 5α-reductase types 1, 2, and 3 (SRD5A1, SRD5A2, and SRD5A3) (Fig. 2).[23]

The majority of testosterone binds to carrier proteins such as the steroid hormone binding globulin and albumin, and only 1–2% of testosterone exists in an unbound form. The free form of testosterone enters prostate cells, and then it is converted into a more active metabolite, DHT, by the 5α-reductase enzyme. Importantly, DHT binds to the AR with higher affinity, and its biological activity exceeds that of testosterone by up to 10 times, which makes DHT the primary ligand for the AR. It has been demonstrated that aberrant regulation of androgens leads to diseases such as androgen insensitivity syndromes and PCa.[20,22,24–26]

5.05.2.2 The Androgen Receptor

The AR gene was first found to be located on chromosome X at Xq11.2 in 1981,[27] and the human AR cDNA was first cloned and sequenced in 1988.[28] The AR gene is more than 90 kb long, and codes for a 110 kDa protein consisting of 919 amino acids.[29] The AR is mainly expressed in androgen target tissues, such as the prostate, muscle, liver, and central nervous system (CNS). It is a key ligand-

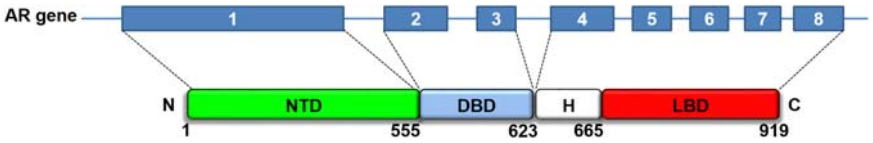

Fig. 3 Structural organization of the AR gene and protein. The exon 1 encodes the N-terminal domain (*NTD*); exons 2 and 3 encode the DNA-binding domain (*DBD*), exons 4–8 encode the hinge and ligand-binding domain (*LBD*).

activated transcription factor in healthy prostate and during neoplastic transformation. In the normal prostate, AR regulates prostate secretory function, stimulates epithelial cell renewal, and maintains cells in a differentiated state. Similar to other SHRs, the AR is organized into four functional parts including the NTD, the DBD, the hinge region, and the LBD (**Fig. 3**). These domains play different roles in the AR activity, and an understanding of these domains is essential for the development of AR-targeted therapeutics.

The NTD is encoded by exon 1, and it accounts for more than half of the size of the AR (residues 1–555), and is highly variable in the sequence compared to other SHRs.[30] This part of the protein is very flexible and intrinsically disordered in solution,[31] which has hampered the elucidation of its three-dimensional (3D) structure. The NTD has the main transactivation function region, termed the activation function 1 (AF1), which contains two transactivation units, TAU1 (residues 100–370) and TAU5 (residues 360–485).[32] The AF1 is indispensable for the full activity of the AR, and is essential for constitutively active truncated AR splice variants (ARVs) that do not contain the LBD portion. Interestingly, two motifs in NTD, the FQNLF (residues 23–27) and the WHTLF (residues 433–437), have been shown to interact with the activation function 2 (AF2) in the AR LBD region, leading to N/C intra- and/or intermolecular interactions, which are important for the transcription of some target genes.[33]

The DBD (residues 556–623) is encoded by exons 2 and 3, and is highly conserved among the SHRs. The DBD consists of two zinc fingers and a loosely structured carboxyl-terminal extension (CTE) region. The first zinc finger is proximal to the NTD, and is responsible for the DNA recognition. The α-helix of the zinc finger, termed the recognition helix, directly interacts with nucleotides in the DNA major groove. There is a P[roximal]-box region (residues 577-GSCKV-581) in the recognition helix, which is responsible for the specific recognition of the DNA response element. The second zinc finger contains the D[istal]-box region (residues 596-ASRND-600), which is the dimerization interface (**Fig. 4**). The CTE is critical for the 3D organization of the DBD, and it mediates the selectivity of the receptor to androgen response elements (AREs) on the DNA.[34] The AR DBD and CTE can recapitulate the DNA binding and dimerization of the full-length AR. The DBD structure has been resolved crystallographically as a DBD dimer bound to a direct repeat of two ARE half-sites.[35]

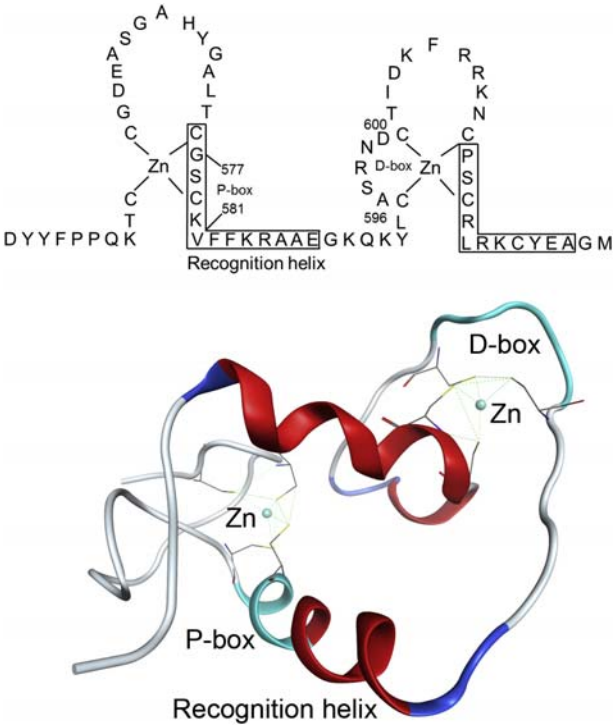

Fig. 4 (*Upper*) A schematic of the AR DBD is given to show two zinc fingers in the core of AR DBD, the P-box, and D-box residues, and residues (in boxes) that constitute two alpha helices. (*Lower*) The 3D structure of the AR DBD monomer with P-box and D-box residues colored in cyan (PDB code: 1R4I).

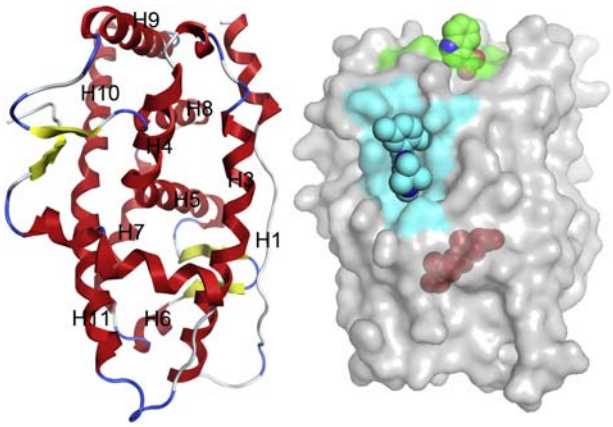

Fig. 5 (*Left*) The AR LBD structure is predominantly composed of 11 α-helices (PDB code: 3X3L). (*Right*) A surface representation of the AR LBD showing the ABS (ligand in *red*), AF2 (*cyan*), and BF3 (*green*) sites with corresponding ligands in each different binding site (PDB code: 2PIP).

The hinge region (residues 624–665) is encoded by exon 4, and it is a flexible linker that connects the LBD and DBD segments. The hinge is known for its role in the nuclear translocation through carrying a ligand-dependent nuclear localization signal (NLS, residues 617–633) spanning the hinge and DBD.[36] The NLS could bind importin-α and translocate the AR from the cytoplasm to the nucleus.[37,38] The NLS consists of two clusters of basic amino acid residues (617-RKCYEAGMTLGARKLKK-633), and this motif is highly conserved among other SHRs.

The LBD section of the AR (residues 666–919) is encoded by five AR exons (exons 4–8, exon 4 encoding both the hinge and part of the LBD) varying from 131 to 288 bp in size. The LBD consists of 11 α-helices (H) and 2 β-sheets that are arranged in three layers to form an antiparallel "α-helical sandwich" (Fig. 5). It is worth noting that the H2 is missing in the AR, but the same numbering for other helices was adopted for easy comparison with other SHRs. The androgen binds to a buried pocket in the LBD, termed the androgen binding site (ABS), which is formed by the N-terminal regions of H3 and H5, and the C-terminal regions of H10 and H11. Upon binding of the androgen, the LBD undergoes conformational changes and the H12 is repositioned to stabilize the complex. This motion allows the formation of a shallow surface groove by residues of H3, loop 3–4, H4, and H12, referred to as the AF2, which is the major interface for the intra- and/or intermolecular N–C interactions and coactivator recruitment.[39] It has been demonstrated that the AF2 preferentially binds to the FXXLF motifs, including the 23-FQNLF-27 present in the NTD, and interacts poorly with LXXLL motifs, which are commonly found in AR coactivators.[40] In recent years, another surface groove consisting of H1, loop 3–4, and H9 residues was identified on the AR LBD, called the binding function 3 (BF3). It was reported to allosterically regulate the AF2 activity;[41] however, the complete functional role of BF3 is not clear yet.

5.05.2.3 Mechanism of AR Activation

The human AR is known as an intracellular ligand-activated transcription factor. In its unliganded state, the AR is inactive and primarily resides in the cytoplasm, where it is bound to cochaperones such as the heat shock protein 90 (HSP90). Upon androgen binding, the AR becomes activated and dissociates from cochaperones. The activated AR then recruits coactivators, and undergoes a series of conformational changes, as well as translocates into the nucleus.[42] In the nucleus, the AR dimerizes via the DBD portions, further binds to AREs in the promoter and enhancer region of target genes, interacts with different coregulators, and initiates the transcription of regulated genes (Fig. 6). Notably, the AR regulates over 1000 genes,[43] including the AR itself, and its target genes such as prostate-specific antigen (PSA), transmembrane protease serine 2 (TMPRSS2), and FK506 binding protein 5 (FKBP5).

The mechanism of AR action is still not entirely clear, and increasing evidence indicates that the function of the AR is also regulated by a complex network of coregulators and cell signaling pathways. The AR serves as a scaffold for the assembly of coregulators in the promoter and enhancer region to activate or repress transcription. The AR coregulators are proteins recruited by the receptor, including coactivators such as the p160 family,[44] and corepressors such as NCOR.[45,46] In addition, the AR could also be activated by kinase signaling pathways in an androgen-independent manner, such as the phosphoinositide 3-kinase (PI3K)/AKT/mammalian target of rapamycin.[47–49]

5.05.3 Conventional Antiandrogens Targeting the AR ABS

5.05.3.1 The AR ABS

The ABS in the AR LBD is a proven druggable site for small-molecule inhibitors. All reported structures of the AR LBD maintain a three-layered sandwich fold; the only observed structural differences lie in subtle conformational changes of side chains of the ABS residues.[42] The AR ABS is a buried site that is mainly composed of hydrophobic side chains, including L701, L704, L707,

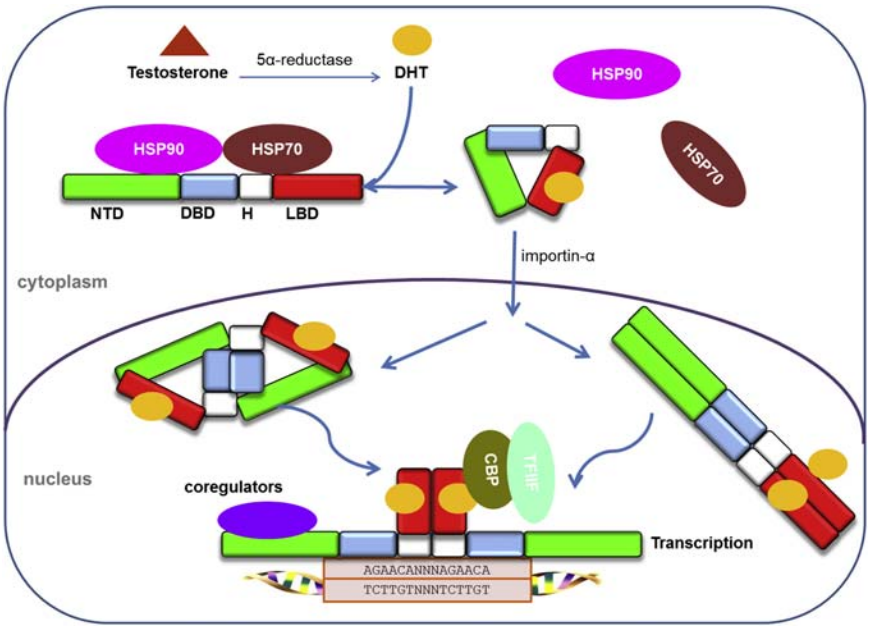

Fig. 6 The classic AR transactivation signaling pathway, involving the androgen conversion, AR activation, nuclear translocation, dimerization, and coregulator recruitment.

Q711, M742, M745, V746, M749, F764, M787, and L873, which interact with AR binders through Van der Waals interactions. There are two pairs of conserved polar patches (R752 and Q711, N705 and T877) located at opposing ends of the site, which may play a pivotal role in anchoring steroidal AR binders (Fig. 7). The ABS is known for its notable plasticity, in that it adjusts the volume to accommodate ligands of various sizes.[50,51]

So far, the agonism and antagonism of the AR have been mainly elaborated from a mechanistic perspective. In brief, the H12 serves as a "switch" to open or close the LBD according to the binding of antagonists or agonists. When agonists bind to the AR ABS,

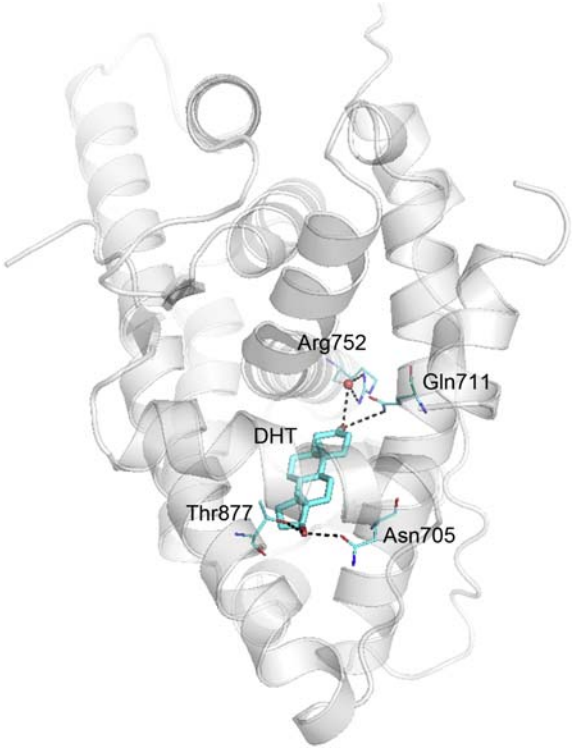

Fig. 7 Crystal structures of the AR LBD with DHT in the ABS (PDB code: 3L3X); hydrogen bond interactions were indicated by black dashes.

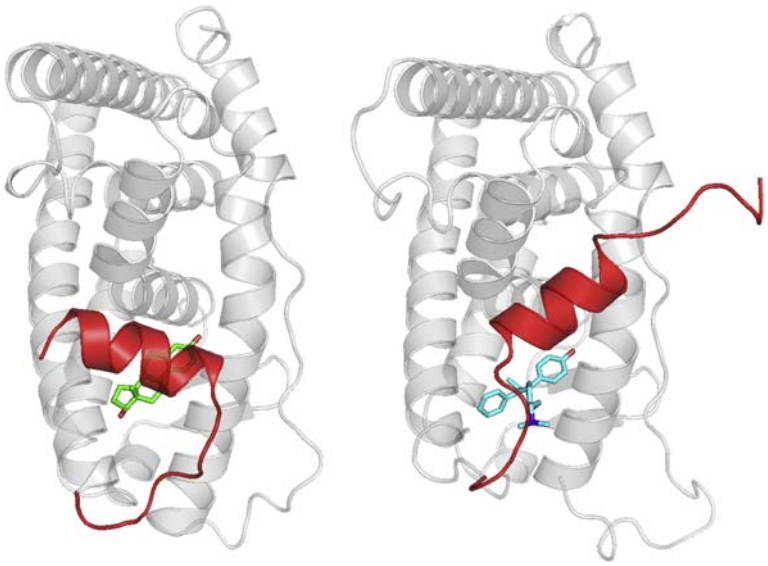

Fig. 8 (*Left*)Crystal structure of ER with estradiol in the agonistic form (PDB code: 1ERE); (*Right*) Crystal structure of ER with tamoxifen in the antagonistic form (PDB code: 3ERT). The H12 was colored in *red*.

the H12 is positioned to cover the LBD in a "closed" state, and then the AF2 is exposed that enables the recruitment of coactivators. Upon antagonist binding, the AR LBD adopts an "open" state by repositioning the H12 to occupy the AF2 site, which prevents the coactivator or recruits repressor binding, and thus blocks the receptor transactivation.[42] The agonistic form of the AR has been revealed by a plethora of crystal structures of wild-type AR LBD with agonists, or mutated AR LBD with "converted" antagonists (Fig. 7).[50–58] This demonstrates the AR LBD in a "closed" state, with coactivators such as SRC attached to the AF2 site of the receptor.

The antagonism of the AR is not clear yet, due to the infeasibility of resolving wild-type AR LBD structures containing antagonists. However, the antagonism of ER (Fig. 8), PR, and GR has been unveiled by cocrystal structures of their wild-type LBD with antagonists,[59–63] demonstrating that the H12 relocates to the AF2 and precludes coactivator binding. Based on the information from other SHRs, the AR may presumably share a similar antagonism. The H12 positioning in the antagonistic forms of SHRs is drastically diverse,[59–62] and thus, it makes realistic homology modeling of H12 in the AR difficult. Although the antagonistic conformation of the AR is absent, the availability of cocrystal structures of the AR LBD with various ligands, as well as a large number of known AR ABS binders, provides a wealth of information for developing new AR ABS inhibitors.[50–58,64,65]

5.05.3.2 First-Generation Antiandrogens

Given the importance of the AR signaling pathway in PCa, the receptor has been recognized as a major drug target for PCa and CRPC. Since the late 1960s, anti-AR drugs, also known as antiandrogens, have been developed which prevent the AR function by competing with androgens for binding to the AR ABS. Antiandrogens can be classified as steroidal or nonsteroidal AR inhibitors based on their structures. Steroidal antiandrogens (such as cyproterone acetate) tend to demonstrate partial agonistic activity, poor oral bioavailability, potential hepatotoxicity, and often exhibit lack of tissue selectivity and cross-activity toward other SHRs.[42] In addition, structural modifications of steroidal ligands are limited by the steroidal scaffold. Thus, steroidal antiandrogens are rarely used in the clinic.

In comparison, nonsteroidal antiandrogens demonstrate better specificity and oral bioavailability, and are more suitable for structural modifications and advancements. A variety of nonsteroidal antiandrogens have been reported to date, including aryl propionamides, hydantoins, phthalimides, and quinolinones. Nonsteroidal antiandrogen monotherapy can be used in advanced PCa as an alternative to castration.[66–68] The first-generation drugs (Fig. 9) such as flutamide (Eulexin®, Schering-Plough), nilutamide (Nilandron®, Sanofi-Avenis), and bicalutamide (Casodex®, AstraZeneca) have been clinically used for decades. They all act on the ABS part of the AR, where they compete with DHT for binding, and therefore block the AR transactivation. Flutamide and nilutamide were found to cause hepatotoxicity, while bicalutamide exhibited fewer side effects and had a longer half-life in patients, so it eventually replaced flutamide and nilutamide as a PCa treatment.[42]

Patients initially respond well to antiandrogens; however, after long-term administration of these drugs, resistance inevitably develops as the disease progresses into CRPC. One of the well-documented mechanisms of antiandrogen resistance is the occurrence of mutation-driven receptor promiscuity and mutation-caused bioconversion of AR antagonists into agonists. T877A and W741L/C mutations in the AR LBD are well-characterized substitutions that drive hydroxyflutamide and bicalutamide to agonize the AR, respectively.[50,69,70] In the cocrystal structures of mutated AR LBDs bound to hydroxyflutamide and bicalutamide in agonistic conformations, hydrogen bond interactions with the polar residue pair Arg752 and Gln711 are maintained, and the hydrogen

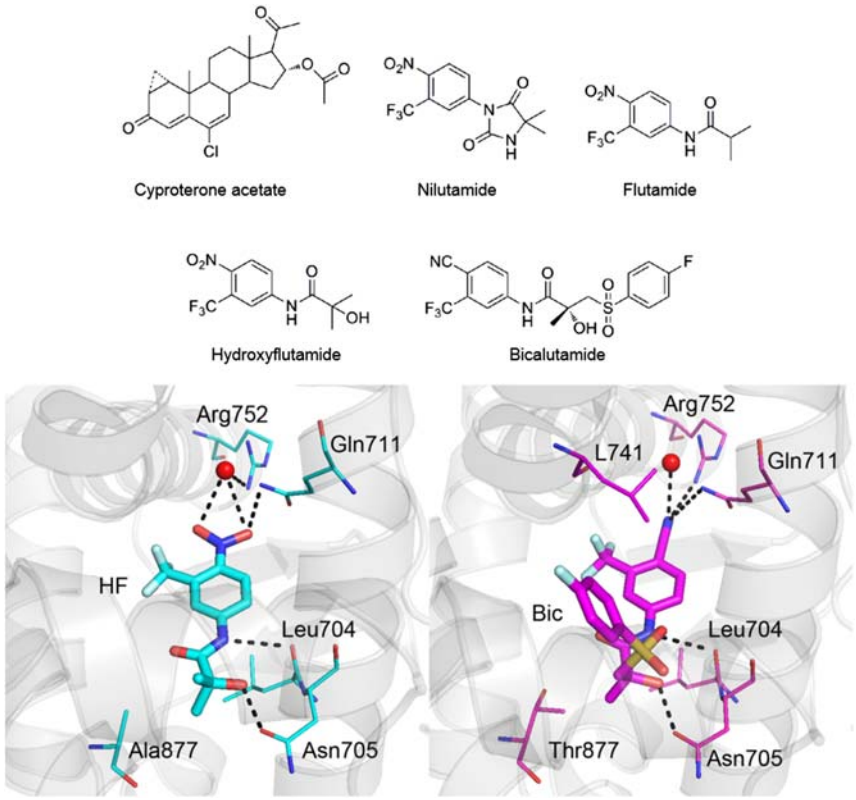

Fig. 9 (*Upper*) Chemical structures of first-generation antiandrogens; (*Lower*) Crystal structures of AR LBD-T877A with hydroxyflutamide (*HF*) and AR LBD-W741L with bicalutamide (*Bic*).

bond contact with Asn705 is also retained while the hydrogen bonding with Thr877 is missing (Fig. 9). In addition, structural modifications on bicalutamide may also lead to the occurrence of AR agonistic properties. For example, the replacement of the aryl sulfonyl in bicalutamide with a phenoxyl group resulted in tissue-selective AR modulators,[71] which act as an antagonist in the prostate, and agonist in the pituitary and muscle.

5.05.3.3 Second- and Next-Generation AR Inhibitors

The development of conventional antiandrogens as PCa therapeutics is the most intensively pursued area. Since resistance occurred with the aforementioned first-generation antiandrogens, the field evolved rapidly, resulting in second- and next-generation antiandrogen drugs aiming to overcome the resistance.[72,73]

5.05.3.3.1 Enzalutamide and ARN509

The second-generation antiandrogens, represented by clinically used enzalutamide (Xtandi®, Astellas), were developed on the basis of a hydantoin compound RU59063 (Fig. 10),[74–76] which has a very high binding affinity to the AR. Enzalutamide is also a competitive AR inhibitor, but in comparison with first-generation antiandrogens, it binds to the AR ABS with higher affinity, and exhibits improved anti-AR potency, better pharmacokinetic (PK) profiles, and better in vivo efficacy.[74] Enzalutamide also exhibits additional mechanisms of anti-AR action, including preventing AR nuclear translocation, impairing DNA binding, and affecting coactivator recruitment.[74] As enzalutamide demonstrated significant overall patient survival benefit (~5 months) for patients with metastatic CRPC,[16] it was approved by FDA for CRPC in 2012.

ARN509 is an investigational drug derived from enzalutamide with greater inhibitory activity on the AR transcription and PCa cell proliferation. As with enzalutamide, ARN509 blocks AR nuclear translocation, impairs AR binding to DNA, and prevents recruitment of coactivators. As an optimized derivative of enzalutamide, ARN509 demonstrated better antitumor effects than enzalutamide in a mouse xenograft model of CRPC.[76] Although both ARN509 and enzalutamide possess an unwanted cross-activity toward the Υ-aminobutyric $acid_A$ ($GABA_A$) receptor at low micromolar concentrations, it has been demonstrated that the steady-state brain level of ARN509 is significantly lower than that of enzalutamide, implying lower seizurogenic potential of ARN509. The phase I and II trials of ARN509 both showed favorable PSA response,[75] and the phase III trial is ongoing.

It should also be noted that despite the survival benefit of enzalutamide in CRPC, resistance is invariably developed to this drug within 1–2 years in patients with metastatic CRPC. Similarly, resistance has already been reported for ARN509. In particular,

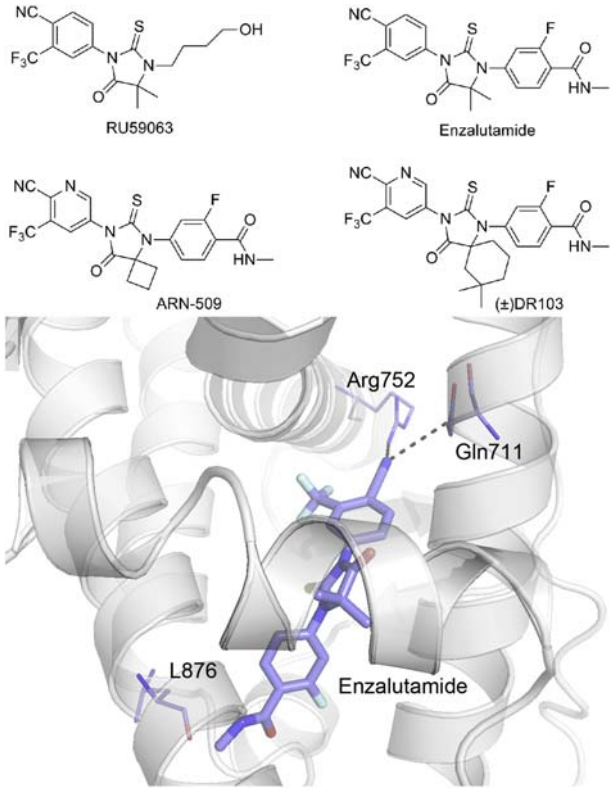

Fig. 10 (*Upper*) Chemical structures of second-generation of antiandrogens; (*Lower*) Docking mode of enzalutamide in the agonistic conformation of AR LBD (PDB code: 3V49) with F876 in the helix 11 mutated to L876.

a mutation F876L in the helix 11 of the AR LBD was implicated in rendering the agonistic effect of enzalutamide and ARN509.[77–79] Molecular dynamics simulation was performed to investigate the structural basis of such antagonist-to-agonist conversion, and it revealed that the F876L mutation could induce H12 to adopt a more agonist-like conformation. In addition, it was observed from the simulation that the geminal-dimethyl group on enzalutamide (**Fig. 10**) and the spirocyclobutyl on ARN509 lie in close proximity to helix 12, and the bulkier spirocyclobutyl moiety elicited greater displacement of the helix 12. This observation provided important insights into structural modifications on enzalutamide and ARN509 to overcome the mutation-induced antagonist-to-agonist conversion. Derivatives were created to replace the geminal-dimethyl in enzalutamide with spirocycles of greater size and complexity, such as (±)DR103, which were reported to be antagonistic to the AR bearing the F876L mutation.[77]

5.05.3.3.2 ODM-201

ODM-201 represents another nonsteroidal antiandrogen that is currently under clinical investigation. ODM-201 has a major pharmacologically active metabolite ORM-15341 (see the chemical structure in **Fig. 11**), and both of them are structurally distinct from all other antiandrogens. When docked into the ABS site of an antagonistic model of the AR LBD, ODM-201 retains the conserved hydrogen bond interactions with Arg752 and Gln711, and might form an additional hydrogen bond contact with Glu709 (**Fig. 11**).

ODM-201 and ORM-15341 have higher binding affinity to the AR with the inhibition constant (Ki) eightfold lower than enzalutamide in a radio-labeled competition assay, and they also inhibit AR transactivation more potently than enzalutamide.[80] In addition, they impair the androgen-induced nuclear translocation to the same extent as enzalutamide.[80] Remarkably, they demonstrated full antagonistic profile upon AR mutations including F876L, T877A, and W741L, which transform the pharmacology of clinically used drugs enzalutamide, flutamide, and bicalutamide, respectively.[80] ODM-201 and ORM-15341 inhibited VCaP cell proliferation in vitro, and did not affect the growth of an AR-negative cell line, suggesting the antiproliferative effect is AR-specific.

ODM-201 and ORM-15341 demonstrated more potent antitumor activity in CRPC mouse models. In comparison with enzalutamide, the PK profile of ODM-201 appeared less favorable (half-life: 1.6 h for ODM-201 vs. 18.3 h for enzalutamide) resulting in higher doses, and more frequent dosing required for ODM-201.[80] Unlike enzalutamide and ARN509, ODM-201 does not penetrate the blood–brain barrier, and no seizures were observed. The phase I/II trial showed a favorable safety profile and PSA response, and the phase III trial is ongoing.[81]

5.05.3.3.3 Abiraterone

Abiraterone acetate (Zytiga®, Johnson & Johnson, New Jersey, USA) is mainly known as an androgen synthesis inhibitor (see the chemical structure in **Fig. 12**), targeting CYP17A1 and other enzymes, which was approved for CRPC in 2009.[82] Of note, it is also

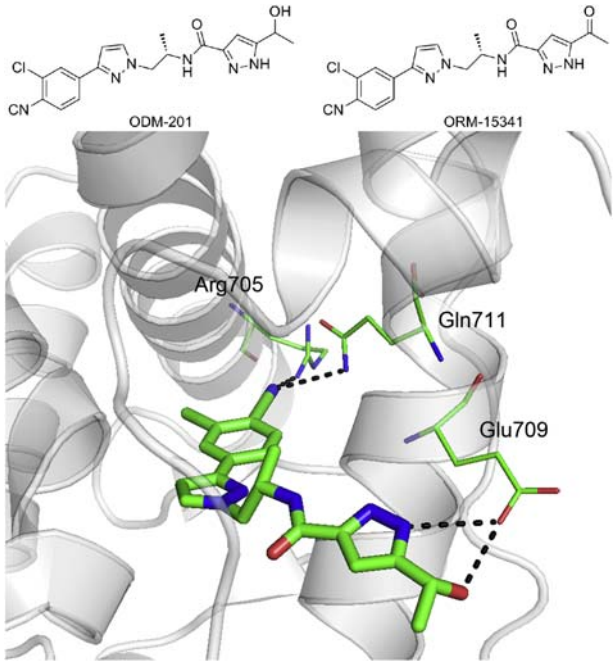

Fig. 11 (*Upper*) Chemical structures of ODM-201 and its main metabolite ORM-15341; (*Lower*) Docked pose of ODM-201 in an antagonistic model of AR LBD.

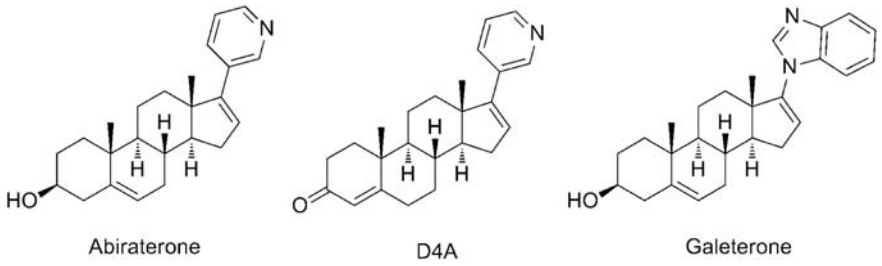

Fig. 12 Chemical structures of next-generation antiandrogens.

considered as an antiandrogen since it competitively binds to the AR as a weak AR antagonist.[83] The anti-AR profile of abiraterone contributes to its antitumoral effects, and abiraterone is clinically used as the pre- and postchemotherapy treatment for metastatic CRPC.[17,84] Resistance to abiraterone has already been reported, and the de novo intratumoral androgen production has been suggested as a mechanism of resistance to abiraterone.[85]

Recently, it has been demonstrated in mice and patients with PCa that abiraterone was converted into a more active metabolite Δ^4-abiraterone (D4A), which blocks enzymes required for androgen synthesis including CYP17A1, 3βHSD, and SRD5A. As for abiraterone, D4A also inhibits AR with potency comparable to enzalutamide.[86] The metabolite D4A has more potent antitumor activity against xenograft tumors than the parent drug abiraterone itself, and thus, direct D4A treatment may offer greater clinical and survival benefits.[86]

5.05.3.3.4 Galeterone

Galeterone (TOK-001 or VN/124-1) is an investigational drug in clinical Phase III study by Tokai Pharmaceuticals (see the chemical structure in Fig. 12). It is a steroidal C17-benzoazole compound based on natural substrates of CYP17A1, such as pregnenolone and progesterone. Galeterone modulates multiple targets in the AR signaling pathway, including CYP17A1 lyase, AR, and 5α-reductase.[87–89] It has been confirmed to disrupt the AR signaling via three distinct mechanisms of action, including: (1) Selectively inhibiting CYP17A1 lyase to prevent androgen synthesis, (2) competing with androgen for binding to the ABS, and (3) causing degradation of full-length and splice variants of the AR.[87–90]

Galeterone is a more potent CYP17A1 inhibitor than abiraterone (IC_{50} of 300 nM for galeterone vs. 800 nM for abiraterone).[87] Different from abiraterone, galeterone selectively inhibits CYP17A1 lyase but not hydroxylyase. The inhibition of hydroxylase results in mineralocorticoid excess, and thus, the selectivity makes galeterone an ideal CYP17A1 inhibitor so that galeterone

does not cause mineralocorticoid excess or require coadministration of steroids as shown in clinical trials. Galeterone competitively binds to the AR ABS, with the binding affinity comparable to bicalutamide. It suppresses AR transactivation with 10-times higher efficiency compared to bicalutamide, while it does not agonize the mutated AR. Galeterone also blocks nuclear translocation and decreases AR-regulated genes such as PSA and TMPRSS2 in CRPC and enzalutamide-resistant cell lines.[91] In addition, galeterone causes marked downregulation of AR protein expression partly due to increased AR degradation in full-length and splice variants of AR, such as AR-V7.[87,88,92] The combined effects of galeterone through CYP17A1 inhibition, AR inactivation, and degradation increase the antitumor efficacy.

Galeterone demonstrated more efficacious in vivo effects in PCa xenograft models than abiraterone or castration.[89] The clinical study phase II demonstrated that galeterone induced PSA and tumor reduction in a majority of patients, and it was well tolerated with an acceptable safety profile.[87] Since galeterone blocks multiple points in the AR signaling pathway, it may help reduce the risk of developing resistance in comparison with other therapeutics targeting the AR signaling.

5.05.3.4 The Resistance Problem of Conventional Antiandrogens

Resistance is the main problem for clinically used drugs targeting the AR signaling, including enzalutamide and abiraterone. Some mechanisms are partly involved in resistance, including AR overexpression,[93–97] gain-of-function mutations,[98–108] the emergence of ARVs lacking the LBD segment,[109–125] alternative pathways,[126–134] and the synthesis of intratumoral androgens and bypass of AR.[135,136]

AR mutations are rare in early-stage untreated PCa patients, but are found in approximately 10–30% of patients previously exposed to bicalutamide and flutamide.[98,101,137] Mutations in the LBD have been intensively studied, and a number of substitutions confer a gain of function by allowing other ligands to bind and activate the AR.[103,104] Aforementioned mutations F876L, W741L, and T877A lead to promiscuous AR activation by antiandrogens through converting AR antagonists into potent agonists.[100,107] Thus, mutations in the AR may account for one of the major mechanisms underlying CRPC progression.

Constitutively active ligand-independent ARVs were first reported in 2009,[121,123] expressed in CRPC cells and clinical samples.[114,121,123,124] So far, there have been 17 ARVs discovered, and all of them contain both NTD and DBD regions, with varying or completely absent LBD parts (**Fig. 13**).[116] Importantly, ARVs could recapitulate the transcriptional program in the absence of androgens or full-length AR.[112,118] It is believed that some ARVs such as AR-V7 are sufficient to drive resistance to antiandrogens, and none of the clinically used drugs are effective against ARVs.[112,122] A recent study of AR-V7 in circulating tumor cells from metastatic CRPC patients (treated with abiraterone and/or enzalutamide) demonstrated that ARVs represent an important predictive biomarker of CRPC and one mechanism of resistance.[113,115]

5.05.4 Novel AR Inhibitors Targeting Alternative Sites

Due to limitations of targeting the ABS, AR inhibitors directed toward alternative functional sites on the receptor (and therefore exhibiting novel mechanisms of action) are expected to circumvent the invariably developed resistance. An ever-increasing number of AR inhibitors has been reported, which target sites beyond the AR ABS, including the AR LBD surface site (AF2, BF3) inhibitors,[138–141] AR NTD binders,[142–145] AR DBD inhibitors,[146,147] and compounds addressing other AR-targeting avenues.[148–150]

5.05.4.1 AR LBD Surface Site Inhibitors

Protein–protein interactions (PPI) play an important role in AR activation, nuclear translocation, and transcription. Thus, PPI sites on the AR represent attractive targets for intervention (**20015. Small-molecule inhibitors of protein–protein interactions**). On the LBD segment of the AR, there have been two adjacent and distinct PPI sites identified—AF2 and BF3, which are important for the coregulator and cochaperone binding, respectively.[151,152] Crystal structures of AR AF2 and BF3 demonstrated that small molecules are able to bind to these large, hydrophobic exposed surface sites, indicating their potential druggability.[53,153,154]

The AF2 site is formed to recruit coactivators containing motifs such as LXXLL and FXXLF when the androgen binds to AR, and the binding of coactivators could enhance the AR activity. The AF2 site is an L-shaped cleft, and LXXLL and FXXLF form short

Fig. 13 The organizational domains of full-length AR and two clinically relevant ARVs.

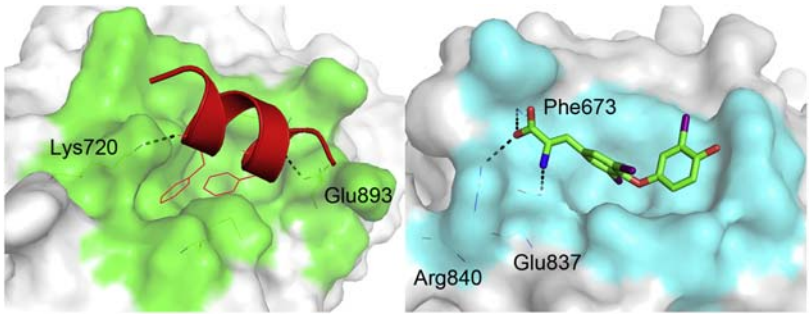

Fig. 14 (*Left*) The crystal structure of the AR LBD with a peptide in the AF2 site (PDB code: 3L3X); (*Right*) The crystal structure of the AR LBD with a small-molecule Triac in the BF3 site (PDB code: 2PIW).

α helices with L+1 (+1 representing the position in the motif), L+5 and F+1, F+5 binding to the hydrophobic cleft, forming electrostatic interactions with Lys720 and Glu893 (Fig. 14). Thus, targeting the AF2 site could disrupt the coregulator modulation of AR transactivation. This type of inhibitor has a distinct mechanism of action from conventional antiandrogens, which may provide opportunities to circumvent the mutation-driven antiandrogen resistance.

Small molecules and peptides were developed to mimic the features of LXXLL or FXXLF motifs to interrupt the AR function.[141,155–157] Small-molecule peptidomimetics (D2 in Fig. 15) were reported as AF2 inhibitors by mimicking the LXXLL motif-containing coregulators,[141] which effectively disrupt interactions of the AR and LXXLL-containing cofactors. D2 demonstrated potent inhibition of AR and PCa cell proliferation, and suppression of tumor growth in vivo. In addition, based on an ensemble of cocrystal structures of the AR LBD with the peptide in AF2, structure-based pharmacophores were generated and used for virtual screening of AF2 disruptors. A series of diarylhydrazides were identified, which inhibit the AR with low micromolar potency,

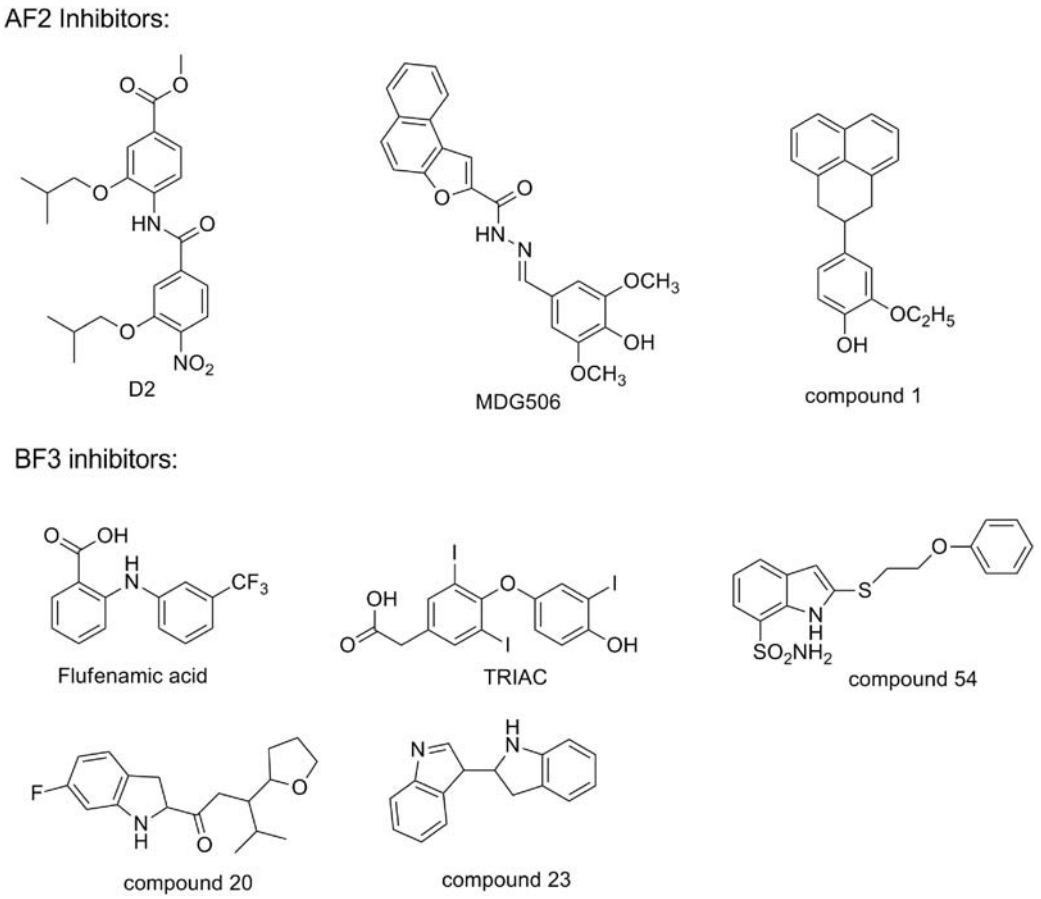

Fig. 15 Chemical structures of AR LBD surface site binders.

and demonstrate selectivity toward other NRs.[156] Molecular docking-based virtual screening also identified active AF2 inhibitors, such as 2,3-dihydro-1*H*-pyrimidines, which inhibit AR transcriptional activity, AR-positive PCa cell growth, and displacement of the SRC2-3 peptide from the AF2 site.[155] In addition to small-molecule inhibitors, peptides that have a Tyr in the +5 position were identified to suppress the AR transactivation through binding to the AF2 site.[157]

In 2007, Fletterick's group reported that some AF2 binders preferentially bind to a previously unknown area—the BF3 site (Fig. 14), which allosterically modulates the AF2 (**20013. Allosteric Inhibitors**), and may function as a PPI site for coregulators.[151,153,158] Little was known about what binds to the BF3 site until recently; it was reported that a duplicated GARRPR motif in Bag-1L functions through the BF3 site, and fine tunes the AR activity.[158] This enables developing a Bag-1L peptide displacement assay to measure the direct binding to BF3, and opens up an opportunity to screen BF3 inhibitors by blocking the AR with cochaperone interaction.[140,41]

A few chemical classes of BF3 inhibitors have been reported to date, which demonstrate potent in vitro and/or in vivo activities, such as dihydropyrimidines,[155] 1*H*-indole-2-carboxamides,[159] benzimidazoles,[139] and indoles[140] (Fig. 15). Notably, the recently reported indole-based AR BF3 inhibitors demonstrate excellent inhibition of AR transcription, PSA expression, and androgen-induced proliferation of androgen-sensitive LNCaP and enzalutamide-resistant MR49F PCa cell lines. Moreover, the reported lead compound (compound 23)[140] effectively reduces AR-dependent gene expression in PCa cells, and importantly, inhibits tumor growth in both LNCaP and MR49F xenograft models. Thus, the BF3-directed AR inhibitors may potentially become alternative therapeutic agents to treat antiandrogen-resistant forms of PCa.

5.05.4.2 AR NTD Inhibitors

The AR NTD has less than 15% sequence similarity with other SHRs. Different from other SHRs, the AF1 region in the NTD is responsible for the majority of AR transcriptional activity, and thus, the ARV lacking the LBD is constitutively active. In addition, the NTD were indicated to play a role in androgen-independent nuclear translocation.[160] Therefore, the AR NTD represents a superior target when compared with AR LBD for PCa and CRPC.[161,162] In contrast with conventional antiandrogens, potential AR NTD inhibitors may not only potently inhibit the AR but possess significant AR specificity, and, more importantly, have the capability to inhibit ARVs. Although targeting the AR NTD is intriguing, the NTD section of the AR is intrinsically disordered, which impedes the structure-based development of AR NTD-targeted therapeutics.

A compound EPI-001 (see the chemical structure in Fig. 16) represents a class of small-molecule inhibitors that interacts with the AF1 region and inhibits the transactivation of the NTD.[142,143,145] EPI-001 was identified from high-throughput screening of a library of marine sponge extracts, and it inhibits the transcriptional activity of the AR as well as ARVs, reduces AR interactions with AREs on the DNA, blocks the N–C interaction as well as PPI, and suppresses the tumor growth of CRPC xenografts.[142] EPI-001 represents a mixture of four stereoisomers due to the presence of two chiral centers in the structure, and the EPI-002 (2*R*, 20*S*) and EIP-005 (2*S*, 20*S*) are the most potent stereoisomers in terms of the in vitro AR transcriptional inhibition, and they also have better antitumor activity when tested in the LNCaP CRPC xenograft model.[143]

Recently, the detailed study of the mechanism of EPI-001 action revealed that all EPI-001 stereoisomers covalently bind to the AF1 in the intrinsically unstructured AR NTD, and that the chlorohydrin in EPI compounds is responsible for the activity and the covalent binding.[143] The EPI compounds do not bind to denatured AF1, and the secondary structure of AF1 is necessary for

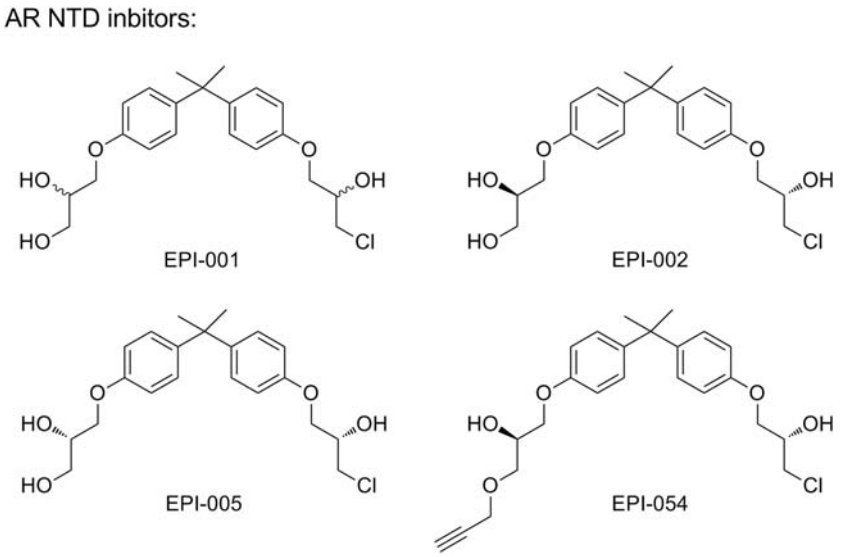

Fig. 16 Representatives of AR NTD inhibitors.

the binding of EPI-001. The effect of EPI-001 isomers was previously claimed to be specific to the AR in vitro and in vivo; however, the latest data demonstrate that EPI-001 is not a specific AR NTD inhibitor but rather is a peroxisome proliferator-activated receptor-gamma modulator with inhibitory effects on AR expression and activity in PCa.[144] In addition, EPI-001 was shown to be a reactive electrophile which forms covalent adducts with thiols.[144] ESSA Pharma Inc. has filed an investigational new drug application for EPI-506 with the FDA, and future reports of its clinical effects are expected.

5.05.4.3 AR DBD Inhibitors

The AR DBD plays an important role in the dimerization and DNA binding of AR transcription, and thus, directly targeting the DBD with small molecules may disrupt AR transactivation. More importantly, selectively targeting the AR DBD could potentially circumvent the resistance of current anti-AR therapy. Firstly, in comparison with the AR LBD and NTD parts, mutations in the DBD may more likely lead to loss of AR transcriptional activity, suggesting a low propensity of mutation-driven resistance.[163] Secondly, the DBD segment plays an important role in the transactivation and gene regulation of both full-length and splice isoforms of the AR, so targeting the DBD may simultaneously inhibit both full-length AR and ARVs. Lastly, the structure of the DBD has been solved by X-ray crystallography since 2004,[35] which provides the structural basis for rational drug discovery and design of AR DBD inhibitors.

Given the above potential advantages of targeting the AR DBD, our group utilized the crystal structure of the AR DBD for the discovery of AR DBD inhibitors. A plausible site was firstly detected underneath the P-box region, which is essential for the DNA binding, and it was hypothesized that the binding of small molecules in that site may disrupt the DBD–DNA interaction and thus inhibits the AR. Virtual screening against the intended site identified a novel chemical class of AR DBD inhibitors, represented by VPC-14228 (4-(4-phenylthiazol-2-yl)morpholine, **Fig. 17**), which potently inhibits the AR transcription in the submicromolar range.[147] Furthermore, this chemical suppresses PSA expression, and blocks AR-positive PCa cell growth as well as the growth of enzalutamide-resistant PCa MR49F cells.[147] More importantly, it inhibits the transcription of ARVs as expected.[146]

The docked pose of VPC-14228 indicates that the compound forms a hydrogen bonding contact with Tyr594 through the morpholine moiety, and the thiazole group may form π–π stacking with Phe583 in the core of the binding site. The anti-AR activity of this chemical class is very sensitive to structural modifications on the benzene ring, presumably due to the hydrophobic interactions with the aliphatic side chain of Arg609 and Lys610.[147] The site-directed mutagenesis study on key binding site residues indicates that these compounds bind to the predicted site, and efforts are underway to provide more direct evidence of binding to the DBD.[146,147]

Since the benzene ring is critical for the AR transcriptional inhibition, structural modifications on the benzene ring displayed a trend that substituents on the para-position are detrimental to the activity which may be exposed to the solvent, and addition of groups on the ortho- and meta- position of the benzene ring could be tolerated. Subsequently, heterocycles were used to replace the benzene ring, and a dibromo-imidazole led to the generation of VPC-14449 with improved cellular activity toward both full-length AR and ARVs.[146,147] These DBD inhibitors do not block the nuclear translocation of AR, which is consistent with DBD targeting in the nucleus, and the chromatin immunoprecipitation assay indicates these compounds block interactions of the AR

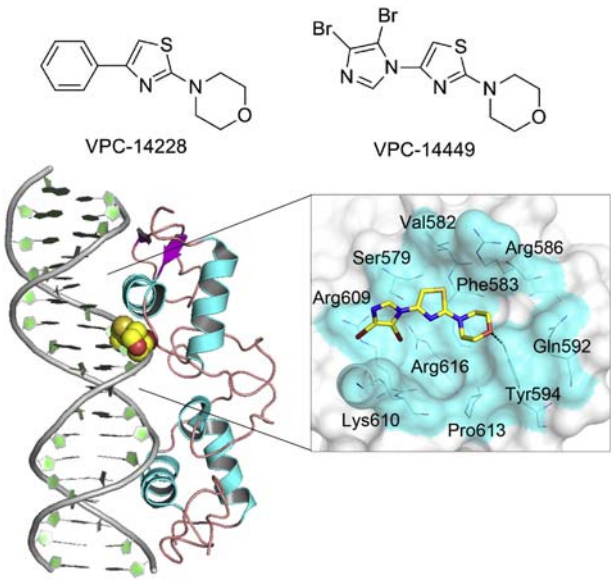

Fig. 17 (*Upper*) Chemical structures of representative AR DBD inhibitors VPC-14228 and VPC-14449; (*Lower*) VPC-14449 in the DBD–DNA interface and a zoomed-in view of VPC-14449 in the binding site.

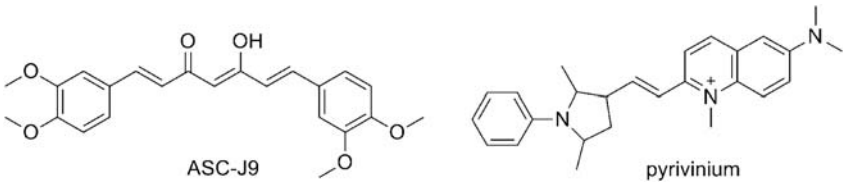

Fig. 18 Chemical structures of miscellaneous compounds targeting the AR.

with the ARE in the nucleus. VPC-14449 was shown to downregulate AR-responsive genes in LNCaP cells in a microarray analysis, and when tested in an LNCaP xenograft model, VPC-14449 reduced tumor growth and blocked PSA production.[146]

5.05.4.4 Other Nonconventional Strategies of Targeting AR Signaling

In addition to conventional and novel ways of targeting of the AR described earlier, there exists a variety of strategies for developing new AR interventions,[149,150,163–167] such as AR degradation, drug repurposing for noncompetitive AR inhibitors, and AR-targeted RNA interference.

The molecule ASC-J9 (see Fig. 18) was identified from natural products as an AR degradation enhancer,[150,167] which selectively degrades AR protein through interruption of the AR–AR selective coregulator interaction. Additionally, the ASC-J9-promoted AR degradation leads to suppression of AR transcription, AR-mediated PCa cell growth, and tumor growth in androgen-dependent and castration-resistant xenograft models.

Pyrivinium pamoate (PP) is an FDA-approved drug, which was identified as a noncompetitive AR inhibitor through drug repurposing (**10002. Drug repurposing: faster drug approval?**).[166] PP was reported to inhibit the transcriptional activity of both full-length AR and ARVs, without preventing DHT binding. However, PP displayed generic toxicity and cross-reactivity with other SHRs,[146] and the fact that PP targets multiple proteins may explain the undesired off-target effects. Recently, it has been reported that PP may inhibit initiation of transcription via the DBD,[163] but the exact mechanism of PP action on the AR is still unclear.

RNA interference is another therapeutic strategy used by silencing critical genes in PCa, such as the AR. The short-hairpin RNA against AR could inhibit tumor growth and suppress PSA,[165] and the lipid nanoparticle small-interfering RNA system and antisense oligonucleotides (**60018. Antisense Drug Discovery: Second-generation antisense oligonucleotide (ASO) mRNA/protein**) have been shown to be effective in silencing the wild-type AR and ARVs.[148,149]

Cochaperones play a critical role in the stability, activation, and maturation of AR, such as HSP90.[168,169] Thus, AR cochaperones were considered as potential targets for PCa, and cotargeting cochaperones and AR may have therapeutic merits. Recently, it was reported that combination therapy of HSP90 inhibitors with antiandrogens enhances the inhibition to AR signaling and prevents ARV-induced resistance.[170,171]

5.05.5 Summary

NRs are strongly associated with a variety of cancers, and SHRs have been extensively studied in the context of the development of anticancer agents. The ligand-binding site of SHRs, such as the AR ABS, is the conventional drug target for a variety of marketed and investigational drugs. However, residues in the ligand-binding site are prone to be mutated, which drives drug resistance. The clinically used antiandrogens target the conventional AR ABS, and they invariably develop resistance when the disease progresses into a lethal form of CRPC. To overcome the resistance, alternative target areas in the AR LBD beyond the ABS were considered, including the AF2 and BF3 sites. The AR AF2 and BF3 inhibitors block the AR function through disrupting critical coregulator binding, which have the potential to circumvent the mutation-induced antagonist-to-agonist conversion arising from targeting the ABS. These sites also exist in other SHRs such as ER, and the ER AF2 has also been targeted by small-molecule inhibitors that act as a potential treatment for ERα-positive, tamoxifen-resistant, and metastatic breast cancers.[172]

The NTD of SHRs is flexible and disordered, which precludes rational drug design of NTD-directed agents. Covalent inhibitors targeting the AR NTD exist; however, they are not very specific, and are believed to have off-target reactivity liabilities. Thus, this type of inhibitor is somewhat disfavored and underdeveloped.

The crystal structures of the DBD portion have been solved for all SHRs, which provides an opportunity for structure-based drug discovery of DBD inhibitors. Our study of targeting the AR DBD demonstrated that the DBD is a viable target for developing small-molecule inhibitors. Compared to antiandrogens as well as AR LBD surface disruptors, AR DBD inhibitors may provide greater advantages regarding addressing resistance, as they are effective in inhibiting ARVs. This strategy for developing DBD-directed drugs could be applied to other SHRs, such as ER and PR, which may provide alternative or complementary therapeutics for existing drugs.

As NR family members share sequence similarity and organizational domains, strategies applied for targeting the human AR could be applied to other NR members. This article reviewed therapeutic targeting of the AR signaling axis, which may provide insights into targeting other NRs.

References

1. Nagy, L.; Schwabe, J. W. Mechanism of the Nuclear Receptor Molecular Switch. *Trends Biochem. Sci.* **2004,** *29,* 317–324.
2. Bookout, A. L.; Jeong, Y.; Downes, M.; Yu, R. T.; Evans, R. M.; Mangelsdorf, D. J. Anatomical Profiling of Nuclear Receptor Expression Reveals a Hierarchical Transcriptional Network. *Cell* **2006,** *126,* 789–799.
3. Sonoda, J.; Pei, L.; Evans, R. M. Nuclear Receptors: Decoding Metabolic Disease. *FEBS Lett.* **2008,** *582,* 2–9.
4. Khan, S.; Lingrel, J. B. Thematic Minireview Series on Nuclear Receptors in Biology and Diseases. *J. Biol. Chem.* **2010,** *285,* 38741–38742.
5. Zhao, X.; Cho, H.; Yu, R. T.; Atkins, A. R.; Downes, M.; Evans, R. M. Nuclear Receptors Rock Around the Clock. *EMBO Rep.* **2014,** *15,* 518–528.
6. Overington, J. P.; Al-Lazikani, B.; Hopkins, A. L. How Many Drug Targets Are There? *Nat. Rev. Drug Discov.* **2006,** *5,* 993–996.
7. Maglich, J. M.; Sluder, A.; Guan, X.; Shi, Y.; McKee, D. D.; Carrick, K.; Kamdar, K.; Willson, T. M.; Moore, J. T. Comparison of Complete Nuclear Receptor Sets from the Human, Caenorhabditis Elegans and Drosophila Genomes. *Genome Biol.* **2001**, 2(8):research0029.1-research0029.7.
8. Helsen, C.; Claessens, F. Looking at Nuclear Receptors From a new Angle. *Mol. Cell. Endocrinol.* **2014,** *382,* 97–106.
9. Rastinejad, F.; Huang, P.; Chandra, V.; Khorasanizadeh, S. Understanding Nuclear Receptor Form and Function Using Structural Biology. *J. Mol. Endocrinol.* **2013,** *51,* T1–T21.
10. Roshan-Moniri, M.; Hsing, M.; Butler, M. S.; Cherkasov, A.; Rennie, P. S. Orphan Nuclear Receptors as Drug Targets for the Treatment of Prostate and Breast Cancers. *Cancer Treat. Rev.* **2014,** *40,* 1137–1152.
11. Kojetin, D. J.; Burris, T. P. Small Molecule Modulation of Nuclear Receptor Conformational Dynamics: Implications for Function and Drug Discovery. *Mol. Pharmacol.* **2013,** *83,* 1–8.
12. Siegel, R.; Ma, J. M.; Zou, Z. H.; Jemal, A. Cancer Statistics, 2014. *CA Cancer J. Clin.* **2014,** *64,* 9–29.
13. Grossmann, M.; Cheung, A. S.; Zajac, J. D. Androgens and Prostate Cancer; Pathogenesis and Deprivation Therapy. *Best Pract. Res. Clin. Endocrinol. Metab.* **2013,** *27,* 603–616.
14. Schroder, F.; Crawford, E. D.; Axcrona, K.; Payne, H.; Keane, T. E. Androgen Deprivation Therapy: Past, Present and Future. *BJU Int.* **2012,** *109* (Suppl 6), 1–12.
15. Denmeade, S. R.; Isaacs, J. T. A History of Prostate Cancer Treatment. *Nat. Rev. Cancer* **2002,** *2,* 389–396.
16. Scher, H. I.; Fizazi, K.; Saad, F.; Taplin, M. E.; Sternberg, C. N.; Miller, K.; de Wit, R.; Mulders, P.; Chi, K. N.; Shore, N. D.; Armstrong, A. J.; Flaig, T. W.; Flechon, A.; Mainwaring, P.; Fleming, M.; Hainsworth, J. D.; Hirmand, M.; Selby, B.; Seely, L.; de Bono, J. S.; Investigators, A. Increased Survival With Enzalutamide in Prostate Cancer After Chemotherapy. *N. Engl. J. Med.* **2012,** *367,* 1187–1197.
17. de Bono, J. S.; Logothetis, C. J.; Molina, A.; Fizazi, K.; North, S.; Chu, L.; Chi, K. N.; Jones, R. J.; Goodman, O. B., Jr.; Saad, F.; Staffurth, J. N.; Mainwaring, P.; Harland, S.; Flaig, T. W.; Hutson, T. E.; Cheng, T.; Patterson, H.; Hainsworth, J. D.; Ryan, C. J.; Sternberg, C. N.; Ellard, S. L.; Flechon, A.; Saleh, M.; Scholz, M.; Efstathiou, E.; Zivi, A.; Bianchini, D.; Loriot, Y.; Chieffo, N.; Kheoh, T.; Haqq, C. M.; Scher, H. I.; Investigators, C.-A. Abiraterone and Increased Survival in Metastatic Prostate Cancer. *N. Engl. J. Med.* **2011,** *364,* 1995–2005.
18. Scher, H. I.; Sawyers, C. L. Biology of Progressive, Castration-Resistant Prostate Cancer: Directed Therapies Targeting the Androgen-Receptor Signaling Axis. *J. Clin. Oncol.* **2005,** *23,* 8253–8261.
19. Mooradian, A. D.; Morley, J. E.; Korenman, S. G. Biological Actions of Androgens. *Endocr. Rev.* **1987,** *8,* 1–28.
20. Cooper, L. A.; Page, S. T. Androgens and Prostate Disease. *Asian J. Androl.* **2014,** *16,* 248–255.
21. Franchimont, P. Regulation of Gonadal Androgen Secretion. *Horm. Res.* **1983,** *18,* 7–17.
22. Rainey, W. E.; Nakamura, Y. Regulation of the Adrenal Androgen Biosynthesis. *J. Steroid Biochem. Mol. Biol.* **2008,** *108,* 281–286.
23. Green, S. M.; Mostaghel, E. A.; Nelson, P. S. Androgen Action and Metabolism in Prostate Cancer. *Mol. Cell. Endocrinol.* **2012,** *360,* 3–13.
24. Penning, T. M. Androgen Biosynthesis in Castration-Resistant Prostate Cancer. *Endocr. Relat. Cancer* **2014,** *21,* T67–T78.
25. Corona, G.; Baldi, E.; Maggi, M. Androgen Regulation of Prostate Cancer: Where Are We Now? *J. Endocrinol. Invest.* **2011,** *34,* 232–243.
26. Chang, K. H.; Ercole, C. E.; Sharifi, N. Androgen Metabolism in Prostate Cancer: From Molecular Mechanisms to Clinical Consequences. *Br. J. Cancer* **2014,** *111,* 1249–1254.
27. Migeon, B. R.; Brown, T. R.; Axelman, J.; Migeon, C. J. Studies of the Locus for Androgen Receptor: Localization on the Human X Chromosome and Evidence for Homology With the Tfm Locus in the Mouse. *Proc. Natl. Acad. Sci. U. S. A.* **1981,** *78,* 6339–6343.
28. Lubahn, D. B.; Joseph, D. R.; Sullivan, P. M.; Willard, H. F.; French, F. S.; Wilson, E. M. Cloning of Human Androgen Receptor Complementary DNA and Localization to the X Chromosome. *Science* **1988,** *240,* 327–330.
29. Gelmann, E. P. Molecular Biology of the Androgen Receptor. *J. Clin. Oncol.* **2002,** *20,* 3001–3015.
30. Davies, P.; Watt, K.; Kelly, S. M.; Clark, C.; Price, N. C.; McEwan, I. J. Consequences of Poly-Glutamine Repeat Length for the Conformation and Folding of the Androgen Receptor Amino-Terminal Domain. *J. Mol. Endocrinol.* **2008,** *41,* 301–314.
31. Lavery, D. N.; McEwan, I. J. Structural Characterization of the Native NH2-Terminal Transactivation Domain of the Human Androgen Receptor: A Collapsed Disordered Conformation Underlies Structural Plasticity and Protein-Induced Folding. *Biochemistry* **2008,** *47,* 3360–3369.
32. Jenster, G.; van der Korput, H. A.; Trapman, J.; Brinkmann, A. O. Identification of Two Transcription Activation Units in the N-Terminal Domain of the Human Androgen Receptor. *J. Biol. Chem.* **1995,** *270,* 7341–7346.
33. He, B.; Lee, L. W.; Minges, J. T.; Wilson, E. M. Dependence of Selective Gene Activation on the Androgen Receptor NH2- and COOH-Terminal Interaction. *J. Biol. Chem.* **2002,** *277,* 25631–25639.
34. Verrijdt, G.; Haelens, A.; Claessens, F. Selective DNA Recognition by the Androgen Receptor as a Mechanism for Hormone-Specific Regulation of Gene Expression. *Mol. Genet. Metab.* **2003,** *78,* 175–185.
35. Shaffer, P. L.; Jivan, A.; Dollins, D. E.; Claessens, F.; Gewirth, D. T. Structural Basis of Androgen Receptor Binding to Selective Androgen Response Elements. *Proc. Natl. Acad. Sci. U. S. A.* **2004,** *101,* 4758–4763.
36. Jenster, G.; Trapman, J.; Brinkmann, A. O. Nuclear Import of the Human Androgen Receptor. *Biochem. J.* **1993,** *293* (Pt 3), 761–768.
37. Ni, L.; Llewellyn, R.; Kesler, C. T.; Kelley, J. B.; Spencer, A.; Snow, C. J.; Shank, L.; Paschal, B. M. Androgen Induces a Switch from Cytoplasmic Retention to Nuclear Import of the Androgen Receptor. *Mol. Cell. Biol.* **2013,** *33,* 4766–4778.
38. Cutress, M. L.; Whitaker, H. C.; Mills, I. G.; Stewart, M.; Neal, D. E. Structural Basis for the Nuclear Import of the Human Androgen Receptor. *J. Cell Sci.* **2008,** *121,* 957–968.
39. Heery, D. M.; Kalkhoven, E.; Hoare, S.; Parker, M. G. A Signature Motif in Transcriptional co-Activators Mediates Binding to Nuclear Receptors. *Nature* **1997,** *387,* 733–736.
40. He, B.; Kemppainen, J. A.; Wilson, E. M. FXXLF and WXXLF Sequences Mediate the NH2-Terminal Interaction With the Ligand Binding Domain of the Androgen Receptor. *J. Biol. Chem.* **2000,** *275,* 22986–22994.
41. Estebanez-Perpina, E.; Arnold, L. A.; Nguyen, P.; Rodrigues, E. D.; Mar, E.; Bateman, R.; Pallai, P.; Shokat, K. M.; Baxter, J. D.; Guy, R. K.; Webb, P.; Fletterick, R. J. A Surface on the Androgen Receptor That Allosterically Regulates Coactivator Binding. *Proc. Natl. Acad. Sci. U. S. A.* **2007,** *104,* 16074–16079.
42. Gao, W.; Bohl, C. E.; Dalton, J. T. Chemistry and Structural Biology of Androgen Receptor. *Chem. Rev.* **2005,** *105,* 3352–3370.
43. Grad, J. M.; Dai, J. L.; Wu, S.; Burnstein, K. L. Multiple Androgen Response Elements and a Myc Consensus Site in the Androgen Receptor (AR) Coding Region Are Involved in Androgen-Mediated Up-Regulation of AR Messenger RNA. *Mol. Endocrinol.* **1999,** *13,* 1896–1911.

44. Fu, M.; Wang, C.; Reutens, A. T.; Wang, J.; Angeletti, R. H.; Siconolfi-Baez, L.; Ogryzko, V.; Avantaggiati, M. L.; Pestell, R. G. p300 and p300/cAMP-Response Element-Binding Protein-Associated Factor Acetylate the Androgen Receptor at Sites Governing Hormone-Dependent Transactivation. *J. Biol. Chem.* **2000,** *275,* 20853–20860.
45. Ghisletti, S.; Huang, W.; Jepsen, K.; Benner, C.; Hardiman, G.; Rosenfeld, M. G.; Glass, C. K. Cooperative NCoR/SMRT Interactions Establish a Corepressor-Based Strategy for Integration of Inflammatory and Anti-Inflammatory Signaling Pathways. *Genes Dev.* **2009,** *23,* 681–693.
46. Heemers, H. V.; Tindall, D. J. Androgen Receptor (AR) Coregulators: A Diversity of Functions Converging on and Regulating the AR Transcriptional Complex. *Endocr. Rev.* **2007,** *28,* 778–808.
47. Wang, Y.; Kreisberg, J. I.; Ghosh, P. M. Cross-Talk Between the Androgen Receptor and the Phosphatidylinositol 3-Kinase/Akt Pathway in Prostate Cancer. *Curr. Cancer Drug Targets* **2007,** *7,* 591–604.
48. Wen, Y.; Hu, M. C.; Makino, K.; Spohn, B.; Bartholomeusz, G.; Yan, D. H.; Hung, M. C. HER-2/neu Promotes Androgen-Independent Survival and Growth of Prostate Cancer Cells Through the Akt Pathway. *Cancer Res.* **2000,** *60,* 6841–6845.
49. Lin, H. K.; Yeh, S.; Kang, H. Y.; Chang, C. Akt Suppresses Androgen-Induced Apoptosis by Phosphorylating and Inhibiting Androgen Receptor. *Proc. Natl. Acad. Sci. U. S. A.* **2001,** *98,* 7200–7205.
50. Bohl, C. E.; Gao, W.; Miller, D. D.; Bell, C. E.; Dalton, J. T. Structural Basis for Antagonism and Resistance of Bicalutamide in Prostate Cancer. *Proc. Natl. Acad. Sci. U. S. A.* **2005,** *102,* 6201–6206.
51. Bohl, C. E.; Miller, D. D.; Chen, J.; Bell, C. E.; Dalton, J. T. Structural Basis for Accommodation of Nonsteroidal Ligands in the Androgen Receptor. *J. Biol. Chem.* **2005,** *280,* 37747–37754.
52. De Jesus-Tran, K. P.; Cote, P. L.; Cantin, L.; Blanchet, J.; Labrie, F.; Breton, R. Comparison of Crystal Structures of Human Androgen Receptor Ligand-Binding Domain Complexed With Various Agonists Reveals Molecular Determinants Responsible for Binding Affinity. *Protein Sci.* **2006,** *15,* 987–999.
53. Zhou, X. E.; Suino-Powell, K. M.; Li, J.; He, Y. Z.; MacKeigan, J. P.; Melcher, K.; Yong, E. L.; Xu, H. E. Identification of SRC3/AIB1 as a Preferred Coactivator for Hormone-Activated Androgen Receptor. *J. Biol. Chem.* **2010,** *285,* 9161–9171.
54. He, B.; Gampe, R. T., Jr.; Kole, A. J.; Hnat, A. T.; Stanley, T. B.; An, G.; Stewart, E. L.; Kalman, R. I.; Minges, J. T.; Wilson, E. M. Structural Basis for Androgen Receptor Interdomain and Coactivator Interactions Suggests a Transition in Nuclear Receptor Activation Function Dominance. *Mol. Cell* **2004,** *16,* 425–438.
55. Nique, F.; Hebbe, S.; Peixoto, C.; Annoot, D.; Lefrancois, J. M.; Duval, E.; Michoux, L.; Triballeau, N.; Lemoullec, J. M.; Mollat, P.; Thauvin, M.; Prange, T.; Minet, D.; Clement-Lacroix, P.; Robin-Jagerschmidt, C.; Fleury, D.; Guedin, D.; Deprez, P. Discovery of Diarylhydantoins as New Selective Androgen Receptor Modulators. *J. Med. Chem.* **2012,** *55,* 8225–8235.
56. Duke, C. B.; Jones, A.; Bohl, C. E.; Dalton, J. T.; Miller, D. D. Unexpected Binding Orientation of Bulky-B-Ring Anti-Androgens and Implications for Future Drug Targets. *J. Med. Chem.* **2011,** *54,* 3973–3976.
57. Nirschl, A. A.; Zou, Y.; Krystek, S. R.; Sutton, J. C.; Simpkins, L. M.; Lupisella, J. A.; Kuhns, J. E.; Seethala, R.; Golla, R.; Sleph, P. G.; Beehler, B. C.; Grover, G. J.; Egan, D.; Fura, A.; Vyas, V. P.; Li, Y. X.; Sack, J. S.; Kish, K. F.; An, Y. M.; Bryson, J. A.; Gougoutas, J. Z.; DiMarco, J.; Zahler, R.; Ostrowski, J.; Hamann, L. G. N-Aryl-oxazolidin-2-imine Muscle Selective Androgen Receptor Modulators Enhance Potency Through Pharmacophore Reorientation. *J. Med. Chem.* **2009,** *52,* 2794–2798.
58. Bohl, C. E.; Wu, Z.; Chen, J.; Mohler, M. L.; Yang, J.; Hwang, D. J.; Mustafa, S.; Miller, D. D.; Bell, C. E.; Dalton, J. T. Effect of B-Ring Substitution Pattern on Binding Mode of Propionamide Selective Androgen Receptor Modulators. *Bioorg. Med. Chem. Lett.* **2008,** *18,* 5567–5570.
59. Madauss, K. P.; Grygielko, E. T.; Deng, S. J.; Sulpizio, A. C.; Stanley, T. B.; Wu, C.; Short, S. A.; Thompson, S. K.; Stewart, E. L.; Laping, N. J.; Williams, S. P.; Bray, J. D. A Structural and in vitro Characterization of Asoprisnil: A Selective Progesterone Receptor Modulator. *Mol. Endocrinol.* **2007,** *21,* 1066–1081.
60. Kauppi, B.; Jakob, C.; Farnegardh, M.; Yang, J.; Ahola, H.; Alarcon, M.; Calles, K.; Engstrom, O.; Harlan, J.; Muchmore, S.; Ramqvist, A. K.; Thorell, S.; Ohman, L.; Greer, J.; Gustafsson, J. A.; Carlstedt-Duke, J.; Carlquist, M. The Three-Dimensional Structures of Antagonistic and Agonistic Forms of the Glucocorticoid Receptor Ligand-Binding Domain: RU-486 Induces a Transconformation that Leads to Active Antagonism. *J. Biol. Chem.* **2003,** *278,* 22748–22754.
61. Shiau, A. K.; Barstad, D.; Loria, P. M.; Cheng, L.; Kushner, P. J.; Agard, D. A.; Greene, G. L. The Structural Basis of Estrogen Receptor/Coactivator Recognition and the Antagonism of this Interaction by Tamoxifen. *Cell* **1998,** *95,* 927–937.
62. Shiau, A. K.; Barstad, D.; Radek, J. T.; Meyers, M. J.; Nettles, K. W.; Katzenellenbogen, B. S.; Katzenellenbogen, J. A.; Agard, D. A.; Greene, G. L. Structural Characterization of a Subtype-Selective Ligand Reveals a Novel Mode of Estrogen Receptor Antagonism. *Nat. Struct. Biol.* **2002,** *9,* 359–364.
63. Delfosse, V.; le Maire, A.; Balaguer, P.; Bourguet, W. A Structural Perspective on Nuclear Receptors as Targets of Environmental Compounds. *Acta Pharmacol. Sin.* **2015,** *36,* 88–101.
64. Couture, J. F.; de Jesus-Tran, K. P.; Roy, A. M.; Cantin, L.; Cote, P. L.; Legrand, P.; Luu-The, V.; Labrie, F.; Breton, R. Comparison of Crystal Structures of Human Type 3 3alpha-Hydroxysteroid Dehydrogenase Reveals an "Induced-Fit" Mechanism and a Conserved Basic Motif Involved in the Binding of Androgen. *Protein Sci.* **2005,** *14,* 1485–1497.
65. Cantin, L.; Faucher, F.; Couture, J. F.; de Jesus-Tran, K. P.; Legrand, P.; Ciobanu, L. C.; Frechette, Y.; Labrecque, R.; Singh, S. M.; Labrie, F.; Breton, R. Structural Characterization of the Human Androgen Receptor Ligand-Binding Domain Complexed With EM5744, a Rationally Designed Steroidal Ligand Bearing a Bulky Chain Directed Toward Helix 12. *J. Biol. Chem.* **2007,** *282,* 30910–30919.
66. Seidenfeld, J.; Samson, D. J.; Hasselblad, V.; Aronson, N.; Albertsen, P. C.; Bennett, C. L.; Wilt, T. J. Single-Therapy Androgen Suppression in Men With Advanced Prostate Cancer: A Systematic Review and Meta-Analysis. *Ann. Intern. Med.* **2000,** *132,* 566–577.
67. Anderson, J. The Role of Antiandrogen Monotherapy in the Treatment of Prostate Cancer. *BJU Int.* **2003,** *91,* 455–461.
68. Abrahamsson, P. A. Treatment of Locally Advanced Prostate Cancer—A New Role for Antiandrogen Monotherapy? *Eur. Urol.* **2001,** *39* (Suppl 1), 22–28.
69. Veldscholte, J.; Ris-Stalpers, C.; Kuiper, G. G.; Jenster, G.; Berrevoets, C.; Claassen, E.; van Rooij, H. C.; Trapman, J.; Brinkmann, A. O.; Mulder, E. A Mutation in the Ligand Binding Domain of the Androgen Receptor of Human LNCaP Cells Affects Steroid Binding Characteristics and Response to Anti-Androgens. *Biochem. Biophys. Res. Commun.* **1990,** *173,* 534–540.
70. Hara, T.; Miyazaki, J.; Araki, H.; Yamaoka, M.; Kanzaki, N.; Kusaka, M.; Miyamoto, M. Novel Mutations of Androgen Receptor: A Possible Mechanism of Bicalutamide Withdrawal Syndrome. *Cancer Res.* **2003,** *63,* 149–153.
71. Dobs, A. S.; Boccia, R. V.; Croot, C. C.; Gabrail, N. Y.; Dalton, J. T.; Hancock, M. L.; Johnston, M. A.; Steiner, M. S. Effects of Enobosarm on Muscle Wasting and Physical Function in Patients With Cancer: A Double-Blind, Randomised Controlled Phase 2 Trial. *Lancet Oncol.* **2013,** *14,* 335–345.
72. Agarwal, N.; Di Lorenzo, G.; Sonpavde, G.; Bellmunt, J. New Agents for Prostate Cancer. *Ann. Oncol.* **2014,** *25,* 1700–1709.
73. De Maeseneer, D. J.; Van Praet, C.; Lumen, N.; Rottey, S. Battling Resistance Mechanisms in Antihormonal Prostate Cancer Treatment: Novel Agents and Combinations. *Urol. Oncol.* **2015,** *33* (7), 310–321.
74. Tran, C.; Ouk, S.; Clegg, N. J.; Chen, Y.; Watson, P. A.; Arora, V.; Wongvipat, J.; Smith-Jones, P. M.; Yoo, D.; Kwon, A.; Wasielewska, T.; Welsbie, D.; Chen, C. D.; Higano, C. S.; Beer, T. M.; Hung, D. T.; Scher, H. I.; Jung, M. E.; Sawyers, C. L. Development of a Second-Generation Antiandrogen for Treatment of Advanced Prostate Cancer. *Science* **2009,** *324,* 787–790.
75. Rathkopf, D. E.; Morris, M. J.; Fox, J. J.; Danila, D. C.; Slovin, S. F.; Hager, J. H.; Rix, P. J.; Chow Maneval, E.; Chen, I.; Gonen, M.; Fleisher, M.; Larson, S. M.; Sawyers, C. L.; Scher, H. I. Phase I Study of ARN-509, a Novel Antiandrogen, in the Treatment of Castration-Resistant Prostate Cancer. *J. Clin. Oncol.* **2013,** *31,* 3525–3530.
76. Clegg, N. J.; Wongvipat, J.; Joseph, J. D.; Tran, C.; Ouk, S.; Dilhas, A.; Chen, Y.; Grillot, K.; Bischoff, E. D.; Cai, L.; Aparicio, A.; Dorow, S.; Arora, V.; Shao, G.; Qian, J.; Zhao, H.; Yang, G.; Cao, C.; Sensintaffar, J.; Wasielewska, T.; Herbert, M. R.; Bonnefous, C.; Darimont, B.; Scher, H. I.; Smith-Jones, P.; Klang, M.; Smith, N. D.; De Stanchina, E.; Wu, N.; Ouerfelli, O.; Rix, P. J.; Heyman, R. A.; Jung, M. E.; Sawyers, C. L.; Hager, J. H. ARN-509: A Novel Antiandrogen for Prostate Cancer Treatment. *Cancer Res.* **2012,** *72,* 1494–1503.

77. Balbas, M. D.; Evans, M. J.; Hosfield, D. J.; Wongvipat, J.; Arora, V. K.; Watson, P. A.; Chen, Y.; Greene, G. L.; Shen, Y.; Sawyers, C. L. Overcoming Mutation-Based Resistance to Antiandrogens With Rational Drug Design. *Elife* **2013,** *2,* e00499.
78. Joseph, J. D.; Lu, N.; Qian, J.; Sensintaffar, J.; Shao, G.; Brigham, D.; Moon, M.; Maneval, E. C.; Chen, I.; Darimont, B.; Hager, J. H. A Clinically Relevant Androgen Receptor Mutation Confers Resistance to Second-Generation Antiandrogens Enzalutamide and ARN-509. *Cancer Discov.* **2013,** *3,* 1020–1029.
79. Korpal, M.; Korn, J. M.; Gao, X.; Rakiec, D. P.; Ruddy, D. A.; Doshi, S.; Yuan, J.; Kovats, S. G.; Kim, S.; Cooke, V. G.; Monahan, J. E.; Stegmeier, F.; Roberts, T. M.; Sellers, W. R.; Zhou, W.; Zhu, P. An F876L Mutation in Androgen Receptor Confers Genetic and Phenotypic Resistance to MDV3100 (Enzalutamide). *Cancer Discov.* **2013,** *3,* 1030–1043.
80. Moilanen, A. M.; Riikonen, R.; Oksala, R.; Ravanti, L.; Aho, E.; Wohlfahrt, G.; Nykanen, P. S.; Tormakangas, O. P.; Palvimo, J. J.; Kallio, P. J. Discovery of ODM-201, a New-Generation Androgen Receptor Inhibitor Targeting Resistance Mechanisms to Androgen Signaling-Directed Prostate Cancer Therapies. *Sci. Rep.* **2015,** *5,* 12007.
81. Fizazi, K.; Massard, C.; Bono, P.; Jones, R.; Kataja, V.; James, N.; Garcia, J. A.; Protheroe, A.; Tammela, T. L.; Elliott, T.; Mattila, L.; Aspegren, J.; Vuorela, A.; Langmuir, P.; Mustonen, M.; group, A. s. Activity and Safety of ODM-201 in Patients With Progressive Metastatic Castration-Resistant Prostate Cancer (ARADES): An Open-Label Phase 1 Dose-Escalation and Randomised Phase 2 Dose Expansion Trial. *Lancet Oncol.* **2014,** *15,* 975–985.
82. Yin, L.; Hu, Q. CYP17 Inhibitors—Abiraterone, C17,20-Lyase Inhibitors and Multi-Targeting Agents. *Nat. Rev. Urol.* **2014,** *11,* 32–42.
83. Richards, J.; Lim, A. C.; Hay, C. W.; Taylor, A. E.; Wingate, A.; Nowakowska, K.; Pezaro, C.; Carreira, S.; Goodall, J.; Arlt, W.; McEwan, I. J.; de Bono, J. S.; Attard, G. Interactions of Abiraterone, Eplerenone, and Prednisolone With Wild-Type and Mutant Androgen Receptor: A Rationale for Increasing Abiraterone Exposure or Combining With MDV3100. *Cancer Res.* **2012,** *72,* 2176–2182.
84. Ryan, C. J.; Smith, M. R.; de Bono, J. S.; Molina, A.; Logothetis, C. J.; de Souza, P.; Fizazi, K.; Mainwaring, P.; Piulats, J. M.; Ng, S.; Carles, J.; Mulders, P. F.; Basch, E.; Small, E. J.; Saad, F.; Schrijvers, D.; Van Poppel, H.; Mukherjee, S. D.; Suttmann, H.; Gerritsen, W. R.; Flaig, T. W.; George, D. J.; Yu, E. Y.; Efstathiou, E.; Pantuck, A.; Winquist, E.; Higano, C. S.; Taplin, M. E.; Park, Y.; Kheoh, T.; Griffin, T.; Scher, H. I.; Rathkopf, D. E.; Investigators, C.-A.-. Biraterone in Metastatic Prostate Cancer Without Previous Chemotherapy. *N. Eng. J. Med.* **2013,** *368,* 138–148.
85. Cai, C.; Chen, S.; Ng, P.; Bubley, G. J.; Nelson, P. S.; Mostaghel, E. A.; Marck, B.; Matsumoto, A. M.; Simon, N. I.; Wang, H.; Chen, S.; Balk, S. P. Intratumoral De Novo Steroid Synthesis Activates Androgen Receptor in Castration-Resistant Prostate Cancer and is Upregulated by Treatment With CYP17A1 Inhibitors. *Cancer Res.* **2011,** *71,* 6503–6513.
86. Li, Z.; Bishop, A. C.; Alyamani, M.; Garcia, J. A.; Dreicer, R.; Bunch, D.; Liu, J.; Upadhyay, S. K.; Auchus, R. J.; Sharifi, N. Conversion of Abiraterone to D4A Drives Anti-Tumour Activity in Prostate Cancer. *Nature* **2015,** *523* (7560), 347–351.
87. Njar, V. C.; Brodie, A. M. Discovery and Development of Galeterone (TOK-001 or VN/124-1) for the Treatment of all Stages of Prostate Cancer. *J. Med. Chem.* **2015,** *58,* 2077–2087.
88. Handratta, V. D.; Vasaitis, T. S.; Njar, V. C.; Gediya, L. K.; Kataria, R.; Chopra, P.; Newman, D., Jr.; Farquhar, R.; Guo, Z.; Qiu, Y.; Brodie, A. M. Novel C-17-Heteroaryl Steroidal CYP17 Inhibitors/Antiandrogens: Synthesis, in vitro Biological Activity, Pharmacokinetics, and Antitumor Activity in the LAPC4 Human Prostate Cancer Xenograft Model. *J. Med. Chem.* **2005,** *48,* 2972–2984.
89. Vasaitis, T.; Belosay, A.; Schayowitz, A.; Khandelwal, A.; Chopra, P.; Gediya, L. K.; Guo, Z.; Fang, H. B.; Njar, V. C.; Brodie, A. M. Androgen Receptor Inactivation Contributes to Antitumor Efficacy of 17{Alpha}-Hydroxylase/17,20-Lyase Inhibitor 3beta-Hydroxy-17-(1H-Benzimidazole-1-yl)Androsta-5,16-Diene in Prostate Cancer. *Mol. Cancer Ther.* **2008,** *7,* 2348–2357.
90. Bruno, R. D.; Vasaitis, T. S.; Gediya, L. K.; Purushottamachar, P.; Godbole, A. M.; Ates-Alagoz, Z.; Brodie, A. M.; Njar, V. C. Synthesis and Biological Evaluations of Putative Metabolically Stable Analogs of VN/124-1 (TOK-001): Head to Head Anti-Tumor Efficacy Evaluation of VN/124-1 (TOK-001) and Abiraterone in LAPC-4 Human Prostate Cancer Xenograft Model. *Steroids* **2011,** *76,* 1268–1279.
91. Nader Al Nakouzi, C. W.; Jacoby, D.; Gleave, M. E.; Zoubeidi, A. Galeterone Suppresses Castration-Resistant and Enzalutamide-Resistant Prostate Cancer Growth in Vitro. Proceedings of the AACR-NCI-EORTC International Conference: Molecular Targets and Cancer Therapeutics, Vol. 12: Boston, MA**;** 2013; p C89.
92. Schayowitz, A.; Sabnis, G.; Goloubeva, O.; Njar, V. C. O.; Brodie, A. M. H. Prolonging Hormone Sensitivity in Prostate Cancer Xenografts Through Dual Inhibition of AR and mTOR. *Br. J. Cancer* **2010,** *103,* 1001–1007.
93. Visakorpi, T.; Hyytinen, E.; Koivisto, P.; Tanner, M.; Keinanen, R.; Palmberg, C.; Palotie, A.; Tammela, T.; Isola, J.; Kallioniemi, O. P. In vivo Amplification of the Androgen Receptor Gene and Progression of Human Prostate Cancer. *Nat. Genet.* **1995,** *9,* 401–406.
94. Koivisto, P.; Kononen, J.; Palmberg, C.; Tammela, T.; Hyytinen, E.; Isola, J.; Trapman, J.; Cleutjens, K.; Noordzij, A.; Visakorpi, T.; Kallioniemi, O. P. Androgen Receptor Gene Amplification: A Possible Molecular Mechanism for Androgen Deprivation Therapy Failure in Prostate Cancer. *Cancer Res.* **1997,** *57,* 314–319.
95. Edwards, J.; Krishna, N. S.; Mukherjee, R.; Watters, A. D.; Underwood, M. A.; Bartlett, J. M. Amplification of the Androgen Receptor May Not Explain the Development of Androgen-Independent Prostate Cancer. *BJU Int.* **2001,** *88,* 633–637.
96. Edwards, J.; Krishna, N. S.; Grigor, K. M.; Bartlett, J. M. Androgen Receptor Gene Amplification and Protein Expression in Hormone Refractory Prostate Cancer. *Br. J. Cancer* **2003,** *89,* 552–556.
97. Holzbeierlein, J.; Lal, P.; LaTulippe, E.; Smith, A.; Satagopan, J.; Zhang, L.; Ryan, C.; Smith, S.; Scher, H.; Scardino, P.; Reuter, V.; Gerald, W. L. Gene Expression Analysis of Human Prostate Carcinoma During Hormonal Therapy Identifies Androgen-Responsive Genes and Mechanisms of Therapy Resistance. *Am. J. Pathol.* **2004,** *164,* 217–227.
98. Taplin, M. E.; Bubley, G. J.; Shuster, T. D.; Frantz, M. E.; Spooner, A. E.; Ogata, G. K.; Keer, H. N.; Balk, S. P. Mutation of the Androgen-Receptor Gene in Metastatic Androgen-Independent Prostate Cancer. *N. Eng. J. Med.* **1995,** *332,* 1393–1398.
99. Tilley, W. D.; Buchanan, G.; Hickey, T. E.; Bentel, J. M. Mutations in the Androgen Receptor Gene Are Associated With Progression of Human Prostate Cancer to Androgen Independence. *Clin. Cancer Res.* **1996,** *2,* 277–285.
100. Fenton, M. A.; Shuster, T. D.; Fertig, A. M.; Taplin, M. E.; Kolvenbag, G.; Bubley, G. J.; Balk, S. P. Functional Characterization of Mutant Androgen Receptors From Androgen-Independent Prostate Cancer. *Clin. Cancer Res.* **1997,** *3,* 1383–1388.
101. Taplin, M. E.; Bubley, G. J.; Ko, Y. J.; Small, E. J.; Upton, M.; Rajeshkumar, B.; Balk, S. P. Selection for Androgen Receptor Mutations in Prostate Cancers Treated With Androgen Antagonist. *Cancer Res.* **1999,** *59,* 2511–2515.
102. Wallen, M. J.; Linja, M.; Kaartinen, K.; Schleutker, J.; Visakorpi, T. Androgen Receptor Gene Mutations in Hormone-Refractory Prostate Cancer. *J. Pathol.* **1999,** *189,* 559–563.
103. Buchanan, G.; Greenberg, N. M.; Scher, H. I.; Harris, J. M.; Marshall, V. R.; Tilley, W. D. Collocation of Androgen Receptor Gene Mutations in Prostate Cancer. *Clin. Cancer Res.* **2001,** *7,* 1273–1281.
104. Steketee, K.; Timmerman, L.; Ziel-van der Made, A. C.; Doesburg, P.; Brinkmann, A. O.; Trapman, J. Broadened Ligand Responsiveness of Androgen Receptor Mutants Obtained by Random Amino Acid Substitution of H874 and Mutation hot Spot T877 in Prostate Cancer. *Int. J. Cancer* **2002,** *100,* 309–317.
105. Gottlieb, B.; Beitel, L. K.; Wu, J. H.; Trifiro, M. The Androgen Receptor Gene Mutations Database (ARDB): 2004 Update. *Hum. Mutat.* **2004,** *23,* 527–533.
106. Duff, J.; McEwan, I. J. Mutation of Histidine 874 in the Androgen Receptor Ligand-Binding Domain Leads to Promiscuous Ligand Activation and Altered p160 Coactivator Interactions. *Mol. Endocrinol.* **2005,** *19,* 2943–2954.
107. Hara, T.; Kouno, J.; Nakamura, K.; Kusaka, M.; Yamaoka, M. Possible Role of Adaptive Mutation in Resistance to Antiandrogen in Prostate Cancer Cells. *Prostate* **2005,** *65,* 268–275.
108. Gottlieb, B.; Beitel, L. K.; Nadarajah, A.; Paliouras, M.; Trifiro, M. The Androgen Receptor Gene Mutations Database: 2012 Update. *Hum. Mutat.* **2012,** *33,* 887–894.
109. Dehm, S. M.; Tindall, D. J. Alternatively Spliced Androgen Receptor Variants. *Endocr. Relat. Cancer* **2011,** *18,* R183–R196.
110. Brand, L. J.; Dehm, S. M. Androgen Receptor Gene Rearrangements: New Perspectives on Prostate Cancer Progression. *Curr. Drug Targets* **2013,** *14,* 441–449.

111. Chan, S. C.; Li, Y.; Dehm, S. M. Androgen Receptor Splice Variants Activate Androgen Receptor Target Genes and Support Aberrant Prostate Cancer Cell Growth Independent of Canonical Androgen Receptor Nuclear Localization Signal. *J. Biol. Chem.* **2012,** *287,* 19736–19749.
112. Li, Y.; Chan, S. C.; Brand, L. J.; Hwang, T. H.; Silverstein, K. A.; Dehm, S. M. Androgen Receptor Splice Variants Mediate Enzalutamide Resistance in Castration-Resistant Prostate Cancer Cell Lines. *Cancer Res.* **2013,** *73,* 483–489.
113. Sartor, O.; Dong, Y. Androgen Receptor Variant-7: An Important Predictive Biomarker in Castrate Resistant Prostate Cancer. *Asian J. Androl.* **2015,** *17* (13), 439–440.
114. Lu, J.; Van der Steen, T.; Tindall, D. J. Are Androgen Receptor Variants a Substitute for the Full-Length Receptor? *Nat. Rev. Urol.* **2015,** *12,* 137–144.
115. Antonarakis, E. S.; Lu, C.; Wang, H.; Luber, B.; Nakazawa, M.; Roeser, J. C.; Chen, Y.; Mohammad, T. A.; Chen, Y.; Fedor, H. L.; Lotan, T. L.; Zheng, Q.; De Marzo, A. M.; Isaacs, J. T.; Isaacs, W. B.; Nadal, R.; Paller, C. J.; Denmeade, S. R.; Carducci, M. A.; Eisenberger, M. A.; Luo, J. AR-V7 and Resistance to Enzalutamide and Abiraterone in Prostate Cancer. *N. Eng. J. Med.* **2014,** *371,* 1028–1038.
116. Ware, K. E.; Garcia-Blanco, M. A.; Armstrong, A. J.; Dehm, S. M. Biologic and Clinical Significance of Androgen Receptor Variants in Castration Resistant Prostate Cancer. *Endocr. Relat. Cancer* **2014,** *21,* T87–T103.
117. Chan, S. C.; Dehm, S. M. Constitutive Activity of the Androgen Receptor. *Adv. Pharmacol.* **2014,** *70,* 327–366.
118. Hu, R.; Lu, C.; Mostaghel, E. A.; Yegnasubramanian, S.; Gurel, M.; Tannahill, C.; Edwards, J.; Isaacs, W. B.; Nelson, P. S.; Bluemn, E.; Plymate, S. R.; Luo, J. Distinct Transcriptional Programs Mediated by the Ligand-Dependent Full-Length Androgen Receptor and Its Splice Variants in Castration-Resistant Prostate Cancer. *Cancer Res.* **2012,** *72,* 3457–3462.
119. Claessens, F.; Helsen, C.; Prekovic, S.; Van den Broeck, T.; Spans, L.; Van Poppel, H.; Joniau, S. Emerging Mechanisms of Enzalutamide Resistance in Prostate Cancer. *Nat. Rev. Urol.* **2014,** *11,* 712–716.
120. Nyquist, M. D.; Dehm, S. M. Interplay Between Genomic Alterations and Androgen Receptor Signaling During Prostate Cancer Development and Progression. *Horm. Cancer* **2013,** *4,* 61–69.
121. Hu, R.; Dunn, T. A.; Wei, S.; Isharwal, S.; Veltri, R. W.; Humphreys, E.; Han, M.; Partin, A. W.; Vessella, R. L.; Isaacs, W. B.; Bova, G. S.; Luo, J. Ligand-Independent Androgen Receptor Variants Derived From Splicing of Cryptic Exons Signify Hormone-Refractory Prostate Cancer. *Cancer Res.* **2009,** *69,* 16–22.
122. Efstathiou, E.; Titus, M.; Wen, S.; Hoang, A.; Karlou, M.; Ashe, R.; Tu, S. M.; Aparicio, A.; Troncoso, P.; Mohler, J.; Logothetis, C. J. Molecular Characterization of Enzalutamide-Treated Bone Metastatic Castration-Resistant Prostate Cancer. *Eur. Urol.* **2015,** *67,* 53–60.
123. Guo, Z. Y.; Yang, X.; Sun, F.; Jiang, R. C.; Linn, D. E.; Chen, H. G.; Chen, H. G.; Kong, X. T.; Melamed, J.; Tepper, C. G.; Kung, H. J.; Brodie, A. M. H.; Edwards, J.; Qiu, Y. A Novel Androgen Receptor Splice Variant Is Up-Regulated During Prostate Cancer Progression and Promotes Androgen Depletion-Resistant Growth. *Cancer Res.* **2009,** *69,* 2305–2313.
124. Dehm, S. M.; Schmidt, L. J.; Heemers, H. V.; Vessella, R. L.; Tindall, D. J. Splicing of a Novel Androgen Receptor Exon Generates a Constitutively Active Androgen Receptor That Mediates Prostate Cancer Therapy Resistance. *Cancer Res.* **2008,** *68,* 5469–5477.
125. Chan, S. C.; Selth, L. A.; Li, Y.; Nyquist, M. D.; Miao, L.; Bradner, J. E.; Raj, G. V.; Tilley, W. D.; Dehm, S. M. Targeting Chromatin Binding Regulation of Constitutively Active AR Variants to Overcome Prostate Cancer Resistance to Endocrine-Based Therapies. *Nucleic Acids Res.* **2015,** *43,* 5880–5897.
126. Hobisch, A.; Eder, I. E.; Putz, T.; Horninger, W.; Bartsch, G.; Klocker, H.; Culig, Z. Interleukin-6 Regulates Prostate-Specific Protein Expression in Prostate Carcinoma Cells by Activation of the Androgen Receptor. *Cancer Res.* **1998,** *58,* 4640–4645.
127. Debes, J. D.; Schmidt, L. J.; Huang, H.; Tindall, D. J. p300 Mediates Androgen-Independent Transactivation of the Androgen Receptor by Interleukin 6. *Cancer Res.* **2002,** *62,* 5632–5636.
128. Engelman, J. A.; Luo, J.; Cantley, L. C. The Evolution of Phosphatidylinositol 3-Kinases as Regulators of Growth and Metabolism. *Nat. Rev. Genet.* **2006,** *7,* 606–619.
129. Soulitzis, N.; Karyotis, I.; Delakas, D.; Spandidos, D. A. Expression Analysis of Peptide Growth Factors VEGF, FGF2, TGFB1, EGF and IGF1 in Prostate Cancer and Benign Prostatic Hyperplasia. *Int. J. Oncol.* **2006,** *29,* 305–314.
130. Wu, Y.; Zhao, W.; Zhao, J.; Pan, J.; Wu, Q.; Zhang, Y.; Bauman, W. A.; Cardozo, C. P. Identification of Androgen Response Elements in the Insulin-Like Growth Factor I Upstream Promoter. *Endocrinology* **2007,** *148,* 2984–2993.
131. Lee, S. O.; Chun, J. Y.; Nadiminty, N.; Lou, W.; Feng, S. T.; Gao, A. C. Interleukin-4 Activates Androgen Receptor Through CBP/p300. *Prostate* **2009,** *69,* 126–132.
132. Taylor, B. S.; Schultz, N.; Hieronymus, H.; Gopalan, A.; Xiao, Y.; Carver, B. S.; Arora, V. K.; Kaushik, P.; Cerami, E.; Reva, B.; Antipin, Y.; Mitsiades, N.; Landers, T.; Dolgalev, I.; Major, J. E.; Wilson, M.; Socci, N. D.; Lash, A. E.; Heguy, A.; Eastham, J. A.; Scher, H. I.; Reuter, V. E.; Scardino, P. T.; Sander, C.; Sawyers, C. L.; Gerald, W. L. Integrative Genomic Profiling of Human Prostate Cancer. *Cancer Cell* **2010,** *18,* 11–22.
133. Carver, B. S.; Chapinski, C.; Wongvipat, J.; Hieronymus, H.; Chen, Y.; Chandarlapaty, S.; Arora, V. K.; Le, C.; Koutcher, J.; Scher, H.; Scardino, P. T.; Rosen, N.; Sawyers, C. L. Reciprocal Feedback Regulation of PI3K and Androgen Receptor Signaling in PTEN-Deficient Prostate Cancer. *Cancer Cell* **2011,** *19,* 575–586.
134. Thomas, C.; Lamoureux, F.; Crafter, C.; Davies, B. R.; Beraldi, E.; Fazli, L.; Kim, S.; Thaper, D.; Gleave, M. E.; Zoubeidi, A. Synergistic Targeting of PI3K/AKT Pathway and Androgen Receptor Axis Significantly Delays Castration-Resistant Prostate Cancer Progression in vivo. *Mol. Cancer Ther.* **2013,** *12,* 2342–2355.
135. Chang, K. H.; Li, R.; Papari-Zareei, M.; Watumull, L.; Zhao, Y. D.; Auchus, R. J.; Sharifi, N. Dihydrotestosterone Synthesis Bypasses Testosterone to Drive Castration-Resistant Prostate Cancer. *Proc. Natl. Acad. Sci. U. S. A.* **2011,** *108,* 13728–13733.
136. Arora, V. K.; Schenkein, E.; Murali, R.; Subudhi, S. K.; Wongvipat, J.; Balbas, M. D.; Shah, N.; Cai, L.; Efstathiou, E.; Logothetis, C.; Zheng, D.; Sawyers, C. L. Glucocorticoid Receptor Confers Resistance to Antiandrogens by Bypassing Androgen Receptor Blockade. *Cell* **2013,** *155,* 1309–1322.
137. Waltering, K. K.; Urbanucci, A.; Visakorpi, T. Androgen Receptor (AR) Aberrations in Castration-Resistant Prostate Cancer. *Mol. Cell. Endocrinol.* **2012,** *360,* 38–43.
138. Lack, N. A.; Axerio-Cilies, P.; Tavassoli, P.; Han, F. Q.; Chan, K. H.; Feau, C.; LeBlanc, E.; Guns, E. T.; Guy, R. K.; Rennie, P. S.; Cherkasov, A. Targeting the Binding Function 3 (BF3) Site of the Human Androgen Receptor Through Virtual Screening. *J. Med. Chem.* **2011,** *54,* 8563–8573.
139. Munuganti, R. S.; Leblanc, E.; Axerio-Cilies, P.; Labriere, C.; Frewin, K.; Singh, K.; Hassona, M. D.; Lack, N. A.; Li, H.; Ban, F.; Tomlinson Guns, E.; Young, R.; Rennie, P. S.; Cherkasov, A. Targeting the Binding Function 3 (BF3) Site of the Androgen Receptor Through Virtual Screening. 2. Development of 2-((2-Phenoxyethyl) Thio)-1H-Benzimidazole Derivatives. *J. Med. Chem.* **2013,** *56,* 1136–1148.
140. Munuganti, R. S. N.; Hassona, M. D. H.; Leblanc, E.; Frewin, K.; Singh, K.; Ma, D.; Ban, F. Q.; Hsing, M.; Adomat, H.; Lallous, N.; Andre, C.; Jonadass, J. P. S.; Zoubeidi, A.; Young, R. N.; Guns, E. T.; Rennie, P. S.; Cherkasov, A. Identification of a Potent Antiandrogen that Targets the BF3 Site of the Androgen Receptor and Inhibits Enzalutamide-Resistant Prostate Cancer. *Chem. Biol.* **2014,** *21,* 1476–1485.
141. Ravindranathan, P.; Lee, T. K.; Yang, L.; Centenera, M. M.; Butler, L.; Tilley, W. D.; Hsieh, J. T.; Ahn, J. M.; Raj, G. V. Peptidomimetic Targeting of Critical Androgen Receptor-Coregulator Interactions in Prostate Cancer. *Nat. Commun.* **2013,** *4,* 1923.
142. Andersen, R. J.; Mawji, N. R.; Wang, J.; Wang, G.; Haile, S.; Myung, J. K.; Watt, K.; Tam, T.; Yang, Y. C.; Banuelos, C. A.; Williams, D. E.; McEwan, I. J.; Wang, Y.; Sadar, M. D. Regression of Castrate-Recurrent Prostate Cancer by a Small-Molecule Inhibitor of the Amino-Terminus Domain of the Androgen Receptor. *Cancer Cell* **2010,** *17,* 535–546.
143. Myung, J. K.; Banuelos, C. A.; Fernandez, J. G.; Mawji, N. R.; Wang, J.; Tien, A. H.; Yang, Y. C.; Tavakoli, I.; Haile, S.; Watt, K.; McEwan, I. J.; Plymate, S.; Andersen, R. J.; Sadar, M. D. An Androgen Receptor N-Terminal Domain Antagonist for Treating Prostate Cancer. *J. Clin. Invest.* **2013,** *123,* 2948–2960.
144. Brand, L. J.; Olson, M. E.; Ravindranathan, P.; Guo, H.; Kempema, A. M.; Andrews, T. E.; Chen, X.; Raj, G. V.; Harki, D. A.; Dehm, S. M. EPI-001 Is a Selective Peroxisome Proliferator-Activated Receptor-Gamma Modulator With Inhibitory Effects on Androgen Receptor Expression and Activity in Prostate Cancer. *Oncotarget* **2015,** *6,* 3811–3824.
145. Banuelos, C. A.; Lal, A.; Tien, A. H.; Shah, N.; Yang, Y. C.; Mawji, N. R.; Meimetis, L. G.; Park, J.; Kunzhong, J.; Andersen, R. J.; Sadar, M. D. Characterization of Niphatenones that Inhibit Androgen Receptor N-Terminal Domain. *PLoS One* **2014,** *9,* e107991.
146. Dalal, K.; Roshan-Moniri, M.; Sharma, A.; Li, H.; Ban, F.; Hassona, M. D.; Hsing, M.; Singh, K.; LeBlanc, E.; Dehm, S.; Tomlinson Guns, E. S.; Cherkasov, A.; Rennie, P. S. Selectively Targeting the DNA-Binding Domain of the Androgen Receptor as a Prospective Therapy for Prostate Cancer. *J. Biol. Chem.* **2014,** *289,* 26417–26429.

147. Li, H.; Ban, F.; Dalal, K.; Leblanc, E.; Frewin, K.; Ma, D.; Adomat, H.; Rennie, P. S.; Cherkasov, A. Discovery of Small-Molecule Inhibitors Selectively Targeting the DNA-Binding Domain of the Human Androgen Receptor. *J. Med. Chem.* **2014,** *57,* 6458–6467.
148. Yamamoto, Y.; Loriot, Y.; Beraldi, E.; Zhang, F.; Wyatt, A. W.; Nakouzi, N. A.; Mo, F.; Zhou, T.; Kim, Y.; Monia, B. P.; MacLeod, A. R.; Fazli, L.; Wang, Y.; Collins, C. C.; Zoubeidi, A.; Gleave, M. Generation 2.5 Antisense Oligonucleotides Targeting the Androgen Receptor and Its Splice Variants Suppress Enzalutamide-Resistant Prostate Cancer Cell Growth. *Clin. Cancer Res.* **2015,** *21,* 1675–1687.
149. Lee, J. B.; Zhang, K.; Tam, Y. Y.; Tam, Y. K.; Belliveau, N. M.; Sung, V. Y.; Lin, P. J.; LeBlanc, E.; Ciufolini, M. A.; Rennie, P. S.; Cullis, P. R. Lipid Nanoparticle siRNA Systems for Silencing the Androgen Receptor in Human Prostate Cancer In Vivo. *Int. J. Cancer* **2012,** *131,* E781–E790.
150. Yamashita, S.; Lai, K. P.; Chuang, K. L.; Xu, D.; Miyamoto, H.; Tochigi, T.; Pang, S. T.; Li, L.; Arai, Y.; Kung, H. J.; Yeh, S.; Chang, C. ASC-J9 Suppresses Castration-Resistant Prostate Cancer Growth Through Degradation of Full-Length and Splice Variant Androgen Receptors. *Neoplasia* **2012,** *14,* 74–83.
151. Grosdidier, S.; Carbo, L. R.; Buzon, V.; Brooke, G.; Nguyen, P.; Baxter, J. D.; Bevan, C.; Webb, P.; Estebanez-Perpina, E.; Fernandez-Recio, J. Allosteric Conversation in the Androgen Receptor Ligand-Binding Domain Surfaces. *Mol. Endocrinol.* **2012,** *26,* 1078–1090.
152. Buzon, V.; Carbo, L. R.; Estruch, S. B.; Fletterick, R. J.; Estebanez-Perpina, E. A Conserved Surface on the Ligand Binding Domain of Nuclear Receptors for Allosteric Control. *Mol. Cell. Endocrinol.* **2012,** *348,* 394–402.
153. Estebanez-Perpina, E.; Arnold, A. A.; Nguyen, P.; Rodrigues, E. D.; Mar, E.; Bateman, R.; Pallai, P.; Shokat, K. M.; Baxter, J. D.; Guy, R. K.; Webb, P.; Fletterick, R. J. A Surface on the Androgen Receptor that Allosterically Regulates Coactivator Binding. *Proc. Natl. Acad. Sci. U. S. A.* **2007,** *104,* 16074, 18874.
154. Askew, E. B.; Gampe, R. T., Jr.; Stanley, T. B.; Faggart, J. L.; Wilson, E. M. Modulation of Androgen Receptor Activation Function 2 by Testosterone and Dihydrotestosterone. *J. Biol. Chem.* **2007,** *282,* 25801–25816.
155. Axerio-Cilies, P.; Lack, N. A.; Nayana, M. R.; Chan, K. H.; Yeung, A.; Leblanc, E.; Guns, E. S.; Rennie, P. S.; Cherkasov, A. Inhibitors of Androgen Receptor Activation Function-2 (AF2) Site Identified Through Virtual Screening. *J. Med. Chem.* **2011,** *54,* 6197–6205.
156. Caboni, L.; Kinsella, G. K.; Blanco, F.; Fayne, D.; Jagoe, W. N.; Carr, M.; Williams, D. C.; Meegan, M. J.; Lloyd, D. G. "True" Antiandrogens-Selective non-Ligand-Binding Pocket Disruptors of Androgen Receptor-Coactivator Interactions: Novel Tools for Prostate Cancer. *J. Med. Chem.* **2012,** *55,* 1635–1644.
157. Hsu, C. L.; Liu, J. S.; Wu, P. L.; Guan, H. H.; Chen, Y. L.; Lin, A. C.; Ting, H. J.; Pang, S. T.; Yeh, S. D.; Ma, W. L.; Chen, C. J.; Wu, W. G.; Chang, C. Identification of a New Androgen Receptor (AR) co-Regulator BUD31 and Related Peptides to Suppress Wild-Type and Mutated AR-Mediated Prostate Cancer Growth via Peptide Screening and X-ray Structure Analysis. *Mol. Oncol.* **2014,** *8,* 1575–1587.
158. Jehle, K.; Cato, L.; Neeb, A.; Muhle-Goll, C.; Jung, N.; Smith, E. W.; Buzon, V.; Carbo, L. R.; Estebanez-Perpina, E.; Schmitz, K.; Fruk, L.; Luy, B.; Chen, Y.; Cox, M. B.; Brase, S.; Brown, M.; Cato, A. C. Coregulator Control of Androgen Receptor Action by a Novel Nuclear Receptor-Binding Motif. *J. Biol. Chem.* **2014,** *289,* 8839–8851.
159. Ban, F.; Leblanc, E.; Li, H.; Munuganti, R. S.; Frewin, K.; Rennie, P. S.; Cherkasov, A. Discovery of 1H-Indole-2-Carboxamides as Novel Inhibitors of the Androgen Receptor Binding Function 3 (BF3). *J. Med. Chem.* **2014,** *57,* 6867–6872.
160. Dar, J. A.; Masoodi, K. Z.; Eisermann, K.; Isharwal, S.; Ai, J.; Pascal, L. E.; Nelson, J. B.; Wang, Z. The N-Terminal Domain of the Androgen Receptor Drives its Nuclear Localization in Castration-Resistant Prostate Cancer Cells. *J. Steroid Biochem. Mol. Biol.* **2014,** *143,* 473–480.
161. Sadar, M. D. Advances in Small Molecule Inhibitors of Androgen Receptor for the Treatment of Advanced Prostate Cancer. *World J. Urol.* **2012,** *30,* 311–318.
162. Sadar, M. D. Small Molecule Inhibitors Targeting the "Achilles' Heel" of Androgen Receptor Activity. *Cancer Res.* **2011,** *71,* 1208–1213.
163. Lim, M.; Otto-Duessel, M.; He, M.; Su, L.; Nguyen, D.; Chin, E.; Alliston, T.; Jones, J. O. Ligand-Independent and Tissue-Selective Androgen Receptor Inhibition by Pyrvinium. *ACS Chem. Biol.* **2014,** *9,* 692–702.
164. Levine, P. M.; Garabedian, M. J.; Kirshenbaum, K. Targeting the Androgen Receptor With Steroid Conjugates. *J. Med. Chem.* **2014,** *57,* 8224–8237.
165. Cheng, H.; Snoek, R.; Ghaidi, F.; Cox, M. E.; Rennie, P. S. Short Hairpin RNA Knockdown of the Androgen Receptor Attenuates Ligand-Independent Activation and Delays Tumor Progression. *Cancer Res.* **2006,** *66,* 10613–10620.
166. Jones, J. O.; Bolton, E. C.; Huang, Y.; Feau, C.; Guy, R. K.; Yamamoto, K. R.; Hann, B.; Diamond, M. I. Non-Competitive Androgen Receptor Inhibition in vitro and In Vivo. *Proc. Natl. Acad. Sci. U. S. A.* **2009,** *106,* 7233–7238.
167. Lai, K. P.; Huang, C. K.; Chang, Y. J.; Chung, C. Y.; Yamashita, S.; Li, L.; Lee, S. O.; Yeh, S.; Chang, C. New Therapeutic Approach to Suppress Castration-Resistant Prostate Cancer Using ASC-J9 via Targeting Androgen Receptor in Selective Prostate Cells. *Am. J. Pathol.* **2013,** *182,* 460–473.
168. Solit, D. B.; Scher, H. I.; Rosen, N. Hsp90 as a Therapeutic Target in Prostate Cancer. *Semin. Oncol.* **2003,** *30,* 709–716.
169. Centenera, M. M.; Fitzpatrick, A. K.; Tilley, W. D.; Butler, L. M. Hsp90: Still a Viable Target in Prostate Cancer. *Biochim. Biophys. Acta* **2013,** *1835,* 211–218.
170. Centenera, M. M.; Carter, S. L.; Gillis, J. L.; Marrocco-Tallarigo, D. L.; Grose, R. H.; Tilley, W. D.; Butler, L. M. Co-Targeting AR and HSP90 Suppresses Prostate Cancer Cell Growth and Prevents Resistance Mechanisms. *Endocr. Relat. Cancer* **2015,** *22,* 805–818.
171. Ku, S.; Lasorsa, E.; Adelaiye, R.; Ramakrishnan, S.; Ellis, L.; Pili, R. Inhibition of Hsp90 Augments Docetaxel Therapy in Castrate Resistant Prostate Cancer. *PLoS One* **2014,** *9,* e103680.
172. Singh, K.; Munuganti, R. S.; Leblanc, E.; Lin, Y. L.; Leung, E.; Lallous, N.; Butler, M.; Cherkasov, A.; Rennie, P. S. In silico Discovery and Validation of Potent Small-Molecule Inhibitors Targeting the Activation Function 2 Site of Human Oestrogen Receptor Alpha. *Breast Cancer Res.* **2015,** *17,* 27.

Relevant Websites

http://androgendb.mcgill.ca/ The androgen receptor gene mutations database World Wide Web server.
https://clinicaltrials.gov/ A service of the U.S. national institutes of health.
http://www.tokaipharma.com/ Mechanisms of action and clinical programs of galeterone released by Tokai.
http://essapharma.com/ESSA, A company focusing on targeting N-terminal domain of androgen receptor.
http://www.pathwaycommons.org/ Androgen synthesis pathway.
http://www.prostatecancer.ca/ Prostate Cancer Canada: information on the testing and diagnosis, treatment, research, and support programs for prostate cancer.

5.06 Protein–Protein Interaction Inhibitors in Cancer

IR Hardcastle, Newcastle University, Newcastle Upon Tyne, United Kingdom

© 2017 Elsevier Ltd. All rights reserved.

5.06.1	**Introduction**	155
5.06.1.1	PPIs as Drug Targets	155
5.06.1.1.1	Structure of PPIs	155
5.06.1.1.2	Advantages of PPIs as drug targets	156
5.06.1.1.3	Identification and validation of PPI targets	157
5.06.1.1.4	Druggability/ligandability of PPIs	157
5.06.2	**Approaches to PPI Inhibitor Discovery**	157
5.06.2.1	Natural Products	157
5.06.2.2	Peptides and Peptidomimetics	159
5.06.2.2.1	Bcl-xL-Bak peptides	159
5.06.2.2.2	MDM2–p53 peptides	159
5.06.2.2.3	Smac-IAP peptides	160
5.06.2.2.4	Stabilized peptides	161
5.06.2.2.5	Peptide mimetics	163
5.06.2.3	High-Throughput Screening	165
5.06.2.4	Virtual Screening	166
5.06.2.5	Fragment Screening	166
5.06.3	**Examples of PPI Inhibitors**	167
5.06.3.1	Inhibitors of Bcl-2 Family PPIs	167
5.06.3.2	Inhibitors of MDM2–p53 and MDMX–p53	171
5.06.3.2.1	MDM2–p53 antagonists	171
5.06.3.2.2	Dual MDM2–p53, MDMX–p53 antagonists	178
5.06.3.3	Inhibitors of Smac-IAP PPIs	178
5.06.3.3.1	Monovalent Smac-mimetic IAP antagonists	180
5.06.3.3.2	Bivalent Smac-mimetic IAP antagonists	183
5.06.3.4	Inhibitors of Other Cancer Related PPIs	186
5.06.3.4.1	14-3-3 proteins	186
5.06.3.4.2	S100 protein inhibitors	186
5.06.3.4.3	Myc/Max inhibitors	186
5.06.3.4.4	PDZ domain inhibitors	186
5.06.3.4.5	SH2 and SH3 domain inhibitors	189
5.06.3.4.6	Ras PPI inhibitors	191
5.06.3.4.7	Other PPI inhibitors	191
5.06.3.5	Challenges in the Optimization of PPI Inhibitors	191
5.06.4	**Outlook**	191
References		194
Relevant Websites		201

Abbreviations

Abu L-2-Aminobutyric acid
AF6 ALL-1 fusion partner on chromosome 6
β2AR β2 adrenergic receptor
Bad Bcl-2 associated death promoter
Bak Bcl-2 homologous antagonist killer
Bcl B-cell lymphoma
Bcl-xL B-cell lymphoma-extra large
BH Bcl homology
Bik Bcl-2 interacting killer
BIR3 Baculoviral inhibitor of apoptosis repeat
BRCA2 Breast cancer 2
c-Abl Abelson murine leukemia viral oncogene homolog 1
CFTR Cystic fibrosis conductance receptor
c-Myc Cellular myleocytomatosis viral oncogene
Dvl Dishevelled
eIF4 ETS-related transcription factor 4
ELISA Enzyme linked immunosorbent assay
EWS-FLI1 Ewings sarcoma-friend leukemia integration 1 transcription factor fusion protein
FKBP12 FK506-binding protein 12
FP Fluorescence polarization
FRET Fluorescence/Förster resonance energy transfer
FtsZ Filamenting temperature-sensitive mutant Z
GDP Guanosine diphosphate

GP130 Glycoprotein 130
Grb Growth factor bound protein
GTP Guanosine triphosphate
HIF-1 Hypoxia inducible factor 1
IAP Inhibitor of apoptosis proteins
IL6 Interleukin 6
ip Intraperitoneal
Max myc-associated factor X
MAGI3 Membrane-associated guanylate kinase 3
Mcl-1 Myeloid Cell Leukemia Sequence 1
MD Molecular dynamics
MDM Mouse double minute
mTOR Mammalian target of rapamycin
NHERF1 Na^+/H^+ exchanger regulatory factor 1
PAINS Pan assay interference compounds
PBX Pre-B cell leukemia transcription factor
PDEδ Phosphodiesterase delta
P-gp P-glycoprotein
PKCε Protein kinase C epsilon
p.o. per os
PPI Protein–protein interaction
pVHL Von Hippel–Lindau tumor suppressor
RACK2 Receptor for activated C-kinase 2
Raf Rapidly accelerated fibrosarcoma
Ral Ras-related protein
RALBP1 RalA-binding protein 1
RIPK1 Receptor-interacting serine/threonine-protein kinase 1
RPA70 Replication protein A subunit
SCLC Small cell lung cancer
SH Src homology
SHP2 Src homology 2 domain-containing phosphatase
SICLOPPS Split intein circular ligation of peptides and proteins
Smac Second mitochondria-derived activator of caspases
SoS Son of Sevenless
SPR Surface plasmon resonance
TRAIL TNF-related apoptosis-inducing ligand
uPA Urokinase-type plasminogen activator
uPAR Urokinase receptor
VS Virtual screening
XIAP X-linked IAP
ZipA FtsZ interacting protein A

5.06.1 Introduction

The search for novel precision medicines for the treatment of cancer has expanded beyond well-established drug targets with good precedent for "druggability," such as enzymes and receptors, to less well-described drug targets, such as protein–protein interactions (PPIs). Detailed investigations of cell-signaling networks linked to the "hallmarks of cancer"[1] have identified many PPIs as important regulatory nodes in important cellular processes. In particular, networks responsible for oncogenic signaling or tumor suppression, including those controlling cell proliferation, survival, and apoptosis, rely on PPIs.[2] The identification of PPIs as key regulators in these networks offers the promise of selective therapeutic intervention through their modulation.

This chapter discusses the structural features of PPIs and their attractiveness as drug targets. Approaches to the identification and validation of PPI targets, in particular peptide-based approaches, are reviewed. Methods for the discovery of small-molecule PPI inhibitors are discussed, such as high-throughput screening, virtual screening (VS), and fragment screens, which have been successful in the discovery of small-molecule PPI inhibitors. Inhibitors of three PPI targets have progressed to clinical trials and are discussed in detail, that is, Bcl-2 family inhibitors, MDM2–p53 inhibitors, and inhibitor of apoptosis protein (IAP) family inhibitors. Examples of inhibitors of other PPI targets in cancer are covered to highlight the biological and chemical diversity that is under investigation.

5.06.1.1 PPIs as Drug Targets

Historically, PPIs have been regarded as difficult or undruggable targets, and consequently drug discovery efforts have focused on other drug targets, such as enzymes or receptors, that have good precedent for success.[3] In contrast to enzyme and receptor drug targets, PPI targets lack intrinsic small-molecule ligand or cofactor binding sites, and the natural, small-molecule, ligands that are commonly used as starting points for drug discovery are not available.[4,5] The growth in interest in PPI targets has coincided with the introduction of many new hit discovery technologies and a reevaluation of the characteristics of screening libraries targeting PPIs. Recently, three cancer PPI inhibitor programs have yielded clinical trial candidates (Sections "**Inhibitors of MDM2–p53 and MDMX–p53**," "**Inhibitors of Smac-IAP PPIs**," and "**Inhibitors of Other Cancer Related PPIs**"). These successes demonstrate the possibility to develop highly potent and druglike small-molecule inhibitors for PPI targets and encourage the examination of other PPI targets.

5.06.1.1.1 Structure of PPIs

Analysis of the structures of PPIs in the protein database has shown that they differ significantly from enzyme active sites.[6–8] They may be significantly larger in area (1500–4660 $Å^2$) than typical drug–protein interfaces (1200–2000 $Å^2$), more circular, and

significantly flatter. Some interactions may require significant conformational change on complex formation, while others appear more rigid.[6] The polarity of PPIs also differs, burial of hydrophobic contacts may provide significant binding energy, with relatively few hydrogen bonds being present.[9] The binding energy of the interaction has also been discussed, suggesting that the usual range of ΔG is -7.0 to -17.2 kcal mol^{-1}.[7] These analyses have not encouraged medicinal chemists to seek inhibitors for such seemingly large, flat, tightly bound interfaces.

In contrast to the unpromising analyses, Bogan and Thorn identified "hot-spots" in PPIs consisting of regions near the center of the interaction, where small numbers of amino acids contribute large amounts to the binding energy.[10,11] Hot-spots frequently include large amino acid side chains, for example, Arg, Tyr, or Trp, bound to small pockets. These hot-spots may be surrounded by more polar residues, possibly to shield the hot-spot residues from solvent.[12] Alanine-scanning mutagenesis is a popular method for the identification of hot-spot epitopes.[13–15] The systematic removal of amino acid side chains by this method allows each side chain's energetic contribution to binding to be quantified. Single amino acids or clusters that give a significant increase in binding energy on mutation (at least 2.0 kcal mol^{-1}) can be defined as hot-spots. Many PPI hot-spots appear to be more compatible with inhibition by small molecules in terms of shape, size, and polarity.[5]

The concept of "hot-segments," or continuous epitopes contributing to the majority of the binding energy, was introduced by London et al.[16] This analysis categorized PPIs into either domain–domain type interactions or domain–peptide interactions, which make up an estimated 15–40% of the total. The authors estimated that more than half of domain–domain interactions include "hot-segments" and are mediated by a continuous sequence of one protein partner interacting with the other. These "hot-segments" resemble the more tractable domain–peptide interactions. In particular, PPIs mediated by α-helix to protein interfaces have been exploited successfully as drug targets, for example, Bcl-2 and MDM2–p53 PPIs (Sections "**Inhibitors of Bcl-2 Family PPIs**" and "**Inhibitors of MDM2–p53 and MDMX–p53**").

The importance of hot-spots as a measure of druggability of PPIs has inspired the development of computational tools for their prediction. The ROBETTA server allows hot-spot prediction via computational alanine scanning of PPIs.[17] HotPoint relies on an empirical model based on sequence conservation, solvent accessible surface area, and pairwise residue potentials to predict hot-spots in PPIs.[18,19] Solvent accessible surface-based hot-spot prediction for protein–protein (SASA-HS-PP) interactions uses solvent accessible surface descriptors and analysis of surface residues to score PPIs.[20]

In addition to hot-spots, small-molecule inhibitors of PPIs have been observed binding to grooves or pockets that are not visible in the free, unbound structures of the target proteins.[21] These transient pockets may become visible during molecular dynamics (MD) simulations of target proteins and are not limited to native binding sites.[22] The constrained geometrical simulation method Framework Rigidity Optimized Dynamics Algorithm (FRODA) is able to predict transient pockets on PPIs, with the advantage of a lower computational cost over conventional simulations.[23] Another analysis indicated that the small-molecule ligands show a preference for binding to pockets close to PPIs.[24] These sites may offer the possibility of growing inhibitors into the interface, or of developing allosteric inhibitors.

Some PPIs are mediated by posttranslational modifications, for example, the 14-3-3 family of proteins binds to phosphoserine within well-defined motifs on a number of protein partners.[25] The structural basis for these interactions has been revealed by X-ray structures of 14-3-3 proteins, indicating that the dimeric proteins form a conserved cleft containing a cluster of basic residues that form salt–bridge interactions with the phosphoserine residue.[26]

Other PPIs can be viewed as interactions between a recognizable domain of one protein and the surface of the partner protein. Examples include PDZ domains, SH3 domain, and WW domain interactions.[27–29]

5.06.1.1.2 Advantages of PPIs as drug targets

Despite the perceived difficulty of targeting PPIs with small molecules, the approach has gained popularity.[5] Drug discovery efforts to date have exploited only a small fraction of the "druggable genome,"[3] thus the novelty of PPIs as targets is attractive in this context from an academic and commercial standpoint. Importantly, inhibition of PPIs may offer routes to inhibit pathways with limited opportunities for intervention by enzyme or receptor targeted small-molecule inhibitors.

Another possible advantage of PPI targets relates to their structural diversity and specificity. Selective inhibition of enzymes via their substrate or cofactor binding sites presents challenges in achieving potency while retaining target selectivity. For example, ATP-competitive kinase inhibitors require profiling against large panels of kinases to establish selectivity and eliminate predictable off-target toxicities, and target selectivity is a central goal in these projects.[30] In contrast, PPIs typically lack such conserved binding sites, and the larger interface can include greater structural diversity. It can be argued that PPIs are required to encode selectivity into their interactions to ensure they bind to the correct partners to exert their biological effects. High selectivity can be observed experimentally for a number of PPI targets that bind to α-helical regions of their cognate proteins, for example, MDM2/p53 and MDMX/p53. Both mouse double minute (MDM) proteins bind to the same α-helical segment of p53, forming interactions with the identical amino acid side chains, and despite the high sequence conservation in the binding cleft of the MDM proteins, both small molecules and peptide mimetics can achieve exquisite selectivity for MDM2 over MDMX (see Section "**Inhibitors of MDM2–p53 and MDMX–p53**").

It has been proposed that PPI targets will offer reduced susceptibility to resistance mutations compared with enzyme inhibitors.[31] Clinical resistance to competitive enzyme inhibitors can occur through mutations in the enzyme active site that reduce the affinity for the inhibitor but not the substrate. It is postulated that mutations at PPIs would be less likely to have an inhibitor specific effect, due to the structural diversity of the interfaces. However, development of resistance to PPI inhibitors has been reported, for example, with MDM2–p53 inhibitors.[32] In this case, treatment with MDM2–p53 inhibitors has been demonstrated

to select for mutations causing loss of p53 function and so induce resistance to the inhibitors. Similar, pathway mutations can be expected for other PPI inhibitors.

5.06.1.1.3 Identification and validation of PPI targets

The growing importance of PPI targets in drug discovery has led to the development of a number of techniques for their identification. Several high-throughput methods have been employed based on the yeast two-hybrid method, affinity purification-mass spectrometry, DNA microarrays, protein microarrays, synthetic lethality screens, or phage display methods, as reviewed in Ref.[33] These methods are designed to evaluate all the interactions within entire genomes. Lower throughput methods have also been used to identify and characterize PPIs relying on methods such as X-ray crystallography, nuclear magnetic resonance (NMR) spectroscopy, fluorescence resonance energy transfer (FRET) assays, and surface plasmon resonance (SPR). Large, publicly accessible databases have been assembled to collate experimental data and curate them computationally.[34] In additional to experimental methods, computational approaches based on three-dimensional (3D) structural data and homology models have been designed to predict PPIs with reasonable accuracy and so identify likely signaling nodes for therapeutic intervention.[35,36]

5.06.1.1.4 Druggability/ligandability of PPIs

As previously described, the structural diversity of PPIs renders some interfaces more suitable for small-molecule inhibition than others. Methods to predict the ability of a PPI to bind small molecules, a property variously described as bindability, ligandability, or druggability, have been developed.[35,37] These approaches frequently assess the surface of the PPI for pockets suitable for binding small-molecule ligands. One such approach assesses pockets or grids in the 3D structures of PPIs to determine "druglike density," a measure of the volume, buriedness, and hydrophobicity of the region, as an indicator of drugability.[38] An alternative determines energetically favorable ligand binding sites and pockets.[39] An extension to the ligandability-based approaches is based on the physicochemical properties of the binding site as related to the ideal druglike properties of the ligand.[40] This method gave a good druggability score for the PPI target MDM2. These approaches do not easily account for the innate plasticity of many PPIs and so may give a low score for PPI targets with inducible pockets.[31]

Three classes of PPI modulators have been described.[41,42] Orthosteric inhibitors occlude the binding site on target protein. Allosteric inhibitors bind at a distant site to the PPI and may induce structural changes that prevent the partner protein binding. Transient stabilizers may interfere with the normal biological function of the PPI by stabilizing the interaction. Interestingly, there are a number of examples of natural products that act as stabilizers of PPIs.

5.06.2 Approaches to PPI Inhibitor Discovery

5.06.2.1 Natural Products

Extensive screening of natural products for cytotoxicity has been used to identify agents for cancer chemotherapy. The molecular targets for many of these compounds were elucidated subsequent to their clinical use. The vinca alkaloids and taxoids were found to share a common target, that is, microtubules formed from α,β-tubulin heterodimers. The mitotic phase (M-phase) of the cell cycle relies on the cycling of microtubules by polymerization and depolymerization of guanosine diphosphate (GDP)-bound α,β-tubulin to control the organization of chromosomes and to effect their separation during the cell division. Disruption of microtubule formation and the mitotic spindle has been shown to activate the metaphase–anaphase checkpoint, and initiate cell death.[43] Destabilization of microtubules in cells during the interphase has also been shown to affect diverse processes, including cell signaling and motility.[44]

Isolated from *Catharanthus roseus*, vinblastine (**Table 1**, **1**) disrupts microtubule polymerization at low concentrations by binding to high-affinity sites at the ends of the microtubules and stabilizing them.[45,46] Each microtubule end can bind 16–17 drug molecules, but only one or two bound molecules are sufficient to disrupt polymerization. At higher drug concentrations depolymerization is induced. An X-ray structure of vinblastine (**1**) bound to a microtubule complex shows that the drug binds into a hydrophobic groove at the interface of the α- and β-subunits and so perturbing microtubule stability.[47] The semisynthetic derivative vinflunine (**2**) has lower toxicity than **1**, possibly due to its lower affinity for tubulin.[48]

Taxol (**3**), isolated from the bark of *Taxus brevifolia* (Pacific yew), was initially thought to share the same mechanism as the vinca alkaloids, but was subsequently shown to bind to α,β-tubulin heterodimers at a different site and to produce distinc effects.[49,50] Analysis of the X-ray structure of **3** bound to GDP-bound α,β-tubulin shows the drug binding to the β-subunit close to the GDP-binding site.[51] The bound drug induces conformational changes in the heterodimer that stabilize polymer formation and override the normal control through guanosine triphosphate (GTP) hydrolysis. The abnormally sticky α,β-tubulin units form unusually stable microtubules, resulting in disruption to the M-phase and cell division. The semisynthetic derivative cabazitaxel (**4**) was selected for development because it shows reduced affinity for cellular efflux pumps such as P-glycoprotein pump-1 (P-gp).[52]

The natural product Halichondrin B (**5**) was isolated from marine sponges.[53] The scarce supply of the compound prohibited its clinical development. A simplified synthetic derivative Erubilin (**6**) showed similar cytotoxicity to the parent via the same antimitotic mechanism. Erubilin (**6**) binds to microtubules at or near the vinca domain and overlaps the GTP binding site on β-tubulin inhibiting GTP hydrolysis.[54] Erubilin **6** suppresses the addition of new α,β-tubulin heterodimers to the plus end of the microtubule but does not affect shortening at the minus end. Overall, the effect of **6** on the dynamic instability of microtubules differs from that of the vinblastine **2**.

Table 1 Natural product derived PPI drugs

Name	*Compound*	*Structure*	*Target*	*References*
Vinblastine	**1**	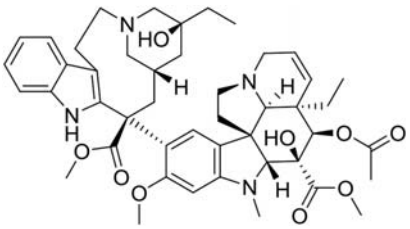	α,β-Tubulin	[45]
Vinflunine	**2**	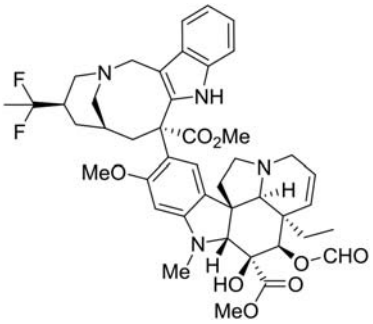	α,β-Tubulin	[48]
Taxol	**3**	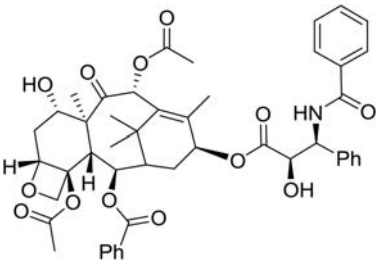	α,β-Tubulin	[50]
Cabazitaxel	**4**	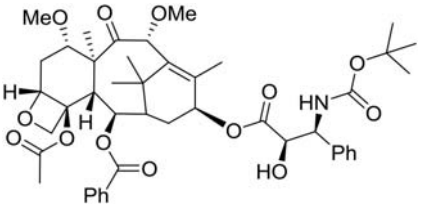	α,β-Tubulin	[52]
Halichondrin B	**5**	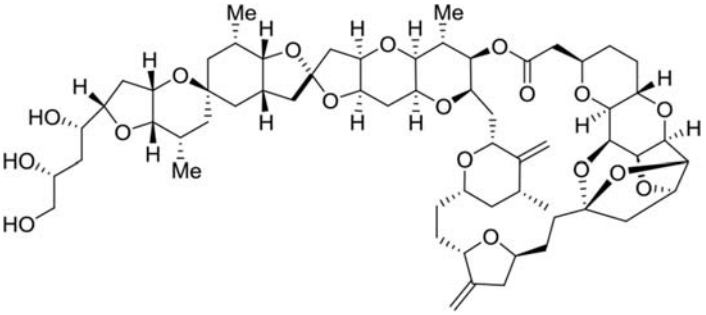	α,β-Tubulin	[53]
Eribulin	**6**	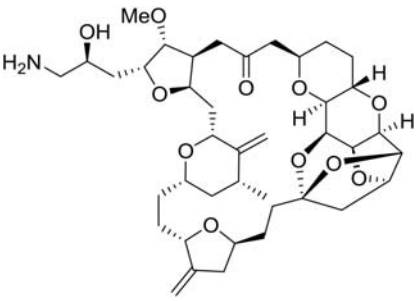	α,β-Tubulin	[53]

Table 1 Natural product derived PPI drugs—cont'd

Name	*Compound*	*Structure*	*Target*	*References*
Epothilone B Ixabepilone	**7**: X = O **8**: X = NH	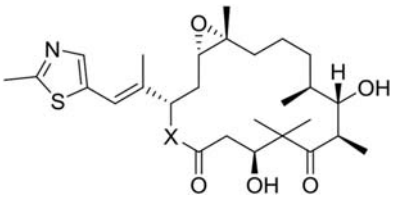	α,β-Tubulin	[55,56]
Temsirolimus	**9**	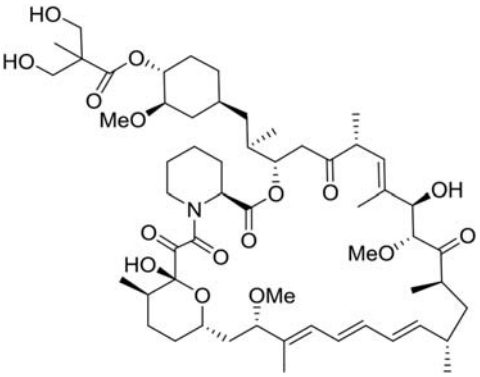	mTOR-FKBP12	[58]

Epothilones, for example, **7** were isolated from the myxobacteria *Sorangium cellulosum* and share a similar mechanism of action to the taxoids as promoters of tubulin polymerization.[55] Epothilones are cytotoxic in P-pg expressing cells and so offer an advantage over taxoids, which suffer from innate and acquired resistance though this mechanism. Ixabepilone **8** is a semisynthetic lactam derivative that overcomes the poor metabolic stability and pharmacokinetic (PK) properties of the corresponding lactone **7**.[56] Ixabepilone **8** showed activity in taxol resistant xenografts resulting from P-gp expression or tubulin mutations, and has shown single-agent activity in patients resistant to a number of chemotherapeutic drugs.

Temsirolimus (**9**) is a semisynthetic derivative of rapamycin, a compound that was initially developed as an antifungal and then as an immunosuppressive agent. The anticancer activity of **9** resides in its inhibition of the kinase activity of the mammalian target of rapamycin (mTOR) protein. The compound forms a complex with FK506-binding protein 12 (FKBP12), which inhibits mTOR activity.[57,58]

5.06.2.2 Peptides and Peptidomimetics

The druggability of PPIs has been assessed by the use of peptide libraries. The information gained has proved important in the validation of a number of targets. In particular, α-helical peptides binding to Bcl-2 or MDM2 have delineated potential small-molecule binding sites. The NMR and X-ray structures of these interactions have been employed in the subsequent design of inhibitors (Sections "Inhibitors of Bcl-2 Family PPIs" and "Inhibitors of MDM2–p53 and MDMX–p53").

5.06.2.2.1 Bcl-xL-Bak peptides

The structure of the Bcl-xL protein was determined by X-ray crystallography and NMR spectroscopy.[59] Further NMR experiments elucidated the structure of the Bcl-xL–Bak BH3 domain peptide interaction.[60] Bak forms an amphipathic α-helix that binds via the hydrophobic side chains of the Val74, Leu78, Ile81, and Ile85 residues into a hydrophobic groove on the surface of Bcl-xL (Fig. 1).

A 16-mer peptide corresponding to the α-helical part of the BH3 domain of Bak bound to avidly to Bcl-xL (Table 2).[60] Shorter peptides bound less tightly, and alanine scanning identified important interactions with the side chains of Val74, Leu78, Ile81, and Ile85 of Bak (highlighted red) and a hydrophobic pocket formed by Tyr101, Leu108, Val126, and Phe146 on the surface of Bcl-xL. An electrostatic interaction between Asp83 of the Bak peptide (highlighted blue) and Arg139 of Bcl-xL stabilizes the complex, and this residue is conserved within the Bcl-family.

5.06.2.2.2 MDM2–p53 peptides

The structure of the p53 and MDM2 interaction has been determined by X-ray crystallography.[61] The p53 peptide binds as an amphipathic α-helix into a twisted trough around a central cleft lined with hydrophobic residues on MDM2. Three p53 residues, Phe19, Trp23, and Leu26, bind to the hydrophobic cleft. Two intermolecular hydrogen bonds stabilize the interaction between the

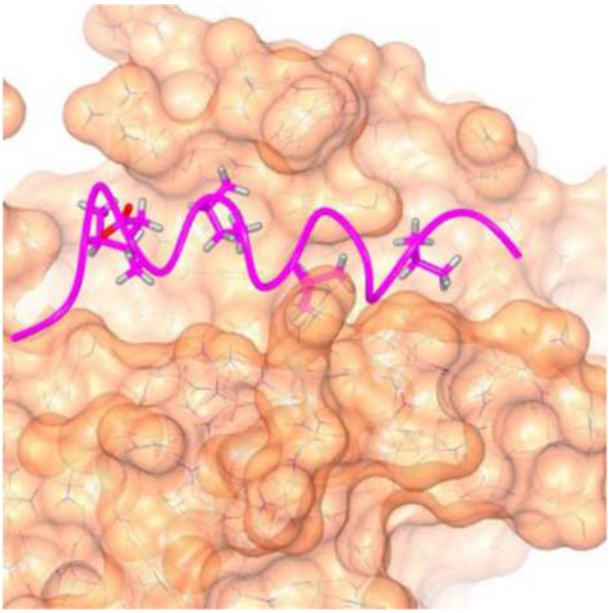

Fig. 1 NMR solution structure of Bcl-xL (ribbon—*blue*, surface—*coral*) bound to a peptide of residues 572–587 of Bak (magenta) showing the key sidechains (pdb 1BXL).

Table 2 Binding affinities of peptides to Bcl-xL

Peptide	*Sequence*[a]	K_d *(μM)*
Bak	72 GQ**V**GRQ**L**AII**G**D**D**INRRYDSEFQ 94	0.2
Bcl-2	91 PVVHLALRQAGDDFSR 106	6.4
Bax	57 KKLSECLKRIGDELDS 72	13
Bik	55 DALALRLACIGDEMDV 70	15
Bcl-xL	84 AAVKQALREAGDEFEL 99	325

[a]Bold indicates the principle side chain interactions.

backbone of Phe19 of p53 and the Gln72 side chain of MDM2, and between the p53 Trp23 indole NH and the backbone carbonyl of Leu54 from MDM2 (Fig. 2).

Peptide inhibitors of MDM2–p53 binding have been identified using phage-display and synthetic peptide libraries, for example, IP3 peptide (Table 3, **10**; $IC_{50}=313$ nM).[62] A shortened versions of the IP3 peptide with stabilized α-helical nature included peptide **12** with fourfold improved inhibitory activity over the corresponding peptide **11**. Switching the tyrosine to a phosphonomethylphenylalanine residue (peptide **13**), to form a salt–bridge interaction with the α-amino group of Lys94 of MDM2, gave a sevenfold improvement in affinity. Optimization of the 6-position of the tryptophan residue with lipophilic groups able to fill a small cavity observed in the X-ray structure, gave a significant increase in affinity. A 6-chloro substituent was optimal, as found in the AP peptide **14** ($IC_{50}=5$ nM).[63]

5.06.2.2.3 Smac-IAP peptides

The IAPs bind to caspases via baculovirus IAP repeat (BIR) domains. In particular, human X-linked IAP (XIAP) binds caspase-9 through an interaction between its BIR3 domain and the amino terminus of the linker peptide on the small subunit of the caspase.[64] Second mitochondrial-derived activator of caspases (Smac) competes with caspases for binding to IAPs to trigger apoptosis through the N-terminal residues (AVPI) binding to the IAP BIR3 domain. Synthetic peptides including seven N-terminal residues of Smac and a cell penetrating TAT domain were found to sensitize TRAIL-induced apoptosis and cytotoxic drug treatment in cells, but did not initiate apoptosis as single agents.[65]

Fluorescently tagged tetrapeptides were used to establish the contribution of each amino acid to BIR3 binding.[66] The results showed that positions 1 and 3 of the peptide were required for affinity, while variations of positions 2 and 4 were tolerated. Peptide libraries were used to determine the SARs for the N-terminal Smac tetrapeptide binding.[67] Position 1 is limited to small L-amino acids, for example, Ala and Abu, and the NH is essential. Position 2 can be substituted with little effect on binding affinity, consistent with this residue pointing into solution, but a D-amino acid is not tolerated. Position 3 was found to require the 5-membered ring of Pro, and only the 4-membered azetidine substitution was tolerated. In position 4, aromatic rings, for example, Phe or Nal,

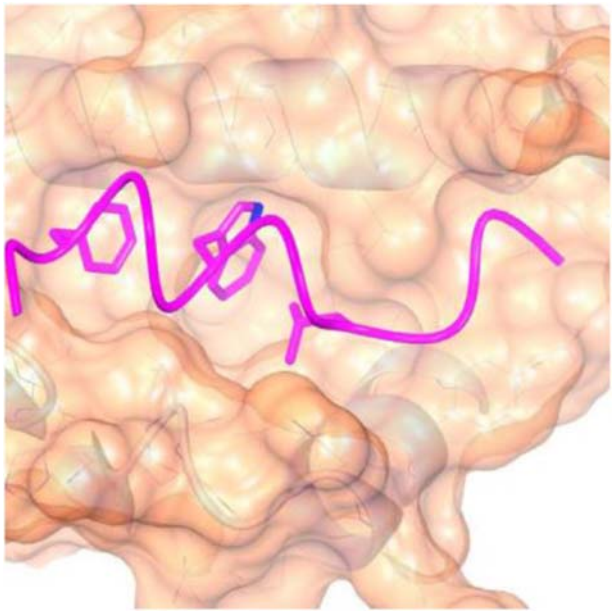

Fig. 2 X-ray structure of MDM2 (ribbon—*blue*, surface—*coral*) bound to a residues 15–29 of p53 (magenta) showing the key hydrophobic side-chains (pdb 1YCR).

Table 3 Peptide inhibitors of the MDM2–p53 interaction

	Peptide	*Sequence*[a]	*IC_{50} (nM)*
	p53 wt	Ac-Gln16-Glu-Thr-**Phe**-Ser-Asp-Leu-**Trp**-Lys-Leu-**Leu**-Pro27-NH_2	8673 ± 164
10	IP3	Ac-Met-Pro-Arg-Phe19-Met-Asp-Tyr-Trp-Glu-Gly-Leu26-Asn-NH_2	313 ± 10
11	8 mer	Ac-Phe19-Met-Asp-Tyr-Trp-Glu-Gly-Leu26-NH_2	8949 ± 85
12		Ac-Phe19-Met-Aib-Tyr-Trp-Glu-Ac_3c-Leu26-NH_2	2210 ± 346
13		Ac-Phe19-Met-Aib-Pmp-Trp-Glu-Ac_3c-Leu26-NH_2	314 ± 88
14	AP	Ac-Phe19-Met-Aib-Pmp-6-Cl-Trp-Glu-Ac3c-Leu26-NH_2[b]	5 ± 1

[a]Bold indicates the principle hydrophobic side chain interactions.
[b]Aib—2-aminoisobutyric acid, Pmp—phosphonomethylphenylalanine, 6-Cl-Trp—6-chlorotryptophan, Ac3c—1-aminocyclopropyl-1-carboxylic acid.

were favored. Introduction of a non-amino acid substituent at position 4 reduced the peptidic nature of the compounds and improved activity, for example, **15** (K_d = 12 nM) (Fig. 3). Introduction of a substituent onto the proline ring resulted in improved potency, for example, **16** (K_d = 5 nM). Similar library optimization, guided by the BIR3 X-ray structure, resulted in potent peptide inhibitors, for example, **17**.[68] These studies helped establish the pharmacophore for inhibitors of the Smac-BIR3 domain interaction (Fig. 4).

5.06.2.2.4 Stabilized peptides

Peptides are naturally subject to metabolism by peptidases and so have limited utility as drugs. Modifications to the peptide backbone, for example, β-peptides;[69] the stereochemistry and sequence, for example, retroinverso peptides; or the introduction of intramolecular cross-links between amino acids known as "staples," can be used to stabilize peptides to metabolism while retaining the key interactions required for tight binding.

β-Peptides incorporate an additional backbone carbon atom, and so are resistant to proteolysis and metabolism. For example, a β_3-decapeptide, which formed a stable 14-residue helix in aqueous solution, was used as the scaffold for the p53 residues Phe19, Trp23, and Leu26 arrayed on sequential turns of the helix. Two β-peptides inhibited MDM2–p53 binding (β53-1 and β53-5) in a fluorescence polarization (FP) assay, albeit with modest IC_{50}s of 94.5 and 80.8 μM.[70,71]

Incorporation of D-amino acids can stabilize peptides to proteolysis. Mirror image phage display identified D-peptides ^{D}PMI-β (TAWYANFEKLLR) and ^{D}PMI-γ (DWWPLAFEALLR) as nanomolar inhibitors of the MDM2–p53 interaction.[72,73] Retroinverso peptides are synthesized from D-amino acids with the reverse sequence of amino acids to the original, and form helices with a left-handed turn. A 14-mer reteroinverso peptide, (D)-H_2N-Ser-Gln-Glu-Thr-Phe-Ser-Asp-Leu-Trp-Lys-Leu-Pro-Gln-Asn-Ac, inhibited MDM2–p53 binding with an IC_{50} of 14 μM compared with the natural 15-mer peptide (IC_{50} = 4.2 μM).[74]

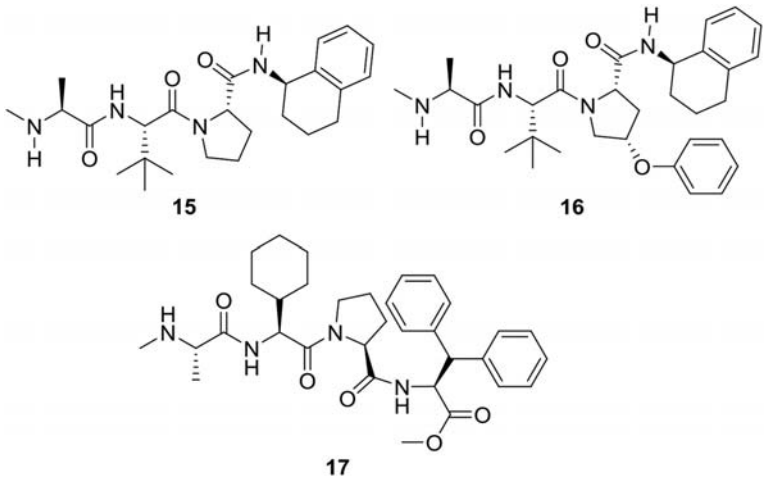

Fig. 3 Smac-mimetic IAP peptide inhibitors (**15–17**).

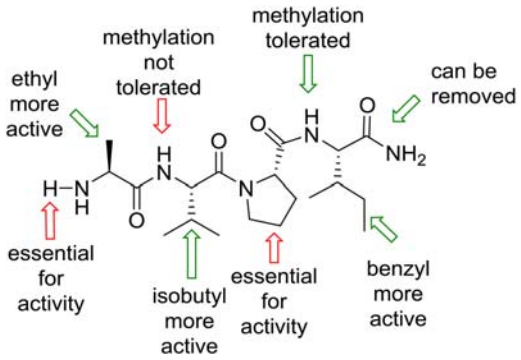

Fig. 4 Pharmacophore for Smac-mimetic IAP inhibitors.

Peptide macrocycles have many advantages as scaffolds for the development of PPI inhibitors. Macrocyclic peptides can adopt a wide range of conformations, are stabilized by intramolecular hydrogen bonding, and present a large interaction surface for comparatively low molecular mass. A variety of methods and linkers have been used to introduce conformational rigidity.

The β-hairpin motif has been used as a scaffold using a D-Pro-L-Pro dipeptide template. Computer modeling was used to design the peptide so that the critical p53 residues are aligned correctly for binding to MDM2. A library of β-hairpin compounds, with variations in the MDM2 binding residues and polar residues to improve water solubility, were evaluated in BIAcore competition assay. The Asp2, 6-Cl-Trp3 analog **18** showed reasonable potency ($IC_{50} = 0.14$ μM) (Fig. 5). The X-ray structure of **16** in complex with MDM2 (PDB code 2AXI) confirmed the β-hairpin conformation and the peptide's amphipathic nature in the bound state.[75,76]

Developed from a disulfide-bridged 11-mer macrocyclic peptide, the bicyclic peptide **19** incorporates a head-to-tail linker and a lactam cross-link. Peptide **19** inhibits the binding of a phosphotyrosine probe to the Grb2-SH2 domain ($IC_{50} = 0.35$ μM) (Fig. 6).[77] The introduction of the cross-link improved potency, selectivity, and plasma stability.

Libraries of cyclic peptides of up to 10^8-members are produced in cells via split intein circular ligation of peptides and proteins (SICLOPPS).[78] The SICLOPPS plasmid codes for a split intein that folds to form an active intein, which undergoes a series of rearrangements to generate a cyclic peptide.[79] Coupling of the SICLOPPS library method to a HIF-1 bacterial reverse two-hybrid system enabled the selection of clones expressing cyclic peptide inhibitors of HIF-1α heterodimerization.[80] One peptide, cyclo-CLLFVY, was shown to bind to the PAS-B domain of HIF-1α and disrupt heterodimerization of HIF-1 with an IC_{50} of 1.3 μM, but HIF2 dimerization was not affected.

The miniature peptide, avian pancreatic polypeptide, is well folded and contains an 18-residue α-helix suitable for modification using protein grafting. The α-helix residues were varied using phage display and the libraries screened against MDM2. Miniature proteins bound to MDM2 with modest potency ($IC_{50} = 1.6$-8.8 μM). Circular dichroism (CD) spectroscopy confirmed a high degree of α-helical structure in the optimized peptides.[81]

Hydrocarbon-stapled peptides offer greater metabolic stability and defined helicity compared with linear peptides.[82] Typically, peptides are stapled by olefin metathesis between two modified alanine residues bearing olefin side chains at the α-carbon, at the i and either $i+4$ or $i+7$ positions.

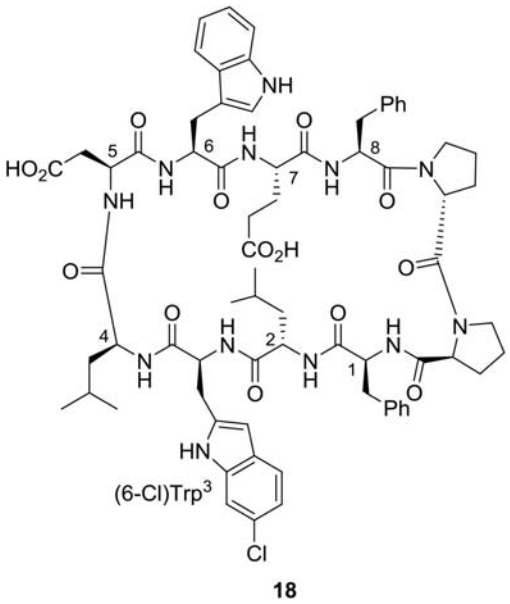

18

Fig. 5 β-Hairpin inhibitor of MDM2–p53.

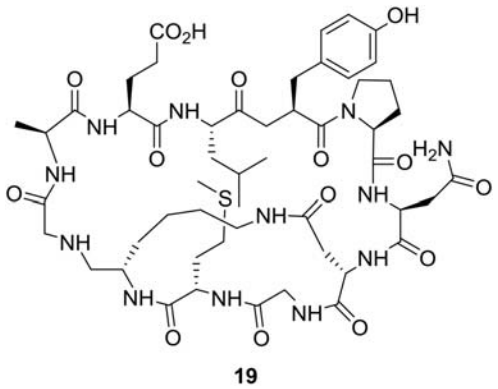

19

Fig. 6 Bridged 11-mer macrocyclic peptide inhibitor of p-Tyr binding to Grb2-SH2 domain.

The stapled peptide SAH-p53-8, Ac-QSQQTF*NLWRLL*QN-NH2 (* indicates the hydrocarbon staple), is a potent inhibitor of MDM2–p53 ($K_d = 55$ nM) and MDMX–p53 ($K_d = 2.3$ nM) and shows excellent helicity and cell permeability.[83,84] The peptide is cytotoxic in cells overexpressing either MDM2 or MDMX in a p53 dependent manner. Similarly, the stapled peptide ATSP-7041 (**20**) (Fig. 7) is a potent dual inhibitor of both MDM2–p53 ($K_i = 0.9$ nM) and MDMX–p53 ($K_i = 6.8$ nM), and was optimized for biophysical properties, for example, solubility and cellular potency.[85] X-ray crystallography shows that the hydrocarbon staple makes significant interactions with the surface of MDMX and contributes to the binding affinity. ATSP-7041 **20** showed activity in vivo in MDM2 and MDMX overexpressing human tumor xenografts.

The B-cell lymphoma-9 (BCL9)–β-catenin interaction is inhibited by peptides incorporating an optimized double triazole (i, $i+4$) staple (**21**) ($K_i = 0.19$ μM) (Fig. 8).[86] The double staple provided the peptide with good stability to proteolysis.

A panel of stabilized alpha-helix of BCL-2 domains (SAHBs), using an i, $i+4$ hydrocarbon staple, was used to identify the BH3 domain of MCL-1 as an inhibitor of the antiapoptotic MCL-1 protein.[87] The MCL-1 BH3 domain peptide $SAHB_A$, KALETLR*VGD*VQRNHETAF, bound avidly to MCL-1 ($K_d = 43$ nM). The peptide was subsequently used in a screen for small-molecule competitive inhibitors of MCL-1.[88]

5.06.2.2.5 Peptide mimetics

An alternative approach to stabilizing peptide PPI inhibitors focuses on the replacement of the peptide bond with more resilient linkers, while maintaining the spatial arrangement of the side chains responsible for the binding affinity. A number of approaches have been investigated and validated against cancer targets, and the p53 α-helix binding to MDM2 has been well studied.[89]

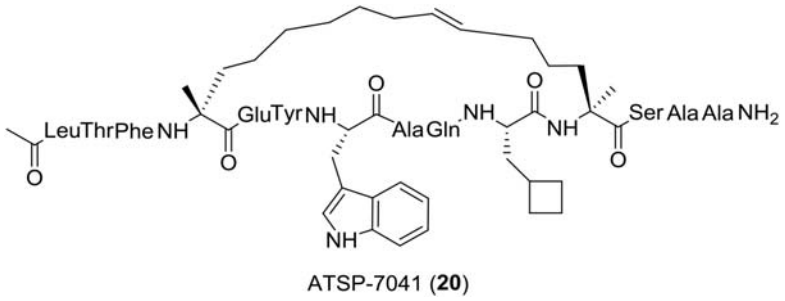

Fig. 7 Stapled peptide dual inhibitor of MDM2–p53 and MDMX–p53.

Fig. 8 Triazole stapled peptide inhibitor of BCL9-β-catenin.

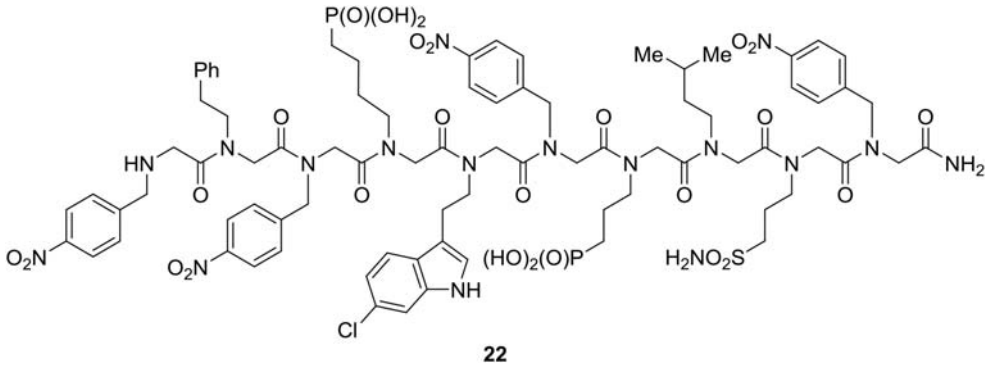

Fig. 9 Oligomeric N-substituted glycine inhibitor of MDM2–p53.

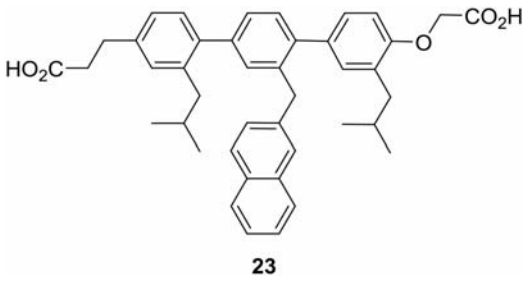

Fig. 10 Terphenyl inhibitor of MDM2–p53.

Peptoids, or oligomeric N-substituted glycines, are resistant to proteolysis, and allow a wide variety of possible side chain substituents. A helical conformation can be introduced using chiral side chains. Peptoids, mimicking the key p53 side chains, for example, (**22**) showed reasonable inhibition of the MDM2–p53 interaction (IC_{50} of 6.6 μM) (Fig. 9).[90]

Terphenyls mimic α-helical structures due to the staggered arrangement of their aromatic rings. The binding of compound **23** to MDM2 was observed by NMR, the 2-naphthylmethylene binding in the Trp23 binding ($K_i = 0.182$ μM) (Fig. 10).[91] The overall hydrophobicity of the terphenyl scaffold limits its utility as a result of which more polar alternatives have been found. Terephthalamide derivatives also act as α-helix mimics, for example, compound **24** inhibits the BH3 domain of Bak binding to Bcl-xL ($K_i = 0.78$ μM) (Fig. 11).[92]

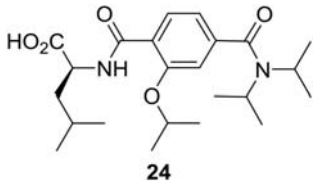

Fig. 11 Terephthalamide inhibitor of Bcl-xL-Bak.

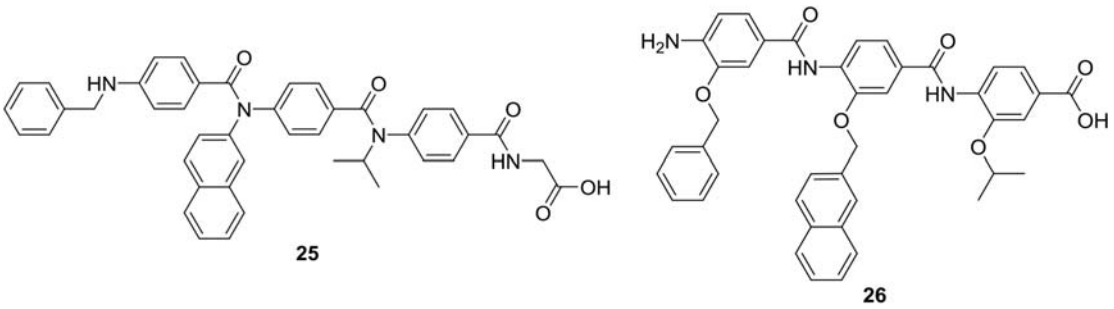

Fig. 12 Oligoamide inhibitors of MDM2–p53.

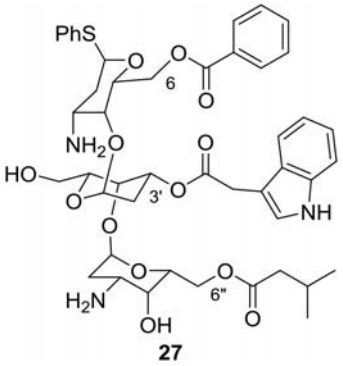

Fig. 13 α-1,4 linked oligogalactose inhibitor of MDM2–p53.

Oligoamides allow a similar orientation of side chains to the terphenyls, with the advantage of improved physicochemical properties. Two series of oligoamides, **25** and **26**, differing in the attachment point of the α-helix mimicking groups, demonstrated modest inhibition of the MDM2–p53 interaction ($IC_{50} = 2.8$ and 1.0 μM, respectively) (Fig. 12).[93,94]

Oligosacharides are alternative scaffolds for α-helix mimics. An α-1,4 linked oligogalactose system was predicted to give the necessary rod-like structure.[95] Functionalization of alternate C-6 and C-3 hydroxyl groups allowed the appendage of p53-like groups. The resulting compound **27** showed weak inhibitory activity in an MDM2 enzyme linked immunosorbent assay (ELISA) (Fig. 13).

5.06.2.3 High-Throughput Screening

High-throughput screening for PPI inhibitors is now commonplace. Screens typically rely on either FP assays that measure the displacement of a fluorescently tagged peptide from the target protein, or proximity-based assays relying on FRET, such as homogeneous time-resolved fluorescence methods. The primary screen is usually accompanied by an orthogonal, biophysical assay, such as SPR or NMR spectroscopy.

Early failures in high throughput screening (HTS) for PPI targets have prompted the rational design of PPI focused libraries.[96] PPI inhibitors may differ significantly from enzyme inhibitors, requiring a more 3D and modular shape than enzyme inhibitors, which may be more linear. PPI inhibitors may also require a higher molecular weight (MW). Statistical analysis of the cocrystal structures of reported PPI inhibitors in databases, for example, 2P2Ichem,[97] proposed a "Rule-of-Four" for generic PPI inhibitors, that is, MW > 400, number of rings > 4, and number of hydrogen bond acceptors > 4.[98] These parameters were used to build a privileged PPI library from commercial sources, and identify privileged scaffolds.[97] VS based on the pharmacophores of known MDM2

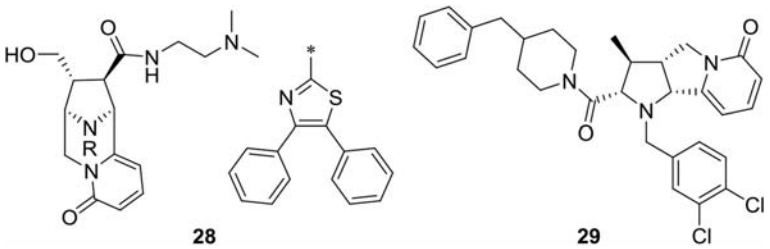

Fig. 14 Bicyclic and tricyclic inhibitors of Bcl2 interactions from DOS.

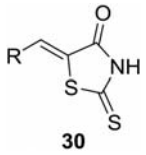

Fig. 15 The PAINS ene-rhodanine motif.

inhibitors has been used to design focused libraries.[99] The 3D characteristics required for PPI inhibitors have been calculated, and critical molecular descriptors defined, including globularity and hydrophobicity.[100]

Diversity oriented synthesis (DOS) generates structurally diverse libraries for screening from a common intermediate building block. This approach has been used to synthesize pyridone libraries as potential inhibitors of the interaction of Bax with Bcl-2 and Bcl-xL.[101] The bridged bicyclic pyridone **28** inhibited Bcl-2 and Bcl-xL ($K_i = 2.0$ and 5.7 μM, respectively), whereas the fused tricyclic pyridone **29** was selective for Bcl-2 ($K_i = 1.2$ and >100 μM, respectively) (Fig. 14).

The challenge of eliminating promiscuous, nonspecific hits, or pan assay interference compounds (PAINS) is particularly relevant for PPI assays.[102–104] A number of chemotypes, such as ene-rhodanines, for example, (**30**), have been identified for compounds, which interfere with HTS assays (Fig. 15). They can act by aggregating proteins through nonspecific interactions, or by covalent modification of proteins. Substructure filters are available for pre- or postassay assessment; however, PAINS substructures still occur regularly in hit compounds from PPI screens. For this reason, follow-up with an orthogonal assay, usually based on a biophysical technique, is necessary to have full confidence in hits from HTS assays for PPI targets.

5.06.2.4 Virtual Screening

VS may be used to identify inhibitors of PPIs in cases where there is good structural information on the target protein's binding sites or hot-spots. Computational methods for docking with PPI targets have been reviewed recently.[105] The open and hydrophobic nature of many PPIs and their limited number of hydrogen bonding opportunities presents a challenge for docking programs. Scoring functions with a component of shape complementarity are more likely to return reasonable hit structures. The flexibility of PPI binding sites also creates additional complexity, so MD simulations have been run in combination with docking.[22] For example, new inhibitory chemotypes for MDM2, for example, **31** (MDM2 $K_i = 9.9$ μM), were identified by docking using multiple structures (Fig. 16).[106] A homology model of Bcl-2 based on the X-ray and NMR structure of Bcl-xL has been used for docking-based VS, and compounds with modest potency are identified.[107,108]

Structure-based methods can establish a ligand pharmacophore, which can be used to search ligand databases. A 3D-pharmacophore of an Annexin A2 derived peptide within the binding site of the S100A10 adapter protein was used to screen a ligand database and identify hits with modest potency, for example, triazole **32** ($IC_{50} = 24$ μM) (Fig. 16).[109] A pharmacophore model of a peptide fragment of PKCε bound to receptor for activated C-kinase 2 was used to screen a compound database and identify quinoline **33** ($IC_{50} = 5.9$ μM) (Fig. 16).[110] The GALAHAD pharmacophore modeling program identified c-Myc-Max heterodimerization inhibitors with modest potency, for example, **34** (Fig. 16).[111] Combined pharmacophore and structure-based searching methods were used to identify possible MDM2 inhibitors, for example, **35** (MDM2 $K_i = 0.12$ μM) from the NCI database of publicly accessible compounds (Fig. 16).[112]

5.06.2.5 Fragment Screening

Fragment-based screening methods generate hits from small, "fragment" compounds, typically with MW <300. Compounds typically have low affinity and so the use of biophysical methods such as NMR or X-ray crystallography is required to detect the hits.[113] These methods have been applied to a number of PPI targets with success. Fig. 17 summarizes the structures of example ligands.

"SAR by NMR" is a two-step method. Firstly, low MW fragments are screened by observing chemical shift changes in the ^{15}N- or ^{1}H-HSQC NMR spectrum of the protein on binding of the ligand. Secondly, ligands in different but close proximity binding sites are

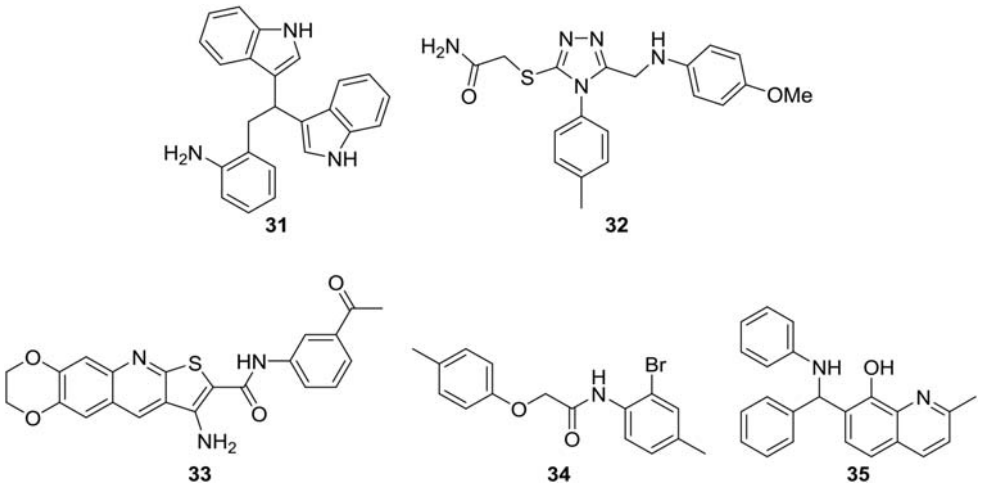

Fig. 16 Protein–protein interaction inhibitors identified using virtual and pharmacophore screening.

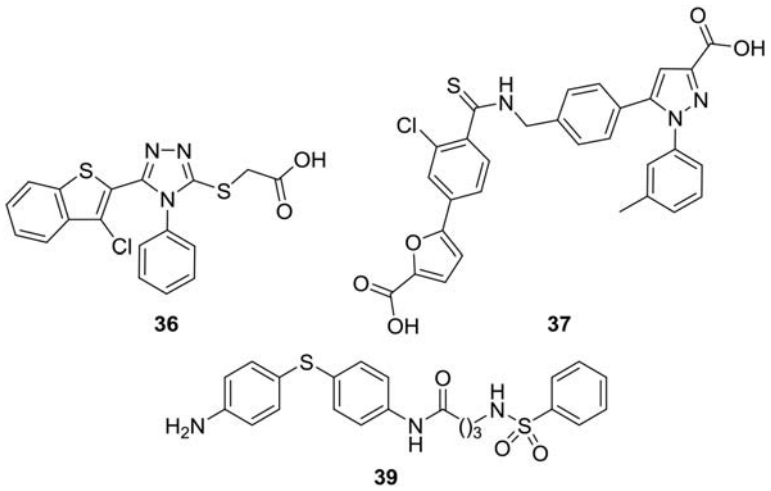

Fig. 17 PPI inhibitors identified using fragment screening.

identified. The location and binding mode of both fragments must be determined by NMR or X-ray crystallography before they can be linked using a suitable group. The goal of linking the fragments is to provide a high-affinity ligand that accesses both binding sites.[114] The structure activity relationships (SAR) by NMR method has been highly successful in identifying high-affinity ligands for Bcl-2 and Bcl-xL proteins as described in Section "**Inhibitors of Bcl-2 Family PPIs**."

Inhibitors of the DNA binding protein–replication protein A subunit (RPA70) PPI were identified from a 15,000 member fragment library using an "SAR-by-NMR" screen.[115,116] Two sets of fragment hits bound in adjacent sites and with good ligand efficiencies (LE >0.3) were selected. For one set, the fragments were "grown" by the purchase of more complex analogs giving compounds, for example, **36**, with improved potency but poorer LE (NMR $K_d = 135$ μM). For the second set, the linking of fragments was guided by X-ray crystallography giving pyrazole **37** ($K_d = 0.19$ μM).

An NMR fragment screen for inhibitors of the proapoptotic Bcl2-family protein Bid BH3 domain identified fragments binding to two adjacent subpockets. Modeling studies and library synthesis allowed the linking of fragments giving rise to sulfonamide **39**.[117] Binding of **39** to the Bid BH3 domain was confirmed by NMR and the compound decreased Smac release in a mitochondrial assay.

5.06.3 Examples of PPI Inhibitors

5.06.3.1 Inhibitors of Bcl-2 Family PPIs

Bcl-2 and related family of proteins form key nodes in the mechanism to regulate apoptosis.[118–120] The antiapoptotic proteins Bcl-2 and Bcl-xL are regulated by proapoptosis proteins (**Fig. 18**). Stimulation of the BH3-only initiator proteins (eg, Bim, Bad, and tBid)

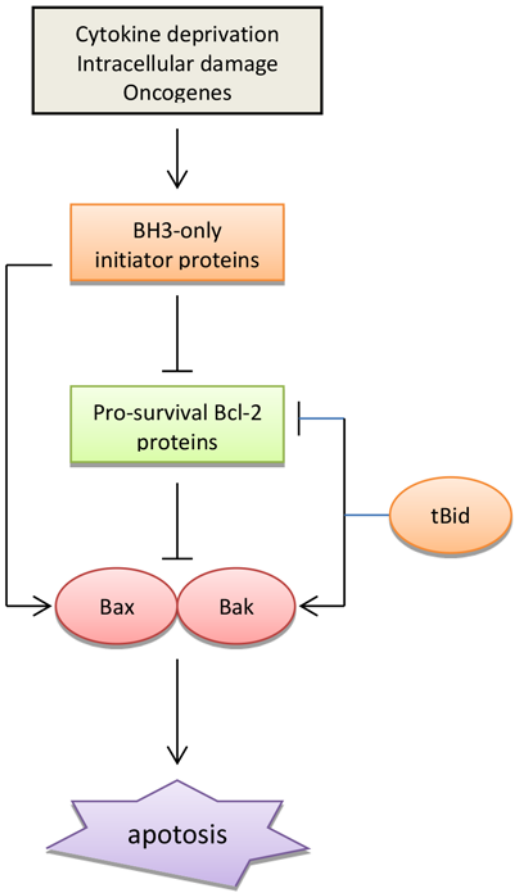

Fig. 18 Bcl-family pathways to apoptosis.

inhibits the prosurvival proteins (eg, Bcl-2 and Bcl-xL), thus allowing activation of proapoptotic effectors Bak and Bax. The proteins share Bcl homology (BH) domains, of which there are 4 (BH1-4). The *Bcl-2* gene is overexpressed in a variety of human tumors, and this has been linked to resistance to chemotherapy and radiotherapy. Inhibition of the Bcl-2-Bax PPI is an attractive target for cancer therapy.

The natural product Gossypol (**40a**) (Table 4) and the derivative Apogossypol (**40b**) are competitive inhibitors of the binding of a labeled BH3 peptide to Bcl-xL ($K_i = 0.3$ and 2.3 μM, respectively), binding to Bcl-xL was confirmed by NMR, and in cells by confocal microscopy.[121,122] Gossypol has a complex pharmacology and exherts multiple cellular effects, at least in part by acting as a BH3 mimetic.[123] In addition, polyphenolic compounds have been shown to have undesirable redox chemistry and protein reactivity.[103] Gossypol and derivatives, for example, AT-101, have been evaluated in clinical trials, but with limited efficacy.[124–126]

The structure of Gossypol docked with Bcl-2 was used as the starting point for the design of TW-37 (**41**).[127] The structure retains the extensive hydrogen bonding of one-half of Gossypol **40a** combined with a larger hydrophobic benzyl group and a hydrophobic amide to access more extensive contacts with the BH3 binding pocket. TW-37 is an inhibitor of Bcl-2, Bcl-xL, and Mcl-1.

Obatoclax (**42**) is a pan-inhibitor of Bcl-2 family proteins, including Bcl-2, Bcl-xL, MCL-1, Bcl-w, A1, and Bcl-b.[128] The inhibitor binds to the BH3 binding groove on the target proteins thus initiating apoptosis. A phase I trial of obatoclax in advanced chronic lymphocytic leukemia and solid tumors demonstrated activation of Bax and Bak, consistent with target engagement, and gave modest single-agent activity.[129,130]

SAR by NMR identified fragments bound to Bcl-xL with millimolar potency. Linking of fragments occupying subpockets in close proximity and further SAR studies enabled the identification of ABT-737 (**43**) (Fig. 19).[131,132] ABT-737 binds avidly to Bcl-xL, Bcl-2, and Bcl-w proteins that have high homology. In cells, ABT-737 antagonized Bcl-2, but did not cause apoptosis, in a similar manner to an apoptosis sensitizing Bad-BH3 peptide. The disruption of Bcl-2 family interactions in cells was confirmed by mammalian two-hybrid experiments. ABT-737 induced tumor regression in Bcl-2 overexpressing small cell lung cancer (SCLC) xenografts (100 mg kg^{-1} day^{-1} ip).[133]

Further structure-guided SAR studies resulted in the identification of Navitoclax (ABT-263, **44**).[134] Modifications to ABT-737 were designed to optimize physicochemical properties, and focused on modulating the acidity of the sulfonamide group to enhance oral bioavailability, and reduction of plasma protein binding by changing the basic amino group to a morpholine. Changes to the

Table 4 Bcl-2 family inhibitors

Compound	*Structure*	*Activity*[a]	*References*
Gossypol **40a** R = CHO **40b** R = H	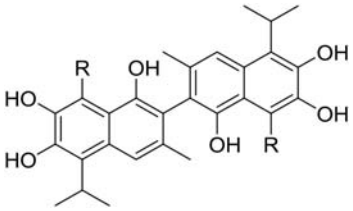	Bcl-2 **40a** $K_i = 0.3\ \mu M$ Bcl-2 **40b** $K_i = 2.3\ \mu M$	121–123
TW-37 **41**	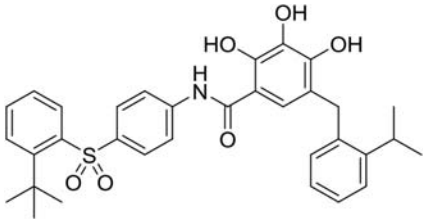	Bcl-2 $K_i = 0.29\ \mu M$ Bcl-xL $K_i = 1.1\ \mu M$ Mcl-1 $K_i = 0.26\ \mu M$	108
Obatoclax **42**	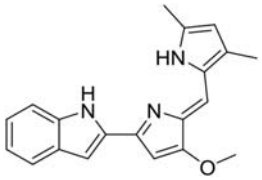	Bcl-2 $IC_{50} = 1.11\ \mu M$ Bcl-xL $IC_{50} = 4.69\ \mu M$ Mcl-1 $IC_{50} = 2.90\ \mu M$	128,130
ABT-737 **43**	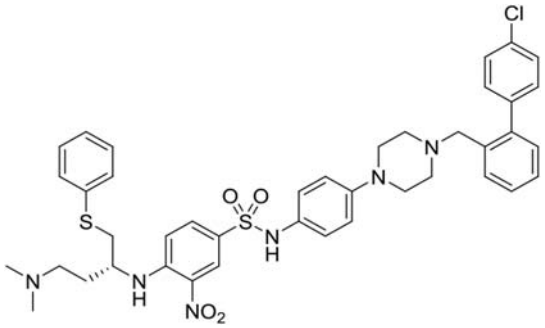	Bcl-2 $K_i < 1$ nM Bcl-xL $K_i < 0.5$ nM Bcl-w $K_i = 0.9$ nM	131,132
Navitoclax ABT-263 **44**	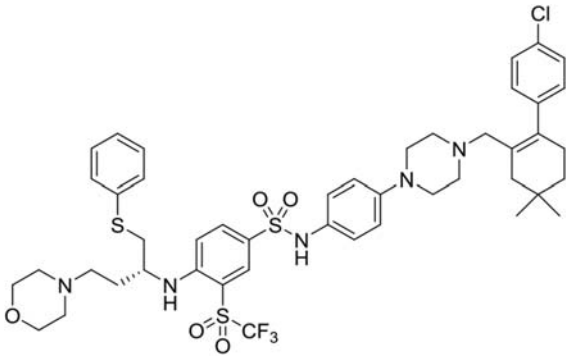	Bcl-2 $K_i < 1$ nM Bcl-xL $K_i < 0.5$ nM Bcl-w $K_i < 1$ nM	134,135
45	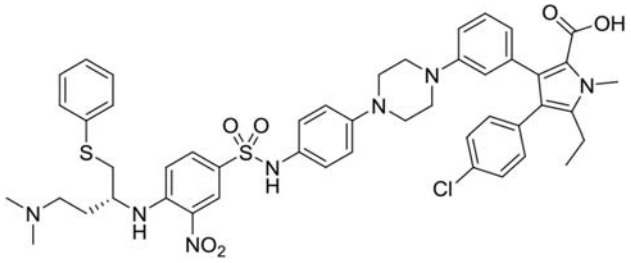	Bcl-2 $K_i = 0.8$ nM Bcl-xL $K_i < 1$ nM Mcl-1 $K_i < 2$ nM	139

(Continued)

Table 4 Bcl-2 family inhibitors—cont'd

Compound	*Structure*	*Activity*[a]	*References*
46	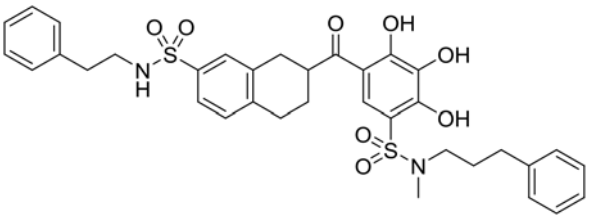	Bcl-2 $K_i = 110$ nM Mcl-1 $K_i = 39$ nM	140
47	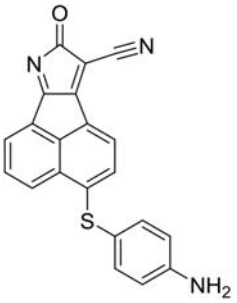	Bcl-2 $IC_{50} = 302$ nM Mcl-1 $IC_{50} = 5$ nM	141
Venetoclax ABT-199 **48**	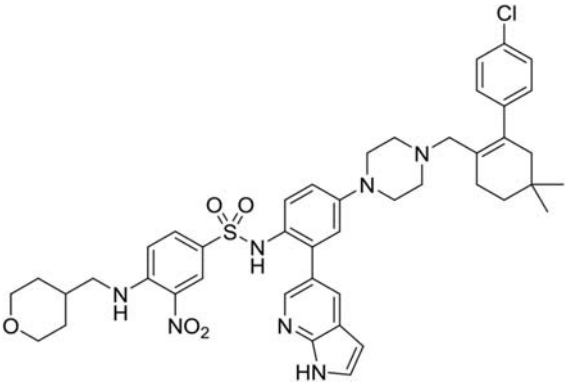	Bcl-2 $K_i < 10$ nM Bcl-xL $K_i = 48$ nM Bcl-w $K_i = 245$ nM Mcl-1 $K_i > 444$ nM	142

[a]Activity in cell-free assays.

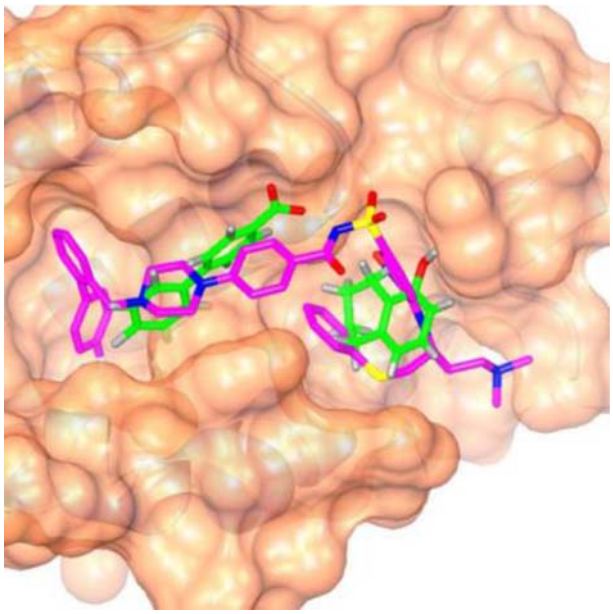

Fig. 19 X-ray structure of Bcl-xL (ribbon—*blue*, surface—*coral*) with ABT-737 (*magenta*) overlayed with the fragment hits (*green*) (pdb 2YXJ and 1YSG).

backbone included switching the undesirable nitro group to trifluoromethylsulfone and replacement of one phenyl ring of the 4-chlorobiphenyl moiety with a cyclohexenyl group. Despite the high MW of the compound (974 Da) ABT-263 has acceptable oral bioavailability and PK properties.[135] ABT-263 shows mechanism-based cytotoxicity in Bcl-2 or Bcl-xL dependent cellular models. In vivo efficacy with complete regressions was observed in SCLC and acute lymphoblastic leukemia xenografts (100 mg kg^{-1} qd p.o.). A mechanism related toxicity, thrombocytopenia, was also seen, but this was reversible. A phase I clinical trial with Navitoclax in SCLC and other solid tumors confirmed the safety of the drug and preliminary efficacy was encouraging.[136] A phase II single-agent trial in SCLC showed limited efficacy so further solid tumor studies are ongoing in combination with other therapies.[137] Bcl-2 family proteins play a central role in the development of many lymphomas. A phase I study in lymphomas showed promising results and phase II studies were initiated.[138]

Structure-based modification of the ABT-737 scaffold, by grafting a celecoxib inspired pyrrole in place of the chlorobiphenyl moiety sought to exploit additional interactions in the BH3 binding site.[139] Compound **45** retained potent Bcl-2 and Bcl-xL activity, and gained Mcl-1 activity, and showed potent cytotoxicity in SCLC cell lines. Alternatively, the triphenolic group of TW-37 was merged with ABT-737 giving (**46**) that inhibits Bcl-2 and Mcl-1.[140]

An alternative scaffold for Bcl-2 and Mcl-1 inhibition was optimized with the aid of molecular modeling studies.[141] Compound **47** is a mixed Bcl-2, Mcl-1 inhibitor with potent cytotoxicity against tumor cell lines.

Preclinical data with navatoclax (**44**) suggested that a selective Bcl-2 inhibitor would induce less thrombocytopenia but retain antitumor activity, compared with mixed Bcl-2, Bcl-xL inhibitors.[142] Structure-based design of venetoclax (ABT-199, **48**) exploited differences in the P4 subpocket on Bcl-2 by moving the hydrophobic group from the thioether linker onto the central phenyl ring giving a Bcl-2 selective inhibitor. Selectivity was confirmed in cells using a mammalian two-hybrid assay. Venetoclax **48** was cytotoxic in Bcl-2 amplified non-Hodgkins lymphoma (NHL) cell lines and induced regressions in hematological tumor xenografts (100 mg kg^{-1} qd^{-1} p.o.). Venetoclax has entered clinical trials as a single agent in NHL and other tumor types with promising results.[143,144]

The Bcl-family PPI inhibitors have been developed by the use of fragment discovery and rational design. Navitoclax can be considered as the first rationally designed PPI inhibitor to enter clinical trials for cancer.

5.06.3.2 Inhibitors of MDM2–p53 and MDMX–p53

MDM2 and MDMX act as negative regulators of p53. Amplification of the *MDM2* gene occurs in around 10% of tumors. Overexpression of MDMX in the absence of gene amplification appears to be more common, observed in breast (19%), uterus (15%), testes (27%), stomach/small intestine (42%), colorectal (19%), larynx (23%), lung (18%), and melanoma (65%).[145–147] Gene amplification of *MDM2* or *MDMX* and p53 mutations appear to be mutually exclusive, suggesting that a single mechanism for disabling the p53 tumor suppressor function is necessary and sufficient for carcinogenesis. MDMX overexpression has been linked with resistance in cell lines to MDM2–p53 inhibition.

Inhibition of the MDM2–p53 PPI will release p53 from the repressive control of MDM2, and activate p53-mediated cell death. Tumor selectivity would be achieved by p53 sensing preexisting DNA-damage or oncogenic activation signals, previously blocked by MDM2. In normal cells, p53 may activate nonapoptotic pathways.

The p53 binding sites of MDM2 and MDMX have been defined by peptide mapping and X-ray crystallography (Section "MDM2–p53 Peptides"). Small-molecule inhibitors mimic the p53 α-helix binding to MDM2, and are required to fill the Phe19, Trp23, and Leu26 subpockets on MDM2 for potency. Inhibitors must also achieve acceptable pharmaceutical properties, usually by the addition of a hydrophilic group.

5.06.3.2.1 MDM2–p53 antagonists

1,4-Benzodiazepine-2,5-dione hits were identified as MDM2 binders from a diverse combinatorial library for binding to MDM2 using the ThermoFluor thermal denaturation affinity assay, and confirmed using an FP assay.[148,149] The X-ray crystal structure of **49a** in complex with MDM2 shows that the inhibitor occupies the hydrophobic p53 binding groove (Fig. 20). Further optimization yielded compounds with improved water solubility, which gave the best combination of cell-free inhibition of MDM2–p53 binding (eg, **49b**, IC_{50} 0.70 μM) (Table 5) in the FP assay and cellular activity as measured by the induction of the p53 inducible gene PIG3, and were selected for further study.[150,151]

The *cis*-imidazoline analogs, named "Nutlins" (eg, **50**, $IC_{50} = 0.09$ μM), were identified by HTS.[152] The compounds inhibit the MDM2–p53 interaction with IC_{50}s in the 100–300 nM range. The X-ray and NMR structures of **50** in complex with MDM2 show the small *cis*-imidazoline scaffold mimics an α-helical peptide by the orientation of its substituents (Fig. 20).[153,154] Nutlin-3a (**50**) has been used as a tool compound in many studies investigating the role of MDM2 and p53 in cells, because of its good potency and selectivity. Structure-guided optimization of potency, selectivity, and pharmacological properties gave improved inhibitors, for example, RG-7112 (**51**). The imidazoline heterocycle and the 4-methoxy group were found to be sites of metabolism and so were modified by two additional *cis*-methyl groups on the heterocycle, and replacement with a 4-*tert*-butyl group, respectively. Additional potency and improved PK properties were gained by modifying the hydrophilic side chain. The X-ray cocrystal structure of MDM2 with **51** shows that it binds in a similar orientation to Nutlin-3a, and the methylsulfone side chain does not make additional interactions with the protein. RG7112 (**51**) has completed phase I clinical trials and demonstrated target engagement and some efficacy with oral dosing.[155]

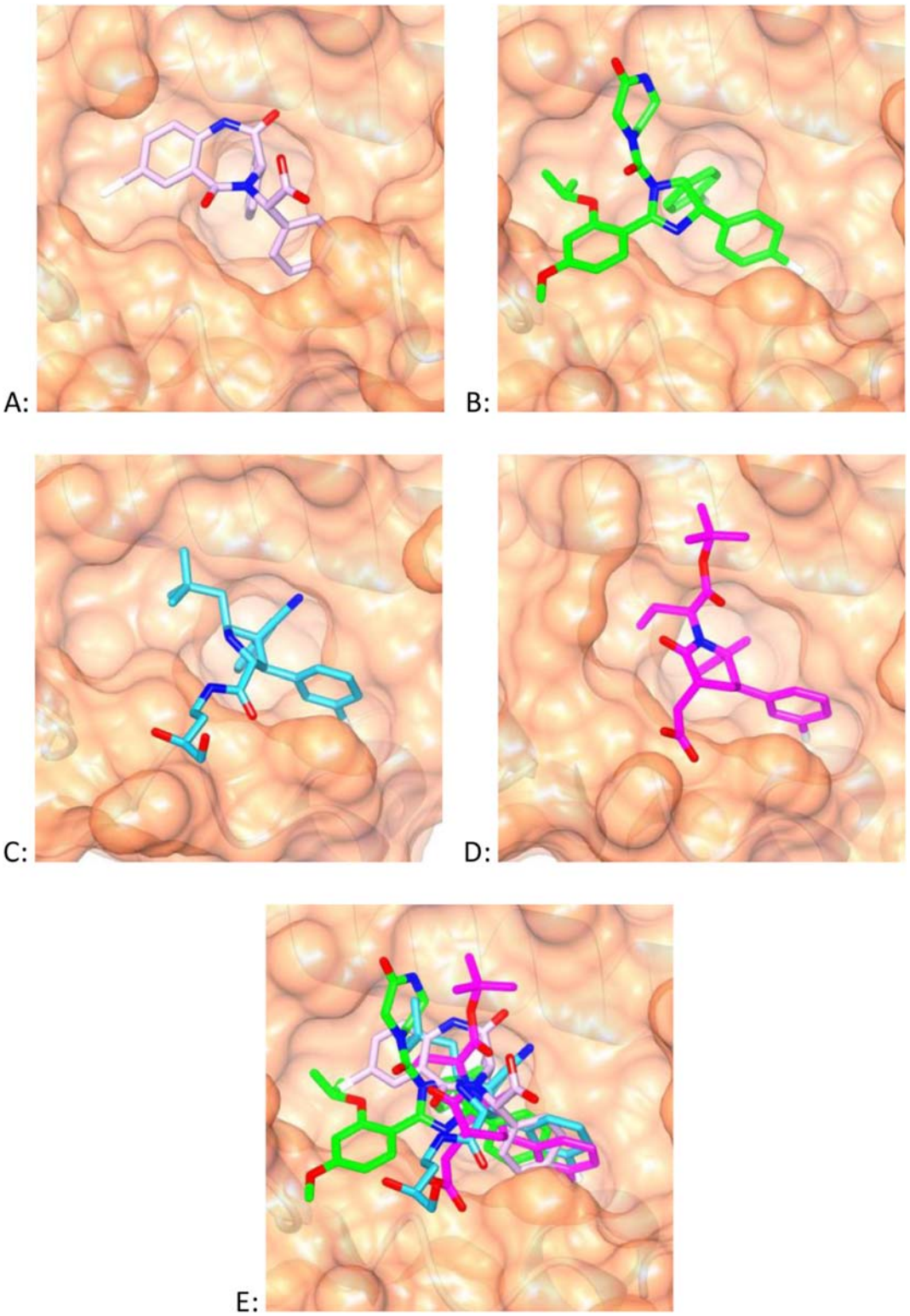

Fig. 20 X-ray crystal structures of MDM2 with ligands bound. (A) Benzodiazepinone **49a** (pdb 1T4E); (B) Nutlin-3a **50** (pdb 4HGJ); (C) RG7388 analog (pdb 4JRG); (D) AMG-232 analog (pdb 4ERE); (E) overlay of structures.

Table 5 MDM2–p53 inhibitors

Compound	*Structure*	*Activity versus MDM2*[a]	*References*
49a **49b**	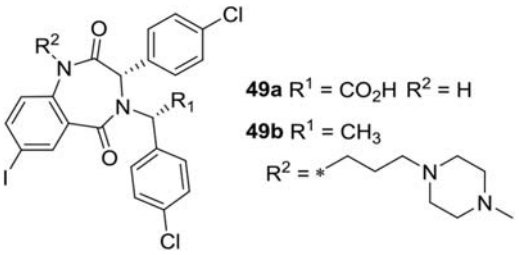	**49a** IC_{50} 0.22 μM **49b** IC_{50} 0.55 μM	145–148, 264, 265
Nutlin-3a **50**	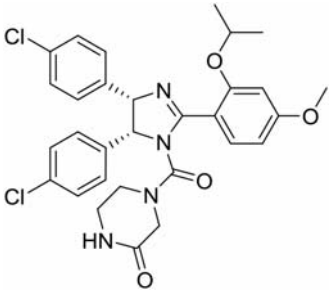	IC_{50} 90 nM	152
RG-7112 **51**	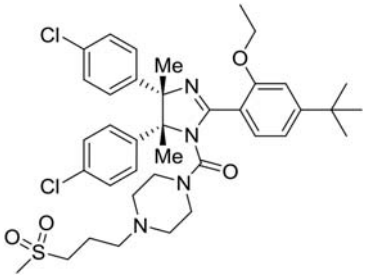	IC_{50} 18 nM	152, 266, 267
52a DS-5272 **52b**	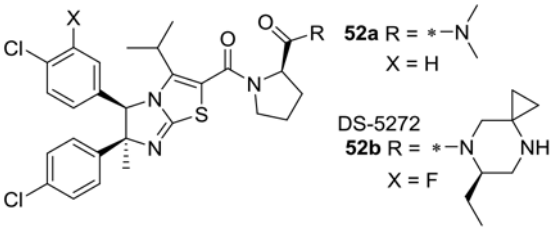	**52a** IC_{50} 92 nM **52b** IC_{50} 24 nM	156–158
53	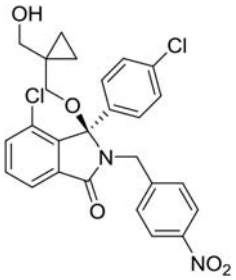	IC_{50} 44 nM	163
54a **54b**	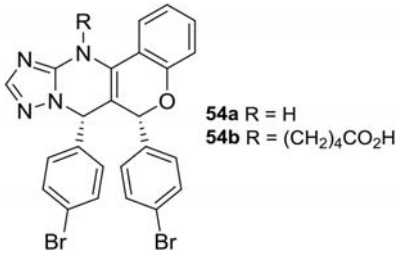	**54a** IC_{50} 1.2 μM **54b** IC_{50} 0.35 μM	161, 162

(Continued)

Table 5 MDM2–p53 inhibitors—cont'd

Compound	*Structure*	*Activity versus MDM2*[a]	*References*
MI-63 **55**	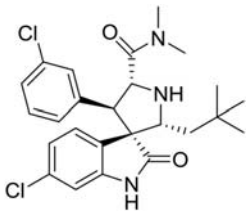	IC_{50} 80 nM	166
SAR405838 (MI-77301) **56**	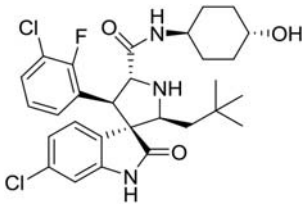	K_i 0.88 nM	170
RG-7388 **57**	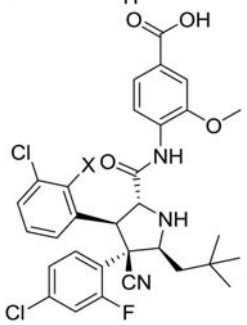	IC_{50} 6 nM	168, 268
RO8994 **57**	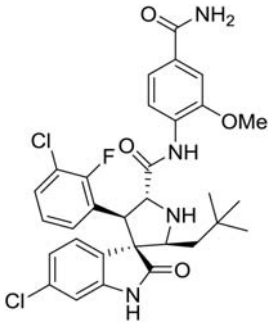	IC_{50} 5 nM	172
RO2468 **58**	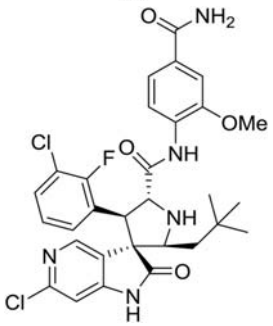	IC_{50} 6 nM	173
RO5353 **59**	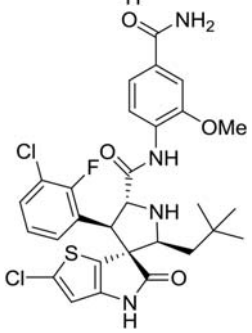	IC_{50} 7 nM	173

Table 5 MDM2–p53 inhibitors—cont'd

Compound	*Structure*	*Activity versus MDM2*[a]	*References*
60	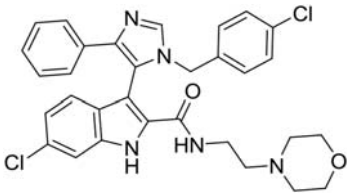	IC_{50} 30 nM	174
61	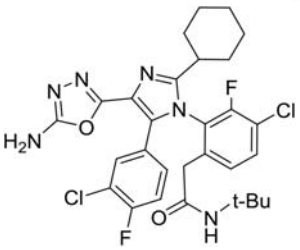	IC_{50} 2 nM	175
62a **62b**	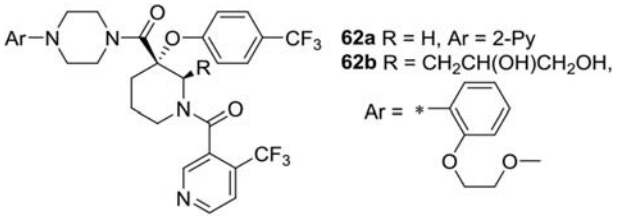 **62a** R = H, Ar = 2-Py **62b** R = $CH_2CH(OH)CH_2OH$, Ar = *	**62a** IC_{50} 2300 nM **62b** IC_{50} 16 nM	173, 174
AM8553 **63**	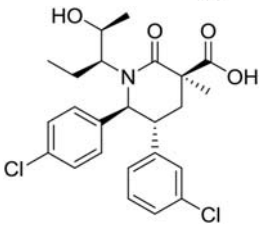	IC_{50} 1.1 nM IC_{50} 72 nM (EdU SJSA-1)	178
64	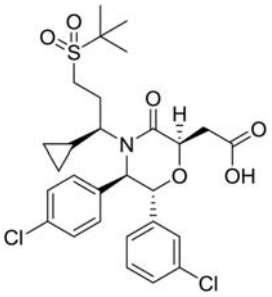	IC_{50} 2 nM IC_{50} 37 nM (EdU SJSA-1)	180
AMG-232 **65**	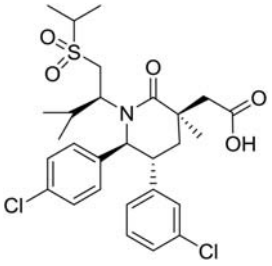	IC_{50} 0.6 nM IC_{50} 9.1 nM (EdU SJSA-1)	181–183
AM6761 **66**	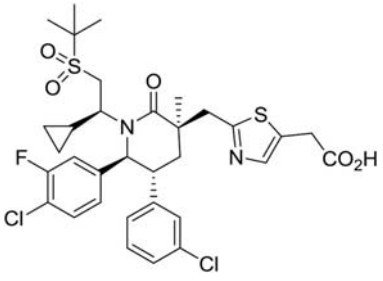	IC_{50} 0.001 nM IC_{50} 16 nM (EdU SJSA-1)	184

(Continued)

Table 5 MDM2–p53 inhibitors—cont'd

Compound	*Structure*	*Activity versus MDM2*[a]	*References*
AM-7209 **67**	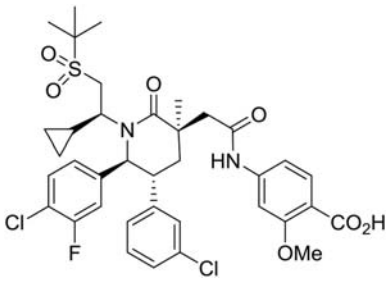	$IC_{50} < 0.1$ nM IC_{50} 1.6 nM (EdU SJSA-1)	185
68	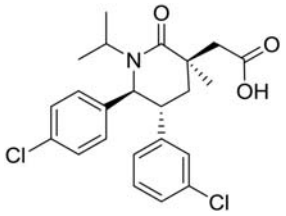	IC_{50} 0.009 nM IC_{50} 380 nM (EdU SJSA-1)	186
NVP-CGM097 **69**	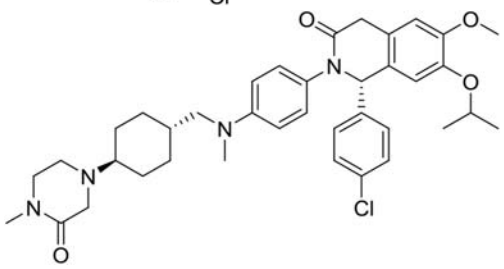	IC_{50} 1.7 nM	184, 185

[a]Activity in cell-free assays.

Dihydroimidazothiazoles, for example, **52a**, were designed by modification to the Nutlin scaffold and have potent MDM2 inhibitory activity. The bicyclic scaffold fixes the 3-isopropyl group in the optimum position for access to the MDM2 Phe19 pocket. Introduction of the 4-position amide gave additional potency, and the 6-methyl group prevents oxidation of the imidazoline ring.[156,157] The X-ray structure of **52a** bound to MDM2 shows the amide side chain occupying a surface groove formed by the movement of a flexible loop. Introduction of a 3-fluoro-4-chlorophenyl group optimized interactions in the Trp23 binding pocket, and further elaboration of the amide group with a 4,7-diazaspiro[2,5]octane group gave DS-5272 (**52b**).[158] The in vitro properties of DS-5272, for example, cellular activity, solubility, and microsomal stability are reasonable. The compound showed in vivo acceptable PK properties and efficacy in a MDM2-amplified mouse xenograft model (50 mg kg^{-1} qdx4^{-1} p.o.).

The isoindolinone series resulted from the development of weak screening hits, optimized using in silico library screening and synthesis.[159,160] NMR studies with a selection of isoindolinones and MDM2 suggested plausible binding modes that were used for the design of improved inhibitors.[161,162] For example, isoindolinone **53** showed improved cellular activity over earlier compounds, inducing transcription of p53 dependent genes at comparable levels to Nutlin-3a (**50**), and was growth inhibitory in p53 wild-type HCT-116 cells ($GI_{50} = 3.7$ μM) and threefold less growth inhibitory in the paired p53 −/− HCT-116 line.[163]

A HTS of 1.4 million compound library identified the chromenotriazolopyrimidine **54a** as a MDM2–p53 inhibitor.[164] The MDM2 cocrystal structure with **54a** shows the 7-(4-bromophenyl) group occupying the Leu26 subpocket, and the 6-(4-bromophenyl) group filling the Trp23 subpocket. The chromenotriazolopyrimidine heterocycle spans the surface of the protein from phenyl "D"-ring in the Phe19 binding site to the triazole ring close to Val93 of MDM2. Potency and PK properties were optimized by introduction of a polar or acidic group at N11.[165] The acid **54b** was moderately orally bioavailable ($F = 54\%$), with improved solubility.

Computational substructure searching for compounds able to mimic the tryptophan of p53 identified the spirooxindole series, for example, MI-63 (**55**).[166,167] Optimization of the series progressed by elaboration of the amide group and addition of a 5-fluoro group, and epimerization to the most stable diastereoisomer under oxidative conditions gave compounds with improved potency and in vivo activity.[168,169] In particular, SAR405838 (**56**) showed potent MDM2 binding affinity and growth inhibitory activity.[170] The X-ray cocrystal structure of **55** bound to MDM2 shows a hydrogen bond between His96 NH and the amide side chain carbonyl group, and movement of the MDM2 N-terminus. In vivo evaluation of spirooxindole **56**, following in vitro PK profiling with mouse, rat, and human liver microsomes, showed **56** induced complete tumor regression in SJSA-1 mouse xenografts with a single oral dose (100 mg kg^{-1}). SAR405838 (**56**) was selected as the clinical candidate from the spirooxindole series and entered phase I clinical trials as a single agent and in combination with the MEK1/2 inhibitor pimasertib.

Replacement of the spirooxindole spirocyclic amide scaffold of **55** with a simpler and more flexible cyanopyrrolidine core gave rise to RG7388 (**57**).[171] The 2-fluoro substituent was important for MDM2 inhibitory potency. The amide side chain substituent modulated the PK profile and the cellular potency of the compounds, and a 4-benzenecarboxylic moiety gave improved PK and cellular potency. Further optimization focused on the introduction of groups with distinct electronic properties, with the ortho-methoxy group, **57** (RG7388), having the ideal combination of MDM2 binding affinity, cellular potency, and selectivity. RG7388 gave complete tumor regression in vivo in an SJSA-1 xenograft model (25 mg kg^{-1} p.o.), and a favorable PK profile. RG7388 (**57**) was selected as the second generation MDM2–p53 clinical trial candidate owing to its improved potency, cellular selectivity, and PK properties over RG7112 (**51**).

A combination of de-novo and structure-based design resulted in the spirooxindole RO8994 (**58**).[172] The same amide substituent as found in **57** was used giving excellent MDM2 inhibition, cellular activity, and PK profile. Compound **58** showed impressive in vivo activity in an SJSA-1 xenograft model, inducing tumor regression (6.25 mg kg^{-1} qd^{-1} p.o.).

Bioisosteric replacement of the oxindole phenyl ring with either five- or six-membered heterocycles resulted in RO2468 (**58**) and RO5353 (**59**), which both showed potent MDM2 inhibitory activity (IC_{50} = 6 and 7 nM, respectively) and excellent cellular activity (GI_{50} = 15 and 7 nM, respectively).[173] Both compounds produced tumor regression in SJSA-1 xenografts (10 mg kg^{-1} qd^{-1} p.o.) with excellent mouse PK properties.

Rational design based on the X-ray structure of the AP peptide (**14**) bound to MDM2 gave rise to the "central valine" concept.[174] An imidazole scaffold makes favorable contacts with Val23 and allows three different substituents into the Phe19, Trp23, and Leu26 subpockets on MDM2. The X-ray crystal structure of MDM2 with (**60**) allowed further structure-based optimization, targeting an interaction with His96, that stacks with the chlorobenzyl group of **60** in the Leu26 pocket.[175] A number of changes to **60** optimized the potency and solubility. Gains in potency were achieved by structure-guided modifications, for example, **61**: addition of an acid isostere to target His96, for example, 2-aminooxadiazole; replacement of the 4-chlorobenzyl with a 3-chloro-2-fluorophenyl substituent; simplification of the indole substituent to a 3-chloro-4-fluorophenyl group; and replacement of the 5-phenyl substituent with a cyclohexyl group. The ortho-methyleneamide group at the 2-position of the imidazole conferred the best combination of inhibitory activity and cellular activity. The cellular activity in this series is low compared with other series displaying similar MDM2–p53 potency, possibly indicating poor cellular uptake.

A FP-based HTS identified substituted piperidines, for example, **62a** as hits.[176] Replacement of the pyridine group with a 2-methoxyethoxyphenyl substituent gave improved potency. Substitution at the 2-position of the piperidine ring, for example, **62b**, improved the PK properties, and favored the bound conformation of the piperidine, giving additional potency.[177]

The piperidone series of inhibitors (eg, **63**) was conceived by analysis of the X-ray cocrystal structures of a number of MDM2 inhibitory chemotypes, highlighting the importance of interacting with His96 and the Leu23 pocket for potency, and efficient filling of the three MDM2 subpockets by the ligand.[178] Structure-guided optimization of the *N*-alkyl group revealed the cyclopropylmethyl group as ideal, for example, **64**.[178] The (3*R*)-carboxyl group at C3 forms a key interaction with His96. Modeling studies suggested the introduction of an additional methyl group at C3 to direct the substituent into the optimal conformation for binding. Similarly, the introduction of a methyl group at C3, to stabilize the conformation of the piperidone ring, gave a modest improvement in potency. Cell potency was optimized for the 3-(2-hydroxypentyl) analogs, for example, **63** (AM8553). AMG8553 had good in vivo PK and pharmacodynamic (PD) properties, and tumor stasis in an SJSA-1 mouse xenograft model was achieved on oral dosing (150 and 100 mg kg^{-1} qd^{-1}).

In parallel to the piperidinone series, a series of related morpholinones (64–69) was identified with acceptable potency and cellular activity.[179] Optimization of this series was guided by the knowledge gained in the piperidone series. The morpholinones showed a 5–10-fold loss of potency compared with the piperidones, but better metabolic stability in hepatocytes derived from human and other mammalian species.[180] The *N*-cyclopropylmethyl compound **64** had the best combination of potency and low clearance in human hepatocytes. **64** induced tumor stasis in SJSA-1 mouse xenografts (100 mg kg^{-1} qd^{-1} p.o.).

Further structure-guided design in the piperidone series targeted the N-substituent to optimize interactions with the "glycine shelf" region, a hydrophobic region on the surface of MDM2 formed by Gly58.[181,182] Sulfone **65** (AMG 232) showed excellent cell-free potency and cell growth inhibitory activity. The X-ray cocrystal structure of a related sulfone showed the sulfone group situated close to the Gly58 CH suggesting a favorable interaction and the Phe19 subpocket occupied by the alkyl group, directed by the α-substituent (**Fig. 20**). Complete tumor regression in SJSA-1 xenografts observed (60 mg kg^{-1} qd^{-1} p.o.), and so AMG 232 was selected for clinical trials.[183]

Alternatives to the carboxylic acid moiety able to retaining the favorable interaction with His96 were sought.[184] Replacement with carboxyl-substituted heterocycles, for example, 2-pyridyl derivative, pyrazole, and thiazoles, for example, **66**, gave equipotent compounds. A hydrogen bond between the His96 NH and heterocycle N was visible in the MDM2 cocrystal structures of the 2-pyridyl and thiazole **65** derivatives. **65** was active in the SJSA-1 xenograft model, inducing tumor stasis (50 mg kg^{-1} qd^{-1} p.o.).

The carboxylic acid group of **65** was modified to an anilide in AM-7209 (**67**), along with modifications to the sulfonamide, replacement of isopropyl chain with cyclopropyl, and addition of a 3-fluoro group to the Trp23 pocket phenyl, giving improved potency and cellular activity over the parent.[185] AM-7209 showed excellent in vivo activity and induced tumor regression in SJSA-1 xenografts (25 mg kg^{-1} qd^{-1} p.o.).

In a parallel approach, the SAR of simplified piperidones was explored by the introduction of heterocyclic and alkyl substituents to the Phe19 subpocket.[186] Compound **68** had the best LE, showed improved metabolic stability, and induced tumor regression in SJSA-1 xenografts (100 mg kg^{-1} qd^{-1} p.o.).

Recently, a series of dihydroisoquinolinones, developed from a VS hit, have been reported.[187,188] X-ray structure-guided optimization gave rise to NVP-CGM097(**69**) with excellent cellular activity and ADME properties. The binding mode of **68** differs from the majority of other potent MDM2 inhibitors, as the Leu26 subpocket is not occupied by a chlorophenyl ring, instead the C7 isopropyl ether and the C6 methyl ether occupy the subpocket. The Trp23 subpocket is filled by the C1 4-chlorophenyl group, and the Phe19 subpocket is occupied and extended by movement of the protein to accommodate the large amine side chain. NVP-CGM097 showed good PK properties in a number of mammalian species and induced tumor regression in SJSA-1 xenografts (30 mg kg^{-1} qd^{-1} p.o.). NVP-CGM097 has been selected for clinical trials.

The design of MDM2–p53 inhibitors has received considerable attention due to the strong target rationale, access to structural biology, and the structural diversity of the hit scaffolds. A number of compounds have entered clinical trials and demonstrated preliminary efficacy.

5.06.3.2.2 Dual MDM2–p53, MDMX–p53 antagonists

Overexpression or gene amplification of MDMX, the paralogue of MDM2, has been observed in a number of tumor types. MDMX acts as a central regulator of p53 activity and overexpression has been linked with resistance in cancer cell lines to MDM2–p53 inhibition. The potent MDM2–p53 inhibitors described above show minimal inhibition of MDMX–p53, and so elevated MDMX levels may produce resistance. Analysis of the peptide bound X-ray structures of MDM2 and MDMX reveals that, although the same three residues of p53 are bound, significant differences in the binding interaction result from differences in the amino acid sequences between MDM2 and MDMX.[189] In particular, differences in the Leu23 subpocket may account for the substantially different SARs. A number of small-molecule dual inhibitors of MDM2 and MDMX interactions with p53 have been reported and are summarized in Table 6.

SJ-172550 (**70**) was identified by HTS as a selective MDMX inhibitor, which showed differential cytotoxicity in a screen using *MDMX* amplified cells.[190] In combination with Nutlin-3a (**50**), SJ-172550 showed additive cytotoxicity in p53 (wt) cells. Mass spectrometry and SPR studies showed evidence of covalent but reversible modification of the MDMX protein by **70**.[191]

The 3-imidazolylindole (**71**) inhibits both MDM2– and MDMX–p53 with modest potency.[192,193] The MDMX cocrystal structure of **71** shows a similar binding mode to that seen for MDM2, the Trp32 subpocket is filled by the chloroindole, the chlorobenzyl group, and the phenyl ring occupy the Leu23 and Phe19 subpockets, respectively. Based on this observation and the SAR of known MDM2 inhibitors, a focused library was synthesized using an Ugi 4-component reaction.[194] Indole amide **72** showed 10-fold selectivity for MDMX inhibition over MDM2.

A series of pyrroles, for example, (**73**) were developed from a screening hit.[195] SAR studies demonstrated that the barbituric acid and triaryl motifs were essential for MDMX activity.

An HTS screen for MDMX–p53 inhibitors identified indolyl hydantoin RO-2443 (**74a**).[196] Analog RO-5963 (**74b**) had improved water solubility. Both compounds are potent inhibitors of MDM2–p53 and MDMX–p53. The MDMX cocrystal structure of **74a** shows an unusual dimeric sandwich-like binding mode. The 3,4-difluorophenyl moiety of one molecule of **74a** occupies the Trp23 pocket, and the Phe19 pocket of the same MDMX binding pocket is overlayed by the indole heterocycle of the other molecule of **74a**. Similarly, the second MDMX binding pocket is occupied by the alternate groups of both **74a** molecules. The more water soluble derivative **74b** activated p53 transcription in MCF7 cells (MDMX overexpressing), and induced apoptosis in SJSA-1 cells and the Nutlin-3a resistant engineered MDMX overexpressing line SJSA-X. In a panel of nine cancer cell lines, enhanced apoptosis was seen with elevated MDMX levels, demonstrating the utility of dual inhibition of MDM2 and MDMX.

The contribution of different regions of MDMX to the binding affinity of Nutlin-3a (**50**) was explored by systematic mutation of the segments to the homologous MDM2 sequence.[197] This knowledge was used in the design of a potent inhibitor dual inhibitor of MDM2 and MDMX based on the Nutlin scaffold (H109, **75**). The gain in MDMX activity was achieved by improving the Trp23 subpocket interaction with the chloroindole substituent, modification of the Leu23 subpocket interaction with the introduction of a carboxylic acid group, and introduction of hydrogen bonding beyond the Phe19 pocket. Compound **75**, inhibited MDMX–p53 binding in cells, and induced the transcription of p53 dependent genes.

Despite significant interest, the design of MDMX–p53 inhibitors has proved to be substantially more challenging than for MDM2–p53. It remains to be seen whether MDMX-selective small-molecule inhibitors can be achieved.

5.06.3.3 Inhibitors of Smac-IAP PPIs

Activation of the intrinsic pathway of apoptosis is controlled by the release of activating proteins such as cytochrome *c* and Smac.[198] Smac binds to IAP family proteins via its four terminal amino acids. XIAP binds to and inhibits caspases 3,7, and 9 via interactions with the N-terminal amino acids of the caspases and the BIR domains of XIAP. The ML-IAP proteins do not bind to caspases, instead they bind to second mitochondria-derived activator of caspases (SMAC), preventing its association with XIAP and so inhibiting apoptosis (Fig. 21).[199] In contrast, c-IAPs negatively regulate the alternative nuclear factor kappa-light-chain-enhancer of activated B cells (NF-kB) pathway by inhibiting NF-kB-inducing kinase, and activating the classical NF-kB pathway by acting on receptor-interacting serine/threonine-protein kinase 1. Amplification or overexpression of XIAP is important in hematological and solid tumors, and is associated with poor response to therapy and poor prognosis. Similarly, amplification or overexpression of c-IAPs has been identified in a large variety of tumor types. Validation of targeting the Smac-IAP interaction as a therapeutic strategy was demonstrated using cell-penetrant Smac peptides.[65] A number of XIAP and c-IAP inhibitors are in clinical trials currently in

Table 6 Dual MDM2–p53, MDMX–p53 inhibitors

Compound	*Structure*	*Activity versus MDM2*[a]	*Activity versus MDMX*[a]	*References*
SJ-172550 **70**	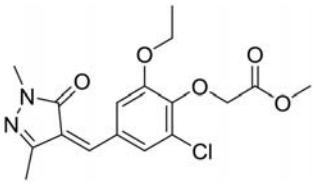	nr[b]	IC_{50} 0.9 μM	98
71	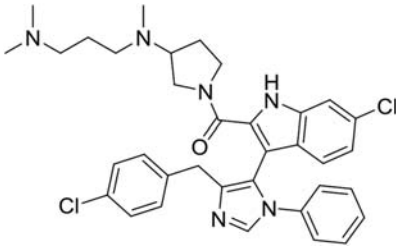	IC_{50} 0.19 μM	IC_{50} 20 μM	192
72	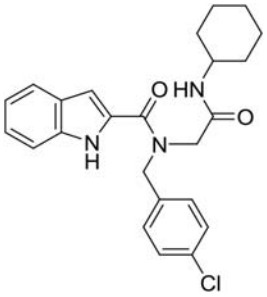	K_i 54 μM	K_i 5.5 μM	194
73	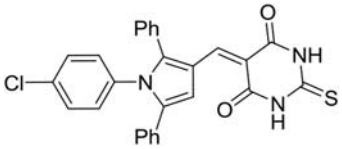	IC_{50} 0.11 μM	IC_{50} 4.2 μM	195
RO-2443 **74a** RO-5963 **74b**	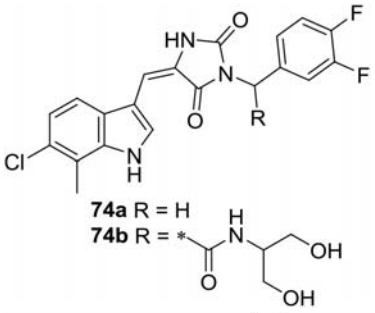	**74a** IC_{50} 33 nM **74b** IC_{50} 17 nM	**74a** IC_{50} 41 nM **74b** IC_{50} 25 nM	196
75	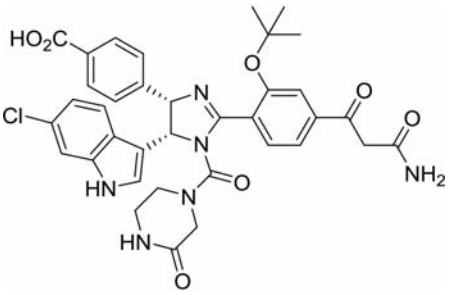	IC_{50} 27 nM	IC_{50} 6 nM	197

[a]Activity in cell-free assays.
[b]*nr*, not recorded.

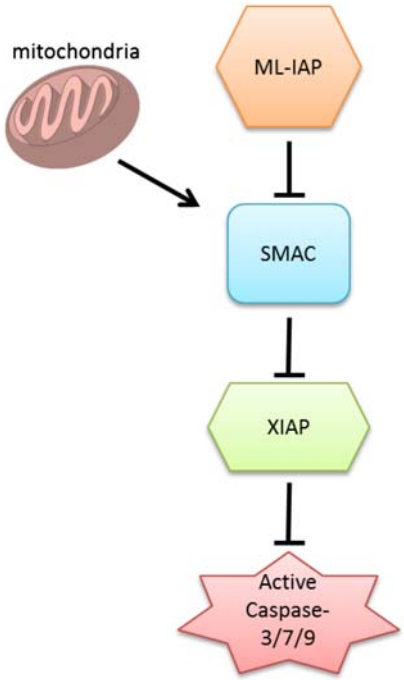

Fig. 21 Pathway for suppression of apoptosis via XIAP.

solid and hematological malignancies, as single agents and in combination with chemotherapy.[200] Preliminary reports indicate that the compounds are well tolerated and some responses have been reported.

5.06.3.3.1 Monovalent Smac-mimetic IAP antagonists

Building on the established pharmacophore for Smac peptide inhibitors,[67,68] a number of structurally diverse of peptido-mimetic scaffolds have been used to develop potent monovalent Smac mimetics with a range of selectivity between cIAP-1 and -2 and XIAP (Table 7). Replacement of the P4 amino acid with a variety of aromatic substituents showed that 2-pyrimidinyl compound (**76**) was a selective inhibitor of cIAP-1 and -2, but >2000-fold less potent versus XIAP.[201] The selectivity was explained by an adverse lone–pair interaction in the P4 binding pocket between the pyrimidine nitrogens and the hydroxyl of Thr308 in XIAP, whereas the corresponding Arg313 in IAP-1 does not make this interaction. In contrast, the pan IAP inhibitor PS1 (**77**) makes favorable hydrophobic and dipolar interactions in the BIR3 binding cleft. Interestingly, the pan-IAP inhibitor **77** was more cytotoxic than the c-IAP-selective compound **76**, indicating that additional apoptotic stimulation is required for the induction of apoptosis by the c-IAP proteins, but not for XIAP. ML101 (**78**) was identified from tripeptide libraries and shows reasonable selectivity for binding to XIAP-BIR2 domain binding over the BIR3 domain.[202]

A number of different bicyclic isosteric replacements have been used to modify the tetrapeptide scaffold in the design of non-peptide Smac mimetics. Structure-based design established the [7,5]-bicycle as a suitable dipeptide replacement for the second and third positions.[203] Compound **79** showed potent inhibition of BIR3-IAP interactions and was cytotoxic as a single agent and in combination with doxorubicin. A [5,6]-fused bicyclic replacement for residues 3 and 4 was used in LBW242 (**80**).[204,205] The compound showed cytotoxity in a panel of leukemia cell lines as a single agent and in combination with the kinase inhibitor midostaurin. Examination of the small-molecule crystal structures of fused-ring bicycles identified the azabicyclooctane system as a suitable scaffold for inhibitors.[206] Reversal of the P3–P4 amide bond and the introduction of a 1-naphthylcarboxamide at P4 gave (**81**) that induced apoptosis in cell lines and inhibited tumor growth in a breast cancer xenograft (50 mg kg^{-1} qd^{-1} p.o.). AT-406 (**82**) was designed as a Smac mimetic incorporating a [5,8]-fused bicyclic replacement for residues 2 and 3 that makes additional hydrophobic contacts from the amide side chain to Trp323 in the XIAP BIR3 domain.[207] AT-406 is a pan-selective IAP inhibitor, and is cytotoxic in a number of cell lines. AT-406 (**82**) shows good oral PK in a number of mammalian species.

Monovalent Smac mimetics have been reported in the patent literature, for example (Table 7, **83–91**).[200] Compounds **83–85** exemplify the simplest AVPI tetrapeptide mimetics, and illustrate the diversity of modifications possible in the hydrophobic P4 subpocket. Bicyclic replacement of either amino acid residues P2 and P3 (**86** and **87**), or P3 and P4 (**88** and **89**) gave inhibitors with good potency, and the capacity to modify the physicochemical properties of the inhibitor. Compound **86** bears an acrylamide group and is reported as an irreversible inhibitor of XIAP. Inhibitor **90** retains only the N-terminal alanine of the Smac peptide, the remaining residues are replaced by a substituted pyridine giving good potency. Inhibitor **91** was discovered by fragment screening, lacks the *N*-methylalanine warhead present in the other examples, and is a potent inhibitor of XIAP and c-IAP1.

Table 7 Monovalent Smac-XIAP inhibitors

ID	*Structure*	*Activity* [a]	*References*
CS3 **76**	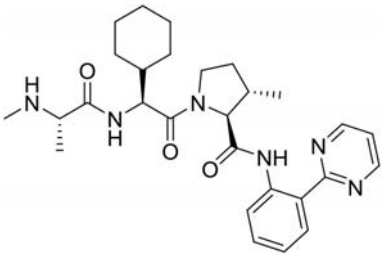	XIAP-BIR3 $K_i > 34$ μMcIAP1-BIR3 K_i 0.016 μMcIAP2-BIR3 K_i 0.085 μM	201
PS1 **77**	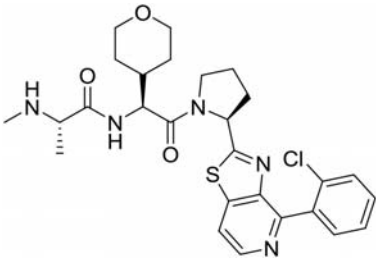	XIAP-BIR3 K_i 0.033 μMcIAP1-BIR3 K_i 0.096 μMcIAP2-BIR3 K_i 0.096 μM	201
ML101 **78**	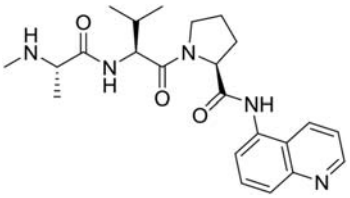	XIAP-BIR2 K_i 1.91 μM XIAP-BIR3 K_i 12.71 μM	202
79	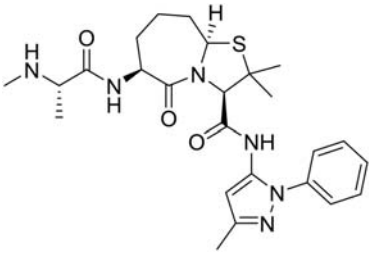	XIAP-BIR3 K_i 0.77 μMML-IAP-BIR3 K_i 0.05 μMcIAP1-BIR3 K_i 0.05 μMcIAP2-BIR3 K_i 0.13 μM	203
LBW242 **80**	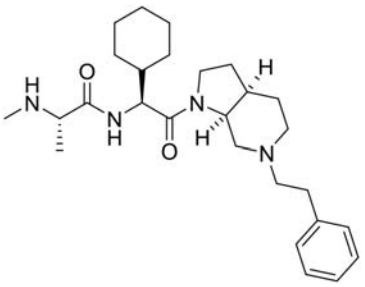	XIAP-BIR3 IC_{50} 0.2 μMcIAP1-BIR3 IC_{50} 0.001 μM	204,205
81	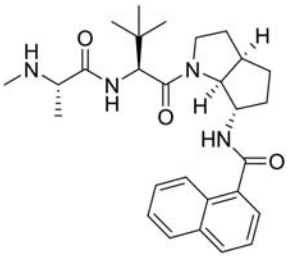	XIAP-BIR3 K_i 0.14 μMMLXBIR3SG K_i 0.05 μM	206

(Continued)

Table 7 Monovalent Smac-XIAP inhibitors—cont'd

ID	*Structure*	*Activity*[a]	*References*
AT-406 **82**	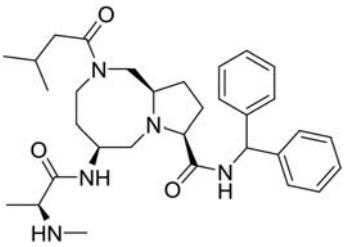	XIAP-BIR3 K_i 0.066 μMcIAP1-BIR3 K_i 0.0019 μMcIAP2-BIR3 K_i 0.0051 μM	207
Aegera Therapeutics **83**	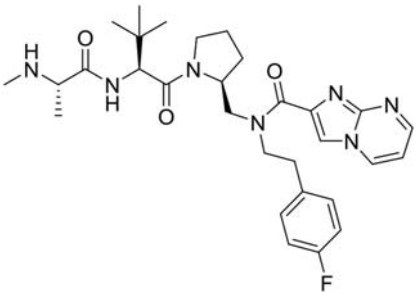	XIAP $K_i < 0.25$ μMcIAP1/2$K_i < 0.025$ μM	200
Allist Pharmaceuticals **84**	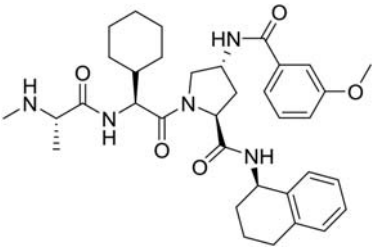	nr[b]	200
Genentech **85**	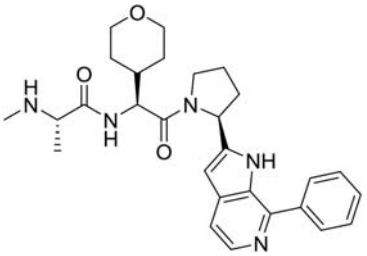	cIAP1-BIR3 $K_i = 0.071$ μM XIAP-BIR3 $K_i = 0.091$ μM	200
Avila Therapeutics **86**	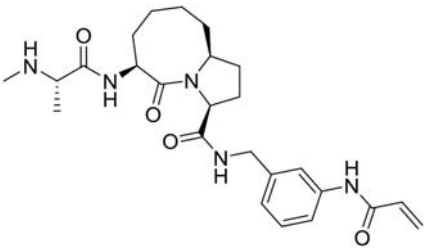	cIAP1 $K_i < 1$ μM XIAP $K_i < 1$ μM ML-IAP$K_i < 1$ μM	200
Roche **87**	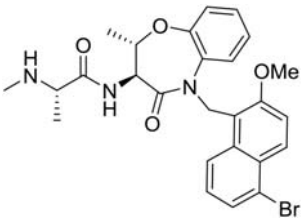	XIAP-BIR2 $IC_{50} = 0.029$ μM XIAP-BIR3 $IC_{50} = 32$ μM	200

Table 7 Monovalent Smac-XIAP inhibitors—cont'd

ID	*Structure*	*Activity* [a]	*References*
Hanmi Holdings **88**	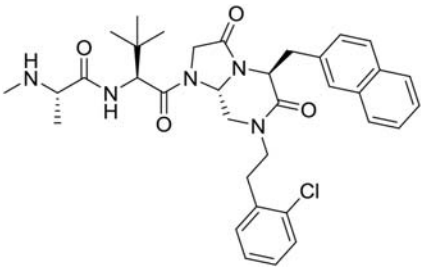	XIAP-BIR3 IC_{50} = 0.1-1 μM	200
Terralogic **89**	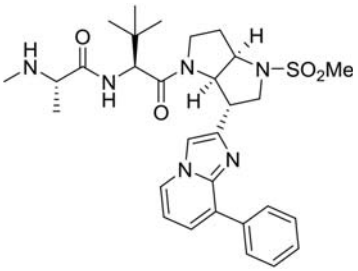	cIAP1-BIR3 K_d < 0.1 μM XIAP-BIR3 K_d < 0.1 μM	200
Boehringer Ingleheim **90**	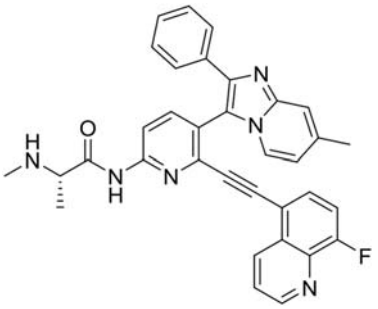	cIAP1-BIR3 IC_{50} = 0.001 μM XIAP-BIR3 IC_{50} = 0.047 μM	200
Astex Pharmaceuticals **91**	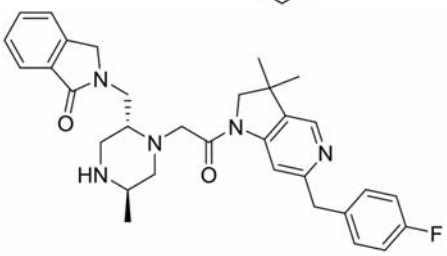	cIAP1-BIR3 K_i < 0.012 μM XIAP-BIR3 K_i < 0.04 μM	200

[a]Activity in cell-free assays.
[b]nr = not recorded.

5.06.3.3.2 Bivalent Smac-mimetic IAP antagonists

The bivalent Smac mimetics were discovered following the adventitious dimerization of an alkynyl Smac mimetic (Table 8).[208] The dimer (**92**) displayed similar activity to the monomer in a FP assay, but greater potency in a cell extract assay. The compound mimics the interaction of Smac that exists as a homodimer with XIAP, and binds to two XIAP BIR domains.

Molecular modeling of the monomer of SM-164 (**93**) bound to XIAP was used to identify a linking point for dimerization and the optimal chain length.[209] The dimer showed a significant gain in potency. Analytical gel filtration and protein NMR studies demonstrated that **93** binds to the BIR3 and BIR2 domain of a single XIAP molecule. Compound **93** induces apoptosis in leukemia cell lines, and is 1000 times more potent than the monomeric compound.

The dimeric Smac-mimetic BV6 (**94**) binds strongly to the BIR2 and BIR3 domains of XIAP and c-IAP1 and 2.[210,211] Treatment of cells with BV6 led to a rapid proteasomal degradation of c-IAP1 and 2, and apoptosis. The bivalent inhibitor **95** binds avidly to XIAP and c-IAP1 and 2.[212] **95** induced apoptosis in sensitive cell lines, and sensitized all cell lines tested to TNFα induced apoptosis. Similar cellular effects were observed with the potent bivalent inhibitor AEG40730 (**96**).[213]

Similarly, the bivalent Smac-mimetic Birinapant (TL32711, **97**) is a potent XIAP and cIAP antagonist, and induces IAP down-regulation in cells.[214,215] Birinapant induced apoptosis in cell lines either as a single agent or in combination with tumor necrosis factor (TNF) and TRAIL. In addition, **97** potentiates some chemotherapy drugs in a p53-independent manner. Birinapant has single-

Table 8 Bivalent Smac-XIAP inhibitors

ID	*Structure*	*Activity*[a]	*References*
92	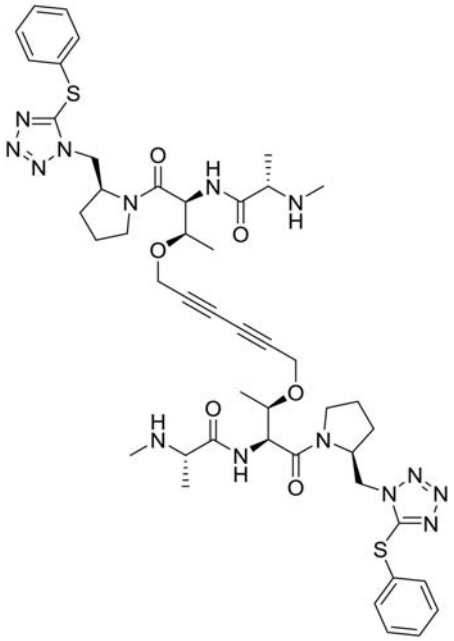	XIAP K_i 0.12 μM	208
SM-164 **93**	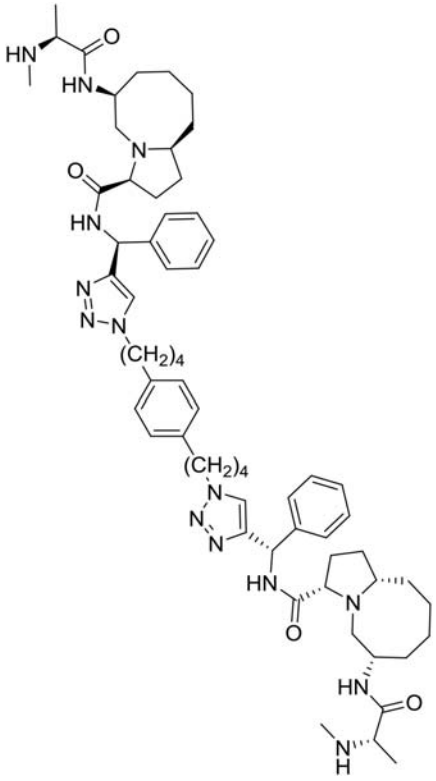	XIAP IC_{50} 0.00139 μM	209

Table 8 Bivalent Smac-XIAP inhibitors—cont'd

ID	*Structure*	*Activity*[a]	*References*
BV6 **94**	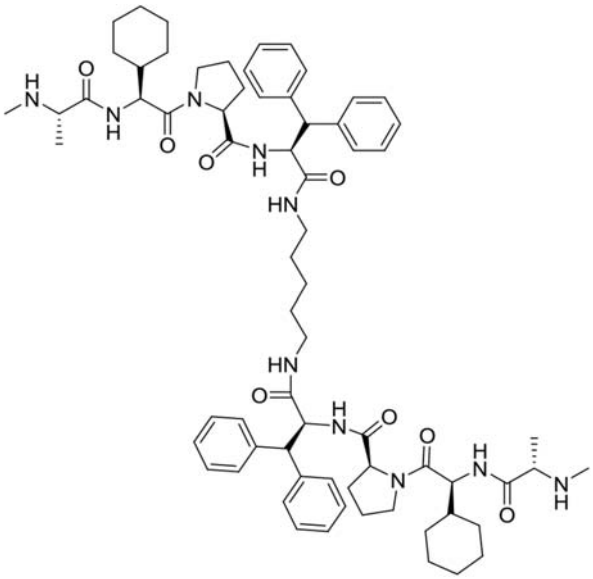	XIAP BIR2 K_i 0.91 μMXIAP BIR3 K_i 0.49 μM c-IAP1 BIR2 K_i 10.5 μM c-IAP1 BIR3 K_i 0.16 μM c-IAP2 BIR2 K_i 2.69 μM c-IAP2 BIR3 K_i 0.23 μM	210,211
95	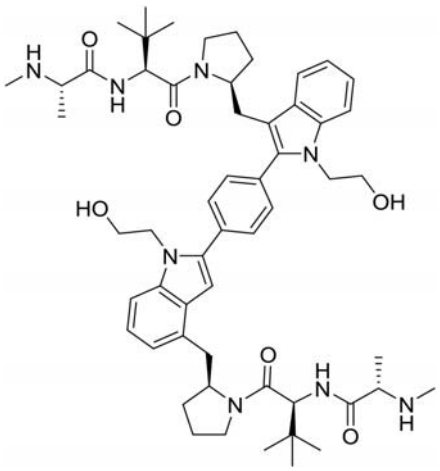	XIAP BIR3 K_d 0.003 μM c-IAP1 BIR3 K_d 0.001 μM	212
AEG40730 **96**	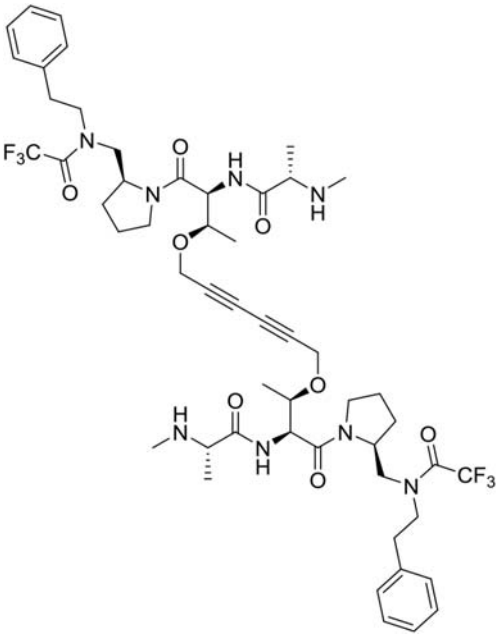	XIAP BIR3 K_d 0.100 μM c-IAP1 BIR3 K_d 0.017 μM c-IAP2 BIR3 K_d 0.034 μM	213

(Continued)

Table 8 Bivalent Smac-XIAP inhibitors—cont'd

ID	Structure	Activity[a]	References
TL32711 **97**	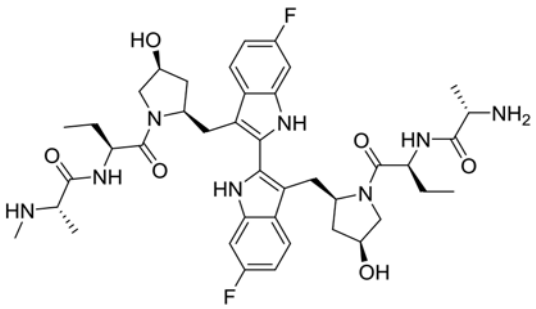	XIAP K_d 45 nM c-IAP1 $K_d < 1$ nM	215

[a]Activity in cell-free assays.

agent antitumor activity in patient derived xenograft models of ovarian cancer, colorectal cancer, and melanoma, and is undergoing clinical trials in solid and hematological malignancies.

5.06.3.4 Inhibitors of Other Cancer Related PPIs

5.06.3.4.1 14-3-3 proteins

The 14-3-3 family of regulatory proteins binds to many signaling proteins, including kinases, phosphatases and receptors, and is involved in mitogenic signaling, apoptosis, and cell cycle control.[216] The protein has a cup-like shape with an inner amphipathic groove, into which the ligand binds in a linear conformation. 14-3-3 proteins form homodimers, and the two inner ligand binding domains bind ligands in an antiparallel orientation. 14-3-3 proteins usually bind phosphoserine containing proteins, but proteins without phosphorylated residues are also reported to bind. The natural products cotylenin (**98**) and fusicoccin (**99**), and the immunosuppressant drug mizoribine (**100**) act to stabilize the 14-3-3 dimer and gave structural insights into the 14-3-3 ligand binding domain (Table 9).[217–219] A number of small-molecule inhibitors of 14-3-3 proteins PPIs with different proteins have been reported (Table 10). Peptide inhibitors, for example, (**101**) were identified using peptide microarrays, and induced apoptosis in cells. VS and docking yielded **102**, an inhibitor of the c-Abl/14-3-3 PPI that showed activity in imatinib resistant chronic myeloid leukaemia (CML) cell lines.[220,221] Inhibitors of 14-3-3/Raf PPI were discovered by library screening, the binding of **103** to 14-3-3 was confirmed by X-ray crystallography, although the diazo group reacted with the protein under the X-ray conditions.[222]

5.06.3.4.2 S100 protein inhibitors

The S100 family of proteins is small acidic calcium-binding proteins that regulate a number of protein partners. Small-molecule inhibitors of S100 family PPIs have been reported (Table 11). VS identified inhibitors of S100B-p53, for example, pentamidine **104**, which inhibited melanoma cell growth ($IC_{50} = 1.2$ μM).[223] The interaction of annexin A2 with S100A10 is important for cancer cell invasion, and annexin A2 is frequently overexpressed in cancers. The interaction has been well characterized by X-ray crystallography allowing the design of inhibitors. A docking-based VS identified a number of inhibitors, for example, **105**, as probe compounds.[224] A 3D pharmacophore model of the S100A10 binding site was used to screen compound databases, and identify triazoles, for example, **106**, with modest potency.

5.06.3.4.3 Myc/Max inhibitors

The oncogenic transcription factor Myc, a member of the basic helix-loop-helix leucine zipper (bHLHLZ) family, is required to dimerize with Max to act as a transcriptional regulator, so inhibitors of the Myc/Max PPI would control Myc activity (Table 12). Compounds inhibiting Myc/Max dimerization were identified from a library screen, for example, **107**, hits were confirmed by ELISA and an electrophoretic mobility-shift assay for DNA binding.[225] A "credit-card" library approach identified naphthalene bis-amides as c-Myc/Max inhibitors with micromolar potency and cellular activity.[226] A screen of 17,298 compounds identified **108** as a Myc/Max dimerization inhibitor, with reasonable selectivity against Jun/Fos heterodimerization, and **109** demonstrated c-Myc-dependant cell growth inhibition.[227] Compound **110** resulted from optimization of a screening hit.[228–231] A 3D pharmacophore model, derived from the structures of the active and inactive compounds described in Ref.,[230] was used to screen the ZINC database.[111] A circular dichroism-based assay for Myc/Max inhibition identified hit compounds, for example, phthalimide **111**, and amide **34** (Fig. 16) showed modest growth inhibitory activity in HL60 cells (IC_{50} 23 μM).

5.06.3.4.4 PDZ domain inhibitors

PDZ domains comprise ~90-amino acids forming six β-strands and two α-helices folded into a β-sandwich.[27] PDZ proteins act as scaffolds for supramolecular complexes and target proteins to specific cellular locations by binding the C-terminus of the target

Table 9 Stabilizers of 14-3-3 protein dimers

Compound	*Target*	*Structure*	*Activity*[a]	*References*
Cotylenin A **98**	14-3-3σ/PMA2	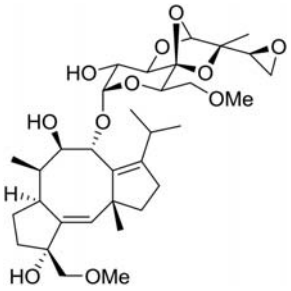	X-ray	217
Fusicoccin A **99**	14-3-3σ/PMA2	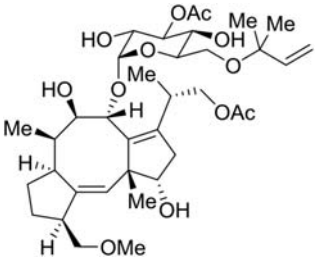	X-ray	217,218
Mizoribine Immunosuppressant **100**	14-3-3/GR	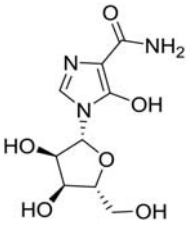	Affinity chromatography	219

[a]Activity in cell-free assays.

Table 10 14-3-3 PPI inhibitors

Compound	*Target*	*Structure*	*Activity*[a]	*References*
101	14-3-3σ	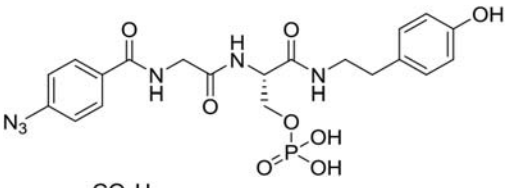	IC_{50} 2.6 μM	272
102	14-3-3σ/c-Abl	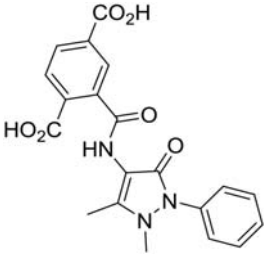	LD_{50} 1.04 μM[b]	220, 221
103	14-3-3σ/Raf	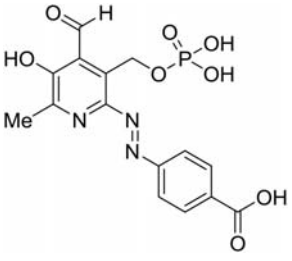	IC_{50} 9.3 μM	222

[a]Activity in cell-free assays.
[b]Clonogenic cytotoxicity in Ba/F3 cells.

Table 11 S100 PPI inhibitors

Compound	*Target*	*Structure*	*Activity*[a]	*References*
104	S100B-p53	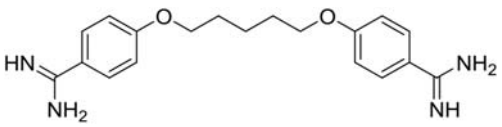	K_d 1.0 μM	223
105	Annexin A2/S100A10	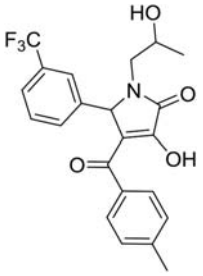	IC_{50} 4 μM	224
106	Annexin A2/S100A10	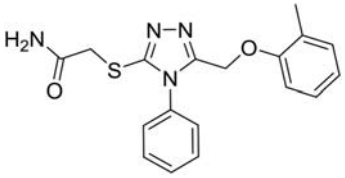	IC_{50} 24 μM	109

[a]Activity in cell-free assays.

Table 12 c-Myc/Max PPI inhibitors

Compound	*Target*	*Structure*	*Activity* [a]	*References*
107	c-Myc/Max	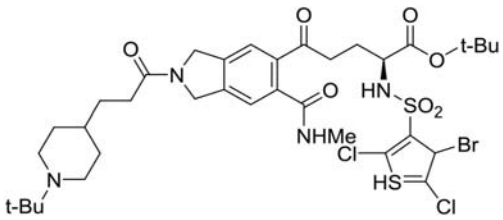	IC_{50} 125 μM	225
108	c-Myc/Max	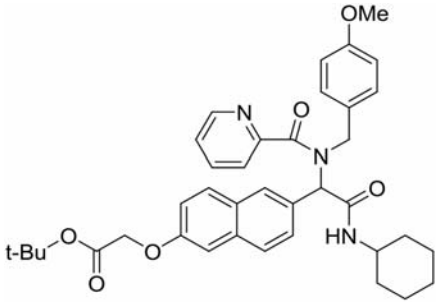	IC_{50} 37 μM	226
109	c-Myc/Max	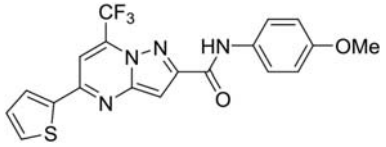	IC_{50} 30 μM	227
110	c-Myc-Max	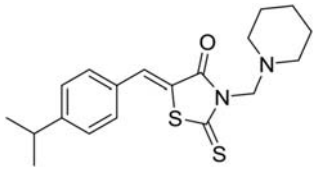	K_{obs} 1.0 μM	228–231
111	c-Myc-Max	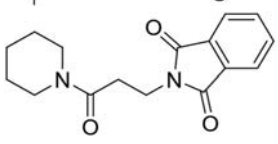	IC_{50} 10 μM	111

[a]Activity in cell-free assays.

Table 13 PDZ domain PPI inhibitors

Compound	*Target*	*Structure*	*Activity* [a]	*References*
112	PTEN/MAGI3 PDZ domain	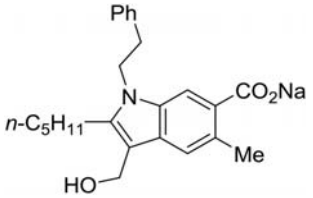	nr [b]	232
113	PTEN/MAGI3 PDZ domain Frz7/hDVL1,3	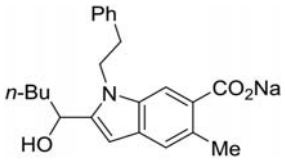	PTEN/MAGI3 $IC_{50} > 100$ μM Frz7/hDvl1 Ki 63 μM Frz7/hDvl1 Ki 29 μM	230, 270
114	NHERF1 PDZ domains	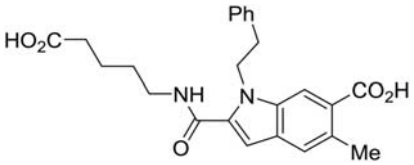	PDZ1: β2AR IC_{50} 15 μM PDZ2: CFTR IC_{50} 170 μM	234
115	DVL PDZ-Tcf	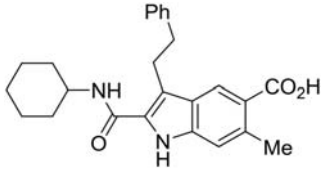	Dvl1 PDZ IC_{50} 157 μM Dvl2 PDZ IC_{50} 309 μM	235
116	AF6-PDZ domain	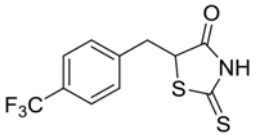	K_d 100 μM	236
117	AF6-PDZ domain	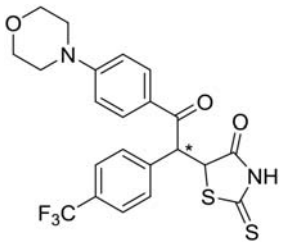	K_d 4.9 μM	237

[a]Activity in cell-free assays.
[b]*nr*, not recorded.

protein. PDZ inhibitors have been discovered by rational design and fragment screening (Table 13). Structure-based design of a mimic for the ITXV peptide motif gave the selective irreversible inhibitor of the second PDZ of MAGI3 (MAGI3-PDZ2) **112** that prevents MAGI3 association with the tumor suppressor protein PTEN.[232] The mechanism of inhibition is reported to be the trapping of histidine by the reactive hydroxymethyl group. Further structure-based design gave rise to the modified indole carbinol scaffold **113**.[233] The indole scaffold was also used to design inhibitors of Na^+/H^+ exchanger regulatory factor 1 (NHERF1) PDZ1, which has an uncertain role in cancer, and inhibition of PDZ1 binding to the β2 adrenergic receptor (β2AR) and cystic fibrosis conductance receptor (CFTR) was demonstrated by **114**.[234] A similar scaffold was used to target the PZD domain of the Dishevelled (Dvl) protein, an activator of the β-catenin/Tcf complex, and compound **115** induced apoptosis in cell lines engineered to overexpress Dvl.[235] The ALL-1 fusion partner on chromosome 6 (AF6) protein interacts with a variety of proteins by its second PDZ domain, including kinases and breakpoint cluster region (BCR).[236] NMR-based screening identified ligands for the AF6 PZD domain, for example, **116**. The lead compound was optimized to **117** that was 25-fold more potent, and was able to inhibit BCR binding in cellular pull-down experiements.[237]

5.06.3.4.5 SH2 and SH3 domain inhibitors

Src homology (SH) domains are noncatalytic protein modules. SH2 domains bind to phosphotyrosine residues, whereas SH3 domains preferentially bind to proline rich regions of target proteins. The natural product UCS15A (Table 14, **118**) was identified

Table 14 SH domain PPI inhibitors

Compound	*Target*	*Structure*	*Activity*[a]	*References*
UCS15A **118**	Stat3 dimerization SH2 domain	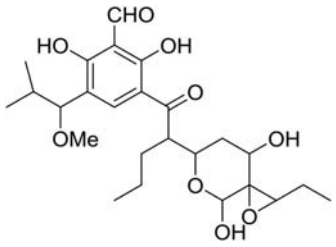	nr[b]	238,239
S3I-2001 **119**	Stat3 dimerization SH2 domain	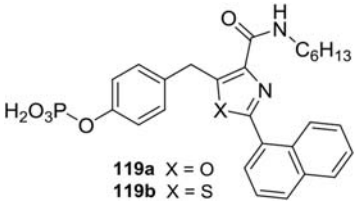 **119a** X = O **119b** X = S	**119a** IC_{50} 58 μM **119b** IC_{50} 25 μM	274,275
120	SHP2	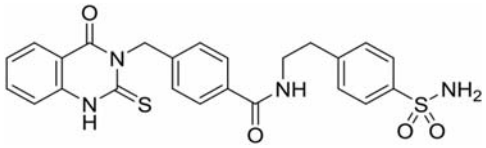	nr	240

[a]Activity in cell-free assays.
[b]*nr*, not recorded.

Table 15 Ras PPI inhibitors

Compound	*Target*	*Structure*	*Activity*[a]	*References*
121	Ras–SoS	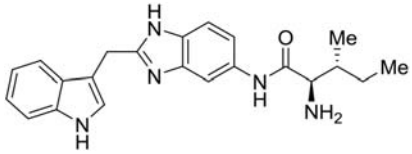	K_d 78 μM	241
122	Ras–SoS	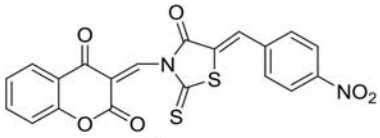	SoS K_d 7 μM IC_{50} 15.4 μM	242
123	Ras–SoS	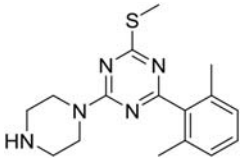	K_d 1.6 mM	243
Deltarasin **124**	K-Ras–PDEδ	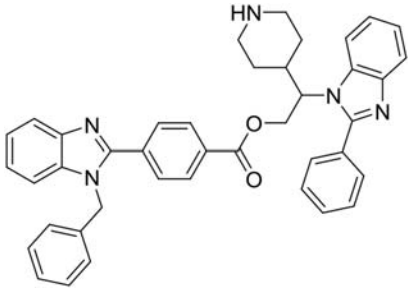	K_d 10 nM	244

[a]Activity in cell-free assays.

from a screen for Src inhibitors, and shown to act in a kinase independent manner by blocking the Src SH3 domain and inhibiting interactions with target proteins.[238,239] Signal transducer and activator of transcription 3 (Stat3) binds phosphotyrosine residues on target proteins via surface hot-spots. Inhibitors based on isoxazole and thiazole scaffolds (**119a** and **119b**) were identified that inhibit the Stat3 dimerization and DNA binding, but had little cellular effect. Src homology 2 domain-containing phosphatase (SHP2) plays a key role in cell signaling, in silico screening using the SHP2 X-ray structure identified hit compounds, for example, **120**, that inhibited SHP2-mediated signaling in cells.[240]

5.06.3.4.6 Ras PPI inhibitors

The small GTP-ase protein Ras regulates cell signaling by binding to extracellular receptors, for example, EGFR, via Son of Sevenless (SoS) and downstream kinases, for example, Raf. Small-molecule inhibitors of the Ras–SoS PPI have been identified through NMR-based fragment screening and X-ray crystallography (Table 15).[241] The indole benzamidazole fragment was developed by the addition of an amino acid to improve potency and solubility, for example, **121**, which showed activity in a SoS-catalyzed nucleotide exchange assay. A Ras–SoS inhibitor was discovered by a docking-based VS, compound **122** binds to SoS and inhibits Ras signaling in cells.[242] A number of fragments including triazine **123** were identified by X-ray-based fragment screening, and bound to three distinct binding pockets, one on SoS, one at the Ras–SoS interface, and one on Ras.[243] The identification of novel allosteric binding sites offers new possibilities for the design of Ras–SoS PPI inhibitors. Deltarasin **124** is a potent inhibitor of the Ras–PDEδ PPI by binding to the prenyl binding site of PDEδ and preventing Ras farnesylation.[244] Deltarasin inhibits Ras signaling in cells, and produced tumor growth delay in Panc-Tu-1 xenografts (10 mg kg^{-1} bid^{-1} ip).

5.06.3.4.7 Other PPI inhibitors

Other PPI inhibitors have been reported against a variety of cancer targets (Table 16). Screening approaches have identified promising lead compounds (**125–130**) for β-catenin/T-cell factor,[245] cyclin-dependent kinase 2 PPIs,[246,247] elF4E/elF4G,[248,249] EWS-FLI1,[250,251] HOX–PBX/DNA,[252]and IL6-GP130.[253] Peptide mimetic compounds **131** and **132** inhibit MLL1/WDR5,[254] and Pin1,[255] respectively. Fragment screening approaches have provided hit compounds (**133–135**) for PPI targets including RAD51/BRCA2,[256] pVHL-HIF-1α,[257,258] and ZipA/FtsZ.[259] VS has been used to provide hit compounds (**136–138**) for PPI targets including IL6-GP130,[253] Ral/RALBP1,[260] and uPAR/uPA.[261]

5.06.3.5 Challenges in the Optimization of PPI Inhibitors

Empirical guidelines for the assessment of likely oral bioavailability of a given molecule have been established. Lipinski's rule of five sets limits for MW (MW < 500), hydrogen bonds (donors ≤ 5, acceptors ≤ 10), and lipophilicity (cLogP < 5).[262] Further refinements to models for oral bioavailability include properties such as rotatable bonds, polar surface area, and pK_a.[263,264] Other useful measures for assessing druglike properties during optimization include LE[265] and lipophilic ligand efficiency.[266]

The challenge for designing druglike PPI inhibitors rests with balancing the extensive lipophilic interactions required for binding affinity to the target, with the need to maintain acceptable physicochemical properties, for example, MW, cLogP, and solubility, in a single compound. Clinical candidates reported to date illustrate different approaches to this problem. The Bcl-2 inhibitor navitoclax (**44**) exceeds the MW threshold (MW 945) and lipophilicity thresholds (cLogP 12.1). In addition to addressing selectivity, the MW and lipophilicity values have been reduced for the second generation Bcl-2 inhibitor venetoclax (**48**), but the compound still falls outside of the thresholds. Despite this both compounds have been effective in clinical trials with oral dosing and so acceptable PK and PD properties can be inferred. Development of the Nutlin series of MDM2–p53 inhibitors resulted in RG7112 (**51**), which exceeds both the MW (MW 728) and lipophilicity thresholds (cLogP 10.6). The PKs of RG7112 showed high levels of interpatient variability in the phase I trial, probably linked to the poor properties of the compound.[155] Other MDM2–p53 inhibitors in the clinic have lower MWs and include either acidic or basic groups to modulate their properties and improve solubility.

The evidence to date suggests that small-molecule PPI inhibitors will frequently fail to fit some of the ideal druglike parameters that have been defined previously. Experience gained from the clinical development of Bcl-2, MDM2–p53, and IAP inhibitors may inform and refine the definitions of druglike properties. Already it seems clear that drug candidates with nonideal physicochemical properties will require exquisite levels of potency against their target to demonstrate clinical efficacy.

5.06.4 Outlook

The importance of PPI inhibitors in cancer is shown by the number of PPI targets that have been explored to date and the diversity of the approaches used. Advances in screening methods, including peptide libraries, high-throughput screening methods, and structure-based fragment discovery have produced significant gains in understanding for PPI inhibitor design. It is likely that our growing understanding of the complexities of cancer cell biology will continue to highlight PPIs as points for therapeutic intervention. As the field matures, the historical view of PPI targets as "undruggable" seems certain to be proved incorrect.[269,271,273]

Table 16 Other PPI inhibitors

Compound	*Target*	*Structure*	*Activity*[a]	*References*
125	β-Catenin/T-cell factor	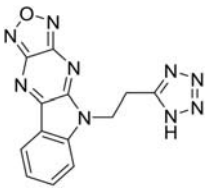	IC_{50} 76 μM	245
126	CDK2-CyclinA	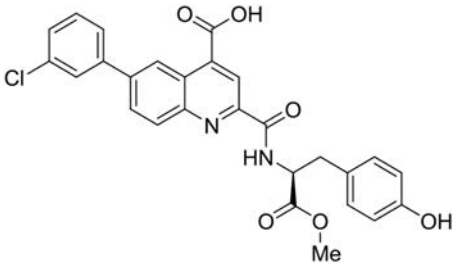	K_i 0.14 μM K_d 0.30 μM K_d 0.30 μM	246
127	CDK2-CKS1	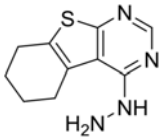	K_d 28 μM	247
128	eIF4E/eIF4G	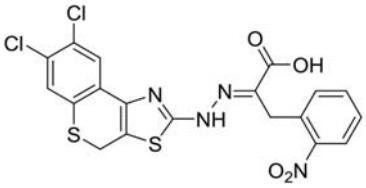	IC_{50} 15 μM	248,249
129	EWS-FLI1	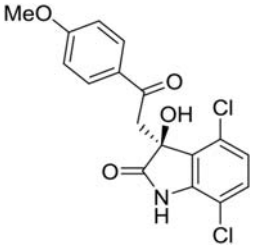	K_d 9.48 μM (*rac*)	250,251
130	HOX–PBX/DNA	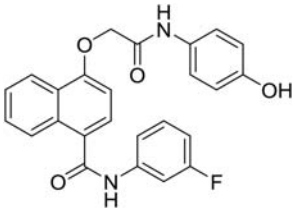	IC_{50} 65 μM	252
131	MLL1/WDR5	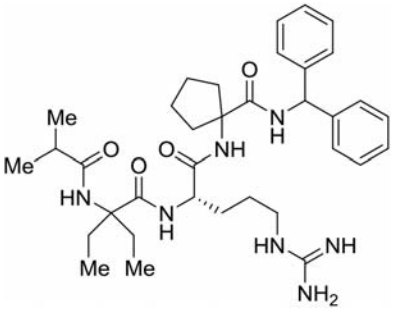	IC_{50} 2.9 μM	254

Table 16 Other PPI inhibitors—cont'd

Compound	*Target*	*Structure*	*Activity*[a]	*References*
132	Pin1	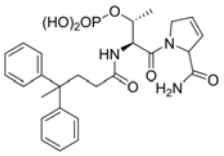	K_d 5 μM	255
133	RAD51/BRCA2	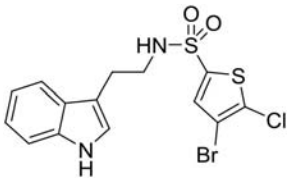	K_d 3.1 μM	256
134	pVHL-HIF-1α	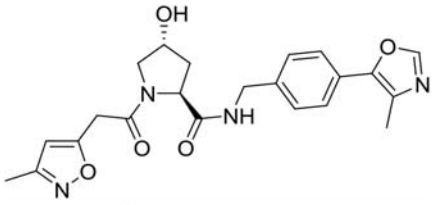	K_d 3.6 μM	257,258
135	ZipA/FtsZ	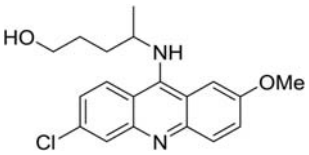	nr[b]	259
136	IL6-GP130	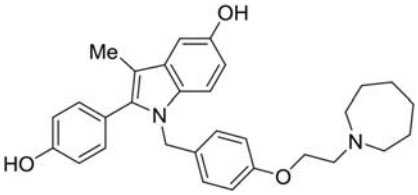	GI_{50} 25 μMSUM159 cells	253
137	Ral/RALBP1	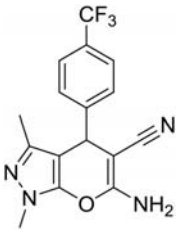	K_d 4.7 μM (SPR)	260
138	uPAR/uPA	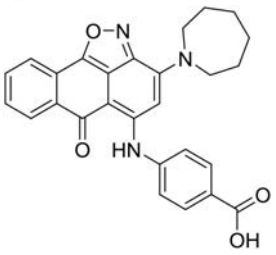	IC_{50} 10 μM	261

[a]Activity in cell-free assays.
[b]*nr*, not recorded.

See also: 2.13. Small-Molecule Inhibitors of Protein–Protein Interactions. 5.07. Targeting Protein Synthesis, Folding, and Degradation Pathways in Cancer. 8.04. The Discovery of First-in-Class Inhibitors of the Nedd8-Activating Enzyme (NAE) and the Ubiquitin-Activating Enzyme (UAE).

References

1. Hanahan, D.; Weinberg, R. A. The Hallmarks of Cancer. *Cell* **2000,** *100* (1), 57–70.
2. Ivanov, A. A.; Khuri, F. R.; Fu, H. Targeting Protein–Protein Interactions as an Anticancer Strategy. *Trends in Pharmacological Sciences* **2013,** *34* (7), 393–400.
3. Overington, J. P.; Al-Lazikani, B.; Hopkins, A. L. How Many Drug Targets Are There? *Nat. Rev. Drug Discov.* **2006,** *5* (12), 993–996.
4. Hopkins, A. L.; Groom, C. R. The Druggable Genome. *Nat. Rev. Drug Discov.* **2002,** *1* (9), 727–730.
5. Wells, J. A.; McClendon, C. L. Reaching for High-Hanging Fruit in Drug Discovery at Protein–Protein Interfaces. *Nature* **2007,** *450* (7172), 1001–1009.
6. Jones, S.; Thornton, J. M. Principles of Protein–Protein Interactions. *Proc. Natl. Acad. Sci.* **1996,** *93* (1), 13–20.
7. Stites, W. E. Protein−Protein Interactions: Interface Structure, Binding Thermodynamics, and Mutational Analysis. *Chem. Rev.* **1997,** *97* (44), 1233–1250.
8. Lo Conte, L.; Chothia, C.; Janin, J. The Atomic Structure of Protein–Protein Recognition Sites. *J. Mol. Biol.* **1999,** *285* (5), 2177–2198.
9. Young, L.; Jernigan, R. L.; Covell, D. G. A Role for Surface Hydrophobicity in Protein–Protein Recognition. *Protein Sci.* **1994,** *3* (5), 717–729.
10. Clackson, T.; Wells, J. A. A Hot Spot of Binding Energy in a Hormone-Receptor Interface. *Science* **1995,** *267* (5196), 383–386.
11. Bogan, A. A.; Thorn, K. S. Anatomy of Hot Spots in Protein Interfaces. *J. Mol. Biol.* **1998,** *280* (1), 1–9.
12. DeLano, W. L. Unraveling Hot Spots in Binding Interfaces: Progress and Challenges. *Curr. Opin. Struct. Biol.* **2002,** *12* (1), 14–20.
13. Wells, J. A. Molecular Design and Modeling: Concepts and Applications Part A: Proteins, Peptides, and Enzymes. In *Methods in Enzymology*; vol. 202; AP academic press: Cambridge, Massachusetts, USA, 1991, .
14. Morrison, K. L.; Weiss, G. A. Combinatorial Alanine-Scanning. *Curr. Opin. Chem. Biol.* **2001,** *5* (3), 302–307.
15. Moreira, I. S.; Fernandes, P. A.; Ramos, M. J. Hot Spots—A Review of the Protein–Protein Interface Determinant Amino-Acid Residues. *Proteins Struct. Funct. Bioinf.* **2007,** *68* (4), 803–812.
16. London, N.; Raveh, B.; Schueler-Furman, O. Druggable Protein–Protein Interactions—From Hot Spots to Hot Segments. *Curr. Opin. Chem. Biol.* **2013,** *17* (6), 952–959.
17. Kim, D. E.; Chivian, D.; Baker, D. Protein Structure Prediction and Analysis Using the Robetta Server. *Nucleic Acids Res.* **2004,** *32* (Web Server issue), W526–W531.
18. Tuncbag, N.; Gursoy, A.; Keskin, O. Identification of Computational Hot Spots in Protein Interfaces: Combining Solvent Accessibility and Inter-Residue Potentials Improves the Accuracy. *Bioinformatics* **2009,** *25* (12), 1513–1520.
19. Tuncbag, N.; Keskin, O.; Gursoy, A. HotPoint: Hot Spot Prediction Server for Protein Interfaces. *Nucleic Acids Res.* **2010,** *38* (Web Server issue), W402–W406.
20. Munteanu, C. R.; Pimenta, A. C.; Fernandez-Lozano, C.; Melo, A.; Cordeiro, M. N. D. S.; Moreira, I. S. Solvent Accessible Surface Area-Based Hot-Spot Detection Methods for Protein–Protein and Protein–Nucleic Acid Interfaces. *J. Chem. Inf. Model.* **2015,** *55* (5), 1077–1086.
21. Arkin, M. R.; Randal, M.; DeLano, W. L.; Hyde, J.; Luong, T. N.; Oslob, J. D.; Raphael, D. R.; Taylor, L.; Wang, J.; McDowell, R. S.; et al. Binding of Small Molecules to an Adaptive Protein–Protein Interface. *Proc. Natl. Acad. Sci. U. S. A.* **2003,** *100* (4), 1603–1608.
22. Eyrisch, S.; Helms, V. What Induces Pocket Openings on Protein Surface Patches Involved in Protein–Protein Interactions? *J. Comput. Aided Mol. Des.* **2009,** *23* (2), 73–86.
23. Metz, A.; Pfleger, C.; Kopitz, H.; Pfeiffer-Marek, S.; Baringhaus, K.-H.; Gohlke, H. Hot Spots and Transient Pockets: Predicting the Determinants of Small-Molecule Binding to a Protein–Protein Interface. *J. Chem. Inf. Model.* **2012,** *52* (1), 120–133.
24. Gao, M.; Skolnick, J. The Distribution of Ligand-Binding Pockets Around Protein–Protein Interfaces Suggests a General Mechanism for Pocket Formation. *Proc. Natl. Acad. Sci. U. S. A.* **2012,** *109* (10), 3784–3789.
25. Fu, H.; Subramanian, R. R.; Masters, S. C. 14-3-3 Proteins: Structure, Function, and Regulation. *Annu. Rev. Pharmacol. Toxicol.* **2000,** *40* (1), 617–647.
26. Yaffe, M. B.; Rittinger, K.; Volinia, S.; Caron, P. R.; Aitken, A.; Leffers, H.; Gamblin, S. J.; Smerdon, S. J.; Cantley, L. C. The Structural Basis for 14-3-3:Phosphopeptide Binding Specificity. *Cell* **1997,** *91* (7), 961–971.
27. Hung, A. Y.; Sheng, M. PDZ Domains: Structural Modules for Protein Complex Assembly. *J. Biol. Chem.* **2002,** *277* (8), 5699–5702.
28. Sudol, M. Structure and Function of the WW Domain. *Prog. Biophys. Mol. Biol.* **1996,** *65* (1–2), 113–132.
29. Cesareni, G.; Panni, S.; Nardelli, G.; Castagnoli, L. Can We Infer Peptide Recognition Specificity Mediated by SH3 Domains? *FEBS Lett.* **2002,** *513* (1), 38–44.
30. Davis, M. I.; Hunt, J. P.; Herrgard, S.; Ciceri, P.; Wodicka, L. M.; Pallares, G.; Hocker, M.; Treiber, D. K.; Zarrinkar, P. P. Comprehensive Analysis of Kinase Inhibitor Selectivity. *Nat. Biotechnol.* **2011,** *29* (11), 1046–1051.
31. Laraia, L.; McKenzie, G.; Spring, D. R.; Venkitaraman, A. R.; Huggins, D. J. Overcoming Chemical, Biological, and Computational Challenges in the Development of Inhibitors Targeting Protein–Protein Interactions. *Chem. Biol.* **2015,** *22* (6), 689–703.
32. Cinatl, J.; Speidel, D.; Hardcastle, I.; Michaelis, M. Resistance Acquisition to MDM2 Inhibitors. *Biochem. Soc. Trans.* **2014,** *42* (4), 752–757.
33. Shoemaker, B. A.; Panchenko, A. R. Deciphering Protein–Protein Interactions. Part I. Experimental Techniques and Databases. *PLoS Comput. Biol.* **2007,** *3* (3), e42.
34. Salwinski, L.; Eisenberg, D. Computational Methods of Analysis of Protein–Protein Interactions. *Curr. Opin. Struct. Biol.* **2003,** *13* (3), 377–382.
35. Fuller, J. C.; Burgoyne, N. J.; Jackson, R. M. Predicting Druggable Binding Sites at the Protein–Protein Interface. *Drug Discov. Today* **2009,** *14* (3–4), 155–161.
36. Zhang, Q. C.; Petrey, D.; Deng, L.; Qiang, L.; Shi, Y.; Thu, C. A.; Bisikirska, B.; Lefebvre, C.; Accili, D.; Hunter, T.; et al. Structure-Based Prediction of Protein–Protein Interactions on a Genome-Wide Scale. *Nature* **2012,** *490* (7421), 556–560.
37. Fauman, E. B.; Rai, B. K.; Huang, E. S. Structure-Based Druggability Assessment—Identifying Suitable Targets for Small Molecule Therapeutics. *Curr. Opin. Chem. Biol.* **2011,** *15* (4), 463–468.
38. Sheridan, R. P.; Maiorov, V. N.; Holloway, M. K.; Cornell, W. D.; Gao, Y.-D. Drug-Like Density: A Method of Quantifying the 'Bindability' of a Protein Target Based on a Very Large Set of Pockets and Drug-Like Ligands From the Protein Data Bank. *J. Chem. Inf. Model.* **2010,** *50* (11), 2029–2040.
39. Laurie, A. T. R.; Jackson, R. M. Q-SiteFinder: An Energy-Based Method for the Prediction of Protein–Ligand Binding Sites. *Bioinformatics* **2005,** *21* (9), 1908–1916.
40. Cheng, A. C.; Coleman, R. G.; Smyth, K. T.; Cao, Q.; Soulard, P.; Caffrey, D. R.; Salzberg, A. C.; Huang, E. S. Structure-Based Maximal Affinity Model Predicts Small-Molecule Druggability. *Nat. Biotechnol.* **2007,** *25* (1), 71–75.
41. Villoutreix, B. O.; Kuenemann, M. A.; Poyet, J.-L.; Bruzzoni-Giovanelli, H.; Labbé, C.; Lagorce, D.; Sperandio, O.; Miteva, M. A. Drug-Like Protein–Protein Interaction Modulators: Challenges and Opportunities for Drug Discovery and Chemical Biology. *Mol. Inf.* **2014,** *33* (6–7), 414–437.
42. Jin, L.; Wang, W.; Fang, G. Targeting Protein–Protein Interaction by Small Molecules. *Annu. Rev. Pharmacol. Toxicol.* **2014,** *54,* 435–456.
43. Torres, K.; Horwitz, S. B. Mechanisms of Taxol-Induced Cell Death Are Concentration Dependent. *Cancer Res.* **1998,** *58* (16), 3620–3626.
44. Schiff, P. B.; Horwitz, S. B. Taxol Stabilizes Microtubules in Mouse Fibroblast Cells. *Proc. Natl. Acad. Sci. U. S. A.* **1980,** *77* (3), 1561–1565.
45. Jordan, M. A.; Margolis, R. L.; Himes, R. H.; Wilson, L. Identification of a Distinct Class of Vinblastine Binding Sites on Microtubules. *J. Mol. Biol.* **1986,** *187* (1), 61–73.
46. Ngan, V. K.; Bellman, K.; Panda, D.; Hill, B. T.; Jordan, M. A.; Wilson, L. Novel Actions of the Antitumor Drugs Vinflunine and Vinorelbine on Microtubules. *Cancer Res.* **2000,** *60* (18), 5045–5051.
47. Cragg, G. M. Paclitaxel (Taxol): A Success Story With Valuable Lessons for Natural Product Drug Discovery and Development. *Med. Res. Rev.* **1998,** *18* (5), 315–331.

48. Mita, A. C.; Denis, L. J.; Rowinsky, E. K.; Debono, J. S.; Goetz, A. D.; Ochoa, L.; Forouzesh, B.; Beeram, M.; Patnaik, A.; Molpus, K.; et al. Phase I and Pharmacokinetic Study of XRP6258 (RPR 116258A), a Novel Taxane, Administered as a 1-Hour Infusion Every 3 Weeks in Patients With Advanced Solid Tumors. *Clin. Cancer Res.* **2009,** *15* (2), 723–730.
49. Towle, M. J.; Salvato, K. A.; Budrow, J.; Wels, B. F.; Kuznetsov, G.; Aalfs, K. K.; Welsh, S.; Zheng, W.; Seletsky, B. M.; Palme, M. H.; et al. In Vitro and in vivo Anticancer Activities of Synthetic Macrocyclic Ketone Analogues of Halichondrin B. *Cancer Res.* **2001,** *61* (3), 1013–1021.
50. Bollag, D. M.; McQueney, P. A.; Zhu, J.; Hensens, O.; Koupal, L.; Liesch, J.; Goetz, M.; Lazarides, E.; Woods, C. M. Epothilones, a New Class of Microtubule-Stabilizing Agents With a Taxol-Like Mechanism of Action. *Cancer Res.* **1995,** *55* (11), 2325–2333.
51. Conlin, A.; Fornier, M.; Hudis, C.; Kar, S.; Kirkpatrick, P. Ixabepilone. *Nat. Rev. Drug Discov.* **2007,** *6* (12), 953–954.
52. Rini, B.; Kar, S.; Kirkpatrick, P. Temsirolimus. *Nat. Rev. Drug Discov.* **2007,** *6* (8), 599–600.
53. Jordan, M. A.; Thrower, D.; Wilson, L. Mechanism of Inhibition of Cell Proliferation by Vinca Alkaloids. *Cancer Res.* **1991,** *51* (8), 2212–2222.
54. Gigant, B.; Wang, C.; Ravelli, R. B. G.; Roussi, F.; Steinmetz, M. O.; Curmi, P. A.; Sobel, A.; Knossow, M. Structural Basis for the Regulation of Tubulin by Vinblastine. *Nature* **2005,** *435* (7041), 519–522.
55. Manfredi, J. J.; Horwitz, S. B. Taxol: An Antimitotic Agent With a New Mechanism of Action. *Pharmacol. Ther.* **1984,** *25* (1), 83–125.
56. Amos, L. A.; Löwe, J. How Taxol® Stabilises Microtubule Structure. *Chem. Biol.* **1999,** *6* (3), R65–R69.
57. Smith, J. A.; Wilson, L.; Azarenko, O.; Zhu, X.; Lewis, B. M.; Littlefield, B. A.; Jordan, M. A. Eribulin Binds at Microtubule Ends to a Single Site on Tubulin to Suppress Dynamic Instability. *Biochemistry* **2010,** *49* (6), 1331–1337.
58. Faivre, S.; Kroemer, G.; Raymond, E. Current Development of mTOR Inhibitors as Anticancer Agents. *Nat. Rev. Drug Discov.* **2006,** *5* (8), 671–688.
59. Muchmore, S. W.; Sattler, M.; Liang, H.; Meadows, R. P.; Harlan, J. E.; Yoon, H. S.; Nettesheim, D.; Chang, B. S.; Thompson, C. B.; Wong, S. L.; et al. X-Ray and NMR Structure of Human Bcl-xL, an Inhibitor of Programmed Cell Death. *Nature* **1996,** *381* (6580), 335–341.
60. Sattler, M.; Liang, H.; Nettesheim, D.; Meadows, R. P.; Harlan, J. E.; Eberstadt, M.; Yoon, H. S.; Shuker, S. B.; Chang, B. S.; Minn, A. J.; et al. Structure of Bcl-xL-Bak Peptide Complex: Recognition Between Regulators of Apoptosis. *Science* **1997,** *275* (5302), 983–986.
61. Kussie, P. H.; Gorina, S.; Marechal, V.; Elenbaas, B.; Moreau, J.; Levine, A. J.; Pavletich, N. P. Structure of the MDM2 Oncoprotein Bound to the p53 Tumor Suppressor Transactivation Domain. *Science* **1996,** *274,* 948–953.
62. Böttger, V.; Böttger, A.; Garcia-Echeverria, C.; Ramos, Y. F. M.; van der Eb, A. J.; Jochemsen, A. G.; Lane, D. P. Comparative Study of the p53–mdm2 and p53–MDMX Interfaces. *Oncogene* **1999,** *18* (1), 189–199.
63. Garcia-Echeverria, C.; Chene, P.; Blommers, M. J. J.; Furet, P. Discovery of Potent Antagonists of the Interaction Between Human Double Minute 2 and Tumor Suppressor p53. *J. Med. Chem.* **2000,** *43* (17), 3205–3208.
64. Srinivasula, S. M.; Hegde, R.; Saleh, A.; Datta, P.; Shiozaki, E.; Chai, J.; Lee, R. A.; Robbins, P. D.; Fernandes-Alnemri, T.; Shi, Y.; et al. A Conserved XIAP-Interaction Motif in Caspase-9 and Smac/DIABLO Regulates Caspase Activity and Apoptosis. *Nature* **2001,** *410* (6824), 112–116.
65. Fulda, S.; Wick, W.; Weller, M.; Debatin, K.-M. Smac Agonists Sensitize for Apo2L/TRAIL- or Anticancer Drug-Induced Apoptosis and Induce Regression of Malignant Glioma In Vivo. *Nat. Med.* **2002,** *8* (8), 808–815.
66. Kipp, R. A.; Case, M. A.; Wist, A. D.; Cresson, C. M.; Carrell, M.; Griner, E.; Wiita, A.; Albiniak, P. A.; Chai, J.; Shi, Y.; et al. Molecular Targeting of Inhibitor of Apoptosis Proteins Based on Small Molecule Mimics of Natural Binding Partners. *Biochemistry* **2002,** *41* (23), 7344–7349.
67. Oost, T. K.; Sun, C.; Armstrong, R. C.; Al-Assaad, A.-S. S.; Betz, S. F.; Deckwerth, T. L.; Ding, H.; Elmore, S. W.; Meadows, R. P.; Olejniczak, E. T.; et al. Discovery of Potent Antagonists of the Antiapoptotic Protein XIAP for the Treatment of Cancer. *J. Med. Chem.* **2004,** *47* (18), 4417–4426.
68. Sharma, S. K.; Straub, C.; Zawel, L. Development of Peptidomimetics Targeting IAPs. *Int. J. Pept. Res. Ther.* **2006,** *12* (1), 21–32.
69. Kritzer, J. A.; Stephens, O. M.; Guarracino, D. A.; Reznik, S. K.; Schepartz, A. β-Peptides as Inhibitors of Protein–Protein Interactions. *Bioorg. Med. Chem.* **2005,** *13* (1), 11–16.
70. Kritzer, J. A.; Lear, J. D.; Hodsdon, M. E.; Schepartz, A. Helical β-Peptide Inhibitors of the p53-hDM2 Interaction. *J. Am. Chem. Soc.* **2004,** *126* (31), 9468–9469.
71. Kritzer, J. A.; Hodsdon, M. E.; Schepartz, A. Solution Structure of a β-Peptide Ligand for hDM2. *J. Am. Chem. Soc.* **2005,** *127* (12), 4118–4119.
72. Liu, M.; Pazgier, M.; Li, C.; Yuan, W.; Li, C.; Lu, W. A Left-Handed Solution to Peptide Inhibition of the p53–MDM2 Interaction. *Angew. Chem. Int. Ed.* **2010,** *49* (21), 3649–3652.
73. Zhan, C.; Zhao, L.; Wei, X.; Wu, X.; Chen, X.; Yuan, W.; Lu, W.-Y.; Pazgier, M.; Lu, W. An Ultrahigh Affinity D-Peptide Antagonist of MDM2. *J. Med. Chem.* **2012,** *55* (13), 6237–6241.
74. Sakurai, K.; Chung, H. S.; Kahne, D. Use of a Retroinverso p53 Peptide as an Inhibitor of MDM2. *J. Am. Chem. Soc.* **2004,** *126* (50), 16288–16289.
75. Fasan, R.; Dias, R. L. A.; Moehle, K.; Zerbe, O.; Obrecht, D.; Mittl, P. R. E.; Grütter, M. G.; Robinson, J. A. Structure-Activity Studies in a Family of β-Hairpin Protein Epitope Mimetic Inhibitors of the p53-HDM2 Protein–Protein Interaction. *ChemBioChem* **2006,** *7* (3), 515–526.
76. Fasan, R.; Dias, R. L. A.; Moehle, K.; Zerbe, O.; Vrijbloed, J. W.; Obrecht, D.; Robinson, J. A. Using a β-Hairpin To Mimic an α-Helix: Cyclic Peptidomimetic Inhibitors of the p53–HDM2 Protein–Protein Interaction. *Angew. Chem. Int. Ed.* **2004,** *43* (16), 2109–2112.
77. Quartararo, J. S.; Wu, P.; Kritzer, J. A. Peptide Bicycles That Inhibit the Grb2 SH2 Domain. *ChemBioChem* **2012,** *13* (10), 1490–1496.
78. Scott, C. P.; Abel-Santos, E.; Jones, A. D.; Benkovic, S. J. Structural Requirements for the Biosynthesis of Backbone Cyclic Peptide Libraries. *Chem. Biol.* **2001,** *8* (8), 801–815.
79. Tavassoli, A.; Lu, Q.; Gam, J.; Pan, H.; Benkovic, S. J.; Cohen, S. N. Inhibition of HIV Budding by a Genetically Selected Cyclic Peptide Targeting the Gag-TSG101 Interaction. *ACS Chem. Biol.* **2008,** *3* (12), 757–764.
80. Miranda, E.; Nordgren, I. K.; Male, A. L.; Lawrence, C. E.; Hoakwie, F.; Cuda, F.; Court, W.; Fox, K. R.; Townsend, P. A.; Packham, G. K.; et al. A Cyclic Peptide Inhibitor of HIF-1 Heterodimerization That Inhibits Hypoxia Signaling in Cancer Cells. *J. Am. Chem. Soc.* **2013,** *135* (28), 10418–10425.
81. Kritzer, J. A.; Zutshi, R.; Cheah, M.; Ran, F. A.; Webman, R.; Wongjirad, T. M.; Schepartz, A. Miniature Protein Inhibitors of the p53-hDM2 Interaction. *ChemBioChem* **2006,** *7* (1), 29–31.
82. Schafmeister, C. E.; Po, J.; Verdine, G. L. An All-Hydrocarbon Cross-Linking System for Enhancing the Helicity and Metabolic Stability of Peptides. *J. Am. Chem. Soc.* **2000,** *122* (24), 5891–5892.
83. Bernal, F.; Wade, M.; Godes, M.; Davis, T. N.; Whitehead, D. G.; Kung, A. L.; Wahl, G. M.; Walensky, L. D. A Stapled p53 Helix Overcomes HDMX-Mediated Suppression of p53. *Cancer Cell* **2010,** *18* (5), 411–422.
84. Bernal, F.; Tyler, A. F.; Korsmeyer, S. J.; Walensky, L. D.; Verdine, G. L. Reactivation of the p53 Tumor Suppressor Pathway by a Stapled p53 Peptide. *J. Am. Chem. Soc.* **2007,** *129* (9), 2456–2457.
85. Chang, Y. S.; Graves, B.; Guerlavais, V.; Tovar, C.; Packman, K.; To, K.-H.; Olson, K. A.; Kesavan, K.; Gangurde, P.; Mukherjee, A.; et al. Stapled α−Helical Peptide Drug Development: A Potent Dual Inhibitor of MDM2 and MDMX for p53-Dependent Cancer Therapy. *Proc. Natl. Acad. Sci. U. S. A.* **2013,** *110* (36), E3445–E3454.
86. Kawamoto, S. A.; Coleska, A.; Ran, X.; Yi, H.; Yang, C.-Y.; Wang, S. Design of Triazole-Stapled BCL9 α-Helical Peptides to Target the β-Catenin/B-Cell CLL/Lymphoma 9 (BCL9) Protein–Protein Interaction. *J. Med. Chem.* **2012,** *55* (3), 1137–1146.
87. Stewart, M. L.; Fire, E.; Keating, A. E.; Walensky, L. D. The MCL-1 BH3 Helix Is an Exclusive MCL-1 Inhibitor and Apoptosis Sensitizer. *Nat. Chem. Biol.* **2010,** *6* (8), 595–601.
88. Cohen, N. A.; Stewart, M. L.; Gavathiotis, E.; Tepper, J. L.; Bruekner, S. R.; Koss, B.; Opferman, J. T.; Walensky, L. D. A Competitive Stapled Peptide Screen Identifies a Selective Small Molecule That Overcomes MCL-1-Dependent Leukemia Cell Survival. *Chem. Biol.* **2012,** *19* (9), 1175–1186.
89. Whitby, L. R.; Boger, D. L. Comprehensive Peptidomimetic Libraries Targeting Protein–Protein Interactions. *Acc. Chem. Res.* **2012,** *45* (10), 1698–1709.

90. Hara, T.; Durell, S. R.; Myers, M. C.; Appella, D. H. Probing the Structural Requirements of Peptoids That Inhibit HDM2–p53 Interactions. *J. Am. Chem. Soc.* **2006,** *128* (6), 1995–2004.
91. Yin, H.; Lee, G. I.; Park, H. S.; Payne, G. A.; Rodriguez, J. M.; Sebti, S. M.; Hamilton, A. D. Terphenyl-Based Helical Mimetics That Disrupt the p53/HDM2 Interaction. *Angew. Chem. Int. Ed.* **2005,** *44* (18), 2704–2707.
92. Yin, H.; Hamilton, A. D. Terephthalamide Derivatives as Mimetics of the Helical Region of Bak Peptide Target Bcl-xL Protein. *Bioorg. Med. Chem. Lett.* **2004,** *14* (6), 1375–1379.
93. Campbell, F.; Plante, J. P.; Edwards, T. A.; Warriner, S. L.; Wilson, A. J. N-Alkylated Oligoamide α-Helical Proteomimetics. *Org. Biomol. Chem.* **2010,** *8* (10), 2344.
94. Plante, J. P.; Burnley, T.; Malkova, B.; Webb, M. E.; Warriner, S. L.; Edwards, T. A.; Wilson, A. J. Oligobenzamide Proteomimetic Inhibitors of the p53-hDM2 Protein–Protein Interaction. *Chem. Commun.* **2009,** *34,* 5091–5093.
95. Sakurai, K.; Kahne, D. Design and Synthesis of Functionalized Trisaccharides as p53-Peptide Mimics. *Tetrahedron Lett.* **2010,** *51* (29), 3724–3727.
96. Kuenemann, M. A.; Sperandio, O.; Labbé, C. M.; Lagorce, D.; Miteva, M. A.; Villoutreix, B. O. In Silico Design of Low Molecular Weight Protein–Protein Interaction Inhibitors: Overall Concept and Recent Advances. *Prog. Biophys. Mol. Biol.* **2015,** *119,* 20–32.
97. Hamon, V.; Brunel, J. M.; Combes, S.; Basse, M. J.; Roche, P.; Morelli, X. 2P2Ichem: Focused Chemical Libraries Dedicated to Orthosteric Modulation of Protein–Protein Interactions. *Med. Chem. Commun.* **2013,** *4* (5), 797.
98. Morelli, X.; Bourgeas, R.; Roche, P. Chemical and Structural Lessons From Recent Successes in Protein–Protein Interaction Inhibition (2P2I). *Curr. Opin. Chem. Biol.* **2011,** *15* (4), 475–481.
99. Koes, D.; Khoury, K.; Huang, Y.; Wang, W.; Bista, M.; Popowicz, G. M.; Wolf, S.; Holak, T. A.; Dömling, A.; Camacho, C. J. Enabling Large-Scale Design, Synthesis and Validation of Small Molecule Protein–Protein Antagonists. *PLoS One* **2012,** *7* (3), e32839.
100. Kuenemann, M. A.; Bourbon, L. M. L.; Labbé, C. M.; Villoutreix, B. O.; Sperandio, O. Which Three-Dimensional Characteristics Make Efficient Inhibitors of Protein–Protein Interactions? *J. Chem. Inf. Model.* **2014,** *54* (11), 3067–3079.
101. Marcaurelle, L. A.; Johannes, C.; Yohannes, D.; Tillotson, B. P.; Mann, D. Diversity-Oriented Synthesis of a Cytisine-Inspired Pyridone Library Leading to the Discovery of Novel Inhibitors of Bcl-2. *Bioorg. Med. Chem. Lett.* **2009,** *19* (9), 2500–2503.
102. Dahlin, J. L.; Nissink, J. W. M.; Strasser, J. M.; Francis, S.; Higgins, L.; Zhou, H.; Zhang, Z.; Walters, M. A. PAINS in the Assay: Chemical Mechanisms of Assay Interference and Promiscuous Enzymatic Inhibition Observed during a Sulfhydryl-Scavenging HTS. *J. Med. Chem.* **2015,** *58* (5), 2091–2113.
103. Baell, J. B.; Holloway, G. A. New Substructure Filters for Removal of Pan Assay Interference Compounds (PAINS) From Screening Libraries and for Their Exclusion in Bioassays. *J. Med. Chem.* **2010,** *53* (7), 2719–2740.
104. Baell, J.; Walters, M. A. Chemistry: Chemical Con Artists Foil Drug Discovery. *Nature* **2014,** *513* (7519), 481–483.
105. Sable, R.; Jois, S. Surfing the Protein–Protein Interaction Surface Using Docking Methods: Application to the Design of PPI Inhibitors. *Molecules* **2015,** *20* (6), 11569–11603.
106. Bowman, A. L.; Nikolovska-Coleska, Z.; Zhong, H.; Wang, S.; Carlson, H. A. Small Molecule Inhibitors of the MDM2–p53 Interaction Discovered by Ensemble-Based Receptor Models. *J. Am. Chem. Soc.* **2007,** *129* (42), 12809–12814.
107. Enyedy, I. J.; Huang, Y.; Long, Y. Q.; Roller, P. P.; Yang, D.; Wang, S.; Ling, Y.; Nacro, K.; Tomita, Y.; Wu, X.; et al. Discovery of Small-Molecule Inhibitors of Bcl-2 Through Structure-Based Computer Screening. *J. Med. Chem.* **2001,** *44* (25), 4313–4324.
108. Wang, J. L.; Liu, D.; Zhang, Z. J.; Shan, S.; Han, X.; Srinivasula, S. M.; Croce, C. M.; Alnemri, E. S.; Huang, Z. Structure-Based Discovery of an Organic Compound That Binds Bcl-2 Protein and Induces Apoptosis of Tumor Cells. *Proc. Natl. Acad. Sci. U. S. A.* **2000,** *97* (13), 7124–7129.
109. Reddy, T. R. K.; Li, C.; Fischer, P. M.; Dekker, L. V. Three-Dimensional Pharmacophore Design and Biochemical Screening Identifies Substituted 1,2,4-Triazoles as Inhibitors of the AnnexinA2-S100A10 Protein Interaction. *ChemMedChem* **2012,** *7* (8), 1435–1446.
110. Rechfeld, F.; Gruber, P.; Kirchmair, J.; Boehler, M.; Hauser, N.; Hechenberger, G.; Garczarczyk, D.; Lapa, G. B.; Preobrazhenskaya, M. N.; Goekjian, P.; et al. Thienoquinolines as Novel Disruptors of the PKCε/RACK2 Protein–Protein Interaction. *J. Med. Chem.* **2014,** *57* (8), 3235–3246.
111. Mustata, G.; Follis, A. V.; Hammoudeh, D. I.; Metallo, S. J.; Wang, H.; Prochownik, E. V.; Lazo, J. S.; Bahar, I. Discovery of Novel Myc-Max Heterodimer Disruptors With a Three-Dimensional Pharmacophore Model. *J. Med. Chem.* **2009,** *52* (5), 1247–1250.
112. Lu, Y.; Nikolovska-Coleska, Z.; Fang, X.; Gao, W.; Shangary, S.; Qiu, S.; Qin, D.; Wang, S. Discovery of a Nanomolar Inhibitor of the Human Murine Double Minute 2 (MDM2)–p53 Interaction Through an Integrated, Virtual Database Screening Strategy. *J. Med. Chem.* **2006,** *49* (13), 3759–3762.
113. Hartshorn, M. J.; Murray, C. W.; Cleasby, A.; Frederickson, M.; Tickle, I. J.; Jhoti, H. Fragment-Based Lead Discovery Using X-Ray Crystallography. *J. Med. Chem.* **2005,** *48* (2), 403–413.
114. Shuker, S. B.; Hajduk, P. J.; Meadows, R. P.; Fesik, S. W. Discovering High-Affinity Ligands for Proteins: SAR by NMR. *Science* **1996,** *274* (5292), 1531–1534.
115. Patrone, J. D.; Kennedy, J. P.; Frank, A. O.; Feldkamp, M. D.; Vangamudi, B.; Pelz, N. F.; Rossanese, O. W.; Waterson, A. G.; Chazin, W. J.; Fesik, S. W. Discovery of Protein–Protein Interaction Inhibitors of Replication Protein A. *ACS Med. Chem. Lett.* **2013,** *4* (7), 601–605.
116. Frank, A. O.; Feldkamp, M. D.; Kennedy, J. P.; Waterson, A. G.; Pelz, N. F.; Patrone, J. D.; Vangamudi, B.; Camper, D. V.; Rossanese, O. W.; Chazin, W. J.; et al. Discovery of a Potent Inhibitor of Replication Protein A Protein–Protein Interactions Using a Fragment-Linking Approach. *J. Med. Chem.* **2013,** *56* (22), 9242–9250.
117. Becattini, B.; Sareth, S.; Zhai, D. Y.; Crowell, K. J.; Leone, M.; Reed, J. C.; Pellecchia, M. Targeting Apoptosis via Chemical Design: Inhibition of Bid-Induced Cell Death by Small Organic Molecules. *Chem. Biol.* **2004,** *11* (8), 1107–1117.
118. Adams, J. M. The Bcl-2 Protein Family: Arbiters of Cell Survival. *Science* **1998,** *281* (5381), 1322–1326.
119. Gross, A.; McDonnell, J. M.; Korsmeyer, S. J. BCL-2 Family Members and the Mitochondria in Apoptosis. *Genes Dev.* **1999,** *13* (15), 1899–1911.
120. Czabotar, P. E.; Lessene, G.; Strasser, A.; Adams, J. M. Control of Apoptosis by the BCL-2 Protein Family: Implications for Physiology and Therapy. *Nat. Rev. Mol. Cell Biol.* **2014,** *15* (1), 49–63.
121. Kitada, S.; Leone, M.; Sareth, S.; Zhai, D.; Reed, J. C.; Pellecchia, M. Discovery, Characterization, and Structure-Activity Relationships Studies of Proapoptotic Polyphenols Targeting B-Cell Lymphocyte/Leukemia-2 Proteins. *J. Med. Chem.* **2003,** *46* (20), 4259–4264.
122. Becattini, B.; Kitada, S.; Leone, M.; Monosov, E.; Chandler, S.; Zhai, D.; Kipps, T. J.; Reed, J. C.; Pellecchia, M.; Jolla, L. Rational Design and Real Time, In-Cell Detection of the Proapoptotic Activity of a Novel Compound Targeting Bcl-X L. *Chem. Biol.* **2004,** *11,* 389–395.
123. Gao, P.; Bauvy, C.; Souquère, S.; Tonelli, G.; Liu, L.; Zhu, Y.; Qiao, Z.; Bakula, D.; Proikas-Cezanne, T.; Pierron, G.; et al. The Bcl-2 Homology Domain 3 Mimetic Gossypol Induces Both Beclin 1-Dependent and Beclin 1-Independent Cytoprotective Autophagy in Cancer Cells. *J. Biol. Chem.* **2010,** *285* (33), 25570–25581.
124. Nguyen, M.; Marcellus, R. C.; Roulston, A.; Watson, M.; Serfass, L.; Murthy Madiraju, S. R.; Goulet, D.; Viallet, J.; Bélec, L.; Billot, X.; et al. Small Molecule Obatoclax (GX15-070) Antagonizes MCL-1 and Overcomes MCL-1-Mediated Resistance to Apoptosis. *Proc. Natl. Acad. Sci. U. S. A.* **2007,** *104* (49), 19512–19517.
125. Zhai, D.; Jin, C.; Satterthwait, A. C.; Reed, J. C. Comparison of Chemical Inhibitors of Antiapoptotic Bcl-2-Family Proteins. *Cell Death Differ.* **2006,** *13* (8), 1419–1421.
126. Oltersdorf, T.; Elmore, S. W.; Shoemaker, A. R.; Armstrong, R. C.; Augeri, D. J.; Belli, B. A.; Bruncko, M.; Deckwerth, T. L.; Dinges, J.; Hajduk, P. J.; et al. An Inhibitor of Bcl-2 Family Proteins Induces Regression of Solid Tumours. *Nature* **2005,** *435* (7042), 677–681.
127. Bruncko, M.; Oost, T. K.; Belli, B. A.; Ding, H.; Joseph, M. K.; Kunzer, A.; Martineau, D.; McClellan, W. J.; Mitten, M.; Ng, S.-C.; et al. Studies Leading to Potent, Dual Inhibitors of Bcl-2 and Bcl-xL. *J. Med. Chem.* **2007,** *50* (4), 641–662.
128. Park, C.-M.; Bruncko, M.; Adickes, J.; Bauch, J.; Ding, H.; Kunzer, A.; Marsh, K. C.; Nimmer, P.; Shoemaker, A. R.; Song, X.; et al. Discovery of an Orally Bioavailable Small Molecule Inhibitor of Prosurvival B-Cell Lymphoma 2 Proteins. *J. Med. Chem.* **2008,** *51* (21), 6902–6915.
129. Tse, C.; Shoemaker, A. R.; Adickes, J.; Anderson, M. G.; Chen, J.; Jin, S.; Johnson, E. F.; Marsh, K. C.; Mitten, M. J.; Nimmer, P.; et al. ABT-263: A Potent and Orally Bioavailable Bcl-2 Family Inhibitor. *Cancer Res.* **2008,** *68* (9), 3421–3428.

130. Zhou, H.; Chen, J.; Meagher, J. L.; Yang, C.-Y.; Aguilar, A.; Liu, L.; Bai, L.; Cong, X.; Cai, Q.; Fang, X.; et al. Correction to Design of Bcl-2 and Bcl-xL Inhibitors With Subnanomolar Binding Affinities Based Upon a New Scaffold. *J. Med. Chem.* **2012,** *55* (12), 5987.
131. Tang, G.; Yang, C.-Y.; Nikolovska-Coleska, Z.; Guo, J.; Qiu, S.; Wang, R.; Gao, W.; Wang, G.; Stuckey, J.; Krajewski, K.; et al. Pyrogallol-Based Molecules as Potent Inhibitors of the Antiapoptotic Bcl-2 Proteins. *J. Med. Chem.* **2007,** *50* (8), 1723–1726.
132. Zhang, Z.; Wu, G.; Xie, F.; Song, T.; Chang, X. 3-Thiomorpholin-8-oxo-8 H-Acenaphtho [1, 2- B] Pyrrole-9-carbonitrile (S1) Based Molecules as Potent, Dual Inhibitors of B-Cell Lymphoma 2 (Bcl-2) and Myeloid Cell Leukemia Sequence 1 (Mcl-1): Structure-Based Design and Structure-Activity Re. *J. Med. Chem.* **2011,** *54* (4), 1101–1105.
133. Souers, A. J.; Leverson, J. D.; Boghaert, E. R.; Ackler, S. L.; Catron, N. D.; Chen, J.; Dayton, B. D.; Ding, H.; Enschede, S. H.; Fairbrother, W. J.; et al. ABT-199, a Potent and Selective BCL-2 Inhibitor, Achieves Antitumor Activity While Sparing Platelets. *Nat. Med.* **2013,** *19* (2), 202–208.
134. Van Poznak, C.; Seidman, A. D.; Reidenberg, M. M.; Moasser, M. M.; Sklarin, N.; Van Zee, K.; Borgen, P.; Gollub, M.; Bacotti, D.; Yao, T.-J.; et al. Oral Gossypol in the Treatment of Patients With Refractory Metastatic Breast Cancer: A Phase I/II Clinical Trial. *Breast Cancer Res. Treat.* **2001,** *66* (3), 239–248.
135. Stein, R. C.; Joseph, A. E.; Matlin, S. A.; Cunningham, D. C.; Ford, H. T.; Coombes, R. C. A Preliminary Clinical Study of Gossypol in Advanced Human Cancer. *Cancer Chemother. Pharmacol.* **1992,** *30* (6), 480–482.
136. Liu, G.; Kelly, W. K.; Wilding, G.; Leopold, L.; Brill, K.; Somer, B. An Open-Label, Multicenter, Phase I/II Study of Single-Agent AT-101 in Men With Castrate-Resistant Prostate Cancer. *Clin. Cancer Res.* **2009,** *15* (9), 3172–3176.
137. Wang, G.; Nikolovska-Coleska, Z.; Yang, C.-Y.; Wang, R.; Tang, G.; Guo, J.; Shangary, S.; Qiu, S.; Gao, W.; Yang, D.; et al. Structure-Based Design of Potent Small-Molecule Inhibitors of Anti-Apoptotic Bcl-2 Proteins. *J. Med. Chem.* **2006,** *49* (21), 6139–6142.
138. Hwang, J. J.; Kuruvilla, J.; Mendelson, D.; Pishvaian, M. J.; Deeken, J. F.; Siu, L. L.; Berger, M. S.; Viallet, J.; Marshall, J. L. Phase I Dose Finding Studies of Obatoclax (GX15-070), a Small Molecule Pan-BCL-2 Family Antagonist, in Patients With Advanced Solid Tumors or Lymphoma. *Clin. Cancer Res.* **2010,** *16* (15), 4038–4045.
139. Hann, C. L.; Daniel, V. C.; Sugar, E. A.; Dobromilskaya, I.; Murphy, S. C.; Cope, L.; Lin, X.; Hierman, J. S.; Wilburn, D. L.; Watkins, D. N.; et al. Therapeutic Efficacy of ABT-737, a Selective Inhibitor of BCL-2, in Small Cell Lung Cancer. *Cancer Res.* **2008,** *68* (7), 2321–2328.
140. Gandhi, L.; Camidge, D. R.; Ribeiro de Oliveira, M.; Bonomi, P.; Gandara, D.; Khaira, D.; Hann, C. L.; McKeegan, E. M.; Litvinovich, E.; Hemken, P. M.; et al. Phase I Study of Navitoclax (ABT-263), a Novel Bcl-2 Family Inhibitor, in Patients With Small-Cell Lung Cancer and Other Solid Tumors. *J. Clin. Oncol.* **2011,** *29* (7), 909–916.
141. Rudin, C. M.; Hann, C. L.; Garon, E. B.; Ribeiro de Oliveira, M.; Bonomi, P. D.; Camidge, D. R.; Chu, Q.; Giaccone, G.; Khaira, D.; Ramalingam, S. S.; et al. Phase II Study of Single-Agent Navitoclax (ABT-263) and Biomarker Correlates in Patients With Relapsed Small Cell Lung Cancer. *Clin. Cancer Res.* **2012,** *18* (11), 3163–3169.
142. Wilson, W. H.; O'Connor, O. A.; Czuczman, M. S.; LaCasce, A. S.; Gerecitano, J. F.; Leonard, J. P.; Tulpule, A.; Dunleavy, K.; Xiong, H.; Chiu, Y.-L.; et al. Navitoclax, a Targeted High-Affinity Inhibitor of BCL-2, in Lymphoid Malignancies: A Phase 1 Dose-Escalation Study of Safety, Pharmacokinetics, Pharmacodynamics, and Antitumour Activity. *Lancet Oncol.* **2010,** *11* (12), 1149–1159.
143. Seymour, J. F.; Gerecitano, J. F.; Kahl, B. S.; Pagel, J. M.; Wierda, W. G.; Anderson, M.-A.; Rudersdorf, N. K.; Gressick, L. A.; Montalvo, N. P.; Yang, J.; et al. The Single-Agent Bcl-2 Inhibitor ABT-199 (GDC-0199) in Patients With Relapsed/Refractory (R/R) Non-Hodgkin Lymphoma (NHL): Responses Observed in All Mantle Cell Lymphoma (MCL) Patients. *Blood* **2013,** *122* (21), 1789.
144. Touzeau, C.; Dousset, C.; Le Gouill, S.; Sampath, D.; Leverson, J. D.; Souers, A. J.; Maïga, S.; Béné, M. C.; Moreau, P.; Pellat-Deceunynck, C.; et al. The Bcl-2 Specific BH3 Mimetic ABT-199: A Promising Targeted Therapy for t(11;14) Multiple Myeloma. *Leukemia* **2014,** *28* (1), 210–212.
145. Danovi, D.; Meulmeester, E.; Pasini, D.; Migliorini, D.; Capra, M.; Frenk, R.; de Graaf, P.; Francoz, S.; Gasparini, P.; Gobbi, A.; et al. Amplification of Mdmx (or Mdm4) Directly Contributes to Tumor Formation by Inhibiting p53 Tumor Suppressor Activity. *Mol. Cell. Biol.* **2004,** *24* (13), 5835–5843.
146. Toledo, F.; Wahl, G. M. Regulating the p53 Pathway: in vitro Hypotheses, in vivo Veritas. *Nat. Rev. Cancer* **2006,** *6* (12), 909–923.
147. Gembarska, A.; Luciani, F.; Fedele, C.; Russell, E. A.; Dewaele, M.; Villar, S.; Zwolinska, A.; Haupt, S.; de Lange, J.; Yip, D.; et al. MDM4 Is a Key Therapeutic Target in Cutaneous Melanoma. *Nat. Med.* **2012,** *18* (8), 1239–1247.
148. Grasberger, B. L.; Lu, T. B.; Schubert, C.; Parks, D. J.; Carver, T. E.; Koblish, H. K.; Cummings, M. D.; LaFrance, L. V.; Milkiewicz, K. L.; Calvo, R. R.; et al. Discovery and Cocrystal Structure of Benzodiazepinedione HDM2 Antagonists That Activate p53 in Cells. *J. Med. Chem.* **2005,** *48* (4), 909–912.
149. Parks, D. J.; LaFrance, L. V.; Calvo, R. R.; Milkiewicz, K. L.; Gupta, V.; Lattanze, J.; Ramachandren, K.; Carver, T. E.; Petrella, E. C.; Cummings, M. D.; et al. 1,4-Benzodiazepine-2,5-diones as Small Molecule Antagonists of the HDM2-p53 Interaction: Discovery and SAR. *Bioorg. Med. Chem. Lett.* **2005,** *15* (3), 765–770.
150. Manallack, D. T.; Prankerd, R. J.; Yuriev, E.; Oprea, T. I.; Chalmers, D. K. The Significance of Acid/Base Properties in Drug Discovery. *Chem. Soc. Rev.* **2013,** *42* (2), 485–496.
151. Hopkins, A. L.; Keserü, G. M.; Leeson, P. D.; Rees, D. C.; Reynolds, C. H. The Role of Ligand Efficiency Metrics in Drug Discovery. *Nat. Rev. Drug Discov.* **2014,** *13* (2), 105–121.
152. Vassilev, L. T. In Vivo Activation of the p53 Pathway by Small-Molecule Antagonists of MDM2. *Science* **2004,** *303* (5659), 844–848.
153. Leeson, P. D.; Springthorpe, B. The Influence of Drug-Like Concepts on Decision-Making in Medicinal Chemistry. *Nat. Rev. Drug Discov.* **2007,** *6* (11), 881–890.
154. Raboisson, P.; Marugan, J. J.; Schubert, C.; Koblish, H. K.; Lu, T. B.; Zhao, S. Y.; Player, M. R.; Maroney, A. C.; Reed, R. L.; Huebert, N. D.; et al. Structure-Based Design, Synthesis, and Biological Evaluation of Novel 1,4-Diazepines as HDM2 Antagonists. *Bioorg. Med. Chem. Lett.* **2005,** *15* (7), 1857–1861.
155. Miyazaki, M.; Kawato, H.; Naito, H.; Ikeda, M.; Miyazaki, M.; Kitagawa, M.; Seki, T.; Fukutake, S.; Aonuma, M.; Soga, T. Discovery of Novel Dihydroimidazothiazole Derivatives as p53-MDM2 Protein–Protein Interaction Inhibitors: Synthesis, Biological Evaluation and Structure-Activity Relationships. *Bioorg. Med. Chem. Lett.* **2012,** *22* (20), 6338–6342.
156. Miyazaki, M.; Naito, H.; Sugimoto, Y.; Kawato, H.; Okayama, T.; Shimizu, H.; Miyazaki, M.; Kitagawa, M.; Seki, T.; Fukutake, S.; et al. Lead Optimization of Novel p53–MDM2 Interaction Inhibitors Possessing Dihydroimidazothiazole Scaffold. *Bioorg. Med. Chem. Lett.* **2013,** *23* (3), 728–732.
157. Miyazaki, M.; Uoto, K.; Sugimoto, Y.; Naito, H.; Yoshida, K.; Okayama, T.; Kawato, H.; Miyazaki, M.; Kitagawa, M.; Seki, T.; et al. Discovery of DS-5272 as a Promising Candidate: A Potent and Orally Active p53-MDM2 Interaction Inhibitor. *Bioorg. Med. Chem.* **2015,** *23* (10), 2360–2367.
158. Watson, A. F.; Liu, J.; Bennaceur, K.; Drummond, C. J.; Endicott, J. A.; Golding, B. T.; Griffin, R. J.; Haggerty, K.; Lu, X.; McDonnell, J. M.; et al. MDM2–p53 Protein–Protein Interaction Inhibitors: A-Ring Substituted Isoindolinones. *Bioorg. Med. Chem. Lett.* **2011,** *21* (19), 5916–5919.
159. Riedinger, C.; Endicott, J. A.; Kemp, S. J.; Smyth, L. A.; Watson, A.; Valeur, E.; Golding, B. T.; Griffin, R. J.; Hardcastle, I. R.; Noble, M. E.; et al. Analysis of Chemical Shift Changes Reveals the Binding Modes of Isoindolinone Inhibitors of the MDM2–p53 Interaction. *J. Am. Chem. Soc.* **2008,** *130* (47), 16038–16044.
160. Riedinger, C.; Noble, M. E.; Wright, D. J.; Mulks, F.; Hardcastle, I. R.; Endicott, J. A.; McDonnell, J. M. Understanding Small-Molecule Binding to MDM2: Insights Into Structural Effects of Isoindolinone Inhibitors From NMR Spectroscopy. *Chem. Biol. Drug Des.* **2011,** *77* (5), 301–308.
161. Ding, K.; Lu, Y.; Nikolovska-Coleska, Z.; Wang, G.; Qiu, S.; Shangary, S.; Gao, W.; Qin, D.; Stuckey, J.; Krajewski, K.; et al. Structure-Based Design of Spiro-Oxindoles as Potent, Specific Small-Molecule Inhibitors of the MDM2–p53 Interaction. *J. Med. Chem.* **2006,** *49* (12), 3432–3435.
162. Wang, S.; Sun, W.; Zhao, Y.; McEachern, D.; Meaux, I.; Barriere, C.; Stuckey, J. A.; Meagher, J. L.; Bai, L.; Liu, L.; et al. SAR405838: An Optimized Inhibitor of MDM2–p53 Interaction That Induces Complete and Durable Tumor Regression. *Cancer Res.* **2014,** *74,* 5855–5865.
163. Zhao, Y.; Liu, L.; Sun, W.; Lu, J.; McEachern, D.; Li, X.; Yu, S.; Bernard, D.; Ochsenbein, P.; Ferey, V.; et al. Diastereomeric Spirooxindoles as Highly Potent and Efficacious MDM2 Inhibitors. *J. Am. Chem. Soc.* **2013,** *135* (19), 7223–7234.
164. Koblish, H. K.; Zhao, S. Y.; Franks, C. F.; Donatelli, R. R.; Tominovich, R. M.; LaFrance, L. V.; Leonard, K. A.; Gushue, J. M.; Parks, D. J.; Calvo, R. R.; et al. Benzodiazepinedione Inhibitors of the Hdm2: p53 Complex Suppress Human Tumor Cell Proliferation in vitro and Sensitize Tumors to Doxorubicin In Vivo. *Mol. Cancer Ther.* **2006,** *5* (1), 160–169.
165. Zhang, Z.; Ding, Q.; Liu, J. J.; Zhang, J.; Jiang, N.; Chu, X. J.; Bartkovitz, D.; Luk, K. C.; Janson, C.; Tovar, C.; et al. Discovery of Potent and Selective Spiroindolinone MDM2 Inhibitor, RO8994, for Cancer Therapy. *Bioorg. Med. Chem.* **2014,** *22* (15), 4001–4009.

166. Zhang, Z.; Chu, X.; Liu, J.; Ding, Q.; Zhang, J.; Bartkovitz, D.; Jiang, N.; Karnachi, P.; So, S.-S.; Tovar, C.; et al. Discovery of Potent and Orally Active p53-MDM2 Inhibitors RO5353 and RO2468 for Potential Clinical Development. *ACS Med. Chem. Lett.* **2014,** *5* (2), 124–127.
167. Furet, P.; Chène, P.; De Pover, A.; Valat, T. S.; Lisztwan, J. H.; Kallen, J.; Masuya, K. The Central Valine Concept Provides an Entry in a New Class of Non Peptide Inhibitors of the p53-MDM2 Interaction. *Bioorg. Med. Chem. Lett.* **2012,** *22* (10), 3498–3502.
168. Vaupel, A.; Bold, G.; De Pover, A.; Stachyra-Valat, T.; Hergovich-Lisztwan, J.; Kallen, J.; Masuya, K.; Furet, P. Tetra-Substituted Imidazoles as a New Class of Inhibitors of the p53–MDM2 Interaction. *Bioorg. Med. Chem. Lett.* **2014,** *24* (9), 2110–2114.
169. Rew, Y.; Sun, D.; Gonzalez-Lopez De Turiso, F.; Bartberger, M. D.; Beck, H. P.; Canon, J.; Chen, A.; Chow, D.; Deignan, J.; Fox, B. M.; et al. Structure-Based Design of Novel Inhibitors of the MDM2–p53 Interaction. *J. Med. Chem.* **2012,** *55* (11), 4936–4954.
170. Gonzalez, A. Z.; Eksterowicz, J.; Bartberger, M. D.; Beck, H. P.; Canon, J.; Chen, A.; Chow, D.; Duquette, J.; Fox, B. M.; Fu, J.; et al. Selective and Potent Morpholinone Inhibitors of the MDM2−p53 Protein−Protein Interaction. *J. Med. Chem.* **2014,** *57,* 2472–2488.
171. Rew, Y.; Sun, D. Discovery of a Small Molecule MDM2 Inhibitor (AMG 232) for Treating Cancer. *J. Med. Chem.* **2014,** *57* (15), 6332–6341.
172. Sun, D.; Li, Z.; Rew, Y.; Gribble, M.; Bartberger, M. D.; Beck, H. P.; Canon, J.; Chen, A.; Chen, X.; Chow, D.; et al. Discovery of AMG 232, a Potent, Selective, and Orally Bioavailable MDM2–p53 Inhibitor in Clinical Development. *J. Med. Chem.* **2014,** *57* (4), 1454–1472.
173. Ye, Q.; Jiang, M.; Huang, W. T.; Ling, Y.; Olson, S. H.; Sun, D.; Xu, G.; Yan, X.; Wong, B. K.; Jin, L. Pharmacokinetics and Metabolism of AMG 232, a Novel Orally Bioavailable Inhibitor of the MDM2–p53 Interaction, in Rats, Dogs and Monkeys: In Vitro–In Vivo Correlation. *Xenobiotica* **2015,** *45,* 681–692.
174. Gonzalez, A. Z.; Li, Z.; Beck, H. P.; Canon, J.; Chen, A.; Chow, D.; Duquette, J.; Eksterowicz, J.; Fox, B. M.; Fu, J.; et al. Novel Inhibitors of the MDM2–p53 Interaction Featuring Hydrogen Bond Acceptors as Carboxylic Acid Isosteres. *J. Med. Chem.* **2014,** *57* (7), 2963–2988.
175. Rew, Y.; Sun, D.; Yan, X.; Beck, H. P.; Canon, J.; Chen, A.; Duquette, J.; Eksterowicz, J.; Fox, B. M.; Fu, J.; et al. Discovery of AM-7209, a Potent and Selective 4-Amidobenzoic Acid Inhibitor of the MDM2–p53 Interaction. *J. Med. Chem.* **2014,** *57* (24), 10499–10511.
176. Yu, M.; Wang, Y.; Zhu, J.; Bartberger, M. D.; Canon, J.; Chen, A.; Chow, D.; Eksterowicz, J.; Fox, B.; Fu, J.; et al. Discovery of Potent and Simplified Piperidinone-Based Inhibitors of the MDM2–p53 Interaction. *ACS Med. Chem. Lett.* **2014,** *5,* 894–899.
177. Parks, D. J.; LaFrance, L. V.; Calvo, R. R.; Milkiewicz, K. L.; Marugan, J. J.; Raboisson, P.; Schubert, C.; Koblish, H. K.; Zhao, S. Y.; Franks, C. F.; et al. Enhanced Pharmacokinetic Properties of 1,4-Benzodiazepine-2,5-dione Antagonists of the HDM2-p53 Protein–Protein Interaction Through Structure-Based Drug Design. *Bioorg. Med. Chem. Lett.* **2006,** *16* (12), 3310–3314.
178. Marugan, J. J.; Leonard, K.; Raboisson, P.; Gushue, J. M.; Calvo, R.; Koblish, H. K.; Lattanze, J.; Zhao, S. Y.; Cummings, M. D.; Player, M. R.; et al. Enantiomerically Pure 1,4-Benzodiazepine-2,5-diones as Hdm2 Antagonists. *Bioorg. Med. Chem. Lett.* **2006,** *16* (12), 3115–3120.
179. Fry, D. C.; Emerson, S. D.; Palmeb, S.; Vua, B. T.; Liua, C.-M.; Podlaskia, F. NMR Structure of a Complex Between MDM2 and a Small Molecule Inhibitor. *J. Biomol. NMR* **2004,** *30,* 163–173.
180. Anil, B.; Riedinger, C.; Endicott, J. A.; Noble, M. E. M. The Structure of an MDM2-Nutlin-3a Complex Solved by the Use of a Validated MDM2 Surface-Entropy Reduction Mutant. *Acta Crystallogr. Sect. D Biol. Crystallogr.* **2013,** *69* (8), 1358–1366.
181. Ray-Coquard, I.; Blay, J.-Y.; Italiano, A.; Le Cesne, A.; Penel, N.; Zhi, J.; Heil, F.; Rueger, R.; Graves, B.; Ding, M.; et al. Effect of the MDM2 Antagonist RG7112 on the P53 Pathway in Patients With MDM2-Amplified, Well-Differentiated or Dedifferentiated Liposarcoma: An Exploratory Proof-of-Mechanism Study. *Lancet Oncol.* **2012,** *13* (11), 1133–1140.
182. Hardcastle, I. R.; Ahmed, S. U.; Atkins, H.; Farnie, G.; Golding, B. T.; Griffin, R. J.; Guyenne, S.; Hutton, C.; Källblad, P.; Kemp, S. J.; et al. Isoindolinone Based Inhibitors of the MDM2–p53 Protein–Protein Interaction. *Bioorg. Med. Chem. Lett.* **2005,** *15,* 1515–1520.
183. Hardcastle, I. R.; Ahmed, S. U.; Atkins, H.; Farnie, G.; Golding, B. T.; Griffin, R. J.; Guyenne, S.; Hutton, C.; Kallblad, P.; Kemp, S. J.; et al. Small-Molecule Inhibitors of the MDM2–p53 Protein–Protein Interaction Based on an Isoindolinone Scaffold. *J. Med. Chem.* **2006,** *49* (21), 6209–6221.
184. Allen, J. G.; Bourbeau, M. P.; Wohlhieter, G. E.; Bartberger, M. D.; Michelsen, K.; Hungate, R.; Gadwood, R. C.; Gaston, R. D.; Evans, B.; Mann, L. W.; et al. Discovery and Optimization of Chromenotriazolopyrimidines as Potent Inhibitors of the Mouse Double Minute 2-Tumor Protein 53 Protein–Protein Interaction. *J. Med. Chem.* **2009,** *52* (22), 7044–7053.
185. Beck, H. P.; DeGraffenreid, M.; Fox, B.; Allen, J. G.; Rew, Y.; Schneider, S.; Saiki, A. Y.; Yu, D.; Oliner, J. D.; Salyers, K.; et al. Improvement of the Synthesis and Pharmacokinetic Properties of Chromenotriazolopyrimidine MDM2–p53 Protein–Protein Inhibitors. *Bioorg. Med. Chem. Lett.* **2011,** *21* (9), 2752–2755.
186. Yu, S.; Qin, D.; Shangary, S.; Chen, J.; Wang, G.; Ding, K.; McEachern, D.; Qiu, S.; Nikolovska-Coleska, Z.; Miller, R.; et al. Potent and Orally Active Small-Molecule Inhibitors of the MDM2−p53 Interaction. *J. Med. Chem.* **2009,** *52* (24), 7970–7973.
187. Zhao, Y.; Yu, S.; Sun, W.; Liu, L.; Lu, J.; McEachern, D.; Shargary, S.; Bernard, D.; Li, X.; Zhao, T.; et al. A Potent Small-Molecule Inhibitor of the MDM2–p53 Interaction (MI-888) Achieved Complete and Durable Tumor Regression in Mice. *J. Med. Chem.* **2013,** *56* (13), 5553–5561.
188. Ding, Q.; Zhang, Z.; Liu, J.-J.; Jiang, N.; Zhang, J.; Ross, T. M.; Chu, X.-J.; Bartkovitz, D.; Podlaski, F.; Janson, C.; et al. Discovery of RG7388, a Potent and Selective p53–MDM2 Inhibitor in Clinical Development. *J. Med. Chem.* **2013,** *56* (14), 5979–5983.
189. Ma, Y.; Lahue, B. R.; Shipps, G. W., Jr.; Brookes, J.; Wang, Y. Substituted Piperidines as HDM2 Inhibitors. *Bioorg. Med. Chem. Lett.* **2014,** *24* (4), 1026–1030.
190. Ma, Y.; Lahue, B. R.; Gibeau, C. R.; Shipps, G. W., Jr.; Bogen, S. L.; Wang, Y.; Guo, Z.; Guzi, T. J.; et al. Pivotal Role of an Aliphatic Side Chain in the Development of an HDM2 Inhibitor. *ACS Med. Chem. Lett.* **2014,** *5* (5), 572–575.
191. Gonzalez-Lopez de Turiso, F.; Sun, D.; Rew, Y.; Bartberger, M. D.; Beck, H. P.; Canon, J.; Chen, A.; Chow, D.; Correll, T. L.; Huang, X.; et al. Rational Design and Binding Mode Duality of MDM2–p53 Inhibitors. *J. Med. Chem.* **2013,** *56* (10), 4053–4070.
192. Gessier, F.; Kallen, J.; Jacoby, E.; Chène, P.; Stachyra-Valat, T.; Ruetz, S.; Jeay, S.; Holzer, P.; Masuya, K.; Furet, P. Discovery of Dihydroisoquinolinone Derivatives as Novel Inhibitors of the p53-MDM2 Interaction With a Distinct Binding Mode. *Bioorg. Med. Chem. Lett.* **2015,** *25,* 3621–3625.
193. Holzer, P.; Masuya, K.; Furet, P.; Kallen, J.; Valat-Stachyra, T.; Ferretti, S.; Berghausen, J.; Bouisset-Leonard, M. M.; Buschmann, N.; Pissot-Soldermann, C.; et al. Discovery of a Dihydroisoquinolinone Derivative (NVP-CGM097): A Highly Potent and Selective MDM2 Inhibitor Undergoing Phase 1 Clinical Trials in p53wt Tumors. *J. Med. Chem.* **2015,** *58* (16), 6348–6358.
194. Popowicz, G. M.; Czarna, A.; Rothweiler, U.; Szwagierczak, A.; Krajewski, M.; Weber, L.; Holak, T. A. Molecular Basis for the Inhibition of p53 by Mdmx. *Cell Cycle* **2007,** *6* (19), 2386–2392.
195. Popowicz, G. M.; Czarna, A.; Wolf, S.; Wang, K.; Wang, W.; Dömling, A.; Holak, T. A. Structures of Low Molecular Weight Inhibitors Bound to MDMX and MDM2 Reveal New Approaches for p53-MDMX/MDM2 Antagonist Drug Discovery. *Cell Cycle* **2010,** *9* (6), 1104–1111.
196. Boltjes, A.; Huang, Y.; van de Velde, R.; Rijkee, L.; Wolf, S.; Gaugler, J.; Lesniak, K.; Guzik, K.; Holak, T. A.; Dömling, A. Fragment-Based Library Generation for the Discovery of a Peptidomimetic p53–Mdm4 Inhibitor. *ACS Comb. Sci.* **2014,** *16* (8), 393–396.
197. Blackburn, T. J.; Ahmed, S.; Coxon, C. R.; Liu, J.; Lu, X.; Golding, B. T.; Griffin, R. J.; Hutton, C.; Newell, D. R.; Ojo, S.; et al. Diaryl- and Triaryl-Pyrrole Derivatives: Inhibitors of the MDM2–p53 and MDMX–p53 Protein–Protein interactions†Electronic Supplementary Information (ESI) Available: Experimental Details for Compound Synthesis, Analytical Data for All Compounds and Intermed. *Med. Chem. Commun.* **2013,** *4* (9), 1297–1304.
198. Graves, B.; Thompson, T.; Xia, M.; Janson, C.; Lukacs, C.; Deo, D.; Di Lello, P.; Fry, D.; Garvie, C.; Huang, K.-S.; et al. Activation of the p53 Pathway by Small-Molecule-Induced MDM2 and MDMX Dimerization. *Proc. Natl. Acad. Sci.* **2012,** *109* (29), 11788–11793.
199. Qin, L.; Yang, F.; Zhou, C.; Chen, Y.; Zhang, H.; Su, Z. Efficient Reactivation of p53 in Cancer Cells by a Dual MdmX/Mdm2 Inhibitor. *J. Am. Chem. Soc.* **2014,** *136,* 18023–18033.
200. Reed, D.; Shen, Y.; Shelat, A. A.; Arnold, L. A.; Ferreira, A. M.; Zhu, F.; Mills, N.; Smithson, D. C.; Regni, C. A.; Bashford, D.; et al. Identification and Characterization of the First Small Molecule Inhibitor of MDMX. *J. Biol. Chem.* **2010,** *285* (14), 10786–10796.

201. Bista, M.; Smithson, D.; Pecak, A.; Salinas, G.; Pustelny, K.; Min, J.; Pirog, A.; Finch, K.; Zdzalik, M.; Waddell, B.; et al. On the Mechanism of Action of SJ-172550 in Inhibiting the Interaction of MDM4 and p53. *PLoS One* **2012,** *7* (6), e37518.
202. Popowicz, G. M.; Dömling, A.; Holak, T. A. The Structure-Based Design of Mdm2/Mdmx–p53 Inhibitors Gets Serious. *Angew. Chem. Int. Ed.* **2011,** *50* (12), 2680–2688.
203. Fulda, S.; Vucic, D. Targeting IAP Proteins for Therapeutic Intervention in Cancer. *Nat. Rev. Drug Discov.* **2012,** *11,* 109–124.
204. LaCasse, E. C.; Mahoney, D. J.; Cheung, H. H.; Plenchette, S.; Baird, S.; Korneluk, R. G. IAP-Targeted Therapies for Cancer. *Oncogene* **2008,** *27* (48), 6252–6275.
205. Hird, A. W.; Aquila, B. M.; Hennessy, E. J.; Vasbinder, M. M.; Yang, B. Small Molecule Inhibitor of Apoptosis Proteins Antagonists: A Patent Review. *Expert Opin. Ther. Pat.* **2015,** *1,* 1–20.
206. Ndubaku, C.; Varfolomeev, E.; Wang, L.; Zobel, K.; Lau, K.; Elliott, L. O.; Maurer, B.; Fedorova, A. V.; Dynek, J. N.; Koehler, M.; et al. Antagonism of c-IAP and XIAP Proteins Is Required for Efficient Induction of Cell Death by Small-Molecule IAP Antagonists. *ACS Chem. Biol.* **2009,** *4* (7), 557–566.
207. González-Lpez, M.; Welsh, K.; Finlay, D.; Ardecky, R. J.; Ganji, S. R.; Su, Y.; Yuan, H.; Teriete, P.; MacE, P. D.; Riedl, S. J.; et al. Design, Synthesis and Evaluation of Monovalent Smac Mimetics That Bind to the BIR2 Domain of the Anti-Apoptotic Protein XIAP. *Bioorg. Med. Chem. Lett.* **2011,** *21* (14), 4332–4336.
208. Zobel, K.; Wang, L.; Varfolomeev, E.; Franklin, M. C.; Elliott, L. O.; Wallweber, H. J. A.; Okawa, D. C.; Flygare, J. A.; Vucic, D.; Fairbrother, W. J.; et al. Design, Synthesis, and Biological Activity of a Potent Smac Mimetic That Sensitizes Cancer Cells to Apoptosis by Antagonizing IAPs. *ACS Chem. Biol.* **2006,** *1* (8), 525–533.
209. Weisberg, E.; Kung, A. L.; Wright, R. D.; Moreno, D.; Catley, L.; Ray, A.; Zawel, L.; Tran, M.; Cools, J.; Gilliland, G.; et al. Potentiation of Antileukemic Therapies by Smac Mimetic, LBW242: Effects on Mutant FLT3-Expressing Cells. *Mol. Cancer Ther.* **2007,** *6* (7), 1951–1961.
210. Gaither, A.; Porter, D.; Yao, Y.; Borawski, J.; Yang, G.; Donovan, J.; Sage, D.; Slisz, J.; Tran, M.; Straub, C.; et al. A Smac Mimetic Rescue Screen Reveals Roles for Inhibitor of Apoptosis Proteins in Tumor Necrosis Factor-Alpha Signaling. *Cancer Res.* **2007,** *67* (24), 11493–11498.
211. Cohen, F.; Alicke, B.; Elliott, L. O.; Flygare, J. A.; Goncharov, T.; Keteltas, S. F.; Franklin, M. C.; Frankovitz, S.; Stephan, J. P.; Tsui, V.; et al. Orally Bioavailable Antagonists of Inhibitor of Apoptosis Proteins Based on an Azabicyclooctane Scaffold. *J. Med. Chem.* **2009,** *52* (6), 1723–1730.
212. Cai, Q.; Sun, H.; Peng, Y.; Lu, J.; Nikolovska-Coleska, Z.; McEachern, D.; Liu, L.; Qiu, S.; Yang, C.-Y.; Miller, R.; et al. A Potent and Orally Active Antagonist (SM-406/AT-406) of Multiple Inhibitor of Apoptosis Proteins (IAPs) in Clinical Development for Cancer Treatment. *J. Med. Chem.* **2011,** *54* (8), 2714–2726.
213. Li, L.; Thomas, R. M.; Suzuki, H.; De Brabander, J. K.; Wang, X.; Harran, P. G. A Small Molecule Smac Mimic Potentiates TRAIL- and TNFalpha-Mediated Cell Death. *Science* **2004,** *305* (5689), 1471–1474.
214. Sun, H.; Nikolovska-Coleska, Z.; Lu, J.; Meagher, J. L.; Yang, C.-Y.; Qiu, S.; Tomita, Y.; Ueda, Y.; Jiang, S.; Krajewski, K.; et al. Design, Synthesis, and Characterization of a Potent, Nonpeptide, Cell-Permeable, Bivalent Smac Mimetic That Concurrently Targets Both the BIR2 and BIR3 Domains in XIAP. *J. Am. Chem. Soc.* **2007,** *129* (49), 15279–15294.
215. Gao, Z.; Tian, Y.; Wang, J.; Yin, Q.; Wu, H.; Li, Y.-M.; Jiang, X. A Dimeric Smac/diablo Peptide Directly Relieves Caspase-3 Inhibition by XIAP. Dynamic and Cooperative Regulation of XIAP by Smac/Diablo. *J. Biol. Chem.* **2007,** *282* (42), 30718–30727.
216. Varfolomeev, E.; Blankenship, J. W.; Wayson, S. M.; Fedorova, A. V.; Kayagaki, N.; Garg, P.; Zobel, K.; Dynek, J. N.; Elliott, L. O.; Wallweber, H. J. A.; et al. IAP Antagonists Induce Autoubiquitination of c-IAPs, NF-kappaB Activation, and TNFalpha-Dependent Apoptosis. *Cell* **2007,** *131* (4), 669–681.
217. Vince, J. E.; Wong, W. W.-L.; Khan, N.; Feltham, R.; Chau, D.; Ahmed, A. U.; Benetatos, C. A.; Chunduru, S. K.; Condon, S. M.; McKinlay, M.; et al. IAP Antagonists Target cIAP1 to Induce TNFalpha-Dependent Apoptosis. *Cell* **2007,** *131* (4), 682–693.
218. Bertrand, M. J. M.; Milutinovic, S.; Dickson, K. M.; Ho, W. C.; Boudreault, A.; Durkin, J.; Gillard, J. W.; Jaquith, J. B.; Morris, S. J.; Barker, P. A. cIAP1 and cIAP2 Facilitate Cancer Cell Survival by Functioning as E3 Ligases That Promote RIP1 Ubiquitination. *Mol. Cell* **2008,** *30* (6), 689–700.
219. Benetatos, C. A.; Mitsuuchi, Y.; Burns, J. M.; Neiman, E. M.; Condon, S. M.; Yu, G.; Seipel, M. E.; Kapoor, G. S.; Laporte, M. G.; Rippin, S. R.; et al. Birinapant (TL32711), a Bivalent SMAC Mimetic, Targets TRAF2-Associated cIAPs, Abrogates TNF-Induced NF-kB Activation, and is Active in Patient-Derived Xenograft Models. *Mol. Cancer Ther.* **2014,** *13* (4), 867–879.
220. Allensworth, J. L.; Sauer, S. J.; Lyerly, H. K.; Morse, M. A.; Devi, G. R. Smac Mimetic Birinapant Induces Apoptosis and Enhances TRAIL Potency in Inflammatory Breast Cancer Cells in an IAP-Dependent and TNF-α-Independent Mechanism. *Breast Cancer Res. Treat.* **2013,** *137* (2), 359–371.
221. Li, J.; Muscarella, P.; Joo, S. H.; Knobloch, T. J.; Melvin, W. S.; Weghorst, C. M.; Tsai, M.-D. Dissection of CDK4-Binding and Transactivation Activities of p34(SEI-1) and Comparison Between Functions of p34(SEI-1) and p16(INK4A). *Biochemistry* **2005,** *44* (40), 13246–13256.
222. Milroy, L.-G.; Brunsveld, L.; Ottmann, C. Stabilization and Inhibition of Protein–Protein Interactions: The 14-3-3 Case Study. *ACS Chem. Biol.* **2013,** *8* (1), 27–35.
223. Würtele, M.; Jelich-Ottmann, C.; Wittinghofer, A.; Oecking, C. Structural View of a Fungal Toxin Acting on a 14-3-3 Regulatory Complex. *EMBO J.* **2003,** *22* (5), 987–994.
224. Takahashi, S.; Wakui, H.; Gustafsson, J. A.; Zilliacus, J.; Itoh, H. Functional Interaction of the Immunosuppressant Mizoribine With the 14-3-3 Protein. *Biochem. Biophys. Res. Commun.* **2000,** *274* (1), 87–92.
225. Wu, H.; Ge, J.; Yao, S. Q. Microarray-Assisted High-Throughput Identification of a Cell-Permeable Small-Molecule Binder of 14-3-3 Proteins. *Angew. Chem. Int. Ed. Engl.* **2010,** *49* (37), 6528–6532.
226. Corradi, V.; Mancini, M.; Manetti, F.; Petta, S.; Santucci, M. A.; Botta, M. Identification of the First Non-Peptidic Small Molecule Inhibitor of the c-Abl/14-3-3 Protein–Protein Interactions Able to Drive Sensitive and Imatinib-Resistant Leukemia Cells to Apoptosis. *Bioorg. Med. Chem. Lett.* **2010,** *20* (20), 6133–6137.
227. Corradi, V.; Mancini, M.; Santucci, M. A.; Carlomagno, T.; Sanfelice, D.; Mori, M.; Vignaroli, G.; Falchi, F.; Manetti, F.; Radi, M.; et al. Computational Techniques are Valuable Tools for the Discovery of Protein–Protein Interaction Inhibitors: The 14-3-3σ Case. *Bioorg. Med. Chem. Lett.* **2011,** *21* (22), 6867–6871.
228. Zhao, J.; Du, Y.; Horton, J. R.; Upadhyay, A. K.; Lou, B.; Bai, Y.; Zhang, X.; Du, L.; Li, M.; Wang, B.; et al. Discovery and Structural Characterization of a Small Molecule 14-3-3 Protein–Protein Interaction Inhibitor. *Proc. Natl. Acad. Sci.* **2011,** *108* (39), 16212–16216.
229. Markowitz, J.; Chen, I.; Gitti, R.; Baldisseri, D. M.; Pan, Y.; Udan, R.; Carrier, F.; MacKerell, A. D.; Weber, D. J. Identification and Characterization of Small Molecule Inhibitors of the Calcium-Dependent S100B-p53 Tumor Suppressor Interaction. *J. Med. Chem.* **2004,** *47* (21), 5085–5093.
230. Reddy, T. R. K.; Li, C.; Guo, X.; Myrvang, H. K.; Fischer, P. M.; Dekker, L. V. Design, Synthesis, and Structure-Activity Relationship Exploration of 1-Substituted 4-aroyl-3-hydroxy-5-phenyl-1H-pyrrol-2(5H)-one Analogues as Inhibitors of the Annexin A2-S100A10 Protein Interaction. *J. Med. Chem.* **2011,** *54* (7), 2080–2094.
231. Berg, T.; Cohen, S. B.; Desharnais, J.; Sonderegger, C.; Maslyar, D. J.; Goldberg, J.; Boger, D. L.; Vogt, P. K. Small-Molecule Antagonists of Myc/Max Dimerization Inhibit Myc-Induced Transformation of Chicken Embryo Fibroblasts. *Proc. Natl. Acad. Sci. U. S. A.* **2002,** *99* (6), 3830–3835.
232. Xu, Y.; Shi, J.; Yamamoto, N.; Moss, J. A.; Vogt, P. K.; Janda, K. D. A Credit-Card Library Approach for Disrupting Protein–Protein Interactions. *Bioorg. Med. Chem.* **2006,** *14* (8), 2660–2673.
233. Kiessling, A.; Sperl, B.; Hollis, A.; Eick, D.; Berg, T. Selective Inhibition of c-Myc/Max Dimerization and DNA Binding by Small Molecules. *Chem. Biol.* **2006,** *13* (7), 745–751.
234. Yin, X.; Giap, C.; Lazo, J. S.; Prochownik, E. V. Low Molecular Weight Inhibitors of Myc-Max Interaction and Function. *Oncogene* **2003,** *22* (40), 6151–6159.
235. Huang, M.-J.; Cheng, Y.; Liu, C.-R.; Lin, S.; Liu, H. E. A Small-Molecule c-Myc Inhibitor, 10058-F4, Induces Cell-Cycle Arrest, Apoptosis, and Myeloid Differentiation of Human Acute Myeloid Leukemia. *Exp. Hematol.* **2006,** *34* (11), 1480–1489.
236. Wang, H.; Hammoudeh, D. I.; Follis, A. V.; Reese, B. E.; Lazo, J. S.; Metallo, S. J.; Prochownik, E. V. Improved Low Molecular Weight Myc-Max Inhibitors. *Mol. Cancer Ther.* **2007,** *6* (9), 2399–2408.
237. Harvey, S. R.; Porrini, M.; Stachl, C.; MacMillan, D.; Zinzalla, G.; Barran, P. E. Small-Molecule Inhibition of c-MYC:MAX Leucine Zipper Formation is Revealed by Ion Mobility Mass Spectrometry. *J. Am. Chem. Soc.* **2012,** *134* (47), 19384–19392.
238. Fujii, N.; Haresco, J. J.; Novak, K. A. P.; Stokoe, D.; Kuntz, I. D.; Guy, R. K. A Selective Irreversible Inhibitor Targeting a PDZ Protein Interaction Domain. *J. Am. Chem. Soc.* **2003,** *125* (40), 12074–12075.

239. Carol, H.; Reynolds, C. P.; Kang, M. H.; Keir, S. T.; Maris, J. M.; Gorlick, R.; Kolb, E. A.; Billups, C. A.; Geier, B.; Kurmasheva, R. T.; et al. Initial Testing of the MDM2 Inhibitor RG7112 by the Pediatric Preclinical Testing Program. *Pediatr. Blood Cancer* **2013,** *60,* 633–641.
240. Mayasundari, A.; Ferreira, A. M.; He, L.; Mahindroo, N.; Bashford, D.; Fujii, N. Rational Design of the First Small-Molecule Antagonists of NHERF1/EBP50 PDZ Domains. *Bioorg. Med. Chem. Lett.* **2008,** *18* (3), 942–945.
241. Mahindroo, N.; Punchihewa, C.; Bail, A. M.; Fujii, N. Indole-2-Amide Based Biochemical Antagonist of Dishevelled PDZ Domain Interaction Down-Regulates Dishevelled-Driven Tcf Transcriptional Activity. *Bioorg. Med. Chem. Lett.* **2008,** *18* (3), 946–949.
242. Joshi, M.; Vargas, C.; Boisguerin, P.; Diehl, A.; Krause, G.; Schmieder, P.; Moelling, K.; Hagen, V.; Schade, M.; Oschkinat, H. Discovery of Low-Molecular-Weight Ligands for the AF6 PDZ Domain. *Angew. Chem. Int. Ed. Engl.* **2006,** *45* (23), 3790–3795.
243. Vargas, C.; Radziwill, G.; Krause, G.; Diehl, A.; Keller, S.; Kamdem, N.; Czekelius, C.; Kreuchwig, A.; Schmieder, P.; Doyle, D.; et al. Small-Molecule Inhibitors of AF6 PDZ-Mediated Protein–Protein Interactions. *ChemMedChem* **2014,** *9* (7), 1458–1462.
244. Fujii, N.; Haresco, J. J.; Novak, K. A. P.; Gage, R. M.; Pedemonte, N.; Stokoe, D.; Kuntz, I. D.; Guy, R. K. Rational Design of a Nonpeptide General Chemical Scaffold for Reversible Inhibition of PDZ Domain Interactions. *Bioorg. Med. Chem. Lett.* **2007,** *17* (2), 549–552.
245. Sharma, S. V.; Oneyama, C.; Yamashita, Y.; Nakano, H.; Sugawara, K.; Hamada, M.; Kosaka, N.; Tamaoki, T. UCS15A, a Non-Kinase Inhibitor of Src Signal Transduction. *Oncogene* **2001,** *20* (17), 2068–2079.
246. Oneyama, C.; Nakano, H.; Sharma, S. V. UCS15A, a Novel Small Molecule, SH3 Domain-Mediated Protein ± Protein Interaction Blocking Drug. *Oncogene* **2001,** *2002* (21), 2037–2050.
247. Siddiquee, K. A. Z.; Gunning, P. T.; Glenn, M.; Katt, W. P.; Zhang, S.; Schrock, C.; Schroeck, C.; Sebti, S. M.; Jove, R.; Hamilton, A. D.; et al. An Oxazole-Based Small-Molecule Stat3 Inhibitor Modulates Stat3 Stability and Processing and Induces Antitumor Cell Effects. *ACS Chem. Biol.* **2007,** *2* (12), 787–798.
248. Gunning, P. T.; Glenn, M. P.; Siddiquee, K. A.; Katt, W. P.; Masson, E.; Sebti, S. M.; Turkson, J.; Hamilton, A. D. Targeting Protein–Protein Interactions: Suppression of Stat3 Dimerization With Rationally Designed Small-Molecule, Nonpeptidic SH2 Domain Binders. *Chembiochem* **2008,** *9* (17), 2800–2803.
249. Yu, W.; Guvench, O.; MacKerell, A. D.; Qu, C. Identification of Small Molecular Weight Inhibitors of Src Homology 2 Domain-Containing Tyrosine Phosphatase 2 (SHP-2) via In Silico Database Screening Combined With Experimental Assay. *J. Med. Chem.* **2008,** *51* (23), 7396–7404.
250. Sun, Q.; Burke, J. P.; Phan, J.; Burns, M. C.; Olejniczak, E. T.; Waterson, A. G.; Lee, T.; Rossanese, O. W.; Fesik, S. W. Discovery of Small Molecules That Bind to K-Ras and Inhibit Sos-Mediated Activation. *Angew. Chem. Int. Ed. Engl.* **2012,** *51* (25), 6140–6143.
251. Evelyn, C. R.; Duan, X.; Biesiada, J.; Seibel, W. L.; Meller, J.; Zheng, Y. Article Rational Design of Small Molecule Inhibitors Targeting the RAS GEF, SOS1. *Chem. Biol.* **2014,** *21* (12), 1618–1628.
252. Winter, J. J. G.; Anderson, M.; Blades, K.; Brassington, C.; Breeze, A. L.; Chresta, C.; Embrey, K.; Fairley, G.; Faulder, P.; Finlay, M. R. V.; et al. Small Molecule Binding Sites on the Ras:SOS Complex Can Be Exploited for Inhibition of Ras Activation. *J. Med. Chem.* **2015,** *58,* 2265–2274.
253. Zimmermann, G.; Papke, B.; Ismail, S.; Vartak, N.; Chandra, A.; Hoffmann, M.; Hahn, S. A.; Triola, G.; Wittinghofer, A.; Bastiaens, P. I. H.; et al. Small Molecule Inhibition of the KRAS-PDEδ Interaction Impairs Oncogenic KRAS Signalling. *Nature* **2013,** *497* (7451), 638–642.
254. Catrow, J. L.; Zhang, Y.; Zhang, M.; Ji, H. Discovery of Selective Small-Molecule Inhibitors for the β-Catenin/T-Cell Factor Protein–Protein Interaction Through the Optimization of the Acyl Hydrazone Moiety. *J. Med. Chem.* **2015,** *58* (11), 4678–4692.
255. Deng, Y.; Shipps, G. W.; Zhao, L.; Siddiqui, M. A.; Popovici-Muller, J.; Curran, P. J.; Duca, J. S.; Hruza, A. W.; Fischmann, T. O.; Madison, V. S.; et al. Modulating the Interaction Between CDK2 and Cyclin A With a Quinoline-Based Inhibitor. *Bioorg. Med. Chem. Lett.* **2014,** *24* (1), 199–203.
256. Hamdi, A.; Lesnard, A.; Suzanne, P.; Robert, T.; Miteva, M. A.; Pellerano, M.; Didier, B.; Ficko-Blean, E.; Lobstein, A.; Hibert, M.; et al. Tampering With Cell Division by Using Small-Molecule Inhibitors of CDK-CKS Protein Interactions. *Chembiochem* **2015,** *16* (3), 432–439.
257. Moerke, N. J.; Aktas, H.; Chen, H.; Cantel, S.; Reibarkh, M. Y.; Fahmy, A.; Gross, J. D.; Degterev, A.; Yuan, J.; Chorev, M.; et al. Small-Molecule Inhibition of the Interaction Between the Translation Initiation Factors eIF4E and eIF4G. *Cell* **2007,** *128* (2), 257–267.
258. Mahalingam, P.; Takrouri, K.; Chen, T.; Sahoo, R.; Papadopoulos, E.; Chen, L.; Wagner, G.; Aktas, B. H.; Halperin, J. A.; Chorev, M. Synthesis of Rigidified eIF4E/eIF4G Inhibitor-1 (4EGI-1) Mimetic and Their in vitro Characterization as Inhibitors of Protein–Protein Interaction. *J. Med. Chem.* **2014,** *57* (12), 5094–5111.
259. Erkizan, H. V.; Kong, Y.; Merchant, M.; Schlottmann, S.; Barber-Rotenberg, J. S.; Yuan, L.; Abaan, O. D.; Chou, T.-H.; Dakshanamurthy, S.; Brown, M. L.; et al. A Small Molecule Blocking Oncogenic Protein EWS-FLI1 Interaction With RNA Helicase A Inhibits Growth of Ewing's Sarcoma. *Nat. Med.* **2009,** *15* (7), 750–756.
260. Barber-Rotenberg, J. S.; Selvanathan, S. P.; Kong, Y.; Erkizan, H. V.; Snyder, T. M.; Hong, S. P.; Kobs, C. L.; South, N. L.; Summer, S.; Monroe, P. J.; et al. Single Enantiomer of YK-4-279 Demonstrates Specificity in Targeting the Oncogene EWS-FLI1. *Oncotarget* **2012,** *3* (2), 172–182.
261. Ji, T.; Lee, M.; Pruitt, S. C.; Hangauer, D. G. Privileged Scaffolds for Blocking Protein–Protein Interactions: 1,4-Disubstituted Naphthalene Antagonists of Transcription Factor Complex HOX-PBX/DNA. *Bioorg. Med. Chem. Lett.* **2004,** *14* (15), 3875–3879.
262. Karatas, H.; Townsend, E. C.; Cao, F.; Chen, Y.; Bernard, D.; Liu, L.; Lei, M.; Dou, Y.; Wang, S. High-Affinity, Small-Molecule Peptidomimetic Inhibitors of mll1/wdr5 Protein–Protein Interaction. *J. Am. Chem. Soc.* **2013,** *135,* 669–682.
263. Smet, C.; Duckert, J.-F.; Wieruszeski, J.-M.; Landrieu, I.; Buée, L.; Lippens, G.; Déprez, B. Control of Protein–Protein Interactions: Structure-Based Discovery of Low Molecular Weight Inhibitors of the Interactions Between Pin1 WW Domain and Phosphopeptides. *J. Med. Chem.* **2005,** *48* (15), 4815–4823.
264. Scott, D. E.; Coyne, A. G.; Venkitaraman, A.; Blundell, T. L.; Abell, C.; Hyvönen, M. Small-Molecule Inhibitors That Target Protein–Protein Interactions in the RAD51 Family of Recombinases. *ChemMedChem* **2015,** *10* (2), 296–303.
265. Van Molle, I.; Thomann, A.; Buckley, D. L.; So, E. C.; Lang, S.; Crews, C. M.; Ciulli, A. Dissecting Fragment-Based Lead Discovery at the von Hippel-Lindau Protein:hypoxia Inducible Factor 1α Protein–Protein Interface. *Chem. Biol.* **2012,** *19* (10), 1300–1312.
266. Buckley, D. L.; Van Molle, I.; Gareiss, P. C.; Tae, H. S.; Michel, J.; Noblin, D. J.; Jorgensen, W. L.; Ciulli, A.; Crews, C. M. Targeting the von Hippel-Lindau E3 Ubiquitin Ligase Using Small Molecules to Disrupt the VHL/HIF-1α Interaction. *J. Am. Chem. Soc.* **2012,** *134* (10), 4465–4468.
267. Tsao, D. H. H.; Sutherland, A. G.; Jennings, L. D.; Li, Y.; Rush, T. S.; Alvarez, J. C.; Ding, W.; Dushin, E. G.; Dushin, R. G.; Haney, S. A.; et al. Discovery of Novel Inhibitors of the ZipA/FtsZ Complex by NMR Fragment Screening Coupled With Structure-Based Design. *Bioorg. Med. Chem.* **2006,** *14* (23), 7953–7961.
268. Li, H.; Xiao, H.; Lin, L.; Jou, D.; Kumari, V.; Lin, J.; Li, C. Drug Design Targeting Protein–Protein Interactions (PPIs) Using Multiple Ligand Simultaneous Docking (MLSD) and Drug Repositioning: Discovery of Raloxifene and Bazedoxifene as Novel Inhibitors of IL-6/GP130 Interface. *J. Med. Chem.* **2014,** *57* (3), 632–641.
269. Yan, C.; Liu, D.; Li, L.; Wempe, M. F.; Guin, S.; Khanna, M.; Meier, J.; Hoffman, B.; Owens, C.; Wysoczynski, C. L.; et al. Discovery and Characterization of Small Molecules That Target the GTPase Ral. *Nature* **2014,** *515* (7527), 443–447.
270. Khanna, M.; Wang, F.; Jo, I.; Knabe, W. E.; Wilson, S. M.; Li, L.; Bum-Erdene, K.; Li, J.; W Sledge, G.; Khanna, R.; et al. Targeting Multiple Conformations Leads to Small Molecule Inhibitors of the uPAR·uPA Protein–Protein Interaction That Block Cancer Cell Invasion. *ACS Chem. Biol.* **2011,** *6* (11), 1232–1243.
271. Lipinski, C. A.; Lombardo, F.; Dominy, B. W.; Feeney, P. J. Experimental and Computational Approaches to Estimate Solubility and Permeability in Drug Discovery and Development Settings. *Adv. Drug Deliv. Rev.* **2001,** *46* (1–3), 3–26.
272. Johnson, T. W.; Dress, K. R.; Edwards, M. Using the Golden Triangle to Optimize Clearance and Oral Absorption. *Bioorg. Med. Chem. Lett.* **2009,** *19* (19), 5560–5564.
273. Vu, B.; Wovkulich, P.; Pizzolato, G.; Lovey, A.; Ding, Q.; Jiang, N.; Liu, J.-J.; Zhao, C.; Glenn, K.; Wen, Y.; et al. Discovery of RG7112: A Small-Molecule MDM2 Inhibitor in Clinical Development. *ACS Med. Chem. Lett.* **2013,** *4* (5), 466–469.
274. Chen, L.; Rousseau, R. F.; Middleton, S. A.; Nichols, G. L.; Newell, D. R.; Lunec, J.; Tweddle, D. A. Pre-Clinical Evaluation of the MDM2–p53 Antagonist RG7388 Alone and in Combination With Chemotherapy in Neuroblastoma. *Oncotarget* **2015,** *6,* 10207–10221.
275. Fujii, N.; You, L.; Xu, Z.; Uematsu, K.; Shan, J.; He, B.; Mikami, I.; Edmondson, L. R.; Neale, G.; Zheng, J.; et al. An Antagonist of Dishevelled Protein–Protein Interaction Suppresses B-Catenin-Dependent Tumor Cell Growth. *Cancer Res.* **2007,** *67* (2), 573–579.

Relevant Websites

http://www.bindingdb.org/bind/index.jsp—BindingDB.
http://mordred.bioc.cam.ac.uk/timbal—TIMBAL.
http://prism.ccbb.ku.edu.tr/hotpoint—HotPOINT.
http://robetta.bakerlab.org/Robetta—Robetta.
http://bio-aims.udc.es/SASA-HS-PP.php—SASA-HS-PP @ Bio-AIMS.

5.07 Targeting Protein Synthesis, Folding, and Degradation Pathways in Cancer

A Elisa Pasqua, B Wilding, MD Cheeseman, and K Jones, The Institute of Cancer Research, London, United Kingdom

© 2017 Elsevier Ltd. All rights reserved.

5.07.1	**Introduction**	203
5.07.2	**Targeting Protein Synthesis**	203
5.07.2.1	Introduction	203
5.07.2.2	Targeting Transcription	204
5.07.2.2.1	Targeting a TF	204
5.07.2.2.2	Targeting RNA polymerases	207
5.07.2.2.3	BRD4 inhibitors	211
5.07.2.3	Targeting Translation	214
5.07.2.3.1	Translational control in cancer	214
5.07.2.3.2	Inhibitors of eIF4F upstream regulators	215
5.07.2.3.3	Direct inhibitors of eIF4F	228
5.07.2.3.4	Inhibitors of ternary complex formation	228
5.07.2.4	Summary	228
5.07.3	**Targeting Protein Folding**	229
5.07.3.1	Introduction to Molecular Chaperones	229
5.07.3.2	HSP70 Inhibitors	229
5.07.3.3	HSP90 Family	231
5.07.3.3.1	HSP90 inhibitors	232
5.07.3.3.2	Isoform selectivity	245
5.07.4	**Targeting Protein Degradation**	246
5.07.4.1	Introduction	246
5.07.4.2	The Ubiquitin–Proteasome System	246
5.07.4.3	Targeting the E1 Activating Enzymes in Cancer Therapy	247
5.07.4.3.1	Pevonedistat (MLN4924)	247
5.07.4.3.2	Targeting the E2 conjugating enzymes in cancer therapy	250
5.07.4.3.3	Targeting E3 ligases	250
5.07.4.4	Targeting the Proteasome in Cancer Therapy	259
5.07.4.4.1	Structure and function of the proteasome	259
5.07.4.4.2	Proteasome inhibitors	260
5.07.4.4.3	Immunoproteasome inhibitors	271
5.07.4.5	Targeting the Deubiquitylating Enzymes in Cancer Therapy	271
5.07.4.6	Degradation of Undruggable Targets in Cancer Therapy	272
5.07.4.6.1	Thalidomide and immunomodulatory drugs	272
5.07.4.7	Summary	273
5.07.5	**Conclusion**	273
References		274

Abbreviations

4EBP eIF4E inhibitory binding protein
ADME Absorption, distribution, metabolism, and excretion
ADP Adenosine diphosphate
AKT Protein kinase B
AML Acute myeloid leukemia
ASCO American Society of Clinical Oncology
ASO Antisense nucleotide
ATP Adenosine triphosphate
CDC37 Cell-division cycle 37 homologue
CDK Cyclin-dependent kinase
CLL Chronic lymphocytic leukemia
CRL Cullin-RING ubiquitin ligase
CRPC Castration resistant prostate cancer
CYP Cytochromes P450
DNA Deoxyribonucleic acid
DUB Deubiquitinating enzyme
eIF Eukaryotic initiation factor
ELISA Enzyme-linked immunosorbent assay
FDA Food and Drug Administration
GIST Gastrointestinal stromal tumors
HOP HSP70–HSP90 organizing protein

HSF1 Heat shock factor 1
HSP Heat shock proteins
HTRF Homogeneous time resolved fluorescence
HTS High-throughput screen
IAP Inhibitor of apoptosis protein
IV Intravenous (administration)
LE Ligand efficiency
MAPK Mitogen-activated protein kinase
MED Minimum effective dose
MM Multiple myeloma
MNK MAPK-interacting kinase
MTD Maximum tolerated dose
mTOR Mammalian target of rapamycin
NAE NEDD8-activating Enzyme
NMR Nuclear magnetic resonance
NSCLC Nonsmall cell lung cancer
PABP Poly(A)-binding protein
PARP Poly ADP ribose polymerase
PD Pharmacodynamic
PDB Protein data bank
PDK Phosphoinositide-dependent kinase
PI3K Phosphoinositide 3-kinase
PK Pharmacokinetic
PO Per os (oral administration)
RAPTOR Regulatory-associated protein of mTOR
RICTOR Rapamycin-insensitive companion of mTOR
RNA Ribonucleic acid
RNAPII RNA polymerase II
SAR Structure–activity relationship
SPR Surface plasmon resonance
TF Transcription factor
TGI Tumor growth inhibition
TOR Target of rapamycin
UPS Ubiquitin–proteasome system
WT Wild-type

5.07.1 Introduction

In order to sustain their uncontrolled growth and proliferation, cancer cells are heavily dependent on maintaining protein homeostasis under challenging cellular conditions. They require an extraordinary level of protein synthesis simply to maintain their growth rate. In addition, they must ensure that the high levels of protein produced do not simply aggregate but are maintained in an active conformation. Finally, cancer cells are heavily dependent on protein degradation processes to balance the intensive protein synthesis and prevent an unsustainable level of protein build up, leading to inevitable cell death. Each of these three areas can be targeted by cancer therapeutics.

Protein synthesis is a fundamental process that all cells must perform and both transcription and translation have been successfully targeted using small-molecule inhibitors. Although transcription has been classically targeted using drugs that interact directly with DNA, significant advances in molecularly targeted therapies designed to inhibit both these processes have been made in the last few years and these are described in "Targeting Protein Synthesis" section. In this broad area, we have seen successful approvals arise from targeting nuclear hormone receptors, for example, tamoxifen and zytiga along with drugs that target translation, such as everolimus.

Understanding of the importance of protein quality control has advanced significantly in the last 20 years. During this period, anticancer drug discovery has moved from the belief that inhibition of molecular chaperones would show no selectivity between cancer cells and normal cells, to proof in the clinic that such inhibitors can have a significant anticancer effect. Heat shock protein 90 (HSP90) has proved to be a druggable protein and has attracted much interest and activity with a range of chemotypes in the clinic but no drugs approved as yet. Heat shock protein 70 (HSP70) provides a clear resistance pathway to HSP90 inhibitors but has proven far more difficult to modulate with small molecules. Progress in the area of targeting molecular chaperones is presented in "Targeting Protein Folding" section.

Finally in this article, the field of protein degradation as a way to target cancer cells is reviewed ("Targeting Protein Degradation" section). The ubiquitin–proteasome system (UPS) has attracted much attention with significant efforts being made to target the E1, E2, and E3 enzymes involved in ubiquitination. Tagging proteins with ubiquitin can target them for proteasomal degradation and inhibition of any of the enzymes involved in this cascade could lead to an unsustainable build up of proteins and cell death. A number of clinical candidates have been disclosed in this area with several compounds entering the clinic. Inhibition of the proteasome has seen real patient benefit, starting with bortezomib (Velcade), which was approved in 2003 in multiple myeloma (MM) followed by carfilmozib in 2012. The discovery of the mode of action of thalidomide has led to an understanding of a very specific form of protein degradation and the potential for this to degrade specific protein targets is an exciting new area that is reviewed in "Degradation of Undruggable Targets in Cancer Therapy" section.

5.07.2 Targeting Protein Synthesis

5.07.2.1 Introduction

One of the hallmarks of transformed cancer cells is their ability to escape the usual checks and balances which stop normal cells undergoing uncontrolled proliferation and survival.[1] The fact that cancer cells display this trait is believed to be derived

from their addiction to oncogenes.[2] Oncogenes allow cancer cells to suppress proapoptotic pathways, manipulate their environment, and avoid immunogenic responses which would otherwise halt the spread of cancer. Targeting oncogenes with small-molecule inhibitors of their resultant proteins has been the primary focus of modern drug discovery efforts to treat cancer with molecularly targeted agents.[3] Because of the dependency of cancer cells on oncogenic proteins, inhibiting their synthesis through the inhibition of gene transcription or translation via the RNA-processing machinery represents a viable strategy for treating cancers, as nonmalignant cells are not reliant on this addiction and can cope with temporary inhibition of protein synthesis, resulting in reduced side effects and an acceptable therapeutic index for these drugs.[4]

5.07.2.2 Targeting Transcription

Excluding compounds that act through interactions with DNA, such as intercalators,[5] there are two opportunities in drug discovery to target protein synthesis, RNA transcription, and translation. RNA transcription is the first step in gene expression, copying a DNA gene sequence of bases into mRNA using RNA polymerase enzymes (Fig. 1). The RNA polymerase creates a transcription bubble by separating the two strands of DNA (Fig. 2). The process of binding the RNA polymerase to the DNA is facilitated by various transcription factors (TFs).[6] Other proteins known as activators and repressors then control the rate of transcription. This complex process affords numerous opportunities in drug discovery to inhibit the synthesis of mRNA molecules. The RNA polymerase could be directly targeted through protein–protein interaction inhibitors, blocking the formation of the transcription bubble. Because the activity of the RNA polymerase is regulated by numerous post-translational modifications, such as phosphorylation, the activity of the RNA polymerase could be controlled indirectly by targeting the enzymes involved in these transformations.[7] Finally, inhibiting the activity of other regulatory proteins within the transcription bubble, such as the TFs, could also reduce or enhance the transcriptional activity of the complex. Each of these strategies has varying potential for drug discovery, dependent on the drugability of the molecular target, selectivity, and therapeutic index.[8]

5.07.2.2.1 Targeting a TF

Since the gene transcription process is tightly regulated by TFs, a viable strategy in oncology to inhibit transcription is to inhibit the function of these proteins. TFs are commonly deregulated in cancer, with many malignant cells showing dependence on either their

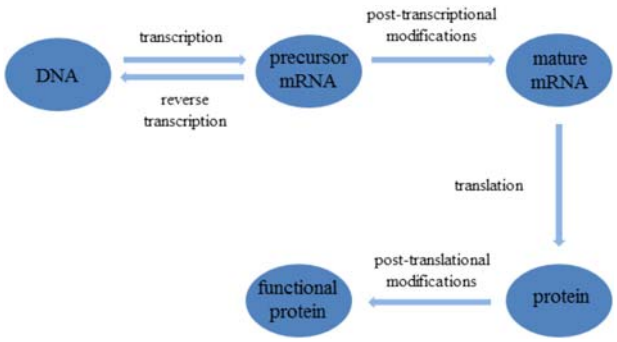

Fig. 1 Process of protein synthesis.

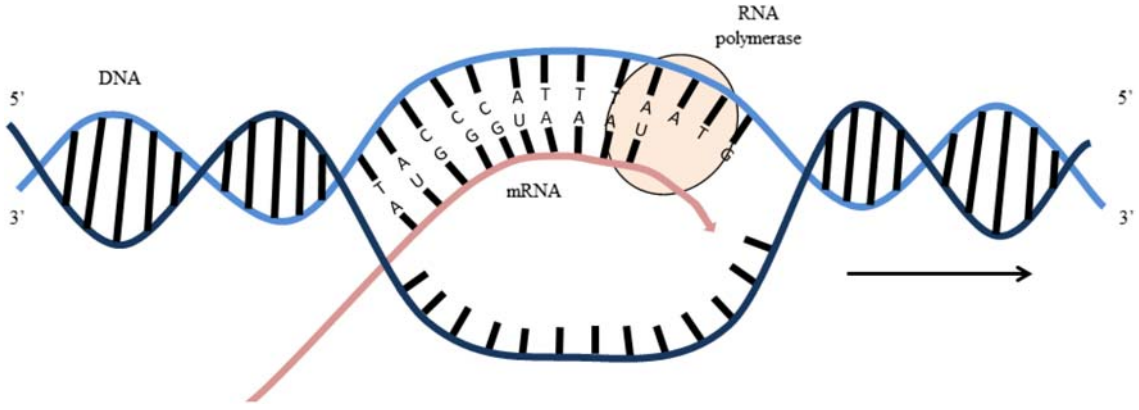

Fig. 2 Process of gene transcription.

activation or repression. Inhibiting TFs can inhibit mRNA synthesis in a gene-specific manner, in contrast to targeting the general transcription machinery.

Some of the most successful treatments realized in oncology have targeted nuclear hormone receptors. In breast cancer, ~70% of tumors rely on estrogen receptors to facilitate cell growth. Two of the compounds that target this reliance on estrogen receptors are tamoxifen **1** and raloxifene **2** (Fig. 3).[9]

Both compounds antagonize estrogen receptor-mediated transcription through direct competition with estrogen for the hormone receptor.[10] Tamoxifen was discovered in 1967 and is in fact a prodrug. The parent compound has little affinity for the estrogen receptor but following oxidation by the metabolizing enzymes CYP3A4 and CYP2D6 (Scheme 1), metabolites such as 4-hydroxytamoxifen (afimoxifene, **3**) bind the receptor with high affinity and stop cancerous cells from dividing.[11]

The increased affinity of the 4-hydroxytamoxifen is clearly explained by the crystal structure of this ligand bound to the estrogen receptor (Fig. 4). The tetrasubstituted alkene forces the three aromatic rings to adopt a propeller-like conformation, giving good complementarity with the binding pocket. This conformation also forces the benzene ring deep into the pocket and in close contact with a hydrophilic region of the protein. The hydroxyl group present in the oxidized tamoxifen metabolite makes multiple hydrogen bond contacts with the arginine-316 and glutamic acid-275 residues and a bound water molecule, interactions that would be absent in tamoxifen itself.

An alternative strategy for targeting nuclear hormone receptor-mediated transcription is to target the synthesis of the endogenous agonist ligand. Androgens, such as testosterone, are often crucial for the proliferation of malignant cells in advanced prostate cancer. To antagonize androgen receptor-mediated transcription, the frontline treatment is chemical castration, which is highly effective at halting disease progression. However, most patients will eventually relapse as despite castration, 10% of circulating testosterone remains due to peripheral conversion of adrenal steroids to testosterone, which continues to drive prostate cancer cell proliferation. By inhibiting the enzyme responsible for residual testosterone synthesis, CYP17α, a new treatment for refractory prostate cancer was developed, the prodrug abiraterone acetate.[12]

The rational design of abiraterone was based on mimicking the endogenous ligand pregenolone but replacing the methyl ketone moiety, which is oxidized by CYP17α by a group that would be resistant to oxidation but could still coordinate the heme cofactor to generate a high affinity ligand (Fig. 5). The pyridine group was designed for this task and it was subsequently revealed that the position of the nitrogen was crucial for inhibitory activity; the 2- and 4-pyridyl groups displayed little activity in contrast with the 3-pyridyl analog which displayed an $IC_{50} = 2.9$ nM. This structure–activity relationship (SAR) can clearly be rationalized with the crystal structure of abiraterone bound to the androgen receptor, as only the 3-pyridyl analog possess the correct geometry to coordinate the iron of the heme cofactor (Fig. 6).

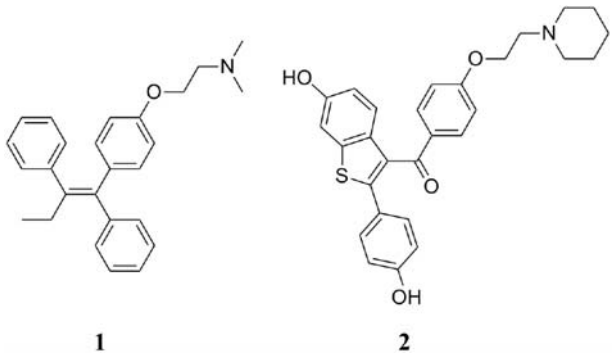

1 2

Fig. 3 Chemical structures of estrogen receptor antagonists.

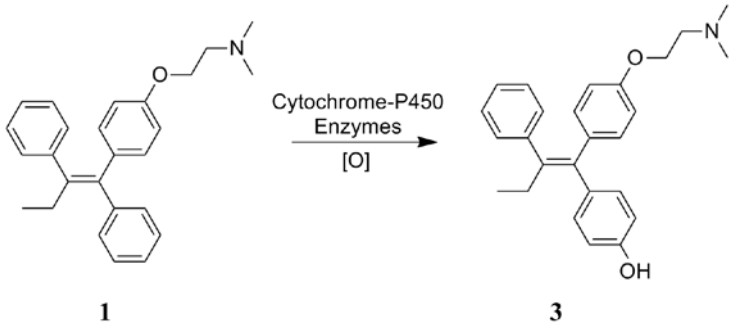

1 3

Scheme 1 Oxidative metabolism of tamoxifen.

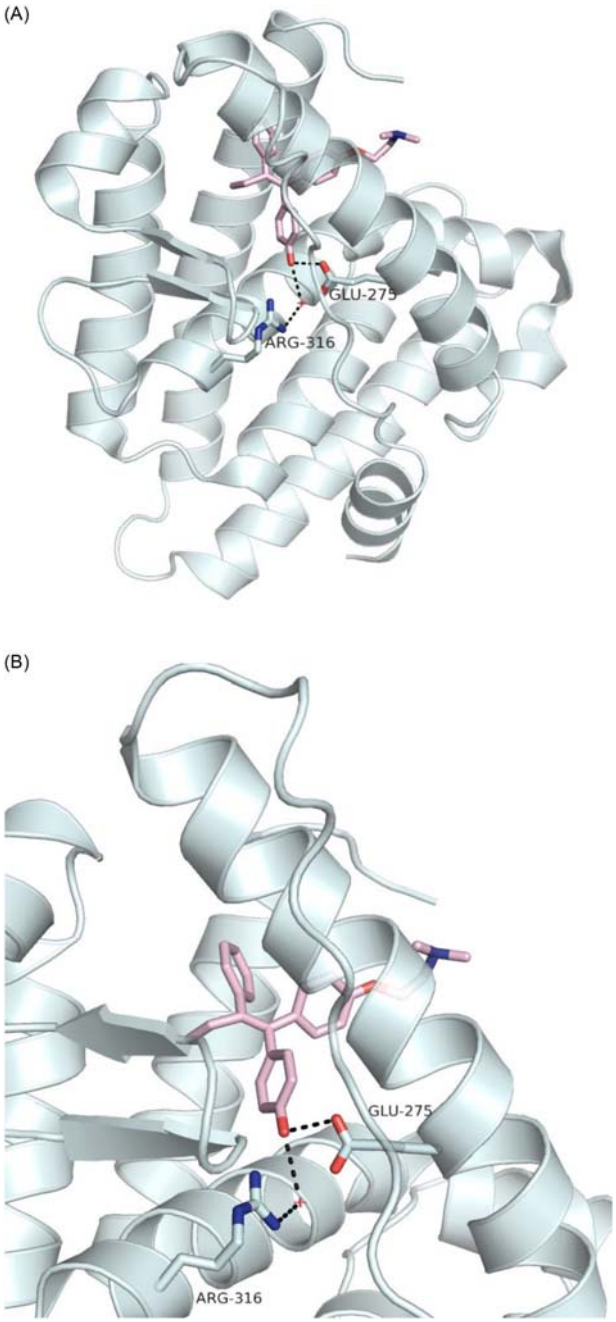

Fig. 4 X-ray crystal structure of estrogen-related receptor gamma (*cyan*) in complex with 4-hydroxytamoxifen (*light pink*), PDB ID: 2P7Z. Panel A: location of the binding site in the protein; panel B: binding site view. The structure of the ligand, and the key binding site residues are shown as sticks. Selected interactions are shown in *black-dashed lines*.

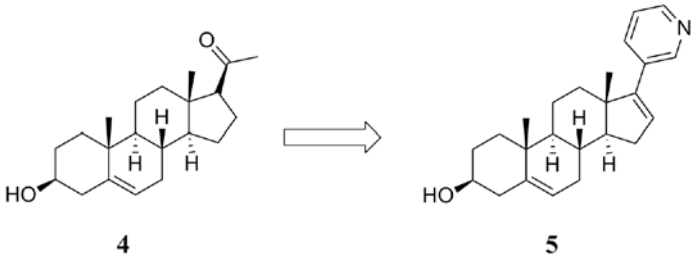

4 5

Fig. 5 Design of abiraterone.

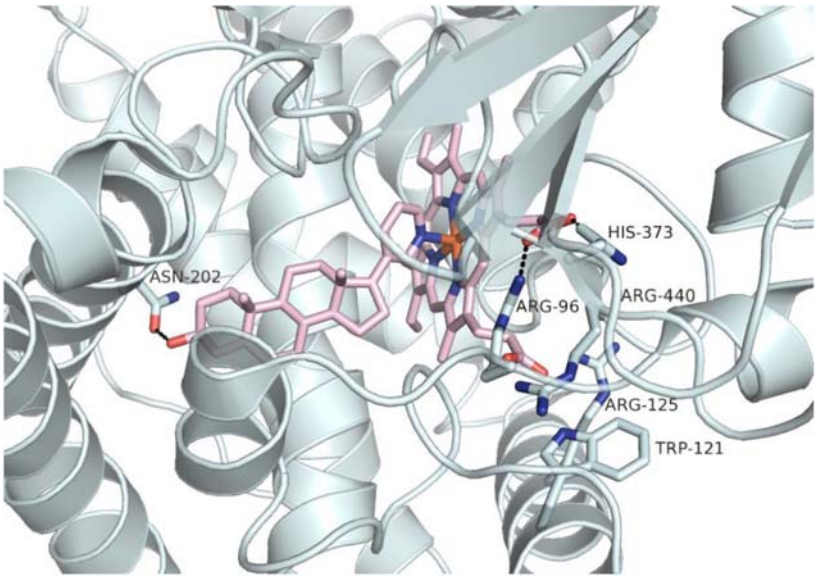

Fig. 6 X-ray crystal structure of human cytochrome P450 CYP17A1 (*cyan*) in complex with abiraterone and heme (*light pink*), PDB ID: 3RUK. The structure of the ligands abiraterone and heme, and the key binding site residues are shown as sticks. Selected interactions are shown in *black-dashed lines*.

There are many other TFs other than the nuclear hormone receptors that have been implicated in cancer. c-Myc is a transcription factor important for cell cycle progression, apoptosis, and cellular transformation and is commonly mutated in cancers to make it constituently active.[13] c-Myc has been a popular molecular target in oncology but because it is ligandless, targeting c-Myc with small molecules has proven particularly challenging, as without a small-molecule binding site, the protein is considered to have low drugability. There are many other TFs which could be potential targets in oncology, such as NRF2,[14] NFkB,[15] and HSF1,[16] which also display this difficulty. Therefore, various alternative strategies have been applied to target the function of TFs rather than relying on direct inhibition. This phenotypic approach has led to a large number of TF pathway inhibitors appearing in the literature; however, their molecular mechanisms of action are often poorly defined.

In contrast, a ligandless transcription factor that has been successfully targeted by small-molecule modulation is the "guardian of the genome" p53.[17] p53 is vital tumor suppressor protein which regulates the transcription of many genes involved in DNA damage and repair. p53 is often mutated in cancer to suppress its function and allow the cancer cell to proliferate; despite the DNA damage in the cell that would normally initiate cell cycle arrest or apoptosis. In cancer cells where p53 is not mutated, its function is often suppressed via continuous degradation by the ubiquitin ligase HDM2. HDM2 binds p53 through a protein–protein interaction and it was proposed that cancer cells that rely on HDM2 to block p53 mediated transcription. Small-molecule inhibitors of the MDM2/p53 interactions will be discussed in the section on protein degradation ("MDM2" section).

5.07.2.2.2 Targeting RNA polymerases

Because of the oncogene addiction of cancer cells to various proteins, inhibiting the general transcription machinery is also a viable strategy in oncology. The RNA polymerases, and in particular RNA polymerase II (RNAPII), are required for most mRNA transcription events. In order to carryout gene transcription, a preinitiation complex is formed by RNAPII and a number of general TFs.[18]

After the first 25–30 nucleotides are transcribed, there is a transition between transcription initiation and elongation resulting in the hyperphosphorylation of RNAPII, which is a requirement for transcription elongation and termination. This complex process gives a number of opportunities to inhibit gene transcription. Actinomycin D is a very large cyclic peptide antibiotic that inhibits RNA synthesis by intercalating DNA. However, since it binds directly to DNA it can also cause DNA damage, leading to a phenotype that differs from general transcription inhibition.[19] Another complex cyclic peptide called alpha-amanitin (**6**) (**Figs. 7** and **8**) is a well-known general transcription inhibitor. Found in the emotively named death-cap mushroom, this highly toxic compound binds RNAPII directly, dramatically slowing its DNA translocation and thus inhibiting mRNA synthesis.[20,21]

α-Amatinin, **6**, is a potent hepatotoxin, resulting in damaging side effects and leaving little therapeutic index against cancer cells versus normal cells, which has prevented its use in cancer therapy. Its complex structure makes analog synthesis a daunting task. The unique mechanism of action of α-amatinin has led to attempts to circumvent the liver toxicity of this compound by using antibody drug conjugates to block uptake into mature hepatocytes and direct the RNAPII inhibitor to cancer cells using tumor-specific antibodies. Despite some encouraging results in mouse models, it is as yet unclear whether this approach will be successful in the clinic.[22]

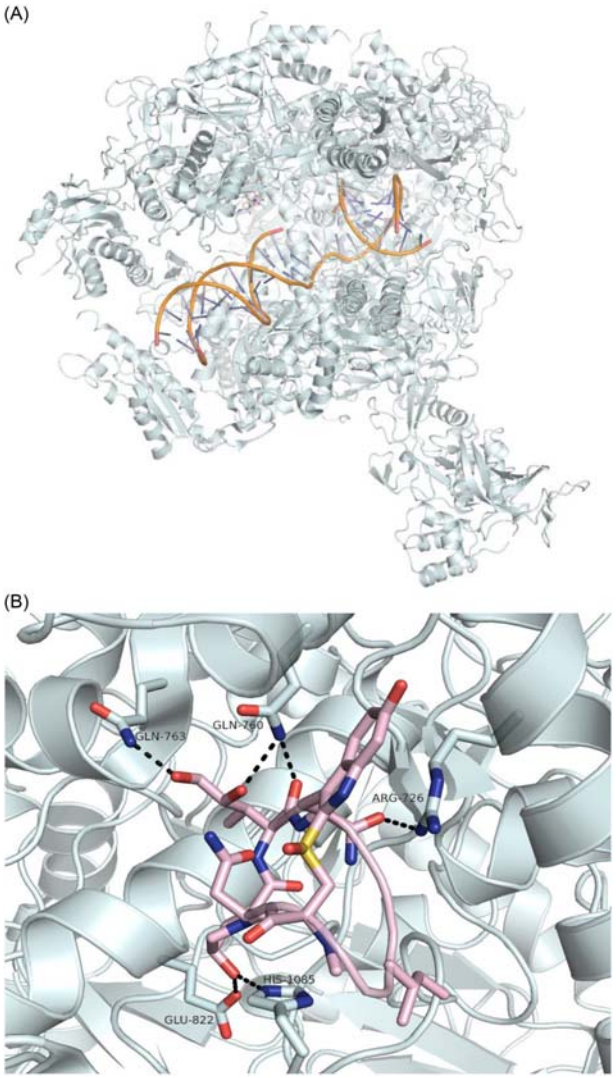

Fig. 7 (A) X-ray crystal structure of α-amanitin-inhibited complete RNA polymerase II elongation complex, DNA shown as *orange ribbon*, PDB ID: 2VUM. (B) Close-up of the α-amanitin binding site. The structure of the ligand α-amanitin (*light pink*), and the key binding site residues are shown as sticks. Selected interactions are shown in *black-dashed lines*.

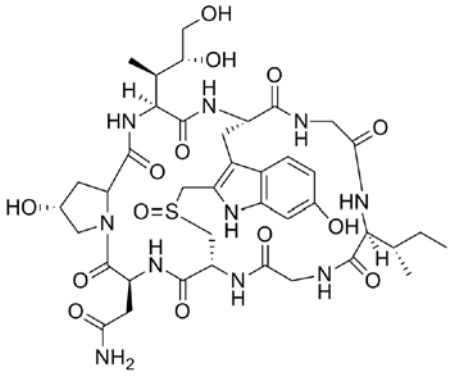

6

Fig. 8 Chemical structure of α-amatinin.

5.07.2.2.2.1 CDK9 inhibitors

Since directly targeting RNAPII to inhibit mRNA transcription has proven particularly challenging, alternative approaches that target proteins which regulate RNAPII have been investigated. Originally discovered as ATP-competitive inhibitors of cyclin-dependent kinase 2 (CDK2),[23] aiming to antagonize cancer proliferation by exploiting CDK2's role in cell cycle arrest, it became clear that many features of the phenotype of CDK2 inhibitors could not be accounted for by the inhibition of that protein, particularly the inhibition of mRNA transcription. The cyclin-dependent kinases are a family of transferases whose function is tightly regulated by cyclins in a dimeric complex.[24] The ATP-binding site of the CDKs is highly conserved across the family, meaning that designing small-molecule CDK-selective inhibitors is challenging.[25] The original CDK2 inhibitors such as roscovitine[26] and flavopiridol, **7**[27] (**Table 1**), were less selective than was originally assumed and it was later discovered they were also inhibiting other CDKs, including the CDK most important for RNAPII-mediated transcription, cyclin-dependent kinase 9 (CDK9). CDK9 directly phosphorylates RNAPII, so inhibiting the catalytic function of CDK9 inhibits the RNAPII hyperphosphorylation crucial for efficient mRNA transcription elongation and therefore mRNA synthesis.[28]

Selectivity between different CDKs is clearly one of the greatest challenges in this field of drug discovery but also represents a big opportunity. The early pan-CDK inhibitors such as flavopiridol suffered from a poor therapeutic index due to their lack of selectivity, including kinases outside of the CDK family. It is now also appreciated that polypharmacology,[29] inhibiting multiple structurally related proteins, is often crucial for potent anticancer effects; while compounds that are too selective can have little effect on cancer progression. The apparent paradox between safety and efficacy resulting from selectivity can be difficult to resolve through rational drug design. Dinaciclib, **9** (**Table 1**), is a potent inhibitor of CDK1, 2, 5, 9 (IC_{50} = 3, 1, 1, 4 nM, respectively) but is highly selective against kinases outside of the CDK family and is a good example of this paradox.[30] Because it is difficult to rationalize the correct balance of CDK inhibition, the discovery of dinaciclib was via an in vivo phenotypic approach to maximize the therapeutic index in tumor bearing nude mice. Presumably, this was because small structural changes altered the balance between the inhibition of the four CDKs. The core scaffold was maintained in each analog, such as compound **8**, with variations focused on the 5-position of the pyrazolopyrimidine core. The ratio of maximum tolerated dose (MTD) to the minimum effective dose was then determined for each analog (**Table 1**).

Table 1 Development of dinaciclib

Compound	*Name*	*MTD (mg kg^{-1})*	*MED (mg kg^{-1})*	*TI[a] (MTD/MED)*
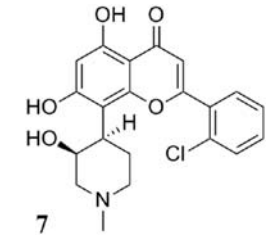 **7**	Flavopiridol	<10	10	<1
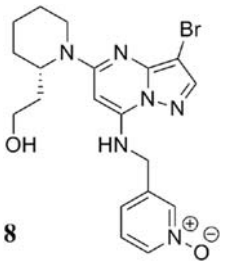 **8**	–	20	4	5
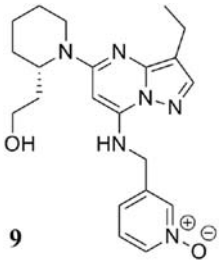 **9**	Dinaciclib	60	5	>10

[a]Relative therapeutic indices (TI) following intraperitoneal (ip) dosing using the in vivo screening paradigm (maximum tolerated dose, MTD = 20% weight loss; minimum effective dose, MED = 50% inhibition of tumour growth; QDx7 = once a day dosing for 7 consecutive days).

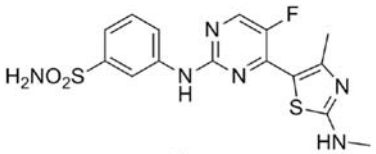

10

Fig. 9 Chemical structure of CDKI-73.

The pan-CDK inhibitor flavopiridol had a poor therapeutic index (<1) in this screen, which was in stark contrast to dinaciclib **9** which was advanced into further study. While this strategy did deliver a compound with an improved therapeutic index compared to flavopiridol, it did mean that PK optimization was not prioritized. Dinaciclib is not orally bioavailable so must be delivered iv, and the unusual pyridinium-*N*-oxide motif means dinaciclib has poor plasma stability. Despite these challenges, dinaciclib was advanced into multiple clinical trials for solid tumors and hematological malignancies.

A variety of core scaffolds have been shown to be good CDK9 inhibitors. CDKI-73, **10**, is a 2-anilino-4-thiazolopyrimidine (Fig. 9) that was rationally designed and optimized using protein crystal structures of CDK9.[31] This chemotype was known to display good CDK9 inhibition ($IC_{50}=4$ nM) but this activity was difficult to uncouple from the CDK2 activity ($IC_{50}=3$ nM).

By analyzing the crystal structure of 2-anilino-4-(thiazole-5-yl)pyrimidine, **11**, bound to CDK2 and through modeling binding to the more open CDK9 structure (Figs. 10 and 11), substitution at both the 5-pyrimidine and *meta*-anilino moieties was proposed to improved selectivity. These design principles lead to **11** which displayed an 80-fold selectivity for CDK9 ($IC_{50}=7$ nM) over CDK2 ($IC_{50}=130$ nM).[32]

However, even though the CDK9 activity of **11** was improved and it could be shown to inhibit RNAPII phosphorylation, its antiproliferative activity was more than 40-fold reduced, so the less selective analog **10** was progressed into further preclinical study.

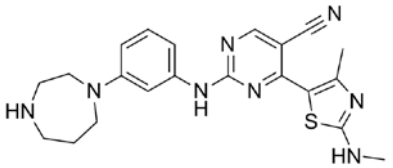

11

Fig. 10 Chemical structure of compound **11**.

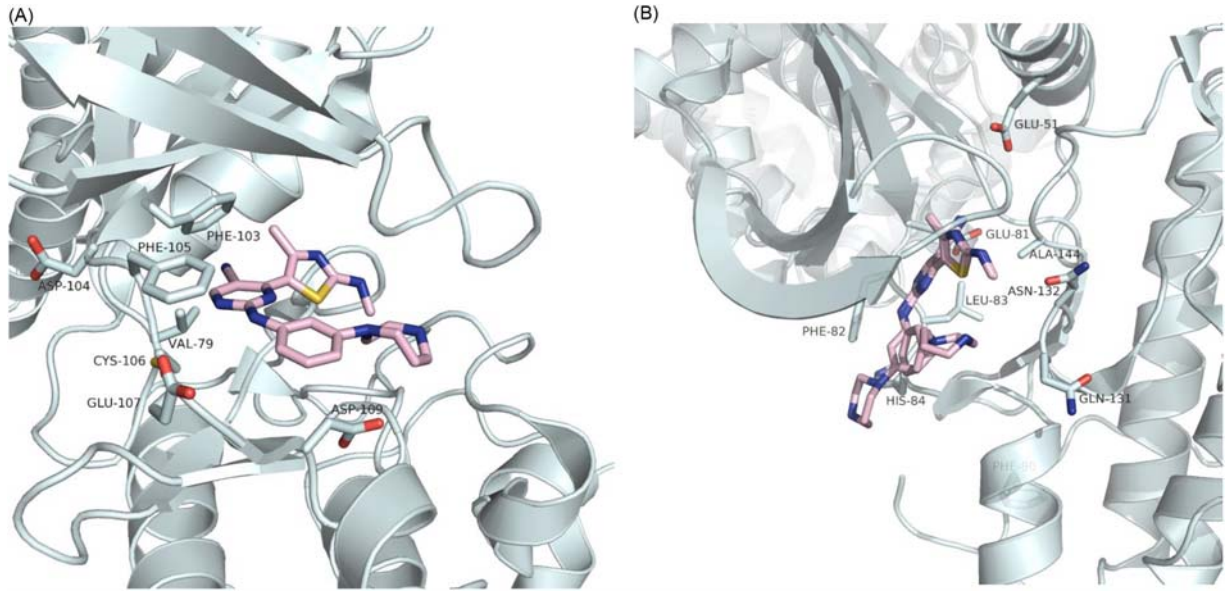

Fig. 11 X-ray crystal structures of CDK9 (Panel A, *cyan*) in complex with cyclin T and a 2-amino-4-heteroaryl- pyrimidine inhibitor (*light pink*), PDB ID: 4BCG, and of CDK2 (Panel B, *cyan*) in complex with cyclin T and a 2-amino-4-heteroaryl-pyrimidine inhibitor (*light pink*), PDB ID: 4BCP. The structure of the ligand, and the key binding site residues are shown as sticks.

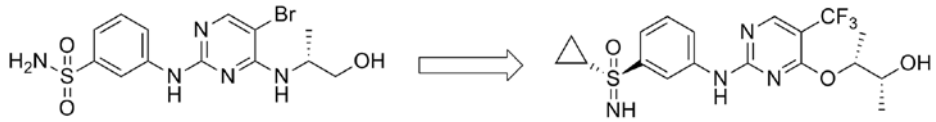

12 13

Fig. 12 Development of ZK3044709.

This contradiction is either a commonly observed example of a biochemical/cell assay disconnect[33] or again demonstrates the importance of polypharmacology to efficacy, especially in the field of kinase drug discovery.

Other CDK9 inhibitors include the pan-CDK inhibitor BAY1000394.[34] Lead optimization of an aminopyrimidine screening hit, **12**, led to ZK3044709[35] **13** (Fig. 12), which although had a promising preclinical profile but was unsuccessful in phase 1 clinical trials due to dose-limiting absorption and high interpatient variability.

The causes of this failure were attributed to the poor aqueous solubility and off-target activity against carbonic anhydrase II. A model of ZK3044709 indicated the importance of the sulfonamide moiety to its affinity to CAII, as this functional group is known to be an excellent zinc(II) ion chelator (Fig. 13).

Modification of this group to a sulfoximide, which can suppress this interaction, followed by optimization of the pyrimidine C5- and C6-substituents to lower lipophilicity and block liver microsome degradation, gave a clinical candidate with nanomolar pan-CDK activity, improved aqueous solubility, and greatly improved predicted human dose.

Another compound that exploits the 2-aminopyrimidine scaffold for CDK9 inhibition is LY2857785[36] **14** (Fig. 14). This CDK9 inhibitor ($IC_{50} = 11$ nM) displayed a good kinase selectivity profile, with only 5 kinases out of the 114 tested displaying an $IC_{50} < 100$ nM. Good aqueous solubility and excellent cellular activity led to numerous in vivo xenograft studies, demonstrating tumor regression from an intravenous (IV) dose.

SNS-032, **15**, is an aminothiazole-derived pan-CDK inhibitor (Fig. 15).[37] Originally designed to be an inhibitor of CDK2, it was subsequently discovered to possess transcription inhibition activity which was attributed to its potent CDK9 inhibition.

5.07.2.2.3 BRD4 inhibitors

BRD4 is a member of the BET family of bromodomains that act as genetic readers of histone acetyl lysine residues to regulate gene transcription. BRD4 has become a popular epigenetic target in oncology. As part of the general transcription machinery, BRD4 interacts with the positive-elongation factor (P-TEFb) complex, which is fundamental for transcription elongation through RNAPII, so can regulate transcription indirectly through control of the transcription preinitiation complex. Also, BRD4 has been

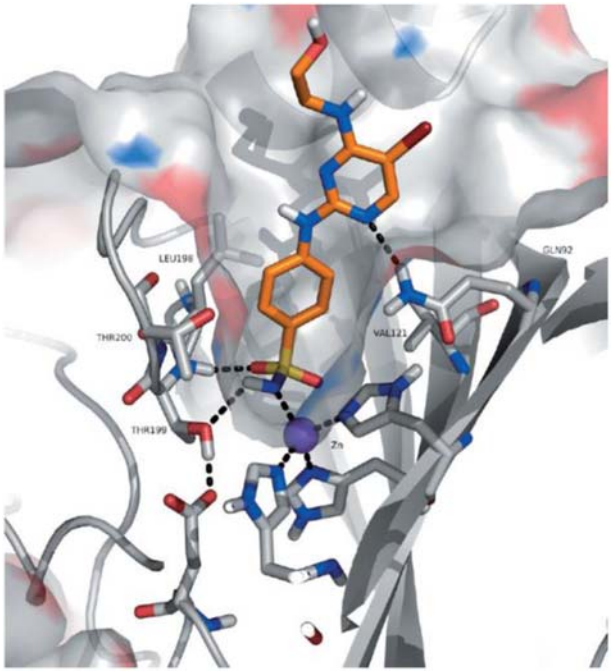

Fig. 13 Model of ZK3044709 in complex with human CAII.[35]

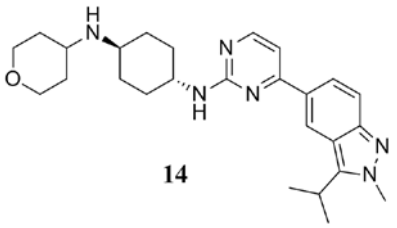

14

Fig. 14 Chemical structure of LY2857785.

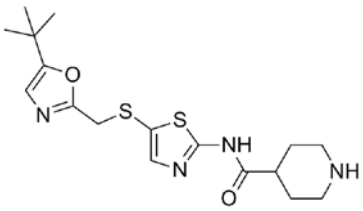

15

Fig. 15 Chemical structure of SNS-032.

proposed to act as an atypical kinase that can phosphorylate serine-2 of RNAPII, regulating transcription through a more direct mechanism.[38,39]

From an antiinflammatory phenotypic study, it was discovered that simple thienodiazepines possessed affinity for BRD4. By inferring SAR derived from molecular modeling of the candidate ligand, the chemical probe (+)-JQ1, **16**, was discovered which displayed a $K_d = 50$ nM (Fig. 16).[40]

Analysis of the co-crystal structure revealed that (+)-JQ1 mimics many of the interactions of the endogenous acetyl lysine complex (Fig. 17). The triazole forms a hydrogen bond with the evolutionarily conserved asparagine 140 and the ligand displayed excellent shape complementarity. Only the (*S*)-enantiomer has affinity for BRD4, which was rationalized using models predicting an energetically unfavorable diazepine conformation and through clashes with the ZA-loop region.

To develop a BRD4 inhibitor that has potential clinical use, the pharmacokinetic profile of the original chemical probe needed to be improved. OTX015, **17**, is a (+)-JQ1 analog, which replaced the t-Bu ester with a para-hydroxyacetamide (Fig. 18).[41] This compound is currently under investigation in human clinical trials for leukemia. No description was given as to why this structural change gave an improved pharmacokinetic profile.

Other chemotypes have been shown to be potent inhibitors of BRD4-mediated transcription and have been progressed to the clinic. I-BET726 (GSK1324726A, **20**, Fig. 19) was discovered via a phenotypic screen to discover upregulators of ApoA1 and most of the SAR development was carried out without knowing that the molecular mechanism of action was through inhibition of the BRD protein family.[42] From the cell-based high-throughput screen, the tetrahydroquinoline was identified to increase ApoA1 activity in a luciferase reporter assay approximately two- to threefold.

The initial hit, **18**, from the HTS contained two stereogenic centers as a mixture of both absolute and relative stereoisomers. Early SAR of the screening hit revealed that the *cis*-stereochemistry was crucial for activity, and the 2*S*,4*R*-enantiomer was more than two orders of magnitude more active than its enantiomer. Substitution at the 6-position of the tetrahydoquinoline was rationalized by

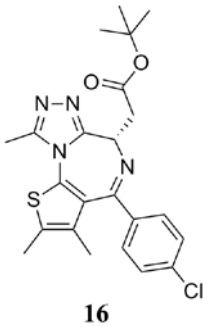

16

Fig. 16 Chemical structure of (+)-JQ1, **16**.

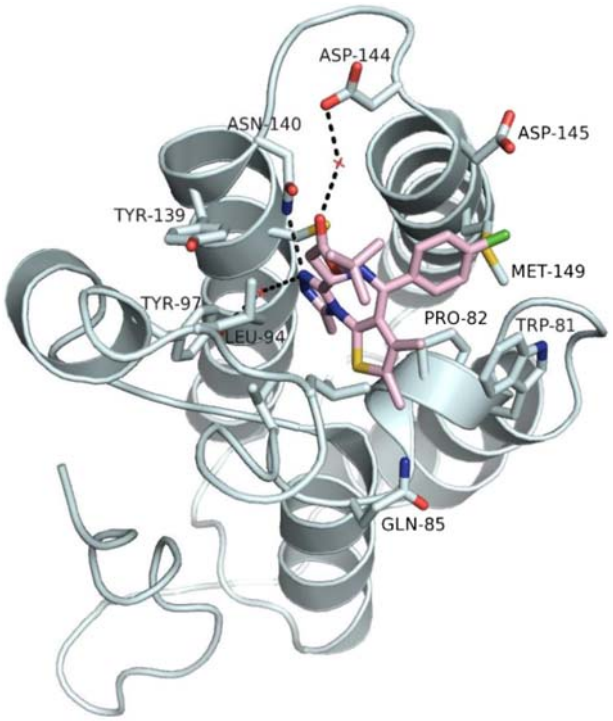

Fig. 17 X-ray crystal structures of bromodomain of human BRD4 (*cyan*) in complex with the inhibitor (+)-JQ1, **16** (*light pink*), PDB ID: 3MXF. The structure of the ligand, and the key binding site residues are shown as sticks. Selected interactions are shown in *black-dashed lines*.

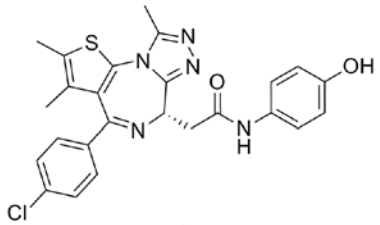

17

Fig. 18 Chemical structure of OTX015.

an overlay with pharmacophores of other ApoA1 upregulators, with substitution of this ring being well-tolerated with various substituents, which facilitated a route to PK optimization (Fig. 19). Interestingly, the carboxylic acid had little effect on cellular activity, despite the expected reduction in permeability this functional group can bring. These features were incorporated into the clinical candidate, which displayed good oral bioavailability across multiple species and activity in an in vivo mouse model. Many of these SAR features were eventually rationalized when the crystal structure of I-BET726 bound to BRD2 was solved

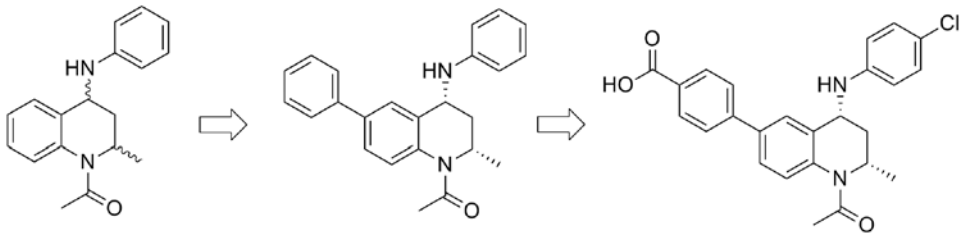

18 **19** **20**

Fig. 19 Development of GSK1324726A.

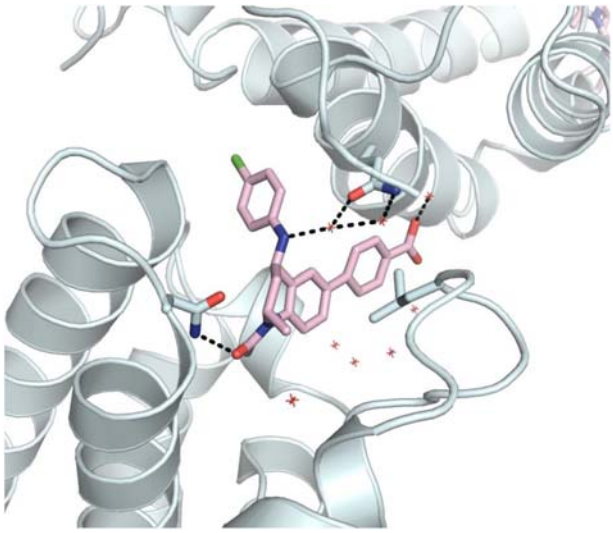

Fig. 20 X-ray crystal structures of bromodomain of human BRD2 (*cyan*) in complex with the inhibitor I-BET726 (*light pink*), PDB ID: 4UYF. The structure of the ligand, and the key binding site residues are shown as sticks. Selected interactions are shown in *black-dashed lines*.

(Fig. 20). The tetrahydroquinoline ring was buried deep in the pocket, while the *para*-chloroaniline and para-benzoic acid were solvent exposed.

Interestingly, a second chemotype was discovered via the ApoA1 phenotypic screen, which was very similar to the (+)-JQ1 series. I-BET762, **22**, was developed from a benzodiazepine, **21**, unsurprisingly since benzene and thiazole are often used as interchangeable bioisosteric replacements, with optimization again focused on the solvent-exposed region. The carbamate was chemically unstable at low gastric pH and was replaced by an ethylamide (Fig. 21).[43]

5.07.2.3 Targeting Translation

5.07.2.3.1 Translational control in cancer

Proteins are synthesized from mRNA through translation by the ribosomes, tRNA, and auxiliary proteins. Translation occurs in four phases: initiation, elongation, termination, and ribosome recycling (Fig. 22). Initiation is the first and generally rate-limiting step of translation, where initiation factors facilitate the positioning of the translation-competent ribosome at the initiator codon of the mRNA. The 43S ribosome preinitiation complex is formed by association of the 40S small ribosomal subunit, the initiating methionyl tRNA, and a group of eukaryotic initiation factors (eIFs). The 43S ribosome complex is then recruited to the 5′ end of the mRNA, marked by a 7-methylguanosine cap. Association of the 43S ribosome complex with the 7-methylguanosine cap, which protects the mRNA from degradation and binds eIF4E, is mediated by the cap-binding complex eIF4F. The eIF4F complex is composed of a 5′mRNA, the cap-binding subunit eIF4E, the large scaffolding protein eIF4G, and the ATP-dependent DEAD box helicase eIF4A. eIF4G also interacts with the poly(A)-binding protein (PABP), which associates with the mRNA 3′ poly(A) tail. Recognition of the initiation codon by the 43S preinitiation complex leads to release of the eIFs and joining of the 60S ribosomal subunit. The formation of a translation-competent 80S ribosome is the end of the initiation and beginning of the elongation phase.[44–46]

The regulation of translation is a mechanism that is used to modulate gene expression in a wide range of biological situations. Two different modes of translational control are known: global control, in which the translation of most mRNAs in the cell is regulated, and mRNA-specific control, where the translation of a defined group of mRNAs is modulated without affecting general

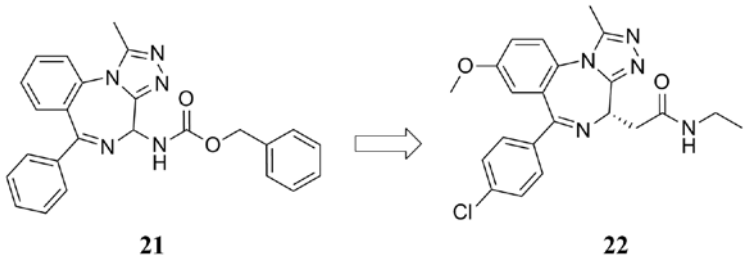

Fig. 21 Development of I-BET762 (**22**).

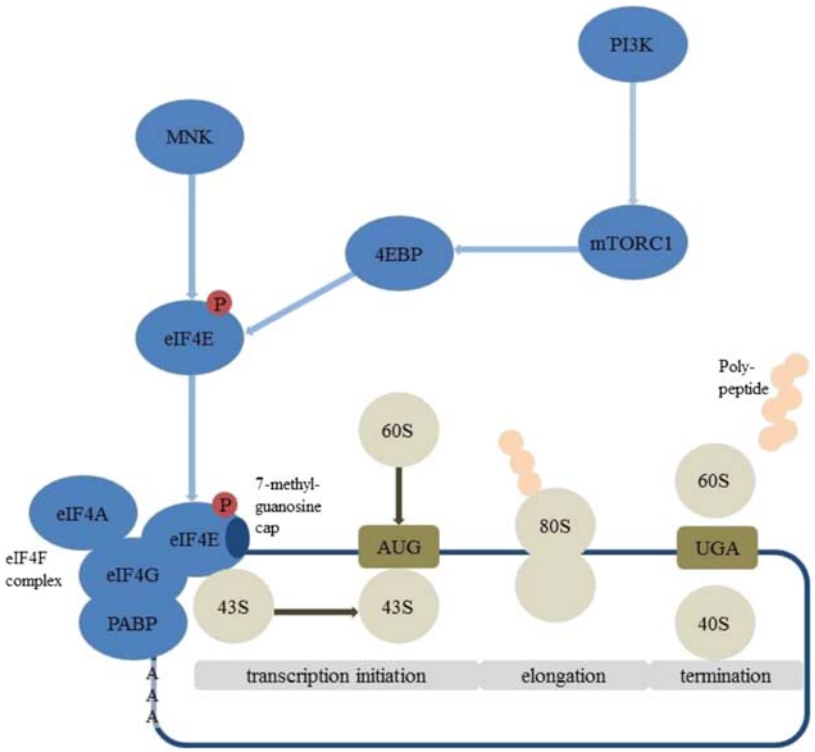

Fig. 22 Oncogenic alterations of mRNA translation. The eukaryotic initiation factor 4F (eIF4F) cap-initiation complex (eIF4G, scaffolding protein for assembly of the translation machinery; eIF4E, cap-binding subunit; eIFA, ATP-dependent DEAD box helicase that unwinds the mRNA) assembles on the 7-methylguanosine cap and interacts with the poly(A) tail binding protein (PABP) at the 3′ end of the mRNA. The 43S preinitiation complex is formed by association of the 40S ribosomal subunit with eukaryotic translation factors and the ternary complex. Recognition of the initiation codon (typically AUG) by the 43S preinitiation complex leads to release of the eIFs and recruitment of the 60S ribosomal subunit, leaving the active 80S ribosome at the initiation codon, primed to begin protein synthesis. The formation of a translation-competent 80S ribosome is the end of the initiation and beginning of the elongation phase. Termination is triggered by a stop codon (UAA, UGA, or UAG). MNK, MAPK-interacting kinase; 4EBP, eIF4E-binding protein; mTORC1, mammalian target of rapamycin complex 1; PI3K, phosphoinositide 3-kinase.

protein biosynthesis. Global regulation mainly occurs by modification of the translation-initiation factors, whereas mRNA-specific regulation is driven by regulatory protein complexes. The translation of most mRNAs is controlled at the initiation step, and involves controlling the assembly of a functional 43S preinitiation complex or altering access of preinitiation complexes to the mRNA template. The assembly and activity of the eIF4F complex is tightly regulated by signaling pathways that are involved in cancer development and progression. eIF4E is regulated by its availability, which is controlled by the eIF4E inhibitory binding proteins (4EBPs), and by its phosphorylation at serine 209 by the MAPK-interacting kinases MNK1 and MNK2. Oncogenic signaling can hyperactivate eIF4E through mTOR complex 1 (mTORC1)-dependent phosphorylation. Translation can also be regulated at the elongation stage by oncogenic signaling.[44–46]

Malignant cells often show augmented translational activity and are believed to become addicted to elevated protein synthesis. This potentially provides a therapeutic window to selectively target cancer cells.[44] Translational control is a crucial component of cancer development and progression. It directs both, global control of protein synthesis, and selective translation of specific mRNAs promoting tumor cell survival, angiogenesis, transformation, invasion, and metastasis. A number of oncogenic signaling pathways affecting translation are known to be deregulated in human cancers, including RAS–MAPK, and PI3K–AKT–mTOR. Alterations of translational control are associated with different types of cancers, disease stages, and tumor microenvironment.[44–46]

5.07.2.3.2 Inhibitors of eIF4F upstream regulators

Most strategies of inhibiting protein translation target the eIF4F complex. These strategies can be categorized into two groups: firstly, targeting upstream regulators of mRNA translation, and secondly, directly targeting the eIF4F complex. The majority of clinical candidates that inhibit protein translation, including mTOR inhibitors, and dual PI3K/mTOR inhibitors are considered upstream regulators of mRNA translation.[44]

5.07.2.3.2.1 Allosteric mTOR inhibitors—rapamycin and rapalogues

Rapamycin (Fig. 23) is a macrolide first isolated in 1972.[47] Rapamycin is produced as a secondary metabolite by *Streptomyces hygroscopius*, a soil bacterium isolated from a sample collected on Easter Island (Rapa Nui). Rapamycin was initially developed

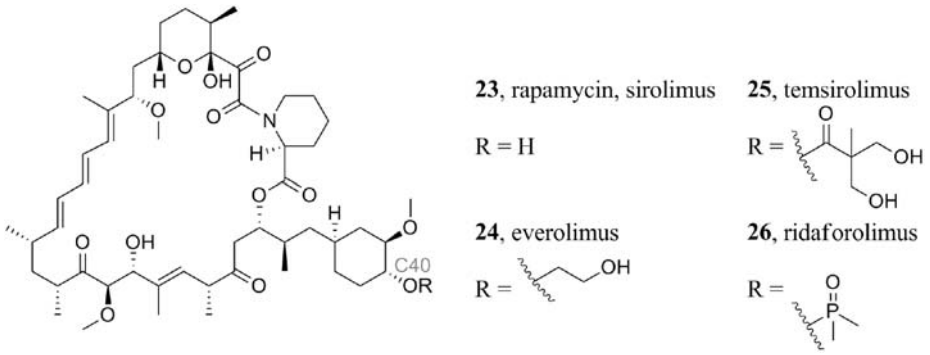

Fig. 23 Rapamycin and rapalogs.

as an antifungal agent, and shows antitumor and immunosuppressive activity in mammalian cell-culture assays. Genetic selection for rapamycin-resistant mutants in *Saccharomyces cerevisiae* (yeast) cells identified FPR1, TOR1, and TOR2 as genes that participate in rapamycin toxicity. The target proteins of rapamycin were collectively named target of rapamycin (TOR).[48] TOR and the mechanism of action were later found to be conserved from yeast to humans.[49]

Mammalian target of rapamycin (mTOR) is a protein kinase that is frequently dysregulated in cancer and metabolic disorders. mTOR belongs to the phosphoinositide 3-kinase (PI3K)-related protein kinase family. This protein family comprises proteins that enable organisms to cope with metabolic, environmental, and genetic stresses. TOR is highly conserved in all eukaryotes and is ubiquitously and constitutively expressed. TOR is a serine/threonine protein kinase that exhibits no lipid kinase activity. The kinase domain is located in the carboxy-terminal region of TOR. mTOR associates with other proteins to generate two distinct complexes called mTOR complex 1 (mTORC1) and mTORC2. mTORC1 is composed of mTOR, regulatory-associated protein of mTOR (RAPTOR), SEC13 protein 8, and proline-rich AKT substrate of 40 kDa (PRAS40, also known as AKT1S1). mTORC1 is involved in protein synthesis and cell progression and is sensitive to inhibition by rapamycin. mTORC2 is composed of mTOR, rapamycin-insensitive companion of mTOR (RICTOR), mLST8, proline-rich protein 5 (PRR5), and mitogen-activated protein kinase-associated protein 1 (MAPKAP1). mTORC2 is involved in cytoskeleton organization and cell survival and is generally insensitive to inhibition by rapamycin. Studies with rapamycin showed that mTOR is involved in translational control. Rapamycin blocks the activation of phosphorylation of S6 kinase by growth factors or nutrient stimuli and promotes the dephosphorylation of 4EBP1, thereby increasing cap-dependent mRNA translation. Both S6 kinase and 4E-BP1 are controlled by multisite phosphorylation.[50]

Inhibition of mTOR by rapamycin is dependent on the formation of a complex with the immunophilin FKBP12, which then binds mTOR in mTORC1. FKBP12 interacts with mTOR through rapamycin, which binds pockets in both proteins.[51] Therefore, rapamycin acts as a protein–protein interaction stabilizer. The requirement for a cofactor makes the mTOR-rapamycin interaction very specific.[49,52] The anticancer activity of rapamycin against a panel of human cancer cell lines was investigated by the US National Cancer Institute (NCI) in the 1980s. Rapamycin showed antitumor effects in several cancer cell lines in vitro and in vivo.[53] Semisynthetic rapamycin analogs (rapalogs) were developed to improve the pharmacokinetic properties of this natural product. The rapalogs all share the same macrocyclic lactone core structure, but differ in their substituents on the C40 hydroxyl group of the cyclohexyl ring, as shown in **Fig. 23**. Temsirolimus is a water-soluble ester derivative for oral and intravenous formulation. Temsirolimus is a prodrug that is metabolized to rapamycin (sirolimus) as the primary active metabolite. Everolimus is a hydroxylethyl ether derivative of rapamycin developed for oral administration. Ridaforolimus (deforolimus) has a phosphate group on the C40 hydroxyl group and was designed for improved aqueous solubility and oral administration. Rapalogs bind at the same binding site for FKBP12 and mTOR as rapamycin with the semisynthetic modifications of the rapalogs located outside the FKBP12- and mTOR-binding domains.[49,52] The rapalogs temsirolimus, everolimus, and rodaforolimus have all been studied in clinical trials. The most promising results have been obtained in renal cell carcinoma when treated with everolimus or temsirolimus, mantle cell lymphoma (MCL), and endometrial cancers. In other tumor types, the clinical performance of rapalogs was disappointing, for example, in glioblastoma, breast cancer, and neuroendocrine carcinoma, the objective response rate with temsirolimus was consistently lower than 10%.[49,52,54] The FDA has approved everolimus for the treatment of renal cell carcinoma, advanced hormone receptor-positive, HER2-negative breast cancer in combination with exemestane and subependymal giant cell astrocytoma (SEGA) tumors. Temsirolimus has also been FDA approved for the treatment of renal cell carcinoma. Ridaforolimus was rejected by the FDA in 2012.

5.07.2.3.2.2 ATP-competitive mTOR inhibitors

A new generation of mTOR inhibitors consists of ATP-competitive compounds that directly inhibit mTOR kinase activity. Unlike rapamycin, these ATP-competitive mTOR kinase inhibitors (TOR-KIs) inhibit both mTORC1 and mTORC2. This blocks feedback activation of PI3K/AKT signaling, thereby offering an advantage over the rapalogs which only inhibit mTORC1.[49,55] The anticancer efficacy of TOR-KIs has been shown superior to that of rapalogs in preclinical settings and a number of these compounds are

investigated in clinical trials.[56] However, mTOR inhibitors remain prone to resistance mechanisms inherent to targeting upstream signaling proteins. Several studies indicate that eIF4E and/or 4EBP expression levels affect the efficacy of PI3K and mTOR inhibitors.[44] Because of the similarity between the kinase domains of mTOR and PI3Ks, a number of ATP-competitive compounds inhibit both mTOR and PI3K. TOR-KIs can be classified into two groups, dual mTOR/PI3K inhibitors, which inhibit both kinases at similar effective concentrations, and pan-mTOR inhibitors, which have a lower IC_{50} for mTOR inhibition than for PI3K.[49]

5.07.2.3.2.2.1 Dual mTOR and PI3K inhibitors

Most of the dual mTOR/PI3K inhibitors currently in clinical trials (Fig. 24) were originally found in drug discovery programs for PI3K inhibitors, but were subsequently shown to also effectively inhibit mTORC1 and mTORC2.[57] However, more recent mTOR/PI3K inhibitors have been developed by simultaneously optimizing compounds against PI3K and mTOR.

5.07.2.3.2.2.1.1 Apitolisib (GDC-0980). Dual mTOR/PI3K inhibitors were originally developed as PI3K inhibitors but were subsequently shown to also inhibit mTORC1 and mTORC2. PI103 was the first dual mTOR/PI3K inhibitor, originally developed from a high-throughput screening for PI3K inhibitors. The original lead compound **34** (Fig. 25) has a quinazoline core structure, substituted with a morpholine and phenyl ring. This compound had an IC_{50} value of 1.3 μM for inhibition of p110α. The focus of the initial SAR investigation was to improve the potency of the lead compound. The morpholine substituent was shown to be essential for activity; any modifications gave at least a ninefold increase in IC_{50}. Substitutions in different positions of the phenyl ring were investigated. A hydroxyl-substituent in the meta-position gave an $IC_{50} = 0.075$ μM, translating into a 17-fold

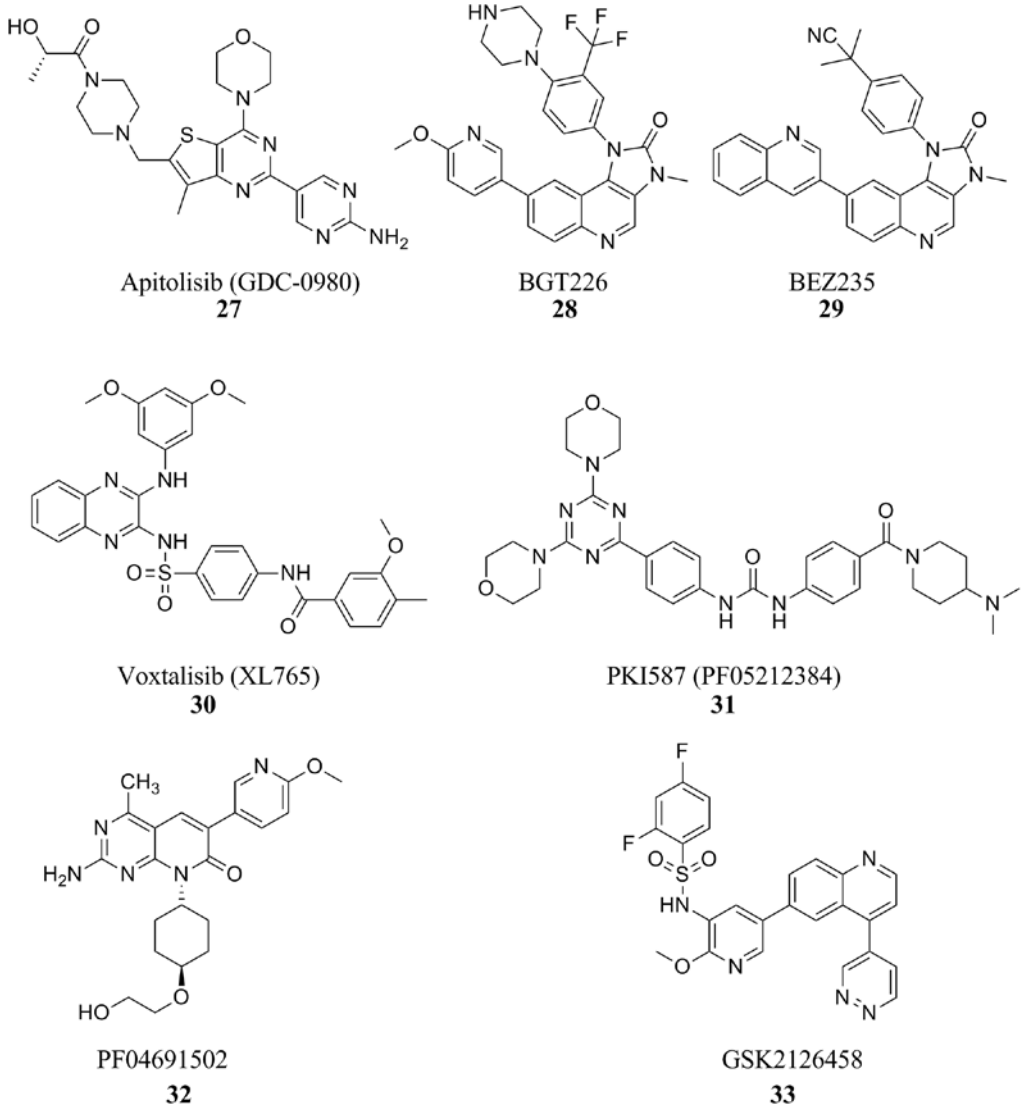

Fig. 24 Overview of dual mTOR/PI3K inhibitors in clinical trials.

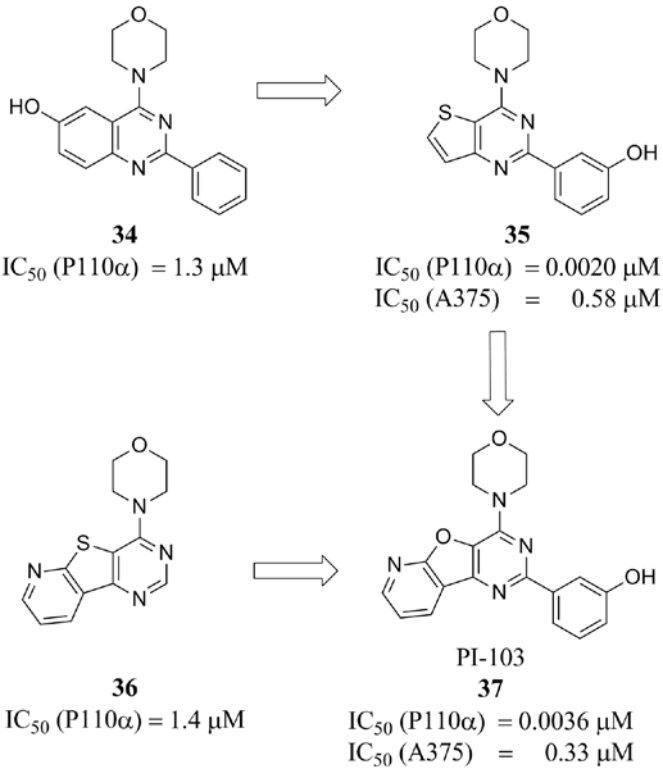

Fig. 25 Development of PI-103, **37**, from lead compounds **34** and **36** obtained in a HTS.

decrease compared to the lead compound **34**. Finally, the effect of the hydroxyl group on the quinazoline ring and replacement of the quinazoline with different bicyclic heterocycles were considered. Replacing the quinazoline ring with a thieno[3,2-*d*]pyrimidine gave compound **35**, which showed the highest activity in this series and a 750-fold improvement in IC_{50} over the original lead compound **34**. Compound **35** suppressed proliferation of A375 melanoma cells with an IC_{50} value of 0.58 μM.[58] However, the PK profile of compound **35** was unsatisfactory; the half-life of **35** was less than 10 min when dosed intraperitoneally (ip) in mice.[59] Compound **36** was identified as another hit compound from the HTS with structural similarity to compound **35**. Modifications of the tricyclic ring of compound **36** were investigated. Replacing the thiophene with a furan resulted in a 2.5-fold increase in activity, while the corresponding pyrrole was found to be inactive. Introduction of a meta-phenol in the same position as in compounds **34** and **35** gave PI-103, **37**, with an IC_{50} of 0.0036 μM (Fig. 25). PI-103 showed a potent in vitro antiproliferative effect on a range of cancer cell lines.[60] PI-103 still showed poor in vivo PK properties, such as high plasma and tissue clearance, and is now used as a tool compound.[49,61]

The crystal structure of p110α in complex with PI-103 has been solved and facilitates a better understanding of the interactions between PI-103 and PI3K (Fig. 26). The ATP-binding pocket is located in a cleft between the N- and C-terminal lobes of the kinase catalytic domain of p110α, similar to the ATP-binding sites in other protein kinases. PI-103 binds to the ATP-binding site on the p110α kinase domain. Three hydrogen bonds are formed between PI-103 and active site residues of p110α. The morpholine oxygen acts as hydrogen bond acceptor to the amide of the hinge residue Val851, explaining the importance of the morpholine substituent for activity. The hydroxyl group of the phenol makes hydrogen bonds to the carboxyl group of Asp810 and to the hydroxyl group of Tyr836. The pyridine ring extends out of the ATP-binding pocket toward solvent.[62]

A multiparameter lead optimization program to develop a drug candidate focused on improving the PK properties while maintaining inhibitory activity on PI3K and the related antiproliferative activity against cancer cells. Substitution with a methyl group in the 6-position of the thieno[3,2-*d*]pyrimidine was well-tolerated, while substitution with a methyl group at the 7-position showed a 2.6-fold decrease in potency. A range of substituents were introduced in the 6-position. The compounds PI-540 and PI-620 (Fig. 27) displayed similar potency to the unsubstituted compound **35** and showed improved in vitro stability in human liver microsomes (compound **35**: 32% remaining after 30 min incubation of 10 μM compound with 1 mg mL^{-1} human microsomes, PI-540: 85%, PI-620: 90%). Despite the encouraging improvement in microsomal stability, PK studies indicated low oral bioavailability of PI-540, **38**, and PI-620, **39**, of $\leq$10% in mouse and rat (based on 10 mg kg^{-1} IV and PO administration), which was mainly attributed to glucuronidation of the phenol group. To overcome this metabolic liability, bioisosters of the phenol group were explored.[63] A homology model of p110α suggested an interaction of the phenolic hydroxyl group with Asp810, as later confirmed in the crystal structure of PI-103, **37**, bound to p110α. Consequently the phenol group was replaced by heterocyclic groups that maintained the potential to act as a hydrogen donor.[62,63] The structurally similar PI3K selective inhibitor GDC-0941

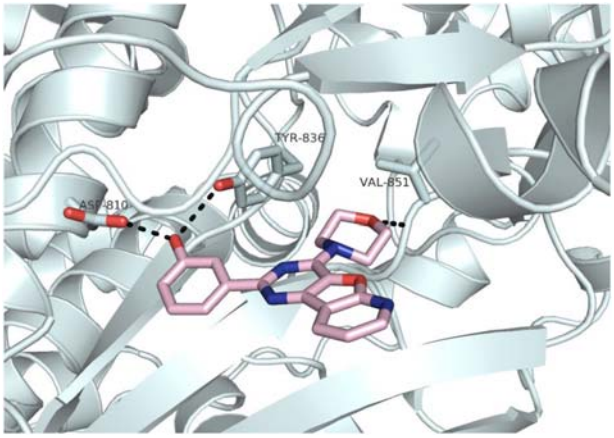

Fig. 26 X-ray crystal structure of p110α (*cyan*) complexed with PI103 (*light pink*), PDB ID: 4L23. The structure of the ligand PI103, and the key binding site residues are shown as sticks. Selected interactions are shown in *black-dashed lines*.

(Pitilisib, **40**) and the dual mTOR/PI3K inhibitor GDC-0980 resulted from this lead optimization program.[64] GDC-0980 is potent across a broad panel of cancer cell lines, with the greatest potency in breast, prostate, and lung cancers, and less potency in melanoma and pancreatic cancers. GDC-0980 has entered Phase I and/or Phase II clinical trials alone and in combination with rapalogs, platins, bevacizumab, abiraterone, and others, in solid cancers, non-Hodgkin lymphoma, breast cancer, prostate cancer, endometrial carcinoma, and renal cell carcinoma.[55,65]

5.07.2.3.2.2.1.2 BGT226 and BEZ235. The dual mTOR/PI3K inhibitor BEZ235, **29**, was generated by the structure-based design starting from a previously identified imidazo[4,5-*c*]quinoline, compound **41**. The imidazo[4,5-*c*]quinoline scaffold is considered a privileged scaffold for inhibiting the ATP-binding site of kinases. This chemotype can adopt different binding modes in the ATP-binding site, so either the quinoline nitrogen or one of the imidazole nitrogen atoms acts as a hydrogen bond acceptor with the kinase hinge region. The structural elements of the compound can then be exploited to reach unique regions of the

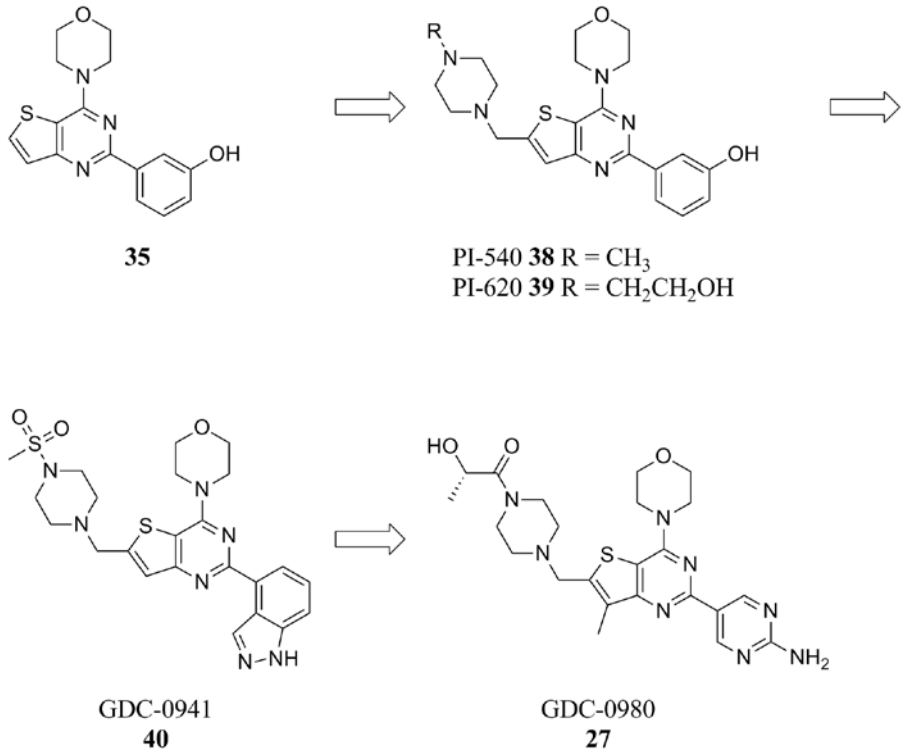

Fig. 27 Development of GDC-0980, **27**, from thieno[3,2-*d*]pyrimidine **25**.

active site of the targeted kinase, in order to achieve selectivity. Compound **41** was shown to be a potent inhibitor of PDK1 (3-phosphoinositide-dependent protein kinase-1, $IC_{50} = 34$ nM), and is also active against class I PI3K ($IC_{50} = 64$ nM for p110α, $IC_{50} < 450$ nM for the isoforms p110β, p110γ, and p110δ). Introduction of a methyl group at the 2-position of the imidazole ring resulted in a 1.5-fold improvement on the proliferation EC_{50} in U87MG (brain glioblastoma) cells, and a threefold increase in PDK1 IC_{50}. Replacing the cyanomethylene moiety, a potential metabolic weak spot, with a dimethyl cyanomethylene group resulted in a 4.4-fold increase in PDK1 IC_{50}, while retaining the effect on proliferation seen with compound **41**. Combining the dimethyl cyanomethylene group with a methyl substituent on the imidazole ring (compound **42**) improved the antiproliferation 2.9-fold. Further modification of compound **42** by changing the imidazole ring to *N*-methyl imidazolinone gave BEZ235 and resulted in further improvement in antiproliferative activity and complete loss of PDK1 inhibitory activity (Fig. 28). BEZ235 retained its activity against PI3K ($IC_{50} < 400$ nM for p110α, p110γ, p110δ, and $IC_{50} = 2.3$ μM p110β). The selectivity between PDK1 and PI3K was rationalized in docking studies, where the docking of compound **41** in the protein structure of ATP-bound PDK1 was compared to the docking of BEZ235 in the protein structure of staurosporine-bound PI3Kγ. These docking studies indicate that a carbonyl group in position-2 of the imidazole ring creates an electronic mismatch with the backbone carbonyl of Leu88 of the P-loop of PDK1. This repulsive interaction is not present in the PI3K active site, because the structural motif corresponding to the P-loop of protein kinases has a spatial arrangement where no residue matches the position of Leu88 in PDK1.[66]

In addition to PI3K inhibition, BEZ235 was also shown to inhibit mTOR activity in a kinase activity ELISA assay, and mTORC1 and mTORC2 kinase activity in immune-kinase assays. In contrast to the conventional PI3K inhibitors wortmannin and LY294002, BEZ235 showed strong antiproliferative activity in a panel of breast cancer cell lines. This antiproliferative effect has been proposed to be due to mTOR inhibition. BEZ235 was found more efficient than LY294002 in blocking AKT activation, again likely reflecting the synergistic inhibitory effects on PI3K and mTORC2. In vivo experiments also supported that mTOR inhibition contributes to the antitumor activity of the compound. In these in vivo experiments, BEZ235 displayed antitumor activity against U87MG (brain glioblastoma) and PC3M (prostate carcinoma) tumor xenografts. The observed effect on S473P-AKT levels correlated with the amount of compound present in the tumor tissue.[67,68]

BEZ235 was effective in preclinical studies as a single agent and in combination with other cancer drugs. It was investigated in several clinical trials of advanced solid tumors and metastatic breast cancer, as single agent or in combination with paclitaxel, trastuzumab, BKM120, or BKM162. The structurally similar compound BGT226 (Fig. 24), also developed by Novartis, was also investigated in clinical trials, but will not be developed further, since BEZ235 is more potent and bioavailable.[49,55]

5.07.2.3.2.2.1.3 Voxtalisib (XL765). Voxtalisib was developed as XL765 by Exelixis and was reported as the first oral dual PI3K/mTOR inhibitor with Phase I clinical trial results.[69] The medicinal chemistry underpinning the discovery of this compound has not been disclosed in the scientific literature so far.

5.07.2.3.2.2.1.4 PKI-587 (PF-05212384). The dual mTOR/PI3K inhibitor PKI-587 was developed from the original imidazolopyrimidine hit (**43**) in an extensive medicinal chemistry effort (Fig. 29). The original hit (**43**) showed high potency against PI3Kα (45 nM), and mTOR (634 nM), and was also active against PI3Kγ (1.1 μM). Replacing the imidazole ring with a triazole improved the activity against PI3Kγ (435 nM) and mTOR (250 nM), while retaining the activity against PI3Kα (83 nM). However, this new compound showed unfavorable physicochemical parameters and poor microsomal stability. The poor microsomal stability was attributed to the hydroxyl group as metabolic hot spot. Incorporation of a urea-substituent in pyrazolopyrimidines has been shown to increase metabolic stability and improve the potency against PI3K and mTOR. Hence, the 3-hydroxymethyl group on the 5-phenylsubsituent of **43** was replaced with a 4-urea group. A number of different urea substituents were explored on *N*-alkyl-7-morpholino-5-phenyltriazolo[4,5-*d*]pyrimidines, while also investigating the different *N*-alkyl groups on the triazole ring. The *N*-ethyl substituent was mostly found to be the best choice as triazole-substituent. A number of heteroaryl substituted urea

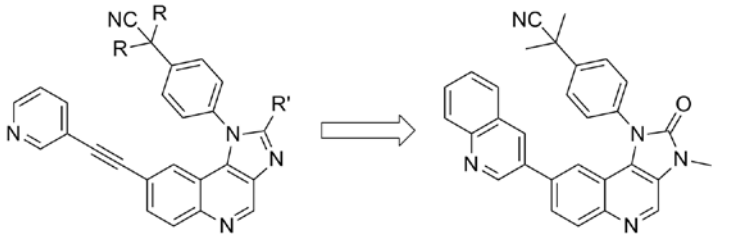

41 R, R' = H; **42** R, R' = CH_3
PDK1 IC_{50} = 34 nM (**41**); 245 nM (**42**)
proliferation EC_{50} = 416 nM (**41**); 143 nM (**42**)

BEZ235
29
PDK1 IC_{50} > 25,000 nM
proliferation EC_{50} = 13 nM

Fig. 28 Development of BEZ235.

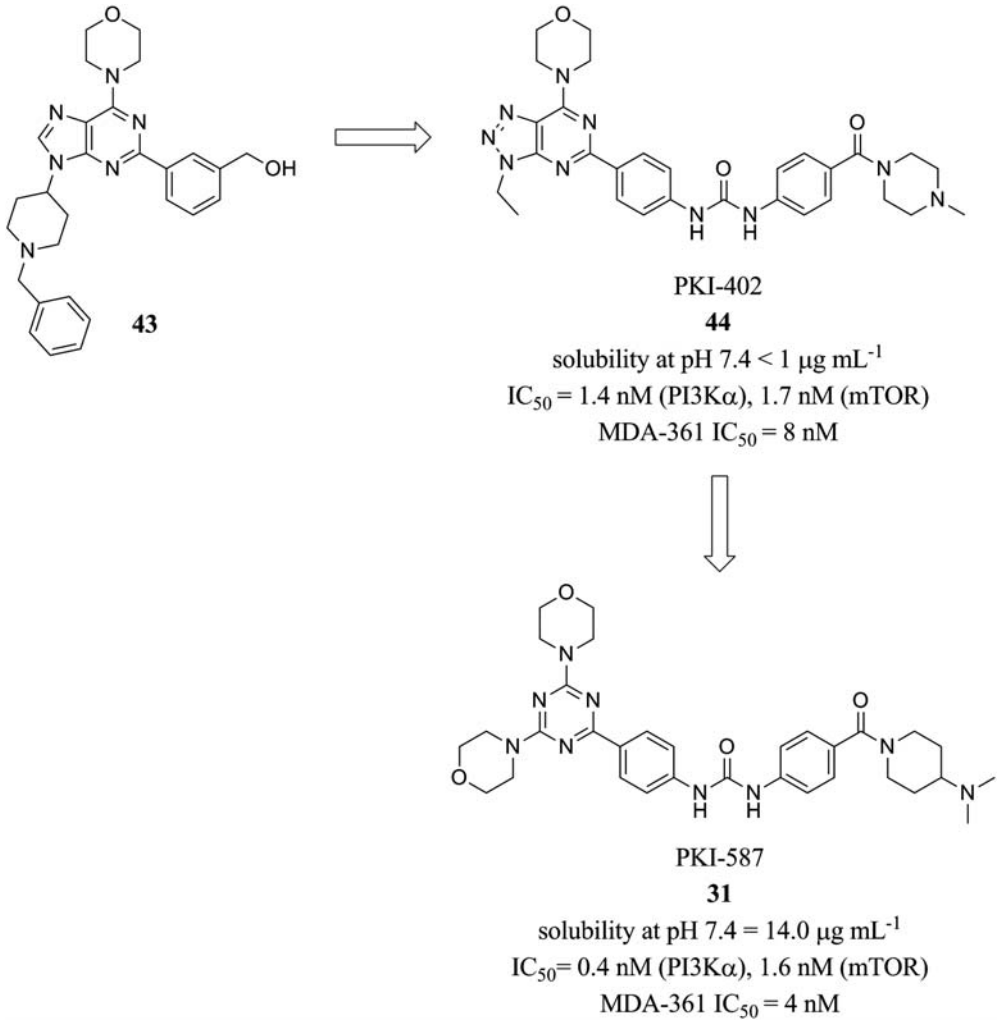

Fig. 29 Development of PKI-587.

analogs were screened as phenyl-substituents. A balance between high potency in biochemical and cellular assays, physicochemical properties, and microsomal stability needed to be achieved. 2-Thiophene substituted urea analogs were highly potent against PI3Kα (2.5 nM), and mTOR (3 nM), as well as MDA-361 (breast adenocarcinoma, 81 nM), and PC3 (prostate carcinoma, 133 nM) cells but showed only modest microsomal stability ($t_{½}$ = 10 min in rat liver microsomes) and poor solubility at physiological pH (1 μg mL^{-1} at pH 7.4). 4-Pyridyl and 3-pyridyl substituted urea analogs retained potency and showed improved microsomal stability ($t_{½}$ = 27 and 19 min in rat liver microsomes). Introduction of a 4-(carboxamido)phenyl moiety in the urea appendage further improved the enzyme and cell potencies (PI3Kα IC_{50} = 2.4 nM, mTOR IC_{50} = 0.39 nM, MDA-361 IC_{50} = 28 nM, and PC3 IC_{50} = 65 nM) and retained microsomal stability ($t_{½}$ = 21 min in rat liver microsomes). Modeling studies of analogs docked in a homology model of PI3Kα based on PI3Kγ crystal structures indicated that the amide moiety is pointing away from the binding pocket toward the solvent. This position is consequently a suitable position to add substituents to improve solubility and/or metabolic stability, which should minimally impact on potency. In a screen of different amines, methylpiperazine emerged as the ideal group. The resulting compound PKI-402, **44**, showed further improvements in cell potencies (MDA-361 IC_{50} = 8 nM and PC3 IC_{50} = 21 nM) and good stability in mouse and human microsomes ($t_{½}$ = 15 min in rat liver microsomes, $t_{½}$ > 30 min nude mouse and human microsomes). PKI-402 showed in vivo efficacy in human xenograft models including MDA-361 (breast cancer), U87 (glioma), and A597 (nonsmall cell lung cancer). PKI-402 was Ames negative and selective for class I PI3K and mTOR. Selectivity was assessed in a panel of 236 human kinases, where no off-target activity (>50% inhibition) was detected at 10 μM. However, PKI-402 was not further pursued because of its poor solubility.[70]

In order to improve the low solubility of PKI-402, different scaffolds that resemble a pyrimidine core, but have lower clogP values than the triazolo[4,5-*d*]pyrimidine in PKI-402, were investigated. The 1,3,5-triazine scaffold was considered as particularly attractive. The 1,3,5-triazine resembles the pyrimidine ring and retains the position of the pyrimidine nitrogens. In addition, this ring allowed retention of the morpholine and phenylurea substituents that were essential for potency. The presence of the three

nitrogens in the 1,3,5-triazine core lowered the clogP values of the designed compounds to about 2 or lower. The morpholine moiety has been reported as essential for activity in several PI3K inhibitors, as the morpholine oxygen was hypothesized to form an essential hydrogen bond with Val851 in the hinge region of the PI3Kα binding pocket. However, the morpholine also presents a metabolic liability via oxidation in the α-position to the morpholine oxygen, causing loss of potency. In PKI-587, **31** (Fig. 29), a bismorpholine-1,3,5-triazine scaffold was envisaged to offer an advantage under conditions where one morpholine gets metabolized, still leaving intact the other morpholine to make the essential hinge region interaction. Different heterocyclic substituents on the urea were investigated. These compounds showed good potencies (PI3Kα $IC_{50} < 3$ nM, mTOR $IC_{50} < 2.3$ nM, PC3 $IC_{50} < 218$ nM) but low solubility at pH 7.4 (< 2 μg mL^{-1}). Compounds bearing a basic amino moiety with an amide linkage exhibited excellent potencies. On the basis of a well-balanced profile of encouraging potency (PI3Kα $IC_{50} = 0.4$ nM, mTOR $IC_{50} = 1.6$ nM, PC3 $IC_{50} = 13.1$ nM), and good solubility (14 μg mL^{-1}), clogP (1.2), microsomal stability and lack of Cyp inhibition, PKI-587 was chosen for further in vitro and in vivo evaluations. In vitro, tumor growth inhibition by PKI-587 correlated with suppression of phosphorylation of PI3K/mTOR signaling pathway proteins in MDA-361 cells. PKI-587 induced cleaved PARP at 30 nM, indicating apoptosis. In vivo, PKI-587 showed potent antitumor efficacy against MDA-361 tumors. PKI-587 is now investigated in several clinical trials against neoplasms, acute myeloid leukemia (AML), breast cancer, and metastatic colorectal cancer.

5.07.2.3.2.2.1.5 PF-04691502. PF-04691502 was developed from a hit from a high-throughput biochemical screen using mouse PI3Kα. Screening hits were tested for activity against mTOR and prioritized according to their ligand efficiency and kinase selectivity profile. A series of 4-methylpyridopyrimidones was chosen for further development. Compound **45** (Fig. 30), one of the early compounds, demonstrated potent activity against mouse PI3Kα ($K_i = 1.4$ nM), modest activity against mTOR ($K_i = 840$ nM), and high ligand efficiency ($LE = 0.48$).

The co-crystal structure of PI3Kγ, as surrogate of PI3Kα, with compound **45** bound into the ATP-binding site was solved (Fig. 30). The aminopyrimidine forms key interactions with the hinge residue Val882. Compared to protein kinases, PI3K has an additional amino acid residue in the hinge region, which results in a small hydrophobic pocket. The 4-methyl substituent of compound **45** fits tightly into this pocket, explaining the selectivity of compound **45** for PI3K over other kinases. As expected, the cyclopentyl substituent is positioned in the ribose binding pocket. The benzylic alcohol group is bound in the selectivity pocket, with the hydroxyl group coordinating to the Tyr867 side chain. Multiparameter optimization of compound **45** was based on physical properties-based optimization of multiple drug-like attributes, guided by structure-based drug design. Compound **45** displayed poor pharmacokinetic properties, such as high in vitro clearance. Design focused on replacing metabolic soft spots while maintaining or improving physical properties. The methyl group on the 2-amino substituent was identified as potential metabolic soft spot for dealkylation and was removed. SAR analysis of analogs indicated that the removal of the methyl group on the 2-amino substituent increased mTOR potency. This observation was supported by structural analysis of a homology model of mTOR derived from the PI3Kγ crystal structure. To address the clearance issues, the benzyl alcohol in compound **45** was replaced with isosteric groups that reduced clogP.[71] A low clogP was shown to correlate with low clearance and consequently higher metabolic stability.[72] Removing the methyl group on the 2-amino substituent and replacing the benzyl alcohol with methoxypyridine changed the clogP from 3.16 (compound **45**) to 2.7. The solubility of this compound was improved by structure-guided design. The compound **45** bound crystal structure of PI3Kγ was used to determine regions of the protein that could accommodate additional polarity. The cyclopentyl ring, binding in the ribose pocket, was identified as a potential target for the introduction of additional polar groups, such as alcohols. Replacing the cyclopentyl group with a cyclohexanol (compound **46**) improved solubility 4- (***trans*-46**) to 15-fold (***cis*-46**) while retaining excellent activity against PI3Kα and improving activity against mTOR. Plasma samples from in vivo rat and mouse PK studies of ***cis*-46** were found to contain significant amounts of ***trans*-46**. In in vivo experiments of ***trans*-46** small amounts

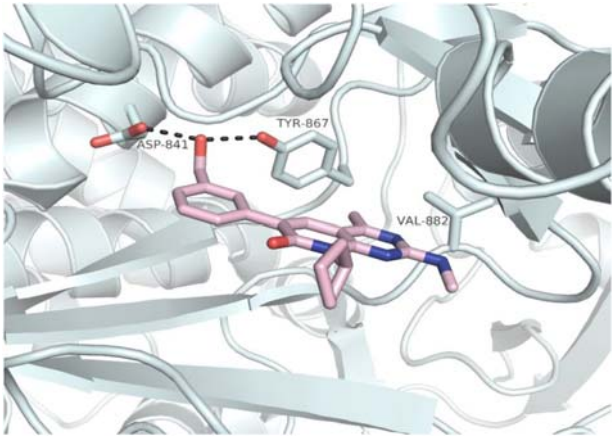

Fig. 30 Co-crystal structure of compound **45** (*light pink*) bound to PI3Kγ (*cyan*), PDB: 3ML8. The ligand structure and key binding site residues are shown as sticks. Selected interactions are shown in *black-dashed lines*.

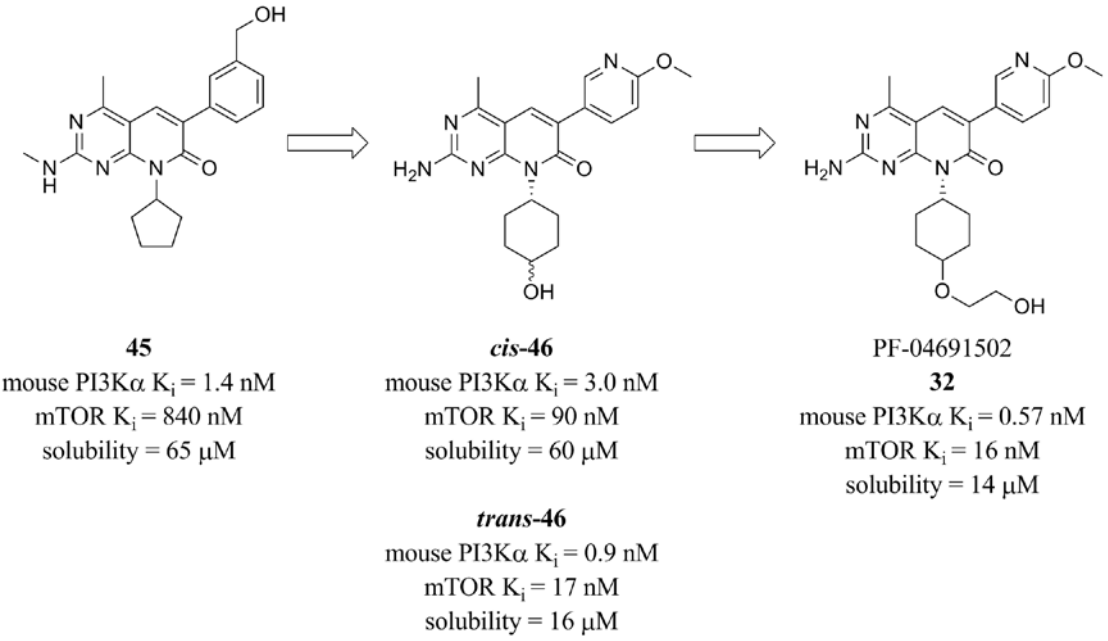

Fig. 31 Development of PF-04691502.

of *cis*-**46** were observed. It was hypothesized that the isomerization occurred by oxidation of the alcohol to the ketone, and subsequent reduction back to the alcohol, with *trans*-**46** being the major product isomer. To avoid potential in vivo isomerization, the hydroxyl group of the cyclohexanol was replaced, and a hydroxyethyl group was found to be the optimum group to give good overall properties (Fig. 31).[71]

PF-04691502 showed good selectivity for class I PI3K and mTOR. No significant inhibitory activity was observed in more than 80 protein kinases at concentrations of up to 10 μM. The cellular activity of PF-04691502 was characterized using tumor cell lines with a hyperactivated PI3K pathway, such as BT20 (breast cancer), SKOV3 (ovarian cancer), and U87MG (glioblastoma) cells. PF-04691502 exhibited good correlation between pharmacokinetics, target modulation, and efficacy in a U87MG xenograft model.[73] PF-04691502 has now been investigated in clinical trials against early breast cancer, breast neoplasms, endometrial neoplasms, and advanced cancer.

5.07.2.3.2.2.1.6 GSK2126458. GSK2126458, **33**, was developed as follow up compound to GSK1059615, **47** (Fig. 32), a dual PI3K/mTOR inhibitor that was investigated in a dose-escalation study in patients with solid tumors, metastatic breast cancer, lymphoma, and endometrial cancer. With the development of a second inhibitor, GSK intended to improve the potency, selectivity, and pharmacokinetic profile of the compound. Development of the compound relied on structure-based design based on the co-crystal structure of GSK1059615-bound PI3Kγ, as a surrogate of PI3Kα. The crystal structure of GSK1059615-bound PI3Kγ showed that the thiazolidinedione formed an interaction with the catalytic lysine (Lys833) in the ATP-binding pocket. The structure also indicated that the thiazolidinedione could potentially be replaced by larger groups and still fit into the binding pocket. Filling the empty space in the binding pocket could lead to inhibitors with improved selectivity and potency. Initial

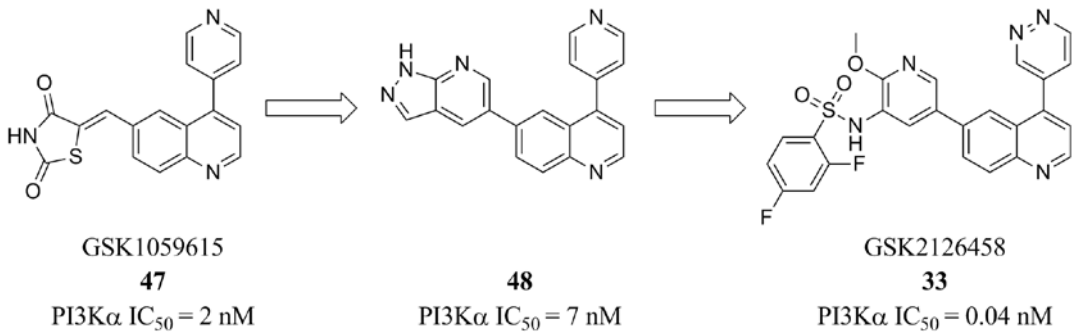

Fig. 32 Development of GSK2126458.

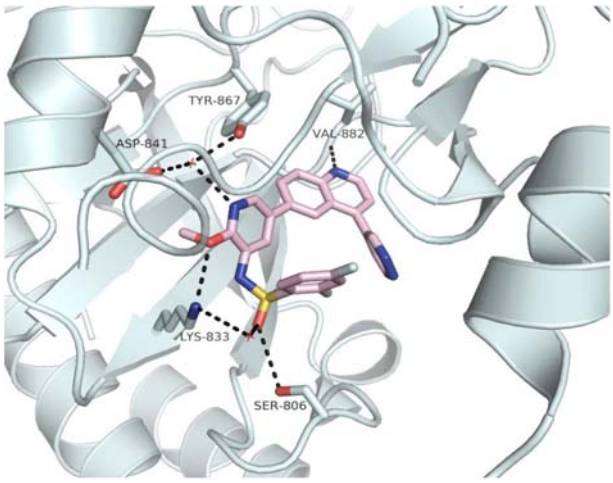

Fig. 33 Co-crystal structure of GSK2126458-bound PI3Kγ, PDB: 3L08. The ligand structure and key binding site residues are shown as sticks. Selected interactions are shown in *black-dashed lines*.

replacements of the thiazolidinedione by a phenyl ring and heterocycles resulted in a dramatic loss of activity. Molecular modeling overlays of different analogs indicated which heteroatoms were most likely to make interactions with the enzyme and aided in the design of a pyrazolo[3,4-*b*]pyridine as replacement of the thiazolidinedione (compound **48**, **Fig. 32**). A co-crystal structure of this compound with PI3Kγ was solved (PDB: 3L54) and confirmed that the nitrogen in 2-position of the pyrazole forms a hydrogen bond with Lys833 and that the pyridine nitrogen interacts with a conserved active site water molecule. Compound **48** showed promising activity; however, it displayed very low aqueous solubility and a poor PK profile, with high clearance, a short half-life, and a lack of oral bioavailability. Opening the pyrazole ring to give 2,3,5-trisubstituted pyridine analogs led to an aminopyridylsulfonamide that retained the potency of compound **48** and showed increased solubility. SAR investigations of the sulfonamide moiety showed that 2-aminoarylsulfonamides achieved oral exposure in rats, while retaining potency. Removing the 2-amino substituent increased exposure and reversal of the sulfonamide connectivity led to a further increase in biochemical and cellular potency, while maintaining the improved oral exposure. Finally, replacing the pyridine substituent in 4-position of the quinoline ring with a pyridazine gave GSK2126458 and resulted in an improvement in the CYP inhibition profile.[74]

GSK2126458 is an extraordinarily potent inhibitor of PI3Kα ($IC_{50} = 0.04$ nM) and more potent than other dual PI3K/mTOR inhibitors in clinical trials. A co-crystal structure of GSK2126458-bound PI3Kγ (**Fig. 33**) shows that the compound binds in the ATP-binding site of the protein. The pyridine nitrogen forms a key hydrogen bond with the conserved water molecule. The sulfonamide interacts with Lys833. The difluorophenyl group fills a hydrophobic region in the back pocket of the enzyme, while the quinoline nitrogen forms a hinge interaction with Val882. GSK2126458 showed excellent selectivity over protein kinases (>10,000-fold over 240 kinases), with the exception of the class IV PI3K family, including mTOR. The PK profile of GSK2126458 was studied in four preclinical species and the compound showed low blood clearance and good oral bioavailability. Efficacy was observed in BT474 (breast cancer) human xenograft models. GSK2126458 is under evaluation in clinical trials against solid tumors and idiopathic pulmonary fibrosis.[74]

5.07.2.3.2.2.1.7 SF1126. SF1126 is a prodrug developed by Semafore and consists of the nonselective PI3K inhibitor LY294002 conjugated to a RGDS peptide fragment. LY294002 is known to inhibit a number of proteins at the concentrations used to inhibit PI3K and is limited by its poor solubility and short half-life. The prodrug SF1126 was designed to improve solubility and to bind specific integrins in the tumor compartment, resulting in improved delivery of the compound to the tumor. SF1126 was tested in a dose-escalation study in patients with advanced solid tumors and was well-tolerated. In 2010, SF1126 was granted orphan drug status by the FDA for the treatment of B-cell chronic lymphocytic leukemia.[75] SF1126 is also investigated in clinical trials for patients with relapsed or refractory neuroblastoma and metastatic squamous neck cancer.

5.07.2.3.2.2.2 Pan-mTOR inhibitors (mTORC1/mTORC2 dual inhibitors)

Pan-mTOR inhibitors inhibit both mTOR complexes and are characterized by an IC_{50} for mTORC1 and mTORC2 that is significantly lower than that for PI3K. A number of pan-mTOR inhibitors are now investigated in clinical trials (**Fig. 34**), however only limited information on their development is available in the scientific literature.[49]

The first pan-mTOR inhibitor reported was PP242. PP242 was found in a screen of tyrosine kinase inhibitors. The primary goal of the screen was to identify molecules that inhibit both tyrosine kinases and PI3Ks. However, in this screen compounds with unexpected selectivity profiles were discovered. In particular, in the pyrazolo[3,4-*d*]pyrimidine scaffold small changes in structure produced considerable alterations in selectivity. One of the compounds displaying an unexpected selectivity profile was PP242. PP242 showed high potency against mTOR ($IC_{50} = 8$ nM), but was much less active against other PI3K family members

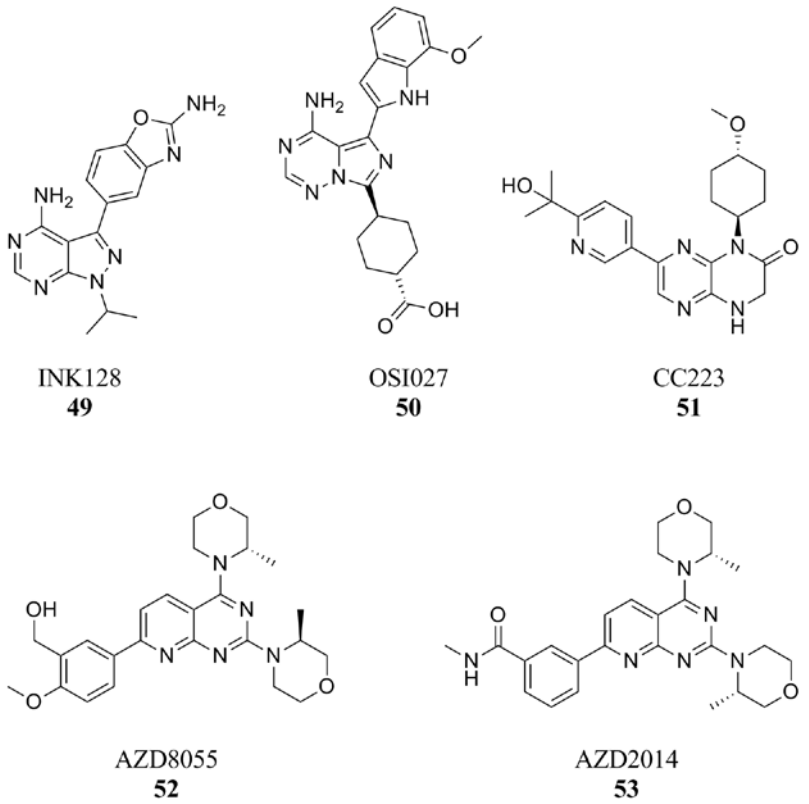

Fig. 34 Overview of pan-mTOR inhibitors in clinical trials.

(PI3Kα, PI3Kβ, PI3Kγ $IC_{50} = 1.3–2.2$ μM; PI3Kδ $IC_{50} = 0.1$ μM). PP242 was tested against 219 protein kinases and revealed remarkable selectivity. At a concentration above 100-fold its IC_{50} for mTOR, PP242 inhibited only one kinase by more than 90% (Ret) and three by more than 75% (PKCα, PKCβII, JAK2, and V617F).[76] PP242 was further developed into INK128 (MLN0128) (Fig. 34), which has been investigated in clinical trials against a number of cancers, including nonsmall cell lung cancer (NSCLC), nonhematologic malignancy, hepatocellular carcinoma, glioblastoma, gliosarcoma, advanced solid malignancies, metastatic breast cancer, and thyroid cancer.[49]

CC223, **52**, and OSI027, **50**, are both dual inhibitors of mTORC1 and mTORC2. The discovery and subsequent medicinal chemistry optimization of these compounds has not been disclosed in the scientific literature. CC223 has been in clinical trials in healthy adults to investigate the metabolism and excretion of CC223, the effect of food on the pharmacokinetics, and drug–drug interactions with ketoconazole. CC223 has also been in safety, pharmacokinetics, and efficacy studies in patients suffering from MM, diffuse large B-cell lymphoma, glioblastoma, hepatocellular carcinoma, nonsmall lung cancer, and others.[77] OSI027 is a selective dual inhibitor of mTORC1 and mTORC2. Biochemical, cellular, and in vivo evidence has been presented that indicates OSI027 is mechanistically and functionally distinct from rapamycin. The antitumor efficacy of OSI027 was evaluated in PIK3CA mutant SKOV3 and KRAS mutant OVCAR5 human ovarian cancer xenograft models. The compound has been investigated in clinical trials in solid tumors and lymphomas.[78]

5.07.2.3.2.2.2.1 AZD8055 and AZD2014. The clinical candidates AZD8055 and AZD2014 were developed from a HTS hit. Inhibition of mTOR kinase was determined in an ELISA-based assay using full-length mTOR with a recombinant 4EBP1 protein substrate and ATP. A pyrido[2,3-*d*]pyrimidine, compound **54** ($IC_{50} = 1.0$ μM, Fig. 35), was chosen as starting point for further medicinal chemistry development. The positioning of the nitrogen in the pyridine ring was essential for activity. The substituents in the 2- and 4-positions were considered for modifications. However, the morpholine substituent in the 4-position is a well precedented motif in PI3K inhibitors, where the morpholine oxygen is involved in a key hydrogen bond interaction in the ATP-binding site of PI3Kγ. By analogy, it was assumed that the morpholine substituent may be involved in a hydrogen bond interaction with Val133 in the hinge region of the mTOR kinase domain. Indeed, replacement of the morpholine by a piperidine, and thereby replacing the oxygen with a carbon, gave a significant reduction in potency. Introducing an additional carbon into the morpholine ring, by replacing the morpholine with 1,4-oxazepane, results in a change of geometry and caused a sevenfold reduction in potency. The original hit, compound **54**, had a racemic 2-methylpiperidine substituent in the 2-position. Investigation of the preferred absolute stereochemistry of the methyl substituent showed a slight improvement in potency for (*S*)-**54** over (*R*)-**54**. In general, substitution on the piperidine was well-tolerated without significant loss of potency.

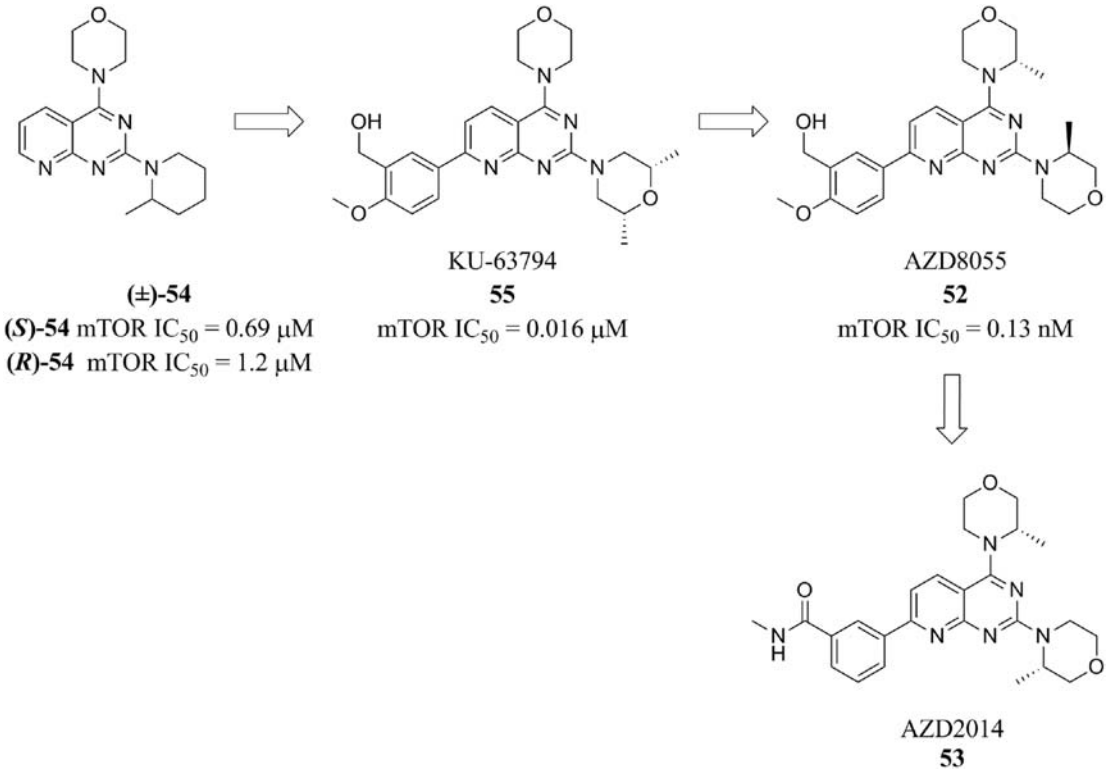

Fig. 35 Development of AZD2014.

To reduce the lipophilicity of the molecule, the piperidine was then replaced by a morpholine. An unsubstituted morpholine in the 2-position led to a dramatic loss in potency, however potency was regained by re-establishing the methyl substituents at the 2- or 3-positions of the morpholine.[79]

Docking studies using an homology model of mTOR based on a crystal structure of PI3Kγ suggested that substituents in the 7-position of the pyrido[2,3-*d*]pyrimidine could access additional space within the ATP-binding site. For the investigations of substituents in the 7-position, the dimethyl-substituted morpholine at the 2-position of the pyrido[2,3-*d*]pyrimidine was chosen, as this compound showed a good balance of potency and lipophilicity. A number of aromatic amino substituents and directly bonded aromatic or heteroaromatic substituents resulted in improved potencies. SAR around substituted analogs of a 7-phenyl substituent showed that electron-donating substituents (hydroxyl, methoxy) in the *para*-position were well-tolerated. A hydroxyl-substituent in the *meta*-position showed similar activity to the corresponding *para*-substituted analog, while for the *meta*-methoxy-substituent a 10-fold decrease in activity was observed. In this case, the presence of a hydrogen bond donor rather than an electron-donating substituent was crucial. Combining an electron-donor in the *para*-position with a hydrogen bond donor in the *meta*-position gave KU-63794, **55**. This compound showed a further increase in potency ($IC_{50} = 0.016$ μM). KU-63794 showed good selectivity over PI3K family members ($IC_{50} = 8.3$ μM for PI3Kα, >5 μM for PI3Kδ, >30 μM for PI3Kβ and PI3Kγ). No significant activity was found against a range of 200 non-PI3K related kinases at a concentration of 10 μM.[79]

Potential limitations for the clinical development of KU-63794 were its relatively low aqueous solubility (2.4 μM) and relatively high potency against the hERG ion channel ($IC_{50} = 8.3$ μM). Consequently, further optimization efforts focused on identifying highly selective compounds with increased cellular potency, improved aqueous solubility, and an improved margin to the hERG IC_{50}. A commonly used strategy to improve aqueous solubility is the introduction of a basic amine. Substituents on the 7-phenyl ring were previously found to be well-tolerated. Replacing the benzyl alcohol with a range of secondary benzyl amines gave a dramatic improvement in solubility (>1000 μM, compared to 2.4 μM for KU-63794) and a reduction in hERG potency, while mTOR inhibition improved in several analogs. Despite improved cellular potency and solubility, little oral exposure was observed, presumably due to compromised permeability and higher efflux. The 4-morpholine substituent was previously found to be essential for activity. However, replacing the morpholine with a thiomorpholine improved cellular potency. A number of analogs were investigated and consistent improvement in cellular potency and solubility was observed. The substituent in position 2 could be a wide range of cyclic and acyclic amines and aromatic substituents. When assessing the overall balance of properties, AZD8055, retaining the substituent in position 7, and bearing 3-methyl morpholine substituents in the 2- and 4-positions, was selected for preclinical development. AZD8055 is a potent inhibitor of mTOR kinase ($IC_{50} = 0.13$ nM) and displays high selectivity against other members of the PI3K family ($IC_{50} > 3$ μM against PI3Kαβγδ) and was inactive against a general panel of 200 kinases when tested at 10 μM. AZD8055 inhibits both mTORC1 and mTORC2 in cells with similar potencies and has been shown to

modulate substrates of both mTORC1 and mTORC2 in vivo. Dose-dependent tumor growth inhibition in U87-MG glioblastoma tumor xenografts was observed. AZD8055 also resulted in significant inhibition of tumor growth and/or regression in breast, lung, colon, prostate, and uterine xenograft models. AZD8055 was evaluated in clinical trials to assess the safety, tolerability, and pharmacokinetics in cancer patients and was also investigated in clinical trials in adults with recurrent gliomas and solid tumors, but is no longer in clinical development.[80,81]

AZD8055 was found to exhibit high turnover in human hepatocytes (36.4 μL min^{-1} per 10^6 cells) and showed lower bioavailability in rat (12%) than in mouse (81%). The benzyl alcohol and aryl-methoxy group on the phenyl substituent on C7 was postulated to be potential metabolic liabilities. Further medicinal chemistry development concentrated on reducing these metabolic liabilities. A primary amide was found to be an appropriate replacement of the benzyl alcohol. Aqueous solubility was further increased to >690 μM, compared to 30 μM for AZD8055. However, the rate of human hepatic turnover remained high. Methyl-substitution on the amide reduced the rate of turnover in human hepatocytes 2.6-fold, but also reduced aqueous solubility. Further reduction in hepatic turnover was achieved for the tertiary amide, however this substitution led to an inacceptable reduction in potency. Strategies to reduce potential metabolism of the methoxy group, including difluorination of the methoxy group or cyclization to give a quinazoline, did not reduce hepatic turnover. Removal of the methoxy group resulted in a compound AZD2014 with good cellular potency and low hepatic turnover (<4.2 μL min^{-1} per 10^6 cells). AZD2014 showed excellent aqueous solubility (>600 μM) and a good margin over the hERG IC_{50}. AZD2014 is now investigated in clinical trials as single agent and in combination with various other cancer medications, such as paclitaxel, ibrutinib, palbociclib, fulvestrant, and abiraterone.[80]

5.07.2.3.2.2.3 Other mTOR inhibitors

WYE132 (Wyeth) was developed from a hit from a high-throughput screen against recombinant mTOR. The original hit compound WAY001 showed sixfold higher potency against PI3Kα than mTOR. Further development led to the compounds WAY600, WYE354 and WYE687 and ultimately WYE132 (**56**, Fig. 31), which displays 5000-fold greater selectivity for mTOR over PI3K. WYE132 showed antitumor activity against MDA361 breast, U87MG glioma, A549 and H1975 lung, and A498 and 786-O renal tumors. Co-administration of WYE132 with bevacizumab achieved regression of MDA361, A498, and A549 tumors.[82]

Torin1 (**57**, Fig. 36) is a potent and selective mTOR inhibitor in vitro and in vivo. Torin 1 is limited by the low yielding synthetic route, its poor aqueous solubility, short half-life, and low oral bioavailability. Medicinal chemistry development of Torin 1 resulted in the discovery of Torin 2 (**58**). Torin 2 retains potency and selectivity of Torin 1 but is easier to produce on scale and shows improved pharmacokinetic properties.[83]

Besides ATP-competitive inhibitors, indirect mTOR inhibitors have been proposed. Metformin, an antidiabetic drug, inhibits mTORC1 and displays a strong antiproliferative effect in a range of cancer cell lines in vitro and in in vivo xenograft models. A number of clinical trials to investigate metformin as single agent or in combination with drugs including vandetanib, simvastatin, placlitaxel, sorafenib, and cisplatin are ongoing.[49]

5.07.2.3.2.3 MNK inhibition

Mitogen-activated protein kinase (MAPK)-interacting serine/threonine protein kinase (MNK) inhibition prevents MNK-mediated signaling and inhibits the phosphorylation of certain regulatory proteins, including eIF4E, that regulate the translation of mRNAs involved in tumor cell proliferation, angiogenesis, survival, and immune signaling. MNK1 and MNK2 are overexpressed in a variety of tumor cells and modulate the function of eIF4E through phosphorylation of a conserved serine (Ser209). This phosphorylation event is necessary for oncogenic transformation, but seems to be dispensable for normal development. Consequently, MNK inhibitors may provide a strategy for anticancer therapeutics.[84] An orally administered inhibitor of MNK1 (BAY1143269) has been developed by Bayer. Neither a structure of the inhibitor nor biological studies have yet been disclosed. The compound is currently under investigation in a Phase I dose-escalation and expansion studies in combination with docetaxel. An orally bioavailable inhibitor of MNK1 and MNK2, eFT508 was developed by eFFECTOR Therapeutics. Again, neither a structure of the inhibitor

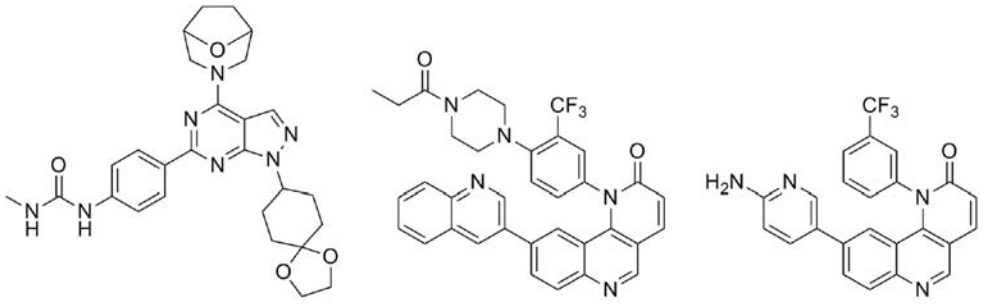

Fig. 36 Chemical structures of mTOR inhibitors.

nor biological studies have yet been disclosed. eFT508 is also currently investigated in Phase I clinical trials, with a dose-escalation and cohort-expansion study in patients with advanced solid tumors.

5.07.2.3.3 Direct inhibitors of eIF4F

Protein expression is controlled at the level of translation primarily through the activity of eIF4E, which is frequently upregulated in tumors. Antisense oligonucleotides (ASOs) targeting eIF4E synthesis showed promising antitumor activities. These ASOs act by reducing eIF4E levels. The antisense oligonucleotide LY2275796 (ISIS183750) was investigated in a Phase I dose-escalation, pharmacokinetic, and pharmacodynamics evaluation and subsequently in a Phase I/II study in combination with irinotecan in irinotecan-refractory colorectal cancer.[85] The antisense oligonucleotide ISIS eIF4E Rx by Ionis Pharmaceuticals has been investigated in safety and tolerability studies in combination with carboplatin, paclitaxel, docetaxel, and prednisone.

Other direct inhibitors of the translational machinery target the eIF4E–cap interaction or inhibit the eIF4E–eIF4G interaction. The ability of eIF4E to cause neoplastic transformation depends on its cap-binding activity. Cap analogs have been used in in vitro studies of eIF4E function, but suffer from poor permeability and stability in vivo. To overcome this limitation, prodrugs or drug delivery using virus-like particles have been explored. A high-throughput screen identified 4EGI-1 (**59**, Fig. 37) as an inhibitor of the eIF4E–eIF4G interaction.[44,86] 4-EGI-1 was shown to directly bind eIF4E by nuclear magnetic resonance (NMR) spectroscopy.[87] 4E1RCat (**60**) and 4E2RCat (**61**, Fig. 37) were found similarly. These compounds downregulate the translation of eI4E-sensitive mRNAs. Disrupting the eIF4E–eIF4G interaction was also achieved by fusion of 4EBPs to the ligand of a cancer-specific cell surface receptor. These approaches of inhibiting the eIF4E–eIF4G interaction have shown promise in preclinical models.[44,86]

The natural products hippuristanol, pateamine A, and silvestrol were initially shown to have strong tumor cell line-specific cytotoxic properties. These compounds were then shown to bind eIF4A in in vitro assays and to affect eIF4A activity. Pateamine A is an irreversible inhibitor of protein synthesis, and was consequently very toxic in vivo. Hippuristanol suffers from poor solubility and low potency. Silvestrol is at present the best studied eIF4A inhibitor and has been investigated in cancer cell xenograft models and oncogene-derived genetic mouse models. In several cases, silvestrol caused tumor regression.[88]

5.07.2.3.4 Inhibitors of ternary complex formation

Although the biochemistry of ternary complex formation and activity is well studied, understanding of the role of the ternary complex in cancer biology and its potential for exploitation as an anticancer target is limited.

5.07.2.4 Summary

Targeting oncogene addiction by inhibiting protein synthesis in cancer cells has great potential in cancer therapy. New targets will continue to emerge as our understanding of the mechanisms of gene transcription and mRNA translation improves, allowing medicinal chemists to generate molecules that more selectively control the synthesis of key oncogenic proteins. There remains an important role for general protein synthesis inhibition, especially as drug delivery techniques improve, helping to increase the therapeutic index of compounds that were previously too toxic to use. Also, our greater understanding of genetic signatures of cancer will allow us to direct compounds to those patients who will see the greatest benefit and with our improved understanding of the role of polypharmacology in the efficacy of cancer drugs, the balance between safety and efficacy can be more rationally addressed.

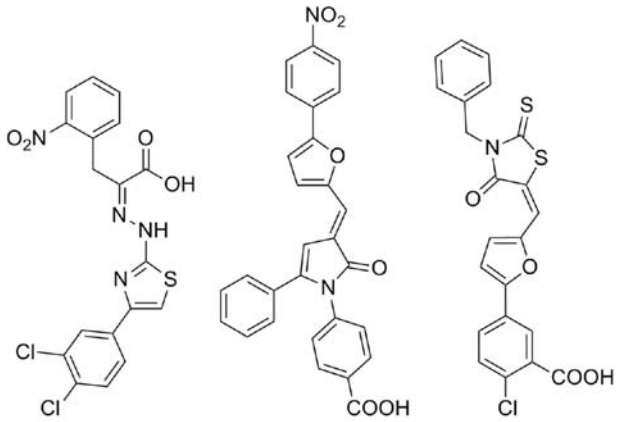

Fig. 37 Chemical structures of 4EFI-1, 4E1RCat, and 4E2RCat.

5.07.3 Targeting Protein Folding

5.07.3.1 Introduction to Molecular Chaperones

The cell is a molecularly crowded environment with a very high total concentration of key macromolecules such as proteins. Estimations of the total concentrations of macromolecules within the cell are in the range of 400 g dm^{-3} meaning that around 5–40% of the total volume of a cell is physically occupied by these important molecules.[89] This is very different from the situation commonly encountered in the laboratory setting where dilute solutions of macromolecules are routinely studied. This high concentration puts a particular strain on the functional macromolecules in a cell and evolution has developed mechanisms for ensuring that proteins can maintain their form and function even under such physically challenging conditions.[90] One of the key mechanisms involved in protein quality maintenance is the heat shock response. This was originally discovered as a response to raising the temperature of organisms and involves the expression and engagement of a range of proteins known as chaperones or heat shock proteins (HSPs).[91] It is now widely recognized that when mammalian cells are exposed to a variety of physiological stresses, including heat, cytotoxic drugs, UV radiation, hypoxia, low pH, or heavy metals, heat shock transcription factor 1 (HSF1) is released from an inhibitory complex with HSP90, trimerizes and binds to the heat shock response element within the promoter regions of *HSP* genes leading to an increased expression of a range of HSPs.[92] This is a vital part of the cell's effort to maintain homeostasis and cell survival.

HSPs are classified into two groups; the high molecular weight HSPs such as HSP90, HSP70, HSP60, and the small HSPs such as HSP27 and αB-crystallin. The key distinguishing feature between these two groups of HSPs is that the high molecular weight chaperones bind ATP and function through an ATPase-mediated mechanism involving a number of co-chaperones, whereas the low molecular weight HSPs do not bind ATP or act as ATPases.

5.07.3.2 HSP70 Inhibitors

There are 13 different genes coding for proteins of the HSP70 family leading to a wider number of isoforms compared to HSP90. The main isoforms are HSC70, which is constitutively expressed; HSP72, which is expressed in response to stress; GRP78 (also known as BiP), which is localized in the endoplasmic reticulum; GRP75 (also known as mortalin), which is localized in the mitochondria. The structure of the HSP70 family shares some similarity to the HSP90s with an N-terminal domain that contains the ATP-binding pocket, a substrate-binding domain, and a C-terminal domain that consists mainly of alpha helices and acts as a "lid" that closes over the bound substrate. The substrate-binding domain contains a hydrophobic groove with sufficient space to bind peptides up to seven residues long. The HSP70s execute their refolding in a similar manner to HSP90 by using the hydrolysis of ATP to ADP.[93] In contrast to the ATP-binding pocket of HSP90, the ATP-binding pocket of HSP70 belongs to the actin ATPase class of proteins[94] which depends heavily on interactions involving the phosphates of the cofactor and as such has delivered little success in finding high affinity ligands.[95] The nature of the ATP-binding pocket also leads to a much tighter binding for ATP/ADP (IC_{50} = 1.2 μM and 670 nM, respectively, in a fluorescence polarization assay) than is the case for HSP90.[96] This requires the involvement of a nucleotide exchange factor, BAG1, to enable release of ADP and catalytic turnover. A recent study has described the binding site as difficult to antagonize with small molecules[97] and a fragment screening campaign returned a very low (0.4%) hit rate indicative of poor ligandability.[98] As a consequence, there has been a variety of chemical tool compounds reported as HSP70 inhibitors but with limited evidence of actual stoichiometric and specific binding to HSP70. A detailed investigation of the reported inhibitor apoptozole has shown that it fails to bind in a specific manner to HSP70 by both SPR and fluorescence polarization, and dynamic light scattering experiments demonstrated aggregation at very low concentrations. This followed a report that the HSP70 inhibitor phenylethynesulfonamide (PES) interacts with the substrate-binding domain of HSP70 in a nonspecific manner.[99] Recently, a covalent inhibitor, novolactone has been characterized which binds between the substrate-binding domain and the ATP-binding site via residue Glu444.[100] Novolactone inhibits both the HSP40-stimulated ATPase activity and refolding activity of HSP70 by inducing a conformational change in the HSP70 protein.

The only compounds that have been shown unequivocally to bind at the ATP-binding site resulted from work at Vernalis in Cambridge. In 2009, they revealed a series of nucleoside analogs based on the structure of ATP.[101] They carried out a "fragment-type" of approach in which they started from adenosine **62** as a fragment of ATP and using a fluorescence polarization assay showed that adenosine **62** binds with an IC_{50} = 560 μM (Fig. 38). The key advance was to recognize that 8-aminoadenosine **63** was 60-fold more potent (IC_{50} = 9.4 μM) and that HSC70 in complex with BAG-1 gave crystals suitable for a structure-based design approach. 8-Aminoadenosine **63** demonstrated potent cell activity, but its biochemical potency and biomarker modulation indicated that this was largely due to off-target effects. Elaboration of the amino group led to 3,4-dichlorobenzyl analog **64** which was equipotent in the biochemical assay (IC_{50} = 9.1 μM) but much less potent in a cell-based assay (GI_{50} = 26 μM in HCT116 colon cancer cells), indicating that previous off-target activity had been reduced. Importantly, a ligand/protein crystal structure of **64** bound to HSC70/BAG-1 (Fig. 39A) showed a key π-stacking interaction of the dichlorophenyl ring with Arg272. This structure also suggested the possibility of growing from the 5′-hydroxy group of the ribose to generate a similar interaction with Tyr15 on the opposite side of the binding site cleft. Several benzyl ethers at the 5′-hydroxyl group were made and tested and the best balance of biochemical potency and cell-based potency was achieved with compound **65** (VER155008) carrying a *p*-cyanobenzyl ester at this position (IC_{50} = 0.5 μM; GI_{50} = 5 μM in HCT116). Although some derivatives possessed marginally improved biochemical IC_{50} values, none showed the same level of cellular activity as **64**. An X-ray structure of **65** (VER155008) bound to HSC70/BAG-1 showed the predicted interaction with Tyr15 and, additionally, an intramolecular hydrogen bond between the 8-amino NH and the 5′-ether

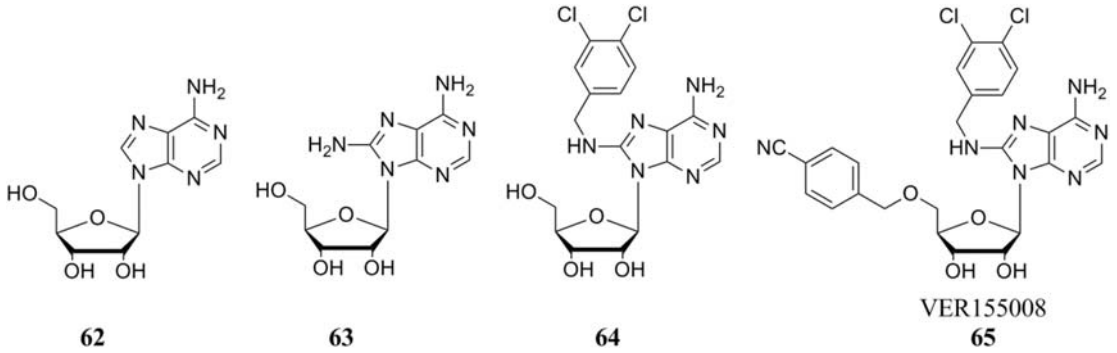

Fig. 38 Chemical structures of Vernalis HSP70 inhibitors **62**, **63**, **64**, **65**.

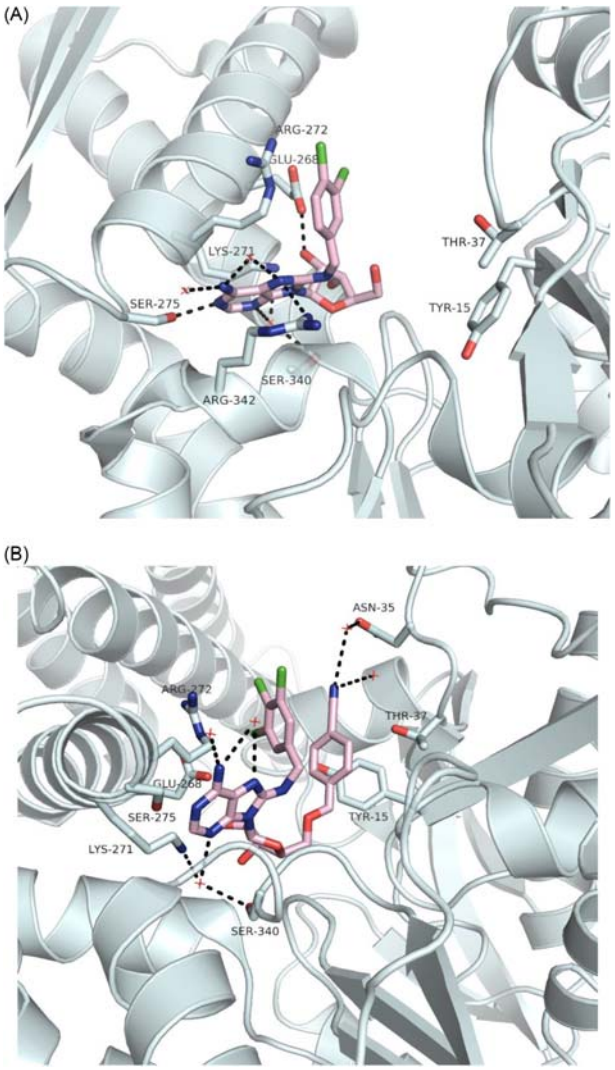

Fig. 39 (A) X-ray structure of **64** (*light pink*) bound to HSC70/BAG-1 (*cyan*), PDB: 3FZK and (B) X-ray structure of **65** (*light pink*) bound to HSC70/BAG-1 (*cyan*), PDB: 3FZW. The structure of the ligand, and the key binding site residues are shown as sticks. Selected interactions are shown in *black-dashed lines*.

oxygen that may contribute to increased potency (Fig. 39B). Exposure of HCT116 colon cancer cells to compound VER155008 led to reduction of cellular levels of HER2 and RAF-1 at concentrations only a little higher than the GI_{50} in agreement with siRNA studies. Although VER155008 was further investigated in cellular experiments,[102] it demonstrated rapid metabolism and clearance unsuitable for progression to in vivo animal model studies.

Vernalis continued development and exploration of these compounds as inhibitors of the endoplasmic reticulum isoform GRP78 but found little selectivity for either isoform except with some simpler versions which demonstrated around a fivefold selectivity for HSP70 over GRP78.[103] The only amino acid change in the ATP-binding pocket in GRP78 is replacement of Thr37 in HSP70 with Ile61 in GRP78 generating a slightly more hydrophobic binding site in GRP78. However, this is probably outweighed by the flexibility of this particular binding pocket that presents a real challenge to finding potent, drug-like compounds. A recent paper has highlighted this issue but also focused attention on a key salt bridge between Glu268 and Lys56 at the top of the binding cleft of HSP70.[104] This work started with the antibiotics sangivamycin ($K_d = 3.3$ μM) and toyocamycin ($K_d = 90$ μM) and carried out a careful analysis of factors leading to potency, identifying desolvation of the salt bridge with suitably placed hydrophobic groups as a key route to a closed conformation and potent binding.

5.07.3.3 HSP90 Family

The most significant of the HSPs is HSP90 which consists of a family of HSPs of around 90 kDa in molecular weight. It is the most abundant of all cellular proteins accounting for 1–2% of all proteins and it is highly conserved in both prokaryotes and eukaryotes.[105] It plays a key role in the proper folding, activation, and stabilization of cellular proteins and targets damaged proteins for either refolding or for ubiquitin-mediated proteasomal degradation.[106] There are four isoforms of HSP90; HSP90α and HSP90β both of which are cytosolic and found in all eukaryotes, GRP94 (glucose-regulated protein 94 kDa) that is expressed in the endoplasmic reticulum and TRAP1 (tumor necrosis factor receptor-associated protein 1) that is expressed in the mitochondria.

The HSP90 monomer consists of three domains; an N-terminal ATP-binding domain (25 kDa), a middle domain (35 kDa), and a C-terminal dimerization domain (12 kDa).[107] Clear proof of the role of the nucleotide-binding domain (NBD) was obtained in 1997 when the X-ray crystal structure of the HSP90 N-terminal domain with ADP bound was published (Fig. 40).[108] The ATP-binding pocket of HSP90 is an example of the unusual Bergerat fold class of ATP-binding site that is found in the GHKL (Gyrase, HSP90, Histidine kinase, MutL) family of ATP-binding proteins.[95] Subsequent work by the Pearl group demonstrated that an ATPase cycle drives a molecular "clamp" mechanism which is crucial for the chaperoning function of HSP90.[109] However, the engagement of HSP90 with client proteins and the fine-tuning of the chaperoning cycle are mediated by a set of co-chaperones as shown in Fig. 41.[110] In addition to chaperones HSP40 and HSP70, a variety of co-chaperones have been implicated in various aspects of the HSP90 machinery. AHA1 (activator of HSP90 ATPase 1) has been shown to activate the ATPase activity of HSP90 and hence controls the efficiency of the HSP90 cycle.[111] CDC37 (cell-division cycle 37 homologue) has been shown by structural and biochemical studies to be involved in the chaperoning of kinase clients.[112] There is evidence that transcription factor clients are delivered by the protein HOP (HSP70–HSP90 organizing protein).[113]

The list of HSP90 client proteins continues to grow and numbers several hundred proteins (https://www.picard.ch). These include a number of key, oncogenic kinases such as BCR-ABL, ERBB2, ALK, BRAF, CRAF, AKT, and CDK4. Additionally, a number of TFs have been shown to be clients, for example, the androgen and estrogen receptors. As might be expected from its range of client proteins, HSP90 has been reported to be overexpressed in both solid tumors and hematological cancers.[114] HSP90 expression levels have been shown to be associated with decreased survival in breast cancer, gastrointestinal stromal tumors (GIST), and NSCLC.[115] It

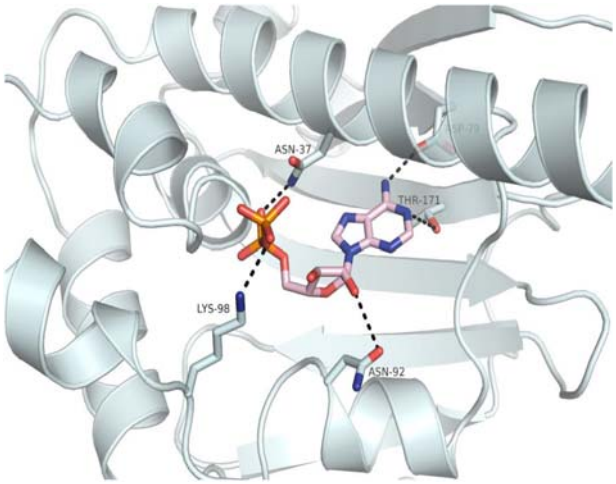

Fig. 40 X-ray crystal structure of the HSP90 NBD (*cyan*) in complex with ADP (*light pink*), PDB: 1AM1. The structure of the ligand, and the key binding site residues are shown as sticks. Selected interactions are shown in *black-dashed lines*.

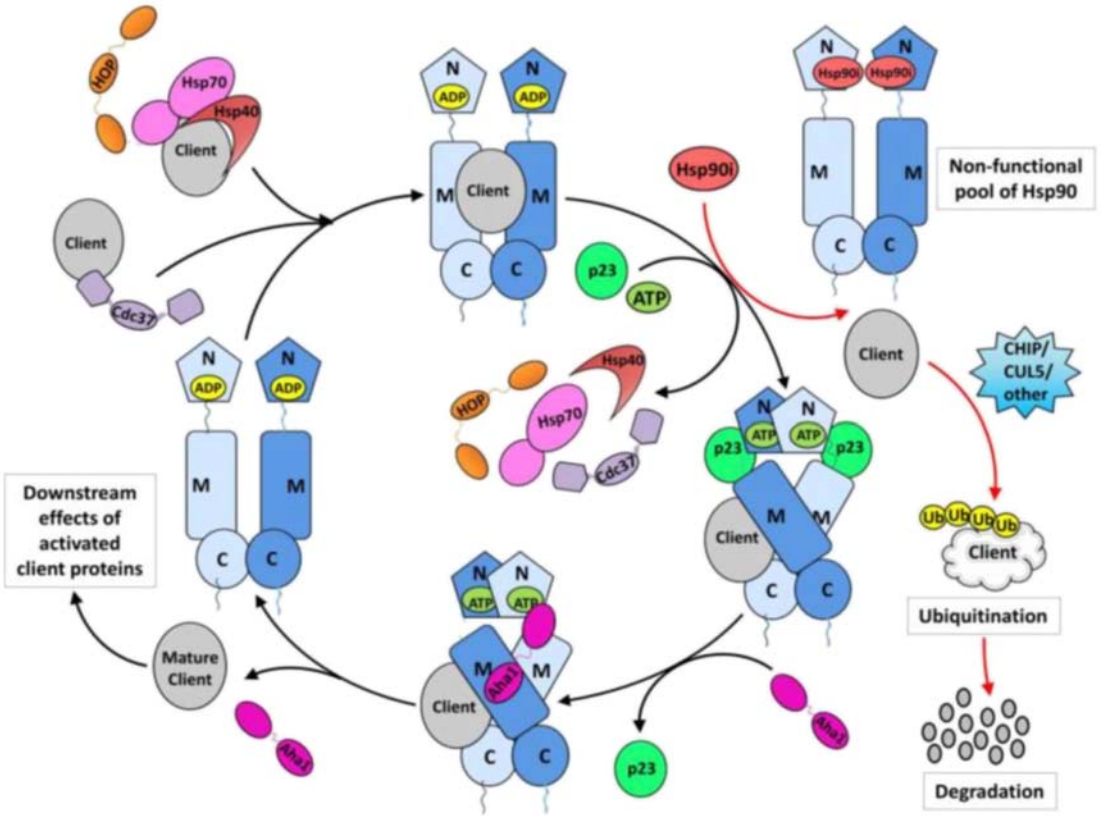

Fig. 41 The chaperone cycle of HSP90 and effects of Hsp90 inhibition. *Light* and *dark blue* indicate the domains of the two monomers of HSP90 that form the active dimer: N = N-terminal domain, M = middle domain, C = C-terminal domain. *Gray circle* represents the client protein. ADP is adenosine diphosphate and ATP is adenosine triphosphate. The client protein is bound to a complex of HSP70 (*purple*) and HSP40 (*red*) with HOP (HSP70–HSP90 organizing protein) also involved for some client proteins. CDC37 (cell-division cycle 37 homologue) delivers kinase clients to HSP90. Client binding to the HSP90 dimer followed by ATP and p23 (*green circle*) binding causes a conformational change. AHA1 (activator of HSP90 ATPase1) binding and p23 displacement promotes ATP hydrolysis and release of mature and active client protein. Competition for the ATP-binding pocket by HSP90i (HSP90 inhibitor—*red oval*) leads to release of immature client which is degraded via ubiquitination.[109]

is also apparent that oncogenic kinases activated by mutation have a greater dependence on HSP90 than wild-type kinases. The common activating BRAF mutation found in many cases of melanoma (V600E) is much more sensitive to HSP90 inhibition than wild-type BRAF.[116] Other mutant proteins that show particular sensitivity include v-SRC, BCR-ABL, mutant EGFR, and rearranged ALK. This clear molecular dependence of cancer cells on functioning HSP90 led to the hypothesis that inhibition of HSP90 would have not only an anticancer effect but would also provide a combinatorial blockade of multiple oncogenic pathways while providing a clear therapeutic window over normal cells.[117] Recently, factors involved in client recognition by HSP90 have been investigated and these shed light on why kinases are such ubiquitous clients of HSP90. It seems that it is their flexible unstructured regions particularly involving the kinase domain that are recognized by the HSP90 machinery.[118]

5.07.3.3.1 HSP90 inhibitors

Over the last 20 years, there have been significant efforts directed toward the discovery and progression of HSP90 inhibitors toward the clinic for the treatment of cancer. This has led to a large number of reviews including some excellent recent reviews to which the reader is referred.[119–121] The fact that ATP hydrolysis is a crucial part of the chaperone cycle makes the N-terminal ATP-pocket of HSP90 an important target for potential small-molecule inhibitors. Indeed, this site has seen most of the drug discovery activity involved in HSP90 inhibition.[120] All the HSP90 inhibitors in clinical trials fall into this category of inhibitor. The C-terminal domain of HSP90 is responsible for dimerization to give the functionally active homodimer and has also been reported to possess an ATP-binding site although there is no direct structural evidence for this. A small group of coumarin-containing antibiotics based on novobiocin have been reported to bind at this site. Finally, the pentapeptide sansalvamide A has been reported to bind to the middle domain of HSP90 and disrupt client protein binding. Although the vast majority of work has focused on pan-HSP90 inhibitors, there has been some recent progress in selective inhibition of HSP90 isoforms as these are differentially expressed and localized and their modulation may lead to different biological outcomes.[122]

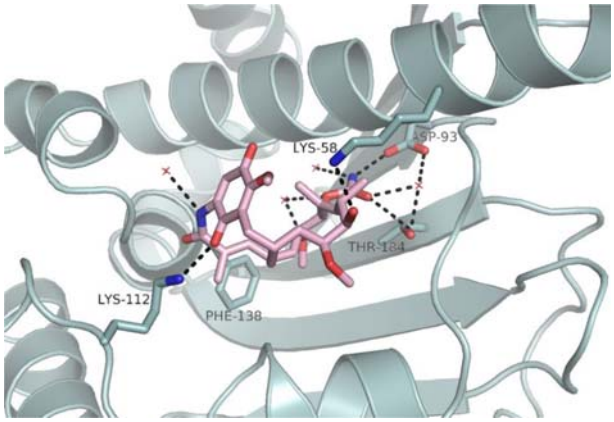

Fig. 42 X-ray crystal structure of the HSP90 NBD (*cyan*) in complex with geldanamycin (*light pink*), PDB: 1YET. The structure of the ligand, and the key binding site residues are shown as sticks. Selected interactions are shown in *black-dashed lines*.

5.07.3.3.1.1 Natural product-based inhibitors

The story of HSP90 inhibitors is a textbook example of how natural product inhibitors led the way in validating the hypothesis that HSP90 inhibition would show an anticancer effect. This effect was first demonstrated in vitro in human cancer cell lines, followed by in vivo experiments in human tumor xenografts in immune-suppressed mice and finally, using semisynthetic derivatives, in the clinic. This was followed by widespread efforts to obtain small-molecule inhibitors using high-throughput screening, fragment-based approaches, and rational approaches using structure-based drug design. This section will describe the natural product-based HSP90 inhibitors and the medicinal chemistry efforts used to progress them toward the clinic.

5.07.3.3.1.1.1 Geldanamycin-based inhibitors

Geldanamycin **66** (**Fig. 43**) is a benzoquinone-containing ansamycin antibiotic from a *Streptomyces* species first reported in 1970.[123] The structure was reported soon afterward.[124] It was originally believed to be a tyrosine kinase inhibitor and shown to cause depletion of the oncoprotein ERBB2.[125] In 1997, soon after the first crystal structure of an HSP90/ADP complex was published,[108] the structure of the HSP90 geldanamycin complex was reported at 1.9 Å resolution.[126] This reveals that geldanamycin neatly mimics the nucleotide binding in the ATP-pocket of HSP90. The macrocyclic ansamycin ring and the carbamate function are oriented toward the bottom of the pocket with the benzoquinone at the top of the pocket with the planes of the macrocycle and the benzoquinone virtually parallel (**Fig. 42**). Critically, there are several water-mediated hydrogen bond interactions which are found repeatedly in HSP90/ligand structures along with key hydrophobic interactions.

Although a potent inhibitor of HSP90 (IC_{50} c.25 nM), geldanamycin shows severe hepatotoxicity in preclinical species which along with its poor solubility rendered it unsuitable for progression into the clinic. This latter issue was addressed by preparing the semisynthetic geldanamycin derivatives 17-AAG (tanespimycin) **67** and 17-DMAG (alvespimycin) **68** by displacement of the 17-methoxy group with the appropriate amine (**Fig. 43**).

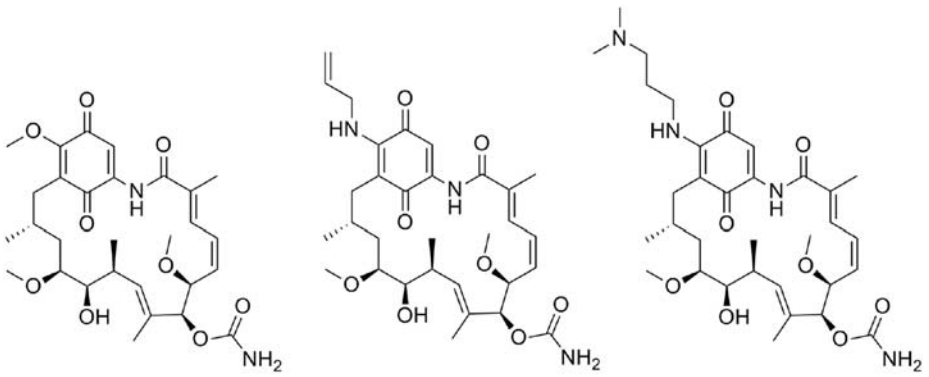

Fig. 43 Chemical structures of geldanamycin, **66**, tanespimycin, **67**, and alvespimycin, **68**.

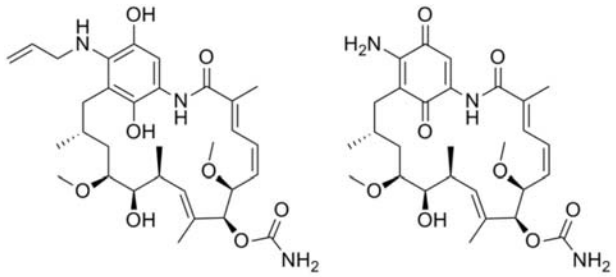

Fig. 44 Chemical structures of retaspimycin, **69**, and IPI-493, **70**.

Tanespimycin is a potent HSP90 inhibitor with an $IC_{50} = 5$ nM in a cell-free assay when HSP90 is isolated from tumor cells compared to c.500 nM when HSP90 is derived from normal cells. It has been suggested that this is due to an activated form of HSP90 in tumor cells.[127] In cell-based experiments, tanespimycin demonstrated an RB-dependent G1 growth arrest in a range of human tumor cell lines with an IC_{50} of 25–45 nM.[128] In in vivo studies in human tumor xenografts in nude mice, tanespimycin showed good growth inhibition at 50 mg kg^{-1} dosed intraperitoneally.[128] In 1999, tanespimycin became the first HSP90 inhibitor to enter the clinic. A Phase I clinical study was able to demonstrate sufficient exposure to cause depletion of key client proteins (CRAF and CDK4) at well-tolerated doses along with induction of HSP72 in both peripheral blood mononucleocytes and tumor biopsies.[129] Therapeutic benefit has been reported in various malignancies including melanoma.[130] Various combination therapies have also shown efficacy in the clinic including a study in ERBB2-positive metastatic breast cancer with traztuzumab[131] and a study in combination with proteasome inhibitor bortezomib in relapsed or refractory MM.[132] Despite these impressive results, the clinical development of tanespimycin was halted; likely due to liver toxicity and formulation issues.[133]

Alvespimycin possesses some potential advantages over tanespimycin including greater solubility leading to easier formulation and greater oral bioavailability.[134] It had similar potency to tanespimycin in a range of human cancer cell lines and showed good efficacy in a gastric cancer xenograft model on dosing at 25 mg kg^{-1} ip three times per week. In the clinic, activity has been reported for IV dosing of alvespimycin in castration resistant prostate cancer (CRPC—a complete response), melanoma (partial response), renal cancer (stable disease), and chondrosarcoma (stable disease).[135] Alvespimycin also showed clinical activity in ERBB2-positive metastatic breast cancer in combination with traztuzumab.[121]

Although tanespimycin and alvespimycin showed some promising results in the clinic, they retain the metabolic issues surrounding the benzoquinone moiety of geldanamycin. It had long been recognized that this moiety is a liability in a pharmaceutical agent owing to redox issues and hepatotoxicity. In addition, it was recognized that reduction of the quinone by the quinone reductase NQO1 (NADPH/quinone oxidoreductase I) led to a much more potent hydroquinone.[136] Loss of expression or expression of a functionally inactive form of this enzyme leads to resistance to tanespimycin and is the mechanism of acquired resistance in preclinical models.[137] Infinity Pharmaceuticals neatly addressed both this problem and the solubility problems by developing the hydroquinone hydrochloride, IPI-504 (**69**, retaspimycin hydrochloride, **Fig. 44**).[138,139] This compound has shown clinical activity in Phase II trials in NSCLC in patients with rearrangements in the anaplastic lymphoma kinase (*ALK*) gene when given intravenously. This is likely due to the fact that ALK is an HSP90 client.[140] The final example of an ansamycin-containing HSP90 inhibitor is IPI-493, **70** (**Fig. 44**), a metabolite of tanespimycin lacking the allyl group and also developed by Infinity Pharmaceuticals. This compound has been developed as an oral formulation and entered Phase I clinical trials.[141]

5.07.3.3.1.1.2 Radicicol-based inhibitors

The 14-membered ring macrolide radicicol, **71** (**Fig. 45**), was isolated from the fungus *Monosporium bonorden* in 1953.[142] In close similarity to geldanamycin, radicicol was originally thought to be a kinase inhibitor but, in 1998, was shown to bind to the

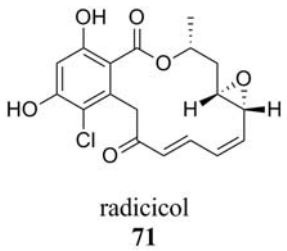

Fig. 45 Chemical structure of radicicol.

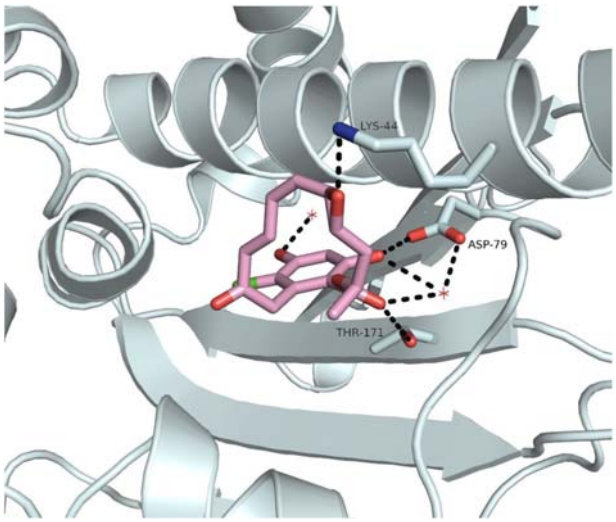

Fig. 46 X-ray crystal structure of the HSP90 NBD (*cyan*) in complex with Radicicol (*light pink*), PDB: 1BGQ. The structure of the ligand, and the key binding site residues are shown as sticks. Selected interactions are shown in *black-dashed lines*.

N-terminal domain of HSP90 and display similar biological activity to geldanamycin.[143] The structural basis of this binding has been revealed[144] and radicicol has been shown to bind in a folded, L-shaped conformation to the N-terminal ATP-binding pocket of HSP90 (Fig. 46). The resorcinol ring is buried deep in the base of the pocket with key interactions involving the hydroxyl groups in a similar manner to geldanamycin.

It will become clear in "**Resorcinol-based inhibitors**" section that the binding of radicicol to the HSP90 ATP-binding site demonstrated at this early stage the key role a resorcinol motif plays in small-molecule binding in this pocket and what an excellent match this simple structural motif is for the unusual ATP-binding site found in HSP90. Isothermal calorimetry was used to determine the K_d for radicicol binding to full-length dimeric HSP90 and a value of 19 nM was obtained. This compares with a $K_d = 1.2$ μM for geldanamycin in the same experiment.[144] Interestingly, thermodynamic analysis of their binding shows a large and favorable enthalpy change in each case, but whereas geldanamycin binding incurs an entropic penalty, radicicol binding leads to a favorable entropy change. In line with its potent HSP90 binding, radicicol exhibits potent antiproliferative activity across a wide range of human tumor cell lines. However, it is inactive in in vivo antitumor models, a fact attributed to its reactive electrophilic groups including a dienone and an epoxide leading to poor plasma stability. An oxime of radicicol, KF58333, **72** (Fig. 47), has been reported to show in vivo antitumor activity in human tumor xenograft experiments without the serious liver toxicity seen with the geldanamycin-based HSP90 inhibitors, but this has not advanced further toward the clinic.[145] The simplified but closely related pochonins isolated from a strain of *Pochonia chlamydosporia*[146] show a wide range of biological activity and pochonin D **73** (Fig. 47) has been shown to be a potent HSP90 inhibitor albeit with poor cellular activity. This led to the synthesis of a library of pochonin-based, resorcinol-containing macrolactones which included the oxime derivative **74**.[147] This compound showed a low nanomolar binding affinity for HSP90 with depletion of HSP90 clients at 35 nM and antiproliferative activity in human cancer cell lines in the range 125–320 nM. Human tumor xenograft experiments using BT474 (a breast cancer cell line) showed regressions using compound **74** dosed on alternate days at 100 mg kg^{-1} with no body weight loss. However, there have been no reports of the progression of radicicol-based HSP90 inhibitors progressing into the clinic.

Synthetic macrolactones and macrolactams inspired by radicicol have also been progressed as HSP90 inhibitors.[148,149] The macrolactams were prepared by a ring-closing metathesis reaction and have been shown to be metabolically more stable than

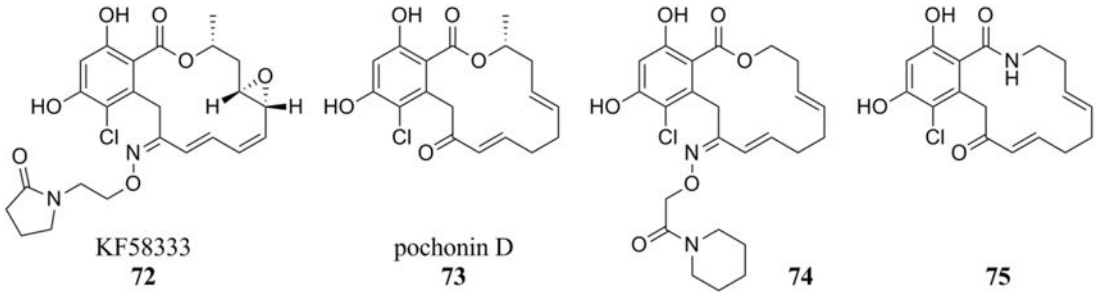

Fig. 47 Chemical structure of compounds **72**, **73**, **74**, and **75**.

the macrolactones in human liver microsome experiments and to be equivalent or superior as HSP90 inhibitors, showing the same client depletion in human colon cancer cells with cellular GI_{50} values of 600 nM. Structures of three of these compounds including macrolactam **75** (Fig. 47) were obtained in complex with HSP90 N-terminal domain and they bind in a similar manner to radicicol although with the ability to form further interactions depending on the nature of the substituents on the macrolactam ring.[149]

5.07.3.3.1.1.3 Novobiocin-based inhibitors

The natural product inhibitors described in the preceding sections all binding in the ATP-pocket in the N-terminal domain of HSP90 to exert their inhibitory effects. However, HSP90 inhibitors are known that have been reported to bind at the C-terminal region of HSP90. Epigallocatechin gallate (EGCG) **76** (Fig. 48) is a flavonoid found in green tea and in 2009 was reported to act as an aryl hydrocarbon receptor (AhR) antagonist via inhibition of HSP90.[150] EGCG showed the classic signature of HSP90 client depletion with reduction of RAF, ERBB2, and pAKT on treatment of the human ovarian cancer cell line SKOV-3 with micromolar concentrations. Using a variety of techniques including proteolysis and immunoprecipitation, EGCG was found to bind at the C-terminal domain of HSP90 and inhibit dimerization to the active form. Subsequently EGCG was tested in a CT26 colon cancer xenograft model and was shown to demonstrate efficacy at 10 mg kg^{-1} ip dosed daily.[151] Recently, Blagg has reported extensive synthetic studies and subsequent SAR around the EGCG structure (Fig. 49).[152] This led to compound **77** which demonstrated a $GI_{50} = 4$ μM in MCF-7 human breast cancer cells, an increase of potency of some 20-fold over EGCG. Compound **77** also showed the classic signature of HSP90 client protein depletion.

The coumarin antibiotics novobiocin, chlorobiocin, and coumermycin A are inhibitors of DNA-gyrase that are known to inhibit the ATPase function. Novobiocin has also been shown to target the C-terminal domain of HSP90 at a putative ATP-binding site leading to changes in interactions between HSP90, co-chaperones, and client proteins.[153] However, novobiocin **78** (Fig. 50) is only weakly active with HSP90 inhibition only observed at concentrations around 700 μM in SKBr3 human breast cancer cells. Blagg has carried out extensive studies on novobiocin in an effort to increase potency and also simplify the complex structure of this natural product.[154] This work led to compound **79** with a simplified coumarin core, a simpler amine-substituent, and unmodified noviose sugar. Subsequent efforts focused on replacing the complex sugar portion of the compound. Following the hypothesis that the noviose could be replaced by aza-sugars, Blagg and colleagues found that replacement with a simple piperidine gave analog **80** with $GI_{50} = 470$ nM in the SKBr3 cell line.[155] This simplified novobiocin analog showed the classic HSP90 inhibition signature of client protein depletion. They subsequently showed that a cyclic amine

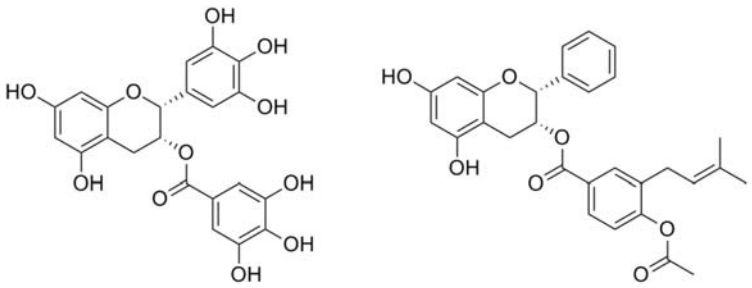

Fig. 48 EGCG **76** and SAR.

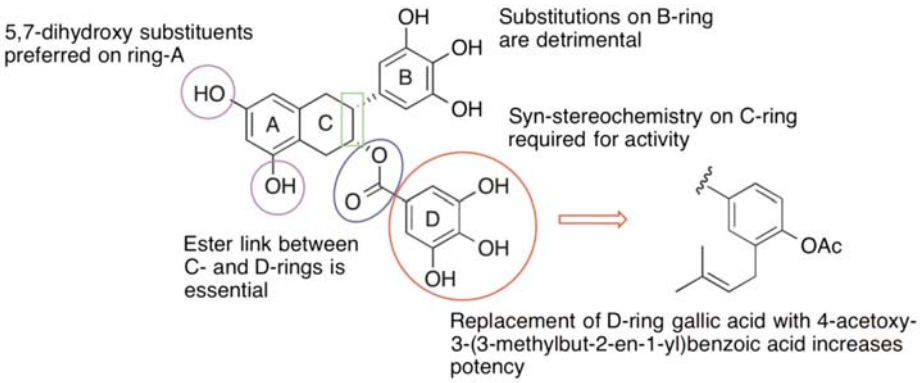

Fig. 49 Chemical structures of compounds **76** and **77**.

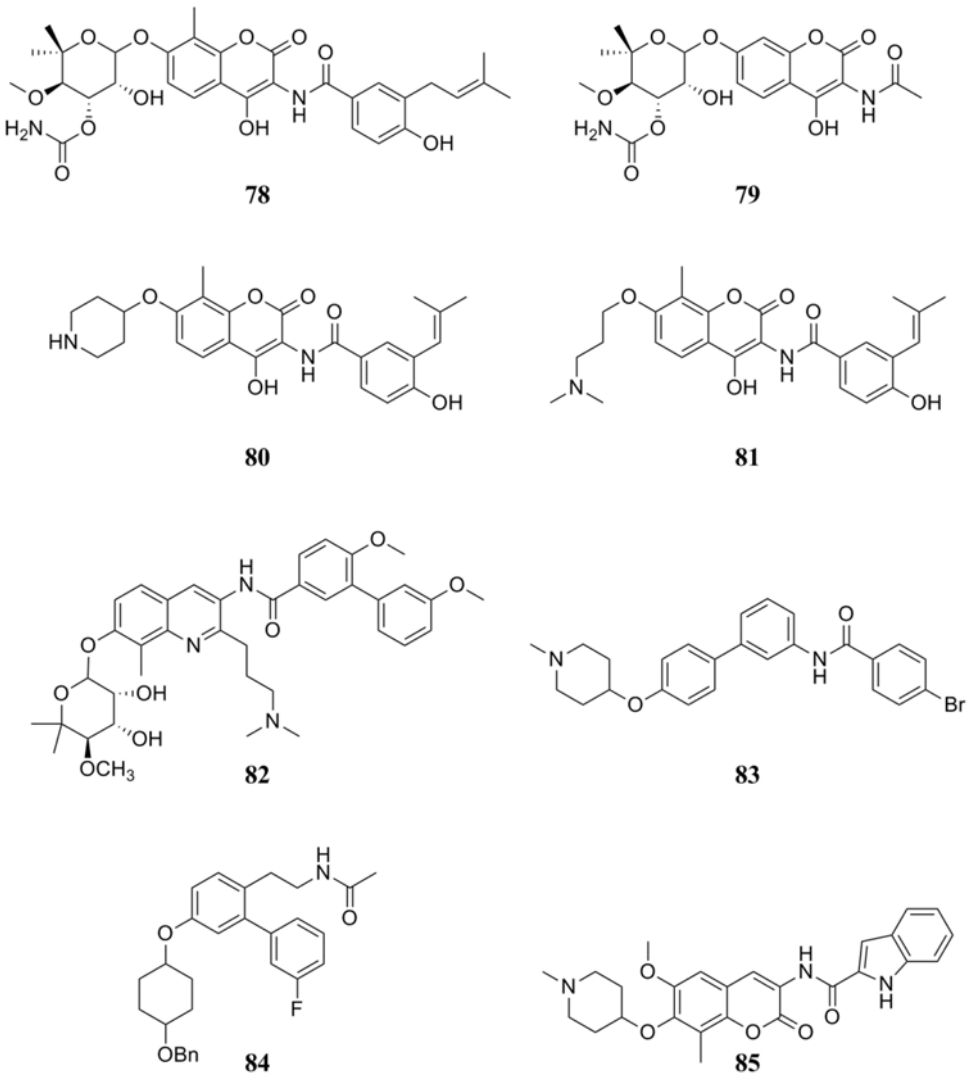

Fig. 50 Chemical structure of compounds **78**, **79**, **80**, **81**, **82**, **83**, **84**, and **85**.

is not required and prepared and tested compound **81**, which showed similar potency in the SKBr3 cell line. A wide range of SAR has been reported for these and related compounds but no compound with significantly greater potency than compounds **80** and **81** was discovered.[156] Replacement of the coumarin core has been explored.[157] Replacement with quinoline or naphthalene rings is possible and the most potent compound obtained was a quinoline derivative **82** that allowed exploration of the vector from the C-2 position which is not possible in the coumarin series. Compound **82** showed a $GI_{50} = 200$ nM in the SKBr3 cell line. Recently, using a molecular modeling approach built on extensive SAR determined around the novobiocin structure, Blagg and colleagues have designed a series of biaryl compounds as C-terminal HSP90 inhibitors.[158] The leading compound from this series, compound **83**, shows a $GI_{50} = 2$ μM in the SKBr3 cell line with the expected client protein depletion signature. Although less potent than the coumarin-containing analogs, the ease of synthesis along with drug-like nature of this compound make it an exciting lead compound from which to develop a C-terminal HSP90 inhibitor compound with in vivo activity. This approach has led to the novobiocin analog **84**, partly designed by molecular modeling using a homology model of the HSP90 C-terminal binding site.[159] It is becoming clear that these C-terminal binders are able to produce different biological effects to the more common N-terminal binders. They have a clear effect on increasing HSP70 expression, while their effect on client proteins such as ERBB2, RAF, and pAKT is notably weaker than N-terminal inhibitors. This is leading to their exploration as neuroprotective agents. Currently, the only report on the in vivo anticancer activity of novobiocin analogs is that for KU363, **85** (Fig. 50), which shows a response in 88% of xenograft tumors in an MDA-1986 head and neck human tumor animal model.[160]

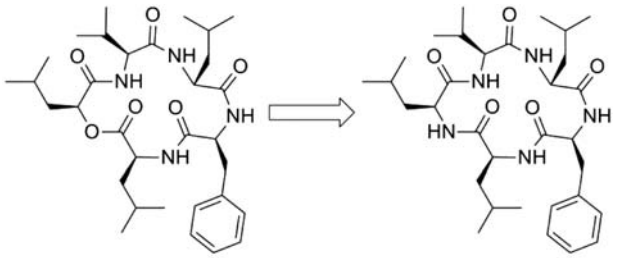

Fig. 51 Chemical structures of San A **86** and San A amide derivative **87**.

5.07.3.3.1.1.4 Other natural product inhibitors of HSP90

Sansalvamide A (San A, **86**) is a cyclic pentapeptide (depsipeptide) isolated from a marine fungus and known to have antitumor activity (Fig. 51). The lactone link in San A is readily hydrolysed leading to ring-opening and was replaced with the more stable amide link to give San A amide derivatives.[161] Out of some 86 derivatives, San A amide **87** (Fig. 51) showed potent antiproliferative activity against a human colon cancer cell line, HCT-116 ($GI_{50} = 700$ nM). The target of San A was investigated in a pull-down experiment using biotinylated San A amide.[162] This suggested HSP90 as the specific binding target and the site of binding was investigated by exploring the effect of San A amide on binding partners of HSP90 known to bind in different regions. This led to the conclusion that San A amide does not bind to the N-terminal domain and subsequent biochemical experiments using different HSP90 constructs showed that San A amide binds to the middle domain. This leads to San A amide possessing a different inhibition profile to not only the N-terminal binders such as geldanamycin but also novobiocin. San A amide does not inhibit the ATPase activity of HSP90, but unlike novobiocin and its analogs, it blocks the binding of FKBP and HOP. Additionally, San A amide is c.100-fold more potent in its inhibition of C-terminal client proteins. This opens up further opportunities for selective inhibition of HSP90 function.

Gambogic acid **88** was identified as an inhibitor of HSP90-mediated luciferase refolding from a screen of natural product libraries (Fig. 52).[163] It had been known for some time to possess a wide range of biological effects including anticancer activity and there is a mention of a Phase I trial in China involving **88** as an anticancer compound.[164] Gambogic acid was shown to demonstrate the classic client depletion signature of an HSP90 inhibitor along with disruption of HSP70 and CDC37 binding to HSP90. Surface plasmon resonance (SPR) was used to show that **88** binds to both full-length and N-terminal domain HSP90 with K_d in the single digit micromolar range but is not competitive with geldanamycin, suggesting an alternative site of binding on the N-terminal domain. There is much interest in gambogic acid as an anticancer agent although its complexity does not render it amenable to the usual medicinal chemistry approaches. A recent report demonstrated in vivo activity in a NSCLC tumor xenograft (NCI-H1993 cells) at doses of 10, 20, and 30 mg kg^{-1} ip once daily without any effect on mouse body weight.[164]

5.07.3.3.1.2 Purine-based inhibitors

As the natural ligand ATP contains an adenine group that is directly involved in the binding to HSP90, it is not surprising that purine-scaffold inhibitors were among the earliest synthetic, small-molecule inhibitors of HSP90 identified. The early work in this area has been reviewed by Taldone and Chiosis[165] and only key points will be presented here. The first purine inhibitor was PU3, **89** (Fig. 54), arrived at by a consideration of the unusual shape of the HSP90 ATP-binding pocket and the bound conformation of ATP itself.[166] Substitution at C-8 of the purine ring was identified as a key site and features in several of the purine-scaffold

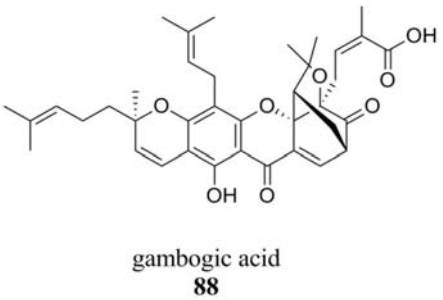

Fig. 52 Chemical structure of gambogic acid **88**.

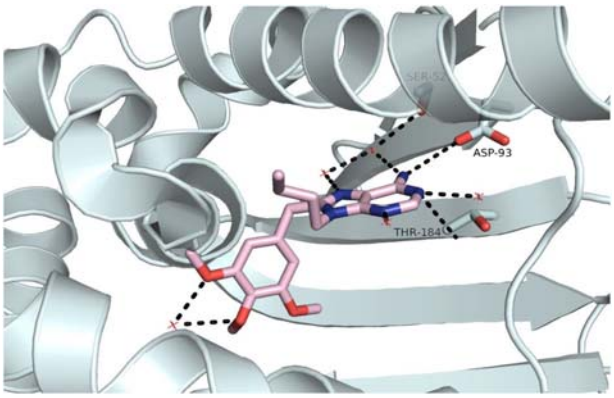

Fig. 53 X-ray crystal structure of the HSP90 NTD (*cyan*) in complex with PU3, **89** (*light pink*), PDB: 1UY6. The structure of the ligand, and the key binding site residues are shown as sticks. Selected interactions are shown in *black-dashed lines*.

inhibitors. PU3, **89**, is significantly less potent than geldanamycin with an EC_{50} value of about 20 μM for binding to purified HSP90 and it exhibited the HSP90 client protein depletion profile at concentrations below 50 μM. The crystal structure of PU3 bound to HSP90 N-terminal domain shows the key role of the C-6 amino group binding to Asp93 and there is the typical water-mediated array of interactions involving other nitrogen atoms of the purine ring[167] (Fig. 53).

The first phase of exploration of SAR around PU3 involved changes to the N-9 alkyl chain, the C-8 linker to the trimethoxyphenyl group, and substitution at C-2 of the purine. Combining the best of all these changes led to PU24FCl, **90**.[168] A key change was introduction of fluorine at C-2 which not only enhanced potency but also led to increased solubility in a chemical series with relatively poor physicochemical properties. PU24FCl showed improved binding to HSP90 with an $EC_{50} = 0.45$ μM and an $IC_{50} = 2$ μM for HER2 depletion in MCF7 human breast cancer cells. More importantly, PU24FCl showed in vivo efficacy in a human breast cancer xenograft (MCF7) model. At 200 mg kg^{-1} iv dosed on alternate days for 30 days, a 72% reduction in tumor volume compared to controls was observed.

The next advance in this area was to change to a sulfur-linker at C-8 and introduce a basic amine in the N-9 alkyl chain to aid solubility. Out of these studies emerged PUH71, **91**, which possessed an EC_{50} for HSP90 binding of 10–55 nM, a GI_{50} in various human cancer cell lines of 50–90 nM, and an IC_{50} for HER2 depletion of 50–80 nM. Interestingly, the 2′-iodo compound is significantly more potent than the 2′-bromo derivative. This has been rationalized by the presence of a lipophilic pocket large enough to accommodate the iodine substituent (PDB: 2FWZ). Salt forms of PUH71 showed good solubility in PBS buffer and improved pharmacokinetic properties including passive permeability as measured in a PAMPA assay. The only cytochrome inhibition found was CYP2D6 ($IC_{50} = 0.89$ μM) and 37% of PUH71 was metabolized to the inactive diphenol after 30 min exposure to human liver microsomes. Extensive in vivo data is available concerning the efficacy of PUH71 in human tumor xenograft experiments across a wide range of tumor types. One of the most compelling involved the treatment of a triple negative breast cancer (TNBC) xenograft in which alternate day dosing of PUH71 at 75 mg kg^{-1} iv led to a complete response in all the mice. In Jul. 2011, PUH71 entered a Phase I clinical trial sponsored by Memorial Sloan Kettering Cancer Centre. Preliminary results were presented at the American Society of Clinical Oncology (ASCO) meeting in 2015[169] and showed PUH71 to be well-tolerated with some signs of activity in a range of cancers.

A team at Myrexis further developed the basic skeleton of PUH71 leading to the clinical candidate MPC-3100,[170] **92**. They focused on optimizing the N-9 alkyl and the C-8 arylsulfide substituents for both potency and pharmacokinetic properties. They discovered that the bromo-version of the halo-methylenedioxyaryl group at C-8 offered the best overall properties at that position and that a pendant piperidine ring in the alkyl chain at N-9 was optimal. A large number of substituents on the piperidine nitrogen were explored leading to MPC-3100. The synthetic chemistry is noteworthy for a novel synthesis of the sulfide by nucleophilic displacement of a C-8 bromide on the adenine unit using in situ deprotection and reaction of a propanoyl ester-protected aryl thiol, thus preventing disulfide formation. In addition to good HSP90 binding in an FP assay ($IC_{50} = 140$ nM), MPC-3100 potently inhibited HER2 expression ($IC_{50} = 60$ nM) and caused growth inhibition in HCT116 human colon cancer cells ($GI_{50} = 540$ nM). It showed good stability in in vitro microsome assays and of the derivatives explored, showed the best C_{max} (c.23 μM), AUC (81,800 h ng mL^{-1}), and oral bioavailability ($F = 37\%$) along with an impressive 53-fold induction of HSP72 expression. Following oral administration of MPC-3100 in a human tumor xenograft model at 200 mg kg^{-1} for 22 days, an average of 48% reduction in tumor volume was observed. MPC-3100 was progressed to a Phase I trial where it demonstrated safety and tolerability with side effects including diarrhea, nausea, and vomiting.

Subsequent exploration of the purine scaffold as HSP90 inhibitors moved away from the C-8 aryl substituent by shifting this benzyl group to N-9 in place of the alkyl chain found in previous inhibitors. It was found that this led to inactive compounds until the C-6 amino group was also moved to become a C-2 amino substituent. The culmination of this work by Biogen Idec/Conforma led to BIIB021, **93**, in which the aryl substituent at N-9 has been changed to a pyridyl unit and a chloro-substituent added at C-2

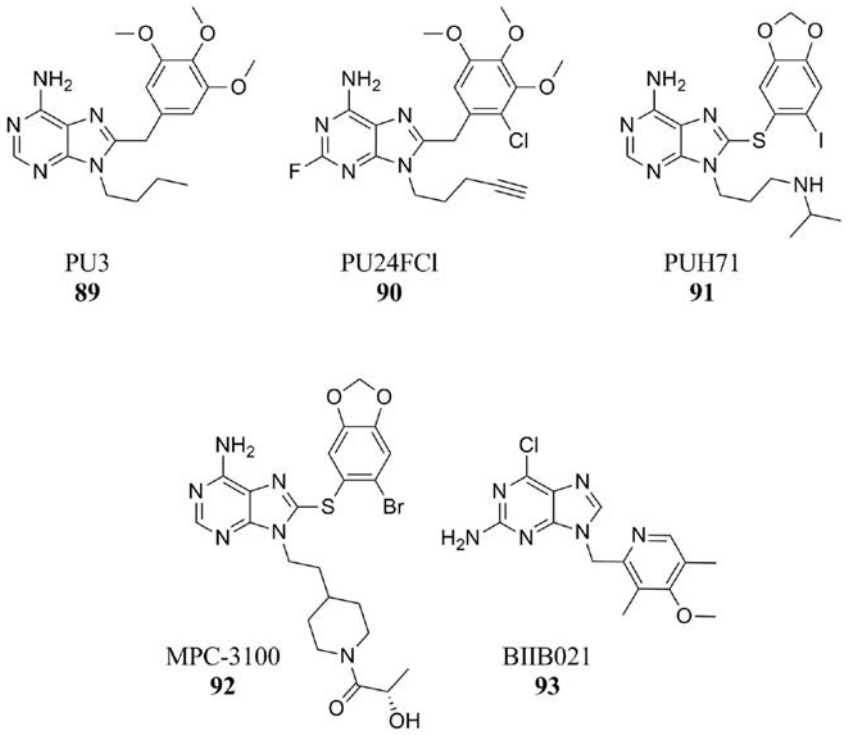

Fig. 54 Chemical structures of compounds **89**, **90**, **91**, **92**, and **93**.

(Fig. 54). BIIB021 displayed good solubility and good oral exposure in mice; its EC_{50} for HSP90 binding is 20 nM and its GI_{50} in various cancer cell lines was 50–150 nM. An in vivo efficacy study using N87 human tumor xenografts gave 87% tumor growth inhibition on dosing at 125 mg kg^{-1} orally 5 days per week for 5 weeks. The observation of oral efficacy in a xenograft study was a clear advance. BIIB021 has entered clinical trials and has shown partial responses as determined by FDG-PET in a Phase II trial in gastrointestinal stromal tumors (GIST).[171]

5.07.3.3.1.3 Resorcinol-based inhibitors

As discussed in "**Radicicol-based inhibitors**" section, the resorcinol motif of radicicol binds deeply in the ATP-binding pocket of the N-terminal domain of HSP90, anchored by water-mediated hydrogen bonds via conserved waters. The drug discovery program to realize the potential of the resorcinol unit arose from a high-throughput screen at The Institute of Cancer Research which identified pyrazole **94** (Fig. 55). This showed an $IC_{50} = 280$ nM for HSP90 binding in a fluorescence polarization assay and a cellular $GI_{50} = 6$ μM. This compound was advanced in a collaboration with Vernalis through addition of an amide at the 5-position of the pyrazole to pick up a binding interaction with Lys58, and gave pyrazole amide **95** with considerably enhanced biochemical and cellular potency. Introduction of a solubilizing group to the 4-aryl substituent and a change to the isoxazole ring to reduce the hydrogen bond donor count gave compound **96** with significantly improved cellular potency. Finally, fine-tuning of the lipophilic group on the resorcinol ring and selection based on pharmacokinetics and pharmacodynamics gave the clinical candidate **97** which was licensed to Novartis and became NVP-AUY922.[172]

NVP-AUY922, **97**, shows significant growth inhibition and/or regressions in both orthotopic and subcutaneous human tumor xenograft experiments in nude mice across a range of cancer types. It is dosed intravenously as it has poor oral bioavailability owing to glucuronidation of the resorcinol. It shows the classic molecular signature of an HSP90 inhibitor with depletion of key oncogenic client proteins and an increase in expression of HSP70. Unlike tanespimycin, activity was independent of NQO1 expression and liver toxicity was avoided.[173] It is entered over 25 clinical trials (www.clinicaltrials.gov) both as a single agent and in combination with other cancer therapeutics. A highlight of these trials so far include a Phase II trial in combination with trastuzumab in ERBB2-positive metastatic breast cancer which achieved a partial response rate of 23% and was well-tolerated with diarrhea and reversible visual disturbance being the main side effects.[174] A Phase II trial is underway in patients with NSCLC carrying an exon 20 insertion mutation in EGFR; which tumors are resistant to EGFR inhibitors such as erlotinib.

A different approach to a resorcinol-based HSP90 inhibitor was taken by the team at Astex. Using the fragment-based approach they have helped pioneer, they uncovered two fragments that bound (by ITC) with a $K_d < 1$ mM. One of these fragments was phenolic benzamide **98** ($K_d = 790$ μM, $LE = 0.26$) and the other was an aminopyrimidine **99** ($K_d = 250$ μM, $LE = 0.38$) (Fig. 56).[175] They pursued both series using protein/ligand structures but although not the most ligand efficient, the phenol series

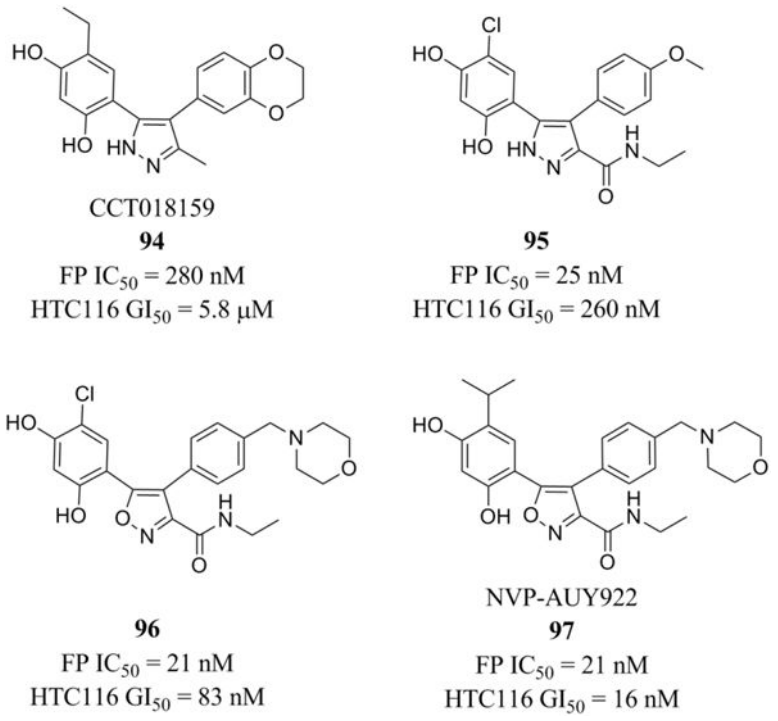

Fig. 55 Chemical structures of compounds **94**, **95**, **96**, and **97**.

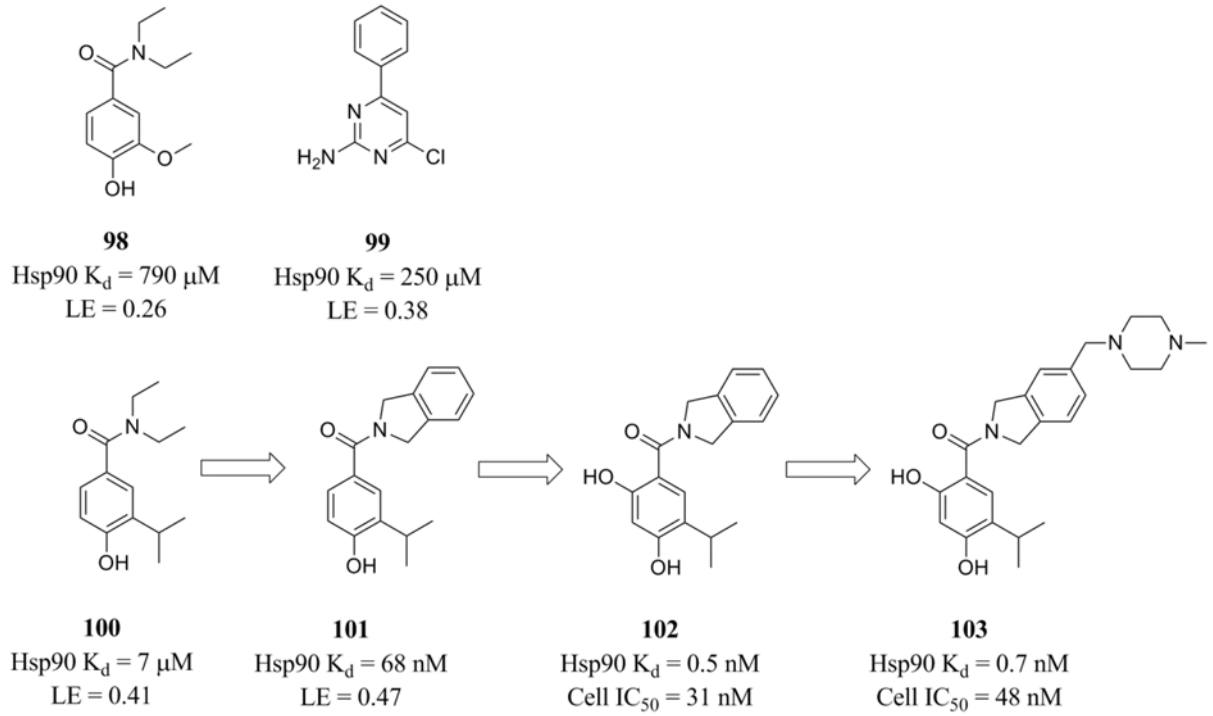

Fig. 56 Fragment-based discovery of AT13387, **103**.

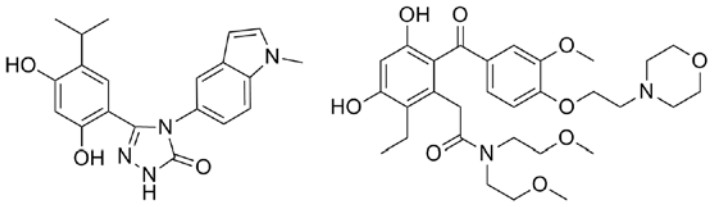

Fig. 57 Chemical structures of compounds **104** and **105**.

led to a clinical candidate. Introduction of an alkyl group to replace the methoxy group and fit into the lipophilic pocket gave compound **100** with a large increase in potency and ligand efficiency (Fig. 56). Replacing the diethylamide with a larger isoindoline group (**101**) moved the Lys58 sidechain and allowed lipophilic interactions with the protein, further enhancing binding. Based on the resorcinol motif, the Astex team then introduced a 2-hydroxy group to **101** to give resorcinol **102** which showed subnanomolar binding and low nanomolar cellular activity. Subsequent exploration of substituents on the isoindoline to enhance the solubility led to the clinical candidate AT13387 (**103**) which retained the binding and growth inhibitory properties of **102** but possessed good pharmacokinetic properties suitable for IV and intraperitoneal administration.[176] In a human colon cancer xenograft experiment in nude mice, compound **103** dosed at 60 mg kg^{-1} ip 3 days on and 3 days off led to 78% tumor growth inhibition. AT13387, **103**, is in some 12 clinical trials covering a range of cancers, as both a single agent and in combinations.

Two further resorcinol-based HSP90 inhibitors have been developed and are in the clinic but much less information has been revealed about their discovery. Ganetespib, **104**, has been developed by Synta and has been shown to be a potent HSP90 inhibitor (Fig. 57).[177] It is currently in some 38 clinical trials as both a single agent and in combination with other cancer therapeutics in a range of cancers. In common with other resorcinols, the mode of administration is iv. The final example of a resorcinol that has reached the clinic is KW-2478, **105**, developed by Kyowa Hakko Kirin Pharma. This compound has entered clinical trials in hematological cancers.[178]

5.07.3.3.1.4 Miscellaneous N-terminal inhibitors

Serenex employed a unique chemoproteomics approach to discover their HSP90 inhibitor SNX-5422.[179] Targeting ATP-binding proteins, they treated immobilized purine-based affinity media with cell lysate and then used a small library of compounds to elute various proteins. They identified proteins eluted by each compound and hence discovered hits to the eluted proteins. The 4-substituted benzamide **106** was discovered in this way and elaborated using structure-based design to give the clinical candidate SNX-5422, **107**, which is a glycine ester prodrug to improve solubility (Fig. 58). This compound was licensed to Pfizer and showed low nanomolar growth inhibition of a wide range of human cancer cell lines in vitro. In a human breast cancer (BT-474) xenograft experiment in nude mice, SNX-5422 was dosed at 40 mg kg^{-1} orally three times per week and led to tumor regressions. This is unlike the previous HSP90 inhibitors described earlier in having orally efficacy in the animal model. SNX-5422 has been in a number of Phase I and Phase I/II trials for both solid and hematological malignancies.[180]

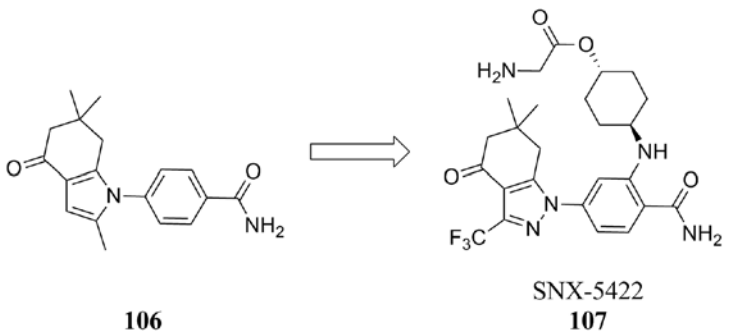

Fig. 58 Development of compound SNX-5422, **107**.

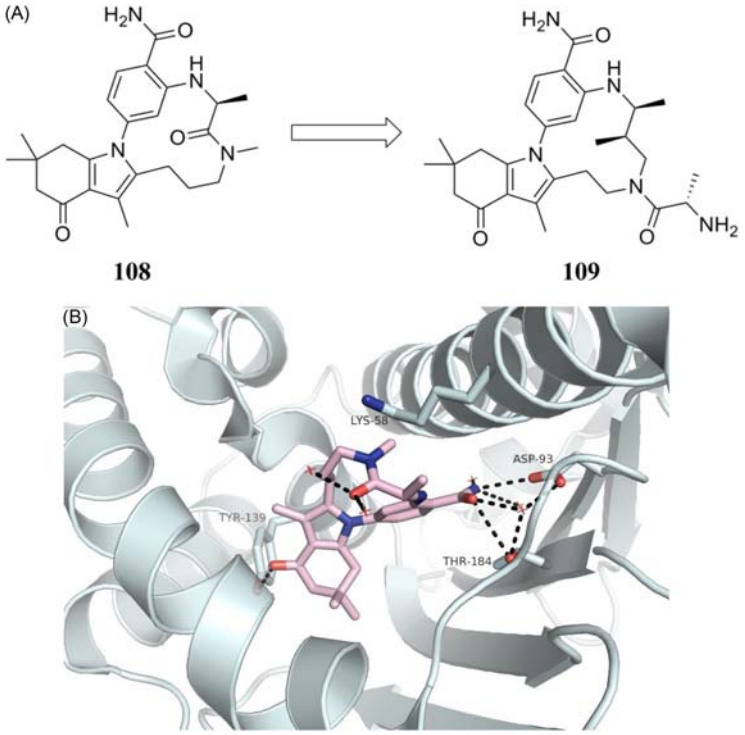

Fig. 59 (A) Chemical structures of **108**, **109**. (B) X-ray crystal structure of the HSP90 NTD (*cyan*) in complex with **108** (*light pink*), PDB: 3R91. The structure of the ligand, and the key binding site residues are shown as sticks. Selected interactions are shown in *black-dashed lines*.

Starting with the structure of SNX-5422, a group at Pfizer used a macrocyclic motif to constrain the conformation leading to compound **108** which showed an $IC_{50} = 92$ nM against the ATPase function of HSP90.[181] A crystal structure showed that the benzamide formed hydrogen bonds with the key Asp93 in the ATP-binding pocket (Fig. 59). This series was progressed to macrocycle **108** (Fig. 59) which showed good in vitro and in vivo pharmacokinetic properties with significant accumulation in the tumor but low oral bioavailability.[182] In a H1975 human lung cancer xenograft in nude mice, **108** dosed daily at 25 mg kg^{-1} iv showed regressions.

Another macrocyclic HSP90 inhibitor, this time based on a 2-aminopyrimidine core, has been disclosed by a group from Chugai.[183] Starting from triazine **110** which was a potent HSP90 inhibitor but with poor pharmacokinetic properties, they developed macrocycle **111** by mimicking the interactions seen in the geldanamycin/HSP90 crystal structure (Fig. 59). Macrocycle **111** showed excellent in vivo pharmacokinetic properties including a high oral bioavailability (71%). In a HCT116 human colon cancer xenograft model, **111** showed tumor growth inhibition of 83% when dosed at 25 mg kg^{-1} po once daily.

A further benzamide-derived HSP90 inhibitor has been discovered and developed by a team at Exelixis.[184] Starting with a high-throughput screen against HSP90 using a fluorescence polarization assay, they screened over 4 million compounds to find two tropane-containing benzamides exemplified by compound **112** (Fig. 61). After a medicinal chemistry campaign in which initially potency was increased followed by a focus on permeability and pharmacokinetics, XL888, **113** (Fig. 61), was obtained with low nanomolar potency in both biochemical and cell-based experiments. Although not the most permeable compound as measured

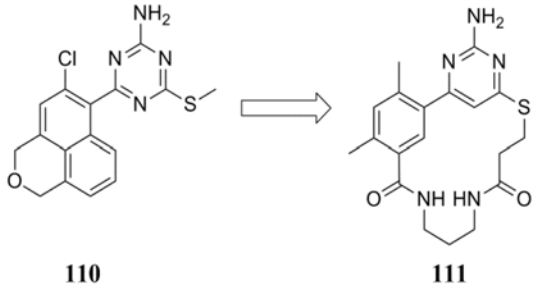

Fig. 60 Chugai compounds: hit **110** and clinical candidate **111**.

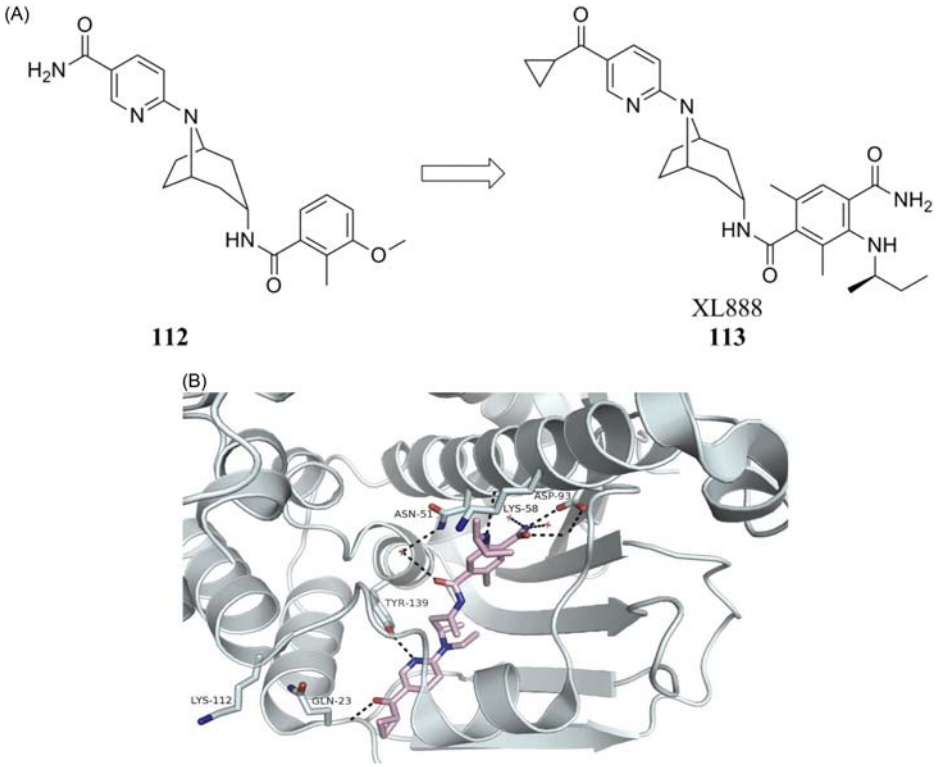

Fig. 61 (A) Structures of Exelixis compounds: hit **112** and clinical candidate **106**. (B) X-ray crystal structure of the HSP90 NTD (*cyan*) in complex with **113** (*light pink*), PDB: 4AWO. The structure of the ligand, and the key binding site residues are shown as sticks. Selected interactions are shown in *black-dashed lines*.

by the MDCK assay, **113** possessed relatively low clearance and 30% oral bioavailability in mice and was chosen for progression to efficacy experiments. Treatment of a NCI-N87 human stomach cancer xenograft in nude mice at 60 mg kg^{-1} orally once a day led to 100% tumor growth inhibition. Interestingly, dosing at 100 mg kg^{-1} once a day on the 3 days out of 7 schedule led to enhanced efficacy with tumor growth inhibition exceeding 100% (21% tumor regression) demonstrating the balance in scheduling between a toxic dose and a therapeutically efficacious dose. XL888 (**113**) has entered clinical trials in solid tumors.

A high-throughput screening effort at Novartis yielded the dihydroquinazolinone **114** with a potency of about 1 μM versus HSP90.[185] With good ligand efficiency ($LE = 0.42$) and good aqueous solubility, a protein/ligand crystal structure for **114** with HSP90 was obtained which enabled structure-based drug design (Fig. 62). A key early step in this work involved a scaffold hop from the carbocyclic ring to a lactam which eased the issue of chiral resolution to obtain the active *R*-series by enabling an enantiospecific synthesis utilizing Ellman chemistry. Exploration mainly focused on the aryl substituent leading to NVP-HSP990 (**115**) which showed an IC_{50} against full-length HSP90 of 1 nM. NVP-HSP990 was found to have a half-life of 146 min in mouse pharmacokinetic experiments with an oral bioavailability of 76%. In a PK–PD experiment following depletion of c-Met as the biomarker, NVP-HSP990 led to prolonged suppression after a single dose. In a GTL-16 human gastrointestinal cancer xenograft, NVP-HSP990 dosed at 5 mg kg^{-1} orally once every 3 days led to 76% tumor growth inhibition. Consequently, NVP-HSP990 (**115**) was chosen for clinical evaluation. A Phase I dose-escalation trial has reported[186] that 50 mg per week is the MTD as a single agent with neurological toxicity being dose limiting. No objective responses were reported although 25/64 patients showed stable disease.

A team at Pfizer has also reported the discovery of a clinical candidate based on a different chemical structure.[187] They started from the hit compound **116**, discovered by a high-throughput screen, and widely explored the structural space using extensive ligand/HSP90 crystal structures to direct the synthetic chemistry (Fig. 63). The hit compound **116** showed a K_i of 1.2 μM against HSP90 but no cellular activity. After multiple rounds of optimization they nominated compound **117** as a clinical candidate. Key drivers of the optimization were decreasing hERG affinity and enhancing in vitro ADME properties. In vivo pharmacokinetics showed an oral bioavailability that corresponded to clearance across species suggesting near complete absorption and also a high volume of distribution leading to a long half-life. Cellular potency was in the low nanomolar range and a xenograft experiment using the A2058 human melanoma cancer cell line with dosing at 25 mg kg^{-1} po once daily gave 96% tumor growth inhibition.

An isolated publication by a team at Sanofi-Aventis reported the design and synthesis of polycyclic HSP90 inhibitor **118** (Fig. 63).[188] This was reported to have arisen from a much simpler resorcinol-containing compound that X-ray crystallography found bound to an induced lipophilic pocket near the ATP-binding site. Compound **118** showed potent cellular activity in terms of both growth inhibition and biomarker modulation and activity in a murine leukemia model.

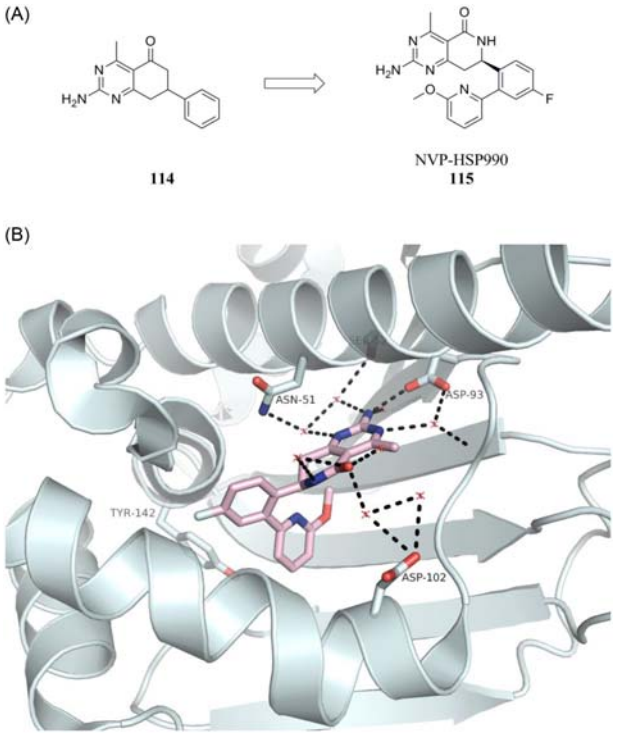

Fig. 62 (A) Structures of Novartis compounds: hit **114** and clinical candidate NVP-HSP990 (**115**). (B) X-ray crystal structure of the HSP90 NTD (*cyan*) in complex with NVP-HSP990 (*light pink*), PDB: 4U93. The structure of the ligand, and the key binding site residues are shown as sticks. Selected interactions are shown in *black-dashed lines*.

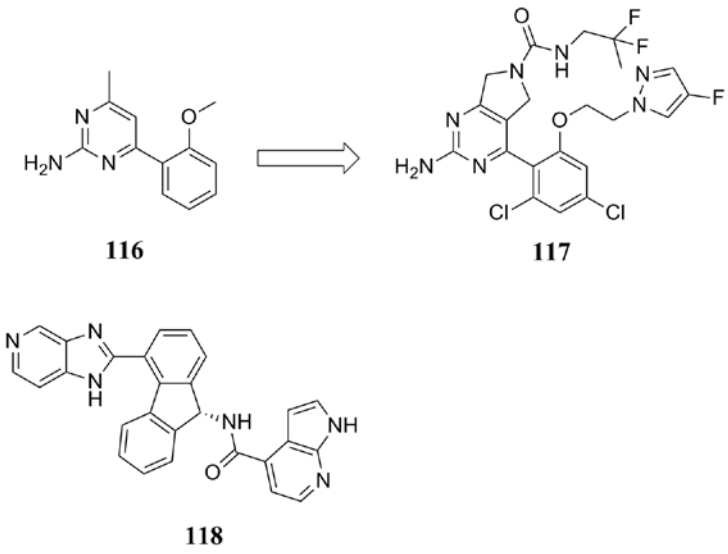

Fig. 63 Structures of Pfizer compounds: hit **116** and clinical candidate **117**. Sanofi-Aventis compound **118**.

5.07.3.3.2 Isoform selectivity

As HSP90 consists of four isoforms distributed differentially (see "HSP90 Family" section), it might be expected that isoform selective inhibitors may display different biology compared to the pan-HSP90 inhibitors. Some insights into this have been reported.[122] Taldone, Chiosis et al. have reported a comprehensive exploration of the binding of a wide variety of inhibitors with all four HSP90 isoforms using a fluorescence polarization assay based on a purine probe compound.[189] They have coupled this with a structural analysis of each of the proteins and the binding modes of the inhibitors using protein/ligand structures where available or modeling if structures were not available. They postulate three binding pockets; pocket A is the ATP-binding region,

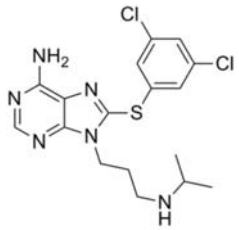

119

Fig. 64 GRP94 selective inhibitor.

pocket B is an adjacent lipophilic region, and pocket C is the exit vector to solvent. Their data suggests that selectivity is achieved via pockets B and C and explain the lower binding of several inhibitors to Trap-1 as being caused by a clash of substituents on the ligands with Lys126 and Phe201 in this pocket of Trap-1. Evidence that selectivity can affect the biology observed has been demonstrated for a purine-based inhibitor **119** (Fig. 64) which is 140-fold selective for GRP94 over HSP90.[190] GRP94 specifically associates with HER2 in SkBr3 cell membranes and compound **119** destabilizes HER2 but does not lead to induction of HSP70. Further recent work exemplifying these principles has recently been reported and the profile of compound **119** investigated in detail.[191] The possibility for further tuning of the pan-HSP90 response by developing selective inhibitors is an exciting area.

5.07.4 Targeting Protein Degradation

5.07.4.1 Introduction

The UPS represents the major quality control pathway for newly synthesized proteins and is a crucial element for maintaining intracellular protein homeostasis and normal cellular functions. The UPS governs proteolytic degradation and other essential cellular processes, such as cell cycle progression, signaling, and antigen processing; therefore, its malfunction is often connected to the development of diseases, including cancer, immune disorders, and neurodegeneration. Thus, targeting the UPS with small-molecule inhibitors represents a viable approach in drug discovery. In particular, the great value of the UPS as a cancer therapeutic target was revealed in 2003 with the FDA approval of the proteasome inhibitor bortezomib, which has become the standard of care for the treatment of relapsed and refractory MM and MCL.[192] Further corroboration arrived the following year as the discovery of the ubiquitin-mediated protein degradation was awarded the Nobel Prize in chemistry.[193]

However, despite the undeniable potential, only a limited number of drugs targeting the UPS have reached FDA approval to date. The main reason for such slow progress is perhaps the difficulty in targeting with small molecules a system that lacks a well-defined enzymatic function and mostly relies on multiple protein–protein interactions. Nevertheless, despite these challenges, improved proteasome inhibitors have been developed and other promising targets within the UPS cascade upstream of the proteasome have emerged with potential for more targeted therapies. These are designed to improve the therapeutic index of the pioneer proteasome inhibitors.[194]

5.07.4.2 The Ubiquitin–Proteasome System

The UPS comprises a series of enzymes, whose aim is to achieve protein ubiquitylation and degradation (Fig. 65). As a whole the cascade includes 2 E1 enzymes, around 40 E2 enzymes, 700 E3 ligases and the proteasome, providing opportunities for both broad and targeted therapeutic approaches.[195]

The process consists of five main steps:

(1) *Activation*: the protagonists in this first step are the E1 activating enzymes, which use the energy derived from ATP hydrolysis to form a thioester bond with the carboxyl terminus of ubiquitin and initiate the cycle.
(2) *Conjugation*: the E2 conjugating enzymes receive the ubiquitin molecule from the E1 enzymes via transthiolation reactions.
(3) *Ubiquitin-conjugate recognition*: the E2-ubiquitin complex is recognized by the E3 ligase enzymes, interacting to transfer the ubiquitin to an acceptor lysine residue present on the substrate protein of E3. This process of ubiquitin-tagging of the target protein is repeated several times and is linked to various physiological processes. The linkage can happen to any of the seven lysine residues of ubiquitin (K6, K11, K27, K29, K33, K48, and K63). Generally, if the polyubiquitin chain is K48-linked, it represents the label which marks the substrate for proteasomal degradation. On the other hand, if poly-ubiquitylation happens at the K63 site, modifications of signal transduction pathways occur.
(4) *Ubiquitin removal*: at this point, the ubiquitylated protein can have two distinct destinies: it can be rescued via deubiquitylation through specific deubiquitylating enzymes (DUBs) or it can proceed toward the final step of degradation.
(5) *Substrate degradation by the proteasome*: the substrates bearing the K48-linked ubiquitin chain are delivered to the 26S proteasome. When the proteasome interacts with the tagged proteins, they are degraded into small peptides, while ubiquitin is released and recycled.

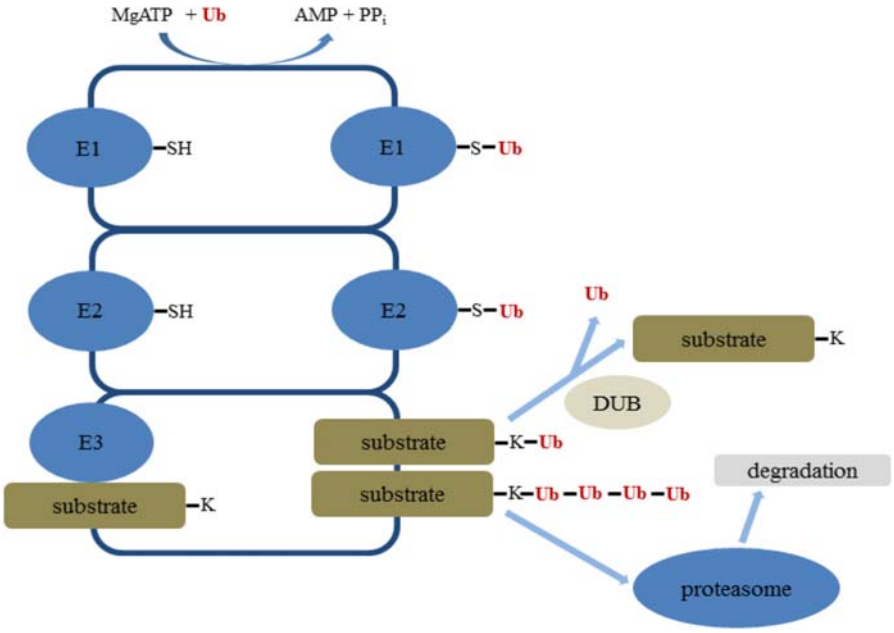

Fig. 65 Schematic representation of the ubiquitination–proteasome degradation cascade. E1: ubiquitin activating enzyme; E2: conjugating enzyme; E3: ligase; Ub: ubiquitin; DUB: deubiquitylating enzyme; –K: lysine residue; –SH: thiol moiety.

It is important to highlight that, although being the first identified and most thoroughly studied, ubiquitin is not the only tag for protein degradation. Subsequently, other tags, called UBLs (ubiquitin-like proteins), have been identified, adding complexity to the proteolytic system.[196,197]

5.07.4.3 Targeting the E1 Activating Enzymes in Cancer Therapy

The E1 (ubiquitin activating enzymes) are at the top of the UPS cascade. Only two different isoforms have been identified in humans, UBA1 and UBA6 (of which UBA1 predominates), which control ubiquitylation of all downstream targets. Due to the low number of isoforms, E1 enzymes are considered challenging broad targets as their lack of specificity could lead to toxic side effects. However, they are also the only enzymes within the UPS cascade with an ATP-dependent mechanism, a feature which may be exploited for the development of selective inhibitors.[192,198]

In their mechanism of action, ATP and ubiquitin interact to form a ubiquitin–AMP intermediate which then reacts with the catalytic cysteine residue of E1 to form a thioester adduct. Another molecule of ATP and ubiquitin bind the enzyme to form a ternary complex from which, via transthiolation, E1 transfers ubiquitin to E2. There are different points of the process in which a small-molecule inhibitor could interfere and the interest in targeting E1 enzymes is increasing.[194,199] To date, there have been mainly two strategies under development: the first strategy focuses on targeting the cysteine residue at the active site of E1 in order to inhibit the transthiolation reaction; the second approach exploits small molecules as AMP mimetics in order to stop the formation of the ubiquitin–AMP complex.

Although delivering early stage irreversible E1 inhibitors, such as the synthetic cell permeable 2-nitro-furan-based inhibitors, PYR41 and PYZD4409,[192] or the natural products himeic acid A and panepophenanthrin[199,200] (Fig. 66), the first approach was unsuccessful for the development of clinical candidates, mainly as a result of selectivity issues, undefined mechanistic characterization, suboptimal potencies, and a lack of drug-like properties, which prevented further progression.

More fruitful, on the other hand, has been the second approach, which led to the development of the clinical candidate pevonedistat.

5.07.4.3.1 Pevonedistat (MLN4924)

Pevonedistat, **125**, is a first-in-class NAE inhibitor with a unique mechanism of substrate-assisted enzymatic inhibition.[195] It targets a specific subclass of E1 enzymes, called NAE (NEDD8-Activating Enzyme, where NEDD8 is an ubiquitin-like protein). In contrast to E1 pan-inhibitors, which were found to be unsuitable for clinical development due to toxicities associated with the broad spectrum E1 inhibition, the great advantage of pevonedistat is its superior selectivity.[201] Importantly, this highlighted that it is possible to target a single UBL pathway without affecting the bulk protein turnover.[202]

Pevonedistat was discovered via a HTS campaign,[201,203,204] and it is an analog of AMP, **126**, a tight binding product of NAE. There are some key structural differences: pevonedistat bears a deazapurine base instead of the adenine base; a carbocycle moiety replaces the ribose sugar and the phosphate group is replaced with a sulfamate, particularly important for its mechanism of action.

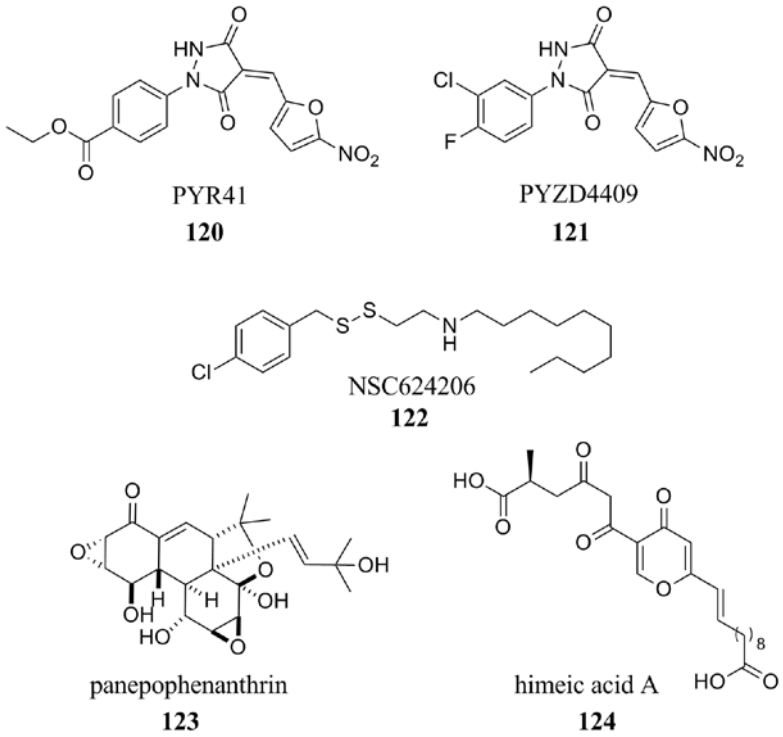

Fig. 66 Chemical structures of some reported synthetic and natural E1 inhibitors.

The stereochemistry, too, is different, with pevonedistat bearing a nonnatural antirelationship between the deazapurine and the sulfamate groups[205] (Fig. 67).

Under normal conditions, the enzyme NAE controls the activity of the E3 Cullin-RING ubiquitin ligases (CRLs) by promoting modification of the NEDD8 protein. ATP and NEDD8 bind to NAE and react to form a covalent complex, NEDD8-AMP. The adduct then reacts with a cysteine residue at the active site of the NAEβ subunit to form a thioester bond between NAE and NEDD8, releasing AMP. Finally, a second NEDD8 molecule is added to form the ternary complex, NEDD8–NAE–NEDD8 (probably more favorable in terms of energy and conformation), which transfers the NEDD8 to specific E2 conjugating enzymes by transthiolation.[206] In turn, the E2 enzymes will transfer NEDD8 to a specific lysine residue at the active site of the E3 ligase. This neddylation reaction is an important posttranslational modification necessary to activate the CRLs. Pevonedistat can exploit the amino group of the sulfamate moiety to perform nucleophilic attack on the thioester bond between NEDD8 and the NAEβ subunit, and form

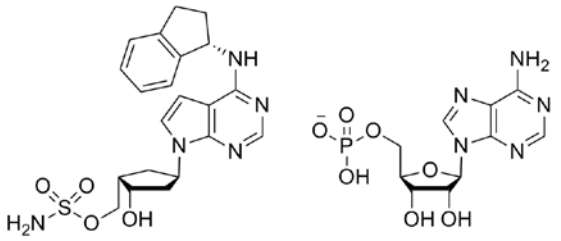

NAE IC50 = 0.004 μM
UAE IC50 = 1.5 μM
SAE IC50 = 18 μM
UBA6 IC50 = 8.2 μM
ATG7 IC50 >10 μM

Fig. 67 Structural features and selectivity profile of pevonedistat/MLN4924, **125**.

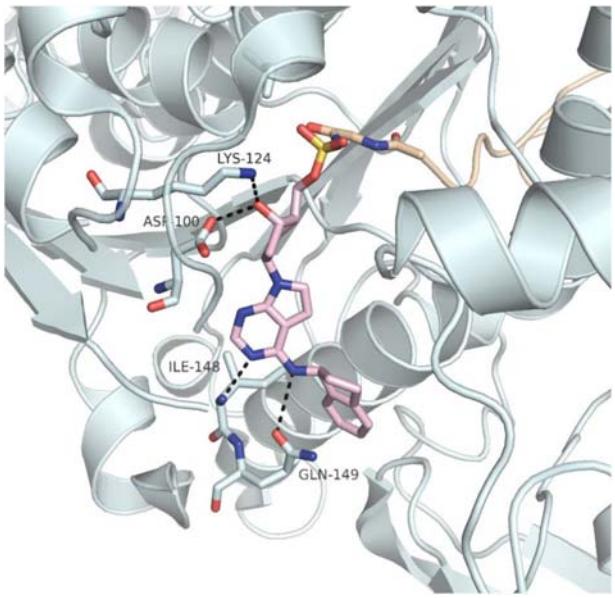

Fig. 68 X-ray crystal structure of NAE (*light cyan*) complexed with NEDD8-MLN4924 (NEDD8 shown in wheat and pevonedistat/MLN4924, **125** shown in *light pink*), PDB: 3GZN. The structure of the ligands NEDD8-MLN4924, and the key binding site residues are shown as sticks. Selected interactions are shown in *black-dashed lines*.

a covalent bond with the C-terminal glycine of NEDD8. This adduct inhibits the cascade. Crystallographic analysis of MLN4924 in complex with the NAEβ subunit has highlighted key interactions which mimic the contacts between the enzyme and ATP. In particular, Asp100 and Lys124 interact with the 3′-OH of the cyclopentane moiety and Ile148 and Gln149 interact with the deazapurine ring. Finally, the sulfamate oxygens interact with Gly79 mimicking the interaction with the α-phosphate oxygens of ATP (Fig. 68). This final interaction is proposed to be responsible for lowering the pK_a of the sulfamate moiety (pK_a 9.35) and promoting nucleophilic attack at the thioester bond of the NEDD8–NAE complex[201] (Scheme 2).

Pevonedistat showed potent inhibition of NAE, with an IC_{50} of 4 nM, and good selectivity with respect to other related enzymes in biochemical assays monitoring the formation of E2-UBL thioester complexes (Fig. 67). The selective NAE inhibitory effect was reconfirmed in cell-based assays that showed apoptosis and selective deregulation of the DNA synthesis (S) phase in cancer cells.[201] This translated in vivo; indeed, pevonedistat displayed high efficacy (growth inhibition and regression) at tolerated doses in multiple human cancer xenograft models when administered daily or at set dosing schedules.[201]

This exciting preliminary data supported the transition of pevonedistat in clinical development.[201] In Phase I studies, pevonedistat displayed a reasonable safety profile with only limited myelosuppression, rendering it suitable for combination therapy with cytotoxic agents. To date, several clinical trials of **125** in multiple solid tumors and hematological cancers have been completed,

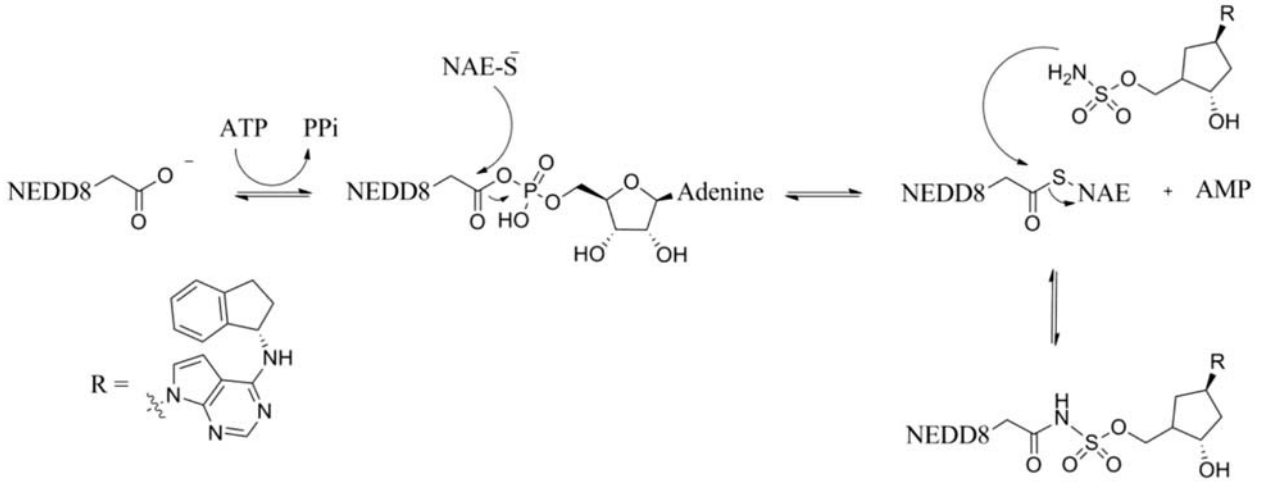

Scheme 2 Mechanism of the NEDD8-MLN4924 complex formation.

with some still ongoing, where pevonedistat is used as a single agent or in combination with cytotoxic agents (gemcitabine, paclitaxel, docetaxel, and carboplatin).[207]

5.07.4.3.2 Targeting the E2 conjugating enzymes in cancer therapy

The E2 conjugating enzymes are not only "ubiquitin-carriers," responsible for the transfer of ubiquitin-tags to the target proteins, but they are also considered key mediators in the chain assembly process and in substrate selectivity.[192,208,209] As the E2 enzymes have been connected to several malignancies including ovarian carcinoma, breast cancer, melanoma, and lung cancer, they may represent an alternative target for cancer therapy.[210] In addition, E2 enzymes are more diverse (there are around 40 isoforms in humans) thus this class might provide the required specificity which is lacking in the E1 enzyme-focused therapies. However, there are some caveats associated with the drugability of E2 enzymes. Firstly, their enzymatic core is highly conserved and possess a reactive cysteine residue, therefore development of selective drugs can be challenging. Secondly, they possess a shallow active site, difficult to target with small molecules.[195]

In theory, as the E2 enzymes function as intermediates between E1 and E3 proteins, and as they bind E1, E3, and ubiquitin, inhibitors could be targeted to different interfaces.[211] Unfortunately, possibly due to the complexity behind the dynamics of the interactions, no potent and selective E2 small-molecule inhibitors have been developed to date. However, some advances have recently been published.[209,212–214] The compound CC0651,[215] **127** (Fig. 69), has been reported as an allosteric inhibitor of the E2 enzyme CDC34, with consequent inhibition of ubiquitination of $p27^{KIP1}$. Also, BAY11-7082, **128**, has been reported as an inhibitor of UBE2N via covalent modification of a cysteine residue in the active site.[216] Another reported small molecule is the NFkB inhibitor, NSC697923, **129**, which specifically targets the E2 enzyme UBE2N and inhibits transfer of ubiquitin to target proteins by blocking the formation of the UBE2N-ubiquitin thioester conjugate.[217] The specificity is related to binding to a cleft in the active pocket not accessible in other E2 enzymes.[209] Also recently reported are selective Rad6 inhibitors, such as TZ8, **130**, and TZ9,[213] **131** (Fig. 69).

5.07.4.3.3 Targeting E3 ligases

More focus has been put on the discovery and development of E3 ligase inhibitors. Probably the main reason for this is that the E3 ligases represent the least promiscuous class of enzymes within the whole ubiquitination–proteasome degradation pathway, thus they are considered safer targets to exploit in cancer therapy. Selective targeting of the E3 ligases with small-molecule inhibitors has been seen as a promising approach in the quest for less toxic anticancer therapies.

The human genome contains around 700 E3 ligases, which are responsible for substrate selectivity in the ubiquitin–proteasome cascade. They are generally divided into four classes: HECT (homology to E6AP C-terminus) domain E3 ligases; U-box E3 ligases; RING (Really Interesting New Gene) finger E3 ligases; multisubunit E3 complexes.[192,218] The E3 ligases are responsible for the ubiquitin–protein conjugation step necessary to obtain targeted proteasomal degradation. As E3 ligases possess specific regions

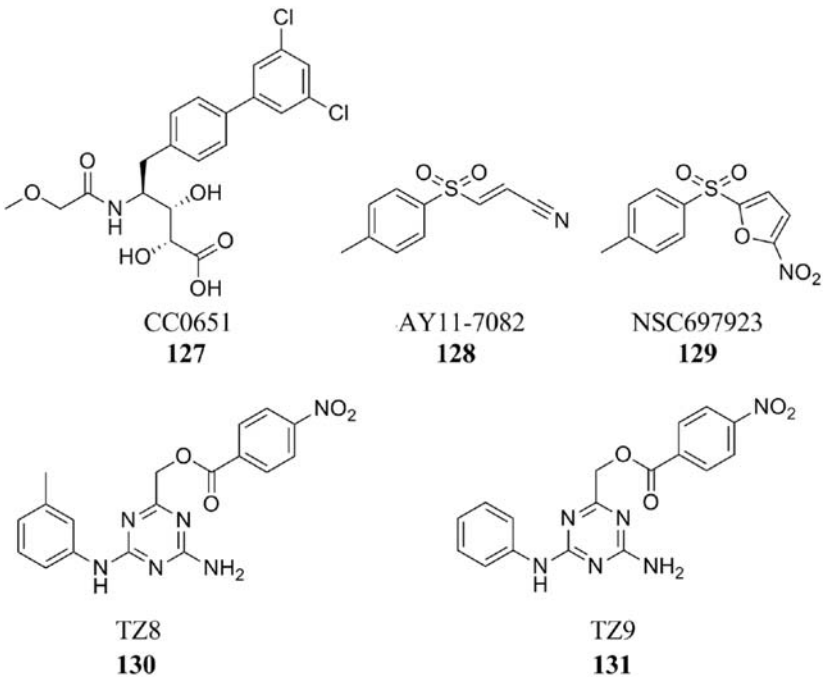

Fig. 69 Chemical structures of recently reported E2 enzyme inhibitors.

for recognition and binding of the target proteins, they determine the substrate specificity and so the selectivity of the proteasome machinery.

Although the principle of targeted E3 ligase cancer therapies is extremely appealing, drug discovery for these proteins is technically challenging as it involves inhibition of protein/protein interactions.[195] The main limitations concern the lack of catalytic activity or recognizable active sites which lead to targeting large protein interfaces with small-molecule inhibitors in order to disrupt the E3 complexes or to achieve allosteric inhibition. Another caveat around inhibition of E3 ligases is the abrogation of auto-ubiquitylation, which would lead to accumulation of a pool of E3 ligases. This excess pool would still bind their substrates without ubiquitylating them, and could result in the possible impairment of the substrate functions.

Nevertheless, several E3 ligase inhibitors[194,219] have been developed and have undergone or are undergoing clinical trials (some examples are: JNJ26854165, LCL161, AEG 35156, AEG 40826, YM155).[192,220]

So far the most druggable E3 ligases appeared to be MDM2 (mouse double minute 2 homolog) and IAPs (inhibitor of apoptosis proteins).[218] More recently, also SCF^{SKP2} (Skp1–Cul1–F-box-protein) is emerging as a possible selective anticancer target. Small molecules capable of binding SCF^{SKP2} and disrupting the interaction between SKP1 and SKP2 have revealed antitumor activity in several animal models and demonstrated synergistic activities with other anticancer agents.[221]

5.07.4.3.3.1 MDM2

MDM2 is an E3 ubiquitin ligase which fulfills the criteria of an ideal cancer target, with low expression in physiological conditions and significant overexpression in a wide variety of tumors including breast, lung, esophageal carcinomas, sarcomas, melanomas, and glioblastomas.[222] MDM2 acts as an E3 ligase and promotes degradation of the oncosuppressor p53. Inhibition of MDM2 is a valid strategy to reactivate p53.[223]

However, protein–protein interactions are one of the most challenging target classes in medicinal chemistry due to the large interfacial area between the two proteins and successful antagonism of these interactions often require small-molecule "hot spots" to be present on the protein surface, where high affinity interactions can be achieved.[224]

Despite the caveats associated with the development of small molecules targeting protein–protein interactions, crystallographic analysis of the MDM2/p53 complex was encouraging as it revealed a deep and well-defined hydrophobic pocket at the N-terminus of MDM2 which is capable of accommodating p53. The N-terminus of the p53 peptide uses three key amino acids (Phe19, Trp23, and Leu26) to interact with MDM2 (**Fig. 70**).[225,226]

It was reasoned that small molecules could insert into this defined cleft, mimic the three key amino acids of p53, and disrupt the protein–protein interaction.

Several MDM2 ligase inhibitors have been reported to date, including compounds identified by in vitro HTS screens (i.e., HL198,[227] TDP521252, and TDP665759[228]), in cell screens (Mel 23[229]), or structure-based design (MI-63[230]).

Through a biochemical high-throughput screen, Roche screened a diverse library of small molecules, from which numerous hits were optimized for potency and selectivity. In particular, one chemical series of *cis*-imidazolines, also termed the nutlins, has been progressed to the clinic.[231]

5.07.4.3.3.1.1 Nutlins

These unusual *cis*-dihydroimidazole compounds bind to the surface of MDM2 by mimicking an alpha-helical segment of p53 in which three key lipophilic residues, Leu26, Trp23, and Phe19, project into lipophilic pockets on the surface of MDM2.[232] The first lead compound, nutlin-3a, **132** (**Fig. 71**), contains two 4-chlorophenyl moieties that perfectly occupy the Leu26 and Trp23 pockets and an isopropoxy substituent which is deeply buried in the Phe19 pocket (**Fig. 70**). Interestingly, only one enantiomer displayed high binding potency ($IC_{50} = 0.09\ \mu M$ vs. $IC_{50} = 13.6\ \mu M$ by SPR).

Nutlin-3a, **132**, exhibits good potency in biochemical HTRF (homogeneous time resolved fluorescence) assay with an IC_{50} of 88 nM, promising IC_{50} of 1.5 μM in a cell viability MTT (3-(4,5-dimethylthiazol-2-yl)-2,5-diphenyltetrazolium bromide) assay against a series of wild-type p53 cancer cell lines (HCT-116, SJSA-1, RKO), and selectivity (defined as ratio between IC_{50} for mutant and WT p53 cell lines) of 15-fold.[225,231] This potency translated in vivo, where in human osteosarcoma SJSA-1 xenograft mouse model nutlin-3a dosed at MTD (200 mg kg^{-1}, po, twice daily) afforded 90% tumor growth inhibition. Albeit a useful chemical tool for the study of the p53/MDM2 complex, nutlin-3a had a suboptimal pharmacological profile which needed to be improved for clinical development.[233]

A second-generation nutlin, RG7112, **133**, was designed (**Fig. 71**). This compound retains the most important structural features of nutlin-3a necessary to bind MDM2, such as the two 4-chlorophenyl groups where the chlorine substituents are crucial to maintain activity, and the third aromatic ring which inserts its alkoxy substituent into the Phe19 pocket. In an effort to reduce the molecular weight, the isopropoxy group was changed to the slightly smaller ethoxy group, without detriment to the interactions with the Phe19 pocket.

In order to prevent oxidation of the imidazoline core, which inactivates the compound, the hydrogens in the 4- and 5-positions of the ring were masked with two methyl groups, whose steric bulk was well-tolerated in terms of binding. Furthermore, the 4-methoxy group on the aromatic ring, which represented another metabolic soft spot, was replaced by a bulkier and more stable *tert*-butyl group. Finally, a solvent-exposed vector was exploited for attachment of a polar sulfone lateral chain. This afforded RG7112, which had improved biochemical activity (HTRF $IC_{50} = 18$ nM), cellular activity (MTT $IC_{50} = 0.4\ \mu M$), and selectivity (33-fold) (**Fig. 71**).

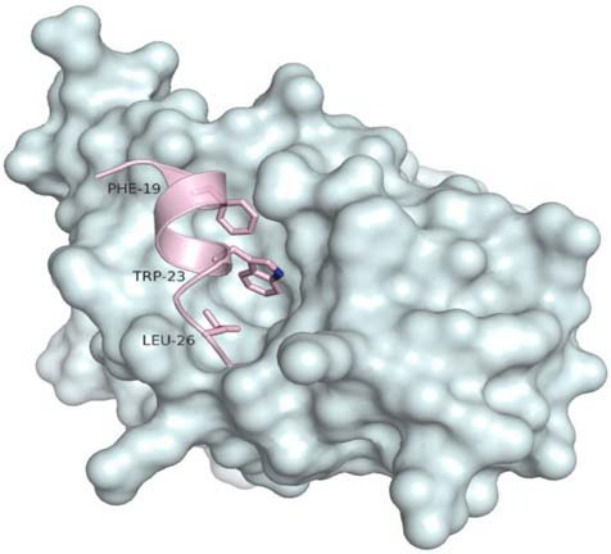

Fig. 70 X-ray crystal structure of the MDM2/p53 complex (PDB: 4HFZ). The structure of MDM2 is shown as surface (*cyan*), p53 is shown as cartoon (*light pink*), and the key binding site residues are shown as sticks.

Comparison of the crystal structures of nutlin-3a, **132**, and RG7112, **133**, bound to MDM2 revealed a very similar binding mode for the two analogs (Fig. 72). The improvement in affinity and consequent antiproliferative activity was attributed to the methyl sulfone substituent on the piperazine ring. Introduction of a polar lateral chain and removal of the metabolic soft spots resulted in a better in vivo PK performance, with high exposure and long half-life (~9 h) in mice.

RG7112 was considered suitable for in vivo efficacy studies in the human osteosarcoma SJSA-1 cell line xenograft mouse model. The compound achieved 74% tumor growth inhibition at a daily oral dose of 50 mg kg^{-1} and tumor regression at 100 mg kg^{-1}. Similar results were obtained in other osteosarcoma cell lines.[233] In addition, RG7112 displayed a good safety profile in preclinical toxicology studies and it was progressed to human clinical trials. To date, RG7112 has undergone six clinical trials, with one still ongoing, for the treatment of both solid and blood cancers.[234]

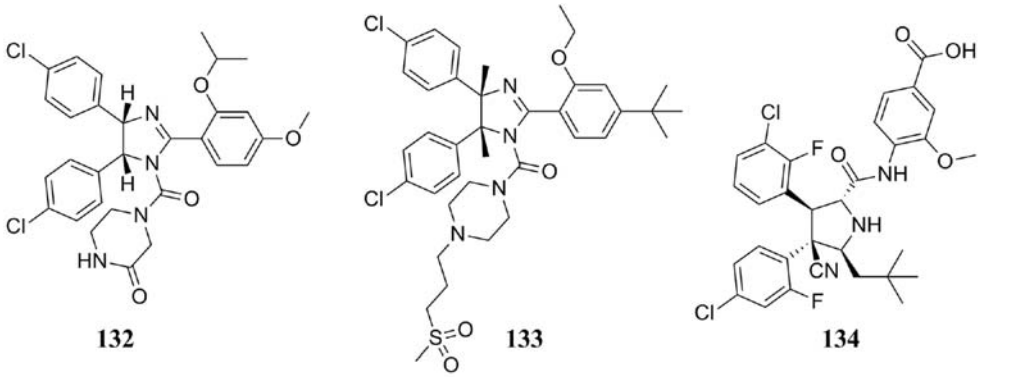

Fig. 71 Evolution of the nutlins from the tool compound, **132**, to the clinical candidates, **133** and **134**.

Unfortunately, some Phase I clinical trials of RG7112 have been rather disappointing due to a lack of response and quite severe side effects, including neutropenia and thrombocytopenia.[235] This highlights the difficulty surrounding a p53 stabilizing therapy which would not affect normal cells. Despite the improvement afforded with the second-generation nutlin, better potency and selectivity were desirable. In order to achieve efficacy in the treatment of AML, RG7112 is administered at the MTD (1500 mg twice daily) which results in some toxicity, such as hematological and gastrointestinal side effects and delirium.[223] For such reasons, Roche continued further optimization of this series, which led to the development of a third generation of nutlins, with increased potency and selectivity.[236]

The key structural feature of this new chemical subseries is a pyrrolidine ring with a "*trans-trans*" configuration, which allows the 3-chlorophenyl and neopentyl substituents to adopt an equatorial position and maintain optimal binding with the hydrophobic pockets (**Fig. 72**).

Structure–property relationship exploration identified introduction of fluorine atoms on the aromatic rings together with the *para*-benzoic acid side chain, as a useful tool to improve the pharmacokinetic profile, leading to compound RG7388, **134**. Interestingly, while lying in proximity to a rather flat region of the protein surface, the *para*-benzoic acid substituent also improved the potency (HTRF $IC_{50} = 6$ nM; MTT $IC_{50} = 30$ nM) and selectivity (344-fold), together with an improvement in the PK profile (mouse $CL = 11\%$ HBF, $F = 80\%$).

Superior potency and pharmacokinetics translated into better efficacy in xenograft models at reduced dose and exposure. Indeed, in human osteosarcoma SJSA1 xenograft mouse model RG7338 displayed tumor regression with TGI > 100% at 25 mg kg^{-1}, while the precursor RG7112, at double dose of 50 mg kg^{-1}, reached a TGI of 74%.

Currently, RG7338 has completed two Phase I clinical trials for the treatment of advanced malignancies and is now undergoing new trials (**Fig. 73**).[237]

5.07.4.3.3.1.2 Other MDM2/p53 inhibitors

The serendipitous discovery of the nutlins established an alpha-helical mimicking pharmacophore as the key design feature for future inhibitors. To mimic the helical conformation of the p53 peptide, a spirooxindole core was designed with similar lipophilic substituents as the original nutlins. This led to the clinical candidate MI77301, **136** (**Fig. 74**), displaying subnanomolar biochemical affinity, $GI_{50} = 70$ nM in wild-type p53 cancer cell lines and regression in human xenograft tumors.[238]

Other small-molecule MDM2/p53 inhibitors have been developed over the past two decades, such as RITA,[239] **137**, MI-63,[230] **138**, and MI-219,[240] **139** (**Fig. 75**), which act on MDM2 E3 ligase by promoting p53 stabilization, or the natural product parthenolide (PN) and its dimethylamino derivative DMAPT,[241] **140**, which induce ubiquitylation and proteasomal degradation of MDM2 with consequent activation of p53. Serdemetan (JNJ-26854165), **141**, is a tryptamine-derived compound which binds to MDM2 and prevents the ubiquitylation and degradation of p53.[194] This compound has undergone Phase I clinical studies in patients with advanced stage or refractory solid tumors.[242]

However, despite the undeniable therapeutic potential, each aforementioned MDM2/p53 inhibitor is only active against WT p53, while p53 mutants are stabilized and remain unaffected by MDM2 ubiquitylation. It might be more efficacious to use small molecules aiming to restore p53 to its native form. In this context, PRIMA-1 and APR-246[243] exploit the covalent alkylation of thiols in mutant p53 in order to restore the wild-type conformation and activity. APR-246, **142**, is currently being evaluated in combination therapy with carboplatin against high-grade serous ovarian cancer[244] (**Fig. 75**).

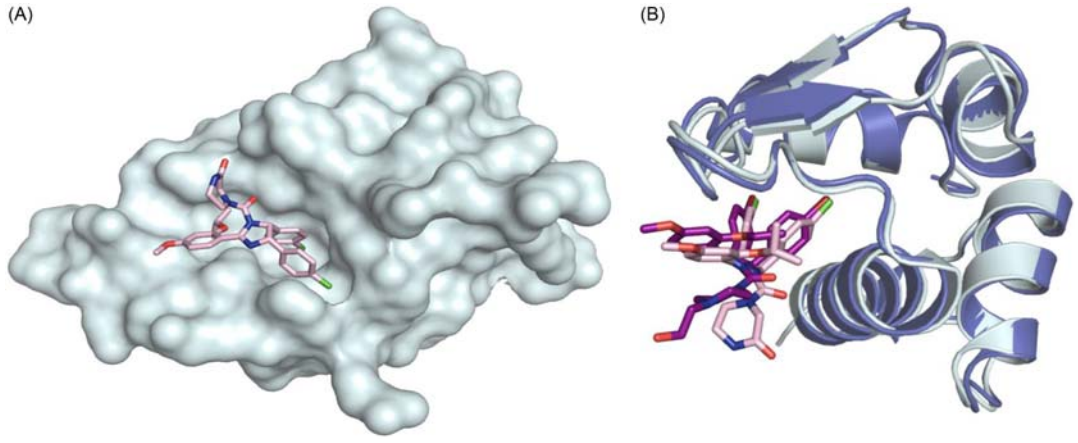

Fig. 72 (A) X-ray crystal structures of the MDM2/nutlin-3a complex (protein shown as surface in *cyan*, ligand shown as sticks in *light pink*, PDB: 4J3E), (B) overlay of the X-ray crystal structures of MDM2/nutlin-3a, **132**, complex (protein shown as cartoon in *cyan*, ligand shown as sticks in *light pink*, PDB: 4J3E) overlayed with the structure of the MDM2/RG7112, **133**, complex (protein shown as cartoon in *blue*, ligand shown as sticks in *magenta*, PDB: 1RV1).

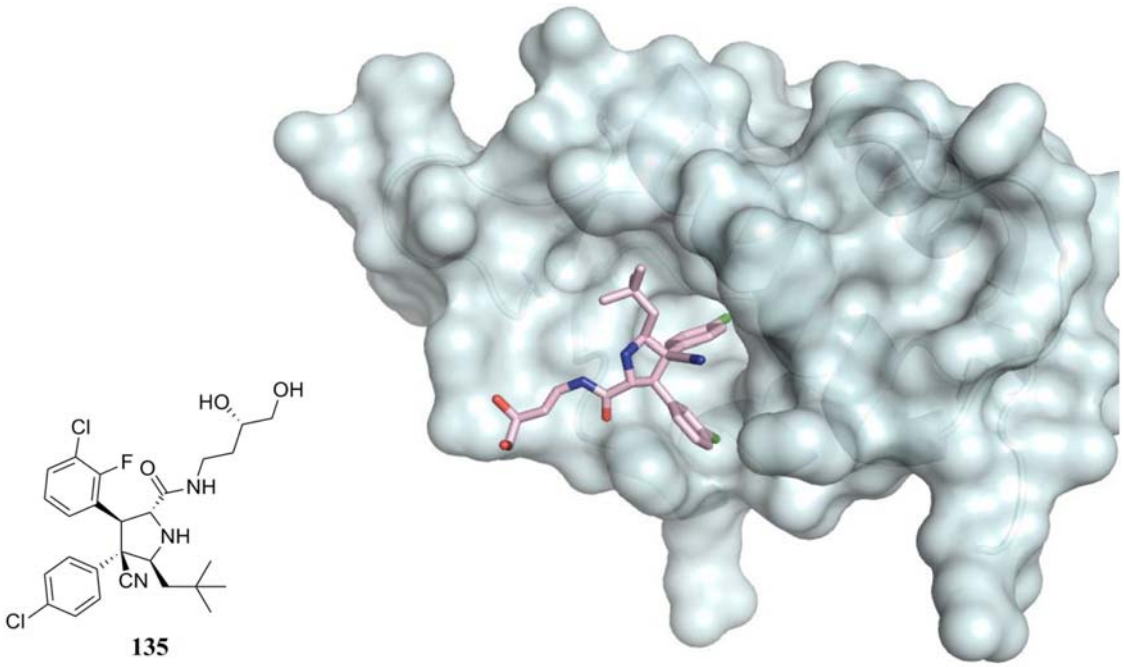

Fig. 73 X-ray crystal structure compound **135** (*light pink*, precursor of RG7388, **134**) bound MDM2 (light *cyan*, PDB: 4JRG). The structure of the ligand is shown as sticks, the protein is shown in a surface representation.

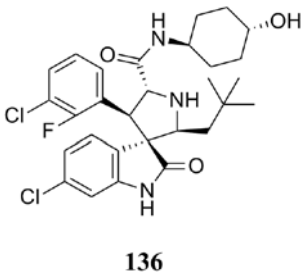

Fig. 74 Chemical structure of the clinical candidate MI77301, **136**.

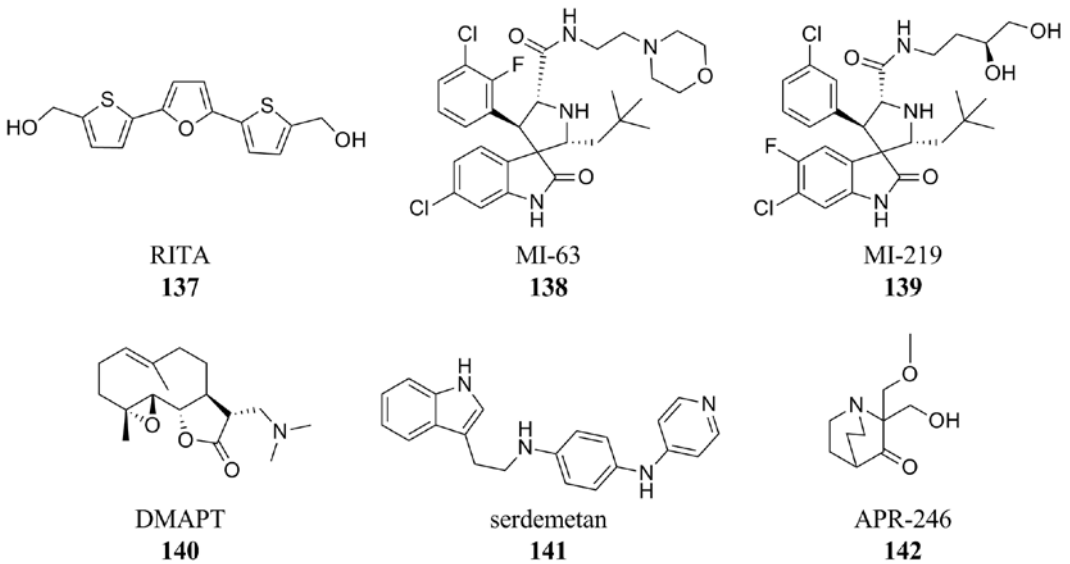

Fig. 75 Chemical structures of other MDM2/p53 inhibitors.

5.07.4.3.3.2 Inhibitor of apoptosis proteins (IAPs)

The Inhibitor of Apoptosis Protein (IAP) E3 ubiquitin ligases are another broad family of ligases of interest for cancer therapy as they are overexpressed in many cancer cells and it has been demonstrated that they contribute to tumor survival, chemoresistance, and disease progression.[194,245,246] Eight IAP isoforms have been identified in humans, among which XIAP, cIAP1, and cIAP2 have been the focus of several drug discovery programs. Their mechanism of action is based on the exploitation of three specific domains (BIR1, BIR2, and BIR3) to bind, ubiquitylate, and degrade caspases 3, 7, and 9.[194] The majority of the small-molecule inhibitors of IAPs developed to date are termed "Smac-mimetics" as they mimic the natural inhibitor of IAP proteins, Smac/DIABLO.[247] The latter is a proapoptotic protein that binds IAP and blocks the interaction with the caspases. Several Smac-mimetics have undergone, or are currently undergoing, Phase I/II clinical trials.[192]

5.07.4.3.3.2.1 AT-406 (SM-406)

AT-406/SM-406, **143**, is a potent and orally bioavailable compound (Fig. 76) discovered by Ascenta Therapeutics as an antagonist of multiple IAP proteins (XIAP, cIAP1, and cIAP2).[248]

The compound was designed using structure-based drug design on the crystal structure of Smac in complex with the XIAP BIR3 domain, with the aim to mimic the interactions between the endogenous Smac AVPI tetrapeptide, **144**, and XIAP BIR3 domain (Fig. 77).

As there are numerous caveats associated to the use of Smac peptides, such as poor permeability, lack of oral bioavailability and metabolic stability, the SAR exploration was focused on nonpeptide analogs. In particular, based on the finding that the isopropyl group of the valine residue of AVPI can be replaced and cyclized in a bicyclic lactam without distorting the binding conformation, constrained lactam analogs were evaluated.[249]

In addition, as the isoleucine residue only exploits the hydrophobic side chain to interact with the protein while the carbonyl moiety is not involved in any specific interaction, this terminal amino acid could be replaced by aromatic substituents with great gain in binding affinity. This led to SM-122, **145**, a highly potent analog. An unfavorable PK profile in rats prevented its further progression. Exploitation of a more polar diazabicyclic core had a dramatic effect on the physicochemical balance of the compound, leading to the candidate compound, SM-406, **143**, characterized by good aqueous solubility (>50 mg mL^{-1}) and adequate oral exposure, consistent across the species (F: mouse = 38%; rat = 45%; NHP = 42%; dog = 55%).[248]

Computational docking simulations revealed that AT-406 can form similar hydrophobic and hydrogen bonding interactions with respect to AVPI (Fig. 77)[250]; however it engages a further hydrophobic interaction with Trp323 of XIAP and exploits its terminal methylamino moiety to insert into a small hydrophobic binding pocket created by Trp310 in XIAP BIR3.[248] Replacement of the methylamino substituent with a bulky 3-methyl-1H-indole motif disrupts the interaction of AT-406 and XIAP BIR3, leading to an inactive compound (SM-428, **146**) used as a negative control. The FP assay revealed that AT-406 has 50- to 100-fold higher

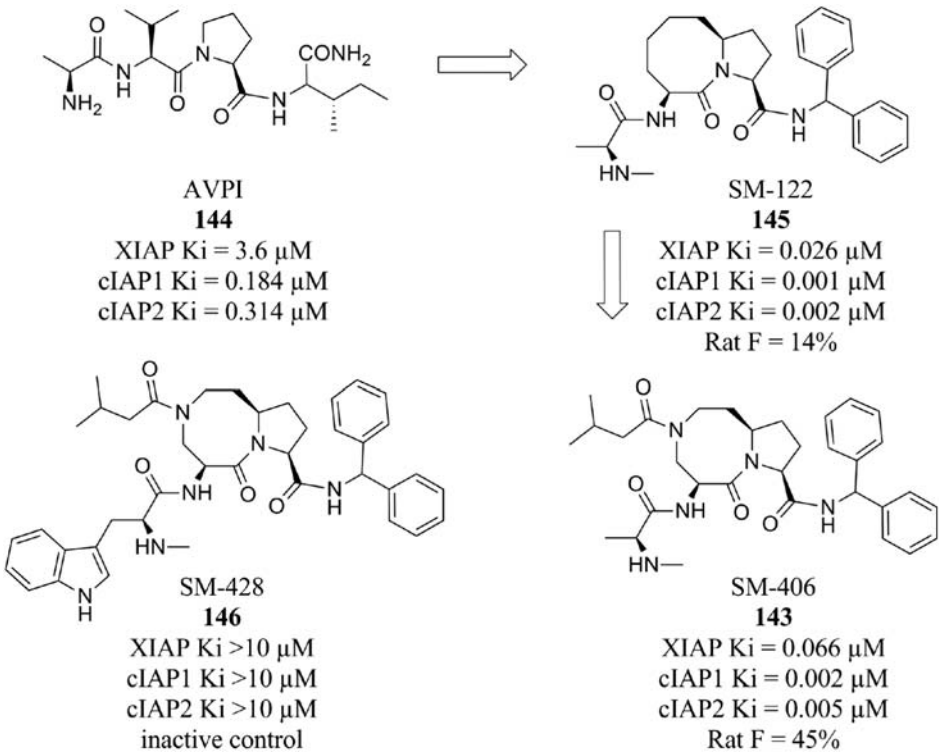

Fig. 76 Structure-based design from the Smac tetrapeptide, **144**, AVPI to the clinical candidate SM-406, **143**. The matched pair negative control SM-428 is also highlighted.

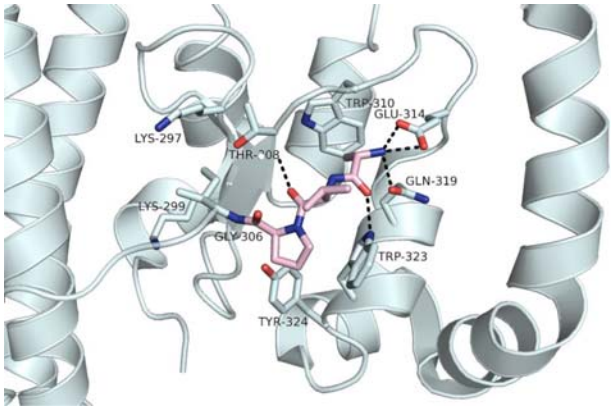

Fig. 77 X-ray crystal structure of XIAP BIR3 (*cyan*) complexed with Smac AVPI, **144** (*light pink*), PDB: 1G73. The structure of the ligand, and the key binding site residues are shown as sticks. Selected interactions are shown in *black-dashed lines*.

affinity than Smac AVPI and binds to XIAP, cIAP1, and cIAP2 with K_i of 66.4, 1.9, and 5.1 nM, respectively. The negative control, as expected, lost affinity for the IAPs (FP IC_{50}s > 10 μM) (Fig. 76).[248] Subsequently, AT-406 and its inactive matched pair were tested in a cell-free functional assay for caspase 9 activity; at 1 μM AT-406 completely antagonized XIAP and reactivated caspase 9 function. The inactive control, on the other hand, showed no activity even at > 100 μM.

AT-406 was screened against more than 100 human cancer cell lines and showed potent growth inhibition for the ovarian SK-OV-3 (IC_{50} = 142 nM) and breast MDA-MB-231 (IC_{50} = 144 nM) by 4-day WT assay, with minimal toxicity toward normal human epithelial cell lines (IC_{50} > 10 μM). In addition, AT-406 displayed high efficacy in MDA-MB-231 breast cancer xenografts, causing tumor growth inhibition after oral dosing at 100 mg kg^{-1} (T/C = 0.30 on day 50) with no toxic effects. A good in vitro safety profile with no hERG ion channel inhibition (IC_{50} > 30 μM) and minimal cytochrome P450 inhibition, coupled to favorable tolerability in dogs, allowed progression of this compound to Phase I clinical trials against ovarian cancer as a single agent, and in combination with carboplatin.[251]

5.07.4.3.3.2.2 GDC-0152

GDC-0152, **147**, is another analog of the endogenous AVPI tetrapeptide (Fig. 78) which was developed as a pan-IAP antagonist, capable of inhibiting cIAP1/2, ML-IAP, and XIAP.[252]

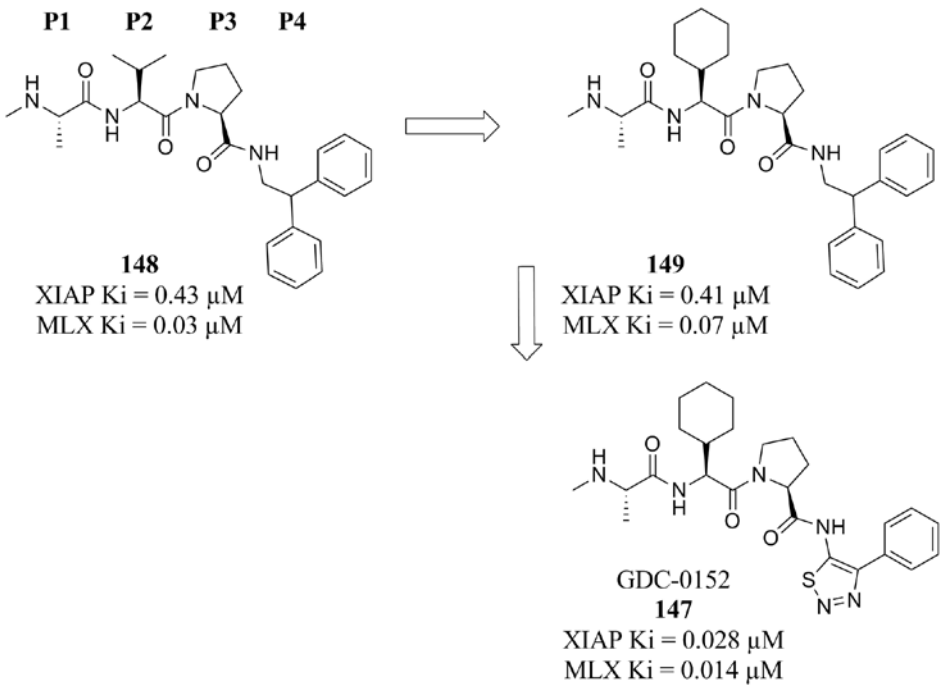

Fig. 78 Development of the clinical candidate GD-0152, **147**, by peptidomimetic approach.

After several unsuccessful large HTS small-molecule screening campaigns (>2,000,000 compounds) which did not deliver any viable hits, a more fruitful peptidomimetic approach was utilized; with the Ala-Val-Pro-2,2-diphenethylamine analog (compound **148**) as a starting point, a systematic approach was undertaken in order to explore different substitutions in the P1–P4 positions with the aim to reduce the peptide character of the compound.[253]

Crystallographic studies revealed that the methyl group of the alanine residue in P1 was deeply inserted into a hydrophobic pocket composed of Leu131, Trp134, and Glu143. As this is a key interaction, it is difficult to replace. At the P2 position, on the other hand, the SAR was broad, with different substitutions being tolerated. The endogenous valine residue only gives weak van der Waals interactions with Ser133 of ML-IAP and it can be easily modified. Substitution with larger, hydrophobic substituents, such as cyclohexyl moieties, provided no differences in binding affinities (compound **149**).

In the P3 position, substitution on the proline ring has been reported as a strategy to tailor selectivity toward specific classes of IAPs, and therefore it would not be suited for a pan-IAP inhibitor approach.[254] As such, the proline residue was left unmodified. Finally, for the P4 position, several aromatic moieties were screened as replacements of the endogenous AVPI isoleucine to occupy the hydrophobic pocket created by Thr116, Gly130, and Glu132 (Fig. 79). Among these substituents, thiadiazole proved to be the moiety of choice.

The resultant candidate, GDC-0152, **147**, binds XIAP-BIR3, cIAP1-BIR3, cIAP2-BIR3, and ML-IAP with $K_i < 50$ nM. This potency translated into cells where the compound was found to activate caspases 3 and 7 in a dose- and time-dependent manner. When tested in a 3-day cell viability assay in the MDA-MB-231 breast cancer cell line, GDC-0152 produced a decrease in viability, with no effect on normal human mammary epithelial cells.

The compound also displayed good kinetic solubility (40 mg mL^{-1} at pH 5.5, 2.0 mg mL^{-1} at pH 6.7, and 4.6 mg mL^{-1} at pH 7.7) and a favorable PK profile with good predictions to man (predicted human $CL = 9.6$ mL min^{-1} kg^{-1}; $V_{ss} = 1.2$ L kg^{-1}) based on allometric scaling from mouse, rat, dog, and monkey. In xenografts of MDA-MB-231 human breast cancer cells, it showed effective tumor reduction when dosed at 100 mg kg^{-1} once per week, with 95% tumor growth inhibition. Such overall promise, combined with a favorable safety profile in preclinical species, led to the selection of GDC-0152 for clinical trials. It has currently undergone Phase I studies with advanced or metastatic solid tumors.[255]

5.07.4.3.3.2.3 Birinapant (TL32711)

Birinapant, **150** (Fig. 80), is another Smac-mimetic IAP-antagonist, developed by Tetralogic Pharmaceuticals.[256] This compound is a bivalent Smac-mimetic, a symmetrical molecule containing two Smac-mimetic monomers tethered by a linker. Dimerization is common among proapoptotic proteins and small-molecule dimers are considered a useful strategy to enhance potency and selectivity with respect to the monovalent counterparts as the dimers can bind multiple BIR3 domains of IAPs.

In contrast to the aforementioned monomeric IAP antagonists, which were developed aiming toward a pan-IAP inhibition as a means to increase efficacy, birinapant was designed to be more selective as part of a strategy to improve tolerability.

SAR exploration around the P2 residue highlighted how the increase in steric bulk at this position increases the selectivity against XIAP; this is detrimental as a strong inhibitory effect on the XIAP pathway is connected to NOD-dependent NFkB activation, inflammatory responses, and lower tolerability.[256] By carefully tailoring the steric bulk around P2, it was possible to achieve strong cIAP1 inhibition with milder effects on cIAP2 and XIAP functional activity, as demonstrated by NOD-dependent NFkB luciferase assay (Fig. 80).

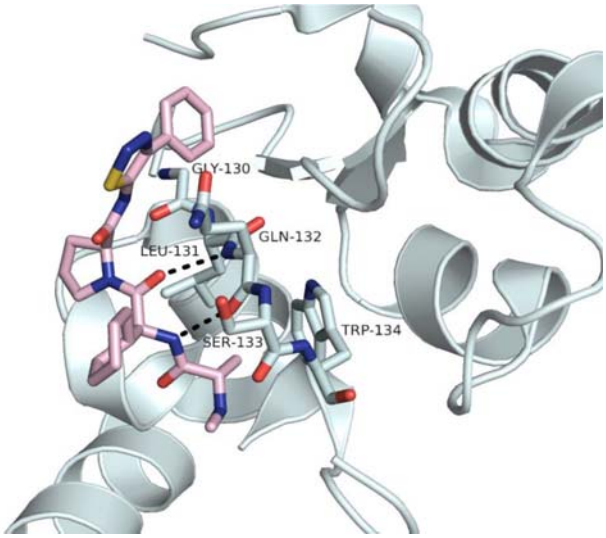

Fig. 79 X-ray crystal structure of the ML-IAP/XIAP chimeric binding domain (*cyan*) complexed with GDC-0152, **147** (*light pink*), PDB: 3UW5. The structure of the ligand, and the key binding site residues are shown as sticks. Selected interactions are shown in *black-dashed lines*.

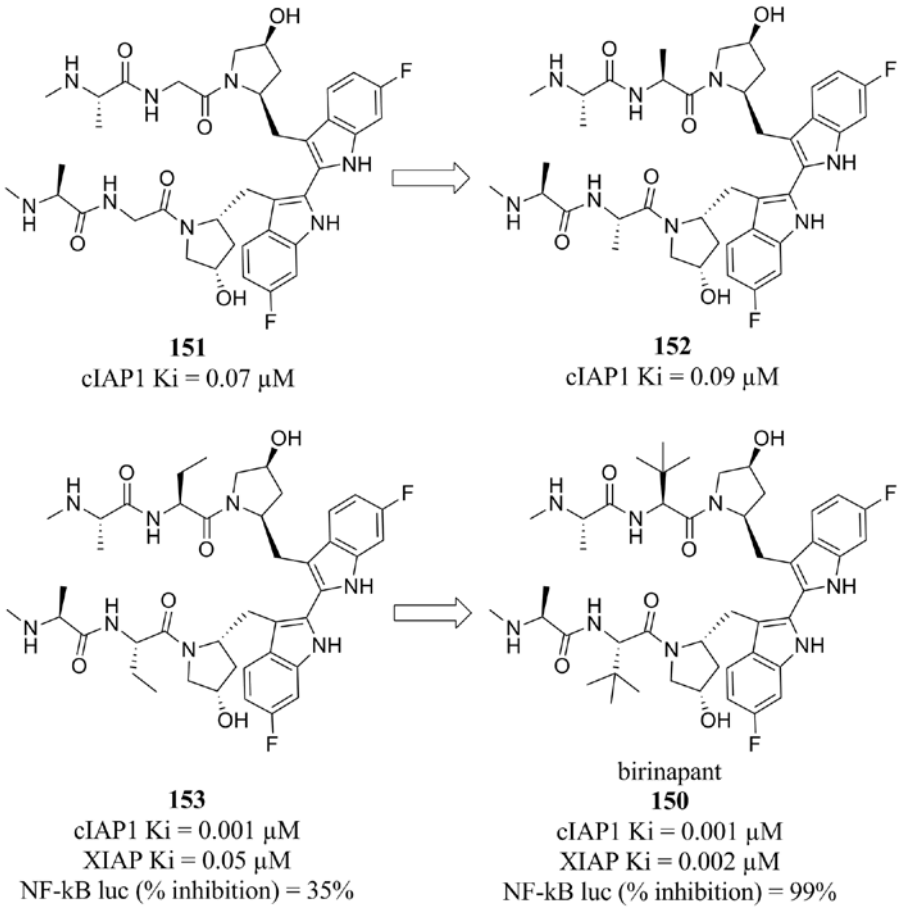

Fig. 80 SAR exploration around the P2 position of the dimeric Smac-mimetics.

Overall the compound maintains the N(Me)Ala at the N-terminal P1 position, common to many Smac-mimetics, an α-aminobutyric acid (Abu) at the P2 position, and a 4(*S*)-hydroxypyrrolidine moiety at P3. A 6-fluoroindole moiety was utilized to occupy the hydrophobic pocket in P4 (Fig. 81). In cell lysate assays the compound gave caspase 3 activation, and treatment of MDA-MB-231 breast cancer cells with TL32711 caused caspase-dependent apoptosis and cell death within 72 h. Efficacy studies conducted in vivo on MDA-MB-231 human xenografts in mice showed dose-dependent tumor regression at well-tolerated doses

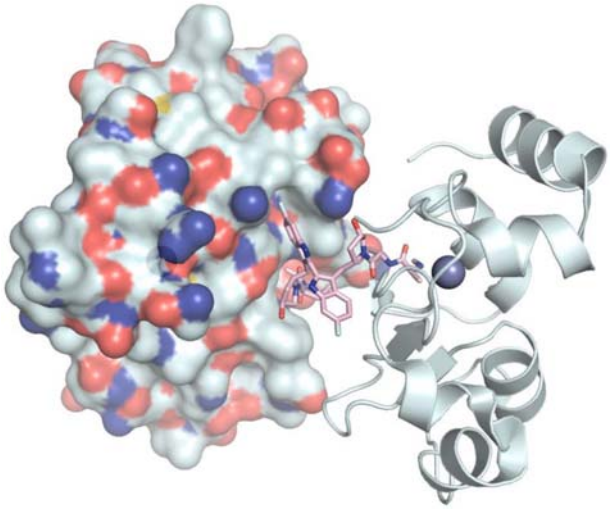

Fig. 81 X-ray crystal structure of birinapant, **150**, (*light pink*, shown as sticks) complexed with two XIAP BIR3 domains (*cyan*, one domain shown as surface, atomic coloring, the other domain is shown as cartoon), PDB: 4KMP.

(5 mg kg^{-1}, iv). Due to the positive profile in a preclinical setting, the compound was advanced to clinical trials. Initial Phase I trials have shown that this compound is well-tolerated without dose-limiting toxicity issues and can lead to anticancer effects both in advanced solid tumors and lymphomas. Further Phase I and Phase II clinical studies are ongoing for solid and hematological tumors.[257]

5.07.4.4 Targeting the Proteasome in Cancer Therapy

The proteasome is involved in the final common step for all the degradative pathways, and therefore is not characterized by high specificity as a therapeutic target.[258] Nevertheless, it remains, to date, the target within the UPS that has afforded the most successful results in anticancer therapy. In fact, the proteasome represents the only UPS target to yield FDA-approved anticancer drugs, namely: bortezomib, carfilzomib, and ixazomib for the treatment of MM. Following the success of bortezomib, a plethora of new promising inhibitors of the proteasome appeared in the literature over the last two decades.[259] In theory, as the proteasome is essential for the physiological homeostasis of cells, it would seem very difficult to succeed in exclusively targeting the proteasome of cancer cells without disrupting normal cellular functions. However, cancer cells possess accelerated proliferation and aberrant cell cycle checkpoints and, as such, can rapidly accumulate a large amount of defective proteins, increasing their susceptibility to proteasome inhibition.[260]

5.07.4.4.1 Structure and function of the proteasome

The 26S proteasome is a 2.4 MDa ATP-dependent multienzyme complex belonging to the Ntn (N-terminal nucleophilic) hydrolase family.[261] The proteasome consists of two subcomplexes: a barrel-shaped 20S core domain containing the protease active site and two 19S regulatory domains which cap the barrel at each end and act as gatekeepers. These domains have the function to recognize, unfold, and translocate the substrates into the cavity of the 20S proteasome[262] (Fig. 82).

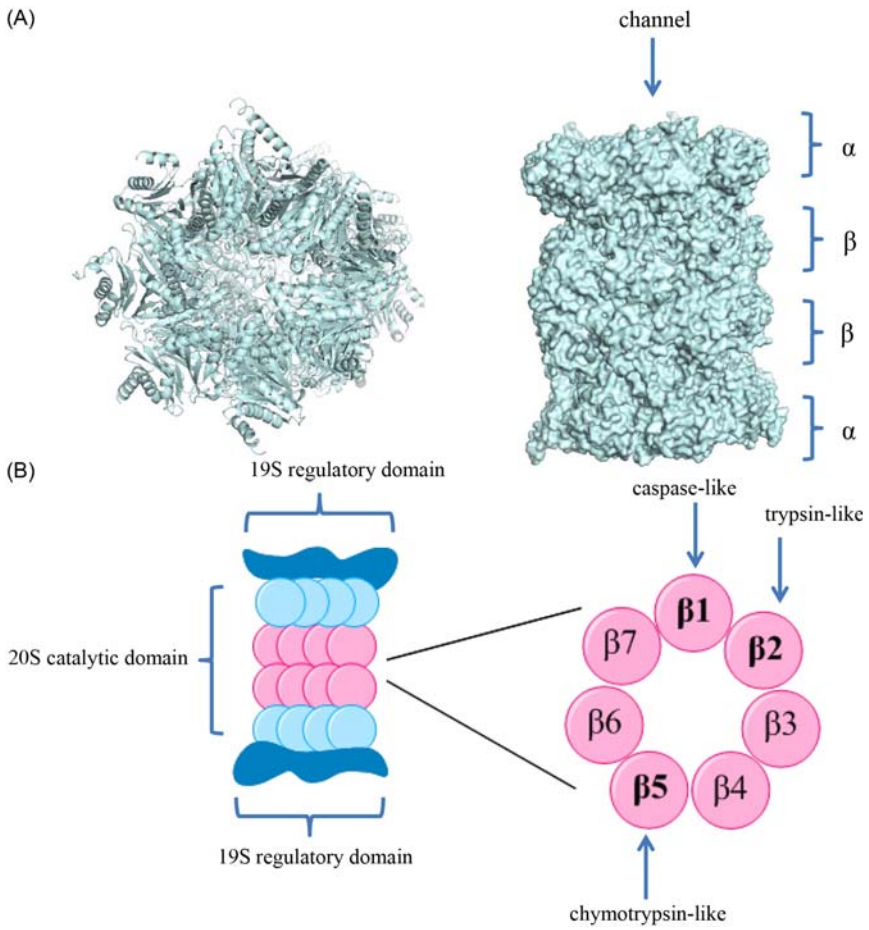

Fig. 82 (A) Crystal structure of the human 20S proteasome (PDB: 4R3O). (B) Schematic representation of the components of the 26S proteasome: the two 19S regulatory domains, the 20S catalytic domain and highlighting the subunits which form the proteolytic active site (β1, β2, and β5).

The central core 20S proteasome is formed by 28 subunits organized into 4 stacked rings, which create the cylindrical structure. The two external rings are formed by seven polypeptides called α-subunits; the two internal rings are composed of seven β-subunits which form the internal core of the complex among which subunits β1 (caspase-like), β2 (trypsin-like), and β5 (chymotrypsin-like) form the proteolytic active site. The proteolytic specificity is determined by the specific (S) pockets of the proteasome, which accommodate side chains (called P sites) of the protein substrate, among which the P1 residue appears to be crucial[263] (**Fig. 83**).

The three proteolytic subunits possess N-terminal threonine residues which act as catalytic nucleophiles in the proteolytic cycle. Nucleophilic Thr1 residues of the proteolytically active β subunits attack the carbonyl carbon of the target peptide bonds affording an acyl-enzyme intermediate which is finally hydrolyzed to release degradation products and restore the active site (**Scheme 3**). Single site mutation studies have identified the β5 subunits as the most important targets for proteasome inhibition and in fact the different classes of proteasome inhibitors mainly act around the chymotrypsin-like proteolytic activity.[265]

Aside from the constitutive proteasome, it is worth also highlighting the importance of the immune proteasome, whose catalytic core 20Si is responsible for the generation of peptides essential in the antigen processing phase of the immune response. Selective immunoproteasome inhibitors are emerging as promising leads for bortezomib-resistant MM therapies.[266]

5.07.4.4.2 Proteasome inhibitors

Proteasome inhibitors can be natural products or synthetic compounds which interact reversibly or irreversibly with Thr1 residues of the proteasome catalytic sites. They are mostly peptidomimetic compounds which mimic the binding mode of natural substrates in the active site channel of the proteasome. Proteasome inhibitors have pleiotropic effects; they stabilize IKB which binds to NFkB

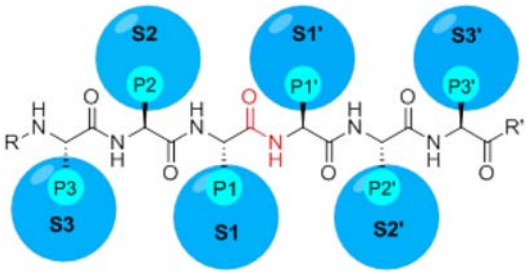

Fig. 83 Specificity pockets of the catalytic site of the proteasome. The scissile bond is highlighted in *red*.

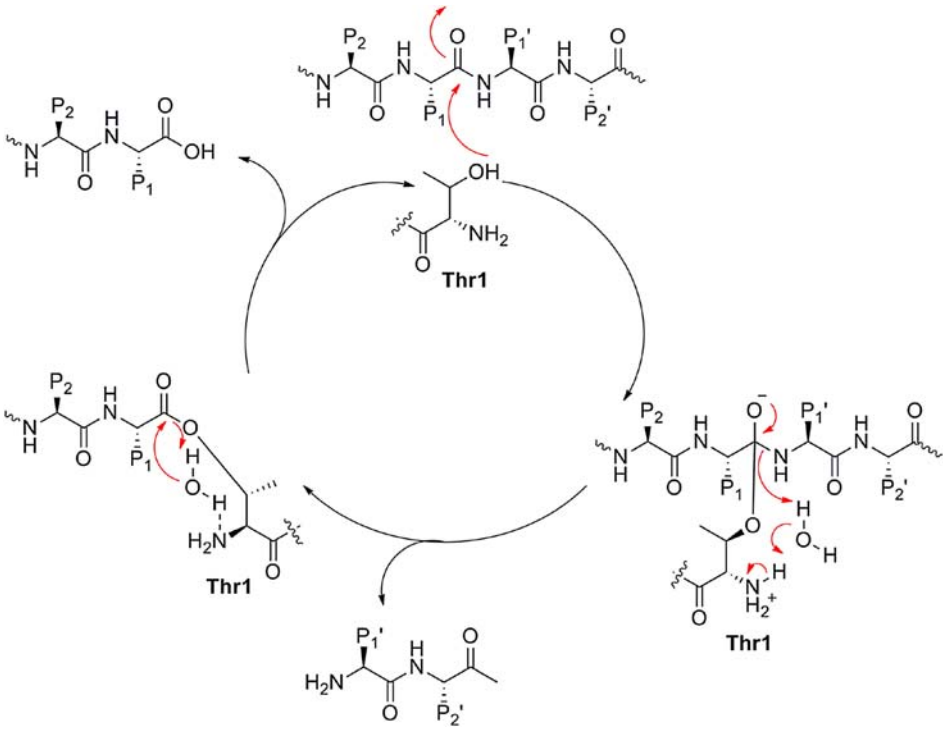

Scheme 3 Catalytic mechanism of the proteasome.[264]

and prevents its activation and nuclear translocation. As a result, the NFkB pathway is repressed with positive consequences on angiogenesis, cell invasion, oncogenesis, proliferation, and suppression of apoptosis. They also stabilize proapoptotic proteins such as p53 and Bax, induce endoplasmic reticulum stress, and activate antiapoptotic cascades.

Proteasome inhibition has proven to be a rational therapeutic approach in single agent therapies and also in combination therapies, being capable of inducing chemosensitization and addressing chemoresistance. Proteasome inhibitors are generally grouped into seven main classes on the basis of the structural properties of their pharmacophore.[192,266]

5.07.4.4.2.1 Peptide aldehydes

Peptide aldehydes (Fig. 84) represented the first class of proteasome inhibitors. They exploit the electrophilic carbonyl carbon atom of the aldehyde to react with the Thr1O$^{\gamma}$ residue of the proteasome and reversibly form a hemiacetal (Scheme 4). Despite being useful tools to study the cellular biochemistry and the mode of action of the proteasome, peptide aldehydes were unsuccessful in clinical development. The highly reactive head groups were successful in achieving high inhibitory potency, but were also detrimental in terms of selectivity. In fact, peptide aldehydes can also target serine and cysteine proteases such as catepsin B and calpains, leading to toxicity issues.

Also, peptide aldehydes display stability concerns: firstly, substituents in the α-position with respect to the aldehyde moiety are not stereochemically stable, due to the acidity of the α-proton; secondly, aldehydes can be rapidly oxidized to inactive carboxylic acids which are effluxed from the cells by multidrug resistance transporters. The consequent poor pharmacokinetic profile, with high clearance and low oral bioavailability, significantly limited the therapeutic potential of this class of inhibitors. As an example, MG132, **154** (Fig. 84), despite being the most widely used proteasome inhibitor tool, was never tested in the clinic due to rapid oxidative metabolism.

5.07.4.4.2.2 Peptide vinyl sulfones

In an attempt to overcome the issues related to the peptide aldehydes, vinyl sulfones were explored as alternative, less reactive head groups. Vinyl sulfones react in a Michael-type 1,4-addition with the Thr1O$^{\gamma}$ to give irreversible formation of an ether bond (Scheme 5 and Fig. 85). This led to a partial improvement in selectivity with respect to aldehydes as the vinyl sulfone head groups act as a Michael acceptor for soft nucleophiles only, and as such do not affect serine proteases. However, the high affinity for cysteine proteases still remained unsolved and this, similar to the peptide aldehydes, prevented in vivo development.

5.07.4.4.2.3 Syrbactins

As with the synthetic peptide vinyl sulfones, the syrbactins were also evaluated as proteasome inhibitors. They are natural products bearing a 12-membered macrolactam ring system in which the vinylamide moiety can undergo 1,4-addition from the Thr1O$^{\gamma}$ residue of the proteasome. Due to the similarity in the mechanism of action, the syrbactins share the same limitations as the vinyl sulfones, which prevented their therapeutic application (Scheme 6 and Fig. 86).

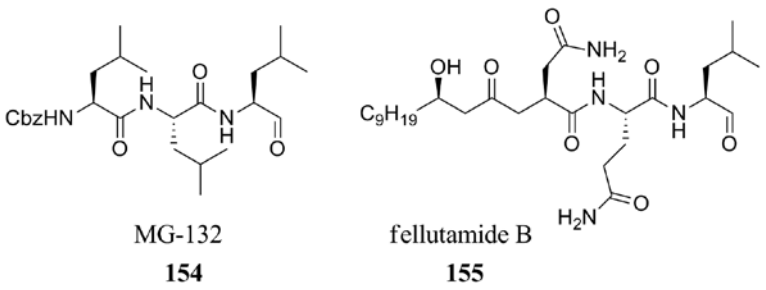

Fig. 84 Examples of peptide aldehydes: MG-132, **154**, and fellutamide B, **155**.

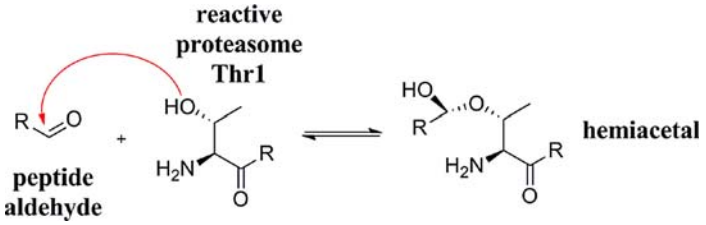

Scheme 4 Reaction mechanism highlighting the interaction between the warhead of the peptide aldehyde and the active site of the proteasome.

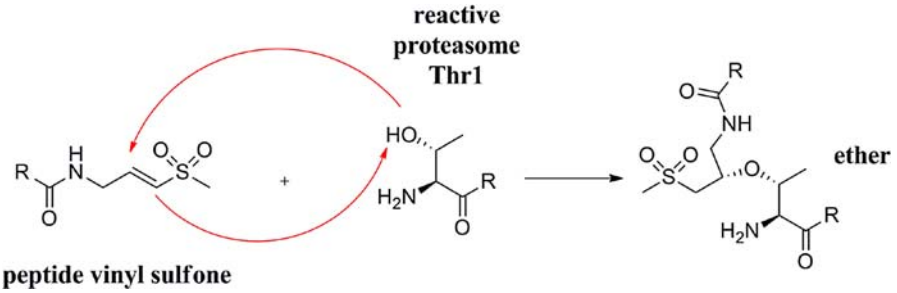

Scheme 5 Reaction mechanism highlighting the interaction between the warhead of the peptide vinyl sulfone and the active site Thr1 of the proteasome.[261,267]

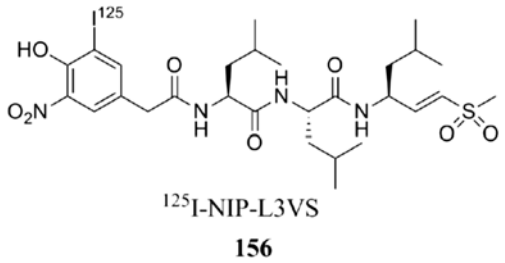

Fig. 85 Example of a peptide vinyl sulfone proteasome inhibitor.

5.07.4.4.2.4 Peptide boronates

The real breakthrough in the development of proteasome inhibitors arrived with the synthesis of boronic acid derivatives, which represent the most important class of proteasome inhibitors to date for several reasons. Firstly, boronate derivatives are more potent inhibitors with respect to the aldehyde precursors as they have significantly slower dissociation rates. Secondly, boronates are highly selective thanks to the nature of their warhead; the boronic acid moiety guarantees high affinity for hard oxygen nucleophiles, rendering the boronate derivatives less prone to interaction with the soft nucleophiles of cysteine proteases. Peptidyl boronic acids were already recognized in the drug discovery scenario as efficient serine protease inhibitors, due to the presence of an empty p-orbital on boron which can accept the lone pair from the serine oxygen residue in the catalytic site. It was reasoned by analogy

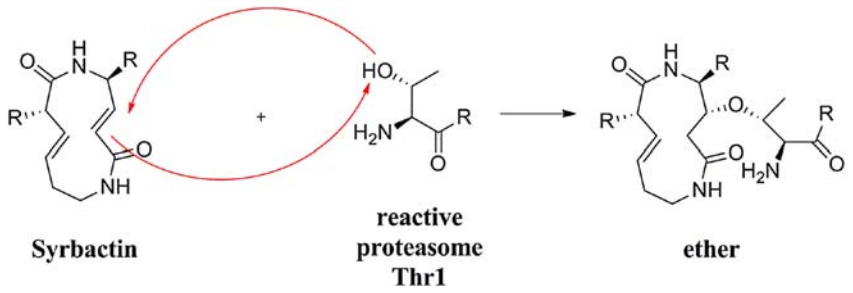

Scheme 6 Reaction mechanism of the syrbactins.[268]

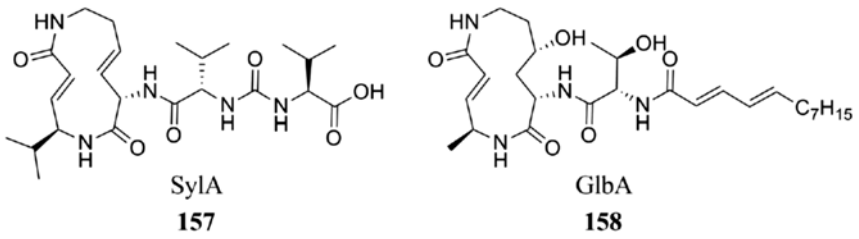

Fig. 86 Examples of Syrbactins, SylA, **157**, and GlbA, **158**.

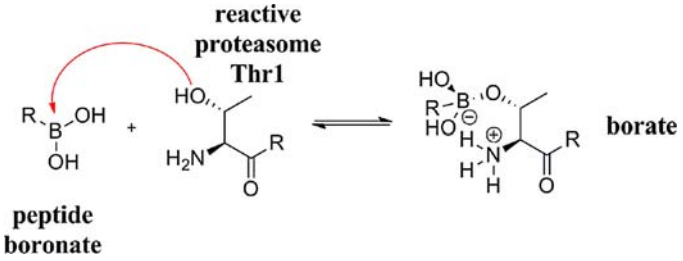

Scheme 7 Reaction mechanism highlighting the interaction between the warhead of the peptide boronate and the active site of the proteasome.

that boronic acid derivatives could form similar interactions with the N-terminal threonine residue present at the β5 subunit of the proteasome active site.

Pleasingly, the peptide boronates displayed higher affinity for the proteasome with limited affinity for the serine proteases and this can be explained by their mode of action. The boron atom forms a covalent bond with the lone pair of the Thr1O$^{\gamma}$ residue of the proteasome, while one hydroxyl of the boronate group forms a hydrogen bond with Gly47N stabilizing the oxyanion hole. The resultant tetrahedral adduct is further stabilized by the second hydroxyl group of the boronate moiety which forms a hydrogen bond with Thr1N (Scheme 7). This extra bond with the active site explains the high selectivity of boronate derivatives for the proteasome with respect to serine proteases.

A third reason for the importance of this compound class is that the peptide boronate inhibitors possess suitable properties for in vivo development due to their higher stability in the physiological environment compared to the previous scaffolds.

5.07.4.4.2.4.1 Bortezomib (MG-341)

The boronic acid derivative bortezomib, **159**, represents the first approved drug targeting the UPS pathway. Structurally, it is a dipeptide boronic acid derivative composed of four main parts: the pyrazinoic acid substituent, the phenylalanine and leucine residues, and the boronic acid warhead (Fig. 87). Mechanistically, bortezomib acts as a reversible inhibitor of the 26S proteasome. In its bound form, the compound adopts an antiparallel β-sheet conformation and the boronic acid head group leads to the tetrahedral adduct formation characteristic of the boronate class.

It was introduced in 1995 with the name MG-341 by Myogenics Company, in an attempt to improve the peptidyl aldehyde inhibitors by finding a good aldehyde surrogate. Preliminary SAR exploration around the tripeptide aldehydes had revealed that leucine was the optimal residue to occupy the P1 position. Starting from this idea and using the common template Cbz-Leu-Leu-R, several R moieties were screened in order to replace the unstable aldehyde motif (Table 2).[269] Trifluoromethyl- and chloromethyl-ketones (compounds **163** and **164**) did not inhibit the proteasome, while the diketo ester and the ketobenzoxazole (compounds **161** and **162**) displayed only modest activity. On the contrary, using a boronic acid as the head group gave 100-fold increase in potency with respect to the aldehyde inhibitor (compound **160**).

As this first tripeptidyl boronate derivative displayed picomolar potency, it was possible to simplify the structure to a truncated version and still maintain good inhibitory activity. Hydrophobic residues were inserted in the P2 and P3 positions and this contributed to the increased potency, leading to the optimized bortezomib, a compound with lower molecular weight, good biochemical activity ($K_i = 0.62$ nM), and very high selectivity for the proteasome with respect to serine proteases.

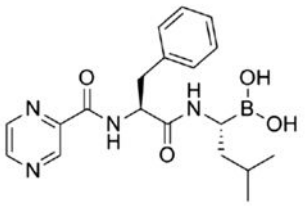

bortezomib

159

20S proteasome K_i = 0.62 nM
thrombin K_i = 13,000 nM
human leukocyte elastase K_i = 2,300 nM
human catepsin G K_i = 630 nM
human chymotripsin K_i = 320 nM

Fig. 87 Chemical structure and selectivity profile of bortezomib, **159**.

Table 2 Screening of aldehyde surrogates with the following structure: Cbz-Leu-Leu-R for proteasome inhibitory activity

Entry	***160***	***159***	***161***	***162***	***163***	***164***
K_i (nM)[a]	0.4	0.03	45	214	1400	22,000
R	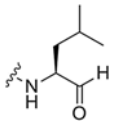	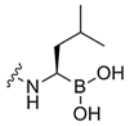	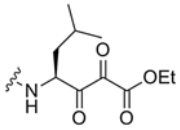	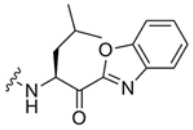	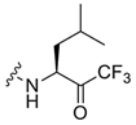	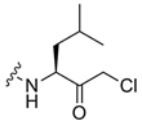

[a]Assay performed using the procedures described by Stein et al. Inhibition of Chymotrypsin-Like Proteolytic Activity of Rabbit Muscle 20S Proteasome. *Biochemistry* **1996**, *35*, 3899.

Bortezomib selectively targets the chymotrypsin-like activity of the proteasome by binding at the β5 subunit active site. Thanks to the P1 leucine side chain, bortezomib creates a shift in the Met45 residue of the β5 subunit affording an induced fit. This structural rearrangement enlarges the S1 specificity pocket allowing further hydrophobic interactions between the P1 leucine side chain and the S1 pocket. The boron atom interacts with the Thr1O$^{\gamma}$, while the remaining two hydroxyl groups of the boronate interact via hydrogen bonds with Thr1N and the Gly47N, respectively. The carbonyl oxygen of Gly47, on the other hand, interacts with the NH of one of the amide moieties, while the second amide interacts with Thr21O. Thr21N, in turn, interacts with a carbonyl of the bortezomib peptide backbone. In addition, one nitrogen atom of the P3 pyrazyl moiety forms a hydrogen bond with the hydroxyl group of Asp114 in the adjacent β6 subunit, further stabilizing the complex. Finally, a series of water-mediated interactions are established with Ala49N and Ala50N and the backbone of bortezomib (Fig. 88).

The anticancer effect of bortezomib is mainly attributed to NOXA upregulation and NFkB suppression. In preclinical studies, bortezomib showed a strong inhibitory effect against a panel of both drug-resistant and drug-sensitive human MM cell lines, with IC_{50}s in the range of 3–40 nM. As this compound showed promising in vitro and in vivo preclinical results, with a strong apoptotic effect in a broad range of cancer types, it entered a Phase I clinical trial in patients with MM under the name PS-341. In clinical setting, patients with refractory MM were treated with bortezomib and showed dose- and time-dependent proteasome inhibition (from 36% to 74% inhibition within 1 h at doses from 0.40 to 1.38 mg m^{-2}).

In 1999, Millennium Pharmaceuticals acquired this promising compound and subjected it to thorough clinical trials. In Phase II trials bortezomib displayed 27% of overall response against MM when administered as an IV bolus at 1.3 mg m^{-2}, with a median duration of response of 12.7 months. In Phase III trials, bortezomib displayed better overall response rate with respect to dexamethasone (43% vs. 18%). Such outcomes led to the approval of **159** in 2003 by the FDA and in 2004 by EMEA under the name bortezomib (Velcade) for the treatment of relapsed and refractory MM as a first-in-class proteasome inhibitor and in 2008 it became the first-line treatment.[270]

The human PK profile showed that after IV dosing the compound has rapid distribution from plasma to tissues (10 min) and has a half-life of 40 h. It can distribute broadly in the body with the exception of the brain and adipose tissue. Metabolism is mostly due to intracellular oxidative deboronation by cytochrome P450 enzymes. Proteasome inhibition induced by bortezomib is reversible and disappears within 72 h of administration.

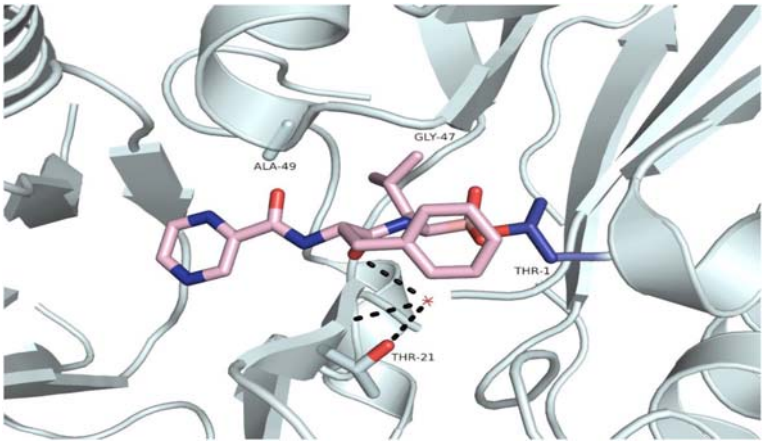

Fig. 88 X-ray crystal structure of the 20S proteasome (*cyan*) complexed with bortezomib, **159** (*light pink*), PDB: 2F16. The structure of the ligand, and the key binding site residues are shown as sticks. Thr-1 is represented in *blue*. Selected interactions are shown in *black-dashed lines*.

Bortezomib also proved advantageous in combination therapy with cytotoxic anticancer drugs (carboplatin, doxorubicin, docetaxel, and prednisone). Bortezomib has a chemosensitizing effect and, as a result, causes increased sensitivity of cancer cells to conventional drugs, allowing dose reduction with respect to monotherapy. However, despite the great success of bortezomib for the treatment of relapsed and refractory MM and for the treatment of MCL, and despite the fact that this drug has given improved response rates and survival compared to other treatments, such as dexamethasone, some limitations have been identified. Bortezomib therapy displayed some disadvantages: IV administration, which reduces patient compliance and dosing flexibility; side effects (thrombocytopenia, neutropenia, gastrointestinal disorders); dose-limiting toxicities, such as tremors, neurotoxicity, fatigue, hypokalemia, hyponatremia, nausea, and especially peripheral neuropathy. This last side effect has been associated with the inhibition of serine (HtrA2) which protects neurons from apoptosis.[195] Another caveat is that bortezomib therapy is hampered by both intrinsic resistance (only 35% of the MM patients treated with bortezomib were sensitive) and acquired resistance (due to β5 mutations and overexpression, together with multidrug resistance).[271]

Although bortezomib displayed great efficacy in the treatment of hematological diseases, the results have been less satisfactory for solid tumors. The issues around bortezomib therapy highlighted the need to develop a second generation of peptide boronates capable of addressing these limitations.

5.07.4.4.2.4.2 Ixazomib (MLN9708)

In an attempt to improve the pharmacokinetic profile and the route of administration, Millennium Pharmaceuticals developed a boronic ester prodrug called Ixazomib, **165**, that in vivo rapidly converts via hydrolysis into its biologically active form MLN2238, **166** (Fig. 89). Ixazomib (Ninlaro, Takeda) was approved by the FDA in 2015 for the treatment of MM in combination with lenalidomide and dexamethasone. The main advantage introduced by ixazomib over bortezomib is that it represents the first orally bioavailable proteasome inhibitor.[272]

While one of the limitations of bortezomib is the lack of efficacy in solid tumors, which has been connected to its inability to penetrate into tissues due to a slow off-rate and high partitioning in red blood cells, ixazomib although slightly less potent than bortezomib in a cellular luciferase assay (MDA-MB-231 4xUb-Luc $EC_{50} = 525$ vs. 310 nM) possesses a shorter 20S proteasome dissociation half-life (18 vs. 110 min) leading to a wider tissue distribution, with a sixfold larger volume of distribution (20 L kg^{-1} vs. 4 L kg^{-1}) in preclinical species (Fig. 90).

Ixazomib possesses an improved pharmacokinetic profile, with an oral bioavailability of 60% in mouse, and stronger antitumor activity than bortezomib in xenograft tumor models in both blood tumors (T/C = 0.2 vs. T/C = 0.8 in lymphoma WSU-DLCL2 for **165** and **159**, respectively) and solid tumors (T/C = 0.4 vs. T/C = 0.8 in prostate CWR22 cancer cell line for **165** and **159**, respectively).

The faster off-rate in blood contributed to a more than 10-fold higher MTD with respect to bortezomib (14 mg kg^{-1} iv vs. 0.8 mg kg^{-1} iv). This improvement was confirmed in human clinical trials, where ixazomib showed superior antitumor activity

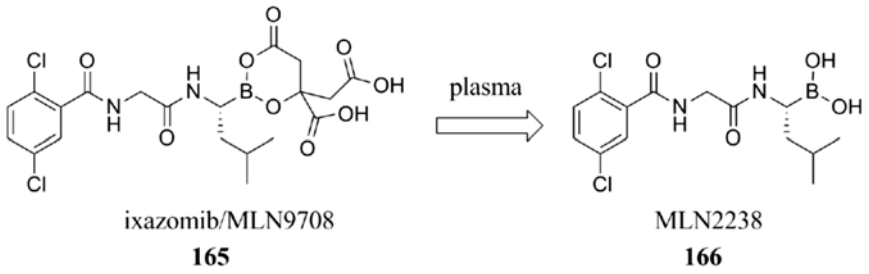

Fig. 89 Conversion of the prodrug ixazomib/MLN9708, **165**, into its active form MLN2238, **166**.

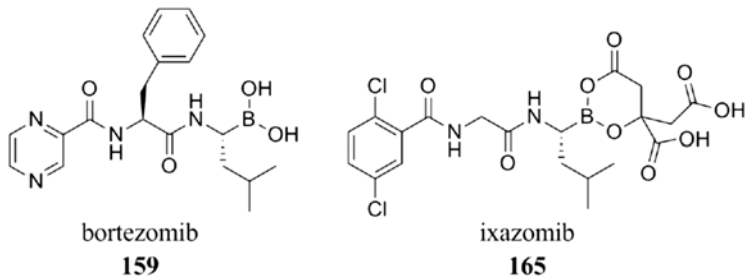

Fig. 90 Comparison between the in vitro and in vivo profiles of bortezomib, **159**, and ixazomib, **165**, in preclinical species.

in hematological malignancies, efficacy in solid tumors and reduced dose-limiting toxicities such as peripheral neuropathy. The lower neurotoxicity has been attributed to lack of inhibition of the serine protease HtrA2.[195] The compound is now undergoing Phase III clinical trials.[273]

5.07.4.4.2.4.3 Delanzomib (CEP-18770)

Delanzomib/CEP18-770, **167**, is another second-generation boronate analog revealing promising results in clinical trials. By leaving untouched the leucine residue in position P1, as crucial for selectivity, the medicinal chemistry efforts focused on amino acid scanning at the P2 position and SAR exploration around the P3 position. A threonine and an aromatic motif, respectively, emerged as the optimal combination in order to improve potency (Fig. 91).[274]

To improve the physicochemical properties of this series, the phenylalanine in the P2 position was replaced by a more polar threonine residue. The consequent loss in potency (see compound **168**; 11-fold loss in enzyme potency and >50-fold loss in cellular activity) was compensated by introduction of a biaryl substituent at the P3 position. Introduction of the 6-phenylpyridin-2-yl motif afforded high potency in biochemical assay (human 20S erythrocyte proteasome fluorimetric kinetic assay of CT-L proteasome activity, HEP $IC_{50}=3.8$ nM), low cross-reactivity (human pancreas α-chymotrypsin activity CHY = 1.5 μM), and high cellular activity (ovarian carcinoma cell line A2780 $IC_{50}=13.7$ nM).

This exploration led to the clinical candidate, called delanzomib or CEP-18770, **167** (Figs. 91 and 92). The compound showed a minimal difference in potency from enzyme to cell-based assay, demonstrating high permeability and potency in antiproliferation assays. In a broad panel of 42 proteases representing all mechanistic classes of these enzymes, the compound displayed high selectivity for the proteasome with no significant inhibition of serine, cysteine, or aspartyl proteases, or metalloproteases. Most importantly, despite being equivalent to bortezomib, **159**, in terms of potency and selectivity, delanzomib also possesses a very good PK profile in rodent species (Fig. 93). In both mouse (CD-1 mouse) and rat (Sprague–Dawley rat), the compound displayed long half-life, large volume of distribution, low clearance, and especially improved oral bioavailability in mice with respect to bortezomib (39% vs. 11%), which translated to improved in vivo efficacy in different human MM xenograft models. At its MTD, delanzomib gave 86% inhibition of proteasome binding compared to 48% given by bortezomib. Also, the safety profile of delanzomib, unlike bortezomib, is not hampered by neuropathy as a dose-limiting toxicity issue. With the improvement demonstrated in preclinical studies, delanzomib has undergone Phase I/II clinical trials for the treatment of myeloma, lymphoma, and solid tumors.[275] Delanzomib yielded an improvement in MM resistant to standard treatment; when used in IV combination with bortezomib, delanzomib afforded complete regression of bortezomib-sensitive tumors and markedly delayed progression of bortezomib-resistant tumors.

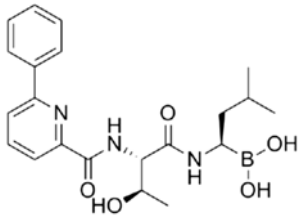

Fig. 91 Chemical structure of delanzomib/CEP-18770, **167**.

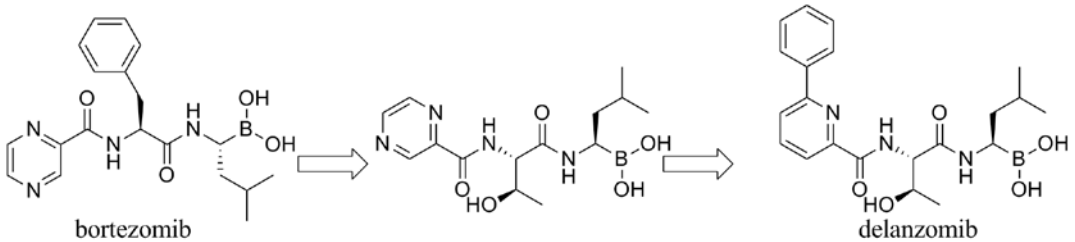

Fig. 92 Development of the clinical candidate delanzomib, **167**.

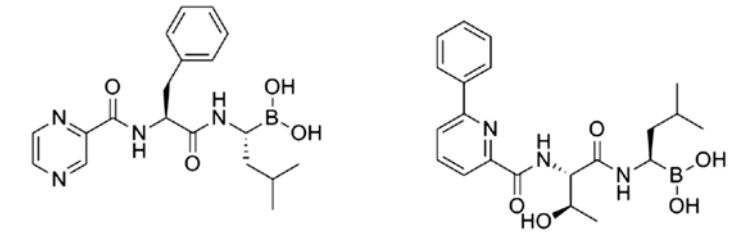

bortezomib
159
Mouse PO AUC_{τ} = 499 ng·h/mL
CL = 0.9 (L/h)/Kg; $t_{½}$ = 98 h
Vd_{ss} = 102 L/Kg; F = 11%

delanzomib
167
Mouse PO AUC_{τ} = 2900 ng·h/mL
CL = 1.4 (L/h)/Kg; $t_{½}$ = 15 h
Vd_{ss} = 10 L/Kg; F = 39%
Rat AUC_{τ} = 2200 ng·h/mL
CL = 0.2 (L/h)/Kg; $t_{½}$ = 86 h
Vd_{ss} = 18 L/Kg; F = 54%

Fig. 93 Comparison between bortezomib, **159**, and delanzomib, **167**, in pharmacokinetic studies in rodent species.

5.07.4.4.2.5 α′,β′-Epoxyketones

Due to the bivalent mode of action involving both Thr1O and Thr1N, α′,β′-epoxyketones are considered the most specific functional groups among the proteasome inhibitors. These inhibitors act through a mechanism very similar to the α-ketoaldehydes. Initial reversible formation of the hemiketal involving the ketone and the Thr1O is followed by nucleophilic attack of Thr1N on the epoxide moiety with irreversible formation of a morpholine ring system (**Scheme 8**). The class of α′,β′-epoxyketones has been particularly fruitful as it has yielded a third marketed proteasome inhibitor named carfilzomib.

5.07.4.4.2.5.1 Carfilzomib

Carfilzomib, **169** (PR-171, Kyprolis), was developed by Proteolix as a more potent proteasome inhibitor. It is a modified peptide related to the family of the natural product epoxomicin. It possesses two key structural features: a peptide portion responsible for selective binding to the proteasome pocket, and an epoxyketone pharmacophore that interacts stereospecifically with the catalytic threonine residue, giving irreversible inhibition of the enzyme. Once carfilzomib is bound to the proteasome, protein turnover is necessary to reestablish proteasomal activity, which explains why carfilzomib has higher potency than bortezomib.[277]

Starting from the natural product epoxomicin, **170**, which showed antitumoral activity, a series of nonnatural α′,β′-epoxyketones was developed. Several residue sequences and lengths were explored as they deeply influence the potency and selectivity for the three main catalytic functions of the proteasome. For example, hydrophobic residues such as leucine and phenylalanine usually give high selectivity for chymotrypsin-like activity, while basic amino acids such as lysine and arginine shift the selectivity toward trypsin-like activity. In order to obtain selective inhibitors of chymotrypsin-like activity, the first round of optimization led to YU-101, **171**, a tetrapeptide epoxyketone bearing a phenylalanine and a leucine at the P2 and P3 positions, respectively. Also, as large hydrophobic side chains have been reported to improve selectivity, an aromatic group was utilized in the P4 position (**Fig. 94**). This compound was a potent and selective inhibitor of the proteasome, however it was flawed by very low aqueous solubility ($<1\ \mu g\ mL^{-1}$) which limited its applicability in vivo.

Carfilzomib, **169**, was developed as an improvement on YU-101, where, thanks to the N-terminal morpholine, the aqueous solubility was greatly increased (>1000-fold). Crystallographic analysis of the human 20S proteasome in complex with carfilzomib revealed a series of key interactions. Thr1O and Thr1N give a dual covalent adduct with the epoxyketone motif to create

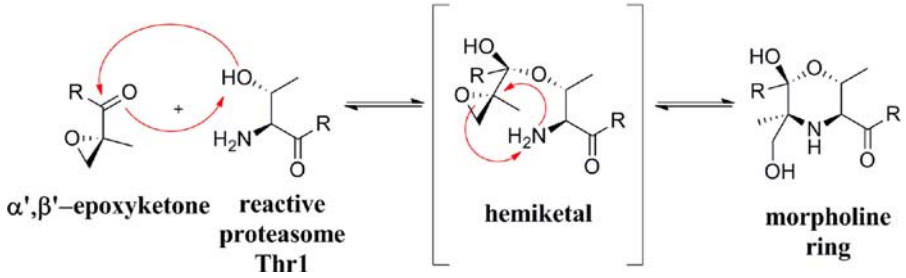

Scheme 8 Reaction mechanism of the α′,β′-epoxyketones.[276]

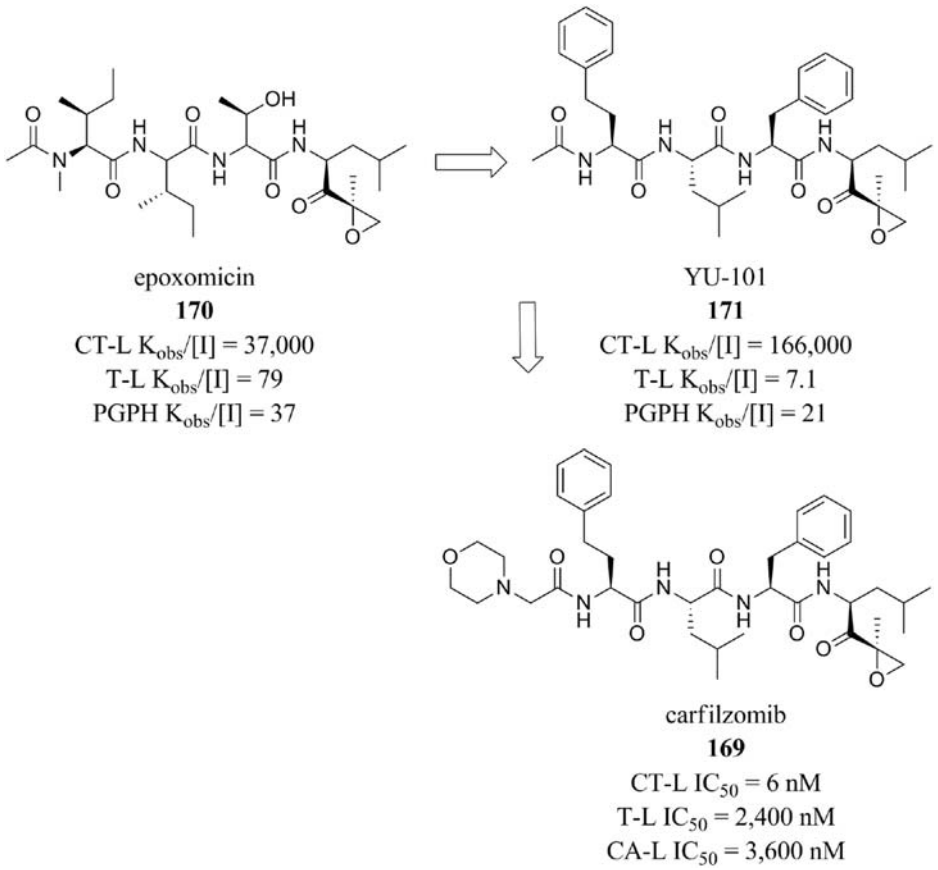

Fig. 94 Evolution of α′,β′-epoxyketones from the natural product epoxomicin, **170**, to the marketed drug PR-171, **169** (Carfilzomib, Proteolix, Inc.).

a morpholine ring. Gly47O, Thr21O, and Thr21N are involved in hydrogen bonds with the peptide backbone of carfilzomib. Finally, water-mediated hydrogen bonds take place with Ala49N and Ala50N (Fig. 95).

Although carfilzomib possesses similar potency to bortezomib, it displayed greater selectivity toward chymotrypsin-like activity over trypsin- and caspase-like activities. Also, because nonproteasomal serine and cysteine proteases do not possess the free α-amino group necessary to form the dual adduct with carfilzomib, this compound displayed higher specificity, giving hope for greater tolerability in vivo.

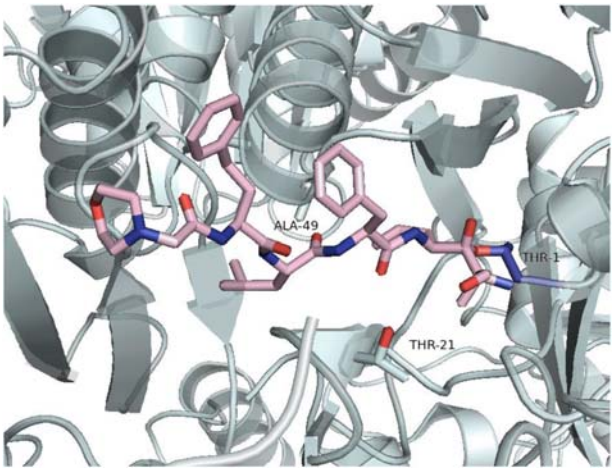

Fig. 95 X-ray crystal structure of the 20S proteasome (*cyan*) complexed with carfilzomib, **169** (*light pink*), PDB: 4R67. The structure of the ligand, and the key binding site residues are shown as sticks. Thr-1 is represented in *blue*.

In animal models, carfilzomib led to a dose-dependent inhibition of chymotrypsin-like activity of the proteasome in a wide range of tissues, with exception of the brain. Carfilzomib is well-tolerated after 2 or 5 days treatment with >80% proteasome inhibition seen in blood and tissues. Due to its potential, Onyx Pharmaceuticals, after acquisition of Proteolix, advanced carfilzomib into several Phase I/II clinical trials. In MM patients treated with 20 mg m^{-2} of carfilzomib, a 47% response rate was obtained with less serious side effects with respect to bortezomib, such as fatigue and cytopenia, but importantly not neuropathy, attributed to the higher selectivity with respect to HtrA2 and other serine proteases. In 2012, the FDA-approved carfilzomib for the treatment of MM in patients not responsive to bortezomib and immunomodulatory therapy.

5.07.4.4.2.5.2 Oprozomib (ONX0912, PR047)

Oprozomib, **172**, was discovered during an effort to find improved analogs of carfilzomib, as orally bioavailable alternatives, with superior patient compliance and dosing flexibility. This work began with the exploration of truncated versions of carfilzomib, **169**. As carfilzomib is a tetrapeptide epoxyketone characterized by poor oral bioavailability and low metabolic stability, the rationale was that truncated forms of carfilzomib would maintain biological activity while improving oral exposure.[278]

Initially, di- and tripeptide analogs (compounds **173** and **174**) were prepared (Fig. 96). In contrast to the dipeptide, the tripeptide epoxyketone proved to be very active both in biochemical and cellular assays (20S proteasome CT-L activity inhibition, $IC_{50}=57$ nM; Molt-4 CT-L $IC_{50}=45$ nM) and represented the starting point for a broad SAR exploration around the tripeptide scaffold. The exploration was performed through a systematic screening of different N-cap groups, coupled with sequential modifications at the P1, P2, and P3 positions, respectively. The first N-cap screening identified five-membered heterocycles as viable substituents for potency optimization. In particular the 5-methyl-isoxazol-3-yl derivative provided good activity (compound **175**, Fig. 97). However, solubility needed to be improved in order to achieve oral exposure. Thus, in a second round of optimization the more polar O-methylserine was identified as the most promising residue for the P3 position with a >12-fold improvement in solubility (compound **176**). In order to increase metabolic stability reduction of lipophilicity through the introduction of a second polar O-methylserine residue was carried out at the P2 position, leading to a twofold improvement in microsomal stability (compound **177**). Finally, by keeping P2 and P3 unchanged, several N-cap groups were screened in combination with leucine or phenylalanine at the P1 position. The best combination was provided by phenylalanine in P1 and 2-methyl-thiazol-5-yl at the N-terminus, giving the final candidate oprozomib/PR047, **172** (Fig. 97).

The candidate showed a favorable profile, with good solubility (1.86 mg mL^{-1} in oral dosing vehicle), metabolic stability in simulated intestinal fluids (90% of parent compound unchanged at 15 min), liver microsomal stability (R_e=liver extraction ratio; mouse $R_e=0.51$; human $R_e=0.60$), and oral bioactivity (mice PO PD=94% inhibition of CT-L activity at 10 mg kg^{-1}).

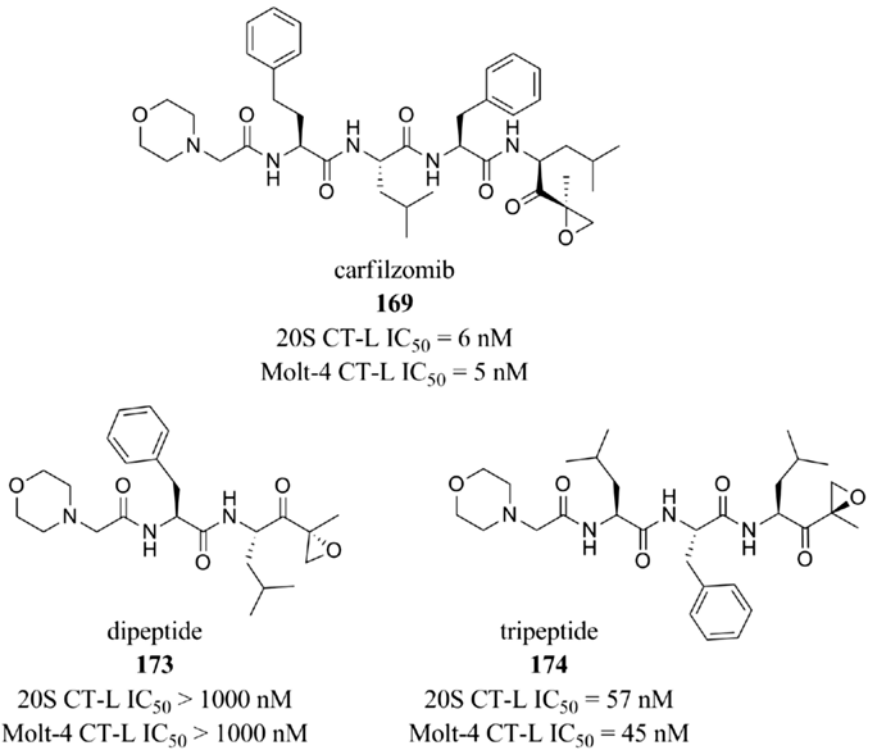

Fig. 96 Structure of carfilzomib, **169**, (PR-171) and its truncated forms. As highlighted in the figure, the dipeptide analog, **173**, lost inhibitory activity against the 20S proteasome chymotrypsin-like activity, while the tripeptide, **174**, represented an encouraging starting point. (From Zhou et al. *J. Med. Chem.* **2009**, *52*, 3028.)

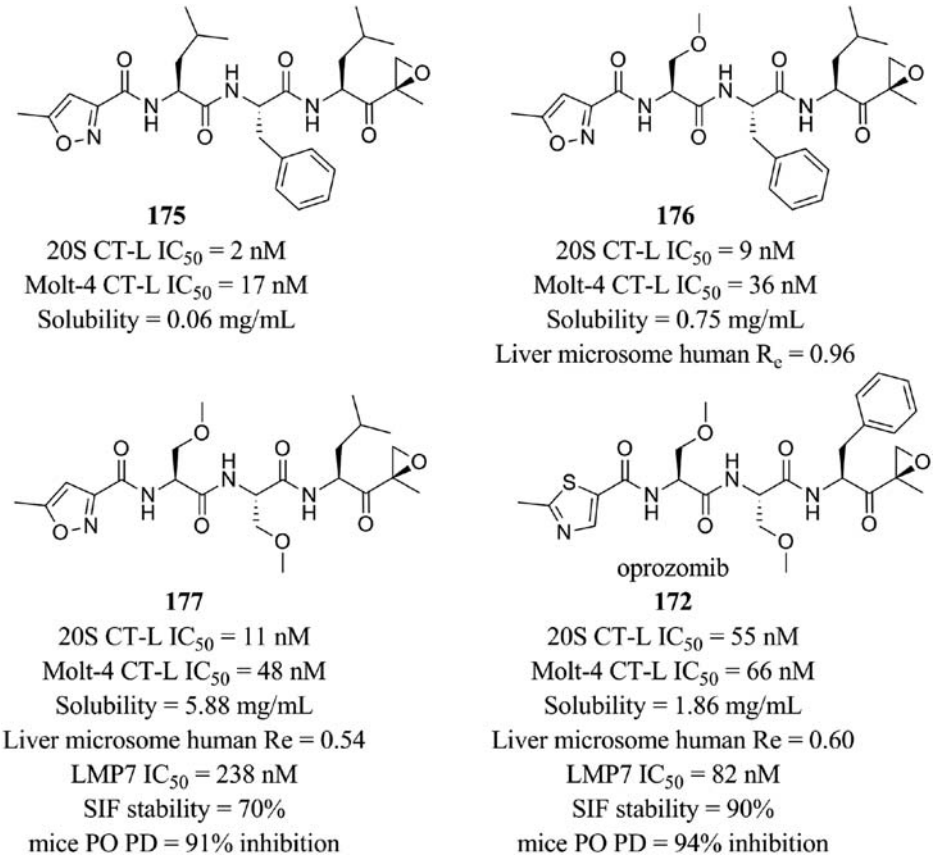

Fig. 97 Development of the clinical candidate PR-047, **172**.

Oprozomib also possessed adequate oral bioavailability across the preclinical species (mouse $F = 17\%$ at 40 mg kg^{-1}; rat $F = 21\%$ at 40 mg kg^{-1}; dog $F = 39\%$, at 19 mg kg^{-1} dose) and enhanced inhibition of the immunoproteasome (LMP7 $IC_{50} = 82$ nM) together with the constitutive proteasome.

Oprozomib was evaluated for antitumor activity in human tumor xenografts (lymphoma and colorectal tumor cell lines) and proved to be very effective. In contrast to carfilzomib, it was administered at a lower dose than its MTD and orally rather than IV, producing the same response in terms of anticancer efficacy. The compound is currently undergoing Phase I/II clinical trials.[279]

5.07.4.4.2.6 β-Lactones

β-Lactones are derivatives of the natural product omuralide (lactacystin) and represent a promising alternative pharmacophore to overcome the limitations associated with bortezomib therapies, especially resistance. The mechanism of action involves nucleophilic attack of the proteasome Thr1O$^{\gamma}$ on the carbonyl which opens the β-lactone ring of the drug to afford an ester product (**Scheme 9**).

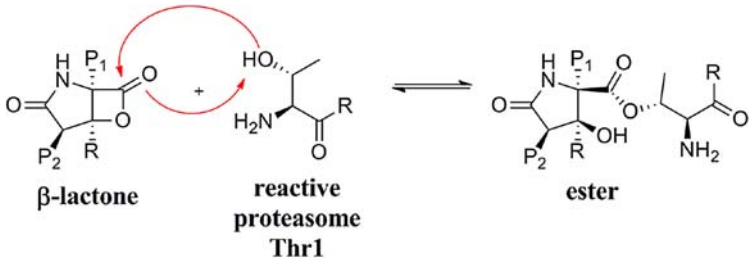

Scheme 9 Reaction mechanism of the β-lactones.[280]

5.07.4.4.2.7 Marizomib (salinosporamide A/NPI-0052)

In contrast to the previously described proteasome inhibitors, the β-lactones are nonpeptide-based compounds. They are natural products of microbial origin among which omuralide, **178**, and salinosporamide A (marizomib), **179**, are the most well-known examples (Fig. 98). Salinosporamide A is a marine natural product extracted from the actinomycete *Salinispora tropica*, which showed high potency as a 20S proteasome inhibitor (IC_{50} in the nanomolar range).[281] In particular, omuralide and salinosporamide A share the β-lactone-γ-lactam bicyclic ring system, but with different substitutions. The common β-lactone unit represents the key pharmacophore. Salinosporamide A, **179**, possesses higher potency with respect to omuralide, **178**, likely deriving from the substituents on the ring (cyclohexene ring and halogenated lateral chain substituents). The necessity of the β-lactone moiety for potency was proven by hydrolysis of the ring which led to complete loss of potency in all assays ($IC_{50} > 20$ μM).

Salinosporamide A exerts its inhibitory activity on the proteasome with a unique two-step mechanism of action. In the first step, the nucleophilic Thr1 residue attacks and opens the lactone ring, then there is cyclization to a tetrahydrofuran ring due to nucleophilic displacement of the chlorine atom.

Salinosporamide A represents a potential replacement therapy to traditional bortezomib as it is able to overcome bortezomib resistance in MM cells. Salinosporamide A has a fairly broad effect as it inhibits all the three catalytic functions of the proteasome (chymotrypsin-like, trypsin-like, and caspase-like) in addition to inhibition of NFkB activation and growth inhibition of human cancer cells. The compound is dosed intravenously twice per week and displays wide tissue distribution (including crossing the BBB). The compound possesses a different toxicology profile to bortezomib and the dose-limiting toxicities are hallucinations, cognitive problems, and loss of balance, probably connected to brain penetration. It is currently undergoing Phase I/II clinical trials as a single agent or in combination therapy in patients with advanced solid and blood cancers.[282]

5.07.4.4.3 Immunoproteasome inhibitors

Selective inhibition of the immunoproteasome is also under evaluation in bortezomib-resistant MM therapies. The aldehyde IPSI-001, **180**, and the epoxyketones ONX0914, **181**, and PR-924, **182** (Fig. 99), are compounds which selectively inhibit the 20Si activity with respect to the competitive proteasome, overcoming bortezomib resistance in a preclinical setting and are therefore appealing as alternative therapeutic approach.

5.07.4.5 Targeting the Deubiquitylating Enzymes in Cancer Therapy

The deubiquitylating enzymes (DUBs) or deubiquitinases share the ability to deconjugate ubiquitin from proteins and provide a regulatory step within the UPS cascade.[192,283] These enzymes specifically cleave the bond between the C-terminal group of ubiquitin and the ε-amino group of lysine side chains or between the α-amino groups of the target proteins.[284] The DUBs are appealing as cancer targets as they are involved in various biological processes essential for cellular homeostasis (protein turnover rate, activation, recycling, and localization). They are less promiscuous than other members of the UPS with around 100 DUBs having already been identified in the human genome.[192,285]

All of this encouraged the development of a series of DUB inhibitors[286] (i.e., HBX 19,818,[287] **183**; P5091,[288] **184**; b-AP15,[289] **185**; IU1,[290] **186**; Fig. 100), however to date no DUB inhibitors have been developed into successful clinical candidates. Perhaps this can be attributed to the fact that, except for JAMMs (JAB1/MPN/MOV34 metalloproteases), all other deubiquitinases are cysteine proteases, known to be more challenging to drug with small-molecule inhibitors due to a lack of specificity and poor pharmacokinetics.[291]

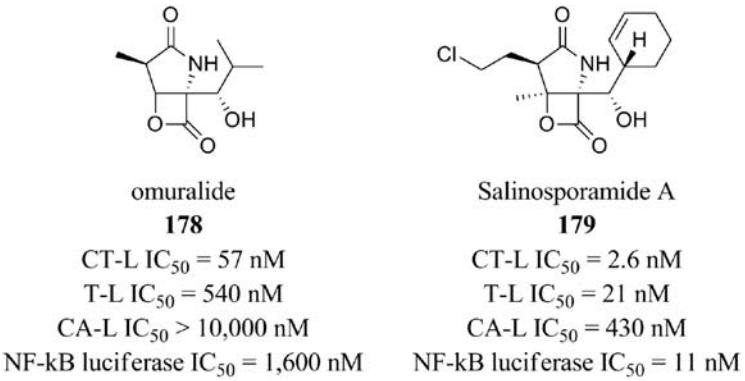

Fig. 98 Chemical structures and in vitro activity/selectivity profiles of omuralide, **178**, and Salinosporamide A, **179**.

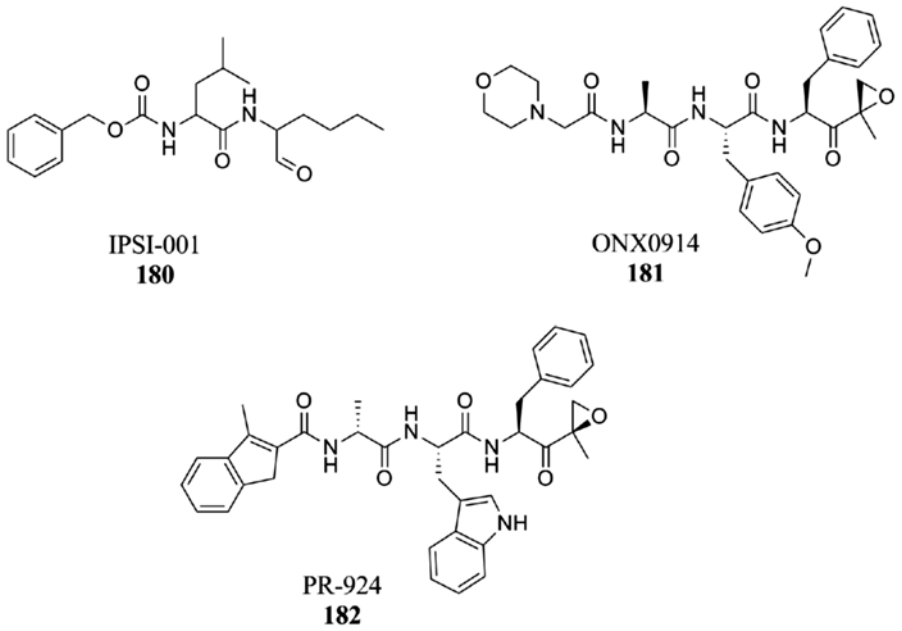

Fig. 99 Chemical structure of selective immunoproteasome inhibitors.

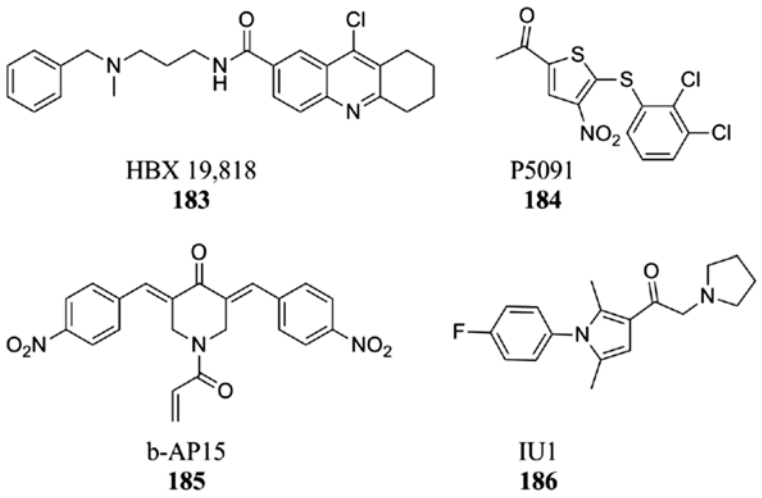

Fig. 100 Chemical structure of some recently reported DUB inhibitors.

5.07.4.6 Degradation of Undruggable Targets in Cancer Therapy

Another emerging strategy focuses on the exploitation of ubiquitination as a tool to enhance degradation of currently undruggable targets, such as MYC, β-catenin, and MCL1.[192] Enhancing the degradation of these targets, for which proteasome degradation is generally impaired in cancer cells, might represent a useful approach to block tumorigenesis.[292] In this context, a series of different classes of small molecules have been explored, such as molecular switches[293] (RNF146 and PAR[294]), PROTACs (protein-targeting chimeric molecules[295]), HyT (hydrophobic tagging[296]), and SERDs (selective estrogen receptor degraders[297]). However, to date, the best results in this field have been achieved with the IMIDs (immunomodulatory drugs).

5.07.4.6.1 Thalidomide and immunomodulatory drugs

The first-in-class compound was thalidomide (Fig. 101), previously known for sedative and antiemetic therapeutic effects, but also for teratogenic side effects. Through high-performance affinity FG beads (FG = ferrite-glycidyl methacrylate), it was demonstrated that thalidomide, **187**, can bind to cereblon (CRBN),[298] a component of the E3 ligase complex $CRL4^{CRBN}$, preventing its ubiquitylation and consequent proteasomal degradation. The interaction between thalidomide and cereblon was deemed responsible for the teratogenicity of the drug.

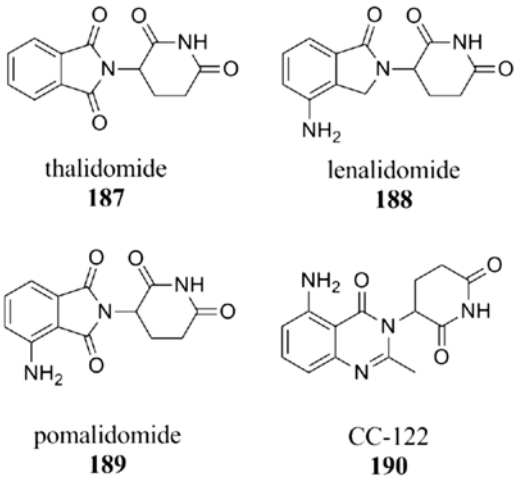

Fig. 101 Chemical structure of thalidomide, **187**, and immunomodulatory drugs.

Subsequently, this interaction has also been connected to the immunomodulatory and antiproliferative effects of thalidomide and of the second-generation immunomodulatory drugs, called IMIDs. The targeting of CRBN and the modulation of its ubiquitylation targets by IMIDs lead to selective degradation of the Ikaros and Aiolos TFs, with consequent strong antiproliferative activity.

This E3 ligase-mediated selective degradation of TF has been exploited in anticancer therapy. In particular, thalidomide displayed good results in the treatment of MM, both as a single agent or in combination therapies with cyclophosphamide or dexamethasone. Thalidomide has also been evaluated in clinical trials for solid malignancies, such as renal cancer, prostate cancer, glioma, and melanoma.[299] While thalidomide showed efficacy in patients with advanced cancer, its use was limited by severe toxic effects, especially teratogenesis. To address the toxicity issues related to thalidomide, second-generation IMIDs analogs were developed. IMIDs proved to be effective against MM[300] and particularly successful were the 4-aminophthalate analogs, developed by Celgene aiming to improve the inhibition of TNF-α. This strategy leads to a 50,000-fold increase in potency against TNF-α, with respect to thalidomide. The best compounds in this series were lenalidomide, **188**, (CC-5013, Remivid) and pomalidomide, **189**, (CC-4047, Actimid). Newer generations of IMIDs, such as CC-122, **190** (Fig. 101), were developed by shifting the focus from TNF-α inhibition to the antiangiogenic and immunomodulatory effect. CC-122 is a nonphthalimide, pleiotropic pathway modifier drug (PPM) with immunomodulatory, antiangiogenic, and antiproliferative effects and was particularly effective in chronic lymphocytic leukemia (CLL) primary cells. CC-122 showed superior performance to lenalidomide, having a broader spectrum of action and efficacy, even in patients nonresponsive to lenalidomide, likely due to CC-122 targeting a new and distinct CLL pathway. CC-122 is currently undergoing Phase I clinical trials.[301]

5.07.4.7 Summary

Protein degradation is an essential process for intracellular homeostasis, being linked to cell cycle progression, signaling, and other vital processes. As cancer cells are highly susceptible to the impairment of the UPS cascade, targeting the UPS system with small-molecule inhibitors is considered a viable strategy for anticancer therapy.

The FDA approval of bortezomib over a decade ago as a first-in-class proteasome inhibitor was welcomed as a sign that the proteasome inhibitors could have undergone a similar fate to kinase inhibitors in anticancer therapy. However, in contrast to the kinase phenomenon, where FDA approval of imatinib initiated an exponential increase in the number of kinase inhibitor candidates reaching the clinic, targeting the UPS cascade has proven more difficult, yielding only three marketed drugs to date. Resistance, dose-limiting toxicities, and selectivity issues are the main limitations challenging this therapeutic area. These caveats highlight that there remains a large window for improvement. In particular, targeting upstream from the proteasome has emerged as a more elegant and useful approach with numerous candidates now reaching the clinic. The UPS pathway is still an open field, with great unexploited potential, and new opportunities may lie just around the corner.

5.07.5 Conclusion

Research to find small-molecule drugs that directly affect protein synthesis, folding, and degradation has proven successful over the last 5–10 years and a wide range of compounds have entered the clinic to treat various cancers along with some significant drug approvals. The underpinning medicinal chemistry has been wide-ranging. Natural products and semisynthetic compounds have featured prominently, in particular as proof of concept compounds that have been taken all the way to the clinic, but also as starting

points for medicinal chemistry. Potent protein/protein interaction inhibitors have been discovered and progressed to the clinic. Selectivity in kinase inhibition has been important as this area matures. Targeting ATPases has been undertaken and considerable success has been achieved in selected cases with challenges remaining in other cases. The recent cereblon-mediated approach provides a potentially new approach to selective degradation of desired proteins in a manner similar to the biological approach of RNAi but using small molecules. In summary, there have been significant advances in the discovery of new molecularly targeted anticancer drugs but there are many remaining challenges. It is clear there will be further exciting advances in the discovery of new cancer therapeutics in this area over the next period.

See also: 5.06. Protein–Protein Interaction Inhibitors in Cancer. 8.04. The Discovery of First-in-Class Inhibitors of the Nedd8-Activating Enzyme (NAE) and the Ubiquitin-Activating Enzyme (UAE). 8.05. The Discovery of p97 Inhibitors.

References

1. Hanahan, D.; Weinberg, R. A. *Cell* **2000,** *100,* 57–70.
2. Weinstein, I. B.; Joe, A. *Cancer Res.* **2009,** *9,* 3077–3080.
3. Sharma, S. V.; Settleman, J. *Genes Dev.* **2007,** *21,* 3214–3231.
4. Martineau, Y.; Muller, D.; Pyronnet, S. *Oncoscience* **2014,** *1,* 484–485.
5. Wheate, N. J.; Brodie, C. R.; Collins, J. G.; Kemp, S.; Aldrich-Wright, J. R. *Mini-Rev. Med. Chem.* **2007,** *7,* 627–648.
6. Villicana, C.; Cruz, G.; Zurita, M. *Cancer Cell Int.* **2014,** *14,* 18.
7. Stellrecht, C. M.; Chen, L. S. *Cancers* **2011,** *3,* 4170–4190.
8. Darnell, J. E. *Nat. Rev. Cancer* **2002,** *10,* 740–749.
9. Jordan, V. C. *Nat. Rev. Drug Discov.* **2003,** *2,* 205–213.
10. Abad, M. C.; Askari, H.; O'Neill, J.; Klinger, A. L.; Milligan, C.; Lewandowski, F.; Springer, B.; Spurlino, J.; Rentzeperis, D. *J. Steroid Biochem. Mol. Biol.* **2008,** *108,* 44–54.
11. Potter, G. A.; Banie, S. E.; Jarman, M.; Rowlands, M. G. *J. Med. Chem.* **1995,** *38,* 2463–2471.
12. Pezaro, C. J.; Mukherji, D.; De Bono, J. S. *Drug Discov. Today* **2012,** *17,* 221–226.
13. Hoffman, B.; Liebermann, D. A. *Oncogene* **2008,** *27,* 6462–6472.
14. Jaramillo, M. C.; Zhang, D. D. *Genes Dev.* **2013,** *27,* 2179–2191.
15. Hoesel, B.; Schmid, J. A. *Mol. Cancer* **2013,** *12,* 86.
16. Jiang, S.; Tu, K.; Fu, Q.; Schmitt, D. C.; Zhou, L.; Lu, N.; Zhao, Y. *Tumour Biol.* **2015,** *36,* 4923–4931.
17. Lane, D. P. *Nature* **1992,** *358,* 15–16.
18. Orphanides, G.; Lagrange, T.; Reinberg, D. *Genes Dev.* **1996,** *10,* 2657–2683.
19. Roots, R.; Smith, K. C. *Cancer Res.* **1976,** *36,* 3654–3658.
20. Bensaude, O. *Transcription* **2011,** *2,* 103–108.
21. Brueckner, F.; Cramer, P. *Nat. Struct. Mol. Biol.* **2008,** *15,* 811–818.
22. Moldenhauer, G.; Salnikov, A. V.; Lüttgau, S.; Herr, I.; Anderl, J.; Faulstich, H. *J. Natl. Cancer Inst.* **2012,** *104,* 622–634.
23. Chohan, T. A.; Qian, H.; Pan, Y.; Chen, J. Z. *Curr. Med. Chem.* **2015,** *22,* 237–263.
24. Mariaule, G.; Belmont, P. *Molecules* **2014,** *19,* 14366–14382.
25. Knight, Z. A.; Lin, H.; Shokat, K. M. *Nat. Rev. Cancer* **2010,** *10,* 130–137.
26. Cicenas, J.; Kalyan, K.; Sorokinas, A.; Stankunas, E.; Levy, J.; Meskinyte, I.; Stankevicius, V.; Kaupinis, A.; Valius, M. *Ann. Transl. Med.* **2015,** *3,* 135.
27. Wirger, A.; Perabo, F. G.; Burgemeister, S.; Haase, L.; Schmidt, D. H.; Doehn, C.; Mueller, S. C.; Jocham, D. *Anticancer Res.* **2005,** *25,* 4341–4347.
28. Sonawane, Y. A.; Taylor, M. A.; Napoleon, J. V.; Rana, S.; Contreras, J. I.; Natarajan, A. *J. Med. Chem.* **2016;** http://dx.doi.org/10.1021/acs.jmedchem.6b00150.
29. Peters, J.-U. *J. Med. Chem.* **2013,** *56,* 8955–8971.
30. Paruch, K.; Dwyer, M. P.; Alvarez, C.; Brown, C.; Chan, T.-Y.; Doll, R. J.; Keertikar, K.; Knutson, C.; McKittrick, B.; Rivera, J.; Rossman, R.; Tucker, G.; Fischmann, T.; Hruza, A.; Madison, V.; Nomeir, A. A.; Wang, Y.; Kirschmeier, P.; Lees, E.; Parry, D.; Sgambellone, N.; Seghezzi, W.; Schultz, L.; Shanahan, F.; Wiswell, D.; Xu, X.; Zhou, Q.; James, R. A.; Paradkar, V. M.; Park, H.; Rokosz, L. R.; Stauffer, T. M.; Guzi, T. J. *ACS Med. Chem. Lett.* **2010,** *1,* 204–208.
31. Frankie, L.; Abdullahi, Y.; AbbasShao, H.; Teo, T.; Adams, J.; Li, P.; Bradshaw, T. D.; Fischer, P. M.; Walsby, E.; Pepper, C.; Chen, Y.; Ding, J.; Wang, S. *Oncotarget* **2014,** *5,* 7691–7704.
32. Shao, H.; Shi, S.; Huang, S.; Hole, A. J.; Abbas, A. Y.; Baumli, S.; Liu, X.; Lam, F.; Foley, D. W.; Fischer, P. M.; Noble, M.; Endicott, J. A.; Pepper, C.; Wang, S. J. *Med. Chem.* **2013,** *56,* 640–659.
33. Moffat, J. G.; Rudolph, J.; Bailey, D. *Nat. Rev. Drug Discov.* **2014,** *13,* 588–602.
34. Lucking, U.; Jautelat, R.; Kruger, M.; Brumby, T.; Lienau, P.; Schafer, M.; Briem, H.; Schulze, J.; Hillisch, A.; Reichel, A.; Wengner, A. M.; Siemeister, G. *ChemMedChem* **2013,** *8,* 1067–1085.
35. Yin, T.; Lallena, M. J.; Kreklau, E. L.; Fales, K. R.; Carballares, S.; Torrres, R.; Wishart, G. N.; Ajamie, R. T.; Cronier, D. M.; Iversen, P. W.; Meier, T. I.; Foreman, R. T.; Zeckner, D.; Sissons, S. E.; Halstead, B. W.; Lin, A. B.; Donoho, G. P.; Qian, Y.; Li, S.; Wu, S.; Aggarwal, A.; Ye, X. S.; Starling, J. J.; Gaynor, R. B.; de Dios, A.; Du, J. *Mol. Cancer Ther.* **2014,** *13,* 1442–1456.
36. Yin, T.; Lallena, M. J.; Kreklau, E. L.; Fales, K. R.; Carballares, S.; Torrres, R.; Wishart, G. N.; Ajamie, R. T.; Cronier, D. M.; Iversen, P. W.; Meier, T. I.; Foreman, R. T.; Zeckner, D.; Sissons, S. E.; Halstead, B. W.; Lin, A. B.; Donoho, G. P.; Qian, Y.; Li, S.; Wu, S.; Aggarwal, A.; Ye, X. S.; Starling, J. J.; Gaynor, R. B.; de Dios, A.; Du, J. *Mol. Cancer Ther.* **2014,** *6,* 1442–1456.
37. Misra, R. N.; Xiao, H.-Y.; Kim, K. S.; Lu, S.; Han, W.-C.; Barbosa, S. A.; Hunt, J. T.; Rawlins, D. B.; Shan, W.; Ahmed, S. Z.; Qian, L.; Chen, B.-C.; Zhao, R.; Bednarz, M. S.; Kellar, K. A.; Mulheron, J. G.; Batorsky, R.; Roongta, U.; Kamath, A.; Marathe, P.; Ranadive, S. A.; Sack, J. S.; Tokarski, J. S.; Pavletich, N. P.; Lee, F. Y. F.; Webster, K. R.; Kimball, S. D. *J. Med. Chem.* **2004,** *47,* 1719–1728.
38. Fu, L.-L.; Tian, M.; Li, X.; Li, J.-J.; Huang, J.; Ouyang, L.; Zhang, Y.; Liu, B. *Oncotarget* **2015,** *6,* 5501–5516.
39. Devaiah, B. N.; Lewis, B. A.; Cherman, N.; Hewitt, M. C.; Albrecht, B. K.; Robey, P. G.; Ozato, K.; Sims, R. J.; Singer, D. S. *Proc. Natl. Acad. Sci. U. S. A.* **2012,** *109,* 6927–6932.
40. Filippakopoulos, P.; Qi, J.; Picaud, S.; Shen, Y.; Smith, W. B.; Fedorov, O.; Morse, E. M.; Keates, T.; Hickman, T. T.; Felletar, I.; Philpott, M.; Munro, S.; McKeown, M. R.; Wang, Y.; Christie, A. L.; West, N.; Cameron, M. J.; Schwartz, B.; Heightman, T. D.; La Thangue, N.; French, C. A.; Wiest, O.; Kung, A. L.; Knapp, S.; Bradner, J. E. *Nature* **2010,** *468,* 1067–1073.
41. Coudé, M.-M.; Braun, T.; Berrou, J.; Dupont, M.; Bertrand, S.; Masse, A.; Raffoux, E.; Itzykson, R.; Delord, M.; Riveiro, M. E.; Herait, P.; Baruchel, A.; Dombret, H.; Gardin, C. *Oncotarget* **2015,** *6,* 17698–17712.

42. Gosmini, R.; Nguyen, V. L.; Toum, J.; Simon, C.; Brusq, J. M.; Krysa, G.; Mirguet, O.; Riou-Eymard, A. M.; Boursier, E. V.; Trottet, L.; Bamborough, P.; Clark, H.; Chung, C. W.; Cutler, L.; Demont, E. H.; Kaur, R.; Lewis, A. J.; Schilling, M. B.; Soden, P. E.; Taylor, S.; Walker, A. L.; Walker, M. D.; Prinjha, R. K.; Nicodème, E. *J. Med. Chem.* **2014,** *57,* 8111–8131.
43. Mirguet, O.; Gosmini, R.; Toum, J.; Clément, C. A.; Barnathan, M.; Brusq, J. M.; Mordaunt, J. E.; Grimes, R. M.; Crowe, M.; Pineau, O.; Ajakane, M.; Daugan, A.; Jeffrey, P.; Cutler, L.; Haynes, A. C.; Smithers, N. N.; Chung, C. W.; Bamborough, P.; Uings, I. J.; Lewis, A.; Witherington, J.; Parr, N.; Prinjha, R. K.; Nicodème, E. *J. Med. Chem.* **2013,** *56,* 7501–7515.
44. Bhat, M.; Robichaud, N.; Hulea, L.; Sonenberg, N.; Pelletier, J.; Topisirovic, I. *Nat. Rev. Drug Discov.* **2015,** *14,* 261–278.
45. Silvera, D.; Formenti, S. C.; Schneider, R. J. *Nat. Rev. Cancer* **2010,** *10,* 254–266.
46. Truitt, M. L.; Ruggero, D. *Nat. Rev. Cancer* **2016,** *16,* 288–304.
47. Vézina, C.; Kudelski, A.; Sehgal, S. N. *J. Antibiot.* **1975,** *28,* 721–726.
48. Heitman, J.; Movva, N. R.; Hall, M. N. *Science* **1991,** *253,* 905–909.
49. Benjamin, D.; Colombi, M.; Moroni, C.; Hall, M. N. *Nat. Rev. Drug Discov.* **2011,** *10,* 868–880.
50. Zoncu, R.; Efeyan, A.; Sabatini, D. M. *Nat. Rev. Mol. Cell Biol.* **2011,** *12,* 21–35.
51. Liang, J.; Choi, J.; Clardy, J. *Acta Cryst* **1999,** *D55,* 736–744.
52. Faivre, S.; Kroemer, G.; Raymond, E. *Nat. Rev. Drug Discov.* **2006,** *5,* 671–688.
53. Douros, J.; Suffness, M. *Cancer Treat. Rev.* **1981,** *8,* 63–87.
54. Zhang, Y.-J.; Duan, Y.; Zheng, X. F. S. *Drug Discov. Today* **2011,** *16,* 325–331.
55. Wander, S. A.; Hennessy, B. T.; Slingerland, J. M. *J. Clin. Invest.* **2011,** *121,* 1231–1241.
56. Zaytseva, Y.; Valentino, J. D.; Gulhati, P.; Evers, B. M. *Cancer Lett.* **2012,** *319,* 1–7.
57. Fruman, D. A.; Rommel, C. *Nat. Rev. Drug Discov.* **2014,** *13,* 140–156.
58. Hayakawa, M.; Kaizawa, H.; Moritomo, H.; Koizumi, T.; Ohishi, T.; Okada, M.; Ohta, M.; Tsukamoto, S.; Parker, P.; Workman, P.; Waterfield, M. *Bioorg. Med. Chem.* **2006,** *14,* 6847–6858.
59. Hayakawa, M.; Kaizawa, H.; Kawaguchi, K.; Ishikawa, N.; Koizumi, T.; Ohishi, T.; Yamano, M.; Okada, M.; Ohta, M.; Tsukamoto, S.; Raynaud, F. I.; Waterfield, M. D.; Parker, P.; Workman, P. *Bioorg. Med. Chem.* **2007,** *15,* 403–412.
60. Hayakawa, M.; Kaizawa, M. H.; Koizumi, T.; Ohishi, T.; Yamano, M.; Okada, M.; Ohta, M.; Tsukamoto, S.; Raynaud, F. I.; Workman, P.; Waterfield, M. D.; Parker, P. *Bioorg. Med. Chem. Lett.* **2007,** *17,* 2438–2442.
61. Raynaud, F. I.; Eccles, S.; Clarke, P. A.; Hayes, A.; Nutley, B.; Alix, S.; Henley, A.; Di-Stefano, F.; Ahmad, Z.; Guillard, S.; Bjerke, L. M.; Kelland, L.; Valenti, M.; Patterson, L.; Gowan, S.; de Haven, B. A.; Hazakawa, M.; Kaizawa, H.; Koizumi, T.; Ohishi, T.; Patel, S.; Saghir, N.; Parker, P.; Waterfield, M.; Workman, P. *Cancer Res.* **2007,** *67,* 5840–5850.
62. Zhao, Y.; Zhang, X.; Chen, Y.; Lu, S.; Peng, Y.; Wang, X.; Guo, C.; Zhou, A.; Zhang, J.; Luo, Y.; Shen, Q.; Ding, J.; Meng, L.; Zhang, J. *ACS Med. Chem. Lett.* **2014,** *5,* 138–142.
63. Folkes, A. J.; Ahmadi, K.; Alderton, W. K.; Alix, S.; Baker, S. J.; Box, G.; Chuckowree, I. S.; Clarke, P. A.; Depledge, P.; Eccles, S. A.; Friedman, L. S.; Hayes, A.; Hancox, T. C.; Kugendradas, A.; Lensun, L.; Moore, P.; Oivero, A. G.; Pang, J.; Patel, S.; Pergl-Wilson, G. H.; Raynaud, F. I.; Robson, A.; Saghir, N.; Salphati, L.; Sohal, S.; Ultsch, M. H.; Valenti, M.; Wallweber, H. J. A.; Chi Wan, N.; Wiesman, C.; Workman, P.; Zhyvoloup, A.; Zvelebil, M. J.; Shuttleworth, S. J. *J. Med. Chem.* **2008,** *51,* 5522–5532.
64. Wallin, J. J.; Edgar, K. A.; Guan, J.; Berry, M.; Prior, W. W.; Lee, L.; Lesnick, J. D.; Lewis, C.; Nonomiya, J.; Pang, J.; Salphati, L.; Olivero, A. G.; Sutherlin, D. P.; O'Brien, C.; Spoerke, J. M.; Patel, S.; Lensun, L.; Kassees, R.; Ross, L.; Lackner, M. R.; Sampath, D.; Belvin, M.; Friedman, L. S. *Mol. Cancer Ther.* **2011,** *10,* 2426–2436.
65. Bauer, T. M.; Patel, M. R.; Infante, J. R. *Pharmacol. Ther.* **2015,** *146,* 53–60.
66. Stauffer, F.; Maira, S.-M.; Furet, P.; García-Echeverría, C. *Bioorg. Med. Chem. Lett.* **2008,** *18,* 1027–1030.
67. Stauffer, F.; Maira, S.-M.; Brueggen, J.; Furet, P.; Schnell, C.; Fritsch, C.; Brachmann, S.; Chène, P.; De Pover, A.; Schoemaker, K.; Fabbro, D.; Gabriel, D.; Simonen, M.; Murphy, L.; Finan, P.; Sellers, W.; García-Echeverría, C. *Mol. Cancer Ther.* **2008,** *7,* 1851–1863.
68. Maira, S.-M.; Stauffer, F.; Schnell, C.; García-Echeverría, C. *Biochem. Soc. Trans.* **2009,** *37,* 265–272.
69. Molckovsky, A.; Siu, L. L. *J. Hematol. Oncol.* **2008,** *1,* 20.
70. Dehnhardt, C. M.; Venkatesan, A. M.; Santos, E. D.; Chen, Z.; Santos, O.; Ayral-Kaloustian, S.; Brooijmans, N.; Mallon, R.; Hollander, I.; Feldberg, L.; Lucas, J.; Chaudhary, I.; Yu, K.; Gibbons, J.; Abraham, R.; Mansour, T. S. J. *Med. Chem.* **2010,** *53,* 798–810.
71. Cheng, H.; Bagrodia, S.; Bailey, S.; Edwards, M.; Hoffman, J.; Hu, Q.; KAnia, R.; Knighton, D. R.; Marx, M. A.; Ninkovic, S.; Sun, S.; Zhang, E. *Med. Chem. Commun.* **2010,** *1,* 139–144.
72. Johnson, T. W.; Dress, K. R.; Edwards, M. *Bioorg. Med. Chem. Lett.* **2009,** *19,* 5560–5564.
73. Yuan, J.; Mehta, P. P.; Yin, M.-J.; Sun, S.; Zou, A.; Chen, J.; Rafidi, K.; Feng, Z.; Nickel, J.; Engebretsen, J.; Hallin, J.; Blasina, A.; Zhang, E.; Nguyen, L.; Sun, M.; Vogt, P. K.; McHarg, A.; Cheng, H.; Christensen, J. G.; Kan, J. L. C.; Bagrodia, S. *Mol. Cancer Ther.* **2011,** *10,* 2189–2199.
74. Knight, S. D.; Adams, N. D.; Burgess, J. L.; Chaudhari, A. M.; Darcy, M. G.; Donatelli, C. A.; Luengo, J. I.; Newlander, K. A.; Parrish, C. A.; Ridgers, L. H.; Sarpong, M. A.; Schmidt, S. J.; Van Aller, G. S.; Carson, J. D.; Diamond, M. A.; Elkins, P. A.; Gardiner, C. M.; Garver, E.; Gilbert, S. A.; Gontarek, R. R.; Jackson, J. R.; Kershner, K. L.; Luo, L.; Raha, K.; Sherk, C. S.; Sung, C.-M.; Sutton, D.; Tummino, P. J.; Wegrzyn, R. J.; Auger, K. R.; Dhanak, D. *ACS Med. Chem. Lett.* **2010,** *1,* 39–43.
75. Garlich, J. R.; De, P.; Dey, N.; Su, J. D.; Peng, X.; Miller, A.; Murali, R.; Lu, Y.; Mills, G. B.; Kundra, V.; Shu, H.-K.; Peng, Q.; Durden, D. L. *Cancer Res.* **2008,** *68,* 206–215.
76. Apsel, B.; Blair, J. A.; Gonzaolz, B.; Nazif, T. M.; Feldman, M. E.; Aizenstein, B.; Hoffman, R.; Williams, R. L.; Shokat, K. M.; Knight, Z. A. *Nat. Chem. Biol.* **2008,** *4,* 691–699.
77. Mortensen, D. S.; Fultz, K. E.; Xu, S.; Xu, W.; Packard, G.; Khambatta, G.; Gamez, J. C.; Leisten, J.; Zhao, J.; Apuy, J.; Ghoreishi, K.; Hickman, M.; Narla, R. K.; Bissonette, R.; Richardson, S.; Peng, S. X.; Perrin-Ninkovic, S.; Tran, T.; Shi, T.; Yang, W. Q.; Tong, Z.; Cathers, B. E.; Moghaddam, M. F.; Canan, S. S.; Worland, P.; Sankar, S.; Raymon, H. K. *Mol. Cancer Ther.* **2015,** *14,* 1295–1305.
78. Bhagwat, S. V.; Gokhale, P. C.; Crew, A. P.; Cooke, A.; Yao, Y.; Mantis, C.; Kahler, J.; Workman, J.; Bittner, M.; Dudkin, L.; Epstein, D. M.; Gibson, N. W.; Wild, R.; Arnold, L. D.; Houghton, P. J.; Pachter, J. A. *Mol. Cancer Ther.* **2011,** *10,* 1394–1406.
79. Malagu, K.; Duggan, H.; Menear, K.; Hummersone, M.; Gomez, S.; Bailey, C.; Edwards, P.; Drzewiecki, J.; Leroux, F.; Quesada, M. J.; Hermann, G.; Maine, S.; Molyneaux, C.-A.; Le Gall, A.; Pullen, J.; Hickson, I.; Smith, L.; Maguire, S.; Martin, N.; Smith, G.; Pass, M. *Bioorg. Med. Chem. Lett.* **2009,** *19,* 5950–5953.
80. Pike, K.; Malagu, K.; Hummersone, M. G.; Menear, K. A.; Duggan, H. M. E.; Gomez, S.; Martin, N. M. B.; Ruston, L.; Pass, S. L.; Pass, M. *Bioorg. Med. Chem. Lett.* **2013,** *23,* 1212–1216.
81. Chresta, C. M.; Davies, B. R.; Hickson, I.; Harding, T.; Cosulich, S.; Critchlow, S. E.; Vincent, J. P.; Ellston, R.; Jones, D.; Sini, P.; James, D.; Howard, Z.; Dudlez, P.; Hughes, G.; Smith, L.; Maguire, S.; Hummersone, M.; Malagu, K.; Menear, K.; Jenkins, R.; Jacobsen, M.; Smith, G. C. M.; Guichard, S.; Pass, M. *Cancer Res.* **2010,** *70,* 288–298.
82. Yu, K.; Shi, C.; Toral-Barza, L.; Lucas, J.; Shor, B.; Kim, J. E.; Zhang, W.-G.; Mahoney, R.; Gaydos, C.; Tardio, L.; Kim, S. K.; Conant, R.; Curran, K.; Kaplan, J.; Verheijen, J.; Azral-Kaloustian, S.; Mansour, T. S.; Abraham, R. T.; Zask, A.; Gibbons, J. J. *Cancer Res.* **2010,** *70,* 621–631.
83. Liu, Q.; Wang, J.; Kang, S. A.; Thoreen, C. C.; Hur, W.; Ahmed, T.; Sabatini, D. M.; Gray, N. S. J. *Med. Chem.* **2011,** *54,* 1473–1480.
84. Hou, J.; Lam, F.; Proud, C.; Wang, S. *Oncotarget* **2012,** *3,* 118–131.
85. Hong, D. S.; Kurzrock, R.; Oh, Y.; Wheler, J.; Naing, A.; Brail, L.; Callies, S.; André, V.; Kadam, S. M.; Nasir, A.; Holzer, T. R.; Meric-Bernstam, F.; Fishman, M.; Simon, G. *Clin. Cancer Res.* **2011,** *17,* 6582–6591.

86. Moerke, N. J.; Aktas, H.; Chen, H.; Cantel, S.; Reibarkh, M. Y.; Fahmy, A.; Gross, J. D.; Degterev, A.; Yuan, J.; Chorev, M.; Halperin, J. A.; Wagner, G. *Cell* **2007,** *128,* 257–267.
87. Papadopoulos, E.; Jenni, S.; Kabha, E.; Takrouri, K. J.; Yi, T.; Salvi, N.; Luna, R. E.; Gavathiotis, E.; Mahalingam, P.; Arthanari, H.; Rodriguez-Mias, R.; Yedfidoff-Freedman, R.; Aktas, B. H.; Chorev, M.; Halperin, J. A.; Wagner, G. *Proc. Natl. Acad. Sci. U. S. A.* **2014,** E3187–E3195.
88. Malina, A.; Mills, J. R.; Pelletier, J. *Cold Spring Harb. Perspect. Biol.* **2012,** *4,* a012377.
89. Ellis, R. J.; Minton, A. P. *Nature* **2003,** *425,* 27–28.
90. Dobson, C. M. *Nature* **2003,** *425,* 884–890.
91. Ritossa, F. *Cell Stress Chaperones* **1996,** *1,* 97–98.
92. Dai, C.; Sampson, S. B. *Trends Cell Biol.* **2016,** *26,* 17–28.
93. Brodsky, J. L.; Chiosis, G. *Curr. Top. Med. Chem.* **2006,** *6,* 1215–1225.
94. Flaherty, K. M.; McKay, D. B.; Kabsch, W.; Holmes, K. *Proc. Natl. Acad. Sci. U. S. A.* **1991,** *88,* 5041–5045.
95. Chene, P. *Nat. Rev. Drug Discov.* **2002,** *1,* 665–673.
96. Evans, L. E.; Cheeseman, M. D.; Yahya, N.; Jones, K. *PLoS ONE* **2015,** *10,* e0140006.
97. Massey, A. J. *J. Med. Chem.* **2010,** *53,* 7280–7286.
98. Hadjuk, P. J.; Huth, J. R.; Fesik, S. W. *J. Med. Chem.* **2005,** *48,* 2518–2525.
99. Schlecht, R.; Scholtz, S. R.; Dahmen, H.; Wegener, A.; Sirrenberg, C.; Musil, D.; Bomke, J.; Eggenweiler, H. M.; Mayer, M. P.; Bukau, B. *PLoS ONE* **2013,** *8*, e78443.
100. Hassan, A. Q.; Kirby, C. A.; Zhou, W.; Schuhmann, T.; Kityk, R.; Kipp, D. R.; Baird, J.; Chen, J.; Chen, Y.; Chung, F.; Hoepfner, D.; Movva, N. R.; Pagliarini, R.; Petersen, F.; Quinn, C.; Quinn, D.; Riedl, R.; Schmitt, E. K.; Schitter, A.; Stams, T.; Studer, C.; Fortin, P. D.; Mayer, M. P.; Sadlish, H. *Chem. Biol.* **2015,** *22,* 87–97.
101. Williamson, D. S.; Borgognoni, J.; Clay, A.; Daniels, Z.; Dokurno, P.; Drysdale, M. J.; Foloppe, N.; Francis, G. L.; Graham, C. J.; Howes, R.; Macias, A. T.; Murray, J. B.; Parsons, R.; Shaw, T.; Surgenor, A. E.; Terry, L.; Wang, Y.; Wood, M.; Massey, A. J. *J. Med. Chem.* **2009,** *52,* 1510–1513.
102. Massey, A. J.; Williamson, D. S.; Browne, H.; Murray, J. B.; Dokurno, P.; Shaw, T.; Macias, A. T.; Daniels, Z.; Geoffroy, S.; Dopson, M.; Lavan, P.; Matassova, N.; Francis, G. L.; Graham, C. J.; Parsons, R.; Wang, Y.; Padfield, A.; Comer, M.; Drysdale, M. J.; Wood, M. *Cancer Chemother. Pharmacol.* **2010,** *66,* 535–545.
103. Macias, A. T.; Williamson, D. S.; Allen, N.; Borgognoni, J.; Clay, A.; Daniels, Z.; Dokurno, P.; Drysdale, M. J.; Francis, G. L.; Graham, C. J.; Howes, R.; Matassova, N.; Murray, J. B.; Parsons, R.; Shaw, T.; Surgenor, A. E.; Terry, L.; Wang, Y.; Wood, M.; Massey, A. J. *J. Med. Chem.* **2011,** *54,* 4034–4041.
104. Cheeseman, M. D.; Westwood, I. M.; Barbeau, O.; Rowlands, M.; Dobson, S.; Jones, A. M.; Jeganathan, F.; Burke, R.; Kadi, N.; Workman, P.; Collins, I.; van Montfort, R. L.; Jones, K. *J. Med. Chem.* **2016,** *59,* 4625–4636.
105. Csermely, P.; Schnaider, T.; Soti, C.; Prohaszka, Z.; Nardai, G. *Pharmacol. Ther.* **1998,** *79,* 129–168.
106. Pearl, L. H.; Prodromou, C.; Workman, P. *Biochem. J.* **2008,** *410,* 439–453.
107. Pearl, L. H.; Prodromou, C. *Annu. Rev. Biochem.* **2006,** *75,* 271–294.
108. Prodromou, C.; Roe, S. M.; O'Brien, R.; Ladbury, J. E.; Piper, P. W.; Pearl, L. H. *Cell* **1997,** *90,* 65–75.
109. Pearl, L. H. *Biopolymers* **2016,** *105,* 594–607.
110. Butler, L. M.; Ferraldeschi, R.; Armstrong, H. K.; Centenera, M. M.; Workman, P. *Mol. Cancer Res.* **2015,** *13,* 1445–1451.
111. Mayer, M. P.; Nikolay, R.; Bukau, B. *Mol. Cell* **2002,** *10,* 1255–1256.
112. Vaughan, C. K.; Mollapour, M.; Smith, J. R.; Truman, A.; Hu, B.; Good, V. M.; Panaretou, B.; Neckers, L.; Clarke, P. A.; Workman, P.; Piper, P. W.; Prodromou, C.; Peral, L. H. *Mol. Cell* **2008,** *31,* 886–895.
113. Dittmar, K. D.; Pratt, W. B. *J. Biol. Chem.* **1997,** *272,* 13047–13054.
114. (a) Yufu, Y.; Nishimura, J.; Nawata, H. *Leuk. Res.* **1992,** *16,* 597–605; (b) McCarthy, M. M.; Pick, E.; Kluger, Y.; Gould-Rothberg, B.; Lazova, R.; Camp, R. L. *Ann. Oncol.* **2008,** *19,* 590–594.
115. (a) Pick, E.; Kruger, Y.; Giltnane, J. M.; Moeder, C.; Camp, R. L.; Rimm, D. L. *Cancer Res.* **2007,** *67,* 2932–2937; (b) Gallegos Ruiz, M. I.; Floor, K.; Poepman, P.; Rodroguez, J. A.; Meijer, G. A.; Mooi, W. J. *PLoS ONE* **2008,** *3,* e0001722; (c) Li, C. F.; Huang, W. W.; Wu, J. M.; Yu, S. C.; Hu, T. H.; Uen, Y. H. *Clin. Cancer Res.* **2008,** *14,* 7822–7831.
116. Grbovic, O. M.; Basso, A. D.; Sawai, A.; Ye, Q.; Friedlander, P.; Solit, D. *Proc. Natl. Acad. Sci. U. S. A.* **2006,** *103,* 57–62.
117. Workman, P.; Burrows, F.; Neckers, L.; Rosen, N. *Ann. N. Y. Acad. Sci.* **2007,** *1113,* 202–216.
118. Taipale, M.; Krykbaeva, I.; Koeva, M.; Kayatekin, C.; Westover, K. D.; Karras, G. I. *Cell* **2012,** *150,* 987–1001.
119. Sharp, S.; Jones, K.; Workman, P.. *Cancer Drug Design and Discovery,* 2nd ed.; Academic Press, 2014; pp. 239–274.
120. Bhat, R.; Tummalapalli, S. R.; Rotella, D. P. J. *Med. Chem.* **2014,** *57,* 8718–8728.
121. Jhaveri, K.; Miller, K.; Rosen, L.; Schneider, B.; Chap, L.; Hannah, A.; Zhong, Z.; Ma, W.; Hudis, C.; Modi, S. *Clin. Cancer Res.* **2012,** *18,* 5090–5098.
122. Chiosis, G.; Dickey, C. A.; Johnson, J. L. *Nat. Struct. Mol. Biol.* **2013,** *20,* 1–4.
123. DeBoer, C.; Meulman, P. A.; Wnuk, R. J.; Peterson, D. H. *J. Antibiot. (Tokyo)* **1970,** *23,* 442–447.
124. Rinehart, K. L.; Sasaki, K.; Slomp, G.; Grostic, M. F.; Olsen, E. C. *J. Am. Chem. Soc.* **1970,** *92,* 7591–7593.
125. Schnur, R. C.; Corman, M. L.; Gallaschun, R. J.; Cooper, B. A.; Dee, M. F.; Doty, J. L.; Muzzi, M. L.; Moyer, J. D.; DiOrio, C. I.; Barbacci, E. G.; et al. *J. Med. Chem.* **1995,** *38,* 3806–3812.
126. Stebbins, C. E.; Russo, A. A.; Schneider, C.; Rosen, N.; Hartl, F. U.; Pavletich, N. P. *Cell* **1997,** *89,* 239–250.
127. Kamal, A.; Thao, L.; Sensintaffar, J.; Zhang, L.; Boehm, M. F.; Fritz, L. C.; Burrows, F. J. *Nature* **2003,** *425* (6956), 407–410.
128. Solit, D. B.; Zheng, F. F.; Drobnjak, M.; Münster, P. N.; Higgins, B.; Verbel, D.; Heller, G.; Tong, W.; Cordon-Cardo, C.; Agus, D. B.; Scher, H. I.; Rosen, N. *Clin. Cancer Res.* **2002,** *8,* 986–993.
129. Banerji, U.; O'Donnell, A.; Scurr, M.; Pacey, S.; Staleton, S.; Asad, Y.; Simmons, L.; Maloney, A.; Raynaud, F.; Cabmpbell, M.; Walton, M.; Lakhani, S.; Kaye, S.; Workman, P.; Judson, I. J. *Clin. Oncol.* **2005,** *23,* 4152–4161.
130. Pacey, S.; Gore, M.; Chao, D.; Banerji, U.; Larkin, J.; Sarker, S.; Owen, K.; Asad, Y.; Raynaud, F.; Walton, M.; Judson, I.; Workman, P.; Eisen, T. *Investig. New Drugs* **2012,** *30,* 341–349.
131. Modi, S.; Stopeck, A.; Linden, H.; Solit, D.; Chandarlapaty, S.; Rosen, N.; D'Andrea, G.; Dickler, M.; Moynahan, M. E.; Sugarman, S.; Ma, W.; Patil, S.; Norton, L.; Hannah, A. L.; Hudis, C. *Clin. Cancer Res.* **2011,** *17,* 5132–5139.
132. Richardson, P. G.; Chanan-Khan, A. A.; Lonial, S.; Krishnan, A. Y.; Carroll, M. P.; Alsina, M.; Albitar, M.; Berman, D.; Messina, M.; Anderson, K. C. *Br. J. Haematol.* **2011,** *153,* 729–740.
133. Artegea, C. L. *Clin. Cancer Res.* **2011,** *17,* 4919–4921.
134. Smith, V.; Sausville, E. A.; Camalier, R. F.; Fiebig, H. H.; Burger, A. M. *Cancer Chemother. Pharmacol.* **2005,** *56,* 126–137.
135. Pacey, S.; Wilson, R. H.; Walton, M.; Eatock, M. M.; Hardcastle, A.; Zetterlund, A.; Arkenau, H. T.; Moreno-Farre, J.; Banerji, U.; Roels, B.; Peachey, H.; Aherne, W.; de Bono, J. S.; Raynaud, F.; Workman, P.; Judson, I. *Clin. Cancer Res.* **2011,** *17,* 1561–1570.
136. Siegel, D.; Yan, C.; Ross, D. *Biochem. Pharmacol.* **2012,** *83,* 1033–1040.
137. Gaspar, N.; Sharp, S. Y.; Pacey, S.; Jones, C.; Walton, M.; Vassal, G.; Eccles, S.; Pearson, A.; Workman, P. *Cancer Res.* **2009,** *69,* 1966–1975.
138. Sydor, J. R.; Normant, E.; Pien, C. S.; Porter, J. R.; Ge, J.; Grenier, L.; Pak, R. H.; Ali, J. A.; Dembski, M. S.; Hudak, J.; Patterson, J.; Penders, C.; Pink, M.; Read, M. A.; Sang, J.; Woodward, C.; Zhang, Y.; Grayzel, D. S.; Wright, J.; Barrett, J. A.; Palombella, V. J.; Adams, J.; Tong, J. K. *Proc. Natl. Acad. Sci. U. S. A.* **2006,** *103,* 17408–17413.

139. Ge, J.; Normant, E.; Porter, J. R.; Ali, J. A.; Dembski, M. S.; Gao, Y.; Georges, A. T.; Grenier, L.; Pak, R. H.; Patterson, J.; Sydor, J. R.; Tibbitts, T. T.; Tong, J. K.; Adams, J.; Palombella, V. J. *J. Med. Chem.* **2006,** *49,* 4606–4615.
140. Sequist, L. V.; Gettinger, S.; Senzer, N. N.; Martins, R. G.; Janne, P. A.; Lilenbaum, R.; Gray, J. E.; Iafrate, A. J.; Katayama, R.; Hafeez, N.; Sweeney, J.; Walker, J. R.; Fritz, C.; Ross, R. W.; Grayzel, D.; Engelman, J. A.; Borger, D. R.; Paez, G.; Natale, R. *J. Clin. Oncol.* **2010,** *28,* 4953–4960.
141. Porter, J. R.; Ge, J.; Lee, J.; Normant, E.; West, K. *Curr. Top. Med. Chem.* **2009,** *9,* 1386–1418.
142. Delmotte, P.; Delmotte-Plaquee, J. *Nature* **1953,** *171,* 344–345.
143. Schulte, T. W.; Akinaga, S.; Soga, S.; Sullivan, W.; Stensgard, B.; Toft, D.; Neckers, L. M. *Cell Stress Chaperones* **1998,** *3,* 100–108.
144. Roe, M. S.; Prodromou, C.; O'Brien, R.; Ladbury, J. E.; Piper, P. W.; Pearl, L. H. *J. Med. Chem.* **1999,** *42,* 260–266.
145. Janin, Y. L. *J. Med. Chem.* **2005,** *48,* 7503–7512.
146. Hellwig, V.; Mayer-Bartschmid, A.; Muller, H.; Greif, G.; Kleymann, G.; Zitzmann, W.; Tichy, H. V.; Stadler, M. *J. Nat. Prod.* **2003,** *66,* 829–837.
147. Barluenga, S.; Wang, C.; Fontaine, J. G.; Aouadi, K.; Beebe, K.; Tsutsumi, S.; Neckers, L.; Winssinger, N. *Angew. Chem. Int. Ed. Engl.* **2008,** *47,* 4432–4435.
148. Proisy, N.; Sharp, S. Y.; Boxall, K.; Connelly, S.; Roe, S. M.; Prodromou, C.; Slawin, A. M.; Pearl, L. H.; Workman, P.; Moody, C. J. *Chem. Biol.* **2006,** *13,* 1203–1215.
149. Day, J. E.; Sharp, S. Y.; Rowlands, M. G.; Aherne, W.; Hayes, A.; Raynaud, F. I.; Lewis, W.; Roe, S. M.; Prodromou, C.; Pearl, L. H.; Workman, P.; Moody, C. J. *ACS Chem. Biol.* **2011,** *6,* 1339–1347.
150. Yin, Z.; Henry, E. C.; Gasiewicz, T. A. *Biochemistry* **2009,** *48,* 336–345.
151. Tran, P. L.; Kim, S.-A.; Choi, H. S.; Yoon, J.-H.; Ahn, S.-G. *BMC Cancer* **2010,** *10,* 276.
152. Khandelwal, A.; Hall, J. A.; Blagg, B. S. J. *Org. Chem.* **2013,** *78,* 7859–7884.
153. Yun, B. G.; Huang, W.; Leach, N.; Hartson, S. D.; Matts, R. L. *Biochemistry* **2004,** *43,* 8217–8229.
154. Donnelly, A.; Blagg, B. S. *Curr. Med. Chem.* **2008,** *15,* 2702–2717.
155. Zhao, H.; Kusuma, B. R.; Blagg, B. S. J. *ACS Med. Chem. Lett.* **2010,** *1,* 311–315.
156. Zhao, H.; Donnelly, A. C.; Kusuma, B. R.; Brandt, G. E.; Brown, D.; Rajewski, R. A.; Vielhauer, G.; Holzbeierlein, J.; Cohen, M. S.; Blagg, B. S. J. *Med. Chem.* **2011,** *54,* 3839–3853.
157. Kusuma, B. R.; Khandelwal, A.; Gu, W.; Brown, D.; Liu, W.; Vielhauer, G.; Holzbeierlein, J.; Blagg, B. S. *Bioorg. Med. Chem.* **2014,** *22,* 1441–1449.
158. Zhao, H.; Moroni, E.; Colombo, G.; Blagg, B. S. J. *ACS Med. Chem. Lett.* **2014,** *5,* 84–88.
159. Anyika, M.; McMullen, M.; Forsberg, L. K.; Dobrowsky, R. T.; Blagg, B. S. J. *ACS Med. Chem. Lett.* **2016,** *7,* 67–71.
160. Cohen, S. M.; Mukerji, R.; Samadi, A. K.; Zhao, H.; Blagg, B. S. J.; Cohen, M. S. *Ann. Surg. Oncol.* **2012,** *19,* 483–490.
161. Otrubova, K.; Lushington, G.; Van der Velde, D.; McGuire, K. L.; McAlpine, S. R. J. *Med. Chem.* **2008,** *51,* 530–544.
162. Vasko, R. C.; Rodriguez, R. A.; Cunningham, C. N.; Ardi, V. C.; Agard, D. A.; McAlpine, S. R. *ACS Med. Chem. Lett.* **2010,** *1,* 4–8.
163. Davenport, J.; Manjarrez, J. R.; Peterson, L.; Krumm, B.; Blagg, B. S.; Matts, R. L. *J. Nat. Prod.* **2011,** *74,* 1085–1092.
164. Li, Y.; Li, W.; Wang, L.; Ma, Z. *Oncol. Lett.* **2015,** *10,* 2802–2806.
165. Taldone, T.; Chiosis, G. *Curr. Top. Med. Chem.* **2009,** *9,* 1436–1446.
166. Chiosis, G.; Timaul, M. N.; Lucas, B.; Munster, P. N.; Zheng, F. F.; Sepp-Lorenzino, L.; Rosen, N. *Chem. Biol.* **2001,** *8,* 289–299.
167. Wright, L.; Barril, X.; Dymock, B.; Sheridan, L.; Surgenor, A.; Beswick, M.; Drysdale, M.; Collier, A.; Massey, A.; Davies, N.; Fink, A.; Fromont, C.; Aherne, W.; Boxall, K.; Sharp, S.; Workman, P.; Hubbard, R. E. *Chem. Biol.* **2004,** *11,* 775–785.
168. Vilenchik, M.; Solit, D.; Basso, A.; Huenzo, H.; Lucas, B.; He, H.; Rosen, N.; Spampinato, C.; Modrich, P.; Chiosis, G. *Chem. Biol.* **2004,** *11,* 787–797.
169. Gerecitano; et al. *J. Clin. Oncol.* **2015,** *33.* abstract 2537.
170. Kim, S. H.; Bajji, A.; Tangallapally, R.; Markovitz, B.; Trovato, R.; Shenderovich, M.; Baichwal, V.; Bartel, P.; Cimbora, D.; McKinnon, R.; Robinson, R.; Papac, D.; Wettstein, D.; Carlson, R.; Yager, K. M. *J. Med. Chem.* **2012,** *55,* 7480–7501.
171. Dickson, M. A.; Okuno, S. H.; Keohan, M. L.; Maki, R. G.; D'Adamo, D. R.; Akhurst, T. J.; Antonescu, C. R.; Schwartz, G. K. *Ann. Oncol.* **2012,** *24,* 252–257.
172. Brough, P. A.; Aherne, W.; Barril, X.; Borgognoni, J.; Boxall, K.; Cansfield, J. E.; Cheung, K. M.; Collins, I.; Davies, N. G.; Drysdale, M. J.; Dymock, B.; Eccles, S. A.; Finch, H.; Fink, A.; Hayes, A.; Howes, R.; Hubbard, R. E.; James, K.; Jordan, A. M.; Lockie, A.; Martins, V.; Massey, A.; Matthews, T. P.; McDonald, E.; Northfield, C. J.; Pearl, L. H.; Prodromou, C.; Ray, S.; Raynaud, F. I.; Roughley, S. D.; Sharp, S. Y.; Surgenor, A.; Walmsley, D. L.; Webb, P.; Wood, M.; Workman, P.; Wright, L. *J. Med. Chem.* **2008,** *51,* 196–218.
173. Eccles, S. A.; Massey, A.; Raynaud, F. I.; Sharp, S. Y.; Box, G.; Valenti, M.; Patterson, L.; de Haven Brandon, A.; Gowan, S.; Boxall, F.; Aherne, W.; Rowlands, M.; Hayes, A.; Martins, V.; Urban, F.; Boxall, K.; Prodromou, C.; Pearl, L.; James, K.; Matthews, T. P.; Cheung, K. M.; Kalusa, A.; Jones, K.; McDonald, E.; Barril, X.; Brough, P. A.; Cansfield, J. E.; Dymock, B.; Drysdale, M. J.; Finch, H.; Howes, R.; Hubbard, R. E.; Surgenor, A.; Webb, P.; Wood, M.; Wright, L.; Workman, P. *Cancer Res.* **2008,** *68,* 2850–2860.
174. Kong, A.; Ahmed, D. R. S.; Beck, J. T.; López, R.; Biganzoli, L.; Armstrong, A.; Aglietta, M.; Alba, E.; Campone, M.; Akimov, M.; Matano, A.; Lefebvre, C.; Lee, S. C. ASCO. Abstract No: 530.
175. Murray, C. W.; Carr, M. G.; Callaghan, O.; Chessari, G.; Congreve, M.; Cowan, S.; Coyle, J. E.; Downham, R.; Fgueroa, E.; Fredrickson, M.; Graham, B.; McMenamin, R.; O'Brien, M. A.; Patel, S.; Phillips, T. R.; Williams, G.; Woodhead, A. J.; Wolloford, A. J.-A. *J. Med. Chem.* **2010,** *53,* 5942–5955.
176. Woodhead, A. J.; Angove, H.; Carr, M. G.; Chessari, G.; Congreve, M.; Coyle, J. E.; Cosme, J.; Graham, B.; Day, P. J.; Downham, R.; Fazal, L.; Feltell, R.; Figueroa, E.; Frederickson, M.; Lewis, J.; McMenamin, R.; Murray, C. W.; O'Brien, M. A.; Parra, L.; Patel, S.; Phillips, T.; Rees, D. C.; Rich, S.; Smith, D. M.; Trewartha, G.; Vinkovic, M.; Williams, B.; Woolford, A. J. J. *Med. Chem.* **2010,** *53,* 5956–5969.
177. Ying, W.; Du, Z.; Sun, L.; Foley, K. P.; Proia, D. A.; Blackman, R. K.; Zhou, D.; Inoue, T.; Tatsuta, N.; Sang, J.; Ye, S.; Acquaviva, J.; Shin Ogawa, L.; Wada, Y.; Barsoum, J.; Koya, K. *Mol. Cancer Ther.* **2012,** *11,* 475–484.
178. Nakashima, T.; Ishii, T.; Tagaya, H.; Seike, T.; Nakagawa, H.; Kanda, Y.; Akinaga, S.; Soga, S.; Shiotsu, Y. *Clin. Cancer Res.* **2010,** *16,* 2792–2802.
179. Fadden, P.; Huang, K. H.; Veal, J. M.; Steed, P. M.; Barabasz, A. F.; Foley, B.; Hu, M.; Partridge, J. M.; Rice, J.; Scott, A.; Dubois, L. G.; Freed, T. A.; Silinski, M. A.; Barta, T. E.; Hughes, P. F.; Ommen, A.; Ma, W.; Smith, E. D.; Spangenberg, A. W.; Eaves, J.; Hanson, G. J.; Hinkley, L.; Jenks, M.; Lewis, M.; Otto, J.; Pronk, G. J.; Verleysen, K.; Haystead, T. A.; Hall, S. E. *Chem. Biol.* **2010,** *17,* 686–694.
180. Infante, J. R.; Weiss, G. J.; Jones, S.; Tibes, R.; Bauer, T. M.; Bendell, J. C.; Hinson, J. M.; Von Hoff, D. D.; Burris, H. A.; Orlemans, E. O.; Ramanathan, R. K. *Eur. J. Cancer* **2014,** *50,* 2897–2904.
181. Zapf, C. W.; Bloom, J. D.; McBean, J. L.; Dushin, R. G.; Nittoli, T.; Otteng, M.; Ingalls, C.; Golas, J. M.; Liu, H.; Lucas, J.; Boschelli, F.; Hu, Y.; Vogan, E.; Levin, J. I. *Bioorg. Med. Chem. Lett.* **2011,** *21,* 3411–3416.
182. Zapf, C. W.; Bloom, J. D.; Li, Z.; Dushin, R. G.; Nittoli, T.; Otteng, M.; Nikitenko, A.; Golas, J. M.; Liu, H.; Lucas, J.; Boschelli, F.; Vogan, E.; Olland, A.; Johnson, M.; Levin, J. I. *Bioorg. Med. Chem. Lett.* **2011,** *21,* 4602–4607.
183. Suda, A.; Koyano, H.; Hayase, T.; Hada, K.; Kawasaki, K.; Komiyama, S.; Hasegawa, K.; Fukami, T. A.; Sato, S.; Miura, T.; Ono, N.; Yamazaki, T.; Saitoh, R.; Shimma, N.; Shiratori, Y.; Tsukuda, T. *Bioorg. Med. Chem. Lett.* **2012,** *22,* 1136–1141.
184. Bussenius, J.; Blazey, C. M.; Aay, N.; Anand, N. K.; Arcalas, A.; Baik, T.; Bowles, O. J.; Buhr, C. A.; Costanzo, S.; Curtis, J. K.; DeFina, S. C.; Dubenko, L.; Heuer, T. S.; Huang, P.; Jaeger, C.; Joshi, A.; Kennedy, A. R.; Kim, A. I.; Lara, K.; Lee, J.; Li, J.; Lougheed, J. C.; Ma, S.; Malek, S.; Manalo, J. C.; Martini, J. F.; McGrath, G.; Nicoll, M.; Nuss, J. M.; Pack, M.; Peto, C. J.; Tsang, T. H.; Wang, L.; Womble, S. W.; Yakes, M.; Zhang, W.; Rice, K. D. *Bioorg. Med. Chem. Lett.* **2012,** *22,* 5396–5404.
185. McBride, C. M.; et al. *J. Med. Chem.* **2014,** *57,* 9124–9129.

186. Spreafico, A.; Delord, J. P.; De Mattos-Arruda, L.; Berge, Y.; Rodon, J.; Cottura, E.; Bedard, P. L.; Akimov, H.; Lu, H.; Pain, S.; Kaag, A.; Siu, L. L.; Cortes, J. *Br. J. Cancer* **2015,** *1120,* 650–659.
187. Zehnder, L.; Bennett, M.; Meng, J.; Huang, B.; Ninkovic, S.; Wang, F.; Braganza, J.; Tatlock, J.; Jewell, T.; Zhou, J. Z.; Burke, B.; Wang, J.; Maegley, K.; Mehta, P. P.; Yin, M. J.; Gajiwala, K. S.; Hickey, M. J.; Yamazaki, S.; Smith, E.; Kang, P.; Sistla, A.; Dovalsantos, E.; Gehring, M. R.; Kania, R.; Wythes, M.; Kung, P. P. *J. Med. Chem.* **2011,** *54,* 3368–3385.
188. Vallee, F.; Carrez, C.; Pilorge, F.; Dupuy, A.; Parent, A.; Bertin, L.; Thompson, F.; Ferrari, P.; Fassy, F.; Lamberton, A.; Thomas, A.; Arrebola, R.; Guerif, S.; Rohaut, A.; Certal, V.; Ruxer, J. M.; Gouyon, T.; Delorme, C.; Jouanen, A.; Dumas, J.; Grepin, C.; Combeau, C.; Goulaouic, H.; Dereu, N.; Mikol, V.; Mailliet, P.; Minoux, H. *J. Med. Chem.* **2011,** *54,* 7206–7219.
189. Taldone, T.; Patel, P. D.; Patel, M.; Patel, H. H.; Evans, C. E.; Rodina, A.; Ochiana, S.; Shah, S. K.; Uddin, M.; Gewirth, D.; Chiosis, G. *J. Med. Chem.* **2013,** *56,* 6803–6818.
190. Patel, P. D.; Yan, P.; Seidler, P. M.; Patel, H. J.; Sun, W.; Yang, C.; Que, N. S.; Taldone, T.; Finotti, P.; Stephani, R. A.; Gewirth, D. T.; Chiosis, G. *Nat. Chem. Biol.* **2013,** *9,* 677–684.
191. Patel, H. J.; Patel, P. D.; Ochiana, S.; Yan, P.; Sun, W.; Patel, M. R.; Shah, S. K.; Tramentozzi, E.; Brooks, J.; Bolaender, A.; Shrestha, L.; Stephani, R. A.; Finotti, P.; Leifer, C.; Li, Z.; Gewirth, D. T.; Taldone, T.; Chiosis, G. *J. Med. Chem.* **2015,** *58,* 3922–3943.
192. (a) Nalepa, G.; Rolfe, M.; Harper, J. W. *Nat. Rev. Drug Discov.* **2006,** *5,* 596–613; (b) Hoeller, D.; Dikic, I. *Nature* **2009,** *458,* 438–444; (c) Ande, S. R.; Chen, J.; Maddika, S. *Eur. J. Pharmacol.* **2009,** *265,* 199–205; (d) Cohen, P.; Tcherpakov, M. *Cell* **2010,** *143,* 686–693; (e) Bedford, L.; Lowe, J.; Dick, L. R.; Mayer, R. J.; Brownell, J. E. *Nat. Rev. Drug Discov.* **2011,** *10,* 29–46; (f) Wilkie, N.; Davies, S. *Drug Discov. World Summer* **2012,** *35–40*; (g) Huang, X.; Dixit, V. M. *Cell Res.* **2016,** *26,* 484–498.
193. The Official Website of the Nobel Prize. Available at: http://www.nobelprize.org/nobel_prizes/chemistry/laureates/2004.
194. Lub, S.; Maes, K.; Menu, E.; De Bruyne, E.; Vanderkerken, K.; Van Valckenborgh, E. *Oncotarget* **2016,** *7,* 6521–6537.
195. Wustrow, D.; Zhou, H. J.; Rolfe, M. *Annu. Rep. Med. Chem.* **2013,** *48,* 205–225.
196. Streich, F. C.; Lima, C. D. *Annu. Rev. Biophys.* **2014,** *43,* 357–379.
197. Van der Veen, A. G.; Ploegh, H. L. *Annu. Rev. Biochem.* **2012,** *81,* 323–357.
198. (a) Yang, Y.; Kitagaki, J.; Dai, R. M.; Tsai, Y. C.; Lorick, K. L.; Ludwig, R. L.; Pierre, S. H.; Jensen, J. P.; Davydov, I. V.; Oberoi, P.; Li, C. C. H.; Kenten, J. H.; Beutler, J. A.; Vousden, K. H.; Weissman, A. M. *Cancer Res.* **2007,** *67,* 9472–9481; (b) Xu, G. W.; Ali, M.; Wood, T. E.; Wong, D.; Maclean, N.; Wang, X.; Gronda, M.; Skrtic, M.; Li, X.; Hurren, R.; Mao, X.; Venkatesan, M.; Zavareh, R. B.; Ketela, T.; Reed, J. C.; Rose, D.; Moffat, J.; Batey, R. A.; Dhe-Paganon, S.; Schimmer, A. D. *Blood* **2010,** *115,* 2251–2259.
199. (a) Tsukamoto, S.; Hirota, H.; Imachi, M.; Fujimuro, M.; Onuki, H.; Ohta, T.; Yokosawa, H. *Bioorg. Med. Chem. Lett.* **2005,** *15,* 191–194; (b) Lu, X.; Olsen, S. K.; Capili, A. D.; Cisar, J. S.; Lima, C. D.; Tan, D. S. J. *Am. Chem. Soc.* **2010,** *132,* 1748–1749; (c) Huang, D. T.; Hunt, H. W.; Ohi, M. D.; Holton, J. M.; Schulman, B. A. *Nature* **2007,** *445,* 394–398; (d) Schulman, B. A.; Harper, J. W. *Nat. Rev. Mol. Cell Biol.* **2009,** *10,* 319–331; (e) Ungermanniova, D.; Parker, S. J.; Nasveschuk, C. G.; Chapnick, D. A.; Phillips, A. J.; Kuchta, R. D.; Liu, X. *J. Biomol. Screen.* **2012,** *17* (4), 421–434; (f) Jin, J.; Li, X.; Gygi, S. P.; Harper, J. W. *Nature* **2007,** *447,* 1135–1138; (g) Streich, F. C.; Lima, C. D. *Annu. Rev. Biophys.* **2014,** *43,* 357–379.
200. Sekizawa, R.; et al. *J. Nat. Prod.* **2002,** *65,* 1491–1493.
201. (a) Soucy, T. A.; Smith, P. G.; Milhollen, M. A.; Berger, A. J.; Gavin, J. M.; Adhikari, S.; Brownell, J. E.; Burke, K. E.; Cardin, D. P.; Critchley, S.; Cullis, C. A.; Doucette, A.; Garnsey, J. J.; Gaulin, J. L.; Gershman, R. E.; Lublinnsky, A. R.; McDonald, A.; Mizutani, H.; Narayanan, U.; Olhava, E. J.; Peluso, S.; Rezaei, M.; Sintachak, M. D.; Talreja, T.; Thomas, M. P.; Traore, T.; Vyskocil, S.; Weatherhead, G. S.; Yu, J.; Zhang, J.; Dick, L. R.; Claiborne, C. F.; Rolfe, M.; Bolen, J. B.; Langston, S. P. *Nature* **2009,** *458,* 732–737; (b) Gallo-Rodriguez, C.; Ji, X.; Melman, N.; Siegman, B. D.; Sanders, L. H.; Orlina, J.; Fischer, B.; Pu, Q.; Olah, M. E.; van Galen, P. J. M.; Stiles, G. L.; Jacobson, K. A. *J. Med. Chem.* **1994,** *37,* 636–646; (c) Brownell, J. E.; Sintchak, M. D.; Gavin, J. M.; Liao, H.; Bruzzese, F. J.; Bump, N. J.; Soucy, T. A.; Milhollen, M. A.; Yang, X.; Burkhardt, A. L.; Ma, J.; Loke, H. K.; Lingaraj, T.; Wu, D.; Hamman, K. B.; Spelman, J. J.; Cullis, C. A.; Langston, S. P.; Vyskocil, S.; Sells, T. B.; Mallender, W. D.; Visiers, I.; Li, P.; Claiborne, C. F.; Rolfe, M.; Bolen, J. B.; Dick, L. R. *Mol. Cell* **2010,** *7,* 102–111; (d) Lukkarila, J. L.; da Silva, S. R.; Ali, M.; Shahani, V. M.; Xu, G. W.; Berman, J.; Roughton, A.; Dhe-Paganon, S.; Schimmer, A. D.; Gunning, P. T. *ACS Med. Chem. Lett.* **2011,** *2,* 577–582; (e) Shah, J. J.; Jakubowiak, A. J.; O'Connor, O. A.; Orlowski, R. Z.; Harvey, R. D.; Smith, M. R.; Lebovic, D.; Diefenbach, C.; Kelly, K.; Hua, Z.; Berger, A. J.; Mulligan, G.; Faessel, H. M.; Tirrell, S.; Dezube, B. J.; Lonial, S. *Clin. Cancer Res.* **2016,** *22,* 34–43; (f) Bhatia, S.; Pavlick, A. C.; Boasberg, P.; Thompson, J. A.; Mulligan, G.; Pickard, M. D.; Faessel, H.; Dezube, B. J.; Hamid, O. *Investig. New Drugs* **2016,** *34,* 439–449.
202. Petroski, M. D. *Chem. Biol.* **2010,** *17,* 6–8.
203. Langston, S.; Olhava, E. J.; Vyskocil, S. Patent Number WO 2007092213.
204. Haas, A. L.; Rose, I. A. *J. Biol. Chem.* **1982,** *257,* 10329–10337.
205. Walden, H.; Podgorski, M. S.; Schulman, B. A. *Nature* **2003,** *422,* 330–334.
206. (a) Gong, L.; Yeh, E. T. *J. Biol. Chem.* **1999,** *274,* 12036–12042; (b) Bohnsack, R. N.; Haas, A. L. *J. Biol. Chem.* **2003,** *278,* 26823–26830; (c) Liakopoulos, D.; Doenges, G.; Matuschewski, K.; Jentsch, S. *EMBO J.* **2005,** *24,* 439–451.
207. https://clinicaltrials.gov/ct2/results?term=MLN4924&Search=Search.
208. (a) Ye, Y.; Rape, M. *Nat. Rev.* **2009,** *10,* 755–764; (b) Cheng, J.; Fan, Y.-H.; Xu, X.; Zhang, H.; Dou, J.; Tang, Y.; Zhong, X.; Rojas, Y.; Yu, Y.; Zhao, Y.; Vasudevan, S. A.; Zhang, H.; Nuchtern, J. G.; Kim, E. S.; Chen, X.; Lu, F.; Yang, J. *Cell Death Dis.* **2014,** *5,* 1–12.
209. Stewart, M. D.; Ritterhoff, T.; Klevit, R. T.; Brzovic, P. S. *Cell Res.* **2016,** *26,* 423–440.
210. Hu, R.; Hochstrasser, M. *Cell Res.* **2016,** *26,* 389–390.
211. (a) Chen, J. J.; Tsu, C. A.; Gavin, J. M.; Milhollen, M. A.; Bruzzese, F. J.; Mallender, W. D.; Sintchak, M. D.; Bump, N. J.; Yang, X.; Ma, J.; Loke, H. K.; Xu, Q.; Li, P.; Bence, N. F.; Brownell, J. E.; Lawrence, R. D. *J. Biol. Chem.* **2011,** *286,* 40867–40877; (b) Huang, H.; Ceccarelli, D. F.; Orlicky, S.; St-Cyr, D. J.; Ziemba, A.; Garg, P.; Plamondon, S.; Auer, M.; Sidhu, S.; Marinier, A.; Kleiger, G.; Tyers, M.; Sicheri, F. *Nat. Chem. Biol.* **2014,** *10,* 156–165; (c) Sanders, M. A.; Brahemi, G.; Nangia-Makker, P.; Balan, V.; Morelli, M.; Kothayer, H.; Westwell, A. D.; Shekhar, M. P. V. *Mol. Cancer Ther.* **2013,** *4* (12), 373–383.
212. Hewitt, W. M.; Lountos, G. T.; Zlotkowski, K.; Dahlhauser, S. D.; Saunders, L. B.; Needle, D.; Tropea, J. E.; Zhan, C.; Wei, G.; Ma, B.; Nussinov, R.; Waugh, D. S.; Schneekloth, J. S. *Angew. Chem. Int. Ed.* **2016,** *55,* 5703–5707.
213. Kothayer, H.; Spencer, S. M.; Tripathi, K.; Westwell, A. D.; Komaraiah, P. *Bioorg. Med. Chem.* **2016,** *26,* 2030–2034.
214. Mulder, M. P. C.; Witting, K.; Berlin, I.; Pruneda, J. N.; Wu, K.; Chang, J. G.; Merkx, R.; Bialas, J.; Groettrup, M.; Vertegaal, A. C. O.; Schulman, B. A.; Komander, D.; Neefjes, J. *Nat. Chem. Biol.* **2016,** *12,* 523–533.
215. Ceccarelli, D. F.; Tang, X.; Pelletier, B.; Orlicky, S.; Xie, W.; Planteviin, V.; Neculai, D.; Chou, Y. C.; Ogunjimi, A.; Al-Hakim, A.; Varelas, X.; Koszela, J.; Wasney, G. A.; Vedadi, M.; Dhe-Paganon, S.; Cox, S.; et al. *Cell* **2011,** *145* (7), 1075–1087.
216. Strickson, S.; Campbell, D. G.; Emmerich, C. H.; et al. *Biochem. J.* **2013,** *451,* 427–437.
217. Pulvino, M.; Liang, Y.; Oleksyn, D.; et al. *Blood* **2012,** *120,* 1668–1677.
218. (a) Jia, L.; Sun, Y. *Curr. Cancer Drug Targets* **2011,** *11,* 347–356; (b) Sun, Y. *Cancer Biol. Ther.* **2003,** *2,* 623–629; (c) Bartlett, J. B.; Dredge, K.; Dalgleish, A. G. *Nat. Rev. Cancer* **2004,** *4,* 314–322; (d) Ito, T.; Ando, H.; Suzuki, T.; Ogura, T.; Hotta, K.; Imamura, Y.; Yamaguchi, Y.; Handa, H. *Science* **2010,** *327,* 1345–1350; (e) Quach, H.; Ritchie, D.; Stewart, A. K.; Neeson, P.; Harrison, S.; Smyth, M. J.; Prince, H. M. *Leukemia* **2010,** *24,* 22–32.
219. (a) Lydeard, J. R.; Harper, J. W. *Nat. Biotechnol.* **2010,** *28,* 682–684; (b) Brahemi, G.; Kona, F. R.; Fiasella, A.; Buac, D.; Soukupova, J.; Brancale, A.; Burger, A. M.; Westwell, A. D. *J. Med. Chem.* **2010,** *53,* 2757–2765.
220. Tcherpacov, M. *BCC Research Report PHM066A,* 2010, 2010.
221. Chan, C. H.; Morrow, J. K.; Li, C. F.; et al. *Cell* **2013,** *154,* 556–568.

222. Momand, J.; Jung, D.; Wilczynski, S.; Niland, J. *Nucleic Acids Res.* **1998,** *15,* 3453–3459.
223. (a) Hoe, K. K.; Verma, C. S.; Lane, D. P. *Nat. Rev. Drug Discov.* **2014,** *13,* 217–235; (b) Brown, C. J.; Lain, S.; Verma, C. S.; Fersht, A. R.; Lane, D. P. *Nat. Rev. Cancer* **2009,** *9,* 862–872; (c) Chene, P. *Nat. Rev. Cancer* **2003,** *3,* 102–109; (d) Drygin, D.; O'Brien, S. E.; Hannan, R. D.; McArthur, G. A.; Von Hoff, D. D. *Drug Discov. Today* **2014,** *19,* 259–265.
224. Arkin, M. R.; Tang, Y.; Wells, J. A. *Cell Chem. Biol.* **2014,** *21,* 1102–1114.
225. Chessum, N.; Jones, K.; Pasqua, E.; Tucker, M. *Prog. Med. Chem.* **2015,** *54,* 1–63.
226. Weinmann, H.; Ottow, E. *Compr. Med. Chem.* **2007,** *7,* 221–251.
227. Yang, Y.; Ludwig, R. L.; Jensen, J. P.; Pierre, S. A.; Medaglia, M. V.; Davydov, I. V.; Safiran, Y. J.; Oberoi, P.; Kenten, J. H.; Phillips, A. C.; Weissman, A. M.; Vousden, K. H. *Cancer Cell* **2005,** *6,* 547–559.
228. Grasberger, B. L.; Lu, T.; Schubert, C.; Parks, D. J.; Carver, T. E.; Koblish, H. K.; Cummings, M. D.; LaFrance, L. V.; Milkiewicz, K. L.; Calvo, R. R.; Maguire, D.; Lattanze, J.; Franks, C. F.; Zhao, S.; Ramachandren, K.; Bylebyl, G. R.; et al. *J. Med. Chem.* **2005,** *48,* 909–912.
229. Herman, A. G.; Hayano, M.; Poyurovsky, M. V.; Shimada, K.; Skouta, R.; Prives, C.; Stockwell, B. R. *Cancer Discov.* **2011,** *4,* 312–325.
230. Ding, K.; Lu, Y.; Nikolovska-Coleska, Z.; Wang, G.; Qiu, S.; Shangary, S.; Gao, W.; Qin, D.; Stuckey, J.; Krajewski, K.; Roller, P. P.; Wang, S. *J. Med. Chem.* **2006,** *12,* 3432–3435.
231. Vassilev, L. T.; Vu, B. T.; Graves, B.; Carvajal, D.; Podlaski, F.; Filipovic, Z.; Kong, N.; Kammlott, U.; Lukacs, C.; Klein, C.; Fotouhi, N.; Liu, E. A. *Science* **2004,** *303,* 844–848.
232. Zhao, Y.; Aguilar, A.; Bernard, D.; Wang, S. *J. Med. Chem.* **2015,** *58,* 1038–1052.
233. Vu, B.; Wovkulich, P.; Pizzolato, G.; Lovey, A.; Ding, Q.; Jiang, N.; Liu, J. J.; Zhao, C.; Glenn, K.; Wen, Y.; Tovar, C.; Packman, K.; Vassilev, L.; Graves, B. *ACS Med. Chem. Lett.* **2013,** *4,* 466–469.
234. https://clinicaltrials.gov/ct2/results?term=RG7112&Search=Search.
235. Andreeff, M.; Kelly, K. R.; Yee, K.; Assouline, S.; Strair, R.; Popplewell, L.; Bowen, D.; Martinelli, G.; Drummond, M. W.; Vyas, P.; Kirschbaum, M.; Iyer, S. P.; Kojima, K.; Geho, D.; Blotner, S.; Cheng, S.; Vassilev, L.; Ding, M.; Zhi, J.; Middleton, S.; Nichols, G. *Blood* **2012,** *120,* 675.
236. Ding, Q.; Zhang, Z.; Liu, J. J.; Jiang, N.; Zhang, J.; Ross, T. M.; Chu, X. J.; Bartkovitz, D.; Podlaski, F.; Janson, C.; Tovar, C.; Filipovic, Z. M.; Higgins, B.; Glenn, K.; Packman, K.; Vassilev, L. T.; Graves, B. *J. Med. Chem.* **2013,** *56,* 5979–5983.
237. https://clinicaltrials.gov/ct2/results?term=RO5503781.
238. Wang, S.; Sun, W.; Zhao, Y.; McEachern, D.; Meaux, I.; Barrière, C.; Stuckey, J. A.; Meagher, J. L.; Bai, L.; Liu, L.; Hoffman-Luca, C. G.; Lu, J.; Shangary, S.; Yu, S.; Bernard, D.; Aguilar, A.; Dos-Santos, O.; Besret, L.; Guerif, S.; Pannier, P.; Gorge-Bernat, D.; Debussche, L. *Cancer Res.* **2014,** *74,* 5855–5865.
239. Issaeva, N.; Bozko, P.; Enge, M.; Protopopova, M.; Verhoef, L.; Masucci, M.; Pramanik, A.; Selivanova, G. *Nat. Med.* **2004,** *10,* 1321–1328.
240. Zheng, M.; Yang, J.; Xu, X.; Sebolt, J. T.; Wang, S.; Sun, Y. *Anticancer Res.* **2010,** *9,* 3321–3331.
241. (a) Siedle, B.; Garcia-Pineres, A. J.; Murillo, R.; Schulte-Monting, J.; Castro, V.; Rungeler, P.; Klaas, C. A.; Da Costa, F. B.; Kisiel, W.; Merfort, I. *J. Med. Chem.* **2004,** *47,* 6042–6054; (b) Long, J.; Zhang, S. F.; Wang, P. P.; Zhang, X. M.; Yang, Z. J.; Zhang, Q.; Chen, Y. *J. Med. Chem.* **2014,** *57,* 7098–7112; (c) Ghantous, A.; Sinjab, A.; Herceg, Z.; Darwiche, N. *Drug Discov. Today* **2013,** *18,* 894–905; (d) Neelakantan, S.; Nasim, S.; Guzman, M. L.; Jordan, C. T.; Crooks, P. A. *Bioorg. Med. Chem. Lett.* **2009,** *19,* 4346–4349.
242. https://clinicaltrials.gov/ct2/results?term=JNJ-26854165&Search=Search.
243. Lambert, J. M.; Gorzov, P.; Veprintsev, D. B.; et al. *Cancer Cell* **2009,** *15,* 376–388.
244. https://clinicaltrials.gov/ct2/results?term=APR-246&Search=Search.
245. (a) Fulda, S.; Vucic, D. *Nat. Rev. Drug Discov.* **2012,** *11,* 109–123; (b) Obexer, P.; Ausserlechner, M. J. *Front. Oncol.* **2014,** *4,* 1–9; (c) Sun, H.; Nikolovska-Coleska, Z.; Lu, J.; Meagher, J. L.; Yang, C. Y.; Qiu, S.; Tomita, Y.; Ueda, Y.; Jiang, S.; Krajewski, K.; Roller, P. P.; Stuckey, J. A.; Wang, S. *J. Am. Chem. Soc.* **2007,** *129,* 15279–15294.
246. Fulda, S.; Vucic, D. *Nat. Rev. Drug Discov.* **2012,** *11,* 109–124.
247. (a) Du, C.; Fang, M.; Li, Y.; Li, L.; Wang, X. *Cell* **2000,** *102,* 33–42; (b) Verhagen, A. M.; Ekert, P. G.; Pakusch, M.; et al. *Cell* **2000,** *102,* 43–53; (c) Varfolomeev, E.; Blankenship, J. W.; Wayson, S. M.; et al. *Cell* **2007,** *131,* 669–681; (d) Dueber, E. C.; Schoeffler, A. J.; Lingel, A.; et al. *Science* **2011,** *334,* 376–380.
248. Cai, Q.; Sun, H.; Peng, Y.; Lu, J.; Nikolovska-Coleska, Z.; McEachern, D.; Liu, L.; Qiu, S.; Yang, C. Y.; Miller, R.; Yi, H.; Zhang, T.; Sun, D.; Kang, S.; Guo, M.; Leopold, L.; Yang, D.; Wang, S. *J. Med. Chem.* **2011,** *54,* 2714–2726.
249. (a) Sun, H.; Nikolovska-Coleska, Z.; Yang, C.-Y.; Xu, L.; Liu, M.; Tomita, Y.; Pan, H.; Yoshioka, Y.; Krajewski, K.; Roller, P. P.; Wang, S. *J. Am. Chem. Soc.* **2004,** *126,* 16686–16697; (b) Sun, H.; Nikolovska-Coleska, Z.; Yang, C.-Y.; Xu, L.; Tomita, Y.; Krajewski, K.; Roller, P. P.; Wang, S. *J. Med. Chem.* **2004,** *47,* 4147–4150; (c) Sun, H.; Nikolovska-Coleska, Z.; Lu, J.; Qiu, S.; Yang, C.-Y.; Gao, W.; Meagher, J.; Stuckey, J.; Wang, S. *J. Med. Chem.* **2006,** *49,* 7916–7920; (d) Sun, H.; Nikolovska-Coleska, Z.; Lu, J.; Meagher, J. L.; Yang, C.-Y.; Qiu, S.; Tomita, Y.; Ueda, Y.; Jiang, S.; Krajewski, K.; Roller, P. P.; Stuckey, J. A.; Wang, S. *J. Am. Chem. Soc.* **2007,** *129,* 15279–15294; (e) Sun, H.; Stuckey, J. A.; Nikolovska-Coleska, Z.; Qin, D.; Meagher, J. L.; Qiu, S.; Lu, J.; Yang, C.-Y.; Saito, N. G.; Wang, S. *J. Med. Chem.* **2008,** *51,* 7169–7180; (f) Peng, Y.; Sun, H.; Nikolovska-Coleska, Z.; Qiu, S.; Yang, C.-Y.; Lu, J.; Cai, Q.; Yi, H.; Wang, S. *J. Med. Chem.* **2008,** *51,* 8158–8162; (g) Zhang, B.; Nikolovska-Coleska, Z.; Zhang, Y.; Bai, L.; Qiu, S.; Yang, C.-Y.; Sun, H.; Wang, S.; Wu, Y. *J. Med. Chem.* **2008,** *51,* 7352–7355; (h) Sun, W.; Nikolovska-Coleska, Z.; Qin, D.; Sun, H.; Yang, C.-Y.; Bai, L.; Qiu, S.; Ma, D.; Wang, S. *J. Med. Chem.* **2009,** *52,* 593–596; (i) Sun, H.; Lu, J.; Liu, L.; Yi, H.; Qiu, S.; Yang, C.-Y.; Deschamps, J. R.; Wang, S. *J. Med. Chem.* **2010,** *53,* 6361–6367.
250. Chai, J.; Du, C.; Wu, J. W.; Kyin, S.; Wang, X.; Shi, Y. *Nature* **2000,** *406,* 855–862.
251. https://clinicaltrials.gov/ct2/results?term=AT-406&Search=Search.
252. Flygare, J. A.; Beresini, M.; Budha, N.; Chan, H.; Chan, I. T.; Cheeti, S.; Cohen, F.; Deshayes, K.; Doerner, K.; Eckhardt, S. G.; Elliott, L. O.; Feng, B.; Franklin, M. C.; Reisner, S. F.; Gazzard, L.; Halladay, J.; Hymowitz, S. G.; La, H.; LoRusso, P.; Maurer, B.; Murray, L.; Plise, E.; Quan, C.; Stephan, J. P.; Young, S. G.; Tom, J.; Tsui, V.; Um, J.; Varfolomeev, E.; Vucic, D.; Wagner, A. J.; Wallweber, H. J. A.; Wang, L.; Ware, J.; Wen, Z.; Wong, H.; Wong, J. M.; Wong, M.; Wong, S.; Yu, R.; Zobel, K.; Fairbrother, W. J. *J. Med. Chem.* **2012,** *55,* 4101–4113.
253. Cohen, F.; Fairbrother, W. J.; et al. *J. Med. Chem.* **2009,** *52,* 1723–1730.
254. Ndubaku, C.; Varfolomeev, E.; Wang, L.; Zobel, K.; Lau, K.; Elliott, L. O.; Maurer, B.; Fedorova, A. V.; Dynek, J. N.; Koehler, M.; Hymowitz, S. G.; Tsui, V.; Deshayes, K.; Fairbrother, W. J.; Flygare, J. A.; Vucic, D. *ACS Chem. Biol.* **2009,** *4,* 557–566.
255. https://clinicaltrials.gov/ct2/results?term=GDC-0152&Search=Search.
256. Condon, S. M.; Mitsuuchi, Y.; Deng, Y.; LaPorte, M. G.; Rippin, S. R.; Haimowitz, T.; Alexander, M. D.; Kumar, P. T.; Hendi, M. S.; Lee, Y. H.; Benetatos, C. A.; Yu, G.; Kapoor, G. S.; Neiman, E.; Seipel, M. E.; Burns, J. M.; Graham, M. A.; McKinlay, M. A.; Li, X.; Wang, J.; Shi, Y.; Feltham, R.; Bettjeman, B.; Cumming, M. H.; Vince, J. E.; Khan, N.; Silke, J.; Day, C. L.; Chunduru, S. K. *J. Med. Chem.* **2014,** *57,* 3666–3677.
257. https://clinicaltrials.gov/ct2/results?term=TL32711&Search=Search.
258. (a) Orlowski, R. Z.; Kuhn, D. J. *Clin. Cancer Res.* **2008,** *14,* 1649–1657; (b) Adams, J. *Cancer Cell* **2004,** *5,* 417–421; (c) Adams, J. *Trends Mol. Med.* **2002,** *8,* S49–S54; (d) Wu, W. K. K.; Cho, C. H.; Lee, C. W.; Wu, K.; Fan, D.; Yu, J.; Sung, J. J. Y. *Cancer Lett.* **2010,** *293,* 15–22; (e) Voorhees, P. M.; Dees, E. C.; O'Neil, B.; Orlowski, R. Z. *Clin. Cancer Res.* **2003,** *9,* 6316–6325.
259. (a) Kawamura, S.; Unno, Y.; List, A.; Mizuno, A.; Tanaka, M.; Sasaki, T.; Arisawa, M.; Asai, A.; Groll, M.; Shuto, S. *J. Med. Chem.* **2013,** *56,* 3689–3700; (b) Geurink, P. P.; van der Linden, W. A.; Mirabella, A. C.; Gallastegui, N.; de Bruin, G.; Blom, A. E. M.; Voges, M. J.; Mock, E. D.; Florea, B. I.; van der Marel, G. A.; Driessen, C.; van der Stelt, M.; Groll, M.; Overkleeft, H. S.; Kisselev, A. F. *J. Med. Chem.* **2013,** *56,* 1262–1275; (c) Azevedo, L. M.; Lansdell, T. A.; Ludwig, J. R.; Mosey, R. A.; Woloch, D. K.; Cogan, D. P.; Patten, G. P.; Kuszpit, M. R.; Fisk, J. S.; Tepe, J. J. *J. Med. Chem.* **2013,** *56,* 5974–5978; (d) Kawamura, S.; Unno, Y.; Asai, A.; Arisawa, M.; Shuto, S. *J. Med. Chem.* **2014,** *57,* 2726–2735; (e) Miller, Z.; Kim, K. S.; Lee, D. M.; Kasam, V.; Baek, S. E.; Lee, K. H.; Zhang, Y. Y.; Ao, L.; Carmony, K.; Lee, N. R.; Zhou, S.; Zhao, Q.; Jang, Y.; Jeong, H. Y.; Zhan, C. G.; Lee, W.; Kim, D. E.; Kim, K. B. *J. Med. Chem.* **2015,** *58,* 2036–2041; (f) Kim, K. B.; Crews, C. M. J. *J. Med. Chem.* **2008,** *51,* 2600–2605; (g) Rydzewski, R. M.; Burrill, L.; Mendonca, R.; Palmer, J. T.; Rice, M.; Tahilramani, R.; Bass, K. E.; Leung, L.; Gjerstad, E.; Janc, J. W.; Pan, L. *J. Med. Chem.* **2006,** *49,* 2953–2968.

260. Hideshima, T.; et al. *Cancer Res.* **2001,** *61,* 3071–3076.
261. (a) Borissenko, L.; Groll, M. *Chem. Rev.* **2007,** *107,* 687–717; (b) Vivier, M.; Jarrousse, A. S.; Bouchon, B.; Galmier, M. J.; Auzeloux, P.; Sauzieres, J.; Madelmont, J. C. *J. Med. Chem.* **2005,** *48,* 6731–6740; (c) Aubin, S.; Martin, B.; Delcros, J. G.; Arlot-Bonnemains, Y.; Baudy-Floc'h, M. *J. Med. Chem.* **2005,** *48,* 330–334.
262. (a) Hough, R.; Pratt, G.; Rechsteiner, M. *J. Biol. Chem.* **1986,** *261,* 2408; (b) Hough, R.; Pratt, G.; Rechsteiner, M. *J. Biol. Chem.* **1987,** *262,* 8303.
263. Huber, E.; Basler, M.; Schwab, R.; Heinemeyer, W.; Kirk, C. J.; Groettrup, M.; Groll, M. *Cell* **2012,** *148,* 727–738.
264. Groll, M.; Huber, R. *Biochim. Biophys. Acta* **2004,** *1695,* 33–44.
265. Verbrugge, S. E.; Assaraf, Y. G.; Dijkmans, B. A.; Scheffer, G. L.; den Uyl, M. A. D.; Oerlemans, R.; Chan, E. T.; Kirk, C. J.; Peters, G. J.; van der Heijden, J. W.; de Gruijl, T. D.; Scheper, R. J.; Jansen, G. J. *Pharmacol. Exp. Ther.* **2012,** *341,* 174–182.
266. (a) Kisselev, A. F.; van der Linden, W. A.; Overkleeft, H. S. *Cell* **2012,** *19,* 99–115; (b) Huber, E. M.; Groll, M. *Angew. Chem. Int. Ed.* **2012,** *51,* 8708–8720.
267. Bogyo, M.; McMaster, J. S.; Gaczynska, M.; Tortorella, D.; Goldberg, A. L.; Ploegh, H. *Proc. Natl. Acad. Sci. U. S. A.* **1997,** *94,* 6629–6634.
268. Groll, M.; Schellenberg, B.; Bachmann, A. S.; Archer, C. R.; Huber, R.; Powell, T. K.; Lindow, S.; Kaiser, M.; Dudler, R. *Nature* **2008,** *452,* 755–759.
269. (a) Adams, J.; Behnke, M.; Chen, S.; Cruickshank, A. A.; Dick, L. R.; Grenier, L.; Klunder, J. M.; Ma, Y. T.; Plamondon, L.; Stein, R. L. *Bioorg. Med. Chem. Lett.* **1998,** *8,* 333–338; (b) Chen, D.; Frezza, M.; Schmitt, S.; Kanwar, J.; Dou, Q. P. *Curr. Cancer Drug Targets* **2011,** *11,* 239–253; (c) Groll, M.; Berkers, C. R.; Ploegh, H. L.; Ovaa, H. *Structure* **2006,** *14,* 451–456.
270. Field-Smith, A.; Morgan, G. J.; Davies, F. E. *Ther. Clin. Risk Manag.* **2006,** *2,* 271–279.
271. Kale, A. J.; Moore, B. S. *J. Med. Chem.* **2012,** *55,* 10317–10327.
272. Kupperman, E.; Lee, E. C.; Cao, Y.; Bannerman, B.; Fitzgerald, M.; Berger, A.; Yu, J.; Yang, Y.; Hales, P.; Bruzzese, F.; Liu, J.; Blank, J.; Garcia, K.; Tsu, C.; Dick, L.; Fleming, P.; Yu, L.; Manfredi, M.; Rolfe, M.; Bolen, J. *Cancer Res.* **2010,** *70,* 1970–1980.
273. https://clinicaltrials.gov/ct2/results?term=MLN2238&Search=Search.
274. Dorsey, B. D.; Iqbal, M.; Chatterjee, S.; Menta, E.; Bernardini, R.; Bernareggi, A.; Cassarà, P. G.; D'Arasmo, G.; Ferretti, E.; De Munari, S.; Oliva, A.; Pezzoni, G.; Allievi, C.; Strepponi, I.; Ruggeri, B.; Ator, M. A.; Williams, M.; Mallamo, J. P. *J. Med. Chem.* **2008,** *51,* 1068–1072.
275. https://clinicaltrials.gov/ct2/results?term=delanzomib&Search=Search.
276. (a) Gräwert, M. A.; Gallastegui, N.; Stein, M.; Schmidt, B.; Kloetzel, P. M.; Huber, R.; Groll, M. *Angew. Chem. Int. Ed.* **2011,** *50,* 542–544; (b) Groll, M.; Kim, K. B.; Kairies, N.; Huber, R.; Crews, C. M. *J. Am. Chem. Soc.* **2000,** *122,* 1237–1238; (c) Crawford, L. J. A.; Walker, B.; Ovaa, H.; Chauhan, D.; Anderson, K. C.; Morris, T. C. M.; Irvine, A. M. *Cancer Res.* **2006,** *66,* 6379–6386.
277. (a) Elofsson, M. *Chem. Biol.* **1999,** *6,* 811–822; (b) Harshbarger, W.; Miller, C.; Diedrich, C.; Sacchettini, J. *Structure* **2015,** *23,* 418–424; (c) Demo, S. D.; Kirk, C. J.; Aujay, M. A.; Buchholz, T. J.; Dajee, M.; Ho, M. N.; Jiang, J.; Laidig, G. J.; Lewis, E. R.; Parlati, F.; Shenk, K. D.; Smyth, M. S.; Sun, C. M.; Vallone, M. K.; Woo, T. M.; Molineaux, C. J.; Bennett, M. K. *Cancer Res.* **2010,** *67,* 6383–6391.
278. Zhou, H. J.; Aujay, M. A.; Bennett, M. K.; Dajee, M.; Demo, S. D.; Fang, Y.; Ho, M. N.; Jiang, J.; Kirk, C. J.; Laidig, G. J.; Lewis, E. R.; Lu, Y.; Muchamuel, T.; Parlati, F.; Ring, E.; Shenk, K. D.; Shields, J.; Shwonek, P. J.; Stanton, T.; Sun, C. M.; Sylvain, C.; Woo, T. M.; Yang, J. *J. Med. Chem.* **2009,** *52,* 3028–3038.
279. https://clinicaltrials.gov/ct2/results?term=ONX0912&Search=Search.
280. (a) Bürgi, H. B.; Dunitz, J. D.; Shefter, E. *J. Am. Chem. Soc.* **1973,** *95,* 5065–5067; (b) Groll, M.; Huber, R.; Potts, B. C. M. *J. Am. Chem. Soc.* **2006,** *128,* 5136–5141.
281. Macherla, V. R.; Mitchell, S. S.; Manam, R. R.; Reed, K. A.; Chao, T. H.; Nicholson, B.; Deyanat-Yazdi, G.; Mai, B.; Jensen, P. R.; Fenical, W. F.; Neuteboom, S. T. C.; Lam, K. S.; Palladino, M. A.; Potts, B. C. M. *J. Med. Chem.* **2005,** *48,* 3684–3687.
282. https://clinicaltrials.gov/ct2/results?term=salinosporamide+A&Search=Search.
283. Fraile, J. M.; Quesada, V.; Rodriguez, D.; Freije, J. M. P.; Lopez-Otin, C. *Oncogene* **2012,** *31,* 2373–2388.
284. Wilkinson, K. D. *FASEB J.* **1997,** *11,* 1245–1256.
285. Hussain, S.; Zhang, Y.; Galardy, P. J. *Cell Cycle* **2009,** *8,* 1688–1697.
286. (a) Colombo, M.; Vallese, S.; Peretto, I.; Jacq, X.; Rain, J. C.; Colland, F.; et al. *ChemMedChem* **2010,** *5,* 552–558; (b) Hirayama, K.; Aoki, S.; Nishikawa, K.; Matsumoto, T.; Wada, K. *Bioorg. Med. Chem.* **2007,** *15,* 6810–6818.
287. Reverdy, C.; Conrath, S.; Lopez, R.; et al. *Chem. Biol.* **2012,** *19,* 467–477.
288. Chauhan, D.; Tian, Z.; Nicholson, B.; et al. *Cancer Cell* **2012,** *22,* 345–358.
289. D'Arcy, P.; Brnjic, S.; Olofsson, M. H.; et al. *Nat. Med.* **2011,** *17,* 1636–1640.
290. Lee, B. H.; Lee, M. J.; Park, S.; et al. *Nature* **2010,** *467,* 179–184.
291. (a) Daviet, L.; Colland, F. *Biochimie* **2008,** *90,* 270–283; (b) Turk, B. *Nat. Rev. Drug Discov.* **2006,** *5,* 785–799.
292. Nero, T. L.; Morton, C. J.; Holien, J. K.; Wielens, J.; Parker, M. W. *Nat. Rev. Cancer* **2014,** *14,* 248–262.
293. Gray, W. M.; Kepinski, S.; Rouse, D.; Leyser, O.; Estelle, M. *Nature* **2001,** *414,* 271–276.
294. DaRosa, P. A.; Wang, Z.; Jinag, X.; et al. *Nature* **2015,** *517,* 223–226.
295. (a) Sakamoto, K. M.; Kim, K. B.; Kumagai, A.; Mercurio, F.; Crews, C. M.; Deshaies, R. J. *Proc. Natl. Acad. Sci. U. S. A.* **2001,** *98,* 8554–8559; (b) Winter, G. E.; Buckley, D. L.; Paulk, J.; et al. *Science* **2015,** *348,* 1376–1381; (c) Buckley, D. L.; Raina, K.; Darricarrere, N.; et al. *ACS Chem. Biol.* **2015,** *10,* 1831–1837; (d) Zengerle, M.; Chan, K. H.; Ciulli, A. *ACS Chem. Biol.* **2015,** *10,* 1770–1777; (e) Bondeson, D. P.; Mares, A.; Smith, I. E.; et al. *Nat. Chem. Biol.* **2015,** *11,* 611–617; (f) Toure, M.; Crews, C. M. *Angew. Chem. Int. Ed.* **2016,** *55,* 1966–1973; (g) Lai, A. C.; Toure, M.; Hellerschmied, D.; Salami, J.; Jaime-Figueroa, S.; Ko, E.; Hines, J.; Crews, C. M. *Angew. Chem. Int. Ed.* **2016,** *55,* 807–810.
296. Neklesa, T. K.; Tae, H. S.; Schneekloth, A. R.; et al. *Nat. Chem. Biol.* **2011,** *7,* 538–543.
297. Lai, A.; Kahraman, M.; Govek, S.; et al. *J. Med. Chem.* **2015,** *58,* 4888–4904.
298. Ito, T.; Ando, H.; Suzuki, T.; Ogura, T.; Hotta, K.; Imamura, Y.; Yamaguchi, Y.; Handa, H. *Science* **2010,** *327,* 1345–1350.
299. Bartlett, J. B.; Dredge, K.; Dalgleish, A. G. *Nat. Rev. Cancer* **2004,** *4,* 314–322.
300. Quach, H.; Ritchie, D.; Stewart, A. K.; Neeson, P.; Harrison, S.; Smyth, M. J.; Prince, H. M. *Leukemia* **2010,** *24,* 22–32.
301. https://clinicaltrials.gov/ct2/results?term=CC122&Search=Search.

5.08 Inhibitors of Epigenetic Regulation in Cancer

D Harvey and M Foley, Epizyme Inc., Cambridge, MA, United States

© 2017 Elsevier Ltd. All rights reserved.

5.08.1	**Introduction**	282
5.08.2	**Epigenetic Modifications**	282
5.08.2.1	Histone Structure	282
5.08.2.2	Role of Chromatin Modifications in Cancer	282
5.08.2.3	Methyl Modifications to Lysine and Arginine	283
5.08.2.4	Writer Enzymes	283
5.08.2.4.1	Histone methyl transferases	283
5.08.2.4.2	Histone acetyl transferases	283
5.08.2.5	Reader Domains	283
5.08.2.6	Eraser Enzymes	284
5.08.2.6.1	Lysine demethylases	284
5.08.2.6.2	Histone deacetylases	284
5.08.3	**Comparison to Kinases**	284
5.08.4	**Challenges in Screening**	285
5.08.4.1	Enzyme Selection	285
5.08.4.2	Substrate Identification	286
5.08.4.3	Assay Conditions	286
5.08.4.4	Hit Validation	286
5.08.4.5	Cellular Assays	286
5.08.5	**Approved and Clinical Stage Epigenetic Regulators**	286
5.08.6	**Case Studies**	286
5.08.6.1	Histone Deacetylases	286
5.08.6.2	Histone Methyltransferases	287
5.08.6.2.1	Arginine methyltransferases	287
5.08.6.2.2	Lysine methyltransferases	290
5.08.6.3	Lysine (K)-Specific Demethylases	300
5.08.6.3.1	Lysine (K)-specific demethylase 1A	300
5.08.6.4	Bromodomains	300
5.08.6.4.1	Bromodomain and extra C-terminal domain	300
5.08.7	**Conclusion**	304
References		305

Abbreviations

ADME Adsorption, distribution, metabolism, excretion
ApoA1 Apolipoprotein A-1
ATP Adenosine triphosphate
BAZ2A Bromodomain next to zinc finger domain 2A
BAZ2B Bromodomain next to zinc finger domain 2B
BET Bromodomain and extra C-terminal domain
BRD Bromodomain testis-specific
CMP Chromatin modifying proteins
DLBCL Diffuse large B-cell lymphoma
DNA Deoxyribonucleic acid
DOT1L Disrupter of telomeric silencing like protein
EHMT1 Euchromatic histone-lysine *N*-methyltransferase 1
EHMT2 Euchromatic histone-lysine *N*-methyltransferase 2
EZH2 Enhancer of zeste homolog 2
FAD Flavin adenine dinucleotide
HAT Histone acetyltransferase
HDAC Histone deacetylase
HMT Histone methyltransferase
HTRF Homogeneous time-resolved fluorescence
H_XK_Y Histone X lysine Y
JAK3 Janus kinase 3
JmjC Jumonji C
KDM Lysine demethylase
KDM1/LSD1 Lysine-specific demethylases
KDM1A Lysine (K)-specific demethylase 1A
KMT Lysine methyltransferase
MELC Murine erythroleukemia cells
MLL Mixed lineage lymphoma
MLL-r MLL rearrangement
p53 Tumor protein p53
PD Pharmacodynamic
PK Pharmacokinetics
PTM Posttranslational modification
PRC2 Polycomb repressive complex 2
PRMT1 protein arginine methyltransferase 1
PRMT5 Protein arginine methyltransferase 5

PRMT6 Protein arginine methyltransferase 6
PRMT8 Protein arginine methyltransferase 8
RMT Arginine methyltransferase
RNA Ribonucleic acid
SAH *S*-Adenosylhomocysteine
SAM *S*-Adenosylmethionine
SAR Structure activity relationship
SET9 SET domain-containing (lysine methyltransferase) 9
SGC Structural Genomics Consortium
SMYD2 SET and MYND domain-containing 2
SMYD3 SET and MYND domain-containing 3
SPA Scintillation proximity assay
TGI Tumor growth inhibition
THIQ Tetrahydroisoquinoline

5.08.1 Introduction

The medical community has been working to understand and treat cancer since before the disease was identified as such. As the field of medicine has advanced so has our understanding of cancer, not as a single uniform disease but as a collection of malignancies united by common hallmarks of aberrant cell growth.[1] In the last decade, the role posttranslational modifications (PTMs) play in driving cancer has been an area of burgeoning research. This article will review how recent advances in our understanding of a subset of the mechanisms by which these modifications drive cancers have led to drug discovery programs, clinical trials, and marketed therapies.

5.08.2 Epigenetic Modifications

5.08.2.1 Histone Structure

Cells store an immense amount of genetic information in the form of deoxyribonucleic acids (DNA). To fit this information into the cell nucleus, the DNA is wound around proteins called histones, of which there are five major families: H1/H5, H2A, H2B, H3, and H4, which come together to form a cylinder shape. Together, the DNA and the histones form the nucleosome which resembles beads on a string. The nucleosomes are further compacted into chromatin which can exist in the open euchromatin form or the highly condensed heterochromatin form (Fig. 1). Utilizing histones in this manner enables 1.8 m of DNA to be compacted into 90 μm of chromatin. Due to the compacted structure of heterochromatin, genes are largely inaccessible to the transcriptional machinery, thus rendering heterochromatin transcriptionally inactive. To initiate protein synthesis, the heterochromatin structure must loosen in a highly controlled manner to reveal specific promoter regions. The relaxing of heterochromatin into euchromatin, and the reverse process, is called chromatin remodeling and is controlled by changes to the structure of the nucleosomes.[2]

The structural changes to the nucleosome are effected through PTMs to the ~30-amino acid tail portion of the histone proteins (Fig. 2). The PTMs include phosphorylation, methylation, and acetylation among others. The enzymes that control the methyl and acetylation states of the lysine residues, and in the case of methylation, arginine residues as well, in histone tails have been the most widely studied to date and will be the subject of this article.[3]

5.08.2.2 Role of Chromatin Modifications in Cancer

It is known that epigenetic regulation is often dysregulated in cancer; however, the precise role chromatin modifying proteins (CMPs) play in driving cancer is postulated for only a small subset of cancers.[3,4] For example, mutations to enhancer of zeste homolog 2 (*EZH2*), which acts as part of a larger complex, can result in an aberrant increase in histone 3 lysine 27 (H3K27) trimethylation activity. Overexpression of EZH2 is also observed in several leukemias and other solid tumors.[2c,3] Methylation of H3K79 by disrupter of telomeric silencing like protein (DOT1L) at ectopic gene locations has also been implicated in leukemia, in which wild-type DOT1L is recruited to mixed lineage lymphoma (MLL) target genes by MLL-fusion proteins. The resulting ectopic methylation at H3K79 leads to overexpression of several genes known to drive leukemogenesis.[5]

Fig. 1 Representation of the two forms of chromatin with permission from Epizyme.

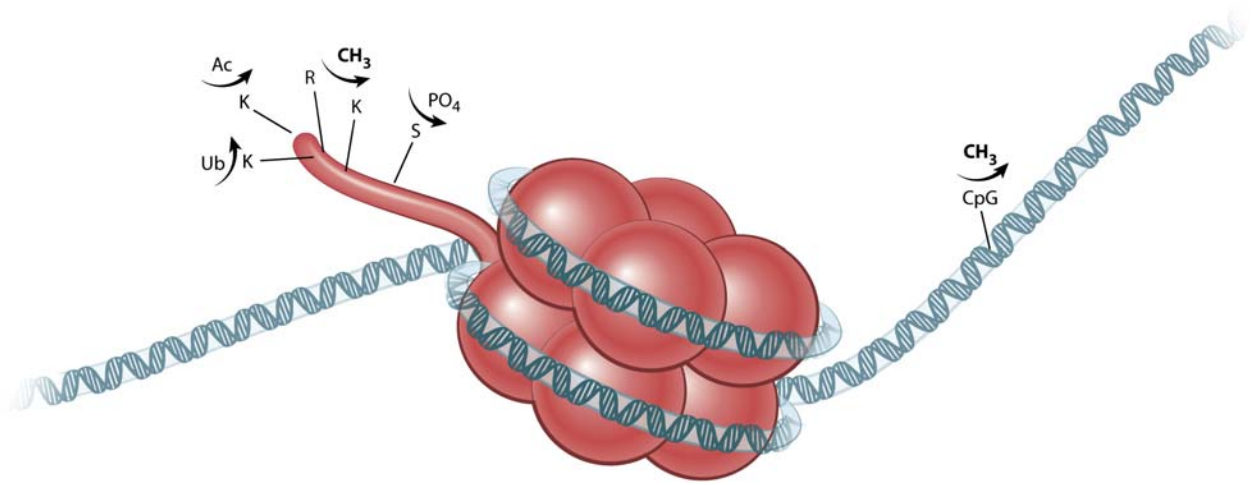

Fig. 2 Representation of the types of PTMs possible on the tail portion of histone proteins: *CH_3*, methylation; *PO_4*, phosphorylation; *Ac*, acetylation; *Ub*, ubiquitination; *K*, lysine; *R*, arginine; *S*, serine; *CpG*, 5′-C-phosphate-G-3′ with permission from Epizyme.

5.08.2.3 Methyl Modifications to Lysine and Arginine

Histone residues can undergo multiple posttranslational modifications. This article will address posttranslational methylation. With respect to methylation, histone-lysine residues can exist in multiple states including the unmodified residue, mono-, di-, or trimethylated (KMe1–3). Likewise, histone arginines can exist in multiple states; they can be mono- or dimethylated and the dimethylation state can either be symmetric or asymmetric (RMe, RMe2sym, and RMe2asym, respectively). The enzymes responsible for these transformations are collectively called writers. There are also reader proteins for both lysine and arginine that recognize the various PTMs and eraser proteins that remove the methyl groups from lysines.[3,4]

5.08.2.4 Writer Enzymes

5.08.2.4.1 Histone methyl transferases

Methyl modifications to histones are catalyzed by histone methyltransferases (HMTs) sometimes more generally referred to as protein methyltransferases. The HMT enzyme class consists of over 50 members and can be divided by target residue into lysine methyltransferases (KMTs) and arginine methyltransferases (RMTs). HMTs use *S*-adenosylmethionine (SAM) as a methyl donor substrate and the methyl group is transferred via an S_N2 mechanism to the side chain nitrogen of the lysine or arginine acceptor substrate.[4] The HMTs vary in substrate specificity; for example, DOT1L is only known to methylate histone H3 lysine 79 (H3K79).[4] On the other hand, H3K9 can be dimethylated by euchromatic histone-lysine *N*-methyltransferase 2 (EHMT2) and trimethylated by SET domain bifurcated 1 enzyme. Protein arginine methyltransferase 5 (PRMT5) is known to methylate H4R3 and H3R8 along with other proteins (http://www.thesgc.org/epigenetics). At the time of writing this article, there are four inhibitors targeted toward two KMTs undergoing clinical trials; tazemetostat, GSK2816126 and CPI-1205 for EZH2, and pinometostat for DOT1L.

5.08.2.4.2 Histone acetyl transferases

In addition to methylation, histone lysines can undergo acetylation mediated by a family of enzymes called histone acetyltransferases (HATs). This 18-member family of enzymes transfers an acetate moiety from acetyl-CoA to the amino group of lysine residues on histones and other proteins. The HATs have not been studied as extensively as some of the other epigenetic regulator families and no HAT inhibitors have advanced to the clinic to date (http://www.thesgc.org/epigenetics).

5.08.2.5 Reader Domains

Histone methyl and acetyl marks are read by proteins containing one of several reader domains. The tudor domain-containing proteins interact with di- and trimethylated lysine, whereas the malignant brain tumor domain-containing proteins bind mono- and dimethylated proteins. Tudor domains are also able to interact with methylated arginine. In contrast, plant homeodomains recognize lysine acetylation and all three methylation states but are specific to H3K4 location for methylation and acetylation and H3K14 for acetylation. H3K4 methylation can also be read by chromodomains. To date, there are no small-molecule inhibitors of methyl reader domains in the clinic (http://www.thesgc.org/epigenetics).

In addition to the proteins mentioned in the previous paragraph, the histone acetyl marks are also read by a family of proteins known as bromodomains. There are over 60 bromodomains encoded in the human genome and 40 bromodomain-containing

proteins.[6] There are currently two compounds in the clinic that target the bromodomain and extra C-terminal domain (BET) subfamily of bromodomains.

5.08.2.6 Eraser Enzymes

5.08.2.6.1 Lysine demethylases

Lysine methyl marks are removed by the lysine demethylase (KDM) family of enzymes in a sequence-dependent manner. The KDMs are divided into two subfamilies, the lysine-specific demethylases (LSD1/KDM1) and the Jumonji C (JmjC)-domain-containing demethylases (KDMs2–7). The lysine-specific demethylase family of enzymes is flavin dependent whereas the JmjC domain-containing enzymes are Fe(II) and 2-oxoglutarate dependent. Jumonji domain-containing 6 (JmjD6) has been reported to have arginine demethylation activity; however, this activity is subject to conflicting reports.[7] Currently, there are three KDM1 inhibitors undergoing clinical trials (Table 1).

5.08.2.6.2 Histone deacetylases

Lysine acetyl marks are removed by a family of enzymes known as histone deacetylases (HDACs). HDACs remove acetyl groups from the lysine residues of histones and other proteins. The HDACs are divided into five broad classes. Class 1 (HDAC 1, 2, 3, and 8), Class IIa (HDAC 4, 5, 7, and 9), Class IIb (HDAC 6 and 10), and Class IV (HDAC 11) are zinc-containing enzymes, whereas Class III are nonzinc-dependent enzymes called sirtuins. The HDACs have historically been the most studied family of histone-modifying proteins to date and as a result there are four approved HDAC inhibitors and numerous others are undergoing clinical trials (Table 1).

5.08.3 Comparison to Kinases

KMTs and RMTs are both members of the broader family of HMTs and both utilize the same methyl donating cofactor (SAM). One can draw an instructive analogy to protein kinases, which also employ a common cofactor, adenosine triphosphate (ATP) to

Table 1 Summary of epigenetic regulators approved and in clinical trials

Drug name	*Target class/enzyme*	*Status*	*Indication*
Belinostat	HDAC/pan-HDAC	Approved	Peripheral T cell lymphoma
Panobinostat	HDAC/pan-HDAC	Approved	Multiple myeloma
Pracinostat	HDAC/class I, II, IV	Approved	AML, T cell lymphoma
Romidepsin	HDAC/Zn dependent HDACS	Approved	Cutaneous T cell lymphoma
Vorinostat	HDAC/pan-HDAC	Approved	Cutaneous T cell lymphoma
Entinostat	HDAC/class I, III	Phase II/III	Multiple cancers
Givinostat	HDAC/class I, II	Phase II	
Mocetinostat	HDAC/pan-HDAC	Phase II	Lymphoma, leukemia
Quisinostat	HDAC/pan-HDAC	Phase II	Leukemia, MLL, lymphoma, solid malignancies
Resminostat	HDAC	Phase II	HCC
Tacedinaline	HDAC/HDAC1, HDAC2	Phase II	Multiple myeloma
Tazemetostat	HMT/EZH2	Phase II	Lymphoma, solid tumors
Valproic acid	HDAC/pan-HDAC	Phase II	Multiple cancers
ACY-1215	HDAC/HDAC6	Phase I/II	Multiple myeloma
AR-42	HDAC/pan-HDAC	Phase I/II	MLL, lymphoma, leukemia
ORY-1001	KDM/KDM1A	Phase I/II	AML
OTX015	Bromodomain/BET	Phase I/II	Glioblastoma
Tranylcypromine	KDM/KDM1A	Phase I/II	AML
ABBV-075	Bromodomain	Phase I	Advanced cancers
Abexinostat	HDAC/pan-HDAC	Phase I	B-cell lymphoma
BAY-1238097	Bromodomain/BET	Phase I	Neoplasms
BMS-986158	Bromodomain/BET	Phase I	Solid tumors
CPI-0610	Bromodomain/BET	Phase I	Lymphoma
CPI-1205	HMT/EZH2	Phase I	B-cell lymphoma
CUDC-907	HDAC/class I, IIB	Phase I	Lymphoma, multiple myeloma, solid tumors
GSK525762	Bromodomain/BDR4	Phase 1	Hematological malignancy, NUT midline carcinoma
GSK2816126	HMT/EZH2	Phase I	B-cell lymphoma, follicular lymphoma
GSK2879552	KDM/KDM1A	Phase I	AML
Pinometostat	HMT/DOT1L	Phase I	Leukemia
TEN-010	Bromodomain/BET	Phase I	AML and solid tumors

accomplish their function. Kinases transfer the terminal phosphoryl group from ATP to a serine, threonine, tyrosine, or histidine residue on the target protein and in doing so generate adenosine diphosphate as a byproduct. Protein kinases have been a vigorous area of pharmaceutical research for the past decade and there are >25 approved kinase inhibitors on the market and a further >50 kinase inhibitors currently in clinical trials. The vast majority of kinase inhibitors that have been clinically examined are ATP competitive and are targeted toward a single kinase. Therefore, kinase specificity is often a challenge for this target class. There is however sufficient structural diversity within the ATP-binding pockets of kinases to enable selective inhibitors to be designed and generated as exemplified by tarceva[8] and imatinib.[9] One could take a parallel approach with HMTs by designing inhibitors that compete with SAM and engender specificity for the HMT of choice by taking advantage of any structural uniqueness within the SAM-binding site (Fig. 3). This has been successfully demonstrated at Epizyme by the production of two selective SAM-competitive HMT inhibitors: tazemetostat,[10] an EZH2 inhibitor, and pinometostat,[11] a DOT1L inhibitor (see Fig. 3).

There are, however, some alternative potential modes of inhibition that can be targeted when drugging HMTs. It is possible to target the protein substrate pocket, interfering where the lysine or arginine residues would bind prior to being methylated. This approach offers certain advantages over SAM competition as proteins with a low K_m for SAM will result in large potential cell shifts when moving from a biochemical assay run under balanced conditions into a cellular context where there may be high intracellular SAM concentration. This is analogous to targeting a kinase with a low K_m for ATP, such as Janus Kinase 3 (JAK3). JAK3 has a reported K_m for ATP of 6 μM,[12] using the Cheng–Prusoff equation and a cellular [ATP] of 1 mM, one would predict that an inhibitor run under balanced condition would see a fold-loss of ~170× when run in a cellular assay. That is a large potency gap that a medicinal chemist would have to anticipate and account for when establishing a desired drug profile. Thus, should the target HMT have a low K_m for SAM relative to the cellular concentrations of SAM, it may be preferable to optimize a noncompetitive SAM inhibitor over a SAM-competitive inhibitor. The screening paradigm would need to be designed, such that it could identify and differentiate a competitive versus noncompetitive profile.

5.08.4 Challenges in Screening

The discovery of small-molecule inhibitors of CMPs is a relatively recent phenomenon. HDAC inhibitors were the first to be discovered but as mentioned in the previous section there are many enzyme classes for which tool compounds are not yet known. Discovering starting points for medicinal chemistry programs has been challenging for a number of reasons.

5.08.4.1 Enzyme Selection

The first step in setting up a screening strategy is determining the protein or protein complex to use in the screen. Even in isolated enzyme screens selecting the enzyme form, full length or truncated, is a crucial step and may influence the hits obtained in the screen. In their SET and MYND domain-containing 2 (SMYD2) program, Eli Lilly used full-length SMYD2 enzyme,[13] in contrast the Structural Genomics Consortium (SGC) used a truncated EHMT2 (913–1193) enzyme in the development of their EHMT2

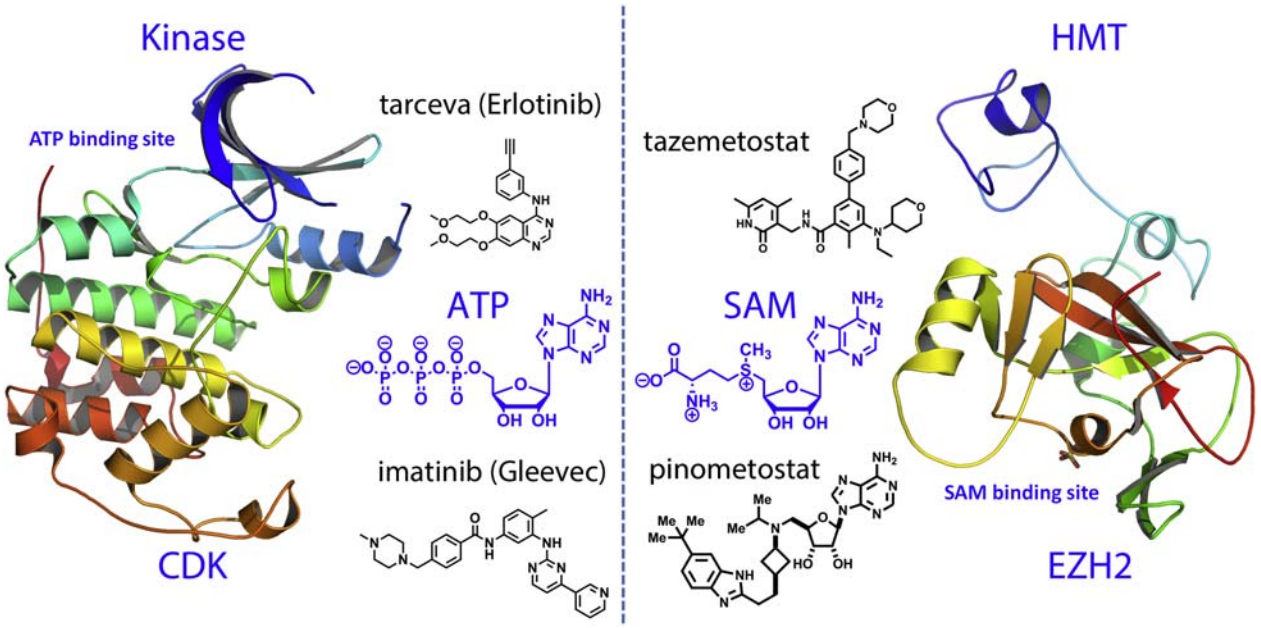

Fig. 3 X-ray representation of CDK and EZH2 and their associated cofactors and published inhibitors.

tool compound.[14] The EZH2 enzyme exists as part of the larger polycomb repressive complex 2 (PCR2) and screening has been carried out using recombinant PCR2 complexes. Constellation (SUZ12, EED, RBBP4, RBBP7, and either wt EZH1, wt EZH2, or Y641N mutated EZH2),[15] Epizyme (EED, SUZ12, RbAP48, and wt EZH2 or Y641C mutant EZH2),[16] GSK (EZH2, EED, SUZ12, AEBP2, and RbAp48),[17] and Novartis[18] (Ezh2, Suz12, EED, RbAP48, and AEBP2) all used a recombinant PRC2 complex in their EZH2 programs.

5.08.4.2 Substrate Identification

Once a protein or protein complex is selected, the substrate for the assay must be identified and validated. The endogenous substrates for these enzymes are the histone proteins that have been compacted into nucleosomes. In their DOT1L program, Epizyme used chicken oligonucleosome as the methylation substrate.[19] However, in their PRMT5 program, Epizyme used an H4 histone tail peptide.[20] Eli Lilly developed both a histone tail (residues 1–24 of H4) assay and a tumor protein p53 (p53) peptide (residues 361–380) assay for their SMYD2 program.[5,13]

5.08.4.3 Assay Conditions

Assay conditions can have a profound influence on the types of hits found during the screening process. For enzymes that have a cofactor, such as the HMTs, HATs, and KDMs, inhibitors can be substrate or cofactor competitive. Running an HMT assay at high SAM concentration, for example, will bias the results toward SAM uncompetitive hits. Boehringer Ingelheim took this approach during their EHMT2 screening campaign.[21] Running an assay under balanced conditions enables the identification of both substrate and cofactor competitive inhibitors.[22]

5.08.4.4 Hit Validation

Both Epizyme and Constellation reported low micromolar potency hits from their PRMT5[20] and EZH2[15] screens, respectively. In this potency range compounds can exhibit a number of behaviors that lead to false positives. For this reason, both companies employed additional assays to identify compounds that were truly inhibitors of the enzymes in question. Epizyme ran the initial screen using a fluorescence assay. Pan-assay interference structures (PAINS)[23] were removed and the remaining compounds were subjected to an orthogonal radiometric PRMT5 assay using ^{3}H SAM followed by a redox assay. These triage steps narrowed the original hit list down to a single prioritized series with potencies ranging from 0.4 to 7 μM. This series was further validated using biophysical methods and X-ray crystallography. Constellation reported 288 confirmed hits in an EZH2 screen, the majority of which were >20 μM in potency. After subjecting these compounds to a number of assays further described in the "**Enhancer of zeste homolog 2**" section, a single weak inhibitor was selected as a starting point for medicinal chemistry optimization.

5.08.4.5 Cellular Assays

Cellular assays are also complicated by the fact that several days of compound treatment can be necessary before effects on histone methyl marks or target genes are observable. Additionally, there is currently a lack of commercially available antibodies for detecting a broad spectrum of specific acylation or methylation events.[5]

5.08.5 Approved and Clinical Stage Epigenetic Regulators

See **Table 1**.

5.08.6 Case Studies

5.08.6.1 Histone Deacetylases

The HDACs have been an area of active research for a number of years and there are currently four approved HDAC inhibitors on the market.[1] Vorinostat, also known as suberoylanilide hydroxamic acid (SAHA), panobinostat, and belinostat are pan-HDAC inhibitors, whereas romidepsin primarily inhibits Class I HDACs (**Fig. 4**).[3] With the exception of romidepsin and valproic acid, both of which are natural product derived, the most advanced HDAC inhibitors can be divided into two different structural classes. Vorinostat, belinostat, panobinostat, and a number of others contain hydroxamides, whereas mocetinostat[24] and entinostat are 2-aminoanilides.

Vorinostat was the first approved HDAC inhibitor, although at the time of discovery the mechanism of action was unknown.[25] Vorinostat evolved from the discovery that murine erythroleukemia cells (MELC) turned red upon treatment with high concentrations of dimethylsulfoxide. A similar result was seen with other highly polar solvents, with amide containing solvents being the most potent. This observation led to the design and synthesis of hexamethylene bisacetamide which inhibited the MELC growth with an IC_{50} of 5 mM (**Fig. 5**). The bisacetamide compound entered clinical trials but was not well-tolerated and it became clear

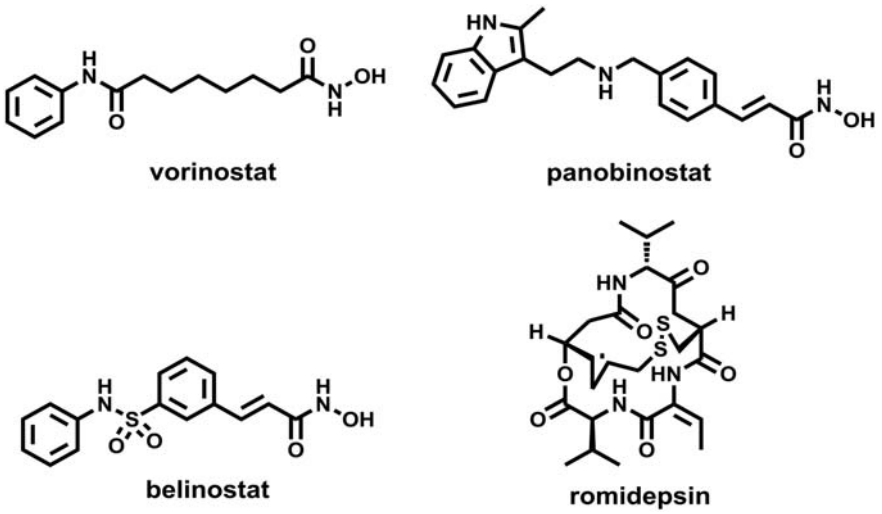

Fig. 4 Structures of approved HDAC inhibitors.

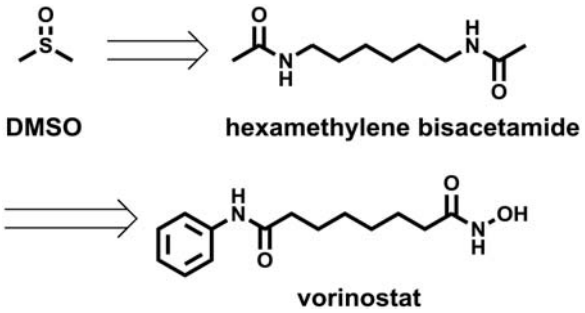

Fig. 5 Chemical iterations toward vorinostat.

that a more potent compound was necessary. Speculating that the amides were binding to a metal containing site on an enzyme, a series of hydroxamide containing compounds were prepared. Vorinostat is not the most potent analog in this series but does strike a balance between efficacy and toxicity. Vorinostat was approved for the treatment of cutaneous T cell lymphoma but due to undesirable side effects has not been approved in other indications.[2a]

Due to the dose limiting toxicity seen with some of the pan-HDAC inhibitors, the next generation of inhibitors has aimed to be more selective, targeting a single HDAC isozyme, or a small subset of isozymes. There are currently several HDAC inhibitor compounds undergoing clinical trials in lymphoma and other indications (**Table 1**).

5.08.6.2 Histone Methyltransferases

5.08.6.2.1 Arginine methyltransferases

5.08.6.2.1.1 Protein arginine methyltransferase 5

PRMT5 is reported to have roles in diverse cellular processes, including tumorigenesis. Overexpression of PRMT5 is observed in cell lines and primary patient samples derived from lymphomas, particularly mantle cell lymphoma (MCL). Epizyme conducted a homogeneous time-resolved fluorescence (HTRF) assay-based HTS campaign monitoring the mono methylation of an H4R3 peptide. A library of 370,000 compounds was profiled and generated a hit rate of 0.7%.[20] A triage funnel was applied (cherry pick retest, PAINS filters, and removal of additional proprietary frequent hitter substructures). This furnished 800 compounds for further follow up. Compounds making it through this preliminary triage were then further culled by utilizing additional screens looking for HTRF artifacts. Examples of these assays were an orthogonal biochemical assay and a redox assay. This further winnowed down the list to a single interesting series, which was further characterized by enzymology experiments, biophysical methods, and X-ray crystallography. EPZ007345 (**Fig. 6**) was an example of a series of 17 compounds with activity against PRMT5 ranging from 0.4 to 7 μM.[26]

The tetrahydroisoquinoline (THIQ) is believed to participate in a π–cation interaction with the charged methyl group of SAM. Altering the electronic properties or the positioning of the aryl ring of the THIQ resulted in compounds with a reduced inhibitory

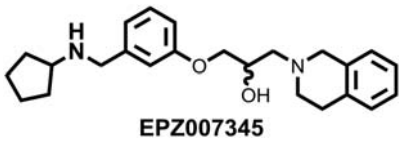

Fig. 6 Structure of EPZ007345.

potency. Initial structure activity relationships (SAR) demonstrated that structural changes distal to the THIQ moiety were well-tolerated and able to show improvements in potency and absorption, distribution, metabolism, and excretion (ADME) properties. Compounds **1** and **2** (Fig. 7) were both active in the cellular methylation assay but compound **2** showed a threefold improvement in cellular antiproliferative assays when compared to **1**. While these compounds represent an improvement in cellular potency, these compounds and others in the chemical series were not stable in human and mouse liver microsome assays.

To address the high clearance in liver microsomes, efforts were directed toward less lipophilic compounds with lower clogD values. Additional attention was paid to compounds with human liver microsome scaled clearance values $\leq$50% of hepatic blood flow. The authors propose that this parameter was likely to lead to chemical space from which a candidate quality compound could be identified. Further assessment of compounds in mouse pharmacokinetic (PK) studies led to the identification of EPZ015666, a 22 nM PRMT5 inhibitor with a favorable in vivo profile (Fig. 8).

EPZ015666 was shown to be competitive with substrate and uncompetitive with SAM. EPZ015666 was also selective versus a panel of 20 other protein methyltransferases, where no inhibition was seen up to 50 μM. The mouse PK profile was also favorable with a plasma clearance of 30 mL $min^{-1} kg^{-1}$ and a volume of distribution of 1.7 L kg^{-1} after intravenous dosing at 2 mg kg^{-1}, and oral bioavailability of 69% following oral administration of 10 mg kg^{-1}. Thus EPZ015666 was used for both in vitro and in vivo studies to explore the biology of PRMT5.

A quaternary crystal structure of PRMT5:MEP50 in complex with EPZ015666 and SAM was obtained (Fig. 9). The THIQ moiety was shown to be involved in a cation–π interaction with the charged methyl group of SAM. The THIQ also made a π–π stacking interaction with Phe327.

EPZ015666 was then profiled in a cellular context. A panel of five MCL cell lines (Z-138, Maver-1, Mino, Granta-519, and Jeko-1) was utilized to characterize target engagement and subsequent effects on cell proliferation upon treatment with a PRMT5 inhibitor. The effects of EPZ015666 treatment on cellular symmetric arginine demethylation in Z-138 cells were tested by immunoblotting using a pan-dimethyl symmetric arginine antibody. A concentration-dependent decrease in the intensity of multiple bands, including one that colocalized with the previously reported PRMT5 substrate small nuclear ribonucleoprotein D3 polypeptide was observed. This effect was further validated using short hairpin ribonucleic acid (RNA). Antiproliferative effects of EPZ015666 were evident after several days of exposure, thus a long-term proliferation assay was established (12 days). EPZ015666 demonstrated potent concentration-dependent antiproliferative effects, with IC_{50} values of 96 and 450 nM for Z-138 and Maver-1 cells, respectively. EPZ015666 is bioavailable and thus suitable for in vivo studies. EPZ015666 was dosed twice-daily to severe combined immune deficiency mice bearing Z-138 or Maver-1 xenografts at doses of 25, 50, 100, and 200 mg kg^{-1} for 21 days. EPZ015666 demonstrated dose-dependent exposure and tumor growth inhibition (TGI) in both models. The 200 mg kg^{-1} cohort induced tumor stasis in Z-138 cells with 93% TGI. In comparison the 200 mg kg^{-1} cohort induced >70% TGI in the Maver-1 study. EPZ015666 was well-tolerated in all models with minimal weights loss in the 200 mg kg^{-1} groups and no other toxicity observations.

5.08.6.2.1.2 Protein arginine methyltransferase-6

Protein arginine methyltransferase-6 (PRMT6) is a member of the 45-enzyme RMT family. PRMT6 is found in the nucleus and can generate mono and asymmetric, dimethyl omega-*N*(G)-arginine derivatives on histones possessing a GAR motif. PRMT6 is the only

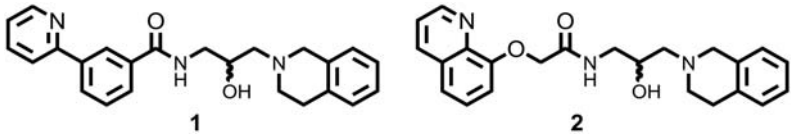

Fig. 7 Published PRMT5 inhibitors from Epizyme.

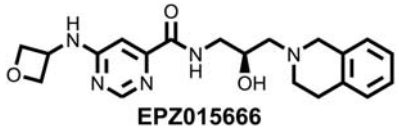

Fig. 8 Structure of EPZ015666.

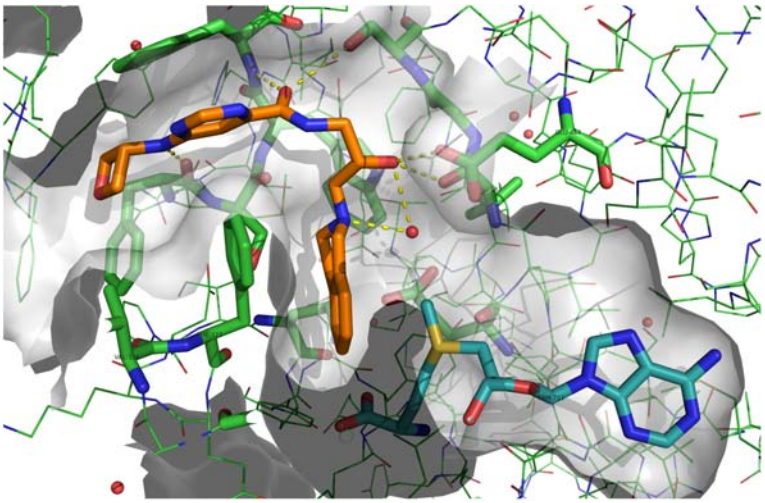

Fig. 9 X-ray pose of PRMT5:MEP50 in complex with EPZ015666 and SAM.

RMT known to methylate the H3R2 mark. Overexpression of PRMT6 has been reported in several cancer types including melanoma, lung, and prostate.[27] The hope is that small-molecule inhibitors of PRMT6 could have utility against these cancer types.

Through screening of its internal compound collection against protein methyltransferase 1 (PRMT1), PRMT6, and protein methyltransferase 8 (PRMT8), Epizyme identified aryl pyrazoles bearing diamine side chains as having inhibitory activity (**3**, Fig. 10).[27]

A ternary crystal structure of compound **3**, *S*-adenosylhomocysteine (SAH) and PRMT6 was generated. The diamine side chain portion of the molecule occupies the putative substrate site. The terminal nitrogen atom gets close to the sulfur atom of SAH and makes multiple direct hydrogen bonds to Glu155 and water-mediated hydrogen bond interaction to Trp156 and Glu164. The X-ray pose of **3** also suggested that there was space in the pocket for further expansion beyond the para-position of the aryl group.

Several analogs of **3** were generated. Analog generation was facilitated by replacement of the *para*-fluorine with an oxygen atom and a series of compounds was prepared. Larger ethers retained activity against PRMT6, PRMT8, and PRMT1. Metachlorination was also tolerated. A different pyrazole isomer and N-methylation of the terminal nitrogen were also well-tolerated. Incorporation of two metasubstituents eroded PRMT6 activity. Epizyme was able to generate some PRMT6 selective compounds by extending further from the phenyl para-position. Various linkers were tolerated such as nitrogen, oxygen, and carbon. After further ADME characterization and in vitro and in vivo studies, EPZ020411 (Fig. 11) was selected as a viable tool compound with a biochemical potency of 10 nM against PRMT6. EPZ020411 demonstrated 10- to 20-fold selectivity for PRMT6 over PRMT8 and PRMT1 and over 100-fold selectivity compared to other HMTs.

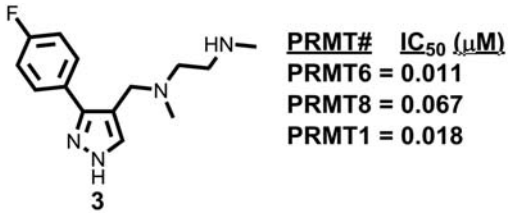

Fig. 10 Published PRMT6 inhibitor from Epizyme.

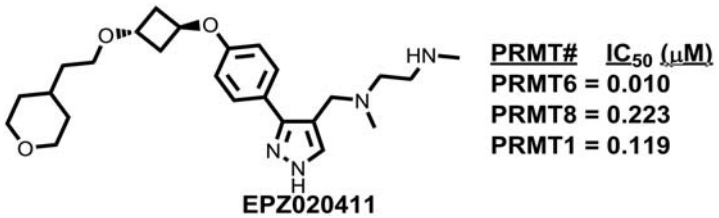

Fig. 11 Structure of EPZ020411.

A ternary crystal structure of EPZ020411, SAH, and PRMT6 was obtained (Fig. 12). The gross topology of the binding pose was similar to that of the previously described compound. The entirety of the oxygen-linked para-substitution was not well-ordered in the structure with electron density not observed for the terminal tetrahydropyran moiety.

The cellular activity of EPZ020411 was investigated in an engineered model in which PRMT6 was transiently expressed in an A375 cell line background. EPZ020411 did not affect levels of PRMT6 expression, but did dose-dependently reduce cellular H3R2 methylation with an $IC_{50} = 0.64\ \mu M$. EPZ020411 was ~10-fold less potent against PRMT1. EPZ020411 demonstrated ~50% free fraction in both human and rat plasma and was poorly permeable in the parallel artificial membrane assay. Subcutaneous dosing of 5 mg kg^{-1} in rats afforded 66% bioavailability with the unbound blood concentration remaining above the PRMT6 biochemical IC_{50} value for >12 h. This suggests that EPZ020411 could be a viable in vivo tool compound with which to explore PRMT6 biology.

5.08.6.2.2 Lysine methyltransferases

5.08.6.2.1.3 Enhancer of zeste homolog 2

HMT EZH2 demonstrates prevalent overexpression in several cancers making it a potential target for drug intervention.[15,17,18,28–32] EZH2 acts as a part of a multiprotein PRC2 complex where it catalyzes the methylation of histone H3 on lysine 27 (H3K27). Increases in H3K27 methylation have been correlated with disease stage and poorer prognosis. Change of function mutations of EZH2 have also been identified in patients with germinal center B-cell diffuse large B-cell lymphoma (DLBCL) and follicular lymphoma. These mutations result in increased levels of H3K27Me3, further implicating EZH2 as an interesting drug target.

Several companies have been active in the area of EZH2 inhibitor design and pyridone-methyl-acetamides have been a dominant chemotype employed (Fig. 13):

Several compounds have advanced into the clinic. Epizyme's inhibitor tazemetostat was the first in Jun. of 2013, followed by GSK with 2816126 and Constellation Pharmaceuticals with CPI-1205 (structure not published).

Epizyme has described the story of the discovery of their clinical candidate tazemetostat.[10] They conducted high-throughput diversity screens against the four-component PRC2 complex containing EZH2, EED, SUZ12, and RbAp48 using chicken oligonucleosomes as the substrate. Epizyme chose to run the screen under balanced conditions (at K_m for SAM and nucleosome) to ensure inhibitors acting via diverse mechanisms of action could be identified, such as competitive with SAM or with nucleosome. Any identified matter was triaged through a rigorous hit validation procedure. Compounds that were redox active, had solubility issues, formed micelles as determined by differential light-scattering, or were known PAINS compounds were removed. This enabled identification of compound **4** as a validated hit (Fig. 14).

Compound **4** contained a 4,6-dimethyl pyridone and demonstrated an EZH2 biochemical IC_{50} of 3.4 μM. Acquisition of commercially available analogs enabled rapid exploration of the chemical space around the initial hit. This effort identified compound **5** as a sub-μM inhibitor of EZH2 (Fig. 15).

Resynthesized compound **5** retained activity and passed a battery of "bad actor" counter screens. Mechanism of action studies demonstrated that compound **2** was SAM-competitive and nucleosome noncompetitive. These data enabled the conclusion that the inhibition mechanism was via direct interaction with the enzyme. Using compound **5** as a starting point, a lead optimization campaign was initiated. Initial modifications were focused on improving the poor ADME profile of compound **5**. Attempts to increase the solubility by incorporation of basic amine moieties were well-tolerated on the 6-position of the 7-azaindazole and improved solubility without substantial loss of potency. After extensive exploration, a benzyl morpholine encompassed the best balance of properties. Epizyme now chose to focus on finding the best central core components. Several 6,5-fused heterocycles

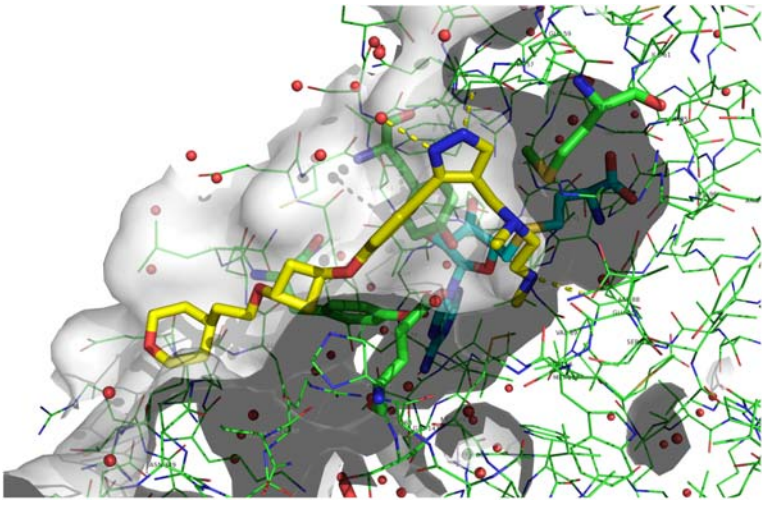

Fig. 12 X-ray pose of PRMT6 in complex with EPZ020411 and SAH.

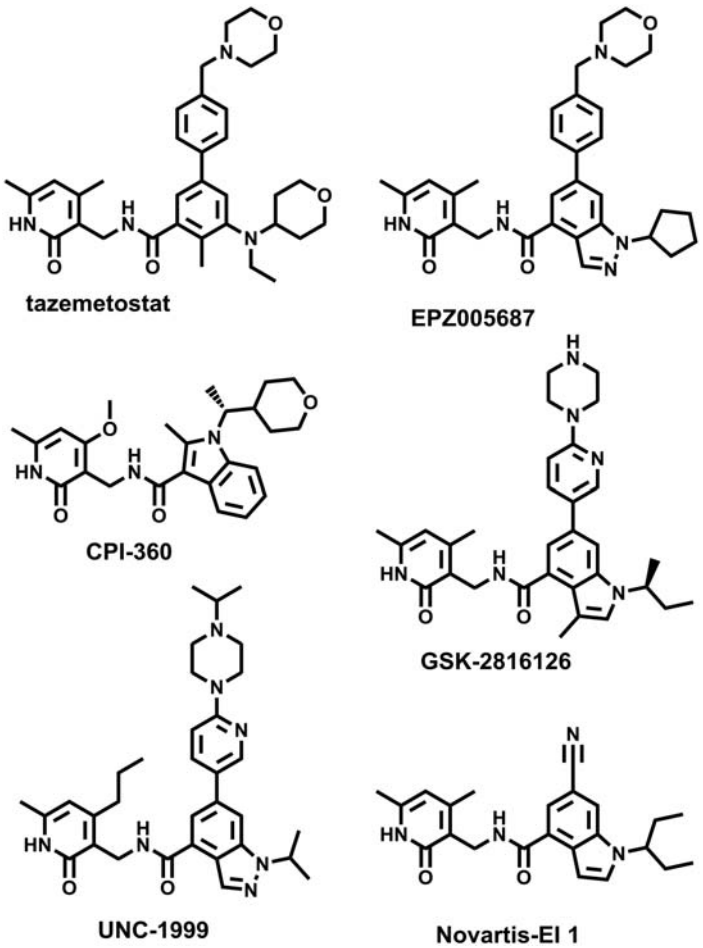

Fig. 13 Published EZH2 inhibitors.

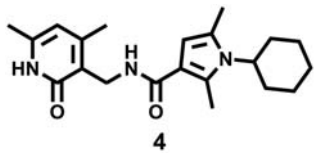

Fig. 14 Published EZH2 inhibitor from Epizyme.

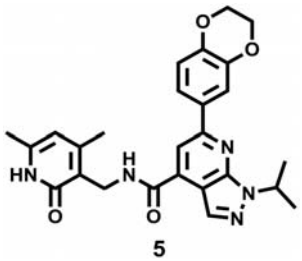

Fig. 15 Published EZH2 inhibitor from Epizyme.

were investigated furnishing the 4-substituted indazole. N1-Alkylation of the indazole with small branched chain alkyl groups was found to be superior for potency, where an *iso*-propyl group was 10× more potent than the ethyl group, which was 10× more potent than the simple methyl group. The team then decided to take a step back and spend some time examining the core ring structure again. Epizyme then "disconnected" the 5,6-bicycle to afford a substituted aniline which enabled access to different vector displacement opportunities. It was then demonstrated that maintaining a substituent on the equivalent position to the carbon of the five-membered ring in the indazole was necessary for potency. This was postulated to be due to a conformational preference for the 6,5-fused hetereocycle systems forcing the amide out of plane relative to the core into a position optimal for binding. The methyl substitution in the ring opened versions was suggested to then mimic that same effect. Other SAR demonstrated a preference for the aniline to be disubstituted. This again was proposed to be due to a conformational effect, where the second substitution would force the aniline to be twisted out of plane relative to the aryl ring. The combination of these two effects enabled Epizyme to reach single digit nM potent compounds for the first time. These efforts culminated in a series exemplified by compound **6** (Fig. 16).[10]

Compound **6** demonstrated acceptable mouse IV clearance, but suffered from poor bioavailability. To optimize the bioavailability, Epizyme considered whether the highly polar benzamidomethyl pyridone could be deleteriously affecting absorption. However, all attempts to further modify or replace the benzamidomethyl pyridone failed to be tolerated for potency. Thus optimization of PK properties remote to the benzamidomethyl pyridone moiety afforded tazemetostat, which had the best balance of potency, clearance, and bioavailability. Tazemetostat was able to show reduction of H3K27Me3 in both tumor and surrogate tissue in mouse xenograft experiments.[33]

Epizyme also disclosed EPZ011989 as a potent, orally available EZH2 inhibitor with robust in vivo activity for the purposes of expanding the known biology of EZH2 (Fig. 17).[28] EPZ011989 was discovered through modification of the pyran substituent of tazemetostat (Fig. 13). The *trans*-*N*,*N*-dimethylcyclohexylamine replacement is able to maintain biochemical activity, but when combined with the morpholine sidechain, the cellular activity of the resulting di-basic compound is negatively impacted. Modulating the pK_a of the amines was proposed as a solution and the resulting SAR validated this approach when adding a methoxyethyl group and replacing the second benzene ring with an acetylene linker to generate EPZ011989.

EPZ011989 was shown to be a very potent EZH2 inhibitor with a biochemical K_i of <3 nM on both mutant and wild-type EZH2. EPZ011989 was also shown to be selective for EZH2, with >15-fold selectivity over EZH1 and with >3000-fold selectivity against a panel of 20 other HMTs. The cellular potency, measured by suppression of the H3K27 methyl mark in an Y641F mutant bearing human lymphoma cell line, WSU-DLCL2, was <100 nM. Further, in vitro characterization suggested that EZP011989 would have reasonable rodent PK, which was then verified when a 1000 mg kg^{-1} oral dose provided target coverage for 24 h. A 7-day pharmacodynamic (PD) study looking at H3K27 methylation in bone marrow showed that a 500 mg kg^{-1} BID dose caused complete ablation of the methyl mark by the end of the seventh day of dosing. EPZ011989 was then reformulated and explored in a 21-day subcutaneous EZH2 mutant KARPAS-422 human DLBCL xenograft TGI study. Both doses, 250 and 500 mg kg^{-1} BID, of EPZ011989 afforded significant tumor regression with nominal effects on body weight. Efficacy at the lower dose was in part due to the superior exposure achieved with the new formulation. Thus EPZ011989 is an excellent tool for both in vitro and in vivo work to further explore EZH2 pathobiology.

Constellation Pharmaceuticals reported a series of EZH2 inhibitors obtained from a conventional high-throughput screen employing a PRC2 enzymatic assay monitoring ^{3}H-labeled methyl group transfer from SAM to oligonucleosome substrate.[32] The HTS assay was run under balanced conditions (i.e., SAM and substrate at K_m) in order to find inhibitors that operate via competitive, noncompetitive, or uncompetitive modes. A total of 150,000 compounds were screened and yielded an initial 288 confirmed

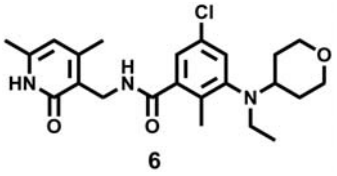

6

Fig. 16 Published EZH2 inhibitor from Epizyme.

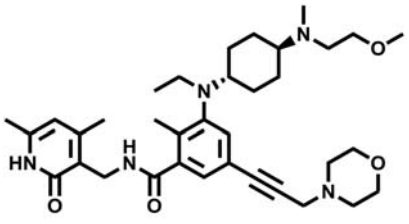

EPZ011989

Fig. 17 Structure of EPZ011989.

hits with potencies generally >20 μM. These were triaged down through several filters (frequent hitters, reactive/toxic moieties, and problem structural features by visual inspection) and then retested in the IC_{50} assay. Any compounds displaying Hill slopes outside a range of 0.7–1.5 were omitted and then several shift assays[32] were employed to remove additional "bad actors" and classify compounds by potential mechanism of action. At this point in the triage funnel, only several weak inhibitors remained (>20 μM) and one of these was the starting point for their optimization campaign (Fig. 17). Shift assay data suggested that the new chemotype was SAM competitive and selective when assayed against other HMTs. Constellation's initial plans were to rapidly explore the inhibitor topology to gauge the quality of the matter. The hit was sectioned into four areas for exploration (Fig. 18).

Initial linker SAR identified that the ether could be replaced by a sulfide. The sulfoxide and sulfone were both inactive, suggesting a preference for a linker that can accept a hydrogen bond. Homologation by methylene insertion next to the central phenyl ring was tolerated, although conversely methylene homologation next to the terminal phenyl ring was not. This was rationalized to be due to a preference for a twist conformation of the bi-aryl system. For the right-hand side SAR, the 2-position was identified as amenable to substitution with cyano being the preferred moiety conveying a 15-fold boost in potency (3.5 μM). The central core was tackled next and while substitution next to the amide of the left-hand side was tolerated, substitution next to the linker ether provided potency enhancements with chlorine providing the best balance of potency and physiochemical effects. Moving back to the right-hand side of the molecule, a para hetero-aromatic ring, specifically a pyridazine, demonstrated an improvement in potency down to 24 nM. This compound **7** (Fig. 19) was poorly permeable in a Caco-2 assay and had a high efflux ratio, which would predict poor oral bioavailability. Attempts to attenuate the pK_a of the piperidine nitrogen were not tolerated nor were any significant modifications to the left-hand side of the molecule. Ultimately compound **7** was selected for further evaluation of EZH2 biology. Compound **7** was evaluated in KARPAS-422 cells and afforded a suppression of global H3K23Me3 levels and growth arrest consistent with previously reported EZH2 inhibitors.

In a follow-up communication to the one described earlier, Constellation Pharmaceuticals reported a class of indole-based EZH2 inhibitors for in vivo dosing.[29] As part of their on-going EZH2 inhibitor program, Constellation also developed a pyridone chemotype, exemplified by compound **9** (Fig. 20). Compound **9** was shown to be SAM competitive and inhibit the PRC2 methyltransferase activity at 39 μM. Due to the structural similarity between the new chemotype (**9**) and the previous series (**8**), Constellation tested the interchangeability of the tetramethyl-piperidine and the dimethylpyridone groups making compound **10**. While **10** was much less potent than the optimized compound from the previous series, it did demonstrate improved potency relative to **7**. Truncation of the chloro, cyano, and pyridazine substituents showed improved potency (**11**).

A scan of various linkers between the two phenyl rings concluded that a carbon linker was the most potent. To maintain the chemical matter in a more drug-like space, Constellation wished to introduce some more polarity into the molecules. This was achieved by swapping the central phenyl group for various heterocycles. The introduction of a 2-methyl group onto an indole linker resulted in a 126-fold increase in potency relative to the des-methyl equivalent (**12** and **13**, Fig. 21). The increase in potency was attributed to an impact on rotational flexibility of the amide, such that the 2-methyl group biases the amide toward a single rotamer.

Replacing the terminal phenyl group with a piperidine ethyl sulfonamide afforded a lower cLogP and good biochemical and cellular potency, but maintained the high microsomal clearance. When this was combined with a change of the dimethylpyridone to a methoxypyridone (Fig. 22), the resulting compound **14** demonstrated a better microsomal stability profile, while retaining its biochemical and cellular potency.

Compound **14** was selected for in vivo profiling. Mouse IV PK showed a clearance of 2.74 $L\,h^{-1}kg^{-1}$, reasonable volume (0.795 $L\,kg^{-1}$), and a short half-life of 0.37 h. Subcutaneous dosing at 200 $mg\,kg^{-1}$ afforded an improved half-life and AUC with plasma adjusted free fraction above the cellular EC_{50} out to 16 h. Constellation was then able to demonstrate a PD response in a KARPAS-422 model. After 17 days of dosing 200 $mg\,kg^{-1}$ BID compound **14** demonstrated an 84% reduction in H3K27Me3

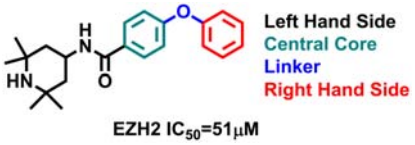

Fig. 18 Published Constellation EZH2 screening hit.

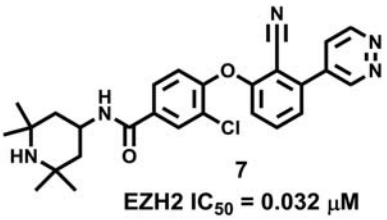

Fig. 19 Published EZH2 inhibitor from Constellation.

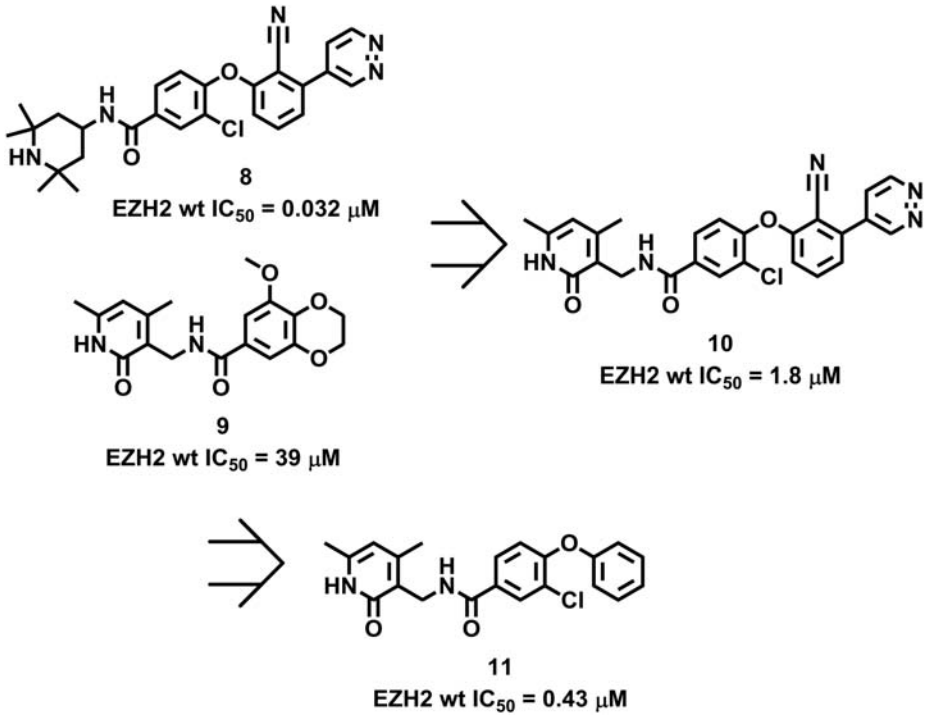

Fig. 20 Published EZH2 pyridone chemotype inhibitor from Constellation.

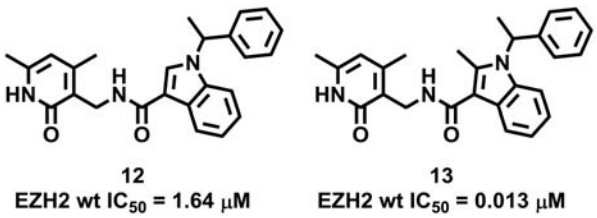

Fig. 21 Published EZH2 inhibitors from Constellation.

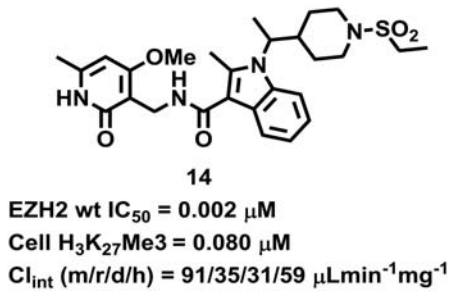

Fig. 22 Published EZH2 inhibitor from Constellation.

mark relative to vehicle control. Compound **14** was then tested in an efficacy model where the 200 mg kg^{-1} dose showed a TGI of $>100\%$. The compound was well-tolerated, suggesting that compound **14** may be a useful tool compound for studying the effect of EZH2 inhibition, both in vitro and in vivo.

5.08.6.2.1.4 Disrupter of telomeric silencing-like 1

DOT1L methylates histone H3 lysine 79 (H3K79) and has been implicated in leukemias bearing MLL rearrangements (MLL-r). MLL is an HMT responsible for the methylation of H3K4. Chromosomal translocations involving the MLL gene result in the expression

of MLL-fusion proteins which lack catalytic activity. It is thought that these fusion proteins are able to recruit DOT1L to a larger MLL containing multiprotein complex which then aberrantly methylates H3K79 leading to enhanced expression of leukemogenic genes.[19,34]

Epizyme initiated a structure-guided approach to discovering a small-molecule, DOT1L inhibitor based on the structure of SAM, and the product of the enzymatic reaction SAH. The initial aim of replacing the polarizable sulfur atom, removing the charged amino acid side chain, and establishing the minimum pharmacophore resulted in EPZ00004 ($K_i = 38$ μM) (Fig. 23). X-ray crystal analysis showed that EPZ0004 bound in the active site with the same configuration as SAM. From this starting point, the program used structure-based design to increase potency by engaging further with the SAM-binding pocket and the adjacent lysine-binding pocket. Systematic modifications to the alkyl side chains appended to the 5′ amine lead to EPZ003696 ($K_i = 13$ nM) (Fig. 23). Changes to the nucleoside portion of the compound were less well-tolerated; however, the nitrogen at position 7 could be replaced with a carbon to give tool compound EPZ004777 ($K_i = 0.3$ nM) (Fig. 23). EPZ004777 demonstrated selectivity over other HMTs, inhibition of intracellular methylation of H3K79, and selective killing of MLL-r leukemia cell lines.[34b] However, poor PK properties, specifically high clearance and low bioavailability, precluded further development. To address these shortfalls, a strategy of reducing the conformational flexibility of the molecule along with the number of hydrogen bond donors was employed.[11] This lead to the discovery of pinometostat (EPZ005676, $K_i = 0.07$ nM), a selective DOT1L inhibitor that demonstrated complete and sustained tumor regression in a nude rat subcutaneous xenograft model of MLL-r leukemia. Pinometostat improved upon EPZ004777; however, both were not orally bioavailable necessitating the use of an IV infusion dosing strategy in the in vivo efficacy studies.[35] Despite the dosing limitations, the preclinical data was compelling and pinometostat has advanced to Phase I clinical trials in pediatric and adult patients.

Initially, it was expected that the extended side chain in EPZ003696 would reach into the proximal lysine-binding channel; however, X-ray crystal structures revealed that the side chain in EPZ003696,[34b] EPZ004777,[34b] and pinometostat[11] accesses a novel subpocket that is not present in structures of the enzyme with SAM, SAH, or EPZ00004. The inhibitors with the extended side chain are able to simultaneously interact with recognition elements in both the SAM pocket and the induced hydrophobic subpocket. This conformational change is unique to DOT1L and thus these compounds demonstrate remarkable selectivity against other HMTs.[34b]

5.08.6.2.1.5 Set and MYND domain-containing protein 2

AstraZeneca reported the discovery and characterization of a SMYD2 inhibitor AZ505 (Fig. 24). The molecule was found as part of an HTS campaign and was then crystallized with the SMYD2 protein (Fig. 25). To establish the optimized HTS assay conditions, AstraZeneca profiled the enzymatic activity of the SMYD2 protein across a panel of standard buffers using peptides derived from two

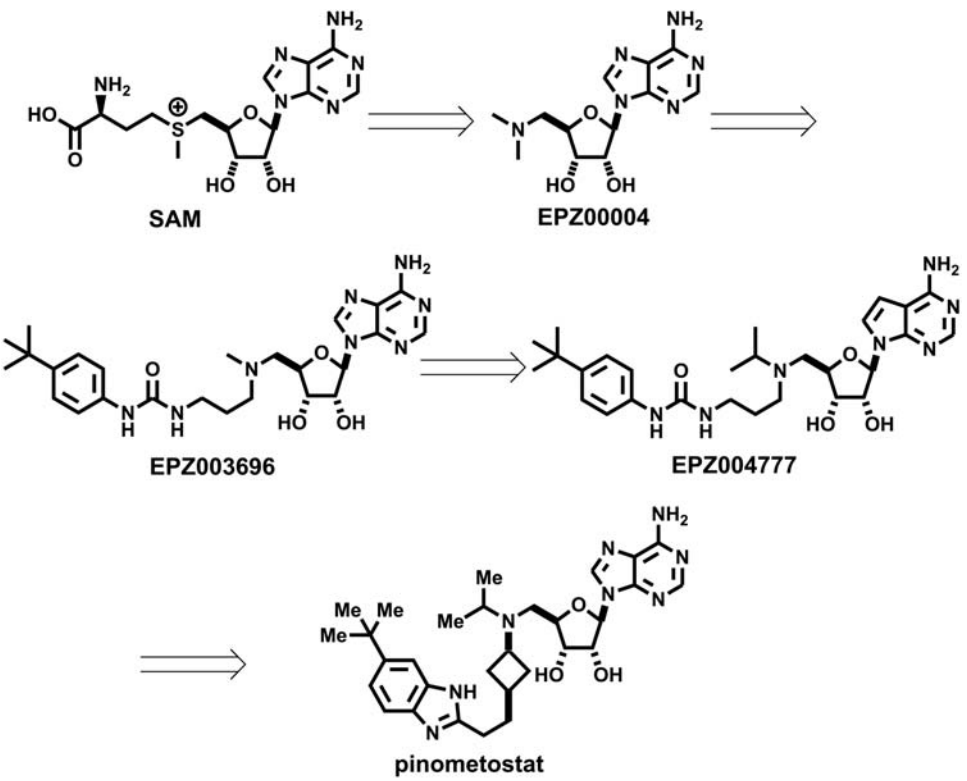

Fig. 23 Chemical developments toward pinometostat.

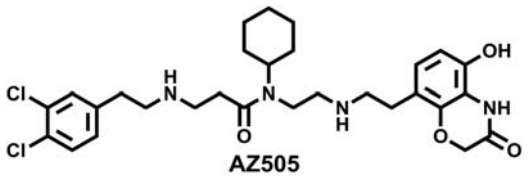

Fig. 24 Structure of AZ505.

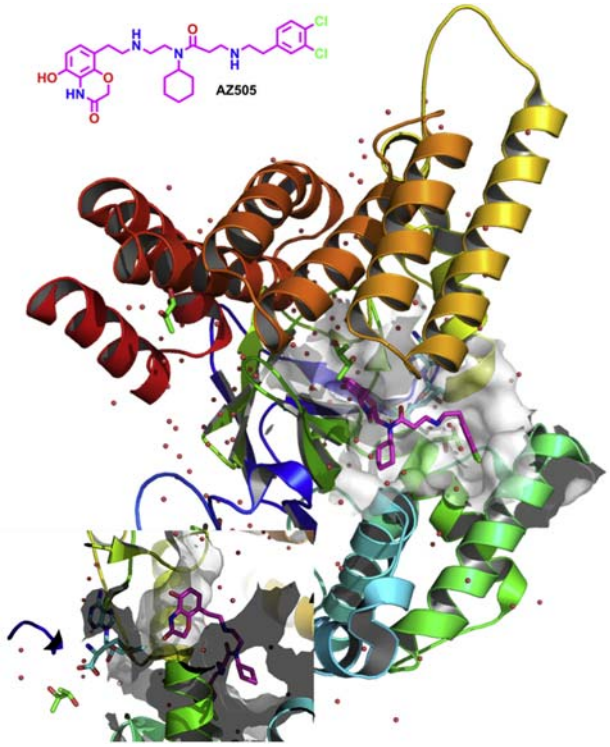

Fig. 25 X-ray representation AZ505 bound to SMYD2.

published substrates (K36 of histone H3 and K370 of transcription factor p53). Tris–HCl with low ionic strength buffer was selected utilizing a p53 substrate peptide as under these conditions SMYD2 demonstrated maximal activity. A small amount of detergent was also utilized to increase protein stability and decrease compound-facilitated protein aggregation.

An AlphaScreen HTS campaign of 1.23 million compounds was completed furnishing a hit rate of 1.2%. As AlphaScreen technology can afford a high false-positive hit rate, a validation cascade was configured. This included an artifact counter screen to invalidate any hits coming from compound interference. A five-point radiometric scintillation proximity assay (SPA) was also employed. A total of 1200 follow-up compounds were then condensed to 25 chemically distinct series along with singletons. Preliminary medicinal chemistry efforts were initiated through purchase of commercially available compounds.

One of the hits, designated AZ505 [*N*-cyclohexyl-3-oxo-3,4-dihydro-2*H*-benzo[b][1,4]oxazin-8-yl)ethylamino)ethyl)propanamide] showed an IC_{50} of 0.12 μM. AZ505 was also shown to be selective over a small panel of KMTs; SET and MYND domain-containing 3 (SMYD3), DOT1L, EZH2, euchromatic histone-lysine *N*-methyltransferase 1 (EHMT1), EHMT2, SET domain-containing (lysine methyltransferase) 7, and SET domain-containing (lysine methyltransferase) 9 having IC_{50}s > 83.3 μM. AZ505 performed well in an isothermal calorimetry assay with a calculated K_d of 0.5 μM. An analysis of the binding kinetics also demonstrated that AZ505 was competitive with substrate and uncompetitive with cofactor (SAM).

AZ505 was also cocrystallized in SMYD2 affording a structure with a resolution of 2.42 Å (Fig. 24). The ternary complex (SMYD2, AZ505, and SAM) showed a single molecule of AZ505 bound in the peptide binding groove. This supported the kinetic evidence that AZ505 is competitive with substrate. The benzoxazinone portion of AZ505 was positioned deep within the lysine-binding channel and showed a series of electronic and hydrophobic packing interactions with the donor methyl group of SAM and surrounding main chain and side chain atoms of SMYD2. The cyclohexyl group of AZ505 binds to a hydrophobic pocket formed at the interface of the core SET and I-SET domains. The terminal dichlorophenethyl moiety slots into another hydrophobic pocket adjacent to the cofactor binding site.

AbbVie also described the identification of a SMYD2 inhibitor, A-893 (Fig. 26). A-893 was developed via a rational design approach based on the, as then, only described small-molecule inhibitor of SMYD2, AZ505. AbbVie described the potency optimizations of the three regions of AZ505 mentioned previously (benzoxazinone, cyclohexylamine, and dichlorophenyl subunits). The SAR was enabled by the utilization of a SPA that measured the SMYD2-mediated methylation of the p53 peptide. The initial premise was that the two moieties occupying the hydrophobic pockets were not significantly contributing to the overall binding efficiency of the molecule (cyclohexylamine and dichlorophenyl subunits). Thus the first targeted analogs were designed to investigate the effects of changes or omissions of these groups. As it turned out, these two regions were sensitive to subtle changes. The initial SAR demonstrated that reducing the size of the cyclohexylamine and dichlorophenyl subunits was generally deleterious to activity. Therefore the team changed focus to the benzoxazinone portion of the molecule. The team wanted to understand the relative importance of each hetero atom in the benzoxazinone lysine channel binding group. They chose to first remove the hydroxyl group. While attempting to synthesize the des-hydroxyl analog, there was a challenge with a reduction reaction resulting in generation of a racemic benzyl hydroxyl compound (Fig. 26). This compound was separated by chiral chromatography to furnish two enantiomers. The measured potencies of the two enantiomers were 2.8 nM (A893) for one enantiomer and 5.8 nM for the other. The mechanism of action was shown to be competitive with peptide, the same as AZ505.

An X-ray structure of A893 in SMYD2 was obtained and showed that the binding mode was very similar to that of AZ505. In the lysine channel, the modified benzyl alcohol accesses a hydrogen bond with the backbone carbonyl of Y240, helping to explain the potency enhancement over AZ505. A893 was shown to be selective for SMYD2 over a panel of 31 other methyltransferases. A893 was also profiled in a human lung carcinoma cell line where incubation at 10 μm for 18 h afforded reduction in the ratio of P53 K370Me1 to overall P53 levels.

Lilly disclosed LLY-507, a potent, cell permeable, and selective small-molecule inhibitor of SMDY2 (Fig. 27).[13] The SMYD2 inhibitory potency of LLY-507 was measured via SPA and found to be <15 nM.[36] LLY-507 binding to SMYD2 was also confirmed by differential scanning fluorometry where 100 μM levels of LLY-507 increased the thermal stability of SMYD2 ($T_m = 49°C$) by 5°C ($T_m = 54°C$). LLY-507 selectively inhibited SMYD2 in a panel of 25 methyltransferases, 454 kinases, 36 G protein-coupled receptors, 14 nuclear hormone receptors, and 3 cytochrome P450 enzyme targets. A high-resolution X-ray structure of LLY-507 in SYMD2 was also generated at 1.63 Å where the binding mode was very similar to that of AZ-505. LLY-507 was examined in a cellular context, where it was demonstrated under three separate sets of conditions and formats that LLY-507 inhibit SMYD2-mediated methylation of p53 with potencies <1 μM.

5.08.6.2.1.6 Set and MYND domain-containing protein 3

SMYD3 is a lysine methyltransferase (KMT) related to SMYD2. Epizyme recently reported the first description of a SMYD3 inhibitor, EPZ031686, that demonstrated good bioavailability in mice upon oral dosing.[37] Epizyme described that SMYD3 is expressed at high levels in several cancer histologies and is associated with a poor clinical prognosis. Epizyme identified compound **15** (Fig. 28) as a micromolar inhibitor of SMYD3 while screening their internal HMT-biased compound library. Compound **15** was able to be crystallized in a ternary complex with SMDY3 and SAM.

The X-ray structure revealed that the oxindole carbonyl formed a hydrogen bond to the side chain Ser202 and was within 2.9 Å of the SAM methyl group. The aromatic ring system formed a π-stacking interaction with Phe183 as well as the oxindole nitrogen making a water-mediated bridge to the protein. The central amide linker made two hydrogen bonds that mimicked a protein substrate interaction. The terminal piperidine was placed into a large solvent-filled peptide binding site and engaged a water-mediated interaction with the side chain reside Glu192. The second molecule of compound **15** present on the periphery of the

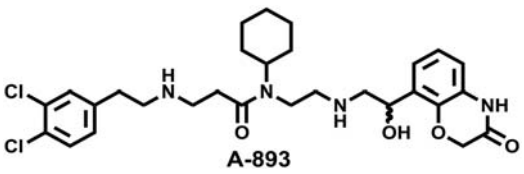

Fig. 26 Structure of A-893.

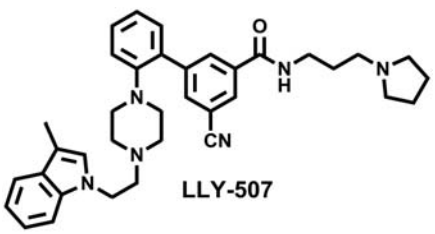

Fig. 27 Structure of LLY-507.

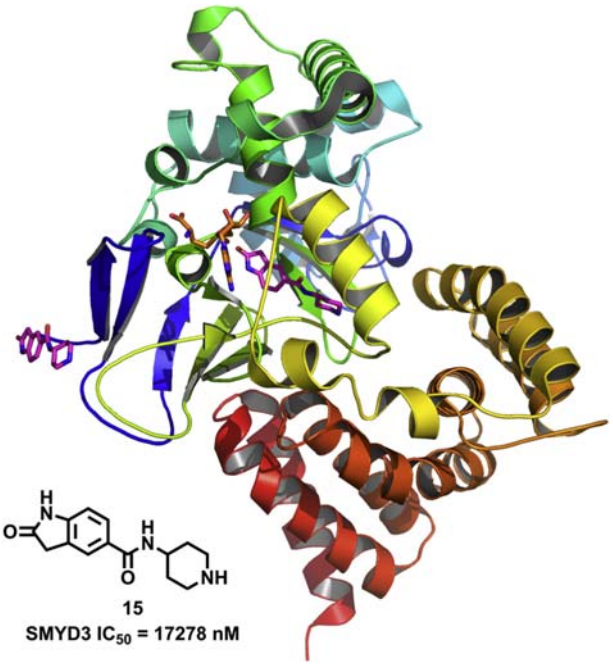

Fig. 28 X-ray representation of SYMD3 inhibitor bound to SMYD3.

structure is a crystal packing artifact. Initial medicinal chemistry efforts were aimed toward exploiting two potential new interactions with Glu192 and Asp241, which were within 3.5 Å of compound **15**'s basic nitrogen. When compound **15** was alkylated on the piperidine nitrogen with a propylamino-sulfonamide moiety, a 10-fold potency boost was observed. Conformational restriction of the terminal amine into a piperidine and the central piperidine core afforded compound **16** (Fig. 29) with a 40-fold potency boost.

However, even though compound **16** had single digit nM potency against SMYD3 in a biochemical assay, the cell potency was still in the single digit micromolar range. This was attributed to poor cell penetration, due to high polarity and too many hydrogen bond donors. Removing hydrogen bond donors successfully increase cell penetration and lowered the biochemical-to-cellular shift, as exemplified by EPZ031686 (Fig. 30), which had an IC_{50} of 36 nM in cell assays. EPZ031686 was profiled against 13 KMTs (including SMYD2), at 10 μM and demonstrated no inhibition >30%. EPZ031686 was examined in mouse oral PKs where a 50 mg kg^{-1} dose was 69% orally bioavailable and the unbound blood concentration remained above the SMYD3 cellular potency

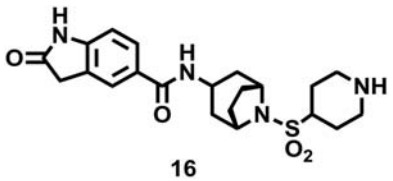

Fig. 29 Published SMYD3 inhibitors from Epizyme.

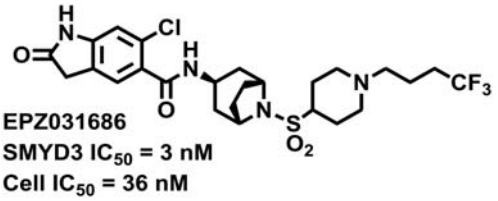

Fig. 30 Structure of EPZ031686.

value for more than 12 h. These data led Mitchell et al. to conclude that EPZ031686 is a suitable tool compound for potential in vivo target validation studies.

5.08.6.2.1.7 Euchromatic histone-lysine-N-methyltransferase 2

EHMT2, also known as G9a, is primarily responsible for the mono and dimethylation of histone 3 lysine 9 (H3K9Me2). Upregulation of EHMT2 is linked to several cancer types[38] and is correlated with a poor prognosis in aggressive lung cancer.[39] At the time of writing, there are no clinical-phase or marketed inhibitors of EHMT2 but several tool compounds have been developed. Boehringer Ingelheim conducted a screen against EHMT2 using a fluoroimmunoassay and a glutathione *S*-transferase-tagged fusion product.[21] The library used in the screen was preselected using an internal algorithm developed using data from publically available HMT inhibitor structures. The resulting ~125,000 compounds were screened at high SAM concentration to bias the results toward substrate competitive hits. Seven potential hits were identified and following additional screening BIX-01294 emerged as the single selective hit (**Fig. 31**). Additional studies showed that BIX-01294 was noncompetitive with SAM, selective against other HMTs, and reduced H3K9Me2 levels in mouse embryonic stem cells and fibroblasts.

In 2009, Chang et al. published an X-ray crystal structure of BIX-01294 bound to the catalytic SET domain of EHMT1.[40] During the course of this work, BIX-01294 was retested against both EHTM1 and EHTM2 using linear conditions for both assays and it was found that BIX-01294 was slightly more potent against EHTM1 (0.7 and 1.9 μM, respectively). The previous EHTM1 assay had been run under saturated conditions resulting in the production of H3K9Me3 rather than the assay end point of H3K9Me2, highlighting that judicious selection of assay conditions is a critical component of a successful program.

In an effort to develop further tool compounds for EHMT2 and to expand the, at the time, sparse knowledge around HMT inhibitors in general, Lui at the University of North Carolina initiated an SAR campaign around the 2,4-diamino-6,7-dimethoxyquinazoline scaffold.[14,41] Replacement of the benzyl group with a simple methyl afforded compound **17** (**Fig. 31**) which was equipotent to BIX01294 in the AlphaScreen assay. This finding is consistent with the X-ray structure of BIX-01294 in EHMT1 which shows the compound bound in the substrate binding groove with the benzyl moiety projecting away from the protein into solvent.

Modifications to the 2-amino moiety of the scaffold were well-tolerated with **17** remaining the most potent. Using the aforementioned X-ray crystal structure as a guide, the 7-methoxy group was replaced with a lysine mimic to generate UNC0224 (**Fig. 31**). The X-ray crystal structure of an EHMT2–UNC0224 complex shows that the 7-dimethylamino side chain is occupying the lysine channel as expected. Compound UNC0224 was found to be significantly more potent than BIX-01294 against EHMT2 in the ThioGlo assay (15 and 109 nM, respectively) but was equipotent to BIX-01294 in the AlphaScreen (298 and 290 nM, respectively). The authors attribute the similar potencies to the compounds reaching the IC_{50} limit of this assay. Using the crystal structure as a guide, compound UNC0224 was then further optimized to UNC0321 (**Fig. 32**).[14] While UNC0321 had single digit nM activity in the in vitro assay, the compound was much less active than BIX-01294 in the cellular assays.

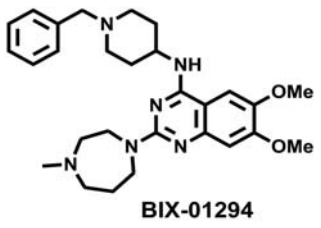

Fig. 31 Structure of BIX-01294.

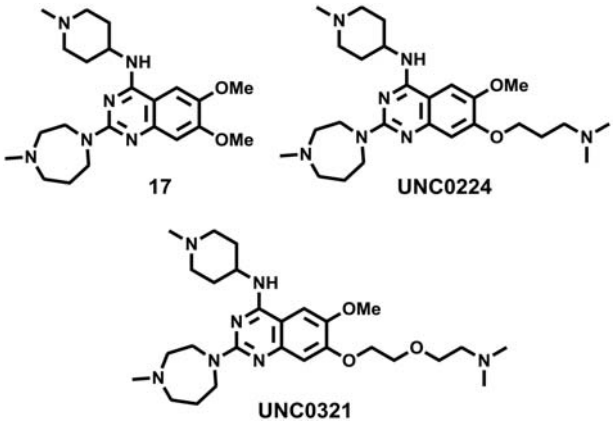

Fig. 32 Published EHMT2 inhibitors.

Extensive SAR exploration around the 2-, 4-, and 7-positions of the quinazoline core led to compound UNC0638 (Fig. 33).[42] The compound bound in a reversible manner and was found to be substrate competitive and SAM uncompetitive. Unlike compound UNC0321, UNC0638 showed activity in a number of cell assays but due to poor in vivo PK properties is not a suitable tool compound for animal studies. Further efforts to improve the properties of the compound resulted in UNC0642 (Fig. 32).[43] The in vitro and cellular potency is similar to UNC0638, but the half-life and clearance in mice is improved.

Following the publication of UNC0638 AbbVie published a structurally distinct inhibitor of EHMT2.[44] A diversity screen using an AlphaLISA assay identified **18** ($IC_{50}=153$ nM) (Fig. 34). The dimethoxy moiety was reminiscent of BIX-01294 and as such the authors postulated that **18** could be binding in a similar fashion. Several lysine mimetic replacements for the 6-methoxy group were prepared. Gratifyingly the pyrrolidine side chain showed a significant improvement in potency (A-366, $IC_{50}=3.3$ nM). A-366 was cell active, showing a reduction in H3K9Me2 at concentrations similar to UNC0638. A-366 represents an alternative chemotype for further exploration of EHMT2 biology. A summary of the SAR around these two chemotypes is presented in Table 2.

5.08.6.3 Lysine (K)-Specific Demethylases

5.08.6.3.1 Lysine (K)-specific demethylase 1A

The first report of a histone demethylase, lysine (K)-specific demethylase 1A (KDM1A), was published in 2004.[45] KDM1A demethylates H3K4Me2 and H3K4Me1 via a flavin adenine dinucleotide (FAD)-dependent oxidative reaction.[46] KDM1A has been of interest as a target for treating a variety of cancers including acute myeloid leukemia and small cell lung cancer.[47]

KDM1A belongs to the monoamine oxidase family and as such known MAO inhibitors were evaluated for KDM1A activity.[48] The antidepressant *trans*-2-phenylcyclopropylamine (tranylcypromine, Parnate) was found to inhibit KDM1A in an irreversible manner (Fig. 35). While promising, tranylcypromine was not selective and was expected to show broad toxicity at the dose necessary for efficacy in a cancer setting.[47a]

Promisingly, crystallographic[49] studies among others suggested that tranylcypromine inhibits the KDM1A–CoREST complex through formation of bridged adduct with FAD. This finding is particularly notable in that the FAD adduct formed in the presence of KDM1A is quite different from the adduct formed in the context of MAO B, suggesting that there is an opportunity to design selective inhibitors of KDM1A.

GlaxoSmithKline screened 2.5 million compounds in a KDM1A biochemical assay and identified a series of molecules containing a cyclopropylamine.[47c] The series was progressed to compound GSK287955 which is currently undergoing Phase I trials in myelocytic leukemia and small cell lung cancer (Fig. 36). A number of other groups have used tranylcypromine as a starting point for developing a KDM1A inhibitor.[50] Oryzon has filed a number of patent applications around tranylcypromine derivatives and has also started clinical trials in Europe in acute leukemia with ORY-1001 (structure not disclosed).

Efforts to identify a reversible KDM1A inhibitor have also been initiated.[47a,b] However, the H3 tail binding site is quite large making identification of a reversible inhibitor particularly challenging. The majority of reversible inhibitors have shown low to mid μM range activity in biochemical assays.

5.08.6.4 Bromodomains

5.08.6.4.1 Bromodomain and extra C-terminal domain

Histone acetylation marks are read by a diverse set of proteins that contain a bromodomain. The bromodomains are structurally diverse, but all share a conserved fold in the vicinity of the acetylated lysine-binding area and the lysine-binding pocket is largely

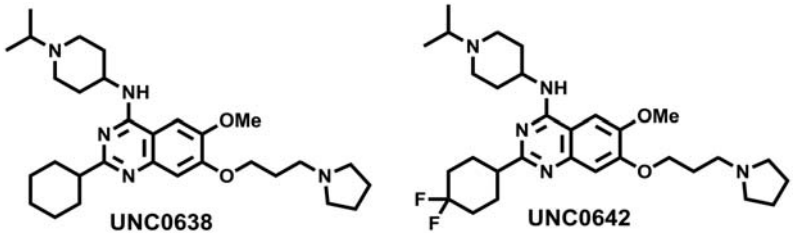

Fig. 33 Structures of UNC0638 and UNC0642.

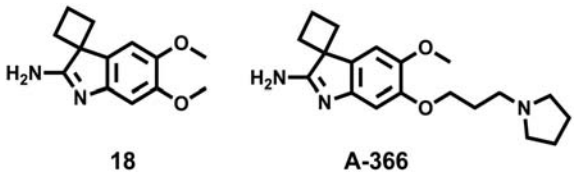

Fig. 34 Published EHMT2 inhibitors from AbbVie.

Table 2 Published EHMT2 inhibitors

Structure	*EHTM2 (μM)*	*EHMT1 (μM)*
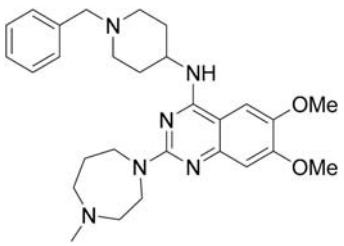	1.7[a] 0.11–0.18[b,c] 0.29[d] 0.25[e]	0.7–38[a] 0.034[c] – 0.027[e]
BIX-01294		
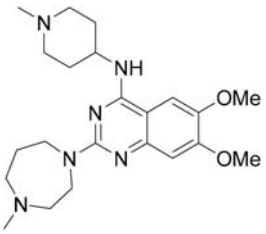	0.33[b,c] 0.23[d,e]	
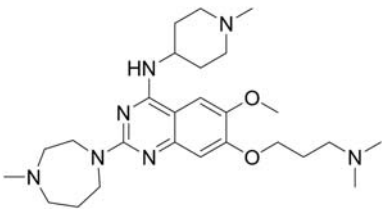	0.043[c] 0.057[e] 0.043[f]	0.050[c] 0.058[e]
UNC0224		
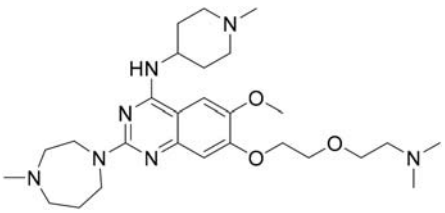	0.009[c] 0.006[e] 0.009[f]	0.015[c] 0.023[e]
UNC0321		
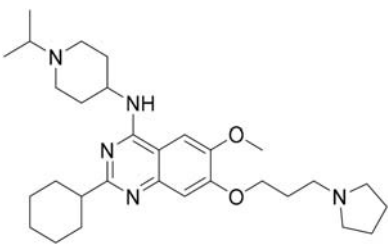	0.012[f] <0.0025[g]	
UNC0638		

(Continued)

Table 2 Published EHMT2 inhibitors—cont'd

Structure	*EHTM2 (μM)*	*EHMT1 (μM)*
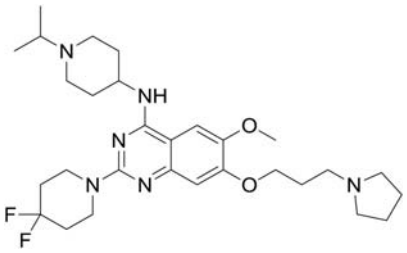 **UNC0642**	<0.0025[g]	
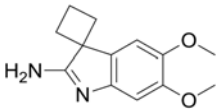 **18**	0.153[h]	
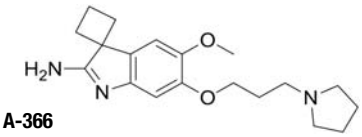 **A-366**	0.0033[h]	0.038[h]

[a]Dissociation-enhanced lanthanide fluorescence immunoassay (DELFIA).
[b]ThioGlo.
[c]Enzyme-coupled SAH detection (ECSD).
[d]AlphaScreen.
[e]Chemiluminescence-based oxygen tunneling assay (CLOT).
[f]SAH hydrolase-coupled assay (SAHH).
[g]Scintillation proximity assay (SPA) SAM-T[3].
[h]AlphaLISA.

Fig. 35 Structure of tranylcypromine.

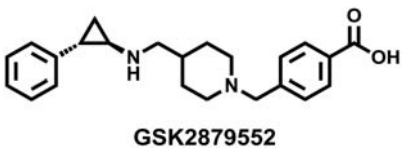

Fig. 36 Structure of GSK2879552.

hydrophobic with a conserved asparagine residue.[51] A subclass of bromodomains, known as BET, simultaneously recognizes two acetylated lysine residues. The BET subclass includes bromodomain 2, bromodomain 3, bromodomain 4, and bromodomain testis-specific (BRD2, BRD3, BRD4, and BRDT).

In 2010, Filippakopoulos et al. and GSK disclosed the structures of diazapine containing, selective BET inhibitors (+)-JQ1[52] and GSK525762A,[53] respectively (Fig. 37). In 2001 GSK launched an effort to identify small molecules that could upregulate Apolipoprotein A-1 (ApoA1) expression. GW841819X was identified through a screening campaign using an ApoA1 luciferase reporter assay and further optimization led to GSK525762A. To determine the mechanism of inhibition of these compounds, GSK screened a large number of structurally related compounds against panels of known drug-target protein classes including kinases, ion channels, and GPCRs. However, the compounds were not active in any of the GSK panels, suggesting they acted on a class of targets not

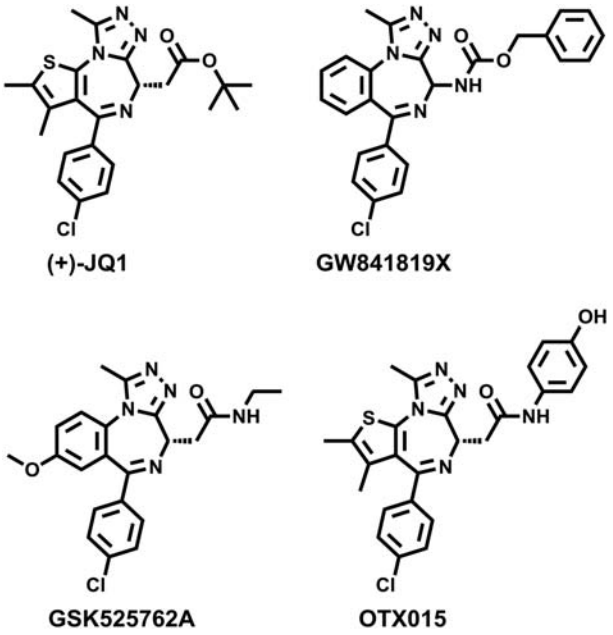

Fig. 37 Published bromodomain inhibitors.

represented in the panels. A chemoproteomics approach revealed that GSK525762A bound to three proteins, BRD2, BRD3, and BRD4. Further biophysical studies demonstrated that the compound could bind simultaneously to each bromodomain of the BET proteins to give an overall 2:1 stoichiometry. The X-ray crystal structure of GSK525762A bound to BRD4 showed the compound positioned at the acetylated lysine pocket with the triazoyl moiety mimicking the key hydrogen bonds made between the AcK substrate and Asp140 and Tyr97. GSK has advanced GSK525762 and the compound is currently undergoing Phase I clinical trials. Oncoethix also has a diazapine containing compound in Phase I/II (OTX015) (Fig. 37).

Additional related tool compounds include CPI-3[54] and CPI203[55] from Constellation (Fig. 38). CPI-3, a close analog of (+)-JQ1, has a short half-life in vivo and was not ideal for animal studies. Efforts to improve the tool compound began with

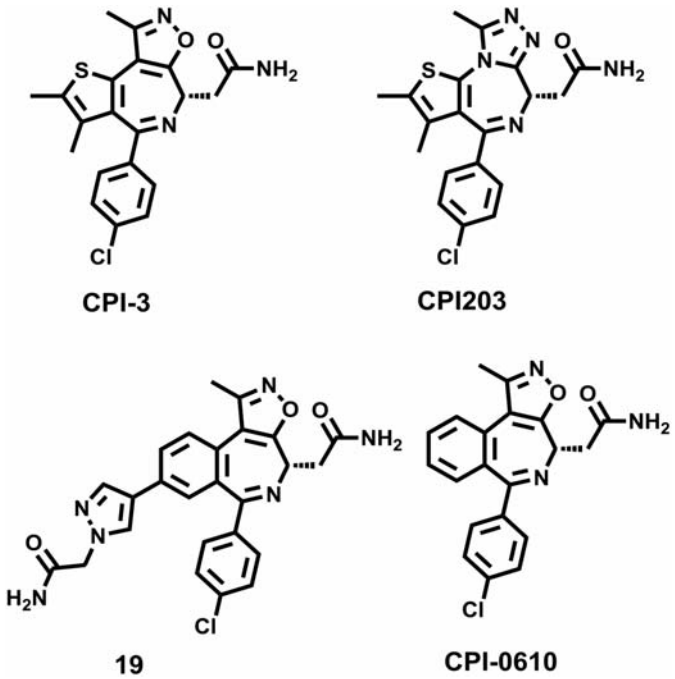

Fig. 38 Published bromodomain inhibitors from Constellation.

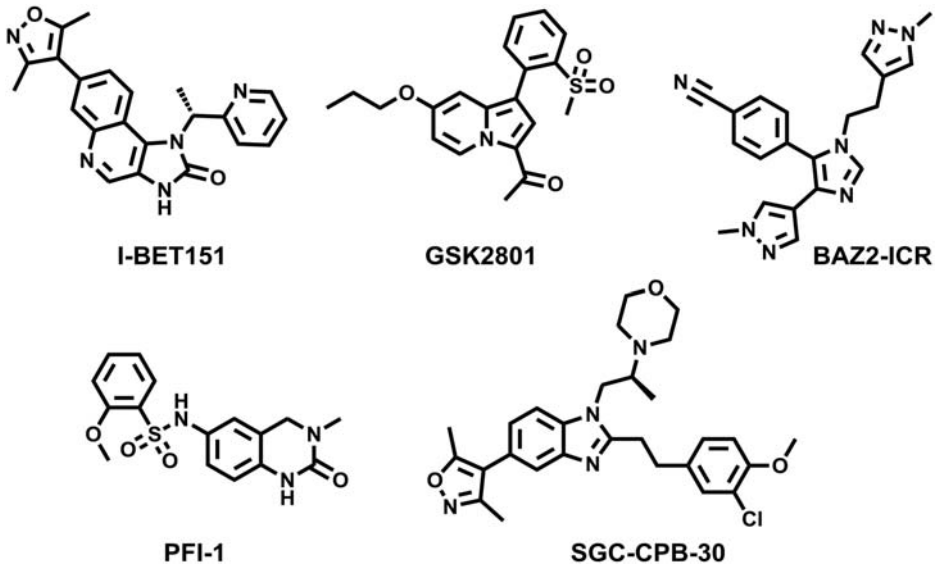

Fig. 39 Published bromodomain inhibitors.

replacement of the thiophene with a phenyl ring. This reduced metabolic liabilities and created a handle for additional substitution. Addition of a pyrazole at the para-position of the new phenyl ring provided a boost in potency and X-ray crystal structures of compounds bound to BRD4 indicated that the pyrazole was making a desired stacking interaction with W81. Compound **19** has an improved PK profile compared with CPI-3 and was selected for further study. The compound is a pan BET inhibitor but did not inhibit other bromodomains. Constellation compound CPI-0610 is currently in a Phase 1 trial for leukemia and other blood disorders.[56]

Much work has also been done to identify nondiazapine and nondiazapine-like bromodomain inhibitors. As part of their ApoA1 program GSK identified I-BET151,[53b] a BET inhibitor that is distinct from GSK525762 (Fig. 39). Additionally, in conjunction with the SGC, GSK has released tool compound GSK2801 which is selective for bromodomain next to zinc finger domain 2A (BAZ2A) and bromodomain next to zinc finger domain 2B (BAZ2B) over the BET proteins (Fig. 39).[57] The SGS in collaboration with Cancer Research UK and the University of Oxford have also published an inhibitor of the BAZ2A and BAZ2B bromodomains (BAZ2-ICR, Fig. 39).[58] Pfizer has also partnered with the SGC to identify PFI-1, a BET domain selective inhibitor.[59] The SGC has released a tool inhibitor for the CREB binding protein and E1A binding protein 300 bromodomains[60](Fig. 39). Abbvie (ABBV-075), BMS (BMS-986158), and Roche (TEN-010) each have inhibitors in the clinic for oncology indications (structures not disclosed).

Recently, Schonbrunn et al. reported that kinase inhibitors BI2536 and TG101209 are potent inhibitors of BET protein BRD4 with high selectivity for the BET family of bromodomains.[6] Building on an earlier discovery that the cyclin-dependent kinase inhibitor dinaciclib bound to BRDT1,[61] a set of 581 kinase inhibitors was screened against BRD4-1 using a high-throughput cocrystallization campaign. Of the 194 crystal structures obtained, 14 showed ligand bound to the KAc site of BRD4-1. The compounds were classified into four groups based on the interactions between BRD4-1 and the kinase hinge binding region of the ligand, Type N (Asn140), Type PZA (Pro82 and ZA channel), Type ZA (ZA channel), and Type I (not involved). The most potent compound, polo-like kinase 1 inhibitor BI2536 (BRDT-4 $IC_{50}=25$ nM), interacts with Asn140 through a carbonyl moiety and the hinge binding region interacts with the ZA channel and Pro82. JAK2 inhibitors TG101209 and TG101348 were the next most potent compounds and are both classified as Type N inhibitors. In addition, these compounds interact with Pro82 via a second aniline group. Taken together, these data suggest that the kinase hinge binding group can interact with the KAc binding area of BET proteins in at least two ways. The new scaffolds identified in this study provide additional starting points for the structure-based design of new BET inhibitors.

5.08.7 Conclusion

Posttranslational modifications of histones have developed into a burgeoning area of research yielding several approved drugs and clinical candidates. HDACs were the first of the histone-modifying enzymes to yield a clinical candidate and there are now more than four HDAC inhibitors on the market and several more in clinical trials. Despite early success, HDAC inhibitors are still an active area of research as, in efforts to reduce toxicity, investigators aim to develop inhibitors that are specific to a single HDAC or class of HDACs.

As the field advanced beyond HDACs toward the discovery of HMT inhibitors, it became clear that each class of enzymes would require new assays and screening paradigms. The collective EHMT2 programs, for example, used a number of different biochemical assays and results were dependent on assay conditions. Pinometostat, a SAM-competitive DOT1L inhibitor, was the first HMT inhibitor to enter clinical trials followed closely by several peptide competitive EZH2 inhibitors. With the exception of EZH2, structure-aided design has played a large role in the development of HMT inhibitors.

Bromodomain and KDMs inhibitors quickly followed the HMT inhibitors with compounds in the clinic from several companies. To date bromodomains, specifically BET domains, are the only reader protein with inhibitors in the clinic. Despite the recent successes, there is much still to understand around histone modifications and the role these changes play in cancer. New tools for discovering key histone-modifying enzymes are being developed and new tool compounds for HATs and other histone-modifying enzymes are emerging in the patent literature.

With the potential for intervention in both methyl and acetyl marks and targets that affect readers, writers and erasers there remain a rich landscape for further investigation. As the science continues to move forward we will see the full fruition of modulating the posttranslational modifications of histones.

See also: 2.12. Novel Therapeutics Targeting Epigenetics.

References

1. Hanahan, D.; Weinberg, R. A. Hallmarks of Cancer: The Next Generation. *Cell* **2011,** *144* (5), 646–674.
2. (a) Dhanak, D.; Jackson, P. Development and Classes of Epigenetic Drugs for Cancer. *Biochem. Biophys. Res. Commun.* **2014,** *455* (1–2), 58–69; (b) McGrath, J.; Trojer, P. Targeting Histone Lysine Methylation in Cancer. *Pharmacol. Ther.* **2015,** *150*, 1–22; (c) Copeland, R. A.; Solomon, M. E.; Richon, V. M. Protein Methyltransferases as a Target Class for Drug Discovery. *Nat. Rev. Drug Discov.* **2009,** *8* (9), 724–732.
3. Arrowsmith, C. H.; Bountra, C.; Fish, P. V.; Lee, K.; Schapira, M. Epigenetic Protein Families: A New Frontier for Drug Discovery. *Nat. Rev. Drug Discov.* **2012,** *11* (5), 384–400.
4. Finley, A.; Copeland, R. A. Small Molecule Control of Chromatin Remodeling. *Chem. Biol.* **2014,** *21* (9), 1196–1210.
5. Campbell, R. M.; Tummino, P. J. Cancer Epigenetics Drug Discovery and Development: The Challenge of Hitting the Mark. *J. Clin. Invest.* **2014,** *124* (1), 64–69.
6. Ember, S. W.; Zhu, J. Y.; Olesen, S. H.; Martin, M. P.; Becker, A.; Berndt, N.; Georg, G. I.; Schonbrunn, E. Acetyl-Lysine Binding Site of Bromodomain-Containing Protein 4 (BRD4) Interacts With Diverse Kinase Inhibitors. *ACS Chem. Biol.* **2014,** *9* (5), 1160–1171.
7. Bottger, A.; Islam, M. S.; Chowdhury, R.; Schofield, C. J.; Wolf, A. The Oxygenase Jmjd6—A Case Study in Conflicting Assignments. *Biochem. J.* **2015,** *468* (2), 191–202.
8. Moyer, J. D.; Barbacci, E. G.; Iwata, K. K.; Arnold, L.; Boman, B.; Cunningham, A.; DiOrio, C.; Doty, J.; Morin, M. J.; Moyer, M. P.; Neveu, M.; Pollack, V. A.; Pustilnik, L. R.; Reynolds, M. M.; Sloan, D.; Theleman, A.; Miller, P. Induction of Apoptosis and Cell Cycle Arrest by CP-358,774, An Inhibitor of Epidermal Growth Factor Receptor Tyrosine Kinase. *Cancer Res.* **1997,** *57* (21), 4838–4848.
9. Druker, B. J.; Lydon, N. B. Lessons Learned From the Development of an Abl Tyrosine Kinase Inhibitor for Chronic Myelogenous Leukemia. *J. Clin. Invest.* **2000,** *105* (1), 3–7.
10. Kuntz, K. W.; Campbell, J. E.; Keilhack, H.; Pollock, R. M.; Knutson, S. K.; Porter Scott, M.; Richon, V. M.; Sneeringer, C. J.; Wigle, T. J.; Allain, C. J.; Majer, C. R.; Moyer, M. P.; Copeland, R. A.; Chesworth, R. The Importance of Being Me: Magic Methyls, Methyltransferase Inhibitors, and the Discovery of Tazemetostat. *J. Med. Chem.* **2016,** *59* (4), 1556–1564.
11. Chesworth, R.; Olhava, E. J.; Kuntz, K. W.; Basavapathruni, A.; Majer, C. R.; Sneeringer, C. J.; Allain, C. J.; Raimondi, A.; Klaus, C. R.; Porter Scott, M. From Protein to Candidate: Discovery of EPZ-5676, A Potent and Selective Inhibitor Off the Histone Methyltransferase DOT1L. 246th ACS National Meeting and Exposition, Indianapolis, IN, United States, September 8–12, 2013.
12. Knight, Z. A.; Shokat, K. M. Features of Selective Kinase Inhibitors. *Chem. Biol.* **2005,** *12* (6), 621–637.
13. Nguyen, H.; Allali-Hassani, A.; Antonysamy, S.; Chang, S.; Chen, L. H.; Curtis, C.; Emtage, S.; Fan, L.; Gheyi, T.; Li, F.; Liu, S.; Martin, J. R.; Mendel, D.; Olsen, J. B.; Pelletier, L.; Shatseva, T.; Wu, S.; Zhang, F. F.; Arrowsmith, C. H.; Brown, P. J.; Campbell, R. M.; Garcia, B. A.; Barsyte-Lovejoy, D.; Mader, M.; Vedadi, M. LLY-507, A Cell-Active, Potent, and Selective Inhibitor of Protein-Lysine Methyltransferase SMYD2. *J. Biol. Chem.* **2015,** *290* (22), 13641–13653.
14. Liu, F.; Chen, X.; Allali-Hassani, A.; Quinn, A. M.; Wigle, T. J.; Wasney, G. A.; Dong, A.; Senisterra, G.; Chau, I.; Siarheyeva, A.; Norris, J. L.; Kireev, D. B.; Jadhav, A.; Herold, J. M.; Janzen, W. P.; Arrowsmith, C. H.; Frye, S. V.; Brown, P. J.; Simeonov, A.; Vedadi, M.; Jin, J. Protein Lysine Methyltransferase G9a Inhibitors: Design, Synthesis, and Structure Activity Relationships of 2,4-Diamino-7-Aminoalkoxy-Quinazolines. *J. Med. Chem.* **2010,** *53* (15), 5844–5857.
15. Garapaty-Rao, S.; Nasveschuk, C.; Gagnon, A.; Chan, E. Y.; Sandy, P.; Busby, J.; Balasubramanian, S.; Campbell, R.; Zhao, F.; Bergeron, L.; Audia, J. E.; Albrecht, B. K.; Harmange, J. C.; Cummings, R.; Trojer, P. Identification of EZH2 and EZH1 Small Molecule Inhibitors With Selective Impact on Diffuse Large B Cell Lymphoma Cell Growth. *Chem. Biol.* **2013,** *20* (11), 1329–1339.
16. Wigle, T. J.; Knutson, S. K.; Jin, L.; Kuntz, K. W.; Pollock, R. M.; Richon, V. M.; Copeland, R. A.; Scott, M. P. The Y641C Mutation of EZH2 Alters Substrate Specificity for Histone H3 Lysine 27 Methylation States. *FEBS Lett.* **2011,** *585* (19), 3011–3014.
17. Verma, S. K.; Tian, X.; LaFrance, L. V.; Duquenne, C.; Suarez, D. P.; Newlander, K. A.; Romeril, S. P.; Burgess, J. L.; Grant, S. W.; Brackley, J. A.; Graves, A. P.; Scherzer, D. A.; Shu, A.; Thompson, C.; Ott, H. M.; Aller, G. S.; Machutta, C. A.; Diaz, E.; Jiang, Y.; Johnson, N. W.; Knight, S. D.; Kruger, R. G.; McCabe, M. T.; Dhanak, D.; Tummino, P. J.; Creasy, C. L.; Miller, W. H. Identification of Potent, Selective, Cell-Active Inhibitors of the Histone Lysine Methyltransferase EZH2. *ACS Med. Chem. Lett.* **2012,** *3* (12), 1091–1096.
18. Qi, W.; Chan, H.; Teng, L.; Li, L.; Chuai, S.; Zhang, R.; Zeng, J.; Li, M.; Fan, H.; Lin, Y.; Gu, J.; Ardayfio, O.; Zhang, J. H.; Yan, X.; Fang, J.; Mi, Y.; Zhang, M.; Zhou, T.; Feng, G.; Chen, Z.; Li, G.; Yang, T.; Zhao, K.; Liu, X.; Yu, Z.; Lu, C. X.; Atadja, P.; Li, E. Selective Inhibition of Ezh2 by a Small Molecule Inhibitor Blocks Tumor Cells Proliferation. *Proc. Natl. Acad. Sci. U. S. A.* **2012,** *109* (52), 21360–21365.
19. Daigle, S. R.; Olhava, E. J.; Therkelsen, C. A.; Majer, C. R.; Sneeringer, C. J.; Song, J.; Johnston, L. D.; Scott, M. P.; Smith, J. J.; Xiao, Y.; Jin, L.; Kuntz, K. W.; Chesworth, R.; Moyer, M. P.; Bernt, K. M.; Tseng, J. C.; Kung, A. L.; Armstrong, S. A.; Copeland, R. A.; Richon, V. M.; Pollock, R. M. Selective Killing of Mixed Lineage Leukemia Cells by a Potent Small-Molecule DOT1L Inhibitor. *Cancer Cell* **2011,** *20* (1), 53–65.
20. Chan-Penebre, E.; Kuplast, K. G.; Majer, C. R.; Boriack-Sjodin, P. A.; Wigle, T. J.; Johnston, L. D.; Rioux, N.; Munchhof, M. J.; Jin, L.; Jacques, S. L.; West, K. A.; Lingaraj, T.; Stickland, K.; Ribich, S. A.; Raimondi, A.; Scott, M. P.; Waters, N. J.; Pollock, R. M.; Smith, J. J.; Barbash, O.; Pappalardi, M.; Ho, T. F.; Nurse, K.; Oza, K. P.; Gallagher, K. T.; Kruger, R.; Moyer, M. P.; Copeland, R. A.; Chesworth, R.; Duncan, K. W. A Selective Inhibitor of PRMT5 With In Vivo and In Vitro Potency in MCL Models. *Nat. Chem. Biol.* **2015,** *11* (6), 432–437.
21. Kubicek, S.; O'Sullivan, R. J.; August, E. M.; Hickey, E. R.; Zhang, Q.; Teodoro, M. L.; Rea, S.; Mechtler, K.; Kowalski, J. A.; Homon, C. A.; Kelly, T. A.; Jenuwein, T. Reversal of H3K9me2 by a Small-Molecule Inhibitor for the G9a Histone Methyltransferase. *Mol. Cell* **2007,** *25* (3), 473–481.

22. (a) Copeland, R. A. Mechanistic Considerations in High-Throughput Screening. *Anal. Biochem.* **2003,** *320* (1), 1–12; (b) Yang, J.; Copeland, R. A.; Lai, Z. Defining Balanced Conditions for Inhibitor Screening Assays That Target Bisubstrate Enzymes. *J. Biomol. Screen.* **2009,** *14* (2), 111–120.
23. Baell, J. B.; Holloway, G. A. New Substructure Filters for Removal of Pan Assay Interference Compounds (PAINS) From Screening Libraries and for Their Exclusion in Bioassays. *J. Med. Chem.* **2010,** *53* (7), 2719–2740.
24. Fournel, M.; Bonfils, C.; Hou, Y.; Yan, P. T.; Trachy-Bourget, M. C.; Kalita, A.; Liu, J.; Lu, A. H.; Zhou, N. Z.; Robert, M. F.; Gillespie, J.; Wang, J. J.; Ste-Croix, H.; Rahil, J.; Lefebvre, S.; Moradei, O.; Delorme, D.; Macleod, A. R.; Besterman, J. M.; Li, Z. MGCD0103, A Novel Isotype-Selective Histone Deacetylase Inhibitor, Has Broad Spectrum Antitumor Activity In Vitro and In Vivo. *Mol. Cancer Ther.* **2008,** *7* (4), 759–768.
25. Marks, P. A.; Breslow, R. Dimethyl Sulfoxide to Vorinostat: Development of This Histone Deacetylase Inhibitor as an Anticancer Drug. *Nat. Biotechnol.* **2007,** *25* (1), 84–90.
26. Duncan, K. W.; Rioux, N.; Boriack-Sjodin, P. A.; Munchhof, M. J.; Reiter, L. A.; Majer, C. R.; Jin, L.; Johnston, L. D.; Chan-Penebre, E.; Kuplast, K. G.; Scott, M. P.; Pollock, R. M.; Waters, N. J.; Smith, J. J.; Moyer, M. P.; Copeland, R. A.; Chesworth, R. Structure and Property Guided Design in the Identification of PRMT5 Tool Compound EPZ015666. *ACS Med. Chem. Lett.* **2016,** *7,* 162–166.
27. Mitchell, L. H.; Drew, A. E.; Ribich, S. A.; Rioux, N.; Swinger, K. K.; Jacques, S. L.; Lingaraj, T.; Boriack-Sjodin, P. A.; Waters, N. J.; Wigle, T. J.; Moradei, O.; Jin, L.; Riera, T.; Porter-Scott, M.; Moyer, M. P.; Smith, J. J.; Chesworth, R.; Copeland, R. A. Aryl Pyrazoles as Potent Inhibitors of Arginine Methyltransferases: Identification of the First PRMT6 Tool Compound. *ACS Med. Chem. Lett.* **2015,** *6* (6), 655–659.
28. Campbell, J. E.; Kuntz, K. W.; Knutson, S. K.; Warholic, N. M.; Keilhack, H.; Wigle, T. J.; Raimondi, A.; Klaus, C. R.; Rioux, N.; Yokoi, A.; Kawano, S.; Minoshima, Y.; Choi, H. W.; Porter Scott, M.; Waters, N. J.; Smith, J. J.; Chesworth, R.; Moyer, M. P.; Copeland, R. A. EPZ011989, A Potent, Orally-Available EZH2 Inhibitor With Robust In Vivo Activity. *ACS Med. Chem. Lett.* **2015,** *6* (5), 491–495.
29. Gehling, V. S.; Vaswani, R. G.; Nasveschuk, C. G.; Duplessis, M.; Iyer, P.; Balasubramanian, S.; Zhao, F.; Good, A. C.; Campbell, R.; Lee, C.; Dakin, L. A.; Cook, A. S.; Gagnon, A.; Harmange, J.-C.; Audia, J. E.; Cummings, R. T.; Normant, E.; Trojer, P.; Albrecht, B. K. Discovery, Design, and Synthesis of Indole-Based EZH2 Inhibitors. *Bioorg. Med. Chem. Lett.* **2015,** *25,* 3644–3649.
30. Bradley, W. D.; Arora, S.; Busby, J.; Balasubramanian, S.; Gehling, V. S.; Nasveschuk, C. G.; Vaswani, R. G.; Yuan, C. C.; Hatton, C.; Zhao, F.; Williamson, K. E.; Iyer, P.; Mendez, J.; Campbell, R.; Cantone, N.; Garapaty-Rao, S.; Audia, J. E.; Cook, A. S.; Dakin, L. A.; Albrecht, B. K.; Harmange, J. C.; Daniels, D. L.; Cummings, R. T.; Bryant, B. M.; Normant, E.; Trojer, P. EZH2 Inhibitor Efficacy in Non-Hodgkin's Lymphoma Does not Require Suppression of H3K27 Monomethylation. *Chem. Biol.* **2014,** *21* (11), 1463–1475.
31. Verma, S. K. Inhibition of the Histone Lysine Methyltransferase EZH2 for the Treatment of Cancer. *Curr. Top. Med. Chem.* **2015,** *15* (8), 714–719.
32. Nasveschuk, C. G.; Gagnon, A.; Garapaty-Rao, S.; Balasubramanian, S.; Campbell, R.; Lee, C.; Zhao, F.; Bergeron, L.; Cummings, R.; Trojer, P.; Audia, J. E.; Albrecht, B. K.; Harmange, J. C. Discovery and Optimization of Tetramethylpiperidinyl Benzamides as Inhibitors of EZH2. *ACS Med. Chem. Lett.* **2014,** *5* (4), 378–383.
33. Knutson, S. K.; Kawano, S.; Minoshima, Y.; Warholic, N. M.; Huang, K. C.; Xiao, Y.; Kadowaki, T.; Uesugi, M.; Kuznetsov, G.; Kumar, N.; Wigle, T. J.; Klaus, C. R.; Allain, C. J.; Raimondi, A.; Waters, N. J.; Smith, J. J.; Porter-Scott, M.; Chesworth, R.; Moyer, M. P.; Copeland, R. A.; Richon, V. M.; Uenaka, T.; Pollock, R. M.; Kuntz, K. W.; Yokoi, A.; Keilhack, H. Selective Inhibition of EZH2 by EPZ-6438 Leads to Potent Antitumor Activity in EZH2-Mutant Non-Hodgkin Lymphoma. *Mol. Cancer Ther.* **2014,** *13* (4), 842–854.
34. (a) Krivtsov, A. V.; Feng, Z.; Lemieux, M. E.; Faber, J.; Vempati, S.; Sinha, A. U.; Xia, X.; Jesneck, J.; Bracken, A. P.; Silverman, L. B.; Kutok, J. L.; Kung, A. L.; Armstrong, S. A. H3K79 Methylation Profiles Define Murine and Human MLL-AF4 Leukemias. *Cancer Cell* **2008,** *14* (5), 355–368; (b) Basavapathruni, A.; Jin, L.; Daigle, S. R.; Majer, C. R.; Therkelsen, C. A.; Wigle, T. J.; Kuntz, K. W.; Chesworth, R.; Pollock, R. M.; Scott, M. P.; Moyer, M. P.; Richon, V. M.; Copeland, R. A.; Olhava, E. J. Conformational Adaptation Drives Potent, Selective and Durable Inhibition of the Human Protein Methyltransferase DOT1L. *Chem. Biol. Drug Des.* **2012,** *80* (6), 971–980.
35. Daigle, S. R.; Olhava, E. J.; Therkelsen, C. A.; Basavapathruni, A.; Jin, L.; Boriack-Sjodin, P. A.; Allain, C. J.; Klaus, C. R.; Raimondi, A.; Scott, M. P.; Waters, N. J.; Chesworth, R.; Moyer, M. P.; Copeland, R. A.; Richon, V. M.; Pollock, R. M. Potent Inhibition of DOT1L as Treatment of MLL-Fusion Leukemia. *Blood* **2013,** *122* (6), 1017–1025.
36. Ferguson, A. D.; Larsen, N. A.; Howard, T.; Pollard, H.; Green, I.; Grande, C.; Cheung, T.; Garcia-Arenas, R.; Cowen, S.; Wu, J.; Godin, R.; Chen, H.; Keen, N. Structural Basis of Substrate Methylation and Inhibition of SMYD2. *Structure* **2011,** *19* (9), 1262–1273.
37. Mitchell, L. H.; Boriack-Sjodin, P. A.; Smith, S.; Thomenius, M.; Rioux, N.; Munchhof, M.; Mills, J. E.; Klaus, C.; Totman, J.; Riera, T. V.; Raimondi, A.; Jacques, S. L.; West, K.; Foley, M.; Waters, N. J.; Kuntz, K. W.; Wigle, T. J.; Scott, M. P.; Copeland, R. A.; Smith, J. J.; Chesworth, R. Novel Oxindole Sulfonamides and Sulfamides: EPZ031686 the First Orally Bioavailable Small Molecule SMYD3 Inhibitor. *ACS Med. Chem. Lett.* **2016,** *7* (2), 134–138.
38. (a) Huang, J.; Dorsey, J.; Chuikov, S.; Perez-Burgos, L.; Zhang, X.; Jenuwein, T.; Reinberg, D.; Berger, S. L. G9a and Glp Methylate Lysine 373 in the Tumor Suppressor p53. *J. Biol. Chem.* **2010,** *285* (13), 9636–9641; (b) Kondo, Y.; Shen, L.; Suzuki, S.; Kurokawa, T.; Masuko, K.; Tanaka, Y.; Kato, H.; Mizuno, Y.; Yokoe, M.; Sugauchi, F.; Hirashima, N.; Orito, E.; Osada, H.; Ueda, R.; Guo, Y.; Chen, X.; Issa, J. P.; Sekido, Y. Alterations of DNA Methylation and Histone Modifications Contribute to Gene Silencing in Hepatocellular Carcinomas. *Hepatol. Res.* **2007,** *37* (11), 974–983; (c) Kondo, Y.; Shen, L.; Ahmed, S.; Boumber, Y.; Sekido, Y.; Haddad, B. R.; Issa, J. P. Downregulation of Histone H3 Lysine 9 Methyltransferase G9a Induces Centrosome Disruption and Chromosome Instability in Cancer Cells. *PLoS ONE* **2008,** *3* (4), e2037; (d) McGarvey, K. M.; Fahrner, J. A.; Greene, E.; Martens, J.; Jenuwein, T.; Baylin, S. B. Silenced Tumor Suppressor Genes Reactivated by DNA Demethylation do not Return to a Fully Euchromatic Chromatin State. *Cancer Res.* **2006,** *66* (7), 3541–3549; (e) Watanabe, H.; Soejima, K.; Yasuda, H.; Kawada, I.; Nakachi, I.; Yoda, S.; Naoki, K.; Ishizaka, A. Deregulation of Histone Lysine Methyltransferases Contributes to Oncogenic Transformation of Human Bronchoepithelial Cells. *Cancer Cell Int.* **2008,** *8,* 15.
39. Chen, M. W.; Hua, K. T.; Kao, H. J.; Chi, C. C.; Wei, L. H.; Johansson, G.; Shiah, S. G.; Chen, P. S.; Jeng, Y. M.; Cheng, T. Y.; Lai, T. C.; Chang, J. S.; Jan, Y. H.; Chien, M. H.; Yang, C. J.; Huang, M. S.; Hsiao, M.; Kuo, M. L. H3K9 Histone Methyltransferase G9a Promotes Lung Cancer Invasion and Metastasis by Silencing the Cell Adhesion Molecule Ep-CAM. *Cancer Res.* **2010,** *70* (20), 7830–7840.
40. Chang, Y.; Zhang, X.; Horton, J. R.; Upadhyay, A. K.; Spannhoff, A.; Liu, J.; Snyder, J. P.; Bedford, M. T.; Cheng, X. Structural Basis for G9a-Like Protein Lysine Methyltransferase Inhibition by BIX-01294. *Nat. Struct. Mol. Biol.* **2009,** *16* (3), 312–317.
41. Liu, F.; Chen, X.; Allali-Hassani, A.; Quinn, A. M.; Wasney, G. A.; Dong, A.; Barsyte, D.; Kozieradzki, I.; Senisterra, G.; Chau, I.; Siarheyeva, A.; Kireev, D. B.; Jadhav, A.; Herold, J. M.; Frye, S. V.; Arrowsmith, C. H.; Brown, P. J.; Simeonov, A.; Vedadi, M.; Jin, J. Discovery of a 2,4-Diamino-7-Aminoalkoxyquinazoline as a Potent and Selective Inhibitor of Histone Lysine Methyltransferase G9a. *J. Med. Chem.* **2009,** *52* (24), 7950–7953.
42. (a) Liu, F.; Barsyte-Lovejoy, D.; Allali-Hassani, A.; He, Y.; Herold, J. M.; Chen, X.; Yates, C. M.; Frye, S. V.; Brown, P. J.; Huang, J.; Vedadi, M.; Arrowsmith, C. H.; Jin, J. Optimization of Cellular Activity of G9a Inhibitors 7-Aminoalkoxy-Quinazolines. *J. Med. Chem.* **2011,** *54* (17), 6139–6150; (b) Vedadi, M.; Barsyte-Lovejoy, D.; Liu, F.; Rival-Gervier, S.; Allali-Hassani, A.; Labrie, V.; Wigle, T. J.; Dimaggio, P. A.; Wasney, G. A.; Siarheyeva, A.; Dong, A.; Tempel, W.; Wang, S. C.; Chen, X.; Chau, I.; Mangano, T. J.; Huang, X. P.; Simpson, C. D.; Pattenden, S. G.; Norris, J. L.; Kireev, D. B.; Tripathy, A.; Edwards, A.; Roth, B. L.; Janzen, W. P.; Garcia, B. A.; Petronis, A.; Ellis, J.; Brown, P. J.; Frye, S. V.; Arrowsmith, C. H.; Jin, J. A Chemical Probe Selectively Inhibits G9a and GLP Methyltransferase Activity in Cells. *Nat. Chem. Biol.* **2011,** *7* (8), 566–574.
43. Liu, F.; Barsyte-Lovejoy, D.; Li, F.; Xiong, Y.; Korboukh, V.; Huang, X. P.; Allali-Hassani, A.; Janzen, W. P.; Roth, B. L.; Frye, S. V.; Arrowsmith, C. H.; Brown, P. J.; Vedadi, M.; Jin, J. Discovery of an In Vivo Chemical Probe of the Lysine Methyltransferases G9a and GLP. *J. Med. Chem.* **2013,** *56* (21), 8931–8942.
44. Sweis, R. F.; Pliushchev, M.; Brown, P. J.; Guo, J.; Li, F.; Maag, D.; Petros, A. M.; Soni, N. B.; Tse, C.; Vedadi, M.; Michaelides, M. R.; Chiang, G. G.; Pappano, W. N. Discovery and Development of Potent and Selective Inhibitors of Histone Methyltransferase G9a. *ACS Med. Chem. Lett.* **2014,** *5* (2), 205–209.
45. Shi, Y.; Lan, F.; Matson, C.; Mulligan, P.; Whetstine, J. R.; Cole, P. A.; Casero, R. A. Histone Demethylation Mediated by the Nuclear Amine Oxidase Homolog LSD1. *Cell* **2004,** *119* (7), 941–953.
46. Culhane, J. C.; Cole, P. A. LSD1 and the Chemistry of Histone Demethylation. *Curr. Opin. Chem. Biol.* **2007,** *11* (5), 561–568.

47. (a) Mould, D. P.; McGonagle, A. E.; Wiseman, D. H.; Williams, E. L.; Jordan, A. M. Reversible Inhibitors of LSD1 as Therapeutic Agents in Acute Myeloid Leukemia: Clinical Significance and Progress to Date. *Med. Res. Rev.* **2014,** *35* (3), 586–618; (b) Hitchin, J. R.; Julian, B.; Burke, R.; Cockerill, M. J.; Fairweather, E. E.; Hutton, C.; Jordan, A. M.; McAndrew, C.; Mould, D.; Mirza, A.; Thompson, G. J.; Waddell, I.; Ogilvie, D. J. Development and Evaluation of Selective, Reversible LSD1 Inhibitors Derived From Fragments. *Med. Chem. Commun.* **2013,** *4,* 1513–1522; (c) Mohammad, H. P.; Smitheman, K. N.; Kamat, C. D.; Soong, D.; Federowicz, K. E.; Van Aller, G. S.; Schneck, J. L.; Carson, J. D.; Liu, Y.; Butticello, M.; Bonnette, W. G.; Gorman, S. A.; Degenhardt, Y.; Bai, Y.; McCabe, M. T.; Pappalardi, M. B.; Kasparec, J.; Tian, X.; McNulty, K. C.; Rouse, M.; McDevitt, P.; Ho, T.; Crouthamel, M.; Hart, T. K.; Concha, N. O.; McHugh, C. F.; Miller, W. H.; Dhanak, D.; Tummino, P. J.; Carpenter, C. L.; Johnson, N. W.; Hann, C. L.; Kruger, R. G. A DNA Hypomethylation Signature Predicts Antitumor Activity of LSD1 Inhibitors in SCLC. *Cancer Cell* **2015,** *28* (1), 57–69.
48. Schmidt, D. M.; McCafferty, D. G. *Trans*-2-Phenylcyclopropylamine is a Mechanism-Based Inactivator of the Histone Demethylase LSD1. *Biochemistry* **2007,** *46* (14), 4408–4416.
49. (a) Yang, M.; Culhane, J. C.; Szewczuk, L. M.; Jalili, P.; Ball, H. L.; Machius, M.; Cole, P. A.; Yu, H. Structural Basis for the Inhibition of the LSD1 Histone Demethylase by the Antidepressant *Trans*-2-Phenylcyclopropylamine. *Biochemistry* **2007,** *46* (27), 8058–8065; (b) Binda, C.; Valente, S.; Romanenghi, M.; Pilotto, S.; Cirilli, R.; Karytinos, A.; Ciossani, G.; Botrugno, O. A.; Forneris, F.; Tardugno, M.; Edmondson, D. E.; Minucci, S.; Mattevi, A.; Mai, A. Biochemical, Structural, and Biological Evaluation of Tranylcypromine Derivatives as Inhibitors of Histone Demethylases LSD1 and LSD2. *J. Am. Chem. Soc.* **2010,** *132* (19), 6827–6833.
50. (a) Khan, M. N.; Suzuki, T.; Miyata, N. An Overview of Phenylcyclopropylamine Derivatives: Biochemical and Biological Significance and Recent Developments. *Med. Res. Rev.* **2013,** *33* (4), 873–910; (b) Mimasu, S.; Umezawa, N.; Sato, S.; Higuchi, T.; Umehara, T.; Yokoyama, S. Structurally Designed *Trans*-2-Phenylcyclopropylamine Derivatives Potently Inhibit Histone Demethylase LSD1/KDM1. *Biochemistry* **2010,** *49* (30), 6494–6503; (c) Valente, S.; Rodriguez, V.; Mercurio, C.; Vianello, P.; Saponara, B.; Cirilli, R.; Ciossani, G.; Labella, D.; Marrocco, B.; Ruoppolo, G.; Botrugno, O. A.; Dessanti, P.; Minucci, S.; Mattevi, A.; Varasi, M.; Mai, A. Pure Diastereomers of a Tranylcypromine-Based LSD1 Inhibitor: Enzyme Selectivity and In-Cell Studies. *ACS Med. Chem. Lett.* **2015,** *6* (2), 173–177.
51. Filippakopoulos, P.; Knapp, S. Targeting Bromodomains: Epigenetic Readers of Lysine Acetylation. *Nat. Rev. Drug Discov.* **2014,** *13* (5), 337–356.
52. Filippakopoulos, P.; Qi, J.; Picaud, S.; Shen, Y.; Smith, W. B.; Fedorov, O.; Morse, E. M.; Keates, T.; Hickman, T. T.; Felletar, I.; Philpott, M.; Munro, S.; McKeown, M. R.; Wang, Y.; Christie, A. L.; West, N.; Cameron, M. J.; Schwartz, B.; Heightman, T. D.; La Thangue, N.; French, C. A.; Wiest, O.; Kung, A. L.; Knapp, S.; Bradner, J. E. Selective Inhibition of BET Bromodomains. *Nature* **2010,** *468* (7327), 1067–1073.
53. (a) Chung, C. W.; Coste, H.; White, J. H.; Mirguet, O.; Wilde, J.; Gosmini, R. L.; Delves, C.; Magny, S. M.; Woodward, R.; Hughes, S. A.; Boursier, E. V.; Flynn, H.; Bouillot, A. M.; Bamborough, P.; Brusq, J. M.; Gellibert, F. J.; Jones, E. J.; Riou, A. M.; Homes, P.; Martin, S. L.; Uings, I. J.; Toum, J.; Clement, C. A.; Boullay, A. B.; Grimley, R. L.; Blandel, F. M.; Prinjha, R. K.; Lee, K.; Kirilovsky, J.; Nicodeme, E. Discovery and Characterization of Small Molecule Inhibitors of the BET Family Bromodomains. *J. Med. Chem.* **2011,** *54* (11), 3827–3838; (b) Mirguet, O.; Lamotte, Y.; Donche, F.; Toum, J.; Gellibert, F.; Bouillot, A.; Gosmini, R.; Nguyen, V. L.; Delannee, D.; Seal, J.; Blandel, F.; Boullay, A. B.; Boursier, E.; Martin, S.; Brusq, J. M.; Krysa, G.; Riou, A.; Tellier, R.; Costaz, A.; Huet, P.; Dudit, Y.; Trottet, L.; Kirilovsky, J.; Nicodeme, E. From ApoA1 Upregulation to BET Family Bromodomain Inhibition: Discovery of I-BET151. *Bioorg. Med. Chem. Lett.* **2012,** *22* (8), 2963–2967.
54. Gehling, V. S.; Hewitt, M. C.; Vaswani, R. G.; Leblanc, Y.; Cote, A.; Nasveschuk, C. G.; Taylor, A. M.; Harmange, J. C.; Audia, J. E.; Pardo, E.; Joshi, S.; Sandy, P.; Mertz, J. A.; Sims, R. J., 3rd; Bergeron, L.; Bryant, B. M.; Bellon, S.; Poy, F.; Jayaram, H.; Sankaranarayanan, R.; Yellapantula, S.; Bangalore Srinivasamurthy, N.; Birudukota, S.; Albrecht, B. K. Discovery, Design, and Optimization of Isoxazole Azepine BET Inhibitors. *ACS Med. Chem. Lett.* **2013,** *4* (9), 835–840.
55. Hewitt, M. C.; Leblanc, Y.; Gehling, V. S.; Vaswani, R. G.; Cote, A.; Nasveschuk, C. G.; Taylor, A. M.; Harmange, J. C.; Audia, J. E.; Pardo, E.; Cummings, R.; Joshi, S.; Sandy, P.; Mertz, J. A.; Sims, R. J., 3rd; Bergeron, L.; Bryant, B. M.; Bellon, S.; Poy, F.; Jayaran, H.; Tang, Y.; Albrecht, B. K. Development of Methyl Isoxazoleazepines as Inhibitors of BET. *Bioorg. Med. Chem. Lett.* **2015,** *25* (9), 1842–1848.
56. Albrecht, B. K.; Gehling, V. S.; Hewitt, M. C.; Vaswani, R. G.; Cote, A.; Leblanc, Y.; Nasveschuk, C. G.; Bellon, S.; Bergeron, L.; Campbell, R.; Cantone, N.; Cooper, M. R.; Cummings, R. T.; Jayaram, H.; Joshi, S.; Mertz, J. A.; Neiss, A.; Normant, E.; O'Meara, M.; Pardo, E.; Poy, F.; Sandy, P.; Supko, J.; Sims, R. J.; Harmange, J. C.; Taylor, A. M.; Audia, J. E. Identification of a Benzoisoxazoloazepine Inhibitor (CPI-0610) of the Bromodomain and Extra-Terminal (BET) Family as a Candidate for Human Clinical Trials. *J. Med. Chem.* **2016,** *59* (4), 1330–1339.
57. Chen, P.; Chaikuad, A.; Bamborough, P.; Bantscheff, M.; Bountra, C.; Chung, C. W.; Fedorov, O.; Grandi, P.; Jung, D.; Lesniak, R.; Lindon, M.; Muller, S.; Philpott, M.; Prinjha, R.; Rogers, C.; Selenski, C.; Tallant, C.; Werner, T.; Willson, T. M.; Knapp, S.; Drewry, D. H. Discovery and Characterization of GSK2801, a Selective Chemical Probe for the Bromodomains BAZ2A and BAZ2B. *J. Med. Chem.* **2016,** *59,* 1410–1424.
58. Drouin, L.; McGrath, S.; Vidler, L. R.; Chaikuad, A.; Monteiro, O.; Tallant, C.; Philpott, M.; Rogers, C.; Fedorov, O.; Liu, M.; Akhtar, W.; Hayes, A.; Raynaud, F.; Muller, S.; Knapp, S.; Hoelder, S. Structure Enabled Design of BAZ2-ICR, a Chemical Probe Targeting the Bromodomains of BAZ2A and BAZ2B. *J. Med. Chem.* **2015,** *58* (5), 2553–2559.
59. (a) Fish, P. V.; Filippakopoulos, P.; Bish, G.; Brennan, P. E.; Bunnage, M. E.; Cook, A. S.; Federov, O.; Gerstenberger, B. S.; Jones, H.; Knapp, S.; Marsden, B.; Nocka, K.; Owen, D. R.; Philpott, M.; Picaud, S.; Primiano, M. J.; Ralph, M. J.; Sciammetta, N.; Trzupek, J. D. Identification of a Chemical Probe for Bromo and Extra C-Terminal Bromodomain Inhibition Through Optimization of a Fragment-Derived Hit. *J. Med. Chem.* **2012,** *55* (22), 9831–9837; (b) Picaud, S.; Da Costa, D.; Thanasopoulou, A.; Filippakopoulos, P.; Fish, P. V.; Philpott, M.; Fedorov, O.; Brennan, P.; Bunnage, M. E.; Owen, D. R.; Bradner, J. E.; Taniere, P.; O'Sullivan, B.; Muller, S.; Schwaller, J.; Stankovic, T.; Knapp, S. PFI-1, A Highly Selective Protein Interaction Inhibitor, Targeting BET Bromodomains. *Cancer Res.* **2013,** *73* (11), 3336–3346.
60. Hay, D. A.; Fedorov, O.; Martin, S.; Singleton, D. C.; Tallant, C.; Wells, C.; Picaud, S.; Philpott, M.; Monteiro, O. P.; Rogers, C. M.; Conway, S. J.; Rooney, T. P.; Tumber, A.; Yapp, C.; Filippakopoulos, P.; Bunnage, M. E.; Muller, S.; Knapp, S.; Schofield, C. J.; Brennan, P. E. Discovery and Optimization of Small-Molecule Ligands for the CBP/p300 Bromodomains. *J. Am. Chem. Soc.* **2014,** *136* (26), 9308–9319.
61. Martin, M. P.; Olesen, S. H.; Georg, G. I.; Schonbrunn, E. Cyclin-Dependent Kinase Inhibitor Dinaciclib Interacts With the Acetyl-Lysine Recognition Site of Bromodomains. *ACS Chem. Biol.* **2013,** *8* (11), 2360–2365.

5.09 Targeting Promoter Quadruplex Nucleic Acids for Cancer Therapy

A Paulo, University of Lisbon, Lisbon, Portugal
CC Castillo and S Neidle*, University College London, London, United Kingdom

© 2017 Elsevier Ltd. All rights reserved.

5.09.1	**Introduction**	308
5.09.1.1	Quadruplex Occurrence and Biological Function	309
5.09.2	**Quadruplex Native Structure Overview**	310
5.09.3	**Quadruplex-Small Molecule Recognition**	313
5.09.4	**Telomeric Quadruplexes as Therapeutic Targets**	314
5.09.5	**Oncogene Expression Control by Small Molecules in Cancer Cells**	316
5.09.5.1	c-*MYC*	316
5.09.5.2	h*TERT*	321
5.09.5.3	The *RAS* Family	322
5.09.5.4	*VEGF* and *VEGFR*	325
5.09.5.5	c-*KIT*	326
5.09.5.6	BCL-2	328
5.09.5.7	HSP-90	330
5.09.5.8	*HIF*α	330
5.09.5.9	The Androgen Receptor	331
5.09.5.10	RET	331
5.09.5.11	MET	332
5.09.5.12	c-*SRC*	332
References		333
Relevant Websites		340

Abbreviations

AR Androgen receptor
BCL-2 B-cell lymphoma 2
CD Circular dichroism
CDK Cyclin-dependent kinase
EGFR Endothelial growth factor receptor
FRET Fluorescence resonance energy transfer
G Guanine
GIST Gastrointestinal stromal tumors
HIF-1 Hypoxia-inducible factor-1
HSP Heat-shock protein
hTERT Human telomerase reverse transcriptase
IRES Internal ribosomal entry sites
MET Hepatocyte growth factor receptor
NCI National Cancer Institute USA
PDB Protein Data Bank
RET Rearranged during transfection
SPR Surface plasmon resonance
TERRA Telomeric RNA sequences
UTRs 5′- and 3′-untranslated regions
VEGF Vascular endothelial growth factor

5.09.1 Introduction

Polynucleotides comprising ribo- or deoxyribo-guanidylic acid repeats have long been known to readily form unusual aggregated structures, especially in the presence of potassium or sodium ions. Fiber diffraction and biophysical studies have established that these are in the form of four-stranded right-handed helical arrangements.[1–4] Analogous arrangements can be formed by specialized sequences comprising several short guanine(G) tracts, which can be found in many eukaryotic and prokaryotic genomes, notably at the ends of chromosomes in telomeric regions.[5,6] Typically such sequences contain four such G-tracts and are of the form $G_{3-5}\ X_n\ G_{3-5}\ X_o\ G_{3-5}\ X_p\ G_{3-5}$ where X_n, X_o, and X_p are loops with one to seven nucleotides. These sequences can readily fold into stable discrete four-stranded structures, termed quadruplexes, with close analogy to the polynucleotide four-stranded helices, although it cannot be assumed that all putative quadruplex-forming sequences actually form stable structures.[7]

*Corresponding author.

Telomeric DNA, the sequences at the ends of eukaryotic chromosomes, comprise tandem repeats of quadruplex-forming sequence—in the case of *homo sapiens*, the telomeric repeat[8] is the hexanucleotide d(TTAGGG), which can form (i) intramolecular quadruplexes with four repeats, and (ii) intermolecular quadruplexes with either one, two, or rarely three repeats.[9–12] Their properties have been extensively characterized by structural (X-ray crystallography and high-field NMR) and biophysical methods [especially UV and fluorescence spectroscopy and circular dichroism (CD)],[13–20] and serve as a paradigm for quadruplexes found in other genomic locations. These methodologies have also been extensively used in the biophysical characterization of quadruplex-small molecule complexes.

The quadruplex field has been well-served by a number of authoritative reviews on various aspects—structural,[16–18] biology,[21–26] and small-molecule binding.[27–37] This article provides a general background to the small-molecule quadruplex field, together with key references. It focuses on the small molecules that have been reported to selectively affect quadruplex function at the level of individual gene promoters, with a view to their potential as anticancer drug candidates, emphasizing those that have promise by virtue of their ability to target particular cancer-selective genes (i.e., oncogenes). It does not aim to catalog all such compounds, but illustrates the main organic compound classes and their known functions. We have for the most part excluded the literature on metallo-containing compounds since although a number of compounds show high potency,[29] their development as potential clinical agents is at present considerably less advanced. Human cancers continue to be the principal area of focus in the therapeutic quadruplex field, but a few studies have indicated the potential of the approach in other therapeutic areas, notably as antibacterial, antiviral, and antiparasitic targets.[38–43]

5.09.1.1 Quadruplex Occurrence and Biological Function

Quadruplex-forming sequences have for some while been identified in a variety of biological contexts in the human genome, notably in immunoglobin switch regions and in the nuclease hypersensitive region of the c-*MYC* oncogene. The availability of the sequence of the human genome has enabled systematic searches of their occurrence to be made using algorithms which employed the general quadruplex-forming sequence shown earlier. Two distinct bioinformatics approaches provided very similar numbers, with a total of c. 350,000 putative occurrences.[44,45] Many of these were found in regions of high G density, with unequal length G-tracts, and multiple overlapping potential quadruplexes. This suggests that some quadruplexes are in dynamic equilibrium, with multiple overlapping species being possible. Validation of actual quadruplex formation is usually made for a particular sequence using data from CD, UV fluorescence melting, and NMR methods[17,19,20]; all need to individually and unequivocally point to quadruplex formation in order for an unambiguous conclusion of quadruplex formation to be made and distinguished from, for example, formation of a stable hairpin structure. To date, this has only been done for a modest number of sequences. There is currently only a limited ability to reliably predict quadruplex folds directly from primary sequence, especially for more complex arrangements since ab initio quadruplex structure prediction approaches are still in their infancy. A recent direct approach to the problem of even predicting validated putative quadruplex-forming sequences, using next-generation DNA sequencing, has not used the assumption of a maximum loop length, of seven nucleotides, inherent in the earlier bioinformatics studies. Instead over 700,000 occurrences have been mapped, with over 450,000 not having been previously predicted.[46] These more recently located occurrences tend to have longer loops and/or sequences that do not conform to the canonical quadruplex sequence shown earlier. Bioinformatics searches in other organisms, notably in prokaryotics such as *Escherichia coli* and in viruses such as HIV, have shown the wide-spread existence of quadruplex sequences,[38–43] although almost all medicinal chemistry effort to date has focussed on quadruplex occurrences in the human genome, especially as potential anticancer targets.

Quadruplex sequences are not randomly distributed in the human genome, outside of telomeres, where they comprise telomeric DNA (of which the 100–150 3′-terminal nucleotides, i.e., 15–25 d(TTAGGG) repeats, are single-stranded). Instead, there is an overabundance of quadruplex sequences in promoter regions, especially close to the transcription start site, and in nuclease hypersensitive regions (notably characterized in the c-*MYC* gene[47]) where they often overlap with SP1 transcription factor sites. A number of these occurrences have been characterized in vitro using biophysical and sometimes structural methods, and shown to be capable of forming stable quadruplexes. The occurrence of an extensive quadruplex sequence in the c-*MYC* promoter is the best-studied and validated.[48–51] Quadruplex characterized in promoter sequences includes *BCL-2*, *VEGF*, h*TERT*, *HSP90*, *HIF*, *k-RAS*, *h-RAS*, *B-RAF*, c-*KIT*, *RET*, and the androgen receptor (AR) as notable examples[52–67]; these are all well-validated genes involved in proliferation and oncogenesis and several are also established anticancer targets at the protein and enzyme levels. Several promoter quadruplexes have full structural assignments, mostly from 2-D NMR studies and in two instances from crystal structure analyses. The targeting of these quadruplexes by small molecules is the focus of much of this article. The approach offers a contrasting alternative to direct gene-product targeting, not least because some of these genes have long been considered to be "undruggable" at the protein level.

Quadruplex-forming sequences are also overrepresented in 5′- and 3′-untranslated regions (UTRs) of a number of genes,[68–73] with some genes having multiple occurrences in promoters as well. These UTR quadruplexes can form very stable RNA quadruplexes, few of which have been characterized to date, although there is evidence that they may play a role in translational regulation. A recent and surprising finding has been that telomeric RNA can be transcribed, to form telomeric RNA sequences (TERRA),[74–78] which in turn can form stable quadruplex multimers.[79] However, the biological function of TERRA is still not clear and thus its potential as a therapeutic target has yet to be determined.

The occurrence of quadruplex sequences and the demonstration that these can fold in vitro to form stable structures does not necessarily mean that they can form in a cell, let alone have biological significance and function. These key issues have been

addressed by the use of quadruplex-specific antibodies to demonstrate their existence, initially in macronuclei of the ciliate organism *Stylonychia lemnae*.[80] Quadruplexes have been shown to play a role in yeast telomere replication and maintenance, possibly with a transient existence once telomeric proteins are released since quadruplexes are effectively unwound by the RecQ helicase. More recently, two distinct quadruplex-specific antibodies have been used to unequivocally demonstrate the existence of DNA and RNA quadruplexes in human cancer cell lines.[81–84] Overall, the evidence strongly suggests that quadruplexes are significantly more prevalent in cancer cells than in normal nontransformed cells. This conclusion has been reinforced by the finding that they are present in primary tumor tissue and not in surrounding normal tissue.[85] A rationale for this selectivity has been provided by the seminal findings[83,86,87] that helicases such as the Werner's syndrome RECQ helicase, the Bloom's syndrome helicase, and FANCJ are all able to unwind quadruplexes during replication, at least in normal cells. Thus quadruplexes normally would have a transient existence, although this may still provide for specific roles in the regulation of transcription within particular genes. However in many cancer cells, the activity of these helicases can be compromised by mutations at their active sites, thus hindering quadruplex unwinding. Also there is evidence from a number of studies that quadruplex formation within the genome induces profound DNA damage responses leading to cancer cell apoptosis[88,89]; the observations that DNA repair pathways in many cancer cells are defective[90] provide a further rationale for promoter quadruplexes being selective and plausible anticancer targets.

The presence of quadruplex elements in the promoters of a number of major cancer-relevant genes has led to the hypothesis, first elaborated for c-*MYC*[48,49] that their stabilization by appropriate small molecules, would result in decreased transcription for that particular gene leading to an anticancer effect.[91] Importantly, such targets include a number long considered to be undruggable, at least at the protein level. A large number of studies have indeed shown such downregulation, accompanied by increased inhibition of cancer cell growth (see Section **Oncogene expression control by small molecules in cancer cells** in this article). It is important though to bear in mind that most studies have only demonstrated correlative relationships between promoter quadruplex affinity and direct effects on the expression of the gene involved. This has been highlighted by a careful cell-based study[92] using the c-*MYC* promoter binding compound 11-piperazinylquindoline which has shown that although c-*MYC* levels are reduced, this is not a consequence of direct c-*MYC* promoter targeting, but is presumed to be a consequence of targeting another gene. On the other hand, a distinct quadruplex-binding compound, this time the dimethylethanamine ellipticine derivative NSC-338258, does have a direct effect on c-*MYC* expression, using the same cell lines and careful approach,[93] emphasizing the importance of the exact nature of the quadruplex-stabilizing ligand.

Although it is not clear that a given small molecule can be specific for a particular quadruplex promoter target, this is of lesser importance if the gene and its gene product is a driver of cancer maintenance and progression in that cell type. Thus c-*KIT* is a major driver of gastrointestinal cancer and *k-RAS* of pancreatic and nonsmall-cell lung cancer. c-*MYC* is of major importance in many cancers, as is h*TERT*. Poly-quadruplex targeting may well offer advantages for the common human cancers, especially when confronted with problems of tumor heterogeneity and single-target resistance. These issues continue to affect more conventional single-protein/enzyme targeting in cancer, notably when using kinase inhibitors and again suggest therapeutic advantage for quadruplex targeting.

Cancer cell selectivity can also arise when targeting telomeric quadruplexes, although the basis for that selectivity is not as clear-cut as the targeting of promoter quadruplexes. The original telomere targeting concept, developed using the first quadruplex-targeting small molecules (disubstituted anthraquinones: see Section **Quadruplex-small molecule recognition**), was that they induce the single-stranded telomeric DNA overhang to fold into quadruplexes, which would resist elongation by the reverse transcriptase enzyme telomerase, whose expression is elevated in almost all tumor cell types and primary tumors. It was subsequently shown that this mode of telomerase inhibition results in cellular senescence and selective cancer cell apoptosis both in cells and in human tumor xenografts. However, telomerase inhibition alone is not the major contributor to the rapidity of observed effects since telomerase enzyme inhibition results in only a relatively small amount of telomeric DNA shortening per round of replication. A number of studies have shown that small molecules can effectively displace bound telomeric proteins and thus directly induce quadruplex formation.[94–96] These quadruplex complexes are not resolved by helicases during cancer cell replication, for the reasons outlined earlier, and the resulting quadruplex-folded telomeric DNA then appears as a DNA damage signal. DNA damage response markers such as γ-H2AX protein and ATM/ATR levels are upregulated both in cells and in xenograft experiments.[89,97–100]

5.09.2 Quadruplex Native Structure Overview

A quadruplex comprises a stable core of two or more G-quartets with four in-plane guanines Hoogsteen hydrogen-bonded together (**Fig. 1**), with intervening loops of general sequence linking the G-quartets. In addition, and uniquely to quadruplexes, the requirement for alkali metal ions is met by a central ion channel which also coordinates to O6 atoms of the guanine bases. The G-quartets are π–π stacked at a 3.4 Å separation. The four strands result in four external grooves, of varying dimensions, whose walls are lined with phosphodiester groups (imparting negative electrostatic potential). The floors of the grooves consist of the edges of the G-quartet core G bases.

The mutual orientations of the four polynucleotide strands in a quadruplex are important determinants of overall structure, and define the nature of the intervening loops.[10,16] A parallel orientation for any two strands requires the connecting loop to be folded back on itself, and is termed "strand-reversal" or "propeller" since it is oriented away from the G-quartets. Other loop types

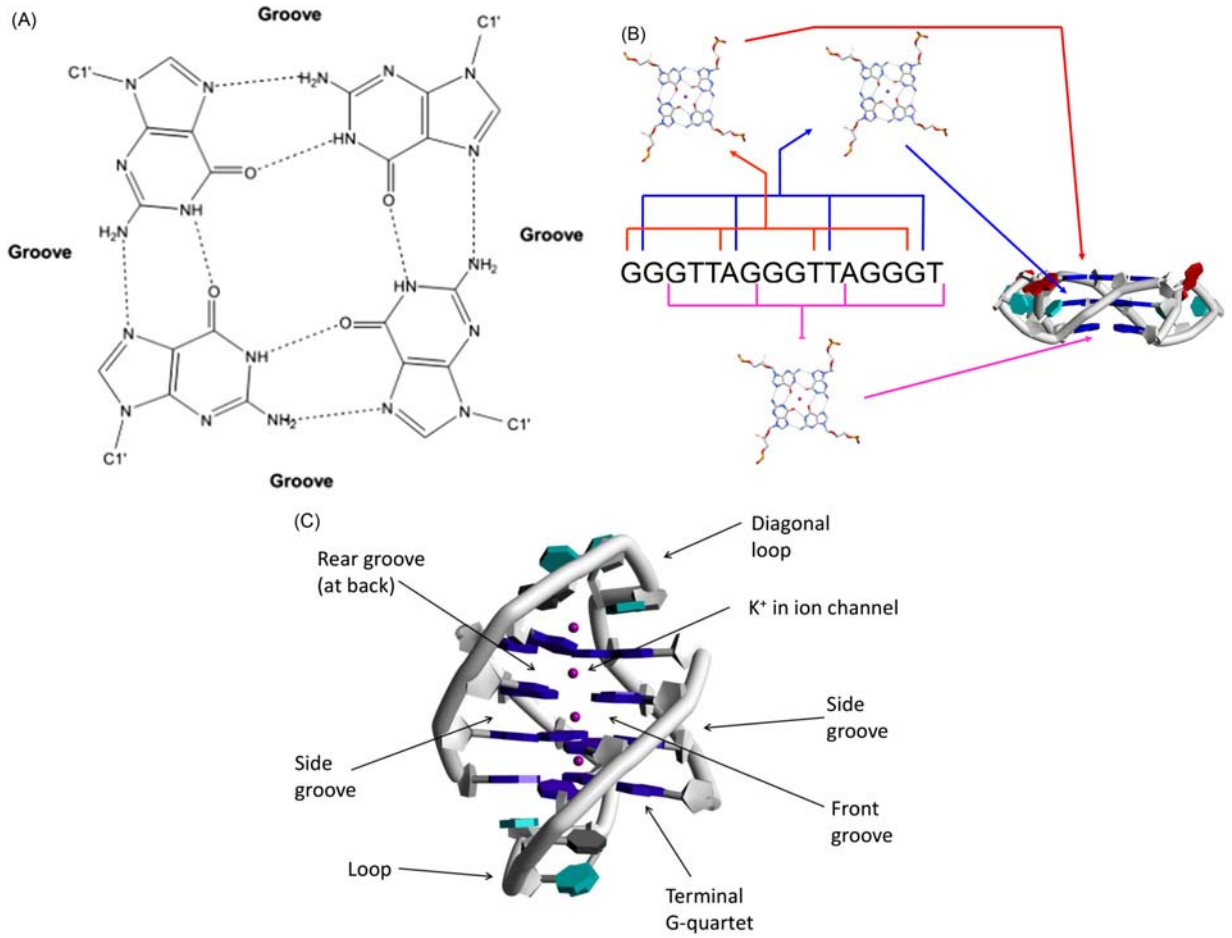

Fig. 1 (A) The G-quartet, showing the four in-plane guanine bases, each involved in four Hoogsteen hydrogen bonds. (B) G-quartet core assembly (in the human telomeric DNA quadruplex,[101]) showing the way in which each G-quartet is built up from a guanine in each G-tract. (C) The grooves and loops of a typical (bimolecular) quadruplex structure. (B, C) Taken with permission from Neidle, S. Quadruplex Nucleic Acids as Novel Therapeutic Targets, *J. Med. Chem.*, **2016**, *59*, 5987–6011.

are diagonal and lateral (edgewise), which connect antiparallel strands (Fig. 2). Diversity in quadruplex tertiary structures occurs with differing patterns of G-tract length, strand orientation, and loop sequence—appropriate longer loop sequences can themselves form stable secondary structural elements involving, for example, duplex and hairpin elements. Examples are where loops comprise repeating AT or AG sequences, which can form stable short duplex stems, as found in one of the c-*KIT* promoter quadruplexes (Fig. 3). In addition, if loop sequences contain G residues, then these can participate in G-quartet formation by inserting themselves into the G-quartet stem, in addition to the Gs in the G-tracts. This results in added complexity to the resulting structures. The human intramolecular telomeric 4-repeat sequence is highly polymorphic, at least in dilute solution, and a variety of quite diverse folds [parallel, antiparallel, and mixed (3 + 1)] have been observed, driven by slight differences in flanking sequence and changes in the coordinating central channel metal ion.[101–108] The exact nature of the biologically relevant quadruplex formed within a single-stranded telomeric DNA sequence continues to be controversial, although solution NMR and CD studies at higher concentrations and/or in crowding conditions tend to favor the parallel form[109,110] as observed in the crystalline state.[101] Considerations of the available surface area on the terminal G-quartets of telomeric quadruplexes have suggested that the preferred topology for a given small-molecule complex is dependent on the size of the bound chromophore moiety of the ligand.[111]

"Simple" quadruplexes based around the canonical quadruplex sequence have overall structural features in common, and all are organized with a single stem of at least two stacked G-quartets. A large number of distinct folds produced as a consequence of variations in loop type and strand direction have been observed experimentally for human telomeric quadruplex sequences.[101–108] In general, the loops connecting the quartets are the most variable feature defining distinct quadruplex folds—the variables of loop length and sequence can in turn result in variable groove dimensions. Table 1 lists some of the crystal and NMR structures of native promoter quadruplexes available from the Protein Data Bank (PDB). Compared to the very large numbers implied by the bioinformatics searches, these can only represent a minute fraction of quadruplex space in the human

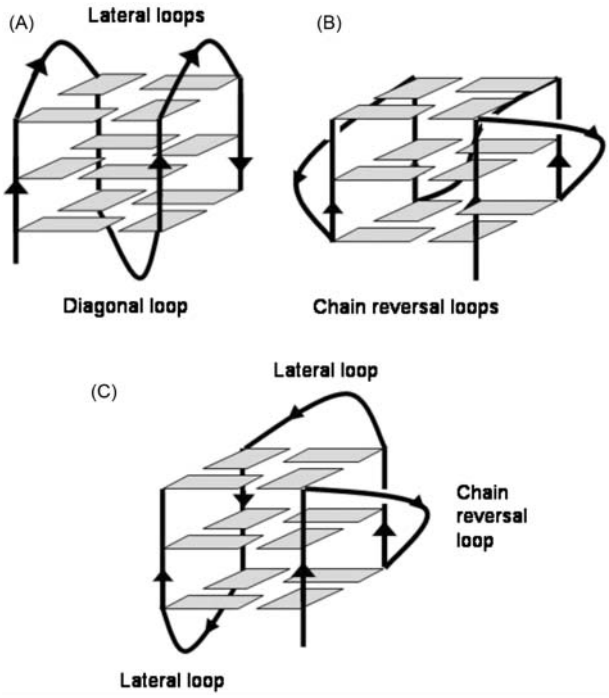

Fig. 2 Simple quadruplex loops in detail, in three distinct quadruplex folds. In each case the phosphodiester chain and its 5′–3′ direction is indicated by the *arrows* on the heavy lines. (a) an antiparallel fold, (b) an all-parallel fold, (c) a hybrid (mixed) fold. All three have used intramolecular human telomeric quadruplexes as exemplars.

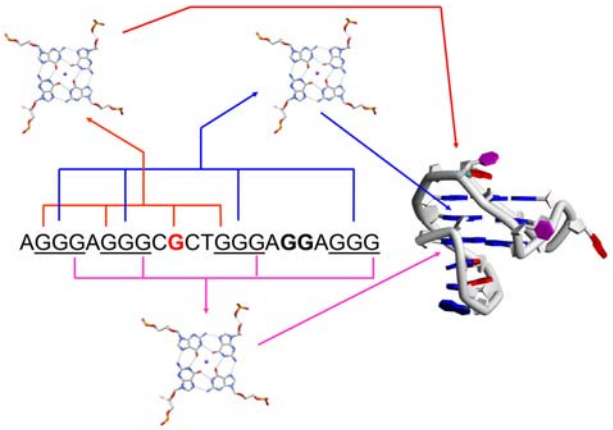

Fig. 3 The structure and assembly of the c-*KIT*1 promoter quadruplex, showing the added complex as a result of a loop guanine (shown in *bold red color*), inserted into the G-quartet stem.[63–65]

genome. A number of loop sizes and sequences are overrepresented in the human genome, with short single-nucleotide loops being common—these result in many quadruplexes having all-parallel strands as a consequence of the steric requirements of propeller loops. More complex quadruplexes are barely represented in the known database of structures; the c-*KIT*1 quadruplex is a notable example of a nonsimple quadruplex, with a guanine from G-tract linkers being inserted into a G-quartet formation so that a large and deep groove is formed.[63–65] The c-*KIT*2 quadruplex sequence can form a dimer as well as an all-parallel monomeric quadruplex,[112,113] in striking contrast to the stability of the unique c-*KIT*1 topology.[114] Polymorphism is not a universal feature of quadruplex structures, and depends on the nature of the sequence itself, with greatest variability shown by those sequences containing more than four G-tracts.

To date, there is little structural information on quadruplexes embedded in a duplex environment, apart from two crystal structures of small molecules bound to RNA quadruplex aptamers embedded within a duplex stem.[115,116] These quadruplexes have highly unusual folds.

Table 1 Selected promoter quadruplexes in the human genome for which NMR and/or crystal structures are available

Gene	*Sequence*	*Topology*	*Loops*	*PDB id*	*Reference*
c-*MYC*	d[TGAG$_3$TG$_3$TAG$_3$TG$_3$TA$_2$]	Parallel	3 × P	1XAV	50
BCL-2	d[G$_3$CGCG$_3$AG$_2$A$_2$T$_2$G$_3$CG$_3$]	Mixed parallel/antiparallel	2 × L, 1 × P	2F8U	52
c-*KIT1*[a]	**d[AG$_3$AG$_3$CGCTG$_3$AG$_2$AG$_3$]**	**Parallel**	**2 × P**	**4W02**	**64, 65**
				4W03	
				3QXR	
c-*KIT1*	d[AG$_3$AG$_3$CGCTG$_3$AG$_2$AG$_3$]	Parallel	2 × P	2O3M	63
c-*KIT2*[a]	d[CG$_3$CG$_3$CGCGAG$_3$AG$_3$T]	Parallel dimer	3 × P	2KYO	112
c-*KIT2*	d[CG$_3$CG$_3$CGCGAG$_3$AG$_3$T]	Parallel	3 × P	2KQG	113
				2KGH	
				2KYP	
VEGF	d[CG$_4$CG$_3$C$_2$T$_2$G$_3$CG$_4$T]	Parallel	3 × P	2M27	53
b-*RAF*	**d[G$_3$CG$_3$GAG$_4$GA$_2$G$_3$A]**	**Parallel dimer**	**2 × P**	**4H29**	59
h*TERT*	d[AG$_3$IAG$_4$CTG$_3$AG$_3$C]	Mixed parallel/antiparallel	2 × L, 1 × P	2KZD	54
h*TERT*	d[AIG$_3$AG$_3$ICTG$_3$AG$_3$C]	Parallel	3 × P	2KZE	54

[a]These are from two quadruplex-forming sequences in the promoter region of the c-*KIT* gene, upstream from and close to the transcription start site.
The structures in *bold type* have been determined by crystallography.

5.09.3 Quadruplex-Small Molecule Recognition

A number of crystal structures of complexes between quadruplexes and small molecules are available in the PDB, as well as several NMR structures (Table 2). All concur in showing the bound molecules stacked on a terminal G-quartet of the stack, most commonly on the 5′ end, regardless of whether the quadruplex itself is tetramolecular, bimolecular, or unimolecular. This surface-binding mode is contrary to early predictions that small-molecule ligands would insert intercalatively in between adjacent G-quartets, analogous to intercalation into duplex DNA, and is in accord with a large number of biophysical studies. Some ligands comprise

Table 2 Crystal and NMR structures of human sequence quadruplex-small molecule complexes

Primary sequence of quadruplex	*Description of quadruplex structure*	*Origin of quadruplex*	*Resolution (Å)*	*R-factor*	*No. of crystallographically unique loops*	*PDB id*	*Reference*
d[U$_{Br}$AG$_3$U$_{Br}$TAG$_3$T]	Native DNA bimolecular	Telomere	2.40	0.193	2[a]	1K8P	101
d[AG$_3$(T$_2$AG$_3$)$_3$]	Native DNA unimolecular	Telomere	2.10	0.231	3	1KF1	101
d[TAG$_3$T$_2$AG$_3$]	Porphyrin TMPyP4 complex	Telomere	2.09	0.208	2	2HRI	117
d[TAG$_3$T$_2$AG$_3$T]	Acridine (BRACO-19) complex	Telomere	2.50	0.184	2	3CE5	118
d[TAG$_3$T$_2$AG$_3$T]	ND[b] complex	Telomere	2.20	0.257	1	3CCO	119
d[TAG$_3$(T$_2$AG$_3$)$_3$]	ND complex	Telomere	2.10	0.234	6	3CDM	119
r(U$_{Br}$AG$_3$U$_2$AG$_3$U)	Native RNA bimolecular	Telomere	2.20	0.216	2[a]	3IBK	120
r(UAG$_3$U$_2$AG$_3$U)	RNA acridine complex	Telomere	2.60	0.236	1	3MIJ	121
d[TAG$_3$T$_2$AG$_3$T]	Acridine complex	Telomere	3.20	0.346	1[c]	3QCR	121
d[AG$_3$(T$_2$AG$_3$)$_3$]	ND complex	Telomere	2.30	0.260	3	3SC8	119
d[AG$_3$(T$_2$AG$_3$)$_3$]	ND complex	Telomere	2.10	0.245	3	3T5E	119
d[AG$_3$T$_2$AG$_3$T$_2$]	Salphen complex	Telomere	2.40	0.214	1	3QSC	122
d[AG$_3$T$_2$AG$_3$T$_2$]	Salphen complex	Telomere	2.40	0.240	1	3QSF	122
d[AG$_3$(T$_2$AG$_3$)$_3$]	ND complex	Telomere	1.95	0.231	3	3UYH	123
d[G$_3$(T$_2$AG$_3$)$_3$]	ND complex	Telomere	2.40	0.242	3	4DA3	123
d[G$_3$(T$_2$AG$_3$)$_3$]	ND complex	Telomere	2.75	0.212	3	4DAQ	123
d[AG$_3$(T$_2$AG$_3$)$_3$]	Berberine complex	Telomere	2.30	0.217	3	3R6R	124
d[AG$_3$(T$_2$AG$_3$)$_3$]	Mesoporphyrin complex	Telomere	2.15	0.239	3	4G0F	125
d[AG$_3$(T$_2$AG$_3$)$_3$]	Mesoporphyrin complex	Telomere	1.65	0.224	3	4FXM	125
d[TGAG$_3$TG$_2$TGAG$_3$TG$_4$A$_2$G$_2$)	**Phen-DC$_3$ complex**	**c-*MYC***				**2MGN**	**126**
d[TGAG$_3$TG$_3$TTAG$_3$TG$_3$TAA]	**Quindoline derivative**	**c-*MYC***				**2L7V**	**127**
d[T2G$_3$(TTAG3)3A]	**Telomestatin derivative**	**Telomere**				**2MB3**	**128**

[a]Chain B loop not resolved in the electron density.
[b]ND, naphthalene diimide.
[c]Loop poorly resolved in the electron density.
The structures in *bold type* have been determined by 2D-NMR methods.

entirely, or almost entirely, a planar chromophore. However, the overwhelming majority also have at least one pendant substituent, which typically terminates in a cationic charge group such as a substituted amine. These substituents reside in the quadruplex grooves, although the crystal structures demonstrate that the cationic groups do not directly interact with phosphate groups, but instead interact indirectly via bridging water molecules in the grooves.

The database of crystal structures involving the human telomeric sequence, either in bimolecular or unimolecular quadruplexes, has them complexed with a diversity of ligands, based for example on acridine,[118,121] porphyrin,[117,125] berberine,[124] square-planar metallo-containing,[122] or naphthalene diimide cores.[119,123,129] Crystal structures of a native RNA telomeric quadruplex[120] and in a complex with a disubstituted acridine compound[121] are also available—this latter structure highlights some significant differences between DNA and RNA telomeric quadruplex recognition in that the latter has a significantly larger end-quartet surface area, enabling two acridine molecules to be bound. The native RNA quadruplex fold as observed in the crystalline state retains its parallel architecture in solution.[130]

The availability of these crystal structures has enabled comparisons to be made of the dependence of quadruplex flexibility on the nature of the bound ligand.[131] In general, the G-quartet core is highly stable and retains its stacked structure in all complexes. Similarly the overall parallel fold seen in the native crystal structure is maintained. However, the 5′-TTA loops have highly variable conformations, which result in changes in groove dimensions and in accessibility to the terminal quadruplex-binding platform. Thus in silico screening of ligand or fragment libraries should take these flexibilities into account in order to obtain meaningful ranking orders of relative affinity. Even so, the marked close similarities in core stacked G-quartets and in overall topology, for example, between the human parallel telomeric quadruplex and the human *VEGF* quadruplex (**Table 1**), suggest that docking with subsequent molecular dynamics simulations could be useful in producing stereochemically and energetically plausible models for small-molecule complexes.

A small number of NMR structures of quadruplex-ligand complexes are currently available in the PDB, with a c-*MYC* quadruplex[126,128] and with an antiparallel human telomeric quadruplex.[127] All three structures show the respective ligand chromophores bound in the conventional end-stacking mode, with substituents neighboring quadruplex grooves. As with the crystal structures, these NMR models provide useful starting points for structure-based design, although there has been rather little such work reported in the literature to date.[123] The overwhelming majority of quadruplex-binding compounds have been obtained either by (i) simple conceptual arguments invoking the terminal planar quartet as the binding platform and the requirement for at least one cationic substituent and (ii) screening of compound libraries.

In silico screens have been undertaken, for example, using the ZINC or NCI (National Cancer Institute, USA) databases, mostly with human telomeric structures, but also with several of the reported c-*MYC* quadruplexes.[132–137] Hits have tended to display the structural characteristics of known quadruplex-binding ligands, although a few studies have resulted in the finding of groove-binding compounds. These tended to have lower quadruplex stabilization effectiveness, as judged by thermal stabilization experiments, and none have been progressed to date as serious drug candidates.

5.09.4 Telomeric Quadruplexes as Therapeutic Targets

The telomere length maintenance enzyme telomerase[138] is a specialized reverse transcriptase, which is expressed in the majority (c. 85%) of cancer cells and primary tumor material and serves to maintain telomere length from attrition and thus plays a major role in cancer cell immortalization.[139,140] There is a close relationship between the upregulated expression of telomerase and early stages of oncogenesis. This has led to a persistent interest in telomerase as a potentially major therapeutic target in cancer,[141] although as yet no antitelomerase drug has reached regulatory approval.

Several ways of inhibiting telomerase action have been reported, most of which involve intervention at the telomerase catalytic subunit (hTERT in humans) active site.[141] This directs the assembly of nascent telomeric DNA onto the 3′ end of telomeric DNA end, which occurs on a complementary RNA template (hTR) and uses a pool of nucleotide triphosphates, with its substrate, the 3′ end of telomeric DNA, hybridizing onto the template. This implies that telomeric DNA must be single-stranded at the point of hybridization, so folding of the 3′ single-stranded end of telomeric DNA (the extreme 100–200 nucleotides at this end) into a quadruplex arrangement has been shown to effectively inhibit hybridization and thus the enzymatic activity of telomerase.[142] Folding can be facilitated by a quadruplex-binding small molecule (first demonstrated with disubstituted anthraquinone derivatives[143]) whose quadruplex affinity is sufficient to compete off telomere-binding proteins, notably hPOT1.[144] Quadruplex-directed telomerase inhibition has been subsequently developed into an anticancer strategy by a large number of studies which have shown[32,36,145–150] that cellular inhibition of telomerase function results in senescence and apoptosis with upregulation of the retinoblastoma pathway via the cyclin-dependent kinase (CDK) inhibitor p21 and increased expression of the tumor suppressor protein $p16^{INK4a.}$

These effects have been frequently observed to occur with much greater rapidity in many cancer cell types than were expected, apparently contradicting the standard model of telomerase-driven telomere maintenance[151] since the onset of replicative senescence normally occurs only when telomeric DNA is shortened to a critical length, requiring an extended time-lag. Mean telomere length in the MCF7 cell line is c. 6 kilobases, and c. 100 nucleotides are lost per round of replication, that is, at least 30 days would be required for the onset of senescence, whereas growth-inhibitory effects are typically observed within a few hours or less. It is now generally concluded, in large part on the basis of data from quadruplex-binding agents (**Figs. 4** and **5**) including quinoline-based triazine compounds,[147] the cyclic oligo oxazole natural product telomestatin,[94] the acridine derivatives RHPS4[98–100] and

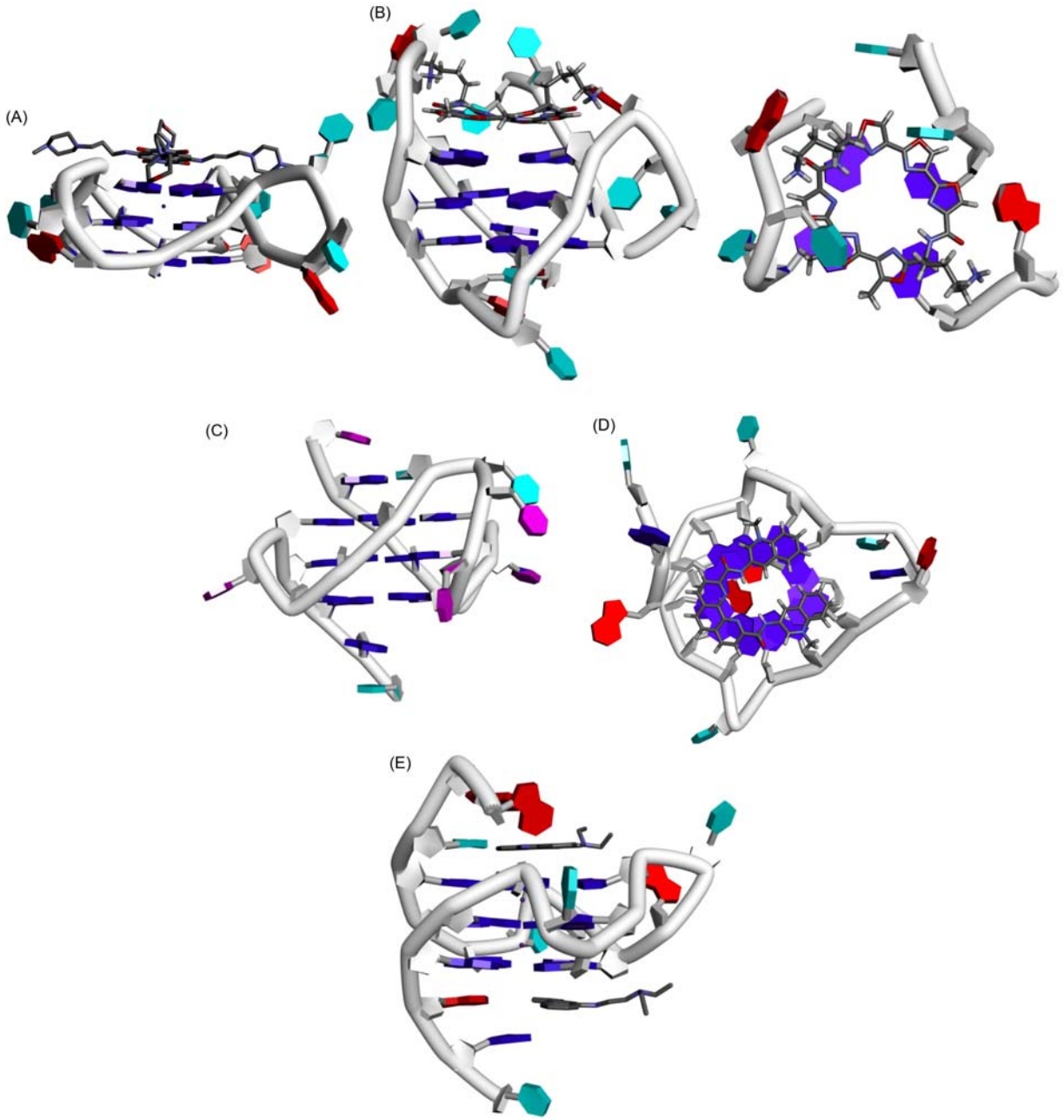

Fig. 4 Cartoon views of various native and ligand-complex quadruplex structures. (A) View showing the crystallographically determined structure of an intramolecular human telomeric DNA G-quadruplex bound by the tetra-substituted naphthalene diimide compound, MM41, shown in stick form (PDB id 3UYH).[123] (B) Two views of the 2D-NMR structure of a complex between a human telomeric quadruplex and a telomestatin analogue, shown in stick representation (PDB id 2MB3).[128] (C) Cartoon view of the parallel quadruplex formed from a sequence in the human VEGF promoter (PDB id 2M27), determined by 2D-NMR. (D) View of the 2D-NMR structure of a c-*MYC* promoter quadruplex, with bound (bisquinolinium) phenanthroline Phen-DC_3 (PDB id 2MGN), projected onto the plane of the G-quartets.[126] Note the extensive π–π overlap between the four guanines of the terminal quartet and the two quinolinium and phenanthroline moieties. (E) View of the 2:1 complex between a monosubstituted quindoline compound (shown in stick representation) and a c-*MYC* promoter complex, determined by 2D-NMR (PDB id 2L7V).[127] Taken with permission from Neidle, S. Quadruplex Nucleic Acids as Novel Therapeutic Targets, *J. Med. Chem.* **2016**, *59*, 5987–6011.

BRACO-19,[150] and the bis(quinolinyl)pyridine-dicarboxamide derivative pyridostatin[152] that rapid telomere uncapping, of associated proteins (including hTERT), is the initial consequence of ligand binding. This then leads to rapid DNA damage responses and a cascade of responses with altered regulation of, in particular, p21/$p16^{INK4a}$ kinases, p53, PARP, and ATM/ATR pathways.[97–100] The DNA damage responses result in senescence and the rapid appearance of phosphorylated histone γ-H2AX foci. Evidence for DNA damage has been obtained following in vivo tumor xenograft experiments with, in particular, RHPS4

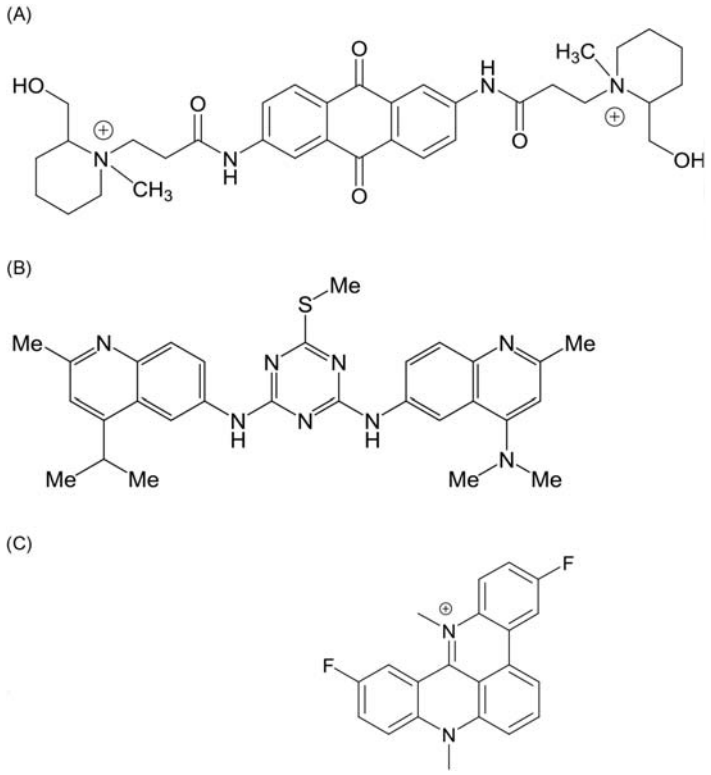

Fig. 5 Molecular structures of some quadruplex-binding small molecules. (A) A disubstituted anthraquinone derivative.[143] (B) A quinoline-based triazine compound.[147] (C) The acridine derivative RHPS4.[98–100] (D) The acridine derivative BRACO-19.[150] (E) The bis(quinolinyl)pyridine-dicarboxamide derivative pyridostatin.[152] (F)The cyclic oligo oxazole natural product telomestatin.[94]

and telomestatin.[97–100] Selectivity for cancer cells may be due to deficiencies of the DNA damage response in many cancer types, as discussed earlier in this article.

5.09.5 Oncogene Expression Control by Small Molecules in Cancer Cells

We discuss in this article examples of the large number of small molecules that have been evaluated against various promoter quadruplex targets and describe the biophysical studies on quadruplex binding in relation to their biological activity.

Many families of small molecules with antiproliferative activity in cancer cell lines have been shown to bind and stabilize strongly in vitro a number of DNA quadruplex structures found in the promoter regions of oncogenes, thus suggesting a potential application of these molecules as new anticancer drugs.[31,36,91] In this section, we review quadruplex-binding small molecules whose mechanism of action has been suggested to be, at least, in part through regulation of oncogene expression. It is hope that the reader will obtain a comprehensive view of the range of targets amenable to the approach. At the same time the current state of the art is that rather few of these small molecules appear to have selectivity for a single quadruplex, although this is hard to directly assess in view of the large number of quadruplexes potentially present in the genome. Even so, data to date does indicate that some selectivity can be achievable, at least for driver oncogenes in a particular cancer type. It is to be hoped that medicinal chemistry optimization of pharmacological properties will lead in the near future to compounds suited to clinical evaluation in several currently hard-to-treat cancers.

5.09.5.1 c-*MYC*

c-*MYC* is a proto-oncogene belonging to the basic helix–loop–helix-leucine zipper (bHLHZip) transcription factor family which includes two other genes (*MYCN* and *MYCL*) originally found in neuronal cells (N) and in lung cancer (L). The c-MYC protein can control the transcription of large numbers of genes involved in cell cycle progression, cell growth, differentiation, apoptosis, metabolism, DNA replication, and mRNA maturation.[153] One of those genes is h*TERT* (the catalytic domain of human telomerase) whose transcription is activated by c-MYC. Cancer genome sequencing analyses revealed that c-*MYC* is one of the most amplified genes across many solid cancers, including almost all serious ovarian and breast carcinomas, a large fraction of lung, and head and neck squamous cell carcinomas, and endometrioid tumors of a more serious subtype.[154] In addition, chromosomal translocation of

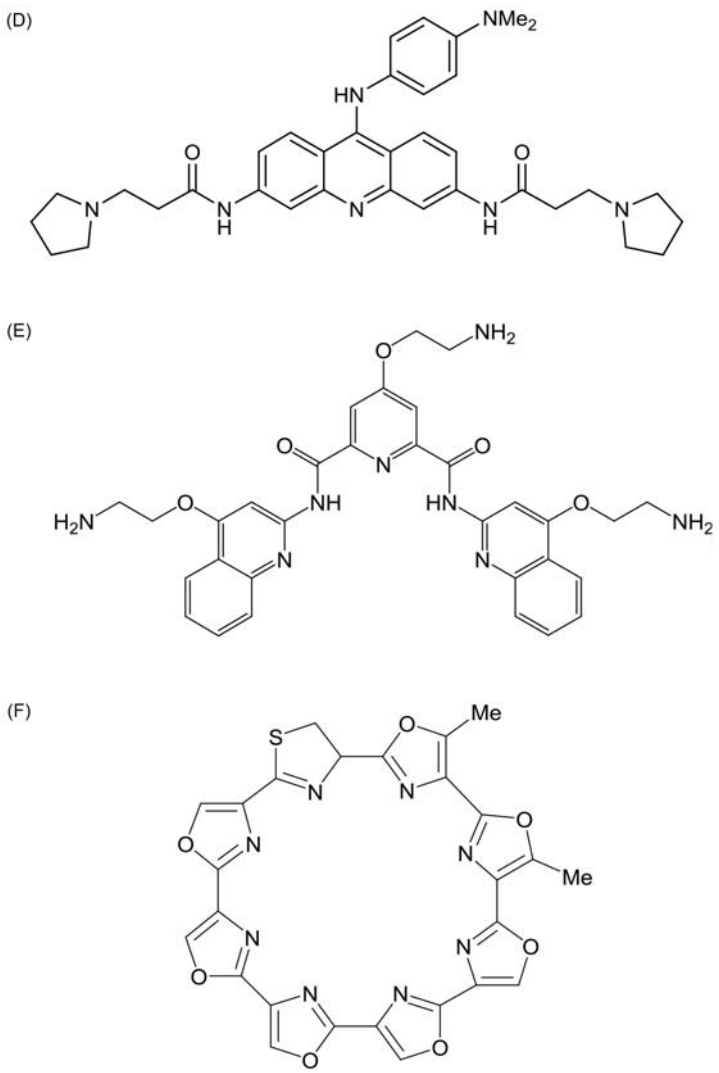

Fig. 5 (*continued*).

c-*MYC* can be particularly found in leukemias and lymphomas such as in Burkitt's lymphoma.[155] The activity of MYC can also be deregulated at the level of expression and stability of *MYC* mRNA and protein.[156]

For these reasons, c-*MYC* has been considered an attractive target for anticancer therapy. Pharmacological inhibition of the c-MYC protein has not been possible to date and it is commonly considered to be an "undruggable" target, although recent studies have provided important proof-of-concept that inhibiting MYC protein–protein interactions may be an effective therapeutic strategy.[157,158] Also, since the discovery of the quadruplex-forming sequence in NHE III1 element of the c-*MYC* promoter and its role in c-*MYC* transcription regulation, several small molecules with the capacity to bind and stabilize c-*MYC* quadruplex DNA structures and to repress c-*MYC* expression in cancer cell lines have been investigated.

The first proof-of-principle that stabilization of quadruplex in the c-*MYC* NHE III1 by small molecules could silence c-*MYC* expression arrived from studies with porphyrins TMPyP4 and TMPyP2 (Fig. 6).[49] In a Taq polymerase stop assay, TMPyP4 at concentrations ranging from 0.5 to 5 μM inhibited transcription of c-*MYC* by stabilization of quadruplex chair conformation, whereas the much weaker quadruplex-ligand isomer TMPyP2 had a lesser effect.[48] To further study the role on gene transcription of the reported quadruplex in the NHE III1 of c-*MYC*, a luciferase reporter assay and two Burkitt's lymphoma cell lines were used. In the Ramos cell line, the quadruplex-forming sequence of the c-*MYC* promoter is preserved after chromosomal translocation, whereas in the CA46 cell line c-*MYC* transcription is no longer regulated by the NHE III1 quadruplex-forming sequence. These studies showed that repression of c-*MYC* expression by TMPyP4 was dependent on the presence of a promoter wild-type sequence or the quadruplex element in the c-*MYC* promoter.[48] In agreement with these studies, it was shown that increasing concentrations of TMPyP4 (1–10 μM) correlated with a decrease in NM23-H2 driven unfolding of the quadruplex, thus justifying the c-*MYC* transcription decrease observed.[159]

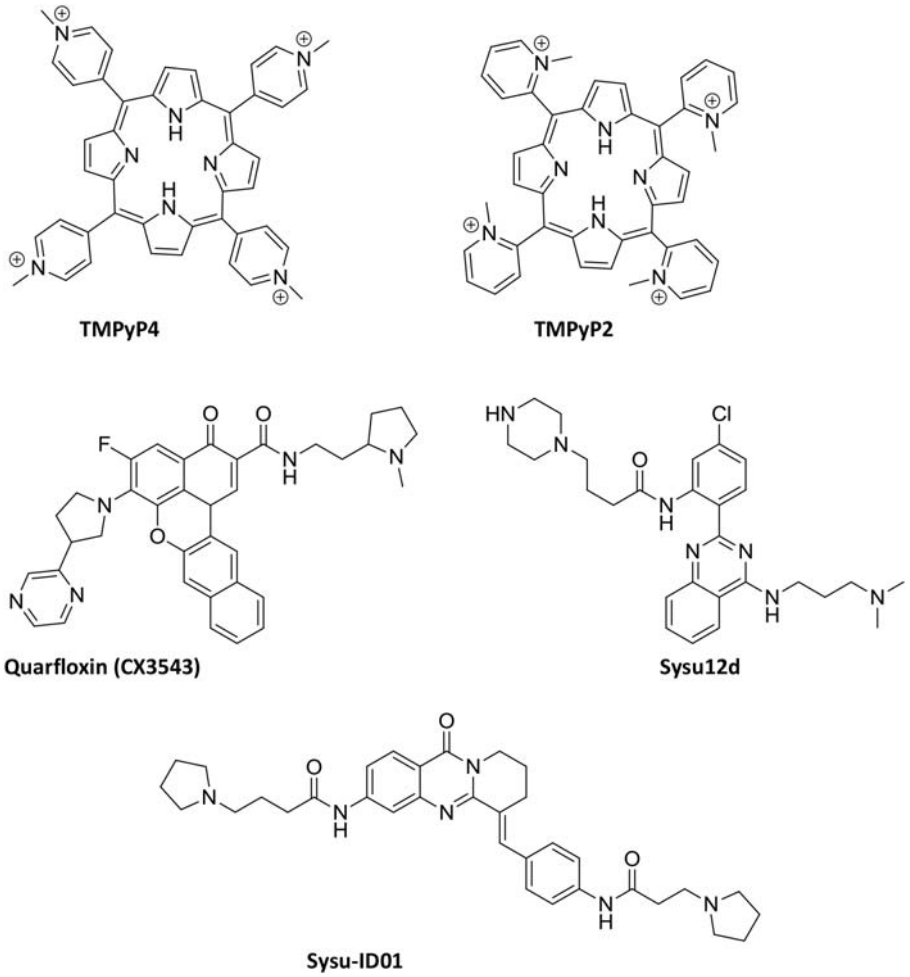

Fig. 6 Structures of porphyrins (TMPyP4 and TMPyP2), quarfloxin, and quinazoline (Sysu12d and Sysu-ID01) derivatives reported as c-*MYC* promoter quadruplex-interactive small molecules and oncogene expression downregulators.

Quarfloxin (also known as CX-3543, Fig. 6) is a first-in-class quadruplex-targeted drug which has reached Phase II clinical trials in human cancers. It is a fluoroquinolone derivative developed from the antibiotic norfloxin via a series of compounds with a larger aromatic surface area and a mechanism of action that involves both topoisomerase II poisoning and quadruplex DNA binding.[160] Further efforts to increase selectivity to quadruplex structures over duplex DNA led to quarfloxin, a compound with an optimized aromatic structure and quadruplex groove-binding side chains. It has greater selectivity than TMPyP4 for parallel quadruplex structures, including that in the c-*MYC* promoter.[91] It has anticancer activity in xenograft models and is devoid of gyrase or topoisomerase II poison activity. However, further studies on the mechanism of action of quarfloxin suggest that its anticancer activity is probably due to an indirect effect on c-*MYC* expression, among other mechanisms, rather than to direct binding to the c-*MYC* promoter quadruplex. Quarfloxin was shown to accumulate in the nucleoli of cancer cells where it can disrupt nucleolin ribosomal DNA quadruplex complexes leading to inhibition of RNA polymerase I and cellular redistribution of nucleolin into the nucleoplasm.[161] This redistribution is a common response to cellular stress, which results in apoptosis through various different pathways.[162–166] Nucleolin has high selectivity for the c-*MYC* promoter quadruplex and inhibits its transcription.[167] This indirect mechanism might explain the observed c-*MYC* transcription inhibition in HCT116 colorectal tumor tissues taken from mice treated with quarfloxin.[91]

The mechanism of action of quarfloxin inspired the studies on anticancer activity of a 2,4-disubstituted quinazoline derivative, Sysu12d (Fig. 6). CD spectroscopy and DNA melting assays have indicated that Syu12d can bind and stabilize the c-*MYC* quadruplex-forming sequence Pu27, and that it is selective for this quadruplex compared to a double-strand DNA sequence. This quinazoline derivative also inhibited c-*MYC* transcription in a PCR-stop assay and in HeLa cancer cells. Sysu12d at a 10 μM concentration was found to downregulate the expression of nucleolin, whose transcription is regulated by c-MYC. Moreover, Sysu12d at concentrations >1 μM disrupted the nucleolin–quadruplex rDNA complex, probably by competing with nucleolin for the quadruplex-binding site. This effect could contribute to the observed repression of RNA polymerase I transcription induced by Sysu12d, which was more evident in HeLa cancer cells than in the nonmalignant HEK293 cell line. Also as a consequence, p53

and caspase-3 were activated leading to apoptosis. Further contributing to the apoptotic effect is the observed BCL-2 downregulation and Bax upregulation induced by Sysu12d. In addition, it is notable that Sysu12d does not phosphorylate H2AX at Ser139, unlike other DNA-damaging agents. Thus, 2,4-disubstituted quinazolines may represent a new anticancer scaffold with a multifunctional mode of action.[168] Interestingly, the related quinazolone Sysu-ID01 (Fig. 6) showed weak quadruplex stabilization activity but high capacity to disrupt the binding of NM23-H2 transcription factor to Pu27, resulting in downregulation of c-*MYC* transcription and other NM23-H2-associated genes, and leading to apoptosis and cell death of HeLa cancer cells. Further studies, including molecular modeling, suggest that Sysu-ID01 inhibits NM23-H2 transcriptional activity by competing with Pu27 DNA for the same pocket of NM23-H2.[169]

The tetracyclic aromatic core indolo[3,2-*b*]quinoline structure (quindoline) with one or two basic side chains has been extensively investigated for binding to c-*MYC* quadruplex and inhibition of oncogene transcription in cancer cells. From all C11-substituted quindoline derivatives tested, IQi (Fig. 7) showed the greatest inhibition of the c-*MYC* quadruplex sequence (Pu27) amplification in a PCR-stop assay and was threefold more selective for the c-*MYC* quadruplex DNA structure than for calf thymus DNA in a competition dialysis experiment. IQi was able to repress c-*MYC* transcription by 25% in HepG2 and Ramos cell lines at 10–12.5 μM after 24 h but not in the CA46 cell line in which c-*MYC* transcription is not regulated by the NHE III1 quadruplex-forming sequence.[170] The solution structure of a 2:1 IQi—c-*MYC* quadruplex complex has been studied by NMR, showing one IQi molecule bound to the top G-quartet and another to the bottom G-quartet of this quadruplex (Fig. 4E). The crescent-shape quindoline structure provided optimal overlay with two guanines of the G-quartet, whereas the diethylamino group of the side chain interacted with the DNA phosphate backbone contributing to the orientation and stabilization of the ligand.[127] Further optimization of IQi led to the close analogue SYUIQ-05 (Fig. 7) which inhibited c-*MYC* transcription and protein expression in the Ramos cell line by approximately 25% after 48 h of drug (0.1 μM) exposure, but not in CA46 cells, probably due to the ability of this compound to disrupt the binding of the NM23H2 protein to the c-*MYC* quadruplex.[171]

The mechanism of action of 11-piperazinylquindoline derivatives has been reported (Fig. 7) to be targeting the c-*MYC* promoter quadruplex.[92] In a competition dialysis experiment, compound PPQ4 demonstrated four- to fivefold selectivity to all quadruplex structures compared to duplex DNA, whereas compound PPQ12 showed notable affinity to the parallel *HIF-1α* quadruplex structure and surprisingly only low affinity to a c-*MYC* quadruplex, or other more complex quadruplex structures. However, other in vitro experiments have suggested that PPQ12 has the capacity to bind to and stabilize the c-*MYC* promoter quadruplex sequence. The effect of compounds on expression of c-*MYC* and on other genes with quadruplex-forming sequences in their promoter sequences has been evaluated in the colorectal cancer HCT116 cell line. PPQ4, at IC_{50} concentrations (23 μM), downregulated the expression of c-*MYC*, h*TERT*, *PDGFRβ*, and *VEGF-A* after 24 h drug exposure, but not of *HIF1-α*. PPQ12 at 31 μM was able to downregulate c-*MYC*, h*TERT*, and *PDGFRβ* after 6 h, but the effects were completely reversed after 24 h. These observations together with results from competition dialysis indicate that these compounds are not selective for the c-*MYC* oncogene. In order to examine the involvement of the c-*MYC* quadruplex structure on mechanism of action, an exon-specific assay was used in CA46 cells. In this assay, amplification of exon 1 is used to monitor the effects on the nontranslocated, quadruplex-maintaining c-*MYC* gene, while amplification of exon 2 predominantly represents c-*MYC* expression from the translocated, quadruplex-lost chromosome. Results from this experiment also indicated that anticancer activity and cellular repression of c-*MYC* by PPQ4, PPQ12, or IQi are not dependent on direct targeting of the quadruplex in the c-*MYC* promoter.[92]

Several small-molecule hits against the c-*MYC* quadruplex have been recently identified using an in silico approach.[172] From these, the phenoxazone derivative B5, the pyrazolo[3,4-*d*]pyrimidine D2, and the triazine C2 (Fig. 7) showed greater inhibitory effect on cell proliferation and a larger decrease in the effects on c-*MYC* mRNA levels in the Ramos cell line than in the CA46 cell line, thus suggesting selectivity for the c-*MYC* quadruplex. The direct effect of compounds on c-*MYC* promoter activity was studied by the PCR-stop assay. Compounds C2 and D2 inhibited the activity of the c-*MYC* wild-type promoter but not of a mutant sequence unable to form quadruplex up to a concentration of 200 μM, whereas B5 showed lower selectivity for the quadruplex structure. In the same assay, none of the three compounds inhibited the activity of quadruplex-forming sequences from the *BCL-2*, *VEGF*, and *HIF-α* promoters. However, by CD, using a molar equivalent of ligand, none of the compounds was able to stabilize the oligonucleotide by increasing its melting temperature or altering the parallel conformation of c-*MYC* quadruplex.[172] Virtual high-throughput screening has identified the natural product-like carbamide (CB1, Fig. 7) as a potent stabilizer of the c-*MYC* quadruplex. Further NMR and molecular modeling experiments indicated a groove-binding mode for CB1. Activity of CB1 via c-*MYC* quadruplex binding was confirmed by its ability to inhibit Taq polymerase-mediated c-*MYC* quadruplex DNA amplification but only at high concentrations of CB1.[173]

The binding affinity and selectivity of three dihydroindolizidino indole derivatives for quadruplex DNAs compared to calf thymus DNA have been studied by a DNA melting assay, isothermal titration calorimetry, and ESI-MS. Compound DHII-4CPh (Fig. 7) was the best quadruplex DNA ligand of the series and the most selective, inducing an increase in 17°C of the human telomeric quadruplex melting temperature and showing a threefold selectivity for this quadruplex compared to duplex calf thymus DNA in the same assay. Selectivity for the c-*MYC* quadruplex was further confirmed by a luciferase reporter and a PCR-stop assay using the c-*MYC* promoter quadruplex-forming sequence and a mutated nonquadruplex forming sequence as control. DHII-4CPh selectively inhibited quadruplex-regulated DNA transcription. Moreover, DHII-4CPh inhibited the proliferation of melanoma cancer cells and reduced c-*MYC* expression by 50% in cells incubated with IC_{50} concentrations of compound (4 μM).[174] The bis-triazolylcarbazole derivative BTC-f (Fig. 7) was also identified as a good stabilizer of promoter quadruplex-forming sequences. This compound showed antiproliferative activity in several cancer cell lines (IC_{50} between 4 and 8 μM) but not in normal mouse myoblast C2C12 cells up to concentrations of 45 μM, and induced a dose-dependent reduction of c-*MYC* mRNA and protein levels

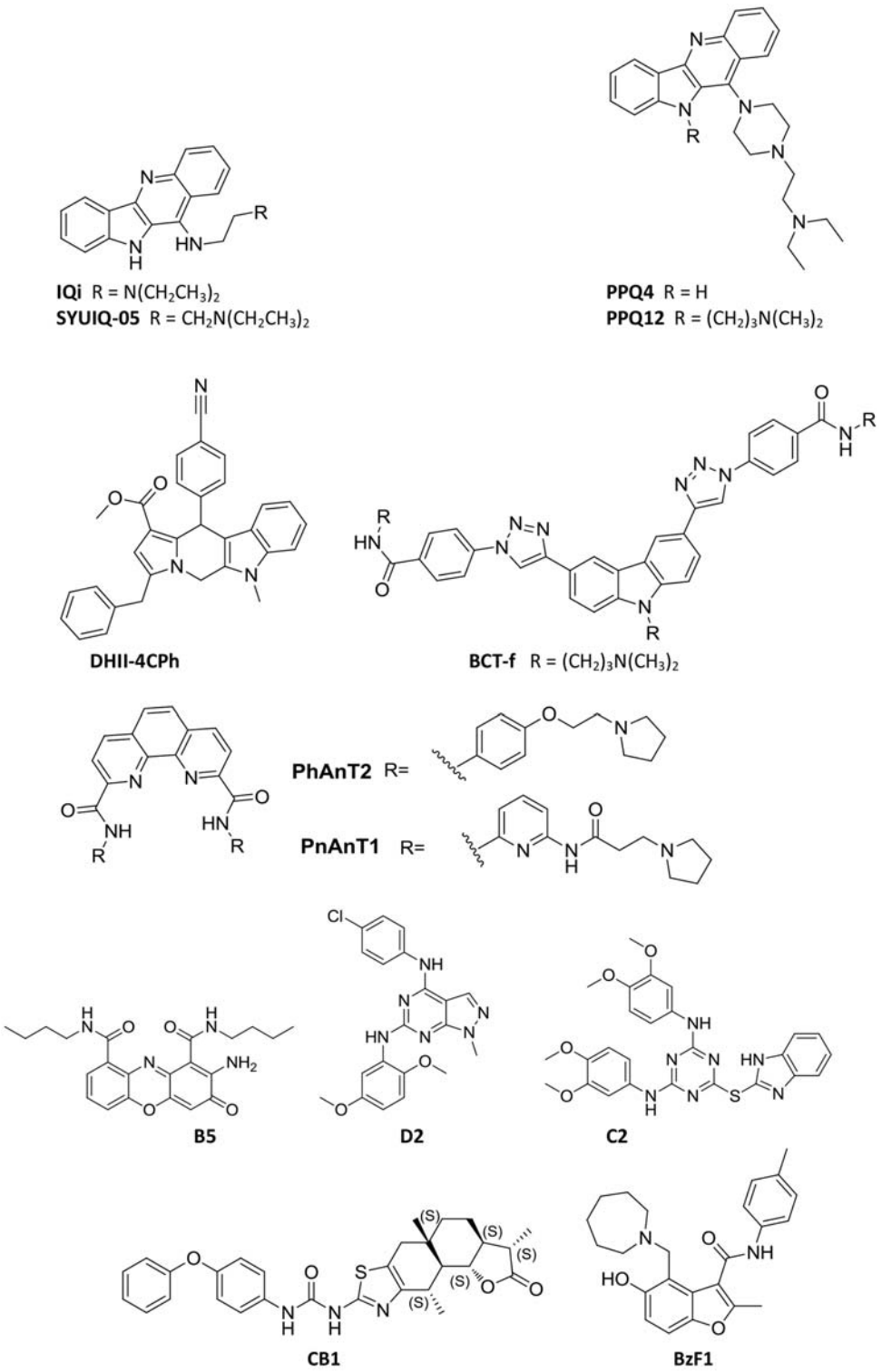

Fig. 7 Structures of quadruplex-interactive small molecules reported as c-MYC expression downregulators.

in liver carcinoma HepG2 cells, as well as triggering apoptosis and cell cycle arrest in the sub-G1 phase.[175] This cancer cell line, which overexpresses c-MYC, was also used to study the anticancer mechanism of two phenanthrolines (PhAnT1 and PnAnT2, Fig. 7) with moderate to weak ability to stabilize the c-*MYC* promoter quadruplex in a melting assay ($\Delta T_m \sim 10°C$ and 5°C, respectively, at 1 μM of ligand).[176,177] Contrary to data obtained by the DNA melting assay, PhAnT2 showed greater antiproliferative

activity than PhAnT1, c-*MYC* gene transcription downregulation, and inhibition of c-MYC, Sp1, and hTERT protein expression.[178] These compounds also increased p53 expression and induced a reduction in cyclin/CDK protein levels, leading to cell cycle arrest in different phases, and apoptosis of HepG2 cells.

In order to identify c-MYC-interactive small molecules with new chemotypes, another screening approach has been used. A small-molecule microarray screen of 20,000 compounds identified the benzofuran derivative BzF1 as a selective ligand of the c-*MYC* promoter quadruplex (Myc22-G14T/G23T) compared to duplex DNA or RNA.[179] Further studies, by surface plasmon resonance (SPR), confirmed that BzF1 (**Fig. 7**) in vitro binds reversibly to c-*MYC* quadruplex but has weaker or no affinity to other gene promoter quadruplexes. Furthermore, decreased c-*MYC* transcription induced by BzF1 correlated with decreased viability across a panel of multiple myeloma cell lines. In addition, the compound at 10 μM has minimal effect on cell viability in a Burkitt's lymphoma cell line harboring a c-*MYC* promoter translocation. Gene expression analysis and qPCR demonstrated that BzF1 is able to reduce the expression of c-*MYC* and c-*MYC* target genes but has no effect on the expression of several other quadruplex-regulated genes, in agreement with biophysical experiments, and demonstrating the selectivity of BzF1 to the c-*MYC* quadruplex.[179]

5.09.5.2 h*TERT*

The h*TERT* gene encodes for the catalytic domain of human telomerase, which is expressed in 85–90% of all cancers but not in somatic cells. Expression of h*TERT* is regulated by the core promoter, which contains a G-rich region of 12 consecutive G-tracts that can form a unique end-to-end stacked quadruplex structure, consisting of an all parallel quadruplex linked to an atypical quadruplex. The formation of this tandem quadruplex structure masks three of the five Sp1-binding sites found in the h*TERT* promoter, thus acting as a transcription repressor. Expression of h*TERT* is also regulated by c-*MYC* which binds to the h*TERT* promoter E-box region activating transcription.[180]

Quadruplex-binding ligands such as TMPyP4 (**Fig. 6**), BRACO-19 (**Fig. 5**), and the triazine 12459 (**Fig. 8**) have been shown to inhibit telomerase activity.[147,150,181] In the case of TMPyP4, this may occur through multiple mechanisms. TMPyP4 might inhibit telomerase activity by preventing telomerase access to telomeres due to induction of quadruplex structures in telomere 3′-overhang, or by stabilizing the quadruplex structure in the c-*MYC* promoter thus leading to decreased levels of c-MYC, a h*TERT* transcription activator. In addition, TMPyP4, but not its positional isomer TMPyP2, induced a dose-dependent decrease of h*TERT* promoter amplification product in a *Taq* polymerase arrest assay.[180] Thus, inhibition of polymerase activity by TMPyP4 may also be due to inhibition of h*TERT* expression[181] by direct targeting and stabilization of the h*TERT* promoter quadruplex. After in vitro and in vivo treatment with BRACO-19, hTERT protein levels in the nuclei of the human uterus carcinoma cell line UXF1138L were

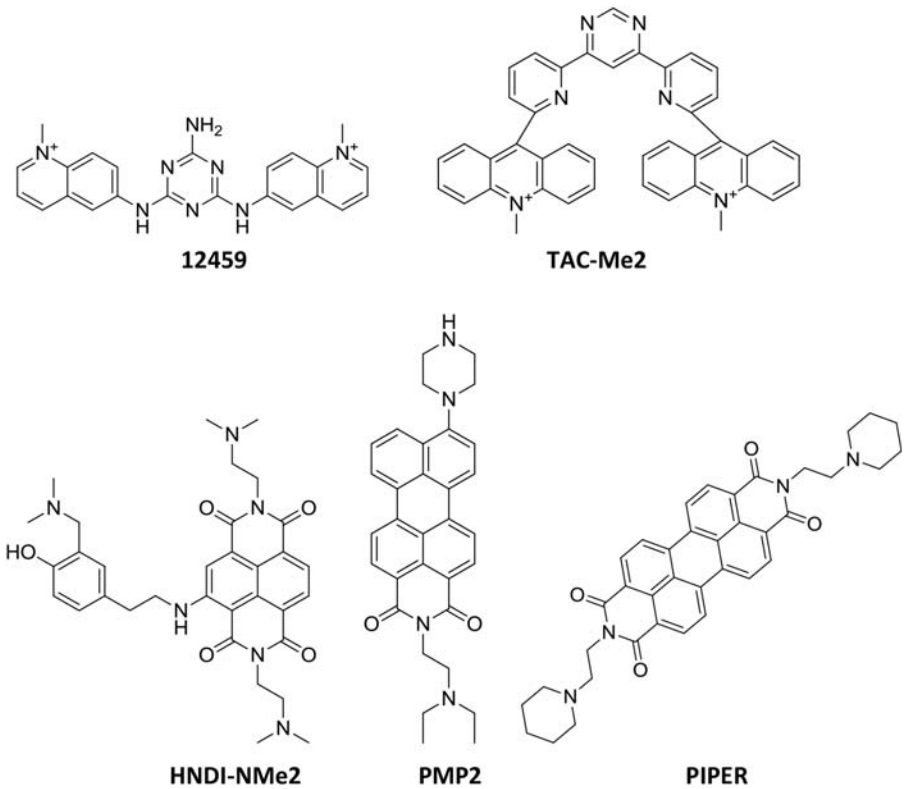

Fig. 8 Structures of G-quadruplex-interactive small molecules with reported h*TERT* expression regulatory activity.

drastically decreased, whereas in the cytoplasm hTERT colocalized with ubiquitin.[150] These observations are consistent with a decrease in h*TERT* expression via stabilization of the h*TERT* promoter quadruplex and hTERT degradation due to BRACO-19-induced displacement of telomerase from telomeres. For the triazine 12459 another mechanism leading to inhibition of telomerase activity has been proposed. Incubation of the human A549 lung carcinoma cell line with 10 μM of 12459 for 48 h induced overexpression of an inactive $-\beta$ h*TERT* transcript and a drastic decrease of the active $(+\alpha,+\beta)$ transcript, which was not observed after cells treated with other quadruplex ligands such as BRACO-19. Thus, triazine 12459 causes an alteration in the h*TERT* mRNA splicing pattern, probably by stabilization of quadruplex structures that can be formed in h*TERT* spliced intron 6.[182]

Not all telomeric quadruplex ligands reduce telomerase activity and/or telomerase expression. The bis-acridine compound TAC–Me2 (Fig. 8) increased the melting temperature of a telomeric quadruplex sequence and showed a twofold selectivity for this compared to duplex DNA in a competitive dialysis assay. At low concentrations (0.5–2.0 μM), TAC-Me2 inhibited the proliferation of glioblastoma multiforme cell lines in a concentration-dependent manner, had minimal effects on cell cycle, apoptosis, and telomere length but increased h*TERT* expression and induced a DNA damage response.[183]

Telomestatin (Fig. 5), in common with TMPyP4, decreased the full-length product of the G-rich sequence in the h*TERT* promoter, in a dose-dependent manner, but it also increased the amount of different premature primer extension products. It was suggested by analysis of these products that telomestatin preferentially recognizes the external G-quartets, while TMPyP4 binds between two tandem h*TERT* quadruplex.[180] Despite the potential of telomestatin to repress h*TERT* expression in vitro, this has not yet been demonstrated in cancer cells. However, telomestatin does potently inhibit telomerase activity and has antitumor activity in vitro and in vivo.[184]

Substituted naphthalene diimides are established quadruplex-binding ligands. The trisubstituted compound HNDI-NMe2 (Fig. 8) has high affinity for the human telomeric quadruplex sequence hTel22.[185] Fluorescence resonance energy transfer (FRET) competition experiments revealed that the best competing sequence to disrupt the complex between HNDI-NMe2 and this quadruplex was the h*TERT* full-length quadruplex sequence, followed by c-*MYC* and *BCL-2* quadruplex sequences. The c-*KIT2* sequence was a poor competitor, whereas both c-*KIT1* and duplex DNA were unable to disrupt the complex.[186] Compound HNDI-NMe2 was able to significantly impair melanoma cell growth by causing telomere dysfunction and inhibition of telomerase activity, likely as a consequence of its induced decrease of mRNA expression levels of c-*MYC* and h*TERT*.[185] However, in the small-cell lung cancer cell line H69, compound HNDI-NMe2 increased mRNA levels of c-*MYC* although it decreased h*TERT*, *BCL-2*, and c-*KIT* transcription. Also, in the same cell line, c-MYC and BCL-2 protein levels were not affected, whereas c-KIT was decreased after cell exposure to HNDI-NMe2. These observations suggest that the effect of HNDI-NMe2 on gene expression is markedly dependent on cell type. Subsequent gene analysis showed cell-dependent modulation of genes implicated in telomere function and cancer mechanisms by this particular naphthalene diimide compound.[186]

The perylene derivatives PMP2 and PIPER (Fig. 8) have been shown to induce in vitro h*TERT* promoter and telomeric quadruplex formation. However, PMP2 is a superior intramolecular quadruplex inducer compared to PIPER and has a preference for the h*TERT1* quadruplex (the parallel quadruplex from G-tracts 1–4 of 26 bp) than to telomeric DNA G-rich sequences. In addition, compounds PMP2 and PIPER, at concentrations higher than 16 μM, induced the formation of an h*TERT2* intermolecular quadruplex (G-tracts 5–12, 44 bp) in the same duplex–quadruplex competition assay. PMP2 is consistently a superior inhibitor of h*TERT* expression than PIPER. At 6 μM, PMP2 reduced h*TERT* mRNA to 37% of the control in A549 lung cancer cells. PMP2 also decreased in vitro telomerase activity in a dose-dependent manner using a crude protein extract of cells treated with the compound. In addition, long-term treatment of A549 lung cancer cells with subcytotoxic concentrations of PMP2 and PIPER induced telomere shortening, reduction of cell proliferation, tumorigenicity, and cellular senescence.[149]

5.09.5.3 The *RAS* Family

The RAS membrane-bound family of G-proteins (k-RAS, h-RAS, and N-RAS) act as switches between the endothelial growth factor receptor (EGFR) and the nucleus, controlling downstream processes associated with cell growth and apoptosis. k-*RAS* is one of the most frequently mutated oncogenes in human cancers, in particular in pancreatic, colorectal, and lung cancers.[154,187,188] k-RAS mutated proteins are locked in the GTP-active state and constitutively transmit signals for cell proliferation to the nucleus, via the MAP-kinase cascade. Importantly, deletion of the mutant k-*RAS* allele in colon cancer cell lines dramatically reduces cellular proliferation,[189] highlighting the fact that many tumors harboring mutant k-*RAS* are k-RAS-dependent. The importance of therapeutic modulation of k-RAS signaling has been widely recognized and several approaches have been reported in the past, but none has led to an approved new anticancer drug to date.[188]

The human k-*RAS* gene promoter contains a 32-mer and a 52-mer sequences upstream of the transcription start site that can form stable quadruplex structures (KRAS32R[58,190] and KRASmid,[191] respectively). KRAS32R can form a mixed parallel and antiparallel quadruplex involving the G-tracts 1-2-3-5, whereas the 21-mer region (21R) can form a three-layer parallel quadruplex, involving the G-tracts 1-2-3-4.[58,190,192,193] Similarly, the h-*RAS* promoter has also two neighboring quadruplex-forming sequences (HRAS-1 and HRAS-2) containing copies of GC-boxes recognized by the MAZ and Sp1 transcription factors.[194] These DNA quadruplex structures have been previously shown to play an important role in the repression of k-*RAS*[58,190] and h-*RAS*[194] transcription. Quadruplex-forming motifs have also been identified in the 5′ UTR of k-*RAS* and N-*RAS* mRNA and shown to be involved in translation inhibition.[195,196]

Three quadruplex-ligand chemical types have been identified as k-*RAS*/h-*RAS* expression downregulators: porphyrins, anthrathiophenediones, and indoloquinolines. The well-established quadruplex ligand TMPyP4 (Fig. 6) and its noninteractive

quadruplex isomer TMPyP2 have been used to probe the role of the promoter quadruplex-forming sequences in the regulation of k-*RAS* expression. FRET melting assays suggest that TMPyP4 is a poorly selective k-*RAS*21R-quadruplex ligand compared to duplex DNA,[197] although it has been reported that this compound is able to repress k-*RAS* transcription. In a dual luciferase assay, TMPyP4 (3–20 μM 24 h prior to transfection) reduced mouse k-*RAS* promoter activity by 80%[190] and also decreased k-*RAS* mRNA levels by 30% in Panc-1 cells incubated by 12 or 24 h with 50 μM of the compound, whereas TMPyP2 had no effect on k-*RAS* transcription in the same assay.[58] In another study, TMPyP4 (3 μM) incubated with cells for 72 h after transfection reduced human k-*RAS* promoter activity by 25% but did not inhibit k-*RAS* transcription in colon cancer HCT116 cells at a 12 μM concentration.[197] However, at the same concentration (12 μM), TMPyP4 reduced the levels of k-RAS protein in HCT116 cells by more than 50%. These results are in agreement with the reported ability of TMPyP4 to preferentially accumulate in cellular cytoplasm[195] and inhibit N-*RAS* translation,[196] due to its capacity to bind and stabilize UTR1 and UTR2 RNA quadruplex-forming sequences.[195,198] However, it has been proposed that this translation inhibitory activity of TMPyP4 is not related to its ability to stabilize the quadruplex motifs in 5′-UTR k-*RAS* mRNA but rather to its nonspecific binding affinity to nucleic acids.[196] Substitution of a methyl group of TMPyP4 by a C14-alkyl chain does not affect binding affinity to RNA quadruplex nor cellular distribution but increases by 25- to 50-fold compound uptake by human pancreatic cancer Panc-1 cells and murine melanoma B78-HI cells, as well as showing k-*RAS* translation inhibition upon photo-activation of cells incubated with nanomolar concentrations of compounds.[195,198] In addition, inhibition of metabolic activity, clonogenic growth, and cell migration of photo-activated melanoma cells by TMPyP4 and its C14 derivative also correlated with their cellular uptake. Peritoneal injection of 3 mg/kg of the C14 derivative or 30 mg/kg of TMPyP4, followed by irradiation 7 h after compound administration, inhibited the growth of the subcutaneous B78-H1 melanoma tumor in C57/BL6 mice. However, contrary to TMPyP4, the C14 derivative also affected in vivo tumor growth even in the absence of irradiation. Analysis of porphyrin biodistribution after peritoneal injection in mice showed that compounds accumulate preferentially in tumor tissues, liver, and kidneys. Moreover, TMPyP4 showed greater subcutaneous tumor accumulation after 9 h injection than the C14 derivative which may reflect the reduced diffusion capacity of the more lipophilic porphyrin C14 derivative.[198]

The guanidine phthalocyanine DIGP (**Fig. 9**) and its zinc-containing analogue (DIGP-Zn) have been studied in a search for quadruplex ligands with superior selectivity and improved cellular uptake and distribution properties compared to TMPyP4. Using a polymerase stop assay, it was shown that DIGP is a good quadruplex-stabilizing ligand for both parallel (k-*RAS*) and antiparallel (h-*RAS*) structures, whereas its zinc-containing analogue is more specific for the parallel structure. DIGP also showed selectivity for quadruplex structures compared with duplex DNA, exhibited good cellular uptake and higher localization in the nuclei and nucleoli, in contrast to DIGP-Zn, which preferentially localizes in the perinuclear region. DIGP (5 μM) has been shown to downregulate h-*RAS* promoter activity to 35 ± 10% of the control in a dual luciferase assay.[199]

A series of anthrathiophenediones with guanidine-alkyl side chains of different length (ATDs, **Fig. 9**) have been investigated for their binding to h-*RAS* DNA quadruplex and N-*RAS* RNA quadruplex structures, together with their cellular uptake, intracellular localization, and repression of h-*RAS* expression in bladder cancer cells.[200] In vitro binding affinities determined by FRET titration and melting assays showed that quadruplex-binding potency increases with the side chain length but surprisingly, cellular uptake experiments have shown that ATD1, with shorter alkyl-guanidino side chains, shows greater accumulation (10-fold) inside bladder cancer cells than analogue ATD13 having longer side chains. Moreover, it was also found that cellular uptake of ATD1 must occur primarily by endocytosis, whereas the more lipophilic analogues (ATD10/12/13) probably cross the cellular membranes by passive diffusion. It was also shown that ATD1 has superior antiproliferative activity ($IC_{50} = 4$ μM) against cancer cells than analogues ATD10/12/13 and is 10-fold more selective for bladder cancer cells than nonmalignant cell lines. Compound ATD1 was shown to localize in the cytoplasm and nucleus of bladder cancer and nonmalignant cells, decreased h-RAS protein levels in bladder cancer cells treated with 5 μM of compound, decreased to 25% of the control h-*RAS* promoter activity, and increased the cell population in the G0/G1 phase in T24 bladder cancer cells. It was also found, using a caspase 3/7 assay, that ATDs do not induce apoptosis in cancer cells, which suggests a cytostatic mechanism of action. The mechanism of h-*RAS* expression downregulation by ATDs has been further investigated. It has been suggested that ATD1 represses *h-RAS* transcription by stabilizing quadruplex structures thus compromising MAZ-GST unfolding activity.[194] More recently, the anticancer activity of a series of chloroacetamidine (CATD) analogues was also studied.[201] Compared to ATDs, these more lipophilic compounds showed superior cell permeation, probably by endocytosis, and induced a large apoptotic response in T24 bladder cancer cells treated with 2.5–5.0 μM of CATDs, as shown by PARP-1, caspases 3/7, and annexin V/propidium iodide assays, accompanied by downregulation of cyclin D1 and blockage of cells in G2 phase. CATD1 (**Fig. 9**), the most potent compound of the series, inhibited metabolic activity ($IC_{50} = 2.7$ μM), colony formation, and h-*RAS* expression, at both mRNA (to ~34% of control) and protein levels (to ~4% of control), in T24 bladder cancer cells exposed to 5 μM of compound for 24 h. To investigate if inhibition of h-*RAS* expression was due, at least in part, to binding of CATD1 to h-*RAS* promoter quadruplexes, a luciferase reporter assay was used. T24 cells were treated with 100 and 200 nM of compound 4 h before transfection with the h-*RAS* promoter and two mutant vectors unable to form quadruplex structures. After 48 h, CATD1 reduced by 40% luciferase expression driven by the h-*RAS* promoter, but had no effect on gene expression driven by mutant promoters. Finally, treatment by intratumoral injection of nude mice bearing a T24 xenograft with 1.7 mg/kg of CATD1, for 4 days (days 1, 8, 15, and 22), inhibited tumor growth and increased median survival time from 32 to 54 days.[201]

Indolo[3,2-*b*]quinolines with three alkylamine side chains (IQ3A1a and 2a, **Fig. 9**) have been shown by a FRET melting assay to efficiently and selectively (10-fold) stabilize the DNA quadruplex motifs present in the k-*RAS* promoter compared to duplex DNA, inhibit the proliferation of HCT116 colon cancer cells with 100-fold selectivity compared to primary rat hepatocytes. They decrease k-RAS protein levels in a dose-dependent manner.[202] A subsequent study showed that increasing the length of side chains in

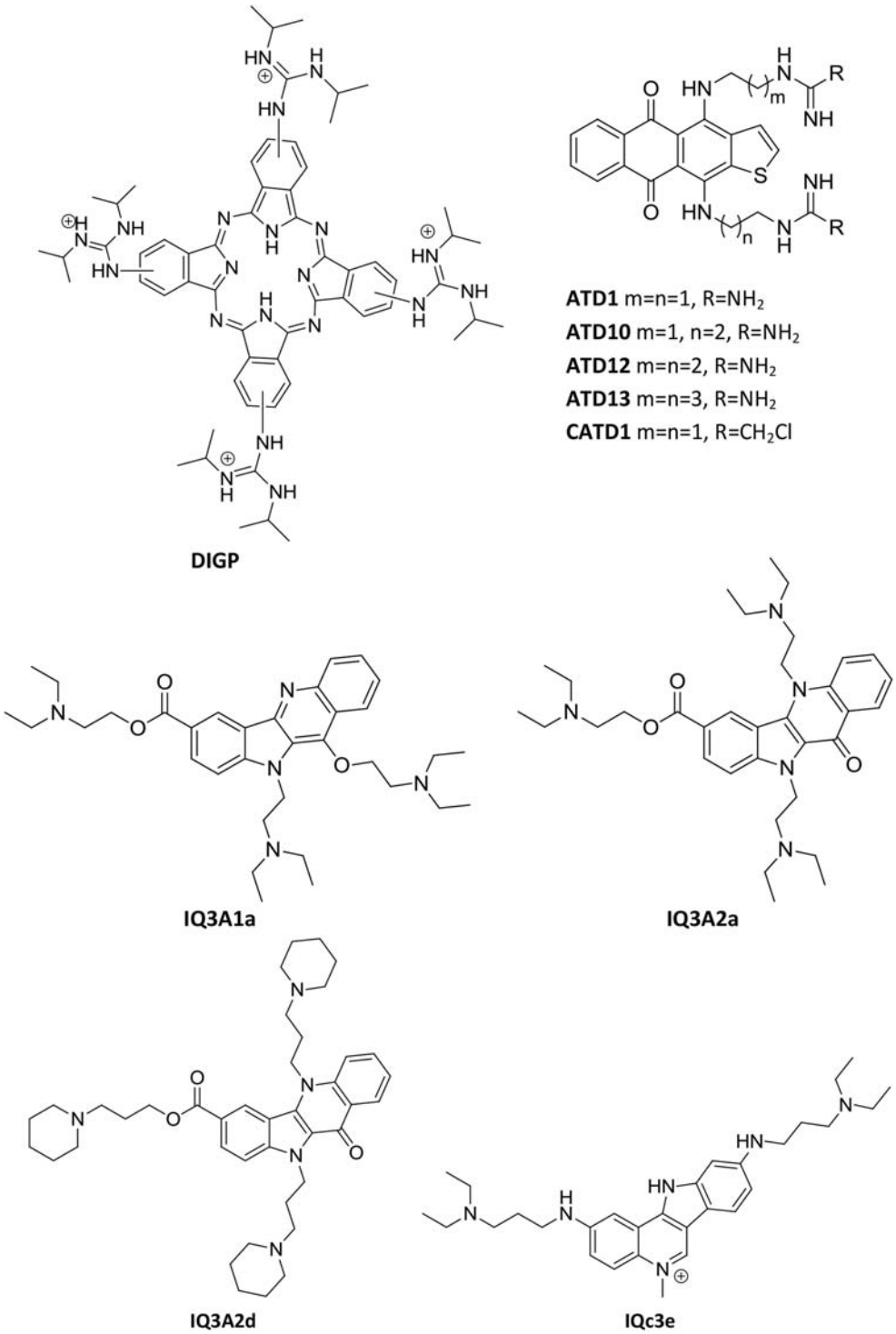

Fig. 9 Structures of guanidine phthalocyanine DIGP, anthrathiophenediones with guanidine-alkyl side chains (ATDs) or chloroacetamidine analogue CATD1 and indoloquinolines (IQ3As and IQc3e) reported as quadruplex-interactive molecules and *RAS* oncogene expression repressors.

compound IQ3A2d increased both the quadruplex thermal stabilization effect and the antiproliferative activity in HCT116 and metastatic SW620 colon cancer cells ($IC_{50} < 2.69$ μM), without producing cell death in nonmalignant HEK293T human embryonic kidney, and CCD18co human colon fibroblast cells. Moreover, IQ3A compounds significantly reduced k-*RAS* promoter activity in a luciferase reporter assay, reduced k-*RAS* mRNA and protein steady-state levels at IC_{50} concentrations, and increased p53 protein steady-state levels and cell death by apoptosis in HCT116 cells (mutant k-*RAS*, wild-type *p53*). Furthermore, induction of apoptosis

and increase in p53 levels were shown to be k-RAS-dependent, as k-*RAS* silencing in HCT116 p53 wild-type [p53(+/+)) and null (p53(−/−)] isogenic cell lines induced a higher level of cell death. A greater level of IQ3A-induced cell death in HCT116 p53(+/+) cells compared to HCT116 p53(−/−) was also observed.[203] The effects of the regioisomeric indolo[3,2-*c*]quinolines (IQcs) (with one and two alkylamine side chains) on selectivity to k-*RAS* DNA and RNA quadruplex motifs and regulation of k-*RAS* expression in colon cancer cell lines were also investigated.[197] FRET melting assays showed that disubstituted indolo[3,2-*c*]quinoline IQc3e (Fig. 9) is the most potent analogue ($\Delta T_m = 22°C$) and a selective DNA quadruplex k-*RAS*21R stabilizer (50-fold selectivity), compared with duplex DNA and telomere quadruplex. The results also suggested that IQc3e is an effective stabilizer of DNA quadruplex k-*RAS*32R, but only a moderate stabilizer of RNA quadruplexes UTR1 and UTR2. CD experiments showed that IQc3e binds to the parallel quadruplex k-*RAS*21R without inducing any change in quadruplex topology, whereas under the same conditions IQc3e induces a topology change from parallel/antiparallel hybrid to an antiparallel form on binding to telomeric quadruplex,[204] which may explain the observed selectivity of IQc3e for the k-*RAS* quadruplex and suggests a more general preference of IQc3e to bind to parallel quadruplexes. Moreover, compound IQc3e preferentially inhibited the proliferation of k-*RAS* mutant cancer cell lines ($1.45 < IC_{50} < 4.80\ \mu M$), downregulated k-*RAS* promoter activity in a luciferase reporter assay, and reduced both k-*RAS* mRNA and protein steady-state levels in mutant k-*RAS* colon cancer cell lines. Additionally, IQcs induced cell death by apoptosis in colon cancer cell lines but not in nonmalignant HEK293T cells.[197]

5.09.5.4 *VEGF* and *VEGFR*

Angiogenesis, the formation of new blood vessels, is essential for tumor growth and progression since it provides oxygen and nutrients to proliferating tumor cells. During tumor growth, these cells can adapt themselves to an angiogenic phenotype, producing and secreting proangiogenic molecules. Among these is the vascular endothelial growth factor (VEGF), particularly VEGF-A, a cytokine with a key role in angiogenesis regulation. VEGF-A binds to tyrosine kinase receptors such as VEGF receptors (VEGFR-1 and VEGFR-2) expressed on the surface of endothelial cells, activating signaling cascades leading to several cellular processes involved in angiogenesis.[205–207] The development of anti-VEGF/VEGFR agents for cancer therapy, including antibodies, engineered proteins, and small molecules targeting VEGFR-2, has been actively pursued but so far with more disappointing results in clinical trials than one would expect from preclinical evidence.[208]

VEGF overexpression in tumor cells can be induced by several factors including the activation of oncogenes, the inactivation of tumor suppressor genes, cis-acting elements, and transcription factors. Studies on *VEGF* transcription activation revealed that the *VEGF* promoter contains a 36-bp G/C-rich sequence (between −85 and −50 of transcription starting site), consisting of at least three SP1 binding sites essential for transcription.[209] The G-rich strand of the *VEGF* promoter is characterized by the presence of five runs of three or more contiguous guanines separated by one or more nucleotides, thus having the potential to form two alternative intramolecular quadruplex structures. The 20-mer sequence containing four 5′ runs of guanines (VEGF-Pu20) was shown by electrophoretic mobility shift assay, the dimethyl sulfate foot-printing technique, the DNA polymerase stop assay, CD spectroscopy, and computer-aided molecular modeling, to form an intramolecular propeller-type parallel-stranded quadruplex structure.[210] Further studies by NMR confirmed the parallel-stranded structure of the 22-mer analogue sequence with G-to-T mutations of two loop residues.[53] There is evidence for the formation of quadruplexes in the polypurine/polypyrimidine tract of the *VEGF* promoter in vitro and in vivo.[211,212] In addition, using a chromatin immunoprecipitation assay it has been shown that nucleolin and hnRPNK can bind to the G-rich and C-rich sequences, respectively, of the *VEGF* promoter in vivo, probably acting as transcription activators.[212,213]

Transcription of *VEGF* can also be controlled by quadruplex-ligand small molecules. Using a DNA polymerase assay, it has been shown that the core-modified expanded porphyrin analogue Se2SAP (Fig. 10) is able to interact in a concentration-dependent manner with the quadruplex (Pu20) in the *VEGF* promoter, being 10-fold more effective in binding than TMPyP4. In addition, Se2SAP (25–50 μM) decreased *VEGF* mRNA levels by 50–80% in kidney (A498 and 786-O), endometrial (HEC1A), and breast (MDA-MB231) cancer cells after 24–48 h treatment, whereas TMPyP4 showed a reduced effect and TMPyP2 was ineffective in the same assays.[210] The perylene derivatives PIPER, PMP1, and PMP2 (Figs. 8 and 10) induced a reduction of both *VEGF* mRNA and protein levels in A549 lung cancer cells incubated for 24 h with compounds at concentrations lower than the respective IC_{50} values (52, 3, and 4 μM, respectively, for PIPER, PMP1, and PMP2). The perylene monoimide derivative PMP2 showed the highest level of transcriptional inhibitory activity followed by PIPER, PMP1, and TMPyP4, being also the compound with the greatest capacity to bind to the *VEGF* promoter quadruplex and stop polymerase product extension. However, duplex/quadruplex competition assays have also shown that all three perylene derivatives have only a slight preference for quadruplex structures over duplex DNA. To demonstrate that these compounds induce transcriptional repression by induction of quadruplex formation in G-rich gene promoters, mRNA levels of other genes containing quadruplex motifs in their promoters (c-*MYC* and *BCL*-2) and of constitutively expressed genes (*Max* and *GADPH*) or inducible genes (*Cox*) were evaluated after treatment of A549 cells with PIPER, PMP1, and PMP2. This key experiment demonstrated that perylene derivatives only repress the transcription of genes with quadruplex-forming sequences in promoter regions (*VEGF*, c-*MYC*, and *BCL*-2), thus supporting the hypothesis of a mechanism of transcription repression by inducing the formation of a quadruplex in promoters and also showing that these perylene-based compounds are not *VEGF*-specific suppressors. Moreover, PMP2 was also shown not to be cell-specific, as it also represses *VEGF* expression in the MCF-7 breast cancer cell line, the HCT-15 colon cancer cell line, and the HeLa cervical cancer cell line.[214]

A series of N5-methyl indolo[3,2-*b*]quinoline derivatives has also been evaluated for its ability to stabilize the *VEGF* quadruplex, downregulate *VEGF* expression in cancer cells, and inhibit angiogenesis.[215] Among the compounds tested SYUIQ-FM05 (Fig. 10)

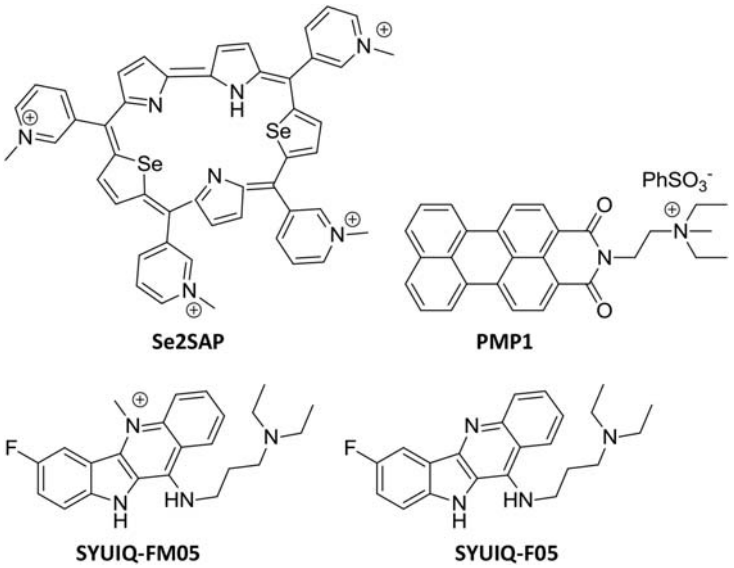

Fig. 10 Structures of G-quadruplex-interactive small molecules with reported *VEGF* expression modulatory activity.

showed the greatest interaction with the *VEGF* promoter quadruplex in a PCR-stop assay and also the highest activity in cancer cells. SYUIQ-FM05 inhibited the short-term proliferation of MCF-7 breast cancer cells ($IC_{50} = 0.96$ μM), downregulated transcription and translation of *VEGF* in MCF-7 cells after 48 h drug exposure, and at 0.5 μM concentration decreased *VEGF* promoter activity by up to 30% in a luciferase reporter assay. SYUIQ-FM05 also showed antiangiogenic potential in a chick embryo assay. The compound showed an inhibitory response to new blood vessels formation in a chorioallantoic membrane of 63% compared with the control, which is higher than that of the control drug thalidomide (53%) and of the analogue SYUIQ-F05 (55%) (**Fig. 10**).

A G-rich sequence within the promoter region of *VEGFR-2* can form an antiparallel quadruplex structure which has been shown to be implicated in the expression of this receptor, thus representing another potential target for anticancer therapy.[216] The well-established quadruplex ligand RHPS4 (**Fig. 5**) has been shown to inhibit tumor angiogenesis by targeting the *VEGFR-2* quadruplex and inhibits the expression of this gene. RHPS4 (0.5 μM) strongly inhibited *VEGFR-2* mRNA and protein levels in human umbilical vein endothelial cells (HUVEC) after 72 h incubation. The transcriptional activity of RHPS4 on other angiogenesis-related genes containing quadruplex sequences in their promoters has also been evaluated. RHPS4 downregulates the expression of *VEGF-A*, *VEGFR-1*, *IL1R*, *CXCR-1*, and *AChRβ1* but not that of *FGFR* and *EGFR*, which may be a consequence of the structural diversity of their quadruplexes. The expression of nonquadruplex-containing genes (*IL10R* and *AChRα1*) was unaffected by RHPS4. Moreover, RHPS4 inhibited HUVEC proliferation and almost completely abrogated VEGF-A stimulated endothelial cell migration. However, RHPS4 did not affect cell viability, apoptosis, or senescence, nor activate the DNA damage response. Finally, RHPS4 impaired angiogenesis in a xenograft model. Immunohistochemical analysis of the tumor tissue after treatment with RHPS4 revealed a massive decrease in the number of blood vessels and *VEGFR-2* expression. In vivo *VEGFR-2* expression inhibition was further confirmed by mRNA quantification.[216]

The 5′-UTR of human *VEGF* contains two internal ribosomal entry sites (IRES A and B) which are involved in cap-independent translation initiation. A 17-nucleotide sequence within the 294-nucleotide fragment of IRES A was shown to fold into a RNA quadruplex with an upregulation effect on translation by direct recruitment and interaction with the 40S ribosomal subunit.[217,218] However, another study indicated that in stress conditions the quadruplex within the VEGF IRES is dispensable for cap-independent function and activation. Moreover, it was also found that stabilization of that RNA quadruplex, including by small molecules, inhibited in vitro the cap-independent translation of *VEGF* mRNA.[219]

5.09.5.5 c-*KIT*

The c-*KIT* proto-oncogene encodes for a tyrosine kinase receptor that upon activation by its ligand (the cytokine stem cell factor) promotes cell proliferation and differentiation.[220,221] Mutations or overexpression of c-*KIT* result in aberrant function that contributes to oncogenicity in melanocytes, mast cells, myeloid cells, and gastrointestinal stromal tumors (GIST). More than 80% of GIST cells express mutated c-KIT proteins that are constitutively activated, thus escaping normal activation control by its natural cytokine ligand.[222] Consequently, inhibition of the c-KIT enzyme domain with kinase inhibitors such as imatinib and sunitinib has become the clinical practice for GIST therapy.[223] However, the emergence of drug resistance due to mutations in the ATP binding site of the enzyme has been a major factor in the search for alternative approaches.

The promoter region of c-*KIT* contains G-rich sequences that can fold into two quadruplexes (c-*KIT1* and c-*KIT2*). Crystal and NMR structures are available for both (see earlier sections in this article). Evidence for the inhibition of c-*KIT* expression in cancer

cells has been provided by selective c-*KIT* promoter quadruplex ligands.[224] A series of 3,8,10-trisubstituted isoalloxazines was designed and synthesized as quadruplex ligands based on a previous observation that oxidized riboflavin (7,8-dimethyl-10-ribityl-isoalloxazine) is a quadruplex ligand. All isoalloxazines examined showed a preference for binding to the c-*KIT2* quadruplex structure over c-*KIT1* (threefold selectivity for compound IAXZ-a, Fig. 11) and also over the human telomere quadruplex sequence (14-fold selectivity for IAXZ-d), but none of the compounds showed significant binding affinity to duplex DNA, as determined by SPR or by a FRET melting assay. At 5 μM concentrations, both IAXZ-a and IAXZ-d were not cytotoxic to the breast cancer cell line MCF-7 or to the GIST cell line HGC-27, but induced a significant reduction or even complete suppression of c-*KIT* expression in both cell lines, as measured by mRNA levels. IAXZ-d showed the greatest inhibitory activity. In the MCF-7 cell line, which shows low basal levels of c-*KIT* expression, IAXZ-d almost completely suppressed the expression of this oncogene after 6 h drug exposure and in the HGC-27 cell line expressing higher levels of c-*KIT*, it reduced the c-*KIT* transcript to a 50% level.[224]

The effects on stabilization of c-*KIT1* and c-*KIT2* quadruplex structures and repression of c-*KIT* expression in cancer cells have also been reported with the known quadruplex ligands TMPyP4, BRACO-19, and the tetra-substituted naphthalene diimide 4-NDII-1[225] (Fig. 11).[226] In a FRET melting assay, all three compounds showed a lower capacity to stabilize c-*KIT1* compared to c-*KIT2* and a telomeric quadruplex, with compound 4-NDII-1 showing the greatest overall ability to stabilize c-*KIT2* and telomeric quadruplexes. A FRET competition assay with increasing concentrations of calf thymus DNA indicated that 4-NDII-1 has modest selectivity (<30-fold) to quadruplexes compared to duplex DNA, similar to TMPyP4 (Fig. 6) and BRACO-19 (Fig. 5). 4-NDII-1 also showed greater short-term growth-inhibitory activity against a range of cancer cell lines ($IC_{50} = 0.02–1.6$ μM), including the primary c-KIT-dependent gastrointestinal tumor cell line GIST882. Moreover, in this cell line the IC_{50} of 4-NDII-1 was comparable to that of the anticancer drug imatinib. Expanding the panel of cancer cell lines, the high level of potency of 4-NDII-1 against c-KIT-dependent GIST cell lines was further confirmed, in contrast with low activity against c-KIT-negative lines. In addition, 4-NDII-1 induced 90% downregulation of c-*KIT* transcription and a complete inhibition of protein expression in the patient-derived GIST882 cell line treated with a concentration of compound (1 μM) close to the IC_{50} value, whereas no significant changes in c-*KIT* transcription were induced by imatinib, BRACO-19, or TMPyP4. Finally, other data supporting the hypothesis of 4-NDII-1 acting at the c-*KIT* gene level comes from the observations of the significantly lower effect of this compound on repressing other cancer-associated genes with quadruplex in promoters, such as c-*MYC*, h*TERT*, and N-*RAS*. However, due to its potent telomeric

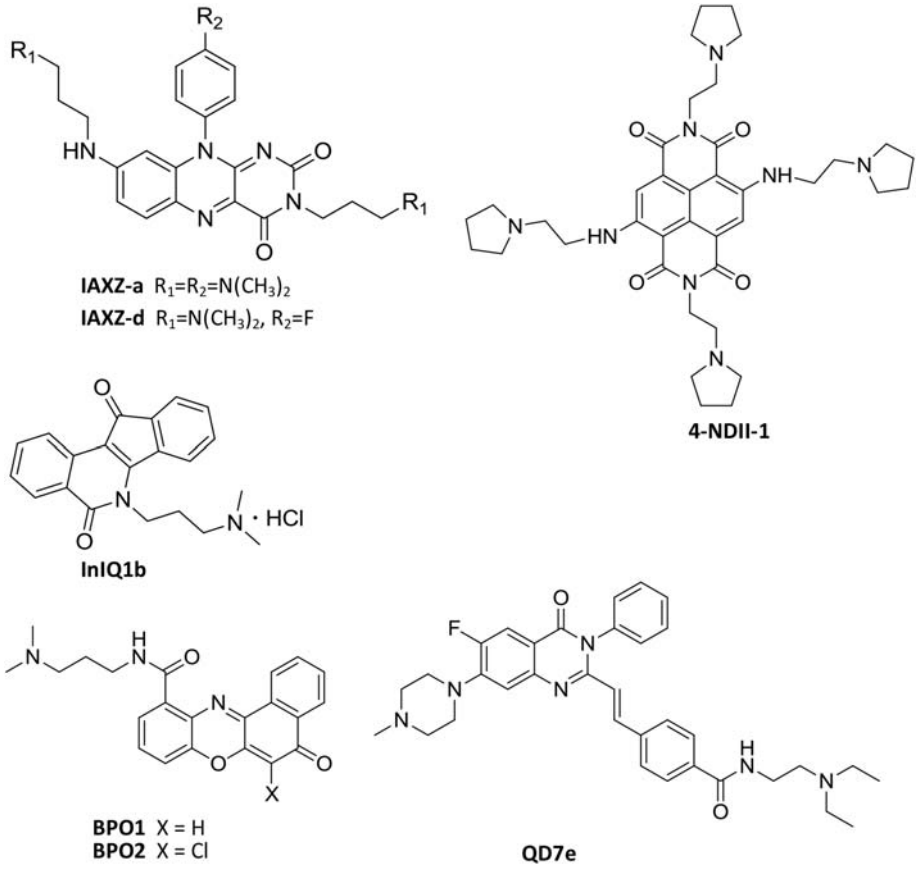

Fig. 11 Structures of G-quadruplex-interactive small molecules with reported c-*KIT* expression modulatory activity.

quadruplex stabilization capacity, level of telomerase inhibitory activity[225] and long-term growth-inhibitory activity, it was suggested that 4-NDII-1 has a dual mechanism of action in GIST882 cells, which also strongly express telomerase.[226]

The benzo[*a*]phenoxazines BPO1 and BPO2 (Fig. 11) were identified as quadruplex selective c-*KIT* promoter targeting molecules, from a library of 173 small molecules interrogated with a luciferase reporter assay driven by the c-*KIT* promoter. The effects of BPO1 and BPO2 on c-*KIT* expression downregulation were further confirmed by incubating human gastric carcinoma HGC-27 cells with 5 μM of each compound. Both compounds reduced by 2.6–2.9-fold the mRNA levels of c-*KIT2*. A greater affinity of both ligands to the c-*KIT2* quadruplex compared to c-*KIT1*, c-*MYC*, and telomere quadruplex sequences was also found by SPR, with selective affinity for the c-*KIT2* quadruplex over duplex DNA.[227]

The established quadruplex ligand and telomerase inhibitor indolo[3,2-*b*]quinoline derivative SYUIQ-FM05 (Fig. 10) with antiproliferative and senescence-induction activities[170,228] has also been examined for c-*KIT* transcription inhibitory activity in c-KIT-positive K562 leukemia cells.[229] SYUIQ-FM05 inhibited cellular growth in this cell line with an IC_{50} of approximately 10 nM and at equitoxic concentrations suppressed c-*KIT* transcription by 7.7-fold, which produced a proportional loss of total c-KIT protein and an apoptotic response. In addition, SYUIQ-FM05, as well as the clinical c-KIT inhibitor imatinib, downregulated downstream MEK and ERK activation. A decrease in *BCL-2* transcription and an increase in *Bax* expression were also found in these treated cells, although these effects were less pronounced than on c-*KIT* expression. These findings support the anticancer potential of SYUIQ-FM05, or related c-*KIT* quadruplex ligands, in the treatment of c-KIT-positive cancers. Other aromatic tetracyclic compounds, the 6-substituted indenoisoquinolines (e.g., InIQ1b, Fig. 11) were also found by a FRET melting assay to be potent and selective quadruplex ligands, particularly of c-*KIT1* compared to c-*KIT2* and telomeric quadruplex sequences.[230] InIQ1b showed antiproliferative activity against two c-KIT-positive cancer cell lines, the primary GIST cells GIST882 and the colorectal cancer cell line HT-29, with IC_{50} values, respectively, of 4.1 and 0.3 μM, which compare with that of imatinib in GIST882 cells ($IC_{50} = 1.7$ μM). Moreover, at IC_{50} concentration, InIQ1b greatly decreased the levels of both c-*KIT* mRNA and c-KIT protein in GIST882 cells.[230]

A series of quinazolone derivatives (QD), constituting a novel unfused aromatic system, has been designed, synthesized, and evaluated for inhibition of c-*KIT* expression in cancer cells, based on previous in vitro evidence of selective binding of compounds with a quinazolone core to quadruplex structures.[231,232] These QDs were designed to include an expansion of the aromatic system via the introduction of a benzene ring and a benzylidene group into the quinazolone moiety, and two protonatable amino side chains (e.g., QD7e, Fig. 11). FRET melting, SPR, and CD experiments demonstrated that QDs, with this adaptive scaffold, could effectively bind and stabilize c-*KIT1* and c-*KIT2* quadruplexes with high selectivity against duplex DNA. From all derivatives tested, compound QD7e has prominent activity in cancer cells, inhibiting the growth of the human gastric carcinoma cell line HGC-27 (having overexpressed c-*KIT*) ($IC_{50} = 8.8$ μM). At a 5 μM concentration, it inhibited by 45% luciferase activity driven by the wild-type c-*KIT* promoter, an inhibitory effect twofold greater than that observed with a mutant construct. It decreased by 52.5% the c-*KIT* mRNA levels in HGC-27 cells incubated with 5 μM of the compound.[232] However, these cellular effects could not be fully explained by c-*KIT* quadruplex interactions (other genomic quadruplex targets could also be involved) and these QDs are apparently less potent quadruplex stabilizers and c-*KIT* transcription inhibitors than other reported fused-aromatic compounds.

5.09.5.6 BCL-2

The *BCL-2* (B-cell lymphoma 2) gene encodes for a mitochondrial membrane protein that functions as an inhibitor of apoptosis. *BCL-2* has been found to be overexpressed, due to gene amplification or translocation,[233] in a wide range of human tumors including B-cell and T-cell lymphomas and breast, prostate, cervical, colorectal, and non-small-cell lung carcinomas.[234–240] Increased BCL-2 levels have also been associated with poor prognosis and resistance to chemotherapy or radiotherapy.[241,242] It has been shown that inhibition of BCL-2 activity or expression by small molecules[243,244] or antisense oligonucleotides[245,246] can decrease cellular proliferation and enhance chemotherapy efficacy. Thus, effective modulation of *BCL-2* expression offers promise for cancer therapeutics. Although targeting the protein directly is challenging, drugs with this mechanism have been developed (e.g., ABT-737, ABT-263, ABT-199), and one (venetoclax, ABT-199) has obtained regulatory approval. These high molecular-weight compounds have significant pharmacological problems and alternatives are still sought.

A 39-bp GC-rich element located 57–19 base pairs upstream of the P1 promoter of *BCL-2* has been reported to be the binding site of multiple transcription factors.[247–249] The 39-mer G-rich strand (Pu39) of this GC-rich element contains six runs of 3–5 consecutive guanines with the potential to form 15 intramolecular quadruplex structures. It has been shown that the quadruplex formed on the central four G-runs (midquadruplex) folds in K^+ solution into a stable three quartet mixed parallel/antiparallel quadruplex with three loops of 1, 7, and 3 nt,[250,251] whereas guanine runs 1, 2, 4, and 5 can fold into another thermodynamically stable quadruplex (1245quadruplex) with a parallel structure and with one 13-nt and two 1-nt chain-reversal loops.[52] The possibility of two interchangeable quadruplex existing within the same region of the *BCL-2* promoter suggests that these two structures may be recognized by different proteins and small molecules which in turn could differentially modulate *BCL-2* gene transcription. Moreover, a second 32-bp GC-rich sequence has been identified −451 bp upstream of the P1 promoter and shown to be implicated in *BCL-2* transcription activation.[252] The G-rich strand of this sequence (labeled p32) can fold into an intramolecular hybrid-type quadruplex and inhibition of its formation through base mutations downregulates *BCL-2* expression.[253]

The indoloquinolines SYUIQ-F05 and SYUIQ-FM05 (Fig. 10) have been shown to decrease *BCL-2* promoter activity in a luciferase assay using the Pu39 construct rather than in the assay with a mutant Pu39 construct. They decrease *BCL-2* transcription and protein levels in HL-60 cells and leukemia K562 cell lines incubated with 0.4 μM concentration of compounds and inhibit cell

proliferation and induce apoptosis in HL-60 tumor cells. SYUIQ-FM05 showed greater activity than SYUIQ-F05 in all assays, in agreement with the observed higher in vitro binding and stabilization of the quadruplex-forming sequence Pu39.[229,254] The 2,4-disubstituted quinazoline SYSU12d (Fig. 6) has also been shown to be a potent quadruplex ligand, able to downregulate c-*MYC* expression which in turn induced a series of cellular events leading to activation of p53 and apoptosis. Contributing to the apoptotic effect is probably the ability of this quinazoline (>2.5 μM) to decrease BCL-2 protein levels in HeLa cells.[168]

As previously mentioned, the quadruplex-mediated regulation of gene expression by the naphthalene diimide derivative HNDI-NMe2 (Fig. 8) depends both on gene and cell type.[186] FRET and CD experiments have shown that HNDI-NMe2 is able to bind to and stabilize the 37mer G-rich strand of the *BCL-2* promoter, maintaining a parallel quadruplex structure, and to decrease mRNA levels in both the melanoma SKMel-5 cell line and the small-cell lung cancer H69 cell line, by 1.6- and 5-fold, respectively, when cells were treated for 48 h with subcytotoxic concentrations of compound (0.6–0.4 μM). However, HNDI-NMe2 did not affect BCL-2 protein levels in the H69 cell line, which, it has been suggested, may be due to compensatory responses activated by cells to cope with the drug.[186] Consistent with the observation that the induced effects of quadruplex-binding ligands on gene expression are cell-type dependent is another study with a related tetra-substituted naphthalene diimide. 4-NDII-MM41 (Fig. 12) has been shown to be a potent stabilizer of several quadruplex structures in vitro and to inhibit cell growth, in particular in pancreatic cancer cells.[123] 4-NDII-MM41 showed an IC_{50} of 10 nM in the MIA PaCa-2 pancreatic adenocarcinoma cell line. Further studies into the mechanism of anticancer activity of this compound revealed that it is not a telomerase inhibitor (in common with other related tetra-substituted naphthalene diimides), does not appear to induce a major DNA damage response in cells, but significantly

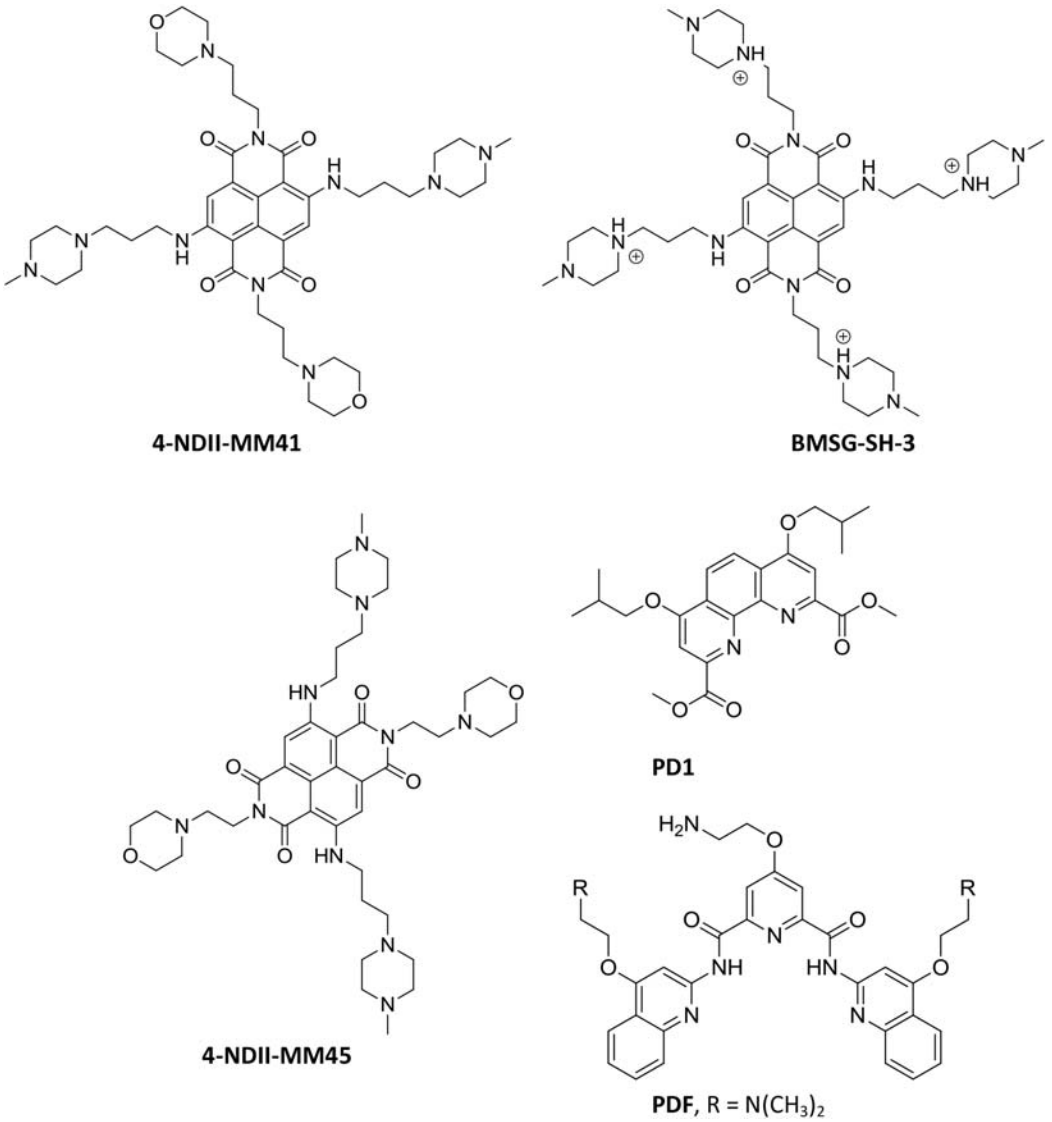

Fig. 12 Structures of tetra-substituted naphthalene diimides (4-NDII-MM41, 4-NDII-MM45, BMSG-SH-3), pyridostatin analogue PDF, and a phenanthroline derivative (PD1) with reported oncogene expression modulatory activity.

downregulates the expression of the antiapoptotic *BCL*-2 gene.[123] Moreover, 4-NDII-MM41 showed in vivo antitumor activity against the MIA PaCa-2 pancreatic cancer xenograft model. Tumor growth decreased by 80% after treatment with 15 mg/kg twice-weekly of 4-NDII-MM41 administered intravenously and levels of BCL-2 and k-RAS proteins were reduced by c. 40% and 30%, respectively, in tumors from treated animals. In addition, whole-animal imaging showed that 4-NDII-MM41 is preferentially localized in the tumor mass 4 h postadministration; it is able to penetrate into the center of the tumor mass and in tumor tissues it is exclusively localized in nuclei.[255]

The p32 G-rich DNA sequence located upstream of the *BCL*-2 P1 promoter has been shown in vitro to form an intramolecular quadruplex hybrid-type structure, which seems to be an essential factor in the binding of transcription factors, thus acting as an activator of gene expression. The phenanthroline dicarboxylate compound PD1 (**Fig. 12**) downregulated *BCL-2* expression in A549 cells, determined by measuring mRNA levels, and in a luciferase assay driven by a constructed vector that included the p32 sequence. Similarly, luciferase activity was also decreased when cells where cotransfected with a pGL vector in which the central guanines in each G-tract of the p32 sequence were mutated to thymine. To further understand the role of p32 on *BCL*-2 expression regulation and how PD1 can affect this, the interaction between PD1 and the p32 quadruplex was studied by fluorescence spectroscopy and CD. It was shown that PD1 can induce a conformational transition in the p32 quadruplex, increasing its antiparallel character, but cannot actually induce quadruplex formation or enhance quadruplex stability. Thus, the design of small molecules targeting the p32 quadruplex in the *BCL*-2 promoter must consider the disruption of the quadruplex structure and not only the increasing of quadruplex stability.[253] The pyridostatin analogue PDF (**Fig. 12**) showed high binding affinity and selectivity (6.5-fold) to the *BCL*-2 quadruplex (MidG4-G15T/G16T) compared to double-strand DNA sequences, as well as antiproliferative activity ($IC_{50} = 1–2$ μM) in human laryngeal squamous carcinoma Hep-2 cells. Moreover, PDF decreased both *BCL*-2 transcription in Hep-2 cells treated with PDF (1–10 μM) and *BCL*-2 promoter activity in a luciferase reporter assay.[256]

5.09.5.7 HSP-90

Heat-shock proteins (HSP) are a family of proteins that act as molecular chaperones, preventing the formation of nonspecific protein aggregates and assisting proteins in their correct folding. HSP90 is the most studied member of this family and it has been found to be overexpressed in several cancers. HSP90 activity has been associated with a larger number of cellular signaling pathways where it has an antiapoptotic role.[257] Moreover, HSP90 also plays a role in telomere maintenance and telomerase regulation.[258,259] HSP90 has been widely recognized as an important target for cancer therapy and several inhibitors are currently under investigation.[260–262] However, emergence of resistance to these inhibitors via mutations in the ATP binding site may occur.[263] Targeting the HSP90 gene rather than the gene product may reduce susceptibility to resistance.

The presence in the promoter region of *HSP90* of a sequence with five short guanine tracts able to form quadruplex structures of mixed topology in high K^+ concentrations has been reported, as well as the possibility of these quadruplex being selectively targeted and stabilized by small molecules.[55] The indoloquinolines IQ3A1a and IQ3A2a (**Fig. 9**) have shown moderate induced thermal stabilization of the 21mer *HSP90*A quadruplex and decreased HSP90 protein expression in HCT116 and SW620 colon cancer cells, although the major effect of these compounds in these cancer cell lines was observed to be on k-*RAS* expression.[202,203]

The naphthalene diimide derivative BMSG-SH-3 (**Fig. 12**), a potent in vitro stabilizer of promoter *HSP90* quadruplex structures, showed significant in vivo antitumor activity against a model for pancreatic cancer. At a dose of 3 mg/kg three times per week, BMSG-SH-3 decreased tumor volume by 50% over the 26 days of the experiment. In addition, the compound localized in tumors and reduced the levels of HSP90 in treated MIA PaCa-2 tumor cells. BMSG-SH-3 has also the capacity to stabilize quadruplex structures in telomeres and inhibit telomerase,[264] which itself is regulated by HSP90. Thus, it has been proposed that the simultaneous targeting of these quadruplex may be an effective antitumor strategy.[265] Moreover, BMSG-SH-3 did not induce a major cellular DNA damage response, nor showed significant hERG activity, and was not localized in the hearts of treated animals, consistent with a lack of cardiotoxicity.[265]

5.09.5.8 *HIFα*

Hypoxia-inducible factor-1 (HIF-1) is a transcription factor that mediates cellular responses to hypoxia, such as increased glycolysis, resistance to apoptosis, and increased angiogenesis. HIF-1 is a heterodimer constituted by a HIF-1β subunit, that is constitutively expressed, and an oxygen-dependent HIF-α subunit. Of the three α isoforms, HIF-1α is the one playing a major role in hypoxia signaling.[266,267] HIF-1α protein has been found to be overexpressed in many human tumors including renal cancers,[268] osteosarcomas, and chondrosarcomas.[269,270] Moreover, levels of serum VEGF, whose gene is a HIF target, were found to be significantly higher in Ewing's sarcoma patients than in healthy controls. HIF-1α is thus an attractive molecular target for the development of novel drugs for these cancers in particular.

Quadruplex-forming sequences have been located in the promoter region of both the *HIF*-1α and the *HIF*-2α genes and shown to be implicated in the regulation of expression of these genes.[56,271–273] A family of naphthalene derivatives with disubstituted triazole side chains has been investigated for their quadruplex binding and stabilizing ability, repression of *HIF*-1α and *HIF*-2α expression and antiproliferative activity in a panel of cancer cell lines. From all the derivatives tested, compound CL67 (**Fig. 13**) showed the optimal binding affinity constants to *HIF*-1α and *HIF*-2α quadruplexes, as determined by SPR, and no significant binding to a control duplex DNA sequence. Further studies by CD showed that CL67 does not induce any conformational change on binding to the parallel *HIF*-1α quadruplex. More importantly, CL67 showed high levels of antiproliferative activity and selectivity for renal,

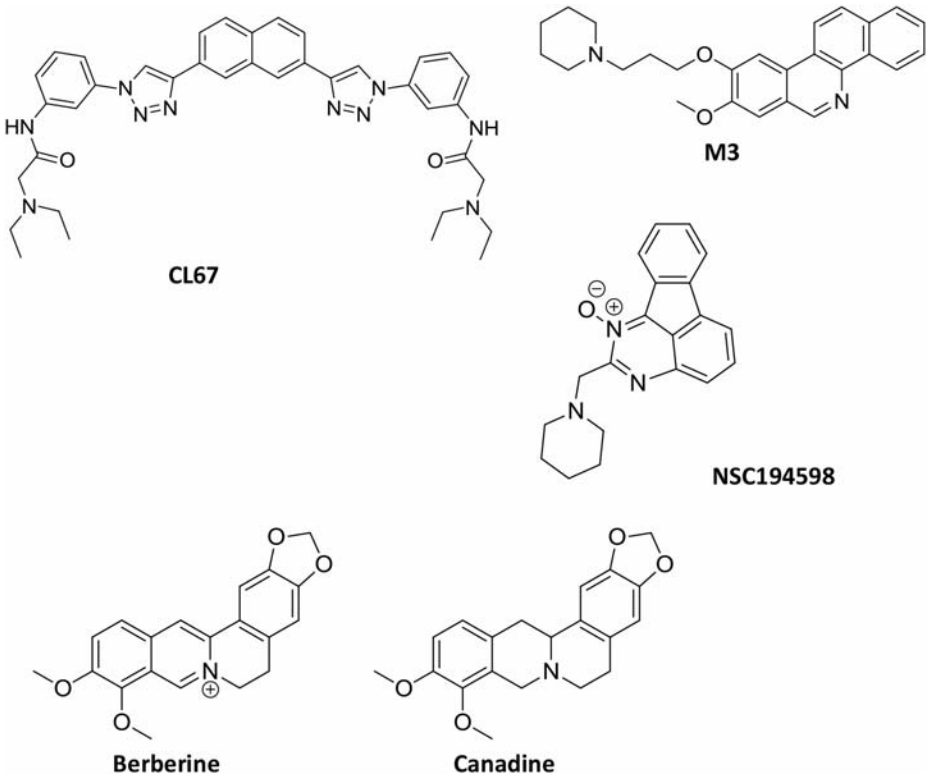

Fig. 13 Structures of G-quadruplex-interactive small molecules with reported effects on expression of *HIF-1α* and *RET*.

osteo-, and Ewing's sarcomas, all of which express HIF-1α protein. It inhibited in a dose-dependent manner both mRNA and HIF-1α and HIF-2α proteins in osteosarcoma and renal carcinoma cell lines, leading to inhibition of HIF transactivation and subsequent reduction in expression of downstream target genes, both in cancer cell lines and in a mouse xenograft model of renal cancer.[271,272] Moreover, this inhibition by CL67 was shown to be independent of pathways controlling oxygen-dependent HIF degradation and expression of HIF-α subunits.[272]

Four other quadruplexes have been identified in the *HIF*-1α promoter and 5′-UTR (S1-S4) by multiple spectroscopic and biochemical methods. The S1-quadruplex has been shown to be the most significant for *HIF*-1α transcription repression by blocking the AP2-binding site. The benzo[*c*]phenanthridine derivative M3 (Fig. 13) was shown to bind preferentially to the S1-quadruplex, inducing conformational change and repressing *HIF*-1α expression in the MCF-7 cell line (which only has low-level expression of *HIF*). M3 also repressed the transcription of several downstream genes such as *VEGF* and *GluT1* but not of upstream regulators such as *AP2*.[273]

5.09.5.9 The Androgen Receptor

An increase in AR protein has been associated with the majority of castrate-resistant prostate cancers in the clinic.[274] Knockdown of AR has been shown to cause cancer cell growth inhibition both in vitro and in a xenograft model of castrate-resistant prostate cancer.[275] Several approaches to downregulate AR transcription have been recently pursued.[276,277] A G-rich sequence able to form a stable quadruplex has been identified 116 bp upstream of the *AR* transcription start site by NMR spectroscopy, CD, UV spectroscopy, and UV thermal melting experiments.[67] The naphthalene diimide derivative 4-NDII-MM45 (Fig. 12) showed potent ability to stabilize the *AR* quadruplex at submicromolar concentrations using a FRET melting assay. It also inhibits prostate cancer cell growth and represses *AR* transcription at the mRNA and protein levels in a dose-dependent manner in these cells, and in a luciferase reporter assay driven by AR promoter. mRNA levels for AR target genes were shown to be downregulated, as well some AR upstream transcription factors that may contribute to repress *AR* transcription, such as c-MYC and SP1, together with upregulation of Jun.[67,274] Thus, a poly-targeting mechanism of action has been suggested for 4-NDII-MM45.

5.09.5.10 RET

The *RET* (rearranged during transfection) proto-oncogene encodes a receptor tyrosine kinase that has been implicated in the development of several human cancers, in particular thyroid cancer.[278,279] In these cancers, RET aberrant function can be due to

mutations or protein overexpression.[280–283] The possibility of targeting RET in these rarer cancers using small molecules, monoclonal antibodies, or gene therapy has been investigated in several studies.[284]

A G-rich sequence containing two GC-boxes essential for SP1-mediated transactivation of the *RET* promoter has been identified[285] and shown to be able to form intramolecular quadruplex structures in vitro,[66,286] which can be stabilized by quadruplex ligands such as TMPyP4, telomestatin, and NSC194598. The indeno[1,2,3]quinazoline derivative NSC194598 (**Fig. 13**) has been shown to more strongly inhibit transcriptional activity in the presence of a wild-type *RET* promoter than in the presence of a quadruplex-mutated one, to inhibit *RET* mRNA expression in a human medullary thyroid carcinoma cell line (TT) harboring a MEN2A-type mutation, but to induce little effect on other genes with known quadruplexes in their promoters (*VEGF*, *HIF*-1α, h-*RAS*). It was also shown that NSC194598 prevents *RET* promoter binding by RNA polymerase II, SP1, and nucleolin, and induces both apoptotic and necrotic cell death in TT cells at concentrations below 2.5 μg/mL.[287]

In another study, berberine, a N^+-containing isoquinoline derivative, was shown by DNA melting and DMS footprint assays to interact more strongly to RET wt quadruplex-forming sequences than the tetrahydro isoquinoline analogue canadine (**Fig. 13**). In agreement with these observations, berberine (2.5 μg/mL) downregulated RET transcription and reduced RET protein levels in a medullary carcinoma TT cell line, without significantly affecting the expression of c-*MYC* and *VEGF*, whereas canadine showed no effect on *RET* expression in the same cell line. Moreover, berberine had minimal effect on *RET* transcription in the papillary thyroid carcinoma TPC1 cell line, which lacks the quadruplex-forming sequence in its *RET* promoter due to chromosomal rearrangement, thus suggesting that oncogene expression is downregulated by quadruplex targeting. However, this was not supported by luciferase reporter assay data since berberine (10 μg/mL) decreased the luciferase expression driven by both the *RET* promoter itself and a *RET* mutated promoter unable to form a quadruplex. Further studies revealed that berberine prevents the binding of SP1 and RNA PolII to the *RET* promoter in TT cells and inhibits the phosphorylation of Akt in a dose-dependent manner, leading to induction of apoptosis. Interestingly, berberine showed no effect on the RET downstream signal transduction pathway MEK/ERK, which could be explained by the fact that this pathway is also governed by other growth factor receptors such as VEGFR and EGFR.[288]

5.09.5.11 MET

Human MET (c-MET or hepatocyte growth factor receptor) is a membrane tyrosine kinase that can be activated by the hepatocyte growth factor, then activating several downstream signaling cascades such as RAS/MAPK, PI3K/Akt, c-SRC, and STAT3/5.[289] MET abnormal activation has been identified in kidney, breast, stomach, liver, and brain cancers, and consequently several approaches to targeting MET have been developed, including the use of receptor antagonists,[290–292] antibodies,[293] and small-molecule inhibitors.[294]

Bioinformatic studies have identified a quadruplex-forming sequence within the proximal promoter region of *MET* (−48 to −26 bp upstream of the TSS) which contains a SP1-binding site. This G-rich sequence (Pu23WT) was confirmed to fold into an intramolecular parallel quadruplex by CD. TMPyP4 (**Fig. 6**) stabilizes this quadruplex structure in vitro and represses luciferase expression driven by Pu23WT but not that driven by MET promoter mutants unable to form stable quadruplexes.[295] Moreover, treatment of liver and gastric cancer cells with 50 μM of TMPyP4 decreased MET expression at both mRNA and protein levels, probably due to TMPyP4 blockage of SP1 recruitment to its binding site in the Pu23WT sequence, as shown by ChIP assays. Treatment of cancer cells with TMPyP4 also results in cell proliferation inhibition, cell cycle arrest in G1 phase, and cell migration retardation, probably due to downregulation of *MET* expression, although other gene promoters containing quadruplex sequences, such as *SRC* and k-*RAS*, may be also targeted by TMPyP4.[295]

5.09.5.12 c-*SRC*

c-SRC (cellular Rous sarcoma) is a nonreceptor tyrosine kinase that has been associated with the initiation and proliferation of several tumors, including melanoma,[296] colon,[297–299] breast,[300,301] and prostate[302] cancers, and is a validated therapeutic target of several tyrosine kinase inhibitors.[302,303]

Pyridostatin (**Fig. 5**) is a pyridine-2,6-bisquinolinedicarboxamide derivative with high affinity and selectivity for DNA quadruplexes (both in telomere and promoters). It is able to induce alteration of shelterin at telomeres,[88] induce a DNA damage response, and produces long-term growth inhibition of cancer cells incubated with IC_{50} concentrations of compound.[152] A chromatin immunoprecipitation sequencing analysis of DNA damage indicated by the damage marker γH2AX showed that pyridostatin targets genes containing clusters of quadruplex-forming sequences.[89] Pyridostatin (2 μM in MRC-5-SV40 cells) downregulated, after 8 h of drug treatment, all the γH2AX-positive target genes, including the oncogenes c-*MYC* and *SRC*, but did not affect the negative controls, such as h-*RAS*. The *SRC* oncogene was the most affected, with its mRNA levels being reduced by over 95%.[89] Importantly, this study allowed the identification of 25 quadruplex-forming sequences in the *SRC* coding region, from which 23 were shown by CD and NMR to form stable quadruplexes of different topologies. Finally, pyridostatin reduced SRC protein levels and SRC-dependent cellular motility in human breast cancer cells, strongly suggesting *SRC* as a target of this compound.[89] More recently, a photo-activated prodrug of pyridostatin was developed by linking a nitroveratryl group to one of the side chain amines. This prodrug upon 10–30 min of UV-light irradiation shows, in common with pyridostatin, high stabilization of a *SRC* quadruplex, cell growth inhibition, and oncogene (c-*MYC*, *SRC*, and *RET*) transcription downregulation activity.[304]

References

1. Gellert, M.; Lipsett, M. N.; Davies, D. R. Helix Formation by Guanylic Acid. *Proc. Natl. Acad. Sci. U. S. A.* **1962,** *48,* 2013–2018.
2. Arnott, S.; Chandrasekaran, R.; Marttila, C. M. Structures for Polyinosinic Acid and Polyguanylic Acid. *Biochem. J.* **1974,** *141,* 537–543.
3. Zimmerman, S. B.; Cohen, G. H.; Davies, D. R. X-ray Fiber Diffraction and Model-Building Study of Polyguanylic Acid and Polyinosinic Acid. *J. Mol. Biol.* **1975,** *92,* 181–192.
4. Howard, F. B.; Miles, H. T. Poly(Inosinic Acid) Helices: Essential Chelation of Alkali Metal Ions in the Axial Channel. *Biochemistry* **1982,** *21,* 6736–6745.
5. Sundquist, W. I.; Klug, A. Telomeric DNA Dimerizes by Formation of Guanine Tetrads Between Hairpin Loops. *Nature* **1989,** *342,* 825–829.
6. Sen, D.; Gilbert, W. A Sodium-Potassium Switch in the Formation of Four-Stranded G4-DNA. *Nature* **1990,** *344,* 410–414.
7. Henderson, E.; Hardin, C. C.; Walk, S. K.; Tinoco, I., Jr.; Blackburn, E. H. Telomeric DNA Oligonucleotides Form Novel Intramolecular Structures Containing Guanine-Guanine Base Pairs. *Biochemistry* **1987,** *51,* 899–908.
8. Meyne, J.; Ratliff, R. L.; Moyzis, R. K. Conservation of the Human Telomere Sequence $(TTAGGG)_n$ Among Vertebrates. *Proc. Natl. Acad. Sci. U. S. A.* **1989,** *86,* 7049–7053.
9. Davis, J. T. G-Quartets 40 Years Later: From 5′-GMP to Molecular Biology and Supramolecular Chemistry. *Angew. Chem. Int. Ed. Engl.* **2004,** *43,* 668–698.
10. Burge, S.; Parkinson, G. N.; Hazel, P.; Todd, A. K.; Neidle, S. Quadruplex DNA: Sequence, Topology and Structure. *Nucleic Acids Res.* **2006,** *34,* 5402–5415.
11. Patel, D. J.; Phan, A. T.; Kuryavyi, V. Human Telomere, Oncogenic Promoter and 5′-UTR G-Quadruplexes: Diverse Higher Order DNA and RNA Targets for Cancer Therapeutics. *Nucleic Acids Res.* **2007,** *35,* 7429–7455.
12. Zhou, J.; Bourdoncle, A.; Rosu, F.; Gabelica, V.; Mergny, J.-L. Tri-G-Quadruplex: Controlled Assembly of a G-Quadruplex Structure from Three G-Rich Strands. *Angew. Chem. Int. Ed. Engl.* **2012,** *51,* 11002–11005.
13. Neidle, S., Balasubramanian, S., Eds. *Quadruplex Nucleic Acids;* RSC Publishing: UK, 2006.
14. Chaires, J. B., Graves, D. E., Eds. *Quadruplex Nucleic Acids;* Springer-Verlag: Berlin, 2013.
15. Neidle, S. *Therapeutic Applications of Quadruplex Nucleic Acids;* Academic Press: San Diego, 2012.
16. Neidle, S. The Structures of Quadruplex Nucleic Acids and Their Drug Complexes. *Curr. Opin. Struct. Biol.* **2009,** *19,* 239–250.
17. Adrian, M.; Heddi, B.; Phan, A. T. NMR Spectroscopy of G-Quadruplexes. *Methods* **2012,** *57,* 11–24.
18. Campbell, N.; Collie, G. W.; Neidle, S. Crystallography of DNA and RNA G-Quadruplex Nucleic Acids and Their Ligand Complexes. *Curr. Protoc. Nucleic Acid Chem.* **2012**. Chapter 17, Unit 17.6. http://dx.doi.org/10.1002/0471142700.nc1706s50.
19. Mergny, J.-L.; Phan, A. T.; Lacroix, L. Following G-Quartet Formation by UV-Spectroscopy. *FEBS Lett.* **1998,** *435,* 74–78.
20. Vorlíčková, M.; Kejnovská, I.; Sagi, J.; Renčiuk, D.; Bednářová, K.; Motlová, J.; Kypr, J. Circular Dichroism and Guanine Quadruplexes. *Methods* **2012,** *57,* 64–75.
21. De, S.; Michor, F. DNA Secondary Structures and Epigenetic Determinants of Cancer Genome Evolution. *Nat. Struct. Mol. Biol.* **2011,** *18,* 950–955.
22. Bochman, M. L.; Paeschke, K.; Zakian, V. A. DNA Secondary Structures: Stability and Function of G-Quadruplex Structures. *Nat. Rev. Genet.* **2012,** *13,* 770–780.
23. Tarsounas, M.; Tijsterman, M. Genomes and G-Quadruplexes: For Better or for Worse. *J. Mol. Biol.* **2013,** *425,* 4782–4789.
24. Maizels, N.; Gray, L. T. The G4 Genome. *PLoS Genet.* **2013,** *9,* e1003468.
25. Murat, P.; Balasubramanian, S. Existence and Consequences of G-Quadruplex Structures in DNA. *Curr. Opin. Genet. Dev.* **2014,** *25,* 22–29.
26. Rhodes, D.; Lipps, H. J. G-Quadruplexes and Their Regulatory Roles in Cancer. *Nucleic Acids Res.* **2015,** *43,* 8627–8637.
27. Monchaud, D.; Teulade-Fichou, M.-P. A hitchhiker's Guide to G-Quadruplex Ligands. *Org. Biomol. Chem.* **2008,** *6,* 627–636.
28. Yang, D.; Okamoto, K. Structural Insights into G-Quadruplexes: Towards New Anticancer Drugs. *Future Med. Chem.* **2010,** *2,* 619–646.
29. Ralph, S. F. Quadruplex DNA: A Promising Drug Target for the Medicinal Inorganic Chemist. *Curr. Top. Med. Chem.* **2011,** *11,* 572–590.
30. Bidzinska, J.; Cimino-Reale, G.; Zaffaroni, N.; Folini, M. G-Quadruplex Structures in the Human Genome as Novel Therapeutic Targets. *Molecules* **2013,** *18,* 12368–91235.
31. Ohnmacht, S. A.; Neidle, S. Small-Molecule Quadruplex-Targeted Drug Discovery. *Bioorg. Med. Chem. Lett.* **2014,** *24,* 2602–2612.
32. Sissi, C.; Palumbo, M. Telomeric G-Quadruplex Architecture and Interactions With Potential Drugs. *Curr. Pharm. Des.* **2014,** *20,* 6489–6509.
33. Müller, S.; Rodriguez, R. G-Quadruplex Interacting Small Molecules and Drugs: From Bench Towards Bedside. *Expert. Rev. Clin. Pharmacol.* **2014,** *7,* 663–679.
34. Cree, S. L.; Kennedy, M. A. Relevance of G-Quadruplex Structures to Pharmacogenetics. *Front. Pharmacol.* **2014,** *5,* 160.
35. Parrotta, L.; Ortuso, F.; Moraca, F.; Rocca, R.; Costa, G.; Alcaro, S.; Artese, A. Targeting Unimolecular G-Quadruplex Nucleic Acids: A New Paradigm for the Drug Discovery? *Expert Opin. Drug Discovery* **2014,** *9,* 1167–1187.
36. Neidle, S. Quadruplex Nucleic Acids as Novel Therapeutic Targets. *J. Med. Chem.* **2016,** *59,* 5987–6011.
37. Islam, M. K.; Jackson, P. J.; Rahman, K. M.; Thurston, D. E. Recent Advances in Targeting the Telomeric G-Quadruplex DNA Sequence With Small Molecules as a Strategy for Anticancer Therapies. *Future Med. Chem.* **2016,** *8,* 1259–1290.
38. Rawal, P.; Kummarasetti, V. B.; Ravindran, J.; Kumar, N.; Halder, K.; Sharma, R.; Mukerji, M.; Das, S. K.; Chowdhury, S. Genome-Wide Prediction of G4 DNA as Regulatory Motifs: Role in *Escherichia Coli* Global Regulation. *Genome Res.* **2006,** *16,* 644–655.
39. Capra, J. A.; Paeschke, K.; Singh, M.; Zakian, V. A. G-Quadruplex DNA Sequences are Evolutionarily Conserved and Associated With Distinct Genomic Features in *Saccharomyces Cerevisiae*. *PLoS Comput. Biol.* **2010,** *6,* e1000861.
40. Holder, I. T.; Hartig, J. S. A Matter of Location: Influence of G-Quadruplexes on *Escherichia Coli* Gene Expression. *Chem. Biol.* **2014,** *21,* 1511–1521.
41. Amrane, S.; Kerkour, A.; Bedrat, A.; Vialet, B.; Andreola, M.-L.; Mergny, J.-L. Topology of a DNA G-Quadruplex Structure Formed in the HIV-1 Promoter: A Potential Target for Anti-HIV Drug Development. *J. Am. Chem. Soc.* **2014,** *136,* 5249–5252.
42. Perrone, R.; Nadai, M.; Poe, J. A.; Frasson, I.; Palumbo, M.; Palù, G.; Smithgall, T. E.; Richter, S. N. Formation of a Unique Cluster of G-Quadruplex Structures in the HIV-1 Nef Coding Region: Implications for Antiviral Activity. *PLoS One* **2013,** *8,* e73121.
43. Smargiasso, N.; Gabelica, V.; Damblon, C.; Rosu, F.; De Pauw, E.; Teulade-Fichou, M.-P.; Rowe, J. A.; Claessens, A. Putative DNA G-Quadruplex Formation Within the Promoters of *Plasmodium Falciparum var* Genes. *BMC Genomics* **2009,** *10,* 362.
44. Todd, A. K.; Johnston, M.; Neidle, S. Highly Prevalent Putative Quadruplex Sequence Motifs in Human DNA. *Nucleic Acids Res.* **2005,** *33,* 2901–2907.
45. Huppert, J. L.; Balasubramanian, S. Prevalence of Quadruplexes in the Human Genome. *Nucleic Acids Res.* **2005,** *33,* 2908–2916.
46. Chambers, V. S.; Marsico, G.; Boutell, J. M.; Di Antonio, M.; Smith, G. P.; Balasubramanian, S. High-Throughput Sequencing of DNA G-Quadruplex Structures in the Human Genome. *Nat. Biotechnol.* **2015,** *33,* 877–881.
47. Simonsson, T.; Pecinka, P.; Kubista, M. DNA Tetraplex Formation in the Control Region of c-MYC. *Nucleic Acids Res.* **1998,** *26,* 1167–1172.
48. Siddiqui-Jain, A.; Grand, C. L.; Bearss, D. J.; Hurley, L. H. Direct Evidence for a G-Quadruplex in a Promoter Region and its Targeting With a Small Molecule to Repress c-MYC Transcription. *Proc. Natl. Acad. Sci. U. S. A.* **2002,** *99,* 11593–11598.
49. Brooks, T. A.; Hurley, L. H. Targeting MYC Expression Through G-Quadruplexes. *Genes Cancer* **2010,** *1,* 641–649.
50. Ambrus, A.; Chen, D.; Dai, J.; Jones, R. A.; Yang, D. Solution Structure of the Biologically Relevant G-Quadruplex Element in the Human c-MYC Promoter. Implications for G-Quadruplex Stabilization. *Biochemistry* **2005,** *44,* 2048–2058.
51. Mathad, R. I.; Hatzakis, E.; Dai, J.; Yang, D. c-MYC Promoter G-Quadruplex Formed at the 5′-End of NHE III1 Element: Insights Into Biological Relevance and Parallel-Stranded G-Quadruplex Stability. *Nucleic Acids Res.* **2011,** *39,* 9023–9033.
52. Agrawal, P.; Lin, C.; Mathad, R. I.; Carver, M.; Yang, D. The Major G-Quadruplex Formed in the Human BCL-2 Proximal Promoter Adopts a Parallel Structure With a 13-nt Loop in K^+ Solution. *J. Am. Chem. Soc.* **2014,** *136,* 1750–1753.
53. Agrawal, P.; Hatzakis, E.; Guo, K.; Carver, M.; Yang, D. Solution Structure of the Major G-Quadruplex Formed in the Human VEGF Promoter in K+: Insights into Loop Interactions of the Parallel G-Quadruplexes. *Nucleic Acids Res.* **2013,** *41,* 10584–10592.

54. Lim, K. W.; Lacroix, L.; Yue, D. J.; Lim, J. K.; Lim, J. M.; Phan, A. T. Coexistence of Two Distinct G-Quadruplex Conformations in the hTERT Promoter. *J. Am. Chem. Soc.* **2010,** *132,* 12331–12342.
55. Ohnmacht, S. A.; Micco, M.; Petrucci, V.; Todd, A. K.; Reszka, A. P.; Gunaratnam, M.; Carvalho, M. A.; Zloh, M.; Neidle, S. A Sequence in the HSP90 Promoter Forms G-Quadruplex Structures With Selectivity for Phenyl bis-Oxazole Derivatives. *Bioorg. Med. Chem. Lett.* **2012,** *22,* 5930–5935.
56. De Armond, R.; Wood, S.; Sun, D.; Hurley, L. H.; Ebbinghaus, S. W. Evidence for the Presence of a Guanine Quadruplex Forming Region Within a Polypurine Tract of the Hypoxia Inducible Factor 1α Promoter. *Biochemistry* **2005,** *44,* 16341–16350.
57. Membrino, A.; Cogoi, S.; Pedersen, E. B.; Xodo, L. E. G4-DNA Formation in the HRAS Promoter and Rational Design of Decoy Oligonucleotides for Cancer Therapy. *PLoS One* **2011,** *6*, e24421.
58. Cogoi, S.; Paramasivam, M.; Spolaore, B.; Xodo, L. E. Structural Polymorphism Within a Regulatory Element of the Human KRAS Promoter: Formation of G4-DNA Recognized by Nuclear Proteins. *Nucleic Acids Res.* **2008,** *36,* 3765–3780.
59. Wei, D.; Todd, A. K.; Zloh, M.; Gunaratnam, M.; Parkinson, G. N.; Neidle, S. Crystal Structure of a Promoter Sequence in the B-Raf Gene Reveals an Intertwined Dimer Quadruplex. *J. Am. Chem. Soc.* **2013,** *135,* 19319–19329.
60. Greco, M. L.; Folini, M.; Sissi, C. Double Stranded Promoter Region of BRAF Undergoes to Structural Rearrangement in Nearly Physiological Conditions. *FEBS Lett.* **2015,** *589,* 2117–2123.
61. Rankin, S.; Reszka, A. P.; Huppert, J.; Zloh, M.; Parkinson, G. N.; Todd, A. K.; Ladame, S.; Balasubramanian, S.; Neidle, S. Putative DNA Quadruplex Formation Within the Human c-*Kit* Oncogene. *J. Am. Chem. Soc.* **2005,** *127,* 10584–10589.
62. Fernando, H.; Reszka, A. P.; Huppert, J.; Ladame, S.; Rankin, S.; Venkitaraman, A. R.; Neidle, S.; Balasubramanian, S. A Conserved Quadruplex Motif Located in a Transcription Activation Site of the Human c-Kit Oncogene. *Biochemistry* **2006,** *45,* 7854–7860.
63. Phan, A. T.; Kuryavyi, V.; Burge, S.; Neidle, S.; Patel, D. J. Structure of an Unprecedented G-Quadruplex Scaffold in the Human *c-Kit* Promoter. *J. Am. Chem. Soc.* **2007,** *129,* 4386–4392.
64. Wei, D.; Parkinson, G. N.; Reszka, A. P.; Neidle, S. Crystal Structure of a c-Kit Promoter Quadruplex Reveals the Structural Role of Metal Ions and Water Molecules in Maintaining Loop Conformation. *Nucleic Acids Res.* **2012,** *40,* 4691–4700.
65. Wei, D.; Husby, J.; Neidle, S. Flexibility and Structural Conservation in a c-Kit G-Quadruplex. *Nucleic Acids Res.* **2015,** *43,* 629–644.
66. Tong, X.; Lan, W.; Zhang, X.; Wu, H.; Liu, M.; Cao, C. Solution Structure of All Parallel G-Quadruplex Formed by the Oncogene RET Promoter Sequence. *Nucleic Acids Res.* **2011,** *39,* 6753–6763.
67. Mitchell, T.; Ramos-Montoya, A.; Di Antonio, M.; Murat, P.; Ohnmacht, S.; Micco, M.; Jurmeister, S.; Fryer, L.; Balasubramanian, S.; Neidle, S.; Neal, D. E. Downregulation of Androgen Receptor Transcription by Promoter G-Quadruplex Stabilization as a Potential Alternative Treatment for Castrate-Resistant Prostate Cancer. *Biochemistry* **2013,** *52,* 1429–1436.
68. Bugaut, A.; Balasubramanian, S. 5′-UTR RNA G-Quadruplexes: Translation Regulation and Targeting. *Nucleic Acids Res.* **2012,** *40,* 4727–4741.
69. Shahid, R.; Bugaut, A.; Balasubramanian, S. The BCL-2 5′ Untranslated Region Contains an RNA G-Quadruplex-Forming Motif That Modulates Protein Expression. *Biochemistry* **2010,** *49,* 8300–8306.
70. Kumari, S.; Bugaut, A.; Huppert, J. L.; Balasubramanian, S. An RNA G-Quadruplex in the 5′ UTR of the NRAS Proto-Oncogene Modulates Translation. *Nat. Chem. Biol.* **2007,** *3,* 218–221.
71. Derecka, K.; Balkwill, G. D.; Garner, T. P.; Hodgman, C.; Flint, A. P.; Searle, M. S. Occurrence of a Quadruplex Motif in a Unique Insert Within Exon C of the Bovine Estrogen Receptor Alpha Gene (ESR1). *Biochemistry* **2010,** *49,* 7625–7633.
72. Morris, M. J.; Basu, S. An Unusually Stable G-Quadruplex Within the 5′-UTR of the MT3 Matrix Metalloproteinase mRNA Represses Translation in Eukaryotic Cells. *Biochemistry* **2009,** *48,* 5313–5319.
73. Agarwala, P.; Pandey, S.; Mapa, K.; Maiti, S. The G-Quadruplex Augments Translation in the 5′ Untranslated Region of Transforming Growth Factor β2. *Biochemistry* **2013,** *52,* 1528–1538.
74. Schoeftner, S.; Blasco, M. A. Developmentally Regulated Transcription of Mammalian Telomeres by DNA-Dependent RNA Polymerase II. *Nat. Cell Biol.* **2008,** *10,* 228–236.
75. Azzalin, C. M.; Reichenbach, P.; Khoriauli, L.; Giulotto, E.; Lingner, J. Telomeric Repeat Containing RNA and RNA Surveillance Factors at Mammalian Chromosome Ends. *Science* **2007,** *318,* 798–801.
76. Cusanelli, E.; Chartrand, P. Telomeric Repeat-Containing RNA TERRA: A Noncoding RNA Connecting Telomere Biology to Genome Integrity. *Front. Genet.* **2015,** *6,* 143.
77. Arora, R.; Azzalin, C. M. Telomere Elongation Chooses TERRA ALTernatives. *RNA Biol.* **2015,** *12,* 938–941.
78. Porro, A.; Feuerhahn, S.; Delafontaine, J.; Riethman, H.; Rougemont, J.; Lingner, J. Functional Characterization of the TERRA Transcriptome at Damaged Telomeres. *Nat. Commun.* **2014,** *5,* 5379.
79. Randall, A.; Griffith, J. D. Structure of Long Telomeric RNA Transcripts: The G-Rich RNA Forms a Compact Repeating Structure Containing G-Quartets. *J. Biol. Chem.* **2009,** *284,* 13980–13986.
80. Schaffitzel, C.; Berger, I.; Postberg, J.; Hanes, J.; Lipps, H. J.; Pluckthun, A. In Vitro Generated Antibodies Specific for Telomeric Guanine-Quadruplex DNA React With *Stylonychia Lemnae* Macronuclei. *Proc. Natl. Acad. Sci. U. S. A.* **2001,** *98,* 8572–8577.
81. Lam, E. Y.; Beraldi, D.; Tannahill, D.; Balasubramanian, S. G-Quadruplex Structures Are Stable and Detectable in Human Genomic DNA. *Nat. Commun.* **2013,** *4,* 1796.
82. Biffi, G.; Tannahill, D.; McCafferty, J.; Balasubramanian, S. Quantitative Visualization of DNA G-Quadruplex Structures in Human Cells. *Nat. Chem.* **2013,** *5,* 182–186.
83. Henderson, A.; Wu, Y.; Huang, Y. C.; Chavez, E. A.; Platt, J.; Johnson, F. B.; Brosh, R. M., Jr.; Sen, D.; Lansdorp, P. M. Detection of G-Quadruplex DNA in Mammalian Cells. *Nucleic Acids Res.* **2013,** *42,* 860–869.
84. Biffi, G.; Di Antonio, M.; Tannahill, D.; Balasubramanian, S. Visualization and Selective Chemical Targeting of RNA G-Quadruplex Structures in the Cytoplasm of Human Cells. *Nat. Chem.* **2014,** *6,* 75–80.
85. Biffi, G.; Tannahill, D.; Miller, J.; Howat, W. J.; Balasubramanian, S. Elevated Levels of G-Quadruplex Formation in Human Stomach and Liver Cancer Tissues. *PLoS One* **2014,** *9,* e102711.
86. Brosh, R. M., Jr.; Cantor, S. B. Molecular and Cellular Functions of the FANCJ DNA Helicase Defective in Cancer and in Fanconi Anemia. *Front. Genet.* **2014,** *5,* 372.
87. Nguyen, G. H.; Tang, W.; Robles, A. I.; Beyer, R. P.; Gray, L. T.; Welsh, J. A.; Schetter, A. J.; Kumamoto, K.; Wang, X. W.; Hickson, I. D.; Maizels, N.; Monnat, R. J., Jr.; Harris, C. C. Regulation of Gene Expression by the BLM Helicase Correlates With the Presence of G-Quadruplex DNA Motifs. *Proc. Natl. Acad. Sci. U. S. A.* **2014,** *111,* 9905–9910.
88. Rodriguez, R.; Müller, S.; Yeoman, J. A.; Trentesaux, C.; Riou, J.-F.; Balasubramanian, S. A Novel Small Molecule That Alters Shelterin Integrity and Triggers a DNA-Damage Response at Telomeres. *J. Am. Chem. Soc.* **2008,** *130,* 15758–15759.
89. Rodriguez, R.; Miller, K. M.; Forment, J. V.; Bradshaw, C. R.; Nikan, M.; Britton, S.; Oelschlaegel, T.; Xhemalce, B.; Balasubramanian, S.; Jackson, S. P. Small-Molecule-Induced DNA Damage Identifies Alternative DNA Structures in Human Genes. *Nat. Chem. Biol.* **2012,** *8,* 301–310.
90. Dietlein, F.; Thelen, L.; Reinhardt, H. C. Cancer-Specific Defects in DNA Repair Pathways as Targets for Personalized Therapeutic Approaches. *Trends Genet.* **2014,** *30,* 326–339.
91. Balasubramanian, S.; Hurley, L. H.; Neidle, S. Targeting G-Quadruplexes in Gene Promoters: A Novel Anticancer Strategy? *Nat. Rev. Drug. Discovery* **2011,** *10,* 261–275.
92. Boddupally, P. V.; Hahn, S.; Beman, C.; De, B.; Brooks, T. A.; Gokhale, V.; Hurley, L. H. Anticancer Activity and Cellular Repression of c-MYC by the G-Quadruplex-Stabilizing 11-Piperazinylquindoline is Not Dependent on Direct Targeting of the G-Quadruplex in the c-MYC Promoter. *J. Med. Chem.* **2012,** *55,* 6076–6086.
93. Brown, R. V.; Danford, F. L.; Gokhale, V.; Hurley, L. H.; Brooks, T. A. Demonstration That Drug-Targeted Down-Regulation of MYC in Non-Hodgkins Lymphoma is Directly Mediated Through the Promoter G-Quadruplex. *J. Biol. Chem.* **2011,** *286,* 41018–41027.

94. Gomez, D.; O'Donohue, M. F.; Wenner, T.; Douarre, C.; Macadré, J.; Koebel, P.; Giraud-Panis, M.-J.; Kaplan, H.; Kolkes, A.; Shin-Ya, K.; Riou, J.-F. The G-Quadruplex Ligand Telomestatin Inhibits POT1 Binding to Telomeric Sequences in vitro and Induces GFP-POT1 Dissociation From Telomeres in Human Cells. *Cancer Res.* **2006,** *66,* 6908–6912.
95. Gunaratnam, M.; Greciano, O.; Martins, C.; Reszka, A. P.; Schultes, C. M.; Morjani, H.; Riou, J.-F.; Neidle, S. Mechanism of Acridine-Based Telomerase Inhibition and Telomere Shortening. *Biochem. Pharmacol.* **2007,** *74,* 679–689.
96. Sabater, L.; Nicolau-Travers, M.-L.; De Rache, A.; Prado, E.; Dejeu, J.; Bombarde, O.; Lacroix, J.; Calsou, P.; Defrancq, E.; Mergny, J.-L.; Gomez, D.; Pratviel, G. The Nickel(II) Complex of Guanidinium Phenyl Porphyrin, a Specific G-Quadruplex Ligand, Targets Telomeres and Leads to POT1 Mislocalization in Culture Cells. *J. Biol. Inorg. Chem.* **2015,** *20,* 729–738.
97. Tauchi, T.; Shin-ya, K.; Sashido, G.; Sumi, M.; Nakajima, A.; Shimamoto, T.; Ohyashiki, J. H.; Ohyashiki, K. Activity of a Novel G-Quadruplex-Interactive Telomerase Inhibitor, Telomestatin (SOT-095), Against Human Leukemia Cells: Involvement of ATM-Dependent DNA Damage Response Pathways. *Oncogene* **2003,** *22,* 5338–5347.
98. Salvati, E.; Leonetti, C.; Rizzo, A.; Scarsella, M.; Mottolese, M.; Galati, R.; Sperduti, I.; Stevens, M. F. G.; D'Incalci, M.; Biasco, M.; Chiorino, G.; Bauwens, S.; Horard, B.; Gilson, E.; Stoppacciaro, A.; Zupi, G.; Biroccio, A. Telomere Damage Induced by the G-Quadruplex Ligand RHPS4 has an Antitumor Effect. *J. Clin. Investig.* **2007,** *117,* 3236–3247.
99. Rizzo, A.; Salvati, E.; Porru, M.; D'Angelo, C.; Stevens, M. F.; D'Incalci, M.; Leonetti, C.; Gilson, E.; Zupi, G.; Biroccio, A. Stabilization of Quadruplex DNA Perturbs Telomere Replication Leading to the Activation of an ATR-Dependent ATM Signaling Pathway. *Nucleic Acids Res.* **2009,** *37,* 5353–5364.
100. Salvati, E.; Scarsella, M.; Porru, M.; Rizzo, A.; Iachettini, S.; Tentori, L.; Graziani, G.; D'Incalci, M.; Stevens, M. F. G.; Orlandi, A.; Passeri, D.; Gilson, E.; Zupi, G.; Leonetti, C.; Biroccio, A. PARP1 is Activated at Telomeres Upon G4 Stabilization: Possible Target for Telomere-Based Therapy. *Oncogene* **2010,** *29,* 6280–6293.
101. Parkinson, G. N.; Lee, M. P. H.; Neidle, S. Crystal Structure of Parallel Quadruplexes From Human Telomeric DNA. *Nature* **2002,** *417,* 876–880.
102. Wang, Y.; Patel, D. J. Solution Structure of the Human Telomeric Repeat $d[AG_3(T_2AG_3)_3]$ G-Tetraplex. *Structure* **1993,** *1,* 263–282.
103. Phan, A. T.; Patel, D. J. Two-Repeat Human Telomeric d(TAGGGTTAGGGT) Sequence Forms Interconverting Parallel and Antiparallel G-Quadruplexes in Solution: Distinct Topologies, Thermodynamic Properties, and Folding/Unfolding Kinetics. *J. Am. Chem. Soc.* **2003,** *125,* 15021–15027.
104. Ambrus, A.; Chen, D.; Dai, J.; Bialis, T.; Jones, R. A.; Yang, D. Human Telomeric Sequence Forms a Hybrid-Type Intramolecular G-Quadruplex Structure With Mixed Parallel/Antiparallel Strands in Potassium Solution. *Nucleic Acids Res.* **2006,** *34,* 2723–2735.
105. Dai, J.; Carver, M.; Punchihewa, C.; Jones, R. A.; Yang, D. Structure of the Hybrid-2 Type Intramolecular Human Telomeric G-Quadruplex in K^+ Solution: Insights Into Structure Polymorphism of the Human Telomeric Sequence. *Nucleic Acids Res.* **2007,** *35,* 4927–4940.
106. Luu, K. N.; Phan, A. T.; Kuryavyi, V.; Lacroix, L.; Patel, D. J. Structure of the Human Telomere in K^+ Solution: An Intramolecular (3 + 1) G-Quadruplex Scaffold. *J. Am. Chem. Soc.* **2006,** *128,* 9963–9970.
107. Lim, K. W.; Amrane, S.; Bouaziz, S.; Xu, W.; Mu, Y.; Patel, D. J.; Luu, K. N.; Phan, A. T. Structure of the Human Telomere in K^+ Solution: A Stable Basket-Type G-Quadruplex With Only two G-Tetrad Layers. *J. Am. Chem. Soc.* **2009,** *131,* 4301–4309.
108. Phan, A. T.; Kuryavyi, V.; Luu, K. N.; Patel, D. J. Structure of Two Intramolecular G-Quadruplexes Formed by Natural Human Telomere Sequences in K^+ Solution. *Nucleic Acids Res.* **2007,** *35,* 6517–6525.
109. Heddi, B.; Phan, A. T. Structure of Human Telomeric DNA in Crowded Solution. *J. Am. Chem. Soc.* **2013,** *133,* 9824–9833.
110. Renčiuk, D.; Kejnovská, I.; Školáková, P.; Bednářová, K.; Motlová, J.; Vorlíčková, M. Arrangements of Human Telomere DNA Quadruplex in Physiologically Relevant K^+ Solutions. *Nucleic Acids Res.* **2009,** *37,* 6625–6634.
111. Haider, S. M.; Autiero, I.; Neidle, S. Surface Area Accessibility and the Preferred Topology of Telomeric DNA Quadruplex-Ligand Complexes. *Biochimie* **2011,** *93,* 1275–1279.
112. Kuryavyi, V.; Phan, A. T.; Patel, D. J. Solution Structures of All Parallel-Stranded Monomeric and Dimeric G-Quadruplex Scaffolds of the Human c-kit2 Promoter. *Nucleic Acids Res.* **2010,** *38,* 6757–6773.
113. Hsu, S. T.; Varnai, P.; Bugaut, A.; Reszka, A. P.; Neidle, S.; Balasubramanian, S. A G-Rich Sequence Within the c-Kit Oncogene Promoter Forms a Parallel G-Quadruplex Having Asymmetric G-Tetrad Dynamics. *J. Am. Chem. Soc.* **2009,** *131,* 13399–13409.
114. Todd, A. K.; Haider, S. M.; Parkinson, G. N.; Neidle, S. Sequence Occurrence and Structural Uniqueness of a G-Quadruplex in the Human *c-Kit* Promoter. *Nucleic Acids Res.* **2007,** *35,* 5799–5808.
115. Warner, K. D.; Chen, M. C.; Song, W.; Strack, R. L.; Thorn, A.; Jaffrey, S. R.; Ferré-D'Amaré, A. R. Structural Basis for Activity of Highly Efficient RNA Mimics of Green Fluorescent Protein. *Nat. Struct. Mol. Biol.* **2014,** *21,* 658–663.
116. Huang, H.; Suslov, N. B.; Li, N. S.; Shelke, S. A.; Evans, M. E.; Koldobskaya, Y.; Rice, P. A.; Piccirilli, J. A. A G-Quadruplex-Containing RNA Activates Fluorescence in a GFP-Like Fluorophore. *Nat. Chem. Biol.* **2014,** *10,* 686–691.
117. Parkinson, G. N.; Ghosh, R.; Neidle, S. Structural Basis for Binding of Porphyrin to Human Telomeres. *Biochemistry* **2007,** *46,* 2390–2397.
118. Campbell, N. H.; Parkinson, G. N.; Reszka, A. P.; Neidle, S. Structural Basis of DNA Quadruplex Recognition by an Acridine Drug. *J. Am. Chem. Soc.* **2008,** *130,* 6722–6724.
119. Collie, G. W.; Promontorio, R.; Hampel, S. M.; Micco, M.; Neidle, S.; Parkinson, G. N. Structural Basis for Telomeric G-Quadruplex Naphthalene Diimide Ligand Targeting. *J. Am. Chem. Soc.* **2012,** *134,* 2723–2731.
120. Collie, G. W.; Haider, S.; Neidle, S.; Parkinson, G. N. A Crystallographic and Modelling Study of a Human Telomeric RNA (TERRA) Quadruplex. *Nucleic Acids Res.* **2010,** *38,* 5569–5580.
121. Collie, G. W.; Sparapani, S.; Parkinson, G. N.; Neidle, S. Structural Basis of Telomeric RNA Quadruplex-Acridine Ligand Recognition. *J. Am. Chem. Soc.* **2011,** *133,* 2721–2728.
122. Campbell, N. H.; Karim, N. H.; Parkinson, G. N.; Gunaratnam, M.; Petrucci, V.; Todd, A. K.; Vilar, R.; Neidle, S. Molecular Basis of Structure-Activity Relationships Between Salphen Metal Complexes and Human Telomeric DNA Quadruplexes. *J. Med. Chem.* **2012,** *55,* 209–222.
123. Micco, M.; Collie, G. W.; Dale, A. G.; Ohnmacht, S. A.; Pazitna, I.; Gunaratnam, M.; Reszka, A. P.; Neidle, S. Structure-Based Design and Evaluation of Naphthalene Diimide G-Quadruplex Ligands as Telomere Targeting Agents in Pancreatic Cancer Cells. *J. Med. Chem.* **2013,** *56,* 2959–2974.
124. Bazzicalupi, C.; Ferraroni, M.; Bilia, A. R.; Scheggi, F.; Gratteri, P. The Crystal Structure of Human Telomeric DNA Complexed With Berberine: An Interesting Case of Stacked Ligand to G-Tetrad Ratio Higher Than 1:1. *Nucleic Acids Res.* **2012,** *41,* 632–638.
125. Nicoludis, J. M.; Miller, S. T.; Jeffrey, P. D.; Barrett, S. P.; Rablen, P. R.; Lawton, T. J.; Yatsunyk, L. A. Optimized End-Stacking Provides Specificity of N-Methyl Mesoporphyrin IX for Human Telomeric G-Quadruplex DNA. *J. Am. Chem. Soc.* **2012,** *134,* 20446–20456.
126. Chung, W. J.; Heddi, B.; Hamon, F.; Teulade-Fichou, M.-P.; Phan, A. T. Solution Structure of a G-Quadruplex Bound to the Bisquinolinium Compound Phen-DC(3). *Angew. Chem. Int. Ed. Engl.* **2014,** *53,* 999–1002.
127. Dai, J.; Carver, M.; Hurley, L. H.; Yang, D. Solution Structure of a 2:1 Quindoline-c-MYC G-Quadruplex: Insights Into G-Quadruplex-Interactive Small Molecule Drug Design. *J. Am. Chem. Soc.* **2011,** *133,* 17673–17680.
128. Chung, W. J.; Heddi, B.; Tera, M.; Iida, K.; Nagasawa, K.; Phan, A. T. Solution Structure of an Intramolecular (3 + 1) Human Telomeric G-Quadruplex Bound to a Telomestatin Derivative. *J. Am. Chem. Soc.* **2013,** *135,* 13495–13501.
129. Parkinson, G. N.; Cuenca, F.; Neidle, S. Topology Conservation and Loop Flexibility in Quadruplex-Drug Recognition: Crystal Structures of Inter- and Intramolecular Telomeric DNA Quadruplex-Drug Complexes. *J. Mol. Biol.* **2008,** *381,* 1145–1156.
130. Martadinata, H.; Phan, A. T. Structure of Propeller-Type Parallel-Stranded RNA G-Quadruplexes, Formed by Human Telomeric RNA Sequences in K^+ Solution. *J. Am. Chem. Soc.* **2009,** *131,* 2570–2578.
131. Collie, G. W.; Campbell, N. H.; Neidle, S. Loop Flexibility in Human Telomeric Quadruplex Small-Molecule Complexes. *Nucleic Acids Res.* **2015,** *43,* 4785–4799.
132. Ma, D. L.; Ma, V. P.; Chan, D. S.; Leung, K. H.; Zhong, H. J.; Leung, C. H. In Silico Screening of Quadruplex-Binding Ligands. *Methods* **2012,** *57,* 106–114.

133. Cosconati, S.; Marinelli, L.; Trotta, R.; Virno, A.; Mayol, L.; Novellino, E.; Olson, A. J.; Randazzo, A. Tandem Application of Virtual Screening and NMR Experiments in the Discovery of Brand new DNA Quadruplex Groove Binders. *J. Am. Chem. Soc.* **2009,** *131,* 16336–16337.
134. Cosconati, S.; Marinelli, L.; Trotta, R.; Virno, A.; De Tito, S.; Romagnoli, R.; Pagano, B.; Limongelli, V.; Giancola, C.; Baraldi, P. G.; Mayol, L.; Novellino, E.; Randazzo, A. Structural and Conformational Requisites in DNA Quadruplex Groove Binding: Another Piece to the Puzzle. *J. Am. Chem. Soc.* **2010,** *132,* 6425–6433.
135. Alcaro, S.; Musetti, C.; Distinto, S.; Casatti, M.; Zagotto, G.; Artese, A.; Parrotta, L.; Moraca, F.; Costa, G.; Ortuso, F.; Maccioni, E.; Sissi, C. Identification and Characterization of New DNA G-Quadruplex Binders Selected by a Combination of Ligand and Structure-Based Virtual Screening Approaches. *J. Med. Chem.* **2013,** *56,* 843–855.
136. Di Leva, F. S.; Zizza, P.; Cingolani, C.; D'Angelo, C.; Pagano, B.; Amato, J.; Salvati, E.; Sissi, C.; Pinato, O.; Marinelli, L.; Cavalli, A.; Cosconati, S.; Novellino, E.; Randazzo, A.; Biroccio, A. Exploring the Chemical Space of G-Quadruplex Binders: Discovery of a Novel Chemotype Targeting the Human Telomeric Sequence. *J. Med. Chem.* **2013,** *56,* 9646–9654.
137. Husby, J.; Todd, A. K.; Platts, J. A.; Neidle, S. Small-Molecule G-Quadruplex Interactions: Systematic Exploration of Conformational Space Using Multiple Molecular Dynamics. *Biopolymers* **2013,** *99,* 989–1005.
138. Greider, C. W.; Blackburn, E. H. Identification of a Specific Telomere Terminal Transferase Activity in *Tetrahymena* Extracts. *Cell* **1985,** *43,* 405–413.
139. Kim, N. W.; Piatyszek, M. A.; Prowse, K. R.; Harley, C. B.; West, M. D.; Ho, P. L.; Corviello, G. M.; Wright, W. E.; Weinrich, S. L.; Shay, J. W. Specific Association of Human Telomerase Activity With Immortal Cells and Cancer. *Science* **1994,** *266,* 2011–2015.
140. Counter, C. M.; Hirte, H. W.; Bacchetti, S.; Harley, C. B. Telomerase Activity in Human Ovarian Carcinoma. *Proc. Natl. Acad. Sci. U. S. A.* **1994,** *91,* 2900–2904.
141. Sekaran, V.; Soares, J.; Jarstfer, M. B. Telomere Maintenance as a Target for Drug Discovery. *J. Med. Chem.* **2014,** *57,* 521–538.
142. Zahler, A. M.; Williamson, J. R.; Cech, T. R.; Prescott, D. M. Inhibition of Telomerase by G-Quartet DNA Structures. *Nature* **1991,** *350,* 718–750.
143. Sun, D.; Thompson, B.; Cathers, B. E.; Salazar, M.; Kerwin, S. M.; Trent, J. O.; Jenkins, T. C.; Neidle, S.; Hurley, L. H. Inhibition of Human Telomerase by a G-Quadruplex-Interactive Compound. *J. Med. Chem.* **1997,** *40,* 2113–2116.
144. Zaug, A. J.; Podell, E. R.; Cech, T. R. Human POT1 Disrupts Telomeric G-Quadruplexes Allowing Telomerase Extension In Vitro. *Proc. Natl. Acad. Sci. U. S. A.* **2005,** *102,* 10864–10869.
145. Jacobs, J. J.; de Lange, T. p16INK4a as a Second Effector of the Telomere Damage Pathway. *Cell Cycle* **2005,** *4,* 1364–1368.
146. Salama, R.; Sadaie, M.; Hoare, M.; Narita, M. Cellular Senescence and Its Effector Programs. *Genes Dev.* **2014,** *28,* 99–114.
147. Riou, J.-F.; Guittat, L.; Mailliet, P.; Laoui, A.; Renou, E.; Petitgenet, O.; Mégnin-Chanet, F.; Hélène, C.; Mergny, J.-L. Cell Senescence and Telomere Shortening Induced by a New Series of Specific G-Quadruplex DNA Ligands. *Proc. Natl. Acad. Sci. U. S. A.* **2002,** *99,* 2672–2677.
148. Incles, C. M.; Schultes, C. M.; Kempski, H.; Koehler, H.; Kelland, L. R.; Neidle, S. A G-Quadruplex Telomere Targeting Agent Produces p16-Associated Senescence and Chromosomal Fusions in Human Prostate Cancer Cells. *Mol. Cancer Ther.* **2004,** *3,* 1201–1206.
149. Taka, T.; Huang, L.; Wongnoppavich, A.; Tam-Chang, S. W.; Lee, T. R.; Tuntiwechapikul, W. Telomere Shortening and Cell Senescence Induced by Perylene Derivatives in A549 Human Lung Cancer Cells. *Bioorg. Med. Chem.* **2013,** *21,* 883–890.
150. Burger, A. M.; Dai, F.; Schultes, C. M.; Reszka, A. P.; Moore, M. J.; Double, J. A.; Neidle, S. The G-Quadruplex-Interactive Molecule BRACO-19 Inhibits Tumor Growth, Consistent With Telomere Targeting and Interference With Telomerase Function. *Cancer Res.* **2005,** *65,* 1489–1496.
151. Hahn, W. C.; Stewart, S. A.; Brooks, M. W.; York, S. G.; Eaton, E.; Kurachi, A.; Beijersbergen, R. L.; Knoll, J. H. M.; Meyerson, M.; Weinberg, R. A. Inhibition of Telomerase Limits the Growth of Human Cancer Cells. *Nat. Med.* **1999,** *10,* 1164–1170.
152. Müller, S.; Sanders, D. A.; Di Antonio, M.; Matsis, S.; Riou, J.-F.; Rodriguez, R.; Balasubramanian, S. Pyridostatin Analogues Promote Telomere Dysfunction and Long-Term Growth Inhibition in Human Cancer Cells. *Org. Biomol. Chem.* **2012,** *10,* 6537–6546.
153. Rohban, S.; Campaner, S. Myc Induced Replicative Stress Response: How to Cope With it and Exploit It. *Biochim. Biophys. Acta, Gene Regul. Mech.* **2015,** *1849* (5), 517–524.
154. Ciriello, G.; Miller, M. L.; Aksoy, B. A.; Senbabaoglu, Y.; Schultz, N.; Sander, C. Emerging Landscape of Oncogenic Signatures Across Human Cancers. *Nat. Genet.* **2013,** *45* (10), 1127–1133.
155. Dalla-Favera, R.; Bregni, M.; Erikson, J.; Patterson, D.; Gallo, R. C.; Croce, C. M. Human c-MYC onc Gene is Located on the Region of Chromosome 8 That is Translocated in Burkitt Lymphoma Cells. *Proc. Natl. Acad. Sci. U. S. A.* **1982,** *79* (24), 7824–7827.
156. Wahlstrom, T.; Henriksson, M. A. Impact of MYC in Regulation of Tumor Cell Metabolism. *Biochim. Biophys. Acta, Gene Regul. Mech.* **2015,** *1849* (5), 563–569.
157. Tu, W. B.; Helander, S.; Pilstal, R.; Hickman, K. A.; Lourenco, C.; Jurisica, I.; Raught, B.; Wallner, B.; Sunnerhagen, M.; Penn, L. Z. Myc and Its Interactors Take Shape. *Biochim. Biophys. Acta, Gene Regul. Mech.* **2015,** *1849* (5), 469–483.
158. Chen, B. J.; Wu, Y. L.; Tanaka, Y.; Zhang, W. Small Molecules Targeting c-MYC Oncogene: Promising Anti-Cancer Therapeutics. *Int. J. Biol. Sci.* **2014,** *10* (10), 1084–1096.
159. Dexheimer, T. S.; Carey, S. S.; Zuohe, S.; Gokhale, V. M.; Hu, X.; Murata, L. B.; Maes, E. M.; Weichsel, A.; Sun, D.; Meuillet, E. J.; Montfort, W. R.; Hurley, L. H. While NM23-H2 May Play an Indirect Role in Transcriptional Activation of c-MYC Gene Expression, It Does Not Cleave the NHE III(1) Element. *Mol. Cancer Ther.* **2009,** *8* (5), 1363–1377.
160. Duan, W.; Rangan, A.; Vankayalapati, H.; Kim, M. Y.; Zeng, Q.; Sun, D.; Han, H.; Fedoroff, O. Y.; Nishioka, D.; Rha, S. Y.; Izbicka, E.; Von Hoff, D. D.; Hurley, L. H. Design and Synthesis of Fluoroquinophenoxazines That Interact With Human Telomeric G-Quadruplexes and Their Biological Effects. *Mol. Cancer Ther.* **2001,** *1* (2), 103–120.
161. Drygin, D.; Siddiqui-Jain, A.; O'Brien, S.; Schwaebe, M.; Lin, A.; Bliesath, J.; Ho, C. B.; Proffitt, C.; Trent, K.; Whitten, J. P.; Lim, J. K. C.; Von Hoff, D.; Anderes, K.; Rice, W. G. Anticancer Activity of CX-3543: A Direct Inhibitor of rRNA Biogenesis. *Cancer Res.* **2009,** *69* (19), 7653–7661.
162. Daniely, Y.; Borowiec, J. A. Formation of a Complex Between Nucleolin and Replication Protein a After Cell Stress Prevents Initiation of DNA Replication. *J. Cell Biol.* **2000,** *149* (4), 799–809.
163. Daniely, Y.; Dimitrova, D. D.; Borowiec, J. A. Stress-Dependent Nucleolin Mobilization Mediated by p53-Nucleolin Complex Formation. *Mol. Cell. Biol.* **2002,** *22* (16), 6014–6022.
164. Wang, Y. Z.; Guan, J.; Wang, H. Y.; Wang, Y.; Leeper, D.; Iliakis, G. Regulation of DNA Replication After Heat Shock by Replication Protein A-Nucleolin Interactions. *J. Biol. Chem.* **2001,** *276* (23), 20579–20588.
165. Saxena, A.; Rorie, C. J.; Dimitrov, D.; Daniely, Y.; Borowiec, J. A. Nucleolin Inhibits Hdm2 by Multiple Pathways Leading to p53 Stabilization. *Oncogene* **2006,** *25* (55), 7274–7288.
166. Ugrinova, I.; Monier, K.; Ivaldi, C.; Thiry, M.; Storck, S.; Mongelard, F.; Bouvet, P. Inactivation of Nucleolin Leads to Nucleolar Disruption, Cell Cycle Arrest and Defects in Centrosome Duplication. *BMC Mol. Biol.* **2007,** *8,* 66.
167. Gonzalez, V.; Guo, K.; Hurley, L.; Sun, D. Identification and Characterization of Nucleolin as a c-MYC G-Quadruplex-Binding Protein. *J. Biol. Chem.* **2009,** *284* (35), 23622–23635.
168. Su, L. J.; Zheng, H. Q.; Li, Z.; Qiu, J.; Chen, S. Q.; Liu, J. G.; Ou, T. M.; Tan, J. H.; Gu, L. Q.; Huang, Z. S.; Li, D. Mechanistic Studies on the Anticancer Activity of 2,4-Disubstituted Quinazoline Derivative. *Biochim. Biophys. Acta, Gen. Subj.* **2014,** *1840* (10), 3123–3130.
169. Shan, C.; Lin, J.; Hou, J. Q.; Liu, H. Y.; Chen, S. B.; Chen, A. C.; Ou, T. M.; Tan, J. H.; Li, D.; Gu, L. Q.; Huang, Z. S. Chemical Intervention of the NM23-H2 Transcriptional Programme on c-MYC via a Novel Small Molecule. *Nucleic Acids Res.* **2015,** *43* (14), 6677–6691.
170. Ou, T. M.; Lu, Y. J.; Zhang, C.; Huang, Z. S.; Wang, X. D.; Tan, J. H.; Chen, Y.; Ma, D. L.; Wong, K. Y.; Tang, J. C. O.; Chan, A. S. C.; Gu, L. Q. Stabilization of G-Quadruplex DNA and Down-Regulation of Oncogene c-MYC by Quindoline Derivatives. *J. Med. Chem.* **2007,** *50* (7), 1465–1474.
171. Ou, T. M.; Lin, J.; Lu, Y. J.; Hou, J. Q.; Tan, J. H.; Chen, S. H.; Li, Z.; Li, Y. P.; Li, D.; Gu, L. Q.; Huang, Z. S. Inhibition of Cell Proliferation by Quindoline Derivative (SYUIQ-05) Through Its Preferential Interaction With c-MYC Promoter G-Quadruplex. *J. Med. Chem.* **2011,** *54* (16), 5671–5679.
172. Kang, H. J.; Park, H. J. In Silico Identification of Novel Ligands for G-Quadruplex in the c-MYC Promoter. *J. Comput. Aid. Mol. Des.* **2015,** *29* (4), 339–348.

173. Ma, D. L.; Chan, D. S. H.; Fu, W. C.; He, H. Z.; Yang, H.; Yan, S. C.; Leung, C. H. Discovery of a Natural Product-Like c-MYC G-Quadruplex DNA Groove-Binder by Molecular Docking. *PLos One* **2012,** *7,* e43278.
174. Nagesh, N.; Raju, G.; Srinivas, R.; Ramesh, P.; Reddy, M. D.; Reddy, C. R. A Dihydroindolizino Indole Derivative Selectively Stabilizes G-Quadruplex DNA and Down-Regulates c-MYC Expression in Human Cancer Cells. *Biochim. Biophys. Acta, Gen. Subj.* **2015,** *1850* (1), 129–140.
175. Panda, D.; Debnath, M.; Mandal, S.; Bessi, I.; Schwalbe, H.; Dash, J. A Nucleus-Imaging Probe That Selectively Stabilizes a Minor Conformation of c-MYC G-Quadruplex and Down-Regulates c-MYC Transcription in Human Cancer Cells. *Sci. Rep.* **2015,** *5,* 13183.
176. Wang, L. H.; Wei, C. Y. Spectroscopic and Biological Studies of Phenanthroline Compounds: Selective Recognition of Gene-Promoter G-Quadruplex DNAs Preferred Over Duplex DNA. *Chem. Biodivers.* **2013,** *10* (6), 1154–1164.
177. Wei, C.; Wang, Y.; Zhang, M. Synthesis and Binding Studies of Novel Di-Substituted Phenanthroline Compounds With Genomic Promoter and Human Telomeric DNA G-Quadruplexes. *Org. Biomol. Chem.* **2013,** *11* (14), 2355–2364.
178. Li, H. Q.; Wei, C. Y. Mechanism Studies on Anti-HepG2 Cell Proliferation of Phenanthroline Derivatives as G-Quadruplex DNA Stabilizers. *Bioorg. Med. Chem. Lett.* **2015,** *25* (18), 3798–3803.
179. Felsenstein, K. M.; Saunders, L. B.; Simmons, J. K.; Leon, E.; Calabrese, D. R.; Zhang, S. L.; Michalowski, A.; Gareiss, P.; Mock, B. A.; Schneekloth, J. S. Small Molecule Microarrays Enable the Identification of a Selective, Quadruplex-Binding Inhibitor of MYC Expression. *ACS Chem. Biol.* **2016,** *11* (1), 139–148.
180. Palumbo, S. L.; Ebbinghaus, S. W.; Hurley, L. H. Formation of a Unique End-to-End Stacked Pair of G-Quadruplexes in the hTERT Core Promoter With Implications for Inhibition of Telomerase by G-Quadruplex-Interactive Ligands. *J. Am. Chem. Soc.* **2009,** *131* (31), 10878–10891.
181. Grand, C. L.; Han, H. Y.; Munoz, R. M.; Weitman, S.; Von Hoff, D. D.; Hurley, L. H.; Bearss, D. J. The Cationic Porphyrin TMPyP4 Down-Regulates c-MYC and Human Telomerase Reverse Transcriptase Expression and Inhibits Tumor Growth In Vivo. *Mol. Cancer Ther.* **2002,** *1* (8), 565–573.
182. Gomez, D.; Lemarteleur, T.; Lacroix, L.; Mailliet, P.; Mergny, J. L.; Riou, J. F. Telomerase Downregulation Induced by the G-Quadruplex Ligand 12459 in A549 Cells is Mediated by hTERT RNA Alternative Splicing. *Nucleic Acids Res.* **2004,** *32* (1), 371–379.
183. Merle, P.; Evrard, B.; Petitjean, A.; Lehn, J. M.; Teulade-Fichou, M. P.; Chautard, E.; De Cian, A.; Guittat, L.; Tran, P. L. T.; Mergny, J. L.; Verrelle, P.; Tchirkov, A. Telomere Targeting With a New G4 Ligand Enhances Radiation-Induced Killing of Human Glioblastoma Cells. *Mol. Cancer Ther.* **2011,** *10* (10), 1784–1795.
184. Miyazaki, T.; Pan, Y.; Joshi, K.; Purohit, D.; Hu, B.; Demir, H.; Mazumder, S.; Okabe, S.; Yamori, T.; Viapiano, M.; Shin-ya, K.; Seimiya, H.; Nakano, I. Telomestatin Impairs Glioma Stem Cell Survival and Growth Through the Disruption of Telomeric G-Quadruplex and Inhibition of the Proto-Oncogene, c-Myb. *Clin. Cancer Res.* **2012,** *18* (5), 1268–1280.
185. Doria, F.; Nadai, M.; Folini, M.; Di Antonio, M.; Germani, L.; Percivalle, C.; Sissi, C.; Zaffaroni, N.; Alcaro, S.; Artese, A.; Richter, S. N.; Freccero, M. Hybrid Ligand-Alkylating Agents Targeting Telomeric G-Quadruplex Structures. *Org. Biomol. Chem.* **2012,** *10* (14), 2798–2806.
186. Nadai, M.; Cimino-Reale, G.; Sattin, G.; Doria, F.; Butovskaya, E.; Zaffaroni, N.; Freccero, M.; Palumbo, M.; Richter, S. N.; Folini, M. Assessment of Gene Promoter G-Quadruplex Binding and Modulation by a Naphthalene Diimide Derivative in Tumor Cells. *Int. J. Oncol.* **2015,** *46* (1), 369–380.
187. Krens, L. L.; Baas, J. M.; Gelderblom, H.; Guchelaar, H. J. Therapeutic Modulation of k-Ras Signaling in Colorectal Cancer. *Drug Discov. Today* **2010,** *15* (13–14), 502–516.
188. Cox, A. D.; Fesik, S. W.; Kimmelman, A. C.; Luo, J.; Der, C. J. Drugging the Undruggable RAS: Mission Possible? *Nat. Rev. Drug Discov.* **2014,** *13* (11), 828–851.
189. Dunn, E. F.; Iida, M.; Myers, R. A.; Campbell, D. A.; Hintz, K. A.; Armstrong, E. A.; Li, C.; Wheeler, D. L. Dasatinib Sensitizes KRAS Mutant Colorectal Tumors to Cetuximab. *Oncogene* **2011,** *30* (5), 561–574.
190. Cogoi, S.; Xodo, L. E. G-Quadruplex Formation Within the Promoter of the KRAS Proto-Oncogene and Its Effect on Transcription. *Nucleic Acids Res.* **2006,** *34* (9), 2536–2549.
191. Morgan, R. K.; Batra, H.; Gaerig, V. C.; Hockings, J.; Brooks, T. A. Identification and Characterization of a New G-Quadruplex Forming Region Within the kRAS Promoter as a Transcriptional Regulator. *Biochim. Biophys. Acta, Gene Regul. Mech.* **2016,** *1859* (2), 235–245.
192. Cogoi, S.; Paramasivam, M.; Filichev, V.; Geci, I.; Pedersen, E. B.; Xodo, L. E. Identification of a New G-Quadruplex Motif in the KRAS Promoter and Design of Pyrene-Modified G4-Decoys With Antiproliferative Activity in Pancreatic Cancer Cells. *J. Med. Chem.* **2009,** *52* (2), 564–568.
193. Paramasivam, M.; Cogoi, S.; Xodo, L. E. Primer Extension Reactions as a Tool to Uncover Folding Motifs Within Complex G-Rich Sequences: Analysis of the Human KRAS NHE. *Chem. Commun. (Camb.)* **2011,** *47* (17), 4965–4967.
194. Cogoi, S.; Shchekotikhin, A. E.; Xodo, L. E. HRAS is Silenced by Two Neighboring G-Quadruplexes and Activated by MAZ, a Zinc-Finger Transcription Factor With DNA Unfolding Property. *Nucleic Acids Res.* **2014,** *42* (13), 8379–8388.
195. Faudale, M.; Cogoi, S.; Xodo, L. E. Photoactivated Cationic Alkyl-Substituted Porphyrin Binding to g4-RNA in the 5 '-UTR of KRAS Oncogene Represses Translation. *Chem. Commun.* **2012,** *48* (6), 874–876.
196. Bugaut, A.; Rodriguez, R.; Kumari, S.; Hsu, S. T.; Balasubramanian, S. Small Molecule-Mediated Inhibition of Translation by Targeting a Native RNA G-Quadruplex. *Org. Biomol. Chem.* **2010,** *8* (12), 2771–2776.
197. Lavrado, J.; Brito, H.; Borralho, P. M.; Ohnmacht, S. A.; Kim, N. S.; Leitao, C.; Pisco, S.; Gunaratnam, M.; Rodrigues, C. M.; Moreira, R.; Neidle, S.; Paulo, A. KRAS Oncogene Repression in Colon Cancer Cell Lines by G-Quadruplex Binding Indolo[3,2-c]Quinolines. *Sci. Rep.* **2015,** *5,* 9696.
198. Rapozzi, V.; Zorzet, S.; Zacchigna, M.; Della Pietra, E.; Cogoi, S.; Xodo, L. E. Anticancer Activity of Cationic Porphyrins in Melanoma Tumour-Bearing Mice and Mechanistic In Vitro Studies. *Mol. Cancer* **2014,** *13,* 75.
199. Membrino, A.; Paramasivam, M.; Cogoi, S.; Alzeer, J.; Luedtke, N. W.; Xodo, L. E. Cellular Uptake and Binding of Guanidine-Modified Phthalocyanines to KRAS/HRAS G-Quadruplexes. *Chem. Commun.* **2010,** *46* (4), 625–627.
200. Cogoi, S.; Shchekotikhin, A. E.; Membrino, A.; Sinkevich, Y. B.; Xodo, L. E. Guanidino Anthrathiophenediones as G-Quadruplex Binders: Uptake, Intracellular Localization, and Anti-Harvey-ras Gene Activity in Bladder Cancer Cells. *J. Med. Chem.* **2013,** *56* (7), 2764–2778.
201. Cogoi, S.; Zorzet, S.; Shchekotilthin, A. E.; Xodo, L. E. Potent Apoptotic Response Induced by Chloroacetamidine Anthrathiophenediones in Bladder Cancer Cells. *J. Med. Chem.* **2015,** *58* (14), 5476–5485.
202. Lavrado, J.; Borralho, P. M.; Ohnmacht, S. A.; Castro, R. E.; Rodrigues, C. M. P.; Moreira, R.; dos Santos, D. J. V. A.; Neidle, S.; Paulo, A. Synthesis, G-Quadruplex Stabilisation, Docking Studies, and Effect on Cancer Cells of Indolo[3,2-b]Quinolines With One, two, or Three Basic Side Chains. *Chemmedchem* **2013,** *8* (10), 1648–1661.
203. Brito, H.; Martins, A. C.; Lavrado, J.; Mendes, E.; Francisco, A. P.; Santos, S. A.; Ohnmacht, S. A.; Kim, N. S.; Rodrigues, C. M. P.; Moreira, R.; Neidle, S.; Borralho, P. M.; Paulo, A. Targeting KRAS Oncogene in Colon Cancer Cells With 7-Carboxylate Indolo[3,2-b]Quinoline tri-Alkylamine Derivatives. *PLos One* **2015,** *10* (5), e126891.
204. Lavrado, J.; Ohnmacht, S. A.; Correia, I.; Leitao, C.; Pisco, S.; Gunaratnam, M.; Moreira, R.; Neidle, S.; dos Santos, D. J. V. A.; Paulo, A. Indolo[3,2-c]Quinoline G-Quadruplex Stabilizers: A Structural Analysis of Binding to the Human Telomeric G-Quadruplex. *Chemmedchem* **2015,** *10* (5), 836–849.
205. Inoue, M.; Hager, J. H.; Ferrara, N.; Gerber, H. P.; Hanahan, D. VEGF-A Has a Critical, Nonredundant Role in Angiogenic Switching and Pancreatic Beta Cell Carcinogenesis. *Cancer Cell* **2002,** *1* (2), 193–202.
206. Ferrara, N.; Gerber, H. P.; LeCouter, J. The Biology of VEGF and Its Receptors. *Nat. Med.* **2003,** *9* (6), 669–676.
207. Olsson, A. K.; Dimberg, A.; Kreuger, J.; Claesson-Welsh, L. VEGF Receptor Signalling—In Control of Vascular Function. *Nat. Rev. Mol. Cell Biol.* **2006,** *7* (5), 359–371.
208. Sitohy, B.; Nagy, J. A.; Dvorak, H. F. Anti-VEGF/VEGFR Therapy for Cancer: Reassessing the Target. *Cancer Res.* **2012,** *72* (8), 1909–1914.
209. Loureiro, R. M. B.; D'Amore, P. A. Transcriptional Regulation of Vascular Endothelial Growth Factor in Cancer. *Cytokine Growth Factor Rev.* **2005,** *16* (1), 77–89.
210. Sun, D.; Liu, W. J.; Guo, K.; Rusche, J. J.; Ebbinghaus, S.; Gokhale, V.; Hurley, L. H. The Proximal Promoter Region of the Human Vascular Endothelial Growth Factor Gene has a G-Quadruplex Structure That Can Be Targeted by G-Quadruplex-Interactive Agents. *Mol. Cancer Ther.* **2008,** *7* (4), 880–889.
211. Sun, D. Y.; Guo, K. X.; Rusche, J. J.; Hurley, L. H. Facilitation of a Structural Transition in the Polypurine/Polypyrimidine Tract Within the Proximal Promoter Region of the Human VEGF Gene by the Presence of Potassium and G-Quadruplex-Interactive Agents. *Nucleic Acids Res.* **2005,** *33* (18), 6070–6080.

212. Sun, D. K.; Guo, K. X.; Shin, Y. J. Evidence of the Formation of G-Quadruplex Structures in the Promoter Region of the Human Vascular Endothelial Growth Factor Gene. *Nucleic Acids Res.* **2011,** *39* (4), 1256–1265.
213. Uribe, D. J.; Guo, K.; Shin, Y. J.; Sun, D. Heterogeneous Nuclear Ribonucleoprotein K and Nucleolin as Transcriptional Activators of the Vascular Endothelial Growth Factor Promoter Through Interaction With Secondary DNA Structures. *Biochemistry* **2011,** *50* (18), 3796–3806.
214. Taka, T.; Joonlasak, K.; Huang, L. M.; Lee, T. R.; Chang, S. W. T.; Tuntiwechapikul, W. Down-Regulation of the Human VEGF Gene Expression by Perylene Monoimide Derivatives. *Bioorg. Med. Chem. Lett.* **2012,** *22* (1), 518–522.
215. Wu, Y.; Zan, L. P.; Wang, X. D.; Lu, Y. J.; Ou, T. M.; Lin, J.; Huang, Z. S.; Gu, L. Q. Stabilization of VEGF G-Quadruplex and Inhibition of Angiogenesis by Quindoline Derivatives. *Biochim. Biophys. Acta* **2014,** *1840* (9), 2970–2977.
216. Salvati, E.; Zizza, P.; Rizzo, A.; Iachettini, S.; Cingolani, C.; D'Angelo, C.; Porru, M.; Randazzo, A.; Pagano, B.; Novellino, E.; Pisanu, M. E.; Stoppacciaro, A.; Spinella, F.; Bagnato, A.; Gilson, E.; Leonetti, C.; Biroccio, A. Evidence for G-Quadruplex in the Promoter of Vegfr-2 and Its Targeting to Inhibit Tumor Angiogenesis. *Nucleic Acids Res.* **2014,** *42* (5), 2945–2957.
217. Morris, M. J.; Negishi, Y.; Pazsint, C.; Schonhoft, J. D.; Basu, S. An RNA G-Quadruplex is Essential for Cap-Independent Translation Initiation in Human VEGF IRES. *J. Am. Chem. Soc.* **2010,** *132* (50), 17831–17839.
218. Bhattacharyya, D.; Diamond, P.; Basu, S. An Independently Folding RNA G-Quadruplex Domain Directly Recruits the 40S Ribosomal Subunit. *Biochemistry* **2015,** *54* (10), 1879–1885.
219. Cammas, A.; Dubrac, A.; Morel, B.; Lamaa, A.; Touriol, C.; Teulade-Fichou, M. P.; Prats, H.; Millevoi, S. Stabilization of the G-Quadruplex at the VEGF IRES Represses Cap-Independent Translation. *RNA Biol.* **2015,** *12* (3), 320–329.
220. Yarden, Y.; Kuang, W. J.; Yang-Feng, T.; Coussens, L.; Munemitsu, S.; Dull, T. J.; Chen, E.; Schlessinger, J.; Francke, U.; Ullrich, A. Human Proto-Oncogene c-Kit: A New Cell Surface Receptor Tyrosine Kinase for an Unidentified Ligand. *EMBO J.* **1987,** *6* (11), 3341–3351.
221. Roskoski, R., Jr. Structure and Regulation of Kit Protein-Tyrosine Kinase—The Stem Cell Factor Receptor. *Biochem. Biophys. Res. Commun.* **2005,** *338* (3), 1307–1315.
222. Sakurai, S.; Fukasawa, T.; Chong, J. M.; Tanaka, A.; Fukayama, M. C-Kit Gene Abnormalities in Gastrointestinal Stromal Tumors (Tumors of Interstitial Cells of Cajal). *Jpn. J. Cancer Res.* **1999,** *90* (12), 1321–1328.
223. Tuveson, D. A.; Willis, N. A.; Jacks, T.; Griffin, J. D.; Singer, S.; Fletcher, C. D. M.; Fletcher, J. A.; Demetri, G. D. STI571 Inactivation of the Gastrointestinal Stromal Tumor c-KIT Oncoprotein: Biological and Clinical Implications. *Oncogene* **2001,** *20* (36), 5054–5058.
224. Bejugam, M.; Sewitz, S.; Shirude, P. S.; Rodriguez, R.; Shahid, R.; Balasubramanian, S. Trisubstituted Isoalloxazines as a New Class of G-Quadruplex Binding Ligands: Small Molecule Regulation of c-Kit Oncogene Expression. *J. Am. Chem. Soc.* **2007,** *129* (43), 12926–12927.
225. Cuenca, F.; Greciano, O.; Gunaratnam, M.; Haider, S.; Munnur, D.; Nanjunda, R.; Wilson, W. D.; Neidle, S. Tri- and Tetra-Substituted Naphthalene Diimides as Potent G-Quadruplex Ligands. *Bioorg. Med. Chem. Lett.* **2008,** *18* (5), 1668–1673.
226. Gunaratnam, M.; Swank, S.; Haider, S. M.; Galesa, K.; Reszka, A. P.; Beltran, M.; Cuenca, F.; Fletcher, J. A.; Neidle, S. Targeting Human Gastrointestinal Stromal Tumor Cells With a Quadruplex-Binding Small Molecule. *J. Med. Chem.* **2009,** *52* (12), 3774–3783.
227. McLuckie, K. I. E.; Waller, Z. A. E.; Sanders, D. A.; Alves, D.; Rodriguez, R.; Dash, J.; McKenzie, G. J.; Venkitaraman, A. R.; Balasubramanian, S. G-Quadruplex-Binding Benzo [a]phenoxazines Down-Regulate c-Kit Expression in Human Gastric Carcinoma Cells. *J. Am. Chem. Soc.* **2011,** *133* (8), 2658–2663.
228. Lu, Y. J.; Ou, T. M.; Tan, J. H.; Hou, J. Q.; Shao, W. Y.; Peng, D.; Sun, N.; Wang, X. D.; Wu, W. B.; Bu, X. Z.; Huang, Z. S.; Ma, D. L.; Wong, K. Y.; Gu, L. Q. 5-N-Methylated Quindoline Derivatives as Telomeric G-Quadruplex Stabilizing Ligands: Effects of 5-N Positive Charge on Quadruplex Binding Affinity and Cell Proliferation. *J. Med. Chem.* **2008,** *51* (20), 6381–6392.
229. Shen, F. H.; Jin, J.; Li, J.; Wang, Y.; Zhu, S. H.; Lu, Y. J.; Ou, T. M.; Huang, Z. S.; Huang, M.; Huang, Z. Y. The G-Quadruplex Ligand, SYUIQ-FM05, Targets Proto-Oncogene c-Kit Transcription and Induces Apoptosis in K562 Cells. *Pharm. Biol.* **2013,** *51* (4), 447–454.
230. Bejugam, M.; Gunaratnam, M.; Muller, S.; Sanders, D. A.; Sewitz, S.; Fletcher, J. A.; Neidle, S.; Balasubramanian, S. Targeting the c-Kit Promoter G-Quadruplexes With 6-Substituted Indenoisoquinolines. *ACS Med. Chem. Lett.* **2010,** *1* (7), 306–310.
231. Hou, J. Q.; Tan, J. H.; Wang, X. X.; Chen, S. B.; Huang, S. Y.; Yan, J. W.; Chen, S. H.; Ou, T. M.; Luo, H. B.; Li, D.; Gu, L. Q.; Huang, Z. S. Impact of Planarity of Unfused Aromatic Molecules on G-Quadruplex Binding: Learning From Isaindigotone Derivatives. *Org. Biomol. Chem.* **2011,** *9* (18), 6422–6436.
232. Wang, X. X.; Zhou, C. X.; Yan, J. W.; Hou, J. Q.; Chen, S. B.; Ou, T. M.; Gu, L. Q.; Huang, Z. S.; Tan, J. H. Synthesis and Evaluation of Quinazolone Derivatives as a New Class of c-KIT G-Quadruplex Binding Ligands. *ACS Med. Chem. Lett.* **2013,** *4* (10), 909–914.
233. Rantanen, S.; Monni, O.; Joensuu, H.; Franssila, K.; Knuutila, S. Causes and Consequences of BCL2 Overexpression in Diffuse Large B-Cell Lymphoma. *Leuk. Lymphoma* **2001,** *42* (5), 1089–1098.
234. Cleary, M. L.; Smith, S. D.; Sklar, J. Cloning and Structural-Analysis of Cdnas for Bcl-2 and a Hybrid Bcl-2/Immunoglobulin Transcript Resulting From the T(14–18) Translocation. *Cell* **1986,** *47* (1), 19–28.
235. Akagi, T.; Kondo, E.; Yoshino, T. Expression of Bcl-2 Protein and Bcl-2 Messenger-Rna in Normal and Neoplastic Lymphoid-Tissues. *Leuk. Lymphoma* **1994,** *13* (1–2), 81–87.
236. Joensuu, H.; Pylkkanen, L.; Toikkanen, S. Bcl-2 Protein Expression and Long-Term Survival in Breast-Cancer. *Am. J. Pathol.* **1994,** *145* (5), 1191–1198.
237. Mcdonnell, T. J.; Troncoso, P.; Brisbay, S. M.; Logothetis, C.; Chung, L. W. K.; Hsieh, J. T.; Tu, S. M.; Campbell, M. L. Expression of the Protooncogene Bcl-2 in the Prostate and its Association With Emergence of Androgen-Independent Prostate-Cancer. *Cancer Res.* **1992,** *52* (24), 6940–6944.
238. Tjalma, W.; De Cuyper, E.; Weyler, J.; Van Marck, E.; De Pooter, C.; Albertyn, G.; van Dam, P. Expression of bcl-2 in Invasive and in Situ Carcinoma of the Uterine Cervix. *Am. J. Obstet. Gynecol.* **1998,** *178* (1), 113–117.
239. Baretton, G. B.; Diebold, J.; Christoforis, G.; Vogt, M.; Muller, C.; Dopfer, K.; Schneiderbanger, K.; Schmidt, M.; Lohrs, U. Apoptosis and Immunohistochemical bcl-2 Expression in Colorectal Adenomas and Carcinomas—Aspects of Carcinogenesis and Prognostic Significance. *Cancer* **1996,** *77* (2), 255–264.
240. Pezzella, F.; Turley, H.; Kuzu, I.; Tungekar, M. F.; Dunnill, M. S.; Pierce, C. B.; Harris, A.; Gatter, K. C.; Mason, D. Y. Bcl-2 Protein in Non-Small-Cell Lung-Carcinoma. *New Engl. J. Med.* **1993,** *329* (10), 690–694.
241. Reed, J. C.; Kitada, S.; Takayama, S.; Miyashita, T. Regulation of Chemoresistance by the Bcl-2 Oncoprotein in Non-Hodgkins-Lymphoma and Lymphocytic-Leukemia Cell-Lines. *Ann. Oncol.* **1994,** *5,* S61–S65.
242. Harima, Y.; Harima, K.; Shikata, N.; Oka, A.; Ohnishi, T.; Tanaka, Y. Bax and Bcl-2 Expressions Predict Response to Radiotherapy in Human Cervical Cancer. *J. Cancer Res. Clin. Oncol.* **1998,** *124* (9), 503–510.
243. Oltersdorf, T.; Elmore, S. W.; Shoemaker, A. R.; Armstrong, R. C.; Augeri, D. J.; Belli, B. A.; Bruncko, M.; Deckwerth, T. L.; Dinges, J.; Hajduk, P. J.; Joseph, M. K.; Kitada, S.; Korsmeyer, S. J.; Kunzer, A. R.; Letai, A.; Li, C.; Mitten, M. J.; Nettesheim, D. G.; Ng, S.; Nimmer, P. M.; O'Connor, J. M.; Oleksijew, A.; Petros, A. M.; Reed, J. C.; Shen, W.; Tahir, S. K.; Thompson, C. B.; Tomaselli, K. J.; Wang, B. L.; Wendt, M. D.; Zhang, H. C.; Fesik, S. W.; Rosenberg, S. H. An Inhibitor of Bcl-2 Family Proteins Induces Regression of Solid Tumours. *Nature* **2005,** *435* (7042), 677–681.
244. Enyedy, I. J.; Ling, Y.; Nacro, K.; Tomita, Y.; Wu, X. H.; Cao, Y. Y.; Guo, R. B.; Li, B. H.; Zhu, X. F.; Huang, Y.; Long, Y. Q.; Roller, P. P.; Yang, D. J.; Wang, S. M. Discovery of Small-Molecule Inhibitors of Bcl-2 Through Structure-Based Computer Screening. *J. Med. Chem.* **2001,** *44* (25), 4313–4324.
245. Marshall, J.; Chen, H.; Yang, D.; Figueira, M.; Bouker, K. B.; Ling, Y.; Lippman, M.; Frankel, S. R.; Hayes, D. F. A Phase I Trial of a Bcl-2 Antisense (G3139) and Weekly Docetaxel in Patients With Advanced Breast Cancer and Other Solid Tumors. *Ann. Oncol.* **2004,** *15* (8), 1274–1283.
246. Klasa, R. J.; Gillum, A. M.; Klem, R. E.; Frankel, S. R. Oblimersen bcl-2 Antisense: Facilitating Apoptosis in Anticancer Treatment. *Antisense Nucleic Acid Drug Dev.* **2002,** *12* (3), 193–213.

247. Seto, M.; Jaeger, U.; Hockett, R. D.; Graninger, W.; Bennett, S.; Goldman, P.; Korsmeyer, S. J. Alternative Promoters and Exons, Somatic Mutation and Deregulation of the Bcl-2-Ig Fusion Gene in Lymphoma. *EMBO J.* **1988,** *7* (1), 123–131.
248. Heckman, C.; Mochon, E.; Arcinas, M.; Boxer, L. M. The WT1 Protein Is a Negative Regulator of the Normal Bcl-2 Allele in t(14;18) Lymphomas. *J. Biol. Chem.* **1997,** *272* (31), 19609–19614.
249. Gomez-Manzano, C.; Mitlianga, P.; Fueyo, J.; Lee, H. Y.; Hu, M.; Spurgers, K. B.; Glass, T. L.; Koul, D.; Liu, T. J.; McDonnell, T. J.; Yung, W. K. A. Transfer of E2F-1 to Human Glioma Cells Results in Transcriptional Up-Regulation of Bcl-2. *Cancer Res.* **2001,** *61* (18), 6693–6697.
250. Dai, J. X.; Chen, D.; Jones, R. A.; Hurley, L. H.; Yang, D. Z. NMR Solution Structure of the Major G-Quadruplex Structure Formed in the Human BCL2 Promoter Region. *Nucleic Acids Res.* **2006,** *34* (18), 5133–5144.
251. Dai, J.; Dexheimer, T. S.; Chen, D.; Carver, M.; Ambrus, A.; Jones, R. A.; Yang, D. An Intramolecular G-Quadruplex Structure With Mixed Parallel/Antiparallel G-Strands Formed in the Human BCL-2 Promoter Region in Solution. *J. Am. Chem. Soc.* **2006,** *128* (4), 1096–1098.
252. Mayo, M. W.; Wang, C. Y.; Drouin, S. S.; Madrid, L. V.; Marshall, A. F.; Reed, J. C.; Weissman, B. E.; Baldwin, A. S. WT1 Modulates Apoptosis by Transcriptionally Upregulating the Bcl-2 Proto-Oncogene. *EMBO J.* **1999,** *18* (14), 3990–4003.
253. Sun, H. X.; Xiang, J. F.; Shi, Y. H.; Yang, Q. F.; Guan, A. J.; Li, Q.; Yu, L. J.; Shang, Q.; Zhang, H.; Tang, Y. L.; Xu, G. Z. A Newly Identified G-Quadruplex as a Potential Target Regulating Bcl-2 Expression. *Biochim. Biophys. Acta, Gen. Subj.* **2014,** *1840* (10), 3052–3057.
254. Wang, X. D.; Ou, T. M.; Lu, Y. J.; Li, Z.; Xu, Z.; Xi, C.; Tan, J. H.; Huang, S. L.; An, L. K.; Li, D.; Gu, L. Q.; Huang, Z. S. Turning Off Transcription of the Bcl-2 Gene by Stabilizing the Bcl-2 Promoter Quadruplex With Quindoline Derivatives. *J. Med. Chem.* **2010,** *53* (11), 4390–4398.
255. Ohnmacht, S. A.; Marchetti, C.; Gunaratnam, M.; Besser, R. J.; Haider, S. M.; Di Vita, G.; Lowe, H. L.; Mellinas-Gomez, M.; Diocou, S.; Robson, M.; Sponer, J.; Islam, B.; Pedley, R. B.; Hartley, J. A.; Neidle, S. A G-Quadruplex-Binding Compound Showing Anti-Tumour Activity in an In Vivo Model for Pancreatic Cancer. *Sci. Rep.* **2015,** *5,* 11385.
256. Feng, Y.; Yang, D. Z.; Chen, H. B.; Cheng, W. L.; Wang, L. X.; Sun, H. X.; Tang, Y. L. Stabilization of G-Quadruplex DNA and Inhibition of Bcl-2 Expression by a Pyridostatin Analog. *Bioorg. Med. Chem. Lett.* **2016,** *26* (7), 1660–1663.
257. Lianos, G. D.; Alexiou, G. A.; Mangano, A.; Mangano, A.; Rausei, S.; Boni, L.; Dionigi, G.; Roukos, D. H. The Role of Heat Shock Proteins in Cancer. *Cancer Lett.* **2015,** *360* (2), 114–118.
258. Keppler, B. R.; Grady, A. T.; Jarstfer, M. B. The Biochemical Role of the Heat Shock Protein 90 Chaperone Complex in Establishing Human Telomerase Activity. *J. Biol. Chem.* **2006,** *281* (29), 19840–19848.
259. Kim, R. H.; Kim, R.; Chen, W.; Hu, S.; Shin, K. H.; Park, N. H.; Kang, M. K. Association of hsp90 to the hTERT Promoter Is Necessary for hTERT Expression in Human Oral Cancer Cells. *Carcinogenesis* **2008,** *29* (12), 2425–2431.
260. Neckers, L.; Workman, P. Hsp90 Molecular Chaperone Inhibitors: Are We There Yet? *Clin. Cancer Res.* **2012,** *18* (1), 64–76.
261. Di, K.; Keir, S. T.; Alexandru-Abrams, D.; Gong, X.; Nguyen, H.; Friedman, H. S.; Bota, D. A. Profiling Hsp90 Differential Expression and the Molecular Effects of the Hsp90 Inhibitor IPI-504 in High-Grade Glioma Models. *J. Neurooncol.* **2014,** *120* (3), 473–481.
262. Fendrich, V.; Wichmann, S.; Wiese, D.; Waldmann, J.; Lauth, M.; Rexin, P.; L-Lopez, C.; Schlitt, H. J.; Bartsch, D. K.; Lang, S. A. Inhibition of Heat Shock Protein 90 With AUY922 Represses Tumor Growth in a Transgenic Mouse Model of Islet Cell Neoplasms. *Neuroendocrinology* **2014,** *100* (4), 300–309.
263. Millson, S. H.; Chua, C. S.; Roe, S. M.; Polier, S.; Solovieva, S.; Pearl, L. H.; Sim, T. S.; Prodromou, C.; Piper, P. W. Features of the Streptomyces Hygroscopicus HtpG Reveal How Partial Geldanamycin Resistance Can Arise With Mutation to the ATP Binding Pocket of a Eukaryotic Hsp90. *FASEB J.* **2011,** *25* (11), 3828–3837.
264. Hampel, S. M.; Sidibe, A.; Gunaratnam, M.; Riou, J. F.; Neidle, S. Tetrasubstituted Naphthalene Diimide Ligands With Selectivity for Telomeric G-Quadruplexes and Cancer Cells. *Bioorg. Med. Chem. Lett.* **2010,** *20* (22), 6459–6463.
265. Gunaratnam, M.; de la Fuente, M.; Hampel, S. M.; Todd, A. K.; Reszka, A. P.; Schatzlein, A.; Neidle, S. Targeting Pancreatic Cancer With a G-Quadruplex Ligand. *Bioorg. Med. Chem.* **2011,** *19* (23), 7151–7157.
266. Hu, C. J.; Wang, L. Y.; Chodosh, L. A.; Keith, B.; Simon, M. C. Differential Roles of Hypoxia-Inducible Factor 1alpha (HIF-1alpha) and HIF-2alpha in Hypoxic Gene Regulation. *Mol. Cell. Biol.* **2003,** *23* (24), 9361–9374.
267. Heikkila, M.; Pasanen, A.; Kivirikko, K. I.; Myllyharju, J. Roles of the Human Hypoxia-Inducible Factor (HIF)-3alpha Variants in the Hypoxia Response. *Cell. Mol. Life Sci.* **2011,** *68* (23), 3885–3901.
268. Jonasch, E.; Futreal, P. A.; Davis, I. J.; Bailey, S. T.; Kim, W. Y.; Brugarolas, J.; Giaccia, A. J.; Kurban, G.; Pause, A.; Frydman, J.; Zurita, A. J.; Rini, B. I.; Sharma, P.; Atkins, M. B.; Walker, C. L.; Rathmell, W. K. State of the Science: An Update on Renal Cell Carcinoma. *Mol. Cancer Res.* **2012,** *10* (7), 859–880.
269. Sadri, N.; Zhang, P. J. Hypoxia-Inducible Factors: Mediators of Cancer Progression; Prognostic and Therapeutic Targets in Soft Tissue Sarcomas. *Cancers* **2013,** *5* (2), 320–333.
270. Chen, C.; Zhou, H.; Wei, F.; Jiang, L.; Liu, X.; Liu, Z.; Ma, Q. Increased Levels of Hypoxia-Inducible Factor-1alpha Are Associated With Bcl-xL Expression, Tumor Apoptosis, and Clinical Outcome in Chondrosarcoma. *J. Orthopaed. Res.* **2011,** *29* (1), 143–151.
271. Lombardo, C. M.; Welsh, S. J.; Strauss, S. J.; Dale, A. G.; Todd, A. K.; Nanjunda, R.; Wilson, W. D.; Neidle, S. A Novel Series of G-Quadruplex Ligands With Selectivity for HIF-Expressing Osteosarcoma and Renal Cancer Cell Lines. *Bioorg. Med. Chem. Lett.* **2012,** *22* (18), 5984–5988.
272. Welsh, S. J.; Dale, A. G.; Lombardo, C. M.; Valentine, H.; de la Fuente, M.; Schatzlein, A.; Neidle, S. Inhibition of the Hypoxia-Inducible Factor Pathway by a G-Quadruplex Binding Small Molecule. *Sci. Rep.* **2013,** *3,* 2799.
273. Chen, H.; Long, H.; Cui, X.; Zhou, J.; Xu, M.; Yuan, G. Exploring the Formation and Recognition of an Important G-Quadruplex in a HIF1alpha Promoter and its Transcriptional Inhibition by a Benzo[c]Phenanthridine Derivative. *J. Am. Chem. Soc.* **2014,** *136* (6), 2583–2591.
274. Shiota, M.; Yokomizo, A.; Naito, S. Increased Androgen Receptor Transcription: A Cause of Castration-Resistant Prostate Cancer and a Possible Therapeutic Target. *J. Mol. Endocrinol.* **2011,** *47* (1), R25–R41.
275. Snoek, R.; Cheng, H.; Margiotti, K.; Wafa, L. A.; Wong, C. A.; Wong, E. C.; Fazli, L.; Nelson, C. C.; Gleave, M. E.; Rennie, P. S. In Vivo Knockdown of the Androgen Receptor Results in Growth Inhibition and Regression of Well-Established, Castration-Resistant Prostate Tumors. *Clin. Cancer Res.* **2009,** *15* (1), 39–47.
276. Welsbie, D. S.; Xu, J.; Chen, Y.; Borsu, L.; Scher, H. I.; Rosen, N.; Sawyers, C. L. Histone Deacetylases Are Required for Androgen Receptor Function in Hormone-Sensitive and Castrate-Resistant Prostate Cancer. *Cancer Res.* **2009,** *69* (3), 958–966.
277. Molife, L. R.; Attard, G.; Fong, P. C.; Karavasilis, V.; Reid, A. H.; Patterson, S.; Riggs, C. E., Jr.; Higano, C.; Stadler, W. M.; McCulloch, W.; Dearnaley, D.; Parker, C.; de Bono, J. S. Phase II, Two-Stage, Single-arm Trial of the Histone Deacetylase Inhibitor (HDACi) Romidepsin in Metastatic Castration-Resistant Prostate Cancer (CRPC). *Ann. Oncol.* **2010,** *21* (1), 109–113.
278. Carter, M. T.; Yome, J. L.; Marcil, M. N.; Martin, C. A.; Vanhorne, J. B.; Mulligan, L. M. Conservation of RET Proto-Oncogene Splicing Variants and Implications for RET Isoform Function. *Cytogenet. Cell Genet.* **2001,** *95* (3–4), 169–176.
279. Runeberg-Roos, P.; Saarma, M. Neurotrophic Factor Receptor RET: Structure, Cell Biology, and Inherited Diseases. *Ann. Med.* **2007,** *39* (8), 572–580.
280. Takaya, K.; Yoshimasa, T.; Arai, H.; Tamura, N.; Miyamoto, Y.; Itoh, H.; Nakao, K. Expression of the RET Proto-Oncogene in Normal Human Tissues, Pheochromocytomas, and Other Tumors of Neural Crest Origin. *J. Mol. Med. (Berl)* **1996,** *74* (10), 617–621.
281. Santoro, M.; Rosati, R.; Grieco, M.; Berlingieri, M. T.; D'Amato, G. L.; de Franciscis, V.; Fusco, A. The ret Proto-Oncogene is Consistently Expressed in Human Pheochromocytomas and Thyroid Medullary Carcinomas. *Oncogene* **1990,** *5* (10), 1595–1598.
282. Sawai, H.; Okada, Y.; Kazanjian, K.; Kim, J.; Hasan, S.; Hines, O. J.; Reber, H. A.; Hoon, D. S.; Eibl, G. The G691S RET Polymorphism Increases Glial Cell Line-Derived Neurotrophic Factor-Induced Pancreatic Cancer Cell Invasion by Amplifying Mitogen-Activated Protein Kinase Signaling. *Cancer Res.* **2005,** *65* (24), 11536–11544.
283. Veit, C.; Genze, F.; Menke, A.; Hoeffert, S.; Gress, T. M.; Gierschik, P.; Giehl, K. Activation of Phosphatidylinositol 3-Kinase and Extracellular Signal-Regulated Kinase is Required for Glial Cell Line-Derived Neurotrophic Factor-Induced Migration and Invasion of Pancreatic Carcinoma Cells. *Cancer Res.* **2004,** *64* (15), 5291–5300.

284. Kodama, Y.; Asai, N.; Kawai, K.; Jijiwa, M.; Murakumo, Y.; Ichihara, M.; Takahashi, M. The RET Proto-Oncogene: A Molecular Therapeutic Target in Thyroid Cancer. *Cancer Sci.* **2005,** *96* (3), 143–148.
285. Andrew, S. D.; Delhanty, P. J.; Mulligan, L. M.; Robinson, B. G. Sp1 and Sp3 Transactivate the RET Proto-Oncogene Promoter. *Gene* **2000,** *256* (1–2), 283–291.
286. Guo, K.; Pourpak, A.; Beetz-Rogers, K.; Gokhale, V.; Sun, D.; Hurley, L. H. Formation of Pseudosymmetrical G-Quadruplex and i-Motif Structures in the Proximal Promoter Region of the RET Oncogene. *J. Am. Chem. Soc.* **2007,** *129* (33), 10220–10228.
287. Shin, Y. J.; Kumarasamy, V.; Camacho, D.; Sun, D. Involvement of G-Quadruplex Structures in Regulation of Human RET Gene Expression by Small Molecules in Human Medullary Thyroid Carcinoma TT Cells. *Oncogene* **2015,** *34* (10), 1292–1299.
288. Kumarasamy, V. M.; Shin, Y. J.; White, J.; Sun, D. Selective Repression of RET Proto-Oncogene in Medullary Thyroid Carcinoma by a Natural Alkaloid Berberine. *BMC Cancer* **2015,** *15,* 599.
289. Cipriani, N. A.; Abidoye, O. O.; Vokes, E.; Salgia, R. MET as a Target for Treatment of Chest Tumors. *Lung Cancer* **2009,** *63* (2), 169–179.
290. Matsumoto, K.; Nakamura, T. Mechanisms and Significance of Bifunctional NK4 in Cancer Treatment. *Biochem. Biophys. Res. Commun.* **2005,** *333* (2), 316–327.
291. Michieli, P.; Mazzone, M.; Basilico, C.; Cavassa, S.; Sottile, A.; Naldini, L.; Comoglio, P. M. Targeting the Tumor and Its Microenvironment by a Dual-Function Decoy Met Receptor. *Cancer Cell* **2004,** *6* (1), 61–73.
292. Kong-Beltran, M.; Stamos, J.; Wickramasinghe, D. The Sema Domain of Met is Necessary for Receptor Dimerization and Activation. *Cancer Cell* **2004,** *6* (1), 75–84.
293. Petrelli, A.; Circosta, P.; Granziero, L.; Mazzone, M.; Pisacane, A.; Fenoglio, S.; Comoglio, P. M.; Giordano, S. Ab-Induced Ectodomain Shedding Mediates Hepatocyte Growth Factor Receptor Down-Regulation and Hampers Biological Activity. *Proc. Natl. Acad. Sci. U. S. A.* **2006,** *103* (13), 5090–5095.
294. Christensen, J. G.; Burrows, J.; Salgia, R. c-Met as a Target for Human Cancer and Characterization of Inhibitors for Therapeutic Intervention. *Cancer Lett.* **2005,** *225* (1), 1–26.
295. Yan, J.; Zhao, X.; Liu, B.; Yuan, Y.; Guan, Y. An Intramolecular G-Quadruplex Structure Formed in the Human MET Promoter Region and Its Biological Relevance. *Mol. Carcinogen.* **2016,** *55* (5), 897–909.
296. Niu, G.; Bowman, T.; Huang, M.; Shivers, S.; Reintgen, D.; Daud, A.; Chang, A.; Kraker, A.; Jove, R.; Yu, H. Roles of Activated Src and Stat3 Signaling in Melanoma Tumor Cell Growth. *Oncogene* **2002,** *21* (46), 7001–7010.
297. Cartwright, C. A.; Kamps, M. P.; Meisler, A. I.; Pipas, J. M.; Eckhart, W. Pp60c-Src Activation in Human-Colon Carcinoma. *J. Clin. Invest.* **1989,** *83* (6), 2025–2033.
298. Cartwright, C. A.; Meisler, A. I.; Eckhart, W. Activation of the Pp60c-Src Protein-Kinase is an Early Event in Colonic Carcinogenesis. *Proc. Natl. Acad. Sci. U. S. A.* **1990,** *87* (2), 558–562.
299. Aligayer, H.; Boyd, D. D.; Heiss, M. M.; Abdalla, E. K.; Curley, S. A.; Gallick, G. E. Activation of Src Kinase in Primary Colorectal Carcinoma: An Indicator of Poor Clinical Prognosis. *Cancer* **2002,** *94* (2), 344–351.
300. Ottenhoff-Kalff, A. E.; Rijksen, G.; van Beurden, E. A.; Hennipman, A.; Michels, A. A.; Staal, G. E. Characterization of Protein Tyrosine Kinases From Human Breast Cancer: Involvement of the c-Src Oncogene Product. *Cancer Res.* **1992,** *52* (17), 4773–4778.
301. Biscardi, J. S.; Belsches, A. P.; Parsons, S. J. Characterization of Human Epidermal Growth Factor Receptor and c-Src Interactions in Human Breast Tumor Cells. *Mol. Carcinogen.* **1998,** *21* (4), 261–272.
302. Nam, S.; Kim, D.; Cheng, J. Q.; Zhang, S.; Lee, J. H.; Buettner, R.; Mirosevich, J.; Lee, F. Y.; Jove, R. Action of the Src Family Kinase Inhibitor, Dasatinib (BMS-354825), on Human Prostate Cancer Cells. *Cancer Res.* **2005,** *65* (20), 9185–9189.
303. Musumeci, F.; Schenone, S.; Brullo, C.; Botta, M. An Update on Dual Src/Abl Inhibitors. *Future Med. Chem.* **2012,** *4* (6), 799–822.
304. Murat, P.; Gormally, M. V.; Sanders, D.; Di Antonio, M.; Balasubramanian, S. Light-Mediated in Cell Downregulation of G-Quadruplex-Containing Genes Using a Photo-Caged Ligand. *Chem. Commun. (Camb.)* **2013,** *49* (76), 8453–8455.

Relevant Websites

http://bioinformatics.ramapo.edu/GQRS/—A quadruplex informatics resource centre.
http://quadbase.igib.res.in/—Provides Quadbase2, a quadruplex mining tool for many genomes.
http://www.quadruplexldb.org/ci2/index.php—A useful quadruplex ligand database which provides browse and docking facilities.
http://scottgroup.med.usherbrooke.ca/quadruplexRNA/—A RNA quadruplex.

5.10 Targeting Pre-mRNA Processing in Cancer

TR Webb, SRI International, Menlo Park, CA, United States
S Stamm, University of Kentucky, Lexington, KY, United States

© 2017 Elsevier Ltd. All rights reserved.

5.10.1	**Introduction**	341
5.10.1.1	Pre-mRNA Splicing and the Spliceosome	344
5.10.1.2	Recognition of Exons	344
5.10.1.3	Circular RNAs	344
5.10.1.4	The Spliceosome	345
5.10.1.5	The Spliceosome is Linked to Other Nuclear Processes	346
5.10.1.6	Mutations in Spliceosomal Proteins	346
5.10.1.7	Mutations in Pre-mRNA	346
5.10.2	**The Spliceosome as a Cancer Target**	347
5.10.2.1	Mechanism of the Selective Antitumor Activity of Spliceosome Targeted Agents	348
5.10.2.1.1	Synthetic lethal spliceosome pairs	348
5.10.2.1.2	Tumors bearing spliceosome mutations are vulnerable to splicing modulation	349
5.10.2.2	Natural Products and Derivatives Targeting *SF3B1*	350
5.10.2.3	Synthetic natural product analogs targeting *SF3B1*	351
5.10.2.4	Inhibitors of the CDC-Like Kinases	351
5.10.3	**Conclusions**	353
References		353

Abbreviations

aa-tRNA Aminoacyl-transfer RNA
AML Acute myeloid leukemia
AS Alternative splicing
BBP Branch-point binding protein
BCL-X BCL-2-like protein 1
BPS Branch-point sequence
CLK Cdc-like kinases
CLL Chronic lymphocytic leukemia
ER Endoplasmic reticulum
ESE Exonic splicing enhancer
GBM Glioblastoma multiforme
GSCs Glioblastoma multiforme stem cells
hnRNP Heterogenous nuclear RNP
MDS Myelodysplastic syndromes
NSCs Neural stem cells
nt Nucleotide
PDX Patient-derived xenografts
PHD Plant homeodomain
RITS RNA-induced transcriptional silencing
RNA Pol II RNA polymerase II
RNP Ribonucleoprotein
RRM RNA recognition motif
scaRNP Small Cajal body RNP
snoRNP Small nucleolar RNP
snRNP Small nuclear RNP
SR Serine-arginine-rich
SRP Signal recognition particle
SS Splice site
tri-snRNP Tri-small nuclear RNP
U2AF U2 auxiliary factor
U-rich Uridine-rich
VEGF Vascular endothelial growth factor

5.10.1 Introduction

The processing of pre-mRNA to mature mRNA in metazoans is one of the numerous critical processes for development and normal functioning of cells that is mediated by ribonucleoproteins (RNPs) (see Fig. 1).[1] The importance of the pre-mRNA splicing process as a source of evolutionary adaptability of metazoans appears to justify the significant burden that is born by each cell that must orchestrate the synthesis and regulation of some 200 proteins and numerous functional RNPs, which are critical for the pre-mRNA splicing process. This process involves the highly regulated combinatorial removal of intervening sequences from pre-mRNA followed by the ligation of exons to form mature mRNA, which is then exported into the cytosol from the nucleus. This splicing process is catalyzed and regulated by a highly complex macromolecular complex called the spliceosome (see Fig. 2).[1–3] The spliceosome is a unique macromolecular machine in its complexity, given that it has thousands of pre-mRNA substrates and potentially millions of

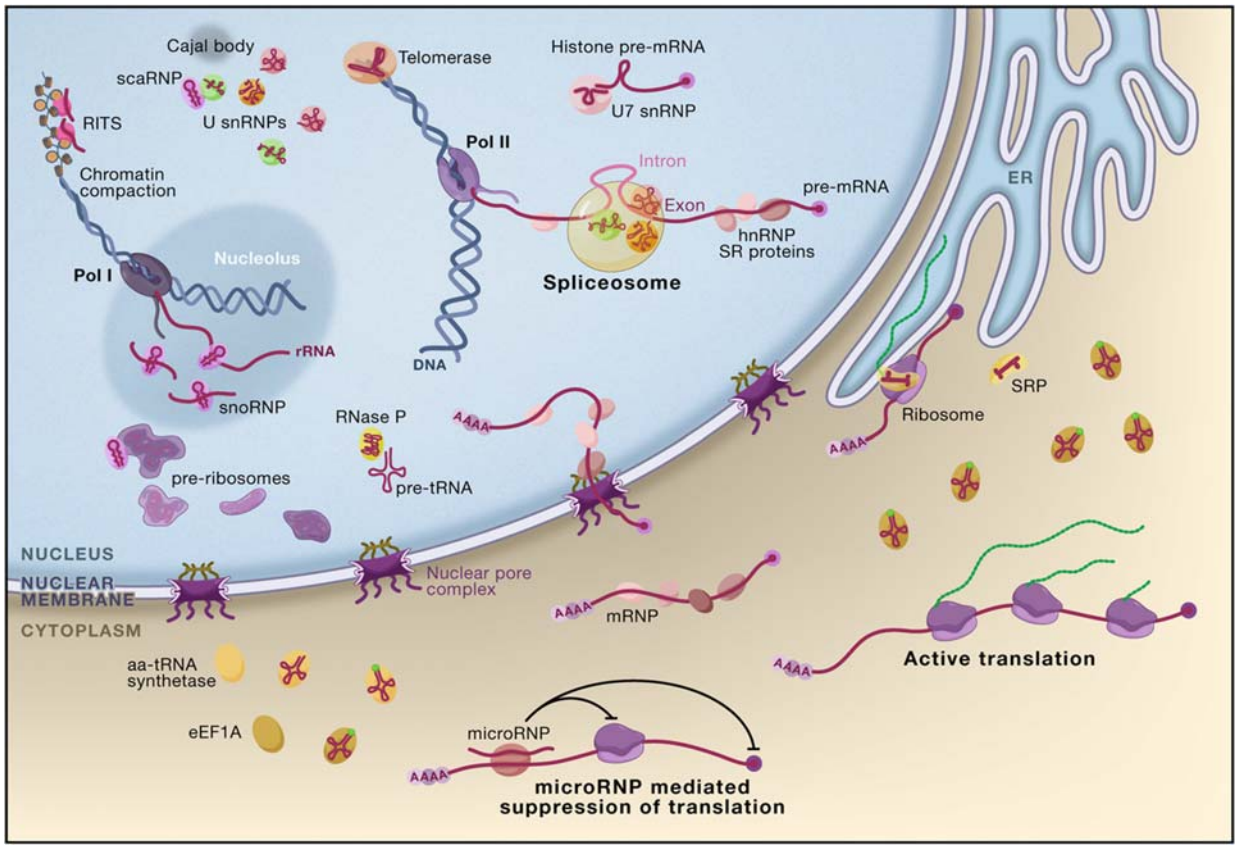

Fig. 1 RNPs in gene expression and its regulation[3]: RNPs play extensive roles in gene expression and its regulation. Here, the major activities of RNPs during gene expression in a eukaryotic cell are depicted. Following transcription by RNA polymerases II (RNA Pol II), pre-mRNAs are bound by diverse proteins, such as hnRNP and SR (serine-arginine-rich) proteins. Pre-mRNAs, containing exons *(red)* and introns *(pink)*, are subjected to processing by a range of RNPs that include uridine-rich (U-rich) small nuclear RNPs (U snRNPs) that make up the spliceosome. Certain RNAs such as pretransfer RNAs and mRNA transcripts encoding histones also undergo processing by specific RNPs (RNase P and U7 snRNP, respectively). Small nucleolar RNPs (snoRNPs) and small Cajal body RNPs (scaRNPs) mediate maturation of RNA components of RNPs such as ribosomal RNAs (transcribed by RNA polymerase I, RNA Pol I) and snRNAs, respectively. Small RNAs can form microRNPs that function to regulate translation. In certain organisms, RNA-induced transcriptional silencing (RITS) complexes, which contain small-interfering RNAs, mediate heterochromatin formation and maintenance. Telomerase, a box H/ACA snoRNP, replenishes the terminal telomeric repeats of chromosomes to maintain genomic stability. In the cytoplasm, the ribosome is the key RNP that directs the translation of mRNA into protein. It also functions with the signal recognition particle (SRP) RNP to direct protein translocation into the endoplasmic reticulum (ER). tRNAs also form complexes in the cytoplasm with aminoacyl-tRNA (aa-tRNA) synthetases, which charge tRNAs with the corresponding amino acid, and with translation elongation factor eEF1A.[3] Reprinted from Wahl, M. C.; Will, C. L.; Luhrmann, R. The Spliceosome: Design Principles of a Dynamic RNP Machine. *Cell* **2009**, *136*, 701–718, with permission from Elsevier.

spliced, and alternately spliced, mature mRNA products that are produced in the transcriptome of each cell; additionally each of these splicing reactions requires regulation that is controlled by the specifics of the environment of the particular cellular phenotype that is undergoing the process of transcription and splicing.[1]

The spliceosome is a complex of five small nuclear RNPs (snRNPs) (U1, U2, U4, U5, and U6) and approximately 200 associated proteins.[2,3] This pre-mRNA maturation process also includes alternative splicing (AS), which is the mechanism that allows for different forms of mature mRNAs to be generated from the same pre-mRNA. Commonly, AS patterns determine the inclusion or exclusion of portions of the coding sequence in the mRNA, giving rise to protein isoforms that differ in their peptide sequence. Alternate splicing is regulated by numerous spliceosomal trans-acting proteins, which are in turn regulated by cis-acting regulatory sites on the pre-mRNA that are the substrates for the spliceosome.[2] Since pre-mRNAs for a given gene may contain many different exon and intron combinations, there are often a very large number of possible mRNAs that can result in a correspondingly large set of resulting proteins that may have very different, even opposing, biological functions within the cell. Numerous genes are subject to splicing events that can be either oncogenic or serve to limit potential tumorigenesis, examples include BCL-2-like protein 1, VEGF-A, Fas Cell Surface Death Receptor (FAS), pyruvate kinase isozymes M1/M2 (PKM), or MDM2 (as described in a recent review).[4]

Recently, there has been a strong acceleration in spliceosome-related research and in the rate of appearance of high-profile publications on this topic, many of which have a significant impact on oncology drug discovery. A search of Pubmed with the query "spliceosome" shows 92 publications in 2000 but 229 publications for 2015. Some of the major recent accomplishments in this

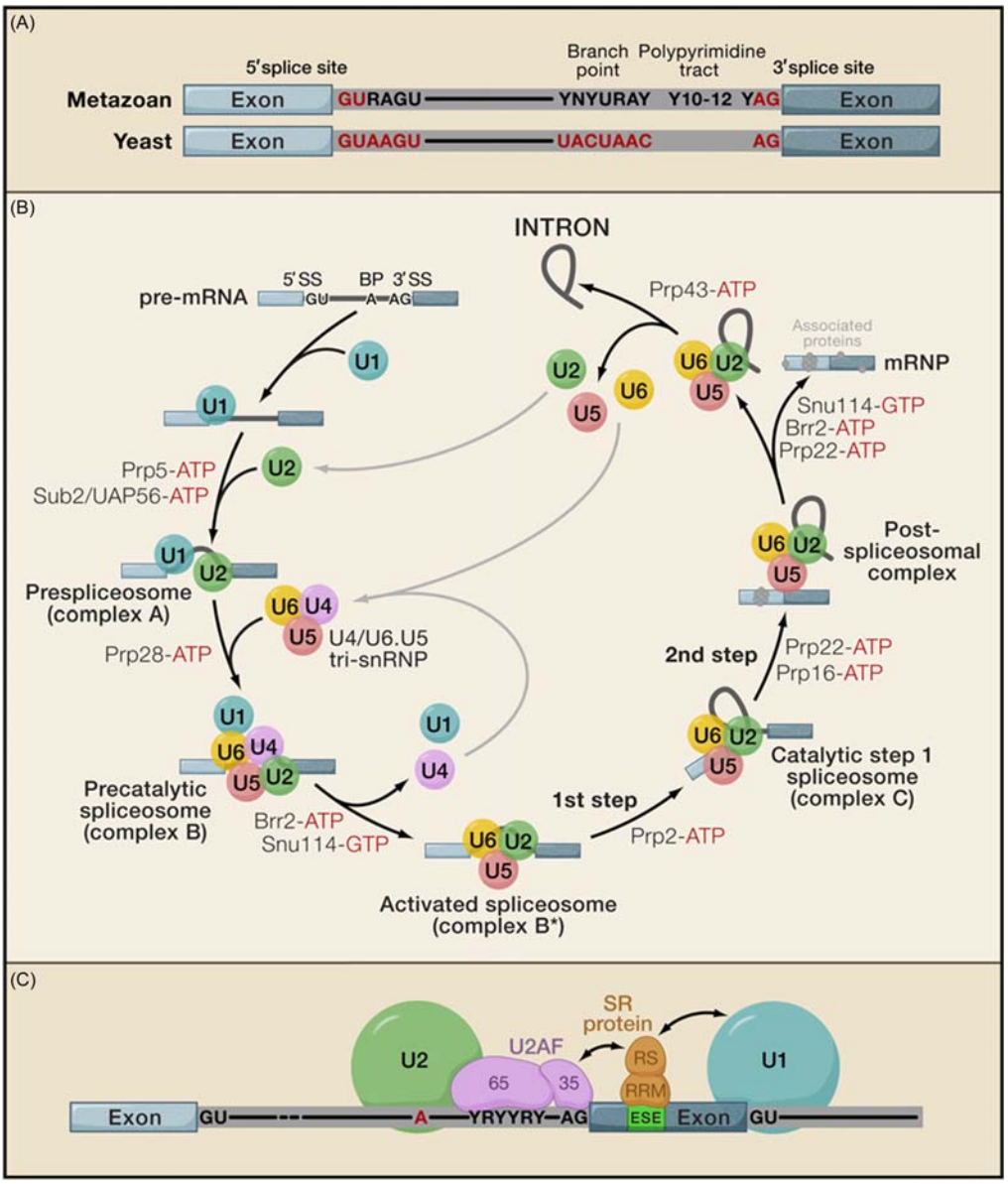

Fig. 2 Pre-mRNA splicing by the major spliceosome[3]: (A) conserved sequence elements of metazoan and yeast pre-mRNAs. Here, two exons *(blue)* are separated by an intron *(gray)*. The consensus sequences in metazoans and yeast at the 5′ splice site (SS), branch point sequence (BPS), and 3′ splice site (SS) are as indicated, where N is any nucleotide, R is a purine, and Y is a pyrimidine. The polypyrimidine tract is a pyrimidine-rich stretch located between the BPS and 3′ SS. (B) Cross-intron assembly and disassembly cycle of the major spliceosome. The stepwise interaction of the spliceosomal snRNPs *(colored circles)*, but not non-snRNP proteins, in the removal of an intron from a pre-mRNA containing two exons *(blue)* is depicted. Only the spliceosomal complexes that can be resolved biochemically in mammalian splicing extracts are shown. Eight evolutionarily conserved DExD/H-type RNA-dependent ATPases/helicases act at specific steps of the splicing cycle to catalyze RNA–RNA rearrangements and RNP remodeling events. These enzymes include Sub2 (UAP56 in humans), Prp5, Prp28, Brr2, Prp2, Prp16, Prp22, and Prp43 (with Brr2 and Prp22 acting at more than one step in the cycle). The GTPase Snu114 also functions at several steps during the cycle. In yeast, Prp28 acts at a later stage during spliceosome activation (the B complex to B* complex transition). Several of these proteins, such as Prp5, Prp16, and Prp22, also carry out proofreading functions at the stages where they are shown. (C) Cross-exon splicing complexes form on long introns during the earliest stage of spliceosome assembly. An SR protein containing a serine-arginine-rich (SR) domain and RRM (RNA recognition motif) is depicted as interacting with an exonic splicing enhancer (ESE). The U1 *(blue)* and U2 *(green)* spliceosomal snRNPs and the two subunits of the U2 auxiliary factor (U2AF), U2AF65 and U2AF35, are also shown interacting with the splice sites flanking the exon.[3] Reprinted from Wahl, M. C.; Will, C. L.; Luhrmann, R. The Spliceosome: Design Principles of a Dynamic RNP Machine. *Cell* **2009**, *136*, 701–718, with permission from Elsevier.

field include the very recent reports of the cryo-EM structures of spliceosome components that have clarified numerous aspects of the splicing process at near (but not at) atomic resolution.[5,6] The complexity of the spliceosome and the current lack of high-resolution structures complicate progress in understanding many of the critically important molecular and functional mechanisms associated with pre-mRNA splicing. Since the splicing process is critical to the normal functioning of the cells of higher organisms,

this area will remain an active area of research for the foreseeable future. However the remaining mysteries surrounding the splicing process do not diminish the importance of this fascinating molecular machine, which is now recognized as a major frontier for molecular biology and, more recently, for oncology target discovery. The discovery of new small molecules that modulate splicing will likely be key in the facilitation of a more detailed understanding of this emerging field. The prominence of pre-mRNA splicing in the regulation of gene expression also makes it an attractive and innovative potential target for therapeutic intervention in numerous diseases, including cancer.[4,7–9] This article will be focus specifically on the numerous developments that have led to the emergence of a new field: *spliceosome medicinal chemistry*.

5.10.1.1 Pre-mRNA Splicing and the Spliceosome

Nearly all human RNA polymerase II (RNA Pol II) transcripts undergo pre-mRNA splicing, a nuclear process where sequences called exons (exported sequences) are joined together and the intervening sequences (introns) are removed.[10] Exons are surrounded by three characteristic sequence elements: the 5′ and 3′ splice sites located at the exon-intron border and the branch point located 18–50 nucleotides (nt) upstream of the 3′ splice site. Two splicing systems operate in humans, a major one where the introns are marked by GU-AG bases and a minor one (accounting for less than 0.5% of introns) marked by AU-AC dinucleotides.[11] The splice sites are recognized through interaction with five small nuclear RNAs (snRNAs), the U1, U2, U4, U5, and U6 snRNAs. Through base complementarity, the U1 snRNA recognizes the 5′ splice site and the U2 snRNA binds to the branch point sequence. The U4/U5 and U6 snRNAs form a complex (the U4/U5/U6 tri-snRNP) involved in splicing catalysis. Human splice sites characteristically adhere weakly to consensus sequences, and only the GU-AG dinucleotides are consistently conserved in the major spliceosome. The removal of introns occurs in two steps: in the first step, the first nucleotide of the intron is ligated to an adenosine branch point by a nucleophilic attack of the branchpoint 2′-OH on phosphorus to form a 5′-2′ phosphodiester bond, and in the second step the two exons are ligated through another nucleophilic attack on phosphorus by the exon 3′-OH to form the phosphodiester bond between the 5′ and 3′ exons.

The vast majority (>95%) and possibly all multiexon genes undergo AS, where an exon is either included or skipped in the final pre-mRNA.[12,13] On average, a human gene contains a median of 26 exons per gene and generates 3.4 isoforms, indicating that AS increases the coding capacity of the human genome more than threefold. AS is more abundant in humans than in other species, for example, mice generate only 2.4 isoforms per gene and *C. elegans* 1.2 isoforms.[10] The overall purpose of AS is to increase the diversity of the mRNA expressed from the genome.[14] A genome-wide analysis showed a large influence of alternative splice variants on protein interaction networks. Within an interaction network, most AS variants behave more like distinct proteins than like minor variants,[15] suggesting that AS generates functionally distinct proteins from a single gene. The deregulation of alternative pre-mRNA splicing is a hallmark of cancer[16] (**Fig. 3**).

5.10.1.2 Recognition of Exons

Exons on average constitute less than 10% of a human pre-mRNA. They have to be recognized with high fidelity, as omission of a single nucleotide will generate a frameshift that usually generates aberrant proteins. Because of the poor conservation of the splice sites, additional RNA sequences (cis elements) are needed for their recognition. These cis-elements bind to proteins that can be subdivided into two classes: serine-arginine-rich (SR)-proteins and heterogenous nuclear RNPs (hnRNPs). SR-proteins are RNA-binding proteins characterized by an RNA-binding domain and an RS domain that interacts with other proteins.[17] hnRNPs are a diverse group of nuclear proteins that bind to pre-mRNA.[18] As a general rule, SR-proteins promote exon inclusion as they bind to components of the spliceosome, whereas hnRNPs antagonize an interaction of the spliceosome with the pre-mRNA, resulting in exon skipping.[19] An increasing number of recent examples showed that in addition to proteins, noncoding RNAs can bind to regulatory cis-elements and change splice site selection.[20] The presence of splicing enhancers can explain the action of synonymous mutations in many cases, if a mutation does not change the predicted open reading frame but causes a disease. In many cases, these mutations act through a change in affinity of a splicing regulatory protein, which causes a modification of alternative exon usage.[21] Similar to the splice sites, splicing enhancers and silencers follow only degenerate consensus sequences. In the case of exonic splicing regulatory elements, this allows for the coexistence of splicing signals and code requirements.[22]

5.10.1.3 Circular RNAs

In nearly all protein-coding mRNAs described so far, the alignment of the exons in mRNAs corresponds to the corresponding sequence in the DNA. However, more than 25 years ago, mRNAs with "scrambled exons" were reported, that is, rather than having exon 1-2-3, mRNAs with exons 1-3-2 were described.[23] This result was not investigated further, since the genesis of these exons had not been elucidated at the time. Subsequent advances in RNAseq technology showed that these "scrambled exons" were part of circular RNAs (circRNAs). Circular RNAs are generated from splicing in large lariats or are generated by intramolecular splicing of RNAs that are constrained through base pairing; for example some are due to strong secondary structures that are present in inverted repeat sequences. The formation of circular RNAs due to strong secondary structures might be important for humans, since 11% of the human genome consists of Alu elements.[24] Because Alu elements originate in structural 7SL RNA, Alu elements can dimerize through the Alu domains that show self-complementarity. Since Alu elements are primate specific, they may generate primate-specific circular RNAs.

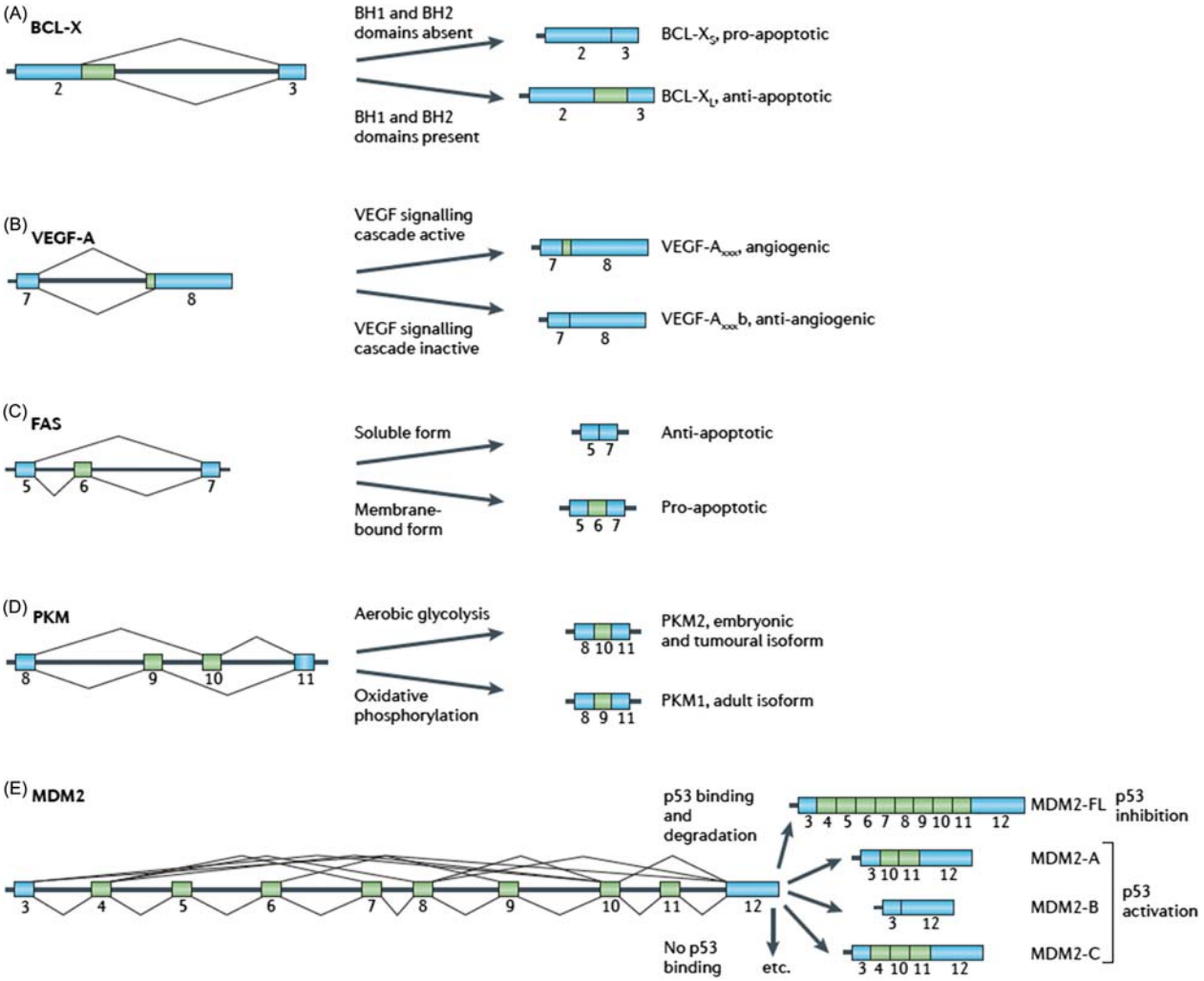

Fig. 3 Examples of regulated alternative splicing (AS) events relevant for cancer progression.[4] Alternative patterns of intron removal are represented, corresponding to alternative 5′- or 3′-splice site usage (A,B) or exon inclusion or skipping, either as cassette single exons (C), mutually exclusive alternative exons (D), or complex patterns of exon skipping (E). Alternative regions of the precursor mRNA are represented as *green boxes*, and constitutive exons are shown in *blue*. The numbers correspond to the exons involved in the AS event for each of the indicated genes. The examples also illustrate the diverse functional outcomes of the encoded alternative protein products, which regulate programmed cell death (A,C), formation of blood vessels (B), the metabolic advantage of tumor cells (D), or inactivation of the tumor suppressor p53 (E). See text for additional explanations. BCL-X, BCL-2-like protein 1; PKM, pyruvate kinase isozymes M1/M2; VEGF, vascular endothelial growth factor.[4] Reprinted by Bonnal, S.; Vigevani, L.; Valcarcel, J. The Spliceosome as a Target of Novel Antitumour Drugs. *Nat. Rev. Drug Discov.* **2012**, *11*, 847–859, with permission from Macmillan Publishers Ltd.

Most circRNAs are less than 1% of the linear mRNAs made from the same locus, but in some cases the circRNA is 10-fold more abundant than the linear mRNA from the locus.[25–27] Studies in cancer showed that circRNAs change their expression more strongly than mRNAs upon cell transformation.[28] circRNAs are mainly cytosolic and can be translated into protein.[25,29] In general, circular RNAs are much more stable than linear mRNAs, as they will not be degraded by the exosome, which acts like an exonuclease. In addition, most circRNAs do not contain 3′ untranslated regions (UTR) that promote deadenylation and exosomal degradation. Due to their circular structure that recapitulates the binding of the poly(A) tail to the mRNA cap in linear RNAs, circRNAs are potentially excellent ribosomal substrates, allowing for efficient translation in vitro and in vivo.[29] Thus, in addition to AS, the generation of circular RNAs, performed by the spliceosome, greatly increases the coding capacity of the human genome.

5.10.1.4 The Spliceosome

As discussed above the splicing reaction of the major spliceosome is performed by the spliceosome, an RNA–protein machine of about 4.8 MDa. The spliceosome contains at least 170 proteins that associate with five RNAs (U1, U2, U4, U5, and U6), generating the U1, U2, U4, U5, and U6 snRNPs.[3,30] Similar to the ribosome, these snRNPs assemble in a step-wise fashion on the pre-mRNA,

and rearrangements of the snRNPs bring together the splice sites allowing for the catalysis to be performed. The substrate of the spliceosome is pre-mRNA that is bound to many regulatory factors, such as SR-proteins and hnRNPs, which expose specific splice sites to the spliceosome. In most human internal exons, the 3′ and 5′ splice sites are paired across the exon through an interaction of U1 and U2 snRNPs, which is referred to as exon definition.[31] In yeast and in a subset of large human exons, the splice site pairing occurs across introns, which is referred to as intron definition. Most of our understanding of the splicing reaction comes from in vitro splicing assays that employ an in vitro RNA with two exons having one splice site each flanking a short intron. These in vitro substrates are recognized according to the intron definition model.

In spliceosome assembly,[3] first U1 snRNP binds to the 5′ splice site, aided by the base complementarity between the U1 snRNA and the 5′ splice site (**Fig. 2**). The branch-point-binding protein (BBP or SF1) binds to the branch point, aided by a protein interaction of RNA recognition motif 3 (RRM3) of the U2 auxiliary factor (U2AF65) binding to the polypyrimidine tract of the 3′ splice site. This protein complex is called the E (early) complex. In the next step the U2 snRNP associates with the complex and replaces BBP, forming the prespliceosome "complex A." The RNA component of U2 snRNP binds to the branch-site, which causes the branch-adenosine to bulge out of a short helix. A protein interaction between the U2 component SF3B1 (SAP155) and the RRM3 of U2AF helps to displace the BBP from its bound form with U2AF65. The entry of the U6/U4/U5 tri-snRNP, catalyzed by prp28, forms the precatalytic spliceosome "complex B." Several RNA helicases (brr2, snu114, and prp2) cause a rearrangement in this complex, which releases U4 and U1, and the U6 snRNA binding to the 5′ splice site. In this activated spliceosome (B* complex), the branch point is brought into close proximity to the 5′ splice site, allowing for the formation of the lariat in the first step of splicing, leading to the catalytic "C complex." The C complex contains the free first exon, and the lariat bound to the second exon. Using the prp8, prp16, prp18, and slu7 components, the second step of splicing, which involves the ligation of the two exons, is carried out. Another RNA helicase, prp22 releases the remaining U6/U2/U5 snRNPs and the lariat from the spliced RNA in the postspliceosome complex. After catalysis, the U6, U2, and U5 snRNPs are removed from the lariat using snu114, Brr2, and prp43, are then recycled for another round of catalysis, and the intron is degraded. In vitro studies using small synthetic U2 and U6 snRNA fractions can generate a phosphodieseter bond using a lariat-analog as a substrate, indicating that the spliceosome is a ribozyme.[32,33]

5.10.1.5 The Spliceosome is Linked to Other Nuclear Processes

The mechanism of the spliceosome has been determined biochemically using a nuclear extract made under high salt conditions.[34] When spliceosomes are prepared using physiological salt conditions larger spliceosome complexes, termed supraspliceosomes are observed.[35–37] These preparations contain other mRNA processing factors, showing that pre-mRNA splicing in vivo is linked to other RNA processing steps. Pre-mRNA splicing occurs during RNA pol II transcription, and there is evidence for cotranscriptional splicing. For example, a fast-moving RNA polymerase promotes alternative exon skipping[38,39] and snRNPs and processing factors are loaded on the carboxy terminal domain of RNA pol II prior to transcription. However, since RNA pol II has an elongation rate of 3–4 kb/min, large introns are likely spliced out after transcription. There is accumulating evidence that chromatin structure is linked to exon selection. The average length of a human cassette exon of 145 nt corresponds well with the length of DNA in a nucleosome and in fact, splice sites preferably correspond to DNA located at the end of a nucleosome.[40,41] Histone modifications, such as H3K4me3, assist in the recruitment of U2 snRNP components to sites of active transcription, which could promote exon recognition.[42] The U2 snRNP component SF3B1 physically interacts with histone H3, suggesting a physiological link.[43] It is possible that pre-mRNA splicing affects chromatin changes, in return, as DNA encoding exons are characterized by the H3K36me3 modification. This modification is lower in DNA corresponding to alternative exons, when compared to constitutive exon. Since on average alternative exons of the same pre-mRNA assemble less spliceosomes than the constitutive exons,[41] this suggests that the activity of the spliceosome is reflected in the H3K36me3 modification. Components of the spliceosome also participate in transcriptome surveillance. The U1 snRNA is more abundant than the other spliceosomal U2, U4, U5, and U6 snRNAs. U1 snRNA binds to specific sites on pre-mRNA that are not recognized as splice sites and which prevents premature cleavage and polyadenylation.[44]

5.10.1.6 Mutations in Spliceosomal Proteins

Similar to the ribosome, the spliceosome is evolutionary, highly conserved from yeast to humans. Underlining its central role in metazoans germ line mutations in core spliceosomal proteins are rare and include PRP3, PRP6, PRP8, Brr2, and PRP31, causing dominant nonsyndromic retinitis Pigmentosa.[45–48] Mutations in the minor spliceosome small nuclear RNA U4atac cause microcephalic osteodysplastic primordial dwarfism type I[49] (**Table 1**). In contrast to germ line mutations, numerous somatic mutations of core spliceosomal and pre-mRNA-associated proteins have been detected in cancer cells using RNAseq (**Table 2**). Interestingly, they cluster in components that recognize the 3′ splice site, namely, U2AF35 (U2AF1), ZRSR2, a binding partner for U2AF[51] and the U2 snRNP component SF3B1 (**Fig. 4**).[54,55] Similarly, mutations in several, but not all proteins binding to splicing regulatory elements on the pre-mRNA have been detected. They include SRSF1 (SF2/ASF); SRSF2 (SC35).[56] These proteins generally promote exon recognition. In addition, SRSF1 plays a role in genome stability.[57]

5.10.1.7 Mutations in Pre-mRNA

In addition to mutations in the spliceosome, mutations on the pre-mRNA that affect splicing are associated with cancer[58–60] (reviewed in Refs. 61 and 62). Lists of alternative exons deregulated in different cancer cells have been compiled in the literature

Table 1 Germ-line mutations of the spliceosome leading to human disease

Gene	*Function*	*Disease*	
PRP3 U4/U6 SnRNP 90 KDa Protein	Part of the U4/U5/U6 tri-snRNP	Retinitis pigmentosa	47
PRP6 U5 SnRNP-Associated 102 KDa Protein	Part of the U4/U5/U6 tri-snRNP	Retinitis pigmentosa	50
PRP8 U5 SnRNP-Specific Protein (220 KD)	Scaffold for snRNPs during the splicing reaction	Retinitis pigmentosa	46
Brr2 U5 SnRNP-Specific 200 KDa Protein	RNA helicase	Retinitis pigmentosa	48
PRP31	U4/U6 SnRNP 61 KDa protein	Retinitis pigmentosa	45
U4atac	snRNA in the minor spliceosome	MOPD type I	49

MOPD, microcephalic osteodysplastic primordial dwarfism

Table 2 Somatic mutations of the spliceosome in cancer cells

SF3B1	U2 component, recognition of 3′ splice site	Chronic lymphocytic leukemia, myelodysplasia	55,76
SF3A1	U2 component, recognition of 3′ splice site	Myelodysplasia	76
PRPF40B	U1 and U2 component	Myelodysplasia	76
SF1	Recognizes branchpoint, 3′ splice site	Myelodysplasia	76
U2AF35	recognition of 3′ splice site	Myelodysplasia	76
U2AF65	recognition of 3′ splice site	Myelodysplasia	76
ZRSR2 zinc finger (CCCH Type), RNA-binding motif and serine/arginine rich 2	Second step of splicing in major splicesome; recognition of 3′ splice site in minor spliceosome	Myelodysplasia	76
SRSF2 (SC35)	Promotes exon inclusion	Myelodysplastic syndromes	129

(see, e.g., Refs. 58, 60, and 63). About 20% of point mutations in cancer are synonymous mutations, that is, mutations located in protein coding exons that do not affect the reading frame.[64] Up to 8% of these somatic mutations are selected in cancer cells, suggesting that they are functional. They frequently affect splicing regulatory sequences (exonic enhancers or silencers) and thus contribute to the deregulation of splicing. Examples include BRCA2 in breast cancer,[65] APC in familial adenomatous polyposis,[66,67] and TP53 in multiple tumors.[64] A much larger number of point mutations are found in intronic regions, but they are mechanistically poorly understood.[68] The best understood effects are the alterations of splice sites. Mutations affecting the conserved AG-GT splice site dinucleotides always abolish usage of the affected splice site, which usually results in the skipping of the exon unless a cryptic splice site is activated. Mutations outside the conserved AG-GT dinucleotides mostly modulate exon usage. However, the mechanistically less well understood mutations are associated with deep intronic alterations that can also affect splice site usage in cancer, usually due to activation of cryptic exons, for example in BRCA2.[69]

5.10.2 The Spliceosome as a Cancer Target

Aberrations in pre-mRNA splicing, in the case of MDM2, for example, were recognized as a feature of tumors as early as 1996,[70] and reviewed in 2002.[71] Subsequently, it was recognized that aberrant pre-mRNA splicing was a global property of the tumor transcriptome; these observations were reviewed as early as 2004 with the prediction that this understanding might lead to new opportunities for the diagnosis[53] and treatment of cancer.[72,73] However, despite much suggestive data, it was difficult to prove that splicing aberrations are actually oncogenic.[61] In the past few years, much more information has been obtained through genomic and transcriptomic studies of tumors.[74,75] Such splicing aberrations are now recognized as another predominant feature of cancer and the spliceosome is now seen as a validated antitumor target.[4,9] In the following, we will explore the history and the evolution of thought regarding the spliceosome as it is relevant to cancer medicinal chemistry by the exploration of applied and basic research studies, which hold the potential to initiate some transformative changes in the treatment of certain cancers.

In parallel to the work described above, strong evidence has continued to mount that aberrant splicing of pre-mRNA is a driver of tumorigenesis[61] and that modulation of this process may be a valid target for cancer therapy.[4,9] It has been known for some time that the deregulation of exon usage is a hallmark of cancer and recent groundbreaking discoveries have identified recurrent mutations in SF3B1 (and/or other splicing factors) in multiple forms of cancer including: myelodysplastic syndromes (MDS),[76,77] chronic lymphocytic leukemia (CLL),[78] acute myeloid leukemia (AML),[79,80] breast cancer,[81,82] lung adenosarcoma,[83] and uveal melanoma.[84] These genetic studies have also fueled complementary research in the therapeutic significance of spliceosome recurrent mutations. Very recently, the selective sensitivity of tumors to agents that target SF3B has also been linked to overexpression of MYC and published as part of a collaborative multidisciplinary effort.[85]

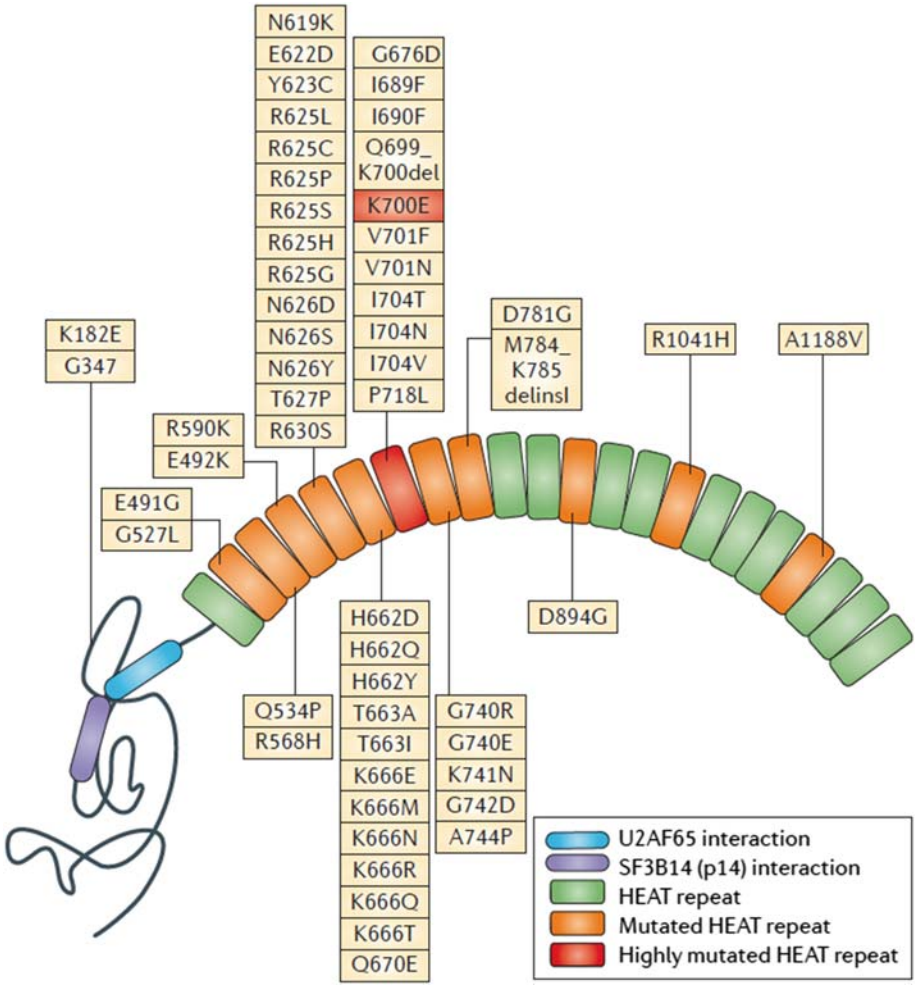

Fig. 4 Recurrent mutations in the drug protein target SF3B1. The scheme depicts the domain organization of splicing factor 3B subunit 1 (SF3B1) according to Ref. 52. The amino-terminal region is involved in interactions with other splicing factors, whereas the carboxy-terminal domain encompasses 22 HEAT (huntingtin, elongation factor 3, protein phosphatase 2A, target of rapamycin 1) repeats. Repeats harboring mutations found in chronic lymphocytic leukemia and/or myelodysplastic syndrome tumor samples are represented in orange, and the most frequent mutation and its corresponding repeat are represented in *red*.[46,53] U2AF65, U2 snRNP auxiliary factor of 65 kDa.[4] Reprinted by Bonnal, S.; Vigevani, L.; Valcarcel, J. The Spliceosome as a Target of Novel Antitumour Drugs. *Nat. Rev. Drug Discov.* **2012**, *11*, 847–859, with permission from Macmillan Publishers Ltd.

5.10.2.1 Mechanism of the Selective Antitumor Activity of Spliceosome Targeted Agents

5.10.2.1.1 Synthetic lethal spliceosome pairs

Since the discovery of the first small molecule antitumor agents that target the spliceosome, there has been substantial confusion in regard to the mechanism of selective activity of the spliceosome-targeted agents. This confusion has been in part due to numerous early reports describing these agents as "splicing inhibitors," which led in turn to the development of an incorrect conceptual framework for understanding the true mechanism of action of these agents. Though it is now well established that these agents act by the modulation of alternate splicing due to a reduction in the fidelity of 3′-splice site selection this confusion remains prevalent even in some recent literature reports. While many mechanisms may play a role in the selective killing of tumor cells by the agents discussed below, it is becoming clear that nononcogene addiction is an important mechanism that can explain the selectivity in many cases.[86] The nononcogene addiction concept provides a platform for the exploration of a large number of potential targets for anticancer therapies, whose change of function could selectively reverse oncogenic phenotypes. Several groups have carried out synthetic lethal RNA interference screens designed to identify genes whose silencing is specifically cytotoxic for cells carrying particular oncogenic mutations, in order to take advantage of this concept in the development of new anticancer approaches and in the elucidation of the mechanism of action of antitumor agents, including those agents that modulate splicing. These latter studies have relied on the use of "synthetic lethal" genetic studies using various screening strategies (e.g., siRNA and shRNA libraries that specifically "knock down" genes) to elucidate the aberrant splicing dependence of tumors bearing certain mutations. This topic has very recently been authoritatively reviewed.[87]

One of the first reports of the synthetic lethal dependence of a specific mutation on splicing function is that of Hubert et al.[85] These investigators searched for glioblastoma multiforme (GBM)-lethal genes using genome-wide RNAi screens in multiple GMB stem cells (GSCs), patient isolates, and neural stem cells (NSCs) in order to classify the genes that are differentially required for GSC expansion. These studies revealed that the plant homeodomain-finger domain protein (PHF5A) was differentially required for expansion and viability of several GSC isolates. Further, molecular studies demonstrated that GSCs have a novel requirement for PHF5A activity. Knockdown of PHF5A resulted in splicing changes in thousands of essential genes, some of which are expected to alter cell division and growth. Also, these authors showed that sensitivity to U2snRNP perturbation could be established in NSCs and fibroblasts overexpressing MYC. Although MYC is not frequency amplified in GBM, MYC is coordinately activated by mutations in p53 and PTEN. In summary, this study established that patient-derived GSCs are vulnerable to perturbation in splicing, which results in a reduction in GSC viability and loss of GBM tumor maintenance. The authors also showed that splicing modulators such as sudemycin C1 showed selective toxicity to GBMs and fibroblasts overexpressing MYC. Since standard of care therapies is ineffective against GBM, the authors concluded that targeting PHF5A and/or U2 snRNP activity offers a new therapeutic inroad for this GBM.

Another more recent study also identified sudemycin sensitivity and a synthetic lethal partner in MYC-driven triple negative breast cancers.[88] In this work, it was found that the spliceosome is a target in MYC-driven cancers. These researchers identified the BUD31 protein as an MYC-synthetic lethal gene in human mammary epithelial cells, and showed that BUD31 was required for spliceosome assembly and catalytic activity. Activity of SF3B1 and other splicing factors associate with BUD31 are also required by oncogenic MYC. MYC activation induces an increase in total pre-mRNA synthesis, suggesting an increased burden on the core spliceosome to process pre-mRNA. In contrast to normal cells, reduction of functional SF3B1 in MYC-hyperactivated cells leads to splicing aberrations, widespread effects on pre-mRNA maturation, and deregulation of many critical cell processes. Genetic or pharmacological modulation of the spliceosome in vivo impairs survival, tumorigenicity, and metastatic inclination of MYC-dependent breast cancers. Importantly, this work showed that a reduction in SF3B1 activity is effective in human MYC-dependent breast cancer patient-derived xenografts (PDX) in vivo using the SF3B1 targeted agent sudemycin D6 (SD6) that was developed in the Webb laboratory.[88]

5.10.2.1.2 Tumors bearing spliceosome mutations are vulnerable to splicing modulation

Following the identification of many common spliceosome recurrent mutations in the MDS, CLL, and AML, there was initially confusion regarding the functional effects of these mutations, since little was known regarding the precise functional consequences of these splicing mutations. The observed recurrent mutations are consistently heterozygous and only very rarely occur together, indicating that one wild-type copy of the normally functional gene product is essential. Given that the spliceosome has important regulatory functions, the standard expectations of "gain of function" or "loss of function" are likely undefined with respect to the splice-site regulatory subunits, given the current understanding that the spliceosome components that are mutated are involved in the *fidelity* of 3′-splice site recognition. Thus, for these proteins a different concept: *change of function*, must be considered. Many researchers hypothesized that such cancers might be particularly sensitive to agents that target SF3B1 since these mutations seemed to produce an oncogenic splicing program. Thus, agents such as SD6 or E7107 were used to test this hypothesis (see **Figs. 5** and **6**).

One of the first such studies that was reported found that the spliceosome modulators sudemycin D1 and D6 showed selective cytotoxicity in primary CLL cells when compared with normal lymphocytes and tumor cells from other B-lymphoid cancers, with a slight bias for CLL cases bearing spliceosome mutations.[107] This work reported that sudemycin exhibited antitumor activity in

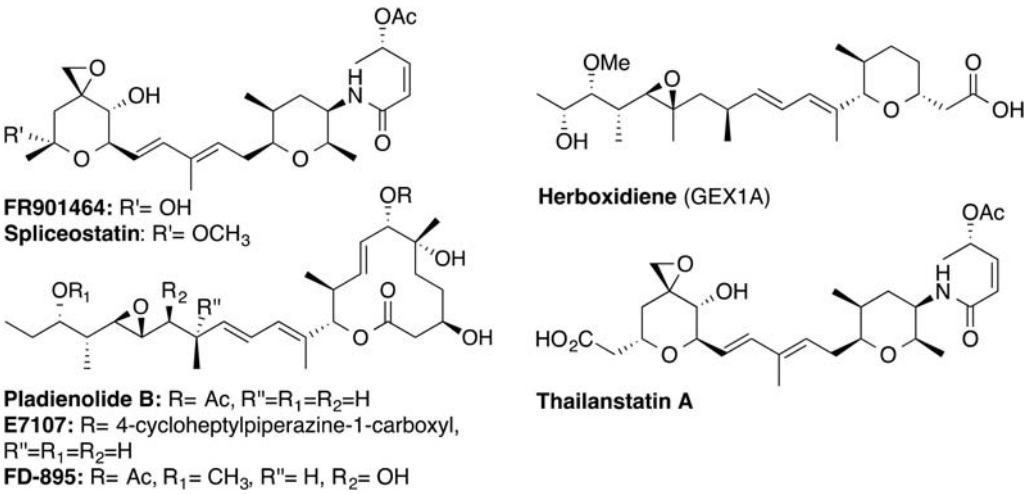

Fig. 5 Natural product spliceosome modulators and active derivatives (FR901464,[89,90] meayamycins,[52] pladienolides,[91,92] FD-895,[93–95] herboxidiene,[96,97] and thailanstatin A).[98]

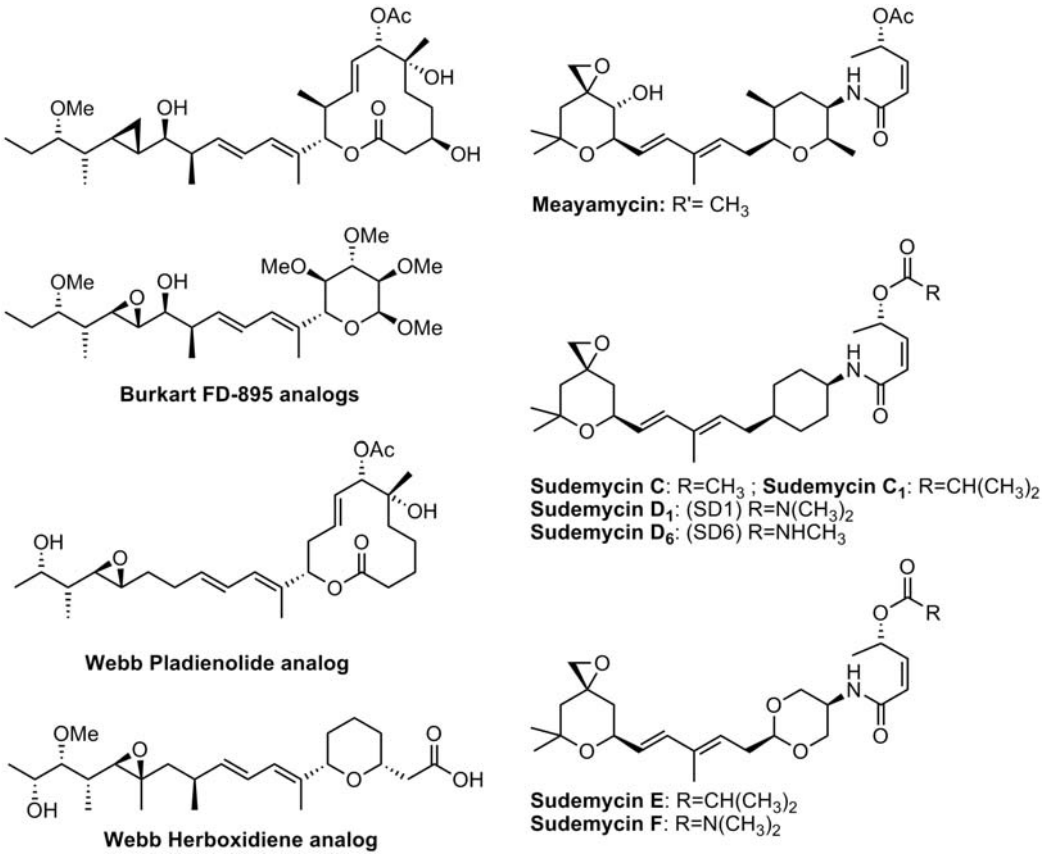

Fig. 6 Active totally synthetic analogs of splicing modulatory natural products discussed in the text. The *left panel* shows the Burkart analogs,[99,100] the weakly active Webb pladienolide analog,[101] and 6-norherboxidiene,[102,103] meayamycin,[52] and the sudemycins.[104–106]

NOD/SCID/IL2Rγ −/− (NSG) mice engrafted with primary cells from CLL patients.[107] This study showed a remarkable selectivity of the SF3B1 targeted agent SD6 for most of the CLL genotypes, which may indicate a common mechanism is driving CLL in addition to the spliceosome mutations and that this common mechanism results in selective susceptibility to any additional reduction in 3′-splice site fidelity. In another conceptually related publication, the authors tested this hypothesis using mice genetically engineered to express a mutated allele of SR splicing factor 2 (Srsf2P95H), which is recurrent in individuals with MDS and AML, in an inducible manner in hematopoietic cells.[108] These mice rapidly succumbed to fatal bone marrow failure, demonstrating that Srsf2-mutated cells depend on the wild-type Srsf2 allele for survival. These authors also showed that treatment with the spliceosome modulator E7107[109,110] specifically showed anticancer activity in both isogenic mouse leukemias and PDX AMLs carrying spliceosomal mutations. Thus, the authors of this publication concluded that:

> Collectively, these data provide genetic and pharmacol evidence that leukemias with spliceosomal gene mutations are preferentially susceptible to addnl. splicing perturbations in vivo as compared to leukemias without such mutations. Modulation of spliceosome function may thus provide a new therapeutic avenue in genetically defined subsets of individuals with MDS or AML.[108]

5.10.2.2 Natural Products and Derivatives Targeting *SF3B1*

In 2007, two research groups (from Astellas Pharma, Inc. and Eisai Co, Ltd., respectively) independently reported two structurally dissimilar bacterial natural products, FR901464 (FR) and pladienolide (Fig. 5), both targeting a similar site on the SF3B subunit of the spliceosome.[109,111] This work proved to be foundational for the field of small molecules that target SF3B1. Subsequent work inspired by these 2007 publications reported additional natural products that were shown to target the SF3B subunit. These subsequent reports include herboxidiene (GEX1A)[97] (isolated from Streptomyces sp. A7847) and the thailanstatins (isolated from *Burkholderia thailandensis*).[98] A similar interaction with the SF3B subunit (which is part of the spliceosomal U2 snRNP that recognizes the branch point and the 3′-splice site) is also likely for the macrolide natural product FD-895, given its potent biological activity

and its high structural and pharmacophore similarity to pladienolide.[95] Many of these bacterial fermentation products show cytotoxic IC_{50}s in the low nanomolar range in several tumor cell lines and have been reported to have a similar distinctive effect on the cell cycle in mammalian cell lines, including cell cycle arrest in the G1 and G2/M phases.[90] Several of these natural products have also been reported to show potent antitumor activity in vitro and in vivo.[89,91]

Work in this area led to the development of the semisynthetic pladienolide analog E7107 (Fig. 5) that entered Phase I clinical studies,[76,109,110] without the benefit of many subsequent recent discoveries relevant to mechanism of action, tumor selectivity, and patient stratification.[4,9] The clinical trials of E7107 were suspended and never reinitiated due to the ocular toxicity of this compound.[110] These results strongly supports the use of pharmacodynamic assays that have recently been reported, as an integral part of the splicing modulatory drug development process, as was used for SD6, since the pharmacodynamics for this class of drugs has unique features. The most notable feature of this class of drugs is the long-lasting cytotoxic effects following drug "washout" in vitro.[104] Though this washout effect is most notable for tumors, we inferred that this is likely to also be the case for sensitive, rapidly dividing normal tissue. We concluded that pulsatile treatment (via slow intravenous infusion) with a fast-acting drug, which possesses a relatively short half-life, is a critical criterion to use in the development of drugs in this class.[105] In contrast to this requirement, observed in our studies, E7107 was optimized on the basis of developing a longer half-life when compared to the parent natural product (pladienolide) series.

Though researchers initially characterized these compounds as "splicing inhibitors," the mechanism was subsequently elucidated and these compounds are now understood to effect alternate splicing,[105] through altering the 3′-splice site selection fidelity of the spliceosome[112] and are correctly understood to be splicing modulators and not general inhibitors of splicing.[4,9] One of our important contributions to this field has been our publication of cell-based splicing assays that use a PCR readout,[104] or a luciferase reporter,[113] and the observation that the *cytotoxicity potency of a range of natural or synthetic splicing modulators correlates to the potency for splicing modulation in this assay*.[102,105] It has also been shown that the potencies of pladienolide, herboxidiene, and sudemycin in cell-based cytotoxicity assays correlate with the potencies in a cell-based luciferase splicing reporter assay.[113] Evidence has been presented that this latter cell-based splicing reporter assay specifically reports on-target spliceosome modulatory pharmacodynamic activity in real time. The structures for the compounds discussed above are presented in Fig. 5.

5.10.2.3 Synthetic natural product analogs targeting *SF3B1*

The initial analogs of the natural product FR901464 were prepared as part of work that examined novel total synthetic routes to this compound first by the Jacobsen group,[114,115] and then by the Koide group[116,117] who also developed more chemically stable analogs (meayamycins),[52] and explored the structure-activity for a set of synthetic analogs of this compound class.[118,119] FD-895 is another natural product that is structurally related to pladienolide, which shows similar splicing modulatory and antitumor activity, and was the target of the successful total synthesis and analoging effort by the Burkart group.[95,100] Most remarkably, the Burkart group recently developed a completely novel, active structural analog, which replaces the macrolide component of FD-895 with a sugar scaffold.[100] This latter work is a tour de force and truly an extraordinary example of natural product molecular design.

As part of an effort to develop a class of drug-like synthetic spliceosome modulators the Webb group reported the design and synthesis of FR analogs that contain only 3 chiral centers (the sudemycins),[104–106,120] pladienolide analogs,[101] and several herboxidiene analogs (including a pladienolide–herboxidiene hybrid),[102] which included many new active compounds that effectively modulate alternate splicing.[104] Additionally, we recently reported our results from a genome-wide array analysis of sudemycin treated tumor cells; we found that sudemycins cause a rapid wide-ranging change in alternate pre-mRNA splicing. This same paper also showed that a biotin-labeled sudemycin probe directly interacts with the SF3B1 protein.[43] Our lead optimization work has primarily focused on the sudemycins, which are chemically stable synthetic molecules that were designed based on the known FR structure–activity relationships and the application of a hypothetical consensus pharmacophore model that is derived from molecular overlays of FR and PD.[106] This work ultimately led to SD6,[105] which is currently in preclinical Investigational New Drug (IND) development, with clinical studies for the treatment of myelodysplastic syndromes expected to start in 2018. The structures for the compounds discussed above are presented in Fig. 6.

5.10.2.4 Inhibitors of the CDC-Like Kinases

Compounds that inhibit members of the cdc-like kinase (CLK) family of kinases are known to modulate pre-mRNA splicing through the inhibition of SR protein phosphorylation.[121] The medicinal chemistry of this emerging area has been extensively reviewed.[121,122] Several diverse marine natural products[122] and synthetic compounds[123,124] have been found to be inhibitors of the CLK family (Figs. 7–9).[122] Several groups have shown that selective CLK inhibitors modulate splicing through their action on spliceosome components.[123,124] This area is nascent and may be fertile ground for the discovery of new compounds for cancer and other diseases that are associated with splicing aberrations. With the recent insights on the biology of the spliceosome medicinal chemistry in this area, as discussed above, drug discovery targeting the various CLKs (especially CLK1 and CLK2) is likely to expand in near future.[121]

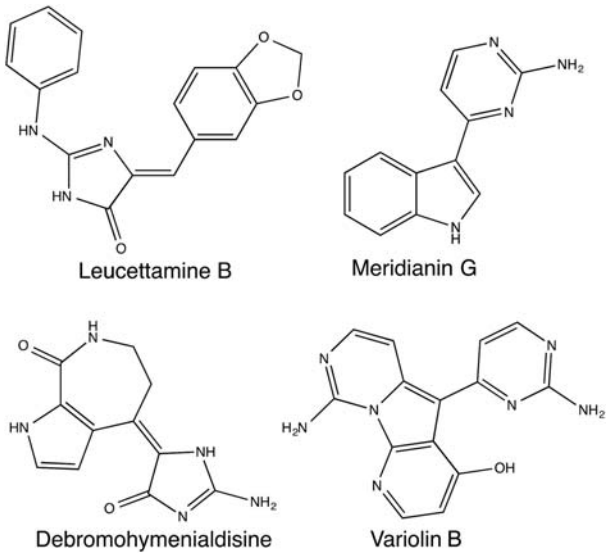

Fig. 7 Examples of marine natural products targeting CLKs.[122]

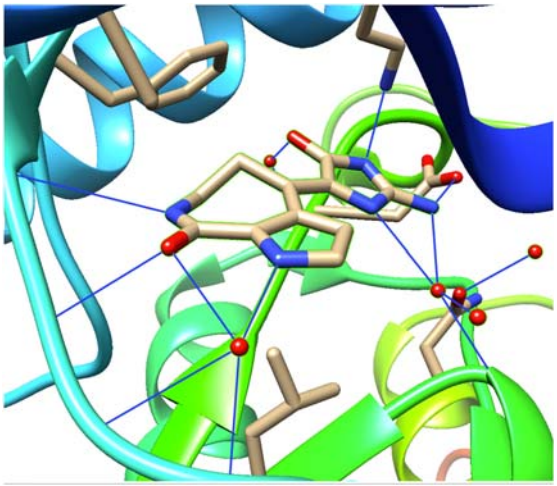

Fig. 8 A representation of the structure of debromohymenialdisine (K0010) bound to CLK1 using the published coordinates,[125] highlighting the hydrogen bonds to the ligand *(as blue lines)*. This figure was prepared using UCSF Chimera.[126]

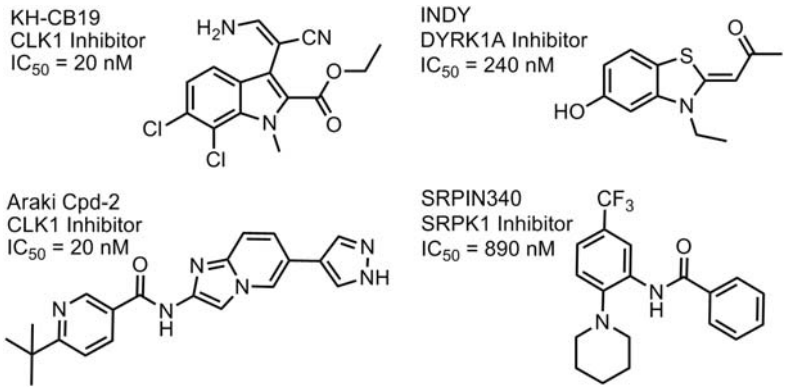

Fig. 9 Synthetic CLK, DYRK1A, and SRPK1 inhibitors showing cell-based activity[121]: KH-CB19,[124] Araki Cpd-2,[123] INDY,[127] and SRPIN340[128]

5.10.3 Conclusions

As discussed earlier, combined progress in natural product screening, target identification, spliceosome-related medicinal chemistry, and high-throughput transcriptome sequencing has led to a remarkable convergence of independent research areas, which have simultaneously identified new oncology drug targets and new small-molecule therapeutic agents. There is good reason to believe that these insights will lead to an expansion of spliceosome medicinal chemistry and the development of many new selective and highly effective chemotherapeutics for a range of cancers.

References

1. Will, C. L.; Luhrmann, R. Spliceosome Structure and Function. *Cold Spring Harb. Perspect. Biol.* **2011,** *3* (7). a003707.
2. Kramer, A. The Structure and Function of Proteins Involved in Mammalian Pre-mRNA Splicing. *Annu. Rev. Biochem.* **1996,** *65,* 367–409.
3. Wahl, M. C.; Will, C. L.; Luhrmann, R. The Spliceosome: Design Principles of a Dynamic RNP Machine. *Cell* **2009,** *136,* 701–718.
4. Bonnal, S.; Vigevani, L.; Valcarcel, J. The Spliceosome as a Target of Novel Antitumour Drugs. *Nat. Rev. Drug Discov.* **2012,** *11,* 847–859.
5. Yan, C.; Hang, J.; Wan, R.; Huang, M.; Wong, C. C.; Shi, Y. Structure of a Yeast Spliceosome at 3.6-Angstrom Resolution. *Science* **2015,** *349,* 1182–1191.
6. Nguyen, T. H.; Galej, W. P.; Bai, X. C.; Savva, C. G.; Newman, A. J.; Scheres, S. H.; Nagai, K. The Architecture of the Spliceosomal U4/U6.U5 Tri-snRNP. *Nature* **2015,** *523,* 47–52.
7. Rymond, B. Targeting the Spliceosome. *Nat. Chem. Biol.* **2007,** *3,* 533–535.
8. van Alphen, R. J.; Wiemer, E. A.; Burger, H.; Eskens, F. A. The Spliceosome as Target for Anticancer Treatment. *Br. J. Cancer* **2009,** *100,* 228–232.
9. Webb, T. R.; Joyner, A. S.; Potter, P. M. The Development and Application of Small Molecule Modulators of SF3b as Therapeutic Agents for Cancer. *Drug Discov. Today* **2013,** *18,* 43–49.
10. Lee, Y.; Rio, D. C. Mechanisms and Regulation of Alternative Pre-mRNA Splicing. *Annu. Rev. Biochem.* **2015,** *84,* 291–323.
11. Turunen, J. J.; Niemela, E. H.; Verma, B.; Frilander, M. J. The Significant Other: Splicing by the Minor Spliceosome. *Wiley Interdiscip. Rev. RNA* **2013,** *4,* 61–76.
12. Merkin, J.; Russell, C.; Chen, P.; Burge, C. B. Evolutionary Dynamics of Gene and Isoform Regulation in Mammalian Tissues. *Science* **2012,** *338,* 1593–1599.
13. Barbosa-Morais, N. L.; Irimia, M.; Pan, Q.; Xiong, H. Y.; Gueroussov, S.; Lee, L. J.; Slobodeniuc, V.; Kutter, C.; Watt, S.; Colak, R.; Kim, T.; Misquitta-Ali, C. M.; Wilson, M. D.; Kim, P. M.; Odom, D. T.; Frey, B. J.; Blencowe, B. J. The Evolutionary Landscape of Alternative Splicing in Vertebrate Species. *Science* **2012,** *338,* 1587–1593.
14. Kelemen, O.; Convertini, P.; Zhang, Z.; Wen, Y.; Shen, M.; Falaleeva, M.; Stamm, S. Function of Alternative Splicing. *Gene* **2013,** *514,* 1–30.
15. Yang, X.; Coulombe-Huntington, J.; Kang, S.; Sheynkman, G. M.; Hao, T.; Richardson, A.; Sun, S.; Yang, F.; Shen, Y. A.; Murray, R. R.; Spirohn, K.; Begg, B. E.; Duran-Frigola, M.; MacWilliams, A.; Pevzner, S. J.; Zhong, Q.; Trigg, S. A.; Tam, S.; Ghamsari, L.; Sahni, N.; Yi, S.; Rodriguez, M. D.; Balcha, D.; Tan, G.; Costanzo, M.; Andrews, B.; Boone, C.; Zhou, X. J.; Salehi-Ashtiani, K.; Charloteaux, B.; Chen, A. A.; Calderwood, M. A.; Aloy, P.; Roth, F. P.; Hill, D. E.; Iakoucheva, L. M.; Xia, Y.; Vidal, M. Widespread Expansion of Protein Interaction Capabilities by Alternative Splicing. *Cell* **2016,** *164,* 805–817.
16. Ladomery, M. Aberrant Alternative Splicing is Another Hallmark of Cancer. *Int. J. Cell Biol.* **2013,** *2013,* 463786.
17. Zhou, Z.; Fu, X. D. Regulation of Splicing by SR Proteins and SR Protein-Specific Kinases. *Chromosoma* **2013,** *122,* 191–207.
18. Busch, A.; Hertel, K. J. Evolution of SR Protein and hnRNP Splicing Regulatory Factors. *Wiley Interdiscip. Rev. RNA* **2012,** *3,* 1–12.
19. Shepard, P. J.; Hertel, K. J. The SR Protein Family. *Genome Biol.* **2009,** *10,* 242.
20. Falaleeva, M.; Pages, A.; Matuszek, Z.; Hidmi, S.; Agranat-Tamir, L.; Korotkov, K.; Nevo, Y.; Eyras, E.; Sperling, R.; Stamm, S. Dual Function of C/D Box Small Nucleolar RNAs in rRNA Modification and Alternative Pre-mRNA Splicing. *Proc. Natl. Acad. Sci. U. S. A.* **2016,** *113,* E1625–E1634.
21. Cooper, T. A.; Mattox, W. The Regulation of Splice-Site Selection, and Its Role in Human Disease. *Am. J. Hum. Genet.* **1997,** *61,* 259–266.
22. Wang, J.; Smith, P. J.; Krainer, A. R.; Zhang, M. Q. Distribution of SR Protein Exonic Splicing Enhancer Motifs in Human Protein-Coding Genes. *Nucleic Acids Res.* **2005,** *33,* 5053–5062.
23. Nigro, J. M.; Cho, K. R.; Fearon, E. R.; Kern, S. E.; Ruppert, J. M.; Oliner, J. D.; Kinzler, K. W.; Vogelstein, B. Scrambled Exons. *Cell* **1991,** *64,* 607–613.
24. Hasler, J.; Samuelsson, T.; Strub, K. Useful 'Junk': Alu RNAs in the Human Transcriptome. *Cell. Mol. Life Sci.* **2007,** *64,* 1793–1800.
25. Jeck, W. R.; Sorrentino, J. A.; Wang, K.; Slevin, M. K.; Burd, C. E.; Liu, J.; Marzluff, W. F.; Sharpless, N. E. Circular RNAs are Abundant, Conserved, and Associated With ALU Repeats. *RNA* **2013,** *19,* 141–157.
26. Lasda, E.; Parker, R. Circular RNAs: Diversity of Form and Function. *RNA* **2014,** *20,* 1829–1842.
27. Salzman, J.; Chen, R. E.; Olsen, M. N.; Wang, P. L.; Brown, P. O. Cell-Type Specific Features of Circular RNA Expression. *PLoS Genet.* **2013,** *9,* e1003777.
28. Bachmayr-Heyda, A.; Reiner, A. T.; Auer, K.; Sukhbaatar, N.; Aust, S.; Bachleitner-Hofmann, T.; Mesteri, I.; Grunt, T. W.; Zeillinger, R.; Pils, D. Correlation of Circular RNA Abundance With Proliferation—Exemplified With Colorectal and Ovarian Cancer, Idiopathic Lung Fibrosis, and Normal Human Tissues. *Sci. Rep.* **2015,** *5,* 8057.
29. Abe, N.; Matsumoto, K.; Nishihara, M.; Nakano, Y.; Shibata, A.; Maruyama, H.; Shuto, S.; Matsuda, A.; Yoshida, M.; Ito, Y.; Abe, H. Rolling Circle Translation of Circular RNA in Living Human Cells. *Sci. Rep.* **2015,** *5,* 16435.
30. Matera, A. G.; Wang, Z. A Day in the Life of the Spliceosome. *Nat. Rev. Mol. Cell Biol.* **2014,** *15,* 108–121.
31. Berget, S. M. Exon Recognition in Vertebrate Splicing. *J. Biol. Chem.* **1995,** *270,* 2411–2414.
32. Valadkhan, S.; Mohammadi, A.; Wachtel, C.; Manley, J. L. Protein-Free Spliceosomal snRNAs Catalyze a Reaction That Resembles the First Step of Splicing. *RNA* **2007,** *13,* 2300–2311.
33. Valadkhan, S.; Manley, J. L. Characterization of the Catalytic Activity of U2 and U6 snRNAs. *RNA* **2003,** *9,* 892–904.
34. Dignam, J. D.; Lebovitz, R. M.; Roeder, R. G. Accurate Transcription Initiation by RNA Polymerase II in a Soluble Extract From Isolated Mammalian Nuclei. *Nucleic Acids Res.* **1983,** *11,* 1475–1489.
35. Muller, S.; Wolpensinger, B.; Angenitzki, M.; Engel, A.; Sperling, J.; Sperling, R. A Supraspliceosome Model for Large Nuclear Ribonucleoprotein Particles Based on Mass Determinations by Scanning Transmission Electron Microscopy. *J. Mol. Biol.* **1998,** *283,* 383–394.
36. Raitskin, O.; Angenitzki, M.; Sperling, J.; Sperling, R. Large Nuclear RNP Particles—the Nuclear Pre-mRNA Processing Machine. *J. Struct. Biol.* **2002,** *140,* 123–130.
37. Azubel, M.; Habib, N.; Sperling, R.; Sperling, J. Native Spliceosomes Assemble With Pre-mRNA to Form Supraspliceosomes. *J. Mol. Biol.* **2006,** *356,* 955–966.
38. Schor, I. E.; Allo, M.; Kornblihtt, A. R. Intragenic Chromatin Modifications: A New Layer in Alternative Splicing Regulation. *Epigenetics* **2010,** *5,* 174–179.
39. Dujardin, G.; Lafaille, C.; Petrillo, E.; Buggiano, V.; Gomez Acuna, L. I.; Fiszbein, A.; Godoy Herz, M. A.; Nieto Moreno, N.; Munoz, M. J.; Allo, M.; Schor, I. E.; Kornblihtt, A. R. Transcriptional Elongation and Alternative Splicing. *Biochim. Biophys. Acta* **2013,** *1829,* 134–140.
40. Andersson, R.; Enroth, S.; Rada-Iglesias, A.; Wadelius, C.; Komorowski, J. Nucleosomes are Well Positioned in Exons and Carry Characteristic Histone Modifications. *Genome Res.* **2009,** *19,* 1732–1741.
41. Schwartz, S.; Meshorer, E.; Ast, G. Chromatin Organization Marks Exon-Intron Structure. *Nat. Struct. Mol. Biol.* **2009,** *16,* 990–995.
42. Sims, R. J., 3rd; Millhouse, S.; Chen, C. F.; Lewis, B. A.; Erdjument-Bromage, H.; Tempst, P.; Manley, J. L.; Reinberg, D. Recognition of Trimethylated Histone H3 Lysine 4 Facilitates the Recruitment of Transcription Postinitiation Factors and Pre-mRNA Splicing. *Mol. Cell* **2007,** *28,* 665–676.

43. Convertini, P.; Shen, M.; Potter, P. M.; Palacidos, G.; Lagisetti, C.; de la Grange, P.; Horinski, C.; Mittendorf, Y.; Webb, T. R.; Stamm, S. Sudemycin E Influences Alternative Splicing and Changes Chromatin Modifications. *Nucleic Acids Res.* **2014,** *42,* 4947–4961.
44. Kaida, D.; Berg, M. G.; Younis, I.; Kasim, M.; Singh, L. N.; Wan, L.; Dreyfuss, G. U1 snRNP Protects Pre-mRNAs From Premature Cleavage and Polyadenylation. *Nature* **2010,** *468,* 664–668.
45. Vithana, E. N.; Abu-Safieh, L.; Allen, M. J.; Carey, A.; Papaioannou, M.; Chakarova, C.; Al-Maghtheh, M.; Ebenezer, N. D.; Willis, C.; Moore, A. T.; Bird, A. C.; Hunt, D. M.; Bhattacharya, S. S. A Human Homolog of Yeast Pre-mRNA Splicing Gene, PRP31, Underlies Autosomal Dominant Retinitis Pigmentosa on Chromosome 19q13.4 (RP11). *Mol. Cell* **2001,** *8,* 375–381.
46. Boon, K. L.; Grainger, R. J.; Ehsani, P.; Barrass, J. D.; Auchynnikava, T.; Inglehearn, C. F.; Beggs, J. D. Prp8 Mutations That Cause Human Retinitis Pigmentosa Lead to a U5 snRNP Maturation Defect in Yeast. *Nat. Struct. Mol. Biol.* **2007,** *14,* 1077–1083.
47. Chakarova, C. F.; Hims, M. M.; Bolz, H.; Abu-Safieh, L.; Patel, R. J.; Papaioannou, M. G.; Inglehearn, C. F.; Keen, T. J.; Willis, C.; Moore, A. T.; Rosenberg, T.; Webster, A. R.; Bird, A. C.; Gal, A.; Hunt, D.; Vithana, E. N.; Bhattacharya, S. S. Mutations in HPRP3, a Third Member of Pre-mRNA Splicing Factor Genes, Implicated in Autosomal Dominant Retinitis Pigmentosa. *Hum. Mol. Genet.* **2002,** *11,* 87–92.
48. Liu, T.; Jin, X.; Zhang, X.; Yuan, H.; Cheng, J.; Lee, J.; Zhang, B.; Zhang, M.; Wu, J.; Wang, L.; Tian, G.; Wang, W. A Novel Missense SNRNP200 Mutation Associated With Autosomal Dominant Retinitis Pigmentosa in a Chinese Family. *PLoS ONE* **2012,** *7,* e45464.
49. He, H.; Liyanarachchi, S.; Akagi, K.; Nagy, R.; Li, J.; Dietrich, R. C.; Li, W.; Sebastian, N.; Wen, B.; Xin, B.; Singh, J.; Yan, P.; Alder, H.; Haan, E.; Wieczorek, D.; Albrecht, B.; Puffenberger, E.; Wang, H.; Westman, J. A.; Padgett, R. A.; Symer, D. E.; de la Chapelle, A. Mutations in U4atac snRNA, a Component of the Minor Spliceosome, in the Developmental Disorder MOPD I. *Science* **2011,** *332,* 238–240.
50. Tanackovic, G.; Ransijn, A.; Ayuso, C.; Harper, S.; Berson, E. L.; Rivolta, C. A Missense Mutation in PRPF6 Causes Impairment of Pre-mRNA Splicing and Autosomal-Dominant Retinitis Pigmentosa. *Am. J. Hum. Genet.* **2011,** *88,* 643–649.
51. Shen, H.; Zheng, X.; Luecke, S.; Green, M. R. The U2AF35-Related Protein Urp Contacts the 3′ Splice Site to Promote U12-Type Intron Splicing and the Second Step of U2-Type Intron Splicing. *Genes Dev.* **2010,** *24,* 2389–2394.
52. Albert, B. J.; Sivaramakrishnan, A.; Naka, T.; Czaicki, N. L.; Koide, K. Total Syntheses, Fragmentation Studies, and Antitumor/Antiproliferative Activities of FR901464 and Its Low Picomolar Analogue. *J. Am. Chem. Soc.* **2007,** *129,* 2648–2659.
53. Brinkman, B. M. Splice Variants as Cancer Biomarkers. *Clin. Biochem.* **2004,** *37,* 584–594.
54. Martin, M.; Masshofer, L.; Temming, P.; Rahmann, S.; Metz, C.; Bornfeld, N.; van de Nes, J.; Klein-Hitpass, L.; Hinnebusch, A. G.; Horsthemke, B.; Lohmann, D. R.; Zeschnigk, M. Exome Sequencing Identifies Recurrent Somatic Mutations in EIF1AX and SF3B1 in Uveal Melanoma With Disomy 3. *Nat. Genet.* **2013,** *45,* 933–936.
55. Quesada, V.; Conde, L.; Villamor, N.; Ordonez, G. R.; Jares, P.; Bassaganyas, L.; Ramsay, A. J.; Bea, S.; Pinyol, M.; Martinez-Trillos, A.; Lopez-Guerra, M.; Colomer, D.; Navarro, A.; Baumann, T.; Aymerich, M.; Rozman, M.; Delgado, J.; Gine, E.; Hernandez, J. M.; Gonzalez-Diaz, M.; Puente, D. A.; Velasco, G.; Freije, J. M.; Tubio, J. M.; Royo, R.; Gelpi, J. L.; Orozco, M.; Pisano, D. G.; Zamora, J.; Vazquez, M.; Valencia, A.; Himmelbauer, H.; Bayes, M.; Heath, S.; Gut, M.; Gut, I.; Estivill, X.; Lopez-Guillermo, A.; Puente, X. S.; Campo, E.; Lopez-Otin, C. Exome Sequencing Identifies Recurrent Mutations of the Splicing Factor SF3B1 Gene in Chronic Lymphocytic Leukemia. *Nat. Genet.* **2012,** *44,* 47–52.
56. Hong, J. Y.; Seo, J. Y.; Kim, S. H.; Jung, H. A.; Park, S.; Kim, K.; Jung, C. W.; Kim, J. S.; Park, J. S.; Kim, H. J.; Jang, J. H. Mutations in the Spliceosomal Machinery Genes SRSF2, U2AF1, and ZRSR2 and Response to Decitabine in Myelodysplastic Syndrome. *Anticancer Res.* **2015,** *35,* 3081–3089.
57. Wang, J.; Takagaki, Y.; Manley, J. L. Targeted Disruption of an Essential Vertebrate Gene: ASF/SF2 is Required for Cell Viability. *Genes Dev.* **1996,** *15,* 2588–2599.
58. Klinck, R.; Bramard, A.; Inkel, L.; Dufresne-Martin, G.; Gervais-Bird, J.; Madden, R.; Paquet, E. R.; Koh, C.; Venables, J. P.; Prinos, P.; Jilaveanu-Pelmus, M.; Wellinger, R.; Rancourt, C.; Chabot, B.; Abou Elela, S. Multiple Alternative Splicing Markers for Ovarian Cancer. *Cancer Res.* **2008,** *68,* 657–663.
59. Misquitta-Ali, C. M.; Cheng, E.; O'Hanlon, D.; Liu, N.; McGlade, C. J.; Tsao, M. S.; Blencowe, B. J. Global Profiling and Molecular Characterization of Alternative Splicing Events Misregulated in Lung Cancer. *Mol. Cell. Biol.* **2011,** *31,* 138–150.
60. Venables, J. P.; Klinck, R.; Koh, C.; Gervais-Bird, J.; Bramard, A.; Inkel, L.; Durand, M.; Couture, S.; Froehlich, U.; Lapointe, E.; Lucier, J. F.; Thibault, P.; Rancourt, C.; Tremblay, K.; Prinos, P.; Chabot, B.; Elela, S. A. Cancer-Associated Regulation of Alternative Splicing. *Nat. Struct. Mol. Biol.* **2009,** *16,* 670–676.
61. David, C. J.; Manley, J. L. Alternative Pre-mRNA Splicing Regulation in Cancer: Pathways and Programs Unhinged. *Genes Dev.* **2010,** *24,* 2343–2364.
62. Kim, E.; Goren, A.; Ast, G. Insights Into the Connection Between Cancer and Alternative Splicing. *Trends Genet.* **2008,** *24,* 7–10.
63. Xu, Q.; Lee, C. Discovery of Novel Splice Forms and Functional Analysis of Cancer-Specific Alternative Splicing in Human Expressed Sequences. *Nucleic Acids Res.* **2003,** *31,* 5635–5643.
64. Supek, F.; Minana, B.; Valcarcel, J.; Gabaldon, T.; Lehner, B. Synonymous Mutations Frequently Act as Driver Mutations in Human Cancers. *Cell* **2014,** *156,* 1324–1335.
65. Raponi, M.; Kralovicova, J.; Copson, E.; Divina, P.; Eccles, D.; Johnson, P.; Baralle, D.; Vorechovsky, I. Prediction of Single-Nucleotide Substitutions That Result in Exon Skipping: Identification of a Splicing Silencer in BRCA1 Exon 6. *Hum. Mutat.* **2011,** *32,* 436–444.
66. Pecina-Slaus, N.; Majic, Z.; Musani, V.; Zeljko, M.; Cupic, H. Report on Mutation in Exon 15 of the APC Gene in a Case of Brain Metastasis. *J. Neuro-Oncol.* **2010,** *97,* 143–148.
67. Pecina-Slaus, N.; Nikuseva Martic, T.; Tomas, D.; Beros, V.; Zeljko, M.; Cupic, H. Meningiomas Exhibit Loss of Heterozygosity of the APC Gene. *J. Neuro-Oncol.* **2008,** *87,* 63–70.
68. Diederichs, S.; Bartsch, L.; Berkmann, J. C.; Frose, K.; Heitmann, J.; Hoppe, C.; Iggena, D.; Jazmati, D.; Karschnia, P.; Linsenmeier, M.; Maulhardt, T.; Mohrmann, L.; Morstein, J.; Paffenholz, S. V.; Ropenack, P.; Ruckert, T.; Sandig, L.; Schell, M.; Steinmann, A.; Voss, G.; Wasmuth, J.; Weinberger, M. E.; Wullenkord, R. The Dark Matter of the Cancer Genome: Aberrations in Regulatory Elements, Untranslated Regions, Splice Sites, Non-Coding RNA and Synonymous Mutations. *EMBO Mol. Med.* **2016,** *8,* 442–457.
69. Anczukow, O.; Buisson, M.; Leone, M.; Coutanson, C.; Lasset, C.; Calender, A.; Sinilnikova, O. M.; Mazoyer, S. BRCA2 Deep Intronic Mutation Causing Activation of a Cryptic Exon: Opening Toward a New Preventive Therapeutic Strategy. *Clin. Cancer Res.* **2012,** *18,* 4903–4909.
70. Sigalas, I.; Calvert, A. H.; Anderson, J. J.; Neal, D. E.; Lunec, J. Alternatively Spliced Mdm2 Transcripts With Loss of p53 Binding Domain Sequences: Transforming Ability and Frequent Detection in Human Cancer. *Nat. Med.* **1996,** *2,* 912–917.
71. Bartel, F.; Taubert, H.; Harris, L. C. Alternative and Aberrant Splicing of MDM2 mRNA in Human Cancer. *Cancer Cell* **2002,** *2,* 9–15.
72. Venables, J. P. Aberrant and Alternative Splicing in Cancer. *Cancer Res.* **2004,** *64,* 7647–7654.
73. Kalnina, Z.; Zayakin, P.; Silina, K.; Line, A. Alterations of Pre-mRNA Splicing in Cancer. *Genes Chromosom. Cancer* **2005,** *42,* 342–357.
74. Nakagawa, H.; Wardell, C. P.; Furuta, M.; Taniguchi, H.; Fujimoto, A. Cancer Whole-Genome Sequencing: Present and Future. *Oncogene* **2015,** *34,* 5943–5950.
75. Patel, L. R.; Nykter, M.; Chen, K.; Zhang, W. Cancer Genome Sequencing: Understanding Malignancy as a Disease of the Genome, Its Conformation, and Its Evolution. *Cancer Lett.* **2013,** *340,* 152–160.
76. Yoshida, K.; Sanada, M.; Shiraishi, Y.; Nowak, D.; Nagata, Y.; Yamamoto, R.; Sato, Y.; Sato-Otsubo, A.; Kon, A.; Nagasaki, M.; Chalkidis, G.; Suzuki, Y.; Shiosaka, M.; Kawahata, R.; Yamaguchi, T.; Otsu, M.; Obara, N.; Sakata-Yanagimoto, M.; Ishiyama, K.; Mori, H.; Nolte, F.; Hofmann, W. K.; Miyawaki, S.; Sugano, S.; Haferlach, C.; Koeffler, H. P.; Shih, L. Y.; Haferlach, T.; Chiba, S.; Nakauchi, H.; Miyano, S.; Ogawa, S. Frequent Pathway Mutations of Splicing Machinery in Myelodysplasia. *Nature* **2011,** *478,* 64–69.
77. Ogawa, S. Splicing Factor Mutations in Myelodysplasia. *Int. J. Hematol.* **2012,** *96,* 438–442.
78. Damm, F.; Nguyen-Khac, F.; Fontenay, M.; Bernard, O. A. Spliceosome and Other Novel Mutations in Chronic Lymphocytic Leukemia and Myeloid Malignancies. *Leukemia* **2012,** *26,* 2027–2031.
79. Murati, A.; Brecqueville, M.; Devillier, R.; Mozziconacci, M. J.; Gelsi-Boyer, V.; Birnbaum, D. Myeloid Malignancies: Mutations, Models and Management. *BMC Cancer* **2012,** *12,* 304.

80. Cancer Genome Atlas Research, N. Genomic and Epigenomic Landscapes of Adult De Novo Acute Myeloid Leukemia. *N. Engl. J. Med.* **2013,** *368,* 2059–2074.
81. Cancer Genome Atlas, N. Comprehensive Molecular Portraits of Human Breast Tumours. *Nature* **2012,** *490,* 61–70.
82. Maguire, S. L.; Leonidou, A.; Wai, P.; Marchio, C.; Ng, C. K.; Sapino, A.; Salomon, A. V.; Reis-Filho, J. S.; Weigelt, B.; Natrajan, R. C. SF3B1 Mutations Constitute a Novel Therapeutic Target in Breast Cancer. *J. Pathol.* **2015,** *235,* 571–580.
83. Imielinski, M.; Berger, A. H.; Hammerman, P. S.; Hernandez, B.; Pugh, T. J.; Hodis, E.; Cho, J.; Suh, J.; Capelletti, M.; Sivachenko, A.; Sougnez, C.; Auclair, D.; Lawrence, M. S.; Stojanov, P.; Cibulskis, K.; Choi, K.; de Waal, L.; Sharifnia, T.; Brooks, A.; Greulich, H.; Banerji, S.; Zander, T.; Seidel, D.; Leenders, F.; Ansen, S.; Ludwig, C.; Engel-Riedel, W.; Stoelben, E.; Wolf, J.; Goparju, C.; Thompson, K.; Winckler, W.; Kwiatkowski, D.; Johnson, B. E.; Janne, P. A.; Miller, V. A.; Pao, W.; Travis, W. D.; Pass, H. I.; Gabriel, S. B.; Lander, E. S.; Thomas, R. K.; Garraway, L. A.; Getz, G.; Meyerson, M. Mapping the Hallmarks of Lung Adenocarcinoma With Massively Parallel Sequencing. *Cell* **2012,** *150,* 1107–1120.
84. Harbour, J. W. Genomic, Prognostic, and Cell-Signaling Advances in Uveal Melanoma. American Society of Clinical Oncology educational book/ASCO. American Society of Clinical Oncology. Meeting**;** 2013; pp 388–391.
85. Hubert, C. G.; Bradley, R. K.; Ding, Y.; Toledo, C. M.; Herman, J.; Skutt-Kakaria, K.; Girard, E. J.; Davison, J.; Berndt, J.; Corrin, P.; Hardcastle, J.; Basom, R.; Delrow, J. J.; Webb, T.; Pollard, S. M.; Lee, J.; Olson, J. M.; Paddison, P. J. Genome-Wide RNAi Screens in Human Brain Tumor Isolates Reveal a Novel Viability Requirement for PHF5A. *Genes Dev.* **2013,** *27,* 1032–1045.
86. Pagliarini, R.; Shao, W.; Sellers, W. R. Oncogene Addiction: Pathways of Therapeutic Response, Resistance, and Road Maps Toward a Cure. *EMBO Rep.* **2015,** *16,* 280–296.
87. Dvinge, H.; Kim, E.; Abdel-Wahab, O.; Bradley, R. K. RNA Splicing Factors as Oncoproteins and Tumour Suppressors. *Nat. Rev. Cancer* **2016,** *16,* 413–430.
88. Hsu, T. Y.; Simon, L. M.; Neill, N. J.; Marcotte, R.; Sayad, A.; Bland, C. S.; Echeverria, G. V.; Sun, T.; Kurley, S. J.; Tyagi, S.; Karlin, K. L.; Dominguez-Vidana, R.; Hartman, J. D.; Renwick, A.; Scorsone, K.; Bernardi, R. J.; Skinner, S. O.; Jain, A.; Orellana, M.; Lagisetti, C.; Golding, I.; Jung, S. Y.; Neilson, J. R.; Zhang, X. H.; Cooper, T. A.; Webb, T. R.; Neel, B. G.; Shaw, C. A.; Westbrook, T. F. The Spliceosome is a Therapeutic Vulnerability in MYC-Driven Cancer. *Nature* **2015,** *525,* 384–388.
89. Nakajima, H.; Hori, Y.; Terano, H.; Okuhara, M.; Manda, T.; Matsumoto, S.; Shimomura, K. New Antitumor Substances, FR901463, FR901464 and FR901465. II. Activities Against Experimental Tumors in Mice and Mechanism of Action. *J. Antibiot.* **1996,** *49,* 1204–1211.
90. Nakajima, H.; Sato, B.; Fujita, T.; Takase, S.; Terano, H.; Okuhara, M. New Antitumor Substances, FR901463, FR901464 and FR901465. I. Taxonomy, Fermentation, Isolation, Physico-Chemical Properties and Biological Activities. *J. Antibiot.* **1996,** *49,* 1196–1203.
91. Mizui, Y.; Sakai, T.; Iwata, M.; Uenaka, T.; Okamoto, K.; Shimizu, H.; Yamori, T.; Yoshimatsu, K.; Asada, M. Pladienolides, New Substances From Culture of Streptomyces Platensis Mer-11107. III. In Vitro and In Vivo Antitumor Activities. *J. Antibiot.* **2004,** *57,* 188–196.
92. Kanada, R. M.; Itoh, D.; Nagai, M.; Niijima, J.; Asai, N.; Mizui, Y.; Abe, S.; Kotake, Y. Total Synthesis of the Potent Antitumor Macrolides Pladienolide B and D. *Angew. Chem. Int. Ed.* **2007,** *46,* 4350–4355.
93. Seki-Asano, M.; Okazaki, T.; Yamagishi, M.; Sakai, N.; Takayama, Y.; Hanada, K.; Morimoto, S.; Takatsuki, A.; Mizoue, K. Isolation and Characterization of a New 12-Membered Macrolide FD-895. *J. Antibiot.* **1994,** *47,* 1395–1401.
94. Mandel, A. L.; Jones, B. D.; La Clair, J. J.; Burkart, M. D. A Synthetic Entry to Pladienolide B and FD-895. *Bioorg. Med. Chem. Lett.* **2007,** *17,* 5159–5164.
95. Villa, R.; Mandel, A. L.; Jones, B. D.; La, C. J. J.; Burkart, M. D. Structure of FD-895 Revealed Through Total Synthesis. *Org. Lett.* **2012,** *14,* 5396–5399.
96. Sakai, Y.; Yoshida, T.; Ochiai, K.; Uosaki, Y.; Saitoh, Y.; Tanaka, F.; Akiyama, T.; Akinaga, S.; Mizukami, T. GEX1 Compounds, Novel Antitumor Antibiotics Related to Herboxidiene, Produced by Streptomyces sp. I. Taxonomy, Production, Isolation, Physicochemical Properties and Biological Activities. *J. Antibiot.* **2002,** *55,* 855–862.
97. Hasegawa, M.; Miura, T.; Kuzuya, K.; Inoue, A.; Won Ki, S.; Horinouchi, S.; Yoshida, T.; Kunoh, T.; Koseki, K.; Mino, K.; Sasaki, R.; Yoshida, M.; Mizukami, T. Identification of SAP155 as the Target of GEX1A (Herboxidiene), an Antitumor Natural Product. *ACS Chem. Biol.* **2011,** *6,* 229–233.
98. Liu, X.; Biswas, S.; Berg, M. G.; Antapli, C. M.; Xie, F.; Wang, Q.; Tang, M.-C.; Tang, G.-L.; Zhang, L.; Dreyfuss, G.; Cheng, Y.-Q. Genomics-Guided Discovery of Thailanstatins A, B, and C As Pre-mRNA Splicing Inhibitors and Antiproliferative Agents From Burkholderia Thailandensis MSMB43. *J. Nat. Prod.* **2013,** *76,* 685–693.
99. Villa, R.; Kashyap, M. K.; Kumar, D.; Kipps, T. J.; Castro, J. E.; La Clair, J. J.; Burkart, M. D. Stabilized Cyclopropane Analogs of the Splicing Inhibitor FD-895. *J. Med. Chem.* **2013,** *56,* 6576–6582.
100. Dhar, S.; La Clair, J. J.; Leon, B.; Hammons, J. C.; Yu, Z.; Kashyap, M. K.; Castro, J. E.; Burkart, M. D. A Carbohydrate-Derived Splice Modulator. *J. Am. Chem. Soc.* **2016,** *138,* 5063–5068.
101. Gundluru, M. K.; Pourpak, A.; Cui, X.; Morris, S. W.; Webb, T. R. Design, Synthesis and Initial Biological Evaluation of a Novel Pladienolide Analog Scaffold. *Med. Chem. Commun.* **2011,** *2,* 904–908.
102. Lagisetti, C.; Yermolina, M. V.; Sharma, L. K.; Palacios, G.; Prigaro, B. J.; Webb, T. R. Pre-mRNA Splicing-Modulatory Pharmacophores: The Total Synthesis of Herboxidiene, a Pladienolide-Herboxidiene Hybrid Analog and Related Derivatives. *ACS Chem. Biol.* **2014,** *9,* 643–648.
103. Ghosh, A. K.; Lv, K.; Ma, N.; Cardenas, E. L.; Effenberger, K. A.; Jurica, M. S. Design, Synthesis and In Vitro Splicing Inhibition of Desmethyl and Carba-Derivatives of Herboxidiene. *Org. Biomol. Chem.* **2016,** *14,* 5263–5271.
104. Fan, L.; Lagisetti, C.; Edwards, C. C.; Webb, T. R.; Potter, P. M. Sudemycins, Novel Small Molecule Analogues of FR901464, Induce Alternative Gene Splicing. *ACS Chem. Biol.* **2011,** *6,* 582–589.
105. Lagisetti, C.; Palacios, G.; Goronga, T.; Freeman, B.; Caufield, W.; Webb, T. R. Optimization of Antitumor Modulators of Pre-mRNA Splicing. *J. Med. Chem.* **2013,** *56,* 10033–10044.
106. Lagisetti, C.; Pourpak, A.; Jiang, Q.; Cui, X.; Goronga, T.; Morris, S. W.; Webb, T. R. Antitumor Compounds Based on a Natural Product Consensus Pharmacophore. *J. Med. Chem.* **2008,** *51,* 6220–6224.
107. Xargay-Torrent, S.; Lopez-Guerra, M.; Rosich, L.; Montraveta, A.; Roldan, J.; Rodriguez, V.; Villamor, N.; Aymerich, M.; Lagisetti, C.; Webb, T. R.; Lopez-Otin, C.; Campo, E.; Colomer, D. The Splicing Modulator Sudemycin Induces a Specific Antitumor Response and Cooperates With Ibrutinib in Chronic Lymphocytic Leukemia. *Oncotarget* **2015,** *6,* 22734–22749.
108. Lee, S. C.; Dvinge, H.; Kim, E.; Cho, H.; Micol, J. B.; Chung, Y. R.; Durham, B. H.; Yoshimi, A.; Kim, Y. J.; Thomas, M.; Lobry, C.; Chen, C. W.; Pastore, A.; Taylor, J.; Wang, X.; Krivtsov, A.; Armstrong, S. A.; Palacino, J.; Buonamici, S.; Smith, P. G.; Bradley, R. K.; Abdel-Wahab, O. Modulation of Splicing Catalysis for Therapeutic Targeting of Leukemia With Mutations in Genes Encoding Spliceosomal Proteins. *Nat. Med.* **2016,** *22,* 672–678.
109. Kotake, Y.; Sagane, K.; Owa, T.; Mimori-Kiyosue, Y.; Shimizu, H.; Uesugi, M.; Ishihama, Y.; Iwata, M.; Mizui, Y. Splicing Factor SF3b as a Target of the Antitumor Natural Product Pladienolide. *Nat. Chem. Biol.* **2007,** *3,* 570–575.
110. Eskens, F. A.; Ramos, F. J.; Burger, H.; O'Brien, J. P.; Piera, A.; de Jonge, M. J.; Mizui, Y.; Wiemer, E. A.; Carreras, M. J.; Baselga, J.; Tabernero, J. Phase I Pharmacokinetic and Pharmacodynamic Study of the First-in-Class Spliceosome Inhibitor E7107 in Patients With Advanced Solid Tumors. *Clin. Cancer Res.* **2013,** *19,* 6296–6304.
111. Kaida, D.; Motoyoshi, H.; Tashiro, E.; Nojima, T.; Hagiwara, M.; Ishigami, K.; Watanabe, H.; Kitahara, T.; Yoshida, T.; Nakajima, H.; Tani, T.; Horinouchi, S.; Yoshida, M. Spliceostatin A Targets SF3b and Inhibits Both Splicing and Nuclear Retention of Pre-mRNA. *Nat. Chem. Biol.* **2007,** *3,* 576–583.
112. Corrionero, A.; Minana, B.; Valcarcel, J. Reduced Fidelity of Branch Point Recognition and Alternative Splicing Induced by the Anti-Tumor Drug Spliceostatin A. *Genes Dev.* **2011,** *25,* 445–459.
113. Shi, Y.; Joyner, A. S.; Shadrick, W.; Palacios, G.; Lagisetti, C.; Potter, P. M.; Sambucetti, L. C.; Stamm, S.; Webb, T. R. Pharmacodynamic Assays to Facilitate Preclinical and Clinical Development of Pre-mRNA Splicing Modulatory Drug Candidates. *Pharmacol. Res. Perspect.* **2015,** *3,* e00158.
114. Thompson, C. F.; Jamison, T. F.; Jacobsen, E. N. Total Synthesis of FR901464. Convergent Assembly of Chiral Components Prepared by Asymmetric Catalysis. *J. Am. Chem. Soc.* **2000,** *122,* 10482–10483.
115. Thompson, C. F.; Jamison, T. F.; Jacobsen, E. N. FR901464: Total Synthesis, Proof of Structure, and Evaluation of Synthetic Analogues. *J. Am. Chem. Soc.* **2001,** *123,* 9974–9983.

116. Albert, B. J.; Koide, K. Synthesis of a C4-epi-C1-C6 Fragment of FR901464 Using a Novel Bromolactolization. *Org. Lett.* **2004,** *6,* 3655–3658.
117. Albert, B. J.; Sivaramakrishnan, A.; Naka, T.; Koide, K. Total Synthesis of FR901464, an Antitumor Agent That Regulates the Transcription of Oncogenes and Tumor Suppressor Genes. *J. Am. Chem. Soc.* **2006,** *128,* 2792–2793.
118. Osman, S.; Albert, B. J.; Wang, Y.; Li, M.; Czaicki, N. L.; Koide, K. Structural Requirements for the Antiproliferative Activity of Pre-mRNA Splicing Inhibitor FR901464. *Chemistry* **2011,** *17,* 895–904.
119. Osman, S.; Waud, W. R.; Gorman, G. S.; Day, B. W.; Koide, K. Evaluation of FR901464 Analogues In Vitro and In Vivo. *Med. Chem. Commun.* **2011,** *2,* 38–43.
120. Lagisetti, C.; Pourpak, A.; Goronga, T.; Jiang, Q.; Cui, X.; Hyle, J.; Lahti, J. M.; Morris, S. W.; Webb, T. R. Synthetic mRNA Splicing Modulator Compounds With In Vivo Antitumor Activity. *J. Med. Chem.* **2009,** *52,* 6979–6990.
121. Ohe, K.; Hagiwara, M. Modulation of Alternative Splicing With Chemical Compounds in New Therapeutics for Human Diseases. *ACS Chem. Biol.* **2015,** *10,* 914–924.
122. Jain, P.; Karthikeyan, C.; Moorthy, N. S.; Waiker, D. K.; Jain, A. K.; Trivedi, P. Human CDC2-Like Kinase 1 (CLK1): A Novel Target for Alzheimer's Disease. *Curr. Drug Targets* **2014,** *15,* 539–550.
123. Araki, S.; Dairiki, R.; Nakayama, Y.; Murai, A.; Miyashita, R.; Iwatani, M.; Nomura, T.; Nakanishi, O. Inhibitors of CLK Protein Kinases Suppress Cell Growth and Induce Apoptosis by Modulating Pre-mRNA Splicing. *PLoS ONE* **2015,** *10,* e0116929.
124. Fedorov, O.; Huber, K.; Eisenreich, A.; Filippakopoulos, P.; King, O.; Bullock, A. N.; Szklarczyk, D.; Jensen, L. J.; Fabbro, D.; Trappe, J.; Rauch, U.; Bracher, F.; Knapp, S. Specific CLK Inhibitors From a Novel Chemotype for Regulation of Alternative Splicing. *Chem. Biol.* **2011,** *18,* 67–76.
125. Bullock, A. N.; Das, S.; Debreczeni, J. E.; Rellos, P.; Fedorov, O.; Niesen, F. H.; Guo, K.; Papagrigoriou, E.; Amos, A. L.; Cho, S.; Turk, B. E.; Ghosh, G.; Knapp, S. Kinase Domain Insertions Define Distinct Roles of CLK Kinases in SR Protein Phosphorylation. *Structure* **2009,** *17,* 352–362.
126. Pettersen, E. F.; Goddard, T. D.; Huang, C. C.; Couch, G. S.; Greenblatt, D. M.; Meng, E. C.; Ferrin, T. E. UCSF Chimera—A Visualization System for Exploratory Research and Analysis. *J. Comput. Chem.* **2004,** *25,* 1605–1612.
127. Ogawa, Y.; Nonaka, Y.; Goto, T.; Ohnishi, E.; Hiramatsu, T.; Kii, I.; Yoshida, M.; Ikura, T.; Onogi, H.; Shibuya, H.; Hosoya, T.; Ito, N.; Hagiwara, M. Development of a Novel Selective Inhibitor of the Down Syndrome-Related Kinase Dyrk1A. *Nat. Commun.* **2010,** *1,* 86.
128. Fukuhara, T.; Hosoya, T.; Shimizu, S.; Sumi, K.; Oshiro, T.; Yoshinaka, Y.; Suzuki, M.; Yamamoto, N.; Herzenberg, L. A.; Herzenberg, L. A.; Hagiwara, M. Utilization of Host SR Protein Kinases and RNA-Splicing Machinery During Viral Replication. *Proc. Natl. Acad. Sci. U. S. A.* **2006,** *103,* 11329–11333.
129. Makishima, H.; Visconte, V.; Sakaguchi, H.; Jankowska, A. M.; Abu Kar, S.; Jerez, A.; Przychodzen, B.; Bupathi, M.; Guinta, K.; Afable, M. G.; Sekeres, M. A.; Padgett, R. A.; Tiu, R. V.; Maciejewski, J. P. Mutations in the Spliceosome Machinery, a Novel and Ubiquitous Pathway in Leukemogenesis. *Blood* **2012,** *119,* 3203–3210.

5.11 Cancer Immunotherapy—An Emerging Field That Bridges Oncology and Immunology Research

JL Adams, KJ Duffy, ML Moore, and J Yang, GlaxoSmithKline, Collegeville, PA, United States

© 2017 Elsevier Ltd. All rights reserved.

5.11.1	**Introduction**	358
5.11.2	**Concept and History of Immuno-Oncology**	358
5.11.3	**Immunity in the Tumor Microenvironment (TME)**	359
5.11.3.1	Modulation of T Cell Activation and Differentiation	360
5.11.3.2	T Regulatory Cells (Tregs)	360
5.11.3.3	Myeloid-Derived Suppressor Cells (MDSCs)	360
5.11.3.4	Tumor-Associated Macrophages (TAMs)	361
5.11.3.5	Modulation of DC Function in Tumor	361
5.11.3.6	Current Status of Immuno-Oncology Therapy	361
5.11.4	**Small Molecule Targets**	361
5.11.4.1	Amino Acid Catabolism	362
5.11.4.1.1	Tryptophan	362
5.11.4.1.2	Arginine	365
5.11.4.2	Purinergic Signaling in Immune Cells	367
5.11.4.2.1	P2X and P2Y receptor modulators	368
5.11.4.2.2	Adenosine receptors (A_1, A_{2A}, A_{2B}, and A_3)	368
5.11.4.2.3	ATP metabolism: CD73 and CD39 nucleotidases	370
5.11.4.2.4	COX-2 and EP2/EP4 receptor antagonists	371
5.11.4.3	Pattern Recognition Receptors (PRRs)	372
5.11.4.3.1	TLR7/8	373
5.11.4.3.2	TLR4	374
5.11.4.3.3	TLR9	375
5.11.4.3.4	TLR agonist in development for IO	375
5.11.4.3.5	STING	376
5.11.4.3.6	Targeted delivery of PRR agonists	377
5.11.4.4	Kinase Inhibitors	378
5.11.4.4.1	TGF-β RI/ALK5 inhibitors	378
5.11.4.4.2	RON inhibitors	380
5.11.4.4.3	CSF-R1 inhibitors	380
5.11.4.4.4	TAM receptor signaling inhibitors	380
5.11.4.4.5	PI3K inhibitors	381
5.11.4.5	Checkpoint Inhibitors	381
5.11.4.5.1	Small molecule inhibitors	382
5.11.4.5.2	Peptide inhibitors	385
5.11.5	**Conclusion**	385
References		386

Abbreviations

ADCC Antibody-dependent cell-mediated cytotoxicity, in which antibody binding to foreign cells recruits cytotoxic effector cells

ADO Adenosine

APCs Antigen-presenting cells, which process and present antigens to T cells

ARG Arginase

CD4 Cell surface marker for activated T helper cells

CD8 Cell surface marker for activated cytotoxic T cells

COX Cyclooxygenase

CTLA4 T-cell checkpoint receptor, modulating immune suppression

DC Dendritic cell, one major subtype of antigen-presenting cells

CGN2 General controlled nonrepressed kinase, an immunosuppressive enzyme which detects cellular amino acid levels

eATP Extracellular ATP

GPI Glycosylphosphatidylinositol, membrane glycolipid which can be covalently attached to protein C-termini to link them to the membrane

IDO Indolamine 2,3-dioxygenase
IFN Interferon
iNOS Inducible nitrogen oxide synthetase
MDSC Myeloid-derived suppressor cell, immunosuppressive immune cells derived from bone marrow
MHC Major histocompatibility complex, surface proteins which present antigens to the TCR
NK cell Natural killer cell, key component of the innate immune system
PD1 T-cell checkpoint receptor, modulating immune suppression
PD-L1 Ligand that activates PD1, often overexpressed in cancer cells
PI3K Phosphatidylinositol-3-kinase
ROS Reactive oxygen species
STING Stimulator of interferon genes, immunostimulatory protein of the innate immune system which responds to cytosolic DNA
TAM Tumor-associated macrophage
TCR T-cell receptor, responsible for antigen recognition
TDO Tryptophan 2,3-dioxygenase
TLR Toll-like receptors, proinflammatory pattern recognition receptors of the innate immune system which recognize conserved elements of pathogens
TME Tumor microenvironment
Treg Regulatory T cell that mediates immunosuppression

5.11.1 Introduction

In 2011 the FDA approved Ipilimumab (anti-CTLA4, trade name Yervoy, Bristol-Myers Squibb) for the treatment of metastatic melanoma. In 2014 anti-PD1 antibodies Keytruda (Merck) and Opdivo (Bristol-Myers Squibb) were approved by the FDA for the same indication. These immune checkpoint inhibitors, as well as their combinations, have demonstrated remarkable clinical activity in multiple cancer types ranging from hematologic tumors to solid malignancies. Furthermore, a significant portion of the patients developed durable responses and remain cancer free years after the treatment. The success of these three agents has firmly established that the immune system plays an important role in the control of tumorigenesis and that the tumor must develop immune escape mechanisms in order to grow. Already cancer immunotherapy is established as one of the important pillars of cancer treatment adding a powerful new intervention in addition to surgery, hormone therapy, radiation therapy, chemotherapy, and cancer targeted therapy. Basic immunology research and pharmaceutical development in the field of immuno-oncology is now intensely focused on understanding the immune escape mechanisms developed by tumors and identifying methods to reestablish an effective immune response to the tumor. A number of approaches are being actively explored including the development of vaccines, recombinant cytokines, antibodies, autologous T cells, and small molecule drugs. Herein we describe the rationale for small molecule drug immunotherapies in cancer, and detail some of the specific targets that should be considered for developing new cancer immunotherapies.

5.11.2 Concept and History of Immuno-Oncology

In the mid-19th century, Rudolf Virchow observed the presence of leukocytes in tumors, providing the first clue of a functional role for the immune system in cancer biology.[1] Several decades later, William Coley made the observation that some cancer patients inadvertently infected by bacteria experienced profound tumor regressions. Based on this observation, he developed and conducted the first immunotherapy treatment of cancer.[2] His treatment, termed Coley's Toxins, contains two bacterial strains of *Streptococcus pyogenes* and *Serratia marcescens*. He and others used this therapy to treat different types of tumors. Although the outcome varied among the patients, the drug induced partial or even complete regression of tumors in a small percentage of patients. The mechanism of action of Coley's Toxins, however, remained a mystery for many decades after its first use which in part impeded its acceptance among immunologists and oncologists. From the late 19th century to the first half of the 20th century, the field of immunology was almost entirely devoted to the development of antitoxins (antibodies) against various diseases through vaccination. This field, which was pioneered by Edward Jenner's groundbreaking work on the development of the first vaccine against smallpox, has greatly advanced medical research and improved public health.[3] Consequently, the humoral immune system (immunity mediated by macromolecules such as antibodies in extracellular fluids) remained the focus of immunology research until the early 1960s when researchers unveiled the cellular arm of the human immune system.[4] It is now clear that cellular immunity, mediated by leukocytes, constitutes the major defense mechanism against cancer. Various types of immune cells such as neutrophils, NK (natural killer) cells, macrophages, dendritic cells (DCs), T cells ($CD4^+$ T helper cells and $CD8^+$ cytotoxic T cells), and B cells form the two lines of the human defense system: the innate immune system (nonspecific immunity) and the adaptive immune system (antigen-specific immunity). These cells work in a highly coordinated fashion both spatially and temporally, through the secretion of signaling molecules such as cytokines and chemokines or through direct cell–cell interactions, to control the body's intricate and highly effective defense system against both foreign and endogenous insults including cancer.

The concept of cancer immune-surveillance was first conceived by Paul Ehrlich in 1909[5] and formally proposed by Sir Macfarlane Burnett and Lewis Thomas in 1957.[6] The key tenet of this hypothesis is that cellular immunity is critical in protecting the body

from neoplastic disease. This concept was initially erroneously challenged owing to a lack of good understanding of the cellular immune system as well as the unavailability of suitable experimental model systems,[7] but has been well validated with various studies carried out since the 1990s. For example, it was shown that endogenously produced IFNγ (interferon γ), a critical cytokine involved in cellular immunity, could protect the host against transplanted tumors and inhibit tumorigenesis of chemically induced or spontaneous tumors in a number of studies carried out on mice.[8] Furthermore, RAG2$^{-/-}$ mice (mice that lack NKT, T and B cells) developed MCA (methylcholanthrene, a potent carcinogen)-induced sarcoma more frequently and rapidly than the wild-type controls.[9] In humans, individuals with severe immune deficiency have a higher probability of developing cancers[10,11] and there is a positive correlation between tumor immune infiltrate and increased survival in patients.[12]

Based on the concept of tumor immune surveillance, the tumor must develop mechanisms to escape immune control in order to grow; hence the concept of cancer immunoediting. There are three phases in this process: elimination, equilibrium, and escape (the three E's of cancer immunoediting).[13] In the elimination phase immune-surveillance results in the detection and destruction of tumors. Tumors that survive the elimination phase enter the equilibrium phase where the immune response is able to contain, but is not sufficient to eradicate the tumor cells. Through genetic mutations and Darwinian selection, newly mutated cancer cells may possess increased resistance to immune attack and these cells will eventually escape the immune surveillance and grow into clinically observable tumors. Cancer cells that successfully escape immune surveillance are conferred a selective growth advantage in the face of an increasingly ineffective adaptive immune response. The goal of cancer immunotherapy is to reestablish immune surveillance by interfering with various cancer immunoediting mechanisms.

5.11.3 Immunity in the Tumor Microenvironment (TME)

Both the innate and the adaptive immune systems participate in tumor immune surveillance. The innate immune system responds to generic signals to elicit rapid immune responses without the need of presensitization. This system is comprised of several different types of immune cells: NK cells, granulocytes (neutrophils, basophils, and eosinophils), mast cells, γδT cells, macrophages, and DCs. Macrophages and DCs are professional antigen-presenting cells (APCs) that serve as an important link between the innate and adaptive immune responses and will be described in more detail in the subsequent section. Among the remaining innate cell types, NK cells have a predominant role in innate immunity against tumor. NK cells express a range of inhibitory and activating receptors that allow them to recognize healthy versus "stressed" cells including tumor cells. The inhibitory KIR and CD94-NKG2A receptors bind to the major histocompatibility complex (MHC) class I molecules on normal cells and prevent the cytolytic activity of NK cells. It is known that certain tumor cells downregulate MHC class I to evade the antigen-specific adaptive immune response. These tumor cells therefore can be recognized as "missing-self" cells and can induce the cytolytic function of NK cells.[14] In addition to inhibitory receptors, NK cells possess a number of activating receptors such as NKG2D, NCRs, and DNAM1. These receptors recognize a range of ligands that typically are not expressed on normal cells but their expression can be upregulated on infected cells and rapidly proliferating cells such as tumor cells (induced-self recognition). For example, NKG2D recognizes MICA, MICB, and ULBP1-ULBP6 that are predominantly expressed on "stressed" cells. NK cells also carry receptor CD16 that recognizes the Fc region of the IgG antibodies, activating antibody-dependent cell-mediated cytotoxicity (ADCC) against antibody-tagged cells. In addition to the direct cytolytic activity, NK cells and other innate cells can also secret cytokines and chemokines to shape the immune response. One of the important cytokines secreted by NK cells is IFNγ which has a critical role in cellular immunity against cancer. Tumor cells may evade NK cell killing by shedding of the activating ligands, or through induction of chronic activation of NK cells leading to NK cell anergy.[15]

The adaptive immune response is a higher level defense system that is initiated by the recognition of specific antigens by B cells and T cells. T cell-mediated adaptive responses play the more critical role in immune surveillance against cancer and will be described in more detail here. Tumor cells, although derived from normal cells, have been shown to express tumor-specific antigens that can be detected by the immune system. These antigens include neoantigens created by mutations in tumor cells, antigens that are overexpressed in tumor cells, and germline antigens that are silent in normal tissue but expressed in cancers.[16] Tumor antigens can be presented directly on the surface of the tumor cells by the MHC class I molecule, or captured by professional APCs such as DCs and macrophages, and presented on the surface by MHC class I and II molecules. APCs possess membrane-associated and intracellular pattern recognition receptors (PRRs) that sense pathogen-associated molecular patterns (PAMPs) such as bacterial lipopolysaccharide (LPS), bacterial or viral nucleic acid, bacterial lipopeptides, fungal glucans, etc., as well as damage-associated molecular patterns (DAMPs) such as cell components released during cell damage and death. APCs actively sample the surrounding tissue antigens and have the ability to engulf cell debris and pathogens through processes such as phagocytosis. Detection of PAMPs initiates the immune response against pathogens whereas detection of DAMPs initiates the immune response against necrotic tissues including necrosis induced by tumor cell growth. In addition, one specific type of apoptosis termed immunogenic cell death (ICD) has gained importance in the field of immuno-oncology. ICD can be induced by certain cytotoxic agents or radiation and can initiate effective immune responses.[17] Recognition of PAMPs and DAMPs by PRRs leads to the activation of APCs with the upregulation of a number of costimulatory molecules such as CD40, CD80, CD86, and MHCs on DCs that interact with specific surface molecules on the T cells and enhance T cell activation. At the same time, activated APCs secret various cytokines/chemokines to boost the immune response, and enhance the antigen processing and presentation activities to T cells. The effector T cells are composed of CD8^{+} cytotoxic T cells and CD4^{+} T helper cells that recognize antigens presented by MHCI and MHCII complexes, respectively. These cells are the main players in the development of effective adaptive immune responses against specific insults.

When APCs carrying the antigens move to the nearby draining lymph nodes, they present antigens to effector T cells with matching T-cell receptor complexes (TCRs). T cells, once activated through antigen recognition, go through clonal expansion. T cells expressing antigen-specific TCRs traffic and infiltrate the tumor bed. Activated $CD4^+$ T cells coordinate actions of various immune cells through secretion of soluble factors and through direct ligand–receptor interactions to ensure an appropriate immune response. $CD8^+$ T cells carry out the mission of direct recognition and killing of tumor cells harboring the same antigens. For effective immune-surveillance, this cycle must operate optimally. Tumors, on the other hand, have developed multiple mechanisms to interfere with various steps in this cycle in a way to promote immune escape and boost tumor growth.[18] Some of the major immune-suppressive mechanisms in the TME are briefly described below.

5.11.3.1 Modulation of T Cell Activation and Differentiation

T cell activation requires the binding of TCR to the matching peptide antigen presented by MHC complexes on APCs or tumor cells. In addition, the level and outcome of T cell activation is further controlled by a number of surface coreceptors that, upon binding to their respective ligands, produce costimulatory (interactions that further boost T cell activation) or coinhibitory/immune checkpoint signals (interactions that dampen the T cell response). Common T cell costimulatory receptors include CD28, ICOS, OX40, and CD137. Notable checkpoint coinhibitory signals are represented by PD1, CTLA-4, TIM3, LAG3, and A2aR.[19] These costimulatory and checkpoint interactions are crucial to ensure the proper level of the immune response toward a specific insult. It is known that tumors directly interfere with the T cell activation process by either downregulating the MHC complexes to make tumor cells less visible to the T cells[14] or inducing the inhibitory immune checkpoint pathway, particularly in the TME, to inhibit the T cell function.[19] PD-L1, the ligand for PD1, one of the major checkpoints during T cell activation, is upregulated in a number of tumors to induce T cell anergy, an induced tolerance state of T cells.[20]

$CD4^+$ T cells, upon activation, can differentiate into various functional classes that lead to different immune outcomes. Two of the major CD4 subtypes are termed Th1 and Th2 $CD4^+$ T cells.[21] The generation of these subtypes of T cells is controlled by the specific cytokine milieu to which the $CD4^+$ T cells are exposed during activation. Specifically, IL-12 and IL-4 are the main cytokines that induce Th1 and Th2 response, respectively.[22] The Th1 response leads to the production of IFNγ and upregulation of T cell surface costimulatory molecules such as CD40 ligand that promote the activation of macrophages and $CD8^+$ T cells and is one of the major cellular immune responses against tumor. The Th2 response leads to the secretion of cytokines such as IL-4, IL-5, IL-10, and IL-13 that have multiple functions including the defense against extracellular parasites, induction of the IgE production of B cells and the allergic reaction, and more relevant to the tumor setting, downregulation of the immune activity and promotion of tissue repair and regeneration. The Th2 response helps with the proper resolution of the immune response and the reestablishment of normal homeostasis. Tumors have developed mechanisms to bias the immune response toward the Th2 polarization by inducing the secretion of Th2 differentiating cytokines, hence suppressing immune attack and boosting tumor cell growth and invasion.

5.11.3.2 T Regulatory Cells (Tregs)

A specific subset of $CD4^+$ T cells called T regulatory cells or Treg cells play a major role in immune regulation to maintain systemic immune homeostasis. The forkhead box P3 (FOXP3) protein is expressed in this subset of cells and is the master transcription factor that controls the expression of genes to mediate the immune suppression function of Tregs.[23] Tregs exert their inhibitory activity through multiple mechanisms: secretion of the inhibitory cytokines such as IL-10 and TGFβ[24]; inhibition of target cells through direct cell–cell interactions[25]; constitutive expression of the T cell activation marker CD25 that results in the depletion of IL-2 (the ligand for CD25 and an essential growth factor for effector T cells) and starvation of effector T cells[26]; expression of additional inhibitory molecules such as CD39 and CD73 that produce extracellular adenosine, an important immune inhibitory molecule that leads to adenosine pathway activation in effector T cells and the inhibition of their functional activity.[27]

5.11.3.3 Myeloid-Derived Suppressor Cells (MDSCs)

Under healthy conditions, immature myeloid cells (IMCs) generated in bone marrow differentiate into granulocytes, macrophages, or DCs. Under certain pathological conditions including cancer, the differentiation of IMCs is partially blocked leading to the accumulation of a heterogeneous population of immature myeloid cells called MDSCs. These MDSCs possess strong immunosuppressive activity. The accumulation of MDSCs in tumors has been shown to inhibit T cell proliferation and activation.[28] There are two types of MDSCs based on their cellular origin, monocytic MDSCs and granulocytic MDSCs, that mediate their suppressive activities through overlapping but differential mechanisms.[29] Both subsets of MDSCs degrade arginine by upregulating the expression of arginase I and inducible nitric oxide synthase (iNOS or NOS2). Arginine is an essential nutrient for T cells and arginine deprivation constitutes one of the major mechanisms of MDSC-mediated immune suppression.[30] MDSCs also have increased expression of reactive oxygen species (ROS).[31] Superoxide anions, together with NO (nitric oxide, another product of iNOS), produce peroxynitrite that can suppress T cell function by nitration and nitrosylation of different amino acids on TCR and CD8 molecules on the surface of T cells, which causes the T cells to become unresponsive to antigen-specific stimulation.[32] In general, monocytic MDSCs generate high levels of NO and low levels of ROS whereas granulocytic MDSCs generate high levels of ROS and low levels of NO.[29] It is important to note that ROS and NO can have a direct cytotoxic effect on tumor cells as well.[33] This needs to be taken into

consideration when evaluating strategies of targeting MDSCs for cancer therapy. One additional mechanism of MDSC-mediated suppression activity is the ability of MDSCs to promote Treg development through secretion of specific cytokines as well as through direct cell–cell interactions.[34]

5.11.3.4 Tumor-Associated Macrophages (TAMs)

Analogous to the Th1 and Th2 $CD4^+$ T cells, macrophages can be stimulated and polarized into M1 and M2 subtypes to represent the two extremes of a continuous spectrum of macrophage phenotypes. M1 macrophages are activated by IFNγ and bacterial products. These macrophages secret IL-12, a major cytokine in the induction of the Th1 polarization of $CD4^+$ T cells. Therefore, M1 macrophages play an important role in mediating the immune attack on tumor. On the other hand, M2 macrophages are activated by Th2 cytokines such as IL-4 and IL-10. They express high levels of IL-10 and low levels of IL-12 and induce Th2 T cell differentiation.[35] TAMs are conditioned by the immune-suppressive tumor environment and have acquired the phenotype of the M2 macrophages. TAMs inhibit T cell activation and function and promote tumor growth and metastasis.[36]

5.11.3.5 Modulation of DC Function in Tumor

Human DCs are mainly derived from monocytes. There are two major DC subsets that are phenotypically and functionally distinct, conventional DCs (cDCs), and plasmacytoid DCs (pDCs). Tissue resident cDCs are immature DCs with high phagocytosis activity, allowing them to actively take up tissue antigens. However, immature DCs have low antigen presentation activity and do not induce T cell activation. Upon engaging PAMPs and DAMPs, DCs are activated with upregulated antigen presentation activity. Multiple factors in the TME inhibit the proper differentiation of DCs in tumor, including immunosuppressive cytokines, hypoxia, and upregulated extracellular adenosine production. These factors collectively induce the differentiation of immunosuppressive DCs with reduced IL-12 and enhanced production of IL-10, IL-6, IL-8, VEGF, COX2, TGFβ and IDO to bias the T cells toward Th2 polarization and T cell anergy.[37] In addition, DCs express a number of costimulatory and coinhibitory molecules on the surface that interact with various T cell coreceptors to fine tune the T cell activation and differentiation process. Immunosuppressive TME tips the balance of these interactions in favor of immune regulation. One notable example is the upregulation of PD-L1 expression on DCs leading to inhibition of T cell function.[38] Plasmacytoid DCs are one of the major producers of IFNα (interferon α), a type I interferon that plays critical role in initiating innate immunity and promoting Th1 adaptive response. Evidence exists that plasmacytoid DCs have impaired ability to produce IFNα in TME through, for example, the downregulation of toll-like receptor 9 (TLR9), a PRR that is selectively expressed on plasmacytoid DCs within DC lineage and induces downstream IFNα production.[39]

5.11.3.6 Current Status of Immuno-Oncology Therapy

Current strategies in the field of immuno-oncology are designed to reverse tumor immune tolerance by boosting the antigen presentation process or by directly activating T cells. Given the importance of the T cell surface receptor–ligand interactions in immune modulation, many antibody drugs are being developed to target these interactions with the goal of stimulating immune responses against tumor. The current marketed antibody drugs include cytotoxic T lymphocyte-associated antigen 4 (CTLA4) blocking antibody ipilimumab (Yervoy; Bristol-Myers Squibb) and programmed cell death protein 1 (PD1) blocking antibodies pembrolizumab (Keytruda; Merck) and nivolumab (Opdivo; Bristol-Myers Squibb). These antibodies work via distinct mechanisms to boost T cell activity. Ipilimumab, a fully human IgG1 mAb, relieves CTLA-4 mediated inhibition at the priming phase of T cell activation. Pembrolizumab and nivolumab are humanized mAbs that help reactivate anergic T cells by blocking the PD1/PD-L1 interaction. The critical importance of tumor control by T cells is further illustrated by autologous cell and gene therapy approaches. For these approaches, TCRs are genetically engineered to either render them high affinity toward a tumor cell-specific surface protein through the chimeric antigen receptor (CAR) technology, or build high affinity and specificity toward the tumor antigen/MHC complexes preferentially expressed on tumor cells. A patient's own T cells are transduced with the engineered TCR and reinfused into the same patient through a process called adoptive cell transfer (ACT).[40] These T cells then selectively bind to and kill the tumor cells possessing the targeted antigen(s).

5.11.4 Small Molecule Targets

While the targeting of cell surface protein–protein interactions is currently best achieved with therapeutic mAbs, there are many alternative processes and pathways that are open to intervention by traditional small-molecule drugs. As detailed by Adams et al.[32b] traditional small molecule medicines offer a number of potential advantages over recombinant protein approaches. These include (1) well developed processes to discover, develop, and advance compounds into the clinic; (2) the potential for orally active drugs that can be fine tuned to deliver a variety of exposure and duration of action profiles; (3) access to the CNS and the potential greater exposure in the TME; (4) access to intracellular targets; and (5) the potential of a pill versus an infusion to provide greater access of these medicines to the patient. Below we detail some of the most promising small-molecule drug targets for immunotherapies in cancer and the current status of discovery efforts.

5.11.4.1 Amino Acid Catabolism

Amino acid levels are a key indicator of cellular fitness to engage in metabolically demanding activities. Amino acids are not only required building blocks for protein synthesis, but their metabolites also provide input into the Krebs cycle as well as nitrogen to support nucleotide and phospholipid synthesis. A number of amino acid sensing systems have evolved which directly regulate key cellular functions.[41] Immune response is sensitive to amino acid levels,[42] and catabolism of cysteine, glutamine, phenylalanine, tryptophan, and arginine have been implicated in regulation of immune responses in tumors, especially through modulation of T-cell proliferation and activation.[17,43]

5.11.4.1.1 Tryptophan

5.11.4.1.1.1 Background

The first and rate-limiting step in tryptophan catabolism is oxidative cleavage of the pyrrole ring to generate *N*-formyl kynurenine. In humans, this is accomplished by one of three heme-containing enzymes. Tryptophan 2,3-dioxygenase (TDO, EC 1.13.11.11) is a tetrameric enzyme constitutively expressed in liver and brain. It has relatively stringent substrate specificity and is thought to be involved in the metabolism of dietary tryptophan to produce nicotinamide adenine dinucleotide (NAD^+) and to limit production of serotonin.[44] Indolamine 2,3-dioxygenase (IDO1, EC 1.13.1.52) is an inducible, monomeric enzyme. While it is widely found throughout the body, high levels are expressed mainly in the antigen-presenting dendritic cells and macrophages, where it is induced by a number of inflammatory stimuli.[45] More recently, IDO2, a paralog of IDO1, has been described. It shares about 40% homology with IDO1 and is constitutively expressed in liver and circulating and plasmacytoid dendritic cells.[44,46] IDO2 is a considerably less active enzyme than IDO1 both in vitro and in cell-based assays,[44,47] and its significance in immune regulation is unclear. Although the three enzymes share the same substrate, there are significant differences in substrate and inhibitor specificity among them,[47,48] suggesting that potent, selective inhibitors will likely be easier to obtain than potent pan-active ones.

IDO1, IDO2, and TDO have been reported to be highly expressed in various tumor types,[49] but most of the target validation has been performed with IDO1. IDO1 is thought to act mostly through induction, activation, or suppression of various T cell and dendritic cell functions, which lead to an immunosuppressive tumor environment.[50] Two mechanisms of action are known to be engaged as the result of oxidative metabolism of tryptophan. The decrease in tryptophan levels activates the stress response GCN2 kinase, which senses uncharged tRNA, and inactivates mTOR, complementary pathways which lead to T cell cycle arrest and apoptosis.[48,51] Additionally, kynurenine, a catabolic product dependent on tryptophan oxidation (**Fig. 1**), is both a regulatory molecule and an endogenous ligand for the aryl hydrocarbon receptor, and is thought to regulate both immune response and IDO activity.[48,52]

5.11.4.1.1.2 IDO1 inhibitors

Among the first IDO1 inhibitors described were tryptophan analogs (**Fig. 2**) like DL-1-methyl tryptophan (DL-1MT, **1**), a substrate-competitive inhibitor which exhibits a modest K_i of 6.6 μM.[53] When the isolated enantiomers of **1** were examined, the L-enantiomer was more potent in the biochemical assay as expected, but it was the D-enantiomer **2** which was significantly more potent in in vivo tumor proliferation assays.[54] This finding suggested that there was an additional target for **2**, and IDO2 was quickly identified as a new protein inhibited by **2**.[55] The consensus now, however, is that **2** is a poor inhibitor of both IDO1 and IDO2,[56] and the mechanism of its in vivo activity is still poorly understood. Despite the ambiguity of the in vivo mechanism of **2**, NewLink Genetics has taken it forward under the name Indoximod into a variety of clinical trials. The most recent data available show a combination of **2** with gemcitabine and nab-paclitaxel giving a 45% objective response rate (ORR) in a Phase 2 trial in metastatic pancreatic

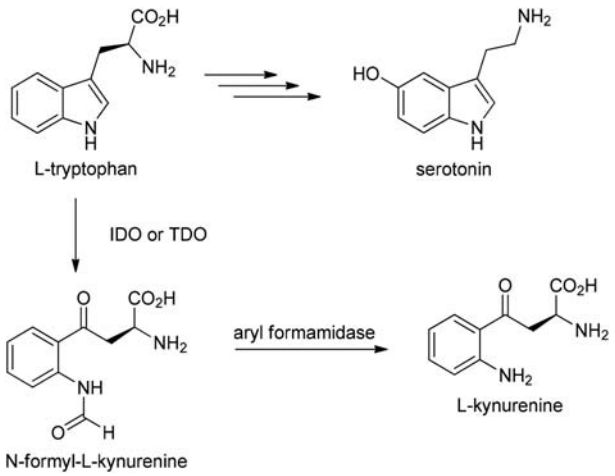

Fig. 1 Relevant pathways of tryptophan metabolism.

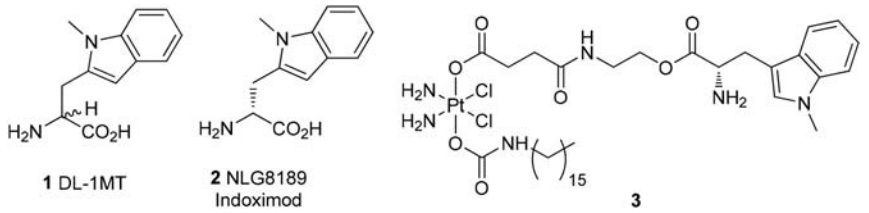

Fig. 2 IDO inhibitors.

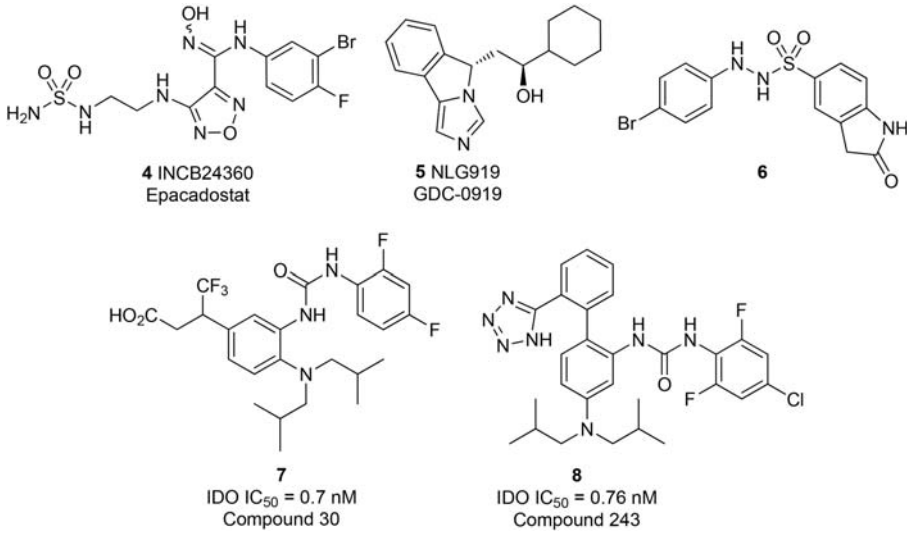

Fig. 3 IDO1 inhibitors.

cancer,[40a] and combinations with checkpoint inhibitors ipilimumab (CTLA-4), pembrolizumab (PD1), and nivolumab (PD1) giving objective response rates of 36–53% in a Phase Ib/II trial of unresectable stage 3 or 4 melanoma.[57] These combinations with **2** were significantly more efficacious than either agent singly. Taking advantage of the observation that **2** selectively accumulates in tumors,[54] the platinum-containing pro-drug **3** was shown to inhibit kynurenine production more potently than **2** and to induce apoptosis in a cis-platin-resistant SKOV3 ovarian cancer cell line.[58]

Investigators at Incyte disclosed the first potent, selective inhibitors of IDO and demonstrated *in vivo activity* in a mouse melanoma model.[59] This led to the development of INCB24360 (Epacadostat, **4**, Fig. 3), which has been advanced into a number of clinical trials.[60] Compound **4** is a potent inhibitor of IDO1 with an IC_{50} of 72 nM, and activity in cell-based kynurenine production assays in the 10–20 nM range. It is active in an in vivo tumor growth model with PAN02 pancreatic cancer cells but only in immunocompetent mice and not immunodeficient mice.[60] It has been in clinical trials in combination with the checkpoint inhibitor pembrolizumab (PD1) and in preliminary results showed a 57% ORR and an 86% disease control rate (DCR) in stage 3/4 melanoma and a 40% ORR and 80% DCR in stage 3/4 renal cell carcinoma.[61] INCB24360 has advanced to Phase III trials in combination with pembrolizumab and also in trials with nivolumab (PD1) and atezolizumab (PD-L1). Investigators at NewLink Genetics have recently disclosed a potent, selective IDO1 inhibitor, NLG919, which displays an IC_{50} of 28 nM against IDO1 and potent activity in cell-based and in vivo tumor models with B16F10 melanoma tumors.[62] While the structure has not been disclosed, it is thought to be **5** or a closely related structure. Investigators are currently recruiting for a clinical trial of **5** in combination with atezolizumab.

The phenylsulfonylhydrazide **6** has recently been described as a potent and selective inhibitor of IDO1, with an IC_{50} of 36 nM.[63] It demonstrates good single agent activity in a mouse CT-26 colorectal cancer model, showing decrease in kynurenine levels, increase in Trp/kynurenine ratio, decrease in tumor volume, and inhibition of tumor growth after oral dosing. Investigators at Bristol-Myers Squibb have recently disclosed potent IDO1 inhibitors **7**[64] and **8**,[65] which appear to be structurally related to **4**.

There is a single crystal structure of a high-affinity ligand, the racemate of **5**, bound to IDO1, shown in Fig. 4.[66] The bound ligand clearly shows the *S* configuration at the pyrrole moiety but the electron density can accommodate either configuration of the alcohol moiety. The imidazole nitrogen interacts with the heme iron as expected, and the phenyl and cyclohexyl moieties occupy distinct hydrophobic binding pockets. The alcohol makes a key hydrogen bond to one of the propionic acid side chains of the heme, but otherwise all the interactions between the ligand and enzyme are hydrophobic.

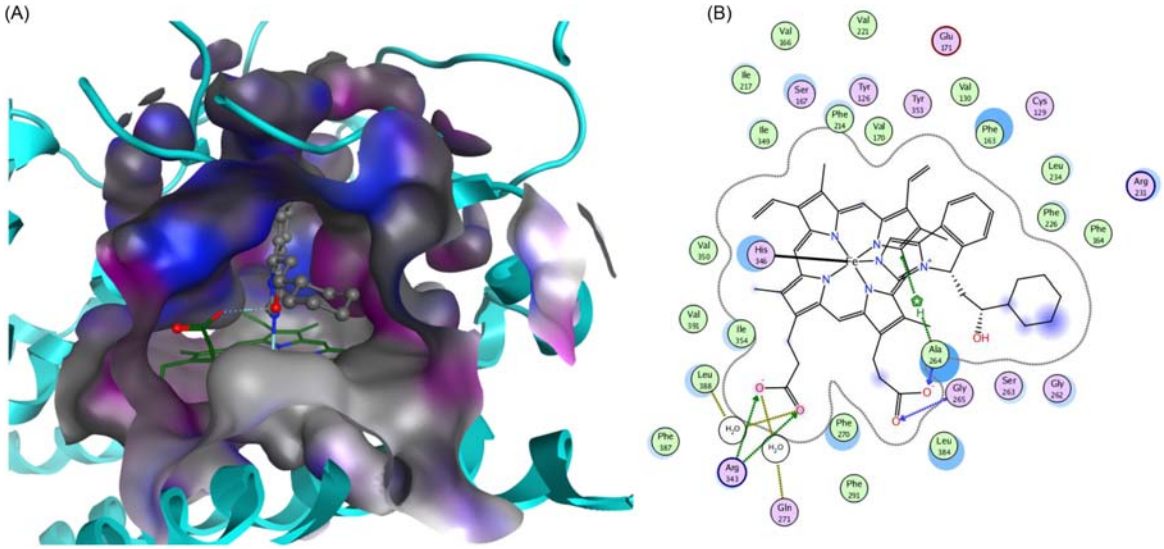

Fig. 4 (A) Racemate of **5** bound to IDO1 (5EK3). The heme is colored *dark green*, and the surface is colored *gray* (hydrophobic), *blue* (polar), and *red* (exposed). (B) Interaction map for rac-**5** bound to IDO. Figures drawn using MOE 2015.1001 (Chemical Computing Group).

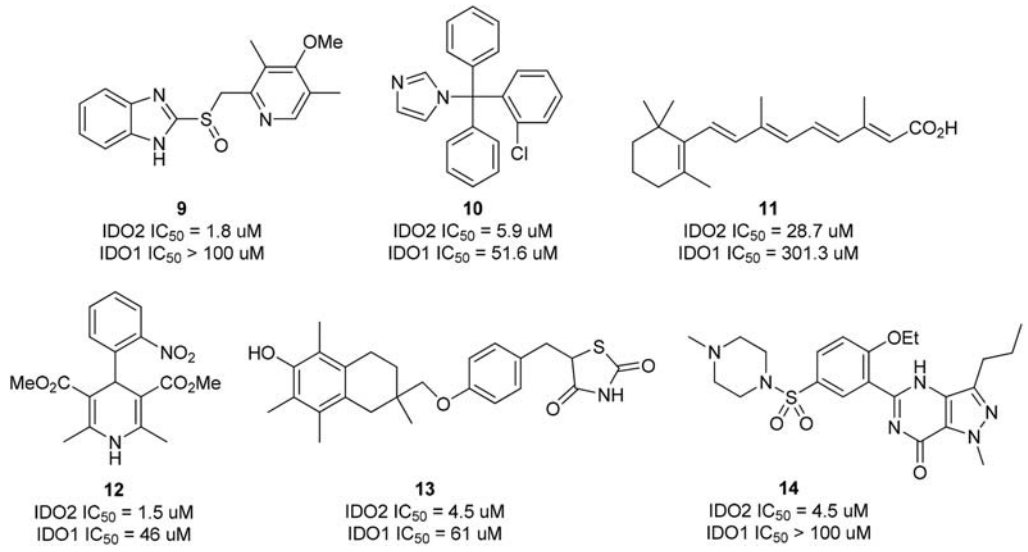

Fig. 5 IDO2-selective inhibitors.

5.11.4.1.1.3 IDO2 inhibitors

It may be due to the low intrinsic activity of IDO2 and its greater sensitivity to its redox partner[44] that few potent IDO2-specific inhibitors have been described. However, this does suggest that IDO2 is unlikely to be an important target for regulation of tryptophan metabolism. Screening of a set of 640 FDA-approved drugs has identified several compounds (Fig. 5) with micromolar potency against IDO2 and about 10-fold or better selectivity against IDO1, including the proton pump inhibitor tenatoprazole (**9**), the antifungal chlortrimazole (**10**), the prototypical retinoic acid nuclear receptor ligand retinoic acid (**11**), the antihypertensive nifedipine (**12**), the PPAR ligand troglitazone (**13**), and the PDE5 inhibitor sildenafil (**14**).[67]

5.11.4.1.1.4 TDO inhibitors

Despite the interest in TDO in brain neurochemistry as a source of serotonin and kynurenine-derived neuroactive compounds,[68] there has been surprisingly little progress in discovering TDO inhibitors. The first potent inhibitor was the pyridyl vinyl indole **15** (Fig. 6),[69] and despite extensive SAR studies around that template, only substitutions of the pyridine with a carboxylate or tetrazole (**16**) have given compounds with significant activity.[70] Structure-based design around the isatin scaffold yielded **17**, which exhibits submicromolar activity against TDO and 10-fold selectivity over IDO1.[71] There is only one crystal structure of a eukaryotic

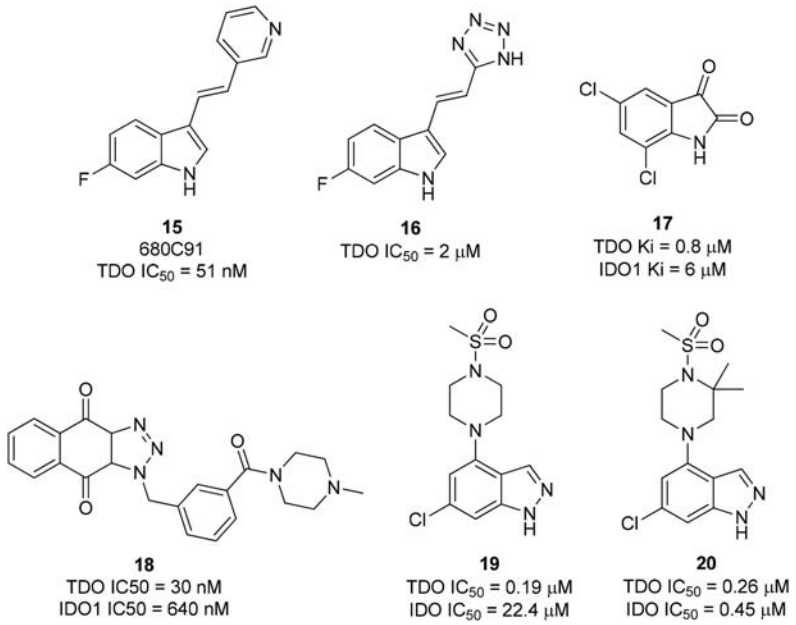

Fig. 6 TDO inhibitors.

TDO, that of the fruit fly *Drosophila melanogaster*,[72] which only shares 59% homology to the human sequence, but it was sufficient to create a homology model which was used for virtual screening by Wu et al.[73] Optimization of screening hits led to the naphthoquinone **18**, which demonstrates a 30 nM IC_{50} against TDO and 20-fold selectivity against IDO1. Investigators at IOmet Pharma (recently acquired by Merck) have disclosed 4-amino substituted indazoles represented by **19** and **20**.[74] They exhibit submicromolar TDO activity, but more interestingly, small changes in structure impart large changes in IDO1 activity, which range from 100-fold selectivity to equipotency, and represent the first potent dual TDO/IDO1 inhibitors reported.

5.11.4.1.2 Arginine

5.11.4.1.2.1 Arginase

Arginine levels are controlled by the activities of two catabolic enzymes, arginase (EC 3.5.3.1) and nitric oxide synthase (EC 1.14.13.39), shown in Fig. 7. ARG1 is a cytosolic enzyme expressed in the liver, and the closely related isoform ARG2 is a mitochondrial enzyme found in diverse number of cells. In the tumor environment ARG1 is highly expressed in, and secreted by, the immunosuppressive MDSCs and TAMs. The depletion of arginine is monitored by the stress response kinase GCN2, which is activated by uncharged transfer RNA, and is a pathway common to both arginine and tryptophan depletion. In addition to regulating transcriptional and translational programs responsible for cell growth and proliferation,[75] GCN2's activation specifically depletes the CD3ζ chain of the TCR receptor, compromising the ability of T cells to mount a response to antigen. Arginase levels are elevated in MSDCs in both renal cell carcinoma and breast cancer,[76] and inhibition of arginase blocks the growth of lung carcinoma in mice.[77]

MDSCs also express inducible nitric oxide synthase (iNOS), which converts arginine to nitric oxide. Nitric oxide is thought to suppress T cell function either by *S*-nitrosylation of critical cysteine residues of proteins or through its regulation of guanylyl cyclase and cyclic GMP-dependent kinases.[75] While the expression of arginase and iNOS is usually mutually exclusive in normal cells, this is not true for MDSCs and TAMs, and the two enzymes compete for available arginine. When arginine levels

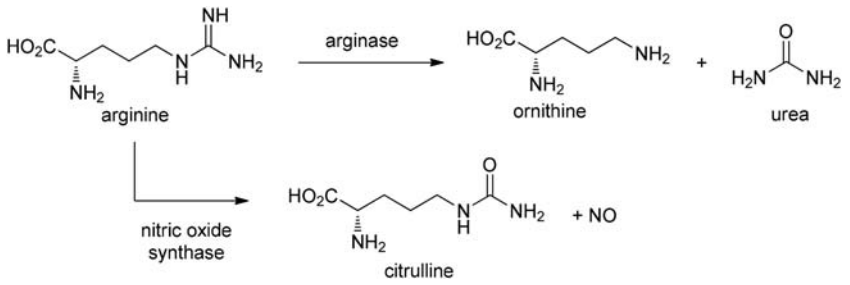

Fig. 7 Arginine catabolism by arginase and nitric oxide synthase.

are depleted by arginase, iNOS switches to superoxide production, ultimately generating reactive oxygen and nitrogen species, which are immunosuppressive in themselves. Given the fact that iNOS activity is immunosuppressive either in the presence or absence of arginine, it was anticipated that dual inhibitors of arginase and iNOS would be optimal for restoring immune function.

5.11.4.1.2.2 Arginase inhibitors

The development of arginase inhibitors quickly followed publication of a crystal structure and elucidation of a mechanism of action.[77] The arginine α-amino and carboxyl groups are anchored to surface residues through networks of water molecules, and the side chain projects down a long tunnel toward a pair of Mn^{2+} ions, which polarize a water molecule positioned to attack the guanidine. This led to the of transition state analogs **21** (2-(*S*)amino-6-boronohexanoic acid, ABH Fig. 8)[76] and its thio analog **22** (S-(2-boronylethyl)-L-cysteine, BEC),[78] in which a trigonal boronic acid mimics the guanidine moiety and accepts the water molecule to form a tetrahedral mimic of the enzymatic transition state, shown clearly in the cocrystal structure of ARG1 with **21** (Fig. 9).[79] Substitution at the α-carbon has been shown to improve potency, with the tropane-containing **23** the most potent inhibitor identified to date. Although ARG1 and ARG2 have only 54% sequence homology, they share very similar active sites,[80] and most inhibitors show very little selectivity between the two isoforms.[81]

N-Hydroxy-L-arginine (**24**) and *N*-hydroxy-L-nor-arginine (**25**) appear more structurally related to nitric oxide synthase intermediates, but they are inhibitors of arginases 1 and 2. X-ray crystallography shows the N-hydroxy group displaces the nucleophilic water that bridges the two manganase atoms, with the shorter nor-arginine analog providing higher potency and the only significant selectivity between ARG1 and ARG2.[82]

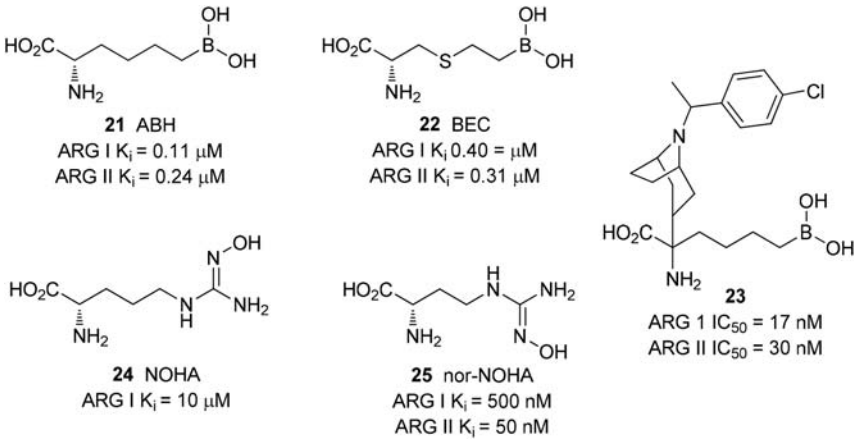

Fig. 8 Arginase inhibitors.

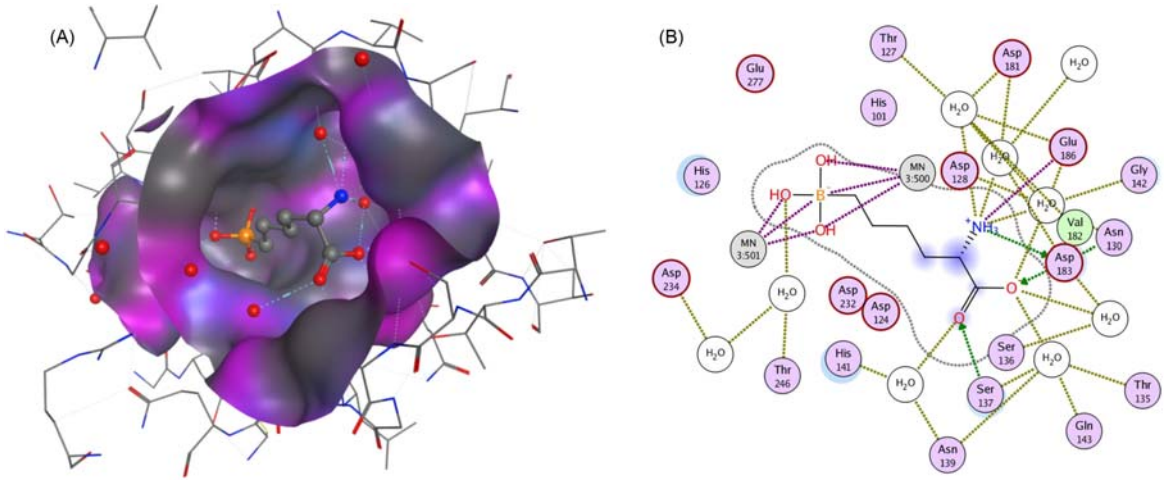

Fig. 9 (A) Crystal structure of **21** in ARG1 (1D3V). Surface is colored polar *(blue)*, hydrogen bonding *(magenta)*, and nonpolar *(gray)*. (B) Interaction map of **21** with ARG I active site. Figures drawn using MOE 2015.1001 (Chemical Computing Group).

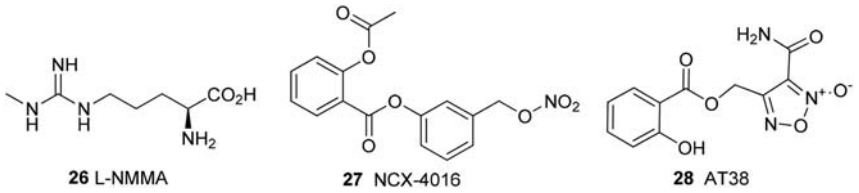

Fig. 10 iNOS inhibitor and dual inhibitors of ARG1 and iNOS function.

5.11.4.1.2.3 Dual inhibitors of arginase/iNOS function

The hypothesis that inhibition of both arginase and iNOS simultaneously would restore T-cell function was demonstrated in collagen gel matrix-supported organ cultures taken from prostate carcinomas treated with a combination of **24** and **26**, an iNOS inhibitor (Fig. 10).[83] Despite the fact that arginase and iNOS utilize the same substrate, generating a dual enzymatic inhibitor has proved elusive.

Compound **27**, NCX-4016, a nitroaspirin that inhibits cyclooxygenase and releases nitric oxide, was the first reported small-molecule drug to inhibit both arginase and iNOS activities in murine in vivo tumor model.[84] The mechanism of action is inhibition of target expression rather than inhibition of enzymatic activity. The more potent nitroaspirin analog **28**, AT38, was identified in a screening protocol using a co-culture of T cells with MDSCs.[85] In vivo, AT38 produced a large influx of T lymphocytes into mouse tumors, and combining AT38 with an adoptive cell transfer of cells recognizing an engineered antigen (EG7-OVA) produced a high number of durable responses.[85]

5.11.4.2 Purinergic Signaling in Immune Cells

The conditioning of the TME toward an antiinflammatory milieu is a major method of immune tolerance.[86] Cellular stress in the form of tissue injury, infection, or ischemia acutely elevates local levels of extracellular ATP (eATP) initiating multiple proinflammatory events, including the recruitment and activation of macrophage and DCs.[87] To reestablish tissue homeostasis, the immune system invokes a number of antiinflammatory pathways. One strategy that invading tumor cells can employ to avoid detection is to upregulate immunosuppressive and downregulate immunostimulatory pathways mediated by purinergic signaling.[88] For example, the sequential hydrolysis of eATP by the ectonucleotidases CD39 and CD73 lowers the levels of proinflammatory eATP and elevates the levels of immunosuppressive extracellular adenosine (eADO). In the TME eADO concentration can increase 10–20-fold above normal levels (Fig. 11)[89] to levels sufficient to activate both A_{2A} and A_{2B} receptor signaling on the infiltrating lymphocytes, thereby initiating a compensatory response that shields the tissue/tumor from excessive inflammation.

The high eADO level has been proposed to maintain the TME in a state of chronic immune suppression, allowing the tumor to grow unconstrained by the immune system.[90] Both CD73 and CD39 are expressed on Tregs and other cells in the TME

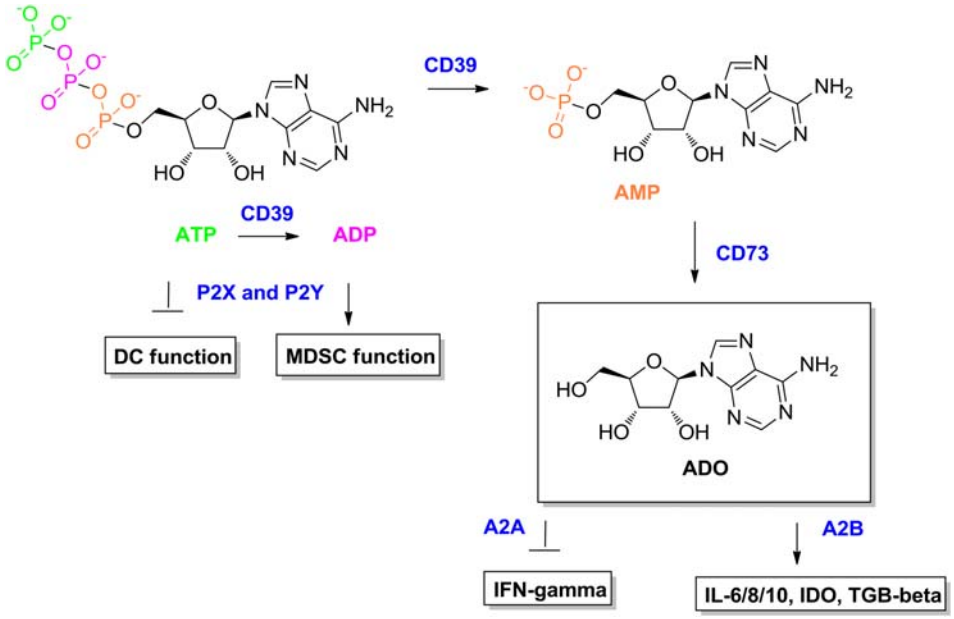

Fig. 11 Adenosinergic signaling pathway.

(B cells and tumor exosomes) providing additional enzymatic capacity to convert eATP to eADO, which can then bind to A_{2A} receptors on Teff cells to silence the antitumor immune response.[27b,91] Tregs also express A_{2A} receptors, which creates an autocrine loop to enhance other immunosuppressive mechanisms of Tregs.[92]

5.11.4.2.1 P2X and P2Y receptor modulators

There are seven subtypes of P2X ion channel receptors (P2X1–7) and eight subtypes of G protein-coupled P2Y receptors, many of which are expressed on immune cells in the TME. Elevated eATP can activate the P2 receptors on DCs to enhance specific $CD8^+$ T cell cytotoxicity.[87] Activation of P2X7R is believed to be an important proinflammatory pathway to stimulate the immune response. If so, a P2X7R agonist or an inhibitor of ATP degradation would boost the antitumor immunity. However, in human tumors overexpression of P2X7R is better correlated with promoting tumor growth and progression.[93] Conversely, P2X7R-deficient mice demonstrate accelerated tumor growth and metastatic spreading.[94] Thus the potential impact of a P2X7R agonist on tumor growth remains unclear. The effect of ATP on P2Y11 receptors present on DCs is to change the cytokine profile toward Th2 immunity and in doing so favor immunosuppressive rather than immunostimulatory pathways.[95]

Potent antagonists of P2X7 have been described, exemplified (Fig. 12) by the bio-isosteric compounds dihydro-[1,2,4]triazolo[4,3-a]pyrazin-8(5H)-one **29** (hP2X7 $IC_{50}=0.7$ nM)[96] and 6,7-dihydro-1H-[1,2,3]triazolo[4,5-c]pyridine **30** (hP2X7 $IC_{50}=4.2$ nM)[97] which demonstrate low-nanomolar antagonism in Ca^{2+} efflux FLIPR assays. Since the majority of researchers have been pursuing mood disorders, the focus has been on improving the CNS-penetration of these antagonists. A detailed exploration of the structural determinants for P2X receptor binding has been published by Dal Ben et al.[98] providing insight into the variations between the P2X 1–7 receptors, the differences between human and rat P2X receptors (important for the interpretation of rat models of CNS disorders) and progress toward the synthesis of subtype selective receptor compounds.

Similarly, detailed reviews of P2Y receptor agonists and antagonists by Jacobson et al.[99] highlight the breadth of research into nucleoside and non nucleoside modulators of this large class of GPCRs. For example, structural modifications within an adenosine template can result in conversion of a potent and selective pyrophosphate-based P2Y1 agonist MRS2365 (**31**; P2Y1 $pEC_{50}=9.4$) into a potent and selective diphosphate-based antagonist MRS2500 (**32**; P2Y1 $pIC_{50}=9.0$) (Fig. 13).[100]

The successful synthesis of both selective agonists and antagonists for those P2 receptor subtypes provides hope that this may prove true for the entire receptor family. As such, we may soon have the tools to discern which P2 receptors may have therapeutic utility to boost the immune response to cancer.

5.11.4.2.2 Adenosine receptors (A_1, A_{2A}, A_{2B}, and A_3)

While the overall impact of eATP on the innate immune response in the TME is unclear, the role of its phospho ester hydrolysis product, ADO, is not: ADO is uniformly immunosuppressive.[101] There are four ADO binding G protein-coupled receptors (A_1, A_{2A}, A_{2B}, and A_3) with different affinities for ADO, enabling cellular responses over a range of physiological levels of ADO. Lymphocytes primarily express the A_{2A} or A_{2B} receptors, whereas tumors may express any one or a combination of these four ADO receptors.[102] Due to the low affinity for ADO, the A_{2B} receptor can only initiate signaling when ADO is outside of the normal physiologic range. Both the A_{2A} and A_{2B} receptors are positively coupled to Gs-dependent adenylyl cyclase, leading to increased production of cAMP as the second messenger for intracellular signal transduction.

5.11.4.2.2.1 A_{2A} receptor antagonists

The A_{2A} receptor is widely expressed on leukocytes, including lymphocytes, DCs, NK cells, and T cells, and binding of ADO suppresses the immune functions of these cells.[103] Of particular interest to immune suppression are the regulatory effects of

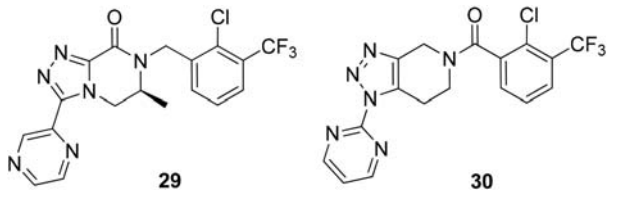

Fig. 12 P2X7 antagonists.

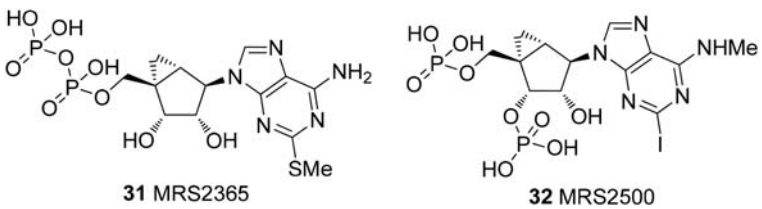

Fig. 13 Conversion of potent P2Y1 agonist into potent and selective P2Y1 antagonist.

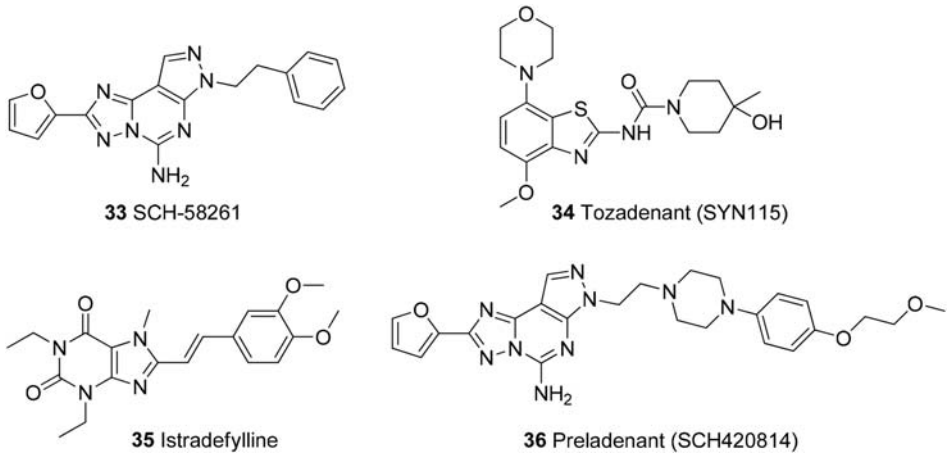

Fig. 14 Selective A_{2A} receptor antagonists.

A_{2A} receptor activation on T cells, in which ADO significantly blunts TCR-mediated cytotoxicity and cytokine production, inhibits T cell proliferation,[27b] and induces the expansion of Tregs that have stronger immunosuppressive activity due to increased expression of CD39, CD73, and CTLA-4.[92]

SCH58261 (**33**) (Fig. 14) is a potent and selective A_{2A} antagonist (bovine A_{2A} $K_i = 2.0$ nM; bovine A_1 $K_i = 201$ nM)[104] which was shown to decrease metastatic spread in murine syngeneic models of metastatic disease (B16F10 melanoma and 4T1.2 breast carcinoma).[105] Furthermore, the combination of an A_{2A} antagonist, either **33** or SYN115 (**34**) (A_{2A} $K_i = 4.9$ nM[106]), with a T cell checkpoint blocker (anti-PD1) was more effective than the individual agents in several murine tumor models.[107] The additional efficacy of an adenosine antagonist with T-cell checkpoint blockade is supportive of a nonredundant role for ADO in the immune response in cancer. Two A_{2A} receptor antagonists, istradefylline (**35**) (A_{2A} $K_i = 12$ nM[106]) and preladenant (**36**) (SCH420814; A_{2A} $K_i = 1.1$ nM[106]), have been studied in phase II and III clinical trials of Parkinson's disease,[106] demonstrating modest efficacy which was sufficient to gain registration approval in Japan for **35**. The preclinical data for A_{2A} antagonists in combination with anti-PD1[108] checkpoint antagonists provide a compelling rationale for testing this combination in the clinic.

5.11.4.2.2.2 A_{2B} receptor antagonists

A_{2B} receptors are expressed at low levels across multiple cell types, but expression is significantly upregulated under hypoxic conditions. The A_{2B} receptor is the least sensitive of the four adenosine receptors, requiring micromolar ADO concentrations that are only achieved under conditions of physiological stress. On classically activated macrophages which release proinflammatory cytokines and are central elements of the cellular immune response, activation of the A_{2B} receptor plays a prominent role in M1 to M2 switching, thereby suppressing the antitumor T cell response and stimulating tumor angiogenesis.[109] Elevated ADO derived from the activity of CD73 also activates A_{2B} receptors on myeloid precursor cells to drive expansion of MDSCs and thereby suppress Teff activity.[110]

The first in vivo demonstration of antitumor activity of a selective A_{2B} receptor antagonist was achieved using intratumoral injections of ATL801 (**37**; A_{2B} $K_i = 19$ nM),[111] to reduce the growth of bladder and breast cancers in mice (Fig. 15).[112] Intratumoral

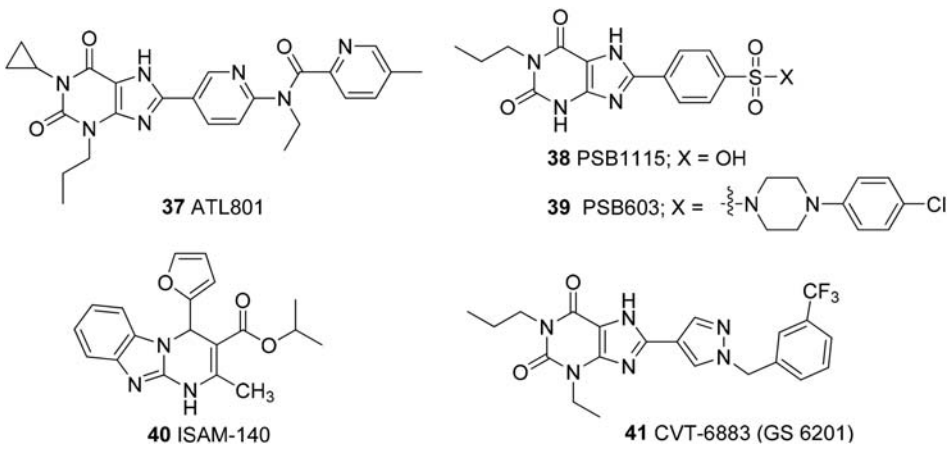

Fig. 15 Selective A_{2B} receptor antagonists.

injection of a different A_{2B} selective antagonist PBS1115 (**38**; A_{2B} $K_i = 53$ nM; A_{2A} $K_i = 24{,}000$ nM)[113] provided in vivo support for an A_{2B} receptor-dependent role in the accumulation of tumor-infiltrating MDSCs.[114] Lastly, both in vitro and in vivo data using the selective A_{2B} antagonist PSB603 (**39**; A_{2B} $K_i = 0.55$ nM; A_{2A} $K_i > 10{,}000$ nM)[115] showed enhanced antitumor immunity due to the inhibition of differentiation of naive $CD4^+$ T cells to Tregs.[116] These results support the prediction that high ADO levels within the TME are sufficient to trigger engagement of low affinity A_{2B} receptors to drive MDSC suppression of tumor immunity and differentiate naive T cells into a Treg suppressive lineage. Researchers from Spain and Sweden synthesized and screened libraries of 3,4-dihydropyrimidin-2(1H)-ones derived through the Biginelli condensation resulting in potent and selective A_{2B} antagonists exemplified by compound ISAM-140 (**40**; A_{2B} $K_i = 3.5$ nM; $A_1/A_{2A}/A_3$ $K_i > 10{,}000$ nM).[117] Several groups are pursuing the clinical development of A_{2B} antagonists for antiinflammatory indications (inflammatory bowel disease [IBD] and chronic obstructive pulmonary disease [COPD]) with one selective antagonist CVT-6883 (**41**; A_{2B} $K_i = 22$ nM; A_{2A} $K_i = 3280$ nM),[118] deemed well tolerated in phase I safety trials.[118]

5.11.4.2.3 ATP metabolism: CD73 and CD39 nucleotidases

The homeostatic extracellular concentration of ADO is low (20–200 nM), but can quickly rise (1000–10,000 nM) under stress.[88,101,119] Such rapid changes require robust mechanisms to synthesize and degrade ADO. The primary pathway for the generation of ADO in the TME is through the sequential phosphate ester hydrolysis of ATP by two ectonucleotidases, CD39 and CD73. Both CD39 and CD73 are plasma membrane anchored phosphatases with active sites that face outward into the extracellular environment.[120]

5.11.4.2.3.1 ENTPD1/CD39 (NTPDase1)

CD39 is expressed on the surface of endothelial cells and subsets of leukocytes, particularly on B cells. CD39 converts eATP first to ADP and then, without release, ADP is converted in a second step to AMP. There are multiple lines of evidence linking elevated CD39 expression to immune suppression and increased tumor susceptibility.[21,27a,b,121] Small molecule inhibitors of CD39 have been used to provide evidence for the CD39 involvement in the production of ADO. ATP-analog ARL 67176 (**42**) is a competitive inhibitor of human CD39 with a $K_i = 11$ μM[122] but also has similar activity versus NTPDase3 ($K_i = 18$ μM) and NPP1 ($K_i = 12$ μM). The 8-butylthio analog of ATP (**43**) was also shown to be a modest inhibitor of CD39 ($K_i = 5.6$ μM) (**Fig. 16**).

These tool inhibitors have many shortcomings[123] with marginal selectivity and potency and while they have been used for in vivo experiments, the pharmacokinetic behavior of these compounds has not been characterized. Polyoxotungstate POM-1 (**44**), a high molecular weight metal complex with a reported CD39 $K_i = 2.6$ μM,[124] raises similar concerns. The lack of potent and selective drug-like CD39 inhibitors may be indicative of the challenge posed by this target.

5.11.4.2.3.2 CD73 (ecto-5′-nucleotidase, e5′NT)

CD73 is a GPI-anchored di-Zn^{2+} metallophosphatase specific for the dephosphorylation of purine and pyrimidine ribo- and deoxyribonucleoside monophosphates with adenosine monophosphate (AMP) being the preferred substrate. Consistent with the proposed nonredundant role of CD73 for the conversion of ATP to ADO, CD73 expression is directly regulated by HIF-1α.[125] CD73 is overexpressed in multiple solid tumor types (colorectal, prostate, and breast) and leukemias, and in a number of aggressive and difficult to treat tumors (glioblastoma and ovarian tumors) (**Fig. 11**).[91]

Adenosine 5′-(α,β-methylene)diphosphate (AMPCP, **46**), a nonhydrolysable ADP-mimetic (**45**), is one of the first potent and selective CD73 inhibitors described and has been widely used as a tool to elucidate the role of CD73 catalytic activity in suppressing immune responses to cancer (**Fig. 17**). In vitro, 40–100 μM concentrations of **46** block ADO production by Tregs,[126] adenosine-dependent chemotaxis of human breast tumor 4T1.2 cells,[127] and glioma derived adenosine-mediated suppression of Teff cell proliferation.[128] Several research groups have published in vivo results showing that **46** (20 mg kg^{-1}, either intraperitoneal or intratumoral injection) reduces tumor growth rates, cytokine production, and metastasis in B16 melanoma.[127,129] A search for more potent AMPCP-derived antagonists resulted in a number of modifications such as the *N*-benzyl analog compound **48**,[130] which is

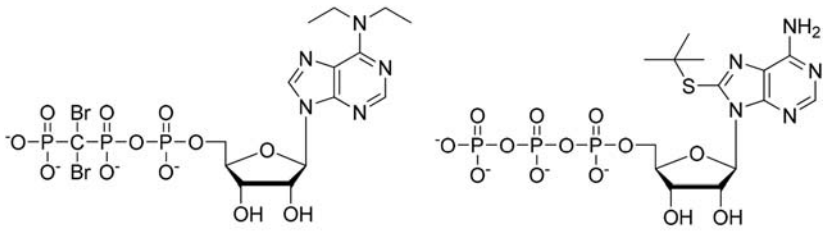

$Na_6[H_2W_{12}O_{40}].21H_2O$

44 POM-1

Fig. 16 CD39 inhibitors.

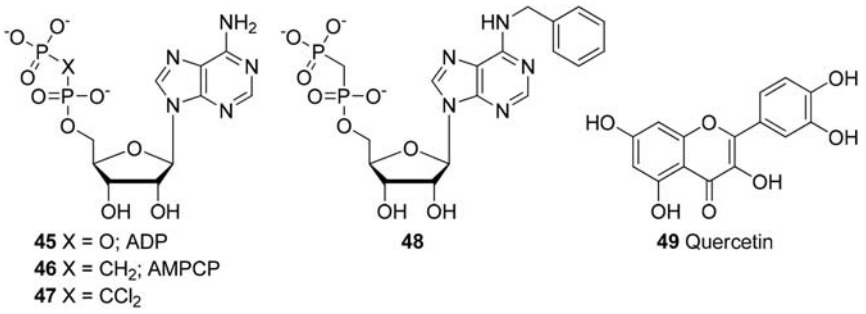

Fig. 17 CD73 inhibitors.

reported to have a K_i for human CD73 of 2.2 nM relative to 88 nM for **46**. The same authors also investigated modifications at the methylene bridge of the nonhydrolysable diphosphate linker, with the best being the α,α-dichloro group, compound **47** having a $K_i = 292$ nM versus rat CD73, showing no improvement over **46** (rat CD73 $K_i = 197$ nM). The availability of active recombinant soluble CD73 has encouraged several groups to develop moderate to high throughput assays suitable for diversity screening to discover new inhibitor classes.[131] The X-ray structure of both free and inhibitor-bound (**46**) forms of human CD73 have recently been published.[132] In the presence of **46**, CD73 adopts a closed conformation bringing the purine binding pocket adjacent to the catalytic zinc centers (**Fig. 18**). This form should mimic relatively closely the state of CD73 when phospho-hydrolysis occurs. Pivoting around the linkage of the two CD73 domains results in an open form of the enzyme.[132] This opening and closing of CD73 allowing reactant to enter; closure to allow catalysis to occur; then reopening to release product must occur rapidly given the high Kcat for this enzyme.[133]

The poly-phenolic compound quercetin (**49**) has been shown to inhibit the conversion of AMP to adenosine by the U138MG glioma cell line ($IC_{50} = 45$ μM)[36] and in the T24 human bladder cancer cell line (48% inhibition at 100 μM after 72 h).[134] This may be due to direct inhibition of CD73 catalysis, disruption of CD73 association with membranes, negative modulation of CD73 mRNA levels, or a combination of the above.[36] That said, a PubMed search for **49** performed in 2016 returned over 13,000 hits referring to a plethora of diverse biological effects, therefore forming conclusions from activities displayed by such molecules should be cautioned against. With the required discovery tools available, further progress in this area may soon be forthcoming.[135]

5.11.4.2.4 COX-2 and EP2/EP4 receptor antagonists

Contrary to the historic observation by Coley that *acute* activation of the immune system stimulates an immune response to cancer,[2] there is an abundant literature linking *chronic* inflammation to tumor promotion and progression.[136] Treatment of IBD and ulcerative colitis patients with NSAIDS (either nonselective COX-1/2 or selective COX-2 inhibitors) slows disease progression. Long-term prophylactic treatment with either nonselective COX-1/2 inhibitors such as indomethacin (**50**) or COX-2 selective

Fig. 18 Open and closed forms of CD73. Catalytic Zn atoms shown as *mustard balls*. Overlay created from PDB codes 4H2I and 4H1Y[132] using MOE 2015.1001 (Chemical Computing Group).

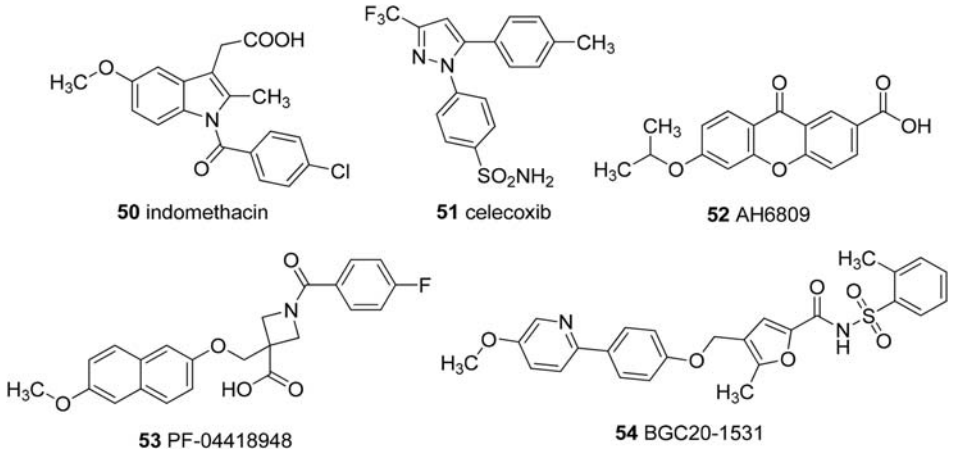

Fig. 19 COX1/2 and EP2/4 antagonists.

inhibitors such as celecoxib (**51**) (COX-2 $IC_{50} = 0.04\ \mu M$; COX-1 $IC_{50} = 15\ \mu M$)[137] led to the regression of adenomas.[138] Prostaglandin E2 (PGE2), a metabolite of COX-2, has direct effects on the immune system favoring a proinflammatory (Th1) immune response acutely,[139] whereas sustained levels enhance the activity of multiple immunosuppressor cells (Fig. 19).[140]

PGE2 signals through a set of four G protein-coupled receptors (EP1–4) which are coupled to different signal transduction pathways. In lymphocytes, PGE2 activation of the EP2 and EP4 receptors is positively coupled to adenylyl cyclase leading to elevated cAMP and subsequent activation of PKA.[141] Treatment of human Tregs with either a nonselective COX inhibitor **50** or an EP2 receptor antagonist AH6809 (**52**; EP2 $K_i = 1150$ nM)[142] decreased Treg-mediated suppression, whereas a selective EP4 receptor antagonist had no effect.[143] As demonstrated by the use of selective EP receptor antagonists, the production of immunosuppressive TGFβ by MDSCs requires the EP2 receptor or a combination of EP2 and EP4 receptors.[144] In murine splenic NK cells, which express all four PGE2 receptors, a selective EP4 agonist inhibited IFN-γ production, whereas selective EP1–3 agonists did not.[144a] These results implicate elevated cAMP as the primary signal leading to immunosuppression, irrespective of which EP receptor is predominant (EP2 or EP4).

Selective PGE2 receptor antagonists have recently been studied clinically for a variety of nononcology indications. Among these agents are selective EP2 antagonists such as compound PF-04418948 (**53**; EP2 $K_i = 16$ nM; cAMP functional assay; EP2 = 1.8 nM; EP1, -2 and -3 > 10,000 nM)[142,145] and EP4 antagonists such as BGC20-1531 (**54**; EP4 $K_i = 12$ nM; EP1–3 > 10,000 nM).[146] Thus far the direct effects of EP antagonists on tumor proliferation and angiogenesis have been the focus of preclinically investigations, but with the recent successes in immuno-oncology and a growing literature highlighting the role of EP signaling in immune tolerance, this emphasis may shift to immune regulation and extend into clinical investigations.[144a]

Upon activation of ADO (A_{2A} and A_{2B}) and PGE2 (EP2 and EP4) receptors, adenylyl cyclase is activated to produce cyclic AMP (cAMP), as a common second messenger. Of the nine transmembrane bound forms of adenylyl cyclase, AC VII is the isoform known to be most highly expressed in lymphocytes and macrophages.[147] The convergence of the ADO and PGE2 pathways on a single isoform of adenylyl cyclase that is preferentially associated with the hematopoietic linage provides an opportunity to block both immunosuppressive pathways with a single agent.[148] Isoform-selective inhibition of AC VII is therefore highly appealing in principle; however, there are currently no known potent, isotype-selective inhibitors for any of the AC isoforms.[149] The availability of structural data for soluble adenylyl cyclases[150] and comparison with the transmembrane ACs holds promise for the future realization of potent and selective AC inhibitors.

5.11.4.3 Pattern Recognition Receptors (PRRs)

The innate immune response to microbial infection relies on a network of pattern recognition receptors that recognize pathogen-associated molecular patterns (PAMPs) as "danger signals" to mobilize both the innate and adaptive immune response to eliminate the invading organism and restore homeostasis. The most well-studied surveillance receptors for bacteria and fungi are the Toll-like receptors (TLRs), which reside on plasma or endosomal membranes.[151] TLRs are expressed on antigen-presenting immune cells, such as monocytes/macrophages, B cells, neutrophils, dendritic cells, and on epithelial cells. TLRs are integral transmembrane glycoproteins possessing either an extracellular (TLR1, -2, -4, -5, -6, and -10) or luminal (TLR3, -7, -8, and -9) ligand-binding domain and a cytoplasmic signaling Toll/interleukin-1 (IL-1) receptor homology domain. They mainly recognize evolutionarily conserved structures on pathogens, such cell surface components of bacteria [lipopolysaccharide (TLR4) and flagellin (TLR5)] or fungi [zymosan (TLR2) and mannan (TLR4)]. Viruses require intracellular access for replication; hence the immune system relies on intracellular receptors to sense these foreign components and mount a defensive response. Multiple sensing mechanisms have evolved to fulfill this role. In the TLR family viral RNAs are recognized by TLR3 (membrane) or TLR7/8 (endosomal) and unmethylated CpG DNA from multiple classes of pathogens can be detected by endosomal TLR9. Recently, the cyclic GMP–AMP synthase (cGAS)/STING

pathway has emerged as an additional intracellular sensing mechanism.[152] When engaged, these PRRs trigger both a proinflammatory (IL-1, TNFα) cytokine response and an innate adaptive type I interferon response. The balance of these pathways determines the nature of the immune surveillance. TLRs and STING are also expressed on tumor cells. The outcome of either TLR or STING stimulation depends which receptors are expressed and the tumor type and can either inhibit or promote tumor growth.[153]

TLR homo- or hetero-dimerization or the formation of higher oligomers upon binding of an agonist is required to initiate the signaling cascade leading to the expression of immunostimulatory cytokines and a subsequent activation of the immune response. The crystal structures of TLR family members have revealed that these receptors share many structural elements, such as the "question mark" or horseshoe-shaped motif containing several leucine-rich repeat units (LRRs) around which two TLRs dimerize.[154] These structures have also revealed the interactions required for ligand binding and signaling and offer promising starting points for the rationale design of new ligands. Until recently small molecule agonists had only been described for TLRs 7/8, thereby limiting the development and type of agonists that have entered into clinical trials. Our discussion of TLR agonist is restricted to the receptors that bind traditional small molecules (TLR7/8 and TLR4) or for which synthetic or semisynthetic ligands are available and have allowed the development of SAR (TLR4 and TLR9).

5.11.4.3.1 TLR7/8

In 2002 Hemmi and coworkers determined TLR7 to be the target of the imidazoquinoline immune response modifiers imiquimod (**55**) and resiquimod (**56**) (Fig. 20).[155] Subsequently both TLR7 and TLR8, which are endosomal TLRs binding the single-stranded RNAs of RNA viruses, were found to be activated by this class of immune modulators molecules. An NF-κB-luciferase reporter assay in HEK 293 cells cotransfected with either TLR7 or TLR8 was first used to identify that 3M-001 (**57**) selectivity activates TLR7 where as 3M-002 (**58**) selectively activates TLR8.[156] Functional differences for the selective stimulation of these receptors were determined in human PBMCs and purified cellular subtypes derived from PBMCs. IFNα is predominately associated with TRL7 activation which is most predominate in plasmoid dendritic cells (pDCs) while TNFα and other proinflammatory cytokines are associated with TLR8 activation in myeloid dendritic cells, monocytes, and monocyte-derived dendritic cells.[156] The luciferase reporter assays are well suited for routine screening and HTS configuration, but they should not be used in place of functional assays which can detect subtle changes in receptor signaling that can be missed in reporter assays. Instead cytokine profiles in human PBMCs[157] are believed to provide a more physiologically relevant readout for activation of the two pathways.

By phylogenetic analysis TLR7, TLR8, and TLR9 form a subfamily within the TLRs. All three bind to single-stranded nucleic acids and as noted above require dimerization to signal. Both TLR7 and TLR8 exist as preformed dimers and are believed to recognize viral uridine- and guanosine-rich ssRNAs. In addition to the imidazoquinolines, guanosine nucleotide analogs, such as loxoribine (**59**) (Fig. 21), are weak agonists which suggest that these small heterocycles are being recognized as mimetics of the natural ligand.

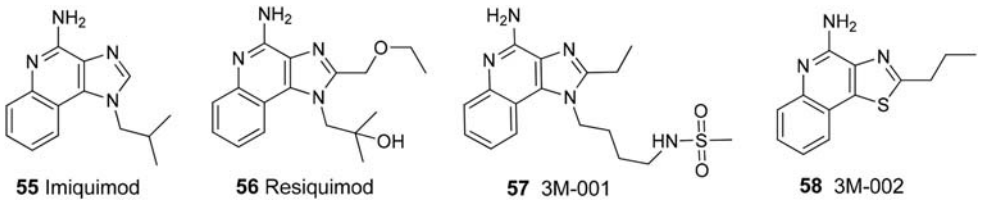

Fig. 20 Early dual and selective TLR7/TLR8 ligands.

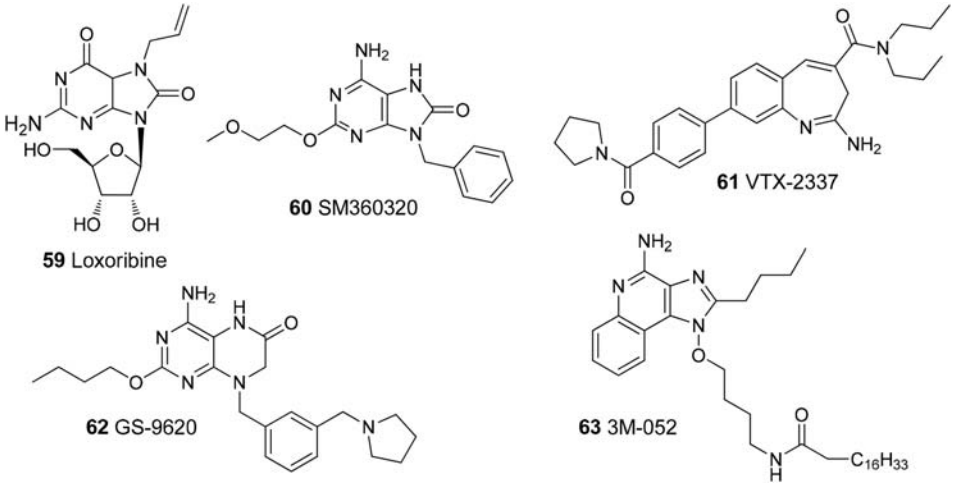

Fig. 21 Additional scaffolds for TLR7/TLR8-selective ligands.

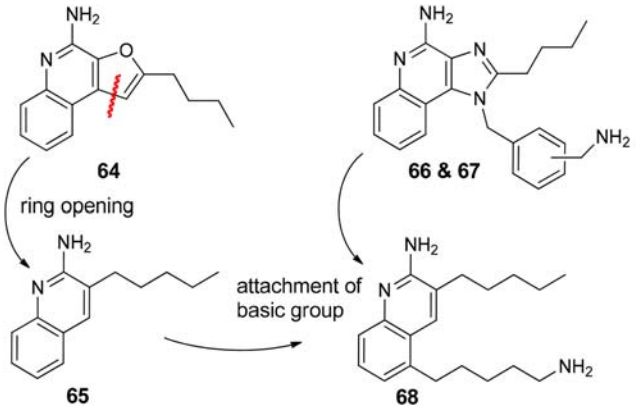

		IC50, nM Luciferase reporter assay	
	sub.	TLR7	TLR8
66	para	50	55
67	ortho	215	14
68		n.d.	9

Fig. 22 Analysis of ligand cocrystal structures (**64–67**) bound to the ectodomain of human TLR8 used to design potent TLR8 selective agonist **68**.

The crystal structures of TLR8 with and without the imidazoquinoline ligand have revealed that the binding of two imidazoquinoline ligands (2:2 complex) induces a conformational change which brings the TIR domains together to activate signaling.[158] X-ray structures imply that activation by the natural ssRNA ligand does not involve binding of the intact oligomer but instead two ssRNA degradation products: uridine which was found to occupy the same site as the imidazoquinoline ligands and a short oligonucleotide which binds at a second site on the receptor thus forming a 2:2:2 complex.[159] Given the dual TLR7/8 agonists properties of the early ligands, one presumes that TLR7 activation follows a similar mechanism, but without an X-ray structure this remains speculative.

Until the 2013 publication of the first ligand-TLR8 structures optimization of potency and selectivity relied upon traditional SAR studies. Functional cellular assays examining the relative potency for induction of IFNα (TLR7) versus TNFα (TLR8) continues to be the preferred method to judge selectivity. New scaffolds discovered include the TLR7 selective 8-oxopurines SM360320 (**60**)[160] which are structural variants of the imidazoquinolines retaining a hydrogen bond donor–acceptor pair and the TLR8 selective benzazepine VTX-2337 (**61**).[161]

One of the first applications of the TLR8 X-ray structural data was the development of a homology model of TLR7 and a docking pose for GS-9620 (**62**) consistent with its high TLR7 selectivity.[162] The new 6,6-scaffold of **62** was derived by ring expansion of the 6,5-ring system of the 8-oxopurine scaffold present in **60** while retaining the two donor acceptor pairs. Further expansion to a 6,7-scaffold resulted in loss of all activity. Several research groups have noted the importance of an N-9 basic group to afford high potency and selectivity for IFNα versus TNF. This cytokine profile is in part a reflection of TLR7 versus TLR8 selectivity of these agonists. An addition consideration is the highly acidic nature of the endosomal compartment which drives endosomal enrichment of these basic amines resulting in enhanced potency/selectivity.[157] For example, **62** has a minimal effective concentration (MEC) for stimulation of IFNα in hPBMCs of 1 nM and is a 100-fold selective versus TNFα compared with a 1000 nM MEC for stimulation of IFNα and 0.3-fold selectivity for TNFα for the analog of **62** lacking the pyrrolidinyl methyl.

The research group of Prof David at the University of Kansas published their initial exploration of TLR7 SAR in 2009. More recently, the emphasis has shifted to TLR8 selective agonist developed using traditional SAR and the application of X-ray structure guided rationale design (Fig. 22). The cocrystal structure of furoquinoline (**64**), a selective TLR8 agonist derived from the imidazoquinoline scaffold, revealed a key salt bridge between the exocyclic 4-amino and Asp543 and suggested disconnections at the furan would be tolerated. The resulting simple bicyclic 3-pentylquinolin-2-amine (**65**) was eightfold more potent ($EC_{50}=200$ nM) and retained the high TLR8 selectivity of **64**.[163] Further structure-guided optimization of this reduced-complexity scaffold was based upon an analysis of the TLR8 cocrystal structures for the *meta*- and *para*-N1-aminomethylbenzyl-substituted imidazoquinolines (**66** and **67**). The differing selectivity and potency of these compounds suggested that the introduction of a basic amine replacement for benzylic amine on the quinolin-2-amine scaffold of **65** could lead to enhanced potency. The resulting optimized n-pentylamine (**68**) is the most potent and selective TLR8 agonist described thus far.[164]

5.11.4.3.2 TLR4

TLR4 was discovered as the primary target mediating the potent inflammatory response to the lipopolysaccharide (LPS) component of the endotoxin produced by gram-negative bacteria. It is the most studied TLR family member. TLR4 is activated by a broad variety of components from infectious organisms, such as fungal mannan and viral glyocoproteins. HMGB1 is an endogenous TLR4-activating DAMP and a key component of immunogenic cell death. HMGB1 release and subsequent activation of TLR4 promotes tumor antigen recognition.[17] The activation by LPS involves the transfer of the TLR4/LPS complex from CD14 to MD-2 resulting in an LPS/MD-2/TLR4 dimeric complex. This dimeric complex, which has been studied both by crystallography and NMR, has 5 of the 6 acyl lipid chains of LPS binding into a hydrophobic pocket on MD-2.[165] The electrostatic interaction of the 4-phosphate of monophosphoryl lipid A (MPLA, **70**) (Fig. 23) with arginine and lysine residues of TLR4 appears critical for activity and explains this requirement for agonist activity in other LPS derivatives.[166] The formation of this intracellular complex

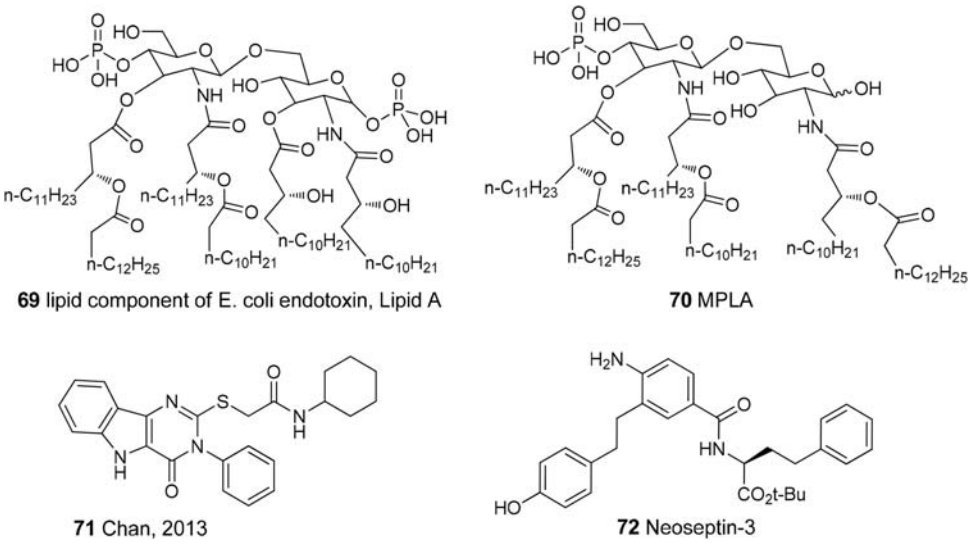

Fig. 23 TLR4 agonist ligands.

activates proinflammatory responses mediated by MyD88 signaling and a TRIF-dependent pathway leading to type I IFN production. Semisynthetic analogs of lipid A (**69**), such **70** have been pursued in order to favor the TRIF over the MyD88 pathway and thereby reduce toxicity and also to improve the pharmaceutical properties.[165]

Until recently all the reported small molecule agonists of TLR4 were modified Lipid A analogs. However, using cellular screens directed to find novel immune stimulants several new classes of TLR4 ligands have been discovered. In 2013 Chan et al. found substituted pyrimido[5,4-b]indoles as potent NFκB activators employing a cell-based high-throughput screen (HTS). The most potent hit compound (**71**) selectively stimulated TLR4 and no other TLR.[167] This same research group of Cottam at the Moores Cancer Center has reported on a second 4-aminoquinazoline hit from HTS. Interestingly, for this second series, the compounds were human but not mouse active. There was no activity with other TLRs and the TLR4 activation was MD-2 dependent and CD14 independent. Computational studies for both hit series indicated that the compounds bind primarily to human MD-2 in the TLR4/MD-2 dimeric complex.[168] Yet a third series has been reported by the Boger group at Scripps Research Institute from screening of compounds libraries for TNFα stimulatory activity in primary mouse peritoneal macrophage cultures. The crystal structure the murine TLR4/MD-2/Neoseptin-3 (**72**) asymmetrical dimer revealed binding within the hydrophobic pocket of MD-2, inducing an active receptor complex similar to that induced by lipid A. Compounds **72** and **69** utilize different residues to achieve receptor activation; demonstrating that TLR4/MD-2 agonists need not mimic the binding of LPS. The Neoseptins, which were discovered by screening against mouse TLR4/MD-2, were in not active the human TLR4. Hence agonist activity for these nonnative ligands, which may utilize nonconserved binding motifs, is not necessarily maintained across species.[169]

5.11.4.3.3 TLR9

TLR9 recognizes bacterial and viral DNA containing the cytosine–phosphate–guanine (CpG) dideoxynucleotide motif. Viral DNA is not methylated and methylated CpG oligos demonstrate reduced binding affinity and ability to activate signaling. X-ray crystal structures of TLR9 with a set of agonist and antagonist DNA-12mers provide a structural basis for understanding receptor activation.[170] Agonistic CpG-DNA binds to form a symmetrical TLR9–CpG-single-stranded DNA complex with 2:2 stoichiometry in which the agonistic DNA binds to two equivalent positions in the dimer, forming a bridge to link both of the TLR9 monomers. Antagonist DNA binds as a monomeric 1:1 complex with TLR9 partially overlapped the agonist binding site. Hence as has been noted for all other TLRs, agonism requires formation of a conformationally active dimer. The unique requirement for agonist bridging to "glue" the TLR9 monomers together to form an active complex may explain why non-DNA agonists have yet to be discovered. Conversely, this new structural information should facilitate the design of non-DNA agonist of TLR9.

5.11.4.3.4 TLR agonist in development for IO

Because of the crucial role played by the TLRs in the innate immune response to infectious pathogens, selective agonists have found utility in multiple indications. For example, as vaccine adjutants to promote maturation of APCs, such as dendritic cells, which in turn directs the induction of adaptive immune responses. TLR agonists have also been used as antiviral and anticancer agents. The imidazoquinoline imiquimod (**55**) was first approved in 1997 as a 5% topical cream for the treatment warts caused by human papillomavirus (HPV) infection and in 2004 FDA approval was obtained for the treatment of superficial basal cell carcinoma. At the time of its initial approval the target (TLR7/8 agonism) responsible for its mechanism of action was unknown and no previous antiviral therapy had been approved that induced the production of antiviral cytokines that enhanced cellular immunity. Our present understanding of TLR7/TLR8 agonists is that the antitumor effects are primarily mediated by activation of DC and NK cells

to directly kill tumor cells, and by the suppression of Tregs.[153a] Compound **57** is a more potent and more selective activator of TLR7 than **55**. In vitro studies have shown that **57** directly activates APCs, such as dendritic cells. The improved solubility of **57** at physiologic pH facilitated i.v. formulations which were used in a phase I trial.[171] Motolimod (**61**) is a small-molecule TLR agonist with 30-fold selectivity for TLR8 over TLR7. The high TLR8 selectivity coupled with the preferential expression of TLR8 in monocytes and myeloid dendritic cells produces a unique pattern of cytokines which activate NK cells and augment ADCC, a property not shared by TLR7 or TLR9 agonist.[161] A phase I trial is complete and phase II trials are ongoing.[172]

In the syngeneic CT-26 tumor model the antitumor response to chemotherapy was dependent on expression of TLR4 in dendritic cells which provided the "danger signal" to break tumor antigen tolerance.[173] This dependence was correlated to the release of high levels of HMGB1 and HSP70, known activators of TLR4. Compound OM-174 (structure not shown), a TLR4 agonist in which three of the six lipid tails of Lipid A have been removed, induced the complete regression of tumors and hemorrhagic ascites in 90% of the tumor bearing rats in a colon cancer metastasis model.[174] Phase I i.v. infusion repeat dose (given twice weekly for a total of 15 doses) studies have determined the maximally tolerated dose.[175] MPLA (**70**) and aminoalkyl glucosamine phosphates have been used as vaccine adjuvants, including a therapeutic cancer vaccine based on the tumor-specific protein melanoma-associated antigen 3 (MAGE-A3).[176] TLR9 agonists induce type 1 IFN secretion in DCs, promoting a Th1 response of cytotoxic DC, NK, and T cells as well as promoting M2 to M1 switching,[177] all of which contribute to tumor-specific immune responses and the reversal of immune suppression. A number of CpG-containing TLR9 agonists (IMO-2055, CPG 7909, and MGN1703; structures not shown) have been evaluated in Phase I/II trials in solid tumors, often in combination with chemotherapy.[153a] To date there has been no clear clinical demonstration of a standalone benefit using any of these systemically administered TLR agonists.

5.11.4.3.5 STING

In 1991 Professors Baguley and Denny of the Cancer Society Research Center, University of Auckland published on a series of xanthenone acetic acids that they were pursing to develop anticancer agents targeting the immature vasculature of solid tumors.[178] In a series of subsequent publications they found that one of these compounds, 5,6-dimethylxanthenone 4-acetic acid (DMXAA, **75**) (Fig. 24), following a single i.p. dose totally eradicated murine MC38 tumors. In addition to the acute effects on tumor vasculature, **75** activated NK cells and induced the release of cytokines, such as TNFα and IFNβ from TAMs. In 2013, Conlon et al. demonstrated the induction of IFNβ to be dependent on the direct binding of **75** to STING.[179]

The recently elucidated STING (stimulator of interferon genes) pathway of cytosolic DNA sensing is an innate immune mechanism driving type I IFN production with particular relevance to the recognition of tumor antigens. STING is an adaptor protein located on the endoplasmic reticulum. Upon binding of a cyclic dinucleotide (CDN) agonist STING dimerizes and binds to TANK-binding kinase 1 (TBK1). This complex then traffics to the perinuclear regions of the cells facilitating TBK1 phosphorylation of transcription factors, IRF3 and NF-κB, leading, respectively, to type I interferon production and proinflammatory cytokine synthesis.[180] The natural mammalian agonist, 2′3′-cGAMP (**73**), is produced by the enzyme cyclic GMP–AMP synthase (cGAS),

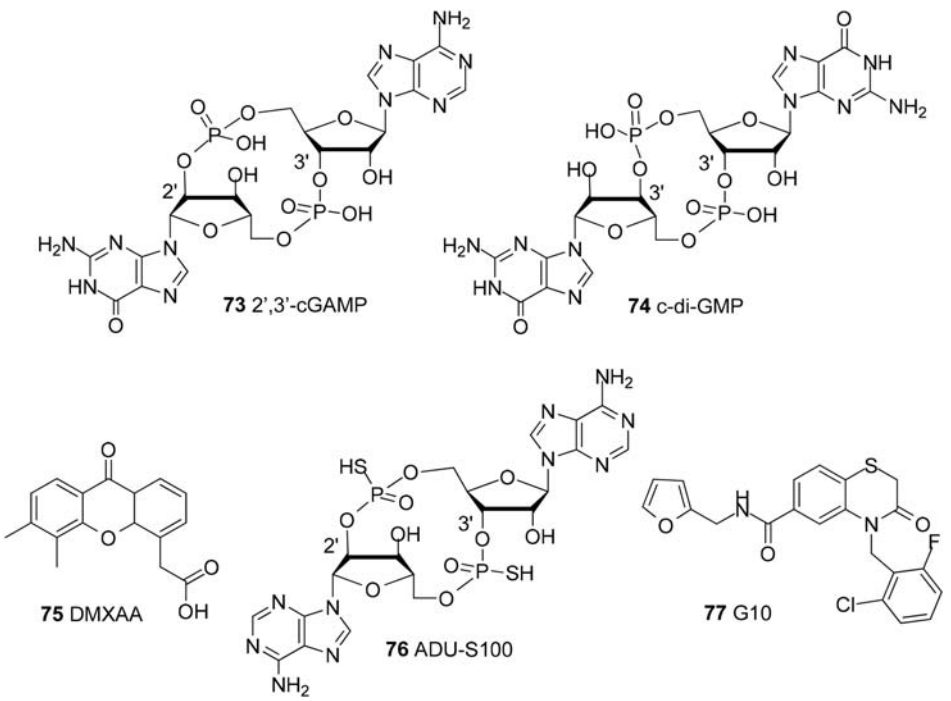

Fig. 24 STING ligands.

which uses ATP and GTP as substrates to produce a CDN with one 2′,5′-phosphodiester linkage and one canonical 3′,5′ linkage. In cells at homeostasis there exist regulatory mechanisms to maintain low levels of cytosolic dsDNA. When the concentration of cytosolic DNA rises sufficiently to form dsDNA-cGAS complex, catalytic active enzyme is formed and the synthesis of **73** is initiated. The recognition of cytosolic DNA appears to be sequence-independent; hence signaling can be initiated by either microbial or mammalian dsDNAs. This mechanism is fundamentally distinct from TLR9, which recognizes unmethylated CpG dsDNAs that are produced only by microbial organisms. Acting in its role as a sentinel to fight off microbial invasion, STING can detect both DNA and RNA viruses, as well as, bacterial DNA. Additionally, bacterially produced second messenger 3′3′-CDNs also bind and activate mammalian STING.[181] It was the X-ray crystallographic elucidation of the binding mode for bacterial CDN (c-di-GMP, **74**),[182] which subsequently led to discovery of cGAS and the unique mammalian ligand **73**.[183] Depending on the organism, the activation of the STING pathway by bacterial CDNs can either enlist the immune system to fight the infection or in some cases to facilitate survival of the bacteria.[184] Several features of the STING pathway suggest that, relative to other PRRs, STING may be uniquely endowed with the ability to detect and defend against tumor antigen. This premise rests upon: (1) the finding that $CD8a^+$ dendritic cells are the key cells essential for tumor antigen-specific $CD8^+$ T cell priming,[185] (2) this priming is dependent on type I IFN production,[185] and (3) the production of type I interferon in response to tumor antigen is uniquely dependent on detection of tumor-derived DNA by STING and not other PRRs.[186] Thus the DNA-cGAS-STING-IFNβ pathway forms the bridge between tumor sensing and a spontaneous adaptive T cell responses. If the STING pathway is an important defense blocking tumorigenesis then one might anticipate that the deregulation of STING signaling could be a trait acquired by tumor cells to avoid detection. Such deregulation has been recently been demonstrated in a majority of the 11 colorectal carcinoma cell lines that were studied which displayed a loss of IFR3 function. The major defect in these cell lines was a loss of cGAS expression. While this study was restricted to colorectal carcinoma cell lines, it may be that the loss of STING pathway during cancer development is a common theme.[187]

Multiple structures of the C-terminal domain of STING show the protein crystallizes as a symmetrical dimer in both free and ligand bound states. The CDN ligands bind into a V-shaped pocket at the dimer interface and are anchored to STING by a network of hydrogen bonds. Depending on the ligand and STING ortholog, ligand binding can induce a subtle conformational shift of the α2-helices which appears coupled to formation of a cap that completely encompasses the ligand. This observation has led to the suggestion that this "closed" form is the active agonist conformation.[188] While all cyclic-GAMP isomers (3′-3′, 2′-3′, or 3′-3′) have the potential to bind and activate both murine and human STING, for human STING this is dependent on which human allelic variant is tested. Xanthenone **75** binds to murine STING in the same V-shaped pocket as the CDNs with 2 molecules of **75** per STING dimer and shares in common with **73** several key contacts. Specifically the ketone groups of **75** hydrogen bond to the hydroxyl of T266 and the carboxylates are anchored with a salt bridge to the guanidine side chain of R237. For **73**, the free oxygens of the phosphodiesters make both these contacts. Human STING is not activated by and does not bind to **75** and related analogs. This surprising discovery, which was first described by Conlon et al.[179], was traced to a single residue, G230, which is an isoleucine in murine STING.[189]

In 2000 before these discoveries were made, **75** began Phase I clinical trials began in New Zealand. The development of **75** was later continued by Novartis into Phase II/III, but to date the results have been disappointing with the failure of two Phase III trials.[190] While it is clear that **75** has some clinical activity, it is also equally clear that the exciting curative results seen in mouse models did not translate into clinical efficacy, a result which is no doubt attributable to the loss of STING agonism in going from mice to human STING. Several researchers have reported preclinical activity for the endogenous CDN ligand (**73**) in murine tumor models. In the CT-26 syngeneic model, Li et al. reported dose-dependent inhibition of tumor growth following continuous subcutaneous dosing (5, 10, and 20 mg kg^{-1}) for 20 days.[191] In the same MC38 murine model which was used to discover **75**, compound **73** was effective when dosed intratumorally on days 2 and 6 following radiation, but had no activity by itself.[192] The initial radiation results in rapid tumor cell death releasing tumor antigen. The addition of a STING agonist provides the type I IFN signal required to prime DCs to the released antigen and initiate an adoptive T cell-mediated immune response. Other than the CDNs, there are no known human active direct STING agonists. However, there has been a report of a STING pathway agonist G10 (**77**) discovered using an HTS to find IRF3 activators.[193] The differing sensitivity of the human polymorphisms to the natural CDNs ligands and the dramatic species sensitivity to **75** are important considerations for researchers considering the development of STING agonists.

5.11.4.3.6 Targeted delivery of PRR agonists

Preclinically multiple drug delivery strategies are being explored for PRR agonists. The goal of these strategies is to maximize delivery and retention in draining lymph nodes where antigen processing and presentation occurs, as well as, T cell priming and activation. An additional consideration for cancer is to maximize the concentration of the PRR agonist in the tumor, the site where tumor antigen is highest. The reliance on endogenous antigen to provide an immune response when boosted by an external adjuvant has been termed "in situ" vaccination.[194] Hence the use of PRR agonists to stimulate the immune response to cancer can be viewed as a therapeutic vaccination which relies primarily on cytotoxic $CD8^+$ T and NK cells and not B cell antibody-mediated immunity normally associated with a vaccine. One additional consideration for targeted delivery is that systemic activation of PRRs is problematic as the ensuing cytokine response can lead to serious toxicity. For example, bacterial toxic shock is largely the result of the cytokine storm (notably TNFα) resulting from the recognition of bacterial endotoxin by the TLR4 receptor. Clinically the maximum tolerated dose of the TLR agonists is typically associated with fever, injection site pain, transient hypotension, and nausea. The lack

of targeted delivery of these agents likely explains the poor clinical results seen as single agent treatments and the same consideration may also contribute to their limited efficacy when used in combination with other therapies.[195]

The simplest form of targeted delivery is direct injection into the tumor. While intratumoral (i.t.) injection limits the types of human cancers that can be treated, researchers have reported multiple preclinical examples of dramatic improvements in efficacy. Examples of TLR agonists being clinically investigated using i.t. administration are IMO-2125 (TLR9, structure not shown)[196] and 3M-052 (**63**, TLR7/8).[197] The synthetic oligonucleotide IMO-2125 is essentially inactive in murine syngeneic models when dosed s.c., but effects a high number of durable responses when dosed i.t. Furthermore, i.t administered IMO-2125 induced tumors to express PD1, which suggests that efficacy would be improved if PD1 were blocked. The combination of IMO-2125 and anti-PD1 demonstrated additive efficacy in mouse models.[196] Compound **63**, a TLR 7/8 agonist, was designed as a slow release drug depot by attachment of an octadecanoic (stearic) amide to the imidazoquinoline scaffold. Similar to IMO-2125, **63** demonstrated additive activity when combined with immune checkpoint inhibitors.[198] The CDNs have relatively short plasma half-lives and as noted earlier provide modest activity when dosed systemically. The short plasma $T_{1/2}$ appears to be primarily the result of phosphodiesterase cleavage of the 2′-5-phosphate linkage. Li et al. demonstrated that the instability of **73** could be significantly improved by replacement of the nonbridging oxygens of the phosphates with sulfur.[199] The resulting bisphosphothioate analog of 2′,3′-cGAMP had similar affinity for hSTING and was 10-fold more potent at inducing IFNβ secretion from human monocytic THP1 cell line. Corrales et al., at Aduro BioTech, extended this observation by preparing and examining the activity of both cyclic-GAMP and cyclic-diAMP bisphosphothioate analogs. Based upon improved stability, good agonist activity across all the major human STING haplotypes, and potent i.t. antitumor activity, dithio-(Rp,Rp)-[cyclic[A(2′,5′)pA(3′,5′)p] (**76**, ADU-S100) was selected as a clinical development candidate.[200]

The development of targeted delivery approaches applicable to all tumor types is a major challenge. While historically these drug delivery technologies have been explored primarily for the delivery of PRR agonists as traditional vaccine adjuvants, many are equally applicable for the development of "in situ" cancer "vaccines." Discussed below are several examples of such approaches that have some promising preclinical results. Covalent incorporation of Imidazoquinoline TLR7/8 agonist into HPMA polymers improved retention at the injection site and draining lymph nodes. However, in order to achieve enhanced vaccine immunogenicity the efficient uptake of the polymer by APCs was required.[201] In addition to its role in immune regulation, the lymphatic system provides a pathway for the transport of dietary lipids. Serum albumin (SA), which is the primary transporter of fatty acids, is preferentially taken up by lymphatic capillaries leading to an accumulation of SA in draining lymph nodes. The Irvine lab at MIT has proposed the concept of albumin "hitchhiking" to achieve selective lymphatic delivery and demonstrated the selective accumulation of an amphiphilic CpG oligonucleotide TLR9 agonist linked to a lipophilic carrier with high SA binding affinity.[202] The same principle that leads to selective transport of SA into the lymphatic system applies to simple liposomal formulations which have long been known to accumulate in the lymphatic system and tumors. Liposomal formulations of Pacitaxel and Doxorubicin have been developed and approved as cancer chemotherapies which offer reduced toxicity and enhanced efficacy. Liposomal formulations of the STING agonist (c-di-GMP **74**) have recently been reported by two research groups. Encapsulation of **74** within PEGylated lipid nanoparticles redirected **74** to dLNs resulting in enhanced adjuvant effectiveness and reduced systemic cytokine induction.[203] Similarly intravenous administration to mice of **74** encapsulated within YSK05-liposomes efficiently induced the production of IFNβ and activation of NK cells, resulting in a significant antitumor effect in the B16-F10 lung metastasis mouse model.[204]

Going forward, important considerations which relate to pro- and antitumor roles attributed to TLR and STING signaling are the strength of the immune stimulation and the duration of the signal.[195] Chronic infection and inflammation resulting in continuous low-level stimulation promotes cytokine signals that lead to Treg stimulation and impaired Teff cells. Conversely, as outlined above, there is compelling preclinical data to suggest that robust acute activation of the PRRs can enhance APC function leading to amplification and activation of tumor-specific Teff cells. The translational of the impressive findings achieved with targeted delivery into the clinic will require drug discovery researchers to match the right agonist with the right delivery system.

5.11.4.4 Kinase Inhibitors

The introduction of the BCR-ABL kinase inhibitor imatinib for the treatment of CML (2001) marked the beginning of targeted personalized treatment of cancer.[205] Mechanistically, imatinib and most other oncology directed kinase inhibitors target oncogenic drivers of tumor growth and survival. However, as discussed by Adams et al., direct immune regulatory effects have also been observed for some of these inhibitors (KIT and BRAF).[32b] Discussed below are several examples of kinases that regulate innate immunity independent of their action on tumor cells and as such could be important targets for the development of new immuno-oncology therapies.

5.11.4.4.1 TGF-β RI/ALK5 inhibitors

Transforming growth factor-β (TGF-β) belongs to a family of cytokines which acts through serine/threonine receptor kinases. Its activity profile is a complex one. It can act directly on tumor cells to promote an antiproliferative effect, but tumors quickly lose their sensitivity to it even as they overexpress TGF-β. It induces a profound immunosuppressive activity via recruitment and activation of regulatory T cells and pro-metastatic MDSCs, and is thought to be a major contributor to the immunosuppressive TME.[206] It is this aspect of TGF-β activity which has made it an attractive immuno-oncology target.

TGF-β's mechanism of action is every bit as complex as its biology. It is synthesized as a precursor molecule but is cleaved in the Golgi before being secreted. It remains noncovalently associated with the propeptide (latency-associated protein, LAP) and forms

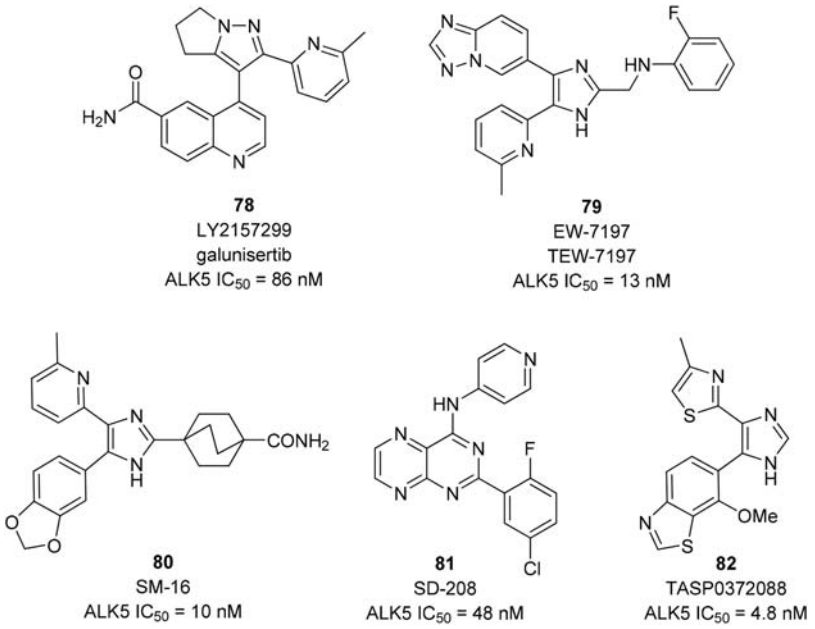

Fig. 25 ALK5 (TGF-β R1) antagonists.

additional interactions with other extracellular proteins (latent transforming growth factor-β binding proteins, LTBPs) to form a complex (large latent complex, LLC), which sequesters the TGF-β. The free cytokine is released from the LLC under a variety of conditions, which include proteolysis as well as interaction with integrins.[207]

There are three TGF-β receptors, two of which are involved in the signal transduction. The catalytically inactive TGF-β RII binds TGF-β, forming a dimeric complex. This is turn recruits the catalytically active TGF-β RI (also known as activin-like receptor kinase 5, ALK5), which then dimerizes and is activated. The active receptor complex is thus a tetramer of two TGF-β RI and two TGF-β RII receptors. The activated complex phosphorylates the downstream targets, the transcription regulators SMAD2 and SMAD3, which then bind to SMAD4 and translocate to the nucleus.[207c] The role of TGF-β RIII is less clear. Like TGF-β RII, it is enzymatically inactive. It is expressed in very high levels and may serve as local reservoir for TGF-β, and it can interact with TGF-β RII to promote formation of the TGF-β RI/TGF-β RII signaling complex.[208]

Because of the strong associations of TGF-β with pathophysiological states, there has been a great deal of activity in the design, synthesis, and evaluation of ALK5 inhibitors, as documented in the cited reviews.[209] While potent and selective ALK5 inhibitors were developed, various toxicities including a worrying hyperplastic valvular heart toxicity was observed in multiple, diverse ALK5 inhibitor chemotypes, suggesting that this was an on-target effect.[210] These results considerably dampened the enthusiasm for further development of ALK5 inhibitors. Researchers at Lilly, noting the reduced cardiac toxicity of LY2157299 (**78**) (Fig. 25), performed an extensive pharmacological study and determined that intermittent dosing or continuous low dosing abrogated the cardiac toxicity in preclinical species,[211] and they were able to advance **78** into clinical trials.[212] Compound **78** is now in Phase III trials both as a single agent and in combination with gemcitabine, and to date has not displayed any Grade 3 or 4 toxicities or cardiotoxicity, while demonstrating a PD response based on measuring reduction in phospho-SMAD2 levels. It is possible that the cardiotoxicity may not be as significant an issue in humans compared with rat or dog.

Researchers at the Ewha Women's University in Seoul developed EW-7197 (**79**), a potent and selective ALK5 inhibitor.[213] They paid particular attention to cardiotoxicity during preclinical development and did not observe any toxicity in rat or dog in 28 day studies at doses 20-fold above pharmacologically active doses. They have just entered Phase I clinical trials in collaboration with MedPacto and OncoVenture.

Compound SM-16 (**80**), developed by Biogen Idec,[214] and SD-208 (**81**), developed by Scios,[215] have been used for preclinical validation of the TGF-β pathway in immune regulation. In a syngeneic AB12 mesothelioma model, **80** has been shown to inhibit tumor growth through $CD8^+$ cytotoxic T cells, with no effect when the model is run in immunodeficient SCID mice.[214] In the same model, **80** also increases the number of tumor infiltrating macrophages, NK cells, and $CD8^+$ CTLs.[216] In an LN-308 glioma model, **81** also increases the number of tumor infiltration NK cells, macrophages, and $CD8^+$ CTLs, and isolated peripheral blood lymphocytes (PBLs) or purified T cells from treated mice show enhanced lytic activity against LN-308 cells in culture compared to PBLs or T cells from naïve mice.[217]

Researchers at Taisho Pharmaceutical Co. have taken a slightly different approach with their ALK5 inhibitor TASP0372088 (**82**). In preclinical work, they have demonstrated a long-lasting PD effect for topically applied **82**.[218] Although their interest is in alopecia rather than an oncology application, topical administration in suitable skin cancers may represent an alternative approach to discharge potential cardiotoxicity risks.

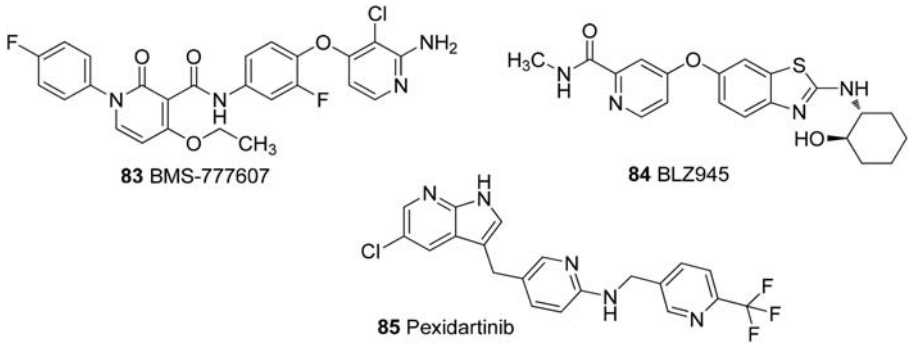

Fig. 26 RON and CSF-R1 inhibitors.

5.11.4.4.2 RON inhibitors

Initially identified on macrophages, RON is a receptor tyrosine kinase belonging to the hepatocyte growth factor receptor family.[219] Activation by macrophage-stimulating protein (MSP) promotes cell proliferation, survival, and chemotaxis.[220] The overexpression of RON protein or activating oncogenic mutants contributes to tumor growth, angiogenesis and chemoresistance.[220] A Met-family-selective inhibitor BMS-777607 (**83**; IC_{50}s for RON/Met/Axl/Tyro3 = 1.8/3.9/1.1/4.3 nM, respectively)[221] has been advanced into clinical trials as tumor-targeted agent (Fig. 26). Loss of RON function has been shown to promote an effective antitumor $CD8^+$ T-cell response which is believed to be the result of repolarization from an M2/TAM phenotype to a proinflammatory M1 macrophage.[222] In the murine PyMT tumor model using cells overexpressing MSP cells **83** significantly reduced outgrowth of lung metastasis, which suggests that clinically Ron inhibitors could prevent the growth of undetectable micrometastases into the overt tumors that are the ultimate cause of cancer mortality.

5.11.4.4.3 CSF-R1 inhibitors

Unlike previous kinase inhibitors which have been advanced primarily based upon their ability to directly inhibit tumor growth, the targeting of innate immunity has been proposed for inhibitors of colony-stimulating factor 1 receptor (CSF-1R) signaling which is exclusively expressed on cells of the myeloid lineage. Within the TME stimulation of CSF-1R promotes M1 to M2 polarization and TAM accumulation which was shown to be blocked by a small molecule CSF-1 kinase inhibitor BLZ945 (**84**; CSF-1R IC_{50} = 1 nM; >3000-fold selective vs 60 tested kinases) in a glioblastoma multiforme[223] and Pexidatrinib (**85**, PLX3397; CSF-1R IC_{50} = 11 nM)[224] in the MMTV-PyMT breast cancer model.[225] The combination of **85** with pacitaxel in the breast cancer model or with checkpoint inhibition (anti-CLT4 or anti-PD1 mAbs) in a mouse pancreatic model[226] afforded a significant increase in response over the monotherapies.

5.11.4.4.4 TAM receptor signaling inhibitors

The TAM (Tyro3/Axl/MerTK) signaling network is a powerful and broadly acting pathway for the inhibition of inflammation and induction of this pathway delimits a cycle of inflammation that governs innate immune system homeostasis.[227] Neutralization of MerTK in allogenic mixed leukocyte reactions, as well as autologous dendritic cell–T cell cultures has been shown to increase T cell proliferation and induce IFN-γ production.[228] Pan-TAM family inhibitors with varying degrees of selectivity, such as the previously mentioned **83** (MerTK IC_{50} = 14 nM),[221] are well known as reviewed by Baladi et al.[229] Recently researchers at UNC have used structure-guided design to discover of a highly potent and selective MerTK inhibitor UNC2881 (**86**; MerTK/Axl/Tyro3 IC_{50} = 4.3/360/250 nM, respectively).[230] Similarly, optimization of an alternative pyrazolopyrimidine scaffold furnished selective MerTK inhibitors such as UNC569 (**87**; MerTK/Axl/Tyro3 IC_{50} = 2.9/37/48 nM, respectively) (Fig. 27).[231] The utility of such selective inhibitors in the clinical setting has yet to be demonstrated.

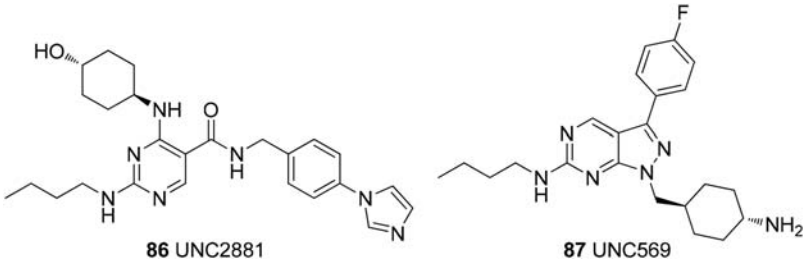

Fig. 27 Selective MerTK inhibitors.

5.11.4.4.5 PI3K inhibitors

The development of inhibitors for oncogenic PI3Kα was an early focus of interventions directed at the lipid kinase family. These initial PI3K inhibitors blocked a number of lipid kinases and were often pan-active across all four human PI3K isoforms. As chemist's knowledge has increased in this area, so has our ability to discover and design more selective lipid kinase inhibitors. While PI3Kα and PI3Kβ are broadly expressed, the expression of PI3Kδ and PI3Kγ is restricted to leukocytes making these isoforms particularly attractive targets to regulate innate and adoptive immunity while minimizing the effects on other tissues. In addition to a potential utility for the treatment of cancer, selective inhibitors are being pursued for the treatment of a variety of immune and inflammatory disorders.[232] Idelalisib (**90**), aPI3Kδ-selective inhibitor, has achieved dramatic responses in certain B cell malignancies, leading to its approval as a second line treatment of chronic lymphocytic leukemia (CLL). In these malignant B cells PI3Kδ activation is a critical component of the B-cell receptor signaling pathway promoting survival and proliferation.[233] Ali et al. have recently uncovered an additional role for PI3Kδ in maintaining the regulatory checkpoint in T cells.[234] The authors propose that immune regulation is due to the effect on cells of the innate immune system differentially impairing Treg and MDSC function, such that the balance shifts from immune tolerance to an enhanced immune response to the tumor. They further speculate that immunoregulatory effects of PI3Kδ inhibition may contribute to the efficacy of idelalisib in CLL and could have potential application across a broad range of solid tumors. PI3Kγ plays an important role in the innate immune response of myeloid cells by mediating integrin (α4β1)-dependent macrophage chemotaxis into tumors. Genetic blockade (p110γ kinase-dead cells/mice) of PI3Kγ in myeloid cells suppressed inflammation, growth, and metastasis of implanted (Lewis lung carcinoma) and spontaneous tumors (PyMT spontaneous breast carcinomas).[235] These results were confirmed with moderately selective PI3Kγ inhibitors that had no direct effect on tumor cells in culture, demonstrating that the PI3Kγ-dependent tumor growth was dependent on myeloid cell which do express PI3Kγ and not a direct effect on the tumor which does not express PI3Kγ.

Similar to protein kinases, ATP-competitive lipid kinase inhibitors make a critical hydrogen bond to a backbone amide NH in the hinge region connecting the upper and lower lobes. The hydrogen bond acceptor on the inhibitor is often a sp^2 heteroaromatic nitrogen, but can also be an oxygen lone pair of a more spatially demanding morpholine hinge binder, as present in the prototypical pan-PI3K inhibitor LY294002 (structure not shown).[236] The spacial placement of the gatekeeper is also slightly different from that of a protein kinase. Both these features contribute to the general observation of nonoverlapping inhibition profiles between these lipid and protein kinase families. Hence while the initial PI3K inhibitors were often pan-active lipid kinase inhibitors, they were in general inactive toward protein kinases. Sadhu et al. reported on the first highly selective PI3Kδ inhibitor (IC87114, **88**) in 2003 (Fig. 28).[237] The structural basis for the selectivity of **88** and PIK-39 (**89**) is the formation of an induced-fit pocket in the phosphate binding P-loop.[238] In the apo enzyme, Met-752 and Trp-760 are packed against each other, but in the presence of idelalisib (**90**) these two residues move 6–7 angstroms apart, opening a hydrophobic specificity pocket.[239] Williams and Shokat present calculations that are in agreement with the X-ray structures which indicate that formation of this specific pocket in the P-loop is energetically more favorable for the delta over the gamma isoform (all PI3K isoforms have these same residues).[240] The orthogonal disposition of the quinazolinone to the plane of the hinge binder motif has been described as a propeller-shaped conformation and is a characteristic of the majority of PI3Kδ selective inhibitors. Examples of propeller-shaped PI3Kδ selectivity inhibitors which utilize the same 4-substituted purine hinge binder are duvelisib (**91**) and AMG-319 (**92**).[241] Related inhibitors employing alternative hinge binders and further modification of the quinazolinone are AM-8508 (**93**)[242] and TGR-1202 (**94**).[243] While the induced-fit pocket favors delta over gamma, researchers at Infinity Pharmaceuticals have recently reported the structure of IPI549 (entire structure not discernible in the view presented in poster) bound to PI3Kγ having this same propeller-binding mode.[244] Hence it does appear that the P-loop of PI3Kγ is sufficiently flexible to make this pocket energetically accessible for the gamma isoform.

While less prevalent, "flat" molecules that do not engage the induced-fit pocket can also achieve high delta selectivity. Examples are **95**,[234] a close analog of GDC-0941 (structure not shown) whose structure in PI3Kδ is known,[240] and the 4,6-diaryl quinazoline (**96**), which was derived using a structure-based design hypothesis from a pan-active PI3K inhibitor (Fig. 29).[245] Interestingly, when cocrystallized in PI3Kδ the structure of **96** revealed a different binding mode from the proposed rationale. Finally, Vertex has reported the design of a highly gamma selective inhibitor (**97**) that does not rely of the induced-fit pocket, but instead on a favorable interaction with glutamate 814, which is unique to the gamma enzyme. This binding mode has not yet been demonstrated in a cocrystal structure.[236]

Clinically trials are currently on going for selective orally active PI3Kδ inhibitors in a number of B-cell-related malignancies and autoimmune disorders.[232] COPD and asthma are also being pursued, but current trials are restricted to inhaled delivery. As might be anticipated dual gamma/delta PI3K inhibition provides potent antiinflammatory activity,[246] but there is concern for increased toxicity as this would effectively block all PI3K activity in lymphocytes. To date no clinical trials have been initiated exploring the potential utility of selective PI3Kδ inhibitors as immunoregulatory agents for solid tumors. Phase I trials in subjects with advanced solid tumors for the first PI3Kγ inhibitor (IPI-549) have recently begun.[244] In mouse syngeneic tumor models IPI-549 demonstrated additive efficacy with both anti-CTLA4 and anti-PD1, providing a strong rationale to pursue this approach in the clinic.

5.11.4.5 Checkpoint Inhibitors

The targeting of T-cell checkpoint receptors and their ligands with inhibitory antibodies has been the first successful therapeutic application of immuno-oncology.[19] Despite the success of antibody-based approaches, there still remains a keen interest in small

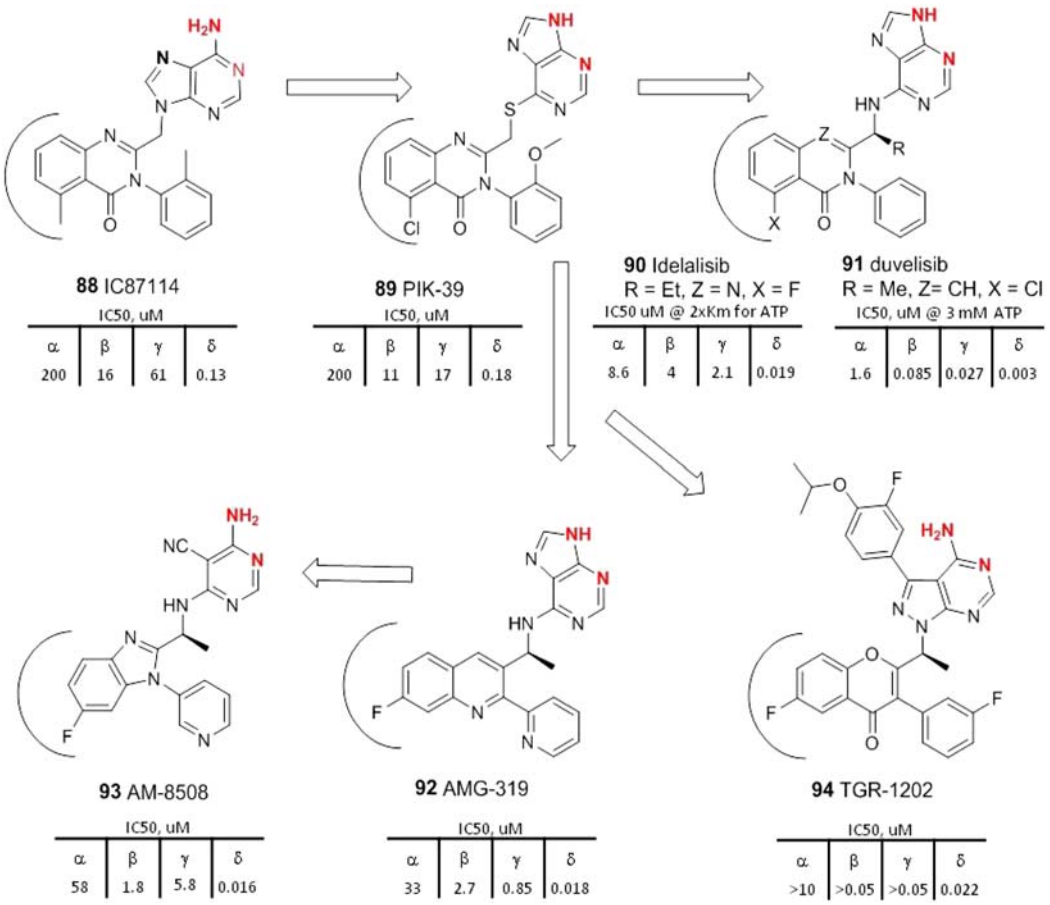

Fig. 28 Progression for discovery of highly selective PI3Kγ inhibitors utilizing the P-loop induced-fit pocket (illustrated with *half circle*). Hinge binder donor–acceptor shown in *bold red*.

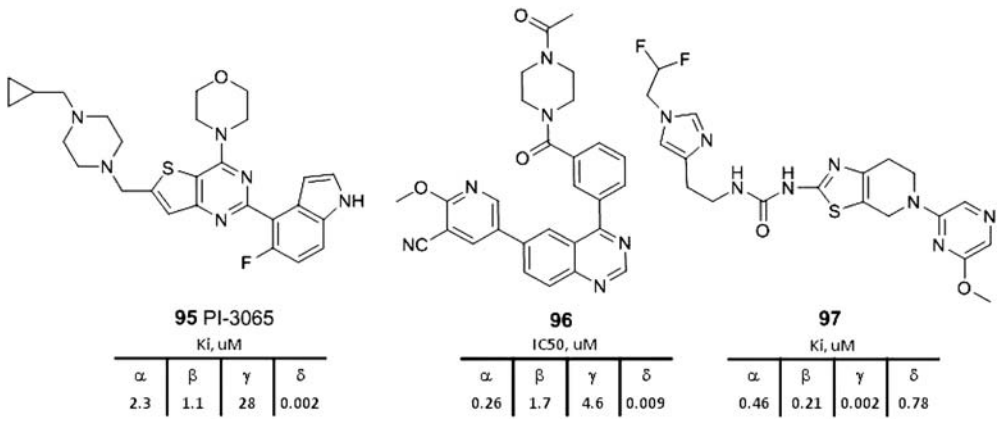

Fig. 29 Isoform-selective PI3K inhibitors.

molecule inhibitors of checkpoint ligand–receptor interactions, which might provide significant advantages in cost of goods, convenience in dosing, and more finely tuned modulation of the immunostimulatory response.

5.11.4.5.1 Small molecule inhibitors

Researchers at Bristol-Myers Squibb recently reported biarylmethoxyphenyl (**99**–**101**) and biarylmethoxpyridiyl (**98**) scaffolds as potent inhibitors of the interaction of PD1 and PD-L1, as measured by a Homogeneous Time-Resolved Fluorescence (HTRF)

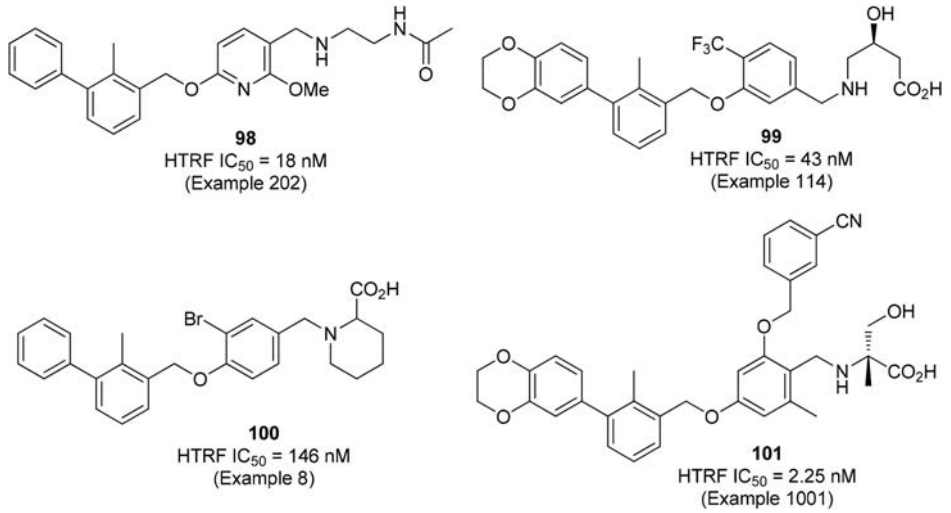

Fig. 30 Small molecule inhibitors of PD1/DP-L1 interaction disclosed by Bristol-Myers Squibb.

binding assay using soluble, extracellular domain constructs of PD1 and PD-L1. Cellular or in vivo data for these compounds has not been reported (Fig. 30).

The mechanism of action of these compounds has been determined by solution studies and X-ray crystallography using soluble, extracellular domain constructs of the two target proteins.[247] The compounds bind selectively to PD-L1 and cause its dimerization, and they are capable of dissociating preformed PD1/PD-L1 complexes. Crystal structures of the PD-L1 dimer complexed with **98** and **100** have been obtained. PD-L1 adopts the same Ig V-type topology that the apo-protein displays. The two PD-L1 monomers are oriented in a C_2 symmetric fashion with the ligand sandwiched between them, as shown in Fig. 31. Interestingly, the binding site of the small molecule is the same as the interaction site with PD1[248] and would completely occlude the interaction of PD1 and PD-L1, as shown in the overlay in Fig. 31B. It is unclear what effect, if any, dimerizing PD-L1 on the presenting tumor cell might have.

Compound **98** binds in a long, cylindrical, hydrophobic cleft at the PD-L1 dimer interface, and most of its interactions with PD-L1 are hydrophobic, as shown in Fig. 32. The biaryl moiety binds in a pocket lined by Ile^{54}, Tyr^{56}, Met^{113}, Ala^{121}, and Tyr^{123} of one monomer and Ile^{54}, Met^{115}, and Ala^{121} of the other monomer. The hydrophobic cylinder is closed across the top by several intermolecular hydrogen bonds between the two monomers. The acetyl ethylene diamine chain projects out of the cylinder toward solvent space, and makes the only hydrophilic interaction, a hydrogen bond with Asp^{122} of one of the monomers. Compound **100** binds in a very analogous manner (5JO8).[247]

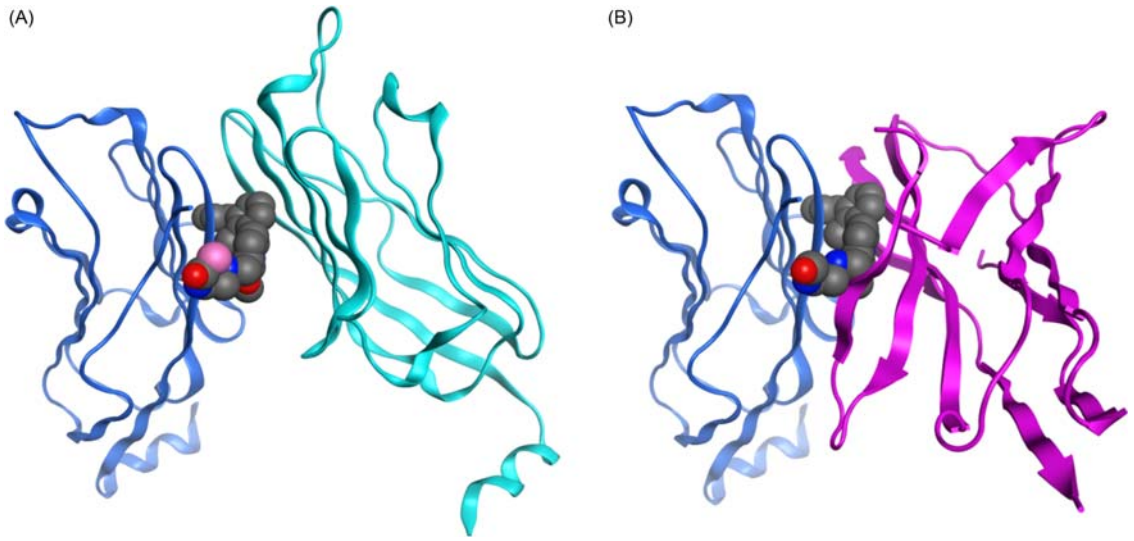

Fig. 31 (A) Ribbon diagram of crystal structure of PD-L1 (monomers in *blue* and *cyan*) with **98** (5J89)[247]; (B) crystal structure of PD1 *(magenta)* and PD-L1 *(blue)* (4ZQK)[248] with **98** overlaid after alignment with PD-L1 from 5J89. Figures drawn using MOE 2015.1001 (Chemical Computing Group).

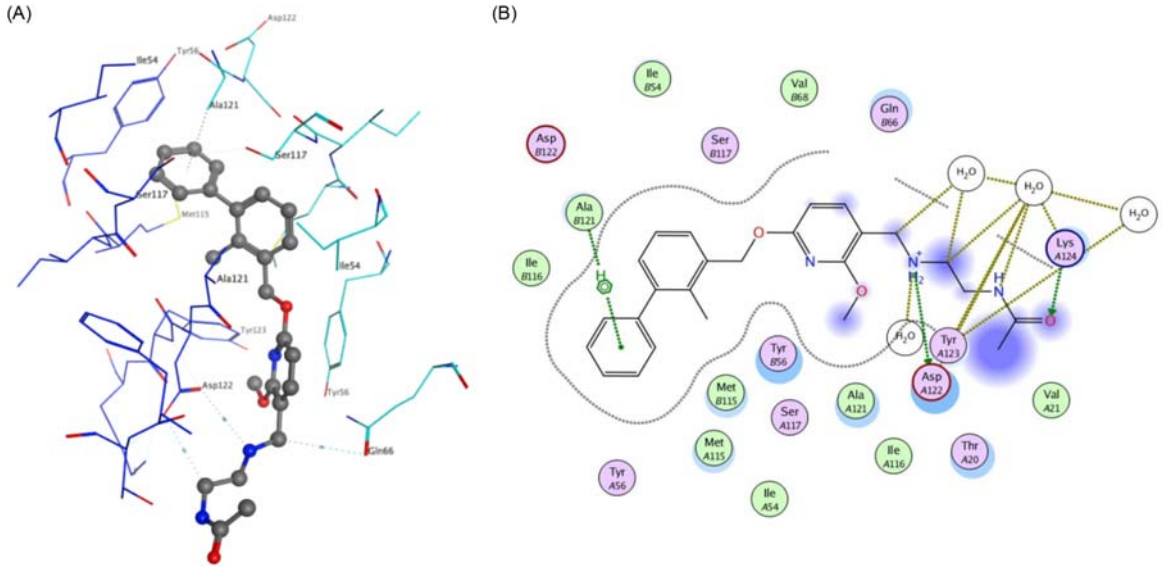

Fig. 32 (A) Binding pocket of 1 in the PD-L1 dimer. Residues from one monomer are colored *blue* and the other monomer *cyan*. (B) Ligand interaction map of **98**. Residues from the *blue* monomer are indicated as A and the cyan monomer as B. Figures drawn using MOE 2015.1001 (Chemical Computing Group).

Researchers at Aurigene Discovery Technologies screened peptides derived from the interaction interface of PD1 and PD-L1 used the results to create pharmacophore models which were in turn used to design small molecule peptidomimetics, which are potent inhibitors of the interactions of PD-L1, PD-L2, and VISTA[249] with PD1.[250] Aurigene has disclosed diacylhydrazine ureas (exemplified by **102**),[251] cyclized diacylhydrazine ureas (**103**),[252] 1,2,4-oxadiazole ureas (**105**),[253] 1,3,4-oxadiazoles (**106**), and thiadiazoles,[254] which exhibit potent inhibition of PD1 in a mouse splenocyte proliferation assay. Mouse splenocytes expressing PD1 are isolated, cultured, and stimulated with murine anti-CD3 and anti-CD28 antibodies. The cells are then treated with a soluble PD-L1 construct in the presence or absence of compound. The amount of proliferation compared to untreated controls is a measure PD1/PD-L1 inhibition. The precise mechanism of action of these compounds has not been disclosed (Fig. 33).

Aurigene has identified a candidate molecule, CA-170 (AUPM-170), which has been licensed to Curis for development and has just entered Phase I clinical trials. CA-170 demonstrates sub-200 nM potency in a number of cell-based assays, is approximately equipotent against PD-L1, PD-L2, and VISTA, and exhibits good in vivo pharmacokinetics, with low clearance, high exposure, and good oral bioavailability.[250] While the structure of CA-170 has not yet been disclosed, it is likely to come from one of the four chemotypes shown above. Aurigene has more recently identified AUPM-327, a dual antagonist of PD-L1 and TIM-3 activation of PD1, which is current undergoing preclinical evaluation.[255] Its structure has also not been disclosed.

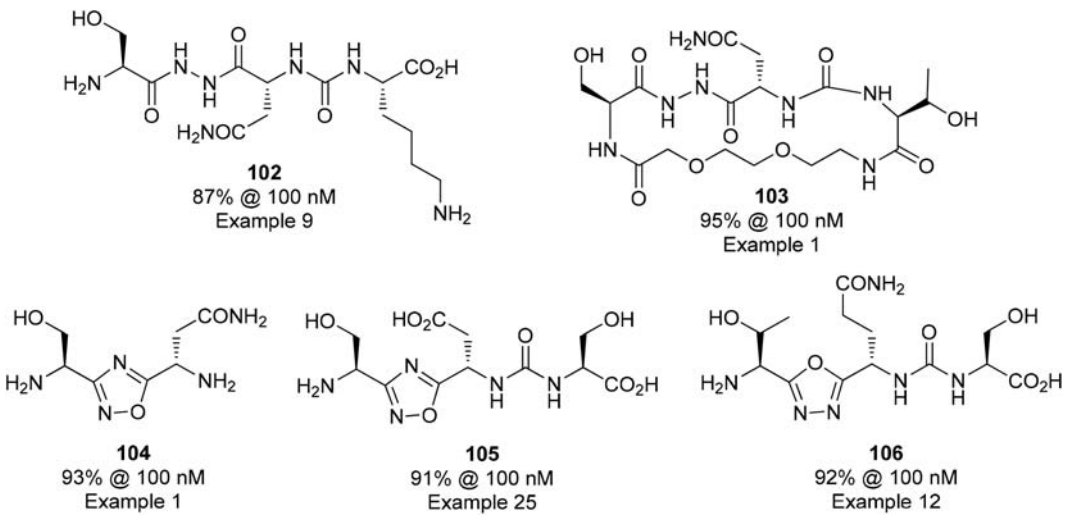

Fig. 33 Small molecule inhibitors of PD1/PD-L1 interaction disclosed by Aurigene.

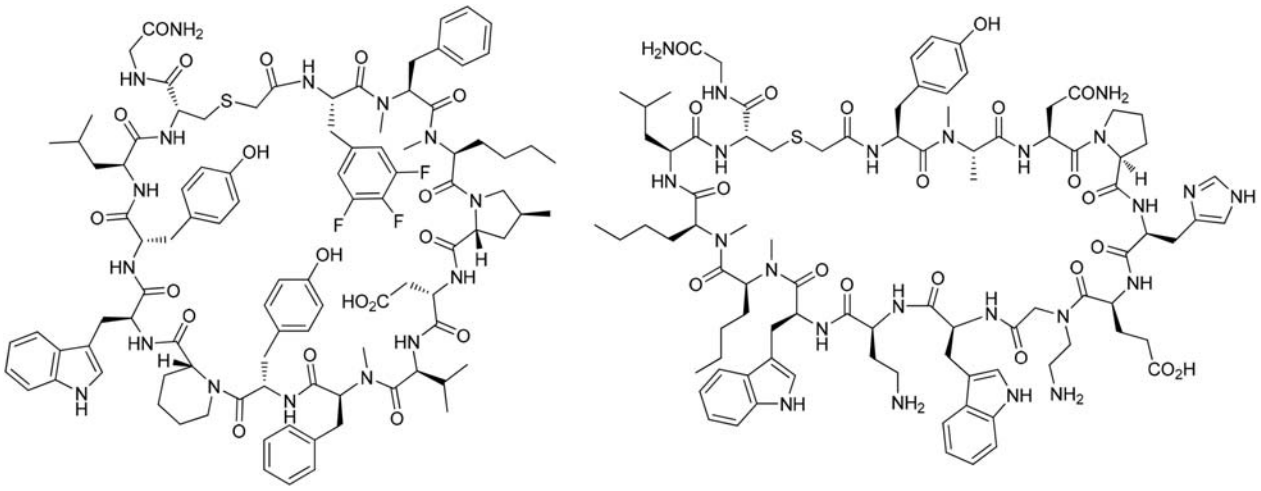

107
HTRF IC_{50} = 4 nM
Cell binding assay IC_{50} = 158 pM
IFNγ production in CMV+ T cells IC_{50} = 620 pM
Example 3592

108
HTRF IC_{50} 6.1 nM
Example 3011

Fig. 34 Cyclic peptide inhibitors of PD1/PD-L1 interaction.

5.11.4.5.2 Peptide inhibitors

Researchers at Bristol-Myers Squibb have reported cyclic 12–14 residue peptides exemplified by **107**[256] and **108**[257] as potent inhibitors of the PD1/PD-L1 and CD80/PD-L1 interactions as measured by the same HTRF assay discussed previously. The macrocyclic rings are generally closed by alkylation of a cysteine side-chain thiol with an amino-terminal chloroacetyl group, but other ring closures such as ring-closing metathesis to generate an olefin are also exemplified. Compound **107** was also evaluated in a cell-based binding assay using a murine B-cell line (LK35.2) that stably overexpresses PD-L1 with a soluble, fluorescently labeled PD1 construct, and in an IFNγ production assay using donor-derived CMV^+ T cells, in both cases generating subnanomolar IC_{50} values. The precise mechanism of action of these macrocyclic peptides has not been disclosed, but since it is known that both PD1 and PD-L1 adopt the primarily β-sheet IG-V fold,[248] it is likely that these peptides are meant provide a complementary docking surface to one of the protein components, most likely PD-L1 (**Fig. 34**).

Chang et al.[258] reported a novel approach to developing a PD-L1 inhibitory ligand using a mirror-image approach.[259] They chemically synthesized an all-D version of the PD-L1 IG-V domain, which provides the PD1 binding element, and used that to screen and optimize a yeast-display library of dodecapeptides for binding. They then synthesized the all-D versions of the peptides they had selected and measured their binding affinity to PD-L1 and their ability to block the PD1/PD-L1 interaction. The compound corresponding to the D-amino acid sequence NYSKPTDRQYHF (^{D}PPA-1), bound to PD-L1 with a affinity of 510 nM in a Surface Plasmon Resonance (SPA) assay and blocked interaction of cellular PD1 with a soluble PD-L1 construct at 1 mg mL^{-1} concentrations. As the D-peptide was completely stable in 10% human serum for 24 h, it was tested in vivo in a mouse CT-26 tumor model. The peptide was injected at 2 mg kg^{-1} either subcutaneously at the site of the tumor or intraperitoneally, and demonstrated a significant antiproliferative effect compared to untreated mice as well as mice treated with 5-FU. While the authors did not demonstrate that their response was due to immune stimulation or compare it to standard PD1 or PD-L1 antibody therapy, it is nevertheless an interesting result.

5.11.5 Conclusion

We began with a summary of the function of the innate and adaptive immune system with respect to tumor recognition and elimination, followed by a discussion of the factors leading to tolerance and the failure of the immune system to eradicate these malignant cells. We then turned to a discussion of selected pathways and targets that have the potential to stimulate an effective immune response to cancer, highlighting those targets most readily amenable to disruption by "traditional" small molecule drugs (nonbiologics). The discussion was not exhaustive, but instead illustrative, of the tremendous potential of medicinal chemistry to impact cancer immunotherapy. For example, not covered was the potential importance of chemokine antagonists[260] and epigenetic regulators.[261]

Our growing understanding of the direct effects of small-molecule drugs on the immune system and the TME provides a basis for exploring small molecule drugs either alone or in combination with a wide range of established oncology drugs. Additionally multiple modalities of non-small molecule drugs are being developed (e.g., mAbs, cellular therapy, oncolytic viruses) with the

goal of boosting the immune system's attack of the tumor.[32b] It is clear that there are multiple intervention points and that drug combination studies offer the advantage of disrupting the cancer immunoediting process simultaneously at different points to maximize the therapeutic effect.[262] Importantly, numerous preclinical studies have demonstrated significant, even synergistic, value in combining immuno-stimulating small molecule drugs with other therapies. Some of these combinations are now being tested in the clinic. Until recently the war on cancer that began in the 60s was devoted almost exclusively to the discovery of cytotoxic agents. Viewing cancer as a failure of immune surveillance promises to greatly enlarge the list of available druggable target. Many of these new targets will be intracellular and as such out of the reach of the therapeutic mAbs that began the new era of cancer immunotherapy. Between the known and those yet to be discovered new targets, medicinal chemists will have multiple opportunities to make a contribution to immuno-oncology therapy, the latest front in the war on cancer.

See also: 6.02. Cancer Immunotherapy.

References

1. Balkwill, F.; Mantovani, A. Inflammation and Cancer: Back to Virchow? *Lancet* **2001,** *357* (9255), 539–545.
2. Coley, W. B. Contribution to the Knowledge of Sarcoma. *Ann. Surg.* **1891,** *14,* 199–220.
3. Riedel, S. Edward Jenner and the History of Smallpox and Vaccination. *Proc. (Baylor Univ. Med. Cent.)* **2005,** *18* (1), 21–25.
4. Gowans, J. L.; McGregor, D. D.; Cowen, D. M.; Ford, C. E. Initiation of Immune Responses by Small Lymphocytes. *Nature* **1962,** *196,* 651–655. Other Information: Orig. Receipt Date: 31-Dec-63 1962, Medium: X.
5. Ehrlich, P. Über den jetzigen stand der karzinomforschung. *Ned. Tijdschr. Geneeskd.* **1909,** *5,* 273–290.
6. Burnet, M. Cancer—A Biological Approach: III. Viruses Associated With Neoplastic Conditions. IV. Practical Applications. *Br. Med. J.* **1957,** *1* (5023), 841–847.
7. (a) Stutman, O. Tumor Development After 3-Methylcholanthrene in Immunologically Deficient Athymic-Nude Mice. *Science* **1974,** *183* (4124), 534–536; (b) Rygaard, J.; Povlsen, C. O. The Mouse Mutant Nude Does Not Develop Spontaneous Tumours. *Acta Pathol. Microbiol. Scand. B: Microbiol. Immunol.* **1974,** *82B* (1), 99–106.
8. Dighe, A. S.; Richards, E.; Old, L. J.; Schreiber, R. D. Enhanced In Vivo Growth and Resistance to Rejection of Tumor Cells Expressing Dominant Negative IFNγ Receptors. *Immunity* **1994,** *1* (6), 447–456.
9. Shankaran, V.; Ikeda, H.; Bruce, A. T.; White, J. M.; Swanson, P. E.; Old, L. J.; Schreiber, R. D. IFN[Gamma] and Lymphocytes Prevent Primary Tumour Development and Shape Tumour Immunogenicity. *Nature* **2001,** *410* (6832), 1107–1111.
10. Penn, I. Malignant Melanoma in Organ Allograft Recipients. *Transplantation* **1996,** *61* (2), 274–278.
11. Pham, S. M.; Kormos, R. L.; Landreneau, R. J.; Kawai, A.; Gonzalez-Cancel, I.; Hardesty, R. L.; Hattler, B. G.; Griffith, B. P. Solid Tumors After Heart Transplantation: Lethality of Lung Cancer. *Ann. Thorac. Surg.* **1995,** *60* (6), 1623–1626.
12. (a) Clemente, C. G.; Mihm, M. C.; Bufalino, R.; Zurrida, S.; Collini, P.; Cascinelli, N. Prognostic Value of Tumor Infiltrating Lymphocytes in the Vertical Growth Phase of Primary Cutaneous Melanoma. *Cancer* **1996,** *77* (7), 1303–1310; (b) Clark, W. H.; Elder, D. E.; Guerry, D.; Braitman, L. E.; Trock, B. J.; Schultz, D.; Synnestvedt, M.; Halpern, A. C. Model Predicting Survival in Stage I Melanoma Based on Tumor Progression. *J. Natl. Cancer Inst.* **1989,** *81* (24), 1893–1904.
13. Dunn, G. P.; Old, L. J.; Schreiber, R. D. The Three Es of Cancer Immunoediting. *Annu. Rev. Immunol.* **2004,** *22* (1), 329–360.
14. Garcia-Lora, A.; Algarra, I.; Garrido, F. MHC Class I Antigens, Immune Surveillance, and Tumor Immune Escape. *J. Cell. Physiol.* **2003,** *195* (3), 346–355.
15. (a) Angulo, I.; Vadas, O.; Garçon, F.; Banham-Hall, E.; Plagnol, V.; Leahy, T. R.; Baxendale, H.; Coulter, T.; Curtis, J.; Wu, C.; Blake-Palmer, K.; Perisic, O.; Smyth, D.; Maes, M.; Fiddler, C.; Juss, J.; Cilliers, D.; Markelj, G.; Chandra, A.; Farmer, G.; Kielkowska, A.; Clark, J.; Kracker, S.; Debré, M.; Picard, C.; Pellier, I.; Jabado, N.; Morris, J. A.; Barcenas-Morales, G.; Fischer, A.; Stephens, L.; Hawkins, P.; Barrett, J. C.; Abinun, M.; Clatworthy, M.; Durandy, A.; Doffinger, R.; Chilvers, E. R.; Cant, A. J.; Kumararatne, D.; Okkenhaug, K.; Williams, R. L.; Condliffe, A.; Nejentsev, S. Phosphoinositide 3-kinase δ gene mutation predisposes to respiratory infection and airway damage. *Science* **2013,** *342* (6160), 866–871; (b) Oppenheim, D. E.; Roberts, S. J.; Clarke, S. L.; Filler, R.; Lewis, J. M.; Tigelaar, R. E.; Girardi, M.; Hayday, A. C. Sustained Localized Expression of Ligand for the Activating NKG2D Receptor Impairs Natural Cytotoxicity in vivo and Reduces Tumor Immunosurveillance. *Nat. Immunol.* **2005,** *6* (9), 928–937; (c) Crane, C. A.; Austgen, K.; Haberthur, K.; Hofmann, C.; Moyes, K. W.; Avanesyan, L.; Fong, L.; Campbell, M. J.; Cooper, S.; Oakes, S. A.; Parsa, A. T.; Lanier, L. L. Immune Evasion Mediated by Tumor-Derived Lactate Dehydrogenase Induction of NKG2D Ligands on Myeloid Cells in Glioblastoma Patients. *Proc. Natl. Acad. Sci.* **2014,** *111* (35), 12823–12828; (d) Salih, H. R.; Rammensee, H.-G.; Steinle, A. Cutting Edge: Down-Regulation of MICA on Human Tumors by Proteolytic Shedding. *J. Immunol.* **2002,** *169* (8), 4098–4102.
16. Coulie, P. G.; Van den Eynde, B. J.; van der Bruggen, P.; Boon, T. Tumour Antigens Recognized by T Lymphocytes: At the Core of Cancer Immunotherapy. *Nat. Rev. Cancer* **2014,** *14* (2), 135–146.
17. Kroemer, G.; Galluzzi, L.; Kepp, O.; Zitvogel, L. Immunogenic Cell Death in Cancer Therapy. *Annu. Rev. Immunol.* **2013,** *31,* 51–72.
18. Motz, G. T.; Coukos, G. Deciphering and Reversing Tumor Immune Suppression. *Immunity* **2013,** *39* (1), 61–73.
19. Pardoll, D. M. The Blockade of Immune Checkpoints in Cancer Immunotherapy. *Nat. Rev. Cancer* **2012,** *12* (4), 252–264.
20. Herbst, R. S.; Soria, J. C.; Kowanetz, M.; Fine, G. D.; Hamid, O.; Gordon, M. S.; Sosman, J. A.; McDermott, D. F.; Powderly, J. D.; Gettinger, S. N.; Kohrt, H. E. K.; Horn, L.; Lawrence, D. P.; Rost, S.; Leabman, M.; Xiao, Y.; Mokatrin, A.; Koeppen, H.; Hegde, P. S.; Mellman, I.; Chen, D. S.; Hodi, F. S. Predictive Correlates of Response to the Anti-PD-L1 Antibody MPDL3280A in Cancer Patients. *Nature* **2014,** *515* (7528), 563–567.
21. Hilchey, S. P.; Kobie, J. J.; Cochran, M. R.; Secor-Socha, S.; Wang, J. C.; Hyrien, O.; Burack, W. R.; Mosmann, T. R.; Quataert, S. A.; Bernstein, S. H. Human Follicular Lymphoma CD39+-Infiltrating T Cells Contribute to Adenosine-Mediated T Cell Hyporesponsiveness. *J. Immunol.* **2009,** *183* (10), 6157–6166.
22. Murphy, K. M.; Reiner, S. L. The Lineage Decisions of Helper T Cells. *Nat. Rev. Immunol.* **2002,** *2* (12), 933–944.
23. (a) Hori, S.; Nomura, T.; Sakaguchi, S. Control of Regulatory T Cell Development by the Transcription Factor Foxp3. *Science* **2003,** *299* (5609), 1057–1061; (b) Fontenot, J. D.; Gavin, M. A.; Rudensky, A. Y. Foxp3 Programs the Development and Function of CD4+CD25+ Regulatory T Cells. *Nat. Immunol.* **2003,** *4* (4), 330–336.
24. (a) Bergmann, C.; Strauss, L.; Zeidler, R.; Lang, S.; Whiteside, T. L. Expansion and Characteristics of Human T Regulatory Type 1 Cells in Co-cultures Simulating Tumor Microenvironment. *Cancer Immunol. Immunother.* **2007,** *56* (9), 1429–1442; (b) Loser, K.; Apelt, J.; Voskort, M.; Mohaupt, M.; Balkow, S.; Schwarz, T.; Grabbe, S.; Beissert, S. IL-10 Controls Ultraviolet-Induced Carcinogenesis in Mice. *J. Immunol.* **2007,** *179* (1), 365–371; (c) Hilchey, S. P.; De, A.; Rimsza, L. M.; Bankert, R. B.; Bernstein, S. H. Follicular Lymphoma Intratumoral CD4+CD25+GITR+ Regulatory T Cells Potently Suppress CD3/CD28-Costimulated Autologous and Allogeneic CD8+CD25− and CD4+CD25− T Cells. *J. Immunol.* **2007,** *178* (7), 4051–4061.
25. (a) Read, S.; Malmström, V.; Powrie, F. Cytotoxic T Lymphocyte–Associated Antigen 4 Plays an Essential Role in the Function of Cd25(+)Cd4(+) Regulatory Cells That Control Intestinal Inflammation. *J. Exp. Med.* **2000,** *192* (2), 295–302; (b) Oderup, C.; Cederbom, L.; Makowska, A.; Cilio, C. M.; Ivars, F. Cytotoxic T Lymphocyte Antigen-4-Dependent Down-Modulation of Costimulatory Molecules on Dendritic Cells in CD4(+) CD25(+) Regulatory T-Cell-Mediated Suppression. *Immunology* **2006,** *118* (2), 240–249.

26. Pandiyan, P.; Zheng, L.; Ishihara, S.; Reed, J.; Lenardo, M. J. CD4+CD25+Foxp3+ Regulatory T Cells Induce Cytokine Deprivation-Mediated Apoptosis of Effector CD4+ T Cells. *Nat. Immunol.* **2007,** *8* (12), 1353–1362.
27. (a) Borsellino, G.; Kleinewietfeld, M.; Di Mitri, D.; Sternjak, A.; Diamantini, A.; Giometto, R.; Höpner, S.; Centonze, D.; Bernardi, G.; Dell'Acqua, M. L.; Rossini, P. M.; Battistini, L.; Rötzschke, O.; Falk, K. Expression of Ectonucleotidase CD39 by Foxp3+ Treg Cells: Hydrolysis of Extracellular ATP and Immune Suppression. *Blood* **2007,** *110* (4), 1225–1232; (b) Deaglio, S.; Dwyer, K. M.; Gao, W.; Friedman, D.; Usheva, A.; Erat, A.; Chen, J. F.; Enjyoji, K.; Linden, J.; Oukka, M.; Kuchroo, V. K.; Strom, T. B.; Robson, S. C. Adenosine Generation Catalyzed by CD39 and CD73 Expressed on Regulatory T Cells Mediates Immune Suppression. *J. Exp. Med.* **2007,** *204* (6), 1257–1265; (c) Allard, B.; Pommey, S.; Smyth, M. J.; Stagg, J. Targeting CD73 Enhances the Antitumor Activity of Anti-PD-1 and Anti-CTLA-4 mAbs. *Clin. Cancer Res.* **2013,** *19* (20), 5626–5635.
28. (a) Almand, B.; Clark, J. I.; Nikitina, E.; Van Beynen, J.; English, N. R.; Knight, S. C.; Carbone, D. P.; Gabrilovich, D. I. Increased Production of Immature Myeloid Cells in Cancer Patients: A Mechanism of Immunosuppression in Cancer. *J. Immunol.* **2001,** *166* (1), 678–689; (b) Diaz-Montero, C. M.; Salem, M.; Nishimura, M.; Garrett-Mayer, E.; Cole, D.; Montero, A. Increased Circulating Myeloid-Derived Suppressor Cells Correlate With Clinical Cancer Stage, Metastatic Tumor Burden, and Doxorubicin–Cyclophosphamide Chemotherapy. *Cancer Immunol. Immunother.* **2009,** *58* (1), 49–59; (c) Kyriakopoulos, C. E.; Montero, A. J.; Diaz-Montero, C. M. Myeloid-Derived Suppressor Cells in Cancer. In *Advances in Tumor Immunology and Immunotherapy;* Rosenblatt, J. D., Podack, E. R., Barber, G. N., Ochoa, A., Eds.; Springer: New York, 2014; pp 3–17.
29. Youn, J.-I.; Nagaraj, S.; Collazo, M.; Gabrilovich, D. I. Subsets of Myeloid-Derived Suppressor Cells in Tumor Bearing Mice. *J. Immunol.* **2008,** *181* (8), 5791–5802.
30. (a) Bronte, V.; Kasic, T.; Gri, G.; Gallana, K.; Borsellino, G.; Marigo, I.; Battistini, L.; Iafrate, M.; Prayer-Galetti, T.; Pagano, F.; Viola, A. Boosting Antitumor Responses of T Lymphocytes Infiltrating Human Prostate Cancers. *J. Exp. Med.* **2005,** *201* (8), 1257–1268; (b) Chioda, M.; Marigo, I.; Mandruzzato, S.; Mocellin, S.; Bronte, V. Arginase, Nitric Oxide Synthase, and Novel Inhibitors of L-Arginine Metabolism in Immune Modulation. *Cancer Immunotherapy: Immune Suppression and Tumor Growth,* 2nd ed.;, 2013; pp. 597–634; (c) Munder, M. Arginase: An Emerging Key Player in the Mammalian Immune System. *Br. J. Pharmacol.* **2009,** *158,* 638–651; (d) Raber, P.; Ochoa, A. C.; Rodríguez, P. C. Metabolism of L-Arginine by Myeloid-Derived Suppressor Cells in Cancer: Mechanisms of T Cell Suppression and Therapeutic Perspectives. *Immunol. Investig.* **2012,** *41* (6–7), 614–634.
31. (a) Kusmartsev, S.; Nefedova, Y.; Yoder, D.; Gabrilovich, D. I. Antigen-Specific Inhibition of CD8+ T Cell Response by Immature Myeloid Cells in Cancer Is Mediated by Reactive Oxygen Species. *J. Immunol.* **2004,** *172* (2), 989–999; (b) Schmielau, J.; Finn, O. J. Activated Granulocytes and Granulocyte-Derived Hydrogen Peroxide are the Underlying Mechanism of Suppression of T-Cell Function in Advanced Cancer Patients. *Cancer Res.* **2001,** *61* (12), 4756–4760; (c) Waris, G.; Ahsan, H. Reactive Oxygen Species: Role in the Development of Cancer and Various Chronic Conditions. *J. Carcinog.* **2006,** *5,* 14.
32. (a) Nagaraj, S.; Gupta, K.; Pisarev, V.; Kinarsky, L.; Sherman, S.; Kang, L.; Herber, D.; Schneck, J.; Gabrilovich, D. I. Altered Recognition of Antigen is a Novel Mechanism of CD8(+) T Cell Tolerance in Cancer. *Nat. Med.* **2007,** *13* (7), 828–835; (b) Adams, J. L.; Smothers, J.; Srinivasan, R.; Hoos, A. Big Opportunities for Small Molecules in Immuno-Oncology. *Nat. Rev. Drug Discov.* **2015,** *14* (9), 603–622.
33. (a) Wiley, J. W. The Many Faces of Nitric Oxide: Cytotoxic, Cytoprotective or Both. *Neurogastroenterol. Motil.* **2007,** *19* (7), 541–544; (b) Auten, R. L.; Davis, J. M. Oxygen Toxicity and Reactive Oxygen Species: The Devil Is in the Details. *Pediatr. Res.* **2009,** *66* (2), 121–127.
34. Huang, B.; Pan, P.-Y.; Li, Q.; Sato, A. I.; Levy, D. E.; Bromberg, J.; Divino, C. M.; Chen, S.-H. Gr-1+CD115+ Immature Myeloid Suppressor Cells Mediate the Development of Tumor-Induced T Regulatory Cells and T-Cell Anergy in Tumor-Bearing Host. *Cancer Res.* **2006,** *66* (2), 1123–1131.
35. Biswas, S. K.; Mantovani, A. Macrophage Plasticity and Interaction With Lymphocyte Subsets: Cancer as a Paradigm. *Nat. Immunol.* **2010,** *11* (10), 889–896.
36. Braganhol, E.; Tamajusuku, A. S.; Bernardi, A.; Wink, M. R.; Battastini, A. M. Ecto-5′-Nucleotidase/CD73 Inhibition by Quercetin in the Human U138MG Glioma Cell Line. *Biochim. Biophys. Acta* **2007,** *1770* (9), 1352–1359.
37. Zou, W. Immunosuppressive Networks in the Tumour Environment and Their Therapeutic Relevance. *Nat. Rev. Cancer* **2005,** *5* (4), 263–274.
38. Curiel, T. J.; Wei, S.; Dong, H.; Alvarez, X.; Cheng, P.; Mottram, P.; Krzysiek, R.; Knutson, K. L.; Daniel, B.; Zimmermann, M. C.; David, O.; Burow, M.; Gordon, A.; Dhurandhar, N.; Myers, L.; Berggren, R.; Hemminki, A.; Alvarez, R. D.; Emilie, D.; Curiel, D. T.; Chen, L.; Zou, W. Blockade of B7-H1 Improves Myeloid Dendritic Cell-Mediated Antitumor Immunity. *Nat. Med.* **2003,** *9* (5), 562–567.
39. Hartmann, E.; Wollenberg, B.; Rothenfusser, S.; Wagner, M.; Wellisch, D.; Mack, B.; Giese, T.; Gires, O.; Endres, S.; Hartmann, G. Identification and Functional Analysis of Tumor-Infiltrating Plasmacytoid Dendritic Cells in Head and Neck Cancer. *Cancer Res.* **2003,** *63* (19), 6478–6487.
40. (a) Bahary, N.; Garrido-Laguna, I.; Cinar, P.; O'Rourke, M. A.; Somer, B. G.; Nyak-Kapoor, A.; Lee, J. S.; Munn, D.; Kennedy, E. P.; Vahanian, N.; Link, C. J.; Wan-Gillam, A. Phase 2 Trial of the IDO Pathway Inhibitor Indoximod Plus Gemcitabine/Nab-Paclitaxel for the Treatment of Metastatic Pancreas Cancer: Interim Analysis. *J. Clin. Oncol. Off. J. Am. Soc. Clin. Oncol.* **2016,** *34.* abstract 3020; (b) Linette, G. P.; Stadtmauer, E. A.; Maus, M. V.; Rapoport, A. P.; Levine, B. L.; Emery, L.; Litzky, L.; Bagg, A.; Carreno, B. M.; Cimino, P. J.; Binder-Scholl, G. K.; Smethurst, D. P.; Gerry, A. B.; Pumphrey, N. J.; Bennett, A. D.; Brewer, J. E.; Dukes, J.; Harper, J.; Tayton-Martin, H. K.; Jakobsen, B. K.; Hassan, N. J.; Kalos, M.; June, C. H. Cardiovascular Toxicity and Titin Cross-Reactivity of Affinity-Enhanced T Cells in Myeloma and Melanoma. *Blood* **2013,** *122* (6), 863–871.
41. Wu, G. Amino Acids: Metabolism, Functions, and Nutrition. *Amino Acids* **2009,** *37,* 1–17.
42. (a) Grohmann, U.; Bronte, V. Control of Immune Response by Amino Acid Metabolism. *Immunol. Rev.* **2010,** *236* (1), 243–264; (b) McGaha, T. L.; Huang, L.; Lemos, H.; Metz, R.; Mautino, M.; Prendergast, G. C.; Mellor, A. L. Amino Acid Catabolism: A Pivotal Regulator of Innate and Adaptive Immunity. *Immunol. Rev.* **2012,** *249,* 135–157.
43. Sikalidis, A. Amino Acids and Immune Response: A Role for Cysteine, Glutamine, Phenylalanine, Tryptophan and Arginine in T-Cell Function and Cancer? *Pathol. Oncol. Res.* **2015,** *21* (1), 9–17.
44. Ball, H. J.; Jusof, F. F.; Bakmiwewa, S. M.; Hunt, N. H.; Yuasa, H. Tryptophan Catabolizing Enzymes—Party of Three. *Front. Immunol.* **2014,** *5,* 1–10. Article 485.
45. Zadori, D.; Veres, G.; Szalardy, L.; Klivenyi, P.; Fulop, F.; Toldi, J.; Vescei, L. Inhibitors of the Kynuernine Pathway as Neurotherapeutics: A Patent Review. *Expert Opin. Ther. Pat.* **2016,** *26* (7), 815–832.
46. Trabinelli, S.; Ocadlikova, D.; Ciciarello, M.; Slalvestrini, V.; Lecciso, M.; Jandus, C.; Metz, R.; Evangelisti, C.; Laury-Kleintop, L. D.; Romero, P.; Prendergast, G. C.; Curti, A.; Lemoli, R. M. The SOCS3-Independent Expression of IDO2 Supports the Homerstatic Generation of T Regulatory Cells by Human Dendritic Cells. *J. Immunol.* **2014,** *192* (3), 1231–1240.
47. Pantouris, G.; Serys, M.; Yuasa, H. J.; Ball, H. J.; Mowat, C. G. Human Indoleamine 2,3-Dioxygenase-2 has Substrate Specificity and Inhibition Characteristics Distinct from Those of Indoleamine 2,3-Dioxygenase-1. *Amino Acids* **2014,** *46,* 2155–2163.
48. Austin, C. J. D.; Rendina, L. M. Targeting Key Dioxygenases in Tryptophan–Kynurenine Metabolism for Immunomodulation and Cancer Chemotherapy. *Drug Discov. Today* **2015,** *20* (5), 609–617.
49. (a) Munn, D. H.; Mellor, A. L. IDO in the Tumor Microenvironment: Inflammation, Counter-Regulation, and Tolerance. *Trends Immunol.* **2016,** *37* (3), 193–207; (b) Witkiewicz, A. K.; Costantino, C. L.; Metz, R.; Muller, A. J.; Prendergast, G. C.; Yeo, C. J.; Brody, J. R. Genotyping and Expression Analysis of IDO2 in Human Pancreatic Cancer: A Novel, Active Target. *J. Am. Coll. Surg.* **2009,** *208* (5), 781–787. discussion 787–789; (c) Pilotte, L.; Larrieu, P.; Stroobant, V.; Colau, D.; Dolušić, E.; Frédérick, R.; De Plaen, E.; Uyttenhove, C.; Wouters, J.; Masereel, B.; Van Den Eynde, B. J. Reversal of Tumoral Immune Resistance by Inhibition of Tryptophan 2,3-Dioxygenase. *Proc. Natl. Acad. Sci. U. S. A.* **2012,** *109* (7), 2497–2502. discussion 787–789.
50. (a) Mellor, A. L.; Munn, D. H. IDO Expression by Dendritic Cells: Tolerance and Tryptophan Catabolism. *Nat. Rev. Immunol.* **2004,** *4* (10), 762–774; (b) Holmgaard, R. B.; Zamarin, D.; Li, Y.; Gasmi, B.; Munn, D. H.; Allison, J. P.; Merghoub, T.; Wolchok, J. D. Tumor-Expressed IDO Recruits and Activates MDSCs in a Treg-Dependent Manner. *Cell Rep.* **2015,** *13* (2), 412–424.
51. Zhai, L.; Spranger, S.; Binder, D. C.; Gritsina, G.; Lauring, K. L.; Giles, F. J.; Wainwright, D. A. Molecular Pathways: Targeting IDO1 and Other Tryptophan Dioxygenases for Cancer Immunotherapy. *Clin. Cancer Res.* **2015,** *21* (24), 7.

52. (a) Belladonna, M. L.; Orabona, C.; Grohmann, U.; Puccetti, P. TGF-β and Kynurenines as the Key to Infectious Tolerance. *Trends Mol. Med.* **2009,** *15* (2), 41–49; (b) Opitz, C. A.; Litzenburger, U. M.; Sahm, F.; Ott, M.; Tritschler, I.; Trump, S.; Schumacher, T.; Jestaedt, L.; Schrenk, D.; Weller, M.; Jugold, M.; Guillemin, G. J.; Miller, C. L.; Lutz, C.; Radlwimmer, B.; Lehmann, I.; Von Deimling, A.; Wick, W.; Platten, M. An Endogenous Tumour-Promoting Ligand of the Human Aryl Hydrocarbon Receptor. *Nature* **2011,** *478* (7368), 197–203; (c) Mandi, Y.; Vecsei, L. The Kynurenine System and Immunoregulation. *J. Neural Transm.* **2012,** *119,* 197–207.
53. (a) Cady, S. G.; Sono, M. 1-Methyl-DL-tryptophan, P-(3-Benzofuranyl)-DL-alanine (the Oxygen Analog of Tryptophan), and b[3-Benzo(b)thienyl]-kalanine (the Sulfur Analog of Tryptophan) are Competitive Inhibitors for Indoleamine 2,3-Dioxygenase. *Arch. Biochem. Biophys.* **1991,** *291* (2), 326–338; (b) Southan, M. D.; Truscott, R. J.; Jamie, J. F.; Pelosi, L.; Walker, M. J.; Maeda, H.; Iwamoto, Y.; Tone, S. Structure Requirements of the Competitive Binding Site of Recombinant Human Indoleamine 2,3-Dioxygenase. *Med. Chem. Res.* **1996,** *6,* 343–352.
54. Hou, D. Y.; Muller, A. J.; Sharma, M. D.; DuHadaway, J.; Banerjee, T.; Johnson, M.; Mellor, A. L.; Prendergast, G. C.; Munn, D. H. Inhibition of Indoleamine 2,3-Dioxygenase in Dendritic Cells by Stereoisomers of 1-Methyl-Tryptophan Correlates With Antitumor Responses. *Cancer Res.* **2007,** *67* (2), 792–801.
55. Metz, R.; Duhadaway, J. B.; Kamasani, U.; Laury-Kleintop, L.; Muller, A. J.; Prendergast, G. C. Novel Tryptophan Catabolic Enzyme IDO2 is the Preferred Biochemical Target of the Antitumor Indoleamine 2,3-Dioxygenase Inhibitory Compound D-1-Methyl-Tryptophan. *Cancer Res.* **2007,** *67* (15), 7082–7087.
56. Austin, C. J. D.; Mailu, B. M.; Maghzal, G. J.; Sanchez-Perez, A.; Rahlfs, S.; Zocher, K.; Yuasa, H. J.; Arthur, J. W.; Becker, K.; Stocker, R.; Hunt, N. H.; Ball, H. J. Biochemical Characteristics and Inhibitor Selectivity of Mouse Indoleamine 2,3-Dioxygenase-2. *Amino Acids* **2010,** *39* (2), 565–578.
57. Zakharia, Y.; Drabick, J. J.; Khleif, S.; McWilliams, R. R.; Munn, D.; Link, C.; Vahanian, N. N.; Kennedy, E.; Shaheen, M. F.; Rixe, O.; Milhem, M. M. Updates on Phase 1b/2 Trial of the IDO Inhibitor Indoximod Plus Checkpoint Inhibitors for the Treatment of Unresectable Stage 3 or 4 Melanoma. *J. Clin. Oncol. Off. J. Am. Soc. Clin. Oncol.* **2016,** *34.* Abstract 3075.
58. Awauh, S. G.; Zheng, Y.-R.; Bruno, P. M.; Hemann, M. T.; Lippard, S. J. A Pt(IV) Pro-Drug Preferentially Targets Indoleamine-2,3-Dioxygenase, Providing Enhanced Ovarian Cancer Immuno-Therapy. *J. Am. Chem. Soc.* **2015,** *137* (47), 14854–14857.
59. Yue, E. W.; Douty, B.; Wayland, B.; Bower, M.; Liu, X.; Leffet, L.; Wang, Q.; Bowman, K. J.; Hansbury, M. J.; Liu, C.; Wei, M.; Li, Y.; Wynn, R.; Burn, T. C.; Koblish, H. K.; Fridman, J. S.; Metcalf, B.; Scherle, P. A.; Combs, A. P. Discovery of Potent Competitive Inhibitors of Indoleamine 2,3-Dioxygenase With In Vivo Pharmacodynamic Activity and Efficacy in a Mouse Melanoma Model. *J. Med. Chem.* **2009,** *52* (23), 7364–7367.
60. Liu, X.; Shin, N.; Koblish, H. K.; Yang, G.; Wang, Q.; Wang, K.; Leffet, L.; Hansbury, M. J.; Thomas, B.; Rupar, M.; Waeltz, P.; Bowman, K. J.; Polam, P.; Sparks, R. B.; Yue, E. W.; Li, Y.; Wynn, R.; Fridman, J. S.; Burn, T. C.; Combs, A. P.; Newton, R. C.; Scherle, P. A. Selective Inhibition of IDO1 Effectively Regulates Mediators of Antitumor Immunity. *Blood* **2010,** *115* (17), 3520–3530.
61. Gangadhar, T.; Hamid, O.; Smith, D.; Bauer, T.; Wasser, J.; Luke, J.; Balmanoukian, A.; Kaufman, D.; Zhao, Y.; Maleski, J.; Leopold, L.; Gajewski, T. Preliminary Results from a Phase I/II Study of Epacadostat (incb024360) in Combination With Pembrolizumab in Patients With Selected Advanced Cancers. *Int. J. Immunother. Cancer* **2015,** *3* (Suppl. 2), 07.
62. (a) Mautino, M.; Jaipuri, F.; Waldo, J.; Kumar, S.; Adams, J.; Van Allen, C.; Marcinowicz-Flick, A.; Munn, D.; Vahanian, N.; Link, C. J. NLG919, a Novel Indoleamine-2,3-Dioxygenase (IDO)-Pathway Inhibitor Drug Candidate for Cancer Therapy. *Cancer Res.* **2013,** *8* (3 Suppl.). Poster 491; (b) Mautino, M.; Kumar, S.; Waldo, J.; Jaipuri, F.; Kesharwani, T. Fused Imidazole Derivatives Useful as IDO Inhibitors. WO 2012142237 A1, 2012.
63. Lin, S.-Y.; Yeh, T.-K.; Kuo, C.-C.; Song, J.-S.; Cheng, M.-F.; Liao, F.-Y.; Chao, M.-W.; Huang, H.-L.; Chen, Y.-L.; Yang, C.-Y.; Wu, M.-H.; Hsieh, C.-L.; Hsiao, W.; Peng, Y.-H.; Wu, J.-S.; Lin, L.-M.; Sun, M.; Chao, Y.-S.; Shih, C.; Wu, S.-Y.; Pan, S.-L.; Hung, M.-S.; Ueng, S.-H. Phenyl Benzenesulfonylhydrazides Exhibit Selective Indoleamine 2,3-Dioxygenase Inhibition With Potent In Vivo Pharmacodynamic Activity and Antitumor Efficacy. *J. Med. Chem.* **2016,** *59* (1), 419–430.
64. Balog, J. A.; Huang, A.; Chen, B.; Chen, L.; Shan, W. IDO Inhibitors. WO 2014150646 A1, 2014.
65. Markwalder, J. A.; Seitz, S. P.; Balog, J. A.; Huang, A.; Williams, D. K.; Chen, L.; Mandal, S.; Srivastava, S. IDO Inhibitors. WO 2015031295 A1, 2015.
66. Peng, Y.-H.; Ueng, S.-H.; Tseng, C.-T.; Hung, M.-S.; Song, J.-S.; Wu, J.-S.; Liao, F.-Y.; Fan, Y.-S.; Wu, M.-H.; Hsiao, W.-C.; Hsueh, C.-C.; Lin, S.-Y.; Cheng, C.-Y.; Tu, C.-H.; Lee, L.-C.; Cheng, M.-F.; Shia, K.-S.; Shih, C.; Wu, S.-Y. Important Hydrogen Bond Networks in Indoleamine 2,3-Dioxygenase 1 (IDO1) Inhibitor Design Revealed by Crystal Structures of Imidazoleisoindole Derivatives With IDO1. *J. Med. Chem.* **2015**.
67. Bakmiwewa, S. M.; Fatokun, A. A.; Tran, A.; Payne, R. J.; Hunt, N. H.; Ball, H. J. Identification of Selective Inhibitors of Indoleamine 2,3-Dioxygenase 2. *Bioorg. Med. Chem. Lett.* **2012,** *22* (24), 7641–7646.
68. (a) Yu, C. P.; Pan, Z. Z.; Luo, D. Y. TDO as a Therapeutic Target in Brain Diseases. *Metab. Brain Dis.* **2016,** *31* (4), 737–747; (b) Badawy, A. A. Tryptophan: The key to Boosting Brain Serotonin Synthesis in Depressive Illness. *J. Psychopharmacol.* **2013,** *27* (10), 878–893.
69. Salter, M.; Hazelwood, R.; Pogson, C. I.; Iyer, R.; Madge, D. J. The Effects of a Novel and Selective Inhibitor of Tryptophan 2,3-Dioxygenase on Tryptophan and Serotonin Metabolism in the Rat. *Biochem. Pharmacol.* **1995,** *49* (10), 1435–1442.
70. Dolusic, E.; Larrieu, P.; Moineaux, L.; Stroobant, V.; Pilotte, L.; Colau, D.; Pochet, L.; Van den Eynde, B.; Masereel, B.; Wouters, J.; Frederick, R. Tryptophan 2,3-Dioxygenase (TDO) Inhibitors. 3-(2-(Pyridyl)Ethenyl)Indoles as Potential Anticancer Immunomodulators. *J. Med. Chem.* **2011,** *54* (15), 5320–5334.
71. Pantouris, G.; Loudon-Griffiths, J.; Mowat, C. G. Insights Into the Mechanism of Inhibition of Tryptophan 2,3-Dioxygenase by Isatin Derivatives. *J. Enzyme Inhib. Med. Chem.* **2016,** *1–9.*
72. Huang, W.; Gong, Z.; Li, J.; Ding, J. Crystal Structure of *Drosophila melanogaster* Tryptophan 2,3-Dioxygenase Reveals Insights into Substrate Recognition and Catalytic Mechanism. *J. Struct. Biol.* **2013,** *181* (3), 291–299.
73. Wu, J. S.; Lin, S. Y.; Liao, F. Y.; Hsiao, W. C.; Lee, L. C.; Peng, Y. H.; Hsieh, C. L.; Wu, M. H.; Song, J. S.; Yueh, A.; Chen, C. H.; Yeh, S. H.; Liu, C. Y.; Lin, S. Y.; Yeh, T. K.; Hsu, J. T.; Shih, C.; Ueng, S. H.; Hung, M. S.; Wu, S. Y. Identification of Substituted Naphthotriazolediones as Novel Tryptophan 2,3-Dioxygenase (TDO) Inhibitors Through Structure-Based Virtual Screening. *J. Med. Chem.* **2015,** *58* (19), 7807–7819.
74. Cowley, P.; Wise, A. Pharmaceutical Compound. WO 2016017293 A1, 2016.
75. Serafini, P. Myeloid Derived Suppressor Cells in Physiological and Pathological Conditions: The Good, the Bad, and the Ugly. *Immunol. Res.* **2013,** *57* (1–3), 172–184.
76. Baggio, R.; Elbaum, D.; Kanyo, Z. F.; Carroll, P. J.; Cavalli, R. C.; Ash, D. E.; Christianson, D. W. Inhibition of Mn^{2+2}-Arginase by Borate Leads to the Design of a Transition State Analogue Inhibitor, 2(*S*)-Amino-6-boronohexanoic Acid. *J. Am. Chem. Soc.* **1997,** *119,* 8107–8108.
77. Kanyo, Z. F.; Scolnik, L. R.; Ash, D. E.; Christianson, D. W. Structure of a Unique Binuclear Manganese Cluster in Arginase. *Nature* **1996,** *383,* 554–557.
78. Kim, N. N.; Cox, J. D.; Baggio, R. F.; Emig, F. A.; Mistry, S. K.; Harper, S. L.; Speicher, D. W.; Morris, J.; Sidney, M.; Ash, D. E.; Traish, A.; Christianson, D. W. Probing Erectile Function: S-(2-Boronoethyl)-L-Cysteine Binds to Arginase as a Transition State Analogue and Enhances Smooth Muscle Relaxation in Human Penile Corpus Cavernosum. *Biochemistry* **2001,** *40,* 2678–2688.
79. D'Amato, N. C.; Rogers, T. J.; Gordon, M. A.; Greene, L. I.; Cochrane, D. R.; Spoelstra, N. S.; Nemkov, T. G.; D'Alessandro, A.; Hansen, K. C.; Richer, J. K. A TDO2-AhR Signaling Axis Facilitates Anoikis Resistance and Metastasis in Triple-Negative Breast Cancer. *Cancer Res.* **2015,** *75* (21), 4651–4664.
80. (a) Cama, C.; Colleluori, D. M.; Emig, F. A.; Shin, H.; Kim, S. W.; Kim, N. N.; Tarish, A. M.; Ash, D. E.; Christianson, D. W. Human Arginase II: Crystal Structure and Physiological Role in Male and Female Sexual Arousal. *Biochemistry* **2003,** *42* (28), 8445–8451; (b) Di Costanzo, L.; Sabio, G.; Mora, A.; Rodriguez, P. C.; Ochoa, A. C.; Centeno, F.; Christianson, D. W. Crystal Structure of Human Arginase I as 1.29-A Resolution and Exploration of Inhibition in the Immune Response. *Proc. Natl. Acad. Sci. U. S. A.* **2005,** *102* (37), 12058–13063.
81. Steppan, J.; Nyhan, D.; Berkowitz, D. E. Development of Novel Arginase Inhibitors for Therapy of Endothelial Dysfunction. *Front. Immunol.* **2013,** *4,* 278.
82. Cox, J. D.; Cama, E.; Colleluori, D. M.; Pethe, S.; Boucher, J.-L.; Mansuy, D.; Ash, D. E.; Christianson, D. W. Mechanistic and Metabolic Inferences from the Binding of Substrate Analogues and Products to Arginase. *Biochemistry* **2001,** *40,* 2689–2701.
83. Bronte, V.; Zanovello, P. Regulation of Immune Responses by L-Arginine Metabolism. *Nat. Rev. Immunol.* **2005,** *5,* 641–654.

84. De Santo, C.; Serafini, P.; Marigo, I.; Dolcetti, L.; Bolla, M.; Del Soldato, P.; Melani, C.; Guiducci, C.; Colombo, M. P.; Iezzi, M.; Musiani, P.; Zanovello, P.; Bronte, V. Nitroaspirin Corrects Immune Dysfunction in Tumor-Bearing Hosts and Promotes Tumor Eradication by Cancer Vaccination. *Proc. Natl. Acad. Sci. U. S. A.* **2005,** *102* (11), 4185–4190.
85. Molon, B.; Ugel, S.; Del Pozzo, F.; Soldani, C.; Zilio, S.; Avella, D.; De Palma, A.; Mauri, P.; Monegal, A.; Rescigno, M.; Savino, B.; Colombo, P.; Jonjic, N.; Pecanic, S.; Lazzarato, L.; Fruttero, R.; Gasco, A.; Bronte, V.; Viola, A. Chemokine Nitration Prevents Intratumoral Infiltration of Antigen-Specific T Cells. *J. Exp. Med.* **2011,** *208* (10), 1949–1962.
86. (a) van der Jeught, K.; Bialkowski, L.; Daszkiewicz, L.; Broos, K.; Goyvaerts, C.; Renmans, D.; van Lint, S.; Heirman, C.; Thielemans, K.; Breckpot, K. Targeting the Tumor Microenvironment to Enhance Antitumor Immune Responses. *Oncotarget* **2015,** *6* (3), 1359–1381; (b) Gajewski, T. F. The Next Hurdle in Cancer Immunotherapy: Overcoming the Non–T-Cell–Inflamed Tumor Microenvironment. *Semin. Oncol.* **2015,** *42* (4), 663–671; (c) Quail, D. F.; Joyce, J. A. Microenvironmental Regulation of Tumor Progression and Metastasis. *Nat. Med.* **2013,** *19* (11), 1423–1437; (d) Gajewski, T. F.; Schumacher, T. Cancer Immunotherapy. *Curr. Opin. Immunol.* **2013,** *25* (2), 259–260; (e) Gajewski, T. F.; Schreiber, H.; Fu, Y.-X. Innate and Adaptive Immune Cells in the Tumor Microenvironment. *Nat. Immunol.* **2013,** *14* (10), 1014–1022.
87. Ghiringhelli, F.; Apetoh, L.; Tesniere, A.; Aymeric, L.; Ma, Y.; Ortiz, C.; Vermaelen, K.; Panaretakis, T.; Mignot, G.; Ullrich, E.; Perfettini, J. L.; Schlemmer, F.; Tasdemir, E.; Uhl, M.; Génin, P.; Civas, A.; Ryffel, B.; Kanellopoulos, J.; Tschopp, J.; André, F.; Lidereau, R.; McLaughlin, N. M.; Haynes, N. M.; Smyth, M. J.; Kroemer, G.; Zitvogel, L. Activation of the NLRP3 Inflammasome in Dendritic Cells Induces IL-1B-Dependent Adaptive Immunity Against Tumors. *Nat. Med.* **2009,** *15* (10), 1170–1178.
88. Cekic, C.; Linden, J. Purinergic Regulation of the Immune System. *Nat. Rev. Immunol.* **2016,** *16* (3), 177–192.
89. Blay, J.; White, T. D.; Hoskin, D. W. The Extracellular Fluid of Solid Carcinomas Contains Immunosuppressive Concentrations of Adenosine. *Cancer Res.* **1997,** *57* (13), 2602–2605.
90. (a) Sitkovsky, M. V.; Kjaergaard, J.; Lukashev, D.; Ohta, A. Hypoxia-Adenosinergic Immunosuppression: Tumor Protection by T Regulatory Cells and Cancerous Tissue Hypoxia. *Clin. Cancer Res.* **2008,** *14* (19), 5947–5952; (b) Sitkovsky, M. V. T Regulatory Cells: Hypoxia-Adenosinergic Suppression and Re-direction of the Immune Response. *Trends Immunol.* **2009,** *30* (3), 102–108.
91. Beavis, P. A.; Stagg, J.; Darcy, P. K.; Smyth, M. J. CD73: A Potent Suppressor of Antitumor Immune Responses. *Trends Immunol.* **2012,** *33* (5), 231–237.
92. Ohta, A.; Kini, R.; Ohta, A.; Subramanian, M.; Madasu, M.; Sitkovsky, M. The Development and Immunosuppressive Functions of CD4+ CD25+ FoxP3+ Regulatory T Cells are Under Influence of the Adenosine-A2A Adenosine Receptor Pathway. *Front. Immunol.* **2012,** *3,* 190.
93. Di Virgilio, F.; Ferrari, D.; Adinolfi, E. P2X7: A Growth-Promoting Receptor—Implications for Cancer. *Purinergic Signalling* **2009,** *5* (2), 251–256.
94. Adinolfi, E.; Capece, M.; Franceschini, A.; Falzoni, S.; Giuliani, A. L.; Rotondo, A.; Sarti, A. C.; Bonora, M.; Syberg, S.; Corigliano, D.; Pinton, P.; Jorgensen, N. R.; Abelli, L.; Emionite, L.; Raffaghello, L.; Pistoia, V.; Di Virgilio, F. Accelerated Tumor Progression in Mice Lacking the ATP Receptor P2X7. *Cancer Res.* **2015,** *75* (4), 635–644.
95. Di Virgilio, F. Purines, Purinergic Receptors, and Cancer. *Cancer Res.* **2012,** *72* (21), 5441–5447.
96. Ameriks, M. K.; Ao, H.; Carruthers, N. I.; Lord, B.; Ravula, S.; Rech, J. C.; Savall, B. M.; Wall, J. L.; Wang, Q.; Bhattacharya, A.; Letavic, M. A. Preclinical Characterization of Substituted 6,7-Dihydro-[1,2,4]Triazolo[4,3-a]Pyrazin-8(5H)-one P2X7 Receptor Antagonists. *Bioorg. Med. Chem. Lett.* **2016,** *26* (2), 257–261.
97. Savall, B. M.; Wu, D.; De Angelis, M.; Carruthers, N. I.; Ao, H.; Wang, Q.; Lord, B.; Bhattacharya, A.; Letavic, M. A. Synthesis, SAR, and Pharmacological Characterization of Brain Penetrant P2X7 Receptor Antagonists. *ACS Med. Chem. Lett.* **2015**.
98. Dal Ben, D.; Buccioni, M.; Lambertucci, C.; Marucci, G.; Thomas, A.; Volpini, R. Purinergic P2X Receptors: Structural Models and Analysis of Ligand-Target Interaction. *Eur. J. Med. Chem.* **2015,** *89,* 561–580.
99. (a) Jacobson, K. A.; Jayasekara, M. P. S.; Costanzi, S. Molecular Structure of P2Y Receptors: Mutagenesis, Modeling, and Chemical Probes. *WIREs Membr. Transport Signaling* **2012,** *1* (6), 815–827; (b) Jacobson, K. A.; Boeynaems, J. M. P2Y Nucleotide Receptors: Promise of Therapeutic Applications. *Drug Discov. Today* **2010,** *15* (13–14), 570–578.
100. (a) Chhatriwala, M.; Ravi, R. G.; Patel, R. I.; Boyer, J. L.; Jacobson, K. A.; Harden, T. K. Induction of Novel Agonist Selectivity for the ADP-Activated P2Y1 Receptor Versus the ADP-Activated P2Y12 and P2Y13 Receptors by Conformational Constraint of an ADP Analog. *J. Pharmacol. Exp. Ther.* **2004,** *311* (3), 1038–1043; (b) Cattaneo, M.; Lecchi, A.; Ohno, M.; Joshi, B. V.; Besada, P.; Tchilibon, S.; Lombardi, R.; Bischofberger, N.; Harden, T. K.; Jacobson, K. A. Antiaggregatory Activity in Human Platelets of Potent Antagonists of the P2Y1 Receptor. *Biochem. Pharmacol.* **2004,** *68* (10), 1995.
101. Young, A.; Mittal, D.; Stagg, J.; Smyth, M. J. Targeting Cancer-Derived Adenosine: New Therapeutic Approaches. *Cancer Discov.* **2014,** *4* (8), 879–888.
102. Gessi, S.; Merighi, S.; Sacchetto, V.; Simioni, C.; Borea, P. A. Adenosine Receptors and Cancer. *Biochim. Biophys. Acta Biomembr.* **2011,** *1808* (5), 1400–1412.
103. Sitkovsky, M.; Ohta, A. Targeting the Hypoxia-Adenosinergic Signaling Pathway to Improve the Adoptive Immunotherapy of Cancer. *J. Mol. Med.* **2013,** *91* (2), 147–155.
104. (a) Zocchi, C.; Ongini, E.; Conti, A.; Monopoli, A.; Negretti, A.; Baraldi, P. G.; Dionisotti, S. The Non-xanthine Heterocyclic Compound SCH 58261 is a New Potent and Selective A2a Adenosine Receptor Antagonist. *J. Pharmacol. Exp. Ther.* **1996,** *276* (2), 398–404; (b) Baraldi, P. G.; Cacciari, B.; Spalluto, G.; Pineda de las Infantas y Villatoro, M. J.; Zocchi, C.; Dionisotti, S.; Ongini, E. Pyrazolo[4,3-e]-1,2,4-triazolo[1,5-c]pyrimidine Derivatives: Potent and Selective A(2A) Adenosine Antagonists. *J. Med. Chem.* **1996,** *39* (5), 1164–1171.
105. Beavis, P. A.; Milenkovski, N.; Stagg, J.; Smyth, M. J.; Darcy, P. K. A2A Blockade Enhances Anti-Metastatic Immune Responses. *OncoImmunology* **2013,** *2* (12), 1–3.
106. Pinna, A. Adenosine A2A Receptor Antagonists in Parkinson's Disease: Progress in Clinical Trials from the Newly Approved Istradefylline to Drugs in Early Development and Those Already Discontinued. *CNS Drugs* **2014,** *28* (5), 455–474.
107. Beavis, P. A.; Milenkovski, N.; Henderson, M. A.; John, L. B.; Allard, B.; Loi, S.; Kershaw, M. H.; Stagg, J.; Darcy, P. K. Adenosine Receptor 2A Blockade Increases the Efficacy of Anti–PD-1 Through Enhanced Antitumor T-Cell Responses. *Cancer Immunol. Res.* **2015,** *3* (5), 506–517.
108. Mittal, D.; Young, A.; Stannard, K.; Yong, M.; Teng, M. W. L.; Allard, B.; Stagg, J.; Smyth, M. J. Antimetastatic Effects of Blocking PD-1 and the Adenosine A2A Receptor. *Cancer Res.* **2014,** *74* (14), 3652–3658.
109. Csóka, B.; Selmeczy, Z.; Koscsó, B.; Németh, Z. H.; Pacher, P.; Murray, P. J.; Kepka-Lenhart, D.; Morris, S. M., Jr.; Gause, W. C.; Leibovich, S. J.; Haskó, G. Adenosine Promotes Alternative Macrophage Activation via A 2A and A 2B Receptors. *FASEB J.* **2012,** *26* (1), 376–386.
110. Ryzhov, S.; Novitskiy, S. V.; Goldstein, A. E.; Biktasova, A.; Blackburn, M. R.; Biaggioni, I.; Dikov, M. M.; Feoktistov, I. Adenosinergic Regulation of the Expansion and Immunosuppressive Activity of CD11b+Gr1+ Cells. *J. Immunol.* **2011,** *187* (11), 6120–6129.
111. Kolachala, V.; Ruble, B.; Vijay-Kumar, M.; Wang, L.; Mwangi, S.; Figler, H.; Figler, R.; Srinivasan, S.; Gewirtz, A.; Linden, J.; Merlin, D.; Sitaraman, S. Blockade of Adenosine A2B Receptors Ameliorates Murine Colitis. *Br. J. Pharmacol.* **2008,** *155* (1), 127–137.
112. Cekic, C.; Sag, D.; Li, Y.; Theodorescu, D.; Strieter, R. M.; Linden, J. Adenosine A 2B Receptor Blockade Slows Growth of Bladder and Breast Tumors. *J. Immunol.* **2012,** *188* (1), 198–205.
113. Hayallah, A. M.; Sandoval-Ramirez, J.; Reith, U.; Schobert, U.; Preiss, B.; Schumacher, B.; Daly, J. W.; Muller, C. E. 1,8-Disubstituted Xanthine Derivatives: Synthesis of Potent A2B-Selective Adenosine Receptor Antagonists. *J. Med. Chem.* **2002,** *45* (7), 1500–1510.
114. Iannone, R.; Miele, L.; Maiolino, P.; Pinto, A.; Morello, S. Blockade of A2b Adenosine Receptor Reduces Tumor Growth and Immune Suppression Mediated by Myeloid-Derived Suppressor Cells in a Mouse Model of Melanoma. *Neoplasia* **2013,** *15* (12), 1400–1409.
115. Borrmann, T.; Hinz, S.; Bertarelli, D. C.; Li, W.; Florin, N. C.; Scheiff, A. B.; Muller, C. E. 1-Alkyl-8-(piperazine-1-sulfonyl)phenylxanthines: Development and Characterization of Adenosine A2B Receptor Antagonists and a New Radioligand With Subnanomolar Affinity and Subtype Specificity. *J. Med. Chem.* **2009,** *52* (13), 3994–4006.
116. Kaji, W.; Tanaka, S.; Tsukimoto, M.; Kojima, S. Adenosine A2B Receptor Antagonist PSB603 Suppresses Tumor Growth and Metastasis by Inhibiting Induction of Regulatory T Cells. *J. Toxicol. Sci.* **2014,** *39* (2), 191–198.
117. El Maatougui, A.; Azuaje, J.; González-Gómez, M.; Miguez, G.; Crespo, A.; Carbajales, C.; Escalante, L.; García-Mera, X.; Gutiérrez-de-Terán, H.; Sotelo, E. Discovery of Potent and Highly Selective A2B Adenosine Receptor Antagonist Chemotypes. *J. Med. Chem.* **2016,** *59* (5), 1967–1983.

118. Kalla, R. V.; Zablocki, J. Progress in the Discovery of Selective, High Affinity A2B Adenosine Receptor Antagonists as Clinical Candidates. *Purinergic Signalling* **2009,** *5* (1), 21–29.
119. Kaku, H.; Cheng, K. F.; Al-Abed, Y.; Rothstein, T. L. A Novel Mechanism of B Cell-Mediated Immune Suppression Through CD73 Expression and Adenosine Production. *J. Immunol.* **2014,** *193* (12), 5904–5913.
120. Clayton, A.; Al-Taei, S.; Webber, J.; Mason, M. D.; Tabi, Z. Cancer Exosomes Express CD39 and CD73, Which Suppress T Cells Through Adenosine Production. *J. Immunol.* **2011,** *187* (2), 676–683.
121. (a) Jie, H. B.; Gildener-Leapman, N.; Li, J.; Srivastava, R. M.; Gibson, S. P.; Whiteside, T. L.; Ferris, R. L. Intratumoral Regulatory T Cells Upregulate Immunosuppressive Molecules in Head and Neck Cancer Patients. *Br. J. Cancer* **2013,** *109* (10), 2629–2635; (b) Serra, S.; Horenstein, A. L.; Vaisitti, T.; Brusa, D.; Rossi, D.; Laurenti, L.; D'Arena, G.; Coscia, M.; Tripodo, C.; Inghirami, G.; Robson, S. C.; Gaidano, G.; Malavasi, F.; Deaglio, S. CD73-Generated Extracellular Adenosine in Chronic Lymphocytic Leukemia Creates Local Conditions Counteracting Drug-Induced Cell Death. *Blood* **2011,** *118* (23), 6141–6152; (c) Sun, X.; Wu, Y.; Gao, W.; Enjyoji, K.; Csizmadia, E.; Müller, C. E.; Murakami, T.; Robson, S. C. CD39/ENTPD1 Expression by CD4+Foxp3+ Regulatory T Cells Promotes Hepatic Metastatic Tumor Growth in Mice. *Gastroenterology* **2010,** *139* (3), 1030–1040; (d) Michaud, M.; Sukkurwala, A. Q.; Martins, I.; Shen, S.; Zitvogel, L.; Kroemer, G. Subversion of the Chemotherapy-Induced Anticancer Immune Response by the Ecto-ATPase CD39. *OncoImmunology* **2012,** *1* (3), 393–395.
122. Lévesque, S. A.; Lavoie, É. G.; Lecka, J.; Bigonnesse, F.; Sévigny, J. Specificity of the Ecto-ATPase Inhibitor ARL 67156 on Human and Mouse Ectonucleotidases. *Br. J. Pharmacol.* **2007,** *152* (1), 141–150.
123. Al-Rashida, M.; Iqbal, J. Therapeutic Potentials of Ecto-Nucleoside Triphosphate Diphosphohydrolase, Ecto-Nucleotide Pyrophosphatase/Phosphodiesterase, Ecto-5′-Nucleotidase, and Alkaline Phosphatase Inhibitors. *Med. Res. Rev.* **2014,** *34* (4), 703–743.
124. (a) Lee, C. F.; Lai, H. L.; Lee, Y. C.; Chien, C. L.; Chern, Y. The A2A Adenosine Receptor is a Dual Coding Gene: A Novel Mechanism of Gene Usage and Signal Transduction. *J. Biol. Chem.* **2014,** *289* (3), 1257–1270; (b) Bastid, J.; Regairaz, A.; Dejou, C.; Laheurte, C.; Cochaud, S.; Alberici, G.; Bonnefoy, N.; Laprevotte, E.; Gros, L.; Bec, N.; Larroque, C.; Eliaou, J.-F.; Guistiniani, J.; Funck-Brentano, E.; Hemon, P.; Bensussan, A. Inhibition of CD39 Enzymatic Function at the Surface of Tumor Cells Alleviates Their Immunosuppressive Activity. *Cancer Immunol. Res.* **2014,** *3* (3), 254–265.
125. Synnestvedt, K.; Furuta, G. T.; Comerford, K. M.; Louis, N.; Karhausen, J.; Eltzschig, H. K.; Hansen, K. R.; Thompson, L. F.; Colgan, S. P. Ecto-5′-Nucleotidase (CD73) Regulation by Hypoxia-Inducible Factor-1 Mediates Permeability Changes in Intestinal Epithelia. *J. Clin. Investig.* **2002,** *110* (7), 993–1002.
126. Mandapathil, M.; Hilldorfer, B.; Szczepanski, M. J.; Czystowska, M.; Szajnik, M.; Ren, J.; Lang, S.; Jackson, E. K.; Gorelik, E.; Whiteside, T. L. Generation and Accumulation of Immunosuppressive Adenosine by Human CD4+CD25highFOXP3+ Regulatory T Cells. *J. Biol. Chem.* **2010,** *285* (10), 7176–7186.
127. Stagg, J.; Divisekera, U.; McLaughlin, N.; Sharkey, J.; Pommey, S.; Denoyer, D.; Dwyer, K. M.; Smyth, M. J. Anti-CD73 Antibody Therapy Inhibits Breast Tumor Growth and Metastasis. *Proc. Natl. Acad. Sci. U. S. A.* **2010,** *107* (4), 1547–1552.
128. Xu, S.; Shao, Q. Q.; Sun, J. T.; Yang, N.; Xie, Q.; Wang, D. H.; Huang, Q. B.; Huang, B.; Wang, X. Y.; Li, X. G.; Qu, X. Synergy Between the Ectoenzymes CD39 and CD73 Contributes to Adenosinergic Immunosuppression in Human Malignant Gliomas. *Neuro-Oncology* **2013,** *15* (9), 1160–1172.
129. Forte, G.; Sorrentino, R.; Montinaro, A.; Luciano, A.; Adcock, I. M.; Maiolino, P.; Arra, C.; Cicala, C.; Pinto, A.; Morello, S. Inhibition of CD73 Improves B Cell-Mediated Anti-Tumor Immunity in a Mouse Model of Melanoma. *J. Immunol.* **2012,** *189* (5), 2226–2233.
130. Bhattarai, S.; Freundlieb, M.; Pippel, J.; Meyer, A.; Abdelrahman, A.; Fiene, A.; Lee, S.; Zimmermann, H.; Yegutkia, G.; Sträter, N.; El-Tayeb, A.; Müller, C. E. α, β-Methylene-ADP Derivatives and Analogs: Development of Potent and Selective Ecto-5′-Nucleotidase (CD73) Inhibitors. *J. Med. Chem.* **2015,** *58* (15), 6248–6263.
131. (a) Sachsenmeier, K. F.; Hay, C.; Brand, E.; Clarke, L.; Rosenthal, K.; Guillard, S.; Rust, S.; Minter, R.; Hollingsworth, R. Development of a Novel Ectonucleotidase Assay Suitable for High-Throughput Screening. *J. Biomol. Screen.* **2012,** *17* (7), 993–998; (b) Freundlieb, M.; Zimmermann, H.; Müller, C. E. A new, Sensitive Ecto-5′-Nucleotidase Assay for Compound Screening. *Anal. Biochem.* **2014,** *446* (1), 53–58.
132. Knapp, K.; Zebisch, M.; Pippel, J.; El-Tayeb, A.; Müller, C. E.; Sträter, N. Crystal Structure of the Human Ecto-5′-Nucleotidase (CD73): Insights into the Regulation of Purinergic Signaling. *Structure* **2012,** *20* (12), 2161–2173.
133. Allard, B.; Turcotte, M.; Stagg, J. Targeting CD73 and Downstream Adenosine Receptor Signaling in Triple-Negative Breast Cancer. *Expert Opin. Ther. Targets* **2014,** *18* (8), 863–881.
134. Longhi, M. S.; Robson, S. C.; Bernstein, S. H.; Serra, S.; Deaglio, S. Biological Functions of Ecto-Enzymes in Regulating Extracellular Adenosine Levels in Neoplastic and Inflammatory Disease States. *J. Mol. Med.* **2013,** *91* (2), 165–172.
135. (a) Antonioli, L.; Yegutkin, G. G.; Pacher, P.; Blandizzi, C.; Haskó, G. Anti-CD73 in Cancer Immunotherapy: Awakening New Opportunities. *Trends Cancer* **2016,** *2* (2), 95–109; (b) Allard, D.; Allard, B.; Gaudreau, P.-O.; Chrobak, P.; Stagg, J. CD73–Adenosine: A Next-Generation Target in Immuno-Oncology. *Immunotherapy* **2016,** *8* (2), 145–163.
136. Ogino, S.; Kirkner, G. J.; Nosho, K.; Irahara, N.; Kure, S.; Shima, K.; Hazra, A.; Chan, A. T.; Dehari, R.; Giovannucci, E. L.; Fuchs, C. S. Cyclooxygenase-2 Expression Is an Independent Predictor of Poor Prognosis in Colon Cancer. *Clin. Cancer Res.* **2008,** *14* (24), 8221–8227.
137. Penning, T. D.; Talley, J. J.; Bertenshaw, S. R.; Carter, J. S.; Collins, P. W.; Docter, S.; Graneto, M. J.; Lee, L. F.; Malecha, J. W.; Miyashiro, J. M.; Rogers, R. S.; Rogier, D. J.; Yu, S. S.; Anderson, G. D.; Burton, E. G.; Cogburn, J. N.; Gregory, S. A.; Koboldt, C. M.; Perkins, W. E.; Seibert, K.; Veenhuizen, A. W.; Zhang, Y. Y.; Isakson, P. C. Synthesis and Biological Evaluation of the 1,5-Diarylpyrazole Class of Cyclooxygenase-2 Inhibitors: Identification of 4-[5-(4-Methylphenyl)-3-(trifluoromethyl)-1H-pyrazol-1-yl]benze Nesulfonamide (SC-58635, Celecoxib). *J. Med. Chem.* **1997,** *40* (9), 1347–1365.
138. Wang, D.; DuBois, R. N. The Role of Anti-Inflammatory Drugs in Colorectal Cancer. *Annu. Rev. Med.* **2013,** *64,* 131–144.
139. Kaidi, A.; Qualtrough, D.; Williams, A. C.; Paraskeva, C. Direct Transcriptional Up-regulation of Cyclooxygenase-2 by Hypoxia-Inducible Factor (HIF)-1 Promotes Colorectal Tumor Cell Survival and Enhances HIF-1 Transcriptional Activity During Hypoxia. *Cancer Res.* **2006,** *66* (13), 6683–6691.
140. (a) Nakanishi, Y.; Nakatsuji, M.; Seno, H.; Ishizu, S.; Akitake-Kawano, R.; Kanda, K.; Ueo, T.; Komekado, H.; Kawada, M.; Minami, M.; Chiba, T. COX-2 Inhibition Alters the Phenotype of Tumor-Associated Macrophages from M2 to M1 in ApcMin/+ Mouse Polyps. *Carcinogenesis* **2011,** *32* (9), 1333–1339; (b) Mahic, M.; Yaqub, S.; Johansson, C. C.; Taskén, K.; Aandahl, E. M. FOXP3+CD4+CD25+ Adaptive Regulatory T Cells Express Cyclooxygenase-2 and Suppress Effector T Cells by a Prostaglandin E2-Dependent Mechanism. *J. Immunol.* **2006,** *177* (1), 246–254; (c) Obermajer, N.; Muthuswamy, R.; Lesnock, J.; Edwards, R. P.; Kalinski, P. Positive Feedback Between PGE2 and COX2 Redirects the Differentiation of Human Dendritic Cells Toward Stable Myeloid-Derived Suppressor Cells. *Blood* **2011,** *118* (20), 5498–5505.
141. Duan, B.; Davis, R.; Sadat, E. L.; Collins, J.; Sternweis, P. C.; Yuan, D.; Jiang, L. I. Distinct Roles of Adenylyl Cyclase VII in Regulating the Immune Responses in Mice. *J. Immunol.* **2010,** *185* (1), 335–344.
142. Ganesh, T. Prostanoid Receptor EP2 as a Therapeutic Target. *J. Med. Chem.* **2014,** *57* (11), 4454–4465.
143. Mandapathil, M.; Szczepanski, M. J.; Szajnik, M.; Ren, J.; Jackson, E. K.; Johnson, J. T.; Gorelik, E.; Lang, S.; Whiteside, T. L. Adenosine and Prostaglandin e2 Cooperate in the Suppression of Immune Responses Mediated by Adaptive Regulatory T Cells. *J. Biol. Chem.* **2010,** *285* (36), 27571–27580.
144. (a) Ma, X.; Holt, D.; Kundu, N.; Reader, J.; Goloubeva, O.; Take, Y.; Fulton, A. M. A Prostaglandin E (PGE) Receptor EP4 Antagonist Protects Natural Killer Cells from PGE2-Mediated Immunosuppression and Inhibits Breast Cancer Metastasis. *OncoImmunology* **2013,** *2* (1), e22647; (b) Mao, Y.; Sarhan, D.; Steven, A.; Seliger, B.; Kiessling, R.; Lundqvist, A. Inhibition of Tumor-Derived Prostaglandin-E2 Blocks the Induction of Myeloid-Derived Suppressor Cells and Recovers Natural Killer Cell Activity. *Clin. Cancer Res.* **2014,** *20* (15), 4096–4106.
145. Af Forselles, K. J.; Root, J.; Clarke, T.; Davey, D.; Aughton, K.; Dack, K.; Pullen, N. In Vitro and in vivo Characterization of PF-04418948, a Novel, Potent and Selective Prostaglandin EP 2 Receptor Antagonist. *Br. J. Pharmacol.* **2011,** *164* (7), 1847–1856.
146. (a) Antonova, M.; Wienecke, T.; Maubach, K.; Thomas, E.; Olesen, J.; Ashina, M. The Pharmacological Effect of BGC20-1531, a Novel Prostanoid EP 4 Receptor Antagonist, in the Prostaglandin E 2 Human Model of Headache. *J. Headache Pain* **2011,** *12* (5), 551–559; (b) Greenhough, A.; Smartt, H. J. M.; Moore, A. E.; Roberts, H. R.; Williams, A. C.; Paraskeva, C.; Kaidi, A. The COX-2/PGE2 Pathway: Key Roles in the Hallmarks of Cancer and Adaptation to the Tumour Microenvironment. *Carcinogenesis* **2009,** *30* (3), 377–386.

147. Jiang, L. I.; Collins, J.; Davis, R.; Fraser, I. D.; Sternweis, P. C. Regulation of cAMP Responses by the G12-13 Pathway Converges on Adenylyl Cyclase VII. *J. Biol. Chem.* **2008,** *283* (34), 23429–23439.
148. Whiteside, T. L.; Jackson, E. K. Adenosine and Prostaglandin E2 Production by Human Inducible Regulatory T Cells in Health and Disease. *Front. Immunol.* **2013,** *4,* 212.
149. Brand, C. S.; Hocker, H. J.; Gorfe, A. A.; Cavasotto, C. N.; Dessauer, C. W. Isoform Selectivity of Adenylyl Cyclase Inhibitors: Characterization of Known and Novel Compounds. *J. Pharmacol. Exp. Ther.* **2013,** *347* (2), 265–275.
150. (a) Steegborn, C. Structure, Mechanism, and Regulation of Soluble Adenylyl Cyclases—Similarities and Differences to Transmembrane Adenylyl Cyclases. *Biochim. Biophys. Acta* **2014,** *1842* (12 Pt B), 2535–2547; (b) Saalau-Bethell, S. M.; Berdini, V.; Cleasby, A.; Congreve, M.; Coyle, J. E.; Lock, V.; Murray, C. W.; O'Brien, M. A.; Rich, S. J.; Sambrook, T.; Vinkovic, M.; Yon, J. R.; Jhoti, H. Crystal Structure of Human Soluble Adenylate Cyclase Reveals a Distinct, Highly Flexible Allosteric Bicarbonate Binding Pocket. *ChemMedChem* **2014,** *9* (4), 823–832; (c) Kleinboelting, S.; van den Heuvel, J.; Steegborn, C. Structural Analysis of Human Soluble Adenylyl Cyclase and Crystal Structures of its Nucleotide Complexes-Implications for Cyclase Catalysis and Evolution. *FEBS J.* **2014,** *281* (18), 4151–4164.
151. Mogensen, T. H. Pathogen Recognition and Inflammatory Signaling in Innate Immune Defenses. *Clin. Microbiol. Rev.* **2009,** *22* (2), 240–273.
152. Barber, G. N. STING: Infection, Inflammation and Cancer. *Nat. Rev. Immunol.* **2015,** *15* (12), 760–770.
153. (a) Pradere, J. P.; Dapito, D. H.; Schwabe, R. F. The Yin and Yang of Toll-Like Receptors in Cancer. *Oncogene* **2014,** *33* (27), 3485–3495; (b) Lemos, H.; Huang, L.; McGaha, T.; Mellor, A. L. STING, Nanoparticles, Autoimmune Disease and Cancer: A Novel Paradigm for Immunotherapy? *Expert. Rev. Clin. Immunol.* **2015,** *11* (1), 155–165.
154. Mancini, R. J.; Stutts, L.; Ryu, K. A.; Tom, J. K.; Esser-Kahn, A. P. Directing the Immune System With Chemical Compounds. *ACS Chem. Biol.* **2014,** *9* (5), 1075–1085.
155. Hemmi, H.; Kaisho, T.; Takeuchi, O.; Sato, S.; Sanjo, H.; Hoshino, K.; Horiuchi, T.; Tomizawa, H.; Takeda, K.; Akira, S. Small Anti-Viral Compounds Activate Immune Cells via the TLR7 MyD88-Dependent Signaling Pathway. *Nat. Immunol.* **2002,** *3* (2), 196–200.
156. Gorden, K. B.; Gorski, K. S.; Gibson, S. J.; Kedl, R. M.; Kieper, W. C.; Qiu, X.; Tomai, M. A.; Alkan, S. S.; Vasilakos, J. P. Synthetic TLR Agonists Reveal Functional Differences Between Human TLR7 and TLR8. *J. Immunol.* **2005,** *174* (3), 1259–1268.
157. Biggadike, K.; Ahmed, M.; Ball, D. I.; Coe, D. M.; Dalmas Wilk, D. A.; Edwards, C. D.; Gibbon, B. H.; Hardy, C. J.; Hermitage, S. A.; Hessey, J. O.; Hillegas, A. E.; Hughes, S. C.; Lazarides, L.; Lewell, X. Q.; Lucas, A.; Mallett, D. N.; Price, M. A.; Priest, F. M.; Quint, D. J.; Shah, P.; Sitaram, A.; Smith, S. A.; Stocker, R.; Trivedi, N. A.; Tsitoura, D. C.; Weller, V. Discovery of 6-Amino-2-{[(1S)-1-Methylbutyl]oxy}-9-[5-(1-piperidinyl)pentyl]-7,9-dihydro-8H-purin-8-one (GSK2245035), a Highly Potent and Selective Intranasal Toll-Like Receptor 7 Agonist for the Treatment of Asthma. *J. Med. Chem.* **2016,** *59* (5), 1711–1726.
158. Tanji, H.; Ohto, U.; Shibata, T.; Miyake, K.; Shimizu, T. Structural Reorganization of the Toll-Like Receptor 8 Dimer Induced by Agonistic Ligands. *Science* **2013,** *339* (6126), 1426–1429.
159. Tanji, H.; Ohto, U.; Shibata, T.; Taoka, M.; Yamauchi, Y.; Isobe, T.; Miyake, K.; Shimizu, T. Toll-Like Receptor 8 Senses Degradation Products of Single-Stranded RNA. *Nat. Struct. Mol. Biol.* **2015,** *22* (2), 109–116.
160. Lee, J.; Wu, C. C. N.; Lee, K. J.; Chuang, T. H.; Katakura, K.; Liu, Y. T.; Chan, M.; Tawatao, R.; Chung, M.; Shen, C.; Cottam, H. B.; Lai, M. M. C.; Raz, E.; Carson, D. A. Activation of Anti-Hepatitis C Virus Responses via Toll-Like Receptor 7. *Proc. Natl. Acad. Sci. U. S. A.* **2006,** *103* (6), 1828–1833.
161. Lu, H.; Dietsch, G. N.; Matthews, M. A. H.; Yang, Y.; Ghanekar, S.; Inokuma, M.; Suni, M.; Maino, V. C.; Henderson, K. E.; Howbert, J. J.; Disis, M. L.; Hershberg, R. M. VTX-2337 is a Novel TLR8 Agonist That Activates NK Cells and Augments ADCC. *Clin. Cancer Res.* **2012,** *18* (2), 499–509.
162. Roethle, P. A.; McFadden, R. M.; Yang, H.; Hrvatin, P.; Hui, H.; Graupe, M.; Gallagher, B.; Chao, J.; Hesselgesser, J.; Duatschek, P.; Zheng, J.; Lu, B.; Tumas, D. B.; Perry, J.; Halcomb, R. L. Identification and Optimization of Pteridinone Toll-Like Receptor 7 (TLR7) Agonists for the Oral Treatment of Viral Hepatitis. *J. Med. Chem.* **2013,** *56* (18), 7324–7333.
163. Kokatla, H. P.; Sil, D.; Tanji, H.; Ohto, U.; Malladi, S. S.; Fox, L. M.; Shimizu, T.; David, S. A. Structure-Based Design of Novel Human Toll-Like Receptor 8 Agonists. *ChemMedChem* **2014,** *9* (4), 719–723.
164. Beesu, M.; Caruso, G.; Salyer, A. C. D.; Khetani, K. K.; Sil, D.; Weerasinghe, M.; Tanji, H.; Ohto, U.; Shimizu, T.; David, S. A. Structure-Based Design of Human TLR8-Specific Agonists With Augmented Potency and Adjuvanticity. *J. Med. Chem.* **2015,** *58* (19), 7833–7849.
165. Peri, F.; Calabrese, V. Toll-Like Receptor 4 (TLR4) Modulation by Synthetic and Natural Compounds: An Update. *J. Med. Chem.* **2014,** *57* (9), 3612–3622.
166. Park, B. S.; Song, D. H.; Kim, H. M.; Choi, B. S.; Lee, H.; Lee, J. O. The Structural Basis of Lipopolysaccharide Recognition by the TLR4-MD-2 Complex. *Nature* **2009,** *458* (7242), 1191–1195.
167. Chan, M.; Hayashi, T.; Mathewson, R. D.; Nour, A.; Hayashi, Y.; Yao, S.; Tawatao, R. I.; Crain, B.; Tsigelny, I. F.; Kouznetsova, V. L.; Messer, K.; Pu, M.; Corr, M.; Carson, D. A.; Cottam, H. B. Identification of Substituted Pyrimido[5,4-b]indoles as Selective Toll-Like Receptor 4 Ligands. *J. Med. Chem.* **2013,** *56* (11), 4206–4223.
168. Nour, A.; Hayashi, T.; Chan, M.; Yao, S.; Tawatao, R. I.; Crain, B.; Tsigelny, I. F.; Kouznetsova, V. L.; Ahmadiiveli, A.; Messer, K.; Pu, M.; Corr, M.; Carson, D. A.; Cottam, H. B. Discovery of Substituted 4-Aminoquinazolines as Selective Toll-Like Receptor 4 Ligands. *Bioorg. Med. Chem. Lett.* **2014,** *24* (21), 4931–4938.
169. Wang, Y.; Su, L.; Morin, M. D.; Jones, B. T.; Whitby, L. R.; Surakattula, M. M. R. P.; Huang, H.; Shi, H.; Choi, J. H.; Wang, K. W.; Moresco, E. M. Y.; Berger, M.; Zhan, X.; Zhang, H.; Boger, D. L.; Beutler, B. TLR4/MD-2 Activation by a Synthetic Agonist With No Similarity to LPS. *Proc. Natl. Acad. Sci. U. S. A.* **2016,** *113* (7), E884–E893.
170. Ohto, U.; Shibata, T.; Tanji, H.; Ishida, H.; Krayukhina, E.; Uchiyama, S.; Miyake, K.; Shimizu, T. Structural Basis of CpG and Inhibitory DNA Recognition by Toll-Like Receptor 9. *Nature* **2015,** *520* (7549), 702–705.
171. Dudek, A. Z.; Yunis, C.; Harrison, L. I.; Kumar, S.; Hawkinson, R.; Cooley, S.; Vasilakos, J. P.; Gorski, K. S.; Miller, J. S. First in Human Phase I Trial of 852A, a Novel Systemic Toll-Like Receptor 7 Agonist, to Activate Innate Immune Responses in Patients With Advanced Cancer. *Clin. Cancer Res.* **2007,** *13* (23), 7119–7125.
172. Northfelt, D. W.; Ramanathan, R. K.; Cohen, P. A.; Von Hoff, D. D.; Weiss, G. J.; Dietsch, G. N.; Manjarrez, K. L.; Randall, T. D.; Hershberg, R. M. A Phase I Dose-Finding Study of the Novel Toll-Like Receptor 8 Agonist VTX-2337 in Adult Subjects With Advanced Solid Tumors or Lymphoma. *Clin. Cancer Res.* **2014,** *20* (14), 3683–3691.
173. Fang, H.; Ang, B.; Xu, X.; Huang, X.; Wu, Y.; Sun, Y.; Wang, W.; Li, N.; Cao, X.; Wan, T. TLR4 is Essential for Dendritic Cell Activation and Anti-Tumor T-Cell Response Enhancement by DAMPs Released From Chemically Stressed Cancer Cells. *Cell. Mol. Immunol.* **2014,** *11* (2), 150–159.
174. Onier, N.; Hilpert, S.; Arnould, L.; Saint-Giorgio, V.; Gwynfor Davies, J.; Bauer, J.; Jeannin, J. F. Cure of Colon Cancer Metastasis in Rats With the New Lipid A OM 174. Apoptosis of Tumor Cells and Immunization of Rats. *Clin. Exp. Metastasis* **1999,** *17* (4), 299–306.
175. Isambert, N.; Fumoleau, P.; Paul, C.; Ferrand, C.; Zanetta, S.; Bauer, J.; Ragot, K.; Lizard, G.; Jeannin, J. F.; Bardou, M. Phase I Study of OM-174, a Lipid A Analogue, With Assessment of Immunological Response, in Patients With Refractory Solid Tumors. *BMC Cancer* **2013,** *13,* 172.
176. Gérard, C.; Baudson, N.; Ory, T.; Louahed, J. Tumor Mouse Model Confirms MAGE-A3 Cancer Immunotherapeutic as an Efficient Inducer of Long-Lasting Anti-Tumoral Responses. *PLoS ONE* **2014,** *9* (5), e94883.
177. Guiducci, C.; Vicari, A. P.; Sangaletti, S.; Trinchieri, G.; Colombo, M. P. Redirecting In Vivo Elicited Tumor Infiltrating Macrophages and Dendritic Cells Towards Tumor Rejection. *Cancer Res.* **2005,** *65* (8), 3437–3446.
178. Rewcastle, G. W.; Atwell, G. J.; Zhuang, L.; Baguley, B. C.; Denny, W. A. Potential Antitumor Agents. 61. Structure-Activity Relationships for in vivo Colon 38 Activity Among Disubstituted 9-Oxo-9H-xanthene-4-acetic Acids. *J. Med. Chem.* **1991,** *34* (1), 217–222.
179. Conlon, J.; Burdette, D. L.; Sharma, S.; Bhat, N.; Thompson, M.; Jiang, Z.; Rathinam, V. A. K.; Monks, B.; Jin, T.; Xiao, T. S.; Vogel, S. N.; Vance, R. E.; Fitzgerald, K. A. Mouse, but not Human STING, Binds and Signals in Response to the Vascular Disrupting Agent 5,6-Dimethylxanthenone-4-acetic Acid. *J. Immunol.* **2013,** *190* (10), 5216–5225.
180. Ishikawa, H.; Barber, G. N. STING is an Endoplasmic Reticulum Adaptor That Facilitates Innate Immune Signalling. *Nature* **2008,** *455* (7213), 674–678.
181. Burdette, D. L.; Monroe, K. M.; Sotelo-Troha, K.; Iwig, J. S.; Eckert, B.; Hyodo, M.; Hayakawa, Y.; Vance, R. E. STING is a Direct Innate Immune Sensor of Cyclic di-GMP. *Nature* **2011,** *478* (7370), 515–518.
182. Huang, Y.-H.; Liu, X.-Y.; Du, X.-X.; Jiang, Z.-F.; Su, X.-D. The Structural Basis for the Sensing and Binding of Cyclic Di-GMP by STING. *Nat. Struct. Mol. Biol.* **2012,** *19* (7), 728–730.

183. Diner, E. J.; Burdette, D. L.; Wilson, S. C.; Monroe, K. M.; Kellenberger, C. A.; Hyodo, M.; Hayakawa, Y.; Hammond, M. C.; Vance, R. E. The Innate Immune DNA Sensor cGAS Produces a Noncanonical Cyclic Dinucleotide That Activates Human STING. *Cell Rep.* **2013,** *3* (5), 1355–1361.
184. Barber, G. N. STING-Dependent Cytosolic DNA Sensing Pathways. *Trends Immunol.* **2014,** *35* (2), 88–93.
185. Fuertes, M. B.; Kacha, A. K.; Kline, J.; Woo, S.-R.; Kranz, D. M.; Murphy, K. M.; Gajewski, T. F. Host Type I IFN Signals are Required for Antitumor CD8+ T Cell Responses Through CD8α+ Dendritic Cells. *J. Exp. Med.* **2011,** *208* (10), 2005–2016.
186. Woo, S.-R.; Fuertes, M. B.; Corrales, L.; Spranger, S.; Furdyna, M. J.; Leung, M. Y. K.; Duggan, R.; Wang, Y.; Barber, G. N.; Fitzgerald, K. A.; Alegre, M.-L.; Gajewski, T. F. STING-Dependent Cytosolic DNA Sensing Mediates Innate Immune Recognition of Immunogenic Tumors. *Immunity* **2014,** *41* (5), 830–842.
187. Xia, T.; Konno, H.; Ahn, J.; Barber, G. N. Deregulation of STING Signaling in Colorectal Carcinoma Constrains DNA Damage Responses and Correlates With Tumorigenesis. *Cell Rep.* **2016,** *14* (2), 282–297.
188. Gao, P.; Ascano, M.; Zillinger, T.; Wang, W.; Dai, P.; Serganov, A. A.; Gaffney, B. L.; Shuman, S.; Jones, R. A.; Deng, L.; Hartmann, G.; Barchet, W.; Tuschl, T.; Patel, D. J. Structure-Function Analysis of STING Activation by c[G(2′,5′) pA(3′,5′)p] and Targeting by Antiviral DMXAA. *Cell* **2013,** *154* (4), 748–762.
189. Gao, P.; Zillinger, T.; Wang, W.; Ascano, M.; Dai, P.; Hartmann, G.; Tuschl, T.; Deng, L.; Barchet, W.; Patel, D. J. Binding-Pocket and Lid-Region Substitutions Render Human STING Sensitive to the Species-Specific Drug DMXAA. *Cell Rep.* **2014,** *8* (6), 1668–1676.
190. LoRusso, P. M.; Boerner, S. A.; Hunsberger, S. Clinical Development of Vascular Disrupting Agents: What Lessons Can We Learn From ASA404? *J. Clin. Oncol.* **2011,** *29* (22), 2952–2955.
191. Li, T.; Cheng, H.; Yuan, H.; Xu, Q.; Shu, C.; Zhang, Y.; Xu, P.; Tan, J.; Rui, Y.; Li, P.; Tan, X. Antitumor Activity of cGAMP via Stimulation of cGAS-cGAMP-STING-IRF3 Mediated Innate Immune Response. *Sci. Rep.* **2016,** *6,* 19049.
192. Deng, L.; Liang, H.; Xu, M.; Yang, X.; Burnette, B.; Arina, A.; Li, X. D.; Mauceri, H.; Beckett, M.; Darga, T.; Huang, X.; Gajewski, T. F.; Chen, Z. J.; Fu, Y. X.; Weichselbaum, R. R. STING-Dependent Cytosolic DNA Sensing Promotes Radiation-Induced Type I Interferon-Dependent Antitumor Immunity in Immunogenic Tumors. *Immunity* **2014,** *41* (5), 543–852.
193. Sali, T. M.; Pryke, K. M.; Abraham, J.; Liu, A.; Archer, I.; Broeckel, R.; Staverosky, J. A.; Smith, J. L.; Al-Shammari, A.; Amsler, L.; Sheridan, K.; Nilsen, A.; Streblow, D. N.; DeFilippis, V. R. Characterization of a Novel Human-Specific STING Agonist That Elicits Antiviral Activity Against Emerging Alphaviruses. *PLoS Pathog.* **2015,** *11* (12), e1005324.
194. Hammerich, L.; Binder, A.; Brody, J. D. In Situ Vaccination: Cancer Immunotherapy Both Personalized and off-the-Shelf. *Mol. Oncol.* **2015,** *9* (10), 1966–1981.
195. Kaczanowska, S.; Joseph, A. M.; Davila, E. TLR Agonists: Our Best Frenemy in Cancer Immunotherapy. *J. Leukoc. Biol.* **2013,** *93* (6), 847–863.
196. Wang, D.; Zhu, F.; Mao, X.; Agrawal, S. B094 Intratumoral Administration of IMO-2125, a Novel TLR9 Agonist, Modulates the Tumor Microenvironment and Exerts Systemic Antitumor Activity Alone and in Combination With an Anti-CTLA-4 mAb. *CRI-CIMT-EATI-AACR—The Inaugural International Cancer Immunotherapy Conference: Translating Science into Survival, Sheraton New York Times Square Hotel, New York, NY.*
197. Singh, M.; Khong, H.; Dai, Z.; Huang, X. F.; Wargo, J. A.; Cooper, Z. A.; Vasilakos, J. P.; Hwu, P.; Overwijk, W. W. Effective Innate and Adaptive Antimelanoma Immunity Through Localized TLR7/8 Activation. *J. Immunol.* **2014,** *193* (9), 4722–4731.
198. Mullins, S.; Grigsby, I.; Harrison, L. I.; Ren, S.; Soukharev, S.; Young, L.; Elvecrog, J. M.; Wilkinson, R. W.; Tomai, M. A.; Herbst, R.; Vasilakos, J. P.; Leishman, A. J. Ocal Immune Activation Resulting in Tumor Growth Inhibition With MEDI9197—An Intratumorally Administered TLR7/8 Agonist. AACR Meeting Abstracts**;** 2016; p 1475.
199. Li, L.; Yin, Q.; Kuss, P.; Maliga, Z.; Millán, J. L.; Wu, H.; Mitchison, T. J. Hydrolysis of 2′3′-cGAMP by ENPP1 and Design of Nonhydrolyzable Analogs. *Nat. Chem. Biol.* **2014,** *10* (12), 1043–1048.
200. Corrales, L.; Glickman, L. H.; McWhirter, S. M.; Kanne, D. B.; Sivick, K. E.; Katibah, G. E.; Woo, S.-R.; Lemmens, E.; Banda, T.; Leong, J. J.; Metchette, K.; Dubensky, T. W., Jr.; Gajewski, T. F. Direct Activation of STING in the Tumor Microenvironment Leads to Potent and Systemic Tumor Regression and Immunity. *Cell Rep.* **2015,** *11* (7), 1018–1030.
201. Lynn, G. M.; Laga, R.; Darrah, P. A.; Ishizuka, A. S.; Balaci, A. J.; Dulcey, A. E.; Pechar, M.; Pola, R.; Gerner, M. Y.; Yamamoto, A.; Buechler, C. R.; Quinn, K. M.; Smelkinson, M. G.; Vanek, O.; Cawood, R.; Hills, T.; Vasalatiy, O.; Kastenmuller, K.; Francica, J. R.; Stutts, L.; Tom, J. K.; Ryu, K. A.; Esser-Kahn, A. P.; Etrych, T.; Fisher, K. D.; Seymour, L. W.; Seder, R. A. In Vivo Characterization of the Physicochemical Properties of Polymer-Linked TLR Agonists That Enhance Vaccine Immunogenicity. *Nat. Biotechnol.* **2015,** *33* (11), 1201–1210.
202. Liu, H.; Moynihan, K. D.; Zheng, Y.; Szeto, G. L.; Li, A. V.; Huang, B.; Van Egeren, D. S.; Park, C.; Irvine, D. J. Structure-Based Programming of Lymph-Node Targeting in Molecular Vaccines. *Nature* **2014,** *507* (7493), 519–522.
203. Hanson, M. C.; Crespo, M. P.; Abraham, W.; Moynihan, K. D.; Szeto, G. L.; Chen, S. H.; Melo, M. B.; Mueller, S.; Irvine, D. J. Nanoparticulate STING Agonists are Potent Lymph Node-Targeted Vaccine Adjuvants. *J. Clin. Investig.* **2015,** *125* (6), 2532–2546.
204. Nakamura, T.; Miyabe, H.; Hyodo, M.; Sato, Y.; Hayakawa, Y.; Harashima, H. Liposomes Loaded With a STING Pathway Ligand, Cyclic Di-GMP, Enhance Cancer Immunotherapy Against Metastatic Melanoma. *J. Control. Release* **2015,** *216,* 149–157.
205. Druker, B. J. STI571 (Gleevec) as a Paradigm for Cancer Therapy. *Trends Mol. Med.* **2002,** *8* (4 Suppl.), S14–S18.
206. (a) Fabregat, I.; Fernando, J.; Mainez, J.; Sancho, P. TGR-Beta Signaling in Cancer Treatment. *Curr. Pharm. Des.* **2014,** *20* (17), 2934–2947; (b) Itoh, S.; Itoh, F. Implication of TGF-Beta as a Survival Factor During Tumour Development. *J. Biochem.* **2012,** *151* (6), 559–562; (c) Lonning, S.; Mannick, J.; McPherson, J. M. Antibody Targeting of TGF-b in Cancer Patients. *Curr. Pharm. Biotechnol.* **2011,** *12,* 2176–2189; (d) Travis, M. A.; Sheppard, D. TGF-Beta Activation and Function in Immunity. *Annu. Rev. Immunol.* **2014,** *32,* 51–82; (e) Bierie, B.; Moses, H. L. Transforming Growth Factor Beta (TGF-Beta) and Inflammation in Cancer. *Cytokine Growth Factor Rev.* **2010,** *21* (1), 49–59.
207. (a) Robertson, I. B.; Horiguchi, M.; Zilberberg, L.; Dabovic, B.; Hadjiolova, K.; Rifkin, D. B. Latent TGF-Beta-Binding Proteins. *Matrix Biol.* **2015,** *47,* 44–53; (b) Hara, M.; Kirita, A.; Kondo, W.; Matusuura, T.; Nagatsuma, K.; Dohmae, N.; Ogawa, S.; Imajoh-Ohmi, S.; Friedman, S. L.; Rifkin, D. B.; Kojima, S. LAP Degradation Product Reflects Plasma Kallikrein-Dependent TGF-β Activation in Patients With Hepatic Fibrosis. *SpringerPlus* **2014,** *3,* 221/1–11; (c) Worthington, J. J.; Fenton, T. M.; Czajkowska, B. I.; Klementowicz, J. E.; Travis, M. A. Regulation of TGFbeta in the Immune System: An Emerging Role for Integrins and Dendritic Cells. *Immunobiology* **2012,** *217* (12), 1259–1265.
208. Gatza, C. E.; Oh, S. Y.; Blobe, G. C. Roles for the Type III TGF-Beta Receptor in Human Cancer. *Cell. Signal.* **2010,** *22* (8), 1163–1174.
209. (a) Ling, L. E.; Lee, W.-C. TGF-Beta Type I Receptor (Alk5) Inhibitors in Oncology. *Curr. Pharm. Biotechnol.* **2011,** *12,* 2190–2202; (b) Wong, D. H.; Higgins, L. S, Small-Molecule Inhibitors of Transforming Growth Factor-b Type I Receptor (ALK5). *Prog. Respir. Res.* **2010,** *10,* 255–259.
210. (a) Frazier, K.; Thomas, R.; Scicchitano, M.; Mirabile, R.; Boyce, R.; Zimmerman, D.; Grygielko, E.; Nold, J.; DeGouville, A. C.; Huet, S.; Laping, N.; Gellibert, F. Inhibition of ALK5 Signaling Induces Physeal Dysplasia in Rats. *Toxicol. Pathol.* **2007,** *35* (2), 284–295; (b) Anderton, M. J.; Mellor, H. R.; Bell, A.; Sadler, C.; Pass, M.; Powell, S.; Steele, S. J.; Roberts, R. R.; Heier, A. Induction of Heart Valve Lesions by Small-Molecule ALK5 Inhibitors. *Toxicol. Pathol.* **2011,** *39* (6), 916–924.
211. (a) Stauber, A. J.; Credille, K. M.; Truex, L. L.; Ehlhardt, W. J.; Young, J. K. Nonclinical Safety Evaluation of a Transforming Growth Factor b Receptor I Kinase Inhibitor in Fischer 344 Rats and Beagle Dogs. *J. Clin. Toxicol.* **2014,** *4* (3), 100196/1–10; (b) Rodón, J.; Carducci, M.; Sepulveda-Sánchez, J. M.; Azaro, A.; Calvo, E.; Seoane, J.; Braña, I.; Sicart, E.; Gueorguieva, I.; Cleverly, A.; Pillay, N. S.; Desaiah, D.; Estrem, S. T.; Paz-Ares, L.; Holdhoff, M.; Blakeley, J.; Lahn, M. M.; Baselga, J. Pharmacokinetic, Pharmacodynamic and Biomarker Evaluation of Transforming Growth Factor-β Receptor I Kinase Inhibitor, Galunisertib, in Phase 1 Study in Patients With Advanced Cancer. *Invest. New Drugs* **2014,** *33* (2), 357–370.
212. Herbertz, S.; Sawyer, J. S.; Stauber, A. J.; Gueorguieva, I.; Driscoll, K. E.; Estrem, S. T.; Cleverly, A. L.; Desaiah, D.; Guba, S. C.; Benhadji, K. A.; Slapak, C. A.; Lahn, M. M. Clinical Development of Galunisertib (LY2157299 Monohydrate), a Small Molecule Inhibitor of Transforming Growth Factor-Beta Signaling Pathway. *Drug Des. Devel. Ther.* **2015,** *9,* 4479–4499.

213. Jin, C. H.; Krishnaiah, M.; Sreenu, D.; Subrahmanyam, V. B.; Rao, K. S.; Lee, H. J.; Park, S.-J.; Park, H.-J.; Lee, K.; Sheen, Y. Y.; Kim, D.-K. Discovery of N-((4-([1,2,4] Triazolo[1,5-a]Pyridin-6-yl)-5-(6-Methylpyridin-2-yl)-1H-Imidazol-2-yl)Methyl)-2-Fluoroaniline (EW-7197): A Highly Potent, Selective, and Orally Bioavailable Inhibitor of TGF-β Type I Receptor Kinase as Cancer Immunotherapeutic/Antifibrotic Agent. *J. Med. Chem.* **2014,** *57* (10), 4213–4238.
214. Suzuki, E.; Kim, S.; Cheung, H. K.; Corbley, M. J.; Zhang, X.; Sun, L.; Shan, F.; Singh, J.; Lee, W. C.; Albelda, S. M.; Ling, L. E. A Novel Small-Molecule Inhibitor of Transforming Growth Factor Beta Type I Receptor Kinase (SM16) Inhibits Murine Mesothelioma Tumor Growth In Vivo and Prevents Tumor Recurrence After Surgical Resection. *Cancer Res.* **2007,** *67* (5), 2351–2359.
215. Kapoun, A. M.; Gaspar, N. J.; Wang, Y.; Damm, D.; Liu, Y.-W.; O'Young, G.; Quon, D.; Lam, A.; Munson, K.; Tran, T.-T.; Ma, J. Y.; Murphy, A.; Dugar, S.; Chakravarty, S.; Protter, A. A.; Wen, F.-Q.; Liu, X.; Rennard, S. I.; Higgins, L. S. Transforming Growth Factor-Beta Receptor Type 1 (TGFbetaR1) Kinase Activity but not p38 Activation is Required for TGFbetaR1-Induced Myofibroblast Differentiation and Gene Expression. *Mol. Pharmacol.* **2006,** *70* (2), 518–531.
216. Kim, S.; Buchlis, G.; Fridlender, Z. G.; Sun, J.; Kapoor, V.; Cheng, G.; Haas, A.; Cheung, H. K.; Zhang, X.; Corbley, M.; Kaiser, L. R.; Ling, L.; Albelda, S. M. Systemic Blockade of Transforming Growth Factor-Beta Signaling Augments the Efficacy of Immunogene Therapy. *Cancer Res.* **2008,** *68* (24), 10247–10256.
217. Uhl, M.; Aulwurm, S.; Wischhusen, J.; Weiler, M.; Ma, J. Y.; Almirez, R.; Mangadu, R.; Liu, Y. W.; Platten, M.; Herrlinger, U.; Murphy, A.; Wong, D. H.; Wick, W.; Higgins, L. S.; Weller, M. SD-208, a Novel Transforming Growth Factor β Receptor I Kinase Inhibitor, Inhibits Growth and Invasiveness and Enhances Immunogenicity of Murine and Human Glioma Cells in vitro and In Vivo. *Cancer Res.* **2004,** *64* (21), 7954–7961.
218. Amada, H.; Asanuma, H.; Koami, T.; Okada, A.; Endo, M.; Ueda, Y.; Naruse, T.; Ikeda, A. Discovery of 7-Methoxy-6-[4-(4-methyl-1,3-thiazol-2-yl)-1*H*-imidazol-5-yl]-1,3-benzothiazole (TASP0382088): A Potent and Selective Transforming Growth Factor-b Type I Receptor Inhibitor as a Topical Drug for Alopecia. *Chem. Pharm. Bull.* **2013,** *61* (3), 286–291.
219. (a) Kurihara, N.; Iwama, A.; Tatsumi, J.; Ikeda, K.; Suda, T. Macrophage-Stimulating Protein Activates STK Receptor Tyrosine Kinase on Osteoclasts and Facilitates Bone Resorption by Osteoclast-Like Cells. *Blood* **1996,** *87* (9), 3704–3710; (b) Gurusamy, D.; Gray, J. K.; Pathrose, P.; Kulkarni, R. M.; Finkleman, F. D.; Waltz, S. E. Myeloid-Specific Expression of Ron Receptor Kinase Promotes Prostate Tumor Growth. *Cancer Res.* **2013,** *73* (6), 1752–1763.
220. Yao, H. P.; Zhou, Y. Q.; Zhang, R.; Wang, M. H. MSP-RON Signalling in Cancer: Pathogenesis and Therapeutic Potential. *Nat. Rev. Cancer* **2013,** *13* (7), 466–481.
221. Schroeder, G. M.; An, Y.; Cai, Z. W.; Chen, X. T.; Clark, C.; Cornelius, L. A.; Dai, J.; Gullo-Brown, J.; Gupta, A.; Henley, B.; Hunt, J. T.; Jeyaseelan, R.; Kamath, A.; Kim, K.; Lippy, J.; Lombardo, L. J.; Manne, V.; Oppenheimer, S.; Sack, J. S.; Schmidt, R. J.; Shen, G.; Stefanski, K.; Tokarski, J. S.; Trainor, G. L.; Wautlet, B. S.; Wei, D.; Williams, D. K.; Zhang, Y.; Zhang, Y.; Fargnoli, J.; Borzilleri, R. M. Discovery of *N*-(4-(2-Amino-3-chloropyridin-4-yloxy)-3-fluorophenyl)-4-ethoxy-1-(4-fluorophenyl)-2-oxo-1,2-dihydropyridine-3-carboxamide (BMS-777607), a Selective and Orally Efficacious Inhibitor of the Met Kinase Superfamily. *J. Med. Chem.* **2009,** *52* (5), 1251–1254.
222. Eyob, H.; Ekiz, H. A.; Welm, A. L. RON Promotes the Metastatic Spread of Breast Carcinomas by Subverting Antitumor Immune Responses. *OncoImmunology* **2013,** *2* (9), e25670.
223. Pyonteck, S. M.; Akkari, L.; Schuhmacher, A. J.; Bowman, R. L.; Sevenich, L.; Quail, D. F.; Olson, O. C.; Quick, M. L.; Huse, J. T.; Teijeiro, V.; Setty, M.; Leslie, C. S.; Oei, Y.; Pedraza, A.; Zhang, J.; Brennan, C. W.; Sutton, J. C.; Holland, E. C.; Daniel, D.; Joyce, J. A. CSF-1R Inhibition Alters Macrophage Polarization and Blocks Glioma Progression. *Nat. Med.* **2013,** *19* (10), 1264–1272.
224. Smith, C. C.; Zhang, C.; Lin, K. C.; Lasater, E. A.; Zhang, Y.; Massi, E.; Damon, L. E.; Pendleton, M.; Bashir, A.; Sebra, R.; Perl, A.; Kasarskis, A.; Shellooe, R.; Tsang, G.; Carias, H.; Powell, B.; Burton, E. A.; Matusow, B.; Zhang, J.; Spevak, W.; Ibrahim, P. N.; Le, M. H.; Hsu, H. H.; Habets, G.; West, B. L.; Bollag, G.; Shah, N. P. Characterizing and Overriding the Structural Mechanism of the Quizartinib-Resistant FLT3 "Gatekeeper" F691L Mutation With PLX3397. *Cancer Discov.* **2015,** *5* (6), 668–679.
225. DeNardo, D. G.; Brennan, D. J.; Rexhepaj, E.; Ruffell, B.; Shiao, S. L.; Madden, S. F.; Gallagher, W. M.; Wadhwani, N.; Keil, S. D.; Junaid, S. A.; Rugo, H. S.; Shelley Hwang, E.; Jirström, K.; West, B. L.; Coussens, L. M. Leukocyte Complexity Predicts Breast Cancer Survival and Functionally Regulates Response to Chemotherapy. *Cancer Discov.* **2011,** *1* (1), 54–67.
226. Zhu, Y.; Knolhoff, B. L.; Meyer, M. A.; Nywening, T. M.; West, B. L.; Luo, J.; Wang-Gillam, A.; Goedegebuure, S. P.; Linehan, D. C.; De Nardo, D. G. CSF1/CSF1R Blockade Reprograms Tumor-Infiltrating Macrophages and Improves Response to T-Cell Checkpoint Immunotherapy in Pancreatic Cancer Models. *Cancer Res.* **2014,** *74* (18), 5057–5069.
227. (a) Lemke, G. Biology of the TAM Receptors. *Cold Spring Harb. Perspect. Biol.* **2013,** *5* (11), a009076; (b) Cook, R. S.; Jacobsen, K. M.; Wofford, A. M.; DeRyckere, D.; Stanford, J.; Prieto, A. L.; Redente, E.; Sandahl, M.; Hunter, D. M.; Strunk, K. E.; Graham, D. K.; Earp Iii, H. S. MerTK Inhibition in Tumor Leukocytes Decreases Tumor Growth and Metastasis. *J. Clin. Investig.* **2013,** *123* (8), 3231–3242; (c) Rothlin, C. V.; Ghosh, S.; Zuniga, E. I.; Oldstone, M. B. A.; Lemke, G. TAM Receptors Are Pleiotropic Inhibitors of the Innate Immune Response. *Cell* **2007,** *131* (6), 1124–1136.
228. Cabezón, R.; Antonio Carrera-Silva, E.; Flórez-Grau, G.; Errasti, A. E.; Calderón-Gómez, E.; Lozano, J. J.; España, C.; Ricart, E.; Panés, J.; Rothlin, C. V.; Benítez-Ribas, D. MERTK as Negative Regulator of Human T Cell Activation. *J. Leukoc. Biol.* **2015,** *97* (4), 751–760.
229. Baladi, T.; Abet, V.; Piguel, S. State-of-the-art of Small Molecule Inhibitors of the TAM Family: The Point of View of the Chemist. *Eur. J. Med. Chem.* **2015,** *105,* 220–237.
230. Zhang, W.; McIver, A. L.; Stashko, M. A.; DeRyckere, D.; Branchford, B. R.; Hunter, D.; Kireev, D.; Miley, M. J.; Norris-Drouin, J.; Stewart, W. M.; Lee, M.; Sather, S.; Zhou, Y.; Di Paola, J. A.; Machius, M.; Janzen, W. P.; Earp, H. S.; Graham, D. K.; Frye, S. V.; Wang, X. Discovery of Mer Specific Tyrosine Kinase Inhibitors for the Treatment and Prevention of Thrombosis. *J. Med. Chem.* **2013,** *56* (23), 9693–9700.
231. Liu, J.; Yang, C.; Simpson, C.; Deryckere, D.; Van Deusen, A.; Miley, M. J.; Kireev, D.; Norris-Drouin, J.; Sather, S.; Hunter, D.; Korboukh, V. K.; Patel, H. S.; Janzen, W. P.; Machius, M.; Johnson, G. L.; Earp, H. S.; Graham, D. K.; Frye, S. V.; Wang, X. Discovery of Novel Small Molecule Mer Kinase Inhibitors for the Treatment of Pediatric Acute Lymphoblastic Leukemia. *ACS Med. Chem. Lett.* **2012,** *3* (2), 129–134.
232. Stark, A. K.; Sriskantharajah, S.; Hessel, E. M.; Okkenhaug, K. PI3K Inhibitors in Inflammation, Autoimmunity and Cancer. *Curr. Opin. Pharmacol.* **2015,** *23,* 82–91.
233. Burger, J. A.; Okkenhaug, K. Haematological Cancer: Idelalisib-Targeting PI3Kδ in Patients With B-Cell Malignancies. *Nat. Rev. Clin. Oncol.* **2014,** *11* (4), 184–186.
234. Ali, K.; Soond, D. R.; Piñeiro, R.; Hagemann, T.; Pearce, W.; Lim, E. L.; Bouabe, H.; Scudamore, C. L.; Hancox, T.; Maecker, H.; Friedman, L.; Turner, M.; Okkenhaug, K.; Vanhaesebroeck, B. Inactivation of PI(3)K p110δ Breaks Regulatory T-Cell-Mediated Immune Tolerance to Cancer. *Nature* **2014,** *510* (7505), 407–411.
235. Schmid, M. C.; Avraamides, C. J.; Dippold, H. C.; Franco, I.; Foubert, P.; Ellies, L. G.; Acevedo, L. M.; Manglicmot, J. R. E.; Song, X.; Wrasidlo, W.; Blair, S. L.; Ginsberg, M. H.; Cheresh, D. A.; Hirsch, E.; Field, S. J.; Varner, J. A. Receptor Tyrosine Kinases and TLR/IL1Rs Unexpectedly Activate Myeloid Cell PI3Kγ, A Single Convergent Point Promoting Tumor Inflammation and Progression. *Cancer Cell* **2011,** *19* (6), 715–727.
236. Collier, P. N.; Messersmith, D.; Le Tiran, A.; Bandarage, U. K.; Boucher, C.; Come, J.; Cottrell, K. M.; Damagnez, V.; Doran, J. D.; Griffith, J. P.; Khare-Pandit, S.; Krueger, E. B.; Ledeboer, M. W.; Ledford, B.; Liao, Y.; Mahajan, S.; Moody, C. S.; Roday, S.; Wang, T.; Xu, J.; Aronov, A. M. Discovery of Highly Isoform Selective Thiazolopiperidine Inhibitors of Phosphoinositide 3-Kinase γ. *J. Med. Chem.* **2015,** *58* (14), 5684–5688.
237. Sadhu, C.; Masinovsky, B.; Dick, K.; Sowell, C. G.; Staunton, D. E. Essential Role of Phosphoinositide 3-Kinase δ in Neutrophil Directional Movement. *J. Immunol.* **2003,** *170* (5), 2647–2654.
238. Knight, Z. A.; Gonzalez, B.; Feldman, M. E.; Zunder, E. R.; Goldenberg, D. D.; Williams, O.; Loewith, R.; Stokoe, D.; Balla, A.; Toth, B.; Balla, T.; Weiss, W. A.; Williams, R. L.; Shokat, K. M. A Pharmacological Map of the PI3-K Family Defines a Role for p110α in Insulin Signaling. *Cell* **2006,** *125* (4), 733–747.
239. Somoza, J. R.; Koditek, D.; Villasenor, A. G.; Novikov, N.; Wong, M. H.; Liclican, A.; Xing, W.; Lagpacan, L.; Wang, R.; Schultz, B. E.; Papalia, G. A.; Samuel, D.; Lad, L.; McGrath, M. E. Structural, Biochemical, and Biophysical Characterization of Idelalisib Binding to Phosphoinositide 3-Kinase δ. *J. Biol. Chem.* **2015,** *290* (13), 8439–8446.
240. Berndt, A.; Miller, S.; Williams, O.; Le, D. D.; Houseman, B. T.; Pacold, J. I.; Gorrec, F.; Hon, W.-C.; Ren, P.; Liu, Y.; Rommel, C.; Gaillard, P.; Ruckle, T.; Schwarz, M. K.; Shokat, K. M.; Shaw, J. P.; Williams, R. L. The p110[Delta] Structure: Mechanisms for Selectivity and Potency of New PI(3)K Inhibitors. *Nat. Chem. Biol.* **2010,** *6* (2), 117–124.

241. Cushing, T. D.; Hao, X.; Shin, Y.; Andrews, K.; Brown, M.; Cardozo, M.; Chen, Y.; Duquette, J.; Fisher, B.; Gonzalez-Lopez de Turiso, F.; He, X.; Henne, K. R.; Hu, Y.-L.; Hungate, R.; Johnson, M. G.; Kelly, R. C.; Lucas, B.; McCarter, J. D.; McGee, L. R.; Medina, J. C.; San Miguel, T.; Mohn, D.; Pattaropong, V.; Pettus, L. H.; Reichelt, A.; Rzasa, R. M.; Seganish, J.; Tasker, A. S.; Wahl, R. C.; Wannberg, S.; Whittington, D. A.; Whoriskey, J.; Yu, G.; Zalameda, L.; Zhang, D.; Metz, D. P. Discovery and In Vivo Evaluation of (*S*)-*N*-(1-(7-Fluoro-2-(pyridin-2-yl)quinolin-3-yl)ethyl)-9H-purin-6-amine (AMG319) and Related PI3Kδ Inhibitors for Inflammation and Autoimmune Disease. *J. Med. Chem.* **2015,** *58* (1), 480–511.
242. Shin, Y.; Suchomel, J.; Cardozo, M.; Duquette, J.; He, X.; Henne, K.; Hu, Y.-L.; Kelly, R. C.; McCarter, J.; McGee, L. R.; Medina, J. C.; Metz, D.; San Miguel, T.; Mohn, D.; Tran, T.; Vissinga, C.; Wong, S.; Wannberg, S.; Whittington, D. A.; Whoriskey, J.; Yu, G.; Zalameda, L.; Zhang, X.; Cushing, T. D. Discovery, Optimization, and In Vivo Evaluation of Benzimidazole Derivatives AM-8508 and AM-9635 as Potent and Selective PI3Kδ Inhibitors. *J. Med. Chem.* **2016,** *59* (1), 431–447.
243. Swaroop Vakkalankaa, S. V., et al. Inhibition of PI3Kδ Kinase by a Selective, Small Molecule Inhibitor Suppresses B-Cell Proliferation and Leukemic Cell Growth. *AACR poster 3741*, **2012**.
244. De Henau, O.; Merghoub, T.; Winkler, D.; Sharma, S.; Pink, M.; Tchaicha, J.; Rausch, M.; Proctor, J.; Kosmider, N.; Soglia, J.; Palombella, V.; Kutok, J. L.; Wolchok, J. D.; McGovern, K., Checkpoint Blockade Therapy is Improved by Altering the Immune Suppressive Microenvironment With IPI-549, a Potent and Selective Inhibitor of PI3K-Gamma, in Preclinical Models. *AACR Poster 554*, **2016**.
245. Hoegenauer, K.; Soldermann, N.; Stauffer, F.; Furet, P.; Graveleau, N.; Smith, A. B.; Hebach, C.; Hollingworth, G. J.; Lewis, I.; Gutmann, S.; Rummel, G.; Knapp, M.; Wolf, R. M.; Blanz, J.; Feifel, R.; Burkhart, C.; Zécri, F. Discovery and Pharmacological Characterization of Novel Quinazoline-Based PI3K Delta-Selective Inhibitors. *ACS Med. Chem. Lett.* **2016,** *7* (8), 762–767.
246. Williams, O.; Houseman, B. T.; Kunkel, E. J.; Aizenstein, B.; Hoffman, R.; Knight, Z. A.; Shokat, K. M. Discovery of Dual Inhibitors of the Immune Cell PI3Ks p110δ and p110γ: A Prototype for New Anti-Inflammatory Drugs. *Chem. Biol.* **2010,** *17* (2), 123–134.
247. Zak, K. M.; Grudnik, P.; Guzik, K.; Zieba, B. J.; Musielak, B.; Domling, A.; Dubin, G.; Holak, T. A. Structural Basis of Small Molecule Targeting of the Programmed Death Ligand 1 (PD-L1). *Oncotarget* **2016,** *7* (21), 30323–30335.
248. Zak, K. M.; Kitel, R.; Przetocka, S.; Golik, P.; Guzik, K.; Musielak, B.; Domling, A.; Dubin, G.; Holak, T. A. Structure of the Complex of Human Programmed Death 1, PD-1, and Its Ligand PD-L1. *Structure* **2015,** *23* (12), 2341–2348.
249. Liu, J.; Yuan, Y.; Chen, W.; Putra, J.; Suriawinata, A. A.; Schenk, A. D.; Miller, H. E.; Guleria, I.; Barth, R. J.; Huang, Y. H.; Wang, L. Immune-Checkpoint Proteins VISTA and PD-1 Nonredundantly Regulate Murine T-Cell Responses. *Proc. Natl. Acad. Sci. U. S. A.* **2015,** *112* (21), 6682–6687.
250. Sasikumar, P. G.; Sudarshan, N. S.; Gowda, N. M.; Samiulla, D. S.; Ramachandra, R. K.; Chandrasekhar, T.; Adurthi, S.; Dhudashia, A. A.; Gowda, N.; Ramachandra, M. AUPM-170: First-in-Class, Oral Immune Checkpoint Inhibitor of PD-L1/2 and VISTA. *AACR Meeting Poster,* **2015**.
251. Sasikumar, P. G.; Ramachandra, M.; Naremaddepalli, S. Immunomodulating Peptidomimetic Derivatives. *WO 2015036927 A1*, **2015**.
252. Sasikumar, P. G.; Ramachandra, M.; Naremaddepalli, S. Cyclic Peptidomimetic Compounds as Immunomodulators. *WO 2015033303 A1*, **2015**.
253. Sasikumar, P. G.; Ramachandra, M.; Naremaddepalli, S. 1,2,4-Oxadizaole Derivatives as Immunomodulators. *WO 2015033299 A1*, **2015**.
254. Sasikumar, P. G.; Ramachandra, M.; Naremaddepalli, S. 1,3,4-Oxadiazole and 1,3,4-Thiadiazole Derivatives as Immunomodulators. *WO 2015033301 A1*, **2015**.
255. Sasikumar, P. G.; Sudarshan, N. S.; Gowda, N. M.; Ramachandra, R. K.; Samiulla, D. S.; Chandrasekhar, T.; Adurthi, S.; Mani, J.; Nair, R.; Singh, S.; Dhudashia, A. A.; Chandranath, D. N.; Ramachandra, M. Oral Immune Checkpoint Antagonists Targeting PD-L1/VISTA and PD-L1/TIM3 for Cancer Therapy. *AACR Meeting Poster*, **2016**.
256. Miller, M. M.; Mapelli, C.; Allen, M. P.; Bowsher, M. S.; Boy, K. M.; Gillis, E. P.; Langley, D. R.; Mull, E.; Poirier, M. A.; Sanghvi, N.; Sun, L.-Q.; Tenney, D. J.; Yeung, K.-S. Macrocyclic Inhibitors of the PD-1/PD-L1 and CD80(B7-1) Protein/Protein Interactions. *WO 2014151634 A1*, **2014**.
257. Mapelli, C.; Gillis, E. P.; Sun, L.-Q.; Zhao, Q.; Allen, M. P.; Mull, E. Immunomodulators. *WO 2016100285 A1*, **2016**.
258. Chang, H.-N.; Liu, B.-Y.; Qi, Y.-K.; Zhou, Y.; Chen, Y.-P.; Pan, K.-M.; Li, W.-W.; Zhou, X.-M.; Ma, W.-W.; Fu, C.-Y.; Qi, Y.-M.; Liu, L.; Gao, Y.-F. Blocking of the DP-1/PD-L1 Interaction by a D-Peptide Antagonist for Cancer Immunotherapy. *Angew. Chem. Int. Ed.* **2015,** *54,* 11760–11764.
259. Schumacher, T. N.; Mayr, L. M.; Minor, D. L., Jr.; Mihollen, M. A.; Burgess, M. W.; Kim, P. S. Identification of D-Peptide Ligands Through Mirror-Image Phage Display. *Science* **1996,** *271* (5257), 1854–1857.
260. Stewart, T. J.; Smyth, M. J. Chemokine—Chemokine Receptors in Cancer Immunotherapy. *Immunotherapy* **2009,** *1* (1), 109–127.
261. Weintraub, K. Take two: Combining Immunotherapy With Epigenetic Drugs to Tackle Cancer. *Nat. Med.* **2016,** *22* (1), 8–10.
262. Smyth, M. J.; Ngiow, S. F.; Ribas, A.; Teng, M. W. L. Combination Cancer Immunotherapies Tailored to the Tumour Microenvironment. *Nat. Rev. Clin. Oncol.* **2016,** *13* (3), 143–158.

5.12 Evolution of Small-Molecule Immunology Research—Changes Since CMC II

TG Murali Dhar and AJ Dyckman, Bristol-Myers Squibb, Research and Development, Princeton, NJ, United States

© 2017 Elsevier Ltd. All rights reserved.

5.12.1	**Introduction**	396
5.12.2	**Clinical Success**	396
5.12.2.1	Everolimus: (Certican/Zortress)-First approval: 2003	396
5.12.2.2	Lumiracoxib: (Prexige)-First approval: 2003	397
5.12.2.3	Ciclesonide: (Omnaris/Alvesco)-First approval: 2004	397
5.12.2.4	Nepafenac: (Nevanac)-First approval: 2005	397
5.12.2.5	Iguratimod: (Iremod)-First approval: 2009	397
5.12.2.6	Dalfampridine: (Ampyra/Fampyra)-First approval: 2010	398
5.12.2.7	Fingolimod: (Gilenya)-First approval: 2010	398
5.12.2.8	Roflumilast: (Daxas/Daliresp)-First approval: 2010	399
5.12.2.9	Bilastine: (Bilaxten)-First approval: 2011	399
5.12.2.10	Teriflunomide: (Aubagio)-First approval: 2012	399
5.12.2.11	Tofacitinib: (Xeljanz)-First approval: 2012	399
5.12.2.12	Dimethyl Fumarate: (Tecfidera)-First approval: 2013	399
5.12.2.13	Apremilast: (Otezla)-First approval: 2014	400
5.12.3	**Clinical Promise**	400
5.12.3.1	CF-101	400
5.12.3.2	Masitinib	400
5.12.3.3	CCX354	401
5.12.3.4	TRK-170	401
5.12.3.5	GLPG0974	401
5.12.3.6	PF-4171327	401
5.12.3.7	GED-0301	402
5.12.3.8	LY3009104 (INCB028050, Baricitinib)	402
5.12.3.9	VX-509	402
5.12.3.10	ACT-128800	402
5.12.3.11	MT-1303	403
5.12.3.12	RPC1063	403
5.12.4	**Clinical and Preclinical Struggles**	403
5.12.4.1	COX2 Inhibitors	403
5.12.4.2	p38 MAP Kinase Inhibitors	404
5.12.4.3	Chemokine Receptor Modulation	404
5.12.4.4	TACE Inhibitors	404
5.12.5	**Emerging Specific Targets**	405
5.12.5.1	Interleukin-1 Receptor-Associated Kinase 4 (IRAK4)	405
5.12.5.2	Receptor-Interacting Protein (RIP)	406
5.12.5.3	Toll-Like Receptors (TLRs)	406
5.12.5.4	Retinoic Acid-Related Orphan Receptor γt (RORγt)	407
5.12.5.5	Tyrosine-Kinase 2 (Tyk2)	407
5.12.5.6	Protein Kinase C Theta (PKCθ)	407
5.12.5.7	Bruton's Tyrosine Kinase (BTK)	408
5.12.5.8	NFkB-Inducing Kinase (NIK)	409
5.12.6	**Emerging Paradigms**	409
5.12.6.1	Targeting Epigenetic Mechanisms to Treat Autoimmune Disorders	409
5.12.6.2	Inflammasome	410
5.12.6.3	Autophagy	411
5.12.6.4	Microbiome	411
5.12.6.5	Targeting the Complement System for Inflammatory Disorders	411
5.12.6.6	Regulatory T Cell Therapy	412
5.12.7	**Conclusion**	412
Acknowledgments		413
References		413

5.12.1 Introduction

In the roughly 10 years that have passed since the previous edition of this work, the medicinal landscape for treating immunology/inflammation disorders has undergone substantial changes. This period witnessed the peak of the selective cyclooxygenase-2 (COX2) antiinflammatory agents and their subsequent decline amid cardiovascular safety concerns, the approval of multiple oral treatments for multiple sclerosis (MS) where previously only injectable therapeutic options existed, and the first new approval for lupus therapy in decades in Benlysta. Perhaps the greatest shift has been the continued emphasis of biopharmaceuticals. Heralded by the introduction of the anti-tumor necrosis factor (TNF) agents in the late 1990s (etanercept, infliximab), the commercialization of biologics for controlling a variety of proinflammatory cytokines (TNFα, IL-6, IL12/IL-23, IL-17) either through direct interaction with the cytokine, or through interaction with the cytokine receptor (eg, IL-6R for tocilizumab), has continued to grow over the past decade. In the following sections, we highlight significant advances and setbacks in the area of immunology research in the past decade with a focus on small molecules.

5.12.2 Clinical Success

While the emphasis of this article is on small-molecule approaches in immunology/inflammation, given the impact that biotherapeutics have had on the field, it is useful to reflect on the large molecules (biologics) approved over the last decade-and-a-half. **Table 1** lists the biologics that have gained marketing approval for immunology/inflammation related indications in this time frame.

Biologic therapies have also set a new standard for small molecules, which now often strive to achieve a "biologic-like efficacy" with the convenience of oral dosing. While this is a challenging goal, it is one that has been met by some of the new small-molecule drugs, as evidenced by comparison of independent clinical trial results and even in head-to-head clinical trials involving biologic comparator arms.[1] Shown in **Table 2** are small molecules that have gained marketing approval since 2003 in the area of immunology/inflammation/allergy. Further details of these new drugs (see **Fig. 1** for structures) are provided in the remainder of this section.

5.12.2.1 Everolimus: (Certican/Zortress)-First approval: 2003

Evirolimus is a close analog of sirolimus (rapamycin), modified by the addition of a hydroxyethyl group on the C40 hydroxyl, an alteration made to enhance solubility as well as improve pharmacokinetic properties.[2] This modification reduced the elimination half-life in comparison to sirolimus, which obviated the need for a loading dose, although the dosing frequency is twice daily, compared to once daily for sirolimus. Everolimus, like sirolimus, exerts its efficacy primarily through initial complexation with the receptor protein FKBP12 and subsequent inhibition of mTORC1 (mechanistic target of rapamycin complex 1). Initially

Table 1 Biologic/large molecule drug approvals: immunology/inflammation

First approval	*Generic name (USAN/INN)*	*Trade name*	*Indication(s)*	*Class/MOA*
2001	Kineret	Anakinra	Rheumatoid arthritis (RA)	IL1-receptor antagonist
2003	Alefacept	Amevive	Chronic plaque psoriasis	Inhibition of LFA-3/CD2 interaction
2004	Natalizumab	Tysabri	Relapsing remitting multiple sclerosis (RRMS)	Anti-a4-integrin mAB
2006	Abatacept	Orencia	(RA)	T cell co-stimulation blocker
2008	Certolizumab pegol	Cimzia	RA, Crohn's disease (CD), psoriatic arthritis (PsA)	Anti-TNF
2008	Rilonacept	Arcalyst	Cryopyrin-associated periodic syndromes (CAPS)	IL-1 trap
2009	Canakinumab	Ilaris	Gout, active systemic juvenile idiopathic arthritis (SJIA), CAPS, familial cold autoinflammatory syndrome (FCAS) and Muckle-Wells syndrome (MWS)	IL1-beta blocker
2009	Ustekinumab	Stelara	Psoriasis (Ps), PsA	Anti-IL-12 IL23
2009	Golimumab	Simponi	RA, PsA, ankylosing spondylitis (AS), ulcerative colitis (UC)	Anti-TNF
2010	Tocilizumab	Actemra	RA, SJIA, PJIA	IL-6 receptor inhibitor
2011	Belatacept	Nulojix	Organ rejection: Kidney transplant	T cell co-stimulation blocker
2011	Belimumab	Benlysta	Lupus	Anti-BAFF antibody
2013	Alemtuzumab	Lemtrada	Multiple sclerosis (MS)	CD52—targeting monoclonal antibody
2013	Anakinra	Kineret	RA	Anti-IL-1
2014	Vedolizumab	Entyvio	UC	Anti-$\alpha_4\beta_7$ integrin
2015	Secukinumab	Cosentyx	Ps, PsA, AS	Anti IL17-A antibody

Table 2 Small-molecule drug approvals: immunology/inflammation/allergy

First approval	*Generic name (USAN/INN)*	*Trade name*	*Indication(s)*	*Class/MOA*
2003	Everolimus	Certican	Transplant rejection	FKB12 FK506 binding inhibitor: derivative of rapamycin
2003	Lumiracoxib	Prexige	Antiinflammatory	Selective Cox-2 inhibitor
2004	Ciclesonide	Alvesco	Asthma, chronic obstructive pulmonary disorder (COPD)	Inhaled corticosteroid
2005	Nepafenac	Nevanac	Antiinflammatory eye drops	Cox-1/Cox-2 inhibitor (prodrug of amfenac)
2009	Iguratimod	Iremod	RA, osteoarthritis (OA)	Antirheumatic agent
2010	Dalfampridine	Ampyra	MS (walking function)	K+ channel blocker
2010	Fingolimod	Gilenya	RRMS	S1P1 agonist
2010	Roflumilast	Daxas; Daliresp	COPD	Phosphodiesterase IV (PDE4) inhibitor
2011	Bilastine	Bilaxten	Allergy	Antihistamine
2012	Teriflunomide	Aubagio	RRMS	Dihydroorotate dehydrogenase inhibitor
2012	Tofacitinib	Xeljanz	RA	JAK3 inhibitor
2013	Dimethyl fumarate	Tecfidera	RRMS	MOA unknown; activates NRF2 pathway
2014	Apremilast	Otezla	Ps, PsA	Phosphodiesterase IV (PDE4) inhibitor

approved for kidney transplant (2003 by European Medicines Agency; 2004 by the Food and Drug Administration), everolimus has continued to gain expanded indications over the years in immunology applications (heart transplant (2010) and liver transplant (2012/2013)), in addition to approval for multiple oncology applications and for use in drug eluting coronary stents.[2–4]

5.12.2.2 Lumiracoxib: (Prexige)-First approval: 2003

Lumiracoxib is an inhibitor of the COX-2 enzyme, with excellent selectivity over COX-1 and therefore was purported to offer improved efficacy without undesired gastrointestinal issues associated with compounds that inhibit COX-1.[5] It is a very close structural analog of the nonsteroidal antiinflammatory drug (NSAID) diclofenac, in which the 2,6-dichloroaniline has been replaced by a 2-chloro-6-fluoroaniline. Under late-stage development at the time the cardiovascular safety profile of selective COX-2 inhibitors (eg, Vioxx) was being called into question, lumiracoxib was the last compound of this class to have received marketing approval to date. The European medicines agency granted marketing authorization in 2003 but the drug was not made available in the United Kingdom because of cardiovascular safety concerns of the class. The approval was granted only in limited regions, and in recent years the approval has been withdrawn by multiple agencies because of concerns about liver toxicity.[6]

5.12.2.3 Ciclesonide: (Omnaris/Alvesco)-First approval: 2004

Ciclesonide is an inhaled corticosteroid (ICS) administered in the form of a nasal spray, intended for the treatment of nasal symptoms associated with allergic rhinitis, or an aerosol inhaler for the control and prevention of asthma. The first worldwide approval for ciclesonide came in Feb. 2004 from the Australian Health Agency (TGA) for the treatment of asthma in adults and adolescents 12 years of age and older.[7] With six other members of the ICS class of drugs, ciclesonide was proposed to differentiate in part based on its prodrug nature, a property shared with just one other member of the class.[8] Exposure to the active moiety (des-ciclesonide), which is formed through hydrolysis of a carboxylic acid ester, would be more restricted as compared to other ICSs, therefore avoiding side effects such as local irritation.

5.12.2.4 Nepafenac: (Nevanac)-First approval: 2005

Nepafenac, a prodrug of the NSAID amefenac in which the carboxylic acid has been replaced by a primary carboxamide, was approved in 2005 for the treatment of inflammation and pain associated with cataract surgery.[9] Intended for ocular administration, nepafenac is able to distribute more deeply into the eye tissue than other ocularly delivered NSAIDs, where the amide then undergoes bioconversion to the carboxylic acid, revealing the cyclooxygenase-1 (COX1)/COX2 inhibitor amefenac.[10]

5.12.2.5 Iguratimod: (Iremod)-First approval: 2009

Iguratimod is a disease-modifying antirheumatic drug (DMARD) that was approved for use in rheumatoid arthritis (RA) patients in China and Japan in 2009. While the mechanism of iguratimod's efficacy is not fully understood, it has been shown to downregulate NFkB and suppress the production of a variety of proinflammatory cytokines.[11] More recently, it has been shown to disrupt IL-17 signaling in fibroblast-like synoviocytes, which is of particular relevance to the demonstrated clinical utility in RA.[12] Iguratimod also has been investigated in the MRL/lpr preclinical mouse model of lupus, where it was found to be protective with respect to kidney injury as well as reducing proteinuria and the appearance of anti-double stranded DNA autoantibodies.[13]

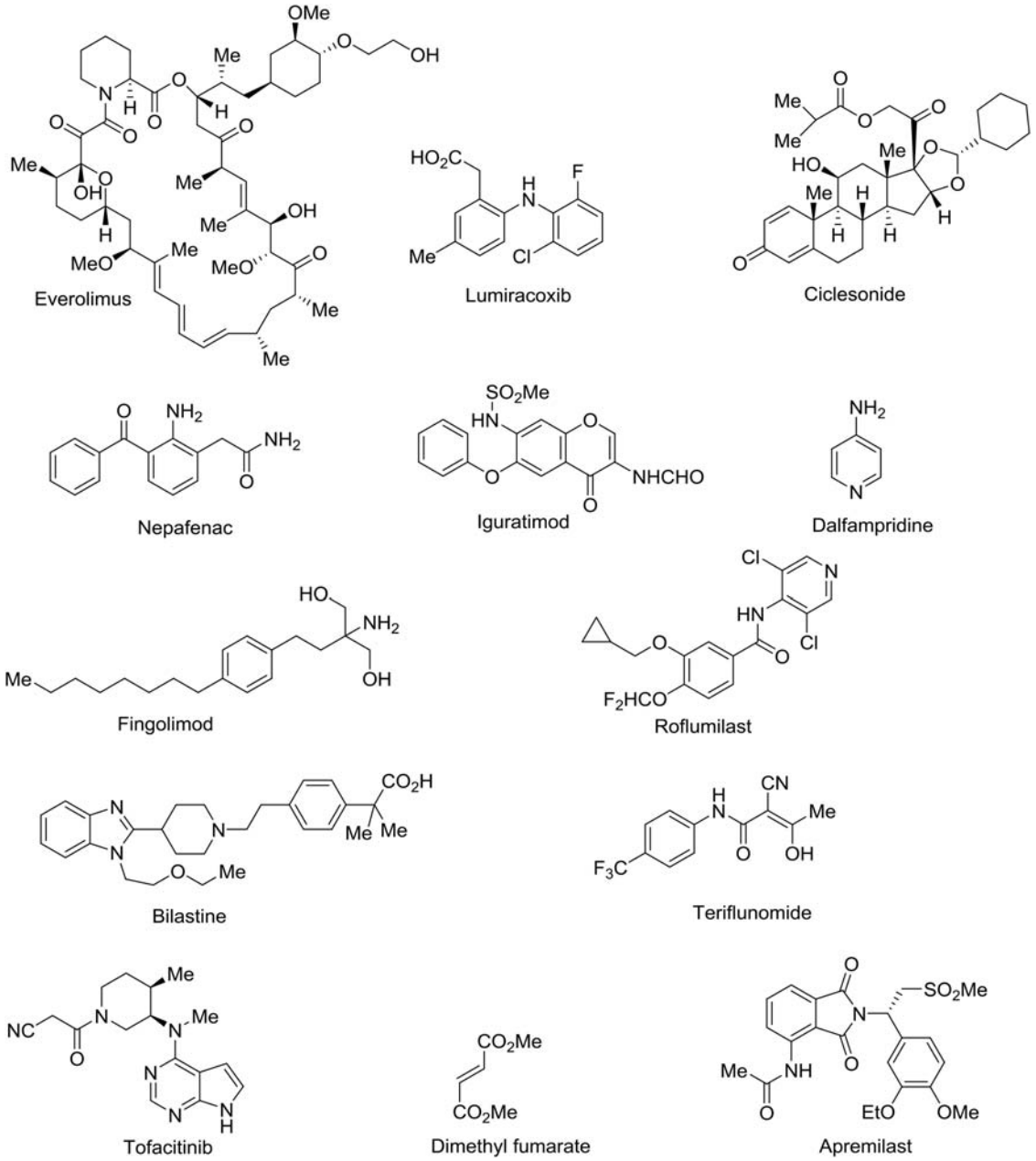

Fig. 1 Structures of small-molecule drugs approved between 2003 and 2014 for autoimmune and inflammatory disorders.

5.12.2.6 Dalfampridine: (Ampyra/Fampyra)-First approval: 2010

Dalfampridine, with the simple structure of 4-aminopyridine, is a broad-spectrum potassium channel blocker that was approved for use in a subset of MS patients. While not disease-modifying, dalfampridine is used to treat a specific symptom (decrease in walking ability) associated with MS.[14] It is believed to achieve the beneficial effects by increasing nerve conduction speed, although the precise mechanism has not been characterized. In Phase 3 trials, administration of an extended release formulation of dalfampridine produced a clinically meaningful improvement in walking ability in a subset of MS patients.[15]

5.12.2.7 Fingolimod: (Gilenya)-First approval: 2010

Fingolimod, the first oral drug approved for the treatment of relapsing remitting multiple sclerosis (RRMS), was shown to be superior to either placebo (FREEDOMS trial) or intramuscular interferon beta-1a (TRANSFORMS trial) at reducing the annualized relapse rate.[16] Acting as a prodrug, fingolimod is converted in vivo to a phosphorylated metabolite that binds to and activates

four of the five S1P (sphingosine-1-phospahte) receptors, S1P-1,3,4,5.[17] Agonism of S1P-1 by fingolimod leads to prolonged internalization and downregulation of this receptor, which disrupts the ability of certain lymphocyte subsets to egress from the lymphatic system, where they remain sequestered. This reduction in circulating lymphocyte levels, preventing autoreactive T cells from reaching the central nervous system (CNS), is believed to be key to fingolimod's efficacy in RRMS, although additional mechanisms involving effects directly on CNS-resident cells also have been investigated.[18,19]

5.12.2.8 Roflumilast: (Daxas/Daliresp)-First approval: 2010

Roflumilast has been approved to reduce the risk of exacerbations in patients with severe chronic obstructive pulmonary disease (COPD).[20] Its activity arises through inhibition of phosphodiesterase-4 (PDE4) enzymes, leading to subsequent accumulation of intracellular cAMP (cyclic adenosine monophosphate) and suppression of inflammatory cell activation. Roflumilast is significantly metabolized through N-oxidation and both the parent and metabolite share similar PDE4 inhibition and pharmacokinetic profiles.[21] Earlier examples of PDE4 inhibitors (eg, rolipram) faltered in development because of a narrow therapeutic window between efficacy and gastrointestinal (GI) effects, with the latter believed to be caused by action on a particular subtype of the enzyme (PDE4D). Although both the parent molecule and the N-oxide metabolite act on multiple PDE4 subtypes, including PDE4D, roflumilast was able to demonstrate an acceptable GI safety profile.

5.12.2.9 Bilastine: (Bilaxten)-First approval: 2011

Bilastine is an antihistamine that was approved for the treatment of allergic rhinitis and urticaria.[22] As a second-generation H1-antihistamine, bilastine has limited CNS penetration and therefore avoids the sedative effects of first-generation antihistamines. Bilastine was shown to bind selectively to the histamine H1 receptors, with a lack of significant activity at a variety of other targets, including H2-, H3-, serotonin, bradykinin, muscarinic, and calcium receptors.[23] In clinical trials, treatment with bilastine was improved versus placebo in reducing nasal symptoms scores of patients with seasonal allergic rhinitis and was associated with an improvement of symptom scores in patients with chronic urticaria.[24]

5.12.2.10 Teriflunomide: (Aubagio)-First approval: 2012

Teriflunomide, approved for the treatment of relapsing MS, is the primary active metabolite of leflunomide (Arava), which had been approved previously for treatment of RA and psoriatic arthritis. An inhibitor of dihydroorotate dehydrogenase, teriflunomide disrupts the de novo synthesis of pyrimidines in rapidly proliferating cells, which reduces the activity of select T and B lymphocytes.[25] Cells that are resting or dividing slowly are spared by teriflunomide. In clinical trials, teriflunomide was noninferior to interferon beta-1a in the prevention of relapses and superior to placebo in both the prevention of relapses and the prevention of disability progression.[26]

5.12.2.11 Tofacitinib: (Xeljanz)-First approval: 2012

Tofacitinib, used in the treatment of RA, was the first approved drug from the Janus kinase (JAK) inhibitor class.[27] The JAK family of nonreceptor tyrosine kinases (JAK1, 2, 3 and TYK2) mediate inflammatory gene transcription via signaling through STAT (signal transducers and activators of transcription) proteins, and their inhibition can control the production of proinflammatory cytokines. In biochemical assays, tofacitinib shows potent activity on JAK1, 2, and 3, with modest selectivity ($\sim$10-fold) against TYK2. In cellular and human whole blood assays, a preference of about 30-fold was noted for JAK1/3 signaling versus JAK2 signaling.[28] Clinical trials of tofacitinib in RA patients demonstrated efficacy similar to that obtained with TNF inhibitors, with ACR20, ACR50, and ACR70 response rates of 66%, 37%, and 20%.[29] Beyond RA, tofacitinib has shown promise in a variety of preclinical models of other diseases and is undergoing trials for lupus, psoriasis, psoriatic arthritis, organ transplant, Crohn's disease, ulcerative colitis (UC), and alopecia.[30]

5.12.2.12 Dimethyl Fumarate: (Tecfidera)-First approval: 2013

Fumaric acid esters (FAEs), mixtures of dimethyl fumarate (DMF) and other FAE salts, have been used as oral treatments of psoriasis for decades.[31] Administration of FAEs to psoriasis patients with concomitant MS showed relief of the MS symptoms.[32] More recently, DMF, with an enteric coated formulation intended to reduce gastrointestinal side effects, was evaluated as a single compound for the treatment of MS, for which it received marketing approval.[33] In vivo, one of the esters of DMF is hydrolyzed rapidly to give monomethyl fumarate (MMF), which serves as the likely bioactive species. Although not completely understood, the mechanism by which DMF (or MMF as the active moiety) exerts its beneficial effects is thought to involve upregulation of the nuclear factor (erythroid-derived 2)-like 2 (Nrf2) pathway.[34]

5.12.2.13 Apremilast: (Otezla)-First approval: 2014

Apremilast was the second drug approved in the PDE4 class, although the approved indications of severe plaque psoriasis or psoriatic arthritis differ from that of roflumilast (approved for COPD). The discovery of apremilast arose from the continued medicinal chemistry efforts on the thalidomide substructure. The observed biologic activity of this modified series (blockade of TNFα release) was discovered to arise through direct inhibition of PDE4 enzymes, with optimization for this activity in cellular and whole blood assay formats, leading to the identification of apremilast.[35] In fact, the modifications led to ablation of activity against the original molecular target of thalidomide (cereblon).[36] Apremilast was found to be selective for the PDE4 family of enzymes relative to other phosphodiesterases (PDE1–3, 5–11) but was found to have relatively little selectivity across the PDE4 subtypes (4A–4D). Despite inhibiting PDE4D, which previously was associated with negative gastrointestinal effects, apremilast was able to demonstrate an acceptable therapeutic window in the clinic. Evaluated in multiple Phase 3 trials for psoriasis, patients receiving 30 mg apremilast twice a day achieved significant improvement over placebo in PASI-50 (55–58% vs. 17–20%) and PASI-75 (29–33% vs. 5–6%) scores.[37] In a separate Phase 3 trial, apremilast was compared against etanercept and was able to approach the activity of the biologic after 16 weeks with PASI-75 response rate of 39.8% versus 48.2% for etanercept (both significantly higher than that of placebo at 11.9%). Ongoing and planned trials with apremilast include investigations for Behcet's disease, UC, atopic dermatitis, and ankylosing spondylitis.[38]

As can be seen by comparing the two tables in this section, the impact of biologic treatments has been quite notable in this therapeutic area. Still, in the preceding decade, patients have gained access to novel small-molecule drugs that are useful for the treatment of a variety of serious autoimmune/inflammatory diseases. In the following sections, we highlight compounds and new pathways that show potential comparable to the marketed drugs, as well as discuss some compounds and targets that have failed to bear out such potential.

5.12.3 Clinical Promise

This section of the article highlights small molecules that are in late-stage clinical trials (completed Phase 2 or in Phase 3) for the treatment of autoimmune disorders with a focus on RA, inflammatory bowel disease (IBD) (UC and Crohn's), psoriasis, lupus, and MS.

5.12.3.1 CF-101

Adenosine is an extracellular signaling molecule that acts via the adenosine receptors and suppresses synaptic transmission. Adenosine receptors belong to the GPCR (G-protein-coupled receptor) family and there are four subtypes: A_1, A_{2A}, A_{2B}, and A_3. The A_3 adenosine receptor (A_3 AR) is overexpressed in inflammatory cells, and A_3AR agonists induce downregulation of the NFkB signaling pathway, resulting in decreased TNF-α levels by monocytes and synoviocytes and leading to antiinflammatory effects.[39] CF-101, an adenosine analog, is a potent agonist of A_3 AR with a K_i of 0.47 nM and with >1000-fold selectivity over A_1. It is also selective versus A_{2A} AR (K_i 560 nM), and A_{2b}AR receptors (K_i of 42,300 nM).[40] Based on its efficacy in preclinical models of RA and IBD,[41] CF-101 was taken into clinical trials for RA and psoriasis. In a 12-week multicenter, randomized, double-blind, placebo-controlled, parallel-group Phase 2b study involving 79 patients with active RA, CF-101 dosed at 1.0 mg achieved ACR20 responses of 48.6% at Week 12 ($p=0.0352$), which was significantly higher statistically than that of the placebo group (25.0%).[42] Phase 3 trials in RA patients are planned. CF-101 was also tested in a Phase 2/3 double-blind, placebo-controlled study in 326 patients with moderate-to-severe plaque psoriasis. However, this study did not achieve its primary efficacy endpoint.[43]

5.12.3.2 Masitinib

Masitinib is a tyrosine kinase inhibitor that inhibits the stem-cell factor (SCF) receptor, KIT (kinase inhibitor targeting) in both biochemical ($IC_{50}=200\pm40$ nM) and cellular assays ($IC_{50}=150\pm80$ nM).[44] Since SCF is upregulated in inflammatory conditions, it represents a potential therapeutic target for the treatment of inflammatory diseases. For example, masitinib treatment at 12.5 and 25 mg kg^{-1} (i.p. twice a day) led to a significant reduction in disease in an experimental autoimmune encephalomyelitis (EAE) mouse model, a preclinical model of human MS.[45] In a multicenter, randomized, placebo-controlled, Phase 2a trial with 35 patients, masitinib treatment orally at 3-6 mg/day had a positive effect in MS-related impairment in primary progressive MS and relapse-free secondary progressive MS patients as evidenced by an improvement in multiple sclerosis functional composite scores (MSFC) relative to baseline, compared with a worsening MSFC score in patients receiving placebo $+103\pm189$% versus -60 ± 190% at month-12, respectively.[45] Based on this data, a Phase 2b/3 study to compare efficacy and safety of masitinib to placebo in the treatment of patients with primary progressive or relapse-free secondary progressive MS is ongoing.[46] In a multicenter, open-label, dose-ranging, Phase 2a study, masitinib treatment administered orally to 43 patients (who had inadequate response to DMARDs) at an initial dose of 3 mg kg^{-1} per day or 6 mg kg^{-1} per day achieved ACR20, ACR50, and ACR70 responses of 54%, 26%, and 8%, respectively.[47] However, it is important to note that the efficacy analysis of this Phase 2 study is hampered by the lack of a placebo group. A Phase 2b/3 study to assess the efficacy and safety of masitinib in comparison to methotrexate in patients with active RA with inadequate response to methotrexate or to any disease-modifying antirheumatic is in progress.[48]

5.12.3.3 CCX354

CC-Chemokine Receptor-1 (CCR1), which belongs to the G-protein coupled receptor family, is expressed on circulating cells such as monocytes, macrophages, T-lymphocytes, and neutrophils that are mobilized during inflammation. CCR1 binds eight chemokine ligands that regulate the processes of cell migration.[49] Synovial joints from patients with chronic RA express high levels of CCR1-expressing monocytes/macrophages and CCR1 associated chemokines like CCL3 and CCL5, suggesting CCR1 antagonists would provide beneficial effects for patients with RA. CCX354 is a potent CCR1 antagonist, which completed a randomized, placebo-controlled ($n=54$) Phase 2 proof-of-concept clinical trial in 160 patients with moderate-to-severe RA who were partially responsive to methotrexate therapy.[50] In this clinical trial, patients were given 100 mg of CCX354 twice daily ($n=53$), or 200 mg once daily ($n=53$) for 12 weeks. All patients continued to receive their regular methotrexate dose. In the patient group satisfying the prespecified criteria of C-reactive protein (CRP) (>5 mg L^{-1}) and tender/swollen joint count (>8), ACR20 response at Week 12 was 30% in the placebo group, 44% in the 100 mg twice daily group ($p=0.17$), and 56% in the 200 mg (once per day) group ($p=0.01$). In the patient group naïve to biological treatment, the 200 mg (once daily) group showed statistical significance for the ACR20 response (62% vs. 26% for placebo, $p=0.002$), while only a trend toward efficacy was observed in the 100 mg (twice daily) group (41% vs. 26%, $p=0.18$). At the time of this writing, no further updates were available regarding Phase 3 clinical trials with CCX354 for the treatment of RA.

5.12.3.4 TRK-170

TRK-170 is an orally active, small-molecule alpha4beta1/alpha4beta7 integrin antagonist. In preclinical studies, TRK-170 dosed at 50 mg kg^{-1} once a day, in a HLA-B27 rat model of chronic colitis (resembling UC), significantly reduced the number of animals with diarrhea and rectal bleeding, and showed a greater reduction in colonic symptoms when compared to prednisolone, which was accompanied with a decrease in the messenger RNA (mRNA) expression of proinflammatory mediators.[51] A two-part, multicenter, randomized, placebo-controlled, double-blind study of TRK-170 for the treatment of Crohn's disease has been completed,[52] but as of this writing, results from this study have not been disclosed.

5.12.3.5 GLPG0974

GPR43 (also referred to as FFA2) is a G-protein coupled receptor that is involved in the mediation of inflammatory responses. GPR43 is activated by short-chain fatty acids (SCFA) resulting in neutrophil activation and migration. In patients suffering from IBD, GPR43 expression is upregulated in the colon. GLPG0974 is a potent small-molecule antagonist of GPR43 and inhibits SCFA-induced neutrophil activation and migration in plasma with an IC_{50} of 27 nM.[53] In addition, GLPG09074 is a potent inhibitor of the FFA2-induced CD11b activated epitope expression ($IC_{50}=483\pm72$ nM). This assay was used to monitor target engagement in healthy volunteers and patients. GLPG09074 was tested in an exploratory, Phase 2, randomized, double-blind, placebo-controlled, proof-of-concept study in 45 patients with mild-to-moderate UC.[54] Patients were treated for 4 weeks with 200 mg twice a day of GLPG09074 or placebo (2:1 randomization). GLPG09074 was safe and well-tolerated and biomarker data indicated that neutrophil activation and influx were reduced, suggesting a role for GPR43 in UC. However, the reduction in neutrophil influx was not accompanied by a measured clinical difference between the GLPG09074 and placebo groups in the four-week treatment period.[55] Galapagos is performing subgroup analyses and considering additional indications for GLPG09074.[56]

5.12.3.6 PF-4171327

PF-4171327 (fosdagrocorat), a phosphate ester prodrug of PF-251802 which is a selective glucocorticoid (GC) receptor agonist, is being developed for the treatment of RA. In preclinical studies, PF-4171327 showed reduced transactivating (TA) potential in comparison to classic GCs while maintaining the ability to transrepress the expression of inflammatory genes, raising the possibility of retaining the beneficial antiinflammatory effects of GCs while minimizing the side effect profile from TA. For example, PF-4171327 did not suppress osteocalcin expression and showed a reduced induction of phosphoenolpyruvate carboxykinase and tyrosine aminotransferase gene expression in primary human hepatocytes, compared to prednisolone. A randomized, double-blind Phase 2 study was conducted to determine the efficacy and safety of PF-04171327 after 8 weeks of treatment. Patients ($n=323$) were randomized to receive oral tablets of PF-04171327 at doses of 1, 5, 10, or 15 mg, prednisone at doses of 5 or 10 mg, or placebo once daily for 8 weeks, in addition to methotrexate.[57] ACR20 scores were superior to placebo at the 10 and 15 mg once daily doses and the 15 mg dose met the criteria for noninferiority to once a day prednisone 10 mg. ACR50 and ACR70 response rates at week 8 showed a similar pattern, with the at 10 mg dose having highest response rate. At the 10 mg dose, PF-04171327 met noninferiority criteria versus once a day prednisone at 5 mg for bone formation biomarker P1NP; the 15 mg dose was comparable to prednisone. There was no dose response for the bone resorption biomarker uNTX/uCr. Glycated hemoglobin (HbA1c) changes for all doses of PF-04171327 were comparable with prednisone 5 mg. At the time of this writing, no further updates were available regarding Phase 3 clinical trials with PF-4171327 for the treatment of RA.

5.12.3.7 GED-0301

One of the characteristics of Crohn's disease is gut inflammation that is accompanied by a decrease in the activity of the immunosuppressive cytokine transforming growth factor (TGF)-β1 and increased levels of the protein SMAD7. SMAD7 binds to the TGF-β receptor and prevents antiinflammatory TGF-β signaling. GED-0301 (morgensen) is a 21-base single-strand phosphorothioate oligonucleotide that hybridizes to the human SMAD7 mRNA and reduces the levels of SMAD7 protein via degradation of its mRNA and restores TGF-β signaling. In preclincal studies, morgensen was shown to alleviate Crohn's disease-like colitis in mice and restore TGF-β signaling in mucosal cells from humans with Crohn's disease.[58] The efficacy of morgensen was tested in a double-blind, placebo-controlled Phase 2 trial. Patients were randomly assigned to receive 10 ($n=41$), 40 ($n=40$), or 160 mg ($n=43$) of GED-0301 or placebo ($n=42$) per day for 2 weeks and then were evaluated at days 15, 28, and 84.[59] Clinical remission (primary endpoint) at both days 15 and 28 were 55% at the 40 mg dose and 65% at the 160 mg dose, compared to 12% for the 10 mg dose and 10% ($p<0.001$) for the placebo groups. Additionally, 67% of patients (6 of 9 patients) reached glucocorticoid-free remission at Day 84 with 160 mg GED-0301 once daily, versus 11% (1 of 9 patients) with placebo ($p=0.04$). Based on this encouraging data, a Phase 3 trial is planned with GED-0301.

5.12.3.8 LY3009104 (INCB028050, Baricitinib)

JAKs, which consist of four family members (JAK1, JAK2, JAK3, and TYK2), play pivotal roles in cytokine receptor signaling and are associated with both adaptive and innate immune responses. Since JAK family kinases regulate the IL-6 and IL-10 pathways, inhibition of JAK kinases provides a novel approach for the treatment of RA. Tofacitinib is the first JAK inhibitor approved for the treatment of RA. Unlike tofacitinib, which is a nonselective JAK family kinase inhibitor (enzyme $IC_{50's}$ for JAK1, JAK2, JAK3, and TYK2 are 3.2, 4.1, 1.6, and 34 nM respectively), LY3009104 (formerly INCB0280050) is a selective inhibitor of JAK1 and JAK2 (enzyme $IC_{50's}$ for JAK1, JAK2, JAK3, and TYK2 are 5.9, 5.7, >400, and 53 nM respectively).[60] Preclincal efficacy with LY3009104 was demonstrated in multiple models of arthritis.[60] A multicenter, randomized, double-blind, placebo-controlled Phase 3 study to evaluate the efficacy and safety of LY3009104 in patients ($n=684$) with inadequate response to conventional DMARDS was conducted. At Week 24, ACR20, ACR50, and ACR70 response rates were 61%, 42%, and 25%, respectively, in the LY3009104 2 mg group (orally, once a day) compared with LY3009104 4 mg group (orally, once a day) (65%, 44%, and 24%, respectively) and placebo (42%, 22%, and 8%, respectively).[61] Additional Phase 3 trials with LY3009104 in RA are ongoing.

LY3009104 also completed Phase 2 trials in psoriasis.[62] In a double-blind, Phase 2b trial, patients ($n=238$) were randomized to receive LY3009104 (2, 4, 8, and 10 mg orally, once a day) or placebo for 12 weeks. At week 12, a significantly greater proportion of patients achieved PASI75 in the 8- and 10-mg LY3009104 groups compared with placebo (43% and 54%, respectively, vs. 15%). Additional information regarding further clinical progression of this compound in psoriasis was unavailable at the time of this writing.

5.12.3.9 VX-509

VX-509 (decernotinib) is a potent JAK3 inhibitor (enzyme $IC_{50}=2.5$ nM) that is being evaluated in clinical trials for RA. Although its biochemical potency for other JAK family members is <10-fold, the cellular selectivity is between 25- and 150-fold.[63] VX-509 was evaluated in a Phase 2b trial for RA at once-daily (100, 150, 200 mg) and twice-daily (100 mg) doses in combination with methotrexate in 350 patients.[64] At 24 weeks, ACR20 scores for the 100 and 150 mg once-daily groups were 60.6% and 61.1%, respectively, compared to 16.9% in the placebo group ($p<0.001$ for both groups). The ACR20 scores for the 200 mg once-daily and the 100 mg twice-daily groups were 61.1% and 62.5%, respectively ($p<0.001$ for both). The ACR50 responses for the four dose groups at six months were 38%, 38.9%, 40.3%, and 47.2%, respectively, compared with 7% of placebo recipients ($p<0.001$). ACR70 responses were seen in 16.9%, 18.1%, 15.3%, and 25%, respectively, compared with 2.8% for placebo ($p<0.01$). Plans for further progression of VX-509 were unavailable at the time of this writing.

5.12.3.10 ACT-128800

ACT-128800 (ponesimod) is an $S1P_1$ receptor modulator that is in clinical trials for the treatment of MS and other autoimmune conditions. Like fingolimod, which was approved for the treatment of MS in 2010, ACT-128800 induces reversible lymphopenia by inhibiting T-cell egress from the thymus and lymph nodes, thereby preventing T-cell infiltration to sites of inflammation. The safety and efficacy of ACT-128800 was evaluated in a double-blind, placebo-controlled, dose-finding Phase 2b study in 464 patients with RRMS.[65] Patients were randomized to receive once-daily oral ACT-128800 10, 20, or 40 mg, or placebo for 24 weeks. ACT-128800 reduced the number of new T1-weighted gadolinium-enhancing lesions by 43%, 83%, and 77% at 10, 20, and 40 mg, respectively, and the number of new or enlarging nonenhancing T2 lesions by 31%, 56%, and 34% at the 10, 20, and 40 mg doses. In addition to being selective for the $S1P_1$ receptor, ACT-128800 differs from fingolimod in other aspects. For example, fingolimod requires a phosphorylation–dephosphorylation cycle in vivo for its activation/deactivation, but this step is not required for ACT-128800 and may contribute to its low pharmacokinetic/pharmacodynamic variability. In addition, ACT-128800 has a terminal half-life of about 32 hours, compared to about 8 days for fingolimod.[65] A multicenter, randomized, double-blind, active-controlled, superiority study to compare the efficacy and safety of ACT-128800 to teriflunomide in subjects with relapsing MS

has been initiated.[66] In addition, an open-label, single-arm, multicenter Phase 2 trial was planned for an expected 30 patients with chronic graft versus host disease (GvHD) to assess the biological activity of ACT-128800.[67]

5.12.3.11 MT-1303

MT-1303 is a selective $S1P_1$ receptor agonist in various clinical trials for the treatment of autoimmune disorders. A multicenter, randomized, double-blind, parallel assignment Phase 2 extension trial is in progress in subjects with RRMS.[68] A multicenter, randomized, double-blind, parallel-group, placebo-controlled, Phase 2a trial was initiated in patients with moderate-to-severe chronic plaque psoriasis to evaluate the safety, tolerability, and efficacy of MT-1303.[69] The compound is also in two Phase 2 trials for the treatment of severe active Crohn's disease.[70,71]

5.12.3.12 RPC1063

RPC1063 (ozanimod) is a selective $S1P_1$ receptor modulator that demonstrates 269-fold selectivity for $S1P_1R$ ($EC_{50} = 0.16$ nM) over $S1P_5R$, and greater than 20,000-fold selectivity over $S1P_2R$, $S1P_3R$, and $S1P_4R$.[72] In a randomized, double-blind, placebo-controlled trial of oral RPC1063 in RRMS, the number of gadolinium-enhanced lesions at Week 24 were reduced by 91% and 94% in doses of 0.5 and 1 mg, respectively, compared with placebo. The cumulative number of new or enlarging T2 lesions from Weeks 12 to 24 also was reduced significantly in the 0.5 mg group (84%) and in the 1 mg group (91%) compared to placebo.[73] A Phase 3, multicenter, randomized, double-blind, double-dummy, active-controlled (beta interferon), parallel-group study to evaluate the efficacy and safety of RPC1063 (0.5 and 1.0 mg doses) in RRMS patients has been initiated.[74] RPC1063 also was tested in a multinational, multicenter, double-blind, randomized, placebo-controlled Phase 2 trial in patients ($n = 199$) with moderate-to-severe UC.[75] Clinical remission (primary endpoint) was met by 16.4% of patients on the 1 mg dose as compared to 6.2% of patients on placebo ($p < 0.05$). Statistical significance was not achieved in the low dose (0.5 mg) group.[76] However, in the maintenance portion of the study, clinical remission at Week 32 was statistically significant at both the 1 mg group and 0.5 mg dose group ($p < 0.05$) compared to placebo. Based on this data, a Phase 3, multicenter, randomized, double-blind, placebo-controlled trial of RPC1063 (1.0 mg) as induction and maintenance therapy for moderate-to-severe UC has been initiated.[77]

It is clear from the discussion above that small-molecule modulators of different targets/pathways that are in advanced clinical trials hold promise for the treatment of various autoimmune disorders. These compounds have the potential to have meaningful impact on the quality of life of patients by providing physicians with a range of therapies that provide the best possible treatment for these disorders. During the past decade, there has been an evolution in disease focus in the autoimmune/inflammation clinical space. While applications toward RA continue to grow in significance, an earlier emphasis on inflammatory pain, allergy, and transplant has diminished, despite the fact that these are not considered to be solved problems. On the rise are therapies directed toward MS and IBDs (Crohn's, UC).

5.12.4 Clinical and Preclinical Struggles

Given the exceptionally difficult path to the discovery and development of new drugs, it is natural that there would be a long list of compounds and targets that did not lead to success. Some of these disappointments are notable because of the stage of development that was reached (late-stage clinical trials, or even reaching market), while others are noted for the perceived potential based on preclinical data and the level of industry engagement that was put forth. This section will outline some of the setbacks that have occurred over the last 10–15 years.

5.12.4.1 COX2 Inhibitors

At the end of the 1990s, a decade or more of research into the identification of safer analgesics, culminated with the first approvals of a new class of compounds, the selective cyclooxygenase-2 (COX2) inhibitors. Targeting the same family of enzymes as aspirin and NSAIDs such as ibuprofen, naproxen, and many others, but sparing activity on COX1, the new inhibitors offered the potential to achieve similar pain management with substantially reduced gastrointestinal side effects. The improved GI tolerability of this class was borne out in multiple trials, and the approved inhibitors (celecoxib, rofecoxib, valdecoxib) quickly achieved blockbuster status, with combined worldwide sales of more than $6 billion in 2004.[78] However, with larger clinical trials, particularly those exploring higher doses, results pointed to increased cardiovascular safety concerns. The specific details of the multiple clinical trials and the resulting FDA and EMEA actions have been reviewed previously,[79] but the result was the removal of market authorization of rofecoxib and valdecoxib and a black box warning for celecoxib.

It is ironic that although cast as a disappointment, the sales of celecoxib, which was allowed to remain on market, were almost $3 billion worldwide in 2014 and the drug was among Pfizer's key products.[78] Maintaining clear blockbuster status a decade after the cardiovascular safety profile of the class was questioned, that drug can hardly be considered a failure. However, the 2004 sales for Pfizer's COX-2 franchise (celecoxib and valdecoxib combined) were $4.6 billion and had been anticipated to rise, so there was clear impact on market potential.[80] In addition to the effect on the marketed drugs of this class, the development of other COX2 inhibitors, exemplified by lumiracoxib and parecoxib, also stalled. Poised for marketing approval in 2004/2005 on the basis of the largest

trial with a COX2 inhibitor, lumiracoxib was unable to garner FDA approval despite showing no difference in myocardial infarction between it and either naproxen or ibuprofen.[5] Lumiracoxib was approved in non-US regions, although issues with liver toxicity subsequently led to marketing withdrawal in some areas.[81] Similarly, the FDA issued a nonapprovable letter for parecoxib (an injectable prodrug of valdecoxib) although it was made available in the European Union and other regions.[82] Development of numerous other COX2 inhibitors in earlier stages was subsequently discontinued in light of the uncertain future of the class.

5.12.4.2 p38 MAP Kinase Inhibitors

In the first decade of the millennium, perhaps no other discreet target in immunology/inflammation received as much attention from the industry as p38 MAP kinase. Significant drug discovery efforts were in place for this kinase at nearly every major pharma company as well as numerous smaller biotech companies. The excitement was driven initially by preclinical data demonstrating a clear role for p38α in the production of a variety of proinflammatory signaling molecules (eg, TNFα).[83] With the success of the anti-TNFα biologics, a small-molecule approach with the potential to match their efficacy seemed to be an opportunity that no one wanted to miss out on. As quality inhibitors of p38α were identified, favorable in vivo data in preclinical models across a range of diseases (autoimmunity and beyond) continued to emerge, bolstering confidence in this target.[84] Early compounds to reach the clinic (SCIO469; BIRB796), aimed at treating RA and Crohn's disease, showed no clear efficacy, and only transient decreases in CRP were observed, suggesting potential escape mechanisms for p38 inhibition.[85,86] Elevation of liver enzymes, an adverse event reported for multiple p38 inhibitors, was found to be dose-limiting for both SCIO469 and BIRB796.[87] Toxicity concerns also plagued VTX-745, which was dropped from clinical development because of CNS toxicity observed in animal studies.[88] The limited and sometimes transient signs of efficacy (tachyphylaxis) demonstrated by the early clinical compounds led to a souring of the field, with articles about the "unfulfilled promise" of p38 and a commentary headlined "Inhibition of p38: has the fat lady sung?" highlighting the prevailing sentiment.[87,89] Nevertheless, trials in RA with some compounds ultimately were able to show sustained efficacy. A dual mechanism of inhibition (blocking both the activation of p38 as well as its activity) was highlighted for BMS-582949, which showed sustained improvement in ACR 20 response in patients with active RA relative to placebo over 12 weeks.[90,91]

With sustained challenges in applying p38 inhibition in RA, companies have turned their attention to a number of alternative indications, with COPD being commonly targeted. Eight p38 inhibitors, four orally administered as well as four inhaled inhibitors, have been evaluated clinically for treating COPD with the available data having been reviewed recently.[92] Of the four oral agents, only acumapimod (BCT-197) remains in development, having recently completed a Phase 2 evaluation as monotherapy or in combination with prednisone although results have not been disclosed.[93] Of the inhaled approaches, three (PF-03715455; AZD-7624; RV-568) appear to be under continued development.[92] Additional indications evaluated with p38 inhibitors include surgical pain (talmapimod), neuropathic pain (dilmapimod), ovarian cancer (LY2228820), and Alzheimer's disease (VX-745). Furthermore, a variety of cardiovascular disorders have been targeted with p38 inhibitors. In one of the most advanced trials with a p38 inhibitor, losmapimod was examined in a Phase 3 study for treatment of acute coronary syndrome.[94] The planned interim review of data from the first part of the stepwise study design did not indicate efficacy against the primary endpoint, casting doubt on the further evaluation in this indication.[95] The development road for p38 kinase inhibitors has been extremely rough, and the tenacity of the industry with regard to this class is noteworthy, although only time will tell if the investment was worthwhile.

5.12.4.3 Chemokine Receptor Modulation

Chemotactic cytokines, or chemokines, are a family of signaling molecules that exert their cellular trafficking abilities through interaction with varied G-protein coupled receptors (GPCRs).[96] Although two small-molecule drugs have been approved in this space (CCR5 antagonist maraviroc and CXCR4 antagonist plerixafor), their indications (HIV infection and mobilization of stem cells, respectively) lie outside of the immunology/inflammation area for which the most effort in CCR development has been directed.

The selection of drug targets within this family could be viewed as daunting, with at least 40 chemokines and 19 functional CCRs identified so far. A few members of this family have emerged as preferred targets and have been the subject of recent reviews.[97,98] As highlighted in those reviews, compounds have reached clinical stage evaluation for CCR1, CCR2, CCR3, CCR4, CCR5, CCR9, CCR1/2 dual, CCR2/5 dual, CXCR1, CXCR1/R2 dual, CXCR3, and CXCR4. The areas of clinical focus include immunology/inflammation indications (MS, RA, psoriasis, COPD, lupus, asthma, allergic rhinitis, Crohn's) as well as conditions outside of that area (HIV, multiple myeloma, atherosclerosis, diabetic retinopathy, pain, stem-cell mobilization, and Type 2 diabetes). While many of the studies are ongoing, or have completed but results are not disclosed, the lack of clear success in RA, for example, is counter to the expectations.[98] Possible reasons for the lack of progression have been debated, with an early hypothesis of redundancy within the chemokine system being challenged by analysis of clinical trial data, suggesting that inadequate target coverage is to blame.[99,100]

5.12.4.4 TACE Inhibitors

As previously discussed, the clinical benefit of controlling TNFα levels has been clearly established for a variety of autoimmune disorders with biologic therapeutics, bringing focus on molecular targets that could achieve the same effect with small-molecule intervention. TACE, or TNF-alpha converting enzyme, plays a key role in the production of active soluble TNFα and is therefore one such promising target. TNFα is a cytokine produced as a membrane-bound form that is cleaved by the zinc-metalloprotease

TACE to liberate the soluble form, which then is able to act on TNFα Receptor I to elicit a variety of proinflammatory responses.[101] Belying the specificity suggested by the name, TACE is involved with the processing of a host of substrates beyond TNFα to reveal their active forms.[101] While this extended role may in some cases lead to enhanced benefit in other diseases, it also may play a role in undesired side effects of TACE inhibition.

Further side effect concerns were potentially related to inhibition of structurally related targets. Early work in the area focused on compounds derived from broad-spectrum inhibitors of matrix metalloproteinases (MMPs) with poor specificity for TACE and whose development was challenged by toxicity.[102] In particular, musculoskeletal toxicity (tendonitis) was attributed to inhibition of MMP1 or MMP14, leading subsequent efforts to be directed at the identification of TACE inhibitors with a more selective MMP inhibition profile.[103,104] Various campaigns were successful in identifying clinical development compounds, the two most advanced of which were progressed to Phase 2 evaluation. Investigations with BMS-561392 (DPC-333) were halted because of hepatotoxicity concerns noted in preclinical studies that were postulated to be mechanism-based.[101,105] While apratastat (TMI-005) completed a Phase 2 evaluation for RA without signs of hepatotoxicity, further development was not undertaken as a lack of efficacy was noted.[106] One recent hypothesis for the lack of clinical efficacy of TACE inhibitors despite good preclinical validation was suggested to be upregulation of caspase-1, which was observed in human cells but not in mice.[107]

Advances in the treatment of autoimmune and inflammation disorders during the last 15 years have accompanied significant struggles in areas that held, or still hold, great potential for human therapeutic application. A number of other targets could be added to the list provided here, including inhibitors of kinases such as spleen tyrosine kinase (SYK), zeta-chain associated protein kinase 70 kDa (ZAP70), or IKK (IkB Kinase) that have proven reluctant to identification of clinically successful molecules or have been challenged by toxicity concerns. Disrupting cell surface interactions such as lymphocyte function-associated antigen 1 (LFA-1) with small-molecule inhibitors was likewise met with clinical disappointment. Dissociated glucocorticoid receptor modulators, able to derive the benefit of steroids while minimizing their varied and often serious side effects represent one version of a holy grail in small-molecule immunotherapy. Despite widespread attention, the desired profile has not yet been fully validated clinically.

5.12.5 Emerging Specific Targets

Despite major success in developing targeted immune therapies in the last decade, there is significant unmet clinical need in therapies directed to a number of autoimmune disorders such as lupus, UC, Crohn's disease, RA, etc. Both small-molecule and biological therapies targeting a number of mechanisms are being investigated to bring successful therapies to the market. We summarize the approaches being taken to target the innate and adaptive immune system by employing small-molecule therapeutics.

5.12.5.1 Interleukin-1 Receptor-Associated Kinase 4 (IRAK4)

IRAK4 belongs to the serine–threonine kinase family and is involved in the signal transduction pathways used by interleukin-1 receptor (IL-1R), interleukin-18 receptor (IL-18R), and toll-like receptors (TLRs) of the innate immune response.[108] Of the four mammalian IRAKs, IRAK-4 is the most important from a drug target perspective since it is indispensable for IL-1R/TLR signaling. When ligands derived from different microorganisms or endogenous stimuli bind to either IL-1R or TLR, the adaptor protein MyD88 binds to the receptor via the intracellular toll and interleukin-1 receptor (TIR) domain present on IL-1R, IL-18R, and TLRs. MyD88 acts as a scaffolding protein and recruits IRAK-4, which subsequently recruits either IRAK-1 or IRAK-2 via death domain interactions. Phosphorylation of IRAK-1 by IRAK-4 results in autophosphorylation and activation of IRAK-1 and the release of IRAK-1 from MyD88. IRAK-1 then binds to TNF receptor-associated factor 6 (TRAF6) leading to the activation of NFkB and the production and secretion of proinflammatory cytokines.[109] In addition, it has been observed that cells derived from IRAK-4 deficient patients exhibit impaired responses to IL-1, IL-18, or exogenous MyD88-dependent TLR ligands.[110] These data suggest that targeting IRAK-4 offers the potential for the development of new therapeutics for the treatment of inflammatory diseases.

The involvement of IRAK-4 in TLR7 and TLR9 induced IFNα production, coupled with the observation that dual inhibition of TLR7 and TLR9 in lupus-prone mice results in amelioration of disease symptoms, suggests that IRAK-4 may be a suitable therapeutic target for lupus.[111] In addition, since IRAK-4 is involved in signal transduction pathways used by IL-1R, IL-18R, IRAK-4 inhibitors have the potential for the treatment of RA, osteoarthritis (OA) (IL-1R),[112] IBD (IL-18R), and inflammasome associated diseases including gout, adult onset Still's disease, systemic juvenile idiopathic arthritis (SJIA), and cryopyrin-associated periodic syndromes (CAPS).[113]

Full-length IRAK-4 has a molecular weight of 52 kDa and is composed of 460 amino acid residues. The kinase domain of IRAK-4 is composed of 269 amino acids. Six crystal structures of the kinase domain of IRAK-4 have been reported, three of which are for the apoenzyme with the other three with small-molecule inhibitors bound. One of the novel structural features related to the kinase domain of IRAK-4 is the presence of a tyrosine gatekeeper residue (Y262). Because of the large tyrosine residue, the entrance to the internal hydrophobic pocket is blocked, resulting in lack of accessibility of inhibitor into the pocket. However, this creates a unique extended front pocket (adenosine triphosphate binding pocket), which allows for the design of highly selective inhibitors.[114]

A potential issue with IRAK-4 inhibition is the susceptibility of children with IRAK-4 deficiency to bacterial infections (*P. aeruginosa*, *S. aureus*). Interestingly, adult patients with this deficiency have decreased susceptibility to infections.[115] Although as of this writing no IRAK-4 inhibitors have entered clinical trials, a number of pharmaceutical companies and academic

laboratories are involved in the identification of potent and selective inhibitors, as judged by the activity in the patent and open literature.[116] Proof-of-principle studies in the clinic with IRAK-4 inhibitors will provide insights into future design and development of therapeutics for the treatment of variety of autoimmune disorders based on IRAK-4 .

5.12.5.2 Receptor-Interacting Protein (RIP)

RIP kinases belong to the serine–threonine kinase family, which has seven members: RIP1, RIP2 (RICK/CARDIAK), RIP3, RIP4 (DIK/PKK), RIP5 (SgK288), RIP6 (LRRK1), and RIP7 (LRRK2).[117] From an immunology/inflammation perspective, there has been significant interest in targeting RIP1, 2, and 3.[118a–c] Less research has focused on RIP4-7, as their physiological functions remain incompletely understood. The RIP kinases share a homologous kinase domain but have different functional (nonkinase) domains.

RIP1 and RIP3 are both critical components of the necroptotic cell-death signal transduction pathway.[119] As both kinases are highly expressed in intestinal epithelial cells, inhibition of either target could protect the intestinal epithelial barrier if necroptosis is active during IBD.[120a,b] RIP1 KO mice die within 1–3 days of birth[121]; however, kinase dead knockin mice have been reported to be healthy and viable,[122a–c] implying that an RIP1 scaffolding function is responsible for the pro-survival role in the nuclear factor kB (NFkB) pathway. RIP3 KO mice are viable and demonstrate protection from disease state.[123]

Although highly specific RIP3 inhibitors are unknown, *in vitro* tool molecules have been reported.[124a,b] Crystal structures of mouse RIP3 kinase domain (mRIP3) and the mRIP3-mixed lineage kinase domain-like complex have been reported.[125] Significant synthetic efforts around both Type II and Type III RIP1 inhibitors have been delineated in a number of patents and publications.[126a–g] Crystal structures for Type II[126a] and Type III[127] inhibitors have been acquired with the kinase domain of human RIP1. Small-molecule inhibitors reported to date have demonstrated *in vivo* activity in a PD model.[126a,b] To date, there is no direct evidence that inhibition of RIP1 or RIP3 will have an impact on IBD disease course or remission in humans.

RIP2 signals through the nucleotide-binding oligomerization domain (NOD)1/2 cytosolic sensors,[117] which are activated by components of the bacterial wall. The NOD/RIP2 signaling pathway has been implicated in a variety of autoimmune diseases, including IBD, MS, and Blau syndrome.[128] RIP2 KO mice are viable and demonstrate a critical role in both adaptive and innate immunity.[129a,b] Loss of function NOD2 mutations are highly associated with Crohn's disease.[130]

A number of RIP2 inhibitors have been reported in the literature.[131] Some of these small-molecule inhibitors have demonstrated efficacy in rodent models of autoimmune diseases.[128] To date, only one crystal structure has been reported for RIP2 with the known Type II inhibitor, ponatinib.[132] Although promising for a number of autoimmune diseases, it remains unknown if inhibition of RIP2 could affect the gut microbiota and/or render patients susceptible to intestinal inflammation.

Within the RIP family of kinases, work around RIP1, 2, and 3 to develop small-molecule tool compounds has led to exciting data in *in vivo* PD (pharmacodynamic) and efficacy studies. Significant work remains to translate this early work into drugs, but the promising results observed to date provide a compelling argument to continue on these targets as an avenue to modulate a number of autoimmune diseases.[133]

5.12.5.3 Toll-Like Receptors (TLRs)

TLRs are Type I transmembrane proteins that are expressed by cells of the innate immune system, such as macrophages, B cells, and dendritic cells and beyond the immune system, including epithelial cells, endothelial cells, and tissue resident cells. TLRs play a critical role in the early innate immune response by recognizing pathogen-associated microbial patterns (PAMPs), which are exclusively expressed by microbial pathogens, or danger-associated molecular patterns (DAMPs) that are endogenous molecules released from necrotic or dying cells. Although 10 TLRs have been characterized in humans, from an autoimmune disorder treatment perspective, there has been most significant interest recently in targeting TLR7, 8, and 9.[134] In addition, it has been shown that in TLR7 and TLR9 double-knockout mice, in TLR7 knockout mice, and in TLR7 and TLR8 double-knockout mice, lupus disease, and disease-associated parameters were abrogated.[135–137] Moreover, activation of TLR7, 8, and 9 by immune complexes leads to the production of proinflammatory cytokines like TNF-α and IL-1β along with Type I interferons.[138] Knockout studies and activation pathways described above for TLR7, 8, and 9 clearly suggest that antagonists of these proteins have the potential to treat autoimmune diseases such as lupus, psoriasis, and RA.

TLR7, 8, and 9 are located in the endosome. TLR7 and 8 bind ssRNA, whereas TLR9 binds (ds)DNA containing unmethylated CG dinucleotides.[139] All TLRs have an extracellular ectodomain and an intracellular Toll/IL-1 receptor homology (TIR) domain. A single stretch of about 20 transmembrane amino acids joins both the domains. The ectodomain of TLRs consists of 19–27 consecutive leucine-rich repeat (LRR) motifs and is responsible for recognizing structural patterns in various microbial molecules, in addition to endogenous nucleic acids (vide supra).[140] Recent advances in obtaining crystal structures of the extracellular domains of TLR8 and TLR9 in the absence and presence of ligands open up new opportunities for drug design.[141,142] This is evidenced in the application of crystallographic information in the discovery of novel small-molecule TLR8 agonists.[143]

Oligonucleotides targeting TLRs are in clinical trials. For example, Idera has a TLR7/9 oligo (IMO3100) and TLR7/8/9 oligo (IMO-8400 IMO-9200) which are in Phase 2 trials for psoriasis.[144] However, Dynavax's TLR7/9 oligo (DV1179) did not meet the pharmacodynamic endpoints related to reduction in interferon alpha-regulated genes in a Phase 1a/2b trial for lupus.[145] A number of pharmaceutical companies (Kowa, Janus, Eisai) and academic labs are involved in the identification of potent and selective inhibitors, as judged by the activity in the patent[146] literature. While the ongoing clinical trials will shed more light on the role of TLRs in innate and adaptive immune signaling, it is clear that targeting TLR7, 8, and 9 offers the promise to address unmet clinical need for diseases such as lupus.

5.12.5.4 Retinoic Acid-Related Orphan Receptor γt (RORγt)

The retinoic acid-related orphan receptor (ROR) nuclear hormone receptor family consists of three members: RORα, RORβ, and RORγ. RORγt is a splice variant of RORγ and plays a central role in the differentiation and proliferation of Th17 T cells.[147] This subset of T cells has been linked to the pathology of a number of autoimmune and inflammatory diseases including psoriasis, IBD, RA, and MS.[148] In addition, genetic data with RORγ/RORγt deficient mice clearly suggests the critical role played by this nuclear hormone receptor in the pathogenesis of multiple autoimmune diseases.[149a–c] Therefore, targeting RORγt has emerged as an important strategy for therapeutic intervention in the treatment of autoimmune disorders.[150]

Full-length RORγt consists of 497 amino acids and like most nuclear hormone receptors has a variable N-terminal A/B domain, a highly conserved DNA-binding domain, a hinge domain that connects the DNA-binding domain to the carboxy-terminal ligand binding domain (LBD). The LBD facilitates coactivator and/or corepressor binding to the receptor and consists of 12 α-helices and two additional helices H2′ and H11″.[151] The structural information of small-molecule modulators bound to the LBD of RORγt along with high throughput screens for hit identification has allowed for the discovery of several novel series of RORγt inverse agonists both in academia and industry.[152]

As of this writing, JPT-151 (Japan Tobacco) and VTP-43742 (Vitae Pharmaceuticals), both small-molecule inverse agonists of RORγt, have entered clinical trials.[153,154] These compounds, along with others at various stages of preclinical development, may provide pharmacological validation of the target both from efficacy an and safety perspective. Given the importance of the IL-17/Th-17 axis in autoimmunity, RORγt inverse agonists have the potential to become standard of care for the treatment of a variety of autoimmune disorders.

5.12.5.5 Tyrosine-Kinase 2 (Tyk2)

Tyk2 belongs to the JAK family of nonreceptor tyrosine kinases, which also includes JAK1, JAK2, and JAK3. Members within this family are known to be critical regulators of signal transduction pathways used by the classical Type I and Type II immune cytokine receptors and, as a result, have emerged as promising targets in the treatment of various cytokine-dependent inflammatory and immune disorders.[155] More specifically, Tyk2 has been linked to the downstream receptor signaling of the p40 containing cytokines IL-23 and IL-12 as well as the Type I interferons (IFNα and IFNβ), IL-6, and IL-10 families.[156] Upon receptor activation, Tyk2, in combination with either JAK1 or JAK2, phosphorylates the intracellular receptor domains, which in turn recruit specific STAT proteins. The STATs subsequently are phosphorylated, causing disassociation from the receptor and the formation of STAT dimers that translocate into the nucleus and trigger gene transcription processes leading to an inflammatory response. Studies in Tyk2-deficient mice have suggested that Tyk2 is required for IL-23, IL-12, and Type I interferon signaling, but not IL-6 and IL-10 responses.[157] In humans, only two patients lacking the Tyk2 protein have been reported, and only one of these patients was thoroughly studied for defective cytokine responses.[158] These studies indicated a potentially broader role of Tyk2 signaling in humans versus mouse since IL-6 and IL-10 pathways also were found to be Tyk2-dependent.

Inhibition of Tyk2 has attracted significant attention within the pharmaceutical industry primarily because of the potential to block the signaling pathways of the p40 cytokines IL-23 and IL-12. IL-23 is known to be critical for the expansion and survival of T_H17 cells, which have been associated with the pathogenesis of serious autoimmune diseases including psoriasis and IBD.[159] In addition, IL-12 is essential for T_H1 cell development and the production of IFNγ, which stimulates the innate and T cell-mediated immune response.[160] Overstimulation of T_H1 cells can lead to tissue damage and chronic inflammation in autoimmune diseases, such as systemic lupus erythematosus (SLE). Clinical validation using monoclonal p40 antibodies, which block the IL-23 and IL-12 pathways, has proven to be beneficial therapeutically in both animal models as well as in patients having various autoimmune diseases.[161] For example, ustekinumab, a p40 antibody, has been approved for the treatment of plaque psoriasis and psoriatic arthritic and also is being investigated in the treatment of Crohn's disease.[162] Tyk2 inhibition is also promising because of the potential to target the type 1 interferon pathways. Elevated levels of interferons have been correlated with disease activity in lupus (SLE) patients and validation of this pathway has been demonstrated with sifalimumab, an IFNα antibody and anifrolumab, an antibody targeting the IFN receptor. Both drugs showed significant inhibition of disease progression compared to placebo in a Phase 2 trial.[163]

Most recent efforts within the industry have focused on the development of small-molecule inhibitors of Tyk2. While a recent report[164] describing studies of ATP-competitive small-molecule inhibitors concluded that inhibition of Tyk2 in humans is restricted to only the IL-12 and IL-23 pathways, more recent studies[165] using ligands that selectively bind to the unique pseudokinase JH2 domain of Tyk2 (rather than the active JH1 kinase domain) have demonstrated that potent inhibition of Type 1 IFN signaling, in addition to inhibition of IL-23 and IL-12 signaling, is possible. Despite these efforts, small-molecule Tyk2 inhibitors have not yet been reported in clinical trials to date. Future efforts likely will clarify the role of Tyk2 inhibition in cytokine signaling and better define the true potential of small-molecule Tyk2 inhibitors in the treatment of autoimmune diseases.

5.12.5.6 Protein Kinase C Theta (PKCθ)

PKCθ is a serine–threonine kinase belonging to the diacylglycerol dependent protein kinase C (PKC) subfamily (PKC δ, ε, η, θ).[166] PKCθ has a limited expression profile being found in muscle, nerves, and T cells. On engagement of the T cell receptor, PKCθ migrates to the immunological synapse, where it interacts with LCK (lymphocyte-specific protein tyrosine kinase) and the

cytoplasmic domain of CD28. Its activation results in downstream activation of the mitogen-activated protein kinase pathway, which in turn activates nuclear factor of activated T cells, activator protein 1, and NFkB.[167,168] This results in activation of effector T cells (T_{eff}). PKCθ also has been shown to mediate the negative feedback in regulatory T cells (T_{reg}) and inhibition of PKCθ promotes T_{reg} proliferation, which may be an alternate or contributory mechanism by which PKCθ inhibition can suppress T_{eff} cell function.[169]

Much of the evidence for the potential therapeutic benefit of PKCθ inhibition comes from PKC$\theta^{(-/-)}$ mouse studies. For example, PKC$\theta^{(-/-)}$ mice showed decreased disease severity in the collagen induced arthritis (CIA)[170] model, and transfer of $CD4^{+}CD45RBhi$ T cells from PKC$\theta^{(-/-)}$ mice failed to induce colitis.[171] It also has been reported that PKC$\theta^{(-/-)}$ mice exhibit decreased severity in myelin oligodendrocyte glycoprotein (MOG) induced EAE;[172] however, in a conflicting report, the disease was exacerbated.[173] Thus there appears to be evidence that PKCθ may be a target for several autoimmune mediated diseases. However, in the absence of PKCθ kinase dead mouse studies, it is difficult to establish whether kinase activity or altered immune synapse composition or both contribute to the observed efficacy in PKC$\theta^{(-/-)}$ animal models.

Full-length PKCθ has a molecular weight of ~110 kDa and is composed of 706 amino acid residues. The kinase domain PKCθ is composed of 254 amino acids. Four crystal structures of the kinase domain of PKCθ have been reported to date, and all the structures have small-molecule inhibitors bound. Novel structural features of the PKC family include a C-terminal tail, which can be either ordered or disordered in crystal structures. It has been hypothesized that if an inhibitor makes optimal contacts with the C-terminal tail of PKCθ that this interaction can contribute to increased selectivity against PKCα.[174]

Sotrastaurin, a nonselective PKC family inhibitor, showed similar efficacy to mycophenolic acid when either agent was combined with tacrolimus, basiliximab, and corticosteroids in clinical kidney transplantation studies. However, as sotrastaurin showed limited benefit over standard of care, its clinical development has been halted.[175] Recently disclosed preclinical selective PKCθ inhibitors were able to inhibit staphylococcal enterotoxin B induced IL-2 production in mice and have demonstrated efficacy in a MOG-induced EAE mouse disease model and a T cell transfer colitis mouse disease model.[176] These results are consistent with the efficacy observed in the PKC$\theta^{(-/-)}$ mouse studies and suggest that selective inhibition of the kinase activity of PKCθ plays a role in blocking signal transduction from the immune synapse. The identification of selective PKCθ inhibitors with good pharmacokinetic profiles will allow for proof-of-principle studies in the clinic and accelerate the development of this class of compounds for the treatment of several T cell mediated diseases.

5.12.5.7 Bruton's Tyrosine Kinase (BTK)

BTK is a member of the TEC family of nonreceptor tyrosine kinases and is expressed in all hematopoietic cells, except T cells and plasma cells. Of the five mammalian TECs, BTK is the most important from a target perspective since it is indispensable for signaling through the B cell receptor (BCR) in B cells.[177] In addition to B cells, BTK is critical for signaling in low affinity activating Fcγ receptors (eg, FcγRIII and FcγRIIa) in monocytic cells as well as for FcεRI signaling in mast cells and basophils, where BTK regulates the expression of proinflammatory cytokines, chemokines, and cell adhesion molecules in response to receptor activation.[178] RANK signaling, which regulates osteoclastogenesis from monocytic precursors, is also BTK-dependent.[179]

B cells are central to the pathogenesis of autoimmune diseases such as RA as evidenced by the clinical data for rituximab (Rituxan), a B cell-depleting anti-CD20 antibody.[180] Besides being a source of autoantibodies, B cells can impact autoimmunity through their role as antigen-presenting cells and as sources of proinflammatory cytokines and chemokines such as IL-6 and TNFα.[181] Since the kinase activity of BTK plays a critical role in BCR-dependent proliferation of B cells, as well as expression of costimulatory molecules (eg, CD86) and proinflammatory cytokines, pharmacological inhibition of BTK is expected to affect many mechanisms by which B cells may mediate autoimmunity. There is a significant body of evidence from genetic and pharmacological studies in animal models supporting the utility of BTK inhibitors against autoimmune indications, such as RA or SLE. BTK-deficient mice are resistant to both CIA as well as the (NZB X NZW)F1 model of lupus.[182] Pharmacological inhibition with BTK inhibitors has demonstrated benefit against the CIA and collagen antibody-induced arthritis models as well as in murine lupus models.[183] The critical role of BTK in B cells also is seen in X-linked agammaglobulinemia (XLA) immunodeficiency in humans. Inactivating mutations in the BTK gene in XLA patients cause loss of mature B cells and circulating antibodies.[184]

Full-length BTK has a molecular weight of 76 kDa and is composed of 659 amino acid residues. The kinase domain of BTK is composed of 258 amino acids. Twenty-four crystal structures of the kinase domain of BTK have been reported to date, of which 4 are for the apoenzyme and 20 are with small-molecule inhibitors bound. The key structural feature related to the kinase domain of BTK is the noncatalytic cysteine (C481) residue in the extended hinge region.[185] There are only 10 other kinases that possess a similar cysteine in the kinase active site, creating an opportunity to design selective covalent inhibitors.[185] Numerous companies have targeted this residue to prepare irreversible BTK inhibitors, with the most successful being Imbruvica (Ibrutinib; Pharmacyclics/J&J), which is approved for various non-Hodgkin's lymphomas.[186,187]

A potential issue with BTK inhibition could be increased infections, also observed in XLA patients.[188] To date, the clinical side effects for Imbruvica do include infections, along with increased bleeding and cytopenias.[189] As of the writing in this article, several BTK inhibitors have entered clinical trials for the treatment of an autoimmune indication, including covalent inhibitors from Celgene (CC-292), Hanmi (HM71224), and Principia (PRN1008),[190a,b] with the most advanced appearing to be CC-292, currently in Phase 2 trials in RA.[191] The efficacy data for these and other compounds entering clinical trials is eagerly awaited, since small-molecule inhibitors of this mechanism have the potential to compete with biologics for the treatment of autoimmune diseases such as RA.

5.12.5.8 NFkB-Inducing Kinase (NIK)

NIK (MAP3K14) is a serine–threonine kinase belonging to the STE group of kinases. NIK plays an important role in the activation of the noncanonical NFkB pathway. This pathway is activated by signals from several receptors including CD40, Lymphotoxin βR and BAFF-R, which are responsible for the development and activation of B cells. In resting cells, NIK is degraded rapidly by a complex of TNF receptor-associated factors (TRAFs) and cellular inhibitors of apoptosis. Upon receptor activation, NIK dissociates from this complex and accumulates in the cytoplasm where it phosphorylates IKKα at Ser_{176}, which activates IKKα to phosphorylate p100 at Ser_{866} and Ser_{870}. This phosphorylation event triggers the processing of p100 to p52, which together with RelB, translocates to the nucleus to effect transcription events associated with the noncanonical NFkB signaling pathway.[192] The importance of NIK in B cell development and secondary lymphoid organ development has been confirmed in mice in which NIK has been deleted conditionally.[193] Studies with $NIK^{(-/-)}$ mice have demonstrated that these mice are resistant to MOG-induced EAE and show defects in Th17 differentiation.[194] While NIK clearly plays an important role in adaptive immunity, it also has been reported to play a role in Type I interferon production as part of the innate immune response to viral pathogens.[195] Immune-compromised patients have been identified[196] who have a single-point mutation in the activation loop of NIK, which renders the kinase incapable of phosphorylation of IKKα. These immune-compromised patients exhibit B cell lymphopenia, impaired memory B cell differentiation, abnormal NK cell development, and decreased development of follicular helper T cells. The NIK transgenic mouse data and the phenotype observed in immune-compromised patients with an inactivating mutation in NIK suggest that NIK inhibitors may provide a therapeutic benefit in the treatment of human autoimmune diseases.

Full-length NIK is composed of 947 amino acid residues containing a TRAF binding domain, a kinase domain, and an IKKα binding domain. The kinase domain of NIK is composed of 280 amino acids. Eight crystal structures of either the human or mouse kinase domain of NIK have been reported, with five of the structures having small-molecule inhibitors bound.[197] Novel structural features for this kinase include a mobile glycine rich loop that exists in multiple conformations in the reported crystal structures and a back pocket beyond the methionine gatekeeper that some inhibitors are able to access.[198]

There are several patents[199] and publications[200] which disclose small-molecule inhibitors of NIK, although little to no pharmacologic proof-of-concept has been reported for these inhibitors. Significant advancements in preclinical and clinical development will be required to determine if selective NIK inhibitors will be useful as therapeutic agents for the treatment of autoimmune diseases.

A number of other targets involved in cellular and signaling pathways that lead to inflammation and autoimmunity are being pursued in academic labs and the pharmaceutical industry. For example, selective PAD4 (protein arginine deiminase 4) inhibitors have been identified,[201] and show the potential for therapeutic intervention in autoimmune disorders like RA. A Phase 1 clinical study with the vascular adhesion protein-1 inhibitor, RTU-1096 having anti-inflammatory and immunomodulatory effects has been completed.[202] There is significant effort targeting macrophage migration inhibitory factor (MIF) inhibitors with either anti-MIF antibody or specific MIF antagonists for the treatment of inflammatory and autoimmune diseases.[203] Other targets that are being pursued include inhibitor of 5-Lipoxygenase Activating Protein, CB2 (Cannabinoid Receptor 2) agonists, adenosine receptor modulators, NOD Inhibitors, EP4 antagonists, P2X7 antagonists for the treatment of inflammatory diseases.

5.12.6 Emerging Paradigms

Genetic, immunological, environmental, and hormonal factors, among others, act in concert and contribute to autoimmunity. This section discusses new mechanisms targeting these factors for the treatment of inflammation and autoimmune disorders. These novel and alternative intervention strategies have the potential to satisfy the unmet medical needs that exist in these diseases. Although these targets are challenging from a small-molecule therapeutic perspective, significant progress has been made in identifying compounds that have advanced to the clinic or are being used as tools for proof-of-principle studies.

5.12.6.1 Targeting Epigenetic Mechanisms to Treat Autoimmune Disorders

Epigenetics is defined as the heritable change or alteration of gene expression without underlying modifications in their nucleotide sequence. Epigenetic processes involve DNA methylation, modifications to histones, and regulation by noncoding RNA. Alterations to these processes can result in autoimmune disorders such as SLE, RA, MS, and systemic sclerosis (SSc).

DNA methylation and demethylation are important processes occurring in cells that contribute to cellular proliferation and differentiation. DNA methyltransferases (DNMT) are a group of enzymes that establish methylation of CpG (cytosine-guanine) dinucleotides and inhibit gene transcription by blocking accessibility to transcriptional activators. Demethylation on the other hand can be induced by inhibiting DNMT. Analysis of $CD4^+$ T cells from patients with SLE, RA, MS, and Sjögren's syndrome (SS) has indicated decreased expression of methylation related genes like DNMT1 and hypomethylation of interferon-regulated genes, such as IRF5, IFIT2, STAT1, and USP18.[204] Therefore, DNMT has been proposed as an epigenetic target to improve the outcome of patients suffering from MS and SSc. In preclinical studies, 5-aza-2′-deoxycytidine, a DNMT inhibitor, was shown to prevent autoimmune encephalomyelitis, suppress CNS inflammation, and increase Treg (regulatory T cell) population in the EAE model in mice.[205] In addition, 5-aza-2′-deoxycytidine reversed the hypermethylation of DKK1, SFRP1, and FLI1 in fibroblasts from patients with SSc.[206] However, nucleoside inhibitors such as 5-aza-2′-deoxycytidine are nonspecific DNMT inhibitors and

therefore have the potential for significant off-target liabilities (eg, myelosuppression). Therefore, the emphasis has shifted to identifying isoform-specific DNMT inhibitors to eliminate nonspecific toxicity while improving clinical outcomes.

Analogous to DNA methylation, histones (H1, H2A, H2B, H3, H4, and H5) are another source of epigenetic alteration. Histones are the major protein components of chromatin and they act as spools around which DNA binds. Posttranslational modifications of histones such as acetylation and methylation are maintained by enzymes like methyltransferases and demethylases, and histone acetyltransferases and deacetylases (HDAC). The $CD4^+$ T cells of SLE patients display hypoacetylation (H3 and H4),[207] whereas H4 is hyperacetylated in B cells of patients with SSc (because of decreased HDAC2 and HDAC7).[208] In clinical trials involving 17 patients, the nonselective HDAC inhibitor, givinostat, showed therapeutic benefit in systemic juvenile idiopathic arthritis, particularly in terms of the arthritic components of the disease.[209] However, nonselective HDAC inhibitors have been associated with serious side effects such as thrombocytopenia and cardiovascular issues, which is why the field is moving toward identifying selective HDAC inhibitors for the treatment of autoimmune disorders.[210a,b] Since each HDAC controls the expression of a large number of genes, it will be interesting to see if isoform-specific HDACs will provide the desired therapeutic benefit without affecting normal physiological functions.

Lysine acetylation is a histone modification that allows bromodomain-containing proteins to bind to and regulate gene expression. Bromodomains are 110-amino acid long and specifically bind to lysine residues in histone tails. The human genome encodes a total of 61 bromodomain proteins. It was shown recently that targeting BET (bromodomain and extra-terminal domain), a member of the bromodomain family, with a small-molecule inhibitor leads to antiinflammatory effects.[211] More recently, it was shown that BET plays an important role in human and murine TH17 differentiation, as well as in the activation of previously differentiated TH17 cells.[212] In vitro, a selective small-molecule inhibitor of BET (JQ1) blocked the expression of signature Th17 cytokines, including IL-17, IL-21, and GM-CSF (granulocyte macrophage colony-stimulating factor) without affecting Th1, Th2, and Tregs. *In vivo*, JQ1 decreased IL-17 production and decreased severity in mouse models of arthritis (CIA model) and MS (EAE) when dosed at 30 mg kg^{-1} twice daily.[212] The *in vitro* results obtained with JQ1 are in contrast with the results obtained with GSK525762, another BET inhibitor, which suppressed the proinflammatory functions of Th1 cells but did not affect Th17 cells.[213] In addition to BET, several bromodomain proteins have been described as potential targets for the treatment or prevention of autoimmune and inflammatory diseases (ATAD2, BAZ1B, SP110, SP140).[214] Since the current inhibitors are relatively unselective and affect multiple immune cells, the tolerability and safety profiles of these compounds are a cause for concern. JQ1 is in clinical trials for oncology indications and the safety data from these trials along with the identification of isoform selective BET and other bromodomain family of inhibitors will be crucial for advancing these compounds into the clinic for treating autoimmune disorders.

MicroRNAs (miRNAs) are small noncoding regulatory RNAs of about 22 nucleotides and are involved in regulating gene expression via translational repression, mRNA destabilization, and degradation. Aberrantly expressed miRNAs modulate multiple genes related to autoimmunity and therefore play a significant role in the pathogenesis of disorders such as SLE, MS, RA, and SSc. Common miRNAs that are dysregulated in autoimmune diseases are miR-21, miR-29a and b, miR-30a and b, miR-146a, miR-155, and let-7a. miRNA sponges and antisense oligonucleotides against miRNAs have been used to demonstrate in vitro and in vivo efficacy by suppressing miRNA function and blocking their effect on the expression of endogenous target genes.[204] Except for one report of a small-molecule inhibitor affecting miR-21 expression,[215] small-molecule approaches have yet to make an impact in this area, although they have the potential to target multiple steps of miRNA assembly and function and provide an alternate approach for the treatment of autoimmune disorders.

5.12.6.2 Inflammasome

The inflammasomes are high molecular weight intracellular protein complexes that activate inflammatory caspases leading to the processing of the proinflammatory cytokines IL-1β and IL-18. Both IL-1β and IL-18 are key players in the initiation and maintenance of a number of pathological processes associated with autoimmune disorders and inflammation. Inflammasome activation has also been associated with several neurologic disorders such as Alzheimer's disease, MS, and Parkinson's disease; metabolic disorders such as atherosclerosis, type 2 diabetes, and obesity; and autoinflammatory diseases such as gout and CAPS.

Unlike other transcriptionally regulated cytokines, which are released in the active form upon induction, IL-1β and IL-18 are synthesized as proforms in response to stimulation of toll-like receptors by pathogen-associated molecular patterns (PAMPs) as well as by damage associated molecular patterns (DAMPs). The proforms require processing for secretion and biologic activity.[216] Four different mammalian inflammasomes have been characterized to date, and they are defined by the LRR–containing Nod-like receptor (NLR) proteins that they contain: the NLRP1/NALP1b inflammasome; the NLRC4/IPAF inflammasome; the NLRP3/NALP3 inflammasome; and the AIM2 containing inflammasome.[217]

Structurally, three domains characterize the NLRs: a C-terminal LRR domain, an intermediate nucleotide-binding and oligomerization domain (NOD, also called NACHT domain), and an N-terminal pyrin (PYD) domain. NLRP1 has an additional C-terminal caspase activation and recruitment domain (CARD). Although the mechanisms have not been described in detail, activation is thought to be triggered by recognition of a stimulus via the LRR domain. This results in recruitment and oligomerization of the adaptor protein ASC via interactions with the PYD domain. ASC also contains a C-terminal CARD domain that subsequently recruits pro-caspase 1, resulting in its autoproteolytic activation.

Small-molecule approaches targeting the inflammasomes have been challenging from a screening perspective because of the tendency of these proteins to form aggregates. Despite this challenge, significant inroads are being made to identify inhibitors of

these targets to fully understand their role in autoimmune diseases. For example, using a recombinant GST-His-Thrombin-NLRP1 protein a diverse set of ATP-competitive inhibitors with micromolar potencies have been identified for NLRP1.[218] In a major breakthrough, two groups recently reported the identification of MCC950 and β-hydroxybutyrate as novel inhibitors of the NLRP3 inflammasome.[219,220] These inhibitors should help clarify the role of NLRP1 and NLRP3 in autoimmunity and inflammation and lead to therapeutics that halt progression of inflammatory diseases.[221]

5.12.6.3 Autophagy

Autophagy is a cellular process that involves sequestration and degradation of intracellular pathogens and damaged organelles in order to maintain cytoplasmic homeostasis.[222] Autophagy plays a multifaceted role in both innate and adaptive immunity leading to protection against disease.[223] In innate immunity, autophagy is involved in regulation of cytokine production, inflammatory transcriptional regulation, oxidative stress and inflammasome activation, in addition to its role in pathogen degradation. In adaptive immunity, autophagy plays an important role in T cell maturation and polarization, T and B lymphocyte homeostasis, and antigen processing and presentation. Given the central role of autophagy in these important immune processes, any dysregulation will lead to the development of autoimmune disorders and inflammation. In addition, genetic association studies have confirmed the link between defects in autophagy and autoimmune diseases, particularly Crohn's[224] and SLE.[225] MTOR inhibitors such as rapamycin have been shown to be protective against intestinal inflammation[226] and SLE[227] both in mouse models and patients.[228] However, the precise role of small-molecule inhibitors in the clinical modulation of autophagy in various diseases is still unclear. For example, compounds such as rapamycin do not directly regulate the autophagy process but rather are involved in activating or inhibiting a number of other cellular processes, raising the question of specificity. Identification of key targets that regulate autophagy will help in the development of selective modulators with an appropriate signaling bias and improved therapeutic index. In addition, because of polymorphism associated with some autoimmune disorders such as Crohn's and SLE (vide supra), identification of predictive biomarkers may be necessary for future autophagy therapy.

5.12.6.4 Microbiome

The microbiome has been defined as the microorganisms that populate the human gut, skin, and other organs of the body. These microorganisms share a commensal, symbiotic, or pathogenic relationship with the human body. Because of the proximity of the microbiome to epithelial and mucosal cells, they affect and regulate the immune, cardiovascular and nervous systems. For example, factors that change the balance and composition of gut bacteria can lead to dysbiosis and changes in immune function. For autoimmune disorders, microbiome research has focused particularly on the treatment of RA, MS, and IBD (UC and Crohn's).[229] Although fecal microbial transplant and microbiota based therapies have garnered significant attention for the treatment of these disorders, research is shifting slowly to the identification of small-molecule drugs as a treatment therapy for autoimmune diseases.[230] One reason for this is the increased understanding of the processes that lead to these diseases by comparing healthy and diseased microbiota from mucosal biopsies and using bioinformatics technology to identify targets that are modulated by the microbiome. For example, SGM-1019 an orally delivered small molecule from Second Genome, Inc. recently completed double-blind, placebo-controlled, single ascending oral dose trial in healthy subjects.[231] Although the target of SGM-1019 has not been disclosed, Second Genome plans to evaluate the compound in Crohn's disease. Enterome is developing EP-8018 for the treatment of Crohn's disease.[232] This compound is supposed to limit binding of a type of bacteria called adherent-invasive *E. coli* to the CEACAM6 receptor leading to the suppression of TNF production. Another area of research gaining momentum is to identify natural product drug leads from small molecules produced by the human microbiome. A success story in this area is FDA approval in 2012 of linaclotide (a homolog of the enterotoxin peptides produced by *E. coli* that cause diarrhea) for the treatment of irritable bowel syndrome. Human microbiome research is expected to take off in the coming years to answer fundamental questions related to the understanding of mechanisms causing disease and identifying targets leading to transformative therapeutics.[233]

5.12.6.5 Targeting the Complement System for Inflammatory Disorders

The complement system was classically defined as being a component of the innate immune system that complements or helps antibodies and phagocytic cells to clear pathogens. However, it has been established that the complement system plays an important role in bridging the innate and adaptive immune responses. Since three different pathways activate the complement cascade (the classical complement pathway, the alternative complement pathway, and the lectin pathway), a number of targets are available for therapeutic intervention. Activation of the complement system results in the release of proinflammatory anaphylatoxins such as C3a and C5a resulting in tissue damage and contributing to the pathogenesis of several autoimmune diseases such as SLE, SS, SSc, dermatomyositis (DM), MS, and RA.[234] Biologic as well as small-molecule strategies have been employed for interfering with the complement system cascade in experimental models of autoimmune disease. For example, PMX53, a small-molecule C5a mimetic that binds to the C5a receptor, showed preclinical efficacy in a rat antigen-induced arthritis model.[235] However, the compound did not reduce synovial inflammation when administered to RA patients in clinical trials.[236] It has been reported that pharmacological inhibition of C5a with PMX205, a small-molecule C5a receptor antagonist, prevented dextran sulfate sodium induced colitis in mice[237] suggesting antagonists of C5a have the potential for the treatment of IBD. Compared to

C5a, therapeutic modulation of C3a with small-molecule antagonists has been challenging, although tool molecules continue to be identified to dissect the role of C3a and its receptor in autoimmune disorders.[238a,b] To the best of our knowledge, no small-molecule complement antagonists are in clinical trials for the treatment of SLE, SS, SSc, DM, MS, or RA. CCX168 (ChemoCentryx), a small-molecule C5a antagonist is being evaluated in Phase 2 clinical trials for antineutrophil cytoplasmic Ab-associated renal vasculitis (NCT01363388).[239] The increasing interest in academia and industry to identify highly specific complement inhibitors will help analyze complement modulation pathways and identify therapies for treating autoimmune disorders in the coming years.[240a,b]

5.12.6.6 Regulatory T Cell Therapy

T regulatory cells (Tregs) are $CD4^+CD25^+$ T cells that express the transcription factor Foxp3 and play a critical role in regulating immune suppression and preventing autoimmune diseases by suppressing self-reactive T cells. In addition to $CD4^+$ T cells, Tregs suppress the proliferation, activation, and cytokine production of $CD8^+$T cells, B cells, antigen-presenting cells, and natural killer cells.[241] Foxp3 knockout mice develop thyroiditis, diabetes, dermatitis, and IBD[242] and a similar phenotype is seen in humans with mutations of the Foxp3 gene.[243] Therefore, there is significant interest in augmenting Treg population to treat human autoimmune disorders. The concept is to isolate Tregs and then adoptively transfer them to patients with autoimmune disorders to potentially suppress the ongoing autoimmune response. Although conceptually simple, the challenge has been to isolate highly pure Tregs using the best cell surface marker, since a small percentage of contaminated T cells potentially can exacerbate the autoimmune disease.[244] However, there is a certain level of plasticity associated with Tregs since cells that are originally $Foxp3^+$ can convert to nonregulatory $Foxp3^-$ pathogenic effector cells.[245,246] This would suggest that the stability of Tregs still would be questioned even if a pure population can be generated and adoptively transferred. Despite these challenges, a strategy to rapidly generate Tregs and adoptively transfer them to suppress immune responses in a mouse model of arthritis has been demonstrated.[247] More importantly, significant success using Treg therapy was achieved in acute graft versus host disease (aGVHD) in a clinical setting.[248,249] The pioneering work using Tregs for treating patients with aGVHD disease has laid the foundation to study Treg therapy in other autoimmune diseases.[250] Although targets for Treg modulation have yet to be validated with small-molecule intervention, one can anticipate significant activity in this area during the next decade.

5.12.7 Conclusion

In addition to the emerging paradigms described above, other innovative approaches are being employed to modulate immunological functions for the treatment of inflammatory and autoimmune disorders. For example, as described above, irreversible BTK inhibitors have opened up a potential new paradigm for the modulation of immunologic pathways relevant to diseases such as RA. Additionally, the application of DNA-encoded chemical library technologies has resulted in the identification of macrocyclic[251] and small-molecule inhibitors[252] of IL-17A with potential utility for the treatment of psoriasis and other autoimmune disorders. Modulation of antibody recognition using antibody-recruiting small molecules is an avenue of research that is being pursued for manipulating immune function.[253]

From an immune tolerance perspective, modulation strategies targeting Tregs (*vide supra*) will continue to remain the focus of attention for therapy in many autoimmune disorders.[254,255] In addition, combination therapies targeting two or more pathways are being considered in order to potentiate efficacy in autoimmune disease.[256] This will be particularly true for diseases that have proven refractory to treatment with single agents, such as lupus nephritis.

Moving forward, precision medicine paradigms will be used increasingly for the treatment of autoimmune disorders. Because of the heterogeneity of inflammatory disorders, identifying patient populations that respond to targeted therapies based on their underlying disease pathogenesis is important (stratified medicine), since patients are likely to receive greater clinical benefit.[257] Bioinformatics, "omics" technologies, and biomarkers are being used as stratification tools for predicting patient subsets that will respond to a particular treatment. For example, transcriptomics (mRNA), metabolomics (metabolites), proteomics (proteins), and genomic technologies, in combination with bioinformatics, are being employed to derive a clear relationship between abnormalities in the immune system and disease pathology. Biomarkers on the other hand are helpful in identifying patients who likely would benefit from treatment (predictive biomarkers) or where patients have an increased risk of disease progression (prognostic biomarker). This will lead to greater clinical benefit for patients with the underlying disease pathophysiology and spare patients from exposure to drugs that carry some risk for whom they would have little benefit.[258] In addition to benefiting the patient, economic benefits over the long term will be quite significant if stratified medicine approaches are considered for the treatment of inflammatory and autoimmune diseases.

It is clear from the discussion throughout this article that the past decade has witnessed our ability to bring forward breakthrough oral therapies for the treatment of autoimmune disorders. Because of the increased understanding of the immune system and the introduction of revolutionary new technologies during the past decade, small-molecule therapeutics have the potential to treat diseases of high unmet medical need and significantly change the clinical landscape of autoimmune disorders during the next decade.

Acknowledgments

The authors would like to sincerely thank Leacy Prior and Tisha Zawisky for literature searches, Dr. Julie Carman for critical review of the article, and Dr. William J. Pitts, Dr. Amy Hart, Dr. Stephen T. Wrobleski, and Dr. Joseph A. Tino for their contributions.

See also: 5.13. Small Molecule Immunosuppressants in Inflammatory Disease. 8.17. Are Two Better Than One in Rheumatoid Arthritis? Development of Dual p38α MAPK/PDE-4 Inhibitors for Treatment of TNFα-Driven Diseases.

References

1. van Vollenhoven, R. F.; Fleischmann, R.; Cohen, S.; Lee, E. B.; Meijide, J. A. G.; Wagner, S.; Forejtova, S.; Zwillich, S. H.; Gruben, D.; Koncz, T.; Wallenstein, G. V.; Krishnaswami, S.; Bradley, J. D.; Wilkinson, B. Tofacitinib or Adalimumab Versus Placebo in Rheumatoid Arthritis. *N. Engl. J. Med.* **2012,** *367,* 508–519.
2. Kirchner, G. I.; Meier-Wiedenbach, I.; Manns, M. P. Clinical Pharmacokinetics of Everolimus. *Clin. Pharmacokinet.* **2004,** *43,* 83–95.
3. Gurk-Turner, C.; Manitpisitkul, W.; Cooper, M. A Comprehensive Review of Everolimus Clinical Reports: A New Mammalian Target of Rapamycin Inhibitor. *Transplantation* **2012,** *15,* 659–668.
4. Whitbeck, M. G.; Applegate, R. J. Second Generation Drug-Eluting Stents: A Review of the Everolimus-Eluting Platform. *Clin. Med. Insights Cardiol.* **2013,** *7,* 115–126.
5. Farkouh, M. E.; Kirshner, H.; Harrington, R. A.; Ruland, S.; Verheugt, F. W. A.; Schnitzer, T. J.; Burmester, G. R.; Mysler, E.; Hochberg, M. C.; Doherty, M.; Ehrsam, E.; Gitton, X.; Krammer, G.; Mellein, B.; Gimona, A.; Matchaba, A.; Hawkey, C. J.; Chesebro, J. H. Comparison of Lumiracoxib With Naproxen and Ibuprofen in the Therapeutic Arthritis Research and Gastrointestinal Event Trial (TARGET), Cardiovascular Outcomes: Randomised Controlled Trial. *Lancet* **2004,** *364,* 675–684.
6. http://www.drugdevelopment-technology.com/projects/prexige/ (accessed 12 January 2016).
7. http://www.businesswire.com/news/home/20040227005158/en/ALTANA-Pharma-Receives-Approval-Market-Alvesco-R—Ciclesonide (accessed 13 January 2016).
8. Chopra, D.; Bhandari, B.; Wardhan, N. Ciclesonide—A Novel Corticosteroid for the Management of Asthma. *Curr. Clin. Pharmacol.* **2012,** *7,* 73–77.
9. Jones, B. M.; Neville, M. W. Nepafenac: An Ophthalmic Nonsteroidal Antiinflammatory Drug for Pain After Cataract Surgery. *Ann. Pharmacother.* **2013,** *47,* 892–896.
10. Gaynes, B. I.; Onyekwuluje, A. Topical Ophthalmic NSAIDs: A Discussion With Focus on Nepafenac Ophthalmic Suspension. *Clin. Ophthalmol.* **2008,** *2,* 355–368.
11. Li, J.; Mao, H.; Liang, Y.; Lu, Y.; Chen, S.; Yang, N.; Shi, G. Efficacy and Safety of Iguratimod for the Treatment of Rheumatoid Arthritis. *Clin. Dev. Immunol.* **2013**. Article ID 310628.
12. Luo, Q.; Sun, Y.; Liu, W.; Qian, C.; Jin, B.; Tao, F.; Gu, Y.; Wu, X.; Shen, Y.; Xu, Q. A Novel Disease-Modifying Antirheumatic Drug, Iguratimod, Ameliorates Murine Arthritis by Blocking IL-17 Signaling, Distinct From Methotrexate and Leflunomide. *J. Immunol.* **2013,** *191,* 4969–4978.
13. Yan, Q.; Du, F.; Huang, X.; Fu, Q.; Chen, S.; Dai, D.; Bao, C. Prevention of Immune Nephritis by the Small Molecular Weight Immunomodulator Iguratimod in MRL/lpr Mice. *PLoS One* **2014,** *9,* e108273.
14. Dunn, J.; Blight, A. Dalfampridine: A Brief Review of Its Mechanism of Action and Efficacy as a Treatment to Improve Walking in Patients With Multiple Sclerosis. *Curr. Med. Res. Opin.* **2011,** *27,* 1415–1423.
15. Goodman, A. D.; Brown, T. R.; Edwards, K. R.; Krupp, L. B.; Schapiro, R. T.; Cohen, R.; Marinucci, L. N.; Blight, A. R. A Phase 3 Trial of Extended Release Oral Dalfampridine in Multiple Sclerosis. *Ann. Neurol.* **2010,** *68,* 494–502.
16. Kappos, L.; Antel, J.; Comi, G.; Montalban, X.; O'Connor, P.; Polman, C. H.; Haas, T.; Korn, A. A.; Karlsson, G.; Radue, E. W. Oral Fingolimod (FTY720) for Relapsing Multiple Sclerosis. *N. Engl. J. Med.* **2006,** *355,* 1124–1140.
17. Mandala, S.; Hajdu, R.; Bergstorm, J.; Quackenbush, E.; Xie, J.; Milligan, J.; Thornton, R.; Shei, G.-J.; Card, D.; Keohane, C. A.; Rosenbach, M.; Hale, J.; Lynch, C. L.; Rupprecht, K.; Parsons, W.; Rosen, H. Alteration of Lymphocyte Trafficking by Sphingosine-1-phosphate Receptor Agonists. *Science* **2002,** *296,* 346–349.
18. Chun, J.; Hartung, H. Mechanism of Action of Oral Fingolimod (FTY720) in Multiple Sclerosis. *Clin. Neuropharmacol.* **2010,** *33,* 91–101.
19. Lee, C. W.; Choi, J. W.; Chun, J. Neurological S1P Signaling as an Emerging Mechanism of Action of Oral FTY720 (Fingolimod) in Multiple Sclerosis. *Arch. Pharm. Res.* **2010,** *33,* 1567–1574.
20. Garnock-Jones, K. P. Roflumilast: A Review in COPD. *Drugs* **2015,** *75,* 1645–1656.
21. Hatzelmann, A.; Morcillo, E. J.; Lungarella, G.; Adnot, S.; Sanjar, S.; Beume, R.; Schudt, C.; Tenor, H. The Preclinical Pharmacology of Roflumilast. *Pulm. Pharmacol. Ther.* **2010,** *23,* 235–256.
22. Ridolo, E.; Montagni, M.; Bonzano, L.; Incorvaia, C.; Canonica, G. W. Bilastine: New Insight Into Antihistamine Treatment. *Clin. Mol. Allergy* **2015,** *13,* 1.
23. Corcóstegui, R.; Labeaga, L.; Innerárity, A.; Berisa, A.; Orjales, A. In Vivo Pharmacological Characterisation of Bilastine, a Potent and Selective Histamine H1 Receptor Antagonist. *Drugs R. D.* **2005,** *6,* 371–384.
24. Carter, N. J. Bilastine in Allergic Rhinitis and Urticaria. *Drugs* **2012,** *72,* 1257–1269.
25. Oh, J.; O'Connor, P. W. An Update of Teriflunomide for Treatment of Multiple Sclerosis. *Ther. Clin. Risk Manag.* **2013,** *9,* 177–190.
26. Garnock-Jones, K. P. Teriflunomide: A Review of Its Use in Relapsing Multiple Sclerosis. *CNS Drugs* **2013,** *12,* 1103–1123.
27. Vyas, D.; O'Dell, K. M.; Bandy, J. L.; Boyce, E. G. Tofacitinib: The First Janus Kinase (JAK) Inhibitor for the Treatment of Rheumatoid Arthritis. *Ann. Pharmacother.* **2013,** *47,* 1524–1531.
28. Flanagan, M. E.; Blumenkopf, T. A.; Brissette, W. H.; Brown, M. F.; Casavant, J. M.; Shang-Poa, C.; Doty, J. L.; Elliott, E. A.; Fisher, M. B.; Hines, M.; Kent, C.; Kudlacz, E. M.; Lillie, B. M.; Magnuson, K. S.; McCurdy, S. P.; Munchhof, M. J.; Perry, B. D.; Sawyer, P. S.; Strelevitz, T. J.; Subramanyam, C.; Sun, J.; Whipple, D. A.; Changelian, P. S. Discovery of CP-690,550: A Potent and Selective Janus Kinase (JAK) Inhibitor for the Treatment of Autoimmune Diseases and Organ Transplant Rejection. *J. Med. Chem.* **2010,** *53,* 8468–8484.
29. Garber, K. Psoriasis: From Bed to Bench and Back. *Nat. Biotechnol.* **2011,** *29,* 467–468.
30. https://clinicaltrials.gov/ct2/results?term=CP-690%2C550+&Search=Search CP-690,550 (tofacitinib) entries on clinicaltrials.gov (accessed 12 January 2016).
31. Gold, R.; Linker, R. M.; Stangel, M. Fumaric Acid and Its Esters: An Emerging Treatment for Multiple Sclerosis With Antioxidative Mechanism of Action. *Clin. Immunol.* **2012,** *142,* 44–48.
32. Ruggieri, S.; Tortorella, C.; Gasperini, G. Pharmacology and Clinical Efficacy of Dimethyl Fumarate (BG-12) for Treatment of Relapsing–Remitting Multiple Sclerosis. *Ther. Clin. Risk Manag.* **2014,** *10,* 229–239.
33. Fox, R. J.; Miller, D. H.; Phillips, J. T.; Hutchinson, M.; Havrdova, E.; Kita, M.; Yang, M.; Raghupathi, K.; Novas, M.; Sweetser, M. T.; Viglietta, V.; Dawson, K. T. Placebo-Controlled Phase 3 Study of Oral BG-12 or Glatiramer in Multiple Sclerosis. *N. Engl. J. Med.* **2012,** *367,* 1087–1097.
34. Linker, R. A.; Lee, D.-H.; Ryan, S.; Van Dam, A. M.; Conrad, R.; Bista, P.; Zeng, W.; Hronowsky, X.; Buko, A.; Chollate, S.; Ellrichmann, G.; Brück, W.; Dawson, K.; Goelz, S.; Wiese, S.; Scannevin, R. H.; Lukashev, M.; Gold, R. Fumaric Acid Esters Exert Neuroprotective Effects in Neuroinflammation via Activation of the Nrf2 Antioxidant Pathway. *Brain* **2011,** *134,* 678–692.

35. Man, H. W.; Schafer, P.; Wong, L. M.; Patterson, R. T.; Corral, L. G.; Raymon, H.; Blease, K.; Leisten, J.; Shirley, M. A.; Tang, Y.; Babusis, D. M.; Chen, R.; Stirling, D.; Muller, G. W. Discovery of (S)-N-[2-[1-(3-Ethoxy-4-methoxyphenyl)-2-methanesulfonylethyl]-1,3-dioxo-2,3-dihydro-1H-isoindol-4-yl] acetamide (Apremilast), a Potent and Orally Active Phosphodiesterase 4 and Tumor Necrosis Factor-Alpha Inhibitor. *J. Med. Chem.* **2009,** *52,* 1522–1524.
36. Schafer, P. H.; Parton, A.; Capone, L.; Cedzik, D.; Brady, H.; Evans, J. F.; Man, H.-W.; Muller, G. W.; Stirling, D. I.; Chopra, R. Apremilast Is a Selective PDE4 Inhibitor With Regulatory Effects on Innate Immunity. *Cell Signal.* **2014,** *26,* 2016–2029.
37. Gooderham, M.; Papp, K. Selective Phosphodiesterase Inhibitors for Psoriasis: Focus on Apremilast. *BioDrugs* **2015,** *29,* 327–339.
38. https://clinicaltrials.gov/ct2/results?term=apremilast&Search=Search Apremilast entries on clinicaltrials.gov (accessed 12 January 2016).
39. Hasko, G.; Linden, J.; Cronstein, B.; Pacher, P. Adenosine Receptors: Therapeutic Aspects for Inflammatory and Immune Diseases. *Nat. Rev. Drug Discov.* **2008,** *7,* 759–770.
40. Bar-Yehuda, S.; Silverman, M.; Kerns, W.; Ochaion, A.; Cohen, A.; Fishman, P. The Anti-Inflammatory Effect of A3 Adenosine Receptor Agonists: A Novel Targeted Therapy for Rheumatoid Arthritis. *Expert Opin. Investig. Drugs* **2007,** *16,* 1601–1613.
41. Fishman, P.; Bar-Yehuda, S.; Liang, B. T.; Jacobson, K. A. Pharmacological and Therapeutic Effects of A3 Adenosine Receptor Agonists. *Drug Discov. Today* **2012,** *17,* 359–366.
42. Stoilov, R. M.; Licheva, R. N.; Mihaylova, M. K.; Reitblat, T.; Dimitrov, E. A.; Shimbova, K. M.; Bhatia, G.; Pispati, A.; Gurman-Balbir, A.; Bagarai, B. R.; Oparanov, B. A.; Fishman, S.; Harpaz, Z.; Farbstein, M.; Cohen, S.; Bristol, D.; Silverman, M. H.; Fishman, P. Therapeutic Effect of Oral CF101 in Patients With Rheumatoid Arthritis: A Randomized, Double-Blind, Placebo-Controlled Phase II Study. *Immunome Res.* **2014,** *10,* 087. http://dx.doi.org/10.4172/17457580.1000087.
43. Can-Fite press release. http://ir.canfite.com/press-releases/detail/714/can-fite-reports-top-line-results-from-phase-iiiii-trial-for-cf101-in-treatment-of-psoriasis (accessed 11 July 2015).
44. Dubreuil, P.; Letard, S.; Ciufolini, M.; Gros, L.; Humbert, M.; Casteran, N.; Borge, L.; Hajem, B.; Lermet, A.; Sippl, W.; Voisset, E.; Arock, M.; Auclair, C.; Leventhal, P. S.; Mansfield, C. D.; Moussy, A.; Hermine, O. Masitinib (AB1010), a Potent and Selective Tyrosine Kinase Inhibitor Targeting KIT. *PLoS One* **2009,** *4,* e7258.
45. Vermersch, P.; Benrabah, R.; Schmidt, N.; Zephir, H.; Clavelou, P.; Vongsouthi, C.; Dubreuil, P.; Moussy, A.; Hermine, O. Masitinib Treatment in Patients With Progressive Multiple Sclerosis: A Randomized Pilot Study. *BMC Neurol.* **2012,** *12,* 36 (see suppl. mat.).
46. ClinicalTrials.gov Identifier: NCT01433497.
47. Tebib, J.; Mariette, X.; Bourgeois, P.; Flipo, R.-M.; Gaudin, P.; Loet, X. L.; Gineste, P.; Guy, L.; Mansfield, C. D.; Moussy, A.; Dubreuil, P.; Hermine, O.; Sibilia, J. Masitinib in the Treatment of Active Rheumatoid Arthritis: Results of a Multicentre, Open-Label, Dose-Ranging, Phase 2a Study. *Arthritis Res. Ther.* **2009,** *11,* R95.
48. ClinicalTrials.gov Identifier: NCT01410695.
49. Zhang, P.; Dairaghi, D. J.; Jaen, J. C.; Powers, J. P. Recent Advances in the Discovery and Development of CCR1 Antagonists. *Annu. Rep. Med. Chem.* **2013,** *48,* 133–147.
50. Tak, P. P.; Balanescu, A.; Tseluyko, V.; Bojin, S.; Drescher, E.; Dairaghi, D.; Miao, S.; Marchesin, V.; Jaen, J.; Schall, T. J.; Bekker, P. Chemokine Receptor CCR1 Antagonist CCX354-C Treatment for Rheumatoid Arthritis: CARAT-2, a Randomised, Placebo Controlled Clinical Trial. *Ann. Rheum. Dis.* **2013,** *72,* 337–344.
51. Hirokawa, H.; Koga, Y.; Sasaki, R.; Hara, S.; Meguro, H.; Kainoh, M. Digestive Disease Week Conference, Chicago, IL, USA, 2014, Abs Mo1706.
52. ClinicalTrials.gov Identifier: NCT01345799.
53. Pizzonero, M.; Dupont, S.; Babel, M.; Beaumont, S.; Bienvenu, N.; Blanque, R.; Cherel, L.; Christophe, T.; Crescenzi, B.; De Lemos, E.; Delerive, P.; Deprez, P.; De Vos, S.; Djata, F.; Fletcher, S.; Kopiejewski, S.; L'Ebraly, C.; Lefrancois, J.-M.; Lavazais, S.; Manioc, M.; Nelles, L.; Oste, L.; Polancec, D.; Quenehen, V.; Soulas, F.; Triballeau, N.; van der Aar, E. M.; Vandeghinste, N.; Wakselman, E.; Brys, R.; Saniere, L. Discovery and Optimization of an Azetidine Chemical Series as a Free Fatty Acid Receptor 2 (FFA2) Antagonist: From Hit to Clinic. *J. Med. Chem.* **2014,** *57,* 10044–10057.
54. ClinicalTrials.gov Identifier: NCT01829321.
55. Vermeire, S.; Kojecky, V.; Knoflicek, V.; Reinisch, W.; Kaem, T. V.; Namour, F.; Beetens, J.; Vanhoutte, F. GLPG0974, an FFA2 Antagonist, in Ulcerative Colitis: Efficacy and Safety in a Multicenter Proof-of-Concept Study. Congress of the European Crohn's and Colitis Organization, Barcelona, Spain, 2015, Abs DOP030.
56. http://www.glpg.com/index.php/randd/pipeline/glpg0974-inflammatory/ (accessed 12 July 2015).
57. Buttgereit, F.; Strand, V.; Lee, E. B.; McCabe, D.; Kolluri, S.; Tammara, B.; Rojo, R.; Hey-Hadavi, J. A Phase 2, Randomized, Double-Blind Comparison of the Efficacy and Safety of PF-04171327 (1, 5, 10, 15 mg QD) Vs 5 and 10 Mg Prednisone QD or Placebo in Subjects With Rheumatoid Arthritis (RA) Over 8 Weeks Followed by a 4-Week Taper of Study Drug. 16th EULAR Annual European Congress in Rome, Italy (June 13), 2015, Abs SAT0221.
58. Boirivant, M.; Pallone, F.; Di Giacinto, C.; Fina, D.; Monteleone, I.; Marinaro, M.; Caruso, R.; Colantoni, A.; Palmieri, G.; Sanchez, M.; Strober, W.; MacDonald, T. T.; Monteleone, G. Inhibition of Smad7 With a Specific Antisense Oligonucleotide Facilitates TGF-Beta1-Mediated Suppression of Colitis. *Gastroenterology* **2006,** *131,* 1786–1798.
59. Monteleone, G.; Neurath, M. F.; Ardizzone, A.; Di Sabatino, A.; Fantini, M. C.; Castiglione, F.; Scribano, M. L.; Armuzzi, A.; Caprioli, F.; Sturniolo, G. C.; Rogai, F.; Vecchi, M.; Atreya, R.; Bossa, F.; Onali, S.; Fichera, M.; Corazza, G. R.; Biancone, L.; Savarino, V.; Pica, R.; Orlando, A.; Pallone, F. Mongersen, an Oral SMAD7 Antisense Oligonucleotide, and Crohn's Disease. *N. Engl. J. Med.* **2015,** *372,* 1104–1113.
60. Fridman, J. S.; Scherle, P. A.; Collins, R.; Burn, T. C.; Li, Y.; Li, J.; Covington, M. B.; Thomas, B.; Collier, P.; Favata, M. F.; Wen, X.; Shi, J.; McGee, R.; Haley, P. J.; Shepard, S.; Rodgers, J. D.; Yeleswaram, S.; Hollis, G.; Newton, R. C.; Metcalf, B.; Friedman, S. M.; Vaddi, K. Selective Inhibition of JAK1 and JAK2 Is Efficacious in Rodent Models of Arthritis: Preclinical Characterization of INCB028050. *J. Immunol.* **2010,** *184,* 5298–5307.
61. Dougados, M.; van der Heijde, D.; Chen, Y.-C.; Greenwald, M.; Drescher, E.; Liu, J.; Beattie, S.; de la Torre, I.; Rooney, T.; Schlichting, D.; de Bono, S.; Emery, P. Baricitinib, an Oral JAK1/JAK2 Inhibitor, in Patients With Active Rheumatoid Arthritis and an Inadequate Response to cDMARDs: Results of the Phase 3 RA-BUILD Study. 16th EULAR Annual European Congress in Rome, Italy (June 13), 2015, Abs LB0001.
62. Menter, A.; Disch, D.; Clemens, J.; Janes, J.; Papp, K.; Macias, W. A Phase 2b Trial of Baricitinib, an Oral JAK Inhibitor, in Patients With Moderate to Severe Psoriasis. 72nd American Academy of Dermatology Annual Meeting in Denver, CO (March), 2014, Abs P7941.
63. Mahajan, S.; Hogan, J. K.; Shlyakhter, D.; Oh, L.; Salituro, F. G.; Farmer, L.; Hoock, T. C. VX-509 (Decernotinib) Is a Potent and Selective Janus Kinase 3 Inhibitor That Attenuates Inflammation in Animal Models of Autoimmune Disease. *J. Pharmacol. Exp. Ther.* **2015,** *353,* 405–414.
64. van Vollenhoven, R.; Genovese, M. C.; Zhang, Y.; Kinnman, N. A Phase 2B, 24-Week Study of VX-509 (Decernotinib), an Oral Selective Janus Kinase 3 Inhibitor, in Combination With Background Methotrexate in Rheumatoid Arthritis. EULAR Annual Meeting Paris, France (June), 2014, Abs OP0151.
65. Olsson, T.; Boster, A.; Fernandez, O.; Freedman, M. S.; Pozzilli, C.; Bach, D.; Berkani, O.; Mueller, M. S.; Sidorenko, T.; Radue, E.-W.; Melanson, M. Oral Ponesimod in Relapsing–Remitting Multiple Sclerosis: A Randomised Phase II Trial. *J. Neurol. Neurosurg. Psychiatry* **2014,** *85,* 1198–1208.
66. ClinicalTrials.gov Identifier: NCT02425644.
67. ClinicalTrials.gov Identifier: NCT02461134.
68. ClinicalTrials.gov Identifier: NCT01890655.
69. EudraCT 2012–005750-27.
70. ClinicalTrials.gov Identifier: NCT02389790.
71. ClinicalTrials.gov Identifier: NCT02378688.
72. Timony, G.; Brooks, J.; Powell, R.; Dedman, H.; Scott, F.; Martinborough, E.; Boehm, M.; Rosen, H.; Peach, R. The Preclinical Safety Profile of RPC1063, A Selective and Potent Sphingosine 1-Phosphate 1 Receptor (S1P1R) Agonist. 65th AAN Annual Meeting in San Diego, CA, 2013, Abs P01.158.
73. Cohen, J.; Arnold, D. L.; Comi, G.; Bar-Or, A.; Gujrathi, S.; Hartung, J. P.; Olson, A.; Cravets, M.; Frohna, P. A.; Selmaj, K. Phase 2 Results of the RADIANCE Trial: A Randomized, Double-Blind, Placebo-Controlled Trial of Oral RPC1063 in Relapsing Multiple Sclerosis. Joint Triennial Congress of the European and Americas Committees for Treatment and Research in Multiple Sclerosis, Boston, MA, September, 2014, Abs LB1.1.
74. ClinicalTrials.gov Identifier: NCT02294058.

75. ClinicalTrials.gov Identifier: NCT01647516.
76. Receptos reports positive phase 2 results for TOUCHSTONE trial of RPC1063 in ulcerative colitis. http://ir.receptos.com/releasedetail.cfm?releaseid=878411 (accessed 11 July 2015).
77. ClinicalTrials.gov Identifier: NCT02435992.
78. Melnikova, I. Future of COX2 Inhibitors. *Nat. Rev. Drug Discov.* **2005,** *4,* 453–454.
79. Hawkey, C. J. COX-2 Chronology. *Gut* **2005,** *54,* 1509–1514.
80. Pfizer 2014 earnings statement. http://www.pfizer.com/system/files/presentation/Q4_2014_PFE_Earnings_Press_Release_alksdjindfls.pdf.
81. Rao, P. N. P.; Knaus, E. E. Evolution of Nonsteroidal Anti-Inflammatory Drugs (NSAIDs): Cyclooxygenase (COX) Inhibition and Beyond. *J. Pharm. Pharm. Sci.* **2008,** *11,* 81s–110s.
82. Gajraj, N. M. COX-2 Inhibitors Celecoxib and Parecoxib: Valuable Options for Postoperative Pain Management. *Curr. Top. Med. Chem.* **2007,** *7,* 235–249.
83. Schieven, G. L. The p38alpha Kinase Plays a Central Role in Inflammation. *Curr. Top. Med. Chem.* **2009,** *9,* 1038–1048.
84. Gupta, J.; Nebreda, A. R. Roles of p38α Mitogen-Activated Protein Kinase in Mouse Models of Inflammatory Diseases and Cancer. *FEBS J.* **2015,** *282,* 1841–1857.
85. Genovese, M. C.; Cohen, S. B.; Wofsy, D.; Weinblatt, M. E.; Firestein, G. S.; Brahn, E.; Strand, V.; Baker, D. G.; Tong, S. E. A 24-Week, Randomized, Double-Blind, Placebo-Controlled, Parallel Group Study of the Efficacy of Oral SCIO-469, a p38 Mitogen-activated Protein Kinase Inhibitor, in Patients with Active Rheumatoid Arthritis. *J. Rheumatol.* **2011,** *38,* 846–854.
86. Schreiber, S.; Feagan, B.; D'Haens, G.; Colombel, J. F.; Geboes, K.; Yurcov, M.; Isakov, V.; Golovenko, O.; Bernstein, C. N.; Ludwig, D.; Winter, T.; Meier, U.; Yong, C.; Steffgen, J. Oral p38 Mitogen-Activated Protein Kinase Inhibition With BIRB 796 for Active Crohn's Disease: A Randomized, Double-Blind, Placebo-Controlled Trial. *Clin. Gastroenterol. Hepatol.* **2006,** *4,* 325–334.
87. Genovese, M. Inhibition of p38: Has the Fat Lady Sung? *Arthritis Rheum.* **2009,** *60,* 317–320.
88. http://www.prnewswire.com/news-releases/vertex-moves-to-re-allocate-resources-from-vx-745-in-p38-map-kinase-program-to-accelerate-development-of-second-generation-drug-candidates-vx-702-and-vx-850-72104487.html (accessed 20 January 2016).
89. Sweeney, S. E. Therapy: The As-Yet Unfulfilled Promise of p38 MAPK Inhibitors. *Nat. Rev. Rheumatol.* **2009,** *5,* 475.
90. Schieven, G.; Zhang, R.; Pitt, S.; Shen, D. R.; Cao, J.; Sack, J.; Doweyko, A.; Ross-MacDonald, P. BMS-582949 Is a Dual Action p38 Kinase Inhibitor Well Suited to Avoid Resistance Mechanisms That Increase p38 Activation in Cells. ACR/ARHP Annual Scientific Meeting, Atlanta, GA, November 7–11, 2010.
91. Genovese, M. C.; Gao, L.; Yin, J.; Smith, S.; Weinblatt, M.; Smolen, J.; Wang, X.; Schieven, G.; Garcia-Meijide, J. A.; Latek, R.; Pasternak, R.; Kaul, S.; Roy, A.; Raymond, R.; Thienel, U.; Wang, J. Proof of Concept Study for a Potent Dual Action p38 Kinase Inhibitor BMS-582949 in Subjects With RA Receiving Concomitant Methotrexate. ACR/ARHP Annual Scientific Meeting, Atlanta, GA, November 7–11, 2010.
92. Norman, P. Investigational p38 Inhibitors for the Treatment of Chronic Obstructive Pulmonary Disease. *Expert Opin. Investig. Drugs* **2015,** *24,* 383–392.
93. Safety & Efficacy of BCT197A2201 in Chronic Obstructive Pulmonary Disease (COPD) Patients Presenting With an Exacerbation. https://clinicaltrials.gov/ct2/show/NCT01332097 (accessed 20 January 2016).
94. A Phase 3 Clinical Outcomes Study to Compare the Incidence of Major Adverse Cardiovascular Events in Subjects Presenting With Acute Coronary Syndrome Treated With Losmapimod Compared to Placebo (LATITUDE-TIMI 60). https://clinicaltrials.gov/ct2/show/NCT02145468 (accessed 20 January 2016).
95. https://www.gsk.com/en-gb/media/press-releases/2015/gsk-provides-update-on-latitude-timi-60-losmapimod-cardiovascular-study/ (accessed 20 January 2016).
96. Bachelerie, F.; Ben-Baruch, A.; Burkhardt, A. M.; Combadiere, C.; Farber, J. M.; Graham, G. J.; Horuk, R.; Sparre-Ulrich, A. H.; Locati, M.; Luster, A. D.; Mantovani, A.; Matsushima, K.; Murphy, P. M.; Nibbs, R.; Nomiyama, H.; Power, C. A.; Proudfoot, A. E.; Rosenkilde, M. M.; Rot, A.; Sozzani, S.; Thelen, M.; Yoshie, O.; Zlotnik, A. International Union of Basic and Clinical Pharmacology. LXXXIX. Update on the Extended Family of Chemokine Receptors and Introducing a New Nomenclature for Atypical Chemokine Receptors. *Pharmacol. Rev.* **2014,** *66,* 1–79.
97. Pease, J.; Horuk, R. Chemokine Receptor Antagonists. *J. Med. Chem.* **2012,** *55,* 9363–9392.
98. Solari, R.; Pease, J.; Begg, M. Chemokine Receptors as Therapeutic Targets: Why Aren't There More Drugs? *Eur. J. Pharmacol.* **2015,** *746,* 363–367.
99. Schall, T. J.; Proudfoot, A. E. Overcoming Hurdles in Developing Successful Drugs Targeting Chemokine Receptors. *Nat. Rev. Immunol.* **2011,** *11,* 355–363.
100. Pease, J. E.; Horuk, R. Chemokine Receptor Antagonists: Part 2. *Expert Opin. Ther. Pat.* **2009,** *19,* 199–221.
101. Brenner, D.; Blaser, H.; Mak, T. W. Regulation of Tumour Necrosis Factor Signalling: Live or Let Die. *Nat. Rev. Immunol.* **2015,** *15,* 362–374.
102. Moss, M. L.; Sklair-Tavron, L.; Nudelman, R. Drug Insight: Tumor Necrosis Factor-Converting Enzyme as a Pharmaceutical Target for Rheumatoid Arthritis. *Nat. Clin. Pract. Rheumatol.* **2008,** *4,* 300–309.
103. Renkiewicz, R.; Qiu, L.; Lesch, C.; Sun, X.; Devalaraja, R.; Cody, T.; Kaldjian, E.; Welgus, H.; Baragi, V. Broad-Spectrum Matrix Metalloproteinase Inhibitor Marimastat-Induced Musculoskeletal Side Effects in Rats. *Arthritis Rheum.* **2003,** *48,* 1742–1749.
104. Murumkar, P. R.; Giridhar, R.; Yadav, M. R. Novel Methods and Strategies in the Discovery of TACE Inhibitors. *Expert Opin. Drug Discov.* **2013,** *8,* 157–181.
105. Lehman-McKeeman, L. D. Mechanism-Based Hepatotoxicity of Tumor Necrosis Factor Alpha (TNFα)-Converting Enzyme Inhibitors. *Toxicol. Sci* **2007,** *96,* 378 (abstract 1827).
106. Thabet, M. M.; Huizinga, T. W. Drug Evaluation: Apratastat, a Novel TACE/MMP Inhibitor for Rheumatoid Arthritis. *Curr. Opin. Investig. Drugs* **2006,** *7,* 1014–1019.
107. Sharma, M.; Mohapatra, J.; Acharya, A.; Deshpande, S. S.; Chatterjee, A.; Jain, M. R. Blockade of Tumor Necrosis Factor-α Converting Enzyme (TACE) Enhances IL-1β and IFN-γ via Caspase-1 Activation: A Probable Cause for Loss of Efficacy of TACE Inhibitors in Humans? *Eur. J. Pharmacol.* **2013,** *701,* 106–113.
108. Li, S.; Strelow, A.; Fontana, E. J.; Wesche, H. IRAK-4: A Novel Member of the IRAK Family With the Properties of an IRAK-Kinase. *Proc. Natl. Acad. Sci.* **2002,** *99,* 5567–5572.
109. Warner, N.; Nunez, G. MyD88: A Critical Adaptor Protein in Innate Immunity Signal Transduction. *J. Immunol.* **2013,** *190,* 3–4.
110. Wang, Z.; Wesche, H.; Srevens, T.; Walker, N.; Yeh, W.-C. IRAK-4 Inhibitors for Inflammation. *Curr. Top. Med. Chem.* **2009,** *9,* 724–737.
111. Isnardi, I.; Ng, Y.-S.; Srdanovic, I.; Motaghedi, R.; Rudchenko, S.; Bernuth, H. V.; Zhang, S.-Y.; Puel, A.; Jouanguy, E.; Picard, C.; Garty, B.-Z.; Camcioglu, Y.; Doffinger, R.; Kumararatne, D.; Davies, G.; Gallin, J. I.; Haraguchi, S.; Day, N. K.; Casanova, J.-L.; Meffre, E. IRAK-4/MyD88-Dependent Pathways Are Essential for the Removal of Developing Autoreactive B Cells in Humans. *Immunity* **2008,** *29,* 746–757.
112. Arend, W. P. The Balance Between IL-1 and IL-1Ra in Disease. *Cytokine Growth Factor Rev.* **2002,** *13,* 323–340.
113. Boraschi, D.; Dinarello, C. A. IL-18 in Autoimmunity: Review. *Eur. Cytokine Netw.* **2006,** *17,* 224–252.
114. Gosu, V.; Choi, S. Structural Dynamic Analysis of apo and ATP-Bound IRAK4 Kinase. *Sci. Rep.* **2014,** *18,* 5748.
115. Ku, C.-L.; von Bernuth, H.; Picard, C.; Zhang, S.-Y.; Chang, H.-H.; Yang, K.; Chrabieh, M.; Issekutz, A. C.; Cunningham, C. K.; Gallin, J.; Holland, S. M.; Roifman, C.; Ehl, S.; Smart, J.; Tang, M.; Barrat, F. J.; Levy, O.; McDonald, D.; Day-Good, N. K.; Miller, R.; Takada, H.; Hara, T.; Al-Hajjar, S.; Al-Ghonaium, A.; Speert, D.; Sanlaville, D.; Li, X.; Geissmann, F.; Vivier, E.; Maródi, L.; Garty, B.-Z.; Chapel, H.; Rodriguez-Gallego, C.; Bossuyt, X.; Abel, L.; Puel, A.; Cassanova, J.-L. Selective Predisposition to Bacterial Infections in IRAK-4-Deficient Children: IRAK-4-Dependent TLRs Are Otherwise Redundant in Protective Immunity. *J. Exp. Med.* **2007,** *204,* 2407–2422.
116. Hynes, J., Jr.; Nair, S. K. Advances in the Discovery of Small-Molecule IRAK4 Inhibitors. *Annu. Rep. Med. Chem.* **2014,** *49,* 117–130.
117. Zhang, D.; Lin, J.; Han, J. Receptor-Interacting Protein (RIP) Kinase Family. *Cell. Mol. Immunol.* **2010,** *7,* 243–249.
118. (a) Ofengeim, D.; Yuan, J. Regulation of RIP1 Kinase Signalling at the Crossroads of Inflammation and Cell Death. *Nat. Rev. Mol. Cell Biol.* **2013,** *14,* 727–736; (b) Jun, J. C.; Cominelli, F.; Abbott, D. E. RIP2 Activity in Inflammatory Disease and Implications for Novel Therapeutics. *J. Leukoc. Biol.* **2013,** *94,* 927–932; (c) Linkermann, A.; Green, D. G. Necroptosis. *N. Engl. J. Med.* **2014,** *370,* 455–465.
119. Cho, Y.; Challa, S.; Moquin, D.; Genga, R.; Ray, T. D.; Guildford, M.; Chan, F. K.-M. Phosphorylation-Driven Assembly of the RIP1-RIP3 Complex Regulates Programmed Necrosis and Virus-Induced Inflammation. *Cell* **2009,** *137,* 1112–1123.

120. (a) Welz, P.-S.; Wullaert, A.; Vlantis, K.; Kondylis, V.; Fernández-Majada, V.; Ermolaeva, M.; Kirsch, P.; Sterner-Kock, A.; van Loo, G.; Pasparakis, M. FADD Prevents RIP3-Mediated Epithelial Cell Necrosis and Chronic Intestinal Inflammation. *Nature* **2011,** *477,* 330–335; (b) Günther, C.; Martini, E.; Wittkopf, N.; Amann, K.; Weigmann, B.; Neumann, H.; Waldner, M. J.; Hedrick, S. M.; Tenzer, S.; Neurath, M. F.; Becker, C. Caspase-8 Regulates TNF-α-Induced Epithelial Necroptosis and Terminal Ileitis. *Nature* **2011,** *477,* 335–340.
121. Kelliher, M. A.; Grimm, S.; Ishida, Y.; Kuo, F.; Stanger, B. Z.; Leder, P. The Death Domain Kinase RIP Mediates the TNF-Induced NF-KappaB Signal. *Immunity* **1998,** *8,* 297–303.
122. (a) Newton, K.; Dugger, D. L.; Wickliffe, K. E.; Kapoor, N.; de Almagro, M. C.; Vucic, D.; Komuves, L.; Ferrando, R. E.; French, D. M.; Webster, J.; Roose-Girma, M.; Warming, S.; Dixit, V. M. Activity of Protein Kinase RIPK3 Determines Whether Cells Die by Necroptosis or Apoptosis. *Science* **2014,** *343,* 1357–1360; (b) Berger, S. B.; Kasparcova, V.; Hoffman, S.; Swift, B.; Dare, L.; Schaeffer, M.; Capriotti, C.; Cook, M.; Finger, J.; Hughes-Earle, A.; Harris, P. A.; Kaiser, W. J.; Mocarski, E. S.; Bertin, J.; Gough, P. J. Cutting Edge: RIP1 Kinase Activity Is Dispensable for Normal Development but Is a Key Regulator of Inflammation in SHARPIN-Deficient Mice. *J. Immunol.* **2014,** *192,* 5476–5480; (c) Polykratis, A.; Hermance, N.; Zelic, M.; Roderick, J.; Kim, C.; Van, T.-M.; Lee, T. H.; Chan, F. K. M.; Pasparakis, M.; Kelliher, M. A. RIPK1 Kinase Inactive Mice are Viable and Protected From TNF-Induced Necroptosis In Vivo. *J. Immunol.* **2014,** *193,* 1539–1543.
123. Newton, K.; Sun, X.; Dixit, V. M. Kinase RIP3 Is Dispensable for Normal NF-kBs, Signaling by the B-cell and T-Cell Receptors, Tumor Necrosis Factor Receptor 1, and Toll-Like Receptors 2 and 4. *Mol. Cell. Biol.* **2004,** *24,* 1464–1469.
124. (a) Kaiser, W. J.; Sridharan, H.; Huang, C.; Mandal, P.; Upton, J. W.; Gough, P. J.; Sehon, C. A.; Marquis, R. W.; Bertin, J.; Mocarski, E. S. Toll-Like Receptor 3-Mediated Necrosis via TRIF, RIP3, and MLKL. *J. Biol. Chem.* **2013,** *288,* 31268–31279; (b) Li, J.-X.; Feng, J.-M.; Wang, Y.; Li, X.-H.; Chen, X.-X.; Su, Y.; Shen, Y.-Y.; Chen, Y.; Xiong, B.; Yang, C.-H.; Ding, J.; Miao, Z.-H. The B-RafV600E Inhibitor Dabrafenib Selectively Inhibits RIP3 and Alleviates Acetaminophen-Induced Liver Injury. *Cell Death Dis.* **2014,** *5,* e1278.
125. Xie, T.; Peng, W.; Yan, C.; Wu, J.; Gong, X.; Shi, Y. Structural Insights Into RIP3-Mediated Necroptotic Signaling. *Cell Rep.* **2013,** *5,* 70–78.
126. (a) Harris, P. A.; Bandyopadhyay, D.; Berger, S. B.; Campobasso, N.; Capriotti, C. A.; Cox, J. A.; Dare, L.; Finger, J. N.; Hoffman, S. J.; Kahler, K. M.; Lehr, R.; Lich, J. D.; Nagilla, R.; Nolte, R. T.; Ouellette, M. T.; Pao, C. S.; Schaeffer, M. C.; Smallwood, A.; Sun, H. H.; Swift, B. A.; Totoritis, R. D.; Ward, P.; Marquis, R. W.; Bertin, J.; Gough, P. J. Discovery of Small Molecule RIP1 Kinase Inhibitors for the Treatment of Pathologies Associated With Necroptosis. *ACS Med. Chem. Lett.* **2013,** *4,* 1238–1243; (b) Najjar, M.; Suebsuwong, C.; Ray, S. S.; Thapa, R. J.; Maki, J. L.; Nogusa, S.; Shah, S.; Saleh, D.; Gough, P. J.; Bertin, J.; Yuan, J.; Balachandran, S.; Cuny, G. D.; Degterev, A. Structure Guided Design of Potent and Selective Ponatinib-Based Hybrid Inhibitors for RIPK1. *Cell Rep.* **2015,** *10,* 1850–1860; (c) Wu, Z.; Li, Y.; Yuan, J.; Yuan, C. A Novel Necroptosis Inhibitor—Necrostatin-21 and its SAR Study. *Bioorg. Med. Chem. Lett.* **2013,** *23,* 4903–4906; (d) Zheng, W.; Degterev, A.; Hsu, E.; Yuan, J.; Yuan, C. Structure-Activity Relationship Study of a Novel Necroptosis Inhibitor, Necrostatin-7. *Bioorg. Med. Chem. Lett.* **2008,** *18,* 4932–4935; (e) Wang, K.; Li, J.; Degterev, A.; Hsu, E.; Yuan, J.; Yuan, C. Structure-Activity Relationship Analysis of a Novel Necroptosis Inhibitor, Necrostatin-5. *Bioorg. Med. Chem. Lett.* **2007,** *17,* 1455–1465; (f) Teng, X.; Degterev, A.; Jagtap, P.; Xing, X.; Choi, S.; Denu, R.; Yuan, J.; Cuny, G. D. Structure–Activity Relationship Study of Novel Necroptosis Inhibitors. *Bioorg. Med. Chem. Lett.* **2005,** *15,* 5039–5044; (g) Degterev, A.; Huang, Z.; Boyce, M.; Li, Y.; Jagtap, P.; Mizushima, N.; Cuny, G. D.; Mitchison, T. J.; Moskowitz, M. A.; Yuan, J. Chemical Inhibitor of Nonapoptotic Cell Death With Therapeutic Potential for Ischemic Brain Injury. *Nat. Chem. Biol.* **2005,** *1,* 112–119.
127. Xie, T.; Peng, W.; Liu, Y.; Yan, C.; Maki, J.; Degterev, A.; Yuan, J.; Shi, Y. Structural Basis of RIP1 Inhibition by Necrostatins. *Structure* **2013,** *21,* 493–499.
128. Tigno-Aranjuez, J. T.; Benderitter, P.; Rombouts, F.; Deroose, F.; Bai, X.; Mattioli, B.; Cominelli, F.; Pizarro, T. T.; Hoflack, J.; Abbott, D. W. In Vivo Inhibition of RIPK2 Kinase Alleviates Inflammatory Disease. *J. Biol. Chem.* **2014,** *289,* 29561–29664.
129. (a) Chin, A. I.; Dempsey, P. W.; Bruhn, K.; Miller, J. F.; Xu, Y.; Cheng, G. Involvement of Receptor-Interacting Protein 2 in Innate and Adaptive Immune Responses. *Nature* **2002,** *416,* 190–194; (b) Magalhaes, J. G.; Lee, J.; Geddes, K.; Rubino, S.; Philpott, D. J.; Girardin, S. E. Essential Role of Rip2 in the Modulation of Innate and Adaptive Immunity Triggered by Nod1 and Nod2 Ligands. *Eur. J. Immunol.* **2011,** *41,* 1445.
130. Strober, W.; Asano, N.; Fuss, I.; Kitani, A.; Watanabe, T. Cellular and Molecular Mechanisms Underlying NOD2 Risk-Associated Polymorphisms in Crohn's Disease. *Immunol. Rev.* **2014,** *260,* 249–260.
131. For example, see, Blom, P.; Françoise, M.; Hoflack, J.; Jozef, M. C.; Benderitter, P.; André, R. "Macrocyclic RIP2 Kinase Inhibitors" WO 14140299 A1, Sep 18, 2014.
132. Canning, P.; Bullock, A. PDB ID: 4C8B.
133. Silke, J.; Rickard, J. A.; Gerlic, M. The Diverse Role of RIP Kinases in Necroptosis and Inflammation. *Nat. Immunol.* **2015,** *16,* 689–697.
134. Krieg, A. M.; Vollmer, J. Toll-Like Receptors 7, 8, and 9: Linking Innate Immunity to Autoimmunity. *Immunol. Rev.* **2007,** *220,* 251–269.
135. Nickerson, K. M.; Christensen, S. R.; Shupe, J.; Kashgarian, M.; Kim, D.; Elkon, K.; Shlomchik, M. J. TLR9 Regulates TLR7- and MyD88-Dependent Autoantibody Production and Disease in a Murine Model of Lupus. *J. Immunol.* **2010,** *184,* 1840–1848.
136. Christensen, S. R.; Nickerson, K. M.; Kashgarian, M.; Flavell, R. A.; Schlomchik, M. J. Toll-Like Receptor 7 and TLR9 Dictate Autoantibody Specificity and Have Opposing Inflammatory and Regulatory Roles in a Murine Model of Lupus. *Immunity* **2006,** *25,* 417–428.
137. Demaria, O.; Pagni, P. P.; Traub, S.; de Gassart, A.; Branzk, N.; Murphy, A. J.; Valenzuela, D. M.; Yancopoulos, G. D.; Flavell, R. A.; Alexopoulou, L. TLR8 Deficiency Leads to Autoimmunity in Mice. *J. Clin. Invest.* **2010,** *120,* 3651–3662.
138. Akira, S.; Takeda, K. Toll-Like Receptor Signaling. *Nat. Rev. Immunol.* **2004,** *4,* 499–511.
139. Kawai, T.; Akira, S. The Role of Pattern-Recognition Receptors in Innate Immunity: Update on Toll-Like Receptors. *Nat. Immunol.* **2010,** *11,* 373–384.
140. Botos, I.; Segal, D. M.; Davies, D. R. The Structural Biology of Toll-Like Receptors. *Structure* **2011,** *19,* 447–459.
141. Tanji, H.; Ohto, U.; Shibata, T.; Miyake, K.; Shimizu, T. Structural Reorganization of the Toll-Like Receptor 8 Dimer Induced by Agonistic Ligands. *Science* **2013,** *339,* 1426–1429.
142. Ohto, U.; Shibata, T.; Tanji, H.; Ishida, H.; Krayukhina, E.; Uchiyama, S.; Miyake, K.; Shimizu, T. Structural Basis of CpG and Inhibitory DNA Recognition by Toll-Like Receptor 9. *Nature* **2015,** *520,* 702–705.
143. Kokatla, H. P.; Sil, D.; Tanji, H.; Ohto, U.; Malladi, S. S.; Fox, L. M.; Shimizu, T.; David, S. A. Structure-Based Design of Novel Human Toll-Like Receptor 8 Agonists. *Chem. Med. Chem.* **2014,** *9,* 719–723.
144. Idera Pharmaceticals press release. http://ir.iderapharma.com/phoenix.zhtml?c=208904&p=irol-newsArticle&ID=1913216&highlight (accessed 20 May 2015).
145. Dynavax press release. http://investors.dynavax.com/releasedetail.cfm?releaseid=885172 (accessed 23 May 2015).
146. WO1308837, WO13161871, WO13180066 (to Kowa); US 20150105370, WO 2013181579 (to Eisai); WO 2008152471, WO 2005007672 (to Coley Pharmaceuticals). WO12167046, WO12167053, WO13052550 (to Janus).
147. Ivanov, I. I.; McKenzie, B. S.; Zhou, L.; Tadokoro, C. E.; Lepelley, A.; Lafaille, J. J.; Cua, D. J.; Littman, D. R. The Orphan Nuclear Receptor RORgammat Directs the Differentiation Program of Proinflammatory IL-17+ T Helper Cells. *Cell* **2006,** *126,* 1121–1133.
148. Bedoya, S. K.; Lam, B.; Lau, K.; Larkin, J., III Th17 Cells in Immunity and Autoimmunity. *Clin. Dev. Immunol.* **2013**. Article ID 986789.
149. (a) Pantelyushin, S.; Haak, S.; Ingold, B.; Kulig, P.; Heppner, F. L.; Navarini, A. A.; Becher, B. Rorγt^{+} Innate Lymphocytes and γδ T Cells Initiate Psoriasiform Plaque Formation in Mice. *J. Clin. Invest.* **2012,** *122,* 2252; (b) Leppkes, M.; Becker, C.; Ivanov, I. I.; Hirth, S.; Wirtz, S.; Neufert, C.; Pouly, S.; Murphy, A. J.; Valenzuela, D. M.; Yancopoulos, G. D.; Becher, B.; Littman, D. R.; Neurath, M. F. RORgamma-Expressing Th17 Cells Induce Murine Chronic Intestinal Inflammation via Redundant Effects of IL-17A and IL-17F. *Gastroenterology* **2009,** *136,* 257–267; (c) Buonocore, S.; Ahern, P. P.; Uhlig, H. H.; Ivanov, I. I.; Littman, D. R.; Maloy, K. J.; Powrie, F. Innate Lymphoid Cells Drive Interleukin-23-Dependent Innate Intestinal Pathology. *Nature* **2010,** *464,* 1371–1375.
150. Dhar, T. G. M.; Zhao, Q.; Markby, D. W. Targeting the Nuclear Hormone Receptor RORγt for the Treatment of Autoimmune and Inflammatory Disorders. *Annu. Rep. Med. Chem.* **2013,** *48,* 169–182.
151. Fujita-Sato, S.; Ito, S.; Isobe, T.; Ohyama, T.; Wakabayashi, K.; Morishita, K.; Ando, O.; Isono, F. Structural Basis of Digoxin That Antagonizes RORγt Receptor Activity and Suppresses Th17 Cell Differentiation and Interleukin (IL)-17 Production. *J. Biol. Chem.* **2011,** *286,* 31409–31417.

152. Fauber, B. P.; Magnuson, S. Modulators of the Nuclear Receptor Retinoic Acid Receptor-Related Orphan Receptor-γ (RORγ or RORc). *J. Med. Chem.* **2014,** *57,* 5871–5892.
153. Japan Tobacco Inc. https://www.jt.com/investors/results/S_information/pharmaceuticals/pdf/P.L.20140130_E.pdf (accessed 23 May 2015).
154. Vitae Pharmaceuticals. http://ir.vitaepharma.com/phoenix.zhtml?c=219654&p=RssLanding&cat=news&id=2063137 (accessed 2 July 2015).
155. O'Shea, J. J.; Plenge, R. JAK and STAT Signaling Molecules in Immunoregulation and Immune-Mediated Disease. *Immunity* **2012,** *36,* 542–550.
156. Strobl, B.; Stoiber, D.; Sexl, V.; Mueller, M. Tyrosine Kinase 2 (TYK2) in Cytokine Signalling and Host Immunity. *Front. Biosci.* **2011,** *16,* 3214–3232.
157. Shaw, M. H.; Boyartchuk, V.; Wong, S.; Karaghiosoff, M.; Ragimbeau, J.; Pellegrini, S.; Muller, M.; Dietrich, W. F.; Yap, G. S. A Natural Mutation in the Tyk2 Pseudokinase Domain Underlies Altered Susceptibility of B10.Q/J Mice to Infection and Autoimmunity. *Proc. Natl. Acad. Sci.* **2003,** *100,* 11594–11599.
158. Minegishi, Y.; Saito, M.; Morio, T.; Watanabe, K.; Agematsu, K.; Tsuchiya, S.; Takada, H.; Hara, T.; Kawamura, N.; Ariga, T.; Kaneko, H.; Kondo, N.; Tsuge, I.; Yachie, A.; Sakiyama, Y.; Iwata, T.; Bessho, F.; Ohishi, T.; Joh, K.; Imai, K.; Kogawa, K.; Shinohara, M.; Fujieda, M.; Wakiguchi, H.; Pasic, S.; Abinum, M.; Ochs, H. D.; Renner, E. D.; Jansson, A.; Belohradsky, B. H.; Metin, A.; Shimzu, N.; Mizutani, S.; Miyawaki, T.; Nonoyama, S.; Karasuyama, M. Human Tyrosine Kinase 2 Deficiency Reveals Its Requisite Roles in Multiple Cytokine Signals Involved in Innate and Acquired Immunity. *Immunity* **2006,** *25,* 745–755.
159. Chung, Y.; Dong, C. Don't Leave Home Without It: The IL-23 Visa to TH-17 Cells. *Nat. Immunol.* **2009,** *10,* 236–238.
160. Trinchieri, G. Interleukin-12: A Proinflammatory Cytokine With Immunoregulatory Functions That Bridge Innate Resistance and Antigen-Specific Adaptive Immunity. *Annu. Rev. Immunol.* **1995,** *13,* 251–276.
161. Clarke, A. W.; Poulton, L.; Wai, H. Y.; Walker, S. A.; Victor, S. D.; Domagala, T.; Mraovic, D.; Butt, D.; Shewmaker, N.; Hennings, P.; Doylce, A. G. A Novel Class of Anti-IL-12p40 Antibodies. *mAbs* **2010,** *2,* 539–549.
162. Benson, J. M.; Sachs, C. W.; Treacy, G.; Zhou, H.; Pendley, C.; Brodmerkel, C. M.; Shankar, G.; Mascelli, M. A. Therapeutic Targeting of the IL-12/23 Pathways: Generation and Characterization of Ustekinumab. *Nat. Biotechnol.* **2011,** *29,* 615–624.
163. Jordan, N.; Lutalo, P. M. K.; D'Cruz, D. P. Progress With the Use of Monoclonal Antibodies for the Treatment of Systemic Lupus Erythematosus. *Immunotherapy* **2015,** *7,* 255–270.
164. Sohn, S. J.; Barrett, K.; Van Abbema, A.; Chang, C.; Kohli, P. B.; Kanda, H.; Smith, J.; Lai, Y.; Zhou, A.; Zhang, B.; Yang, W.; Williams, K.; Macleod, C.; Hurley, C. A.; Kulagowski, J. J.; Lewin-Koh, N.; Dengler, H. S.; Johnson, A. R.; Ghilardi, N.; Zak, M.; Liang, J.; Blair, W. S.; Magnuson, S.; Wu, L. C. A Restricted Role for TYK2 Catalytic Activity in Human Cytokine Responses Revealed by Novel TYK2-Selective Inhibitors. *J. Immunol.* **2013,** *191,* 2205–2216.
165. Tokarski, J. S.; Zupa-Fernandez, A.; Tredup, J. A.; Pike, K.; Chang, C. Y.; Xie, D.; Cheng, L.; Pedicord, D.; Muckelbauer, J.; Johnson, S. R.; Wu, S.; Edavettal, S. C.; Hong, Y.; Witmer, M. R.; Elkin, L. L.; Blat, Y.; Pitts, W. J.; Weinstein, D. S.; Burke, J. R. Tyrosine Kinase 2-Mediated Signal Transduction in T Lymphocytes Is Blocked by Pharmacological Stabilization of Its Pseudokinase Domain. *J. Biol. Chem.* **2015,** *290,* 11061–11074.
166. Newton, A. C. Protein Kinase C: Structural and Spatial Regulation by Phosphorylation, Cofactors, and Macromolecular Interactions. *Chem. Rev.* **2001,** *101,* 2353–2364.
167. Dustin, M. L. What Counts in the Immunological Synapse? *Mol. Cell* **2014,** *54,* 255–262.
168. Wachowicz, K.; Baier, G. Protein Kinase Cθ: The Pleiotropic T-Cell Signalling Intermediate. *Biochem. Soc. Trans.* **2014,** *42,* 1512–1518.
169. Zanin-Zhorov, A.; Ding, Y.; Kumari, S.; Attur, M.; Hippen, K. L.; Brown, M.; Blazar, B. R.; Abrahamson, S. B.; Lafaille, J. J.; Dustin, M. L. Protein Kinase C-Theta Mediates Negative Feedback on Regulatory T Cell Function. *Science* **2010,** *328,* 372–376.
170. Healy, A. M.; Izmailova, E.; Fitzgerals, R. W.; Hattersly, M.; Silva, M.; Siebert, E.; Terkelsen, J.; Picarella, D.; Pickard, M. D.; LeClair, B.; Chandra, S.; Jaffee, B. PKC-θ-Deficient Mice Are Protected From Th1-Dependent Antigen-Induced Arthritis. *J. Immunol.* **2006,** *177,* 1886–1893.
171. Anderson, K.; Fitzgerald, M.; Dupont, M.; Wang, T.; Paz, N.; Dorsch, M.; Healym, A.; Xu, Y.; Ocain, T.; Schopf, L. The Kinase GLK Controls Autoimmunity and NF-kB Signaling by Activating the Kinase PKC-θ in T Cells. *Autoimmunity* **2006,** *39,* 469–478.
172. Salek-Ardakani, S.; So, T.; Halteman, B. S.; Altman, A.; Croft, M. Protein Kinase C-θ Controls Th1 Cells in Experimental Autoimmune Encephalomyelitis. *J. Immunol.* **2005,** *175,* 7635–7641.
173. Wachowicz, K.; Hermann-Kleiter, N.; Meisel, M.; Siegmund, K.; Thuille, N.; Baier, G. Protein Kinase C-θ Regulates the Phenotype of Murine CD4+ Th17 Cells. *PLoS One* **2014,** *9,* e96401.
174. George, D. M.; Breinlinger, E. C.; Friedman, M.; Zhang, Y.; Wang, J.; Argiriadi, M.; Bansal-Pakala, P.; Barth, M.; Duignan, D. B.; Honore, P.; Lang, Q.-Y.; Mittelstadt, S.; Potin, D.; Rundell, L.; Edmunds, J. J. Discovery of Selective and Orally Bioavailable Protein Kinase C-θ (PKCθ) Inhibitors From a Fragment Hit. *J. Med. Chem.* **2015,** *58,* 222–236.
175. Russ, G. R.; Tedesco-Silva, H.; Kuypers, D. R.; Cohney, S.; Langer, R. M.; Witzke, O.; Eris, J.; Sommerer, C.; von Zur-Muhlen, B.; Woodle, E. S.; Gill, J.; Ng, J.; Klupp, J.; Chodoff, L.; Budde, K. Efficacy of Sotrastaurin Plus Tacrolimus After De Novo Kidney Transplantation: Randomized, Phase II Trial Results. *Am. J. Transplant.* **2013,** *13,* 1746–1756.
176. Curnock, A.; Bolton, C.; Chiu, P.; Doyle, E.; Fraysse, D.; Heese, M.; Jones, J.; Weber, P.; Jimenez, J.-M. Selective Protein Kinase Cθ (PKCθ) Inhibitors for the Treatment of Autoimmune Diseases. *Biochem. Soc. Trans.* **2014,** *42,* 1524–1528.
177. (a) Mohamed, A.; Yu, L.; Bäckesjö, C.; Vargas, L.; Faryal, R.; Aints, A.; Christensson, B.; Berglöf, A.; Vihinen, M.; Nore, B. F.; Smith, C. I. E. Bruton's Tyrosine Kinase (Btk): Function, Regulation, and Transformation With Special Emphasis on the PH Domain. *Immunol. Rev.* **2009,** *228,* 58–73; (b) Mohamed, A. J.; Nore, B. F.; Christensson, B.; Smith, C. I. E. Signalling of Bruton's Tyrosine Kinase Btk. *Scand. J. Immunol.* **1999,** *49,* 113–118.
178. (a) Jongstra-Bilen, J.; Puig Cano, A.; Hasija, M.; Xiao, H.; Smith, C. I.; Cybulsky, M. I. Dual Functions of Bruton's Tyrosine Kinase and Tec Kinase During Fcγ Receptor-Induced Signaling and Phagocytosis. *J. Immunol.* **2008,** *181,* 288–298; (b) Kuehn, H. S.; Radinger, M.; Brown, J. M.; Ali, K.; Vanhaesebroeck, B.; Beaven, M. A.; Metcalfe, D. D.; Gilfillan, A. M. Btk-Dependent Rac Activation and Actin Rearrangement Following FcεRI Aggregation Promotes Enhanced Chemotactic Responses of Mast Cells. *J. Cell Sci.* **2010,** *123,* 2576–2585; (c) Tsukada, S.; Rawlings, D. J.; Witte, O. N. Role of Bruton's Tyrosine Kinase in Immunodeficiency. *Curr. Opin. Immunol.* **1994,** *6,* 623–630.
179. Lee, S. H.; Kim, T.; Jeong, D.; Kim, N.; Choi, Y. The Tec Family Tyrosine Kinase Btk Regulates RANKL-Induced Osteoclast Maturation. *J. Biol. Chem.* **2008,** *283,* 11526–11534.
180. Mease, P. J. B Cell-Targeted Therapy in Autoimmune Disease: Rationale, Mechanisms, and Clinical Application. *J. Rheumatol.* **2008,** *35,* 1245–1255.
181. Goldstein, M. D.; Debenedette, M. A.; Hollenbaugh, D.; Watts, T. H. Induction of Costimulatory Molecules B7-1 and B7-2 in Murine B Cells. The CBA/N Mouse Reveals a Role for Bruton's Tyrosine Kinase in CD40-Mediated B7 Induction. *Mol. Immunol.* **1996,** *33,* 541–552.
182. (a) Jansson, L.; Holmdahl, R. Genes on the X Chromosome Affect Development of Collagen-Induced Arthritis in Mice. *Clin. Exp. Immunol.* **1993,** *94,* 459–465; (b) Steinberg, B. J.; Smathers, P. A.; Frederiksen, K.; Steinberg, A. D. Ability of the xid Gene to Prevent Autoimmunity in (NZB X NZW)F1 Mice During the Course of Their Natural History, After Polyclonal Stimulation, or Following Immunization With DNA. *J. Clin. Invest.* **1982,** *70,* 587–597.
183. (a) Xu, D.; Kim, Y. K.; Postelnek, J.; Vu, M. D.; Hu, D.; Liao, C.; Bradshaw, M.; Hsu, J.; Zhang, J.; Pashine, A.; Srinivassan, D.; Woods, J.; Levin, A.; O'Mahony, A.; Owens, T. D.; Lou, Y.; Hill, R. J.; Narula, S.; DeMartino, J.; Fine, J. S. RN486, a Selective Bruton's Tyrosine Kinase Inhibitor, Abrogates Immune Hypersensitivity Responses and Arthritis in Rodents. *J. Pharmacol. Exp. Ther.* **2012,** *341,* 90–103; (b) Rankin, A. L.; Seth, N.; Keegan, S.; Andreyeva, T.; Cook, T. A.; Edmonds, J.; Mathialagan, N.; Benson, M. J.; Syed, J.; Zhan, Y.; Benoit, S. E.; Miyashiro, J. S.; Wood, N.; Mohan, S.; Peeva, E.; Ramaiah, S. K.; Messing, D.; Homer, B. L.; Dunussi-Joannopoulos, K.; Nickerson-Nutter, C. L.; Schnute, M. E.; Douhan, J., III Selective Inhibition of BTK Prevents Murine Lupus and Antibody-Mediated Glomerulonephritis. *J. Immunol.* **2013,** *193,* 4540–4550.
184. (a) Puck, J. M. Molecular and Genetic Basis of X-Linked Immunodeficiency Disorders. *J. Clin. Immunol.* **1994,** *14,* 81–89; (b) Hendriks, R. W.; Bredius, R. G. M.; Pike-Overzet, K.; Staal, F. J. T. Biology and Novel Treatment Options for XLA, the Most Common Monogenetic Immunodeficiency in Man. *Expert Opin. Ther. Targets* **2011,** *15,* 1003–1021.

185. (a) Cohen, M. S.; Zhang, C.; Shokat, K. M.; Taunton, J. Structural Bioinformatics-Based Design of Selective, Irreversible Kinase Inhibitors. *Science* **2005,** *308,* 1318–1321; (b) Leproult, E.; Barluenga, S.; Moras, D.; Wurtz, J. M.; Winssinger, N. Cysteine Mapping in Conformationally Distinct Kinase Nucleotide Binding Sites: Application to the Design of Selective Covalent Inhibitors. *J. Med. Chem.* **2011,** *54,* 1347–1355.
186. Honigberg, L. A.; Smith, A. M.; Sirisawad, M.; Verner, E.; Loury, D.; Chang, B.; Li, S.; Pan, Z.; Thamm, D. H.; Miller, R. A.; Buggy, J. J. The Bruton Tyrosine Kinase Inhibitor PCI-32765 Blocks B-Cell Activation and Is Efficacious in Models of Autoimmune Disease and B-Cell Malignancy. *Proc. Natl. Acad. Sci.* **2010,** *107,* 13075–13080.
187. (a) Burger, J. A. Bruton's Tyrosine Kinase (BTK) Inhibitors in Clinical Trials. *Curr. Hematol. Malig. Rep.* **2014,** *9,* 44–49; (b) Whang, J. A.; Chang, B. Y. Bruton's Tyrosine Kinase Inhibitors for the Treatment of Rheumatoid Arthritis. *Drug Disc. Today* **2014,** *19,* 1200–1204.
188. Lederman, H. M.; Winkelstein, J. A. X-Linked Agammaglobulinemia and Gastric Adenocarcinoma. An Analysis of 96 Patients. *Medicine* **1985,** *64,* 145–156.
189. Pharmacyclics Inc. Imbruvica® prescribing information. 2015. http://www.imbruvica.com/docs/librariesprovider3/default-document library/prescribing_information.pdf?sfvrsn=2 (accessed 27 June 2015).
190. (a) Bradshaw, J. M.; McFarland, J. M.; Paavilainen, V. O.; Bisconte, A.; Tam, D.; Phan, V. T.; Romanov, S.; Finkle, D.; Shu, J.; Patel, V.; Ton, T.; Li, X.; Loughhead, D. G.; Nunn, P. A.; Karr, D. E.; Gerritsen, M. E.; Funk, J. O.; Owens, T. D.; Verner, E.; Brameld, K. A.; Hill, R. J.; Goldstein, D. M.; Taunton, J. Prolonged and Tunable Residence Time Using Reversible Covalent Kinase Inhibitors. *Nat. Chem. Biol.* **2015,** *11,* 525–531; (b) Phase 1 clinical trial results for PRN1008. http://www.principiabio.com/news/061515/ (accessed 21 June 2015).
191. Evans, E. K.; Tester, R.; Aslanian, S.; Karp, R.; Sheets, M.; Labenski, M. T.; Witowski, S. R.; Lounsbury, H.; Chaturvedi, P.; Mazdiyasni, H.; Zhu, Z.; Nacht, M.; Freed, M. I.; Petter, R. C.; Dubrovskiy, A.; Singh, J.; Westlin, W. F. Inhibition of Btk With CC-292 Provides Early Pharmacodynamic Assessment of Activity in Mice and Humans. *J. Pharmacol. Exp. Ther.* **2013,** *346,* 219–228.
192. Gray, C. M.; Remouchamps, C.; McCorkell, K. A.; Solt, L. A.; Dehardin, E.; Orange, J. S.; May, M. J. Non-Canonical NF-kB Signaling Is Limited by Classical IKK Activity and Dysregulated in NEMO-ID. *Sci. Signal.* **2014,** *7.* ra13/1-ra13/11.
193. Brightbill, H. D.; Jackman, J. K.; Suto, E.; Kennedy, H.; Jones, C., III; Chalasani, S.; Lin, Z.; Tam, L.; Roose-Girma, M.; Balazs, M.; Austin, C. D.; Lee, W. P.; Wu, L. C. Conditional Deletion of NF-kB-Inducing Kinase (NIK) in Adult Mice Disrupts Mature B Cell Survival and Activation. *J. Immunol.* **2015,** *195,* 953–964.
194. Jin, W.; Zhou, X.-F.; Yu, J.; Chen, X.; Sun, S.-C. Regulation of Th17 Cell Differentiation and EAE Induction by MAP3K NIK. *Blood* **2009,** *113,* 6603–6610.
195. Jin, J.; Hu, H.; Li, H.; Yu, J.; Xiao, Y.; Brittain, G. C.; Zou, Q.; Cheng, X.; Mallette, F. A.; Watowich, S. S.; Sun, S.-C. Noncanonical NF-kB Pathway Controls the Production of Type I Interferons in Antiviral Innate Immunity. *Immunity* **2014,** *40,* 342–354.
196. Willmann, K. L.; Klaver, S.; Dogu, F.; Santos-Valente, E.; Garncarz, W.; Bilic, I.; Mace, E.; Salzer, E.; Conde, C.; Sic, H.; Majek, P.; Banerjee, P. P.; Vladimer, G. I.; Haskologu, S.; Bolkent, M. G.; Kupesiz, A.; Condino-Neto, A.; Colinge, J.; Superti-Furga, G.; Pickl, W. F.; van Zelm, M. C.; Eibel, H.; Orange, J. S.; Ikinciogullari, A.; Boztug, K. Biallelic Loss-of-Function Mutation in NIK Causes a Primary Immunodeficiency With Multifaceted Aberrant Lymphoid Immunity. *Nat. Commun.* **2014,** *5,* 5360. http://dx.doi.org/10.1038/ncomms6360.
197. NIK PDB ID = 4DN5, 4GC3, 4G3F,4G3G, 4G3D, 4G3E,4IDT,4IDV.
198. de Leon-Boenig, G.; Bowman, K. K.; Geng, J. A.; Crawford, T.; Everett, C.; Franke, Y.; Oh, A.; Stanley, M.; Staben, S. T.; Starovasnik, M. A.; Wallweber, H. J. A.; Wu, J.; Wu, L. C.; Johnson, A. R.; Hymowitz, S. G. The Crystal Structure of the Catalytic Domain of the NF-kB Inducing Kinase Reveals a Narrow but Flexible Active Site. *Structure* **2012,** *20,* 1704–1714.
199. For example see: (a) Chen, G.; Cushing, T.D.; Fisher, B.; He, X.; Li, K.; Li, Z.; McGee, L.R.; Pattaropong, V.; Faulder, P.; Seganish, J.L.; Shin, Y. WO 200915801.(b) Castanedo, G.; Feng, J.; Montalbetti, C.; Staben, S. WO2013120980.(c) Hynd, G.; Tisselli, P.; Clark, D.E.; Kulagowski, J.J.; Macleaod, C.; Mann, S.E.; Panchal, T.A.; Price, S.C.; Montana, J.G. WO2015044267.
200. Li, K.; McGee, L. R.; Fisher, B.; Sudom, A.; Liu, J.; Rubenstein, S. M.; Anwer, M. K.; Cushing, T. D.; Shin, Y.; Ayres, M.; Lee, F.; Eksterowicz, J.; Faulder, P.; Waszkowycz, B.; Plotnikova, O.; Farrylley, E.; Xiao, S.-H.; Chen, G.; Wang, Z. Inhibiting NF-kB-Inducing Kinase (NIK): Discovery, Structure-Based Design, Synthesis, Structure-Activity Relationship, and Co-Crystal Structures. *Bioorg. Med. Chem. Lett.* **2013,** *23,* 1238–1244.
201. Lewis, H. D.; Liddle, J.; Coote, J. E.; Atkinson, S. J.; Barker, M. D.; Bax, B. D.; Bicker, K. L.; Bingham, R. P.; Campbell, M.; Chen, Y. H.; Chung, C.-W.; Craggs, P. D.; Davis, R. P.; Eberhard, D.; Joberty, G.; Lind, K. E.; Locke, K.; Maller, C.; Martinod, K.; Patten, C.; Polyakova, O.; Rise, C. E.; Rudiger, M.; Sheppard, R. J.; Slade, D. J.; Thomas, P.; Thorpe, J.; Yao, G.; Drewes, G.; Wagner, D. D.; Thompson, P. R.; Prinjha, R. K.; Wilson, D. M. Inhibition of PAD4 Activity Is Sufficient to Disrupt Mouse and Human NET Formation. *Nat. Chem. Biol.* **2015,** *11,* 189–191.
202. R-Tech Ueno: Announcement on Completion of the Phase I Single-Dose Clinical Trial for the Novel VAP-1 Inhibitor RTU-1096. http://www.businesswire.com/news/home/20150524005057/en/R-Tech-Ueno-Announcement-Completion-Phase-Single-Dose-Clinical#.VZRBhGDbKEg (accessed 4 July 2015).
203. Xu, L.; Li, Y.; Sun, H.; Zhen, X.; Qiao, C.; Tian, S.; Hou, T. Current Developments of Macrophage Migration Inhibitory Factor (MIF) Inhibitors. *Drug Discov. Today* **2013,** *18,* 592–600.
204. Zhang, Z.; Zhang, R. Epigenetics in Autoimmune Diseases: Pathogenesis and Prospects for Therapy. *Autoimmun. Rev.* **2015,** *14,* 854–863.
205. Chan, M. W.; Chang, C. B.; Tung, C. H.; Sun, J.; Suen, J. L.; Wu, S. F. Low-Dose 5-Aza-2′-deoxycytidine Pretreatment Inhibits Experimental Autoimmune Encephalomyelitis by Induction of Regulatory T Cells. *Mol. Med.* **2014,** *20,* 248–256.
206. Dees, C.; Schlottmann, I.; Funke, R.; Distler, A.; Palumbo-Zerr, K.; Zerr, P.; Lin, N. Y.; Beyer, C.; Distler, O.; Schett, G.; Distler, J. H. The Wnt Antagonists DKK1 and SFRP1 Are Downregulated by Promoter Hypermethylation in Systemic Sclerosis. *Ann. Rheum. Dis.* **2014,** *73,* 1232–1239.
207. Hu, N.; Qiu, X.; Luo, Y.; Yuan, J.; Li, Y.; Lei, W.; Zhang, G.; Zhou, Y.; Su, Y.; Lu, Q. Abnormal Histone Modification Patterns in Lupus CD4+ T Cells. *J. Rheumatol.* **2008,** *35,* 804–810.
208. Wang, Y.; Yang, Y.; Luo, Y.; Yin, Y.; Wang, Q.; Li, Y.; Kanekura, T.; Wang, J.; Liang, G.; Zhao, M.; Lu, Q.; Xiao, R. Aberrant Histone Modification in Peripheral Blood B Cells From Patients With Systemic Sclerosis. *Clin. Immunol.* **2013,** *149,* 46–54.
209. Vojinovic, J.; Damjanov, N.; D'Urzo, C.; Furlan, A.; Susic, G.; Pasic, S.; Iagaru, N.; Stefan, M.; Dinarello, C. A. Safety and Efficacy of an Oral Histone Deacetylase Inhibitor in Systemic-Onset Juvenile Idiopathic Arthritis. *Arthritis Rheum.* **2011,** *63,* 1452–1458.
210. (a) Regna, N. L.; Reilly, C. M. Isoform-Selective HDAC Inhibition in Autoimmune Disease. *J. Clin. Cell Immunol.* **2014,** *5,* 1–8; (b) Falkenberg, K. J.; Johnstone, R. W. Histone Deacetylases and Their Inhibitors in Cancer, Neurological Diseases and Immune Disorders. *Nat. Rev. Drug Discov.* **2014,** *13,* 673–691.
211. Nicodeme, E.; Jeffrey, K. L.; Schaefer, U.; Beinke, S.; Dewell, S.; Chung, C. W.; Chandwani, R.; Marazzi, I.; Wilson, P.; Coste, H.; White, J.; Kirilovsky, J.; Rice, C. M.; Lora, J. M.; Prinjha, R. K.; Lee, K.; Tarakhovsky, A. Suppression of Inflammation by a Synthetic Histone Mimic. *Nature* **2010,** *468,* 1119–1123.
212. Mele, D. A.; Salmeron, A.; Ghosh, S.; Huang, H.-R.; Bryant, B. M.; Lora, J. M. BET Bromodomain Inhibition Suppresses TH17-Mediated Pathology. *J. Exp. Med.* **2013,** *210,* 2181–2190.
213. Bandukwala, H. S.; Gagnon, J.; Togher, S.; Greenbaum, J. A.; Lamperti, E. D.; Parr, N. J.; Molesworth, A. M.; Smithers, N.; Lee, K.; Witherington, J.; Tough, D. F.; Prinjha, R. K.; Peters, B.; Rao, A. Selective Inhibition of CD4+ T-Cell Cytokine Production and Autoimmunity by BET Protein and c-Myc Inhibitors. *Proc. Natl. Acad. Sci. U.S.A.* **2012,** *109,* 14532–14537.
214. Laurens, K.; Lee, K.; Tough, D.F.; Wilson, D.M. WO2012055880.
215. Gumireddy, K.; Young, D. D.; Xiong, X.; Hogenesch, J. B.; Huang, Q.; Deiters, A. Small-Molecule Inhibitors of Microrna miR-21 Function. *Angew. Chem. Int. Ed.* **2008,** *47,* 7482–7484.
216. Shaw, P. J.; McDermott, M. F.; Kanneganti, T.-D. Inflammasomes and Autoimmunity. *Trends Mol. Med.* **2011,** *17,* 57–64.
217. Davis, B. K.; Wen, H.; Ting, J. P. The Inflammasome NLRs in Immunity, Inflammation, and Associated Diseases. *Annu. Rev. Immunol.* **2011,** *29,* 707–735.

218. Harris, P. A.; Duraiswami, C.; Fisher, D. T.; Fornwald, J.; Hoffman, S. J.; Hofmann, G.; Jiamg, M.; Lehr, R.; McCormick, P. M.; Nickels, L.; Schwartz, B.; Wu, Z.; Zhang, G.; Marquis, R. W.; Bertin, J.; Gough, P. J. High Throughput Screening Identifies ATP-Competitive Inhibitors of the NLRP1 Inflammasome. *Bioorg. Med. Chem. Lett.* **2015,** *25,* 2739–2743.
219. Coll, R. C.; Robertson, A. A. B.; Chae, J. J.; Higgins, S. C.; Planillo, R. M.; Inserra, M. C.; Vetter, I.; Dungan, L. S.; Monks, B. G.; Stutz, A.; Croker, D. E.; Butler, M. S.; Haneklaus, M.; Sutton, C. E.; Nunez, G.; Latz, E.; Kastner, D. L.; Mills, K. H. G.; Masters, S. L.; Schroder, K.; Cooper, M. A.; O'Neill, L. A. J. A Small-Molecule Inhibitor of the NLRP3 Inflammasome for the Treatment of Inflammatory Diseases. *Nat. Med.* **2015,** *21,* 248–255.
220. Youm, Y.-H.; Nguyen, K. Y.; Grant, R. W.; Goldberg, E. L.; Bodogai, M.; Kim, D.; D'Agostino, D.; Planavsky, N.; Lupfer, C.; Kanneganti, T. D.; Kang, S.; Horvath, T. L.; Fahmy, T. M.; Crawford, P. A.; Biragyn, A.; Alnemri, E.; Dixit, V. D. The Ketone Metabolite β-Hydroxybutyrate Blocks NLRP3 Inflammasome-Mediated Inflammatory Disease. *Nat. Med.* **2015,** *21,* 263–269.
221. Guo, H.; Callaway, J. B.; Ting, J. P. Inflammasomes: Mechanism of Action, Role in Disease, and Therapeutics. *Nat. Med.* **2015,** *21,* 677–687.
222. Cheng, Y.; Ren, X.; Hait, W. N.; Yang, J.-M. Therapeutic Targeting of Autophagy in Disease: Biology and Pharmacology. *Pharmacol. Rev.* **2013,** *65,* 1162–1197.
223. Jones, S. A.; Mills, K. H. G.; Harris, J. Autophagy and Inflammatory Diseases. *Immunol. Cell Biol.* **2013,** *91,* 250–258.
224. Brinar, M.; Vermeire, S.; Cleynen, I.; Lemmens, B.; Sagaert, X.; Henckaerts, L.; Assche, G. V.; Geboes, K.; Rutgeerts, P.; Hertogh, G. D. Genetic Variants in Autophagy-Related Genes and Granuloma Formation in a Cohort of Surgically Treated Crohn's Disease Patients. *J. Crohns Colitis* **2012,** *6,* 43–50.
225. Pierdominici, M.; Vomero, M.; Barbati, C.; Colasanti, T.; Maselli, A.; Vacirca, D.; Giovannetti, A.; Malorni, W.; Ortona, E. Role of Autophagy in Immunity and Autoimmunity, With a Special Focus on Systemic Lupus Erythematosus. *FASEB J.* **2012,** *26,* 1400–1412.
226. Massey, D. C.; Bredin, F. Use of Sirolimus (Rapamycin) to Treat Refractory Crohn's Disease. *Gut* **2008,** *57,* 1294–1296.
227. Lui, S. L.; Tsang, R.; Chan, K. W.; Zhang, F.; Tam, S.; Yung, S.; Chan, T. M. Rapamycin Attenuates the Severity of Established Nephritis in Lupus-Prone NZB/WF1 Mice. *Nephrol. Dial. Transplant.* **2008,** *23,* 2768–2776.
228. Rapamycin is currently in Phase II trials for the treatment of SLE. https://clinicaltrials.gov/ct2/results?term=NCT00779194 (accessed 13 June 2015).
229. Barin, J. G.; Tobias, L. D.; Peterson, D. A. The Microbiome and Autoimmune Disease: Report From a Noel R. Rose Colloquium. *Clin. Immunol.* **2015,** *159,* 183–188.
230. Garber, K. Drugging the Gut Microbiome. *Nat. Biotechnol.* **2015,** *33,* 228–231.
231. http://www.secondgenome.com/2015/01/second-genome-advances-lead-microbiome-drug-development-program-in-phase-i-clinical-trial-as-a-treatment-for-inflammatory-bowel-disease/ (accessed 14 June 2015).
232. http://www.clinica.co.uk/home/supplements/Clinica-Medtech-Ventures-Enterome-355942?autnID=/contentstore/clinica/escenic/355942.xml (accessed 14 June 2015).
233. Waldor, M. K.; Tyson, G.; Borenstein, E.; Ochman, H.; Moeller, A.; Finlay, B. B.; Komg, H. H.; Gordon, J. I.; Nelson, K. E.; Dabbagh, K.; Smith, H. Where Next for Microbiome Research. *PLoS Biol.* **2015,** *13,* e1002050.
234. Chen, M.; Daha, M. R.; Kallenberg, C. G. The Complement System in Systemic Autoimmune Disease. *J. Autoimmun.* **2010,** *34,* J276–J286.
235. Williams, A. S.; Mizuno, M.; Richards, P. J.; Holt, D. S.; Morgan, B. P. Deletion of the Gene Encoding CD59a in Mice Increases Disease Severity in a Murine Model of Rheumatoid Arthritis. *Arthritis Rheum.* **2004,** *50,* 3035–3044.
236. Vergunst, C. E.; Gerlag, D. M.; Dinat, H.; Schulz, L.; Vinkenoog, M.; Smeets, T. J. M.; Sanders, M. E.; Reedquist, K. A.; Tak, P. P. Blocking the Receptor for C5a in Patients With Rheumatoid Arthritis Does Not Reduce Synovial Inflammation. *Rheumatology* **2007,** *4,* 1773–1778.
237. Jain, U.; Woodruff, T. M.; Stadnyk, A. W. The C5a Receptor Antagonist PMX205 Ameliorates Experimentally Induced Colitis Associated With Increased IL-4 and IL-10. *Br. J. Pharmacol.* **2013,** *168,* 488–501.
238. (a) Mathieu, M.-C.; Sawyer, N.; Greig, G. M.; Hamel, M.; Kargman, S.; Ducharme, Y.; Lau, C. K.; Friesen, R. W.; O'Neill, G. P.; Gervais, F. G.; Therien, A. G. The C3a Receptor Antagonist SB 290157 Has Agonist Activity. *Immunol. Lett.* **2005,** *100,* 139–145; (b) Reid, R. C.; Yau, M. K.; Singh, R.; Hamidon, J. K.; Lim, J.; Stoermer, M. J.; Fairlie, D. P. Potent Heterocyclic Ligands for Human Complement C3a Receptor. *J. Med. Chem.* **2014,** *57,* 8459–8470.
239. A Study to Evaluate the Safety and Efficacy of CCX168 in Subjects With ANCA-Associated Vasculitis. https://clinicaltrials.gov/ct2/show/NCT01363388?term=NCT01363388&rank=1 (accessed 14 June 2015).
240. (a) Ricklin, D.; Lambris, J. D. Complement in Immune and Inflammatory Disorders: Therapeutic Interventions. *J. Immunol.* **2013,** *190,* 3839–3847; (b) Ballanti, E.; Perricone, C.; Greco, E.; Ballanti, M.; Muzio, G. D.; Chimenti, M. S.; Perricone, R. Complement and Autoimmunity. *Immunol. Res.* **2013,** *56,* 477–491.
241. Sakaguchi, S.; Yamaguchi, T.; Nomura, T.; Ono, M. Regulatory T Cells and Immune Tolerance. *Cell* **2008,** *133,* 775–787.
242. Hori, S.; Nomura, T.; Sakaguchi, S. Control of Regulatory T Cell Development by the Transcription Factor Foxp3. *Science* **2003,** *299,* 1057–1061.
243. Michels, A. W.; Gottlieb, P. A. Autoimmune Polyglandular Syndromes. *Nat. Rev. Endocrinol.* **2010,** *6,* 270–277.
244. Rosenblum, M. D.; Gratz, I. K.; Paw, J. S.; Abbas, A. K. Treating Human Autoimmunity: Current Practice and Future Prospects. *Sci. Transl. Med.* **2012,** *4,* 125sr1.
245. Zhou, X.; Bailey-Bucktrout, S.; Jeker, L. T.; Penaranda, C.; Martínez-Llordella, M.; Ashby, M.; Nakayama, M.; Rosenthal, W.; Bluestone, J. A. Foxp3 Instability Leads to the Generation of Pathogenic Memory T Cells In Vivo. *Nat. Immunol.* **2009,** *10,* 1000–1007.
246. Voo, K. S.; Wang, Y. H.; Santori, F. R.; Boggiano, C.; Wang, Y. H.; Arima, K.; Bover, L.; Hanabuchi, S.; Khalili, J.; Marinova, E.; Zheng, B.; Littman, D. R.; Liu, Y. J. Identification of IL-17-Producing FOXP3+ Regulatory T Cells in Humans. *Proc. Natl. Acad. Sci. U.S.A.* **2009,** *106,* 4793–4798.
247. Wright, G. P.; Notley, C. A.; Xue, S.-A.; Bendle, G. M.; Holler, A.; Schumacher, T. N.; Ehrenstein, M. R.; Stauss, H. J. Adoptive Therapy With Redirected Primary Regulatory T Cells Results in Antigen-Specific Suppression of Arthritis. *Proc. Natl. Acad. Sci. U.S.A.* **2009,** *106,* 19078–19083.
248. Di Ianni, M.; Falzetti, F.; Carotti, A.; Terenzi, A.; Castellino, F.; Bonifacio, E.; Del Papa, B.; Zei, T.; Ostini, R. I.; Cecchini, D.; Aloisi, T.; Perruccio, K.; Ruggeri, L.; Balucani, C.; Pierini, A.; Sportoletti, P.; Aristei, C.; Falini, B.; Reisner, Y.; Velardi, A.; Aversa, F.; Martelli, M. F. Tregs Prevent GVHD and Promote Immune Reconstitution in HLA-Haploidentical Transplantation. *Blood* **2011,** *117,* 3921–3928.
249. Brunstein, C. G.; Miller, J. S.; Cao, Q.; McKenna, D. H.; Hippen, K. L.; Curtsinger, J.; Defor, T.; Levine, B. L.; June, C. H.; Rubinstein, P.; McGlave, P. B.; Blazar, B. R.; Wagner, J. E. Infusion of ex vivo Expanded T Regulatory Cells in Adults Transplanted With Umbilical Cord Blood: Safety Profile and Detection Kinetics. *Blood* **2011,** *117,* 1061–1070.
250. Tang, Q.; Bluestone, J. A. Regulatory T-Cell Therapy in Transplantation: Moving to the Clinic. *Cold Spring Harb. Perspect. Med.* **2013,** *3,* a015552.
251. Terrett, N. K. Macrocycles for Drug Discovery—Identification of Small Molecule Synthetic Macrocycle Antagonists of Human IL-17A. 245th ACS National Meeting & Exposition, New Orleans, LA, United States, April 7–11, 2013. BIOL-120.
252. Larsen, L. K.; Blakskjaer, P.; Dietvorst, J.; Sloek, F.; Christensen, A. B.; Petersen, L. K.; Holmkvist, J.; Heitner, T. R.; Hansen, N. Discovery of the First Small Molecule IL-17A Blockers. Poster # 188, Protein-Protein Interaction Conference October 23–25, 2013 San Diego, CA.
253. McEnaney, P. J.; Parker, C. G.; Zhang, A. X.; Spiegel, D. A. Antibody-Recruiting Molecules: An Emerging Paradigm for Engaging Immune Function in Treating Human Disease. *ACS Chem. Biol.* **2012,** *7,* 1139–1151.
254. Yadav, M.; Stephan, S.; Bluestone, J. A. Peripherally Induced Tregs—Role in Immune Homeostasis and Autoimmunity. *Front. Immunol.* **2013,** *4,* 232.
255. Bluestone, J. A.; Bour-Jordan, H. Current and Future Immunomodulation Strategies to Restore Tolerance in Autoimmune Diseases. *Cold Spring Harb. Perspect. Biol.* **2012,** *4,* a007542.
256. Smilek, D. E.; Ehlers, R. M.; Nepom, G. T. Restoring the Balance: Immunotherapeutic Combinations for Autoimmune Disease. *Dis. Model. Mech.* **2014,** *7,* 503–513.
257. Arron, J. R.; Townsend, M. J.; Keir, M. E.; Yaspan, B. L.; Chan, A. C. Stratified Medicine in Inflammatory Disorders: From Theory to Practice. *Clin. Immunol.* **2015,** *161,* 11–22.
258. Willis, J. C. D.; Lord, G. M. Immune Biomarkers: The Promises and Pitfalls of Personalized Medicine. *Nat. Rev. Immunol.* **2015,** *15,* 323–329.

5.13 Small Molecule Immunosuppressants in Inflammatory Disease

R Fleischmann, University of Texas, Southwestern Medical Center, Metroplex Clinical Research Center, Dallas, TX, United States

© 2017 Elsevier Ltd. All rights reserved.

5.13.1	**Small Molecule Immunosuppressants in Inflammatory Disease**	421
5.13.1.1	Cytokine Signaling	421
5.13.1.2	MAP Kinases	421
5.13.1.2.1	MAP kinase pathway	421
5.13.1.2.2	MAP kinase inhibitors in RA	421
5.13.2	**Jakinibs in RA**	422
5.13.2.1	Tofacitinib	422
5.13.2.1.1	Clinical development of tofacitinib	422
5.13.2.1.2	Pivotal clinical trial results with use of tofacitinib as monotherapy	423
5.13.2.1.3	Use of tofacitinib in combination with csDMARDs	423
5.13.2.1.4	Long-term efficacy (LTE) of tofacitinib	423
5.13.2.1.5	Safety	423
5.13.3	**Baricitinib**	425
5.13.3.1	Phase 2b Clinical Trial of Baricitinib I	425
5.13.3.2	Four Pivotal Phase 3 Clinical Trials Have Been Reported	425
5.13.3.2.1	Use of baricitinib as monotherapy compared to combination therapy in MTX naïve patients	425
5.13.3.2.2	Baricitinib in combination with csDMARDs	425
5.13.3.3	Baricitinib Long-Term Extension Study	426
5.13.3.4	Safety of Baricitinib	426
5.13.4	**Filgotinib**	427
5.13.4.1	Filgotinib as Monotherapy	427
5.13.4.2	Filgotinib in Combination With MTX	428
5.13.4.3	Safety of Filgotinib	428
5.13.5	**ABT 494**	428
5.13.5.1	Efficacy of ABT-494 (Upadacitinib)	429
5.13.5.1.1	ABT-494 in MTX-IR	429
5.13.5.1.2	ABT-494 in TNF IR	429
5.13.5.2	Safety of ABT-494	429
5.13.5.2.1	MTX-IR	429
5.13.6	**Peficitinib (ASP015K)**	430
5.13.6.1	Peficitinib as Monotherapy	430
5.13.6.2	Peficitinib in MTX-IR	430
5.13.6.3	Peficitinib in MTX-IR	430
5.13.6.4	Peficitinib Summary	431
5.13.7	**VX-509 (Decernotinib) Oral-Selective JAK3 Inhibitor**	431
5.13.7.1	VX-509 as Monotherapy	431
5.13.7.2	VX-509 in MTX-IR	431
5.13.8	**Ruxolitinib**	431
5.13.9	**Syk Inhibitors**	432
5.13.10	**Btk Inhibitors**	432
5.13.11	**PDE4 Inhibitors**	433
5.13.11.1	Psoriatic Arthritis	433
5.13.11.2	Psoriasis	434
5.13.12	**Behçet's Disease**	434
5.13.13	**Conclusion**	435
References		435

Abbreviations

ACR American College of Rheumatology
AE Adverse events
BtK Bruton's tyrosine kinase
cAMP Cyclic adenosine monophosphate
cGMP Cyclic guanosine monophosphate
CPK Creatine phosphokinase
CRP C-reactive protein
DAS Disease activity score

DMARD Disease-modifying antirheumatic drugs
ERK Extracellular signal-regulated kinase
HAQ-DI Health assessment questionnaire-disability index
HZ Herpes Zoster
IL Interleukin
JaK, JAK Janus kinase
JNK c-Jun N-terminal kinase
KAK-STAT Janus kinase-signal transducer and activator of transcription proteins
LDA Low disease activity
LTE Long-term extension study
MAPK Mitogen-activated protein kinase
MTX Methotrexate
PDE Phosphodiesterase
PsA Psoriatic arthritis
RA Rheumatoid arthritis
SAE Serious adverse events
SIE Serious infection events
SyK Spleen tyrosine kinase
TEAE Treatment-emergent adverse event
TNF Tumor necrosis factor
VAS Visual analog scale
VDhMTSS van der Heijde modified total sharp score

5.13.1 Small Molecule Immunosuppressants in Inflammatory Disease

5.13.1.1 Cytokine Signaling

In chronic inflammatory diseases such as rheumatoid arthritis (RA), there is pathologic activation of cytokine signaling in affected tissues. Several key signaling pathways are involved in the pathogenesis of RA and other inflammatory diseases, many of which use intracellular protein kinases for signal transduction.[1] Inhibiting these kinases modulates the inflammatory reaction and reduces disease activity. Specifically inhibiting intracellular signal transduction pathways that modulate immune cell functions such as surface receptors, signaling proteins, and transcription of nuclear proteins was postulated as a reasonable approach to treating chronic inflammation conditions such as RA and psoriatic arthritis (PsA).[2] There are a number of intracellular signaling pathways implicated in RA and other inflammatory diseases: JaK-STAT, MAPK, SyK, Btk, and PDE4 inhibitors and drugs targeting these pathways are in various stages of development; a JaK inhibitor for use in RA and a PDE4 inhibitor for use in PsA and psoriasis (PsO) are approved in many countries. This section will provide a summary of what is currently known about their clinical efficacy and safety.

5.13.1.2 MAP Kinases

5.13.1.2.1 MAP kinase pathway

The MAPK pathway is a critical regulator of processes such as cell proliferation, differentiation, growth, and survival.[3,4] Cytokines that signal through the MAPK pathway include tumor necrosis factor (TNF)-α, interleukin (IL)-1, IL-2, IL-6, IL-7, and IL-10.[5–7] MAPKs make up a family of more than 20 serine/threonine kinases.[8] The three groups of MAPKs that have been well characterized include the extracellular signal-regulated kinases (ERKs), the c-Jun N-terminal kinases (JNKs), and the p38 MAPKs.[9] Upon receptor activation, MAPKs are activated by sequential phosphorylation of upstream MAPKs and MAPKs. The MAPK pathway is activated in RA and psoriasis.[10,11] Activated ERK, JNK, and p38 MAPKs have been detected in synovial tissue isolated from patients with RA but not in synovial tissue isolated from patients with osteoarthritis. Significantly higher levels of activated MAPK-4 and MAPK-7 were observed in synovial samples from patients with RA compared to patients with osteoarthritis. In psoriasis, epidermal sections from psoriatic lesions show elevated levels of activated MAPK and ERK compared with healthy skin.[12]

5.13.1.2.2 MAP kinase inhibitors in RA

Several MAPK inhibitors have been developed and studied in RA. As a group, they have had disappointing efficacy, possibly because of the redundancy in the systems, and/or significant toxicity. Compounds that did not demonstrate efficacy include pamapimod (1), an oral inhibitor of the p38 MAPK α-isoform, SCIO-469 (2), and VX-702 (3).[13–18] Two of these p38 inhibitors were efficacious in RA, BMS-582949 (4) and VX-745 (5). The development of both compounds was halted because of neurologic adverse events noted in animal studies. At this time, no MAPK inhibitors are under development for the treatment of RA.

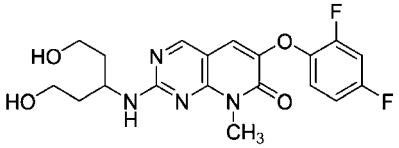

pamapimod, **1**

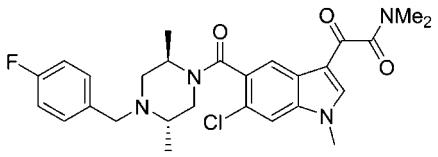

SCIO-469, **2**

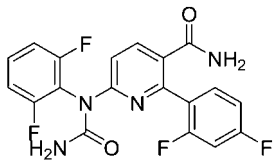

VX-702, **3**

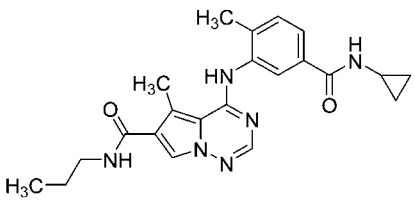

BMS-582949, **4**

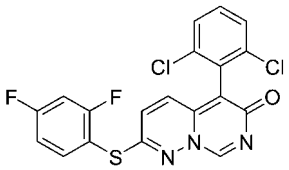

VX-745, **5**

5.13.2 Jakinibs in RA

5.13.2.1 Tofacitinib

Tofacitinib (**6**) is a small-molecule chemical pan JaK inhibitor.[19] By binding to Jak3/1/2, tofacitinib inhibits activation of STAT molecules and downstream signaling, resulting in modulation of inflammatory responses.[20,21]

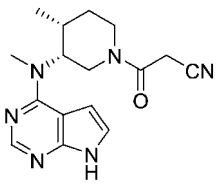

tofacitinib, **6**

5.13.2.1.1 Clinical development of tofacitinib

The approved dose of tofacitinib in most countries is 5 mg orally twice daily and may be used as monotherapy or in combination with conventional synthetic disease-modifying antirheumatic drugs (csDMARD) including methotrexate (MTX); its approvals have been based on the results of 6 pivotal, randomized, double-blind, placebo-controlled phase III trials.[22–27] An 11 mg once-daily tablet has recently been introduced. Tofacitinib has not been tested, and is not approved for use, in combination with biologic disease-modifying antirheumatic drugs (bDMARDs). Clinical studies evaluating the use of tofacitinib in patients with ankylosing

spondylitis, juvenile idiopathic arthritis, ulcerative colitis, and PsA are currently under way; the full results of these trials have not been presented prior to submission of this article for publication. An additional study comparing tofacitinib as monotherapy or in combination with MTX to adalimumab plus MTX should be available in 2017.

5.13.2.1.2 Pivotal clinical trial results with use of tofacitinib as monotherapy

ORAL Solo Phase 3 study investigated tofacitinib 5 and 10 mg BID compared to placebo as monotherapy over 6 months in patients with active RA who had had an inadequate response to at least 1 csDMARD or bDMARDs.[22] At 3 months, significantly more patients treated with either dose of tofacitinib achieved an American College of Rheumatology 20%, 50%, and 70% (ACR20/50/70) improvement response and improvement in physical function, as measured by the health assessment questionnaire-disability index (HAQ-DI), compared with placebo.

ORAL Start study investigated the efficacy of 5 and 10 mg tofacitinib monotherapy versus MTX monotherapy in patients with active RA who were naïve (93%) or received no more than 3 doses of MTX (7%) over 24 months. In this study, clinical, functional, and radiographic responses were assessed.[23] Both doses of tofacitinib monotherapy demonstrated significant improvements in ACR20/50/70 responses, disease activity score (DAS)28-erythrocyte sedimentation rate (DAS28-ESR) < 2.6, and HAQ-DI responses compared to MTX monotherapy. In addition, both doses achieved significance in preventing structural damage compared with MTX, as assessed by change in van der Heijde-modified total sharp score (vdHmTSS) as early as 6 months, which was maintained at 24 months.

5.13.2.1.3 Use of tofacitinib in combination with csDMARDs

ORAL Sync clinical trial investigated the efficacy and safety of tofacitinib 5 and 10 mg on background csDMARDs compared to patients on background csDMARDs taking placebo in a 12-month trial; all patients had active RA in spite of background csDMARDs.[24] Patients treated with either dose of tofacitinib plus csDMARDs achieved significantly greater ACR20 responses and DAS28(ESR) < 2.6 at 6 months compared with placebo plus csDMARDs. At 3 months, significantly more patients improved their HAQ-DI with either dose of tofacitinib compared with placebo.

ORAL Standard study compared patients with active RA in spite of MTX therapy, which was continued, treated with tofacitinib 5 or 10 mg orally BID to patients treated with placebo. In this trial, an additional comparator arm included adalimumab (ADA) plus MTX which was also compared to placebo plus MTX but not to tofacitinib.[25] Patients treated with either dose of tofacitinib plus MTX or ADA plus MTX achieved significantly greater ACR20/50/70 responses and percentages of patients achieving DAS28-ESR < 2.6 at 6 months than placebo plus MTX. At month 3, HAQ-DI improvement was significantly greater in patients treated with combination of tofacitinib and MTX as well as ADA plus MTX compared to placebo plus MTX. The clinical and functional responses achieved with tofacitinib were similar to those achieved with ADA compared with placebo, although the responses were numerically higher with tofacitinib.

ORAL Scan clinical study investigated the efficacy and safety of tofacitinib 5 and 10 mg orally BID with background MTX compared to patients on background MTX taking placebo in a 12-month study which assessed the clinical, functional, and radiographic efficacy of tofacitinib 5 and 10 mg BID in patients with active RA in spite of MTX, to placebo. Structural damage was assessed by the vdHmTSS.[26] At 6 months, patients treated with either dose of tofacitinib achieved statistically significant improvements in ACR20/50/70, DAS28-ESR < 2.6 at month 6 and HAQ-DI scores at month 3.The 10 mg dose of tofacitinib plus MTX statistically significantly inhibited structural damage compared with placebo plus MTX; the 5 mg tofacitinib dose did not. Tofacitinib also achieved significant improvements in patient-reported outcomes, including Patient Global Assessment of disease activity, patient-reported pain, HAQ-DI, and health-related quality of life at months 3 and 24 vs baseline.[27]

ORAL Step clinical study evaluated tofacitinib 5 and 10 mg orally BID in patients with active RA who were on background MTX who had failed ≥ 1 TNF antagonist.[28] At 3 months, statistically significantly more patients treated with tofacitinib—MTX combination therapy achieved ACR20/50/70 responses, DAS28-ESR < 2.6, and HAQ-DI improvement compared with patients treated with placebo plus MTX. Tofacitinib was also associated with significant improvements in Patient Global Assessment of Disease Activity and Short Form 36 Health Survey version 2 physical and mental component summary scores vs placebo.[29]

5.13.2.1.4 Long-term efficacy (LTE) of tofacitinib

Long-term efficacy of tofacitinib, both 5 and 10 mg BID, either as monotherapy or in combination with csDMARDs, from pooled data of 2 open-label extension trials (LTE) including 4858 patients with RA showed sustained ACR20/50/70 responses, maintenance of DAS28 < 2.6, and improvement in HAQ-DI up to month 72. Approximately 36% of the patients in the LTE discontinued treatment over this time frame, 2.7% for lack of efficacy.[30,31]

5.13.2.1.5 Safety (Table 1)

The safety of tofacitinib has been assessed in 12 phase 2 and 3 trials and two LTE of 5671 patients with median tofacitinib exposure of 2.35 years[22–26,28,32–34]

5.13.2.1.5.1 Infections

The most common adverse event (AE) reported during the first 3 months of treatment was infection, occurring in 20% of patients in the 5-mg BID groups and 22% in the 10-mg BID groups compared with 18% in the placebo groups.[34] Serious infection events (SIE) were reported in 11 patients who received tofacitinib compared with 1 patient who received placebo in the phase 3 studies. In the

Table 1 OLE studies up to 7 years[32]

	All tofacitinib n = *4867*	*Tofacitinib 5 mg bid* n = *1471*	*Tofacitinib 10 mg bid* n = *3396*	*All tofacitinib + csDMARDs* n = *3117*	*All tofacitinib monotherapy* n = *1750*
Patient-years	14,926	5278	9648	9651	5275
Mean Rx LTE days	1107	1297	1025	1117	1088
Pts with AEs, *n* (%)	4366 (89.7)	1354 (92.0)	3012 (88.7)	2803 (89.9)	1563 (89.3)
D/C for AE, *n* (%)	1082 (22.2)	385 (26.2)	697 (20.5)	743 (23.8)	352 (20.1)
Exposure-adjusted incidence rate					
SAEs	9.7 (9.2, 10.2)	9.1 (8.3, 10.1)	10.0 (9.3, 10.7)	10.0 (9.3, 10.7)	9.1 (8.3, 10.0)
Serious infections	2.8 (2.5, 3.0)	2.4 (2.0, 2.8)	3.0 (2.6, 3.3)	2.9 (2.5, 3.2)	2.6 (2.2, 3.1)
Malignancies	1.0 (0.8, 1.1)	1.1 (0.8, 1.4)	0.9 (0.7, 1.1)	1.0 (0.8, 1.2)	0.9 (0.7, 1.2)
NMSC	0.7 (0.6, 0.9)	0.5 (0.3, 0.8)	0.8 (0.6, 1.0)	0.8 (0.6, 1.0)	0.5 (0.3, 0.8)
OI (excl. TB)	0.3 (0.3, 0.5)	0.3 (0.2, 0.5)	0.4 (0.3, 0.5)	0.4 (0.2, 0.5)	0.3 (0.2, 0.5)
Tuberculosis	0.2 (0.1, 0.3)	0.1 (0.1, 0.3)	0.2 (0.1, 0.3)	0.2 (0.1, 0.3)	0.2 (0.1, 0.3)
HZ (nonserious + serious)	4.0 (3.7, 4.3)	3.8 (3.2, 4.3)	4.1 (3.7, 4.6)	4.1 (3.7, 4.6)	3.8 (3.2, 4.3)

LTE, SIE occurred in 4.5–7.2% of patients with an incidence rate of 2.9–3.1/100 patient-years.[30,31,33] The most frequent investigator-reported infection and infestation AE were nasopharyngitis (12.7–16.3%), upper respiratory tract infection (10.5–14.5%), and urinary tract infection (6.6–10.3%). Tuberculosis (TB) has been reported in the LTE of tofacitinib, primarily in countries with high endemic rates of TB. For this reason, patients should be screened for latent TB prior to initiating therapy.[34] Other opportunistic infections, similar to those observed with bDMARD therapy, have been reported as well. Herpes zoster (HZ) was reported in ~4% of patients receiving tofacitinib.[30,31,34] with an incidence of closer to 8% in Japan. The incidence of serious HZ (multidermatomes or systemic involvement) has been reported as occurring in ~1% of patients.[34] Although HZ is also reported in patients receiving bDMARDs, the incidence is lower than with tofacitinib.

5.13.2.1.5.2 Malignancies

Of 5671 tofacitinib-treated patients, 107 developed malignancies; the most common were lung cancer in 24 patients, breast cancer in 19, and lymphoma in 10. Twenty of the lung cancer patients were current or former smokers. This incidence is not different than what has been reported in patients with active RA. The types of malignancies and the overall incidence rates have remained stable over time with continued tofacitinib exposure. The standardized incidence ratio as compared with the US National Cancer Institute Surveillance, Epidemiology, and End Results database is ~1[35] The rate of occurrence is similar to what has been reported with the use of bDMARDs.

5.13.2.1.5.3 Hematology

In the LTE, a decrease in hemoglobin and neutrophils in 4.6% and 1% of patients, respectively, were reported.[30] The neutropenia has not been associated with infections or SIE. Importantly, lymphopenia of <500 cells/mm^3 was seen in $<1.0\%$ of patients; ~50% of patients with lymphopenia developed an SIE.[30,36]

5.13.2.1.5.4 Liver tests

Elevated liver aminotransferases >3 times the upper limit of normal were reported in 2.0% (alanine aminotransferase) and 0.9% (aspartate aminotransferase) of patients treated with tofacitinib in combination with a csDMARD, primarily MTX.[30] In contrast, elevated liver tests did not occur more frequently than with placebo in patients treated with tofacitinib monotherapy.

5.13.2.1.5.5 Lipids and cardiovascular events

Elevated lipids occurred in ~20% of patients treated with either 5 or 10 mg tofacitinib BID.[34] The elevations occurred rapidly but can be treated effectively with the use of lipid-lowering agents.[37] It is not clear, however, if the increase is pathogenic.[38] A 3-year follow-up of patients with RA suggests that tofacitinib does not appear to increase the risk of cardiovascular events or lead to changes in blood pressure; the question is still not resolved, however, as longer follow-up with many more patients is needed to answer this question definitively.[39]

5.13.2.1.5.6 Tofacitinib in other autoimmune diseases

Additional clinical studies of tofacitinib in patients with juvenile idiopathic arthritis, ulcerative colitis, and PsA are currently under way; results have not yet been reported.

5.13.3 Baricitinib

Baricitinib (7) is an investigational oral, once-daily Jak1/2 inhibitor currently in development for the treatment of RA.

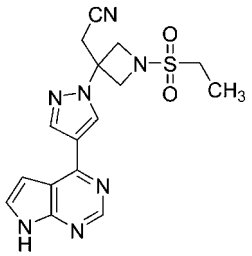

baricitinib, **7**

5.13.3.1 Phase 2b Clinical Trial of Baricitinib I

A dose-ranging, placebo-controlled, phase 2b study investigated baricitinib in combination with MTX; placebo 1, 2, 4, and 8 mg doses were evaluated. The 4 and 8 mg doses plus MTX demonstrated significant clinical improvement with ACR20 responses at 12 weeks of 76% with either 4 or 8 mg compared to 41% with placebo ($p < .001$) with a safety profile that favored the 4 mg dose.[40]

5.13.3.2 Four Pivotal Phase 3 Clinical Trials Have Been Reported

5.13.3.2.1 Use of baricitinib as monotherapy compared to combination therapy in MTX naïve patients

RA-BEGIN was a phase 3 study of baricitinib in 584 patients administered as monotherapy or in combination with MTX in patients with early active RA who had limited or no prior treatment with csDMARDs.[41] Patients were randomized to MTX, baricitinib 4 mg QD as monotherapy, or baricitinib 4 mg QD + MTX for up to 52 weeks. The primary endpoint was the noninferiority of baricitinib 4 mg monotherapy to MTX on ACR20 response at week 24. ACR20 response at week 24 favored baricitinib 4 mg monotherapy vs MTX (77% vs 62%, $p \leq .01$). Compared to MTX, baricitinib 4 mg monotherapy produced significantly greater improvements in multiple secondary measures of disease activity including ACR50/70 response, DAS28(ESR), CDAI and SDAI remission, and low disease activity (LDA). MTX in combination with baricitinib 4 mg had similar efficacy as baricitinib monotherapy, suggesting that baricitinib does not require MTX for clinical or functional efficacy. Radiographic progression was assessed in this trial. Baricitinib in combination with MTX was statistically superior to MTX monotherapy; Baricitinib monotherapy was numerically, but not statistically, superior to MTX. Clinically, the change in all three groups (MTX, baricitinib plus MTX, and baricitinib monotherapy) was all very similar. Patient-reported outcomes were statistically superior with baricitinib as monotherapy or in combination with MTX, compared to MTX, many as early as week 1.[42] Rates of treatment-emergent adverse events (TEAEs) and serious adverse events (SAEs) were similar across groups although there were more laboratory abnormalities in patients treated with MTX either as monotherapy or in combination.

5.13.3.2.2 Baricitinib in combination with csDMARDs

5.13.3.2.2.1 Baricitinib in patients who failed a TNFi

RA-BEACON enrolled 527 patients with active RA on csDMARDs with an inadequate response to at least one TNF inhibitor.[43] Patients were treated with either 2 or 4 mg of baricitinib or placebo. Both doses of baricitinib were superior to placebo with ACR20 responses achieved in 49% and 55% of patients on 2- and 4-mg doses, respectively, compared with 27% of patients receiving placebo at week 12 (either dose vs placebo $p \leq .001$). DAS28(ESR) < 2.6 was improved in both baricitinib arms vs placebo.

5.13.3.2.2.2 Baricitinib in csDMARD-IR with evaluation of radiographic progression

RA-BUILD study enrolled 684 patients with active RA and an inadequate response to csDMARDs therapy.[44] Patients were treated with either 2 or 4 mg of baricitinib or placebo. Both doses of baricitinib were superior to placebo with ACR20 responses in 66% and 62% of patients on 2- and 4-mg doses of baricitinib vs 40% of patients receiving placebo (either dose vs placebo $p \leq .001$). Radiographic progression, measured by the vdHmTSS, was significantly less with both doses of baricitinib vs the placebo arm.

5.13.3.2.2.3 Baricitinib in csDMARD-IR compared to adalimumab (ADA)

RA-BEAM enrolled 1305 patients with active RA despite stable background MTX who were randomized to placebo, baricitinib 4 mg QD, or adalimumab 40 mg biweekly.[45] The primary endpoint was ACR20 response at week 12. ACR20 response at week 12 for baricitinib vs PBO was 70% vs 40%, $p \leq .001$. At weeks 12 and 24, statistically significant improvements in ACR 20/50/70 & HAQ-DI response rates, and DAS28, CDAI, and SDAI LDA and remission rates were seen for baricitinib vs PBO. Compared to adalimumab, baricitinib was superior with respect to ACR20/50/70 response, improvement in DAS28-CRP, and HAQ-DI

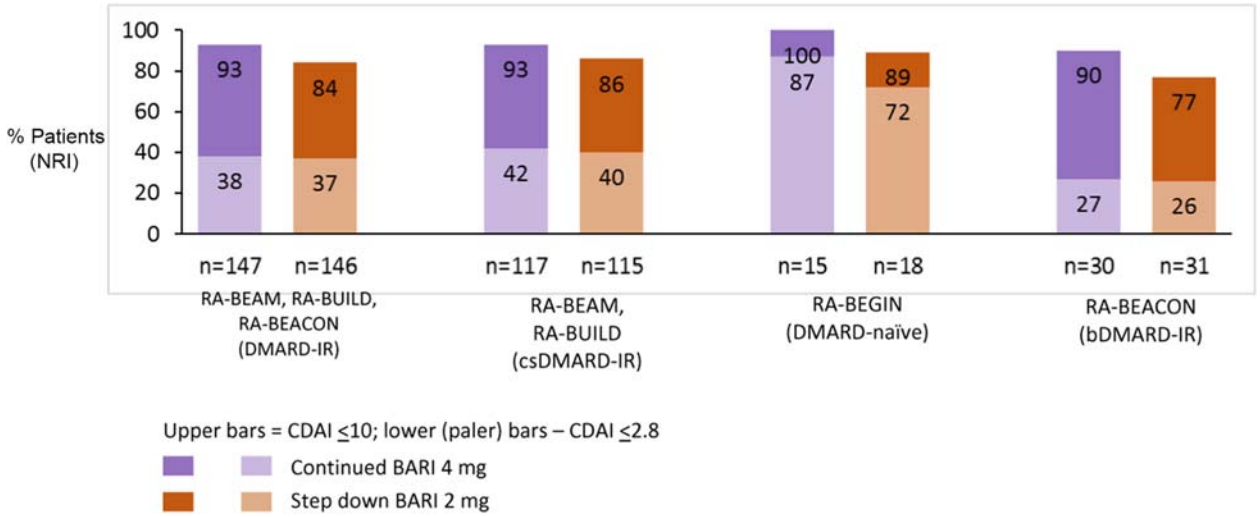

Fig. 1 Baricitinib dose step-down following disease control in patients with rheumatoid arthritis.[46] Upper bars, CDAI <10; lower (paler) bars, CDAI <2.8.

improvement. Compared to placebo, daily diary measures of morning joint stiffness duration and severity, worst tiredness, and worst joint pain were significantly improved in patients receiving baricitinib.

The phase 3 studies of baricitinib demonstrated clinical efficacy of both 2 and 4 mg QD dose in patients with active and an inadequate response to csDMARDs or bDMARDs. In general, greater, more rapid, and more consistent treatment effects were observed for the 4 mg dose across multiple measures.

5.13.3.3 Baricitinib Long-Term Extension Study

In the LTE, RA-BEYOND, the effects of baricitinib dose step-down in patients who had achieved sustained CDAI <10 in csDMARD-IR or CDAI <2.8 in RA-BEGIN, was investigated.[46] Patients who completed a baricitinib phase 3 trial (RA-BEGIN, RA-BEAM, RA-BUILD, or RA-BEACON) could enter the LTE and those patients who had received baricitinib 4 mg for at least 15 months and who had achieved sustained LDA or remission (defined by CDAI score at 2 consecutive visits at least 3 months apart) were rerandomized in a double-blind manner to continue receiving baricitinib 4 mg or to step down to 2 mg QD (RA-EXTEND).[46] At the time of this report, disease activity was assessed at the 12-week time point following rerandomization. Among the patients who achieved satisfactory and sustained disease control with the 4 mg QD dose, randomized, double-blind dose reduction to 2 mg QD there was a modest, statistically significant increase in disease activity across measures at the subsequent 12-week time point. However, many patients in both the continued 4 mg and reduced to 2 mg groups retained a state of LDA or remission that had initially led to their re-randomization (Fig. 1). These data suggest that 4 mg QD is the most efficacious dose for patients with RA and most patients who achieve sustained disease control with baricitinib 4 mg maintained sustained LDA or remission 12 weeks after being rerandomized, in a blinded manner, to 2 mg QD.

5.13.3.4 Safety of Baricitinib

The integrated safety analysis of baricitinib has been reported in abstract form on six studies of baricitinib 4 mg QD compared to placebo and dose-response assessments on four studies with baricitinib 2 and 4 mg QD and PBO arms.[47] Three thousand four hundred and sixty-four patients were exposed to baricitinib (4214 pt-yrs (PY); 2166 patients >1 year and 467 >2 years. In the controlled periods of these studies, there were no increases seen in deaths, AEs leading to study drug discontinuation, malignancies, major cardiac events, or serious infection for baricitinib vs placebo. HZ was reported more frequently for baricitinib vs placebo. In randomized, controlled periods of the studies, TB was reported in two patients, one treated with baricitinib and one with adalimumab. In the LTE, 6 TB events were reported (baricitinib 4 mg: two with incomplete TB screening, three without organism confirmed). All TB occurred in endemic areas. Two GI perforations were reported (0.05/100 PY). No confirmed opportunistic infections were reported. Baricitinib treatment was associated with neutropenia, liver test abnormalities, and lipid elevation, similar to tofacitinib; few patients (<1%) discontinued due to abnormal lab results (Table 2).

Table 2 Integrated safety analysis arms[47]

	Death	*AE → perm DC*	*Malignancy*	*MACE*	*SIE*	*HZ*
6 Study weeks 0–24						
PBO (n=1070)	2 (0.5)	35 (8.9)	2 (0.5)	2 (0.5)	17 (4.2)	4 (1.0)
BARI 4 mg (n=997)	3 (0.7)	47 (11.5)	2 (0.5)	2 (0.5)	16 (3.8)	18 (4.3)*
4 Study weeks 0–24						
PBO (n=551)	2 (1.0)	21 (11.1)	0	2 (1.2)	10 (5.1)	2 (1.0)
Bari 2 mg (n=479)	0	20 (10.8)	1 (0.5)	0	8 (4.2)	6 (3.1)
Bari 4 mg (n=479)	1 (0.5)	26 (13.9)	0	2 (1.1)	11 (5.7)	10 (5.2)
All bari						
Phases 1–3 (n=3464)	13 (0.3)	255 (6.1)	29 (0.7)	16 (0.5)	137 (3.2)	143 (3.4)

Primary safety analysis was based on six studies with bari 4 mg QD and placebo (PBO) arms and dose-response assessments on four studies with bari 2 and 4 mg QD and PBO arms. In addition, the all-bari RA set included all patients exposed to any bari dose. Two studies contained active comparators. Data reported as "n" and IR = incidence rate/100 PY.
*Significantly different vs comparator (95% CI: 2.6, 6.8).

Safety by study

	Death	*AE → perm DC*	*Malignancy*	*MACE*	*SIE*	*HZ*
RA-BEGIN weeks 0–52						
MTX (n=210)	3 (1.7)	11 (6.4)	1 (0.6)	2 (1.1)	8 (4.6)	2 (1.1)
Bari 4 mg (n=159)	0	11 (7.7)	1 (0.7)	1 (0.7)	6 (4.1)	4 (2.7)
Bari 4 mg + MTX (n=215)	0	23 (12.2)	3 (1.6)	0	5 (2.6)	5 (2.6)
RA-BEAM weeks 0–24						
PBO (n=488)	0	17 (8.6)	2 (1.0)	0	7 (3.5)	2 (1.0)
Bari 4 mg (n=487)	2 (0.9)	25 (11.6)	2 (0.9)	1 (0.5)	5 (2.3)	7 (3.2)
Adalimumab (n=330)	0	7 (4.9)	0	0	2 (1.4)	4 (2.8)
RA-BEAM weeks 0–52						
Bari 4 mg (n=487)	2 (0.5)	36 (8.4)	3 (0.7)	2 (0.5)	10 (2.3)	11 (2.5)
Adalimumab (n=330)	1 (0.4)	15 (5.5)	0	1 (0.4)	5 (1.8)	5 (1.8)

Data reported as "n" and IR = incidence rate/100 PY.

5.13.4 Filgotinib

Filgotinib (GLPG0634; **8**) is an oral, once-daily Jak1-selective inhibitor that was found to improve response to MTX in a 4-week proof-of-concept study.[48] After 4 weeks of treatment with GLPG0634 200 mg once daily or 100 mg twice daily, significantly higher ACR20 scores and improvement in DAS28(CRP) and CRP were seen compared with placebo.

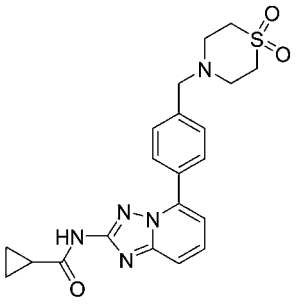

filgotinib, **8**

5.13.4.1 Filgotinib as Monotherapy[49]

The efficacy and safety of filgotinib as monotherapy versus placebo were evaluated in 283 patients with active RA with inadequate response to MTX in a phase 2B study. Patients were randomized to placebo, 50, 100, or 200 mg of filgotinib once daily for 24 weeks. At week 12, a statistically significant higher ACR20 response versus placebo was observed with all three doses of filgotinib. For other key efficacy endpoints (ACR50, ACR-N, DAS28 (CRP), CDAI, SDAI) all doses showed significant difference versus placebo. By week 12, 24–45% of patients on filgotinib achieved DAS28(CRP) $\leq$ 3.2 in a dose-dependent manner, compared to 14% in placebo-treated patients. Safety was similar to tofacitinib and baricitinib (Table 2).

Table 3 DARWIN 2 monotherapy in MTX-IR—Week 24 safety[52]

	PBO → 100 mg		*Cont. 50 mg (n = 57)*	*50 → 100 mg (n = 15)*	*Cont. 100 mg (n = 70)*	*Cont. 200 mg (n = 69)*
	Pbo W0-12 *N* = 72	100 mg W13-24 *N* = 66				
TEAE	28 (39%)	10 (15%)	30 (53%)	8 (53%)	31 (44%)	35 (51%)
SAE	1 (1%)	1 (2%)	2 (4%)	0	2 (3%)	3 (4%)
SIE	0	1 (2%)	1 (2%)	0	1 (1%)	1 (1%)
	PBO → mg (n = 72)		*Cont. 50 mg (n = 57)*	*50 → 100 mg*	*Cont. 100 mg*	*Cont. 200 mg*
ALT						
Grade 1 (1.0, 2.5) × ULN	1 (1.4%)		3 (5.3%)	1 (6.7%)	8 (11.4%)	4 (5.8%)
Grade 2 (2.5, 5.0) × ULN	0		0	0	1 (1.4%)	0
Grade 3 (5.0, 20.0) × ULN	0		1 (1.8)	0	0	0
AST						
Grade 2 (2.5, 5.0) × ULN	0		0	0	0	0
Grade 3 (5.0, 20.0) × ULN	0		1 (1.8%)	0	1 (1.4%)	0
Cholesterol						
Grade 2 (7.5, 10.34)	2 (2.8%)		4 (7.0%)	1 (6.7%)	5 (7.1%)	6 (8.7%)
≥Grade 3 > 10.34	0		0	0	1 (1.4%)	1 (1.4%)

5.13.4.2 Filgotinib in Combination With MTX[50]

The efficacy and safety of filgotinib in combination with MTX versus placebo were evaluated in 594 patients with active RA with inadequate response to MTX in a phase 2b study. Patients were randomized to placebo or one of three doses of filgotinib (50, 100, or 200 mg) QD or BID for 24 weeks. At week 12, a statistically significant higher ACR20 response versus placebo was observed with 200 mg daily dose of filgotinib. For other key efficacy endpoints (ACR50, ACR-N, DAS28(CRP), CDAI, SDAI) all doses showed significant differences versus placebo. No statistically significant difference between QD and BID regimens was seen. By week 12, 24–50% of patients on filgotinib achieved DAS28(CRP) ≤ 3.2 in a dose-dependent manner, compared to 14% on PBO. The 100 mg BID and 200 mg QD doses appeared to have the best efficacy. Safety was similar to the monotherapy study. Patient-reported outcomes were reported from these 2 phase 2b studies.[51] Filgotinib therapy led to a rapid improvement in all assessed PROs including patient's visual analog scale (VAS) disease activity, patient's VAS pain, HAQ-DI, FACIT-F, SF-36 PCS, and SF-36 MCS. After 24 weeks of treatment, filgotinib in combination with MTX as QD or bid or as monotherapy demonstrated comparable benefit.

5.13.4.3 Safety of Filgotinib[52]

At week 24 of the phase 2b program, SAE and TEAE were seen in all dose groups; 39% of PBO and 41% of filgotinib (TEAE) and 1% of PBO and 4% of filgotinib (SAE). Infections occurred in 10% PBO and 19% filgotinib groups. No opportunistic infections, cancers, or deaths occurred. In the filgotinib groups, for the first 4 weeks, a dose-dependent decrease in mean neutrophil and a small reduction in platelet counts were seen; mild increase in mean creatinine was apparent which remained stable up to week 24. A dose-dependent increase in hemoglobin was seen during the first 12 weeks which was stable up to week 24. No meaningful increase in transaminase was seen. Neutropenia, lymphopenia, decreased NK cells, and decreased creatinine were seen as with other Jakinibs. With the higher dose, JAK2 effects were seen on hemoglobin. There has been no mention of HZ in the filgotinib program as yet (Table 3).

5.13.5 ABT 494

ABT-494 (**9**) is an oral Jak1-selective inhibitor that was investigated in two-phase 2b studies.

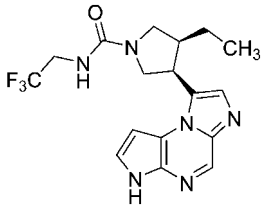

ABT-494, **9**

5.13.5.1 Efficacy of ABT-494 (Upadacitinib)

5.13.5.1.1 ABT-494 in MTX-IR[53]

In a 12-week double-blind placebo-controlled study phase 2b study, the safety, efficacy, and dose response of ABT-494 on background MTX were characterized vs placebo in 299 patients with active RA and an inadequate response to MTX. Patients were randomized to ABT-494 3, 6, 12, or 18 mg BID, 24 mg QD, or matching placebo. ACR20 response rates at week 12 were significantly higher with ABT-494 at 6 mg BID (68%), 12 mg BID (80%), and 24 mg QD (76%) vs placebo (46%); ACR50 and ACR70 response rates and change from baseline in DAS28(CRP) were also statistically significantly improved for all ABT-494 doses (except ACR70 in 12 mg BID) vs placebo. ACR responses were seen within 2 weeks. DAS28(CRP) <2.6 was achieved by significantly more patients on ABT-494 (except 24 mg QD) vs placebo. DAS28(CRP) ≤ 3.2 and CDAI ≤ 10 were achieved by significantly more patients on ABT-494 (except 24 mg QD for CDAI) vs placebo.

5.13.5.1.2 ABT-494 in TNF IR[54]

In a 12-week double-blind placebo-controlled study phase 2B study, the safety, efficacy, and dose response of ABT-494 were characterized vs placebo in 276 patients with active RA and an inadequate response to ≥ 1 anti-TNF bDMARD on background MTX. All patients had failed ≥ 1 anti-TNF therapy prior to enrolment; 28% ≥ 2 anti-TNFi and 20% had also received non-anti-TNF bDMARD. Patients were randomized to ABT-494 3, 6, 12, or 18 mg BID or matching placebo. The proportion achieving ACR20 at week 12 was significantly higher for all ABT-494 groups vs placebo ($p<.01$). ACR50 and ACR70 responses were statistically significantly higher at doses of ≥ 6 mg BID. Changes in DAS28(CRP) from baseline were significantly greater for all doses of ABT-494 vs placebo. There were significant differences in ACR20 response and change in DAS28(CRP) from baseline at week 2 ($p\leq .007$) for 6, 12, and 18 mg BID vs placebo. DAS28(CRP) <2.6 and ≤ 3.2 were achieved statistically significantly more often in the 12-mg BID dose group vs PBO.

5.13.5.2 Safety of ABT-494

5.13.5.2.1 MTX-IR[53]

AE incidence was numerically higher with ABT-494, with a trend of dose dependence (Table 4). The incidence of infections was similar across groups. One serious infection (community-acquired pneumonia) occurred with ABT-494 12 mg BID. One patient receiving ABT-494 3 mg BID and 2 receiving 24 mg QD had nonserious zoster infections (single dermatomes). No deaths occurred during the study. ABT-494 treatment resulted in dose-dependent increases in both low and high density lipoprotein cholesterol. Liver function test elevations were sporadic, with no clear dose dependence. Mean hemoglobin values remained stable or increased at lower doses, most notably in patients with an elevated CRP at baseline. Dose-dependent decreases in hemoglobin were seen at higher doses.

In TNF-IR, the incidences of AEs were numerically higher in ABT-494 dose groups, with some trend toward dose dependency (Table 5)[54] The majority of infections were mild. There was one SIE (bronchiectasis) in the placebo group and none in the

Table 4 ABT-494: MTX-IR—Safety[53]

% Patients	*PBO*	*3 mg*	*6 mg*	*12 mg*	*18 mg*	*24 mg*
Any AE	25	40	45	58	50	35
SAE	0	0	4	2	5	4
AE → D/C	2	2	2	2	10	2
SIE	0	0	0	2	0	0
HZ	0	2	0	0	0	4
Hepatic	0	2	0	0	4	0
Neutropenia	2	0	0	0	0	0

Table 5 ABT-494: TNF-IR—Safety[54]

n *(%)*	*PBO*	*3 mg b.i.d.*	*6 mg b.i.d.*	*12 mg b.i.d.*	*18 mg b.i.d.*
TEAE	25 (45)	26 (47)	31 (56)	37 (67)	39 (71)
SAE	1 (2)	2 (4)	2 (4)	0	1 (2)
AE → DC	2 (4)	0	6 (11)	2 (4)	1 (2)
Infections	13 (23)	11 (20)	12 (22)	22 (40)	21 (38)
SIE	1 (2)	0	0	0	0
Anemia	0	0	0	0	1 (2)
HZ	1 (2)	0	0	0	2 (4)
Neutropenia	0	0	0	1 (2)	1 (2)
Hepatic	1 (2)	0	0	0	2 (4)
Malignancy	0	0	1 (2)	0	0

ABT-494 treatment groups. Five patients had nonserious events of HZ: one patient each in the ABT-494 3, 12, and 18 mg BID treatment groups, and two patients in the placebo group. One patient in the 6-mg BID dose group reported two events of nonmelanoma skin cancer (basal cell and squamous cell carcinomas). There was one report of anemia in the 18-mg BID dose group. No deaths were reported during the study.

5.13.6 Peficitinib (ASP015K)

Peficitinib (**10**) has selectivity for Jak1/3 with more selectivity over JAK2; it is dosed once daily (QD).

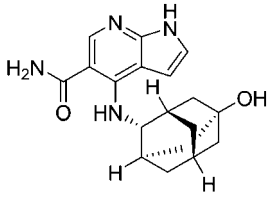

peficitinib, **10**

5.13.6.1 Peficitinib as Monotherapy

The efficacy, safety, and dose response of peficitinib monotherapy in 281 Japanese patients with active RA were evaluated in a 12-week, double-blind study.[55] Patients, 25.3% of whom had previously used an anti-TNF therapy, were randomized equally to once-daily peficitinib 25, 50, 100, 150 mg or placebo. Peficitinib 50, 100, and 150 mg QD each achieved a statistically significantly higher ACR20-CRP response at week 12 compared to placebo, with a dose response. ACR50/70 response and DAS28-CRP < 2.6 were significantly higher in the 100 and 150 mg dose groups. Dose-dependent improvement in DAS28-CRP was also seen. AE incidence was similar between placebo and combined peficitinib groups (64.3% vs 64.0%). The most frequently reported AEs in the combined treatment groups as compared to placebo were nasopharyngitis (13.3% vs 5.4%), RA (12.4% vs 32.1%), blood creatine phosphokinase (CPK) increase (4.9% vs 0%), and diarrhea (3.6% vs 1.8%). The incidence of infections and SIE were similar between placebo and peficitinib (21.4% vs 24.9% and 1.8% vs 2.7%, respectively). The safety profile was generally comparable among the peficitinib groups.

5.13.6.2 Peficitinib in MTX-IR

The efficacy, safety, and dose response of once-daily peficitinib in 289 patients with active RA with an inadequate response/intolerance to csDMARDs and not currently on concomitant MTX (although concomitant hydroxychloroquine and sulfasalazine were allowed) was evaluated in a 12-week, double-blind, placebo-controlled trial.[56] Patients were treated with 25, 50, 100, 150 mg or placebo. Allowed concomitant csDMARD therapies were antimalarials and/or sulfasalazine. A statistically significant dose response at week 12 was seen for ACR20 with the highest response seen in the peficitinib 100 and 150 mg groups. ACR50/70 response and DAS28-CRP < 2.6 were also higher in the 100 and 150 mg dose groups as compared to placebo. Dose-dependent improvement in DAS28-CRP was seen, with statistically significant differences shown in the 100 and 150 mg dose groups by week 4. The incidence of AEs was similar between combined peficitinib groups and placebo (41.6% vs 43.1%). The most frequently reported AEs with peficitinib as compared to placebo were upper respiratory tract infection (5.5% vs 3.9%), nausea (5.0% vs 0%), and diarrhea (3.8% vs 2.0%). The incidence of infections and SAE was similar between peficitinib and placebo (13.4% vs 13.7% and 4.2% vs 3.9%, respectively). No meaningful differences in absolute neutrophil and lymphocyte counts or hemoglobin were seen between peficitinib and placebo. The safety profile was comparable among the peficitinib dose groups, except for a higher incidence of dyspepsia, headache, and CPK increased in the 100 and 150 mg groups.

5.13.6.3 Peficitinib in MTX-IR

The efficacy, safety, and dose response of once-daily peficitinib in 378 patients with active RA with an inadequate response to MTX study were evaluated in a 12-week, double-blind, placebo-controlled study.[57] In this study, a dose response on ACR20 was not shown. Numerically greater ACR20 responses than placebo were seen in the peficitinib 50 and 150 mg groups, with statistical significance shown in the 50 mg group only. A statistically significant dose response was demonstrated in change in DAS28-CRP and DAS28-ESR, with effects seen as early as week 1. AE was similar between combined peficitinib groups and placebo (47.7% vs 47.2%). The most frequently reported AE in the combined peficitinib groups' vs placebo were headache (2.9% vs 1.4%) and hypercholesterolemia (2.0% vs 1.4%). The overall incidence of infections and SAE were similar between peficitinib and placebo (18.3% vs 26.4% and 1.0% vs 0%, respectively). No meaningful differences in absolute neutrophil and lymphocyte counts and hemoglobin

were seen between peficitinib and placebo. More AEs leading to study drug discontinuation and all three SAEs occurred in the 100 and 150 mg groups.

5.13.6.4 Peficitinib Summary

Because of the disparate results between the monotherapy and MTX-IR study, the development of peficitinib was halted on a global basis although there are continuing phase 3 studies being conducted in Japan.

5.13.7 VX-509 (Decernotinib) Oral-Selective JAK3 Inhibitor

VX-509 (**11**) has been developed as a more specific inhibitor of JaK 3 compared to tofacitinib.

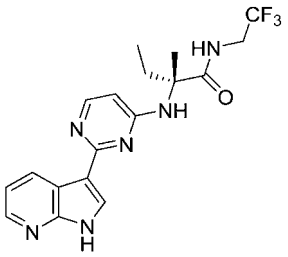

VX-509, **11**

5.13.7.1 VX-509 as Monotherapy

As monotherapy, VX-509 achieved improvement in the signs and symptoms of RA in a 12-week dose-ranging phase 2 study in 204 patients who were csDMARD-IR; patients were treated with VX-509 25, 50, 100, or 150 mg BID or placebo.[58] Primary endpoints at week 12 included the ACR20 response and degree of DAS28(CRP) improvement. DAS28-CRP scores were significantly decreased in patients treated with VX-509 at doses of 50, 100, and 150 mg BID daily compared with placebo ($p \leq .001$). ACR20 responses were 61%, 65%, and 66% in patients treated with VX-509 50, 100, and 150 mg twice daily, respectively, compared with 29% in patients given placebo ($p < .007$). Patients receiving VX-509 achieved clinically meaningful improvements in patient-reported outcomes including HAQ-DI, VAS assessment of general health, and the Short Form-36 Health Survey (all $p < .001$).[59] The safety of VX-509 appeared to be similar to tofacitinib.

5.13.7.2 VX-509 in MTX-IR

In a 24-week, randomized, placebo-controlled, double-blind, phase 2 study, four dosing regimens of VX-509 in combination with MTX were administered to 358 patients with active RA who were MTX-IR.[60] Patients were treated with placebo or VX-509 100 mg QD, 150 mg QD, 200 mg QD, or 100 mg BID. After 24 weeks of treatment the proportion of patients achieving ACR20/50/70, DAS28(CRP) < 2.6, and DAS28(ESR) < 2.6 and the decrease from baseline in DAS28(CRP) were statistically significantly greater in each of the VX-509 dose groups compared to the placebo group. Over 24 weeks, the percentage of patients with any AE was higher in all VX-509 dose groups combined (59.9%) relative to placebo (42.3%) and led to study discontinuation in 9.1% and 8.5% of patients in the VX-509 and placebo groups, respectively. The most common AEs in the VX-509 group were headache (8.7%), hypercholesterolemia (5.2%), and diarrhea (4.5%). SAEs occurred in similar proportions of patients receiving VX-509 (7.3%) or placebo (5.6%), but there were more SIE in the VX-509 group (3.5%) compared with placebo (1.4%). Through 24 weeks there were two SAEs that resulted in death; one was cardiac failure in the VX-509 100 mg BID group and one was pancytopenia in a patient with pneumonia in the VX-509 200 mg QD group. Elevations in transaminase levels and decreases in median neutrophil and lymphocyte counts were observed in the VX-509 groups and were generally mild. Safety profiles were comparable across groups receiving VX-509.

5.13.8 Ruxolitinib

Ruxolitinib (INCB018424; **12**) is an oral Jak1/2 inhibitor that is currently approved by the US Food and Drug Administration for the treatment of myelofibrosis. This agent has shown suggested efficacy in several preclinical models of arthritis. In a small phase 2a study of 16 patients, ruxolitinib demonstrated increased rates of ACR20 response and a decrease in DAS28 at a dose of 15 mg twice daily.[61]

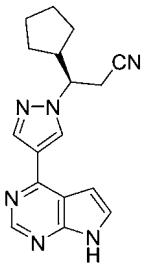

ruxolitinib, **12**

5.13.9 Syk Inhibitors

Syk is expressed in many different cell types and is essential in the development and activation of T-cell, B-cell, and Fc receptor signaling; mast cell degranulation; neutrophil and macrophage phagocytosis; and platelet activation.[62–65]

The oral Syk inhibitor fostamatinib (R788; **13**) was assessed in combination with MTX in 2 randomized, placebo-controlled, double-blind phase II trials of patients with RA.[66,67] In both trials, fostamatinib-treated patients achieved significantly improved clinical responses compared with placebo. Significant diarrhea and hypertension were seen in a number of patients. A randomized, placebo-controlled phase II trial of fostamatinib in patients with RA, who experienced treatment failure during previous biologic disease-modifying antirheumatic drug therapy, failed to show a difference between fostamatinib and placebo.[68] A randomized, placebo-controlled phase IIb trial of the safety and efficacy of fostamatinib as monotherapy did show that fostamatinib was superior to placebo at week 6 in decreasing DAS28(CRP) but was inferior to adalimumab monotherapy at week 24.[69] The results of two published randomized, double-blind, placebo-controlled phase III trials evaluating fostamatinib in patients with RA and inadequate response to TNFi or MTX demonstrated limited efficacy and relatively high rates of diarrhea and hypertension.[70,71] Because of the failure of these studies, and its adverse event profile, development of fostamatinib was suspended as of Jun. 2013.

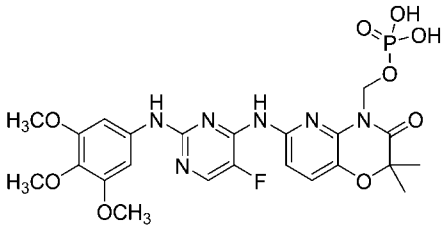

fostamatinib, **13**

5.13.10 Btk Inhibitors

Btk, a member of the Tec family of cytoplasmic protein tyrosine kinases, is predominantly expressed in hematopoietic cells including B-cells and those of myeloid lineage (e.g., macrophages). These cell lineages are thought to be important contributors to the development of inflammatory arthritis and other autoimmune diseases.[72,73] Animal models suggest that Btk inhibition can lead to inhibition of B-cell receptor-dependent cell proliferation and a reduction of inflammatory cytokine production from myeloid cells. This is due to prevention of signaling through the FCyRIII receptor.[73,74] Because these target cells play important roles in autoimmunity, there is interest in testing Btk inhibition in patients with RA.

The Btk inhibitor ibrutinib (PCI-32765; **14**) has demonstrated efficacy in animal models of arthritis and is currently in phase II trials for treatment of B-cell lymphomas.[2,75,76] A second Btk inhibitor, CC-292 (**15**), has also exhibited efficacy in a collagen-induced arthritis animal model and is in early clinical trials for treatment of B-cell lymphomas.[2]

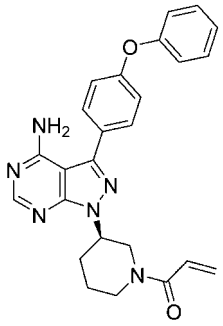

ibrutinib, **14**

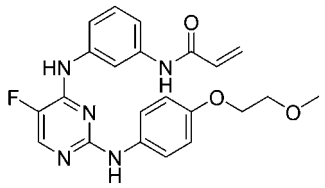

CC-292, **15**

5.13.11 PDE4 Inhibitors

In addition to targeting intracellular protein kinases, small-molecule inhibitors of phosphodiesterase signaling pathways are under development to treat autoimmune and inflammatory diseases.[73] Phosphodiesterases are enzymes that hydrolyze the 3′ phosphate bond of cyclic adenosine monophosphate (cAMP) and cyclic guanosine monophosphate (cGMP) and, through degradation of these intracellular secondary messengers, regulate many downstream biologic processes. They are classified into 11 different subfamilies (PDE1-PDE11), each exhibiting different degrees of specificity for cAMP and cGMP.[77,78] PDE4 demonstrates specificity for cAMP and is expressed in many tissues including the brain, heart, lungs, and inflammatory cells such as B- and T-cells, neutrophils, eosinophils, macrophages, and mast cells.[79–81]

Apremilast (**16**) has been approved by the US Food and Drug Administration for the treatment of adults with active PsA.

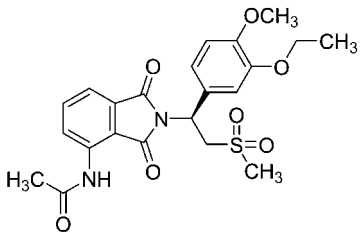

apremilast, **16**

5.13.11.1 Psoriatic Arthritis

The efficacy and safety of apremilast to treat PsA have been evaluated in four randomized, double-blind, placebo-controlled phase III trials (PALACE-1-4).[82–85] In these studies, patients were randomized to receive either apremilast 20 or 30 mg BID or placebo for 24 weeks. The primary endpoint for the trials was achievement of an ACR20 response at week 16. Patients with poor response at week 16 were randomized to 20 or 30 mg apremilast; all patients receiving placebo were randomized to active treatment by week 24–52. Patients receiving csDMARDs were allowed to continue stable doses of MTX, sulfasalazine, leflunomide, or a combination of these.

PALACE-1 was a 52-week double-blind, placebo-controlled phase 3 study which enrolled 504 patients with active PsA who were csDMARD or bDMARD-IR.[82] Significantly more patients in the apremilast 20- and 30-mg BID groups achieved the primary endpoint of ACR20 response at week 16 compared with placebo (30.4%, 38.1%, and 19.0%, respectively). AE occurring in $\geq$5% of patients included diarrhea, nausea, headache, and urinary tract infection. Diarrhea was generally, but not always, self-limited. A dose escalation strategy at the initiation of therapy appeared to ameliorate this toxicity. After week 52, patients could continue open-label apremilast treatment for up to 4 years. An analysis at week 104 demonstrated sustained improvements with continued therapy and no additional safety concerns.[86]

PALACE-2 was a 52-week double-blind, placebo-controlled phase 3 study, which enrolled 484 patients with active PsA.[83] Significantly more patients treated with apremilast 20 and 30 BID achieved the primary endpoint of ACR20 at 16 weeks compared with placebo (38.4% and 34.4% vs 19.5%, respectively). At 52 weeks, patients receiving apremilast 20 and 30 from randomization achieved multiple endpoints including observed ACR20 responses (52.9% and 52.6%, respectively), mean change in health assessment questionnaire-disability index (HAQ-DI) from baseline (-0.192 and -0.330, respectively), and mean change from baseline in Short Form-36 Physical Functioning domain score (5.05 and 6.35, respectively). In addition, patients with baseline psoriasis body surface area of $\geq$3% achieved significant psoriasis area and severity index (PASI)-75/PASI-50 results (27.1%/49.2% and 39.3%/58.9%, respectively). Through week 52, adverse events occurring in $\geq$5% of apremilast-exposed patients were diarrhea, nausea, upper respiratory tract infection, headache, and nasopharyngitis.

PALACE-3 was a 52-week double-blind, placebo-controlled phase 3 study, which enrolled 506 with PsA and $\geq$1psoriatic lesion $\geq$2 cm at baseline.[84] Significantly more patients receiving apremilast 20 and 30 achieved an ACR20 at 16 weeks compared with placebo (29.4% and 42.8% vs 18.9%, respectively). At 52 weeks, patients originally randomized to receive apremilast 20 and

Table 6 Safety over 2 years[92]

AEs (%)	*Apremilast 30 mg, 0–52 weeks (n = 721)*	*Apremilast 30 mg, 52–104 weeks (n = 520)*
≥1 SAE	6.5	6.3
Diarrhea	16	4
Nausea	15	2
Headache	10	3

30 achieved multiple endpoints including ACR20 responses (56% and 63%, respectively), mean change in HAQ-DI from baseline (−0.332 and −0.350, respectively), and mean change from baseline in Short Form-36 Physical Functioning domain score (5.05 and 6.35, respectively). In addition, patients with baseline psoriasis body surface area of ≥3% achieved significant PASI-75/PASI-50 results (28.6%/49.2% for apremilast 20 and 39.1%/54.7% for apremilast 30). Overall, patients receiving apremilast 30 achieved higher responses than those receiving apremilast 20, and placebo patients randomized to apremilast at weeks 16 or 24 achieved similar results with those originally randomized to apremilast. Apremilast was generally well tolerated, and AE occurring through 52 weeks in ≥5% of apremilast-exposed patients were diarrhea, nausea, upper respiratory tract infection, headache, nasopharyngitis, and vomiting. Data through week 104 showed sustained disease activity decreases and symptom relief and improved physical function.[87]

PALACE-4 evaluated apremilast in 527 patients with PsA who had not received previous csDMARDs.[85] Significantly more patients treated with apremilast 20 and 30 BID achieved an ACR20 at 16 weeks compared with placebo (28.0% and 30.7% vs 15.9%, respectively). At 52 weeks, using an as observed analysis, 55% of patients randomized to receive apremilast 20 and 58% of patients randomized to receive apremilast 30 achieved ACR20 responses. Responders, through week 104, showed sustained outcomes including ACR response, HAQ-DI improvement, changes in dactylitis severity scores, and PASI responses.

In a pooled 52- and 104-week efficacy post hoc analyses of PALACE 1-3, apremilast improved enthesitis, dactylitis, swollen joint and tender join counts, HAQ-DI, Short Form-36 Physical Functioning domain, and work productivity (Work Limitations Questionnaire).[88–90]

The safety of apremilast has been assessed in a pooled analysis of 1493 patients from PALACE 1–3.[91] No additional safety findings were identified. The most common adverse events reported were diarrhea (weeks 0–52: 13.9%; weeks 53–104: 2.9%), nausea (weeks 0–52: 12.2%; weeks 53–104: 1.8%), headache (weeks 0–52: 9.4%; weeks 53–104: 3%), upper respiratory tract infections (weeks 0–52: 9.1%; weeks 53–104: 6.5%), and nasopharyngitis (weeks 0–52: 6.2%; weeks 53–104: 5.8%). The incidence of diarrhea, nausea, and headache were greater at the apremilast 30 dose. Serious adverse events occurred in 5.6% of patients receiving apremilast 20 and 6.5% in patients receiving apremilast 30 through week 52 (**Table 6**)[92]

Apremilast did not appear to have any significant effects on laboratory measurements.[93] Abnormal hematology and chemistry laboratory values were reported infrequently, and median values did not change significantly from baseline. Changes were transient and did not require specific treatment or lead to study discontinuation. Laboratory changes included alanine aminotransferase and aspartate aminotransferase values ≥1 times the upper limit of normal, and alanine aminotransferase and aspartate aminotransferase values ≥3 times the upper limit of normal, which returned to normal or baseline in most patients even with continued apremilast treatment. No cases of liver function test elevations meeting Hy's law were reported.

5.13.11.2 Psoriasis

Apremilast has been evaluated for the treatment of psoriasis in several phase III trials. In the double-blinded, placebo-controlled phase 3 ESTEEM 1 and 2 trials, patients with moderate to severe plaque psoriasis were randomized to apremilast 30 mg BID or placebo.[94,95] At week 16, patients randomized to receive placebo were switched to apremilast through study week 32. Patients randomized to apremilast who experienced a ≥75% PASI reduction in ESTEEM 1 and ≥50% PASI reduction in ESTEEM 2 at week 32 were rerandomized to continue receiving apremilast or to switch to placebo with switch back to apremilast if PASI response was lost. Patients randomized to placebo at baseline and switched to apremilast at week 16 who experienced the predefined response at week 32 continued apremilast for up to 5 years. All patients without predefined response at week 32 continued apremilast with the option to add topical agents and/or ultraviolet B phototherapy, based on investigator discretion. The results from both trials demonstrated significantly higher rates of PASI response at week 16 with apremilast vs placebo ($p < .0001$). Among patients rerandomized at week 32 to apremilast or placebo, most of those who continued apremilast (61% in ESTEEM 1 and 80.3% in ESTEEM 2) maintained their PASI response through week 52, whereas 48.4% (ESTEEM 2) to 83.1% (ESTEEM 1) of those rerandomized to placebo lost PASI response and switched to apremilast before week 52. Additionally, in ESTEEM 1 and 2, nail disease improvement was investigated. At week 16 the response was NAPSI50, 33% and 45% APREMILAST vs 15% and 19% PBO (week 16).

5.13.12 Behçet's Disease

Apremilast showed improvement in the signs and symptoms of Behçet's disease in a 12-week randomized, placebo-controlled phase 2 trial in 111 patients with active oral ulcers.[96] Patients without major organ involvement and with ≥2 oral ulcers were

randomized to either apremilast 30 mg BID or placebo. The primary endpoint was the number of oral ulcers at week 12. At 12 weeks, the mean number of oral ulcers for patients receiving apremilast was 0.5 ± 1.0 compared with 2.1 ± 2.6 for patients receiving placebo ($p < .001$). A higher rate of patients receiving apremilast reported improvements in oral ulcer pain, complete response (oral ulcer free), and reduction in genital ulcers compared with patients receiving placebo.

5.13.13 Conclusion

Small molecule oral agents affecting the kinase and PDE4 pathways have been shown to be of value in the treatment of patients with rheumatic disease including RA and PsA. One Jakinib (pan JAK inhibitor), tofacitinib, is FDA approved for the treatment of RA, either as monotherapy or in combination with csDMARDs. Tofacitinib has been shown to be more effective than MTX clinically, functionally, and radiographically as monotherapy in MTX naïve patients, effective in patients who are csDMARD-IR as monotherapy or combined with a csDMARD, and effective in combination with MTX after incomplete response to a TNFi. In a trial which compared tofacitinib plus MTX to MTX in a MTX-IR population, an adalimumab plus MTX arm was included. Adalimumab plus MTX was superior to MTX plus placebo in this same population. Although not powered to be a head-to-head comparison of tofacitinib to adalimumab, tofacitinib appeared to be numerically superior to adalimumab clinically and functionally. A phase 3B study is currently underway to compare tofacitinib monotherapy to tofacitinib plus MTX to adalimumab plus MTX in a powered head-to-head comparison in MTX naïve patients. The results should be available in 2017.

Other Jakinibs in development, including baricitinib, ABT-494, and filgotinib, have shown similar efficacy so far. Baricitinib has completed its phase 3 program and will be evaluated by the FDA and EMA for approval in early 2017. Baricitinib is distinctive in that in a head-to-head trial against adalimumab, both with background MTX, baricitinib was more effective than adalimumab clinically and functionally with similar radiographic effects. Also, in a trial comparing baricitinib monotherapy to combination with MTX, there did not appear to be a difference between the two clinically or functionally; the combination was statistically superior radiographically but the difference was not significant clinically. ABT-494 and filgotinib are currently in phase 3 studies. Peficitinib has shown mixed results. In phase 2 studies, monotherapy appears to be effective as well as in combination with sulfasalazine and/or hydroxychloroquine. A study in MTX-IR failed. Phase 3 studies are in progress.

An oral small molecule inhibitor of PDE4, apremilast, has been approved for use in PsA. Although its efficacy is not as dramatic as the TNFi or inhibitors of IL17 on the joints and skin, its favorable safety profile has led to widespread acceptance of its use prior to bDMARDs.

Other small molecules working intracellularly, with different mechanisms of action, are being investigated in a number of rheumatic diseases. If they are successful in their clinical trials, they have the potential to be additional valuable agents for our therapeutic armamentarium.

Unfortunately, not all small molecules affecting intracellular mechanisms have been successful. A number of inhibitors on the MAPK pathways and of the SyK pathway have failed, either for lack of efficacy or tolerability.

Much still needs to be done to find the optimal inhibition of these pathways both with respect to efficacy and safety. Second- and third-generation molecules may have better results and be effective in other rheumatic diseases. The future should be interesting.

See also: 5.16. Small-Molecule Drugs for the Treatment of Inflammatory Bowel Disease. 8.17. Are Two Better Than One in Rheumatoid Arthritis? Development of Dual p38α MAPK/PDE-4 Inhibitors for Treatment of TNFα–Driven Diseases.

References

1. Ghoreschi, K.; Laurence, A.; O'Shea, J. Janus Kinases in Immune Cell Signaling. *Immunol. Rev.* **2009,** *228,* 273–287.
2. O'Shea, J.; Laurence, A.; McInnes, I. Back to the Future: Oral Targeted Therapy for RA and Other Autoimmune Diseases. *Nat. Rev. Rheumatol.* **2013,** *9,* 173–182.
3. Bonilla-Hernán, M.; Miranda-Carús, M.; Martin-Mola, E. New Drugs Beyond Biologics in Rheumatoid Arthritis: The Kinase Inhibitors. *Rheumatology* **2011,** *50,* 1542–1550.
4. Sweeney, S.; Firestein, G. Primer: Signal Transduction in Rheumatic Disease—A Clinician's Guide. *Nat. Clin. Pract. Rheumatol.* **2007,** *3,* 651–660.
5. Winston, B.; Lange-Carter, C.; Gardner, A.; Johnson, G.; Riches, D. Tumor Necrosis Factor Alpha Rapidly Activates the Mitogen-Activated Protein Kinase (MAPK) Cascade in a MAPK Kinase Kinase-Dependent, c-Raf-1-Independent Fashion in Mouse Macrophages. *Proc. Natl. Acad. Sci. U. S. A.* **1995,** *2,* 1614–1618.
6. Crawley, J.; Rawlinson, L.; Lali, F.; Page, T.; Saklatvala, J.; Foxwell, B. T Cell Proliferation in Response to Interleukins 2 and 7 Requires p38 MAP Kinase Activation. *J. Biol. Chem.* **1997,** *272,* 15023–15027.
7. Foey, A.; Parry, S.; Williams, L.; Feldmann, M.; Foxwell, B.; Brennan, F. Regulation of Monocyte IL-10 Synthesis by Endogenous IL-1 and TNF-Alpha: Role of the p38 and p42/44 Mitogen-Activated Protein Kinases. *J. Immunol.* **1998,** *160,* 920–928.
8. Pearson, G.; Robinson, F.; Beers, A.; Gibson, T.; Xu, B.; Karandikar, M.; Berman, K.; Cobb, M. Mitogen-Activated Protein (MAP) Kinase Pathways: Regulation and Physiological Functions. *Endocr. Rev.* **2001,** *22,* 153–183.
9. Zhang, Y.; Dong, C. MAP Kinases in Immune Responses. *Cell. Mol. Immunol.* **2005,** *2,* 20–27.
10. Schett, G.; Tohidast-Akrad, M.; Smolen, J.; Schmid, B.; Steiner, C.; Bitzan, P.; Zenz, P.; Redlich, K.; Xu, Q.; Steiner, G. Activation, Differential Localization, and Regulation of the Stress-Activated Protein Kinases, Extracellular Signal-Regulated Kinase, c-JUN N-Terminal Kinase, and p38 Mitogen-Activated Protein Kinase, in Synovial Tissue and Cells in Rheumatoid Arthritis. *Arthritis Rheum.* **2000,** *43,* 2501–2512.
11. Sundarrajan, M.; Boyle, D.; Chabaud-Riou, M.; Hammaker, D.; Firestein, G. Expression of the MAPK Kinases MKK-4 and MKK-7 in Rheumatoid Arthritis and Their Role as Key Regulators of JNK. *Arthritis Rheum.* **2003,** *48,* 2450–2460.

12. Haase, I.; Hobbs, R.; Romero, M.; Broad, S.; Watt, F. A Role for Mitogen-Activated Protein Kinase Activation by Integrins in the Pathogenesis of Psoriasis. *J. Clin. Invest.* **2001,** *108,* 527–536.
13. Cohen, S.; Cheng, T.; Chindalore, V.; Damjanov, N.; Burgos-Vargas, R.; Delora, P.; Zimany, K.; Travers, H.; Caulfield, J. Evaluation of the Efficacy and Safety of Pamapimod, a p38 MAP Kinase Inhibitor, in a Double-Blind, Methotrexate-Controlled Study of Patients With Active Rheumatoid Arthritis. *Arthritis Rheum.* **2009,** *60,* 335–344.
14. Alten, R.; Zerbini, C.; Jeka, S.; Irazoque, F.; Khatib, F.; Emery, P.; Bertasso, A.; Rabbia, M.; Caulfield, J. Efficacy and Safety of Pamapimod in Patients With Active Rheumatoid Arthritis Receiving Stable Methotrexate Therapy. *Ann. Rheum. Dis.* **2010,** *69,* 364–367.
15. Genovese, M.; Cohen, S.; Wofsy, D.; Weinblatt, M.; Firestein, G.; Brahn, E.; Strand, V.; Baker, D.; Tong, S. A 24-Week, Randomized, Double-Blind, Placebo-Controlled, Parallel Group Study of the Efficacy of Oral SCIO-469, a p38 Mitogen-Activated Protein Kinase Inhibitor, in Patients With Active Rheumatoid Arthritis. *J. Rheumatol.* **2011,** *38,* 846–854.
16. Damjanov, N.; Kauffman, R.; Spencer-Green, G. Efficacy, Pharmacodynamics, and Safety of VX-702, a Novel p38 MAPK Inhibitor, in Rheumatoid Arthritis: Results of Two Randomized, Double-Blind, Placebo-Controlled Clinical Studies. *Arthritis Rheum.* **2009,** *60,* 1232–1241.
17. Genovese, M.; Gao, L.; Yin, J.; Smith, S.; Weinblatt, M.; Smolen, J.; Wang, X.; Schieven, G.; Garcia-Meijiede, J.; Latck, R.; Pasternak, R.; Kaul, S.; Roy, A.; Raymond, R.; Thienel, U.; Wang, J. Proof of Concept Study for a Potent p38 MAPK Dual Action Inhibitor BMS-582949 in Subjects With RA Receiving Concomitant Methotrexate. *Arthritis Rheum.* **2010,** *62,* S469.
18. Weisman, M.; Furst, D.; Schiff, M.; Kauffman, R.; Merica, E.; Martin-Munley, S. A Double-Blind, Placebo-Controlled Trial of VX-745, an Oral p38 Mitogen Activated Protein Kinase (MAPK) Inhibitor, in Patients With Rheumatoid Arthritis (RA). *Ann. Rheum. Dis.* **2002,** *61. FRI0018.*
19. Changelian, P.; Flanagan, M.; Ball, D.; Kent, C.; Magnuson, K.; Martin, W.; Rizzuti, B.; Sawyer, P.; Perry, B.; Brissette, W.; McCurdy, S.; Kudlacz, E.; Conklyn, M.; Elliott, E.; Koslov, E.; Fisher, M.; Strelevitz, T.; Yoon, K.; Whipple, D.; Sun, J.; Munchhof, M.; Doty, J.; Casavant, J.; Blumenkopf, T.; Hines, M.; Brown, M.; Lillie, B.; Subramanyam, C.; Shang-Poa, C.; Milici, A.; Beckius, G.; Moyer, J.; Su, C.; Woodworth, T.; Gaweco, A.; Beals, C.; Littman, B.; Fisher, D.; Smith, J.; Zagouras, P.; Magna, H.; Saltarelli, M.; Johnson, K.; Nelms, L.; Des Etages, S.; Hayes, L.; Kawabata, T.; Finco-Kent, D.; Baker, D.; Larson, M.; Si, M.; Paniagua, R.; Higgins, J.; Holm, B.; Reitz, B.; Zhou, Y.; Morris, R.; O'Shea, J.; Borie, D. Prevention of Organ Allograft Rejection by a Specific Janus Kinase 3 Inhibitor. *Science* **2003,** *302,* 875–878.
20. Kudlacz, E.; Conklyn, M.; Andresen, C.; Whitney-Pickett, C.; Changelian, P. The JAK-3 Inhibitor CP-690550 is a Potent Anti-Inflammatory Agent in a Murine Model of Pulmonary Eosinophilia. *Eur. J. Pharmacol.* **2008,** *582,* 154–161.
21. Ghoreschi, K.; Jesson, M.; Li, X.; Lee, J.; Ghosh, S.; Alsup, J.; Warner, J.; Tanaka, M.; Steward-Tharp, S.; Gadina, M.; Thomas, C.; Minnerly, J.; Storer, C.; LaBranche, T.; Radi, Z.; Dowty, M.; Head, R.; Meyer, D.; Kishore, N.; O'Shea, J. Modulation of Innate and Adaptive Immune Responses by Tofacitinib (CP-690,550). *J. Immunol.* **2011,** *186,* 4234–4243.
22. Fleischmann, R.; Kremer, J.; Cush, J.; Schulze-Koops, H.; Connell, C.; Bradley, J.; Gruben, D.; Wallenstein, G.; Zwillich, S.; Kanik, K. Placebo-Controlled Trial of Tofacitinib Monotherapy in Rheumatoid Arthritis. *N. Engl. J. Med.* **2012,** *367,* 495–507.
23. Lee, E.; Fleischmann, R.; Hall, S.; Wilkinson, B.; Bradley, J.; Gruben, D.; Koncz, T.; Krishnaswami, S.; Wallenstein, G.; Zang, C.; Zwillich, S.; van Vollenhoven, R. Tofacitinib Versus Methotrexate in Rheumatoid Arthritis. *N. Engl. J. Med.* **2014,** *370,* 2377–2386.
24. Kremer, J.; Li, Z.; Hall, S.; Fleischmann, R.; Genovese, M.; Martin-Mola, E.; Isaacs, J.; Gruben, D.; Wallenstein, G.; Krishnaswami, S.; Zwillich, S.; Koncz, T.; Riese, R.; Bradley, J. Tofacitinib in Combination With Non-Biologic Disease-Modifying Antirheumatic Drugs in Patients With Active Rheumatoid Arthritis: A Randomized Trial. *Ann. Intern. Med.* **2013,** *159,* 253–261.
25. van Vollenhoven, R.; Fleischmann, R.; Cohen, S.; Lee, E.; Garcia Meijide, J.; Wagner, S.; Forejtova, S.; Zwillich, S.; Gruben, D.; Koncz, T.; Wallenstein, G.; Krishnaswami, S.; Bradley, J.; Wilkinson, B. Tofacitinib or Adalimumab Versus Placebo in Rheumatoid Arthritis. *N. Engl. J. Med.* **2012,** *367,* 508–519.
26. van der Heijde, D.; Tanaka, Y.; Fleischmann, R.; Keystone, E.; Kremer, J.; Zerbini, C.; Cardiel, M.; Cohen, S.; Nash, P.; Song, Y.; Tegzova, D.; Wyman, T.; Gruben, D.; Benda, B.; Wallenstein, G.; Krishnaswami, S.; Zwillich, S.; Bradley, J.; Connell, C. Tofacitinib (CP-690,550) in Patients With Rheumatoid Arthritis on Methotrexate: 12-Month Data From a 24-Month Phase 3 Randomized Radiographic Study. *Arthritis Rheum.* **2013,** *65,* 559–570.
27. Strand, V.; van der Heijde, D.; Zerbini, C.; Connell, C.; Gruben, D.; Riese, R.; Wallenstein, G. ORAL SCAN: Effects of the Oral JAK Inhibitor Tofacitinib in Combination With Methotrexate on Patient Reported Outcomes in a 24-Month Phase 3 Trial of Active Rheumatoid Arthritis. *Arthritis Rheum.* **2013,** *65,* S996.
28. Burmester, G.; Blanco, R.; Charles-Schoeman, C.; Wollenhaupt, J.; Zerbini, C.; Benda, B.; Gruben, D.; Wallenstein, G.; Krishnaswami, S.; Zwillich, S.; Koncz, T.; Soma, K.; Bradley, J.; Mebus, C. Tofacitinib (CP-690,550) in Combination With Methotrexate in Patients With Active Rheumatoid Arthritis With an Inadequate Response to Tumour Necrosis Factor Inhibitors: A Randomised Phase 3 Trial. *Lancet* **2013,** *381,* 451–460.
29. Strand, V.; Burmester, G.; Zerbini, C.; Mebus, C.; Zwillich, S.; Gruben, D.; Wallenstein, G. Tofacitinib With Methotrexate in Third-Line Treatment of Patients With Active Rheumatoid Arthritis: Patient-Reported Outcomes From a Phase III Trial. *Arthritis Care Res.* **2015,** *67,* 475–483.
30. Wollenhaupt, J.; Silverfield, J.; Lee, E.; Curtis, J.; Wood, S.; Soma, K.; Nduaka, C.; Benda, B.; Gruben, D.; Nakamura, H.; Komuro, Y.; Zwillich, S.; Wang, L.; Riese, R. Safety and Efficacy of Tofacitinib, an Oral Janus Kinase Inhibitor, for the Treatment of Rheumatoid Arthritis in Open-Label, Long-Term Extension Studies. *J. Rheumatol.* **2014,** *41,* 837–852.
31. Wollenhaupt, J.; Silverfield, J.; Lee, E.; Wood, S.; Terry, K.; Nakamura, H.; Kwok, K.; Anisfeld, A.; Nduaka, C.; Riese, R.; Wang, L. Tofacitinib, an Oral Janus Kinase Inhibitor, in the Treatment of Rheumatoid Arthritis: Safety and Efficacy in Open-Label, Long-Term Extension up to 6 Years. *Arthritis Rheum.* **2014,** *66,* S375.
32. Wollenhaupt, J.; Silverfield, J.; Lee, E.; Terry, K.; Kwok, K.; Lazariciu, I.; Nduaka, C.; Connell, C.; DeMasi, R.; Wang, L. Tofacitinib, an Oral JaK Inhibitor, in the Treatment of Rheumatoid Arthritis: Safety and Clinical and Radiographic Efficacy in Open-Label, Long-Term Extension Studies Over 7 Years. *Ann. Rheum. Dis.* **2016,** *75* (Supplement 2), 252.
33. Cohen, S.; Radominski, S.; Gomez-Reino, J.; Wang, L.; Krishnaswami, S.; Wood, S.; Soma, K.; Nduaka, C.; Kwok, K.; Valdez, H.; Benda, B.; Riese, R. Analysis of Infections and All-Cause Mortality in Phase II, Phase III, and Long-Term Extension Studies of Tofacitinib in Patients With Rheumatoid Arthritis. *Arthritis Rheumatol.* **2014,** *66,* 2924–2937.
34. US Food and Drug Administration. Tofacitinib citrate. http://labeling.pfizer.com/ShowLabeling.aspx?id=959, (assessed August 9, 2016).
35. Curtis, J.; Lee, E.; Kaplan, I.; Kwok, K.; Geier, J.; Benda, B.; Soma, K.; Wang, L.; Riese, R. Tofacitinib, an Oral Janus Kinase Inhibitor: Analysis of Malignancies Across the Rheumatoid Arthritis Clinical Development Programme. *Ann. Rheum. Dis.* **2015,** *75,* 831–841.
36. van Vollenhoven, R.; Riese, R.; Krishnaswami, S.; Kawabata, T.; Fosser, C.; Rottinghaus, S.; Lamba, S.; Zwillich, S. Relationship Between Lymphocyte Count and Risk of Infection in Rheumatoid Arthritis Patients Treated With Tofacitinib. *Arthritis Rheum.* **2013,** *65,* S994.
37. McInnes, I.; Kim, H.; Lee, S.; Mandel, D.; Song, Y.; Connell, C.; Luo, Z.; Brosnan, M.; Zuckerman, A.; Zwillich, S.; Bradley, J. Open-Label Tofacitinib and Double-Blind Atorvastatin in Rheumatoid Arthritis Patients: A Randomised Study. *Ann. Rheum. Dis.* **2014,** *73,* 124–131.
38. Charles-Schoeman, C.; Fleischmann, R.; Davignon, J.; Schwartz, H.; Turner, S.; Beysen, C.; Milad, M.; Hellerstein, M.; Luo, Z.; Kaplan, I.; Riese, R.; Zuckerman, A.; McInnes, I. Potential Mechanisms Leading to the Abnormal Lipid Profile in Patients With Rheumatoid Arthritis Versus Healthy Volunteers and Reversal by Tofacitinib. *Arthritis Rheumatol.* **2015,** *67,* 616–625.
39. Charles-Schoeman, C.; Wicker, P.; Gonzalez-Gay, M.; Wood, S.; Boy, M.; Grier, J.; Gruben, D.; Soma, K.; Riese, R. Cardiovascular Safety Findings in Rheumatoid Arthritis Patients Treated With Tofacitinib, a Novel, Oral Janus Kinase Inhibitor. *Arthritis Rheum.* **2013,** *65,* S191.
40. Keystone, E.; Taylor, P.; Drescher, E.; Schlichting, D.; Beattie, S.; Berclaz, P.; Lee, C.; Fidelus-Gort, R.; Luchi, M.; Rooney, T.; Macias, W.; Genovese, M. Safety and Efficacy of Baricitinib at 24 Weeks in Patients With Rheumatoid Arthritis Who Have Had an Inadequate Response to Methotrexate. *Ann. Rheum. Dis.* **2015,** *74,* 333–340.
41. Fleischmann, R.; Schiff, M.; van der Heijde, D.; Ramos, C.; Spindler, A.; Stanislav, M.; Zerbini, C.; Gurbuz, S.; Dickson, C.; de Bono, S.; Schlichting, D.; Beattie, S.; Kuo, W.; Rooney, T.; Macias, W.; Takeuchi, T. Baricitinib, Methotrexate, or Combination in Patients With Rheumatoid Arthritis and No or Limited Prior Disease-Modifying Antirheumatic Drug Treatment. *Arthritis Rheumatol.* **2016** (in press).

42. Schiff, M.; Takeuchi, T.; Gaich, C.; DeLozier, A.; Schlichting, D.; Kuo, W.; Durez, P.; Carmack, T.; Won, J.; Fleischmann, R. Patient-Reported Outcomes From a Phase 3 Study of Baricitinib in Patients With Early Rheumatoid Arthritis Who Had Received Limited or No Treatment With Disease-Modifying Anti-Rheumatic Drugs. *Ann. Rheum. Dis.* **2016,** *75* (Suppl. 2), 419.
43. Genovese, M.; Kremer, J.; Zamani, O.; Ludivico, C.; Krogulec, M.; Xie, L.; Beattie, S.; Koch, A.; Cardillo, T.; Rooney, T.; Macias, W.; de Bono, S.; Schlichting, D.; Smolen, J. Baricitinib in Patients With Refractory Rheumatoid Arthritis. *N. Engl. J. Med.* **2016,** *374,* 1243–1252.
44. Dougados, M.; van der Heijde, D.; Chen, Y.; Greenwald, M.; Drescher, E.; Liu, J.; Beattie, S.; de la Torre, I.; Rooney, T.; Schlichting, D.; de Bono, S.; Emery, P. Baricitinib, an Oral Janus Kinase (JAK)1/JAK2 Inhibitor, in Patients With Active Rheumatoid Arthritis (RA) and an Inadequate Response to csDMARD Therapy: Results of the Phase 3 RA-BUILD Study. *Ann. Rheum. Dis.* **2015,** *74* (Supplement 2), 79.
45. Taylor, P.; Keystone, E.; van der Heijde, D.; Tanaka, Y.; Ishii, T.; Emoto, K.; Yang, T.; Arora, V.; Gaich, C.; Rooney, T.; Schlichting, D.; Macias, W.; de Bono, S.; Weinblatt, M. Baricitinib versus placebo or adalimumab in patients with active rheumatoid arthritis (RA) and an inadequate response to background methotrexate therapy: Results of a phase 3 study. *Arthritis Rheumatol.* **2015,** *67.* http://acrabstracts.org/abstract/baricitinib-versus-placebo-or-adalimumab-in-patients-with-active-rheumatoid-arthritis-ra-and-an-inadequate-response-to-background-methotrexate-therapy-results-of-a-phase-3-study/, (accessed August 10, 2016).
46. Takeuchi, T.; Genovese, M.; Xie, L.; Issa, M.; Pinto Correia, A.; Rooney, T.; Emoto, K.; Smolen, J. Baricitinib Dose Step-Down Following Disease Control in Patients With Rheumatoid Arthritis. *Ann. Rheum. Dis.* **2016,** *75* (Supplement 2), 144.
47. Smolen, J.; Genovese, M.; Takeuchi, T.; Hyslop, D.; Macias, W.; Rooney, T.; Chen, L.; Dickson, C.; Riddle, J.; Cardillo, T.; Winthrop, K. Safety Profile of Baricitinib in Patients With Active RA: An Integrated Analysis. *Ann. Rheum. Dis.* **2016,** *75* (Supplement 2), 243.
48. Vanhoutte, F.; Mazur, M.; Van der Aa, A.; Wiegerinck, P.; van't Klooster, G. Selective JAK1 Inhibition in the Treatment of Rheumatoid Arthritis: Proof of Concept With GLPG0634. *Arthritis Rheum.* **2012,** *64,* S1051.
49. Kavanaugh, A.; Ponce, L.; Cseuz, R.; Reshetko, O.; Stanislavchuk, M. A.; Greenwald, M.; Van der Aa, A.; Vanhoutte, F.; Tasset, C.; Harrison, P. Filgotinib (GLPG0634), an oral JAK1 selective inhibitor is effective as monotherapy in patients with active rheumatoid arthritis: Results from a phase 2B dose ranging study. *Arthritis Rheumatol.* **2015,** *67.* http://acrabstracts.org/abstract/filgotinib-glpg0634-an-oral-jak1-selective-inhibitor-is-effective-as-monotherapy-in-patients-with-active-rheumatoid-arthritis-results-from-a-phase-2b-dose-ranging-study/. (accessed August 10, 2016).
50. Westhovens, R.; Alten, R.; Pavlova, D.; Enríquez-Sosa, F.; Mazur, M.; Greenwald, M.; Van der Aa, A.; Vanhoutte, F.; Tasset, C.; Harrison, P. Filgotinib (GLPG0634), an Oral JAK1 Selective Inhibitor Is Effective in Combination With Methotrexate In Patients With Active Rheumatoid Arthritis: Results From A Phase 2B Dose Ranging Study. *Arthritis Rheumatol.* **2015,** *67* (Supplement 10). Abstract 1048. http://acrabstracts.org/abstract/filgotinib-glpg0634-an-oral-jak1-selective-inhibitor-is-effective-in-combination-with-methotrexate-in-patients-with-active-rheumatoid-arthritis-results-from-a-phase-2b-dose-ranging-study/, (accessed August 10, 2016).
51. Genovese, M.; Westhovens, R.; Kavanaugh, A.; Meuleners, L.; Van der Aa, A.; Harrison, P.; Tasset, C. The Effect of Filgotinib (GLG0634), an Oral JaK1 Selective Inhibitor on Patient-Reported Outcomes: Results From Two 24-Week Phase 2b Dose Ranging Studies. *Ann. Rheum. Dis.* **2016,** *75* (Supplement 2), 244.
52. Kavanaugh, A.; Ponce, L.; Cseuz, R.; Reshetko, O.; Stanislavchuk, M.; Greenwald, M.; Van der Aa, A.; Vanhoutte, F.; Tasset, C.; Harrison, P. Filgotinib (GLPG0634), an Oral JaK1 Selective Inhibitor Is Effective as Monotherapy in Patients With Active Rheumatoid Arthritis: Results From a 24-Week Phase 2b dos Ranging Study. *Ann. Rheum. Dis.* **2016,** *75* (Supplement 2), 247.
53. Genovese, M.; Smolen, J.; Weinblatt, M.; Burmester, G.; Meerwein, S.; Camp, H.; Wang, L.; Othman, A.; Khan, N.; Pangan, A.; Jungerwirth, S. Safety and Efficacy of ABT-494, a Novel Selective JaK1 Inhibitor, in Patients With Active Rheumatoid Arthritis With an Inadequate Response to Methotrexate. *Arthritis Rheumatol.* **2016.** http://dx.doi.org/10.1002/art.39808 [Epub ahead of print].
54. Kremer, J.; Keystone, E.; Emery, P.; Camp, H.; Friedman, A.; Wang, L.; Othman, A.; Khan, N.; Jungerwirth, S. Safety and Efficacy of ABT-494, a Novel Selective JAK1 Inhibitor, in Patients With Active Rheumatoid Arthritis and Inadequate Response or Intolerance to Anti-TNF Biologic Therapy. *Arthritis Rheumatol.* **2015,** *67* (Supplement 10). http://acrabstracts.org/abstract/safety-and-efficacy-of-abt-494-a-novel-selective-jak1-inhibitor-in-patients-with-active-rheumatoid-arthritis-and-inadequate-response-or-intolerance-to-anti-tnf-biologic-therapy, (accessed August 17, 2016).
55. Takeuchi, T.; Tanaka, Y.; Iwasaki, M.; Ishikura, H.; Saeki, S.; Kaneko, Y. Efficacy and Safety of the Oral Janus Kinase Inhibitor Peficitinib (ASP015K) Monotherapy in Patients With Moderate to Severe Rheumatoid Arthritis in Japan: A 12-Week, Randomised, Double-Blind, Placebo-Controlled Phase IIb Study. *Ann. Rheum. Dis.* **2016,** *75,* 1057–1064.
56. Genovese, M.; Greenwald, M.; Codding, C.; Cardiel, M.; Zubrzycka-Sienkiewicz, A.; Kivitz, A.; Wisseh, S.; Shay, K.; Garg, J. A Phase 2b, Randomized, Double-Blind, Parallel-Group, Placebo-Controlled, Dose-Finding, Multi-Center Study to Evaluate the Safety and Efficacy of ASP015K in Moderate to Severe Rheumatoid Arthritis Subjects not on Concomitant Methotrexate. *Arthritis Rheum.* **2014,** *66,* S1234.
57. Kivitz, A.; Zubrzycka-Sienkiewicz, A.; Gutierrez-Uren, S.; Poiley, J.; Kristy, R.; Shay, K.; Garg, J. A Phase 2b, Randomized, Double-Blind, Parallel-Group, Placebo-Controlled, Dose-Finding, Multi-Center Study to Evaluate the Safety and Efficacy of ASP015K in Moderate to Severe Rheumatoid Arthritis Subjects who Have had an Inadequate Response to Methotrexate. *Arthritis Rheum.* **2014,** *66,* S421.
58. Fleischmann, R.; Damjanov, N.; Kivitz, A.; Legedza, J.; Hoock, A.; Kinnman, N. A Double-Blind, Placebo-Controlled, Randomized, 12-Week, Dose-Ranging Study of VX-509 (Decernotinib), an Oral Selective Janus Kinase 3 (JAK3) Inhibitor, as Monotherapy in Patients With Active Rheumatoid Arthritis. *Arthritis Rheumatol.* **2015,** *67,* 334–343.
59. Strand, V.; Suthoff, E.; Fleischmann, R.; Vera-Llonch, M.; Jiang, J.; Zhang, Y.; Kinman, N. Effects of VX-509, An Investigational Oral Selective Janus Kinase 3 (JAK3) Inhibitor, on Patient-Reported Outcomes in a Phase 2A Study of Patients With Active Rheumatoid Arthritis **2013,** *66* (10 (Supplement)). S1004 Abstract 2350.
60. Genovese, M.; van Vollenhoven, R.; Pacheco-Tena, C.; Zhang, Y.; Kinnman, N. VX-509 (Decernotinib), an Oral Selective JAK-3 Inhibitor, in Combination With Methotrexate in Patients With Rheumatoid Arthritis. *Arthritis Rheumatol.* **2016,** *68,* 46–55.
61. Williams, W.; Scherle, P.; Shi, J. A Randomized Placebo-Controlled Study of INCB018424, a Selective Janus Kinase 1& 2 (JAK1&2) Inhibitor in Rheumatoid Arthritis (RA. *Arthritis Rheum.* **2008,** *58* (10 (Supplement)), S431. Abstract 714.
62. Riccaboni, M.; Bianchi, I.; Petrillo, P. Spleen Tyrosine Kinases: Biology, Therapeutic Targets and Drugs. *Drug Discov. Today* **2010,** *15,* 517–530.
63. Pamuk, O.; Tsokos, G. Spleen Tyrosine Kinase Inhibition in the Treatment of Autoimmune, Allergic and Auto-Inflammatory Diseases. *Arthritis Res. Ther.* **2010,** *12,* 222–228.
64. Tohyama, Y.; Yamamura, H. Protein Tyrosine Kinase, Syk: A Key Player in Phagocytic Cells. *J. Biochem.* **2009,** *145,* 267–273.
65. Mocsai, A.; Ruland, J.; Tybulewicz, L. The Syk Tyrosine Kinase: A Crucial Player in Diverse Biological Functions. *Nat. Rev. Immunol.* **2010,** *10,* 387–402.
66. Weinblatt, M.; Kavanaugh, A.; Burgos-Vargas, R.; Dikranian, A.; Medrano-Ramirez, G.; Morales-Torres, J.; Murphy, F.; Musser, T.; Straniero, N.; Vicente-Gonzales, A.; Grossbard, E. Treatment of Rheumatoid Arthritis With a Syk Kinase Inhibitor: A Twelve-Week, Randomized, Placebo-Controlled Trial. *Arthritis Rheum.* **2008,** *58,* 3309–3318.
67. Weinblatt, M.; Kavanaugh, A.; Genovese, M.; Musser, T.; Grossbard, E.; Magilavy, D. An Oral Spleen Tyrosine Kinase (Syk) Inhibitor for Rheumatoid Arthritis. *N. Engl. J. Med.* **2010,** *363,* 1303–1312.
68. Genovese, M.; Kavanaugh, A.; Weinblatt, M.; Peterfy, C.; DiCarlo, J.; White, M.; O'Brien, M.; Grossbard, E.; Magilavy, D. An Oral Syk Kinase Inhibitor in the Treatment of Rheumatoid Arthritis: A Three-Month Randomized, Placebo-Controlled, Phase II Study in Patients With Active Rheumatoid Arthritis That Did Not Respond to Biologic Agents. *Arthritis Rheum.* **2011,** *63,* 337–345.
69. Taylor, P.; Genovese, M.; Greenwood, M.; Ho, M.; Nasonov, E.; Oemar, B.; Stoilov, R.; Vencovsky, J.; Weinblatt, M. OSKIRA-4: A Phase IIb Randomised, Placebo-Controlled Study of the Efficacy and Safety of Fostamatinib Monotherapy. *Ann. Rheum. Dis.* **2015,** *74,* 2123–2129.
70. Weinblatt, M.; Genovese, M.; Ho, M.; Hollis, S.; Rosiak-Jedrychowicz, K.; Kavanaugh, A.; Millson, D.; Leon, G.; Wang, M.; van der Heijde, D. Effects of Fostamatinib, an Oral Spleen Tyrosine Kinase Inhibitor, in Rheumatoid Arthritis Patients With an Inadequate Response to Methotrexate: Results From a Phase III, Multicenter, Randomized, Double-Blind, Placebo-Controlled, Parallel-Group Study. *Arthritis Rheumatol.* **2014,** *66,* 3255–3264.
71. Genovese, M.; van der Heijde, D.; Keystone, E.; Spindler, A.; Benhamou, C.; Kavanaugh, A.; Fudman, E.; Lampi, K.; O'Brien, C.; Duffield, E.; Poiley, J.; Weinblatt, M. A Phase III, Multicenter, Randomized, Double-Blind, Placebo-Controlled, Parallel-Group Study of 2 Dosing Regimens of Fostamatinib in Patients With Rheumatoid Arthritis With an Inadequate Response to a Tumor Necrosis Factor-α Antagonist. *J. Rheumatol.* **2014,** *41,* 2120–2128.

72. Lindvall, J.; Blomberg, K.; Valiaho, J.; Vargas, L.; Heinonen, J.; Berglof, A.; Mohamed, A.; Nore, B.; Vihinen, M.; Smith, C. Bruton's Tyrosine Kinase: Cell Biology, Sequence Conservation, Mutation Spectrum, siRNA Modifications, and Expression Profiling. *Immunol. Rev.* **2005,** *203,* 200–215.
73. Kelly, V.; Genovese, M. Novel Small Molecule Therapeutics in Rheumatoid Arthritis. *Rheumatology* **2013,** *52,* 1155–1162.
74. Di Paolo, J.; Huang, T.; Balazs, M.; Barbosa, J.; Barck, K.; Bravo, B.; Carano, R.; Darrow, J.; Davies, D.; DeForge, L.; Diehl, L.; Ferrando, R.; Gallion, S.; Giannetti, A.; Gribling, P.; Hurez, V.; Hymowitz, S.; Jones, R.; Kropf, J.; Lee, W.; Maciejewski, P.; Mitchell, S.; Rong, H.; Staker, B.; Whitney, J.; Yeh, S.; Young, W.; Yu, C.; Zhang, J.; Reif, K.; Currie, K. Specific Btk Inhibition Suppresses B Cell- and Myeloid Cell-Mediated Arthritis. *Nat. Chem. Biol.* **2011,** *7,* 41–50.
75. Chang, B.; Huang, M.; Francesco, M.; Chen, J.; Sokolove, J.; Magadala, P.; Robinson, W.; Buggy, J. The Bruton Tyrosine Kinase Inhibitor PCI-32765 Ameliorates Autoimmune Arthritis by Inhibition of Multiple Effector Cells. *Arthritis Res. Ther.* **2011,** *13,* R115–R121.
76. Honigberg, L.; Smith, A.; Sirisawad, M.; Verner, E.; Loury, D.; Chang, B.; Li, S.; Pan, Z.; Thamm, D.; Miller, R.; Buggy, J. The Bruton Tyrosine Kinase Inhibitor PCI-32765 Blocks B-Cell Activation and Is Efficacious in Models of Autoimmune Disease and B-Cell Malignancy. *Proc. Natl. Acad. Sci. U. S. A.* **2010,** *107,* 13075–13080.
77. Bender, A.; Beavo, A. Cyclic Nucleotide Phosphodiesterases: Molecular Regulation to Clinical Use. *Pharmacol. Rev.* **2006,** *58,* 488–520.
78. Boswell-Smith, V.; Spina, D.; Page, C. P. Phosphodiesterase Inhibitors. *Br. J. Pharmacol.* **2006,** *147* (Supplement 1), S252–S257.
79. Page, C.; Spina, D. Phosphodiesterase Inhibitors in the Treatment of Inflammatory Diseases. *Handb. Exp. Pharmacol.* **2011,** *204,* 391–414.
80. Rao, Y.; Xi, L. Pivotal Effects of Phosphodiesterase Inhibitors on Myocyte Contractility and Viability in Normal and Ischemic Hearts. *Acta Pharmacol. Sin.* **2009,** *30,* 1–24.
81. McCann, F.; Palfreeman, A.; Andrews, M.; Perocheau, D.; Inglis, J.; Schafer, P.; Feldmann, M.; Williams, R.; Brennan, F. Apremilast, a Novel PDE4 Inhibitor, Inhibits Spontaneous Production of Tumour Necrosis Factor-Alpha from Human Rheumatoid Synovial Cells and Ameliorates Experimental Arthritis. *Arthritis Res. Ther.* **2010,** *12,* R107–R112.
82. Kavanaugh, A.; Mease, P.; Gomez-Reino, J.; Adebajo, A.; Wollenhaupt, J.; Gladman, D.; Hochfeld, M.; Teng, L.; Schett, G.; Lespessailles, E.; Hal, S. Long-Term (52-Week) Results of a Phase III Randomized, Controlled Trial of Apremilast in Patients With Psoriatic Arthritis. *J. Rheumatol.* **2015,** *4,* 479–488.
83. Cutolo, M.; Myerson, G.; Fleischmann, R.; Liote, F.; Diaz-Gonzalez, F.; Van den Bosch, F.; Marzo-Ortega, H.; Feist, E.; Shah, K.; Hu, C.; Stevens, R.; Poder, A. A Phase III, Randomized, Controlled Trial of Apremilast in Patients With Psoriatic Arthritis: Results of the PALACE 2 Trial. *J. Rheumatol.* **2016,** *43* (9), 1724–1734.
84. Edwards, C.; Blanco, F.; Crowley, J.; Birbara, C.; Jaworski, J.; Aelion, J.; Stevens, R.; Vessey, A.; Zhan, X.; Bird, P. Apremilast, an Oral Phosphodiesterase 4 Inhibitor, in Patients With Psoriatic Arthritis and Current Skin Involvement: A Phase III, Randomised, Controlled Trial (PALACE 3). *Ann. Rheum. Dis.* **2016,** *75,* 1065–1073.
85. Wells, A.; Adebajo, A.; Aelion, J.; Bird, P.; Kivitz, A.; Liote, F.; Sarzi-Puttini, P.; Hu, C.; Stevens, R.; Edwards, C. Apremilast, an Oral Phosphodiesterase 4 Inhibitor, Is Associated With Long-Term (52-Week) Improvement in the Signs and Symptoms of Psoriatic Arthritis in DMARD-Naive Patients: Results From a Phase 3, Randomized, Controlled Trial. *Arthritis Rheum.* **2014,** *66,* S680.
86. Kavanaugh, A.; Adebajo, A.; Gladman, D.; Gomez-Reino, J.; Hall, S.; Lespessailles, E.; Mease, P.; Schett, G.; Shah, K.; Hu, C.; Wollenhaupt, J. Long-Term (104-Week) Efficacy and Safety Profile of Apremilast, an Oral Phosphodiesterase 4 Inhibitor, in Patients With Psoriatic Arthritis: Results From a Phase III, Randomised, Controlled Trial and Open-Label Extension (PALACE 1). *Ann. Rheum. Dis.* **2015,** *74* (Supplement 2), 350.
87. Edwards, C.; Blanco, F.; Crowley, J.; Hu, C.; Shah, K.; Birbara, C. Disease Activity and Safety During Long-Term (104-Week) Treatment With Apremilast, an Oral Phosphodiesterase 4 Inhibitor, in Patients With Psoriatic Arthritis: Results From a Phase III, Randomized, Controlled Trial and Open-Label Extension (PALACE 3). *Ann. Rheum. Dis.* **2016,** *75* (Supplement 2), 347.
88. Gladman, D.; Kavanaugh, A.; Adebajo, A.; Gomez-Reino, J.; Wollenhaupt, J.; Cutolo, M.; Schett, G.; Lespessailles, E.; McIlraith, M.; Hu, C.; Edwards, C.; Birbara, C.; Mease, P. Apremilast, an Oral Phosphodiesterase 4 Inhibitor, Is Associated With Long-Term (104-Week) Improvements in Enthesitis and Dactylitis in Patients With Psoriatic Arthritis: Pooled Results From Three Phase 3, Randomized, Controlled Trials. *Ann. Rheum. Dis.* **2015,** *74* (Supplement 2), 133.
89. Zhang, F.; Clancy, Z.; Li, S. Long-Term Work Productivity Improvement Associated With Apremilast, an Oral Phosphodiesterase 4 Inhibitor, in Patients With Psoriatic Arthritis: Pooled Analysis of 3 Phase 3 Studies. *Ann. Rheum. Dis.* **2015,** *74* (Supplement 2), 866.
90. Edwards, C.; Blanco, F.; Crowley, J.; McIlraith, M.; Shah, K.; Teng, T.; Birbara, C. DAS-28 Remission and Improvements in Skin Disease Over 3 Years of Treatment With Apremilast: Results From the Palace 3 Study in DMARD/Biologic-Experienced Active PsA Patients. *Ann. Rheum. Dis.* **2016,** *75* (Supplement2), 347.
91. Mease, P.; Kavanaugh, A.; Gladman, D.; Adebajo, A.; Gomez-Reino, J.; Wollenhaupt, J.; Cutolo, M.; Schett, G.; Lespessailles, E.; Shah, K.; Hu, C.; Stevens, R.; Edwards, C.; Birbara, C. Long-Term Safety and Tolerability of Apremilast, an Oral Phosphodiesterase 4 Inhibitor, in Patients With Psoriatic Arthritis: Pooled Safety Analysis of Three Phase 3, Randomized, Controlled Trials. *Arthritis Rheum.* **2013,** *65,* S131.
92. Mease, P.; Adebajo, A.; Gladman, D.; Gomez-Reino, J.; Hal, S.; Kavanaugh, A.; Lespessailles, E.; Schett, G.; Shah, K.; Teng, L.; Wollenhaupt, J. Laboratory Abnormalities in Patients With Psoriatic Arthritis Receiving Apremilast, an Oral Phosphodiesterase 4 Inhibitor: Pooled Safety Analysis of Three Phase 3, Randomized, Controlled Trials. *Ann. Rheum. Dis.* **2015,** *74* (Supplement 2), 355.
93. Mease, P.; Kavanaugh, A.; Adebajo, A.; Gomez-Reino, J.; Wollenhaupt, J.; Gladman, D.; Cutolo, M.; Schett, G.; Lespessailles, E.; Shah, K.; Hu, C.; Stevens, R.; Edwards, C.; Birbara, C. *Arthritis Rheum.* **2013,** *65,* S151.
94. Papp, K.; Reich, K.; Leonardi, C.; Kircik, L.; Chimenti, S.; Langley, R.; Hu, C.; Stevens, R.; Day, R.; Gordon, K.; Korman, N.; Griffiths, C. Apremilast, an Oral Phosphodiesterase 4 (PDE4) Inhibitor, in Patients With Moderate to Severe Plaque Psoriasis: Results of a Phase III, Randomized, Controlled Trial (Efficacy and Safety Trial Evaluating the Effects of Apremilast in Psoriasis [ESTEEM] 1). *J. Am. Acad. Dermatol.* **2015,** *73,* 37–49.
95. Paul, C.; Cather, J.; Gooderham, M.; Poulin, Y.; Mrowietz, U.; Ferrandiz, C.; Crowley, J.; Hu, C.; Stevens, R.; Shah, K.; Day, R.; Girolomoni, G.; Gottlieb, A. Efficacy and Safety of Apremilast, an Oral Phosphodiesterase 4 Inhibitor, in Patients With Moderate to Severe Plaque Psoriasis Over 52 Weeks: A Phase III, Randomized, Controlled Trial (ESTEEM 2). *Br. J. Dermatol.* **2015,** *173,* 1387–1399.
96. Hatemi, G.; Melikoglu, M.; Tunc, R.; Korkmaz, C.; Turgut-Ozturk, B.; Mat, C.; Merkel, P.; Calamia, K.; Liu, Z.; Pineda, L.; Stevens, R.; Yazici, H.; Yazici, Y. Apremilast for Behçet's Syndrome—A Phase 2, Placebo-Controlled Study. *N. Engl. J. Med.* **2015,** *372,* 1510–1518.

5.14 Therapeutic Approaches to MS and Other Neurodegenerative Diseases

LP Kotra and J Park, University of Toronto and University Health Network, Toronto, ON, Canada

© 2017 Elsevier Ltd. All rights reserved.

5.14.1	**Introduction**	441
5.14.1.1	Citrullination and Neurodegeneration	442
5.14.1.2	Calcium Imbalance	442
5.14.1.3	Acute Neuronal Injury	442
5.14.1.4	Chronic Neurodegeneration	443
5.14.2	**Therapeutic Approaches in MS**	444
5.14.2.1	Fingolimod	446
5.14.2.2	Teriflunomide	447
5.14.2.3	Dimethyl Fumarate	447
5.14.2.4	Laquinimod	447
5.14.2.5	Interferon β-1b	448
5.14.2.6	Interferon β-1a (IFN-β-1a; Avonex, and Rebif)	448
5.14.2.7	Peginterferon β-1a	449
5.14.2.8	Natalizumab	449
5.14.2.9	Alemtuzumab	450
5.14.2.10	Glatiramer Acetate	450
5.14.2.11	Mitoxantrone	450
5.14.2.12	Rituximab	451
5.14.2.13	Cyclophosphamide	451
5.14.2.14	Adrenocorticotropin Hormone (ACTH)	451
5.14.2.15	Methotrexate	452
5.14.2.16	Cladribine	452
5.14.3	**Other Neurodegenerative Disorders**	453
5.14.3.1	Alzheimer's Disease	453
5.14.3.2	Therapeutic Approaches in AD	454
5.14.3.2.1	Donepezil	455
5.14.3.2.2	Rivastigmine	456
5.14.3.2.3	Galanthamine	456
5.14.3.2.4	Memantine	456
5.14.3.2.5	Select drugs in development for AD treatment	457
5.14.3.3	Parkinson's Disease	458
5.14.3.4	Therapeutic Approaches in PD	458
5.14.3.4.1	Carbidopa/levodopa	458
5.14.3.4.2	Pramipexole	459
5.14.3.4.3	Ropinirole	459
5.14.3.4.4	Bromocriptine	459
5.14.3.4.5	Cabergoline	459
5.14.3.4.6	Pergolide	459
5.14.3.4.7	Rotigotine	462
5.14.3.4.8	Anticholinergics (trihexyphenidyl and benzotropine)	462
5.14.3.4.9	Apomorphine	462
5.14.3.4.10	Amantadine	462
5.14.3.4.11	COMT inhibitors (entacapone and tolcapone)	462
5.14.3.4.12	MAO-B inhibitors (selegiline and rasagiline)	463
5.14.3.4.13	Istradefylline	463
5.14.3.4.14	Levodopa formulations	463
5.14.4	**Conclusion**	464
References		464
Relevant Websites		473

Abbreviations

A2a Adenosine 2a receptor
AADC Aromatic-L-amino-acid decarboxylase
Ach Acetylcholine
AchE Acetylcholine esterase
ACTH Adrenocorticotropin hormone
AD Alzheimer's disease
ADCC Antibody-directed cell cytolysis
ADL Activities of daily living
ALS Amyotrophic lateral sclerosis
AMD Age-related macular degeneration
AMPK AMP-activated protein kinase
ANLS Astrocyte neuron lactate shuttle
APC Antigen-presenting cell
ARR Annualized rate of relapse
AV Atrioventricular
Aβ Amyloid-β
BuChE Butyrylcholinesterase
cAMP Cyclic adenosine monophosphate
CDC Complement directed cytolysis
CDMS Clinically definite MS
CGIC Clinician evaluation
CHO Chinese hamster ovary
CIS clinically isolated syndrome
CLARITY Cladribine tablets treating multiple sclerosis orally
CNS Central nervous system
COMT Catechol-*O*-methyltransferase
CONFIRM Comparator and an oral fumarate in relapsing–remitting multiple sclerosis
CSF Cerebrospinal fluid
DE Diabetic encephalopathy
DEFINE Determination of the efficacy and safety of oral fumarate in relapsing–remitting MS
DHFR Dihydrofolate reductase
DHODH Dihydroorotate dehydrogenase
DIREQT Duodopa infusion: randomized efficacy and quality of life trail
DMD Disease-modifying drug
DMF Dimethyl fumarate
DMT Disease-modifying therapy
DS Down's syndrome
EAE Experimental autoimmune encephalomyelitis
EDSS Expanded disability status scale
FDA Food and Drug Administration
GA Glatiramer acetate
Gd Gadolinium
GFAP Glial fibrillary acidic protein
GSK-3 Glycogen synthase kinase 3
HD Huntington's disease
HERV Human endogenous retrovirus
HI Hypoxic ischemia
IBO Ibotenic acid
IFN Interferon
IL Interleukin
IVMP Intravenous methylprednisolone
LCIG Levodopa/carbidopa intestinal gel
LRRK2 Leucine-rich repeat kinase 2
MAO-B Monoamine oxidase type B
MBP Myelin basic protein
MCI Mild cognitive impairment
MMSE Mini-mental state examination
MPP + 1-Methyl-4-phenylpyridinium
MPTP *N*-Methyl-4-phenyl-1,2,3,6-tetrahydropyridine
MRI Magnetic resonance imaging
MS Multiple sclerosis
MTR Magnetization transfer ratio
MTX Mitoxantrone
NAWM Normal-appearing white matter
NET Neutrophil extracellular trap
NMDA *N*-Methyl-D-aspartate
NMO Neuromyelitis optica
NMR Nuclear magnetic resonance spectroscopy
nNOS Neuronal nitric oxide synthase
OCT Optical coherence tomography
ORACLE MS Oral cladribine for early MS
PAD Protein arginine deiminase
PBMC Peripheral blood mononuclear cell
PD Parkinson's disease
PEG Percutaneous endoscopic gastrostomy
PGC-1α Peroxisome proliferator-activated receptor γ coactivator-1α
PI3K Phosphoinositide 3-kinase
PML Progressive multifocal leukoencephalopathy
pMOG Peptide of myelin oligodendrocyte glycoprotein
PPMS Primary progressive MS
PROUD Pramipexole on underlying disease
PTCD2 Pentatricopeptide repeat domain 2
QOL-P Quality-of-life scores assessed by the patient
RCT Randomized controlled trial
RRMS Relapsing–remitting MS
S1P Sphingosine-1-phosphate
SIRT1 Sirtuin 1
SNRS Scripps neurological rating scale
SPMS Secondary progressive MS
SSRI Serotonin selective reuptake inhibitor
TB Tuberculosis
Th T-helper
TSQM Treatment satisfaction questionnaire for medication
UPDRS Unified Parkinson's disease rating scale
VCAM Vascular adhesion molecule
VGCC Voltage-gated calcium channel

5.14.1 Introduction

Multiple sclerosis (MS) is the most common chronic inflammatory disease of the central nervous system (CNS), with distinct demyelination of axons and brain atrophy with an early onset that affects young to middle-aged adults.[1] Recent studies suggest that the disease progression in MS integrally involves neurodegeneration along with autoinflammatory component.[2] MS is diagnosed usually late after the disease onset based on gadolinium (Gd)-enhanced magnetic resonance imaging (MRI), and until recently, definitive diagnosis was difficult due to the lack of diagnostic tools.[3] The exact causes of MS are still unknown, but MS is considered to be a disease of multifactorial origin with a strong inflammatory component based on the detection of autoreactive T cells, B cells, and macrophages in active MS lesions.[4] In the past 20 years, significant progress was accomplished in understanding and moderating the acute inflammatory components of MS, but the pathophysiological mechanisms of the underlying neurodegeneration, which causes irreversible damage to the CNS and physical disability, are still not completely understood. MS is gaining acceptance as a neurodegenerative disease, and in general, many neurodegenerative diseases are challenging to diagnose early and to identify a unique target for the development of therapeutics.

The complex patterns involved in the onset and progression of the disease and diagnostic challenges in MS historically are related to a number of controversies and differences in opinions in various aspects of MS.[5] These challenges are also due to the poor understanding of the molecular mechanisms and relationship between relapses and disability progression due to neurodegeneration. MS has classically been considered as an autoimmune, white matter disease. Overall, physical disability progression and brain and spinal cord atrophy were regarded as consequences of global inflammation of normal-appearing white matter (NAWM), and gray matter involvement was considered secondary. Recent histopathology studies and MRI techniques indicated that the pathology in MS is a prominent gray and white matter disease.[6] Inflammatory demyelination of gray matter occurs early in MS, and following this observation, immunomodulatory drugs were introduced and became the main therapeutic option for the treatment of MS. Although early therapy of MS with immunomodulatory drugs protects the CNS from the consequential damage due to inflammatory attacks, disability progression and neurodegeneration continue to deteriorate the clinical status of the patient. This indicates that antiinflammatory treatment is not adequate to treat and/or manage MS successfully. Due to the lack of a single target responsible for the disease onset and/or progression and complex factors involved during the clinical course of MS, it is now well recognized that therapeutic approaches must manage the disease and prevent worsening of the disability, achieved through so-called disease-modifying therapies (DMTs). There is now considerable understanding and acceptance that chronic inflammatory processes continuously disturb neuroaxonal homeostasis and promote neurodegeneration. Clinical outcomes in these situations depend on the balance of damage due to inflammation and any remaining capacity for neuronal self-protection. Hence, suitable drugs that promote the remyelination are also considered to be potentially efficacious.

There are four clinical types of MS, all of which are characterized on the basis of inflammatory and neurodegenerative disease states using MRI-based diagnostic tools. This measurement system is recently introduced and updated from the previously established measurement system.[7,8] These four types are the following: (1) *Clinically isolated syndrome (CIS)*: CIS is the first episode of neurological symptoms caused by inflammation and demyelination in the CNS. Although this does not meet the criteria for definitive MS diagnosis, when CIS is accompanied by brain lesions on MRI, the patient has a high likelihood of a second attack leading to the diagnosis of MS. It is also reported that optic neuritis many times is one of these CISs that often leads to clinically diagnosed MS.[9] (2) *Relapsing–remitting MS (RRMS)*: In the RRMS stages of the disease, clearly defined attacks, in the form of relapses or inflammatory exacerbations, are experienced by the patients. These attacks are episodes of acute worsening of clinical symptoms, followed by partial or complete recovery for a period of time with no disease progression. RRMS is further characterized as active stage with CNS lesions and/or relapses, not active and worsening stage with increased disability resulting from symptoms that do not completely disappear following a relapse, or not worsening stage. RRMS is the most common form of MS when patients are diagnosed, and almost 85% of patients are diagnosed at this stage.[10] (3) *Primary progressive MS (PPMS)*: A slow and continuous worsening of the disease from the onset of symptoms is observed in the patients with the PPMS, almost with no relapses or remissions. The rates of progression over time may vary among different patients with occasional plateaus and minor, albeit temporary, improvements in the clinical symptoms. Similar to RRMS, PPMS is further characterized as active with MRI activity and/or relapses, not active and progressing—exhibiting a confirmed increase in disability over a given period of time, or not progressing. PPMS is the second most commonly diagnosed form of MS, amounting to up to 15% of MS diagnoses. (4) *Secondary progressive MS (SPMS):* This type of MS is characterized by a combination of RRMS-like and PPMS-like disease courses; patients experience an initial period of RRMS, followed by a steadily worsening disease course with or without occasional flare-ups, minor recoveries (remissions), or plateaus. It must be noted that majority of patients with RRMS will eventually transition to SPMS. However, early diagnosis and early and ongoing treatment with a DMT have been shown to delay SPMS, and age plays an important role for the onset of progressive phase of the disease.[11]

The role of immune system in MS has been explored in-depth over the past several decades, and a number of immunomodulatory approaches are used to develop novel therapeutics. This article is particularly interested in looking into neurodegeneration and nonimmunologic mechanisms that are emerging and gaining traction with a focus on protein citrullination. These nonimmunologic mechanisms are also known to play a role in other neurodegenerative diseases such as Parkinsons' disease (PD) and Alzheimer's disease (AD). Thus, in the latter sections of this article, therapeutic approaches in these two diseases are described in the context of neurodegeneration.

5.14.1.1 Citrullination and Neurodegeneration

Protein arginine deiminases (PADs) are a family of five isozymes, PAD1–4 and PAD6, and these are comparatively less-studied enzymes for their role in various disease conditions.[12] They are involved in the posttranslational modification of peptidyl Arg residues, specifically those on the surface of the proteins and accessible for a biochemical transformation. They hydrolyze the terminal guanidinium moiety of peptidyl Arg into peptidyl citrulline residue, altering the surface charges on the protein surface. PADs have a wide range of tissue distribution and play a role in many physiological processes. PAD2 and PAD4 are in general associated with neuronal cells and neurodegeneration. PAD2 is expressed broadly in the skeletal muscle, brain, spleen, and secretory glands.[13–16] In particular and of relevance, PAD2 is found in various compartments of the brain such as in the cerebral cortex, hippocampus, and cerebellum.[17] PAD2 is present in myelin basic protein (MBP)-producing oligodendrocytes and is implied to play a role in myelin formation and plasticity within the CNS.[18] Elevated PAD2 and PAD4 activities are associated with hypercitrullinated MBP (and other cellular proteins in the neurons) and neurodegeneration.[19] PAD4, the only isozyme with a nuclear localization signal, is also expressed in white blood cells[20] and has been implicated in the immune response by initiating neutrophil extracellular traps (NETs) via chromatin remodeling.[21] The ability of PAD4 to enter the nucleus indicates a role for genetic regulation via epigenetic modification of histones, especially histone H3.[20] Overall, elevated levels of active PAD2/PAD4 enzymes and hypercitrullination play a definitive role in driving neuronal cell death and neurodegeneration in MS.

PADs cause the deimination of peptidyl arginine residues in a stepwise mechanism utilizing the two catalytic residues, Asp350 and Asp473 (PAD4 amino acid numbering) in the active site of these enzymes. Interaction of the positively charged guanidinium group with the negatively charged Asp side chains yields to the nucleophilic attack of Cys645 onto the guanidine group, followed by the displacement of ammonia with a water molecule. His471, which is in proximity to Cys645, participates as a proton donor and a proton acceptor in various steps of this hydrolysis process.[22] The formation of a tetrahedral intermediate with ammonia is the rate-limiting catalytic event, and this ammonia molecule is the leaving group during hydrolysis.[23] PADs are entirely Ca^{2+}-dependent enzymes. In fact, up to six Ca^{2+} ions are required for the optimal function of these enzymes. Mechanistic and mutagenesis studies of PAD4 confirmed that Ca^{2+} ions play a role in the organization and integrity of the active site at the C-terminal domain and in catalysis.[22–26]

5.14.1.2 Calcium Imbalance

Abnormal calcium influx is being considered at the root of a number of disease conditions in the recent times. Under various stress conditions, such as hypoxia and chemically induced ischemia,[27,28] the reversal of Ca^{2+}/Na^{+} exchange is seen in partially demyelinated axons due to overaccumulation of intracellular Na^{+} ions.[29,30] This phenomena is also seen upon interactions of immune cells with axons.[31] Due to its importance in activating PADs in vivo and the necessity of sufficient Ca^{2+} concentrations that are approximately 100 times greater than homeostatic cytosolic levels,[14] there is a high likelihood that PADs are dysregulated leading to their hyperactivity.[32–34] There is also emerging evidence of voltage-gated calcium channels (VGCCs) involvement in neurodegeneration via Ca^{2+} regulatory mechanisms. These channels may not carry high amounts of Ca^{2+} in neurons due to toxicity.[35] Some of these channels, such as L-type channels, are essential for Ca^{2+}-dependent regulation of prosurvival gene programs in the cells. However, there is a strong evidence that VGCC-dependent neurotoxicities are involved in a number of neurodegenerative diseases, adversely affecting the neurons, microglia, and neurovasculature. Data show a beneficial effect of drugs acting on VGCCs in several neurodegenerative and neurovascular diseases.[35] In particular, within the scope of this article, enhanced expression and activities of L-type Ca^{2+} channels were observed with Ca^{2+} overload in AD and chronic hypoxia conditions. On the other hand, in PD, VGCC-dependent neurotoxicity is observed without Ca^{2+} overload in the neurons. In MS, enhanced chemokine release and associated pathogenic mechanisms in the microglial compartments are shown to play a role in the VGCC-dependent neurotoxicity. Thus, VGCCs, which are usually required for neuronal survival, may take part in neurodegeneration under certain abnormal conditions. For example, high concentrations of Ca^{2+} could in turn activate normally quiescent or moderately active systems such as PADs, which leads to an apoptotic state of the neuronal cell (vide infra). VGCCs may also promote neuronal cell death without carrying excess Ca^{2+} in instances when they carry metal ions into neuronal cytoplasm or when a pathological decrease in their activity weakens Ca^{2+}-dependent prosurvival gene programs.[35]

Citrullination of proteins (or deimination of Arg residues on protein surfaces) increases with age even under normal conditions, and its potential significance to neurodegeneration may be relevant although must be proved further.[17,36] Shimada et al. showed that PAD2 protein and its corresponding mRNA levels steadily increased in the mouse brains up to 30 months of age.[17] In another study, a western blot analysis of citrullinated proteins in brain extracts from 8-week-old and 10- to 12-month-old mice and from humans in the ages of 29–40 years and 67–71 years showed an increase in deimination in the tissue from older subjects compared with that from younger subjects.[37] Such observations make one to consider the relationship between neurodegeneration and aging and any synergistic relationship for most of the neurodegenerative diseases to occur in aged population. Overall, evidence supports that hypercitrullination and elevated PAD activity are associated with neurodegeneration. Such a molecular insult to neuronal cells could be acute in nature, such as in hypoxic ischemia (HI), or chronic, such as in MS, PD, and AD.

5.14.1.3 Acute Neuronal Injury

Although this book article does not deal with neuronal injury, following discussion is somewhat relevant to events that may lead to neurodegeneration and subsequent manifestation of neurodegenerative conditions. HI occurs when the blood flow to cells and

organs becomes reduced; this lower concentration of oxygen due to decreased blood flow is insufficient for healthy function. The pathophysiology of HI involves membrane depolarization, brain edema, increased neurotransmitter release with inhibition of uptake, increased intracellular Ca^{2+}, and other events that eventually may lead to neuronal death.[38] Survivors of HI insult may show permanent neurological consequences including mental retardation, cerebral palsy, epilepsy, or learning disability.[39]

Increased intracellular calcium and its relevance in HI insult indicate a potential association of PADs and citrullination with HI. Indeed, protein citrullination has been observed in neonatal murine models of HI. Following HI induction, Lange et al. found an increase in deiminated (or citrullinated) proteins due to PAD enzymes, accompanied by cell death, activated microglia, and neuronal loss.[40] A direct relationship between HI insult and the induction of PAD activity was established using a covalent PAD inhibitor, Cl-amidine, where cell death and the levels of deiminated histones decreased in the presence of this PAD inhibitor.[40] *N*-methyl-D-aspartate (NMDA) glutamate receptors mediate the accumulation of calcium within the myelin sheath when chemical ischemia is induced, and this clearly affects the calcium levels and thus PAD activity in the neurons.[27] This process is similar to the aforementioned discussion leading to Ca^{2+} balance in the cells and potentially leading one to consider NMDA receptors as drug targets for the treatment of demyelinating diseases such as MS. This mechanism could be an independent mechanism for drug targeting.[27]

5.14.1.4 Chronic Neurodegeneration

MS is one of the common chronic demyelinating diseases with an early onset that affects young to middle-aged adults.[1] MS is often diagnosed late after the disease onset due to the lack of appropriate and accurate diagnostic tools, but MRI is helping to change that.[3] The exact causes of MS are quite debated and could be multifactorial, but MS is considered to be a disease of multifactorial origin with a strong inflammatory component based on the detection of autoreactive T cells, B cells, and macrophages in active MS lesions.[4] There is significant evidence that MS is composed of neurodegenerative and inflammatory components.[2] Majority of the current therapeutics are immunomodulatory, and the leading theory is an autoimmune theory for the root causes of MS. However, in the past decade, causes other than autoimmune in nature are put forward to account for the progressive neurodegenerative nature of this disease. One such molecular mechanism involves PAD enzymes, and hypercitrullination has been found to be associated with MS and its progression in studies of patient brain samples. It is observed that citrullination was more prominent in lesions compared to NAWM in both animal models and in human.[41,42] Other most prominently hypercitrullinated proteins found in tissues isolated from patients with MS include glial fibrillary acidic protein (GFAP),[43] MBP,[44,45] and histones.[46] Citrullinated MBP is also found in large spinal cord and small white matter extracellular brain lesions in addition to the brain lesions surrounded by astrocytes with peptidyl citrulline that colocalized with GFAP in murine models of MS.[43]

Of the five PAD isoforms, PAD2 and PAD4 may be the most relevant to MS, as both were found to be significantly upregulated in MS NAWM.[47] In rodent species, specifically in rats, PAD2 localizes to oligodendrocytes and is responsible for the citrullination of MBP when external Ca^{2+} is added in vitro to brain homogenates.[19] Studies on PAD2 knockout mice demonstrated that the enzyme was necessary for the citrullination of MBP and GFAP.[48] On the other hand, transgenic mice with overexpressed PAD2 cDNA showed thinning of myelin sheath and its degradation.[49] These data suggested that in rodents, upregulated PAD2 preceded MS-like disease progression. Enzyme activity levels of PAD2 and PAD4 were found to be elevated in peripheral blood mononuclear cells (PBMCs) isolated from MS patients, although this does not directly connect to the changes in the CNS.[50,51] With these data, one is led to the broad conclusion that the development and progression of MS may be associated with PAD dysregulation and hypercitrullination, which in turn may be related to the intracellular Ca^{2+} aberrations.

The MHC class II HLA-DRB1*1501 loci is highly associated with an increased risk of developing MS, and environmental factors such as vitamin D may also play a role in this context.[52,53] However, there seems to be no link between PAD genes and HLA-DRB1*15.[54] Nevertheless, epigenetic regulation appears to exist, and the two CpG islands in the promoter region of PAD2 have been found to be significantly hypomethylated in NAWM[55] and the PBMCs[50] of MS patients. These were positively correlated with increased transcription of PAD2 and associated enhanced citrullination, leading to hypercitrullination of proteins in the cell.

A link between PAD enzymes, the citrullination process they are responsible for, and hypercitrullination that contributes to MS pathogenesis via the generation of immunogenic antigens could be conceived where these modified or citrullinated proteins cause an inflammatory response and a break in autoimmunity. Although current evidence in animals does not fully support this idea and more evidence is needed, intent here is to provide a plausible explanation that MS may not be an autoimmune disease entirely and could have CNS origins. MBP is one of the most prominently citrullinated proteins associated with MS, and it plays a key role in maintaining the structural integrity of the myelin sheath via synergistic interactions with phospholipids.[56] The hypercitrullinated form of MBP, due to changes in the surface charges, was found to loosen the myelin sheath from its native C-shaped curvature. Such structural elements trigger digestion enzymes such as cathepsin D,[57] an aspartic protease that is known to be upregulated in the brains of patients with MS in regions around plaques.[58,59] Such digested myelin proteins and others generate potentially immunodominant epitopes with tertiary structures such as α-helical structure.[60,61] These modified protein epitopes may be protected from further digestion, allowing these epitopes to leave the CNS to interact and activate the peripheral immune system. Interestingly, citrullinated MBP was found to be more reactive to T cells than its noncitrullinated counterpart.[60] Furthermore, citrullinated epitopes of MBP were found to cause a Th1 polarized response in T cells isolated from patients with MS.[62] As described earlier, elevated PAD2 in the periphery has been associated with its epigenetic regulation in PBMCs.[50] Thus, to bring this all together, one can conceive that PAD2 primes the peripheral immune system for attack against citrullinated MBP in the CNS by generating citrullinated epitopes from the MBP, which is elevated in lymphoid tissues during experimental autoimmune

encephalomyelitis (EAE), typically induced in mice.[63] Typically, peptide of myelin oligodendrocyte glycoprotein (pMOG) is used as an antigen to induce EAE in mice. Evidence supports that citrullinated brain proteins in EAE mice generate neoantigens in due time, ultimately leading to nonspecific anticitrulline autoantibodies.[64] Citrullinated pMOG, however, cannot induce EAE in mice but can prime T cells to cause a relapse of EAE that was previously in remission in the EAE mice.[65] This leads one to suggest that hypercitrullination can exacerbate the inflammatory response in the mouse models of MS, and autoantibodies may also play a role in this event. While further studies are needed to identify the proteins involved in immune reactivities, which is no trivial task, IgG sensitivity to citrullinated MBP does not appear to be one of the significant components in the immunoreactive role played by citrullinated MBP in MS.[66]

Interestingly, PAD2, which is present in the nucleus, and PAD4, due to its nuclear localization signal, can citrullinate nuclear peptidyl Arg residues. Histone citrullination has been associated with MS, as the accumulation of citrullinated histones in NAWM of MS is suggested to lead to cellular apoptosis.[46] In these studies, translocation of PAD4 from cytosol into the nucleus was shown to be regulated by TNF-α in human oligodendroglial cells prior to demyelination. The apoptosis of oligodendrocytes may also initiate an autoimmune response if cellular debris is not cleared.[67–69] PAD4 upregulates the transcription of several human endogenous retroviruses (HERVs) and immune-related genes including TNF-α and IL-8, as a part of its epigenetic control. Citrullination of histone H3R8 reduces the binding affinity of the repressor protein HP1-α to the promoter regions of the aforementioned genes in PBMCs isolated from the MS patients.[51] Mastronardi et al. also noted a functional deficiency of HP1-α repressor protein in studies involving PAD4 and histones,[46] and interestingly, covalent inhibition of PAD4 reversed the derepression of HERVs and the cytokines. Increased transcription of cytokines may provide feedback for the priming of neutrophils.[72] Its worth noting that under normal conditions, histone H3 citrullination by PAD4 triggers a number of nuclear events leading to the formation of NETs in response to inflammatory stimuli for the trapping and killing of bacteria.[21,70,71] Furthermore, patients with MS were found to possess greater quantities of overactive neutrophils possibly because of the chronic inflammatory environment in MS.[72] These studies connect the PAD enzymes and immune reactivity to neurodegeneration or the loss of neurons overall via apoptosis and epigenetic control, primarily with evidence from in vitro studies and in vivo mouse models in MS. While it is not yet clear if these events occur in the human form of MS, inhibitors of PAD in the animal models of MS provide indirect evidence for the validity of these pathways in MS.[73] In fact, an in silico screening of PAD4 active site using chemical libraries led to a hydantoin-based derivative that inhibited these enzymes noncovalently.[74] This PAD inhibitor also exhibited good in vivo efficacy reducing the physical disability in the autoimmune encephalomyelitis mouse model and immune cells infiltration into the brains of the treated mice.[74] Preclinical and clinical development of compounds targeting nonimmunologic targets such as in the preceding text remains to be seen in the coming years.

Astrocytes play an important role in neuronal metabolism through the activation of the astrocyte–neuron lactate shuttle (ANLS). Their role is also significant in controlling the levels of extracellular glutamate, production of antioxidant molecules, disposal of neuronal waste products, storage of energy in the form of glycogen, and expression of neurotrophic factors. These mechanisms are essential for brain activity and cognition, and they also contribute to neuronal degeneration.

New DMTs can potentially be designed to regulate mechanisms and targets such as NMDA receptors, VGCCs, neuronal nitric oxide synthase (nNOS), oxidative stress from reactive oxygen species, and protein aggregation. Neurodegenerative diseases such as AD and PD are characterized by progressive neuroaxonal injury, indicating that they share a common pathophysiological pathway.[75] Due to the advanced neuroaxonal compromise at the time of initial onset of clinical symptoms, identification and development of neuroprotective therapies have proved to be challenging. Therefore, in order to ensure immediate neuroprotective therapies, methods for early identification of neurodegeneration are essential. The role of neuroaxonal injury in MS is more sufficiently understood, and the earlier manifestation in life and the earlier diagnosis in the course of the disease can be achieved in comparison with AD and PD. Therefore, MS can potentially be used as a model disease to study the degeneration and regeneration of the CNS. It is generally believed that inflammation leads to neurodegeneration in MS, but the reverse mechanism of neuroaxonal injury may also be true; the neuroaxonal degeneration leads to inflammation. Animal models of AD and PD displayed the initial inflammation that is followed by a degenerative process in most cases, indicating the similarity between MS and the classic neurodegenerative diseases. Other similarities between MS and the neurodegenerative diseases include iron and mitochondrial dysregulation, abnormalities in α-synuclein and tau protein, and a number of immune mediators. Using MS as a clinical model to study the course of neuroaxonal injury in the brain may signify a progress in treatment strategy development for AD and PD.

MRI techniques, such as nuclear magnetic resonance spectroscopy (NMR), magnetization transfer ratio (MTR), and myelin water imaging, aid in providing more pathology-specific data in MS studies. Moreover, optical coherence tomography (OCT) is used to quantify optic nerve integrity and retinal ganglion cell loss as markers of neuroaxonal injury. This is a non-MRI technique that still needs to be assessed on the reliability of the information obtained from the technique. Potentially, these techniques can be used to follow degeneration and regeneration longitudinally in MS patients and differentiate the effects of various drugs under investigation.

5.14.2 Therapeutic Approaches in MS

Therapeutic approaches in MS have evolved over the past several decades, from small molecules with immunomodulatory properties to monoclonal antibodies reducing the autoimmune insults, and the current treatment objective to delay or halt the progression of irreversible disability.[76] Disease-modifying drugs or disease-modifying therapeutics (DMDs or DMTs) including β-interferon and glatiramer acetate (Copaxone) have been shown to reduce relapse rates in RRMS as detected by MRI (Table 1). However, the

Table 1 Chemical structures of drugs for the treatment of multiple sclerosis

Drug name	*Chemical structure*
Fingolimod	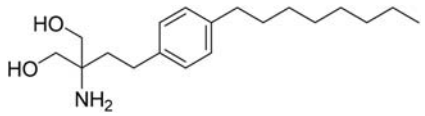
Teriflunomide	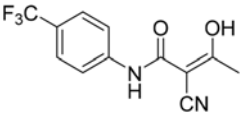
Dimethyl fumarate	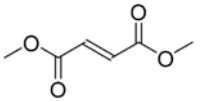
Laquinimod	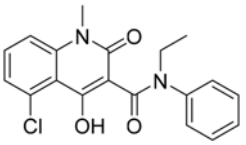
Interferon β-1b	Biologic drug
Interferon β-1a	Biologic drug
Peginterferon β-1a	Biologic drug
Natalizumab	Biologic drug
Alemtuzumab	Biologic drug
Glatiramer acetate	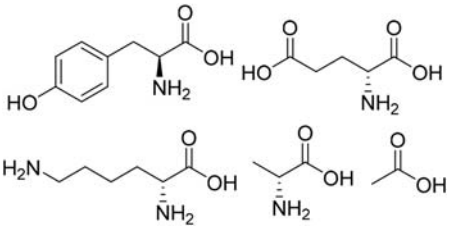
Mitoxantrone	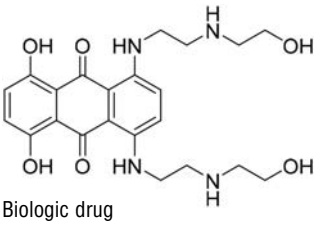
Rituximab	Biologic drug
Cyclophosphamide	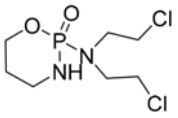
Adrenocorticotropin hormone (ACTH)	Peptide drug
Methotrexate	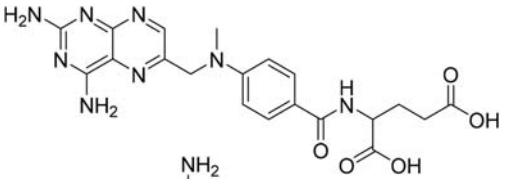
Cladribine	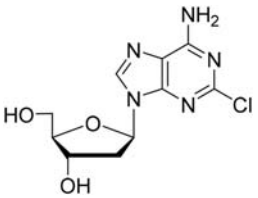

long-term effects of DMTs on MS progression are not very clear, and majority of the immunomodulators do not help with the progressive MS disease and delaying the disability progression.[76] Most of the current research efforts are directed at the discovery and development of agents that will help progressive phases of MS and those that delay or prevent disability in the MS patients. Later, a number of drugs currently marketed for MS are described providing an overview of the current therapeutic approaches (Table 1).

5.14.2.1 Fingolimod

Fingolimod is a sphingosine-1-phosphate (S1P) receptor modulator that prevents T and B lymphocyte egress from lymph nodes,[77,78] reducing peripheral blood lymphocyte counts by 70% of baseline within 3 months of treatment initiation.[79,80] Fingolimod is the first oral therapy approved as a first-line treatment in various countries during 2010–11.[81,82] In the European Union, fingolimod is approved as a second-line treatment, except for patients with highly active RRMS, for whom it can be prescribed as a first-line therapy.

In an analysis of six randomized clinical trials including a total of 5152 participants, three doses of fingolimod were investigated. In this study, 1621 were control patients, and 3531 patients were treated with oral fingolimod at three doses: 2061 patients with 0.5 mg/day, 1376 patients with 1.25 mg/day, and 94 patients with 5.0 mg/day.[79] In the control group, 923 participants were treated with placebo and 698 with others DMTs. The treatment duration was 6 months in three trials, 12 months in one trial, and 24 months in two trials. When fingolimod 0.5 mg/day treatment was compared to that with placebo, the drug at 24 months increased the probability of being relapse-free, but it did not prevent disability progression. Clinical benefit was observed for other measures of inflammatory disease activity including much reduced ARR, MRI activity, and Gd-enhancing lesions. The mean change of MRI/T2-weighted lesion load was reduced when treated with fingolimod at 12 and 24 months. No significant increased risk of discontinuation due to adverse events was observed for fingolimod 0.5 mg/day compared to placebo at 6 and 24 months. Serious adverse events were not observed for fingolimod at 0.5 mg dose compared to placebo at 6 and 24 months, but at 1.25 mg/day dose for 12 months, there is a higher risk of discontinuation of fingolimod treatment due to adverse effects. Even at 0.5 mg/day dose of fingolimod, a significant increased risk of discontinuation due to serious adverse events was observed compared to placebo at 6 months.

When fingolimod 0.5 mg/day was compared with intramuscular interferon β-1a, the drug treatment with fingolimod for 12 months slightly increased the number of participants free from relapse or from Gd-enhancing lesions and decreased the relapse rate, but in these cases, disability progression was not affected. Higher number of patients chose to continue fingolimod as compared with other DMTs due to favorable adverse events profile in the 6-month term, but there was no significant difference in the 12-month term when compared with treatment with interferon β-1a. Overall, the treatment with fingolimod in RRMS patients is effective in reducing inflammatory disease activity compared to placebo, but it may lead to little or no difference in preventing disability worsening, due to neurodegenerative component of MS. Over a 24-month period, brain volume loss was reduced in fingolimod-treated patients compared with both placebo-treated patients[79] and interferon β-1a-treated patients.[83] Three major clinical trials and their extensions investigated the safety profile of fingolimod, including 3916 patients altogether with up to 7 years of treatment.[79,80,84,85] Adverse effects related to the immunosuppressive properties of fingolimod included a moderately increased risk of lower respiratory tract infections compared to placebo.[80] No increase in risk of malignancy was observed in patients treated with fingolimod compared to placebo in these studies.

Serious cardiac side effects due to fingolimod therapy have been reported in the literature, including cases of asystole or cardiac arrest.[86,87] S1P receptors, the targets for fingolimod, are expressed in many tissues including the cardiovascular system and have roles in heart rate and blood pressure regulation. These effects are responsible for the cardiovascular adverse events when treated with fingolimod.[88] Upon treatment initiation, fingolimod leads to a dose-dependent bradycardia. This effect is transient, with heart rate reaching its nadir 4–5 h after the first dose. In most cases, bradycardia is asymptomatic, and heart rate is back to baseline after a month of continuous treatment.[79,80] Other cardiac side effects include first- and second-degree atrioventricular (AV) conduction blocks, with a pooled incidence in both phase III trials of 4.7% (1.7% in the placebo group) and 0.2% (0% in the placebo group), respectively.[84] Absolute contraindications for fingolimod therapy within the 6-month period prior to initiating treatment include incidences of myocardial infarction, unstable angina, stroke or transient ischemic attack, class III/IV heart failure or heart decompensation, Mobitz II second-degree or third-degree AV block, sick-sinus syndrome, and prolonged QTc or treatment with class Ia or III antiarrythmic drugs.

A recent study suggests subtle subclinical macular oedema may occur more frequently in fingolimod-treated patients compared to placebo.[79,80,89,90] Elevation of liver enzymes three times above the upper limit was reported in 8% of fingolimod-treated patients compared with 1.9% in the placebo group, and any higher titers of the liver enzymes require treatment cessation.[84] More recently, several cases of atypical, tumefactive demyelinating lesions have been reported in fingolimod-treated MS patients, suggesting fingolimod may have a paradoxical effect in some MS patients.[91,92] MS patients on fingolimod have similar cellular and humoral immune responses to influenza vaccination compared with healthy controls.[93] For safety reasons, live attenuated vaccines are contraindicated while on fingolimod treatment, and immunization status (including VZV) should be checked prior to treatment initiation.

Preclinical studies with fingolimod have demonstrated embryotoxicity and teratogenicity. Female patients are therefore advised not to become pregnant while treated with fingolimod, and a 3-month washout period with normalization of blood tests before conception is recommended.[94]

5.14.2.2 Teriflunomide

Teriflunomide is the active metabolite of leflunomide, an antirheumatic small-molecule drug. Teriflunomide inhibits a key enzyme, dihydroorotate dehydrogenase (DHODH), in the de novo pyrimidine synthesis pathway.[95] De novo pathway is favored over the salvage pathway in rapidly proliferating cells such as activated lymphocytes. Immunomodulatory properties of teriflunomide are manifested by the inhibition of lymphocyte proliferation.[96] Teriflunomide is approved as a first-line treatment of RRMS by the FDA, EMA, and Swissmedic.

In the TEMSO phase III study, teriflunomide 14 mg/day reduced ARR by 31.5%, which was confirmed subsequently by a second phase III study, TOWER.[97,98] In both studies, the risk of sustained accumulation of disability was significantly reduced in patients taking 14 mg/day teriflunomide.[97,98] In TEMSO trial, MRI evidence of disease activity was significantly reduced in patients taking 14 mg teriflunomide. However, brain volume loss did not differ significantly between teriflunomide and placebo-treated groups.[97] The efficacy of teriflunomide, in terms of ARR reduction, is comparable with that of the first-line injectable treatments interferon β-1a, but "treatment satisfaction questionnaire for medication (TSQM)" scores were higher for teriflunomide, underscoring the benefit of an oral formulation on patient's quality of life.[99] A phase II study showed no benefit of teriflunomide as an add-on therapy in patients receiving interferon β-1a.[100]

In phase II trials, long-term follow-up of patients from phase II trials up to 8.5 years, and phase III trials, no serious adverse events were observed. Side effects included nausea, diarrhea, and reversible hair thinning.[97,101,102] Tuberculosis (TB) reactivation was reported in patients treated with leflunomide, and if the TB test was positive, treatment was mandatory prior to teriflunomide initiation. A slight increase in blood pressure and elevated transaminase levels were reported.[97,101,102] Teriflunomide activates cytochrome P450, and drug–drug interactions with other drugs could occur, including with warfarin, antibiotics, and antiepileptics. Patients treated with teriflunomide were shown to have a normal response to influenza vaccine, but live attenuated vaccines are contraindicated.[103] Preclinical studies with teriflunomide in rats, rabbits, and mice have demonstrated embryotoxicity and teratogenicity,[94] and female patients are advised not to become pregnant while treated with teriflunomide.

5.14.2.3 Dimethyl Fumarate

Dimethyl fumarate (DMF), a fumaric acid ester (**Table 1**), exhibits both immunomodulatory and neuroprotective effects, but the exact mechanisms of action remains to be elucidated.[104] In vitro studies on PBMCs showed that DMF and its metabolite, monomethylfumarate, stimulate cyclic adenosine monophosphate (cAMP) production.[107] cAMP is a small-molecule second messenger that has been shown to modulate immune response. These findings suggest that DMF may provide protection against MS by inhibiting immune cell function via the cAMP signaling pathway.[107] More research is needed to understand the complete molecular mechanisms responsible for the clinical efficacy of DMF. Fumaric acid esters in fact have been in clinical use in Germany for psoriasis treatment under the brand name Fumaderm.[105] An oral formulation of DMF, delayed-release DMF, also known as gastroresistant DMF, is a recently approved oral DMT for RRMS.[106–108] Two randomized clinical trials, viz. *Determination of the efficacy and safety of oral fumarate in relapsing–remitting MS* (DEFINE) and *Comparator and an oral fumarate in relapsing–remitting multiple sclerosis* (CONFIRM), demonstrated significant efficacy in reducing relapse rate and disease activity based on MRI scans, due to DMF treatment. The DEFINE study also indicated a significant effect of DMF on disability worsening, although low incidences of disability worsening in the CONFIRM trial render the reduction in disability worsening among the DMF-treated groups statistically insignificant when compared to that with placebo treatment. In DEFINE study, oral DMF 240 mg *b.i.d.* reduced ARR by 53% compared to placebo.[109] Risk of disability progression was reduced by 38% compared to placebo in the DEFINE study but did not reach significance in the second phase III trial, CONFIRM.[109,110] Brain volume loss was not assessed in either phase III trials.

Overall, DMF demonstrated a good safety profile and acceptable tolerability, and no serious side effects were reported in phase II and III trials.[109–111] Most common side effects such as gastrointestinal events and flushing reactions are transient with moderate severity.[108] Most frequent side effects included flushing (31%), diarrhea (13%), nausea (11%), and abdominal pain (10%).[110] Patients enrolled in phase III trials were allowed to be vaccinated. However, available data are insufficient to assess safety or efficacy of vaccines in combination with DMF. Animal studies showed embryolethality and teratogenicity in various animals, and female patients taking DMF are advised not to become pregnant.[94] Patients switching from interferons or glatiramer acetate to DMF exhibited greater benefit, whereas patients pretreated with more potent immunotherapies did not benefit. This opened up the possibility for using DMF as switching treatment or as an add-on strategy in patients with breakthrough disease. In a retrospective analysis of medical records at two German MS centers, 644 MS patients treated with DMF were studied for safety and efficacy; the ARR decreased from 0.52 at baseline to 0.35 and the annualized disability progression from 0.15 to 0.10. This postmarketing, retrospective study concluded that DMF is an overall safe and effective drug that reduces relapse rate and disability progression in MS patients.[106]

5.14.2.4 Laquinimod

Laquinimod is a quinolone-3-carboxamide derivative approved for RRMS treatment (**Table 1**). In Jan. 2014, it received a negative evaluation from the EMA, due to potential risks observed in animal studies.[81] Laquinimod is a CNS and peripheral immunomodulator with both antiinflammatory and neuroprotective properties.[112–114] Laquinimod seems to modulate CNS immunity

independent of effects on the peripheral immune system, which is a potentially different mechanism than the current immunomodulators.[112,115] The exact mechanisms of action of laquinimod remain to be fully understood as well.

In ALLEGRO phase III study, laquinimod 0.6 mg *q.d.* reduced ARR by 23% compared to placebo.[116] MRI markers of disease activity reduction and reduction in confirmed disability progression by 36% and 48% at 3 and 6 months, respectively, compared to placebo were observed in the ALLEGRO study.[116] Brain volume loss over a 24-month period was reduced in laquinimod-treated patients compared with patients receiving placebo.[116] In BRAVO phase III trial, laquinimod 0.6 mg *q.d.* treatment was compared to that with placebo and interferon β-1a (Avonex) *q.d.*[117] Compared to placebo, there was no significant reduction in ARR in patients receiving laquinimod, thereby failing to reproduce the results of ALLEGRO.[117] However, similarly to what was observed in ALLEGRO,[117] brain volume loss over a 24-month period was reduced in laquinimod-treated patients. No serious adverse events were reported in phase II and III trials.[80,116–118] Side effects included a moderate increase in the risk of urinary tract infection, abdominal pain, back pain, and elevated liver transaminase.[80,116,118]

5.14.2.5 Interferon β-1b

Interferon β-1b (Betaseron) was first introduced in 1993 for the treatment of RRMS and is a recombinant IFN-β produced in *Escherichia coli*.[119] The amino acid structure of Betaseron is slightly modified from that of the native human IFN-β molecule. The Met1 is absent, and a Ser residue is substituted for Cys17. IFNβ-1b is also not glycosylated, unlike natural interferon-β. The mechanism of action of IFN-β in MS is not known. Interferons are cytokines and accordingly are immunomodulatory agents. Numerous immune system abnormalities are identified in MS patients, and IFN-β treatment helps modulate the immune-mediated inflammatory responses.[125] HLA-DR expression on circulating blood cells increases abnormally during MS disease activity, and when treated with IFN-β, this is gradually reduced. CD8 regulatory cell function is deficient when MS is active, and IFN-β treatment partially reverses this deficiency. Interestingly, treatment with IFN-β lowers the production of interferon-γ (IFN-γ), which exaggerates the MS attack. Despite a clear understanding of IFN-β effects on the immune system at the molecular level, it is still unclear how this drug achieves therapeutic effect in MS patients.

In a phase III double-blind placebo-controlled trial in patients with RRMS, the Betaseron reduced MS attack frequency by 34% and 30% during 2 and 5 years, respectively, of the course of the treatment.[120,121] Mean attack duration and steroid use were reduced significantly in the drug-treated group. Progression of permanent disability was reduced in Betaseron-treated group when compared with the placebo group, although statistically insignificant. Based on the annual MRI scans on all patients, disease burden increased ~5% annually over the five-year course of the trial, but the disease burden did not change in the treated patients.[122] Subsequent studies using Gd-enhanced MRI scans showed an 85% reduction in disease activity in patients receiving Betaseron.[123] Betaseron treatment also helped improve few select measures of cognition in MS patients.[124] Based on the clinical outcomes using two dose regimens (1.6 and 8 MU *s.c.* every other day) for Betaseron, higher doses of the drug were more effective than the lower doses.[120,121] All the early studies were primarily confined to RRMS patients only.

A recent placebo-controlled study in SPMS over a 2-year period showed MRI findings similar to the earlier ones. Patients with continued attacks superimposed on progressive disease had 33% reduction in attack frequency, which is comparable with those observed in the earlier trial. Median time to progression to disability has reduced by 38% ($p=0.0007$), a significant beneficial effect on progression of disability, and this was consistent regardless of disability status at entry into the trial, when treated with Betaseron. As is with other cytokine and interferon treatments, systemic side effects in the form of flu-like symptoms including fever, chills, sweating, and muscle aches are common with interferon β-1b treatment. Lower doses of interferon β-1b (3–4 MU *s.c.*) and subsequently increasing to the recommended dose could be considered, as well as evening administration of the drug to alleviate some of the suffering due to side effects. Acetaminophen can be used as an adjuvant therapy to lessen systemic side effects.[120,121,125]

5.14.2.6 Interferon β-1a (IFN-β-1a; Avonex, and Rebif)

Two interferon β-1a products are approved, one marketed by Biogen and the other by Merck Serono. Avonex, a Biogen product, is a recombinant IFN-β preparation and is a close structural mimic of betaseron and the sequence of native IFN-β. A portion of the preparation may lack the first amino acid, Met1 in the full native IFN-β sequence, and the protein is glycosylated. It is produced in Chinese hamster ovary (CHO) cells. The drug was approved in 1996 at the dose of 6 MU and is given intramuscularly once weekly. Avonex reduced MS attack frequency by 9% in the first year and by 18% over the 2-year span of a clinical trial conducted on RRMS patients with very mild early MS disease.[126] In a subgroup analysis with 87 patients who were treated with Avonex for 2 years, MS attack frequency was reduced by 32% ($p=0.03$), and treated patients had significantly less projected accumulating disability than placebo-treated patients. MRI scans showed 35% fewer Gd-enhancing lesions and, in turn, 35% less disease activity in treated patients than that in the placebo group after first year of treatment ($p=0.02$) and 52% less disease activity after second year of treatment ($p=0.05$). Only minimal changes in blood parameters were noted. Side effects such as flu-like symptoms were comparable but less frequent to those seen with Betaseron treatment.

Rebif (EMD Merck Serono) is also an IFN-β-1a preparation, very similar to Avonex. It is also produced in CHO cells. Rebif is not currently marketed in the United States but is available in other countries. Preliminary studies had shown that subcutaneous and intramuscular administration gave comparable responses for a range of biologic markers that are induced by IFN-β, and subcutaneous administration is convenient for the patients. Rebif was evaluated in clinical trials at two doses, 6 and 12 MU *s.c.* three times

a week over 2 years in RRMS patients. Both doses of Rebif reduced attack frequency, by 29% for the 6-MU dose and by 32% for the 12-MU dose, when compared with the patients receiving placebo.[127] At the higher dose, there was a 37.5% reduction in major MS attack. Time to progression of disability based on expanded disability status scale (EDSS) was 18.2 months for the Rebif 6-MU dose group versus 11.8 months for the placebo group. In the 12-MU dose arm, time to progression of disability was 21 months, slightly higher than that for the 6-MU Rebif dose. The accumulation of disease burden was significantly lessened in Rebif treatment groups: 1.2% improvement in the 6-MU treatment arm and 3.8% improvement in the 12-MU treatment arm in comparison with 10.9% worsening in the placebo arm after 24-month treatment with Rebif. CNS lesions and disease activity were 81% and 87.5% lower for the 6- and 12-MU Rebif treatment arms, respectively.[128] Overall, the effect of the higher dose was only slightly better than that of the lower dose for the majority of parameters evaluated.

5.14.2.7 Peginterferon β-1a

US Food and Drug Administration (FDA) approved peginterferon β-1a in 2014 for RRMS and marketed as Plegridy by Biogen Idec. Peginterferon β-1a is the pegylated follow-on biologic of Avonex (interferon β-1a).[129,130] Pegylation extends the half-life of interferon β-1a permitting a less frequent administration of the drug than that of the unpegylated product.[131] The recommended dosage of peginterferon β-1a is 125 μg *s.c.* every 14 days with a prefilled pen-type syringe.[132] The FDA's approval of this drug was based on results of the 2-year, randomized phase III double-blind clinical trial, ADVANCE study, in which efficacy and safety were evaluated. One-year ADVANCE study results indicated that after 48 weeks of treatment with peginterferon β-1a, patients had a significantly reduced relapse rate and might be an effective treatment of RRMS with less frequent administration.[133]

In a placebo-controlled multicenter study, patients with RRMS were randomly assigned to receive subcutaneous injection of placebo or 125 μg of peginterferon β-1a once every 2 weeks or every 4 weeks. Out of the 1512 patients, 1332 patients completed 48 weeks of treatment.[133] In the first year of the study, ARR for peginterferon β-1a once every 2 weeks treatment was lower (0.256) than that of placebo recipients (0.397) ($p=0.0007$). For those who took peginterferon β-1a every 4 weeks, the annualized relapse rate was 0.288. This 2-year study confirmed the clinical benefits of peginterferon β-1a.[134] The most common adverse events associated with peginterferon β-1a are minor in general such as injection-site reactions, flu-like symptoms, pyrexia, and headache.[133] There is no significant difference between the placebo and drug-treated groups in serious adverse events such as relapse, pneumonia, and urinary tract infection.[133]

5.14.2.8 Natalizumab

Natalizumab is a humanized monoclonal antibody that targets the lymphocyte adhesion molecule, α4β1 integrin. Binding of this monoclonal antibody disrupts the interaction of α4β1 integrin with vascular adhesion molecule VCAM-1 and interferes with the migration of the peripheral lymphocytes from blood vessels into the CNS.[135] Natalizumab (Tysabri) is approved for treatment of active RRMS in Europe, North America, and other countries globally.[81,136]

Natalizumab was approved by the FDA in 2004 before the completion of phase III trials SENTINEL[137] and AFFIRM due to its remarkable efficacy.[138] However, it was withdrawn from the US market after two patients were diagnosed with progressive multifocal leukoencephalopathy (PML) in natalizumab treatment groups.[139,140] Both phase III trials confirmed high efficacy of natalizumab 300 mg infusion every month, and the treatment reduced ARR by 68% compared to placebo.[138] Natalizumab also reduced the accumulation of new and enlarging T2 lesions, Gd-enhancing lesions,[141] and the risk of sustained disability progression.[110,138] Besides the risk of PML, other serious adverse events included hypersensitivity reactions. Additional research and analyses of risks and benefits of natalizumab treatment eventually led to the recommercialization of natalizumab in more than 65 countries globally.

In a recent Danish study involving RRMS patients who started their first second-line treatment with natalizumab or fingolimod between 2011 and 2015, no differences were found in clinical disease activity between natalizumab- and fingolimod-treated RRMS patients, and EDSS was similar between the two groups.[136] It must be noted that, despite recommercialization of natalizumab after the risk–benefit analysis, more than 370 cases of PML have been diagnosed worldwide among the 700,000 natalizumab recipients.[142] In phase III trials, the presence of antinatalizumab antibodies was noted potentially affecting its clinical efficacy, and majority of these cases appear to be neutralizing antibodies.[138] The incidence of antinatalizumab antibodies was measured in 9% of natalizumab-treated patients; one third of these patients were transiently positive with no clinical significance, and the remaining were persistently positive with loss of clinical efficacy of natalizumab.[143] Natalizumab treatment is not effective in antiaquaporin 4-positive neuromyelitis optica (NMO) patients and must be excluded before the initiation of natalizumab treatment.[144–146] Live-attenuated vaccines are permitted in natalizumab-treated patients, unlike other immunomodulating drugs for MS treatment, and vaccination against influenza in patients treated with natalizumab yields effective humoral immune response.[147] Animal studies show teratogenicity when treated with natalizumab; thus, female patients on natalizumab are advised not to become pregnant.[148] In general, increased susceptibility for infections and the development of anti-antibody antibodies with or without clinical implications when treated with monoclonal antibody therapeutics are some of the common concerns. Thus, these factors would have to be monitored on a continuing basis when antibody treatments are used.

5.14.2.9 Alemtuzumab

Alemtuzumab (Lemtrada) is a humanized monoclonal antibody targeting CD52 antigen on mature lymphocytes specifically depleting T and B lymphocytes, and it is a fast-acting drug.[81,149] After the treatment initiation, B cells are replenished to baseline within 3–6 months with a distinct pattern, and T-cell counts slowly rise toward normal within 12 months, without returning to baseline.[150] These changes lead to long-lasting changes in adaptive immunity. In 2013, alemtuzumab was approved by the EMA for RRMS.

Two phase III studies, CARE-MS I and CARE-MS II, evaluated the efficacy of alemtuzumab and compared with interferon-β-1a (Rebif). In CARE-MS I and its extension CAMMS223, alemtuzumab reduced ARR by 54.9% and 66% at 2 and 5 years, respectively, compared with that with Rebif treatment.[151] In CARE-MS II, which included MS patients who relapsed on prior interferon or glatiramer acetate (Copaxone) therapy, alemtuzumab reduced ARR by 49.4% compared with that with Rebif.[152] A significant reduction in sustained disability progression was observed in alemtuzumab-treated patients compared with interferon-treated patients in CARE-MS II.[150,152] A significant reduction in new or enlarging T2 lesions and Gd-enhancing lesions in alemtuzumab-treated patients compared with those treated with Rebif was also observed.[150,152] Brain volume loss was reduced in alemtuzumab-treated patients compared to placebo- and interferon β-1a-treated patients.[150,152]

Studies involving six clinical trials and their extensions investigated safety profile of alemtuzumab; 90% of patients reported infusion-associated reactions including headache, skin rash, and pyrexia; an increased risk of autoimmune conditions including autoimmune thyroid disease, immune thrombocytic purpura, hematologic, renal, and dermatologic autoimmune diseases was also observed.[150–154] Cumulative risk of autoimmune disease in MS patients following alemtuzumab treatment was about 22.2% at 12–18 months after the initiation of the treatment and is due to the change in the balance of the immune system from a Th1-mediated response toward a Th2-mediated response. Upper respiratory tract, urinary tract, herpes (predominantly cutaneous), and localized fungal infections were more frequent in alemtuzumab-treated patients.[150,152] The benefit–risk ratio of alemtuzumab should be assessed for each patient due to its relatively high rate of side effects and complex administration requiring herpes simplex prophylaxis, methylprednisolone premedication, and antipyretic and antihistaminic coadministration.

In a meta-analysis of three randomized clinical trials in patients with RRMS, treatment with alemtuzumab 12 mg was better than subcutaneous interferon β-1a at 24 months; outcomes for relapse-free survival, sustained disease progression-free survival, number of participants with at least one adverse event, and number of participants with new or enlarging T2-hyperintense lesions on MRI were all better in patients receiving alemtuzumab.[155]

5.14.2.10 Glatiramer Acetate

Glatiramer acetate (GA; Copaxone, Teva Pharma) is an acetate salt of a random polymer of four amino acids, L-alanine, L-lysine, L-glutamic acid, and L-tyrosine at a molar ratio of 4.2:3.4:1.4:1.0, respectively (**Table 1**).[156,157] This drug may capture the antibodies or may reduce inflammatory response targeted toward antigenic epitopes from MBP; thus, GA carries similar charge to that of MBP and shares some cross-reactivity with MBP. GA is approved as a DMT for the treatment of relapsing forms of MS.[156,158,159] Pretreatment with GA is known to decrease the incidence and severity of EAE in mouse models of MS.[156] The postulated mechanisms of action include desensitization, enhanced production of antigen-specific suppressor T cells, inhibition of MBP-specific effector T cells, and competition for the peptide-binding site of the MHC class II antigen.[156,160,161] Its mechanism of action is only being elucidated in recent times, and GA modulates both the innate and adaptive immune systems.[162] These mechanisms include alteration of regulatory T-cell function[163–165] with induction of a T-helper 1 (Th1) to Th2 cell shift. This T-cell subtype shift results in an enhanced antiinflammatory cytokine profile,[166–170] alterations in the function of antigen-presenting cells (APC),[163] and modulation of B-cell function.[162] GA exhibits neuroprotective effects that are mediated by neurotrophic factors, and GA treatment exhibits reduction in demyelination and promotes remyelination.[162] GA is administered for extended periods of time.[171,172] Glatiramer acetate and similar therapies are indicated to reduce the frequency of exacerbations in patients with relapsing MS and are commonly initiated when patients show signs of relapsing MS.[158,172–176]

Initial trials demonstrated the safety but did not convincingly prove the efficacy of GA in the treatment of MS.[161,177] A 2-year multicenter placebo-controlled phase III trial of GA in 251 patients with RRMS demonstrated a beneficial treatment effect.[156] There was observable reduction in ARR (0.59 relapses in the treatment group vs. 0.84 relapses in the placebo group), percentage of patients remaining relapse-free at 2 years (78.4% in the treatment group vs. 75.4% in the placebo group), and median time to first relapse (287 days in the treatment group vs. 198 days in the placebo group). As with other immunomodulators, progression of the disease and worsening of the lesions were not altered in the treatment group when compared with that receiving placebo.[178] On the other hand, side effects in the GA-treated patients are mild and infrequent and are generally well tolerated. GA produced a systemic reaction in about 15% of patients receiving GA, characterized by flushing, chest tightness, and palpitations, and these reactions are resolved spontaneously in less than 30 min. GA is one of the first-line therapies for RRMS.

5.14.2.11 Mitoxantrone

Mitoxantrone (MTX) is a synthetic anthracycline with antineoplastic, immunomodulatory, and antiinflammatory effects.[179,180] Due to its mode of action and the chemical class of compound, it has direct applications as an anticancer agent and is used in treatment of breast, prostate, ovarian, stomach, and liver cancer. MTX is used as a second line of treatment for SPMS and RRMS in patients such

as those who do not respond to treatment with IFN-β-1a and GA.[181] This drug inhibits the activity of T lymphocytes, B lymphocytes, and macrophages and also affects the synthesis of antibodies. MTX is currently approved for aggressive, adult RRMS or SPMS and pediatric MS and has shown efficacy in several clinical trials.[182–184] However, it is not widely used due to safety concerns including high incidence of cardiotoxicity, liver toxicity, amenorrhea, and treatment-related leukemia due to its primary effects on cell topoisomerase II and triggering apoptosis.[185–188] Interestingly, cardiomyopathy and leukemia may occur many years after treatment cessation.[189] The most dangerous side effects of MTX treatment are cardiotoxicity, induction of leukemia, and colorectal cancer.[190] There is the lack of studies describing MTX effectiveness and safety in treatment of PPMS.

5.14.2.12 Rituximab

Rituximab is a genetically engineered, chimeric monoclonal antibody that targets the CD20 cell-surface antigen on B lymphocytes, and it induces antibody-directed cell cytolysis (ADCC) and complement-directed cytolysis (CDC) of the target cells.[191] Proof-of-concept data for the B-cell depletion upon treatment with the drug in RRMS patients were obtained in the HERMES trial, essentially one of the first clinical studies to evaluate rituximab in adults with RRMS (NCT00097188). In a randomized study with 104 patients in a 2:1 ratio to rituximab 1000 mg or placebo infusions on study days 1 and 15, rituximab-treated patients had a 91% reduction in the brain lesions at weeks 12, 16, 20, and 24 (primary end point) compared with those treated with placebo ($p < 0.001$). The ARR at 24 weeks with rituximab treatment was 56% lower than that on placebo (0.37 vs. 0.84, $p = 0.04$).[192] Safety concerns with rituximab in phase II trial included primarily infusion-related reactions (78.3% vs. 40% on placebo), but there was no increase in serious infection-related adverse events. Other adverse events were minor as well.[192]

Rituximab was not superior to placebo in preventing 12-week confirmed disability progression in a 96-week OLYMPUS trial of 439 PPMS patients (NCT00087529).[193] However, in a preplanned subgroup analysis, patients under age 51 with Gd-enhancing brain lesions at baseline were less likely to progress in disability on rituximab than placebo.

5.14.2.13 Cyclophosphamide

Cyclophosphamide was first used in an MS patient in 1966.[194] Cyclophosphamide is an immunosuppressive agent that was commonly used in the treatment of MS.[195] Cyclophosphamide is an alkylating agent (**Table 1**) and belongs to the class of nitrogen mustard agents that bind to DNA and disrupts cell replication. Cyclophosphamide is converted to active metabolites in the liver, one of the major active metabolites being 4-hydroxycyclophosphamide, and targets rapidly proliferating malignant cells. It has been used in the treatment of cancer, immune-mediated disorders such as Wegener's granulomatosis, nephrotic syndrome, multiple myeloma, and disorders of the peripheral nervous system.[196] The mechanism of action of cyclophosphamide lends itself to serve as a general immune suppressant inhibiting both cell-mediated and humoral immunity. Cyclophosphamide suppresses interleukin-12 (IL-12) and Th1-type responses[197] and enhances Th2 and Th3 activity, potentiating inflammatory mediators such as IL-4, IL-10, transforming growth factor-β, and eosinophils that further help suppress immune response.[196,198] Cyclophosphamide upregulates antiinflammatory CCR4+ IL-4-producing T cells while normalizing CCR5+ and CXCR3+ T cells in SPMS patients,[199] favoring a Th2-type response. Overall, its mode of action and in vivo efficacy indicate that cyclophosphamide has a more selective immune therapeutic effect rather than serving solely as a general immune suppressant.[195]

Hommes et al. conducted an open-label clinical study on 32 patients diagnosed with chronic progressive MS, investigating the efficacy of cyclophosphamide 400 mg *i.v.* combined with prednisone 100 mg *q.d.*[200] More than 50% of the treated patients showed clinical improvements in neurological signs and disability measures, and sustained improvements were observed following treatment up to 3 years. In a larger cohort of 110 patients treated with cyclophosphamide *i.v.* with up to 2 g exposure over a 1- to 2-week period, improvements in clinical measures were observed in most cases, and 62% of patients have shown stabilization of disease over 2–4 years. These data suggest that immunosuppression may interfere with the MS disease pathology and perhaps prevent disease progression.[201]

Cyclophosphamide was evaluated for its efficacy in pediatric MS as well. Pediatric MS has a different temporal profile of the disease with potentially more clinical relapses than one observes in adult MS.[202] There are also significant differences in structural neuroimaging of the brain and the disease-associated cerebrospinal fluid (CSF) inflammatory profiles.[203–205] A smaller multicenter clinical study involved the retrospective evaluation of 17 children with RRMS. Patients were treated with various regimens of cyclophosphamide, with doses in the range of 600–1000 mg/m^2.[206] In the majority of patients 1 year post treatment, relapse rate and EDSS have reduced, and the treatment was well tolerated. The general side effects include nausea, vomiting, alopecia, transient immunosuppression, amenorrhea, hemorrhagic cystitis, gonadal toxicity (in both men and women), bladder cancer, and future risk for malignancies. Overall, one can conclude that cyclophosphamide may be an appropriate therapeutic for pediatric MS disease that may be refractory to routine immunomodulatory treatments. The risk of bladder carcinoma appears to be associated with cumulative exposures of over 100 g of the drug and the long duration of exposure to cyclophosphamide.[207,208]

5.14.2.14 Adrenocorticotropin Hormone (ACTH)

ACTH first received new drug application approval from US FDA in 1952, and later in 1972, its use for the treatment of MS was added. Recently, in 2010, FDA approved ACTH gel under an orphan drug designation for infantile spasms and permitted the new label to include MS in addition to 17 other indications.[209] ACTH influences both the corticotropic and melanocortin

pathways.[210] ACTH induces cortisol production and exerts antiinflammatory actions by targeting melanocortin receptors present on immune cells. The endogenous agonists for these receptors, viz. ACTH, α-, β-, and γ-melanocyte stimulating hormones, are also produced locally by immune cells. These agonists act on the endogenous antiinflammatory tissue-protective pathway involving the melanocortin system. Thus, drugs such as ACTH and ACTH-like melanocortin drugs are devoid of steroidogenic actions and associated side effects.

ACTH, in a gel formulation, is a gelatin suspension administered intramuscularly or subcutaneously.[211] In a double-blind randomized controlled study in 1989, relative efficacy of intravenous methylprednisolone (IVMP) was compared with ACTH for the treatment of MS relapses.[212] The study included 61 patients randomized to receive treatment with either IVMP (1 g daily) for 3 days or ACTH *i.m.* (80 units for 7 days, 40 units for 4 days, and 20 units for 3 days). Both groups improved over the course of the study without a significant difference in the rate of recovery or final outcome at 3 months. A 2000 Cochrane Collaboration review concluded that both IVMP and ACTH result in acceleration of recovery and improvement in relapse-related disability.[213]

5.14.2.15 Methotrexate

Methotrexate is an antimetabolite and has been used in the treatment of neoplastic diseases, psoriasis, and rheumatoid arthritis for several decades. It is a potent oral immunosuppressant as well and has been commonly used as an "off-label" treatment for MS. Methotrexate inhibits dihydrofolate reductase (DHFR), an enzyme responsible for the conversion of dihydrofolate into tetrahydrofolate, thus inhibits cell proliferation and growth. Other beneficial antiinflammatory effects within the immune system are theorized, and the exact mechanism by which this is accomplished is currently unknown. Overall, the mechanism of action provides a rationale for its use in cancer and autoimmune disease.

In a randomized trial with 45 patients with RRMS, chronic progressive MS, and progressive MS, methotrexate treatment was evaluated over 18 months.[214] The aim was to study the efficacy of methotrexate in MS by assessing differences in relapse rate and EDSS. Patients were randomized to receive either methotrexate 2.5 mg every 12 h for three consecutive doses once a week (7.5 mg/week) or placebo. There was no difference between the treatment group and placebo group in suppressing exacerbations; however, when evaluating the subgroup of RRMS patients, there was a suggested benefit with fewer relapses observed in the treated versus untreated group (36% vs. 41%, $p=0.05$). Overall, methotrexate treatment was well tolerated, with minor side effects including nausea, elevation in liver function tests, and hair thinning.

Further studies on the impact of methotrexate treatment on chronic progressive MS also confirmed the efficacy of methotrexate for its immunosuppressive activity. In a study of 60 patients with clinically definite chronic progressive MS, participants were stratified by EDSS score (3.0–5.5 and 6.0–6.5) and were randomized to receive either methotrexate (7.5 mg/week) or placebo for 2 years, followed by an observation period of 1 year.[215] The principal finding of this investigation was that there was less progression of impairment in patients with EDSS greater than 6.0. Adverse effects were found to be similar between methotrexate- and placebo-treated groups. Although the number of patients evaluated was modest, this study provided data that methotrexate may have promise in MS patients with chronic progressive MS who have more disability. The mechanisms as to why this may occur are unclear but may be related to an immunosuppressive, antiinflammatory, or immunoregulatory effect. Contrast-enhanced MRI was performed every 6 weeks for 6 months on 31 chronic progressive MS patients, among which 16 patients received methotrexate (7.5 mg/week) and 15 patients received placebo.[216] Overall, there was no significant difference in the lesions between the two groups.

The effects of intrathecal methotrexate in patients with refractory MS disease were evaluated in a retrospective study.[217] The hypothesis for this study is grounded in the idea that orally administered therapy may be suboptimal for the treatment of spinal cord disease, the area of the CNS believed to be principally responsible for clinical impairment in progressive MS patients. SPMS subgroup ($n=87$) exhibited improvement in EDSS scores when compared with baseline data ($p=0.014$). This significant benefit was not observed in the PPMS subgroup ($n=34$) despite recording stable EDSS scores in 82% of subjects. Intrathecal methotrexate was well tolerated and may have benefits in progressive patients with treatment-unresponsive MS. It is possible that intrathecal delivery might provide this additional benefit over oral administration of methotrexate.[218,219]

A review of the data on oral methotrexate and its effects on relapse prevention and benefits due to sustained EDSS progression scores strongly suggest that methotrexate alters the course of the disease in progressive MS patients.[205,220] Methotrexate treatment is primarily used due to the convenience that it is orally administered weekly, but newer oral immunomodulatory therapeutics such as fingolimod and others with better outcomes have gained the market in recent times.

5.14.2.16 Cladribine

Although this drug failed to show efficacy, it is included in this section to highlight the strategy behind the development of cladribine, a nucleoside drug, and its efficacy as an immunomodulator. Cladribine (2-chloro-2′-deoxyadenosine) is an adenosine deaminase-resistant purine nucleoside drug licensed for the treatment of hairy cell leukemia (**Table 1**).[221] This drug was evaluated for efficacy via parenteral route for the treatment of progressive MS and an oral dosage form for the treatment of RRMS.[222] This molecule is a prodrug and enters the cell via the purine nucleoside transporters. Cladribine is then phosphorylated by deoxycytidine kinase.[223,224] In cells in which the ratio of deoxycytidine kinase to deoxynucleotidase is high, such as lymphocytes and monocytes, cladribine is phosphorylated to its corresponding triphosphate derivative, 2-chloro-2′-deoxy-ATP, which is the active form. Accumulation of this triphosphate form disrupts cellular metabolism and damages DNA, causing cell death.[225] These processes lead

to lymphocyte depletion and long-lasting lymphopenia, essentially leading to immunomodulation. Two phase II clinical trials involving progressive MS patients published in 1994 and 1996 showed that treatment with four monthly courses of 0.7 mg/kg cladribine was associated with significant disease stabilization measured with the EDSS and scripps neurological rating scale (SNRS).[226,227] In a multicenter study, however, cladribine did not have any significant clinical improvements for the treatment of progressive MS.[228]

The outcomes in RRMS patients, when treated with cladribine, were more encouraging than those in progressive MS patients. In the first double-blind, placebo-controlled, randomized trial with 52 RRMS patients, both the frequency and severity of relapses were reduced, and MRI enhanced lesions were completely suppressed by 6 months of treatment with cladribine.[229] In the CLARITY phase III trial (cladribine tablets treating multiple sclerosis orally), the long-term efficacy and safety of cladribine tablets (either 3.5 or 5.25 mg/kg) versus placebo were analyzed.[230] The annualized rate of relapse (ARR) values (the primary end points) were 0.14 and 0.15, respectively, in the two cladribine groups, compared with 0.33 in the placebo group, translating to relative ARR reductions of 57.6% and 54.5%, respectively. The risk of 3-month sustained progression of disability was also lower in the cladribine group (hazard ratio, 0.67 for the 3.5 mg/kg group and 0.69 for the 5.25 mg/kg group). Brain MRI revealed significant reductions in the extent of T2-weighted lesions (by 73.4% and 76.9%, respectively) and Gd-enhanced lesions (by 85.7% and 87.9%, respectively) in the aforementioned two groups. Overall, treatment with cladribine tablets for 96 weeks significantly reduced relapse rates in the RRMS patients, the risk of disability progression, and MRI measures of disease activity.[230]

Preliminary findings of the phase III ORACLE MS (oral cladribine for early MS) trial on the efficacy of cladribine in delaying conversion to clinically definite MS (CDMS) were released in 2014.[231] The treated groups exhibited significant delays in such conversion, accompanied by risk reductions of 67.3% and 61.9% in the two dose groups, 3.5 and 5.25 mg/kg, respectively, relative to placebo. Moreover, such treatment also significantly delayed the time to conversion to McDonald MS, compared with the placebo, echoing the efficacy seen in the CLARITY trial. Although cladribine may be more effective than the traditional drugs used for MS treatment, several adverse effects have limited its use. Dose-dependent myelosuppression, opportunistic infections (herpes zoster and TB), and malignancies have been linked to cladribine use and potentially limiting its use for the treatment of RRMS.[230] Benign uterine leiomyomas (smooth muscle tumors) and three cases of cancer were noted in patients in the CLARITY study.[232] Furthermore, secondary exacerbation of latent TB and latent herpes zoster led to implementation of screening measures in all ongoing trials using cladribine. Due to the negative feedback from the FDA and the European Medicines Agency, cladribine tablets were not further pursued for global approvals for marketing.[233]

Aforementioned therapeutics more or less capture the most popular therapeutic strategies deployed for the treatment of MS. While RRMS condition can be treated successfully with DMTs with various drugs available today, it is still a challenge to address the progressive forms of MS. Intense research and efforts are dedicated to develop novel DMTs that can prevent or reverse neurodegeneration in the progressive MS. There are no drugs yet that are directly addressing the neurodegeneration and progressive decline or loss of function in MS.

5.14.3 Other Neurodegenerative Disorders

In line with the concept of neurodegeneration due to progressive deterioration of the structure and/or function of neurons, other neurodegenerative diseases could include AD, PD, amyotrophic lateral sclerosis (ALS), Huntington's disease (HD), Down's syndrome (DS), glaucoma, age-related macular degeneration (AMD), and diabetic encephalopathy (DE). Clinical symptoms, disease progression and prognosis, and therapeutic approaches are quite diverse addressing these diseases. They do share similar biochemical reactions that lead to neurodegeneration. AD, ALS, and PD all share common features that include elevated oxidative stress levels and impaired energy metabolism in the nervous system.[234] Here, we will focus on PD and AD primarily and cover therapeutic options briefly in the context of neurodegeneration. Much of the treatments currently in market are only effective in alleviating some of the pathological symptoms, but most are unsuccessful at preventing neurodegeneration. Therefore, more innovative treatments are required for neurodegenerative disorders.

5.14.3.1 Alzheimer's Disease

The clinical manifestations in AD include irreversible loss of memory and thinking ability. Neuritic plaques, neurofibrillary tangles, and degeneration of several neural systems and neurotransmitters have all been connected to AD pathology. The difficulty in determining a singular neural pathway, affected by the disease leading to the deterioration of cholinergic system, suggests that there is an underlying mechanism for the degeneration and dysfunction of more than one of these neural pathways.[235] Moreover, the neuritic plaques found in the brains of AD patients have been associated with neuroinflammation through the colocalization of inflammatory peptides.[236,237] In AD, much of senile plaques were found to be composed of amyloid-β (Aβ), and Aβ is also believed to assist the onset of neurodegeneration.[235] The apparent relationship between PAD expression and AD progression signifies the potential use of citrullinated proteins as markers for neurodegeneration.[238–243]

It also appears that PAD enzymes are involved in neurodegenerative pathways associated with AD also, although more investigations are needed. Aβ peptides can increase the concentration of cytosolic Ca^{2+}, and PADs are calcium-dependent, hence, the suggestion of a link between PADs and AD progression.[239] Therefore, an increase in PAD activity, mediated by Aβ peptides, may be associated with the neuroinflammation mechanism of the disease. In the study conducted by Arif and Kato, increased activity

and higher levels of PAD2 within the hippocampus were observed in the rat model of AD after amyloid peptides were infused into the brain; however, PAD2 enzyme activation was inhibited by the administration of memantine (an NMDA antagonist used in the treatment of AD).[239] One can deduce that Aβ inhibits glutamate uptake in neurons, resulting in its accumulation and subsequent activation of NMDA receptor-induced Ca^{2+} influx into the cell, which activates the PAD2 enzyme. Arif and Kato also proposed the activation of glial cells by Aβ as an alternative mechanism leading to the activation of PAD2 due to their colocalization in astrocytes and microglia.[239] The study conducted by Nicholas showed immunohistological evidence of deimination within extracellular amyloid plaques in humans with AD.[240] Deiminated proteins were detected in the nuclei of neurons whose cytoplasm was immunoreactive for phosphorylated tau, implicating that histones may be a target for this process in these cells.

Along with amyloid proteins catalyzing increased PAD levels and their activation, the citrullinated forms of other proteins, such as vimentin and GFAP, were found in hippocampal tissues from patients with AD. In healthy humans, the citrullinated proteins were not observed.[238] PAD2 also citrullinates GFAP in AD which was shown using monoclonal antibodies against citrullinated GFAP. In addition to elevated PAD2 levels in AD patients, the role of PADs in AD pathogenesis and neurodegeneration then becomes apparent.[238,239] PTCD2, an antigen target of an AD diagnostic antibody, was found as the citrullinated form in the AD brains.[329] Therefore, potentially citrullinated proteins and their degraded fragments may enter the blood and lymphatic circulation and cause an immune response that produces the autoantibodies observed in AD.[329] More studies must be executed in order to determine the exact molecular mechanism of PAD enzymes in AD.

5.14.3.2 Therapeutic Approaches in AD

Current treatments in market for AD are designed to alleviate the symptoms and improve the quality of life of the patients temporarily (Table 2). In older patients suffering with AD, dementia and disability are commonly caused by AD.[244] Targeting cell-signaling pathways associated with neurodegeneration could be a potential strategy in decreasing neuroinflammation and excitotoxicity and improving cognitive functions. Molecular mechanism of each drug is briefly described later along with clinical evidence, to draw attention to therapeutic approaches employed for the treatment of AD and associated clinical conditions.

Table 2 Chemical structures of drugs for the treatment of Alzheimer's disease

Drug name	*Chemical structure*
Donepezil	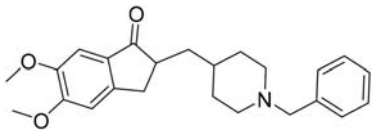
Rivastigmine	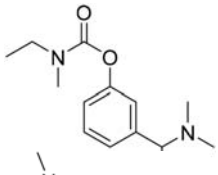
Galanthamine	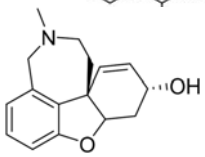
Memantine	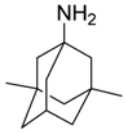
Solanezumab	Biologic drug
Gantenerumab	Biologic drug
Resveratrol	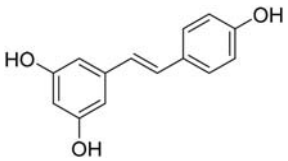

5.14.3.2.1 Donepezil

Neuroprotective agents with multiple mechanisms of action are used for the treatment of AD, and donepezil mechanism of action is related to the neuroprotective effects of this compound.[245] Donepezil is a potent, noncompetitive, and reversible acetylcholine esterase (AChE) inhibitor (**Table 2**).[246] In an in vitro study using neuroblastoma SH-SY5Y cells against okadaic acid or $A\beta_{25-35}$, donepezil exhibited neuroprotective effects along with galanthamine and rivastigmine.[247] The blocker of phosphoinositide 3-kinase (PI3K)-Akt reversed the protective effects of galanthamine and donepezil but not the effect of rivastigmine.[247] It is suggested that the mechanism of action of donepezil is likely not related to AChE inhibition, but possibly to the inhibition of the activation of glycogen synthase kinase 3 (GSK-3) and Akt enzymes.[247,248] Incubation of cortical neurons in the presence of donepezil prevented glutamate-induced apoptosis and consequently apoptotic neuronal death.[249,250] It was observed that donepezil causes loss of $\Delta\psi_m$, increases the release of cytochrome *c* to the cytosol, and modulates the expressions of Bcl-2 family proteins and the activation of caspase-9.[251] The loss of $\Delta\psi_m$ is usually associated with the formation of mPTPs followed by the diffusion of cyt *c* into the cytosol, which is normally associated with the inner membrane in mitochondria. Cytosolic cyt *c* activates procaspase-9 by binding to Apaf-1, which leads to caspase-9 activation and the subsequent activations of downstream executioner caspases (caspases-3, caspases-6, and caspases-7)—a well-established cascade of events.[251] Levels of cytosolic cyt *c* were elevated by donepezil in HL-60 cells, which suggested the involvement of the mitochondrial pathway in donepezil-induced apoptosis. These findings suggest that donepezil modulates the protein levels of Bid, Bax, Bcl-2, and Bcl-xl and that this results in loss of $\Delta\psi_m$ and release of cyt *c* from mitochondria.[251] This supports the mechanism that donepezil induces apoptosis in HL-60 cells via a mitochondria-mediated, caspase-dependent pathway. In vivo, it was found to increase the extracellular acetylcholine levels in the cerebral cortex and hippocampus of the rat.[250]

In three clinical studies investigating the efficacy and safety of donepezil,[252,253] patients were considered to have AD if they met the standard criteria: (1) diagnostic and statistical manual of mental disorders (third edition, revised) and National Institute of Neurological and Communicative Disorders and Stroke criteria for probable AD, (2) a minimental state examination (MMSE) score between 10 and 26 inclusive, and (3) a clinical dementia rating score of 1 or 2.[254] In a phase II multicenter, double-blind, placebo-controlled trial, dose-ranging study, among 161 patients of 96% white, aged 55–85 years randomized into four treatment arms, donepezil 5 mg once daily for 12 weeks exhibited significant clinical improvements in cognitive function in patients with mild to moderately severe AD.[252] Treatment arms consisted of placebo or 1, 3, or 5 mg/day of donepezil, respectively, for 12 weeks and then 2 weeks of single-blind, placebo washout period.[252] The efficacy of donepezil was acquired using ADAS-cog and CGIC as a primary measure and uniform activities of daily living (ADL), MMSE, Clinical Dementia Rating-Sum of the Boxes, and quality-of-life scores assessed by the patient (QOL-P) or the caregiver as a secondary measure. Patients receiving 5 mg/day had a significant improvement in their ADAS-cog scores ($p < 0.01$) at 3, 9, and 12 weeks as well as after the 2-week washout period compared to the placebo.[252] Some of the common adverse events included gastrointestinal events such as nausea, vomiting, diarrhea, gastric upset, constipation, and dizziness.

In the aforementioned study, an intent-to-treat analysis was conducted.[252] The adjusted mean changes in the ADAS-cog from baseline for placebo and treatment with the 5-mg/day groups were 0.7 (clinical decline) and −2.5 (clinical improvement), respectively ($p < 0.02$). A dose–response relationship was observed.[252] Based on the clinician evaluation (CGIC), most of the study patients did not have a change in their condition over the course of the 12-week study, and likely explanation is that AD patients do not show significant cognitive decline in 12 weeks.[252] In therapeutics development for AD, it necessary to have a longer evaluation period to detect a change based on clinician assessment (CGIC) scores. Fewer treatment failures also occurred in the donepezil-treated group (11%) compared with the placebo group (20%). Treatment with donepezil did not result in a significant improvement in the secondary measures of efficacy. Although there was an improvement in QOL-P, donepezil treatment was not any better than the placebo due to extensive patient variability.[252] The promising results from the phase II trials prompted the completion of two phase III randomized, double-blind, placebo-controlled trials, 15 and 30 weeks' duration.[253] Patients were randomized to receive placebo or donepezil at two doses: 5 or 10 mg/day. Efficacy was measured by using the ADAS-cog and the CIBIC-Plus. Baseline scores on the ADAS-cog ranged from 4 to 61 units (mean 26 units). Patients ranged in age from 50 to 94 years (mean 73 years); 62% were women, and most (95%) were white. In the 30-week study, 473 patients were randomized to the three treatment arms, placebo or donepezil, 5 or 10 mg. The trial was divided into a 24-week treatment phase followed by a 6-week single-blind, placebo washout phase. After 24 weeks of treatment, the mean differences in the ADAS-cog change scores for the 5-mg/day group and the 10-mg/day group compared with placebo were 2.8 and 3.1 units ($p < 0.001$), respectively. Thus, the difference between the two treatment groups was not significantly different, and the effects of the treatment were similar to that of placebo after the washout period. This suggests that the disease continues to progress during drug therapy and that donepezil did not alter the underlying disease process. Majority of patients (62–68%) taking donepezil showed no change or improvement in the CIBIC-Plus rating compared with those taking placebo (47%). Because of the progressive nature of AD, one can consider the "no-change status" in clinical condition over a 6-month period as a positive treatment effect. Donepezil treatment did not show any correlation to the outcomes based on the age, gender, and ethnicity of patients. In a subpopulation of the patients who completed the 30-week phase III trial and those that were on treatment for a long-term, an open-label study with 5–10 mg/day was investigated to understand the long-term efficacy of donepezil.[255] Patients maintained performance levels above the baseline scores for up to 40 weeks on an average, and collected ADAS-cog scores of 2 years suggested this benefit could extend as long as 2 years supporting the long-term use of donepezil in AD.[255]

5.14.3.2.2 Rivastigmine

Rivastigmine is another AChE inhibitor and is a potent compound that has been used for the treatment of a variety of neurological disorders. This compound has found its use for the treatment of AD, due to its AChE inhibitory activity. This is a noncompetitive pseudoirreversible inhibitor (Table 2). The pharmacokinetic properties of rivastigmine are quite different from donepezil due to this reason.[256–258] Rivastigmine inhibits AChE activity in the CSF of AD patients.[259–261] It allows greater selectivity of AChE inhibition in the CNS than in the periphery.[257,262] Thus, AD patients who are deteriorating on selective AChE inhibitor or those who cannot tolerate donepezil could potentially benefit from switching to rivastigmine.[263,264] Rivastigmine inhibits AChE with a long binding to its active site, up to 10 h, and it inhibits butyrylcholinesterase (BuChE) as well. As rivastigmine is a dual inhibitor, it can provide longer sustained efficacy than selective inhibitors and also can delay the formation of amyloidogenic proteins.[265] During the degeneration of primary rat neurons, rivastigmine reduced the secretion of Aβ while increasing α-secretase cleaved, secreted APP.[266] The increase in α-secretase cleaved secreted APP levels may potentially take part in cellular metabolic activity and enhanced neuronal survival.[266]

Rivastigmine exhibits effects on lymphocyte mitochondria. Biochemical analyses suggest that rivastigmine has a role in attenuating 3-nitropropionic acid-induced (complex II inhibitor) behavioral, biochemical, and cellular alterations.[267] Additionally, rivastigmine significantly reduced the oxidative damage while improving mitochondrial complex enzyme activities in different regions of the rat brain such as striatum, cortex, and hippocampus. This means that rivastigmine can potentially be an effective therapeutic agent for managing several neurodegenerative diseases beyond AD. When rivastigmine-treated AD patients were compared to control or untreated patients, higher oxidative and enzymatic activities were observed, including oxidation of pyruvate–malate (substrate of complex I) and glycerol-3-phosphate (substrate of complex III) and enzymatic activities of complexes II, III, and IV. The difference between treated and untreated AD patients and between treated patients of AD and controls was apparent.

5.14.3.2.3 Galanthamine

Galanthamine is a competitive inhibitor of AChE and allosteric activator of nicotinic acetylcholine receptors.[268,269] Its later activity, the allosteric modulation of nicotinic ACh receptors that is responsible for its therapeutic benefit in AD (Table 2).[270] Increased density of α7 nicotinic receptors and upregulation of antiapoptotic protein Bcl-2 after the incubation with galanthamine were observed in human neuroblastoma SH-SY5Y cells.[271] Furthermore, it was shown that galanthamine protected PC12 cells against the Aβ-induced apoptosis. It prevented Aβ aggregation, morphological changes of endoplasmic reticulum and mitochondria, and loss of $\Delta\psi_m$, as well as accumulation of ROS.[272] Galanthamine-induced cytotoxicity was not observed in human HepG cells, and also the oxidative stress markers were not affected at concentrations lower than 100 μM.[273] In an in vivo study in mice, galanthamine restored complex I and complex II activity and protected the mice brains from neurodegeneration, where the neurodegeneration was induced by intrahippocampal administration of kainic acid.[274] Thus, in vitro and in vivo studies indicate the prospects for galanthamine in the treatment of AD.

In vivo data in humans on galanthamine appear to have some variations, especially in the pharmacokinetics parameters. Surgical patients were given *i.v.* injection of galanthamine to reverse neuromuscular blockade after a surgery.[275] In these patients, maximum plasma concentration (C_{max}) of galanthamine was achieved at 2 min, and the serum concentration decreased rapidly between 2 and 30 min and then decreased slowly. The half-life ($t_{½}$) was found to be 4.4 h, and the mean cumulative urinary excretion was observed to be 28% of the administered dose, while biliary excretion was found to be 0.2%. Moreover, it is noted that only negligible amounts of the metabolites, epigalanthamine, and galanthaminone were detected.[276] In a study by Mihailova et al.,[276] young male volunteers were subjected to single oral and subcutaneous injection doses of galanthamine. Unlike previous studies, this study showed a quite dissimilar result where the C_{max} range was about 20 times greater than previous records. Although the reason for the diverse result is unclear, it may be due to different assay methods used in the study. T_{max} was observed to be 2 h for both types of doses, and the absorption kinetics exhibited a slow phase followed by a fast phase. Moreover, both doses achieved bioequivalence in rate and extent of absorption, and $t_{½}$ was not significantly different from the previously reported values.[275] In a study comparing an elderly AD patient and a healthy volunteer, it was observed that multiple oral doses of 15–55 mg galanthamine in the AD patient resulted in a steady-state near-peak plasma concentration of 32–182 ng/L.[277] Furthermore, in the healthy volunteer, 10 mg of *i.v.* injection resulted in a peak plasma concentration of about 180 ng/mL which correlated with the values obtained in the AD patient. It was concluded that galanthamine concentrations were dose-dependent, and the overall $t_{½}$ for galanthamine observed in this study was 8–10 h which is significantly longer than the $t_{½}$ values obtained in the other studies.

5.14.3.2.4 Memantine

Memantine is a noncholinergic alternative to AChE inhibitors such as rivastigmine and a low-affinity uncompetitive antagonist of NMDA receptors (Table 2). Memantine is used for treatment of moderate-to-severe stage of AD.[278] Memantine blocks the extensive activity of NMDA receptors but does not accumulate to interfere with normal synaptic transmission, and hence no disruption of normal physiological activity.[279,280] Via inhibition of NMDA receptors, memantine prevents the mitochondrial swelling, increases oxidative stress, and decreases $\Delta\psi_m$ induced by berberine in vitro in primary neurons from mice and rats.[281] In vitro, it prevents irreversible electrophysiological changes induced by the inhibitor of complex II (3-nitropropionic acid). However, it was shown to be ineffective in protecting complex I as the rotenone toxicity (complex I inhibitor) was not influenced in spiny striatal neurons.[282] Memantine is similar to AChE inhibitors in that it reduces Aβ levels in neuronal cultures in APP/PS1 transgenic mice.[283] Moreover, memantine is also neuroprotective as it inhibits Aβ-induced neurodegeneration and enhanced cerebral glucose utilization[268] and decreases brain glucose metabolism.[284] Memantine reduces the mitochondrial dysfunctions and mitochondrial

calcium, reverses $\Delta\psi_m$, and reduces ROS production induced by okadaic acid in the rat brain mitochondria. In a study that investigated the effect of memantine in ibotenic acid (IBO)-treated AD model in rats, it was found that glial cell activation can potentially play a significant role in the AD pathology and correlate with the changes of neuropeptide levels in the AD brain that is recovered by memantine treatment.[285] In a different study that examined the protective effects of memantine on $A\beta_{25-35}$-induced changes in peptidergic and glial systems,[286] it was found that treatment with memantine significantly increased $A\beta_{25-35}$-induced changes of neuropeptides, their metabolizing enzymes, and glial marker proteins. It was suggested that memantine exerts its protective effects by modulating the neuropeptide system as a consequence of suppressing the glial cells and oxidative stress in the AD model rat brain. Moreover, it was revealed that memantine protects against Aβ-induced neurotoxicity and learning impairment in rats.[287] Therefore, it was concluded that memantine protects against neurodegeneration induced by Aβ at therapeutic concentrations. Memantine also showed protection of cultured neurons against Aβ-induced toxicity by reducing the tau phosphorylation and its related signaling mechanisms.[288] However, memantine did not change either the conformation or the internalization of $A\beta_{1-42}$, and it was unable to reduce Aβ-induced potentiation of extracellular glutamate levels.

In a study that examined memantine as a NMDA receptor antagonist for the treatment of AD, patients with moderate-to-severe AD were randomly assigned to receive either placebo or 20 mg/day of memantine for 28 weeks. This multicenter study included 252 patients where 67% were women and the mean age was 76 years. According to CIBIC-Plus scores, patients under treatment showed better outcome than placebo. Memantine did not exhibit any significant adverse events in this study, and therefore, it was concluded that memantine reduced clinical deterioration, a phase associated with distress for patients and burden on caregivers, in moderate-to-severe AD.

5.14.3.2.5 Select drugs in development for AD treatment

Immunotherapy is a promising strategy for a variety of diseases, and AD treatment is seeing several strategies as well. Antibodies directed against Aβ are among the popular because they clear plaques and reverse cognitive deficits in mouse models. However, their clinical success has been limited due to side effects. Here, two antibodies, solanezumab and gantenerumab, are described and the ongoing efforts to develop this new class of AD therapeutics. In addition, a small-molecule drug, resveratrol, is gaining much popularity and is explored for the treatment of AD. Resveratrol is discussed in the context of its potential for the treatment of AD.

5.14.3.2.5.1 Solanezumab

Solanezumab, an IgG1 antiamyloid monoclonal antibody, binds to the mid-domain of the Aβ peptide.[289] It is shown to increase the clearance of soluble Aβ, and in preclinical studies, it was observed that murine anti-Aβ monoclonal antibody, from which solanezumab was derived, reduced brain amyloid plaque deposition in the transgenic APP^{V717F} mice.[290,291] Another correlation between plasma Aβ accumulation and plaque deposition was also apparent. Phase I and phase II studies done on patients with mild-to-moderate AD revealed that target engagement was present due to dose-dependent increases in plasma and CSF total Aβ.[292,293] This may be because during solanezumab movement from plasma to the CNS, it binds to Aβ in the compartment with accumulation of measureable total Aβ in CSF.[292] More complex effects of solanezumab on unbound Aβ in CSF were observed. In a phase II study with AD patients, 12-week treatment with solanezumab showed a dose-dependent increase in CSF free $A\beta_{1-42}$ while showing dose-dependent decrease in CSF free $A\beta_{1-40}$ although the cause of the difference is not yet apparent. $A\beta_{1-42}$ is the predominant form of Aβ, while $A\beta_{1-40}$ is a much less abundant form in amyloid plaque.[293] One possible hypothesis is that solanezumab may be altering equilibria so that concentrations of free $A\beta_{1-42}$ in CSF might be different from those of free $A\beta_{1-40}$. Solanezumab is known to have similar affinity for the two Aβ isoforms, and the relative abundance of each isoform is different in amyloid plaque consisting primarily of $A\beta_{1-42}$.[293,294] Mouse model of AD benefited from both active and passive immunizations by Aβ peptide, showing clearance of aggregated Aβ deposits and improving memory and learning. When a similar study was done on humans using solanezumab, it was observed that the drug only showed significant beneficial effect in mild AD cases in the secondary outcome, but not in the primary end point.[295] Two phase III studies, EXPEDITION and EXPEDITION2, are identical placebo-controlled studies to assess the effects of solanezumab on cognitive and functional decline over 80 weeks in patients with mild-to-moderate AD. These studies used secondary analyses of efficacy, biomarker, and safety end points. The results showed that cognitive and functional decline was less when under treatment for patients with AD compared to placebo using various clinical measurement scales, ADASC subscale, MMSE, and ADCSA of Daily Living functional scale Instrumental ADLs. Baseline-to-end point changes did not exhibit any difference between treatment groups. Plasma/CSF biomarker findings indicated target engagement by solanezumab, and the drug also showed adequate safety. This drug is a biologic molecule, and it remains to be seen if any neuroprotective effects or prevention and reversal of neurodegeneration would be seen as a result of the treatment with solanezumab.

5.14.3.2.5.2 Gantenerumab

Gantenerumab, a monoclonal antibody drug, binds an epitope in the N-terminus of oligomeric and fibrillar Aβ, which leads to microglia-mediated phagocytic clearance of plaques.[296] It showed a failure in one of the phase III trials in patients with mild-to-moderate AD, and it is currently in phase III trials (Scarlet RoAD and Marguerite RoAD) in patients with earlier stages.[297] It was shown that gantenerumab decreases the tau levels in the CSF significantly. However, it did not have much effect in reducing Aβ levels. It is believed that higher concentration of gantenerumab can potentially achieve clinical significance.

5.14.3.2.5.3 Resveratrol

Resveratrol (trans-3,4′,5-trihydroxystilbene) is a naturally occurring polyphenol that is being explored for its potential to treat AD by mimicking the caloric restriction through extending the lifespan of several small organisms (Table 2).[298–302] Resveratrol can also delay various age-related phenotypes such as abnormal glucose metabolism,[303] and patients with AD can benefit from its effect on cognitive deterioration under this treatment.[304,305] It is currently under investigation to determine its benefits in treating dementia in patients with mild cognitive impairment (MCI), which could progress to AD. The direct molecular targets of resveratrol have yet to be identified in vitro and in vivo. However, it has been hypothesized that resveratrol modulates cellular processes by activating key metabolic sensor or effector proteins, such as AMP-activated protein kinase (AMPK), sirtuin 1 (SIRT1), and peroxisome proliferator-activated receptor γ coactivator-1α (PGC-1α).[306–308] Binding of resveratrol to SIRT1 in vitro leads to the activation of deacetylase activity of the enzyme.[309] However, recent studies have indicated that the relationship between resveratrol and SIRT1 in vitro may be an artificial observation and that in vivo, resveratrol may target other proteins,[310,311] although it appears that SIRT1 is still required in resveratrol metabolic functions in vivo by taking parts in energy sensing network involving AMPK and PGC-1α.[306,312]

Although many studies support the beneficial effects of resveratrol in AD in vitro and in vivo, large-scale clinical trials have yet to be completed to prove its benefits. However, it appears that resveratrol is well tolerated and no marked toxicity was reported. On the other hand, resveratrol exhibits poor bioavailability, low water solubility, and chemically unstable.[313,314] With oral administration or *i.v.* injection in humans, resveratrol was quickly metabolized within 2 h.[315] Various studies in animals and in humans have shown that resveratrol has poor intestinal uptake, and unmetabolized form of resveratrol was difficult to detect in plasma.[313] The pharmacokinetics of *trans*-resveratrol (200 mg *t.i.d.* oral administration) was shown to be independent of age but with relatively low plasma concentrations.[316] In animal models, resveratrol appears to be bioavailable and bioactive.[317] Although recent studies have attempted in finding the most effective route of administration for resveratrol,[318–321] none of them appeared to be efficacious.

Various clinical trials are underway to determine the benefits of resveratrol on neurodegenerative diseases such as AD even though there are many difficulties.[322] One study (a double-blind, placebo-controlled, and crossover trial) on healthy young volunteers consuming 500 mg resveratrol showed that the levels of total hemoglobin were remarkably higher in the frontal cortex during task performance,[323] but it failed to show its effect on cognitive performance.[322,324] In a randomized controlled trial (RCT) versus placebo, 60 AD patients were given liquid resveratrol with glucose and malate as a dietary supplement delivered in grape juice. The ADAS-cog scores were assessed at regular intervals up to 1 year after study commencement.[324,325] In another multi-interventional clinical trial in MCI, resveratrol supplementation or caloric restriction or omega-3 supplementation or placebo was provided for 6 months, and then, the ADAS-cog scores would be assessed.[325] In a separate, but similar randomized, double-blind, placebo-controlled study with 119 patients, patients received 500 mg daily with dose escalation by 500 mg every 13 weeks.[326] In this 52-week phase II trial, resveratrol and its major metabolites were measurable in plasma and CSF, contrary to the earlier studies. Aβ40 levels in the CSF and plasma declined more in the placebo group than the resveratrol-treated group with a significant difference by the end of study. Interestingly, brain volume loss was increased in the resveratrol-treated group compared to placebo. Overall, this study provided plausible evidence that resveratrol is reasonably safe and is well tolerated in AD patients. It also alters biomarker levels. Additional studies are needed to confirm any beneficial effects of resveratrol.

5.14.3.3 Parkinson's Disease

PD is a neurological disease that exhibits several motor and nonmotor neuron-related symptoms. Unlike the studies in MS, the link between PAD enzymes and PD is only recently being discovered. Neurodegenerative aspects of this disease are caused by the death of dopaminergic neurons in the substantia nigra region of the brain and the presence of Lewy bodies (intraneuronal protein aggregates).[327] In another independent study, using the brain tissue from the PAD patients, immunoreactivity for the deiminated (hypercitrullinated) proteins was shown to be localized to GFAP and in the cytoplasm of dopamine neurons within the substantia nigra region.[328] These studies indicated the involvement of substantia nigra and hypercitrullination of proteins within this region as one of the biochemical consequences. One of the most useful target antigens for the antibody diagnosis of AD and PD, known as pentatricopeptide repeat domain 2 (PTCD2), was discovered in the citrullinated form in the brain.[329] However, the root cause of such neurodegeneration associated with hypercitrullination and PAD activity still needs to be explored.[330] In addition to many factors associated with neurodegeneration in PD, neuroinflammation also contributes to the degeneration of dopaminergic neurons; one of the factors is shown to be a mutated kinase, leucine-rich repeat kinase 2 (LRRK2) potentially exacerbating inflammation and leading to the neurodegeneration seen in PD.[331]

5.14.3.4 Therapeutic Approaches in PD

5.14.3.4.1 Carbidopa/levodopa

Levodopa is now widely used as a PD treatment.[332] Some of the drawbacks of the treatment includes large daily dosage, delayed onset of 1–2 months prior to showing therapeutic benefits, and numerous side effects. In PD, substantia nigra degenerates, which leads to the disruption of nigrostriatal pathway and reduction of striatal dopamine.[333] This reduction or loss of dopamine and denegeration of the brain lead to the clinical symptoms seen in PD. Dopamine is a polar molecule and cannot cross the blood–brain barrier. Thus, a precursor of dopamine, levodopa, has been developed, which delivers dopamine into the brain, and levodopa

is commonly discussed as a prodrug due to this character (Table 3). Levodopa becomes absorbed in the small bowel and quickly becomes catabolized by aromatic L-amino-acid decarboxylase (AADC) and catechol-*O*-methyltransferase (COMT). It was observed that gastric AADC and COMT can degrade levodopa. Therefore, levodopa is usually given with AADC inhibitor, carbidopa. Thus, when levodopa/carbidopa is administered, levodopa enters the brain and is decarboxylated to generate dopamine. The exact site of decarboxylation of exogenous levodopa to dopamine in the brain has yet to be determined. However, most of striatal AADC is found in nigrostriatal dopaminergic nerve terminals where dopamine is synthesized and stored in the terminals and becomes released to stimulate the postsynaptic dopamine receptors and mediates the antiparkinsonian action of levodopa. Metabolic conversion, storage, and release are omitted since dopamine agonists act directly on postsynaptic dopamine receptors.

5.14.3.4.2 Pramipexole

Along the lines of addressing dopamine deficiency, a variety of dopamine receptor agonists are deployed for the treatment of PD. Pramipexole is a dopamine D2/D3 receptor agonist that is used for treating PD symptoms (Table 3).[334] In vitro and in vivo models have shown that pramipexole can potentially have disease-modifying properties in PD.[335–337] The ability of pramipexole to protect against cell death in dopaminergic and nondopaminergic cells was investigated in vitro.[335,338] Preincubation of dopaminergic SHSY-5Y cells and nondopaminergic JK cells with either the active (−)- or inactive (+)-enantiomer forms of pramipexole at 10 μM concentration decreased cell death in response to 1-methyl-4-phenylpyridinium (MPP+) and rotenone, and the cells were protected. Interestingly, the protective effect was not prevented by dopamine receptor blockade using sulpiride or clozapine. Concentration of pramipexole for its protective effect was less than that required for its antioxidant activity. Supporting its antiapoptotic action in these cell lines, pramipexole reduced caspase-3 activation, decreased the release of cytochrome *c*, and prevented the fall in the mitochondrial membrane potential. From this study, it is suggested that pramipexole may be exhibiting neuroprotective effects independent of dopamine receptor occupation or antioxidant activity. Further studies must be established to conclude whether this neuroprotective action represents disease-modifying effect in PD. An RCT with a group of patients with early PD, receiving an early start of treatment, another group receiving a delayed start, and another group receiving just placebo, also known as Pramipexole On Underlying Disease (PROUD), was established to determine the disease-modifying effects of pramipexole.[339] From this investigation, it was suggested that pramipexole lacks disease-modifying effects, although it is still an effective option for symptomatic treatment for PD.[340]

5.14.3.4.3 Ropinirole

Ropinirole (Requip, GlaxoSmithKline) is indicated for the treatment of early and advanced Parkinson's disease.[341] Ropinirole, a nonergoline dopamine agonist, binds to dopamine D2-like receptors (Table 3).[342] Similar to dopamine, its selectivity toward dopamine receptors is in the order of D3 > D2 > D4. A randomized, placebo-controlled, double-blind, parallel-group, 6-month study was established to determine the efficacy and safety of ropinirole in early PD patients with limited or no prior dopaminergic therapy.[343] Patients ($n = 241$; Hoehn and Yahr stages I–III, mean age 62.8 years), stratified by concomitant use of selegiline, were randomized to ropinirole ($n = 116$) or placebo ($n = 125$). The starting dose of ropinirole was 0.25 mg *t.i.d.* with titration to at least 1.5 mg *t.i.d.* Primary efficacy end point was the percentage improvement in unified Parkinson's disease rating scale (UPDRS) motor score. Ropinirole-treated patients had a significantly greater percentage improvement in UPDRS motor score than patients who received placebo (+24% vs. −3%; $p < 0.001$). Ropinirole showed high-tolerability and infrequent withdrawals, with most of adverse events being related to peripheral dopaminergic activity. This drug is metabolized by the liver, and its elimination half-life is 5.8 h.[341] As a monotherapy, ropinirole improves signs and symptoms in early PD. In advanced PD with motor fluctuations, employed as an adjunct to levodopa, ropinirole reduces off time and allows for a reduction of levodopa dose in these patients.

5.14.3.4.4 Bromocriptine

Bromocriptine is a potent dopamine agonist that directly stimulates dopamine receptors and alleviates numerous symptoms of PD (Table 3).[344] Its pharmacological effects are similar to those of levodopa with respect to benefits and adverse effects. Bromocriptine can mitigate the drawbacks of chronic use of levodopa such as decline in efficacy, fluctuations in therapeutic response, and development of disabling abnormal involuntary movements. Bromocriptine achieved safety in dosages of up to 100 mg/day for 2 years, although some of the adverse effects are common to those due to levodopa.

5.14.3.4.5 Cabergoline

Cabergoline is a synthetic ergoline dopamine agonist and has a high affinity for D2 receptors.[345] It also has longer elimination half-life, thus continuously providing dopaminergic stimulation with once-daily administration. Furthermore, cabergoline has high tolerability and effectiveness in controlling PD symptoms. It is comparable with levodopa in that levodopa exhibits fluctuations in response during long-term use, but cabergoline appears to be less fluctuating. Cabergoline can also reduce the risk of developing drug-induced motor complications.

5.14.3.4.6 Pergolide

Pergolide is an agonist of D1 and D2 dopaminergic receptors.[346] In comparison with levodopa, which gradually loses its effectiveness during chronic use, pergolide at a dose of 2 mg/day improved PD symptoms and allowed patients to reduce the intake of levodopa dosage by as much as 50%. The adverse events of pergolide, although are manifested frequently, are mild and reversible.

Table 3 Chemical structures of drugs for the treatment of Parkinson's disease

Drug name	*Chemical structure*
Levodopa	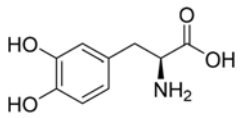
Carbidopa	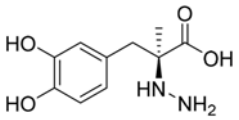
Pramipexole	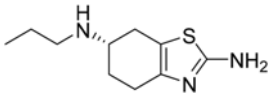
Ropinirole	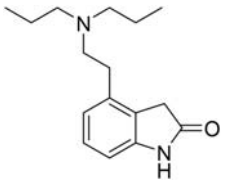
Bromocriptine	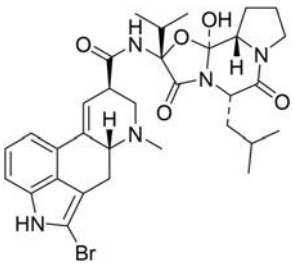
Cabergoline	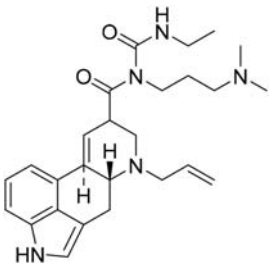
Pergolide	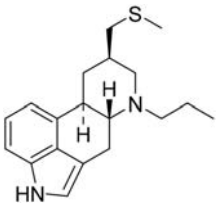
Rotigotine	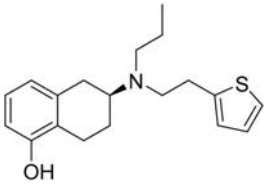

Table 3 Chemical structures of drugs for the treatment of Parkinson's disease—cont'd

Drug name	*Chemical structure*
Trihexyphenidyl hydrochloride	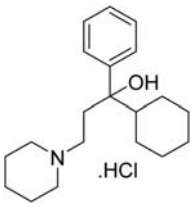
Benzotropine	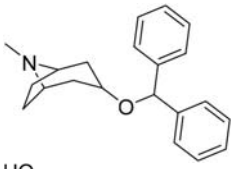
Apomorphine	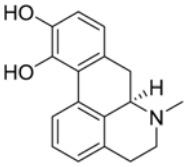
Amantadine	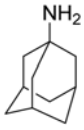
Entacapone	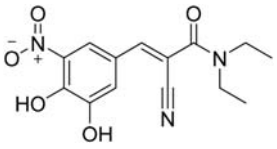
Tolcapone	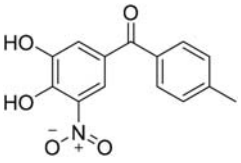
Selegiline	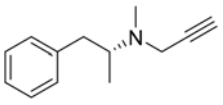
Rasagiline	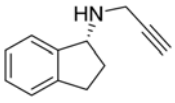
Istradefylline	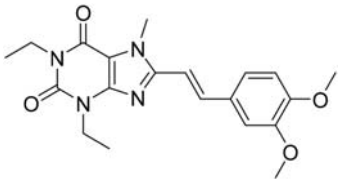

5.14.3.4.7 Rotigotine

Rotigotine, a lipid-soluble, nonergot, D3, D2, or D1, dopaminergic receptor agonist, is effective in early and advanced PD treatments.[347] Rotigotine is unique due to its transdermal patch formulation that allows for continuous, once-daily administration leading to higher patient compliance. Rotigotine was shown to achieve high tolerability, and it can also be used as a combination with levodopa for patients with advanced PD.

5.14.3.4.8 Anticholinergics (trihexyphenidyl and benzotropine)

Anticholinergic drugs currently in market include benzotropine (Cogentin) and trihexyphenidyl hydrochloride (Artane) (Table 3). Deployment of this class of drugs goes back to 1940s and 1950s, where the use of benzotropine sulfonate was described for the treatment of PD symptoms.[348] Anticholinergic drugs are used as PD treatment to reduce the acetylcholine activity and to balance the production of dopamine and acetylcholine. Anticholinergic drugs antagonize the hyperactive cholinergic transmission via blockade of postsynaptic muscarinic receptors and restore the balance between DA and acetylcholine (Ach) systems in the striatum. ACh controls movement, and anticholinergic drugs are used in combination with levodopa, described earlier, to treat mild symptoms of tremors and rigidity without alterations in bradykinesia.[349,350] Anticholinergics were commonly employed in a number of conditions related to dystonia in the recent years.

Some of the adverse events that can be caused by anticholinergics include blurred vision, dry mouth, and urinary retention. Moreover, reactions in CNS such as confusion, dementia, and psychiatric symptoms can be seen in elderly patients. Anticholinergic drugs are not to be used with other drugs, and they are rarely used as primary drug therapy. There is also no evidence that these drugs provide neuroprotective effects, in the context of preventing or reversing neurodegeneration associated with PD.

5.14.3.4.9 Apomorphine

Apomorphine is a potent D1 and D2 dopaminergic agonist and is administered through subcutaneous injection at doses from 15 to 180 μg/kg.[351] Intranasal, sublingual, and rectal routes of administration have shown to cause local allergic effects and thus limited the use of other dosage forms. Apomorphine is able to achieve rapid onset of action and short-duration effect, and the maximal plasma concentration is established in 8–16 min. Its plasma half-life was observed to be 34–70 min, and the bioavailability was approximately 100%. Diminished sensitivity (tolerance) can also be observed in patients with repeated use of the drug. Due to this reason, it is discretely employed for routine therapeutic use. Apomorphine is also used in differential diagnosis between idiopathic PD, other Parkinson plus syndromes, and as a predictive test for dopaminergic responsiveness. Apomorphine was shown to alleviate akinesia, rigidity, and tremor. Either a continuous apomorphine subcutaneous infusion or multiple subcutaneous injections of apomorphine may be beneficial when levodopa treatment was temporarily interrupted. The side effects of apomorphine include nausea and hypotension. However, these adverse effects can be prevented with the use of domperidone, a peripheral dopaminergic antagonist. It was also shown that cutaneous fibrous nodules and psychiatric symptoms may occur at high dosages and with continuous infusion of this drug.

5.14.3.4.10 Amantadine

Amantadine, an NMDA receptor antagonist, is used alone to treat early PD or as an adjunct to treat advanced PD.[352] Amantadine, similar to memantine, belongs to the class of adamantine derivatives (Table 3). The mechanism of action for this drug in PD has yet to be discovered. Unlike other dopaminergic treatments, amantadine was shown to effectively control tremor and muscle rigidity (classified together under "impulse control"), although these symptomatic benefits could only be a short-term effect. The dose could range from 100 mg once daily to 100 mg three times daily. Some of the adverse effects include nausea, dizziness, insomnia, confusion, hallucinations, peripheral edema, and livedo reticularis. It was also shown that high serum concentrations could potentially cause severe psychosis in elderly, and it can also lead to additive adverse effects on mental function. Sudden withdrawal from the treatment could potentially cause exacerbation of PD symptoms or neuroleptic malignant syndrome and acute delirium. Patients with liver or renal dysfunction and older adults may require dosage adjustment and close monitoring.[353] A very recent study in 2016 concluded that amantadine and selective serotonin reuptake inhibitors (SSRIs), antipsychotics, anticonvulsants, opioid antagonists, etc. have insufficient proof on the efficacy of this drug based on the current literature evidence.[354] Additional research is necessary to confirm the utility of this drug for the treatment of PD symptoms.

5.14.3.4.11 COMT inhibitors (entacapone and tolcapone)

COMT inhibitors are shown to improve motor fluctuations and block the breakdown of levodopa, which allows increased levodopa level to reach the brain.[349,355,356] This class of drugs is primarily employed as an adjunct therapy with levodopa. It has been observed that using COMT inhibitors along with levodopa therapy reduces the end-of-dose failure patients experience as the effect of levodopa decreases and also decreases the motor fluctuations.[355,357] COMT inhibitors currently in market include entacapone (Comtan) and tolcapone (Tasmar), both of which are structurally related analogs (Table 3). Adverse effects of entacapone include increase in dyskinesias, gastrointestinal upset, dizziness, and drowsiness. Stalevo is still under investigation by the US Food and Drug Administration due to possible increased risk of prostate cancer.[358] Adverse effects of tolcapone include dizziness, drowsiness, excessive dreaming, nausea, vomiting, diarrhea, and increased sweating. Tolcapone may also cause life-threatening liver damage, and hence, patients under this treatment must be monitored with care.[359]

5.14.3.4.12 MAO-B inhibitors (selegiline and rasagiline)

Monoamine oxidase type B (MAO-B) inhibitors are intended to prevent the catabolism of dopamine in the brain and enhance dopamine levels (Table 3). Selegiline and rasagiline are two irreversible MAO-B inhibitors used alone to treat early PD or with levodopa for treatment of advanced PD.[360,361] Both compounds share similar structural features, with a prop-2-ynyl amino group as the active entity is responsible for their inhibitory activity. Selegiline is available in various dosage forms such as classical tablet, capsule, and in a lower-dose, orally disintegrating tablet formulation. Using orally disintegrating tablet formulation allows the drug to be absorbed through the oral mucosa, and it minimizes first-pass metabolism, increasing bioavailability and reducing serum concentrations of amphetamine metabolites. Rasagiline was shown to delay its progression of PD. In a double-blind, delayed-start trial of rasagiline, patients receiving 1 mg daily of the drug had significantly less disability after 72 weeks than those who received placebo, but those receiving 2-mg doses did not.[362] While the mode of action of this class of compounds appear to show prospects for neuroprotection in in vitro and in animal models of neurodegeneration, recent evidence suggests that MAO-A also must be playing a role in the neuroprotection.[363]

5.14.3.4.13 Istradefylline

Adenosine 2a (A2a) receptors antagonists are nondopaminergic drugs that have been under investigation to assess their effects on treating symptoms of PD for several years.[364] A2a receptors in the striatum can colocalize with dopamine D2 receptors on GABAergic striatopallidal output neurons of the indirect pathway and to GABAergic recurrent collaterals.[365] Adenosine A2a antagonists reduce the overactivity of the striatopallidal pathway and play a role in motor control.[366] In nonhuman *N*-methyl-4-phenyl-1,2,3,6-tetrahydropyridine (MPTP)-lesioned primates, A2a antagonists have improved motor neuron control with little development of dyskinesia. In levodopa-primed animals, treatment with A2a antagonists was also observed to improve motor function without worsening dyskinesia.[367–370] Furthermore, in rodent models, nonmotor functions such as memory, olfaction, and mood were also showing improvements.[371] Lastly, neuroprotective effects have been demonstrated in numerous models.[372,373] Istradefylline is the first one to complete phase III development, and it is now marketed for the treatment of PD.[374] In an early proof-of-concept, placebo-controlled study, istradefylline was used as an adjunctive therapy with levodopa in 15 PD patients with motor complications.[375] Istradefylline alone did not exhibit antiparkinsonian response to a low-dose, suboptimal levodopa infusion. At a dose of 80 mg/day, istradefylline with a low-dose levodopa infusion showed 36% increase in motor function UPDRS and with 45% less dyskinesia compared with an optimal-dose levodopa infusion alone. Clinical benefits of istradefylline were shown to last 76% longer after stopping levodopa infusion, when coadministered with levodopa infusion.[375]

In a separate study consisting of 83 PD patients with motor fluctuations and dyskinesia, 20 or 40 mg *q.d.* of istradefylline showed 1.7 h reduction in the off time compared to placebo ($p=0.004$).[376] Similarly, in one phase II study, patients with motor fluctuations that were given 40 mg/day istradefylline experienced 1.2 h reduction of off time compared with placebo ($p=0.005$).[377] In another phase II study, istradefylline 20 mg/day was observed to reduce off time by 0.64 h (4.35%, $p=0.026$), and istradefylline 60 mg/day reduced off time by 0.77 h (4.49%, $p=0.024$).[378] In this study, an increase in on time with dyskinesia was noted but was considered to be insignificant as it was an increase in nontroublesome dyskinesia. In a phase III trial, istradefylline 20 mg/day reduced off time compared with placebo by 0.7 h ($p=0.03$).[379] On the other hand, another phase III trial of istradefylline (10, 20, and 40 mg/day) has shown insignificant reductions in off time compared with placebo.[380] The reason for the failure of this study is unknown; istradefylline received a not approval letter from FDA in 2008 due to its efficacy results being insufficient enough to support its clinical utility, although phase III trials were carried out in Japan and other countries.[381–383] As a monotherapy in treating early PD, istradefylline was not able to show any significant improvement in UPDRS motor scores compared with placebo (-1.11, $p=0.228$).[384] Nonetheless, istradefylline showed high tolerability and mild efficacy in reducing off time in PD patients with motor fluctuations. In general, evidence for the use of A2a antagonists in early PD is very limited and is not supportive. However, patients already treated with dopaminergic drugs and exhibiting compromised efficacy in late-stage disease have benefitted from this class of drugs.[374]

5.14.3.4.14 Levodopa formulations

Due to the high efficacy of levodopa and its direct mechanism of action, significant effort was dedicated to new formulations for levodopa and adjunct therapies primarily to improve the pharmacokinetic properties of these drugs and ultimately lead to better patient compliance and/or comfort.

5.14.3.4.14.1 Levodopa/carbidopa intestinal gel (LCIG; duodopa)

Duodopa or LCIG is an aqueous intestinal gel which contains 20 mg/mL of levodopa and 5 mg/mL of carbidopa, and this gel is administered via a portable pump.[385] A 100 mL cassette contains 2000 mg of levodopa, which is enough for a full day of treatment. The cassette is used to attach to a portable infusion pump, and the gel is pumped through a transabdominal tube connected to a percutaneous endoscopic gastrostomy (PEG) tube with the tip positioned in the proximal jejunum or duodenum. The gel can be infused during waking hours or around-the-clock. It was shown to be effective in reducing motor fluctuations and dyskinesia in advanced PD.[385–387] In a randomized, crossover trial, nasoduodenal infusion of LCIG was compared with carbidopa/levodopa controlled release tablets 50/200 mg/and immediate release 12.5/50 mg.[388] The pharmacokinetics of LCIG revealed that the intra-individual variation for plasma levodopa concentration was 34% with oral medication compared with 14% with LCIG infusion ($p<0.01$). Also, motor assessments have shown increased near-normal state observations (80% vs. 61%, $p<0.01$) with LCIG compared with oral medication. Bradykinesia and dyskinesia have also shown reduction with LCIG.

A study named DIREQT (Duodopa infusion: randomized efficacy and quality of life trial) was conducted to compare the naso-duodenal infusion of LCIG to individually optimized combinations of pharmacotherapy in a randomized crossover trial using two 3-week treatment periods for 25 patients.[389] This study revealed that the median percentage of ratings in the functional on state increased significantly with LCIG compared to standard pharmacotherapy (100% vs. 81%, $p < 0.01$). Dyskinesia appeared to be uncommon and not different for the two treatment periods. Quality-of-life scores achieved significantly higher scores with LCIG. Multiple longer-duration open-label studies have also demonstrated benefit with LCIG delivered via PEG. In the HORIZON study, a 12-week, randomized, double-blind, double-dummy, double-titration phase III trial, LCIG showed a promising option for control of advanced Parkinson's disease with motor complications.[390] In this multicenter study, the primary end point was the change in motor off time from baseline to final visit. Patients receiving LCIG showed superior outcomes in the off times, and 14% of the patients showed significant adverse events mainly associated with the percutaneous gastrojejunostomy tube and related issues. In the United States, this drug was approved by US FDA in 2015. The main drawbacks of LCIG use is the invasiveness of the procedure, the inconvenience of carrying the pump, and the problems associated with managing device malfunctions, including tube dislocations and obstructions.

5.14.3.4.14.2 IPX066

IPX066 is an extended-release oral formulation of carbidopa/levodopa. In an open-label crossover study, IPC066 was compared with carbidopa/levodopa immediate-release (carbidopa/levodopa IR) formulation.[391] At a single dose, time to on was similar for both medications, but UPDRS motor scores were significantly better with IPX066 from hours 3 to 6 ($p < 0.05$), which indicated longer duration of action. The mean daily dosing frequency for IPX066 was 3.5 compared with 5.4 for carbidopa/levodopa IR. It was also observed that patients experienced 2 h less off time per day with IPX066 ($p < 0.0001$) despite the reduced frequency of drug administration. In a randomized double-blind phase III trial, 393 patients with fluctuations on carbidopa/levodopa IR were enrolled.[392] Patients were given a 3-week dose adjustment period of carbidopa/levodopa IR. They were then switched to IPX066 and underwent a 6-week adjustment phase using IPX066. And in the last 13 weeks, they were randomized to their adjusted IPX066 or carbidopa/levodopa IR regimen using a double-dummy design. The mean daily dosing frequency was 3.6 for IPX066 compared with 5.1 for carbidopa/levodopa IR. Results demonstrated that IPX066 provided a 1.1-h improvement in on time without troublesome dyskinesia compared with carbidopa/levodopa IR ($p < 0.001$). Thirty-nine percent of patients rated themselves as much or very much improved with IPX066 compared with 17% with carbidopa/levodopa IR ($p < 0.0001$). IPX066 maintains therapeutic levodopa concentrations for an extended period of time compared with carbidopa/levodopa IR. Although IPX066 has shown to be effective in early PD, the ultimate value of IPX066 in early disease may depend on whether more continuous dopamine stimulation can reduce the development of dyskinesia.[393]

5.14.4 Conclusion

While the well-established therapeutics for these diseases are still grounded in the theories and observations from the past century primarily focusing on the clinical symptoms, prevention and, if possible, reversal of neurodegeneration and disease progression are a priority for the new generation of therapeutics. MS and various neurodegenerative disorders such as AD and PD have benefitted tremendously due to the introduction of new diagnostic tools driving new avenues of research in the new millennium. Definitions of the disease states, a closer alignment with the progressive stages of the diseases and neurodegeneration, are introduced in the recent years, and they facilitate focused research efforts for novel drug targets and development of novel therapeutics. DMTs are considered to be the best course, once the disease is diagnosed appropriately, because disease onset takes several years and the root causes of the disease onset are complex. New DMTs addressing these diseases and neurodegeneration is the new frontier in research and therapeutics.

References

1. McFarlin, D. E.; McFarland, H. F. Multiple Sclerosis (First of Two Parts). *N. Engl. J. Med.* **1982,** *307* (19), 1183–1188.
2. Stys, P. K. Pathoetiology of Multiple Sclerosis: Are We Barking Up the Wrong Tree? *F1000Prime Rep.* **2013,** *5,* 20.
3. Gonzalez-Scarano, F.; Grossman, R. I.; Galetta, S.; Atlas, S. W.; Silberberg, D. H. Multiple Sclerosis Disease Activity Correlates with Gadolinium-Enhanced Magnetic Resonance Imaging. *Ann. Neurol.* **1987,** *21* (3), 300–306.
4. Hafler, D. A. Multiple Sclerosis. *J. Clin. Invest.* **2004,** *113* (6), 788–794.
5. Brinar, V. V.; Barun, B. Challenges in Multiple Sclerosis; How to Define Occurence of Progression. *Clin. Neurol. Neurosurg.* **2013,** *115* (Suppl. 1), S30–S40.
6. Jacobsen, C. O.; Farbu, E. MRI Evaluation of Grey Matter Atrophy and Disease Course in Multiple Sclerosis: An Overview of Current Knowledge. *Acta Neurol. Scand. Suppl.* **2014,** *198,* 32–36.
7. Plantone, D.; De Angelis, F.; Doshi, A.; Chataway, J. Secondary Progressive Multiple Sclerosis: Definition and Measurement. *CNS Drugs* **2016,** *30* (6), 517–526.
8. Hawker, K. Progressive Multiple Sclerosis: Characteristics and Management. *Neurol. Clin.* **2011,** *29* (2), 423–434.
9. Swanton, J. K.; Fernando, K. T.; Dalton, C. M.; Miszkiel, K. A.; Altmann, D. R.; Plant, G. T.; Thompson, A. J.; Miller, D. H. Early MRI in Optic Neuritis: The Risk for Clinically Definite Multiple Sclerosis. *Mult. Scler.* **2010,** *16* (2), 156–165.
10. Lublin, F. D.; Cutter, G.; Giovannoni, G.; Pace, A.; Campbell, N. R.; Belachew, S. Natalizumab Reduces Relapse Clinical Severity and Improves Relapse Recovery in MS. *Mult. Scler. Relat. Disord.* **2014,** *3* (6), 705–711.

11. Tutuncu, M.; Tang, J.; Zeid, N. A.; Kale, N.; Crusan, D. J.; Atkinson, E. J.; Siva, A.; Pittock, S. J.; Pirko, I.; Keegan, B. M.; et al. Onset of Progressive Phase is an age-Dependent Clinical Milestone in Multiple Sclerosis. *Mult. Scler.* **2013,** *19* (2), 188–198.
12. Tu, R.; Grover, H.; Kotra, L. P. Peptidyl Arginine Deiminase (PADs) and Neurodegenerative Diseases. *Curr. Med. Chem.* **2016,** *23* (2), 104–114.
13. Terakawa, H.; Takahara, H.; Sugawara, K. Three Types of Mouse Peptidylarginine Deiminase: Characterization and Tissue Distribution. *J. Biochem.* **1991,** *110* (4), 661–666.
14. Vossenaar, E. R.; Zendman, A. J. W.; van Venrooij, W. J.; Pruijn, G. J. M. PAD, A Growing Family of Citrullinating Enzymes: Genes, Features and Involvement in Disease. *Bioessays* **2003,** *25* (11), 1106–1118.
15. Watanabe, K.; Akiyama, K.; Hikichi, K.; Ohtsuka, R.; Okuyama, A.; Senshu, T. Combined Biochemical and Immunochemical Comparison of Peptidylarginine Deiminases Present in Various Tissues. *Biochim. Biophys. Acta* **1988,** *966* (3), 375–383.
16. Nagata, S.; Yamagiwa, M.; Inoue, K.; Senshu, T. Estrogen Regulates Peptidylarginine Deiminase Levels in a Rat Pituitary Cell Line in Culture. *J. Cell. Physiol.* **1990,** *145* (2), 333–339.
17. Shimada, N.; Handa, S.; Uchida, Y.; Fukuda, M.; Maruyama, N.; Asaga, H.; Choi, E. K.; Lee, J.; Ishigami, A. Developmental and Age-Related Changes of Peptidylarginine Deiminase 2 in the Mouse Brain. *J. Neurosci. Res.* **2010,** *88* (4), 798–806.
18. György, B.; Tóth, E.; Tarcsa, E.; Falus, A.; Buzás, E. I. Citrullination: A Posttranslational Modification in Health and Disease. *Int. J. Biochem. Cell Biol.* **2006,** *38* (10), 1662–1677.
19. Akiyama, K.; Sakurai, Y.; Asou, H.; Senshu, T. Localization of Peptidylarginine Deiminase Type II in a Stage-Specific Immature Oligodendrocyte from Rat Cerebral Hemisphere. *Neurosci. Lett.* **1999,** *274* (1), 53–55.
20. Nakashima, K.; Hagiwara, T.; Yamada, M. Nuclear Localization of Peptidylarginine Deiminase V and Histone Deimination in Granulocytes. *J. Biol. Chem.* **2002,** *277* (51), 49562–49568.
21. Wang, Y.; Li, M.; Stadler, S.; Correll, S.; Li, P.; Wang, D.; Hayama, R.; Leonelli, L.; Han, H.; Grigoryev, S. A.; et al. Histone Hypercitrullination Mediates Chromatin Decondensation and Neutrophil Extracellular Trap Formation. *J. Cell Biol.* **2009,** *184* (2), 205–213.
22. Arita, K.; Hashimoto, H.; Shimizu, T.; Nakashima, K.; Yamada, M.; Sato, M. Structural Basis for Ca^{2+}-Induced Activation of Human PAD4. *Nat. Struct. Mol. Biol.* **2004,** *11* (8), 777–783.
23. Leopoldini, M.; Marino, T.; Toscano, M. Theoretical Investigation of the Catalytic Mechanism of the Protein Arginine Deiminase 4 Enzyme. *Theor. Chem. Acc.* **2008,** *120* (4–6), 459–466.
24. Kearney, P. L.; Bhatia, M.; Jones, N. G.; Yuan, L.; Glascock, M. C.; Catchings, K. L.; Yamada, M.; Thompson, P. R. Kinetic Characterization of Protein Arginine Deiminase 4: A Transcriptional Corepressor Implicated in the Onset and Progression of Rheumatoid Arthritis. *Biochemistry* **2005,** *44* (31), 10570–10582.
25. Liu, Y. L.; Tsai, I. C.; Chang, C. W.; Liao, Y. F.; Liu, G. Y.; Hung, H. C. Functional Roles of the Non-Catalytic Calcium-Binding Sites in the N-Terminal Domain of Human Peptidylarginine Deiminase 4. *PLoS One* **2013,** *8* (1), e51660.
26. Slade, D. J.; Fang, P.; Dreyton, C. J.; Zhang, Y.; Fuhrmann, J.; Rempel, D.; Bax, B. D.; Coonrod, S. A.; Lewis, H. D.; Guo, M.; et al. Protein Arginine Deiminase 2 Binds Calcium in an Ordered Fashion: Implications for Inhibitor Design. *ACS Chem. Biol.* **2015,** *10* (4), 1043–1053.
27. Micu, I.; Jiang, Q.; Coderre, E.; Ridsdale, A.; Zhang, L.; Woulfe, J.; Yin, X.; Trapp, B. D.; McRory, J. E.; Rehak, R.; et al. NMDA Receptors Mediate Calcium Accumulation in Myelin during Chemical Ischaemia. *Nature* **2006,** *439* (7079), 988–992.
28. Petrescu, N.; Micu, I.; Malek, S.; Ouardouz, M.; Stys, P. K. Sources of Axonal Calcium Loading during In Vitro Ischemia of Rat Dorsal Roots. *Muscle Nerve* **2007,** *35* (4), 451–457.
29. Craner, M. J.; Hains, B. C.; Lo, A. C.; Black, J. A.; Waxman, S. G. Co-Localization of Sodium Channel Nav1.6 and the Sodium-Calcium Exchanger at Sites of Axonal Injury in the Spinal Cord in EAE. *Brain* **2004,** *127* (Pt 2), 294–303.
30. Craner, M. J.; Newcombe, J.; Black, J. A.; Hartle, C.; Cuzner, M. L.; Waxman, S. G. Molecular Changes in Neurons in Multiple Sclerosis: Altered Axonal Expression of Nav1.2 and Nav1.6 Sodium Channels and Na^{+}/Ca^{2+} Exchanger. *Proc. Natl. Acad. Sci. U. S. A.* **2004,** *101* (21), 8168–8173.
31. Siffrin, V.; Birkenstock, J.; Luchtman, D. W.; Gollan, R.; Baumgart, J.; Niesner, R. A.; Griesbeck, O.; Zipp, F. FRET Based Ratiometric Ca^{2+} Imaging to Investigate Immune-Mediated Neuronal and Axonal Damage Processes in Experimental Autoimmune Encephalomyelitis. *J. Neurosci. Methods.* **2015,** *249,* 8–15.
32. Riggs, J. E. Neurologic Manifestations of Electrolyte Disturbances. *Neurol. Clin.* **2002,** *20* (1), 227–239.
33. Asaga, H.; Ishigami, A. Protein Deimination in the Rat Brain After Kainate Administration: Citrulline-Containing Proteins as a Novel Marker of Neurodegeneration. *Neurosci. Lett.* **2001,** *299* (1–2), 5–8.
34. Asaga, H.; Akiyama, K.; Ohsawa, T.; Ishigami, A. Increased and Type II-Specific Expression of Peptidylarginine Deiminase in Activated Microglia but Not Hyperplastic Astrocytes Following Kainic Acid-Evoked Neurodegeneration in the Rat Brain. *Neurosci. Lett.* **2002,** *326* (2), 129–132.
35. Cataldi, M. The Changing Landscape of Voltage-Gated Calcium Channels in Neurovascular Disorders and in Neurodegenerative Diseases. *Curr. Neuropharmacol.* **2013,** *11* (3), 276–297.
36. Bhattacharya, S. K.; Sinicrope, B.; Rayborn, M. E.; Hollyfield, J. G.; Bonilha, V. L. Age-Related Reduction in Retinal Deimination Levels in the F344BN Rat. *Aging Cell* **2008,** *7* (3), 441–444.
37. Nicholas, A. P.; Lu, L.; Heaven, M.; Kadish, I.; van Groen, T.; Accavitti-Loper, M. A.; Wewering, S.; Kofskey, D.; Gambetti, P.; Brenner, M. Ongoing Studies of Deimination in Neurodegenerative Diseases Using the F95 Antibody. In *Protein Deimination in Human Health and Disease;* Nicholas, A., Bhattacharya, S., Eds.; Springer: New York, 2014; pp 257–280. ISBN: 1461483166.
38. Calvert, J. W.; Zhang, J. H. Pathophysiology of an Hypoxic-Ischemic Insult During the Perinatal Period. *Neurol. Res.* **2005,** *27* (3), 246–260.
39. Vannucci, S. J.; Hagberg, H. Hypoxia–Ischemia in the Immature Brain. *J. Exp. Biol.* **2004,** *207* (Pt 18), 3149–3154.
40. Lange, S.; Rocha-Ferreira, E.; Thei, L.; Mawjee, P.; Bennett, K.; Thompson, P. R.; Subramanian, V.; Nicholas, A. P.; Peebles, D.; Hristova, M.; et al. Peptidylarginine Deiminases: Novel Drug Targets for Prevention of Neuronal Damage Following Hypoxic Ischemic Insult (HI) in Neonates. *J. Neurochem.* **2014,** *130* (4), 555–562.
41. Bradford, C. M.; Ramos, I.; Cross, A. K.; Haddock, G.; McQuaid, S.; Nicholas, A. P.; Woodroofe, M. N. Localisation of Citrullinated Proteins in Normal Appearing White Matter and Lesions in the Central Nervous System in Multiple Sclerosis. *J. Neuroimmunol.* **2014,** *273* (1–2), 85–95.
42. Oguz, K. K.; Kurne, A.; Aksu, A. O.; Karabulut, E.; Serdaroglu, A.; Teber, S.; Haspolat, S.; Senbil, N.; Kurul, S.; Anlar, B. Assessment of Citrullinated Myelin by (1)H-MR Spectroscopy in Early-Onset Multiple Sclerosis. *Am. J. Neuroradiol.* **2009,** *30* (4), 716–721.
43. Nicholas, A. P.; Sambandam, T.; Echols, J. D.; Tourtellotte, W. W. Increased Citrullinated Glial Fibrillary Acidic Protein in Secondary Progressive Multiple Sclerosis. *J. Comp. Neurol.* **2004,** *473* (1), 128–136.
44. Moscarello, M. A.; Wood, D. D.; Ackerley, C.; Boulias, C. Myelin in Multiple Sclerosis Is Developmentally Immature. *J. Clin. Invest.* **1994,** *94* (1), 146–154.
45. Wood, D. D.; Bilbao, J. M.; O'Connors, P.; Moscarello, M. A. Acute Multiple Sclerosis (Marburg Type) Is Associated With Developmentally Immature Myelin Basic Protein. *Ann. Neurol.* **1996,** *40* (1), 18–24.
46. Mastronardi, F. G.; Wood, D. D.; Mei, J.; Raijmakers, R.; Tseveleki, V.; Dosch, H.-M.; Probert, L.; Casaccia-Bonnefil, P.; Moscarello, M. A. Increased Citrullination of Histone H3 in Multiple Sclerosis Brain and Animal Models of Demyelination: A Role for Tumor Necrosis Factor-Induced Peptidylarginine Deiminase 4 Translocation. *J. Neurosci.* **2006,** *26* (44), 11387–11396.
47. Wood, D. D.; Ackerley, C. A.; van den Brand, B.; Zhang, L.; Raijmakers, R.; Mastronardi, F. G.; Moscarello, M. A. Myelin Localization of Peptidylarginine Deiminases 2 and 4: Comparison of PAD2 and PAD4 Activities. *Lab. Invest.* **2008,** *88* (4), 354–364.
48. Raijmakers, R.; Vogelzangs, J.; Raats, J.; Panzenbeck, M.; Corby, M.; Jiang, H.; Thibodeau, M.; Haynes, N.; Van Venrooij, W. J.; Pruijn, G. J. M.; et al. Experimental Autoimmune Encephalomyelitis Induction in Peptidylarginine Deiminase 2 Knockout Mice. *J. Comp. Neurol.* **2006,** *498* (2), 217–226.

49. Musse, A. A.; Li, Z.; Ackerley, C. A.; Bienzle, D.; Lei, H.; Poma, R.; Harauz, G.; Moscarello, M. A.; Mastronardi, F. G. Peptidylarginine Deiminase 2 (PAD2) Overexpression in Transgenic Mice Leads to Myelin Loss in the Central Nervous System. *Dis. Model. Mech.* **2008,** *1* (4–5), 229–240.
50. Calabrese, R.; Zampieri, M.; Mechelli, R.; Annibali, V.; Guastafierro, T.; Ciccarone, F.; Coarelli, G.; Umeton, R.; Salvetti, M.; Caiafa, P. Methylation-Dependent PAD2 Upregulation in Multiple Sclerosis Peripheral Blood. *Mult. Scler.* **2012,** *18* (3), 299–304.
51. Sharma, P.; Azebi, S.; England, P.; Christensen, T.; Møller-Larsen, A.; Petersen, T.; Batsché, E.; Muchardt, C. Citrullination of Histone H3 Interferes With HP1-Mediated Transcriptional Repression. *PLoS Genet.* **2012,** *8* (9), e1002934.
52. Ramagopalan, S. V.; Ebers, G. C. Genes for Multiple Sclerosis. *Lancet* **2008,** *371* (9609), 283–285.
53. Ramagopalan, S. V.; Maugeri, N. J.; Handunnetthi, L.; Lincoln, M. R.; Orton, S. M.; Dyment, D. A.; DeLuca, G. C.; Herrera, B. M.; Chao, M. J.; Sadovnick, A. D.; et al. Expression of the Multiple Sclerosis-Associated MHC Class II Allele HLA-DRB1*1501 Is Regulated by Vitamin D. *PLoS Genet.* **2009,** *5* (2), e1000369.
54. Tommasi, C.; Petit-Teixeira, E.; Cournu-Rebeix, I.; Caponi, L.; Pierlot, C.; Fontaine, B.; Cornelis, F.; Migliorini, P. PADI4 Gene in Multiple Sclerosis: A Family-Based Association Study. *J. Neuroimmunol.* **2006,** *177* (1–2), 142–145.
55. Mastronardi, F. G.; Noor, A.; Wood, D. D.; Paton, T.; Moscarello, M. A. Peptidyl Argininedeiminase 2 CpG Island in Multiple Sclerosis White Matter Is Hypomethylated. *J. Neurosci. Res.* **2007,** *85* (9), 2006–2016.
56. Hu, Y.; Doudevski, I.; Wood, D.; Moscarello, M.; Husted, C.; Genain, C.; Zasadzinski, J. A.; Israelachvili, J. Synergistic Interactions of Lipids and Myelin Basic Protein. *Proc. Natl. Acad. Sci. U. S. A.* **2004,** *101* (37), 13466–13471.
57. Pritzker, L. B.; Joshi, S.; Gowan, J. J.; Harauz, G.; Moscarello, M. A. Deimination of Myelin Basic Protein. 1. Effect of Deimination of Arginyl Residues of Myelin Basic Protein on Its Structure and Susceptibility to Digestion by Cathepsin D. *Biochemistry* **2000,** *39* (18), 5374–5381.
58. Cuzner, M. L.; Davison, A. N. Changes in Cerebral Lysosomal Enzyme Activity and Lipids in Multiple Sclerosis. *J. Neurol. Sci.* **1973,** *19* (1), 29–36.
59. Einstein, E. R.; Csejtey, J.; Dalal, K. B.; Adams, C. W. M.; Bayliss, O. B.; Hallpike, J. F. Proteolytic Activity and Basic Protein Loss in and Around Multiple Sclerosis Plaques: Combined Biochemical and Eiistochemical Observations. *J. Neurochem.* **1972,** *19* (3), 653–662.
60. Cao, L. G.; Goodin, R.; Wood, D.; Moscarello, M. A.; Whitaker, J. N. Rapid Release and Unusual Stability of Immunodominant Peptide 45–89 from Citrullinated Myelin Basic Protein. *Biochemistry* **1999,** *38* (19), 6157–6163.
61. Bates, I. R.; Feix, J. B.; Boggs, J. M.; Harauz, G. An Immunodominant Epitope of Myelin Basic Protein Is an Amphipathic α-Helix. *J. Biol. Chem.* **2004,** *279* (7), 5757–5764.
62. Deraos, G.; Chatzantoni, K.; Matsoukas, M. T.; Tselios, T.; Deraos, S.; Katsara, M.; Papathanasopoulos, P.; Vynios, D.; Apostolopoulos, V.; Mouzaki, A.; et al. Citrullination of Linear and Cyclic Altered Peptide Ligands From Myelin Basic Protein (MBP(87–99)) Epitope Elicits a Th1 Polarized Response by T Cells Isolated From Multiple Sclerosis Patients: Implications in Triggering Disease. *J. Med. Chem.* **2008,** *51* (24), 7834–7842.
63. MacKenzie-Graham, A. J.; Pribyl, T. M.; Kim, S.; Porter, V. R.; Campagnoni, A. T.; Voskuhl, R. R. Myelin Protein Expression Is Increased in Lymph Nodes of Mice With Relapsing Experimental Autoimmune Encephalomyelitis. *J. Immunol.* **1997,** *159* (9), 4602–4610.
64. Kidd, B. A.; Ho, P. P.; Sharpe, O.; Zhao, X.; Tomooka, B. H.; Kanter, J. L.; Steinman, L.; Robinson, W. H. Epitope Spreading to Citrullinated Antigens in Mouse Models of Autoimmune Arthritis and Demyelination. *Arthritis Res. Ther.* **2008,** *10* (5), R119.
65. Carrillo-Vico, A.; Leech, M. D.; Anderton, S. M. Contribution of Myelin Autoantigen Citrullination to T Cell Autoaggression in the Central Nervous System. *J. Immunol.* **2010,** *184* (6), 2839–2846.
66. de Seze, J.; Dubucquoi, S.; Lefranc, D.; Virecoulon, F.; Nuez, I.; Dutoit, V.; Vermersch, P.; Prin, L. IgG Reactivity against Citrullinated Myelin Basic Protein in Multiple Sclerosis. *J. Neuroimmunol.* **2001,** *117* (1–2), 149–155.
67. Botto, M.; Dell'Agnola, C.; Bygrave, A. E.; Thompson, E. M.; Cook, H. T.; Petry, F.; Loos, M.; Pandolfi, P. P.; Walport, M. J. Homozygous C1q Deficiency Causes Glomerulonephritis Associated With Multiple Apoptotic Bodies. *Nat. Genet.* **1998,** *19* (1), 56–59.
68. Gaultier, A.; Wu, X.; Le Moan, N.; Takimoto, S.; Mukandala, G.; Akassoglou, K.; Campana, W. M.; Gonias, S. L. Low-Density Lipoprotein Receptor-Related Protein 1 is an Essential Receptor for Myelin Phagocytosis. *J. Cell Sci.* **2009,** *122* (Pt 8), 1155–1162.
69. Fernandez-Castaneda, A.; Arandjelovic, S.; Stiles, T. L.; Schlobach, R. K.; Mowen, K. A.; Gonias, S. L.; Gaultier, A. Identification of the Low Density Lipoprotein (LDL) Receptor-Related Protein-1 Interactome in Central Nervous System Myelin Suggests a Role in the Clearance of Necrotic Cell Debris. *J. Biol. Chem.* **2013,** *288* (7), 4538–4548.
70. Li, P.; Li, M.; Lindberg, M. R.; Kennett, M. J.; Xiong, N.; Wang, Y. PAD4 Is Essential for Antibacterial Innate Immunity Mediated by Neutrophil Extracellular Traps. *J. Exp. Med.* **2010,** *207* (9), 1853–1862.
71. Neeli, I.; Khan, S. N.; Radic, M. Histone Deimination as a Response to Inflammatory Stimuli in Neutrophils. *J. Immunol.* **2008,** *180* (3), 1895–1902.
72. Naegele, M.; Tillack, K.; Reinhardt, S.; Schippling, S.; Martin, R.; Sospedra, M. Neutrophils in Multiple Sclerosis Are Characterized by a Primed Phenotype. *J. Neuroimmunol.* **2012,** *242* (1–2), 60–71.
73. Moscarello, M. A.; Lei, H.; Mastronardi, F. G.; Winer, S.; Tsui, H.; Li, Z.; Ackerley, C.; Zhang, L.; Raijmakers, R.; Wood, D. D. Inhibition of Peptidyl-Arginine Deiminases Reverses Protein-Hypercitrullination and Disease in Mouse Models of Multiple Sclerosis. *Dis. Model. Mech.* **2013,** *6* (2), 467–478.
74. Wei, L.; Wasilewski, E.; Chakka, S. K.; Bello, A. M.; Moscarello, M. A.; Kotra, L. P. Novel Inhibitors of Protein Arginine Deiminase With Potential Activity in Multiple Sclerosis Animal Model. *J. Med. Chem.* **2013,** *56* (4), 1715–1722.
75. Bar-Or, A.; Rieckmann, P.; Traboulsee, A.; Yong, V. W. Targeting Progressive Neuroaxonal Injury: Lessons From Multiple Sclerosis. *CNS Drugs* **2011,** *25* (9), 783–799.
76. Katrych, O.; Simone, T. M.; Azad, S.; Mousa, S. A. Disease-Modifying Agents in the Treatment of Multiple Sclerosis: A Review of Long-Term Outcomes. *CNS Neurol. Disord. Drug Targets* **2009,** *8* (6), 512–519.
77. Brinkmann, V.; Davis, M. D.; Heise, C. E.; Albert, R.; Cottens, S.; Hof, R.; Bruns, C.; Prieschl, E.; Baumruker, T.; Hiestand, P.; et al. The Immune Modulator FTY720 Targets Sphingosine 1-Phosphate Receptors. *J. Biol. Chem.* **2002,** *277* (24), 21453–21457.
78. Matloubian, M.; Lo, C. G.; Cinamon, G.; Lesneski, M. J.; Xu, Y.; Brinkmann, V.; Allende, M. L.; Proia, R. L.; Cyster, J. G.; et al. Lymphocyte Egress From Thymus and Peripheral Lymphoid Organs is Dependent on S1P Receptor 1. *Nature* **2004,** *427* (6972), 355–360.
79. Kappos, L.; Radue, E. W.; O'Connor, P.; Polman, C.; Hohfeld, R.; Calabresi, P.; Selmaj, K.; Agoropoulou, C.; Leyk, M.; Zhang-Auberson, L.; et al. A Placebo-Controlled Trial of Oral Fingolimod in Relapsing Multiple Sclerosis. *N. Engl. J. Med.* **2010,** *362* (5), 387–401.
80. Cohen, J. A.; Barkhof, F.; Comi, G.; Hartung, H. P.; Khatri, B. O.; Montalban, X.; Pelletier, J.; Capra, R.; Gallo, P.; Izguierdo, G.; et al. Oral Fingolimod or Intramuscular Interferon for Relapsing Multiple Sclerosis. *N. Engl. J. Med.* **2010,** *362* (5), 402–415.
81. Bridel, C.; Lalive, P. H. Update on Multiple Sclerosis Treatments. *Swiss Med. Wkly.* **2014,** *144,* w14012.
82. La Mantia, L.; Tramacere, I.; Firwana, B.; Pacchetti, I.; Palumbo, R.; Filippini, G. Fingolimod for Relapsing-Remitting Multiple Sclerosis. *Cochrane Database Syst. Rev.* **2016,** *4,* CD009371.
83. Khatri, B.; Barkhof, F.; Comi, G.; Hartung, H. P.; Kappos, L.; Montalban, X.; Pelletier, J.; Stites, T.; Wu, S.; Holdbrook, F.; et al. Comparison of Fingolimod With Interferon Beta-1a in Relapsing-Remitting Multiple Sclerosis: A Randomised Extension of the TRANSFORMS Study. *Lancet Neurol.* **2011,** *10* (6), 520–529.
84. Kappos, L.; Antel, J.; Comi, G.; Montalban, X.; O'Connor, P.; Poman, C. H.; Haas, T.; Korn, A. A.; Karlsson, G.; Radue, E. W.; et al. Oral Fingolimod (FTY720) for Relapsing Multiple Sclerosis. *N. Engl. J. Med.* **2006,** *355* (11), 1124–1140.
85. Singer, B. A. Fingolimod for the Treatment of Relapsing Multiple Sclerosis. *Expert. Rev. Neurother.* **2013,** *13* (6), 589–602.
86. Lindsey, J. W.; Haden-Pinneri, L.; Memon, N. B.; Buja, L. M.; et al. Sudden Unexpected Death on Fingolimod. *Mult. Scler.* **2012,** *18* (10), 1507–1508.
87. Espinosa, P. S.; Berger, J. R. Delayed Fingolimod-Associated Asystole. *Mult. Scler.* **2011,** *17* (11), 1387–1389.
88. Means, C. K.; Brown, J. H. Sphingosine-1–Phosphate Receptor Signalling in the Heart. *Cardiovasc. Res.* **2009,** *82* (2), 193–200.
89. Nolan, R.; Gelfand, J. M.; Green, A. J. Fingolimod Treatment in Multiple Sclerosis Leads to Increased Macular Volume. *Neurology* **2013,** *80* (2), 139–144.
90. Dinkin, M.; Paul, F. Higher Macular Volume in Patients With MS Receiving Fingolimod: Positive Outcome or Side Effect? *Neurology* **2013,** *80* (2), 128–129.

91. Pilz, G.; Harrer, A.; Wipfler, P.; Oppermann, K.; Sellner, J.; Fazekas, F.; Trinka, E.; Kraus, J.; et al. Tumefactive MS Lesions Under Fingolimod: A Case Report and Literature Review. *Neurology* **2013,** *81* (19), 1654–1658.
92. Paul, F.; Bourdette, D. Tumefactive Multiple Sclerosis and Fingolimod: Immunotherapies and Unintended Consequences. *Neurology* **2013,** *81* (19), 1648–1689.
93. Mehling, M.; Hilbert, P.; Fritz, S.; et al. Antigen-Specific Adaptive Immune Responses in Fingolimod-Treated Multiple Sclerosis Patients. *Ann. Neurol.* **2011,** *69* (2), 408–413.
94. Lu, E.; et al. Safety of Disease-Modifying Drugs for Multiple Sclerosis in Pregnancy: Current Challenges and Future Considerations for Effective Pharmacovigilance. *Expert. Rev. Neurother.* **2013,** *13* (3), 251–260. quiz 261.
95. Cherwinski, H. M.; et al. Leflunomide Interferes With Pyrimidine Nucleotide Biosynthesis. *Inflamm. Res.* **1995,** *44* (8), 317–322.
96. Papadopoulou, A.; Kappos, L.; Sprenger, T. Teriflunomide for Oral Therapy in Multiple Sclerosis. *Expert. Rev. Clin. Pharmacol.* **2012,** *5* (6), 617–628.
97. O'Connor, P.; et al. Randomized Trial of Oral Teriflunomide for Relapsing Multiple Sclerosis. *N. Engl. J. Med.* **2011,** *365* (14), 1293–1303.
98. Confavreux, C.; O'Connor, P.; Comi, G.; Freedman, M. S.; Miller, A. E.; Olsson, T. P.; Wolinsky, J. S.; Bagulho, T.; Delhay, J. L.; Dukovic, D.; et al. Oral Teriflunomide for Patients With Relapsing Multiple Sclerosis (TOWER): A Randomised, Double-Blind, Placebo-Controlled, Phase 3 Trial. *Lancet Neurol.* **2014,** *13* (3), 247–256.
99. Vermersch, P.; Czlonkowska, A.; Grimaldi, L. M.; Confavreux, C.; Comi, G.; Kappos, L.; Olsson, T. P.; Benamor, M.; Bauer, D.; Truffinet, P.; et al. Teriflunomide Versus Subcutaneous Interferon Beta-1a in Patients With Relapsing Multiple Sclerosis: A Randomised, Controlled Phase 3 Trial. *Mult. Scler.* **2013,** *20* (6), 705–716.
100. Freedman, M. S.; Wolinsky, J. S.; Wamil, B.; Confavreux, C.; Comi, G.; Kappos, L.; Olsson, T. P.; Miller, A.; Benzerdjeb, H.; Li, H.; et al. Teriflunomide Added to Interferon-Beta in Relapsing Multiple Sclerosis: A Randomized Phase II Trial. *Neurology* **2012,** *78* (23), 1877–1885.
101. O'Connor, P. W.; Li, D.; Freedman, M. S.; Bar-Or, A.; Rice, G. P.; Confavreux, C.; Paty, D. W.; Stewart, J. A.; Scheyer, R.; et al. A Phase II Study of the Safety and Efficacy of Teriflunomide in Multiple Sclerosis With Relapses. *Neurology* **2006,** *66* (6), 894–900.
102. Confavreux, C.; Li, D. K.; Freedman, M. S.; Truffinet, P.; Benzerdjeb, H.; Wang, D.; Bar-Or, A.; Traboulsee, A. L.; Reiman, L. E.; O'Connor, P. W.; et al. Long-Term Follow-up of a Phase 2 Study of Oral Teriflunomide in Relapsing Multiple Sclerosis: Safety and Efficacy Results up to 8.5 Years. *Mult. Scler.* **2012,** *18* (9), 1278–1289.
103. Bar-Or, A.; Freedman, M. S.; Kremenchutzky, M.; Menguy-Vacheron, F.; Bauer, D.; Jodl, S.; Truffinet, P.; Benamor, M.; Chambers, S.; O'Connor, P. W. Teriflunomide Effect on Immune Response to Influenza Vaccine in Patients With Multiple Sclerosis. *Neurology* **2013,** *81* (6), 552–558.
104. Fox, R. J.; Kita, M.; Cohan, S. L.; Henson, L. J.; Zmbrano, J.; Scannevin, R. H.; O'Gorman, J.; Novas, M.; Dawson, K. T.; Phillips, J. T. BG-12 (Dimethyl Fumarate): A Review of Mechanism of Action, Efficacy, and Safety. *Curr. Med. Res. Opin.* **2013,** *30* (2), 251–262.
105. Meissner, M.; Valesky, E. M.; Kippenberger, S.; Kaufmann, R. Dimethyl Fumarate—Only an Anti-Psoriatic Medication? *J. Dtsch. Dermatol. Ges.* **2012,** *10* (11), 793–801.
106. Miclea, A.; Leussink, V. I.; Hartung, H. P.; Gold, R.; Hoepner, R. Safety and Efficacy of Dimethyl Fumarate in Multiple Sclerosis: A Multi-Center Observational Study. *Ther. Clin. Risk Manag.* **2016,** *12,* 339–350.
107. Fiedler, S. E.; Kerns, A. R.; Tsang, C.; Tsang, V.; Bourdette, D.; Salinthone, S. Dimethyl Fumarate Activates the Prostaglandin EP2 Receptor and Stimulates cAMP Signaling in Human Peripheral Blood Mononuclear Cells. *Biochem. Biophys. Res. Commun.* **2016,** *475* (1), 19–24.
108. Prosperini, L.; Pontecorvo, S. Dimethyl Fumarate in the Management of Multiple Sclerosis: Appropriate Patient Selection and Special Considerations. *Ther. Clin. Risk Manag.* **2016,** *12,* 339–350.
109. Gold, R.; Kappos, L.; Arnold, D. L.; Bar-Or, A.; Giovannoni, G.; Selmaj, K.; Tornatore, C.; Sweetser, M. T.; Yang, M.; Sheikh, S. I.; et al. Placebo-Controlled Phase 3 Study of Oral BG-12 for Relapsing Multiple Sclerosis. *N. Engl. J. Med.* **2012,** *367* (12), 1098–1107.
110. Fox, R. J.; Miller, D. H.; Phillips, J. T.; Hutchinson, M.; Havrdova, E.; Kita, M.; Yang, M.; Raghupathi, K.; Novas, M.; Sweetser, M. T.; et al. Placebo-Controlled Phase 3 Study of Oral BG-12 or Glatiramer in Multiple Sclerosis. *N. Engl. J. Med.* **2012,** *367* (12), 1087–1097.
111. Kappos, L.; Gold, R.; Miller, D. H.; Macmanus, D. G.; Havrdova, E.; Limmroth, V.; Polman, C. H.; Schmierer, K.; Yousry, T. A.; Yang, M.; et al. Efficacy and Safety of Oral Fumarate in Patients With Relapsing-Remitting Multiple Sclerosis: A Multicentre, Randomised, Double-Blind, Placebo-Controlled Phase IIb Study. *Lancet* **2008,** *372* (9648), 1463–1472.
112. Bruck, W.; Wegner, C. Insight into the Mechanism of Laquinimod Action. *J. Neurol. Sci.* **2011,** *306* (1–2), 173–179.
113. Filippi, M.; Rocca, M. A.; Pagani, E.; De Stefano, N.; Jeffery, D.; Kappos, L.; Montalban, X.; Boyko, A. A.; Comi, G.; et al. Placebo-Controlled Trial of Oral Laquinimod in Multiple Sclerosis: MRI Evidence of an Effect on Brain Tissue Damage. *J. Neurol. Neurosurg. Psychiatry* **2013,** *85* (8), 851–858.
114. Tur, C. Oral Laquinimod for Multiple Sclerosis: Beyond the Anti-Inflammatory Effect. *J. Neurol. Neurosurg. Psychiatry* **2014,** *85* (8), 832.
115. Bruck, W.; Vollmer, T. Multiple Sclerosis: Oral Laquinimod for MS-Bringing the Brain Into Focus. *Nat. Rev. Neurol.* **2013,** *9* (12), 664–665.
116. Comi, G.; Jeffery, D.; Kappos, L.; Montalban, X.; Boyko, A.; Rocca, M. A.; Filippi, M.; ALLEGRO Study Group. Placebo-Controlled Trial of Oral Laquinimod for Multiple Sclerosis. *Med. N. Engl. J.* **2012,** *366* (11), 1000–1009.
117. Vollmer, T. L.; Sorensen, P. S.; Selmaj, K.; Zipp, F.; HAvrdova, E.; Cohen, J. A.; Sasson, N.; Gilgun-Sherki, Y.; Arnold, D. L.; BRAVO Study Group. A Randomized Placebo-Controlled Phase III Trial of Oral Laquinimod for Multiple Sclerosis. *J. Neurol.* **2014,** *261* (4), 773–783.
118. Comi, G.; Pulizzi, A.; Rovaris, M.; Abramsky, O.; Arbizu, T.; Boiko, A.; Gold, R.; Havrdova, E.; Komoly, S.; Selmaj, K.; et al. Effect of Laquinimod on MRI-Monitored Disease Activity in Patients With Relapsing-Remitting Multiple Sclerosis: A Multicentre, Randomised, Double-Blind, Placebo-Controlled Phase IIb Study. *Lancet* **2008,** *371* (9630), 2085–2092.
119. Arnason, B. G. Immunologic Therapy of Multiple Sclerosis. *Annu. Rev. Med.* **1999,** *50,* 291–302.
120. IFNβ Multiple Sclerosis Study Group.; University of British Columbia MS/MRI Analysis Group. Interferon Beta-1b is Effective in Relapsing-Remitting Multiple Sclerosis. I. Clinical Results of a Multicenter, Randomized, Double-Blind, Placebo-Controlled Trial. *Neurology* **1993,** *43,* 655–661.
121. IFNβ Multiple Sclerosis Study Group.; University of British Columbia MS/MRI Analysis Group. Interferon Beta-1b in the Treatment of Multiple Sclerosis: Final Outcome of the Randomized Controlled Trial. *Neurology* **1995,** *44,* 1277–1285.
122. Paty, D. W.; Li, D. K.; University of British Columbia MS/MRI Study Group.; IFNB Multiple Sclerosis Study Group. Interferon Beta-1b is Effective in Relapsing-Remitting Multiple Sclerosis. II. MRI Analysis Results of a Multicenter, Randomized, Double-Blind, Placebo-Controlled Trial. *Neurology* **1993,** *43,* 662–667.
123. Stone, L. A.; Frank, J. A.; Albert, P. S.; et al. The Effect of Interferon-b on Blood–Brain Barrier Disruptions Demonstrated by Contrast-Enhanced Magnetic Resonance Imaging in Relapsing-Remitting Multiple Sclerosis. *Ann. Neurol.* **1995,** *37,* 611–619.
124. Pliskin, N. H.; Hamer, D. P.; Goldstein, D. S.; Towle, V. L.; Reder, A. T.; Noronha, A.; Arnason, B. G. Improved Neuropsychological Function in Multiple Sclerosis Patients Receiving Interferon Beta-1b. *Neurology* **1996,** *47* (6), 1463–1468.
125. Arnason, B. G. W. Interferon Beta in Multiple Sclerosis. *Clin. Immun. Immunopathol.* **1996,** *81,* 1–11.
126. Jacobs, L. D.; Cookfair, D. L.; Rudick, R. A.; et al. Intramuscular Interferon Beta-1a for Disease Progression in Relapsing Multiple Sclerosis. The Multiple Sclerosis Collaborative Research Group (MSCRG). *Ann. Neurol.* **1996,** *3* (9), 285–294.
127. The PRISMS (Prevention of Relapses and Disability by Interferon-Beta 1a Subcutaneously in Multiple Sclerosis) Study Group. Randomised, Double-Blind, Placebo-Controlled Study of Interferon-Beta 1a in Relapsing-Remitting Multiple Sclerosis: Clinical Results. *Lancet* **1998,** *352* (9139), 1498–1504.
128. Li, D. K. B.; Paty, D.; UBC MS/MRI Analysis Research Group.; The PRISMS (Prevention of Relapses and Disability by Interferon-Beta 1a Subcutaneously in Multiple Sclerosis) Study Group. Randomised, Double-Blind, Placebo-Controlled Study of Interferon-Beta 1a in Relapsing-Remitting Multiple Sclerosis: MRI Results. *Ann. Neurol.* **1999,** *46* (2), 197–206.
129. Radick, L.; Mehr, S. R. The Latest Innovations in the Drug Pipeline for Multiple Sclerosis. *Am. Health Drug Benefits* **2015,** *8* (8), 448–453.
130. Biogen Idec. Avonex Prescribing Information. August 2014. www.avonex.com/pdfs/Avonex_Prescribing_Information.pdf (Accessed June, 2016).
131. Biogen Idec. Biogen Idec's Plegridy (Peginterferon Beta-1a) Approved in the US for the Treatment of Multiple Sclerosis. http://media.biogen.com/press-release/multiple-sclerosis-ms/biogen-idecs-plegridypeginterferon-beta-1a-approved-us-treatment (Accessed June, 2016).
132. Biogen Idec. Plegridy Prescribing Information. www.plegridy.com/pdfs/plegridy-prescribing-information.pdf (Accessed June, 2016).

133. Calabresi, P. A.; Kieseier, B. C.; Arnold, D. L.; Balcer, L. J.; Boyko, A.; Pelletier, J.; Liu, S.; Zhu, Y.; Seddighzadeh, A.; Hung, S.; et al. Pegylated Interferon β-1a for Relapsing-Remitting Multiple Sclerosis (ADVANCE): A Randomised, Phase 3, Double-Blind Study. *Lancet Neurol.* **2014,** *13* (7), 657–665.
134. Kieseier, B. C.; Arnold, D. L.; Balcer, L. J.; Boyko, A. A.; Pelletier, J.; Liu, S.; Zhu, Y.; Seddighzadeh, A.; Hung, S.; Deykin, A.; et al. Peginterferon Beta-1a in Multiple Sclerosis: 2-Year Results From ADVANCE. *Mult. Scler.* **2015,** *21* (8), 1025–1035.
135. Niino, M.; Bodner, C.; Simard, M. L.; Alatab, S.; Gano, D.; Kim, H. J.; Trigueiro, M.; Racicot, D.; Guerette, C.; Antel, J. P.; et al. Natalizumab Effects on Immune Cell Responses in Multiple Sclerosis. *Ann. Neurol.* **2006,** *59* (5), 748–754.
136. Koch-Henriksen, N.; Magyari, M.; Sellebjerg, F.; Soelberg Sørensen, P. A Comparison of Multiple Sclerosis Clinical Disease Activity Between Patients Treated With Natalizumab and Fingolimod. *Mult. Scler.* **2016,** http://dx.doi.org/10.1177/1352458516643393.
137. Rudick, R. A.; Stuart, W. H.; Calabresi, P. A.; Confavreux, C.; Galetta, S. L.; Radue, E. W.; Lublin, F. D.; Weinstock-Guttman, B.; Wynn, D. R.; Lynn, F.; et al. Natalizumab Plus Interferon Beta-1a for Relapsing Multiple Sclerosis. *N. Engl. J. Med.* **2006,** *354* (9), 911–923.
138. Polman, C. H.; O'Connor, P. W.; Havrdova, E.; Hutchinson, M.; Kappos, L.; Miller, D. H.; Phillips, J. T.; Lublin, F. D.; Giovannoni, G.; Wajgt, A.; et al. A Randomized, Placebo-Controlled Trial of Natalizumab for Relapsing Multiple Sclerosis. *N. Engl. J. Med.* **2006,** *354* (9), 899–910.
139. Langer-Gould, A.; Atlas, S. W.; Green, A. J.; Bollen, A. W.; Pelletier, D. Progressive Multifocal Leukoencephalopathy in a Patient Treated With Natalizumab. *N. Engl. J. Med.* **2005,** *353* (4), 375–381.
140. Kleinschmidt-DeMasters, B. K.; Tyler, K. L. Progressive Multifocal Leukoencephalopathy Complicating Treatment With Natalizumab and Interferon Beta-1a for Multiple Sclerosis. *N. Engl. J. Med.* **2005,** *353* (4), 369–374.
141. Miller, D. H.; Soon, D.; Fernando, K. T. I.; MacManus, D. G.; Barker, G. J.; Yousry, T. A.; Fisher, E.; O'Connor, P. W.; Phillips, J. T.; Polman, C. H.; et al. MRI Outcomes in a Placebo-Controlled Trial of Natalizumab in Relapsing MS. *Neurology* **2007,** *68* (17), 1390–1401.
142. Plavina, T. E. A. In The 27th Annual Meeting of the Consortium of Multiple Sclerosis Centers, 2013.
143. Calabresi, P. A.; Giovannoni, G.; Confavreux, C.; Galetta, S. L.; HAvrdova, E.; Hutchinson, M.; Kappos, L.; Miller, D. H.; O'Connor, P. W.; Phillips, J. T.; et al. The Incidence and Significance of Anti-Natalizumab Antibodies: Results From AFFIRM and SENTINEL. *Neurology* **2007,** *69* (14), 1391–1403.
144. Kleiter, I.; Hellwig, K.; Berthele, A.; Kumpfel, T.; Linker, R. A.; Hartung, H. P.; Paul, F.; Aktas, O.; Neuromyelitis Optica Study Group. Failure of Natalizumab to Prevent Relapses in Neuromyelitis Optica. *Arch. Neurol.* **2012,** *69* (2), 239–245.
145. Barnett, M. H.; Prineas, J. W.; Buckland, M. E.; Parratt, J. D.; Pollard, J. D. Massive Astrocyte Destruction in Neuromyelitis Optica Despite Natalizumab Therapy. *Mult. Scler.* **2012,** *18* (1), 108–112.
146. Kitley, J.; Evangelou, N.; Kuker, W.; Jacob, A.; Leite, M. I.; Palace, J. Catastrophic Brain Relapse in Seronegative NMO After a Single Dose of Natalizumab. *J. Neurol. Sci.* **2014,** *339* (1–2), 223–225.
147. Vagberg, M.; Kumlin, U.; Svenningsson, A. Humoral Immune Response to Influenza Vaccine in Natalizumab-Treated MS Patients. *Neurol. Res.* **2012,** *34* (7), 730–733.
148. Houtchens, M. K.; Kolb, C. M. Multiple Sclerosis and Pregnancy: Therapeutic Considerations. *J. Neurol.* **2013,** *260* (5), 1202–1214.
149. Freedman, M. S.; Kaplan, J. M.; Markovic-Plese, S. Insights into the Mechanisms of the Therapeutic Efficacy of Alemtuzumab in Multiple Sclerosis. *J. Clin. Cell. Immunol.* **2013,** *4* (4).
150. Cohen, J. A.; Coles, A. J.; Arnold, D. L.; Confavreux, C.; Fox, E. J.; Hartung, H. P.; Havrdova, E.; Selmaj, K. W.; Weiner, H. L.; Fisher, E.; et al. Alemtuzumab Versus Interferon Beta 1a as First-Line Treatment for Patients With Relapsing-Remitting Multiple Sclerosis: A Randomised Controlled Phase 3 Trial. *Lancet* **2012,** *380* (9856), 1819–1828.
151. Coles, A. J.; Compston, D. A.; Selmaj, K. W.; Lake, S. L.; Moran, S.; Margolin, D. H.; Norris, K.; Tandon, P. K.; CAMMS223 Trial Investigators. Alemtuzumab vs. Interferon Beta-1a in Early Multiple Sclerosis. *N. Engl. J. Med.* **2008,** *359* (17), 1786–1801.
152. Coles, A. J.; Twyman, C. L.; Arnold, D. L.; Cohen, J. A.; Confavreux, C.; Fox, E. J.; Hartung, H. P.; Havrdova, E.; Selmaj, K. W.; Weiner, H. L.; et al. Alemtuzumab for Patients With Relapsing Multiple Sclerosis After Disease-Modifying Therapy: A Randomised Controlled Phase 3 Trial. *Lancet* **2012,** *380* (9856), 1829–1839.
153. Fox, E. J.; Sullivan, H. C.; Gazda, S. K.; Mayer, L.; O'Donnell, L.; Melia, K.; Lake, S. L. A Single-arm, Open-Label Study of Alemtuzumab in Treatment-Refractory Patients With Multiple Sclerosis. *Eur. J. Neurol.* **2012,** *19* (2), 307–311.
154. Coles, A. J.; Wing, M.; Smith, S.; Coraddu, F.; Greer, S.; Taylor, C.; Weetman, A.; Hale, G.; Chatterjee, V. K.; Waldmann, H.; et al. Pulsed Monoclonal Antibody Treatment and Autoimmune Thyroid Disease in Multiple Sclerosis. *Lancet* **1999,** *354* (9191), 1691–1695.
155. Riera, R.; Porfírio, G. J.; Torloni, M. R. Alemtuzumab for Multiple Sclerosis. *Cochrane Database Syst. Rev.* **2016,** *4*, CD011203.
156. Bashir, K.; Whitaker, J. N. Current Immunotherapy in Multiple Sclerosis. *Immunol. Cell Biol.* **1998,** *76* (1), 55–64.
157. Johnson, K. P.; Brooks, B. R.; Cohen, J. A.; et al. Copolymer-1 Reduces Relapse Rate and Improves Disability in Relapsing-Remitting Multiple Sclerosis: Results of a Phase III Multicenter, Double Blind, Placebo-Controlled Trial. The Copolymer-1 Multiple Sclerosis Study Group. *Neurology* **1995,** *45,* 1268–1276.
158. *Product Monogram on Copaxone (Glatiramer Acetate Injection) for Subcutaneous Use.* Teva Pharmaceuticals: North Wales, PA, January 2014.
159. Anderson, J.; Bell, C.; Bishop, J.; Capila, I.; Ganguly, T.; Glajch, J.; Iyer, M.; Kaundinya, G.; Lansing, J.; Pradines, J.; et al. Demonstration of Equivalence of a Generic Glatiramer Acetate (Glatopa™). *J. Neurol. Sci.* **2015,** *359* (1–2), 24–34.
160. Becker, C. C.; Gidal, B. E.; Fleming, J. O. Immunotherapy in Multiple Sclerosis, Part 2. *Am. J. Health-Syst. Pharm.* **1995,** *52,* 2105–2120.
161. Bornstein, M. B.; Miller, A.; Slagle, S.; et al. A Pilot Trial of Cop 1 in Exacerbating-Remitting Multiple Sclerosis. *N. Engl. J. Med.* **1987,** *317,* 408–414.
162. Lalive, P. H.; Neuhaus, O.; Benkhoucha, M.; Burger, D.; Hohlfeld, R.; Zamvil, S. S.; Weber, M. S. Glatiramer Acetate in the Treatment of Multiple Sclerosis: Emerging Concepts Regarding its Mechanism of Action. *CNS Drugs* **2011,** *25,* 401–414.
163. Racke, M. K.; Lovett-Racke, A. E.; Karandikar, N. J. The Mechanism of Action of Glatiramer Acetate Treatment in Multiple Sclerosis. *Neurology* **2010,** *74* (Suppl. 1), S25–S30.
164. Hong, J.; Li, N.; Zhang, X.; Zheng, B.; Zhang, J. Z. Induction of CD4+ CD25+ Regulatory T Cells by Copolymer-I Through Activation of Transcription Factor Foxp3. *Proc. Natl. Acad. Sci. U. S. A.* **2005,** *102,* 6449–6454.
165. Aharoni, R. The Mechanism of Action of Glatiramer Acetate in Multiple Sclerosis and Beyond. *Autoimmun. Rev.* **2013,** *12,* 543–553.
166. Vieira, P. L.; Heystek, H. C.; Wormmeester, J.; Wierenga, E. A.; Kapsenberg, M. L. Glatiramer Acetate (Copolymer-1, Copaxone) Promotes Th2 Cell Development and Increased IL-10 Production Through Modulation of Dendritic Cells. *J. Immunol.* **2003,** *170,* 4483–4488.
167. Neuhaus, O.; Farina, C.; Wekerle, H.; Hohlfeld, R. Mechanisms of Action of Glatiramer Acetate in Multiple Sclerosis. *Neurology* **2001,** *56,* 702–708.
168. Arnon, R.; Aharoni, R. Mechanism of Action of Glatiramer Acetate in Multiple Sclerosis and its Potential for the Development of New Applications. *Proc. Natl. Acad. Sci. U. S. A.* **2004,** *101* (Suppl. 2), 14593–14598.
169. Kimby, E. Tolerability and Safety of Rituximab (MabThera). *Cancer Treat. Rev.* **2005,** *31,* 456–473.
170. Farina, C.; Then, B. F.; Albrecht, H.; Meinl, E.; Yassouridis, A.; Neuhaus, O.; et al. Treatment of Multiple Sclerosis With Copaxone (COP): Elispot Assay Detects COP-Induced Interleukin-4 and Interferon-Gamma Response in Blood Cells. *Brain* **2001,** *124,* 705–719.
171. Stuart, W. H. Clinical Management of Multiple Sclerosis: The Treatment Paradigm and Issues of Patient Management. *J. Manag. Care Pharm.* **2004,** *10* (3 Suppl. B), S19–S25.
172. Miller, R. M.; Happe, L. E.; Meyer, K. L.; Spear, R. J. Approaches to the Management of Agents Used for the Treatment of Multiple Sclerosis: Consensus Statements from a Panel of U.S. Managed Care Pharmacists and Physicians. *J. Manag. Care Pharm.* **2012,** *18,* 54–62.
173. *Extavia (Interferon Beta-1b).* Novartis Pharmaceuticals Corporation: East Hanover, NJ, 2014.
174. *Betaseron (Interferon Beta-1b) for Injection, for Subcutaneous Use.* Bayer HealthCare Pharmaceuticals Inc.: Whippany, NJ, January 2014.
175. *Avonex (Interferon Beta-1a) Injection, for Intramuscular Injection [Package Insert].* Biogen Idec Inc.: Cambridge, MA, March 2013.
176. *Rebif (Interferon Beta-1a), for Subcutaneous Injection [Package Insert].* EMD Serono Inc.: Rockland, MA, April 2014.

177. Bornstein, M. B.; Miller, A.; Slagle, S.; et al. A Placebo-Controlled, Double-Blind, Randomized, Two-Center, Pilot Trial of Cop 1 in Chronic Progressive Multiple Sclerosis. *Neurology* **1991,** *41,* 533–539.
178. Cohen, J. A.; Grossman, R. I.; Udupa, J. K.; et al. Assessment of the Efficacy of Copolymer-1 in the Treatment of Multiple Sclerosis by Quantitative MRI (Abstract). *Neurology* **1995,** *45* (Suppl. 4), A418.
179. Pastuszak, Ż.; Stępień, A.; Tomczykiewicz, K.; Piusińska-Macoch, R.; Durka-Kęsy, M. Mitoxantrone Role in Treatment of Primary Progressive Multiple Sclerosis. *Pol. Merkur. Lekarski.* **2016,** *40* (235), 66–99.
180. Koffman, B. M.; Hacker, M.; Gunning, W. T., 3rd; Quinn, A. Something Old, New, Borrowed, Blue: Anthracenedione Agents for Treatment of Multiple Sclerosis. *Clin. Neuropharmacol.* **2016,** *39* (2), 102–111.
181. Simone, M.; Chitnis, T. Use of Disease-Modifying Therapies in Pediatric MS. *Curr. Treat. Options Neurol.* **2016,** *18* (8), 36.
182. Millefiorini, E.; et al. Randomized Placebo-Controlled Trial of Mitoxantrone in Relapsing-Remitting Multiple Sclerosis: 24-Month Clinical and MRI Outcome. *J. Neurol.* **1997,** *244* (3), 153–159.
183. Edan, G.; et al. Therapeutic Effect of Mitoxantrone Combined With Methylprednisolone in Multiple Sclerosis: A Randomised Multicentre Study of Active Disease Using MRI and Clinical Criteria. *J. Neurol. Neurosurg. Psychiatry* **1997,** *62* (2), 112–118.
184. Hartung, H. P.; et al. Mitoxantrone in Progressive Multiple Sclerosis: A Placebo-Controlled, Double-Blind, Randomised, Multicentre Trial. *Lancet* **2002,** *360* (9350), 2018–2025.
185. Martinelli, V.; et al. Acute Myeloid Leukemia in Italian Patients With Multiple Sclerosis Treated With Mitoxantrone. *Neurology* **2011,** *77* (21), 1887–1895.
186. Mulroy, E.; et al. Long-Term Risk of Leukaemia or Cardiomyopathy After Mitoxantrone Therapy for Multiple Sclerosis. *Eur. Neurol.* **2012,** *67* (1), 45–47.
187. Kornek, B.; et al. Long-Term Follow-up of Pediatric Patients Treated With Mitoxantrone for Multiple Sclerosis. *Neuropediatrics* **2011,** *42* (1), 7–12.
188. Arnold, M.; Bissinger, R.; Lang, F. Mitoxantrone-Induced Suicidal Erythrocyte Death. *Cell. Physiol. Biochem.* **2014,** *34* (5), 1756–1767.
189. Marriott, J. J.; Miyasaki, J.; Gronseth, G.; O'Connor, P. W. Therapeutics and Technology Assessment Subcommittee of the American Academy of Neurology. Evidence Report: The Efficacy and Safety of Mitoxantrone (Novantrone) in the Treatment of Multiple Sclerosis: Report of the Therapeutics and Technology Assessment Subcommittee of the American Academy of Neurology. *Neurology* **2010,** *74,* 1463–1470.
190. Buttmann, M.; Seuffert, L.; Mäder, U.; Toyka, K. V. Malignancies After Mitoxantrone for Multiple Sclerosis: A Retrospective Cohort Study. *Neurology* **2016,** *86* (23), 2203–2207.
191. Singer, B. A. Parenteral Treatment of Multiple Sclerosis: The Advent of Monoclonal Antibodies. *Semin. Neurol.* **2016,** *36* (2), 140–147.
192. Hauser, S. L.; Waubant, E.; Arnold, D. L.; et al. HERMES Trial Group. B-Cell Depletion With Rituximab in Relapsing-Remitting Multiple Sclerosis. *N. Engl. J. Med.* **2008,** *358* (7), 676–688.
193. Hawker, K.; O'Connor, P.; Freedman, M. S.; et al. OLYMPUS Trial Group. Rituximab in Patients With Primary Progressive Multiple Sclerosis: Results of a Randomized Double-Blind Placebo-Controlled Multicenter Trial. *Ann. Neurol.* **2009,** *66* (4), 460–471.
194. Aimard, G.; Girard, P. F.; Raveau, J. Multiple Sclerosis and the Autoimmunization Process. Treatment by Antimitotics. *Lyon. Med.* **1966,** *215* (6), 345–352.
195. Okuda, D. T. Immunosuppressive Treatments in Multiple Sclerosis. *Handbook Clin. Neurol.* **2014,** *122,* 503–511.
196. Weiner, H. L. Immunosuppressive Treatment in Multiple Sclerosis. *J. Neurol. Sci.* **2004,** *223,* 1–11.
197. Balashov, K. E.; Smith, D. R.; Khoury, S. J.; et al. Increased Interleukin 12 Production in Progressive Multiple Sclerosis: Induction by Activated CD4+ T Cells via CD40 Ligand. *Proc. Natl. Acad. Sci. U. S. A.* **1997,** *94,* 599–603.
198. Smith, D. R.; Balashov, K. E.; Hafler, D. A.; et al. Immune Deviation Following Pulse Cyclophosphamide/Methylprednisolone Treatment of Multiple Sclerosis: Increased Interleukin-4 Production and Associated Eosinophilia. *Ann. Neurol.* **1997,** *42,* 313–318.
199. Karni, A.; Balashov, K.; Hancock, W. W.; et al. Cyclophosphamide Modulates CD4+ T Cells into a T Helper Type 2 Phenotype and Reverses Increased IFN-Gamma Production of CD8+ T Cells in Secondary Progressive Multiple Sclerosis. *J. Neuroimmunol.* **2004,** *146,* 189–198.
200. Hommes, O. R.; Prick, J. J.; Lamers, K. J. Treatment of the Chronic Progressive Form of Multiple Sclerosis With a Combination of Cyclophosphamide and Prednisone. *Clin. Neurol. Neurosurg.* **1975,** *78,* 59–72.
201. Gonsette, R. E.; Demonty, L.; Delmotte, P. Intensive Immunosuppression With Cyclophosphamide in Multiple Sclerosis. Follow up of 110 Patients for 2–6 Years. *J. Neurol.* **1977,** *214,* 173–181.
202. Gorman, M. P.; Healy, B. C.; Polgar-Turcsanyi, M.; et al. Increased Relapse Rate in Pediatric-Onset Compared With Adult-Onset Multiple Sclerosis. *Arch. Neurol.* **2009,** *66,* 54–59.
203. Waubant, E.; Chabas, D.; Okuda, D. T.; et al. Difference in Disease Burden and Activity in Pediatric Patients on Brain Magnetic Resonance Imaging at Time of Multiple Sclerosis Onset vs. Adults. *Arch. Neurol.* **2009,** *66,* 967–971.
204. Chabas, D.; Ness, J.; Belman, A.; et al. Younger Children With MS Have a Distinct CSF Inflammatory Profile at Disease Onset. *Neurology* **2010,** *74,* 399–405.
205. Goodin, D. S.; Frohman, E. M.; Garmany, G. P., Jr.; et al. Disease Modifying Therapies in Multiple Sclerosis: Report of the Therapeutics and Technology Assessment Subcommittee of the American Academy of Neurology and the MS Council for Clinical Practice Guidelines. *Neurology* **2002,** *58,* 169–178.
206. Makhani, N.; Gorman, M. P.; Branson, H. M.; et al. Cyclophosphamide Therapy in Pediatric Multiple Sclerosis. *Neurology* **2009,** *72,* 2076–2082.
207. Talar-Williams, C.; Hijazi, Y. M.; Walther, M. M.; et al. Cyclophosphamide-Induced Cystitis and Bladder Cancer in Patients With Wegener Granulomatosis. *Ann. Intern. Med.* **1996,** *124,* 477–484.
208. Radis, C. D.; Kahl, L. E.; Baker, G. L.; et al. Effects of Cyclophosphamide on the Development of Malignancy and on Long-Term Survival of Patients With Rheumatoid Arthritis. A 20-Year Followup Study. *Arthritis Rheum.* **1995,** *38,* 1120–1127.
209. U.S. Food and Drug Administration. Center for Drug Evaluation and Research. Application number 022432Orig1s000 Risk Assessment and Risk Mitigation Review(s). 2010. http://www.accessdata.fda.gov/17 Page 12 of 14 Curr Treat Options Neurol (2015) 17: 17drugsatfda_docs/nda/2010/022432Orig1s000RiskR.pdf (Accessed June, 2016).
210. Arnason, B. G.; et al. Mechanisms of Action of Adrenocorticotropic Hormone and Other Melanocortins Relevant to the Clinical Management of Patients With Multiple Sclerosis. *Mult. Scler.* **2013,** *19* (2), 130–136.
211. Bevan, C.; Gelfand, J.; MGelfand, J. M. Therapeutic Management of Severe Relapses in Multiple Sclerosis. *Curr. Treat. Opt. Neurol.* **2015,** *17* (4), 345–356.
212. Thompson, A. J.; Kennard, C.; Swash, M.; Summers, B.; Yuill, G. M.; Shepherd, D. I.; Roche, S.; Perkin, G. D.; Loizou, L. A.; Ferner, R.; et al. Relative Efficacy of Intravenous Methylprednisolone and ACTH in the Treatment of Acute Relapse in MS. *Neurology* **1989,** *39* (7), 969–971.
213. Filippini, G.; Brusaferri, F.; Sibley, W. A.; Citterio, A.; Ciucci, G.; Midgard, R.; Candelise, L. Corticosteroids or ACTH for Acute Exacerbations in Multiplesclerosis. *Cochrane Database Syst. Rev.* **2000,** *4,* CD001331.
214. Currier, R. D.; Haerer, A. F.; Meydrech, E. F. Low Dose Oral Methotrexate Treatment of Multiple Sclerosis: A Pilot Study. *J. Neurol. Neurosurg. Psychiatry* **1993,** *56,* 1217–1218.
215. Goodkin, D. E.; Rudick, R. A.; Vanderbrug Medendorp, S.; et al. Low-Dose (7.5 mg) Oral Methotrexate Reduces the Rate of Progression in Chronic Progressive Multiple Sclerosis. *Ann. Neurol.* **1995,** *37,* 30–40.
216. Goodkin, D. E.; Rudick, R. A.; Vanderbrug Medendorp, S.; et al. Low-Dose Oral Methotrexate in Chronic Progressive Multiple Sclerosis: Analyses of Serial MRIs. *Neurology* **1996,** *47,* 1153–1157.
217. Sadiq, S. A.; Simon, E. V.; Puccio, L. M. Intrathecal Methotrexate Treatment in Multiple Sclerosis. *J. Neurol.* **2010,** *257,* 1806–1811.
218. Serafini, B.; Rosicarelli, B.; Magliozzi, R.; et al. Detection of Ectopic B-Cell Follicles With Germinal Centers in the Meninges of Patients With Secondary Progressive Multiple Sclerosis. *Brain Pathol.* **2004,** *14,* 164–174.
219. Franciotta, D.; Salvetti, M.; Lolli, F.; et al. B Cells and Multiple Sclerosis. *Lancet Neurol.* **2008,** *7,* 852–858.
220. Gray, O. M.; McDonnell, G. V.; Forbes, R. B. A Systematic Review of Oral Methotrexate for Multiple Sclerosis. *Mult. Scler.* **2006,** *12,* 507–510.

221. Huynh, E.; Sigal, D.; Saven, A. Cladribine in the Treatment of Hairy Cell Leukemia: Initial and Subsequent Results. *Leuk. Lymphoma* **2009,** *50* (Suppl. 1), 12–17.
222. Kim, W.; Zandoná, M. E.; Kim, S. H.; Kim, H. J. Oral Disease-Modifying Therapies for Multiple Sclerosis. *J. Clin. Neurol.* **2015,** *11* (1), 9–19.
223. Hartung, H. P.; Aktas, O.; Kieseier, B.; Giancarlo Comi, G. C. Development of Oral Cladribine for the Treatment of Multiple Sclerosis. *J. Neurol.* **2010,** *257* (2), 163–170.
224. Liliemark, J. The Clinical Pharmacokinetics of Cladribine. *Clin. Pharmacokinet.* **1997,** *32* (2), 120–131.
225. Beutler, E. Cladribine (2-Chlorodeoxyadenosine). *Lancet* **1992,** *340* (8825), 952–956.
226. Sipe, J. C.; Romine, J. S.; Koziol, J. A.; McMillan, R.; Zyroff, J.; Beutler, E. Cladribine in Treatment of Chronic Progressive Multiple Sclerosis. *Lancet* **1994,** *344* (8914), 9–13.
227. Beutler, E.; Sipe, J. C.; Romine, J. S.; Koziol, J. A.; McMillan, R.; Zyroff, J. The Treatment of Chronic Progressive Multiple Sclerosis With Cladribine. *Proc. Natl. Acad. Sci. U. S. A.* **1996,** *93* (4), 1716–1720.
228. Rice, G. P.; Filippi, M.; Comi, G. Cladribine and Progressive MS: Clinical and MRI Outcomes of a Multicenter Controlled Trial. Cladribine MRI Study Group. *Neurology* **2000,** *54* (5), 1145–1155.
229. Romine, J. S.; Sipe, J. C.; Koziol, J. A.; Zyroff, J.; Beutler, E. A Double-Blind, Placebo-Controlled, Randomized Trial of Cladribine in Relapsing-Remitting Multiple Sclerosis. *Proc. Assoc. Am. Physicians* **1999,** *111* (1), 35–44.
230. Giovannoni, G.; Comi, G.; Cook, S.; Rammohan, K.; Rieckmann, P.; Soelberg Sørensen, P.; Vermersche, P.; Chanp, P.; Hamlett, A.; Musch, B.; et al. A Placebo-Controlled Trial of Oral Cladribine for Relapsing Multiple Sclerosis. *N. Engl. J. Med.* **2010,** *362* (5), 416–426.
231. Leist, T. P.; Comi, G.; Cree, B. A.; Coyle, P. K.; Freedman, M. S.; Hartung, H. P.; et al. Effect of Oral Cladribine on Time to Conversion to Clinically Definite Multiple Sclerosis in Patients With a First Demyelinating Event (ORACLE MS): A Phase 3 Randomised Trial. *Lancet Neurol.* **2014,** *13* (3), 257–267.
232. Cook, S.; Vermersch, P.; Comi, G.; Giovannoni, G.; Rammohan, K.; Rieckmann, P.; et al. Safety and Tolerability of Cladribine Tablets in Multiple Sclerosis: The CLARITY (CLAdRIbine Tablets Treating Multiple Sclerosis orallY) Study. *Mult. Scler.* **2011,** *17* (5), 578–593.
233. Killestein, J.; Rudick, R. A.; Polman, C. H. Oral Treatment for Multiple Sclerosis. *Lancet Neurol.* **2011,** *10* (11), 1026–1034.
234. Finsterwald, C.; Magistretti, P. J.; Lengacher, S. Astrocytes: New Targets for the Treatment of Neurodegenerative Diseases. *Curr. Pharm. Des.* **2015,** *21* (25), 3570–3581.
235. Selkoe, D. J. Alzheimer's Disease: Genes, Proteins, and Therapy. *Physiol. Rev.* **2001,** *81* (2), 741–766.
236. Rozemuller, A. J. M.; van Gool, W. A.; Eikelenboom, P. The Neuroinflammatory Response in Plaques and Amyloid Angiopathy in Alzheimer's Disease: Therapeutic Implications. *Curr. Drug Targets CNS Neurol. Disord.* **2005,** *4* (3), 223–233.
237. Rogawski, M. A.; Wenk, G. L. The Neuropharmacological Basis for the Use of Memantine in the Treatment of Alzheimer's Disease. *CNS Drug Rev.* **2003,** *9* (3), 275–308.
238. Ishigami, A.; Ohsawa, T.; Hiratsuka, M.; Taguchi, H.; Kobayashi, S.; Saito, Y.; Murayama, S.; Asaga, H.; Toda, T.; Kimura, N.; et al. Abnormal Accumulation of Citrullinated Proteins Catalyzed by Peptidylarginine Deiminase in Hippocampal Extracts from Patients With Alzheimer's Disease. *J. Neurosci. Res.* **2005,** *80* (1), 120–128.
239. Arif, M.; Kato, T. Increased Expression of PAD2 After Repeated Intracerebroventricular Infusions of Soluble Abeta(25–35) in the Alzheimer's Disease Model Rat Brain: Effect of Memantine. *Cell. Mol. Biol. Lett.* **2009,** *14* (4), 703–714.
240. Nicholas, A. P. Dual Immunofluorescence Study of Citrullinated Proteins in Alzheimer Diseased Frontal Cortex. *Neurosci. Lett.* **2013,** *545,* 107–111.
241. Prusiner, S.; Prions, B. *Proc. Natl. Acad. Sci. U. S. A.* **1998,** *95* (23), 13363–13383.
242. Whiteley, C. G. Arginine Metabolising Enzymes as Targets Against Alzheimers' Disease. *Neurochem. Int.* **2014,** *67,* 23–31.
243. Louw, C.; Gordon, A.; Johnston, N.; Mollatt, C.; Bradley, G.; Whiteley, C. G. Arginine Deiminases: Therapeutic Tools in the Etiology and Pathogenesis of Alzheimer's Disease. *J. Enzyme Inhib. Med. Chem.* **2007,** *22* (1), 121–126.
244. Folch, J.; Petrov, D.; Ettcheto, M.; Pedrós, I.; Abad, S.; Beas-Zarate, C.; Lazarowski, A.; Marin, M.; Olloquequi, J.; Auladell, C.; et al. Masitinib for the Treatment of Mild to Moderate Alzheimer's Disease. *Expert Rev. Neurother.* **2015,** *15* (6), 587–596.
245. Hroudová, J.; Singh, N.; Fišar, Z.; Ghosh, K. K. Progress in Drug Development for Alzheimer's Disease: An Overview in Relation to Mitochondrial Energy Metabolism. *Eur. J. Med. Chem.* **2016,** *S0223-5234* (16), 30266–30275.
246. Bryson, H. M.; Benfield, P. Donepezil. *Drugs Aging* **1997,** *10* (3), 234–239.
247. Arias, E.; Gallego-Sandin, S.; Villarroya, M.; Garcia, A. G.; Lopez, M. G. Unequal Neuroprotection Afforded by the Acetylcholinesterase Inhibitors Galantamine, Donepezil, and Rivastigmine in SH-SY5Y Neuroblastoma Cells: Role of Nicotinic Receptors. *J. Pharmacol. Exp. Ther.* **2005,** *315,* 1346–1353.
248. Noh, M. Y.; Koh, S. H.; Kim, Y.; Kim, H. Y.; Cho, G. W.; Kim, S. H. Neuroprotective Effects of Donepezil Through Inhibition of GSK-3 Activity in Amyloid-Beta-Induced Neuronal Cell Death. *J. Neurochem.* **2009,** *108,* 1116–1125.
249. Takada, Y.; Yonezawa, A.; Kume, T.; Katsuki, H.; Kaneko, S.; Sugimoto, H.; Akaike, A. Nicotinic Acetylcholine Receptor-Mediated Neuroprotection by Donepezil Against Glutamate Neurotoxicity in rat Cortical Neurons. *J. Pharmacol. Exp. Ther.* **2003,** *306,* 772–777.
250. Kamat, P. K.; Tota, S.; Shukla, R.; Ali, S.; Najmi, A. K.; Nath, C. Mitochondrial Dysfunction: A Crucial Event in Okadaic Acid (ICV) Induced Memory Impairment and Apoptotic Cell Death in Rat Brain. *Pharmacol. Biochem. Behav.* **2011,** *100* (2), 311–319.
251. Ki, Y. S.; Park, E. Y.; Lee, H. W.; Oh, M. S.; Cho, Y. W.; Kwon, Y. K.; Moon, J. H.; Lee, K. T. Donepezil, A Potent Acetylcholinesterase Inhibitor, Induces Caspase-Dependent Apoptosis in Human Promyelocytic Leukemia HL-60 Cells. *Biol. Pharm. Bull.* **2010,** *33* (6), 1054–1059.
252. Rogers, S. L.; Friedhoff, L. T.; Donepezil Study Group. The Efficacy and Safety of Donepezil in Patients With Alzheimer's Disease: Results of a US Multicentre, Randomized, Double-Blind, Placebo-Controlled Trial. *Dementia* **1996,** *7* (6), 293–303.
253. Rogers, S. L.; Doody, R.; Mohs, R.; Friedhoff, L. T. E2020 Produces Both Clinical Global and Cognitive Test Improvements in Patients With Mild to Moderately Severe Alzheimer's Disease: Result of a 30-Week Phase III Trial (Abstract). *Neurology* **1996,** *46* (suppl), A217.
254. McKhann, G.; Drachman, D.; Folstein, M.; Katzman, R.; Price, D.; Stadlan, E. M. Clinical Diagnosis of Alzheimer's Disease: Report of the NINCDSADRDA Work Group Under the Auspices of Department of Health and Human Services Task Force on Alzheimer's Disease. *Neurology* **1984,** *34,* 939–944.
255. Rogers, S. L.; Friedhoff, L. T. The Efficacy and Safety of Donepezil in Patients With Alzheimer's Disease: Results of a US Multicentre, Randomized, Double-Blind, Placebo-Controlled Trial, The Donepezil Study Group. *Dementia* **1996,** *7* (6), 293–303.
256. Ellis, J. M. Cholinesterase Inhibitors in the Treatment of Dementia. *J. Am. Osteopath. Assoc.* **2005,** *105,* 145–158.
257. Jann, M. W. Rivastigmine, A New-Generation Cholinesterase Inhibitor for the Treatment of Alzheimer's Disease. *Pharmacotherapy* **2000,** *20* (1), 1–12.
258. Hroudová, J.; Singh, J.; Fišar, N.; Ghosh, K. K. Progress in Drug Development for Alzheimer's Disease: An Overview in Relation to Mitochondrial Energy Metabolism. *Eur. J. Med. Chem.* **2016,** *121,* 774–784.
259. Parnetti, L.; Amici, S.; Lanari, A.; Romani, C.; Antognelli, C.; Andreasen, N.; Minthon, L.; Davidsson, P.; Pottel, H.; Blennow, K.; et al. Cerebrospinal Fluid Levels of Biomarkers and Activity of Acetylcholinesterase (AChE) and Butyrylcholinesterase in AD Patients Before and After Treatment With Different AChE Inhibitors. *Neurol. Sci.* **2002,** *23* (Suppl. 2), S95–S96.
260. Amici, S.; Lanari, A.; Romani, R.; Antognelli, C.; Gallai, V.; Parnetti, L. Cerebrospinal Fluid Acetylcholinesterase Activity After Long-Term Treatment With Donepezil and Rivastigmina. *Mech. Ageing Dev.* **2001,** *122* (16), 2057–2062.
261. Hellstrom-Lindahl, E.; Moore, A.; Nordberg, A. Increased Levels of tau Protein in SH-SY5Y Cells After Treatment With Cholinesterase Inhibitors and Nicotinic Agonists. *J. Neurochem.* **2000,** *74* (2), 777–784.
262. Polinsky, R. J. Clinical Pharmacology of Rivastigmine: A New-Generation Acetylcholinesterase Inhibitor for the Treatment of Alzheimer's Disease. *Clin. Ther.* **1998,** *20* (4), 634–647.
263. Bartorelli, L.; Giraldi, C.; Saccardo, M.; Cammarata, S.; Bottini, G.; Fasanaro, A. M.; Trequattrini, A. Effects of Switching From an AChE Inhibitor to a Dual AChE-BuChE Inhibitor in Patients With Alzheimer's Disease. *Curr. Med. Res. Opin.* **2005,** *21* (11), 1809–1818.
264. Auriacombe, S.; Pere, J. J.; Loria-Kanza, Y.; Vellas, B. Efficacy and Safety of Rivastigmine in Patients With Alzheimer's Disease Who Failed to Benefit from Treatment With Donepezil. *Curr. Med. Res. Opin.* **2002,** *18,* 129–138.

265. Ballard, C. G. Advances in the Treatment of Alzheimer's Disease: Benefits of Dual Cholinesterase Inhibition. *Eur. Neurol.* **2002,** *47* (1), 64–70.
266. Bailey, J. A.; Ray, B.; Greig, N. H.; Lahiri, D. K. Rivastigmine Lowers Abeta and Increases sAPPalpha Levels, Which Parallel Elevated Synaptic Markers and Metabolic Activity in Degenerating Primary Rat Neurons. *PloS ONE* **2011,** *6* (7), e21954.
267. Kumar, P.; Kumar, A. Protective Effect of Rivastigmine Against 3-Nitropropionic Acid-Induced Huntington's Disease Like Symptoms: Possible Behavioural, Biochemical and Cellular Alterations. *Eur. J. Pharmacol.* **2009,** *615* (1–3), 91–101.
268. Rogawski, M. A. What is the Rationale for new Treatment Strategies in Alzheimer's Disease? *CNS Spectr.* **2004,** *9* (7 Suppl. 5), 6–12.
269. Sramek, J. J.; Frackiewicz, E. J.; Cutler, N. R. Review of the Acetylcholinesterase Inhibitor Galanthamine. *Expert. Opin. Investig. Drugs* **2000,** *10,* 2393–2402.
270. Maelicke, A. Allosteric Modulation of Nicotinic Receptors as a Treatment Strategy for Alzheimer's Disease. *Dement. Geriatr. Cogn. Disord.* **2000,** *11* (Suppl. 1), 11–18.
271. Arias, E.; Ales, E.; Gabilan, N. H.; Cano-Abad, M. F.; Villarroya, M.; Garcia, A. G.; Lopez, M. G. Galantamine Prevents Apoptosis Induced by Beta-Amyloid and Thapsigargin: Involvement of Nicotinic Acetylcholine Receptors. *Neuropharmacology* **2004,** *46* (1), 103–114.
272. Liu, X.; Xu, K.; Yan, M.; Wang, Y.; Zheng, X. Protective Effects of Galantamine Against Abeta-Induced PC12 Cell Apoptosis by Preventing Mitochondrial Dysfunction and Endoplasmic Reticulum Stress. *Neurochem. Int.* **2010,** *57* (5), 588–599.
273. Ezoulin, M. J.; Li, J.; Wu, G.; Dong, C. Z.; Ombetta, J. E.; Chen, H. Z.; Massicot, F.; Heymans, F. Differential Effect of PMS777, a new Type of Acetylcholinesterase Inhibitor, and Galanthamine on Oxidative Injury Induced in Human Neuroblastoma SK-N-SH Cells. *Neurosci. Lett.* **2005,** *389* (2), 61–65.
274. Kumar, A.; Prakash, A.; Pahwa, D. Galantamine Potentiates the Protective Effect of Rofecoxib and Caffeic Acid Against Intrahippocampal Kainic Acid-Induced Cognitive Dysfunction in Rat. *Brain Res. Bull.* **2011,** *85* (3–4), 158–168.
275. Westra, P.; van Thiel, M. J.; Vermeer, G. A.; Soeterbroek, A. M.; Scaf, A. H.; Claessens, H. A. Pharmacokinetics of Galanthamine (A Long-Acting Anticholinesterase Drug) in Anaesthetized Patients. *Br. J. Anaesth.* **1986,** *58* (11), 1303–1307.
276. Mihailova, D.; Yamboliev, I.; Zhivkova, Z.; Tencheva, J.; Jovovich, V. Pharmacokinetics of Galanthamine Hydrobromide After Single Subcutaneous and Oral Dosage in Humans. *Pharmacology* **1989,** *39* (1), 50–58.
277. Thomsen, T.; Bicker, U.; Fischer, J. P.; Kewitz, H. Galanthamine Hydrobromide in a Long-Term Treatment of Alzheimer's Disease. *Dementia* **1990,** *1,* 46–51.
278. Reisberg, B.; Doody, R.; Stöffler, A.; Schmitt, F.; Ferris, S.; Möbius, H. J. Memantine Study Group. Memantine in Moderate-to-Severe Alzheimer's Disease. *N. Engl. J. Med.* **2003,** *348* (14), 1333–1341.
279. Lipton, S. A. Paradigm Shift in NMDA Receptor Antagonist Drug Development: Molecular Mechanism of Uncompetitive Inhibition by Memantine in the Treatment of Alzheimer's Disease and Other Neurologic Disorders. *J. Alzheimer's Dis.* **2004,** *6* (6 Suppl.), S61–S74.
280. Lipton, S. A. The Molecular Basis of Memantine Action in Alzheimer's Disease and Other Neurologic Disorders: Low-Affinity, Uncompetitive Antagonism. *Curr. Alzheimer Res.* **2005,** *2* (2), 155–165.
281. Kysenius, K.; Brunello, C. A.; Huttunen, H. J. Mitochondria and NMDA Receptor-Dependent Toxicity of Berberine Sensitizes Neurons to Glutamate and Rotenone Injury. *PloS One* **2014,** *9* (9), e107129.
282. Tozzi, A.; Costa, C.; Di Filippo, M.; Tantucci, M.; Siliquini, S.; Belcastro, V.; Parnetti, L.; Picconi, B.; Calabresi, P. Memantine Reduces Neuronal Dysfunctions Triggered by In Vitro Ischemia and 3-Nitropropionic Acid. *Exp. Neurol.* **2007,** *207* (2), 218–226.
283. Alley, G. M.; Bailey, J. A.; Chen, D.; Ray, B.; Puli, L. K.; Tanila, H.; Banerjee, P. K.; Lahiri, D. K. Memantine Lowers Amyloid-Beta Peptide Levels in Neuronal Cultures and in APP/PS1 Transgenic Mice. *J. Neurosci. Res.* **2010,** *88* (1), 143–154.
284. Picco, A.; Polidori, M. C.; Ferrara, M.; Cecchetti, R.; Arnaldi, D.; Baglioni, M.; Morbelli, S.; Bastiani, P.; Bossert, I.; Fiorucci, G.; et al. Plasma Antioxidants and Brain Glucose Metabolism in Elderly Subjects With Cognitive Complaints. *Eur. J. Nucl. Med. Mol. Imaging* **2014,** *41* (4), 764–775.
285. Ahmed, M. M.; Hoshino, H.; Chikuma, T.; Yamada, M.; Kato, T. Effect of Memantine on the Levels of Glial Cells, Neuropeptides, and Peptide-Degrading Enzymes in Rat Brain Regions of Ibotenic Acid-Treated Alzheimer's Disease Model. *Neuroscience* **2004,** *126* (3), 639–649.
286. Arif, M.; Chikuma, T.; Ahmed, M. M.; Nakazato, M.; Smith, M. A.; Kato, T. Effects of Memantine on Soluble Alphabeta(25–35)-Induced Changes in Peptidergic and Glial Cells in Alzheimer's Disease Model Rat Brain Regions. *Neuroscience* **2009,** *164,* 1199–1209.
287. Miguel-Hidalgo, J. J.; Alvarez, X. A.; Cacabelos, R.; Quack, G. Neuroprotection by Memantine Against Neurodegeneration Induced by Beta-Amyloid(1–40). *Brain Res.* **2002,** *958,* 210–221.
288. Song, M. S.; Rauw, G.; Baker, G. B.; Kar, S. Memantine Protects rat Cortical Cultured Neurons Against Beta-Amyloid-Induced Toxicity by Attenuating tau Phosphorylation. *Eur. J. Neurosci.* **2008,** *28* (10), 1989–2002.
289. Tabira, T. Immunotherapy for Alzheimer's Disease Targeting Aβ. *Nihon Rinsho* **2016,** *74* (3), 423–426.
290. DeMattos, R. B.; Bales, K. R.; Cummins, D. J.; Dodart, J. C.; Paul, S. M.; Holtzman, D. M. Peripheral Anti-Aβ Antibody Alters CNS and Plasma Aβ Clearance and Decreases Brain Aβ Burden in a Mouse Model of Alzheimer's Disease. *Proc. Natl. Acad. Sci. U. S. A.* **2001,** *98,* 8850–8855.
291. DeMattos, R. B.; Bales, K. R.; Cummins, D. J.; Paul, S. M.; Holtzman, D. M. Brain to Plasma Amyloid-β Efflux: A Measure of Brain Amyloid Burden in a Mouse Model of Alzheimer's Disease. *Science* **2002,** *295* (5563), 2264–2267.
292. Siemers, E. R.; Friedrich, S.; Dean, R. A.; Gonzales, C.; Farlow, M. R.; Paul, S. M.; et al. Safety and Changes in Plasma and Cerebrospinal Fluid Aβ Following a Single Administration of an Aβ Monoclonal Antibody in Subjects With Alzheimer's Disease. *Clin. Neuropharmacol.* **2010,** *33* (2), 67–73.
293. Farlow, M.; Arnold, S. E.; van Dyck, C. H.; Aisen, P. S.; Snider, B. J.; Porsteinsson, A. P.; et al. Safety and Biomarker Effects of Solanezumab in Patients With Alzheimer's Disease. *Alzheimers Dement.* **2012,** *8* (4), 261–271.
294. Karran, E.; Hardy, J. Antiamyloid Therapy for Alzheimer's Disease—Are We on the Right Road? *N. Engl. J. Med.* **2014,** *370,* 377–378.
295. Siemers, E. R.; Sundell, K. L.; Carlson, C.; Case, M.; Sethuraman, G.; Liu-Seifert, H.; Dowsett, S. A.; Pontecorvo, M. J.; Dean, R. A.; Demattos, R. Phase 3 Solanezumab Trials: Secondary Outcomes in Mild Alzheimer's Disease Patients. *Alzheimers Dement.* **2016,** *12* (2), 110–120.
296. Qian, X.; Hamad, B.; Dias-Lalcaca, G. The Alzheimer Disease Market. *Nat. Rev. Drug Discov.* **2015,** *14* (10), 675–676.
297. Panza, F.; Solfrizzi, V.; Imbimbo, B. P.; Giannini, M.; Santamato, A.; Seripa, D.; Logroscino, G. Efficacy and Safety Studies of Gantenerumab in Patients With Alzheimer's Disease. *Expert Rev. Neurother.* **2014,** *14* (9), 973–986.
298. Pasinetti, G. M.; Wang, J.; Ho, L.; Zhao, W.; Dubner, L. Roles of Resveratrol and Other Grape-Derived Polyphenols in Alzheimer's Disease Prevention and Treatment. *Biochim. Biophys. Acta* **2015,** *1852* (6), 1202–1208.
299. Baur, J. A.; et al. Resveratrol Improves Health and Survival of Mice on a High-Calorie Diet. *Nature* **2006,** *444* (7117), 337–342.
300. Lagouge, M.; Argmann, C.; Gerhart-Hines, Z.; Meziane, H.; Lerin, C.; Daussin, F.; Messadeq, N.; Milne, J.; Lambert, P.; Elliott, P.; et al. Resveratrol Improves Mitochondrial Function and Protects Against Metabolic Disease by Activating SIRT1 and PGC-1α. *Cell* **2006,** *127* (6), 1109–1122.
301. Baur, J. A.; Sinclair, D. A. Therapeutic Potential of Resveratrol: The In Vivo Evidence. *Nat. Rev. Drug Discov.* **2006,** *5* (6), 493–506.
302. Greet, E. L.; Brunet, A. Different Dietary Restriction Regimens Extend Lifespan by Both Independent and Overlapping Genetic Pathways in *C. elegans*. *Aging Cell* **2009,** *8* (2), 113–127.
303. Poulsen, M. M.; Jørgensen, J. O.; Jessen, N.; Richelsen, B.; Pedersen, S. B. Resveratrol in Metabolic Health: An Overview of the Current Evidence and Perspectives. *Ann. N. Y. Acad. Sci.* **2013,** *1290,* 74–82.
304. Ranney, A.; Petro, M. S. Resveratrol Protects Spatial Learning in Middle-Aged C57BL/6 Mice From Effects of Ethanol. *Behav. Pharmacol.* **2009,** *20* (4), 330–336.
305. Abraham, J.; Johnson, R. W. Consuming a Diet Supplemented With Resveratrol Reduced Infection-Related Neuroinflammation and Deficits in Working Memory in Aged Mice. *Rejuvenation Res.* **2009,** *12* (6), 445–453.
306. Cantó, C.; Auwerx, J. PGC-1alpha, SIRT1 and AMPK, an Energy Sensing Network That Controls Energy Expenditure. *Curr. Opin. Lipidol.* **2009,** *20* (2), 98–105.

307. Um, J. H.; Park, S. J.; Kang, H.; Yang, S.; Foretz, M.; McBurney, M. W.; Kim, M. K.; Viollet, B.; Chung, J. H. AMP-Activated Protein Kinase-Deficient Mice are Resistant to the Metabolic Effects of Resveratrol. *Diabetes* **2010,** *59* (3), 554–563.
308. Vingtdeux, V.; Davies, P.; Dickson, D. W.; Marambaud, P. AMPK is Abnormally Activated in Tangle- and Pre-Tangle-Bearing Neurons in Alzheimer's Disease and Other Tauopathies. *Acta Neuropathol.* **2011,** *121* (3), 337–349.
309. Howitz, K. T.; et al. Small Molecule Activators of Sirtuins Extend *Saccharomyces cerevisiae* Lifespan. *Nature* **2003,** *425* (6954), 191–196.
310. Borra, M. T.; Smith, B. C.; Denu, J. M. Mechanism of Human SIRT1 Activation by Resveratrol. *J. Biol. Chem.* **2005,** *280* (17), 17187–17195.
311. Pacholec, M.; et al. SRT1720, SRT2183, SRT1460, and Resveratrol are not Direct Activators of SIRT1. *J. Biol. Chem.* **2010,** *285* (11), 8340–8351.
312. Ruderman, N. B.; Xu, X. J.; Nelson, L.; Cacicedo, J. M.; Saha, A. K.; Lan, F.; Ido, Y. AMPK and SIRT1: A Long-Standing Partnership? *Am. J. Physiol. Endocrinol. Metab.* **2010,** *298* (4), 751–760.
313. Walle, T. Bioavailability of Resveratrol. *Ann. N. Y. Acad. Sci.* **2011,** *1215* (1), 9–15.
314. Cottart, C.-H.; Nivet-Antoine, V.; Laguillier-Morizot, C.; Beaudeux, J. L. Resveratrol Bioavailability and Toxicity in Humans. *Mol. Nutr. Food Res.* **2010,** *54* (1), 7–16. http://dx.doi.org/10.1002/mnfr.200900437.
315. Anekonda, T. S. Resveratrol—A Boon for Treating Alzheimer's Disease? *Brain Res. Rev.* **2006,** *52* (2), 316–326.
316. Nunes, T.; Almeida, L.; Rocha, J. F.; Falcão, A.; Fernandes-Lopes, C.; Loureiro, A. I.; Wright, L.; Vaz-Da-Silva, M.; Soares-Da-Silva, P. Pharmacokinetics of Trans-Resveratrol Following Repeated Administration in Healthy Elderly and Young Subjects. *J. Clin. Pharmacol. Pharmacol.* **2009,** *49* (12), 1477–1482.
317. Vingtdeux, V.; Giliberto, L.; Zhao, H.; Chandakkar, P.; Wu, Q.; Simon, J. E.; Janle, E. M.; Lobo, J.; Ferruzzi, M. G.; Davies, P.; et al. AMP-Activated Protein Kinase Signaling Activation by Resveratrol Modulates Amyloid-β Peptide Metabolism. *J. Biol. Chem.* **2010,** *285* (12), 9100–9113.
318. Amiot, M. J.; Romier, B.; Anh Dao, T. M.; Fanciullino, R.; Ciccolini, J.; Burcelin, R.; Pechere, L.; Emond, C.; Savouret, J. F.; Seree, E. Optimization of Trans-Resveratrol Bioavailability for Human Therapy. *Biochimie* **2013,** *95* (6), 1233–1238.
319. Sessa, M.; Balestrieri, M. L.; Ferrari, G.; Castaldo, D.; D'Onofrio, N.; Donsì, F.; Tsao, R. Bioavailability of Encapsulated Resveratrol Into Nanoemulsion-Based Delivery Systems. *Food ChemChem* **2014,** *147,* 42–50.
320. Planas, J. M.; Alfaras, I.; Colom, H.; Juan, M. E. The Bioavailability and Distribution of Trans-Resveratrol are Constrained by ABC Transporters. *Arch. Biochem. Biophys.* **2012,** *527* (2), 67–73.
321. Neves, A. R.; Lúcio, M.; Martins, S.; Lima, J. L. C.; Reis, S. Novel Resveratrol Nanodelivery Systems Based on Lipid Nanoparticles to Enhance its Oral Bioavailability. *Int. J. Nanomed.* **2013,** *8,* 177–187.
322. Pasinetti, G. M.; Wang, J.; Marambaud, P.; Ferruzzi, M.; Gregor, P.; Knable, L. A.; Ho, L. Neuroprotective and Metabolic Effects of Resveratrol: Therapeutic Implications for Huntington's Disease and Other Neurodegenerative Disorders. *Exp. Neurol.* **2011,** *232* (1), 1–6.
323. Patel, K. R.; Scott, E.; Brown, V. A.; Gescher, A.; Steward, W. P.; Brown, K. Clinical Trials of Resveratrol. *Ann. N. Y. Acad. Sci.* **2011,** *1215* (1), 161–169.
324. Kennedy, D. O.; Wightman, E. L.; Reay, J. L.; Lietz, G.; Okello, E. J.; Wilde, A.; Haskell, C. F. Effects of Resveratrol on Cerebral Blood Flow Variables and Cognitive Performance in Humans: A Double-Blind, Placebo-Controlled, Crossover Investigation. *Am. J. Clin. Nutr.* **2010,** *91* (6), 1590–1597.
325. Mecocci, P.; Polidori, M. C. Antioxidant Clinical Trials in Mild Cognitive Impairment and Alzheimer's Disease. *Biochim. Biophys. Acta* **2012,** *1822* (5), 631–638.
326. Turner, R. S.; Thomas, R. G.; Craft, S.; van Dyck, C. H.; Mintzer, J.; Reynolds, B. A.; Brewer, J. B.; Rissman, R. A.; Raman, R.; Aisen, P. S. Alzheimer's Disease Cooperative Study. A Randomized, Double-Blind, Placebo-Controlled Trial of Resveratrol for Alzheimer Disease. *Neurology* **2015,** *85* (16), 1383–1391.
327. Jankovic, J. Parkinson's Disease: Clinical Features and Diagnosis. *J. Neurol. Neurosurg. Psychiatry* **2008,** *79* (4), 368–376.
328. Nicholas, A. P. Dual Immunofluorescence Study of Citrullinated Proteins in Parkinson Diseased Substantia Nigra. *Neurosci. Lett.* **2011,** *495* (1), 26–29.
329. Acharya, N. K.; Nagele, E. P.; Han, M.; Coretti, N. J.; DeMarshall, C.; Kosciuk, M. C.; Boulos, P. A.; Nagele, R. G. Neuronal PAD4 Expression and Protein Citrullination: Possible Role in Production of Autoantibodies Associated With Neurodegenerative Disease. *J. Autoimmun.* **2012,** *38* (4), 369–380.
330. Dauer, W.; Przedborski, S. Parkinson's Disease: Mechanisms and Models. *Neuron* **2003,** *39* (6), 889–909.
331. Russo, I.; Bubacco, L.; Greggio, E. LRRK2 and Neuroinflammation: Partners in Crime in Parkinson's Disease? *J. Neuroinflammation* **2014,** *11,* 52.
332. Celesia, G. G.; Wanamaker, W. M. L-Dopa-Carbidopa: Combined Therapy for the Treatment of Parkinson's Disease. *Dis. Nerv. Syst.* **1976,** *37* (3), 123–125.
333. Koller, W. C.; Rueda, M. G. Mechanism of Action of Dopaminergic Agents in Parkinson's Disease. *Neurology* **1998,** *50* (6 Suppl. 6), S11–S14.
334. Kalia, L. V.; Kalia, S. K.; Lang, A. E. Disease-Modifying Strategies for Parkinson's Disease. *Mov. Disord.* **2015,** *30* (11), 1442–1450.
335. Gu, M.; Iravani, M. M.; Irvani, M.; et al. Pramipexole Protects Against Apoptotic Cell Death by Non-Dopaminergic Mechanisms. *J. Neurochem.* **2004,** *91,* 1075–1081.
336. Iravani, M. M.; Haddon, C. O.; Cooper, J. M.; et al. Pramipexole Protects Against MPTP Toxicity in Non-Human Primates. *J. Neurochem.* **2006,** *96,* 1315–1321.
337. Iravani, M. M.; Sadeghian, M.; Leung, C. C. M.; et al. Continuous Subcutaneous Infusion of Pramipexole Protects Against Lipopolysaccharide-Induced Dopaminergic Cell Death Without Affecting the Inflammatory Response. *Exp. Neurol.* **2008,** *212,* 522–531.
338. Gu, M.; Iravani, M. M.; Cooper, J. M.; King, D.; Jenner, P.; Schapira, A. H. Pramipexole Protects Against Apoptotic Cell Death by Non-Dopaminergic Mechanisms. *J. Neurochem.* **2004,** *91* (5), 1075–1081.
339. Schapira, A. H.; McDermott, M. P.; Barone, P.; et al. Pramipexole in Patients With Early Parkinson's Disease (PROUD): A Randomised Delayed-Start Trial. *Lancet Neurol.* **2013,** *12,* 747–755.
340. Fox, S. H.; Katzenschlager, R.; Lim, S. The Movement Disorder Society Evidence-Based Medicine Review Update: Treatments for the Motor Symptoms of Parkinson's Disease. *Mov. Disord.* **2011,** *26* (Suppl. 3), S2–S41.
341. Pahwa, R.; Lyons, K. E.; Hauser, R. A. Ropinirole Therapy for Parkinson's Disease. *Expert Rev. Neurother.* **2004,** *4* (4), 581–588.
342. Tulloch, I. F. Pharmacologic Profile of Ropinirole: A Nonergoline Dopamine Agonist. *Neurology* **1997,** *49* (1 Suppl. 1), S58–S62.
343. Adler, C. H.; Sethi, K. D.; Hauser, R. A.; Davis, T. L.; Hammerstad, J. P.; Bertoni, J.; Taylor, R. L.; Sanchez-Ramos, J.; O'Brien, C. F. Ropinirole for the Treatment of Early Parkinson's Disease. The Ropinirole Study Group. *Neurology* **1997,** *49* (2), 393–399.
344. Hoehn, M. M. Bromocriptine and Its Use in Parkinsonism. *J. Am. Geriatr. Soc.* **1981,** *29* (6), 251–258.
345. Curran, M. P.; Perry, C. M. Cabergoline: A Review of Its Use in the Treatment of Parkinson's Disease. *Drugs* **2004,** *64* (18), 2125–2141.
346. Gonce, M.; Delwaide, P. J. Clinical Study of Pergolide in Parkinson's Disease. *Presse. Med.* **1985,** *14* (26), 1409–1411.
347. Morgan, J. C.; Sethi, K. D. Rotigotine for the Treatment of Parkinson's Disease. *Expert Rev. Neurother.* **2006,** *6* (9), 1275–1282.
348. O'Doherty, D.; Forster, F. M. The Use of Benzotropine Sulfonate in the Treatment of Parkinsonism. *Med. Ann. Dist. Columbia* **1953,** *22* (5), 221–223.
349. Cranwell-Bruce, L. A. Drugs for Parkinson's Disease. *Medsurg. Nurs.* **2010,** *19* (6), 347–349.
350. Yuan, H.; Zhang, Z. W.; Liang, L. W.; Shen, Q.; Wang, X. D.; Ren, S. M.; Ma, H. J.; Jiao, S. J.; Liu, P. Treatment Strategies for Parkinson's Disease. *Neurosci. Bull.* **2010,** *26* (1), 66–76.
351. Muguet, D.; Broussolle, E.; Chazot, G. Apomorphine in Patients With Parkinson's Disease. *Biomed. Pharmacother.* **1995,** *49* (4), 197–209.
352. Spilovska, K.; Zemek, F.; Korabecny, J.; Nepovimova, E.; Windisch, O. S.; Kuca, K. Adamantane—A Lead Structure for Drugs in Clinical Practice. *Curr. Med. Chem.* **2016,** *23* (29), 3245–3266.
353. Edmunds, M. W.; Mayhew, M. S. *Pharmacology for the Primary Care Provider;* St. Mosby Elsevier: Louis, MO, 2009.
354. Zhang, S.; Dissanayaka, N. N.; Dawson, A.; O'Sullivan, J. D.; Mosley, P.; Hall, W.; Carter, A. Management of Impulse Control Disorders in Parkinson's Disease. *Int. Psychogeriatr.* **2016,** 1–18.
355. Chan, K. Y.; Cordato, D. J.; O'Rouke, F. Management for Motor and Non-Motor Complications in Late Parkinson's Disease. *Geriatrics* **2008,** *63* (5), 22–27.
356. Rascol, O.; Perez-Lloret, S.; Ferreira, J. J. New Treatments for Levodopa-Induced Motor Complications. *Mov. Disord.* **2015,** *30* (11), 1451–1460.

357. Damier, R.; Viallet, F.; Ziegler, M.; Bourdeix, I.; Rerat, K. Levodopa/DDCI and Entacapoine is the Preferred Treatment for Parkinson's Disease Patients With Motor Fluctuations in Routine Practice: A Retrospective, Observational Analysis of a Large French Cohort. *Eur. J. Neurol.* **2008,** *15* (7), 643–648.
358. Muller, T. *Entacapone. Expert Opin. Drug Metabol. Toxicol.* **2010,** *6* (8), 983–993.
359. Hasiko, K. Toxicology and safety of COMT inhibitors. *Intl. Rev. Neurobiol.* **2010,** *95,* 163–189.
360. Rasagiline (Azilect) for Parkinson's Disease. *Med. Lett. Drugs. Ther.* **2006,** *48* (1249/1250), 97–99.
361. Elmer, L. W. Rasagiline Adjunct Therapy in Patients With Parkinson's Disease: Post hoc Analyses of the PRESTO and LARGO Trials. *Parkinsonism Relat. Disord.* **2013,** *19* (11), 930–936.
362. Olanow, C. W.; et al. ADAGIO Study Investigators: A Double-Blind, Delayed-Start Trial of Rasagiline in Parkinson's Disease. *N. Engl. J. Med.* **2009,** *361* (13), 1268–1278.
363. Naoi, M.; Maruyama, W.; Inaba-Hasegawa, K. Type A and B Monoamine Oxidase in Age-Related Neurodegenerative Disorders: Their Distinct Roles in Neuronal Death and Survival. *Curr. Top. Med. Chem.* **2012,** *12* (20), 2177–2188.
364. Jenner, P. An Overview of Adenosine A2A Receptor Antagonists in Parkinson's Disease. *Int. Rev. Neurobiol.* **2014,** *119,* 71–86.
365. Jenner, P.; Mori, A.; Hauser, R.; Morelli, M.; Fredholm, B. B.; Chen, J. F. Adenosine, Adenosine A 2A Antagonists, and Parkinson's Disease. *Parkinsonism Relat. Disord.* **2009,** *15,* 406–413.
366. Hauser, R. A.; Schwarzschild, M. A. Adenosine A2A Receptor Antagonists for Parkinson's Disease: Rationale, Therapeutic Potential and Clinical Experience. *Drugs Aging.* **2005,** *22,* 471–482.
367. Kanda, T.; Jackson, M. J.; Smith, L. A.; Pearce, R. K.; Nakamura, J.; Kase, H.; Kuwana, Y.; Jenner, P. Adenosine A2A Antagonist: A Novel Antiparkinsonian Agent That Does Not Provoke Dyskinesia in Parkinsonian Monkeys. *Ann. Neurol.* **1998,** *43,* 507–513.
368. Kanda, T.; Jackson, M. J.; Smith, L. A.; Pearce, R. K.; Nakamura, J.; Kase, H.; Kuwana, Y.; Jenner, P. Combined Use of the Adenosine A(2A) Antagonist KW-6002 With L-DOPA or With Selective D1 or D2 Dopamine Agonists Increases Antiparkinsonian Activity But Not Dyskinesia in MPTP-Treated Monkeys. *Exp. Neurol.* **2000,** *162,* 321–327.
369. Grondin, R.; Bedard, P. J.; Hadj Tahar, A.; Gregoire, L.; Mori, A.; Kase, H. Antiparkinsonian Effect of a New Selective Adenosine A2A Receptor Antagonist in MPTP-Treated Monkeys. *Neurology* **1999,** *52* (2), 1673–1677.
370. Hodgson, R. A.; Bedard, P. J.; Varty, G. B.; Kazdoba, T. M.; Di Paolo, T.; Grzelak, M. E.; Pond, A. J.; Hadjtahar, A.; Belanger, N.; Gregoire, L.; et al. Preladenant, A Selective A(2A) Receptor Antagonist, is Active in Primate Models of Movement Disorders. *Exp. Neurol.* **2010,** *225,* 384–390.
371. Prediger, R. D. Effects of Caffeine in Parkinson's Disease: From Neuroprotection to the Management of Motor and Non-Motor Symptoms. *J. Alzheimers Dis.* **2010,** *20* (Suppl. 1), S205–S220.
372. Ikeda, K.; Kurokawa, M.; Aoyama, S.; Kuwana, Y. Neuroprotection by Adenosine A2A Receptor Blockade in Experimental Models of Parkinson's Disease. *J. Neurochem.* **2002,** *80,* 262–270.
373. Kalda, A.; Yu, L.; Oztas, E.; Chen, J. F. Novel Neuroprotection by Caffeine and Adenosine A(2A) Receptor Antagonists in Animal Models of Parkinson's Disease. *J. Neurol. Sci.* **2006,** *248,* 9–15.
374. Dungo, R.; Deeks, E. D. Istradefylline: First Global Approval. *Drugs* **2013,** *73* (8), 875–882.
375. Bara-Jimenez, W.; Sherzai, A.; Dimitrova, T.; Favit, A.; Bibbiani, F.; Gillespie, M.; Morris, M. J.; Mouradian, M. M.; Chase, T. N. Adenosine A(2A) Receptor Antagonist Treatment of Parkinson's Disease. *Neurology* **2003,** *61,* 293–296.
376. Hauser, R. A.; Hubble, J. P.; Truong, D. D.; Istradefylline US-001 Study Group. Randomized Trial of the Adenosine A(2A) Receptor Antagonist Istradefylline in Advanced PD. *Neurology* **2003,** *61,* 297–303.
377. LeWitt, P. A.; Guttman, M.; Tetrud, J. W.; Tuite, P. J.; Mori, A.; Chaikin, P.; Sussman, N. M.; 6002-US-005 Study Group. Adenosine A2A Receptor Antagonist Istradefylline (KW-6002) Reduces "Off" Time in Parkinson's Disease: A Double-Blind, Randomized, Multicenter Clinical Trial (6002-US-005). *Ann. Neurol.* **2008,** *63,* 295–302.
378. Stacy, M.; Silver, D.; Mendis, T.; Sutton, J.; Mori, A.; Chaikin, P.; Sussman, N. M. A 12-Week, Placebo-Controlled Study (6002US-006) of Istradefylline in Parkinson Disease. *Neurology* **2008,** *70,* 2233–2240.
379. Hauser, R. A.; Shulman, L. M.; Trugman, J. M.; Roberts, J. W.; Mori, A.; Ballerini, R.; Sussman, N. M.; Istradefylline 6002-US-013 Study Group. Study of Istradefylline in Patients With Parkinson's Disease on Levodopa With Motor Fluctuations. *Mov. Disord.* **2008,** *23,* 2177–2185.
380. Guttman, M. Efficacy of Istradefylline in Parkinson's Disease Patients Treated With Levodopa With Motor Fluctuations. *Mov. Disord.* **2006,** *21* (Suppl. 15), S585.
381. FDA Issues Not Approvable Letter for Istradefylline. http://www.kyowa.co.jp/eng/netext/er080228_01.htm
382. Hauser, R. A.; Auinger, P.; Parkinson Study Group. Determination of Minimal Clinically Important Change in Early and Advanced Parkinson's Disease. *Mov. Disord.* **2011,** *26,* 813–818.
383. Kyowa Pharmaceutical Inc. *Kyowa Pharmaceutical Suspends Development of Istradefylline in North America [Internet].* http://www.michaeljfox.org/newsEvents_parkinsonsInTheNews_article.cfm?ID=353, 2008 (cited 2011 Feb 24).
384. Fernandez, H. H.; Greeley, D. R.; Zweig, R. M.; Wojcieszek, J.; Mori, A.; Sussman, N. M.; 6002-US-051 Study Group. Istradefylline as Monotherapy for Parkinson Disease: Results of the 6002-US-051 Trial. *Parkinsonism Relat. Disord.* **2010,** *16* (1), 16–20.
385. Samanta, J.; Hauser, R. A. Duodenal Levodopa Infusion for the Treatment of Parkinson's Disease. *Expert. Opin. Pharmacother.* **2007,** *8* (5), 657–664664.
386. Nyholm, D. Enteral Levodopa/Carbidopa Gel Infusion for the Treatment of Motor Fluctuations and Dyskinesias in Advanced Parkinson's Disease. *Expert. Rev. Neurother.* **2006,** *6* (10), 1403–1411.
387. Fernandez, H. H.; Odin, P. Levodopa-Carbidopa Intestinal Gel for Treatment of Advanced Parkinson's Disease. *Curr. Med. Res. Opin.* **2011,** *7,* 907–919.
388. Nyholm, D.; Askmark, H.; Gomes-Trolin, C.; Knutson, T.; Lennernas, H.; Nystrom, C.; Aquilonius, S. M. Optimizing Levodopa Pharmacokinetics: Intestinal Infusion Versus Oral Sustained-Release Tablets. *Clin. Neuropharmacol.* **2003,** *26,* 156–163.
389. Nyholm, D.; Nilsson Remahl, A. I.; Dizdar, N.; Constantinescu, R.; Holmberg, B.; Jansson, R.; Aquilonius, S. M.; Askmark, H. Duodenal Levodopa Infusion Monotherapy vs. Oral Polypharmacy in Advanced Parkinson Disease. *Neurology* **2005,** *64* (4), 216–223.
390. Olanow, C. W.; Kieburtz, K.; Odin, P.; Espay, A. J.; Standaert, D. G.; Fernandez, H. H.; Vanagunas, A.; Othman, A. A.; Widnell, K. L.; Robieson, W. Z.; et al. Continuous Intrajejunal Infusion of Levodopa-Carbidopa Intestinal Gel for Patients With Advanced Parkinson's Disease: A Randomised, Controlled, Double-Blind, Double-Dummy Study. *Lancet Neurol.* **2014,** *13* (2), 141–149.
391. Hauser, R. A.; Ellenbogen, A. L.; Metman, L. V.; Hsu, A.; O'Connell, M. J.; Modi, N. B.; Yao, H. M.; Kell, S. H.; Gupta, S. K. Crossover Comparison of IPX066 and a Standard Levodopa Formulation in Advanced Parkinson's Disease. *Mov. Disord.* **2011,** *26* (12), 2246–2252.
392. Hauser, R. A.; Nausieda, P.; Ondo, W.; Espay, A. J.; Hsu, A.; O'Connell, M.; Kell, S.; Gupta, S. Double-Blind, Controlled Trial of IPX066, A Novel Carbidopa–Levodopa Extended-Release Formulation, in Advanced Parkinson's Disease (ADVANCE-PD Trial). Movement Disorder Society Meeting 2011 (late breaking abstract LB9).
393. Olanow, C. W.; Obeso, J. A.; Stocchi, F. Continuous Dopamine Receptor Treatment of Parkinson's Disease: Scientific Rationale and Clinical Implications. *Lancet Neurol.* **2006,** *5,* 677–687.

Relevant Websites

http://www.neurodegenerationresearch.eu/—EU Joint Program-Neurodegenerative Disease Research.
https://www.msif.org/—International MS Federation.
http://msj.sagepub.com/—Multiple Sclerosis Journal.

5.15 Lupus and Lupus Overlap Diseases: Emerging Therapies

VC Kyttaris, Beth Israel Deaconess Medical Center, Boston, MA, United States

© 2017 Elsevier Ltd. All rights reserved.

5.15.1	**Introduction**	474
5.15.2	**Loss of Tolerance and Development of Systemic Autoimmunity**	475
5.15.3	**Etiology and Pathophysiology of SLE**	477
5.15.4	**Clinical Presentation of SLE: Challenges for Clinical Trial Design**	477
5.15.5	**Current Therapeutic Paradigm in SLE**	479
5.15.6	**Novel Lupus Therapeutics: The Role of Small Molecules**	479
5.15.6.1	Kinases and Phosphatases	479
5.15.6.1.1	Janus kinases/signal transducer and activator of transcription	479
5.15.6.1.2	Spleen tyrosine kinase	481
5.15.6.1.3	Rho kinase (ROCK)	482
5.15.6.1.4	Calcium/calmodulin-dependent kinase IV	482
5.15.6.1.5	Calcineurin/nuclear factor of activated T cells	483
5.15.6.1.6	Mammalian target of rapamycin	484
5.15.6.1.7	Phosphaditylinositol-3 kinase	484
5.15.6.1.8	Bruton's tyrosine kinase	485
5.15.6.2	Modifiers of Chromatin	486
5.15.6.3	Proteasome Inhibitors	487
5.15.6.4	Quinoline Derivatives	488
5.15.7	**Conclusion and Future Directions**	489
References		490
Relevant Websites		494

Abbreviations

AP-1 Activator protein-1
BCR B-cell receptor
BICLA BILAG-based combined lupus assessment
BILAG British Isles Lupus Assessment Group
BLyS B lymphocyte stimulator
Btk Bruton's tyrosine kinase
CaMK Calcium/calmodulin-dependent kinase
CREM c-AMP regulatory element modulator
DNMT DNA methyl-transferase
HDAC Histone deacetylase
IFN Interferon
IL Interleukin
ITAM Immunoreceptor tyrosine activating motifs
ITP Immune thrombocytopenia
Jak Janus kinase
MHC Major histocompatibility complex
MS Multiple sclerosis
MTOR Mammalian target of rapamycin
NAC *N*-acetyl cysteine
NFAT Nuclear factor of activated T cells
NZBW F1 F1 mouse from crossing New Zealand Black and New Zealand White mice
PASLI p110δ Activating mutation causing senescent T cells, lymphadenopathy, and immunodeficiency
PI3K Phosphaditylinositol 3-kinase
RA Rheumatoid arthritis
SLE Systemic lupus erythematosus
SLEDAI SLE disease activity index
SRI SLEDAI response index
STAT Signal transducer and activator of transcription
Syk Spleen tyrosine kinase
TCR T-cell receptor
Th T-helper cells
TLR Toll-like receptor
Treg Regulatory T cells
TSA Trichostatin A

5.15.1 Introduction

One can broadly categorize the diseases that affect the immune system into states of immune deficiency and those of unnecessary activation. The latter category of diseases can be further divided into allergic, autoimmune, and the more recently described category of autoinflammatory diseases. Autoimmunity is characterized by an aberrant immune attack to organs and tissues without a clear initiating or sustaining external factor, such as an allergen or a microbe.[1] Moreover, although genetics contribute to the pathogenesis of autoimmune diseases, most diseases are not caused by single-gene mutations as is the case for autoinflammatory conditions.[2]

It is precisely this characteristic of autoimmunity that makes treatment challenging; there is no underlying mutation that can be either directly or indirectly targeted; there is no allergen that can be avoided or desensitized against; there is no missing immunoglobulin that can be substituted. The events that eventually lead to the development of autoimmune diseases are rather slow without a specific causative factor readily identifiable in the vast majority of cases. Although epidemiologic and genetic studies have shed little light into the etiology of these diseases, the use of both animal models and in vitro studies using blood cells and biopsy materials from patients has identified several key pathways that are important for the pathogenesis of these diseases.

This lack of a definite cause has made the treatment of these diseases to rely on nonspecific suppression of the activated immune system, in hopes that after a period of time the immune-suppression can be stopped with the immune system having reset itself in a more normal condition. This strategy causes significant problems, not the least of which are overwhelming infections in the immunosuppressed host. Recent advances in our understanding of the pathogenesis of certain autoimmune diseases though have allowed the design of rationale therapies that target key aspects of the autoimmune response allowing for control of the disease without global immune-suppression. This approach has already yielded significant improvements in the treatment of certain conditions such as rheumatoid arthritis (RA)[3] and vasculitis.[4] It has to be emphasized that these treatment regimens remain disease modifying and not curative as the autoimmune response is suppressed but not necessarily abolished.

In the case of systemic lupus erythematosus (SLE), target-specific disease-modifying therapies are still elusive. Several new molecules have been studied in animal models and early human studies with promising results leading for the first time after several decades to the approval of a new medication for SLE, with albeit modest efficacy. To understand the role of new therapeutics in SLE, we will discuss herein SLE pathogenesis, the current treatment paradigm, and the approach to move new medications from the bench to the bedside.

5.15.2 Loss of Tolerance and Development of Systemic Autoimmunity

Systemic autoimmunity is a disease that primarily arises from a dysfunctional adaptive immune system. The adaptive immune system is comprised by T and B lymphocytes that recognize foreign material in a specific manner and are able to mount well-coordinated responses to eliminate threats.

The central axiom of the nascent field of immunology in the early 21st century was that the main characteristic of adaptive immune system is the recognition of one's self from foreign material. Autoimmunity, or as it was called then "horror autotoxicus," happened when the immune system started recognizing self-proteins as foreign resulting in inflammatory damage of the tissues and organs where those proteins were found. This theory had its own merits but failed to recognize that the healthy immune system does not only contain specialized cells and molecules that recognize foreign proteins–antigens but also self-antigens. Rather than completely eliminating these self-reactive cell clones and antibodies, the immune system limits their reactivity by employing a variety of checks and balances. This mechanism is called immunologic tolerance and does not only refer to self-antigens but also any antigen that the immune system has learned to accept as nonharmful (reviewed in Ref. 5). Tolerance is achieved primarily in the central lymphoid organs, that is, the bone marrow for B cells and the thymus for T cells. In Figs. 1 and 2 the two-step process of T-cell education is shown. T cells that are not useful by not being able to recognize any antigen or T cells that react very strongly against self-antigens are eliminated from the lymphocyte pool and never populate the secondary immune organs, that is the spleen

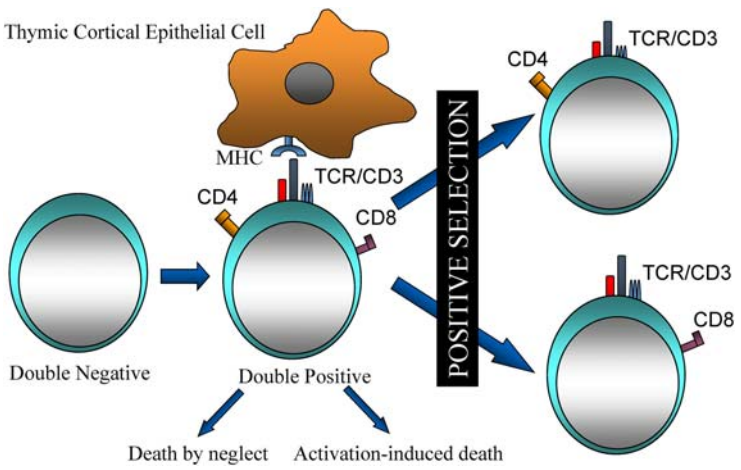

Fig. 1 Positive selection of T cells in the thymus. Immature T cells that have yet to express surface markers (double negative) evolve into TCR/CD3+CD4+CD8+ double positive T cells. At this stage the T cell has to prove that is functioning properly by interacting with the MHC complex on epithelial cells in the thymus. Incompetent T cells that do not recognize the MHC or cells that overreact to it die by neglect or activation-induced cell death. The double positive T cells that are selected become functional CD3+CD4+ or CD3+CD8+ T cells.

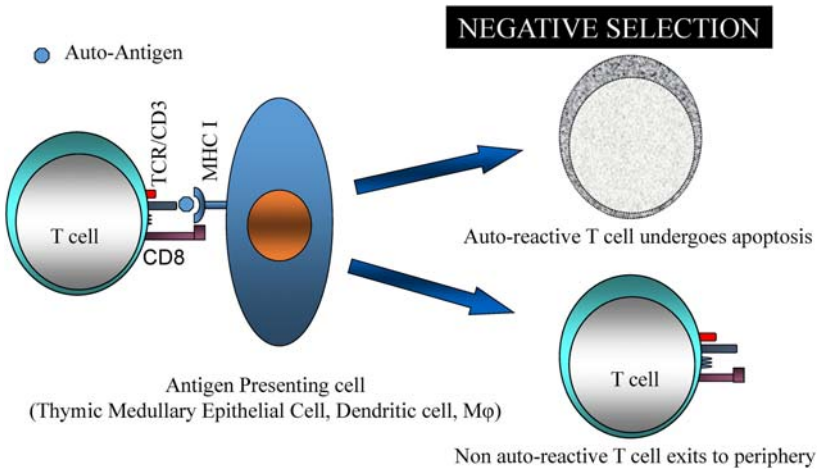

Fig. 2 Negative selection. Following the positive selection process the selected CD3+CD4+ or CD3+CD8+ T cells (here the CD8+ are shown) interact in the thymus with self-antigens that are presented to them by local cells. The cells that do not recognize self-antigens migrate to the secondary lymphoid organs (spleen, lymph nodes), while the autoreactive cells undergo cell death (apoptosis).

and lymph nodes. B cells undergo similar but not identical education in the bone marrow. Some T (and B) cells that are self-reactive do escape though from the primary (central) lymphoid organs, and hence a separate set of peripheral tolerance mechanisms is needed. One of the most important mechanisms is the regulatory T cells (Treg) that suppress aberrant activation of T cells and keep the immune system balanced.[6]

These regulatory check and balances can fail at various levels leading from benign autoimmunity to the appearance of detectable autoimmune reactions, inflammation, and end-organ damage. The first step in that process is the escape of autoreactive cells or clones (T or B cells) of the adaptive immune system from the regulatory constraints of the immune system: a process called loss of tolerance. This can be detected by the presence of autoantibodies and cytokines in the blood of otherwise healthy individuals as they are on their way to develop systemic autoimmune disease. Indeed, autoantibodies such as antinuclear or Sjogren syndrome-associated antibodies exist in the serum of patients with SLE several years before the clinical presentation of the disease.[7] In the second phase of this process, the autoimmune reaction evolves with recruitment of effector cells and molecules in various tissues resulting in inflammation. This second phase, called disease flare, besides causing symptoms and signs of the disease, if left untreated, may result in permanent tissue damage. The regulatory mechanisms of the immune system can limit the disease flare even without pharmacologic intervention bringing about the third phase of the disease, a period of clinical quiescence until the next flare. Some autoimmune diseases such as multiple sclerosis (MS) behave in this relapsing-remitting way, while others such as systemic vasculitis do not spontaneously remit without therapy. SLE has relapsing-remitting characteristics, but severe flares, such as nephritis, do not remit without therapeutic interventions (Fig. 3). The factors that contribute to the generation of autoimmunity (phase I), disease flare (phase II), and spontaneous resolution (phase III) are unclear for most autoimmune diseases in general and SLE in particular. In the case of SLE, the interplay between genetics, hormonal factors,[8] and viruses such as Ebstein Barr (EBV)[9] have been implicated in the development of autoimmunity, while ultraviolet light has been shown to cause disease flares.[10] It has to be noted that in the vast majority of cases of SLE neither the initiating nor the sustaining factors are identifiable.

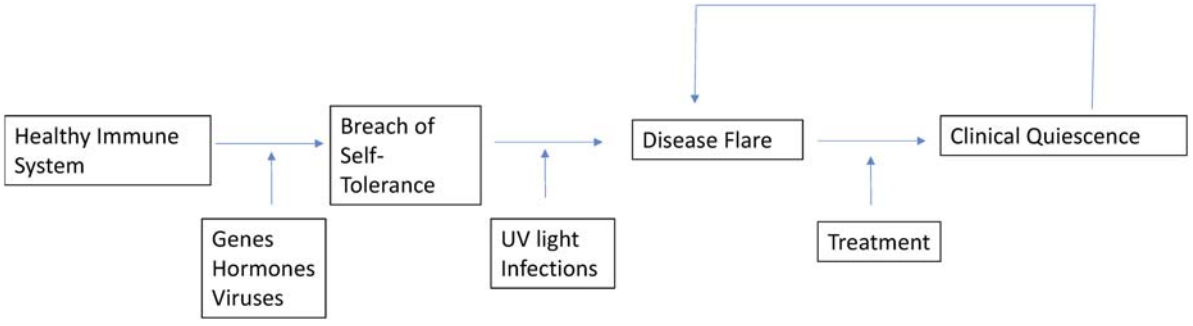

Fig. 3 Schematic representation of the etiology and pathophysiology of SLE.

5.15.3 Etiology and Pathophysiology of SLE

SLE is a relatively rare disease with a prevalence of 0.04–0.05% in the United States[11] and affects primarily women of childbearing years. Epidemiologic studies suggest that SLE is more common in women of Hispanic or African ancestry than Northern Europeans.[12] Genome-wide searches recognized several genes that increase the risk for SLE. Besides a strong association with the major histocompatibility complex (MHC) class II molecules DR2 and DR3, several genes that code for immune-regulatory molecules are associated with the disease (reviewed in Ref. 13). Genes are only one part of the puzzle of SLE pathogenesis though; as discussed above hormonal, environmental, and infectious factors have been implicated in disease pathogenesis, but their relative importance and contribution is heatedly debated. The rarity of the condition, the heterogeneity of presentation, and the long preclinical phase make the determination of disease etiology difficult.

Although lupus etiology is still unclear, the use of both murine models that approximate lupus and ex vivo studies using peripheral blood cells from patients with SLE and biopsy material from inflamed skin and kidneys has led to significant breakthroughs in our understanding of how damage occurs.

The sine-qua-non of SLE is the production of autoantibodies against cellular components and in particular DNA and RNA containing protein complexes. The immune complexes that are generated through the binding of these high-affinity antibodies to their cognate antigens are deposited in the target tissues and especially in the glomerular basement membrane of the kidney and the dermal–epidermal junction of the skin. The antibodies that are thought to be particularly important in this process are anti-double-stranded DNA antibodies. The levels of these antibodies in the serum rise and fall in parallel to disease activity and in particular kidney inflammation[14]; this makes their measurement particularly important for prediction of flares and response to therapy. The immune complexes either after depositing or while circulating lead to complement system activation, which in turn causes accumulation of inflammatory cells, initially polymorphonuclear leucocytes and later lymphocytes, in the tissues. Moreover, mononuclear cells either circulating or resident in the tissues get activated by the immune complexes or complement and produce an array of cytokines and chemokines that perpetuate the inflammatory response. The accumulation and deposition of all these cells and soluble mediators in the tissues leads to their eventual damage; characteristically this takes the form of destruction of the glomerular tuft in the kidney, and untreated or after repeated flares may lead to kidney failure.[15]

The production of autoantibodies by specialized B cells that become antibody-forming cells (AFC) is key for the initiation of the autoimmune response in lupus. The B-cell population as it matures in the bone marrow and gradually exits to the periphery contains autoreactive clones that are eliminated by a variety of mechanisms such as lack of help by other cells (such as T cells), or editing of their receptors. Extensive work in both animals and humans has clearly shown that autoreactive B cells can escape these checkpoints[16] during their ontogeny and eventually become autoreactive AFC that produce high-affinity pathogenic antibodies such as anti-dsDNA antibodies. The cytokine B lymphocyte stimulator (BLyS) plays an important role in the survival and maturation of early autoreactive B cells. Indeed, BLyS transgenic mice develop a lupus-like illness.[17] After extensive preclinical and clinical studies, the anti-BLyS antibody belimumab was found effective in reducing disease activity in patients with active lupus, becoming in 2011 the first drug to be approved for SLE after several decades. Complete elimination of mature B cells in SLE patients though using the depleting anti-CD20 antibody rituximab did not improve the outcomes when added to standard of care[18] suggesting a more complex picture.

The failure to contain autoreactive B cells is not only due to intrinsic B-cell factors but also to aberrant T cell:B cell interaction. T cells are critical for the production of pathogenic high-affinity autoantibodies by B cells through help they provide via a set of complementary molecules termed costimulatory molecules (Fig. 4). One such molecule is CD154 (also known as CD40 ligand, CD40L) that is expressed on activated T cells and is essential for the maturation, differentiation, and eventual antibody production by activated B cells. CD154 was therefore an early target for biologic therapy in SLE; BG9588, a humanized anti-CD154 antibody, was injected in patients with lupus nephritis[19] showing effectiveness in improving immunologic and kidney injury parameters. A few patients unfortunately developed thromboembolic events, possibly due to off target effects, halting further development of this therapy. Despite this setback, several anti-CD154 are currently in early stages of development.

Circulating immune complexes and/or nucleic acids can directly activate immune cells that bear Fc receptors and toll-like receptors (TLR), respectively. The monocyte system as well as B cells can therefore be activated via this mechanism as they express both types of receptors on their surface. The activated cells in turn produce an array of proinflammatory cytokines. One such cytokine that has been recognized to be ubiquitously expressed in SLE is interferon α (IFNα). Indeed, circulating white cells in the blood of patients with SLE have upregulated a certain set of genes that are influenced by IFNα; This transcriptional signature, called the interferon signature, may be important for the pathophysiology of the disease as attempts to block IFNα showed promising results in early trials.[20]

The complex autoimmune response that underlies SLE pathophysiology is schematically summarized in Fig. 4. It is the interaction of this abnormally activated system with the tissue targets that leads to the signs and symptoms of lupus that can be highly variable, difficult to treat, and even more challenging to predict.

5.15.4 Clinical Presentation of SLE: Challenges for Clinical Trial Design

Broadly autoimmune diseases are divided into organ specific, such as Hashimoto's thyroiditis or MS, and systemic, such as SLE. In the first category the autoimmune response targets a small number of localized self-antigens, while in the latter the

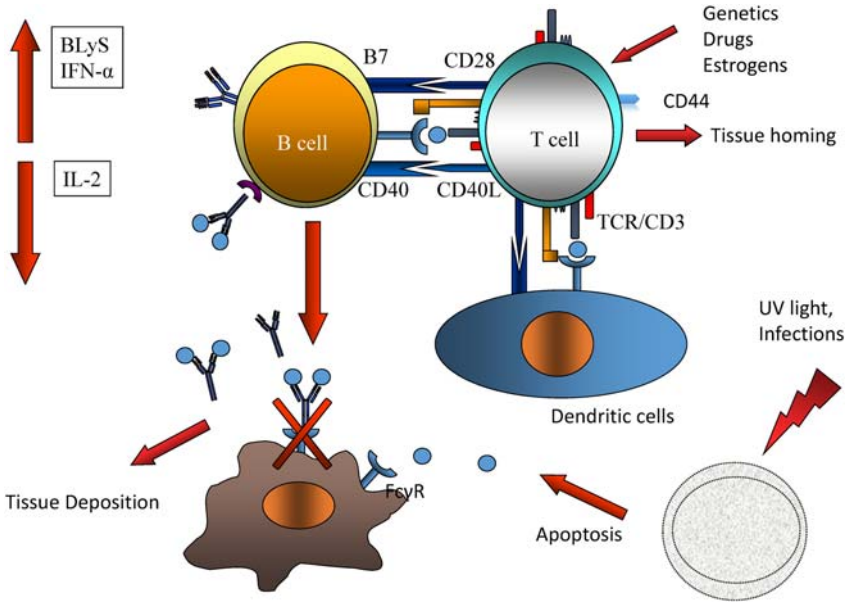

Fig. 4 The pathophysiology of systemic lupus erythematosus.

inflammatory response is widespread with numerous antigenic targets. SLE is the prototypic systemic autoimmune disease and is characterized by the presence of numerous autoantibodies against self-antigens that are primarily found in the nuclei of cells.[21] This complexity inevitably leads to a heterogeneous clinical presentation. Various organs and tissues are affected with the skin, joints, serosal surfaces (pericardium, pleura), kidneys, nervous system, and hematologic systems (neutrophils, red cells, platelets) being the most common.[22] Moreover, the type of tissue inflammation varies among individuals; for example, there are six different classes of lupus nephritis that differ widely in their presentation, prognosis, and treatment[23]; or the discoid variant of lupus dermatitis that leads to skin scarring differs substantially from the generally nonscarring malar rash.

A consensus has been reached in what constitutes SLE by using a set of criteria that are useful in clinical settings and indispensable in clinical trial design.[24] It is important to stress that a significant number of patients have a clinical picture consistent with SLE but do not fulfill the strict SLE criteria. Moreover, patients may exhibit clinical and laboratory findings that are consistent with more than one systemic autoimmune disease, such as lupus arthritis and myositis or skin lupus and erosive (rheumatoid) arthritis. These overlap syndromes can vary in severity and manifestations and are generally treated similar to the prototypic syndrome, that is, RA or SLE. A well-described overlap syndrome is mixed connective tissue disease, which is defined by the presence of an autoantibody against ribonuclear protein[25] and shares clinical characteristics with SLE, RA, myositis, and scleroderma.

Given these disease characteristics, rarity, heterogeneity, and unpredictability, clinical trial design has been challenging. The most successful trials have been the ones targeting the subgroup of patients with lupus nephritis. Class III and IV nephritis patients have similar enough presentations and courses of their disease to make the design of clinical trials easier. Starting in the 1970s, patients with nephritis were treated using unifying outcomes such as levels of creatinine concentrations in the serum, a measurement of kidney filtrating capability, and protein concentration in the urine, a measurement of glomerular membrane damage. The real challenge has been though to design an outcome measure for nonrenal lupus. At the end of the last century, the SLE disease activity index (SLEDAI) was validated as a good albeit imperfect composite index to capture disease activity in almost all the systems affected by SLE.[26] Another more complicated index, the British Isles Lupus Assessment Group (BILAG),[27] has also been extensively validated. These two indexes were used in the design of two new outcome measures that aim at capturing broadly disease activity changes in various tissues and organs in SLE patients. The SLEDAI-based SRI (SLEDAI response index) and the BILAG-based BICLA (BILAG-based Combined Lupus Assessment) are nowadays the standard outcome measure in clinical trials of generalized lupus. An improvement of the SLEDAI after treatment by 4, 5, or 6 points is regarded as significant (SRI-4, 5, or 6, respectively) allowing to report the outcome of a placebo controlled clinical trial in a meaningful manner. For example, in the study of the BLyS inhibitor belimumab in SLE, 52 weeks into treatment, 58% of patients on belimumab had an improvement in their baseline SLEDAI by 4 points or more (SRI-4) as opposed to 44% of the placebo group; this outcome led to the approval of belimumab for the treatment on nonrenal lupus.[28]

Besides the composite indexes SRI and BICLA, outcome measures pertaining specifically to tissue targets such as the kidneys (discussed earlier), skin (area and extent of skin damage), and joints are also significant. In addition, therapeutic trials are also evaluating future flare prevention and corticosteroid sparring. These new unifying outcome measures have allowed the exponential increase of clinical trials in SLE testing several biologics and small molecules.

5.15.5 Current Therapeutic Paradigm in SLE

As described earlier, the current therapeutic approaches in SLE consist primarily of nonspecific immune-suppressive medications. Treatment aims at (a) inducing remission of acute flares, (b) reducing frequency of flares, and (c) ultimately preventing organ and tissue damage.

Since their discovery, corticosteroids have been the mainstay of treatment of SLE. As a general principle, corticosteroids are used for induction of remission of all but the very mild lupus flares, in which case nonsteroidal antiinflammatory medications and antimalarial medications are used. In moderate and severe lupus flares, besides using higher doses of corticosteroids, remission is achieved with the concomitant use of immune-modulator drugs such as mycophenolate, azathioprine, and methotrexate. In very severe flares, primarily affecting the kidneys and central nervous system, the alkylating agent cyclophosphamide is used as well. The use of immune-modulator drugs together with steroids has not been conclusively shown to improve short-term outcomes but helps (a) reduce the amount of corticosteroids used and (b) bridge the patient's treatment to the consolidation phase of therapy that may last for years following the induction phase.

These therapeutic phases have been best studied in patients who present with lupus nephritis. The current standard of care in these patients consists of a 6-month induction, followed by (at least) 18 months of consolidation. The goal of the induction period is to normalize kidney function and to prevent damage in the kidneys as measured by the amount of protein that is abnormally found in the urine. The standard of care for the induction period consists of corticosteroids and cyclophosphamide or corticosteroids and mycophenolate mofetil. In the consolidation period that lasts for at least one and a half years, patients are treated with mycophenolate mofetil or azathioprine. The goal of the treatment is complete renal remission characterized by normal kidney function and minimal proteinuria.

5.15.6 Novel Lupus Therapeutics: The Role of Small Molecules

In the era of targeted therapies, soluble mediators, such as cytokines and chemokines, and surface molecules are targeted primarily using an antibody or a modified decoy ligand against them. These biologic drugs have revolutionized the treatment of several autoimmune diseases, such as RA or Crohn's disease, but have been only marginally successful in SLE as discussed earlier.

The success of tofacitinib (**1**) in treating RA by blocking the Janus kinases (Jak)[29] clearly shows that blocking signaling molecules that are distal to a receptor:ligand interaction can be a viable alternative to biologics. Below we will discuss, important signaling pathways that affect the (auto)-immune response, and the effectiveness of small molecular inhibitors targeting them.

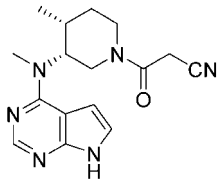

tofacitinib, **1**

5.15.6.1 Kinases and Phosphatases

5.15.6.1.1 Janus kinases/signal transducer and activator of transcription

The cytokine milieu influences the way immune cells respond to antigenic stimuli. In the so-called three-signal model, lymphocytes bind to a presented antigen in a specific manner through their receptor; for this first signal to translate into a productive immune response, a second costimulatory response has to be delivered by a molecule on the antigen-presenting cell to its ligand on the lymphocyte. This response is further refined by circulating cytokines that bind to their receptor. This third signal makes the lymphocyte respond in different ways depending on the circumstances: for example, in the presence of interleukin-6 (IL-6), T cells may differentiate into proinflammatory T-helper cells-17 (Th17 cells), while in the presence of TGF-β, the same specificity T cells may differentiate into counter-inflammatory Treg cells.

There are several types of cytokine receptors that employ different intracytoplasmic molecules to transduce the signals inwards. Type I/II cytokine receptors use the Jak/signal transducer and activator of transcription (STAT) molecules (reviewed in Ref. 30). Numerous cytokine receptors belong to this category and regulate both proinflammatory (e.g., IL-6, IL-21, IL-23, IL-22) and regulatory processes (e.g., IL-2, IL-10). Importantly for SLE, Jak/STAT mediate IFNα signaling. This system is also used by hormone and hormone-like molecules that direct important functions, such as hematopoiesis,[31] which may result in significant side effects such as neutropenia or anemia when this system is blocked. There are four different Jak (Jak1, Jak2, Jak3, and Tyk2) and six STAT molecules. Proinflammatory molecules employ primarily Jak1 and Jak3, while erythropoietin and other hematopoietic hormones signal through Jak2.

Following the realization that several of the proinflammatory cytokines such as IL-6 and IL-23 that play a role in autoimmune diseases, signal through the Jak/STAT pathway, the Jak inhibitor tofacitinib (**1**) was successfully introduced as a potent treatment in RA.[29] Tofacitinib (3-((3R,4R)-4-methyl-3-(methyl(7H-pyrrolo[2,3-d]pyrimidin-4-yl)amino)piperidin-1-yl)-3-oxopropanenitrile, **1**) is a potent inhibitor of Jak3 but also blocks less potently Jak1 and Jak2, theoretically blocking more IL-2, IL-4, and IL-21 than IL-6 signaling. Baricitinib (2-(3-(4-(7H-pyrrolo[2,3-d]pyrimidin-4-yl)-1H-pyrazol-1-yl)-1-(ethylsulfonyl)azetidin-3-yl)acetonitrile, **2**), a preferential Jak1/2 inhibitor, is also efficacious in RA, even in severe refractory cases.[32] The side effects of these compounds besides infections included elevation of cholesterol and cytopenias. Generally, these are potent antiinflammatory compounds that contain RA activity within few weeks from the initiation of therapy.

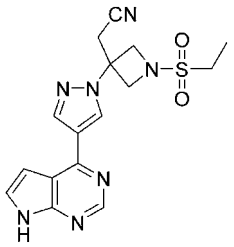

baricitinib, **2**

In the case of SLE, several pathogenic cytokines, such as the IFNs, Th17 related cytokines (IL-6, IL-23), and antibody production inducing cytokines (IL-21) signal through this Jak/STAT system. Tofacitinib (**1**) that blocks Jak1 and Jak3 is therefore an attractive option for SLE. In the murine lupus model MRL/*lpr*, tofacitinib (**1**), given before disease onset, resulted in a significant improvement of nephritis, by affecting antibody and proinflammatory cytokine production.[33] It did result in a decrease in red blood cell concentration in the blood, suggesting that it does block to some extent Jak2 as well. Tofacitinib (**1**) was effective even after the disease onset, suggesting that it may be beneficial in patients with SLE as well.

Jak/STAT inhibition can also be achieved by blocking the STAT molecules, potentially bypassing the nonspecific effects of Jak inhibitors. The importance of this pathway in SLE was shown in an early study of lupus-prone B6.Sle1ab mice, which had increased STAT3 expression in their B cells.[34] STAT3 was found to be essential for antinuclear antibody production, a hallmark of the disease in these mice. Later it was found that SLE T-cell migration to target tissues depends on STAT3 that is abnormally upregulated.[35] STAT3 plays a broader role in T-cell function, being critically important for the development of the proinflammatory Th17 subset,[36] T follicular helper cells,[37] and Treg cells[38]; these T-cell subsets are central in the pathophysiology of SLE in both humans and murine models of the disease. The importance of STAT3 in SLE was further underlined by a study comparing the genetic signatures of kidney tissues from three different murine models of lupus[39]; this study identified STAT3 as the top gene-regulating candidate in these mice. Stattic (6-nitro-1-benzothiophene 1,1-dioxide; 6-nitrobenzo[b]thiophene 1,1-dioxide, **3**), a STAT3 blocker, delayed the onset of disease in MRL/*lpr* mice.[40] Moreover, Stattic blocked the migration of T cells from SLE patients in response to chemokines, recapitulating earlier findings using gene silencing of STAT3. These preclinical results supported the inhibition of this pathway in SLE.

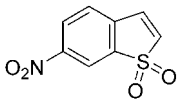

stattic, **3**

The first trial of Jak inhibition in SLE was done using specific Jak1 inhibitor solcitinib (**4**); the patients enrolled in the study had high baseline interferon signature,[41] as high IFNα is thought to play a role in SLE pathogenesis and it signals through Jak. This trial was stopped prematurely as there was no change in the IFN-related gene expression in an interim analysis. Two patients developed a reversible syndrome of fever, eosinophilia, and liver test abnormalities (DRESS syndrome).[42] The negative result of the study does not reflect on Jak inhibition in general as this compound failed to show biologic activity at least as this pertains to the IFN system. Further studies are needed given the positive preclinical data to assess the clinical usefulness of Jak inhibitors in SLE.

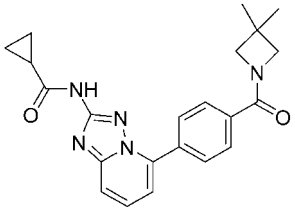

solcitinib, **4**

5.15.6.1.2 Spleen tyrosine kinase

The tyrosine kinase Syk (spleen tyrosine kinase) is a member of Src kinases and is expressed in various types of hematopoietic cells, such as T cells, B cells, osteoclasts, monocytes, and neutrophils (reviewed in Ref. 43). A wide range of membrane-bound receptors on these cells closely associate with signaling molecules that bear the immuno-receptor tyrosine activating motifs (ITAM) structures containing the amino acid tyrosine. Once the receptor engages its ligand, tyrosines are phosphorylated and recruit Syk by binding to its Src homology 2 (SH2) domain. The engaged Syk activates downstream molecules such as Vav, phospholipase C-γ2 (PLCγ2), and PI3 kinase among others, starting a transcriptional program that differs depending on the cell type and surface receptor.

Receptors that are known to engage Syk via their ITAM include the Fc receptors that are expressed on B cells, monocytes, and neutrophils among other cells. These receptors engage IgG and are pivotal in phagocytosis of opsonized material, an essential step in elimination of infectious agents. Moreover, Syk associates with the main receptor of B cells, the B-cell receptor (BCR),[44] and transduces an activating signal inwards upon engagement of the BCR with its cognate antigen. In addition to the process of recognizing exogenous material, Syk kinase may also play a role in neutrophil effector functions that are necessary for host defense.[45]

Given the widespread expression of Syk in inflammatory cells, it became one of the first treatment targets in autoimmune diseases. The small molecule *N*4-(2,2-dimethyl-3-oxo-4H-pyrid[1,4]-oxazin-6-yl)-5-fluoro-N2-(3,4,5-trimethoxyphenyl)-2,4-pyrimidinediamine (R406, **5**)[46] blocks Syk kinase activity and was shown to be effective in vitro and in animals in inhibiting Syk-mediated signaling in a variety of cells. Given the importance of Syk in B-cell signaling through the BCR and antibody responsiveness through the Fc receptors, R406 (**5**) was developed into fostamatinib (**6**), a small-molecule kinase inhibitor with the intention to treat several autoimmune diseases. Late-phase clinical trials in patients with RA with fostamatinib (**6**) although encouraging initially showed a rather modest effect.[47] The main side effects included neutropenia and increase in the blood pressure. Currently the RA program has been abandoned, but trials are conducted in patients with immune thrombocytopenia (ITP) and hemolytic anemia.

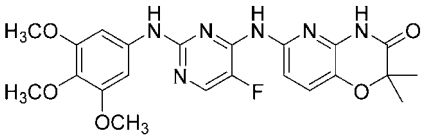

R406, **5**

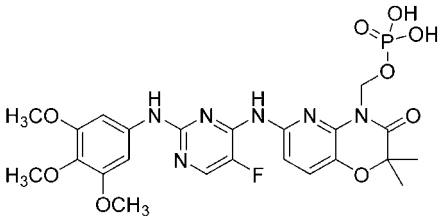

fostamatinib, **6**

In SLE, Syk was found to be abnormally expressed in peripheral blood T cells[48] from patients with both active and inactive SLE as part of a broader "rewiring" of the surface T-cell receptor (TCR) that employed FcRγ in lieu of CD3ζ chain as the main ITAM-containing signaling molecule. This change in SLE T cells is not merely substitution of one molecule for another but has significant implications in the way the SLE T cells handle cognate signals that are transmitted through their TCR. SLE T cells mobilize calcium in a very robust way once activated,[49] thus exhibiting an overexcitable phenotype as compared to healthy T cells; this phenotype is in turn associated with a different transcriptional program that enhances T cell help to B cells and production of proinflammatory cytokines.[50]

SLE therefore stands out from other autoimmune diseases in that Syk is not only playing a role in the production and handling of antibodies and immune complexes but is ectopically expressed in T cells and is a pivotal molecule in their aberrant function. A series of in vitro experiments showed that R406 (**5**) can indeed block TCR-mediated signaling in SLE but not healthy T cells.[51] Deng et al then used R788 (R406 orally available prodrug, **6**) to treat lupus-prone mice before the onset of the disease but also after disease initiation.[52] The investigators showed that there was complete abrogation of the inflammatory damage to the kidneys and the skin even when the drug was given after the disease was established in the target organs. Importantly, this effect of Syk inhibition persisted for several weeks after the discontinuation of the treatment.

Syk overexpression in SLE T cells and its prominent role in antibody production and handling by the B cell and monocyte compartments make it a very interesting therapeutic target in SLE. The preclinical studies support this line of thought and provided the necessary rationale for human trials that although initially planned have yet to be conducted.

5.15.6.1.3 Rho kinase (ROCK)

Rho kinase (ROCK) is an important cytosolic node that integrates activating signals from surface receptors leading to both cell proliferation and migration. ROCK is a 160 KDa serine/threonine kinase,[53] that is the target of the small GTPase Rho. There are two isoforms, ROCK1 and ROCK2, that are widely distributed in tissues, such as the eye, the central nervous system, and the spleen. Once Rho binds to ROCK, ROCK is activated and leads to downstream phosphorylation of target proteins that control the cytoskeleton arrangement and gene transcription.

The first indication that ROCK may be important in SLE came after the observation that SLE T cells freshly isolated from patients showed an enhanced potential to adhere to hyaluronic acid migrate in response to chemokines.[54] This was proven to be secondary to the overexpression of the surface molecule CD44 that binds hyaluronic acid and spontaneous cytoskeletal rearrangements that enabled the formation of polar caps. The ezrin/radixin/moiesin (ERM) protein is the key molecule that precipitates those two processes. Indeed, phosphorylated ERM-containing T cells were present not only in the peripheral blood of patients but also in the kidneys of patients with nephritis. ROCK is directly responsible for the phosphorylation of ERM, and in vitro ROCK inhibition using the inhibitor Y27632 (**7**) resulted in a reversal of this process and "normalization" of the SLE T-cell phenotype. The proposed model postulated that TCR-mediated signals activated ROCK which through ERM phosphorylation enhanced the ability of SLE T cells to adhere and migrate to tissues.

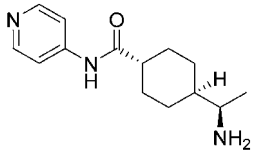

Y27632, **7**

Parallel work in murine lupus models showed that ROCK2 phosphorylates the transcription factor interferon regulatory factor 4 (IRF4), an important factor for the polarization of T cells into the proinflammatory subset Th17.[55] ROCK2 through regulation of the IRF4 enables the spontaneous production of IL-17 and IL-21 by murine lupus T cells. IRF4 also influences B-cell responsiveness to IL-21,[56] an important step for the production of autoantibodies. ROCK therefore is playing a broad role in the aberrant T:B cell interaction in lupus and the production of high-affinity pathogenic autoantibodies.

The ROCK inhibitor fasudil (5-(1,4-diazepan-1-ylsulfonyl) isoquinoline, **8**) is the first inhibitor extensively studied in murine lupus. Fasudil (**8**) was shown to be efficacious when given to female MRL/*lpr* mice[55] and F1 mouse from crossing New Zealand Black and New Zealand White mice (NZBW F1 mice),[57] both murine models of lupus. The effect was more pronounced when given early in the disease course in NZBW F1 mice, suggesting a protective role against the disease; the effect on established nephritis though, where the cells have already migrated in the kidney may not be as pronounced. Fasudil (**8**) causes also vasodilation, and it is for this property that it has been evaluated in clinical trials of patients with angina pectoris[58] and pulmonary hypertension.[59] Fasudil (**8**) was generally well tolerated in these studies with only mild-to-moderate side effects attributable to the drug. A small but statistically significant elevation of the creatinine was observed in the angina pectoris study. Fasudil (**8**) was also tried in patients with vasospasm (Raynaud's) due to systemic sclerosis.[60] Fasudil (**8**) did improve blood flow to the digital arteries that are narrowed in this condition but did not have a significant clinical effect in this short trial.

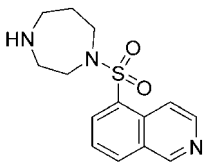

fasudil, **8**

Overall, ROCK inhibition has clear antiinflammatory effects blocking the autoimmune response at several checkpoints (T-cell differentiation, T:B cell interaction, lymphocyte migration) in preclinical studies. Its added vasodilatory effect is of particular interest as it can improve compromised blood flow in patients with systemic autoimmune diseases. Fasudil (**8**), a clinically tried drug with acceptable safety profile, represents therefore an attractive agent for trials in SLE.

5.15.6.1.4 Calcium/calmodulin-dependent kinase IV

Signaling through the abnormally wired TCR that employs the Syk kinase as discussed earlier is associated with increased calcium influx into the T-cell cytosol. Early on it was observed that one of the kinases that depends on calcium, the serine/threonine kinase calcium/calmodulin-dependent kinase IV (CaMKIV) but not CaMKII, is abnormally activated in SLE T cells; it is not only found as expected in the cytosol of SLE T cells but also in the nucleus.[61] There it associates with the transcription factor c-AMP regulatory element modulator (CREM).[62] CREM in turn limits the production of the regulatory IL-2 cytokine and boosts the production of the proinflammatory cytokine IL-17.[63] The activation of CaMKIV in SLE T cells could be replicated in normal T cells by incubating

them with SLE patient-derived serum supporting the notion that the inflammatory milieu in SLE can prime the T cells, rendering them proinflammatory.

Following these early experiments, CaMKIV was targeted genetically[64] in lupus-prone mice, showing that its deletion can prevent the development of lupus. The small molecule 2-[*N*-(2-hydroxyethyl)-*N*-(4-methoxybenzenesulfonyl)]amino-*N*-(4-chlorocinnamyl)-*N*-methylbenzylamine (KN-93, **9**)[65] is a potent inhibitor of the kinase activity of CaMK. KN-93 (**9**) was therefore used in experiments in lupus-prone mice showing significant effect in alleviating disease.[66] The effect of the genetic deletion of CaMKIV was thought to be mediated by a boost in the Treg population.[64] KN-93's effect was somewhat different as it inhibited costimulatory molecule expression and proinflammatory cytokine production[66] and mesangial cell proliferation in the kidneys.[67] KN-93 (**9**) has therefore an effect on both circulating immune cells and local cells in the target organs, making it an interesting therapeutic option albeit with the potential for off target effects.

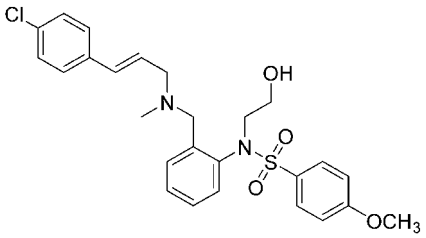

KN-93, **9**

5.15.6.1.5 Calcineurin/nuclear factor of activated T cells

Besides cytosolic kinases, calcium also activates the phosphatase calcineurin. Calcineurin, one of the first phosphatases to be targeted for therapy, then activates by dephosphorization the transcription factor nuclear factor of activated T cells (NFAT).[68] NFAT in cooperation with other transcriptional activators, such as the activator protein-1 (AP-1), initiates the transcription of several key genes, including IL-2 and CD154 among others. SLE T cells, when evaluated in vitro, express high levels of CD154, but because of skewed partnership between NFAT and AP-1, IL-2 production lags.[50] This transcriptional aberration is characteristic of T cells; it renders them good helpers for B cells (through CD154) to produce antibodies, whereas the support for counter-inflammatory Treg through IL-2 is limited. The calcineurin-NFAT duet therefore represents a good molecular target for therapy in SLE that can help normalize the SLE T cells phenotype.

Calcineurin inhibitors cyclosporine and tacrolimus[69] have been extensively used for transplant rejection prevention for several decades. They are well tolerated in general but have been associated with nephrotoxicity among other toxic effects.[70] In SLE and in particular lupus nephritis, they have been used off label for many years but are considered third or fourth line agents behind mycophenolate mofetil, cyclophosphamide, and azathioprine.[71] A recent study comparing tacrolimus to mycophenolate proved noninferiority of tacrolimus to mycophenolate as an induction agent.[72] In a limited number of patients with lupus nephritis, a strategy using low-dose mycophenolate mofetil and tacrolimus was found superior to cyclophosphamide.[73] Besides being an antiinflammatory agent, tacrolimus can be helpful in nephritis by stabilizing the podocytes,[74] thus limiting protein leak in the urine space, which in by itself can be nephrotoxic. These studies and especially the combination studies open the window for the use of these agents in lupus nephritis and in particular in patients who cannot tolerate the chemotherapeutic agent cyclophosphamide or high doses of mycophenolate.

To avoid some of the side effects of calcineurin inhibition, one could try to interfere specifically with the interaction of calcineurin and the NFAT molecule without globally inhibiting calcineurin phosphatase activity. In a chemical screen of such molecules the already approved drug dipyridamole (2-[[2-[bis(2-hydroxyethyl)amino]-4,8-di(piperidin-1-yl)pyrimido[5,4-d]pyrimidin-6-yl]-(2-hydroxyethyl)amino]ethanol, **10**), which is used for its vasodilator properties, was shown to be a calcineurin–NFAT interaction blocker.[75] SLE T cells treated with dipyridamole (**10**) in vitro were unable to help B cells produce excess immunoglobulins. Moreover MRL/*lpr* mice injected with dipyridamole (**10**) showed delayed onset of nephritis compared to placebo-treated mice.[76] Dipyridamole (**10**) is in general well tolerated, making this drug a good alternative to traditional calcineurin inhibitors as an add-on therapy in lupus nephritis.

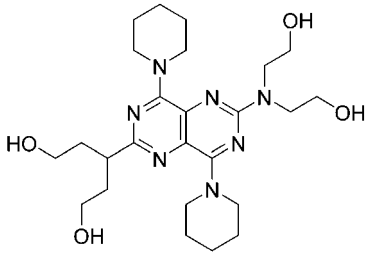

dipyridamole, **10**

5.15.6.1.6 Mammalian target of rapamycin

The serine/threonine kinase mammalian target of rapamycin (mTOR) took its name when it was recognized as the target of the antibiotic/immune-modulatory molecule rapamycin or sirolimus.[77] mTOR is central in a variety of cellular functions including cell metabolism, proliferation, and differentiation. As a drug, rapamycin has been used with great success in allograft rejection prevention, acting synergistically with cyclosporine to improve kidney allograft survival.[78] It has also been used in drug-eluting stents to delay reocclusion of atherosclerotic vessels.[79]

mTOR serves as a censor of the metabolic conditions and coordinates cell growth and proliferation.[80] When activated, mTOR phosphorylates several substrates including STAT3, S6 kinase (S6K), eukaryotic translation initiation factor 4E binding protein 1 (4EBP-1), and activating molecule in BECN1-regulated autophagy protein 1 (AMBRA-1) (reviewed in Ref. 81). mTOR has two interacting isoforms mTORc1 and mTORc2 that play a proinflammatory role by supporting CD4+ T cells[82] differentiation (Th1 and Th17 for mTORc1 and Th2 for mTORc2). SLE T cells are characterized by an enhanced mitochondrial hyperpolarization that upregulates mTOR activity in these cells.[83] This high mTOR activity may therefore contribute to the observed enhanced Th1, Th17 activity, and loss of Treg activity in SLE.

As mTOR links metabolism and cell activation/differentiation, it was targeted in a variety of autoimmune diseases, such as RA[84] with limited success. In SLE after positive animal trials, rapamycin was given in nine SLE patients who failed other therapies and had active disease.[85] In this proof of concept study, rapamycin was well tolerated and proved efficacious in reducing disease activity and the need for steroids. Importantly the overexcitable T-cell phenotype that is characteristic of SLE was reversed with the use of rapamycin.

Besides inhibition with rapamycin, mTOR activation can be targeted indirectly by glutathione (**11**), an antioxidant that regulates mitochondrial hyperpolarization and shown to be decreased in SLE.[86] Glutathione (**11**) can be boosted by its precursor *N*-acetyl cysteine (NAC, **12**), a compound used primarily for its antioxidant properties, such as in preventing contrast-induced nephropathy[87] and the treatment of acetaminophen overdose. In a double-blind placebo control trial, 36 patients were randomized to take NAC (**12**) at three different doses (1.2, 2.4, and 4.8 g/day) or placebo.[88] The highest dose of NAC (**12**) caused significant nausea. NAC (**12**) had the expected biologic effect of reducing mTOR activity by reversing mitochondrial hyperpolarization in T cells. There was a moderate effect on disease activity especially with the two higher doses of NAC (**12**); patients on the highest doses had the most benefit with five of six patients in that group achieving an improvement of three or more on the SLEDAI scale. That group also had the only dropouts (three) because of headache, nausea, and heartburn. Overall, NAC (**12**) has modest effects on disease activity with good tolerance in the medium but not the highest doses.

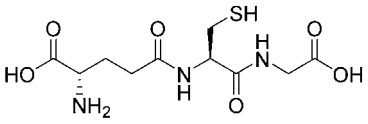

glutathione, **11**

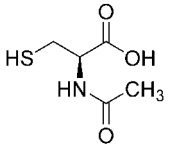

N-acetyl cysteine (NAC), **12**

In conclusion, the mTOR pathway is activated in SLE, and its targeting with traditional or novel agents can be beneficial. Given the modest effectiveness of these drugs, their primary role would be in combination regimens with other immunosuppressives such as the calcineurin inhibitors as is commonly done for transplant rejection prevention.

5.15.6.1.7 Phosphaditylinositol-3 kinase

Class I phosphaditylinositol-3 kinase (PI3K) are heterodimeric kinases that are formed by a regulatory and a p110 catalytic subunit. They catalyze the formation of phosphatidyl-inositol-3,4-diphosphate and phosphatidyl-inositol-3,4,5-triphosphate.[89] They are subcategorized based on the catalytic subunit into: (a) class IA lipid kinases PI3K (p110α, β, δ) that are activated in response to 1st (TCR), 2nd (costimulatory), and 3rd (cytokine) activation signals; and (b) class IB (p110γ) that associates with G-coupled receptors.[90] The lipid second messengers that are generated by these kinases are prosurvival molecules. The main isoforms that are found in hematopoietic cells are p110δ (class IA) and p110γ (class IB). A rare disease called PASLI (p110δ-activating mutation causing senescent T cells, lymphadenopathy, and immunodeficiency) is due, as implied by its name, to an activating mutation of p110δ.

The importance of these kinases in autoimmunity is shown by a transgenic mouse that overexpresses the regulatory subunit and developed a lupus-like illness.[91] PI3K overactivity decreased cell death, accumulation of memory CD4+ T cells, and nephritis. The same research group used the MRL/*lpr* mouse model of lupus to test whether direct inhibition of the class IB PI3K p110γ with the compound AS605240 ((5Z)-5-(quinoxalin-6-ylmethylidene)-1,3-thiazolidine-2,4-dione, **13**) can improve disease outcomes.[92]

Both male and female mice (female mice have more severe disease) responded to the compound with decreased T-cell activation and resulting glomerulonephritis. AS605240 (**13**) also improved survival and overall had a result analogous to dexamethasone.

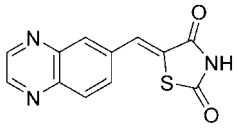

AS605240, **13**

Since p110δ is the other isoform found in hematopoietic cells and is known to regulate B- and T-cell activation, Suarez-Fueyo et al. asked whether it contributes to SLE pathology.[93] p110δ was upregulated in both total peripheral mononuclear cells and T cells of lupus patients, with a tendency to be higher in patients who had higher disease activity. This increase was correlated with increased survival of T cells upon activation and increased proportion of memory T cells. Inhibition of p110δ with AS252424 ((5Z)-5-[[5-(4-fluoro-2-hydroxyphenyl)furan-2-yl]methylidene]-1,3-thiazolidine-2,4-dione, **14**), but not p110γ, resulted in normalization of apoptosis by SLE T cells. The discrepancy between the relative importance of the two isoforms in human T cells (p110δ) and mouse models (p110γ) may be due to the different experimental condition (in vitro vs. in vivo) or in true differences in the role of these isoforms in mice and humans.

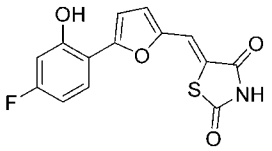

AS252424, **14**

Overall, the PI3K system plays an important role in the survival of T cells after activation and the generation of memory cells, two processes that are clearly abnormal in SLE and represents a promising therapeutic target in this disease. Since PI3K is important in cell survival numerous compounds targeting these enzymes are in trials for cancer but not for autoimmune diseases. A drug that inhibits p110δ, CDZ173 (structure not disclosed), which is currently in trials for PASLI, is also being tested in an early phase trial for the autoimmune disease Sjogren syndrome (clinicaltrials.gov; NCT02775916).

5.15.6.1.8 Bruton's tyrosine kinase

As B cells are the source of autoantibody production, limiting their activity is key in the treatment of the disease. Elimination of B cells with rituximab though did not result in significant outcome improvements suggesting that a more refined approach to B-cell modulation is needed. Targeting B-cell signaling is an important alternative to B-cell depletion therapies.

Bruton's tyrosine kinase (Btk) is a Tec family kinase that is activated following engagement of the BCR complex. *Btk* gene mutations are responsible for the X-linked agamma-globulinemia.[94] Following BCR engagement, Lyn is recruited and, by phosphorylating the BCR ITAM, recruits Syk. Syk in turn recruits and phosphorylates Btk. The activated Btk leads to the translocation of NfkB to the nucleus of B cells.[95] Btk may also bridge the BCR signal with a second signal from the nucleic acid sensing receptor TLR9.[96] Moreover, Btk is involved in Fc receptor signaling in monocytes, suggesting a crucial role for this kinase in the production and handling of antibodies.[97] As the importance of Btk became apparent, it was targeted with small-molecule inhibitors in cancer and autoimmunity. After a series of successful preclinical studies, the Btk inhibitor ibrutinib (**15**) became the first in class drug to show significant efficacy in the treatment of chronic lymphocytic leukemia among other B-cell malignancies.[98] Serious side effects were rare and included hypertension and cytopenias. Atrial fibrillation and hemorrhage were also observed in a minority of patients.

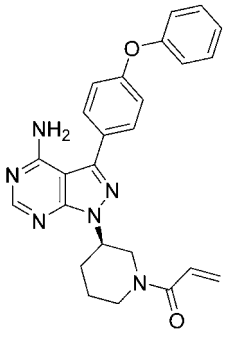

ibrutinib, **15**

Another Btk inhibitor, PF-06250112 ((R)-5-amino-1-(1-cyanopiperidin-3-yl)-3-(4-[2,4-difluorophenoxy]phenyl)-1H-pyrazole-4-carboxamide, **16**), was used in various doses in NZBW F1 mice starting at the age where autoimmunity was apparent, but clinical disease was still not evident. The compound significantly improved renal pathology, preventing complement and antibody deposition in the kidneys. Moreover, it inhibited cell accumulation in the kidneys and kidney damage, in an induced nephritis model, where animals were injected with nephrotoxic serum. In the murine lupus study, low-dose PF-06250112 (**16**) prevented kidney damage without affecting dsDNA antibody production to a significant extent. This speaks to the fact that as important the effect of this drug in the development of germinal centers and anti-dsDNA antibodies may be, limiting Fc receptor-mediated response to immune complexes may be equally or more critical.[99] Ibrutinib (PCI-32765, **15**) was also evaluated in B6.Sle1 and B6.Sle1.Sle3 murine models of lupus. It did limit humoral autoimmunity in both models. In the B6.Sle1.Sle3 that develops severe glomerulonephritis, ibrutinib (**15**) had a moderate effect in limiting kidney damage.[100]

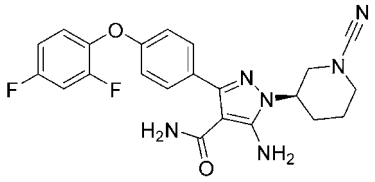

PF-06250112, **16**

The fact that Btk inhibition is successful in murine models of the disease and Btk inhibitors have a good safety profile led to a phase Ib double-blind clinical trial (NCT02537028) of another inhibitor, MSC2364447C (structure not disclosed), in patients with lupus. This is a 4-week trial of two doses of the drug (25 or 75 mg) or placebo to determine safety conducted in patients with mild to moderately active disease with positive autoantibodies excluding patients with active central nervous disease. Overall, Btk inhibition may prove to be very important in the therapeutic armamentarium in SLE as it not only targets B cells and production of antibodies but also the interaction of Fc receptor bearing cells with these antibodies.

5.15.6.2 Modifiers of Chromatin

Ever since the realization that the lupus-inducing drugs procainamide and hydralazine can cause the disease by altering the methylation status of DNA,[101] there has been significant interest in epigenetic changes in the DNA and chromatin structure in SLE patients. Although genetics contribute to disease susceptibility, it is clear that cues from the environment are necessary for both disease initiation and flares. These environmental factors can cause epigenetic changes including methylation of cytosine on the DNA that is catalyzed by the DNA methyl-transferases (DNMT) and histone acetylation/deacetylation mediated by the histone acetylases and histone deacetylases (HDAC).

In SLE, and not only drug-induced lupus which is a somewhat different syndrome, T cells are characterized by an altered DNA methylation status. This change allows for more robust gene expression in the case of demethylated IL-17[63] or protein phosphatase 2A[102] and limited production of the overmethylated IL-2.[103] This change in the methylation status is directed by the aberrant expression of transcription factors such as CREM-α that silences IL-2 while increasing IL-17 production via methylation changes in the respective genes.[103,63]

CREM-α besides altering the methylation status of genes by recruiting DNMT enzymes, alters the histone acetylation status (as in the case of *IL-2*) by promoting histone deacetylation in the gene promoter area, limiting the ability of transcription factors to access the chromatin.[104] HDAC inhibition can therefore correct the underlying inability of SLE T cells to produce sufficient amounts of IL-2, a cytokine critical for the survival of Treg cells. Given these data, trichostatin A (TSA, **16**), a nonspecific HDAC inhibitor, was given in lupus-prone female NZBW F1 mice starting at 14–16 weeks of age.[105] TSA (**16**) improved renal pathology in mice as compared to controls, limiting autoantibody production. Importantly and in line with the in vitro human experiments, the main effect of TSA (**16**) was induction of Treg. The same group also showed that TSA (**16**) improved disease pathology in MRL/*lpr* mice by limiting proinflammatory cytokine production.[106]

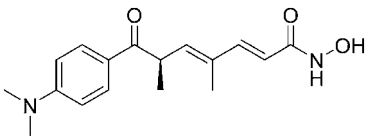

trichostatin A, **16**

Currently, HDAC inhibitors such as Vorinostat (suberoylanilide hydroxamic acid (SAHA, **17**)) are in clinical use for hematologic malignancies, such as cutaneous T-cell lymphoma.[107] Givinostat, another oral HDAC inhibitor, was successful in treating systemic onset juvenile RA in a short 12-week trial with good safety profile.[108] This trial paved the way for the evaluation of HDAC inhibitors in other inflammatory diseases, such as SLE.

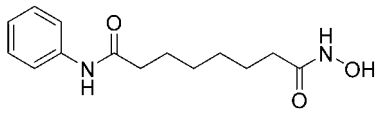

SAHA, **17**

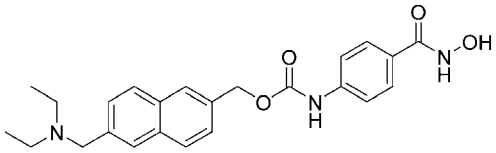

givinostat, **18**

5.15.6.3 Proteasome Inhibitors

Immune cells and especially antigen-presenting cells play an important role in disposing of degradation products from proteins that are either intrinsically produced in the cell or phagocytosed. The immune cell has to critically distinguish between microbial and self-products in this process as it has to dispose them differently. Proteins are degraded by the proteasome, a complex of large proteins in the cell that is crucial in cell homeostasis. In the immune cells, a specialized immunoproteasome is responsible for generating protein fragments to be presented in association with the MHC molecules. The interferons can also induce the immunoproteasome assembly in nonimmune cells.

Plasma cells, the terminally differentiated antibody-forming cells, depend on the proper assembly of the proteasome for their function and survival: The production of significant amounts of immunoglobulin by these cells leads inevitably to a large number of mis- or unfolded proteins that need to be degraded by the proteasome. In the absence or misassembly of the proteasome, these proteins may cause endoplasmic reticulum stress and subsequent programmed cell death (apoptosis).[109] This apparent reliance on the proteasome for their proper function led the successful clinical application of proteasome inhibitors, such as bortezomib (**19**), in the treatment of plasma cell dyscrasias, such as multiple myeloma.[110]

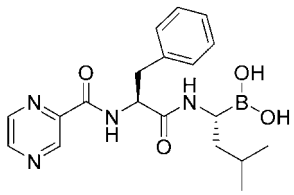

bortezomib, **19**

As I mentioned earlier, elimination of B cells (with anti-CD20 antibodies) or manipulation of B-cell signaling (with anti-BLyS, anti-CD22 antibodies, or Btk inhibitors) is not sufficiently efficacious in controlling SLE pathology. One explanation could be that all these medications do not directly affect the plasma cells, and especially the long-lived plasma cells.[111] Proteasome inhibitors represent exactly such medications.

Bortezomib (**19**) was evaluated in NZBW F1 and MRL/*lpr* lupus-prone mice where it was directly compared to cyclophosphamide and the corticosteroid dexamethasone.[112] The treatment was successful in limiting production of pathogenic autoantibodies, deposition of immunoglobulin to the glomeruli of the kidneys, preventing kidney damage and prolonging survival. The treatment was successful not only to prevent disease but to treat already established disease in these mice. Bortezomib (**19**) was also shown not only to affect plasma cells but also to prevent podocyte damage by preserving its ultrastructure. Whether that is a direct or indirect effect is still unclear though.[113]

Bortezomib's effectiveness in treating multiple myeloma has spurred the creation and marketing of several proteasome inhibitors. Carfilzomib (**20**)[114] and delanzomib (**21**),[115] two newer inhibitors, were shown to be efficacious in the preclinical models of lupus NZBW F1 and MRL/*lpr* just as Bortezomib (**19**). Importantly, these studies showed the specific immunoproteasome inhibitor ONX 0914 (**22**) to be as effective as dual-specificity classic proteasome inhibitors.[114] In these studies, it became also apparent that besides inhibiting autoantibody production, Bortezomib (**19**) also blocked the production of IFNα, an important cytokine for lupus pathogenesis.

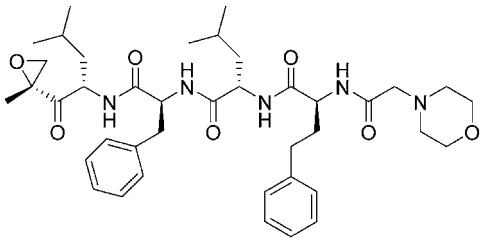

carfilzomib, **20**

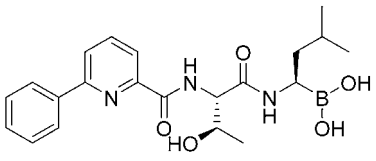

delanzomib, **21**

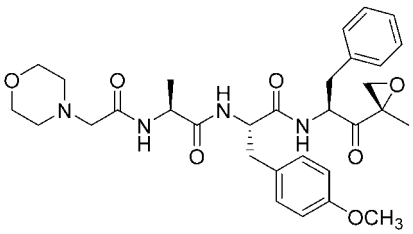

ONX-0914, **22**

Given the wealth of preclinical results, 12 patients with refractory SLE were treated with 1–4 (median 2) cycles of intravenous Bortezomib (**19**). The treatment of these highly refractory patients resulted in impressive[116] improvement in most manifestations including pericarditis, rashes, proteinuria, and arthritis. The drug resulted in a decrease in both short- and long-lived plasma cell-derived autoantibodies but also in significant decreases in protective antibody titers. Bortezomib (**19**) caused significant side effects including neuropathy (two cases). A phase II clinical study on SLE, RA, and myasthenia gravis is under way (NCT02102594). The overall evidence with proteasome inhibitors in SLE is positive, but their usefulness may be limited by their significant neurotoxicity and nonspecific immunosuppression.

5.15.6.4 Quinoline Derivatives

Linomide (**23**), a quinolone derivative, was the prototypic drug of this category of immunomodulators that although efficacious for MS[117] was withdrawn because of toxicity. Two more safe compounds related to linomide (**23**), Laquinimod (**24**) and Paquinimod (**25**), have since been developed.

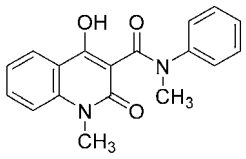

linomide, **23**

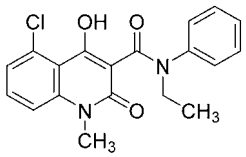

laquinimod, **24**

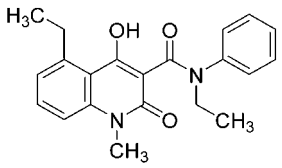

paquinimod, **25**

The exact mechanism of quinolone derivatives remains unclear. Recently it was proposed that they may be targeting the interaction of the proinflammatory molecule S100A9 with the TLR4 and the RAGE (receptor for advanced glycation end products).[118] The danger sensing proinflammatory proteins S100 are upregulated in SLE[119] and may induce the production of the proinflammatory cytokine IL-17 by CD8+ T cells.[120]

Late-phase trials have shown that laquinimod (5-chloro-*N*-ethyl-4-hydroxy-1-methyl-2-oxo-*N*-phenyl-1,2-dihydroquinoline-3-carboxamide, **24**) has modest effects in MS.[121] Murine studies showed that laquinimod (**24**) was as effective as mycophenolate in preventing and treating established nephritis in NZBW F1 mice.[122] Moreover, in advanced disease laquinimod (**24**) was more effective than mycophenolate in prolonging survival. Subsequently, a phase IIa trial in patients with lupus nephritis was conducted using two different doses of laquinimod (**24**) 0.5, 1 mg or placebo. All patients received standard of care with mycophenolate mofetil and corticosteroids. The results favored the laquinimod (**24**) arms with 64% of the patients having a renal response at 24 weeks in the 0.5 mg dose arm versus 50% in 1 mg dose arm versus 33.3% in the placebo arm.[123] Cardiovascular side effects have also plagued the laquinimod (**24**) trials for MS, so the future of its development for SLE remains unclear.

Paquinimod (*N*,5-diethyl-4-hydroxy-1-methyl-2-oxo-*N*-phenylquinoline-3-carboxamide, **25**) is the other quinolone derivative used in SLE. It was successful in preventing disease in MRL/*lpr* mice[124] to a degree comparable to mycophenolate. In a proof of concept study that did not address efficacy to a significant extent, it was also given in SLE patients and was relatively well tolerated; mild-to-moderate side effects such as arthralgias and myalgias were observed in patients who received higher doses.[124]

Overall, the quinoline derivatives may be effective in a variety of autoimmune diseases, but a lot is yet to be learned-regarding their mode of action. The side-effect profile and especially cardiovascular toxicity remains a significant barrier to the full clinical deployment of these compounds decades after their initial introduction as immunomodulatory medications.

5.15.7 Conclusion and Future Directions

Extensive basic science work in vitro and in animal models has uncovered much of the immunopathology of SLE. Treatment options have largely though remained static with an emphasis in global immunosuppression with extensive use of corticosteroids. The development of new agents follows two trends: the first one is to block easily accessible surface molecules and circulating mediators. This approach using biologics has been very effective in rheumatoid and psoriatic arthritis but in the case of SLE has had modest success, such as with belimumab or no effect such as with epratuzumab or abatacept. The second approach targets intracellular enzymes and other factors using small molecules that penetrate the cell membrane. As discussed earlier and shown in **Table 1**, various agents show promise. The problem of selectivity does remain though given that most of the targets are generally expressed in a variety of cells and tissues.

A major hurdle to move these drugs from preclinical studies to the clinic is the appropriate design of trials. SLE trials have been difficult to conduct not only because of the rarity of the disease but also its heterogeneity. This has been to a degree improved but not resolved, by the use of novel outcome measures, BICLA (a BILAG-based measure) and SRI (a SLEDAI-based measure). The second hurdle is the use of background immunosuppressive therapies in SLE. The introduction of new therapies should not only improve outcomes but also decrease the side effects (immune-suppressive and metabolic) of current therapies. Corticosteroid and other immunosuppressives sparing strategies should therefore be taken into account when designing clinical trials with novel agents The Biomarkers in lupus disease (BOLD) study design (https://www.clinicaltrials.gov/ct2/show/NCT00987831) is one example where patients without life threatening disease are taken off major immunosuppressives, and thus the drug in question can be examined in a more thorough way for effectiveness and toxicity.

In conclusion, several novel small molecules discussed earlier show promise in becoming effective treatments for SLE, either alone or more likely in combination with traditional disease-modifying agents and corticosteroids.

Table 1 Emerging small-molecule treatments for SLE

Target	*Compound*	*Stage of development in SLE*
Jak/STAT	Tofacitinib (**1**)	Positive mouse studies
	Solcitinib (**4**)	Early human study stopped because of lack of biologic effect
	Stattic (**3**)	Positive mouse studies
Syk	Fostamatinib (**6**)	Positive mouse studies; clinical development for ITP
ROCK	Fasudil (**8**)	Positive mouse studies; clinical development for vascular diseases
CaMKIV	KN-93 (**9**)	Positive mouse studies
Calcineurin	Tacrolimus	Successful trials in nephritis
	Dipyridamole (**10**)	Positive mouse studies
mTOR	Rapamycin	Effective in case series
	N-acetyl cysteine (**12**)	Positive early studies in patients
PI3K	AS605240 (**13**)	Positive mouse studies
	AS252424 (**14**)	Human in vitro trial
	CDZ173	Clinical trial in Sjogren syndrome
Btk	Ibrutinib (**15**)	Positive mouse studies
	PF-06250112 (**16**)	Positive mouse studies
	MSC2364447C	Ongoing phase Ib trial
HDAC	Vorinostat (**17**)	Positive mouse studies
	Givinostat (**18**)	Effective in systemic juvenile rheumatoid arthritis
	Trischostatin-A (**16**)	Positive mouse studies
Proteasome	Bortezomib (**19**)	Effective in case series
	Carfilzomib (**20**)	Positive mouse studies
	Delanzomib (**21**)	Positive mouse studies
	ONX 0914 (**22**)	Positive mouse studies
S100A9 (?)	Laquinimod (**24**)	Pilot study in SLE; long-term toxicity risk unclear
	Paquinimod (**25**)	Pilot study in SLE

See also: 8.17. Are Two Better Than One in Rheumatoid Arthritis? Development of Dual p38α MAPK/PDE-4 Inhibitors for Treatment of TNFα-Driven Diseases.

References

1. Mackay, I. R. Travels and Travails of Autoimmunity: A Historical Journey From Discovery to Rediscovery. *Autoimmun. Rev.* **2010,** *9* (5), A251–A258.
2. Stoffels, M.; Kastner, D. L. Old Dogs, New Tricks: Monogenic Autoinflammatory Disease Unleashed. *Annu. Rev. Genomics Hum. Genet.* **2016,** *17,* 245–272.
3. Singh, J. A.; Saag, K. G.; Bridges, S. L., Jr.; Akl, E. A.; Bannuru, R. R.; Sullivan, M. C.; Vaysbrot, E.; McNaughton, C.; Osani, M.; Shmerling, R. H.; Curtis, J. R.; Furst, D. E.; Parks, D.; Kavanaugh, A.; O'Dell, J.; King, C.; Leong, A.; Matteson, E. L.; Schousboe, J. T.; Drevlow, B.; Ginsberg, S.; Grober, J.; St Clair, E. W.; Tindall, E.; Miller, A. S.; McAlindon, T. 2015 American College of Rheumatology Guideline for the Treatment of Rheumatoid Arthritis. *Arthritis Rheumatol.* **2016,** *68* (1), 1–26.
4. Stone, J. H.; Merkel, P. A.; Spiera, R.; Seo, P.; Langford, C. A.; Hoffman, G. S.; Kallenberg, C. G.; St Clair, E. W.; Turkiewicz, A.; Tchao, N. K.; Webber, L.; Ding, L.; Sejismundo, L. P.; Mieras, K.; Weitzenkamp, D.; Ikle, D.; Seyfert-Margolis, V.; Mueller, M.; Brunetta, P.; Allen, N. B.; Fervenza, F. C.; Geetha, D.; Keogh, K. A.; Kissin, E. Y.; Monach, P. A.; Peikert, T.; Stegeman, C.; Ytterberg, S. R.; Specks, U.; RAVE-ITN Research Group. Rituximab Versus Cyclophosphamide for ANCA-Associated Vasculitis. *N. Engl. J. Med.* **2010,** *363* (3), 221–232.
5. Kamradt, T.; Mitchison, N. A. Tolerance and Autoimmunity. *N. Engl. J. Med.* **2001,** *344* (9), 655–664.
6. Sakaguchi, S. Regulatory T Cells: History and Perspective. *Methods Mol. Biol.* **2011,** *707,* 3–17.
7. Arbuckle, M. R.; McClain, M. T.; Rubertone, M. V.; Scofield, R. H.; Dennis, G. J.; James, J. A.; Harley, J. B. Development of Autoantibodies Before the Clinical Onset of Systemic Lupus Erythematosus. *N. Engl. J. Med.* **2003,** *349* (16), 1526–1533.
8. Costenbader, K. H.; Feskanich, D.; Stampfer, M. J.; Karlson, E. W. Reproductive and Menopausal Factors and Risk of Systemic Lupus Erythematosus in Women. *Arthritis Rheum.* **2007,** *56* (4), 1251–1262.
9. McClain, M. T.; Poole, B. D.; Bruner, B. F.; Kaufman, K. M.; Harley, J. B.; James, J. A. An Altered Immune Response to Epstein-Barr Nuclear Antigen 1 in Pediatric Systemic Lupus Erythematosus. *Arthritis Rheum.* **2006,** *54* (1), 360–368.
10. Lehmann, P.; Holzle, E.; Kind, P.; Goerz, G.; Plewig, G. Experimental Reproduction of Skin Lesions in Lupus Erythematosus by UVA and UVB Radiation. *J. Am. Acad. Dermatol.* **1990,** *22* (2 Pt 1), 181–187.
11. Lawrence, R. C.; Helmick, C. G.; Arnett, F. C.; Deyo, R. A.; Felson, D. T.; Giannini, E. H.; Heyse, S. P.; Hirsch, R.; Hochberg, M. C.; Hunder, G. G.; Liang, M. H.; Pillemer, S. R.; Steen, V. D.; Wolfe, F. Estimates of the Prevalence of Arthritis and Selected Musculoskeletal Disorders in the United States. *Arthritis Rheum.* **1998,** *41* (5), 778–799.
12. McCarty, D. J.; Manzi, S.; Medsger, T. A., Jr.; Ramsey-Goldman, R.; LaPorte, R. E.; Kwoh, C. K. Incidence of Systemic Lupus Erythematosus. Race and Gender Differences. *Arthritis Rheum.* **1995,** *38* (9), 1260–1270.
13. Kyttaris, V. C. Systemic Lupus Erythematosus: From Genes to Organ Damage. *Methods Mol. Biol.* **2010,** *662,* 265–283.

14. ter Borg, E. J.; Horst, G.; Hummel, E. J.; Limburg, P. C.; Kallenberg, C. G. Measurement of Increases in Anti-Double-Stranded DNA Antibody Levels as a Predictor of Disease Exacerbation in Systemic Lupus Erythematosus. A Long-Term, Prospective Study. *Arthritis Rheum.* **1990,** *33* (5), 634–643.
15. Parikh, S. V.; Nagaraja, H. N.; Hebert, L.; Rovin, B. H. Renal Flare as a Predictor of Incident and Progressive CKD in Patients With Lupus Nephritis. *Clin. J. Am. Soc. Nephrol.* **2014,** *9* (2), 279–284.
16. Yurasov, S.; Wardemann, H.; Hammersen, J.; Tsuiji, M.; Meffre, E.; Pascual, V.; Nussenzweig, M. C. Defective B Cell Tolerance Checkpoints in Systemic Lupus Erythematosus. *J. Exp. Med.* **2005,** *201* (5), 703–711.
17. Mackay, F.; Woodcock, S. A.; Lawton, P.; Ambrose, C.; Baetscher, M.; Schneider, P.; Tschopp, J.; Browning, J. L. Mice Transgenic for BAFF Develop Lymphocytic Disorders Along With Autoimmune Manifestations. *J. Exp. Med.* **1999,** *190* (11), 1697–1710.
18. Merrill, J. T.; Neuwelt, C. M.; Wallace, D. J.; Shanahan, J. C.; Latinis, K. M.; Oates, J. C.; Utset, T. O.; Gordon, C.; Isenberg, D. A.; Hsieh, H. J.; Zhang, D.; Brunetta, P. G. Efficacy and Safety of Rituximab in Moderately-to-Severely Active Systemic Lupus Erythematosus: The Randomized, Double-Blind, Phase II/III Systemic Lupus Erythematosus Evaluation of Rituximab Trial. *Arthritis Rheum.* **2010,** *62* (1), 222–233.
19. Boumpas, D. T.; Furie, R.; Manzi, S.; Illei, G. G.; Wallace, D. J.; Balow, J. E.; Vaishnaw, A. A Short Course of BG9588 (Anti-CD40 Ligand Antibody) Improves Serologic Activity and Decreases Hematuria in Patients With Proliferative Lupus Glomerulonephritis. *Arthritis Rheum.* **2003,** *48* (3), 719–727.
20. Khamashta, M.; Merrill, J. T.; Werth, V. P.; Furie, R.; Kalunian, K.; Illei, G. G.; Drappa, J.; Wang, L.; Greth, W.; CD1067 Study Investigators. Sifalimumab, an Anti-Interferon-Alpha Monoclonal Antibody, in Moderate to Severe Systemic Lupus Erythematosus: A Randomised, Double-Blind, Placebo-Controlled Study. *Ann. Rheum. Dis.* **2016** (Epub ahead of print).
21. Sherer, Y.; Gorstein, A.; Fritzler, M. J.; Shoenfeld, Y. Autoantibody Explosion in Systemic Lupus Erythematosus: More Than 100 Different Antibodies Found in SLE Patients. *Semin. Arthritis Rheum.* **2004,** *34* (2), 501–537.
22. Boumpas, D. T.; Austin, H. A., 3rd; Fessler, B. J.; Balow, J. E.; Klippel, J. H.; Lockshin, M. D. Systemic Lupus Erythematosus: Emerging Concepts. Part 1: Renal, Neuropsychiatric, Cardiovascular, Pulmonary, and Hematologic Disease. *Ann. Intern. Med.* **1995,** *122* (12), 940–950.
23. Weening, J. J.; D'Agati, V. D.; Schwartz, M. M.; Seshan, S. V.; Alpers, C. E.; Appel, G. B.; Balow, J. E.; Bruijn, J. A.; Cook, T.; Ferrario, F.; Fogo, A. B..; Ginzler, E. M.; Hebert, L.; Hill, G.; Hill, P.; Jennette, J. C.; Kong, N. C.; Lesavre, P.; Lockshin, M.; Looi, L.-M.; Makino, H.; Moura, L. A.; Nagata, M. The Classification of Glomerulonephritis in Systemic Lupus Erythematosus Revisited. *J. Am. Soc. Nephrol.* **2004,** *15* (2), 241–250.
24. Hochberg, M. C. Updating the American College of Rheumatology Revised Criteria for the Classification of Systemic Lupus Erythematosus. *Arthritis Rheum.* **1997,** *40* (9), 1725.
25. Sharp, G. C.; Irvin, W. S.; Tan, E. M.; Gould, R. G.; Holman, H. R. Mixed Connective Tissue Disease—An Apparently Distinct Rheumatic Disease Syndrome Associated With a Specific Antibody to an Extractable Nuclear Antigen (ENA). *Am. J. Med.* **1972,** *52* (2), 148–159.
26. Bombardier, C.; Gladman, D. D.; Urowitz, M. B.; Caron, D.; Chang, C. H. Derivation of the SLEDAI. A Disease Activity Index for Lupus Patients. The Committee on Prognosis Studies in SLE. *Arthritis Rheum.* **1992,** *35* (6), 630–640.
27. Isenberg, D. A.; Rahman, A.; Allen, E.; Farewell, V.; Akil, M.; Bruce, I. N.; D'Cruz, D.; Griffiths, B.; Khamashta, M.; Maddison, P.; McHugh, N.; Snaith, M.; Teh, L. S.; Yee, C. S.; Zoma, A.; Gordon, C. BILAG 2004. Development and Initial Validation of an Updated Version of the British Isles Lupus Assessment Group's Disease Activity Index for Patients With Systemic Lupus Erythematosus. *Rheumatology* **2005,** *44* (7), 902–906.
28. Furie, R.; Petri, M.; Zamani, O.; Cervera, R.; Wallace, D. J.; Tegzová, D.; Sanchez-Guerrero, J.; Schwarting, A.; Merrill, J. T.; Chatham, W. W.; Stohl, W.; Ginzler, E. M.; Hough, D. R.; Zhong, Z. J.; Freimuth, W.; van Vollenhoven, R. F.; BLISS-76 Study Group. A Phase III, Randomized, Placebo-Controlled Study of Belimumab, a Monoclonal Antibody That Inhibits B Lymphocyte Stimulator, in Patients With Systemic Lupus Erythematosus. *Arthritis Rheum.* **2011,** *63* (12), 3918–3930.
29. Fleischmann, R.; Kremer, J.; Cush, J.; Schulze-Koops, H.; Connell, C. A.; Bradley, J. D.; Gruben, D.; Wallenstein, G. V.; Zwillich, S. H.; Kanik, K. S. Placebo-Controlled Trial of Tofacitinib Monotherapy in Rheumatoid Arthritis. *N. Engl. J. Med.* **2012,** *367* (6), 495–507.
30. Schwartz, D. M.; Bonelli, M.; Gadina, M.; O'Shea, J. J. Type I/II Cytokines, JAKs, and New Strategies for Treating Autoimmune Diseases. *Nat. Rev. Rheumatol.* **2016,** *12* (1), 25–36.
31. Witthuhn, B. A.; Quelle, F. W.; Silvennoinen, O.; Yi, T.; Tang, B.; Miura, O.; Ihle, J. N. JAK2 Associates With the Erythropoietin Receptor and Is Tyrosine Phosphorylated and Activated Following Stimulation With Erythropoietin. *Cell* **1993,** *74* (2), 227–236.
32. Genovese, M. C.; Kremer, J.; Zamani, O.; Ludivico, C.; Krogulec, M.; Xie, L.; Beattie, S. D.; Koch, A. E.; Cardillo, T. E.; Rooney, T. P.; Macias, W. L.; de Bono, S.; Schlichting, D. E.; Smolen, J. S. Baricitinib in Patients With Refractory Rheumatoid Arthritis. *N. Engl. J. Med.* **2016,** *374* (13), 1243–1252.
33. Furumoto, Y.; Smith, C. K.; Blanco, L.; Zhao, W.; Brooks, S. R.; Thacker, S. G.; Zarzour, A.; Sciume, G.; Tsai, W. L.; Trier, A. M.; Nunez, L.; Mast, L.; Hoffmann, V.; Remaley, A. T.; O'Shea, J. J.; Kaplan, M. J.; Gadina, M. Tofacitinib Ameliorates Murine Lupus and Its Associated Vascular Dysfunction. *Arthritis Rheumatol.* **2016** (Epub ahead of print).
34. Liu, K.; Liang, C.; Liang, Z.; Tus, K.; Wakeland, E. K. Sle1ab Mediates the Aberrant Activation of STAT3 and Ras-ERK Signaling Pathways in B Lymphocytes. *J. Immunol.* **2005,** *174* (3), 1630–1637.
35. Harada, T.; Kyttaris, V.; Li, Y.; Juang, Y. T.; Wang, Y.; Tsokos, G. C. Increased Expression of STAT3 in SLE T Cells Contributes to Enhanced Chemokine-Mediated Cell Migration. *Autoimmunity* **2007,** *40* (1), 1–8.
36. Harris, T. J.; Grosso, J. F.; Yen, H. R.; Xin, H.; Kortylewski, M.; Albesiano, E.; Hipkiss, E. L.; Getnet, D.; Goldberg, M. V.; Maris, C. H.; Housseau, F.; Yu, H.; Pardoll, D. M.; Drake, C. G. Cutting Edge: An In Vivo Requirement for STAT3 Signaling in TH17 Development and TH17-Dependent Autoimmunity. *J. Immunol.* **2007,** *179* (7), 4313–4317.
37. Nurieva, R. I.; Chung, Y.; Hwang, D.; Yang, X. O.; Kang, H. S.; Ma, L.; Wang, Y. H.; Watowich, S. S.; Jetten, A. M.; Tian, Q.; Dong, C. Generation of T Follicular Helper Cells Is Mediated by Interleukin-21 but Independent of T Helper 1, 2, or 17 Cell Lineages. *Immunity* **2008,** *29* (1), 138–149.
38. Laurence, A.; Amarnath, S.; Mariotti, J.; Kim, Y. C.; Foley, J.; Eckhaus, M.; O'Shea, J. J.; Fowler, D. H. STAT3 Transcription Factor Promotes Instability of nTreg Cells and Limits Generation of iTreg Cells During Acute Murine Graft-Versus-Host Disease. *Immunity* **2012,** *37* (2), 209–222.
39. Bethunaickan, R.; Berthier, C. C.; Zhang, W.; Kretzler, M.; Davidson, A. Comparative Transcriptional Profiling of 3 Murine Models of SLE Nephritis Reveals Both Unique and Shared Regulatory Networks. *PLoS One* **2013,** *8* (10), e77489.
40. Edwards, L. J.; Mizui, M.; Kyttaris, V. Signal Transducer and Activator of Transcription (STAT) 3 Inhibition Delays the Onset of Lupus Nephritis in MRL/lpr Mice. *Clin. Immunol.* **2015,** *158* (2), 221–230.
41. Kahl, L.; Patel, J.; Layton, M.; Binks, M.; Hicks, K.; Leon, G.; Hachulla, E.; Machado, D.; Staumont-Salle, D.; Dickson, M.; Condreay, L.; Schifano, L.; Zamuner, S.; van Vollenhoven, R. F.; JAK115919 Study Team. Safety, Tolerability, Efficacy and Pharmacodynamics of the Selective JAK1 Inhibitor GSK2586184 in Patients With Systemic Lupus Erythematosus. *Lupus* **2016** (Epub ahead of print).
42. van Vollenhoven, R. F.; Layton, M.; Kahl, L.; Schifano, L.; Hachulla, E.; Machado, D.; Staumont-Salle, D.; Patel, J.; JAK115919 Study Team. DRESS Syndrome and Reversible Liver Function Abnormalities in Patients With Systemic Lupus Erythematosus Treated With the Highly Selective JAK-1 Inhibitor GSK2586184. *Lupus* **2015,** *24* (6), 648–649.
43. Mocsai, A.; Ruland, J.; Tybulewicz, V. L. The SYK Tyrosine Kinase: A Crucial Player in Diverse Biological Functions. *Nat. Rev. Immunol.* **2010,** *10* (6), 387–402.
44. Takata, M.; Sabe, H.; Hata, A.; Inazu, T.; Homma, Y.; Nukada, T.; Yamamura, H.; Kurosaki, T. Tyrosine Kinases Lyn and Syk Regulate B Cell Receptor-Coupled Ca2+ Mobilization Through Distinct Pathways. *EMBO J.* **1994,** *13* (6), 1341–1349.
45. Mocsai, A.; Abram, C. L.; Jakus, Z.; Hu, Y.; Lanier, L. L.; Lowell, C. A. Integrin Signaling in Neutrophils and Macrophages Uses Adaptors Containing Immunoreceptor Tyrosine-Based Activation Motifs. *Nat. Immunol.* **2006,** *7* (12), 1326–1333.
46. Braselmann, S.; Taylor, V.; Zhao, H.; Wang, S.; Sylvain, C.; Baluom, M.; Qu, K.; Herlaar, E.; Lau, A.; Young, C.; Wong, B. R.; Lovell, S.; Sun, T.; Park, G.; Argade, A.; Jurcevic, S.; Pine, P.; Singh, R.; Grossbard, E. B.; Payan, D. G.; Masuda, E. S. R406, an Orally Available Spleen Tyrosine Kinase Inhibitor Blocks fc Receptor Signaling and Reduces Immune Complex-Mediated Inflammation. *J. Pharmacol. Exp. Ther.* **2006,** *319* (3), 998–1008.

47. Weinblatt, M. E.; Genovese, M. C.; Ho, M.; Hollis, S.; Rosiak-Jedrychowicz, K.; Kavanaugh, A.; Millson, D. S.; Leon, G.; Wang, M.; van der Heijde, D. Effects of Fostamatinib, an Oral Spleen Tyrosine Kinase Inhibitor, in Rheumatoid Arthritis Patients With an Inadequate Response to Methotrexate: Results From a Phase III, Multicenter, Randomized, Double-Blind, Placebo-Controlled, Parallel-Group Study. *Arthritis Rheumatol.* **2014,** *66* (12), 3255–3264.
48. Krishnan, S.; Warke, V. G.; Nambiar, M. P.; Tsokos, G. C.; Farber, D. L. The FcR Gamma Subunit and Syk Kinase Replace the CD3 Zeta-Chain and ZAP-70 Kinase in the TCR Signaling Complex of Human Effector CD4 T Cells. *J. Immunol.* **2003,** *170* (8), 4189–4195.
49. Vassilopoulos, D.; Kovacs, B.; Tsokos, G. C. TCR/CD3 Complex-Mediated Signal Transduction Pathway in T Cells and T Cell Lines From Patients With Systemic Lupus Erythematosus. *J. Immunol.* **1995,** *155* (4), 2269–2281.
50. Kyttaris, V. C.; Wang, Y.; Juang, Y.-T.; Weinstein, A.; Tsokos, G. C. Increased Levels of NF-ATc2 Differentially Regulate CD154 and IL-2 Genes in T Cells From Patients With Systemic Lupus Erythematosus. *J. Immunol.* **2007,** *178* (3), 1960–1966.
51. Krishnan, S.; Juang, Y. T.; Chowdhury, B.; Magilavy, A.; Fisher, C. U.; Nguyen, H.; Nambiar, M. P.; Kyttaris, V.; Weinstein, A.; Bahjat, R.; Pine, P.; Rus, V.; Tsokos, G. C. Differential Expression and Molecular Associations of Syk in Systemic Lupus Erythematosus T Cells. *J. Immunol.* **2008,** *181* (11), 8145–8152.
52. Deng, G. M.; Liu, L.; Bahjat, F. R.; Pine, P. R.; Tsokos, G. C. Suppression of Skin and Kidney Disease by Inhibition of Spleen Tyrosine Kinase in Lupus-Prone Mice. *Arthritis Rheum.* **2010,** *62* (7), 2086–2092.
53. Nakagawa, O.; Fujisawa, K.; Ishizaki, T.; Saito, Y.; Nakao, K.; Narumiya, S. ROCK-I and ROCK-II, Two Isoforms of Rho-Associated Coiled-Coil Forming Protein Serine/Threonine Kinase in Mice. *FEBS Lett.* **1996,** *392* (2), 189–193.
54. Li, Y.; Harada, T.; Juang, Y. T.; Kyttaris, V. C.; Wang, Y.; Zidanic, M.; Tung, K.; Tsokos, G. C. Phosphorylated ERM Is Responsible for Increased T Cell Polarization, Adhesion, and Migration in Patients With Systemic Lupus Erythematosus. *J. Immunol.* **2007,** *178* (3), 1938–1947.
55. Biswas, P. S.; Gupta, S.; Chang, E.; Song, L.; Stirzaker, R. A.; Liao, J. K.; Bhagat, G.; Pernis, A. B.. Phosphorylation of IRF4 by ROCK2 Regulates IL-17 and IL-21 Production and the Development of Autoimmunity in Mice. *J. Clin. Invest.* **2010,** *120* (9), 3280–3295.
56. Biswas, P. S.; Gupta, S.; Stirzaker, R. A.; Kumar, V.; Jessberger, R.; Lu, T. T.; Bhagat, G.; Pernis, A. B. Dual Regulation of IRF4 Function in T and B Cells Is Required for the Coordination of T-B Cell Interactions and the Prevention of Autoimmunity. *J. Exp. Med.* **2012,** *209* (3), 581–596.
57. Stirzaker, R. A.; Biswas, P. S.; Gupta, S.; Song, L.; Bhagat, G.; Pernis, A. B. Administration of Fasudil, a ROCK Inhibitor, Attenuates Disease in Lupus-Prone NZB/WF1 Female Mice. *Lupus* **2012,** *21* (6), 656–661.
58. Vicari, R. M.; Chaitman, B.; Keefe, D.; Smith, W. B.; Chrysant, S. G.; Tonkon, M. J.; Bittar, N.; Weiss, R. J.; Morales-Ballejo, H.; Thadani, U.; Fasudil Study Group. Efficacy and Safety of Fasudil in Patients With Stable Angina: A Double-Blind, Placebo-Controlled, Phase 2 Trial. *J. Am. Coll. Cardiol.* **2005,** *46* (10), 1803–1811.
59. Fukumoto, Y.; Yamada, N.; Matsubara, H.; Mizoguchi, M.; Uchino, K.; Yao, A.; Kihara, Y.; Kawano, M.; Watanabe, H.; Takeda, Y.; Adachi, T.; Osanai, S.; Tanabe, N.; Inoue, T.; Kubo, A.; Ota, Y.; Fukuda, K.; Nakano, T.; Shimokawa, H. Double-Blind, Placebo-Controlled Clinical Trial With a Rho-Kinase Inhibitor in Pulmonary Arterial Hypertension. *Circ. J.* **2013,** *77* (10), 2619–2625.
60. Fava, A.; Wung, P. K.; Wigley, F. M.; Hummers, L. K.; Daya, N. R.; Ghazarian, S. R.; Boin, F. Efficacy of Rho kinase inhibitor fasudil in secondary Raynaud's Phenomenon. *Arthritis Care Res. (Hoboken)* **2012,** *64* (6), 925–929.
61. Juang, Y. T.; Wang, Y.; Solomou, E. E.; Li, Y.; Mawrin, C.; Tenbrock, K.; Kyttaris, V. C.; Tsokos, G. C. Systemic Lupus Erythematosus Serum IgG Increases CREM Binding to the IL-2 Promoter and Suppresses IL-2 Production Through CaMKIV. *J. Clin. Invest.* **2005,** *115* (4), 996–1005.
62. Solomou, E. E.; Juang, Y. T.; Gourley, M. F.; Kammer, G. M.; Tsokos, G. C. Molecular Basis of Deficient IL-2 Production in T Cells From Patients With Systemic Lupus Erythematosus. *J. Immunol.* **2001,** *166* (6), 4216–4222.
63. Rauen, T.; Hedrich, C. M.; Juang, Y. T.; Tenbrock, K.; Tsokos, G. C. cAMP-Responsive Element Modulator (CREM)alpha Protein Induces Interleukin 17A Expression and Mediates Epigenetic Alterations at the Interleukin-17A Gene Locus in Patients With Systemic Lupus Erythematosus. *J. Biol. Chem.* **2011,** *286* (50), 43437–43446.
64. Koga, T.; Ichinose, K.; Mizui, M.; Crispin, J. C.; Tsokos, G. C. Calcium/Calmodulin-Dependent Protein Kinase IV Suppresses IL-2 Production and Regulatory T Cell Activity in Lupus. *J. Immunol.* **2012,** *189* (7), 3490–3496.
65. Sumi, M.; Kiuchi, K.; Ishikawa, T.; Ishii, A.; Hagiwara, M.; Nagatsu, T.; Hidaka, H. The Newly Synthesized Selective Ca2+/Calmodulin Dependent Protein Kinase II Inhibitor KN-93 Reduces Dopamine Contents in PC12h Cells. *Biochem. Biophys. Res. Commun.* **1991,** *181* (3), 968–975.
66. Ichinose, K.; Juang, Y. T.; Crispin, J. C.; Kis-Toth, K.; Tsokos, G. C. Suppression of Autoimmunity and Organ Pathology in Lupus-Prone Mice Upon Inhibition of Calcium/Calmodulin-Dependent Protein Kinase Type IV. *Arthritis Rheum.* **2011,** *63* (2), 523–529.
67. Ichinose, K.; Rauen, T.; Juang, Y. T.; Kis-Toth, K.; Mizui, M.; Koga, T.; Tsokos, G. C. Cutting Edge: Calcium/Calmodulin-Dependent Protein Kinase Type IV Is Essential for Mesangial Cell Proliferation and Lupus Nephritis. *J. Immunol.* **2011,** *187* (11), 5500–5504.
68. Muller, M. R.; Rao, A. NFAT, Immunity and Cancer: A Transcription Factor Comes of Age. *Nat. Rev. Immunol.* **2010,** *10* (9), 645–656.
69. Liu, J.; Farmer, J. D., Jr.; Lane, W. S.; Friedman, J.; Weissman, I.; Schreiber, S. L. Calcineurin Is a Common Target of Cyclophilin-Cyclosporin A and FKBP-FK506 Complexes. *Cell* **1991,** *66* (4), 807–815.
70. Jacobson, P. A.; Schladt, D.; Israni, A.; Oetting, W. S.; Lin, Y. C.; Leduc, R.; Guan, W.; Lamba, V.; Matas, A. J.; De, K. A. F. I. Genetic and Clinical Determinants of Early, Acute Calcineurin Inhibitor-Related Nephrotoxicity: Results From a Kidney Transplant Consortium. *Transplantation* **2012,** *93* (6), 624–631.
71. Bertsias, G. K.; Tektonidou, M.; Amoura, Z.; Aringer, M.; Bajema, I.; Berden, J. H.; Boletis, J.; Cervera, R.; Dorner, T.; Doria, A.; Ferrario, F.; Floege, J.; Houssiau, F. A.; Ioannidis, J. P.; Isenberg, D. A.; Kallenberg, C. G.; Lightstone, L.; Marks, S. D.; Martini, A.; Moroni, G.; Neumann, I.; Praga, M.; Schneider, M.; Starra, A.; Tesar, V.; Vasconcelos, C.; van Vollenhoven, R. F.; Zakharova, H.; Haubitz, M.; Gordon, C.; Jayne, D.; Boumpas, D. T.; European League Against Rheumatism and European Renal Association-European Dialysis and Transplant Association. Joint European League Against Rheumatism and European Renal Association-European Dialysis and Transplant Association (EULAR/ERA-EDTA) Recommendations for the Management of Adult and Paediatric Lupus Nephritis. *Ann. Rheum. Dis.* **2012,** *71* (11), 1771–1782.
72. Mok, C. C.; Ying, K. Y.; Yim, C. W.; Siu, Y. P.; Tong, K. H.; To, C. H.; Ng, W. L. Tacrolimus Versus Mycophenolate Mofetil for Induction Therapy of Lupus Nephritis: A Randomised Controlled Trial and Long-Term Follow-Up. *Ann. Rheum. Dis.* **2016,** *75* (1), 30–36.
73. Liu, Z.; Zhang, H.; Liu, Z.; Xing, C.; Fu, P.; Ni, Z.; Chen, J.; Lin, H.; Liu, F.; He, Y.; He, Y.; Miao, L.; Chen, N.; Li, Y.; Gu, Y.; Shi, W.; Hu, W.; Liu, Z.; Bao, H.; Zeng, C.; Zhou, M. Multitarget Therapy for Induction Treatment of Lupus Nephritis: A Randomized Trial. *Ann. Intern. Med.* **2015,** *162* (1), 18–26.
74. Wakamatsu, A.; Fukusumi, Y.; Hasegawa, E.; Tomita, M.; Watanabe, T.; Narita, I.; Kawachi, H. Role of Calcineurin (CN) in Kidney Glomerular Podocyte: CN Inhibitor Ameliorated Proteinuria by Inhibiting the Redistribution of CN at the Slit Diaphragm. *Physiol. Rep.* **2016,** *4* (6), e12679.
75. Mulero, M. C.; Aubareda, A.; Orzaez, M.; Messeguer, J.; Serrano-Candelas, E.; Martinez-Hoyer, S.; Messeguer, A.; Perez-Paya, E.; Perez-Riba, M. Inhibiting the Calcineurin-NFAT (Nuclear Factor of Activated T Cells) Signaling Pathway With a Regulator of Calcineurin-Derived Peptide Without Affecting General Calcineurin Phosphatase Activity. *J. Biol. Chem.* **2009,** *284* (14), 9394–9401.
76. Kyttaris, V. C.; Zhang, Z.; Kampagianni, O.; Tsokos, G. C. Calcium Signaling in Systemic Lupus Erythematosus T Cells: A Treatment Target. *Arthritis Rheum.* **2011,** *63* (7), 2058–2066.
77. Vezina, C.; Kudelski, A.; Sehgal, S. N. Rapamycin (AY-22,989), a New Antifungal Antibiotic. I. Taxonomy of the Producing Streptomycete and Isolation of the Active Principle. *J. Antibiot. (Tokyo)* **1975,** *28* (10), 721–726.
78. Kahan, B. D.; Julian, B. A.; Pescovitz, M. D.; Vanrenterghem, Y.; Neylan, J. Sirolimus Reduces the Incidence of Acute Rejection Episodes Despite Lower Cyclosporine Doses in Caucasian Recipients of Mismatched Primary Renal Allografts: A Phase II Trial. Rapamune Study Group. *Transplantation* **1999,** *68* (10), 1526–1532.
79. Kaiser, C.; Galatius, S.; Erne, P.; Eberli, F.; Alber, H.; Rickli, H.; Pedrazzini, G.; Hornig, B.; Bertel, O.; Bonetti, P.; De Servi, S.; Brunner-La Rocca, H. P.; Ricard, I.; Pfisterer, M.; BASKET–PROVE Study Group. Drug-Eluting Versus Bare-Metal Stents in Large Coronary Arteries. *N. Engl. J. Med.* **2010,** *363* (24), 2310–2319.

80. (a) Sarbassov, D. D.; Sabatini, D. M. Redox Regulation of the Nutrient-Sensitive Raptor-mTOR Pathway and Complex. *J. Biol. Chem.* **2005,** *280* (47), 39505–39509; (b) Zoncu, R.; Bar-Peled, L.; Efeyan, A.; Wang, S.; Sancak, Y.; Sabatini, D. M. mTORC1 Senses Lysosomal Amino Acids Through an Inside-Out Mechanism That Requires the Vacuolar H(+)-ATPase. *Science* **2011,** *334* (6056), 678–683.
81. Perl, A. Activation of mTOR (Mechanistic Target of Rapamycin) in Rheumatic Diseases. *Nat. Rev. Rheumatol.* **2016,** *12* (3), 169–182.
82. Delgoffe, G. M.; Pollizzi, K. N.; Waickman, A. T.; Heikamp, E.; Meyers, D. J.; Horton, M. R.; Xiao, B.; Worley, P. F.; Powell, J. D. The Kinase mTOR Regulates the Differentiation of Helper T Cells Through the Selective Activation of Signaling by mTORC1 and mTORC2. *Nat. Immunol.* **2011,** *12* (4), 295–303.
83. Fernandez, D. R.; Telarico, T.; Bonilla, E.; Li, Q.; Banerjee, S.; Middleton, F. A.; Phillips, P. E.; Crow, M. K.; Oess, S.; Muller-Esterl, W.; Perl, A. Activation of Mammalian Target of Rapamycin Controls the Loss of TCRzeta in Lupus T Cells Through HRES-1/Rab4-Regulated Lysosomal Degradation. *J. Immunol.* **2009,** *182* (4), 2063–2073.
84. Bruyn, G. A.; Tate, G.; Caeiro, F.; Maldonado-Cocco, J.; Westhovens, R.; Tannenbaum, H.; Bell, M.; Forre, O.; Bjorneboe, O.; Tak, P. P.; Abeywickrama, K. H.; Bernhardt, P.; van Riel, P. L.; RADD Study Group. Everolimus in Patients With Rheumatoid Arthritis Receiving Concomitant Methotrexate: A 3-Month, Double-Blind, Randomised, Placebo-Controlled, Parallel-Group, Proof-of-Concept Study. *Ann. Rheum. Dis.* **2008,** *67* (8), 1090–1095.
85. Fernandez, D.; Bonilla, E.; Mirza, N.; Niland, B.; Perl, A. Rapamycin Reduces Disease Activity and Normalizes T Cell Activation-Induced Calcium Fluxing in Patients With Systemic Lupus Erythematosus. *Arthritis Rheum.* **2006,** *54* (9), 2983–2988.
86. Gergely, P., Jr.; Grossman, C.; Niland, B.; Puskas, F.; Neupane, H.; Allam, F.; Banki, K.; Phillips, P. E.; Perl, A. Mitochondrial Hyperpolarization and ATP Depletion in Patients With Systemic Lupus Erythematosus. *Arthritis Rheum.* **2002,** *46* (1), 175–190.
87. Ali-Hassan-Sayegh, S.; Mirhosseini, S. J.; Ghodratipour, Z.; Sarrafan-Chaharsoughi, Z.; Rahimizadeh, E.; Karimi-Bondarabadi, A. A.; Haddad, F.; Shahidzadeh, A.; Mahdavi, P.; Dehghan, A. M.; Tahernejad, M.; Shahidzadeh, A.; Dehghan, H.; Ghanei, A.; Lotfaliani, M.; Weymann, A.; Zeriouh, M.; Popov, A. F.; Sabashnikov, A. Strategies Preventing Contrast-Induced Nephropathy After Coronary Angiography: A Comprehensive Meta-Analysis and Systematic Review of 125 Randomized Controlled Trials. *Angiology* **2016** (Epub ahead of print).
88. Lai, Z. W.; Hanczko, R.; Bonilla, E.; Caza, T. N.; Clair, B.; Bartos, A.; Miklossy, G.; Jimah, J.; Doherty, E.; Tily, H.; Francis, L.; Garcia, R.; Dawood, M.; Yu, J.; Ramos, I.; Coman, I.; Faraone, S. V.; Phillips, P. E.; Perl, A. *N*-acetylcysteine Reduces Disease Activity by Blocking Mammalian Target of Rapamycin in T Cells From Systemic Lupus Erythematosus Patients: A Randomized, Double-Blind, Placebo-Controlled Trial. *Arthritis Rheum.* **2012,** *64* (9), 2937–2946.
89. Fruman, D. A.; Bismuth, G. Fine Tuning the Immune Response With PI3K. *Immunol. Rev.* **2009,** *228* (1), 253–272.
90. Vanhaesebroeck, B.; Ali, K.; Bilancio, A.; Geering, B.; Foukas, L. C. Signalling by PI3K Isoforms: Insights From Gene-Targeted Mice. *Trends Biochem. Sci.* **2005,** *30* (4), 194–204.
91. Borlado, L. R.; Redondo, C.; Alvarez, B.; Jimenez, C.; Criado, L. M.; Flores, J.; Marcos, M. A.; Martinez, A. C.; Balomenos, D.; Carrera, A. C. Increased Phosphoinositide 3-Kinase Activity Induces a Lymphoproliferative Disorder and Contributes to Tumor Generation In Vivo. *FASEB J.* **2000,** *14* (7), 895–903.
92. Barber, D. F.; Bartolome, A.; Hernandez, C.; Flores, J. M.; Redondo, C.; Fernandez-Arias, C.; Camps, M.; Ruckle, T.; Schwarz, M. K.; Rodriguez, S.; Martinez, A. C.; Balomenos, D.; Rommel, C.; Carrera, A. C. PI3Kgamma Inhibition Blocks Glomerulonephritis and Extends Lifespan in a Mouse Model of Systemic Lupus. *Nat. Med.* **2005,** *11* (9), 933–935.
93. Suarez-Fueyo, A.; Barber, D. F.; Martinez-Ara, J.; Zea-Mendoza, A. C.; Carrera, A. C. Enhanced Phosphoinositide 3-Kinase Delta Activity Is a Frequent Event in Systemic Lupus Erythematosus That Confers Resistance to Activation-Induced T Cell Death. *J. Immunol.* **2011,** *187* (5), 2376–2385.
94. Thomas, J. D.; Sideras, P.; Smith, C. I.; Vorechovsky, I.; Chapman, V.; Paul, W. E. Colocalization of X-Linked agammaglobulinemia and X-Linked Immunodeficiency Genes. *Science* **1993,** *261* (5119), 355–358.
95. Kurosaki, T. Regulation of BCR Signaling. *Mol. Immunol.* **2011,** *48* (11), 1287–1291.
96. Kenny, E. F.; Quinn, S. R.; Doyle, S. L.; Vink, P. M.; van Eenennaam, H.; O'Neill, L. A. Bruton's Tyrosine Kinase Mediates the Synergistic Signalling Between TLR9 and the B Cell Receptor by Regulating Calcium and Calmodulin. *PLoS One* **2013,** *8* (8), e74103.
97. Jongstra-Bilen, J.; Puig Cano, A.; Hasija, M.; Xiao, H.; Smith, C. I.; Cybulsky, M. I. Dual Functions of Bruton's Tyrosine Kinase and Tec Kinase During Fcgamma Receptor-Induced Signaling and Phagocytosis. *J. Immunol.* **2008,** *181* (1), 288–298.
98. Burger, J. A.; Tedeschi, A.; Barr, P. M.; Robak, T.; Owen, C.; Ghia, P.; Bairey, O.; Hillmen, P.; Bartlett, N. L.; Li, J.; Simpson, D.; Grosicki, S.; Devereux, S.; McCarthy, H.; Coutre, S.; Quach, H.; Gaidano, G.; Maslyak, Z.; Stevens, D. A.; Janssens, A.; Offner, F.; Mayer, J.; O'Dwyer, M.; Hellmann, A.; Schuh, A.; Siddiqi, T.; Polliack, A.; Tam, C. S.; Suri, D.; Cheng, M.; Clow, F.; Styles, L.; James, D. F.; Kipps, T. J.; RESONATE-2 Investigators. Ibrutinib as Initial Therapy for Patients With Chronic Lymphocytic Leukemia. *N. Engl. J. Med.* **2015,** *373* (25), 2425–2437.
99. Rankin, A. L.; Seth, N.; Keegan, S.; Andreyeva, T.; Cook, T. A.; Edmonds, J.; Mathialagan, N.; Benson, M. J.; Syed, J.; Zhan, Y.; Benoit, S. E.; Miyashiro, J. S.; Wood, N.; Mohan, S.; Peeva, E.; Ramaiah, S. K.; Messing, D.; Homer, B. L.; Dunussi-Joannopoulos, K.; Nickerson-Nutter, C. L.; Schnute, M. E.; Douhan, J., 3rd. Selective Inhibition of BTK Prevents Murine Lupus and Antibody-Mediated Glomerulonephritis. *J. Immunol.* **2013,** *191* (9), 4540–4550.
100. Hutcheson, J.; Vanarsa, K.; Bashmakov, A.; Grewal, S.; Sajitharan, D.; Chang, B. Y.; Buggy, J. J.; Zhou, X. J.; Du, Y.; Satterthwaite, A. B.; Mohan, C. Modulating Proximal Cell Signaling by Targeting Btk Ameliorates Humoral Autoimmunity and End-Organ Disease in Murine Lupus. *Arthritis Res. Ther.* **2012,** *14* (6), R243.
101. Cornacchia, E.; Golbus, J.; Maybaum, J.; Strahler, J.; Hanash, S.; Richardson, B. Hydralazine and Procainamide Inhibit T Cell DNA Methylation and Induce Autoreactivity. *J. Immunol.* **1988,** *140* (7), 2197–2200.
102. Sunahori, K.; Juang, Y. T.; Kyttaris, V. C.; Tsokos, G. C. Promoter Hypomethylation Results in Increased Expression of Protein Phosphatase 2A in T Cells From Patients With Systemic Lupus Erythematosus. *J. Immunol.* **2011,** *186* (7), 4508–4517.
103. Hedrich, C. M.; Rauen, T.; Tsokos, G. C. cAMP-Responsive Element Modulator (CREM)alpha Protein Signaling Mediates Epigenetic Remodeling of the Human Interleukin-2 Gene: Implications in Systemic Lupus Erythematosus. *J. Biol. Chem.* **2011,** *286* (50), 43429–43436.
104. Tenbrock, K.; Juang, Y. T.; Tolnay, M.; Tsokos, G. C. The Cyclic Adenosine 5′-Monophosphate Response Element Modulator Suppresses IL-2 Production in Stimulated T cells by a Chromatin-Dependent Mechanism. *J. Immunol.* **2003,** *170* (6), 2971–2976.
105. Reilly, C. M.; Thomas, M.; Gogal, R., Jr.; Olgun, S.; Santo, A.; Sodhi, R.; Samy, E. T.; Peng, S. L.; Gilkeson, G. S.; Mishra, N. The Histone Deacetylase Inhibitor Trichostatin A Upregulates Regulatory T Cells and Modulates Autoimmunity in NZB/WF1 Mice. *J. Autoimmun.* **2008,** *31* (2), 123–130.
106. Mishra, N.; Reilly, C. M.; Brown, D. R.; Ruiz, P.; Gilkeson, G. S. Histone Deacetylase Inhibitors Modulate Renal Disease in the MRL-lpr/lpr Mouse. *J. Clin. Invest.* **2003,** *111* (4), 539–552.
107. Olsen, E. A.; Kim, Y. H.; Kuzel, T. M.; Pacheco, T. R.; Foss, F. M.; Parker, S.; Frankel, S. R.; Chen, C.; Ricker, J. L.; Arduino, J. M.; Duvic, M. Phase IIb Multicenter Trial of Vorinostat in Patients With Persistent, Progressive, or Treatment Refractory Cutaneous T-Cell Lymphoma. *J. Clin. Oncol.* **2007,** *25* (21), 3109–3115.
108. Vojinovic, J.; Damjanov, N.; D'Urzo, C.; Furlan, A.; Susic, G.; Pasic, S.; Iagaru, N.; Stefan, M.; Dinarello, C. A. Safety and Efficacy of an Oral Histone Deacetylase Inhibitor in Systemic-Onset Juvenile Idiopathic Arthritis. *Arthritis Rheum.* **2011,** *63* (5), 1452–1458.
109. Meister, S.; Schubert, U.; Neubert, K.; Herrmann, K.; Burger, R.; Gramatzki, M.; Hahn, S.; Schreiber, S.; Wilhelm, S.; Herrmann, M.; Jack, H. M.; Voll, R. E. Extensive Immunoglobulin Production Sensitizes Myeloma Cells for Proteasome Inhibition. *Cancer Res.* **2007,** *67* (4), 1783–1792.
110. San Miguel, J. F.; Schlag, R.; Khuageva, N. K.; Dimopoulos, M. A.; Shpilberg, O.; Kropff, M.; Spicka, I.; Petrucci, M. T.; Palumbo, A.; Samoilova, O. S.; Dmoszynska, A.; Abdulkadyrov, K. M.; Schots, R.; Jiang, B.; Mateos, M. V.; Anderson, K. C.; Esseltine, D. L.; Liu, K.; Cakana, A.; van de Velde, H.; Richardson, P. G.; VISTA Trial Investigators. Bortezomib Plus Melphalan and Prednisone for Initial Treatment of Multiple Myeloma. *N. Engl. J. Med.* **2008,** *359* (9), 906–917.
111. Slifka, M. K.; Ahmed, R. Long-Lived Plasma Cells: A Mechanism for Maintaining Persistent Antibody Production. *Curr. Opin. Immunol.* **1998,** *10* (3), 252–258.
112. Neubert, K.; Meister, S.; Moser, K.; Weisel, F.; Maseda, D.; Amann, K.; Wiethe, C.; Winkler, T. H.; Kalden, J. R.; Manz, R. A.; Voll, R. E. The Proteasome Inhibitor Bortezomib Depletes Plasma Cells and Protects Mice With Lupus-Like Disease From Nephritis. *Nat. Med.* **2008,** *14* (7), 748–755.

113. Hainz, N.; Thomas, S.; Neubert, K.; Meister, S.; Benz, K.; Rauh, M.; Daniel, C.; Wiesener, M.; Voll, R. E.; Amann, K. The Proteasome Inhibitor Bortezomib Prevents Lupus Nephritis in the NZB/WF1 Mouse Model by Preservation of Glomerular and Tubulointerstitial Architecture. *Nephron Exp. Nephrol.* **2012,** *120* (2), e47–e58.
114. Ichikawa, H. T.; Conley, T.; Muchamuel, T.; Jiang, J.; Lee, S.; Owen, T.; Barnard, J.; Nevarez, S.; Goldman, B. I.; Kirk, C. J.; Looney, R. J.; Anolik, J. H. Beneficial Effect of Novel Proteasome Inhibitors in Murine Lupus via Dual Inhibition of Type I Interferon and Autoantibody-Secreting Cells. *Arthritis Rheum.* **2012,** *64* (2), 493–503.
115. Seavey, M. M.; Lu, L. D.; Stump, K. L.; Wallace, N. H.; Ruggeri, B. A. Novel, Orally Active, Proteasome Inhibitor, Delanzomib (CEP-18770), Ameliorates Disease Symptoms and Glomerulonephritis in Two Preclinical Mouse Models of SLE. *Int. Immunopharmacol.* **2012,** *12* (1), 257–270.
116. Alexander, T.; Sarfert, R.; Klotsche, J.; Kuhl, A. A.; Rubbert-Roth, A.; Lorenz, H. M.; Rech, J.; Hoyer, B. F.; Cheng, Q.; Waka, A.; Taddeo, A.; Wiesener, M.; Schett, G.; Burmester, G. R.; Radbruch, A.; Hiepe, F.; Voll, R. E. The Proteasome Inhibitior Bortezomib Depletes Plasma Cells and Ameliorates Clinical Manifestations of Refractory Systemic Lupus Erythematosus. *Ann. Rheum. Dis.* **2015,** *74* (7), 1474–1478.
117. Andersen, O.; Lycke, J.; Tollesson, P. O.; Svenningsson, A.; Runmarker, B.; Linde, A. S.; Astrom, M.; Gjorstrup, P.; Ekholm, S. Linomide Reduces the Rate of Active Lesions in Relapsing-Remitting Multiple Sclerosis. *Neurology* **1996,** *47* (4), 895–900.
118. Bjork, P.; Bjork, A.; Vogl, T.; Stenstrom, M.; Liberg, D.; Olsson, A.; Roth, J.; Ivars, F.; Leanderson, T. Identification of Human S100A9 as a Novel Target for Treatment of Autoimmune Disease via Binding to Quinoline-3-Carboxamides. *PLoS Biol.* **2009,** *7* (4), e97.
119. Lood, C.; Stenstrom, M.; Tyden, H.; Gullstrand, B.; Kallberg, E.; Leanderson, T.; Truedsson, L.; Sturfelt, G.; Ivars, F.; Bengtsson, A. A. Protein Synthesis of the Pro-inflammatory S100A8/A9 Complex in Plasmacytoid Dendritic Cells and Cell Surface S100A8/A9 on Leukocyte Subpopulations in Systemic Lupus Erythematosus. *Arthritis Res. Ther.* **2011,** *13* (2), R60.
120. Loser, K.; Vogl, T.; Voskort, M.; Lueken, A.; Kupas, V.; Nacken, W.; Klenner, L.; Kuhn, A.; Foell, D.; Sorokin, L.; Luger, T. A.; Roth, J.; Beissert, S. The Toll-Like Receptor 4 Ligands Mrp8 and Mrp14 Are Crucial in the Development of Autoreactive CD8+ T Cells. *Nat. Med.* **2010,** *16* (6), 713–717.
121. Hainke, U.; Thomas, K.; Ziemssen, T. Laquinimod in the Treatment of Relapsing Remitting Multiple Sclerosis. *Expert Opin. Drug Metab. Toxicol.* **2016,** *12* (6), 701–709.
122. Lourenco, E. V.; Wong, M.; Hahn, B. H.; Palma-Diaz, M. F.; Skaggs, B. J. Laquinimod Delays and Suppresses Nephritis in Lupus-Prone Mice and Affects Both Myeloid and Lymphoid Immune Cells. *Arthritis Rheumatol.* **2014,** *66* (3), 674–685.
123. Jayne, D.; Appel, G.; Chan, T. M.; Barkay, H.; Weiss, R.; Wofsy, D. A Randomized Controlled Study of Laquinimod in Active Lupus Nephritis Patients in Combination With Standard of Care. *Ann. Rheum. Dis.* **2013,** *72* (Suppl. 3), 164.
124. Bengtsson, A. A.; Sturfelt, G.; Lood, C.; Ronnblom, L.; van Vollenhoven, R. F.; Axelsson, B.; Sparre, B.; Tuvesson, H.; Ohman, M. W.; Leanderson, T. Pharmacokinetics, Tolerability, and Preliminary Efficacy of Paquinimod (ABR-215757), a New Quinoline-3-Carboxamide Derivative: Studies in Lupus-Prone Mice and a Multicenter, Randomized, Double-Blind, Placebo-Controlled, Repeat-Dose, Dose-Ranging Study in Patients With Systemic Lupus Erythematosus. *Arthritis Rheum.* **2012,** *64* (5), 1579–1588.

Relevant Websites

125. www.rheumatology.org—Information on Treatment Guidelines and Conference Abstracts From the American College of Rheumatology Meetings.
126. http://www.lupusresearchinstitute.org—Information on New Therapies and Ongoing Trials.
127. www.eular.org—The European League Against Rheumatism Website: Guidelines and Abstracts From the EULAR Conference.

5.16 Small-Molecule Drugs for the Treatment of Inflammatory Bowel Disease

LR Fitzpatrick and T Woldemariam, California Northstate University College of Pharmacy, Elk Grove, CA, United States

© 2017 Elsevier Ltd. All rights reserved.

5.16.1	**General Characteristics of IBD**	496
5.16.2	**Small-Molecule Approaches for IBD: Drugs in Clinical Trials**	496
5.16.2.1	S1P Receptor Modulators	496
5.16.2.2	JAK Inhibitors	499
5.16.2.3	CCR9 Antagonists	499
5.16.2.4	Alpha (α)-4 Integrin Antagonists	500
5.16.2.5	Immunomodulator Drugs	500
5.16.2.6	Mucosal Barrier Enhancer Drug	501
5.16.3	**Novel Small-Molecule Approaches for IBD: Preclinical Results**	501
5.16.3.1	Synthetic Triterpenoids	501
5.16.3.2	ROR-γT Inhibitors	502
5.16.3.3	Sphingosine Kinase Inhibitors	502
5.16.3.4	Immunoproteasome Subunit Inhibitors	503
5.16.3.5	Melanin-Concentrating Hormone (MCH) Receptor 1 Antagonists	503
5.16.3.6	Receptor-Interacting Protein Kinase 1 (RIP1 and RIP3) Inhibitors	503
5.16.4	**Natural Product-Derived Small-Molecule Approaches for IBD**	504
5.16.4.1	Curcumin	504
5.16.4.2	Berberine	504
5.16.4.3	Silibinin	505
5.16.4.4	Triterpene Ganoderic Acid C1 (GAC1)	505
5.16.4.5	Gallic Acid	506
5.16.4.6	Diallyl Sulfide	506
5.16.4.7	6-Gingerol	506
5.16.4.8	Rutin	507
5.16.5	**Summary: Small-Molecule Compounds for IBD Therapy**	507
References		507
Relevant Websites		510

Abbreviations

AMPK adenosine monophosphate-activated protein kinase
CAC colitis-associated cancer
CCL20 chemokine (C-C motif) ligand 20
CCL25 chemokine (C-C motif) ligand 25
CCR9 C-C chemokine receptor type 9
CD Crohn's disease
CDDO-Im 1[2-cyano-3,12-dioxooleana-1,9(11)-dien-28-oyl]imidazole
CDDO-Me 2-cyano-3,12-dioxooleana-1,9(11)-dien-28-oic acid, methyl ester
COX-2 cyclooxygenase-2
DAS diallyl sulfide
DHODH dihydroorotate dehydrogenase
DSS dextran sulfate sodium
ERK extracellular receptor kinase
FDA Food and Drug Administration
GI gastrointestinal
IBD inflammatory bowel disease
IFN-γ interferon-gamma
IL-10 interleukin 10
IL-13 interleukin 13
IL-17 interleukin 17
IL-1β interleukin 1-beta
IL-21 interleukin 21
IL-23R interleukin 23 receptor
iNOS inducible nitric oxide synthase
IV intravenous
JAK Janus kinase
LMP2 low molecular mass polypeptide 2
LMP7 low molecular mass polypeptide 7
LOX lipoxygenase
MAPK mitogen-activated protein kinase
MCH melanin-concentrating hormone
MPO myeloperoxidase
MS multiple sclerosis
NF-κB nuclear factor-kappa B
NK natural killer cell
NKT natural killer T cells
PC phosphatidylcholine
PML progressive multifocal leukoencephalopathy
RIP receptor-interacting protein kinase
ROR-γT retinoic acid-related orphan nuclear receptor gamma T
ROS reactive oxygen species

S1P sphingosine-1-phosphate
S1PR sphingosine-1-phosphate receptor
SK sphingosine kinase
STAT3 signal transducer and activator of transcription 3
Th1 T-helper 1 cells
Th17 T-helper 17 cells
TNBS trinitrobenzene sulfonic acid
TNF-α tumor necrosis factor-alpha
UC ulcerative colitis
α-4Integrin alpha-4 integrin
5-ASA 5-amino salicylic acid

5.16.1 General Characteristics of IBD

There are two major types of inflammatory bowel disease (IBD): ulcerative colitis (UC) and Crohn's disease (CD). These are chronic inflammatory diseases affecting the gastrointestinal (GI) tract. The general characteristics of UC and CD are summarized in Table 1.[1–5]

The exact causes of IBD are currently not fully understood. IBD is likely due to a combination of genetic variations and alterations in the bacterial flora, which can subsequently drive a dysregulated immune response resulting in chronic intestinal inflammation.

Scientific evidence suggests that UC is associated with an atypical Th2 response mediated by natural killer T (NKT) cells producing interleukins 5 and 13. Interleukin 13 is of particular importance because it exerts cytotoxic functions against epithelial cells, including induction of apoptosis and alteration of the protein composition of tight junctions.[1] In addition, NK T cells upon activation may be directly cytotoxic to epithelial cells.[2]

CD is characterized by T lymphocytes producing the signature cytokines IFN-γ and IL-17, respectively. Recent studies have identified T cells that produce both IFN-γ and IL-17.[3] Also, these dual Th17/Th1 cells can be converted into nonclassic Th1 cells. These T lymphocytes, which produce mainly IFN-γ, may also be involved in the pathogenesis of CD.[4,5]

When considering the characteristics of IBD, it becomes clear that suppression (during active disease) or prevention (acute flares of IBD) related to an exaggerated immune response is critical when considering new therapeutic approaches for IBD. This article will primarily address recent small-molecule approaches, which have resulted in drugs that have entered clinical trials for CD and/or UC. Secondarily, we will discuss certain novel small-molecule approaches that have shown efficacy in animal models of IBD. Finally, we will summarize results with some natural product-derived small molecules, which could have future utility for the treatment of IBD.

5.16.2 Small-Molecule Approaches for IBD: Drugs in Clinical Trials

During the past 5 years, several small-molecule drugs have entered clinical trials for IBD. These drugs have actions against various targets such as Janus kinase (JAK1 and JAK3 inhibitors), sphingosine 1 phosphate (S1P), alpha 4 integrin, C-C chemokine receptor type 9 (CCR9), and IL-17.

5.16.2.1 S1P Receptor Modulators

S1P is formed intracellularly by the phosphorylation of sphingosine, a process that is controlled by two sphingosine kinases: SK1 and SK2. S1P is then exported out of cells where it can act on five specific receptors (S1P receptor 1 (S1PR1) to S1PR5).[6] *Fingolimod* (Gilenya, Novartis AG) is a sphingosine analog that is phosphorylated primarily by SK2 to form phosphorylated fingolimod, which is an agonist at all of the S1PRs except for S1PR2. It is a functional antagonist, which prevents lymphocyte egress from lymphoid organs and induces immunosuppression. Fingolimod is an approved drug for relapsing-remitting multiple sclerosis (MS).[6,7] It has shown efficacy in various murine models of IBD.[8–12]

Fingolimod has unique pharmacokinetic properties. Its absorption is slow, reaching peak concentrations 8–36 h after oral administration. It has a large volume of distribution (1116–1737 L) and a clearance of about 123–383 mL min^{-1}, resulting in

Table 1 General characteristics of IBD

Ulcerative colitis	*Crohn's disease*
Disease is limited to colon	Disease throughout GI tract (ileum is a common site)
Continuous disease	Discontinuous disease (skip lesions)
Disease affects the mucosa and submucosa	Disease is transmural (affects all layers including the muscularis propria)
Classified as an atypical Th2 disease with a Th17 component (increased IL-13 and IL-17)	Classified as a transitional Th17 to Th1 disease (increased IL-17 and IFN-γ)

a long elimination half-life of about 108 h (4.5 days).[13] Since it is given once a day, seemingly it takes about 4 weeks to reach steady-state concentration, with 11–19-fold accumulation in tissues compared to first-dose administration.

Fingolimod belongs to the class of organic compounds known as phenylpropylamines. These are compounds containing a phenylpropylamine moiety, which consists of a phenyl group substituted at the third carbon by a propan-1-amine. It is derived from myriocin (ISP-1), a metabolite of the fungus *Isaria sinclairii* broth.[14] The structures of these compounds are shown here.

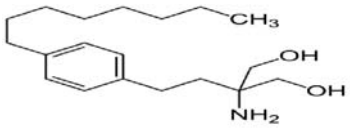

Fingolimod (FTY720) [Compound1]

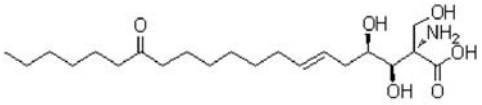

Myriocin [Compound 2]

APD-334 (Arena Pharmaceuticals) is a potent functional antagonist of S1PR1.[15] APD-334 is an orally available agonist of the S1P1 receptor. S1P1 receptors have been demonstrated to be involved in the modulation of several biological responses, including lymphocyte trafficking from lymph nodes to the peripheral blood. This compound (structure shown in the succeeding text) has entered phase 2 clinical trials for UC (see **Fig. 1**).

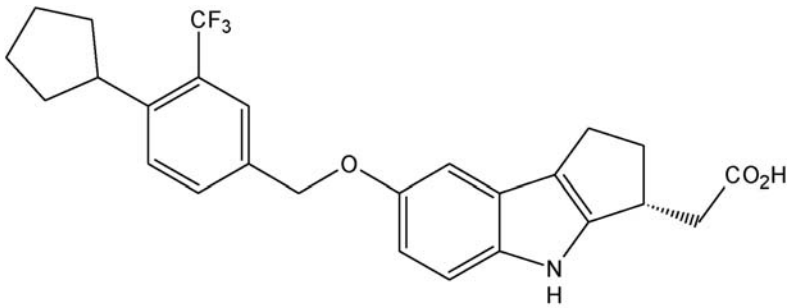

ADP-334 [Compound 3]

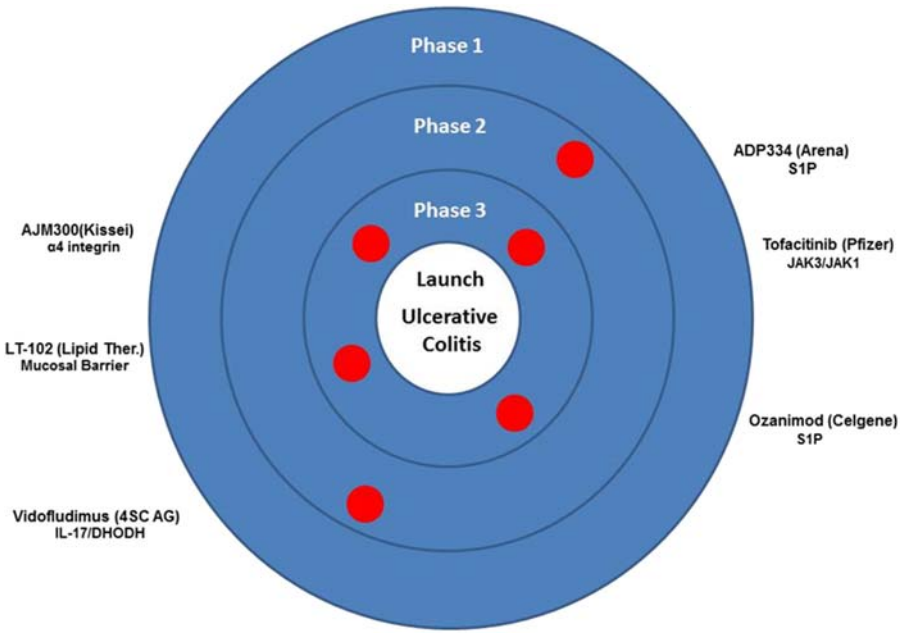

Fig. 1 This figure shows drugs that are currently in clinical trials for the treatment of ulcerative colitis (UC). The red circles within the figure show the phase of development that the drug is currently in as an UC therapeutic agent. The applicable drug, drug target, and relevant company are indicated parallel to the red circles within the figure.

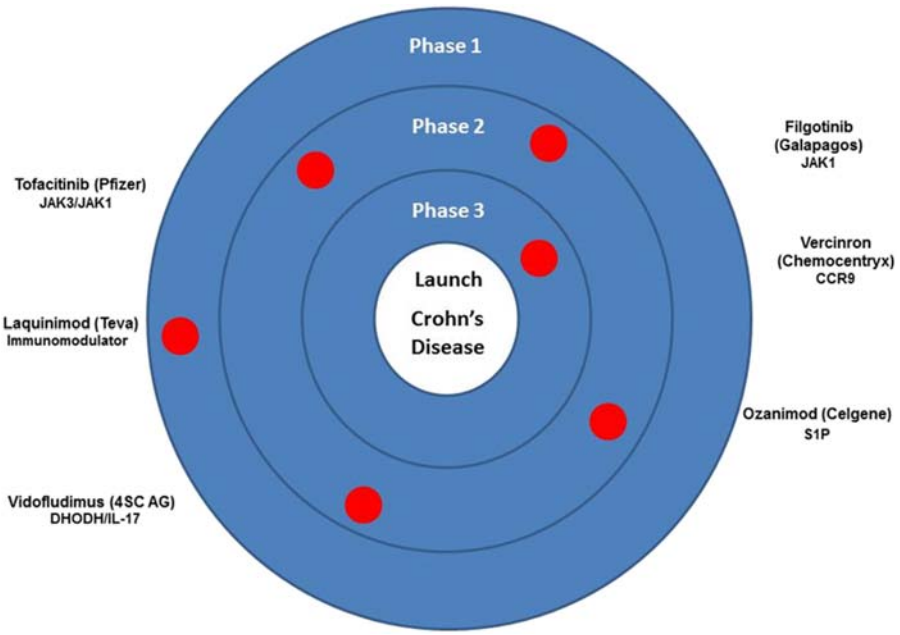

Fig. 2 This figure shows drugs that are currently in clinical trials for the treatment of Crohn's disease (CD). The *red circles* within the figure show the phase of development that the drug is currently in as a CD therapeutic agent. The applicable drug, drug target, and relevant company are indicated parallel to the *red circles* within the figure.

Ozanimod (RPC1063) is another S1PR1 modulator. It was discovered by Receptos (a spin-off company from Scripps Research Institute) and is currently being developed by Celgene.[6] Ozanimod has advanced to phase 3 clinical trials for UC patients (Fig. 1), as well as phase 2 clinical trials for CD (Fig. 2).

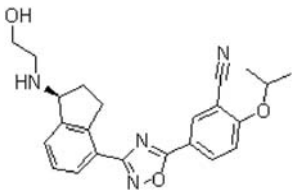

Ozanimod [Compound 4]

KRP-203 (Kyorin Pharmaceutical) is a S1P receptor 1, 4, 5 prodrug. Specifically, KRP-203, 2-amino-2-(2-(4-(3-benzyloxyphenylthio)-2-chlorophenyl)ethyl)-1,3-propanediol hydrochloride, is an immunosuppressant that has been identified as an agonist for S1PR1 and appears to behave similarly to fingolimod, by sequestering lymphocytes in lymphoid tissues.[16] It was effective in dextran sulfate sodium (DSS) and IL-10 knockout mouse models of IBD.[7] This compound progressed to phase 2 clinical trials. However, clinical development of the drug has apparently been discontinued in Europe and Japan.

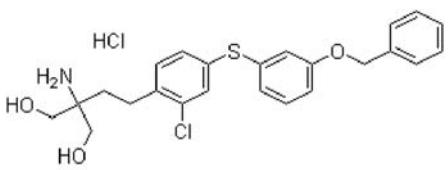

KRP-203 [Compound 5]

5.16.2.2 JAK Inhibitors

In Nov. 2012, the Food and Drug Administration (FDA) approved *tofacitinib* (Xeljanz, Pfizer), which is a JAK inhibitor for the treatment of rheumatoid arthritis (RA). Oral tofacitinib is indicated for the treatment of active RA, in adult patients who had inadequate responses to methotrexate and/or other DMARDs. Tofacitinib is primarily a JAK1/JAK 3 inhibitor.[17] Therefore, this drug would block the production of various key cytokines (IL-2, IL-6, IFN-γ, and IL-17), which have been implicated in the pathogenesis of IBD.[17,18]

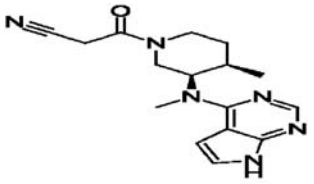

Tofacitinib [Compound 6]

Tofacitinib has shown good clinical results in a phase 2 UC trial. Specifically, Pfizer reported positive phase 2 (OCTAVE trials) results in patients with moderate to severe UC. Tofacitinib has now entered phase 3 trials (Fig. 1). In contrast, the phase 2 clinical results with tofacitinib in CD patients were not as positive. Therefore, tofacitinib is being tested in a larger phase 2B trial for CD (Fig. 2).[19]

Filgotinib (Galapagos NV) is a selective JAK1 inhibitor in clinical development for CD. It is currently in a phase 2 clinical trial, which is evaluating efficacy as both an induction and maintenance therapy.[20]

Filgotinib belongs to the class of compounds known as *n*-phenylbenzamides. These are benzamides that are N-linked to a phenyl group via the carboxamide group. The structure of filgotinib is shown in the succeeding text.

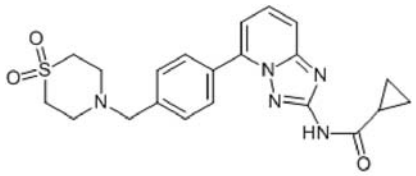

Filgotinib [Compound 7]

Peficitinib (Astellas Pharma) is another JAK1 inhibitor that was in clinical development for IBD.[18] However, phase 2 clinical trials for UC have been discontinued. It is interesting that unlike filgotinib, the clinical testing of this compound focused on UC (instead of CD) patients.

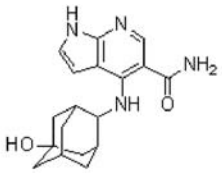

Peficitinib (ASP 015K) [Compound 8]

5.16.2.3 CCR9 Antagonists

CCR9 is a chemokine receptor expressed on memory/effector CD4 + T cells and selectively binds the chemokine CCL25. Inhibition of the CCR9/CCL25 interaction has been proposed as a therapeutic approach for CD.[21] CCR9 is a tissue-specific lymphocyte trafficking molecule that selectively attracts T lymphocytes to the intestine.

Vercirnon is an oral small-molecule CCR9 antagonist. It is a selective antagonist of the CCR9 and is being developed by GlaxoSmithKline under license from ChemoCentryx Inc. for the potential treatment of intestinal inflammatory diseases, including CD and celiac disease. Vercirnon may hasten the elimination of inflammatory T cells from the intestines, thus potentially speeding

clinical recovery by reducing the longevity of flare-ups associated with IBD.[22] This drug has advanced to phase 3 clinical trials for CD.[23] The chemical structure of vercirnon is shown in the succeeding text.

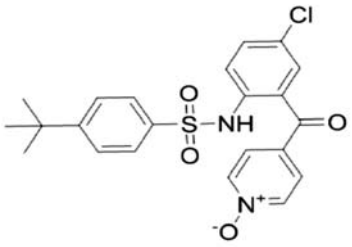

Vercirnon (GSK-1605786; CCX282-B, Vercimon, Traficet-EN) [Compound 9]

5.16.2.4 Alpha (α)-4 Integrin Antagonists

AJM300 is an orally active small-molecule inhibitor of the α-4 integrin. Similarly to vedolizumab (Entyvio, Millennium Pharmaceuticals, Inc.), which is a marketed α4β7 integrin antagonist, the pharmacological goal of this approach is to block lymphocyte trafficking (via adhesion molecules) into the inflamed intestine. This compound showed efficacy in a murine IL-10-deficient T-cell transfer model of colitis.[24] AJM300 showed efficacy as an induction therapy for patients with active UC, in a phase 2a clinical trial.[25] As indicated in **Fig. 1**, AJM300 has entered phase 3 clinical studies in Japan, for the treatment of UC. Safety issues (i.e., progressive multifocal leukoencephalopathy (PML)) may be a potential concern with this pharmacological approach.[26] However, PML was not reported to be a problem in the aforementioned phase 2a clinical trial.[25]

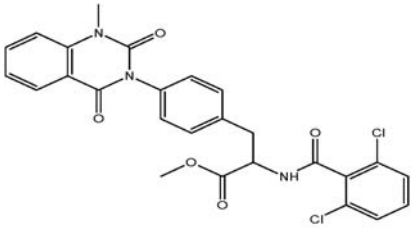

AJM300 [Compound 10]

5.16.2.5 Immunomodulator Drugs

Laquinimod is an interesting orally active small-molecule immunomodulatory drug. This drug is being developed by Teva Pharmaceuticals for the treatment of various autoimmune diseases. Using an IL-10-deficient mouse model of colitis, investigators showed that laquinimod ameliorated colitis. The reduction in colonic inflammation was associated with a restoration of colonic barrier function, as well as a decrease in NF-kB signaling.[27] A recent phase 2 study demonstrated the efficacy and safety of this drug in CD patients. Laquinimod is currently in phase 3 trials for the treatment of moderate to severe CD.[28]

Laquinimod is the successor of Active Biotech's failed experimental immunomodulator linomide (Roquinimex). *Linomide* is a quinoline derivative immunostimulant that increases NK cell activity and macrophage cytotoxicity. It also inhibits angiogenesis and reduces the secretion of TNF-α. Linomide had been investigated as a treatment for some cancers (including as adjuvant therapy after bone marrow transplantation in acute leukemia) and autoimmune diseases, such as multiple sclerosis and recent-onset type I diabetes. Several trials of this drug have been terminated due to serious cardiovascular toxicity.[29]

Previous preclinical publications by the lead author demonstrated that vidofludimus (a novel immunomodulatory from 4SC AG) has a dual mechanism of action. Specifically, vidofludimus can (1) reduce colonic IL-17 production by inhibiting STAT3 and NF-kB activation and (2) act as a DHODH (dihydroorotate dehydrogenase) inhibitor, which attenuates T-cell expansion in the colon.[30,31] This compound was effective in mouse DSS and TNBS models, as well as a rat model of TNBS-induced colitis.[30,31] Vidofludimus showed good efficacy and safety in an initial phase 2A European IBD clinical trial, involving both CD and UC

patients.[32] This clinical trial showed an 88.5% response rate for patients with IBD.[32] Further clinical testing of vidofludimus is anticipated in 2016.

The structures of these three immunomodulatory drugs are shown in the succeeding text.

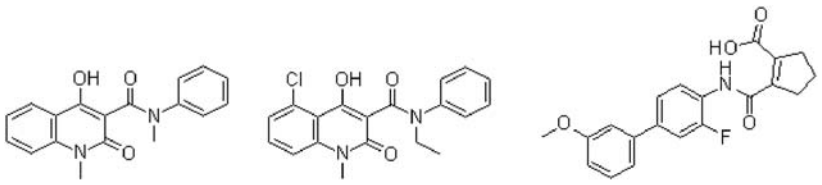

Linomide (Roquinimex) [Compound 11]

Laquinimod [Compound 12]

Vidofludimus [Compound 13]

5.16.2.6 Mucosal Barrier Enhancer Drug

LT-102 is an interesting small-molecule compound that is under development for IBD by Lipid Therapeutics. Essentially, it is a retarded-release phosphatidylcholine-rich phospholipid agent. In this regard, the mucus layer coating the GI tract is predominantly composed of water, glycoproteins, lipids, other proteins, and nucleic acids.[33] Phospholipids, although minor constituents of the GI mucus, are indispensable for the maintenance of an intact barrier function where they play a role in establishing the hydrophobic surface by virtue of their amphipathic nature.[34] Phosphatidylcholine (PC), the major mucus phospholipid, has been found to be substantially reduced in the mucus of patients with UC compared with patients with CD and healthy controls, independent of the state of inflammation.[35] A lack of PC could result in a reduction in surface hydrophobicity, enabling the invasion of luminal noxious agents. However, by virtue of being integrated in the plasma membranes of enterocytes, PC also participates in various potential pro-inflammatory pathways including tumor necrosis factor-α (TNF-α) signaling, activation of NF-kB cytokine expression, and mitogen-activated protein kinase.[36] Based on its inherent structural role in the colonic mucosa, it has been hypothesized that PC reconstitution (by LT-102) in the colonic mucus of patients with UC could help to restore the structure and density of the mucus, improving the barrier function and preventing inflammation in UC.[37] The goal of this phosphatidylcholine agent is to improve mucosal barrier function in patients with mild/moderate UC. According to a company release statement, LT-102 will enter phase 3 trials for UC in 2016.[38]

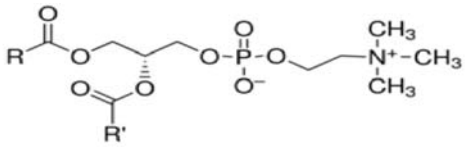

R, R' = fatty acid residues

L-α-Phosphatidylcholine (LT-102) [Compound 14]

5.16.3 Novel Small-Molecule Approaches for IBD: Preclinical Results

5.16.3.1 Synthetic Triterpenoids

Synthetic triterpenoids (like *CDDO-Im/CDDO imidazolide*, Geisel School of Medicine, Dartmouth College) can inhibit activation of the STAT3 and NF-kB pathways.[39,40] Interestingly, synthetic triterpenoids also upregulate the expression of nuclear factor E2-related factor 2 (Nrf2), which positively regulates the levels of important antioxidant enzymes like heme oxygenase-1 (HO-1).[41] Previous results from the lead author's laboratory showed that CDDO-Im could effectively inhibit colonic STAT3 activation and attenuate various parameters of acute DSS-induced colitis in mice.[42] Another synthetic triterpenoid (*CDDO-Me/bardoxolone*) suppressed the development of colitis-associated cancer (CAC) in mice.[43] As a whole, these data suggest that synthetic triterpenoids could be an interesting therapeutic approach in patients with IBD. However, a phase 3 clinical trial (by Reata Pharmaceuticals) evaluating bardoxolone for the treatment of chronic kidney disease was terminated, when drug-treated patients were found to have a higher rate of heart-related adverse events.[44] In a more recent phase 2 study for patients with pulmonary arterial hypertension, the drug was relatively well tolerated with no serious adverse events.[45] Nevertheless, with regard to the potential development of any synthetic triterpenoids for IBD, safety considerations would be a top priority during ongoing clinical trials.

From a chemical perspective, compounds belonging to the most potent molecules of oleanolic derivatives include 2-cyano-3,12-dioxooleana-1,9(11)-dien-28-oic acid (CDDO) and its C-28 methyl ester, CDDO-Me. Both compounds have enone functions in their A- and C-rings and an electron-withdrawing nitrile group at the C-2 position in the A-ring.[46] A chemical feature shown to be essential for the activity of the synthetic triterpenoids focuses on the electron-withdrawing nitrile group that activates the A-ring enone, thereby allowing it to serve as an acceptor of a Michael addition to covalently, but reversibly, bind activated sulfhydryl groups of cysteine residues in protein targets.[47] Relevant chemical structures are shown in the succeeding text.

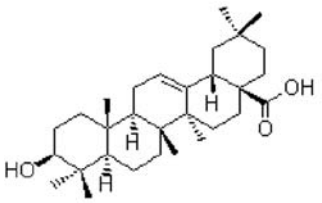

Oleanolic acid (Oleanic acid)

[Compound 15]

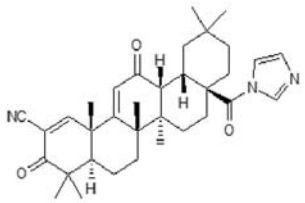

CDDO Im

[Compound 16]

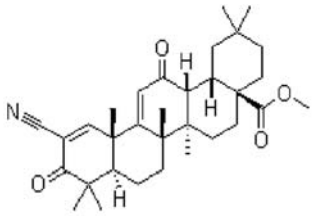

Bardoxolone methyl (CDDO-Methyl ester)

[Compound 17]

5.16.3.2 ROR-γT Inhibitors

Retinoic acid-related orphan nuclear receptor gamma T (ROR-γT) is the key transcription factor for IL-17 expressing cells. Importantly, ROR-γT expression is upregulated in various animal models of colitis.[48] Recent data showed that various parameters of TNBS-induced colitis were improved by treatment with VPR-7 (a specific small-molecule ROR-γT inverse agonist, discovered by Visionary Pharmaceuticals).[48] Theoretically, VPR-7 could also block the transcription of possible pro-inflammatory receptors (IL-23R) cytokines (IL-17 and IL-21) and chemokines (CCL20) putatively involved in the pathogenesis of IBD.[48,49] Development of ROR-γT inhibitors may be an interesting approach for IBD (particularly as a maintenance therapy), as recent data suggest that Th17 cells (due to plasticity) can be converted to atypical Th1 cells during the pathogenesis of IBD.[4,5] Various pharmaceutical companies have focused on ROR-γT as a therapeutic target during the past 5 years. In this regard, Lycera and Merck previously announced an agreement (in 2011) to develop an alliance targeting ROR-γT for the treatment of autoimmune disease.[50]

5.16.3.3 Sphingosine Kinase Inhibitors

As mentioned earlier, sphingosine kinase (SK) catalyzes the formation of S1P from sphingosine. SK inhibitors like ABC294640 (discovered by Apogee Biotechnology and being developed by RedHill Biopharma) have shown efficacy in rodent models of colitis and colitis-associated cancer.[51–53] The potential utility of SK inhibitors as drugs for IBD was discussed in previous papers.[54,55] Selective small-molecule inhibitors of SK1, like *RB-005* and analogs (originally discovered by Queens College, The City University of New York), would be interesting compounds to test in IBD models.[56] RB-005 is selective inhibitor of SK1 over SK2. The hydroxyl group in the heterocyclic ring is important for inhibition of SK1 by RB-005. Replacement of the 4-OH group with a 4-methyl group yields a moderate inhibitor of both SK1 and SK2, whereas the 3-OH region isomer is a selective but less potent SK1 inhibitor.[57] The structure of RB-005 is shown in the succeeding text.

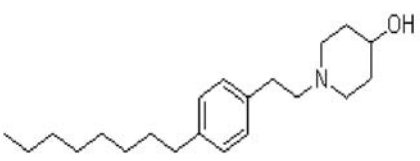

RB-005 (1-(4-octylphenethyl) piperidin-4-ol)

[Compound 18]

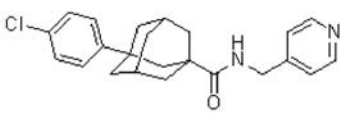

ABC294640

[Compound 19]

5.16.3.4 Immunoproteasome Subunit Inhibitors

Exposure of cells to pro-inflammatory cytokines (IFN-γ, IL-1β, and TNF-α) causes the replacement of constitutive catalytic proteasome subunits with immunoproteasome subunits. These immunoproteasome subunits (low molecular mass polypeptide (LMP)2 (b1i), multicatalytic endopeptidase complex-like-1 (b2i), and LMP7 (b5i)) have been implicated in the pathogenesis of colitis.[58,59]

Of note, a novel small-molecule LMP7-selective inhibitor (*PR-957*, or *ONX-0914*, which was originally discovered by Proteolix Inc.) strongly reduced the symptoms of DSS-induced colitis in mice, following IV administration of the compound.[59] Interestingly, treatment with PR-957 also attenuated the expression of key cytokines (IL-6, TNF-α, IL-23, and IL-17) associated with this colitis.[60] Some previous review papers have discussed the potential utility of immunoproteasome subunit inhibitors for the treatment of chronic inflammatory diseases like IBD.[54,61]

Carfilzomib (PR-171, discovered by Proteolix Inc. and developed by Onyx Pharmaceuticals) is an approved drug for multiple myeloma. It is a modified tetrapeptidyl epoxide and an analog of epoxomicin (see structures in the succeeding text).

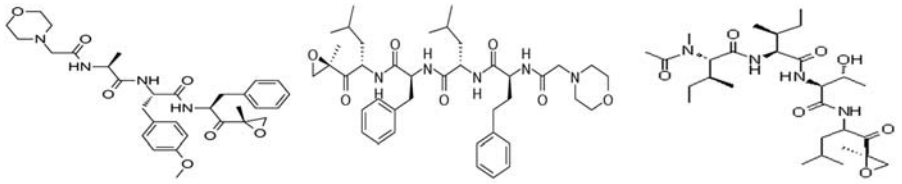

PR-957 (ONX-0914) [Compound 20]

Carfilzomib (PR-171) [Compound 21]

Epoxomicin [Compound 22]

It is also a selective proteasome inhibitor. Carfilzomib irreversibly and selectively binds to *N*-terminal threonine-containing active sites of the 20S proteasome, the proteolytic core particle within the 26S proteasome. This 20S core has 3 catalytic active sites: the chymotrypsin, trypsin, and caspase-like sites. Inhibition of the chymotrypsin-like site by carfilzomib (particularly the β5i subunit) is the most effective target in decreasing cellular proliferation, ultimately resulting in cell cycle arrest and apoptosis of cancerous cells. At higher doses, carfilzomib reportedly will also inhibit both the trypsin- and caspase-like sites.[62]

5.16.3.5 Melanin-Concentrating Hormone (MCH) Receptor 1 Antagonists

MCH is a peptide that is produced in both the brain and the GI tract.[63] Previous work from the lead author's laboratory showed that two small-molecule MCH receptor 1 antagonists (DABA-821 and DABA-822, originally discovered by Procter & Gamble Pharmaceuticals, Inc.) attenuated various parameters of TNBS-induced colitis in mice.[64] However, DABA-822 was not effective in mice with established colitis due to IL-10 deficiency.[65] Further studies with specific MCH receptor 1 antagonists are needed in other animal models of IBD, in order to better understand the true clinical potential of this pharmacological approach.[66–68] The structures of these DABA compounds are shown here.

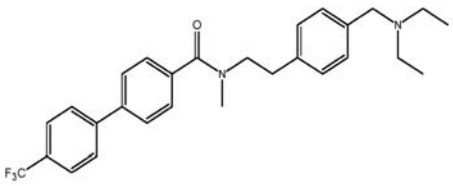

DABA-821 [Compound 23]

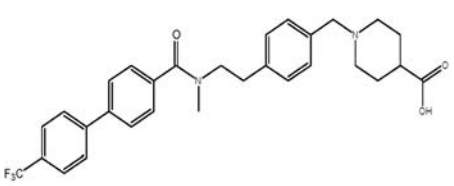

DABA-822 [Compound 24]

5.16.3.6 Receptor-Interacting Protein Kinase 1 (RIP1 and RIP3) Inhibitors

A recent review paper suggested that receptor-interacting protein kinase 1 (RIP1 and RIP3) played a role in the control of apoptosis and inflammatory cytokine production, independent of the traditional role in necrosis.[69] Liu and colleagues found that necrostatin 1 (a specific inhibitor of RIP1 and RIP3) attenuated various parameters of acute DSS-induced colitis in mice.[70] Other investigators have suggested that the development of RIP kinase 1 inhibitors may be an effective pharmacological approach for the treatment of

IBD.[71] Necrostatin 1 was originally discovered by academic investigators at Tufts University. The structure of necrostatin1 is shown in the succeeding text.

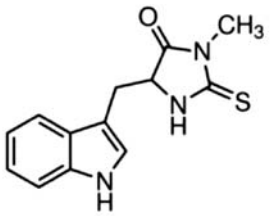

Necrostatin 1 or 5-(1H-indol-3-ylmethyl)-3-methyl-2-thioxo-4-Imidazolidinone [Compound 25]

5.16.4 Natural Product-Derived Small-Molecule Approaches for IBD

An excellent review article recently summarized various botanical drugs, which may be potentially used in the treatment of IBD.[72] When considering this approach, it is important to remember that the development of natural products as primary therapies for IBD would likely require the isolation of an individual active component from the plane extract. An example is curcumin.[72]

5.16.4.1 Curcumin

Curcumin is the main active component of *Curcuma longa* (Zingiberaceae), commonly known as turmeric. Several pharmacological activities have been reported for curcumin, including antioxidant, antimicrobial, anticancer, and anti-inflammatory properties.[73] It has three vital functionalities central to its biological activities including an aromatic *o*-methoxy phenolic group, α, β-unsaturated β-diketo moiety, and a seven-carbon linker (see structure in the succeeding text). Extensive research in the last two decades has provided evidence for the role of these different functional groups in its crucial biological activities.

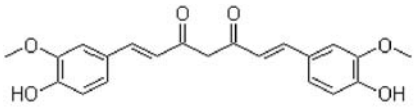

Curcumin (Diferuloylmethane) [Compound 26]

Curcumin has demonstrated efficacy in different experimental models of colitis.[74–77] The anticolitis mechanism of action for curcumin may be related to the inhibition of p38 MAPK and/or NF-kB.[72,77] Of note, clinical studies have shown that curcumin has demonstrated some evidence of efficacy for the treatment of IBD.[72,78] A very recent clinical study showed that curcumin plus mesalamine therapy was superior to the combination of placebo and mesalamine for inducing remission in patients with mild/moderate UC.[79] Other postulated mechanisms of actions for curcumin are due to its ability to scavenge free radicals and modify multiple signaling pathways (especially MAPK and ERK), thereby affecting the expression of different proteins implicated in the intestinal inflammatory cascade, like MPO, COX-2, iNOS, or LOX.[80]

5.16.4.2 Berberine

Berberine is an interesting compound, which is derived from various plants. It is an alkaloid isolated mainly from *Hydrastis canadensis*. Berberine is also found in many other plants. It is relatively toxic parenterally but has been used orally for various parasitic and fungal infections and as antidiarrheal agent.[81] Berberine belongs to the class of organic compounds known as protoberberine alkaloids and derivatives. These are alkaloids with a structure based on a protoberberine moiety, which consists of a 5,6-dihydrodibenzene moiety fused to a quinolizinium and forming the 5, 6-dihydrodibenzo (a, g) quinolizinium skeleton (see the structure in the succeeding text).

Berberine inhibits both NF-kB and STAT3 pathways.[82] The lead author (and others) proposed that these two intracellular pathways could be important in the pathogenesis of IBD and CAC.[54,83] Numerous studies have shown berberine to

be effective in rodent models of IBD.[82,84–87] This compound would appear to be an interesting candidate for future testing in IBD patients.

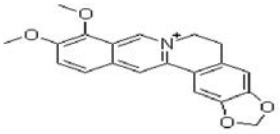

Berberine (5,6-Dihydro-9,10-dimethoxybenzo[g]-1,3-benzodioxolo[5,6-a]quinolizinium) [Compound 27]

5.16.4.3 Silibinin

Silymarin is an extract of milk thistle seeds. Silymarin's primary constituents are the flavonolignan isomers silybins A and B, isosilybins A and B, silychristin (also known as silichristin), silydianin (also known as silidianin), and their flavonoid precursor, taxifolin. In the literature, the mixture of the silybins A and B is often referred to as silibinin. These compounds exist as equimolar mixtures as trans diastereoisomers. These diastereomers have very similar ^{1}H and ^{13}C NMR spectra and have no characteristic signals for facile identification of the individual isomers.[88] A number of other chemically related compounds have been found in the fruits including dehydrosilybin, desoxysilychristin, desoxysilydianin, silandrin, silybinome, silyhermin, and neosilymermin. The common feature of these compounds is a flavonolignan skeleton ($C_{25}H_{22}O_{10}$, MW 482). Basically, flavonolignan nucleus consists of the dihydroflavonol taxifolin linked to coniferyl alcohol moiety through an oxeran ring. The oxeran ring is responsible for the biological activity of silymarin, and opening of this ring results in loss of activity. Only silybins and isosilybins contain the 1,4-dioxane ring system in their structure. Silybin and isosilybin have the same trans conformation of C-2, C-3, and C-7′ and C-8′. Silybin is considered the major and most active component in silymarin.[89]

These compounds are known for their antioxidant and anti-inflammatory properties.[90] Human clinical trials have investigated milk thistle or silymarin primarily in individuals with hepatitis or cirrhosis, although small studies have been reported about individuals with acute lymphoblastic leukemia, prostate cancer, breast cancer, and hepatocellular carcinoma.[91] With relevance to this article, silibinin was effective in a rat model of hapten-induced colitis.[92] The chemical structure of silibinin and other silymarin constituents is shown in the succeeding text.

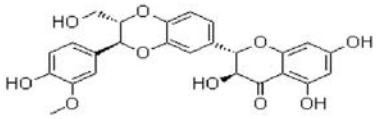

Silibinin (Silybin) [Compound 28]

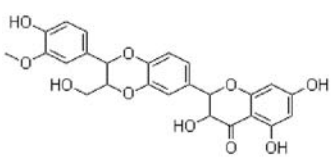

Isosilybin (Isosilibinin) [Compound 29]

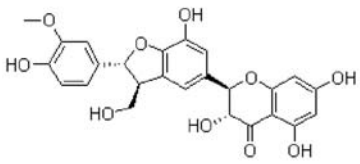

Silychristin (Silicristin) [Compound 30]

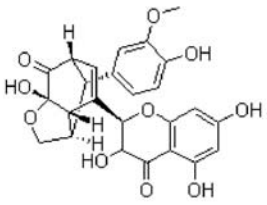

Silydianin (Silidianin) [Compound 31]

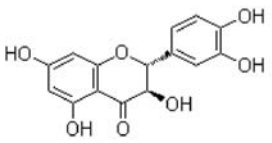

Taxifolin [Compound 32]

5.16.4.4 Triterpene Ganoderic Acid C1 (GAC1)

Ganoderic acid C1 (GAC1) is a triterpenoid that has been isolated from *Ganoderma lucidum* (*reishi*), which is the lingzhi mushroom.[93] There are many ganoderic acids that have been isolated and characterized, of which ganoderic acid A and ganoderic acid B are the best characterized. GAC1 belongs to the class of compounds known as tirucallane and euphane triterpenoids with

a structure based on either the tirucallane or the euphane skeleton. These compounds are obtained by backbone rearrangement of a dammarane-based precursor molecule.[94]

GAC1 decreased TNF-α production by macrophages from CD patients. It also decreased pro-inflammatory cytokine production (TNF-α, IL-17, and IFN-γ) by inflamed colonic biopsied from CD patients. These effects were related to inhibition of the NF-kB pathway.[93] GAC1 should undergo future testing in animal models of IBD.

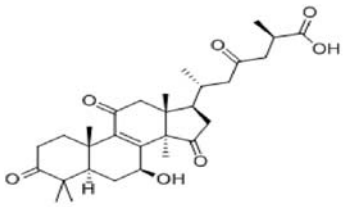

Ganoderic Acid C1 (GAC1) [Compound 33]

5.16.4.5 Gallic Acid

Gallic acid is a phenolic compound also known as 3,4,5-trihydroxybenzoic acid. It is found both as a free state and as a constituent of tannins, namely, gallotannin. Gallic acid and its derivatives are present in nearly every part of the plant, such as bark, wood, leaf, fruit, root, and seed.[95] Gallic acid has been shown to effectively suppress DSS-induced colitis in mice. Intriguingly, the anticolitis effect was attributed to the suppression of colonic NF-kB and STAT3 activation.[54,96] Here is the structure of gallic acid.

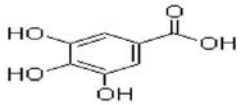

Gallic acid (3, 4, 5-Trihydroxybenzoic acid; Pyrogallol-5-carboxylic acid) [Compound 34]

5.16.4.6 Diallyl Sulfide

Diallyl sulfide (di-2-propenyl sulfide, DAS) belongs to the class of organosulfur compounds known as dialkylthioethers, containing a thioether group that is substituted by two alkyl groups. Diallyl sulfide is found in animal foods, *Allium* species (garlic oil), Japanese horseradish (*Wasabia japonica*), and black mustard (*Brassica nigra*) powder and cooked beef. Diallyl sulfide has antioxidant and anti-inflammatory activities. Like other natural product-derived compounds cited in this article, the compound inhibits inflammatory signaling mediated by NF-kB and STAT3.[97,98] This small-molecule compound was also effective after oral administration for attenuating DSS-induced colitis in mice.[98]

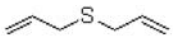

Diallyl sulfide (Allyl sulfide) [Compound 35]

5.16.4.7 6-Gingerol

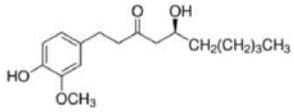

6-Gingerol [Compound 36]

Gingerols are phenolic compounds in ginger (*Zingiber officinale Roscoe*, *Zingiberaceae*). Gingerols are the most abundant pungent compounds in fresh roots, and several gingerols of various chain lengths (n6 to n10) are present in ginger, with the most abundant being 6-gingerol.[99] These compounds have antioxidant and anti-inflammatory activities.[100] 6-Gingerol, a pungent ingredient of ginger, has a wide array of pharmacologic effects. 6-Gingerol has been tested in the murine DDS-colitis model. Two separate

laboratories demonstrated the efficacy of 6-gingerol against this colitis. One group attributed the anticolitis activity to activation of adenosine monophosphate-activated protein kinase (AMPK) activity.[100,101]

5.16.4.8 Rutin

Rutin (rutoside or quercetin-3-*O*-rutinoside) is a flavonoid contained in many plants. The major sources of rutin for medical use include buckwheat, Japanese pagoda tree, and *Eucalyptus macrorhyncha*. It is thought to be an antioxidant, a free radical scavenger, and an iron-chelator working similarly to the antioxidant mechanism of 5-ASA.[102,103] After oral administration, rutin is hydrolyzed in the GI tract to release quercetin, which is responsible for many of the actions of rutin. The structure of rutin is shown here.

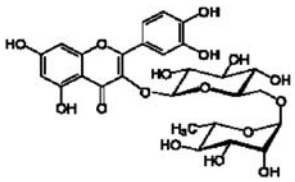

Rutin (quercetin-3ß-D-rutinoside) [Compound 37]

Animal studies suggest rutin has anti-inflammatory activity against TNBS-induced colitis in rats, as well as T-cell transfer colitis in mice.[104,105]

The inhibitory effects of natural products on the expression of pro-inflammatory cytokines (e.g., tumor necrosis factor-α (TNF-α)), intercellular adhesion molecule expression and pro-inflammatory mediators (such as inducible nitric oxide synthase (iNOS) and cyclooxygenase 2 (COX2)), master transcription factors (such as nuclear factor-kB (NF-kB)), and reactive oxygen species (ROS) (summarized earlier) and their utmost safety profile suggest that they have encouraging potential for the treatment of IBD. However, randomized controlled clinical investigations in large cohorts of patients are needed to fully evaluate the clinical potential of these compounds. It is possible that some of these natural products may find utility as adjunct therapies in IBD patients. In this regard, clinical trials that examine the efficacy of natural products in combination with traditional IBD drugs (e.g., 5-aminosalicylate derivatives and corticosteroids) are eagerly anticipated in the future.

5.16.5 Summary: Small-Molecule Compounds for IBD Therapy

Over the last decade, some degree of success has been achieved in developing biological drugs (monoclonal antibodies) for treating patients with IBD. Recently, new small-molecule inhibitors have also been developed for chronic inflammatory diseases like IBD. It is anticipated that over the next 5 years, some of the small-molecule drug approaches described in this article will find utility for the treatment of IBD. In this regard, the results of relevant and ongoing clinical studies are eagerly awaited in 2016.

References

1. Ordas, I.; Eckmann, L.; Talamini, M.; et al. Ulcerative Colitis. *Lancet* **2013,** *380* (9853), 1606–1619.
2. Fuss, I.; Strober, W. The Role of IL-13 and NKT Cells in Experimental and Human Ulcerative Colitis. *Mucosal Immunol.* **2008,** *1* (Suppl. 1), S31–S33.
3. Kleinschek, M. A.; Boniface, K.; Sadevoka, S.; et al. Circulating and Gut Resident Human Th17 Cells Express CD161 and Promote Intestinal Inflammation. *J. Exp. Med.* **2009,** *206* (3), 525–534.
4. Annunziato, F.; Santarlasci, V.; Maggi, L.; et al. Reasons for Rarity of Th17 Cells in Inflammatory Sites of Human Disorders. *Semin. Immunol.* **2013,** *25,* 299–304.
5. Cosmi, L.; Liotta, F.; Maggi, E.; et al. Th17 and Non-Classic Th1 Cells in Chronic Inflammatory Disorders: Two Sides of the Same Coin. *Int. Arch. Immunol.* **2014,** *164,* 171–177.
6. Kunkel, G. T.; Maceyka, M.; Milstein, S.; et al. Targeting the Sphingosine-1-Phosphate Axis in Cancer, Inflammation and Beyond. *Nat. Rev. Drug Discov.* **2013,** *12,* 688–702.
7. Gonzalez-Cabrera, P. J.; Brown, S.; Studer, S. M.; et al. SIP Signaling: New Therapies and Opportunities. *F1000 Prime Rep.* **2014,** *6* (109), 1–7.
8. Daniel, C.; Sartory, N. A.; Zahn, N.; et al. FTY20 Ameliorates Oxazolone Colitis in Mice by Directly Affecting T Helper Type 2 Functions. *Mol. Immunol.* **2007,** *44* (13), 3305–3316.
9. Daniel, C.; Sartory, N. A.; Zahn, N.; et al. FTY20 Ameliorates Th-1 Mediated Colitis in Mice by Directly Affecting the Functional Activity of CD4 + CD25 + Regulatory T Cells. *J. Immunol.* **2007,** *178* (4), 2458–2468.
10. Deguchi, Y.; Andoh, A.; Yagi, Y.; et al. The S1P Modulator FTY720 Prevents the Development of Experimental Colitis in Mice. *Oncol. Rep.* **2006,** *16* (4), 699–703.
11. Fujii, R.; Kana, T.; Nemoto, Y.; et al. FTY720 Suppresses CD4 + CD44highCD62L-Effector Memory T Cell Mediated Colitis. *Am. J. Physiol. Gastointest. Liver Physiol.* **2006,** *291* (2), G267–G274.
12. Mizushima, T.; Ito, T.; Kishi, D.; et al. Therapeutic Effects of a New Lymphocyte Homing Reagent FTY720 in Interleukin-10-Gene Deficient Mice With Colitis. *Inflamm. Bowel Dis.* **2004,** *10* (3), 189–192.
13. Budde, K.; Schmouder, R. L.; Brunkhorst, R.; et al. Pharmacodynamics of Single Doses of the Novel Immunosuppressant FTY720 in Stable Renal Transplant Patients. *Am. J. Transplant.* **2003,** *3,* 846–854.
14. Fujita, T.; Inoue, K.; Yamamoto, S.; et al. Fungal Metabolites. Part 11. A Potent Immunosuppressive Activity Found in Isaria Sinclairii Metabolite. *J. Antibiot.* **1994,** *47,* 208–215.

15. Buzard, D. J.; Kim, S. H.; Lopez, L.; et al. Discovery of ADP334: Design of a Clinical Stage Functional Antagonist of the Sphingosine-1-Phosphate-1 Receptor. *ACS Med. Chem. Lett.* **2004,** *5* (12), 1313–1317.
16. Chi, H. Sphingosine-1-Phosphate and Immune Regulation: Trafficking and Beyond. *Trend. Pharmacol. Sci.* **2011,** *32* (1), 16–24.
17. Tanaka, Y.; Yamaoka, K. Jak Inhibitor Tofacitinib for Treating Rheumatoid Arthritis: From Basic to Clinical. *Mod. Rheumatol.* **2013,** *23* (3), 415–424.
18. Amiot, A.; Biroulet, L. P. Current, New and Future Biological Agents on the Horizon for the Treatment of Inflammatory Bowel Diseases. *Ther. Adv. Gastroenterol.* **2015,** *8* (2), 66–82.
19. Sandborn, W. J. New Targets for Small Molecules in Inflammatory Bowel Disease. *Gastroenterol. Hepatol.* **2015,** *11* (5), 338–340.
20. Goodwin E. Patient Recruitment Completed in FITZROY Phase 2 Crohn's Disease Study With Filgotinib. *Galapagos NV*, Aug 6, 2015.
21. Arseneu, K. O.; Cominelli, F. Vercirnon for the Treatment of Crohn's Disease. *Expert Opin. Invest. Drugs* **2013,** *22* (7), 907–913.
22. Bekker, P.; Ebsworth, K.; Walters, M. J. CCR9 Antagonists in the Treatment of Ulcerative Colitis. *Mediat. Inflamm.* **2015,** *2015,* 628340.
23. Feagan, B. F.; Sandborn, W. J.; D'Haens, G. D.; et al. Randomized Clinical Trial: Vercirnon, an Oral CCR9 Antagonist, vs. Placebo as Induction Therapy in Active Crohn's Disease. *Aliment. Pharmacol. Ther.* **2015,** *42,* 1170–1181.
24. Sugiura, T.; Kageyama, S.; Androu, A.; et al. Oral Treatment With a Novel Small Molecule Alpha 4 Integrin Antagonist, AJM300, Prevents the Development of Experimental Colitis in Mice. *J. Crohn's Colitis* **2013,** *7* (11), e533–e542.
25. Yoshimura, N.; Watanabe, M.; Motoya, S.; et al. Safety and Efficacy of AJM300, an Oral Antagonist of α4 Integrin, in Induction Therapy for Patients With Active Ulcerative Colitis. *Gastroenterology* **2015,** *149* (7), 1775–1783.
26. Goldsmith, J. R.; Higgins, P. D. R. The Current Status of the Inflammatory Bowel Disease Drug Pipeline: A Promising Time. *Pract. Gastroenterol.* **2015,** 20–27.
27. Sun, J.; Shen, X.; Dong, J.; et al. Laquinimod Ameliorates Spontaneous Colitis in Interleukin-10-Gene-Deficient Mice With Improved Barrier Function. *Int. Immunopharmacol.* **2015,** *29,* 423–432.
28. D'Haens, G.; Sandborn, W. J.; Colombel, J. F.; et al. A Phase II Study of Laquinimod in Crohn's Disease. *Gut* **2015,** *64,* 1227–1235.
29. Tan, I. L.; Lycklama, A.; Nijeholt, G. J.; et al. Linomide in the Treatment of Multiple Sclerosis: MRI Results from Prematurely Terminated Phase-III Trials. *Mult. Scler.* **2000,** *6* (2), 99–104.
30. Fitzpatrick, L. R.; Demi, L.; Hoffmann, C.; et al. 4SC-101, a Novel Immunosuppressive Drug, Inhibits IL-17 and Attenuates Colitis in two Murine Models of Inflammatory Bowel Disease. *Inflamm. Bowel Dis.* **2010,** *16* (10), 1763–1777.
31. Fitzpatrick, L. R.; Small, J. S.; Doblhofer, R.; et al. Vidofludimus Inhibits Colonic Interleukin-17 and Improves Hapten-Induced Colitis in Rats by a Unique Dual Mode of Action. *J. Pharmacol. Exp. Ther.* **2012,** *342* (3), 850–860.
32. Herrlinger, K. R.; Dicluseu, M.; Fellerman, K.; et al. Efficacy, Safety and Tolerability of Vidofludimus in Patients With Inflammatory Bowel Disease: The ENTRANCE Study. *J. Crohn's Colitis* **2013,** *7,* 636–643.
33. Braun, A.; Treede, I.; Gotthardt, D.; et al. Alterations of Phospholipid Concentration and Species Composition of the Intestinal Mucus Barrier in Ulcerative Colitis: A Clue to Pathogenesis. *Inflamm. Bowel Dis.* **2009,** *15,* 1705–1720.
34. Treede, I.; Braun, A.; Sparla, R.; et al. Anti-Inflammatory Effects of Phosphatidylcholine. *J. Biol. Chem.* **2007,** *282,* 27155–27156.
35. Ehehalt, R.; Wagenblast, J.; Erben, G.; et al. Phosphatidylcholine and Lysophosphatidylcholine in Intestinal Mucus of Ulcerative Colitis Patients: A Quantitative Approach by Nanoelectrospray-Tandem Mass Spectrometry. *Scand. J. Gastroenterol.* **2004,** *39,* 737–742.
36. Schneider, H.; Braun, A.; Fullekrug, J.; et al. Lipid Based Therapy for Ulcerative Colitis-Modulation of Intestinal Mucus Membrane Phospholipids as a Tool to Influence Inflammation. *Int. J. Mol. Sci.* **2010,** *11,* 4149–4164.
37. Stremmel, W.; Merle, U.; Zahn, A.; et al. Retarded Release Phosphatidylcholine Benefits Patients With Chronic Active Ulcerative Colitis. *Gut* **2005,** *54,* 966–971.
38. Semedo, D. Nestle Health Science Licenses Rights for LT-02 as Ulcerative Colitis Therapy. *IBD News Today*, September 21, 2015.
39. Yore, M. M.; Liby, K. T.; Honda, T.; et al. The Synthetic triterpenoid1-[2-Cyano3, 12-Dioxooleana-1,9 (11)-Dien-28-oyl)-Dien-28-oyl]Imidazole Blocks Nuclear Factor-kB Activation Through Direct Inhibition of IkB Kinase b. *Mol. Cancer Ther.* **2006,** *5,* 3232–3239.
40. Liby, K.; Voong, N.; Williams, C. R.; et al. The Synthetic Triterpenoid CDDO-Imidazole Suppresses STAT Phosphorylation and Induces Apoptosis in Myeloma and Lung Cancer Cells. *Clin. Cancer Res.* **2006,** *12,* 4288–4293.
41. Yates, M. S.; Kwak, M. K.; Egner, P. A.; et al. Potent Protection Against Aflatoxin-Induced Tumorigenesis Through Induction of Nrf2-Regulated Pathways by the Triterpenoid 1-[2-cyano3, 12-Dioxooleana-1,9 (11)-Dien-28-oyl)-Dien-28-oyl] Imidazole. *Cancer Res.* **2006,** *66,* 2488–2494.
42. Fitzpatrick, L. R.; Stonesifer, E.; Small, J. S.; et al. The Synthetic Triterpenoid (CDDO-Im) Inhibits STAT3, as Well as IL-17, and Improves DSS-Induced Colitis in Mice. *Inflammopharmacology* **2014,** *22* (6), 341–349.
43. Choi, S. H.; Kim, B. G.; Robinson, J.; et al. Synthetic Triterpenoid Induces 15-PGDH Expression and Suppresses Inflammation-Driven Colon Carcinogenesis. *J. Clin. Invest.* **2014,** *124* (6), 2472–2482.
44. de Zeeuw, D.; Akizawa, T.; Audhya, P.; et al. Bardoxolone Methyl in Type 2 Diabetes and Stage 4 Chronic Kidney Disease. *N. Engl. J. Med.* **2013,** *369,* 2492–2503.
45. Reata Pharmaceuticals. Reata Announces Initial Phase 2 Pulmonary Arterial Hypertension Data for Bardoxolone Methyl and Planned Initiation of a Phase 3 Study. *Reata Pharmaceuticals*, Oct 27, 2015.
46. Honda, T.; Rounds, B. V.; Gribble, G. W.; et al. Pharmacodynamic Characterization of Chemopreventive Triterpenoids as Exceptionally Potent Inducers of Nrf2-Regulated Genes. *Mol. Cancer Ther.* **2007,** *6,* 154–162.
47. Liby, K. T.; Yore, M. M.; Sporn, M. B. Triterpenoids and Rexinoids as Multifunctional Agents for the Prevention and Treatment of Cancer. *Nat. Rev. Cancer* **2007,** *7,* 357–369.
48. Fitzpatrick, L. R. Ror-Gamma T Inhibition as a Pharmacological Approach for Inflammatory Bowel Disease. *Med. Res. Arch.* **2015,** *2* (2). http://dx.doi.org/10.18103/mra.v0i4.334.
49. Fitzpatrick, L. R.; Zapf, J.; Flood, E. M.; et al. Efficacy of a Novel Small Molecule Rorγt Inverse Agonist in Mouse DSS and TNBS Models of Inflammatory Bowel Disease. *Gastroenterology* **2015,** *148* (4 Suppl. 1), S-26.
50. Sheridan, C. Footrace to Clinic Heats up for T-Cell Nuclear Receptor Inhibitors. *Nat. Biotechnol.* **2013,** *31,* 370.
51. Maines, L. W.; Fitzpatrick, L. R.; French, K. J.; et al. Suppression of Ulcerative Colitis in Mice by Orally Available Inhibitors of Sphingosine Kinase. *Dig. Dis. Sci.* **2008,** *53* (4), 997–1012.
52. Maines, L. W.; Fitzpatrick, L. R.; Green, C. L.; et al. Efficacy of a Novel Sphingosine Kinase Inhibitor in Experimental Crohn's Disease. *Inflammopharmacology* **2010,** *18* (2), 73–85.
53. Chumanevich, A. A.; Poudyal, D.; Cui, X.; et al. Suppression of Colitis-Driven Colon Cancer in Mice by a Novel Small Molecule Inhibitor of Sphingosine Kinase. *Carcinogenesis* **2010,** *31* (10), 1787–1793.
54. Fitzpatrick, L. R. Novel Pharmacological Approaches for Inflammatory Bowel Disease: Targeting Key Intracellular Pathways and the IL-23/IL-17 Axis. *Int. J. Inflamm.* **2012,** *389404.*
55. Snider, A. J.; Ali, W. H.; Sicca, J. A.; et al. Distinct Roles for Hematopoietic and Extra-Hematopoietic Sphingosine Kinase-1 in Inflammatory Bowel Disease. *PLoS One* **2014,** *9* (12), e113998.
56. Baeek, D. J.; MacRitchie, N.; Anthony, N. G.; et al. Structure–Activity Relationships and Molecular Modeling of Sphingosine Kinase Inhibitors. *J. Med. Chem.* **2015,** *56* (22), 9310–9327.
57. Baeek, D. J.; MacRitchie, N.; Pyne, N. J.; et al. Synthesis of Selective Inhibitors of Sphingosine Kinase 1. *Chem. Commun. (Camb.)* **2013,** *49* (21), 2136–2138.
58. Fitzpatrick, L. R.; Small, J. S.; Poritz, L. S.; et al. Enhanced Intestinal Expression of the Proteasome Subunit low Molecular Mass Polypeptide 2 in Patients With Inflammatory Bowel Disease. *Dis. Colon Rectum* **2007,** *50* (3), 337–348.

59. Visekruna, A.; Joeris, T.; Seidel, D.; et al. Proteasome-Mediated Degradation of IkappaB Alpha and Processing of p105 in Crohn's Disease and Ulcerative Colitis. *J. Clin. Invest.* **2006,** *116* (12), 3195–3203.
60. Baisler, M.; Dajee, M.; Moll, C.; et al. Prevention of Experimental Colitis by a Selective Inhibitor of the Immunoproteasome. *J. Immunol.* **2010,** *185* (1), 634–641.
61. Miller, Z.; Ao, L.; Kim, K. B.; et al. Inhibitors of the Immunoproteasome: Current Status and Future Directions. *Curr. Pharm. Des.* **2013,** *19* (22), 41404151.
62. Kuhn, D. J.; Chen, Q.; Voorhees, P. M.; et al. Potent Activity of Carfilzomib, a Novel, Irreversible Inhibitor of the Ubiquitin-Proteasome Pathway, Against Preclinical Models of Multiple Myeloma. *Blood* **2007,** *110* (9), 3281–3290.
63. Kokkotou, E.; Moss, A. C.; Torres, D.; et al. Melanin-Concentrating Hormone as a Mediator of Intestinal Inflammation. *Proc. Natl. Acad. Sci. U. S. A.* **2008,** *105* (30), 10613–10618.
64. Fitzpatrick, L. R.; Small, J. S.; Zhang, G. Melanin-Concentrating Hormone Receptor 1 Antagonists Attenuate TNBS-Induced Colitis in Mice. *Gastroenterology* **2009,** *136,* A403.
65. Ziogas, D. C.; Karagiannis, A. K.; Geiger, B. M.; et al. Inflammation-Induced Functional Connectivity of Melanin-Concentrating Hormone and IL-10. *Peptides* **2014,** *55,* 58–64.
66. Ziogas, D. C.; Gras-Miralles, B.; Mustafa, S.; et al. Anti-Melanin-Concentrating Hormone Treatment Attenuates Chronic Experimental Colitis and Fibrosis. *Am. J. Physiol. Gastrointest. Liver Physiol.* **2013,** *304* (10), G876–G884.
67. Moore, N. A.; Sargent, B. J.; Guzzo, P. R.; et al. From Preclinical to Clinical Development: The Example of a Novel Treatment for Obesity. *Neurobiol. Dis.* **2014,** *61,* 47–54.
68. Szali, K. K.; Beke, G.; Eles, J.; et al. Recent Patents on Novel MCH1 Receptor Antagonists as Potential Anti-Obesity Drugs. *Rec. Pat. CNS Drug. Discov.* **2014,** *9* (2), 122–140.
69. Morlwaski, K.; Chan, F. K. Necrosis-Dependent and Independent Signaling of the RIP Kinases in Inflammation. *Cytokine Growth Factor Rev.* **2014,** *25* (2), 167–174.
70. Liu, Z. Y.; Wu, B.; Guo, Y. S.; et al. Necrostatin-1 Reduces Intestinal Inflammation and Colitis-Associated Tumorigenesis in Mice. *Am. J. Cancer Res.* **2015,** *5* (10), 3174–3185.
71. Vlantis, K.; Wullaert, A.; Polykratis, A.; et al. NEMO Prevents RIP Kinase 1-Mediated Epithelial Cell Death and Chronic Intestinal Inflammation by NF-kB-Dependent and -Independent Functions. *Immunity* **2016,** *44,* 533–567.
72. Algieri, F.; Nogales, A. R.; Cabezs, M. E. R.; et al. Botanical Drugs as an Emerging Strategy in Inflammatory Bowel Disease: A Review. *Mediat. Inflamm.* **2015,** 1–14.
73. Hatcher, H.; Planalp, R.; Cho, J.; et al. Curcumin: From Ancient Medicine to Current Clinical Trials. *Cell. Mol. Life Sci.* **2008,** *65* (11), 1631–1652.
74. Salh, B.; Assi, K.; Templeman, V.; et al. Curcumin Attenuates DNB-Induced Murine Colitis. *Am. J. Physiol. Gastrointest. Liver Physiol.* **2003,** *285* (1), G235–G243.
75. Deguchi, Y.; Andoh, A.; Inatomi, O.; et al. Curcumin Prevents the Development of Dextran Sulfate Sodium (DSS)-Induced Experimental Colitis. *Dig. Dis. Sci.* **2007,** *52* (11), 2993–2998.
76. Ukil, A.; Maity, S.; Karmakar, S.; et al. Curcumin, the Major Component of Food Flavor Turmeric, Reduces Mucosal Injury in Trinitrobenzene Sulphonic Acid-Induced Colitis. *Br. J. Pharmacol.* **2003,** *139* (2), 209–218.
77. Camacho-Barquero, L.; Villegas, I.; Sanchez-Calvo, J. M.; et al. Curcumin, a *Curcuma longa* Constituent, Acts on MAPK p38 Pathway Modulating COX-2 and iNOS Expression in Chronic Experimental Colitis. *Int. Immunopharmacol.* **2007,** *7* (3), 333–342.
78. Brumatti, L. V.; Marcuzzi, A.; Tricarico, P. M.; et al. Curcumin and Inflammatory Bowel Disease: Potential and Limits of Innovative Treatments. *Molecules* **2014,** *19,* 2127–21153.
79. Lang, A.; Salomon, N.; Wu, J. C. Y.; et al. Curcumin in Combination With Mesalamine Induces Remission in Patients With Mild-to-Moderate Ulcerative Colitis in a Randomized Controlled Trial. *Clin. Gastroenterol. Hepatol.* **2015,** *18,* 1444–1449.
80. Epstein, J.; Docena, G.; MacDonald, T. T.; et al. Curcumin Suppresses p38 Mitogen-Activated Protein Kinase Activation, Reduces IL-1β and Matrix Metalloproteinase-3 and Enhances IL-10 in the Mucosa of Children and Adults With Inflammatory Bowel Disease. *Br. J. Nutr.* **2010,** *103* (6), 824–832.
81. Overington, J. P.; Al-Lazikani, B.; Hopkins, A. L. How Many Drug Targets are There? *Nat. Rev. Drug Discov.* **2006,** *5* (12), 993–996.
82. Li, C.; Yebin, X.; Li, S.; et al. Berberine Ameliorates TNBS Induced Colitis by Inhibiting Inflammatory Responses and Th1/Th17 Differentiation. *Mol. Immunol.* **2015,** *67* (2 Pt B), 444–454.
83. Liang, J.; Nagahashi, M.; Kim, E. Y.; et al. Sphingosine-1-Phosphate Links Persistent STAT3 Activation, Chronic Intestinal Inflammation, and Development of Colitis-Associated Cancer. *Cancer Cell* **2014,** *23* (1), 107–120.
84. Li, Y. H.; Zhang, M.; Xiao, H. T.; et al. Addition of Berberine to 5-Aminosalicylic Acid for Treatment of Dextran Sulfate Sodium-Induced Chronic Colitis in C57BL/6 Mice. *PLoS One* **2015,** *10* (12), e0144101.
85. Hong, T.; Yang, Z.; Lu, C. F.; et al. Suppressive Effect of Berberine on Experimental Dextran Sulfate Sodium Induced Colitis. *Immunopharmacol. Immunotoxicol.* **2012,** *34* (3), 391–397.
86. Minaiyan, M.; Ghannadi, A.; Mahzouni, P.; et al. Comparative Study of Berberis Vulgaris and Berberine Chloride Effects on Acetic Acid-Induced Colitis in Rats. *Iran J. Pharm. Res.* **2011,** *10* (1), 97–104.
87. Lee, I. A.; Hyun, Y. J.; Kim, D. H. Berberine Ameliorates TNBS-Induced Colitis by Inhibiting Lipid Peroxidation, Enterobacterial Growth and NF-κB Activation. *Eur. J. Pharmacol.* **2010,** *648* (1-3), 162–170.
88. Lee, D. Y. W.; Liu, Y. Molecular Structure and Stereochemistry of Silybin A, Silybin B, Isosilybin A, and Isosilybin B, Isolated from *Silybum marianum* (Milk Thistle). *J. Nat. Prod.* **2003,** *66,* 1171–1174.
89. Kim, S.; Choi, J. H.; Lim, H. I.; et al. Silibinin Prevents TPA-Induced MMP-9 Expression and VEGF Secretion by Inactivation of the Raf/MEK/ERK Pathway in MCF-7 Human Breast Cancer Cells. *Phytomedicine* **2009,** *16,* 573–580.
90. Zhu, H. J.; Brinda, B. J.; Chavin, K. D.; et al. An Assessment of Pharmacokinetics and Antioxidant Activity of Free Silymarin Flavonolignans in Health Volunteers: A Dose Escalation Study. *Drug Metab. Dispos.* **2013,** *41,* 1469–1475.
91. Scambia, G.; De Vincenzo, R.; Ranelletti, F. O.; et al. Antiproliferative Effect of Silybin on Gynaecological Malignancies: Synergism With Cisplatin and Doxorubicin. *Eur. J. Cancer* **1996,** *5* (32A), 877–882.
92. Esmaily, H.; Vaziri-Bami, A.; Miroliaee, A. E.; et al. The Correlation Between NF-κB Inhibition and Disease Activity by Coadministration of Silibinin and Ursodeoxycholic Acid in Experimental Colitis. *Fundam. Clin. Pharmacol.* **2011,** *25,* 723–733.
93. Liu, C.; Dunkin, D.; Lai, J.; et al. Anti-Inflammatory Effects of *Ganoderma lucidum* Triterpenoid in Human Crohn's Disease Associated With Downregulation of NF-κB Signaling. *Inflamm. Bowel Dis.* **2015,** *23* (8), 1918–1925.
94. Yannai, S. *Dictionary of Food Compounds With CD-ROM: Additives, Flavors, and Ingredients;* Chapman & Hall: Boca Raton, 2004.
95. Daglia, M.; Di Lorenzo, A.; Nabavi, S. F.; Talas, Z. S.; Nabavi, S. M. Polyphenols: Well Beyond the Antioxidant Capacity: Gallic Acid and Related Compounds as Neuroprotective Agents: You are What You Eat!. *Curr. Pharm. Biotechnol.* **2014,** *15* (4), 362–372.
96. Pandurangan, A. K.; Mohebali, N.; Esa, N. M.; et al. Gallic Acid Suppresses Inflammation in Dextran Sodium Sulfate-Induced Colitis in Mice; Possible Mechanisms. *Int. ImmunoPharmacol.* **2013,** *28,* 1034–1043.
97. Bai, A. P.; Ouyang, Q.; Hu, R. W. Diallyl Trisulfide Inhibits Tumor Necrosis Factor-Alpha Expression in Inflamed Mucosa of Ulcerative Colitis. *Dig. Dis. Sci.* **2005,** *8,* 1426–1431.
98. Lee, H. J.; Lee, H. G.; Choi, K. S.; et al. Diallyl Trisulfide Suppresses Dextran Sodium Sulfate-Induced Mouse Colitis: NF-kB and STAT3 as Potential Targets. *Biochem. Biophys. Res. Commun.* **2013,** *437,* 267–273.
99. Chrubasik, S.; Pittler, M. H.; Roufogalis, B. D. Zingiberis Rhizoma: A Comprehensive Review on the Ginger Effect and Efficacy Profiles. *Phytomedicine* **2005,** *12,* 1684–1701.
100. Alayi, B. O.; Adadara, I. A.; Farombi, E. O. Pharmacological Activity of 6-Gingerol in Dextran Sulphate Sodium-Induced Ulcerative Colitis in BALB/c Mice. *Phytother. Res.* **2015,** *29* (4), 566–572.
101. Chang, K. W.; Kuo, C. Y. 6-Gingerol Modulates Proinflammatory Responses in Dextran Sodium Sulfate (DSS)-Treated CACO-2 Cells and Experimental Colitis in Mice Through Adenosine Monophosphate-Activated Protein Kinase (AMPK) Activation. *Food Funct.* **2015,** *6* (10), 3334–3341.

102. Kostyuk, V. A.; Potapovich, A. I. Antiradical and Chelating Effects in Flavonoid Protection Against Silica-Induced Cell Injury. *Arch. Biochem. Biophys.* **1998,** *355,* 43–48.
103. Escarpa, A.; Gonzalez, M. C. High-Performance Liquid Chromatography With Diode-Array Detection for the Determination of Phenolic Compounds in Peel and Pulp from Different Apple Varieties. *J. Chromatogr. A* **1998,** *823,* 331–337.
104. Cruz, T.; Galvez, J.; Ocete, M. A.; et al. Oral Administration of Rutoside can Ameliorate Inflammatory Bowel Disease in Rats. *Life Sci.* **1998,** *62,* 687–695.
105. Mascaraque, C.; Aranda, C.; Ocon, B. Rutin has Intestinal Anti-Inflammatory Effects in the CD4+ CD62L+ T Cell Transfer Model of Colitis. *Pharmacol. Res.* **2014,** *90,* 48–57.

Relevant Websites

https://www.nlm.nih.gov/—National Library of Medicine. Collection of Scientific Holdings. It is an US Government Web-site.
http://www.ncbi.nlm.nih.gov/pubmed/—PubMed. PubMed comprises more than 25 million citations for biomedical literature from MEDLINE, life science journals, and online books. Citations may include links to full-text content from PubMed Central and publisher web sites.
http://reatapharma.com/—Reata Pharmaceuticals. This is a US-based pharmaceutical company, which is developing Bardoxolone.
http://www.visionarypharmaceutical.com/—Visionary Pharmaceuticals. This is a US-Based company that is involved in the development of ROR-γT Inhibitors.
http://www.4sc.de/—4SC AG. This is a German-based biotech company that was involved in the pre-clinical and clinical development of Vidofludimus.

5.17 Recent Epidemiological Changes in Infectious Diseases

MJ Pucci, Spero Therapeutics, Cambridge, MA, United States
C Callebaut and A Cathcart, Gilead Sciences Inc., Foster City, CA, United States
K Bush, Indiana University, Bloomington, IN, United States

© 2017 Elsevier Ltd. All rights reserved.

5.17.1 Introduction 512
5.17.2 Antibacterial Resistance 514
5.17.2.1 Selected Drug Classes 514
5.17.2.1.1 β-Lactam resistance 514
5.17.2.1.2 β-Lactamase Inhibitor Resistance 516
5.17.2.1.3 Aminoglycoside resistance 517
5.17.2.1.4 Quinolone resistance 518
5.17.2.1.5 Macrolide resistance 519
5.17.2.1.6 Tetracycline resistance 520
5.17.2.1.7 Glycopeptide resistance 522
5.17.2.1.8 Oxazolidinone resistance 523
5.17.2.1.9 Colistin resistance 524
5.17.2.1.10 Trimethoprim resistance 525
5.17.2.1.11 Daptomycin resistance 526
5.17.2.2 Selected Key Pathogens 526
5.17.2.2.1 Carbapenem-resistant Enterobacteriaceae 526
5.17.2.2.2 Antibiotic-resistant *N. gonorrhoeae* 527
5.17.2.2.3 Clostridium difficile 527
5.17.2.2.4 Multidrug-resistant *Acinetobacter* 529
5.17.2.2.5 Methicillin-resistant *Staphylococcus aureus* 529
5.17.2.2.6 Multidrug-resistant *Pseudomonas aeruginosa* 530
5.17.2.2.7 Mycobacterium tuberculosis 530
5.17.3 Antifungal Resistance 532
5.17.4 Antiviral Resistance 532
5.17.4.1 Human Immunodeficiency Virus 534
5.17.4.1.1 HIV reverse transcriptase 534
5.17.4.1.2 HIV protease 535
5.17.4.1.3 HIV integrase 536
5.17.4.1.4 HIV envelope (ENV) 536
5.17.4.1.5 Drug combinations 537
5.17.4.2 Hepatitis B Virus 537
5.17.4.2.1 Nucleos(t)ide reverse transcriptase inhibitors 537
5.17.4.2.2 New viral targets 538
5.17.4.3 Hepatitis C Virus 538
5.17.4.3.1 Nucleotide analogue NS5B inhibitors 538
5.17.4.3.2 Nonnucleotide NS5B inhibitors 539
5.17.4.3.3 NS5A inhibitors 539
5.17.4.3.4 NS3/4A protease inhibitors 539
5.17.4.3.5 Drug combinations 539
5.17.4.4 Influenza 540
5.17.4.4.1 M2 inhibitors (adamantanes) 540
5.17.4.4.2 Neuraminidase inhibitors 540
5.17.4.4.3 New influenza antivirals 542
5.17.5 Conclusions 542
References 542

Abbreviations

ABSSSI acute bacterial skin and soft tissue infection
ADV adefovir
AIDS acquired immunodeficiency syndrome
AME aminoglycoside-modifying enzyme

ANSORP Asian Network for Surveillance of Resistant Pathogens
ARV antiretroviral drug
BLI β-lactamase inhibitor
CA-MRSA community-associated-MRSA
cART combination antiretroviral therapy
cccDNA covalently closed circular DNA
CDC Centers for Disease Control and Prevention
CDI *Clostridium difficile* infection
CF cystic fibrosis
CHB chronic hepatitis B
C_{min} minimum (trough) plasma concentrations
CRE carbapenem-resistant Enterobacteriaceae
cSSSI complicated skin and skin structure infection
DAA direct-acting antiviral agent
DHFR dihydrofolate reductase
DTG dolutegravir
EC_{95} antiviral activity as effective inhibitory concentration
ENV envelope gene product
ESBL extended-spectrum β-lactamase
ETV entecavir
EVG elvitegravir
FDA Food and Drug Administration
HAART highly active antiretroviral therapy
HBV hepatitis B virus
HCAP healthcare-associated infections
HCV hepatitis C virus
HIV human immunodeficiency virus
IAI intraabdominal infection
IN integrase
INSTI integrase strand transfer inhibitor
IQ inhibitory quotient
LAM lamivudine
LdT telbivudine
LPS lipopolysaccharide
MBL metallo-β-lactamase
MDR multidrug-resistant
MDR-TB multidrug-resistant tuberculosis
MIC minimum inhibitory concentration
MIC_{90} minimum inhibitory concentrations for 90% of the isolates tested
MLS macrolide–lincosamide–streptogramin B
MRSA methicillin-resistant *Staphylococcus aureus*
MSSA methicillin-susceptible staphylococci
MTB *Mycobacterium tuberculosis*
N[t]RTI nucleos(t)ide reverse transcriptase inhibitor
NAI neuraminidase inhibitor
NDM New Delhi metallo-β-lactamase
NNRTI nonnucleoside reverse transcriptase inhibitor
NRTI nucleoside reverse transcriptase inhibitor
PBP penicillin-binding protein
PI protease inhibitor
PK pharmacokinetics
PR protease
RAL raltegravir
RAV resistance-associated variants
RMT rRNA methyl transferase
RND resistance-nodulation-cell division
RT reverse transcriptase
SSTI skin and soft tissue infection
SVR sustained virologic response
SXT trimethoprim–sulfamethoxazole
TB tuberculosis
TDF tenofovir prodrug
TFV tenofovir
UTI urinary tract infection
VAP ventilator-associated pneumonia
VRE vancomycin-resistant enterococci
VRSA vancomycin-resistant *Staphylococcus aureus*
WHO World Health Organization
XDR-TB extensively drug-resistant tuberculosis

5.17.1 Introduction

Since their introduction into clinical medicine over 70 years ago, perhaps no drugs have had more impact on both quantity and quality of human life than antibiotics.[1] Formerly fatal bacterial infections could now be cured relatively rapidly and completely in the majority of cases. Yet very soon after antibiotics were introduced, resistance to these drugs was observed in a number of pathogens.[2] The pharmaceutical industry was able to keep ahead of this resistance issue by a combination of discovery and development of new agents/novel classes and modifications of old ones. However, as we move into the early 21st century, the bacteria are steadily gaining ground such that occasional clinical isolates are now observed that are essentially untreatable.[3–6] There is increasing discussion of the possibility of returning to a pre-antibiotic era with increased incidence of mortality due to previously curable infections.

Antibiotic resistance genes are located both on the bacterial chromosome and, increasingly, on transmissible extrachromosomal elements.[7] Important resistant clones such as methicillin-resistant *Staphylococcus aureus* (MRSA) USA300,[8] *Escherichia coli* ST131,[9] and *Klebsiella pneumoniae* ST258[10] have disseminated rapidly worldwide in recent years. This spread has been facilitated by a combination of factors including interspecies gene transmission, poor sanitation and hygiene in communities and hospitals, and the increasing frequency of global travel. Diseases that formerly would have remained isolated are now just a plane ride away from the rest of the world.

Table 1 Overview of major bacterial resistance concerns[a]

Drug class/pathogen	*Drug*	*Elevated resistance rates (%) (country, year)*
Aminoglycosides		
E. coli	Amikacin	60 (India, 2009)
P. aeruginosa	Gentamicin	84 (India, 2010)
K. pneumoniae		91 (Romania, 2006)
Carbapenems		
E. coli		13 (India, 2012)
P. aeruginosa		54 (Greece, 2013)
K. pneumoniae		60 (India, 2013)
A. baumannii		71 (Greece, 2011)
		43 (United States, 2012)
Cephalosporins (expanded spectrum)		
E. coli		87 (Belarus, 2012)
K. pneumoniae		90 (India, 2011)
		94 (Romania, 2006)
		69 (Romania, 2013)
P. aeruginosa	Ceftazidime	89 (India, 2010)
Fluoroquinolones		
E. coli		89 (India, 2011)
P. aeruginosa		84 (India, 2010)
K. pneumoniae		87 (Belarus, 2012)
N. gonorrhoeae		99.8 (China, 2012–13)[11]
A. baumannii		91 (Serbia, 2014)
Glycopeptides		
E. faecalis	Vancomycin	7 (Greece, 2013)
E. faecium	Ampicillin	89 (United States, 2012)
	Vancomycin	76 (United States, 2012)
Macrolides		
S. pneumoniae		45 (Malta, 2006)
		42 (Turkey, 2013)
Penicillins		
S. aureus (MRSA)	Oxacillin	55 (United States, 2006)
		44 (United States, 2012)
S. pneumoniae		87 (Thailand, 2010)
Piperacillin/tazobactam		
Enterobacter spp.		65 (India, 2014)
P. aeruginosa		62 (India, 2014)
Tetracycline		
N. gonorrhoeae		23 (United States, 2013)[12]
		50 (Korea, 2011–13)[13]

[a]Data from Center for Disease Dynamics, Economics & Policy http://resistancemap.cddep.org/ except where noted.

Key recent examples of notable resistance spread are summarized on a topline level in **Table 1**.[11,13] These examples include antibiotic-resistant *Neisseria gonorrhoeae*, which emerged in Vietnam in 1967, then spread to the Philippines, and finally to the United States and other parts of the world where it is becoming a major health concern.[14–16] The New Delhi metallo-β-lactamase-1 (NDM-1) enzyme, first reported in 2008, has now spread worldwide.[17] A study found NDM-1-producing bacteria (including *Shigella boydii* and *Vibrio cholera*) in 2 (4%) of 50 drinking water samples and 51 (30%) of 171 seepage samples in New Delhi, India, indicating the possibility of acquiring resistance outside healthcare facilities.[18] Finally, increasing rates of resistance to colistin and polymyxin B, often treatments of last resort for Gram-negative organisms, are being reported from countries around the world, including South Korea, Italy, Greece, and Saudi Arabia.[19] The recent discovery of the plasmid-encoded *mcr-1* gene, conferring colistin resistance, in animals and humans in China is a truly disturbing finding and this gene has since been found in other areas of the world as well.[20] Moreover, there is some evidence of cross-resistance to colistin and host antimicrobial peptides that are part of the body's immune response.[21] More detailed descriptions of these examples along with others are found here.

Other factors influence the continued spread of antibiotic resistance in the world today. The sheer breadth of antibiotic usage is itself an important driver: these drugs are among the most commonly purchased and are widely available in a number of countries without a physician's prescription. As a result worldwide antibiotic consumption continues to increase, exerting constant selective pressure for expanded resistance. There have been attempts at antibiotic stewardship in recent years by curbing the unnecessary use of these drugs and some successes have been achieved in recent years.[22] However, the usage trends remain of concern, and certainly more needs to be done to preserve the utility of these valuable agents. In this article, recent resistance trends for major antibacterial,

antifungal, and antiviral agents will be described as well as additional updates on selected key pathogens. For bacteria, we have divided the discussion into updates for selected drug classes and updates on selected key pathogens.

5.17.2 Antibacterial Resistance

5.17.2.1 Selected Drug Classes

5.17.2.1.1 β-Lactam resistance

β-Lactam antibiotics represent one of the oldest, and currently most prescribed classes of antibacterial agents in clinical use (Fig. 1).[23] The β-lactams include penicillins (**1**), cephalosporins (**2**), carbapenems (**3**), and monobactams (**4**), all of which are originated from natural products. Most pathogenic bacteria are intrinsically susceptible to at least one of the β-lactam subgroups, although serious resistance to these drugs has emerged in all bacterial species. The β-lactams are bactericidal agents that kill bacteria by interrupting peptidoglycan (cell wall) biosynthesis. Their targets are penicillin-binding proteins (PBPs) that exhibit transglycosylase/transpeptidase or carboxypeptidase activities in both Gram-positive and Gram-negative bacteria.[24] The PBPs are found anchored in the cytoplasmic membrane but are extracytoplasmic; in Gram-negative bacteria, they extend into the periplasmic space. Thus, access to the killing targets for β-lactams is somewhat more facile than for other antibiotics that must enter the cytoplasm.

Penicillins such as penicillin G (**5**) and cloxacillin (**6**) were initially developed to treat infections caused by Gram-positive bacteria, but as Gram-negative bacteria became more prominent, broad-spectrum penicillins such as amoxicillin (**7**) and antipseudomonal penicillins such as piperacillin (**8**) were introduced. Cephalosporins with activity against methicillin-susceptible staphylococci (MSSA) included the early agents like cefazolin (**9**), but have recently been displaced by the "anti-MRSA cephalosporins" ceftobiprole (**10**) and ceftaroline (**11**). The early cephalosporins were followed by the introduction of "expanded-spectrum" cephalosporins cefotaxime (**12**), ceftazidime (**13**), and cefepime (**14**) with potent activity against Gram-negative bacteria. The monobactam aztreonam (**15**) has dedicated anti-Gram-negative activity similar to ceftazidime, but with less potency against current *Pseudomonas aeruginosa* strains. Carbapenems, such as imipenem (**16**) and meropenem (**17**), are considered to be the most potent of the β-lactams, with broad-spectrum activity encompassing MSSA, the streptococci, enteric bacteria, nonfermentative bacteria, and anaerobes.[23]

Because β-lactams are found commonly in the environment,[25] it was not unexpected that β-lactam resistance determinants were identified in ancient sources.[26] Resistance can be due to any or all of the three major factors: (a) modification of an essential PBP target; (b) decreased concentration of the antibiotic at the target site due to increased efflux or decreased penetrability; and (c) enzymatic inactivation of the β-lactam. In the staphylococci, the major β-lactam resistance determinant is conferred by the *mecA* gene that encodes PBP2a, a PBP with low affinity for almost all β-lactam antibiotics with the exception of the recently introduced ceftobiprole and ceftaroline. It is assumed that the *mecA* gene was originally introduced into MRSA from environmental isolates of *Staphylococcus sciuri*.[27] Decreased cellular β-lactam concentrations are important in Gram-negative bacteria, where defective outer membrane proteins can limit the amount of β-lactam that can enter the periplasmic space where the PBPs are located, or where efflux mechanisms serve to pump out intact β-lactam molecules. However, the most common β-lactam resistance mechanism is enzymatic hydrolysis of the β-lactam ring by β-lactamases. Before penicillin was introduced for use in the military during World War II, resistance due to the production of a penicillin-inactivating enzyme had been reported in a strain of "*Bacillus coli*" (or *E. coli*) that had not been exposed to penicillin.[28] Similar penicillin-inactivating activity was soon recognized in staphylococcal clinical isolates from patients treated with the drug.[29] Today β-lactamases are found in $>80\%$ of staphylococcal clinical isolates[30] and are the most frequent β-lactam resistance determinant identified in Gram-negative bacteria. To date more than 2100 unique, naturally occurring β-lactamases have been identified (Bush, personal communication). The most important classes include the penicillinases in staphylococci and many enteric bacteria, the chromosomal AmpC cephalosporinases in Gram-negative bacteria, the extended-spectrum β-lactamases (ESBLs), and the carbapenemases, which encompass those with serine at the active and those that are zinc-containing metallo-β-lactamases (MBLs).[31]

Epidemiological studies show that penicillins are still effective therapeutic agents against some Gram-positive bacteria, including β-hemolytic streptococci.[32–34] Ampicillin (**18**) retains $>90\%$ susceptibility among *Enterococcus faecalis* worldwide,[35,36] but has little useful activity against vancomycin-resistant strains, especially *Enterococcus faecium*.[37] Among the staphylococci, MSSA is usually susceptible to the penicillinase-stable penicillins such as cloxacillin and to cephalosporins such as cefazolin and carbapenems,[38,39] but, with the exception of ceftaroline and ceftobiprole, β-lactams are not effective against MRSA.[40] The "anti-MRSA cephalosporins" generally exhibit susceptibility against $>85\%$ of isolates at their respective susceptible breakpoints (minimum inhibitory concentrations, or MICs <1 μg mL^{-1} for ceftaroline[41,42] and <2 μg mL^{-1} for ceftobiprole[43]). However, recent studies have identified a set of MRSA isolates in Switzerland, the Asia-Pacific region and Africa with MICs for these cephalosporins elevated two- to fourfold higher than the susceptibility breakpoints in strains with missense mutations in PBP2a.[42,43] Susceptibility to penicillin in *Streptococcus pneumoniae* varies by geographic location, with susceptibility as low as 42.9% in Japan[40] to 91% in Europe.[44] Recent increases in penicillin susceptibility in Europe and the United States have been attributed to the introduction of the 13-valent pneumococcal conjugate vaccine.[44,45]

β-Lactamase-mediated resistance is a major factor in the Gram-negative bacteria. Most enteric and nonfermentative bacteria produce a species-specific AmpC-type cephalosporinase that can be produced constitutively at high enzyme concentrations, or that can be induced by β-lactam antibiotics.[46] AmpC enzymes have escaped onto high copy plasmids that ensure elevated levels of these enzymes that confer resistance to many penicillins and cephalosporins, as well as carbapenems when combined with a porin defect. In addition, production of the ESBLs has ensured resistance to almost all β-lactam antibiotics with the exception of the

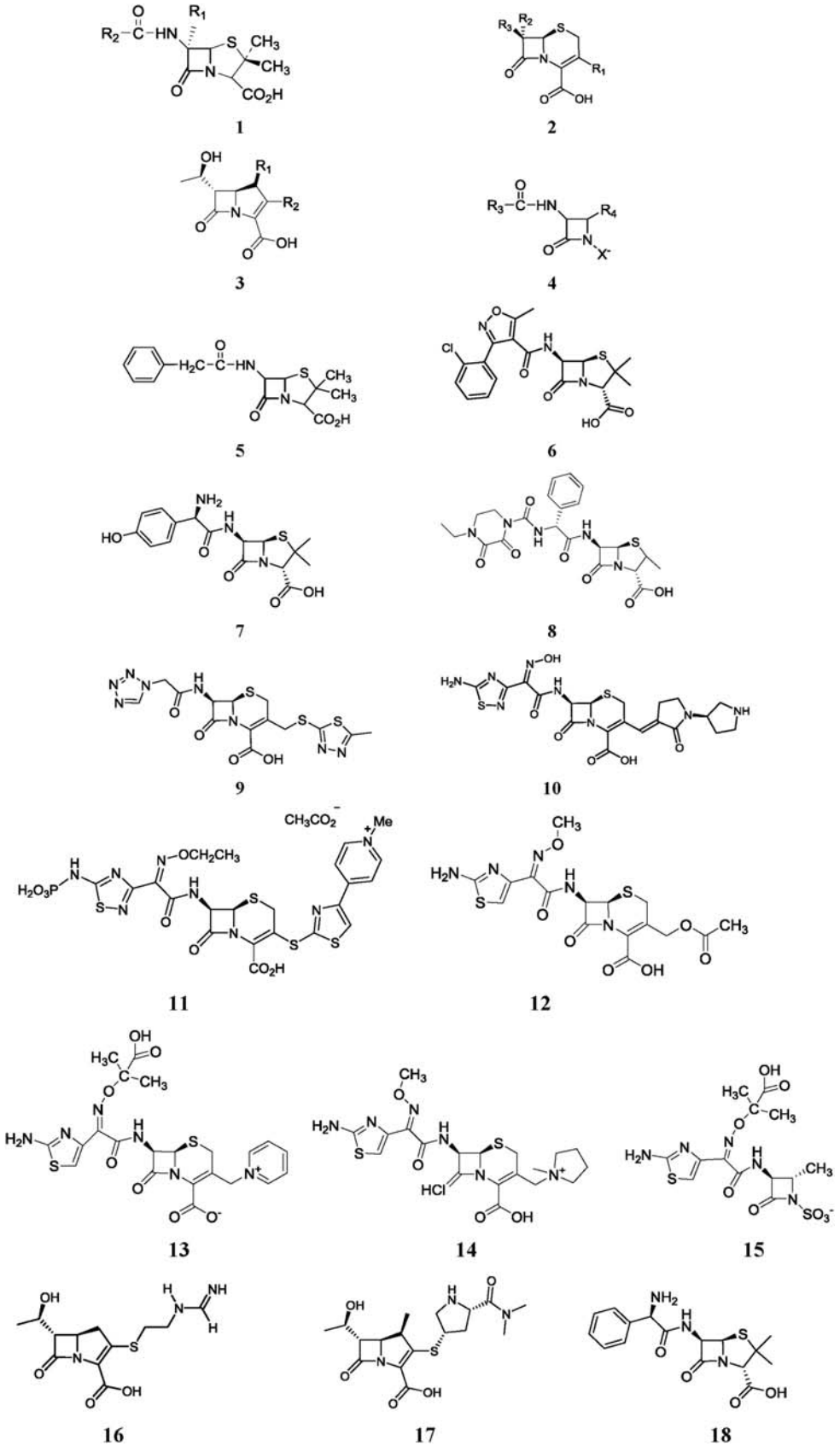

Fig. 1 β-Lactam antibiotics: **1** penicillins, **2** cephalosporins, **3** carbapenems, **4** monobactams, **5** penicillin G, **6** cloxacillin, **7** amoxicillin, **8** piperacillin, **9** cefazolin, **10** ceftobiprole, **11** ceftaroline, **12** cefotaxime, **13** ceftazidime, **14** cefepime, **15** aztreonam, **16** imipenem, **17** meropenem, **18** ampicillin.

carbapenems.[47] These enzymes are usually found on mobile elements that can be readily transferred among the enteric and nonfermentative bacteria. Cephalosporin resistance due to ESBL-producing Enterobacteriaceae isolated from healthy individuals ranges from 2% in the Americas to 46% in the Western Pacific region.[48] In Japan, $<5\%$ of *K. pneumoniae* isolates from complicated urinary tract infections (UTIs) produce ESBLs,[49] compared to China (60%) and Thailand (71.4%) for similar isolates.[50] These latter rates are similar to southern European countries like Greece and Bulgaria where 70–75% of invasive *K. pneumoniae* isolates exhibit resistance to expanded-spectrum cephalosporins (European Centre for Disease Prevention and Control, 2015). ESBL-related resistance in *E. coli* is similar to that seen for *K. pneumoniae* for the Asia-Pacific region, but is generally less in European isolates; Greece and Bulgaria report 21.0% and 40.4% cephalosporin resistance in invasive *E. coli* isolates, respectively (European Centre for Disease Prevention and Control, 2015). Notably, ESBL-producing isolates usually retain full susceptibility to carbapenems.[50] Unfortunately, the latter have become the latest to fall victim to the critical β-lactamase-related resistance mechanisms in Gram-negative pathogens, as plasmid-encoded serine and zinc-containing MBLs have emerged capable of hydrolyzing virtually all β-lactams and especially carbapenems.[51] These enzymes usually travel with other resistance determinants to create Gram-negative pathogens that are multidrug-resistant (MDR).[52] Further information about these β-lactamases is discussed in Section **β-Lactamase Inhibitor Resistance** in this article.

5.17.2.1.2 β-Lactamase Inhibitor Resistance

In an attempt to circumvent the hydrolytic activity of the β-lactamases, novel β-lactamase-inactivating molecules were introduced in combination with β-lactamase-labile penicillins (**Fig. 2**).[53] The first of these inactivating agents was clavulanic acid (**19**), a potent suicide inhibitor of the penicillinases that was combined with amoxicillin (**7**) in an orally bioavailable form and with ticarcillin (**20**) for nosocomial infections. Sulfone-containing β-lactams soon followed, with sulbactam (**21**) combined with ampicillin (**18**), and tazobactam (**22**) combined with piperacillin (**8**). These inhibitors serve to acylate the active site serine of class A penicillinases, with limited hydrolysis of the inhibitor occurring before the enzymes are rendered inactive.[53] They are not effective inhibitors of the AmpC cephalosporinases or of carbapenemases.[54] Resistance to the β-lactamase inhibitor (BLI) combinations has been due largely to the emergence of enzymes inherently resistant to the action of the inhibitors, or to the production of multiple β-lactamases in an organism. To a lesser extent, mutational changes leading to a previously susceptible enzyme becoming resistant to the inhibitor have been seen particularly in TEM and SHV penicillinase variants that have decreased affinities for clavulanic acid or tazobactam.[53] In ESBL-producing *E. coli* UTI isolates from the Asia-Pacific area (2010–13), susceptibility to piperacillin–tazobactam was 88–92%, but only 53–65% of similar ESBL-producing *K. pneumoniae* isolates were susceptible.[50] In studies of US and European pneumonia isolates (2009–12), susceptibility to piperacillin–tazobactam was 29.5% in *Acinetobacter* spp., 72.9% in *P. aeruginosa*, 84.4% in *K. pneumoniae*, and 90.4% in *E. coli*.[55]

New BLI combinations have recently emerged. Tazobactam has been combined with the antipseudomonal cephalosporin ceftolozane (**23**) to provide increased coverage of *P. aeruginosa* and to inhibit some ESBL-producing enteric bacteria.[56,57] Resistance in the enteric bacteria is usually due to the inefficiency of tazobactam to inhibit AmpC cephalosporinases, some ESBLs and the carbapenemases. In *P. aeruginosa*, the primary resistance mechanism that has been identified in vitro is the result of multiple mutations affecting the structure and high-level expression of the AmpC enzyme.[58] Susceptibility to ceftolozane–tazobactam has been reported to be 94–97% in *P. aeruginosa* and 98–100% in *E. coli*, even in ESBL-producing isolates.[56,57] Lower susceptibility occurs in *K. pneumoniae* with 86–89% susceptibility for all isolates, and 44% in isolates with an ESBL phenotype.[57]

Avibactam (**24**) is a novel non-β-lactam diazabicyclooctane BLI[59] that has been approved for marketing in combination with ceftazidime (**13**), but that is also in development with ceftaroline (**11**) and aztreonam (**15**).[54] Unlike the other BLIs, its main mechanism of action is to form reversible covalent bonds with the active site serine in those β-lactamases that utilize serine to facilitate β-lactam hydrolysis.[60,61] Its activity expands the spectrum from the previous BLIs by inhibiting not only the narrow-spectrum

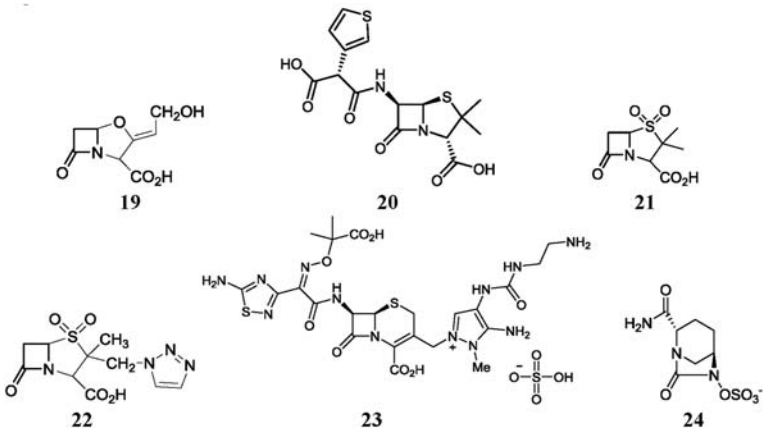

Fig. 2 β-Lactamase inhibitors (BLIs): **19** clavulanic acid, **20** ticarcillin, **21** sulbactam, **22** tazobactam, **23** ceftolozane, **24** avibactam.

penicillinases, but also AmpC cephalosporinases, ESBLs, serine carbapenemases, and some OXA β-lactamases[61]; MBLs are not inhibited.[62] In addition to its β-lactamase inhibitory activity, it binds to essential PBPs in both Gram-positive and Gram-negative bacteria, leading to enhanced synergistic antibacterial activity when avibactam is combined with other cell wall active agents.[63] MICs for ceftazidime, ceftaroline, and aztreonam are frequently decreased up to 128-fold in MDR enteric bacteria when avibactam is present.[64] Ceftazidime susceptibility in a set of 34,062 Enterobacteriaceae isolates increased from 75.6% to 99.5% when tested with avibactam; a subset of non-MBL-producing isolates that were not susceptible to meropenem exhibited 91.4% resistance to ceftazidime, but only 2.3% resistance after the addition of avibactam.[62] In *P. aeruginosa*, the addition of avibactam to ceftazidime increases ceftazidime susceptibility from 84.0% to 96.3%.[65] Resistance to the combination reported from clinical isolates has often been due to mechanisms related to the accompanying β-lactam. In historical *P. aeruginosa* patient isolates, resistance to the ceftazidime–avibactam combination has been observed as a result of permeability barriers and efflux mechanisms.[66] Among recent French carbapenem-nonsusceptible Enterobacteriaceae, the highest MIC for ceftazidime when tested with avibactam was 4 $\mu g\,mL^{-1}$, occurring in porin-deficient *K. pneumoniae* isolates. A novel aztreonam–avibactam resistance mechanism observed in a set of *E. coli* isolates producing the NDM MBL is an insertion in PBP3, thus leading to resistance to an accompanying cephalosporin or monobactam, not to the BLI.[67] Only future use will determine whether the new BLI combinations will select for resistance more frequently than their predecessors.

5.17.2.1.3 Aminoglycoside resistance

Aminoglycosides (Fig. 3; **25**) were among the first antibiotics to be developed as antibacterial drugs with the discovery of streptomycin by Waksman in the early 1940s.[68] This class of drugs has been widely utilized for decades due to broad-spectrum activity encompassing staphylococci and Gram-negative bacteria,[69] but also mycobacteria.[70] Aminoglycosides act by binding to the aminoacyl tRNA site (A-site) of the bacterial ribosome,[71] resulting in the cessation of protein synthesis. They are generally considered to be bactericidal agents,[72] although cidality is often enhanced in the presence of β-lactam antibiotics.[73] The most frequently used agents are gentamicin (**26**), tobramycin (**27**), and amikacin (**28**). They have been utilized for treatment of a variety of bacterial infections including sepsis, skin and soft tissue infections (SSTIs), serious infections of the respiratory tract, serious bone and joint infections, intraabdominal infections (IAIs) (including peritonitis), postoperative infections (including postvascular surgery), ophthalmic disease, the management of cystic fibrosis (CF) with inhaled tobramycin, and tuberculosis (TB) (streptomycin [**29**]) (https://dailymed.nlm.nih.gov/dailymed/search.cfm?startswith=amikacin&x=14&y=12). Because of the potential for ototoxicity[74] and nephrotoxicity,[75] as well as the increasing resistance seen for all antibiotics, aminoglycosides are currently not utilized as frequently

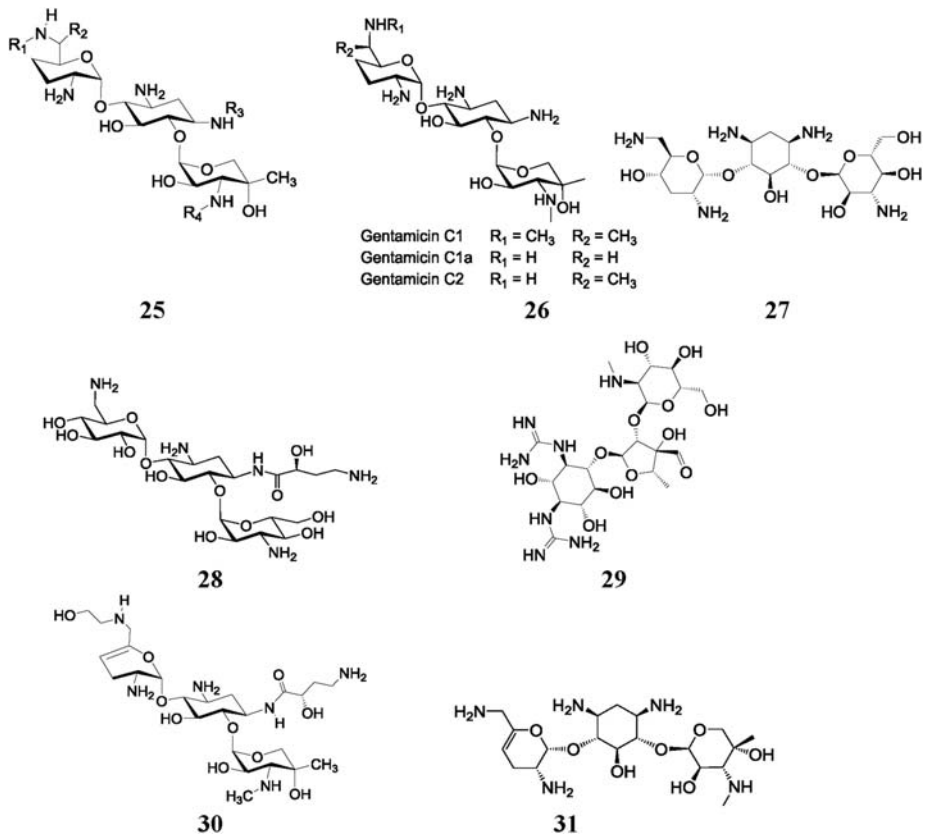

Fig. 3 Aminoglycoside antibiotics: **25** aminoglycosides, **26** gentamicin, **27** tobramycin, **28** amikacin, **29** streptomycin, **30** plazomicin, **31** sisomicin.

as other drugs such as the β-lactams, unless the appearance of aminoglycoside susceptibility in highly resistant Gram-negative bacteria suggests that an aminoglycoside may be a reasonable therapeutic option. Encouraging results have recently been reported for the investigational aminoglycoside plazomicin (**30**), a semisynthetic aminoglycoside based on sisomicin (**31**), designed to avoid common aminoglycoside resistance mechanisms, particularly those related to aminoglycoside-modifying enzymes (AMEs).[76] This novel aminoglycoside is currently under development for the treatment of serious antibiotic-resistant infections caused by enteric bacteria.[77]

Aminoglycoside resistance can be caused by three major mechanisms. Production of AMEs is the most common, occurring in both staphylococci and Gram-negative bacteria. Enzymes that modify specific drugs either by N-acetylation, O-adenylation, or O-phosphorylation can cause aminoglycoside inactivation.[78] Multiple AMEs may exist in a single bacterial strain, with two or three AMEs frequently appearing in aminoglycoside-resistant Enterobacteriaceae or *Acinetobacter* spp.[78] Plazomicin evades most AMEs, except for an uncommon chromosomal acetylase that inactivates plazomicin and gentamicin,[76] and has been identified only in *Providencia stuartii*.[78] In staphylococci, a limited number of AMEs may be produced alone or in combination[76,79,80] resulting in resistance to amikacin and tobramycin, but generally showing lower MICs for gentamicin and plazomicin. A second common aminoglycoside resistance mechanism is alteration of the ribosomal binding, often through 16S rRNA methyl transferases (RMTs) in the Enterobacteriaceae.[78,81] Both AMEs and RMTs can be found on transferable elements that may be circulated among species, thus increasing the proliferation of resistance. Dissemination may be due to both clonal spread and plasmidic transfer of mobile resistance determinants. RMTs may travel on the same plasmids as ESBL-encoding genes[82] or quinolone resistance proteins[83] and are often associated with insertion sequences.[83] One of the most disconcerting appearances of these methylases has been the identification of RMTs in highly antibiotic-resistant Gram-negative pathogens that produce the NDM-1.[84] A third aminoglycoside mechanism, primarily in Gram-negative bacteria, involves decreased penetration and/or increased efflux. Membrane alterations that affect aminoglycoside permeability are infrequently encountered in most enteric bacteria with the exception of the Proteae, which typically have an outer membrane that impedes the aminoglycoside entry[85] (including plazomicin[78]). In *P. aeruginosa*, aminoglycosides often exhibit higher MICs as a result of hyperproduction of the MexXY efflux pump,[86] whereas in *Acinetobacter baumannii*, increased expression of the AdeB efflux system may contribute to reduced sensitivity to plazomicin.[87]

In recent surveillance studies, aminoglycoside susceptibilities have remained relatively steady from 2009 to 2012 among the Enterobacteriaceae in both the United States and Europe, with amikacin resistance usually $<10\%$ and gentamicin resistance $<20\%$[55] except for ESBL-producing *Klebsiella* spp. where resistance was as high as 39% (amikacin) and 46% (gentamicin). These data contrast with historical data collected in 2001 from intensive care patients in which aminoglycoside resistance ranged from 2.2% to 5.4% in *Klebsiella* spp. with confirmed ESBLs.[88] Aminoglycoside susceptibility in *P. aeruginosa* ranged from 87% to 96% in the United States ($n=1439$) and from 75% to 89% in Europe and the Mediterranean region ($n=1250$) in patients hospitalized with pneumonia from 2009 to 2012.[55] In *Acinetobacter* spp., amikacin and gentamicin susceptibility is lower than in pseudomonal isolates, with 41–49% amikacin susceptibility and 30% gentamicin susceptibility in US patients, and 32–35% amikacin susceptibility and 28% gentamicin susceptibility in European/Mediterranean patients.[55] Interestingly, susceptibility to aminoglycosides in nonfermentative bacteria has not changed dramatically for pseudomonal isolates since the period 1997–2001, when 76–89% susceptibility was reported for gentimicin, tobramycin, or amikacin in a global collection of *P. aeruginosa* isolates[89]; however, slightly higher aminoglycoside susceptibilities were observed in a similar older collection of *Acinetobacter* isolates that reported 48–62% susceptibility to the three aminoglycosides tested.[89]

5.17.2.1.4 Quinolone resistance

Quinolones (Fig. 4; **32**) represent a class of potent, broad-spectrum antibiotics with good bioavailability that has enabled both oral and intravenous formulations.[90] These drugs target the essential bacterial enzymes DNA gyrase and topoisomerase IV, which are involved in DNA replication and recombination and control the topology of the bacterial chromosome.[91] Initially used mainly in the treatment of UTIs, newer generations of fluoroquinolones were optimized to gain sufficient antibacterial activity for the treatment of systemic Gram-negative infections as well as Gram-positive respiratory tract infections.[92] Although antibacterial activity gains were achieved for newer quinolones against Gram-positive pathogens, ciprofloxacin (**33**), introduced in 1987, still remains

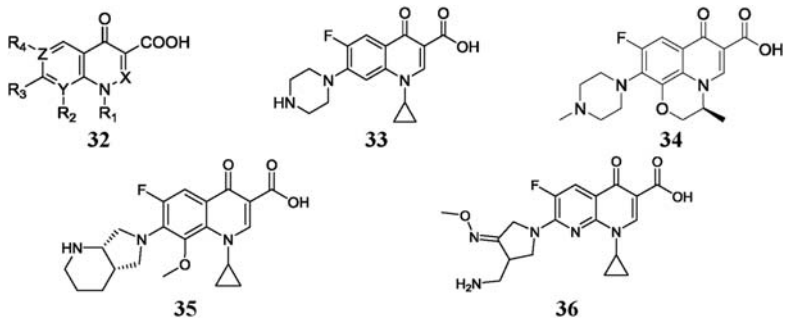

Fig. 4 Quinolone antibiotics: **32** quinolones, **33** ciprofloxacin, **34** levofloxacin, **35** moxifloxacin, **36** gemifloxacin.

the most active against Gram-negative pathogens. Additional clinical indications now include SSTIs, IAIs, sexually transmitted diseases, bone and joint infections, and gastrointestinal infections, and in recent years several quinolones have been explored for the treatment of TB.[93]

Not surprisingly, the growing popularity of these drugs led to increased usage, particularly in the 1990s, and subsequently to resistance development that was first chromosomally mediated through target-based mutations and/or mutations that affect drug accumulation (permeability or efflux) in the bacterial cell.[91,94] Target-based mutations are found in the *gyrA* and *parC* genes encoding DNA gyrase and topoisomerase IV enzymes, respectively. More recently, the emergence of several mechanisms of plasmid-mediated resistance has occurred as well.[95] A key plasmid-encoded gene designated *qnr* has been discovered that encodes a protein that can bind to and protect both DNA gyrase and topoisomerase IV from inhibition by quinolones.[96] Most *qnr* genes are found on multidrug resistance plasmids linked to genes for ESBLs, AmpC β-lactamase, and resistance to aminoglycosides, sulfonamides, trimethoprim, and other antimicrobial agents, thus adding to treatment issues in patients infected with these organisms. Changes in quinolone resistance over the past decade for several clinical indications are captured here.

The overall resistance rate of ciprofloxacin for outpatient *E. coli* urinary isolates in the United States and Canada during 2003–04 was reported to be 5.4%, though some areas reported rates in excess of 20%.[97] A similar study performed in 2003–06 in nine European countries including Russia and Brazil found that the ciprofloxacin resistance rate for *E. coli* isolates in the healthy women having uncomplicated lower UTIs was 8.3%, although again higher rates (up to 13.6%) were observed in several areas.[98] A more recent (2010–12) Korean study reported ciprofloxacin resistance in *E. coli* isolates from women having community-acquired acute pyelonephritis was 20.0%,[99] while a second study showed similar (22.5%) ciprofloxacin resistance in *E. coli* isolates from women with community-associated acute pyelonephritis.[100] Most studies have indicated that prior exposure to quinolones is a significant risk factor for the development of quinolone resistance in uropathogenic *E. coli*.[100,101] Of additional concern is the high association of quinolone resistance with ESBL production in Enterobacteriaceae in UTI patients, which limits treatment options.[102]

Pneumococcal resistance to β-lactam and macrolide antibiotics has led to increased use of quinolones such as levofloxacin (**34**), moxifloxacin (**35**), and gemifloxacin (**36**) for the treatment of patients with community-acquired pneumonia. As the use of quinolones has increased, fluoroquinolone-resistant *S. pneumoniae* has emerged in many countries.[103] Quinolone resistance rates for *S. pneumoniae* in North America remain low (<2%).[104] In Europe, pneumococcal resistance to quinolones was reported to be 5.2% in 2012 (European Centre for Disease Prevention and Control); however, rates were much lower (<0.7%) in two German multicenter studies (MOXIAKTIV Study and German CAPNETZ surveillance study).[105,106] In Asia, the Asian Network for Surveillance of Resistant Pathogens (ANSORP) also showed relatively low resistance rates of 1.7% and 0.4% for levofloxacin and moxifloxacin, respectively, with highest rates of levofloxacin resistance at 6.5% and 4.6% in Taiwan and Korea, respectively.[107]

Haemophilus influenzae and *Moraxella catarrhalis* have largely remained highly susceptible to quinolones.[108] For other respiratory pathogens isolated from healthcare-associated pneumonia, such as Enterobacteriaceae, *P. aeruginosa*, and *A. baumannii*, quinolone resistance rates have been substantially higher with isolates frequently MDR. A prospective surveillance study by the ANSORP from 2008 to 2009 also showed high ciprofloxacin resistance in *K. pneumoniae* (31.2%), *P. aeruginosa* (30.1%), and *Acinetobacter* spp. (80.7%) in Asian countries.[109]

5.17.2.1.5 Macrolide resistance

The macrolides (Fig. 5; **37**) and ketolides (**38**) represent a class of antibiotics with antibacterial activities against most Gram-positive and selected Gram-negative as well as atypical pathogens including penicillin-resistant microorganisms.[110] Macrolides belong to the polyketide class of natural products that reversibly bind to the 50S subunit of the bacterial ribosome blocking protein synthesis, thereby preventing bacterial growth and replication. These drugs are primarily bacteriostatic, but at higher concentrations can be bactericidal.[111] Erythromycin (**39**), clarithromycin (**40**), and azithromycin (**41**), the most extensively used examples, have proven useful in a variety of clinical indications including both upper and lower respiratory tract infections as well as skin and skin structure and ophthalmic infections. The introduction of clarithromycin and azithromycin provided both increased pathogen coverage and a significant improvement in adverse event profiles when compared with the first macrolide agent, erythromycin. However, as might be expected, widespread usage led to the development of resistance including a global increase in macrolide-resistant *S. pneumoniae*, thus limiting their effectiveness. By 2005, 29.5% of *S. pneumoniae* strains isolated in the United States were found nonsusceptible to macrolides.[112]

Solithromycin (**42**), a next-generation oral and intravenous fluoroketolide currently in Phase 3 clinical development, has been reported to possess improved effectiveness against macrolide-resistant bacteria because of the ability to bind to three sites on the bacterial ribosome, as opposed to one or two for the current macrolides. This binding to three ribosomal sites is also expected to limit resistance development (http://www.cempra.com/products/Solithromycin-cem-101/). In vitro and in vivo studies have shown potent activity against *S. pneumoniae* as well as an extended spectrum of activity against community-associated-MRSA (CA-MRSA), enterococci, *Mycobacterium avium* and in malaria. It is also active against atypical bacteria such as *Legionella*, *Chlamydia*, *Mycoplasma*, and *Ureaplasma* and against gonococci and other organisms that cause genitourinary tract infections. It is 8–16 times more potent than azithromycin and is active against azithromycin-resistant strains.

Soon after the introduction of erythromycin into clinical use in the 1950s, bacterial resistance to this antibiotic was reported for the first time in staphylococci.[113] In addition to ribosomal mutations, there are three major gene-encoded mechanisms by which bacteria become resistant to macrolides: rRNA methylases, efflux, and inactivating enzymes[114,115] that include esterases, lyases, phosphorylases, and transferases. The cluster of macrolides with two other classes, lincosamides and streptogramin B, has been

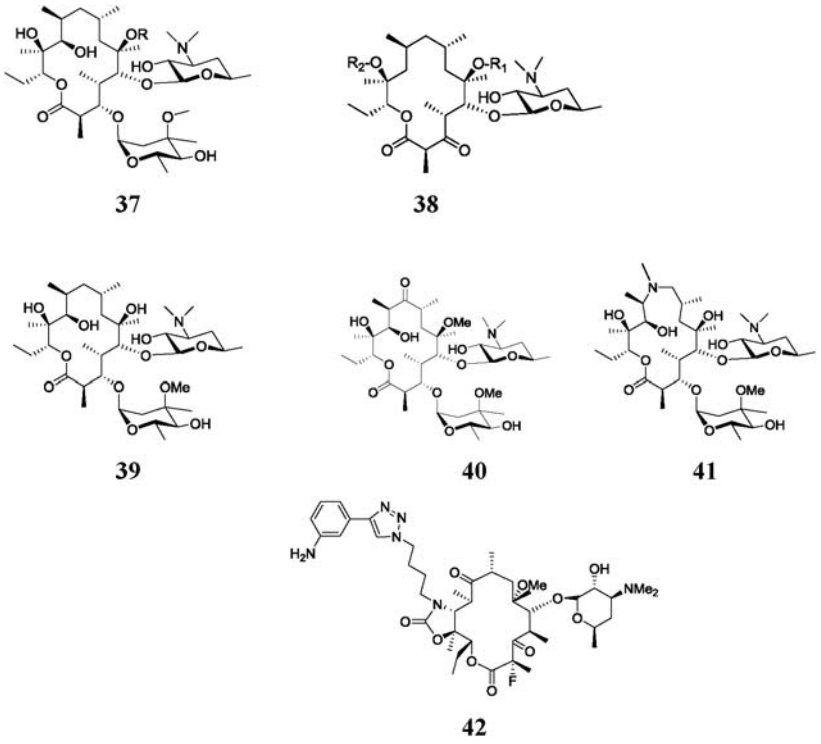

Fig. 5 Macrolide antibiotics: **37** macrolides, **38** ketolides, **39** erythromycin, **40** clarithromycin, **41** azithromycin, **42** solithromycin.

designated the macrolide–lincosamide–streptogramin B (MLS) antibiotics, and resistance to these drugs is termed MLS resistance.[116] More than 60 MLS resistance genes have been identified to date.

Erythromycin resistance is widespread in MRSA, with 87.9% erythromycin resistance reported for these isolates (compared with 8.2% for MSSA).[117] Due to the apparent inability of ketolides to act as inducers of methylase production, they maintain good in vitro activity against *S. aureus* strains with inducible methylase, but lose activity against strains constitutively producing ermA or ermC methylase.[118] With regard to pneumococci, even though macrolide MICs typically increase along with those of penicillin, ketolides remain consistently active irrespective of penicillin susceptibility. In contrast, 71% of penicillin-nonsusceptible pneumococci were nonsusceptible to erythromycin and azithromycin.[119] Macrolides have poor activity against *Enterococcus* spp. with ketolides exhibiting better activity. However, neither demonstrated activity against erythromycin- or vancomycin-resistant *E. faecalis* and *E. faecium*.[120,121] *Listeria monocytogenes* and *Corynebacterium* spp. showed susceptibility to macrolides and ketolides, with the latter having superior activity compared with macrolides.[121–123] In regard to Gram-negative pathogens, *P. aeruginosa*, Enterobacteriaceae, and *Acinetobacter* are intrinsically nonsusceptible to macrolides and ketolides. However, both classes were active against *H. influenzae* and *M. catarrhalis* and their in vitro activities were not affected by the presence of β-lactamase production or by ampicillin susceptibility.[121,123]

5.17.2.1.6 Tetracycline resistance

Tetracycline (Fig. 6; **43**) antibiotics have been widely used in the treatment of bacterial infections for more than 60 years. These drugs inhibit bacterial growth by inhibiting protein synthesis through binding to the bacterial 30S ribosomal subunit, preventing aminoacyl-t-RNA binding to the ribosomal A-site and subsequent addition of amino acids to the growing polypeptide chain. Because of the widespread use of tetracyclines over many years, resistance developed in many pathogens leading to limitations in their utility. Efforts to identify new analogs in this class that could overcome bacterial resistance issues resulted in the discovery of the glycylcyclines (**44**),[124] exemplified by tigecycline (**45**), which was approved by the USA Food and Drug Administration (FDA) in 2005 and by the European Medicines Agency in 2006 for the treatment of adults with complicated IAIs and complicated skin and skin structure infections (cSSSI).[125,126] Tigecycline also received FDA approval for the treatment of community-acquired bacterial pneumonia in adults.[127] This drug offers expanded broad-spectrum coverage of such problem pathogens as MRSA, vancomycin-resistant enterococci (VRE), *A. baumannii*, and ESBL-producing Gram-negative strains.[128] It is also active against anaerobes and "atypical" bacteria including *Mycoplasma*, *Legionella*, and *Chlamydia* species. Tigecycline exhibits a low MIC against *Clostridium difficile* in vitro and may be able to affect the pathogenesis of the disease in a mouse model of *C. difficile* infection (CDI).[129]

In vitro susceptibility data for tigecycline against Gram-positive organisms was collected between 2004 and 2009 from the Tigecycline Evaluation and Surveillance Trial[130] and indicated that activity was maintained against the organisms tested, including MRSA and other antibiotic-resistant pathogens.[131] Tigecycline has continued to maintain this in vitro antibacterial activity against MSRA

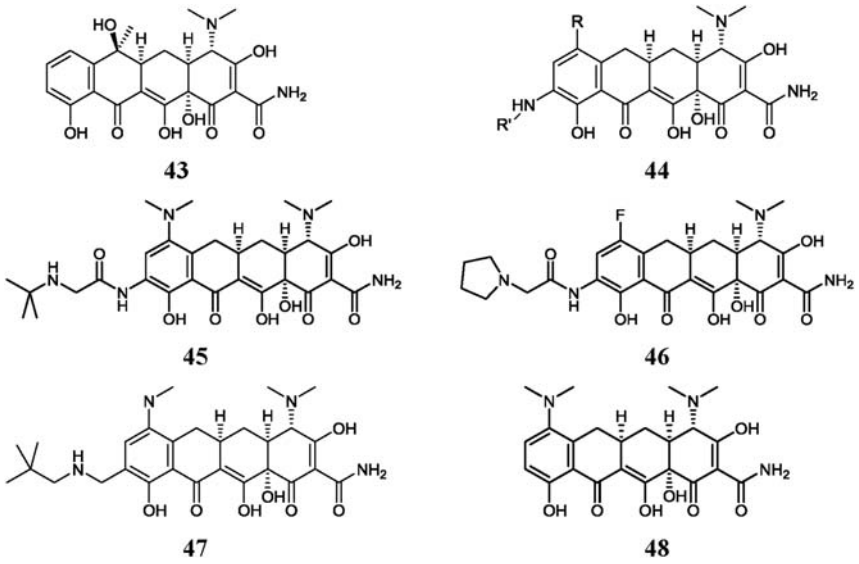

Fig. 6 Tetracycline antibiotics: **43** tetracyclines, **44** glycylcyclines, **45** tigecycline, **46** eravacycline, **47** omadacycline, **48** minocycline.

into 2012.[132] In vitro activity against Gram-negative organisms has also continued independent of ESBL phenotype or resistance to other antimicrobials.[133] For example, 97.9% of ESBL-producing *Klebsiella* spp. and 98.2% of imipenem nonsusceptible strains remained susceptible to tigecycline (minimum inhibitory concentrations for 90% of the isolates tested, MIC_{90}, 0.5/1.0 mg L^{-1} for both subsets) in data through 2009. Another study of European blood culture isolates from 2004 to 2009 showed no decline in tigecycline susceptibility against Gram-negative organisms.[134] A more recent survey indicates that tigecycline has maintained this excellent broad-spectrum pathogen coverage through 2014.[135] However, it is not active against *P. aeruginosa* and *Proteus* spp., *Morganella* and *Providencia* species.[136]

Tigecycline is often considered as a drug of last resort against MDR *A. baumannii*. However, increasing resistance has been observed following growing usage of the drug to treat infections caused by this pathogen, primarily due to efflux mediated by the resistance-nodulation-cell division (RND)-type transporters AdeABC, AdeFGH, and AdeIJK. Other resistance mechanisms may contribute as well.[137] Comparative evaluation of the tigecycline resistance rates reported worldwide has been difficult due to differences in vitro susceptibility methodologies used, with broth microdilution being considered the reference method. The high concentrations of manganese in Mueller–Hinton agar have been associated with increased MICs determined by both Etest® and disk diffusion.[138] Since the concentration of manganese in human serum is much lower than levels found in standard bacterial media, tigecycline MICs in media with low manganese content are considered more clinically relevant.

Because tigecycline has broad-spectrum antibacterial activity against both Gram-positive and Gram-negative pathogens, there has been some confusion in how to best position the drug for clinical usage.[139,140] There have been multiple clinical investigations of tigecycline for the treatment of both community-acquired and hospital-acquired infections. Despite some resistance observed for *A. baumannii*, the drug possesses good tissue distribution and effective levels of activity against most current MDR pathogens. There is even a case for its use in *A. baumannii* infections, since most isolates show MICs of ≤ 2 μg mL^{-1} and can be resistant to almost all other antibiotics, but a susceptibility breakpoint for *Acinetobacter* spp. has not yet been adequately established for the reasons discussed earlier. Despite the apparent positive microbiology data, there are several issues that must be considered prior to clinical use. Tigecycline is bacteriostatic against Gram-negative bacteria, and while good clinical successes have been reported by some investigators, others have reported high clinical failure rates.[141] Also, standard tigecycline doses can result in serum concentrations that are below the MICs of most Gram-negative pathogens, making it risky for use in bloodstream infections. Warnings of increased mortality have been raised by meta-analyses based on heterogeneous infections encompassing ventilator-associated pneumonia (VAP), hospital-acquired pneumonia, diabetic foot infections, and infections by MDR bacteria.[142,143]

Two other tetracycline derivatives are in late stages of clinical development. Eravacycline (**46**) (in Phase 3) is a synthetic fluorocycline antibacterial agent that is structurally similar to tigecycline with two modifications to the D-ring of its tetracycline core: a fluorine atom replaces the dimethylamine moiety at C-7 and a pyrrolidineacetamido group replaces the 2-tertiary-butyl glycylamido at C-9.[144] Eravacycline is two- to fourfold more potent than tigecycline versus Gram-positive cocci and two- to eightfold more potent than tigecycline versus Gram-negative bacilli. This drug demonstrates broad-spectrum antimicrobial activity against Gram-positive, Gram-negative, and anaerobic bacteria with the exception of *P. aeruginosa*. Omadacycline (**47**), representative of another class of tetracycline analogs, the aminomethylcyclines that are C-9 derivatives of minocycline (**48**),[145] is also in advanced clinical development (III3). Both of these compounds are reported to have advantages against isolates with current tetracycline resistance mechanisms.[146,147]

5.17.2.1.7 Glycopeptide resistance

Vancomycin (Fig. 7; 49), first isolated in 1957, is a cell wall antibiotic that inhibits a late stage of peptidoglycan biosynthesis by binding to the D-ala-D-ala termini of murein monomers, blocking the activity of glycosyltransferase leading to inhibition of the incorporation of the murein monomers to the growing peptidoglycan chain. This prevents further transpeptidation and continued cell wall synthesis. Vancomycin is a tricyclic glycopeptide consisting of seven-membered peptide chains forming the tricyclic structure with attached disaccharide composed of vancosamine and glucose. It has a relatively high molecular weight of 1485 similar to that of

Fig. 7 Glycopeptide antibiotics: **49** vancomycin, **50** avoparcin, **51** dalbavancin, **52** oritavancin, **53** televancin.

daptomycin and possesses a bactericidal mechanism of action with the exceptions of enterococci, where it is bacteriostatic, and MSSA, where it is only slowly bactericidal, sometimes leading to poorer clinical outcomes.[148]

The drug has an impressive spectrum of activity against Gram-positive aerobic pathogens including staphylococci (including both MSSA and MRSA), streptococci, enterococci, and pneumococci as well as *Corynebacterium*, *Listeria*, *Bacillus* spp., *Clostridia*, and oral Gram-positive anaerobes. Strains of *Leuconosoc*, *Lactobacillus*, *Pediococcus*, and *Erysipelothrix* possess inherent resistance to vancomycin. Even after many decades of use, vancomycin remains an inexpensive first-line agent for MRSA and MRSE infections, including bacteremia, endocarditis, pneumonia, cellulitis, and osteomyelitis. In addition, it is used to treat serious Gram-positive infections among patients who are allergic to β-lactam antibiotics.[149]

Due to the widespread emergence of MRSA and MRSE in the 1970s, vancomycin usage increased dramatically, which led to the subsequent appearance of vancomycin resistance among enterococci by the mid-1980s and patient treatment failures.[150] In the late 1990s, staphylococcal strains with intermediate susceptibility to vancomycin (VISA), vancomycin-resistant *S. aureus* (VRSA),[150–152] and vancomycin-resistant *S. epidermidis*[153] were reported. Fortunately, the occurrence of these difficult-to-treat staphylococci remains rare. Typically, MICs of vancomycin against *S. aureus* are ≤ 2 μg mL^{-1} and it has been repeatedly shown that clinical failures in patients with endocarditis, bacteremia, and pneumonia occur when the *S. aureus* isolates causing these infections have MIC of ≥ 2 μg mL^{-1}.[154,155] However, even within the range of MICs below 2 μg mL^{-1}, high failure rates have been observed in patients infected with strains that have vancomycin MICs of 1.5 μg mL^{-1}.[156] A phenomenon designated "vancomycin creep" has been described in recent years, denoting a slow but steady increase in vancomycin MIC observed over time from values of 0.5–0.75 μg mL^{-1} to levels of 1.25–1.5 μg mL^{-1}.[157] In some parts of the world, however, this phenomenon does not seem to occur.[158]

VRE isolates were first encountered in England and France in 1986 followed by isolation of VRE *E. faecalis* in the United States in 1987.[159–161] In Europe, the rise of VRE was mostly in the community and the selective pressure was believed to derive from transmission from animals and animal food products to humans through the use of the glycopeptide antibiotic avoparcin (**50**) as a growth promoter in livestock.[162] In contrast, in the United States the predominance of VRE was in the hospital setting, believed to be due to the increasing use of vancomycin.[163] A rapid spread of VRE occurred in US hospitals in the 1990s, followed by a VRE increase in Europe in the 2000s. Changes in the D-Ala-D-Ala peptidoglycan precursors to D-Ala-D-Lac or D-Ala-D-Ser resulted in significant decreases in vancomycin binding affinities to bacterial cell wall, allowing for cell survival.[164] Currently *E. faecium* displays more resistance, with the more pathogenic *E. faecalis* lagging behind. Eight phenotypic variants of acquired glycopeptide resistance in enterococci have been described (VanA, VanB, VanD, VanE, VanG, VanL, VanM, and VanN), as well as one intrinsic resistance (VanC). VanA is responsible for most human VRE disease around the world, principally in *E. faecium*.

Around the world, rates of VRE are at their highest in the United States, with 35.5% of enterococcal hospital-associated infections resistant to vancomycin from 2009 to 2010, ranking as the second most common cause of nosocomial infections.[165] In Europe, VRE is much less prevalent (4% in 2013), but on the rise. However, prevalence depended on the country, ranging from less than 1% (France, Spain, Sweden) to greater than 20% (Greece, Ireland, Portugal, United Kingdom).[166] Infections often target the immunosuppressed, causing bacteremia, IAIs, UTIs, SSSIs, and other clinical manifestations. Due to the multiple resistance mechanisms found in VRE, treatment options are often limited.

Three other glycopeptide antibiotics have been approved since 2009.[167,168] Dalbavancin (**51**) inhibits the late stages of peptidoglycan synthesis by mainly impairing transglycosylase activity, while oritavancin (**52**) and telavancin (**53**) anchor in the bacterial membrane by the lipophilic side chain linked to their disaccharidic moiety and disrupt membrane integrity leading to bacteriolysis. The long half-lives of oritavancin and dalbavancin allow for infrequent dosing compared to vancomycin and televancin. Televancin was approved in 2009 for cSSSI, and in 2013 for hospital-acquired and ventilator-associated bacterial pneumonia caused by *S. aureus*.[169] Dalbavancin was approved in 2014 for the treatment of acute bacterial skin and soft tissue infection (ABSSSI) caused by certain susceptible bacteria such as *S. aureus* (including MSSA and MRSA) and *Streptococcus pyogenes*.[170] Oritavancin was approved for ABSSSI in 2014.[171] A recent study of skin and soft tissue clinical isolates from the United States and Europe showed 97.9–100% susceptibility for staphylococci, streptococci, and enterococci with MIC_{90} values ranging from 0.008 to 0.5 μg mL^{-1}.[172]

5.17.2.1.8 Oxazolidinone resistance

Oxazolidones (Fig. 8; **54**) represent one of only three novel antibacterial structural classes (the others are fidaxomicin and daptomycin) approved by the FDA in the last 30 years. Linezolid (**55**) was approved in 2000 and is available both intravenously and orally for several clinical indications, including infections caused by VRE, nosocomial pneumonia, CAP, and both uncomplicated and complicated SSSIs.[173] A second oxazolidinone, tedizolid (**56**), was approved by the FDA in 2014 for the treatment of ABSSSI caused by certain susceptible bacteria including *S. aureus* (both MSSA and MRSA), various *Streptococcus* species (including *S. pyogenes* and *S. agalactiae*),

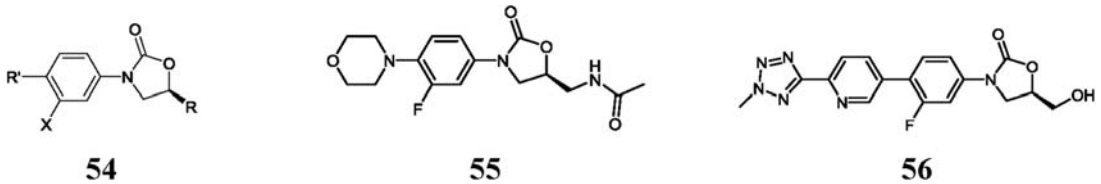

54 **55** **56**

Fig. 8 Oxazolidinone antibiotics: **54** oxazolidinones, **55** linezolid, **56** tedizolid.

and *E. faecalis*.[174] This second-generation oxazolidinone derivative has been reported to be 4- to 16-fold more potent against staphylococci and enterococci compared to linezolid. Mechanism of action data indicates that oxazolidinones interact with the 50S ribosomal subunit and inhibit the initiation phase of translation by binding at the A-site of the peptidyl transferase center. This leads to interference with the binding of the amino acyl moiety of the incoming aminoacyl tRNA.[175] Crystal structure data of linezolid bound to the *Haloarcula marismortui* 50S subunit supports this inhibition mechanism of competition with the incoming A-site substrates.[176]

The spontaneous frequency of resistance to oxazolidinones is quite low compared to other antibiotics, probably due to the necessity of mutating multiple copies of the 23S rRNA gene target. The frequency of linezolid resistance in staphylococci and enterococci has been reported to be $<10^{-9}$, while tedizolid was found to possess an even more impressive mutation frequency, $\sim$16-fold lower mean spontaneous mutation than linezolid.[177] Linezolid resistance was first seen clinically in *E. faecium* infections in patients from two early compassionate use programs, and soon after its launch in 2000 additional resistant staphylococci and enterococci strains were identified. Analyses of linezolid-resistant mutants indicated a limited spectrum of mutations in the 23S rRNA along with mutations in ribosomal proteins L3 and L4.[178]

Another mechanism of resistance, mediated by the *cfr* gene, was originally identified in veterinary staphylococcal isolates as early as 1997.[179] This gene encodes a methyltransferase that abolishes drug binding and confers resistance to a set of structurally diverse compounds that target the peptidyl transfer region including phenicols, lincosamides, oxazolidinones, pleuromutilins, streptogramin A, and 16-membered macrolides. The *cfr* gene was discovered to be often associated with additional antibiotic resistance genes, including *erm* (resistance to macrolides, lincosamides, and streptogramin B), *lsaB* (reduced susceptibility to lincosamides), and *fexA* (resistance to phenicols).[180] Strains carrying *cfr* in combination with ribosomal mutations also have been observed. However, MIC values for tedizolid were reported to be unchanged against strains that carried the *cfr* gene compared with two- to eightfold increases for linezolid, suggesting better clinical effectiveness against these *cfr* isolates.[181]

In regard to clinical linezolid resistance, the 2009 LEADER study reported no significant increases in rates between 2004 and 2009 among six groups of Gram-positive organisms, with resistance rates in the United States for *S. aureus* 0.15%, coagulase-negative staphylococci 1.47%, and enterococci 0.49%.[182] A similar 2010 study that included isolates from Canada, Europe, Latin America, and the Asia-Pacific regions reported stable linezolid resistance rates for coagulase-negative staphylococci, streptococci, and enterococci.[183] Increases in the rate of resistance have, however, been observed in local outbreaks of linezolid-resistant strains. For example, a Spanish multicenter surveillance program showed that the frequency of linezolid resistance among coagulase-negative staphylococci increased from 1.6% in 2008 to 8% in 2010.[184] In the most recent data update from LEADER 2014, susceptibility testing of $>$6000 Gram-positive pathogens demonstrated excellent linezolid activity and a sustained susceptibility rate of 99.78% overall (99.62–99.83% during 2008–13).[185] There were 15 nonsusceptible isolates, 8 of which (8/15 (53.3%)) carried *cfr*. Even though these numbers are very low, the increase in the presence of *cfr* in linezolid nonsusceptible isolates is a concern and merits monitoring in the future due to its transmissible properties.[186] However, it is encouraging that the linezolid-resistant and nonsusceptible rate (0.22%) is essentially the same as in 2005 (0.24%). Linezolid MIC distributions have remained stable without evidence of "MIC creep" in these studies.

In regard to tedizolid, nearly 7000 Gram-positive clinical isolates collected from multiple US and European sites as part of the Surveillance of Tedizolid Activity and Resistance Program in 2011 and 2012 were assayed for in vitro susceptibilities.[187] MIC_{90} values were 0.25 μg mL^{-1} for *S. epidermidis* and beta-hemolytic streptococci and 0.5 μg mL^{-1} for *S. aureus*, other CoNS, and enterococci. Of 16 isolates with elevated tedizolid or linezolid MIC values (intermediate or resistant isolates), 10 had mutations in the genes encoding 23S rRNA, 5 had mutations in the genes encoding ribosomal proteins L3 or L4, and 5 carried the *cfr* multidrug resistance gene. Overall, tedizolid showed excellent activity against Gram-positive bacteria and was at least fourfold more potent than linezolid against wild-type and linezolid-resistant isolates.[187]

5.17.2.1.9 Colistin resistance

Colistin (**57**) belongs to the family of polymyxins (Fig. 9), cationic polypeptides with broad-spectrum activity against Gram-negative bacteria, including most current MDR isolates. The two polymyxins currently in clinical use are polymyxin B (**58**) and

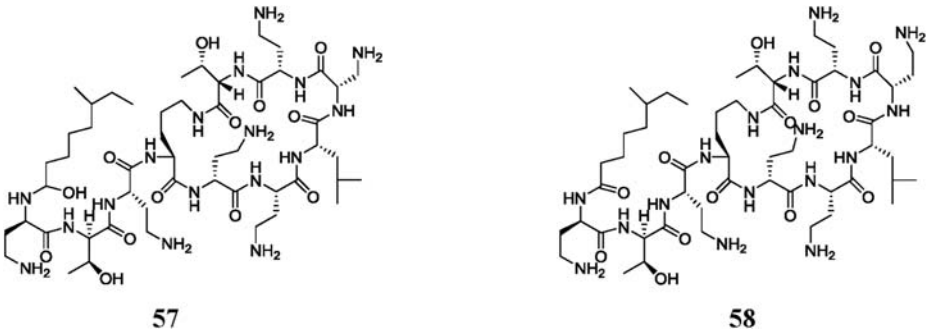

Fig. 9 Polymyxin antibiotics: **57** colistin, **58** polymyxin B.

colistin (polymyxin E), which differ only by one amino acid and have similar biological activity. The initial target of polymyxins is the lipopolysaccharide (LPS) content of the bacterial outer membrane. Polymyxins bind selectively to LPS, and consequently are active against only Gram-negative bacteria.[188,189] It is generally believed that the polymyxins kills bacteria through membrane lysis, first crossing the outer membrane and then destroying the physical integrity of phospholipid bilayer of inner membrane.[189]

Colistin was used clinically from the late 1950s into the 1970s, and then rarely until the 2000s, when it was revived as a last resort for treating MDR Gram-negative infections with few other treatment options. However, because it was originally developed decades ago, there was little information about dosing regimens with regard to both efficacy and adverse effects. Toxicity was the main reason use declined, as serious nephrotoxicity and neurotoxicity was often seen after parenteral administration and safer alternatives became available.

The mechanism of resistance to polymyxins is modification of lipid A, resulting in reduction of polymyxin affinity.[190] Until recently, all reported polymyxin resistance mechanisms were chromosomally mediated, involving modulation of two component regulatory systems (e.g., pmrAB, and phoPQ and its negative regulator mgrB in the case of *K. pneumoniae*). However, *mcr-1*, a plasmid-mediated gene that confers colistin resistance in *E. coli* and *K. pneumoniae*, was recently identified in isolates cultured from animals and patients in China.[20] The *mcr-1* gene was found to encode a phosphoethanolamine transferase able to cationically modify the lipid A moiety of LPS with phosphoethanolamine, leading to reduced electrostatic interaction between colistin and LPS.[191] Following this discovery, this gene has been shown to be present outside of China, in other parts of Asia, Europe, Africa, and South America, and in other Enterobacteriaceae species. Additional studies have found that it is more widespread than initially believed and has been around since the 1980s.[192] A major concern is that the *mcr-1* gene has already established itself in highly antibiotic-resistant Enterobacteriaceae, including carbapenem-resistant strains carrying an NDM-5 resistance plasmid.[193] Such an isolate possesses a pandrug-resistant phenotype where even colistin and the new β-lactam–BLI combination ceftazidime–avibactam are rendered ineffective.

5.17.2.1.10 Trimethoprim resistance

Trimethoprim (Fig. 10; **59**) is a completely synthetic drug belonging to the diaminopyrimidine group of compounds, and is a competitive inhibitor of the enzyme dihydrofolate reductase (DHFR).[194] In the folic acid biosynthetic pathway, DHFR catalyzes the NADPH-dependent reduction of dihydrofolate acid to the active coenzyme tetrahydrofolate. Trimethoprim can be considered as a structural analog of folic acid, therefore, through inhibition of DHFR, affects DNA synthesis and replication leading to the death of the bacterial cell. The folate biosynthetic pathway has been recognized for more than 60 years as an outstanding target for the development of antibacterial compounds[195] although resistance soon emerged when a single folate antagonist was used therapeutically.

Sulfamethoxazole (**60**) also interferes with folate biosynthesis by competing with *p*-aminobenzoic acid to block the biogenesis of dihydrofolate. The combination trimethoprim–sulfamethoxazole (SXT) has been used clinically since the 1960s for the treatment of MRSA and UTIs. Recent clinical practice guidelines recommend SXT as first-line therapy for uncomplicated UTIs, SSTIs, and CA-MRSA infections.[196,197] No significant changes in the rates of susceptibility among CA-MRSA clinical isolates were reported over a 10-year period despite a significant increase in usage of SXT, although decreased susceptibility was observed for *E. coli* and *Proteus* species.[198] There was also no evidence for selection of isolates with increased resistance to other antibiotics correlating with this increased SXT use. However, this drug combination has been associated with the spread of resistant microorganisms on a population level through selection of a transferable class 1 integron, resulting in MDR Enterobacteriaceae in the intestinal flora of children.[199]

While intrinsic resistance to TMP has limited the useful spectrum, the emergence of resistance threatens to reduce the bacterial spectrum even further. Low-level resistance to trimethoprim can occur through chromosomal mutations in the *folA* gene that encodes DHFR.[200,201] Because the drug is synthetic, enzymes that degrade or modify it would not be expected in nature. High-level resistance occurs by a bypass mechanism through the action of an acquired gene that is a drug-nonsusceptible variant of a chromosomal DHFR. These plasmid-mediated DHFRs emerged in Gram-negative bacteria within several years of the clinical introduction of the drug.[202] These acquired alternative DHFR genes were first classified into two distinct gene families, *dfrA* and *dfrB*.[203] Currently six plasmid-mediated families have been reported, with relatively few *dfr* determinants originating from Gram-positive sources.[7,204]

Iclaprim (**61**), a next-generation diaminopyrimidine, is a potent and selective inhibitor of DHFR that was resulted from a rational design approach based on TMP structural information.[205,206] It has been shown to have good antibacterial activity against Gram-positive pathogens that are susceptible to TMP. Iclaprim inhibits bacterial DHFR in a manner similar to TMP but possesses higher affinity due to increased hydrophilic interactions with the protein.[207] It exhibits some activity against TMP-resistant isolates, but lower than that against TMP-susceptible strains. Iclaprim has been shown to be rapidly bactericidal and to possess a low potential for resistance development when used as monotherapy without the synergistic combination of

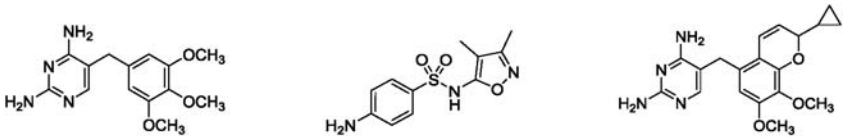

59 60 61

Fig. 10 Dihydrofate reductase (DHFR) inhibitors: **59** trimethoprim, **60** sulfamethoxazole, **61** iclaprim.

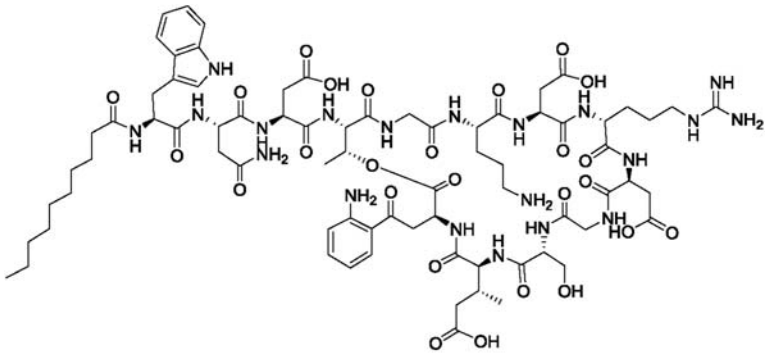

62

Fig. 11 Daptomycin.

a sulfonamide agent.[208] Iclaprim completed Phase 3 clinical trials for the treatment of complicated SSTIs but was denied approval until additional clinical data demonstrate efficacy and safety. New Phase 3 trials are currently in progress.

5.17.2.1.11 Daptomycin resistance

Daptomycin (Fig. 11; **62**) is a bactericidal lipopeptide antibiotic active against a wide range of Gram-positive clinical pathogens. The mechanism of action involves perturbation of the cell membrane in a calcium-dependent manner, interacting with its target mostly at the bacterial division septum.[209,210] Although daptomycin was first discovered in the late 1980s, it did not gain FDA approval until 2003. The drug is approved in the United States for the treatment of cSSSI at a 4 mg kg^{-1} day^{-1} dose and for treatment of bacteremia and right-sided endocarditis caused by *S. aureus* at 6 kg^{-1} day^{-1}. Because daptomycin represents a new antibiotic class and targets membranes, widespread resistance has been slow to emerge.

Most *S. aureus* isolates remain susceptible to daptomycin, but there are reports of resistance to the drug. Although resistance mechanisms are still not completely understood, current data suggest that they are complex and multifactorial involving mutational changes.[210,211] Risk factors for selection of these isolates appear to include infections with high bacterial loads such as endocarditis, catheter-related bacteremia, or an undrained abscess and/or exposure to vancomycin.[212] In *S. aureus*, the mechanism of resistance can involve electrostatic repulsion of the drug–calcium complex via an increase in the positive charge of the bacterial cell surface,[213] although other causes have been implicated.[214] Enterococci are intrinsically more resistant to daptomycin compared with staphylococci (Clinical Laboratory Standards Institute MIC breakpoint of ≤ 4 vs. ≤ 1 μg mL^{-1}). Genes involved in daptomycin resistance in enterococci appear to encode either regulatory systems that control cell-envelope homeostasis and stress response or those involved in cell membrane phospholipid metabolism.[215,216] In particular, the LiaFSR three-component regulatory system that controls cell-envelope response to antimicrobial and host defense peptide stress[217] and is analogous to the vraSR regulatory system in *S. aureus* has been implicated. Mutation to this system has been identified in daptomycin-nonsusceptible *E. faecalis*.[218] Transmissible resistance has not been observed for daptomycin to date.

5.17.2.2 Selected Key Pathogens

5.17.2.2.1 Carbapenem-resistant Enterobacteriaceae

Carbapenems (reviewed in section "Antibacterial resistance") are the most potent broad-spectrum β-lactam antibiotics active against Gram-negative organisms. Due to slow or negligible hydrolysis by the majority of β-lactam-hydrolyzing enzymes, this class has been used successfully against MDR Gram-negative organisms since their introduction in the early 1980s, often as a last line of defense. Their utility, however, has been eroding due to increased resistance, especially in the Enterobacteriaceae. Isolates have become MDR; mortality rates associated with carbapenem-resistant Enterobacteriaceae (CRE) infections are as high as 65% in patients with hematologic malignancies.[219] Carbapenemases, the major resistance factors, were known to be produced by the Gram-positive bacilli in the 1960s,[220] but were first detected in Enterobacteriaceae in the mid-1980s[221]; however, there was no significant detection of these enzymes for more than 20 years.[222] These first carbapenemases known were all chromosomally encoded, with any dissemination due to clonal spread. Transferable imipenem resistance due to an MBL was first noted in Japan in *P. aeruginosa*,[223] signaling the beginning of an era when carbapenemases became mobile among Gram-negative bacteria. Widespread carbapenemase production in the Enterobacteriaceae began to be reported in the early 2000s after the first carbapenem-resistant *K. pneumoniae* carrying a new carbapenemase, KPC, was reported in 2001.[224] In addition to carbapenemase production, carbapenem resistance can be caused by increased levels of other β-lactamases such as ESBLs or the AmpC cephalosporinases, accompanied by porin defects leading to decreased penetration of the drug.[225] The National Healthcare Safety Network reported in 2008 that among the nosocomial pathogens reported during 2006–07 from 463 hospitals throughout the United States, 10–11% of all *K. pneumoniae* isolates causing central line-associated bloodstream infections or UTIs were resistant to

carbapenems.[226] From 2005 onward, there were reports of KPC-producing strains in multiple countries with notable nationwide outbreaks in Israel, Greece, and Italy.[227–229]

As of 2014, areas with endemic KPC enzymes are China, Israel, Greece, Italy, Poland, Colombia, Argentina, Brazil, and some states in the United States. In India, the NDM family of MBLs is identified in 75–88% of CRE, often appearing with other carbapenemases such as KPC or OXA enzymes in as many as 19% of the isolates.[230,231] In Turkey OXA-48 carbapenemases are prevalent. It has become evident that without stringent infection control measures these organisms can rapidly become endemic. In New York City 38% of *K. pneumoniae* isolates produced a KPC enzyme in 2006; after stricter infection control measures were implemented, this number was reduced to 29% in 2009, indicating improvement, but not eradication of these pathogens.[232] There are limited treatment options today for CRE, although the avibactam-BLI combinations and some of the newer investigational drugs such as plazomicin and eravacycline have potentially useful antibacterial activity against many of these isolates. Overall, it is clear that CRE have become a challenge to our healthcare systems due to their rapid spread, poor treatment options, and often severe outcomes.[233]

5.17.2.2.2 *Antibiotic-resistant* N. gonorrhoeae

The World Health Organization (WHO) estimated in 2008 that 106 million new gonorrhea cases occur among adults annually worldwide causing significant morbidity and socioeconomic consequences globally.[234] Previously relatively easily treatable, the prevalence of *N. gonorrhoeae* strains with resistance to most antimicrobial agents, including sulfonamides, penicillins, earlier cephalosporins, tetracyclines, macrolides, and fluoroquinolones is now increasing.[235] In most countries, the only options for first-line empirical antibiotic monotherapy are currently the extended-spectrum cephalosporins, oral cefixime (**Fig. 12**; **63**), and particularly, the more potent injectable ceftriaxone (**64**).[236] The dual-antimicrobial treatment regimens with ceftriaxone and azithromycin introduced in the United States and Europe[237,238] appear currently to be highly effective. Recent gonorrhea treatment failures with the extended-spectrum cephalosporins cefixime and ceftriaxone and the emergence of gonococcal strains exhibiting high-level clinical resistance combined with resistance to nearly all other available antimicrobials are quite troubling. Resistance to azithromycin has been reported in Asia and Canada at rates $\leq 5\%$, but emerges more rapidly where there is frequent use of this drug.[235] There is a significant contribution of drug efflux pumps in clinical isolates of *N. gonorrhoeae* that express extensively drug-resistant or MDR phenotypes.[239] Furthermore, gonococcal strains with decreased susceptibility or resistance to both ceftriaxone and azithromycin have already been observed around the world.

Future therapy might not be affordable for lower economic-level individuals where the highest gonorrhea burdens are often found. From a global public health perspective, new antimicrobials for effective monotherapy or for inclusion in a new combination regimen are desperately needed. Some other currently marketed or late stage drugs with potential for use include tigecycline and eravacycline, solithromycin, dalbavancin, and delafloxacin (**65**).[235] Older antimicrobials have also been considered for future empirical monotherapy of gonorrhea.[236] These include the injectable carbapenem ertapenem (**66**),[240] oral fosfomycin (**67**),[241] and the injectable aminoglycoside gentamicin, which has been used as first-line treatment in Malawi for more than 20 years without any reported emergence of in vitro resistance.[242] However, it is important to note that *N. gonorrhoeae* has developed resistance to all antimicrobials introduced as first-line therapy over the last 70 years; for more sustainable future treatment, combination therapies or new compounds with truly novel mechanisms of action are needed.

5.17.2.2.3 *Clostridium difficile*

C. difficile is recognized as the major cause of healthcare antibiotic-associated diarrhea[243] and is correlated with antibiotic therapy, particularly with broad-spectrum agents that disrupt the protective intestinal microbiota allowing acquired or resident *C. difficile* to colonize the gastrointestinal tract and infect the host. CDI has significantly increased in incidence across the United States, Canada, and Europe over the last decade, adding a large financial burden on healthcare systems.[244–247] The emergence of highly virulent

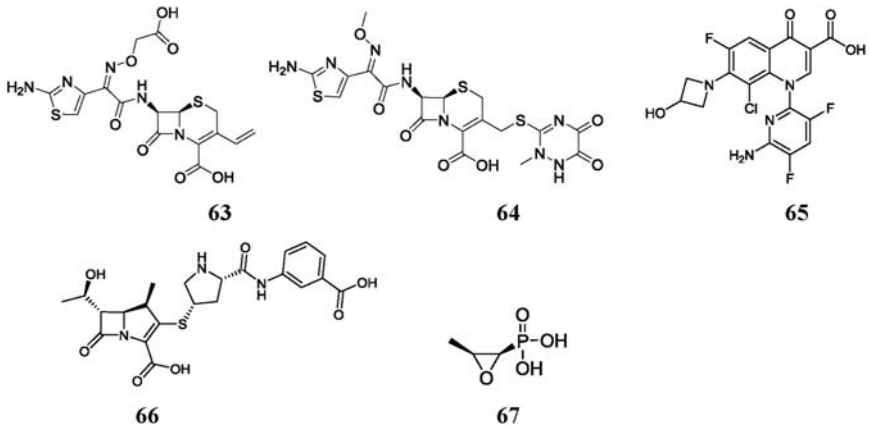

Fig. 12 Antibiotics for the treatment of *Neisseria gonorrhoeae* infections: **63** cefixime, **64** ceftriaxone, **65** delafloxacin, **66** ertapenem, **67** fosfomycin.

strains, particularly ribotype RT027, has led to severe infections characterized by a high recurrence rate recurrences, increased mortality, and less responsiveness to traditional therapies.[243,248] These strains have spread globally over recent years[249,250] including into previous low-risk populations such as young individuals, healthy peripartum women, antibiotic-naive patients, or those with no recent healthcare exposure.[251–253] Paralleling the increased CDI incidence, increased morbidity and mortality was observed and associated with the emergence and spread of the hypervirulent type RT027 strain. CDI caused by RT027 is characterized by increased severity, being refractory to traditional therapy and greater risk of relapse.

Antibiotic resistance has played a key role in driving this current epidemic. The emergence and spread of *C. difficile* RT027 has been correlated with the widespread use of fluoroquinolones and the acquisition of fluoroquinolone resistance, since this resistance was not observed in ancestral strains of the same type.[254] Antibiotic resistance rates vary considerably in different studies, often dependent on locations and antibiotic usage. Recent data extrapolated from 30 studies published between 2012 and 2015 indicate that resistance to clindamycin (Fig. 13; **68**) and cephalosporins is very common in *C. difficile* clinical isolates (55% and 51%, respectively), as is the resistance to erythromycin and fluoroquinolones (47%).[255] Most of the strains tested for susceptibility to second-generation cephalosporins such as cefotetan (**69**) and cefoxitin (**70**) were resistant (79%), whereas resistance to expanded-spectrum cephalosporins such as ceftriaxone and cefotaxime is present in a lower number of isolates (38%). For quinolones, resistance to ciprofloxacin was widespread in *C. difficile* (99% of the strains tested), while resistance to fourth-generation fluoroquinolones such as moxifloxacin and gatifloxacin (**71**) was observed in 34% of the tested strains.[255]

Ribosomal methylation is the most widespread mechanism of *C. difficile* resistance to MLS antibiotics. ErmB erythromycin ribosomal methylases commonly mediate resistance, while other *erm* genes are rarely detected in *C. difficile* isolates.[256–258] Quinolone resistance is due to alterations in the quinolone resistance determining region (QRDR) of either the GyrA or GyrB DNA gyrase subunits.[259–261]

Metronidazole (**72**) is considered first-line treatment for mild to moderate CDI.[262,263] However, although resistance rates remain low, treatment failures are observed.[264] Vancomycin is used as the first-line antibiotic for moderate to severe CDI.[263] Although resistance to this drug is not common, a number of strains with reduced susceptibility (MICs $>$ 2–16 μg mL^{-1}) have recently been reported. The clinical significance of reduced susceptibility to vancomycin is not clear, since the fecal concentration of drug can be over 2 mg mL^{-1}.[265] Since there has been an increased rate of treatment failure and infection recurrence with either vancomycin or metronidazole treatment, other therapy options have been investigated.[264] Rifamycins, in particular rifaximin (**73**), have recently

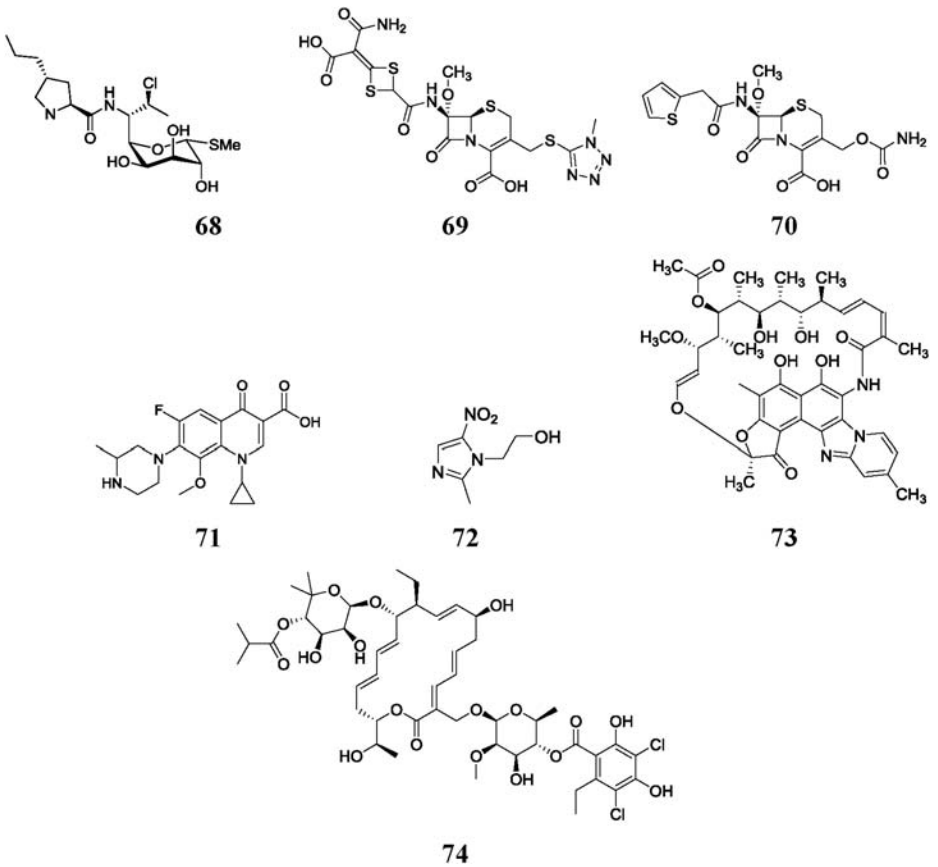

Fig. 13 Antibiotics for the treatment of *Clostridium difficile* infections: **68** clindamycin, **69** cefotetan, **70** cefoxitin, **71** gatifloxacin, **72** metronidazole, **73** rifaximin, **74** fidaxomicin.

been suggested for treatment of relapsing CDI,[266] while fidaxomicin (**74**) is a bactericidal narrow-spectrum macrocyclic antibiotic that is used for the management of CDI with high risk for recurrences.[267] Both rifamycins and fidaxomycin inhibit bacterial transcription but with different RNA polymerase target sites. Fidaxomicin provides cure rates not inferior to vancomycin and is associated with a significantly lower rate of recurrence of CDI.[268] It also has a minimal impact on the composition of the gut microbiome, in particular Bacteroides species,[12] despite high local concentration in the gut and feces.

5.17.2.2.4 *Multidrug-resistant* Acinetobacter

Acinetobacter spp. are strictly aerobic, nonfermentative, Gram-negative organisms frequently isolated in soil and water that can exist as part of normal skin flora. There has been a significant increase in the incidence of infections caused by *A. baumannii* in recent years. Most of the nosocomial outbreaks by this microorganism have occurred in intensive care units, where there is substantial use of antimicrobial agents that select for the emergence of MDR strains. There has been a large increase in *A. baumannii* resistance to all antimicrobial agents in recent years. For example, resistance to ceftazidime is >85% and to ciprofloxacin is >90%.[269] About 63% of *Acinetobacter* are considered MDR to at least three different classes of antibiotics and approximately 2% of healthcare-associated infections are caused by this organism with the proportion higher among critically ill patients on mechanical ventilators (about 7%).[270] The result is an estimated 12,000 healthcare-associated *Acinetobacter* infections in the United States each year with nearly 7000 (or 63%) MDR, and about 500 deaths are attributed to these infections.

Resistance to β-lactams occurs in several ways, including upregulation of inherent chromosomal AmpC and carbapenemase (bla_{OXA-51}) genes by insertion sequences, OXA carbapenemases, and NDM carbapenemases.[271] The presence of a specific IS element ISAba1 upstream of the naturally occurring *ampC* gene generates promoter sequences that enhance expression, providing resistance to broad-spectrum cephalosporins. The most common ESBLs identified in *A. baumannii* are the PER-, GES- and VEB-type β-lactamases. Despite wide dissemination among Enterobacteriaceae, only a few KPC-type β-lactamases have been identified in *A. baumannii*.

Quinolone resistance in *A. baumannii* arises by a single mutation in the *gyrA* gene, resulting in high-level resistance clinically. This is due to the fact that *A. baumannii* also has some intrinsic resistance due to decreased permeability or constitutive expression of efflux pumps.[272] Plasmid-mediated *qnr* genes have not been identified in this organism. Tigecycline has shown good antibacterial activity against *A. baumannii* with successful clinical outcomes.[273] Two mechanisms of resistance to colistin have been reported in *A. baumannii*: alterations of the lipid A component of LPS resulting from mutations in the PmrAB two-component system,[274] and complete loss of LPS production resulting from mutations in the *lpxA*, *lpxC*, and *lpxD* genes encoding the enzymes that catalyze the first steps in LPS biosynthesis.[275]

In a recent study, 5477 *A. baumannii* and other relevant Gram-negative organisms (collected 2007–11) were tested for susceptibility to tetracycline, doxycycline (**Fig. 14**; **75**), and other broad-spectrum antimicrobial agents.[276] *A. baumannii* strains were highly resistant to all agents tested with the exception of minocycline (79.1% susceptible) and colistin (98.8% susceptible).

5.17.2.2.5 *Methicillin-resistant* Staphylococcus aureus

S. aureus continues to be one of the most common bacterial pathogens in the world and causes a broad spectrum of diseases in both community and hospital settings.[277] More recently, highly virulent CA-MRSA strains such as USA300 have emerged. Over time treatment of *S. aureus* infections has become more challenging, with an increasing frequency of MDR isolates, particularly in MRSA. Clinical isolates with reduced susceptibility to glycopeptides, particularly vancomycin, have been reported.[278] However, unlike for MDR Gram-negative pathogens, there are now a number of treatment options available for MRSA infections.

Overall rates of *S. aureus* bacteremia appear to have stabilized over the past 20 years while the contribution MRSA has fluctuated.[277,279] Since 2005 many regions have seen significant reductions in rates of MRSA bacteremia, usually correlated with improvements in infection control procedures. These reductions were especially evident in the United Kingdom, where rates of MRSA bacteremia were halved between 2004 and 2011.[280] The United States has also seen such reductions.[281] While *S. aureus* has traditionally been the leading cause of SSTIs, its importance has been magnified in the past 15 years with the emergence of a worldwide epidemic of CA-MRSA SSTIs.[282,283] Recent US data suggest that the MRSA SSTI incidence may have peaked around 2007–08; for example, the proportion of all community-onset SSTIs due to MRSA in the US military health system declined from 62% to 52% from 2005 to 2010, although overall *S. aureus* SSTI rates did not change.[284]

The increased prevalence of cardiac device implantations has led to an increased incidence of cardiac device *S. aureus* infections.[285] The impact of these infections is high and those due to MRSA are generally, but not invariably, associated with higher mortality rates than those caused by MSSA.[286] *S. aureus* is an important cause of pneumonia in both community and hospital settings. In particular, *S. aureus* has consistently been shown to be one of the most common pathogens in healthcare-associated infections (HCAP). A recent study found MRSA as the cause of 28% of VAP cases in 31 US community hospitals,[287] and patients

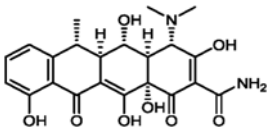

Fig. 14 Doxycycline.

with MRSA VAP tend to incur increased costs of care compared to patients with MSSA pneumonia.[288] Fortunately, the overall incidence of MDR pathogens, including MRSA, is relatively low in patients with HCAP[289] and rates are lower in most parts of Europe compared with the United States.[290] *S. aureus* is becoming a common pathogen in CF patients, an increasing proportion of which are MRSA. *S. aureus* may form biofilms in the airways of patients with CF,[291] contributing to the persistence of colonization and antibiotic failure.

The worldwide emergence of methicillin-resistant staphylococci (MRSA and MRSE) in the 1970s brought vancomycin to the forefront for treatment of staphylococcal infections. The drug remains as first-line therapy for methicillin-resistant coagulase-negative and coagulase-positive staphylococcal infections, including bacteremia, endocarditis, pneumonia, cellulitis, and osteomyelitis.[292] Vancomycin exhibits slower bactericidal activity against MSSA compared to β-lactams, and this slow activity may contribute to the worse clinical outcomes seen with cases of MSSA bacteremia and pneumonia treated with vancomycin.[293] In 2002, the first vanA-mediated vancomycin-resistant strain was reported and, since that time only 13 isolates have been reported in the United States,[294] with a few others in India, Iran, and Brazil.

One more recent treatment option is daptomycin,[209] for which no *S. aureus* MIC "creep" (such as reported for vancomycin) has been observed since its approval for clinical use.[157] In fact, daptomycin MIC distributions have changed little for any of the Gram-positive pathogens for which it is approved[295] and the MIC_{90} remains 0.5 μg mL^{-1} among staphylococci. However, there have been reports of emergence of daptomycin-nonsusceptible *S. aureus* isolates during unsuccessful therapy with the drug.[296,297] *S. aureus* nonsusceptibility to daptomycin appears to be multifactorial, involving alterations to both cell membrane and cell wall through adaptations in metabolic and stress response regulatory pathways.[298]

Clinical infections with *S. aureus*, especially MRSA, will likely remain both common and serious, with waves of increasing antimicrobial resistance.[299] Over the past 20 years, two clear shifts in the epidemiology of *S. aureus* infections have occurred: first, growth in the number of healthcare-associated infections such as those associated with prosthetic device procedures, and second, an epidemic of community-associated SSTIs driven by strains with particular virulence factors.[277] Further epidemiology shifts are probable in the future, with MRSA maintaining its role as a key human pathogen.

5.17.2.2.6 *Multidrug-resistant* Pseudomonas aeruginosa

P. aeruginosa is an important pathogen frequently involved in a variety of healthcare-associated infections, especially in critically ill or immunocompromised patients. Intrinsic antibiotic resistance is a particular problem with *P. aeruginosa* due to a combination of reduced cell wall permeability and the ability to acquire and express multiple resistance mechanisms including porin deletions and overexpression of efflux pumps.[300,301] Although the prevalence of *P. aeruginosa* in the last two decades has remained relatively stable, the incidence of antibiotic-resistant strains has increased dramatically.[302,303] *P. aeruginosa* infections caused by resistant isolates are associated with higher mortality, increased morbidity, and extensive resource utilization and associated costs. These MDR isolates make effective treatment much more challenging and limited available treatment options can lead to inappropriate empiric therapy often associated with poor clinical and economic outcomes.[304]

P. aeruginosa currently shows resistance to the following antibiotics at varying levels: penicillins, including those combined with BLIs; early cephalosporins; piperacillin; piperacillin and tazobactam; cefepime; ceftazidime; aminoglycosides; the quinolones; and the carbapenems, as well as colistin and fosfomycin. Therefore, monitoring resistance trends for *P. aeruginosa* becomes important for choosing the optimal antibiotic, as this organism has become one of the leading causes of pneumonia. Carbapenem resistance in *P. aeruginosa* is mostly attributable to porin (OprD) deficiency, often combined with derepressed expression of the chromosomal AmpC cephalosporinase, and more rarely to carbapenemases—mainly the IMP, VIM, SPM, and GIM MBLs.[305] NDM-1-producing *P. aeruginosa* isolates were first reported in 2011, with two strains recovered from Serbia.[306] NDM-1-positive *P. aeruginosa* isolates have since been identified in India, Italy, Egypt, and Slovakia.[305] A *P. aeruginosa* isolate producing both the IMP-18 MBL and the KPC-2 serine carbapenemase has been reported from Puerto Rico.[307] With regard to aminoglycoside resistance, the first 16S rRNA methylase, RmtA, recovered in *P. aeruginosa* was identified in 2003 in a clinical isolate from Japan.[308] Fluoroquinolone resistance in *P. aeruginosa* is mainly related to the MexAB–OprM RND-type efflux system, whose expression is constitutive. This system also confers reduced susceptibility to chloramphenicol (Fig. 15; **76**), tetracyclines and β-lactams.[309] The emergence of colistin-resistant *P. aeruginosa* isolates associated with modifications of the lipid A component of LPS has been reported worldwide.[310] Several two-component regulatory systems, such as PmrAB, PhoPQ, ParRS, CprRS, and ColRS, are involved in resistance to polymyxins in *P. aeruginosa*.[311]

5.17.2.2.7 *Mycobacterium tuberculosis*

Tuberculosis (TB) continues to be the world's leading cause of death by a single infectious agent. The WHO estimates that in 2014, 9.6 million people became ill with active TB and 1.5 million died from the disease, including 140,000 children.[312] Most new cases

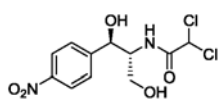

75

Fig. 15 Chloramphenicol.

of TB occur in Asia and Africa (58% and 28%, respectively). South Africa is particularly affected, as TB represents the single largest cause of mortality with nearly 9% of all deaths in 2013,[313] and TB continues to be a major killer of human immunodeficiency virus (HIV)-infected individuals in Africa and elsewhere around the world causing 400,000 of the 1.2 million HIV deaths reported in 2014.[312]

Antibiotic treatment regimens are available, but the emergence of drug-resistant TB complicates efforts to control the epidemic fully. In 2014, 3.3% of these cases resulted from MDR tuberculosis (MDR-TB) and extensively drug-resistant tuberculosis (XDR-TB) strains.[314] MDR-TB are resistant to both of the first-line drugs of standard TB treatment isoniazid (**Fig. 16**; **77**) and rifampicin (**78**), while XDR-TB are resistant to isoniazid, rifampin, at least one fluoroquinolone, and any of the second-line injectable treatments (amikacin, capreomycin [**79**], kanamycin [**80**]).[315] Other drugs considered to be in first-line combination therapy are ethambutol (**81**) and pyrazinamide (**82**).[316] The cost of treating these resistant TB strains can be as much as 25 times higher and take three times longer than for drug-susceptible strains.[317] In 2014, there were 480,000 new cases of MDR-TB with especially significant incidence in Eastern Europe and central Asia. Approximately 9.7% of MDR-TB cases are caused by XDR-TB strains globally, with the highest rates of XDR-TB among MDR-TB cases occurring in Belarus (29%), Lithuania (25%), Latvia (19%), and Georgia (15%) in 2014.[312] In the United States in 2014, the proportional incidence of MDR-TB remains relatively low at 1.3%, and overall TB incidence in the United States remained approximately 3.0 cases per 100,000 persons during 2013–15.[318]

Drug resistance to *Mycobacterium tuberculosis* (MTB) generally results from inadequate drug treatment of active TB caused by lack of patient compliance, inadequate drug levels, drug shortages, or other factors. New antibiotic regimens with novel drugs are needed that can potentially shorten the current treatment course of 6 months or more. Treatment of MDR- or XDR-TB strains can take 18 months and cost more than $150,000 in the United States. With the increased toxicity of second-line agents, patient compliance over the entire treatment period can be even more challenging. Treatment of patients in less developed countries is often beyond the means of governments, ensuring that MDR- and XDR-TB strains will remain with us and possibly increase in incidence in the future.

Recent years have seen the first regulatory approvals for new TB drugs bedaquiline and delamanid, in more than 40 years.[319] Bedaquiline (**83**) is a diarylquinoline that was granted accelerated approval for the treatment of MDR-TB by the US FDA in Dec. 2012,

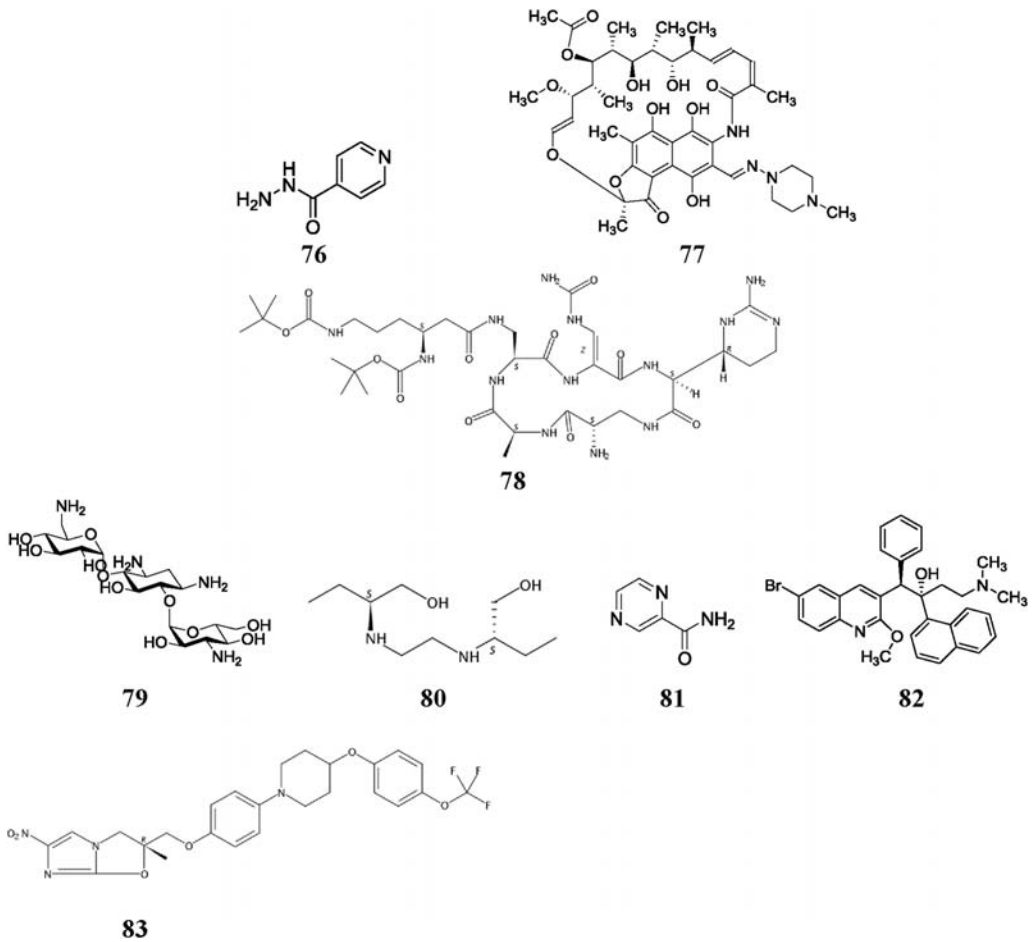

Fig. 16 Antibiotics for the treatment of *Mycobacterium tuberculosis*: **77** isoniazid, **78** rifampicin, **79** capreomycin, **80** kanamycin, **81** ethambutol, **82** pyrazimide, **83** bedaquiline.

based on data generated by Phase 2b trials. This is the first new drug approved specifically for TB. Bedaquiline has a unique mechanism of action that targets the proton pump for ATP synthase.[320] Delamanid (**84**), a nitro-dihydro-imidazooxazole, is an orally dosed prodrug whose primary metabolites likely kill mycobacteria by blocking the synthesis of mycolic acids and disrupt cell wall synthesis.[321,322] Nitroimidazoles also appear to kill the TB bacteria by poisoning them with nitric oxide, which the drugs release when metabolized. Delamanid received its first global approval for the treatment of MDR-TB in the European Union (EU), for use in combination with optimized background therapy, and also has been granted orphan drug status in both the EU and Japan.[323]

5.17.3 Antifungal Resistance

Candida species and *Aspergillus* are the key pathogenic fungi whose incidence and resistance trends have been carefully monitored. Over the past decade, decreases in bacterial causes have led to *Candida* becoming the most common cause of healthcare-associated bloodstream infections in many US hospitals.[324] *Candida* spp. are becoming increasingly resistant to current antifungal drugs (Fig. 17) such as the azole fluconazole (**85**) and the echinocandin glucan synthetase inhibitor caspofungin (**86**); however, overall resistance rates are relatively low compared with what has been observed for bacteria. Fluconazole resistance in particular has remained relatively constant over the past 20 years.[325,326]

A 2016 publication described 1846 fungal clinical isolates from 31 countries. Echinocandin resistance in *Candida* spp. ranged from 0.0% to 2.8% (highest for anidulafungin [**87**] vs. *C. glabrata*), and fluconazole resistance was noted among 11.9% and 11.6% of the *C. glabrata* and *Candida tropicalis* isolates, respectively.[327] Other US studies have followed the development of echinocandin resistance in *Candida* species, particularly *C. glabrata*. The majority of these resistant isolates have specific mutations in one of two "hot spot" regions of the FKS1 or FKS2 genes, which encode a subunit of the 1,3-β-D-glucan synthase target protein.[328,329] There is also evidence that many echinocandin-resistant *C. glabrata* isolates are also resistant to fluconazole.[330] One recent study reported several significant findings. First, despite a decreasing number of *C. glabrata* candidemia, the level of echinocandin resistance remained steady or has increased. Second, elevated MIC values and echinocandin resistance are caused by an increasing number of distinct mutations in *C. glabrata*, primarily in the FKS1 and FKS2 genes. Third, MDR among *C. glabrata* isolates was high (>3%) and may indicate future problems with this pathogen.[328]

Other studies showed that immunocompromised patients, particularly those undergoing bone marrow or organ transplants, were found to develop *Candida* infections after receiving micafungin (**88**) prophylaxis. The rate of echinocandin-resistant *C. glabrata* increased from 4.9% to 12.3% and fluconazole-resistant isolates from 18% to 30% over a 10-year period through 2010.[331] Echinocandin resistance among US *C. glabrata* isolates is a concern, especially in light of the fact that one-third of those isolates may be MDR. Because treatment options for fungal infections remain limited, this potential new resistance trend needs to be closely monitored.

Azole resistance in *Aspergillus fumigatus* has become an issue in recent years. It has been known that in patients with chronic exposure to azoles, such as those with chronic pulmonary aspergillosis, resistance to this class of agents can occur. The first reports came from isolates collected from patients who had been treated with itraconazole in the 1990s in the United States and Sweden (**89**).[332] As seen with *Candida* species, resistance in *Aspergillus* can be due to point mutations in the CYP51A gene, which encodes the enzyme responsible for the demethylation of lanosterol in the final step in ergosterol biosynthesis. Rates of azole resistance in the United Kingdom were reported to have increased from 5% to 7% to up to 20% from 2004 to 2009, with these isolates primarily coming from patients with chronic pulmonary aspergillosis combined with long-term azole exposure.[333,334]

Fluconazole inhibits the fungal cytochrome P450 enzyme 14α-demethylase. Selectivity occurs since the mammalian demethylase activity is much less sensitive to fluconazole than fungal demethylase. This inhibition prevents the conversion of lanosterol to ergosterol, an essential component of the fungal cytoplasmic membrane, with consequent accumulation of 14α-methyl sterols. Of note, in documented invasive aspergillosis, azole-resistant *A. fumigatus* isolates have been reported in patients without previous azole exposure with tandem repeats in the promoter region of CYP51A, in addition to point mutations found within this gene. Environmental isolates with these changes have also been recovered, including the indoor environment of hospitals and areas in direct proximity to the medical centers along with areas where azole fungicides are used in agriculture.[335,336] The rise in azole resistance rates in *A. fumigatus* isolates in the United States and in other countries around the world and the discovery of mechanisms of resistance associated with environmental exposure are causes for concern.[337] Even more troubling is the appearance of multidrug *Candida* infections resistant to both echinocandins and fluconazole, leaving few treatment options other than amphotericin B (**89**). Such limited treatment options for infections due to resistant isolates may be associated with a higher probability of treatment failure.[338,339]

5.17.4 Antiviral Resistance

By comparison with the antibacterials and antifungals, antiviral drug discovery took longer to gain momentum as the dogma in the early days was that because viruses are obligatory parasites their replication could not be blocked selectively. Initial antiviral treatments were not specific and were mostly derived from the development of polymers (including polyanions). Antiviral development was also influenced by the emergence of interferon therapy and by research on innate and acquired immunity. Additionally, synthetic polyanions initially thought to act as direct-acting antiviral agents (DAAs) were later discovered to induce interferon. Since the first antiviral treatments were nonspecific, had low selectivity, and were frequently targeting cellular factors, they were not prone

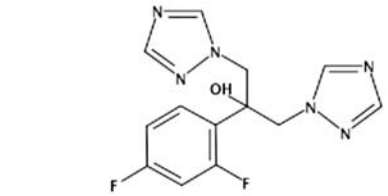

84

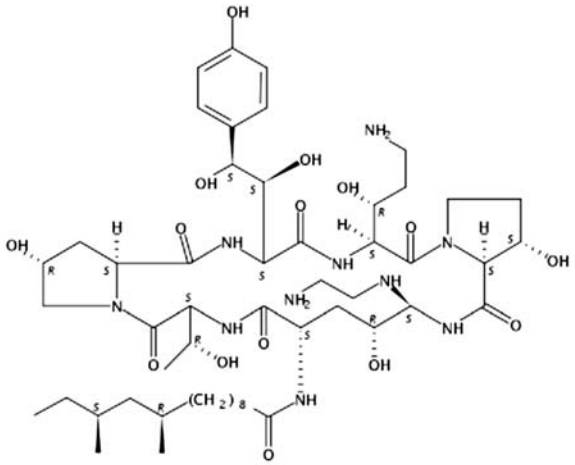

85

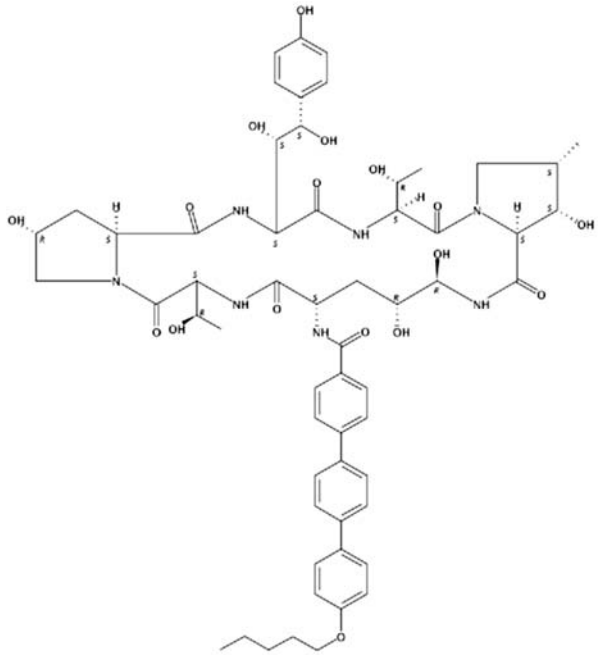

86

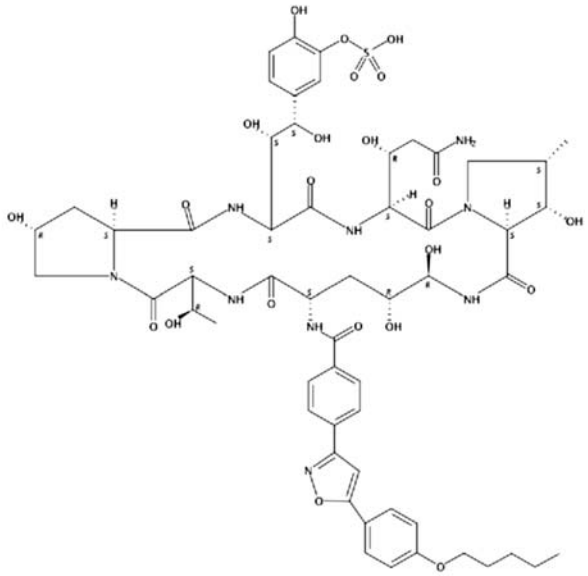

87

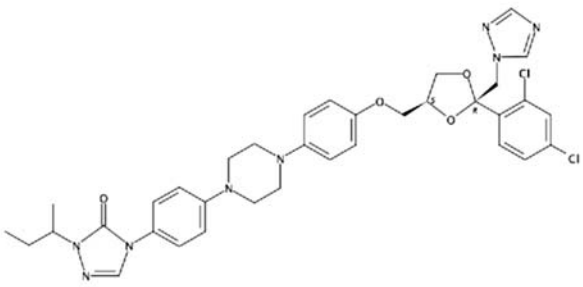

88

Fig. 17 Antibiotics for the treatment of fungal infections.

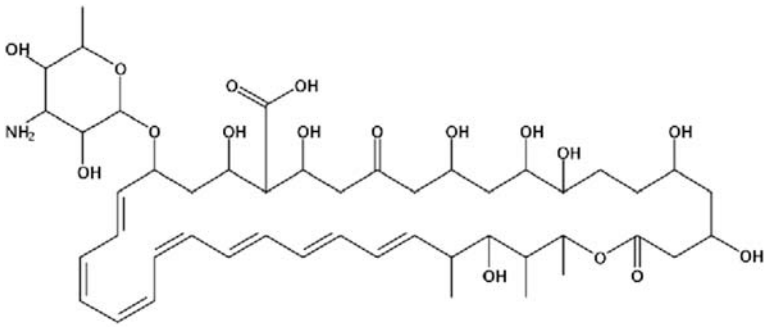

89

Fig. 17 (*continued*).

to resistance. With the development of DAAs targeting specific viral gene products, better selectivity was achieved but at the cost of selective pressure against the less genetically stable viral targets. This led to the emergence of drug resistance to viral pathogens, in particular those with high genetic variability arising from low polymerase fidelity or from high levels of viral genome recombination. The discovery of acyclovir, the first selective antiviral, as a treatment for herpes simplex infection stimulated a further quest for novel antiviral agents with narrow selectivity and high activity.[340]

As the number of DAAs in clinical usage increased, so resistance emerged. This emergence was also more pronounced for lethal diseases such as acquired immunodeficiency syndrome (AIDS), as treatment to prevent patient health worsening or death was obviously urgent, and initial regimens provided suboptimal antiviral effects. For long-term treatments, patient fatigue or side effects led to reduced treatment adherence, suboptimal drug levels, and a consequent increase in the development of resistance. Overall, resistance to antiviral drugs has emerged as one of the most important barriers to efficacy in the treatment of chronic infections.[341] This section discusses only the resistance issues encountered with the most frequently used drugs, focusing on the last 10–15 years and the major pathogens HIV, hepatitis B virus (HBV), hepatitis C virus (HCV), and influenza.

5.17.4.1 Human Immunodeficiency Virus

HIV is a lentivirus, a member of the Retroviridae family. Two types of HIV, HIV-1 and HIV-2, were discovered in the early 1980s and were rapidly identified as the causative agents of AIDS.[342–344] HIV-1 is found worldwide, and HIV-2 is mostly prevalent in sub-Saharan Africa. HIV has a unique viral cycle characterized by an RNA-to-DNA step executed by an unusual polymerase, the reverse transcriptase (RT), offering an opportunity for the development of nucleoside analogs able to target viral replication relatively specifically. Additionally, and in contrast to retroviruses discovered previously, a function map of the HIV genome was quickly established after discovery and sequencing, allowing the identification of potential targets and leading to intensified drug development.

The drugs currently approved to treat HIV target the viral proteins RT, protease (PR), and integrase (IN), all three of which generated from the pol polyprotein, as well as the envelope gene product (ENV). All current antiretroviral drugs (ARVs) are DAAs, and representatives from several classes are usually combined to treat HIV infection for life, as no curative treatment is available. The well-established high mutation rate of HIV is linked to its error-prone polymerase, the RT. Although frequently deleterious for the viruses, some mutations are fit enough to allow transmission of drug-resistant isolates, one of the modern challenges for HIV treatment.[341] Consequently, screening for HIV drug resistance before the start of a new regimen is now standard of care in most developed countries.

Modern antiretroviral regimens are adjusted to the presence or potential emergence of resistance mutations by preferentially selecting drugs with higher minimum (trough) plasma concentrations (C_{min}) that largely exceed the antiviral activity (EC_{95}). These properties are captured by their inhibitory quotient (IQ), the ratio of the clinical drug concentration (such as C_{min}) to the EC_{95} ($IQ = C_{min}/EC_{95}$).[345–348] The IQ can be advantageously modified by adjustment of the drug dosage when available for clinical use.[349] The most commonly used ARVs, their respective HIV targets, and their resistance profiles are described here.

5.17.4.1.1 HIV reverse transcriptase

HIV RT inhibitors were the first class of drug to be developed. These drugs bind directly to the HIV RT, an RNA-dependent DNA polymerase, blocking its function in viral replication. Early drugs were derivatives of natural nucleosides and included examples with simple chemical modifications such as zidovudine, zalcitabine, didanosine, and stavudine. With limited selectivity between the viral and cellular polymerases, many had significant side effects, but they played a key role in delaying AIDS for some patients, allowing for the discovery of new drugs.[350] Next generations of RT inhibitors were further developed, are mostly in use today and discussed here.

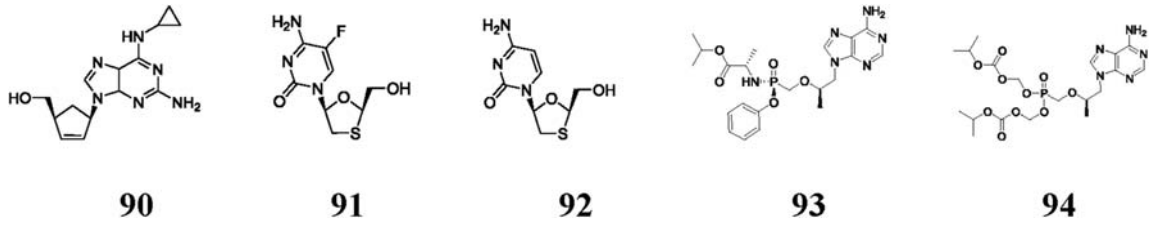

Fig. 18 HIV nucleoside RT inhibitor (NRTI).

5.17.4.1.1.1 Nucleoside RT inhibitors

Drugs in the nucleoside reverse transcriptase inhibitor (NRTI) class were designed as derivatives of natural nucleosides or nucleotides (Fig. 18). All are phosphorylated by cellular host enzymes to produce their triphosphate analogs. The most frequently used drugs in this class include abacavir (**90**), emtricitabine (**91**), lamivudine (LAM) (**92**), and tenofovir (TFV). For each, the active metabolite can inhibit RT by incorporation into viral DNA, causing a termination of DNA chain elongation. The most recent NRTI to be FDA-approved is TFV alafenamide (**93**), a novel prodrug of TFV, with more selective safety and pharmacokinetics (PK) properties than the current tenofovir prodrug, TDF (**94**).[351] The resistance barrier to NRTIs is usually low, as a single point mutation can render the virus less susceptible or drug-resistant, such as M184V or K65R (reviewed in Ref. [352]). Resistance can also be conferred through accumulation of multiple mutations, such as the Q151M complex or thymidine analog mutations, as well as insertion multiple residues at position T69.

5.17.4.1.1.2 Nonnucleoside RT inhibitors

Nonnucleoside reverse transcriptase inhibitors (NNRTIs) do not originate from natural products but from synthetic screening libraries. Unlike NRTIs, NNRTIs act as allosteric inhibitors by reducing the catalytic activity of RT without binding the polymerase catalytic pocket.[353] Interestingly, the NNRTI binding site is not observed crystallographically in the absence of ligand. Current NNRTIs (Fig. 19) are only active against HIV-1. Drugs in this class are very potent, and include nevirapine, delavirdine, and efavirenz (**95**). Etravirine (**96**) and rilpivirine (**97**) are second-generation NNRTIs, which were designed to be active against HIV strains with mutations that confer resistance to the most commonly prescribed first-generation NNRTIs such as K103N, although their IQ is lower than some of the first-generation drugs in this class.

5.17.4.1.2 HIV protease

HIV PR plays a central role in the viral cycle, as it is responsible for the processing of all the viral products produced in the gag-pol polyprotein, including auto-processing to generate the free PR. The enzyme has different levels of activity against the several substrate sequences it needs to cleave, allowing coordinated cuts in specific order, important for the production of viral PARTICLES with optimal infectivity.

5.17.4.1.2.1 Protease inhibitors

Protease inhibitors (PIs) are early examples of peptido-mimetic drugs. Their structures were based on tetrapeptides, mimicking amino acid residues around the cleavage sites (P2–P1–P1′–P2′) in the enzyme substrates (gag and pol products). First-generation PIs were very hydrophobic, with an entropy-based binding to the PR heavily relying on desolvation. These properties led to fast emergence of resistance.[354] Moreover, high structural similarities between the first-generation PIs and their extensive use led to the emergence of HIV-1 isolates with cross-resistance to all members of this class,[355] leading to their combination in attempts to obtain better antiviral activity. An important outcome was the observation of improved PK wherein one PI (ritonavir, which irreversibly inhibits CYP3A) boosted the PK properties of the others.[356] This led to the extensive use of boosted-PIs in the clinic,[357] allowing higher drug systemic exposures through an increased IQ and better antiviral activity against isolates with PR resistance-associated mutations such as D30N, M46I, G48V, I50V, V82A, I84V, N88S, and L90M.[358] Second-generation PIs (Fig. 20) such as lopinavir (**98**), atazanavir (**99**), and darunavir (**100**) were developed to reduce serum binding, resistance to

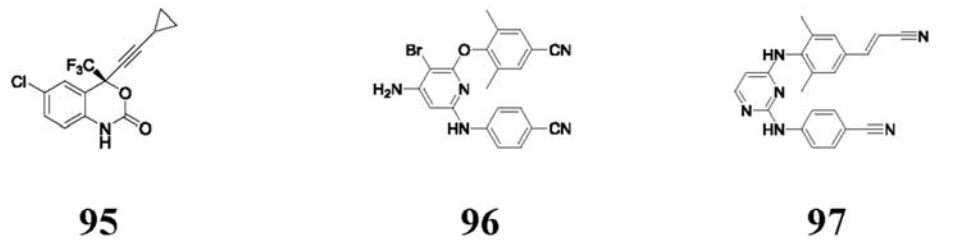

Fig. 19 HIV nonnucleoside RT inhibitors (NNRTIs).

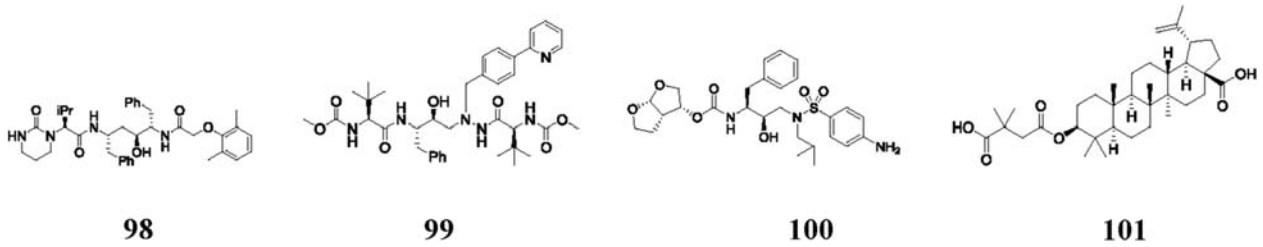

Fig. 20 HIV protease inhibitors and maturation inhibitors.

some primary mutations, and adverse metabolic profiles such as elevation of serum lipids, and these are currently the most commonly prescribed agents, although they still require boosting to achieve high IQs.[359]

5.17.4.1.2.2 Gag maturation inhibitors

A second locus involved in HIV resistance to PIs was identified outside of the PR gene, with mutations emerging in the gag polyprotein precursor, close to cleavage sites.[360] This discovery led to the development of a novel class of gag-pol polyprotein maturation inhibitors, with beviramat (Fig. 20; **101**) as the prototypical example. Bevirimat has not reached FDA approval, but analogs are being investigated in clinical studies.

5.17.4.1.3 HIV integrase

HIV IN is also produced from the gag-pol polyprotein. After penetration of the HIV preintegration complex into the cell nucleus, IN catalyzes the integration of viral DNA into host DNA. Although several inhibitory modes have been identified, only one resulted in FDA-approved drugs, known as integrase strand transfer inhibitors (INSTIs). Currently, three INSTIs are available (Fig. 21): raltegravir (RAL) (**102**), elvitegravir (EVG) (**103**), and dolutegravir (DTG) (**104**). INSTIs bind to the IN active site, preventing the DNA strand transfer step essential for the HIV replication. EVG retains activity against some IN mutants (such as L74M, G140S, Y143R/H/C) that are resistant to RAL.[361] Similarly, DTG retains activity against IN mutants that are resistant to EVG and RAL (such as T66I, E92Q, N155H).[362,363]

5.17.4.1.4 HIV envelope (ENV)

HIV ENV is produced as a highly glycosylated precursor polyprotein, gp160. The gp160 is then processed by the cellular enzyme furin into two subunits, the surface (SU) subunit gp120 and the transmembrane (TM) subunit gp41. Mature functional ENV consists of a trimer of gp120/41 (SU/TM) heterodimers. The viral envelope controls entry into selected permissive target cells. Entry inhibitors preventing envelope functioning have been the focus of intense research, such as small molecules or peptides[364]; the few entry inhibitors FDA-approved are described here.

5.17.4.1.4.1 Fusion inhibitors

The TM protein gp41 contains a fusion peptide at its NH_2-terminal end, allowing fusion of the virus and cell membranes. The fusion peptide contains two helical heptad repeat regions that control the fusion process, and adopts a triple helix secondary structure, allowing conformational changes enabling membrane fusion. Exploration of peptidic analogs of the triple helix led to the approved drug T-20 (enfuvirtide; Fig. 22) (**105**).[365] The drug needs to be injected, limiting its attractiveness in comparison to oral treatments, but has been frequently used in salvage therapy.

5.17.4.1.4.2 Cellular receptor antagonists

Before fusion, HIV needs to bind to cells expressing the CD4 protein, which is used as a receptor by the virus. Along with CD4, a coreceptor is necessary for initiation of fusion process. Either of the chemokine receptors CCR5 or CXCR4 can serve as coreceptor, and the interaction triggers conformational changes in the gp120/gp41 envelope glycoprotein complex leading to the fusion of the virus with cell membranes. Maraviroc (MVC) (Fig. 22; **106**) is an antagonist of CCR5 and is active against HIV strains that depend upon CCR5 for cell entry (the large majority) but not those that depend on CXCR4.[366] Consequently, it is only recommended for

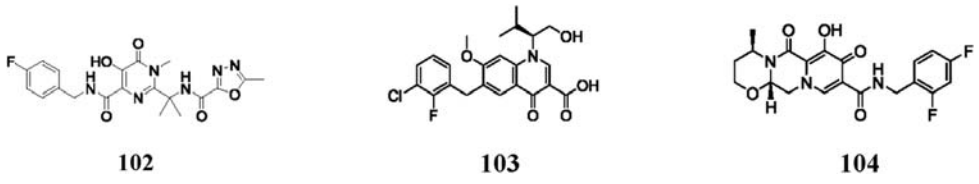

Fig. 21 HIV integrase strand transfer inhibitors (INSTIs).

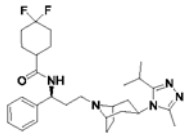

[acetyl]-YTSLIHSLIEESQNQQEKNEQELLELDKWASLWNWF-[NH_2]

105 **106**

Fig. 22 HIV entry inhibitors.

treating HIV infections with CCR5-tropic viruses.[341] Although resistance data to MVC is limited, resistance has been associated with mutations in the V3 loop of gp120 such as positions 308, 316, and 323. Substitutions outside the V3 loop may also contribute to reduced susceptibility and could be classified as resistant mutations.[367]

5.17.4.1.5 Drug combinations

Antiviral drug resistance emerged rapidly when ARVs were used alone early in the AIDS epidemic. This led to the exploration of combinations of multiple drugs, which initially showed a significantly increased reduction of HIV viral load, preventing damage to the immune system and significantly lowering the risk of developing AIDS. The approach was widely adopted in clinical practice, and combinations of three ARVs from at least two different classes became the standard of care (initially defined as highly active antiretroviral therapy, HAART, and later as combination antiretroviral therapy, cART). Consistent HIV treatment with cART led to better adherence to the regimen, improved drug steady-state levels, and sustained viral suppression in the majority of the patients. A large diversity of ARVs are currently available and several have been formulated as fixed-dose combinations, administered as single tablets once daily, that enable adherence.[368] These efforts have resulted in clinical efficacy rates for chronic viral suppression of above 90%, consequently reducing the incidence of drug resistance. However, management of HIV infection still requires lifelong therapy as the regimens are not curative.[369]

5.17.4.2 Hepatitis B Virus

HBV is a double-stranded DNA virus of the Hepadnaviridae family and is the causative agent of chronic hepatitis B (CHB). Currently, the only two drug classes approved for treatment CHB are a finite course of interferon and continuous therapy with oral nucleos(t)ide analogues. Treatment response to interferon varies, but the host and viral factors that contribute to differences in treatment response are not fully elucidated. Given that interferon is not a DAA, no resistance mutations have been established against interferon and only direct-acting pol/RT inhibitors will be discussed here.

While treatment of CHB often results in suppression of HBV DNA levels in the serum, current regimens are rarely effective at eliminating the viral genetic reservoir covalently closed circular DNA (cccDNA), which remains in the nucleus of infected hepatocytes and allows for an increase of viral load after cessation of treatment. The cccDNA reservoir is established early during the course of CHB infection. Current DAAs against HBV inhibit the transcription of RNA from viral DNA and thus do not target the established cccDNA reservoir (reviewed in Ref. [370]). This viral reservoir, along with the long half-life of infected hepatocytes, creates a lifelong risk of viral rebound if treatment is suspended. Because of the need for long-term treatment of patients with CHB, antiviral resistance is an important consideration for therapy.

5.17.4.2.1 Nucleos(t)ide reverse transcriptase inhibitors

The HBV polymerase is a multifunctional protein encoding four domains, including an RT and RNase H domain. The pol/RT domain of HBV shares structural homology to that of HIV,[371] and this similarity is reflected by the overlapping antivirals used in HIV and HBV therapy. There are currently five oral antivirals available for treatment of CHB. Unlike HIV therapy, antivirals for HBV are routinely prescribed as monotherapy.

Nucleos(t)ide reverse transcriptase inhibitors (N[t]RTIs) approved for treatment of CHB (Fig. 23) include nucleosides (LAM (**92**) and telbivudine (LdT) (**107**)), phosphonate analogs (adefovir (ADV) (**108**) and TDF (**94**)), and entecavir (ETV) (**109**), a nucleoside analog with a carbocyclic replacement for the ribose ring.[372] The first antiviral to be approved for the treatment of HBV was LAM, marketed in 1998. Increased suppression of viral DNA was achieved with LAM compared to interferon treatment; however, rates of resistance mutations in the pol/RT (rtM204V/I/S) were as high as 20% after 1 year, to 70% through 5 years of treatment.[373] Beginning with ADV in 2002 and through the 2000s, several novel agents were approved, with varying levels of resistance development. Unlike LAM, resistance to ADV is typically associated with two mutations (rtA181T/V, rtN236T) leading to a higher barrier to resistance. Despite this, rates of resistance were as high as 29% after 5 years of treatment.[374,375] Initial studies with LdT demonstrated increased rates of HBV DNA suppression compared to LAM. Unfortunately, like ADV, rates of resistance were high with 25% of subjects developing LdT resistance mutation (rtM204I/V, rtA181T/V) after only 2 years of treatment.[376]

The third-generation CHB antivirals ETV and TDF are characterized by higher potency, low rates of resistance, and rates of HBV DNA suppression over 90% after 5 years in treatment-naïve patients. In N[t]RTI-naïve patients, resistance to ETV is low, with 1.2% of patients with resistance after 5 years.[377,378] Resistance to ETV requires the rtL180M + rtM204V/I LAM-associated resistance

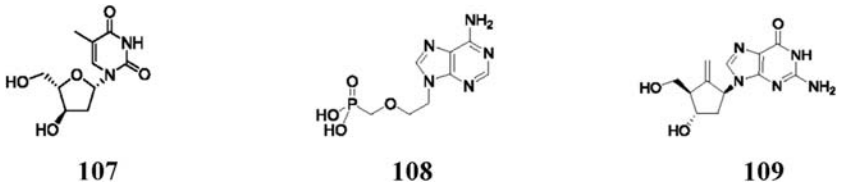

Fig. 23 HBV nucleos(t)ide reverse transcriptase inhibitors (N[t]RTI).

mutations as well as additional ETV-specific substitutions (rtI169 T, rtS184G, rtS202G/I, or rtM250V). Unfortunately, treatment-experienced patients that have developed resistance or compensatory mutations to other antivirals have a lower barrier to resistance development to ETV. Conversely, despite the structural similarity of TDF and ADV, no clinical antiviral resistance has been detected in treatment-naïve patients through at least 6 years of treatment.[379] TDF was also effective in patient populations with preexisting resistance mutations, although the time to viral suppression may be slower in ADV experienced patients.[380–383] TDF can therefore be used in patient populations who have failed previous treatments with other N[t]RTIs. Due to the high rates of resistance, the first- and second-generation antivirals LAM, ADV, and LdT have been replaced in the American Association for the Study of Liver Diseases and the European Association for the Study of the Liver treatment guidelines by third-generation agents that have lower rates of resistance even with long-term therapy.[384,385]

5.17.4.2.2 New viral targets

Although antiviral therapeutics with no known associated resistance mutations are available, the rate of clearance of the viral cccDNA reservoir is low and new viral targets must be identified to achieve a CHB cure. Multiple pathways to cccDNA clearance have been envisioned, including direct targeting of the cccDNA (histone modification, siRNA), activation of the immune system (TLR agonists, therapeutic vaccines), and inhibition of viral spread (capsid inhibitors, egress inhibitors) (reviewed in Ref. [386]).

5.17.4.3 Hepatitis C Virus

Discovered in 1989 as a causative agent of hepatitis, HCV is a single-stranded positive enveloped virus and the only member of the Hepacivirus genus, which constitutes at least seven distinct genotypic variants. Infection can result in acute hepatitis, but over 70% of infections establish chronic HCV that can lead to cirrhosis and hepatocellular carcinoma.[387] In contrast to other chronic viral infections such as HIV and HBV, HCV does not have a viral reservoir and elimination of viral replication can result in a complete cure, or sustained virologic response (SVR).

The first therapies for HCV, based on a 24-week regimen of interferon and the guanosine analog ribavirin, achieved approximately 55% SVR.[388] Greater understanding of the viral enzymes encoded by HCV (including the NS3/4A proteinase, NS5B polymerase, and multifunctional NS5A protein) were afforded by the development of replicon systems for in vitro study and allowed for direct targeting of viral processes by DAAs.[389] Since the introduction of HCV-specific DAAs into clinical practice in the 2010s, SVR rates have steadily risen to as high as 100% in some patient populations (reviewed in Ref. [390]). In general, DAAs with or without ribavirin are now the recommended therapy for most patients.[391,392] Four classes of DAAs are currently approved for chronic HCV, including nucleotide analogues and nonnucleotide NS5B inhibitors, NS5A inhibitors, and NS3/4A proteinase inhibitors. Mutations associated with drug resistance to HCV are referred to as resistance-associated variants (RAVs), and are briefly discussed here.

5.17.4.3.1 Nucleotide analogue NS5B inhibitors

Nucleotide analogues against HCV target the viral RNA-dependent RNA polymerase NS5B, and the only approved drug as of 2016 is the uridine analogue sofosbuvir (Fig. 24; **110**). Viruses with the S282T sofosbuvir resistance substitution within the highly conserved NS5B active site have lower viral fitness. Additionally, resistance to sofosbuvir is rarely seen prior to treatment and is not stable in the viral population after treatment cessation.[393–395] Few mutations have been determined to confer resistance clinically (L159F, S282T, and L320F), and the occurrence of these substitutions varies by genotype (reviewed in Ref. [396]).

Fig. 24 HCV NS5B inhibitors.

5.17.4.3.2 Nonnucleotide NS5B inhibitors

Many nonnucleotide NS5B inhibitors are in development, but dasabuvir (Fig. 24; **111**) is the only approved example. This class of drugs has a lower barrier to resistance than nucleotides and is therefore used in combination therapy, as in the Viekira Pak™. Established resistance-associated sites include C316, M441, Y448, and S556. Mutations at these positions have limited impact on viral fitness, allowing them to persist off treatment.[397,398]

5.17.4.3.3 NS5A inhibitors

Although it lacks any known enzymatic activities, the viral protein NS5A is required for HCV replication, modulates the cellular immune response, and alters the membranous environment via unknown mechanisms. Daclatasvir (Fig. 25; **112**) was the first NS5A inhibitor approved for HCV treatment and was followed by additional NS5A-targeted antivirals including ledipasvir (**113**), ombitasvir (**114**), and elbasvir (**115**), with additional examples currently in development. This drug class is characterized by high potency, perhaps due to the inhibition of multiple NS5A-dependent steps of the HCV replication cycle. Amino acids that can harbor resistance mutations (including M28, Q30, L31, and Y93) are located at the NS5A dimer interface, suggesting that one consequence of drug binding is to block dimerization.[389,392]

Polymorphic sites with preexisting resistance to NS5A inhibitors are common and are detected in upwards of 10% of patients prior to treatment.[399] When a patient develops resistance to NS5A on treatment, the mutation often becomes fixed in the viral population. This may be due to a high viral fitness levels, additional compensatory mutations, or a barrier to reversion back to wild type (reviewed in Ref. [390]).

5.17.4.3.4 NS3/4A protease inhibitors

The NS3 protein encodes multiple enzymatic components including the N-terminal proteinase responsible for cleavage of the viral polyprotein, and the C-terminal helicase and NTPase. At the C-terminal end, the covalently bound NS4A acts both to target the viral proteinase to cellular membranes and as a cofactor to the viral PR. The first approved NS3/4A inhibitors (Fig. 26) telaprevir (**116**) and boceprevir (**117**) act by binding directly to the catalytic serine of NS3. Additional drugs in this class include paritaprevir (**118**) and grazoprevir (**119**).

5.17.4.3.5 Drug combinations

Due to the prevalence of some RAVs in viral populations, combination therapies with or without ribavirin or interferon are the preferred treatment options for both treatment-naïve and treatment-experienced patients and lead to higher overall SVR rates. A number of combination therapies are approved for treatment and the recommended regimens are determined by viral genotype, preexisting RAVs, and presence of cirrhosis. For example, commonly prescribed combination therapies include ledipasvir/sofosbuvir, ombitasvir/paritaprevir/ritonavir/dasabuvir, and grazoprevir/elbasvir.[391,392]

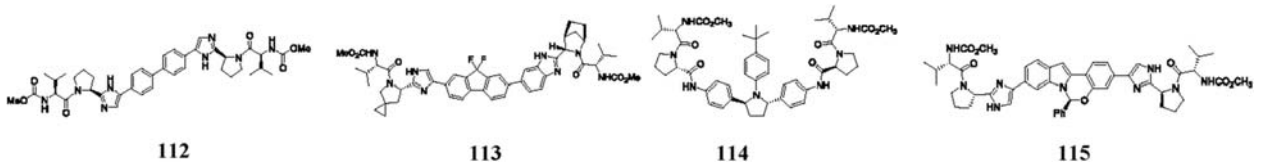

112 113 114 115

Fig. 25 HCV NS5A inhibitors.

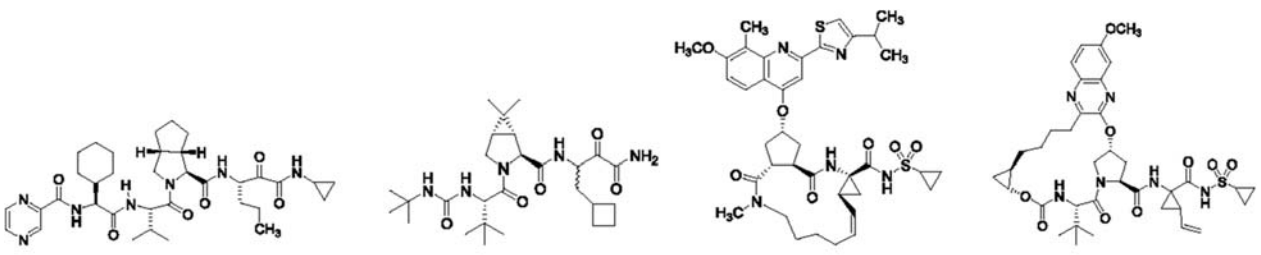

116 117 118 119

Fig. 26 HCV protease inhibitors.

5.17.4.4 Influenza

Influenza viruses are negative-sense, single-stranded, segmented RNA viruses of the orthomyxovirus family. Of the three types of influenza viruses (A, B, and C), Influenza A viruses are the major cause of influenza symptoms in humans. Influenza B and C viruses are less common, cause milder symptoms, and do not result in pandemics.

The high error rate of the viral polymerase as well as the inclusion of eight genome segments makes influenza uniquely primed for the development of antiviral resistance mutations.[400] In addition to mutation, reassortment of gene segments during coinfections with multiple influenza viruses leads to the rapid acquisition of new genes. This allows for rapid spread of resistance mutations, and is also typically the origin of novel pandemics.

While vaccination is the most effective method for prevention of influenza epidemics, antivirals are used as treatment in severe cases as well as to prevent spread of the disease in closed populations or early in the course of pandemics when vaccines are unavailable.[401] Currently, only two classes of influenza antivirals are approved: adamantanes and neuraminidase inhibitors (NAIs).

5.17.4.4.1 M2 inhibitors (adamantanes)

The first antiviral drugs developed for treatment of influenza were the adamantane class of compounds (Fig. 26; **120**), targeted against the viral protein M2. This protein is only found in influenza A virus, so the class is ineffective against influenza B. The M2 protein is a transmembrane ion channel responsible for both the release of viral RNA from the virion after entry as well as regulating viral maturation. Adamantane-based antivirals block M2 function by binding to the pore of the channel to displace a water molecule, resulting in disruption of the pH-sensing residues of the transmembrane domain.[402] Two adamantane-based antivirals are approved for use: amantadine and rimantadine.

Three dominant adamantane-resistant mutations (S31N, V27A, L26F) have been observed clinically and additional mutations (A30T, G34E) have been reported to confer resistance in vitro.[403] A single point mutation is sufficient to confer resistance to both marketed adamantanes, and all mutations are naturally occurring variations at the drug binding site. In vitro and animal studies demonstrated that adamantane resistance does not decrease viral fitness,[404,405] allowing resistance to become fixed in currently circulating influenza viruses.

Resistance to adamantanes rose rapidly in the early 2000s, with resistance mutations detected in nearly all currently circulating H3N2 influenza. The prevalence of adamantane resistance in H1N1 influenza was rare in the 2007–08 seasonal strain, but the 2009 pandemic H1N1 that remains the dominant H1N1 in circulation has resistance rates of over 99%. Due to the high prevalence of resistance to adamantanes in circulating influenza A viruses, this class of antiviral drugs is not recommended for treatment by Centers for Disease Control and Prevention (CDC) guidelines.[406,407]

5.17.4.4.2 Neuraminidase inhibitors

Along with hemagglutinin, the neuraminidase of influenza makes up one of two glycoproteins on the surface of the viral envelope. It is required for cleavage of sialic acid from the cell surface during the release of progeny virions from infected cells and is highly conserved across influenza and B viruses, making it an attractive antiviral target. NAIs are structural analogs of the natural substrate of neuraminidase, sialic acid, and bind directly to the enzymatic site.[406] Two NAIs (Fig. 27), oseltamivir (**121**) and zanamivir (**122**), are currently widely approved for treatment of influenza, with an additional two, peramivir (**123**) and laninamivir (**124**), available in selected countries. Peramivir shares structural similarities to both oseltamivir and zanamivir, while laninamivir is similar to zanamivir.[408]

Resistance to NAIs can occur either through mutations at the highly conserved active site of the neuraminidase or to the surrounding structural amino acids. The H274Y mutation (N1 numbering) is the only one considered to have proven clinical resistance by the WHO and confers complete resistance to oseltamivir, with reduced susceptibility to zanamivir. A number of additional substitutions detected in clinical isolates have been implicated in antiviral resistance (E119G, E119V, R224K, R292K, N294S), with others often associated with the H274Y mutation (I222R, I222V, S246N) (reviewed in Ref. [408]).

As with the adamantanes, drug resistance to NAIs was detected soon after the introduction of treatment in the early 2000s. While most frequently detected in children or immune-compromised adults, resistance has also been found in patients without previous exposure to influenza antivirals. Although NAI resistance occurs at lower levels than that to adamantanes, prevalence can reach up to 100%, as was seen with oseltamivir resistance in the 2007–08 H1N1 seasonal strain. Currently, resistance to all NAIs remains low, at less than 10% globally.[406]

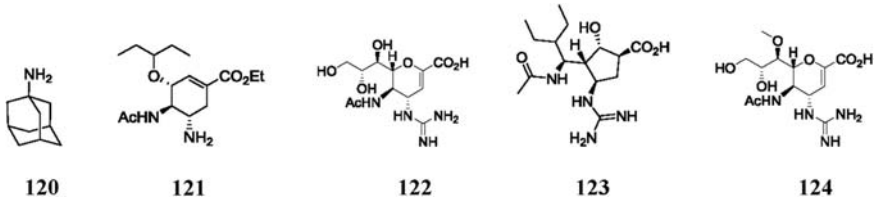

120 121 122 123 124

Fig. 27 Influenza inhibitors.

Table 2 Infectious disease threats as defined by the Centers for Disease Prevention and Control in 2013[12]

CDC threat level	*Pathogen*	*Recent status*
Urgent	Carbapenem-resistant Enterobacteriaceae (CRE)	Endemic in many US states and in many countries worldwide Treatment options becoming more limited New agents in late development may provide protection against many CRE
	Clostridium difficile	Cephalosporin, fluoroquinolone, clindamycin, erythromycin resistance common Increased treatment failures with vancomycin and metronidazole
	Neisseria gonorrhoeae	Strains identified with resistance to most available antimicrobials New antibiotics effective as monotherapy or in combinations needed Late stage investigational agents are in development
Serious	MDR *Acinetobacter*	Significant increase in the incidence of *Acinetobacter* infections Large increase in resistance to all antimicrobial agents in recent years New antibiotics effective as monotherapy or in combinations urgently needed
	Extended-spectrum β-lactamase-producing (ESBL) Enterobacteriaceae	Steady increase in rates in United States since 2000 Treatment options becoming more limited as multidrug resistance is common Carbapenems and new β-lactamase inhibitor combinations often effective
	MDR *Pseudomonas aeruginosa*	Prevalence of infections has remained relatively stable Incidence of multidrug-resistant strains has increased dramatically in recent years
	Drug-resistant tuberculosis	TB now the most prevalent infectious disease in the world Incidence of TB has been relatively stable in United States in recent years but increasing in other parts of the world MDR and XDR remain a concern Important global cause of death per year
	Methicillin-resistant *Staphylococcus aureus* (MRSA)	Rates of bacteremia and SSTIs have stabilized in recent years A leading cause of healthcare-associated infections especially involving devices Resistance rates for linezolid, daptomycin, and other new anti-Gram-positive antibiotics remain very low[416]
	Vancomycin-resistant enterococcus (VRE)	High rates in United States, prevalence still relative low elsewhere[339] Limited treatment options, especially for *Enterococcus faecium*
	Drug-resistant *Streptococcus pneumoniae*	Despite vaccine availability, invasive pneumococcal disease (IPD) remains a problem worldwide[417] IPD mortality has not changed significantly in the past decades[159]
	Fluconazole-resistant *Candida*	Fluconazole resistance has remained relatively low and constant over the past 20 years
Concerning	Vancomycin-resistant *Staphylococcus aureus* (VRSA)	14 cases in four states 2002–15 Still rare in occurrence Cases mainly in patients with other underlying conditions Many newer anti-Gram-positive agents effective

Initial in vitro and animal studies on drug resistance mutations in the neuraminidase gene determined that resistance had a detrimental effect on viral replication, with viruses encoding H274Y being highly attenuated.[409] Recent in vitro work suggests that the H274Y compensatory mutations R194G and V234M/R222Q can increase viral fitness while maintaining resistance to oseltamivir.[410] These permissive mutations may account for the high frequency of resistance seen in seasonal influenza in 2007.[410,411]

5.17.4.4.3 New influenza antivirals

The rapid development of antiviral resistance in influenza viruses could potentially be overcome through the use of combination therapies, much as for HIV and HCV therapy. Given the high frequency of adamantane resistance and the relative paucity of influenza antiviral classes, new drugs are necessary to provide an effective combination therapy. Research into the design of M2 or NA inhibitors with higher thresholds of antiviral resistance is underway, although far from market approval.[412] The many other viral enzymes of influenza make attractive antiviral targets, including the three components of the viral polymerase (PB1, PB2, and PA) (reviewed in Ref. [413]). Indeed, one polymerase inhibitor (favipiravir) is licensed for limited use in Japan.[414] The nucleoside analog ribavirin has demonstrated inhibition of influenza in vitro; however, clinical results have been inconclusive. In addition to DAAs, multiple therapeutic antibodies and host-targeting drugs are in preclinical and early clinical trials for use in influenza treatment.[415]

5.17.5 Conclusions

Antimicrobial resistance is a critical threat that affects agents in all areas of infectious disease. **Table 2** lists the most important threats described by the CDC in 2013.[12,159,416–418] Many of these threats have only increased in severity, whereas others such as MDR-*S. pneumoniae* and fluconazole-resistant *Candida* spp. remain virtually unchanged. Somewhat optimistically, for some threats such as those posed by the ESBL-producing Enterobacteriaceae, treatment options are improving.

Drug discovery efforts and adaptiveness over the past few decades, in all antimicrobial fields, have been up to the challenge of fighting emerging resistant strains. Drug combinations played a key role in constraining resistance. However, the need for innovation is still there, since new drug combinations will be limited by the diversity of drugs available.

Overall, resistance is still a major challenge to our antimicrobial armamentarium, and needs to be monitored on a continuing basis.[182,419–427]

See also: 5.18. Direct-Acting Antiviral Agents for the Treatment of Hepatitis C Virus Infection. 5.19. New Antiretrovirals for HIV and Antivirals for HBV. 5.20. Antiviral Drugs for Acute Infections. 5.21. New Drugs and Emerging Leads in Antibacterial Drug Discovery. 5.22. Antifungal Chemistry Review.

References

1. Aminov, R. I. A Brief History of the Antibiotic Era: Lessons Learned and Challenges for the Future. *Front. Microbiol.* **2010,** *1,* 134.
2. Laxminarayan, R.; Duse, A.; Wattal, C.; Zaidi, A. K. M.; Wertheim, H. F. L.; Sumpradit, N.; Vlieghe, E.; Hara, G. L.; Gould, I. M.; Goossens, H.; Greko, C.; So, A. D.; Bigdeli, M.; Tomson, G.; Woodhouse, W.; Ombaka, E.; Peralta, A. Q.; Qamar, F. N.; Mir, F.; Kariuki, S.; Bhutta, Z. A.; Coates, A.; Bergstrom, R.; Wright, G. D.; Brown, E. D.; Cars, O. Antibiotic Resistance—The Need for Global Solutions. *Lancet Infect. Dis.* **2013,** *13,* 1057–1098.
3. Walsh, F. *Antibiotic Resistance: Cameron Warns of Medical 'Dark Ages'.* http://www.bbc.co.uk/news/health-28098838, 2014 (accessed March 17, 2016).
4. Center for Disease Dynamics, Economics & Policy. *State of the World's Antibiotics, 2015;* CDDEP: Washington, DC, 2015.
5. Livermore, D. M. Current Epidemiology and Growing Resistance of Gram-Negative Pathogens. *Korean J. Intern. Med.* **2012,** *27,* 128–142.
6. Livermore, D. M. Fourteen Years in Resistance. *Int. J. Antimicrob. Agents* **2012,** *39,* 283–294.
7. van Hoek, A. H. A. M.; Mevius, D.; Guerra, B.; Mullany, P.; Roberts, A. P.; Aarts, H. J. M. Acquired Antibiotic Resistance Genes: An Overview. *Front. Microbiol.* **2011,** *2,* 1–27.
8. King, M. D.; Humphrey, B. J.; Wang, Y. F.; Kourbatova, E. V.; Ray, S. M.; Blumberg, H. M. Emergence of *Community*-Acquired Methicillin-Resistant *Staphylococcus aureus* USA 300 Clone as the Predominant Cause of Skin and Soft-Tissue Infections. *Ann. Intern. Med.* **2006,** *144,* 309–317.
9. Rogers, B. A.; Sidjabat, H. E.; Paterson, D. L. *Escherichia coli* O25b-ST131: A Pandemic, Multiresistant, Community-Associated Strain. *J. Antimicrob. Chemother.* **2011,** *66,* 1–14.
10. Woodford, N.; Turton, J. F.; Livermore, D. M. Multiresistant Gram-Negative Bacteria: The Role of High-Risk Clones in the Dissemination of Antibiotic Resistance. *FEMS Microbiol. Rev.* **2011,** *35,* 736–755.
11. Chen, S.-C.; Yin, Y.-P.; Dai, X.-Q.; Unemo, M.; Chen, X.-S. First Nationwide Study Regarding Ceftriaxone Resistance and Molecular Epidemiology of *Neisseria gonorrhoeae* in China. *J. Antimicrob. Chemother.* **2016,** *71,* 92–99.
12. Louie, T.; Cannon, K.; Byrne, B.; Emery, J.; Ward, L.; Eyben, M.; et al. Fidaxomicin Preserves the Intestinal Microbiome During and After Treatment of *Clostridium difficile* Infection (CDI) and Reduces Both Toxin Reexpression and Recurrence of CDI. *Clin. Infect. Dis.* **2012,** *55* (Suppl. 2), S132–S142.
13. Lee, H.; Unemo, M.; Kim, H. J.; Seo, Y.; Lee, K.; Chon, Y. Emergence of Decreased Susceptibility and Resistance to Extended-Spectrum Cephalosporins in *Neisseria gonorrhoeae* in Korea. *J. Antimicrob. Chemother.* **2015,** *70,* 2536–2542.
14. Holmes, K. K.; Johnson, D. W.; Floyd, T. M. Studies of Venereal Disease. I. Probenecid-Procaine Penicillin G Combination and Tetracycline Hydrochloride in the Treatment of "Penicillin-Resistant" Gonorrhea in Men. *JAMA* **1967,** *202,* 461–473.
15. Ohnishi, M.; Golparian, D.; Shimuta, K.; Saika, T.; Hoshina, S.; Iwasaku, K.; Nakayama, S.; Kitawaki, J.; Unemo, M. Is *Neisseria gonorrhoeae* Initiating a Future era of Untreatable Gonorrhea?: Detailed Characterization of the First Strain With High-Level Resistance to Ceftriaxone. *Antimicrob. Agents Chemother.* **2011,** *55,* 3538–3545.
16. Unemo, M.; Golparian, D.; Nicholas, R.; Ohnishi, M.; Gallay, A.; Sednaoui, P. High-Level Cefixime- and Ceftriaxone-Resistant *N. gonorrhoeae* in France: Novel penA Mosaic Allele in a Successful International Clone Causes Treatment Failure. *Antimicrob. Agents Chemother.* **2012,** *56,* 1273–1280.
17. Nordmann, P.; Naas, T.; Poirel, L. Global Spread of Carbapenemase Producing Enterobacteriaceae. *Emerg. Infect. Dis.* **2011,** *17,* 1791–1798.
18. Walsh, T. R.; Weeks, J.; Livermore, D. M.; Toleman, M. A. Dissemination of NDM-1 Positive Bacteria in the New Delhi Environment and Its Implications for Human Health: An Environmental Point Prevalence Study. *Lancet Infect. Dis.* **2011,** *11,* 355–362.
19. Capone, A.; Giannella, M.; Fortini, D.; Giordano, A.; Meledandri, M.; Ballardini, M.; Venditti, M.; Bordi, E.; Capozzi, D.; Balice, M. P.; Tarasi, A.; Parisi, G.; Lappa, A.; Carattoli, A.; Petrosillo, N.; SEERBIO-GRAB network. High Rate of Colistin Resistance Among Patients With Carbapenem-Resistant *Klebsiella Pneumoniae* Infection Accounts for an Excess of Mortality. *Clin. Microbiol. Infect.* **2013,** *19,* 23–30.
20. Liu, Y. Y.; Wang, Y.; Walsh, T. R.; Yi, L. X.; Zhang, R.; Spencer, J.; Doi, Y.; Tian, G.; Dong, B.; Huang, X.; Yu, L. F.; Gu, D.; Ren, H.; Chen, X.; Lv, L.; He, D.; Zhou, H.; Liang, Z.; Liu, J. H.; Shen, J. Emergence of Plasmid-Mediated Colistin Resistance Mechanism MCR-1 in Animals and Human Beings in China: A Microbiological and Molecular Biological Study. *Lancet Infect. Dis.* **2016,** *16,* 161–168.

21. Napier, B. A.; Burd, E. M.; Satola, S. W.; Cagle, S. M.; Ray, S. M.; McGann, P.; Pohl, J.; Lesho, E. P.; Weiss, D. S. Clinical use of Colistin Induces Cross-Resistance to Host Antimicrobials in *Acinetobacter baumannii*. *MBio* **2013,** *4.* e00021-13.
22. Weiner, L. M.; Fridkin, S. K.; Aponte-Torres, Z.; Avery, L.; Coffin, N.; Dudeck, M. A.; Edwards, J. R.; Jernigan, J. A.; Konnor, R.; Soe, M. M.; Peterson, K.; McDonald, L. C. Vital Signs: Preventing Antibiotic-Resistant Infections in Hospitals—United States, 2014. *MMWR* **2016,** *65,* 235–241.
23. Bush, K.; Bradford, P. A. β-Lactams and β-Lactamase Inhibitors: An Overview. In *Antibiotic Resistance;* Silver, L. L., Bush, K., Eds.; *Perspective Medicine;* Cold Spring Harbor Laboratory Press: Cold Spring Harbor, NY, 2016.
24. Spratt, B. G. Penicillin-Binding Proteins and the Future of β-Lactam Antibiotics. *J. Gen. Microbiol.* **1983,** *129,* 1247–1260.
25. Wells, J. S.; Hunter, J. C.; Astle, G. L.; Sherwood, J. C.; Ricca, C. M.; Trejo, W. H.; Bonner, D. P.; Sykes, R. B. Distribution of β-Lactam and β-Lactone Producing Bacteria in Nature. *J. Antibiot.* **1982,** *35,* 814–821.
26. D'Costa, V. M.; King, C. E.; Kalan, L.; Morar, M.; Sung, W. W.; Schwarz, C.; Froese, D.; Zazula, G.; Calmels, F.; Debruyne, R.; Golding, G. B.; Poinar, H. N.; Wright, G. D. Antibiotic Resistance is Ancient. *Nature* **2011,** *477,* 457–461.
27. Couto, I.; de Lencastre, H.; Severina, E.; Kloos, W.; Webster, J. A.; Hubner, R. J.; Sanches, I. S.; Tomasz, A. Ubiquitous Presence of a *mecA* Homologue in Natural Isolates of *Staphylococcus sciuri*. *Microb. Drug Resist.* **1996,** *2,* 377–391.
28. Abraham, E. P.; Chain, E. An Enzyme From Bacteria Able to Destroy Penicillin. *Nature* **1940,** *146,* 837.
29. Kirby, W. M. N. Extraction of a Highly Potent Penicillin Inactivator from Penicillin Resistant Staphylococci. *Science* **1944,** *99,* 452–453.
30. Medeiros, A. A. Evolution and Dissemination of β-Lactamases Accelerated by Generations of Beta-Lactam Antibiotics. *Clin. Infect. Dis.* **1997,** *24,* S19–S45.
31. Bush, K.; Jacoby, G. A. Updated Functional Classification of Beta-Lactamases. *Antimicrob. Agents Chemother.* **2010,** *54,* 969–976.
32. Karlowsky, J. A.; Biedenbach, D. J.; Bouchillon, S. K.; Iaconis, J. P.; Reiszner, E.; Sahm, D. F. In Vitro Activity of Ceftaroline Against Bacterial Pathogens Isolated from Skin and Soft Tissue Infections in Europe, Russia and Turkey in 2012: Results From the Assessing Worldwide Antimicrobial Resistance Evaluation (AWARE) Surveillance Programme. *J. Antimicrob. Chemother.* **2016,** *71,* 162–169.
33. Torumkuney, D.; Chaiwarith, R.; Reechaipichitkul, W.; Malatham, K.; Chareonphaibul, V.; Rodrigues, C.; Chitins, D. S.; Dias, M.; Anandan, S.; Kanakapura, S.; Park, Y. J.; Lee, K.; Lee, H.; Kim, J. Y.; Lee, Y.; Lee, H. K.; Kim, J. H.; Tan, T. Y.; Heng, Y. X.; Mukherjee, P.; Morrissey, I. Results from the Survey of Antibiotic Resistance (SOAR) 2012–14 in Thailand, India, South Korea and Singapore. *J. Antimicrob. Chemother.* **2016,** *71* (Suppl. 1), i3–i19.
34. Villasenor-Sierra, A.; Katahira, E.; Jaramillo-Valdivia, A. N.; Barajas-Garcia Mde, L.; Bryant, A.; Morfin-Otero, R.; Marquez-Diaz, F.; Tinoco, J. C.; Sanchez-Corona, J.; Stevens, D. L. Phenotypes and Genotypes of Erythromycin-Resistant *Streptococcus pyogenes* Strains Isolated from Invasive and Non-Invasive Infections from Mexico and the USA During 1999–2010. *Int. J. Infect. Dis.* **2012,** *16,* e178–e181.
35. Mendes, R. E.; Sader, H. S.; Farrell, D. J.; Jones, R. N. Telavancin Activity Tested Against a Contemporary Collection of Gram-Positive Pathogens from USA Hospitals (2007–2009). *Diagn. Microbiol. Infect. Dis.* **2012,** *72,* 113–117.
36. Coombs, G. W.; Pearson, J. C.; Daley, D. A.; Le, T.; Robinson, O. J.; Gottlieb, T.; Howden, B. P.; Johnson, P. D.; Bennett, C. M.; Stinear, T. P.; Turnidge, J. D.; Australian Group on Antimicrobial Resistance. Molecular Epidemiology of Enterococcal Bacteremia in Australia. *J. Clin. Microbiol.* **2014,** *52,* 897–905.
37. Toner, L.; Papa, N.; Aliyu, S. H.; Dev, H.; Lawrentschuk, N.; Al-Hayek, S. Vancomycin Resistant Enterococci in Urine Cultures: Antibiotic Susceptibility Trends Over a Decade at a Tertiary Hospital in the United Kingdom. *Investig. Clin. Urol.* **2016,** *57,* 129–134.
38. Turner, P. J. Trends in Antimicrobial Susceptibilities Among Bacterial Pathogens Isolated from Patients Hospitalized in European Medical Centers: 6-Year Report of the MYSTIC Surveillance Study (1997–2002). *Diagn. Microbiol. Infect. Dis.* **2005,** *51,* 281–289.
39. Wong, D.; Wong, T.; Romney, M.; Leung, V. Comparative Effectiveness of Beta-Lactam Versus Vancomycin Empiric Therapy in Patients With Methicillin-Susceptible *Staphylococcus aureus* (MSSA) Bacteremia. *Ann. Clin. Microbiol. Antimicrob.* **2016,** *15,* 27.
40. Yanagihara, K.; Kadota, J.; Aoki, N.; Matsumoto, T.; Yoshida, M.; Yagisawa, M.; Oguri, T.; Sato, J.; Ogasawara, K.; Wakamura, T.; Sunakawa, K.; Watanabe, A.; Iwata, S.; Kaku, M.; Hanaki, H.; Ohsaki, Y.; Watari, T.; Toyoshima, E.; Takeuchi, K.; Shiokoshi, M.; Takeda, H.; Miki, M.; Kumagai, T.; Nakanowatari, S.; Takahashi, H.; Utagawa, M.; Nishiya, H.; Kawakami, S.; Kobayashi, N.; Takasaki, J.; Mezaki, K.; Konosaki, H.; Aoki, Y.; Yamamoto, Y.; Shoji, M.; Goto, H.; Saraya, T.; Kurai, D.; Okazaki, M.; Niki, Y.; Yoshida, K.; Kawana, A.; Saionji, K.; Fujikura, Y.; Miyazawa, N.; Kudo, M.; Sato, Y.; Yamamoto, M.; Yoshida, T.; Nakamura, M.; Tsukada, H.; Imai, Y.; Tsukada, A.; Kawasaki, S.; Honma, Y.; Yamamoto, T.; Ban, N.; Mikamo, H.; Sawamura, H.; Miyara, T.; Toda, H.; Sato, K.; Nakamura, T.; Fujikawa, Y.; Mitsuno, N.; Mikasa, K.; Kasahara, K.; Sano, R.; Sugimoto, K.; Asari, S.; Nishi, I.; Toyokawa, M.; Miyashita, N.; Koguchi, Y.; Kusano, N.; Mihara, E.; Kuwabara, M.; Watanabe, Y.; Kawasaki, Y.; Takeda, K.; Tokuyasu, H.; Masui, K.; Negayama, K.; Hiramatsu, K.; Aoki, Y.; Fukuoka, M.; Magarifuchi, H.; Nagasawa, Z.; Suga, M.; Muranaka, H.; Morinaga, Y.; Honda, J.; Fujita, M. Nationwide Surveillance of Bacterial Respiratory Pathogens Conducted by the Surveillance Committee of Japanese Society of Chemotherapy, the Japanese Association for Infectious Diseases, and the Japanese Society for Clinical Microbiology in 2010: General View of the Pathogens' Antibacterial Susceptibility. *J. Infect. Chemother.* **2015,** *21,* 410–420.
41. Flamm, R. K.; Sader, H. S.; Jones, R. N. Ceftaroline Activity Against Organisms Isolated From Respiratory Tract Infections in USA Hospitals: Results From the AWARE Program, 2009–2011. *Diagn. Microbiol. Infect. Dis.* **2014,** *78,* 437–442.
42. Biedenbach, D. J.; Alm, R. A.; Lahiri, S. D.; Reiszner, E.; Hoban, D. J.; Sahm, D. F.; Bouchillon, S. K. In Vitro Activity of Ceftaroline Against *Staphylococcus aureus* Isolated in 2012 from Asia-Pacific Countries as Part of the AWARE Surveillance Program. *Antimicrob. Agents Chemother.* **2016,** *60,* 343–347.
43. Schaumburg, F.; Peters, G.; Alabi, A.; Becker, K.; Idelevich, E. Missense Mutations of PBP2a are Associated With Reduced Susceptibility to Ceftaroline and Ceftobiprole in African MRSA. *J. Antimicrob. Chemother.* **2016,** *71,* 41–44.
44. Navarro Torne, A.; Dias, J. G.; Quinten, C.; Hruba, F.; Busana, M. C.; Lopalco, P. L.; Gauci, A. J.; Pastore-Celentano, L. European Enhanced Surveillance of Invasive Pneumococcal Disease in 2010: Data from 26 European Countries in the Post-Heptavalent Conjugate Vaccine Era. *Vaccine* **2014,** *32,* 3644–3650.
45. Kaplan, S. L.; Center, K. J.; Barson, W. J.; Ling-Lin, P.; Romero, J. R.; Bradley, J. S.; Tan, T. Q.; Hoffman, J. A.; Peters, T. R.; Gurtman, A.; Scott, D. A.; Trammel, J.; Gruber, W. C.; Hulten, K. G.; Mason, E. O. Multicenter Surveillance of *Streptococcus pneumoniae* Isolates from Middle Ear and Mastoid Cultures in the 13-Valent Pneumococcal Conjugate Vaccine Era. *Clin. Infect. Dis.* **2015,** *60,* 1339–1345.
46. Jacoby, G. A. AmpC β-Lactamases. *Clin. Microbiol. Rev.* **2009,** *22,* 161–182.
47. Bradford, P. A. Extended-Spectrum β-Lactamases in the 21st Century: Characterization, Epidemiology, and Detection of This Important Resistance Threat. *Clin. Microbiol. Rev.* **2001,** *14,* 933–951.
48. Karanika, S.; Karantanos, T.; Arvanitis, M.; Grigoras, C.; Mylonakis, E. Fecal Colonization With Extended-Spectrum Beta-Lactamase-Producing Enterobacteriaceae and Risk Factors Among Healthy Individuals: A Systematic Review and Meta-Analysis. *Clin. Infect. Dis.* **2016,** *63* (3), 310–318.
49. Ishikawa, K.; Hamasuna, R.; Uehara, S.; Yasuda, M.; Yamamoto, S.; Hayami, H.; Takahashi, S.; Matsumoto, T.; Minamitani, S.; Kadota, J.; Iwata, S.; Kaku, M.; Watanabe, A.; Sunakawa, K.; Sato, J.; Hanaki, H.; Tsukamoto, T.; Kiyota, H.; Egawa, S.; Deguchi, T.; Matsumoto, M.; Tanaka, K.; Arakawa, S.; Fujisawa, M.; Kumon, H.; Kobayashi, K.; Matsubara, A.; Wakeda, H.; Amemoto, Y.; Onodera, S.; Goto, H.; Komeda, H.; Yamashita, M.; Takenaka, T.; Fujimoto, Y.; Tsugawa, M.; Takahashi, Y.; Maeda, H.; Onishi, H.; Ishitoya, S.; Nishimura, K.; Mitsumori, K.; Ito, T.; Togo, Y.; Nakamura, I.; Ito, N.; Kanamaru, S.; Hirose, T.; Muranaka, T.; Yamada, D.; Ishihara, S.; Oka, H.; Inatomi, H.; Matsui, T.; Kobuke, M.; Kunishima, Y.; Kimura, T.; Ichikawa, T.; Kagara, I.; Matsukawa, M.; Takahashi, K.; Mita, K.; Kato, M.; Okumura, K.; Kawanishi, H.; Hashimura, T.; Aoyama, T.; Shigeta, M.; Koda, S.; Taguchi, K.; Matsuda, Y. Japanese Nationwide Surveillance in 2011 of Antibacterial Susceptibility Patterns of Clinical Isolates from Complicated Urinary Tract Infection Cases. *J. Infect. Chemother.* **2015,** *21,* 623–633.
50. Jean, S. S.; Coombs, G.; Ling, T.; Balaji, V.; Rodrigues, C.; Mikamo, H.; Kim, M. J.; Rajasekaram, D. G.; Mendoza, M.; Tan, T. Y.; Kiratisin, P.; Ni, Y.; Weinman, B.; Xu, Y.; Hsueh, P. R. Epidemiology and Antimicrobial Susceptibility Profiles of Pathogens Causing Urinary Tract Infections in the Asia-Pacific Region: Results From the Study for Monitoring Antimicrobial Resistance Trends (SMART), 2010–2013. *Int. J. Antimicrob. Agents* **2016,** *47,* 328–334.
51. Nordmann, P.; Poirel, L. The Difficult-to-Control Spread of Carbapenemase Producers in Enterobacteriaceae Worldwide. *Clin. Microbiol. Infect.* **2014,** *20,* 821–830.

52. Bush, K. Carbapenemases: Partners in Crime. *J. Global Antimicrob. Resist.* **2013,** *1,* 7–16.
53. Drawz, S. M.; Bonomo, R. A. Three Decades of Beta-Lactamase Inhibitors. *Clin. Microbiol. Rev.* **2010,** *23,* 160–201.
54. Bush, K. A. Resurgence of β-Lactamase Inhibitor Combinations Effective Against Multidrug-Resistant Gram-Negative Pathogens. *Int. J. Antimicrob. Agents* **2015,** *46,* 483–493.
55. Sader, H. S.; Farrell, D. J.; Flamm, R. K.; Jones, R. N. Antimicrobial Susceptibility of Gram-Negative Organisms Isolated From Patients Hospitalised With Pneumonia in US and European Hospitals: Results from the SENTRY Antimicrobial Surveillance Program, 2009–2012. *Int. J. Antimicrob. Agents* **2014,** *43,* 328–334.
56. Sutherland, C. A.; Nicolau, D. P. Susceptibility Profile of Ceftolozane/Tazobactam and Other Parenteral Antimicrobials Against *Escherichia coli*, *Klebsiella pneumoniae*, and *Pseudomonas aeruginosa* from US Hospitals. *Clin. Therapeut.* **2015,** *37,* 1564–1571.
57. Tato, M.; Garcia-Castillo, M.; Bofarull, A. M.; Canton, R.; Group, C. S. In Vitro Activity of Ceftolozane/Tazobactam Against Clinical Isolates of *Pseudomonas aeruginosa* and Enterobacteriaceae Recovered in Spanish Medical Centres: Results of the CENIT Study. *Int. J. Antimicrob. Agents* **2015,** *46,* 502–510.
58. Cabot, G.; Bruchmann, S.; Mulet, X.; Zamorano, L.; Moya, B.; Juan, C.; Haussler, S.; Oliver, A. *Pseudomonas aeruginosa* Ceftolozane–Tazobactam Resistance Development Requires Multiple Mutations Leading to Overexpression and Structural Modification of AmpC. *Antimicrob. Agents Chemother.* **2014,** *58,* 3091–3099.
59. Stachyra, T.; Levasseur, P.; Pechereau, M. C.; Girard, A. M.; Claudon, M.; Miossec, C.; Black, M. T. In Vitro Activity of the β-Lactamase Inhibitor NXL104 Against KPC-2 Carbapenemase and Enterobacteriaceae Expressing KPC Carbapenemases. *J. Antimicrob. Chemother.* **2009,** *64,* 326–329.
60. Ehmann, D. E.; Jahic, H.; Ross, P. L.; Gu, R. F.; Hu, J.; Kern, G.; Walkup, G. K.; Fisher, S. L. Avibactam is a Covalent, Reversible, non-Beta-Lactam Beta-Lactamase Inhibitor. *Proc. Natl. Acad. Sci. U. S. A.* **2012,** *109,* 11663–11668.
61. Ehmann, D. E.; Jahić, H.; Ross, P. L.; Gu, R.-F.; Hu, J.; Durand-Réville, T. F.; Lahiri, S.; Thresher, J.; Livchak, S.; Gao, N.; Palmer, T. K.; Walkup, G.; Fisher, S. L. Kinetics of Avibactam Inhibition Against Class A, C, and D β-Lactamases. *J. Biol. Chem.* **2013,** *288,* 27960–27971.
62. de Jonge, B. L.; Karlowsky, J. A.; Kazmierczak, K. M.; Biedenbach, D. J.; Sahm, D. F.; Nichols, W. W. In Vitro Susceptibility to Ceftazidime–Avibactam of Carbapenem-Nonsusceptible Enterobacteriaceae Isolates Collected During the INFORM Global Surveillance Study (2012 to 2014). *Antimicrob. Agents Chemother.* **2016,** *60,* 3163–3169.
63. Asli, A.; Brouillette, E.; Krause, K. M.; Nichols, W. W.; Malouin, F. Distinctive Binding of Avibactam to Penicillin-Binding Proteins of Gram-Negative and Gram-Positive Bacteria. *Antimicrob. Agents Chemother.* **2016,** *60,* 52–756.
64. Testa, R.; Canton, R.; Giani, T.; Morosini, M. I.; Nichols, W. W.; Seifert, H.; Stefanik, D.; Rossolini, G. M.; Nordmann, P. In Vitro Activity of Ceftazidime, Ceftaroline and Aztreonam Alone and in Combination With Avibactam Against European Gram-Negative and Gram-Positive Clinical Isolates. *Int. J. Antimicrob. Agents* **2015,** *45,* 641–646.
65. Huband, M. D.; Castanheira, M.; Flamm, R. K.; Farrell, D. J.; Jones, R. N.; Sader, H. S. In Vitro Activity of Ceftazidime–Avibactam Against Contemporary *Pseudomonas aeruginosa* Isolates from U.S. Medical Centers by Census Region, 2014. *Antimicrob. Agents Chemother.* **2016,** *60,* 2537–2541.
66. Winkler, M. L.; Papp-Wallace, K. M.; Hujer, A. M.; Domitrovic, T. N.; Hujer, K. M.; Hurless, K. N.; Tuohy, M.; Halld, G.; Bonomo, R. A. Unexpected Challenges in Treating Multidrug-Resistant Gram-Negative Bacteria: Resistance to Ceftazidime–Avibactam in Archived Isolates of *Pseudomonas aeruginosa*. *Antimicrob. Agents Chemother.* **2015,** *59,* 1020–1029.
67. Alm, R. A.; Johnstone, M. R.; Lahiri, S. D. Characterization of *Escherichia coli* NDM Isolates With Decreased Susceptibility to Aztreonam/Avibactam: Role of a Novel Insertion in PBP3. *J. Antimicrob. Chemother.* **2015,** *70,* 1420–1428.
68. Schatz, A.; Bugie, E.; Waksman, S. Streptomycin: A Substance Exhibiting Antibiotic Activity Against Gram-Positive and Gram-Negative Bacteria. *Proc. Soc. Exp. Biol. Med.* **1944,** *55,* 66–69.
69. Miller, G. H.; Arcieri, G.; Weinstein, M. J.; Waitz, J. A. Biological Activity of Netilmicin, a Broad-Spectrum Semisynthetic Aminoglycoside Antibiotic. *Antimicrob. Agents Chemother.* **1976,** *10,* 827–836.
70. Smith, D. G.; Waksman, S. A. Tuberculostatic and Tuberculocidal Action of Streptomycin. *J. Bacteriol.* **1947,** *54,* 67.
71. Vicens, Q.; Westhof, E. Molecular Recognition of Aminoglycoside Antibiotics by Ribosomal RNA and Resistance Enzymes: An Analysis of X-ray Crystal Structures. *Biopolymers* **2003,** *70,* 42–57.
72. Fung-Tomc, J. C.; Lincourt, W.; Thater, C.; Kessler, R. E. Comparison of the Inhibitory and Bactericidal Activity of Aztreonam and Amikacin Against Gram Negative Aerobic Bacilli. *Ann. Clin. Lab. Sci.* **1988,** *18,* 463–467.
73. Giamarellou, H.; Evagelopoulou, V.; Lelekis, M. Enhanced In-Vitro Bactericidal Activity of Amikacin Combined With Latamoxef, Cefotaxime and Aztreonam Against Multi-Resistant *Enterobacter cloacae*. *J. Antimicrob. Chemother.* **1989,** *23,* 537–545.
74. Xie, J.; Talaska, A. E.; Schacht, J. New Developments in Aminoglycoside Therapy and Ototoxicity. *Hear. Res.* **2011,** *281,* 28–37.
75. Wargo, K. A.; Edwards, J. D. Aminoglycoside-Induced Nephrotoxicity. *J. Pharm. Pract.* **2014,** *27,* 573–577.
76. Aggen, J. B.; Armstrong, E. S.; Goldblum, A. A.; Dozzo, P.; Linsell, M. S.; Gliedt, M. J.; Hildebrandt, D. J.; Feeney, L. A.; Kubo, A.; Matias, R. D.; Lopez, S.; Gomez, M.; Wlasichuk, K. B.; Diokno, R.; Miller, G. H.; Moser, H. E. Synthesis and Spectrum of the Neoglycoside ACHN-490. *Antimicrob. Agents Chemother.* **2010,** *54,* 4636–4642.
77. Bassetti, M.; Righi, E. New Antibiotics and Antimicrobial Combination Therapy for the Treatment of Gram-Negative Bacterial Infections. *Curr. Opin. Crit. Care* **2015,** *21,* 402–411.
78. Armstrong, E. S.; Miller, G. H. Combating Evolution With Intelligent Design: The Neoglycoside ACHN-490. *Curr. Opin. Microbiol.* **2010,** *13,* 565–573.
79. Lopez, M. C.; Picazo, J. J.; Simaluiza, J. R.; Rodriguez-Avial, I.; Culebras, E. Plazomicin has Potent In Vitro Activity Against Methicillin-Resistant *Staphylococcus aureus* (MRSA) Isolates Carrying Different Aminoglycoside-Modifying Enzymes. 25th *ECCMID*; European Society for Clinical Microbiology and Infectious Disease: Copenhagen, Denmark, 2015.
80. Tenover, F. C.; Tickler, I.; Armstrong, E. S.; Kubo, A.; Lopez, S.; Persing, D. H.; Miller, G. H. Activity of ACHN-490 Against Meticillin-Resistant *Staphylococcus aureus* (MRSA) Isolates From Patients in US Hospitals. *Int. J. Antimicrob. Agents* **2011,** *38,* 352–354.
81. Doi, Y.; Yokoyama, K.; Yamane, K.; Wachino, J.; Shibata, N.; Yagi, T.; Shibayama, K.; Kato, H.; Arakawa, Y. Plasmid-Mediated 16S rRNA Methylase in *Serratia marcescens* Conferring High-Level Resistance to Aminoglycosides. *Antimicrob. Agents Chemother.* **2004,** *48,* 491–496.
82. Ma, L.; Lin, C. J.; Chen, J. H.; Fung, C. P.; Chang, F. Y.; Lai, Y. K.; Lin, J. C.; Siu, L. K.; Taiwan Surveillance of Antimicrobial Resistance Project. Widespread Dissemination of Aminoglycoside Resistance Genes *armA* and *rmt*B in *Klebsiella pneumoniae* Isolates in Taiwan Producing CTX-M-Type Extended-Spectrum Beta-Lactamases. *Antimicrob. Agents Chemother.* **2009,** *53,* 104–111.
83. Wei, D. D.; Wan, L. G.; Yu, Y.; Xu, Q. F.; Deng, Q.; Cao, X. W.; Liu, Y. Characterization of Extended-Spectrum Beta-Lactamase, Carbapenemase, and Plasmid Quinolone Determinants in *Klebsiella pneumoniae* Isolates Carrying Distinct Types of 16S rRNA Methylase Genes, and Their Association With Mobile Genetic Elements. *Microb. Drug Resist.* **2015,** *21,* 186–193.
84. Livermore, D. M.; Mushtaq, S.; Warner, M.; Zhang, J. C.; Maharjan, S.; Doumith, M.; Woodford, N. Activity of Aminoglycosides, Including ACHN-490, Against Carbapenem-Resistant Enterobacteriaceae Isolates. *J. Antimicrob. Chemother.* **2011,** *66,* 48–53.
85. Waitz, J. A.; Miller, G. H.; Moss, E., Jr.; Chiu, P. J. Chemotherapeutic Evaluation of 5-Episisomicin (Sch 22591), a New Semisynthetic Aminoglycoside. *Antimicrob. Agents Chemother.* **1978,** *13,* 41–48.
86. Sobel, M. L.; McKay, G. A.; Poole, K. Contribution of the MexXY Multidrug Transporter to Aminoglycoside Resistance in *Pseudomonas aeruginosa* Clinical Isolates. *Antimicrob. Agents Chemother.* **2003,** *47,* 3202–3207.
87. Georgescu, C.; Martin, D.; Bratu, S.; Quale, J.; Landman, D. Activity of ACHN-490, a Novel Neoglycoside Antibiotic, Against Contemporary Gram-Negative Clinical Isolates from Brooklyn, NY Hospitals. *49th ICAAC*; American Society for Microbiology: San Francisco, 2009.
88. Streit, J. M.; Jones, R. N.; Sader, H. S.; Fritsche, T. R. Assessment of Pathogen Occurrences and Resistance Profiles Among Infected Patients in the Intensive Care Unit: Report from the SENTRY Antimicrobial Surveillance Program (North America, 2001). *Int. J. Antimicrob. Agents* **2004,** *24,* 111–118.

89. Jones, R. N.; Sader, H. S.; Beach, M. L. Contemporary In Vitro Spectrum of Activity Summary for Antimicrobial Agents Tested Against 18569 Strains Non-Fermentative Gram-Negative Bacilli Isolated in the SENTRY Antimicrobial Surveillance Program (1997–2001). *Int. J. Antimicrob. Agents* **2003,** *22,* 551–556.
90. Andriole, V. T. The Quinolones: Past, Present, and Future. *Clin. Infect. Dis.* **2005,** *41* (Suppl. 2), S113–S119.
91. Redgrave, L. S.; Sutton, S. B.; Webber, M. A.; Piddock, L. J. V. Fluoroquinolone Resistance: Mechanisms, Impact on Bacteria, and Role in Evolutionary Success. *Trends Microbiol.* **2014,** *22,* 438–445.
92. Ball, P. Quinolone Generations: Natural History or Natural Selection? *J. Antimicrob. Chemother.* **2000,** *46,* 17–24.
93. Kim, E. S.; Hooper, D. C. Clinical Importance and Epidemiology of Quinolone Resistance. *Infect. Chemother.* **2014,** *46,* 226–238.
94. Hooper, D. C.; Jacoby, G. A. Mechanisms of Drug Resistance: Quinolone Resistance. *Ann. N. Y. Acad. Sci.* **2015,** *1354,* 12–31.
95. Martõnez-Martõnez, L.; Pascual, A.; Jacoby, G. A. Quinolone Resistance From a Transferable Plasmid. *Lancet* **1998,** *351,* 797–799.
96. Jacoby, G. A.; Strahilevitz, J.; Hooper, D. C. Plasmid-Mediated Quinolone Resistance. *Microbiol. Spectr.* **2014,** *2,* 1–42.
97. Zhanel, G. G.; Hisanaga, T. L.; Laing, N. M.; DeCorby, M. R.; Nichol, K. A.; Weshnoweski, B.; Johnson, J.; Noreddin, A.; Low, D. E.; Karlowsky, J. A.; NAUTICA Group; Hoban, D. J. Antibiotic Resistance in *Escherichia coli* Outpatient Urinary Isolates: Final Results from the North American Urinary Tract Infection Collaborative Alliance (NAUTICA). *Int. J. Antimicrob. Agents* **2006,** *27,* 468–475.
98. Schito, G. C.; Naber, K. G.; Botto, H.; Palou, J.; Mazzei, T.; Gualco, L.; Marchese, A. The ARESC Study: An International Survey on the Antimicrobial Resistance of Pathogens Involved in Uncomplicated Urinary Tract Infections. *Int. J. Antimicrob. Agents* **2009,** *34,* 407–413.
99. Kim, Y.; Wie, S. H.; Chang, U. I.; Kim, J.; Ki, M.; Cho, Y. K.; Lim, S. K.; Lee, J. S.; Kwon, K. T.; Lee, H.; Cheong, H. J.; Park, D. W.; Ryu, S. Y.; Chung, M. H.; Pai, H. Comparison of the Clinical Characteristics of Diabetic and Non-Diabetic Women With Community-Acquired Acute Pyelonephritis: A Multicenter Study. *J. Infect.* **2014,** *69,* 244–251.
100. Park, K. H.; Oh, W. S.; Kim, E. S.; Park, S. W.; Hur, J. A.; Kim, Y. K.; Moon, C.; Lee, J. H.; Lee, C. S.; Kim, B. N. Factors Associated With Ciprofloxacin-and Cefotaxime-Resistant *Escherichia coli* in Women With Acute Pyelonephritis in the Emergency Department. *Int. J. Infect. Dis.* **2014,** *23,* 8–13.
101. van der Starre, W. E.; van Nieuwkoop, C.; Paltansing, S.; van't Wout, J. W.; Groeneveld, G. H.; Becker, M. J.; Koster, T.; Wattel-Louis, G. H.; Delfos, N. M.; Ablij, H. C.; Leyten, E. M.; Blom, J. W.; van Dissel, J. T. Risk Factors for Fluoroquinolone-Resistant *Escherichia coli* in Adults With Community-Onset Febrile Urinary Tract Infection. *J. Antimicrob. Chemother.* **2011,** *66,* 650–656.
102. Paterson, D. L.; Mulazimoglu, L.; Casellas, J. M.; Ko, W. C.; Goossens, H.; Von, G. A.; Mohapatra, S.; Trenholme, G. M.; Klugman, K. P.; McCormack, J. G.; Yu, V. L. Epidemiology of Ciprofloxacin Resistance and Its Relationship to Extended-Spectrum Beta-Lactamase Production in *Klebsiella pneumoniae* Isolates Causing Bacteremia. *Clin. Infect. Dis.* **2000,** *30,* 473–478.
103. Low, D. E. Quinolone Resistance Among Pneumococci: Therapeutic and Diagnostic Implications. *Clin. Infect. Dis.* **2004,** *38* (Suppl. 4), S357–S362.
104. Patel, S. N.; McGeer, A.; Melano, R.; Tyrrell, G. J.; Green, K.; Pillai, D. R.; Low, D. E.; Canadian Bacterial Surveillance Network. Susceptibility of *Streptococcus pneumoniae* to Fluoroquinolones in Canada. *Antimicrob. Agents Chemother.* **2011,** *55,* 3703–3708.
105. Jacobs, E.; Dalhoff, A.; Korfmann, G. Susceptibility Patterns of Bacterial Isolates From Hospitalised Patients With Respiratory Tract Infections (MOXIAKTIV Study). *Int. J. Antimicrob. Agents* **2009,** *33,* 52–57.
106. Pletz, M. W.; van der Linden, M.; von Baum, H.; Duesberg, C. B.; Klugman, K. P.; Welte, T.; CAPNETZ Study Group. Low Prevalence of Fluoroquinolone Resistant Strains and Resistance Precursor Strains in *Streptococcus pneumoniae* From Patients With Community-Acquired Pneumonia Despite High Fluoroquinolone Usage. *Int. J. Med. Microbiol.* **2011,** *301,* 535–537.
107. Kim, S. H.; Song, J. H.; Chung, D. R.; ThamLikitkul, V.; Yang, Y.; Wang, H.; Lu, M.; So, T. M.; Hsueh, P. R.; Yasin, R. M.; Carlos, C. C.; Pham, H. V.; Lalitha, M. K.; Shimono, N.; Perera, J.; Shibl, A. M.; Baek, J. Y.; Kang, C. I.; Ko, K. S.; Peck, K. R.; ANSORP Study Group. Changing Trends in Antimicrobial Resistance and Serotypes of *Streptococcus pneumoniae* Isolates in Asian Countries: An Asian Network for Surveillance of Resistant Pathogens (ANSORP) Study. *Antimicrob. Agents Chemother.* **2012,** *56,* 1418–1426.
108. Pfaller, M. A.; Farrell, D. J.; Sader, H. S.; Jones, R. N. AWARE Ceftaroline Surveillance Program (2008–2010): Trends in Resistance Patterns Among *Streptococcus pneumoniae*, *Haemophilus influenzae*, and *Moraxella catarrhalis* in the United States. *Clin. Infect. Dis.* **2012,** *55* (Suppl. 3), S187–S193.
109. Chung, D. R.; Song, J. H.; Kim, S. H.; ThamLikitkul, V.; Huang, S. G.; Wang, H.; So, T. M.; Yasin, R. M.; Hsueh, P. R.; Carlos, C. C.; Hsu, L. Y.; Buntaran, L.; Lalitha, M. K.; Kim, M. J.; Choi, J. Y.; Kim, S. I.; Ko, K. S.; Kang, C. I.; Peck, K. R.; Asian Network for Surveillance of Resistant Pathogens Study Group. High Prevalence of Multidrug-Resistant Nonfermenters in Hospital-Acquired Pneumonia in Asia. *Am. J. Respir. Crit. Care Med.* **2011,** *184,* 1409–1417.
110. Zuckerman, J. M. Macrolides and Ketolides: Azithromycin, Clarithromycin, Telithromycin. *Infect. Dis. Clin. North Am.* **2004,** *18,* 621–649.
111. Retsema, J. A.; Girard, A. E.; Girard, D.; Milisen, W. B. Relationship of High Tissue Concentrations of Azithromycin to Bactericidal Activity and Efficacy In Vivo. *J. Antimicrob. Chemother.* **1990,** *25* (Suppl. A), 83–89.
112. Doern, G. V. Macrolide and Ketolide Resistance With *Streptococcus pneumoniae. Med. Clin. North Am.* **2006,** *90,* 1109–1124.
113. Weisblum, B. Erythromycin Resistance by Ribosome Modification. *Antimicrob. Agents Chemother.* **1995,** *39,* 577–585.
114. Roberts, M. C.; Sutcliffe, J.; Courvalin, P.; Jensen, L. B.; Rood, J.; Seppala, H. Nomenclature for Macrolide and Macrolide–Lincosamide–Streptogramin B Resistance Determinants. *Antimicrob. Agents Chemother.* **1999,** *43,* 2823–2830.
115. Roberts, M. C. Update on Macrolide–Lincosamide–Streptogramin, Ketolide, and Oxazolidinone Resistance Genes. *FEMS Microbiol. Lett.* **2008,** *282,* 147–159.
116. Roberts, M. C. Resistance to Tetracycline, Macrolide–Lincosamide–Streptogramin, Trimethoprim, and Sulfonamide Drug Classes. *Mol. Biotechnol.* **2002,** *20,* 261–283.
117. Henwood, C. J.; Livermore, D. M.; Johnson, A. P.; James, D.; Warner, M.; Gardiner, A.; The Linezolid Study Group. Susceptibility of Gram-Positive Cocci From 25 UK Hospitals to Anti-Microbial Agents Including Linezolid. *J. Antimicrob. Chemother.* **2000,** *46,* 931–940.
118. Chancey, S. T.; Zähner, D.; Stephens, D. S. Acquired Inducible Antimicrobial Resistance in Gram-Positive Bacteria. *Future Microbiol.* **2012,** *7,* 959–978.
119. Mason, E. O., Jr.; Lamberth, L. B.; Wald, E. R.; Bradley, J. S.; Barson, W. J.; Kaplan, S. L. In Vitro Activities of Cethromycin (ABT-773), a New Ketolide, Against *Streptococcus pneumoniae* Strains That are Not Susceptible to Penicillin or Macrolides. *Antimicrob. Agents Chemother.* **2003,** *47,* 166–169.
120. Singh, K. V.; Malathum, K.; Murray, B. E. In Vitro Activities of a New Ketolide, ABT-773, Against Multidrug-Resistant Gram-Positive Cocci. *Antimicrob. Agents Chemother.* **2001,** *45,* 3640–3643.
121. Barry, A. L.; Fuchs, P. C.; Brown, S. D. In Vitro Activity of the Ketolide ABT-773. *Antimicrob. Agents Chemother.* **2001,** *45,* 2922–2924.
122. Nilius, A. M.; Bui, M. H.; Almer, L.; Hensey-Rudloff, D.; Beyer, J.; Ma, Z.; Or, Y. S.; Flamm, R. K. Comparative in vitro Activity of ABT-773, a Novel Antibacterial Ketolide. *Antimicrob. Agents Chemother.* **2001,** *45,* 2163–2168.
123. Goldstein, E. J.; Citron, D. M.; Merriam, C. V.; Warren, Y.; Tyrrell, K. Comparative In Vitro Activities of ABT-773 Against Aerobic and Anaerobic Pathogens Isolated From Skin and Soft-Tissue Animal and Human Bite Wound Infections. *Antimicrob. Agents Chemother.* **2001,** *44,* 2525–2529.
124. Olson, M. W.; Ruzin, A.; Feyfant, E.; Rush, T. S., III; O'Connell, J.; Bradford, P. A. Functional, Biophysical, and Structural Bases for Antibacterial Activity of Tigecycline. *Antimicrob. Agents Chemother.* **2006,** *50,* 2156–2166.
125. Babinchak, T.; Ellis-Grosse, E.; Dartois, N.; Rose, G. M.; Loh, E.; Tigecycline 301 and 306 Study Groups. The Efficacy and Safety of Tigecycline for the Treatment of Complicated Intra-Abdominal Infections: Analysis of Pooled Clinical Trial Data. *Clin. Infect. Dis.* **2005,** *41,* S354–S367.
126. Ellis-Grosse, E. J.; Babinchak, T.; Dartois, N.; Rose, G.; Loh, E.; Tigecycline 300 and 305 cSSSI Study Groups. The Efficacy and Safety of Tigecycline in the Treatment of Skin and Skin-Structure Infections: Results of 2 Double-Blind Phase 3 Comparison Studies With Vancomycin-Aztreonam. *Clin. Infect. Dis.* **2005,** *41,* S341–S353.
127. Tanaseanu, C.; Bergallo, C.; Teglia, O.; Jasovich, A.; Oliva, M. E.; Dukart, G.; Dartois, N.; Cooper, C. A.; Gandjini, H.; Mallick, R.; 308 and 313 Study Group. Integrated Results of 2 Phase 3 Studies Comparing Tigecycline and Levofloxacin in Community-Acquired Pneumonia. *Diagn. Microbiol. Infect. Dis.* **2008,** *61,* 329–338.
128. Noskin, G. A. Tigecycline: A New Glycylcycline for Treatment of Serious Infections. *Clin. Infect. Dis.* **2005,** *41,* S303–S314.

129. Theriot, C. M.; Schumacher, C. A.; Bassis, C. M.; Seekatz, A. M.; Young, V. B. Effects of Tigecycline and Vancomycin Administration on Established *Clostridium difficile* Infection. *Antimicrob. Agents Chemother.* **2015,** *59,* 1596–1604.
130. TEST. Tigecycline Evalauation and Surveillance Trial. http://www.testsurveillance.com (accessed March 24, 2016).
131. Dowzicky, M. J.; Chmelarova, E. Global in vitro Activity of Tigecycline and Linezolid Against Gram-Positive Organisms Collected Between 2004 and 2009. *Int. J. Antimicrob. Agents* **2011,** *37,* 562–566.
132. Stein, G. E.; Babinchak, T. Tigecycline: An Update. *Diagn. Microbiol. Infect. Dis.* **2013,** *75,* 331–336.
133. Sader, H. S.; Farrell, D. J.; Jones, R. N. Tigecycline Activity Tested Against Multidrug-Resistant Enterobacteriaceae and *Acinetobacter* spp. Isolated in US Medical Centers (2005–2009). *Diagn. Microbiol. Infect. Dis.* **2011,** *69,* 223–227.
134. Andrasevic, A. T.; Dowzicky, M. J. In Vitro Activity of Tigecycline and Comparators Against Gram-Negative Pathogens Isolated from Blood in Europe (2004–2009). *Int. J. Antimicrob. Agents* **2012,** *39,* 115–123.
135. Sader, H. S.; Flamm, R. K.; Mendes, R. E.; Farrell, D. J.; Jones, R. N. Antimicrobial Activity of Ceftaroline and Comparator Agents Tested Against Bacterial Organisms Causing Bacteremia in Patients With Skin and Skin Structure Infections in United States Medical Centers (2008–2014). *Antimicrob. Agents Chemother.* **2016,** *60,* 2558–2563.
136. Bradford, P. A.; Petersen, P. J.; Young, M.; Jones, C. H.; Tischler, M.; O'Connell, J. Tigecycline MIC Testing by Broth Dilution Requires use of Fresh Medium or Addition of the Biocatalytic Oxygen-Reducing Reagent Oxyrase to Standardize the Test Method. *Antimicrob. Agents Chemother.* **2005,** *49,* 3903–3909.
137. Pournaras, S.; Koumaki, V.; Gennimata, V.; Kouskouni, E.; Tsakris, A. In Vitro Activity of Tigecycline Against *Acinetobacter baumannii*: Global Epidemiology and Resistance Mechanisms. *Adv. Exp. Med. Biol.* **2016,** *897,* 1–14.
138. Fernández-Mazarrasa, C.; Mazarrasa, O.; Calvo, J.; del Arco, A.; Martínez-Martínez, L. High Concentrations of Manganese in Mueller–Hinton Agar Increase MICs of Tigecycline Determined by Etest. *J. Clin. Microbiol.* **2009,** *47,* 827–829.
139. Livermore, D. M. Tigecycline: What is it, and Where Should it be Used? *J. Antimicrob. Chemother.* **2005,** *56,* 611–614.
140. Nathwani, D. Tigecycline: Clinical Evidence and Formulary Positioning. *Int. J. Antimicrob. Agents* **2005,** *25,* 185–192.
141. Cai, Y.; Bai, N.; Liu, X.; Liang, B.; Wang, J.; Wang, R. Tigecycline: Alone or in Combination? *Infect. Dis. (Lond.)* **2016,** *16,* 1–12.
142. De Rosa, F. G.; Corcione, S.; Di Perri, G.; Scaglione, F. Critical Issues for *Klebsiella pneumoniae* KPC-Carbapenemase Producing *K. pneumoniae* Infections: A Critical Agenda. *New Microbiol.* **2015,** *38,* 121–136.
143. FDA. *FDA Drug Safety Communication: Increased Risk of Death With Tygacil (Tigecycline) Compared to Other Antibiotics Used to Treat Similar Infections*. Available at: http://www.fda.gov/drugs/drugsafety/ucm224370.htm, 2010 (accessed March 24, 2016).
144. Zhanel, G. G.; Cheung, D.; Adam, H.; Zelenitsky, S.; Golden, A.; Schweizer, F.; Gorityala, B.; Lagacé-Wiens, P. R.; Walkty, A.; Gin, A. S.; Hoban, D. J.; Karlowsky, J. A. Review of Eravacycline, a Novel Fluorocycline Antibacterial Agent. *Drugs* **2016,** *76,* 567–588.
145. Honeyman, L.; Ismail, M.; Nelson, M. L.; Bhatia, B.; Bowser, T. E.; Chen, J.; Mechiche, R.; Ohemeng, K.; Verma, A. K.; Cannon, E. P.; Macone, A.; Tanaka, S. K.; Levy, S. Structure–Activity Relationship of the Aminomethylcyclines and the Discovery of Omadacycline. *Antimicrob. Agents Chemother.* **2015,** *59,* 7044–7053.
146. Grossman, T. H.; Starosta, A. L.; Fyfe, C.; O'Brien, W.; Rothstein, D. M.; Mikolajka, A.; Wilson, D. N.; Sutcliffe, J. A. Target- and Resistance-Based Mechanistic Studies With TP-434, a Novel Fluorocycline Antibiotic. *Antimicrob. Agents Chemother.* **2012,** *56,* 2559–2564.
147. Draper, M. P.; Weir, S.; Macone, A.; Donatelli, J.; Trieber, C. A.; Tanaka, S. K.; Levy, S. B. Mechanism of Action of the Novel Aminomethylcycline Antibiotic Omadacycline. *Antimicrob. Agents Chemother.* **2014,** *58,* 1279–1283.
148. Rubinstein, E.; Keynan, Y. Vancomycin Revisited—60 Years Later. *Front. Public Health* **2014,** *2,* 1–7.
149. Liu, C.; Bayer, A.; Cosgrove, S. E.; Daum, R. S.; Fridkin, S. K.; Gorwitz, R. J.; Kaplan, S. L.; Karchmer, A. W.; Levine, D. P.; Murray, B. E.; Rybak, M.; Talan, D. A.; Chambers, H. F. Clinical Practice Guidelines by the Infectious Diseases Society of America for the Treatment of Methicillin-Resistant *Staphylococcus aureus* Infections in Adults and Children. *Clin. Infect. Dis.* **2011,** *52,* 285–292.
150. Fridkin, S. K.; Hageman, J.; McDougal, L. K.; Mohammed, J.; Jarvis, W. R.; Perl, T. M.; Tenover, F. C.; Vancomycin-Intermediate *Staphylococcus aureus* Epidemiology Study Group. Epidemiological and Microbiological Characterization of Infections Caused by *Staphylococcus aureus* With Reduced Susceptibility to Vancomycin, United States, 1997–2001. *Clin. Infect. Dis.* **2003,** *36,* 429–439.
151. Hiramatsu, K. Vancomycin-Resistant *Staphylococcus aureus*: A new Model of Antibiotic Resistance. *Lancet Infect. Dis.* **2001,** *1,* 147–155.
152. Howden, B. P.; Davies, J. K.; Johnson, P. D.; Stinear, T. P.; Grayson, M. L. Reduced Vancomycin Susceptibility in *Staphylococcus aureus*, Including Vancomycin-Intermediate and Heterogeneous Vancomycin-Intermediate Strains: Resistance Mechanisms, Laboratory Detection, and Clinical Implications. *Clin. Microbiol. Rev.* **2010,** *23,* 99–139.
153. Biavasco, F.; Vignaroli, C.; Varaldo, P. E. Glycopeptide Resistance in Coagulase-Negative Staphylococci. *Eur. J. Clin. Microbiol. Infect. Dis.* **2000,** *19,* 403–417.
154. Sakoulas, G.; Moise-Broder, P. A.; Schentag, J.; Forrest, A.; Moellering, R. C., Jr.; Eliopoulos, G. M. Relationship of MIC and Bactericidal Activity to Efficacy of Vancomycin for Treatment of Methicillin-Resistant *Staphylococcus aureus* Bacteremia. *J. Clin. Microbiol.* **2004,** *42,* 2398–2402.
155. Lodise, T. P.; Graves, J.; Evans, A.; Graffunder, E.; Helmecke, M.; Lomaestro, B. M.; Stellrecht, K. Relationship Between Vancomycin MIC and Failure Among Patients With Methicillin-Resistant *Staphylococcus aureus* Bacteremia Treated With Vancomycin. *Antimicrob. Agents Chemother.* **2008,** *52,* 3315–3320.
156. van Hal, S. J.; Lodise, T. P.; Paterson, D. L. The Clinical Significance of Vancomycin Minimum Inhibitory Concentration in *Staphylococcus aureus* Infections: A Systematic Review and Meta-Analysis. *Clin. Infect. Dis.* **2012,** *54,* 755–771.
157. Sader, H. S.; Fey, P. D.; Limaye, A. P.; Madinger, N.; Pankey, G.; Rahal, J.; Rybak, M. J.; Snydman, D. R.; Steed, L. L.; Waites, K.; Jones, R. N. Evaluation of Vancomycin and Daptomycin Potency Trends (MIC Creep) Against Methicillin-Resistant *Staphylococcus aureus* Isolates Collected in Nine U.S. Medical Centers From 2002 to 2006. *Antimicrob. Agents Chemother.* **2009,** *53,* 4127–4132.
158. Reynolds, R.; Hope, R.; Warner, M.; MacGowan, A. P.; Livermore, D. M.; Ellington, M. J.; BSAC Extended Working Party on Resistance Surveillance. Lack of Upward Creep of Glycopeptide MICs for Methicillin-Resistant *Staphylococcus aureus* (MRSA) Isolated in the UK and Ireland 2001–07. *J. Antimicrob. Chemother.* **2012,** *67,* 2912–2918.
159. O'Driscoll, T.; Crank, C. W. Vancomycin-Resistant Enterococcal Infections: Epidemiology, Clinical Manifestations, and Optimal Management. *Infect. Drug Resist.* **2015,** *24,* 217–230.
160. Uttley, A. H.; Collins, C. H.; Naidoo, J.; George, R. C. Vancomycin-Resistant Enterococci. *Lancet* **1988,** *1,* 57–58.
161. Sahm, D. F.; Kissinger, J.; Gilmore, M. S.; Murray, P. R.; Mulder, R.; Solliday, J.; Clarke, B. In Vitro Susceptibility Studies of Vancomycin-Resistant *Enterococcus faecalis*. *Antimicrob. Agents Chemother.* **1989,** *33,* 1588–1591.
162. Acar, J.; Casewell, M.; Freeman, J.; Friis, C.; Goossens, H. Avoparcin and Virginiamycin as Animal Growth Promoters: A Plea for Science in Decision-Making. *Clin. Microbiol. Infect.* **2000,** *6,* 477–482.
163. Kirst, H. A.; Thompson, D. G.; Nicas, T. I. Historical Yearly Usage of Vancomycin. *Antimicrob. Agents Chemother.* **1998,** *42,* 1303–1304.
164. Courvalin, P. Vancomycin Resistance in Gram-Positive Cocci. *Clin. Infect. Dis.* **2006,** *42* (Suppl. 1), S25–S34.
165. Sievert, D. M.; Ricks, P.; Edwards, J. R.; Schneider, A.; Patel, J.; Srinivasan, A.; Kallen, A.; Limbago, B.; Fridkin, S.; National Healthcare Safety Network (NHSN) Team and Participating NHSN Facilities. Antimicrobial-Resistant Pathogens Associated With Healthcare-Associated Infections: Summary of Data Reported to the National Healthcare Safety Network at the Centers for Disease Control and Prevention, 2009–2010. *Infect. Control Hosp. Epidemiol.* **2013,** *34,* 1–14.
166. The European Antimicrobial Resistance Surveillance System. *EARS-Net Results*. Available from: http://www.ecdc.europa.eu/en/healthtopics/antimicrobial_resistance/database/Pages/database.aspx, 2015 (accessed April 29, 2016).
167. Klinker, K. P.; Borgert, S. J. Beyond Vancomycin: The Tail of the Lipoglycopeptides. *Clin. Ther.* **2015,** *37,* 2619–2636.
168. Van Bambeke, F. Lipoglycopeptide Antibacterial Agents in Gram-Positive Infections: A Comparative Review. *Drugs* **2015,** *75,* 2073–2095.
169. Smith, W. J.; Drew, R. H. Telavancin: A new Lipoglycopeptide for Gram-Positive Infections. *Drugs Today (Barc.)* **2009,** *45,* 159–173.
170. Ramdeen, S.; Boucher, H. W. Dalbavancin for the Treatment of Acute Bacterial Skin and Skin Structure Infections. *Expert Opin. Pharmacother.* **2015,** *16,* 2073–2081.

171. Messina, J. A.; Fowler, V. G., Jr.; Corey, G. R. Oritavancin for Acute Bacterial Skin and Skin Structure Infections. *Expert Opin. Pharmacother.* **2015,** *16,* 1091–1098.
172. Mendes, R. E.; Farrell, D. J.; Sader, H. S.; Flamm, R. K.; Jones, R. N. Activity of Oritavancin Against Gram-Positive Clinical Isolates Responsible for Documented Skin and Soft-Tissue Infections in European and US Hospitals (2010–13). *J. Antimicrob. Chemother.* **2015,** *70,* 498–504.
173. Shaw, K. J.; Barbachyn, M. The Oxazolidinones: Past, Present, and Future. *Ann. N. Y. Acad. Sci.* **2011,** *1241,* 48–70.
174. Hui, Y.; Xiaoju, L. Tedizolid for Treatment of Acute Bacterial Skin and Skin Structure Infections. *Expert Rev. Anti Infect. Ther.* **2015,** *13,* 1051–1060.
175. Shinabarger, D. Mechanism of Action of the Oxazolidinone Antibacterial Agents. *Expert Opin. Investig. Drugs* **1999,** *8,* 1195–1202.
176. Ippolito, J. A.; Kanyo, Z. F.; Wang, D.; Franceschi, F. J.; Moore, P. B.; Steitz, T. A.; Duffy, E. M. Crystal Structure of the Oxazolidinone Antibiotic Linezolid Bound to the 50S Ribosomal Subunit. *J. Med. Chem.* **2008,** *51,* 3353–3356.
177. Locke, J. B.; Hilgers, M.; Shaw, K. J. Novel Ribosomal Mutations in *Staphylococcus aureus* Strains Identified Through Selection With the Oxazolidinones Linezolid and Torezolid (TR-700). *Antimicrob. Agents Chemother.* **2009,** *53,* 5265–5274.
178. Locke, J. B.; Hilgers, M.; Shaw, K. J. Mutations in Ribosomal Protein L3 are Associated With Oxazolidinone Resistance in Staphylococci of Clinical Origin. *Antimicrob. Agents Chemother.* **2009,** *53,* 5275–5278.
179. Toh, S. M.; Xiong, L.; Arias, C. A.; Villegas, M. V.; Lolans, K.; Quinn, J.; Mankin, A. S. Acquisition of a Natural Resistance Gene Renders a Clinical Strain of Methicillin-Resistant *Staphylococcus aureus* Resistant to the Synthetic Antibiotic Linezolid. *Mol. Microbiol.* **2007,** *64,* 1506–1514.
180. Long, K. S.; Poehlsgaard, J.; Kehrenberg, C.; Schwarz, S.; Vester, B. The Cfr rRNA Methyltransferase Confers Resistance to Phenicols, Lincosamides, Oxazolidinones, Pleuromutilins, and Streptogramin A Antibiotics. *Antimicrob. Agents Chemother.* **2006,** *50,* 2500–2505.
181. Locke, J. B.; Finn, J.; Hilgers, M.; Morales, G.; Rahawi, S.; Picazo, J. J.; Im, W.; Shaw, K. J.; Stein, J. L. Structure–Activity Relationships of Diverse Oxazolidinones for Linezolid-Resistant *Staphylococcus aureus* Strains Possessing the *cfr* Methyltransferase Gene or Ribosomal Mutations. *Antimicrob. Agents Chemother.* **2010,** *54,* 5337–5343.
182. Farrell, D. J.; Mendes, R. E.; Ross, J. E.; Sader, H. S.; Jones, R. N. LEADER Program Results for 2009: An Activity and Spectrum Analysis of Linezolid Using 6,414 Clinical Isolates from 56 Medical Centers in the United States. *Antimicrob. Agents Chemother.* **2011,** *55,* 3684–3690.
183. Flamm, R. K.; Farrell, D. J.; Mendes, R. E.; Ross, J. E.; Sader, H. S.; Jones, R. N. ZAAPS Program Results for 2010: An Activity and Spectrum Analysis of Linezolid Using Clinical Isolates From 75 Medical Centres in 24 Countries. *J. Chemother.* **2012,** *24,* 328–337.
184. Picazo, J. J.; Betriu, C.; Rodríguez-Avial, I.; Culebras, E.; López-Fabal, F.; Gómez, M.; VIRA Study Group. Comparative Activities of Daptomycin and Several Agents Against Staphylococcal Blood Isolates. Glycopeptide Tolerance. *Diagn. Microbiol. Infect. Dis.* **2011,** *70,* 373–379.
185. Flamm, R. K.; Mendes, R. E.; Hogan, P. A.; Streit, J. M.; Ross, J. E.; Jones, R. N. Linezolid Surveillance Results for the United States (LEADER Surveillance Program 2014). *Antimicrob. Agents Chemother.* **2016,** *60,* 2273–2280.
186. Gu, B.; Kelesidis, T.; Tsiodras, S.; Hindler, J.; Humphries, R. M. The Emerging Problem of Linezolid-Resistant *Staphylococcus*. *J. Antimicrob. Chemother.* **2013,** *68,* 4–11.
187. Sahm, D. F.; Deane, J.; Bien, P. A.; Locke, J. B.; Zuill, D. E.; Shaw, K. J.; Bartizal, K. F. Results of the Surveillance of Tedizolid Activity and Resistance Program: In Vitro Susceptibility of Gram-Positive Pathogens Collected in 2011 and 2012 From the United States and Europe. *Diagn. Microbiol. Infect. Dis.* **2015,** *81,* 112–118.
188. Vaara, M. Polymyxins and Their Novel Derivatives. *Curr. Opin. Microbiol.* **2010,** *13,* 574–581.
189. Biswas, S.; Brunel, J. M.; Dubus, J. C.; Reynaud-Gaubert, M.; Rolain, J. M. Colistin: An Update on the Antibiotic of the 21st Century. *Expert Rev. Anti Infect. Ther.* **2012,** *10,* 917–934.
190. Olaitan, A. O.; Morand, S.; Rolain, J. M. Mechanisms of Polymyxin Resistance: Acquired and Intrinsic Resistance in Bacteria. *Front. Microbiol.* **2014,** *5.* Article 643.
191. Telke, A. A.; Rolain, J. M. Functional Genomics to Discover Antibiotic Resistance Genes: The Paradigm of Resistance to Colistin Mediated by Ethanolamine Phosphotransferase in *Shewanella algae* MARS 14. *Int. J. Antimicrob. Agents* **2015,** *46,* 648–652.
192. Shen, Z.; Wang, Y.; Shen, Y.; Shen, J.; Wu, C. Early Emergence of *mcr-1* in *Escherichia coli* from Food-Producing Animals. *Lancet Infect. Dis.* **2016,** *16,* 293.
193. Poirel, L.; Kieffer, N.; Liassine, N.; Thanh, D.; Nordmann, P. Plasmid-Mediated Carbapenem and Colistin Resistance in a Clinical Isolate of *Escherichia coli*. *Lancet Infect. Dis.* **2016,** *16,* 281.
194. Baccanari, D. P.; Kuyper, L. F. Basis of Selectivity of Antibacterial Diaminopyrimidines. *J. Chemother.* **1993,** *5,* 393–399.
195. Hawser, S.; Lociuro, S.; Islam, K. Dihydrofolate Reductase Inhibitors as Antibacterial Agents. *Biochem. Pharmacol.* **2006,** *71,* 941–948.
196. Gupta, K.; Hooton, T. M.; Naber, K. G.; Wullt, B.; Colgan, R.; Miller, L. G.; Moran, G. J.; Nicolle, L. E.; Raz, R.; Schaeffer, A. J.; Soper, D. E.; Infectious Diseases Society of America; European Society for Microbiology and Infectious Diseases. International Clinical Practice Guidelines for the Treatment of Acute Uncomplicated Cystitis and Pyelonephritis in Women: A 2010 Update by the Infectious Diseases Society of America and the European Society for Microbiology and Infectious Diseases. *Clin. Infect. Dis.* **2011,** *52,* e103–e120.
197. Stevens, D. L.; Bisno, A. L.; Chambers, H. F.; Dellinger, E. P.; Goldstein, E. J.; Gorbach, S. L.; Hirschmann, J. V.; Kaplan, S. L.; Montoya, J. G.; Wade, J. C.; Infectious Diseases Society of America. Practice Guidelines for the Diagnosis and Management of Skin and Soft Tissue Infections: 2014 Update by the Infectious Diseases Society of America. *Clin. Infect. Dis.* **2014,** *59,* e10–e52.
198. Wood, J. B.; Smith, D. B.; Baker, E. H.; Brecher, S. M.; Gupta, K. Has the Emergence of Community-Associated Methicillin-Resistant *Staphylococcus aureus* Increased Trimethoprim–Sulfamethoxazole use and Resistance?: A 10-Year Time Series Analysis. *Antimicrob. Agents Chemother.* **2012,** *56,* 5655–5660.
199. van der Veen, E. L.; Schilder, A. G.; Timmers, T. K.; Rovers, M. M.; Fluit, A. C.; Bonten, M. J.; Leverstein-van Hall, M. A. Effect of Long-Term Trimethoprim/Sulfamethoxazole Treatment on Resistance and Integron Prevalence in the Intestinal Flora: A Randomized, Double-Blind, Placebo-Controlled Trial in Children. *J. Antimicrob. Chemother.* **2009,** *63,* 1011–1016.
200. Huovinen, P.; Sundström, L.; Swedberg, G.; Sköld, O. Trimethoprim and Sulfonamide Resistance. *Antimicrob. Agents Chemother.* **1995,** *39,* 279–289.
201. Sköld, O. Resistance to Trimethoprim and Sulfonamides. *Vet. Res.* **2001,** *32,* 261–273.
202. Thomson, C. J. Trimethoprim and Brodimoprim Resistance of Gram-Positive and Gram-Negative Bacteria. *J. Chemother.* **1993,** *5,* 458–464.
203. Howell, E. E. Searching Sequence Space: Two Different Approaches to Dihydrofolate Reductase Catalysis. *ChemBioChem* **2005,** *6,* 590–600.
204. Kadlec, K.; Schwarz, S. Identification of a Novel Trimethoprim Resistance Gene, dfrK, in a Methicillin-Resistant *Staphylococcus aureus* ST398 Strain and its Physical Linkage to the Tetracycline Resistance Gene tet(L). *Antimicrob. Agents Chemother.* **2009,** *53,* 776–778.
205. Kohlhoff, S. A.; Sharma, R. Iclaprim. *Expert Opin. Investig. Drugs* **2007,** *16,* 1441–1448.
206. Schneider, P.; Hawser, S.; Islam, K. Iclaprim, a Novel Diaminopyrimidine With Potent Activity on Trimethoprim Sensitive and Resistant Bacteria. *Bioorg. Med. Chem. Lett.* **2003,** *13,* 4217–4221.
207. Oefner, C.; Bandera, M.; Haldimann, A.; Laue, H.; Schulz, H.; Mukhija, S.; Parisi, S.; Weiss, L.; Lociuro, S.; Dale, G. E. Increased Hydrophobic Interactions of Iclaprim With *Staphylococcus aureus* Dihydrofolate Reductase are Responsible for the Increase in Affinity and Antibacterial Activity. *J. Antimicrob. Chemother.* **2009,** *63,* 687–698.
208. Sader, H. S.; Fritsche, T. R.; Jones, R. N. Potency and Bactericidal Activity of Iclaprim Against Recent Clinical Gram-Positive Isolates. *Antimicrob. Agents Chemother.* **2009,** *53,* 2171–2175.
209. Humphries, R. M.; Pollett, S.; Sakoulasc, G. A Current Perspective on Daptomycin for the Clinical Microbiologist. *Clin. Microbiol. Rev.* **2013,** *26,* 759–780.
210. Tran, T. T.; Munita, J. M.; Arias, C. A. Mechanisms of Drug Resistance: Daptomycin Resistance. *Ann. N. Y. Acad. Sci.* **2015,** *1354,* 32–53.
211. Song, Y.; Rubio, A.; Jayaswal, R. K.; Silverman, J. A.; Wilkinson, B. J. Additional Routes to *Staphylococcus aureus* Daptomycin Resistance as Revealed by Comparative Genome Sequencing, Transcriptional Profiling, and Phenotypic Studies. *PLoS One* **2013,** *8,* e58469.
212. Moise, P. A.; North, D.; Steenbergen, J. N.; Sakoulas, G. Susceptibility Relationship Between Vancomycin and Daptomycin in *Staphylococcus aureus*: Facts and Assumptions. *Lancet Infect. Dis.* **2009,** *9,* 617–624.
213. Bayer, A. S.; Schneider, T.; Sahl, H. G. Mechanisms of Daptomycin Resistance in *Staphylococcus aureus*: Role of the Cell Membrane and Cell Wall. *Ann. N. Y. Acad. Sci.* **2013,** *1277,* 139–158.

214. Peleg, A. Y.; Miyakis, S.; Ward, D. V.; Earl, A. M.; Rubio, A.; Cameron, D. R.; Pillai, S.; Moellering, R. C., Jr.; Eliopoulos, G. M. Whole Genome Characterization of the Mechanisms of Daptomycin Resistance in Clinical and Laboratory Derived Isolates of *Staphylococcus aureus*. *PLoS One* **2012,** *7,* e28316.
215. Friedman, L.; Alder, J. D.; Silverman, J. A. Genetic Changes That Correlate With Reduced Susceptibility to Daptomycin in *Staphylococcus aureus*. *Antimicrob. Agents Chemother.* **2006,** *50,* 2137–2145.
216. Munita, J. M.; Panesso, D.; Diaz, L.; Tran, T. T.; Reyes, J.; Wanger, A.; Murray, B. E.; Arias, C. A. Correlation Between Mutations in liaFSR of *Enterococcus faecium* and MIC of Daptomycin: Revisiting Daptomycin Breakpoints. *Antimicrob. Agents Chemother.* **2012,** *56,* 4354–4359.
217. Panesso, D.; Reyes, J.; Gaston, E. P.; Deal, M.; Londoño, A.; Nigo, M.; Munita, J. M.; Miller, W. R.; Shamoo, Y.; Tran, T. T.; Arias, C. A. Deletion of liaR Reverses Daptomycin Resistance in *Enterococcus faecium* Independent of the Genetic Background. *Antimicrob. Agents Chemother.* **2015,** *59,* 7327–7334.
218. Arias, C. A.; Panesso, D.; McGrath, D. M.; Qin, X.; Mojica, M. F.; Miller, C.; Diaz, L.; Tran, T. T.; Rincon, S.; Barbu, E. M.; Reyes, J.; Roh, J. H.; Lobos, E.; Sodergren, E.; Pasqualini, R.; Arap, W.; Quinn, J. P.; Shamoo, Y.; Murray, B. E.; Weinstock, G. M. Genetic Basis for in vivo Daptomycin Resistance in Enterococci. *New Engl. J. Med.* **2011,** *365,* 892–900.
219. Satlin, M. J.; Jenkins, S. G.; Walsh, T. J. The Global Challenge of Carbapenem-Resistant Enterobacteriaceae in Transplant Recipients and Patients With Hematologic Malignancies. *Clin. Infect. Dis.* **2014,** *58,* 1274–1283.
220. Sabath, L. D.; Abraham, E. P. Zinc as a Cofactor for Cephalosporinase From *Bacillus cereus* 569. *Biochem. J.* **1966,** *98,* 11c–13c.
221. Medeiros, A. A.; Hare, R. S. Beta-Lactamase Mediated Resistance to Penems and Carbapenems Amongst Enterobacteriaceae. Abstract No. 116. 26th Interscience Conference on Antimicrobial Agents and Chemotherapy; American Society for Microbiology: New Orleans, LA, 2016.
222. Temkin, E.; Adler, A.; Lerner, A.; Carmeli, Y. Carbapenem-Resistant Enterobacteriaceae: Biology, Epidemiology, and Management. *Ann. N. Y. Acad. Sci.* **2014,** *1323,* 22–42.
223. Watanabe, M.; Iyobe, S.; Inoue, M.; Mitsuhashi, S. Transferable Imipenem Resistance in *Pseudomonas aeruginosa*. *Antimicrob. Agents Chemother.* **1991,** *35,* 147–151.
224. Yigit, H.; Queenan, A. M.; Anderson, G. J.; Domenech-Sanchez, A.; Biddle, J. W.; Steward, C. D.; Alberti, S.; Bush, K.; Tenover, F. C. Novel Carbapenem-Hydrolyzing Beta-Lactamase, KPC-1, From a Carbapenem-Resistant Strain of *Klebsiella pneumoniae*. *Antimicrob. Agents Chemother.* **2001,** *45,* 1151–1161.
225. Dupont, H.; Gaillot, O.; Goetgheluck, A.-S.; Plassart, C.; Emond, J.-P.; Lecuru, M.; Gaillard, N.; Derdouri, S.; Lemaire, B.; de Courtilles, M. G.; Mammeri, H.; Cattoir, V. Molecular Characterization of Carbapenem-Nonsusceptible Enterobacterial Isolates Collected During a Prospective Interregional Survey in France and Susceptibility to the Novel Ceftazidime–Avibactam and Aztreonam–Avibactam Combinations. *Antimicrob. Agents Chemother.* **2016,** *60,* 215–221.
226. Hidron, A. I.; Edwards, J. R.; Patel, J.; Horan, T. C.; Sievert, D. M.; Pollock, D. A.; Fridkin, S. K.; National Healthcare Safety Network Team; Participating National Healthcare Safety Network Facilities. NHSN Annual Update: Antimicrobial-Resistant Pathogens Associated With Healthcare-Associated Infections: Annual Summary of Data Reported to the National Healthcare Safety Network at the Centers for Disease Control and Prevention, 2006–2007. *Infect. Control Hosp. Epidemiol.* **2008,** *29,* 996–1011.
227. Leavitt, A.; Navon-Venezia, S.; Chmelnitsky, I.; Schwaber, M. J.; Carmeli, Y. Emergence of KPC-2 and KPC-3 in Carbapenem-Resistant *Klebsiella pneumoniae* Strains in an Israeli Hospital. *Antimicrob. Agents Chemother.* **2007,** *51,* 3026–3029.
228. Pournaras, S.; Protonotariou, E.; Voulgari, E.; Kristo, I.; Dimitroulia, E.; Vitti, D.; Tsalidou, M.; Maniatis, A. N.; Tsakris, A.; Sofianou, D. Clonal Spread of KPC-2 Carbapenemase-Producing *Klebsiella pneumoniae* Strains in Greece. *J. Antimicrob. Chemother.* **2009,** *64,* 348–352.
229. Mezzatesta, M. L.; Gona, F.; Caio, C.; Petrolito, V.; Sciortino, D.; Sciacca, A.; Santangelo, C.; Stefani, S. Outbreak of KPC-3-Producing, and Colistin-Resistant, *Klebsiella pneumoniae* Infections in Two Sicilian Hospitals. *Clin. Microbiol. Infect.* **2011,** *17,* 1444–1447.
230. Sood, S. Identification and Differentiation of Carbapenemases in *Klebsiella pneumoniae*: A Phenotypic Test Evaluation Study From Jaipur, India. *JCDR* **2014,** *8,* DC01–DC03.
231. Kazi, M.; Drego, L.; Nikam, C.; Ajbani, K.; Soman, R.; Shetty, A.; Rodrigues, C. Molecular Characterization of Carbapenem-Resistant Enterobacteriaceae at a Tertiary Care Laboratory in Mumbai. *Eur. J. Clin. Microbiol. Infect. Dis.* **2015,** *34,* 467–472.
232. Landman, D.; Babu, E.; Shah, N.; Kelly, P.; Olawole, O.; Backer, M.; Bratu, S.; Quale, J. Transmission of Carbapenem-Resistant Pathogens in New York City Hospitals: Progress and Frustration. *J. Antimicrob. Chemother.* **2012,** *67,* 1427–1431.
233. van Duin, D.; Kaye, K. S.; Neuner, E.; Bonomo, R. A. Carbapenem-Resistant Enterobacteriaceae: A Review of Treatment and Outcomes. *Diagn. Microbiol. Infect. Dis.* **2013,** *75,* 115–120.
234. World Health Organization (WHO). *Global Incidence and Prevalence of Selected Curable Sexually Transmitted Infections—2008;* World Health Organization: Geneva, 2012.
235. Unemo, M.; Shafer, W. M. Antimicrobial Resistance in *Neisseria gonorrhoeae* in the 21st Century: Past, Evolution, and Future. *Clin. Microbiol. Rev.* **2014,** *27,* 587–613.
236. Unemo, M. Current and Future Antimicrobial Treatment Of Gonorrhoea—The Rapidly Evolving *Neisseria gonorrhoeae* Continues to Challenge. *BMC Infect. Dis.* **2015,** *15,* 364.
237. Centers for Disease Control and Prevention (CDC). Cephalosporin-Resistant *Neisseria gonorrhoeae* Public Health Response Plan, 2012; pp 1–43. http://www.cdc.gov/std/gonorrhea/default.htm (date last accessed March 29, 2015).
238. Bignell, C.; Unemo, M. European Guideline on the Diagnosis and Treatment of Gonorrhoea in Adults. *Int. J. STD AIDS* **2012,** *2013* (24), 85–92.
239. Unemo, M.; Golparian, D.; Shafer, W. M. Importance of Multidrug Efflux Pumps in the Antimicrobial Resistance Property of Clinical Multidrug-Resistant Isolates of *Neisseria gonorrhoeae*. *Antimicrob. Agents Chemother.* **2014,** *58,* 3556–3559.
240. Quaye, N.; Cole, M. J.; Ison, C. A. Evaluation of the Activity of Ertapenem Against Gonococcal Isolates Exhibiting a Range of Susceptibilities to Cefixime. *J. Antimicrob. Chemother.* **2014,** *69,* 1568–1571.
241. Hauser, C.; Hirzberger, L.; Unemo, M.; Furrer, H.; Endimiani, A. In Vitro Activity of Fosfomycin Alone and in Combination With Ceftriaxone or Azithromycin Against Clinical *Neisseria gonorrhoeae* Isolates. *Antimicrob. Agents Chemother.* **2015,** *59,* 1605–1611.
242. Brown, L. B.; Krysiak, R.; Kamanga, G.; Mapanje, C.; Kanyamula, H.; Banda, B.; Mhango, C.; Hoffman, M.; Kamwendo, D.; Hobbs, M.; Hosseinipour, M. C.; Martinson, F.; Cohen, M. S.; Hoffman, I. F. *Neisseria gonorrhoeae* Antimicrobial Susceptibility in Lilongwe, Malawi, 2007. *Sex. Transm. Dis.* **2010,** *37,* 169–172.
243. To, K.; Napolitano, L. *Clostridium difficile* Infection: Update on Diagnosis, Epidemiology, and Treatment Strategies. *Surg. Infect.* **2014,** *15,* 490–502.
244. Bauer, M.; Notermans, D.; van Benthem, B.; Brazier, J.; Wilcox, M.; Rupnik, M.; Monnet, D. L.; van Dissel, J. T.; Kuijper, E. J.; ECDIS Study Group. *Clostridium difficile* Infection in Europe: A Hospital-Based Survey. *Lancet* **2011,** *377,* 63–73.
245. Burckhardt, F.; Friedrich, A.; Beier, D.; Eckmanns, T. *Clostridium difficile* Surveillance Trends, Saxony, Germany. *Emerg. Infect. Dis.* **2008,** *14,* 691–692.
246. Gravel, D.; Miller, M.; Simor, A.; Taylor, G.; Gardam, M.; McGeer, A.; Hutchinson, J.; Moore, D.; Kelly, S.; Canadian Nosocomial Infection Surveillance Program. Health Care-Associated *Clostridium difficile* Infection in Adults Admitted to Acute Care Hospitals in Canada: A Canadian Nosocomial Infection Surveillance Program Study. *Clin. Infect. Dis.* **2009,** *48,* 568–576.
247. Lessa, F.; Mu, Y.; Bamberg, W.; Beldavs, Z.; Dumyati, G.; Dunn, J.; Farley, M. M.; Holzbauer, S. M.; Meek, J. I.; Phipps, E. C.; Wilson, L. E.; Winston, L. G.; Cohen, J. A.; Limbago, B. M.; Fridkin, S. K.; Gerding, D. N.; McDonald, L. C. Burden of *Clostridium difficile* Infection in the United States. *New Engl. J. Med.* **2015,** *372,* 825–834.
248. Redelings, M.; Sorvillo, F.; Mascola, L. Increase in *Clostridium difficile*-Related Mortality Rates, United States, 1999–2004. *Emerg. Infect. Dis.* **2007,** *13,* 1417–1419.
249. Clements, A.; Magalhaes, R.; Tatem, A.; Paterson, D.; Riley, T. *Clostridium difficile* PCR Ribotype 027: Assessing the Risks of Further Worldwide Spread. *Lancet Infect. Dis.* **2010,** *10,* 395–404.
250. Pepin, J.; Valiquette, M.; Clossette, B. Mortality Attributed to Nosocomial *Clostridium difficile* Associated Disease During an Epidemic Caused by a Hypervirulent Strain in Quebec. *CMAJ* **2005,** *173,* 1037–1042.
251. Kim, J.; Smathers, S.; Prasad, P.; Leckerman, K.; Coffin, S.; Zaoutis, T. Epidemiological Features of *Clostridium difficile*-Associated Disease Among Inpatients at Children's Hospitals in the United States, 2001–2006. *Pediatrics* **2008,** *122,* 1266–1270.
252. Pituch, H. *Clostridium difficile* is No Longer Just Anosocomial Infection or an Infection of Adults. *Int. J. Antimicrob. Agents* **2009,** *33,* S42–S45.
253. Freeman, J.; Bauer, M.; Baines, S.; Corver, J.; Fawley, W.; Goorhuis, B. The Changing Epidemiology of *Clostridium difficile* Infections. *Clin. Microbiol. Rev.* **2010,** *23,* 529–549.

254. He, M.; Miyajima, F.; Roberts, P.; Ellison, L.; Pickard, D.; Martin, M.; Connor, T. R.; Harris, S. R.; Fairley, D.; Bamford, K. B.; D'Arc, S.; Brazier, J.; Brown, D.; Coia, J. E.; Douce, G.; Gerding, D.; Kim, H. J.; Koh, T. H.; Kato, H.; Senoh, M.; Louie, T.; Michell, S.; Butt, E.; Peacock, S. J.; Brown, N. M.; Riley, T.; Songer, G.; Wilcox, M.; Pirmohamed, M.; Kuijper, E.; Hawkey, P.; Wren, B. W.; Dougan, G.; Parkhill, J.; Lawley, T. D. Emergence and Global Spread of Epidemic Healthcare-Associated *Clostridium difficile*. *Nat. Genet.* **2013,** *45,* 109–113.
255. Spigaglia, P. Recent Advances in the Understanding of Antibiotic Resistance in *Clostridium difficile* Infection. *Ther. Adv. Infect. Dis.* **2016,** *3,* 23–42.
256. Roberts, M.; McFarland, L.; Mullany, P.; Mulligan, M. Characterization of the Genetic Basis of Antibiotic Resistance in *Clostridium difficile*. *J. Antimicrob. Chemother.* **1994,** *33,* 419–429.
257. Spigaglia, P.; Carucci, V.; Barbanti, F.; Mastrantonio, P. ErmB Determinants and Tn916-Like Elements in Clinical Isolates of *Clostridium difficile*. *Antimicrob. Agents Chemother.* **2005,** *49,* 2550–2553.
258. Schmidt, C.; Loffler, B.; Ackermann, G. Antimicrobial Phenotypes and Molecular Basis in Clinical Strains of *Clostridium difficile*. *Diagn. Microbiol. Infect. Dis.* **2007,** *59,* 1–5.
259. Ackermann, G.; Tang, Y.; Kueper, R.; Heisig, P.; Rodloff, A.; Silva, J.; Cohen, S. H. Resistance to Moxifloxacin in Toxigenic *Clostridium difficile* Isolates is Associated With Mutations in gyr A. *Antimicrob. Agents Chemother.* **2001,** *45,* 2348–2353.
260. Dridi, L.; Tankovic, J.; Burghoffer, B.; Barbut, F.; Petit, J. *GyrA* and *gyrB* Mutations are Implicated in Cross-Resistance to Ciprofloxacin and Moxifloxacin in *Clostridium difficile*. *Antimicrob. Agents Chemother.* **2002,** *46,* 3418–3421.
261. Drudy, D.; Kyne, L.; O'Mahony, R.; Fanning, S. *gyrA* Mutations in Fluoroquinolone-Resistant *Clostridium difficile* PCR-027. *Emerg. Infect. Dis.* **2007,** *13,* 504–505.
262. Lyras, D.; Cooper, M. *Clostridium difficile* Drug Pipeline: Challenges in Discovery and Development of New Agents. *J. Med. Chem.* **2015,** *58,* 5164–5185.
263. Debast, S.; Bauer, M.; Kuijper, E. European Society of Clinical Microbiology and Infectious Diseases: Update of the Treatment Guidance Document for *Clostridium difficile* Infection. *Clin. Microbiol. Infect.* **2014,** *20,* 1–26.
264. Vardakas, K.; Polyzos, K.; Patouni, K.; Rafailidis, P.; Samonis, G.; Falagas, M. Treatment Failure and Recurrence of *Clostridium difficile* Infection Following Treatment With Vancomycin or Metronidazole: A Systematic Review of the Evidence. *Int. J. Antimicrob. Agents* **2012,** *40,* 1–8.
265. Young, G. P.; Ward, P. B.; Bayley, N.; Gordon, D.; Higgins, G.; Trapani, J. A.; McDonald, M. I.; Labrooy, J.; Hecker, R. Antibiotic-Associated Colitis due to *Clostridium difficile*: Double-Blind Comparison of Vancomycin With Bacitracin. *Gastroenterology* **1985,** *89,* 1038–1045.
266. Oldfield, E., IV; Oldfield, E., III; Johnson, D. Clinical Update for the Diagnosis and Treatment of *Clostridium difficile* Infection. *World J. Gastrointest. Pharmacol. Ther.* **2014,** *5,* 1–26.
267. Chaparro-Rojas, F.; Mullane, K. Emerging Therapies for *Clostridium difficile* Infection—Focus on Fidaxomicin. *Infect. Drug Resist.* **2013,** *6,* 41–53.
268. Louie, T.; Miller, M.; Mullane, K.; Weiss, K.; Lentnek, A.; Golan, Y.; et al. Fidaxomicin Versus Vancomycin for *Clostridium difficile* Infection. *New Engl. J. Med.* **2011,** *364,* 422–431.
269. Vila, J.; Pachon, J. Therapeutic Options for *Acinetobacter baumannii* Infections. *Expert Opin. Pharmacother.* **2008,** *9,* 587–599.
270. Centers for Disease Control and Prevention (CDC). Antibiotic Resistance Threats in the United States; CDC: Atlanta, 2013. Available from: http://www.cdc.gov/drugresistance/threat-report-2013/pdf/ar-threats-2013-508.pdf.
271. Bonnin, R. A.; Nordmann, P.; Poirel, L. Screening and Deciphering Antibiotic Resistance in *Acinetobacter baumannii*: A State of the Art. *Expert Rev. Anti Infect. Ther.* **2013,** *11,* 571–583.
272. Damier-Piolle, L.; Magnet, S.; Brémont, S.; Lambert, T.; Courvalin, P. AdeIJK, a Resistance-Nodulation-Cell Division Pump Effluxing Multiple Antibiotics in *Acinetobacter baumannii*. *Antimicrob. Agents Chemother.* **2008,** *52,* 557–562.
273. Hawkey, P.; Finch, R. Tigecycline: In-Vitro Performance as a Predictor of Clinical Efficacy. *Clin. Microbiol. Infect.* **2007,** *13,* 354–362.
274. Beceiro, A.; Llobet, E.; Aranda, J.; Bengoechea, J. A.; Doumith, M.; Hornsey, M.; Dhanji, H.; Chart, H.; Bou, G.; Livermore, D. M.; Woodford, N. Phosphoethanolamine Modification Of Lipid A in Colistin-Resistant Variants of *Acinetobacter baumannii* Mediated by the pmrAB Two-Component Regulatory System. *Antimicrob. Agents Chemother.* **2011,** *55,* 3370–3379.
275. Moffatt, J. H.; Harper, M.; Harrison, P.; Hale, J. D.; Vinogradov, E.; Seemann, T.; Henry, R.; Crane, B.; St Michael, F.; Cox, A. D.; Adler, B.; Nation, R. L.; Li, J.; Boyce, J. D. Colistin Resistance in *Acinetobacter baumannii* is Mediated by Complete Loss of Lipopolysaccharide Production. *Antimicrob. Agents Chemother.* **2010,** *54,* 4971–4977.
276. Castanheira, M.; Mendes, R. E.; Jones, R. N. Update on *Acinetobacter* species: Mechanisms of Antimicrobial Resistance and Contemporary In Vitro Activity of Minocycline and Other Treatment Options. *Clin. Infect. Dis.* **2014,** *59* (Suppl. 6), S367–S373.
277. Tong, S. Y.; Davis, J. S.; Eichenberger, E.; Holland, T. L.; Fowler, V. G., Jr. *Staphylococcus aureus* Infections: Epidemiology, Pathophysiology, Clinical Manifestations, and Management. *Clin. Microbiol. Rev.* **2015,** *28,* 603–661.
278. Nannini, E.; Murray, B. E.; Arias, C. A. Resistance or Decreased Susceptibility to Glycopeptides, Daptomycin, and Linezolid in Methicillin-Resistant *Staphylococcus aureus*. *Curr. Opin. Pharmacol.* **2010,** *10,* 516–521.
279. Laupland, K. B.; Lyytikainen, O.; Sogaard, M.; Kennedy, K. J.; Knudsen, J. D.; Ostergaard, C.; Galbraith, J. C.; Valiquette, L.; Jacobsson, G.; Collignon, P.; Schonheyder, H. C.; International Bacteremia Surveillance Collaborative. The Changing Epidemiology of *Staphylococcus aureus* Bloodstream Infection: A Multinational Population-Based Surveillance Study. *Clin. Microbiol. Infect.* **2013,** *19,* 465–471.
280. Johnson, A. P.; Davies, J.; Guy, R.; Abernethy, J.; Sheridan, E.; Pearson, A.; Duckworth, G. Mandatory Surveillance Of Methicillin-Resistant *Staphylococcus aureus* (MRSA) Bacteraemia in England: The First 10 Years. *J. Antimicrob. Chemother.* **2012,** *67,* 802–809.
281. Kallen, A. J.; Mu, Y.; Bulens, S.; Reingold, A.; Petit, S.; Gershman, K.; Ray, S. M.; Harrison, L. H.; Lynfield, R.; Dumyati, G.; Townes, J. M.; Schaffner, W.; Patel, P. R.; Fridkin, S. K. Health Care-Associated Invasive MRSA Infections, 2005–2008. *JAMA* **2010,** *304,* 641–648.
282. DeLeo, F. R.; Otto, M.; Kreiswirth, B. N.; Chambers, H. F. Community-Associated Methicillin-Resistant *Staphylococcus aureus*. *Lancet* **2010,** *375,* 1557–1568.
283. Otto, M. Community-Associated MRSA: What Makes Them Special? *Int. J. Med. Microbiol.* **2013,** *303,* 324–330.
284. Landrum, M. L.; Neumann, C.; Cook, C.; Chukwuma, U.; Ellis, M. W.; Hospenthal, D. R.; Murray, C. K. Epidemiology of *Staphylococcus aureus* Blood and Skin and Soft Tissue Infections in the US Military Health System, 2005–2010. *JAMA* **2012,** *308,* 50–59.
285. Greenspon, A. J.; Patel, J. D.; Lau, E.; Ochoa, J. A.; Frisch, D. R.; Ho, R. T.; Pavri, B. B.; Kurtz, S. M. 16-Year Trends in the Infection Burden for Pacemakers and Implantable Cardioverter-Defibrillators in the United States 1993 to 2008. *J. Am. Coll. Cardiol.* **2011,** *58,* 1001–1006.
286. Zahar, J. R.; Clech, C.; Tafflet, M.; Garrouste-Orgeas, M.; Jamali, S.; Mourvillier, B.; De Lassence, A.; Descorps-Declere, A.; Adrie, C.; Costa de Beauregard, M. A.; Azoulay, E.; Schwebel, C.; Timsit, J. F.; Outcomerea Study Group. Is Methicillin Resistance Associated With a Worse Prognosis in *Staphylococcus aureus* Ventilator-Associated Pneumonia? *Clin. Infect. Dis.* **2005,** *41,* 1224–1231.
287. Lee, M. S.; Walker, V.; Chen, L. F.; Sexton, D. J.; Anderson, D. J. The Epidemiology of Ventilator-Associated Pneumonia in a Network of Community Hospitals: A Prospective Multicenter Study. *Infect. Control Hosp. Epidemiol.* **2013,** *34,* 657–662.
288. Shorr, A. F.; Tabak, Y. P.; Gupta, V.; Johannes, R. S.; Liu, L. Z.; Kollef, M. H. Morbidity and Cost Burden of Methicillin-Resistant *Staphylococcus aureus* in Early Onset Ventilator-Associated Pneumonia. *Crit. Care* **2006,** *10,* R97.
289. Garcia-Vidal, C.; Viasus, D.; Roset, A.; Adamuz, J.; Verdaguer, R.; Dorca, J.; Gudiol, F.; Carratala, J. Low Incidence of Multidrug-Resistant Organisms in Patients With Healthcare-Associated Pneumonia Requiring Hospitalization. *Clin. Microbiol. Infect.* **2011,** *17,* 1659–1665.
290. Aliberti, S.; Cilloniz, C.; Chalmers, J. D.; Zanaboni, A. M.; Cosentini, R.; Tarsia, P.; Pesci, A.; Blasi, F.; Torres, A. Multidrug-Resistant Pathogens in Hospitalised Patients Coming From the Community With Pneumonia: A European Perspective. *Thorax* **2013,** *68,* 997–999.
291. Cakir Aktas, N.; Erturan, Z.; Karatuna, O.; Karahasan Yagci, A. Panton Valentine Leukocidin and Biofilm Production of *Staphylococcus aureus* Isolated From Respiratory Tract. *J. Infect. Dev. Ctries* **2013,** *7,* 888–891.
292. Rubinstein, E.; Keynan, Y. Vancomycin Revisited—60 Years Later. *Front. Public Health* **2014,** *2,* 217.

293. Holmes, N. E.; Howden, B. P. What's New in the Treatment of Serious MRSA Infection? *Curr. Opin. Infect. Dis.* **2014,** *27,* 471–478.
294. Limbago, B. M.; Kallen, A. J.; Zhu, W.; Eggers, P.; McDougal, L. K.; Albrecht, V. S. Report of the 13th Vancomycin-Resistant *Staphylococcus aureus* Isolate From the United States. *J. Clin. Microbiol.* **2014,** *52,* 998–1002.
295. Sader, H. S.; Jones, R. N. Antimicrobial Activity of Daptomycin in Comparison to Glycopeptides and Other Antimicrobials When Tested Against Numerous Species of Coagulase-Negative *Staphylococcus*. *Diagn. Microbiol. Infect. Dis.* **2012,** *73,* 212–214.
296. Mariani, P. G.; Sader, H. S.; Jones, R. N. Development of Decreased Susceptibility to Daptomycin and Vancomycin in a *Staphylococcus aureus* Strain During Prolonged Therapy. *J. Antimicrob. Chemother.* **2006,** *58,* 481–483.
297. Sharma, M.; Riederer, K.; Chase, P.; Khatib, R. High Rate of Decreasing Daptomycin Susceptibility During the Treatment of Persistent *Staphylococcus aureus* Bacteremia. *Eur. J. Clin. Microbiol. Infect. Dis.* **2008,** *27,* 433–437.
298. Fischer, A.; Yang, S. J.; Bayer, A. S.; Vaezzadeh, A. R.; Herzig, S.; Stenz, L.; Girard, M.; Sakoulas, G.; Scherl, A.; Yeaman, M. R.; Proctor, R. A.; Schrenzel, J.; François, P. Daptomycin Resistance Mechanisms in Clinically Derived *Staphylococcus aureus* Strains Assessed by a Combined Transcriptomics and Proteomics Approach. *J. Antimicrob. Chemother.* **2011,** *66,* 1696–1711.
299. Chambers, H. F.; Deleo, F. R. Waves of Resistance: *Staphylococcus aureus* in the Antibiotic Era. *Nat. Rev. Microbiol.* **2009,** *7,* 629–641.
300. Livermore, D. M. Multiple Mechanisms of Antimicrobial Resistance in *Pseudomonas aeruginosa*: Our Worst Nightmare? *Clin. Infect. Dis.* **2002,** *34,* 634–640.
301. Breidenstein, E. B.; de la Fuente-Nunez, C.; Hancock, R. E. *Pseudomonas aeruginosa*: All Roads Lead to Resistance. *Trends Microbiol.* **2011,** *19,* 419–426.
302. Tam, V.; Chang, K. T.; Abdelraouf, K.; Brioso, C. G.; Ameka, M.; McCaskey, L. A.; Weston, J. S.; Caeiro, J. P.; Garey, K. W. Prevalence, Resistance Mechanisms, and Susceptibility of Multidrug-Resistant Bloodstream Isolates of *Pseudomonas aeruginosa*. *Antimicrob. Agents Chemother.* **2010,** *54,* 1160–1164.
303. Morrow, B. J.; Pillar, C. M.; Deane, J.; Sahm, D. F.; Lynch, A. S.; Flamm, R. K.; Peterson, J.; Davies, T. A. Activities of Carbapenem and Comparator Agents Against Contemporary US *Pseudomonas aeruginosa* Isolates From the CAPITAL Surveillance Program. *Diagn. Microbiol. Infect. Dis.* **2013,** *75,* 412–416.
304. Nathwani, D.; Raman, G.; Sulham, K.; Gavaghan, M.; Menon, V. Clinical and Economic Consequences of Hospital-Acquired Resistant and Multidrug-Resistant *Pseudomonas aeruginosa* Infections: A Systematic Review and Meta-Analysis. *Antimicrob. Resist. Infect. Control* **2014,** *3,* 32.
305. Potron, A.; Poirel, L.; Nordmann, P. Emerging Broad-Spectrum Resistance in *Pseudomonas aeruginosa* and *Acinetobacter baumannii*: Mechanisms and Epidemiology. *Int. J. Antimicrob. Agents* **2015,** *45,* 568–585.
306. Jovcic, B.; Lepsanovic, Z.; Suljagic, V.; Rackov, G.; Begovic, J.; Topisirovic, L.; Kojic, M. Emergence of NDM-1 Metallo-Beta-Lactamase in *Pseudomonas aeruginosa* Clinical Isolates From Serbia. *Antimicrob. Agents Chemother.* **2011,** *55,* 3929–3931.
307. Martínez, T.; Vazquez, G. J.; Aquino, E. E.; Goering, R. V.; Robledo, I. E. Two Novel Class I Integron Arrays Containing IMP-18 Metallo-B-Lactamase Gene in *Pseudomonas aeruginosa* Clinical Isolates From Puerto Rico. *Antimicrob. Agents Chemother.* **2012,** *56,* 2119–2121.
308. Yamane, K.; Doi, Y.; Yokoyama, K.; Yagi, T.; Kurokawa, H.; Shibata, N.; Yagi, T.; Shibayama, K.; Kato, H.; Arakawa, Y. Genetic Environments of the rmtA Gene in *Pseudomonas aeruginosa* Clinical Isolates. *Antimicrob. Agents Chemother.* **2004,** *48,* 2069–2074.
309. Li, X. Z.; Nikaido, H.; Poole, K. Role of *mexA–mexB–oprM* in Antibiotic Efflux in *Pseudomonas aeruginosa*. *Antimicrob. Agents Chemother.* **1995,** *39,* 1948–1953.
310. Lee, J. Y.; Song, J. H.; Ko, K. S. Identification of Nonclonal *Pseudomonas aeruginosa* Isolates With Reduced Colistin Susceptibility in Korea. *Microb. Drug Resist.* **2011,** *17,* 299–304.
311. Barrow, K.; Kwon, D. H. Alterations in Two-Component Regulatory Systems of phoPQ and pmrAB are Associated With Polymyxin B Resistance in Clinical Isolates of *Pseudomonas aeruginosa*. *Antimicrob. Agents Chemother.* **2009,** *53,* 5150–5154.
312. World Health Organization. *Global Tuberculosis Report 2015*. http://www.who.int/tb/publications/global_report/en/, 2015 (accessed April 13, 2016).
313. Statistics South Africa. *What are South Africans Dying of?*. http://www.statssa.gov.za/?p=1023, 2013 (accessed April 13, 2016).
314. Manjelievskaia, J.; Erck, D.; Piracha, S.; Schrager, L. Drug-Resistant TB: Deadly, Costly and in Need of a Vaccine. *Trans. R. Soc. Trop. Med. Hyg.* **2016,** *110,* 186–191.
315. Millard, J.; Ugarte-Gil, C.; Moore, D. A. Multidrug Resistant Tuberculosis. *BMJ* **2015,** *350,* h882.
316. http://www.cdc.gov/tb/topic/treatment/tbdisease.htm.
317. Marks, S. M.; Flood, J.; Seaworth, B.; Hirsch-Moverman, Y.; Armstrong, L.; Mase, S.; Salcedo, K.; Oh, P.; Graviss, E. A.; Colson, P. W.; Armitige, L.; Revuelta, M.; Sheeran, K.; TB Epidemiologic Studies Consortium. Treatment Practices, Outcomes, and Costs of Multidrug-Resistant and Extensively Drug-Resistant Tuberculosis, United States, 2005–2007. *Emerg. Infect. Dis.* **2014,** *20,* 812–821.
318. Salinas, J. L.; Mindra, G.; Haddad, M. B.; Pratt, R.; Price, S. F.; Langer, A. J. Leveling of Tuberculosis Incidence—United States, 2013–2015. *MMWR* **2016,** *65,* 273–278.
319. Hoagland, D.; Liu, J.; Lee, R. B.; Lee, R. E. New Agents for the Treatment of Drug-Resistant *Mycobacterium tuberculosis*. *Adv. Drug Deliv. Rev.* **2016,** *102,* 55–72.
320. Hards, K.; Robson, J. R.; Berney, M.; Shaw, L.; Bald, D.; Koul, A.; Andries, K.; Cook, G. M. Bactericidal Mode of Action of Bedaquiline. *J. Antimicrob. Chemother.* **2015,** *70,* 2028–2037.
321. Matsumoto, M.; Hashizume, H.; Tomishige, T.; Kawasaki, M.; Tsubouchi, H.; Sasaki, H.; Shimokawa, Y.; Komatsu, M. OPC-67683, a Nitrodihydro-Imidazooxazole Derivative With Promising Action Against Tuberculosis In Vitro and in Mice. *PLoS Med.* **2006,** *3,* e466.
322. Rustomjee, R.; Zumla, A. Delamanid Expanded Access Novel Treatment of Drug Resistant Tuberculosis. *Infect. Drug Resist.* **2015,** *8,* 359–366.
323. Ryan, N. J.; Lo, J. H. Delamanid: First Global Approval. *Drugs* **2014,** *74,* 1041–1045.
324. Magill, S. S.; Edwards, J. R.; Bamberg, W.; Beldavs, Z. G.; Dumyati, G.; Kainer, M. A.; Lynfield, R.; Maloney, M.; McAllister-Hollod, L.; Nadle, J.; Ray, S. M.; Thompson, D. L.; Wilson, L. E.; Fridkin, S. K. Multistate Point-Prevalence Survey of Health Care-Associated Infections. *New Engl. J. Med.* **2014,** *370,* 1198–1208.
325. Hajjeh, R. A.; Sofair, A. N.; Harrison, L. H.; Lyon, G. M.; Arthington-Skaggs, B. A.; Mirza, S. A.; Phelan, M.; Morgan, J.; Lee-Yang, W.; Ciblak, M. A.; Benjamin, L. E.; Sanza, L. T.; Huie, S.; Yeo, S. F.; Brandt, M. E.; Warnock, D. W. Incidence of Bloodstream Infections due to *Candida* Species and In Vitro Susceptibilities of Isolates Collected From 1998 to 2000 in a Population-Based Active Surveillance Program. *J. Clin. Microbiol.* **2004,** *42,* 1519–1527.
326. Lockhart, S. R.; Iqbal, N.; Cleveland, A. A.; Farley, M. M.; Harrison, L. H.; Bolden, C. B.; Baughman, W.; Stein, B.; Hollick, R.; Park, B. J.; Chiller, T. Species Identification and Antifungal Susceptibility Testing of *Candida* Bloodstream Isolates From Population-Based Surveillance Studies in Two U.S. Cities From 2008 to 2011. *J. Clin. Microbiol.* **2012,** *50,* 3435–3442.
327. Castanheira, M.; Messer, S. A.; Rhomberg, P. R.; Pfaller, M. A. Antifungal Susceptibility Patterns of a Global Collection of Fungal Isolates: Results of the SENTRY Antifungal Surveillance Program (2013). *Diagn. Microbiol. Infect. Dis.* **2016,** *85* (2), 200–204.
328. Pham, C. D.; Iqbal, N.; Bolden, C. B.; Kuykendall, R. J.; Harrison, L. H.; Farley, M. M.; Schaffner, W.; Beldavs, Z. G.; Chiller, T. M.; Park, B. J.; Cleveland, A. A.; Lockhart, S. R. Role of FKS Mutations in *Candida glabrata*: MIC Values, Echinocandin Resistance, and Multidrug Resistance. *Antimicrob. Agents Chemother.* **2014,** *58,* 4690–4696.
329. Garcia-Effron, G.; Chua, D. J.; Tomada, J. R.; DiPersio, J.; Perlin, D. S.; Ghannoum, M.; Bonilla, H. Novel FKS Mutations Associated With Echinocandin Resistance in *Candida* Species. *Antimicrob. Agents Chemother.* **2010,** *54,* 2225–2227.
330. Pfaller, M. A.; Castanheira, M.; Lockhart, S. R.; Ahlquist, A. M.; Messer, S. A.; Jones, R. N. Frequency of Decreased Susceptibility and Resistance to Echinocandins Among Fluconazole-Resistant Bloodstream Isolates of *Candida glabrata*. *J. Clin. Microbiol.* **2012,** *50,* 1199–1203.
331. Alexander, B. D.; Johnson, M. D.; Pfeiffer, C. D.; Jiménez-Ortigosa, C.; Catania, J.; Booker, R.; Castanheira, M.; Messer, S. A.; Perlin, D. S.; Pfaller, M. A. Increasing Echinocandin Resistance in *Candida glabrata*: Clinical Failure Correlates With Presence of FKS Mutations and Elevated Minimum Inhibitory Concentrations. *Clin. Infect. Dis.* **2013,** *56,* 1724–1732.
332. Denning, D. W.; Venkateswarlu, K.; Oakley, K. L.; Anderson, M. J.; Manning, N. J.; Stevens, D. A.; Warnock, D. W.; Kelly, S. L. Itraconazole Resistance in *Aspergillus fumigatus*. *Antimicrob. Agents Chemother.* **1997,** *41,* 1364–1368.
333. Bueid, A.; Howard, S. J.; Moore, C. B.; Richardson, M. D.; Harrison, E.; Bowyer, P.; Denning, D. W. Azole Antifungal Resistance in *Aspergillus fumigatus*: 2008 and 2009. *J. Antimicrob. Chemother.* **2010,** *65,* 2116–2118.

334. Howard, S. J.; Pasqualotto, A. C.; Denning, D. W. Azole Resistance in Allergic Bronchopulmonary Aspergillosis and *Aspergillus bronchitis*. *Clin. Microbiol. Infect.* **2010,** *16,* 683–688.
335. van der Linden, J. W.; Camps, S. M.; Kampinga, G. A.; Arends, J. P.; Debets-Ossenkopp, Y. J.; Haas, P. J.; Rijnders, B. J.; Kuijper, E. J.; van Tiel, F. H.; Varga, J.; Karawajczyk, A.; Zoll, J.; Melchers, W. J.; Verweij, P. E. Aspergillosis due to Voriconazole Highly Resistant *Aspergillus fumigatus* and Recovery of Genetically Related Resistant Isolates From Domiciles. *Clin. Infect. Dis.* **2013,** *57,* 513–520.
336. Snelders, E.; Huis Int Veld, R. A.; Rijs, A. J.; Kema, G. H.; Melchers, W. J.; Verweij, P. E. Possible Environmental Origin of Resistance of *Aspergillus fumigatus* to Medical Triazoles. *Appl. Environ. Microbiol.* **2009,** *75,* 4053–4057.
337. Wiederhold, N. P.; Patterson, T. F. Emergence of Azole Resistance in *Aspergillus*. *Semin. Respir. Crit. Care Med.* **2015,** *36,* 673–680.
338. Seyedmousavi, S.; Mouton, J. W.; Melchers, W. J.; Brüggemann, R. J.; Verweij, P. E. The Role of Azoles in the Management of Azole-Resistant Aspergillosis: From the Bench to the Bedside. *Drug Resist. Update* **2014,** *17,* 37–50.
339. van Hal, S. J.; Chen, S. C.; Sorrell, T. C.; Ellis, D. H.; Slavin, M.; Marriott, D. M. Support for the EUCAST and Revised CLSI Fluconazole Clinical Breakpoints by Sensititre® YeastOne® for *Candida albicans*: A Prospective Observational Cohort Study. *J. Antimicrob. Chemother.* **2014,** *69,* 2210–2214.
340. Field, H. J.; DeClercq, E. Antiviral Drugs—A Short History of Their Discovery and Development. *Microbiol. Today* **2004,** *31,* 58.
341. Shafer, R. W.; Schapiro, J. M. HIV-1 Drug Resistance Mutations: An Updated Framework for the Second Decade of HAART. *AIDS Rev.* **2008,** *10* (2), 67–84.
342. Barre-Sinoussi, F.; et al. Isolation of a T-Lymphotropic Retrovirus From a Patient at Risk for Acquired Immune Deficiency Syndrome (AIDS). *Science* **1983,** *220* (4599), 868–871.
343. Gallo, R. C.; Montagnier, L. The Discovery of HIV as the Cause of AIDS. *New Engl. J. Med.* **2003,** *349* (24), 2283–2285.
344. Gottlieb, M. S.; et al. *Pneumocystis carinii pneumonia* and Mucosal Candidiasis in Previously Healthy Homosexual Men: Evidence of a New Acquired Cellular Immunodeficiency. *New Engl. J. Med.* **1981,** *305* (24), 1425–1431.
345. Duval, X.; et al. Amprenavir Inhibitory Quotient and Virological Response in Human Immunodeficiency Virus-Infected Patients on an Amprenavir-Containing Salvage Regimen Without or With Ritonavir. *Antimicrob. Agents Chemother.* **2002,** *46* (2), 570–574.
346. la Porte, C. Inhibitory Quotient in HIV Pharmacology. *Curr. Opin. HIV AIDS* **2008,** *3* (3), 283–287.
347. Acosta, E. P.; et al. Novel Method to Assess Antiretroviral Target Trough Concentrations Using in vitro Susceptibility Data. *Antimicrob. Agents Chemother.* **2012,** *56* (11), 5938–5945.
348. Ellner, P. D.; Neu, H. C. The inhibitory Quotient. A Method for Interpreting Minimum Inhibitory Concentration Data. *JAMA* **1981,** *246* (14), 1575–1578.
349. Hoefnagel, J. G. M.; et al. Role of the Inhibitory Quotient in HIV Therapy. *Antivir. Ther.* **2005,** *10* (8), 879–892.
350. Young, F. E. The Role of the FDA in the Effort Against AIDS. *Public Health Rep.* **1988,** *103* (3), 242–245.
351. Sax, P. E.; et al. Tenofovir Alafenamide Versus Tenofovir Disoproxil Fumarate, Coformulated With Elvitegravir, Cobicistat, and Emtricitabine, for Initial Treatment of HIV-1 Infection: Two Randomised, Double-Blind, Phase 3, Non-Inferiority Trials. *Lancet* **2015,** *385,* 2606–2615.
352. Wensing, A. M.; et al. 2014 Update of the Drug Resistance Mutations in HIV-1. *Top. Antivir. Med.* **2014,** *22* (3), 642–650.
353. Sluis-Cremer, N.; Tachedjian, G. Mechanisms of Inhibition of HIV Replication by Non-Nucleoside Reverse Transcriptase Inhibitors. *Virus Res.* **2008,** *134* (1–2), 147–156.
354. Velazquez-Campoy, A.; Kiso, Y.; Freire, E. The Binding Energetics of First- and Second-Generation HIV-1 Protease Inhibitors: Implications for Drug Design. *Arch. Biochem. Biophys.* **2001,** *390* (2), 169–175.
355. Hertogs, K.; et al. Phenotypic and Genotypic Analysis of Clinical HIV-1 Isolates Reveals Extensive Protease Inhibitor Cross-Resistance: A Survey of Over 6000 Samples. *AIDS* **2000,** *14* (9), 1203–1210.
356. Wensing, A. M.; van Maarseveen, N. M.; Nijhuis, M. Fifteen years of HIV Protease Inhibitors: Raising the Barrier to Resistance. *Antivir. Res.* **2010,** *85* (1), 59–74.
357. Naggie, S.; Hicks, C. Protease Inhibitor-Based Antiretroviral Therapy in Treatment-Naive HIV-1-Infected Patients: The Evidence Behind the Options. *J. Antimicrob. Chemother.* **2010,** *65* (6), 1094–1099.
358. Morse, G. D.; Catanzaro, L. M.; Acosta, E. P. Clinical Pharmacodynamics of HIV-1 Protease Inhibitors: Use of Inhibitory Quotients to Optimise Pharmacotherapy. *Lancet Infect. Dis.* **2006,** *6* (4), 215–225.
359. Lambert-Niclot, S.; et al. Pharmacokinetics, Protein-Binding-Adjusted Inhibitory Quotients for Atazanavir/Ritonavir 300/100 mg in Treatment-Naive HIV-Infected Patients. *HIV Med.* **2010,** *11* (10), 666–669.
360. Doyon, L.; et al. Second Locus Involved in Human Immunodeficiency Virus Type 1 Resistance to Protease Inhibitors. *J. Virol.* **1996,** *70* (6), 3763–3769.
361. Abram, M. E.; et al. Impact of Primary Elvitegravir Resistance-Associated Mutations in HIV-1 Integrase on Drug Susceptibility and Viral Replication Fitness. *Antimicrob. Agents Chemother.* **2013,** *57* (6), 2654–2663.
362. Castagna, A.; et al. Dolutegravir in Antiretroviral-Experienced Patients With Raltegravir- and/or Elvitegravir-Resistant HIV-1: 24-Week Results of the Phase III VIKING-3 Study. *J. Infect. Dis.* **2014,** *210* (3), 354–362.
363. Hofstra, L. M.; et al. Use of Dolutegravir in Two INI-Experienced Patients With Multiclass Resistance Resulted in Excellent Virological and Immunological Responses (Abstract P223) *JIAS* **2014,** *17* (4 Suppl. 3), 19755.
364. Haqqani, A. A.; Tilton, J. C. Entry Inhibitors and Their Use in the Treatment of HIV-1 Infection. *Antiviral Res.* **2013,** *98* (2), 158–170.
365. Cervia, J. S.; Smith, M. A. Enfuvirtide (T-20): A Novel Human Immunodeficiency Virus Type 1 Fusion Inhibitor. *Clin. Infect. Dis.* **2003,** *37* (8), 1102–1106.
366. Woollard, S. M.; Kanmogne, G. D. Maraviroc: A Review of Its Use in HIV Infection and Beyond. *Drug Des. Dev. Ther.* **2015,** *9,* 5447–5468.
367. Pfizer Labs. *SELZENTRY™ (maraviroc) tablets;* US Prescribing Information: New York, NY, November 2009.
368. Cihlar, T.; Fordyce, M. Current Status and Prospects of HIV Treatment. *Curr. Opin. Virol.* **2016,** *18,* 50–56.
369. Tseng, A.; Seet, J.; Phillips, E. J. The Evolution of Three Decades of Antiretroviral Therapy: Challenges, Triumphs and the Promise of the Future. *Br. J. Clin. Pharmacol.* **2015,** *79* (2), 182–194.
370. Nassal, M. HBV cccDNA: Viral Persistence Reservoir and Key Obstacle for a Cure of Chronic Hepatitis B. *Gut* **2015,** *64* (12), 1972–1984.
371. Xiong, Y.; Eickbush, T. H. Origin and Evolution of Retroelements Based Upon Their Reverse Transcriptase Sequences. *EMBO J.* **1990,** *9* (10), 3353–3362.
372. Revill, P.; Locarnini, S. The Basis for Antiviral Therapy: Drug Targets, Cross-Resistance, and Novel Small Molecule Inhibitors. In *Hepatitis B Virus in Human Diseases;* Liaw, Y. F., Zoulim, F., Eds.; *Molecular and Translational Medicine;* Humana Press: Switzerland, 2016; pp 303–324 (Chapter 14).
373. Lok, A. S. F.; et al. Long-Term Safety of Lamivudine Treatment in Patients With Chronic Hepatitis B. *Gastroenterology* **2003,** *125* (6), 1714–1722.
374. Hadziyannis, S. J.; et al. Long-Term Therapy With Adefovir Dipivoxil for HBeAg-Negative Chronic Hepatitis B for up to 5 Years. *Gastroenterology* **2006,** *131* (6), 1743–1751.
375. Angus, P.; et al. Resistance to Adefovir Dipivoxil Therapy Associated With the Selection of a Novel Mutation in the HBV Polymerase. *Gastroenterology* **2003,** *125* (2), 292–297.
376. Liaw, Y. F.; et al. 2-Year GLOBE Trial Results: Telbivudine is Superior to Lamivudine in Patients With Chronic Hepatitis B. *Gastroenterology* **2009,** *136* (2), 486–495.
377. Tenney, D. J.; et al. Long-Term Monitoring Shows Hepatitis B Virus Resistance to Entecavir in Nucleoside-Naive Patients is Rare Through 5 Years of Therapy. *Hepatology* **2009,** *49* (5), 1503–1514.
378. Colonno, R. J.; et al. Entecavir Resistance is Rare in Nucleoside Naive Patients With Hepatitis B. *Hepatology* **2006,** *44* (6), 1656–1665.
379. Kitrinos, K. M.; et al. No Detectable Resistance to Tenofovir Disoproxil Fumarate After 6 Years of Therapy in Patients With Chronic Hepatitis B. *Hepatology* **2014,** *59* (2), 434–442.
380. Lim, Y. S.; et al. Tenofovir Monotherapy Versus Tenofovir and Entecavir Combination Therapy in Patients With Entecavir-Resistant Chronic Hepatitis B With Multiple Drug Failure: Results of a Randomised Trial. *Gut* **2016,** *65* (5), 852–860.
381. Corsa, A. C.; et al. No Resistance to Tenofovir Disoproxil Fumarate Through 96 Weeks of Treatment in Patients With Lamivudine-Resistant Chronic Hepatitis B. *Clin. Gastroenterol. Hepatol.* **2014,** *12,* 2106–2112.

382. Fung, S.; et al. Randomized Comparison of Tenofovir Disoproxil Fumarate vs Emtricitabine and Tenofovir Disoproxil Fumarate in Patients With Lamivudine-Resistant Chronic Hepatitis B. *Gastroenterology* **2014,** *146* (4), 980–988. e1.
383. Lim, Y. S.; et al. Tenofovir Monotherapy Versus Tenofovir and Entecavir Combination Therapy in Patients With Entecavir-Resistant Chronic Hepatitis B With Multiple Drug Failure: Results of a Randomised Trial. *Gut* **2016,** *65* (5), 852–860.
384. Terrault, N. A.; et al. AASLD Guidelines for Treatment of Chronic Hepatitis B. *Hepatology* **2016,** *63* (1), 261–283.
385. European Association for the Study of the Liver (EASL). EASL Clinical Practice Guidelines: Management of Chronic Hepatitis B Virus Infection. *J. Hepatol.* **2012,** *57,* 167–185.
386. Revill, P.; et al. Global Strategies are Required to Cure and Eliminate HBV Infection. *Nat. Rev. Gastroenterol. Hepatol.* **2016,** *13* (4), 239–248.
387. Bowen, D. G.; Walker, C. M. Adaptive Immune Responses in Acute and Chronic Hepatitis C Virus Infection. *Nature* **2005,** *436* (7053), 946–952.
388. Pearlman, B. L.; Traub, N. Sustained Virologic Response to Antiviral Therapy for Chronic Hepatitis C Virus Infection: A Cure and So Much More. *Clin. Infect. Dis.* **2011,** *52* (7), 889–900.
389. Bartenschlager, R.; Lohmann, V.; Penin, F. The Molecular and Structural Basis of Advanced Antiviral Therapy for Hepatitis C Virus Infection. *Nat. Rev. Microbiol.* **2013,** *11* (7), 482–496.
390. Pawlotsky, J. M. Hepatitis C Virus Resistance to Direct-Acting Antiviral Drugs in Interferon-Free Regimens. *Gastroenterology* **2016,** *151* (1), 70–86.
391. European Association for the Study of the Liver. EASL Recommendations on Treatment of Hepatitis C 2015. *J. Hepatol.* **2015,** *63,* 199–236 (1).
392. Aasld Idsa Hcv Guidance Panel. Hepatitis C Guidance: AASLD-IDSA Recommendations for Testing, Managing, and Treating Adults Infected With Hepatitis C Virus. *Hepatology* **2015,** *62,* 932–954 (3).
393. Gane, E. J.; et al. Efficacy of Ledipasvir and Sofosbuvir, With or Without Ribavirin, for 12 Weeks in Patients With HCV Genotype 3 or 6 Infection. *Gastroenterology* **2015,** *149* (6), 1454–1461.
394. Svarovskaia, E. S.; et al. L159F and V321A Sofosbuvir-Associated Hepatitis C Virus NS5B Substitutions. *J. Infect. Dis.* **2016,** *213* (8), 1240–1247.
395. Svarovskaia, E. S.; et al. Infrequent Development of Resistance in Genotype 1-6 Hepatitis C Virus-Infected Subjects Treated With Sofosbuvir in Phase 2 and 3 Clinical Trials. *Clin. Infect. Dis.* **2014,** *59* (12), 1666–1674.
396. Gotte, M.; Feld, J. J. Direct-Acting Antiviral Agents for Hepatitis C: Structural and Mechanistic Insights. *Nat. Rev. Gastroenterol. Hepatol.* **2016,** *13* (6), 338–351.
397. Krishnan, P.; et al. In Vitro and In Vivo Antiviral Activity and Resistance Profile of Ombitasvir, an Inhibitor of Hepatitis C Virus NS5A. *Antimicrob. Agents Chemother.* **2015,** *59* (2), 979–987.
398. Kati, W.; et al. In Vitro Activity and Resistance Profile of Dasabuvir, a Nonnucleoside Hepatitis C Virus Polymerase Inhibitor. *Antimicrob. Agents Chemother.* **2015,** *59* (3), 1505–1511.
399. Zeuzem, S.; et al. *Prevalence of Pre-Treatment NS5A Resistance Associated Variants in Genotype 1 Patients Across Different Regions Using Deep Sequencing and Effect on Treatment Outcome With LDV/SOF* (Presentation); American Association for the Study of Liver Diseases (AASLD): San Francisco, CA, 2015.
400. Nobusawa, E.; Sato, K. Comparison of the Mutation Rates of Human Influenza A and B Viruses. *J. Virol.* **2006,** *80* (7), 3675–3678.
401. Beyleveld, G.; et al. New-Generation Screening Assays for the Detection of Anti-Influenza Compounds Targeting Viral and Host Functions. *Antivir. Res.* **2013,** *100* (1), 120–132.
402. Cady, S.; Wang, T.; Hong, M. Membrane-Dependent Effects of a Cytoplasmic Helix on the Structure and Drug Binding of the Influenza Virus M2 Protein. *J. Am. Chem. Soc.* **2011,** *133* (30), 11572–11579.
403. Hayden, F. G.; Hay, A. J. Emergence and Transmission of Influenza A Viruses Resistant to Amantadine and Rimantadine. *Curr. Top. Microbiol. Immunol.* **1992,** *176,* 119–130.
404. Abed, Y.; Goyette, N.; Boivin, G. Generation and Characterization of Recombinant Influenza A (H1N1) Viruses Harboring Amantadine Resistance Mutations. *Antimicrob. Agents Chemother.* **2005,** *49* (2), 556–559.
405. Sweet, C.; et al. Virulence of Rimantadine-Resistant Human Influenza A (H3N2) Viruses in Ferrets. *J. Infect. Dis.* **1991,** *164* (5), 969–972.
406. Hurt, A. C. The Epidemiology and Spread of Drug Resistant Human Influenza Viruses. *Curr. Opin. Virol.* **2014,** *8,* 22–29.
407. Fiore, A. E.; et al. Antiviral Agents for the Treatment and Chemoprophylaxis of Influenza—Recommendations of the Advisory Committee on Immunization Practices (ACIP). *MMWR Recomm. Rep.* **2011,** *60* (1), 1–24.
408. Samson, M.; et al. Influenza Virus Resistance to Neuraminidase Inhibitors. *Antiviral Res.* **2013,** *98* (2), 174–185.
409. Aoki, F. Y.; Boivin, G.; Roberts, N. Influenza Virus Susceptibility and Resistance to Oseltamivir. *Antivir. Ther.* **2007,** *12* (4 Pt B), 603–616.
410. Bloom, J. D.; Gong, L. I.; Baltimore, D. Permissive Secondary Mutations Enable the Evolution of Influenza Oseltamivir Resistance. *Science* **2010,** *328* (5983), 1272–1275.
411. Butler, J.; et al. Estimating the Fitness Advantage Conferred by Permissive Neuraminidase Mutations in Recent Oseltamivir-Resistant A(H1N1)pdm09 Influenza Viruses. *PLoS Pathog.* **2014,** *10* (4), e1004065.
412. Gu, R. X.; Liu, L. A.; Wei, D. Q. Structural and Energetic Analysis of Drug Inhibition of the Influenza A M2 Proton Channel. *Trends Pharmacol. Sci.* **2013,** *34* (10), 571–580.
413. Das, K. Antivirals Targeting Influenza A Virus. *J. Med. Chem.* **2012,** *55* (14), 6263–6277.
414. Li, T. C.; Chan, M. C.; Lee, N. Clinical Implications of Antiviral Resistance in Influenza. *Viruses* **2015,** *7* (9), 4929–4944.
415. Wathen, M. W.; Barro, M.; Bright, R. A. Antivirals in Seasonal and Pandemic Influenza—Future Perspectives. *Influenza Other Respir. Viruses* **2013,** *7* (Suppl. 1), 76–80.
416. Torres, A.; Bonanni, P.; Hryniewicz, W.; Moutschen, M.; Reinert, R. R.; Welte, T. Pneumococcal Vaccination: What Have We Learnt So Far and What Can We Expect in the Future? *Eur. J. Clin. Microbiol. Infect. Dis.* **2015,** *34,* 19–31.
417. Welte, T. How Can We Reduce the Mortality of Invasive Pneumococcal Disease? *Eur. Respir. Rev.* **2012,** *21,* 6–7.
418. Walters, M. S.; Eggers, P.; Albrecht, V.; Travis, T.; Lonsway, D.; Hovan, G.; Taylor, D.; Rasheed, K.; Limbago, B.; Kallen, A. Vancomycin-Resistant *Staphylococcus aureus*—Delaware, 2015. *MMWR* **2015,** *64,* 1056.
419. Landman, D.; Babu, E.; Shah, N.; Kelly, P.; Backer, M.; Bratu, S.; Quale, J. Activity of a Novel Aminoglycoside, ACHN-490, Against Clinical Isolates of *Escherichia coli* and *Klebsiella pneumoniae* from New York City. *J. Antimicrob. Chemother.* **2010,** *65,* 2123–2127.
420. Landman, D.; Kelly, P.; Backer, M.; Babu, E.; Shah, N.; Bratu, S.; Quale, J. Antimicrobial Activity of a Novel Aminoglycoside, ACHN-490, Against *Acinetobacter baumannii* and *Pseudomonas aeruginosa* from New York City. *J. Antimicrob. Chemother.* **2011,** *66,* 332–334.
421. Galani, I.; Souli, M.; Daikos, G. L.; Chrysouli, Z.; Poulakou, G.; Psichogiou, M.; Panagea, T.; Argyropoulou, A.; Stefanou, I.; Plakias, G.; Giamarellou, H.; Petrikkos, G. Activity of Plazomicin (ACHN-490) Against MDR Clinical Isolates of *Klebsiella pneumoniae*, *Escherichia coli*, and *Enterobacter* spp. from Athens, Greece. *J. Chemother.* **2012,** *24,* 191–194.
422. Walkty, A.; Adam, H.; Baxter, M.; Denisuik, A.; Lagace-Wiens, P.; Karlowsky, J. A.; Hoban, D. J.; Zhanel, G. G. In vitro Activity of Plazomicin Against 5,015 Gram-Negative and Gram-Positive Clinical Isolates Obtained From Patients in Canadian Hospitals as Part of the CANWARD Study, 2011–2012. *Antimicrob. Agents Chemother.* **2014,** *58,* 2554–2563.
423. Castanheira, M.; Watters, A. A.; Rhomberg, P. R.; Jones, R. N. Plazomicin (PLZ) Activity Against Contemporary Clinical Isolates Collected in USA Hospitals. In 55th ICAAC American Society for Microbiology: San Diego, CA, 2015.
424. Rodriguez-Avial, I.; Pena, I.; Picazo, J. J.; Rodriguez-Avial, C.; Culebras, E. In Vitro Activity of the Next-Generation Aminoglycoside Plazomicin Alone and in Combination With Colistin, Meropenem, Fosfomycin or Tigecycline Against Carbapenemase-Producing Enterobacteriaceae Strains. *Int. J. Antimicrob. Agents* **2015,** *46,* 616–621.
425. Hitchings, G. H. Mechanism of Action of Trimethoprim–Sulfamethoxazole: I. *J. Infect. Dis.* **1973,** *128* (Suppl. 3), S433–S436.
426. Nguyen, L. T.; et al. Baseline Prevalence and Emergence of Protease Inhibitor Resistance Mutations Following Treatment in Chronic HCV Genotype-1-Infected Individuals. *Antivir. Ther.* **2015,** *20* (8), 865–869.
427. Summa, V.; et al. MK-5172, a Selective Inhibitor of Hepatitis C Virus NS3/4a Protease With Broad Activity Across Genotypes and Resistant Variants. *Antimicrob. Agents Chemother.* **2012,** *56* (8), 4161–4167.

5.18 Direct-Acting Antiviral Agents for the Treatment of Hepatitis C Virus Infection

NA Meanwell, Department of Discovery Chemistry and Molecular Technologies, Bristol-Myers Squibb Research and Development, 5 Research Parkway, Wallingford, CT 06492

© 2017 Elsevier Ltd. All rights reserved.

5.18.1	**Introduction**	554
5.18.1.1	Inhibitors of HCV Core (Capsid) Protein Function	556
5.18.1.2	Inhibitors of HCV Entry: E1 and E2	558
5.18.1.3	Inhibitors of the Ion Channel Activity of p7	561
5.18.1.4	HCV NS2 Protease Inhibitors	563
5.18.1.5	HCV NS3 Protease Inhibitors	563
5.18.1.6	HCV NS3 Helicase Inhibitors	575
5.18.1.7	HCV NS4A Inhibitors	576
5.18.1.8	HCV NS4B Inhibitors	577
5.18.1.9	HCV NS5A Inhibitors	580
5.18.1.10	HCV NS5B Inhibitors	587
5.18.1.10.1	Background	587
5.18.1.10.2	Nucleoside inhibitors of HCV NS5B RdRp activity	588
5.18.1.10.3	Nonnucleoside inhibitors of HCV NS5B RdRp activity	592
5.18.1.10.4	Thumb site I nonnucleoside inhibitors of HCV NS5B RdRp activity	592
5.18.1.10.5	Thumb site II nonnucleoside inhibitors of HCV NS5B RdRp activity	596
5.18.1.10.6	Palm site (primer grip) nonnucleoside inhibitors of HCV NS5B RdRp activity	598
5.18.1.10.7	Palm site I nonnucleoside inhibitors of HCV NS5B RdRp activity	598
5.18.1.10.8	Palm site II nonnucleoside inhibitors of HCV NS5B RdRp activity	601
5.18.1.11	HCV Internal Ribosome Entry Site (IRES) Inhibitors	604
5.18.2	**Drug Combinations in Clinical Trials**	605
5.18.3	**Conclusion**	607
Acknowledgment		607
References		607
Relevant Websites		627

Abbreviations

AAG Alpha-1-acid glycoprotein
AMP Adenosine monophosphate
ADP Adenosine diphosphate
ATP Adenosine triphosphate
BID Bis in die (twice a day)
BVDV Bovine viral diarrhea virus
CLDN1 Claudin 1
DAA Direct-acting antiviral agent
Dif 3,3-Diphenylalanine
EGFR Epidermal growth factor receptor
EphA2 Ephrin type-A receptor 2
ER Endoplasmic reticulum
FBDD Fragment-based drug design
GSH Glutathione
GST Glutathione S-transferase
GT Genotype
GTP Guanosine triphosphate
HCV Hepatitis C virus
HCVcc HCV cell culture
HCVpp HCV pseudoparticle
HAS Human serum albumin
HTS High-throughput screening
ID Intraduodenal
IRES Internal ribosome entry site
LE Ligand efficiency
MAPK Mitogen-activated protein kinase
PEG-IFN-α Pegylated interferon-α
NDPK Nucleoside-diphosphate kinase
NMR Nuclear magnetic resonance
NPC1L1 Niemann–Pick C1-like 1 protein
NHVs Normal healthy volunteers
PK Pharmacokinetic
PSA Polar surface area
QD Quaque die (once a day)
RdRp RNA-dependent RNA polymerase
RT-PCR Reverse transcriptase polymerase chain reaction
SR-B1 Scavenger receptor class B type 1
STD Saturation transfer difference

SVR Sustained virologic response
TID Ter in die (three times a day)
TM Transmembrane
UGT1A1 UDP glucuronosyltransferase 1 polypeptide A1
uPA-SCID Urokinase plasminogen activator–severe combined immunodeficiency

5.18.1 Introduction

Remarkable progress has been made in the treatment of hepatitis C virus (HCV) infection since the 2007 edition of *Comprehensive Medicinal Chemistry* when the optimal therapy was a combination of pegylated interferon-α-2a (PEG-IFN-2α) administered subcutaneously once weekly and ribavirin (**1**) taken twice daily orally for 48 weeks.[1–5] This drug regimen was poorly tolerated, with essentially all patients experiencing side effects so severe that many were unable to complete the course of therapy, with some refusing to start therapy based on the anticipated ordeal.[3,6–9] In addition, cure rates were low, of the order of 40–50% for genotype (GT) 1 virus, which proved to be the most challenging for this therapeutic regimen.[4] In 2014, the first direct-acting antiviral drug combinations were approved, providing regimens able to cure HCV infection in GT-1-infected patients after 8–24 weeks of therapy depending on clinical background, with the convenience of oral dosing and a marked reduction in the side effects that are associated with the use of PEG-IFN-α and **1**.[10] Nevertheless, therapy continues to evolve toward the development of oral regimens capable of treating all genotypes of HCV infection, and for the first time in history, we are in a position to be able to cure a chronic virus infection solely with small-molecule inhibitors.[11–16]

The development of combinations of direct-acting antiviral agents (DAAs) for the treatment of HCV has been described as a medical triumph based on the high cure rates in GT-1-infected patients, a circumstance subtended by the elegant medicinal chemistry associated with the design and development of effective drug candidates.[14–17]

The HCV genome is encoded by a single strand of positive RNA composed of approximately 9600 nucleotides that was first characterized in 1989 by the cloning of a cDNA from an infected patient, the first virus to be identified using molecular biology techniques.[18–21] The genetic organization of the ~3000 residue polyprotein that was encoded by the viral RNA (captured in Fig. 1) was quickly mapped, providing the first glimpse of potential targets for drug discovery including the NS3 serine protease, the NS3 helicase, and the NS5B RNA-dependent RNA polymerase (RdRp).[22–29] The structural and nonstructural proteins and the 5′- and 3′-untranslated regions were subsequently defined more precisely and the mode and order of cleavage of the polypeptide determined, as summarized in Fig. 2.[30–32] These developments set the stage for drug discovery programs, which initially were focused on the NS3 protease and NS5B RdRp since biochemical assays were readily recapitulated in vitro and were aided considerably by the availability of structural information for these enzymes by X-ray crystallographic analysis.[33–37] However, a major impediment to rapid progress was the lack of a cell culture system that would allow demonstration of target engagement by lead inhibitors under the more authentic circumstances associated with a complex cellular milieu. This situation changed in 1999 with the development of the first subgenomic replicon based on a genotype 1b sequence, with subsequent advances broadening these systems to include replicons that encompassed the full genomes and extending to genotype 1a and 2a viruses.[38–43] The development of replicons facilitated the implementation of phenotypic screening, an approach that led to the identification of the first HCV NS5A inhibitors that were optimized into a clinically important drug class that has taken its place as a mainstay of therapy when used in combination with NS3 and/or NS5B RdRp inhibitors.[44–46] Careful study and optimization of cell culture systems ultimately culminated in the identification of fully replicating systems that extended the interrogation of the virus life cycle to include the processes of entry, uncoating, assembly, and release of virions.[47–51] These developments have led to the current circumstance where a combination of in vitro assays, replicons, and infectious viruses have been utilized to identify and/or characterize small-molecule inhibitors of all of the structural and nonstructural proteins of HCV and the HCV internal ribosome entry site (IRES).

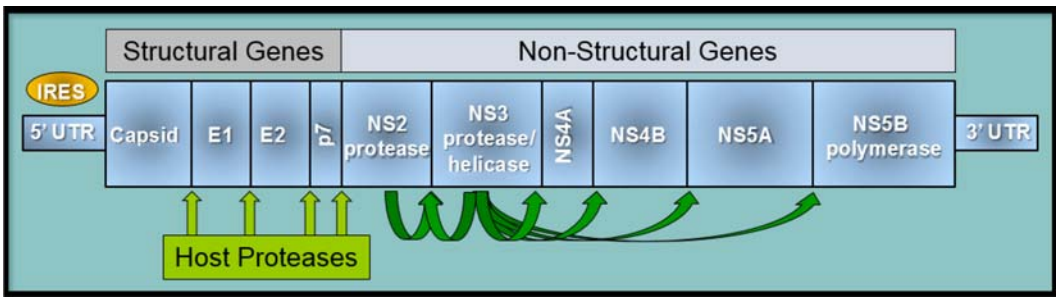

Fig. 1 Genetic organization of HCV depicting the untranslated regions, the structural and nonstructural genes, and the sites of cleavage in the polypeptide by host cell and viral proteases.

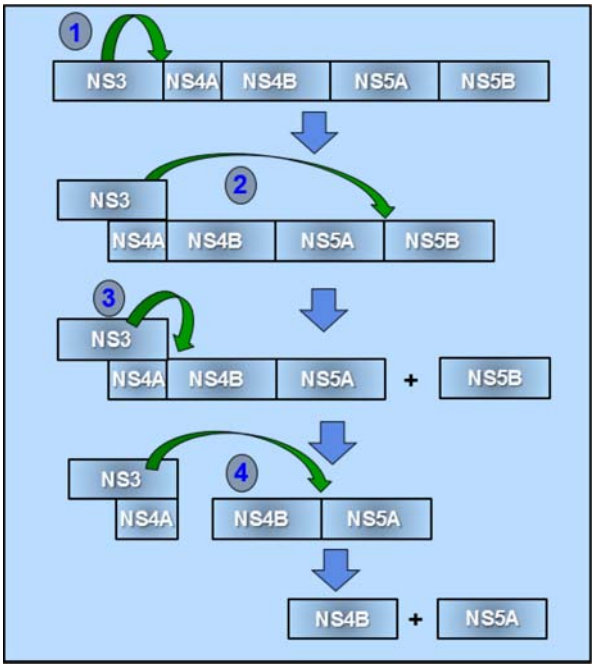

Fig. 2 Order of cleavage of the HCV nonstructural proteins by the NS3 protease.

The need for combinations of DAAs to treat HCV was anticipated based on the experience with human immunodeficiency virus-1 (HIV-1) drug development, setting the stage for a considerable effort that was expended across both the pharmaceutical industry and academia, which focused on developing antiviral agents acting by complementary mechanisms. More recently, the scientific basis for combination therapy has been articulated based on studies that assessed virus replication rates in vivo in the context of the frequency of errors of reproduction attributed to the limited fidelity of the HCV NS5B RdRp.[52–57] These analyses estimated that the average individual infected with HCV produces up to 10^{12} virions per day, 10–100-fold higher than the reproduction rate of HIV-1, and that the fidelity of reproduction is one base error incorporated for every 10 genomes that are synthesized. Taken together, these figures predict that 91% of the virus is reproduced faithfully, while 8.7% of the genomes produced incorporate a single mutation that equates to a daily production of 87 billion virus particles (data summarized in Table 1). Viruses with two mutations are estimated to be produced at a rate of 4.2 billion per day, while triply mutant viruses constitute only 0.013% of the daily output, although that still represents 130 million virus particles in the average infected individual. These calculations suggest that with a genome composed of $<10{,}000$ RNA bases, every possible single mutant is produced every day and predict that the use of drug monotherapy will lead to the rapid emergence of resistant virus. This was indeed observed in practice in early clinical trials with NS3, NS5A, and NS5B RdRp inhibitors, which were administered for up to 14 days as monotherapy.[58–63]

While the first DAAs to be approved, the NS3 protease inhibitors telaprevir (**2**) and boceprevir (**3**), were licensed for use in combination with PEG-IFN-α and ribavirin (**1**), the approval of the nucleoside-based NS5B RdRp inhibitor sofosbuvir (**4**) and the NS3 protease inhibitor simeprevir (**5**) set the stage for the use of DAAs in combination (Figs. 3 and 4).[64–68] This was formalized in 2014 with the regulatory approval of the combination of the NS3 protease inhibitor asunaprevir (**6**) and the NS5A inhibitor daclatasvir (**7**) for the treatment of GT-1b infection in Japan in July.[69] Further advances came in Nov. 2014 with the licensing by the Food and Drug Administration (FDA) of a fixed-dose combination comprising 400 mg of sofosbuvir (**4**) with 90 mg of the NS5A inhibitor ledipasvir (**8**), marketed as Harvoni™.[70] Shortly thereafter, Viekira Pak™, a fixed-dose combination of 12.5 mg of the NS5A inhibitor ombitasvir (**9**), 75 mg of the NS3 protease inhibitor paritaprevir (**10**), and the cytochrome P450

Table 1 Estimated kinetics of HCV reproduction in vivo

Number of mutations	*% of viruses produced daily*	*Virions produced per day*
0	91	910×10^9
1	8.7	87×10^9
2	0.42	4.2×10^9
3	0.013	0.13×10^9

Based on 10^{12} virions produced per day with 0.1 changes per RNA synthesized.

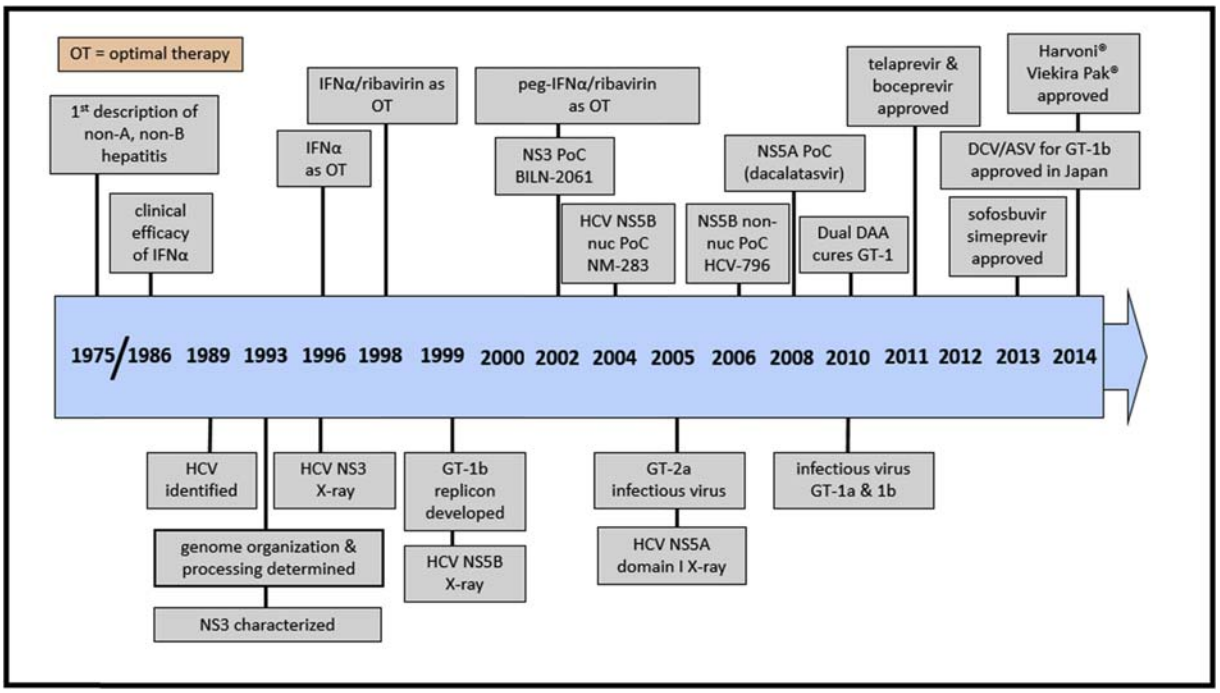

Fig. 3 Timelines for HCV drug approvals and key developments in biochemical pharmacology.

inhibitor ritonavir (**11**) taken quaque die (QD) along with the allosteric NS5B inhibitor dasabuvir (**12**) (which is administered on a bis in die (BID) schedule of 250 mg), was approved for the treatment of GT-1 infection (Fig. 4).[71] For those with GT-1a infections or cirrhosis, adding ribavirin (**1**) at doses of 1 or 1.2 g BID based on body weight to Viekira Pak™ improved cure rates.[71] A fixed-dose combination of 50 mg of the NS5A inhibitor elbasvir (**13**) and 100 mg of the NS3 protease inhibitor grazoprevir (**14**) has completed phase 3 clinical trials in patients infected with GT-1, GT-4, and GT-6 HCV, and a new drug application (NDA) for the marketing of Zepatier TM was approved by the FDA on Jan. 28, 2016.[72] However, achieving this level of clinical success with DAAs has been arduous, relying upon the development of a large number of compounds examined preclinically and clinically, with many failing for reasons of either poor efficacy or unacceptable levels of toxicity.[73] It has been estimated that 712 individual drug candidates were examined between 1995 and 2014 from which 12 drugs had been marketed, while 588 failed and 112 remain in development, statistics that translate to an overall success rate at the end of 2015 of just 2%.[74]

5.18.1.1 Inhibitors of HCV Core (Capsid) Protein Function

The HCV core or capsid protein is composed of approximately 177 residues in its mature form and is cleaved from the 191 residue precursor protein by removal of the C-terminal transmembrane residues that form the signal sequence for the E1 protein (Fig. 5).[75–77] Little is known about the specific three-dimensional structure of the core protein, although about half of the protein adopts an α-helical conformation, and the basic functional unit appears to be a dimer that is disulfide-linked via Cys128.[75–78] The protein has been divided into two domains with the hydrophilic domain D1 composed of residues 1–117, while the remainder of the protein is more hydrophobic and designated as domain D2. Within D1, there are three clusters of basic residues, designated as BD1 (AAs 2–23), BD2 (AAs 38–74), and BD3 (AAs 101–121). Domain D1 is involved in both RNA binding and oligomerization, with the first 82 residues of the protein highly disordered but capable of forming ordered nucleocapsid-like particles in the presence of structured RNA. The D2 domain mediates association with the endoplasmic reticulum and lipid droplet membranes and contains two regions that form amphipathic helices—helix I (AAs 119–136) and helix II (AAs 148–164)—that are separated by a hydrophobic loop.[75] The process of HCV capsid assembly and release involves complex choreography between viral (core, E1, E2, p7, NS2, NS3, NS4A, NS5A, and NS5B) and host cell proteins, with roles for diacylglycerol *O*-acyltransferase (DGAT), the mitogen-activated protein kinase-regulated cytosolic phospholipase A2, endosomal sorting complex required for transport, microsomal triglyceride transfer protein, apolipoprotein E, and the assembly of very-low-density lipoprotein documented, but many others remain to be identified.[77]

While therapeutic intervention with agents targeting some of these host cell processes has been described, direct inhibitors of core protein have focused on identifying compounds that interfere with dimerization.[75,76,79,80] An in vitro assay was developed that assessed the binding of an FLAG-tagged core protein to an immobilized glutathione S-transferase (GST)–core protein construct, in which the core protein of each partner was identical and composed of residues 1–106 to avoid the precipitation and aggregation problems associated with full-length protein.[76] The protein–protein interaction was assessed by fluorophore-labeled antibodies

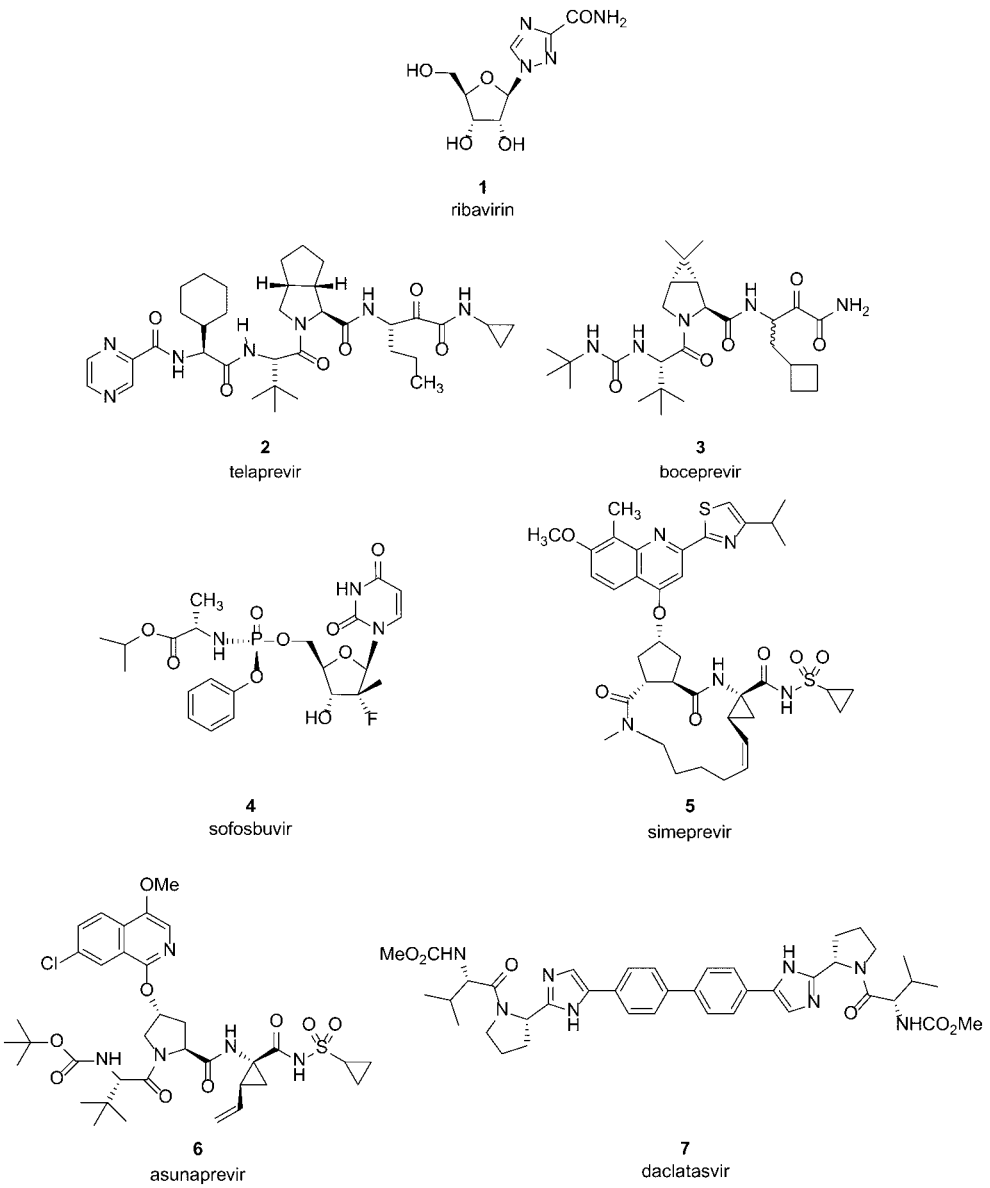

Fig. 4 The structures of drugs approved to treat HCV infection.

against GST and the FLAG tag, and this assay was used as the basis for a high-throughput screen.[76,78] SL175 (**15**), a 15-amino acid peptide that represents residues 92–106 of the core sequence, inhibited protein association in this assay with an IC_{50} of 21.9 μM, while a control peptide composed of the reverse sequence was inactive (Fig. 6).[76,79] SL175 (**15**) was shown to bind to a core protein fragment comprising residues 1–106 with a K_d of 1.9 μM using a fluorophore-tagged derivative of the peptide, and this molecule was displaced by unlabeled SL175 (**15**) with an IC_{50} of 18.7 μM.[76,79] The core 1–106 protein association assay was used to screen for additional small-molecule inhibitors, leading to the identification of the racemic pyrido[4,3-*b*]indole derivative SL209 (**16**) as a lead, $IC_{50} = 1.4$ μM.[76,80] This compound demonstrated antiviral activity in a GT-2a virus replication assay with EC_{50} values of 2.3 and 3.2 μM when viral RNA levels were determined early and late, respectively, using a real-time reverse transcriptase polymerase chain reaction (RT-PCR) assay.[76,80] The EC_{50} values determined for **16** are well separated from the concentration at which cytotoxicity toward the host cell was evident, reported as a CC_{50} value of 127 μM, consistent with an effect on the virus rather than the host cell. Further studies with SL209 (**16**) attempted to exploit the dimeric nature of the core protein by preparing symmetrical dimeric inhibitors that demonstrated markedly enhanced potency, results that catalyzed the synthesis of the asymmetrical triazole derivative **17**, which blocked core association with an $IC_{50} = 92$ nM (Fig. 6).[81] However, the potency of **17** in the virus replication assay was comparable with **16** with EC_{50} values of 1.4 and 1.1 μM, measured early and late, respectively, and a CC_{50} of > 100 μM.[81] A member of this series was shown to interfere with HCV NS3 helicase association with an oligomeric form of the core protein and to block the production of infectious virus but not the replication of a subgenomic replicon, consistent with an inhibitory effect on virus

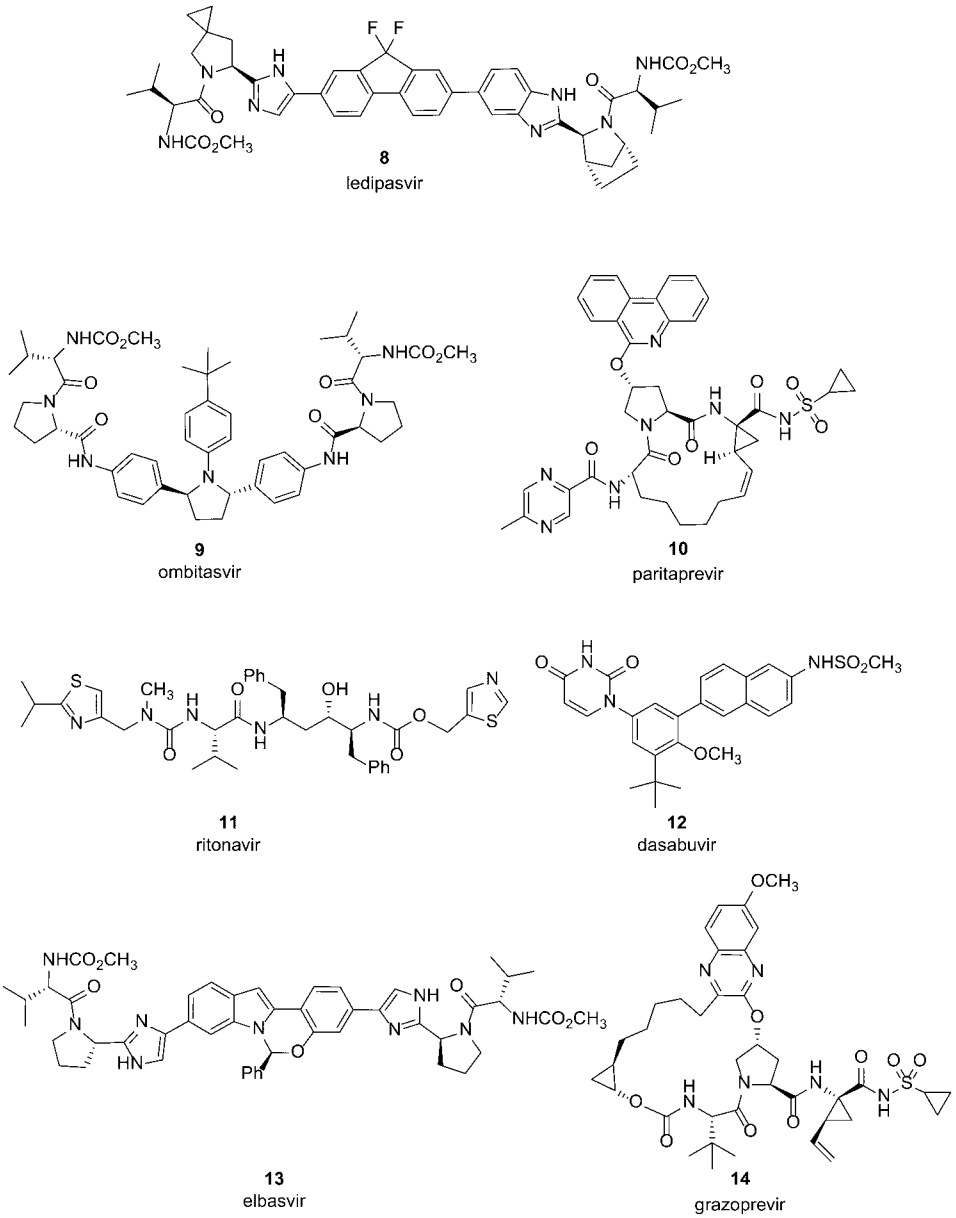

Fig. 4 (*continued*).

assembly.[82] The biotinylated analog SL209 (**18**), which inhibited core dimerization with an IC_{50} of 2.8 μM and virus replication with an EC_{50} value of 3.2 μM, was utilized as an affinity probe to screen lysates of HCV-infected cells and recombinant HCV proteins.[83] When lysates were passed over SL209 (**18**) bound to streptavidin-coated agarose beads, core protein was pulled down along with NS3, NS5A, and NS5B, proteins known to associate with core; however, neither NS5A nor NS5B adhered to the SL209-coated beads in the absence of core protein. While intracellular labeling studies with SL209 (**18**) were consistent with the core protein as the target, the precise mode of action of this compound remains to be determined since the in vitro experiments could not distinguish between an effect on capsid assembly and an effect on capsid disassembly.

5.18.1.2 Inhibitors of HCV Entry: E1 and E2

HCV entry into hepatocytes is mediated by the viral E1 and E2 surface glycoproteins interacting with multiple host cell proteins, but the precise mechanism and sequence of events are complex and not fully understood.[77,84–86] The most coherent current view suggests that the first step of the entry process involves a low-affinity association between the virus particle and the basolateral membrane of hepatocytes that is mediated by interactions with highly sulfated heparan sulfate proteoglycans (HSPGs), the LDL

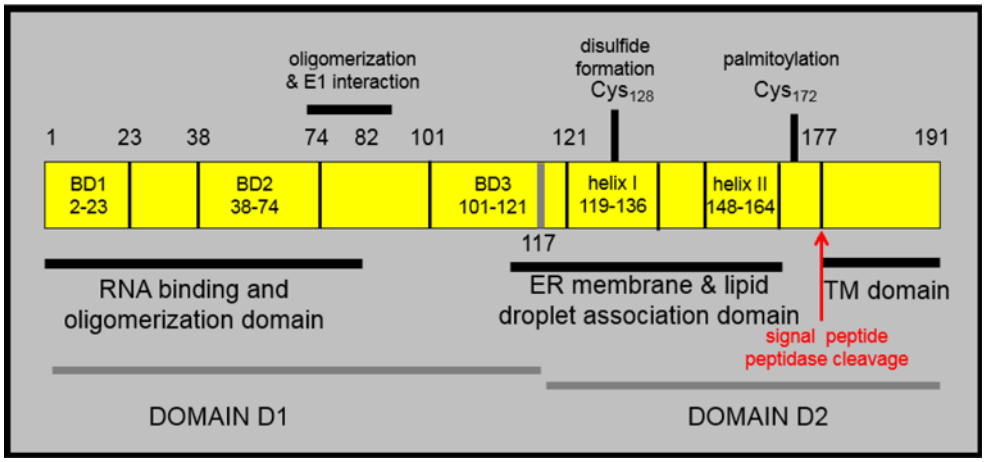

Fig. 5 Structural features of the HCV core protein.

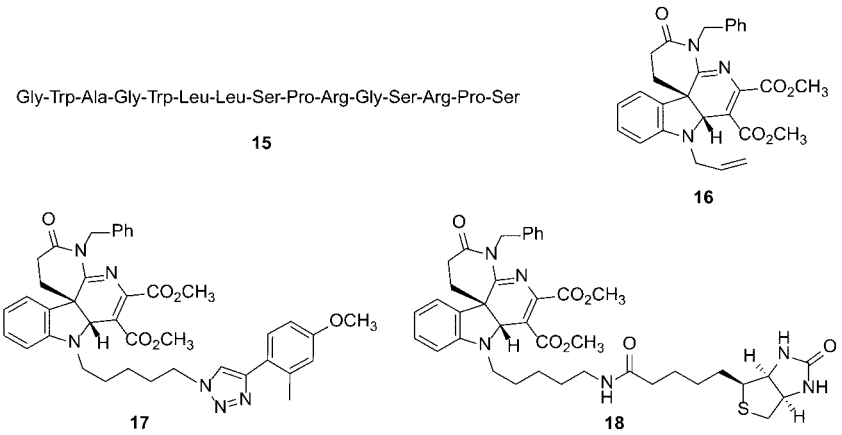

Fig. 6 HCV core protein inhibitors.

receptor, and the scavenger receptor class B type 1 (SR-B1).[77] SR-B1 may stimulate the dissociation of lipoproteins from the virus particle to expose the CD81 binding domain of the E2 glycoprotein. An important step in the entry process is the lateral migration of the CD81-bound particles to tight junctions where claudin 1 (CLDN1) is located; CLDN1 is believed to interact with CD81 to form a complex competent for clathrin-mediated endocytosis. Occludin has also been implicated in this step of the process but its precise function is unknown. The movement of the HCV particles to tight junctions and the interaction of CD81 with CLDN1 are facilitated by the activation of several intracellular signaling pathways triggered by CD81 engagement, a repertoire that includes the receptor tyrosine kinases epidermal growth factor receptor (EGFR) and the ephrin type-A receptor 2 (EphA2). This leads to activation of Rho and Ras GTPases, which promote remodeling of actin and the cell membrane, thereby facilitating migration of the HCV particle to tight junctions. After endocytosis, the virus particle is trafficked to an endosomal compartment containing the Ras-related protein Rab5A where the lipoprotein content of the virus may be further modified by SR-B1 and Niemann–Pick C1-like 1 protein (NPC1L1), a mediator of cholesterol absorption, as a prelude to membrane fusion. The low pH of the endosomal compartment triggers a conformational rearrangement of the HCV E1 and E2 glycoprotein heterodimer that leads to the formation of a trimeric fusion spike and exposure of the fusion peptide, resulting in convergence of the viral and endosomal membranes to release the viral RNA into the cytosol.

The identification of host factors involved in the entry process provides a rational basis for the selection and study of potential sites for intervention. The EGFR inhibitor erlotinib (**19**) inhibits HCV pseudoparticle (HCVpp) entry and HCV cell culture (HCVcc) infection in human hepatoma Huh7.5.1 cells with EC_{50} values of 0.45 and 0.53 μM, respectively, while dasatinib (**20**), a potent EphA2 inhibitor, blocks HCVpp entry and HCVcc infection with EC_{50} values of 0.53 and 0.50 μM, respectively.[87,88] Both compounds were effective only when present during in the early stages of infection, blocked cell-to-cell transmission, and interacted synergistically with a range of DAAs, data consistent with an inhibitory effect on the entry process.[87,89] Erlotinib (**19**) (Fig. 7) demonstrated antiviral activity in the chimeric urokinase plasminogen activator–severe combined immunodeficiency (uPA-SCID) mouse model of HCV infection, reducing viremia by 90% compared with the placebo control group.[87] The

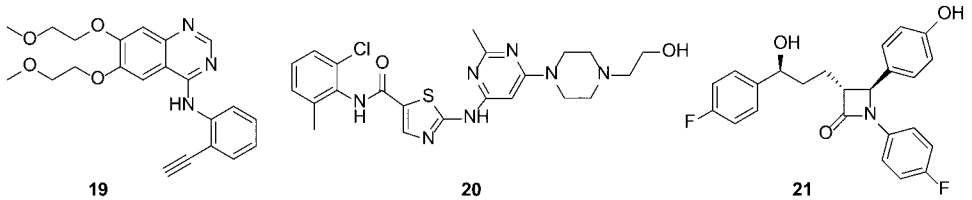

Fig. 7 Structure of the EGFR inhibitor erlotinib (**19**), dasatinib (**20**), and ezetimibe (**21**).

determination of a role for NPC1L1 in HCV entry prompted evaluation of the cholesterol absorption inhibitor ezetimibe (**21**), and this compound was shown to dose-dependently interfere with infection of all of the major genotypes in an HCVcc assay if added at the time of inoculation with virus but not at later time points.[90] In the uPA-SCID mouse model, pretreatment with ezetimibe (**21**) for 2 weeks delayed the establishment of HCV GT-1b infection.[90] A single clinical observation has described the resolution of a chronic HCV GT-1b infection unresponsive to multiple treatments with PEG-IFN-α and ribavirin (**1**) after several months of therapy with **21** in combination with a 3-hydroxy-3-methylglutaryl coenzyme A reductase inhibitor.[91]

Intervention at the entry step mediated by SR-B1 has been probed with ITX-5061 (**22**), which half-maximally prevents infection of Huh7 hepatoma cells by an HCV GT-2a chimeric virus at a concentration of 0.1 nM, a profile preserved in an unidentified analog that is associated with reduced p38 mitogen-activated kinase (p38 MAPK) and UDP glucuronosyltransferase 1, polypeptide A1 (UGT1A1) inhibition (Fig. 8).[92–95] ITX-5061 (**22**) interacts synergistically with IFN-α, ribavirin (**1**), and HCV NS3 and NS5B RdRp inhibitors to inhibit GT-2a virus infection of Huh7.5.1 cells.[95] Resistance mapping experiments identified an Asn415Asp change in the E2 protein as a mutation that conferred >1000-fold resistance, $EC_{50} > 20$ μM, compared with an EC_{50} value of 20 nM for the wild-type Jc1-Luc virus used in these experiments.[95] ITX-5061 (**22**) exhibits 10-fold lower activity toward the Gly451Arg mutant that shows a reduced dependence on SR-B1 for entry, data that taken together with the results described in the preceding text are consistent with SR-B1 as the pharmacological target. When administered to subjects with low HDL levels at doses of 150 and 300 mg daily for 6 weeks, ITX-5061 (**22**) was associated with a 20% increase in HDL levels in plasma, an effect also observed in wild-type and human apoA-1 transgenic but not in SR-B1$^{-/-}$ mice.[96] Although this result demonstrated a clinical effect, in a phase 2a clinical trial conducted in HCV-infected subjects administered with 150 mg of ITX-5061 (**22**) per day for 3, 14, and 28 days, no significant effect on viral load was observed, with the exception of one patient in the 28-day arm who experienced a 1.49 $\log_{10}$ IU mL^{-1} reduction in viremia from a baseline value of 5.58 $\log_{10}$ IU mL^{-1} to 4.09 $\log_{10}$ IU mL^{-1}.[97] There was no clearly apparent reason why ITX-5061 (**22**) failed to demonstrate an antiviral effect in this study, a particularly perplexing outcome considering that genetically humanized SR-B1$^{-/-}$ mice exhibited reduced HCV infectivity consistent with a role for this protein in virus entry.[98] Structurally disparate SR-B1 antagonists have been described, including ITX-4520 (**23**), which inhibits both GT-1a and GT-2a HCV infectious viruses with EC_{50} values of 1.5 nM, but these compounds do not appear to have been advanced into development.[99,100]

The advent of cell culture infectious HCV and the development of pseudoparticles facilitated the implementation of phenotypic screening campaigns, which have identified several classes of HCV entry inhibitors. EI-1 (**24**), identified using a pseudoparticle assay, inhibits a GT-1a/2a and GT-1b/2a Rluc HCVcc with EC_{50} values of 24 and 12 nM, respectively, with an excellent therapeutic index based on a CC_{50} of >50 μM toward the host Huh7.5 cell line.[101] The results of time of addition experiments are consistent with inhibition of virus entry at a post-attachment step prior to endosomal acidification, and **24** prevents cell-to-cell spread of virus in vitro. Resistance mapping studies identified Val719Phe and Val719Gly substitutions in a residue located in the transmembrane region of the carboxy terminus of the E2 protein that conferred a 50- to 90-fld shift in the EC_{50}.[101] Resistance to the HCV entry inhibitor **25**, which prevents HCV infection in vitro with EC_{50} values of 30 nM toward a GT-1b/2a chimeric virus and 40 nM toward a GT-2a virus, also maps to the E2 protein with a Pro687Ser substitution that is 20-fold less sensitive.[102] This compound rapidly inactivates infectious HCV while allowing the release of only noninfectious particles and prevents the fusion of the viral and endosomal membranes. However, the precise modes of action of both **24** and **25** will require further experimentation, with studies directed toward developing a deeper understanding of the role and function of the enigmatic E1 and E2 proteins, optimally aided by analyses of the solid-state structures of these proteins in complex with an inhibitor.[103–107]

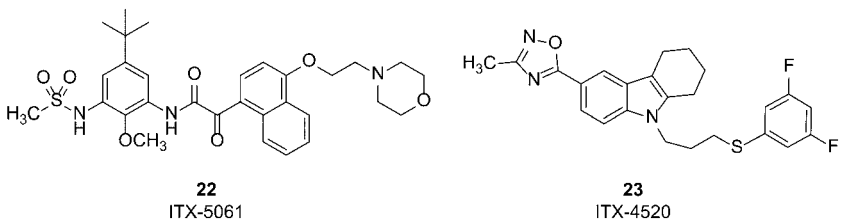

Fig. 8 SR-B1 inhibitors.

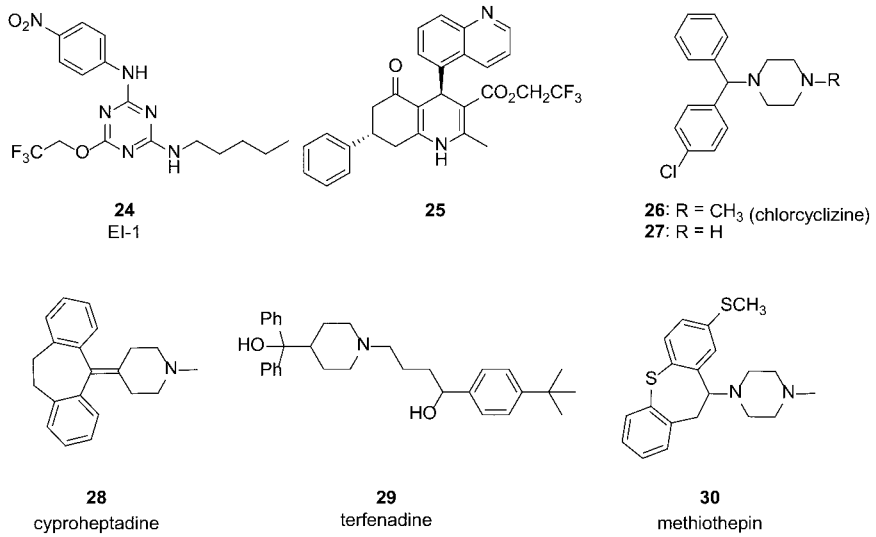

Fig. 9 HCV entry inhibitors.

The HCV entry inhibitors **26–29**, which share some common structural features and mechanistic attributes, were discovered using phenotypic screens (Fig. 9).[108–110] The antihistamine agent chlorcyclizine (**26**) and its major in vivo metabolite norchlorcyclizine (**27**) are potent HCV entry inhibitors in cell culture with EC_{50} values ranging from 2.3 to 44 nM, activity that is insensitive to the absolute configuration at the chiral center.[108–110] Cyproheptadine (**28**) inhibits infectious GT-1a and GT-2a viruses with EC_{50} values of less than 1 μM, while terfenadine (**29**) and the 5-HT_2 antagonist methiothepin (**30**) were identified as modestly potent inhibitors of HCV infectivity using assays designed to detect inhibitors of the interaction of E2 with CD81.[108–112] Attempts to probe the mode of action of chlorcyclizine (**26**) by the development of resistant virus in vitro were unsuccessful, leading to the conclusion that the compound may act by interfering with a host cell target; however, as a potential complicating factor, it has been noted that lipophilic amines can interfere with endosomal maturation.[108,109] In a chimeric mouse model infected with either a GT-1b or GT-2a virus, chlorcyclizine (**26**) administered at daily IP doses of 50 mg kg^{-1} for 4 weeks (GT-1b) and 10 mg kg^{-1} for 6 weeks (GT-2a) suppressed viremia by 1.5 to 2 $\log_{10}$IU mL^{-1}, with rebound occurring only after cessation of drug dosing.[109]

However, against the backdrop of the failure of the SR-B1 antagonist ITX-5061 (**22**) and JTK-652 (a pyrrolopyridazine derivative of undisclosed structure and entry inhibition mechanism) to demonstrate significant antiviral activity in HCV-infected patients, the potential for inhibitors of HCV entry to emerge as clinically relevant therapeutic agents remains to be determined.[97,113]

5.18.1.3 Inhibitors of the Ion Channel Activity of p7

HCV p7 is a small hydrophobic protein composed of 63 residues that include three helical segments embedded in the membrane domains, residues 2–14 (H1), 19–32 (H2), and 40–52 (H3) (Fig. 10).[114–117] The p7 protein is predicted to adopt an overall topology that projects the N- and C-termini into the ER lumen with the cytoplasmic loop composed of residues 33–39, which incorporates a dibasic Lys–Gly–Arg motif. The p7 protein has been shown to be critical for virus propagation in vitro and in vivo in chimpanzees and plays a crucial role in virus infectivity and capsid assembly but not replication.[118–122]

In vitro, p7 oligomerizes into hexamers and heptamers, with the N-terminus helical domains forming the pore of an ion channel that selectively conducts cations (Ca^{2+}, K^+, Na^+, and H^+) across an artificial membrane.[114–117,123–128] Using single-particle electron microscopy that mapped a detergent-solubilized, cross-linked, hexameric channel from GT-1b virus to ~16 Å resolution, a flower-shaped architecture was observed in which the N- and C-termini sequences projected like petals into the ER lumen.[124] Nuclear magnetic resonance (NMR) studies have provided deeper insight into channel structure and function, with improved detail revealing the three helical segments and confirming the flower-shaped hexamer structure, data that have facilitated analysis of

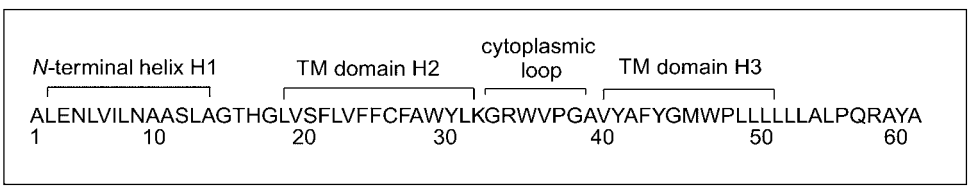

Fig. 10 Structure of HCV p7 with the N-terminal helix, the transmembrane (TM) domains, and the cytoplasmic loop demarcated.

the interaction of p7 with inhibitors.[125–128] The channel from GT-5a virus exhibited some difference from that of the GT-1b protein, adopting an overall funnel architecture, with H1 forming the narrow conical region and H2 the wide cylindrical element of the pore, whereas H3 faced the lipid membrane.[127] Ile6 was suggested to form the hydrophobic filter that prevents water from passing through the channel, while Asn9, conserved in all HCV genotypes with the exception of GT-2, was proposed as a selectivity filter that recruits cations and removes the associated water molecules and is located close to the funnel exit. A second key polar residue is Arg35, located at the wide end of the funnel, which has been hypothesized to associate with anions at the entrance to the pore and interfere with their passage.

The ion channel function of p7 has led to its classification as a member of the viroporin family that includes the Vpu protein of HIV-1, the picornavirus 2B protein, and the influenza M2 proton channel. Indeed, HCV p7 can substitute for the influenza M2 channel in a cell-based assay where it facilitates the transport of hemagglutinin to the cell surface.[115] The cation-conducting properties of p7 have formed the basis for the development of assays to facilitate the identification of inhibitors, with further advances assisted by structural information derived from detailed NMR analyses.[125–128] The influenza M2 inhibitors amantadine (**31**) and rimantadine (**32**) have been characterized as modestly potent inhibitors of HCV p7 channel activity in vitro that show genotype dependency; however, both compounds exhibit poor antiviral activity in cell culture assays (**Fig. 11**).[125,130–132] The antiviral effects of amantadine (**31**) have been studied clinically since the original observation of a beneficial effect, but more recent studies have concluded that the benefit is minimal at best.[133–135] Nevertheless, amantadine (**31**) has been shown to associate with the p7 hexamer by NMR, binding to a hydrophobic pocket between the pore and lipid-facing helices defined by Phe20, Val25, and Val26 from H2 and Leu52, Val53, and Leu56 from H3, with six of these symmetrically distributed within the hexamer.[127] This is concordant with resistance data that have associated changes at Phe20 with modulating sensitivity to inhibition by amantadine (**31**), with a Leu substitution found in GT-1b and GT-2a strains more sensitive to **31**, leading to consideration of this region as a binding site that modulates channel function by an allosteric mechanism.[136]

Other inhibitors of p7 ion channel function in vitro include the iminosugar *N*-nonyl-deoxynojirimycin (**33**), which also expresses antiviral activity via α-glucosidase inhibition, and the acyl guanidine BIT225 (**34**), which also inhibits HIV-1 Vpu function.[136–139] Resistance to **33** maps to a Phe25Ala change that suggested an inhibitory effect on proper channel oligomerization.[136] BIT225 (**34**) has been evaluated clinically where a preliminary study evaluated a dose of 400 mg BID in conjunction with PEG-IFN-α and ribavirin (**1**), with the result that the observed decline in viremia was enhanced by 10-fold compared with the control group administered with PEG-IFN-α and ribavirin (**1**) alone.[117,139] The quinazoline LDS25 (**35**) was one of several compounds identified as a potent p7 inhibitor based on a structure-guided drug design exercise that used the solution structure of monomeric GT-1b protein to develop a model of a heptameric channel.[128] This exercise was part of a broader effort to more precisely define the binding site for adamantine (**31**) and rimantadine (**32**), information that would be useful for in silico compound screening.[128] Twelve of the hits identified in this fashion inhibited GT-1b p7 ion channel activity with IC_{50} values of ~250 nM, considerably more potent than rimantadine (**32**), IC_{50} = 40 μM. LDS25 (**35**) is reported to demonstrate antiviral activity in cell culture with an EC_{50} value of ~300 nM.[117,128]

The challenges associated with identifying and characterizing HCV p7 inhibitors preclinically have impeded progress toward this target, and although clinical evaluation of BIT225 (**34**) is ongoing, the potential for a p7 inhibitor to be approved as a component of combination therapy against a rapidly evolving clinical landscape remains to be determined.[117]

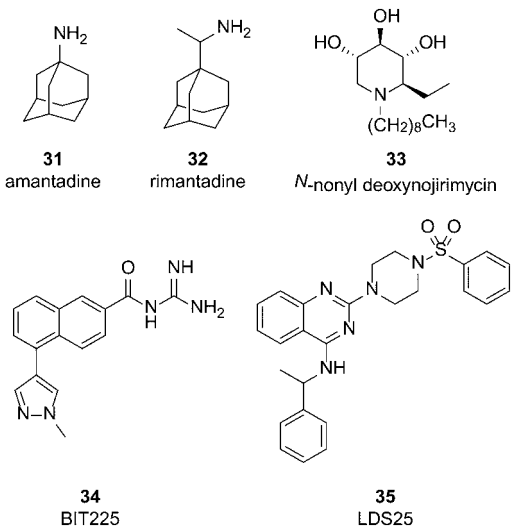

Fig. 11 HCV p7 ion channel inhibitors.

5.18.1.4 HCV NS2 Protease Inhibitors

The HCV NS2 cysteine protease is a 217-residue peptide that is essential for viral replication, cleaving the viral polypeptide at the NS2–NS3 junction in a fashion that is dependent on the presence of the NS3 protein.[140–142] NS2 forms complexes with both structural (E1, E2, and p7) and nonstructural (NS3 and NS5A) proteins that contribute to a central role in virion assembly, although the precise function and choreography of these interactions remain to be determined.[140,141,119] In addition, NS2 interacts with several host cell proteins that allow the virus to modulate the cellular environment in its favor. Biochemical studies have revealed that the N-terminal hydrophobic region anchors the peptide in the endoplasmic reticulum membrane via three putative transmembrane domains and that residues His143, Glu163, and Cys184 are associated with proteolytic catalysis.[140,141] HCV NS2 protease is, however, unusual in that in the crystalline form, the postcleavage protein (residues 94–217) assembles as a dimer that shows little resemblance to other viral proteases, with two composite active sites in which Cys184 from one monomer combines with His143 and Glu163 from the other.[143] Experimental data are consistent with the protease functioning as a dimeric species, and once cleavage has occurred, Leu217 in the C-terminus associates with the active site residues of the dimer to stabilize the enzyme in an inactive configuration, thereby regulating the function of the protease during viral replication.

Inhibitors of the HCV NS2 protease have been explored only sparsely.[140,141] As a cysteine protease, NS2 is sensitive to inhibition by the thiol modifiers *N*-ethylmaleimide and iodoacetamide but, surprisingly, not the *trans*-configured epoxide E-64 (**36**), which has been utilized as a general inhibitor of cysteine proteases (Fig. 12).[140,141,144,145] However, the *cis*-disposed epoxy bis-amide **37** has been characterized as a modestly potent inhibitor of autoproteolysis of the GT-2a JFH1 NS2–NS3, $IC_{50} = 93$ μM, while the prototype **38** is inactive.[146] This provided a matched pair of compounds with which to explore effects in a cell-based assay where **37** was active in a subgenomic replicon system only when processing of the polyprotein was dependent on NS2 autoprotease activity, determined by comparison of NS2–NS5 and NS3–NS5 constructs.[146] Epoxide **38** was inactive both in this context and toward a transient GT-2a chimeric infectious clone, whereas **37** reduced replication to 15% of control at a concentration of 90 μM.

The HCV NS2 protease inhibitors that have been described to date have not been the subject of attempts to refine these leads into more potent and specific agents, a reflection of the difficulties associated with this protein as a therapeutic target. As a consequence, the current understanding of the biochemical pharmacology of the NS2 protease and its inhibition is immature and with several very effective drug combinations already approved as HCV therapeutics, this circumstance seems unlikely to change.

5.18.1.5 HCV NS3 Protease Inhibitors

The HCV NS3 serine protease has been extensively explored as a drug target since its original identification and characterization, facilitated by the development of biochemical assays suitable for screening and further enhanced by the solving of solid-state structures that have been exploited in rational drug design.[24–27,32–34,147] This protease comprises the first 181 residues of the 631-residue bifunctional NS3 protease/helicase and is characterized by an extended and exposed substrate-binding groove that is largely shallow and featureless, originally viewed as providing limited opportunity for optimizing drug–target affinity.[32–34] The catalytic activity of the native enzyme is poor in comparison with mammalian serine proteases with a $K\text{cat}/K\text{m} = 30$–$2000\ M^{-1}\ s^{-1}$ for peptide-based substrates (versus a $K\text{cat}/K\text{m} = 10^{15}\ M^{-1}\ s^{-1}$ for thrombin); however, NS3 is markedly stimulated by association with NS4A, a cofactor that increases $K\text{cat}/K\text{m}$ values to 10,000–55,000 $M^{-1}\ s^{-1}$.[147–151] The catalytic triad of the enzyme is composed of His57, Asp81, and Ser139 that in the solid state lie in a cleft between two β-barrel subdomains and is deployed in a chymotrypsin-like fold.[31,32] The enzyme is further stabilized by coordination of a Zn^{2+} ion by Cys97, Cys99, Cys145, and His149, a structural element of importance to the cleavage of the polyprotein by NS2. The central portion of the NS4A cofactor, residues 21–32, adopts a β-strand structure that associates with the N-terminal β-barrel of the protease, thereby favoring the correct folding of NS3. The hydrophobic α-helix located at the amino terminus of NS4A anchors the complex to the membrane, while the acidic carboxy terminal region of the protease interacts with the helicase domain. Substrate specificity is relatively low, governed primarily by recognition of Cys at the cleavage site, a small residue at P1′, and an acidic amino acid at P6.[31,32] In addition to processing the viral polyprotein, the NS3 protease also acts on several host cell substrates that provide the virus with a measure of control over the host cell immune response. Mitochondrial antiviral-signaling protein (MAVS, formerly known as CARDIF, VISA, and IPS1) and Toll/interleukin-1 receptor (TIR) domain-containing adaptor inducing IFN-β (TRIF) are the two host substrates that have been characterized most thoroughly, and both are involved in the induction of an innate immune response.[152–155]

The biochemical properties and structural features of the NS3 protease are such that the identification of lead small-molecule inhibitors using high-throughput screening protocols was unsuccessful, focusing drug design on substrate-based approaches. An

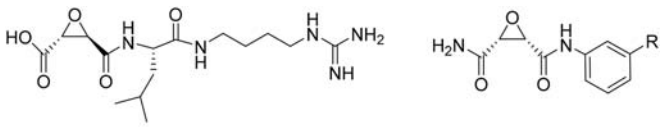

36
E-64

37: R = Cl
38: R = H

Fig. 12 HCV NS2 protease inhibitors.

important discovery toward that objective was the observation that the NS3 enzyme was subject to product inhibition by the carboxylic acid products of cleavage, providing a basis for the optimization of product-based peptides into potent inhibitors.[156–158] The hexapeptide **39**, which is derived from the NS4A–NS4B junction, inhibited the protease with a K_i of 600 nM, a potent but challenging lead template from which to design more drug-like molecules based on the size, the polyacidic nature of the molecule, and the presence of the Cys at the C-terminus (**Fig. 13**).[157] The latter problem was solved initially in an elegant fashion in the context of the more potent analog **40**, $K_i = 40$ nM, in which the P2 glutamate residue is substituted by a cyclohexylalanine (Cha) moiety and the P3 Met residue is elaborated to 3,3,-diphenylalanine (Dif).[158] Capitalizing on the known but underappreciated H-bond-donating properties of an alkyl difluoride and the similarity in shape, size, and molecular electrostatic potential compared with a thiol moiety, a difluoro-Abu P1 residue was examined.[159,160] This afforded **41** as a compound with potency comparable with **40** that was superior to the simple Abu analog **42**, indicative of effective functional mimicry of the thiol moiety.[161,162] The keto acid **45** is a smaller, slow-binding analog of the more potent aldehyde **43** and keto acid **44** and displays a K_i of 17 μM and a K_i* of 27 nM. These inhibitors take advantage of the electrophilicity of the keto carbonyl of **45**, the *Si*-face of which reacts with the hydroxyl of the catalytic Ser139 to form a covalently bound, tetrahedral intermediate, as observed in the cocrystal structure. In the P1 pocket, the CF_2H moiety makes hydrophobic contacts with Val132, Leu135, and part of the side chain of Lys136, while the hydrogen atom is oriented toward the backbone amide oxygen of Lys136, confirming the bioisosteric mimicry of the cysteine thiol moiety.[159,162] In addition, one of the fluorine atoms is in contact with the *para*-hydrogen atom of Phe154 at the base of the pocket.

As the understanding of the activity and SARs associated with substrate-based inhibitors of NS3 evolved, two avenues for drug discovery were pursued that focused on optimizing either activated ketone-containing peptide derivatives or carboxylic acid-based product inhibitors. The former approach led to the approval of the first HCV NS3 protease inhibitors telaprevir (**2**) and boceprevir (**3**), which were licensed in May 2011, although both were taken on a TID dosing schedule in combination with PEG-IFN-α and ribavirin (**1**).[64,65,163–165] The discovery of telaprevir (**2**) has its origins in the tetrapeptidic aldehyde **46**, a modestly potent inhibitor of NS3, $K_i = 12$ μM (**Fig. 14**).[166–169] Further optimization of **46** to the α-keto amide **47**, $K_i = 0.22$ μM, took advantage of interactions with the S′ subpockets of the enzyme. Both **46** and **47** incorporate large aromatic-containing moieties attached via a 4-hydroxy proline at P2 that project beyond the substrate-binding groove of the enzyme, frequently designated as P2* elements. However, further modification focused on fused bicyclic rings at this site, culminating in the discovery of **48**, $K_i = 0.04$ μM. Subsequent adjustments to the structure systematically optimized the bicycloproline, P4, and ketoamide moieties to arrive at telaprevir (**2**), $K_i = 0.007$ μM.[166,167,170] Telaprevir (**2**) undergoes facile racemization at the P1 residue in vivo to afford a diastereomeric mixture with 30-fold weaker potency, an observation that prompted a study of the deuterated analog **49**.[171,172] This compound sought to take advantage of the kinetic isotope effect associated with deuterium and its design was based on the hypothesis that proton removal was the rate-determining step in racemization. Compound **49** was characterized as a twofold more potent NS3 inhibitor than telaprevir (**2**) and exhibited slower racemization at P1 in phosphate buffer and human plasma, producing only 10% of the epimer over 1 hour compared with 35% for the parent drug. Consistent with increased stability, the AUC of **49** following oral dosing to rats was 13% higher than for telaprevir (**2**), suggestive of slower racemization at P1 in vivo.[171]

By way of contrast, boceprevir (**3**) was developed as the racemate at P1 due to the facility with which racemization at P1 occurred, particularly in biological assays.[173] Optimization charted a similar pathway of truncation from an undecapeptide-based lead inhibitor, initially to the pentapeptide derivative **50**, K_i* = 15 nM, which like telaprevir relies upon the α-ketoamide

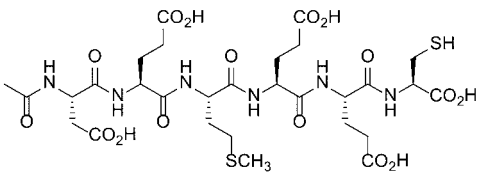

39: *Ki* = 600 nM

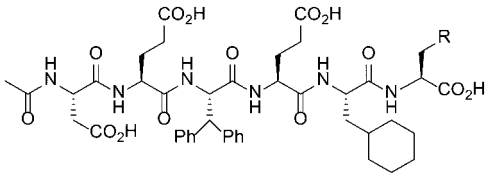

40: R = SH: K_i = 40 nM
41: R = CHF_2: K_i = 30 nM
42: R = CH_3: K_i = 700 nM

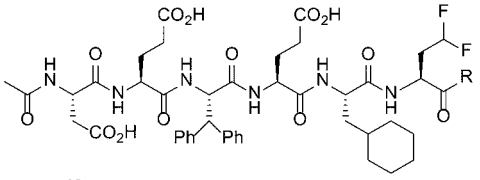

43: R = H: K_i = 0.5 nM
44: R = CO_2H: K_i = 4 nM, K_i* = 0.01 nM

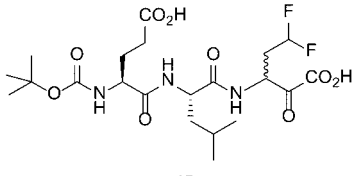

45

Fig. 13 HCV NS3 protease inhibitors **39–45**.

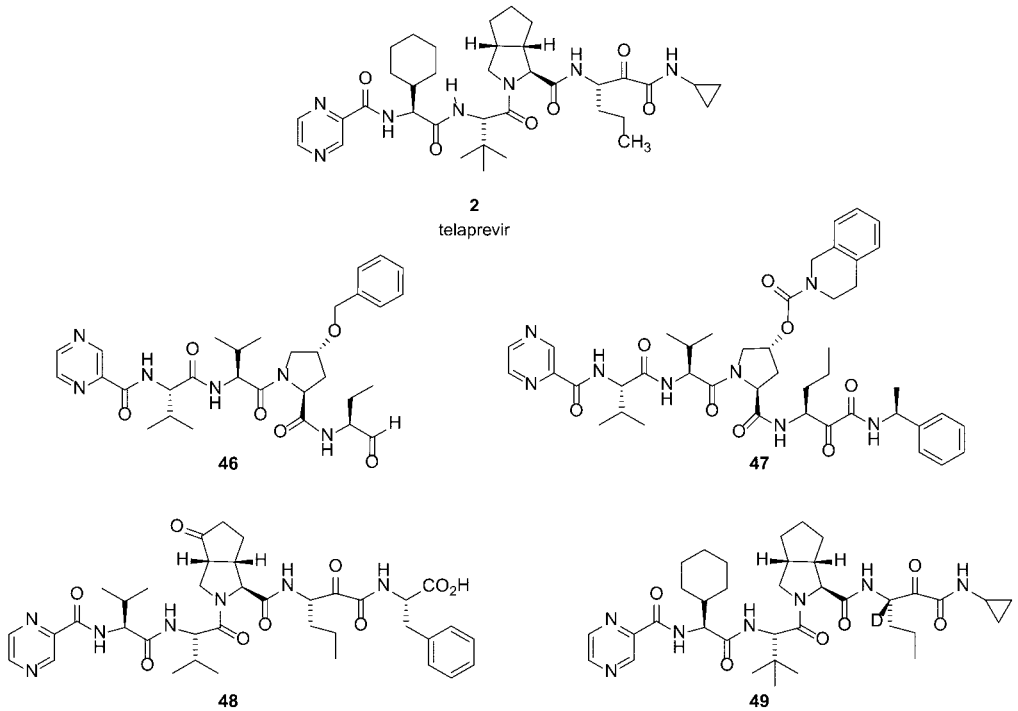

Fig. 14 HCV NS3 protease inhibitors telaprevir (**2**) and precursor molecules **46–49**.

motif to react with the serine hydroxyl of NS3 (Fig. 15).[173–176] The introduction of a *gem*-dimethylcyclopropylproline at P2, which was observed to interact closely with the CH_3 of Ala156 in the cocrystal structure, coupled with modification of the amide terminus provided **51**, $K_i^* = 15$ nM, with measurable inhibitory activity in a replicon assay, $EC_{90} = 100$ nM, but poor PK properties in rats. The latter was addressed by further truncation at the P′ side of the scissile bond mimic and modification of the P3 moiety to give **52**, $K_i^* = 25$ nM and $EC_{90} = 400$ nM. The final structural adjustments were made at P1, P3, and the amino terminus by combining optimal elements identified from the extensive SAR studies that had been conducted, leading to boceprevir (**3**), $K_i^* = 15$ nM and $EC_{90} = 350$ nM, which demonstrated oral bioavailability in the mouse, rat, dog, and cynomolgus monkey.[173–176]

The alternative pathway focused on optimizing peptidic carboxylic acid derivatives and resulted in the discovery of BILN-2061 (**53**), a macrocyclic tripeptide-based inhibitor that was the first NS3 protease inhibitor to demonstrate antiviral activity following oral dosing to HCV-infected subjects (Fig. 16).[177–181] A 200 mg dose of **53** administered twice daily orally as a solution in PEG 400 and ethanol for 2 days to eight GT-1-infected subjects resulted in a rapid reduction in viremia, amounting to 2–3 $\log_{10}$ IU mL^{-1} in all patients, with most achieving undetectable levels of HCV RNA by 48 hours after the first dose of drug.[177]

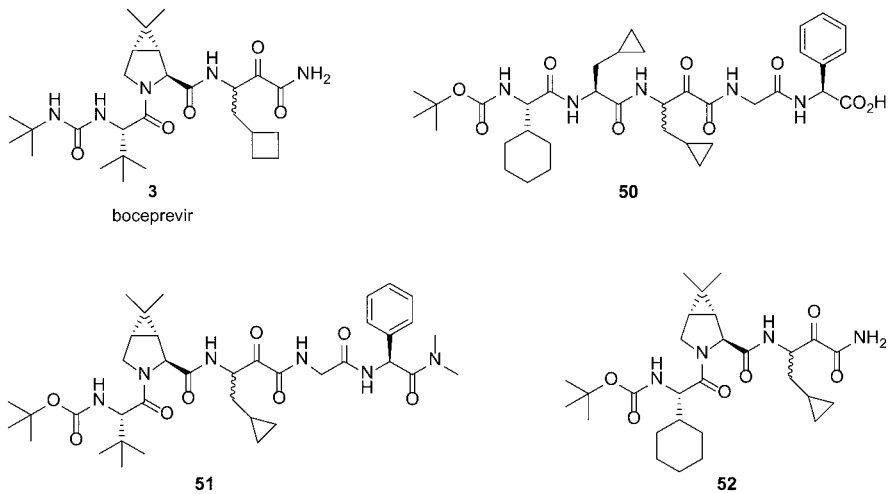

Fig. 15 HCV NS3 protease inhibitors boceprevir (**3**) and precursor molecules **50–52**.

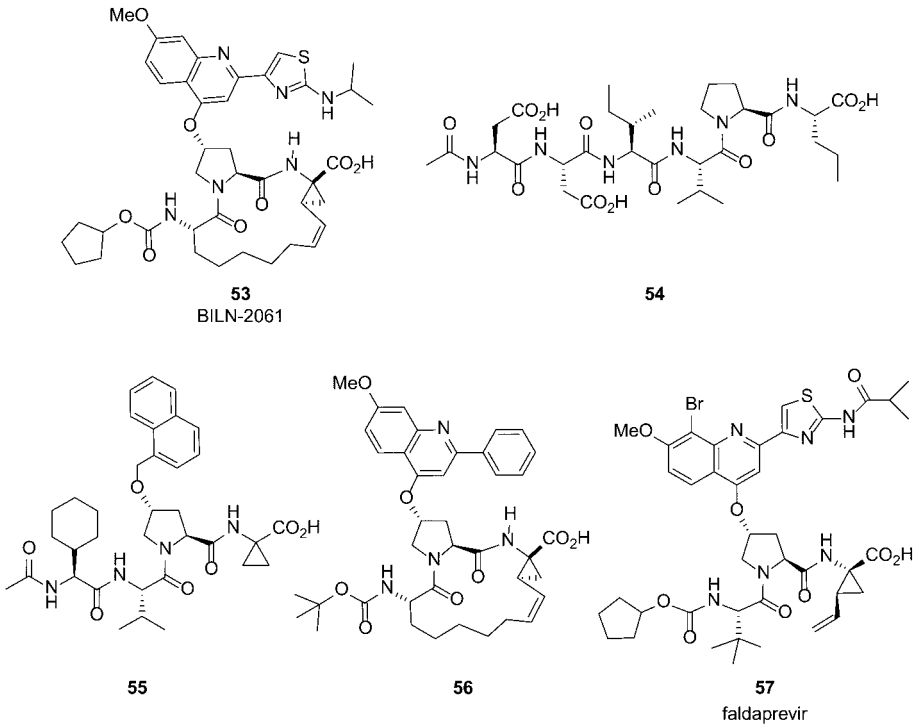

Fig. 16 HCV NS3 protease inhibitors **53–57**.

The origin of **53** was the polyacidic hexapeptide **54**, $IC_{50} = 150$ μM, for which systematic SAR studies established that the installation of 1-aminocyclopropane-1-carboxylic acid at P1 enhanced potency by threefold, while the introduction of a large lipophilic P2* element at the 4-position of the P2 proline produced a more dramatic 350-fold enhancement.[181] A combination of these SAR observations gave potent inhibitors in the context of a platform that facilitated truncation to afford the tetrapeptide **55**, which contains only a single acidic moiety and which inhibited NS3 with an IC_{50} value of 3.5 μM. Further optimization of **55** relied upon systematic variation of each amino acid residue, aided by NMR analysis of representative inhibitor–protease complexes that revealed an extended β-strand conformation of the inhibitor that placed P1 and P3 proximal.[182–184] This is a common binding mode for protease substrates and provided the inspiration to link the P1 and P3 elements as a means of preorganizing the bound conformation and improving the negative entropic aspect of the binding event.[185] The interest in this approach was heightened by the observation that when free in solution, the P1 moiety of unconstrained inhibitors adopted a conformation different to that recognized by the protease, while the P2–P3 amide existed as a *cis–trans* mixture. These studies reinforced the potential for enhanced potency in macrocycle-based inhibitors, an anticipation that was realized in the context of **56**, which inhibited NS3 with an IC_{50} of 11 nM, 30-fold more potent than a structurally similar acyclic analog.[178–180,186] An X-ray cocrystal structure of **56** bound to NS3 illuminated the key drug–target interactions, which included H bonds between the P1–P2 amide NH and the backbone carbonyl of Arg155 and between the P2–P3 carbonyl oxygen atom and the NH of Ala157.[178–180] At the C-terminus, one of the oxygen atoms of the carboxylic acid was bound in the oxyanion hole of the protease, interacting with the backbone NHs of Gly137 and Ser139, while the other interacted with the NH of the imidazole of His57. In addition, there appeared to be a bifurcated H bond between the carboxylate moiety and the side-chain OH of Ser139. The methoxyphenyl group of the P2* quinoline interacted with the guanidinium moiety of Arg155 in a π-stacking-type interaction that helped to stabilize the salt bridge association between Arg155 and Asp168 of the enzyme.[187] This provided an understanding of the emergence of resistance associated with Arg155Gln and Asp168Val—mutations in which disruption of the salt bridge removes the conformational constraint on these residues leading to a steric clash with the P2* moiety of the inhibitor.

The fully optimized molecule BILN-2061 (**53**) inhibited NS3 with IC_{50} value of 3.0 nM, which translated efficiently into potent antiviral activity in a replicon ($EC_{50} = 1.2$ nM), while dosing to rats demonstrated an oral bioavailability of 42%.[178,179,181] These data provided the basis for advancing BILN-2061 (**53**) into clinical trials, but development was terminated as a consequence of the occurrence of cardiac toxicity in rhesus monkeys.[188] Myocytic vacuolation and mitochondrial swelling resulted in left ventricular dysfunction after 28 days of exposure, and cardiac effects were observable after three or more doses of drug, a toxicity profile found to be common to two other macrocycle-based NS3 inhibitors. This led to a refocus on nonmacrocyclic alternatives from which faldaprevir (**57**) emerged as a candidate that successfully completed phase 3 clinical trials in conjunction with PEG-IFN-α and ribavirin (**1**) before development was halted for business reasons in June 2014.[189–191] Faldaprevir (**57**) is a slow-binding inhibitor of NS3 with K_i values of 2.6 and 2.0 nM toward GT-1a and GT-1b proteases, respectively, that translate into potent antiviral effects in

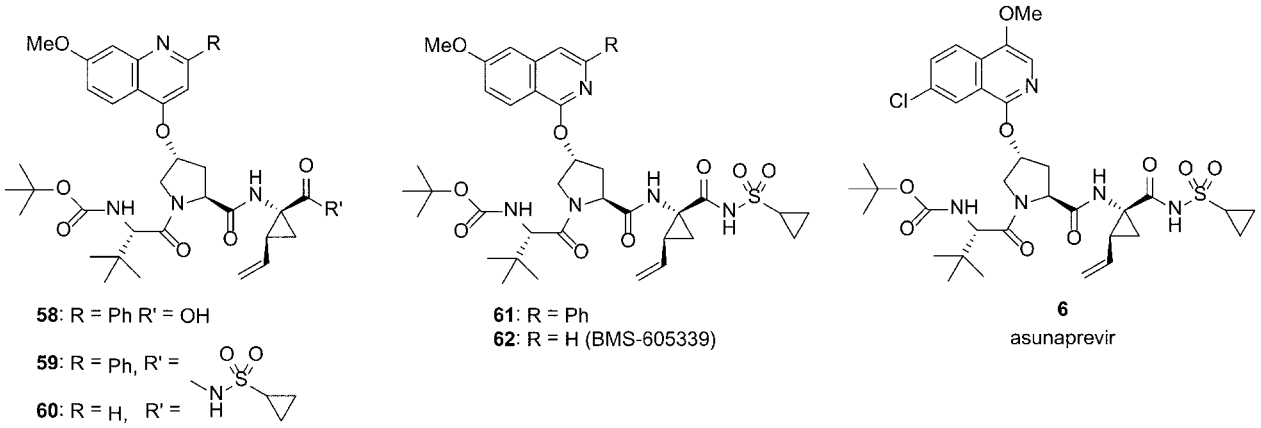

Fig. 17 HCV NS3 protease inhibitors **58–62** and asunaprevir (**6**).

replicons with EC_{50} values of 6.5 and 3.1 nM for GT-1a and GT-1b, respectively (Fig. 16).[189,190] The cocrystal structure of **57** bound to NS3 revealed an interesting halogen bonding interaction between the bromine atom and the backbone carbonyl of Asp79.[191,192] In addition, the sulfur atom of the thiazole heterocycle engaged in a close chalcogen interaction with the pendent acyl oxygen atom (the S to O distance is 2.87 Å, almost 0.5 Å less than the 3.32 Å sum of the van der Waals radii of S and O), which stabilizes the observed topology in an overall planar arrangement.[191,193]

A significant advance in the optimization of carboxylic acid-based NS3 inhibitors came with the advent of the cyclopropyl acylsulfonamide moiety, which was designed to enhance potency by preserving the acidic nature of the C-terminus motif while allowing access to the small but well-defined S1′ pocket that is lined, in part, by the side chains of Phe43, Val55, and Gly58.[194,195] The effectiveness of this approach is amply illustrated by comparing the enzyme and replicon inhibitory data for the matched pairs **58** and **59** (Fig. 17), results that reflect a 50–100 potency gain in the acylsulfonamide (Table 2).[194] An X-ray cocrystal structure revealed the origin of the enhancement, with the acylsulfonamide nitrogen atom rather than the oxygen atom engaging the catalytic His57 in a salt bridge interaction—a regiochemistry supported by electrostatic potential calculations, which favor residence of the charge on nitrogen—while the carbonyl oxygen atom accepts a H bond from the NH of Gly137.[194] Both sulfonamide oxygen atoms interact closely with the oxyanion hole with each accepting a H bond, one from Gly137 and one from Ser139, while the cyclopropyl ring is an optimal fit in the small, lipophilic S1′ pocket.

In this series, oral bioavailability in rats demonstrated a remarkable sensitivity to the identity of the P2* heterocycle, most effectively illustrated by comparing the rat exposure data following intraduodenal (ID) dosing of the quinolines **59** and **60** with their matched isoquinoline partners **61** and **62**, respectively (Table 2).[194] The ratios of AUC and liver levels measured at 4 hours after dosing **59** and **61** are ~10-fold in favor of the isoquinoline **61**, an advantage that is amplified to 100–600-fold for the simpler-substituted 6-methoxy isoquinoline BMS-605339 (**62**) compared with **60**. An in-depth evaluation of BMS-605339 (**62**) in a series of preclinical studies revealed an overall profile that supported advancing this compound into phase 1 clinical trials.[194] A single ascending dose study conducted initially in healthy volunteers and subsequently in subjects infected with HCV GT-1 demonstrated a dose-related increase in plasma exposure accompanied by a dose-dependent reduction in viremia, with a mean maximal decline of 1.8 $\log_{10}$IU mL^{-1} following a single oral dose of 120 mg.[194] However, mild bradycardia, PR interval prolongation, and junctional rhythm disturbances that were observed in two subjects resulted in further development being halted. Asunaprevir (**6**), which differs from BMS-605339 (**62**) by structural changes only to the isoquinoline P2* moiety and adds only a single chlorine atom to the molecular formula, was identified as a second clinical candidate that exhibits similar in vitro potency to **62**, a more hepatotropic in vivo disposition in rats (Table 2) and an improved cardiac profile, the result of rigorous triaging of candidate compounds through a Langendorff isolated perfused heart preparation.[195]

Table 2 In vitro antiviral activity and in vivo rat PK parameters for NS3 inhibitors **58–62** and asunaprevir (**6**)

	In vitro profiling		*Rat PK data following dosing of 15 mg kg^{-1} ID*	
Compound	*IC_{50} GT-1a enzyme (nM)*	*GT-1b replicon (nM)*	*AUC (μM•h) 0–4 h*	*Liver concentration at 4 h (μg g^{-1})*
58	54	550	0.027	0.838
59	1	4	0.077	7.85
60	5	26	0.015	0.62
61	1	4	1.11	72.91
62	2	12	10.40	64.71
6	1	6	1.90	67.41

The advantages offered by the cyclopropyl acylsulfonamide moiety have resulted in this structural element being prominently deployed in many clinically evaluated NS3 inhibitors that explore a range of interesting drug design principles. Sovaprevir (**63**) is an acyclic protease inhibitor that incorporates a succinic acid moiety as the P3–P4 element and was advanced into clinical trials (Fig. 18).[196] However, development of this compound was halted in favor of the P1–P3 macrocycle neceprevir (**64**), which incorporates the same P2* moiety as simeprevir (**5**) and demonstrates activity toward a broader range of HCV genotypes.[197] The design of simeprevir (**5**) relies upon the use of a *trans*-disposed cyclopentane dicarboxylic acid as a mimic of the P2 proline that is constrained within a 14-membered macrocycle linking P1 to P3.[198–201] Although this compound does not contain functionality that projects into P4, it is a potent, time-dependent NS3 inhibitor with K_i values estimated at 0.5 and 0.4 nM toward GT-1a and GT-1b proteases, respectively, which translates into potent inhibition in cell-based assays, $EC_{50} = 28$ and 25 nM in GT-1a and GT-1b replicons, respectively.[200,202] Resistance studies mapped virus escape to mutations at Asp168 with a Val or Ile substitution at this position associated with ~2000-fold reduced sensitivity to simeprevir (**5**), while Gly or Asn substitutions exhibited a less than 10-fold shift in the EC_{50} values.[203] In the cocrystal structure with NS3, the thiazole moiety of simeprevir (**5**) adopts a coplanar arrangement with the quinolone ring that juxtaposes the sulfur atom with the quinolone nitrogen atom.[201] This is the result of an attractive interaction between these two atoms, which are just 3.0 Å apart (less than the sum of the respective van der Waals radii), that stabilizes the observed conformation.[193,201] Simeprevir (**5**) gained regulatory approval in Japan in Sep. of 2013, in the United States in Nov. 2013, and by the European Commission in May 2014 with an indication for the treatment of HCV GT-1 infection to be used in conjunction with PEG-IFN-α and ribavirin (**1**).[67,204]

Two other protease inhibitors that are based on a P1–P3 macrocyclic tripeptidic acylsulfonamide backbone but incorporate different structural elements at P2* and P4 are danoprevir (**65**) and paritaprevir (**10**).[205–212] Danoprevir (**65**) (Fig. 18) is a potent

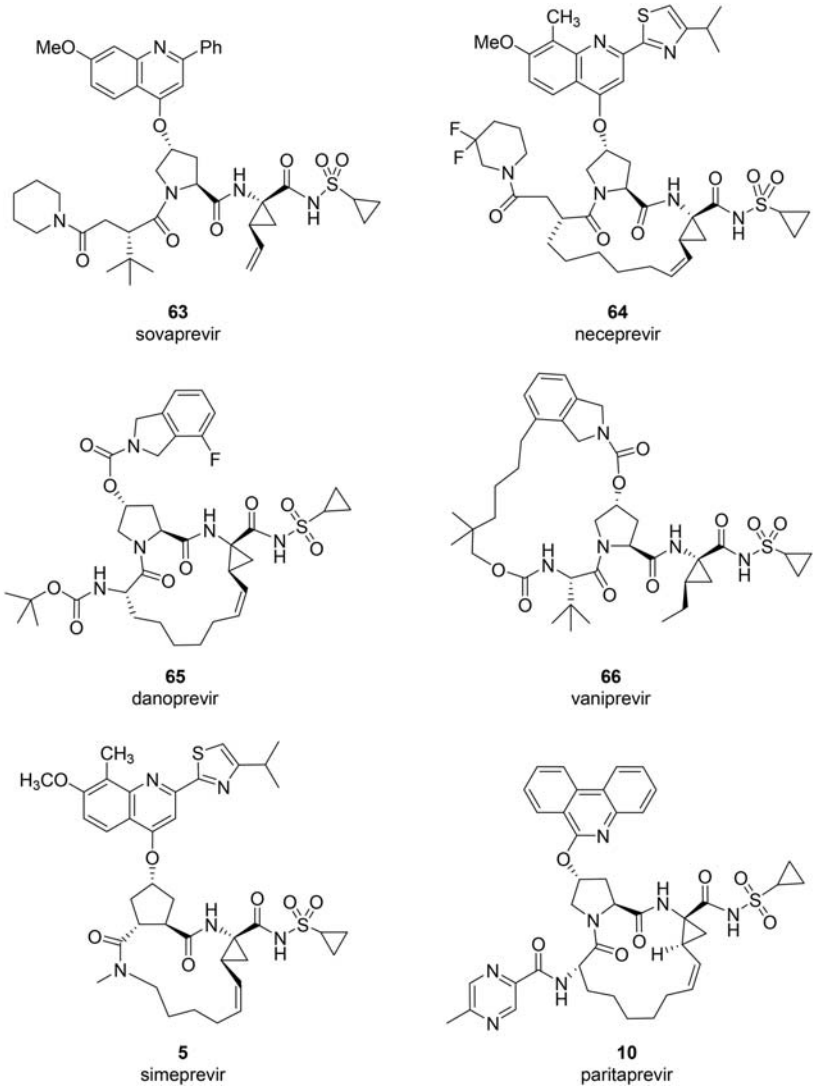

Fig. 18 HCV NS3 protease inhibitors **63–66**, simeprevir (**5**), and paritaprevir (**10**).

NS3 inhibitor, $IC_{50} = 0.2–3.5$ nM dependent upon genotype, that exhibits a slow off rate from the enzyme and displays potent antiviral activity in replicons, $EC_{50} = 1.6$ nM (GT-1b) and 20 nM (GT-2 and GT-3).[205–207] Danoprevir (**65**) deploys a carbamate moiety at P2* that was initially derived by probing a virtual library of potential targets based on an acyclic tetrapeptide carboxylic acid core and synthesizing representative examples of those with the most promising scores.[205] Subsequent optimization focused on identifying compounds that reduced the peptidic nature of the molecules while combining potent antiviral activity in replicons with good liver exposure in rats following oral dosing, with the latter varying markedly within the chemotype. A 30 mg kg^{-1} dose of danoprevir (**65**) administered orally to rats and cynomolgus monkeys provided liver levels of drug at 12 hours that exceeded the replicon EC_{50} values, with levels 10-fold higher in the rat than the monkey.[205,207] In a 14-day monotherapy study in HCV-infected subjects, 200 mg doses of danoprevir (**65**) administered on a BID and TID schedule were associated with declines in viremia of 3.2 $\log_{10}$ and 3.9 $\log_{10}$ IU mL^{-1}, respectively.[208,209] Virus rebound was observed in ~20% of the patients, with sequencing revealing an Arg155Lys mutation as the predominant change that reduced susceptibility by over 400-fold.[210] Since danoprevir (**65**) is metabolized by CYP 3A4, a PK-boosting strategy by coadministration with the potent CYP 3A4 inhibitor ritonavir (**11**) has been pursued for more advanced clinical studies.[208]

The design parameters and preclinical challenges that subtend the discovery and development of paritaprevir (**10**) have not been described in detail.[211] However, the compound is a potent antiviral agent in GT-1a, GT-1b, GT-2a, GT-3a, GT-4a, and GT-6a HCV replicons, with EC_{50} values ranging from 0.09 nM (GT-4a) to 19 nM (GT-3a) in the absence of human serum, while in GT-1a replicons, the EC_{50} value shifts by 17–25-fold in the presence of human serum.[211,212] Resistance mapping studies in vitro identified Asp168Val as a key mutation, conferring 96- and 159-fold reduced susceptibility toward GT-1a and GT-1b replicons, respectively, and this mutation, along with Arg155Lys, was observed in a 3-day monotherapy study.[212] Since paritaprevir (**10**) is metabolized primarily by CYP 3A4, it, like danoprevir (**65**), is coadministered with ritonavir (**11**) to boost the C_{trough} of the drug and minimize the emergence of resistant virus.[211,212]

Vaniprevir (**66**) and grazoprevir (**14**) are the result of an examination of an alternative macrocyclization topology that takes advantage of the proximity of the P2* moiety to elements that bind in the S4 pocket in cocrystal structures, a design principle explored by modeling studies.[213–215] The seminal study examined the concept in the context of tripeptidic carboxylic acids incorporating a quinoline heterocycle at P2*, from which **67** emerged with the optimal linker length and point of attachment to the quinoline, inhibiting a GT-1b protease with a K_i of 8.5 nM and active in a GT-1b replicon, $EC_{50} = 1.15$ μM.[213] In this molecule, the P4–P2* linker occupies the site occupied by Glu628 of the C-terminus of the helicase domain in the X-ray of the full-length protein, an observation that was instrumental in the original design concept. Installation of the cyclopropyl acylsulfonamide terminus to give **68** improved intrinsic potency by more than 500-fold, $K_i = < 0.016$ nM, accompanied by a 170-fold increase in replicon inhibitory activity, $EC_{50} = 6.7$ nM. However, **68** demonstrated poor plasma and liver exposure in rats following oral dosing, a shortcoming only partially resolved by rearranging the P3 substituent to that of a *tert*-butyl moiety. These results prompted the examination of an isoquinoline P2* heterocycle, with the prototype **69** preserving the in vitro profile of **68**, $K_i = 0.07$ nM, $EC_{50} = 4.5$ nM, but demonstrating a 36-fold higher plasma $AUC_{0-4\ h}$ and 4.75-fold higher liver levels 4 hours after a single 5 mg kg^{-1} oral dose, recapitulating observations in the acyclic series.[194,213]

Further optimization of this chemotype focused on variation of the P2* moiety, which enabled additional probing of linker length, level of saturation, and substitution in conjunction with modifications to P3 and P1.[214] While saturation of the linker had no effect on potency, saturation of the P1 vinyl moiety led to a 10-fold reduction in potency but increased liver levels after oral dosing to rats. Interestingly, saturation of both the linker and the P1 vinyl moiety restored potency toward the sentinel GT-1b virus and led to improved liver levels, but activity toward a GT-2a replicon was modest (EC_{50} ~ 100 nM), stimulating additional optimization in pursuit of a broader inhibitory profile. This was accomplished by the installation of a gem-dimethyl substituent on the linker proximal to the P3–P4 carbamate, a modification leading to the identification of vaniprevir (**66**), which exhibits improved GT-2a inhibition ($EC_{50} = 9–15$ nM).[214–216] Vaniprevir (**66**) exhibited high liver concentrations 24 hours after an

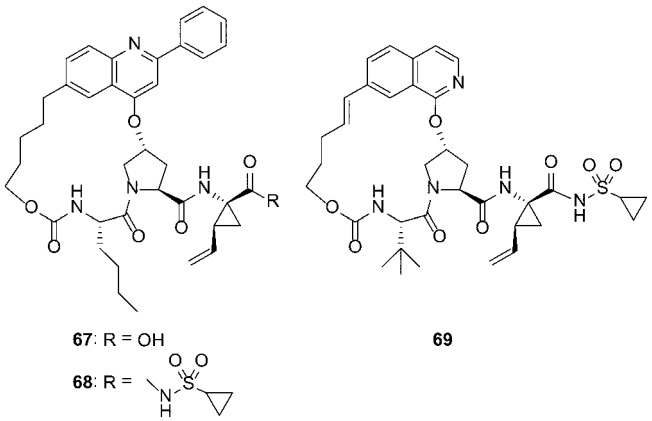

Fig. 19 HCV NS3 protease inhibitors **67–69**.

oral dose of 5 mg kg^{-1} to rats (400 nM), dogs (600 nM), and rhesus monkeys (200 nM), although plasma exposure was not sustained in the rat and rhesus monkey.[216] In addition, a 10 mg kg^{-1} dose administered to chimpanzees afforded a liver concentration of 31 μM. In patients chronically infected with GT-1 HCV and administered doses of vaniprevir (**66**) ranging from 25–700 mg BID to 125 and 600 mg QD for 8 days, viral load declined by 1.8 to 4.6 $\log_{10}$ IU mL^{-1}.[217] Plasma and liver levels of the drug were determined in a cohort of three treatment-experienced subjects administered with 300 or 600 mg on a BID schedule, with liver biopsy samples taken at 6 or 12 hours after the final dose.[218] Liver levels ranged from 84.6 to 169 μM at 6 hours and 29.4 to 54 μM at 12 hours, concentrations well above the replicon EC_{50}s of 2.9 to 27 nM, with liver/plasma ratios ranging from 20 to 280. These data are consistent with transporter-mediated hepatic uptake of vaniprevir (**66**), and the results contrast markedly with the profile of telaprevir (**2**), which demonstrates a hepatotropic disposition in preclinical species but a very different profile in HCV-infected patients where liver/plasma ratios were <1 and absolute drug concentrations in the liver were much lower at $\sim$7 ng g^{-1}.[219]

The antiviral activity of vaniprevir (**66**) was diminished toward replicons harboring resistant mutations that arose during combination therapy, with EC_{50} values of 350 nM for Arg155Lys, 430 nM for Asp168Tyr, and 200 nM for Ala156Thr, while the K_i toward a GT-3a enzyme was 54 nM, over 100-fold higher than for a GT-1b protease.[217,220–223] This provided focus for subsequent studies that led to the identification of grazoprevir (**14**), a molecule with an improved antiviral profile that inhibits a GT-3a protease with a K_i of 0.7 nM, while the three mutant proteases described in the preceding text are inhibited with K_i values ranging from 0.07 to 5.3 nM.[215,221] The optimization campaign leading to grazoprevir (**14**) was directed toward topological modifications of the P2* heterocycle that would increase contact with the GT-3a protease. This approach relied upon building into a conserved region of the protease in a fashion that also reduced contact of the P2* element with the Arg155–Asp168 salt bridge, which when compromised by mutations leads to conformationally more mobile side chains that sterically interfere with inhibitor binding. The topology of the P2*–P4 linker was also altered to avoid polymorphisms unique to GT-3a in this region of the protease, a design exercise that provided a compound with a significantly improved antiviral profile.[215,221–225] Grazoprevir (**14**) has completed phase 3 clinical studies as a fixed-dose combination with the NS5A inhibitor elbasvir (**13**), and an NDA was filed on 28 May 2015 seeking approval for marketing to treat of GT-1, GT-4, and GT-6 infection, which was granted in Jan. 2016.[223]

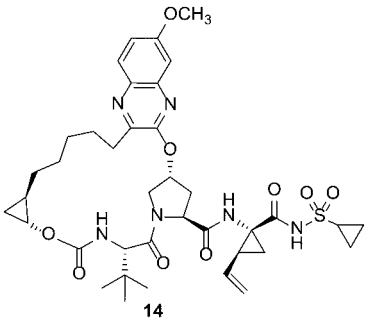

14
grazoprevir

The simultaneous incorporation of both a P4–P2* and a P1–P3 macrocycle was explored in the context of MK-6325 (**70**) (Fig. 20).[226] This compound demonstrated subnanomolar IC_{50} values toward proteases representative of GT-1 to GT-6a and those with mutations at Arg155, Ala156, and Asp168, a profile that translated into potent antiviral activity in replicons, with EC_{50} values ranging from 0.4 nM (Arg155Lys) to 5.5 nM (Ala156Thr). This analog, which incorporates a methyl substituent in the cyclopropylsulfonamide moiety, exhibited a liver concentration of 20 μM in rats 24 hours following a 5 mg kg^{-1} oral

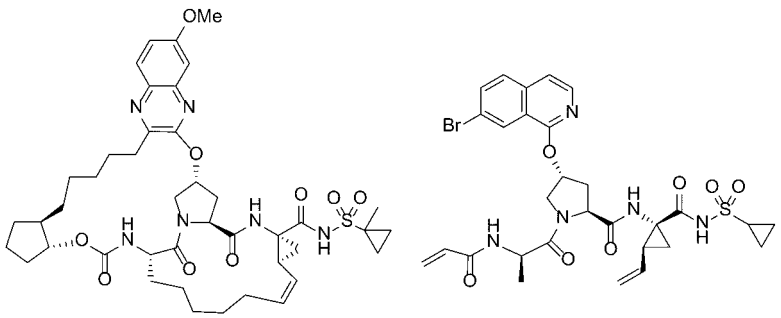

70
MK-6325

71

Fig. 20 HCV NS3 protease inhibitors **70** and **71**.

dose and 9.9 μM in dogs 24 hours after a 3 mg kg^{-1} dose, although oral bioavailability in both species was poor at 8% and 12%, respectively.

Irreversible inhibition of NS3 protease by targeting a reactive cysteine, Cys159, in the substrate-biding groove remote from the catalytic site and proximal to the S4 pocket, inspired the design of tripeptidic inhibitors that incorporate a Michael acceptor with low intrinsic chemical reactivity, as exemplified by **71** (Fig. 20).[227] A structure-based design approach suggested that a D-Ala P3 moiety would provide the necessary conformational bias to help present the acrylamide element of **71** to Cys159, a residue highly conserved in NS3 sequences. Compound **71** potently inhibited HCV NS3 protease activity with an IC_{50} of 2 nM, whereas the saturated propylamide homologue was a much weaker inhibitor, IC_{50} of 1.15 μM, and **71** poorly inhibited a protease incorporating a Cys159Ser mutation, $IC_{50} = 1.8$ μM. In an HCV replicon assay, **71** half-maximally inhibited luciferase activity at a concentration of 6 nM, while the propylamide analog was inactive, collective data that are consistent with a covalent mechanism of action. Adduct formation was confirmed by mass spectrometric and X-ray crystallographic analysis of the complex of **71** with the wild-type enzyme. Despite the presence of an unsubstituted acrylamide moiety, **71** demonstrated good discrimination with respect to inhibition of a panel of mammalian proteases and was not overtly reactive with glutathione.

Boronic acid derivatives are an established class of serine protease inhibitor that have been shown by X-ray cocrystal structural data to form a covalent adduct in which the catalytic serine hydroxyl adds to the boron to afford a stable tetrahedral intermediate.[228,229] Peptide-based boronic acid derivatives were examined for their potential as a platform for NS3 inhibitor design with the P1-phenethyl-substituted pentapeptide derivative **72** a representative example, $K_i = 8$ nM (Fig. 21).[230–232] The introduction of a para-CF_3 substituent gave **73**, which exhibited improved NS3 protease inhibition, $K_i = 2$ nM, while reducing affinity for human leukocyte elastase by twofold, $IC_{50} = 3.5$ μM, and chymotrypsin by 200-fold, $IC_{50} = 16$ μM.[232] The most successful boron-based NS3 protease inhibitor was PHX-1766 (**74**), which demonstrated potent ($IC_{50} = 8$ nM; $K_i = 0.05$ nM), selective, and reversible inhibitory activity toward GT-1, GT-2a, and GT-3a proteases.[233,234] This compound retained activity against the most common resistance mutations at Ala156, Arg155, and Asp168, although replicon EC_{50} values have not been reported. PHX-1766 (**74**) was advanced into phase 1 clinical studies where doses of 50–1000 mg were administered to normal healthy volunteers (NHVs) to establish the safety and exposure of the compound. This was followed by a study conducted in 6 HCV-infected patients, which assessed single doses of 100 and 500 mg QD and 250 mg BID and a multiple-dose study of 400 and 800 mg BID administered to 7 subjects.[234] However, plasma levels at trough in the 800 mg BID dose group were only threefold higher than the in vitro IC_{50} of 8 nM, and the observed reduction in viral load, 1.5 $\log_{10}$ IU mL^{-1} after 6 days of dosing, was considered to be a modest antiviral effect when compared with contemporary inhibitors. As a consequence, further development of PHX-1766 (**74**) was abandoned.[234]

An interesting variation on the boronic acid motif that has been explored focused on several series of cyclic α-amino oxaborole derivatives, with **75** and **76** as representative examples.[235,236] NS3 inhibitory activity exhibited some sensitivity to the size of the oxaborole ring, with the 6-membered homologue severalfold weaker than the prototypical 5-membered example, although a 7-membered ring largely retained activity; however, substitution of the ring was poorly tolerated.[235] The isoquinoline-based inhibitor **75** inhibited GT-1a NS3 protease with an $IC_{50} = 120$ nM but was poorly active in a replicon system. The binding mode

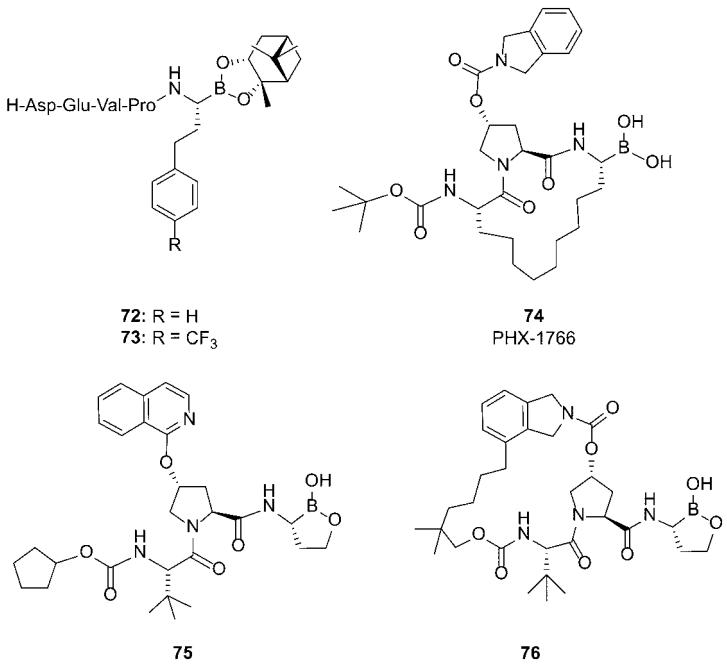

Fig. 21 Boron-based HCV NS3 protease inhibitors **72–76**.

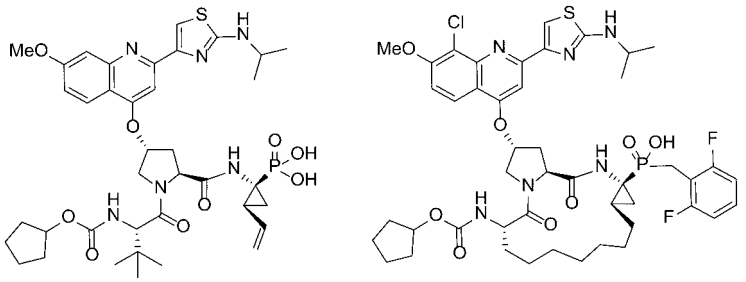

Fig. 22 Phosphorus-based HCV NS3 protease inhibitors **77**–**78**.

was confirmed by an X-ray cocrystal structure that revealed a covalent bond between the boronic acid and the hydroxyl moiety of Ser139 while the intramolecular boron–oxygen bond was cleaved. An X-ray cocrystal of **75** with a Ser139Ala mutant protease revealed a similar overall binding topography, but in this structure, the oxaborole ring remained intact.[235] The formation of the observed adduct with the wild-type enzyme was proposed to proceed by addition of the serine hydroxyl to the cyclic oxaborole followed by hydrolytic cleavage of the ring.[236] This cyclic α-amino oxaborole P1 moiety was subsequently incorporated into more potent macrocycle-based NS3 protease inhibitor chemotypes exemplified by **76**, which hybridizes the boronic acid motif with the macrocyclic ring system found in vaniprevir (**66**). This compound inhibits a GT-1a NS3 protease with an IC_{50} value of 43 nM, displays a binding mode analogous to **75**, and is active in GT-1a and GT-1b replicons with EC_{50} values of 780 and 520 nM, respectively, representing an improvement over the acyclic series.[236] However, these values are several hundredfold weaker than those recorded for vaniprevir (**66**), which was used as the control, $EC_{50} < 1$ nM.

Phosphonic acids are another C-terminus motif that have been probed, designed to take advantage of the observation of product inhibition and interact with the catalytic elements of the protease.[237] This concept was explored initially in the context of the acyclic tripeptide **77**, which inhibited NS3 protease activity with an IC_{50} of 900 nM, threefold more potent than the corresponding carboxylic acid (**Fig. 22**). However, **77** exhibited poor potency in a replicon assay, $EC_{50} = 92$ μM, and further optimization focused initially on structural modifications of the phosphonic acid to a phosphinic acid, designed to allow the introduction of lipophilic moieties that would help mask the overtly acidic polarity.[238,239] Further optimization took advantage of P1–P3 macrocycles and culminated in the identification of GS-9256 (**78**), which inhibited a GT-1b NS3 protease activity with an IC_{50} of 4 nM, exhibited rapid association and slow dissociation kinetics, and was potently active in a replicon, $EC_{50} = 20$ nM.[239,240] The 2,6-difluoro substitution was determined to be important for membrane permeability, while the introduction of the chlorine atom to the P2* isoquinoline heterocycle improved oral bioavailability in the dog to 21%, an eightfold improvement over the unsubstituted congener.[239] GS-9256 (**78**) was advanced into clinical trials where single doses of 150, 300, and 450 mg administered to HCV GT-1-infected subjects were associated with reductions in viremia of 1.8, 2.4, and 2.8 $\log_{10}$ IU mL^{-1}, respectively. However, in a phase 2a clinical trial evaluating GS-9256 (**78**) in combination with an NS5B polymerase inhibitor with and without PEG-IFN-α and ribavirin (**1**), bilirubin elevation was seen in all patients, leading to discontinuation of the compound.[241–243]

An interesting approach to serine protease inhibitor design, discovered originally in the context of trypsin inhibitors, relies upon the incorporation of two metal-binding elements appropriately disposed to combine with the catalytic histidine and serine side chains to create a tetrahedral coordination site that can bind a Zn^{2+} ion.[244–246] This kind of metal-binding motif is presented by *bis*-benzimidazolemethane derivatives, and a library screening campaign identified **79** as a lead inhibitor that inhibited full-length NS3 protease activity with a K_i of 200 nM in the presence of Zn^{2+} ion (**Fig. 23**).[247,248] In the presence of EDTA, which sequesters the

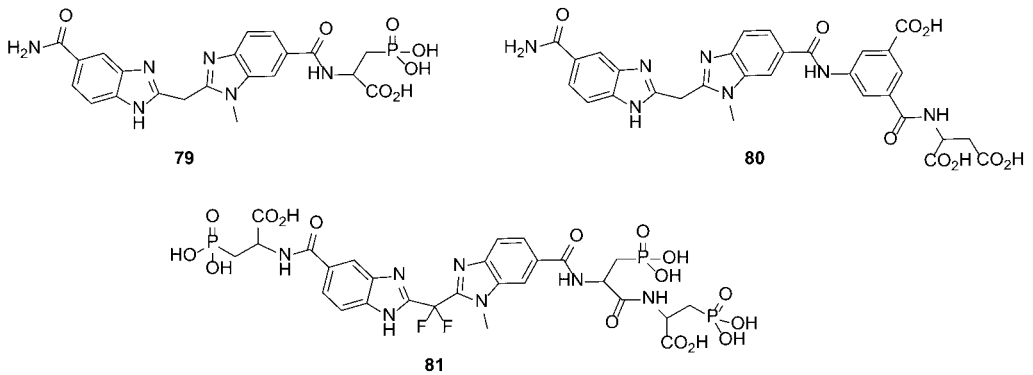

Fig. 23 Zn^{2+}-dependent HCV NS3 protease inhibitors **79**–**81**.

metal, the K_i increased by over 800-fold to 167 μM, providing an index for the effect of stabilization of the complex by the Zn^{2+} ion. Structure–activity studies directed toward finding replacements for the polar phosphonate moiety were only partially successful with **80**, the most potent compound identified from the initial survey, $K_i = 1$ μM in the presence of Zn^{2+}.[247] The highly charged nature of **79** proved to be of importance since partial masking of the charge led to compounds with reduced potency. Polyacidic compounds, exemplified by the tri-phosphonoalanine derivative **81**, which displayed K_i values of 27 nM and 1 μM in the presence and absence of Zn^{2+} ion, respectively, exhibited the optimal potency.[248] These findings appear to reflect the natural substrate selection process, which relies upon multiple acidic residues proximal to the cleavage site, although the SARs developed for this bis-benzimidazolemethane series exhibited some divergence in the presence and absence of Zn^{2+} ion, suggestive of different binding modes dependent on the conditions.

The ring strain associated with a pyrrolidine-5,5-*trans*-lactam presents a chemically reactive carbonyl moiety with some analogy to the well-known β-lactams that interact with serine-containing penicillin-binding proteins.[249] Pyrrolidine-5,5-*trans*-lactams react with serine proteases as mechanism-based inhibitors that engage with the catalytic serine hydroxyl, and the inherent chemical reactivity can readily be modulated by the lactam nitrogen substituent where sulfonylation or acylation enhances electrophilicity.[249] The design of this chemotype was inspired by a family of euphane triterpene-based serine protease inhibitors for which activity is dependent on an unusual trans γ-lactone moiety, with modification to the pyrrolidine-5,5-*trans*-lactam core providing vectors suitable for both derivatization and modulation of carbonyl electrophilicity. This chemical platform has been exploited in the design of inhibitors of a range of mammalian and viral proteases, including HCV NS3.[249–256] In order to identify lead inhibitors of HCV NS3 protease, the amine moiety of **82** (**Fig. 24**) was coupled with a series of carboxylic acid derivatives to provide a library of 200 amides; however, none of these compounds demonstrated significant inhibitory activity, necessitating a more refined analysis of the design priniciples.[250] To improve recognition by the protease, the pyrrolidine amine was acylated with the tetrapeptide Ac-EDVV, which mimics the NS5A-5B cleavage sequence—a modification that gave a time-dependent inhibitor that exhibited a modest IC_{50} of 19 μM after incubation with the enzyme for 18 hours. Systematic SAR studies focused initially on separation of the pyrrolidinone diastereomers, which revealed similar overall inhibitory activity, although the α-isomer was found to react with the protease more rapidly. The next phase of optimization examined truncation of the peptide element to afford **83**, which inhibited NS3 activity with an IC_{50} value of 20 μM after 18 hours of incubation. A cocrystal of **83** with a truncated NS3 protease bound to the NS4A cofactor provided key insights to guide further structural modification, despite being solved at a modest 2.6 Å resolution.[252] It was established that the lactam moiety had reacted covalently with Ser139 and that the ethyl substituent was projecting into the S1 pocket of the enzyme. In addition, the carbamate nitrogen atom was proximal to the carbonyl of Ala157, although beyond H-bonding distance, and the *tert*-butyl moiety was close to the S4 pocket. Further modification focused on optimization of the P1 ethyl group to a spirocyclobutane, while the sulfonyl moiety was replaced with a less electrophilic acyl group. This design exercise afforded **84** as a compound with modest potency in a replicon assay, $EC_{50} = 9$ μM, improved plasma stability, and reasonable clearance in the dog following IV administration.[252,253] Further adjustments were required to more effectively balance the biochemical and replicon properties, affording GW0014 (**85**), which demonstrated an EC_{50} of 1 μM in a replicon, a moderated K_{obs}/I value of 270 $M^{-1}s^{-1}$, and reasonable IV PK in the dog.[255] Although human leukocyte elastase and human cytomegalovirus protease inhibitors derived from this chemotype were developed that exhibited oral bioavailability in the dog, no oral PK data were described for any of the HCV NS3 inhibitors, and more advanced molecules have not been described.[249]

Fragment-based drug design (FBDD) has evolved into an effective strategy for ligand discovery and optimization that relies upon the identification of compact, efficient molecules that bind weakly to specific sites of interest on target proteins.[257,258] This is followed by structural elaboration that, when practiced optimally, takes advantage of insights provided by X-ray crystallographic and isothermal titration calorimetry data in a fashion that allows for the careful optimization of ligands while paying close attention to maintaining a high ligand-binding efficiency index. The application of FBDD to the identification of inhibitors of HCV NS3 activity has provided a compelling example of the power of this approach to identify functionally useful and mechanistically novel molecules that, in this case, act via a unique allosteric mechanism.[259] The screening campaign to identify ligands that bind to NS3

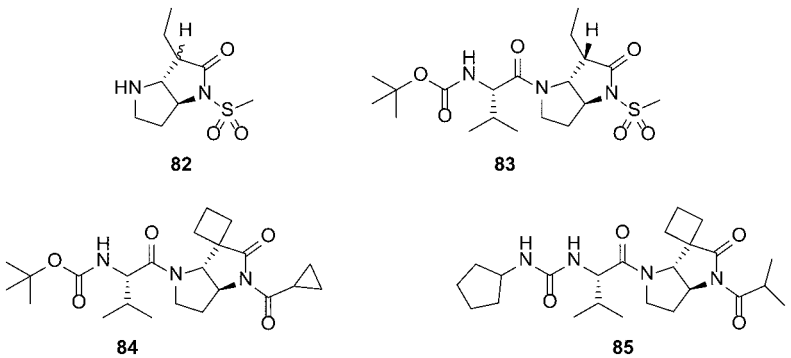

Fig. 24 Pyrrolidine-5,5-*trans*-lactam-based HCV NS3 protease inhibitors **82–85**.

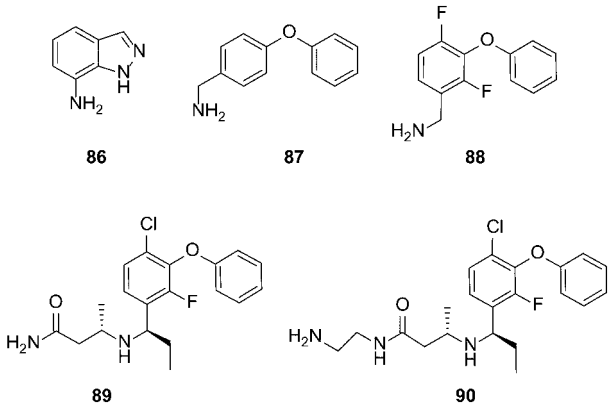

Fig. 25 Optimization of HCV NS3 protease inhibitors **86–90** by fragment-based drug design.

utilized a full-length GT-1b protease/helicase enzyme comprising residues 3–631 with a fragment, residues 21–32, of the NS4A cofactor incorporated at the amino terminus. In this structure, the active site of the protease was occupied by the C-terminus of the helicase domain, a construct that, by definition, would focus on the identification of compounds binding to allosteric sites. Crystals of the NS3 protein construct were soaked for up to 10 days with a total of 176 fragments, presented to the protein as cocktails of 4 compounds that were screened at an individual concentration of 50 mM before the complex was subjected to X-ray crystallographic analysis. Two compounds, **86** and **87**, were found to occupy a hydrophobic site located at the interface of the protease and helicase domains (Fig. 25). These ligands were within van der Waals contact of residues Met485, Val524, Cys525, Glu526, and Val630 from the helicase domain and Val78, Asp79, Arg155, His57, and Asp81 of the protease domain, the latter two residues being functional elements of the catalytic triad. (Note that Arg155, Met485, Val524, and Glu526 are proximal to the region occupied by the typically large P2* element of the more conventional tripeptide-based active site ligands.) Although the indazole **86** showed no significant inhibition of protease activity at a concentration of 5 mM, the benzyl amine **87** weakly inhibited the enzyme, reducing activity by 55% at 500 μM, a result that encouraged further study. Moving the aminomethyl moiety to the *meta* position relative to the ethereal oxygen atom allowed engagement of the acid side chain of Glu628, while the addition the two *ortho* fluorine atoms afforded **88**, which exhibited detectable enzyme inhibition, $IC_{50} = 20$ μM, and represented a favorable increase in ligand efficiency (LE), defined as the log of the IC_{50} value divided by the heavy atom count of the inhibitor, from 0.30 to 0.38 kcal per heavy atom.[259] Further optimization included the introduction of an ethyl substituent at the benzylic position, designed to limit the rotational freedom of the amine-containing side chain, which, in this context, engaged the NS3 protein via H bonds to Glu628, mediated via a bound H_2O molecule, and the carbonyl moiety of Cys525. Elaboration of the phenyl substitution pattern and the amine moiety led to the primary amide **89**, which inhibited NS3 protease activity with an IC_{50} of 100 nM and exhibited promising antiviral activity in a GT-1b replicon, $EC_{50} = 400$ nM. The key interactions between **89** and the full-length NS3 are depicted in Fig. 26, with the primary amide adding to the binding energy and efficiency by engaging the NH of Cys525 and the C=O of Leu517 in H-bonding interactions. The absolute configuration of the CH_3 in the propionamide element was found to be critical, since inversion reduced binding affinity by over 250-fold. Extension of the primary amide of **89** with functionality designed to probe interactions with Asp79, Thr519, and Leu522 gave **90**, which displayed an IC_{50} of < 10 nM, a K_d of 22 nM, and an EC_{50} in a GT-1b replicon of 8 nM.[259]

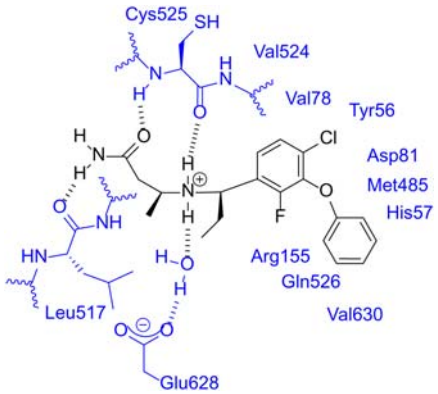

Fig. 26 Key interactions between **89** and the full-length HCV NS3 protein.

Isothermal titration calorimetry data indicated a trend toward reduced conformational flexibility of the protein in the presence of this class of inhibitor, while sedimentation analysis revealed that the NS3 protein populates two conformations in solution, attributed to the closed form observed in the X-ray and an extended, open form in which the helicase C-terminus vacates the protease active site to allow entry of substrate. These data suggested a mode of action in which the compounds interfere with articulation of NS3 between the closed inhibited state and the protease competent open form by stabilizing the auto-inhibited conformation.[259]

Passaging of **89** in increasing drug concentrations for 39 days resulted in the isolation of resistant viruses that upon sequencing revealed Met485Val and Val630Leu mutations in the helicase domain, both of which interact with the phenyl ether ring of the inhibitor. Full-length NS3 protein incorporating these mutations exhibited reduced sensitivity to **89**, with an X-ray cocrystal with the Val630Leu mutant protein clearly demonstrating the effects of the smaller binding pocket that results from the larger side chain presented by the leucine substitution upon inhibitor binding. An analysis of available NS3 sequences indicated 75–96% conservation of identity of the key residues in the binding pocket, suggestive of broad genotype inhibition. This was confirmed experimentally using hybrid proteins incorporating sequences from GT-1a, GT-2a, GT-3a, GT-4, GT-5, and GT-6, which revealed preservation of the activity of **89** toward all but GT-2a, for which inhibition was substantially compromised, and GT-4, where inhibitory activity was modestly reduced. These results are in accord with the sequence differences in the binding pocket, with the Val630Met mutation expressed by GT-2a and the Leu517Phe associated with GT-4 anticipated to compromise inhibitor binding.[259] While **89** offers a unique approach to NS3 protease inhibition and presents an interesting antiviral profile, further studies with this compound have not been described.

The successful development of potent and clinically effective HCV NS3 protease inhibitors offers a compelling example of contemporary drug discovery in which significant advances in the understanding of inhibitor design were based on a combination of developing fundamental structure–activity relationships in conjunction with iterative analyses of X-ray cocrystallographic structures to guide optimization. This class of HCV inhibitor has had a significant impact on HCV drug discovery and development and has taken its place as an important component of therapeutic drug regimens that are curative.

5.18.1.6 HCV NS3 Helicase Inhibitors

The HCV NS3 helicase, which resides in the C-terminus domain of NS3, has proved to be a challenging target for drug discovery, with few well-characterized inhibitors and no clinically relevant compounds described in the literature.[260,261] The HCV helicase is composed of three domains that allows it to traverse RNA or single-stranded DNA from the 3′ to 5′ direction, with energy derived from adenosine triphosphate (ATP) hydrolysis. The role of helicase in HCV replication has not been precisely defined, but it is thought that it may either unwind the duplex RNA formed when the NS5B polymerase duplicates the single-stranded genome or modulate the conformation of viral RNA to facilitate processing by the NS5B RdRp. The helicase is essential for viral replication since mutation of the Asp in the DECH motif, which abrogates ATP hydrolytic function, gave virus incapable of establishing an infection in chimpanzees.[261,262] Inhibitors of the binding of ATP to kinases have proved to be a successful approach to drug discovery, but the ATP-binding site in HCV helicase has been recalcitrant to the identification of potent and selective inhibitors.

A strategy that integrated biophysical and structural approaches was used to characterize and triage low-molecular-weight fragments that bound to a conserved lipophilic pocket in the enzyme.[263] This pocket was identified by a combination of in silico and bioinformatic analyses that initially characterized 8 potential binding sites. After high-throughput screening (HTS) failed to identify an inhibitor lead, a 1000-member fragment library was screened using a saturation transfer difference (STD) NMR assay, which identified an indole-3-acetic acid derivative that bound to the targeted site. An initial round of optimization afforded **91** (**Fig. 27**), an inhibitor of NS3-mediated RNA duplex unwinding with an $IC_{50} = 14\ \mu M$, that was cocrystallized with NS3 helicase in order to characterize the binding mode. The X-ray structure suggested that substitution at the 6-position of the indole ring would be beneficial, a fruitful hypothesis since the 3,5-diaminophenyl derivative **92** was the most potent inhibitor of the series, $IC_{50} = 3\ \mu M$, accompanied by only a modest reduction in ligand efficiency.[263] In the cocrystal structure of **92** bound to helicase, the diaminophenyl moiety projected into solvent, but one of the amines interacted with the backbone carbonyl of Trp501 by donating a H bond, while the 2-methoxy-5-nitrobenzene moiety bound closer to the lipophilic pocket when compared with **91** but still maintained a productive $\pi - \pi$ interaction with Trp501.

Two series of acridones, represented by the optimized compounds **93** and **94**, have been described as HCV helicase inhibitors, with **93** half-maximally inhibiting helicase-mediated unwinding of a double-stranded DNA substrate at a concentration of 8.6 μM, while the IC_{50} value for **94** was 110 μM.[264,265] Both compounds exhibited antiviral activity in a replicon assay, with EC_{50} values of < 1 and 6.7 μM for **93** and **94**, respectively; however, the precise mode of action of these compounds in the cell-based assay remains to be determined.

The symmetrical *bis*-amide **95** inhibits HCV helicase-mediated strand separation of both RNA and DNA duplexes with IC_{50} values ranging from 0.7 to 5 μM but lacked virus selectivity, also inhibiting helicases from dengue virus, Japanese encephalitis virus, and humans.[266,267] SARs indicated the importance of the benzimidazole NH and the phenyl ring at the two position, while mechanistic studies suggested that **95** inhibits helicase-mediated ATP hydrolysis by competing with RNA binding to the protein.[266,267]

HCV NS3 helicase inhibitor design has been challenging, and the molecules that have been described to date that interfere with the function of this enzyme lack inherent intrinsic potency. Thus, the potential of this approach as an antiviral strategy remains unfulfilled.

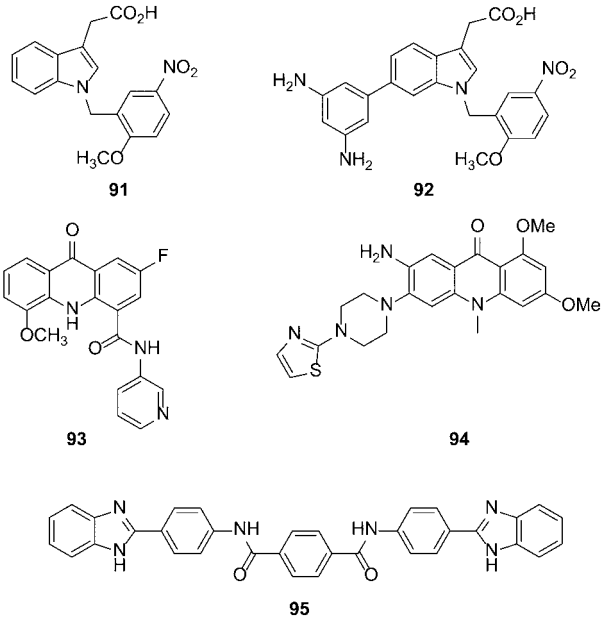

Fig. 27 HCV NS3 helicase inhibitors **91**–**95**.

5.18.1.7 HCV NS4A Inhibitors

The HCV NS4A protein is a 54-residue cofactor for NS3 that catalyzes protease activity by increasing the K_{cat} and K_{cat}/K_m and promotes the binding of peptide-based inhibitors.[268,269] Inhibitors of NS4A function have been identified using replicon-based screening, with the acylated thiourea derivative ACH-806 (GS-9132, **96**) an optimized molecule that was advanced into clinical trials.[270–273] ACH-806 (**96**) is a potent inhibitor of HCV replication in GT-1a and GT-1b replicons, EC_{50} values = 10–50 nM that does not directly inhibit NS3 protease and interacts synergistically with protease and polymerase inhibitors.[270,271] The selection of replicons resistant to ACH-806 (**96**) led to the isolation of cell lines with EC_{50} values 10- to 20-fold higher than for the wild-type parent, with Cys16Ser and Ala39Val mutations in NS3 shown to confer 12- to 14-fold resistance when reverse engineered into replicons. These replicons retained replicative capacity comparable with wild-type and remained sensitive to a direct inhibitor of protease and both a nucleoside and nonnucleoside NS5B polymerase inhibitor. The mutations mapped to the amino terminus of NS3 and these residues are in close contact (4.1–7.3 Å) with NS4A. In more detailed mechanism of action studies, ACH-806 (**96**) had no effect on polyprotein processing or NS5B polymerase activity but reduced the amount of NS3 and NS4A in replicons, attributed to an accelerated degradation that resulted in an altered composition of the replication complex.[272,273] ACH-806 (**96**) treatment led to the appearance of a 14 kDa protein determined to be a dimer of NS4A, while an analog containing an azide photoaffinity element selectively labeled NS4A. These observations were interpreted as a scenario in which ACH-806 (**96**) binds to NS4A to promote dimer formation, thereby reducing its association with NS3 and compromising protease function and leading to the degradation of both proteins and the formation of defective replication complexes. The antiviral activity of ACH-806 (**96**) was determined to be dependent on the presence of the thiourea moiety since comparison of a matched thiourea/urea pair revealed the latter to be inactive, although NS4A dimer association did not appear to rely upon the formation of a disulfide bond.[272]

ACH-806 (**96**) was advanced into clinical trials where a dose of 300 mg BID was administered to 10 GT-1-infected subjects for 5 days in a proof-of-concept study.[272] A reduction in viremia was detected by day 2 and all patients experienced a >0.5 $\log_{10}$IU mL^{-1} decline in viral load by day 5, with a mean change of -0.91 $\log_{10}$IU mL^{-1}. However, reversible kidney toxicity was observed in this study, detected by increased creatinine levels in treated subjects and attributed to renal tubular dysfunction, toxicity concerns that prevented further development of the compound, which was terminated in Feb. 2007.[272]

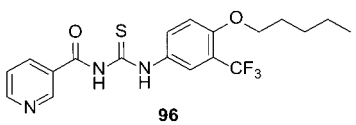

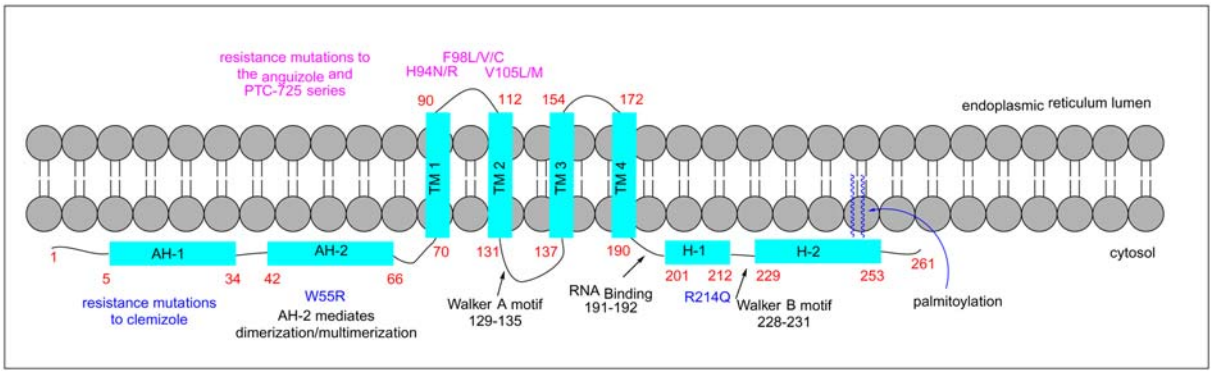

Fig. 28 Topology of the HCV NS4B protein with demarcation of the transmembrane domains in accord with Gouttenoire et al.[274] Key residues are noted, including those associated with resistance to small-molecule inhibitors.

5.18.1.8 HCV NS4B Inhibitors

HCV NS4B is a hydrophobic 261-residue protein whose integration into the endoplasmic reticulum (ER) membrane is predicted by four putative transmembrane domains located in the central region of the protein, with a topology that projects the N- and C-terminal regions toward the cytosol (Fig. 28).[274–277] More recent studies suggest that the N-terminus can translocate to the endoplasmic reticulum (ER) lumen, while the precise location of the transmembrane domain boundaries is not clear, with those shown in Fig. 28 based on those proposed in a review article.[274] NS4B is a critical component of the HCV replication complex that appears to oligomerize and has been shown to induce the formation of the membranous web that acts as a platform for viral replication. It associates with the viral nonstructural proteins and viral RNA in the replication complex as well as with several host cell proteins.[274–278] NS4B appears to express enzymatic activity, binding to and hydrolyzing both ATP and guanosine triphosphate (GTP) as well as catalyzing the formation of ATP and adenosine monophosphate (AMP) from two molecules of adenosine diphosphate (ADP), described as an adenylate kinase activity.[279] However, the enigmatic role(s) of NS4B in virus replication initially limited the utility of specific biochemical assays designed to identify lead inhibitors, directing screening campaigns toward a phenotypic approach. The seminal description of such a strategy identified leads by using a cell line expressing NS4B to screen for compounds capable of reversing its antiapoptotic activity, with hits triaged by discarding those that induced death in cells not expressing NS4B.[280] Several active series were identified that were confirmed to bind to purified NS4B using an assay that evaluated quenching of the fluorescence of tryptophan residues upon compound association, with measured K_d values ranging from 0.31 to 10 μM. The profile of the triazino[5,6-*b*]indole **97** (Fig. 29), one of 12 examples of this chemotype disclosed, was examined in some detail, demonstrating antiviral activity in an HCV GT-1b replicon with an EC_{50} value of 1.13 μM. Resistance mapped to Lys52Arg, Gly120Val, and Ala210Ser in the NS4B protein, although these were not confirmed by reverse engineering the mutations into replicons.[278,280] Several aminothiophenes related to **98**, EC_{50} = 700 nM, were also claimed but it was the pyrazolopyrimidine anguizole (**99**), EC_{50} = 630 nM, that attracted further attention.[280–284]

Initial studies related to anguizole (**99**) focused on a modified imidazo[1,2-*a*]pyridine core, with optimization designed to enhance potency and divest of the problematic furan and thiophene rings that can be associated with metabolic activation.[282] A critical element for enhancing potency was the presence of a H-bond acceptor in the amide moiety, fulfilled by the piperazinamide carbonyl in **100**, a potent inhibitor of GT-1a and GT-1b replication in replicons, EC_{50} values = 0.81 and 5.4 nM, respectively.[282] The *trans*-hydroxyl substituent of **100** (Fig. 30) was introduced to the cyclohexane ring to improve metabolic stability, inspired by biotransformation studies of the parent unsubstituted cyclohexane that indicated this to be a metabolic hot spot. Resistance mapping for earlier compounds in the series had identified His94Asn/Arg, Phe98Leu, and Val105Leu/Met in NS4B as mutations conferring reduced sensitivity to inhibition, and **100** was 5- to 160-fold less active in stable and transiently transfected replicons incorporating the individual changes, although mutations associated with resistance to NS3, NS5A, and NS5B inhibitors remained

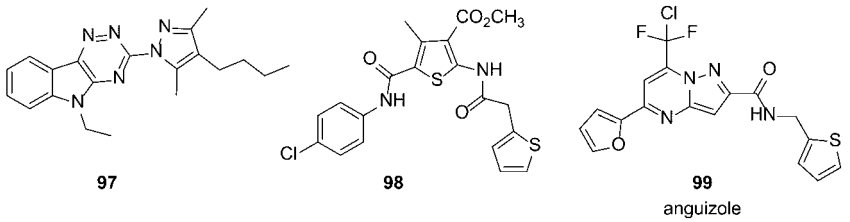

Fig. 29 HCV NS4B inhibitors **97**–**99**.

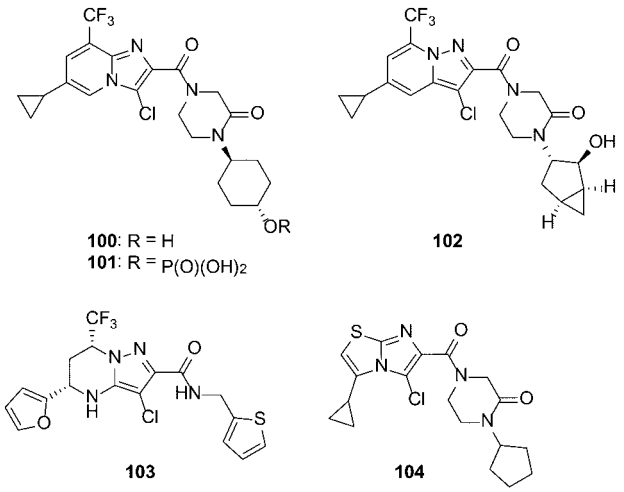

Fig. 30 HCV NS4B inhibitors **100–104**.

fully sensitive. All of these mutations reside in the endoplasmic reticulum lumen-facing loop located between transmembrane (TM) domains I and II (Fig. 28), dependent on the precise boundaries of transmembrane domain I (*vide infra*).[274] Of particular note, residue 94 of NS4B of wild-type GT-2a virus is Thr, while both residues 98 and 105 are Leu, providing a potential explanation for the poor antiviral activity toward this genotype.

Although **100** demonstrated good oral exposure in rats and dogs following a 5 mg kg^{-1} dose, higher doses failed to achieve the exposure margins required by safety studies, despite the evaluation of several formulations.[282,283] This problem was successfully addressed by the phosphate prodrug **101,** which was used to establish efficacy in the PXB mouse model of GT-1a HCV infection. In this model, oral doses of 10 and 30 mg kg^{-1} of **101** administered on a BID schedule for 7 days were associated with a reduction in viremia of 4 $\log_{10}$ IU mL^{-1} by day 4, superior to a clinically effective NS5B inhibitor used as the control.[283,284] However, a 7-day toxicological evaluation of **101** in rats revealed an adverse cardiovascular finding that led to termination of the compound, providing a clear focus for the profile of a replacement compound. An initial survey probed the effect of isosteric variation of the core heterocycle using a binding assay that was developed with a tritiated NS4B inhibitor from an earlier series, with inhibitory activity confirmed in a GT-1b replicon.[282,283] After consideration of the lipophilic ligand efficiency and binding efficiency index of lead inhibitors, a pyrazolo[1,5-*a*]pyridine core was selected as a vehicle that offered the optimum combination of physical and antiviral properties.[283–286] Variation in the amide terminus modulated lipophilicity, antiviral activity, and PK properties from which **102** was identified as a compound meeting the targeted profile.[283] The binding of **102** to NS4B and the antiviral activity in replicons were found to be quite sensitive to the configuration of the [3.1.0]bicyclohexanol moiety. In GT-1a and GT-1b replicons, the EC_{50} values recorded for **102** were 0.6 and 0.3 nM, respectively, and 5 and 38 nM for GT-1b replicons harboring His94Asn and Val105Met mutations, respectively. PK studies with **102** revealed low to moderate clearance in the mouse, rat, dog, and cynomolgus monkey and >90% oral bioavailability, with exposure margins for safety evaluation achieved without resort to a prodrug moiety. In a humanized mouse model of HCV infection in which **102** was administered over 7 days, viremia declined by 3 $\log_{10}$ IU mL^{-1}, but sequencing of virus at the end of the dosing period revealed several resistance mutations in the NS4B protein including Asn56Ile and Asn99His, which had not been observed with in vitro studies. While the overall profile of **102** appears to be encouraging, the fate of the molecule has not been disclosed.

A high-throughput screen using a GT-1b replicon identified the racemate of AP80978 (**103**) as an HCV inhibitor with an EC_{50} of 1.78 μM that was resolved by chiral chromatography to identify the active species shown, EC_{50} = 0.63 μM, with the absolute configuration determined by analysis of a single crystal X-ray structure.[287] This compound bears a significant structural resemblance to anguizole (**99**) and exhibits a similar antiviral profile, with poor activity toward a GT-2a replicon (EC_{50} > 25 μM) and resistance mapping to Phe98Val and Phe98Leu mutations in NS4B that increase EC_{50} values to >20 μM.

The imidazo[1,2-*a*]pyridine-based NS4B inhibitor **100** provided inspiration for the design of a series of imidazo[2,1-*b*]thiazole derivatives giving rise to **104**, which half-maximally inhibited a GT-1b replicon at a concentration of 16 nM.[288] This compound was profiled in transient replicons harboring single mutations in NS4B known to confer resistance to anguizole-like compounds, with His94Arg (EC_{50} = 4 μM), Phe98Cys (EC_{50} = 27.1 μM), and Val105Met (EC_{50} = 27.3 μM) all showing significantly reduced sensitivity. However, mutations in the amino (His3Arg, EC_{50} = 1.1 μM) and carboxy (Gln26Arg, EC_{50} = 350 nM) termini of NS4B also compromised the potency of **104**. Replicons with mutations associated with resistance to NS3, NS5A, and NS5B inhibitors remained sensitive, and combination studies between **104** and representatives of these mechanistically different HCV inhibitors revealed synergistic antiviral interactions.[288]

The precise mode of action of anguizole (**99**) and related compounds remains obscure, although studies have revealed an inhibitory effect of the compound on vesicle aggregation induced by a peptide derived from the NS4B AH2 domain.[281,290] This observation was attributed to interference of anguizole (**99**) with the AH2 of the full-length protein associating with the membrane,

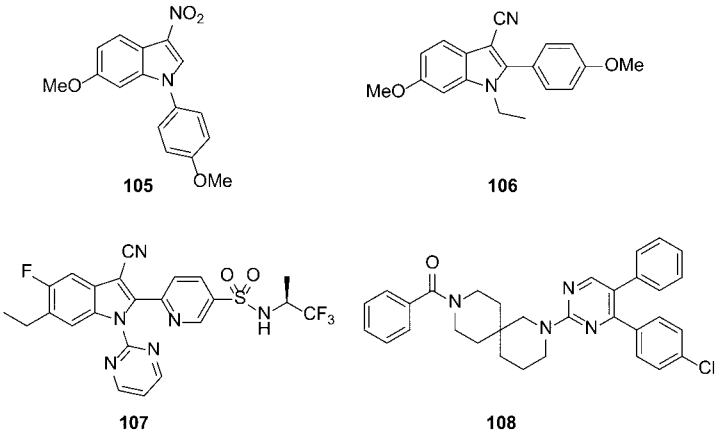

Fig. 31 HCV NS4B inhibitors **105–108**.

but no effect was observed on the multimerization of NS4B. However, more recent studies conducted in cell-based settings have provided evidence that the AH2 domain of NS4B is a mediator of both multimerization and the correct subcellular localization of the protein, in addition to an interaction with NS5A, and that anguizole (**99**) interferes with all of these events.[291]

Another series of NS4B inhibitors originated with the indole **105** (Fig. 31), identified as a weakly potent inhibitor of HCV replication in a GT-1b replicon, $EC_{50} = 50$ μM, that was optimized to **106**, $EC_{50} = 4.1$ μM, after an initial survey of SARs.[292] A refined and more potent compound was used to probe the mode of action by developing resistant virus, which mapped to a Phe98Cys change in NS4B. These studies facilitated the identification of PTC-725 (**107**) as an advanced molecule with moderate oral bioavailability in mice, rats, dogs, and cynomolgus monkeys and liver to plasma ratios of 15 in mice and 23 in rats.[293–296] This compound inhibits GT-1a and GT-1b replicons with EC_{50} values of 7 and 1.7 nM, respectively, but is much less potent toward JFH1 GT-2a infectious virus, $EC_{50} = 2.2$ μM.[296] More detailed resistance mapping studies confirmed Phe98Cys and also identified Phe98Leu and Vla105Leu, along with His94Arg, as sensitivity determinants for **107**, data that were rationalized based on these residues being present in transmembrane domain I and localized proximally on the same face of a helical wheel representation of residues 93–109.[296] Interestingly, immunofluorescence studies indicated that PTC-725 (**107**) did not affect subcellular localization of NS4B in replicons.

Using a radioligand displacement assay that monitored the association of a tritiated NS4B inhibitor related to **100** to purified GT-1b protein immobilized on resin via an FLAG–His-tagged sequence, 28 DNA-encoded combinatorial libraries of small molecules were screened in an effort to identify structurally novel binders that might offer the potential to be optimized into compounds demonstrating inhibitory activity toward GT-2a virus.[297] A chemotype based on a 2,9-diazaspiro[5.5]undecane core was identified that after several cycles of optimization resulted in the characterization of GSK0109 (**108**), which displayed a K_i of 46 nM in the biochemical assay and was active in a GT-1b replicon, $EC_{50} = 20$ nM. Although this molecule exhibited more modest activity in GT-1a ($EC_{50} = 803$ nM) and transient GT-3a, GT-4a, and GT-5a replicons, it showed no significant activity toward two GT-2a transient replicons at concentrations of 10 μM. As a result of this profile, which is analogous to the anguizole-based series of inhibitors, this chemotype was not pursued further.[297]

The piperazinone **109** (Fig. 32) is representative of another class of NS4B inhibitor that was optimized from a screening lead discovered using a GT-1b replicon assay.[298] Compound **109** is a potent antiviral agent, exhibiting EC_{90} values of 22 and 6 nM

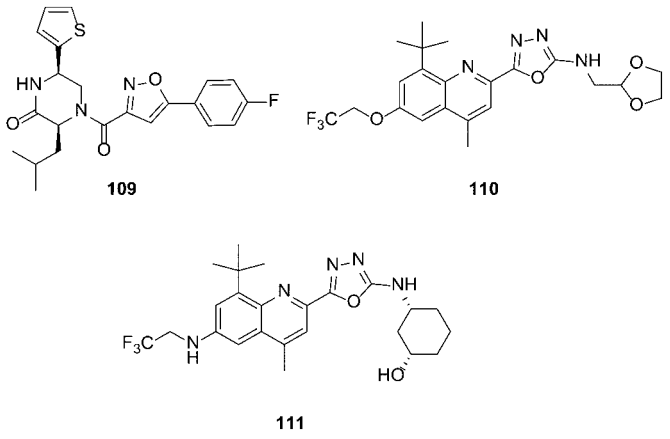

Fig. 32 HCV NS4B inhibitors **109–111**.

in GT-1a and GT-1b replicons, respectively.[298] While specific resistance mapping studies were not conducted, this compound was inactive in a GT-2a replicon, although a Leu98Phe mutation partially restored sensitivity to an analog in the series. However, the antiviral profile fell short of the sought-after pan-genotypic inhibitor, resulting in diminished interest in further pursuit of the chemotype.

The absence of GT-2a activity with NS4B inhibitors provided a key focal point for the optimization of a series of quinolone-based compounds derived from the early lead **110,** which inhibits GT-1a and GT-1b replicons with EC_{50} values of 0.9 and 1.3 nM, respectively.[299] This compound binds to NS4B with a K_d of 31 nM; retains activity toward a GT-1b His94Asn mutant virus, $EC_{50} = 54$ nM; and exhibits modest potency in a GT-2a replicon, $EC_{50} = 3.6$ μM. Optimization studies sought to reduce the Log *D* to 3.5 while improving GT-2a inhibition on the path to a goal of achieving a lipophilic ligand efficiency (LLE; pIC_{50}—Log *D*) value of 4.5 using a screening tier that evaluated activity in GT-1a, GT-1b, GT-1b His94Asn, and GT-2a replicon assays. The *tert*-butyl substituent in **110** improved potency in GT-1b and GT-2a replicons by fourfold compared with the CF_3 analog, while systematic exploration of the SAR associated with the amide moiety arrived at **111** as a potent GT-1a and GT-1b inhibitor, EC_{50} values = 0.08 and 0.10 nM, respectively. This compound was inhibitory toward the His94Asn/Ser mutants and GT-2b and GT-4a viruses while inhibiting GT-2a JFH, GT-3a, and GT-6a replicons with EC_{50} values of 3.0–3.7 nM.[299] While the antiviral properties and preliminary PK profile of **111** in rats appear to be promising, further studies with **111** have not been forthcoming.

An analysis of HCV NS4B binding to RNA using a microfluidic affinity assay demonstrated an associative interaction, $K_d = 3.4$ nM, corroborated using an RNA filter binding assay with recombinant NS4B protein.[300] The interacting elements were mapped to the 3′-terminus of negative strand viral RNA and to an arginine-rich motif located in the last 71 residues of the C-terminus of NS4B that projects from the cytosolic side of the membrane. The microfluidic affinity assay offered a screening capability with which to identify potential inhibitors of the NS4B–RNA interaction, with 104 active hits identified from a library of 1280 compounds and 110 compounds that showed some discordance between replicate experiments.[300–302] These 214 compounds were tested at a lower concentration in a secondary assay, a triage that left 18 confirmed hits of which 5 demonstrated specificity for NS4B and were evaluated in replicons. This screening cascade distilled the hits to the histamine H_1 receptor antagonist clemizole (**112**) as an inhibitor of GT-1b replication, $EC_{50} = 8$ μM, with activity extending to GT-2a infectious virus. Resistance mapping using the GT-1b replicon identified Trp55Arg and Arg214Gln mutations in NS4B that reduced potency by 2.25- and fivefold, respectively. The Trp55Arg protein demonstrated a fourfold increased affinity for RNA ($K_d = 0.75$ nM) comparable to the Arg214Gln mutant where the K_d was determined to be 0.6 nM, providing an understanding of the mode of resistance.[300–302] Clemizole (**112**) exhibited a synergistic interaction with the NS3 protease inhibitors telaprevir (**2**) and boceprevir (**3**) and was additive in conjunction with ribavirin (**1**), PEG-IFN-α, and both a nucleoside and a nonnucleoside NS5B polymerase inhibitor.[302] A clinical trial in subjects chronically infected with HCV and naive to therapy was conducted between July 2009 and Aug. 2010 but the results have not been disclosed.[303]

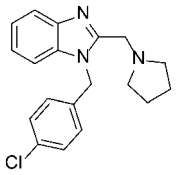

112

Screening leads for which resistance maps to the NS4B protein have been optimized into compounds demonstrating impressively potent antiviral activity in replicons. However, despite the expenditure of considerable effort that has led to several compounds being evaluated in advanced preclinical studies, there are no examples of NS4B inhibitors that have demonstrated clinical efficacy and the full potential of this class of antiviral agent remains to be determined.

5.18.1.9 HCV NS5A Inhibitors

HCV NS5A inhibitors are characterized by remarkable potency in cell-based assays where refined compounds typically express subnanomolar EC_{50} values toward a broad range of genotypes, and this class has assumed prominence as an important component of clinically effective drug combination regimens.[304–312] Despite this, the precise mode of action of NS5A inhibitors remains enigmatic since the protein does not express enzymatic activity. However, NS5A is critically involved in both virus replication and assembly and also plays a key role in modulating the host cell environment to favor the virus, leading to its designation as a master regulator protein.[313–317] The NS5A protein is structurally organized into three domains, with domain I incorporating an amphipathic helix (residues 5–25) that mediates association with the membrane and a Zn^{2+}-binding motif (**Fig. 33**). Protein constructs derived from domain I crystallize as dimers, with one interfacial arrangement forming a U-shaped domain in which the interior is rich in basic amino acids, leading to the proposal that this motif binds RNA, although all three domains appear to be involved in viral RNA recognition.[318–323] Concordant with the crystal structural data, NS5A dimerization has been shown to be important for virus replication in vitro.[324] Domain I contains a segment that binds to NS5B, while the 4 serine residues that are subject to phosphorylation, including the conserved Ser222, reside in the segment intervening between domains I and II. Phosphorylation of NS5A has been proposed as a mechanism to regulate the activities of the protein at different stages of the virus life cycle,

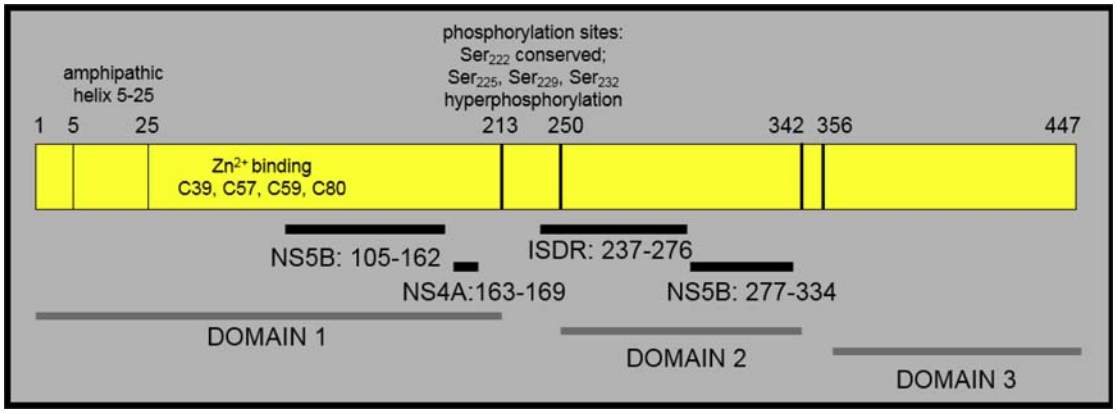

Fig. 33 Structural organization of the HCV NS5A protein, with protein interaction sites and residues that are phosphorylated noted. ISDR = interferon sensitivity-determining region.

with the basally phosphorylated protein (referred to as P56) involved in replication. Hyperphosphorylation (to generate P58) may disrupt this function and the lipid kinase phosphatidylinositol 4-kinase IIIα has been implicated as playing an important role in this respect.[325–328] Domain II contains a second sequence that interacts with NS5B and a region that is believed to be involved in countering the effects of interferon on the host cell, although this function is somewhat controversial.[329–334] Domain III contributes to HCV replication but is also associated with an essential role in virion assembly.[77,335,336]

The initial disclosure of HCV inhibitors for which resistance mapped to the NS5A protein claimed a series of C-5-arylated iminothiazolidinones.[44,45,337] These compounds were discovered using a dual-replicon assay screen format that evaluated for inhibition of HCV and bovine viral diarrhea virus (BVDV) in a single well with host cell cytotoxicity also determined, allowing for a rapid and rigorous triaging of hit compounds. The prototype lead, BMS-858 (**113**), inhibited a wild-type GT-1b replicon with an EC_{50} value of 0.5 μM ($CC_{50} > 5$ μM) while the homologue BMS-824 (**114**) was 100-fold more potent ($EC_{50} = 5$ nM) (Fig. 34).[45,337] Resistance mapping with BMS-858 (**113**) identified a Tyr93His change in the NS5A protein that conferred at least 10-fold reduced sensitivity that was amplified with BMS-824 (**114**) for which the EC_{50} value was > 5 μM, representing greater than 1000-fold reduction in inhibitory activity. Studies with BMS-824 (**114**) identified additional mutations in NS5A associated with resistance, mapped to Leu31Val (60x) and Gln54Leu (9x) changes, with the combination 354-fold less sensitive to the inhibitory effect of the compound.[45] Additional studies revealed that BMS-824 (**114**) exhibited poor inhibition of a GT-1a replicon ($EC_{50} > 5$ μM), while evaluation of GT-1a/1b hybrid replicons confirmed that sensitivity mapped to the N-terminus of NS5A. These NS5A inhibitors altered the phosphorylation state of NS5A, preventing the formation of the P58 hyperphosphorylated form without affecting its stability—a profile that was, interestingly, mimicked by a NS3 protease inhibitor but not an inhibitor of the NS5B RdRp.

The exploratory optimization of this series of NS5A inhibitors took an interesting turn when it was discovered that BMS-824 (**114**) was chemically unstable, completely degrading under the assay conditions but, remarkably, without a significant effect on the potency of replicon inhibition.[338–340] Detailed studies using a biogram-based analysis of extracted fractions of compound that had been incubated in cell culture assay medium for 48 hours identified several degradation products, with two high-molecular-weight species equating with potent replicon inhibition.[339] These compounds were determined to be dimers (**115**) using spectroscopic methodologies that established the connectivity to be at C-5 of the iminothiazolidinone heterocycle.[339] A

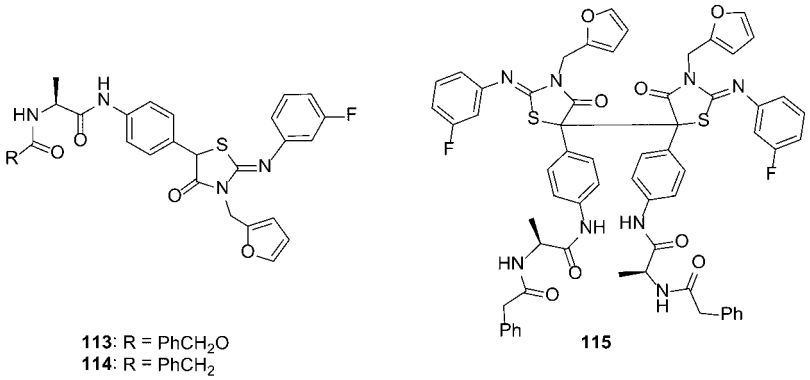

Fig. 34 HCV NS5A inhibitors **113–115**.

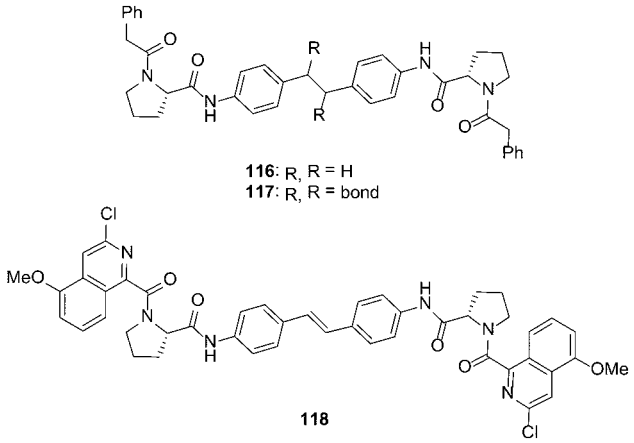

Fig. 35 Dimeric HCV NS5A inhibitors **116–118**.

radical-mediated mechanism of dimerization was proposed that was attributed to an initial abstraction of the C-5 H-atom by molecular oxygen, which is a diradical in the ground state, with the resultant radical stabilized by the captodative properties of the C-5 methine substituents.[340,341] Based on the somewhat nebulous SARs associated with the iminothiazolidinone *N*-substituents in contrast to the precise requirement exhibited by the amino acid moiety, which was restricted to alanine and proline and was highly sensitive to absolute configuration, it was hypothesized that the inhibitory pharmacophore was defined by the bibenzyl **116**.[340] This compound demonstrated an EC_{50} value of 30 nM in the GT-1b replicon, while the more planar, unsaturated stilbene precursor **117** (Fig. 35) was almost 350-fold more potent, $EC_{50} = 86$ pM. Confirmation that **116** and **117** preserved the NS5A-inhibiting activity of the original lead molecules was obtained by testing **117** in the GT-1b Tyr93His mutant replicon where the EC_{50} value was determined to be more than 10,000-fold higher at 4 μM.[338,340] The symmetry inherent to this pharmacophore elegantly complemented that subsequently observed in the crystal structures of the domain I proteins and the observation that HCV replication depends upon NS5A dimerization.[318–320,324]

While **117** was a potent inhibitor of GT-1b replication, the compound was inactive toward a GT-1a replicon, necessitating further structural manipulation in order to broaden the antiviral spectrum. These studies sought to concomitantly address the liabilities associated with the stilbene moiety, which offered the complication of facile *cis–trans* isomerization, and the embedded anilines, where concern revolved around the possible safety issues associated with the potential for unmasking to occur in vivo. Optimization was broad-based and studied the effects on structural manipulation of both the stilbene core, viewed as a scaffold on which to deploy the peripheral structural elements, and the phenylacetic acid moiety, which was determined to be a critical and sensitive modulator of potency.[338,342–346] The key breakthrough in expanding the genotype inhibition to encompass GT-1a was made with the synthesis and profiling of the isoquinolinamide **118**, a balanced inhibitor with EC_{50} values of 19 and 7 nM toward GT-1a and GT-1b replicons, respectively.[344] This discovery inspired an examination of α-substituted phenylacetic acid derivatives, with the substituents designed to mimic the H-bond-accepting capability of the isoquinoline heteroatom while also relaxing the conformational constraint imposed by the fused heterocyclic ring system. A series of mandelic acids productively probed the installation of an α-hydroxyl substituent but it was dimethylamine and methylcarbamate moieties that emerged as the preferred elements. These substituents conferred broad genotype inhibition when examined in the context of the alkynes **119** (Fig. 36), which exhibited EC_{50} values of ~8 and <4.6 nM toward GT-1a and GT-1b replicons, respectively, and **120**, which displayed EC_{50} values of 26 and 0.013 nM toward GT-1a and GT-1b, replicons, respectively.[343–345] The potentially problematic anilide moiety was addressed by replacing it with a benzimidazole heterocycle, as in **121**, which preserved the H-bond acceptor and donor properties but modified the topological presentation of the terminal phenylglycine moieties.[346] This change compromised potency, particularly toward GT-1a, $EC_{50} = 108$ nM, although potent GT-1b inhibition was maintained, $EC_{50} = 0.055$ nM. The final steps that culminated in the discovery of daclatasvir (**7**) involved replacing the diphenyl alkyne core of **121** with a biphenyl moiety, which recapitulates the linear topology, accompanied by deannelation of the benzimidazole ring to compensate for the reduced distance between the termini, affording **122**. These modifications produced a potent and balanced inhibitor of GT-1a and GT-1b replicons, $EC_{50} = 28$ and 6.7 pM, respectively, but **122** demonstrated poor oral bioavailability in rats, prompting truncation of the phenyl ring to an isopropyl moiety, explored in the context of the D-valine derivative **123**. However, this structural change had a dramatically deleterious effect on inhibition of both HCV genotype replicons, with EC_{50} values of 1.24 μM and 1.22 nM toward GT-1a and GT-1b, respectively.[347] This was addressed with a final structural adjustment, inverting the stereo-configuration of the valine moiety of **123** to that of the natural amino acid, which afforded daclatasvir (**7**) as a potent HCV inhibitor that demonstrated antiviral activity toward a broad range of genotypes in replicons and also inhibited replicating GT-2a virus.[46,338,347]

The initial clinical study with daclatasvir (**7**) evaluated single oral doses of 1, 10, and 100 mg in GT-1-infected patients and revealed a significant reduction in viremia at all dose levels.[46,63] Notably, the decline in viral load was more rapid than had been observed with either HCV NS3 protease or NS5B RdRp inhibitors, subsequently attributed to an inhibitory effect of daclatasvir

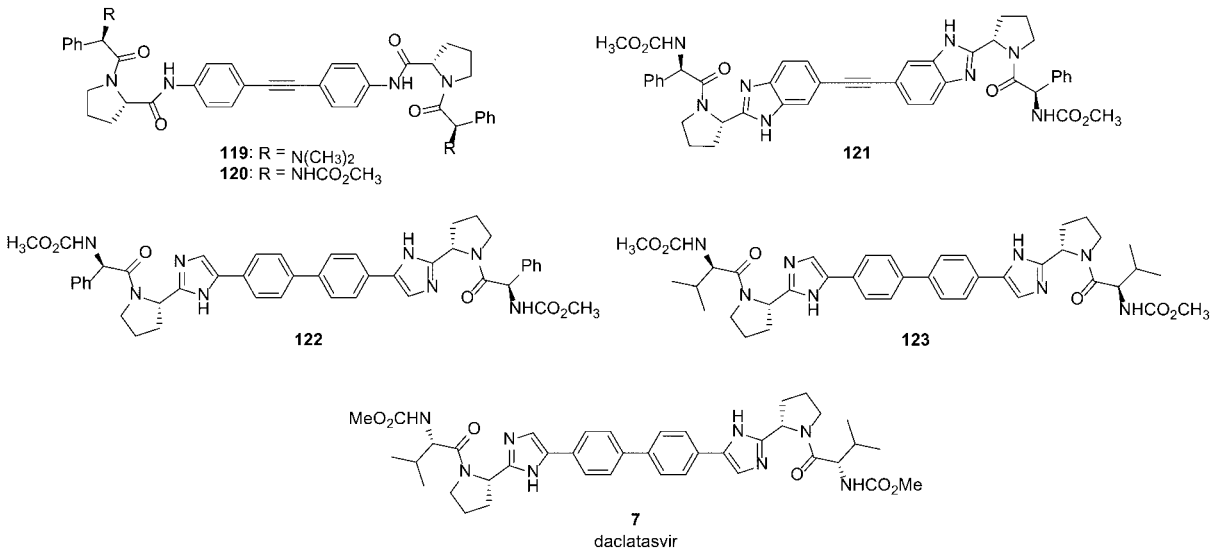

Fig. 36 Symmetrically dimeric HCV NS5A inhibitors **119–123**, precursors to daclatasvir (**7**).

(7) on virion assembly and/or production in addition to interfering with virus replication.[348] This effect was not detectable in the initial replicon screen but was subsequently observed in studies of replicating virus and indicates that although daclatasvir (7) appears to act by binding to domain I of NS5A, the interaction compromises the activity of the protein in virion assembly.[349,350] A careful analysis of the clinical data led to a revision of the half-life of the virus in plasma to approximately 45 minutes, significantly lower than the 2.7 hours originally estimated.[52,348]

Evidence of the binding of NS5A inhibitors to the protein was probed with the biotinylated compounds **124** and **125** and the photoaffinity probes **126** and **127**.[46,350–352] The biotin derivative **124**, based on natural proline, inhibited HCV GT-1b replication in a replicon with an EC_{50} value ranging from 33 to 150 nM, an activity that was sensitive to the Tyr93His mutation, $EC_{50} \geq 10$ μM.[46,338,350,352] The (*R*,*R*)-isomer **125** is inactive, $EC_{50} > 10$ μM, SARs that mirror that of symmetrical NS5A inhibitors.[46,352] An attempted pull-down experiment using **124** in which GT-1b replicons were lysed, incubated with the probe, and then passed over streptavidin beads failed to enrich a bound protein. However, when **124** was incubated in GT-1b replicons for 18 hours before passing the cell lysate over streptavidin beads, HCV NS5A was selectively pulled down, while the inactive diastereomer **125** was ineffective. This indicates that the association of **124** with NS5A occurs during formation of the replication complex. Most intriguingly, when **124** was incubated in replicons harboring the Tyr93His resistance mutation, NS5A protein was still enriched in pull-down experiments. This observation indicated that resistance mutations do not lead to exclusion of the inhibitor from the binding site but rather that the NS5A protein appears to be capable of restoring function in the presence of a bound molecule.[352] Direct binding of daclatasvir (7) to the NS5A protein has been demonstrated using an in vitro microscale thermophoresis assay, which indicated that drug binding prevented the association of the protein with RNA, while ledipasvir (8) has also been shown to bind to NS5A protein.[349,353] Binding models for the interaction of NS5A inhibitors with the dimeric form of the protein have been proposed based on an analysis of structure–target interactions, the location of resistance mutations, and structure–activity relationships associated with the core and proline elements, which are thought to be proximal to Leu31 and Gln54, while the valine cap moiety is believed to associate with Tyr93.[352–355] Although the symmetry of daclatasvir (7) complements that of the crystal structure of domain I of NS5A, symmetry is not required and unsymmetrical binding modes have also been contemplated.[354] Interestingly, and in contrast to the results with the biotin derivative **124** (Fig. 37), in the

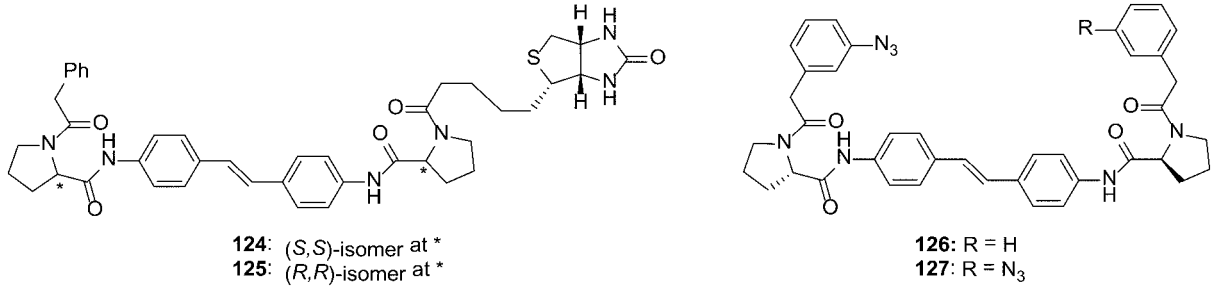

Fig. 37 HCV NS5A biotin-based and photoaffinity probes **124–127**.

microscale thermophoresis assay, daclatasvir (**7**) binds less effectively to NS5A protein incorporating Leu31Val and Tyr93His mutations, while ledipasvir (**8**) has been shown to bind less effectively to protein incorporating a Tyr93His mutation.[349,353] Studies with the photoaffinity probes **126** and **127**, EC_{50} values of 7 and 55 nM toward GT-1b replicons, respectively, provided additional insight into drug–target interactions: Photolysis of the monoazide **126** in replicons selectively labeled NS5A, whereas a similar experiment conducted with the symmetrical homologue **127** resulted in the labeling of bands corresponding to both dimers and to higher-order multimers, indicative of a more complex drug–target interaction.[352] Using NS5A fluorescently labeled at either the N- or C-terminus, active inhibitors have been shown to disrupt the intramolecular and intermolecular proximity of both domain I and domain III by altering the conformation of the protein.[356] This results in the formation of large aggregates of NS5A with altered subcellular distribution.[350,351] The collective data have been interpreted to suggest of a mode of action in which the binding of an inhibitor to an oligomeric form of NS5A is able to disrupt its function, providing an explanation for the remarkable potency and stoichiometry of inhibition; it has been estimated that the NS5A protein exceeds inhibitor concentration by several thousand-fold.[309,350–353,357]

The NS5A inhibitor pharmacophore defined by daclatasvir (**7**) has been explored extensively in the literature, with structural modifications focused primarily on the 4,4′-di(1*H*-imidazol-5-yl)-1,1′-biphenyl core scaffolding element that appears to project the dipeptide-based cap moieties in a spatial arrangement that complements the dimeric domain I of NS5A.[309,354,355] These studies have revealed some latitude in functionalization of the proline ring, exemplified by ledipasvir (**8**) and GSK2336805 (**128**) (Fig. 38).[358,359] However, the methoxycarbonyl valine moiety is largely invariant in those compounds that retain potent and

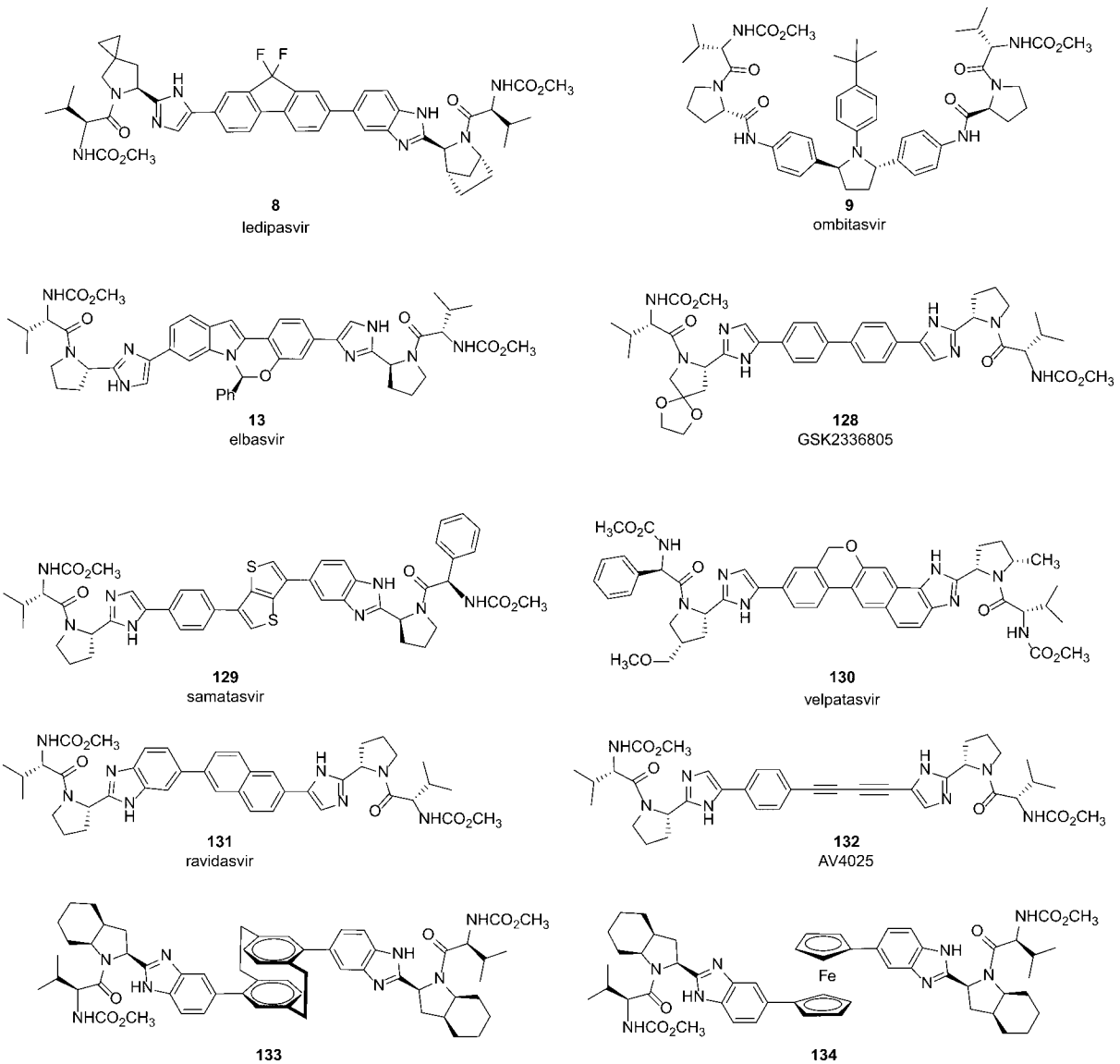

Fig. 38 HCV NS5A inhibitors ledipasvir (**8**), ombitasvir (**9**), elbasvir (**13**), and **128–134**.

balanced inhibitory activity toward a broad range of genotypes although the phenylglycine moiety that was discovered with **120**–**122**, antecedents of daclatasvir (**7**), is exploited effectively in samatasvir (**129**) and velpatasvir (**130**).[360,361] Both of these molecules combine asymmetrical caps with unsymmetrical core elements that incorporate a benzimidazole heterocycle as one of the H-bond donor/acceptor elements that in the case of **129**, presumably compensates for the increased length of the molecule imposed by the changes to the scaffold. Ravidasvir (**131**) and AV4025 (**132**) are also assembled on asymmetrical cores that effectively project the key methoxycarbonyl valine–proline moieties; a benzimidazole and imidazole-naphthyl pharmacophore is exploited in **131**, while the buta-1,3-diyne moiety of **132** recapitulates the linear geometry of a phenyl ring, although with a slightly extended reach.[309,362] Other interesting cores that have been explored include the *N*-phenylated pyrrolidine in ombitasvir (**9**), the substituted indole moiety in elbasvir (**13**), the cyclophane in odalasvir (**133**), and the ferrocene in **134**, although very little has been disclosed about the specific antiviral profiles of the latter two compounds.[363–365]

Several additional chemotypes for which resistance was mapped to NS5A have been discovered by phenotypic screening, but the antiviral activity of these compounds has generally been restricted to the GT-1b virus strain utilized in the original screen.[309] Prominent examples include AZD-7295 (A-689, **135**), which was evaluated clinically, and GL-100953 (**136**) and its homologue **136**, which exhibited improved GT-1b inhibitory activity but not GT-1a inhibition (**Fig. 39**).[304,308,309,359,366] AZD-7295 (**135**) inhibits GT-1b replication with an EC_{50} value of 7 nM but activity toward a chimeric GT-1a replicon was significantly weaker, $EC_{50} = 1.24$ μM, while the EC_{50} value for **137** in a GT-1b replicon is 400 pM; however, this compound is essentially inactive toward GT-1a virus, $EC_{50} > 50$ μM.

The screening hit **138** (**Fig. 40**), which inhibited a GT-1b replicon with an EC_{50} value of 18 nM but was 100-fold less active in a GT-1a replicon, $EC_{50} = 1.8$ μM, was elaborated into a series of quinazoline-based HCV inhibitors.[367,368] A prototype molecule, **139**, demonstrated improved potency toward a GT-1a replicon, $EC_{50} = 170$ nM, while maintaining GT-1b inhibition, $EC_{50} = 16$ nM. In this molecule, the *iso*-propyl moiety exerts a significant influence on potency and is optimal, with the cyclopropyl and *iso*-butyl homologues >100-fold weaker toward the GT-1b replicon and 50-fold less active toward GT-1a virus.[367] Further elaboration afforded **140**, which exhibited more a balanced inhibitory profile, $EC_{50} = 45$ and 7 nM toward GT-1a and GT-1b, respectively, with this enantiomer 4- to 13-fold more potent than the (*R*)-isomer.[368] The homologue **141**, although a little less potent than **140**, possessed adequate solubility to be administered IV to a chimpanzee infected with HCV GT-1b virus.[368] Five 2.5 mg kg^{-1} doses of **141** were infused at 8 hour intervals, with viremia falling by 1.65 $\log_{10}$ IU mL^{-1} over 32 hours. Sequencing of the virus at the end of the experiment identified resistance mutations emerging in the NS5A gene, notably Leu28Met and Tyr93Cys + Lys26Arg. Reverse engineering of the Tyr93Cys mutation into a GT-1b replicon resulted in a 900-fold increase in the EC_{50} value for **141**, implicating NS5A as the drug target. However, this chemotype bears some structural resemblance to AZD-2836 (**142**), for which resistance initially mapped to NS5A, but subsequent experiments and reverse genetic engineering studies were far less definitive.[366] The structurally related compound AL-9 (**143**) has been shown to interfere with HCV replication by inhibiting the host cell enzyme phosphatidylinositol 4-kinase IIIα (PI4KIIIα), $IC_{50} = 570$ nM, with fivefold selectivity over the β-isoform.[369] Kinase inhibition correlated with replicon potency, and it was shown that cells exposed to **143** had reduced plasma membrane levels of phosphatidylinositol 4-phosphate. AZD-2836 (A-831, **142**) was advanced into clinical trials but was subsequently abandoned due to low plasma levels following oral dosing that were attributed to the poor pharmaceutical properties of the compound.[366]

Adding to the biochemical complexity and intrigue associated with the inhibition of HCV NS5A, further experiments with the biotinylated probe **124** have led to the identification of molecules that modulate the protein in an allosteric fashion that resensitizes resistant viruses to restore full inhibition by daclatasvir (**7**).[370] That **124** bound to both wild-type and Tyr93His NS5A in replicons with similar affinity and was competed out in both circumstances by an NS5A inhibitor with similar EC_{50} values led to the

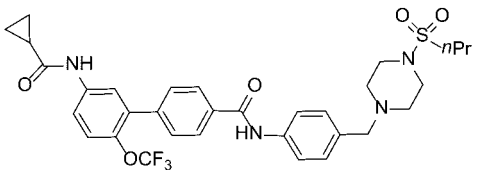

135

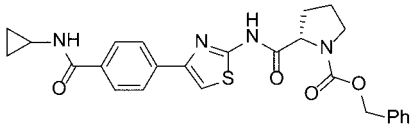

136

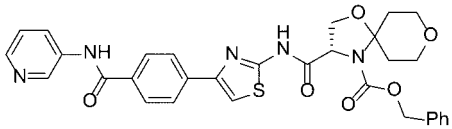

137

Fig. 39 HCV NS5A inhibitors **135**–**137**.

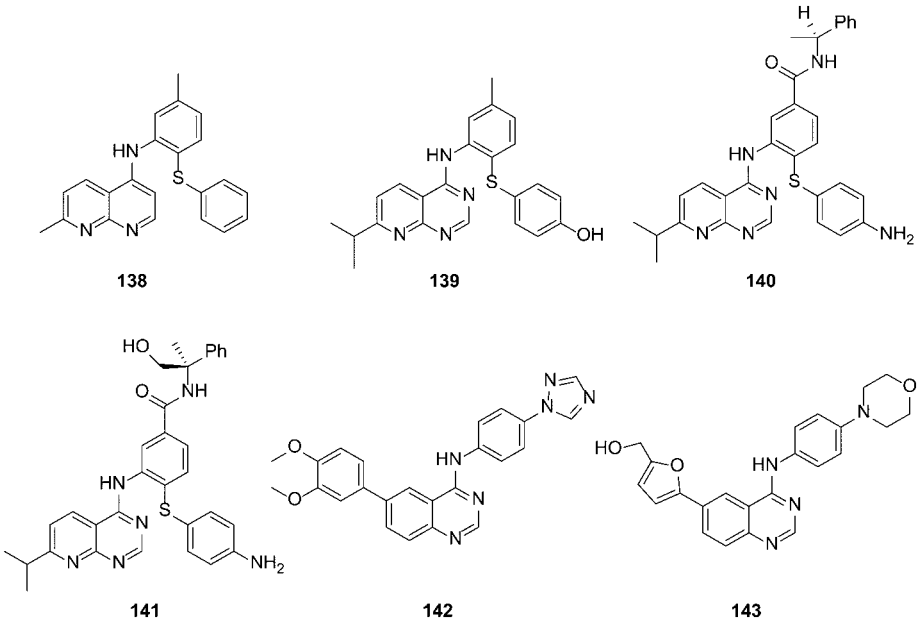

Fig. 40 HCV NS5A inhibitors **138–142** and the phosphatidylinositol 4-kinase IIIα inhibitor **143**.

hypothesis that the binding of a second molecule to NS5A at an adjacent site may be capable of restoring inhibition by bound **7**. Using a Tyr93Asn GT-1a replicon to screen weakly active and inactive compounds structurally related to **7** that would restore inhibition, the tert-butyl glycine derivative **144** was identified as a synergistic inhibitor. The EC_{50} value for **7** toward the Tyr93Asn GT-1a replicon was 339 nM, over 10,000-fold higher than the half-maximal inhibition of wild-type replicon, $EC_{50} = 0.033$ nM, while the synergist **144** was poorly active in both replicons, EC_{50} values of 214 nM (wild-type) and 215 nM (Tyr93Asn). However, in the presence of 40 nM of **144**, a concentration of 0.13 nM of **7** is required to half-maximally inhibit replication of the Tyr93Asn GT-1a replicon, representing a 2600-fold increase in sensitivity. As might be anticipated, the interaction between **7** and **144** is reciprocal in nature with the EC_{50} value for **144** measured as 7 nM in the presence of 1.37 nM of **7**. In HCV elimination studies conducted in GT-1a replicons, synergist **144** was an effective replacement for either an NS3 protease or an NS5B polymerase inhibitor in triple-drug combinations. Moreover, the combination of **7** and **144** resulted in a higher genetic barrier to the emergence of resistance in GT-1a replicons and mapping experiments revealed that linked substitutions, including Met28Thr-Gln30Arg and Met28Thr-Ser38Phe, were required for a resistant phenotype. Studies in vivo in chimeric mice in which the liver is largely replaced with normal human hepatocytes that support an HCV infection, combination therapy with close analogs of **7** and **144** delayed the emergence of resistant virus compared with monotherapy with the individual drugs.[370] The model proposed to explain both the high potency of NS5A inhibitors, and the phenomenon of cooperativity between **7** and **144** suggested that in the replication complex, the protein functions in an oligomeric form and that the individual monomers communicate with each other in a fashion in which changes in one dimer are transmitted to adjacent dimers. Thus, the conformational changes associated with accommodation of bond inhibitors by resistant NS5A protein are communicated throughout the oligomeric chain in a manner that allows a second inhibitor molecule to bind with restoration of inhibition.

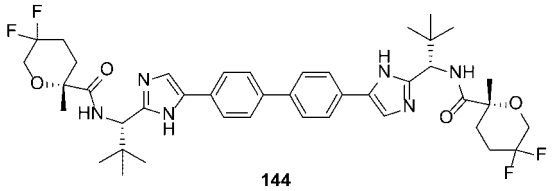

The discovery and development of HCV NS5A inhibitors represents a compelling example of the value of phenotypic screening to identify and optimize important and mechanistically interesting antiviral agents. In the absence of screening leads, the poor understanding of NS5A function and an inability to develop a useful biochemical assay basically rendered this protein in the class of undruggable targets, with no apparent rational or practical approach to the design inhibitors de novo. While the mechanistic underpinnings of daclatasvir (**7**) and related compounds remain as enigmatic as the function of the NS5A protein, this class of HCV antiviral agent has developed into an important contributor to the clinical landscape since all of the approved HCV combination therapies include a drug from this class.

5.18.1.10 HCV NS5B Inhibitors

5.18.1.10.1 Background

Viral polymerases represent a classic target for antiviral drug discovery, with nucleoside analog synthesis a universal design strategy that originates with the demonstration that idoxuridine (**145**) selectively inhibits herpesvirus replication.[371–376] Nucleoside analogs rely upon metabolic activation to an unnatural nucleoside triphosphate or triphosphate analog that is incorporated into the growing oligomeric chain to block elongation in either an obligate (no 3′-OH) or nonobligate fashion.[371–375] However, host toxicity with nucleoside analogs is an ever-present and frequently unpredictable concern, and nucleoside-based inhibitors of the HCV NS5B RNA-dependent RNA polymerase (RdRp) have not been an exception.[377–380] However, the HCV RdRp offers multiple opportunities for intervention since two major allosteric inhibitor binding regions have been characterized.[377,381–386] The thumb domain, where closing of the fingers is required to initiate polymerase activity, contains two sites where inhibitor ligands have been characterized. The palm site region, sometimes referred to as the primer grip site, is adjacent to the active site of the enzyme and presents an extended pocket to which several structurally diverse inhibitor chemotypes have been shown to bind. Inhibitors that bind at both thumb and palm domains block initiation of viral RNA polymerization, while nucleoside analogs primarily act by interfering with elongation of the growing RNA chain after incorporation.

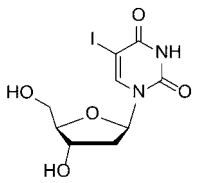

145
idoxuridine

The HCV NS5B polymerase is composed of ~590 amino acids and incorporates the GDD motif that is a hallmark of viral RNA polymerases at residues Gly317, Asp318, and Asp319.[377] Initial studies focused on characterization of the biochemical and kinetic properties of the polymerase as a prelude to developing assays suitable for screening for lead inhibitors, while X-ray crystallographic studies of apo GT-1b proteins from which the C-terminal membrane-binding domain had been deleted revealed key molecular details of the enzyme.[29,35–37,386–391] In the solid state, the apoprotein adopted the shape of a right hand in common with several classes of polymerase enzyme, with loops from the fingers subdomain associated with the thumb subdomain in what is the closed and active form of the enzyme, while the palm domain contained the catalytic elements of the active site (**Fig. 41**).[35–37,389–391] The key active site residues Asp318 and Asp319 combine with Asp220 and the carbonyl oxygen atom of Thr221 to coordinate the two metal ions, either Mg^{2+} or Mn^{2+}, with the former likely to be the physiological relevant element that catalyzes the polymerization reaction. These metal ions coordinate with the α- and β-phosphate moieties of the incoming nucleotide, as determined from X-ray structures of ternary complexes of the enzyme with dinucleotide primers and nucleoside diphosphates as substrate mimics.[389–392] The priming dinucleotide is stabilized by salt bridge interactions between Arg386 and Arg394 located on the primer grip helix and

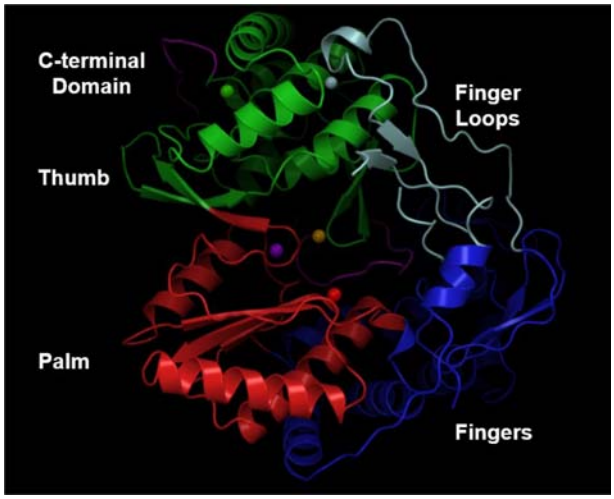

Fig. 41 Domain structure and location of inhibitor binding sites in HCV NS5B RdRp. The palm (red), thumb (green), fingers (blue), and C-terminal (magenta) domains and finger loops (cyan) are shown in cartoon representation. Locations of the active site (red), thumb site I (cyan), thumb site II (green), and palm sites I (magenta) and II (yellow) are denoted with colored spheres. Image generated with the PyMOL Molecular Graphics System (Version 1.7.6 Schrödinger, LLC) using coordinates in the Protein Data Bank, entry 1C2P.[35]

the 5′-phosphate of the primer.[392] The ternary complex structures reveal that the selectivity of NS5B for ribonucleotide triphosphates resides in the establishment of a H-bonding network in which the OH of Ser282 engages both the 2′-hydroxyl of the substrate and the carboxylate of Asp225 in H-bonding interactions, further stabilized by an interaction of the 2′-*O* atom with the side-chain amide NH of Asn291. Mutation of Ser282 to Thr282 of NS5B leads to resistance to 2′-CH_3-based nucleoside analogs, attributed to a steric clash of this moiety with the CH_3 of Thr282. Analysis of ternary complexes representing the primed initiation and elongation states of the enzyme has suggested a mechanism of function that is initiated by entry into the active site of both the 3′-nucleotide of the viral RNA template and the nucleotides that will form the primer. The dinucleotide primer is generated de novo by the initial phosphoryl transfer reaction but the primed complex is thought to be unstable until the dinucleotide primer is extended by an additional 1–3 bases. This results in the β-loop of the finger domain and the C-terminus residues of NS5B that are bound into the active site cavity being expelled, thereby allowing the enzyme to transition into its fully processive elongation state.[392]

5.18.1.10.2 Nucleoside inhibitors of HCV NS5B RdRp activity

The first HCV-inhibiting nucleoside analog to be advanced into clinical trials was 2′-*C*-methylcytidine (NM-107, **146**) that was developed as valopicitabine (NM-283, **147**), a valine ester prodrug designed to improve oral bioavailability (**Fig. 42**).[393–396] NM-107 (**146**) was discovered as an inhibitor of a range of RNA viruses in cell culture that included BVDV (EC_{50} = 670 nM), the closest flavivirus to HCV that was used as a surrogate in the early days of drug discovery before the advent of HCV replicons, yellow fever virus (EC_{50} = 3.1 μg mL^{-1}), and West Nile virus (98% inhibition at 5 μg mL^{-1}). In a GT-1b HCV replicon, NM-107 (**146**) was modestly potent, EC_{50} = 270 nM, and although synergistic when combined with IFN-α, the combination with ribavirin (**1**) was antagonistic.[393,396,397] Resistance to BVDV was mapped to a Ser405Thr mutation in the viral polymerase that is equivalent to a Ser282Thr change in HCV NS5B.[396] Daily administration of **147** to chimpanzees chronically infected with GT-1b HCV at a dose of 8.3 and 16.6 mg kg^{-1} each to 2 animals for 7 days resulted in mean reductions in viremia measured at day 7 of 0.83 and 1.05 $\log_{10}$IU mL^{-1}, respectively, with no significant change in the placebo control group.[396] In a phase 1 clinical trial, a dose of 800 mg of **147** administered QD for 15 days to subjects chronically infected with HCV produced a 0.73 $\log_{10}$IU mL^{-1} decline in viral load, while combination of this dosing regimen with PEG-IFN-α-2b afforded more than a 2 $\log_{10}$IU mL^{-1} reduction in viremia in 93% of the patients after 4 weeks of therapy. Although this compound established proof of concept for nucleoside-based inhibitors of NS5B RdRp in a clinical setting, development was halted by the FDA on 13 July 2007 due to gastrointestinal toxicity that could not be obviated by codosing with an antiemetic, and the compound was subsequently abandoned.

Both 2′-*C*-methyladenine (**148**) and 2′-*C*-methylguanine (**149**) inhibit HCV replication in replicons with EC_{50} values of 0.25 and 3.5 μM, respectively, with conversion to the active triphosphate determined to be a limitation for **149** (**Fig. 43**).[398–400] The phosphoramidate prodrug **150** of the 5′-monophosphate of **148** failed to significantly improve potency in a replicon, EC_{50} = 0.25 μM, but application of the same ProTide prodrug technology to **149** led to **151**, which exhibits >10-fold enhanced antiviral activity, EC_{50} = 0.28 μM.[401–404] The activity of **151** was further improved by modification of the guanosine base to afford INX-08189 (**152**), which inhibits HCV replication in a GT-1b replicon with an EC_{50} of 10 nM.[405–408] Administration of a single 3 mg kg^{-1} oral dose of **152** to rats revealed that the liver concentration of 2′-*C*-Me-GTP was equivalent to the EC_{90} in replicons and further increased in proportion to doses ranging from 5 to 300 mg kg^{-1}.[408] The complex sequence of intracellular metabolism of **152** has been elucidated and relies upon carboxylesterase cleavage of the ester moiety to initiate the cascade of prodrug unmasking reactions, with the released acid **153** reacting intramolecularly at phosphorus to eject β-naphthol and generate the unstable cyclic acyl phosphoramidate **154** (**Scheme 1**).[403,404,409,410] This is believed to hydrolyze spontaneously to the phosphonamide **155,** which is processed, at least in part, by histidine triad nucleotide-binding protein 1 (Hint1) to afford the monophosphate **156**.[409] The monophosphate **156** is a substrate for adenosine deaminase-like protein 1 (ADAL1), which metabolizes the base to the guanine moiety to afford 2′-*C*-methylguanine monophosphate (**157**). Sequential phosphorylation of **157** by guanylate kinase and nucleoside-diphosphate kinase (NDPK) is believed to complete metabolism to **158**, the active triphosphate species (**Fig. 44**).

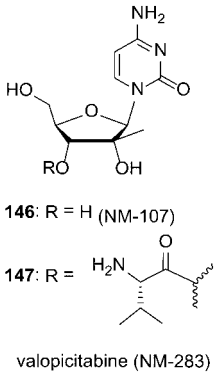

Fig. 42 HCV NS5B inhibitor NM-107 (**146**) and its prodrug valopicitabine (**147**).

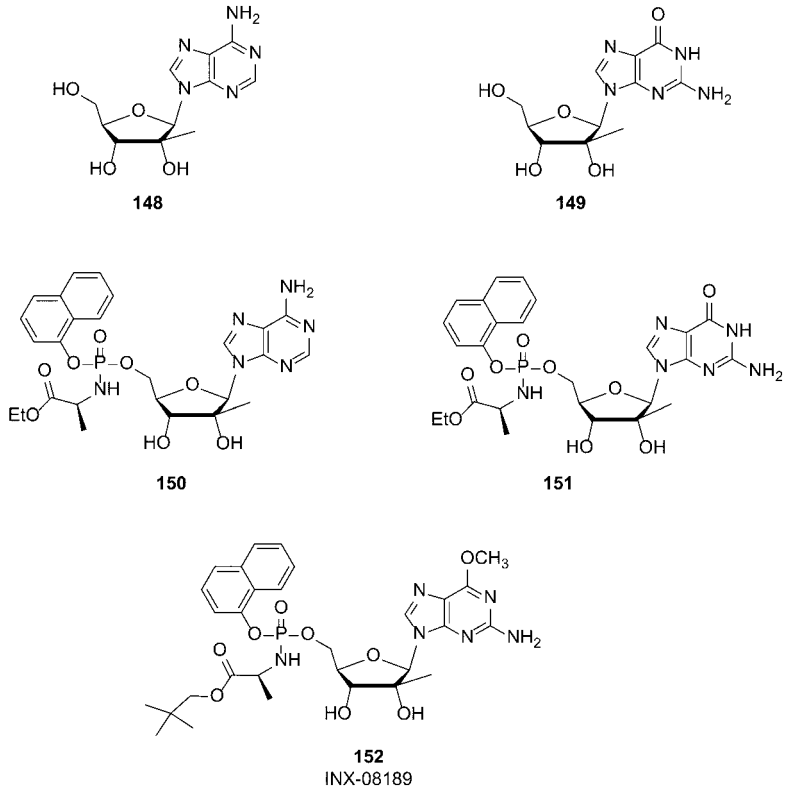

Fig. 43 Nucleoside-based HCV NS5B inhibitors **148–152**.

Since the resolved isomers of INX-08189 (**152**) exhibited equivalent antiviral activity in vitro, this compound was advanced into clinical trials as a mixture of diastereomers at the phosphorus center where daily doses of 9–200 mg for 7 days were associated with dose-dependent reductions in viremia ranging from 0.64 to 4.25 $\log_{10}$IU mL^{-1}.[402] However, development of this compound was terminated in Aug. 2012 after the observation of unexpected cardiac toxicity in a phase 2 clinical trial in combination with daclatasvir (**7**), manifested as an ST-segment and T-wave abnormalities on the surface ECG, with one patient suffering a rapidly progressive heart failure that was ultimately fatal.[379,411]

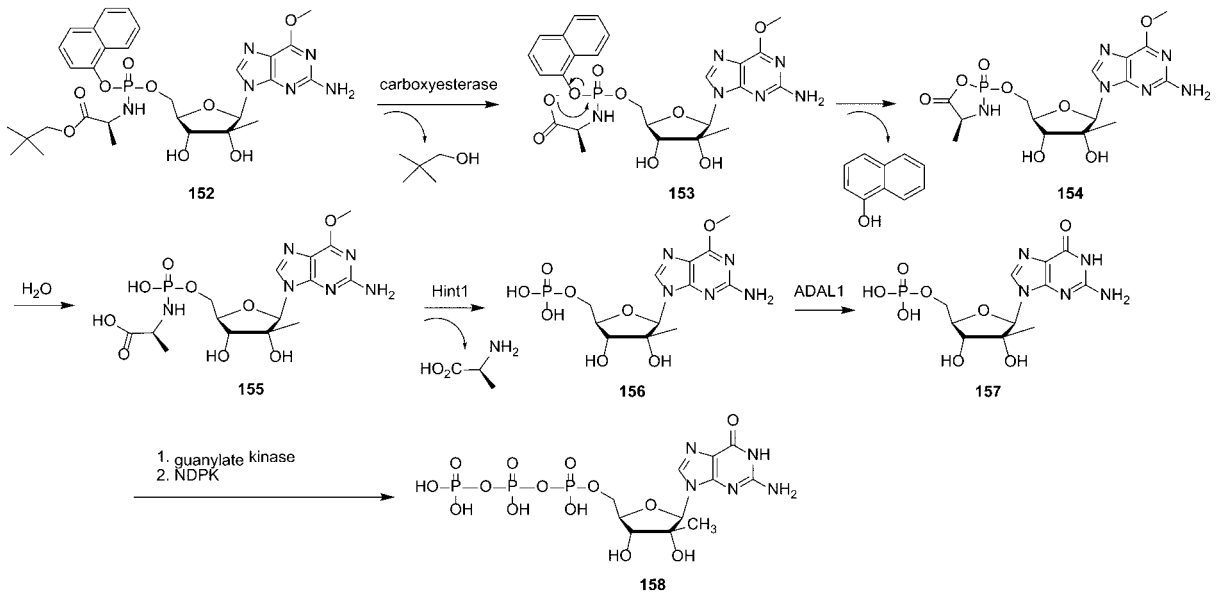

Scheme 1 Intracellular metabolism of INX-08189 (152) to generate 2′-*C*-methylguanine triphosphate (158).

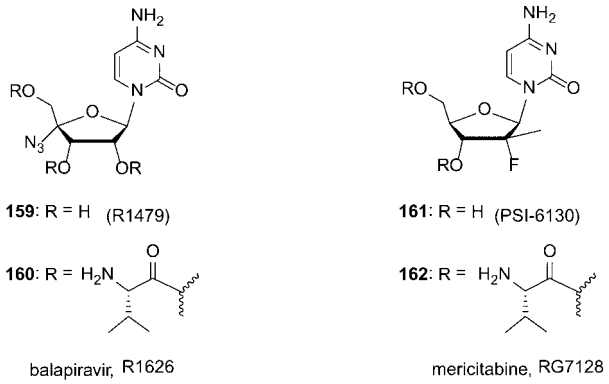

Fig. 44 Nucleoside-based HCV NS5B inhibitors **159–162**.

R1479 (**159**) is a 4′-azido cytidine derivative that is an effective although modestly potent inhibitor of HCV replication in a GT-1b replicon, $EC_{50} = 1.28\ \mu M$, for which antiviral activity was not significantly improved by the preparation of prodrugs of the monophosphate derivative.[412–414] R1479 (**159**) was advanced into clinical trials as the trivaline ester prodrug **160** (R1626, balapiravir), which improved drug absorption in the gut.[415] HCV-infected subjects were treated with doses of 1500, 3000, and 4500 mg of **160** administered on a BID regimen for 14 days, which produced viral load reductions of 1.2, 2.6, and 3.7 $\log_{10}$-IU mL^{-1}, respectively.[416] A subsequent study evaluated a 1500 mg BID dose of **160** administered for 28 days in conjunction with PEG-IFN-α and ribavirin (**1**) and resulted in a 5.2 $\log_{10}$IU mL^{-1} reduction in viremia.[417] While these patients subsequently continued with PEG-IFN-α and ribavirin (**1**) therapy for 44 weeks, high relapse rates were seen at 72 weeks, and this compound was discontinued after a phase 2 clinical trial revealed an unacceptable benefit-to-risk ratio.[418,419]

The presence of a 2′-hydroxyl on the ribose ring is not an essential recognition element for nucleoside-based inhibitors of HCV NS5B.[376,420,421] 2′-Deoxy-2′-fluoro-2′-*C*-methylcytidine (PSI-6130, **161**) is an active antiviral agent in HCV replicons, $EC_{50} = 1.3\ \mu M$, that is not cross-resistant with R1479 (**159**) and was formulated as the bis-valine ester **162** (RG7128, mericitabine) for clinical development, a modification designed to improve the poor pharmacokinetic properties associated with the parent drug.[422–426] In early clinical trials in patients infected with GT-1, GT-2, or GT-3 viruses, a dose of 1500 mg BID of **162** for 14 days was associated with a reduction in viremia of 2.7 $\log_{10}$IU mL^{-1} while QD doses of 750 mg and 1500 mg were less effective, reducing viral load by 2.1 and 1.5 $\log_{10}$IU mL^{-1}, respectively.[427] A 4-week clinical trial in which a 1500 mg BID dose of **162** was added to a regimen of PEG-IFN-α and ribavirin (**1**) for 4 weeks produced a maximal mean viral load reduction of 5.1 $\log_{10}$IU mL^{-1}, with no evidence of the emergence of resistance.[427,428] These studies set the stage for longer trials of the combination therapy, explored in context of 8-week, 12-week (PROPEL), and 24-week (JUMP-C) phase 2b regimens in which doses of 500 or 1000 mg BID of **162** with PEG-IFN-α and **1** were compared with a combination of PEG-IFN-α and **1** with a placebo control.[429,430] In the shorter studies, there was no difference in SVR across the drug regimens, while in the longer study, **162** improved SVR to 56.8% compared with 36.5% with placebo, although relapse rates in the two groups were similar, results anticipating combination studies with direct-acting antiviral agents.[429–431] However, the clinical development of **162** was apparently abandoned in Jan. 2015.

A comprehensive analysis of the intracellular metabolism of **161** identified a complex, bifurcated pathway that resulted in the production of the fluorinated uridine triphosphate **167**, a potent inhibitor of the HCV NS5B enzyme that has a much longer intracellular half-life than the cytidine triphosphate derivative **164** (Scheme 2).[432,433] Conversion of **161** to the uridine **165** by cytidine deaminase was observed in vitro but the latter compound is not metabolized to the monophosphate **166** in hepatocytes, providing an explanation for the absence of antiviral activity with **165** in cell-based assays. However, the monophosphate **163** is also a substrate for cytidine deaminase, generating **166**, which, analogous to **163**, is phosphorylated sequentially by cytidine monophosphate (UMP-CMP) kinase 1 and NDPK to afford the active triphosphate **167**.

In order to circumvent the metabolic block preventing **165** from being converted to the active species **167**, phosphoramidate-based prodrugs of **165** were explored, with optimization of the prodrug elements guided by antiviral potency in a subgenomic replicon assay.[409,434] The result of this process was the identification of PSI-7851 (**168**) (Fig. 45) as a potent inhibitor of replication, $EC_{90} = 0.52\ \mu M$.[434] PSI-7851 (**168**), which was subsequently renamed GS-9851, was advanced into clinical trials as the mixture of diastereomers at phosphorus after preclinical profiling established that oral administration of this compound to rats and dogs resulted in the formation of high levels of the triphosphate in the liver.[434,435] In phase 1 clinical studies, **168** was well tolerated with dose-related effects on viral load observed: 3 daily doses of 400 mg effected a mean maximal reduction in viremia of 1.95 $\log_{10}$IU mL^{-1} compared with 0.09 $\log_{10}$IU mL^{-1} in the placebo group.[377,436,437] Resolution of **168** identified the *Sp* diastereomer **4** (PSI-7977, sofosbuvir) as the preferred species, $EC_{90} = 0.42\ \mu M$, while the *Rp* diastereomer was over 10-fold less active, $EC_{90} = 7.5\ \mu M$.[434] Sofosbuvir (**4**) exhibits pan-genotypic inhibitory activity in replicons expressing GT-1 to GT-6 sequences, with EC_{50} values ranging from 14 to 110 nM, and a high genetic barrier to resistance, with 16-fold reduced sensitivity to replicons expressing the Ser282Thr mutation.[435,66] In a phase 2 clinical study, a 400 mg daily dose of **4** administered as monotherapy for 14 days to GT-1-infected subjects resulted in a decline in viral load of 5.0 $\log_{10}$IU mL^{-1}.[377]

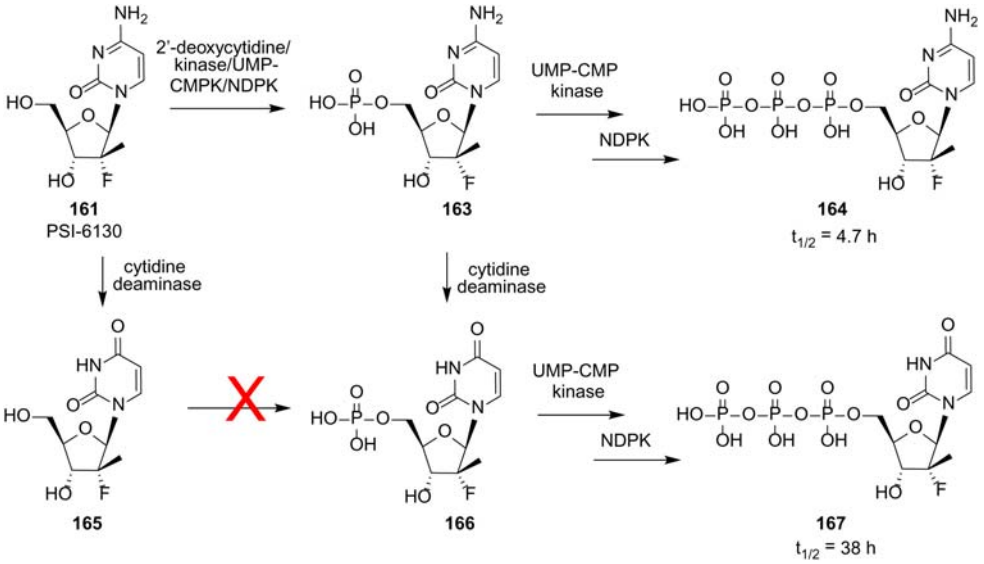

Scheme 2 Intracellular metabolism of PSI-6130 (161).

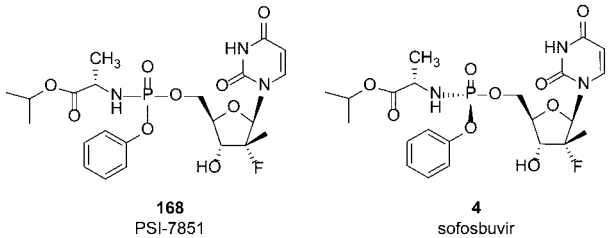

Fig. 45 Nucleoside-based HCV NS5B inhibitors **168** and sofosbuvir (**4**).

2′-Fluoro-2′-C-methyl guanosine (**169**) is a modestly potent HCV inhibitor in a subgenomic replicon, $EC_{90} = 56–69$ μM, while the adenosine homologue is inactive with an EC_{90} value of > 100 μM (Fig. 46).[438–440] However, not only was triphosphate derived from **169** a potent inhibitor of wild-type GT-1b, GT-2a, GT-3a, and GT-4a NS5B polymerase activity with IC_{50} values ranging from 1 to 4.7 μM, but also it inhibited the Ser282Thr mutant polymerase with only twofold reduced sensitivity, $IC_{50} = 9.2$ μM, an improved profile compared with the pyrimidine-based triphosphate **167**.[377,440] Based on the premise that the initial

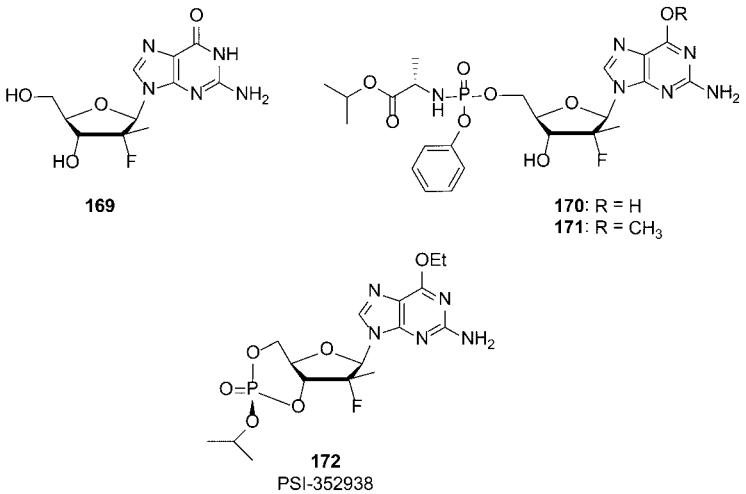

Fig. 46 Nucleoside-based HCV NS5B inhibitors **169–172**.

phosphorylation of the 5′-alcohol was limiting cellular production of the triphosphate of **168**, the phosphoramidate prodrug **170** was prepared and evaluated.[439] This compound offered significantly increased potency in cell-based assays with an EC_{90} of 0.75 μM in a GT-1b wild-type replicon. Further optimization focused on the C-6 substituent of the guanine base, with small alkoxy and alkylamine substituents offering improved potency. The observation that more lipophilic compounds were more cytotoxic precipitated a focus on the methoxy analog **171**, $EC_{90} = 0.02$ μM, as an optimal compromise.[439] The *Sp* diastereomer of **171**, isolated initially by crystallization, was the more potent, $EC_{90} = 8$ nM, offering a threefold advantage over the *Rp* isomer, $EC_{90} = 27$ nM, a structure–activity relationship that mirrors observations with **168**. The metabolic activation pathway for the *Sp* diastereomer of **171** was determined to be analogous to that elucidated for **152,** and the compound afforded high levels of the triphosphate of **169** in primary human hepatocytes.[377,439,440] However, although this compound was selected for clinical development, it appears to have been abandoned in favor of the cyclic phosphate analog PSI-352938 (**172**).[377,441,442] PSI-352938 (**172**) is the thermodynamically more stable *Rp* (*cis*) isomer and inhibits a GT-1b replicon with an EC_{90} value of 1.37 μM, while the *Sp* (*trans*) diastereomer is twofold more potent, $EC_{90} = 0.69$ μM.[441] However, **172** was able to deliver higher levels of the triphosphate metabolite of **169** in primary human hepatocytes than in replicon cells, and high levels of triphosphate were measured in the livers of rats following oral administration of the drug.[441,443,444] The metabolic pathway unmasking **172** has been elucidated and is initiated by CYP 3A4-mediated removal of the *iso*-propyl ester moiety with other CYP enzymes being incompetent, a mechanism that may underlie the modest replicon potency since the parent cell lines only poorly express this enzyme.[444] Ring opening of the cyclic phosphate is mediated by phosphodiesterases 2A1, 5A, 9A, and 11A4, all of which are expressed in the liver, with the next step the removal of the 6-ethoxy moiety of the guanine base by ADAL1 to afford the monophosphate of **169**. The final steps of activation are sequential phosphorylation of the monophosphate of **169** by guanylate kinase 1 and NDPK to give the triphosphate.[444] In a multiple ascending dose study in which GT-1-infected subjects were administered with 100, 200, and 300 mg of **172** daily for 7 days, mean viral load declined by 4.31, 4.65, and 3.94 $\log_{10}$ IU mL^{-1}, respectively, measured at the end of the study, with no viral breakthrough observed.[376] This reflects a high genetic barrier to resistance in which multiple mutations in the NS5B gene are required for virus escape.[445] Clinical development of **172** was focused on combination with sofosbuvir (**4**), but this compound was abandoned after a phase 2a trial in which liver enzyme elevation of greater than threefold was observed in a monotherapy arm of the study, reflective of hepatotoxicity.[378,380]

5.18.1.10.3 Nonnucleoside inhibitors of HCV NS5B RdRp activity

Lead nonnucleoside HCV NS5B polymerase inhibitors that act via an allosteric mechanism were discovered by high-throughput screening campaigns, and structural studies have provided further details on modes of binding in the thumb and palm regions described in the preceding text.[377] The thumb domain contains two distinct sites, designated as thumb sites I and II, that are separated by approximately 15 Å. The palm domain has also been classified into 2 main sites based on inhibitor binding, but these form part of an extended, contiguous binding site that is ~15 Å long and ~20 Å wide and demonstrates considerable conformational plasticity.[377] Perhaps not surprisingly given its size, HCV NS5B inhibitors that have been characterized as interacting with the palm site represent multiple structurally diverse themes.

5.18.1.10.4 Thumb site I nonnucleoside inhibitors of HCV NS5B RdRp activity

Prototypical ligands for thumb domain I are represented by the indoles deleobuvir (**173**) and JTK-109 (**174**), while filibuvir (**175**), lomibuvir (**176**), and radalbuvir (**177**, GS-9669) are ligands that bind to thumb site II (Fig. 47).[377,386–338,446–449] Thumb domain site I of HCV NS5B is located 30 Å away from the active site of the enzyme and X-ray crystallographic structures reveal that in the apo enzyme, this binding site is occupied by a short α-helix, located at the tip of the N-terminal loop of the enzyme, that serves to connect the fingers and thumb domains.[450,451] Thumb domain I inhibitors interfere with this interaction, thereby preventing the enzyme from articulating correctly during viral RNA synthesis. However, thumb domain I is proximal to a GTP-binding site and inhibitors that act at this domain indirectly compromise GTP association.

The benzimidazole-based thumb domain I inhibitor leads **178** and **179** were discovered independently by high-throughput screening campaigns, and both demonstrated modest enzyme inhibitory potency, IC_{50} values = 14 and ~10 μM, respectively, and neither were active in HCV replicons (Fig. 48).[452,453] In both cases, the minimum pharmacophore was deduced to be the embedded *N*-alkyl-1*H*-benzo[*d*]imidazole-5-carboxylic acid, with initial SAR studies directed in complementary directions that led to the identification of BILB 1941 (**180**), which is based on a more lipophilic indole core, and the benzimidazole JTK-109 (**174**) as clinical candidates.[447,454,455] Both compounds were profiled as potent antiviral agents in HCV replicons with EC_{50} values of 153 and 84 nM for **180** toward GT-1a and GT-1b replicons, respectively.[455,456] JTK-109 (**174**) inhibited GT-1a and GT-1b replicons with EC_{50} values of 62 and 320 nM for GT-1a and GT-1b, respectively, although this compound was poorly active in replicons based on GT-2a and GT-2b sequences.[447] Moreover, both compounds were the result of drug discovery campaigns that optimized for both intrinsic antiviral potency and oral exposure, with a specific focus on liver exposure where concentrations of both were ~10-fold higher than in plasma following oral administration to rats.[447,455]

In the case of BILB 1941 (**180**), the optimized spirocyclobutane moiety was confirmed using parallel synthesis methodology starting from a *gem*-dimethyl substituent that functioned to provide a distinct stereo-orientation by taking advantage of the Thorpe–Ingold effect and favoring an L-shaped topology that complements the enzyme binding site.[457–459] Resistance to **180** mapped to changes at Pro495, Pro496, and Val499 in the thumb region, residues that are proximal to the aromatic ring of the indole core.[451] Clinical evaluation of **180** established proof of concept for this inhibitory mechanism with doses of 10–450 mg administered on a TID schedule for 5 days to GT-1-infected subjects.[456] A robust antiviral response was observed only in the

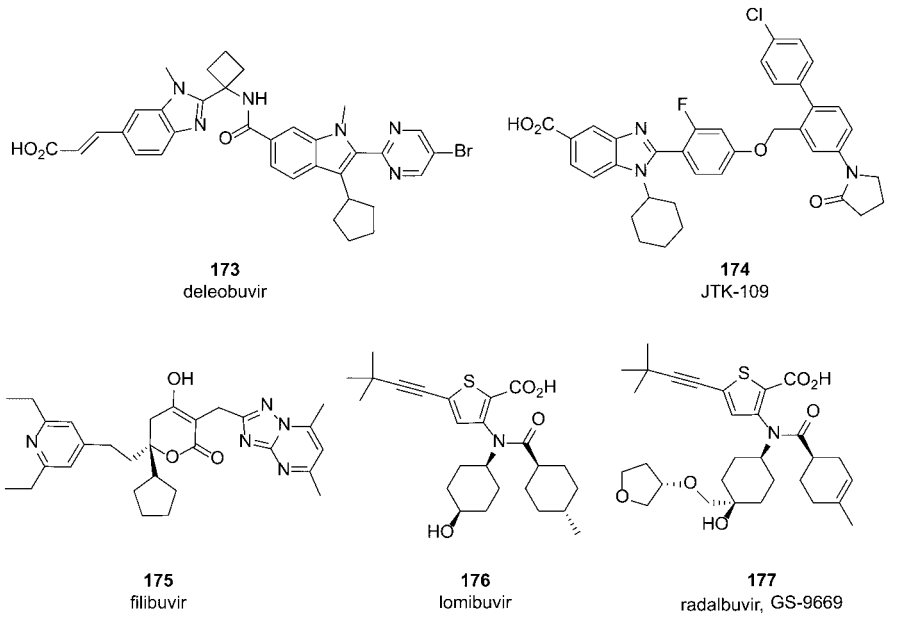

Fig. 47 Nonnucleoside-based HCV NS5B inhibitors **173–177**.

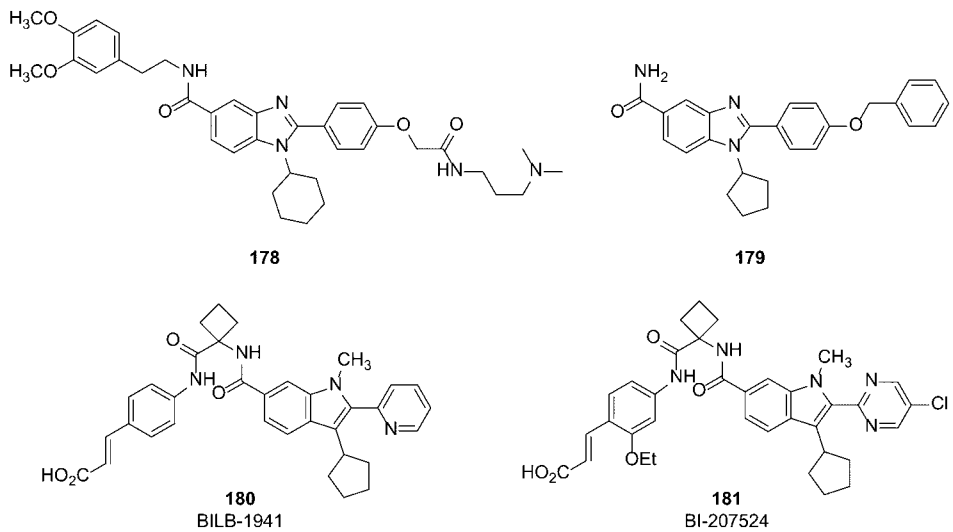

Fig. 48 Nonnucleoside-based HCV NS5B inhibitors **173–177**.

450 mg dose cohort, with 4 of 5 patients experiencing a >1 $\log_{10}$ IU mL^{-1} decline in viremia. However, at this dose, GI intolerance in 4 of the subjects and liver enzyme elevation in the remaining patient prevented further dose escalation and development of this compound was abandoned.[457,458] Follow-up studies were focused on identifying compounds with improved potency, and BI-207524 (**181**), a compound with a less acidic carboxylic acid moiety by virtue of the *ortho*-ethoxy substituent, fulfilled the improved targeted antiviral criteria with EC_{50} values of 29 and 11 nM for GT-1a and GT-1b replicons, respectively, while maintaining the PK profile of **180**.[460,461] Unfortunately, development of this compound was precluded by the observation that the embedded aniline, a genotoxin, was released in vitro in both rat and human liver microsomes.[461,462] While the genotoxicity problem was addressed by replacing the aniline with a 2-aminopyridine, compounds in this class failed to achieve antiviral and PK profiles predictive of reasonable doses in humans, necessitating further optimization, ultimately arriving at deleobuvir (**173**) in which the anilide is replaced by a benzimidazole ring.[446] The design of **173** relied upon extensive NMR and computational studies of conformational preferences of **180** that illuminated the role of the individual substituents and identified potential sites for rigidification as an approach to optimizing complementarity with the protein binding site. This analysis, which carefully assessed key rotatable bonds, also suggested that the role of the pyridyl moiety of **180** was to influence the orientation of the cyclopentyl ring, a critical element of the pharmacophore.[446,463] The orientation of the amide carbonyl attached to the indole

ring is also of importance since the oxygen atom establishes a H-bonding interaction with the guanidinium moiety of Arg503. However, attempts to influence conformation of the amide to that in the bound state (which is as depicted in **173** and **178–181**) by installing an *ortho*-CH_3 or introducing a nitrogen atom into the phenyl ring of the core heterocycle of a benzimidazole series were associated with poorer inhibition, despite achieving the desired control of the preferred topology.[446] Ultimately, a focus on modulating the conformation of the anilide element of **180** and **181** precipitated the idea of exploiting benzimidazole as an anilide isostere, leading to the identification of deleobuvir (**173**). This compound inhibited a GT-1b NS5B RdRp with an IC_{50} value of 50 nM; was active in both GT-1a and GT-1b replicons with EC_{50} values of 23 and 11 nM, respectively; and was active toward representative GT-2a, GT-2b, GT-3a, GT-4a, GT-5a, and GT-6a replicons, with EC_{50} values of <100 nM.[446,464] Resistance mapping experiments identified mutations in the thumb domain, with reduced sensitivity associated with changes at Pro495, Pro496, and Val499 and with the Pro495Leu variant 120- to 310-fold resistant.[464,465] In a phase 1b clinical trial conducted in GT-1-infected subjects, doses of 100, 200, 400, 800, or 1200 mg of **173** administered TID for 5 days to those without cirrhosis were associated with a dose-dependent reductions in viral load that ranged from 0.4 to 3.8 $\log_{10}$ IU mL^{-1}, with the maximal effect seen at the 800 mg dose.[377,465] Subjects with cirrhotic livers received doses of 400 or 600 mg TID for 5 days and had mean HCV RNA reductions of approximately 3.0 $\log_{10}$ IU mL^{-1}. Although deleobuvir (**173**) was advanced into phase 3 clinical trials in combination with the NS3/4A inhibitor faldaprevir (**57**), development was abandoned in early 2014 after a preliminary analysis of the data revealed a higher rate of premature drug discontinuations that compromised drug efficacy.[466] A similar fate befell JTK-109 (**174**), which was advanced into phase 2 clinical studies but abandoned late in 2003 for reasons that have not been disclosed.[377]

Further evolution of this chemotype focused on indole derivatives, which allowed for simultaneous 1,2,3-trisubstitution to probe the effects of structural constraint between the core heterocycle and the 2-aryl substituent.[377] The acetamide **182** (**Fig. 49**) inhibited a C-terminus truncated NS5B polymerase with an IC_{50} value of 26 nM and was active in a GT-1b replicon, $EC_{50} = 800$ nM.[450] A cocrystal structure of **182** with the NS5B protein revealed the key drug–target interactions and provided a rational basis for further structural exploration. The carboxylic acid moiety formed a salt bridge with the guanidinium of Arg503, with the proximal His428 imidazole adding to the positive electrostatic potential in this region, while the cyclohexyl and phenyl rings occupied adjacent hydrophobic pockets in the thumb domain. An initiative focused on surveying carboxylic acid isosteres was embarked upon based on the premise of solving the problem of acyl glucuronide formation in vivo, a metabolite that can be problematic from a toxicity perspective.[467,468] However, this tactic also allows extension of the pharmacophore into the region probed by the amino acid amide moieties of **173**, **180**, and **181** while preserving acidic functionality at this important site. The success of this approach is exemplified by the acyl-*N*,*N*-dimethylsulfamide **183**, which inhibits the N-terminal truncated GT-1b enzyme with an IC_{50} of 4 nM and is active in a GT-1b replicon with an EC_{50} value of 120 nM.[467]

The construction of a ring between the indole heterocycle and the 2-phenyl substituent was explored by several groups as a means of conferring conformational constraint to the core and providing some control over the topological vectors explored by substituents extending from the bridging element.[469–474] These studies gave rise to MK-3281 (**184**) as a compound with potent in vitro

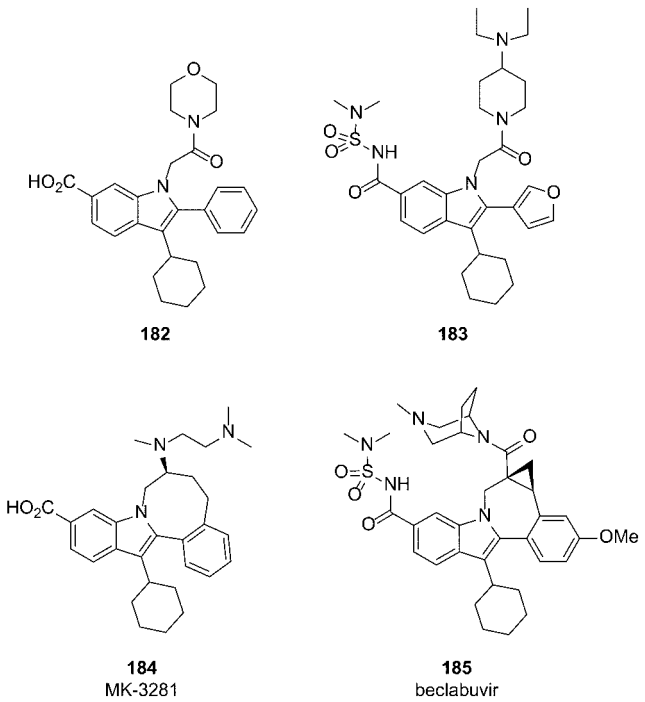

Fig. 49 Nonnucleoside-based HCV NS5B inhibitors **182–185**.

activity, $IC_{50} = 6$ nM toward a GT-1b enzyme, with EC_{50} values of 28, 38, and 37 nM in GT-1a, GT-1b, and GT-3a replicons, respectively, that was six- to ninefold more potent than its enantiomer.[473] However, MK-3281 (**184**) was a weaker inhibitor of GT-2a and GT-2b replication, $EC_{50} = 2$ and 1.8 μM, respectively. In a cocrystal structure of **184** with a GT-1b polymerase, the dihedral angle between the phenyl and indole rings was measured at 46°, the carboxylic acid moiety engaged Arg503, and the amine-containing side chain projected into solvent, leading to the suggestion that the poorer activity of the enantiomer could be attributed to unfavorable steric interactions between enzyme and ligand. This compound demonstrated oral bioavailability in rat, dog, and cynomolgus monkeys, with liver levels in the rat fivefold higher than plasma levels.[473] In vivo antiviral activity was demonstrated in HCV-infected chimeric mice following a dose of 50 mg kg^{-1} administered intraperitoneally twice a day for 4 days, which led to a mean decrease in viremia of 3.13 ± 0.7 $\log_{10}$ IU mL^{-1}. A 10 mg kg^{-1} dose was associated with reduced efficacy, with a mean decrease in viremia of 1.4 ± 0.25 $\log_{10}$ IU mL^{-1}. MK-3281 (**184**) was evaluated in a phase 1b clinical trial where a dose of 800 mg BID for 7 days as monotherapy resulted in a decrease in viral load of 1.28 $\log_{10}$ IU mL^{-1} in GT-1a-infected subjects and 3.75 $\log_{10}$ IU mL^{-1} in those infected with GT-1b virus.[376] Development of **184** was, however, suspended for reasons that have not been disclosed.

Beclabuvir (**185**) resulted from extensive optimization of a tetracyclic chemotype that traces its origins to the benzodiazepinone **186**, a potent GT-1b enzyme inhibitor, $IC_{50} = 70$ nM, that prevents replication of a GT-1b replicon with an EC_{50} value of 240 nM.[474–476] The exocyclic amide **187** (**Fig. 50**) offered comparable potency with balanced GT-1a and GT-1b replicon inhibition, EC_{50} values = 404 and 359 nM, respectively.[476] The acyl-*N*,*N*-dimethylsulfamide **188** provided an optimized solution to metabolic modification of the carboxylic acid of **186** by glucuronidation and improved antiviral potency by twofold, EC_{50} values for GT-1a and GT-1b replicons of 119 and 148 nM, respectively. A focus on structural modification of the morpholine ring required considerable iterative evolution through a series of heterocycles in order to circumvent pregnane X receptor transactivation while preserving potency and PK properties compatible with oral delivery.[476,477] The site of the bridge in the bicyclic piperazine moiety of **185** was determined to be important since the isomer in which the bridge is proximal to the tertiary amine demonstrated higher clearance and poorer exposure in rats.[476] The absolute configuration of the cyclopropyl moiety in **185** was also important with selection based on a significant 15- to 30-fold advantage for the more active enantiomer in potency in replicons. Beclabuvir (**185**) was active in cell culture, inhibiting GT-1a and GT-1b HCV replicons with EC_{50} values of 3 and 6 nM, respectively, with similar activity toward GT-3a, GT-4a, and GT-5a replicons, although GT-2a and GT-6a replicons were less potently inhibited.[476,478] The PK characteristics of **185** in rat, dog, and cynomolgus monkey revealed a hepatotropic disposition, with liver to plasma ratios ranging from 1.6 to 60, and plasma levels in all species were ≥10-fold above the protein binding-adjusted EC_{50} values after a single, orally administered dose. Interestingly, beclabuvir (**185**) is metabolized by CYP 3A4 to the desmethyl derivative **189**, which is a major circulating metabolite that exhibits an antiviral profile similar to the parent drug but exhibits much lower oral bioavailability.[479] Mechanistic studies revealed that **185** is a time-dependent, noncompetitive NS5B inhibitor that interacts with resistant mutants in a fashion that is indicative of a two-step inhibition process.[480] For the Pro495Leu variant, the rates of association with and dissociation from the enzyme are similar to wild-type, but the second step leading to the final tight-binding complex is significantly faster, indicating that this mutation results in a less stable initial complex. In contrast, the Leu30Ser mutant shows seven- to 10-fold higher association/dissociation kinetics but the forward and reverse rates of final complex formation are comparable to the wild-type enzyme.[480] In a phase 1b clinical trial conducted in HCV GT-1-infected subjects, a single 300 mg oral dose of **185** resulted in a mean 2.5 $\log_{10}$-IU mL^{-1} decline in viral load measured at 24 hours post dose.[481]

Conformational constraint in which the acyl-*N*,*N*-dimethylsulfamide element is linked back to the core via a macrocyclic ring has been explored as an approach to simultaneously addressing the metabolism issues associated with simple carboxylic acids while improving drug–target interactions by favoring the bound topology of the acyl-*N*,*N*-dimethylsulfamide moiety.[482–484] Macrocycle motifs that linked the acyl-*N*,*N*-dimethylsulfamide to the indole *N* atom or to the 2-phenyl substituent provided lead compounds **190** and **191**, respectively, which demonstrate sub-micromolar EC_{50} values in a GT-1b replicon (**Fig. 51**). However, early compounds from this series displayed poor in vivo PK profiles, leading to a focus on a third topological design in which macrocyclization linked the acyl-*N*,*N*-dimethylsulfamide to an amide moiety projecting from the bridged ring that was originally explored

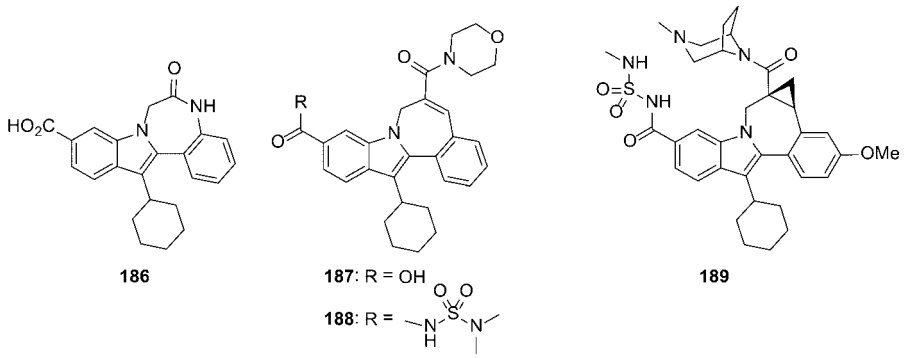

Fig. 50 Nonnucleoside-based HCV NS5B inhibitors **186–189**.

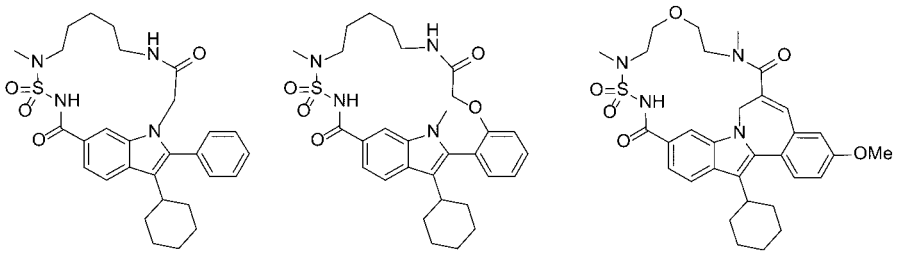

190: EC_{50} = 430 nM **191**: EC_{50} = 180 nM **192** TMC647055

Fig. 51 Nonnucleoside-based HCV NS5B inhibitors **190–192**.

with **184**, **185**, and **188**.[482–484] TMC647055 (**192**) emerged from this effort as an optimized compound after careful examination of the linker length and composition of the bridge olefin.[484,485] A 16- or 17-membered macrocycle provided higher potency than either a 15- or 18-membered ring, while the amide moiety attached to the bridge was important for potency since reduction to the amine was associated with a 25-fold increase in the IC_{50} value. The identity of the bridge motif was particularly influential on the PK profile since the unsaturated analog exhibited lower bioavailability and reduced liver levels, while the cyclopropane analogous to beclabuvir (**185**) was associated with higher clearance in vivo. TMC647055 (**192**) inhibits GT-1a, GT-1b, GT-3a, GT-4a, and GT-6a replicons with EC_{50} values ranging from 27 to 113 nM but is markedly less potent toward GT-2a and GT-2b replicons with EC_{50} values >10 μM.[484,485] The NS5B Pro495Leu mutation conferred a 370-fold reduction in sensitivity in a GT-1b background, while the EC_{50} values for Leu392Ile and Val494Ala were nine- and threefold higher, respectively. Phase 1 clinical trials with **192** examined escalating doses of 300, 1000, and 1250 mg BID in NHVs and doses of 500 and 1000 mg BID were selected for the phase 1b study in HCV-infected subjects who were administered with the drug for 6 days. Exposure was twofold higher in the HCV-infected individuals and mean trough concentrations after oral dosing exceeded the EC_{50} values measured in GT-1a and GT-1b replicons. In GT-1a-infected subjects, the median maximal decline in viremia was 1.4 $\log_{10}$ and 2.4 $\log_{10}$ IU mL^{-1} at the 500 and 1000 mg dose, respectively, while in GT-1b-infected subjects, the median maximal decline in viremia was 3.3 $\log_{10}$ and 3.4 $\log_{10}$ IU mL^{-1}, respectively. Preliminary phase 2 studies of **192** in combination with the NS3 protease inhibitor simeprevir (**5**) have been completed, with antiviral effects superior to the individual drugs although the emergence of Arg155Lys in the NS3 protein was observed in GT-1a-infected subjects, reducing sensitivity to simeprevir (**5**) by 30-fold.[484] Ongoing trials evaluating combinations of TMC647055 (**192**) and simeprevir (**5**) include the CYP 3A4 inhibitor ritonavir (**11**) in order to offset the induction of CYP 3A4 by **192**, which promotes its own metabolism.

5.18.1.10.5 Thumb site II nonnucleoside inhibitors of HCV NS5B RdRp activity

The discovery of filibuvir (**175**) has its genesis with the HTS hit **193** (Fig. 52), a modestly potent NS5B inhibitor, $IC_{50} = 0.93$ μM, that is derived from a series of HIV-1 protease inhibitors.[486] An X-ray cocrystal structure of **193** with a genotype 1b BK strain ΔC21 C-terminal truncated NS5B polymerase protein identified the binding site in the thumb domain. The key drug–target interactions were revealed to be a direct H bond between the enol and the backbone NH of Ser476 in conjunction with three additional H-bonding interactions, all of which were mediated by H_2O molecules: the enol moiety with the NH of Tyr477, the lactone C=O with the guanidinium of Arg501, and the phenol with the NH of Leu497.[486] The phenol ring occupied a hydrophobic pocket, while the aniline ring appeared to make limited contact with the protein. The optimization of **193** focused on enhancing potency while retaining the sulfide linker, with structural modifications guided by X-ray cocrystal data; however, while the initial iterations improved potency by 30-fold, this was not accompanied by demonstrable antiviral activity in a replicon. Subsequent studies probed replacing the aniline moiety with fused heterocycles and modifying the phenol ring, changes that led to compounds with antiviral activity in replicon screens.[487] Substituting the sulfur atom with a CH_2 led to a 10-fold increase in replicon potency in a matched pair comparison, attributed to reduced acidity of the enol, with the added benefit of improved PK properties. Compound **194** emerged as an advanced prototype that inhibited GT-1a and GT-1b polymerases with IC_{50} values of 3 and 70 nM, respectively;

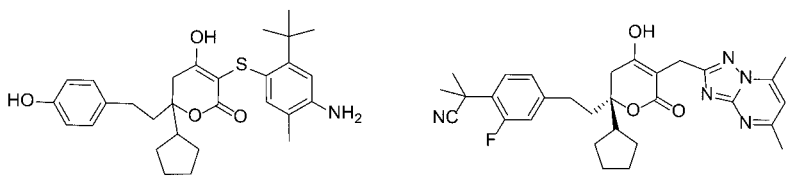

193 **194**

Fig. 52 Nonnucleoside-based HCV NS5B inhibitors **193** and **194**.

was active in a GT-1b replicon with an EC_{50} value of 15 nM; and demonstrated favorable oral bioavailability and clearance in rats.[487,488] However, development of **194** was abandoned due to potent CYP 2D6 inhibition, $IC_{50}=300$ nM, and the identification of a more stable polymorph during the scale-up process that was associated with 80-fold lower solubility.[448,488] The CYP 2D6 inhibition was determined to be associated with the cyano moiety attached to the fluorophenyl ring, an important structural element since it engaged the NH of Leu497 of NS5B in a direct H-bonding interaction, replacing the H_2O that mediated this interaction with the phenol **193**. A focus on modifications of the cyano phenyl moiety led to the identification of filibuvir (**175**) as a compound meeting criteria for advancement into clinical trials.[448,489] Preclinical profiling of **175** in a panel of chimeric subgenomic reporter replicons incorporating polymerase proteins from GT-1a and GT-1b clinical isolates revealed potent in vitro antiviral activity toward 95.8% of the strains, with an overall mean EC_{50} value of 0.59 nM.[489] In vitro resistance mapping studies identified Met423Thr as a mutation conferring 760-fold reduced susceptibility. In phase 1 clinical trials, antiviral efficacy with **175** was established at doses of 100, 300, and 450 mg BID and 300 mg TID for 8 days that were associated with mean maximal reductions in viremia of 0.97, 1.84, 1.73, and 2.13 $\log_{10}$ IU mL^{-1}, respectively.[490] Viral breakthrough was observed in almost half of the patients, mapped to changes of Met423 to Ile, Thr, or Val, although a small number of subjects harbored virus with mutations at Arg422 and Met426 that were also associated with reduced susceptibility in vitro.[490,491] Although **175** was advanced into phase 2b clinical trials where it was studied in conjunction with PEG-IFN-α and **1**, development was abandoned in Mar. 2013 for strategic reasons.[379]

The second major chemotype that binds to the thumb site II domain is a series of carboxylic acid derivatives that originated in two screening hits, the substituted phenylalanine **195**, $IC_{50}=1.8$ μM, and the thiophene carboxamide **196**, $IC_{50}=14$ μM (**Fig. 53**).[492–496] While optimization of both chemotypes was investigated, advancing the potency of the thiophene-based series, particularly in the replicon, was more facile and guided by NMR and X-ray cocrystal structure data.[494–498] Replacing the amide of **196** with a CO_2H enhanced potency by threefold and further optimization afforded VCH-759 (**197**) for which the presence of an *N*-alkyl substituent enhanced potency, particularly in replicons.[496] The key drug–target interactions between the NS5B enzyme and **195** and analogs of **197** were determined to be direct H-bonding interactions between the CO_2H moieties and the backbone N–H atoms of Ser476 and Tyr477, thus acting as functional isosteres of the acidic enol moiety of **193** and **194** and the intermediary H_2O molecule.[494,498,499] VCH-759 (**197**) exhibits antiviral activity in a GT-1b replicon, $EC_{50}=150$ nM, with major resistant mutations identified as Leu419Met and Met423Thr, which conferred eight- to 20-fold reduced susceptibility.[500] VCH-759 (**197**) was evaluated in phase 1 clinical trials where the maximal effect was observed at a dose of 800 mg BID, which reduced viremia by 2.46 $\log_{10}$ IU mL^{-1}.[377,501]

Further structural refinement afforded lomibuvir (**176**) that exhibits higher potency in replicons; EC_{50} values of 23 nM (GT-1a), 5–12 nM (GT-1b), and 4.6 μM (GT-2a); and good preclinical oral bioavailability in the rat and dog.[377,502] In a phase 1b clinical trial, lomibuvir (**176**) was administered to GT-1-infected subjects at a dose of 750 mg on a BID regimen for 3 days, which resulted in a 3.7 $\log_{10}$ IU mL^{-1} reduction in viral load.[377,379] However, development of **176** was halted in Mar. 2013 after results from a phase 2 clinical trial evaluating combination therapy with ribavirin (**1**) and telaprevir (**2**) suggested that the efficacy and safety profile of the combination would not be competitive with other drug regimens in development at that time.[380]

Radalbuvir (**177**) exhibits high-affinity binding to wild-type GT-1b polymerase, $K_D=1.35$ nM, which translates into potent HCV inhibition with EC_{50} values of <11 nM toward GT-1 and GT-5 replicons.[449,503] However, GT-2a, GT-2b, and GT-3a replicons are significantly less susceptible to **177**, with EC_{50} values of ≥ 30 μM, while GT-4a is more sensitive, $EC_{50}=348$ nM. The resistance profile for radalbuvir (**177**) is different to the other thumb site II inhibitors **175** and **176**, with selective pressure producing mutations primarily at Ile482Leu in GT-1a replicons and at Arg422Lys and Leu419Met in GT-1b replicons, while the Met423Thr is only threefold less susceptible.[503,504] Detailed mechanism of action studies has revealed that in order for binding by radalbuvir (**177**) to the polymerase to result in potent enzyme inhibition, both the β-loop and C-terminus regulatory elements must be present, suggesting that the compound stabilizes the full-length protein in a closed, inactive conformation that is dependent on intramolecular interactions mediated by the regulatory elements.[505] In a phase 1b clinical trial conducted in GT-1a- and GT-1b infected individuals, radalbuvir (**177**) was administered at doses ranging from 50 to 500 mg on either a BID or QD regimen.[504] Mean maximal reductions in viremia ranged from 2.18 $\log_{10}$ to 4.02 $\log_{10}$ IU mL^{-1} with doses of 100 mg BID associated with 3.4 $\log_{10}$ and 3.47 $\log_{10}$ IU mL^{-1} declines in viremia in GT-1a and GT-1b patients, respectively.

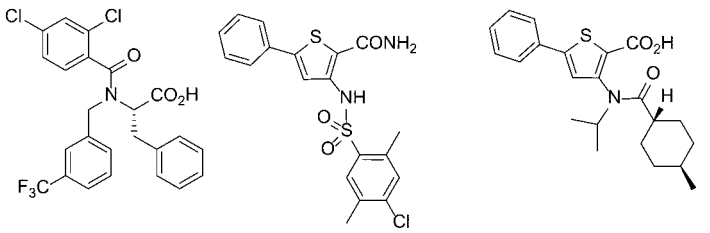

195 **196** **197** VCH-759

Fig. 53 Thiophene-based nonnucleoside HCV NS5B inhibitors **195–197**.

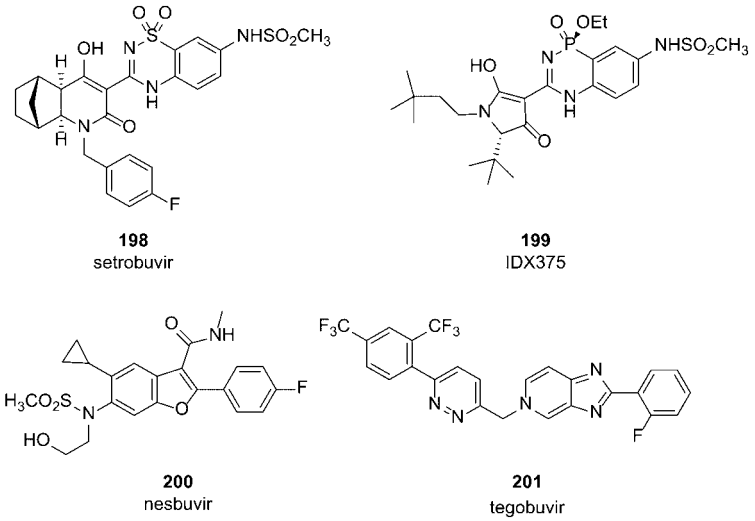

Fig. 54 Nonnucleoside HCV NS5B inhibitors **198–201**.

5.18.1.10.6 Palm site (primer grip) nonnucleoside inhibitors of HCV NS5B RdRp activity

Palm domain binding site inhibitors present a structurally diverse group of allosteric NS5B inhibitors that have been categorized based on their binding location, either palm site region I or II. The most prominent clinically evaluated palm site I HCV NS5B inhibitors are dasabuvir (**12**), setrobuvir (**198**), and IDX375 (**199**), while nesbuvir (HCV-796, **200**) and tegobuvir (**201**) are representative of inhibitors acting at palm site II that have demonstrated clinical efficacy (Fig. 54).[506–512]

5.18.1.10.7 Palm site I nonnucleoside inhibitors of HCV NS5B RdRp activity

The first palm site I inhibitor to be characterized was the benzo-1,2,4-thiadiazine **202**, discovered by high-throughput screening, which inhibited HCV polymerase with an IC_{50} of 100 nM and demonstrated antiviral activity in a GT-1b replicon, $EC_{50}=550$ nM (Fig. 55).[513,514] Preliminary SAR studies indicated the importance of the quinolone *N*-substituent since its absence or contraction to a methyl group resulted in an inactive compound, while the expansion of the side chain to the branched derivative **203** retained activity.[513–515] Resistance mapping studies with **202** identified Met414Thr as a key mutation that reduced susceptibility by 4 orders of magnitude.[516] Mode of action studies with **202** determined it to be an inhibitor of the initiation of RNA synthesis with no effect on elongation, potentially the result of the formation of a ternary complex composed of the inhibitor, the enzyme, and the RNA template.[517] The introduction of polarity into the *N*-alkyl side chain was generally detrimental to potency, while activity was preserved with an *N*-benzyl substituent but, interestingly, not the *N*-phenethyl homologue.[514,518] Substitution on the quinolone ring was largely restricted to small atoms or groups at C-5 and C-6, with C-6 more tolerant; substituents at C-7 led to reduced potency, while a fluorine was acceptable at C-8 but not NO_2. The enol moiety was critical for potency with a range of modifications or deletion leading to inactive compounds. *N*-Methylation of the benzo-1,2,4-thiadiazine was detrimental, attributed to the disruption of an intramolecular H-bonding interaction that stabilized the overall planar conformation observed in the cocrystal (a 20° twist between thiadiazine and quinolone rings). The cyclopropyl derivative **204** (SB-711845) was identified as a clinical candidate based on its in vitro inhibitory potency, $IC_{50}=49$ and 10 nM toward GT-1a and GT-1b enzymes, respectively; activity in a GT-1b replicon, $EC_{50}=38$ nM; and a preclinical PK profile that revealed low clearance and >35% oral bioavailability when dosed as a suspension in rat, dog, and monkey.[514] However, the potency of **204** in a replicon assay in the presence of 45 mg mL^{-1} of human serum albumin (HSA) and 1 mg mL^{-1} of alpha-1-acid glycoprotein (AAG) was significantly reduced, EC_{50} value of

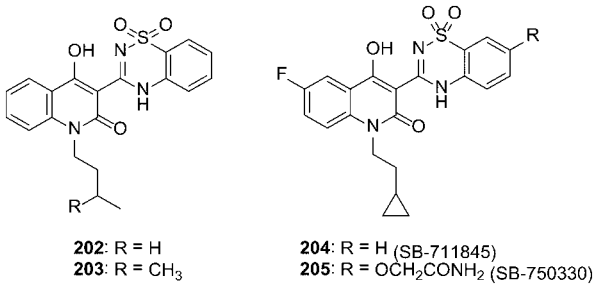

Fig. 55 Palm site nonnucleoside HCV NS5B inhibitors **202–205**.

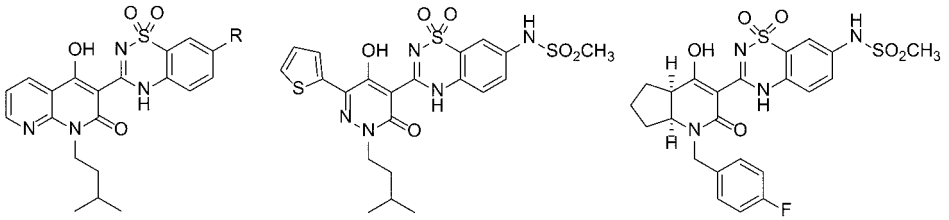

Fig. 56 Palm site I nonnucleoside HCV NS5B inhibitors **206–209**.

13 μM, providing a focus for further optimization that probed the effects of substitution of the benzo-1,2,4-thiadiazine ring.[518] Polar moieties at C-7 were found to be beneficial and SB-750330 (**205**) was selected as a second clinical candidate. This compound was 20-fold more potent in a GT-1b replicon than **204**, $EC_{50}=2$ nM, attributed to the oxyacetamide moiety more effectively occupying the pocket and the amide C=O engaging a side-chain NH of Asn291 in a H-bonding interaction, while potency in presence of HSA and AAG was also improved, $EC_{50}=1.48$ μM.[518]

Although neither of these compounds progressed into advanced clinical trials, the antiviral activity and favorable PK properties of this chemotype attracted considerable attention, and SARs associated with this class of NS5B inhibitor have been extensively explored.[515] The advantage of a sulfonamide substituent at C-7 of the benzo-1,2,4-thiadiazine was demonstrated in the context of the matched pair of naphthyridones **206** and **207** where the addition of this C-7 substituent conferred potent antiviral activity in GT-1a and GT-1b enzyme assays, IC_{50} values for **207** = 2 and 6 nM, respectively (Fig. 56).[519] Of particular importance was the enhanced GT-1a inhibition associated with **207** (since **206** exhibited only modest activity, $IC_{50}=310$ nM), which translated into potent antiviral activity in a GT-1a replicon, $EC_{50}=3$ nM. The importance of the sulfonamide moiety was recognized in a series of pyridazinones that formed the basis of an extensive set of studies where the focus was on optimizing potency and oral bioavailability.[520–523] Compound **208** potently inhibited replication of GT-1a and GT-1b replicons with respective EC_{50} values of 22 and 5 nM and demonstrated good metabolic stability in rat liver microsomes, $t_{1/2}=60$ minutes.[522] After oral administration of a single 3 mg kg^{-1} dose to rats, liver levels of **208** were ~1 μg g^{-1} at 4 hours post dose, over 240-fold higher than the concentration in plasma, while at 12 hours post dose, liver levels were ~40 ng g^{-1}, 64-fold higher than in plasma and 24-fold above the EC_{50} value for the GT-1b replicon.[522] However, the oral bioavailability of **208** in cynomolgus monkeys was poor despite good IV PK, attributed to poor absorption from the gastrointestinal tract due to the high polar surface area (PSA) of the molecule and P-gp-mediated efflux, necessitating further optimization. Fused pyridinones were explored as a vehicle for reducing PSA, with **209** characterized as a compound with good permeability in vitro, favorable PK properties in rats and monkeys, and potent antiviral activity in a GT-1b replicon, $EC_{50}=16$ nM.[524] However, despite being a potent inhibitor of a GT-1a enzyme, $IC_{50}<25$ nM, this compound was considerably less active in a GT-1a replicon, $EC_{50}=550$ nM, providing a key objective for the next phase of optimization of this chemotype.[508]

A cocrystal structure of **209** bound to GT-1b HCV NS5B revealed the key drug–target interactions (Fig. 57), providing an explanation for the beneficial effect of the sulfonamide moiety, which formed two direct H-bonding interactions with the enzyme

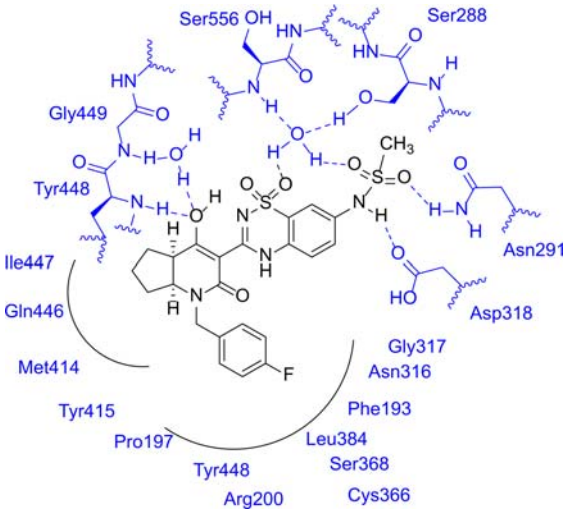

Fig. 57 Key drug–target interactions between **209** and the HCV NS5B GT-1b polymerase enzyme.

and one through the intermediacy of a H_2O molecule.[508,522] The structure also suggested that potency might be improved by probing the third dimension around the cyclopenta[*b*]pyridin-2-one ring by incorporating a bicyclic ring system designed to more effectively fill this pocket of the enzyme. Since the pocket is of a defined size, the preparation of only a limited series of target molecules was necessary in order to examine the concept and the preferred stereochemistry of the bicyclic ring system was quickly established as favoring the (2*S*,7*R*)-enantiomers found in setrobuvir (**198**).[508] Setrobuvir (**198**) was characterized as a potent inhibitor of the replication of GT-1b HCV, EC_{50} 3 nM, but the activity toward GT-1a is more variable with reported EC_{50} values ranging from 8 to 52 nM.[377,510,525–527] This has been attributed to the presence of Phe at residue 415 of the GT-1a RdRp that reduces susceptibility but which is Tyr in GT-1b sequences. Nevertheless, setrobuvir (**198**) is 7- to 30-fold more potent than the prototype **209**, confirming the design premise. Resistance development studies with setrobuvir (**198**) identified Met414Thr (EC_{50} = 470 nM), Met314Leu (EC_{50} = 300 nM), Gly554Asp (EC_{50} = 634 nM), and the dual combination of Met414Thr with Gly554Asp (EC_{50} = 20 μM) as mutants with reduced sensitivity.[509] Preclinical efficacy was established in HCV-infected chimpanzees, with a single dose of 30 mg kg^{-1} administered orally to two GT-1a-infected animals producing reductions in viremia amounting to 0.5 and 1.5 log_{10} IU mL^{-1}. A multiple-dose study in which two GT-1b-infected chimpanzees were administered with 30 mg kg^{-1} doses of **198** daily for 4 days resulted in a maximal viral load decline of 2.1 and 2.6 log_{10} IU mL^{-1}.[509] One animal maintained viral suppression throughout the dosing period, while the second experienced rebound beginning on day 2; sequencing of the viral RNA in each animal revealed the presence of the Gly544Asp mutation. In a phase 1b clinical study, doses of 200, 400, and 800 mg of setrobuvir (**198**) were administered orally on a BID dosing regimen for 3 days to subjects chronically infected with GT-1 and the effect on viremia compared with a placebo control.[528] At the end of the treatment period, viral load was reduced by 2.1, 2.2, and 2.9 log_{10} IU mL^{-1} in the 200, 400, and 800 mg cohorts, respectively, with GT-1b-infected subjects experiencing greater efficacy (range: 2.7 to 3.1 log_{10} IU mL^{-1}) than GT-1a-infected patients (range: 1.3 to 2.7 log_{10} IU mL^{-1}); no viral breakthrough was observed during therapy. Although setrobuvir (**198**) was advanced into combination trials with PEG-IFN-α and ribavirin (**1**), development of this compound appears to have been halted in early 2015.

IDX375 (**199**) is a palm site I inhibitor that combines a tetramic acid moiety with an unusual benzo[*c*][1,5,2]diazaphosphinine 1-oxide heterocycle that was formulated as its choline salt for clinical studies.[510,529] This compound expresses relatively balanced GT-1a and GT-1b inhibition in replicons with EC_{50} values of ~6.2 and 2.3 nM, respectively, and IC_{50} values of 30 and 18 nM toward the respective polymerase enzymes. IDX375 (**199**) is not overtly cytotoxic to a range of cell lines but its spectrum of inhibitory activity is restricted since it is much less active toward GT-2a, GT-3a, and GT-4a polymerases. In PK profiling, **199** exhibited 16–42% oral bioavailability in preclinical species, and the compound was successfully advanced through IND toxicology studies. In a small phase 1b study of **199** conducted in three HCV-infected subjects administered with two 200 mg doses, plasma exposure was fourfold higher than in NHVs and viral load declined by 0.5–1.1 log_{10} IU mL^{-1}.[528]

The second major class of palm site I inhibitor that has been evaluated in clinical studies originated with the high-throughput screening lead **210**, a dihydrouracil derivative that provided the template from which dasabuvir (**12**) and ABT-072 (**211**) were identified (**Fig. 58**).[506,513,530] Compound **210** inhibited GT1-a and GT-1b polymerases with IC_{50} values of 0.58 and 0.36 μM, respectively, but was inactive toward GT-2a, GT-2b, and GT-3a enzymes.[530] Mechanistic studies indicated that the compound was not interfering with RNA binding, and testing against a panel of mutant polymerases revealed reduced susceptibility to enzymes with mutations in the palm site I pocket. The Cys316Tyr mutant exhibited 100-fold resistance, while Met414Thr and Thr448Tyr were 24- and 41-fold less susceptible, respectively, but changes in the thumb region—Met423Thr and Pro495Ala—conferred only a fivefold reduced sensitivity. Details of the optimization of **210** to arrive at dasabuvir (**12**) and ABT-072 (**211**) have not been shared but both compounds were advanced into clinical trials and the preclinical profile of dasabuvir (**12**) has been described in some detail.[377,506] The in vitro biochemical and antiviral profiles of dasabuvir (**12**) and ABT-072 (**211**) are summarized in **Table 3** and reveal potent inhibition of GT-1 polymerases and replicons, with modest eight- to 17-fold shifts in the presence of 40% human serum, but much weaker activity toward GT-2a, GT-2b, GT-3, and GT-4a RdRp enzymes.[506,531,532] Both compounds exhibited high membrane permeability and their preclinical PK profiles indicated good oral exposure in rat and dog and preferential distribution to the liver.[531,532] In dose-ranging phase 2a clinical trials, dasabuvir (**12**) and ABT-072 (**211**) were evaluated briefly as monotherapy followed by 12 weeks of combination therapy with PEG-IFN-α and ribavirin (**1**).[533] ABT-072 (**211**) at doses of 100, 300, and 600 mg QD was associated with reductions in viremia ranging from 1.07 to 1.57 log_{10} IU mL^{-1} after 3 days, while administration of dasabuvir (**12**) at doses of 400 and 800 mg BID for 3 days produced mean maximum decreases in viral load of 1.08 and 0.97 log_{10} IU mL^{-1}, respectively. After completion of the study, SVR_{24} was achieved in 50%, 25%, and 86% of the subjects receiving

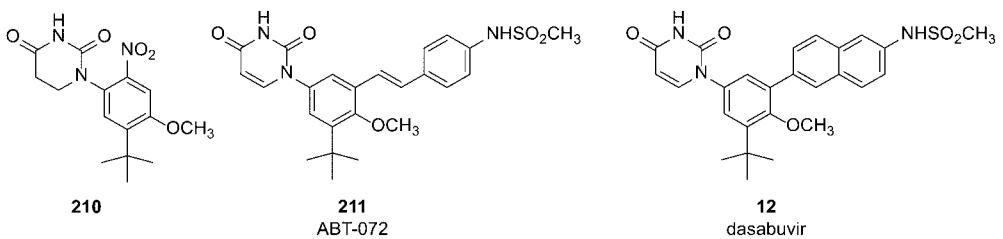

210 **211** ABT-072 **12** dasabuvir

Fig. 58 Palm site I nonnucleoside HCV NS5B inhibitors **210** and **211** and dasabuvir (**12**).

Table 3 The in vitro biochemical and antiviral profiles of dasabuvir (**12**) and ABT-072 (**211**)

Compound	*HCV NS5B RdRp inhibition IC_{50} (nM)*						*Replicon EC_{50} (nM)*	
	GT-1a	*GT-1b*	*GT-2a*	*GT-2b*	*GT-3a*	*GT-4a*	*GT-1a*	*GT-1b*
12	2.4–2.8	2.2–10.7	16,400	16,100 and >20,000	5600 and 11,900	900 and 3700	7.7 99[a]	1.8 21[a]
211	4.2–8.4	6.2–16.7	23,000	7500 and >20,000	1800–4700	2800 and 5400	1.1 19[a]	0.3 2.4[a]

[a]With 40% human plasma.

ABT-072 (**211**) and in 63% of both cohorts administered with dasabuvir (**12**), which compared with 9% in the placebo control group receiving PEG-IFN-α and ribavirin (**1**) alone.

There are many additional chemotypes that either bind to palm site I or bind in a fashion that is partially overlapping with it. The pyrrolidine diacid **212** (Fig. 59) available synthetically via a [3 + 2] cycloaddition between imines of amino acid esters and *tert*-butyl acrylate was deconvoluted from a combinatorial library mixture of 168 racemic compounds that inhibited a truncated GT-1b HCV NS5B enzyme, with the pure compound active in the biochemical screen with an $IC_{50} = 700$ nM.[534] The active enantiomer was determined to be as depicted in **212**, and further optimization was focused on modulating physical properties in an effort to identify compounds active in replicons.[535] The 2-carboxylate was demonstrably of importance since the ester was inactive and the primary amide over 10-fold less potent, leading to a focus on the C-4 and C-5 positions, which were explored via the preparation of combinatorial arrays of racemic compounds. These studies identified a 2-linked thiazole as the preferred C-5 element and replicon activity was initially detected with C-4 amide derivatives. Refinement of this structure was aided by X-ray cocrystallographic structures, which identified H bonds between the C-2 carboxylate and the NH of Gly449 and the benzamide C = O and the NH of Tyr448 as the key drug–target interactions. Further optimization focused on manipulating the benzamide substitution pattern while reducing polarity at C-4 in order to enhance membrane permeability, an enterprise that identified **213** as a homochiral compound displaying good oral bioavailability (59%) and low clearance (5 mL $min^{-1} kg^{-1}$) in the rat.[536] This compound inhibited a full-length GT-1b NS5B enzyme with an $IC_{50} = 440$ nM, potency that translated effectively into antiviral activity in a GT-1b replicon, $EC_{50} = 390$ nM, and was selected for clinical development.[537] However, this compound was subsequently replaced with GSK625433 (**214**), a more potent inhibitor that exhibited EC_{50} values of 290 and 3 nM in GT-1a and GT-1b replicons, respectively, and a modest three- to fourfold shift in potency in the presence of 40% human serum.[538] The difference in potency between the GT-1a and GT-1b enzymes was ascribed to the Tyr415Phe mutation in GT-1a that removes a water-mediated H bond between the phenol moiety and the thiazole nitrogen atom. GSK625433 (**214**) was also much less active toward GT-2a, GT-3a, GT-3b, and GT-4a enzymes, while resistance mapping experiments conducted in a GT-1b replicon identified Met414Thr and Ile447Phe as mutations with 83- and 170-fold reduced susceptibility, respectively.[538] Although GSK625433 (**214**) was advanced into clinical studies, development was terminated for reasons unknown.[539]

5.18.1.10.8 Palm site II nonnucleoside inhibitors of HCV NS5B RdRp activity

Nesbuvir (**200**) is a potent inhibitor of GT-1a and GT-1b replication in replicons, EC_{50} values = 5 and 9 nM, respectively, and of NS5B enzymatic activity with IC_{50} values ranging from 20 to 140 nM for GT-1a and 10 to 40 nM for GT-1b.[511] Representative GT-2, GT-3, and GT-4 polymerases were less susceptible with IC_{50} values of 1700, 220, and 570 nM, respectively. Resistance was mapped to mutations within palm site II, specifically changes at Cys316 and Ser365 that conferred substantial changes in sensitivity. Mutation of Cys316 to Asn, Phe, and Tyr was associated with 73-, 130-, and 167-fold changes, respectively, while Ser365Ala and Ser365Thr enzymes are, respectively, 41- and 212-fold less sensitive to inhibition. These residues are proximal to nesbuvir (**200**) in a cocrystal structure where the oxygen atom of Ser365 was observed to engage the N–H of the benzamide moiety in a H-bonding interaction, while larger side chains at Cys316 sterically interfere with the association of the core benzofuran heterocycle to the enzyme.[540,541] Indeed, the Cys316Asn mutation reduces the affinity of **200** for an NS5B enzyme construct by 2 orders of magnitude from a K_i value of 70 nM to 7 μM.[542,543] The Cys316Asn mutation occurs in 11–13% of GT-1b clinical samples isolated

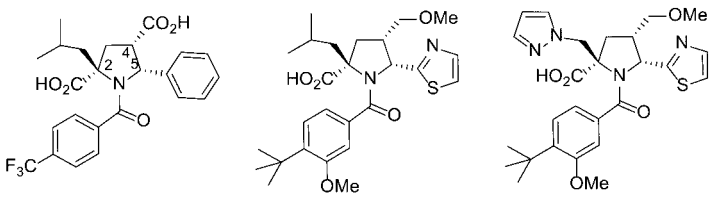

212 **213** **214** GSK625433

Fig. 59 Nonnucleoside HCV NS5B inhibitors **212–214**.

from DAA-naive subjects, although prevalence can be higher, potentially limiting the therapeutic efficacy of nesbuvir (**200**) in some patient populations.[544–546] In a phase 1b clinical trial, nesbuvir (**200**) was administered to HCV-infected patients at doses of 50, 100, 250, 500, 1000, and 1500 mg twice daily for 14 days as monotherapy, with the highest dose associated with a maximal fall in viremia (on day 4) of 1.4 $\log_{10}$ IU mL^{-1}.[511,547] However, viral rebound was observed, and by day 14, viral load was only 0.7 $\log_{10}$ IU mL^{-1} below baseline, coincident with the emergence of a Cys316Tyr mutation in the NS5B protein. In a subsequent phase 2 study of nesbuvir (**200**) administered at 500 mg BID in conjunction with PEG-IFN-α and ribavirin (**1**), serum ALT concentrations increased to three times the upper limit of normal in 13 of 162 patients after 8 weeks of dosing compared with ~1% of patients in the control group receiving only PEG-IFN-α and ribavirin (**1**).[511,548] Two patients who were described in some detail developed severe symptoms of liver toxicity after more than 15 weeks of dosing at which point therapy was suspended and both went on to recover. Notably, neither patient had detectable HCV RNA in their serum 6 months after the end of treatment.[546] The specter of hepatotoxicity, however, in a patient population already managing a liver insult presented a significant problem and clinical development of nesbuvir (**200**) was abandoned in 2008.[511,549]

The identification of the palm site II inhibitor GSK2485852 (**215**) relied upon a computer-aided drug design approach that sought to hybridize the unique chemical properties of a boronic acid moiety with the antiviral attributes of nesbuvir (**200**) in a fashion that would overcome some of the limitations of this compound associated with its resistance profile.[550–552] The site of installation of the boronic acid functionality on the nesbuvir (**200**) template was guided by the principle of placing this structural element proximal to the incoming nucleoside triphosphate where it was anticipated to interfere with RNA processing or modulate the conformation of the protein.[550] This analysis suggested the hydroxyethyl side chain as the optimal location, and a series of compounds were prepared that installed a boronic acid-containing moiety at the sulfonamide *N* atom. Biological evaluation was guided by an initial focus on introducing potent antiviral activity toward the Cys316Asn and Cys361Tyr mutant viruses with subsequent studies directed toward improving PK properties. GSK2485852 (**215**) was identified as a compound meeting the targeted antiviral criteria with EC_{50} values of 3 and 1.7 nM toward WT GT-1a and GT-1b replicons, 1.9 nM toward the GT-1b Cys316Asn mutant, and 3.2 and 1.4 nM in GT-1a and GT-1b Cys316Tyr mutants, respectively (Fig. 60).[550,553] This molecule takes full advantage of the unique properties of the boronic acid since replacing it with carboxylic, sulfonic, and phosphonic acid moieties resulted in compounds with markedly inferior profiles in replicons. Kinetic analysis of the interaction of GSK2485852 (**215**) with a GT-1b Cys316Asn mutant NS5B indicated a 40-fold slower dissociation rate compared with nesbuvir (**200**) and preservation of the initiation inhibitory mechanism observed with the prototype. X-ray cocrystallographic structures with WT GT-1a, Cys316Tyr GT-1a, and Cys316Asn GT-1b NS5B enzymes revealed the molecular basis for the potent antiviral activity toward these viruses.[550] Interestingly, association of **215** with the RdRp protein did not depend on covalent bond formation between the boronic acid and the protein, perhaps surprising based on the chemical reactivity of this moiety, but rather, a network of H-bonding interactions with Met414 and Tyr488 in addition to bound H_2O molecules. GSK2485852 (**215**) exhibited potent antiviral activity toward GT-3a, GT-4a, and GT-5a chimeric replicons with EC_{50} values close to that of the wild-type GT-1b replicon, while a GT-2a replicon was somewhat less sensitive but still half-maximally inhibited at a drug concentration of <10 nM.[553] Although GSK2485852 (**215**) was advanced into clinical trials where a single orally administered 420 mg dose resulted in 1.33 $\log_{10}$ IU mL^{-1} decline in viremia, development was terminated in Aug. 2012 due to poor human PK properties associated with rapid metabolism and the observation of an undisclosed toxicity on repeat dosing.[380,550,554]

The HCV inhibitor tegobuvir (**201**) was developed using a phenotypic approach to lead identification based on the BVDV inhibitor **216**, and SAR optimization was guided by replicon inhibitory activity.[512,555–557] The *ortho*-fluoro substituent on the 2-phenyl ring of tegobuvir (**201**) was found to be important for conferring HCV inhibition but SARs for inhibition of the two viruses were found to be divergent, although molecules with dual activity were identified.[512,556,557] Tegobuvir (**201**) inhibited GT-1a and GT-1b replicons with EC_{50} values of 13.8 and 0.8 nM, respectively, but chimeric replicons incorporating GT-2 to GT-6 polymerase sequences were much less susceptible to inhibition, EC_{50} values of >100 nM, with sensitivity traced to a Cys445Phe mutation present in the latter genotypes.[558,559] Resistance mapped to mutations in the NS5B polymerase, most notably Cys316Tyr, Tyr448-His, Tyr452His, and Cys445Phe, which when individually reverse engineered into a GT-1b replicon conferred 7- to 36-fold reduced sensitivity. However, tegobuvir (**201**) presented an interesting mechanistic conundrum since it failed to inhibit NS5B enzymatic activity in biochemical assays and biophysical analyses failed to detect binding of the compound to the protein.[512,558,560] A Western blot analysis of HCV nonstructural proteins in a GT-1b replicon exposed to tegobuvir (**201**) revealed two NS5B species, with the size of the unnatural band correlating with inhibitor potency. Mass spectrometric analysis of the additional protein indicated a mass

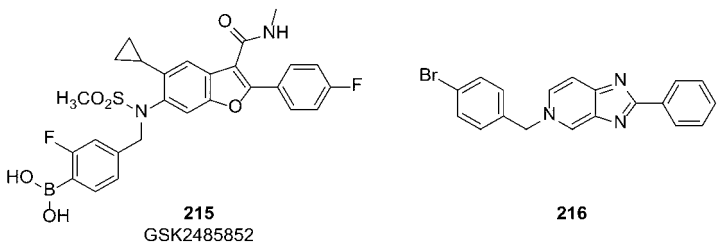

215
GSK2485852

216

Fig. 60 Palm site II nonnucleoside HCV NS5B inhibitors **215** and **216**.

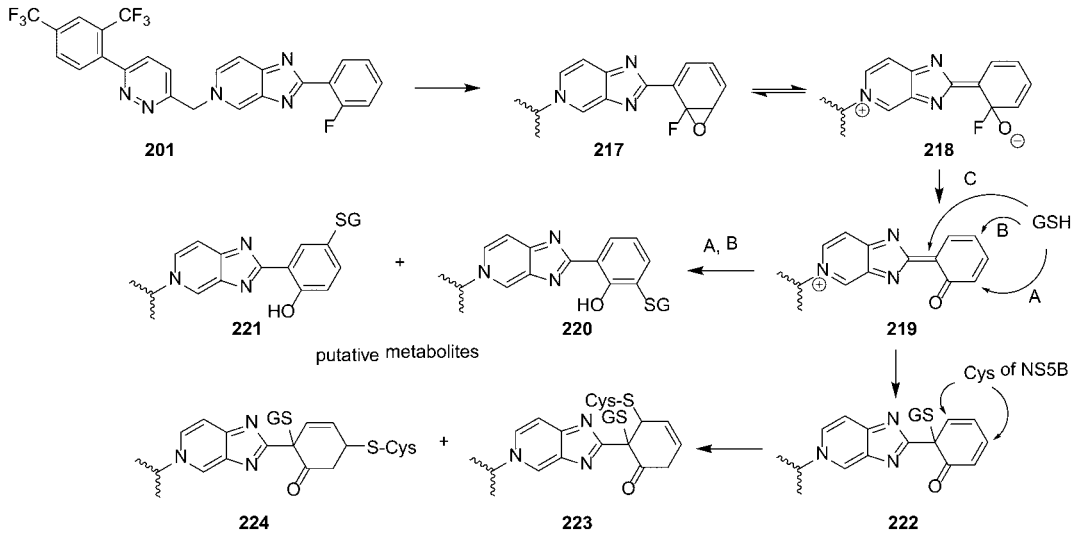

Scheme 3 Proposed mechanism of bioactivation and HCV NS5B inhibition by tegobuvir (201).

increase of 820 Da, a difference that correlated with the molecular weight of a tegobuvir (**201**) metabolite that involved the addition of glutathione (GSH) coupled with the loss of fluorine, leading to the hypothesis that a metabolite of **201** was responsible for the antiviral acitivity.[560] This was corroborated by the observation that CYP inhibitors abrogated the activity of tegobuvir (**201**), narrowed to CYP 1A1 when it was observed that expression of this enzyme in HeLa cells carrying HCV replicons restored inhibitory activity.[558,560] The mechanism proposed to account for these observations is summarized in **Scheme 3** and relies upon an initial metabolic activation of the fluorophenyl ring to the epoxide **217**. Epoxide **217** is thought to undergo ring opening and loss of fluoride via **218**, a process assisted by the extended electronic interaction with the dihydropyridine ring, to afford the highly reactive electrophile **219**. Addition of GSH to **219** via path A or B followed by rearomatization affords the suspected metabolites **220** or **221**, while addition of GSH to the exocyclic double bond (path C) does not allow rearomatization of the ring but rather preserves electrophilicity, allowing **222** to react with a Cys of HCV NS5B to afford the putative adducts **223** or **224**.[560] The identity of the amino acid residue reacting with **222** has not been identified but speculation has implicated Cys366 since this has been shown to be susceptible to modification by soft electrophiles and sulfenylating agents that inhibit NS5B polymerase.[561–563]

In a phase 1 clinical trial conducted in HCV GT-1-infected subjects who were administered with 40 or 120 mg of tegobuvir (**201**) on a BID schedule for 8 days, viremia declined by 1.61 and 1.95 $\log_{10}$ IU mL^{-1}, respectively.[241,377] In a follow-up phase 2 study, dosing of tegobuvir (**201**) was restricted to 40 mg BID due to concerns over QT prolongation, and this dosing regimen was examined in combination with the NS3 protease inhibitor **78** (75 mg BID) with and without ribavirin (**1**) or PEG-IFN-α for 28 days at which point all patients were switched to **1** and PEG-IFN-α.[377] In the dual DAA therapy arm, viral load declined by a median 4.1 $\log_{10}$ IU mL^{-1} but significant breakthrough was observed and only 13% of the cohort achieved RVR, while all patients receiving quadruple therapy achieved RVR.[241,377] Although tegobuvir (**201**) was the subject of several additional clinical studies in combination with other DAAs, development of the compound was ended in 2013.[564]

An interesting variation on the structure of tegobuvir (**201**) that was designed to address the hERG liability associated with this compound focused on reducing basicity.[565] This approach was studied in the context of the imidazopyridazine **225** (**Fig. 61**), which has a calculated pK_a for the core scaffold that is 3.6 units lower than the identically substituted imidazopyridine. Systematic SAR studies that examined all elements of the molecule identified the phenol ether **226** as an optimized compound, $EC_{50} = 22$ and 3 nM toward GT-1a and GT-1b replicons, respectively. The ester **227** was prepared as part of the SAR survey and found to exhibit comparable antiviral activity to **226** but several attempts to prepare the corresponding carboxylic acid by saponification always resulted in isolation of **226**. This suggested that under the assay conditions, **227** was converting to **226**, a thesis confirmed by analysis of the replicon supernatant, and the compound was determined to be unstable in biological media but stable in aqueous medium at pH 2 or 7. This fortuitous finding proved to be useful since the PK of **226** was less than optimal, with 33% and 12% oral bioavailability in

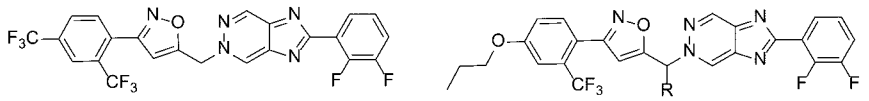

Fig. 61 Palm site II nonnucleoside HCV NS5B inhibitors **225**–**227**.

the rat and dog, respectively. However, administering **227** resulted in a significant increase in the plasma exposure of **226**, with F = 80% and 51% in the rat and the dog, respectively; moreover, the ester exhibited improved exposure on dose escalation. Plasma exposure was further enhanced by manipulating the identity of the ester moiety, which acts as a traceless prodrug moiety.[565]

5.18.1.11 HCV Internal Ribosome Entry Site (IRES) Inhibitors

The initiation of HCV polyprotein translation relies upon an IRES that extends from position 40 to 372 of the 5′ untranslated region of the viral RNA and is well conserved across virus genotypes.[566] This region of the viral genome adopts a highly structured fold that is defined by two major domains, labeled II and III, that contain the structural elements responsible for recognizing and recruiting the two initiation factors eIF2 and eIF3 and the 40S ribosome.[567–569] Flexible interconnecting linkers intervene between these domains and between domain III and domain IV where the AUG start codon is located in a stem loop structure at positions 342–344.[567–569] The earliest approach to targeting the HCV IRES relied upon antisense technology and ISIS-14803, a 20-unit phosphorothioate oligodeoxynucleotide designed to complement nucleotides 330–349 of the HCV IRES, inhibited HCV protein expression and replication in cell culture, and was active in a mouse model of HCV infection.[570,571] ISIS-14803 was evaluated in a phase 1 clinical trial where it was administered to subjects chronically infected with HCV as a 2 hr IV infusion at doses of 0.5, 1, and 2 mg kg^{-1} three times per week for 4 weeks with a 7-day washout period following the first dose.[572] However, plasma viral RNA was not reduced in the majority of the patients with just 3 of the 20 treated individuals experiencing transient reductions of 1.2–1.7 $\log_{10}$ IU mL^{-1} that persisted for up to 32 days. A follow-up phase 2 study conducted in GT-1-infected subjects evaluated doses of 0.5, 1, 2, and 3 mg kg^{-1} administered IV or subcutaneously 3 times a week for 4 weeks and produced a qualitatively similar result with only limited efficacy observed in 11 of 24 patients, while 17 subjects experienced ALT flares, a profile that that led to the development of the compound being terminated.[573,574]

The design of small molecules that target the various forms of RNA is an underexploited approach to drug discovery and an area of considerable contemporary interest where the focus is on developing a deeper understanding of the structure of RNA motifs and specifically the kinds of interactions that can be taken advantage of with small molecules.[575,576] The observation from cryoelectron microscopy studies that domain II of the HCV IRES induces a conformational change in the 40S ribosomal subunit once it is bound to elements of domain III, an event that is important for initiating translation, provided the basis of a high-throughput screen that sought small molecules binding to domain IIa.[577,578] A 29-mer derived from **228** (**Fig. 62**), which represents the stem loop of domain IIa, was prepared along with a 33-mer structured RNA used as a control and compounds selectively binding to **228** were identified using mass spectrometry. The 2-aminobenzimidazole **229** was characterized as an initial lead that bound to the 29-mer RNA with a K_d of 100 μM and exhibited a threefold selectivity compared with binding to the control RNA.[578] An optimization campaign found that introducing a second basic amine moiety at C-6 of the core improved affinity, and further refinement involved the introduction of conformational constraint. This design process arrived at **230**, a racemic mixture of *cis* and *trans* diastereomers, that bound to the 29-mer RNA with a K_d of 0.72 μM, representing a 25-fold improvement over the lead. Compound **230** exhibited antiviral activity in a subgenomic replicon, reducing HCV RNA levels with an EC_{50} value of 5.4 μM without overt cytotoxicity, $CC_{50} > 100$ μM. Mapping of the binding site using protection against RNase-mediated degradation of a larger 40-mer RNA identified uridine-55 and cytosine-56, residues in the bulge of **228**, as the ligand-binding region. Subsequent NMR studies with an analog of **230** binding to a 38-mer RNA that encompassed the sequence defined by **227** determined that inhibitor association with the bulge resulted in a structural reorganization of the RNA.[579] This study revealed that in the presence of the small-molecule ligand, the helical regions adjacent to the binding site adopted a coaxial structure that in the fuller IRES would be expected to orient the domain II apical loop away from the ribosomal E-site where eIF5 binds to the 40S

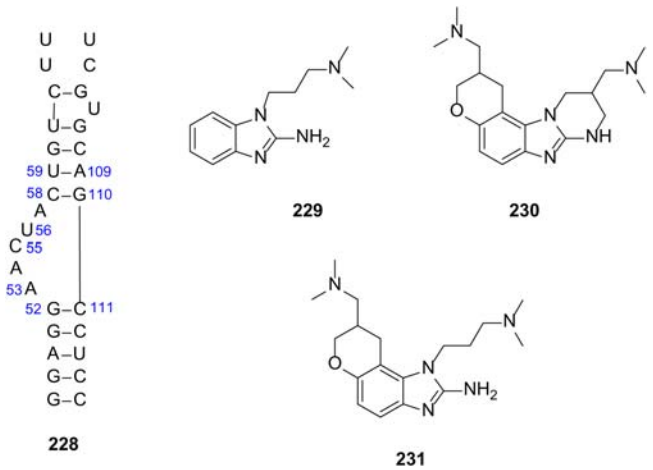

Fig. 62 Structure of a stem loop of domain IIa of the HCV IRES (**228**) and HCV IRES inhibitors **229–231**.

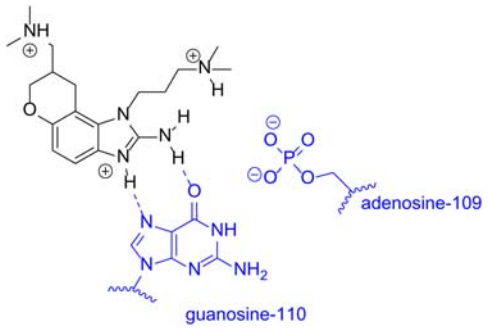

Fig. 63 Key interactions between **231** and elements of domain IIa of the HCV IRES.

subunit. X-ray crystallographic studies of the native domain IIa revealed an L-shaped structural motif that plays a key role in positioning the domain II hairpin into the ribosomal E-site. In the presence of inhibitor **231**, which binds into a deep cavity, domain II is stabilized in a more linear architecture that prevents it from associating with the ribosomal E-site.[569,580–582] The inhibitor **231** associates with the heterocycle of the guanine of the cytosine-58–guanosine-110 base pair via H-bonding interactions and engages adenosine-53, which forms the ceiling of the binding pocket (Fig. 63).[569,582] In addition, the guanosine-52–cytosine-111 base pair, which forms the floor of the binding cavity, is involved in stacking interactions with the heterocycle of **231**, while the protonated dimethylamine side chain attached to the benzimidazole core interacts with the phosphate moiety of adenosine-109. The essential nature of guanosine-110 in ligand recognition was confirmed by analyzing two double mutants in which the crucial cytosine-58–guanosine-110 base pair was replaced by either a guanosine58–cytosine-110 or uridine-58–adenosine-110 base pair, with neither undergoing a conformational change in the presence of **231**.[582]

In contrast to the observations with the benzimidazoles **229–231**, the substituted lysine derivative **232** appears to act in a complementary fashion by competing with structurally important Mg^{2+} ions to stabilize the domain IIa RNA in the L-shaped conformation, with speculation suggesting that this interaction interferes with ribosome release.[569,583] Compound **232** was identified using an RNA-binding screen similar to that described earlier in the text, and no change in conformation of the RNA using a FRET assay was detected, in contrast to the observations with **229–231**.[583] In a cell-based replicon assay, **232** inhibited HCV IRES-mediated translation of a luciferase reporter at low micromolar concentrations that were not overtly toxic to the host cell line.

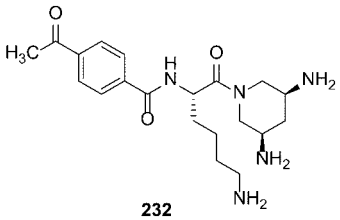

232

The residues that surround the binding site of **230** are >99% conserved across 1600 HCV clinical isolates, with adenosine-109 and cytosine-111 completely conserved and only three residues within domain IIa, adenosine-57, cytosine-104, and guanosine-107, exhibiting polymorphisms. These observations suggest that IRES inhibitors may be have a high genetic barrier to the emergence of resistance since mutations would be expected to compromise IRES function.[582] However, while these HCV IRES inhibitors are mechanistically interesting and provide some insight into approaches to productively targeting RNA, as HCV inhibitors in cell-based assays, they offer limited potency and thus remain prototypes that require considerable additional optimization if they are to be transformed into potential drug candidates.

5.18.2 Drug Combinations in Clinical Trials

The drug discovery programs that began in the decade after the identification and characterization of HCV in 1989 developed in parallel with the evolution of HCV therapy from poorly effective daily doses of INF-α alone to weekly subcutaneous administration of PEG-IFN-α along with daily oral doses of ribavirin (**1**). This combination offered improved but still far from ideal cure rates (~50%) and with the burden of a significant incidence of unpleasant side effects over the 24–72 weeks of therapy associated with each drug. These early drug discovery efforts were hampered by the lack of a convenient cell culture system that supported HCV replication and the only animal model available was the chimpanzee, which could not be used routinely because of the expense. The advent of subgenomic replicons in 1999 represented a crucial advance that catalyzed drug discovery initiatives by providing a cell-based system that assessed the antiviral activity of candidate compounds in a more relevant environment while generating a target for plasma concentrations in vivo.[38] The impediment presented by the dearth of animal models was

circumvented by advancing compounds directly into clinical trials, where the efficacy of inhibitors could typically be assessed after just a few days of dosing to chronically infected subjects. Preclinical profiling of candidate compounds generally assessed PK parameters in several species and demonstrated liver exposure, typically in rats, with human dosing projections based on attaining plasma and/or liver levels that exceeded the replicon EC_{50} value. During much of the early period of DAA discovery and development, it was not clear if DAA combinations would be sufficient to cure HCV in the absence of the immune stimulation contributed by PEG-IFN-α and the indirect antiviral effects associated with **1**, particularly in difficult-to-treat populations.[584,585] There were also a large number of failures along the way with many of the early DAAs; indeed, almost all of the molecules that provided clinical proof of concept for a specific mechanism of action were terminated because of either preclinical or clinical toxicity or efficacy issues, the sole exception being the NS5A inhibitor daclatasvir (**7**).[73,74] It was estimated that by Mar. 2015, 712 candidate drugs had been considered for the treatment of HCV infection, of which 588 had failed, 12 had achieved marketed status and 112 were still in development.[74] However, the issues encountered by the pioneering molecules were of value in as much as they provided follow-on compounds with a clearer path toward clinical success.

Clinical trials with the early HCV DAAs **2** and **3** were by necessity studies of these drugs as add-on therapy to PEG-IFN-α and ribavirin (**1**), with both drugs approved based on improving response rates in GT-1-infected naive and experienced subjects from 45–55% to 65–75%.[586–589] However, therapy was still based on 48 weeks of treatment, the DAAs were administered on a TID schedule and each brought an additional tolerability burden, with **2** associated with a significant occurrence of rash and pruritus (35–59%), while **3** resulted in a worsening of anemia and a higher incidence of thrombocytopenia.[590,591] The first step toward DAA-only therapy was a small, 13-day clinical trial evaluating the combination of danoprevir (**65**) and mericitabine (**162**) in treatment-naive subjects and null responders.[592] The highest dose tested resulted in a 5.1 $\log_{10}$ IU mL^{-1} reduction in viral load measured on day 14 and all of these patients then continued on PEG-IFN-α and ribavirin (**1**) for 46 weeks. However, a key turning point in the development HCV DAAs occurred in 2012 with the publication of the results of a small phase 2a clinical study evaluating the combination of the NS3 inhibitor asunaprevir (**6**) and the NS5A inhibitor daclatasvir (**7**) in GT-1-infected subjects who either had failed to respond to PEG-IFN-α and ribavirin (**1**) (null responders) or experienced an initial reduction in viral load but ultimately failed therapy.[593] This study evaluated the combination of **6** and **7** with and without PEG-IFN-α and **1** for 24 weeks in what was considered to be the most difficult patient population to treat. All patients in the cohort of 10 receiving the quadruple therapy achieved SVR_{12} and 9 achieved SVR_{24}, while in the dual-therapy arm, 4 of 11 patients achieved SVR_{12} and SVR_{24}. Two of these subjects were infected with GT-1b virus and two were infected with a GT-1a strain, while the remaining seven patients, all of whom experienced viral breakthrough during therapy, were infected with GT-1a virus. The rapid emergence of resistance in the GT-1a-infected subjects can be attributed to the lower genetic barrier to resistance of this genotype that frequently requires only a single base pair change in order to code for a different amino acid, while genotype 1b generally requires two changes.[594–596] These results were important because they demonstrated for the first time that a chronic HCV infection could be cured without the use of immune stimulation by PEG-IFN-α and/or the inclusion of ribavirin (**1**) and were described as *a watershed moment in the treatment of hepatitis C*.[597] This clinical trial set the stage for what subsequently became an extensive study of DAA combinations that were evaluated in a wide range of patient populations extending to genotypes beyond GT-1 and including patients with and without cirrhosis, the renally impaired, those coinfected with HIV-1, and those in the post-liver transplant setting in addition to evaluating the effects of shortening the duration of therapy.

Whereas the combination of **6** and **7** would require a third agent to enhance efficacy in the treatment of GT-1a infections, the results with GT-1b-infected subjects provided the basis for a focus on phase 2 and phase 3 clinical trials in Japan where GT-1b is the predominant infecting strain, studies that ultimately led to this being the first DAA combination to achieve regulatory approval that occurred in July 2014.[69,598,599] In combination with the NS5B inhibitor beclabuvir (**185**), **6** and **7** effect high rates of cure (≥87%) in noncirrhotic and cirrhotic patients, while the combination of **7** with sofosbuvir (**4**) is an effective treatment of GT-1, GT-2, and GT-3 infections in subjects who are naive to or experienced with therapy, HIV-1-coinfected subjects, and those in the post-liver transplant patient population.[600–604]

The combination of sofosbuvir (**4**) and ledipasvir (**8**) is associated with >90% cure rates in GT-1 infections against a range of background conditions that include those naive to therapy or previously treated, those with or without cirrhosis, and subjects who are coinfected with HIV-1.[605–610] In a phase 2a clinical study conducted in therapy-naive GT-1-infected patients without cirrhosis, intensifying this dual-combination therapy to include either the NS5B inhibitor radalbuvir (**177**) or vedroprevir (GS-9451, **233**), a potent inhibitor of GT-1 HCV NS3 protease, resulted in 19 of 20 subjects achieving SVR_{12} in each arm after just 6 weeks of therapy.[611–614]

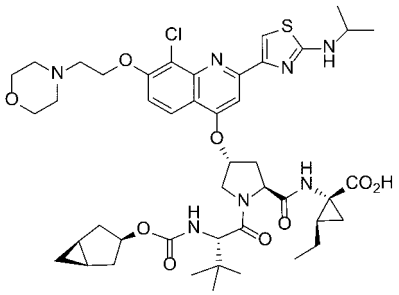

233
vedroprevir (GS-9451)

The fixed-dose combination of sofosbuvir (**4**) and ledipasvir (**8**) is an effective therapy for GT-4 infections, but GT-2 and GT-3 infections require the addition of ribavirin (**1**) in order to achieve high SVR_{12} rates, although GT-2 and GT-3 infections can be treated effectively with sofosbuvir (**5**) and ribavirin (**1**) alone.[70,615,616] However, 12 weeks of therapy of a fixed-dose combination of sofosbuvir (**4**) and velpatasvir (**130**) provided SVR_{12} rates of 95 to >99% in HCV genotypes 1–6, providing a well-tolerated pan-genotypic drug regimen.[617–620] In patients with advanced cirrhosis or those who had failed previous therapy, the SVR_{12} rates ranged from 89 to 91%, while for those with decompensated cirrhosis, the cure rates were 83% in the absence of **1** and 94% when this drug was included in the regimen.

Viekira Pak™ was developed for the treatment of GT-1 infections and is associated with high rates of cure in treatment-naive and treatment-experienced patients with and without cirrhosis, those coinfected with HIV-1, and those in a post-liver transplant setting where SVR_{12} rates are in excess of 85%.[71,621–625] Cirrhotics fare better with the addition of ribavirin (**1**) to the regimen and this therapy is also effective in those infected with GT-4, where SVR_{12} rates in excess of 95% were achieved in a phase 2b clinical trial conducted in experienced patients and those naive to therapy.[626]

There are several additional drug combinations in advanced clinical studies or that have completed phase 3 trials that are designed to be effective against all genotypes and that, if successful, will add to the available options to treat HCV infection.[564,627,628]

5.18.3 Conclusion

The advent of combination antiretroviral therapy in 1995 had a significant impact on mortality due to HIV-1 infection, with a rapid and marked decline in death rates following the approval of the first protease inhibitors that were combined with existing nucleoside analogs.[629,630] By 2007, HCV infection had surpassed HIV-1 as a cause of mortality in the United States.[631] Predictions of morbidity and mortality as a consequence of HCV infection in the absence of effective therapy suggested a continuous rise in the incidence of serious complications arising from the disease that would peak between 2030 and 2035 before subsiding.[632–634] This analysis estimated 38,600 cases of end-stage liver disease, 3200 liver transplant referrals, and 36,100 deaths that would occur annually during the peak years. The successful development of orally acting DAAs that are well tolerated and lead to high rates of cure of HCV infection after 8–24 weeks of therapy has the potential to significantly alter the course of these predictions and reduce the significant morbidity and mortality that was anticipated in their absence.[15,635,636] However, many questions remain concerning the precise outcome of curing HCV infection for individual patients as a fuller understanding of the effects of chronic infection on the liver and the potential for fibrosis and cirrhosis to reverse as well as the outcome of the insult placed on extrahepatic sites becomes more apparent from experience.[637] While the DAA combinations that have been approved or are in late stages of clinical testing offer high rates of cure are well tolerated and cost-effective, the scope of the epidemic is presenting a significant financial challenge for health authorities to manage.[638–642] Nevertheless, the development of DAAs that cure chronic HCV infection with well-tolerated drugs administered orally on convenient dosing schedules represents a medical triumph that has its roots firmly in the basic science and intellectual creativity associated with contemporary drug design and development.[11–16]

Acknowledgment

Dr. Brett Beno (Department of Computer-Assisted Drug Design, Bristol-Myers Squibb Research and Development, Wallingford, CT) is thanked for providing Fig. 41 and Dr. Makonen Belema (Department of Discovery Chemistry, Bristol-Myers Squibb Research and Development, Wallingford, CT) is acknowledged for his careful review of the manuscript.

See also: 5.20. Antiviral Drugs for Acute Infections. 8.23. Harvoni: A Combination Therapy for Curing HCV. 8.24. Discovery of Boceprevir and Narlaprevir: Ketoamide-Derived HCV NS3 Serine Protease Inhibitors for the Treatment of Chronic Hepatitis C.

References

1. Asselah, T.; Marcellin, P. Optimal IFN-Free Therapy in Treatment-Naïve Patients With HCV Genotype 1 Infection. *Liver Int.* **2015,** *35* (Suppl. 1), 56–64.
2. Peter, J.; Nelson, D. R. Optimal Interferon-Free Therapy in Treatment-Experienced Chronic Hepatitis C Patients. *Liver Int.* **2015,** *35* (Suppl. 1), 65–70.
3. Keam, S. J.; Cvetkovíc, R. S. Peginterferon-α-2a (40 kD) Plus Ribavirin. A Review of Its Use in the Management of Chronic Hepatitis C Mono-Infection. *Drugs* **2008,** *68,* 1273–1317.
4. Aghemo, A.; Grazia Rumi, M.; Colombo, M. Pegylated Interferons α2a and α2b in the Treatment of Chronic Hepatitis C. *Nat. Rev. Gastroenterol. Hepatol.* **2010,** *7,* 485–494.
5. Ghany, M. G.; Strader, D. B.; Thomas, D. L.; Seeff, L. B. Diagnosis, Management, and Treatment of Hepatitis C: An Update. *Hepatology* **2009,** *49,* 1335–1374.
6. Bota, S.; Sporea, I.; Şirli, R.; Popescu, A.; Neghină, A. M.; Dănilă, M.; Sträin, M. Severe Adverse Events During Antiviral Therapy in Hepatitis C Virus Cirrhotic Patients: A Systematic Review. *World J. Hepatol.* **2013,** *5,* 120–126.
7. Dusheiko, G. Side Effects of Alpha Interferon in Chronic Hepatitis C. *Hepatology* **1997,** *26* (Suppl 1), 112S–121S.
8. Manns, M. P.; Wedemeyer, H.; Cornberg, M. Treating Viral Hepatitis C: Efficacy, Side Effects, and Complications. *Gut* **2006,** *55,* 1350–1359.
9. Fried, M. W. Side Effects of Therapy of Hepatitis C and Their Management. *Hepatology* **2002,** *36,* S237–S244.

10. European Association for the Study of the Liver. EASL Recommendations on Treatment of Hepatitis C 2015. *J. Hepatol.* **2015,** *63,* 199–236.
11. Pawlotsky, J.-M. Hepatitis C Virus: From Discovery to Eradication in 40 Years? *Clin. Microbiol. Infect.* **2011,** *17,* 105–106.
12. Pawlotsky, J.-M. New Hepatitis C Therapies: The Toolbox, Strategies, and Challenges. *Gastroenterology* **2014,** *146,* 1176–1192.
13. Heim, M. H. 25 Years of Interferon-Based Treatment of Chronic Hepatitis C: An Epoch Coming to an End. *Nat. Rev. Immunol.* **2013,** *13,* 535–542.
14. Gane, E. Hepatitis C Beware — The End Is Nigh. *Lancet* **2014,** *384,* 1557–1560.
15. Chung, R. T.; Baumert, T. F. Curing Chronic Hepatitis C — The Arc of a Medical Triumph. *N. Engl. J. Med.* **2014,** *370,* 1576–1578.
16. Edlin, B. R.; Winkelstein, E. R. Can Hepatitis C be Eradicated in the United States? *Antivir. Res.* **2014,** *110,* 79–93.
17. Sheridan, C. FDA Approvals Usher in the Post-Interferon Era in HCV. *Nat. Biotechnol.* **2014,** *32,* 3–5.
18. Choo, Q. L.; Kuo, G.; Weiner, A. J.; Overby, L. R.; Bradley, D. W.; Houghton, M. Isolation of a cDNA Clone Derived from a Blood-Borne Non-A, Non-B Viral Hepatitis Genome. *Science* **1989,** *244,* 359–362.
19. Trepo, C. A Brief History of Hepatitis Milestones. *Liver Int.* **2014,** *34* (Suppl 1), 29–37.
20. Houghton, M. Discovery of the Hepatitis C Virus. *Liver Int.* **2009,** *29,* 82–88.
21. Houghton, M. The Long and Winding Road Leading to the Identification of the Hepatitis C Virus. *J. Hepatol.* **2009,** *51,* 939–948.
22. Choo, Q. L.; Richman, K. H.; Han, J. H.; Berger, K.; Lee, C.; Dong, C.; Gallegos, C.; Coit, D.; Medina-Selby, R.; Barr, P. J.; Weiner, A. J.; Bradley, D. W.; Kuo, G.; Houghton, M. Genetic Organization and Diversity of the Hepatitis C Virus. *Proc. Natl. Acad. Sci. U. S. A.* **1991,** *88,* 2451–2455.
23. Kato, N.; Hijikata, M.; Ootsuyama, Y.; Nakagawa, M.; Ohkoshi, S.; Sugimura, T.; Shimotohno, K. Molecular Cloning of the Human Hepatitis C Virus Genome From Japanese Patients With Non-A, Non-B Hepatitis. *Proc. Natl. Acad. Sci. U. S. A.* **1990,** *87,* 9524–9528.
24. Grakoui, A.; McCourt, D. W.; Wychowski, C.; Feinstone, S. M.; Rice, C. M. Characterization of the Hepatitis C Virus-Encoded Serine Proteinase: Determination of Proteinase-Dependent Polyprotein Cleavage Sites. *J. Virol.* **1993,** *67,* 2832–2843.
25. Bartenschlager, R.; Ahlborn-Laake, R.; Mous, J.; Jacobsen, H. Nonstructural Protein 3 of the Hepatitis C Virus Encodes a Serine Type Proteinase Required for Cleavage at the NS3/4 and NS4/5 Junctions. *J. Virol.* **1993,** *67,* 3835–3844.
26. Hijikata, M.; Mizushima, H.; Akagi, T.; Mori, S.; Kakiuchi, N.; Kato, N.; Tanaka, T.; Kimura, K.; Shimotohno, K. Two Distinct Proteinase Activities Required for the Processing of a Putative Nonstructural Precursor Protein of Hepatitis C Virus. *J. Virol.* **1993,** *67,* 4665–4675.
27. Eckart, M. R.; Selby, M.; Masiarz, F.; Lee, C.; Berger, K.; Crawford, K.; Kuo, C.; Kuo, G.; Houghton, M.; Choo, Q. L. The Hepatitis C Virus Encodes a Serine Protease Involved in Processing of the Putative Nonstructural Proteins From the Viral Polyprotein Precursor. *Biochem. Biophys. Res. Commun.* **1993,** *192,* 399–406.
28. Suzich, J. A.; Tamura, J. K.; Palmer-Hill, F.; Warrener, P.; Grakoui, A.; Rice, C. M.; Feinstone, S. M.; Collett, M. S. Hepatitis C Virus NS3 Protein Polynucleotide Stimulated Nucleoside Triphosphatase and Comparison With the Related Pestivirus and Flavivirus Enzymes. *J. Virol.* **1993,** *67,* 6152–6158.
29. Lohmann, V.; Körner, F.; Herian, U.; Bartenschlager, R. Biochemical Properties of Hepatitis C Virus NS5B RNA-Dependent RNA Polymerase and Identification of Amino Acid Sequence Motifs Essential for Enzymatic Activity. *J. Virol.* **1997,** *71,* 8416–8428.
30. Moradpour, D.; Penin, F.; Rice, C. M. Replication of Hepatitis C Virus. *Nat. Rev. Microbiol.* **2007,** *5,* 453–463.
31. Bartenschlager, R.; Lohmann, V.; Penin, F. The Molecular and Structural Basis of Advanced Antiviral Therapy for Hepatitis C Virus Infection. *Nat. Rev. Microbiol.* **2013,** *11,* 482–496.
32. Morikawa, K.; Lange, C. M.; Gouttenoire, J.; Meylan, E.; Brass, V.; Penin, F.; Moradpour, D. Nonstructural Protein 3-4A: The Swiss Army Knife of Hepatitis C Virus. *J. Viral Hepat.* **2011,** *18,* 305–315.
33. Love, R. A.; Parge, H. E.; Wickersham, J. A.; Hostomsky, Z.; Habuka, N.; Moomaw, E. W.; Adachi, T.; Hostomska, Z. The Crystal Structure of Hepatitis C Virus NS3 Proteinase Reveals a Trypsin-Like Fold and a Structural Zinc Binding Site. *Cell* **1996,** *87,* 331–342.
34. Kim, J. L.; Morgenstern, K. A.; Lin, C.; Fox, T.; Dwyer, M. D.; Landro, J. A.; Chambers, S. P.; Markland, W.; Lepre, C. A.; O'Malley, E. T.; Harbeson, S. L.; Rice, C. M.; Murcko, M. A.; Caron, P. R.; Thomson, J. A. Crystal Structure of the Hepatitis C Virus NS3 Protease Domain Complexed With a Synthetic NS4A Cofactor Peptide. *Cell* **1996,** *87,* 343–355.
35. Lesburg, C. A.; Cable, M. B.; Ferrari, E.; Hong, Z.; Mannarino, A. F.; Weber, P. C. Crystal Structure of the RNA-Dependent RNA Polymerase From Hepatitis C Virus Reveals a Fully Encircled Active Site. *Nat. Struct. Biol.* **1999,** *6,* 937–943.
36. Ago, H.; Adachi, T.; Yoshida, A.; Yamamoto, M.; Habuka, N.; Yatsunami, K.; Miyano, M. Crystal Structure of the RNA-Dependent RNA Polymerase of Hepatitis C Virus. *Structure* **1999,** *7,* 1417–1426.
37. Bressanelli, S.; Tomei, L.; Roussel, A.; Incitti, I.; Vitale, R. L.; Mathieu, M.; De Francesco, R.; Rey, F. A. Crystal Structure of the RNA-Dependent RNA Polymerase of Hepatitis C Virus. *Proc. Natl. Acad. Sci. U. S. A.* **1999,** *96,* 13034–13039.
38. Lohmann, V.; Korner, F.; Koch, J.; Herian, U.; Theilmann, L.; Bartenschlager, R. Replication of Subgenomic Hepatitis C Virus RNAs in a Hepatoma Cell Line. *Science* **1999,** *285,* 110–113.
39. Blight, K. J.; McKeating, J. A.; Rice, C. M. Highly Permissive Cell Lines for Subgenomic and Genomic Hepatitis C Virus RNA Replication. *J. Virol.* **2002,** *76,* 13001–13014.
40. Kato, T.; Date, T.; Miyamoto, M.; Furusaka, A.; Tokushige, K.; Mizokami, M.; Wakita, T. Efficient Replication of the Genotype 2a Hepatitis C Virus Subgenomic Replicon. *Gastroenterology* **1808–1817,** *2003,* 125.
41. Bartenschlager, R. Hepatitis C Virus Replicons: Potential Role for Drug Development. *Nat. Rev. Drug Discov.* **2002,** *1,* 911–916.
42. Bartenschlager, R. The Hepatitis C Virus Replicon System: From Basic Research to Clinical Application. *J. Hepatol.* **2005,** *43,* 210–216.
43. Taylor, D. R. Evolution of Cell Culture Systems for HCV. *Antivir. Ther.* **2013,** *18,* 523–530.
44. O'Boyle, D. R., II; Nower, P. T.; Lemm, J. A.; Valera, L.; Sun, J.-H.; Rigat, K.; Colonno, R.; Gao, M. Development of a Cell-Based High-Throughput Specificity Screen Using a Hepatitis C Virus-Bovine Viral Diarrhea Virus Dual Replicon Assay. *Antimicrob. Agents Chemother.* **2005,** *49,* 1346–1353.
45. Lemm, J. A.; O'Boyle, D. R., II; Liu, M.; Nower, P. T.; Colonno, R.; Deshpande, M. S.; Snyder, L. B.; Martin, S. W.; St.Laurent, D. R.; Serrano-Wu, M. H.; Romine, J. L.; Meanwell, N. A.; Gao, M. Identification of Hepatitis C Virus NS5A Inhibitors. *J. Virol.* **2010,** *84,* 482–491.
46. Gao, M.; Nettles, R. E.; Belema, M.; Snyder, L. B.; Nguyen, V. N.; Fridell, R. A.; Serrano-Wu, M. H.; Langley, D. R.; Sun, J.-H.; O'Boyle, D. R., II; Lemm, J. A.; Wang, C.; Knipe, J. O.; Chien, C.; Colonno, R. J.; Grasela, D. M.; Meanwell, N. A.; Hamann, L. G. Chemical Genetics Strategy Identifies an HCV NS5A Inhibitor With a Potent Clinical Effect. *Nature* **2010,** *465,* 96–100.
47. Lohmann, V.; Bartenschlager, R. On the History of Hepatitis C Virus Cell Culture Systems. *J. Med. Chem.* **2014,** *57,* 1627–1642.
48. Lindenbach, B. D.; Evans, M. J.; Syder, A. J.; Wölk, B.; Tellinghuisen, T. L.; Liu, C. C.; Maruyama, T.; Hynes, R. O.; Burton, D. R.; McKeating, J. A.; Rice, C. M. Complete Replication of Hepatitis C Virus in Cell Culture. *Science* **2005,** *309,* 623–626.
49. Zhong, J.; Gastaminza, P.; Cheng, G.; Kapadia, S.; Kato, T.; Burton, D. R.; Wieland, S. F.; Uprichard, S. L.; Wakita, T.; Chisari, F. V. Robust Hepatitis C Virus Infection In Vitro. *Proc. Natl. Acad. Sci. U. S. A.* **2005,** *102,* 9294–9299.
50. Wakita, T.; Pietschmann, T.; Kato, T.; Date, T.; Miyamoto, M.; Zhao, Z.; Murthy, K.; Habermann, A.; Kraeusslich, H.-G.; Mizokami, M.; Bartenschlager, R.; Liang, T. J. Production of Infectious Hepatitis C Virus in Tissue Culture From a Cloned Viral Genome. *Nat. Med.* **2005,** *11,* 791–796.
51. Bartenschlager, R.; Pietschmann, T. Efficient Hepatitis C Virus Cell Culture System: What a Difference the Host Cell Makes. *Proc. Natl. Acad. Sci. U. S. A.* **2005,** *102,* 9739–9740.
52. Neumann, A. U.; Lam, N. P.; Dahari, H.; Gretch, D. R.; Wiley, T. E.; Layden, T. J.; Perelson, A. S. Hepatitis C Viral Dynamics in vivo and the Antiviral Efficacy of Interferon-α Therapy. *Science* **1998,** *282,* 103–107.
53. Perelson, A. S.; Herrmann, E.; Micol, F.; Zeuzem, S. New Kinetic Models for the Hepatitis C Virus. *Hepatology* **2005,** *42,* 749–754.

54. Shudo, E.; Ribeiro, R. M.; Perelson, A. S. Modeling HCV Kinetics Under Therapy Using PK and PD Information. *Exp. Opin. Drug. Metab. Toxicol.* **2009,** *5,* 321–332.
55. Rong, L.; Perelson, A. S. Treatment of Hepatitis C Virus Infection With Interferon and Small Molecule Direct Antivirals: Viral Kinetics and Modeling. *Crit. Rev. Immunol.* **2010,** *30,* 131–148.
56. Ribeiro, R. M.; Li, H.; Wang, S.; Stoddard, M. B.; Learn, G. H.; Korber, B. T.; Bhattacharya, T.; Guedj, J.; Parrish, E. H.; Hahn, B. H.; Shaw, G. M.; Perelson, A. S. Quantifying the Diversification of Hepatitis C Virus (HCV) During Primary Infection: Estimates of the in vivo Mutation Rate. *PLoS Pathog.* **2012,** *8* (8), e1002881. http://dx.doi.org/10.1371/journal.ppat.1002881.
57. Chatterjee, A.; Guedj, J.; Perelson, A. S. Mathematical Modeling of HCV Infection: What Can It Teach Us in the Era of Direct-Acting Antiviral Agents? *Antivir. Ther.* **2012,** *17,* 1171–1182.
58. Guedj, J.; Dahari, H.; Shudo, E.; Smith, P.; Perelson, A. S. Hepatitis C Viral Kinetics With the Nucleoside Polymerase Inhibitor Mericitabine (RG7128). *Hepatology* **2012,** *55,* 1030–1037.
59. Rong, L.; Guedj, J.; Dahari, H.; Coffield, D. J., Jr.; Levi, M.; Smith, P.; Perelson, A. S. Analysis of Hepatitis C Virus Decline During Treatment With the Protease Inhibitor Danoprevir Using a Multiscale Model. *PLoS Comput. Biol.* **2013,** *9* (3), e1002959. http://dx.doi.org/10.1371/journal.pcbi.1002959.
60. Sarrazin, C.; Kieffer, T. L.; Bartels, D.; Hanzelka, B.; Müh, U.; Welker, M.; Wincheringer, D.; Zhou, Y.; Chu, H.-M.; Lin, C.; Weegink, C.; Reesink, H.; Zeuzem, S.; Kwong, A. D. Dynamic Hepatitis C Virus Genotypic and Phenotypic Changes in Patients Treated With the Protease Inhibitor Telaprevir. *Gastroenterology* **2007,** *132,* 1767–1777.
61. Rong, L.; Dahari, H.; Ribeiro, R. M.; Perelson, A. S. Rapid Emergence of Protease Inhibitor Resistance in Hepatitis C Virus. *Sci. Transl. Med.* **2010,** *2,* 1–9.
62. Susser, S.; Welsch, C.; Wang, Y.; Zettler, M.; Domingues, F. S.; Karey, U.; Hughes, E.; Ralston, R.; Tong, X.; Herrmann, E.; Zeuzem, S.; Sarrazin, C. Characterization of Resistance to the Protease Inhibitor Boceprevir in Hepatitis C Virus-Infected Patients. *Hepatology* **2009,** *50,* 1709–1718.
63. Nettles, R. E.; Gao, M.; Bifano, M.; Chung, E.; Persson, A.; Marbury, T. C.; Goldwater, R.; DeMicco, M. P.; Rodriguez-Torres, M.; Vutikullird, A.; Fuentes, E.; Lawitz, E.; Lopez-Talavera, J. C.; Grasela, D. M. Multiple Ascending Dose Study of BMS-790052, a Nonstructural Protein 5A Replication Complex Inhibitor, in Patients Infected With Hepatitis C Virus Genotype 1. *Hepatology* **2011,** *54,* 1956–1965.
64. Perry, C. M. Telaprevir—A Review of Its Use in the Management of Genotype 1 Chronic Hepatitis C. *Drugs* **2012,** *72,* 619–641.
65. Garnock-Jones, K. P. Boceprevir—A Review of Its Use in the Management of Chronic Hepatitis C Genotype 1 Infection. *Drugs* **2012,** *72,* 2431–2456.
66. Keating, G. M. Sofosbuvir: A Review of Its Use in Patients With Chronic Hepatitis C. *Drugs* **2014,** *74,* 1127–1146.
67. Vaidya, A.; Perry, C. M. Simeprevir: First Global Approval. *Drugs* **2013,** *73,* 2093–2106.
68. Childs-Kean, L. M.; Hand, E. O. Simeprevir and Sofosbuvir for Treatment of Chronic Hepatitis C Infection. *Clin. Ther.* **2015,** *37,* 243–267.
69. Poole, R. M. Daclatasvir + Asunaprevir: First Global Approval. *Drugs* **2014,** *74,* 1559–1571.
70. Keating, G. M. Ledipasvir/Sofosbuvir: A Review of Its Use in Chronic Hepatitis C. *Drugs* **2015,** *75,* 675–685.
71. Arezou Minaei, A.; Kowdley, K. V. ABT-450/Ritonavir and ABT-267 in Combination With ABT-333 for the Treatment of Hepatitis C Virus. *Expert. Opin. Pharmacother.* **2015,** *16,* 929–937.
72. Zeuzem, S.; Ghalib, R.; Reddy, K. R.; Pockros, P. J.; Ari, Z. B.; Zhao, Y.; Brown, D. D.; Wan, S.; DiNubile, M. J.; Nguyen, B.-Y.; Robertson, M. N.; Wahl, J.; Barr, E.; Butterton, J. R. Grazoprevir-Elbasvir Combination Therapy for Treatment-Naïve Cirrhotic and Noncirrhotic Patients With Chronic HCV Genotype 1, 4, or 6 Infection: A Randomized Trial. *Ann. Intern. Med.* **2015,** *163,* 1–13.
73. Meanwell, N. A.; Koszalka, G. W. 2007—A Difficult Year for HCV Drug Development. *Curr. Opin. Investig. Drugs* **2008,** *9,* 128–131.
74. Calcoen, D.; Elias, L.; Yu, X. What Does It Take to Produce a Breakthrough Drug? *Nat. Rev. Drug Discov.* **2015,** *14,* 161–162.
75. Gawlik, K.; Gallay, P. A. HCV Core Protein and Virus Assembly: What We Know Without Structures. *Immunol. Res.* **2014,** *60,* 1–10.
76. Strosberg, A. D.; Kota, S.; Takahashi, V.; Snyder, J. K.; Mousseau, G. Core as a Novel Viral Target for Hepatitis C Drugs. *Viruses* **2010,** *2,* 1734–1751.
77. Lindenbach, B. D.; Rice, C. M. The Ins and Outs of Hepatitis C Virus Entry and Assembly. *Nat. Rev. Microbiol.* **2013,** *11,* 688–700.
78. Kushima, Y.; Wakita, T.; Hijikata, M. A Disulfide-Bonded Dimer of the Core Protein of Hepatitis C Virus Is Important for Virus-Like Particle Production. *J. Virol.* **2010,** *84,* 9118–9127.
79. Kota, S.; Coito, C.; Mousseau, G.; Lavergne, J.-P.; Strosberg, A. D. Peptide Inhibitors of Hepatitis C Virus Core Oligomerization and Virus Production. *J. Gen. Virol.* **2009,** *90,* 1319–1328.
80. Wei, W.; Cai, C.; Kota, S.; Takahashi, V.; Ni, F.; Strosberg, A. D.; Snyder, J. K. New Small Molecule Inhibitors of Hepatitis C Virus. *Bioorg. Med. Chem. Lett.* **2009,** *19,* 6926–6930.
81. Ni, F.; Kota, S.; Takahashi, V.; Strosberg, A. D.; Snyder, J. K. Potent Inhibitors of Hepatitis C Core Dimerization as New Leads for Anti-Hepatitis C Agents. *Bioorg. Med. Chem. Lett.* **2011,** *21,* 2198–2202.
82. Mousseau, G.; Kota, S.; Takahashi, V.; Frick, D. N.; Strosberg, D. A. Dimerization-Driven Interaction of Hepatitis C Virus Core Protein With NS3 Helicase. *J. Gen. Virol.* **2011,** *92,* 101–111.
83. Kota, S.; Takahashi, V.; Ni, F.; Snyder, J. K.; Strosberg, A. D. Direct Binding of a Hepatitis C Virus Inhibitor to the Viral Capsid Protein. *PLoS One* **2012,** *7,* e32207. http://dx.doi.org/10.1371/journal.pone.0032207.
84. Samreen, B.; Khaliq, S.; Ashfaq, U. A.; Khan, M.; Afzal, N.; Shahzad, M. A.; Riaz, S.; Jahan, S. Hepatitis C Virus Entry: Role of Host and Viral Factors. *Infect. Genet. Evol.* **2012,** *12,* 1699–1709.
85. Colpitts, C. C.; Verrier, E. R.; Baumert, T. F. Targeting Viral Entry for Treatment of Hepatitis B and C Virus Infections. *ACS Infect. Dis.* **2015,** *1,* 420–427.
86. Zeisel, M. B.; Fofana, I.; Fafi-Kremer, S.; Baumert, T. F. Hepatitis C Virus Entry Into Hepatocytes: Molecular Mechanisms and Targets for Antiviral Therapies. *J. Hepatol.* **2011,** *54,* 566–576.
87. Lupberger, J.; Zeisel, M. B.; Xiao, F.; Thumann, C.; Fofana, I.; Zona, L.; Davis, C.; Mee, C. J.; Turek, M.; Gorke, S.; Royer, C.; Fischer, B.; Zahid, M. N.; Lavillette, D.; Fresquet, J.; Cosset, F.-L.; Rothenberg, S. M.; Pietschmann, T.; Patel, A. H.; Pessaux, P.; Doffoël, M.; Raffelsberger, W.; Poch, O.; McKeating, J. A.; Brino, L.; Baumert, T. F. EGFR and EphA2 Are Host Factors for Hepatitis C Virus Entry and Possible Targets for Antiviral Therapy. *Nat. Med.* **2011,** *17,* 589–595.
88. Patricelli, M. P.; Nomanbhoy, T. K.; Wu, J.; Brown, H.; Zhou, D.; Zhang, J.; Jagannathan, S.; Aban, A.; Okerberg, E.; Herring, C.; Nordin, B.; Weissig, H.; Yang, Q.; Lee, J.-D.; Gray, N. S.; Kozarich, J. W. In Situ Kinase Profiling Reveals Functionally Relevant Properties of Native Kinases. *Chem. Biol.* **2011,** *18,* 699–710.
89. Xiao, F.; Fofana, I.; Thumann, C.; Mailly, L.; Alles, R.; Robinet, E.; Meyer, N.; Schaeffer, M.; Habersetzer, F.; Doffoël, M.; Leyssen, P.; Neyts, J.; Zeisel, M. B.; Baumert, T. F. Synergy of Entry Inhibitors With Direct-Acting Antivirals Uncovers Novel Combinations for Prevention and Treatment of Hepatitis C. *Gut* **2015,** *64,* 483–494.
90. Sainz, B., Jr.; Barretto, N.; Martin, D. N.; Hiraga, N.; Imamura, M.; Hussain, S.; Marsh, K. A.; Yu, X.; Chayama, K.; Alrefai, W. A.; Uprichard, S. L. Identification of the Niemann-Pick C1-Like 1 Cholesterol Absorption Receptor as a New Hepatitis C Virus Entry Factor. *Nat. Med.* **2012,** *18,* 281–285.
91. Soza, A. Hepatitis C RNA Clearance After Treatment With Ezetimibe. *Liver Int.* **2012,** *32,* 1323–1324.
92. Scarselli, E.; Ansuini, H.; Cerino, R.; Roccasecca, R. M.; Acali, S.; Filocamo, G.; Traboni, C.; Nicosia, A.; Cortese, R.; Vitelli, A. The Human Scavenger Receptor Class B Type I Is a Novel Candidate Receptor for the Hepatitis C Virus. *EMBO J.* **2002,** *21,* 5017–5025.
93. Zeisel, M. B.; Koutsoudakis, G.; Schnober, E. K.; Haberstroh, A.; Blum, H. E.; Cosset, F.-L.; Wakita, T.; Jaeck, D.; Doffoel, M.; Royer, C.; Soulier, E.; Schvoerer, E.; Schuster, C.; Stoll-Keller, F.; Bartenschlager, R.; Pietschmann, T.; Barth, H.; Baumert, T. F. Scavenger Receptor Class B Type I Is a Key Host Factor for Hepatitis C Virus Infection Required for an Entry Step Closely Linked to CD81. *Hepatology* **2007,** *46,* 1722–1731.
94. Syder, A. J.; Lee, H.; Zeisel, M. B.; Grove, J.; Soulier, E.; Macdonald, J.; Chow, S.; Chang, J.; Baumert, T. F.; McKeating, J. A.; McKelvy, J.; Wong-Staal, F. Small Molecule Scavenger Receptor BI Antagonists Are Potent HCV Entry Inhibitors. *J. Hepatol.* **2011,** *54,* 48–55.
95. Zhu, H.; Wong-Staal, F.; Lee, H.; Syder, A.; McKelvy, J.; Schooley, T. T.; Wyles, D. L. Evaluation of ITX 5061, a Scavenger Receptor B1 Antagonist: Resistance Selection and Activity in Combination With Other Hepatitis C Virus Antivirals. *J. Infect. Dis.* **2012,** *205,* 656–662.

96. Masson, D.; Koseki, M.; Ishibashi, M.; Larson, C. J.; Miller, S. G.; King, B. D.; Tall, A. R. Increased HDL Cholesterol and ApoA-I in Humans and Mice Treated With a Novel SR-BI Inhibitor. *Arterioscler. Thromb. Vasc. Biol.* **2009,** *29,* 2054–2060.
97. Sulkowski, M. S.; Kang, M.; Matining, R.; Wyles, D.; Johnson, V. A.; Morse, G. D.; Amorosa, V.; Bhattacharya, D.; Coughlin, K.; Wong-Staal, F.; Glesby, M. J.; For the AIDS Clinical Trials Group A5277 Protocol Team. Safety and Antiviral Activity of the HCV Entry Inhibitor ITX5061 in Treatment-Naive HCV-Infected Adults: A Randomized, Double-Blind, Phase 1b Study. *J. Infect. Dis.* **2014,** *209,* 658–667.
98. Dorner, M.; Horwitz, J. A.; Robbins, J. B.; Barry, W. T.; Feng, Q.; Mu, K.; Jones, C. T.; Schoggins, J. W.; Catanese, M. T.; Burton, D. R.; Law, M.; Rice, C. M.; Ploss, A. A Genetically Humanized Mouse Model for Hepatitis C Virus Infection. *Nature* **2011,** *474,* 208–211.
99. Mittapalli, G. P.; Jackson, A.; Zhao, F.; Lee, H.; Chow, S.; McKelvy, J.; Wong-Staal, F.; Macdonald, J. E. Discovery of Highly Potent Small Molecule Hepatitis C Virus Entry Inhibitors. *Bioorg. Med. Chem. Lett.* **2011,** *21,* 6852–6855.
100. Mittapalli, G. P.; Zhao, F.; Jackson, A.; Gao, H.; Lee, H.; Chow, S.; Pal Kaur, M.; Nguyen, N.; Zamboni, R.; McKelvy, J.; Wong-Staal, F.; Macdonald, J. E. Discovery of ITX 4520: A Highly Potent Orally Bioavailable Hepatitis C Virus Entry Inhibitor. *Bioorg. Med. Chem. Lett.* **2012,** *22,* 4955–4961.
101. Baldick, C. J.; Wichroski, M.; Pendri, A.; Walsh, A. W.; Fang, J.; Mazzucco, C.; Pokornowski, K.; Rose, R.; Eggers, B.; Hsu, M.; Zhai, G.; Gerritz, S. W.; Poss, M.; Meanwell, N. A.; Cockett, M. I.; Tenney, D. J. Identification of a Small Molecule Antiviral Inhibitor of the Entry Stage of Hepatitis C Virus Infection. *PLoS Pathog.* **2010,** *6,* e1001086. http://dx.doi.org/10.1371/journal.ppat.1001086.
102. Bush, C. O.; Pokrovskii, M. V.; Saito, R.; Morganelli, P.; Canales, E.; Clarke, M. O.; Lazerwith, S. E.; Golde, J.; Reid, B. G.; Babaoglu, K.; Pagratis, N.; Zhong, W.; Delaney, W. E., IV; Paulson, M. S.; Beran, R. F. K. A Small-Molecule Inhibitor of Hepatitis C Virus Infectivity. *Antimicrob. Agents Chemother.* **2014,** *58,* 386–396.
103. Kong, L.; Giang, E.; Nieusma, T.; Kadam, R. U.; Cogburn, K. E.; Hua, Y.; Dai, X.; Stanfield, R. L.; Burton, D. R.; Ward, A. B.; Wilson, I. A.; Law, M. Hepatitis C Virus E2 Envelope Glycoprotein Core Structure. *Science* **2013,** *342,* 1090–1094.
104. Ghafoor Khan, A.; Whidby, J.; Miller, M. T.; Scarborough, H.; Zatorski, A. V.; Cygan, A.; Price, A. A.; Yost, S. A.; Bohannon, D. D.; Jacob, J.; Grakoui, A.; Marcotrigiano, J. Structure of the Core Ectodomain of the Hepatitis C Virus Envelope Glycoprotein 2. *Nature* **2014,** *509,* 381–384.
105. Sabahi, A.; Uprichard, S. L.; Wimley, W. C.; Dash, S.; Garry, R. F. Unexpected Structural Features of the Hepatitis C Virus Envelope Protein 2 Ectodomain. *J. Virol.* **2014,** *88,* 10280–10288.
106. Castelli, M.; Clementi, N.; Sautto, G. A.; Pfaff, J.; Kahle, K. M.; Barnes, T.; Doranz, B. J.; Dal Peraro, M.; Clementi, M.; Burioni, R.; Mancini, N. HCV E2 Core Structures and mAbs: Something Is Still Missing. *Drug Discov. Today* **2014,** *19,* 1964–1970.
107. El Omari, K.; Iourin, O.; Kadlec, J.; Sutton, G.; Harlos, K.; Grimes, J. M.; Stuart, D. I. Unexpected Structure for the N-Terminal Domain of Hepatitis C Virus Envelope Glycoprotein E1. *Nat. Commun.* **2014,** *5,* 4874. http://dx.doi.org/10.1038/ncomms5874.
108. Chamoun-Emanuelli, A. M.; Pécheur, E.-I.; Chen, Z. Benzhydrylpiperazine Compounds Inhibit Cholesterol-Dependent Cellular Entry of Hepatitis C Virus. *Antivir. Res.* **2014,** *109,* 141–148.
109. He, S. L. B.; Chu, V.; Hu, Z.; Hu, X.; Xiao, J.; Wang, A. Q.; Schweitzer, C. J.; Li, Q.; Imamura, M.; Hiraga, N.; Southall, N.; Ferrer, M.; Zheng, W.; Chayama, K.; Marugan, J. J.; Liang, T. J. Repurposing of the Antihistamine Chlorcyclizine and Related Compounds for Treatment of Hepatitis C Virus Infection. *Sci. Transl. Med.* **2015,** *7,* 282ra49.
110. Gastaminza, P.; Whitten-Bauer, C.; Chisari, F. V. Unbiased Probing of the Entire Hepatitis C Virus Life Cycle Identifies Clinical Compounds That Target Multiple Aspects of the Infection. *Proc. Natl. Acad. Sci. U. S. A.* **2010,** *107,* 291–296.
111. Holzer, M.; Ziegler, S.; Albrecht, B.; Kronenberger, B.; Kaul, A.; Bartenschlager, R.; Kattner, L.; Klein, C. D.; Hartmann, R. W. Identification of Terfenadine as an Inhibitor of Human CD81-Receptor HCV-E2 Interaction: Synthesis and Structure Optimization. *Molecules* **2008,** *13,* 1081–1110.
112. Al Olaby, R. R.; Cocquerel, L.; Zemla, A.; Saas, L.; Dubuisson, J.; Vielmetter, J.; Marcotrigiano, J.; Ghafoor Khan, A.; Vences Catalan, F.; Perryman, A. L.; Freundlich, J. S.; Forli, S.; Levy, S.; Balhorn, R.; Azzazy, H. M. Identification of a Novel Drug Lead That Inhibits HCV Infection and Cell-to-Cell Transmission by Targeting the HCV E2 Glycoprotein. *PLoS One* **2014,** *9,* e111333. http://dx.doi.org/10.1371/journal.pone.0111333.
113. de Bruijne, J.; Bergmann, J. F.; Weegink, C. J.; van Nieuwkerk, C. M. J.; de Knegt, R. J.; Komoda, Y.; van de Wetering de Rooji, J. J.; van Vliet, A.; Jansen, P. L. M.; Molenkamp, R.; Schinke, J.; Reesink, H.; Janssen, H. L. A. Safety and Antiviral Activity of JTK-652: A Novel HCV Infection Inhibitor. *Antivir. Ther.* **2010,** *15,* 765–773.
114. Griffin, S. Inhibition of HCV p7 as a Therapeutic Target. *Curr. Opin. Investig. Drugs* **2010,** *11,* 175–181.
115. Steinmann, E.; Pietschmann. Hepatitis C Virus p7–A Viroporin Crucial for Virus Assembly and an Emerging Target for Antiviral Therapy. *Viruses* **2010,** *2,* 2078–2095.
116. Madan, V.; Bartenschlager, R. Structural and Functional Properties of the Hepatitis C Virus p7 Viroporin. *Viruses* **2015,** *7,* 4461–4481.
117. Griffin, S. 'Too Little, Too Late?' Will Inhibitors of the Hepatitis C Virus p7 Ion Channel Ever be Used in the Clinic? *Fut. Med. Chem.* **2014,** *6,* 1893–1907.
118. Sakai, A.; St. Claire, M.; Faulk, K.; Govindarajan, S.; Emerson, S. U.; Purcell, R. H.; Bukh, J. The p7 Polypeptide of Hepatitis C Virus Is Critical for Infectivity and Contains Functionally Important Genotype-Specific Sequences. *Proc. Natl. Acad. Sci. U. S. A.* **2003,** *100,* 11646–11651.
119. Jones, C. T.; Murray, C. L.; Eastman, D. K.; Tassello, J.; Rice, C. M. Hepatitis C Virus p7 and NS2 Proteins Are Essential for Production of Infectious Virus. *J. Virol.* **2007,** *81,* 8374–8383.
120. Steinmann, E.; Penin, F.; Kallis, S.; Patel, A. H.; Bartenschlager, R.; Pietschmann, T. Hepatitis C Virus p7 Protein Is Crucial for Assembly and Release of Infectious Virions. *PLoS Pathog.* **2007,** *3* (7), e103. http://dx.doi.org/10.1371/journal.ppat.0030103.
121. Bentham, M. J.; Foster, T. L.; McCormick, C.; Griffin, S. Mutations in Hepatitis C Virus p7 Reduce Both the Egress and Infectivity of Assembled Particles via Impaired Proton Channel Function. *J. Gen. Virol.* **2013,** *94,* 2236–2248.
122. Gentzsch, J.; Brohm, C.; Steinmann, E.; Friesland, M.; Menzel, N.; Vieyres, G.; Monteiro Perin, P.; Frentzen, A.; Kaderali, L.; Pietschmann, T. Hepatitis C Virus p7 Is Critical for Capsid Assembly and Envelopment. *PLoS Pathog.* **2013,** *9* (5), e1003355. http://dx.doi.org/10.1371/journal.ppat.1003355.
123. Chew, C. F.; Vijayan, R.; Chang, J.; Zitzmann, N.; Biggin, P. C. Determination of the Pore-Lining Residues of the Hepatitis C Virus p7 Protein. *Biophys. J.* **2009,** *96,* L10–L12.
124. Luik, P.; Chew, C.; Aittoniemi, J.; Chang, J.; Wentworth, P., Jr.; Dwek, R. A.; Biggin, P. C.; Vénien-Bryand, C.; Zitzmann, N. The 3-Dimensional Structure of a Hepatitis C Virus p7 Ion Channel by Electron Microscopy. *Proc. Natl. Acad. Sci. U. S. A.* **2009,** *106,* 12712–12716.
125. Montserret, R.; Saint, N.; Vanbelle, C.; Salvay, A. G.; Simorre, J. P.; Ebel, C.; Sapay, N.; Renisio, J. G.; Böckmann, A.; Steinmann, E.; Pietschmann, T.; Dubuisson, J.; Chipot, C.; Penin, F. NMR Structure and Ion Channel Activity of the p7 Protein From Hepatitis C Virus. *J. Biol. Chem.* **2010,** *285,* 31446–31461.
126. Cook, G. A.; Dawson, L. A.; Tian, Y.; Opella, S. J. Three-Dimensional Structure and Interaction Studies of Hepatitis C Virus p7 in 1,2-Dihexanoyl-sn-Glycero-3-Phosphocholine by Solution Nuclear Magnetic Resonance. *Biochemistry* **2013,** *52,* 5295–5303.
127. OuYang, B.; Xie, S.; Berardi, M. J.; Zhao, X.; Dev, J.; Yu, W.; Sun, B.; Chou, J. J. Unusual Architecture of the p7 Channel From Hepatitis C Virus. *Nature* **2013,** *498,* 521–525.
128. Foster, T. L.; Thompson, G. S.; Kalverda, A. P.; Kankanala, J.; Bentham, M.; Wetherill, L. F.; Thompson, J.; Barker, A. M.; Clarke, D.; Noerenberg, M.; Pearson, A. R.; Rowlands, D. J.; Homans, S. W.; Harris, M.; Foster, R.; Griffin, S. Structure-Guided Design Affirms Inhibitors of Hepatitis C Virus p7 as a Viable Class of Antivirals Targeting Virion Release. *Hepatology* **2014,** *59,* 408–422.
129. StGelais, C.; Tuthill, T. J.; Clarke, D. S.; Rowlands, D. J.; Harris, M.; Griffin, S. Inhibition of Hepatitis C Virus p7 Membrane Channels in a Liposome-Based Assay System. *Antivir. Res.* **2007,** *76,* 48–58.
130. Griffin, S. D.; Beales, L. P.; Clarke, D. S.; Worsfold, O.; Evans, S. D.; Jaeger, J.; Harris, M. P.; Rowlands, D. J. The p7 Protein of Hepatitis C Virus Forms an Ion Channel That Is Blocked by the Antiviral Drug Amantadine. *FEBS Lett.* **2003,** *535,* 34–38.
131. Steinmann, E.; Whitfield, T.; Kallis, S.; Dwek, R. A.; Zitzmann, N.; Pietschmann, T.; Bartenschlager, R. Antiviral Effects of Amantadine and Iminosugar Derivatives Against Hepatitis C Virus. *Hepatology* **2007,** *46,* 330–338.
132. Griffin, S.; StGelais, C.; Owsianka, A. M.; Patel, A. H.; Rowlands, D.; Harris, M. Genotype-Dependent Sensitivity of Hepatitis C Virus to Inhibitors of the p7 Ion Channel. *Hepatology* **2008,** *48,* 1779–1790.

133. Smith, J. P. Treatment of Chronic Hepatitis C With Amantadine. *Dig. Dis. Sci.* **1997,** *42,* 1681–1687.
134. van Soest, H.; van der Schaar, P. J.; Koek, G. H.; de Vries, R. A.; van Ooteghem, N. A.; van Hoek, B.; Drenth, J. P.; Vrolijk, J. M.; Lieverse, R. J.; Houben, P.; van der Sluys Veer, A.; Siersema, P. D.; Schipper, M. E.; van Erpecum, K. J.; Boland, G. J. No Beneficial Effects of Amantadine in Treatment of Chronic Hepatitis C Patients. *Dig. Liver Dis.* **2010,** *42,* 496–502.
135. Piccolo, P. Amantadine for Treatment of Hepatitis C: Time to Say "Enough Is Enough"? *Dig. Liver Dis.* **2010,** *42,* 468–469.
136. Foster, T. L.; Verow, M.; Wozniak, A. L.; Bentham, M. J.; Thompson, J.; Atkins, E.; Weinman, S. A.; Fishwick, C.; Foster, R.; Harris, M.; Griffin, S. Resistance Mutations Define Specific Antiviral Effects for Inhibitors of the Hepatitis C Virus p7 Ion Channel. *Hepatology* **2011,** *54,* 79–90.
137. Pavlovic, D.; Neville, D. C. A.; Argaud, O.; Blumberg, B.; Dwek, R. A.; Fischer, W. B.; Zitzmann, N. The Hepatitis C Virus p7 Protein Forms an Ion Channel That Is Inhibited by Long-Alkyl-Chain Iminosugar Derivatives. *Proc. Natl. Acad. Sci. U. S. A.* **2003,** *100,* 6104–6108.
138. Luscombe, C. A.; Huang, Z.; Murray, M. G.; Miller, M.; Wilkinson, J.; Ewart, G. D. A Novel Hepatitis C Virus p7 Ion Channel Inhibitor, BIT225, Inhibits Bovine Viral Diarrhea Virus in vitro and Shows Synergism With Recombinant Interferon-Alpha-2b and Nucleoside Analogues. *Antivir. Res.* **2010,** *86,* 144–153.
139. Gazina, E. V.; Petrou, S. Viral Targets of Acylguanidines. *Drug Discov. Today* **2012,** *17,* 1039–1043.
140. Welbourn, S.; Pause, A. The Hepatitis C Virus NS2/3 Protease. *Curr. Issues Mol. Biol.* **2007,** *9,* 63–70.
141. Lorenz, I. C. The Hepatitis C Virus Nonstructural Protein 2 (NS2): An Up-and-Coming Antiviral Drug Target. *Viruses* **2010,** *2,* 1635–1646.
142. Schregel, V.; Jacobi, S.; Penin, F.; Tautz, N. Hepatitis C Virus NS2 Is a Protease Stimulated by Cofactor Domains in NS3. *Proc. Natl. Acad. Sci. U. S. A.* **2009,** *106,* 5342–5347.
143. Lorenz, I. C.; Marcotrigiano, J.; Dentzer, T. G.; Rice, C. M. Structure of the Catalytic Domain of the Hepatitis C Virus NS2-3 Protease. *Nature* **2006,** *442,* 831–835.
144. Thibeault, D.; Maurice, R.; Pilote, L.; Lamarre, D.; Pause, A. In Vitro Characterization of a Purified NS2/3 Protease Variant of Hepatitis C Virus. *J. Biol. Chem.* **2001,** *276,* 46678–46684.
145. Matsumoto, K.; Mizoue, K.; Kitamura, K.; Tse, W.-C.; Huber, C. P.; Ishida, T. Structural Basis of Inhibition of Cysteine Proteases by E-64 and Its Derivatives. *Biopolymers* **1999,** *51,* 99–107.
146. Shaw, J.; Fishwick, C. W. G.; Harris, M. Epoxide Based Inhibitors of the Hepatitis C Virus Non-Structural 2 Autoprotease. *Antivir. Res.* **2015,** *117,* 20–26.
147. Raney, K. D.; Sharma, S. D.; Moustafa, I. M.; Cameron, C. E. Hepatitis C Virus Non-Structural Protein 3 (HCV NS3): A Multifunctional Antiviral Target. *J. Biol. Chem.* **2010,** *285,* 22725–22731.
148. Steinkühler, C.; Tomei, L.; De Francesco, R. In Vitro Activity of Hepatitis C Virus Protease NS3 Purified From Recombinant Baculovirus-Infected Sf9 Cells. *J. Biol. Chem.* **1996,** *271,* 6367–6373.
149. Zhang, R.; Durkin, J.; Windsor, W. T.; McNemar, C.; Ramanathan, L.; Le, H. V. Probing the Substrate Specificity of Hepatitis C Virus NS3 Serine Protease by Using Synthetic Peptides. *J. Virol.* **1997,** *71,* 6208–6213.
150. Gallinari, P.; Paolini, C.; Brennan, D.; Nardi, C.; Steinkühler, C.; De Francesco, R. Modulation of Hepatitis C Virus NS3 Protease and Helicase Activities Through the Interaction With NS4A. *Biochemistry* **1999,** *38,* 5620–5632.
151. Urbani, A.; Bianchi, E.; Narjes, F.; Tramontano, A.; De Francesco, R.; Steinkühler, C.; Pessi, A. Substrate Specificity of the Hepatitis C Virus Serine Protease NS3. *J. Biol. Chem.* **1997,** *272,* 9204–9209.
152. Meylan, E.; Curran, J.; Hofmann, K.; Moradpour, D.; Binder, M.; Bartenschlager, R.; Tschopp, R. Cardif Is an Adaptor Protein in the RIG-I Antiviral Pathway and Is Targeted by Hepatitis C Virus. *Nature* **2005,** *437,* 1167–1172.
153. Li, X. D.; Sun, L. R.; Seth, B.; Pineda, G.; Chen, Z. J. Hepatitis C Virus Protease NS3/4A Cleaves Mitochondrial Antiviral Signaling Protein Off the Mitochondria to Evade Innate Immunity. *Proc. Natl. Acad. Sci. U. S. A.* **2005,** *102,* 17717–17722.
154. Li, K.; Foy, E. J.; Ferreon, C.; Nakamura, M.; Ferreon, A. C.; Ikeda, M.; Ray, S. C.; Gale, M., Jr.; Lemon, S. M. Immune Evasion by Hepatitis C Virus NS3/4A Protease-Mediated Cleavage of the Toll-Like Receptor 3 Adaptor Protein TRIF. *Proc. Natl. Acad. Sci. U. S. A.* **2005,** *102,* 2992–2997.
155. Johnson, C. L.; Owen, D. M.; Gale, M., Jr. Functional and Therapeutic Analysis of Hepatitis C Virus NS3 · 4A Protease Control of Antiviral Immune Defense. *J. Biol. Chem.* **2007,** *282,* 10792–10803.
156. Llinàs-Brunet, M.; Bailey, M.; Fazal, G.; Goulet, S.; Halmos, T.; Laplante, S.; Maurice, R.; Poirier, M.; Poupart, M.-A.; Thibeault, D.; Wernic, D.; Lamarre, D. Peptide-Based Inhibitors of the Hepatitis C Virus Serine Protease. *Bioorg. Med. Chem. Lett.* **1998,** *8,* 1713–1718.
157. Steinkühler, C.; Biasiol, G.; Brunetti, M.; Urbani, A.; Koch, U.; Cortese, R.; Pessi, A.; De Francesco, R. Product Inhibition of the Hepatitis C Virus NS3 Protease. *Biochemistry* **1998,** *37,* 8899–8905.
158. Ingallinella, P.; Altamura, S.; Bianchi, E.; Taliani, M.; Ingenito, R.; Cortese, R.; De Francesco, R.; Steinkühler, C.; Pessi, A. Potent Peptide Inhibitors of Human Hepatitis C Virus NS3 Protease Are Obtained by Optimizing the Cleavage Products. *Biochemistry* **1998,** *37,* 8906–8914.
159. Narjes, F.; Koehler, K. F.; Koch, U.; Gerlach, B.; Colarusso, S.; Steinkühler, C.; Brunetti, M.; Altamura, S.; De Francesco, R.; Matassa, V. G. A Designed P1 Cysteine Mimetic for Covalent and Non-Covalent Inhibitors of HCV NS3 Protease. *Bioorg. Med. Chem. Lett.* **2002,** *12,* 701–704.
160. Erickson, J. A.; McLoughlin, J. I. Hydrogen Bond Donor Properties of the Difluoromethyl Group. *J. Org. Chem.* **1995,** *60,* 1626–1631.
161. Narjes, F.; Brunetti, M.; Colarusso, S.; Gerlach, B.; Koch, U.; Biasiol, G.; Fattori, D.; Francesco, R. D.; Matassa, V. G.; Steinkühler, C. α-Ketoacids Are Potent Slow Binding Inhibitors of the Hepatitis C Virus NS3 Protease. *Biochemistry* **2000,** *39,* 1849–1861.
162. Di Marco, S.; Rizzi, M.; Volpari, C.; Walsh, M. A.; Narjes, F.; Colarusso, S.; De Francesco, R.; Matassa, V. G.; Sollazzo, M. Inhibition of the Hepatitis C Virus NS3/4A Protease: The Crystal Structures of Two Protease-Inhibitor Complexes. *J. Biol. Chem.* **2000,** *275,* 7152–7157.
163. Garber, K. Hepatitis C: Move Over Interferon. *Nat. Biotechnol.* **2011,** *29,* 963–966.
164. Williams, S. C. P. New HCV Drugs Trigger Race for More Tolerable Therapies. *Nat. Med.* **2011,** *17,* 1526.
165. Butt, A. A.; Kanwal, F. Boceprevir and Telaprevir in the Management of Hepatitis C Virus-Infected Patients. *Clin. Infect. Dis.* **2012,** *54,* 96–104.
166. Lin, C.; Kwong, A. D.; Perni, R. B. Discovery and Development of VX-950, a Novel, Covalent, and Reversible Inhibitor of Hepatitis C Virus NS3-4A Serine Protease. *Infect. Disord. Drug Targets* **2006,** *6,* 3–16.
167. Kwong, A. D.; Kauffman, R. S.; Hurter, P.; Mueller, P. Discovery and Development of Telaprevir: An NS3-4A Protease Inhibitor for Treating Genotype 1 Chronic Hepatitis C Virus. *Nat. Biotechnol.* **2011,** *29,* 993–1003.
168. Perni, R. B.; Britt, S. D.; Court, J. C.; Courtney, L. F.; Deininger, D. D.; Farmer, L. J.; Gates, C. A.; Harbeson, S. L.; Kim, L. J.; Landro, J. A.; Levin, R. B.; Luong, Y.-P.; O'Malley, E.; Pitlik, J.; Rao, B. G.; Schairer, W. C.; Thomson, J. A.; Tung, R. D.; Van Drie, J. H.; Wei, Y. Inhibitors of Hepatitis C Virus NS3-4A Protease 1. Non-Charged Tetrapeptide Variants. *Bioorg. Med. Chem. Lett.* **2003,** *13,* 4059–4063.
169. Perni, R. B.; Pitlik, J.; Britt, S. D.; Courte, J. J.; Courtney, L. F.; Deininger, D. D.; Farmer, L. J.; Gates, C. A.; Habeson, S. L.; Levin, R. B.; Lin, C.; Lin, K.; Moon, Y.-C.; Luong, Y.-P.; O'Malley, E. T.; Rao, G.; Thomson, J. A.; Tung, R. D.; Van Drie, J. H.; Wei., Y. Inhibitors of Hepatitis C Virus NS3-4A Protease 2. Warhead SAR and Optimization. *Bioorg. Med. Chem. Lett.* **2004,** *14,* 1441–1446.
170. Yip, Y.; Victor, F.; Lamar, J.; Johnson, R.; Wang, Q. M.; Barket, D.; Glass, J.; Jin, L.; Liu, L.; Venable, D.; Wakulchik, M.; Xie, C.; Heinz, B.; Villarreal, E.; Colacino, J.; Yumibe, N.; Munroe, M. T. J.; Chen, S.-H. Discovery of Novel Bicycloproline P2 Bearing Peptidyl α-Ketoamide LY514962 as HCV Protease Inhibitor. *Bioorg. Med. Chem. Lett.* **2004,** *14,* 251–256.
171. Maltais, F.; Chun Jung, Y.; Chen, M.; Tanoury, J.; Perni, R. B.; Mani, N.; Laitinen, L.; Huang, H.; Liao, S.; Gao, H.; Tsao, H.; Block, E.; Ma, C.; Shawgo, R. S.; Town, C.; Brummel, C. L.; Howe, D.; Pazhanisamy, S.; Raybuck, S.; Namchuk, M.; Bennani, Y. L. In Vitro and in vivo Isotope Effects With Hepatitis C Protease Inhibitors: Enhanced Plasma Exposure of Deuterated Telaprevir Versus Telaprevir in Rats. *J. Med. Chem.* **2009,** *52,* 7993–8001.
172. Gant, T. G. Using Deuterium in Drug Discovery: Leaving the Label in the Drug. *J. Med. Chem.* **2014,** *57,* 3595–3611.

173. Njoroge, F. G.; Chen, K. X.; Shih, N.-Y.; Piwinski, J. J. Challenges in Modern Drug Discovery: A Case Study of Boceprevir, an HCV Protease Inhibitor for the Treatment of Hepatitis C Virus Infection. *Acc. Chem. Res.* **2008,** *41,* 50–59.
174. Venkatraman, S. Discovery of Boceprevir, a Direct-Acting NS3/4A Protease Inhibitor for Treatment of Chronic Hepatitis C Infections. *Trends Pharmacol. Sci.* **2012,** *33,* 289–294.
175. Venkatraman, S.; Bogen, S. L.; Arasappan, A.; Bennett, F.; Chen, K.; Jao, E.; Liu, Y.-T.; Lovey, R.; Hendrata, S.; Huang, Y.; Pan, W.; Parekh, T.; Pinto, P.; Popov, V.; Pike, R.; Ruan, S.; Santhanam, B.; Vibulbhan, B.; Wu, W.; Yang, W.; Kong, J.; Liang, X.; Wong, J.; Liu, R.; Butkiewicz, N.; Chase, R.; Hart, A.; Agrawal, S.; Ingravallo, P.; Pichardo, J.; Kong, R.; Baroudy, B.; Malcolm, B.; Guo, Z.; Prongay, A.; Madison, V.; Broske, L.; Cui, X.; Cheng, K.-C.; Hsieh, Y.; Brisson, J.-M.; Prelusky, D.; Korfmacher, W.; White, R.; Bogdanowich-Knipp, S.; Pavlovsky, A.; Bradley, P.; Saksena, A. K.; Ganguly, A.; Piwinski, J.; Girijavallabhan, V.; Njoroge, F. G. Discovery of (1R,5S)-N-[3-Amino-1-(cyclobutylmethyl)-2,3-dioxopropyl]-3-[2(S)-[[[(1,1-dimethylethyl)amino]carbonyl]amino]-3,3-dimethyl-1-oxobutyl]-6,6-dimethyl-3-azabicyclo[3.1.0]hexan-2(S)-carboxamide (SCH 503034), a Selective, Potent, Orally Bioavailable Hepatitis C Virus NS3 Protease Inhibitor: A Potential Therapeutic Agent for the Treatment of Hepatitis C Infection. *J. Med. Chem.* **2006,** *49,* 6074–6086.
176. Prongay, A. J.; Guo, Z.; Yao, N.; Pichardo, J.; Fischmann, T.; Strickland, C.; Myers, J., Jr.; Weber, P. C.; Beyer, B. M.; Ingram, R.; Hong, Z.; Prosise, W. W.; Ramanathan, L.; Taremi, S. S.; Yarosh-Tomaine, T.; Zhang, R.; Senior, M.; Yang, R.-S.; Malcolm, B.; Arasappan, A.; Bennett, F.; Bogen, S. L.; Chen, K.; Jao, E.; Liu, Y.-T.; Lovey, R. G.; Saksena, A. K.; Venkatraman, S.; Girijavallabhan, V.; Njoroge, F. G.; Madison, V. Discovery of the HCV NS3/4A Protease Inhibitor (1R,5S)-N-[3-Amino-1-(cyclobutylmethyl)-2,3-dioxopropyl]-3-[2(S)-[[[(1,1-dimethylethyl)amino]carbonyl]amino]-3,3-dimethyl-1-oxobutyl]-6,6-dimethyl-3-azabicyclo[3.1.0]hexan-2(S)-carboxamide (Sch 503034) II. Key Steps in Structure-Based Optimization. *J. Med. Chem.* **2007,** *50,* 2310–2318.
177. Lamarre, D.; Anderson, P. C.; Bailey, M.; Beaulieu, P.; Bolger, G.; Bonneau, P.; Bös, M.; Cameron, D. R.; Cartier, M.; Cordingley, M. G.; Faucher, A. M.; Goudreau, N.; Kawai, S. H.; Kukolj, G.; Lagace, L.; LaPlante, S. R.; Narjes, H.; Poupart, M. A.; Rancourt, J.; Sentjens, R. E.; St George, R.; Simoneau, B.; Steinmann, G.; Thibeault, D.; Tsantrizos, Y. S.; Weldon, S. M.; Yong, C. L.; Llinàs-Brunet, M. An NS3 Protease Inhibitor With Antiviral Effects in Humans Infected With Hepatitis C Virus. *Nature* **2003,** *426,* 186–189.
178. Tsantrizos, Y. S. The Design of a Potent Inhibitor of the Hepatitis C Virus NS3 Protease: BILN 2061—From the NMR Tube to the Clinic. *Biopolymers* **2004,** *76,* 309–323.
179. Tsantrizos, Y. Peptidomimetic Therapeutic Agents Targeting the Protease Enzyme of the Human Immunodeficiency Virus and Hepatitis C Virus. *Acc. Chem. Res.* **2008,** *41,* 1252–1263.
180. Tsantrizos, Y. S.; Bolger, G.; Bonneau, P.; Cameron, D. R.; Goudreau, N.; Kukolj, G.; LaPlante, S. R.; Llinàs-Brunet, M.; Nar, H.; Lamarre, D. Macrocyclic Inhibitors of the NS3 Protease as Potential Therapeutic Agents of Hepatitis C Virus Infection. *Angew. Chem. Int. Ed.* **2003,** *42,* 1355–1360.
181. Llinàs-Brunet, M.; Bailey, M. D.; Bolger, G.; Brochu, C.; Faucher, A.-M.; Ferland, J. M.; Garneau, M.; Ghiro, E.; Gorys, V.; Grand-Maître, C.; Halmos, T.; Lapeyre-Paquette, N.; Liard, F.; Poirier, M.; Rhéaume, M.; Tsantrizos, Y. S.; Lamarre, D. Structure-Activity Study on a Novel Series of Macrocyclic Inhibitors of the Hepatitis C Virus NS3 Protease Leading to the Discovery of BILN 2061. *J. Med. Chem.* **2004,** *47,* 1605–1608.
182. Llinàs-Brunet, M.; Bailey, M.; Fazal, G.; Ghiro, E.; Gorys, V.; Goulet, S.; Halmos, T.; Maurice, R.; Poirier, M.; Poupart, M.-A.; Rancourt, J.; Thibeault, D.; Wernic, D.; Lamarre, D. Highly Potent and Selective Peptide-Based Inhibitors of the Hepatitis C Virus Serine Protease: Towards Smaller Inhibitors. *Bioorg. Med. Chem. Lett.* **2000,** *10,* 2267–2270.
183. LaPlante, S. R.; Cameron, D. R.; Aubry, N.; Lefebvre, S.; Kukolj, G.; Maurice, R.; Thibeault, D.; Lamarre, D.; Llinàs-Brunet, M. Solution Structure of Substrate-Based Ligands When Bound to Hepatitis C Virus NS3 Protease Domain. *J. Biol. Chem.* **1999,** *274,* 18618–18624.
184. LaPlante, S. R.; Aubry, N.; Déziel, R.; Ni, F.; Xu, P. Transferred 13C T1 Relaxation at Natural Isotopic Abundance: A Practical Method for Determining Site-Specific Changes in Ligand Flexibility Upon Binding to a Macromolecule. *J. Am. Chem. Soc.* **2000,** *122,* 12530–12535.
185. Tyndall, J. D. A.; Nall, T.; Fairlie, D. P. Proteases Universally Recognize Beta Strands in Their Active Sites. *Chem. Rev.* **2005,** *105,* 973–999; Madala, P. K.; Tyndall, J. D. A.; Nall, T.; Fairlie, D. P. Update 1 of: Proteases Universally Recognize Beta Strands in Their Active Sites. *Chem. Rev.* **2010,** *110,* PR1–PR31.
186. LaPlante, S. R.; Nar, H.; Lemke, C. T.; Jakalian, A.; Aubry, N.; Kawai, S. H. Ligand Bioactive Conformation Plays a Critical Role in the Design of Drugs That Target the Hepatitis C Virus NS3 Protease. *J. Med. Chem.* **2013,** *57,* 1777–1789.
187. Lu, L.; Pilot-Matias, T. J.; Stewart, K. D.; Randolph, J. T.; Pithawalla, R.; He, W.; Huang, P. P.; Klein, L. L.; Mo, H.; Molla, A. Mutations Conferring Resistance to a Potent Hepatitis C Virus Serine Protease Inhibitor In Vitro. *Antimicrob. Agents Chemother.* **2004,** *48,* 2260–2266.
188. Stoltz, J. H.; Stern, J. O.; Huang, Q.; Seidler, R. W.; Pack, F. D.; Knight, B. L. A Twenty-Eight-Day Mechanistic Time Course Study in the Rhesus Monkey With Hepatitis C Virus Protease Inhibitor BILN 2061. *Toxicol. Pathol.* **2011,** *39,* 496–501.
189. Llinàs-Brunet, M.; Bailey, M.; Goudreau, D. N.; Bhardwaj, P. K.; Bordeleau, J.; Bös, M.; Bousquet, Y.; Cordingley, M. G.; Duan, J.; Forgione, P.; Garneau, M.; Ghiro, E.; Gorys, V.; Goulet, S.; Halmos, T.; Kawai, S. H.; Naud, J.; Poupart, M. A.; White, P. W. Discovery of a Potent and Selective Noncovalent Linear Inhibitor of the Hepatitis C Virus NS3 Protease (BI 201335). *J. Med. Chem.* **2010,** *53,* 6466–6476.
190. White, P. W.; Llinàs-Brunet, M.; Amad, M.; Bethell, R. C.; Bolger, G.; Cordingley, M. G.; Duan, J.; Garneau, M.; Lagace, L.; Thibeault, D.; Kukolj, G. Preclinical Characterization of BI 201335, a C-Terminal Carboxylic Acid Inhibitor of the Hepatitis C Virus NS3-NS4A Protease. *Antimicrob. Agents Chemother.* **2010,** *54,* 4611–4618.
191. Lemke, C. T.; Goudreau, N.; Zhao, S.; Hucke, O.; Thibeault, D.; Llinàs-Brunet, M.; White, P. W. Combined X-ray, NMR, and Kinetic Analyses Reveal Uncommon Binding Characteristics of the Hepatitis C Virus NS3-NS4A Protease Inhibitor BI 201335. *J. Biol. Chem.* **2011,** *286,* 11434–11443.
192. Wilcken, R.; Zimmermann, M. O.; Lange, A.; Joerger, A. C.; Boeckler, F. M. Principles and Applications of Halogen Bonding in Medicinal Chemistry and Chemical Biology. *J. Med. Chem.* **2013,** *56,* 1363–1388.
193. Beno, B. R.; Yeung, K.-S.; Bartberger, M. D.; Pennington, L. D.; Meanwell, N. A. A Survey of the Role of Noncovalent Sulfur Interactions in Drug Design. *J. Med. Chem.* **2015,** *58,* 4383–4438.
194. D'Andrea, S.; Zheng, B.; Hewawasam, P.; Ding, M.; Thuring, J.; Li, J.; Hernandez, D.; Yu, F.; Falk, P.; Zhai, G.; Sheaffer, A. K.; Chen, C.; Lee, M. S.; Barry, D.; Knipe, J. O.; Li, W.; Han, Y.-H.; Jenkins, S.; Gesenberg, C.; Gao, Q.; Sinz, M. W.; Santone, K. S.; Zvyaga, T.; Rajamani, R.; Klei, H. E.; Colonno, R. J.; Grasela, D. M.; Hughes, E.; Chien, C.; Adams, S.; Levesque, P. C.; Li, D.; Zhu, J.; Meanwell, N. A.; McPhee, F. Discovery and Early Clinical Evaluation of BMS-605339, a Potent and Orally Efficacious Tripeptidic Acylsulfonamide NS3 Protease Inhibitor for the Treatment of Hepatitis C Virus Infection. *J. Med. Chem.* **2014,** *57,* 1708–1729.
195. Scola, P. M.; Sun, L.-Q.; Wang, A. X.; Chen, J.; Sin, N.; Venables, B. L.; Sit, S.-Y.; Chen, Y.; Cocuzza, A.; Bilder, D. M.; D'Andrea, S. V.; Zheng, B.; Hewawasam, P.; Tu, Y.; Friborg, J.; Falk, P.; Hernandez, D.; Levine, S.; Chen, C.; Yu, F.; Sheaffer, A. K.; Zhai, G.; Barry, D.; Knipe, J. O.; Han, Y.-H.; Schartman, R.; Donoso, M.; Mosure, K.; Sinz, M. W.; Zvyaga, T.; Good, A. C.; Rajamani, R.; Kish, K.; Tredup, J.; Klei, H. E.; Gao, Q.; Mueller, L.; Colonno, R. J.; Grasela, D. M.; Adams, S. P.; Loy, J.; Levesque, P. C.; Sun, H.; Shi, H.; Sun, L.; Warner, W.; Li, D.; Zhu, J.; Meanwell, N. A.; McPhee, F. The Discovery of Asunaprevir (BMS-650032), an Orally Efficacious NS3 Protease Inhibitor for the Treatment of Hepatitis C Virus Infection. *J. Med. Chem.* **2014,** *57,* 1730–1752.
196. De Clercq, E. Current Race in the Development of DAAs (Direct-Acting Antivirals) Against HCV. *Biochem. Pharmacol.* **2014,** *89,* 441–452.
197. Thompson, J. R. Emerging Therapeutic Options for the Management of Hepatitis C Infection. *World J. Gastroenterol.* **2014,** *20,* 7079–7088.
198. Johansson, P.-O.; Bäck, M.; Kvarnström, I.; Vrang, L.; Hamelink, E.; Hallberg, A.; Rosenquist, Å.; Samuelsson, B. Potent Inhibitors of the Hepatitis C Virus NS3 Protease: Use of a Novel P2 Cyclopentane-Derived Template. *Bioorg. Med. Chem.* **2006,** *14,* 5136–5151.
199. Raboisson, P.; de Kock, H.; Rosenquist, Å.; Nilsson, M.; Salvador-Oden, L.; Lin, T. I.; Roue, N.; Ivanov, V.; Wahling, H.; Wickstrom, K.; Hamelink, E.; Edlund, M.; Vrang, L.; Vendeville, S.; Van de Vreken, W.; McGowan, D.; Tahri, A.; Hu, L.; Boutton, C.; Lenz, O.; Delouvroy, F.; Pille, G.; Surleraux, D.; Wigerinck, P.; Samuelsson, B.; Simmen, K. Structure-Activity Relationship Study on a Novel Series of Cyclopentane-Containing Macrocyclic Inhibitors of the Hepatitis C Virus NS3/4A Protease Leading to the Discovery of TMC435350. *Bioorg. Med. Chem. Lett.* **2008,** *18,* 4853–4858.
200. Rosenquist, Å.; Samuelsson, B.; Johansson, P.-O.; Cummings, M. D.; Lenz, O.; Raboisson, P.; Simmen, K.; Vendeville, S.; de Kock, H.; Nilsson, M.; Horvath, A.; Kalmeijer, R.; de la Rosa, G.; Beumont-Mauviel, M. Discovery and Development of Simeprevir (TMC435), a HCV NS3/4A Protease Inhibitor. *J. Med. Chem.* **2014,** *57,* 1673–1693.

201. Cummings, M. D.; Lindberg, J.; Lin, T.-I.; de Kock, H.; Lenz, O.; Lilja, E.; Fellander, S.; Baraznenok, V.; Nystrom, S.; Nilsson, M.; Vrang, L.; Edlund, M.; Rosenquist, Å.; Samuelsson, B.; Raboisson, P.; Simmen, K. Induced-Fit Binding of the Macrocyclic Noncovalent Inhibitor TMC435 to Its HCV NS3/NS4A Protease Target. *Angew. Chem. Int. Ed.* **2010,** *49,* 1652–1655.
202. Lin, T. I.; Lenz, O.; Fanning, G.; Verbinnen, T.; Delouvroy, F.; Scholliers, A.; Vermeiren, K.; Rosenquist, Å.; Edlund, M.; Samuelsson, B.; Vrang, L.; de Kock, H.; Wigerinck, P.; Raboisson, P.; Simmen, K. In Vitro Activity and Preclinical Profile of TMC435350, a Potent Hepatitis C Virus Protease Inhibitor. *Antimicrob. Agents Chemother.* **2009,** *53,* 1377–1385.
203. Lenz, O.; Verbinnen, T.; Lin, T. I.; Vijgen, L.; Cummings, M. D.; Lindberg, J.; Berke, J. M.; Dehertogh, P.; Fransen, E.; Scholliers, A.; Vermeiren, K.; Ivens, T.; Raboisson, P.; Edlund, M.; Storm, S.; Vrang, L.; de Kock, H.; Fanning, G. C.; Simmen, K. A. In Vitro Resistance Profile of the Hepatitis C Virus NS3/4A Protease Inhibitor TMC435. *Antimicrob. Agents Chemother.* **2010,** *54,* 1878–1887.
204. Takehara, T. Simeprevir for the Treatment of Chronic Hepatitis C Genotype 1 Infection. *Expert Rev. Anti-Infect. Ther.* **2014,** *12,* 909–917.
205. Jiang, Y.; Andrews, S. W.; Condroski, K. R.; Buckman, B.; Serebryany, V.; Wenglowsky, S.; Kennedy, A. L.; Madduru, M. R.; Wang, B.; Lyon, M.; Doherty, G. A.; Woodard, B. T.; Lemieux, C.; Geck Do, M.; Zhang, H.; Ballard, J.; Vigers, G.; Brandhuber, B. J.; Stengel, P.; Josey, J. A.; Beigelman, L.; Blatt, L.; Seiwert, S. D. Discovery of Danoprevir (ITMN-191/R7227), a Highly Selective and Potent Inhibitor of Hepatitis C Virus (HCV) NS3/4A Protease. *J. Med. Chem.* **2014,** *57,* 1753–1769.
206. Rajagopalan, R.; Misialek, S.; Stevens, S. K.; Myszka, D. G.; Brandhuber, B. J.; Ballard, J. A.; Andrews, S. W.; Seiwert, S. D.; Kossen, K. Inhibition and Binding Kinetics of the Hepatitis C Virus NS3 Protease Inhibitor ITMN-191 Reveals Tight Binding and Slow Dissociative Behavior. *Biochemistry* **2009,** *48,* 2559–2568.
207. Seiwert, S. D.; Andrews, S. W.; Jiang, Y.; Serebryany, V.; Tan, H.; Kossen, K.; Rajagopalan, P. T. R.; Misialek, S.; Stevens, S. K.; Stoycheva, A.; Hong, J.; Lim, S. R.; Qin, X.; Rieger, R.; Condroski, K. R.; Zhang, H.; Do, M. G.; Lemieux, C.; Hingorani, G. P.; Hartley, D. P.; Josey, J. A.; Pan, L.; Beigelman, L.; Blatt, L. M. Preclinical Characteristics of the Hepatitis C Virus NS3/4A Protease Inhibitor ITMN-191 (R7227). *Antimicrob. Agents Chemother.* **2008,** *52,* 4432–4441.
208. Deutsch, M.; Papatheodoridis, G. V. Danoprevir, a Small-Molecule NS3/4A Protease Inhibitor for the Potential Oral Treatment of HCV Infection. *Curr. Opin. Investig. Drugs* **2010,** *11,* 951–963.
209. Forestier, N.; Larrey, D.; Guyader, D.; Marcellin, P.; Rouzier, R.; Patat, A.; Smith, P.; Bradford, W.; Porter, S.; Blatt, L.; Seiwert, S. D.; Zeuzem, S. Treatment of Chronic Hepatitis C Patients With the NS3/4A Protease Inhibitor Danoprevir (ITMN-191/RG7227) Leads to Robust Reductions in Viral RNA: A Phase 1b Multiple Ascending Dose Study. *J. Hepatol.* **2011,** *54,* 1130–1136.
210. Lim, S. R.; Qin, X.; Susser, S.; Nicholas, J. B.; Lange, C.; Herrmann, E.; Hong, J.; Arfsten, A.; Hooi, L.; Bradford, W.; Najera, I.; Smith, P.; Zeuzem, S.; Kossen, K.; Sarrazin, C.; Seiwert, S. D. Virologic Escape During Danoprevir (ITMN-191/RG7227) Monotherapy Is Hepatitis C Virus Subtype Dependent and Associated With R155K Substitution. *Antimicrob. Agents Chemother.* **2012,** *56,* 271–279.
211. Carrion, A. F.; Gutierrez, J.; Martin, P. New Antiviral Agents for the Treatment of Hepatitis C: ABT-450. *Expert. Opin. Pharmacother.* **2014,** *15,* 711–716.
212. Pilot-Matias, T.; Tripathi, R.; Cohen, D.; Gaultier, I.; Dekhtyar, T.; Lu, L.; Reisch, T.; Irvin, M.; Hopkins, T.; Pithawalla, R.; Middleton, T.; Ng, T.; McDaniel, K.; Or, Y. S.; Menon, R.; Kempf, D.; Molla, A.; Collins, C. In Vitro and in vivo Antiviral Activity and Resistance Profile of the Hepatitis C Virus NS3/4A Protease Inhibitor ABT-450. *Antimicrob. Agents Chemother.* **2015,** *59,* 988–997.
213. Liverton, N. J.; Holloway, M. K.; McCauley, J. A.; Rudd, M. T.; Butcher, J. W.; Carroll, S. S.; DiMuzio, J.; Fandozzi, C.; Gilbert, K. F.; Mao, S.-S.; McIntyre, C. J.; Nguyen, K. T.; Romano, J. J.; Stahlhut, M.; Wan, B.-L.; Olsen, D. B.; Vacca, J. P. Molecular Modeling Based Approach to Potent P2-P4 Macrocyclic Inhibitors of Hepatitis C NS3/4A Protease. *J. Am. Chem. Soc.* **2008,** *130,* 4607–4609.
214. McCauley, J. A.; McIntyre, C. J.; Rudd, M. T.; Nguyen, K. T.; Romano, J. J.; Butcher, J. W.; Gilbert, K. F.; Bush, K. J.; Holloway, M. K.; Swestock, J.; Wan, B.-L.; Carroll, S. S.; DiMuzio, J. M.; Graham, D. J.; Ludmerer, S. W.; Mao, S.-S.; Stahlhut, M. W.; Fandozzi, C. M.; Trainor, N.; Olsen, D. B.; Vacca, J. P.; Liverton, N. J. Discovery of Vaniprevir (MK-7009), a Macrocyclic Hepatitis C Virus NS3/4a Protease Inhibitor. *J. Med. Chem.* **2010,** *53,* 2443–2463.
215. Harper, S.; McCauley, J. A.; Rudd, M. T.; Ferrara, M.; DiFilippo, M.; Crescenzi, B.; Koch, U.; Petrocchi, A.; Holloway, M. K.; Butcher, J. W.; Romano, J. J.; Bush, K. J.; Gilbert, K. F.; McIntyre, C. J.; Nguyen, K. T.; Nizi, E.; Carroll, S. S.; Ludmerer, S. W.; Burlein, C.; DiMuzio, J. M.; Graham, D. J.; McHale, C. M.; Stahlhut, M. W.; Olsen, D. B.; Monteagudo, E.; Cianetti, S.; Giuliano, C.; Pucci, V.; Trainor, N.; Fandozzi, C. M.; Rowley, M.; Coleman, P. J.; Vacca, J. P.; Summa, V.; Liverton, N. J. Discovery of MK-5172, a Macrocyclic Hepatitis C Virus NS3/4a Protease Inhibitor. *ACS Med. Chem. Lett.* **2012,** *3,* 332–336.
216. Liverton, N. J.; Carroll, S. S.; Di Muzio, J.; Fandozzi, C.; Graham, D. J.; Hazuda, D.; Holloway, M. K.; Ludmerer, S. W.; McCauley, J. A.; McIntyre, C. J.; Olsen, D. B.; Rudd, M. T.; Stahlhut, M.; Vacca, J. P. MK-7009, a Potent and Selective Inhibitor of Hepatitis C Virus NS3/4A Protease. *Antimicrob. Agents Chemother.* **2010,** *54,* 305–311.
217. Lawitz, E.; Sulkowski, M.; Jacobson, I.; Kraft, W. K.; Maliakkal, B.; Al-Ibrahim, M.; Gordon, S. C.; Kwo, P.; Rockstroh, J. K.; Panorchan, P.; Miller, M.; Caro, L.; Barnard, R.; Hwang, P. M.; Gress, J.; Quirk, E.; Mobashery, N. Characterization of Vaniprevir, a Hepatitis C Virus NS3/4A Protease Inhibitor, in Patients With HCV Genotype 1 Infection: Safety, Antiviral Activity, Resistance, and Pharmacokinetics. *Antivir. Res.* **2013,** *99,* 214–220.
218. Wright, D. H.; Caro, L.; Cerra, M.; Panorchan, P.; Du, L.; Anderson, M.; Potthoff, A.; Nachbar, R. B.; Wagner, J.; Manns, M. P.; Talal, A. H. Liver-to-Plasma Vaniprevir (MK-7009) Concentration Ratios in HCV-Infected Patients. *Antivir. Ther.* **2015,** *20,* 843–848.
219. Talal, A. H.; Dimova, R. B.; Zhang, E. Z.; Jiang, M.; Penney, M. S.; Sullivan, J. C.; Botfield, M. C.; Chakilam, A.; Sawant, R.; Cervini, C. M.; Zeremski, M.; Jacobson, I. M.; Kwong, A. D. Telaprevir-Based Treatment Effects on Hepatitis C Virus in Liver and Blood. *Hepatology* **2014,** *60,* 1826–1837.
220. Barnard, R. J. O.; McHale, C. M.; Newhard, W.; Cheney, C. A.; Graham, D. J.; Himmelberger, A. L.; Strizki, J.; Hwang, P. M. T.; Rivera, A. A.; Reeves, J. D.; Nickle, D.; DiNubile, M. J.; Hazuda, D. J.; Mobashery, N. Emergence of Resistance-Associated Variants After Failed Triple Therapy With Vaniprevir in Treatment-Experienced Non-Cirrhotic Patients With Hepatitis C-Genotype 1 Infection: A Population and Clonal Analysis. *Virology* **2013,** *443,* 278–284.
221. Summa, V.; Ludmerer, S. W.; McCauley, J. A.; Fandozzi, C.; Burlein, C.; Claudio, G.; Coleman, P. J.; DiMuzio, J. M.; Ferrara, M.; Di Filippo, M.; Gates, A. T.; Graham, D. J.; Harper, S.; Hazuda, D. J.; McHale, C.; Monteagudo, E.; Pucci, V.; Rowley, M.; Rudd, M. T.; Soriano, A.; Stahlhut, M. W.; Vacca, J. P.; Olsen, D. B.; Liverton, N. J.; Carroll, S. MK-5172, a Selective Inhibitor of Hepatitis C Virus NS3/4a Protease With Broad Activity Across Genotypes and Resistant Variants. *Antimicrob. Agents Chemother.* **2012,** *56,* 4161–4167.
222. Gottwein, J. M.; Scheel, T. K. H.; Jensen, T. B.; Ghanem, L.; Bukh, J. Differential Efficacy of Protease Inhibitors Against HCV Genotypes 2a, 3a, 5a, and 6a NS3/4A Protease Recombinant Viruses. *Gastroenterology* **2011,** *141,* 1067–1079.
223. Gentile, I.; Buonomo, A. R.; Borgia, F.; Zappulo, E.; Castaldo, G.; Borgia, G. MK-5172: A Second-Generation Protease Inhibitor for the Treatment of Hepatitis C Virus Infection. *Exp. Opin. Invest. Drugs* **2014,** *23,* 719–728.
224. Romano, K. P.; Ali, A.; Aydin, C.; Soumana, D.; Özen, A.; Deveau, L. M.; Silver, C.; Cao, H.; Newton, A.; Petropoulos, C. J.; Huang, W.; Schiffer, C. A. The Molecular Basis of Drug Resistance Against Hepatitis C Virus NS3/4A Protease Inhibitors. *PLoS Pathog.* **2012,** *8,* e1002832. http://dx.doi.org/10.1371/journal.ppat.1002832.
225. Ali, A.; Aydin, C.; Gildemeister, R.; Romano, K. P.; Cao, H.; Özen, A.; Soumana, D.; Newton, A.; Petropoulos, C. J.; Huang, W.; Schiffer, C. A. Evaluating the Role of Macrocycles in the Susceptibility of Hepatitis C Virus NS3/4A Protease Inhibitors to Drug Resistance. *ACS Chem. Biol.* **2013,** *8,* 1469–1478.
226. Rudd, M. T.; Butcher, J. W.; Nguyen, K. T.; McIntyre, C. J.; Romano, J. J.; Gilbert, K. F.; Bush, K. J.; Liverton, N. J.; Holloway, M. K.; Harper, S.; Ferrara, M.; DiFilippo, M.; Summa, V.; Swestock, J.; Fritzen, J.; Carroll, S. S.; Burlein, C.; DiMuzio, J. M.; Gates, A.; Graham, D. J.; Huang, Q.; McClain, S.; McHale, C.; Stahlhut, M. W.; Black, S.; Chase, R.; Soriano, A.; Fandozzi, C. M.; Taylor, A.; Trainor, N.; Olsen, D. B.; Coleman, P. J.; Ludmerer, S. W.; McCauley, J. A. P2-Quinazolinones and Bis-Macrocycles as New Templates for Next-Generation Hepatitis C Virus NS3/4a Protease Inhibitors: Discovery of MK-2748 and MK-6325. *ChemMedChem* **2015,** *10,* 727–735.
227. Hagel, M.; Niu, D.; St Martin, T.; Sheets, M. P.; Qiao, L.; Bernard, H.; Karp, R. M.; Zhu, Z.; Labenski, M. T.; Chaturvedi, P.; Nacht, M.; Westlin, W. F.; Petter, R. C.; Singh, J. Selective Irreversible Inhibition of a Protease by Targeting a Noncatalytic Cysteine. *Nat. Chem. Biol.* **2011,** *7,* 22–24.
228. Matthews, D. A.; Alden, R. A.; Birktoft, J. J.; Freer, S. T.; Kraut, J. The X-ray Crystallographic Study of Boronic Acid Adducts With Subtilisin BPN' (Novo). Model for the Catalytic Transition State. *J. Biol. Chem.* **1975,** *250,* 7120–7126.
229. Smoum, R.; Rubinstein, A.; Dembitsky, V. M.; Srebnik, M. Boron Containing Compounds as Protease Inhibitors. *Chem. Rev.* **2012,** *112,* 4156–4220.

230. Attwood, M. R.; Bennett, J. M.; Campbell, A. D.; Canning, G. G. M.; Carr, M. G.; Dunsdon, R. M.; Greening, J. R.; Jones, P. S.; Kay, P. B.; Handa, B. K.; Hurst, D. N.; Jennings, N. S.; Jordan, S.; Keech, E.; O'Brian, M. A.; Overton, N. H.; King-Underwood, J.; Raynham, T. M.; Stenson, K. P.; Wilkinson, C. S.; Wilkinson, T. C. I.; Wilson, F. X. The Design and Synthesis of Potent Inhibitors of Hepatitis C Virus NS3-4A Proteinase. *Antivir. Chem. Chemoth.* **1999,** *10,* 259–273.
231. Dunsdon, R. M.; Greening, J. R.; Jones, P. S.; Jordan, S.; Wilson, F. X. Solid Phase Synthesis of Aminoboronic Acids: Potent Inhibitors of the Hepatitis C Virus NS3 Proteinase. *Bioorg. Med. Chem. Lett.* **2000,** *10,* 1577–1579.
232. Priestley, E. S.; De Lucca, I.; Ghavimi, B.; Erickson-Viitanen, S.; Decicco, C. P. P1 Phenethyl Peptide Boronic Acid Inhibitors of HCV NS3 Protease. *Bioorg. Med. Chem. Lett.* **2002,** *12,* 3199–3202.
233. Boloor, A.; Hanway, D.; Joshi, M.; Winn, D. T.; Mendez, G.; Walls, M.; Wei, P.; Qian, F.; Zhang, X.; Zhang, Y.; Hepperle, M. E.; Li, X.; Campbell, D. A.; Betancort, J. M. Synthesis and Antiviral Activity of HCV NS3/4A Peptidomimetic Boronic Acid Inhibitors. *Bioorg. Med. Chem. Lett.* **2009,** *19,* 5708–5711.
234. Hotho, D. M.; de Bruijne, J.; O'Farrell, A. M.; Boyea, T.; Li, J.; Bracken, M.; Li, X.; Campbell, D.; Guler, H.-P.; Weegink, C. J.; Schinkel, J.; Molenkamp, R.; van de Wetering de Rooij, J.; van Vliet, A.; Janssen, H. L. A.; de Knegt, R. J.; Reesink, H. W. Pharmacokinetics and Antiviral Activity of PHX1766, a Novel HCV Protease Inhibitor, Using an Accelerated Phase I Study Design. *Antivir. Ther.* **2012,** *17,* 365–375.
235. Li, X.; Zhang, Y.-K.; Liu, Y.; Ding, C. Z.; Li, Q.; Zhou, Y.; Plattner, J. J.; Baker, S. J.; Qian, X.; Fan, D.; Liao, L.; Ni, Z.-J.; White, G. V.; Mordaunt, J. E.; Lazarides, L. X.; Slater, M. J.; Jarvest, R. L.; Thommes, P.; Ellis, M.; Edge, C. M.; Hubbard, J. A.; Somers, D.; Rowland, P.; Nassau, P.; McDowell, B.; Skarzynski, T. J.; Kazmierski, W. M.; Grimes, R. M.; Wright, L. L.; Smith, G. K.; Zou, W.; Wright, J.; Pennicott, L. E. Synthesis and Evaluation of Novel α-Amino Cyclic Boronates as Inhibitors of HCV NS3 Protease. *Bioorg. Med. Chem. Lett.* **2010,** *20,* 3550–3556.
236. Li, X.; Zhang, Y.-K.; Liu, Y.; Ding, C. Z.; Zhou, Y.; Li, Q.; Plattner, J. J.; Baker, S. J.; Zhang, S.; Kazmierski, W. M.; Wright, L. L.; Smith, G. K.; Grimes, R. M.; Crosby, R. M.; Creech, K. L.; Carballo, L. H.; Slater, M. J.; Jarvest, R. L.; Thommes, P.; Hubbard, J. A.; Convery, M. A.; Nassau, P. M.; McDowell, W.; Skarzynski, T. J.; Qian, X.; Fan, D.; Liao, L.; Ni, Z.-J.; Pennicott, L. E.; Zou, W.; Wright, J. Novel Macrocyclic HCV NS3 Protease Inhibitors Derived From α-Amino Cyclic Boronates. *Bioorg. Med. Chem. Lett.* **2010,** *20,* 5695–5700.
237. Sheng, X. C.; Pyun, H.-J.; Chaudhary, K.; Wang, J.; Doerffler, E.; Fleury, M.; McMurtrie, D.; Chen, X.; Delaney, W. E., IV; Kim, C. U. Discovery of Novel Phosphonate Derivatives as Hepatitis C Virus NS3 Protease Inhibitors. *Bioorg. Med. Chem. Lett.* **2009,** *19,* 3453–3457.
238. Clarke, M. O.; Chen, X.; Cho, A.; Delaney, W. E., IV; Doerffler, E.; Fardis, M.; Ji, M.; Mertzman, M.; Pakdaman, R.; Pyun, H.-J.; Rowe, T.; Yang, C. Y.; Sheng, X. C.; Kim, C. U. Novel, Potent, and Orally Bioavailable Phosphinic Acid Inhibitors of the Hepatitis C Virus NS3 Protease. *Bioorg. Med. Chem. Lett.* **2011,** *21,* 3568–3572.
239. Sheng, X. C.; Casarez, A.; Cai, R.; Clarke, M. O.; Chen, X.; Cho, A.; Delaney, W. E., IV; Doerffler, E.; Ji, M.; Mertzman, M.; Pakdaman, R.; Pyun, H.-J.; Rowe, T.; Wu, Q.; Xu, J.; Kim, C. U. Discovery of GS-9256: A Novel Phosphinic Acid Derived Inhibitor of the Hepatitis C Virus NS3/4A Protease With Potent Clinical Activity. *Bioorg. Med. Chem. Lett.* **2012,** *22,* 1394–1396.
240. Barauskas, O.; Corsa, A. C.; Wang, R.; Hluhanich, S.; Jin, D.; Hung, M.; Yang, H.; Delaney, W. E.; Schultz, B. E. Binding Kinetics, Potency, and Selectivity of the Hepatitis C Virus NS3 Protease Inhibitors GS-9256 and Vedroprevir. *Biochim. Biophys. Acta* **2014,** *1840,* 3292–3298.
241. Zeuzem, S.; Buggisch, P.; Agarwal, K.; Marcellin, P.; Sereni, D.; Klinker, H.; Moreno, C.; Zarski, J. P.; Horsmans, Y.; Mo, H.; Arterburn, S.; Knox, S.; Oldach, D.; McHutchison, J. G.; Manns, M. P.; Foster, G. R. The Protease Inhibitor, GS-9256, and Non-Nucleoside Polymerase Inhibitor Tegobuvir Alone, With Ribavirin, or Pegylated Interferon Plus Ribavirin in Hepatitis C. *Hepatology* **2012,** *55,* 749–758.
242. Nelson, D.; Yoshida, E. M.; Paulson, M. S.; Hengen, P. N.; Ge, D.; Kanwar, B.; McNally, J.; Pang, P. S.; Subramanian, G. M.; McHutchison, J. G.; Urbanek, P.; Lawitz, E.; Urban, T. J. Genome-Wide Association Study to Characterize Serum Bilirubin Elevations in Patients With HCV Treated With GS-9256, an HCV NS3 Serine Protease Inhibitor. *Antivir. Ther.* **2014,** *19,* 679–686.
243. Vachon, M.-L.; Dieterich, D. T. The Era of Direct-Acting Antivirals has Begun: The Beginning of the End for HCV? *Semin. Liver Dis.* **2011,** *31,* 399–409.
244. Katz, B. A.; Clark, J. M.; Finer-Moore, J. S.; Jenkins, T. E.; Johnson, C. R.; Ross, M. J.; Luong, C.; Moore, W. R.; Stroud, R. M. Design of Potent Selective Zinc-Mediated Serine Protease Inhibitors. *Nature* **1998,** *391,* 608–612.
245. Katz, B. A.; Luong, C. Recruiting Zn^{2+} to Mediate Potent, Specific Inhibition of Serine Proteases. *J. Mol. Biol.* **1999,** *292,* 669–684.
246. Janc, J. W.; Clark, J. M.; Warne, R. L.; Elrod, K. C.; Katz, B. A.; Moore, W. R. A Novel Approach to Serine Protease Inhibition: Kinetic Characterization of Inhibitors Whose Potencies and Selectivities Are Dramatically Enhanced by Zinc(II). *Biochemistry* **2000,** *39,* 4792–4800.
247. Yeung, K.-S.; Meanwell, N. A.; Qiu, Z.; Hernandez, D.; Zhang, S.; McPhee, F.; Weinheimer, S.; Clark, J. M.; Janc, J. W. Structure-Activity Relationship Studies of a Bisbenzimidazole-Based, Zn^{2+}-Dependent Inhibitor of HCV NS3 Serine Protease. *Bioorg. Med. Chem. Lett.* **2001,** *11,* 2355–2359.
248. Sperandio, D.; Gangloff, A. R.; Litvak, J.; Goldsmith, R.; Hataye, J. M.; Wang, V. R.; Shelton, E. J.; Elrod, K.; Janc, J. W.; Clark, J. M.; Rice, K.; Weinheimer, S.; Yeung, K.-S.; Meanwell, N. A.; Hernandez, D.; Staab, A. J.; Venables, B. L.; Spencer, J. R. Highly Potent Non-Peptidic Inhibitors of the HCV NS3/NS4A Serine Protease. *Bioorg. Med. Chem. Lett.* **2002,** *12,* 3129–3133.
249. Borthwick, A. D. Design of Translactam HCMV Protease Inhibitors as Potent Antivirals. *Med. Res. Rev.* **2005,** *25,* 427–452.
250. Slater, M. J.; Andrews, D. M.; Baker, G.; Bethell, S. S.; Carey, S.; Chaignot, H.; Clarke, B.; Coomber, B.; Ellis, M.; Good, A.; Gray, N.; Hardy, G.; Jones, P.; Mills, G.; Robinson, E. Design and Synthesis of Ethyl Pyrrolidine-5,5-*Trans*-Lactams as Inhibitors of Hepatitis C Virus NS3/4A Protease. *Bioorg. Med. Chem. Lett.* **2002,** *12,* 3359–3362.
251. Andrews, D. M.; Carey, S. J.; Chaignot, H.; Coomber, B. A.; Gray, N. M.; Hind, S. L.; Jones, P. S.; Mills, G.; Robinson, J. E.; Slater, M. J. Pyrrolidine-5,5-*Trans*-Lactams. 1. Synthesis and Incorporation Into Inhibitors of Hepatitis C Virus NS3/4A Protease. *Org. Lett.* **2002,** *4,* 4475–4478.
252. Andrews, D. M.; Chaignot, H.; Coomber, B. A.; Good, A. C.; Hind, S. L.; Johnson, M. R.; Jones, P. S.; Mills, G.; Robinson, J. E.; Skarzynski, T.; Slater, M. J.; O'N Somers, D. Pyrrolidine-5,5-*Trans*-Lactams. 2. The Use of X-ray Crystal Structure Data in the Optimization of P3 and P4 Substituents. *Org. Lett.* **2002,** *4,* 4479–4482.
253. Andrews, D. M.; Chaignot, H. M.; Coomber, B. A.; Dowle, M. D.; Hind, S. L.; Johnson, M. R.; Jones, P. S.; Mills, G.; Patikis, A.; Pateman, T. J.; Robinson, J. E.; Slater, M. J.; Trivedi, N. The Design of Potent, Non-Peptidic Inhibitors of Hepatitis C Protease. *Eur. J. Med. Chem.* **2003,** *38,* 339–343.
254. Slater, M. J.; Amphlett, E. M.; Andrews, D. M.; Bamborough, P.; Carey, S. J.; Johnson, M. R.; Jones, P. S.; Mills, G.; Parry, N. R.; Somers, O.'. N.; Stewart, A. J.; Skarzynski, T. Pyrrolidine-5,5-*Trans*-Lactams. 4. Incorporation of a P3/P4 Urea Leads to Potent Intracellular Inhibitors of Hepatitis C Virus NS3/4A Protease. *Org. Lett.* **2003,** *45,* 4627–4630.
255. Andrews, D. M.; Barnes, M. C.; Dowle, M. D.; Hind, S. L.; Johnson, M. R.; Jones, P. S.; Mills, G.; Patikis, S.; Pateman, T. J.; Redfern, T. J.; Robinson, J. E.; Slater, M. J.; Trivedi, N. Pyrrolidine-5,5-*Trans*-Lactams. 5. Pharmacokinetic Optimization of Inhibitors of Hepatitis C Virus NS3/4A Protease. *Org. Lett.* **2003,** *5,* 4631–4634.
256. Andrews, D. M.; Jones, P. S.; Mills, G.; Hind, S. L.; Slater, M. J.; Trivedi, N.; Wareing, K. J. Design and Synthesis of Spiro-Cyclopentenyl and Spiro-[1,3]-Dithiolanyl Substituted Pyrrolidine-5,5-*Trans*-Lactams as Inhibitors of Hepatitis C Virus NS3/4A Protease. *Bioorg. Med. Chem. Lett.* **2003,** *13,* 1657–1660.
257. Murray, C. W.; Verdonk, M. L.; Rees, D. C. Experiences in Fragment-Based Drug Discovery. *Trends Pharmacol. Sci.* **2012,** *33,* 224–232.
258. Scott, D. E.; Coyne, A. G.; Hudson, S. A.; Abell, C. Fragment-Based Approaches in Drug Discovery and Chemical Biology. *Biochemistry* **2012,** *51,* 4990–5003.
259. Saalau-Bethell, S. M.; Woodhead, A. J.; Chessari, G.; Carr, M. G.; Coyle, J.; Graham, B.; Hiscock, S. D.; Murray, C. W.; Pathuri, P.; Rich, S. J.; Richardson, C. J.; Williams, P. A.; Jhoti, H. Discovery of an Allosteric Mechanism for the Regulation of HCV NS3 Protein Function. *Nat. Chem. Biol.* **2012,** *8,* 920–925.
260. Kwong, A. D.; Rao, B. G.; Jeang, K.-T. Viral and Cellular RNA Helicases as Antiviral Targets. *Nat. Rev. Drug Discov.* **2005,** *4,* 845–853.
261. Frick, D. N. HCV Helicase: Structure, Function, and Inhibition. In *Hepatitis C Viruses: Genomes and Molecular Biology;* Tan, S. L., Ed.; *Horizon Bioscience;* Norfolk: U.K, 2006.
262. Kolykhalov, A. A.; Mihalik, K.; Feinstone, S. M.; Rice, C. M. Hepatitis C Virus-Encoded Enzymatic Activities and Conserved RNA Elements in the 3'-Nontranslated Region Are Essential for Virus Replication In Vivo. *J. Virol.* **2000,** *74,* 2046–2051.
263. LaPlante, S. R.; Padyana, A. K.; Abeywardane, A.; Bonneau, P.; Cartier, M.; Coulombe, R.; Jakalian, A.; Wildeson-Jones, J.; Li, X.; Liang, S.; McKercher, G.; White, P.; Zhang, Q.; Taylor, S. J. Integrated Strategies for Identifying Leads That Target the NS3 Helicase of the Hepatitis C Virus. *J. Med. Chem.* **2014,** *57,* 2074–2090.

264. Stankiewicz-Drogoń, A.; Dörner, B.; Erker, T.; Boguszewska-Chachulska, A. M. Synthesis of New Acridone Derivatives, Inhibitors of NS3 Helicase, Which Efficiently and Specifically Inhibit Subgenomic HCV Replication. *J. Med. Chem.* **2010,** *53,* 3117–3126.
265. Manfroni, G.; Paeshuyse, J.; Massari, S.; Zanoli, S.; Gatto, B.; Maga, G.; Tabarrini, O.; Cecchetti, V.; Fravolini, A.; Neyts, J. Inhibition of Subgenomic Hepatitis C Virus RNA Replication by Acridone Derivatives: Identification of an NS3 Helicase Inhibi tor. *J. Med. Chem.* **2009,** *52,* 3354–3365.
266. Phoon, C. W.; Ng, P. Y.; Ting, A. E.; Yeo, S. L.; Sim, M. M. Biological Evaluation of Hepatitis C Virus Helicase Inhibitors. *Bioorg. Med. Chem. Lett.* **2001,** *11,* 1647–1650.
267. Belon, C. A.; High, Y. D.; Lin, T. I.; Pauwels, F.; Frick, D. N. Mechanism and Specificity of a Symmetrical Benzimidazolephenylcarboxamide Helicase Inhibitor. *Biochemistry* **2010,** *49,* 1822–1832.
268. Lin, C.; Thomson, J. A.; Rice, C. M. A Central Region in the Hepatitis C Virus NS4A Protein Allows Formation of an Active NS3-NS4A Serine Proteinase Complex in vivo and In Vitro. *J. Virol.* **1995,** *69,* 4373–4380.
269. Landro, J. A.; Raybuck, S. A.; Luong, Y. P. C.; O'Malley, E. T.; Harebeson, S. L.; Morgenstern, K. A.; Rao, G.; Livingston, D. J. Mechanistic Role of an NS4A Peptide Cofactor With the Truncated NS3 Protease of Hepatitis C Virus: Elucidation of the NS4A Stimulatory Effect via Kinetic Analysis and Inhibitor Mapping. *Biochemistry* **1997,** *36,* 9340–9348.
270. Yang, W.; Zhao, Y.; Fabrycki, J.; Hou, X.; Nie, X.; Sanchez, A.; Phadke, A.; Deshpande, M.; Agarwal, A.; Huang, M. Selection of Replicon Variants Resistant to ACH-806, a Novel Hepatitis C Virus Inhibitor With no Cross-Resistance to NS3 Protease and NS5B Polymerase Inhibitors. *Antimicrob. Agents Chemother.* **2008,** *52,* 2043–2052.
271. Wyles, D. L.; Kaihara, K. A.; Schooley, R. T. Synergy of a Hepatitis C Virus (HCV) NS4A Antagonist in Combination With HCV Protease and Polymerase Inhibitors. *Antimicrob. Agents Chemother.* **2008,** *52,* 1862–1864.
272. Yang, W.; Sun, Y.; Hou, X.; Zhao, Y.; Fabrycki, J.; Chen, D.; Wang, X.; Agarwal, A.; Phadke, A.; Deshpande, M.; Huang, M. ACH-806, an NS4A Antagonist, Inhibits Hepatitis C Virus Replication by Altering the Composition of Viral Replication Complexes. *Antimicrob. Agents Chemother.* **2013,** *57,* 3168–3177.
273. Gottwein, J. M.; Jensen, S. B.; Serre, S. B. N.; Ghanem, L.; Scheel, T. K. H.; Jensen, T. B.; Krarup, H.; Uzcategui, N.; Mikkelsen, L. S.; Bukh, J. Adapted J6/JFH1-Based Hepatitis C Virus Recombinants With Genotype-Specific NS4A Show Similar Efficacies Against Lead Protease Inhibitors, Alpha Interferon, and a Putative NS4A Inhibitor. *Antimicrob. Agents Chemother.* **2013,** *57,* 6034–6049.
274. Gouttenoire, J.; Penin, F.; Moradpour, D. Hepatitis C Virus Nonstructural Protein 4B: A Journey Into Unexplored Territory. *Rev. Med. Virol.* **2010,** *20,* 117–129.
275. Dvory-Sobol, H.; Pang, P. S.; Glenn, J. S. The Future of HCV Therapy: NS4B as an Antiviral Target. *Viruses* **2010,** *2,* 2481–2492.
276. Rai, R.; Deval, J. New Opportunities in Anti-Hepatitis C Virus Drug Discovery—Targeting NS4B. *Antivir. Res.* **2011,** *90,* 93–101.
277. Cannalire, R.; Letizia Barreca, M.; Manfroni, G.; Cecchetti, V. A Journey Around the Medicinal Chemistry of Hepatitis C Virus Inhibitors Targeting NS4B: From Target Validation to Preclinical Drug Candidates. *J. Med. Chem.* **2016,** *59,* 16–41.
278. Li, S.; Yu, X.; Guo, Y.; Kong, L. Interaction Networks of Hepatitis C Virus NS4B: Implications for Antiviral Therapy. *Cell. Microbiol.* **2012,** *14,* 994–1002.
279. Thompson, A. A.; Zou, A.; Yan, J.; Duggal, R.; Hao, W.; Molina, D.; Cronin, C. N.; Wells, P. A. Biochemical Characterization of Recombinant Hepatitis C Virus Nonstructural Protein 4B: Evidence for ATP/GTP Hydrolysis and Adenylate Kinase Activity. *Biochemistry* **2009,** *48,* 906–916.
280. Chunduru, S. K.; Benetatos, C. A.; Nitz, T. J.; Bailey, T. R. Compounds, Compositions and Methods for Treatment and Prophylaxis of Hepatitis C Viral Infections and Associated Diseases. World Patent Application WO-2005/051318 A2, **2005**.
281. Bryson, P. D.; Cho, N.-J.; Einav, S.; Lee, C.; Tai, V.; Bechtel, J.; Sivaraja, M.; Roberts, C.; Schmitz, U.; Glenn, J. S. A Small Molecule Inhibits HCV Replication and Alters NS4B's Subcellular Distribution. *Antivir. Res.* **2010,** *87,* 1–8.
282. Shotwell, J. B.; Baskaran, S.; Chong, P.; Creech, K. L.; Crosby, R. M.; Dickson, H.; Fang, J.; Garrido, D.; Mathis, A.; Maung, J.; Parks, D. J.; Pouliot, J. J.; Price, D. J.; Rai, R.; Seal, J. W., 3rd; Schmitz, U.; Tai, V. W.; Thomson, M.; Xie, M.; Xiong, Z. Z.; Peat, A. J. Imidazo[1,2-*a*]Pyridines That Directly Interact With Hepatitis C NS4B: Initial Preclinical Characterization. *ACS Med. Chem. Lett.* **2012,** *3,* 565–569.
283. Miller, J. F.; Chong, P. Y.; Shotwell, J. B.; Catalano, J. G.; Tai, V. W.-F.; Fang, J.; Banka, A. L.; Roberts, C. D.; Youngman, M.; Zhang, H.; Xiong, Z.; Mathis, A.; Pouliot, J. J.; Hamatake, R. K.; Price, D. J.; Seal, J. W., 3rd; Stroup, L. L.; Creech, K. L.; Carballo, L. H.; Todd, D.; Spaltenstein, A.; Furst, S.; Hong, Z.; Peat, A. J. Hepatitis C Replication Inhibitors That Target the Viral NS4B Protein. *J. Med. Chem.* **2014,** *57,* 2107–2120.
284. Pouliot, J. J.; Thomson, M.; Xie, M.; Horton, J.; Johnson, J.; Krull, D.; Mathis, A.; Morikawa, Y.; Parks, D.; Peterson, R.; Shimada, T.; Thomas, E.; Vamathevan, J.; Van Horn, S.; Xiong, Z.; Hamatake, R.; Peat, A. J. Preclinical Characterization and in vivo Efficacy of GSK8853, a Small Molecule Inhibitor of the Hepatitis C Virus NS4B Protein. *Antimicrob. Agents Chemother.* **2015,** *59,* 6539–6550.
285. Leeson, P. D.; Springthorpe, B. The Influence of Drug-Like Concepts on Decision Making in Medicinal Chemistry. *Nat. Rev. Drug Discov.* **2007,** *6,* 881–890.
286. Meanwell, N. A. Improving Drug Candidates by Design: A Focus on Physicochemical Properties as a Means of Improving Compound Disposition and Safety. *Chem. Res. Toxicol.* **2011,** *24,* 1420–1456.
287. Dufner-Beattie, J.; O'Guin, A.; O'Guin, S.; Briley, A.; Wang, B.; Balsarotti, J.; Roth, R.; Starkey, G.; Slomczynska, U.; Noueiry, A.; Olivo, P. D.; Rice, C. M. Identification of AP80978, a Novel Small-Molecule Inhibitor of Hepatitis C Virus Replication That Targets NS4B. *Antimicrob. Agents Chemother.* **2014,** *58,* 3399–3410.
288. Wang, N.-Y.; Xu, Y.; Zuo, W.-Q.; Xiao, K.-J.; Liu, L.; Zeng, X.-X.; You, X.-Y.; Zhang, L.-D.; Gao, C.; Liu, Z.-H.; Ye, T. H.; Xia, Y.; Xiong, Y.; Song, X. J.; Lei, Q.; Peng, C. T.; Tang, H.; Yang, S. Y.; Wei, Y. Q.; Yu, L. T. Discovery of Imidazo[2,1-*b*]Thiazole HCV NS4B Inhibitors Exhibiting Synergistic Effect With Other Direct-Acting Antiviral Agents. *J. Med. Chem.* **2015,** *58,* 2764–2778.
289. Tai, V. W.-F.; Garrido, D.; Price, D. J.; Maynard, A.; Pouliot, J. J.; Xiong, Z.; Seal, J. W.; Creech, K. L.; Kryn, L. H.; Baughman, T. M.; Peat, A. J. Design and Synthesis of Spirocyclic Compounds as HCV Replication Inhibitors by Targeting Viral NS4B Protein. *Bioorg. Med. Chem. Lett.* **2014,** *24,* 2288–2294.
290. Cho, N.-J.; Dvory-Sobol, H.; Lee, C.; Cho, S.-J.; Bryson, P.; Masek, M.; Elazar, M.; Frank, C. W.; Glenn, J. S. Identification of a Class of HCV Inhibitors Directed Against the Nonstructural Protein NS4B. *Sci. Transl. Med.* **2010,** *2,* 15ra6. http://dx.doi.org/10.1126/scitranslmed.3000331.
291. Choi, M.; Lee, S.; Choi, T.; Lee, C. A Hepatitis C Virus NS4B Inhibitor Suppresses Viral Genome Replication by Disrupting NS4B's Dimerization/Multimerization as Well as Its Interaction With NS5A. *Virus Genes* **2013,** *47,* 395–407.
292. Chen, G.; Ren, H.; Turpoff, A.; Arefolov, A.; Wilde, R.; Takasugi, J.; Khan, A.; Almstead, N.; Gu, Z.; Komatsu, T.; Freund, C.; Breslin, J.; Colacino, J.; Hedrick, J.; Weetall, M.; Karp, G. M. Discovery of *N*-(4'-(Indol-2-yl)Phenyl)Sulfonamides as Novel Inhibitors of HCV Replication. *Bioorg. Med. Chem. Lett.* **2013,** *23,* 3942–3946.
293. Zhang, X.; Zhang, N.; Chen, G.; Turpoff, A.; Ren, H.; Takasugi, J.; Morrill, C.; Zhu, J.; Li, C.; Lennox, W.; Paget, S.; Liu, Y.; Almstead, N.; Njoroge, F. G.; Gu, Z.; Komatsu, T.; Clausen, V.; Espiritu, C.; Graci, J.; Colacino, J.; Lahser, F.; Risher, N.; Weetall, M.; Nomeir, A.; Karp, G. M. Discovery of Novel HCV Inhibitors: Synthesis and Biological Activity of 6-(Indol-2-yl)Pyridine-3-Sulfonamides Targeting Hepatitis C Virus NS4B. *Bioorg. Med. Chem. Lett.* **2013,** *23,* 3947–3953.
294. Chen, G.; Ren, H.; Zhang, N.; Lennox, W.; Turpoff, A.; Paget, S.; Li, C.; Almstead, N.; Njoroge, F. G.; Gu, Z.; Jung, S. P.; Colacino, J.; Lahser, F.; Zhao, X.; Weetall, M.; Nomeir, A.; Karp, G. M. 6-(Azaindol-2-yl)Pyridine-3-Sulfonamides as Potent and Selective Inhibitors Targeting Hepatitis C Virus NS4B. *Bioorg. Med. Chem. Lett.* **2015,** *25,* 781–786.
295. Zhang, N.; Zhang, X.; Zhu, J.; Turpoff, A.; Chen, G.; Morrill, C.; Huang, S.; Lennox, W.; Kakarla, R.; Liu, R.; Li, C.; Ren, H.; Almstead, N.; Venkatraman, S.; Njoroge, F. G.; Gu, Z.; Clausen, V.; Graci, J.; Jung, S. P.; Zheng, Y.; Colacino, J. M.; Lahser, F.; Sheedy, J.; Mollin, A.; Weetall, M.; Nomeir, A.; Karp, G. M. Structure-Activity Relationship (SAR) Optimization of 6-(Indol-2-yl)Pyridine-3-Sulfonamides: Identification of Potent, Selective, and Orally Bioavailable Small Molecules Targeting Hepatitis C (HCV) NS4B. *J. Med. Chem.* **2014,** *57,* 2121–2135.
296. Gu, Z.; Graci, J. D.; Lahser, F. C.; Breslin, J. J.; Jung, S. P.; Crona, J. H.; McMonagle, P.; Xia, E.; Liu, S.; Karp, G.; Zhu, J.; Huang, S.; Nomeir, A.; Weetall, M.; Almstead, N. G.; Peltz, S. W.; Tong, X.; Ralston, R.; Colacino, J. M. Identification of PTC725, an Orally Bioavailable Small Molecule That Selectively Targets the Hepatitis C Virus NS4B Protein. *Antimicrob. Agents Chemother.* **2013,** *57,* 3250–3261.
297. Arico-Muendel, C.; Zhu, Z.; Dickson, H.; Parks, D.; Keicher, J.; Deng, J.; Aquilani, L.; Coppo, F.; Graybill, T.; Lind, K.; Peat, A.; Thomson, M. Encoded Library Technology Screening of Hepatitis C Virus NS4B Yields a Small-Molecule Compound Series With in vitro Replicon Activity. *Antimicrob. Agents Chemother.* **2015,** *59,* 3450–3459.

298. Kakarla, R.; Liu, J.; Naduthambi, D.; Chang, W.; Mosley, R. T.; Bao, D.; Steuer, H. M.; Micolochick, K. M.; Bansal, S.; Lam, A. M.; Seibel, W.; Neilson, S.; Furman, P. A.; Sofia, M. J. Discovery of a Novel Class of Potent HCV NS4B Inhibitors: SAR Studies on Piperazinone Derivatives. *J. Med. Chem.* **2014,** *57,* 2136–2160.
299. Phillips, B.; Cai, R.; Delaney, W.; Du, Z.; Ji, M.; Jin, H.; Lee, J.; Li, J.; Niedziela-Majka, A.; Mish, M.; Pyun, H. J.; Saugier, J.; Tirunagari, N.; Wang, J.; Yang, H.; Wu, Q.; Sheng, C.; Zonte, C. Highly Potent HCV NS4B Inhibitors With Activity Against Multiple Genotypes. *J. Med. Chem.* **2014,** *57,* 2161–2166.
300. Einav, S.; Gerber, D.; Bryson, P. D.; Sklan, E. H.; Elazar, M.; Maerkl, S. J.; Glenn, J. S.; Quake, S. R. Discovery of a Hepatitis C Target and Its Pharmacological Inhibitors by Microfluidic Affinity Analysis. *Nat. Biotechnol.* **2008,** *26,* 1019–1027.
301. Welsch, C.; Zeuzem, S. RNA-Binding Activity of Hepatitis C Virus NS4B: A Novel Target for Small Molecule Inhibitors. *Gastroenterology* **2009,** *137,* 2170–2172.
302. Einav, S.; Dvory-Sobol, H.; Gehrig, E.; Glenn, J. S. The Hepatitis C Virus (HCV) NS4B RNA Binding Inhibitor Clemizole Is Highly Synergistic With HCV Protease Inhibitors. *J. Infect. Dis.* **2010,** *202,* 65–74.
303. A Phase 1b, Open Label Study of the Safety, Tolerability Pharmacokinetics and Pharmacodynamics of 100 mg Clemizole Hydrochloride Administered Orally Twice a Day for 28 Days Immediately Prior to Initiation of Treatment With HCV Standard of Care Therapy in Treatment-Naïve Subjects Chronically Infected With HCV. Safety and Tolerability Study of Clemizole Hydrochloride to Treat Hepatitis C in Subjects Who are Treatment-Naïve (CLEAN-1). https://clinicaltrials.gov/ct2/show/NCT00945880 (accessed on July 11th, 2015).
304. Schmitz, U.; Tan, S.-L. NS5A—From Obscurity to New Target for HCV Therapy. *Recent Patents Anti-Infect. Drug Disc.* **2008,** *3,* 77–92.
305. Cordek, D. G.; Bechtel, J. T.; Maynard, A. T.; Kazmierski, W. M.; Cameron, C. E. Targeting the NS5A Protein of HCV: An Emerging Option. *Drugs Future* **2011,** *36,* 691–711.
306. Gish, R. G.; Meanwell, N. A. The NS5A Replication Complex Inhibitors—Difference Makers? *Cl. Liver Disc.* **2011,** *15,* 627–639.
307. Belda, O.; Targett-Adams, P. Small Molecule Inhibitors of the Hepatitis C Virus-Encoded NS5A Protein. *Virus Res.* **2012,** *170,* 1–14.
308. Hamatake, R.; Maynard, A.; Kazmierski, W. M. HCV Inhibition Mediated Through the Non-Structural Protein 5A (NS5A) Replication Complex. *Ann. Rep. Med. Chem.* **2012,** *47,* 331–345.
309. Belema, M.; Lopez, O. D.; Bender, J. A.; Romine, J. L.; St.Laurent, D. R.; Langley, D. R.; Lemm, J. A.; O'Boyle, D. R., II; Sun, J.-H.; Wang, C.; Fridell, R. A.; Meanwell, N. A. Discovery and Development of Hepatitis C Virus NS5A Replication Complex Inhibitors. *J. Med. Chem.* **2014,** *57,* 1643–1672.
310. Kohler, J. J.; Nettles, J. H.; Amblard, F.; Hurwitz, S. J.; Bassit, L.; Stanton, R. A.; Ehteshami, M.; Schinazi, R. F. Approaches to Hepatitis C Treatment and Cure Using NS5A Inhibitors. *Infect. Drug Resist.* **2014,** *7,* 41–56.
311. Pawlotsky, J.-M. NS5A Inhibitors in the Treatment of Hepatitis C. *J. Hepatol.* **2013,** *59,* 375–382.
312. Janardhan, S. V.; Reau, N. S. Should NS5A Inhibitors Serve as the Scaffold for All-Oral Anti-HCV Combination Therapies? *Hepatic Med.* **2015,** *7,* 11–20.
313. Macdonald, A.; Harris, M. Hepatitis C Virus NS5A: Tales of a Promiscuous Protein. *J. Gen. Virol.* **2004,** *85,* 2485–2502.
314. Ross-Thriepland, D.; Harris, M. Hepatitis C Virus NS5A: Enigmatic but Still Promiscuous 10 Years On!. *J. Gen. Virol.* **2015,** *96,* 727–738.
315. Tripathi, L. P.; Kambara, H.; Chen, Y.-A.; Nishimura, Y.; Moriishi, K.; Okamoto, T.; Morita, E.; Abe, T.; Mori, T.; Matsuura, Y.; Mizuguchi, K. Understanding the Biological Context of NS5A-Host Interactions in HCV Infection: A Network-Based Approach. *Proteome Res.* **2013,** *12,* 2537–2551.
316. Dolan, P. T.; Zhang, C.; Khadka, S.; Arumugaswami, V.; Vangeloff, A. D.; Heaton, N. S.; Sahasrabudhe, S.; Randall, G.; Sun, R.; LaCount, D. J. Identification and Comparative Analysis of Hepatitis C Virus-Host Cell Protein Interactions. *Mol. Biosyst.* **2013,** *9,* 3199–3209.
317. Szabo, G. Hepatitis C Virus NS5A Protein—A Master Regulator? *Gastroenterology* **2006,** *130,* 996–999.
318. Tellinghuisen, T. L.; Marcotrigiano, J.; Rice, C. M. Structure of the Zinc-Binding Domain of an Essential Component of the Hepatitis C Virus Replicase. *Nature* **2005,** *435,* 374–379.
319. Love, R. A.; Brodsky, O.; Hickey, M. J.; Wells, P. A.; Cronin, C. N. Crystal Structure of a Novel Dimeric Form of NS5A Domain I Protein From Hepatitis C Virus. *J. Virol.* **2009,** *83,* 4395–4403.
320. Lambert, S. M.; Langley, D. R.; Garnett, J. A.; Angell, R.; Hedgethorne, K.; Meanwell, N. A.; Matthews, S. J. The Crystal Structure of NS5A Domain 1 From Genotype 1a Reveals New Clues to the Mechanism of Action for Dimeric HCV Inhibitors. *Protein Sci.* **2014,** *23,* 723–734.
321. Huang, L.; Hwang, J.; Sharma, S. D.; Hargittai, M. R. S.; Chen, Y.; Arnold, J. J.; Raney, K. D.; Cameron, C. E. Hepatitis C Virus Nonstructural Protein 5A (NS5A) Is an RNA-Binding Protein. *J. Biol. Chem.* **2005,** *280,* 36417–36428.
322. Hwang, J.; Huang, L.; Cordek, D. G.; Vaughan, R.; Reynolds, S. L.; Kihara, G.; Raney, K. D.; Kao, C. C.; Cameron, C. E. Hepatitis C Virus Nonstructural Protein 5A: Biochemical Characterization of a Novel Structural Class of RNA-Binding Proteins. *J. Virol.* **2010,** *84,* 12480–12491.
323. Foster, T. L.; Belyaeva, T.; Stonehouse, N. J.; Pearson, A. R.; Harris, M. All Three Domains of the Hepatitis C Virus Nonstructural NS5A Protein Contribute to RNA Binding. *J. Virol.* **2010,** *84,* 9267–9277.
324. Lim, P. J.; Chatterju, U.; Cordek, D.; Sharma, S. D.; Garcia-Rivera, J. A.; Cameron, C. E.; Lin, K.; Targett-Adams, P.; Gallay, P. A. Correlation Between NS5A Dimerization and HCV Replication. *J. Biol. Chem.* **2012,** *287,* 30861–30873.
325. Huang, Y.; Staschke, K.; De Francesco, R.; Tan, S.-L. Phosphorylation of Hepatitis C Virus NS5A Nonstructural Protein: A New Paradigm for Phosphorylation-Dependent Viral RNA Replication? *Virology* **2007,** *364,* 1–9.
326. Colpitts, C. C.; Lupberger, J.; Doerig, C.; Baumert, T. F. Host Cell Kinases and the Hepatitis C Virus Life Cycle. *Biochim. Biophys. Acta* **2015,** *1854,* 1657–1662.
327. Tellinghuisen, T. L.; Foss, K. L.; Treadaway, J. Regulation of Hepatitis C Virion Production via Phosphorylation of the NS5A Protein. *PLoS Pathog.* **2008,** *4,* e1000032. http://dx.doi.org/10.1371/journal.ppat.1000032.
328. Reiss, S.; Harak, C.; Romero-Brey, I.; Radujkovic, D.; Klein, R.; Ruggieri, A.; Rebhan, I.; Bartenschlager, R.; Lohmann, V. The Lipid Kinase Phosphatidylinositol-4 Kinase III Alpha Regulates the Phosphorylation Status of Hepatitis C Virus NS5A. *PLoS Pathog.* **2013,** *9,* e1003359.
329. Shirota, Y.; Luo, H.; Qin, W. P.; Kaneko, S.; Yamashita, T.; Kobayashi, K.; Murakami, S. Hepatitis C Virus (HCV) NS5A Binds RNA-Dependent RNA Polymerase (RdRp) NS5B and Modulates RNA-Dependent RNA Polymerase Activity. *J. Biol. Chem.* **2002,** *277,* 11149–11155.
330. Sklan, E. H.; Charuworn, P.; Pang, P. S.; Glenn, J. S. Mechanisms of HCV Survival in the Host. *Nat. Rev. Gastroenterol. Hepatol.* **2009,** *6,* 217–227.
331. Hofmann, W. P.; Zeuzem, S.; Sarrazin, C. Hepatitis C Virus-Related Resistance Mechanisms to Interferon Alpha-Based Antiviral Therapy. *J. Clin. Virol.* **2005,** *32,* 86–91.
332. El-Shamy, A.; Nagano-Fujii, M.; Sasase, N.; Imoto, S.; Kim, S. R.; Hotta, H. Sequence Variation in Hepatitis C Virus Nonstructural Protein 5A Predicts Clinical Outcome of Pegylated Interferon/Ribavirin Combination Therapy. *Hepatology* **2008,** *48,* 38–47.
333. Brillet, R.; Penin, F.; Hezode, C.; Chouteau, P.; Dhumeaux, D.; Pawlotsky, J.-M. The Nonstructural 5A Protein of Hepatitis C Virus Genotype 1b Does not Contain an Interferon Sensitivity-Determining Region. *J. Infect. Dis.* **2007,** *195,* 432–441.
334. Hiet, M.-S.; Bauhofer, O.; Zayas, M.; Roth, H.; Tanaka, Y.; Schirmacher, P.; Willemsen, J.; Grünvogel, O.; Bender, S.; Binder, M.; Lohmann, V.; Lotteau, V.; Ruggieri, A.; Bartenschlager, R. Control of Temporal Activation of Hepatitis C Virus-Induced Interferon Response by Domain 2 of Nonstructural Protein 5A. *J. Hepatol.* **2015,** *63,* 829–837.
335. Hughes, M.; Griffin, S.; Harris, M. Domain III of NS5A Contributes to Both RNA Replication and Assembly of Hepatitis C Virus Particles. *J. Gen. Virol.* **2009,** *90,* 1329–1334.
336. Appel, N.; Zayas, M.; Miller, S.; Krijnse-Locker, J.; Schaller, T.; Friebe, P.; Kallis, S.; Engel, U.; Bartenschlager, R. Essential Role of Domain III of Nonstructural Protein 5A for Hepatitis C Virus Infectious Particle Assembly. *PLoS Pathog.* **2008,** *4,* e1000035. http://dx.doi.org/10.1371/journal.ppat.1000035.
337. Romine, J. L.; Martin, S. W., Snyder, L. B.; Serrano-Wu, M.; Deshpande, M.; Whitehouse, D.; Lemm, J.; O'Boyle, D. R.; Gao, M.; Colonno, R. Iminothiazolidinones as Inhibitors of HCV Replication. *World Patent Application* WO-2004/014852. February 19th, **2004**.
338. Belema, M.; Nicholas, A.; Meanwell, N. A. Discovery of Daclatasvir, a Pan-Genotypic Hepatitis C Virus NS5A Replication Complex Inhibitor With Potent Clinical Effect. *J. Med. Chem.* **2014,** *57,* 5057–5071.
339. Lemm, J. A.; Leet, J. E.; O'Boyle, D. R., II; Romine, J. L.; Huang, X. S.; Schroeder, D. R.; Alberts, J.; Cantone, J. L.; Sun, J.-H.; Nower, P. T.; Martin, S. W.; Serrano-Wu, M. H.; Meanwell, N. A.; Snyder, L. B.; Gao, M. Discovery of Potent Hepatitis C Virus NS5A Inhibitors With Dimeric Structures. *Antimicrob. Agents Chemother.* **2011,** *55,* 3795–3802.

340. Romine, J. L.; St.Laurent, D. R.; Leet, J. E.; Martin, S. W.; Serrano-Wu, M. H.; Yang, F.; Gao, M.; O'Boyle, D. R., II; Lemm, J. A.; Sun, J.-H.; Nower, P. T.; Huang, X.; Deshpande, M. S.; Meanwell, N. A.; Snyder, L. B. Inhibitors of HCV NS5A: From Iminothiazolidinones to Symmetrical Stilbenes. *ACS Med. Chem. Lett.* **2011,** *2,* 224–229.
341. Viehe, H. G.; Janousek, Z.; Merenyi, R.; Stella, L. The Captodative Effect. *Acc. Chem. Res.* **1985,** *18,* 148–154.
342. St.Laurent, D. R.; Belema, M.; Gao, M.; Goodrich, J.; Kakarla, R.; Knipe, J. O.; Lemm, J. A.; Liu, M.; Lopez, O. D.; Nguyen, V. N.; Nower, P. T.; O'Boyle, D. R., II; Qiu, Y.; Romine, J. L.; Serrano-Wu, M. H.; Sun, J.-H.; Valera, L.; Yang, F.; Yang, X.; Meanwell, N. A.; Snyder, L. B. HCV NS5A Replication Complex Inhibitors. Part 2: Investigation of Stilbene Prolinamides. *Bioorg. Med. Chem. Lett.* **2012,** *22,* 6063–6066.
343. Lopez, O. D.; Nguyen, V. N.; St.Laurent, D. R.; Belema, M.; Serrano-Wu, M. H.; Goodrich, J. T.; Yang, F.; Qiu, Y.; Ripka, A. S.; Nower, P. T.; Valera, L.; Liu, M.; O'Boyle, D. R., II; Sun, J.-H.; Fridell, R. A.; Lemm, J. A.; Gao, M.; Good, A. C.; Meanwell, N. A.; Snyder, L. B. HCV NS5A Replication Complex Inhibitors. Part 3: Discovery of Potent Analogs With Distinct Core Topologies. *Bioorg. Med. Chem. Lett.* **2013,** *23,* 779–784.
344. St.Laurent, D. R.; Serrano-Wu, M. H.; Belema, M.; Ding, M.; Fang, H.; Gao, M.; Goodrich, J. T.; Krause, R. G.; Lemm, J. A.; Liu, M.; Lopez, O. D.; Nguyen, V. N.; Nower, P. T.; O'Boyle, D. R., II; Pearce, B. C.; Romine, J. L.; Valera, L.; Sun, J.-H.; Wang, Y.-K.; Yang, F.; Yang, X.; Meanwell, N. A.; Snyder, L. B. HCV NS5A Replication Complex Inhibitors. Part 4: Optimization for Genotype 1a Replicon Inhibitory Activity. *J. Med. Chem.* **2014,** *57,* 1976–1994.
345. Belema, M.; Nguyen, V. N.; St.Laurent, D. R.; Lopez, O. D.; Qiu, Y.; Good, A. C.; Nower, P. T.; Valera, L.; O'Boyle, D. R., II; Sun, J.-H.; Fridell, R. A.; Lemm, J. A.; Gao, M.; Knipe, J.; Meanwell, N. A.; Snyder, L. B. HCV NS5A Replication Complex Inhibitors. Part 5: Discovery of Potent and Pan-Genotypic HCV NS5A Replication Complex Inhibitors. *Bioorg. Med. Chem. Lett.* **2013,** *23,* 4428–4435.
346. Belema, M.; Nguyen, V. N.; Romine, J. L.; St.Laurent, D. R.; Lopez, O. D.; Goodrich, J.; Nower, P. T.; O'Boyle, D. R., II; Lemm, J. A.; Fridell, R. A.; Gao, M.; Fang, H.; Krause, R. G.; Wang, Y.-K.; Oliver, A. J.; Good, A. C.; Knipe, J. O.; Meanwell, N. A.; Snyder, L. B. Hepatitis C Virus NS5A Replication Complex Inhibitors. Part 6: The Discovery of a Novel and Highly Potent Biarylimidazole Chemotype With Inhibitory Activity Toward Genotype 1a and 1b Replicons. *J. Med. Chem.* **2014,** *57,* 1995–2012.
347. Belema, M.; Nguyen, V. N.; Bachand, C.; Deon, D. H.; Goodrich, J. T.; Lavoie, R.; James, C. A.; Lopez, O. D.; Martel, A.; Romine, J. L.; Ruediger, E. H.; Snyder, L. B.; St.Laurent, D. R.; Good, A. C.; Langley, D. R.; Chimalakonda, A.; Fura, A.; Knipe, J. O.; Nower, P. T.; O'Boyle, D. R., II; Lemm, J. A.; Fridell, R. A.; Gao, M.; Meanwell, N. A.; Hamann, L. G. Hepatitis C Virus NS5A Replication Complex Inhibitors: The Discovery of Daclatasvir. *J. Med. Chem.* **2014,** *57,* 2013–2032.
348. Guedj, J.; Dahari, H.; Rong, L.; Sansone, N. D.; Nettles, R. E.; Cotler, S. J.; Layden, T. J.; Uprichard, S. L.; Perelson, A. S. Modeling Shows That the NS5A Inhibitor Daclatasvir Has Two Modes of Action and Yields a Shorter Estimate of the Hepatitis C Virus Half-Life. *Proc. Natl. Acad. Sci. U. S. A.* **2013,** *110,* 3991–3996.
349. Ascher, D. B.; Wielens, J.; Nero, T. L.; Doughty, L.; Morton, C. J.; Parker, M. W. Potent Hepatitis C Inhibitors Bind Directly to NS5A and Reduce Its Affinity for RNA. *Sci. Rep.* **2014,** *4,* 4765. http://dx.doi.org/10.1038/srep04765.
350. Targett-Adams, P.; Graham, E. J. S.; Middleton, J.; Palmer, A.; Shaw, S. M.; Lavender, H.; Brain, P.; Tran, T. D.; Jones, L. H.; Wakenhut, F.; Stammen, B.; Pryde, D.; Pickford, C.; Westby, M. Small Molecules Targeting Hepatitis C Virus-Encoded NS5A Cause Subcellular Redistribution of Their Target: Insights Into Compound Modes of Action. *J. Virol.* **2011,** *85,* 6353–6368.
351. Lee, C.; Ma, H.; Hang, J. Q.; Leveque, V.; Sklan, E. H.; Elazar, M.; Klumpp, K.; Glenn, J. S. The Hepatitis C Virus NS5A Inhibitor (BMS-790052) Alters the Subcellular Localization of the NS5A Non-Structural Viral Protein. *Virology* **2011,** *414,* 10–18.
352. O'Boyle, D. R., II; Sun, J.-H.; Nower, P. T.; Lemm, J. A.; Fridell, R. A.; Wang, C.; Romine, J. L.; Belema, M.; Nguyen, V. N.; St.Laurent, D. R.; Serrano-Wu, M.; Snyder, L. B.; Meanwell, N. A.; Langley, D. R.; Gao, M. Characterization of HCV NS5A Replication Complex Inhibitors. *Virology* **2013,** *444,* 343–354.
353. Kwon, H. J.; Xing, W.; Chan, K.; Niedziela-Majka, A.; Brendza, K. M.; Kirschberg, T.; Kato, D.; Link, J. O.; Cheng, G.; Liu, X.; Sakowicz, R. Direct Binding of Ledipasvir to HCV NS5A: Mechanism of Resistance to an HCV Antiviral Agent. *PLoS One* **2015,** *10* (4), e0122844. http://dx.doi.org/10.1371/journal.pone.0122844.
354. Nettles, J. H.; Stanton, R. A.; Broyde, J.; Amblard, F.; Zhang, H.; Zhou, L.; Shi, J.; McBrayer, T. R.; Whitaker, T.; Coats, S. J.; Kohler, J. J.; Schinazi, R. F. Asymmetric Binding to NS5A by Daclatasvir (BMS-790052) and Analogs Suggests Two Novel Modes of HCV Inhibition. *J. Med. Chem.* **2014,** *57,* 10031–10043.
355. Barakat, K. H.; Anwar-Mohamed, A.; Tuszynski, J. A.; Robins, M. J.; Tyrrell, D. L.; Houghton, M. A Refined Model of the HCV NA5A Protein Bound to Daclatasvir Explains Drug-Resistant Mutations and Activity Against Divergent Genotypes. *J. Chem. Inf. Model.* **2015,** *55,* 362–373.
356. Bhattacharya, D.; Ansari, I. H.; Hamatake, R.; Walker, J.; Kazmierski, W. M.; Striker, R. Pharmacological Disruption of Hepatitis C NS5A Protein Intra- and Intermolecular Conformations. *J. Gen. Virol.* **2014,** *95,* 363–372.
357. Appel, N.; Schaller, T.; Penin, F.; Bartenschlager, R. From Structure to Function: New Insights Into Hepatitis C Virus RNA Replication. *J. Biol. Chem.* **2006,** *281,* 9833–9836.
358. Link, J. O.; Taylor, J. G.; Xu, L.; Mitchell, M.; Guo, H.; Liu, H.; Kato, D.; Kirschberg, T.; Sun, J.; Squires, N.; Parrish, J.; Keller, T.; Yang, Z.-Y.; Yang, C.; Matles, M.; Wang, Y.; Wang, K.; Cheng, G.; Tian, Y.; Mogalian, E.; Mondou, E.; Cornpropst, M.; Perry, J.; Desai, M. C. The Discovery of Ledipasvir (GS-5885), a Potent Once-Daily Oral NS5A Inhibitor for the Treatment of Hepatitis C Virus Infection. *J. Med. Chem.* **2014,** *57,* 2033–2046.
359. Kazmierski, W. M.; Maynard, A.; Duan, M.; Baskaran, S.; Botyanszki, J.; Crosby, R.; Dickerson, S.; Tallant, M.; Grimes, R.; Hamatake, R.; Leivers, M.; Roberts, C. D.; Walker, J. Novel Spiroketal Pyrrolidine GSK2336805 Potently Inhibits Key Hepatitis C Virus Genotype 1b Mutants: From Lead to Clinical Compound. *J. Med. Chem.* **2014,** *57,* 2058–2073.
360. Bilello, J. P.; Lallos, L. B.; McCarville, J. F.; La Colla, M.; Serra, I.; Chapron, C.; Gillum, J. M.; Pierra, C.; Standring, D. N.; Seifer, M. In Vitro Activity and Resistance Profile of Samatasvir, a Novel NS5A Replication Inhibitor of Hepatitis C Virus. *Antimicrob. Agents Chemother.* **2014,** *58,* 4431–4442.
361. Lawitz, E.; Freilich, B.; Link, J.; German, P.; Mo, H.; Han, L.; Brainard, D. M.; McNally, J.; Marbury, T.; Rodriguez-Torres, M. A Phase 1, Randomized, Dose-Ranging Study of GS-5816, a Once-Daily NS5A Inhbitor, in Patients With Genotype 1-4 Hepatitis C Virus. *J. Viral Hepatitis* **2015,** *22,* 1011–1109.
362. Ivachtchenko, A. V.; Mitkin, O. D.; Yamanushkin, P. M.; Kuznetsova, I. V.; Bulanova, E. A.; Shevkun, N. A.; Koryakova, A. G.; Karapetian, R. N.; Bichko, V. V.; Trifelenkov, A. S.; Kravchenko, D. V.; Vostokova, N. V.; Veselov, M. S.; Chufarova, N. V.; Ivanenkov, Y. A. Discovery of Novel Highly Potent Hepatitis C Virus NS5A Inhibitor (AV4025). *J. Med. Chem.* **2014,** *57,* 7716–7730.
363. DeGoey, D. A.; Randolph, J. T.; Liu, D.; Pratt, J.; Hutchins, C.; Donner, P.; Krueger, A. C.; Matulenko, M.; Patel, S.; Motter, C. E.; Nelson, L.; Keddy, R.; Tufano, M.; Caspi, D. D.; Krishnan, P.; Mistry, N.; Koev, G.; Reisch, T. J.; Mondal, R.; Pilot-Matias, T.; Gao, Y.; Beno, D. W. A.; Maring, C. J.; Molla, A.; Dumas, E.; Campbell, A.; Williams, L.; Collins, C.; Wagner, R.; Kati, W. M. Discovery of ABT-267, a Pan-Genotypic Inhibitor of HCV NS5A. *J. Med. Chem.* **2014,** *57,* 2047–2057.
364. Coburn, C. A.; Meinke, P. T.; Chang, W.; Fandozzi, C. M.; Graham, D. J.; Hu, B.; Huang, Q.; Kargman, S.; Kozlowski, J.; Liu, R.; McCauley, J. A.; Nomeir, A. A.; Soll, R. M.; Vacca, J. P.; Wang, D.; Wu, H.; Zhong, B.; Olsen, D. B.; Ludmerer, S. W. Discovery of MK-8742: An HCV NS5A Inhibitor With Broad Genotype Activity. *ChemMedChem* **2013,** *8,* 1930–1940.
365. Wiles, J. A.; Wang, Q.; Hashimoto, A.; Pais, G.; Chen, D.; Wang, X.; Gadhachanda, V.; Phadke, A.; Deshpande, M. Substituted Aliphanes, Cyclophanes, Heteraphanes, Heterophanes, Hetero-Heteraphanes and Metallocenes Useful for Treating HCV Infections. *World Patent Application* WO-2012/166716 A2. December 6th, **2012**.
366. Najarro, P.; Mathews, N.; Cockerill, S. NS5A Inhibitors. Hepatitis C Viruses. In *Horizon Bioscience;* Tan, S.-L., Ed.; Wymondham: UK, 2006; pp 271–292.
367. Krueger, A. C.; Madigan, D. L.; Beno, D. W.; Betebenner, D. A.; Carrick, R.; Green, B. E.; He, W.; Liu, D.; Maring, C. J.; McDaniel, K. F.; Mo, H.; Molla, A.; Motter, C. E.; Pilot-Matias, T. J.; Tufano, M. D.; Kempf, D. J. Novel Hepatitis C Virus Replicon Inhibitors: Synthesis and Structure–Activity Relationships of Fused Pyrimidine Derivatives. *Bioorg. Med. Chem. Lett.* **2012,** *22,* 2212–2215.
368. DeGoey, D. A.; Betebenner, D. A.; Grampovnik, D. J.; Liu, D.; Pratt, J. K.; Tufano, M. D.; He, W.; Krishnan, P.; Pilot-Matias, T. J.; Marsh, K. C.; Molla, A.; Kempf, D. J.; Maring, C. J. Discovery of Pyrido[2,3-*d*]Pyrimidine-Based Inhibitors of HCV NS5A. *Bioorg. Med. Chem. Lett.* **2013,** *23,* 3627–3630.
369. Bianco, A.; Reghellin, V.; Donnici, L.; Fenu, S.; Alvarez, R.; Baruffa, C.; Peri, F.; Pagani, M.; Abrignani, S.; Neddermann, P.; De Francesco, R. Metabolism of Phosphatidylinositol 4-Kinase IIIα-Dependent PI4P Is Subverted by HCV and Is Targeted by a 4-Anilino Quinazoline With Antiviral Activity. *PLoS Pathog.* **2012,** *8,* e1002576. http://dx.doi.org/10.1371/journal.ppat.1002576.
370. Sun, J.-H.; O'Boyle, D. R., II; Fridell, R. A.; Langley, D. R.; Wang, C.; Roberts, S. B.; Nower, P.; Johnson, B. M.; Moulin, F.; Nophsker, M. J.; Wang, Y.-K.; Liu, M.; Rigat, K.; Tu, Y.; Hewawasam, P.; Kadow, J.; Meanwell, N. A.; Cockett, M.; Lemm, J. A.; Kramer, M.; Belema, M.; Gao, M. Resensitizing Daclatasvir-Resistant Hepatitis C Variants by Allosteric Modulation of NS5A. *Nature* **2015,** *527,* 245–258.

371. De Clercq, E. Strategies in the Design of Antiviral Drugs. *Nat. Rev. Drug Discov.* **2002,** *1,* 13–25.
372. Tsai, C. H.; Lee, P. Y.; Stollar, V.; Li, M. L. Antiviral Therapy Targeting Viral Polymerase. *Curr. Pharm. Des.* **2006,** *12,* 1339–1355.
373. Choi, K. H. Viral Polymerases. In *Viral Molecular Machines;* Rossmann, M. G., Rao, V. B., Eds.; *Adv. Exp. Med. Biol.* 2012, 726; pp 267–304.
374. te Velthuis, A. J. W. Common and Unique Features of Viral RNA-Dependent Polymerase. *Cell Mol. Life Sci.* **2014,** *71,* 4403–4442.
375. Jordheim, L. P.; Durantel, D.; Zoulim, F.; Dumontet, C. Advances in the Development of Nucleoside and Nucleotide Analogues for Cancer and Viral Diseases. *Nat. Rev Drug Disc.* **2013,** *12,* 447–464.
376. Perkins, E. S.; Wood, R. M.; Sears, M. L.; Prusoff, W. H.; Welch, A. D. Anti-Viral Activities of Several Iodinated Pyrimidine Deoxyribonucleosides. *Nature* **1962,** *194,* 985–986.
377. Sofia, M. J.; Chang, W.; Furman, P. A.; Mosley, R. T.; Ross, B. S. Nucleoside, Nucleotide, and Non-Nucleoside Inhibitors of Hepatitis C Virus NS5B RNA-Dependent RNA-Polymerase. *J. Med. Chem.* **2012,** *55,* 2481–2531.
378. Coats, S. J.; Garnier-Amblard, E. C.; Amblard, F.; Ehteshami, M.; Amiralaei, S.; Zhang, H.; Zhou, L.; Boucle, S. R.; Lu, X.; Bondada, L.; Shelton, J. R.; Li, H.; Liu, P.; Li, C.; Cho, J. H.; Chavre, S. N.; Zhou, S.; Mathew, J.; Schinazi, R. F. Chutes and Ladders in Hepatitis C Nucleoside Drug Development. *Antivir. Res.* **2014,** *102,* 119–147.
379. Arnold, J. J.; Sharma, S. D.; Feng, J. Y.; Ray, A. S.; Smidansky, E. D.; Kireeva, M. L.; Cho, A.; Perry, J.; Vela, J. E.; Park, Y.; Xu, Y.; Tian, Y.; Babusis, D.; Barauskus, O.; Peterson, B. R.; Gnatt, A.; Kashlev, M.; Zhong, W.; Cameron, C. E. Sensitivity of Mitochondrial Transcription and Resistance of RNA Polymerase II Dependent Nuclear Transcription to Antiviral Ribonucleosides. *PLoS Pathog.* **2012,** *8* (11), e1003030. http://dx.doi.org/10.1371/journal.ppat.1003030.
380. Gentile, I.; Buonomo, A. R.; Zappulo, E.; Borgia, G. Discontinued Drugs in 2012-2013: Hepatitis C Virus Infection. *Expert Opin. Invest. Drugs* **2015,** *24,* 239–251.
381. Powdrill, M. H.; Bernatchez, J. A.; Götte, M. Inhibitors of the Hepatitis C Virus RNA-Dependent RNA Polymerase NS5B. *Viruses* **2010,** *2,* 2169–2195.
382. Watkins, W. J.; Ray, A. S.; Chong, L. S. HCV NS5B Polymerase Inhibitors. *Curr. Opin. Drug Discov. Dev.* **2010,** *13,* 441–465.
383. Legrand-Abravanel, F.; Nicot, F.; Izopet, J. New NS5B Polymerase Inhibitors for Hepatitis C. *Exp. Opin. Invest. Drugs* **2010,** *19,* 963–975.
384. Mayhoub, A. S. Hepatitis C RNA-Dependent RNA Polymerase Inhibitors: A Review of Structure-Activity and Resistance Relationships; Different Scaffolds and Mutations. *Bioorg. Med. Chem.* **2012,** *20,* 3150–3161.
385. Haudecoeur, R.; Peuchmaur, M.; Ahmed-Belkacem, A.; Pawlotsky, J.-M.; Boumendjel, A. Structure-Activity Relationships in the Development of Allosteric Hepatitis C Virus RNA-Dependent RNA Polymerase Inhibitors: Ten Years of Research. *Med. Res. Rev.* **2013,** *33,* 934–984.
386. Zhao, F.; Liu, N.; Zhan, P.; Jiang, X.; Liu, X. Discovery of HCV NS5B Thumb Site I Inhibitors: Core-Refining From Benzimidazole to Indole Scaffold. *Eur. J. Med. Chem.* **2015,** *94,* 218–228.
387. Behrens, S.-E.; Tomei, L.; De Francesco, R. Identification and Properties of the RNA-Dependent RNA Polymerase of Hepatitis C Virus. *EMBO J.* **1996,** *15,* 12–22.
388. Lohmann, V.; Roos, A.; Körner, F.; Koch, J. O.; Bartenschlager, R. Biochemical and Kinetic Analyses of NS5B RNA-Dependent RNA Polymerase of the Hepatitis C Virus. *Virology* **1998,** *249,* 108–118.
389. O'Farrell, D.; Trowbridge, R.; Rowlands, D.; Jäger, J. Substrate Complexes of Hepatitis C Virus RNA Polymerase (HC-J4): Structural Evidence for Nucleotide Import and De-Novo Initiation. *J. Mol. Biol.* **2003,** *326,* 1025–1035.
390. Mosley, R. T.; Edwards, T. E.; Murakami, E.; Lam, A. M.; Grice, R. L.; Du, J.; Sofia, M. J.; Furman, P. A.; Otto, M. J. Structure of Hepatitis C Virus Polymerase in Complex With Primer-Template RNA. *J. Virol.* **2012,** *86,* 6503–6511.
391. Caillet-Saguy, C.; Lim, S. P.; Shi, P.-Y.; Lescar, J.; Bressanelli, S. Polymerases of Hepatitis C Viruses and Flaviviruses: Structural and Mechanistic Insights and Drug Development. *Antivir. Res.* **2014,** *105,* 8–16.
392. Appleby, T. C.; Perry, J. K.; Murakami, E.; Barauskas, O.; Feng, J.; Cho, A.; Fox, D., III; Wetmore, D. R.; McGrath, M. E.; Ray, A. S.; Sofia, M. J.; Swaminathan, S.; Edwards, T. E. Structural Basis for RNA Replication by the Hepatitis C Virus Polymerase. *Science* **2015,** *347,* 771–775.
393. Pierra, C.; Amador, A.; Benzaria, S.; Cretton-Scott, E.; D'Amours, M.; Mao, J.; Mathieu, S.; Moussa, A.; Bridges, E. G.; Standring, D. N.; Sommadossi, J.-P.; Storer, R.; Gosselin, G. Synthesis and Pharmacokinetics of Valopicitabine (NM283), an Efficient Prodrug of the Potent Anti-HCV Agent 2′-*C*-Methylcytidine. *J. Med. Chem.* **2006,** *49,* 6614–6620.
394. Pierra, C.; Benzaria, S.; Amador, A.; Moussa, A.; Mathieu, S.; Storer, R.; Gosselin, G. NM-283, an Efficient Prodrug of the Potent Anti-HCV Agent 2′-*C*-Methylcytidine. *Nucleosides Nucleotides Nucleic Acids* **2005,** *24,* 767–770.
395. Sorbera, L. A.; Castaner, J.; Leeson, P. A. Valopicitabine: Anti-Hepatitis C Virus Drug RNA-Directed RNA Polymerase (NS5B) Inhibitor. *Drugs Future* **2006,** *31,* 320–324.
396. Toniutto, P.; Fabris, C.; Bitetto, D.; Fornasiere, E.; Rapetti, R.; Pirisi, M. Valopicitabine Dihydrochloride: A Specific Polymerase Inhibitor of Hepatitis C Virus. *Curr. Opin. Investig. Drugs* **2007,** *8,* 150–158.
397. Coelmont, L.; Paeshuyse, J.; Windisch, M. P.; De Clercq, E.; Bartenschlager, R.; Neyts, J. Ribavirin Antagonizes the in vitro Anti-Hepatitis C Virus Activity of 2′-*C*-Methylcytidine, the Active Component of Valopicitabine. *Antimicrob. Agents Chemother.* **2006,** *50,* 3444–3446.
398. Eldrup, A. B.; Allerson, C. R.; Bennett, C. F.; Bera, S.; Bhat, B.; Bhat, N.; Bosserman, M. R.; Brooks, J.; Burlein, C.; Carroll, S. S.; Cook, P. D.; Getty, K. L.; MacCoss, M.; McMasters, D. R.; Olsen, D. B.; Prakash, T. P.; Prhavc, M.; Song, Q.; Tomassini, J. E.; Xia, J. Structure-Activity Relationship of Purine Ribonucleosides for Inhibition of Hepatitis C Virus RNA-Dependent RNA Polymerase. *J. Med. Chem.* **2004,** *47,* 2283–2295.
399. Tomassini, J. E.; Getty, K.; Stahlhut, M. W.; Shim, S.; Bhat, B.; Eldrup, A. B.; Prakash, T. P.; Carroll, S. S.; Flores, O.; MacCoss, M.; McMasters, D. R.; Migliaccio, G.; Olsen, D. B. Inhibitory Effect of 2′-Substituted Nucleosides on Hepatitis C Virus Replication Correlates With Metabolic Properties in Replicon Cells. *Antimicrob. Agents Chemother.* **2005,** *49,* 2050–2058.
400. Eldrup, A. B.; Prhavc, M.; Brooks, J.; Bhat, B.; Prakash, T. P.; Song, Q.; Bera, S.; Bhat, N.; Dande, P.; Cook, P. D.; Bennett, C. F.; Carroll, S. S.; Ball, R. G.; Bosserman, M.; Burlein, C.; Colwell, L. F.; Fay, J. F.; Flores, O. A.; Getty, K.; LaFemina, R. L.; Leone, J.; MacCoss, M.; McMasters, D. R.; Tomassini, J. E.; Von, L. D.; Wolanski, B.; Olsen, D. B. Structure-Activity Relationship of Heterobase-Modified 2′-C-Methyl Ribonucleosides as Inhibitors of Hepatitis C Virus RNA Replication. *J. Med. Chem.* **2004,** *47,* 5284–5297.
401. McGuigan, C.; Perrone, P.; Madela, K.; Neyts, J. The Phosphoramidate Protide Approach Greatly Enhances the Activity of β-2′-*C*-Methylguanosine Against Hepatitis C Virus. *Bioorg. Med. Chem. Lett.* **2009,** *19,* 4316–4320.
402. Sofia, M. J. Nucleotide Prodrugs for HCV Therapy. *Antivir. Chem. Chemoth.* **2011,** *22,* 23–49.
403. Pertusati, F.; Serpi, M.; McGuigan, C. Medicinal Chemistry of Nucleoside Phosphonate Prodrugs for Antiviral Therapy. *Antivir. Chem. Chemoth.* **2012,** *22,* 181–203.
404. Pradere, U.; Garnier-Amblard, E. C.; Coats, S. J.; Amblard, F.; Schinazi, R. F. Synthesis of Nucleoside Phosphate and Phosphonate Prodrugs. *Chem. Rev.* **2014,** *114,* 9154–9218.
405. McGuigan, C.; Madela, K.; Aljarah, M.; Gilles, A.; Brancale, A.; Zonta, N.; Chamberlain, S.; Vernachio, J.; Hutchins, J.; Hall, A.; Ames, B.; Gorovits, E.; Ganguly, B.; Kolykhalov, A.; Wang, J.; Muhammad, J.; Patti, J. M.; Henson, G. Design, Synthesis and Evaluation of a Novel Double Pro-Drug: INX-08189. A New Clinical Candidate for Hepatitis C Virus. *Bioorg. Med. Chem. Lett.* **2010,** *20,* 4850–4854.
406. McGuigan, C.; Madela, K.; Aljarah, M.; Gilles, A.; Battina, S. K.; Ramamurty, C. V.; Rao, C. S.; Vernachio, J.; Hutchins, J.; Hall, A.; Kolykhalov, A.; Henson, G.; Chamberlain, S. Dual Pro-Drugs of 2′-*C*-Methyl Guanosine Monophosphate as Potent and Selective Inhibitors of Hepatitis C Virus. *Bioorg. Med. Chem. Lett.* **2011,** *21,* 6007–6012.
407. McGuigan, C.; Gilles, A.; Madela, K.; Aljarah, M.; Holl, S.; Jones, S.; Vernachio, J.; Hutchins, J.; Ames, B.; Bryant, K. D.; Gorovits, E.; Ganguly, B.; Hunley, D.; Hall, A.; Kolykhalov, A.; Liu, Y.; Muhammad, J.; Raja, N.; Walters, R.; Wang, J.; Chamberlain, S.; Henson, G. Phosphoramidate ProTides of 2′-*C*-Methylguanosine as Highly Potent Inhibitors of Hepatitis C Virus. Study of Their in vitro and in vivo Properties. *J. Med. Chem.* **2010,** *53,* 4949–4957.
408. Vernachio, J. H.; Bleiman, B.; Bryant, K. D.; Chamberlain, S.; Hunley, D.; Hutchins, J.; Ames, B.; Gorovits, E.; Ganguly, B.; Hall, A.; Kolykhalov, A.; Liu, Y.; Muhammad, J.; Raja, N.; Walters, C. R.; Wang, J.; Williams, K.; Patti, J. M.; Henson, G.; Madela, K.; Aljarah, M.; Gilles, A.; McGuigan, C. INX-08189, a Phosphoramidate Prodrug Of 6-O-Methyl-2′-C-Methyl Guanosine, Is a Potent Inhibitor of Hepatitis C Virus Replication With Excellent Pharmacokinetic and Pharmacodynamic Properties. *Antimicrob. Agents Chemother.* **2011,** *55,* 1843–1851.

409. Murakami, E.; Tolstykh, T.; Bao, H.; Niu, C.; Steuer, H. M.; Bao, D.; Chang, W.; Espiritu, C.; Bansal, S.; Lam, A. M.; Otto, M. J.; Sofia, M. J.; Furman, P. A. Mechanism of Activation of PSI-7851 and Its Diastereoisomer PSI-7977. *J. Biol. Chem.* **2010,** *285,* 34337–34347.
410. Murakami, E.; Bao, H.; Mosley, R. T.; Du, J.; Sofia, M. J.; Furman, P. A. Adenosine Deaminase-Like Protein 1 (ADAL1): Characterization and Substrate Specificity in the Hydrolysis of *N*6- or *O*6-Substituted Purine or 2-Aminopurine Nucleoside Monophosphates. *J. Med. Chem.* **2011,** *54,* 5902–5914.
411. Ahmad, T.; Yin, P.; Saffitz, J.; Pockros, P. J.; Lalezari, J.; Shiffman, M.; Freilich, B.; Zamparo, J.; Brown, K.; Dimitrova, D.; Kumar, M.; Manion, D.; Heath-Chiozzi, M.; Wolf, R.; Hughes, E.; Muir, A. J.; Hernandez, A. F. Cardiac Dysfunction Associated With a Nucleotide Polymerase Inhibitor for Treatment of Hepatitis C. *Hepatology* **2015,** *62,* 409–416.
412. Smith, D. B.; Martin, J. A.; Klumpp, K.; Baker, S. J.; Blomgren, P. A.; Devos, R.; Granycome, C.; Hang, J.; Hobbs, C. J.; Jiang, W.-R.; Laxton, C.; Le, P. S.; Leveque, V.; Ma, H.; Maile, G.; Merrett, J. H.; Pichota, A.; Sarma, K.; Smith, M.; Swallow, S.; Symons, J.; Vesey, D.; Najera, I.; Cammack, N. Design, Synthesis, and Antiviral Properties of 4-Substituted Ribonucleosides as Inhibitors of Hepatitis C Virus Replication: The Discovery of R1479. *Bioorg. Med. Chem. Lett.* **2007,** *17,* 2570–2576.
413. Klumpp, K.; Leveque, V.; Le Pogam, S.; Ma, H.; Jiang, W. R.; Kang, H.; Granycome, C.; Singer, M.; Laxton, C.; Hang, J. Q.; Sarma, K.; Smith, D. B.; Heindl, D.; Hobbs, C. J.; Merrett, J. H.; Symons, J.; Cammack, N.; Martin, J. A.; Devos, R.; Najera, I. The Novel Nucleoside Analog R1479 (4′-Azidocytidine) Is a Potent Inhibitor of NS5B-Dependent RNA Synthesis and Hepatitis C Virus Replication in Cell Culture. *J. Biol. Chem.* **2006,** *281,* 3793–3799.
414. McGuigan, C.; Kelleher, M. R.; Perrone, P.; Mulready, S.; Luoni, G.; Daverio, F.; Rajyaguru, S.; Le Pogam, S.; Najera, I.; Martin, J. A.; Klumpp, K.; Smith, D. B. The Application of Phosphoramidate Protide Technology to the Potent Anti-HCV Compound 4′-Azidocytidine (R1479). *Bioorg. Med. Chem. Lett.* **2009,** *19,* 4250–4254.
415. Brandl, M.; Wu, X.; Holper, M.; Hong, L.; Jia, Z.; Birudaraj, R.; Reddy, M.; Alfredson, T.; Tran, T.; Larrabee, S.; Hadig, X.; Sarma, K.; Washington, C.; Hill, G.; Smith, D. B. Physicochemical Properties of the Nucleoside Prodrug R1626 Leading to High Oral Bioavailability. *Drug Dev. Ind. Pharm.* **2008,** *34,* 683–691.
416. Roberts, S. K.; Cooksley, G.; Dore, G. J.; Robson, R.; Shaw, D.; Berns, H.; Hill, G.; Klumpp, K.; Najera, I.; Washington, C. Robust Antiviral Activity of R1626, a Novel Nucleoside Analog: A Randomized, Placebo-Controlled Study in Patients With Chronic Hepatitis C. *Hepatology* **2008,** *48,* 398–406.
417. Pockros, P. J.; Nelson, D.; Godofsky, E.; Rodriguez-Torres, M.; Everson, G. T.; Fried, M. W.; Ghalib, R.; Harrison, S.; Nyberg, L.; Shiffman, M. L.; Najera, I.; Chan, A.; Hill, G. R1626 Plus Peginterferon Alfa-2a Provides Potent Suppression of Hepatitis C Virus RNA and Significant Antiviral Synergy in Combination With Ribavirin. *Hepatology* **2008,** *48,* 385–397.
418. Pockros, P. J.; Nelson, D.; Godofsky, E.; Rodriguez-Torres, M.; Everson, G. T.; Fried, M. W.; Ghalib, R.; Harrison, S.; Nyberg, L.; Shiffman, M. L.; Chan, A.; Hill, G. High Relapse Rate Seen at Week 72 for Patients Treated With R1626 Combination Therapy. *Hepatology* **2008,** *48,* 1349–1350.
419. Nelson, D. R.; Zeuzem, S.; Andreone, P.; Ferenci, P.; Herring, R.; Jensen, D. M.; Marcellin, P.; Pockros, P. J.; Rodríguez-Torres, M.; Rossaro, L.; Rustgi, V. K.; Sepe, T.; Sulkowski, M.; Thomason, I. R.; Yoshida, E. M.; Chan, A.; Hill, G. Balapiravir Plus Peginterferon Alfa-2a (40KD)/Ribavirin in a Randomized Trial of Hepatitis C Genotype 1 Patients. *Ann. Hepatol.* **2012,** *11,* 15–31.
420. Klumpp, K.; Kalayanov, G.; Ma, H.; Le Pogam, S.; Leveque, V.; Jiang, W. R.; Inocencio, N.; De Witte, A.; Rajyaguru, S.; Tai, E.; Chanda, S.; Irwin, M. R.; Sund, C.; Winqist, A.; Maltseva, T.; Eriksson, S.; Usova, E.; Smith, M.; Alker, A.; Najera, I.; Cammack, N.; Martin, J. A.; Johansson, N. G.; Smith, D. B. 2′-Deoxy-4′-Azido Nucleoside Analogs Are Highly Potent Inhibitors of Hepatitis C Virus Replication Despite the Lack of 2′-α-Hydroxyl Groups. *J. Biol. Chem.* **2008,** *283,* 2167–2175.
421. Clark, J. L.; Hollecker, L.; Mason, J. C.; Stuyver, L. J.; Tharnish, P. M.; Lostia, S.; McBrayer, T. R.; Schinazi, R. F.; Watanabe, K. A.; Otto, M. J.; Furman, P. A.; Stec, W. J.; Patterson, S. E.; Pankiewicz, K. W. Design, Synthesis, and Antiviral Activity of 2′-Deoxy-2′-Fluoro-2′-*C*-Methyl-Cytidine, a Potent Inhibitor of Hepatitis C Virus Replication. *J. Med. Chem.* **2005,** *48,* 5504–5508.
422. Stuyver, L. J.; McBrayer, T. R.; Tharnish, P. M.; Clark, J.; Hollecker, L.; Lostia, S.; Nachman, T.; Grier, J.; Bennett, M. A.; Xie, M.-Y.; Schinazi, R. F.; Morrey, J. D.; Julander, J. L.; Furman, P. A.; Otto, M. J. Inhibition of Hepatitis C Replicon RNA Synthesis by β-D-2′-Deoxy-2′-Fluoro-2′-*C*-Methylcytidine: A Specific Inhibitor of Hepatitis C Virus Replication. *Antivir. Chem. Chemoth.* **2006,** *17,* 79–87.
423. Murakami, E.; Bao, H.; Ramesh, M.; McBrayer, T. R.; Whitaker, T.; Micolochick Steuer, H. M.; Schinazi, R. F.; Stuyver, L. J.; Obikhod, A.; Otto, M. J.; Furman, P. A. Mechanism of Activation of β-D-2′-Deoxy-2′-Fluoro-2′-*C*-Methylcytidine and Inhibition of Hepatitis C Virus NS5B RNA Polymerase. *Antimicrob. Agents Chemother.* **2007,** *51,* 503–509.
424. Ali, S.; Leveque, V.; Le Pogam, S.; Ma, H.; Philipp, F.; Inocencio, N.; Smith, M.; Alker, A.; Kang, H.; Najera, I.; Klumpp, K.; Symons, J.; Cammack, N.; Jiang, W. R. Selected Replicon Variants With Low-Level in vitro Resistance to the Hepatitis C Virus NS5B Polymerase Inhibitor PSI-6130 Lack Cross-Resistance With R1479. *Antimicrob. Agents Chemother.* **2008,** *52,* 4356–4369.
425. Cole, P.; Castaner, R.; Bolos, J. R-7128: RNA-Directed RNA Polymerase (NS5B) Inhibitor, Treatment of Hepatitis C Virus Infection. *Drugs Future* **2009,** *34,* 282–290.
426. Asif, G.; Hurwitz, S. J.; Shi, J.; Hernandez-Santiago, B. I.; Schinazi, R. F. Pharmacokinetics of the Antiviral Agent β-D-2′-Deoxy-2′-Fluoro-2′-*C*-Methylcytidine in Rhesus Monkeys. *Antimicrob. Agents Chemother.* **2007,** *51,* 2877–2882.
427. Le Pogam, S.; Seshaadri, A.; Ewing, A.; Kang, H.; Kosaka, A.; Yan, J. M.; Berrey, M.; Symonds, B.; De La Rosa, A.; Cammack, N.; Nájera, I. RG7128 Alone or in Combination With Pegylated Interferon-α2a and Ribavirin Prevents Hepatitis C Virus (HCV) Replication and Selection of Resistant Variants in HCV-Infected Patients. *J. Infect. Dis.* **2010,** *202,* 1510–1519.
428. Pawlotsky, J. M.; Najera, I.; Jacobson, I. Resistance to Mericitabine, a Nucleoside Analogue Inhibitor of HCV RNA-Dependent RNA Polymerase. *Antivir. Ther.* **2012,** *17,* 411–423.
429. Wedemeyer, H.; Jensen, D.; Herring, R., Jr.; Ferenci, P.; Ma, M. M.; Zeuzem, S.; Rodriguez-Torres, M.; Bzowej, N.; Pockros, P.; Vierling, J.; Ipe, D.; Munson, M. L.; Chen, Y. C.; Najera, I.; Thommes, J.; The PROPEL Investigators. PROPEL: A Randomized Trial of Mericitabine Plus Peginterferon Alpha-2a/Ribavirin Therapy in Treatment-Naïve HCV Genotype 1/4 Patients. *Hepatology* **2013,** *58,* 524–537.
430. Pockros, P. J.; Jensen, D.; Tsai, N.; Taylor, R.; Ramji, A.; Cooper, C.; Dickson, R.; Tice, A.; Kulkarni, R.; Vierling, J. M.; Munson, M. L.; Chen, Y. C.; Najera, I.; Thommes, J.; The JUMP-C Investigators. JUMP-C: A Randomized Trial of Mericitabine Plus Pegylated Interferon Alpha-2a/Ribavirin for 24 Weeks in Treatment-Naïve HCV Genotype 1/4 Patients. *Hepatology* **2013,** *58,* 514–523.
431. Torres, D. M.; Harrison, S. A. Small Steps Toward a Better Treatment for Chronic Hepatitis C Infection: Mericitabine, Pegylated Interferon, and Ribavirin in the PROPEL and JUMP-C Trials. *Hepatology* **2013,** *58,* 488–490.
432. Ma, H.; Jiang, W. R.; Robledo, N.; Leveque, V.; Ali, S.; Lara-Jaime, T.; Masjedizadeh, M.; Smith, D. B.; Cammack, N.; Klumpp, K.; Symons, J. Characterization of the Metabolic Activation of Hepatitis C Virus Nucleoside Inhibitor β-D-2′-Deoxy-2′-Fluoro-2′-*C*-Methylcytidine (PSI-6130) and Identification of a Novel Active 5′-Triphosphate Species. *J. Biol. Chem.* **2007,** *282,* 29812–29820.
433. Murakami, E.; Niu, C.; Bao, H.; Micolochick, S. H. M.; Whitaker, T.; Nachman, T.; Sofia, M. A.; Wang, P.; Otto, M. J.; Furman, P. A. The Mechanism of Action of β-D-2′-Deoxy-2′-Fluoro-2′-*C*-Methylcytidine Involves a Second Metabolic Pathway Leading to β-D-2′-Deoxy-2′-Fluoro-2′-*C*-Methyluridine 5′-Triphosphate, a Potent Inhibitor of the Hepatitis C Virus RNA-Dependent RNA Polymerase. *Antimicrob. Agents Chemother.* **2008,** *52,* 458–464.
434. Sofia, M. J.; Bao, D.; Chang, W.; Du, J.; Nagarathnam, D.; Rachakonda, S.; Reddy, P. G.; Ross, B. S.; Wang, P.; Zhang, H. R.; Bansal, S.; Espiritu, C.; Keilman, M.; Lam, A. M.; Steuer, H. M.; Niu, C.; Otto, M. J.; Furman, P. A. Discovery of a β-D-2′-Deoxy-2′-α-fluoro-2′-β-*C*-methyluridine Nucleotide Prodrug (PSI-7977) for the Treatment of Hepatitis C Virus. *J. Med. Chem.* **2010,** *53,* 7202–7218.
435. Lam, A. M.; Murakami, E.; Espiritu, C.; Steuer, H. M.; Niu, C.; Keilman, M.; Bao, H.; Zennou, V.; Bourne, N.; Julander, J. G.; Morrey, J. D.; Smee, D. F.; Frick, D. N.; Heck, J. A.; Wang, P.; Nagarathnam, D.; Ross, B. S.; Sofia, M. J.; Otto, M. J.; Furman, P. A. PSI-7851, a Pronucleotide of β-D-2′-Deoxy-2′-Fluoro-2′-*C*-Methyluridine Monophosphate, Is a Potent and Pan-Genotype Inhibitor of Hepatitis C Virus Replication. *Antimicrob. Agents Chemother.* **2010,** *54,* 3187–3196.
436. Denning, J.; Cornpropst, M.; Flach, S. D.; Berrey, M. M.; Symonds, W. T. Pharmacokinetics, Safety, and Tolerability of GS-9851, a Nucleotide Analog Polymerase Inhibitor for Hepatitis C Virus, Following Single Ascending Doses in Healthy Subjects. *Antimicrob. Agents Chemother.* **2013,** *57,* 1201–1208.

437. Lawitz, E.; Rodriguez-Torres, M.; Denning, J. M.; Albanis, E.; Cornpropst, M.; Berrey, M. M.; Symonds, W. T. Pharmacokinetics, Pharmacodynamics, and Tolerability of GS-9851, a Nucleotide Analog Polymerase Inhibitor, Following Multiple Ascending Doses in Patients With Chronic Hepatitis C Infection. *Antimicrob. Agents Chemother.* **2013,** *57,* 1209–1217.
438. Clark, J. L.; Mason, J. C.; Hollecker, L.; Stuyver, L. J.; Tharnish, P. M.; McBrayer, T. R.; Otto, M. J.; Furman, P. A.; Schinazi, R. F.; Watanabe, K. A. Synthesis and Antiviral Activity of 2′-Deoxy-2′-fluoro-2′-*C*-methyl Purine Nucleosides as Inhibitors of Hepatitis C Virus RNA Replication. *Bioorg. Med. Chem. Lett.* **2006,** *16,* 1712–1715.
439. Chang, W.; Bao, D.; Chun, B.-K.; Naduthambi, D.; Nagarathnam, D.; Rachakonda, S.; Reddy, P. G.; Ross, B. S.; Zhang, H.-R.; Bansal, S.; Espiritu, C. L.; Keilman, M.; Lam, A. M.; Niu, C.; Steuer, H. M.; Furman, P. A.; Otto, M. J.; Sofia, M. J. Discovery of PSI-353661, a Novel Purine Nucleotide Prodrug for the Treatment of HCV Infection. *ACS Med. Chem. Lett.* **2011,** *2,* 130–135.
440. Furman, P. A.; Murakami, E.; Niu, C.; Lam, A. M.; Espiritu, C.; Bansal, S.; Bao, H.; Tolstykh, T.; Micolochick Steuer, H.; Keilman, M.; Zennou, V.; Bourne, N.; Veselenak, R. L.; Chang, W.; Ross, B. S.; Du, J.; Otto, M. J.; Sofia, M. J. Activity and the Metabolic Activation Pathway of the Potent and Selective Hepatitis C Virus Pronucleotide Inhibitor PSI-353661. *Antivir. Res.* **2011,** *91,* 120–132.
441. Reddy, P. G.; Bao, D.; Chang, W.; Chun, B.-K.; Du, J.; Nagarathnam, D.; Rachakonda, S.; Ross, B. S.; Zhang, H.-R.; Bansal, S.; Espiritu, C. L.; Keilman, M.; Lam, A. M.; Niu, C.; Steuer, H. M.; Furman, P. A.; Otto, M. J.; Sofia, M. J. 2′-Deoxy-2′-α-fluoro-2′-β-C-methyl 3′,5′-cyclic Phosphate Nucleotide Prodrug Analogs as Inhibitors of HCV NS5B Polymerase: Discovery of PSI-352938. *Bioorg. Med. Chem. Lett.* **2010,** *20,* 7376–7380.
442. Du, J.; Bao, D.; Chun, B.-K.; Jiang, Y.; Reddy, P. G.; Zhang, H.-R.; Ross, B. S.; Bansal, S.; Bao, H.; Espiritu, C.; Lam, A. M.; Murakami, E.; Niu, C.; Micolochick Steuer, H. M.; Furman, P. A.; Otto, M. J.; Sofia, M. J. β-D-2′-α-F-2′-β-*C*-Methyl-6-*O*-substituted 3′,5′-Cyclic Phosphate Nucleotide Prodrugs as Inhibitors of Hepatitis C Virus Replication: A Structure-Activity Relationship Study. *Bioorg. Med. Chem. Lett.* **2012,** *22,* 5924–5929.
443. Lam, A. M.; Espiritu, C.; Murakami, E.; Zennou, V.; Bansal, S.; Steuer, H. M.; Niu, C.; Keilman, M.; Bao, D.; Bourne, N.; Veselenek, R. L.; Reddy, P. G.; Chang, W.; Du, J.; Nagarathnam, D.; Sofia, M. J.; Otto, M. J.; Furman, P. A. Inhibition of Hepatitis C Virus Replicon RNA Synthesis by PSI-352938, a Cyclic Phosphate Prodrug of β-D-2′-Deoxy-2′-α-fluoro-2′-β-*C*-methylguanosine. *Antimicrob. Agents Chemother.* **2011,** *55,* 2566–2575.
444. Niu, C.; Tolstykh, T.; Bao, H.; Park, Y.; Babusis, D.; Lam, A. M.; Bansal, S.; Du, J.; Chang, W.; Reddy, P. G.; Zhang, H. R.; Woolley, J.; Wang, L. Q.; Chao, P. B.; Ray, A. S.; Otto, M. J.; Sofia, M. J.; Furman, P. A.; Murakami, E. Metabolic Activation of the Anti-Hepatitis C Virus Nucleotide Prodrug PSI-352938. *Antimicrob. Agents Chemother.* **2012,** *56,* 3767–3775.
445. Lam, A. M.; Espiritu, C.; Bansal, S.; Micolochick Steuer, H. M.; Zennou, V.; Otto, M. J.; Furman, P. A. HCV Nucleotide Inhibitors PSI-352938 and PSI-353661 Exhibit a Novel Mechanism of Resistance Requiring Multiple Mutations Within Replicon RNA. *J. Virol.* **2011,** *85,* 12334–12342.
446. LaPlante, S. R.; Bös, M.; Brochu, C.; Chabot, C.; Coulombe, R.; Gillard, J. R.; Jakalian, A.; Poirier, M.; Rancourt, J.; Stammers, T.; Thavonekham, B.; Beaulieu, P. L.; Kukolj, G.; Tsantrizos, Y. S. Conformation-Based Restrictions and Scaffold Replacements in the Design of Hepatitis C Virus Polymerase Inhibitors: Discovery of Deleobuvir (BI 207127). *J. Med. Chem.* **2014,** *57,* 1845–1854.
447. Hirashima, S.; Suzuki, T.; Ishida, T.; Noji, S.; Yata, S.; Ando, I.; Komatsu, M.; Ikeda, S.; Hashimoto, H. Benzimidazole Derivatives Bearing Substituted Biphenyls as Hepatitis C Virus NS5B RNA-Dependent RNA Polymerase Inhibitors: Structure–Activity Relationship Studies and Identification of a Potent and Highly Selective Inhibitor JTK-109. *J. Med. Chem.* **2006,** *49,* 4721–4736.
448. Li, H.; Tatlock, J.; Linton, A.; Gonzalez, J.; Jewell, T.; Patel, L.; Ludlum, S.; Drowns, M.; Rahavendran, S. V.; Skor, H.; Hunter, R.; Shi, S. T.; Herlihy, K. J.; Parge, H.; Hickey, M.; Yu, X.; Chau, F.; Nonomiya, J.; Lewis, C. Discovery of (R)-6-cyclopentyl-6-(2-(2,6-diethylpyridin-4-yl)ethyl)-3-((5,7-dimethyl-[1,2,4]triazolo[1,5-a]pyrimidin-2-yl) methyl)-4-hydroxy-5,6-dihydropyran-2-one (PF-00868554) as a Potent and Orally Available Hepatitis C Virus Polymerase Inhibitor. *J. Med. Chem.* **2009,** *52,* 1255–1288.
449. Lazerwith, S. E.; Lew, W.; Zhang, J.; Morganelli, P.; Liu, Q.; Canales, E.; Clarke, M. O.; Doerffler, E.; Byun, D.; Mertzman, M.; Ye, H.; Chong, L.; Xu, L.; Appleby, T.; Chen, X.; Fenaux, M.; Hashash, A.; Leavitt, S. A.; Mabery, E.; Matles, M.; Mwangi, J. W.; Tian, Y.; Lee, Y. J.; Zhang, J.; Zhu, C.; Murray, B. P.; Watkins, W. J. Discovery of GS-9669, a Thumb Site II Non-Nucleoside Inhibitor of NS5B for the Treatment of Genotype 1 Chronic Hepatitis C Infection. *J. Med. Chem.* **2014,** *57,* 1893–1901.
450. Di Marco, S.; Volpari, C.; Tomei, L.; Altamura, S.; Harper, S.; Narjes, F.; Koch, U.; Rowley, M.; De Francesco, R.; Migliaccio, G.; Carfi, A. Interdomain Communication in Hepatitis C Virus Polymerase Abolished by Small Molecule Inhibitors Bound to a Novel Allosteric Site. *J. Biol. Chem.* **2005,** *280,* 29765–29770.
451. Kukolj, G.; McGibbon, G. A.; McKercher, G.; Marquis, M.; Lefebvre, S.; Thauvette, L.; Gauthier, J.; Goulet, S.; Poupart, M.-A.; Beaulieu, P. L. Binding Site Characterization and Resistance to a Class of Non-Nucleoside Inhibitors of the Hepatitis C Virus NS5B Polymerase. *J. Biol. Chem.* **2005,** *280,* 39260–39267.
452. Beaulieu, P. L.; Bös, M.; Bousquet, Y.; Fazal, G.; Gauthier, J.; Gillard, J.; Goulet, S.; LaPlante, S.; Poupart, M. A.; Lefebvre, S.; McKercher, G.; Pellerin, C.; Austel, V.; Kukolj, G. Non-Nucleoside Inhibitors of the Hepatitis C Virus NS5B Polymerase: Discovery and Preliminary SAR of Benzimidazole Derivatives. *Bioorg. Med. Chem. Lett.* **2004,** *14,* 119–124.
453. Ando, I.; Ikeda, S.; Adachi, T.; Hashimoto, H. Benzimidazole Inhibitors of Hepatitis C Virus NS5B Polymerase: Identification of 2-[(4-Diarylmethoxy)phenyl]-benzimidazole. *Bioorg. Med. Chem. Lett.* **2006,** *16,* 1859–1863.
454. Beaulieu, P. L.; Gillard, J.; Bykowski, D.; Brochu, C.; Dansereau, N.; Duceppe, J.-S.; Hache, B.; Jakalian, A.; Lagace, L.; LaPlante, S.; McKercher, G.; Moreau, E.; Perreault, S.; Stammers, T.; Thauvette, L.; Warrington, J.; Kukolj, G. Improved Replicon Cellular Activity of Non-Nucleoside Allosteric Inhibitors of HCV NS5B Polymerase: From Benzimidazole to Indole Scaffolds. *Bioorg. Med. Chem. Lett.* **2006,** *16,* 4987–4993.
455. Beaulieu, P. L.; Bös, M.; Cordingley, M. G.; Chabot, C.; Fazal, G.; Garneau, M.; Gillard, J. R.; Jolicoeur, E.; LaPlante, S.; McKercher, G.; Poirier, M.; Poupart, M. A.; Tsantrizos, Y. S.; Duan, J.; Kukolj, G. Discovery of the First Thumb Pocket 1 NS5B Polymerase Inhibitor (BILB 1941) With Demonstrated Antiviral Activity in Patients Chronically Infected With Genotype 1 Hepatitis C Virus (HCV). *J. Med. Chem.* **2012,** *55,* 7650–7666.
456. Erhardt, A.; Deterding, K.; Benhamou, Y.; Reiser, M.; Forns, X.; Pol, S.; Calleja, J. L.; Ross, S.; Spangenberg, H. C.; Garcia- Samaniego, J.; Fuchs, M.; Enriquez, J.; Wiegand, J.; Stern, J.; Wu, K.; Kukolj, G.; Marquis, M.; Beaulieu, P.; Nehmiz, G.; Steffgen, J. Safety, Pharmacokinetics and Antiviral Effect of BILB 1941, a Novel Hepatitis C Virus RNA Polymerase Inhibitor, After 5 Days Oral Treatment. *Antivir. Ther.* **2009,** *14,* 23–32.
457. LaPlante, S. R.; Gillard, J. R.; Jakalian, A.; Aubry, N.; Coulombe, R.; Brochu, C.; Tsantrizos, Y. S.; Poirier, M.; Kukolj, G.; Beaulieu, P. L. Importance of Ligand Bioactive Conformation in the Discovery of Potent Indole-Diamide Inhibitors of the Hepatitis C Virus NS5B. *J. Am. Chem. Soc.* **2010,** *132,* 15204–15212.
458. Beaulieu, P. L.; Chabot, C.; Duan, J.; Garneau, M.; Gillard, J.; Jolicoeur, E.; Poirier, M.; Poupart, M. A.; Stammers, T. A.; Kukolj, G.; Tsantrizos, Y. S. Indole 5-Carboxamide Thumb Pocket I Inhibitors of HCV NS5B Polymerase With Nanomolar Potency in Cell-Based Subgenomic Replicons (Part 2): Central Amino Acid Linker and Right-Hand-Side SAR Studies. *Bioorg. Med. Chem. Lett.* **2011,** *21,* 3664–3670.
459. Jung, M. E.; Piizzi, G. *Gem*-Disubstituent Effect: Theoretical Basis and Synthetic Applications. *Chem. Rev.* **2005,** *105,* 1735–1766.
460. Beaulieu, P. L.; Anderson, P. C.; Bethell, R.; Bös, M.; Bousquet, Y.; Brochu, C.; Cordingley, M. G.; Fazal, G.; Garneau, M.; Gillard, J. R.; Kawai, S.; Marquis, M.; McKercher, G.; Poupart, M. A.; Stammers, T.; Thavonekham, B.; Wernic, D.; Duan, J.; Kukolj, G. Discovery of BI 207524, an Indole Diamide NS5B Thumb Pocket 1 Inhibitor With Improved Potency for the Potential Treatment of Chronic Hepatitis C Virus Infection. *J. Med. Chem.* **2014,** *57,* 10130–10143.
461. Beaulieu, P. L.; Bolger, G.; Duplessis, M.; Gagnon, A.; Garneau, M.; Stammers, T.; Kukolj, G.; Duan, J. Aza Follow-Ups to BI 207524, a Thumb Pocket 1 HCV NS5B Polymerase Inhibitor. Part 1: Mitigating the Genotoxic Liability of an Aniline Metabolite. *Bioorg. Med. Chem. Lett.* **2015,** *25,* 1135–1139.
462. Beaulieu, P. L.; Bolger, G.; Deon, D.; Duplessis, M.; Fazal, G.; Gagnon, A.; Garneau, M.; LaPlante, S.; Stammers, T.; Kukolj, G.; Duan, J. Multi-Parameter Optimization of Aza-Follow-Ups to BI 207524, a Thumb Pocket 1 HCV NS5B Polymerase Inhibitor. Part 2: Impact of Lipophilicity on Promiscuity and in vivo Toxicity. *Bioorg. Med. Chem. Lett.* **2015,** *25,* 1140–1145.
463. LaPlante, S. R.; Jakalian, A.; Aubry, N.; Bousquet, Y.; Ferland, J.-M.; Gillard, J.; Lefebvre, S.; Poirier, M.; Tsantrizos, Y. S.; Kukolj, G.; Beaulieu, P. L. Drug Design: Binding Mode Determination of Benzimidazole Inhibitors of the Hepatitis C Virus RNA Polymerase by a Structure and Dynamics Strategy. *Angew. Chem. Int. Ed.* **2004,** *43,* 4306–4311.

464. Beaulieu, P. L.; Anderson, P. C.; Brochu, C.; Bös, M.; Cordingley, M. G.; Duan, J.; Garneau, M.; Lagacé, L.; Marquis, M.; McKercher, G.; Poupart, M.-A.; Rancourt, J.; Stammers, T.; Tsantrizos, Y. S.; Kukolj, G. Preclinical Characterization of the Hepatitis C Virus NS5B Polymerase Non-Nucleoside Inhibitor BI 207127. *J. Hepatol.* **2012,** *56* (Suppl. 2), S321.
465. Larrey, D.; Lohse, A. W.; Trepo, C.; Bronowicki, J. P.; Arastéh, K.; Bourlière, M.; Calleja, J. L.; Stern, J. O.; Nehmiz, G.; Abdallah, N.; Berger, K. L.; Marquis, M.; Steffgen, J.; Kukolj, G.; The BI 207127 Study Group. Antiviral Effect, Safety, and Pharmacokinetics of Five-Day Oral Administration of Deleobuvir (BI 207127), an Investigational Hepatitis C Virus RNA Polymerase Inhibitor, in Patients With Chronic Hepatitis C. *Antimicrob. Agents Chemother.* **2013,** *57,* 4727–4735.
466. Boehringer-Ingelheim 2013 Annual Report, page 11 available at: https://www.boehringer-ingelheim.com/content/dam/internet/opu/com_EN/document/01_news/08_APC/APC_2014/BoehringerIngelheim_Annual_Report_2013.pdf.
467. Stansfield, I.; Pompei, M.; Conte, I.; Ercolani, C.; Migliaccio, G.; Jairaj, M.; Giuliano, C.; Rowley, M.; Narjes, F. Development of Carboxylic Acid Replacements in Indole-*N*-Acetamide Inhibitors of Hepatitis C Virus NS5B Polymerase. *Bioorg. Med. Chem. Lett.* **2007,** *17,* 5143–5149.
468. Regan, S. L.; Maggs, J. L.; Hammond, T. G.; Lambert, C.; Williams, D. P.; Park, B. K. Acyl Glucuronides: The Good, the Bad and the Ugly. *Biopharm. Drug Dispos.* **2010,** *31,* 367–395.
469. Ikegashira, K.; Oka, T.; Hirashima, S.; Noji, S.; Yamanaka, H.; Hara, Y.; Adachi, T.; Tsuruha, J.; Doi, S.; Hase, Y.; Noguchi, T.; Ando, I.; Ogura, N.; Ikeda, S.; Hashimoto, H. Discovery of Conformationally Constrained Tetracyclic Compounds as Potent Hepatitis C Virus NS5B RNA Polymerase Inhibitors. *J. Med. Chem.* **2006,** *49,* 6950–6953.
470. Hirashima, S.; Oka, T.; Ikegashira, K.; Noji, S.; Yamanaka, H.; Hara, Y.; Goto, H.; Mizojiri, R.; Niwa, Y.; Noguchi, T.; Ando, I.; Ikeda, S.; Hashimoto, H. Further Studies on Hepatitis C Virus NS5B RNA Dependent RNA Polymerase Inhibitors Toward Improved Replicon Cell Activities: Benzimidazole and Structurally Related Compounds Bearing the 2-Morpholinophenyl Moiety. *Bioorg. Med. Chem. Lett.* **2007,** *17,* 3181–3186.
471. Stansfield, I.; Ercolani, C.; Mackay, A.; Conte, I.; Pompei, M.; Koch, U.; Gennari, N.; Giuliano, C.; Rowley, M.; Narjes, F. Tetracyclic Indole Inhibitors of Hepatitis C Virus NS5B-Polymerase. *Bioorg. Med. Chem. Lett.* **2009,** *19,* 627–632.
472. Habermann, J.; Capito, E.; del Rosario Rico Ferreira, M.; Koch, U.; Narjes, F. Discovery of Pentacyclic Compounds as Potent Inhibitors of Hepatitis C Virus NS5B RNA Polymerase. *Bioorg. Med. Chem. Lett.* **2009,** *19,* 633–638.
473. Narjes, F.; Crescenzi, B.; Ferrara, M.; Habermann, J.; Colarusso, S.; Ferreira, M.d. R. R.; Stansfield, I.; Mackay, A. C.; Conte, I.; Ercolani, C.; Zaramella, S.; Palumbi, M.-C.; Meuleman, P.; Leroux-Roels, G.; Giuliano, C.; Fiore, F.; Di, M. S.; Baiocco, P.; Koch, U.; Migliaccio, G.; Altamura, S.; Laufer, R.; De, F. R.; Rowley, M. Discovery of (7R)-14-Cyclohexyl-7-{[2-(dimethylamino)ethyl]-(methyl)amino}-7,8-dihydro-6H-indolo[1,2-e][1,5]benzoxazocine-11-carboxylic acid (MK-3281), a Potent and Orally Bioavailable Finger-Loop Inhibitor of the Hepatitis C Virus NS5B Polymerase. *J. Med. Chem.* **2011,** *54,* 289–301.
474. Zheng, X.; Hudyma, T. W.; Martin, S. W.; Bergstrom, C.; Ding, M.; He, F.; Romine, J.; Poss, M. A.; Kadow, J. F.; Chang, C. H.; Wan, J.; Witmer, M. R.; Morin, P.; Camac, D. M.; Sheriff, S.; Beno, B. R.; Rigat, K. L.; Wang, Y. K.; Fridell, R.; Lemm, J.; Qiu, D.; Liu, M.; Voss, S.; Pelosi, L.; Roberts, S. B.; Gao, M.; Knipe, J.; Gentles, R. G. Syntheses and Initial Evaluation of a Series of Indolo-Fused Heterocyclic Inhibitors of the Polymerase Enzyme (NS5B) of the Hepatitis C Virus. *Bioorg. Med. Chem. Lett.* **2011,** *21,* 2925–2929.
475. Ding, M.; He, F.; Hudyma, T. W.; Zheng, X.; Poss, M. A.; Kadow, J. F.; Beno, B. R.; Rigat, K. L.; Wang, Y. K.; Fridell, R. A.; Lemm, J. A.; Qiu, D.; Liu, M.; Voss, S.; Pelosi, L. A.; Roberts, S. B.; Gao, M.; Knipe, J.; Gentles, R. G. Synthesis and SAR Studies of Novel Heteroaryl Fused Tetracyclic Indole-Diamide Compounds: Potent Allosteric Inhibitors of the Hepatitis C Virus NS5B Polymerase. *Bioorg. Med. Chem. Lett.* **2012,** *22,* 2866–2871.
476. Zheng, X.; Chao, S.; Sun, J.-H.; Beno, B. R.; Camac, D. M.; Chang, C.-H.; Gao, M.; Morin, P. E.; Sheriff, S.; Tredup, J.; Wan, J.; Witmer, M. R.; Xie, D.; Hanumegowda, U.; Knipe, J.; Mosure, K.; Santone, K. S.; Parker, D. D.; Zhuo, X.; Lemm, J.; Liu, M.; Pelosi, L.; Rigat, K.; Voss, S.; Wang, Y.; Wang, Y.-K.; Colonno, R. J.; Gao, M.; Roberts, S. B.; Gao, Q.; Ng, A.; Meanwell, N. A.; Kadow, J. F. Discovery and Preclinical Characterization of the Cyclopropylindolobenzazepine BMS-791325, a Potent Allosteric Inhibitor of the Hepatitis C Virus NS5B Polymerase. *J. Med. Chem.* **2014,** *57,* 1855–1879.
477. Sinz, M. W. Pregnane X Receptor: Prediction and Attenuation of Human CYP3A4 Enzyme Induction and Drug–Drug Interactions. *Ann. Rep. Med. Chem.* **2008,** *43,* 405–418.
478. Lemm, J. A.; Liu, M.; Gentles, R. G.; Ding, M.; Voss, S.; Pelosi, L. A.; Wang, Y. K.; Rigat, K. L.; Mosure, K. W.; Bender, J. A.; Knipe, J. O.; Colonno, R.; Meanwell, N. A.; Kadow, J. F.; Santone, K. S.; Roberts, S. B.; Gao, M. Preclinical Characterization of BMS-791325, an Allosteric Inhibitor of Hepatitis C Virus NS5B Polymerase. *Antimicrob. Agents Chemother.* **2014,** *58,* 3485–3495.
479. Yuan, L.; Jiang, H.; Zheng, N.; Xia, Y. Q.; Ouyang, Z.; Zeng, J.; Akinsanya, B.; Valentine, J. L.; Moehlenkamp, J. D.; Deng, Y.; Aubry, A. F.; Arnold, M. E. A Validated LC-MS/MS Method for the Simultaneous Determination of BMS-791325, a Hepatitis C Virus NS5B RNA Polymerase Inhibitor, and Its Metabolite in Plasma. *J. Chromatogr. B Anal. Technol. Biomed. Life Sci.* **2014,** *973,* 1–8.
480. Rigat, K. L.; Lu, H.; Wang, Y. K.; Argyrou, A.; Fanslau, C.; Beno, B.; Wang, Y.; Marcinkeviciene, J.; Ding, M.; Gentles, R. G.; Gao, M.; Abell, L. M.; Roberts, S. B. Mechanism of Inhibition for BMS-791325, a Novel Non-Nucleoside Inhibitor of Hepatitis C Virus NS5B Polymerase. *J. Biol. Chem.* **2014,** *289,* 33456–33468.
481. Sims, K. D.; Lemm, J.; Eley, T.; Liu, M.; Berglind, A.; Sherman, D.; Lawitz, E.; Vutikullird, A. B.; Tebas, P.; Gao, M.; Pasquinelli, C.; Grasela, D. M. Randomized, Placebo-Controlled, Single-Ascending-Dose Study of BMS-791325, a Hepatitis C Virus (HCV) NS5B Polymerase Inhibitor, in HCV Genotype 1 Infection. *Antimicrob. Agents Chemother.* **2014,** *58,* 3496–3503.
482. Cummings, M. D.; Lin, T. I.; Hu, L.; Tahri, A.; McGowan, D.; Amssoms, K.; Last, S.; Devogelaere, B.; Rouan, M. C.; Vijgen, L.; Berke, J. M.; Dehertogh, P.; Fransen, E.; Cleiren, E.; van der Helm, L.; Fanning, G.; Van Emelen, K.; Nyanguile, O.; Simmen, K.; Raboisson, P.; Vendeville, S. Structure-Based Macrocyclization Yields Hepatitis C Virus NS5B Inhibitors With Improved Binding Affinities and Pharmacokinetic Properties. *Angew. Chem. Int. Ed. Engl.* **2012,** *51,* 4460–4637.
483. Vendeville, S.; Lin, T. I.; Hu, L.; Tahri, A.; McGowan, D.; Cummings, M. D.; Amssoms, K.; Canard, M.; Last, S.; Van den Steen, I.; Devogelaere, B.; Rouan, M. C.; Vijgen, L.; Berke, J. M.; Dehertogh, P.; Fransen, E.; Cleiren, E.; van der Helm, L.; Fanning, G.; Van Emelen, K.; Nyanguile, O.; Simmen, K.; Raboisson, P. Finger. Loop Inhibitors of the HCV NS5b Polymerase. Part II. Optimization of Tetracyclic Indole-Based Macrocycle Leading to the Discovery of TMC647055. *Bioorg. Med. Chem. Lett.* **2012,** *22,* 4437–4443.
484. Cummings, M. D.; Lin, T. I.; Hu, L.; Tahri, A.; McGowan, D.; Amssoms, K.; Last, S.; Devogelaere, B.; Rouan, M. C.; Vijgen, L.; Berke, J. M.; Dehertogh, P.; Fransen, E.; Cleiren, E.; van der Helm, L.; Fanning, G.; Nyanguile, O.; Simmen, K.; Van Remoortere, P.; Raboisson, P.; Vendeville, S. Discovery and Early Development of TMC647055, a Non-Nucleoside Inhibitor of the Hepatitis C Virus NS5B Polymerase. *J. Med. Chem.* **2014,** *57,* 1880–1892.
485. Devogelaere, B.; Berke, J. M.; Vijgen, L.; Dehertogh, P.; Fransen, E.; Cleiren, E.; van der Helm, L.; Nyanguile, O.; Tahri, A.; Amssoms, K.; Lenz, O.; Cummings, M. D.; Clayton, R. F.; Vendeville, S.; Raboisson, P.; Simmen, K. A.; Fanning, G. C.; Lin, T. I. TMC647055, a Potent Nonnucleoside Hepatitis C Virus NS5B Polymerase Inhibitor With Cross-Genotypic Coverage. *Antimicrob. Agents Chemother.* **2012,** *56,* 4676–4684.
486. Li, H.; Tatlock, J.; Linton, A.; Gonzalez, J.; Borchardt, A.; Dragovich, P.; Jewell, T.; Prins, T.; Zhou, R.; Blazel, J.; Parge, H.; Love, R.; Hickey, M.; Doan, C.; Shi, S.; Duggal, R.; Lewis, C.; Fuhrman, S. Identification and Structure-Based Optimization of Novel Dihydropyrones as Potent HCV RNA Polymerase Inhibitors. *Bioorg. Med. Chem. Lett.* **2006,** *16,* 4834–4838.
487. Li, H.; Linton, A.; Tatlock, J.; Gonzalez, J.; Borchardt, A.; Abreo, M.; Jewell, T.; Patel, L.; Browns, M.; Ludlum, S.; Goble, M.; Yang, M.; Blazel, J.; Rahavendran, R.; Skor, H.; Shi, S.; Lewis, C.; Fuhrman, S. Allosteric Inhibitors of Hepatitis C Polymerase: Discovery of Potent and Orally Bioavailable Carbon-Linked Dihydropyrones. *J. Med. Chem.* **2007,** *50,* 3672–3969.
488. Camp, D.; Matthews, C. F.; Neville, S. T.; Rouns, M.; Scott, R. W.; Truong, Y. Development of a Synthetic Process Towards a Hepatitis C Polymerase Inhibitor. *Org. Process Res. Dev.* **2006,** *10,* 814–821.
489. Shi, S. T.; Herlihy, K. J.; Graham, J. P.; Nonomiya, J.; Rahavendran, S. V.; Skor, H.; Irvine, R.; Binford, S.; Tatlock, J.; Li, H.; Gonzalez, J.; Linton, A.; Patick, A. K.; Lewis, C. Preclinical Characterization of PF-00868554, a Potent Nonnucleoside Inhibitor of the Hepatitis C Virus RNA-Dependent RNA Polymerase. *Antimicrob. Agents Chemother.* **2009,** *53,* 2544–2552.

490. Wagner, F.; Thompson, R.; Kantaridis, C.; Simpson, P.; Troke, P. J.; Jagannatha, S.; Neelakantan, S.; Purohit, V. S.; Hammond, J. L. Antiviral Activity of the Hepatitis C Virus Polymerase Inhibitor Filibuvir in Genotype 1-Infected Patients. *Hepatology* **2011,** *54,* 50–59.
491. Troke, P. J.; Lewis, M.; Simpson, P.; Gore, K.; Hammond, J.; Craig, C.; Westby, M. Characterization of Resistance to the Nonnucleoside NS5B Inhibitor Filibuvir in Hepatitis C Virus-Infected Patients. *Antimicrob. Agents Chemother.* **2012,** *56,* 1331–1341.
492. Chan, L.; Reddy, T. J.; Proulx, M.; Das, S. K.; Pereira, O.; Wang, W.; Siddiqui, A.; Yannopoulos, C. G.; Poisson, C.; Turcotte, N.; Drouin, A.; Alaoui-Ismaili, M. H.; Bethell, R.; Hamel, M.; L'Heureux, L.; Bilimoria, D.; Nguyen-Ba, N. Identification of N, N-Disubstituted Phenylalanines as a Novel Class of Inhibitors of Hepatitis C NS5B Polymerase. *J. Med. Chem.* **2003,** *46,* 1283–1285.
493. Reddy, T. J.; Chan, L.; Turcotte, N.; Proulx, M.; Pereira, O. Z.; Das, S. K.; Siddiqui, A.; Wang, W.; Poisson, C.; Yannopoulos, C. G.; Bilimoria, D.; L'Heureux, L.; Alaoui, H. M.; Nguyen-Ba, N. Further SAR Studies on Novel Small Molecule Inhibitors of the Hepatitis C (HCV) NS5B Polymerase. *Bioorg. Med. Chem. Lett.* **2003,** *13,* 3341–3344.
494. Wang, M.; Ng, K. K.; Cherney, M. M.; Chan, L.; Yannopoulos, C. G.; Bedard, J.; Morin, N.; Nguyen-Ba, N.; Alaoui-Ismaili, M. H.; Bethell, R. C.; James, M. N. Non-Nucleoside Analogue Inhibitors Bind to an Allosteric Site on HCV NS5B Polymerase. Crystal Structures and Mechanism of Inhibition. *Biol. Chem.* **2003,** *278,* 9489–9495.
495. Chan, L.; Das, S. K.; Reddy, T. J.; Poisson, C.; Proulx, M.; Pereira, O.; Courchesne, M.; Roy, C.; Wang, W.; Siddiqui, A.; Yannopoulos, C. G.; Nguyen-Ba, N.; Labrecque, D.; Bethell, R.; Hamel, M.; Courtemanche-Asselin, P.; L'Heureux, L.; David, M.; Nicolas, O.; Brunette, S.; Bilimoria, D.; Bedard, J. Discovery of Thiophene-2-Carboxylic Acids as Potent Inhibitors of HCV NS5B Polymerase and HCV Subgenomic RNA Replication. Part 1: Sulfonamides. *Bioorg. Med. Chem. Lett.* **2004,** *14,* 793–796.
496. Chan, L.; Pereira, O.; Reddy, T. J.; Das, S. K.; Poisson, C.; Courchesne, M.; Proulx, M.; Siddiqui, A.; Yannopoulos, C. G.; Nguyen-Ba, N.; Roy, C.; Nasturica, D.; Moinet, C.; Bethell, R.; Hamel, M.; L'Heureux, L.; David, M.; Nicolas, O.; Courtemanche-Asselin, P.; Brunette, S.; Bilimoria, D.; Bedard, J. Discovery of Thiophene-2-Carboxylic Acids as Potent Inhibitors of HCV NS5B Polymerase and HCV Subgenomic RNA Replication. Part 2: Tertiary Amides. *Bioorg. Med. Chem. Lett.* **2004,** *14,* 797–800.
497. Yannopoulos, C. G.; Xu, P.; Ni, F.; Chan, L.; Pereira, O. Z.; Reddy, T. J.; Das, S. K.; Poisson, C.; Nguyen-Ba, N.; Turcotte, N.; Proulx, M.; Halab, L.; Wang, W.; Bédard, J.; Morin, N.; Hamel, M.; Nicolas, O.; Bilimoria, D.; L'Heureux, L.; Bethell, R.; Dionne, G. HCV NS5B Polymerase-Bound Conformation of a Soluble Sulfonamide Inhibitor by 2D Transferred NOESY. *Bioorg. Med. Chem. Lett.* **2004,** *14,* 5333–5337.
498. Biswal, B. K.; Cherney, M. M.; Wang, M.; Chan, L.; Yannopoulos, C. G.; Bilimoria, D.; Nicolas, O.; Bedard, J.; James, M. N. Crystal Structures of the RNA-Dependent RNA Polymerase Genotype 2a of Hepatitis C Virus Reveal Two Conformations and Suggest Mechanisms of Inhibition by Non-Nucleoside Inhibitors. *J. Biol. Chem.* **2005,** *280,* 18202–18210.
499. Biswal, B. K.; Wang, M.; Cherney, M. M.; Chan, L.; Yannopoulos, C. G.; Bilimoria, D.; Bedard, J.; James, M. N. Non-Nucleoside Inhibitors Binding to Hepatitis C Virus NS5B Polymerase Reveal a Novel Mechanism of Inhibition. *J. Mol. Biol.* **2006,** *361,* 33–45.
500. Le Pogam, S.; Kang, H.; Harris, S. F.; Leveque, V.; Giannetti, A. M.; Ali, S.; Jiang, W. R.; Rajyaguru, S.; Tavares, G.; Oshiro, C.; Hendricks, T.; Klumpp, K.; Symons, J.; Browner, M. F.; Cammack, N.; Najera, I. Selection and Characterization of Replicon Variants Dually Resistant to Thumb- and Palm-Binding Nonnucleoside Polymerase Inhibitors of the Hepatitis C Virus. *J. Virol.* **2006,** *80,* 6146–6154.
501. Cooper, C.; Lawitz, E. J.; Ghali, P.; Rodriguez-Torres, M.; Anderson, F. H.; Lee, S. S.; Bédard, J.; Chauret, N.; Thibert, R.; Boivin, I.; Nicolas, O.; Proulx, L. Evaluation of VCH-759 Monotherapy in Hepatitis C Infection. *J. Hepatol.* **2009,** *51,* 39–46.
502. Yi, G.; Deval, J.; Fan, B.; Cai, H.; Soulard, C.; Ranjith-Kumar, C. T.; Smith, D. B.; Blatt, L.; Beigelman, L.; Kao, C. C. Biochemical Study of the Comparative Inhibition of Hepatitis C Virus RNA Polymerase by VX-222 and Filibuvir. *Antimicrob. Agents Chemother.* **2012,** *56,* 830–837.
503. Fenaux, M.; Eng, S.; Leavitt, S. A.; Lee, Y. J.; Mabery, E. M.; Tian, Y.; Byun, D.; Canales, E.; Clarke, M. O.; Doerffler, E.; Lazerwith, S. E.; Lew, W.; Liu, Q.; Mertzman, M.; Morganelli, P.; Xu, L.; Ye, H.; Zhang, J.; Matles, M.; Murray, B. P.; Mwangi, J.; Zhang, J.; Hashash, A.; Krawczyk, S. H.; Bidgood, A. M.; Appleby, T. C.; Watkins, W. J. Preclinical Characterization of GS-9669, a Thumb Site II Inhibitor of the Hepatitis C Virus NS5B Polymerase. *Antimicrob. Agents Chemother.* **2013,** *57,* 804–810.
504. Dvory-Sobol, H.; Voitenleitner, C.; Mabery, E.; Skurnac, T.; Lawitz, E. J.; McHutchison, J.; Svarovskaia, E. S.; Delaney, W.; Miller, M. D.; Mo, H. Clinical and in vitro Resistance to GS-9669, a Thumb Site II Nonnucleoside Inhibitor of the Hepatitis C Virus NS5B Polymerase. *Antimicrob. Agents Chemother.* **2014,** *58,* 6599–6606.
505. Boyce, S. E.; Tirunagari, N.; Niedziela-Majka, A.; Perry, J.; Wong, M.; Kan, E.; Lagpacan, L.; Barauskas, O.; Hung, M.; Fenaux, M.; Appleby, T.; Watkins, W. J.; Schmitz, U.; Sakowicz, R. Structural and Regulatory Elements of HCV NS5B Polymerase—β-Loop and C-Terminal Tail—Are Required for Activity of Allosteric Thumb Site II Inhibitors. *PLoS One* **2014,** *9* (1), e84808. http://dx.doi.org/10.1371/journal.pone.0084808.
506. Kati, W.; Koev, G.; Irvin, M.; Beyer, J.; Liu, Y.; Krishnan, P.; Reisch, T.; Mondal, R.; Wagner, R.; Molla, A.; Maring, C.; Collins, C. In Vitro Activity and Resistance Profile of Dasabuvir, a Nonnucleoside Hepatitis C Virus Polymerase Inhibitor. *Antimicrob. Agents Chemother.* **2015,** *59,* 1505–1511.
507. Trivella, J. P.; Gutierrez, J.; Martin, P. Dasabuvir: A New Direct Antiviral Agent for the Treatment of Hepatitis C. *Expert. Opin. Pharmacother.* **2015,** *16,* 617–624.
508. Ruebsam, F.; Murphy, D. E.; Tran, C. V.; Li, L. S.; Zhao, J.; Dragovich, P. S.; McGuire, H. M.; Xiang, A. X.; Sun, Z.; Ayida, B. K.; Blazel, J. K.; Kim, S. H.; Zhou, Y.; Han, Q.; Kissinger, C. R.; Webber, S. E.; Showalter, R. E.; Shah, A. M.; Tsan, M.; Patel, R. A.; Thompson, P. A.; Lebrun, L. A.; Hou, H. J.; Kamran, R.; Sergeeva, M. V.; Bartkowski, D. M.; Nolan, T. G.; Norris, D. A.; Khandurina, J.; Brooks, J.; Okamoto, E.; Kirkovsky, L. Discovery of Tricyclic 5,6-Dihydro-1H-Pyridin-2-Ones as Novel, Potent, and Orally Bioavailable Inhibitors of HCV NS5B Polymerase. *Bioorg. Med. Chem. Lett.* **2009,** *19,* 6404–6412.
509. Kapelusznik, I.; Heil, E. L.; Temesgen, Z.; Talwani, R. Setrobuvir. *Drugs Future* **2012,** *37,* 725–733.
510. de Bruijne, J.; van de Wetering de Rooij, J.; van Vliet, A. A.; Zhou, X. J.; Temam, M. F.; Molles, J.; Chen, J.; Pietropaolo, K.; Sullivan-Bólyai, J. Z.; Mayers, D.; Reesink, H. W. First-in-Human Study of the Pharmacokinetics and Antiviral Activity of IDX375, a Novel Nonnucleoside Hepatitis C Virus Polymerase Inhibitor. *Antimicrob. Agents Chemother.* **2012,** *56,* 4525–4528.
511. Kneteman, N. M.; Howe, A. Y.; Gao, T.; Lewis, J.; Pevear, D.; Lund, G.; Douglas, D.; Mercer, D. F.; Tyrrell, D. L.; Immermann, F.; Chaudhary, I.; Speth, J.; Villano, S. A.; O'Connell, J.; Collett, M. HCV796: A Selective Nonstructural Protein 5B Polymerase Inhibitor With Potent Anti-Hepatitis C Virus Activity In Vitro, in Mice With Chimeric Human Livers, and in Humans Infected With Hepatitis C Virus. *Hepatology* **2009,** *49,* 745–752.
512. Vliegen, I.; Paeshuyse, J.; De Burghgraeve, T.; Lehman, L. S.; Paulson, M.; Shih, I. H.; Mabery, E.; Boddeker, N.; De Clercq, E.; Reiser, H.; Oare, D.; Lee, W. A.; Zhong, W.; Bondy, S.; Purstinger, G.; Neyts, J. Substituted Imidazopyridines as Potent Inhibitors of HCV Replication. *J. Hepatol.* **2009,** *50,* 999–1009.
513. Dhanak, D.; Duffy, K. J.; Johnston, V. K.; Lin-Goerke, J.; Darcy, M.; Shaw, A. N.; Gu, B.; Silverman, C.; Gates, A. T.; Nonnemacher, M. R.; Earnshaw, D. L.; Casper, D. J.; Kaura, A.; Baker, A.; Greenwood, C.; Gutshall, L. L.; Maley, D.; DelVecchio, A.; Macarron, R.; Hofmann, G. A.; Alnoah, Z.; Cheng, H. Y.; Chan, G.; Khandekar, S.; Keenan, R. M.; Sarisky, R. T. Identification and Biological Characterization of Heterocyclic Inhibitors of the Hepatitis C Virus RNA-Dependent RNA Polymerase. *J. Biol. Chem.* **2002,** *277,* 38322–38327.
514. Tedesco, R.; Shaw, A. N.; Bambal, R.; Chai, D.; Concha, N. O.; Darcy, M. G.; Dhanak, D.; Fitch, D. M.; Gates, A.; Gerhardt, W. G.; Halegoua, D. L.; Han, C.; Hofmann, G. A.; Johnston, V. K.; Kaura, A. C.; Liu, N.; Keenan, R. M.; Lin-Goerke, J.; Sarisky, R. T.; Wiggall, K. J.; Zimmerman, M. N.; Duffy, K. J. 3-(1,1-Dioxo-2*H*-(1,2,4)-benzothiadiazin-3-yl)-4-hydroxy-2(1*H*)-quinolinones, Potent Inhibitors of Hepatitis C Virus RNA-Dependent RNA Polymerase. *J. Med. Chem.* **2006,** *49,* 971–983.
515. Das, D.; Hong, J.; Chen, S. H.; Wang, G.; Beigelman, L.; Seiwert, S. D.; Buckman, B. O. Recent Advances in Drug Discovery of Benzothiadiazine and Related Analogs as HCV NS5B Polymerase Inhibitors. *Bioorg. Med. Chem.* **2011,** *19,* 4690–4703.
516. Nguyen, T. T.; Gates, A. T.; Gutshall, L. L.; Johnston, V. K.; Gu, B.; Duffy, K. J.; Sarisky, R. T. Resistance Profile of a Hepatitis C Virus RNA-Dependent RNA Polymerase Benzothiadiazine Inhibitor. *Antimicrob. Agents Chemother.* **2003,** *47,* 3525–3530.
517. Gu, B.; Johnston, V. K.; Gutshall, L. L.; Nguyen, T. T.; Gontarek, R. R.; Darcy, M. G.; Tedesco, R.; Dhanak, D.; Duffy, K. J.; Kao, C. C.; Sarisky, R. T. Arresting Initiation of Hepatitis C Virus RNA Synthesis Using Heterocyclic Derivatives. *J. Biol. Chem.* **2003,** *278,* 16602–16607.
518. Shaw, A. N.; Tedesco, R.; Bambal, R.; Chai, D.; Concha, N. O.; Darcy, M. G.; Dhanak, D.; Duffy, K. J.; Fitch, D. M.; Gates, A.; Johnston, V. K.; Keenan, R. M.; Lin-Goerke, J.; Liu, N.; Sarisky, R. T.; Wiggall, K. J.; Zimmerman, M. N. Substituted Benzothiadizine Inhibitors of Hepatitis C Virus Polymerase. *Bioorg. Med. Chem. Lett.* **2009,** *19,* 4350–4353.

519. Rockway, T. W.; Zhang, R.; Liu, D.; Betebenner, D. A.; McDaniel, K. F.; Pratt, J. K.; Beno, D.; Montgomery, D.; Jiang, W. W.; Masse, S.; Kati, W. M.; Middleton, T.; Molla, A.; Maring, C. J.; Kempf, D. J. Inhibitors of HCV NS5B Polymerase: Synthesis and Structure-Activity Relationships of *N*-1-Benzyl and *N*-1-[3-methylbutyl]-4-hydroxy-1,8-naphthyridon-3-yl Benzothiadiazine Analogs Containing Substituents on the Aromatic Ring. *Bioorg. Med. Chem. Lett.* **2006,** *16,* 3833–3838.
520. Zhou, Y.; Webber, S. E.; Murphy, D. E.; Li, L.-S.; Dragovich, P. S.; Tran, C. V.; Sun, Z.; Ruebsam, F.; Shah, A. M.; Tsan, M.; Showalter, R. E.; Patel, R.; Li, B.; Zhao, Q.; Han, Q.; Hermann, T.; Kissinger, C. R.; LeBrun, L.; Sergeeva, M. V.; Kirkovsky, L. Novel HCV NS5B Polymerase Inhibitors Derived From 4-(1',1'-Dioxo-1,4'-dihydro-1'λ6-benzo[1',2',4']thiadiazin-3'-yl)-5-hydroxy-2H-pyridazin-3-ones. Part 1: Exploration of 7'-Substitution of Benzothiadiazine. *Bioorg. Med. Chem. Lett.* **2008,** *18,* 1413–1418.
521. Zhou, Y.; Li, L.-S.; Dragovich, P. S.; Murphy, D. E.; Tran, C. V.; Ruebsam, F.; Webber, S. E.; Shah, A. M.; Tsan, M.; Averill, A.; Showalter, R. E.; Patel, R.; Han, Q.; Zhao, Q.; Hermann, T.; Kissinger, C. R.; LeBrun, L.; Sergeeva, M. V. Novel HCV NS5B Polymerase Inhibitors Derived From 4-(1',1'-Dioxo-1',4'-dihydro-1'λ^6-benzo[1',2',4']thiadiazin-3'-yl)-5-hydroxy-2*H*-pyridazin-3-ones. Part 2: Variation of the 2- and 6-Pyridazinone Substituents. *Bioorg. Med. Chem. Lett.* **2008,** *18,* 1419–1424.
522. Li, L.-S.; Zhou, Y.; Murphy, D. E.; Stankovic, N.; Zhao, J.; Dragovich, P. S.; Bertolini, T.; Sun, Z.; Ayida, B.; Tran, C. V.; Ruebsam, F.; Webber, S. E.; Shah, A. M.; Tsan, M.; Showalter, R. E.; Patel, R.; LeBrun, L. A.; Bartkowski, D. M.; Nolan, T. G.; Norris, D. A.; Kamran, R.; Brooks, J.; Sergeeva, M. V.; Kirkovsky, L.; Zhao, Q.; Kissinger, C. R. Novel HCV NS5B Polymerase Inhibitors Derived From 4-(1',1'-Dioxo-1',4'-dihydro-1'λ6-benzo[1',2',4'] thiadiazin-3'-yl)-5-hydroxy-2H-pyridazin-3-ones. Part 3: Further Optimization of the 2-, 6-, and 7'-Substituents and Initial Pharmacokinetic Assessments. *Bioorg. Med. Chem. Lett.* **2008,** *18,* 3446–3455.
523. Sergeeva, M. V.; Zhou, Y.; Bartkowski, D. M.; Nolan, T. G.; Norris, D. A.; Okamoto, E.; Kirkovsky, L.; Kamran, R.; LeBrun, L. A.; Tsan, M.; Patel, R.; Shah, A. M.; Lardy, M.; Gobbi, A.; Li, L.-S.; Zhao, J.; Bertolini, T.; Stankovic, N.; Sun, Z.; Murphy, D. E.; Webber, S. E.; Dragovich, P. S. Novel HCV NS5B Polymerase Inhibitors Derived From 4-(1',1'-Dioxo-1',4'-dihydro-1' λ^6-benzo[1',2',4']thiadiazin-3'-yl)-5-hydroxy-2*H*-pyridazin-3-ones: Part 4. Optimization of DMPK Properties. *Bioorg. Med. Chem. Lett.* **2008,** *18,* 3421–3426.
524. Ruebsam, F.; Tran, C. V.; Li, L. S.; Kim, S. H.; Xiang, A. X.; Zhou, Y.; Blazel, J. K.; Sun, Z.; Dragovich, P. S.; Zhao, J.; McGuire, H. M.; Murphy, D. E.; Tran, M. T.; Stankovic, N.; Ellis, D. A.; Gobbi, A.; Showalter, R. E.; Webber, S. E.; Shah, A. M.; Tsan, M.; Patel, R. A.; Lebrun, L. A.; Hou, H. J.; Kamran, R.; Sergeeva, M. V.; Bartkowski, D. M.; Nolan, T. G.; Norris, D. A.; Kirkovsky, L. 5,6-Dihydro-1*H*-pyridin-2-ones as Potent Inhibitors of HCV NS5B Polymerase. *Bioorg. Med. Chem. Lett.* **2009,** *19,* 451–458.
525. Showalter, R. E.; Thompson, P. A.; Steffy, K. R.; Appleman, J. R. ANA598 Displays Potent in vitro Antiviral Activity Against Diverse Clinical Isolates of Genotype 1 HCV in a Transient Replicon Shuttle Vector System. 60th Annual Meeting of the American Association for the Study of Liver Diseases, Boston, MA, U.S., October 30–November 3, 2009. Abstract No. 1586.
526. Nyanguile, O.; Devogelaere, B.; Vijgen, L.; Van den Broeck, W.; Pauwels, F.; Cummings, M. D.; De Bondt, H. L.; Vos, A. M.; Berke, J. M.; Lenz, O.; Vandercruyssen, G.; Vermeiren, K.; Mostmans, W.; Dehertogh, P.; Delouvroy, F.; Vendeville, S.; VanDyck, K.; Dockx, K.; Cleiren, E.; Raboisson, P.; Simmen, K. A.; Fanning, G. C. 1a/1b Subtype Profiling of Nonnucleoside Polymerase Inhibitors of Hepatitis C Virus. *J. Virol.* **2010,** *84,* 2923–2934.
527. Sun, S. C.; Bae, A.; Qi, X.; Harris, J.; Wong, K. A.; Miller, M. D.; Mo, H. Natural Variation in Drug Susceptibility to HCV Polymerase Inhibitors in Treatment-Naïve HCV Patient Isolates. *J. Viral Hepatitis* **2011,** *18,* 861–870.
528. Mallalieu, N. L.; Rahimy, M. H.; Crowley, C. A.; Appleman, J. R.; Smith, P. F.; Freddo, J. L. Pharmacokinetics and Pharmacodynamics of Setrobuvir, an Orally Administered Hepatitis C Virus Non-Nucleoside Analogue Inhibitor. *Clin. Ther.* **2014,** *36,* 2047–2063.
529. Evans, K. A.; Chai, D.; Graybill, T. L.; Burton, G.; Sarisky, R. T.; Lin-Goerke, J.; Johnston, V. K.; Rivero, R. A. An Efficient, Asymmetric Solid-Phase Synthesis of Benzothiadiazine-Substituted Tetramic Acids: Potent Inhibitors of the Hepatitis C Virus RNA-Dependent RNA Polymerase. *Bioorg. Med. Chem. Lett.* **2006,** *16,* 2205–2208.
530. Liu, Y.; Lim, B. H.; Jiang, W. W.; Flentge, C. A.; Hutchinson, D. K.; Madigan, D. L.; Randolph, J. T.; Wagner, R.; Maring, C. J.; Kati, W. M.; Molla, A. Identification of Aryl Dihydrouracil Derivatives as Palm Initiation Site Inhibitors of HCV NS5B Polymerase. *Bioorg. Med. Chem. Lett.* **2012,** *22,* 3747–3750.
531. Maring, C.; Wagner, R.; Hutchinson, D.; Flentge, C.; Kati, W.; Koev, G.; Liu, Y.; Beno, D.; Shen, J.; Lau, Y.; Gao, Y.; Fischer, J.; Vaidyanathan, S.; Lim, H.; Beyer, J.; Mondal, R.; Molla, A. Preclinical Potency, Pharmacokinetic and ADME Characterization of ABT-333, a Novel Non-nucleoside HCV Polymerase Inhibitor. 44th Annual Meeting of the European Association for the Study of the Liver, Copenhagen, Denmark, April 22–26, 2009. Abstract 955.
532. Wagner, R.; Maring, C.; Donner, P. L.; Randolph, J. T.; Krueger, A. C.; Rockway, T. W.; Pratt, J. K.; Liu, D.; Tufano, M.; Kati, W. M.; Liu, Y.; Lim, H. B.; Koev, G.; Beyer, J. M.; Mondal, R.; Reisch, T. J.; Krishnan, P.; Beno, D. W. A.; Lau, Y. Y.; Shen, J.; Fischer, J. S.; Gao, Y.; Molla, A. Preclinical Characterization of ABT-072: A Novel Non-nucleoside HCV Polymerase Inhibitor. 44th Annual Meeting of the European Association for the Study of the Liver, Copenhagen, Denmark, April 22–26, 2009. Abstract 970.
533. Poordad, F.; Lawitz, E.; DeJesus, E.; Kowdley, K.; Gaultier, I.; Cohen, D.; Xie, W.; Larsen, L.; Pilot-Matias, T.; Koev, G.; Dumas, E.; Podsadecki, T.; Bernstein, B. ABT-072 or ABT-333 Combined With Pegylated Interferon/Ribavirin After 3-day Monotherapy in HCV Genotype 1 (GT1)-Infected Treatment-Naïve Subjects: 12-Week Sustained Virologic Response (SVR12) and Safety Results. 47th Annual Meeting of the European Association for the Study of the Liver, Barcelona, Spain, April 18–22, 2012. Abstract 1206.
534. Burton, G.; Ku, T. W.; Carr, T. J.; Kiesow, T.; Sarisky, R. T.; Lin-Goerke, J.; Baker, A.; Earnshaw, D. L.; Hofmann, G. A.; Keenan, R. M.; Dhanak, D. Identification of Small Molecule Inhibitors of the Hepatitis C Virus RNA-Dependent RNA Polymerase From a Pyrrolidine Combinatorial Mixture. *Bioorg. Med. Chem. Lett.* **2005,** *15,* 1553–1556.
535. Burton, G.; Ku, T. W.; Carr, T. J.; Kiesow, T.; Sarisky, R. T.; Lin-Goerke, J.; Hofmann, G. A.; Slater, M. J.; Haigh, D.; Dhanak, D.; Johnson, V. K.; Parry, N. R.; Thommes, P. Studies on Acyl Pyrrolidine Inhibitors of HCV RNA-Dependent RNA Polymerase to Identify a Molecule With Replicon Antiviral Activity. *Bioorg. Med. Chem. Lett.* **2007,** *17,* 1930–1933.
536. Slater, M. J.; Amphlett, E. M.; Andrews, D. M.; Bravi, G.; Burton, G.; Cheasty, A. G.; Corfield, J. A.; Ellis, M. R.; Fenwick, R. H.; Fernandes, S.; Guidetti, R.; Haigh, D.; Hartley, C. D.; Howes, P. D.; Jackson, D. L.; Jarvest, R. L.; Lovegrove, V. L.; Medhurst, K. J.; Parry, N. R.; Price, H.; Shah, P.; Singh, O. M.; Stocker, R.; Thommes, P.; Wilkinson, C.; Wonacott, A. Optimization of Novel Acyl Pyrrolidine Inhibitors of Hepatitis C Virus RNA-Dependent RNA Polymerase Leading to a Development CANDIDATE. *J. Med. Chem.* **2007,** *50,* 897–900.
537. Flanagan, R. C.; Xie, S.; Millar, A. A Catalyzed and Highly Selective Ester Reduction in the Synthesis of an *N*-Acylpyrrolidine: Safe Design Through Reaction Calorimetry and Modeling. *Org. Process Res. Dev.* **2008,** *12,* 1307–1312.
538. Gray, F.; Amphlett, E.; Bright, H.; Chambers, L.; Cheasty, A.; Fenwick, R.; Haigh, D.; Hartley, D.; Howes, P.; Jarvest, R.; Mirzai, F.; Nerozzi, F.; Parry, N.; Slater, M.; Smith, S.; Thommes, P.; Wilkinson, C.; Williams, E. A Novel and Highly Potent Inhibitor of the HCV NS5B Polymerase. GSK625433. 42nd Annual Meeting of the European Association for the Study of the Liver, Barcelona, Spain, April 11-15, 2007. Abstract 594.
539. Monotherapy Versus Placebo Over 14 or 17 Days in Healthy and Hepatitis C Infected Adults. Clinicaltrials.gov/ct2/show/study/NCT00439959 (accessed September 29th, 2015).
540. Howe, A. Y.; Cheng, H.; Johann, S.; Mullen, S.; Chunduru, S. K.; Young, D. C.; Bard, J.; Chopra, R.; Krishnamurthy, G.; Mansour, T.; O'Connell, J. Molecular Mechanism of Hepatitis C Virus Replicon Variants With Reduced Susceptibility to a Benzofuran Inhibitor, HCV-796. *Antimicrob. Agents Chemother.* **2008,** *52,* 3327–3338.
541. Flint, M.; Mullen, S.; Deatly, A. M.; Chen, W.; Miller, L. Z.; Ralston, R.; Broom, C.; Emini, E. A.; Howe, A. Y. Selection and Characterization of Hepatitis C Virus Replicons Dually Resistant to the Polymerase and Protease Inhibitors HCV-796 and Boceprevir (SCH 503034). *Antimicrob. Agents Chemother.* **2009,** *53,* 401–411.
542. Reich, S.; Golbik, R. P.; Geissler, R.; Lilie, H.; Behrens, S. E. Mechanisms of Activity and Inhibition of the Hepatitis C Virus RNA-Dependent RNA Polymerase. *J. Biol. Chem.* **2010,** *285,* 13685–13693.
543. Hang, J. Q.; Yang, Y.; Harris, S. F.; Leveque, V.; Whittington, H. J.; Rajyaguru, S.; Ao-leong, G.; McCown, M. F.; Wong, A.; Giannetti, A. M.; Le Pogam, S.; Talamás, F.; Cammack, N.; Nájera, I.; Klumpp, K. Slow Binding Inhibition and Mechanism of Resistance of Non-Nucleoside Polymerase Inhibitors of Hepatitis C Virus. *J. Biol. Chem.* **2009,** *284,* 15517–15529.
544. Bartels, D. J.; Sullivan, J. C.; Zhang, E. Z.; Tigges, A. M.; Dorrian, J. L.; De Meyer, S.; Takemoto, D.; Dondero, E.; Kwong, A. D.; Picchio, G.; Kieffer, T. L. Hepatitis C Virus Variants With Decreased Sensitivity to Direct Acting Antivirals (DAAs) Were Rarely Observed in DAA Naive Patients Prior to Treatment. *J. Virol.* **2013,** *87,* 1544–1553.
545. Paolucci, S.; Fiorina, L.; Mariani, B.; Gulminetti, R.; Novati, S.; Barbarini, G.; Bruno, R.; Baldanti, F. Naturally Occurring Resistance Mutations to Inhibitors of HCV NS5A Region and NS5B Polymerase in DAA Treatment-Naïve Patients. *J. Virol.* **2013,** *10,* 355.

546. McCown, M. F.; Rajyaguru, S.; Kular, S.; Cammack, N.; Najera, I. GT-1a or GT-1b Subtype-Specific Resistance Profiles for Hepatitis C Virus Inhibitors Telaprevir and HCV-796. *Antimicrob. Agents Chemother.* **2009,** *53,* 2129–2132.
547. Villano, S.; Howe, A.; Raible, D.; Harper, D.; Speth, J.; Bichier, G. Analysis of HCV NS5B Genetic Variants Following Monotherapy With HCV-796, a Non-Nucleoside Polymerase Inhibitor, in Treatment-Naïve HCV-Infected Patients. 57th Annual Meeting of the American Association for the Study of Liver Diseases, Boston, MA, October 27-31, 2006. Abstract 1127*Hepatology* **2006,** *44 (SUppl. 1)*; pp 606A–607A.
548. Feldstein, A.; Kleiner, D.; Kravetz, D.; Buck, M. Severe Hepatocellular Injury With Apoptosis Induced by a Hepatitis C Polymerase Inhibitor. *J. Clin. Gastroenterol.* **2009,** *43,* 374–381.
549. Ryder, N. S. Discontinued Drugs in 2008: Anti-Infectives. *Exp. Opin. Invest. Drugs* **2010,** *19,* 1–21.
550. Maynard, A.; Crosby, R. M.; Ellis, B.; Hamatake, R.; Hong, Z.; Johns, B. A.; Kahler, K. M.; Koble, C.; Leivers, A.; Leivers, M. R.; Mathis, A.; Peat, A. J.; Pouliot, J. J.; Roberts, C. D.; Samano, V.; Schmidt, R. M.; Smith, G. K.; Spaltenstein, A.; Stewart, E. L.; Thommes, P.; Turner, E. M.; Voitenleitner, C.; Walker, J. T.; Waitt, G.; Weatherhead, J.; Weaver, K.; Williams, S.; Wright, L.; Xiong, Z. Z.; Haigh, D.; Shotwell, J. B. Discovery of a Potent Boronic Acid Derived Inhibitor of the HCV RNA-Dependent RNA Polymerase. *J. Med. Chem.* **2014,** *57,* 1902–1913.
551. Baker, S. J.; Ding, C. Z.; Akama, T.; Zhang, Y. K.; Hernandez, V.; Xia, Y. Therapeutic Potential of Boron-Containing Compounds. *Future Med. Chem.* **2009,** *1,* 1275–1288.
552. Trippier, P. C.; McGuigan, C. Boronic Acids in Medicinal Chemistry: Anticancer, Antibacterial and Antiviral Applications. *Med. Chem. Commun.* **2010,** *1,* 183–198.
553. Voitenleitner, C.; Crosby, R.; Walker, J.; Remlinger, K.; Vamathevan, J.; Wang, A.; You, S.; Johnson, J., III; Woldu, E.; Van Horn, S.; Horton, J.; Creech, K.; Shotwell, J. B.; Hong, Z.; Hamatake, R. *In Vitro* Characterization of GSK2485852, a Novel Hepatitis C Virus Polymerase Inhibitor. *Antimicrob. Agents Chemother.* **2013,** *57,* 5216–5224.
554. Baughman, T. M.; Lee, D.; Losos, J.; Moss, L.; Sigafoos, J.; Talarico, C.; Wagner, D. Determining Metabolism Differences in Preclinical Species and Human in vitro and in vivo for GSK2485852, a NS5B HCV Inhibitor. *The Role of Drug Metabolism in Immune Mediated Drug Toxicity: Molecular, Clinical and Mechanistic Aspects*, April 17–19, 2013, Cambridge, MA. Poster P14. Available at: http://c.ymcdn.com/sites/issx.site-ym.com/resource/resmgr/Workshop_Poster_Abstracts-Fl.pdf. Accessed September, 30th, 2015.
555. Paeshuyse, J.; Leyssen, P.; Mabery, E.; Boddeker, N.; Vrancken, R.; Froeyen, M.; Ansari, I. H.; Dutartre, H.; Rozenski, J.; Gil, L. H.; Letellier, C.; Lanford, R.; Canard, B.; Koenen, F.; Kerkhofs, P.; Donis, R. O.; Herdewijn, P.; Watson, J.; De Clercq, E.; Puerstinger, G.; Neyts, J. A Novel, Highly Selective Inhibitor of Pestivirus Replication That Targets the Viral RNA-Dependent RNA Polymerase. *J. Virol.* **2006,** *80,* 149–160.
556. Puerstinger, G.; Paeshuyse, J.; De Clercq, E.; Neyts, J. Antiviral 2,5-Disubstituted Imidazo[4,5-*c*]Pyridines: From Anti-Pestivirus to Anti-Hepatitis C Virus Activity. *Bioorg. Med. Chem. Lett.* **2007,** *17,* 303–390.
557. Puerstinger, G.; Paeshuyse, J.; Heinrich, S.; Mohr, J.; Schraffl, N.; De Clercq, E.; Neyts, J. Antiviral 2,5-Disubstituted Imidazo[4,5-*c*]Pyridines: Further Optimization of Anti-Hepatitis C Virus Activity. *Bioorg. Med. Chem. Lett.* **2007,** *17,* 5111–5114.
558. Shih, I.-h.; Vliegen, I.; Peng, B.; Yang, H.; Hebner, C.; Paeshuyse, J.; Pürstinger, G.; Fenaux, M.; Tian, Y.; Mabery, E.; Qi, X.; Bahador, G.; Paulson, M.; Lehman, L. S.; Bondy, S.; Tse, W.; Reiser, H.; Lee, W. A.; Schmitz, U.; Neyts, J.; Zhong, W. Mechanistic Characterization of GS-9190 (Tegobuvir), a Novel Nonnucleoside Inhibitor of Hepatitis C Virus NS5B Polymerase. *Antimicrob. Agents Chemother.* **2011,** *55,* 4196–4203.
559. Wong, K. A.; Xu, S.; Martin, R.; Miller, M. D.; Mo, H. Tegobuvir (GS-9190) Potency Against HCV Chimeric Replicons Derived From Consensus NS5B Sequences From Genotypes 2b, 3a, 4a, 5a, and 6a. *Virology* **2012,** *429,* 57–62.
560. Hebner, C. M.; Han, B.; Brendza, K. M.; Nash, M.; Sulfab, M.; Tian, Y.; Hung, M.; Fung, W.; Vivian, R. W.; Trenkle, J.; Taylor, J.; Bjornson, K.; Bondy, S.; Liu, X.; Link, J.; Neyts, J.; Sakowicz, R.; Zhong, W.; Tang, H.; Schmitz, U. The HCV Non-Nucleoside Inhibitor Tegobuvir Utilizes a Novel Mechanism of Action to Inhibit NS5B Polymerase Function. *PLoS One* **2012,** *7* (6), e39163. http://dx.doi.org/10.1371/journal.pone.0039163.
561. Powers, J. P.; Piper, D. E.; Li, Y.; Mayorga, V.; Anzola, J.; Chen, J. M.; Jaen, J. C.; Lee, G.; Liu, J.; Peterson, M. G.; Tonn, G. R.; Ye, Q.; Walker, N. P.; Wang, Z. SAR and Mode of Action of Novel Non-Nucleoside Inhibitors of Hepatitis C NS5B RNA Polymerase. *J. Med. Chem.* **2006,** *49,* 1034–1046.
562. Yan, S.; Appleby, T.; Gunic, E.; Shim, J. H.; Tasu, T.; Kim, H.; Rong, F.; Chen, H.; Hamatake, R.; Wu, J. Z.; Hong, Z.; Yao, N. Isothiazoles as Active-Site Inhibitors of HCV NS5B Polymerase. *Bioorg. Med. Chem. Lett.* **2007,** *17,* 28–33.
563. Chen, K. X.; Lesburg, C. A.; Vibulbhan, B.; Yang, W.; Chan, T. Y.; Venkatraman, S.; Velazquez, F.; Zeng, Q.; Bennett, F.; Anilkumar, G. N.; Duca, J.; Jiang, Y.; Pinto, P.; Wang, L.; Huang, Y.; Selyutin, O.; Gavalas, S.; Pu, H.; Agrawal, S.; Feld, B.; Huang, H. C.; Li, C.; Cheng, K. C.; Shih, N. Y.; Kozlowski, J. A.; Rosenblum, S. B.; Njoroge, F. G. A Novel Class of Highly Potent Irreversible Hepatitis C Virus NS5B Polymerase Inhibitors. *J. Med. Chem.* **2012,** *55,* 2089–2101.
564. Manns, M. P.; von Hahn, T. Novel Therapies for Hepatitis C—One Pill Fits All? *Nat. Rev. Drug Discov.* **2013,** *12,* 595–610.
565. Leivers, M.; Miller, J. F.; Chan, S. A.; Lauchli, R.; Liehr, S.; Mo, W.; Ton, T.; Turner, E. M.; Youngman, M.; Falls, J. G.; Long, S.; Mathis, A.; Walker, J. Imidazopyridazine Hepatitis C Virus Polymerase Inhibitors. Structure-Activity Relationship Studies and the Discovery of a Novel, Traceless Prodrug Mechanism. *J. Med. Chem.* **2014,** *57,* 1964–1975.
566. Tsukiyama-Kohara, K.; Iizuka, N.; Kohara, M.; Nomoto, A. Internal Ribosome Entry Site Within Hepatitis C Virus RNA. *J. Virol.* **1992,** *66,* 1476–1483.
567. Fraser, C. S.; Doudna, J. A. Structural and Mechanistic Insights Into Hepatitis C Viral Translation Initiation. *Nat. Rev. Microbiol.* **2007,** *5,* 29–38.
568. Davis, D. R.; Seth, P. P. Therapeutic Targeting of HCV Internal Ribosomal Entry Site RNA. *Antivir. Chem. Chemoth.* **2010,** *21,* 117–128.
569. Dibrov, S. M.; Parsons, J.; Carnevali, M.; Zhou, S.; Rynearson, K. D.; Ding, K.; Garcia Sega, E.; Brunn, N. D.; Boerneke, M. A.; Castaldi, M. P.; Hermann, T. Hepatitis C Virus Translation Inhibitors Targeting the Internal Ribosomal Entry Site. *J. Med. Chem.* **2014,** *57,* 1694–1707.
570. Hanecak, R.; Brown-Driver, V.; Fox, M. C.; Azad, R. F.; Furusako, S.; Nozaki, C.; Ford, C.; Sasmor, H.; Anderson, K. P. Antisense Oligonucleotide Inhibition of Hepatitis C Virus Gene Expression in Transformed Hepatocytes. *J. Virol.* **1996,** *70,* 5203–5212.
571. Zhang, H.; Hanecak, R.; Brown-Driver, V.; Azad, R.; Conklin, B.; Fox, M. C.; Anderson, K. P. Antisense Oligonucleotide Inhibition of Hepatitis C Virus (HCV) Gene Expression In Livers of Mice Infected With an HCV-Vaccinia Virus Recombinant. *Antimicrob. Agents Chemother.* **1999,** *43,* 347–353.
572. McHutchison, J. G.; Patel, K.; Pockros, P.; Nyberg, L.; Pianko, S.; Yu, R. Z.; Dorr, F. A.; Kwoh, T. J. A Phase I Trial of an Antisense Inhibitor of Hepatitis C Virus (ISIS 14803), Administered to Chronic Hepatitis C Patients. *J. Hepatol.* **2006,** *44,* 88–96.
573. Soler, M.; McHutchison, J. G.; Kwoh, T. J.; Dorr, F. A.; Pawlotsky, J.-M. Virological Effects of ISIS 14803, an Antisense Oligonucleotide Inhibitor of Hepatitis C Virus (HCV) Internal Ribosome Entry Site (IRES), on HCV IRES in Chronic Hepatitis C Patients and Examination of the Potential Role of Primary and Secondary HCV Resistance in the Outcome of Treatment. *Antivir. Ther.* **2004,** *9,* 953–968.
574. Georgopapadakou, N. Discontinued Drugs in 2005: Anti-Infectives. *Exp. Opin. Invest. Drugs* **2007,** *16,* 1–10.
575. Thomas, J. R.; Hergenrother, P. J. Targeting RNA With Small Molecules. *Chem. Rev.* **2008,** *108,* 1171–1224.
576. Guan, L.; Disney, M. D. Recent Advances in Developing Small Molecules Targeting RNA. *ACS Chem. Biol.* **2012,** *7,* 73–86.
577. Spahn, C. M.; Kieft, J. S.; Grassucci, R. A.; Penczek, P. A.; Zhou, K.; Doudna, J. A.; Frank, J. Hepatitis C Virus IRES RNA-Induced Changes in the Conformation of the 40s Ribosomal Subunit. *Science* **2001,** *291,* 1959–1962.
578. Seth, P. P.; Miyaji, A.; Jefferson, E. A.; Sannes-Lowery, K. A.; Osgood, S. A.; Propp, S. S.; Ranken, R.; Massire, C.; Sampath, R.; Ecker, D. J.; Swayze, E. E.; Griffey, R. H. SAR by MS: Discovery of a New Class of RNA-Binding Small Molecules for the Hepatitis C Virus: Internal Ribosome Entry Site IIA Subdomain. *J. Med. Chem.* **2005,** *48,* 7099–7102.
579. Paulsen, R. B.; Seth, P. P.; Swayze, E. E.; Griffey, R. H.; Skalicky, J. J.; Cheatham, T. E., III; Davis, D. R. Inhibitor-Induced Structural Change in the HCV IRES Domain IIa RNA. *Proc. Natl. Acad. Sci. U. S. A.* **2010,** *107,* 7263–7268.
580. Dibrov, S. M.; Johnston-Cox, H.; Weng, Y. H.; Hermann, T. Functional Architecture of HCV IRES Domain II Stabilized by Divalent Metal Ions in the Crystal and in Solution. *Angew. Chem. Int. Ed.* **2007,** *46,* 226–229.
581. Zhao, Q.; Han, Q.; Kissinger, C. R.; Hermann, T.; Thompson, P. A. Structure of Hepatitis C Virus IRES Subdomain IIa. *Acta Crystallogr. Sect. D: Biol. Crystallogr.* **2008,** *64,* 436–443.

582. Dibrov, S. M.; Ding, K.; Brunn, N. D.; Parker, M. A.; Bergdahl, B. M.; Wyles, D. L.; Hermann, T. Structure of a Hepatitis C Virus RNA Domain in Complex With a Translation Inhibitor Reveals a Binding Mode Reminiscent of Riboswitches. *Proc. Natl. Acad. Sci. U. S. A.* **2012,** *109,* 5223–5228.
583. Carnevali, M.; Parsons, J.; Wyles, D. L.; Hermann, T. A Modular Approach to Synthetic RNA Binders of the Hepatitis C Virus Internal Ribosome Entry Site. *ChemBioChem* **2010,** *11,* 1364–1367.
584. Garber, K. Hepatitis C: Staying The Course. *Nat. Biotechnol.* **2007,** *25,* 1379–1381.
585. Melnikova, I. Hepatitis C Therapies. *Nat. Rev. Drug Discov.* **2008,** *7,* 799–800.
586. Jacobson, I. M.; McHutchison, J. G.; Dusheiko, G.; Di Bisceglie, A. M.; Reddy, K. R.; Bzowej, N. H.; Marcellin, P.; Muir, A. J.; Ferenci, P.; Flisiak, R.; George, J.; Rizzetto, M.; Shouval, D.; Sola, R.; Terg, R. A.; Yoshida, E. M.; Adda, N.; Bengtsson, L.; Sankoh, A. J.; Kieffer, T. L.; George, S.; Kauffman, R. S.; Zeuzem, S.; Zeuzem.; ADVANCE Study Team. Telaprevir for Previously Untreated Chronic Hepatitis C Virus Infection. *N. Engl. J. Med.* **2011,** *364,* 2405–2416.
587. Zeuzem, S.; Andreone, P.; Pol, S.; Lawitz, E.; Diago, M.; Roberts, S.; Focaccia, R.; Younossi, Z.; Foster, G. R.; Horban, A.; Ferenci, P.; Nevens, F.; Müllhaupt, B.; Pockros, P.; Terg, R.; Shouval, D.; van Hoek, B.; Weiland, O.; Van Heeswijk, R.; De Meyer, S.; Luo, D.; Boogaerts, G.; Polo, R.; Picchio, G.; Beumont, M.; REALIZE Study Team. Telaprevir for Retreatment of HCV Infection. *N. Engl. J. Med.* **2011,** *364,* 2417–2428.
588. Poordad, F.; McCone, J., Jr.; Bacon, B. R.; Bruno, S.; Manns, M. P.; Sulkowski, M. S.; Jacobson, I. M.; Reddy, K. R.; Goodman, Z. D.; Boparai, N.; DiNubile, M. J.; Sniukiene, V.; Brass, C. A.; Albrecht, J. K.; Bronowicki, J. P.; For the SPRINT-2 Investigators. Boceprevir for Untreated Chronic HCV Genotype 1 Infection. *N. Engl. J. Med.* **2011,** *364,* 1195–1206.
589. Bacon, B. R.; Gordon, S. C.; Lawitz, E.; Marcellin, P.; Vierling, J. M.; Zeuzem, S.; Poordad, F.; Goodman, Z. D.; Sings, H. L.; Boparai, N.; Burroughs, M.; Brass, C. A.; Albrecht, J. K.; Esteban, R.; For the HCV Respond-2 Investigators. Boceprevir for Previously Treated Chronic HCV Genotype 1 Infection. *N. Engl. J. Med.* **2011,** *364,* 1207–1217.
590. Ridjuero, E. Safety of Direct-Acting Antivirals in the Treatment of Chronic Hepatitis C. *Expert Opin. Drug Saf.* **2014,** *13,* 307–319.
591. Smith, M. A.; Love, B. L.; Mohammad, R. A. The Changing Landscape fo Adverse Drug Events Associated With Chronic Hepatitis C Virus Therapy. *Expert Opin. Drug Saf.* **2015,** *14,* 1649–1652.
592. Gane, E. J.; Roberts, S. K.; Stedman, C. A.; Angus, P. W.; Ritchie, B.; Elston, R.; Ipe, D.; Morcos, P. N.; Baher, L.; Najera, I.; Chu, T.; Lopatin, U.; Berrey, M. M.; Bradford, W.; Laughlin, M.; Shulman, N. S.; Smith, P. F. Oral Combination Therapy With a Nucleoside Polymerase Inhibitor (RG7128) and Danoprevir for Chronic Hepatitis C Genotype 1 Infection (INFORM-1): A Randomised, Double-Blind, Placebo-Controlled, Dose-Escalation Trial. *Lancet* **2010,** *376,* 1467–1475.
593. Lok, A. S.; Gardiner, D. F.; Lawitz, E.; Martorell, C.; Everson, G. T.; Ghalib, R.; Reindollar, R.; Rustgi, V.; McPhee, F.; Wind-Rotolo, M.; Persson, A.; Zhu, K.; Dimitrova, D. I.; Eley, T.; Guo, T.; Grasela, D. M.; Pasquinelli, C. Preliminary Study of Two Antiviral Agents for Hepatitis C Genotype 1. *N. Engl. J. Med.* **2012,** *366,* 216–224.
594. Powdrill, M. H.; Tchesnokov, E. P.; Kozak, R. A.; Russell, R. S.; Martin, R.; Svarovskaia, E. S.; Mo, H.; Kouyos, R. D.; Götte, M. Contribution of a Mutational Bias in Hepatitis C Virus Replication to the Genetic Barrier in the Development of Drug Resistance. *Proc. Natl. Acad. Sci. U. S. A.* **2011,** *108,* 20509–20513.
595. Wyles, D. L. Antiviral Resistance and the Future Landscape of Hepatitis C Virus Infection Therapy. *J. Infect. Dis.* **2013,** *207* (S1), S33–S399.
596. Wyles, D. L.; Gutierrez, J. A. Importance of HCV Genotype 1 Subtypes for Drug Resistance and Response to Therapy. *J. Viral Hepatitis* **2014,** *21,* 229–240.
597. Chung, R. T. A Watershed Moment in the Treatment of Hepatitis C. *N. Engl. J. Med.* **2012,** *366,* 273–275.
598. Kumada, H.; Suzuki, Y.; Ikeda, K.; Toyota, J.; Karino, Y.; Chayama, K.; Kawakami, Y.; Ido, A.; Yamamoto, K.; Takaguchi, K.; Izumi, N.; Koike, K.; Takehara, T.; Kawada, N.; Sata, M.; Miyagoshi, H.; Eley, T.; McPhee, F.; Damokosh, A.; Ishikawa, H.; Hughes, E. Daclatasvir Plus Asunaprevir for Chronic HCV Genotype 1b Infection. *Hepatology* **2014,** *2083–2091,* 59.
599. Manns, M.; Pol, S.; Jacobson, I. M.; Marcellin, P.; Gordon, S. C.; Peng, C.-Y.; Chang, T.-T.; Everson, G. T.; Heo, J.; Gerken, G.; Yoffe, B.; Towner, W. J.; Bourliere, M.; Metivier, S.; Chu, C.-J.; Sievert, W.; Bronowicki, J.-P.; Thabut, D.; Lee, Y.-J.; Kao, J.-H.; McPhee, F.; Kopit, J.; Mendez, P.; Linaberry, M.; Hughes, E.; Noviello, S.; On behalf of the hallmark-DUAL Study Team. All-Oral Daclatasvir Plus Asunaprevir for Hepatitis C Virus Genotype 1b: A Multinational, Phase 3, Multicohort Study. *Lancet* **2014,** *384,* 1597–1605.
600. Poordad, F.; Sievert, W.; Mollison, L.; Bennett, M.; Tse, E.; Brau, N.; Levin, J.; Sepe, T.; Lee, S. S.; Angus, P.; Conway, B.; Pol, S.; Boyer, N.; Bronowicki, J.; Jacobson, I.; Muir, A. J.; Reddy, K. R.; Tam, E.; Ortiz-Lasanta, G.; de Ledinghen, V.; Sulkowski, M.; Boparai, N.; McPhee, F.; Hughes, E.; Swenson, E. S.; Yin, P. D.; For the UNITY-1 Study Group. Fixed-Dose Combination Therapy With Daclatasvir, Asunaprevir, and Beclabuvir for Noncirrhotic Patients With HCV Genotype 1 Infection. *JAMA* **2015,** *313,* 1728–1735.
601. Muir, A. J.; Poordad, F.; Lalezari, J.; Everson, G.; Dore, G. J.; Herring, R.; Sheikh, A.; Kwo, P.; Hézode, C.; Pockros, P. J.; Tran, A.; Yozviak, J.; Reau, N.; Ramji, A.; Stuart, K.; Thompson, A. J.; Vierling, J.; Freilich, B.; Cooper, J.; Ghesquiere, W.; Yang, R.; McPhee, F.; Hughes, E. A.; Swenson, E. S.; Yin, P. D. Daclatasvir in Combination With Asunaprevir and Beclabuvir for Hepatitis C Virus Genotype 1 Infection With Compensated Cirrhosis. *JAMA* **2015,** *313,* 1736–1744.
602. Sulkowski, M. S.; Gardiner, D. F.; Rodriguez-Torres, M.; Reddy, K. R.; Hassanein, T.; Jacobson, I.; Lawitz, E.; Lok, A. S.; Hinestrosa, F.; Thuluvath, P. J.; Schwartz, H.; Nelson, D. R.; Everson, G. T.; Eley, T.; Wind-Rotolo, M.; Huang, S.-P.; Gao, M.; Hernandez, D.; McPhee, F.; Sherman, D.; Hindes, R.; Symonds, W.; Pasquinelli, C.; Grasela, D. M.; For the AI444040 Study Group. Daclatasvir Plus Sofosbuvir for Previously Treated or Untreated Chronic HCV Infection. *N. Engl. J. Med.* **2014,** *370,* 211–221.
603. Wyles, D. L.; Ruane, P. J.; Sulkowski, M. S.; Dieterich, D.; Luetkemeyer, A.; Morgan, T. R.; Sherman, K. E.; Dretler, R.; Fishbein, D.; Gathe, J. C., Jr.; Henn, S.; Hinestrosa, F.; Huynh, C.; McDonald, C.; Mills, A.; Overton, E. T.; Ramgopal, M.; Rashbaum, B.; Ray, G.; Scarsella, A.; Yozviak, J.; McPhee, F.; Liu, Z.; Hughes, E.; Yin, P. D.; Noviello, S.; Ackerman, P.; For the ALLY-2 Investigators. Daclatasvir Plus Sofosbuvir for HCV in Patients Coinfected With HIV-1. *N. Engl. J. Med.* **2015,** *373,* 714–725.
604. Leroy, V.; Dumortier, J.; Coilly, A.; Sebagh, M.; Fougerou-Leurent, C.; Radenne, S.; Botta, D.; Durand, F.; Silvain, C.; Lebray, P.; Houssel-Debry, P.; Kamar, N.; d'Alteroche, L.; Petrov-Sanchez, V.; Diallo, A.; Pageaux, G.-P.; Duclos-Vallee, J.-C. Efficacy of Sofosbuvir and Daclatasvir in Patients With Fibrosing Cholestatic Hepatitis C After Liver Transplantation. *Clin. Gastroenterol. Hepatol.* **2015,** *13,* 1993–2001.
605. Afdhal, N.; Zeuzem, S.; Kwo, P.; Chojkier, M.; Gitlin, N.; Puoti, M.; Romero-Gomez, M.; Zarski, J.-P.; Agarwal, K.; Buggisch, P.; Foster, G. R.; Bräu, N.; Buti, M.; Jacobson, I. M.; Subramanian, G. M.; Ding, X.; Mo, H.; Yang, J. C.; Pang, P. S.; Symonds, W. T.; McHutchison, J. G.; Muir, A. J.; Mangia, A.; Marcellin, P.; For the ION-1 Investigators. Ledipasvir and Sofosbuvir for Untreated HCV Genotype 1 Infection. *N. Engl. J. Med.* **2014,** *370,* 1889–1898.
606. Afdhal, N.; Reddy, K. R.; Nelson, D. R.; Lawitz, E.; Gordon, S. C.; Schiff, E.; Nahass, R.; Ghalib, R.; Gitlin, N.; Herring, R.; Lalezari, J.; Younes, Z. H.; Pockros, P. J.; Di Bisceglie, A. M.; Arora, S.; Subramanian, G. M.; Zhu, Y.; Dvory-Sobol, H.; Yang, J. C.; Pang, P. S.; Symonds, W. T.; McHutchison, J. G.; Muir, A. J.; Sulkowski, M.; Kwo, P.; For the ION-2 Investigators. Ledipasvir and Sofosbuvir for Previously Treated HCV Genotype 1 Infection. *N. Engl. J. Med.* **2014,** *370,* 1483–1493.
607. Kowdley, K. V.; Gordon, S. C.; Reddy, K. R.; Rossaro, L.; Bernstein, D. E.; Lawitz, E.; Shiffman, M. L.; Schiff, E.; Ghalib, R.; Ryan, M.; Rustgi, V.; Chojkier, M.; Herring, R.; Di Bisceglie, A. M.; Pockros, P. J.; Subramanian, G. M.; An, D.; Svarovskaia, E.; Hyland, R. H.; Pang, P. S.; Symonds, W. T.; McHutchison, J. G.; Muir, A. J.; Pound, D.; Fried, M. W.; For the ION-3 Investigators. Ledipasvir and Sofosbuvir for 8 or 12 Weeks for Chronic HCV Without Cirrhosis. *N. Engl. J. Med.* **2014,** *370,* 1879–1888.
608. Alqahtani, S. A.; Afdhal, N.; Zeuzem, S.; Gordon, S. C.; Mangia, A.; Kwo, P.; Fried, M.; Yang, J. C.; Ding, X.; Pang, P. S.; McHutchison, J. G.; Pound, D.; Reddy, K. R.; Marcellin, P.; Kowdley, K. V.; Sulkowski, M. Safety and Tolerability of Ledipasvir/Sofosbuvir With and Without Ribavirin in Patients With Chronic Hepatitis C Virus Genotype 1 Infection: Analysis Of Phase III ION Trials. *Hepatology* **2015,** *62,* 25–30.
609. Naggie, S.; Cooper, C.; Saag, M.; Workowski, K.; Ruane, P.; Towner, W. J.; Marks, K.; Luetkemeyer, A.; Baden, R. P.; Sax, P. E.; Gane, E.; Santana-Bagur, J.; Stamm, L. M.; Yang, J. C.; German, P.; Dvory-Sobol, M.; Ni, L.; Pang, P. S.; McHutchison, J. G.; Stedman, C. A. M.; Morales-Ramirez, J. O.; Bräu, N.; Jayaweera, D.; Colson, A. E.; Tebas, P.; Wong, D. K.; Dieterich, D.; Sulkowski, M.; For the ION-4 Investigators. Ledipasvir and Sofosbuvir for HCV in Patients Coinfected With HIV-1. *N. Engl. J. Med.* **2015,** *373,* 705–713.
610. Kumari, R.; Nguyen, M. H. Fixed-Dose Combination of Sofosbuvir and Ledipasvir for the Treatment of Chronic Hepatitis C Genotype 1. *Exp. Opin. Pharmacother.* **2015,** *16,* 739–748.

611. Sheng, X. C.; Appleby, T.; Butler, T.; Cai, R.; Chen, X.; Cho, A.; Clarke, M. O.; Cottell, J.; Delaney, W. E. I. V.; Doerffler, E.; Link, J.; Ji, M.; Pakdaman, R.; Pyun, H.-J.; Wu, Q.; Xu, J.; Kim, C. U. Discovery of GS-9451: An Acid Inhibitor of the Hepatitis C Virus NS3/4A Protease. *Bioorg. Med. Chem. Lett.* **2012,** *22,* 2629–2634.
612. Yang, H.; Robinson, M.; Corsa, A. C.; Peng, B.; Cheng, G.; Tian, Y.; Wang, Y.; Pakdaman, R.; Shen, M.; Qi, X.; Mo, H.; Tay, C.; Krawczyk, S.; Sheng, X. C.; Kim, C. U.; Yang, C.; Delaney, W. E., IV Preclinical Characterization of the Novel Hepatitis C Virus NS3 Protease Inhibitor GS-9451. *Antimicrob. Agents Chemother.* **2014,** *58,* 647–653.
613. Lawitz, E. J.; Hill, J. M.; Marbury, T.; Demicco, M. P.; Delaney, W.; Yang, J.; Moorehead, L.; Mathias, A.; Mo, H.; McHutchison, J. G.; Rodriguez-Torres, M.; Gordon, S. C. A Phase 1, Randomized, Placebo-Controlled, 3-day, Ascending-Dose Study of GS-9451, an NS3/4A Protease Inhibitor, in Genotype 1 Hepatitis C Patients. *Antivir. Ther.* **2013,** *18,* 311–319.
614. Kohli, A.; Osinusi, A.; Sims, Z.; Nelson, A.; Meissner, E. G.; Barrett, L. L.; Bon, D.; Marti, M. M.; Silk, R.; Kotb, C.; Gross, C.; Jolley, T. A.; Sidharthan, S.; Petersen, T.; Townsend, K.; Egerson, D.'. A.; Kapoor, R.; Spurlin, E.; Sneller, M.; Proschan, M.; Herrmann, E.; Kwan, R.; Teferi, G.; Talwani, R.; Diaz, G.; Kleiner, D. E.; Wood, B. J.; Chavez, J.; Abbott, S.; Symonds, W. T.; Subramanian, G. M.; Pang, P. S.; McHutchison, J.; Polis, M. A.; Fauci, A. S.; Masur, H.; Kottilil, S. Virological Response After 6 Week Triple-Drug Regimens for Hepatitis C: A Proof-of-Concept Phase 2a Cohort Study. *Lancet* **2015,** *385,* 1107–1113.
615. Kohli, A.; Kapoor, R.; Sims, Z.; Nelson, A.; Sidharthan, S.; Lam, B.; Silk, R.; Kotb, C.; Gross, C.; Teferi, G.; Sugarman, K.; Pang, P. S.; Osinusi, A.; Polis, M. A.; Rustgi, V.; Masur, H.; Kottilil, S. Ledipasvir and Sofosbuvir for Hepatitis C Genotype 4: A Proof-of-Concept, Single-Centre, Open-Label Phase 2a Cohort Study. *Lancet Infect. Dis.* **2015,** *15,* 1049–1054.
616. Jacobson, I. M.; Gordon, S. C.; Kowdley, K. V.; Yoshida, E. M.; Rodriguez-Torres, M.; Sulkowski, M. S.; Shiffman, M. L.; Lawitz, E.; Everson, G.; Bennett, M.; Schiff, E.; Tarek Al-Assi, M.; Subramanian, G. M.; An, D.; Lin, M.; McNally, J.; Brainard, D.; Symonds, W. T.; McHutchison, J. G.; Patel, K.; Feld, J.; Pianko, S.; Nelson, D. R. Sofosbuvir for Hepatitis C Genotype 2 or 3 in Patients Without Treatment Options. *N. Engl. J. Med.* **2013,** *368,* 1867–1877.
617. Feld, J. J.; Jacobson, I. M.; Hézode, C.; Asselah, T.; Ruane, P. J.; Gruener, N.; Abergel, A.; Mangia, A.; Lai, C. L.; Chan, H. L.; Mazzotta, F.; Moreno, C.; Yoshida, E.; Shafran, S. D.; Towner, W. J.; Tran, T. T.; McNally, J.; Osinusi, A.; Svarovskaia, E.; Zhu, Y.; Brainard, D. M.; McHutchison, J. G.; Agarwal, K.; Zeuzem, S.; For the ASTRAL-1 Investigators. Sofosbuvir and Velpatasvir for HCV Genotype 1, 2, 4, 5, and 6 Infection. *N. Engl. J. Med.* **2015,** *373,* 2599–2607.
618. Foster, G. R.; Afdhal, N.; Roberts, S. K.; Bräu, N.; Gane, E. J.; Pianko, S.; Lawitz, E.; Thompson, A.; Shiffman, M. L.; Cooper, C.; Towner, W. J.; Conway, B.; Ruane, P.; Bourlière, M.; Asselah, T.; Berg, T.; Zeuzem, S.; Rosenberg, W.; Agarwal, K.; Stedman, C. A. M.; Mo, H.; Dvory-Sobol, H.; Han, L.; Wang, J.; McNally, J.; Osinusi, A.; Brainard, D. M.; McHutchison, J. G.; Mazzotta, F.; Tran, T. T.; Gordon, S. C.; Patel, K.; Reau, N.; Mangia, A.; Sulkowski, M.; For the ASTRAL-2 ASTRAL-3 Investigators. Sofosbuvir and Velpatasvir for HCV Genotype 2 and 3 Infection. *N. Engl. J. Med.* **2015,** *373,* 2608–2617.
619. Everson, G. T.; Towner, W. J.; Davis, M. N.; Wyles, D. L.; Nahass, R. G.; Thuluvath, P. J.; Etzkorn, K.; Hinestrosa, F.; Tong, M.; Rabinovitz, M.; McNally, J.; Brainard, D. M.; Han, L.; Doehle, B.; McHutchison, J. G.; Morgan, T.; Chung, R. T.; Tran, T. T. Sofosbuvir With Velpatasvir in Treatment-Naive Noncirrhotic Patients With Genotype 1 to 6 Hepatitis C Virus Infection: A Randomized Trial. *Ann. Intern. Med.* **2015,** *163,* 818–826.
620. Curry, M. P.; O'Leary, J. G.; Bzowej, N.; Muir, A. J.; Korenblat, K. M.; Fenkel, J. M.; Reddy, K. R.; Lawitz, E.; Flamm, S. L.; Schiano, T.; Teperman, L.; Fontana, R.; Schiff, E.; Fried, M.; Doehle, B.; An, D.; McNally, J.; Osinusi, A.; Brainard, D. M.; McHutchison, J. G.; Brown, R. S.; Charlton, M.; For the ASTRAL-4 Investigators. Sofosbuvir and Velpatasvir for HCV in Patients With Decompensated Cirrhosis. *N. Engl. J. Med.* **2015,** *373,* 2618–2628.
621. Ferenci, P.; Bernstein, D.; Lalezari, J.; Cohen, D.; Luo, Y.; Cooper, C.; Tam, E.; Marinho, R. T.; Tsai, N.; Nyberg, A.; Box, T. D.; Younes, Z.; Enayati, P.; Green, S.; Baruch, Y.; Bhandari, B. R.; Alexandru Caruntu, F.; Sepe, T.; Chulanov, V.; Janczewska, E.; Rizzardini, G.; Gervain, J.; Planas, R.; Moreno, C.; Hassanein, T.; Xie, W.; King, M.; Podsadecki, T.; Reddy, K. R. ABT-450/r-Ombitasvir and Dasabuvir With or Without Ribavirin for HCV. *N. Engl. J. Med.* **2014,** *370,* 1892–1983.
622. Poordad, F.; Hezode, C.; Trinh, R.; Kowdley, K. V.; Zeuzem, S.; Agarwal, K.; Shiffman, M. L.; Wedemeyer, H.; Berg, T.; Yoshida, E. M.; Forns, X.; Lovell, S. S.; Da Silva-Tillmann, B.; Collins, C. A.; Campbell, A. L.; Podsadecki, T.; Bernstein, B. ABT-450/r-Ombitasvir and Dasabuvir With Ribavirin for Hepatitis C With Cirrhosis. *N. Engl. J. Med.* **2014,** *370,* 1973–1982.
623. Zeuzem, S.; Jacobson, I. M.; Baykal, T.; Marinho, R. T.; Poordad, F.; Bourlière, M.; Sulkowski, M. S.; Wedemeyer, H.; Tam, E.; Desmond, P.; Jensen, D. M.; Di Bisceglie, A. M.; Varunok, P.; Hassanein, T.; Xiong, J.; Pilot-Matias, T.; DaSilva-Tillmann, B.; Larsen, L.; Podsadecki, T.; Bernstein, B. Retreatment of HCV With ABT-450/r-Ombitasvir and Dasabuvir With Ribavirin. *N. Engl. J. Med.* **2014,** *370,* 1604–1614.
624. Sulkowski, M. S.; Eron, J. J.; Wyles, D.; Trinh, R.; Lalezari, J.; Wang, C.; Slim, J.; Bhatti, L.; Gathe, J.; Ruane, P. J.; Elion, R.; Bredeek, F.; Brennan, R.; Blick, G.; Khatri, A.; Gibbons, K.; Hu, Y. B.; Fredrick, L.; Schnell, G.; Pilot-Matias, T.; Tripathi, R.; Da Silva-Tillmann, B.; McGovern, B.; Campbell, A. L.; Podsadecki, T. O. Paritaprevir Co-Dosed With Ritonavir, Dasabuvir, and Ribavirin for Hepatitis C in Patients Co-Infected With HIV-1. A Randomized Trial. *JAMA* **2015,** *313,* 1223–1231.
625. Kwo, P. Y.; Mantry, P. S.; Coakley, E.; Te, H. S.; Vargas, H. E.; Brown, R., Jr.; Gordon, F.; Levitsky, J.; Terrault, N. A.; Burton, J. R., Jr.; Xie, W.; Setze, C.; Badri, P.; Pilot-Matias, T.; Vilchez, R. A.; Forns, X. An Interferon-Free Antiviral Regimen for HCV After Liver Transplantation. *N. Engl. J. Med.* **2014,** *371,* 2375–2382.
626. Hézode, C.; Asselah, T.; Reddy, K. R.; Hassanein, T.; Berenguer, M.; Fleischer-Stepniewska, K.; Marcellin, P.; Hall, C.; Schnell, G.; Pilot-Matias, T.; Mobashery, N.; Redman, R.; Vilchez, R. A.; Pol, S. Ombitasvir PLUS Paritaprevir Plus ritonavir With or Without Ribavirin in Treatment-Naive and Treatment-Experienced Patients With Genotype 4 Chronic Hepatitis C Virus Infection (PEARL-I): A Randomised, Open-Label Trial. *Lancet* **2015,** *385,* 2502–2509.
627. Azvolinsky, A. Industry Chases Pan-Genotypic and Shorter HCV Treatments. *Nat. Biotechnol.* **2015,** *33,* 575–576.
628. Nyalakonda, H.; Utay, N. S. A New Era of Therapy for Hepatitis C Virus Infection. *Curr. Opin. Infect. Dis.* **2015,** *28,* 471–478.
629. Lichtenberg, F. R. The Effect of New Drug Approvals on HIV Mortality in the US, 1987-1998. *Econ. Hum. Biol.* **2003,** *1,* 259–266.
630. Lichtenberg, F. R. Pharmaceutical Innovation and Longevity Growth in 30 Developing and High-Income Countries, 2000-2009. *Health Policy Technol.* **2014,** *3,* 36–58.
631. Rein, D. B.; Wittenborn, J. S.; Weinbaum, C. M.; Sabin, M.; Smith, B. D.; Lesesne, S. B. Forecasting the Morbidity and Mortality Associated With Prevalent Cases of pre-Cirrhotic Chronic Hepatitis C in the United States. *Dig. Liver Dis.* **2011,** *43,* 66–72.
632. Tanaka, Y.; Hanada, K.; Mizokami, M.; Yeo, A. E.; Shih, J. W.-K.; Gojobori, T.; Alter, H. J. A Comparison of the Molecular Clock of Hepatitis C Virus in the United States and Japan Predicts That Hepatocellular Carcinoma Incidence in the United States Will Increase Over the Next Two Decades. *Proc. Natl. Acad. Sci. U. S. A.* **2002,** *99,* 15584–15589.
633. Ly, K. N.; Xing, J.; Klevens, M.; Jiles, R. B.; Ward, J. W.; Holmberg, S. D. The Increasing Burden of Mortality From Viral Hepatitis in the United States Between 1999 and 2007. *Ann. Intern. Med.* **2012,** *156,* 271–278.
634. Klevens, R. M.; Hu, D. J.; Jiles, R.; Holmberg, S. D. Evolving Epidemiology of Hepatitis C Virus in the United States. *Clin. Infect. Dis.* **2012,** *55,* S3–S9.
635. Pawlotsky, J.-M.; Feld, J. J.; Zeuzem, S.; Hoofnagle, J. H. From Non-A, Non-B Hepatitis to Hepatitis C Virus Cure. *J. Hepatol.* **2015,** *62,* S87–S89.
636. Razavi, H.; Waked, I.; Sarrazin, C.; Myers, R. P.; Idilman, R.; Calinas, F.; Vogel, W.; Mendes Correa, M. C.; Hézode, C.; Lázaro, P.; Akarca, U.; Aleman, S.; Balõk, I.; Berg, T.; Bihl, F.; Bilodeau, M.; Blasco, A. J.; Brandão Mello, C. E.; Bruggmann, P.; Buti, M.; Calleja, J. L.; Cheinquer, H.; Christensen, P. B.; Clausen, M.; Coelho, H. S. M.; Cramp, M. E.; Dore, G. J.; Doss, W.; Duberg, A. S.; El-Sayed, M. H.; Ergör, G.; Esmat, G.; Falconer, K.; Félix, J.; Ferraz, M. L. G.; Ferreira, P. R.; Frankova, S.; García-Samaniego, J.; Gerstoft, J.; Giria, J. A.; Gonçales, F. L., Jr.; Gower, E.; Gschwantler, M.; Guimarães Pessôa, M.; Hindman, S. J.; Hofer, H.; Husa, P.; Kåberg, M.; Kaita, K. D. E.; Kautz, A.; Kaymakoglu, S.; Krajden, M.; Krarup, H.; Laleman, W.; Lavanchy, D.; Marinho, R. T.; Marotta, P.; Mauss, S.; Moreno, C.; Murphy, K.; Negro, F.; Nemecek, V.; Örmeci, V.; Øvrehus, A. L. H.; Parkes, J.; Pasini, K.; Peltekian, K. M.; Ramji, A.; Reis, N.; Roberts, S. K.; Rosenberg, W. M.; Roudot-Thoraval, F.; Ryder, S. D.; Sarmento-Castro, R.; Semela, D.; Sherman, M.; Shiha, G. E.; Sievert, W.; Sperl, J.; Stärkel, P.; Stauber, R. E.; Thompson, A. J.; Urbanek, P.; Van Damme, P.; van Thiel, I.; Van Vlierberghe, H.; Vandijck, D.; Wedemeyer, D.; Weis, N.; Wiegand, J.; Yosry, A.; Zekry, A.; Cornberg, M.; Müllhaupt, B.; Estes, C. The Present and Future Disease Burden of Hepatitis C Virus (HCV) Infection With Today's Treatment Paradigm. *J. Viral Hepatitis* **2014,** *21* (Suppl. 1), 34–59.
637. Shiffman, M. L.; Benhamou, Y. Cure of HCV Related Liver Disease. *Liver Int.* **2015,** *35* (Suppl. 1), 71–77.
638. Brennan, T.; Shrank, W. New Expensive Treatments for Hepatitis C Infection. *JAMA* **2014,** *312,* 593–594.
639. Rein, D. B.; Wittenborn, J. S.; Smith, B. D.; Liffmann, D. K.; Ward, J. W. The Cost-Effectiveness, Health Benefits, and Financial Costs of New Antiviral Treatments for Hepatitis C Virus. *Clin. Infect. Dis.* **2015,** *61,* 157–168.

640. Chhatwal, J.; Kanwal, F.; Roberts, M. S.; Dunn, M. A. Cost-Effectiveness and Budget Impact of Hepatitis C Virus Treatment With Sofosbuvir and Ledipasvir in the United States. *Ann. Intern. Med.* **2015,** *162,* 397–406.
641. Reau, N. S.; Jensen, D. M. Sticker Shock and the Price of New Therapies for Hepatitis C: Is It Worth It. *Hepatology* **2014,** *59,* 1246–1249.
642. Ward, J. W.; Mermin, J. H. Simple, Effective, but Out of Reach? Public Health Implications of HCV Drugs. *Nat. Eng. J. Med.* **2015,** *373,* 2678–2680.

Relevant Websites

Centers for Disease Control and Prevention: http://www.cdc.gov/hepatitis/hcv/ provides statistics and surveillance relating to HCV infection, answers to common questions for health professionals and the public, information about laboratory testing and patient education resources.

HCV Advocate: http://hcvadvocate.org/ provides information for those newly diagnosed with infection, links to clinical trial information, fact sheets and general resources including community events and support groups.

American Association for the Study of Liver Diseases (AASLD): http://www.aasld.org/ provides information on publications, programs research and research awards and abstracts for annual sponsored conferences.

European Association for the Study of the Liver (EASL): Fosters public awareness of the management of liver diseases and acts as an advisor to European Health authorities. This site provides information for all who are involved with liver disease and focused on cure and prevention, a link to the sponsored journal Hepatology and information on research in the science of liver disease. EASL facilitates scientific exchange, catalyzes multi-site European clinical trials and provides, state-of-the-art education materials for physicians and scientists.

Hepatitis Central: http://www.hepatitiscentral.com/ provides a range of resources and practical advice for those infected with HCV.

All the virology on the www: http://www.virology.net/garryfavwebvirlabs.html provides links to U.S.-based and international laboratories involved in virology research, information on scientific meetings, companies and societies.

5.19 New Antiretrovirals for HIV and Antivirals for HBV

SE Lazerwith, D Siegel, RM McFadden, MR Mish, and WC Tse, Gilead Sciences, Inc., Foster City, CA, United States

© 2017 Elsevier Ltd. All rights reserved.

5.19.1	**Human Immunodeficiency Virus**	629
5.19.1.1	HIV Life Cycle and Drug Targets	630
5.19.1.2	Current Regimens—Evolution of Treatment Guidelines 2006 Versus 2014	630
5.19.1.3	Adherence and Resistance	632
5.19.1.4	Integrase Inhibitors	632
5.19.1.4.1	Raltegravir	632
5.19.1.4.2	Elvitegravir	633
5.19.1.4.3	Dolutegravir	634
5.19.1.4.4	Other clinical- and preclinical-stage integrase inhibitors	635
5.19.1.5	Nucleoside Reverse Transcriptase Inhibitors	636
5.19.1.5.1	Tenofovir alafenamide	637
5.19.1.5.2	Investigational NRTIs	638
5.19.1.6	Nonnucleoside Reverse Transcriptase Inhibitors	640
5.19.1.6.1	Rilpivirine	640
5.19.1.6.2	Doravirine	641
5.19.1.7	Protease Inhibitors	642
5.19.1.7.1	Darunavir	642
5.19.1.7.2	Other protease inhibitors	644
5.19.1.8	Other Mechanisms	644
5.19.1.8.1	Attachment inhibitors	644
5.19.1.8.2	Capsid inhibitors	645
5.19.1.8.3	Maturation inhibitors	645
5.19.1.8.4	Noncatalytic integrase inhibitors	646
5.19.1.9	Simplified Regimens and Nonstandard Regimen Research	646
5.19.1.10	Boosters and Cobicistat	647
5.19.1.11	Preexposure Prophylaxis (PreP)	647
5.19.1.12	HIV Cure	648
5.19.1.12.1	Kick and kill	648
5.19.1.12.2	Direct-acting antivirals for functional cure	650
5.19.2	**Hepatitis B Virus**	651
5.19.2.1	HBV Replication Cycle and Potential Drug Targets (New Section)	651
5.19.2.2	Nucleoside Reverse Transcriptase Inhibitors	653
5.19.2.2.1	Investigational HBV RT inhibitors	654
5.19.2.3	Capsid Assembly Inhibitors	655
5.19.2.4	Immunomodulators	656
5.19.2.5	Biologics-Based Approaches: RNAi and Entry Inhibition	657
5.19.3	**Conclusion**	658
References		658

Abbreviations

3TC Lamivudine
4′-Ed4T Festinavir
ABC Abacavir
ADV Adefovir dipivoxil
AIDS Acquired immune deficiency syndrome
ATC Apricitabine
ATZ Atazanivir
AZT Azidothymidine or zidovudine
BID Bis in die (Latin, two times a day)
C Cobicistat
CA Capsid protein
cccDNA Covalent circular closed DNA
CCR5 C−C Chemokine receptor type 5
CNS Central nervous system
COBI Cobicistat
CTD C-Terminal domain
CXCR4 C-X-C Chemokine receptor type 4
CYP3A4 Cytochrome P450 3A4
d4T Stavudine
DAP Diaminopurine
DAPD Amdoxovir
dCA Dehydrocortistatin A

ddC Zalcitabine
ddI Didanosine
DRV Darunavir
DTG Dolutegravir
E Elvitegravir
eAg E-antigen
EC50 Half maximal effective concentration
EFV Efavirenz
ETV Entecavir
EVG Elvitegravir
F% Oral bioavailability
FLT Alovudine
FTC Emtricitabine
gp120 Envelope glycoprotein gp120
HAART Highly active antiretroviral therapy
HAPs Heteroaryldihydropyrimidines
HBcAg Hepatitis B core antigen
HBsAg Hepatitis B surface antigen
HBV Hepatitis B virus
HBx Hepatitis B X protein
HCC Hepatocellular carcinoma
HCV Hepatitis C virus
HDACi Histone deacetylase inhibitor
HDACs Histone deacetylases
HIV Human immunodeficiency virus
IC50 Half maximal inhibitory concentration
INF Interferon
INSTIs Integrase strand-transfer inhibitors
IRBM Integrated Research Biotech Model
L-d4FC Elvucitabine
L-dT Telbivudine
L-FMAU Clevudine
MEC Minimum effective concentration
mtDNA Mitochondrial DNA polymerase gamma
NCINIs Noncatalytic integrase inhibitors
NFV Nelfinavir
NNRTIs Nonnucleoside reverse transcriptase inhibitors
NRTIs Nucleoside reverse transcriptase inhibitors
NS5B Nonstructural protein 5B
NTCP Sodium-taurocholate cotransporting polypeptide
NTD N-Terminal domain
OAT1 Organic anion transporter 1
OAT3 Organic anion transporter 3
p24 HIV capsid protein
PBMCs Peripheral blood mononuclear cells
PD Pharmacodynamic
PIs Protease inhibitors
PK Pharmacokinetic
PKC Protein kinase C
PMA Phorbol-12-myristate-13-acetate
PreP Preexposure prophylaxis
PTEN Phosphatase and tensin homolog
QD Quaque die (Latin, once a day)
R Rilpivirine
RAL Raltegravir
rcDNA Relaxed-circular DNA
RT Reverse transcriptase
RTV Ritonavir
sAg Surface antigen
SQV Saquinavir
STRs Single-tablet regimens
TAF Tenofovir alafenamide
TAMs Thymidine analog mutations
TAR Trans-activation region
TDF Tenofovir disoproxil fumarate
TFV Tenofovir
THF Tetrahydrofuran
TID Ter in die (Latin, three times a day)
TLR7 Toll-like receptor 7
TLRs Toll-like receptors
TNF Tumor necrosis factor
WHV Woodchuck hepatitis virus

5.19.1 Human Immunodeficiency Virus

The advent of highly active antiretroviral therapy (HAART) for human immunodeficiency virus (HIV) infection has transformed acquired immune deficiency syndrome (AIDS) from a fatal disease to a manageable, long-term, chronic condition.[1] As treatment regimens have improved, the life expectancy of HIV patients has increased dramatically.[2,3] This transformation represents one of the great accomplishments of medicinal chemistry, and indeed of biomedical research, in the last century. When the first antiretrovirals for HIV were used clinically, it quickly became clear that single agents were inadequate for long-term suppression of the virus due to rapid emergence of HIV strains resistant to the drugs being administered. But greater understanding of the viral life cycle subsequently enabled the discovery of antiretroviral agents whose combination suppressed resistance and led to long-term control over viral replication (see Chapter 50017).[4] Much of the history of this momentous accomplishment was detailed in the previous iteration of *Comprehensive Medicinal Chemistry*, published in 2007, including the development of nucleoside reverse transcriptase inhibitors (NRTIs), nonnucleoside reverse transcriptase inhibitors (NNRTIs), protease inhibitors (PIs), and entry inhibitors, as well as newer areas of research including integrase and maturation inhibitors.[5] In this update, new medicinal chemistry research in these and other drug classes is described. This work has led to more powerful, better-tolerated, and simplified treatment regimens for HIV patients. In addition, recent strategies and efforts aimed at true eradication or cure of HIV are reviewed.

5.19.1.1 HIV Life Cycle and Drug Targets

The life cycle of HIV is both one of the most complex and most well-studied processes in virology (Fig. 1). Researchers have attempted to target nearly every step in the process with small-molecule drugs. The life cycle commences with a mature HIV virion binding to a CD4 cell via the CD4 receptor and co-receptors CCR5 and CXCR4. This initial binding has been targeted by entry inhibitors such as maraviroc. This is followed by fusion to the cell membrane, a process targeted by fusion inhibitors (enfuvirtide), and uncoating of the viral capsid releasing the viral RNA. Reverse transcription of this RNA to viral DNA (targeted by both NRTIs and NNRTIs), formation of the preintegration complex, and translocation to the nucleus is followed by integration of the viral DNA to the host genome by the viral integrase [targeted by both integrase strand-transfer inhibitors (INSTIs) and noncatalytic integrase inhibitors (NCINIs)]. Transcription of the viral DNA to new viral RNA and proteins is followed by assembly as new immature virus. After budding and release, the viral protease cleaves the polyprotein to form the mature Gag protein (targeted by PIs), and the resultant mature HIV virions are ready to infect new cells.[6,7]

5.19.1.2 Current Regimens—Evolution of Treatment Guidelines 2006 Versus 2014

The last decade has seen significant improvements in both individual agents and clinical regimens for HIV, and these are reflected in a comparison of the treatment guidelines published by the International Antiviral Society—USA Panel from 2006[9] versus 2014[10] (Tables 1 and 2). In both sets of recommendations, treatments with two NRTIs plus a third agent with a different mechanism were preferred. In 2006, three nucleoside combinations were included along, with two NNRTIs and four PIs. Choices were based on many factors, including the side effect profile of the drugs involved as well as the viral genotype of the patient to determine which drug combinations would prove most effective.

In 2006, the side effect profile for many of the individual agents and regimens were daunting and likely played a role in limiting adherence. The choice of third agent (NNRTI or PI) was nuanced: NNRTIs showed higher tolerability, but a greater propensity for development of resistance, whereas PIs showed worse tolerability, but a significantly stronger resistance profile. Also, although some agents were dosed once daily (QD), several recommended agents were twice daily, resulting in many different complicated regimens. Taken together, the combination of side effects and complicated dosing protocols for many of the better regimens in 2006 limited overall efficacy.

By 2014, several agents with the least favorable tolerability profiles, dosing schedules and efficacy were dropped from the recommended list. These include the NNRTI nevirapine, the PIs lopinavir, fosamprenavir and saquinavir, and the nucleoside combination zidovudine/lamivudine. In addition, each recommendation now constitutes a complete regimen containing two NRTIs and a third agent; overall, the recommendations are considerably simplified.

The biggest change in the recommendations was the inclusion of INSTIs as a new third agent class. Regimens containing the three approved INSTIs raltegravir, elvitegravir, and dolutegravir show good efficacy with generally improved tolerability compared with

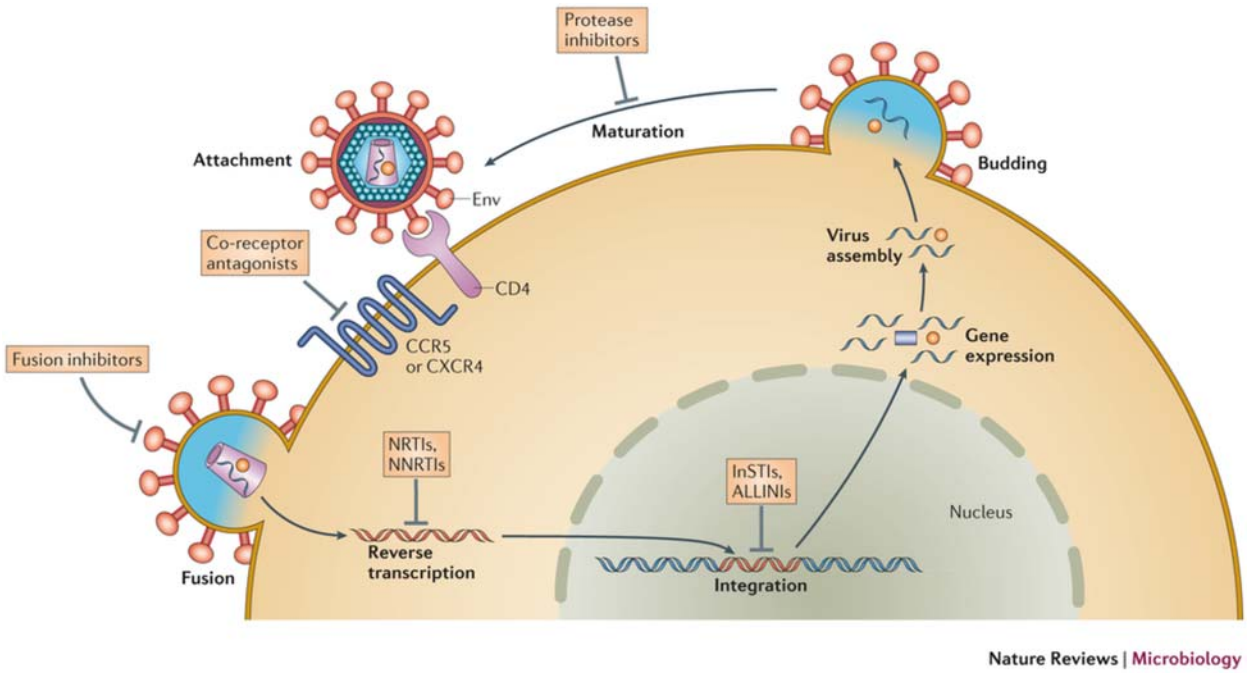

Fig. 1 The HIV life cycle and drug targets.[8] http://www.nature.com/reprints/permission-requests.html.

Table 1 Recommended components of initial antiviral therapy taken from the 2006 International Antiviral Society recommendations[7]

Component	*Considerations*	*Major toxic effects and cautions*	*Resistance considerations*
NRTIs	Well tolerated	Baseline renal function should be evaluated	M184V and K65R
Tenofovir disoproxil fumarate (TDF)/ emtricitabine	Efficacy > zidovudine/lamivudine or stavudine/lamivudine Spares thymidine analogs Fixed dose, QD	before initiating Use with caution or avoid in patients with renal dysfunction	
Zidovudine/lamivudine	Most extensive clinical trial data set and Phase IV experience supporting use Standard-of-care comparator in many trials Fixed dose, BID	Headache, nausea Anemia Liopatrophy	M184V and thymidine-analog-associated mutations
Abacavir/lamivudine	Supportive clinical trial data Spares thymidine analogs Fixed dose, QD	Hypersensitivity syndrome in 5–8% of persons (greater risk in person with the HLA-B5701 genotype)	M184V and K65R
NNRTIs	Efficacy proven in controlled trials	CNS toxic effects may be limiting	Single-step high-level resistance occurs with treatment failure with cross-resistance to nevirapine
Efavirenz	Standard-of-care comparator in many trials Fixed dose	Teratogenic in the first trimester of pregnancy	
Nevirapine	Efficacy proved in controlled trials Safe to fetus	Rash Hepatotoxicity Hypersensitivity syndrome Avoid in women with > 250 CD4 cell mL^{-1} and men with > 400 CD4 cells mL^{-1}	Single-step high-level resistance occurs with treatment failure with cross-resistance to efavirenz
Ritonavir-boosted protease inhibitors	Substantial clinical trial data set and Phase IV experience supporting	Gastrointestinal adverse events Hyperlipidemia	Protease inhibitor mutations are rare in treatment failure if virus is fully susceptible at baseline
Ritonavir-boosted Lopinavir	efficacy Heat-stable formulation available QD or BID for treatment naive BID for treatment experienced	Lipodystrophy Insulin resistance	
Ritonavir-boosted Atazanavir	Decreased potential for hyperlipidemia than with other protease inhibitors QD	Hyperbilirubinemia (UGT1A1-28 alleles and T3435C polymorphism in MDR1 gene) Avoid concomitant antacid use (separate dosing times) Do not use concomitant proton pump inhibitors	Limited data on resistance mutations in previously antiretroviral-naive patients
Ritonavir-boosted Fosamprenavir	No food restrictions	Rash	Limited data on resistance mutations in previously antiretroviral-naive patients
Ritonavir-boosted Saquinavir	Lower lipid effects(?) Soft-gel formulation is less effective than ritonavir-lopinavir	Gastrointestinal toxic effects with soft-gel formulation; incidence diminished with hard-gel formulation	Limited data on resistance mutations in previously antiretroviral-naive patients

Table 2 Initial antiviral regimens taken from the 2014 International Antiviral Society recommendations[8]

Regimen type	*Combination*	*Considerations*
INSTI plus 2 NRTIs	Dolutegravir plus tenofovir disoproxil fumarate (TDF)/ emtricitabine	Dolutegravir associated with modest increases in creatinine levels
	Dolutegravir plus abacavir/lamivudine	
	Elvitegravir/cobicistat/TDF/emtricitabine	Cobicistat is associated with modest increases in creatinine levels; has similar drug interactions to ritonavir
	Raltegravir plus TDF/emtricitabine	Raltegravir is taken twice daily
NNRTI plus 2 NRTIs	Efavirenz/TDF/emtricitabine	Efavirenz is associated with CNS side effects
	Efavirenz plus abacavir/lamivudine	Efavirenz is associated with CNS side effects
	Rilpivirine/TDF/emtricitabine	Rilpivirine-based therapy is not recommended in patients with baseline viral load > 100,000 copies mL^{-1}
Ritonavir-boosted PI plus 2 NRTIs	Atazanavir plus TDF/emtricitabine	Atazanavir is associated with nephrolithiasis, cholelithiasis, and chronic kidney injury
	Atazanavir plus abacavir/lamivudine	Atazanavir is associated with nephrolithiasis, cholelithiasis, and chronic kidney injury
	Darunavir plus TDF/emtricitabine	

PI-based regimens. Notably, nearly all the recommended third agents are dosed QD (with the exception of raltegravir), though PIs still require a boosting agent. Four of the 10 regimens are available as single-tablet regimens (STRs)—a simplification that can lead to improved adherence.

The other significant change that occurred between 2006 and 2014 is the recommendation to begin HIV treatment as soon as the patient is diagnosed and not wait for the immune system to show signs of failure (low CD4 counts).

5.19.1.3 Adherence and Resistance

The development of viral resistance has long been recognized as the main obstacle for the long-term suppression of HIV.[11] Maintaining viral suppression and inhibiting resistance require both potent drug combinations and high levels of adherence, and in the early days of HIV treatment this was difficult due to complicated and poorly tolerated regimens.[12]

Over the last 10 years, improvements in the efficacy and tolerability of HIV agents have led to both higher levels of adherence and viral suppression. Further, as the regimens have improved it has been recognized that complete adherence may no longer be necessary to maintain suppression. In 2007, near perfect levels (95% and up) of adherence to prescribed regimens were required to achieve the highest levels of viral suppression.[13] However, a 2015 study showed that somewhat lower levels of adherence (85–90%) with newer agents can still be associated with high levels of viral suppression.[14] This is likely due in part to improved overall characteristics of the individual agents and regimens (more potent compounds, longer half-lives, higher individual barriers to resistance, and better tolerability). Further, there is now significant evidence that simplification to STRs leads to higher adherence and better outcomes as well.[15,16]

5.19.1.4 Integrase Inhibitors

The discovery and development of INSTIs has led to one of the most significant changes to HIV treatment over the past decade—INSTIs have become the third agent of choice for most of the currently recommended HIV regimens. Prior to 2007, nearly all naive HIV patients were treated with a triple combination containing two NRTIs and either a PI or an NNRTI. Though these regimens are efficacious for many patients, they have limitations—patients on NNRTI-based regimens tend to develop viral resistance more quickly, and patients on PI-based regimens are subject to more frequent and severe adverse events. In addition, development of resistance to the NNRTI- and PI-based regimens was still causing some patients to fail therapy. In this context, researchers were eager to discover new antivirals targeting other parts of the viral life cycle. Indeed, efforts targeting many vital aspects of the life cycle were undertaken, and out of these efforts INSTIs have emerged with the best combination of efficacy and tolerability. Three INSTIs have been approved for the treatment of HIV: raltegravir (**1**, 2007), elvitegravir (**2**, 2012), and dolutegravir (**3**, 2014). Due to their great efficacy and relatively good tolerability they have rapidly become the first choice of regimens. Indeed, a recent meta-analysis of 48 clinical studies suggests that regimens containing INSTIs are superior to others.[17]

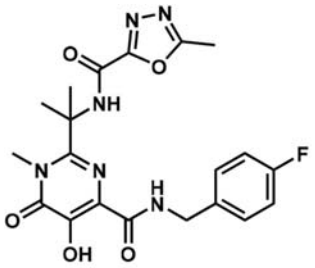

Raltegravir, RAL, MK-0518
1

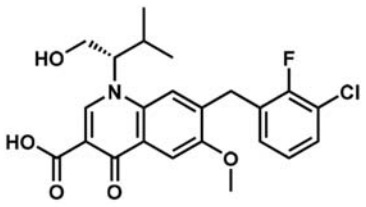

Elvitegravir, EVG, GS-9137
2

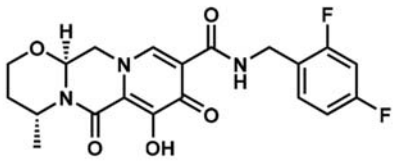

Dolutegravir, DTG, GSK-572
3

5.19.1.4.1 Raltegravir

Raltegravir (**1**) was the first FDA-approved INSTI, and its discovery has been described extensively.[18–20] High-throughput screening campaigns led to the identification of diketo acids like **4** (Fig. 2). These compounds are divalent cation binders and were found to bind to and inhibit HIV integrase and, subsequently, HCV NS5B. A collaboration between Integrated Research Biotech Model

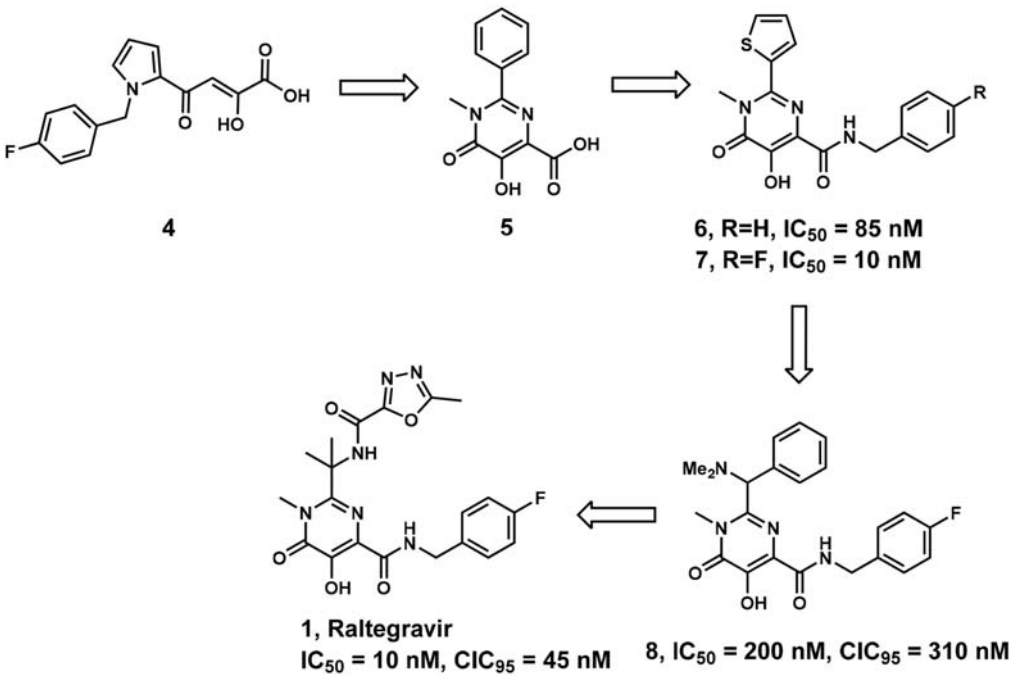

Fig. 2 Discovery of raltegravir.

(IRBM) in Rome and Merck West Point found a suitable replacement for the diketo acids in dihydroxypyrimidine **5**. Though this compound lacked cell-based activity, it was further optimized by the addition of a 4-fluorobenzylamide giving compound **7** with a biochemical potency of 10 nM. The addition of a basic substituent at the 2-position of the core gave the first compound with cell-based activity (**8**, $CIC_{95} = 310$ nM). Finally, an extensive investigation of the 2-position was undertaken with an eye toward finding the optimal level of plasma protein binding. High protein binding led to unacceptably high potency shift under high serum conditions. Lower levels led to higher clearance in animals. The methyl-oxadiazole analog **1** provided for optimal protein binding and became raltegravir.

Clinical studies with raltegravir show impressive response rates. In naive patients in combination with tenofovir disoproxil fumarate (TDF)/emtricitabine, twice daily administration led to a higher suppression rate compared to the NNRTI efavirenz: virologic suppression was observed in 86.1% of patients in the raltegravir group compared with 81.9% in the efavirenz group.[21] In the same combination context, Phase III studies established that twice daily administration of raltegravir was more efficacious than QD: 89% of patients on the twice daily regimen responded versus 83% of patients in the QD cohort.[22] In a study of multidrug-resistant HIV patients, twice daily raltegravir (400 mg) added to regimens containing an average of four other antiretrovirals brought 53.3% of patients to full suppression (<50 copies mL^{-1}).[23] Raltegravir was approved in 2007.

5.19.1.4.2 Elvitegravir

The discovery of elvitegravir (EVG) began with a different divalent cation-binding motif—the monoketo acid **9** (Fig. 3). Though this compound had only weak integrase activity (1.6 μM) and no measurable cellular activity, it was found that potency could be improved dramatically with the addition of two halogens on the benzyl group and an ethanol moiety attached to the pyridine (**10**). Further exploration of the SAR in this series revealed that the addition of an isopropyl group to the ethanol side chain or the attachment of a methoxy group to core each increased cellular potency significantly (10- and 4-fold, respectively). Combination of these motifs gave EVG with a cellular potency of 0.9 nM.[24] EVG shows high potency against many wild-type HIV strains with potencies below 1 nM in most cases. In vitro resistance selection experiments demonstrated that selection pressure with EVG can lead to single-point mutants with >30-fold resistance (T66I and E92Q).[25]

Elvitegravir was co-formulated with the booster cobicistat (COBI) to allow for QD dosing, and when combined with the NRTIs TDF and FTC in Phase III studies, the four-drug regimen was found to be equally as effective (noninferior) as the NNRTI-based regimen EFV/FTC/TDF,[26] as well as the PI-based regimen ATZ/RTV + FTC/TDF.[27] In addition, significantly lower rates of neurological side effects were observed for the EVG-based regimen as compared to the EFV-based regimen, and lower rates of bilirubin abnormalities as compared with the ATZ-based regimen. The EVG combination showed a higher incidence of nausea compared with the EFV combination. EVG/COBI/FTC/TDF was approved by the FDA in 2012 as the first STR containing an integrase inhibitor.[28]

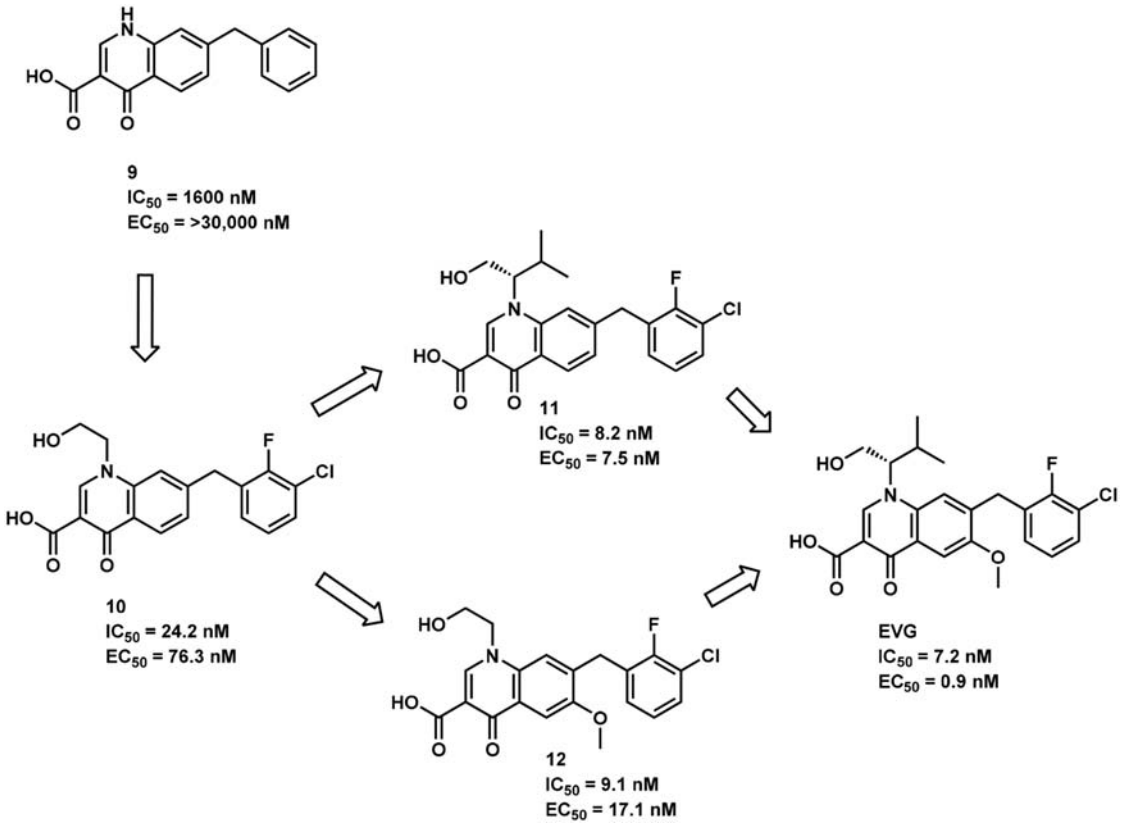

Fig. 3 Discovery of elvitegravir.

5.19.1.4.3 Dolutegravir

An extensive analysis of known integrase inhibitor scaffolds including raltegravir, elvitegravir, and others based on quinolones provided the basis for the discovery of dolutegravir (DTG, Fig. 4). Using data from foamy virus integrase crystal structures as a guide, a pyridine scaffold was incorporated to orient the divalent metal-binding motif and lipophilic tail optimally (compound **13**, $IC_{50} = 10$ nM).[29] Cyclization to bicycle **14** resulted in an increase in wild-type potency (1.6 nM), but this compound shows a significant loss in potency to the known integrase mutant Q148K (22-fold change).[30] At the same time, it was found that hemiaminal **15** showed good wild-type potency (3.8 nM) with only a small Q148K shift (2.1). This compound suffered from low bioavailability in

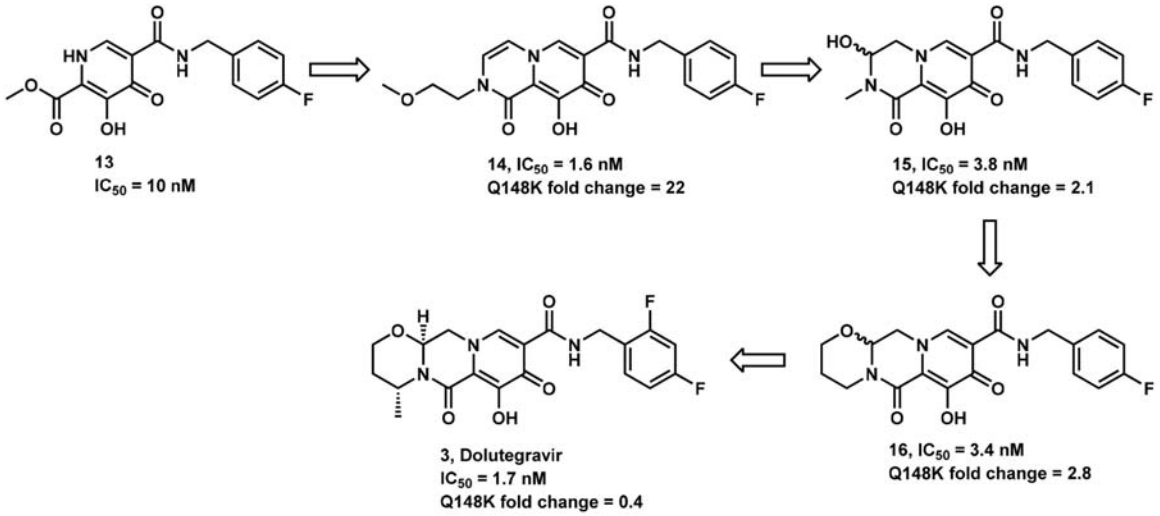

Fig. 4 Discovery of dolutegravir.

Table 3 Activity of DTG and RAL against RAL-resistant HIV strains

		Fold change	
Patient # (week at RAL failure)	*Genotype*	*DTG*	*RAL*
1 (8)	Y143K	1.26	10.5
1 (8)	E138K and Q148K	3.01	50.12
2 (24)	T97A and Y143C	1.72	45.3
3 (24)	V72I, Y143R, and T206S	1.92	72.41
4 (24)	G140S and Q148H	10.39	327.84

rat as well as stereochemical instability. The addition of a third ring gave racemate **16**, a compound with good potency (3.4 nM) and small Q148K shift (2.8) and very good pharmacokinetics profile in rats ($t_{1/2} = 17$ h, $F(\%) = 51$). Investigation of different substitutions around the aminal ring afforded monomethyl analog **3**, which became dolutegravir. This compound showed excellent potency against WT virus as well as Q148K, and pharmacokinetic profiles in preclinical studies suggestive of a QD profile in humans.[31]

DTG shows a significantly improved resistance profile compared with first-generation integrase inhibitors, maintaining significant potency against many of RAL-resistant clinical isolates (Table 3).[32]

In a large Phase III trial, QD DTG (50 mg) regimens achieved noninferiority to twice daily raltegravir regimens (400 mg twice daily).[33] Frequency and severity of adverse events were similar in both groups. In another trial, the combination of DTG with abacavir and lamivudine was shown to provide a superior level of viral suppression compared with efavirenz-TDF–FTC (88% vs. 81%), though this difference was primarily due to a greater number of discontinuations in the efavirenz group.[34] Similarly, DTG regimens have shown superiority over darunavir regimens—also primarily due to fewer discontinuations.[35] Further, the improved resistance profile of DTG has been demonstrated in a clinical trial of treatment-experienced patients in which DTG was shown to provide effective viral suppression for 75% of patients with preexisting RAL and EVG mutations when given twice daily.[36] The improved resistance profile for DTG has been attributed to the kinetics of enzyme inhibition; DTG has much longer k_{off} rates than first-generation integrase inhibitors RAL and EVG.[37] DTG has recently been approved as part of a STR with abacavir and lamuvidine, and this is currently the only unboosted, STR containing an integrase inhibitor.[38]

5.19.1.4.4 Other clinical- and preclinical-stage integrase inhibitors

Work on new integrase inhibitors continues. Cabotegravir, discovered concurrently with dolutegravir,[39] has a very long human half-life and is being investigated clinically as a long acting injectable in combination with the NNRTI rilpivirine (Fig. 5).[40] Bictegravir (GS-9883), a new INSTI shows a longer human half-life and improved resistance profile compared to currently approved INSTIs.[41] In a 10-day Phase I study, QD bictegravir showed a >2 $\log_{10}$ viral load reduction at doses at or above 25 mg day^{-1}, and the compound is being studied in Phase II in combination with tenofovir alafenamide (TAF) and emtricitabine.[42] MK-8970, a prodrug of RAL, shows improved bioavailability in the colon, effectively lengthening the time absorption that takes place, and thus has potential for QD dosing.[43] PF-47765480, containing an N-hydroxyl-amide chelator, showed good potency and an improved

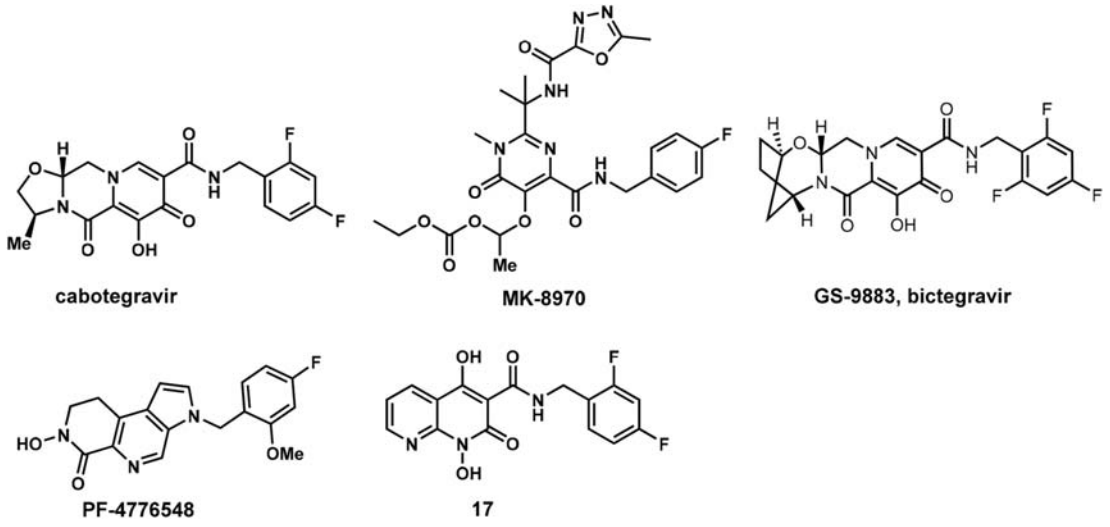

Fig. 5 Structures of recent clinical- and preclinical-stage INSTIs.

resistance profile compared to RAL and EVG. However, a human PK study using a microdose of the compound revealed higher than expected human clearance and a short human half-life (2.8 h).[44] An N-hydroxyquinolone series exemplified by **17** has also been reported to exhibit single-digit nanomolar potencies and improved coverage of some RAL-resistant mutants.[45]

5.19.1.5 Nucleoside Reverse Transcriptase Inhibitors

Since the regulatory approval of the first nucleoside analog zidovudine (AZT) in 1987 as a monotherapy for HIV, nucleoside or NRTIs have been established as the backbone for therapeutic regimens for the treatment of HIV infection.[46–48] NRTIs mimic endogenous 2′-deoxy-nucleosides and nucleotides and require intracellular phosphorylation by host cell kinases[49,50] to form their respective active triphosphate metabolites, which are incorporated by and inhibit reverse transcription. Each of the approved antiretroviral NRTIs (**Fig. 6** and **Table 4**) lack the 3′-hydroxyl moiety and thus cause obligate chain termination of the viral reverse transcripts. The standard of care for the treatment of HIV, known as HAART, includes combinations of three or more drugs of which two are typically NRTIs owing to their high genetic barrier to resistance, potent activity, and in general long intracellular persistence, which translates to lower dosing frequency. Limitations of NRTI's, however, include drug-drug interactions,[51] emergence of resistance,[52,53] and especially adverse events,[54] which have had the greatest impact on guidelines for current HAART.[55]

A majority of the adverse events observed with NRTIs, especially pertaining to AZT, zalcitabine (ddC), stavudine (d4T), and didanosine (ddI), have been associated with inhibition of mitochondrial DNA polymerase gamma (mtDNA).[56] The thymidine-based NRTIs stavudine (d4T) and AZT have both been associated with lipoatrophy.[57,58] AZT has also been associated with myopathy, cardiomyopathy, and anemia, all of which are attributed to indirect depletion of mitochondrial DNA through inhibition of thymidine phosphorylating enzymes, affecting endogenous mitochondrial thymidine triphosphate concentrations.[59] As well as causing lipodystrophy, stavudine has also been associated with peripheral neuropathy[60] and as a result is no longer considered an appropriate treatment for patients. The cytidine-based NRTI zalcitabine (ddC), while highly potent,[61] has a short half-life requiring three times daily dosing, and has also been associated with adverse events resulting from depletion of mitochondrial DNA.[62] The sale and distribution of ddC has been discontinued. Didanosine (ddI) has been associated with short-term toxicities including lactic acidosis, pancreatitis, peripheral neuropathy,[54] and myocardial infarction,[63] as well as with noncirrhotic portal hypertension in patients on long-term therapy.[64]

Modern antiretroviral therapies have shifted away from NRTIs that exhibit high potential for mitochondrial toxicity and have moved toward the use of TDF, 3TC, emtricitabine (FTC), and abacavir (ABC), which exhibit improved safety profiles. TDF and FTC are the two NRTIs that are preferred for first-line combination regimens by virtue of their potent and durable efficacy and established long-term safety in combination therapies.[65–69] TDF is a bis(isopropyloxycarbonyloxymethyl) ester prodrug of tenofovir (TFV), employed to improve oral bioavailability of the parent, and is the most widely prescribed antiretroviral drug worldwide. While it has a favorable safety profile, long-term TDF therapy has been associated with renal adverse events[70] as well as bone density loss,[71,72] in small patient populations. These adverse events are attributed to the high plasma exposures of TFV, a consequence of the low plasma stability of the prodrug moiety. TFV accumulation in renal proximal tubule cells due to transport by human OAT1 has been implicated in the renal insufficiency observed.[73] A prodrug of TFV, tenofovir alafenamide (TAF, vide infra), which has improved plasma stability to mitigate this toxicity, has recently received regulatory approval.

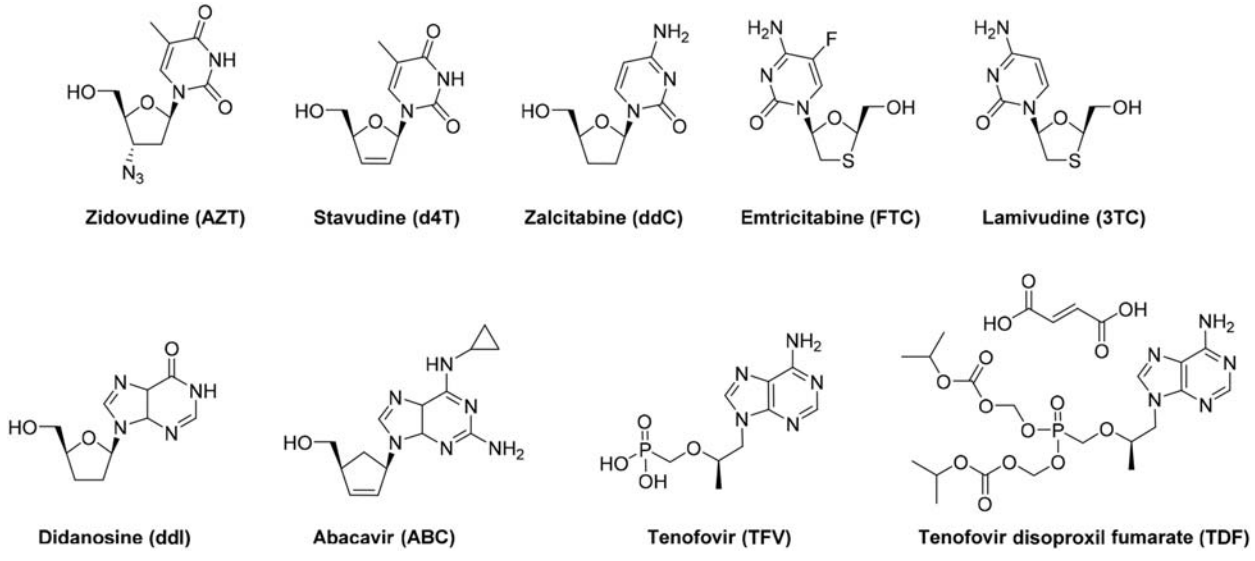

Fig. 6 Structures of approved pyrimidine- and purine-based NRTIs.

Table 4 FDA-approved NRTIs

Drug	Approval year	Dosage (mg)	Dose frequency[a]	F%[b,47]	Plasma $t_{1/2}$ (h)[48]	Intracellular TP $t_{1/2}$ (h)[c,48]	Resistance mutations[52]	Adverse effects[54]
AZT	1987	300 200	bid tid	75%[82]	0.5–3	7[83]	Q151M	Dyslipidemia, myopathy, anemia, nausea, and rash
ddI	1991	250–400 125–200	qd bid	30–42%	1.5	24[84]	K65R, L74V, and Q151M	Lipoatrophy, dyslipidemia, lactic acidosis, pancreatitis, distal sensory polyneuropathy, and hepatic steatosis
ddC	1992	0.75	tid	>80%[85]	1–3[86]		Q151M	Lactic acidosis, pancreatitis, peripheral neuropathy, myocardial infarction, and portal hypertension
d4T	1994	30–40	bid	99%[87]	1.2	7[84]	V75T and Q151M	Lipoatrophy, dyslipidemia, lactic acidosis, pancreatitis, DSPN, and hepatic steatosis
3TC	1995	300 150	qd bid	86–87%	5–7	22[83]	M184VI and K65R	Negligible
ABC	1998	600 300	qd bid	83%	1.54	21[79]	M184V, K65R, L74V, and Q151M	Hypersensitivity, hepatotoxicity, and heart disease
TDF	2001	300	qd	25–39%	~17	>60[88]	K65R and K70E	Renal insufficiency and bone loss
FTC	2003	200	qd	93%	10	39[89]	M184VI and K65R	Skin discoloration

[a]qd, once daily; bid, twice daily; tid, three times daily.
[b]*F*%, oral bioavailability.
[c]Terminal half-life in PBMCs.

FTC is a fluorinated cytidine analog featuring an oxathiolane replacement for the ribose ring. Importantly, the FTC conformation is in the unnatural L-enantiomeric form, which is more potent and less toxic than the S-antipode and provides an excellent selectivity profile.[74] FTC is relatively well tolerated in patients with side effects that include headache, insomnia, diarrhea, nausea, vomiting, rash as well as hyperpigmentation on the palms and/or soles.[75,76]

Lamivudine (3TC) is closely related in structure to FTC but lacks the 5-fluoro substitution on the cytidine base, and the two have very similar profiles. Compared to FTC, 3TC is slightly less potent in in vitro assays, has a shorter serum and intracellular half-lives, and has lower bioavailability which translates to a moderately higher dose.[74,77] ABC is a diaminopurine-based nucleoside with a cyclopentene in place of the ribose ring.[78]

ABC is a prodrug that undergoes intracellular metabolism to the monophosphate by adenosine phosphotransferase followed by further enzymatic conversion of the cyclopropyl diaminopurine to guanosine to afford carbovir monophosphate.[79] ABC causes a hypersensitivity reaction in approximately 8% of treated patients, related to histocompatibility complex class 1 human leukocyte antigen 57.1 haplotype.[80] Genetic testing is available to prescreen patients that may be predisposed to this hypersensitivity. ABC has also been associated with an increased risk of myocardial infarction.[63]

In therapeutic practice, the resistance profiles of the NRTIs discussed above are weighed against their potential side effects. The most common resistance mutations include M184V/I, arising from FTC and 3TC use, as well as thymidine analog mutations (TAMs)—see Chapter 50017.[52,53] Although the prevalence of M184V/I mutants is high their fitness is greatly reduced,[81] and FTC and 3TC are still used in first-line treatment with TDF or ABC.

5.19.1.5.1 Tenofovir alafenamide

TAF is the phenoxy isopropyl L-alaninate phosphoramidate prodrug of TFV (Fig. 7), and the first reports of synthesis and isolation appeared in 2001.[90,91] The EC_{50} of TAF in MT-2 cells is 0.005 μM, compared to 5 μM for the parent TFV and 0.05 μM for TDF, and it has been shown to more efficiently load lymphoid cells and tissues as compared to TDF.[92] The improved pharmacology of TAF is

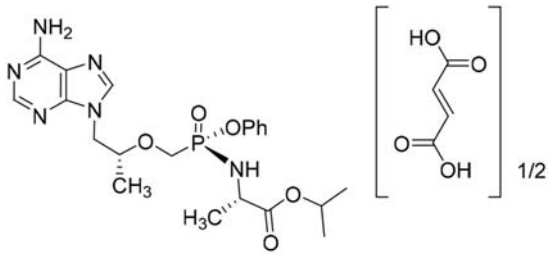

Fig. 7 Structure of tenofovir alafenamide (TAF) in the hemifumarate form.

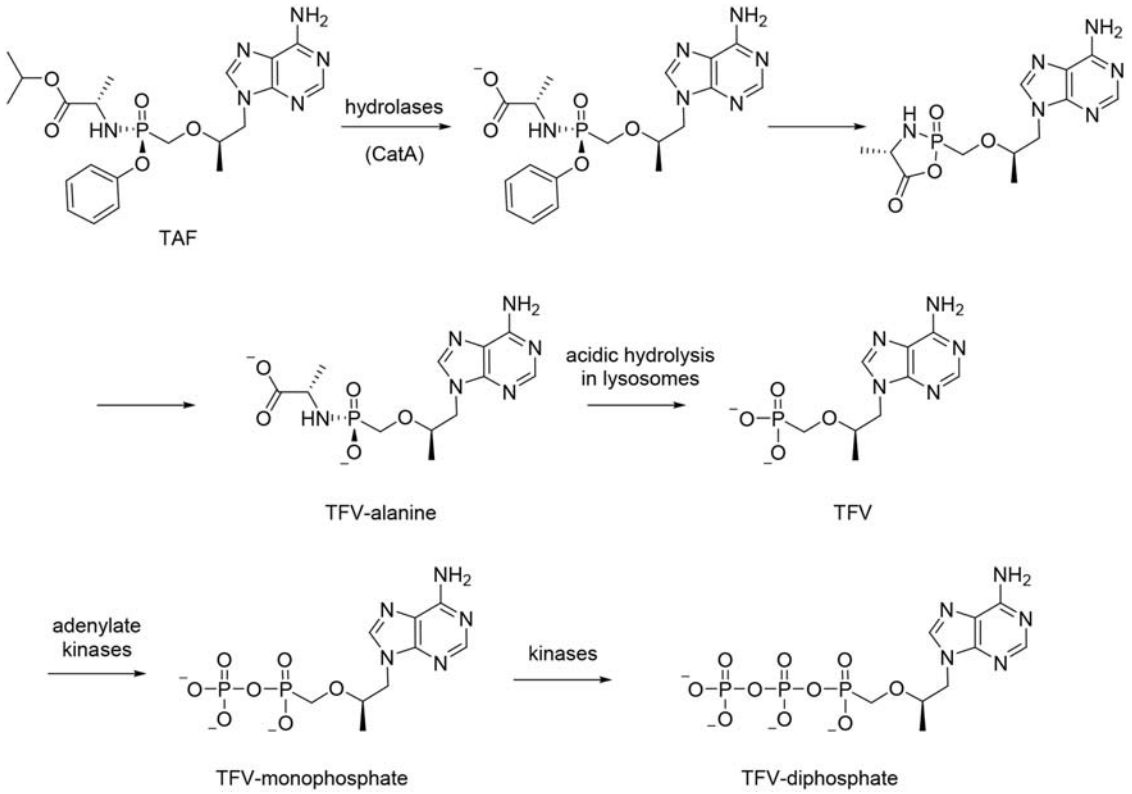

Fig. 8 Mechanism of the intracellular activation of TAF.

attributed to its distinct mechanism of activation (Fig. 8). In peripheral blood mononuclear cells (therapeutically relevant target cells of HIV-1 infection), intracellular metabolism of TAF begins with the hydrolysis of the ester moiety by hydrolases localized in lysosomes.[93–96] The serine protease cathepsin A, which is highly expressed in lymphoid tissue,[97] has been established as primarily responsible for this initial bond cleavage. The metastable carboxylate metabolite then spontaneously cyclizes to expel phenol, and subsequent hydrolysis of the cyclic acyl phosphate affords the TFV-alanine metabolite. Chemical or enzymatic cleavage of the alanine reveals the parent TFV, which is anabolized to the active TFV-diphosphate. As for TDF, the fact that TFV is a phosphonic acid precludes any metabolism to an uncharged species (such as a nucleoside), and consequently the intracellular half-life is enhanced.

In addition to exhibiting higher intracellular concentrations of TFV-diphosphate, TAF shows greater stability in human plasma, resulting in lower parent TFV plasma exposures as compared to TDF and thereby reducing the potential for renal and bone toxicity. Furthermore, TAF does not interact with OAT1 or OAT3 and exhibits no OAT-dependent cytotoxicity and thus is unlikely to actively accumulate in renal proximal tubules.[98] TAF has been evaluated in combination with other direct-acting antiviral agents (Fig. 9). The first TAF-based combination regimen, Genvoya (elvitegravir (E), 150 mg/cobicistat (C), 150 mg/emtricitabine (FTC) 200 mg/TAF 10 mg), was approved by the FDA in Nov. 2015 for the treatment of HIV-1 infection. The efficacy of E/C/FTC/TAF provided noninferior virological suppression as compared to the standard of care E/C/FTC/TDF, and both regiments maintained a high barrier to resistance.[99,100] Patients receiving E/C/FTC/TAF had significant improvements in serum creatinine, renal tubular proteinuria, and bone mineral density as compared to E/C/FTC/TDF.[99,100] In March 2016, a STR containing rilpivirine (R) with FTC/TAF was approved as the second TAF-based STR.[101]

Additional clinical studies with TAF are ongoing. The beneficial resistance profile of darunavir and the safety profile of TAF make for an attractive combination that in a Phase II clinical study has been shown to provide comparable efficacy to the E/C/FTC/TAF regimen.[102] Subdermal implants containing TAF for long-acting HIV prophylaxis have also been reported.[103]

5.19.1.5.2 Investigational NRTIs

The currently approved NRTIs have demonstrated efficacy and a high degree of safety in long-term treatments and will continue to play an important role for HAART in the future. However, some limitations in the safety, resistance, and pharmacology of these NRTIs remain, and several investigational alternatives are currently in development (Fig. 10). Apricitabine (ATC) is the natural (−)-enantiomer 2′-deoxy-3′-oxa-4′-thiocytidine analog of 3TC.[104] It is less active than the unnatural (+)-enantiomer but has an improved toxicity profile.[105] While it is less potent than other NRTIs, it maintains broad activity against HIV-1 resistance mutants

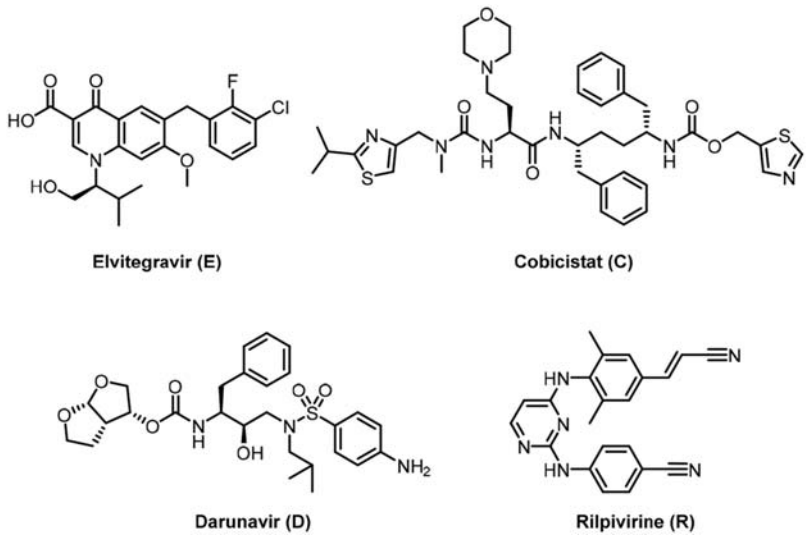

Fig. 9 Structures of antiretrovirals being evaluated in combination regimens with TAF.

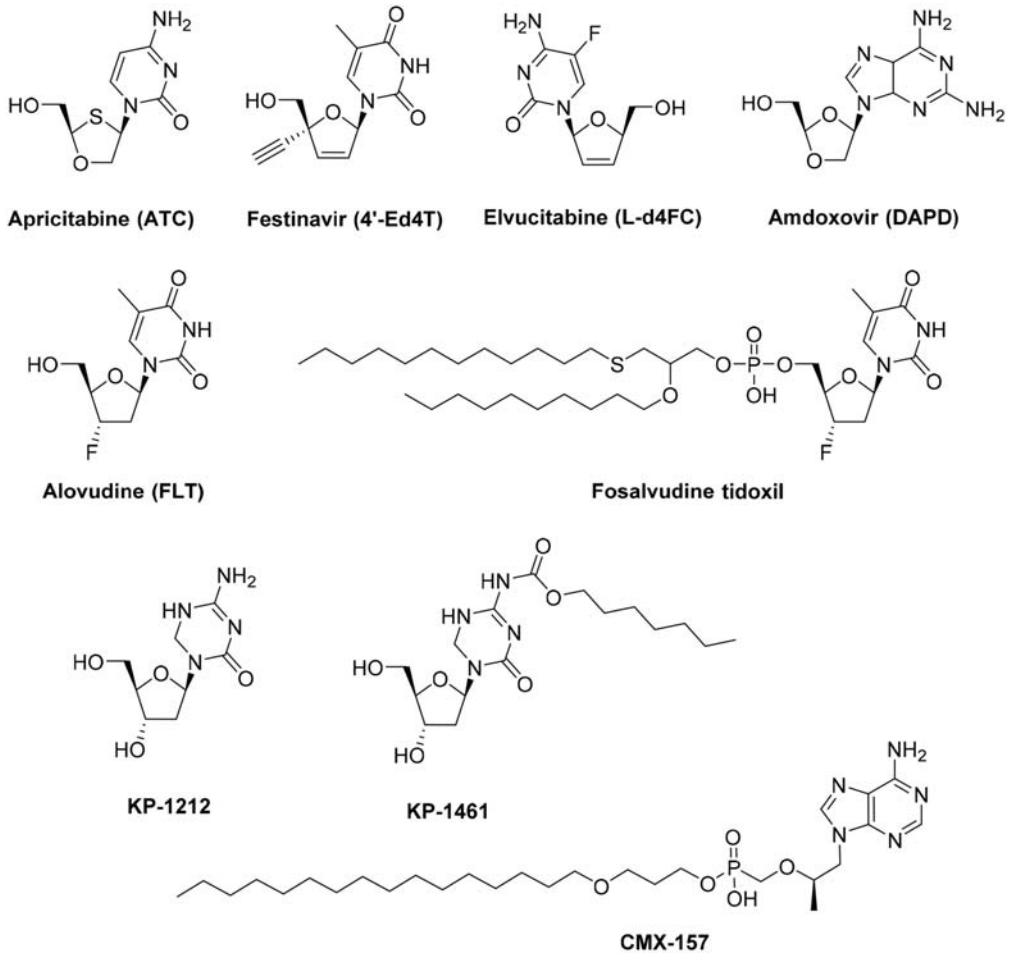

Fig. 10 Structures of investigational NRTIs in clinic trials.

which provides a potential advantage for the treatment of NRTI-experienced patients who failed prior therapies.[106] The efficacious dose of ATC is 800 mg twice daily and it is currently in the final stages of Phase III clinical development.

Festinavir (4′-Ed4T, BMS-986001) is a d4T analog with a 4′-ethynyl substitution[107] that exhibits an EC_{50} of 250 nM in MT-2 cells.[108] The 4′-ethynyl substitution confers selectivity against incorporation by host mitochondrial DNA and has a significantly improved in vitro toxicity profile as compared to d4T.[109] Festinivir has reached Phase II clinical development.

Elvucitabine (L-d4FC) is of the unnatural L-nucleoside configuration, with a dideoxy ribose ring and a 5-fluoro cytidine base. While highly potent, L-d4FC shows in vitro cytotoxicity despite having little effect on mitochondrial DNA.[110,111] Observations of hematological toxicity in the clinic limits the dose[112] and lower $CD4^+$ cell recovery was observed as compared to 3TC.[113] Elvucitabine has reached Phase II clinical evaluation, but there have been no recent developments reported.

Amdoxovir (DAPD) is a diaminopurine (DAP) dioxolane prodrug that is converted to the corresponding guanosine base (DXG) through the action of adenosine deaminase. DXG has an EC_{50} of 85 nM in MT-2 cells and has little effect on mitochondrial DNA.[114] Notably, DAPD retains the activity of M184V and TAMs resistance mutants.[115,116] Amdoxovir has reached Phase II clinical evaluation.

Alovudine (FLT) is a 3′-deoxy-3′-fluorothymidine analog that has comparable potency to AZT, but maintains activity against NRTI-resistant mutants including TAMs.[117] FLT does affect mitochondrial DNA[118] and has been shown to cause hematopoietic toxicity,[119] which restricts doses to levels that only achieved moderate suppression of viral load in a Phase II clinical study.[120] The development of FLT has been discontinued. In order to overcome the dose limitations, the phospholipid prodrug fosalvudine tidoxil was investigated. In a Phase II study for 14 days, a 40 mg dose provided a 1.00 $\log_{10}$ reduction in viral titer with no dose-dependent adverse effects.[121] The long-term potential for toxicity of fosalvudine tidoxil has yet to be addressed and there have been no recent developments reported.

KP-1212 is a deoxycytidine analog with a 5-aza-5,6-dihydro cytidine-modified base. The 3′-hydroxyl group enables stable incorporation by reverse transcriptase and the trizazinone base efficiently base-pairs with both G and A which increases the rate of random transitional mutations in the viral genome and leads to clearance of the virus.[122] KP-1212 is a substrate for mitochondrial DNA polymerase γ,[123] which potentially can lead to long-term mitochondrial toxicity; however, this toxicity has not been observed thus far in in vitro cell-based assays.[122] KP-1461 is the N^4-heptyloxycarbonyl prodrug of KP-1212, designed to enhance oral bioavailability. In a Phase IIa study, KP-1461 was dosed orally at 1600 mg twice daily and was generally well tolerated, but it did not significantly affect viral load or CD4 lymphocyte count.[124] However, alteration of the mutation spectrum of HIV consistent with the mechanism of action of KP-1461 was observed.[125]

CMX-157 is the hexadecyloxypropyl prodrug of TFV designed to mimic natural phospholipids, and exhibits excellent potency with an $EC_{50} < 1$ nM in MT-2 cells.[126] The prodrug moiety enhances gastrointestinal absorption and cell permeability as compared to TFV, and provides a plasma-stable prodrug that is well tolerated in rats and monkeys.[127] CMX-157 is currently being developed in Phase II clinical trials assessing safety, tolerability, and pharmacokinetics.

5.19.1.6 Nonnucleoside Reverse Transcriptase Inhibitors

Early NNRTIs were plagued by the rapid development of resistance.[128] The discovery of TMC-125 (etravirine) came from an effort to develop new NNRTIs that retained activity against many of the strains known to be resistant to earlier generations of NNRTIs, and began with a healthy dose of good fortune.[129,130] Though many varied types of chemical scaffolds were known to inhibit HIV reverse transcriptase, iminothiourea **18** was one of the first to retain appreciable activity against many of the known single mutant-resistant strains (Fig. 11). After a problematic liability in the metabolism of **18** (oxidative cyclization to a thiadiazole) became apparent, an attempt to synthesize the cyano-guanidine analog **19** resulted in the unexpected formation of amino-triazole **20**. This compound retained nearly all of the activity of the thiourea lead, including its potency against many single-point mutants. Specific removal of one of the nitrogens in the core led to amino-pyrimidine **21**, which had greater potency, and the addition of a second cyano group (as well as swapping methyls for chlorines) gave the exquisitely potent compound **22**. This compound retained low nanomolar potency against many single mutants and even had some activity versus some problematic double mutants. Finally, the addition of bromine atom on the core further improved the resistant mutant profile, giving TMC-125 (etravirine). Etravirine showed good efficacy, even in treatment-experienced patients,[131] and was approved by the FDA in 2008.

5.19.1.6.1 Rilpivirine

Further work in the diaminopyrimine series resulted in the discovery of rilpivirine (TMC278).[132] Rilpivirine shows even greater potency against wild-type and mutant strains of HIV than efavirenz or etravirine, and this enhanced activity has been attributed to a new specific interaction between the vinyl-extended cyano group and Trp229. It is speculated that some of the improved activity against resistant strains may derive from additional torsional freedom in the bonds to the aniline ring in TMC278 compared to

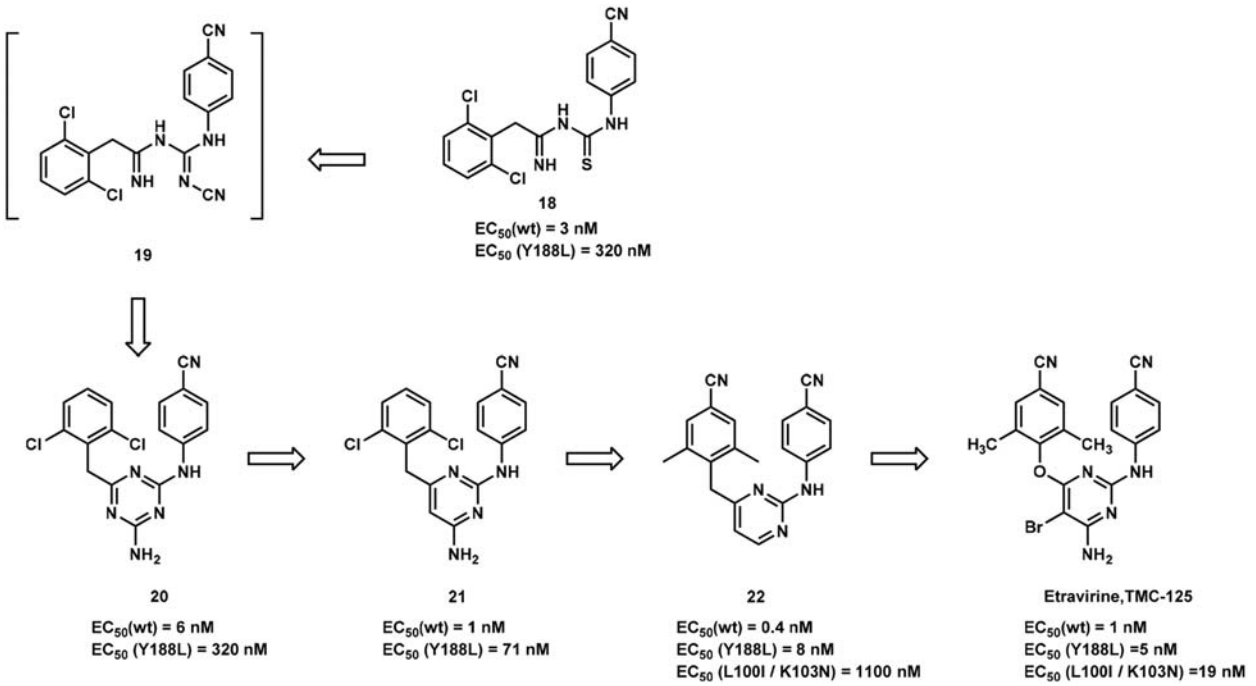

Fig. 11 Optimization of diaryltriazines to TMC-125 (etravirine).

previous analogs. In vitro studies for rilpivirine suggest that it has a higher genetic barrier and a more robust resistance profile than either efavirenz or nevirapine.[133]

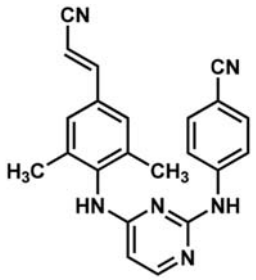

Clinical studies show rilpivirine has comparable efficacy to efavirenz with better tolerability (reduced incidences of several adverse events—neurological events, rash, and lower lipid elevations).[134,135] Though patients with high viral load ($>500{,}000$ copies mL^{-1}) showed higher rates of virologic failure than efavirenz, rilpivirine regimens showed superiority in patients with lower initial viral loads ($<100{,}000$ copies mL^{-1}) with fewer adverse events and discontinuations.[136] Rilpivirine dosing is limited to 25 mg by a hERG interaction at higher doses.[137] Rilpivirine was approved by the FDA in 2011. It is included in multiple STRs and is also being studied as a long-acting injectable treatment in combination with the second-generation integrase inhibitor cabotegravir.[138]

5.19.1.6.2 Doravirine

Recent work on NNRTIs with pyridone cores led to the discovery of doravirine (MK-1439).[139] Early compounds in this series showed much improved activity against NNRTI-resistant strains such as K103N/Y181C, but poor pharmacokinetics. Optimization of both the heterocycle and substituents on the pyridone core led to doravirine.

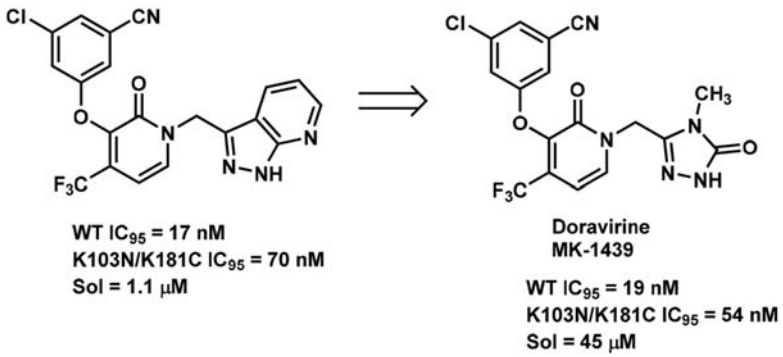

Doravirine shows improved potency against both wild-type HIV as well as key resistant strains (Table 5), and also lacks the dose-limiting hERG liability of rilpivirine.

Currently in Phase III studies, doravirine (100 mg QD) shows comparable efficacy to efavirenz (600 mg QD) and a significantly improved tolerability profile with only half as many patients experiencing a CNS-related adverse event (22.2% for doravirine vs. 43.5% for efavirenz). The most common CNS adverse events were dizziness (doravirine 9.3% and efavirenz 27.8%) and abnormal dreams (doravirine 5.6% and efavirenz 16.7%).[140]

5.19.1.7 Protease Inhibitors

PIs have historically been one of the most important and widely used third agents contained in HIV regimens. Though they have generally have had more onerous side effect profiles than NNRTIs, they exhibit a stronger barrier to resistance. Darunavir, approved by the FDA in 2006, is the newest PI to reach the market, and it, along with atazanavir (approved in 2003, and described extensively in Comprehensive Medicinal Chemistry II) have become the PIs of choice for modern HIV regimens.

5.19.1.7.1 Darunavir

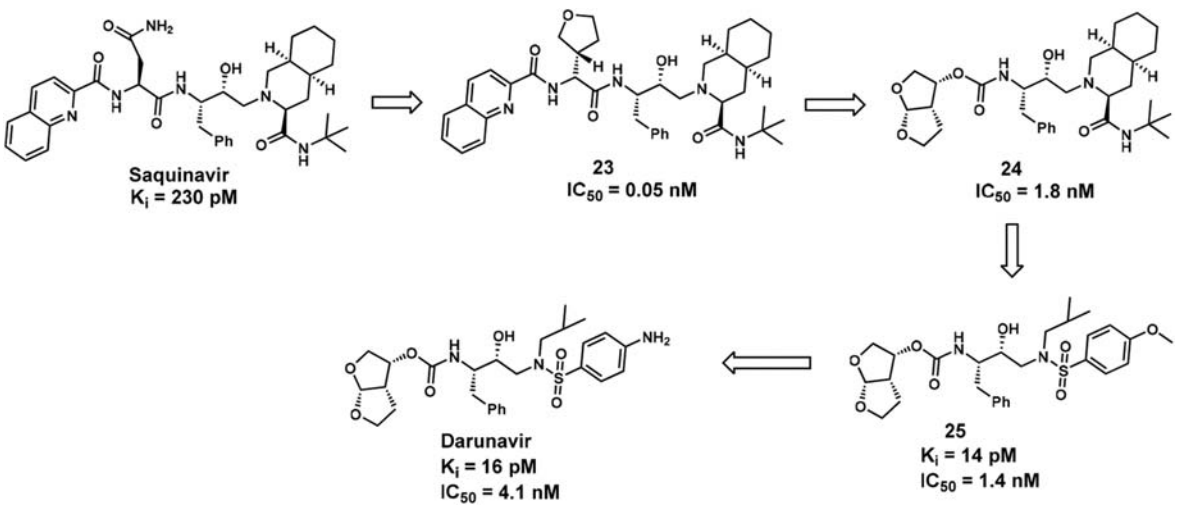

Table 5 Resistance profiles of NNRTIs

	Spread IC95 (μM) with 50% NHS			
Compound	*WT*	*K103N*	*Y181C*	*K103N/Y181C*
Efavirenz	0.039	1.4	0.089	3.2
Rilpivirine	0.036	0.044	0.120	0.37
MK-1439	0.019	0.042	0.025	0.054

The discovery of darunavir came out of an effort to improve both the pharmacokinetic properties and the resistance profile of existing PIs. Starting from the crystal structure of the known PI saquinavir, researchers sought to improve PK properties by reducing the peptidic character of the molecules (by removing amides and other hydrogen bond donors) and further improve the resistance profile by increasing contacts with the backbone of the enzyme.[141,142] Initial replacement of the P2-asparagine with a tetrahydrofuran led to the highly potent compound **23**. Removal of the quinolinyl-amide led to a significant loss of potency ($IC_{50} = 160$ nM), but optimization of the THF moiety led to the discovery of bis-THF **24**, and the recovery of much of the potency. The bis-THF motif (in the proper *R,S,R* stereochemistry) was shown to improve binding through two new hydrogen bonds to backbone residues Asp29 and Asp30. In the context of this motif, reoptimization of the remainder of the molecule led to the discovery of *p*-methoxyphneylsulfonamide as a potent element for P2 binding. Compound **25** (TMC-126), containing both of these pieces, showed extraordinary potency against WT (14 pM) and much improved potency against many PI-resistant strains. The oxygen atom of the methoxy group was shown to make two more important hydrogen bonds including one to the backbone. Finally, replacement of the methoxyphenyl with aniline provided darunavir, a compound with significantly improved pharmacokinetics compared with **25**. A crystal structure of darunavir bound to HIV-PI clearly shows the backbone hydrogen bonds believed to be responsible for its improved potency and resistance profile (Fig. 12).

A clear advantage of darunavir over the earlier PIs saquinavir and nelfinavir can be seen in comparing their potencies against both wild-type HIV strains and multidrug-resistant strains (Table 6).[143]

Early Phase II studies showed that darunavir boosted with ritonavir provided a much greater response in protease-experienced patients than control PIs (45% vs. 10% reaching <50 viral copies mL^{-1}), with 9% of darunavir-treated patients discontinuing treatment due to an AE- or HIV-related event (compared to 5% in the PI control arm) and 8% of darunavir patients discontinuing as a result of virologic failure (compared to 67% of PI control patients).[144]

More recent clinical data shows that darunavir regimens are superior to lopinavir regimens[145] as well as atazanavir regimens,[146] though in both cases the improvement is primarily a result of fewer discontinuations due to adverse events. Lower rates of

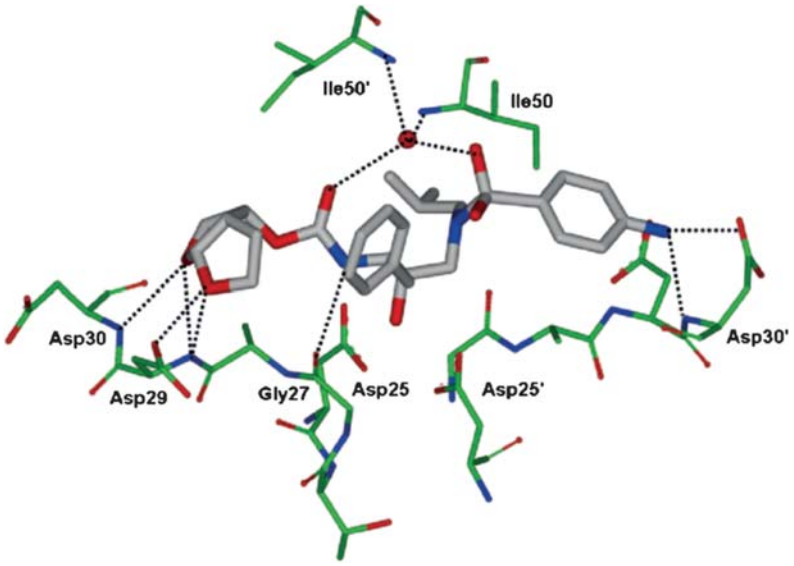

Fig. 12 Crystal structure of darunavir bound to HIV protease showing key hydrogen bonds including backbone hydrogen bonds to both the bis-THF moiety and the aniline nitrogen.

Table 6 Comparison of the potency against WT and protease-resistant HIV isolates for darunavir (DRV) with older protease inhibitors saquinavir (SQV) and nelfinavir (NFV)

Virus	*IC_{50} (μM)*		
	SQV	*NFV*	*DRV*
HIV-1 (wild-type X4)	0.010 ± 0.004	0.019 ± 0.002	0.003 ± 0.0003
HIV-1 (wild-type R5)	0.004 ± 0.001	0.033 ± 0.008	0.003 ± 0.0005
HIV-1 (MDR X4)	0.23 ± 0.02 (23)	0.54 ± 0.01 (28)	0.004 ± 0.0008 (1)
HIV-1 (MDR R5)	0.30 ± 0.04 (30)	>1 (>53)	0.02 ± 0.009 (7)
HIV-1 (MDR R5)	0.35 ± 0.16 (35)	>1 (>53)	0.029 ± 0.007 (10)

Adapted from Koh, AAC, 2003.

gastrointestinal side effects, lipid level increases, and hyperbilirubinemia in the darunavir arms appeared to contribute to its statistical superiority.

5.19.1.7.2 Other protease inhibitors

Beyond darunavir, newer PI research has led to compounds like brecanavir, an extremely potent PI[147] which was studied clinically and ultimately abandoned due to difficulty in developing an effective oral formulation (Fig. 13). The addition of a third fused THF (**26**) was shown to result in an excellent antiviral profile against both wild-type and drug-resistant strains.[148] TMC310911, a newer PI from Tibotec, shows further improvements in resistance profile compared with darunavir. It retains activity (less than a fourfold potency shift) for 71% (879/1233) of a large set of clinical isolates which show decreased susceptibility to DRV and early PIs.[149]

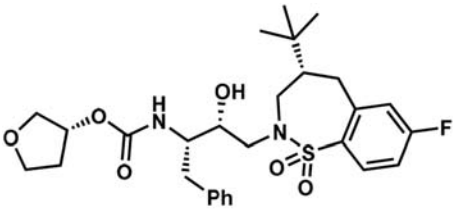

27
K_i = 0.26 nM

Additional structural diversity in the PI class is seen in compounds like cyclic sulfonamide **27**,[150] as well as PI's containing heterocyclic cores[151] including benzodiazapenes[152] and other nonpeptidomimetic alternatives.[153] Somewhat weaker activity has been seen with macrocyclic approaches.[154]

5.19.1.8 Other Mechanisms

5.19.1.8.1 Attachment inhibitors

HIV attachment inhibitors are a class of anti-HIV compounds that prevent HIV entry. The process by which HIV gains entry into uninfected cells is a sequential series of events initiated by the binding of the viral surface glycoprotein gp120 to the host cell CD4 receptor. Upon binding, gp120 undergoes a conformational change that helps promote a cascade of events involving gp41-promoted pore formation and membrane fusion. Distinct from fusion inhibitors such as enfuvirtide, which inhibit gp41-mediated fusion, and CCR5 antagonists such as maraviroc, which inhibit the binding of the essential cofactor CCR5, attachment inhibitors appear to stabilize a conformation of gp120 that inhibits binding of CD4 and prevents attachment to CD4 cells. The exact mechanism of action remains a subject of investigation.[155]

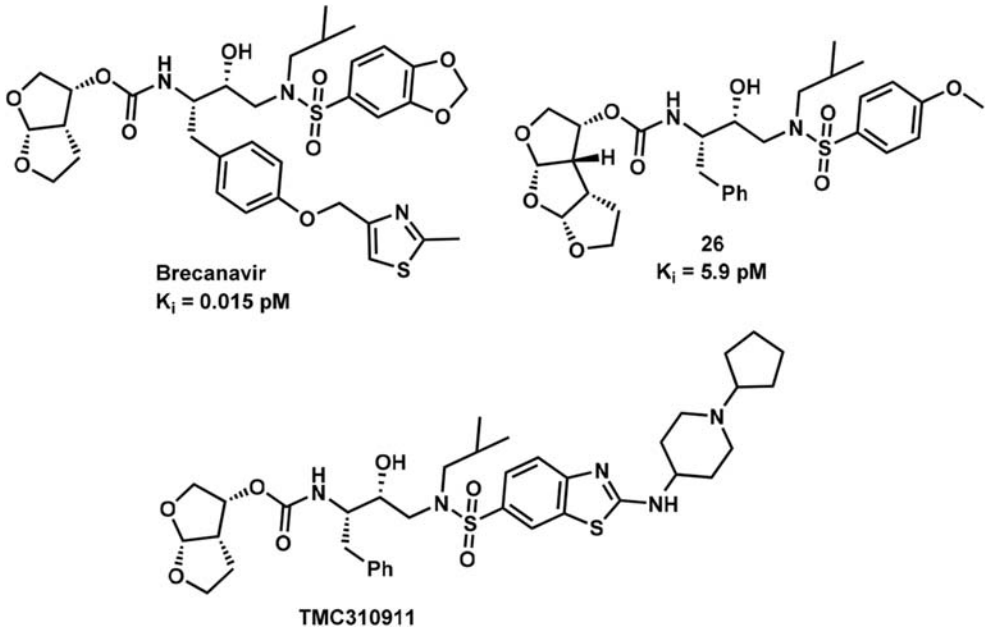

Fig. 13 Newer HIV protease research has led to compounds with further enhanced profiles.

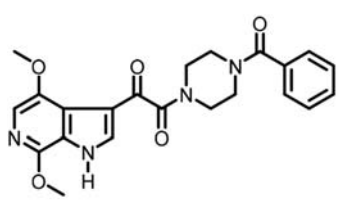

BMS-488043

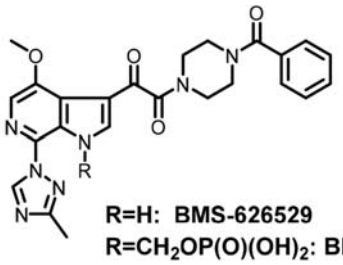

R=H: BMS-626529
R=$CH_2OP(O)(OH)_2$: BMS-663068

Initial proof of concept for targeting gp120 to prevent virus entry was provided by positive results in clinical trials of PRO542, a tetravalent CD4-IgG_2 fusion protein.[156] Small-molecule gp120 inhibitors were identified from a broad cell-based anti-HIV screen. Evaluation of BMS-488043 in HIV-1-infected subjects provided oral proof of concept for this class, albeit with modest antiviral potency. A next generation compound was sought to address limited oral bioavailability, suboptimal pharmacokinetics and insufficient inhibitory potency in the context of gp120 heterogeneity. BMS-626529 displays improved potency against a broader spectrum of HIV-1 viruses than its predecessor. BMS-663068 (fostemsavir) entered clinical development as the phosphonooxymethyl prodrug of BMS-626529, successfully addressing the low solubility and poor intrinsic dissolution properties of the active parent molecule.[157] In early-stage clinical trials, fostemsavir has demonstrated good antiviral activity and found to be well tolerated. It is currently in late-stage clinical evaluation. The FDA has granted Breakthrough Therapy Designation to fostemsavir in part due to the novel mechanism of action and its efficacy in treatment-experienced HIV patients.

5.19.1.8.2 Capsid inhibitors

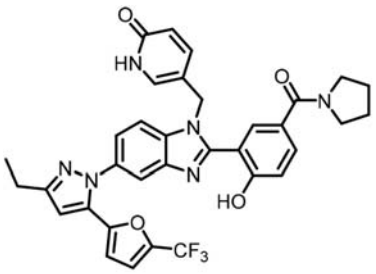

BI-060

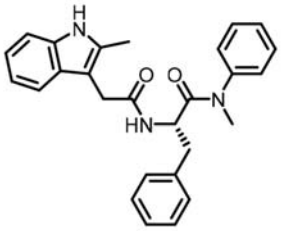

PF-3450074

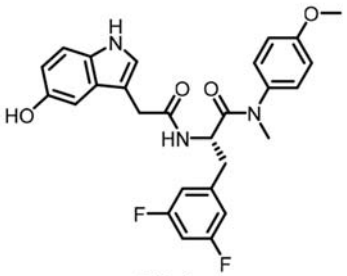

GS-2

In recent years, significant advances have been made in understanding the role of the HIV-1 capsid protein (CA) in the HIV life cycle. In addition to its key role in virus maturation, it is becoming increasingly apparent that the capsid protein has important functions during the early stages of infection. Capsid protein is now associated with impacting the kinetics of virus uncoating, recognition by restriction factors, and nuclear import and integration.[158] As such, there has been increasing attention toward targeting CA as a novel mechanism of intervention.

Multiple CA small-molecule binding sites have been identified on both NTD and CTD domains. The most notable inhibitors described thus far are shown below. BI-060 was discovered by BI to bind at the NTD site I, inhibiting the ability of CA to form higher order multimeric species necessary for proper core formation, and established proof of concept for potent anti-HIV activity through capsid binding.[159] Although less potent, PF-3450074 may provide a more intriguing starting point for potential drug discovery. Also binding the Capsid NTD, it does so at an orthogonal site 2, with drastic mechanistic consequences. Current evidence suggests that PF-3450074 and the more potent analog GS-2 possess a unique multimodal antiviral mechanism involving potent early-stage (nuclear import block) and late-stage (improper capsid assembly) effects on virus replication.[160] To date, no capsid inhibitors have been evaluated in human clinical trials.

5.19.1.8.3 Maturation inhibitors

The first-generation maturation inhibitor, bevirimat, demonstrated efficacy in HIV-infected subjects in early-phase clinical trials. Maturation inhibitors of this class target the Gag polyprotein, inhibiting the action of HIV protease at its last cleavage event between capsid (CA) protein p24 and SP1. This mechanism of action constitutes the inhibition of a single cleavage event, and stands in contrast to PIs, which directly target the active site of the viral protease. Due to naturally occurring polymorphisms in Gag, ~50% of patients exhibited reduced viral susceptibility to bevirimat, thus limiting its potential clinical utility.[161] Work toward a maturation inhibitor with improved virologic profile has been ongoing with BMS and GSK both reporting second-generation compounds. BMS-955176 possesses improved potency, antiviral spectrum, and Gag polymorphic coverage.[162] In a proof-of-concept study, 10 days of BMS-955176 monotherapy at 40 mg QD resulted in maximum median declines in HIV-1 RNA of

$\sim$1.70 $\log_{10}$c mL^{-1}.[163] Further evaluation of BMS-955176 in Phase II trials is ongoing. GSK2838232 displays an improved virologic profile with a reported MT4 $IC_{50} < 1$ nM that appears not to be affected by the presence of human serum.[164] GSK2838232 was advanced into human clinical trials.

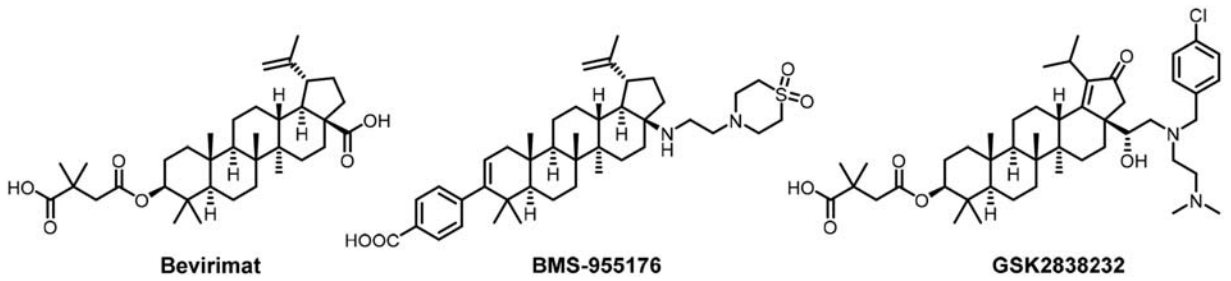

5.19.1.8.4 Noncatalytic integrase inhibitors

NCINIs bind to the viral integrase in an allosteric pocket within the catalytic core domain. The most advanced NCINI is BI 224436 (**28**). This compound, a stable atropisomer bearing a carboxylic acid that binds the peptide backbone in the integrase dimer cleft, shows high potency, a low serum shift, and a long half-life in rat pharmacokinetics (8.8 h). The discovery of this compound relied on structure-based drug design and X-ray crystallography of the catalytic core domain of integrase.[165] The upper tricyclic quinoline motif stacks against the protein and provides improved metabolic stability. Contrary to initial hypotheses surrounding the antiviral mechanisms of NCINIs, these compounds do not derive their potency by blocking integration. Instead, NCINIs promote improper integrase oligomerization during viral particle formation, leading to defective virion production.[166] Compound **28** was progressed into Phase I clinical studies.

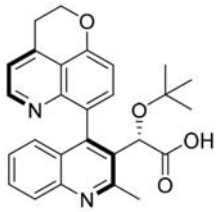

28

5.19.1.9 Simplified Regimens and Nonstandard Regimen Research

To improve adherence and outcomes, researchers have long sought to simplify regimens. Some simplification has occurred naturally as the dosing frequency of preferred individual agents has moved more and more to QD administration. Further, as the potency of the preferred agents has increased, the tablet sizes have gone down, and more agents have been combined into single tablets. The convergence of these two trends has allowed for the creation of STRs—three or more medicines constituting complete HIV regimens, co-formulated into single pills. Since 2006, five STRs for QD administration have been approved by the FDA (**Table 7**).[167]

Although standard regimens have long contained two nucleosides and a third agent, clinical researchers have continued to investigate innovations beyond this convention. The motivations behind this research are twofold—to find effective regimens for patients resistant to certain drugs classes (NRTIs, NNRTIs, and others), and to find regimens with better tolerability profiles. In one case, researchers investigated the addition of a fourth agent for patients with high viremia.[168] This study showed no benefit to patients with four drugs over three. Much of the research in this area involves regimens which are either nuc sparing[169] or

Table 7 Approved single-table regimens for HIV

Generic names	*Brand name*	*FDA approval date*
Efavirenz, emtricitabine, and tenofovir disoproxil fumarate	Atripa	Jul. 12, 2006
Emtricitabine, rilpivirine, and tenofovir disoproxil fumarate	Complera	Aug. 10, 2011
Elvitegravir, cobicistat, emtricitabine, and tenofovir disoproxil fumarate	Stribild	Aug. 27, 2012
Abacavir, dolutegravir, and lamivudine	Triumeq	Aug. 22, 2014
Elvitegravir, cobicistat, emtricitabine, and tenofovir alafenamide	Genvoya	Nov. 5, 2015
Rilpivirine, emtricitabine, and tenofovir alafenamide	Odefsey	Mar. 1, 2016

both nuc- and protease sparing.[170,171] Currently, evidence supports the use of these simpler nuc-sparing regimens in patients failing standard regimens. However, evidence for the use of nuc-sparing regimens in naive patients is more sparse.[172] And none are currently recommended for first-line therapy.

5.19.1.10 Boosters and Cobicistat

Ritonavir, a first-generation PI, was originally approved in 1996 and used in combination with two NRTIs for several years until it was gradually replaced by more efficacious and better-tolerated PIs such as fosamprenavir and lopinavir, and more recently by atazanavir and darunavir.[173] However, since it was recognized as a potent irreversible CYP3A4 inhibitor, its use as a "boosting" agent for other PIs has continued.[174] Due to concerns for generation of resistance—especially at this lower dose—ritonavir's use a booster is limited to PI-based regimens.

In this context, the need for a CYP3A4 inhibitor, or booster, without HIV protease inhibition was recognized. A booster without protease activity could be used to enhance the pharmacokinetics of drugs with other mechanisms (such as INSTIs). An effort to discover an agent of this type was undertaken and resulted in the discovery of cobicistat. Starting from the structure of ritonavir, removal of the central hydroxyl group of ritonavir led to >20-fold reduction in HIV protease activity without affecting CYP3A inhibition.[175] Further, it was found that the addition of polar groups at P2, as exemplified by **31**, gave compounds with little or no remaining HIV protease activity.[176] When **31** was shown to have poor permeability and bioavailability, alternative basic groups at P2 with fewer hydrogen bond donors were shown to give acceptable pharmacokinetics. This led to cobicistat (COBI) **32**, a CYP3A inhibitor (or pharmacoenhancer) devoid of HIV protease activity.[177]

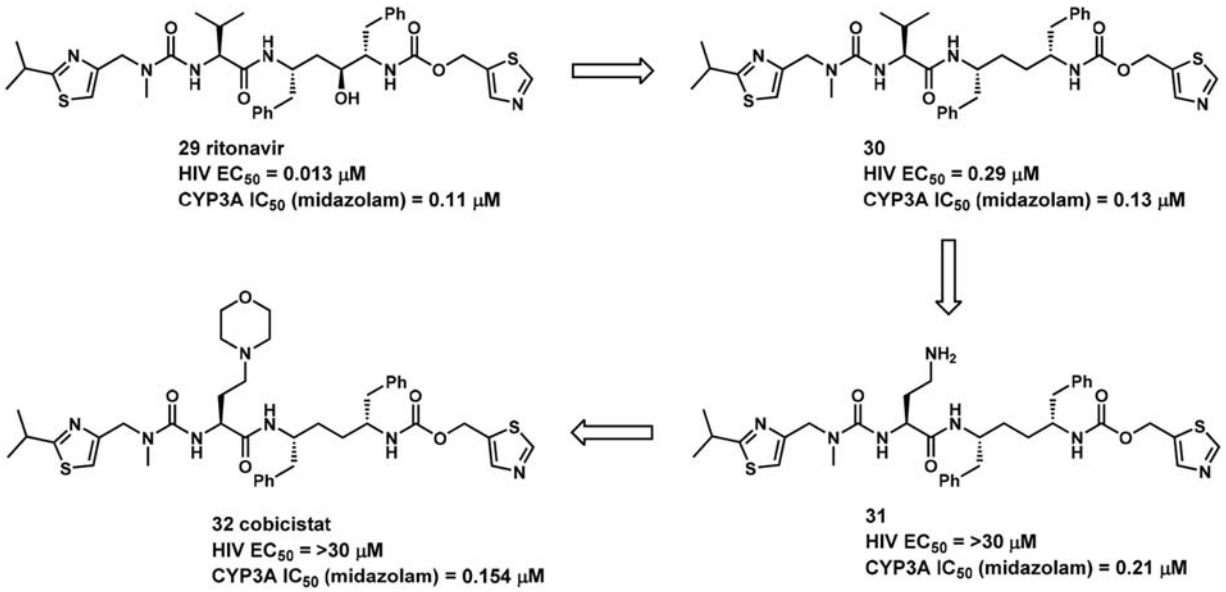

In a Phase II clinical study, 150 mg of COBI was shown to produce a strong pharmacokinetic boosting effect on EVG, allowing for the latter to be dosed QD.[178] The four-drug combination of EVG/COBI and TDF/FTC was studied in multiple Phase III trials. This combination showed noninferiority to EFV/TDF/FTC with fewer of the CNS-related side effects that are characteristic of EFV-containing regimens (abnormal dreams and dizziness), and a larger increase in serum creatinine.[179] Further, EVG/COBI/TDF/FTC showed noninferiority to the protease-based regimen ATZ/RTV/TDF/FTC, with fewer reports of abnormal liver function tests.[180] EVG/COBI/TDF/FTC was approved by the FDA in 2012 as the first integrase-containing STR.[181] In 2015, the four-drug combination of EVG/COBI/TAF/FTC (containing the newer low-dose NRTI TAF in place of TDF) was approved by the FDA.[182] Further, COBI has been shown to effectively enhance the pharmacokinetics of the PIs darunavir and atazanavir.[183] These fixed-dose combinations have also been approved by the FDA and STR-containing darunavir/cobicistat/TAF/FTC is also being studied clinically.[184] If approved, this would be the first protease-containing STR.

5.19.1.11 Preexposure Prophylaxis (PreP)

In 2010, clinical studies were published showing that a combination of TDF and FTC was effective in preventing HIV infection in humans—both in men who have sex with men,[185] as well as by heterosexual transmission.[186] These data were supported by subsequent monkey studies.[187] Though seen as controversial due to its perceived potential to reduce compliance with other HIV prevention strategies, TDF/FTC was approved as an HIV preventative in 2012.[188] In addition, the integrase inhibitor cabotegravir, formulated as a long-acting injectable suspension, is also being evaluated for PreP.[189]

5.19.1.12 HIV Cure

Although current HIV treatments can effectively deter resistance emergence, reduce viral load, and are better tolerated than older treatments, HIV patients are aging and new cases continue to emerge. As a result, a significant amount of scientific effort has focused on approaches toward HIV cure, with the ultimate goal of pathogen eradication.

The pursuit of HIV cure has been approached from several angles, and this section focuses on the two dominant paradigms. The first strategy, known as the "kick-and-kill" approach, is designed to tackle the problem of viral latency. HIV infects multiple cell types, integrating copies of proviral DNA into the host. When infected cells undergo transition into a dormant state, viral latency is achieved. Patients who discontinue HAART will nearly always experience a rapid and strong viral rebound that is presumed to originate from viral propagation out of this latent reservoir. The first strategy seeks to "kick" this latent reservoir of infected cells into an active state with a small molecule or biologic, and then to "kill" them with further therapy. In this way, purging the viral reservoirs could lead to viral eradication or sustained viral control by the host immune system.

Even in the absence of a complete cure, it is desirable for patients to reduce the frequency of dosing associated with HAART. Lowering the total amount of drug in the body could benefit patients on life-long therapy.[190] This alternative to "kick and kill" for managing care is referred to as "functional cure."

5.19.1.12.1 Kick and kill

Epigenetic control of DNA transcription has been shown to contribute to many pathogenic states, including HIV. Because integration of proviral HIV DNA occurs in many cell types, one "kick" approach involves removing epigenetic regulators that block viral transcription in latently infected cells. The most well-studied targets in this area are histone deacetylases (HDACs)—zinc-containing metalloproteins that catalyze the removal of acetyl groups from lysine residues of histones, which is a process known to downregulate the transcription of select genes, and which may contribute to the latency of integrated HIV. Small-molecule HDAC inhibitor (HDACi) research in the context of oncology has served to provide momentum for this approach.

HDACi's which have been tested in vitro or in vivo for latency reversal are shown in **Fig. 14**. **33–36** have all been tested in multiple in vitro models.[195,196] To avoid the known off-target liabilities of the hydroxamic acid class, the macrobicyclic depsipeptide Romidepsin (**37**) was also investigated.[191] Romidepsin is a prodrug that undergoes disulfide bioreduction to provide a free thiol that coordinates to the zinc atom in the active site of HDACs.[192–194]

Despite their potential to deliver the clinical "kick," there is evidence that HDACi's may lead to latent reservoir reseeding. A further concern is the potential for HDACi's to produce undesirable side effects due to nonspecific epigenetic effects.

In latency reversal models of HIV in $CD4^+$ T cells derived from patients, Vorinostat (**33**)[195] and Romidepsin (**37**)[192] have both shown latency reactivation with proviral transcription, but belinostat (**34**), gavinostat (**35**), and panobinostat (**36**) have not yet demonstrated efficacy.[196]

Vorinostat (**33**), the most advanced hydroxamic acid-based HDACi, has been tested in HIV patients.[197] Though there was a 4.8-fold increase in viral mRNA production (potential evidence of a "kick"), concerns regarding reservoir reseeding remained.[198] Although HDAC inhibitors may achieve the "kick" portion of latency reversal approach, a "kill" is also needed. Activation of the innate and adaptive immune systems of the host may aid this process. TLR7 agonists such as compounds (**38–40**) can stimulate the release of interferon and immunomodulatory cytokines, and awaken the innate immune system. Thus, TLR7 agonists are being pursued as potential components of an HIV cure.

SAR studies revealed two important factors governing the potency of TLR7 agonists (**Table 8**).[199] First, a basic amine on the distal portion of the molecule was critical for achieving a potent minimal effective concentration (MEC, defined as the minimal agonist concentration requires threefold stimulation of IFNα over baseline). Thus, **39** displayed greater MEC potency than **38**. Additionally, **39** was more selective for stimulation of IFN-α relative to TNF-α. Second, the addition of a lipophilic n-butoxy side chain led to GS-

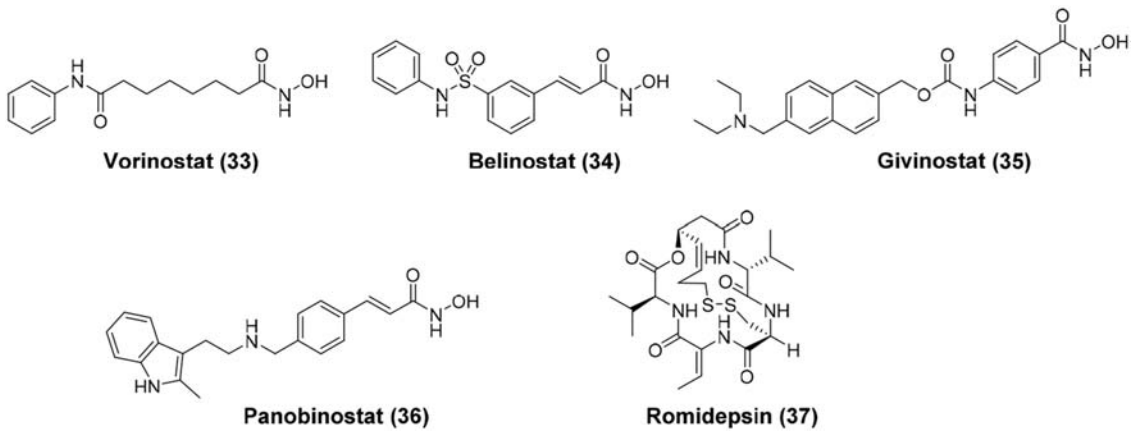

Fig. 14 HDAC inhibitors.

Table 8 TLR7 agonists

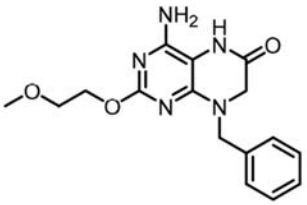

38

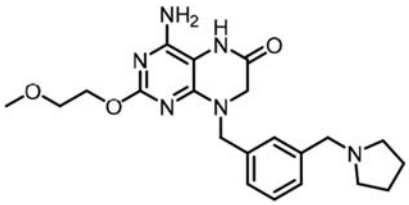

39

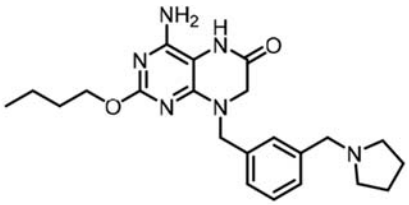

40

Compound	*IFN-α MEC (nM)*	*Fold TNF-α MEC over IFN-α MEC*
38	1000	0.3
39	10	1000
40	3	100

9620 (**40**), which showed further increased potency and also favorable pharmacodynamics in cynomolgus monkeys. GS-9620 is currently in a Phase I clinical trial in HIV-infected patients.[200]

One challenge with modulation of the innate or adaptive immune system is the activation of unwanted pathways during the "kick" process. Indeed, antiviral IFNα-based therapies are associated with undesirable side effects. Thus, some research has been directed toward agents that affect a "kill" without activating the latent infected cells (i.e., no "kick"). A high-throughput screen for CD4/8T-cell killing agents that do not broadly activate the immune system revealed disulfiram (antabuse) (**9**) as a candidate molecule (Table 9).[201] While the precise mechanism of HIV "killing" is unknown, evidence suggests the inhibition of PTEN, which is important in the regulation of the Akt pathway.[202] The human metabolism of disulfiram (**9**) is complex, making it difficult to assess whether biological activity derives from the parent or metabolite(s).[203] Disulfiram (**41**) and its primary thiocarbamic acid metabolite (**42**) are both active in a latency reversal assay, but the S-oxide metabolite (**43**) and thioester analog (**44**) are both inactive (Table 9). Disulfiram (**41**) was tested in HIV-infected adults, and although latency reversal was observed, there was no statistically significant change in the size of the viral reservoir.[204]

HDAC inhibitors can act at the level of chromatin remodeling and epigenetic control, functionally close to the production of viral mRNA. Disulfiram is believed to act further upstream, at the level of PTEN signaling in the cytosol.[202] The TLR7 receptor is yet further upstream, expressed in the early endosomal compartment, and activates immunity in response to pathogen-associated molecular patterns. Another target in the "kick and/or kill" strategy, protein kinase C (PKC), lies even farther upstream. PKC is a cell-membrane-associated enzyme capable of T-cell activation via the NF-kB pathway when stimulated by small molecules.[205] Exploration of PKC activation has spanned multiple cell classes including primary $CD4^+$ T cells, J-Lat cells, and QVOA patient cell isolates.

One PKC activator, phorbol-12-myristate-13-acetate (PMA, **45**), showed some activity in three different models of latent cellular activation, reaching full activation in J-Lat clone cells (Table 10). The natural product prostratin (**46**) can also induce virus from latently infected primary $CD4^+$ T cells.[205] As with **45**, the response to **46** across cell types was highly variable. The macrolide

Table 9 Disulfuram and SAR

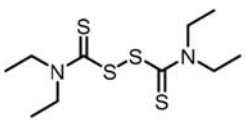

Disulfiram (41)

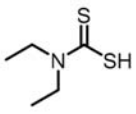

42

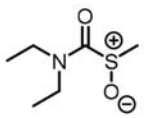

43

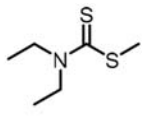

44

Compound	*Capable of latency reversal?*
41	Yes
42	Yes
43	No
44	No

Table 10 Protein kinase C activators % latent cellular activation (normalized to maximal level)

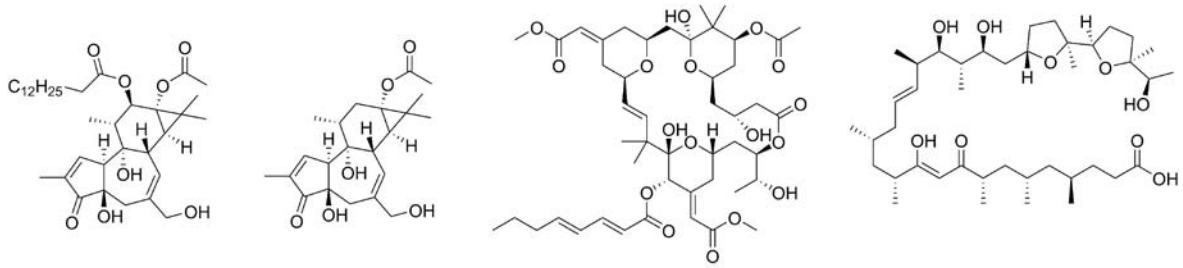

Compound	*Primary CD4$^+$ T cells* [a] *(%)*	*J-Lat clone cells* [b] *(%)*	*QVOA cells* [c] *(%)*
45	4–70	40–100	30
46	15–70	10–90	40
47	−5 to 100	5–60	0
45 + 48	20–90	100	90
48	5–30	0	25

[a]Primary CD4$^+$ T-cell methods: Greene, Lewin, Planelles, Siliciano, and Spina.
[b]J-Lat clone cell lineages: 5A8, 6.3, 8.4, and 11.1.
[c]QVOA cells are HIV patient-derived cells.

bryostatin-1 (**47**) and related analogs can also engage PKC via binding to the diacetylglycerol-binding region.[205] Bryostatin-1 (**47**) exhibited extreme variability in primary CD4$^+$ T cells depending on the specific model, but failed to activate QVOA cells.

Because calcium regulation is important within the PKC activation pathway, PKC activators such as PMA (**45**) have been paired with the calcium ionophore ionomycin (**48**). In the Greene and Siliciano versions of the HIV latent CD4$^+$ T-cell assay, the combination of **45** and **48** gives more robust activation than for either compound alone (**Table 4**).

5.19.1.12.2 Direct-acting antivirals for functional cure

Several HIV targets have been investigated specifically due to their unusual PK/PD potential—they may provide more effective treatments with less frequent dosing regimens. Among targets of this type are tat and rev (**Fig. 15**).

HIV tat regulates the transcription of integrated proviral DNA.[206] One of its functions is to bind a DNA segment called the trans-activation region (TAR) to enable viral DNA transcription. When tat binds to TAR a feedback signaling loop is initiated, amplifying the transcription of full-length viral mRNA. Dehydrocortistatin A (dCA, **49**), a synthetic analog of the natural product cortistatin A (**50**), binds to the TAR-binding domain of tat (**Fig. 15**) suppressing the formation of p24 (HIV capsid protein) with an EC_{50} of 0.7 pM[207] and thereby repressing the feedback trans-activation loop. In contrast to the "kick" approach, which aims to reverse latency, **49** *promotes* latency. Hence, in a separate experiment, CD4$^+$-HeLa cells infected with HIV were treated with **49** for a period of 60 days, followed by cessation of treatment. No viral rebound was observed for up to 27 days postcessation, in contrast to the rebound seen with current HAART.[208] This phenomenon has been attributed to long-term silencing of key HIV-transcriptional systems.[207,209] Notably, HIV-infected cells treated with **49** were resistant or even recalcitrant to "kick" reactivation by the HDAC

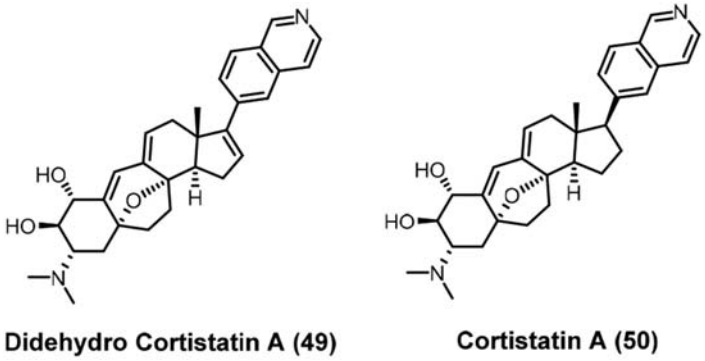

Fig. 15 Selected small molecules targeting HIV tat.

inhibitor **33**, the PKC activator **46,** or the PKC activator combination of **45** and **48**. To provide further evidence that the silencing effect of **49** is mediated via inhibition of the TAR domain of HIV-tat, the introduction of a plasmid containing the *Tat* gene into silenced HIV-infected cells was shown to result in a rapid rebound in viremia.[209] Taken together, these studies suggest dCA (**49**) administration could help achieve a "functional cure" alone or in combination with other therapies by reducing therapeutic dosing frequency.

HIV-tat is responsible for transcription activation, leading to the production of full-length 9 kB viral mRNA. The next stage in the viral life cycle requires both partial and complete splicing to the 4 and 2 kB viral mRNAs that encode select viral proteins. Regulation of this splicing is directed by the HIV rev protein, which binds to the rev response element (RRE) present on 4 and 9 kB viral mRNA transcripts. Rev also coordinates the export of viral mRNA by binding directly to cap-binding-complex (CBC) proteins.[210] Tetracycle **51** (IDC16) was found to disrupt the action of HIV-rev by controlling splicing factors.[211] However, IDC16 is nonspecific in its binding to RNA and DNA, giving rise to cytotoxicity. ABX-464 (**52**) was devised as a less planar version of **51** and retained the favorable disruption of rev in HIV-infected macrophages while imparting lowered cytotoxicity (**Table 11**).[211] In a humanized mouse model of HIV, mice were virally suppressed either with HAART or **52**. When therapies were removed, viral rebound was rapid in mice treated with HAART, but delayed (sometimes by greater than a month) in those treated with **52**. ABX-464 (**52**) is currently in Phase II clinical trial as part of a "functional cure" approach toward HIV.

The field of HIV cure research is growing, and clinical work has begun. Key to the "kick-and-kill" approach will be increased understanding of the interactions between HIV and the host immune system. Combination therapy has evolved as STRs have emerged for HAART, and combinations could play a valuable role in the "kick-and-kill" strategy as well. This may also be true for "functional cure" regimens, which could allow patients the option of less frequent dosing.

5.19.2 Hepatitis B Virus

Hepatitis B virus (HBV) is a DNA virus that targets hepatocytes and causes a chronic liver infection which, like that of hepatitis C virus (HCV), slowly causes liver damage and can eventually lead to liver fibrosis, cirrhosis, and hepatocellular carcinoma (HCC).[212] Although HBV is a small and relatively simple virus,[213] the search for effective treatments has been surprisingly difficult. This is likely due to an unusual viral life cycle, which involves a long-lived covalent, circular closed DNA (cccDNA) genetic template, as well as the virus's apparent ability to dampen the host immune response.[214] In this section, current treatment regimens, the life cycle of HBV and efforts to develop improved small molecule and biologic treatments are described.

There are approximately 240 million chronically infected HBV patients worldwide,[215] for whom current treatment options are quite limited and based on interferon- and nucleoside-based regimens.[216] Both approaches lead to improvements in disease severity (HBV DNA reductions and often ALT normalization) in many patients, with nucleoside regimens well tolerated and effective for long-term viral suppression, but neither leads to significant rates of cure (defined as S-antigen seroconversion or HBsAg loss) (**Table 12**); indeed, no currently approved HBV regimen leads to HBsAg loss in >10% of patients. As a consequence of this limited efficacy, patients are generally not recommended for treatment until the severity of disease becomes problematic (increased ALT levels and/or detectable fibrosis or cirrhosis).

5.19.2.1 HBV Replication Cycle and Potential Drug Targets (New Section)

In contrast to HIV, HBV is a small and relatively simple DNA virus. The virus consists of viral DNA and the viral polymerase enclosed within an icosahedral nucleocapsid composed of core antigen protein (HBcAg). The surface of the nucleocapsid is covered by

Table 11 Disruption of the HIV rev protein

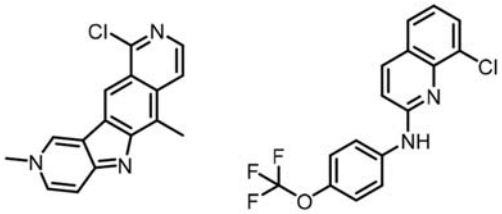

IDC16 (51) **ABX-464 (52)**

Compound	*IC_{50} (μM) in macrophages*	*CC_{50} (μM) in macrophages*	*IC_{50} (μM) in PBMCs*	*CC_{50} (μM) in PBMCs*
51	0.1–0.5	>1.0	0.1–0.5	>2.5
52	0.1–0.5	>50	0.1–0.5	>63

Table 12 Results of main studies for the treatment of HBeAg-positive chronic hepatitis B at 6 months following 12 months (48 or 52 weeks) of pegylated interferon alpha (PEG-IFN) and at 12 months (48 or 52 weeks) of nucleos(t)ide analog therapy[217]

	PEG-INF		*Nucleosides*			*Nucleotides*	
	PEG-INF-2a	*PEG-INF-2b*	*Lamivudine*	*Telbivudine*	*Entecavir*	*Adefovir*	*TDF*
Dose	180 mg	100 mg	100 mg	600 mg	0.5 mg	10 mg	245 mg
Anti-HBe seroconversion (%)	32	29	16–18	22	21	12–18	21
HBV DNA $<$60–80 IU mL^{-1} (%)	14	7	36–44	60	67	13–21	76
ALT normalization (%)	41	32	41–72	77	68	48–54	68
HBsAg loss (%)	3	7	0–1	0.5	2	0	3

surface antigen (HBsAg). The replication cycle commences when HBV binds the sodium-taurocholate cotransporting polypeptide (NTCP) receptor on a hepatocyte (Fig. 16). After receptor-mediated endocytosis, the nucleocapsid is released into the cell. This is followed by import into the nucleus, after which viral DNA (in the form of relaxed-circular DNA or rcDNA) is converted by the covalently attached viral polymerase to the stable viral genetic template—covalently closed circular DNA or cccDNA. Transcription of cccDNA, which may be aided by host transcription factors as well as viral proteins such as HBcAg and HBx, leads to the formation of three classes of mRNAs which include genome-length pregenomic and precore RNAs (coding for core protein, the viral polymerase, and e-antigen) and subgenomic mRNAs (coding for S antigens and HBx protein). After translation to form viral proteins (core, polymerase, eAg, sAg, and X), pregenomic RNA and polymerase are encapsidated. Reverse transcription to form the viral DNA

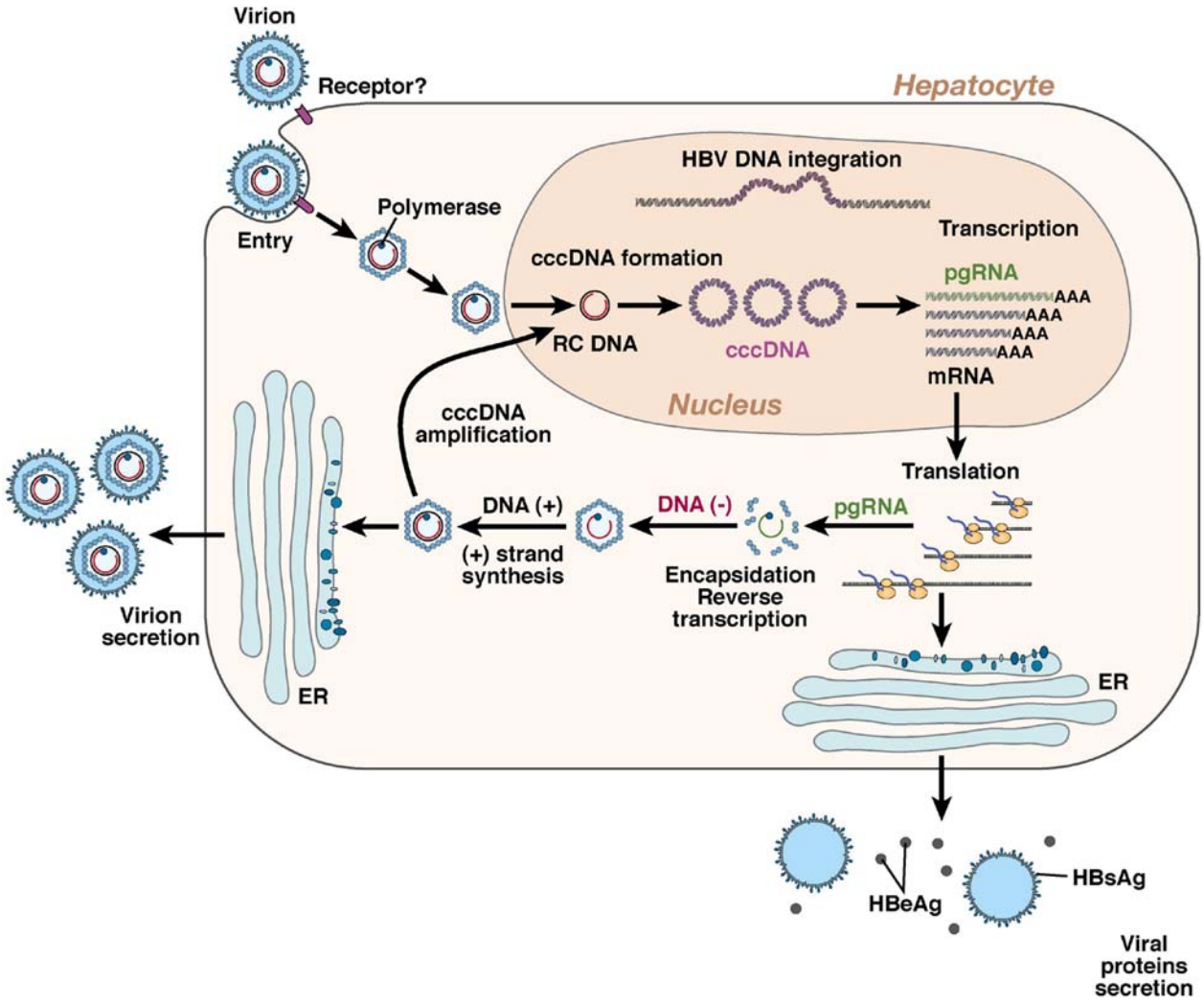

Fig. 16 The HBV replication cycle.[220]

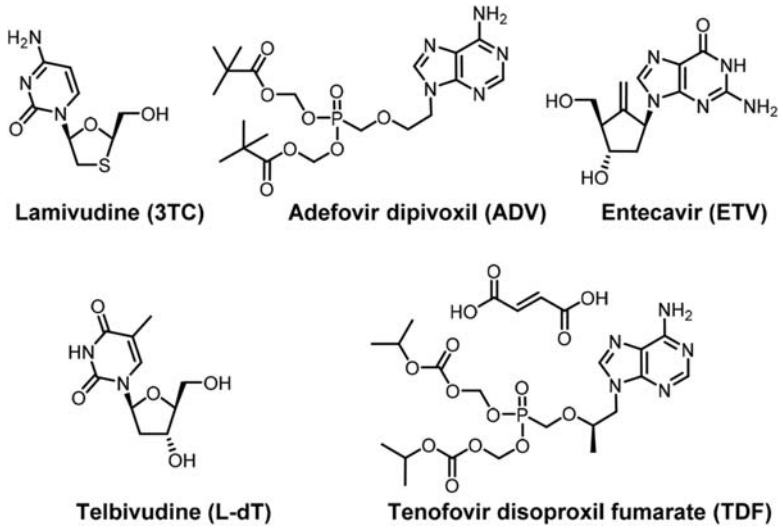

Fig. 17 Structures of approved nucleoside HBV reverse transcriptase inhibitors.

occurs inside the nucleocapsid, and this immature virion can either be recycled back to the nucleus for potential cccDNA amplification or enveloped with sAg and secreted as an infectious virion.[218,219]

5.19.2.2 Nucleoside Reverse Transcriptase Inhibitors

Nucleoside or nucleotide reverse transcriptase (RT) inhibitors have become widely used for the treatment of chronic HBV infection.[221–224] There are five approved anit-HBV nucleoside or nucleotide therapeutics: lamivudine (3TC), adefovir dipivoxil (ADV), entecavir (ETV), telbivudine (L-dT), and TDF (Fig. 17 and Table 13). These agents undergo phosphorylation to their active triphosphate (ETV, 3TC, and L-dT) or diphosphate (ADV and TDF) metabolites which are then incorporated by the viral polymerase and inhibit phases of reverse transcription. 3TC inhibits (+)RNA-dependent (−)DNA synthesis,[225,226] whereas ADV and TDF inhibit both priming of RT and (+)RNA-dependent (−)DNA synthesis.[227–230] ETV and L-dT interact with priming, (+)RNA-dependent (−)DNA synthesis, and subsequent (−)DNA-dependent (+)DNA synthesis.[231–233] The goal of HBV treatment with nucleoside or nucleotide agents is to achieve sustained viral suppression of HBV replication without the emergence of resistance, and thereby to decrease the risk of liver cirrhosis and HCC.

Table 13 FDA-approved nucleoside HBV reverse transcriptase inhibitors

Drug	*Approval year*	*Dosage (mg)*	*Dose frequency* [a]	F% [b]	*Plasma* $t_{1/2}$ *(h)*	*Intracellular NTP* $t_{1/2}$ *(h)* [c]	*Resistance mutations*[234]	*Resistance/ at year*[224]	*Adverse effects*
3TC	1998	100	qd	86–87%	5–7	17–19[235]	V173L, L183M, A181T/V, and M204V/I	70%/5	Negligible
ADV	2002	10	qd	59%	7.48[f]	33[236]	A181T/V and N236T	29%/5	Potential nephrotoxicity
ETV	2005	0.5[d] 1.0[e]	qd dq	>70%	130	15[237]	L180M, T184, M204I/V, S202, and M250I/V	1%/5	Negligible
L-dT	2006	600	qd	52%	29.5–43[238]	15[239]	V173L, L183M, A181T/V, and M204V/I	17%/2	Negligible
TDF	2008	300	qd	25–39%	~17	95[227]	A181T/V and N236T	0%/6	Renal insufficiency and bone loss

[a]qd, once daily; bid, twice daily; tid, three times daily.
[b]*F*%, oral bioavailability.
[c]Half-life in HepG2 cells.
[d]For treatment-naive patients.
[e]For treatment experience patients.
[f]Adefovir terminal elimination half-life.

3TC was the first HBV RT inhibitor to be approved by the FDA (in 1998). It inhibits HBV replication with an EC_{50} of approximately 10 nM in HepG2 2.2.15 cells,[240,241] and is dosed orally at 100 mg QD and is well tolerated with negligible adverse effects. The drawback of 3TC therapy is the rapid onset of resistance, with only a single mutation sufficient to compromise efficacy significantly.[242] Thus, other antivirals with higher barriers to resistance are prescribed preferentially.[234] The related 5-fluoro analog, emtricitabine (FTC, not shown), is also potent against HBV[241] and has an excellent safety profile. FTC, has been evaluated as both monotherapy[243] and in combination with TDF,[244,245] for the treatment of HBV. In both combination studies, FTC/TDF treatment resulted in higher rates of viral suppression than TDF alone. However, rates of e- or s seroconversion were low and not improved with combination therapy.

ADV, the bis-(pivaloylmethyl) ester prodrug of adefovir designed to improve oral absorption, was approved in 2002 for the treatment of HBV. The parent adefovir inhibits HBV replication with an IC_{50} of 0.7 μM in HepG2 cells.[246] ADV exhibits an EC_{50} of 0.1 μM in HepG2 2.2.15 cells[227] and is dosed orally at 10 mg QD. ADV has been associated with renal toxicity at higher (30 mg) or more frequent doses; while the 10 mg dose has minimal effects, close monitoring of renal function is required.[222] While improved compared to 3TC, ADV still has a low genetic barrier with high-level resistance occurring from a single mutation.[234,242] The resistance profile coupled with the potential for renal toxicity has led to a decrease in use of ADV.

ETV is a 2′-deoxyguanosine nucleoside analog featuring a cyclopentyl ring with an exocyclic olefin replacement for the oxygen of the ribose moiety, and was approved in 2005 for the treatment of chronic HBV infection. ETV is a highly potent and selective inhibitor of HBV with an EC_{50} of 3.75 nM in the HepG2 2.2.15 cells, and is dosed orally QD at 0.5 or 1.0 mg in treatment-naive or -experienced patients, respectively.[247,248] Unlike the other approved anti-HBV nucleoside inhibitors, ETV is a nonobligate delayed chain terminator,[249] which reduces the potential for subsequent excision.[232] ETV is well tolerated, and has a very high genetic barrier with a very low incidence of resistance that requires three point mutations.[234,250,251] ETV is currently prescribed as a first line of therapy for the treatment of HBV.[221,223]

L-dT is the unnatural L-isomer of thymidine approved for the treatment of HBV in 2006. L-dT has selective anti-HBV activity with an EC_{50} of 0.19 μM in HepG2 2.2.15 cells, and is dosed orally at 600 mg once daily.[252] L-dT has an excellent safety profile and has been implicated in the suppression of mother-to-child transmission of HBV during pregnancy.[253] While the barrier to resistance is higher than 3TC, resistance to L-dT can still develop through a single point mutation[234,242] and thus it is not recommended as a first-line therapy.

TDF is the most recent RT inhibitor to be approved for the treatment of HBV (2008). It shows comparable clinical efficacy to ETV and is also prescribed as a first-line agent.[221,223,254] TDF is the bis(isopropyloxycarbonyloxymethyl) ester prodrug of the parent nucleotide TFV. The ester prodrug is required for adequate oral absorption. TFV-diphosphate is a potent competitive inhibitor of HBV polymerase ($K_i = 0.18$ μM), and TDF inhibits HBV replication with an EC_{50} of 0.02 μM in HepG2 2.2.15 cells.[227] TDF is dosed orally at 300 mg QD, and while generally well tolerated, TDF therapy has been associated with renal adverse events[255] as well as bone density loss,[256,257] in some patients. Despite this potential for toxicity, discontinuation of therapy with TDF was less prevalent than with ETV therapy.[254] Remarkably, TDF shows a very high barrier to resistance and no resistance mutations have been identified after up to 6 years of treatment.[258]

5.19.2.2.1 Investigational HBV RT inhibitors

Even with the success of existing anti-HBV nucleoside and nucleotide therapeutics, efforts have continued to identify novel RT inhibitors that may have additional benefits as compared to the existing agents (**Fig. 18**). TAF is the orally bioavailable isopropylalanilyl phenyl ester prodrug of TFV and was approved in 2015 for the treatment of HIV (vide supra). TAF exhibits greater stability in human plasma than TDF and leads to much lower exposure of the parent TFV in plasma. As a result, TAF shows lower potential for renal and bone toxicity. TAF also provides efficient delivery of the active metabolite TFV-diphosphate to hepatocytes, where the prodrug is primarily activated by carboxylesterase 1.[259] TAF is safe and well tolerated, with similar efficacy to TDF even at much lower doses (from 8 to 120 mg),[260] and is currently being evaluated in Phase III clinical trials.

Besifovir is the dipivoxil prodrug of a novel acyclic guanine phosphonate nucleoside analog which features a cyclopropyl group in the backbone. Besifovir is a potent and selective anti-HBV agent with an EC_{50} of 50 nM in HepG2 2.2.15 cells.[261] Besifovir is currently being evaluated clinically at once daily oral doses of 90 or 150 mg, and has demonstrated good safety profile with carnitine depletion noted as the most common side effect.[262] No virological breakthrough has been observed over 2 years of treatment and the efficacy is comparable to ETV. Besifovir is in Phase III clinical trials.

Pradefovir is a prodrug of adefovir that was designed to be selectively activated in the liver to improve the therapeutic index as compared to ADV.[263,264] The prodrug is oxidatively cleaved by CYP3A4 in hepatocytes.[265] Pradefovir has demonstrated good efficacy as compared to ADV and appears to be well tolerated up to 48 weeks of administration.[266] Pradefovir is currently being evaluated in Phase II clinical trials.

CMX-157 is the hexadecycloxypropyl phospholipid prodrug of TFV and is in development for the treatment of HBV as well as for HIV (vide supra). It inhibits HBV replication with an EC_{50} of 1.6 μM in HepG2 2.2.15 cells.[267] The prodrug is designed to mimic natural phospholipids and improves oral bioavailability and cell permeability as compared to the parent TFV. Like TAF, the prodrug is stable in plasma and is intended to reduce the potential for renal and bone toxicity by lowering plasma

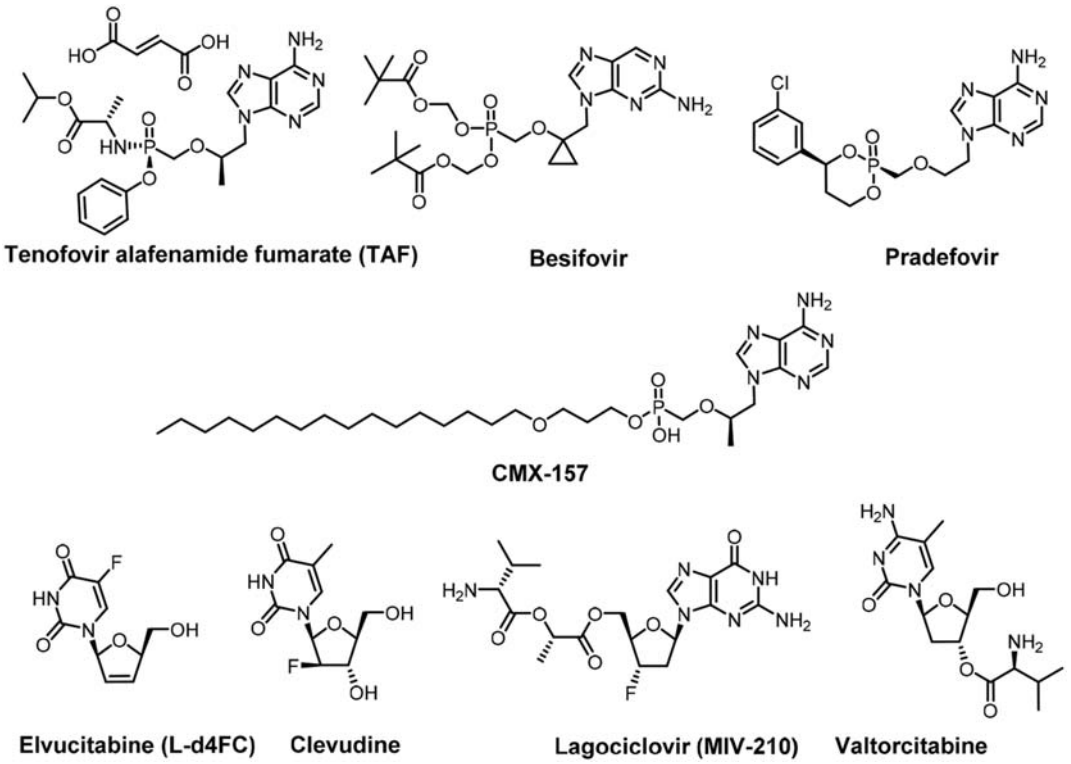

Fig. 18 Structures of investigational nucleoside HBV reverse transcriptase inhibitors.

exposure of the parent TFV. CMX-157 is currently being evaluated for safety, tolerability, and pharmacokinetics in Phase I clinical trials.

Elvucitabine (L-d4FC) is a 5-fluoro cytidine dideoxy ribose L-nucleoside that has also been explored clinically for the treatment of both HIV (vide supra) and HBV. L-d4FC inhibits HBV replication with an EC_{50} of 2-8 nM in HepG2 2.2.15 cells.[268–270] At oral doses up to 100 mg L-d4FC was well tolerated, without apparent drug-related adverse events, and showed potent antiviral activity in patients with hepatitis B infection.[271–274] L-d4FC has reached Phase II clinical development; however, there have been no recent reports of its clinical progress.

Clevudine (L-FMAU) is a 2′-fluoro-5-methyl-β-L-arabinofuranosyl uracil analog that exhibits an EC_{50} of 0.1 μM against HBV in HepG2 2.2.15 cells.[275] L-FMAU was launched in several Asian countries; however, in the United States, it was associated with the onset of myopathy in Phase III clinical trials[276] and its development was discontinued. Additionally, Lagociclovir[277] and Valtorcitabine[278] are two further investigational anti-HBV nucleosides that reached Phase II clinical evaluation, but whose development has recently been discontinued.

5.19.2.3 Capsid Assembly Inhibitors

Beyond NRTIs, the mechanism that has elicited the most interest from small-molecule drug discovery groups has been capsid inhibition. Capsid modulators are believed to act by changing the kinetics of capsid assembly, resulting in malformed or noninfectious particles.[279] Further, because the core protein is involved in multiple parts of the viral life cycle, it is believed that capsid assembly modulators can affect HBV infection in more ways that simply reducing viral load. It has been reported that capsid inhibitors, in addition to causing misassembly of the capsid, also cause improper packaging of RNA and interfere with the establishment of new cccDNA.[280] At least four classes of small molecules have been shown to interfere with the viral capsid assembly process: heteroaryldihydropyrimidines (HAPs), phenyl sulfonamides, oxazolidinones,[281] and propenamides.[282] Of these the most extensively studied are the HAPs, which were discovered in the late 1990s. An important early HAP lead is BAY-41,[283,284] which showed activity in cellular assays as well as in an HBV transgenic mouse model. Later the more potent GLS-

4[285] was disclosed, and this analog has completed Phase I clinical studies.[286] More recent work on the HAP chemotype includes bicyclic variants.[287]

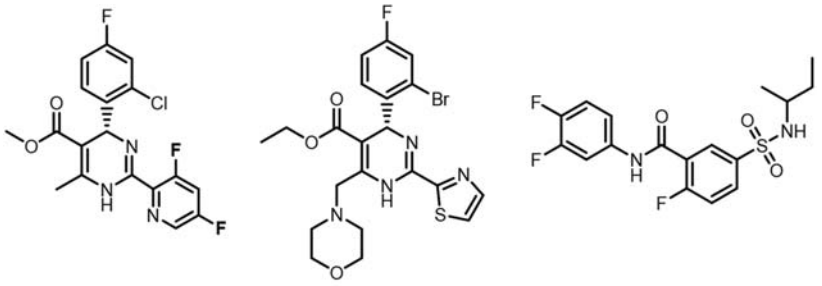

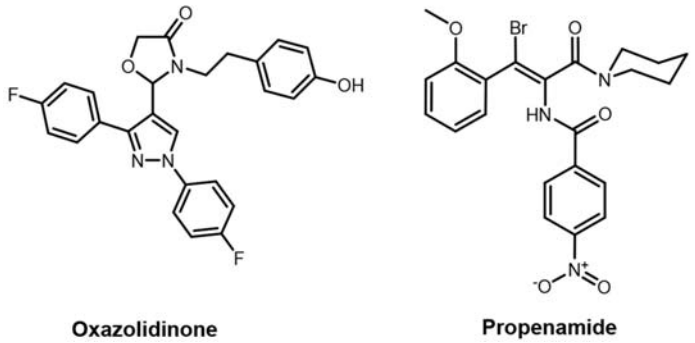

The sulfonamide class of capsid modulators originated from a high-throughput screening effort resulting in compounds, such as DRV-23, with sub-micromolar potency in cellular assays.[288] Optimization of this class has continued, and one compound, NVR-3-778 (structure not disclosed) has entered clinical trials. The first human clinical proof of concept for this mechanism was established with this compound: oral administration of 600 mg twice daily for 28 days led to a 1.7 log reduction of HBV DNA in the plasma of chronically infected patients.[289]

5.19.2.4 Immunomodulators

A coordinated action of both the innate and adaptive immune response is understood to be a requirement for effective host control of viral infection.[290] Pattern recognition receptors such as the Toll-like receptors (TLRs) serve as first responders in signaling and activation of the innate immune system and additionally provide a link to adaptive immune system T- and B-cell responses.[291] Of particular relevance as a therapeutic target for the treatment of HBV infection, TLR7 has been identified as a member of this receptor class with single-stranded RNA of viral origin as its native ligand.[292]

A family of pteridinone TLR7 receptor agonists including **53**, **54**, and **55** was reported, and their properties described in terms of immunomodulatory activity, selectivity versus other TLRs, and the resulting induction of antiviral cytokines such as IFN-α and TNF-α in assays characterizing the in vitro response of peripheral blood mononuclear cell culture (PBMC) assays. Compound **55** (GS-9620) exhibited an IFN-α MEC of 3 nM and a selectivity ratio of 100 for the observed IFN-α/TNF-α response. Appending the pyrrolidine ring onto the scaffold conferred higher potency and selectivity as compared to related compound **55** (**Fig. 19**).[293]

Compound **55** is highly soluble at low pH and is rapidly metabolized in mouse, rat, dog, monkey, and human hepatic microsomes (with a human microsomal $t_{1/2}$ of 30.5 min). Compound **55** was tested in both chimpanzee and woodchuck efficacy models for HBV. In chimpanzees, every-other-day dosing at 1 mg kg^{-1} for 4 weeks followed by a 1 week rest and then 4 weeks at 2 mg kg^{-1} led to a mean maximal HBV viral reduction of 2.2 logs.[294] In a WHV[295] woodchuck efficacy study, sustained antiviral response to compound **55**, including long-term sAg loss and s-antibody seroconversion was reported in animals treated with dose regimens of 2.5 mg kg^{-1} every other day for 9 weeks as well as in animals receiving 5 mg kg^{-1} weekly for 8 weeks.[296]

In human Phase Ib clinical trials recently reported for compound **55**, chronically infected HBV patients received 0.3, 1, 2, or 4 mg as either a single dose or with a second dose repeated 7 days later. Dose-dependent peripheral mRNA expression of interferon-stimulated gene 15 was detected, although no clinically significant reductions in plasma HBV DNA levels were observed in treatment-naive patients, and no clinically significant HBsAg reduction was observed for either treatment naive or virally suppressed

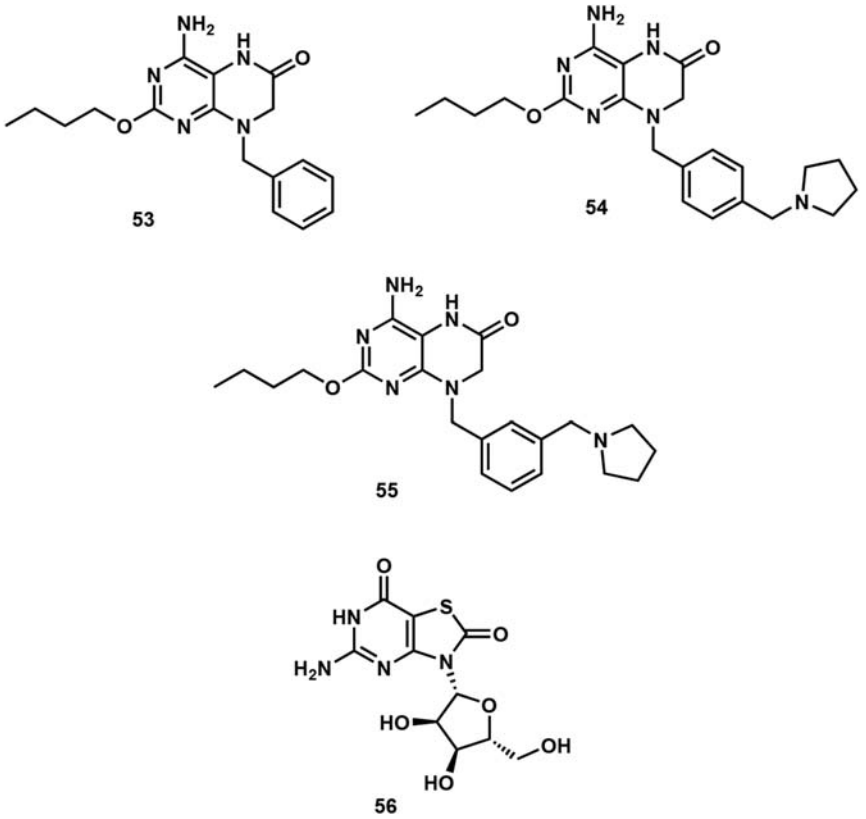

Fig. 19 Immunomodulators for HBV.

subjects.[297] Compound **55** is currently the subject of Phase II clinical trials examining longer dosing durations in chronically infected HBV patients.[298]

Another immunomodulator under examination for its potential to treat HBV is RG-7795 (formerly ANA-773), a prodrug of the nucleoside analog isatoribine (**56**). The prodrug moiety for **56** remains undisclosed, but its active metabolite has been characterized for TLR7 agonism, as well as for in vitro activation of the innate and adaptive immune response.[299] Following earlier clinical trials for the treatment of HCV, its efficacy in the context of virally suppressed, chronically infected HBV patients is the subject of Phase II clinical trials.[300]

5.19.2.5 Biologics-Based Approaches: RNAi and Entry Inhibition

Though nucleoside polymerase inhibitors have provided durable viral suppression and improved outcomes for HBV patients, a cure has remained elusive. Beginning in the early 2000s, some researchers turned their attention to biologic-based approaches. Foremost among these is the use of small-interfering RNAs (siRNAs) to block viral transcription. One early report showed that siRNA reduced viral DNA, RNA, and antigens in vitro (up to 80%) and when delivered by plasmid was also active in a mouse model.[301] Soon after, another group showed that siRNA delivered in liposomes elicited a >1.0 log reduction in viral DNA in a mouse model of HBV.[302] Adenovirus delivery of siRNA was also shown to reduce HBV gene expression and replication to near undetectable levels for at least 26 days in mouse.[303] Still it was recognized that for RNAi silencing to become an effective HBV treatment in humans, several limitations needed to be addressed. These include poor siRNA stability, difficulties in cellular uptake, and off-target effects.[304]

Several groups are actively pursuing this line of research,[305] and the most advanced siRNAs for HBV are ARC-520 and ARC-521—both designed to address the difficulties in delivery that generally plague siRNA therapy. The novel delivery method in both cases involves a siRNA conjugated to a cholesterol derivative (for liver targeting), coinjected with a hepatocyte-targeted endosomolytic polymer (which facilitates siRNA escape from endosomes).[306–308] In Phase II clinical trials in HBV patients, ARC-520 administration was recently reported to result in a mean viral DNA reduction in plasma of 2.2 logs, with a mean maximal HBsAg reduction of 1.1 logs in eAg-positive patients.[309]

In addition to drugs targeting transcription, agents which block viral entry have also been pursued. The most effective and well studied of these is myrcludex B, a lipopeptide that targets the critical entry host factor NTCP.[310] In HBV infected uPA/SCID mice, myrcludex B was shown to block viral spread and hinder amplification of cccDNA.[311] Myrcludex B was recently reported to be in clinical trials in combination with pegylated interferon-alpha-2a.[312]

5.19.3 Conclusion

The results of decades of drug discovery and development for treatments of HIV and HBV have greatly improved the lives of millions of patients. Medicinal chemistry research directed at HIV has resulted in many classes of effective drugs that, in proper combinations, lead to a long-term suppression of HIV. The newest of these drugs are more potent, result in fewer side effects, have longer half-lives, and are often combined into convenient STRs. In addition to ever more effective oral antivirals, treatments requiring less frequent dosing including once-monthly injectables are being tested. Efforts are now intensifying toward the even greater challenge of discovery of a safe and effective curative approach.

HBV research is at a less advanced stage. Though several nucleoside- and interferon-based treatments are in common use and can improve liver function, few patients achieve cure (sAg seroconversion), and no other classes of HBV drugs have yet been approved. Current work on HBV includes direct-acting antivirals (capsid inhibitors), immunomodulators (TLR7), and biologics that block viral translation (RNAi). If an HBV cure is to be found, it may require the combination of several of these approaches.

References

1. Deeks, S. G.; Lewin, S. R.; Havlir, D. V. *Lancet* **2013,** *382,* 1525–1533.
2. The Antiretroviral Therapy Cohort Collaboration. *Lancet* **2008,** *372,* 293–299.
3. Lima, V. D.; Hogg, R. S.; Harrigan, P. R.; Moore, D.; Yip, B.; Wood, E.; Montaner, J. S. G. *AIDS* **2007,** *21,* 685–692.
4. Mehellou, Y.; DeClerq, E. *J. Med. Chem.* **2010,** *53,* 521–538.
5. Comprehensive Medicinal Chemistry, vol.7; 2007. pp. 329–371; Chapter 12.
6. DeClercq, E. *Nat. Rev. Drug Discov.* **2002,** *1,* 13–25.
7. Barre-Sinoussi, F.; Ross, A. L.; Delfraissy, J.-F. *Nat. Rev. Microbiol.* **2013,** *11,* 877–883.
8. Laskey, S. B.; Siliciano, R. F. *Nat. Rev. Microbiol.* **2014,** *12,* 772–780.
9. Hammer, S. M.; Saag, M. S.; Schechter, M.; Montaner, J. S. G.; Schooley, R. T.; Jacobsen, D. M.; Thompson, M. A.; Carpenter, C. C. J.; Fischl, M. A.; Gazzard, B. G.; Gatell, J. M.; Hirsch, M. S.; Katzenstein, D. A.; Richman, D. D.; Vella, S.; Yenni, P. G.; Voldberding, P. A. *JAMA* **2006,** *296,* 827–843.
10. Gunthard, H. F.; Aberg, J. A.; Eron, J. J.; Hoy, J. F.; Telenti, A.; Benson, C. A.; Burger, D. M.; Cahn, P.; Gallant, J. E.; Glesby, M. J.; Reiss, P.; Saag, M. S.; Thomas, D. L.; Jacobsen, D. M.; Volberding, P. A. *JAMA* **2014,** *312,* 410–425.
11. Little, S. J.; Holte, S.; Routy, J.-P.; Daar, E. S.; Markowitz, M.; Collier, A. C.; Koup, R. A.; Mellors, J. W.; Connick, E.; Conway, B.; Kilby, M.; Wang, L.; Whitcomb, J. M.; Hellmann, N. S.; Richman, D. D. *N. Engl. J. Med.* **2002,** *347,* 385–394.
12. Chesney, M. *AIDS Patient Care STDs* **2003,** *17,* 169–188.
13. Nachega, J. B.; Hislop, M.; Dowdy, D. W.; Chalsson, R. E.; Regensberg, L.; Maartens, G. *Ann. Intern. Med.* **2007,** *146,* 564–573.
14. Viswanathan, S.; Justice, A. M.; Alexander, C.; Brown, T. T.; Gandhi, N. R.; McNicholl, I. R.; Rimland, D.; Rodriguez-Barradas, M. C.; Jacobson, L. P. *J. Acquir. Immune Defic. Syndr.* **2015,** *69,* 493–498.
15. Bangsberg, D. R.; Ragland, K.; Monk, A.; Deeks, S. G. *AIDS* **2010,** *24,* 2835–2840.
16. DeJesus, E.; Young, B.; Morales-Ramirez, J. O.; Sloan, L.; Ward, D. J.; Flaherty, J. F.; Ebrahimi, R.; Maa, J.-F.; Reilly, K.; Ecker, J.; McColl, D.; Seekins, D.; Farajallah, A. *JAIDS* **2009,** *51,* 163–174.
17. Messiaen, P.; Wensing, A. M. J.; Fun, A.; Nijhuis, M.; Brusselaers, N.; Vandekerckhove, L. *PLoS ONE* **2013,** *8,* 1–16.
18. Rowley, M. *Prog. Med. Chem.* **2008,** *46,* 1–28.
19. Summa, V.; Pace, P. *Antiviral Drugs: From Basic Discovery Through Clinical Trials;* John Wiley & Sons, Inc., 2011; pp. 181–195.
20. Summa, V.; Petrocchi, A.; Bonelli, F.; Crescenzi, B.; Donghi, M.; Ferrara, M.; Fiore, F.; Gardelli, C.; Gonzalez Paz, O.; Hazuda, D. J.; Jones, P.; Kinzel, O.; Laufer, R.; Monteagudo, E.; Muraglia, E.; Nizi, E.; Orvieto, F.; Pace, P.; Pescatore, G.; Scarpelli, R.; Stillmock, K.; Witmer, M. V.; Rowley, M. *J. Med. Chem.* **2008,** *51,* 5843–5855.
21. Lennox, J. L.; De Jesus, E.; Lazzarin, A.; Pollard, R. B.; Valez Ramalho Madruga, J.; Berger, D. S.; Zhao, J.; Xu, X.; Williams-Diaz, A.; Rodgers, A. J.; Barnard, R. J. O.; Miller, M. D.; Di Nubile, M. J.; Nguyen, B.-Y.; Leavitt, R.; Sklar, P. *Lancet* **2009,** *374,* 796–806.
22. Eron, J. J.; Rockstroh, J. K.; Reynes, J.; Andrade-Villanueva, J.; Ramalho-Madruga, J. V.; Bekker, L.-G.; Young, B.; Katlama, C.; Gatell-Artigas, J. M.; Arribas, J. R.; Nelson, M.; Campbell, H.; Zhao, J.; Rodgers, A. J.; Rizk, M. L.; Wenning, L.; Miller, M. D.; Hazuda, D.; DiNubile, M. J.; Leavitt, R.; Isaacs, R.; Robertson, M. N.; Sklar, P.; Nguyen, B.-Y. *Lancet Infect. Dis.* **2011,** *11,* 907–915.
23. Grinsztejn, B.; Nguyen, B.-Y.; Katlama, C.; Gatell, J. M.; Lazzarin, A.; Vittecoq, D.; Gonzalez, C. J.; Chen, J.; Harvey, C. M.; Isaacs, R. D. *Lancet* **2007,** *369,* 1261–1269.
24. Shinkai, H.; Sato, M.; Matsuzaki, Y. *Antiviral Drugs: From Basic Discovery Through Clinical Trials;* John Wiley & Sons, Inc., 2011; pp. 197–205.
25. Shimura, K.; Kodama, E.; Sakagami, Y.; Matsuzaki, Y.; Watanabe, W.; Yamataka, K.; Watanabe, Y.; Ohata, Y.; Doi, S.; Sato, M.; Kano, M.; Ikeda, S.; Matsuoka, M. *J. Virol.* **2008,** *82,* 764–774.
26. DeJesus, E.; Rockstroh, J. K.; Henry, K.; Molina, J.-M.; Gathe, J.; Ramanathan, S.; Wei, X.; Yale, K.; Szwarcberg, J.; White, K.; Cheng, A. K.; Kearney, B. P. *Lancet* **2012,** *379,* 2429–2438.
27. Sax, P. E.; De Jesus, E.; Mills, A.; Zolopa, A.; Calvin, C.; Wohl, D.; Gallant, J. E.; Liu, H. C.; Zhong, L.; Yale, K.; White, K.; Kearney, B. P.; Szwarcberg, J.; Quirk, E.; Cheng, A. K. *Lancet* **2012,** *379,* 2439–2448.
28. https://aidsinfo.nih.gov/education-materials/fact-sheets/21/58/fda-approved-hiv-medicines.
29. Kawasuji, T.; Johns, B. A.; Yoshida, H.; Taishi, T.; Taoda, Y.; Murai, H.; Kiyama, R.; Fuji, M.; Yoshinaga, T.; Seki, T.; Kobayashi, M.; Sato, A.; Fujiwara, T. *J. Med. Chem.* **2012,** *55,* 8735–8744.
30. Kawasuji, T.; Johns, B. A.; Yoshida, H.; Weatherhead, J. G.; Akiyama, T.; Taishi, T.; Taoda, Y.; Mikamiyama-Iwata, M.; Murai, H.; Kiyama, R.; Fuji, M.; Yoshinaga, T.; Seki, T.; Kobayashi, M.; Sato, A.; Garvey, E. P.; Fujiwara, T. *J. Med. Chem.* **2013,** *56,* 1124–1135.
31. Johns, B. A.; Kawasuji, T.; Weatherhead, J. G.; Taishi, T.; Temelkoff, D. P.; Yoshida, H.; Akiyama, T.; Taoda, Y.; Murai, H.; Kiyama, R.; Fuji, M.; Tanimoto, N.; Jeffrey, J.; Foster, S. A.; Yoshinaga, T.; Seki, T.; Kobayashi, M.; Sato, A.; Johnson, M. N.; Garvey, E. P.; Fujiwara, T. *J. Med. Chem.* **2013,** *56,* 5901–5916.
32. Canducci, F.; Ceresola, E. R.; Boeri, E.; Spagnuolo, V.; Cossarini, F.; Castagna, A.; Lazzarin, A.; Clementi, M. *J. Infect. Dis.* **2011,** *204,* 1811–1815.
33. Raffi, F.; Rachlis, A.; Stellbrink, H.-J.; Hardy, W. D.; Torti, C.; Orkin, C.; Bloch, M.; Podzamczer, D.; Pokrovsky, V.; Pulido, F.; Almond, S.; Margolis, D.; Brennan, C.; Min, S. *Lancet* **2013,** *381,* 735–743.
34. Walmsley, S. L.; Antela, A.; Clumeck, N.; Duiculescu, D.; Eberhard, A.; Gutierrez, F.; Hocqueloux, L.; Maggiolo, F.; Sandkovsky, U.; Granier, C.; Pappa, K.; Wynne, B.; Min, S.; Nichols, G. *N. Engl. J. Med.* **2013,** *369,* 1807–1818.
35. Molina, J. M.; Clotet, B.; van Lunzen, A.; Cavassini, M.; Henry, K.; Kulagin, V.; Givens, N.; Brennan, C.; de Oliveira, C. F. *J. Int. AIDS Soc.* **2014,** *17* (Suppl. 3), 4.

36. Eron, J.; Clotet, B.; Durant, J.; Katlama, C.; Kumar, P.; Lazzarin, A.; Poizot-Martin, I.; Richmond, G.; Soriano, V.; Ait-Khaled, M.; Fujiwara, T.; Huang, J.; Min, S.; Vavro, C.; Yeo, J.; Walmsley, S. L.; Cox, J.; Reynes, J.; Morlat, P.; Vittecoq, D.; Livrozet, J.-M.; Fernandez, P. V.; Gatell, J. M.; DeJesus, E.; DeVente, J.; Lalezari, J. P.; McCurdy, L. H.; Sloan, L. A.; Young, B.; LaMarca, A.; Hawkins, T. *J. Infect. Dis.* **2013,** *207,* 740–748.
37. Hightower, K. E.; Wang, R.; Deanda, F.; Johns, B. A.; Weaver, K.; Shen, Y.; Tomberlin, G. H.; Carter, H. L., 3rd; Broderick, T.; Sigethy, S.; Seki, T.; Kobayashi, M.; Underwood, M. R. *Antimicrob. Agents Chemother.* **2011,** *55,* 4552–4559.
38. https://aidsinfo.nih.gov/drugs/534/triumeq/0/patient.
39. Johns, B. A.; Kawasuji, T.; Weatherhead, J. G.; Taishi, T.; Temelkoff, D. P.; Yoshida, H.; Akiyama, T.; Taoda, Y.; Murai, H.; Kiyama, R.; Fuji, M.; Tanimoto, N.; Jeffrey, J.; Foster, S. A.; Yoshinaga, T.; Seki, T.; Kobayashi, M.; Sato, A.; Johnson, M. N.; Garvey, E. P.; Fujiwara, T. *J. Med. Chem.* **2013,** *56,* 5901–5916.
40. Margolis, D. A.; Brinson, C. C.; Smith, G. H. R.; de Vente, J.; Hagins, D. P.; Eron, J. J.; Griffith, S. K.; Clair, M. H. S.; Ford, S. L.; Stancil, B. S.; Bomar, M. M.; Hudson, K. J.; Spreen, W. R.; Stevens, M. C.; Williams, P. E.; Smith, K. Y. *Lancet* **2015,** *15,* 1145–1155.
41. (a) Lazerwith, S. E.; et al. *ASM Microbe 2016*, Poster #414; (b) Tsiang, M.; et al. *ASM Microbe 2016*, Poster #416.
42. Gallant, J.; et al. *ASM Microbe 2016*, Poster #415.
43. Walji, A. M.; Sanchez, R. I.; Clas, S.-D.; Nofsinger, R.; de Lera Ruiz, M.; Li, J.; Bennet, A.; John, C.; Bennett, D. J.; Sanders, J. M.; Di Marco, C. N.; Kim, S. H.; Balsells, J.; Ceglia, S. S.; Dang, Q.; Manser, K.; Nissley, B.; Wai, J. S.; Hafey, M.; Wang, J.; Chessen, G.; Templeton, A.; Higgins, J.; Smith, R.; Wu, Y.; Grobler, J.; Coleman, P. J. *ChemMedChem* **2015,** *10,* 245–252.
44. Pryde, D. C.; Webster, R.; Butler, S. L.; Murray, E. J.; Whitby, K.; Pickford, C.; Westby, M.; Palmer, M. J.; Bull, D. J.; Vuong, H.; Blakemore, D. C.; Stead, D.; Ashcroft, C.; Gardner, I.; Bru, C.; Cheung, W.-Y.; Roberts, I. O.; Morton, J.; Bissel, R. A. *Med. Chem. Commun.* **2013,** *4,* 709–719.
45. Zhao, X. Z.; Smith, S. J.; Metifiot, M.; Johnson, B. C.; Marchand, C.; Pommier, Y.; Hughes, S. H.; Burke, T. R., Jr. *J. Med. Chem.* **2014,** *57,* 1573–1582.
46. Gandhi, M.; Gandhi, R. T. N. *Engl. J. Med.* **2014,** *371,* 248–259.
47. Permpalung, N.; Putcharoen, O.; Avihingsanon, A.; Ruxrungtham, K. *Expert Opin. Pharmacother.* **2012,** *13,* 2301–2317.
48. Cihlar, T.; Ray, A. S. *Antiviral Res.* **2010,** *85,* 39–58.
49. Balzarini, J. *Pharm. World Sci.* **1994,** *16,* 113–126.
50. Stein, D. S.; Moore, K. H. *Pharmacotherapy* **2001,** *21,* 11–34.
51. Dickinson, L.; Khoo, S.; Back, D. *Antivir. Res.* **2010,** *85,* 176–189.
52. Menendez-Arias, L. *Antivir. Res.* **2010,** *85,* 210–231.
53. McColl, D. J.; Chappey, C.; Parkin, N. T.; Miller, M. D. *Antivir. Ther.* **2008,** *13,* 189–197.
54. Hawkins, T. *Antivir. Res.* **2010,** *85,* 201–209.
55. DHHS Guidelines. https://aidsinfo.nih.gov/guidelines.
56. Brinkman, K.; ter Hofstede, H. J.; Burger, D. M.; Smeitink, J. A.; Koopmans, P. P. *AIDS* **1998,** *12,* 1735–1744.
57. Carr, A.; Miller, J.; Law, M.; Cooper, D. A. *AIDS* **2000,** *14,* F25–F32.
58. van der Valk, M.; Casula, M.; Weverlingz, G. J.; van Kuijk, K.; van Eck-Smit, B.; Hulsebosch, H. J.; Nieuwkerk, P.; van Eeden, A.; Brinkman, K.; Lange, J.; de Ronde, A.; Reiss, P. *Antivir. Ther.* **2004,** *9,* 385–393.
59. McKee, E. E.; Bentley, A. T.; Hatch, M.; Gingerich, J.; Susan-Resiga, D. *Cardiovasc. Toxicol.* **2004,** *4,* 155–167.
60. Scarsella, A.; Coodley, G.; Shalit, P.; Anderson, R.; Fisher, R. L.; Liao, Q.; Ross, L. L.; Hernandez, J. E. *Adv. Ther.* **2002,** *19,* 1–8.
61. Mitsuya, H.; Broder, S. *Proc. Natl. Acad. Sci. U. S. A.* **1986,** *83,* 1911–1915.
62. Walker, U. A.; Bauerle, J.; Laguno, M.; Murillas, J.; Mauss, S.; Schmutz, G.; Setzer, B.; Miquel, R.; Gatell, J. M.; Mallolas, J. *Hepatology* **2004,** *39,* 311–317.
63. D:A:D Study Group; Sabin, C. A.; Worm, S. W.; Weber, R.; Reiss, P.; El-Sadr, W.; Dabis, F.; De Wit, S.; Law, M.; D'Arminio Monforte, A.; Friis-Moller, N.; Kirk, O.; Pradier, C.; Weller, I.; Phillips, A. N.; Lundgren, J. D. *Lancet* **2008,** *371,* 1417–1426.
64. Maida, I.; Nunez, M.; Rios, M. J.; Martin-Carbonero, L.; Sotgiu, G.; Toro, C.; Rivas, P.; Barreiro, P.; Mura, M. S.; Babudieri, S.; Garcia-Samaniego, J.; Gonzalez-Lahoz, J.; Soriano, V. *J. Acquir. Immune Defic. Syndr.* **2006,** *42,* 177–182.
65. Arribas, J. R.; Pozniak, A. L.; Gallant, J. E.; Dejesus, E.; Gazzard, B.; Campo, R. E.; Chen, S. S.; McColl, D.; Holmes, C. B.; Enejosa, J.; Toole, J. J.; Cheng, A. K. *J. Acquir. Immune Defic. Syndr.* **2008,** *47,* 74–78.
66. Cassetti, I.; Madruga, J. V.; Suleiman, J. M.; Etzel, A.; Zhong, L.; Cheng, A. K.; Enejosa, J.; Study, E. T. *HIV Clin. Trials* **2007,** *8,* 164–172.
67. Gallant, J. E.; Staszewski, S.; Pozniak, A. L.; DeJesus, E.; Suleiman, J. M.; Miller, M. D.; Coakley, D. F.; Lu, B.; Toole, J. J.; Cheng, A. K.; Study, G. *JAMA* **2004,** *292,* 191–201.
68. Gallant, J. E.; DeJesus, E.; Arribas, J. R.; Pozniak, A. L.; Gazzard, B.; Campo, R. E.; Lu, B.; McColl, D.; Chuck, S.; Enejosa, J.; Toole, J. J.; Cheng, A. K.; Study, G. *N. Engl. J. Med.* **2006,** *354,* 251–260.
69. Smith, K. Y.; Patel, P.; Fine, D.; Bellos, N.; Sloan, L.; Lackey, P.; Kumar, P. N.; Sutherland-Phillips, D. H.; Vavro, C.; Yau, L.; Wannamaker, P.; Shaefer, M. S.; Team, H. S. *AIDS* **2009,** *23,* 1547–1556.
70. Nelson, M. R.; Katlama, C.; Montaner, J. S.; Cooper, D. A.; Gazzard, B.; Clotet, B.; Lazzarin, A.; Schewe, K.; Lange, J.; Wyatt, C.; Curtis, S.; Chen, S. S.; Smith, S.; Bischofberger, N.; Rooney, J. F. *AIDS* **2007,** *21,* 1273–1281.
71. Grigsby, I. F.; Pham, L.; Mansky, L. M.; Gopalakrishnan, R.; Mansky, K. C. *Ther. Clin. Risk Manag.* **2010,** *6,* 41–47.
72. Bedimo, R.; Maalouf, N. M.; Zhang, S.; Drechsler, H.; Tebas, P. *AIDS* **2012,** *26,* 825–831.
73. Cihlar, T.; Ho, E. S.; Lin, D. C.; Mulato, A. S. *Nucleosides Nucleotides Nucleic Acids* **2001,** *20,* 641–648.
74. Schinazi, R. F.; McMillan, A.; Cannon, D.; Mathis, R.; Lloyd, R. M.; Peck, A.; Sommadossi, J. P.; St. Clair, M.; Wilson, J.; Furman, P. A.; Painter, G.; Choi, W. B.; Liotta, D. C. *Antimicrob. Agents Chemother.* **1992,** *36,* 2423–2431.
75. Benson, C. A.; van der Horst, C.; Lamarca, A.; Haas, D. W.; McDonald, C. K.; Steinhart, C. R.; Rublein, J.; Quinn, J. B.; Mondou, E.; Rousseau, F.; Group, F. T. C. W. *AIDS* **2004,** *18,* 2269–2276.
76. Saag, M. S.; Cahn, P.; Raffi, F.; Wolff, M.; Pearce, D.; Molina, J. M.; Powderly, W.; Shaw, A. L.; Mondou, E.; Hinkle, J.; Borroto-Esoda, K.; Quinn, J. B.; Barry, D. W.; Rousseau, F.; Team, F.-A. S. *JAMA* **2004,** *292,* 180–189.
77. Frampton, J. E.; Perry, C. M. *Drugs* **2005,** *65,* 1427–1448.
78. Daluge, S. M.; Good, S. S.; Faletto, M. B.; Miller, W. H.; St Clair, M. H.; Boone, L. R.; Tisdale, M.; Parry, N. R.; Reardon, J. E.; Dornsife, R. E.; Averett, D. R.; Krenitsky, T. A. *Antimicrob. Agents Chemother.* **1997,** *41,* 1082–1093.
79. Faletto, M. B.; Miller, W. H.; Garvey, E. P.; St Clair, M. H.; Daluge, S. M.; Good, S. S. *Antimicrob. Agents Chemother.* **1997,** *41,* 1099–1107.
80. Mallal, S.; Nolan, D.; Witt, C.; Masel, G.; Martin, A. M.; Moore, C.; Sayer, D.; Castley, A.; Mamotte, C.; Maxwell, D.; James, I.; Christiansen, F. T. *Lancet* **2002,** *359,* 727–732.
81. White, K. L.; Margot, N. A.; Wrin, T.; Petropoulos, C. J.; Miller, M. D.; Naeger, L. K. *Antimicrob. Agents Chemother.* **2002,** *46,* 3437–3446.
82. Moore, K. H.; Raasch, R. H.; Brouwer, K. L.; Opheim, K.; Cheeseman, S. H.; Eyster, E.; Lemon, S. M.; van der Horst, C. M. *Antimicrob. Agents Chemother.* **1995,** *39,* 2732–2737.
83. Anderson, P. L.; Kakuda, T. N.; Kawle, S.; Fletcher, C. V. *AIDS* **2003,** *17,* 2159–2168.
84. Becher, F.; Landman, R.; Mboup, S.; Kane, C. N.; Canestri, A.; Liegeois, F.; Vray, M.; Prevot, M. H.; Leleu, G.; Benech, H. *AIDS* **2004,** *18,* 181–187.
85. Gustavson, L. E.; Fukuda, E. K.; Rubio, F. A.; Dunton, A. W. *J. Acquir. Immune Defic. Syndr.* **1990,** *3,* 28–31.
86. Balzarini, J.; Cooney, D. A.; Dalal, M.; Kang, G. J.; Cupp, J. E.; DeClercq, E.; Broder, S.; Johns, D. G. *Mol. Pharmacol.* **1987,** *32,* 798–806.
87. Horton, C. M.; Dudley, M. N.; Kaul, S.; Mayer, K. H.; Squires, K.; Dunkle, L.; Anderson, R. *Antimicrob. Agents Chemother.* **1995,** *39,* 2309–2315.

88. Hawkins, T.; Veikley, W.; St Claire, R. L., 3rd; Guyer, B.; Clark, N.; Kearney, B. P. *J. Acquir. Immune Defic. Syndr.* **2005,** *39,* 406–411.
89. Wang, L. H.; Begley, J.; St. Claire, R. L., 3rd; Harris, J.; Wakeford, C.; Rousseau, F. S. *AIDS Res. Hum. Retroviruses* **2004,** *20,* 1173–1182.
90. Chapman, H.; Kernan, M.; Prisbe, E.; Rohloff, J.; Sparacino, M.; Terhorst, T.; Yu, R. *Nucleosides Nucleotides Nucleic Acids* **2001,** *20,* 621–628.
91. Chapman, H.; Kernan, M.; Rohloff, J.; Sparacino, M.; Terhorst, T. *Nucleosides Nucleotides Nucleic Acids* **2001,** *20,* 1085–1090.
92. Lee, W. A.; He, G. X.; Eisenberg, E.; Cihlar, T.; Swaminathan, S.; Mulato, A.; Cundy, K. C. *Antimicrob. Agents Chemother.* **2005,** *49,* 1898–1906.
93. Eisenberg, E. J.; He, G. X.; Lee, W. A. *Nucleosides Nucleotides Nucleic Acids* **2001,** *20,* 1091–1098.
94. Birkus, G.; Kutty, N.; He, G. X.; Mulato, A.; Lee, W.; McDermott, M.; Cihlar, T. *Mol. Pharmacol.* **2008,** *74,* 92–100.
95. Babusis, D.; Phan, T. K.; Lee, W. A.; Watkins, W. J.; Ray, A. S. *Mol. Pharm.* **2013,** *10,* 459–466.
96. Bam, R. A.; Birkus, G.; Babusis, D.; Cihlar, T.; Yant, S. R. *Antivir. Ther.* **2014,** *19,* 669–677.
97. Birkus, G.; Wang, R.; Liu, X.; Kutty, N.; MacArthur, H.; Cihlar, T.; Gibbs, C.; Swaminathan, S.; Lee, W.; McDermott, M. *Antimicrob. Agents Chemother.* **2007,** *51,* 543–550.
98. Bam, R. A.; Yant, S. R.; Cihlar, T. *Antivir. Ther.* **2014,** *19,* 687–692.
99. Sax, P. E.; Zolopa, A.; Brar, I.; Elion, R.; Ortiz, R.; Post, F.; Wang, H.; Callebaut, C.; Martin, H.; Fordyce, M. W.; McCallister, S. *J. Acquir. Immune Defic. Syndr.* **2014,** *67,* 52–58.
100. Sax, P. E.; Wohl, D.; Yin, M. T.; Post, F.; DeJesus, E.; Saag, M.; Pozniak, A.; Thompson, M.; Podzamczer, D.; Molina, J. M.; Oka, S.; Koenig, E.; Trottier, B.; Andrade-Villanueva, J.; Crofoot, G.; Custodio, J. M.; Plummer, A.; Zhong, L.; Cao, H.; Martin, H.; Callebaut, C.; Cheng, A. K.; Fordyce, M. W.; McCallister, S.; Team, G.-U.-S. *Lancet* **2015,** *385,* 2606–2615.
101. http://content.govdelivery.com/accounts/USFDA/bulletins/139b577 (retrieved .23.06.16).
102. Mills, A.; Crofoot, G., Jr.; McDonald, C.; Shalit, P.; Flamm, J. A.; Gathe, J., Jr.; Scribner, A.; Shamblaw, D.; Saag, M.; Cao, H.; Martin, H.; Das, M.; Thomas, A.; Liu, H. C.; Yan, M.; Callebaut, C.; Custodio, J.; Cheng, A.; McCallister, S. *J. Acquir. Immune Defic. Syndr.* **2015,** *69,* 439–445.
103. Gunawardana, M.; Remedios-Chan, M.; Miller, C. S.; Fanter, R.; Yang, F.; Marzinke, M. A.; Hendrix, C. W.; Beliveau, M.; Moss, J. A.; Smith, T. J.; Baum, M. M. *Antimicrob. Agents Chemother.* **2015,** *59,* 3913–3919.
104. Cox, S.; Southby, J. *Expert Opin. Investig. Drugs* **2009,** *18,* 199–209.
105. de Muys, J. M.; Gourdeau, H.; Nguyen-Ba, N.; Taylor, D. L.; Ahmed, P. S.; Mansour, T.; Locas, C.; Richard, N.; Wainberg, M. A.; Rando, R. F. *Antimicrob. Agents Chemother.* **1999,** *43,* 1835–1844.
106. Bethell, R. C.; Lie, Y. S.; Parkin, N. T. *Antivir. Chem. Chemother.* **2005,** *16,* 295–302.
107. Haraguchi, K.; Takeda, S.; Tanaka, H.; Nitanda, T.; Baba, M.; Dutschman, G. E.; Cheng, Y. C. *Bioorg. Med. Chem. Lett.* **2003,** *13,* 3775–3777.
108. Nitanda, T.; Wang, X.; Kumamoto, H.; Haraguchi, K.; Tanaka, H.; Cheng, Y. C.; Baba, M. *Antimicrob. Agents Chemother.* **2005,** *49,* 3355–3360.
109. Dutschman, G. E.; Grill, S. P.; Gullen, E. A.; Haraguchi, K.; Takeda, S.; Tanaka, H.; Baba, M.; Cheng, Y. C. *Antimicrob. Agents Chemother.* **2004,** *48,* 1640–1646.
110. Dutschman, G. E.; Bridges, E. G.; Liu, S. H.; Gullen, E.; Guo, X.; Kukhanova, M.; Cheng, Y. C. *Antimicrob. Agents Chemother.* **1998,** *42,* 1799–1804.
111. Lin, T. S.; Luo, M. Z.; Liu, M. C.; Zhu, Y. L.; Gullen, E.; Dutschman, G. E.; Cheng, Y. C. *J. Med. Chem.* **1996,** *39,* 1757–1759.
112. Dunkle, L. M.; Gathe, J. C.; Pedevillano, D. E.; Robison, H. G.; Rice, W. G.; Pottage, J. C. *12th International HIV Drug Resistance Workshop: Basic Principles & Clinical Implications, Los Cabos, Mexico,* 2003 (abstract 2).
113. DeJesus, E.; Saple, D.; Morales-Ramirez, J.; Kumarasamy, N.; Jefferson, T.; Bellos, N.; Wade, B. H.; Gugliotti, R.; Robison, H.; Olek, E. *48th Interscience Conference on Antimicrobial Agents and Chemotherapy (ICAAC), Washington, DC*. Available at: http://www.natap.org/2008/ICAAC/ICAAC_22.htm, 2008.
114. Furman, P. A.; Jeffrey, J.; Kiefer, L. L.; Feng, J. Y.; Anderson, K. S.; Borroto-Esoda, K.; Hill, E.; Copeland, W. C.; Chu, C. K.; Sommadossi, J. P.; Liberman, I.; Schinazi, R. F.; Painter, G. R. *Antimicrob. Agents Chemother.* **2001,** *45,* 158–165.
115. Gu, Z.; Wainberg, M. A.; Nguyen-Ba, N.; L'Heureux, L.; de Muys, J. M.; Bowlin, T. L.; Rando, R. F. *Antimicrob. Agents Chemother.* **1999,** *43,* 2376–2382.
116. Mewshaw, J. P.; Myrick, F. T.; Wakefield, D. A.; Hooper, B. J.; Harris, J. L.; McCreedy, B.; Borroto-Esoda, K. *J. Acquir. Immune Defic. Syndr.* **2002,** *29,* 11–20.
117. Kim, E. Y.; Vrang, L.; Oberg, B.; Merigan, T. C. *AIDS Res. Hum. Retroviruses* **2001,** *17,* 401–407.
118. Martin, J. L.; Brown, C. E.; Matthews-Davis, N.; Reardon, J. E. *Antimicrob. Agents Chemother.* **1994,** *38,* 2743–2749.
119. Flexner, C.; van der Horst, C.; Jacobson, M. A.; Powderly, W.; Duncanson, F.; Ganes, D.; Barditch-Crovo, P. A.; Petty, B. G.; Baron, P. A.; Armstrong, D.; et al. *J. Infect. Dis.* **1994,** *170,* 1394–1403.
120. Ghosn, J.; Quinson, A. M.; Sabo, N.; Cotte, L.; Piketty, C.; Dorleacq, N.; Bravo, M. L.; Mayers, D.; Harmenberg, J.; Mardh, G.; Valdez, H.; Katlama, C. *HIV Med.* **2007,** *8,* 142–147.
121. Cahn, P.; Schuermann, D.; Reuss, F.; Wit, F.; Boehm, E.; Lange, J. *4th IAS Conference on Pathogenesis, Treatment, and Prevention, Sydney, Australia,* 2007 (abstract WEBEP114LB).
122. Harris, K. S.; Brabant, W.; Styrchak, S.; Gall, A.; Daifuku, R. *Antivir. Res.* **2005,** *67,* 1–9.
123. Murakami, E.; Basavapathruni, A.; Bradley, W. D.; Anderson, K. S. *Antivir. Res.* **2005,** *67,* 10–17.
124. Hicks, C.; Clay, P.; Redfield, R.; Lalezari, J.; Liporace, R.; Schneider, S.; Sension, M.; McRae, M.; Laurent, J. P. *AIDS Res. Hum. Retroviruses* **2013,** *29,* 250–255.
125. Mullins, J. I.; Heath, L.; Hughes, J. P.; Kicha, J.; Styrchak, S.; Wong, K. G.; Rao, U.; Hansen, A.; Harris, K. S.; Laurent, J. P.; Li, D.; Simpson, J. H.; Essigmann, J. M.; Loeb, L. A.; Parkins, J. *PLoS ONE* **2011,** *6*, e15135.
126. Painter, G. R.; Almond, M. R.; Trost, L. C.; Lampert, B. M.; Neyts, J.; De Clercq, E.; Korba, B. E.; Aldern, K. A.; Beadle, J. R.; Hostetler, K. Y. *Antimicrob. Agents Chemother.* **2007,** *51,* 3505–3509.
127. Lanier, E. R.; Ptak, R. G.; Lampert, B. M.; Keilholz, L.; Hartman, T.; Buckheit, R. W., Jr.; Mankowski, M. K.; Osterling, M. C.; Almond, M. R.; Painter, G. R. *Antimicrob. Agents Chemother.* **2010,** *54,* 2901–2909.
128. De Clercq, E. *Antivir. Res.* **1998,** *38,* 153–179.
129. De Corte, B. L. *J. Med. Chem.* **2005,** *48,* 1689–1696.
130. Janssen, P. A. J.; Lewi, P. J.; Arnold, E.; Daeyaert, F.; de Jonge, M.; Heeres, J.; Koymans, L.; Vinkers, M.; Guillemont, J.; Pasquier, E.; Kukla, M.; Ludovici, D.; Andries, K.; de Bethune, M.-P.; Pauwels, R.; Das, K.; Clark, A. D., Jr.; Frenkel, Y. V.; Hughes, S. H.; Medaer, B.; De Knaep, F.; Bohets, H.; De Clerck, F.; Lamp, A.; Williams, P.; Stoffels, P. *J. Med. Chem.* **2005,** *48,* 1901–1909.
131. Lazzarin, A.; Campbell, T.; Clotet, B.; Johnson, M.; Katlama, C.; Moll, A.; Towner, W.; Trottier, B.; Peeters, M.; Vingerhoets, J.; De Smedt, G.; Baeten, B.; Beets, G.; Sinha, R.; Woodfall, B. *Lancet* **2007,** *370,* 39–48.
132. Lennox, J. L.; De Jesus, E.; Lazzarin, A.; Pollard, R. B.; Valez Ramalho Madruga, J.; Berger, D. S.; Zhao, J.; Xu, X.; Williams-Diaz, A.; Rodgers, A. J.; Barnard, R. J. O.; Miller, M. D.; Di Nubile, M. J.; Nguyen, B.-Y.; Leavitt, R.; Sklar, P. *Lancet* **2009,** *374,* 796–806.
133. Azjin, H.; Tirry, I.; Vingerhoets, J.; de Bethune, M.-P.; Kraus, G.; Boven, K.; Jochmans, D.; Van Craenenbroeck, E.; Picchio, G.; Rimsky, L. T. *Antimicrob. Agents Chemother.* **2010,** *54,* 718–727.
134. Pozniak, A. L.; Morales-Ramirez, J.; Katabira, E.; Steyn, D.; Lupo, S. H.; Santoscoy, M.; Grinsztejn, B.; Ruxrungtham, K.; Rimsky, L. T.; Vanveggel, S.; Boven, K. *AIDS* **2010,** *24,* 55–65.
135. Schafer, J. J.; Short, W. R. *Antivir. Ther.* **2012,** *17,* 1495–1502.
136. Cohen, C.; Wohl, D.; Arribas, J. R.; Henry, K.; Van Lunzen, J.; Bloch, M.; Towner, W.; Wilkins, E.; Ebrahimi, R.; Porter, D.; White, K.; Walker, I.; Chuck, S.; De-Oertel, S.; Fralich, T. *AIDS* **2014,** *28,* 989–997.
137. Pharmacology Review(s). Rilpivirine, Edurant. FDA Approval package for NDA 202022. May 20, 2011, http://www.accessdata.fda.gov/drugsatfda_docs/nda/2011/202022Orig1s000PharmR.pdf (accessed 20.12.15).

138. Margolis, D. A.; Boffito, M. *Curr. Opin. HIV AIDS* **2015,** *10,* 246–252.
139. Cote, B.; Burch, J. D.; Asante-Appiah, E.; Bayly, C.; Bedard, L.; Blouin, M.; Campeau, L.-C.; Cauchon, E.; Chan, M.; Chefson, A.; Coulombe, N.; Cromlish, W.; Debnath, S.; Deschenes, D.; Dupont-Gaudet, K.; Falgueyret, J.-P.; Forget, R.; Gagne, S.; Gauvreau, D.; Girardin, M.; Guiral, S.; Langlois, E.; Li, C. S.; Nguyen, N.; Papp, R.; Plamondon, S.; Roy, A.; Roy, S.; Seliniotakis, R.; St-Onge, M.; Ouellet, S.; Tawa, P.; Truchon, J.-F.; Vacca, J.; Wrona, M.; Yan, Y.; Ducharme, Y. *Bioorg. Med. Chem. Lett.* **2014,** *24,* 917–922.
140. Gatell, J. M.; Morales-Ramirez, J. O.; Hagins, D. P.; Thompson, M.; Keikawus, A.; Hoffmann, C.; Rugina, S.; Osiyemi, O.; Escoriu, S.; Dretler, R.; Harvey, C.; Xu, X.; Teppler, H. *J. Int. AIDS Soc.* **2014,** *17* (Suppl. 3), 19532.
141. Ghosh, A. K.; Anderson, D. D.; Weber, I. T.; Mitsuya, H. *Angew. Chem. Int. Ed.* **2012,** *51,* 1778–1802.
142. Ghosh, A. K.; Chapsal, B. D. *Introduction to Biological and Small Molecule Drug Research and Development;* Elsevier, 2013; pp 355–384.
143. Koh, Y.; Nakata, H.; Maeda, K.; Ogata, H.; Bilcer, H. G.; Devasamudram, T.; Kincaid, J. F.; Boross, P.; Wang, Y. F.; Tie, Y.; Volarath, P.; Gaddis, L.; Harrison, R. W.; Weber, I. T.; Ghosh, A. K.; Mitsuya, H. *Antimicrob. Agents Chemother.* **2003,** *47,* 3123–3129.
144. Clotet, B.; Bellos, N.; Molina, J.-M.; Cooper, D.; Goffard, J.-C.; Lazzarin, A.; Wohrmann, A.; Katlama, C.; Wilkin, T.; Haubrich, R.; Cohen, C.; Fathing, C.; Jayaweera, D.; Markowitz, M.; Ruane, P.; Guzman-Spinosa, S.; Lefebvre, E. *Lancet* **2007,** *369,* 1169–1178.
145. Orkin, C.; DeJesus, E.; Khanlou, H.; Stoehr, A.; Supparatpinyo, K.; Lathouwers, E.; Lefebvre, E.; Opsomer, M.; de Casteele, T. V.; Tomaka, F. *HIV Med.* **2013,** *14,* 49–59.
146. Lennox, J. L.; Landovitz, R. J.; Ribaudo, H. J.; Ofotokun, I.; Na, L. H.; Godfrey, C.; Kuritzkes, D. R.; Sagar, M.; Brown, T. T.; Cohn, S. E.; McComsey, G. A.; Aweeka, F.; Fichtenbaum, C. J.; Presti, R. M.; Koletar, S. L.; Haas, D. W.; Patterson, K. B.; Benson, C. A.; Baugh, B. P.; Leavitt, R. Y.; Rooney, J. F.; Seekins, D.; Currier, J. S. *Ann. Intern. Med.* **2014,** *161,* 461–471.
147. Miller, J. F.; Furfine, E. S.; Hanlon, M. H.; Hazen, R. J.; Ray, J. A.; Robinson, L.; Samano, V.; Spaltenstein, A. *Bioorg. Med. Chem. Lett.* **2004,** *14,* 959–963.
148. Ghosh, A. K.; Parham, G. L.; Martyr, C. D.; Nyalapatla, P. R.; Osswald, H. L.; Agniswamy, J.; Wang, Y.-F.; Amano, M.; Weber, I. T.; Mitsuya, H. *J. Med. Chem.* **2013,** *56,* 6792–6802.
149. (a) Dierynck, I.; Marck, H. V.; Ginderen, M. V.; Jonckers, T. H. M.; Nalam, M. N. L.; Schiffer, C. A.; Raoof, A.; Kraus, G.; Picchio, G. *Antimicrob. Agents Chemother.* **2011,** *55,* 5723–5731.
150. Ganguly, A. K.; Alluri, S. S.; Wang, C.-H.; Antropow, A.; White, A.; Caroccia, D.; Biswas, D.; Kang, E.; Zhang, L.-K.; Carroll, S. S.; Burlein, C.; Fay, J.; Orth, P.; Strickland, C. *Tetrahedron* **2014,** *70,* 2894–2904.
151. Calugi, C.; Guarna, A.; Trabocchi, A. *Curr. Med. Chem.* **2013,** *20,* 3693–3701.
152. Schimer, J.; Cigler, P.; Vesely, J.; Saskova, K. G.; Lepsik, M.; Brynda, J.; Rezacova, P.; Kozisek, M.; Cisarova, I.; Oberwinkler, H.; Kraeusslich, H.-G.; Konvalinka, J. *J. Med. Chem.* **2012,** *55,* 10130–10135.
153. Pang, X.; Liu, Z.; Zhai, G. *Curr. Med. Chem.* **2014,** *21,* 1–15.
154. Joshi, A.; Verson, J.-B.; Unge, J.; Rosenquist, A.; Wallberg, H.; Samuelsson, B.; Hallberg, A.; Larhed, M. *J. Med. Chem.* **2013,** *56,* 8999–9007.
155. Wilen, C. B.; Tilton, J. C.; Doms, R. W. *Cold Spring Harb. Perspect. Med.* **2012,** *2,* 1–13.
156. Jacobson, J. M.; Israel, R. J.; Lowy, I.; Ostrow, N. A.; Vassilatos, L. S.; Barish, M.; Tran, D. N. H.; Sullivan, B. M.; Ketas, T. J.; O'Neill, T. J.; Nagashima, K. A.; Huang, W.; Petropoulos, C. J.; Moore, J. P.; Maddon, P. J.; Olson, W. C. *Antimicrob. Agents Chemother.* **2004,** *48,* 423–429.
157. Nowicka-Sans, B.; Gong, Y.-F.; McAuliffe, B.; et al. *Antimicrob. Agents Chemother.* **2012,** *56,* 3498–3507.
158. Campbell, E. M.; Hope, T. J. *Nat. Rev. Microbiol.* **2015,** *13,* 471–483.
159. Lemke, C. T.; Titolo, S.; von Schwedler, U.; Goudreau, N.; Mercier, J.-F.; Wardrop, E.; Faucher, A.-M.; Coulombe, R.; Banik, S. S. R.; Fader, L.; Gagnon, A.; Kawai, S. H.; Rancourt, J.; Tremblay, M.; Yoakim, C.; Simoneau, B.; Archambault, J.; Sundquist, W. I.; Mason, S. W. *J. Virol.* **2012,** *86* (12), 6643–6655.
160. Yant, S. R.; Tsai, L.; Jin, D.; Bam, R. A.; Mulato, A.; Niedziela-Majka, A.; Hung, M.; Chou, C.-H.; Wong, M.; Halcomb, R.; Sundquist, W. I.; Cihlar, T. Poster 534 Presented at: 21st Conference on Retroviruses and Opportunistic Infections, 2014 Mar. 3–6, Boston, MA.
161. Van Baelen, K.; Salzwedel, K.; Rondelez, E.; Van Eygen, V.; De Vos, S.; Verheyen, A.; Steegen, K.; Verlinden, Y.; Allaway, G. P.; Stuyver, L. J. *Antimicrob. Agents Chemother.* **2009,** *53,* 2185–2188.
162. Nowicka-Sans, B.; Protack, T.; Lin, Z.; et al. *Antimicrob. Agents Chemother.* **2016,** *60,* 3956–3965.
163. Hwang, C.; Schürmann, D.; Sobotha, C.; Sevinsky, H.; Ravindran, P.; Xiao, H.; Ray, N.; Krystal, M.; Dicker, I. B.; Lataillade, M. Abstract 114LB Presented at: 22nd Conference on Retroviruses and Opportunistic Infections, 2015 Feb. 23–26, Seattle, WA.
164. Jeffrey, J. L.; Wang, P.; McDanal, C.; Schipper, P. J.; Brown, K.; Galardi, C.; Tang, J.; Nijhuis, M.; Johns, B. A. Poster 538 Presented at: 22nd Conference on Retroviruses and Opportunistic Infections, 2015 Feb. 23–26, Seattle, WA.
165. (a) Fenwick, C.; Amad, M.; Bailey, M. D.; Bethel, R.; Bos, M.; Bonneau, P.; Cordingley, M.; Coulombe, R.; Duan, J.; Edwards, P.; Fader, L. D.; Faucher, A.-M.; Garneau, M.; Jakalian, A.; Kawai, S.; Lamorte, L.; LaPlante, S.; Luo, L.; Mason, S.; Poupart, M.-A.; Rioux, N.; Schroeder, P.; Simoneau, B.; Tremblay, S.; Tsantrizos, Y.; Witvrouw, M.; Yoakim, C. *Antimicrob. Agents Chemother.* **2014,** *58,* 3233–3244; (b) Fader, L. D.; Malenfant, E.; Parisien, M.; Carson, R.; Bilodeau, F.; Landry, S.; Pesant, M.; Brochu, C.; Morin, S.; Chabot, C.; Halmos, T.; Bousquet, Y.; Bailey, M. D.; Kawai, S. H.; Coulombe, R.; LaPlante, S.; Jakalian, A.; Bhardwaj, P. K.; Wernic, D.; Schroeder, P.; Amad, M.; Edwards, P.; Garneau, M.; Duan, J.; Cordingley, M.; Bethell, R.; Mason, S. W.; Bos, M.; Bonneau, P.; Poupart, M.-A.; Faucher, A.-M.; Simoneau, B.; Fenwick, C.; Yoakim, C.; Tsantrizos, Y. *ACS Med. Chem. Lett.* **2014,** *5,* 422–427.
166. (a) van Bel, N.; van der Velden, Y.; Bonnard, D.; Le Rouzic, E.; Das, A. T.; Benarous, R.; Berkhout, B. *PLoS ONE* **2014,** *9,* e103552; (b) Balakrishnan, M.; Yant, S. R.; Tsai, L.; O'Sullivan, C.; Bam, R. A.; Tsai, A.; Niedziela-Majka, A.; Stray, K. M.; Sakowicz, R.; Cihlar, T. *PLoS ONE* **2013,** *8,* e74163.
167. https://aidsinfo.nih.gov/education-materials/fact-sheets/21/58/fda-approved-hiv-medicines.
168. Grijsen, M. L.; Holman, R.; Gras, L.; Wit, F. W. N. M.; Hoepelman, A. I. M.; van den Berk, G. E.; de Wolf, F.; Prins, J. M. *Antivir. Ther.* **2012,** *17,* 1609–1613.
169. Mills, A.; Mildvan, D.; Podzamczer, D.; Fatkenheuer, G.; Leal, M.; Than, S.; Valluri, S. R.; Craig, C.; McFadyen, L.; Vourvahis, M.; Heera, J.; Valdez, H.; Rinehart, A. R.; Portsmouth, S. *J. Acquir. Immune Defic. Syndr.* **2013,** *62,* 164–170.
170. Reliquet, V.; Chirouze, C.; Allavena, C.; Muret, P.; Peytavin, G.; Andre-Garnier, E.; Bettinger, D.; Ferre, V.; Hoen, B.; Raffi, F. *Antivir. Ther.* **2014,** *19,* 117–123.
171. Nozza, S.; Galli, L.; Bigoloni, A.; Gianotti, N.; Spagnuolo, V.; Carbone, A.; Chiappetta, S.; Ripa, M.; Tambussi, G.; Lazzarin, A.; Castagna, A. *New Microbiol.* **2014,** *37,* 145–151.
172. Achhra, A. C.; Boyd, M. A. *AIDS Res. Ther.* **2013,** *10,* 33.
173. Wensing, A. M. J.; van Maarseveen, N. M.; Nijhuis, M. *Antivir. Res.* **2010,** *85,* 59–74.
174. van Heeswijk, R. P.; Veldkamp, A.; Mulder, J. W.; Meenhorst, P. L.; Lange, J. M.; Beijnen, J. H.; Hoetelmans, R. M. *Antivir. Ther.* **2001,** *6,* 201–229.
175. Liu, H.; Xu, L.; Hui, H.; Vivian, R.; Callebaut, C.; Murray, B. P.; Hong, A.; Lee, M. S.; Tsai, L. K.; Chau, J. K.; Stray, K. M.; Cannizzaro, C.; Choi, Y.-C.; Rhodes, G. R.; Desai, M. C. *Bioorg. Med. Chem. Lett.* **2014,** *24,* 989–994.
176. Xu, L.; Liu, H.; Hong, A.; Vivian, R.; Murray, B. P.; Callebaut, C.; Choi, Y.-C.; Lee, M. S.; Chau, J.; Tsai, L. K.; Stray, K. M.; Strickley, R. G.; Wang, J.; Tong, L.; Swaminathan, S.; Rhodes, G. R.; Desai, M. C. *Bioorg. Med. Chem. Lett.* **2014,** *24,* 995–999.
177. Xu, L.; Liu, H.; Murray, B. P.; Callebaut, C.; Lee, M. S.; Hong, A.; Strickley, R. G.; Tsai, L. K.; Stray, K. M.; Wang, Y.; Rhodes, G. R.; Desai, M. C. *ACS Med. Chem. Lett.* **2010,** *1,* 209–213.
178. German, P.; Warren, D.; West, S.; Hui, J.; Kearney, B. P. *J. Acquir. Immune Defic. Syndr.* **2010,** *55,* 323–329.
179. Sax, P. E.; De Jesus, E.; Mills, A.; Zolopa, A.; Cohen, C.; Wohl, D.; Gallant, J. E.; Liu, H. C.; Zhong, L.; Yale, K.; White, K.; Kearney, B. P.; Szwarcberg, J.; Quirk, E.; Cheng, A. K. *Lancet* **2012,** *379,* 2439–2448.

180. De Jesus, E.; Rockstroh, J. K.; Henry, K.; Molina, J.-M.; Gathe, J.; Ramanathan, S.; Wei, X.; Yale, K.; Szwarcberg, J.; White, K.; Cheng, A. K.; Kearney, B. P. *Lancet* **2012,** *379,* 2429–2438.
181. https://aidsinfo.nih.gov/education-materials/fact-sheets/21/58/fda-approved-hiv-medicines.
182. https://aidsinfo.nih.gov/education-materials/fact-sheets/21/58/fda-approved-hiv-medicines.
183. Kakuda, T. N.; Opsomer, M.; Timmers, M.; Iterbeke, K.; Van de Casteele, T.; Hillewaert, V.; Petrovic, R.; Hoetelmans, R. M. W. *J. Clin. Pharmacol.* **2014,** *54,* 949–957.
184. Mills, A.; Crofoot, G., Jr.; McDonald, C.; Shalit, P.; Flamm, J. A.; Gathe, J., Jr.; Scribner, A.; Shamblaw, D.; Saag, M.; Cao, H.; Martin, H.; Das, M.; Thomas, A.; Liu, H. C.; Yan, M.; Callebaut, C.; Custodio, J.; Cheng, A.; McCallister, S. *J. Acquir. Immune Defic. Syndr.* **2015,** *69,* 439–445.
185. Grant, R. M.; Lama, J. R.; Anderson, P. L.; McMahan, V.; Liu, A. Y.; Vargas, L.; Goicochea, P.; Casapia, M.; Guanira-Carranza, J. V.; Ramirez-Cardich, M. E.; Montoya-Herrera, O.; Fernandez, T.; Veloso, V. G.; Buchbinder, S. P.; Suwat, C.; Schechter, M.; Bekker, L.-G.; Mayer, K. H.; Kallas, E.; Georges, A. K. R.; Mulligan, K.; Bushman, L. R.; Hance, R. J.; Ganoza, C.; Defechereux, P.; Postle, B.; Wang, F.; McConnell, J. J.; Zheng, J.-H.; Lee, J.; Rooney, J. F.; Jaffe, H. S.; Martinez, A. I.; Burns, D. N.; Glidden, D. V. *N. Engl. J. Med.* **2010,** *363,* 2587–2599.
186. Baeten, J. M.; Donnell, D.; Ndase, P.; Mugo, N. R.; Campbell, J. D.; Wangisi, J.; Tappero, J. W.; Bukusi, E. A.; Cohen, C. R.; Katabira, E.; Ronald, A.; Tumwesigye, E.; Were, E.; Fife, K. H.; Kiarie, J.; Farquhar, C.; John-Stewart, G.; Kakia, A.; Odoyo, J.; Mucunguzi, A.; Nakku-Joloba, E.; Twesigye, R.; Ngure, K.; Apaka, C.; Tamooh, H.; Gabona, F.; Mujugira, A.; Panteleeff, D.; Thomas, K. K.; Kidoguchi, L.; Krows, M.; Revall, J.; Morrison, S.; Haugen, H.; Emmanuel-Ogier, M.; Ondrejcek, L.; Coombs, R. W.; Frenkel, L.; Hendrix, C.; Bumpus, N. N.; Bangsberg, D.; Haberer, J. E.; Stevens, W. S.; Lingappa, J. R.; Celum, C. *N. Engl. J. Med.* **2010,** *367,* 399–410.
187. Cong, M.; Youngpairoj, A. S.; Zheng, Q.; Aung, W.; Mitchell, J.; Sweeney, E.; Hanson, D. L.; Hendry, R. M.; Dobard, C.; Heneine, W.; Garcia-Lerma, J. G. *J. Virol.* **2011,** *85,* 7933–7936.
188. http://www.fda.gov/NewsEvents/Newsroom/PressAnnouncements/ucm312210.htm.
189. Andrews, C. D.; Walid, H. *Curr. Opin. HIV AIDS* **2015,** *10,* 258–263.
190. (a) For an example of an HIV-protease inhibitor containing regimen, see: Mills, A.; Crofoot, G., Jr.; McDonald, C.; Shalit, P.; Flamm, J. A.; Gathe, J., Jr.; Scribner, A.; Shamblaw, D.; Saag, M.; Cao, H.; Martin, H.; Das, M.; Thomas, A.; Liu, H. C.; Yan, M.; Callebaut, C.; Custodio, J.; Cheng, A.; McCallister, S. *J. Acquir. Immune Defic. Syndr.* **2015,** *69* (4), 439–445; (b) For an example of an HIV-integrase inhibitor containing regimen, see: Sax, P. E.; Wohl, D.; Yin, M. T.; Post, F.; De Jesus, E.; Saag, M.; Pozniak, A.; Thomson, M.; Podzamczer, D.; Molina, J. M.; Oka, S.; Koenig, E.; Trottier, B.; Andrade-Villanueva, J.; Crofoot, G.; Custodio, J. M.; Plummer, A.; Zhong, L.; Cao, H.; Martin, H.; Callebaut, C.; Cheng, A. K.; Fordyce, M. W.; McCallister, S. *Antimicrob. Agents Chemother.* **2015,** *59* (2), 838–845.
191. (a) Ueda, H.; Nakajima, H.; Hori, Y.; Fujita, T.; Nishimura, M.; Goto, T.; Okuhara, M. *J. Antibiotics* **1994,** *47,* 301–310; (b) For the total synthesis of Romidepsin, see: Li, K. W.; Wu, J.; Xing, W.; Simon, J. A. *J. Am. Chem. Soc.* **1996,** *118,* 7237–7238; (c) For characterization of Romidepsin as an HDACi, see: Nakajima, H.; Kim, Y. B.; Terano, H.; Yoshida, M.; Horinouchi, S. *Exper. Cell. Res.* **1998,** *241,* 126–133.
192. Wei, D. G.; Chiang, V.; Fyne, E.; Balakrishnan, M.; Barnes, T.; Graupe, M.; Hesselgesser, J.; Irrinki, A.; Murry, J. P.; Stepan, G.; Stray, K. M.; Tsai, A.; Yu, H.; Sindler, J.; Kearney, M.; Spina, C. A.; McMahon, D.; Lalezari, J.; Sloan, D.; Mellors, J.; Geleziunas, R.; Cihlar, T. *PLoS Pathog.* **2014,** *10,* e1004071.
193. Ueda, H.; Nakajima, H.; Hori, Y.; Fujita, T.; Nishimura, M.; Goto, T.; Okuhara, M. J. *Antibiotics* **1994,** *47,* 301–310.
194. (a) Shigematsu, N.; Ueda, H.; Takase, S.; Tanaka, H.; Yamamoto, K.; Tada, T. *J. Antibiotics* **1994,** *47,* 311–314; (b) Ueda, H.; Manda, T.; Matsumoto, S.; Mukumoto, S.; Nishigaki, F.; Kawamura, I.; Shinomura, K. *J. Antibiotics* **1994,** *47,* 315–323.
195. Archin, N. M.; Liberty, A. L.; Kashuba, A. D.; Choudhary, S. K.; Kuruc, J. D.; Crooks, A. M.; Parker, D. C.; Anderson, E. M.; Kearney, M. F.; Strain, M. C.; Richman, D. D.; Hudgens, M. G.; Bosch, R. J.; Coffin, J. M.; Eron, J. J.; Hazuda, D. J.; Margolis, D. M. *Nature* **2012,** *487,* 482–485.
196. Campbell, G. R.; Bruckman, R. S.; Chu, Y.-L.; Spector, S. A. J. *Biol. Chem.* **2015,** *290,* 5028–5040.
197. For studies of HDACi's in macrophages, see: (a) Campbell, G. R.; Bruckman, R. S.; Chu, Y.-L.; Spector, S. A. *J. Biol. Chem.* **2015,** *290* (8), 5028–5040; For clinical work on Vorinostat, see: (b) Archin, N. M.; Liberty, A. L.; Kashuba, A. D.; Choudhary, S. K.; Kuruc, J. D.; Crooks, A. M.; Parker, D. C.; Anderson, E. M.; Kearney, M. F.; Strain, M. C.; Richman, D. D.; Hudgens, M. G.; Bosch, R. J.; Coffin, J. M.; Eron, J. J.; Hazuda, D. J.; Margolis, D. M. *Nature* **2012,** *487,* 482–485; (c) Lucera, M.; Tilton, C. A.; Mao, H.; Dobrowolski, C.; Tabler, C. O.; Haqqani, A. A.; Karn, J.; Tilton, J. C. *J. Virol.* **2012,** *88,* 10803–10812; For studies on HIV expression in $CD4^+$ T cells induced by HDACi's see: (d) Wei, D. G.; Chiang, V.; Fyne, E.; Balakrishnan, M.; Barnes, T.; Graupe, M.; Hesselgesser, J.; Irrinki, A.; Murry, J. P.; Stepan, G.; Stray, K. M.; Tsai, A.; Yu, H.; Sindler, J.; Kearney, M.; Spina, C. A.; McMahon, D.; Lalezari, J.; Sloan, D.; Mellors, J.; Geleziunas, R.; Cihlar, T. *PLoS Pathog.* **2014,** *10,* e1004071.
198. Lucera, M.; Tilton, C. A.; Mao, H.; Dobrowolski, C.; Tabler, C. O.; Haqqani, A. A.; Karn, J.; Tilton, J. C. *J. Virol.* **2012,** *88,* 10803–10812.
199. Roethle, P. A.; McFadden, R. M.; Yang, H.; Hrvatin, P.; Hui, H.; Graupe, M.; Gallagher, B.; Chao, J.; Hesselgesser, J.; Duatschek, P.; Zheng, J.; Lu, B.; Tumas, D. B.; Perry, J.; Halcomb, R. L. *J. Med. Chem.* **2013,** *56* (18), 7324–7333.
200. (a) Lopatin, U.; Wolfgang, G.; Tumas, D.; Frey, C. R.; Ohmstede, C.; Hesselgesser, J.; Kearney, B.; Moorehead, L.; Subramanian, G. M.; McHutchinson, J. G. *Antivir. Ther.* **2013,** *18* (3), 409–418; (b) Fosdick, A.; Zheng, J.; Pflanz, S.; Frey, C. R.; Hesselgesser, J.; Halcomb, R. L.; Wolfgang, G.; Tumas, D. B. *J. Pharmacol. Exp. Ther.* **2014,** *348,* 96–105.
201. Xing, S.; Bullen, C. K.; Shroff, N. S.; Shan, L.; Yang, C.-H.; Manucci, J. L.; Bhat, S.; Zhang, H.; Margolick, J. B.; Quinn, T. C.; Margolis, D. M.; Siliciano, J. D.; Siliciano, R. F. *J. Virol.* **2011,** *85,* 6060–6064.
202. Doyon, G.; Zerbato, J.; Mellors, J. W.; Sluis-Cremer, N. *AIDS* **2013,** *27,* F7–F11.
203. (a) Petersen, E. N. *Acta Psychaitr. Scand. Suppl.* **1992,** *369,* 7–13; (b) Pike, M. G.; Mays, D. C.; Macomber, D. W.; Lipsky, J. J. *Drug Metab. Dispos.* **2001,** *29,* 127–132.
204. Spivak, A. M.; Andrade, A.; Eisele, E.; Hoh, R.; Bacchetti, P.; Bumpus, N. N.; Emad, F.; Buckheit, R., III; McCance-Katz, E. F.; Lai, J.; Kennedy, M.; Chander, G.; Siliciano, R. F.; Siliciano, J. D.; Deeks, S. G. *Clin. Infect. Dis.* **2014,** *58,* 883–890.
205. Spina, C. A.; Anderson, J.; Archin, N. M.; Bosque, A.; Chan, J.; Famiglietti, M.; Greene, W.; Kashuba, A.; Lewin, S. R.; Margolis, D. M.; Mau, M.; Ruelas, D.; Saleh, S.; Shirakawa, K.; Siliciano, R. F.; Singhania, A.; Soto, P. C.; Terry, V. H.; Verdin, E.; Woelk, C.; Wooden, S.; Xing, S.; Planelles, V. *PLOS Pathog.* **2013,** *9,* 1–15.
206. (a) Okamoto, T.; Wong-Staal, F.; et al. *Cell* **1986,** *47,* 29–35; (b) Selby, M. J.; Bain, E. S.; Luciw, P. A.; Peterlin, B. M. *Genes Dev.* **1989,** *3,* 547–558; (c) Sodroski, J.; Rosen, C.; Wong-Staal, F.; Salahuddin, S. Z.; Popovic, M.; Arya, S.; Gallo, R. C.; Haseltine, W. A. *Science* **1985,** *227,* 171–173.
207. Mousseau, G.; Clementz, M. A.; Bakeman, W. N.; Nagarsheth, N.; Cameron, M.; Shi, J.; Baran, P.; Fromentin, R.; Chomont, N.; Valente, S. T. *Cell Host Microbe* **2012,** *12,* 97–108.
208. Certain HIV patients do not experience the rapid rebound seen with HAART cessation. For details, see: Hocquelouz, L.; Prazuck, T.; Avettand-Fenoel, V.; Lafeuillade, A.; Cardon, B.; Viard, J. P.; Rouzioux, C. *AIDS* **2010,** *24,* 1598–1601.
209. Mousseau, G.; Kessing, C. F.; Fromentin, R.; Trautmann, L.; Chomont, N. Valente. *S. mBio* **2015,** *6,* e00465-15.
210. Campos, N.; Myburgh, R.; Garcel, A.; Vautrin, A.; Lapasset, L.; Nadal, E. S.; Mahuteau-Betzer, F.; Najman, R.; Fornarelli, P.; Tantale, K.; Basyuk, E.; Seveno, M.; Venables, J. P.; Pau, B.; Bertrand, E.; Wainberg, M. A.; Speck, R. F.; Scherrer, D.; Tazi, J. *Retrovirology* **2015,** *12,* 1–31.
211. (a) Tazi, J.; Bakkour, N.; Marchand, V.; Ayadi, L.; Aboufirassi, A.; Branlant, C. *FEBS J.* **2010,** *277,* 867–876; (b) Bakkour, N.; Lin, Y.-L.; Maire, S.; Ayadi, L.; Mahuteau-Betzer, F.; Nguyen, C. H.; Mettling, C.; Portales, P.; Grierson, D.; Chabot, B.; Jeanteur, P.; Branlant, C.; Corbeau, P.; Tazi, J. *PLoS Pathogens* **2007,** *3,* 1530–1539; (c) Soret, J.; Bakkour, N.; Maire, S.; Durand, S.; Zekri, L.; Gabut, M.; Fic, W.; Divita, G.; Rivalle, C.; Dauzonne, D.; Nguyen, C. H.; Jeanteur, P.; Tazi, J. *Proc. Natl. Acad. Sci. U. S. A.* **2005,** *102,* 8764–8769.
212. Chen, C.-J.; Yang, H.-I.; Su, J.; Jen, C.-L.; You, S.-L.; Lu, S.-N.; Huang, G.-T.; Iloeje, U. H. *JAMA* **2006,** *295,* 65–73.
213. Seeger, C.; Mason, W. S. *Microbiol. Mol. Biol. Rev.* **2000,** *64,* 51–68.
214. Stoop, J. N.; van der Molen, R. G.; Baan, C. C.; van der Laan, L. J. W.; Kuipers, E. J.; Kusters, J. G.; Janssen, H. L. A. *Hepatology* **2005,** *41,* 771–778.
215. Ott, J. J.; Stevens, G. A.; Groeger, J.; Wiersma, S. T. *Vaccine* **2012,** *30,* 2212–2219.
216. European Association for the Study of the Liver *J. Hepatol.* **2012,** *57,* 167–185.

217. European Association for the Study of the Liver *J. Hepatol.* **2012,** *57,* 167–185.
218. Liang, T. J.; Block, T. M.; McMahon, B. J.; Ghany, M. G.; Urban, S.; Guo, J.-T.; Locarnini, S.; Zoulim, F.; Chang, K.-M.; Lok, A. S. *Hepatology* **2015,** *62,* 1893–1908.
219. Urban, S.; Schulze, A.; Dandri, M.; Peterson, J. J. *Hepatology* **2010,** *52,* 282–284.
220. Zoulim, F.; Locarnini, S. *Gastroenterology* **2009,** *137. 1593-608.e1–2.*
221. Lok, A. S.; McMahon, B. J. *Hepatology* **2009,** *50,* 661–662.
222. Liaw, Y. F.; Kao, J. H.; Piratvisuth, T.; Chan, H. L.; Chien, R. N.; Liu, C. J.; Gane, E.; Locarnini, S.; Lim, S. G.; Han, K. H.; Amarapurkar, D.; Cooksley, G.; Jafri, W.; Mohamed, R.; Hou, J. L.; Chuang, W. L.; Lesmana, L. A.; Sollano, J. D.; Suh, D. J.; Omata, M. *Hepatol. Int.* **2012,** *6,* 531–561.
223. European Association for the Study of the Liver *J. Hepatol.* **2012,** *57,* 167–185.
224. Han, S. H.; Tran, T. T. J. *Am. Board. Fam. Med.* **2015,** *28,* 822–837.
225. Severini, A.; Liu, X. Y.; Wilson, J. S.; Tyrrell, D. L. *Antimicrob. Agents Chemother.* **1995,** *39,* 1430–1435.
226. Zoulim, F.; Dannaoui, E.; Borel, C.; Hantz, O.; Lin, T. S.; Liu, S. H.; Trepo, C.; Cheng, Y. C. *Antimicrob. Agents Chemother.* **1996,** *40,* 448–453.
227. Delaney, W. E.t.; Ray, A. S.; Yang, H.; Qi, X.; Xiong, S.; Zhu, Y.; Miller, M. D. *Antimicrob. Agents Chemother.* **2006,** *50,* 2471–2477.
228. Peters, M. G.; Singer, G.; Howard, T.; Jacobsmeyer, S.; Xiong, X.; Gibbs, C. S.; Lamy, P.; Murray, A. *Transplantation* **1999,** *68,* 1912–1914.
229. Seigneres, B.; Pichoud, C.; Martin, P.; Furman, P.; Trepo, C.; Zoulim, F. *Hepatology* **2002,** *36,* 710–722.
230. Jacquard, A. C.; Brunelle, M. N.; Pichoud, C.; Durantel, D.; Carrouee-Durantel, S.; Trepo, C.; Zoulim, F. *Antimicrob. Agents Chemother.* **2006,** *50,* 955–961.
231. Seifer, M.; Hamatake, R. K.; Colonno, R. J.; Standring, D. N. *Antimicrob. Agents Chemother.* **1998,** *42,* 3200–3208.
232. Tchesnokov, E. P.; Obikhod, A.; Schinazi, R. F.; Gotte, M. J. *Biol. Chem.* **2008,** *283,* 34218–34228.
233. Standring, D. N.; Bridges, E. G.; Placidi, L.; Faraj, A.; Loi, A. G.; Pierra, C.; Dukhan, D.; Gosselin, G.; Imbach, J. L.; Hernandez, B.; Juodawlkis, A.; Tennant, B.; Korba, B.; Cote, P.; Cretton-Scott, E.; Schinazi, R. F.; Myers, M.; Bryant, M. L.; Sommadossi, J. P. *Antivir. Chem. Chemother.* **2001,** *12* (Suppl. 1), 119–129.
234. Gish, R.; Jia, J. D.; Locarnini, S.; Zoulim, F. *Lancet Infect. Dis.* **2012,** *12,* 341–353.
235. Johnson, M. A.; Moore, K. H.; Yuen, G. J.; Bye, A.; Pakes, G. E. *Clin. Pharmacokinet.* **1999,** *36,* 41–66.
236. Ray, A. S.; Vela, J. E.; Olson, L.; Fridland, A. *Biochem. Pharmacol.* **2004,** *68,* 1825–1831.
237. Yamanaka, G.; Wilson, T.; Innaimo, S.; Bisacchi, G. S.; Egli, P.; Rinehart, J. K.; Zahler, R.; Colonno, R. J. *Antimicrob. Agents Chemother.* **1999,** *43,* 190–193.
238. Zhou, X. J.; Lim, S. G.; Lloyd, D. M.; Chao, G. C.; Brown, N. A.; Lai, C. L. *Antimicrob. Agents Chemother.* **2006,** *50,* 874–879.
239. Hernandez-Santiago, B.; Placidi, L.; Cretton-Scott, E.; Faraj, A.; Bridges, E. G.; Bryant, M. L.; Rodriguez-Orengo, J.; Imbach, J. L.; Gosselin, G.; Pierra, C.; Dukhan, D.; Sommadossi, J. P. *Antimicrob. Agents Chemother.* **2002,** *46,* 1728–1733.
240. Sells, M. A.; Zelent, A. Z.; Shvartsman, M.; Acs, G. *J. Virol.* **1988,** *62,* 2836–2844.
241. Furman, P. A.; Davis, M.; Liotta, D. C.; Paff, M.; Frick, L. W.; Nelson, D. J.; Dornsife, R. E.; Wurster, J. A.; Wilson, L. J.; Fyfe, J. A.; et al. *Antimicrob. Agents Chemother.* **1992,** *36,* 2686–2692.
242. Qi, X.; Xiong, S.; Yang, H.; Miller, M.; Delaney, W. E.t. *Antivir. Ther.* **2007,** *12,* 355–362.
243. Lim, S. G.; Ng, T. M.; Kung, N.; Krastev, Z.; Volfova, M.; Husa, P.; Lee, S. S.; Chan, S.; Shiffman, M. L.; Washington, M. K.; Rigney, A.; Andersen, J.; Mondou, E.; Snow, A.; Sorbel, J.; Guan, R.; Rousseau, F. *Arch. Intern. Med.* **2006,** *166,* 49–56.
244. Chan, H. L. Y.; Chan, C. K.; Hui, A. J.; Chan, S.; Poordad, F.; Chang, T.-T.; Mathurin, P.; Flaherty, J. F.; Lin, L.; Corsa, A.; Gaggar, A.; Subramanian, G. M.; McHutchison, J. G.; Lee, S.; Gane, E. J. *Gastroenterology* **2014,** *146,* 1240–1248.
245. Liaw, Y.-F.; Sheen, I.-S.; Lee, C.-M.; Akarca, U. S.; Papatheodoridis, G. V.; Wong, F. S.-H.; Chang, T.-T.; Horban, A.; Wang, C.; Kwan, P.; Buti, M.; Prieto, M.; Berg, T.; Kitrinos, K.; Peschell, K.; Mondou, E.; Frederick, D.; Rousseau, F.; Schiff, E. R. *Hepatology* **2011,** *53,* 62–72.
246. Heijtink, R. A.; De Wilde, G. A.; Kruining, J.; Berk, L.; Balzarini, J.; De Clercq, E.; Holy, A.; Schalm, S. W. *Antiviral Res.* **1993,** *21,* 141–153.
247. Innaimo, S. F.; Seifer, M.; Bisacchi, G. S.; Standring, D. N.; Zahler, R.; Colonno, R. J. *Antimicrob. Agents Chemother.* **1997,** *41,* 1444–1448.
248. Bisacchi, G. S.; Chao, S. T.; Bachard, C.; Daris, J. P.; Innaimo, S.; Jacobs, G. A.; Kocy, O.; Lapointe, P.; Martel, A.; Merchant, Z.; Slusarchyk, W. A.; Sundeen, J. E.; Young, M. G.; Colonno, R.; Zahler, R. *Bioorg. Med. Chem. Lett.* **1997,** *7,* 127–132.
249. Langley, D. R.; Walsh, A. W.; Baldick, C. J.; Eggers, B. J.; Rose, R. E.; Levine, S. M.; Kapur, A. J.; Colonno, R. J.; Tenney, D. J. *J. Virol.* **2007,** *81,* 3992–4001.
250. Tenney, D. J.; Levine, S. M.; Rose, R. E.; Walsh, A. W.; Weinheimer, S. P.; Discotto, L.; Plym, M.; Pokornowski, K.; Yu, C. F.; Angus, P.; Ayres, A.; Bartholomeusz, A.; Sievert, W.; Thompson, G.; Warner, N.; Locarnini, S.; Colonno, R. J. *Antimicrob. Agents Chemother.* **2004,** *48,* 3498–3507.
251. Villet, S.; Ollivet, A.; Pichoud, C.; Barraud, L.; Villeneuve, J. P.; Trepo, C.; Zoulim, F. *J. Hepatol.* **2007,** *46,* 531–538.
252. Bryant, M. L.; Bridges, E. G.; Placidi, L.; Faraj, A.; Loi, A. G.; Pierra, C.; Dukhan, D.; Gosselin, G.; Imbach, J. L.; Hernandez, B.; Juodawlkis, A.; Tennant, B.; Korba, B.; Cote, P.; Marion, P.; Cretton-Scott, E.; Schinazi, R. F.; Sommadossi, J. P. *Antimicrob. Agents Chemother.* **2001,** *45,* 229–235.
253. Wu, Q.; Huang, H.; Sun, X.; Pan, M.; He, Y.; Tan, S.; Zeng, Y.; Li, L.; Deng, G.; Yan, Z.; He, D.; Li, J.; Wang, Y. *Clin. Gastroenterol. Hepatol.* **2015,** *13,* 1170–1176.
254. Ozaras, R.; Mete, B.; Ceylan, B.; Ozgunes, N.; Gunduz, A.; Karaosmanoglu, H.; Cagatay, A.; Gokturk, K.; Erdem, L.; Kocak, F.; Senates, E.; Tabak, F. *Eur. J. Gastroenterol. Hepatol.* **2014,** *26,* 774–780.
255. Nelson, M. R.; Katlama, C.; Montaner, J. S.; Cooper, D. A.; Gazzard, B.; Clotet, B.; Lazzarin, A.; Schewe, K.; Lange, J.; Wyatt, C.; Curtis, S.; Chen, S. S.; Smith, S.; Bischofberger, N.; Rooney, J. F. *AIDS* **2007,** *21,* 1273–1281.
256. Grigsby, I. F.; Pham, L.; Mansky, L. M.; Gopalakrishnan, R.; Mansky, K. C. *Ther. Clin. Risk Manag.* **2010,** *6,* 41–47.
257. Bedimo, R.; Maalouf, N. M.; Zhang, S.; Drechsler, H.; Tebas, P. *AIDS* **2012,** *26,* 825–831.
258. Kitrinos, K. M.; Corsa, A.; Liu, Y.; Flaherty, J.; Snow-Lampart, A.; Marcellin, P.; Borroto-Esoda, K.; Miller, M. D. *Hepatology* **2014,** *59,* 434–442.
259. Murakami, E.; Wang, T.; Park, Y.; Hao, J.; Lepist, E. I.; Babusis, D.; Ray, A. S. *Antimicrob. Agents Chemother.* **2015,** *59,* 3563–3569.
260. Agarwal, K.; Fung, S. K.; Nguyen, T. T.; Cheng, W.; Sicard, E.; Ryder, S. D.; Flaherty, J. F.; Lawson, E.; Zhao, S.; Subramanian, G. M.; McHutchison, J. G.; Gane, E. J.; Foster, G. R. *J. Hepatol.* **2015,** *62,* 533–540.
261. Kim, J.; Cho, W. Y.; Cho, Y. G.; Kim, G. W.; Lee, M. K.; Kim, C. M.; Han, M. J.; Choi, J.; Hwang, J.; Cho, D. G.; Roh, K. Y.; Kim, Y. Z. *42nd Interscience Conference on Antimicrobial Agents and Chemotherapy (ICAAC), San Diego, CA* (abstract F-1690).
262. Yuen, M. F.; Ahn, S. H.; Lee, K. S.; Um, S. H.; Cho, M.; Yoon, S. K.; Lee, J. W.; Park, N. H.; Kweon, Y. O.; Sohn, J. H.; Lee, J.; Kim, J. A.; Lai, C. L.; Han, K. H. *J. Hepatol.* **2015,** *62,* 526–532.
263. Reddy, K. R.; Matelich, M. C.; Ugarkar, B. G.; Gomez-Galeno, J. E.; DaRe, J.; Ollis, K.; Sun, Z.; Craigo, W.; Colby, T. J.; Fujitaki, J. M.; Boyer, S. H.; van Poelje, P. D.; Erion, M. D. *J. Med. Chem.* **2008,** *51,* 666–676.
264. Erion, M. D.; van Poelje, P. D.; Mackenna, D. A.; Colby, T. J.; Montag, A. C.; Fujitaki, J. M.; Linemeyer, D. L.; Bullough, D. A. *J. Pharmacol. Exp. Ther.* **2005,** *312,* 554–560.
265. Lin, C. C.; Fang, C.; Benetton, S.; Xu, G. F.; Yeh, L. T. *Antimicrob. Agents Chemother.* **2006,** *50,* 2926–2931.
266. Lee, K. S.; Lim, S. G.; Chuang, W. L.; Hwang, S. G.; Cho, M.; Lai, M. Y.; Chao, Y. C.; Chang, T. T.; Han, K. H.; Lee, C. M.; Um, S. H.; Yeon, J. E.; Yang, S. S.; Teo, E. K.; Peng, C. Y.; Lin, H. H.; Yang, S. S.; Huo, T. I.; Nguyen, T.; Chen, T. Y.; Hu, K. Q.; Xu, Y.; Sullivan-Bolyai, J. Z. *J. Hepatol.* **2006,** *44,* S274.
267. Painter, G. R.; Almond, M. R.; Trost, L. C.; Lampert, B. M.; Neyts, J.; De Clercq, E.; Korba, B. E.; Aldern, K. A.; Beadle, J. R.; Hostetler, K. Y. *Antimicrob. Agents Chemother.* **2007,** *51,* 3505–3509.
268. Lin, T. S.; Luo, M. Z.; Liu, M. C.; Zhu, Y. L.; Gullen, E.; Dutschman, G. E.; Cheng, Y. C. *J. Med. Chem.* **1996,** *39,* 1757–1759.
269. Chen, S. H.; Lin, S.; King, I.; Spinka, T.; Dutschman, G. E.; Gullen, E. A.; Cheng, Y. C.; Doyle, T. W. *Bioorg. Med. Chem. Lett.* **1998,** *8,* 3245–3250.
270. Zhu, Y. L.; Dutschman, D. E.; Liu, S. H.; Bridges, E. G.; Cheng, Y. C. *Antimicrob. Agents Chemother.* **1998,** *42,* 1805–1810.

271. Afdhal, N. H.; O'Brien, C. B.; Oshana, S. C.; Dunkle, L. M. *53rd Annual Meeting of the American Association for the Study of Liver Disease (AASLD), Boston, MA* (abstract 837).
272. Afdhal, N.; O'Brien, C. B.; Oshana, S. C.; Dunkle, L. *42nd Interscience Conference on Antimicrobial Agents and Chemotherapy (ICAAC), San Diego, CA* (abstract V-690).
273. Pottage, J. C., Jr.; Oshana, S. C.; Yen, P. T.; Delic, D.; Rehak, V.; Plisek, S.; Mechkov, G. M.; Dunkle, L. M. *J. Hepatol.* **2003,** *38,* 136.
274. Dunkle, L. M.; Oshana, S. C.; Rice, W. G. *Hepatology* **2001,** *34* (abstract 1814).
275. Balakrishna Pai, S.; Liu, S. H.; Zhu, Y. L.; Chu, C. K.; Cheng, Y. C. *Antimicrob. Agents Chemother.* **1996,** *40,* 380–386.
276. Tak, W. Y.; Park, S. Y.; Cho, C. M.; Jung, M. K.; Jeon, S. W.; Kweon, Y. O.; Park, J. Y.; Sohn, Y. K. J. *Hepatol.* **2010,** *53,* 261–266.
277. Harmenberg, J.; Larsson, T.; Boettiger, D.; Augustsson, E.; Mardh, G.; Oeberg, B. 15th International Conference on Antiviral Research (ICAR), Prague (abstract 148).
278. Lai, C. L.; Brown, N. A.; Yuen, M. F.; Wai, C. T.; Lloyd, D.; Pietropaolo, K.; Zhou, X. J.; Chao, G.; Lim, S. G. 55th Annual Meeting of the American Association for the Study of Liver Disease (AASLD), Boston, MA (abstract 24).
279. Bourne, C.; Lee, S.; Venkataiah, B.; Lee, A.; Korba, B.; Finn, M. G.; Zlotnick, A. *J. Virol.* **2008,** *82,* 10262–10270.
280. Zlotnick, A.; Venkatakrishnan, B.; Tan, Z.; Lewellyn, E.; Turner, W.; Francis, S. *Antiviral Res.* **2015,** *121,* 82–93.
281. Chen, H.; Raney, A. K.; Allan, M. J.; Song, J.; Lang, S. A. Thiazolidinones, Oxazolidinones, and Pyrrolidinones for HBV, International Patent Application WO 2007/014023 A1, February 1, 2007.
282. Perni, R. B.; Conway, S. C.; Ladner, S. K.; Zaifert, K.; Otto, M. J.; King, R. W. *Bioorg. Med. Chem.* **2000,** *10,* 2687–2690.
283. Deres, K.; Schroder, C. H.; Paessens, A.; Goldmann, S.; Hacker, H. J.; Weber, O.; Kramer, T.; Niewohner, U.; Pleiss, U.; Stoltefuss, J.; Graef, E.; Koletzki, D.; Masantschek, R. N. A.; Reimann, A.; Jaeger, R.; Grob, R.; Beckermann, B.; Schlemmer, K.-H.; Haebich, D.; Rubsamen-Waigmann, H. *Science* **2003,** *299,* 893–896.
284. Weber, O.; Schlemmer, K.-H.; Hartmann, E.; Hagelschuer, I.; Paessens, A.; Graef, E.; Deres, K.; Goldmann, S.; Niewoehner, U.; Stoltefuss, J.; Haebich, D.; Ruebsamen-Waigmann, H.; Wohlfeil, S. *Antiviral Res.* **2002,** *54,* 69–78.
285. Wu, G.; Liu, B.; Zhang, Y.; Li, J.; Arzumanyan, A.; Clayton, M. M.; Schinzi, R. F.; Wang, Z.; Goldmann, S.; Ren, Q.; Zhang, F.; Feitelson, M. A. *Antimicrob. Agents Chemother.* **2013,** *57,* 5344–5354.
286. http://www.hecpharm.com/research-and-development/pipeline.html#.V1IVs0-jNcZ (retrieved 06.03.16).
287. Zhu, X.; Zhao, G.; Zhou, W.; Xu, W.; Xia, G.; Zheng, Z.; Wang, L.; Yang, X.; Li, S. *Bioorg. Med. Chem. Lett.* **2010,** *20,* 299–301.
288. Campagna, M. R.; Liu, F.; Mao, R.; Mills, C.; Cai, D.; Guo, F.; Zhao, X.; Ye, H.; Cuconati, A.; Guo, H.; Chang, J.; Xu, X.; Block, T. M.; Guo, J.-T. *J. Virol.* **2013,** *87,* 6931–6942.
289. Yuen, M.-F.; Kim, D. J.; Weilert, F.; Chan, H. L.-Y.; Lalezari, J.; Hwang, S. G.; Nguyen, T.; Liaw, S.; Brown, N.; Klumpp, K.; Flores, L.; Hartman, G.; Gane, E. J. *AASLD* **2015** (Phase 1b Efficacy and Safety of NVR 3-778, a First-In-Class HBV Core Inhibitor, in HBeAg-Positive Patients With Chronic HBV Infection).
290. Bertoletti, A.; Ferrari, C. *Gut* **2012,** *61,* 1754–1764.
291. Zoulim, F.; Luangsay, S.; Durantel, D. *Gastroenterology* **2013,** *144,* 1342–1344.
292. Diebold, S. S.; Alexopolou, L.; Hemmi, H.; Reis e Sousa, C. *Science* **2004,** *303,* 1529–1531.
293. Roethle, P. A.; Ryan, M.; McFadden, R. M.; Yang, H.; Hrvatin, P.; Hui, H.; Graupe, M.; Gallagher, B.; Chao, J.; Hesselgesser, J.; Duatschek, P.; Zheng, J.; Lu, B.; Tumas, D. B.; Perry, J.; Halcomb, R. H. *J. Med. Chem.* **2013,** *56,* 7324–7333.
294. Lanford, R. E.; Guerra, B.; Chavez, D.; Giavedoni, L.; Hodara, V. L.; Brasky, K. M.; Fosdick, A.; Frey, C. R.; Zheng, J.; Wolfgang, G.; Halcomb, R. L.; Tumas, D. B. *Gastroenterology* **2013,** *144,* 1508–1517.
295. Woodchuck hepatitis virus (WHV) is frequently used as a model for HBV.
296. Menne, S.; Tumas, D. B.; Liu, K. H.; Thampi, L.; AlDeghaither, D.; Baldwin, B. H.; Bellezza, C. A.; Cote, P. J.; Zheng, J.; Halcomb, R.; Fosdick, A.; Fletcher, S. P.; Daffis, S.; Li, L.; Yue, P.; Wolfgang, G. H. I.; Tennant, B. C. J. *Hepatol.* **2015,** *62,* 1237–1245.
297. Gane, E. J.; Lim, Y. S.; Gordon, S. C.; Kumar, V.; Sicard, E.; Fedorak, R. N.; Roberts, S.; Massetto, B.; Ye, Z.; Pflanz, S.; Garrison, K. L.; Gaggar, A.; Subramanian, G. M.; MCHutchison, J. G.; Kottilil, S.; Freilich, B.; Coffin, C. S.; Cheng, W.; Kim, Y. J. *J. Hepatol.* **2015,** *63,* 320–328.
298. https://clinicaltrials.gov/ct2/show/NCT02579382 (retrieved 06.03.16).
299. Bergmann, J. F.; de Bruijne, J.; Hotho, D. M.; de Knegt, R. J.; Boonstra, A.; Weegink, C. J.; van Vliet, A. A.; van de Wetering, J.; Fletcher, S. P.; Bauman, L. A.; Rahimy, M.; Appleman, J. R.; Freddo, J. L.; Janssen, H. L. A.; Reesink, H. W. *Aliment. Pharmacol. Ther.* **2011,** *34,* 443–453.
300. http://www.roche.com/irp2q15e-annex.pdf (retrieved 06.02.16).
301. Giladi, H.; Ketzinel-Gilad, M.; Rivkin, L.; Felig, Y.; Nussbaum, O.; Galun, E. *Mol. Ther.* **2003,** *8,* 769–776.
302. Morrissey, D. V.; Lockridge, J. A.; Shaw, L.; Blanchard, K.; Jensen, K.; Breen, W.; Hartsough, K.; Machemer, L.; Radka, S.; Jadhav, V.; Vaish, N.; Zinnen, S.; Vargeese, C.; Bowman, K.; Shaffer, C. S.; Jeffs, L. B.; Judge, A.; MacLachlan, I.; Bolisky, B. *Nat. Biotechnol.* **2005,** *23,* 1002–1007.
303. Uprichard, S. L.; Boyd, B.; Althage, A.; Chisari, F. V. *PNAS* **2005,** *102,* 773–778.
304. Chen, Y.; Cheng, G.; Mahato, R. I. *Pharm. Res.* **2008,** *25,* 72–86.
305. http://arbutusbio.com/portfolio/tkm-hbv.php (retrieved 05.01.16).
306. Wooddell, C. I.; Rozema, D. B.; Hossbach, M.; John, M.; Hamilton, H. L.; Chu, Q.; Hegge, J. O.; Klein, J. J.; Wakefield, D.; Oropeza, C.; Deckert, J.; Roehl, I.; Jahn-Hofmann, K.; Hadwiger, P.; Vornlocher, H.-P.; McLachlan, A.; Lewis, D. L. *Mol. Ther.* **2013,** *21,* 973–985.
307. Gish, R. G.; Yuen, M.-F.; Chan, H. L. Y.; Given, B. D.; Lai, C.-L.; Locarnini, S. A.; Lau, J. Y. N.; Woodell, C. I.; Schleup, T.; Lewis, D. L. *Antivir. Res.* **2015,** *121,* 97–108.
308. Wong, S. C.; Klein, J. J.; Hamilton, H. L.; Chu, Q.; Frey, C. L.; Trubetskoy, V. S.; et al. *Nucleic Acid Ther.* **2012,** *22,* 380–390.
309. Yuen, M.; Liu, S.; Lai, C.; Locarnini, S.; Lau, J. Y.; Ferrari, C.; Gish, R. *AASLD* **2015,** *LB-9.*
310. Urban, S.; Bartenschlager, R.; Kubitz, R.; Zoulim, F. *Gastroenterology* **2014,** *147,* 48–64.
311. Volz, T.; Allweiss, L.; Ben Mbarek, M.; Warlich, M.; Lohse, A. W.; Pollock, J. M.; Alexandrov, A.; Urban, S.; Peterson, J.; Luetgehetmann, M.; Dandri, M. *J. Hepatol.* **2013,** *58,* 861–867.
312. https://clinicaltrials.gov/ct2/show/NCT02637999 (retrieved 06.01.16).

5.20 Antiviral Drugs for Acute Infections

KL Powell and E Thomas, ReViral Ltd, Stevenage Bioscience Catalyst, Stevenage, United Kingdom
GS Cockerill, Durham University, Stockton on Tees, United Kingdom; and ReViral, Stevenage Bioscience Catalyst, Stevenage, United Kingdom

© 2017 Elsevier Ltd. All rights reserved.

5.20.1 Introduction 665
5.20.2 Respiratory Virus Targets of Research Into Acute Viral Infections 666
5.20.3 Rhinoviruses 667
5.20.3.1 Reasons to Develop Antiviral Drugs for Rhinovirus Infections 667
5.20.3.2 Classes of Rhinovirus Agents 667
5.20.3.2.1 Capsid binders 667
5.20.3.2.2 Protease inhibitors 669
5.20.3.2.3 Polymerase inhibitors 669
5.20.3.3 Opportunities for Combination Therapies 669
5.20.4 Influenza Viruses 670
5.20.4.1 Reasons to Develop Antiviral Drugs for Influenza Virus Infections 670
5.20.4.2 Classes of Influenza Agents 670
5.20.4.2.1 Ion channel blockers 670
5.20.4.2.2 Fusion inhibitors 670
5.20.4.2.3 Neuraminidase inhibitors 670
5.20.4.2.4 Polymerase inhibitors 671
5.20.4.3 Combination Therapy for Influenza 672
5.20.5 Adenoviruses 672
5.20.5.1 Reasons to Develop Antiviral Drugs for Adenovirus Infections 672
5.20.5.2 Classes of Adenovirus Agents 672
5.20.5.2.1 Polymerase inhibitors 672
5.20.5.2.2 Other targets 673
5.20.6 Paramyxoviruses 673
5.20.6.1 Reasons to Develop Antiviral Drugs for Paramyxovirus Infections 673
5.20.6.1.1 Intervention opportunities 673
5.20.6.2 Antiviral Agents for RSV 673
5.20.6.2.1 Fusion protein inhibitors 673
5.20.6.2.2 RSV RNA replication 676
5.20.6.3 Combination Therapy for RSV Infection 676
5.20.7 Emerging Virus Infections 677
5.20.7.1 Coronaviruses 677
5.20.7.2 Ebola 677
5.20.7.3 Nipah and Hendra Viruses 678
5.20.7.4 Zika Virus 678
5.20.7.5 Yellow Fever 679
5.20.7.6 Alternative Approach to Emerging Infections 679
5.20.8 Conclusions 679
References 679

5.20.1 Introduction

The purpose of this article is to review the unique challenges that are offered by the development of treatments for acute as opposed to chronic viral diseases. To an extent, the outstanding success of treatments for chronic virus infections including human immunodeficiency virus (HIV) and hepatitis C virus (HCV) detailed in previous articles has served to encourage investment in research and development aimed at the treatment of acute viral infections.

Each acute viral infection offers a unique set of epidemiological and technical characteristics that contribute to the overall possibility of the discovery of useful therapeutic agents. It would be impossible in the space available to examine all acute virus infections so we have chosen to compare and contrast the apparently similar respiratory virus infections caused by orthomyxoviruses (influenza (flu)), rhinoviruses, adenoviruses, and paramyxoviruses including respiratory syncytial virus (RSV). We will consider the challenges of drug discovery in each virus family and how these are being overcome.

We will review in detail the discovery efforts aimed at RSV as a general example of an acute viral infection. This virus illuminates the challenges and promise of working in the field. RSV is also the acute virus infection of most current interest to the industry post the emergence of multiple potent therapeutic combinations to treat HCV.

Finally, we will review the interesting challenges of emerging viral infections. Global warming, the subsequent migrations of viral vectors, and the popularity of global travel are all combining to spread little known viruses around the world and to threaten its human populations.

5.20.2 Respiratory Virus Targets of Research Into Acute Viral Infections

The graph later (Fig. 1) shows an overlay of the epidemics of four common respiratory virus families in the United Kingdom over a 10-year period. The RSV epidemic (*black line*) is a consistent feature every winter. Other paramyxoviruses assume less importance. The rhinoviruses (of which there are more than 150 serotypes) are present through much of the year, while influenza virus epidemics are much less predictable. From this timeline, it is clear that the feared global pandemic of influenza is very much overdue. Adenoviruses become important when groups of seronegative individuals congregate (e.g., army recruits or college students) or when the virus attacks the immunocompromised.

The differences seen in the epidemiology of these four virus families show that one cannot generalize on the "respiratory virus" theme and that each virus needs to be considered from multiple aspects before embarking on a drug discovery project.

The key issues to consider when initiating a discovery project are the following:

- *Prevalence*: the significance of the disease burden caused by the virus
- *Diagnosis*: specimen accessibility and speed and accuracy of testing
- *Alternative therapeutic approaches*: vaccines, immunotherapy, etc.
- *Therapeutic window*: ability to intervene in a timely fashion to significantly improve the outcome for patients
- *Competition*: relative progress of other discovery projects and the opportunity/threat they offer

A common issue for all therapeutic areas in the drug industry has for many years been the choice of target protein(s) suitable for each disease. In the virology field, this has become much less complex. For each virus, multiple targets are available and are well understood. Often, the limiting step in starting an antiviral discovery project is making the commercial case that the return on investment will be sufficient to justify the work. This issue is particularly the case for acute viral infections. The history of such projects is often that they fail to get off the ground because the commercial case is based on attempting to treat the "otherwise healthy" population. This approach is often superficially attractive simply because the numbers of such patients are so large. The real medical need *and* the commercial opportunity lie in finding the patient groups where an acute infection can be catastrophic. These patients may be the very young, the elderly or the immunocompromised.

Table 1 lists the four virus families we have chosen to illustrate the issues in discovery of agents to combat acute virus infections. We will discuss each in turn, followed by the issues around emerging virus infections.

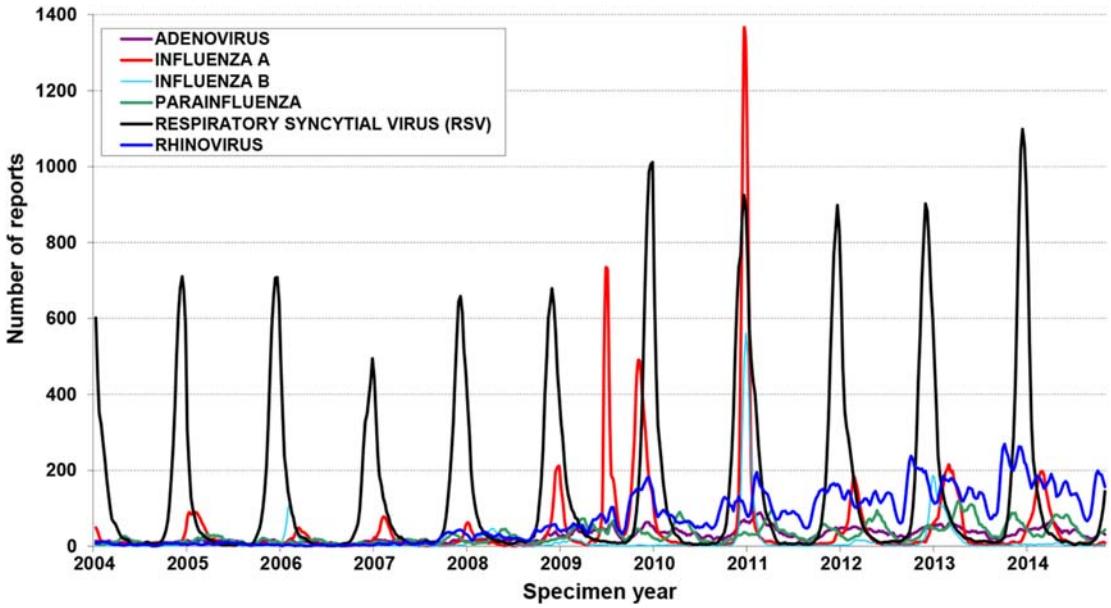

Fig. 1 Six major respiratory viruses reported from PHE and NHS laboratories (LabBase) in England and Wales between weeks 01/2004 and 44/2014 (3-week moving average).

Table 1 Respiratory viruses as targets of drug discovery

Virus family	*Vaccine status*	*Prevalence*	*Approved drugs*	*Active discovery research*
Rhinovirus	None (multiple serotypes)	Very widely distributed; common infection	None	Limited
Orthomyxovirus (influenza)	Multiple	Epidemic and potential for pandemics	Multiple targeting different viral functions	Limited
Adenovirus	Limited (largely for army personnel)	Limited	None	Limited
Paramyxovirus	Passive immunotherapy with Synagis for RSV; multiple vaccines in research phases	Seasonal epidemics with a reliable periodicity	Ribavirin	Active

5.20.3 Rhinoviruses

5.20.3.1 Reasons to Develop Antiviral Drugs for Rhinovirus Infections

Rhinoviruses are known as the cause of the common cold—one of the mildest infections known to medicine. Most adults see two to five infections a year, and although they may cause irritation and some morbidity, they generally are well tolerated. Attempts to treat the common cold with agents like interferons or capsid binders have generally been targeted at the "otherwise healthy" populations. This approach has led to failure, with limited benefits not compensating for the side effects observed. It has also led to a widespread reluctance from the industry to invest in antiviral discovery programs for "the common cold."

Severe outcomes of rhinovirus infections are now widely appreciated in asthmatics, chronic obstructive pulmonary disease (COPD) patients, and those with cystic fibrosis. The problems of developing vaccines or passive immunotherapies for patients who are infected by a virus that may be one of >150 serotypes mandate efforts to develop pan-rhinovirus inhibitors.

Rhinoviruses are a member of the picornavirus family of small single-stranded RNA viruses, and lessons learned through discovery efforts for this group provide useful starting points for research into newly discovered or appreciated small RNA viruses causing significant disease burdens. These include the coronaviruses (SARS-CoV and MERS-CoV) and enteroviruses, which share similar target proteins. A broad-spectrum inhibitor of these viruses would be attractive for use in the life-threatening diseases they can cause.

5.20.3.2 Classes of Rhinovirus Agents

5.20.3.2.1 Capsid binders

Early discovery efforts in several companies identified different types of hydrophobic small molecules that inhibited rhinovirus replication. These compounds were shown to bind to the virus particle and to interfere with the early stages of viral replication. Classic experiments by Rossmann's group determined the three-dimensional structure of example inhibitors bound to virus particles and showed that they were bound to a canyon in the external structure of the viral capsid protein VP1.[1]

A number of structural studies subsequently have confirmed this binding mode with more recently developed compounds on poliovirus[2] and enterovirus 71,[3,4] as well as rhinovirus. In rhinovirus itself, a consistent binding mode can be observed for inhibitors, with a range of interactions with key residues postulated, most notably H-bonding and π interactions with residue Y152. The mutations Y152P and V191L were observed in naturally derived serotypes, and alongside the A150V mutation that is observed across multiple serotypes, all these changes overcome the antiviral effect of inhibitors by reducing the binding affinity of the drug modification at or proximal to the binding site.

In the case of the recently described LPCRW_0005, the distance of the A150 residue from the binding position of the compound (>8 Å) suggests a different effect. The hypothesis proposed is that this mutation stabilizes a collapsed conformation of a portion of the protein that impedes inhibitor access.[5]

As rational as these structural arguments appear, the major feature of drug development in this structural type has been the modification of features that have an effect on both binding affinity and the pharmacokinetic profile. The structures of these inhibitors are long, with multiple freely rotating bonds (Fig. 2). In addition, metabolically labile groups, for example, ester and oximes, are common (CA603 (7), pirodavir (2), and BTA188 (4); Fig. 2). Pleconaril was the first molecule in which these issues were addressed (through the incorporation of the trifluoromethyl-substituted oxadiazole system) and demonstrated satisfactory oral pharmacokinetics.[6] The latest inhibitor BTA798 (5) (vapendavir)[7] utilizes a benzisoxazole replacement for the labile functionality. This isostere appears to provide an orally bioavailable compound, although the bioavailability of 94% in rats is reported at a rather large dose of 50 mg kg^{-1} and retains the potential for the saturation of any metabolic processes that may occur at lower doses closer to the therapeutic range.

The most recently described inhibitor type (6) (LPCRW_0005)[5] certainly demonstrates a different perspective on site binding mode for capsid inhibitors. Due to the compound's decreased size over other inhibitors, it occupies a fraction of the conventional binding pocket. As such, it provides an interesting new template for further medicinal optimization.[8]

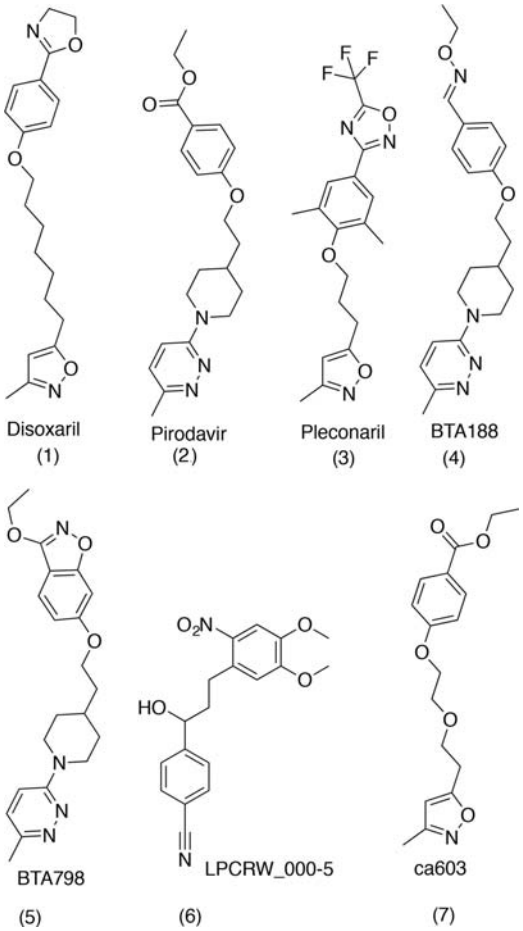

Fig. 2 Capsid inhibitor structures.

The Janssen group developed a series of capsid binders that showed potent activity against selected strains of rhinovirus. As the series developed, an appreciation emerged of variation in the sensitivity of various rhinovirus serotypes and the need for compounds with a wider spectrum of activity.[9] This work culminated in pirodavir (2) (R77,975), which entered clinical trials in challenge studies.[10] As with most capsid binders, the physicochemical properties of the compound made formulation difficult, and an intranasal spray was developed. The compound was tested both in the prophylaxis and treatment modes. There was a clear antiviral effect when the compound was used six times a day in the prophylactic mode, but the treatment data and the effect on the symptoms of the "cold" were disappointing.

Pleconaril originated from research at Winthrop that was later acquired by Sanofi, and pleconaril was licensed to ViroPharma. Using clinical trial data obtained with an oral formulation of the drug ViroPharma attempted to obtain an new drug application (NDA). The trials[11] showed a clear effect on the outcome of a common cold with a benefit of about a day in the resolution of clinical symptoms. Unfortunately, the side effects, although moderate (largely GI-related), were considered too severe by the FDA for the limited benefit. The drug also induced the metabolism of contraceptives, and two women on the trial became pregnant. This outcome very clearly demonstrates the uphill task of developing a medicine for what is considered to be a "trivial" infection.

Detailed analysis of the clinical trial and laboratory data on pleconaril highlights some other interesting challenges for this type of rhinovirus inhibitor. There was very wide variation in the sensitivity of the various serotypes of rhinovirus to the drug, with some insensitive to inhibition. Resistant virus variants were readily isolated during therapy although their relative "fitness" was not assessed (in a recent paper extending the interest in capsid binders to other picornaviruses, Kelly et al.[12] clearly demonstrate the fitness cost of VP1 resistance mutations to the virus.).

In 2007, Schering-Plough in-licensed pleconaril from ViroPharma and began developing an intranasal formulation for the prevention of rhinovirus-induced exacerbation of asthma. A recent update of the results on the https://clinicaltrials.gov website (NCT00394914) show that although patients were entered on the trial when they came into contact with a family member with a proven rhinovirus infection, only 8 out about 600 recruits were found to be infected.

Vapendavir (5) (from Aviragen Therapeutics, previously known as Biota Pharmaceuticals), described earlier, is currently in a phase II trial in asthmatics. Vapendavir displays a broader spectrum of activity against virus isolates than pleconaril. The phase

II study seeks to monitor moderate-to-severe asthmatics during the rhinovirus season and to start dosing with drug or placebo when they are proven to be infected, and its outcome, including measurements of asthma exacerbation, is anticipated in late 2016 (http://www.aviragentherapeutics.com).

Various groups are exploring the possibility of challenge studies in asthmatics to provide more controlled and hence more clear-cut results. The Rega group is continuing to explore the possibility of more advanced capsid binders.[3] Further work in this area is also exploring the possibility of extending the activity to other members of the picornavirus family.[12,13] Mello et al.[14] showed that some rhinovirus isolates in group C (which do not replicate in traditional monolayer cell culture) may not be inhibited by capsid binders. This information will need to be taken into account in the design of new agents.

5.20.3.2.2 Protease inhibitors

Picornaviruses encode a protease encoded by the 3C gene. The 3C protease is essential for replication and is responsible for cleavage of the viral polyprotein into the active enzymes and structural components. Viral encoded proteases have been extensively explored as targets for chronic viral infections. These efforts inspired pioneering work on the equivalent rhinovirus enzyme by the Agouron group (later acquired by Pfizer). This team used a structure-based approach to optimize 3C protease inhibitors, culminating in ruprintivir (8) (formerly AG-7088), a potent agent active against all the rhinovirus isolates tested and some other picornaviruses.[15] The compound is a peptidomimetic whose design is based upon the picornaviral cleavage-site recognition characteristics. In these proteases, most cleavages occur between glutamine and glycine residues. In addition, the rhinovirus 3C protease catalytic triad of cysteine, histidine, and glutamic acid with a geometry similar to those observed in trypsin-like serine proteases suggested the incorporation of a covalent modifier warhead, specifically the α,β-unsaturated ester present in AG-7088. Incorporation of a cyclic butyramide at P1 provided the optimal structure shown in Fig. 3. A detailed description of the optimization of the structural elements P2, P3, and P4 has been published.[16]

The poor aqueous solubility of ruprintivir rendered formulation challenging, but adopting a nasal spray formulation enabled a clinical challenge study to explore the effectiveness of the drug against experimentally acquired infection.[17] While significant effects on some viral parameters were seen (especially with five times a day prophylactic dosing), there was little effect on the development of rhinovirus colds. As high concentrations of drug were reached in the nasal epithelium, this raises questions concerning the bioavailability of such drugs in the upper respiratory tract (URT) on one hand and the relevance of the experimental challenge model on the other.

5.20.3.2.3 Polymerase inhibitors

All picornaviruses encode an RNA polymerase (3D gene product) that in principle appears an ideal target for broad-spectrum inhibitors, as all share a somewhat invariant RNA sequence (reviewed in Ref. 18). An enormous amount of academic work has explored the structure of RNA polymerases from many picornaviruses and in many states (for review, see Ref. 19). A variety of picornavirus polymerase inhibitors have been discovered though screening programs or testing of nucleoside libraries, encompassing both purine and pyrimidine nucleosides[14,20] as well as potential nonnucleoside inhibitors.[18] The clinical impact of inhibitors of polymerases for chronic viral infections suggests that optimized versions of these leads might have high utility.

5.20.3.3 Opportunities for Combination Therapies

Given the extreme plasticity of the picornavirus genome due to its error-prone RNA polymerase, combination therapy will undoubtedly be important in the development of effective broad-spectrum treatments. These may include not only improved small-molecule inhibitors of the types discussed earlier but also biological agents like interferons and soluble viral receptors.

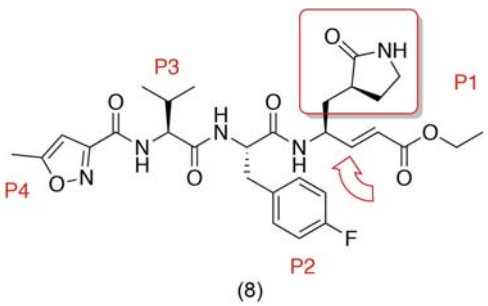

Fig. 3 Ruprintivir (8), showing the position of cysteine attack (*red arrow*) and key butyramide modification (*red box*) in P1. P2–4 indicate other optimization pockets.

5.20.4 Influenza Viruses

5.20.4.1 Reasons to Develop Antiviral Drugs for Influenza Virus Infections

There has been considerable success in the development of both vaccines and antiviral drugs to treat influenza infections, but the unmet medical need is still high. This is largely due to the plasticity of the viral genome that both mandates the manufacture of new vaccines for each virus "season" and allows for the rapid development of resistant virus. The impetus to develop new approaches to influenza comes largely from the potential emergence of a new "pandemic" virus to which the population has little resistance.

As with other respiratory viruses, influenza is already a significant problem in the elderly, the immunocompromised, and the asthmatic population. According to the WHO, influenza occurs globally with an annual attack rate estimated at 5–10% in adults and 20–30% in children. Worldwide, annual epidemics are estimated to result in about 3–5 million cases of severe illness and about 250,000–500,000 deaths.

5.20.4.2 Classes of Influenza Agents

5.20.4.2.1 Ion channel blockers

From early discovery efforts using phenotypic cellular screens for antiinfluenza activity, amantadine was discovered to have potent inhibitory effects. At the time of this discovery, little was known about virus genes and the proteins they encode. In the clinic, the drug was shown to have modest efficacy. Analogs of amantadine were synthesized and found to have a slightly improved profile. The most widely studied was rimantidine, which was extensively used in the former Soviet Union (reviewed by Zlydnikov et al.[21]).

Resistant mutants were easily isolated and mapped to the viral M2 protein. We now know that this protein is an ion channel encoded within the viral genome. With the discovery of the more active neuraminidase (NA) inhibitors and the development of widespread resistance to both amantadine and rimantadine in the clinic, the interest in this target has reduced. Molecular studies of resistant mutants have identified the mechanism of resistance within the structure of the M2 protein, and the area is deserving of more attention as the interest in combination therapies for this virus family grows. Recently, work has been reported on novel scaffolds working on the same target[22] and on novel adamantine analogs.[23]

5.20.4.2.2 Fusion inhibitors

The fusion activity of the influenza hemagglutinin has been shown to be essential for the release of the viral particle from endosomes, allowing replication to begin. Arbidol (**Fig. 4** (9)) is a small indole derivative that was discovered and developed in Russia and is approved and used there and in China,[24] which acts (at least in part) through this mechanism. The clinical trial data reported from the Russian and Chinese studies are not dissimilar to those obtained with the NA inhibitors, but only one clinical study is reported on https://clinicaltrials.gov (NCT01651663). Unfortunately, the compound is clearly suboptimal with relatively poor activity and off-target effects. There have been some attempts to improve on Arbidol's selectivity and activity using its indole scaffold, but as yet, no candidate compounds have emerged.[25,26] The target remains to be exploited but probably through a new lead discovery exercise.

5.20.4.2.3 Neuraminidase inhibitors

By far, the most widely used antivirals for influenza are the NA inhibitors. The NA enzyme is encoded by the viral genome and is present in the external surface of the virus particle. NA has roles in both entry and exit of the virus from the host cell and in the passage of virus through mucus-rich surfaces. Inhibitors of the enzyme are natural substrate analogs based around the structure

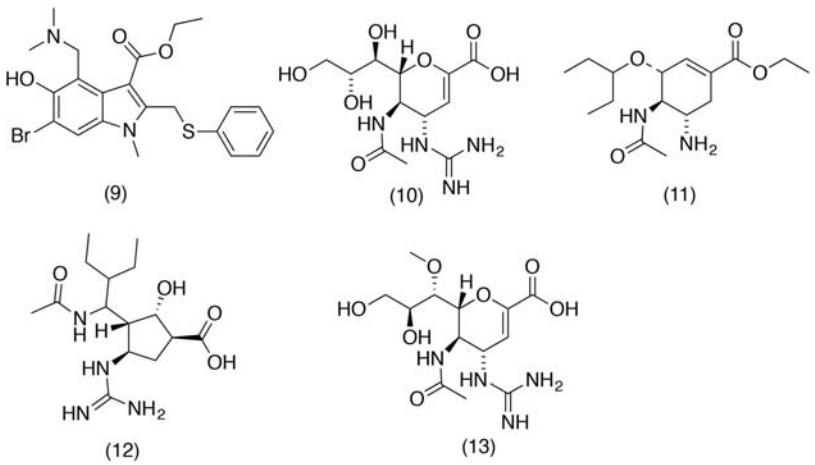

Fig. 4 Arbidol (9), zanamivir (10), oseltamivir (11), peramivir (12), and laninamivir octanoate (13).

of the viral receptor, sialic acid. The approved NA inhibitors zanamivir (Fig. 4 (10)) (Relenza) and oseltamivir (Fig. 4 (11)) (Tamiflu) are potent inhibitors of the enzyme[27,28] and of virus replication in tissue culture. Zanamivir has poor physicochemical characteristics and was formulated for intranasal dosing, while oseltamivir is an oral prodrug that has seen more widespread use. Both drugs showed clear effects in well-controlled experimental challenge models of influenza infection in volunteers.[29,30] It has been far more difficult to prove that the compounds have a significant effect on naturally acquired influenza infections. Indeed, the controversy is still active; while the drugs clearly have an effect on viral load, their effects on URT symptoms do not seem to relate to virus infection as they are seen in patients without proven infection.[31]

At the time of the discovery and development of these drugs, attention was focused on the treatment of seasonal influenza, but anxiety about potential pandemics of newly emerging influenza strains led to extensive stockpiling by government agencies of both agents. This stockpiling activity has had a significant effect on the return on investment on the development of the drugs and illustrates well how the commercial environment can vary for different viruses causing URT infections.

Another significant factor in the use of NA inhibitors has been concern with the development of significant levels of resistance to the drugs. This was enhanced by the emergence of an H1N1 influenza during the 2007–08 influenza season that carried a mutation for oseltamivir resistance and that spread rapidly.[32] Together with the mutation for oseltamivir resistance, this virus carried compensatory mutations that allowed it to replicate normally. The virus spread around the world even in the absence of selective pressure with the drug, but subsequent seasons have not seen a rise in oseltamivir resistance rates above the background level of about 3% of all isolates. The level of resistance to other NA inhibitors is even lower (<1%), but it is not clear if this is due to a real difference in the ease of mutant generation or to the much lower use of the other drugs.[33]

Efforts have continued to develop improved NA inhibitors with enhanced activity, physicochemical properties, and ability to inhibit virus isolates resistant to other NA inhibitors. Peramivir (Fig. 4 (12)), developed by BioCryst, is a more costly NA inhibitor that can be given by infusion and is recommended in cases where oral or IV administration is difficult.[34] Laninamivir octanoate (Fig. 4 (13)) is a long-acting NA inhibitor developed by Biota in collaboration with Daiichi Sankyo. This drug is approved for use in Japan but remains in phase II trials in the rest of the world. The compound is given by the inhaled route as a single administration, and drug levels are maintained over a 5-day period.[35]

5.20.4.2.4 Polymerase inhibitors

As with all other viruses, the RNA polymerase of influenza makes an attractive target for new drugs. Polymerase inhibitors for the influenza virus have been identified either by screening programs, through nucleoside chemistry or more recently through target-driven approaches to the subunits of the enzyme.

Favipiravir (T-705) (Fig. 5 (14)) is the polymerase inhibitor in most advanced development for influenza infections. This compound was discovered at Toyama Chemical in Japan through lead optimization of a screening program hit. The compound is activated by cellular enzymes to a triphosphate form, which then inhibits the viral polymerase.[36] Its activity against influenza is in the range of 0.2–10 μM in in vitro assays. Favipiravir has shown activity in two Japanese phase III trials and is licensed in Japan for stockpiling against pandemic influenza. Currently, the drug is in phase III trials in the United States to treat influenza in adults, using a much higher dose (Japanese dose is a 1.6 g loading dose followed by 400 mg twice a day, while the US dose is a loading dose of 3.6 g plus 400 mg four times a day). Favipiravir has weak activity against a wide variety of RNA viruses, including Ebola virus. Clinical trial data are awaited on the efficacy of the drug against the latter.

A wide variety of pyrimidine and purine nucleosides have been claimed to have activity against influenza viruses. Unfortunately, to date, none of these have been found to be sufficiently selective for the virus over host cell enzymes to develop further.

A nonnucleoside polymerase inhibitor VX-787 was developed by Vertex and licensed to Johnson & Johnson in 2014 and renamed JNJ-872. This compound was discovered as an inhibitor of the "cap-snatching" activity of the PB2 subunit of the viral

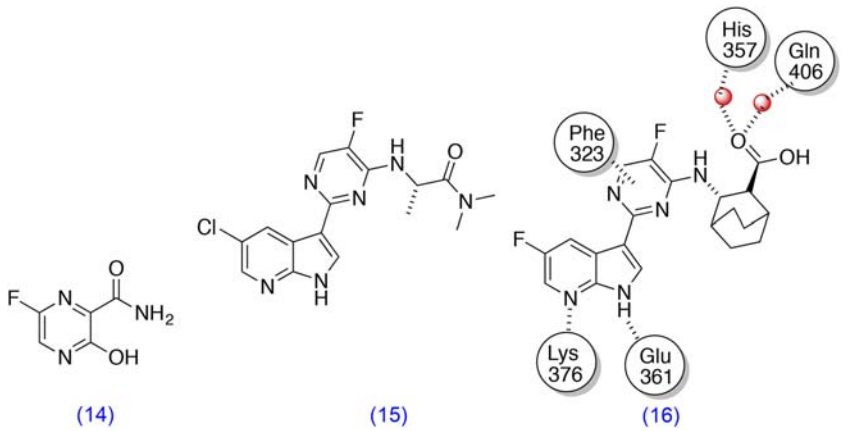

Fig. 5 Favipiravir (14). A representative hit (15) from the phenotypic screening program undertaken at Vertex and its optimization, showing the key interactions of VX-787 (16) with residues within the cap-binding domain.

RNA polymerase and indeed occupies the 7-methyl GTP cap-binding site.[37] In preclinical studies, the compound showed excellent activity against influenza in animal models of the disease. Unfortunately, the compound has no activity against influenza B strains. Interesting activity over a longer window of activity than that seen with NA inhibitors stimulated investment by BARDA in the phase III program on this compound for treatment of patients hospitalized with influenza infection.

As with many influenza programs, VX-787 was discovered utilizing a phenotypic cellular assay.[38] The initial screen was limited to 1000 compounds but identified several with measurable antiviral activity. The identification of a kinase inhibitor template as a hit was perhaps not only a reflection of the focused source of compounds but also an example of the successful reuse of drug-like compound types provided by kinase-based screening sets. Specifically, a series of pyrimidine azaindoles emerged from the screen with significant activity and are represented by compound 15 (**Fig. 5**). The project was supported by crystallography, with several structures generated of compounds bound to the GTP cap-binding domain revealing key hydrogen-bonding interactions between the azaindole and lysine and glutamic acid side chains in the binding site. Further interactions were delineated in the clinical compound for the carboxylic acid, introduced as part of the optimization process and resulting in VX-787 (**Fig. 5** (16)).

The endonuclease activity of the PA subunit of the polymerase was targeted by the Merck group in the 1990s.[39] Although this project did not lead to clinical candidates, the leads became an excellent starting point for the very successful program that led to HIV integrase inhibitors (the enzyme shares a similar active site). Two companies have PA inhibitors in clinical trials: S-0033188, from Shionogi, is in phase 1 in Japan, and Alios (J&J) has AL794 in a challenge study in the United States (https://clinicaltrials.gov, NCT02588521).

5.20.4.3 Combination Therapy for Influenza

Clear clinical needs and interesting opportunities exist for further antiinfluenza research. For a truly effective approach to pandemic management, a combination regimen using different inhibitor classes would be appropriate, and in this context, the concept of combining polymerase PA and PB2 inhibitors to provide a broad-spectrum therapeutic is appealing.

5.20.5 Adenoviruses

5.20.5.1 Reasons to Develop Antiviral Drugs for Adenovirus Infections

Adenoviruses are the cause of a variety of important human and animal infections, and yet, there has been little progress in the development of antiviral drugs to treat these diseases. Given the size of the adenovirus genome, the number of attractive targets encoded therein, and the stability of a double-stranded DNA viral genome, antiviral drugs could clearly be developed were sufficient commercial incentive to exist. The three major opportunities are infectious viral conjunctivitis, lung infections in the immunocompromised (especially in transplant patients), and epidemics of adenovirus pneumonia in young adults (especially military recruits or students brought into close proximity due to enlistment or starting college).

Conjunctivitis is an ocular inflammation that can be caused by a virus, a bacterium, or an allergen. Adenovirus infections account for up to 90% of all viral conjunctivitis. Rapid diagnostic tests at point of care are now available and would aid rapid treatment. There are signs of interest in this area from specialist ophthalmic companies. It is difficult to get accurate estimates of the numbers of patients, as in most countries infection is not notifiable.

Adenovirus infection in the immunocompromised patient is a major threat. Infection is especially common in young recipients of stem cell transplants. Given the otherwise excellent prognosis for these patients, their significant numbers, and the complete lack of treatment options, this indication may represent an "orphan drug" designation with an attractive price to support development.

Military support has enabled the development of a vaccine against adenovirus types 4 and 7 that is used extensively by the US army. The complex nature of the adenovirus family mitigates against the development of a pan-family vaccine.

5.20.5.2 Classes of Adenovirus Agents

5.20.5.2.1 Polymerase inhibitors

Cidofovir is a nucleotide analog that was discovered in Prague by Holy's group[40] and developed by Gilead as a treatment for cytomegalovirus (CMV) retinitis in AIDS patients (a major problem before the development of effective combination regimens). It was the first nucleotide analog to be approved for human use. The compound was active against a range of DNA viruses, including adenovirus, but its use was limited by its nephrotoxicity and lack of oral availability.

Chimerix used a proprietary lipid conjugate technology to produce an orally available prodrug of cidofovir, brincidofovir (CMX001), with the primary aim of reducing the impact of CMV in the immunocompromised. Brincidofovir is orally available and avoids some of the issues with cidofovir therapy. During its development, the compound became the target of a social media campaign for its compassionate use in a young patient with adenovirus infection, as no other therapy was available. Data from an ongoing open label phase III trial in 20 stem cell transplant patients with adenovirus infection that completed enrollment in Aug. 2015 are awaited (https://clinicaltrials.gov, NCT02087306). Unfortunately, this trial appears not to have shown a therapeutic benefit, although viral load was reduced (http://www.chimerix.com, May 9, 2016).

5.20.5.2.2 Other targets

Nicox is developing NCX 4240 for viral conjunctivitis. NCX 4240 is Carragelose (iota-carrageenan), a sulfated galactose polymer derived from red seaweed with antiviral properties. Carragelose inhibits viruses from binding to and entering human cells, reducing viral replication and associated symptoms. Carragelose is already available without prescription for the treatment of respiratory viral infections. Antiviral activity has been demonstrated in preclinical studies, including three of the most important adenoviruses causing conjunctivitis. Nicox plans to conduct clinical investigation of NCX 4240 as a medical device (http://www.nicox.com, 2016).

5.20.6 Paramyxoviruses

5.20.6.1 Reasons to Develop Antiviral Drugs for Paramyxovirus Infections

The paramyxoviruses are quite distinct from the orthomyxoviruses (Influenza viruses) and have a completely different genomic structure and epidemiology, despite both groups causing infections of the respiratory tract. RSV is clinically the most important member of the Paramyxoviridae family and was first isolated in 1956. There are two major serotypes of RSV, A & B, which alternate with each other and which cause similar disease. RSV is highly infectious and is transmitted through respiratory secretions via close contact with infected individuals, through droplets or through contaminated surfaces. In healthy adults, RSV is one of the causes of "winter colds," but in infants, the virus causes 1–2 weeks of respiratory tract disease. Infants can continue to excrete virus for several weeks. By age 2, virtually all children have been infected by the virus. Infection by RSV induces only partial protection, and subsequent infection can occur even in the same winter season. RSV is a significant pathogen of the very young, the immunocompromised, and the elderly:

- *RSV in new born infants*: In the United States, between 100,000 and 126,000 infants under 1 year have been hospitalized in each of the last 5 years. There are about 2.1 million outpatient consultations for the under 5 s with RSV each and every year. Each of these infants is a prime candidate for a safe and effective oral therapy. The mortality rate in the very young at risk infants is between 2% and 3% in most developed countries including the United States. Care of babies with RSV infection imposes a major burden on the hospital sector and limits capacity to undertake routine surgery.
- *RSV in the immunocompromised or other medically compromised patients*: RSV is a major issue in those who are immunocompromised through natural causes, by cancer or chemotherapy, or deliberately for transplantation. Although numerically less significant, the considerable investment in such patients mandates their treatment.
- *RSV in the elderly*: There is increasing awareness of the burden caused by RSV in the elderly. In years without a major influenza epidemic (i.e., most years; see **Fig. 1**), RSV is a more significant cause of morbidity and mortality in the over 60s. There are more than 2 million consultations with physicians in the United States each year due to RSV infection. The virus is also a significant problem in adults with COPD, where it is a major cause of exacerbations. In care homes, RSV causes annual epidemics during the winter season.

5.20.6.1.1 Intervention opportunities

As for influenza infections, otherwise healthy adults will develop a severe cold but will normally recover unaided. Consequently, therapies are being developed to treat firstly infants and those children where the disease is more severe both in terms of duration and the severity of the possible outcomes. Studies have shown that such children see up to three physicians prior to hospital admission, presenting multiple prescribing opportunities.[41] Secondly, in the "compromised" adult patients, the treating physician would generally be well aware of the need to survey his or her patients for RSV infection and to use effective remedies quickly and efficiently. Finally, in the adult population, treatment during a local epidemic would be of use to prevent the spread of this life-threatening infection. The concept that there is insufficient time for therapeutic intervention during respiratory virus infections, derived from the influenza field, is now regarded as outmoded.[42] Due to the longer duration of RSV disease in both infants and adults, it is now widely accepted by the experts in the field that a small-molecule drug could be effective either for treatment or for prophylaxis.[43]

5.20.6.2 Antiviral Agents for RSV

Two agents are approved for the treatment of RSV infections. The first, ribavirin, is a nucleoside analog that was discovered to have anti-RSV activity in a screening program. Its clinical use is restricted due to limited antiviral potency, inherent toxicity, and teratogenic potential. The other approved agent is the prophylactic monoclonal antibody Synagis (paluvizimab), marketed by AstraZeneca. This antibody, which interacts with the F glycoprotein of the virus (see in the succeeding text), has been shown to provide protection in infants and has gained widespread use to protect premature babies. The cost of therapy (about $5000 per infant for the winter season) limits wider uptake.[43–45] There is thus an obvious clinical need for new small-molecule inhibitors of the virus.

5.20.6.2.1 Fusion protein inhibitors

RSV encodes two surface glycoproteins, the F and G proteins. G is dispensable in tissue culture, but its deletion attenuates virus infectivity. The F protein is essential for the entry of the virus into the host cell. Expression of the protein at the cell membrane causes

cell-to-cell fusion, leading to the giant syncytia characteristic of RSV infection. Since the early discovery that inhibitors of the fusion of RSV virus particles and host cells could be readily identified by high-throughput screening, a great deal of work has been done to refine the potency and selectivity of a variety of structural types of inhibitor. Early work in the field has been surveyed in previous reviews.[46,47] More contemporary research has led to a high-resolution, three-dimensional understanding of the fusion process and its inhibition.

For an excellent detailed overview of F protein structure and function, see Battles et al.,[48] who described a structural analysis of inhibitor interaction with the prehairpin structure of the RSV fusion protein. In that work, a number of inhibitor structures were docked into a trimeric model of the fusion complex based upon the crystal structure of JNJ-250685 bound to a prefusion construct. Although not all-encompassing, a rational description of the binding of these drug-like and structurally diverse inhibitors is evident from these studies. **Fig. 6** provides an annotated version of the binding modes of JNJ-2408068 (17), Biota-9881 (substituting in this analysis for the structurally related BTA-C585 (18) and GS-5806 (19)). Most evident is the hydrophobic π/π nature of the binding of the Biota compound (18), with JNJ-258606 and presumably GS-5806 taking advantage in addition of further energetically beneficial polar interactions by virtue of the amines they incorporate.

All of these inhibitors exhibit potency against laboratory strains of RSV and are orally bioavailable. The discovery and progress toward clinical evaluation of presatovir (GS-5806) have been described recently.[49] A moderately active screening hit (20, **Fig. 7**) with a poor oral pharmacokinetic profile was transformed in an efficient manner into the clinical compound. Of note is the role of the pendant amine in presatovir, perhaps incorporated to target potential salt-bridge binding interactions as described earlier. A further recent disclosure[50] draws a comparison between the improved lung distribution properties of presatovir and its alcohol analog (21, **Fig. 7**). This advantage of the basic amine-containing compound is rationalized as product of the interaction at lung epithelial cells with phospholipids, phosphatidyl choline, or fatty acids in the pulmonary surfactant.

To date, less information is available regarding the Biota compound BTA-C585. In 2014, Draffan et al.[51] disclosed a generic structure for a compound that is potent in the human epithelial airway model (EC_{50} 8.4 nM), but with some variability in clinical isolate data (most EC_{50}s appear around 100 nM), and exhibits oral bioavailability (59% is quoted in rat and 107% in dog at a dose of 20 mg kg^{-1}). Efficacy in the cotton rat model is described, with a 99% reduction in viral titer observed at 100 mg kg^{-1}. A 2011 patent supporting this generic structure describes example 22 (**Fig. 8**) as one of the more potent examples (2.2 nM in an RSVA2 cytopathic effect assay).[52]

The failure of a single fusion inhibitor to reach the market may reflect an attrition rate typical of pharmaceutical development in general but leaves open the question of clinical validation. In that context, the first successful clinical study with a fusion inhibitor was recently reported by Gilead with GS-5806.[53] This compound given rapidly reduced viral load and symptoms of RSV disease in volunteers with confirmed RSV infection. The compound is leading a group of fusion programs from J&J, Biota Holdings, Teva, ARK Therapeutics, and ReViral. **Table 2** gives an overview of the stage of development of these efforts, all of which are or will be in clinical studies in 2016.

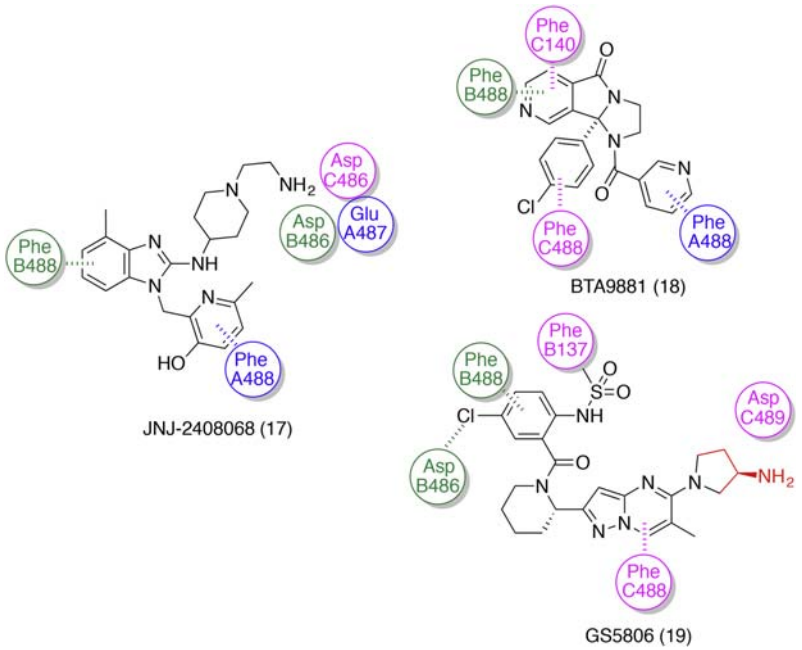

Fig. 6 An annotated schematic of the proposed binding modes of JNJ-2408068 (17), BTA-9881 (18), and GS-5806 (19).[48] Key binding interactions are shown for each inhibitor with colors indicating an individual component of the trimeric fusion protein complex.

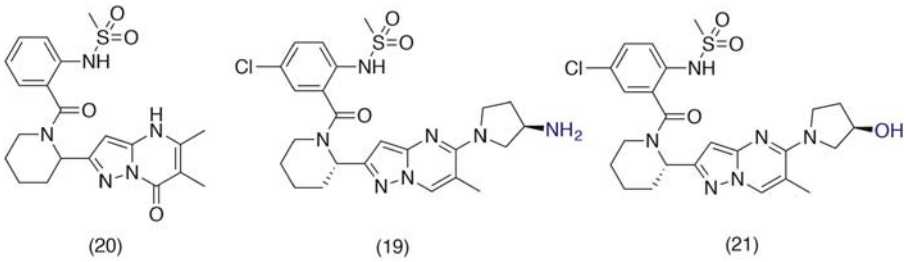

Compound	EC_{50} (RSVA2)	PPB (Human, %)	EC_{50} Fold shift in plasma	F (%, rat)
20	65	93.5	13	2
19	1.5	94.4	13	67
21	1.5	94.5	10	42

Fig. 7 Selected pharmacokinetic and potency data for hit compound (20), presatovir (19), and the hydroxyl analog (21).

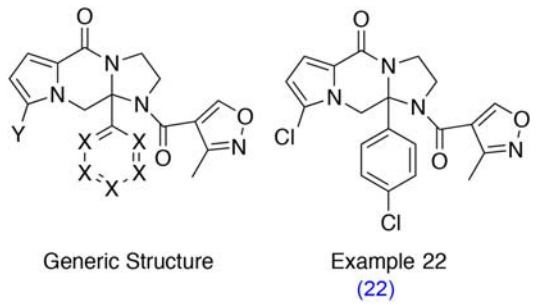

Fig. 8 Generic structure and potent example from Biota.

Table 2 Fusion inhibitors under pharmaceutical development

Compound	*Company*	*Status*
GS-5806 Presatovir	Gilead	Completed a challenge study and now in phase II study in stem cell transplant patients
JNJ-2408068	Johnson & Johnson	Extensively studied preclinical candidate with suboptimal PK characteristics. Superseded by TMC-353121 and a new fusion inhibitor JNJ-53718678 for which little data are in the public domain. A phase I study in hospitalized infants is underway
VP-14637/MDT-637	Teva—MicroDose Therapeutx (MDT)	Difficult to formulate compound discovered by ViroPharma and licensed to MDT. Reformulated and partnered with Gilead but returned. MDT acquired by Teva. A challenge study was undertaken but no data yet released
BTA-C585	Biota	Completed phase I in 2015. Challenge study underway in Apr. 2016 at relatively high doses. Clinical hold reported on Aviragen (Biota) website (http://www.aviragen.com, May 2016) due to a cardiovascular issue
AK0529	Ark Biosciences Inc.	Out-licensed by Roche, no challenge study was undertaken but a phase Ib study in hospitalized infants underway in Australia
RV521	ReViral	Entering phase I in 2016

There is an active debate about the ultimate clinical utility of fusion inhibitors given the relatively rapid emergence of resistance mutants during in vitro studies. This was first observed in the pioneering work of the BMS group.[54] Subsequently, Yan et al.[55] showed that mutants obtained to a novel fusion inhibitor structure mapped to the same region of the protein as other fusion inhibitor mutants. This group claimed that one of their mutants was equally pathogenic to the wild-type virus in a murine model of RSV.

Extensive use has been made of the differentiated human airway epithelium model of RSV replication to measure the "fitness" of resistant mutants[48] where mutants that had become less sensitive to fusion inhibitors paid a cost in replication efficiency. Clinical

data further showed that although resistant mutants do occur when humans are treated with fusion inhibitors, Gilead's GS-5806 was very effective in reducing both virus load and the signs and symptoms of disease.[53]

5.20.6.2.2 RSV RNA replication

To replicate its RNA, RSV requires four viral proteins—the M2-1 protein (only required for transcription), the nucleocapsid (N), phosphoprotein (P), and large (L) proteins. This complex provides a variety of potential targets for viral inhibition. In vitro replicon systems are now available, which measure the role of N, P, and L in RNA duplication. The role of the three proteins is gradually becoming clearer, and we are starting to see the fruit of research in emerging development programs aimed at these targets. A recent publication, for example, examines a druggable pocket at the N–P interface using high-resolution 3D structures.[56] This group identified compounds based on docking studies using this structure, which confirm that the site is a viable target.

Several compounds targeting different aspects of RSV replication are in various stages of preclinical and clinical development (see **Table 3**).

The Alios research program[58] was directed toward the identification of nucleosides that could inhibit RSV polymerase by chain termination. A large number (>100) of structurally diverse nucleosides were designed and screened in a cell-based RSV assay. The nucleoside analogs were also converted to their 5′-triphosphates and screened for inhibition of RSV RNA-dependent RNA polymerase activity. One compound, 4′-azido-2′-deoxy-2′,2′-difluorocytidine (23, **Fig. 9**), exhibited potent inhibition of the cytopathic effect of long-strain RSV, with an EC_{50} of 1 μM. Furthermore, the corresponding triphosphate was identified as a potent RSV polymerase inhibitor with an IC_{50} of 0.3 μM.

An intensive, primarily safety-guided optimization process furnished a selective inhibitor of RSV. The isobutyryl prodrug of this inhibitor, termed ALS008176 (24, **Fig. 9**), showed acceptable oral bioavailability in hamsters, rats, and monkeys and has progressed into clinical trials.

PC786, most likely the subject of a recent patent filing by Pulmocide Ltd.,[59] appears to be a derivative of a series of RSV inhibitors exemplified by YM-53403 (25), originally described by Yamanouchi[60] and further elaborated by Gilead[61] and AstraZeneca.[62] They are high-molecular-weight, low-solubility compounds that in their AstraZeneca and Gilead guises can be characterized as weak bases. The structural modifications in this evolution are shown in **Fig. 10**.

PC786 is intended for inhaled dosing, presumably through increasing molecular weight and clogP, and in this context, the addition of a fluoro toluidine fragment into the molecule is noteworthy; an earlier representative of this chemotype, however, was retained poorly in lung tissue.[59]

5.20.6.3 Combination Therapy for RSV Infection

Although treatment of RSV infections will likely be short term, longer-term regimens will be optimal for the elderly where prophylaxis may be required. Combination therapies targeting multiple different viral targets would optimize antiviral effect and reduce the risk of significant resistance emerging.

Table 3 Other small-molecule inhibitors of RSV replication in development

Compound	*Company*	*Status*
ALS-008176	Alios (now part of J&J)	Nucleoside analog that inhibits RNA polymerase activity. Potent activity in viral challenge studies. Currently in early phase II trials in infants
PC786	Pulmocide	A nonnucleoside RNA polymerase inhibitor with physical characteristics suitable for inhaled administration. Currently in formal preclinical studies
Ribavirin	M,S&D and multiple generics	Licensed medicine whose limited activity against RSV is still a matter of controversy. Major mechanism against RSV is probably hypermutation via the RNA replication complex[57]
RSV604	Novartis	RSV 604 interacts with the N protein and proved to be effective in early clinical studies

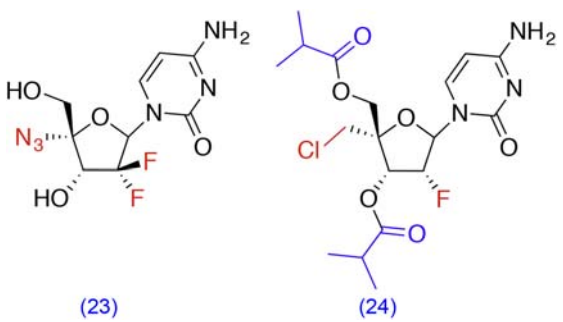

Fig. 9 The initial hit nucleoside (23) discovered by Alios and its optimized prodrug ALS-008176 (24). The isobutyryl prodrug functionality is shown in blue. Key optimization modifications are highlighted in red.

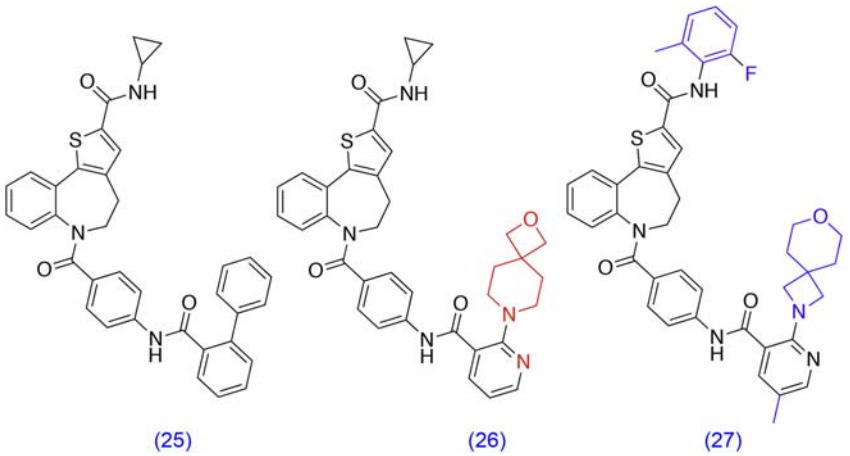

Fig. 10 The optimization of the original Yamanouchi series (25) to the Pulmocide compound (27) via AZ (26).

5.20.7 Emerging Virus Infections

As the impact of climate change on the spread of insect vectors grows, viruses are emerging, which are well-documented human pathogens but whose geographic range has been limited. The large increase in global travel for business and leisure has also created the opportunity for any virus to be transported around the world in hours and days.[63]

When any new virus emerges, a clamor arises for a new vaccine or drug to control the infection and hurried clinical trials using agents with limited preclinical validation result. Rarely do such repurposing efforts prove useful; genomic and functional diversity across viral pathogens mandates specific drug optimization efforts, despite the precedent from broad-spectrum antibacterial agents. An alternative approach is to identify antiviral agents working through host targets, but this field remains in its infancy. Here, we present a brief overview of recent viral epidemics to illustrate these points and end with an alternative scenario for pandemic preparedness.

5.20.7.1 Coronaviruses

SARS-CoV appeared in 2003. It appears to have spread from small mammals in China to humans and then to have passed from human to human via close contact with respiratory secretions either directly or through fomites.[64] The virus is a member of the corona virus family some members of which were known to cause mild symptoms like those of the common cold. The SARS epidemic spread rapidly by air travel of infected patients and caused about 8000 infections, with a mortality rate of about 10% (http://www.WHO.int). The epidemic was controlled by strict public health measures—isolating patients and providing high-quality support. The virus has caused no new case since 2004.

Coronaviruses are small RNA viruses that encode a replicase and a protease most similar to the rhinoviruses (see in the preceding text) and other targets. Attempts have been made to utilize the knowledge gained from the latter to accelerate drug development,[65] but more than a decade later, no strong candidate molecule has emerged. The coronavirus replicase complex has been studied extensively since 2003 and is quite different from other small RNA viruses.

The failure to go from promising ideas to candidate drugs probably resulted from a lack of commercial market for a SARS drug, but then, in 2012 another Coronavirus, MERS-CoV, emerged. This virus is thought to have transferred to humans from bats (bats are a natural reservoir for many coronaviruses) with camels as a major intermediate host. MERS-CoV does not spread readily from human to human. Nevertheless, the virus has caused small epidemics, mainly in Saudi Arabia. In total, there have been about 1644 cases and 590 related deaths. Cases have been exported to several countries including South Korea, where more than 100 cases resulted though infection in a healthcare setting. Good infection control measures are very effective. The arrival of a second coronavirus with significant healthcare impact has reawakened interest in both vaccine and drug research.

5.20.7.2 Ebola

Ebola is caused by a filovirus and was first recognized in 1976 in Sudan and the Congo. The most recent outbreak began in 2014 and is the largest to date (>28,657 cases and 11,325 deaths). The infection has about a 50% mortality rate and has been transported via air travel. The natural hosts of Ebola virus are thought to be fruit bats. Infection of humans occurs through contact with dead animal tissue or body fluids; human-to-human transmission occurs by similar routes. Ebola virus belongs to the Filoviridae family of the Mononegavirales, in the same order as the Paramyxoviridae family. Given clinical precedent with these related viruses, the viral RNA polymerase is a logical target for drug discovery. Several groups have screened nucleoside libraries to identify leads. Of existing nucleoside antivirals, favipiravir (see section "**Influenza Viruses**"), brincidofovir (see section "**Adenovirus**"), and BCX4430

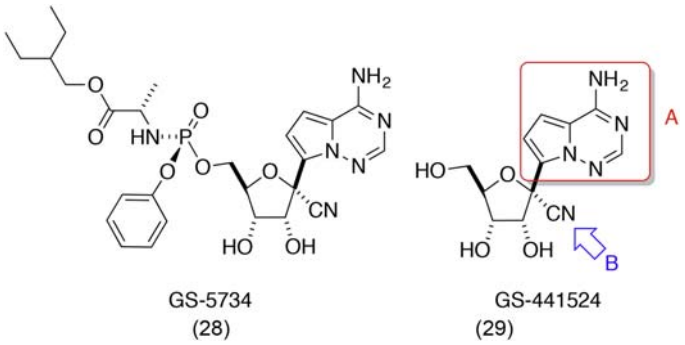

Fig. 11 The phosphoramidate prodrug GS-5734 (28) and its parent nucleoside GS-441524 (29).

(BioCryst)[66] have all shown some activity in animal models. Unfortunately, none were used early enough in the epidemic to obtain indications of clinical efficacy. Further work is underway to look for selective Ebola virus nucleoside inhibitors.

GS-441524 was identified as a novel inhibitor of the West African Ebola strain and other Ebola species. The 1′-cyano group (29, Fig. 11) provided potency and selectivity for viral polymerases, while the C-linked pyrrolo[2,1-f][1,2,4]-triazin-4-amine base fragment (28, Fig. 10) is stable to deglycosylation. A program to identify a suitable prodrug of GS-441524 provided GS-5734, a monophosphoramidate, which has potent in vitro activity against multiple filoviruses, with EC_{50} values in the 0.1–0.2 μM range (Ref. 67; http://www.usamriid.army.mil, Oct. 9, 2015). In a rhesus monkey model of Ebola infection, the compound was effective in a therapeutic mode.[68] GS-5734 has activity against not only filoviruses but also arenaviruses and coronaviruses. The compound's clinical potential mandated its use in a Scottish nurse who had contracted the Ebola infection while working with patients in Sierra Leone. She was treated at the Royal Free Hospital in London and discharged Jan. 2015 but was readmitted to the same hospital in Oct. 2015, when her Ebola virus infection relapsed in the form of acute meningitis.

As a consequence of the successful in vivo testing, Gilead filed an IND July for the use of GS-5734 to treat Ebola virus disease, and phase I testing in healthy human volunteers began in August. When the Scottish nurse was hospitalized in early October, sufficient data had been obtained to support compassionate use of the drug.

5.20.7.3 Nipah and Hendra Viruses

These viruses belong to the Paramyxoviridae family in the order Mononegavirales, and as such are quite closely related to RSV. Both viruses' natural hosts are fruit bats. Hendra virus was first described in 1994 as the causative agent of an equine epidemic in Hendra, a town in Queensland, Australia. The fatality rate is high—74% in horses and 60% in humans, infected by contact with diseased horses. More than 50 outbreaks of Hendra have occurred since the virus emerged. A vaccine is available for horses, but there are little data on efficacy. Nipah virus emerged in 1998 on pig farms in Malaysia with 257 human infections and 105 deaths. The virus may have the ability for transfer between humans as it causes respiratory infections. Again, the virus's natural host is thought to be a fruit bat. Fruit bats excrete the virus in urine, which probably contaminates pig feed. Since 1998, eight further outbreaks have occurred in Bangladesh and the neighboring areas of India.

The emergence of both viruses probably relates to the loss and change of habitat due to human encroachment. Both viruses would appear to have the potential for widespread dissemination, and further discovery work is justified. Ribavirin has been used in experimental animal models and patients with equivocal results.[69] The discovery efforts described earlier for the related RSV provide a rationale for exploration of fusion inhibitors and nucleosides.

5.20.7.4 Zika Virus

Although Zika virus was discovered in the 1940s during surveys of arthropod-borne viruses in Uganda, it received very little attention until the recent outbreak in South America. The virus moved across the Pacific from about 2007 and arrived in South America in 2014 and Brazil in 2015. It is thought that between 0.4 and 1.3 million cases were infected in 2015 in Brazil. The virus appears to be spreading much more rapidly in the Americas than was seen in Africa, giving little opportunity for the development of countermeasures.

Zika is a member of the Flavivirus genera of the Flaviviridae family, other members of which include yellow fever virus (YFV), West Nile virus, and dengue virus. As such, there are good reasons to think that effective vaccines and antiviral medications will be developed for the infection. In the most recent outbreak, manifestations of Guillain–Barre syndrome and fetal abnormalities have been associated with Zika infection, and it is unclear whether these result from the larger patient population or whether the virus evolved CNS tropism during its spread. The rapid spread of Zika is probably due to increased human travel and the northerly spread of the viral vectors *Aedes aegypti* and *Aedes albopictus*.[70–72]

The very successful antiviral discovery programs for the related flavivirus hepatitis C provide a solid platform for the discovery of anti-Zika compounds.

5.20.7.5 Yellow Fever

A recent resurgence of YFV in Angola has already spread to China, Kenya, and the Congo and has reawakened awareness of the infection. YFV is a flavivirus (the name derives from yellow fever) that causes between 81,000 and 170,000 cases per year and about 60,000 deaths, despite the availability of an effective and affordable vaccine. A current shortage of vaccine stocks has precipitated a lively debate about increasing the number of people protected by diluting the vaccine (an untested measure). This outbreak illustrates the dangers of complacency in infectious disease; an antiviral treatment for YFV would be very useful in such a rapid-response context.

5.20.7.6 Alternative Approach to Emerging Infections

The previous section illustrates the growing threat from viruses emerging or reemerging from reservoirs in the changing environment. Each new emergence stimulates fresh research efforts, but these frequently lack the sustained commitment and investment to provide clinically effective agents and the episodic threat abates. Greater coordination between international agencies might provide for discovery programs at relatively nominal cost to produce credible lead molecules for the identifiable viruses that threaten us. Such a small investment could save thousands of lives in future emerging viral epidemics.

5.20.8 Conclusions

The aim of this article was to survey the progress in the discovery of new antiviral drugs to treat acute viral infections. The antiviral therapeutic area is one of the great success stories of the pharmaceutical industry. In the case of HIV infections, we have seen the introduction of more than 20 new drugs used in ever more sophisticated combinations and formulations to extend the life span of infected individuals to near normal, with a good quality of life. In hepatitis C, we have seen effective cures for patients, reducing treatment times from a year to a few weeks. This success can now be applied to acute viral infections. Using four examples of respiratory tract infection, we have sought to illustrate the different challenges that need to be overcome to bring a new medicine to patients. Although the scientific challenge is far from trivial, the greater problem is to make the investment case support the discovery effort.

See also: 5.18. Direct-Acting Antiviral Agents for the Treatment of Hepatitis C Virus Infection.

References

1. Smith, T. J.; Kremer, M. J.; Luo, M.; Vriend, G.; Arnold, E.; Kamer, G.; Rossmann, M. G.; McKinlay, M. A.; Diana, G. D.; Otto, M. J. The Site of Attachment in Human Rhinovirus 14 for Antiviral Agents That Inhibit Uncoating. *Science* **1986,** *233* (4770), 1286–1293.
2. Hiremath, C. N.; Filman, D. J.; Grant, R. A.; Hogle, J. M. Ligand-Induced Conformational Changes in Poliovirus-Antiviral Drug Complexes. *Acta Crystallogr. D Biol. Crystallogr.* **1997,** *53* (Pt 5), 558–570.
3. Lacroix, C.; Laconi, S.; Angius, F.; Coluccia, A.; Silvestri, R.; Pompei, R.; Neyts, J.; Leyssen, P. In Vitro Characterisation of a Pleconaril/Pirodavir-Like Compound With Potent Activity Against Rhinoviruses. *Virol. J.* **2015,** *12,* 106.
4. Tijsma, A.; Franco, D.; Tucker, S.; Hilgenfeld, R.; Froeyen, M.; Leyssen, P.; Neyts, J. The Capsid Binder Vapendavir and the Novel Protease Inhibitor SG85 Inhibit Enterovirus 71 Replication. *Antimicrob. Agents Chemother.* **2014,** *58* (11), 6990–6992.
5. Lacroix, C.; Querol-Audí, J.; Roche, M.; Franco, D.; Froeyen, M.; Guerra, P.; Terme, T.; Vanelle, P.; Verdaguer, N.; Neyts, J.; Leyssen, P. A Novel Benzonitrile Analogue Inhibits Rhinovirus Replication. *J. Antimicrob. Chemother.* **2014,** *69* (10), 2723–2732.
6. Pevear, D. C.; Tull, T. M.; Seipel, M. E.; Groarke, J. M. Activity of Pleconaril Against Enteroviruses. *Antimicrob. Agents Chemother.* **1999,** *43* (9), 2109–2115.
7. Feil, S. C.; Hamilton, S.; Krippner, G. Y.; Lin, B.; Luttick, A.; McConnell, D. B.; Nearn, R.; Parker, M. W.; Ryan, J.; Stanislawski, P. C.; Tucker, S. P.; Watson, K. G.; Morton, C. J. An Orally Available 3-Ethoxybenzisoxazole Capsid Binder With Clinical Activity Against Human Rhinovirus. *ACS Med. Chem. Lett.* **2012,** *3* (4), 303–307.
8. Smith, G. F. Designing Drugs to Avoid Toxicity. *Prog. Med. Chem.* **2011,** *50,* 1–47.
9. Andries, K.; Dewindt, B.; Snoeks, J.; Willebrords, R.; van Eemeren, K.; Stokbroekx, R.; Janssen, P. A. In Vitro Activity of Pirodavir (R 77975), a Substituted Phenoxy-Pyridazinamine with Broad-Spectrum Antipicornaviral Activity. *Antimicrob. Agents Chemother.* **1992,** *36* (1), 100–107.
10. Hayden, F. G.; Hipskind, G. J.; Woerner, D. H.; Eisen, G. F.; Janssens, M.; Janssen, P. A.; Andries, K. Intranasal Pirodavir (R77,975) Treatment of Rhinovirus Colds. *Antimicrob. Agents Chemother.* **1995,** *39* (2), 290–294.
11. Pevear, D. C.; Hayden, F. G.; Demenczuk, T. M.; Barone, L. R.; McKinlay, M. A.; Collett, M. S. Relationship of Pleconaril Susceptibility and Clinical Outcomes in Treatment of Common Colds Caused by Rhinoviruses. *Antimicrob. Agents Chemother.* **2005,** *49* (11), 4492–4499.
12. Kelly, J. T.; De Colibus, L.; Elliott, L.; Fry, E. E.; Stuart, D. I.; Rowlands, D. J.; Stonehouse, N. J. Potent Antiviral Agents Fail to Elicit Genetically-Stable Resistance Mutations in Either Enterovirus 71 or Coxsackievirus A16. *Antiviral Res.* **2015,** *124,* 77–82.
13. De Colibus, L.; Wang, X.; Spyrou, J. A.; Kelly, J.; Ren, J.; Grimes, J.; Puerstinger, G.; Stonehouse, N.; Walter, T. S.; Hu, Z.; Wang, J.; Li, X.; Peng, W.; Rowlands, D. J.; Fry, E. E.; Rao, Z.; Stuart, D. I. More-Powerful Virus Inhibitors from Structure-Based Analysis of HEV71 Capsid-Binding Molecules. *Nat. Struct. Mol. Biol.* **2014,** *21* (3), 282–288.

14. Mello, C.; Aguayo, E.; Rodriguez, M.; Lee, G.; Jordan, R.; Cihlar, T.; Birkus, G. Multiple Classes of Antiviral Agents Exhibit In Vitro Activity Against Human Rhinovirus Type C. *Antimicrob. Agents Chemother.* **2014,** *58* (3), 1546–1555.
15. Patick, A. K.; Binford, S. L.; Brothers, M. A.; Jackson, R. L.; Ford, C. E.; Diem, M. D.; Maldonado, F.; Dragovich, P. S.; Zhou, R.; Prins, T. J.; Fuhrman, S. A.; Meador, J. W.; Zalman, L. S.; Matthews, D. A.; Worland, S. T. In Vitro Antiviral Activity of AG7088, a Potent Inhibitor of Human Rhinovirus 3C Protease. *Antimicrob. Agents Chemother.* **1999,** *43* (10), 2444–2450.
16. Matthews, D. A.; Dragovich, P. S.; Webber, S. E.; Fuhrman, S. A.; Patick, A. K.; Zalman, L. S.; Hendrickson, T. F.; Love, R. A.; Prins, T. J.; Marakovits, J. T.; Zhou, R.; Tikhe, J.; Ford, C. E.; Meador, J. W.; Ferre, R. A.; Brown, E. L.; Binford, S. L.; Brothers, M. A.; DeLisle, D. M.; Worland, S. T. Structure-Assisted Design of Mechanism-Based Irreversible Inhibitors of Human Rhinovirus 3C Protease With Potent Antiviral Activity Against Multiple Rhinovirus Serotypes. *Proc. Natl. Acad. Sci. U. S. A.* **1999,** *96* (20), 11000–11007.
17. Hayden, F. G.; Turner, R. B.; Gwaltney, J. M.; Chi-Burris, K.; Gersten, M.; Hsyu, P.; Patick, A. K.; Smith, G. J.; Zalman, L. S. Phase II, Randomized, Double-Blind, Placebo-Controlled Studies of Ruprintrivir Nasal Spray 2-Percent Suspension for Prevention and Treatment of Experimentally Induced Rhinovirus Colds in Healthy Volunteers. *Antimicrob. Agents Chemother.* **2003,** *47* (12), 3907–3916.
18. Van der Linden, L.; Vives-Adrián, L.; Selisko, B.; Ferrer-Orta, C.; Liu, X.; Lanke, K.; Ulferts, R.; De Palma, A. M.; Tanchis, F.; Goris, N.; Lefebvre, D.; De Clercq, K.; Leyssen, P.; Lacroix, C.; Pürstinger, G.; Coutard, B.; Canard, B.; Boehr, D. D.; Arnold, J. J.; Cameron, C. E.; Verdaguer, N.; Neyts, J.; Van Kuppeveld, F. J. The RNA Template Channel of the RNA-Dependent RNA Polymerase as a Target for Development of Antiviral Therapy of Multiple Genera within a Virus Family. *PLoS Pathog.* **2015,** *11* (3), e1004733.
19. Ferrer-Orta, C.; Ferrero, D.; Verdaguer, N. RNA-Dependent RNA Polymerases of Picornaviruses: From the Structure to Regulatory Mechanisms. *Viruses* **2015,** *7* (8), 4438–4460.
20. Kelley, J. L.; Linn, J. A.; Selway, J. W. Synthesis and Antirhinovirus Activity of 8-Substituted Analogues of 6-(Dimethylamino)-9-(4-Methylbenzyl)-2-(Trifluoromethyl)-9H-Purine. *J. Med. Chem.* **1991,** *34* (1), 157–160.
21. Zlydnikov, D. M.; Kubar, O. I.; Kovaleva, T. P.; Kamforin, L. E. Study of Rimantadine in the USSR: A Review of the Literature. *Rev. Infect. Dis.* **1981,** *3* (3), 408–421.
22. Rey-Carrizo, M.; Barniol-Xicota, M.; Ma, C.; Frigolé-Vivas, M.; Torres, E.; Naesens, L.; Llabrés, S.; Juárez-Jiménez, J.; Luque, F. J.; DeGrado, W. F.; Lamb, R. A.; Pinto, L. H.; Vázquez, S. Easily Accessible Polycyclic Amines that Inhibit the Wild-Type and Amantadine-Resistant Mutants of the M2 Channel of Influenza A Virus. *J. Med. Chem.* **2014,** *57* (13), 5738–5747.
23. Li, F.; Ma, C.; DeGrado, W. F.; Wang, J. Discovery of Highly Potent Inhibitors Targeting the Predominant Drug-Resistant S31N Mutant of the Influenza A Virus M2 Proton Channel. *J. Med. Chem.* **2016,** *59* (3), 1207–1216.
24. Boriskin, Y. S.; Leneva, I. A.; Pécheur, E. I.; Polyak, S. J. Arbidol: A Broad-Spectrum Antiviral Compound That Blocks Viral Fusion. *Curr. Med. Chem.* **2008,** *15* (10), 997–1005.
25. Leneva, I. A.; Russell, R. J.; Boriskin, Y. S.; Hay, A. J. Characteristics of Arbidol-Resistant Mutants of Influenza Virus: Implications for the Mechanism of Anti-influenza Action of Arbidol. *Antiviral Res.* **2009,** *81* (2), 132–140.
26. Brancato, V.; Peduto, A.; Wharton, S.; Martin, S.; More, V.; Di Mola, A.; Massa, A.; Perfetto, B.; Donnarumma, G.; Schiraldi, C.; Tufano, M. A.; de Rosa, M.; Filosa, R.; Hay, A. Design of Inhibitors of Influenza Virus Membrane Fusion: Synthesis, Structure–Activity Relationship and In Vitro Antiviral Activity of a Novel Indole Series. *Antiviral Res.* **2013,** *99* (2), 125–135.
27. Woods, J. M.; Bethell, R. C.; Coates, J. A.; Healy, N.; Hiscox, S. A.; Pearson, B. A.; Ryan, D. M.; Ticehurst, J.; Tilling, J.; Walcott, S. M. 4-Guanidino-2,4-Dideoxy-2,3-Dehydro-N-Acetylneuraminic Acid Is a Highly Effective Inhibitor both of the Sialidase (Neuraminidase) and of Growth of a Wide Range of Influenza A and B Viruses In Vitro. *Antimicrob. Agents Chemother.* **1993,** *37* (7), 1473–1479.
28. Li, W.; Escarpe, P. A.; Eisenberg, E. J.; Cundy, K. C.; Sweet, C.; Jakeman, K. J.; Merson, J.; Lew, W.; Williams, M.; Zhang, L.; Kim, C. U.; Bischofberger, N.; Chen, M. S.; Mendel, D. B. Identification of GS 4104 as an Orally Bioavailable Prodrug of the Influenza Virus Neuraminidase Inhibitor GS 4071. *Antimicrob. Agents Chemother.* **1998,** *42* (3), 647–653.
29. Hayden, F. G.; Treanor, J. J.; Betts, R. F.; Lobo, M.; Esinhart, J. D.; Hussey, E. K. Safety and Efficacy of the Neuraminidase Inhibitor GG167 in Experimental Human Influenza. *JAMA* **1996,** *275* (4), 295–299.
30. Hayden, F. G.; Osterhaus, A. D.; Treanor, J. J.; Fleming, D. M.; Aoki, F. Y.; Nicholson, K. G.; Bohnen, A. M.; Hirst, H. M.; Keene, O.; Wightman, K. Efficacy and Safety of the Neuraminidase Inhibitor Zanamivir in the Treatment of Influenzavirus Infections. GG167 Influenza Study Group. *N. Engl. J. Med.* **1997,** *337* (13), 874–880.
31. Jones, M.; Jefferson, T.; Doshi, P.; Del Mar, C.; Heneghan, C.; Onakpoya, I. Commentary on Cochrane Review of Neuraminidase Inhibitors for Preventing and Treating Influenza in Healthy Adults and Children. *Clin. Microbiol. Infect.* **2015,** *21* (3), 217–221.
32. Meijer, A.; Lackenby, A.; Hungnes, O.; Lina, B.; van-der-Werf, S.; Schweiger, B.; Opp, M.; Paget, J.; van-de-Kassteele, J.; Hay, A.; Zambon, M.; Scheme, E. I. S. Oseltamivir-Resistant Influenza Virus A (H1N1), Europe, 2007–08 Season. *Emerg. Infect. Dis.* **2009,** *15* (4), 552–560.
33. Lin, C.; Sun, C.; Liu, X.; Zhou, Y.; Hussain, M.; Wan, J.; Li, M.; Li, X.; Jin, R.; Tu, Z.; Zhang, J. Design, Synthesis, and In Vitro Biological Evaluation of Novel 6-Methyl-7-Substituted-7-Deaza Purine Nucleoside Analogs as Anti-influenza A Agents. *Antiviral Res.* **2016,** *129,* 13–20.
34. de Jong, M. D.; Ison, M. G.; Monto, A. S.; Metev, H.; Clark, C.; O'Neil, B.; Elder, J.; McCullough, A.; Collis, P.; Sheridan, W. P. Evaluation of Intravenous Peramivir for Treatment of Influenza in Hospitalized Patients. *Clin. Infect. Dis.* **2014,** *59* (12), e172–e185.
35. Ikematsu, H.; Kawai, N. Laninamivir Octanoate: A New Long-Acting Neuraminidase Inhibitor for the Treatment of Influenza. *Expert Rev. Anti Infect. Ther.* **2011,** *9* (10), 851–857.
36. Furuta, Y.; Gowen, B. B.; Takahashi, K.; Shiraki, K.; Smee, D. F.; Barnard, D. L. Favipiravir (T-705), a Novel Viral RNA Polymerase Inhibitor. *Antiviral Res.* **2013,** *100* (2), 446–454.
37. Byrn, R. A.; Jones, S. M.; Bennett, H. B.; Bral, C.; Clark, M. P.; Jacobs, M. D.; Kwong, A. D.; Ledeboer, M. W.; Leeman, J. R.; McNeil, C. F.; Murcko, M. A.; Nezami, A.; Perola, E.; Rijnbrand, R.; Saxena, K.; Tsai, A. W.; Zhou, Y.; Charifson, P. S. Preclinical Activity of VX-787, a First-in-Class, Orally Bioavailable Inhibitor of the Influenza Virus Polymerase PB2 Subunit. *Antimicrob. Agents Chemother.* **2015,** *59* (3), 1569–1582.
38. Clark, M. P.; Ledeboer, M. W.; Davies, I.; Byrn, R. A.; Jones, S. M.; Perola, E.; Tsai, A.; Jacobs, M.; Nti-Addae, K.; Bandarage, U. K.; Boyd, M. J.; Bethiel, R. S.; Court, J. J.; Deng, H.; Duffy, J. P.; Dorsch, W. A.; Farmer, L. J.; Gao, H.; Gu, W.; Jackson, K.; Jacobs, D. H.; Kennedy, J. M.; Ledford, B.; Liang, J.; Maltais, F.; Murcko, M.; Wang, T.; Wannamaker, M. W.; Bennett, H. B.; Leeman, J. R.; McNeil, C.; Taylor, W. P.; Memmott, C.; Jiang, M.; Rijnbrand, R.; Bral, C.; Germann, U.; Nezami, A.; Zhang, Y.; Salituro, F. G.; Bennani, Y. L.; Charifson, P. S. Discovery of a Novel, First-in-Class, Orally Bioavailable Azaindole Inhibitor (VX-787) of Influenza PB2. *J. Med. Chem.* **2014,** *57* (15), 6668–6678.
39. Blair, W.; Cox, C. Current Landscape of Antiviral Drug Discovery. *F1000Res.* **2016,** *5.* Rev-202.
40. Holý, A. Antiviral Acyclic Nucleoside Phosphonates Structure Activity Studies. *Antiviral Res.* **2006,** *71* (2–3), 248–253.
41. DeVincenzo, J. P.; Aitken, J. B.; Harrison, L. G. Opportunities for Early Therapy of Respiratory Syncytial Virus (RSV) Infection: What Happens Before Hospitalization. *Antiviral Res.* **2004,** *62* (1), 47–51.
42. Bagga, B.; Woods, C. W.; Veldman, T. H.; Gilbert, A.; Mann, A.; Balaratnam, G.; Lambkin-Williams, R.; Oxford, J. S.; McClain, M. T.; Wilkinson, T.; Nicholson, B. P.; Ginsburg, G. S.; Devincenzo, J. P. Comparing Influenza and RSV Viral and Disease Dynamics in Experimentally Infected Adults Predicts Clinical Effectiveness of RSV Antivirals. *Antivir. Ther.* **2013,** *18* (6), 785–791.
43. Simões, E. A.; DeVincenzo, J. P.; Boeckh, M.; Bont, L.; Crowe, J. E.; Griffiths, P.; Hayden, F. G.; Hodinka, R. L.; Smyth, R. L.; Spencer, K.; Thirstrup, S.; Walsh, E. E.; Whitley, R. J. Challenges and Opportunities in Developing Respiratory Syncytial Virus Therapeutics. *J. Infect. Dis.* **2015,** *211* (Suppl. 1), S1–S20.
44. Bentley, A.; Filipovic, I.; Gooch, K.; Büsch, K. A Cost-Effectiveness Analysis of Respiratory Syncytial Virus (RSV) Prophylaxis in Infants in the United Kingdom. *Health Econ. Rev.* **2013,** *3* (1), 18.
45. Joint Committee on Vaccination and Immunisation. http://webarchive.nationalarchives.gov.uk/20130107105354/http:/www.dh.gov.uk/prod_consum_dh/groups/dh_digitalassets/@dh/@ab/documents/digitalasset/dh_120395.pdf.

46. Powell, K. L.; Alber, D. Development of Antivirals Against Respiratory Syncytial Virus. In *Perspectives in Medical Virology;* Cane, P., Ed.; Elsevier: Amsterdam, 2007; pp 279–297.
47. Najarro, P.; Angell, R.; Powell, K. The Prophylaxis and Treatment With Antiviral Agents of Respiratory Syncytial Virus Infections. *Antivir. Chem. Chemother.* **2012,** *22* (4), 139–150.
48. Battles, M. B.; Langedijk, J. P.; Furmanova-Hollenstein, P.; Chaiwatpongsakorn, S.; Costello, H. M.; Kwanten, L.; Vranckx, L.; Vink, P.; Jaensch, S.; Jonckers, T. H.; Koul, A.; Arnoult, E.; Peeples, M. E.; Roymans, D.; McLellan, J. S. Molecular Mechanism of Respiratory Syncytial Virus Fusion Inhibitors. *Nat. Chem. Biol.* **2016,** *12* (2), 87–93.
49. Mackman, R. L.; Sangi, M.; Sperandio, D.; Parrish, J. P.; Eisenberg, E.; Perron, M.; Hui, H.; Zhang, L.; Siegel, D.; Yang, H.; Saunders, O.; Boojamra, C.; Lee, G.; Samuel, D.; Babaoglu, K.; Carey, A.; Gilbert, B. E.; Piedra, P. A.; Strickley, R.; Iwata, Q.; Hayes, J.; Stray, K.; Kinkade, A.; Theodore, D.; Jordan, R.; Desai, M.; Cihlar, T. Discovery of an Oral Respiratory Syncytial Virus (RSV) Fusion Inhibitor (GS-5806) and Clinical Proof of Concept in a Human RSV Challenge Study. *J. Med. Chem.* **2015,** *58* (4), 1630–1643.
50. Eisenberg, E. J.; Wang, W. K.; Carey, C.; Gershwin, L.; Perron, M.; Mackman, R. Presatovir (GS-5806), a Novel Fusion Inhibitor of Respiratory Syncytial Virus, Delivers High Respiratory Tract Levels in Nonclinical Specie. ID Week 2015, San Diego, CA.
51. Draffan, A.; Bond, S.; Fenner, J.; Hamilton, S.; Harding, M.; Iswaran, J.; Jahangiri, S.; Lambert, J.; Lin, B.; Luttick, A.; Mayes, P.; Morton, C.; McAllister, D.; Pitt, G.; Porter, K.; Tucker, S.; Patti, J. Preclinical Characterization of an Orally Bioavailable Fusion Inhibitor, BTA-C585, for the Treatment of RSV infections. ICAAC, Washington, DC.
52. Mitchell, J.; Pitt, G.; Draffan, A. G.; Mayes, P. A.; Andrau, L.; Anderson, K. Compounds for Treating Respiratory Syncytial Virus Infections. WO2011094823 A1, 2011.
53. DeVincenzo, J. P.; Whitley, R. J.; Mackman, R. L.; Scaglioni-Weinlich, C.; Harrison, L.; Farrell, E.; McBride, S.; Lambkin-Williams, R.; Jordan, R.; Xin, Y.; Ramanathan, S.; O'Riordan, T.; Lewis, S. A.; Li, X.; Toback, S. L.; Lin, S. L.; Chien, J. W. Oral GS-5806 Activity in a Respiratory Syncytial Virus Challenge Study. *N. Engl. J. Med.* **2014,** *371* (8), 711–722.
54. Cianci, C.; Langley, D. R.; Dischino, D. D.; Sun, Y.; Yu, K. L.; Stanley, A.; Roach, J.; Li, Z.; Dalterio, R.; Colonno, R.; Meanwell, N. A.; Krystal, M. Targeting a Binding Pocket Within the Trimer-of-Hairpins: Small-Molecule Inhibition of Viral Fusion. *Proc. Natl. Acad. Sci. U. S. A.* **2004,** *101* (42), 15046–15051.
55. Yan, D.; Lee, S.; Thakkar, V. D.; Luo, M.; Moore, M. L.; Plemper, R. K. Cross-Resistance Mechanism of Respiratory Syncytial Virus Against Structurally Diverse Entry Inhibitors. *Proc. Natl. Acad. Sci. U. S. A.* **2014,** *111* (33), E3441–E3449.
56. Ouizougun-Oubari, M.; Pereira, N.; Tarus, B.; Galloux, M.; Lassoued, S.; Fix, J.; Tortorici, M. A.; Hoos, S.; Baron, B.; England, P.; Desmaële, D.; Couvreur, P.; Bontems, F.; Rey, F. A.; Eléouët, J. F.; Sizun, C.; Slama-Schwok, A.; Duquerroy, S. A Druggable Pocket at the Nucleocapsid/Phosphoprotein Interaction Site of Human Respiratory Syncytial Virus. *J. Virol.* **2015,** *89* (21), 11129–11143.
57. Thomas, E.; Ghany, M. G.; Liang, T. J. The Application and Mechanism of Action of Ribavirin in Therapy of Hepatitis C. *Antivir. Chem. Chemother.* **2013,** *23* (1), 1–12.
58. Wang, G.; Deval, J.; Hong, J.; Dyatkina, N.; Prhavc, M.; Taylor, J.; Fung, A.; Jin, Z.; Stevens, S. K.; Serebryany, V.; Liu, J.; Zhang, Q.; Tam, Y.; Chanda, S. M.; Smith, D. B.; Symons, J. A.; Blatt, L. M.; Beigelman, L. Discovery of 4'-Chloromethyl-2'-Deoxy-3',5'-Di-O-Isobutyryl-2'-Fluorocytidine (ALS-8176), a First-in-Class RSV Polymerase Inhibitor for Treatment of Human Respiratory Syncytial Virus Infection. *J. Med. Chem.* **2015,** *58* (4), 1862–1878.
59. Hunt, S. F.; Onions, S. T.; Sherbukhin, V.; Fordyce, E. A. F.; Murray, P. J.; Brookes, D. W.; Ito, K.; Strong, P.; Teuten, A. Novel 5,6-Dihydro-4H-Benzo[b]thieno-[2,3-d]azepine Derivative. WO/2016/055791, 2016.
60. Sudo, K.; Miyazaki, Y.; Kojima, N.; Kobayashi, M.; Suzuki, H.; Shintani, M.; Shimizu, Y. YM-53403, a Unique Anti-respiratory Syncytial Virus Agent With a Novel Mechanism of Action. *Antiviral Res.* **2005,** *65* (2), 125–131.
61. Mackman, R. L.; Sperandio, D.; Yang, H. Anti-RSV Compounds. WO/2011/005842, 2011.
62. Xiong, H.; Foulk, M.; Aschenbrenner, L.; Fan, J.; Tiong-Yip, C. L.; Johnson, K. D.; Moustakas, D.; Fleming, P. R.; Brown, D. G.; Zhang, M.; Ferguson, D.; Wu, D.; Yu, Q. Discovery of a Potent Respiratory Syncytial Virus RNA Polymerase Inhibitor. *Bioorg. Med. Chem. Lett.* **2013,** *23* (24), 6789–6793.
63. Browne, A.; Ahmad, S. S.; Beck, C. R.; Nguyen-Van-Tam, J. S. The Roles of Transportation and Transportation Hubs in the Propagation of Influenza and Coronaviruses: A Systematic Review. *J. Travel Med.* **2016,** *23* (1). tav002.
64. Dowell, S. F.; Simmerman, J. M.; Erdman, D. D.; Wu, J. S.; Chaovavanich, A.; Javadi, M.; Yang, J. Y.; Anderson, L. J.; Tong, S.; Ho, M. S. Severe Acute Respiratory Syndrome Coronavirus on Hospital Surfaces. *Clin. Infect. Dis.* **2004,** *39* (5), 652–657.
65. Anand, K.; Ziebuhr, J.; Wadhwani, P.; Mesters, J. R.; Hilgenfeld, R. Coronavirus Main Proteinase (3CLpro) Structure: Basis for Design of Anti-SARS Drugs. *Science* **2003,** *300* (5626), 1763–1767.
66. Julander, J. G.; Bantia, S.; Taubenheim, B. R.; Minning, D. M.; Kotian, P.; Morrey, J. D.; Smee, D. F.; Sheridan, W. P.; Babu, Y. S. BCX4430, a Novel Nucleoside Analog, Effectively Treats Yellow Fever in a Hamster Model. *Antimicrob. Agents Chemother.* **2014,** *58* (11), 6607–6614.
67. Warren, T.; Jordan, R.; Lo, M.; Soloveva, V.; Ray, A.; Bannister, R.; Mackman, R.; Perron, M.; Stray, K.; Feng, J.; Xu, Y.; Chun, K.; Hiu, H.; Neville, S.; Lew, W.; Park, Y.; Babusis, D.; Strickley, R.; Wong, P.; Swaminathan, S.; Lee, W.; Mayers, D.; Cihar, T.; Bavari, S. Nucleotide Prodrug GS-5734 Is a Broad-Spectrum Filovirus Inhibitor That Provides Complete Therapeutic Protection Against the Development of Ebola Virus Disease (EVD) in Infected Non-human Primates. ID Week 2015, San Diego, CA.
68. Warren, T. K.; Jordan, R.; Lo, M. K.; Ray, A. S.; Mackman, R. L.; Soloveva, V.; Siegel, D.; Perron, M.; Bannister, R.; Hui, H. C.; Larson, N.; Strickley, R.; Wells, J.; Stuthman, K. S.; Van Tongeren, S. A.; Garza, N. L.; Donnelly, G.; Shurtleff, A. C.; Retterer, C. J.; Gharaibeh, D.; Zamani, R.; Kenny, T.; Eaton, B. P.; Grimes, E.; Welch, L. S.; Gomba, L.; Wilhelmsen, C. L.; Nichols, D. K.; Nuss, J. E.; Nagle, E. R.; Kugelman, J. R.; Palacios, G.; Doerffler, E.; Neville, S.; Carra, E.; Clarke, M. O.; Zhang, L.; Lew, W.; Ross, B.; Wang, Q.; Chun, K.; Wolfe, L.; Babusis, D.; Park, Y.; Stray, K. M.; Trancheva, I.; Feng, J. Y.; Barauskas, O.; Xu, Y.; Wong, P.; Braun, M. R.; Flint, M.; McMullan, L. K.; Chen, S. S.; Fearns, R.; Swaminathan, S.; Mayers, D. L.; Spiropoulou, C. F.; Lee, W. A.; Nichol, S. T.; Cihlar, T.; Bavari, S. Therapeutic Efficacy of the Small Molecule GS-5734 Against Ebola Virus in Rhesus Monkeys. *Nature* **2016,** *531* (7594), 381–385.
69. Broder, C. C. Henipavirus Outbreaks to Antivirals: The Current Status of Potential Therapeutics. *Curr. Opin. Virol.* **2012,** *2* (2), 176–187.
70. Lambrechts, L.; Scott, T. W.; Gubler, D. J. Consequences of the Expanding Global Distribution of *Aedes albopictus* for Dengue Virus Transmission. *PLoS Negl. Trop. Dis.* **2010,** *4* (5), e646.
71. Kraemer, M. U.; Sinka, M. E.; Duda, K. A.; Mylne, A. Q.; Shearer, F. M.; Barker, C. M.; Moore, C. G.; Carvalho, R. G.; Coelho, G. E.; Van Bortel, W.; Hendrickx, G.; Schaffner, F.; Elyazar, I. R.; Teng, H. J.; Brady, O. J.; Messina, J. P.; Pigott, D. M.; Scott, T. W.; Smith, D. L.; Wint, G. R.; Golding, N.; Hay, S. I. The Global Distribution of the Arbovirus Vectors *Aedes aegypti* and *Ae. albopictus. Elife* **2015,** *4,* e08347.
72. Altizer, S.; Ostfeld, R. S.; Johnson, P. T.; Kutz, S.; Harvell, C. D. Climate Change and Infectious Diseases: From Evidence to a Predictive Framework. *Science* **2013,** *341* (6145), 514–519.

5.21 New Drugs and Emerging Leads in Antibacterial Drug Discovery

DG Brown, AstraZeneca Neurosciences, Innovative Medicines and Early Development Unit, Cambridge, United Kingdom

© 2017 Elsevier Ltd. All rights reserved.

5.21.1	**New Drugs and Economic Incentives**	683
5.21.1.1	New Drug Approvals	683
5.21.1.2	Economic Incentives: The Generating Antibiotic Incentives Now Act and Innovative Medicines Initiative	683
5.21.2	**Current Technical Challenges for New Antibacterial Lead Discovery**	683
5.21.2.1	Understanding the Physical Property Determinants of Antibacterial Chemical Space	683
5.21.2.2	Understanding Translocation and Efflux at a Molecular Level	685
5.21.2.3	Siderophore-Mediated Bacterial Cell-Wall Translocation	686
5.21.3	**β-Lactamase Inhibitors**	687
5.21.3.1	MBL Inhibition Strategies	687
5.21.3.1.1	Direct MBL inhibitors	689
5.21.3.1.2	Exploiting monobactam insensitivity to MBLs	690
5.21.3.2	Serine β-Lactamase Inhibitors	690
5.21.3.2.1	Oxaboroles as β-lactamase inhibitors	690
5.21.3.2.2	Diazabicyclooctanes	690
5.21.4	**Beyond β-Lactams and β-Lactamase Inhibitors**	691
5.21.4.1	Protein Synthesis Inhibitors	691
5.21.4.1.1	Ribosome binders	691
5.21.4.1.2	Leucine-tRNA synthetase inhibitors and oxaboroles	693
5.21.4.2	DNA Synthesis: Novel Topoisomerase Inhibitors	693
5.21.4.3	Cell-Wall Biosynthesis Inhibitors	694
5.21.4.4	LptD Inhibitors	694
5.21.4.5	LpxC Inhibitors	694
5.21.5	***Clostridium difficile* Infections**	695
5.21.5.1	Surotomycin From Daptomycin	696
5.21.5.1.1	Cadazolid	696
5.21.5.1.2	LFF571	696
5.21.6	**Finding New Drug Leads**	697
5.21.6.1	Natural Products	697
5.21.6.1.1	Novel screening approaches	697
5.21.6.1.2	New natural products from legacy screening approaches	697
5.21.6.2.3	New natural products with new chemistry applied	698
5.21.6.2	Screening Libraries	698
5.21.7	**Nontraditional Approaches: Host Factors and Virulence Targets**	699
5.21.8	**Conclusions**	700
References		700
Relevant Websites		702

Abbreviations

ABSSSI Acute bacterial skin and skin structure infections
AccAD Carboxytransferase activity of acetyl-CoA carboxylase
CAP Community-acquired pneumonia
CDAD *Clostridium difficile*-associated disease
cIAI Complicated intra-abdominal infections
CoaD Pantetheine-phosphate adenylyltransferase
cSSSI Complicated skin and skin structure infections
cUTI Complicated urinary tract infection
CWR Cell wall reporter gene assay in *E. coli*
FDA Food and Drug Administration
GAIN Generating Antibiotic Incentives Now
HAP Hospital-acquired pneumonia
IMI Innovative medicines initiative
KPC *Klebsiella pneumoniae* carbapenemases
MBL Metallo-β-lactamase
MDR TB Multidrug-resistant tuberculosis
MIC Minimum inhibitory concentration
MurC UDP-*N*-acetylmuramic acid: L-alanine ligase
ND4BB New drugs for bad bugs
NDM New Delhi metallo-β-lactamase
PAE Postantibiotic effect
ParE Topoisomerase IV ATP-hydrolyzing subunit
QIDP Qualified infectious disease product
TT Transcription and translation phenotypic screen
VAP Ventilator-associated pneumonia

5.21.1 New Drugs and Economic Incentives

5.21.1.1 New Drug Approvals

Between 2007 and 2014, only eight new drugs or new drug combinations were approved by the Food and Drug Administration (FDA) for treatment of bacterial infections (Table 1 and Figs. 1 and 2).[1] With four of these eight approvals occurring in 2014, an upward trend appears to be emerging in antibacterial drug discovery, perhaps signaling a welcome resurgence in productive research. However, most of the recent approvals are indicated for infections caused by Gram-positive pathogens, with only two new drugs approved for the treatment of Gram-negative infections (ceftaroline in 2010 and ceftolozane + tazobactam in 2014). A recent report by the World Health Organization cited an alarming rise in resistance against certain infections caused by Gram-negative pathogens, with few treatment options remaining.[2] The paucity of new drugs coming to the market for infections caused by Gram-negative pathogens is likely due to economic disincentives for their development (e.g., low predicted return on investment if physicians are reluctant to prescribe new and expensive medications), combined with the high discovery and development hurdles in identifying novel treatments for these infections.[3] Further to this, such expensive medications will not be affordable in resource-limited nations, where resistance to common antibiotics is already approaching critical levels.[2] Ultimately, these factors have resulted in a lack of new Gram-negative drugs emerging from pharmaceutical R&D.[3]

From a structural point of view, most of the new drug approvals stem from legacy antibacterial scaffolds. Fig. 1 depicts the three vancomycin analogs **1**, **2**, and **3** that have been approved to treat specific Gram-positive infections. Fig. 2 includes two recently approved cephalosporins (ceftolozane **8** and ceftaroline **9**), the latest in a long line of such antibiotics. Tedizolid **4** is member of the oxazolidinones, originating from linezolid (approved in 1988). Only fidaxomicin **5** and bedaquiline **6** represent new chemical classes to enter the market. These examples serve to highlight the difficulty across the industry in identifying truly novel antibacterial mechanisms or new chemical classes acting via previously established targets. The remainder of this article will discuss new initiatives that are helping to promote innovation in this area as well as some examples of important new scaffolds that are emerging in the field.

5.21.1.2 Economic Incentives: The Generating Antibiotic Incentives Now Act and Innovative Medicines Initiative

A significant legislative change in the United States that provides economic incentives to develop new antibacterials is the Generating Antibiotic Incentives Now (GAIN) Act passed in 2011.[4] This legislation provides for 5 years of exclusivity and fast-track approval for antibiotics termed "qualified infectious disease products (QIDP)."[4] The QIDP designation is applicable to exploratory agents for the treatment of serious or life-threatening infections from pathogens such as vancomycin-resistant *Enterococcus* spp., methicillin-resistant *Staphylococcus aureus*, vancomycin-resistant *S. aureus*, *Acinetobacter baumannii*, *Klebsiella pneumoniae*, *Pseudomonas aeruginosa*, and *E. coli*. Collectively, these have been given the acronym the ESKAPE pathogens, and they now form the core of most new drug discovery antibacterial research programs and government-funded initiatives.[5] The first drug approved under this act was dalbavancin for treatment of acute bacterial skin and skin structure infections in May 2014.[6,7] Beyond the United States, European initiatives such as the Innovative Medicines Initiative New Drugs for Bad Bugs (IMI ND4BB) have allocated over €600 M toward structured partnerships between academia and industry[8] addressing basic research into some of the most fundamental problems of new antibiotic drug discovery, such as bacterial resistance (COMBACTE) and drug translocation across bacterial membranes (TRANSLOCATION).

5.21.2 Current Technical Challenges for New Antibacterial Lead Discovery

5.21.2.1 Understanding the Physical Property Determinants of Antibacterial Chemical Space

The structures in Fig. 1 reveal that of the eight new compounds approved by the FDA since 2007, five are natural products in origin (dalbavancin, fidaxomicin, telavancin, and the β-lactams ceftaroline and ceftolozane). Only two were truly synthetic in origin

Table 1 Approved antibacterial drugs 2007–2014

Year	*Name*	*Indication, spectrum*
2014	Dalbavancin	ABSSSI, Gram-positive-related infections
	Tedizolid	ABSSSI, Gram-positive-related infections
	Ceftolozane + tazobactam	cUTI and cIAI-, Gram-positive- and Gram-negative-related infections
	Oritavancin	ABSSSI-, Gram-positive-related infections
2012	Bedaquiline	MDR TB
2011	Fidaxomicin	*C. difficile*-associated diarrhea
2010	Ceftaroline	cSSSI, CAP, Gram-positive- and Gram-negative-related infections
2009	Telavancin	cSSSI and HAP, VAP by *S. aureus*
2007 and 2008	No FDA approvals	

ABSSSI, acute bacterial skin and skin structure infections; *cSSSI*, complicated skin and skin structure infections; *cUTI*, complicated urinary tract infection; *cIAI*, complicated intra-abdominal infections; *MDR TB*, multidrug-resistant tuberculosis; *CAP*, community-acquired pneumonia; *HAP*, hospital-acquired pneumonia; and *VAP*, ventilator-associated pneumonia.

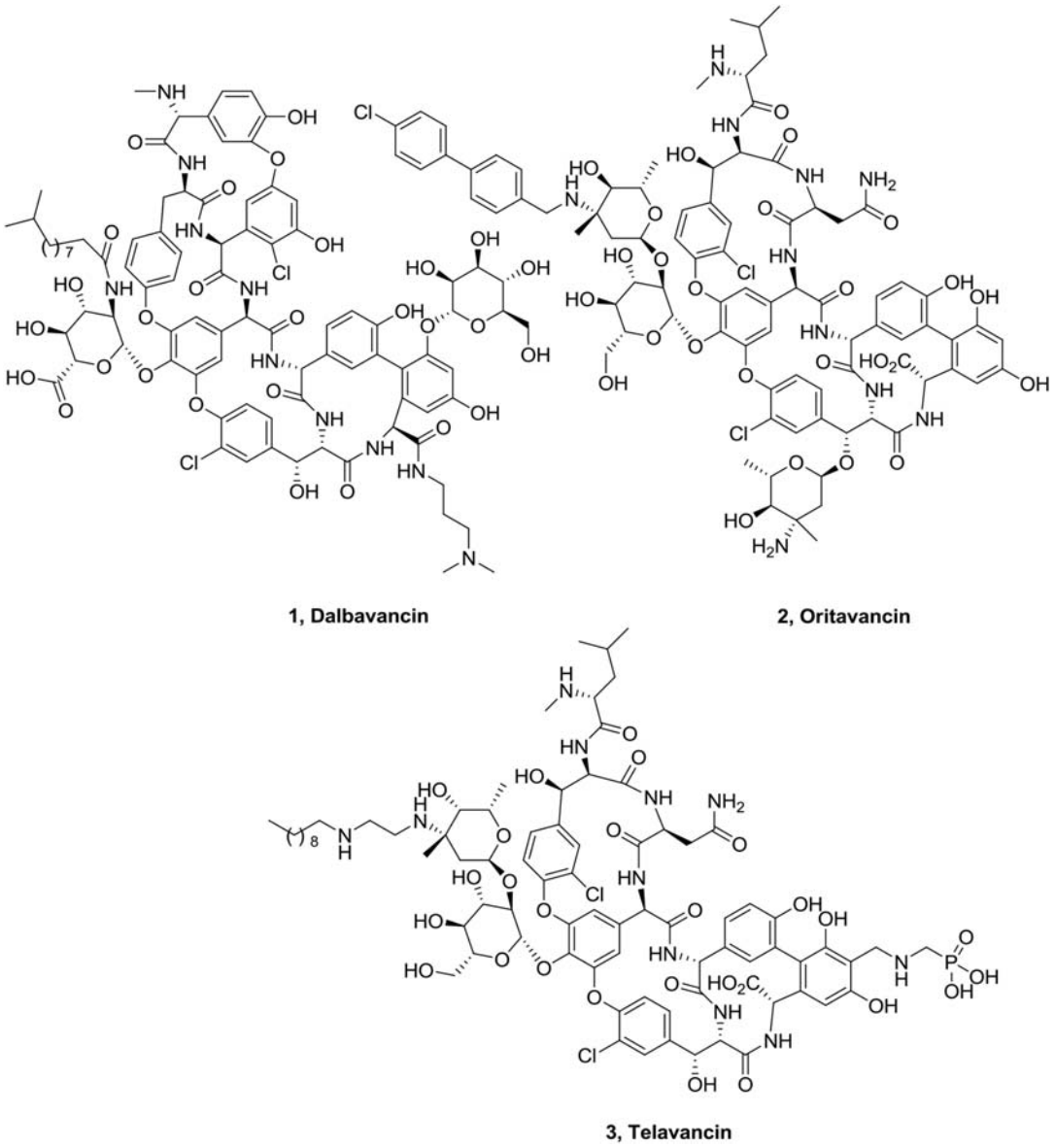

Fig. 1 FDA-approved vancomycin analogs 2007–2014.

(tedizolid and bedaquiline). It is widely recognized that many of the established antibacterial drug classes were discovered through natural product screening.[9] However, with the explosive recent growth of biochemical tools and the complete sequencing of the bacterial genome in 1995, discovery strategies shifted away from traditional phenotypic cell-based natural product screens. A significant investment was made instead in target-based approaches, coupled with high-throughput screening (HTS), in an effort to find new antibacterial leads. At the outset, this approach offered the prospect of efficient and productive discovery of many new antibacterial drugs. However, this turned out not to be the case. Researchers at GSK in 2007 were the first to report that the new strategy had failed to meet its high expectations.[10] They concluded that the major reasons for failure were the inability to find antibacterial-like leads from within the corporate screening collection, coupled with the challenges of requiring broad-spectrum (i.e., both Gram-positive and Gram-negative) activity. These themes were further reinforced by Moser et al., who analyzed antibacterial drug-like space as being much more polar than oral drug-like space for human targets.[9] In further exploration of this topic, the profiles of antibacterial actives across species were compared by authors at AstraZeneca to those emerging from HTS (Fig. 3A and B).[11] The authors concluded that antibacterial HTS screening hits were typically very lipophilic compounds (in fact, often more so than the screening collection average), inconsistent with antibacterial drug-like space. The difficulty in achieving optimal physical properties (e.g., often logD <0) for antibacterial cellular activity while maintaining biochemical potency is enormous and is perhaps a unique challenge for antibacterial drug discovery. Furthermore, simply optimizing to a low logD range does not guarantee

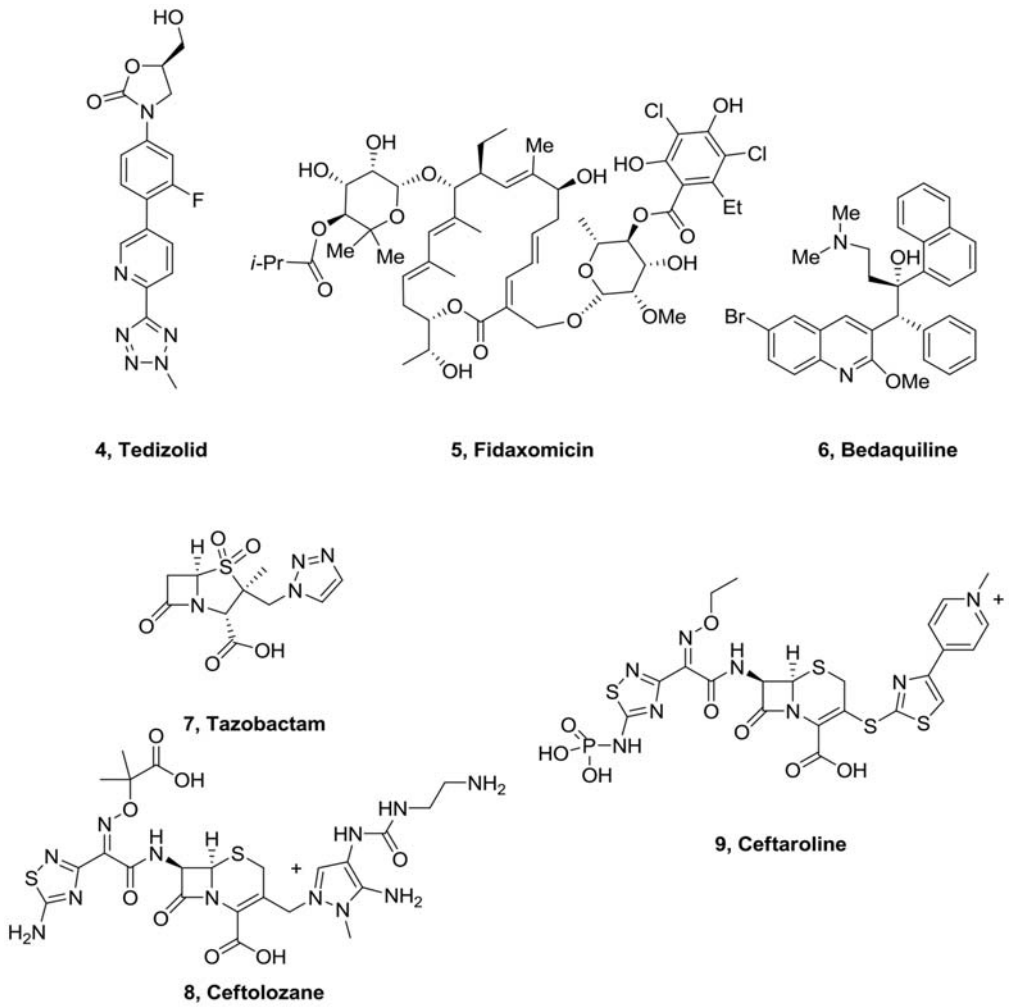

Fig. 2 Other FDA-approved antibacterial drugs 2007–2014. (Note that tazobactam **7** was already an approved β-lactamase inhibitor prior to 2014. It is included here for completeness since it was approved in combination with ceftolozane.)

antibacterial activity. The nature of the outer membrane in Gram-negative organisms and the wide variety of efflux pumps expressed present a complex barrier whose penetration is not assured merely by addressing one simple chemical descriptor such as logD. Tomassi and coauthors at AstraZeneca published a further review on their experiences with HTS screening and antibacterial drug discovery.[12] Their experience contrasted with GSK[10] in that many hits and leads were found by HTS screening, but the lack of viable medicinal chemistry tactics to engineer penetration of Gram-negative outer membranes proved to be the key limitation.[12] The importance of understanding translocation phenomena at a molecular level and the development of potential Structure activity relationships (SAR) rules would provide life to many of these abandoned hits and open up new frontiers in antibacterial drug discovery.

5.21.2.2 Understanding Translocation and Efflux at a Molecular Level

In order to develop a fundamental understanding of medicinal chemistry tactics to enable penetration of bacterial cell membranes, it is critical to understand the various barriers and entry mechanisms and in particular those in Gram-negative bacteria. The barriers for compounds to penetrate the outer membrane of Gram-negative bacteria are the following: (a) a highly polar outer membrane, (b) small narrow openings for nutrient transport (porins), and (c) promiscuous efflux pumps.[13,14] One strategy to overcome these barriers has been to develop compounds that are amphiphilic and highly cationic and can thereby disrupt the membrane, but these may also be cytotoxic if they exhibit similar properties in mammalian cells. An example of this approach can be found in the field of amphiphilic cationic homopolymers, which work through bacterial membrane disruption but can also give rise to hemolysis in mammalian cells.[15] Other strategies include translocation through porins, but the structure of these channels places severe constraints on molecular characteristics for efficient passage to take place. The crystal structure of the *P. aeruginosa* porin OccD1 is shown in the succeeding text to illustrate the β-barrel type topography and specific arrangement of charged amino acids, with

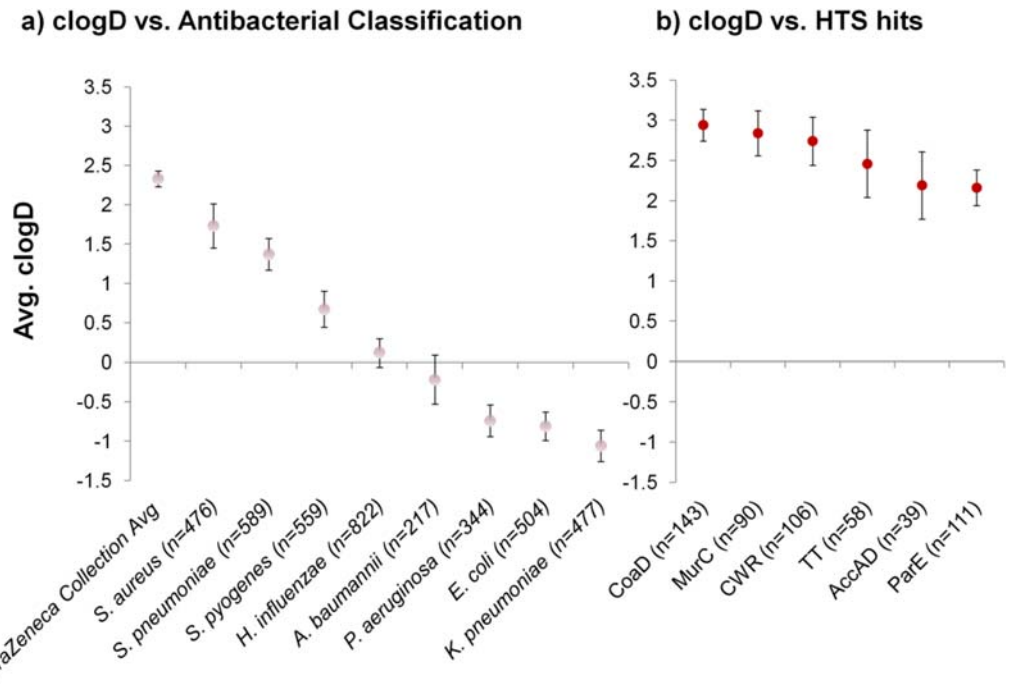

Fig. 3 Physical property analysis of antibacterial actives compared with HTS actives. Panel (A) is the average calculated logD (clogD) of antibacterial actives from AstraZeneca projects for specific pathogens (active defined as minimum inhibitory concentration (MIC) $\leq 8\ \mu g\ mL^{-1}$). Vertical bars represent the $\pm 99\%$ confidence interval of the mean. Numbers in parentheses indicate the number of actives included in the analysis. The "AstraZeneca Collection Avg" is the average of a random sample of 45 K compounds from the corporate screening collection. Panel (B) illustrates actives identified by HTS screening of a representative sample of HTS campaigns. *CoaD*, pantetheine-phosphate adenylyltransferase; *MurC*, UDP-*N*-acetylmuramic acid: L-alanine ligase; CWR, cell wall reporter gene assay in *E. coli*; TT, transcription and translation phenotypic screen; AccAD, carboxytransferase activity of acetyl-CoA carboxylase; ParE, topoisomerase IV ATP-hydrolyzing subunit.

consequent narrow openings (Fig. 4).[16] Passive diffusion is thought to be severely diminished for compounds with MW > 600 Da, since porin channels in the bacterial outer membrane are quite narrow.[17] However, a recent example by van den Berg and coauthors identified the passive diffusion of very large cyclodextrins in *K. oxytoca* via a monomeric 14-stranded β-barrel large pore, which appears to be gated on the periplasmic side by the N-terminal domain of the protein.[17] In other recent studies in outer membrane transport, Tommasi and Isabella et al. used an integrated genetics and computational approach to characterize the translocation of meropenem through the *P. aeruginosa* porins OccD1 and OccD3.[18] Meropenem analogs were then designed to retain critical binding features to the intended penicillin-binding protein target and also test SAR around the molecular dynamic simulation models. This is the first reported example of a rational approach to enhance permeation through a bacterial porin channel and offers a glimpse into the next generation of antibacterial drug design.

A much needed tool in the arsenal of antibacterial medicinal chemists is a biophysical method to understand bacterial cell penetration across a range of similar compounds, thus establishing permeation–structure relationships, which can be applied across programs. A review of electrophysiology and molecular modeling methods by Winterhalter and Ceccarelli suggested that advances in nanotechnology and electrophysiology coupled with molecular modeling might prove of benefit in optimizing translocation of hits.[19] This work is also significant in that it highlights the emerging impact of the innovative medicines initiative (IMI)-funded initiatives described earlier.

5.21.2.3 Siderophore-Mediated Bacterial Cell-Wall Translocation

Another strategy for bacterial translocation is to incorporate a structural motif into the drug molecule that is recognized by a transporter that is essential for bacterial nutrition, thereby facilitating uptake. One of the most well-studied such approaches exploits siderophores, which transport Fe^{3+} (required for bacterial survival and replication) from the host to the pathogen.[20] Although this approach has been studied on many antibacterial scaffolds, the tactic has been most widely applied with β-lactams. This combination confers the advantage that the putative drugs need to only penetrate the bacterial outer membrane, given that the targets (penicillin-binding proteins) are located within the periplasmic space. (Bacterial targets such as the ribosome that reside in the cytoplasm would require that these highly polar molecules, which would also be coordinated to Fe^{3+}, must penetrate the hydrophobic inner cytosolic membrane and the polar outer membrane.) Some of the more advanced programs were published by a Pfizer-led team (Fig. 5), where three scaffolds incorporating siderophore motifs were studied – the lactivicins (**10** → **11**),[21] monocarbams

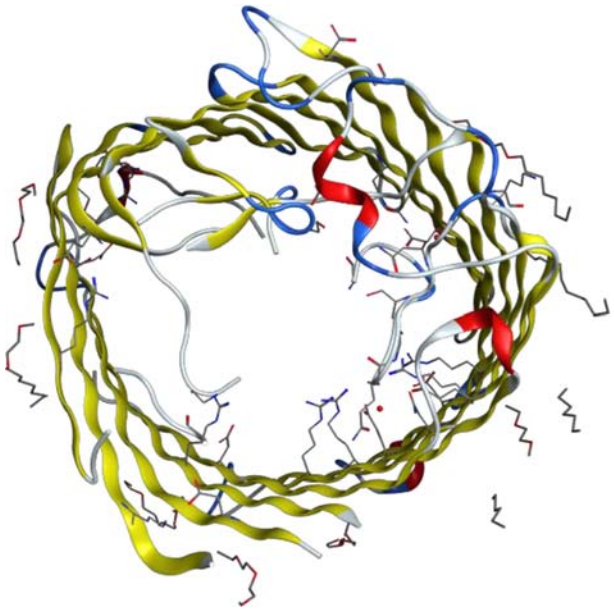

Fig. 4 X-ray crystal structure of *P. aeruginosa* OccD1 (PDB code, 4FOZ).

(**12**),[22a] and monobactams (**13**).[22b] Dramatic improvements in antibacterial activities were illustrated with the lactivicins (**10** → **11**), where a 64-fold shift in minimum inhibitory concentration was engineered through incorporation of the siderophore with no change in the biochemical activity. Despite these promising in vitro results, the tactic failed to translate in preclinical in vivo models. Despite adequate free systemic drug levels, the monobactam **12** (MB-1) did not generate the antibacterial effect predicted by in vitro assays. The drop-off in activity was attributed to adaptation-based resistance within these animal models of infection. These discouraging results have left serious concerns about the potential of siderophore-based approaches for circumventing the Gram-negative outer membrane. A study revealed that combination dosing with an efflux pump inhibitor (reserpine) could potentiate and circumvent the proposed adaptive in vivo resistance mechanism and perhaps rescue this type of approach.[23]

Another noteworthy example of the siderophore approach is the clinical development candidate BAL30072 from Basilea (**14**). This compound has reached Ph1 human clinical trials, but little has been published since that disclosure.[24] When this agent demonstrates clinical activity, it would validate not only Gram-negative penetration through siderophore-mediated uptake but also the avoidance of monobactam cleavage by class B metallo-β-lactamases (MBLs) (discussed further in the succeeding text).

5.21.3 β-Lactamase Inhibitors

Since the introduction of penicillin, resistant strains of bacteria have emerged with an enormous number of enzymes capable of hydrolyzing β-lactams. These enzymes are termed β-lactamases, and they are divided into four major classes (A, B, C, and D). The currently marketed β-lactamase inhibitors clavulanic acid, tazobactam, and sulbactam are all derived from a β-lactam core (Fig. 6)[25,26] and are becoming less effective against a rising tide of extended-spectrum β-lactamase-producing organisms. Class A, C, and D β-lactamases are serine-based proteases and as such hydrolyze the β-lactam rings in these molecules in a suicide-based mechanism. Furthermore, established β-lactamase inhibitors offer no protection against class B (metallo-) β-lactamases, because the metalloprotease mechanism and active site are very different from class A, C, and D enzymes.

5.21.3.1 MBL Inhibition Strategies

The rise of bacteria-producing class B MBLs has triggered significant alarm within the health community, with very few treatment options available to the physician should an outbreak occur.[27] MBLs are promiscuous enzymes that rapidly hydrolyze most β-lactam antibiotics and thus render them useless before they can bind to penicillin-binding proteins within bacteria.[28,29] Among the β-lactam classes, only the monobactams such as aztreonam are not hydrolyzed and thus are resistant to these enzymes. However, the relatively weak intrinsic antibacterial efficacy and the susceptibility of most monobactams to serine β-lactamases limit the general utility of the class.[30] Worse, MBLs are typically coexpressed with serine β-lactamases, such that any clinically effective regimen must address the impact of both simultaneously.[26] Over the past few years, two different approaches have been taken to try and develop new drugs against MBL-expressing bacteria: (a) direct inhibition of the MBL and (b) potentiation of monobactam potency with new-generation β-lactamase inhibitors.

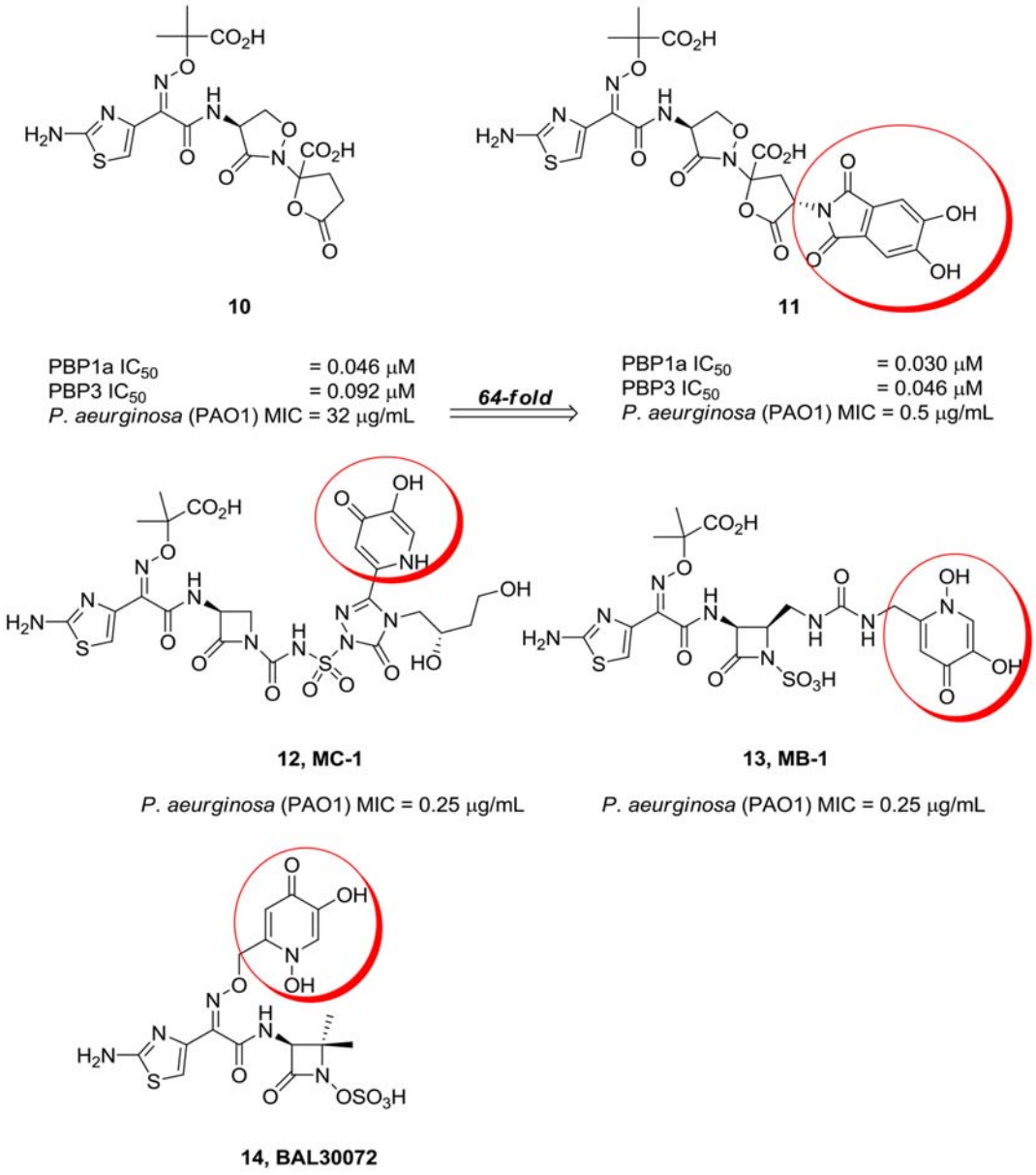

Fig. 5 Representative examples of siderophore-containing antibacterial compounds. The siderophores are highlighted in red circles.

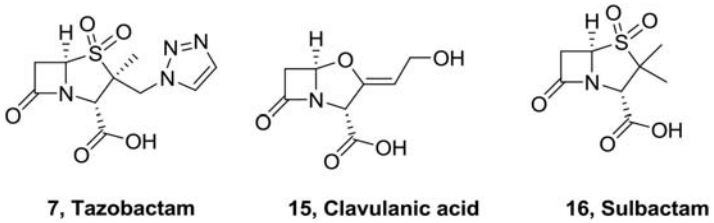

Fig. 6 Marketed β-lactamase inhibitors.

5.21.3.1.1 Direct MBL inhibitors

Direct, specific inhibition of an MBL is an attractive option since it can be enabled by structure-based discovery, and inhibition of metalloenzymes is precedented in other therapeutic contexts. However, such an approach would necessitate triple combination therapy, since a serine β-lactamase inhibitor and the intrinsic antibacterial β-lactam would also be required for clinical effectiveness. There would almost certainly be the need for rapid diagnostics in such an approach, since such a regimen would not be used unless a physician could confirm the presence of an MBL drug-resistant strain. This is further complicated in that most of the concern with MBLs is found in developing nations, where implementing such a diagnostic and treatment protocol would be particularly problematic. Furthermore, the MBL inhibitor would likely need to cover all genetic variants of MBLs. In spite of these hurdles, investments in this area continue, and the field continues to grow. As an example of the types of scaffolds being explored, a group at Goethe University has explored the potential of current marketed thiol-containing drugs (which might interact with the active-site Zn^{2+}) to prevent hydrolysis of β-lactams such as imipenem (Fig. 7).[31] Several MBL inhibitors were identified (exemplified by **17** and **18**) that demonstrated potentiation against imipenem-resistant Gram-negative clinical isolates and genetically altered *E. coli* strains (Fig. 7). The authors point out that one component in further optimization of molecules of this type may be to assess limitations in bacterial translocation.

A novel discovery strategy was adopted by Hu and coworkers at AstraZeneca using a cell-based NMR screen for MBL inhibitors.[32] In this assay, the hydrolysis product of meropenem is expelled into the supernatant by New Delhi metallo-β-lactamase (NDM-1)-expressing bacteria and can be monitored in real time using 1-D NMR methods. The method also allowed the opportunity to screen small libraries in 96-well format for potential inhibitors. From this approach, novel inhibitors of NDM-1 were identified (e.g., **19**) that like **17** and **18** contain thiols. Other classes of molecules that have been identified as MBL inhibitors are EDTA-like moieties, which function to sequester the Zn^{2+} from the active site. One interesting example is the natural product AMA (**20**), which has been shown to remove both Zn^{2+} atoms in NDM-1.[33] The diversity of potential MBL inhibitors is highlighted by an unusual selenium-containing class of inhibitors (**21,** ebselen) discovered by a cell-based screening approach. The lead compound was found to be a potent irreversible inhibitor with limited cytotoxicity.[34]

The first report of potent dual serine and MBL inhibition has been disclosed by The Medicines Company with the oxaborole-based inhibitors exemplified by **22** (KPC2 $IC_{50} = 0.01$ μM and OXA-48 $IC_{50} = 0.01$ μM).[35] As revealed by crystal structures, the boronate oxygen and the carboxylate both bind to the MBI Zn^{2+} ion. As mentioned previously, the potential clinical advantage of such a compound is considerable. The two-drug antibacterial combinations are well established, whereas three-drug regimens are likely to be significantly more problematic.

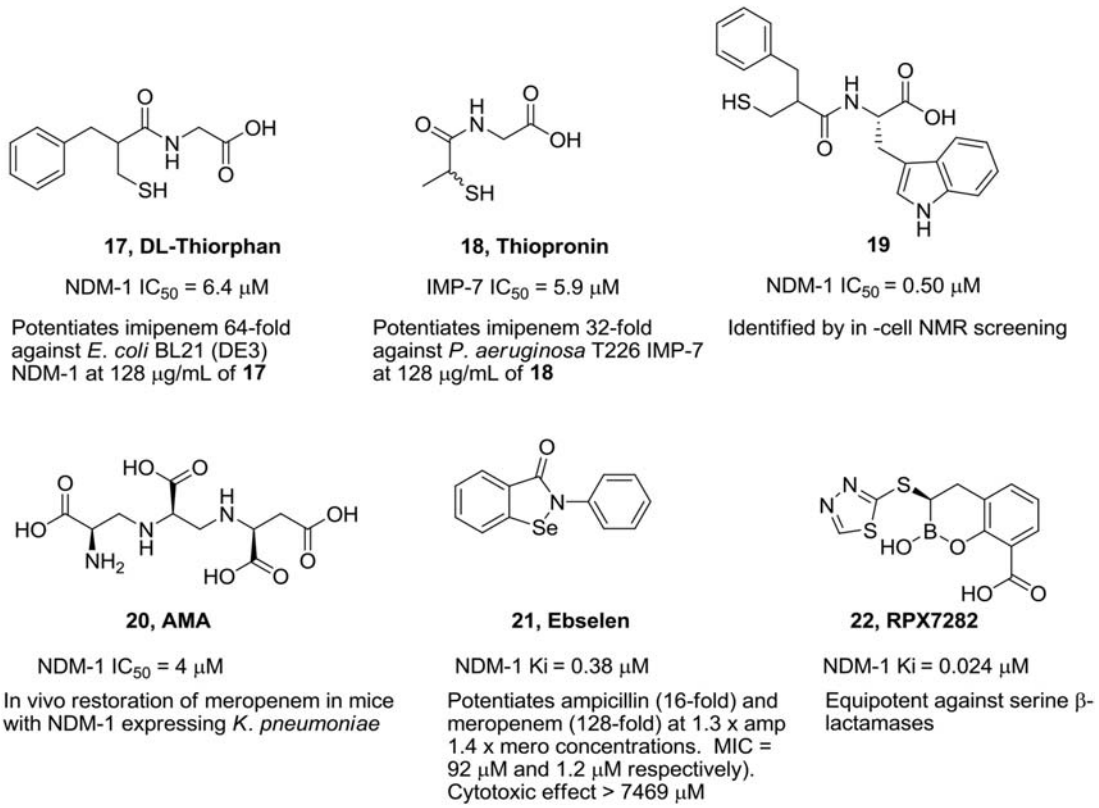

Fig. 7 Representative examples of metallo-β-lactamase inhibitors.

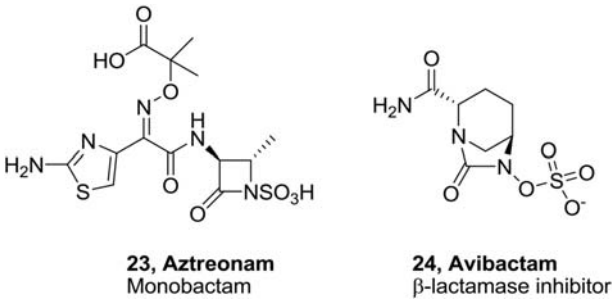

Fig. 8 Current combination in development for treatment of MBLs.

5.21.3.1.2 Exploiting monobactam insensitivity to MBLs

Aztreonam is now a generic drug, but its clinical use has been limited due to its narrow spectrum of activity as a single agent and its susceptibility to serine-based β-lactamases.[30] However, its lack of susceptibility to MBL-mediated hydrolysis has stimulated a search for more effective serine-based β-lactamase inhibitors for combination therapy. A combination currently in clinical development is aztreonam–avibactam (Fig. 8).[36] The aforementioned BAL30072 also belongs in this category in that it is a monocyclic β-lactam that is not susceptible to class B β-lactamases.[24]

5.21.3.2 Serine β-Lactamase Inhibitors

Not only will the world need to address the emergence of MBLs, but also the serine β-lactamases are also becoming more and more resistant to the inhibitors currently used in clinical practice. As a result, substantial effort has been invested in novel chemotypes, a subset of which is discussed in the succeeding text.

5.21.3.2.1 Oxaboroles as β-lactamase inhibitors

Oxaboroles have a dual role in antibacterial research, as they can function as both β-lactamase inhibitors and intrinsic antibacterial agents. Their mechanism of action as serine β-lactamase inhibitors involves reversible covalent complexation with the active-site nucleophile, which is distinct from their mechanism of intrinsic antibacterial activity (inhibition of leucine-tRNA synthetase, discussed in section "Leucine-tRNA synthetase inhibitors and oxaboroles"). Two classes of oxaborole-based β-lactamase inhibitors are shown in Fig. 9. Compounds **25** and **26** represent fused aromatic oxaboroles, which demonstrate potent activity in biochemical assays (e.g., inhibition of nitrocefin degradation by β-lactamases) and potentiation of β-lactams in *E. coli*- and *K. pneumoniae*-resistant strains.[37,38] A cocrystal structure revealed **26** anchored as a stable borate species in the active site of the enzyme by virtue of an interaction of the nucleophilic serine with the boron atom. The second class of oxaborole inhibitors is the aliphatic type as exemplified by **27** (RXP7009, The Medicines Company). RPX7009 demonstrates high selectivity over mammalian serine proteases (>100 μM against 11 representative enzymes) with potent activities at bacterial β-lactamases such as *K. pneumoniae* carbapenemases (KPC $IC_{50}=0.069$ μM), CTX-M ($IC_{50}=0.044$ μM), SHV ($IC_{50}=0.029$ μM), and CMY ($IC_{50}=0.099$ μM).[39] The compound also restores the MIC for *Enterobacteriaceae* expressing class A carbapenemases for carbapenems (e.g., in *E. coli* 1007 KPC-3, the MIC of meropenem was improved from 4 to <0.06 μg mL^{-1} in combination with 4 μg mL^{-1} of RPX7009). RPX7009 also restored imipenem activity in a carbapenem-resistant *K. pneumoniae* mouse lung infection model strain (two-log reduction in CFU at 50 mg kg^{-1} RPX7009 and 100 mg kg^{-1} meropenem). The potential for general electrophilicity of the oxaborole has not translated into demonstrable toxicity: The compound was tolerated at doses up to 1000 mg kg^{-1} in preclinical rodent studies,[40] and in phase 1 studies, the compound was well tolerated at 1500 mg kg^{-1} infused over 3 h.[39] RPX7009 is currently under investigation in a phase III trial in combination with meropenem for treatment of carbapenem-resistant *Enterobacteriaceae*.[41]

5.21.3.2.2 Diazabicyclooctanes

Another class of novel β-lactamase inhibitors is the diazabicyclooctanes (DABCOs), as shown in Fig. 10. The discovery that highly strained five-membered ring ureas could mimic the reactivity of a β-lactam has delivered a brand new weapon in the arsenal against drug-resistant bacteria.[42] The urea in these compounds is stable under physiological conditions but behaves in a similar manner to β-lactams in that it is hydrolyzed by the active-site serine of the class A, C, and D β-lactamases. The leading examples in the field are avibactam (**24**),[43] which was the first in class to be approved (in combination with ceftazidime), and relebactam **28**, which is currently in phase III trials in triple combination with imipenem/cilastatin.[44] Relebactam was designated fast-track QIDP approval by the FDA for the study of complicated urinary tract infections (cUTIs).

Another member of the DABCO class of β-lactamase inhibitors has been disclosed by Fedora as FPI-1465.[45] This compound, like other members of the class, also inhibits penicillin-binding protein 2, which provides intrinsic antibacterial activity and β-lactamase inhibition.[45]

A unique feature of at least one member of the chemical class of the DABCOs is the reversibility of covalent binding of the strained urea, a phenomenon that has not been reported for the β-lactams (Fig. 11). Ehmann et al. demonstrated that avibactam

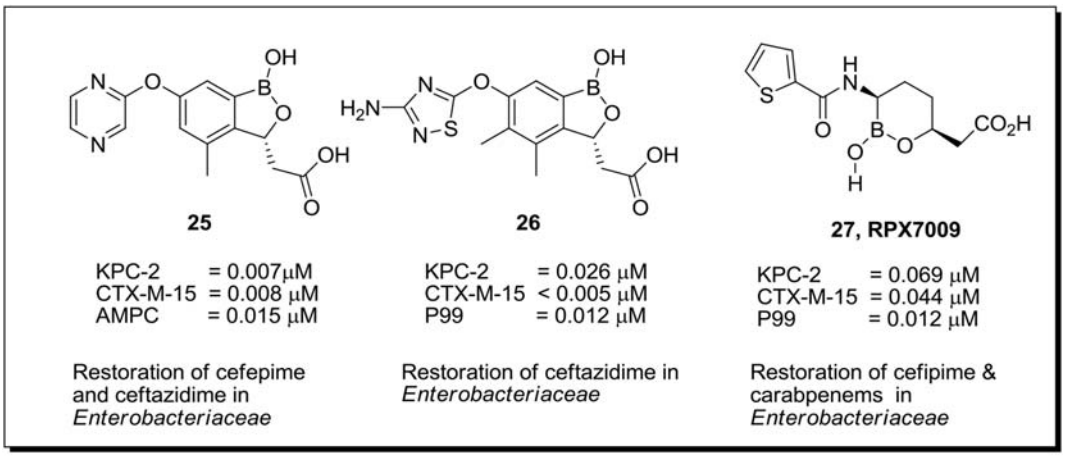

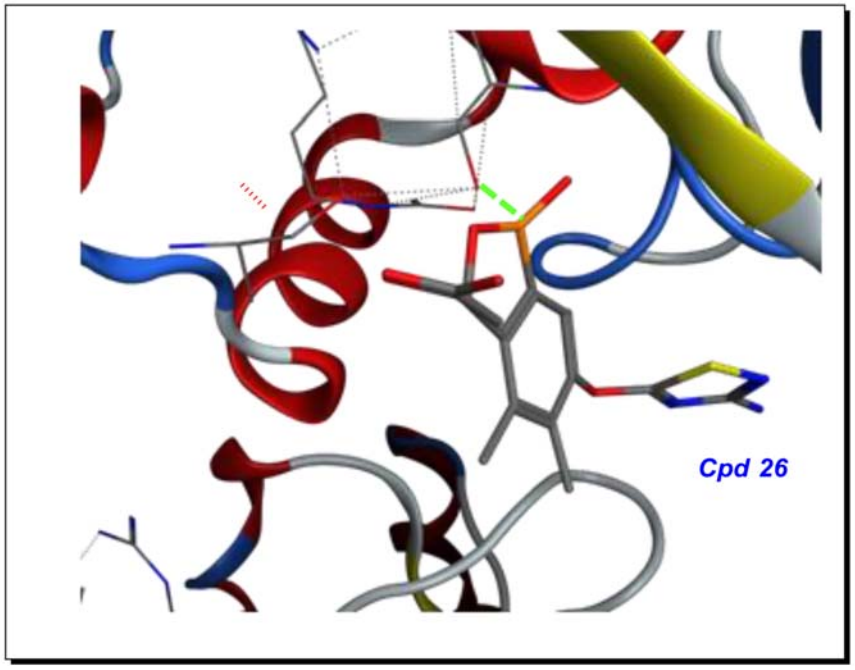

Fig. 9 Oxaborole β-lactamase inhibitor **26** bound to active site of a β-lactamase.[37] The dashed green line indicates the serine OH covalent bond with the boron atom of the oxaborole.

binds in covalent fashion to the active-site serine residues of TEM-1 and AmpC, but, that surprisingly, the urea could be regenerated and subsequently binds to another β-lactamase in the vicinity.[46] It is not yet known to what extent this feature contributes to the efficacy and resistance mechanisms of avibactam, but the discovery has opened up significant new ideas on β-lactamase inhibitor design.

5.21.4 Beyond β-Lactams and β-Lactamase Inhibitors

This section will review some of the most important examples of new approaches to antibacterial agents outside of the β-lactam class and will highlight some of the unique developments that are changing the field.

5.21.4.1 Protein Synthesis Inhibitors

5.21.4.1.1 Ribosome binders

Disruption of bacterial protein synthesis through binding to the ribosome is the basis of action for many successful drug classes, including aminoglycosides, tetracyclines, oxadiazoles, and macrolides.[47] New representatives in these classes continue to advance

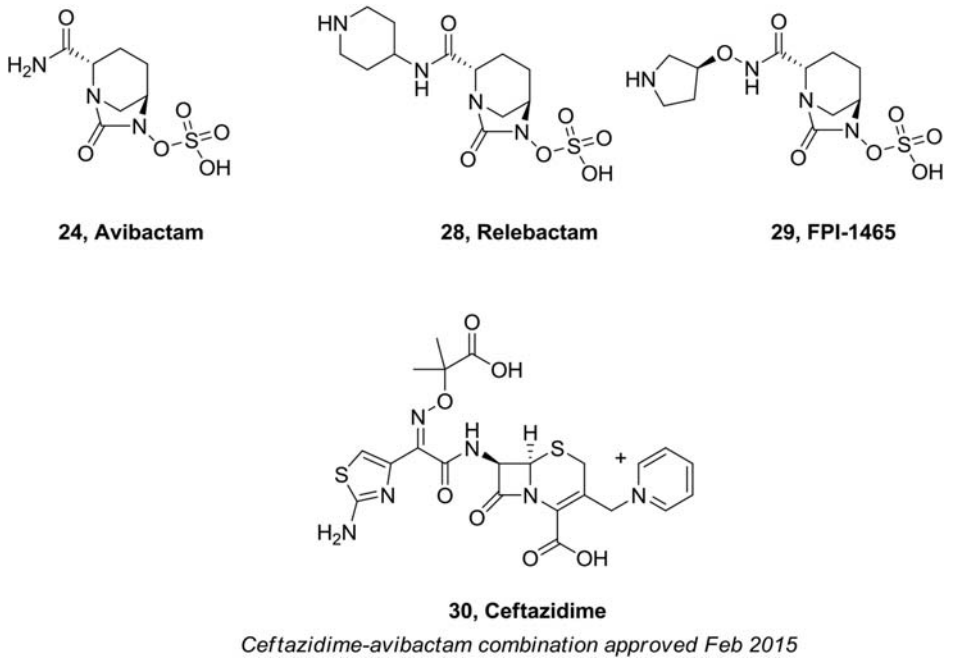

Fig. 10 Examples of diazabicyclooctane-based β-lactamase inhibitors (**24**, **28**, and **29**).

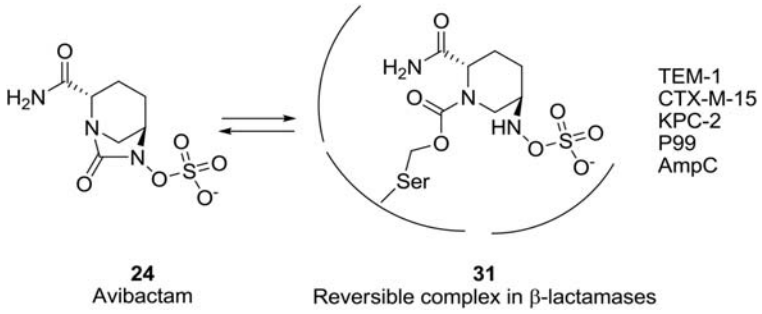

Fig. 11 Reversibility of avibactam.

into clinical development (e.g., the next-generation aminoglycoside plazomicin, currently in phase III trials).[48] This section will not review these legacy classes, but rather examine some of the new technology and chemical series that have emerged recently.

One major breakthrough in the past decade for ribosome-based targets has been the incorporation of high-resolution X-ray crystallography in drug discovery programs. For many years, the size and complexity of the ribosome prevented routine deployment of the technology, and challenges still remain.[49] However, several recent examples illustrate the power of this technique to identify novel binding modes and chemical starting points. A group at Rib-X Pharmaceuticals has made use of the 50S subunit of the ribosome from *Haloarcula marismortui*.[50] This archaeon, isolated from the Dead Sea in Israel, grows in high salt conditions and generates ribosomes that are structurally robust enough to be amenable for crystallography.[51] Using the structural information gained in this way, scaffolds such as **32** (Fig. 12) were optimized to deliver very potent broad-spectrum anti-Gram-negative activity, in particular against *P. aeruginosa*. This is significant, since compounds working at this site have to penetrate not only the highly polar outer membrane (while also avoiding efflux mechanisms) but also the inner cytosolic membrane (thus requiring sufficient hydrophobicity). The mechanism by which these molecules reach the cytosol has not been reported, but further analysis would certainly be of interest.

Another chemical class known to bind to the ribosome is derived from the natural product negamycin (**33**). Originally discovered in 1970, the antibacterial activity of this compound was subsequently attributed to inhibition of bacterial protein synthesis.[52–54] Crystal structures have been reported wherein negamycin binds to the nascent chain exit tunnel of the *H. marismortui* 50S ribosome subunit, but analogous binding in the more relevant pathogen *E. coli* has not been established.[55] Instead, the application of ribosome crystallography in *E. coli* and small molecule FRET techniques has revealed that in this species, negamycin acts by causing translational stalling and miscoding.[56] The crystal structure was different from that reported in *H. marismortui* and was found to

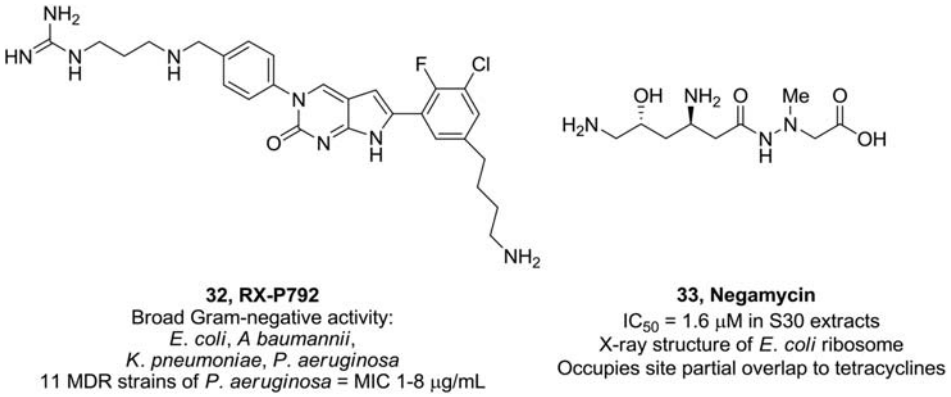

Fig. 12 Inhibitors of bacterial ribosomes.

partially overlap with the tetracycline-binding site, thus highlighting the critical relevance of high-resolution *E. coli* ribosome crystallography. Furthermore, two potential mechanisms of negamycin transport across the hydrophobic inner membrane of *E. coli* were characterized (a high-affinity route facilitated by the Dpp dipeptide transporter and a low-affinity energetically driven change in membrane potential).[57] This study nicely illustrates the benefit of understanding the mode of bacterial translocation, which may in principle be applicable across multiple drug classes.

5.21.4.1.2 Leucine-tRNA synthetase inhibitors and oxaboroles

The oxaboroles represent a novel and versatile chemical motif in the fight against drug-resistant bacteria. Not only are they potential inhibitors of β-lactamases, as discussed previously, but also they can be optimized for intrinsic antibacterial activity, especially through inhibition of leucine-tRNA synthetase.[58] This enzyme is responsible for transferring leucine to growing peptide chains, and, as such, inhibition results in a disruption of normal protein synthesis and bacterial cell death. Oxaboroles function by formation of a covalent borate complex with the ribose alcohols on the adenine moiety within the active site, and, uniquely, they exhibit relatively weak biochemical activity that nonetheless translates to potent antibacterial activity in vitro (Fig. 13).[59] This phenomenon may be related to slow but tight binding kinetics on the enzyme. For example, tavaborole (**35**) has a half-life of ~424 min on yeast cytoplasmic leucyl-tRNA synthetase, despite modest potency in conventional inhibitory assays (IC_{50} = 2.1 μM).[60] However, one of the leading oxaboroles in development for bacterial infections, AN3365, was halted in phase II cUTI clinical trials due to the development of resistance.[61] Although this was a setback for this target class, it should be noted that tavaborole has reached the market as a topical antifungal for treatment of onychomycosis of the toenail.[60]

5.21.4.2 DNA Synthesis: Novel Topoisomerase Inhibitors

Similar to the ribosome, inhibition of bacterial topoisomerase function has provided a rich legacy of antibacterial drugs, including the fluoroquinolones (e.g., ciprofloxacin) and novobiocin.[62] The search for potent topoisomerase inhibitors that are safe and do not show cross-resistance to fluoroquinolones has been at the center of many recent research efforts. The identification of several unique binding modes distinct from fluoroquinolones has enabled the discovery of several novel chemical classes and advanced clinical compounds, leading examples of which are shown in Fig. 14. The spiropyrimidinetrione EXT0914 (formerly AZD0914) **36** exploits a binding site that was first reported in 2007 with PNU-286607.[63] The mechanism of action is attributed to inhibition of DNA synthesis via accumulation of double-strand cleavages by stabilization of the cleaved DNA complex, thus preventing religation to circular DNA. EXT0914 was optimized for potency against Gram-positive bacteria and also *N. gonorrhoeae*.[64] The recent

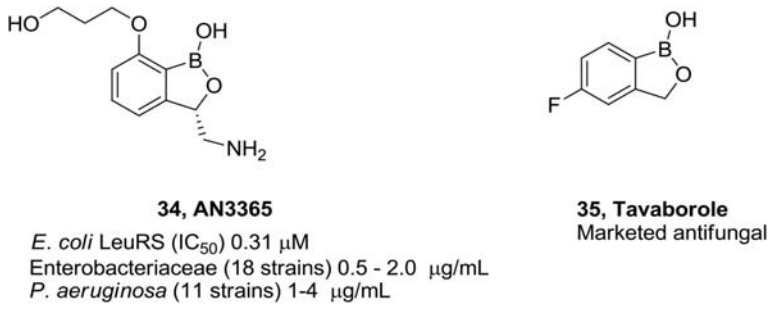

Fig. 13 Examples of oxaborole leucyl-tRNA synthetase inhibitors.

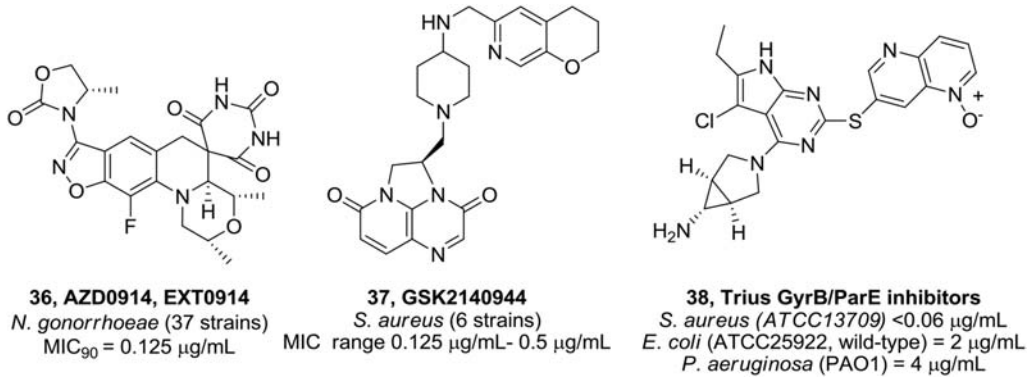

Fig. 14 Topoisomerase inhibitors.

emergence of drug-resistant *N. gonorrhoeae* infections has prompted the Centers for Disease Control and Prevention to call attention to this crisis.[65] EXT0914 lacks cross-resistance to clinical isolates resistant to fluoroquinolones[63,64] and is currently under investigation in patients in a phase II trial.

Another unique mode of interaction for type II topoisomerase inhibition is exemplified by GSK2140944 (**37**).[66,67] Compounds of this type work by stabilization of the precleavage DNA topoisomerase-DNA complex, thus leading to single-strand DNA breaks. GSK2140944 is also currently in phase II clinical trials.

A third mechanistic approach involves the dual inhibition of DNA gyrase (GyrB) and topoisomerase IV (ParE). Compounds that are known to inhibit these targets do so by binding to the ATPase subunits of the complex and interfere with supercoiling processes of bacterial DNA. Trius reported on a series of pyrrolopyrimidines, exemplified by **38**, which demonstrate potent broad-spectrum Gram-negative activity by virtue of this dual-inhibition mechanism.[68]

Collectively, these three mechanisms offer an opportunity to further exploit DNA synthesis as a target for antibacterial drugs while circumventing the increasingly widespread resistance to fluoroquinolones.

5.21.4.3 Cell-Wall Biosynthesis Inhibitors

Inhibition of cell-wall biosynthesis is the mechanism of action of many marketed drugs, divided into two major classes: (a) β-lactams, which target penicillin-binding proteins and (b) glycopeptides of the vancomycin family, which bind to D-Ala-Ala precursors.[69] This section will cover some of the emerging cell-wall biosynthesis targets that are distinct from those exploited by established agents.

5.21.4.4 LptD Inhibitors

A group at Polyphor AG has recently described their work originating from protegrin-1 (**39**, Fig. 15).[70] Naturally occurring protegrins were identified as antimicrobials but were limited by hemolytic activity. Through the use of a D-proline–L-proline template for stabilization of β-turns, potent *P. aeruginosa*-specific compounds were identified as exemplified by POL7001 (**40**). These compounds bind to the β-barrel protein LptD and thereby disrupt the translocation of lipopolysaccharide from the periplasm to the outer membrane. From this effort, a clinical candidate was identified (POL7080, structure not disclosed; *P. aeruginosa* (ATCC 27853) MIC = 0.008 μg mL^{-1}; and hemolytic activity > 100 μg mL^{-1}). This compound acts exclusively on *P. aeruginosa* and is inactive against other Gram-negative and Gram-positive bacteria. In a phase 1 trial, no adverse events were seen upon 6-day dosing of POL7080 (2–3 h infusion up to three times daily at up to 10 mg kg^{-1} day^{-1}).[71]

5.21.4.5 LpxC Inhibitors

A promising class of agents that demonstrate activity in wild-type strains of *P. aeruginosa* is those that target UDP-3-*O*-(*R*-3-hydroxymyristoyl)-*N*-acetylglucosamine deacetylase, encoded by *LpxC*.[72] This is the first committed step in the lipid A biosynthetic pathway, which has been shown to be essential in Gram-negative bacteria. All of the known LpxC inhibitors are characterized by a hydroxamic acid, which coordinates the active-site Zn^{2+}, and by a lipophilic tail, which mimics the natural lipid A precursor substrates. As mentioned earlier, lipophilic molecules are not typically found to be active against Gram-negative pathogens, even when they have very potent biochemical activity at their intended target. However, despite a wide logD range, many LpxC inhibitors provide potent wild-type activity in *P. aeruginosa*[11,12] with a yet unknown mechanism of cellular penetration. Potent examples are **41**, **42**, **43**, and **44** (Fig. 16).[73–75] These compounds have also been used to demonstrate the different resistance phenotypes, which can be manifested across species: for example, efflux is the primary first-step mechanism of resistance in *P. aeruginosa* but not in *K. pneumoniae* (where it is mutation in *fabZ*). Further to the mechanism of action, a collaborative study by

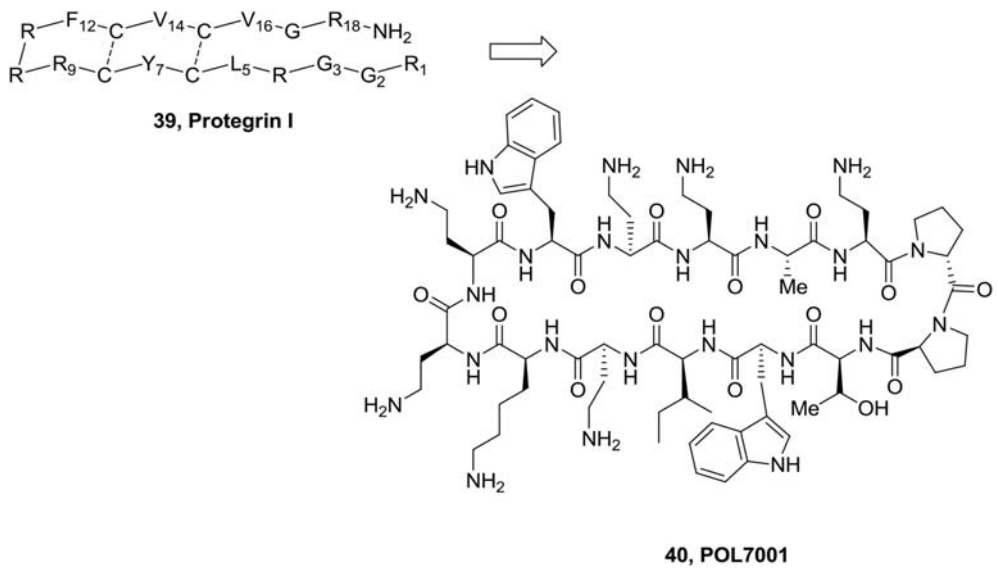

Fig. 15 Protegrin LptD inhibitors.

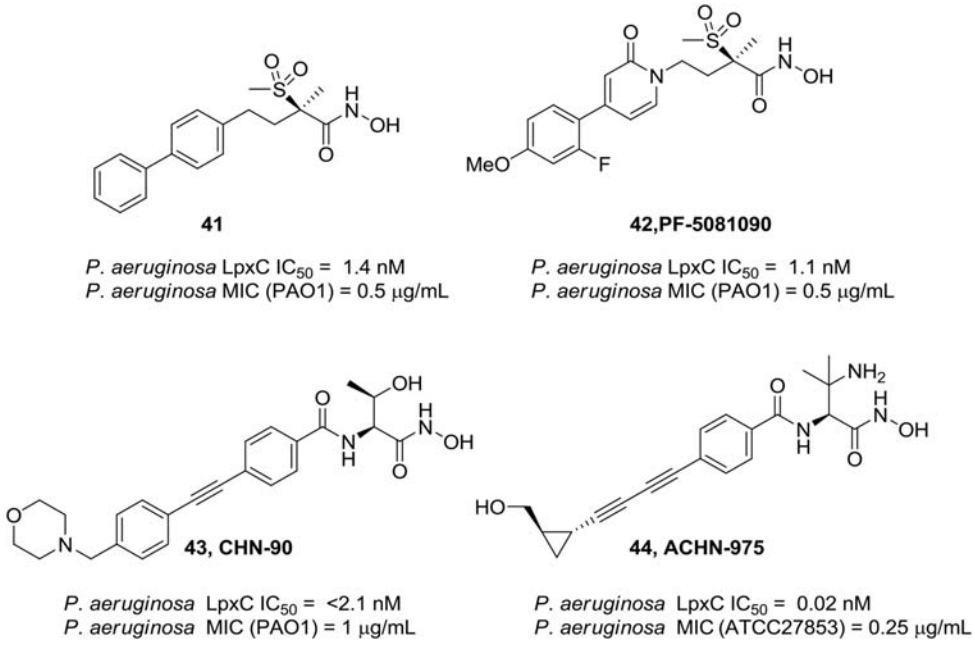

Fig. 16 LpxC inhibitors.

AstraZeneca and Stony Brook University has demonstrated that some LpxC inhibitors demonstrate slow-binding kinetics and a prolonged postantibiotic effect (PAE).[76] The off rate was correlated with the PAE, which in turn was incorporated into a model to predict efficacy in a mouse thigh model of infection. The first compound in the class to enter clinical trials was ACHN-975.[77] This compound was withdrawn due to inflammation at the infusion site in some phase 1 subjects.[78] It is hoped that this promising target can eventually lead to new antibacterial drugs, but no examples have yet reached late-stage clinical trials.

5.21.5 *Clostridium difficile* Infections

Over recent years, *Clostridium difficile* has emerged as an important gut pathogen that causes colitis due to the toxins it secretes. The treatment presents unique technical challenges: the therapy not only needs to target the intestinal tract but also should be pathogen

specific to avoid perturbing the normal enteric bacterial population.[79] The current oral use of vancomycin fulfills the first criterion (by virtue of its low oral bioavailability) but is suboptimal due to its lack of bacterial selectivity.[80]

5.21.5.1 Surotomycin From Daptomycin

Surotomycin **46** is a new clinical candidate that is currently in a phase III trial for the treatment of *C. difficile*-associated disease (CDAD).[81] Surotomycin **46** is a semisynthetic analog of daptomycin **45**, a natural product antibiotic (Fig. 17).[82] Granted fast-track QIDP designation in 2012, surotomycin represents a further example of the influence of the GAIN Act in support of the development of new antibacterial agents. Like daptomycin, surotomycin acts to depolarize (but not to permeabilize) bacterial membranes.[81] However, surotomycin also demonstrated less disruption of gastrointestinal microbiota and improved antibacterial activity against daptomycin-resistant strains of *E. faecium* and *E. faecalis*, as well as nonsusceptible strains of *S. aureus*.

5.21.5.1.1 Cadazolid

Another approach to the treatment of CDAD is the "chimeric" molecule cadazolid **47** (Fig. 18), which bears the features of an oxazolidinone ribosome inhibitor and those of a fluoroquinolone topoisomerase-type inhibitor and has recently completed a phase 1 clinical trial.[83] Cadazolid demonstrates potent in vitro activity against linezolid (oxazolidinone)- and fluoroquinoline-resistant or nonsusceptible strains of *C. difficile*.[84,85] Mechanistically, it has been established that it acts predominantly via inhibition of protein synthesis (attributable to the oxazolidinone moiety) and to a lesser extent by interfering with DNA synthesis.

5.21.5.1.2 LFF571

LFF571 (**48**) is derived from a series of thiopeptide-based secondary metabolites that interfere with bacterial protein synthesis by inhibition of elongation factor EF-Tu (Fig. 18).[86] Through semisynthesis, the poor solubility of the lead natural product structures was dramatically improved (original lead <0.001 mg mL^{-1}) while maintaining activity against *C. difficile*.[87,88] In a phase II trial, LFF571 was generally safe and well tolerated and demonstrated noninferiority to vancomycin (clinical cure 90.6% vs. 78.3%).[88]

Overall, several new approaches to treating CDAD are moving through advanced clinical studies. It is expected that these will serve to alleviate patient suffering and decrease the hospitalization stays caused by these troublesome infections.

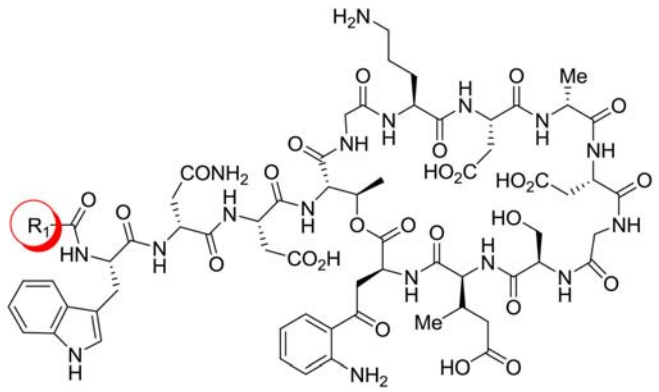

Cpd	R1	Name	*C. difficile* MIC_{90} (30 isolates)
45	$CH_3(CH_2)_8$-	Daptomycin	2.0 μg/mL
46	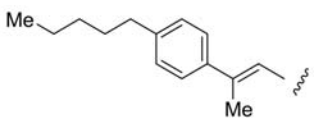	Surotomycin	0.5 μg/mL

Fig. 17 Surotomycin for *C. difficile* infections.

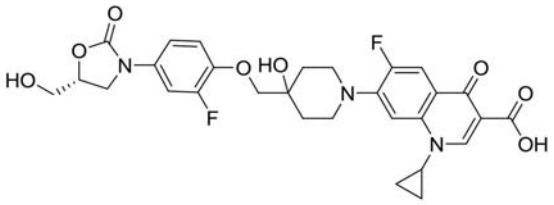

47, Cadazolid

C. difficile MIC_{90} (23 strains) = 0.25 μg/mL

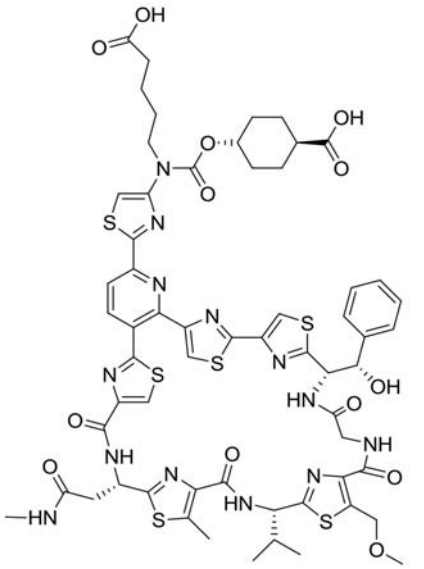

48, LFF571

Aqueous solubility = 12 mg/mL
EF-Tu IC_{50} = 6 nM
C. difficile MIC = 0.03 μg/mL

Fig. 18 Cadazolid and LFF571 for *C. difficile* infections.

5.21.6 Finding New Drug Leads

5.21.6.1 Natural Products

5.21.6.1.1 Novel screening approaches

It is estimated that 99% of microbes are "unculturable."[89] A team from NovoBiotic, Northeastern University, and the University of Bonn has developed methods to culture some of these organisms and, by doing so, isolated the novel antibacterial agent teixobactin (Fig. 19) from *Eleftheria terrae*.[90] Teixobactin has potent broad-spectrum Gram-positive activity, with MICs for most strains well below 1 μg mL^{-1}. Remarkably, no resistant strains emerged in either *S. aureus* or *M. tuberculosis* in the presence of the compound over a period of 27 days. The compound was not toxic to mammalian cells even at high concentrations (100 μg mL^{-1}) and was active in murine septicemia (*S. aureus*, PD_{50} 0.2 mg kg^{-1}), thigh (*S. aureus*), and lung (*S. pneumoniae*) models of infection. Mechanistically, the activity was attributed to binding of lipid II and lipid III, precursors of cell-wall synthesis.

5.21.6.1.2 New natural products from legacy screening approaches

Promysalin **50** (Fig. 20) is an amphipathic salicylate produced by *P. putida*.[91] Notably, it is one of the few natural products with activity reported against *Pseudomonas*: among 16 species tested, sensitive strains were found in 12. The initial report of promysalin did not identify the active stereoisomer from among the eight possible stereoisomers. A total synthesis was completed by Wuest in order to establish the stereochemistry and provide pure material for further mechanistic investigation.[92] It was assumed that the (*S*) configuration at C-16 was likely since no epimerase or thioesterase was found in the biosynthetic gene cluster. Thus, the synthetic investigation was narrowed to four stereoisomers, and all were synthesized to ultimately identify the bioactive ones (2*R*, 8*R*, and 16*S*). Further investigation identified two antivirulence phenotypes: mature biofilm dispersion and inhibition of pyoverdine production.

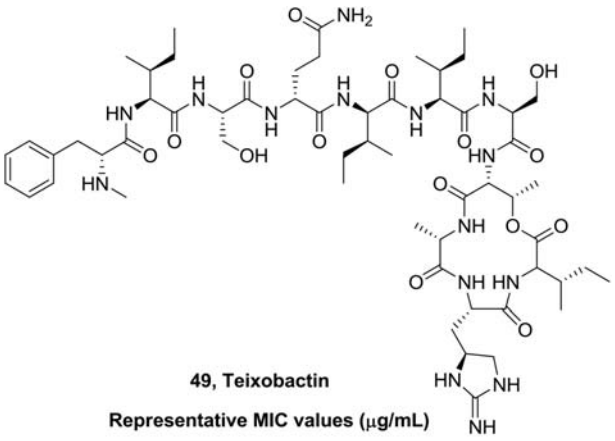

49, Teixobactin

Representative MIC values (μg/mL)

S. aureus (MSSA)	= 0.25
S. aureus + 10% serum	= 0.25
S. aureus (MRSA)	= 0.25
C. difficile	= 0.005
M. tuberculosis H37Rv	= 0.125
E. coli	= 25
P. aeruginosa	>32

Fig. 19 Profile of teixobactin, a natural product from a previously unculturable organism.

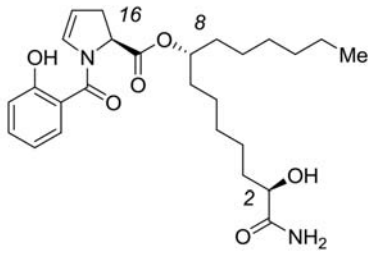

50, Promysalin

P. aeruginosa PA 14 IC_{50} = 0.16 μg/mL

Fig. 20 Promysalin, a unique natural product targeting *P. aeruginosa*.

5.21.6.2.3 New natural products with new chemistry applied

An example of an emerging class of natural products with potent Gram-positive activity is the cyclic acyldepsipeptides called enopeptins (Fig. 21).[93] Simplification of the acyl side chain present in the natural products served to improve solubility and metabolic stability, leading to ADEP4 (**53**).[94] The scaffold was further modified by a group at Brown University, incorporating methyl substituents as illustrated in **54** in order to further stabilize the hypothetical, transannular H-bond-dependent bioactive conformation.[95] These structural modifications led to a 1200-fold improvement in potency.

5.21.6.2 Screening Libraries

Being mindful of the challenges in identifying high-quality antibacterial leads from existing screening libraries,[10] Houghten and Shaw recently demonstrated that large libraries can be designed incorporating some of the key molecular properties required for cellular penetration in Gram-negative bacteria (e.g., amphiphilic and highly basic).[96] In this work (Fig. 22), the authors generated mixtures (exploiting 37 unique cores) totaling six million compounds. Using a scanning positional approach, they identified a library of 45864 individual compounds, constituted in 110 mixtures, with activity against the ESKAPE pathogens. The systematic library structure enabled efficient deconvolution, leading to a preferred series illustrated by **56**. Despite the high clogD, this compound still displays Gram-negative activity. The authors note that the potency of these molecules is limited by bacterial efflux mechanisms, and the use of an efflux pump inhibitor would improve their intrinsic activity.

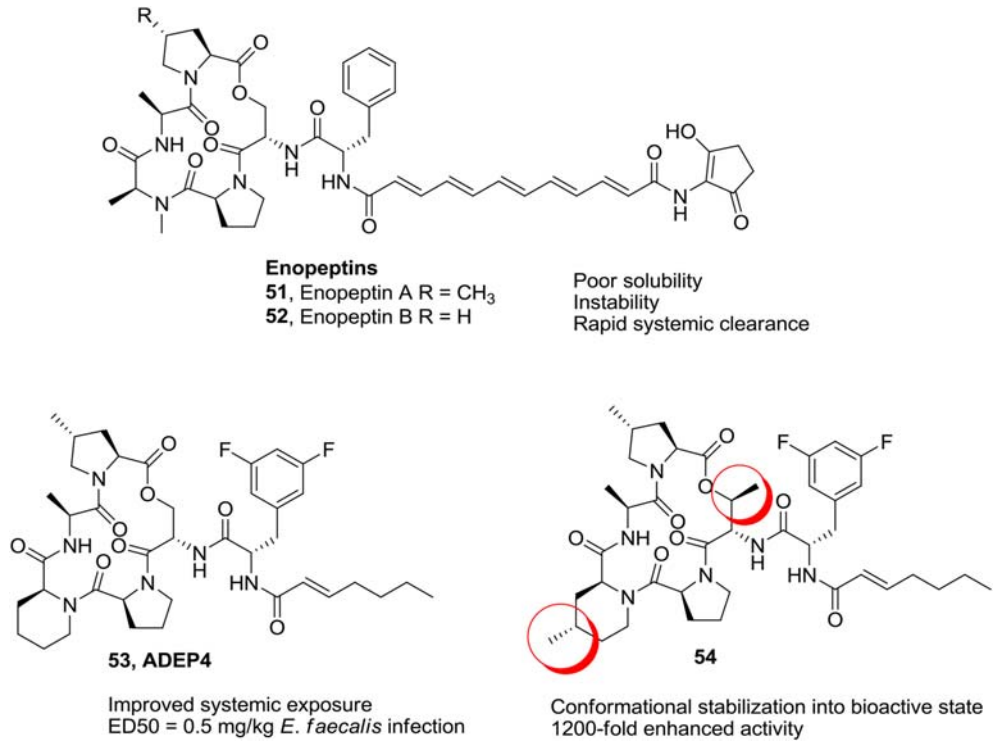

Fig. 21 Progression of enopeptins to stable and potent antibacterial lead structures.

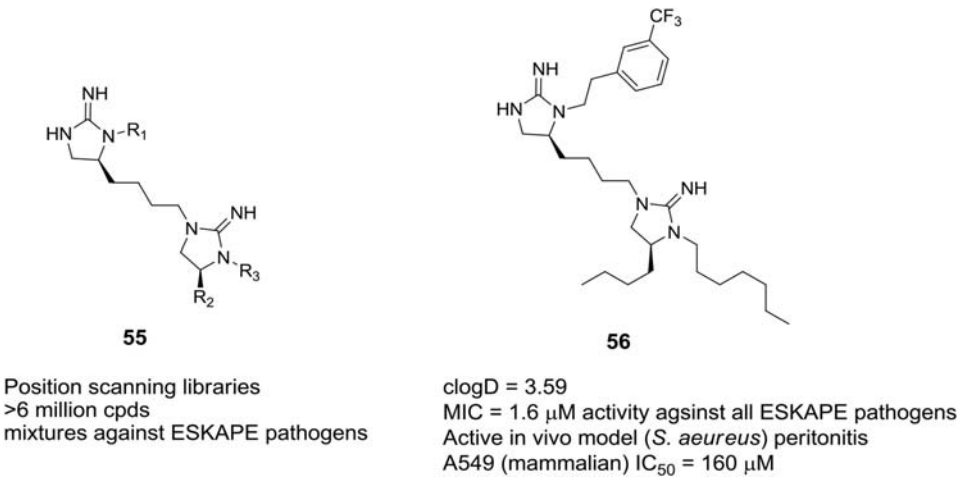

Fig. 22 Synthetic libraries leading to new Gram-negative scaffolds.

5.21.7 Nontraditional Approaches: Host Factors and Virulence Targets

The topics reviewed earlier can be considered classical antibacterial approaches in that their discovery and clinical development are based upon MICs in relevant strains as an indicator of antibacterial potential. Although the challenges in identifying new leads and drugs in this way are substantial, their path to regulatory approval is well precedented. However, diseases resulting from bacterial infections are complex and multifactorial, and modulation of host factors and bacterial gene products that affect virulence might well prove to be of clinical benefit. Unfortunately, it is the lack of clinical precedence of such approaches that makes the discovery, development, and regulatory path unclear. The reader is directed to a recent review in this area,[97] which is not addressed further here. Success against any of these types of targets might unlock significant new potential for sustained management of antibacterial diseases.

5.21.8 Conclusions

Over the past decade, clinical trends in antibacterial therapy have changed in several significant ways, and these have influenced the direction of antibacterial research as outlined earlier. Economic and regulatory incentives have helped to push new drugs forward into the clinic, which might never otherwise would have found traction. A focus on narrow spectrum agents, illustrated in particular by those directed toward infections caused by *C. difficile*, *P. aeruginosa* (POL70082), and *N. gonorrhoeae* (EXT0914), may point toward the future of the industry. The increasing rise of β-lactamases and especially MBLs requires new tools to combat these emerging outbreaks, and the discovery of DABCOs and boron-based β-lactamase inhibitors offers hope for their clinical management. It is also likely that these approaches will benefit greatly from a companion diagnostic method to enable the physician to rapidly determine the most appropriate antibiotic agent to prescribe. These new and emerging trends provide evidence of a path forward in the search for lifesaving treatments for serious drug-resistant bacterial infections.

References

1. http://www.centerwatch.com/drug-information/fda-approved-drugs/year/.
2. World Health Organization. Antimicrobial Resistance Global Report on Surveillance, 2014.
3. Butler, M. S.; Blaskovich, M. A.; Cooper, M. A. Antibiotics in the Clinical Pipeline in 2013. *J. Antibiot.* **2013,** *66,* 571–591.
4. GAIN Act: H.R.2182 – Generating Antibiotic Incentives Now Act of 2011112th Congress (2011–2012). https://www.congress.gov/bill/112th-congress/house-bill/2182.
5. Rice, L. B. Federal Funding for the Study of Antimicrobial Resistance in Nosocomial Pathogens: No ESKAPE. *J. Infect. Dis.* **2009,** *197,* 1079–1081.
6. http://www.fda.gov/NewsEvents/Newsroom/PressAnnouncements/ucm398724.htm. May 23, 2014. U.S. Food and Drug Administration, Silver Spring, MD.
7. Boucher, H. W.; Wilcox, M.; Talbot, G. H.; Puttagunta, S.; Das, A. F.; Dunne, M. W. Once-Weekly Dalbavancin Versus Daily Conventional Therapy for Skin Infection. *N. Engl. J. Med.* **2014,** *370,* 2169–2179.
8. Rex, J. ND4BB: Addressing the Antimicrobial Resistance Crisis. *Nat. Rev. Microbiol.* **2014,** *12,* 231–232.
9. O'Shea, R.; Moser, H. E. Physical Properties of Antibacterial Compounds: Implications for Drug Discovery. *J. Med. Chem.* **2008,** *51,* 2871–2878.
10. Payne, D. J.; Gwynn, M. N.; Holmes, D. J.; Pompliano, D. L. Drugs for Bad Bugs: Confronting the Challenges of Antibacterial Discovery. *Nat. Rev. Drug Discov.* **2007,** *6,* 29–40.
11. Brown, D. G.; May-Dracka, T. L.; Gagnon, M.; Tommasi, R. Trends and Exceptions of Physical Properties on Antibacterial Activity for Gram-Positive and Gram-Negative Pathogens. *J. Med. Chem.* **2014,** *57,* 10144–10161.
12. Tommasi, R.; Brown, D. G.; Walkup, G. K.; Manchester, J. I.; Miller, A. A. ESKAPEing the Labyrinth of Antibacterial Discovery. *Nat. Rev. Drug Discov.* **2015,** *14,* 529–542.
13. Nikaido, H.; Pagès, J.-M. Broad-Specificity Efflux Pumps and Their Role in Multidrug Resistance of Gram-Negative Bacteria. *FEMS Microbiol. Rev.* **2012,** *36,* 340–363.
14. Efren, E.; Vijayaraghavan, J.; Liu, J.; Cheneke, B. R.; Touw, D. S.; Lepore, B. W.; Indic, M.; Movileanu, L.; van den Berg, B. Substrate Specificity Within a Family of Outer Membrane Carboxylate Channels. *PLoS Biol.* **2012,** *10*, e1001242.
15. Wang, H.; Shi, X.; Yu, D.; Zhang, J.; Yang, G.; Cui, Y.; Sun, K.; Wang, J.; Yan, H. Antibacterial Activity of Geminized Amphiphilic Cationic Homopolymers. *Langmuir* **2015,** *31,* 13469–13477.
16. Eren, E.; van den Berg, B. Toward Understanding the Outer Membrane Uptake of Small Molecules by *Pseudomonas aeruginosa*. *J. Biol. Chem.* **2013,** *288,* 12042–12053. PDB code: 4FOZ.
17. van den Berg, B.; Bhamidimarri, S. P.; Prajapati, J. D.; Kleinekathofer, U.; Winterhalter, M. Outer-Membrane Translocation of Bulky Small Molecules by Passive Diffusion. *Proc. Natl. Acad. Sci.* **2015,** *112,* E2991–E2999. http://dx.doi.org/10.1073/pnas.1424835112.
18. Isabella, V. M.; Campbell, A. J.; Manchester, J.; Sylvester, M.; Nayar, A. S.; Ferguson, K. E.; Tommasi, R.; Miller, A. A. Toward Rational Design of Carbapenem Uptake in *P. aeruginosa*. *Chem. Biol.* **2015,** *22,* 535–547.
19. Winterhalter, M.; Ceccarelli, M. Physical Methods to Quantify Small Antibiotic Molecules Uptake into Gram-Negative Bacteria. *Eur. J. Pharm. Biopharm.* **2015,** *95, Part A,* 63–67. http://dx.doi.org/10.1016/j.ejpb.2015.05.006 (Article in press).
20. Page, M. G. P. Siderophore Conjugates. *Ann. N. Y. Acad. Sci.* **2013,** *1277,* 115–126.
21. Starr, J.; Brown, M. F.; Aschenbrenner, L.; Caspers, N.; Che, Y.; Gerstenberger, B. S.; Huband, M.; Knafels, J. D.; Lemmon, M. M.; Li, C.; McCurdy, S. P.; McElroy, E.; Rauckhorst, M. R.; Tomaras, A. P.; Young, J. A.; Zaniewski, R. P.; Shanmugasundaram, V.; Han, S. Siderophore Receptor-Mediated Uptake of Lactivicin Analogs in Gram-Negative Bacteria. *J. Med. Chem.* **2014,** *57,* 3845–3855.
22. (a) Tomaras, A. P.; Crandon, J. L.; McPherson, C. J.; Banevicius, M. A.; Finegan, S. M.; Irvine, R. L.; Brown, M. F.; O'Donnell, J. P.; Nicolau, D. P. Adaptation-Based Resistance to Siderophore-Conjugated Antibacterial Agents by *Pseudomonas aeruginosa*. *Antimicrob. Agents Chemother.* **2013,** *57,* 4197–4207; (b) McPherson, C. J.; Aschenbrenner, L. M.; Lacey, B. M.; Fahnoe, K. C.; Lemmon, M.; Finegan, S. M.; Tadakamalla, B.; O'Donnell, J. P.; Mueller, J. P.; Tomaras, A. P. Clinically Relevant Gram-Negative Resistance Mechanisms Have No Effect on the Efficacy of MC-1, a Novel Siderophore-Conjugated Monocarbam. *Antimicrob. Agents Chemother.* **2012,** *56,* 6334–6342.
23. Tomaras, A. P.; Crandon, J. L.; McPherson, C. J.; Nicolau, D. P. Potentiation of Antibacterial Activity of the MB-1 Siderophore-Monobactam Conjugate Using an Efflux Pump Inhibitor. *Antimicrob. Agents Chemother.* **2015,** *59,* 2439–2442.
24. Page, M. G. P.; Dantier, C.; Desarbre, E. In Vitro Properties of BAL30072, a Novel Siderophore Sulfactam With Activity Against Multiresistant Gram-Negative Bacteria. *Antimicrob. Agents Chemother.* **2010,** *54,* 2291–2302.
25. Drawz, S. M.; Bonomo, R. A. Three Decades of β-Lactamase Inhibitors. *Clin. Microbiol. Rev.* **2010,** *23,* 160–201.
26. Watkins, R. R.; Papp-Wallace, K. M.; Drawz, S. M.; Bonomo, R. A. Novel β-Lactamase Inhibitors: A Therapeutic Hope Against the Scourge of Multidrug Resistance. *Front. Microbiol.* **2013,** *4,* 1–8.
27. Jacoby, G. A.; Munoz-Price, L. S. The New β-Lactamases. *N. Eng. J. Med.* **2005,** *352,* 380–391.
28. Rogers, B. A.; Sidjabat, H. E.; Silvey, A.; Anderson, T. L.; Perera, S.; Li, J.; Paterson, D. Treatment Options for New Delhi Metallo-β-Lactamase-Harboring *Enterobacteriaceae*. *Microb. Drug Resist.* **2013,** *19,* 100–103.
29. Crowder, M. W.; Spencer, J.; Vila, A. J. Metallo-β-Lactamases: Novel Weaponry for Antibiotic Resistance in Bacteria. *Acc. Chem. Res.* **2006,** *39,* 721–728.
30. Westley-Horton, E.; Koestner, J. A. Aztreonam: A Review of the First Monobactam. *Am. J. Med. Sci.* **1991,** *302,* 46–49.
31. Klinger, F.-M.; Wichelhasu, T. A.; Frank, D.; Cuesta-Bernal, J.; El-Delik, J.; Müller, H. F.; Sjuts, H.; Göttig, S.; Koenigs, A.; Pos, K. M.; Pogoryelov, D.; Proschak, E. Approved Drugs Containing Thiols as Inhibitors of Metallo-β-Lactamases: Strategy to Combat Multidrug-Resistant Bacteria. *J. Med. Chem.* **2015,** *58,* 3626–3630.
32. Ma, J.; Cao, Q.; McLeod, S. M.; Ferugson, K.; Gao, N.; Breeze, A. L.; Hu, J. Target-Based Whole Cell Screening by ^{1}H NMR Spectroscopy. *Angew. Chem. Int. Ed.* **2015,** *54,* 4764–4767.
33. King, A. M.; Reid-Yu, S. A.; Wang, W. L.; King, D. T.; De Pascale, K. G.; Strynadka, N. C.; Walsh, T. R.; Coombes, B. K.; Wright, G. D. Aspergillomarasmine A Overcomes Metallo-β-Lactamase Antibiotic Resistance. *Nature* **2014,** *510,* 503.

34. Chiou, J.; Wan, S.; Chan, K. F.; So, P.-K.; He, D.; Chan, E. W.-C.; Chan, T.-H.; Wong, K.-y.; Tao, J.; Chen, S. Ebselen as a Potent Covalent Inhibitor of New Delhi Metallo-B-Lactamase (NDM-1). *Chem. Commun.* **2015,** *51,* 9543–9546.
35. Hecker, S. J.; Reddy, K. R.; Glinka, T. W.; Totrov, M.; Lomovskaya, O.; Tsivkovski, R.; Rubio-Aparicio, D.; Clifton, M. C.; Atkins, K.; Fairman, J. W.; Griffith, D.; Dudley, M. N. Discovery of a New Series of Broad-Spectrum Carbapenemase Inhibitors (Bcis) With Activity vs. Serine and Beta-Lactamases. 55th Interscience Conference on Antimicrobial Agents and Chemotherapy, F-270, San Diego, CA, Sep. 17–21, 2015.
36. Biedenbach, D. J.; Kazmierczak, K.; Bouchillon, S. K.; Sahm, D. F.; Bradford, P. A. In Vitro Activity of Aztreonam-Avibactam Against a Global Collection of Gram-Negative Pathogens from 2012 and 2013. *Antimicrob. Agents Chemother.* **2015,** *59,* 4239–4248.
37. McKinney, D. C.; Zhou, F.; Eyermann, C. J.; Ferguson, A. D.; Prince, B. D.; Breen, J.; Giacobbe, R. A.; Lahiri, S.; Verheijen, J. C. 4,5-Disubstituted 6-Aryloxy-1,3-dihydrobenzo [c][1,2]oxaboroles Are Broad-Spectrum Serine β-Lactamase Inhibitors. *ACS Infect. Dis.* **2015,** *1,* 310–316.
38. Xia, Y.; Aley, M. R. K.; Zhou, Y.; Singh, R.; Ding, C.; Cao, K.; Plattner, J. J.; Ou, L.; Jia, G.; Saraswat, N.; Ramachandran, S.; Zhou, D. Trisubstituted Boron-Containing Molecules, WO 2011/017125 A1, Feb. 10, 2011.
39. Hecker, S. J.; Reddy, K. R.; Totrov, M.; Hirst, G. C.; Lomovskaya, O.; Griffith, D. C.; King, P.; Tsivkovski, R.; Sun, D.; Sabet, M.; Tarazi, Z.; Clifton, M. C.; Atkins, K.; Raymond, A.; Potts, K. T.; Abendroth, J.; Boyer, S. H.; Loutit, J. S.; Morgan, E. E.; Durso, S.; Dudley, M. N. Discovery of a Cyclic Boronic Acid β-Lactamase Inhibitor (RPX7009) With Utility vs. Class A Serine Carbapenemases. *J. Med. Chem.* **2015,** *58,* 3682–3692.
40. Griffith, D. C.; Sabet, M.; Tarazi, Z.; Tsivkovski, R.; Lomovskaya, O.; Hecker, S. J.; Dudley, M. N. Nonclinical Toxicology and Safety Profile of the Beta-Lactamase Inhibitor RPX7009. Presented at the 52nd Interscience Conference on Antimicrobial Agents and Chemotherapy, San Francisco, CA; No. F-852.
41. Phase III: https://clinicaltrials.gov/ct2/show/NCT02168946.
42. Garber, K. A β-Lactamase Inhibitor Revival Provides New Hope for Old Antibiotics. *Nat. Rev. Drug Discov.* **2015,** *14,* 445–447.
43. Coleman, K. Diazobicyclooctanes (DBO's): A Potent New Class of Non-β-lactam β-lactamase Inhibitors. *Curr. Opin. Microbiol.* **2011,** *14,* 550–555.
44. Relebactam: https://clinicaltrials.gov/ct2/show/NCT02452047.
45. Salama, S. M.; Brouillette, E.; Malouin, F.; Parr, T. R., Jr. Mechanistic Studies of FPI-1465 Novel B-Lactamase Inhibitors. 53rd Interscience Conference on Antimicrobial Agents and Chemotherapy, F-1191, Denver, CO, Sep. 10–13, 2013.
46. Ehmann, D. E.; Jahic, H.; Ross, P. L.; Gu, R.-F.; Hu, J.; Kern, G.; Walkup, G. K.; Fisher, S. L. Avibactam Is a Covalent, Reversible Non-β-Lactam β-Lactamase Inhibitor. *Proc. Natl. Acad. Sci.* **2012,** *109,* 11663–11668.
47. Poehlsgaard, J.; Douthwaite, S. The Bacterial Ribosome as a Target for Antibiotics. *Nat. Rev. Microbiol.* **2005,** *3,* 870–881.
48. Karaiskos, I.; Souli, M.; Giamarellou, H. Plazomicin: An Investigational Therapy for the Treatment of Urinary Tract Infections. *Expert Opin. Investig. Drugs* **2015,** *24,* 1501–1511.
49. Moore, P. B. The Ribosome Returned. *J. Biol.* **2009,** *8.* http://dx.doi.org/10.1186/jbiol103.
50. Kanyo, Z.; Bhattacharjee, A.; Chen, S.; Collin, F.; Dalton, J.; DeVito, J.; DeVito, M.; Lou, R.; O'Dowd, H.; Martynow, J.; Paik, I.; Remy, J.; Scheideman, M.; Sinishtaj, S.; Skripkim, E.; Tang, Y.; Wimberly, B.; Wu, Y.; Duffy, E. Three Completely Novel Antibiotic Scaffolds for Treating Multidrug-Resistant Gram-Negative Infections. PosterP-1166, 21st ECCMID, Milan, Italy, May 7–10, 2011.
51. Ban, N.; Nissen, P.; Hansen, J.; Moore, P. B.; Steitz, T. A. The Complete Atomic Structure of the Large Ribosomal Subunit at 2.4 Å Resolution. *Science* **2000,** *289,* 905–920.
52. Hamada, M.; Takeuchi, T.; Kondo, S.; Ikeda, Y.; Naganawa, H. A New Antibiotic, Negamycin. *J. Antibiot. (Tokyo)* **1970,** *23,* 170–171.
53. Mizuno, S.; Nitta, K.; Umezawa, H. Mechanism of Action of Negamycin in *Escherichia coli* K12, I. Inhibition of Initiation of Protein Synthesis. *J. Antibiot. (Tokyo)* **1970,** *23,* 581–588.
54. Mizuno, S.; Nitta, K.; Umezawa, H. Mechanism of Action of Negamycin in *Escherichia coli* K12, II. Miscoding Activity in Polypeptide Synthesis Directed by Synthetic Polynucleotide. *J. Antibiot. (Tokyo)* **1970,** *23,* 589–594.
55. Schroeder, S. J.; Blaha, G.; Moore, P. B. Negamycin Binds to the Wall of the Nascent Chain Exit Tunnel of the 50S Ribosomal Subunit. *Antimicrob. Agents Chemother.* **2007,** *51,* 4462–4465.
56. Olivier, N. B.; Altman, R. B.; Noeske, J.; Basarab, G. S.; Code, E.; Ferguson, A. D.; Gao, N.; Huang, J.; Juette, M. F.; Livchak, S.; Miller, M. D.; Prince, D. B.; Cate, J. H. D.; Buurman, E. T.; Blanchard, S. C. Negamycin Induces Translational Stalling and Miscoding by Binding to the Small Subunit Head Domain of the *Escherichia coli* Ribosome. *Proc. Natl. Acad. Sci. U. S. A.* **2014,** *111,* 16274–16279.
57. McKinney, D. C.; Bezdenejnih-Snyder, N.; Farrington, K.; Guo, J.; McLaughlin, R. E.; Ruvinsky, A.; Singh, R.; Basarab, G. S.; Narayan, S.; Buurman, E. T. Illicit Transport via Dipeptide Transporter Is Irrelevant to the Efficacy of Negamycin in Mouse Thigh Models of *Escherichia coli*. *ACS Infect. Dis.* **2015,** *1,* 222–230.
58. Hurdle, J. G.; O'Neill, A. J.; Chopra, I. Prospects for Aminoacyl-tRNA Synthetase Inhibitors as New Antimicrobial Agents. *Antimicrob. Agents Chemother.* **2005,** *49,* 4821–4833.
59. Hernandez, V.; Crépin, T.; Palencia, A.; Cusack, S.; Akama, T.; Baker, S. J.; Bu, W.; Feng, L.; Freund, Y. R.; Liu, L.; Meewan, M.; Mohan, M.; Mao, W.; Rock, F. L.; Sexton, H.; Sheoran, A.; Zhang, Y.; Zhang, Y.-K.; Zhou, Y.; Nieman, J. A.; Anugula, M. R.; Keramane, E. M.; Savariraj, K.; Reddy, D. S.; Sharma, R.; Subedi, R.; Singh, R.; O'Leary, A.; Simon, N. L.; De Marsh, P. L.; Mushtaq, S.; Warner, M.; Livermore, D. M.; Alley, M. R. K.; Plattner, J. J. Discovery of a Novel Class of Boron-Based Antibacterials With Activity Against Gram-Negative Bacteria. *Antimicrob. Agents Chemother.* **2013,** *57,* 1394–1403.
60. Rock, F. L.; Mao, W.; Yaremchuk, A.; Tukalo, M.; Crépin, T.; Zhou, H.; Zhang, Y.-K.; Hernandez, V.; Akama, T.; Baker, S. J.; Plattner, J. J.; Shapiro, L.; Martinis, S. A.; Benkovic, S. J.; Cusak, S.; Alley, M. R. K. An Antifungal Agent Inhibits an Aminoacyl-tRNA Synthetase by Trapping tRNA in the Editing Site. *Science* **2007,** *316,* 1759–1761.
61. https://www.clinicaltrials.gov/ct2/show/results/NCT01381549?term=gsk2251052&rank=5.
62. Kohanski, M. A.; Dwyer, D. J.; Collins, J. J. How Antibiotics Kill Bacteria: From Targets to Networks. *Nat. Rev. Microbiol.* **2010,** *8,* 423–435.
63. Huband, M. D.; Bradford, P. A.; Otteson, L. G.; Basarab, G. S.; Kutschke, A. C.; Giacobbe, R. A.; Patey, S. A.; Alm, R. A.; Johnstone, M. R.; Potter, M. E.; Miller, P. F.; Mueller, J. P. In Vitro Antibacterial Activity of AZD0914, a New Spiropyrimidine DNA Gyrase/Topoisomerase Inhibitors With Potent Activity Against Gram-Positive, Fastidious Gram-Negative, and Atypical Bacteria. *Antimicrob. Agents Chemother.* **2015,** *59,* 467–474.
64. Basarab, G. S.; Doig, P.; Galullo, V.; Kern, G.; Kimzey, A.; Kutschke, A.; Newman, J.; Morningstar, M.; Mueller, J.; Otterson, L.; Vishwanathan, K.; Zhou, F.; Gowravaram, M. Discovery of Novel DNA Gyrase Inhibiting Spiropyrimidinetriones—Benzisoxazole Fusion With N-Linked Oxazolidinone Substituents Leading to a Clinical Candidate (EXT0914). *J. Med. Chem.* **2015;** http://dx.doi.org/10.1021/acs.jmedchem.5b00863.
65. Deguchi, T.; Nakane, K.; Ysuda, M.; Maeda, S. Emergence and Spread of Drug Resistant *Neisseria gonorrhoeae*. *J. Urol.* **2010,** *184,* 851–858.
66. Ross, J. E.; Scangarella-Oman, N. E.; Flamm, R. K.; Jones, R. N. Determination of Disk Diffusion and MIC Quality Control Guidelines for GSK2140944, a Novel Bacterial Type II Topoisomerase Inhibitor Antimicrobial Agent. *J. Clin. Microbiol.* **2014,** *52,* 2629–2632.
67. So, W.; Crandon, J. L.; Nicolau, D. P. Pharmacodynamic Profile of GSK2140944 Against Methicillin-Resistant *Staphylococcus aureus* in a Murine Lung Infection Model. *Antimicrob. Agents Chemother.* **2015,** *59,* 4956–4961.
68. Trzoss, M.; Bensen, D. C.; Li, X.; Chen, Z.; Lam, T.; Zhang, J.; Creighton, C. J.; Cunningham, M. L.; Kwan, B.; Stidham, M.; Nelson, K.; Brown-Driver, V.; Castellano, A.; Shaw, K. J.; Lightstone, F. C.; Wong, S. E.; Nguyen, T. B.; Finn, J.; Tari, L. W. Pyrrolopyrimidine Inhibitors of DNA Gyrase (GyrB) and Topoisomerase IV (ParE), Part II: Development of Inhibitors With Broad Spectrum, Gram-Negative Antibacterial Activity. *Bioorg. Med. Chem. Lett.* **2013,** *23,* 1537–1543.
69. Schneider, T.; Sahl, H. G. An Oldie But Goodie—Cell Wall Biosynthesis as Antibiotic Target Pathway. *Int. J. Med. Microbiol.* **2010,** *300,* 161–169.
70. Srinivas, N.; Jetter, P.; Ueberbacher, B. J.; Werneburg, M.; Zerbe, K.; Steinmann, J.; Van der Meijden, B.; Bernardini, F.; Lederer, A.; Dias, R. L. A.; Misson, P. E.; Henze, H.; Zumbrunn, J.; Gombert, F. O.; Obrecht, D.; Hunziker, P.; Schauer, S.; Ziegler, U.; Käch, A.; Eberl, L.; Riedel, K.; DeMarco, S. J.; Robinson, J. A. Peptidomimetic Antibiotics Target Outer-Membrane Biogenesis in *Pseudomonas aeruginosa*. *Science* **2010,** *327,* 1010.
71. Polyphor. March 4, 2013, Polyphor Reports Successful Phase 1 Results for Its Pseudomonas Selective Inhibitor POL7080 [Press release]. Retrieved from http://www.nabativi.org/upload/file/Polyphor%20POL7080_Press%20Release_.pdf.

72. Barb, A. W.; Zhou, P. Mechanism and Inhibition of LpxC: An Essential Zinc-Dependant Deacetylase of Bacterial Lipid A Synthesis. *Curr. Pharm. Biotechnol.* **2008,** *9,* 9–15.
73. Tomaras, A. P.; McPherson, C. J.; Kuhn, M.; Carifa, A.; Mullins, L.; George, D.; Desbonnet, C.; Eidem, T. M.; Montgomery, J. I.; Brown, M. F.; Reilly, U.; Miller, A. A.; O'Donnell, J. P. JLpxC Inhibitors as New Antibacterial Agents and Tools for Studying Regulation of Lipid A Biosynthesis in Gram-Negative Pathogens. *mBio* **2014,** *5,* e01551–e01554.
74. Brown, M. F.; Reilly, U.; Abramite, J. A.; Arcari, J. T.; Oliver, R.; Barham, R.; Che, Y.; Chen, J. M.; Collantes, E. M.; Chung, S. W.; Desbonnet, C.; Doty, J.; Doroski, M.; Engtrakul, J. J.; Harris, T. M.; Huband, M.; Knafels, J. D.; Leach, K. L.; Liu, S.; Marfat, A.; Marra, A.; McElroy, E.; Melnick, M.; Menard, C. A.; Montgomery, J. I.; Mullins, L.; Noe, M. C.; O'Donnell, J.; Penzien, J.; Plummer, M. S.; Price, L. M.; Shanmugasundaram, V.; Thoma, C.; Uccello, D. P.; Warmus, J. S.; Wishka, D. G. Potent Inhibitors of LpxC for the Treatment of Gram-Negative Infections. *J. Med. Chem.* **2012,** *55,* 914–923.
75. Montgomery, J. I.; Brown, M. F.; Reilly, U.; Price, L. M.; Abramite, J. A.; Arcari, J.I.; Barham, R.; Che, Y.; Chen, J. M.; Chung, S. W.; Collantes, E. M.; Desbonnet, C.; Doroski, M.; Doty, J.; Engtrakul, J. J.; Harris, T. M.; Huband, M.; Knafels, J. D.; Leach, K. L.; Liu, S.; Marfat, A.; McAllister, L.; McElroy, E.; Menard, C. A.; Mitton-Fry, M.; Mullins, L.; Noe, M. C.; O'Donnell, J.; Oliver, R.; Penzien, J.; Plummer, M.; Shanmugasundaram, V.; Thoma, C.; Tomaras, A. P.; Uccello, D. P.; Vaz, A.; Wishka, D. G. Pyridone Methylsulfone Hydroxamate LpxC Inhibitors for the Treatment of Serious Gram-Negative Infections. *J. Med. Chem.* **2012,** *55,* 1662–1670.
76. Walkup, G. K.; You, Z.; Ross, P. L.; Allen, E. K. H.; Daryaee, F.; Hale, M. R.; O'Donnell, J.; Ehmnann, D. E.; Schuck, V. J. A.; Buurman, E. T.; Coy, A. L.; Hajec, L.; Murphy-Benenato, K.; Marone, V.; Patey, S. A.; Grosser, L. A.; Johnstone, M.; Walker, S. G.; Tonge, P. J.; Fisher, S. L. Translating Slow-Binding Inhibition Kinetics Into Cellular and in vivo Effects. *Nat. Chem. Biol.* **2015,** *11,* 416–426.
77. Serio, A. W.; Kubo, A.; Lopez, S.; Gomez, M.; Corey, V. C.; Andrews, L.; Schwartz, M. A.; Kasar, R.; McEnroe, G.; Aggen, J.; Miller, G.; Armstrong, E. S. Structure, Potency and Bactericidal Activity of ACHN-975, a First-in-Class LpxC Inhibitor. 53rd Interscience Conference on Antimicrobial Agents and Chemotherapy, F-1227, Denver, CO.
78. ACHN-975 completed December 2012. Clinicaltrials.gov, NCT01597947. SEC form S-1 Registration Statement on ACHN-975, January 24, 2014. http://www.sec.gov/Archives/edgar/data/1301501/000119312514020548/d623715ds1.htm.
79. Leffler, D. A.; Lamont, T. *Clostridium difficile* Infection. *N. Engl. J. Med.* **2015,** *372,* 1539–1548.
80. Fekety, R.; Silva, J.; Kauffman, C.; Buggy, B.; Deery, H. G. Treatment of Antibiotic-Associated *Clostridium difficile* Colitis With Oral Vancomycin: Comparison of Two Dosage Regimens. *Am. J. Med.* **1989,** *86,* 15–19.
81. Mascio, C. T.; Mortin, L. I.; Howland, K. T.; Van Praagh, A. D.; Zhang, S.; Arya, A.; Chuong, C. L.; Kang, C.; Li, T.; Silverman, J. A. In Vitro and in vivo Characterization of CB-183,315, a Novel Lipopeptide Antibiotic for Treatment of *Clostridium difficile*. *Antimicrob. Agents Chemother.* **2012,** *56,* 5023–5030.
82. Yin, N.; He, Y.; Herradura, P.; Pearson, A.; Mesleh, M. F.; Mascio, C. T.; Howland, K.; Steenbergen, J.; Thorne, G. M.; Citron, D.; Van Praagh, A. D. G.; Mortin, L. I.; Keith, D.; Silverman, J.; Metcalf, C. Structure-Activity Relationship Studies of a Series of Semisynthetic Lipopeptides Leading to the Discovery of Surotomycin, a Novel Cyclic Lipopeptide Being Developed for the Treatment of *Clostridium difficile*-Associated Diarrhea. *J. Med. Chem.* **2015,** *58,* 5137–5142.
83. Baldoni, D.; Gutierrez, M.; Timmer, W.; Dingemanse, J. Cadazolid, a Novel Antibiotic With Potent Activity Against *Clostridium difficile*: Safety, Tolerability and Pharmacokinetics in Healthy Subjects Following Single and Multiple Oral Doses. *J. Antimicrob. Chemother.* **2014,** *69,* 706–714.
84. Locher, H. H.; Seller, P.; Chen, X.; Schroeder, S.; Pfaff, P.; Enderlin, M.; Klenk, A.; Fournier, E.; Hubschwerlen, C.; Ritz, D.; Kelly, C. P.; Keck, W. In Vitro and in vivo Antibacterial Evaluation of Cadazolid, a New Antibiotic for Treatment of *Clostridium difficile* Infections. *Antimicrob. Agents Chemother.* **2014,** *58,* 892–900.
85. Locher, H. H.; Caspers, P.; Bruyère, T.; Schroeder, S.; Pfaff, P.; Knezevic, A.; Keck, W.; Ritz, D. Investigations of the Mode of Action and Resistance Development of Cadazolid, a New Antibiotic for Treatment of *Clostridium difficile* Infections. *Antimicrob. Agents Chemother.* **2014,** *58,* 901–908.
86. Leeds, J. A.; Sachdeva, M.; Mullin, S.; Dzink-Fox, J.; Lamarche, M. J. Mechanism of Action of and Mechanism of Reduced Susceptibility to the Novel Anti-*Clostridium difficile* Compound LFF571. *Antimicrob. Agents Chemother.* **2012,** *56,* 4463–4465.
87. LaMarche, M. J.; Leeds, J. A.; Amaral, A.; Brewer, J. T.; Bushell, S. M.; Deng, G.; Dewhurst, J. M.; Ding, J.; Dzink-Fox, J.; Gamber, G.; Jain, A.; Lee, K.; Lee, L.; Lister, T.; McKenney, D.; Mullin, S.; Osborne, C.; Palestrant, D.; Patane, M. A.; Rann, E. M.; Sachdeva, M.; Shao, J.; Tiamfook, S.; Trzasko, A.; Whitehead, L.; Yifru, A.; Yu, D.; Yan, W.; Zhu, Q. Discovery of LFF571: An Investigational Agent for *Clostridium difficile* Infection. *J. Med. Chem.* **2012,** *55,* 2376–2387.
88. Mullane, K.; Lee, C.; Bressler, A.; Buitrago, M.; Weiss, K.; Dabovic, K.; Praestgaard, J.; Leeds, J. A.; Blias, J.; Pertel, P. Multicenter, Randomized Clinical Trial to Compare the Safety and Efficacy of LFF571 and Vancomycin for *Clostridium difficile* Infections. *Antimicrob. Agents Chemother.* **2015,** *59,* 1435–1440.
89. Stewart, E. J. Growing Unculturable Bacteria. *J. Bacteriol.* **2012,** *194,* 4151–4160.
90. Ling, L. L.; Schneider, T.; Peoples, A. J.; Spoering, A. L.; Engels, I.; Conlon, B. P.; Mueller, A.; Schäberle, T. F.; Hughes, D. E.; Epstein, S.; Jones, M.; Lazarides, L.; Steadman, V. A.; Cohen, D. R.; Felix, C. R.; Fetterman, K. A.; Millett, W. P.; Nitti, A. G.; Zullo, A. M.; Chen, C.; Lewis, K. A New Antibiotic Kills Pathogens Without Detectable Resistance. *Nature* **2015,** *517,* 455–459.
91. Li, W.; Estrada-de los Santos, P.; Matthijs, S.; Xie, G.-L.; Busson, R.; Cornelis, P.; Rozenski, J.; De Mot, R. Promysalin, a Salicylate-Containing *Pseudomonas putida* Antibiotic, Promotes Surface Colonization and Selectively Targets Other *pseudomonas*. *Chem. Biol.* **2011,** *18,* 1320–1330.
92. Steele, A. D.; Knouse, K. W.; Keohane, C. E.; Wuest, W. M. Total Synthesis and Biological Investigation of (–) Promysalin. *J. Am. Chem. Soc.* **2015,** *137,* 7314–7317.
93. Koshino, H.; Osada, H.; Yano, T.; Uzawa, J.; Isono, K. The Structure of Enopeptins A and B, Novel Depsipeptide Antibiotics. *Tetrahedron Lett.* **1991,** *32,* 7707–7710.
94. Brötz-Oesterhelt, H.; Beyer, D.; Kroll, H.-P.; Endermann, R.; Ladel, C.; Schroeder, W.; Hinzen, B.; Raddatz, S.; Paulsen, H.; Henninger, K.; Bandow, J. E.; Sahl, H.-G.; Labischinski, H. Dysregulation of Bacterial Proteolytic Machinery by a New Class of Antibiotics. *Nat. Med.* **2005,** *11,* 1082–1087.
95. Carney, D. W.; Schmitz, K. R.; Truong, J. V.; Sauer, R. T.; Sello, J. K. Restriction of Conformational Dynamics of the Cyclic Acyldepsipeptide Antibiotics Improves Their Antibacterial Activity. *J. Am. Chem. Soc.* **2014,** *136,* 1922–1929.
96. Fleeman, R.; LaVoi, T. M.; Santos, R. G.; Morlaes, A.; Nefzi, A.; Welmaker, G. S.; Medina-Franco, J. L.; Giulianotti, M. A.; Houghten, R. A.; Shaw, L. N. Combinatorial Libraries as a Tool for the Discovery of Novel, Broad-Spectrum Antibacterial Agents Targeting the ESKAPE Pathogens. *J. Med. Chem.* **2015,** *58,* 3340–3355.
97. Phoenix, D. A., Harris, F., Dennison, S. R., Eds. *Novel Antimicrobial Agents and Strategies;* Wiley-VCH Verlag GmbH & Co. KGaA: Weinheim, Germany, 2015.

Relevant Websites

http://www.centerwatch.com/drug-information/fda-approved-drugs/year/—This website provides summary information on FDA approved drugs from 1995 to 2015.
http://www.imi.europa.eu/content/nd4bb—This website provides content and overview of the European Union IMI initiaitive New Drugs for Bad Bugs (ND4BB).

5.22 Antifungal Chemistry Review

M Birch and G Sibley, F2G Ltd, Manchester, United Kingdom

© 2017 Elsevier Ltd. All rights reserved.

5.22.1	**Introduction to Fungal Disease**	703
5.22.2	**Current Systemic Antifungal Agents**	705
5.22.2.1	Polyenes	705
5.22.2.2	Flucytosine	705
5.22.2.3	Azoles	706
5.22.2.4	Allylamines	708
5.22.2.5	Echinocandins	708
5.22.3	**Notable Others**	708
5.22.3.1	Nikkomycin Z	708
5.22.3.2	Tavaborole	709
5.22.3.3	Sordarins	710
5.22.4	**New Antifungals in Clinical Development**	710
5.22.4.1	VT-1161	710
5.22.4.2	SCY-078	711
5.22.4.3	CD101	711
5.22.4.4	F901318	712
5.22.4.5	E1210	713
5.22.4.6	VL-2397	713
5.22.5	**Summary**	714
References		714

5.22.1 Introduction to Fungal Disease

Over the last decade infectious diseases have been consistently making headlines in the world news. Whether it be the global rise of methicillin resistant Staphylococcus aureus (MRSA) and antibiotic resistance, epidemics due to SARS, Ebola, and hepatitis C or the threat of malaria and tuberculosis to the health of the world's poorest people, infectious diseases have been constantly in the global consciousness.

One group of microorganisms have had little of the global infectious disease limelight—the fungi.

This is perhaps surprising because it is estimated that 300 million people suffer from a fungal infection with up to 1.5 million deaths annually.[1] Indeed cryptococcal infections are estimated to kill over 500,000 people in sub Saharan Africa and this is as high a death toll as that due to tuberculosis, a disease which is widely recognized.

Fungal diseases can be divided into two broad categories: superficial and invasive.

Superficial fungal infections are by far the most common mycoses, with dermatophytes representing the most common fungi isolated from immunocompetent people. Dermatophyte infections occur within the stratum corneum of the skin and other keratin-containing structures such as hair and nails. Dermatophyte infections are ubiquitous and it is estimated that 20–25% of the world's population suffers from some form of dermatophyte infections, making it one of the commonest infections in humans.[2] Whilst considered trivial, dermatophyte infections can cause significant stress and psychological impact. Superficial fungal infections may require extended periods of dosing for effective treatment: for onychomycosis, treatment periods of up to 12 months are common.

Fungal infections by *Candida* species are also common, with mucocutaneous candidiasis a typical presentation.

Oesophageal candidiasis or oral thrush, is a common infection in immunocompromised patients, particularly HIV patients not receiving Highly Active antiretroviral therapy (HAART) therapy, whilst vulvovaginal candidiasis (VVC) occurs in up to 70% of premenopausal women, with 5–9% having recurrent infection.[1,3]

Serious systemic fungal infections are predominantly infections of the immunocompromised host, and increased globally in the latter half of the 20th century as a result of the enhanced use of immunosuppressive therapies in transplant and for the treatment of cancers in an aging population. Major advances in diagnostic tests for invasive fungal disease have also contributed to the increase in recording of disease.

Three genera of fungi, *Candida*, *Aspergillus*, and *Cryptococcus*, are responsible for the vast majority of invasive fungal infections.

Candida are commensal dimorphic fungi that reside on mucosa and in the gastrointestinal tract of healthy individuals. Along with superficial skin infections, *Candida* spp. can also cause life threatening invasive disease. Invasive *Candida* infections are the most prevalent systemic fungal infections worldwide, with *Candida* the fifth most common cause of blood stream infection in the United States. Mortality for candidemia approaches 40% but can be higher depending on the underlying disease.[4]

Aspergillus species are ubiquitous environmental saprophytic molds whose ecological niche is the soil, where they are important in the decay of biological matter. Aspergilli are spore-forming organisms that produce aerial reproductive structures called conidiophores, which in turn produce many smaller spores or conidia. These hydrophobic conidia are released into the air in vast numbers in order to propagate the organism, and infection occurs when they are inhaled by a susceptible host. A spectrum of disease associated with *Aspergillus* infections exists, ranging from noninvasive colonization of the upper airways, localized growth within the lung, allergic disease exacerbating preexisting respiratory disease, to full disseminated invasive infection. The extent of disease is related to the immune status of the host. Invasive aspergillosis is predominantly a disease of the neutropenic host, and people with hematological malignancies are at the greatest risk. Additionally, solid organ transplant and hematopoietic stem cell transplant recipients and patients on prolonged corticosteroid therapy are also at considerable risk.[5] Mortality of invasive aspergillosis at one time ranged from 40% to 90% dependent on the underlying medical condition responsible for the immunosuppressed state, but with the advent of modern antifungal therapy this has been reduced to 20–30%.[6]

Of the 200 species of aspergilli known, only around 20 cause infections in man and of these, four are isolated more frequently than the rest. *A. fumigatus* is by far the most common species infecting man and resistance to first line antifungal therapy is now emerging. Resistance to the azole class of antifungals is now recognized globally and carries very high mortality of over 80%.[7]

Cryptococcosis is a severe fungal infection that is primarily caused by two species of capsulated yeast, *Cryptococcus gattii* and *Cryptococcus neoformans*. The disease has been recognized for over a 100 years but the incidence has increased dramatically as a result of the Acquired immune deficiency syndrome (AIDS) pandemic with over 600,000 deaths in the Human Immunodeficiency virus (HIV) population in Africa annually.[8] *Cryptococcus* is also a disease of the immunocompromised patient, with mortalities of up to 30% in organ transplant and cancer patients.[9] Recently an outbreak of hypervirulent *C. gattii* infections occurred in north western United States in an immunocompetent patient population.[10]

At the turn of the 21st century there was a significant global decline in antiinfective drug research and development. Antifungal drug discovery was one of the most affected areas, with almost no new discovery undertaken at this time, particularly by large pharmaceutical companies. Instead discovery research became the almost exclusive remit of biotechnology companies supported in part by academia. In this period the only antifungal products to make significant progress were those already established in clinical development. A few new antifungal drug registrations did result, most notably voriconazole in 2002. At this time the echinocandins became the first new class of systemic antifungal agents to be marketed for over a decade (**Fig. 1**).

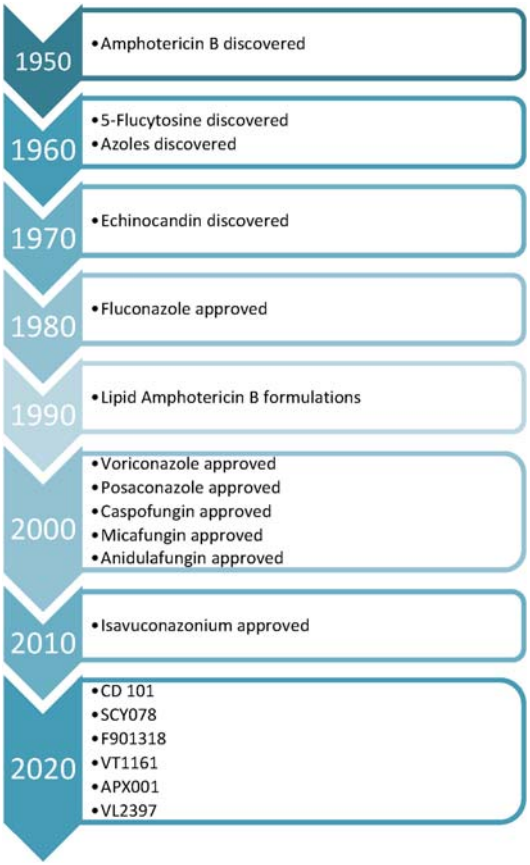

Fig. 1 Timeline of systemic antifungal drug discovery.

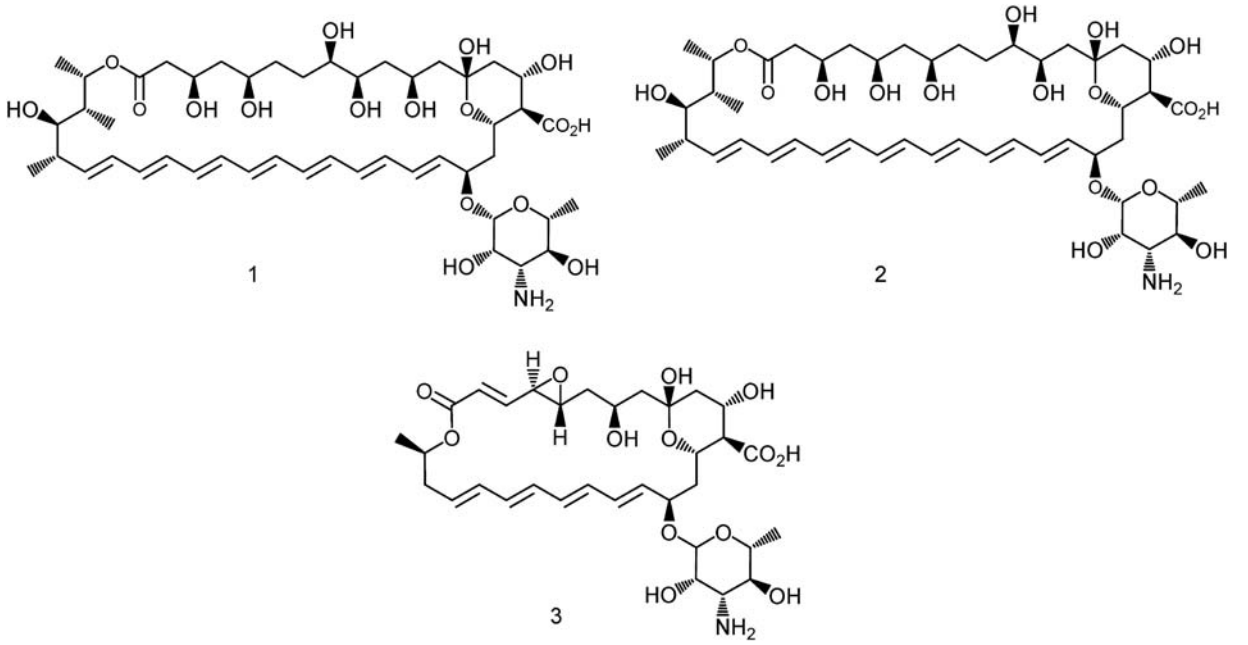

Fig. 2 **1**, Amphotericin B; **2**, nystatin; and **3**, natamycin.

5.22.2 Current Systemic Antifungal Agents

5.22.2.1 Polyenes

Polyenes are a class of broad spectrum antifungal compounds with a cyclic amphiphilic macrolide substructure which are derived from a species of *Streptomyces* bacteria.[11] The polyenes are antifungal by virtue of binding to ergosterol, which is a prevalent steroid in the fungal cell wall, resulting in depolarization of the membrane leading to increased K^+ and Na^+ permeability and ultimately cell death.[12]

The main polyene drug used in the treatment of fungal infections is amphotericin B (AmB, **1**) (Fig. 2), with other compounds within the class being nystatin (**2**) and natamycin (**3**). The polyene class possess a slight affinity for binding to human cholesterol which in turn leads to toxic effects mainly associated with the kidneys and liver.[13] The polyenes are not orally bioavailable, and nystatin (**2**) and natamycin (**3**) use is limited to treatment of fungal infections of the oral cavity. AmB is the only polyene that is dosed systemically, via intravenous (IV) infusion, with infusion-related adverse effects and dose limiting nephrotoxicity being problematic. An improved toxicity profile has been achieved through lipid and nanoparticulate formulations, which allow the administration of larger doses with a reduction in renal toxicity.[14]

Its broad spectrum of activity, encompassing both most yeasts and filamentous fungi,[15] and inherent low propensity for the development of resistance has led to AmB being widely regarded as the gold standard for the treatment of systemic fungal infections for many years.

5.22.2.2 Flucytosine

Flucytosine or 5-fluorocytosine (5-FC, **4**) (Fig. 3) was initially intended as an antitumor agent[16] but was later found to be an effective antimycotic.[17] 5-FC is transported into fungal cells by cytosine permease and the active form is only formed upon conversion into 5-fluorouracil (5-FU, **5**) by cytosine deaminase in susceptible fungal cells. 5-FU is in turn converted to active metabolites by uracil phosphoribosyltransferase, giving 5-fluorouridine monophosphate (5-fluoro-UMP) which inhibits the synthesis of fungal DNA by targeting thymidylate synthetase.[18] Further conversion of 5-fluoro-UMP to 5-fluorouridine triphosphate also perturbs protein synthesis by incorporation into fungal RNA, leading to cell death. Mammalian cells are not subjected to the toxic effects of 5-FC as they lack the requisite cytosine deaminase.[19,20]

5-FC displays good activity against *Candida* and *Cryptococcus* species, but activity against *Aspergillus* species is far more limited.[19]

5-FC is usually only dosed in combination with other antifungal agents such as AmB or an azole, as the development of resistance is a common problem when used as monotherapy.[21] 5-FC is orally bioavailable but elicits some problematic side effects such as bone marrow suppression, GI disturbances, and hepatotoxicity. It continues to be used for the initial management of severe cryptococcal pneumonia and meningoencephalitis infections[22] and (less frequently) in select invasive candidal infections.

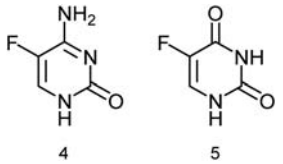

Fig. 3 **4**, Flucytosine and **5**, fluorouracil.

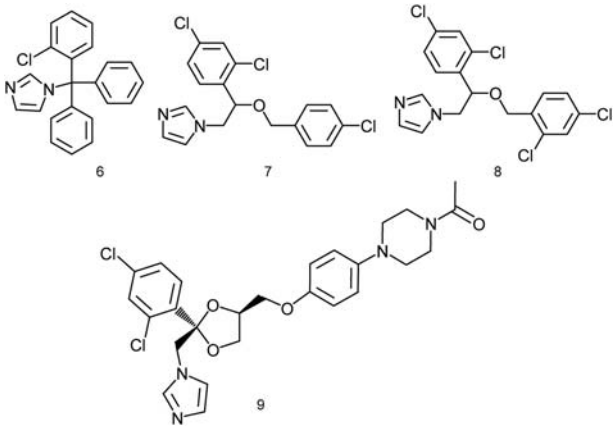

Fig. 4 **6**, Clotrimazole; **7**, econazole; **8**, miconazole; and **9**, ketoconazole.

5.22.2.3 Azoles

In recent years the azole class of antifungal compounds has been the richest source of antifungal discovery leading to new therapies for clinical use.[23] They are typified by the presence of an imidazole or triazole ring.

The azoles elicit an antifungal effect by inhibition of lanosterol 14α-demethylase, the cytochrome P450 3A enzyme that is responsible for the conversion of lanosterol to ergosterol. This has the effect of disrupting the fungal cell membrane integrity and ultimately cell death.[24,25]

The initial imidazole azole antifungals clotrimazole (**6**), econazole (**7**), and miconazole (**8**) (Fig. 4) became available in the late 1960s. However, due to their toxicity profiles their use was primarily in topical administration as an alternative to nystatin for the treatment of cutaneous and mucocutaneous dermatophyte and *Candida* infections. At the time only miconazole found an application for IV therapy for the treatment of cryptococcal meningitis and disseminated candidiasis. However significant adverse effects now limit its use to the nonsystemic treatment of oropharyngeal candidiasis, VVC and tinea corporis, and pedis and cruris infections, administered in gels, creams, and buccal patches.

In the 1980s a new imidazole azole called ketoconazole (**9**) was developed which displayed a spectrum of activity similar to miconazole but showed improved tolerability over both miconazole and AmB and therefore became the preferred treatment. However it was only available for oral administration and displayed variable absorption. Ketoconazole also displayed significant toxicity, such as a dose-dependent reduction in testosterone and cortisol levels due to inhibition of the human CYP450 enzymes required for hormone synthesis.[26,27] This and other adverse effects resulted in the Food and Drug Administration (FDA) recommending that ketoconazole be restricted to instances where alternative therapies have failed.[28]

The imidazole azoles demonstrate good activity against a number, but not all, yeast infections and no activity against mold species such as *A. fumigatus*. Currently the use of imidazole azole antifungals is limited almost exclusively to the treatment of nonsystemic infections.[29]

During the 1990s a new class of azole antifungals, the triazoles, emerged in the form of the first-generation agents itraconazole (**10**) and fluconazole (**11**) (Fig. 5). Fluconazole was the first approved for clinical use, in 1990, and represented a huge advance for the treatment of mucosal and invasive candidiasis, via IV and oral dosage forms, with an improved pharmacokinetic and safety profiles over ketoconazole. Nonetheless, the treatment of clinically important fungal infections such as aspergillosis remained a problem, as although fluconazole had good activity against many *Candida* and *Cryptococcus* spp., *C. krusei*, and *C. glabrata* are less susceptible and activity is completely lacking against molds such as *A. fumigatus*.

Itraconazole was approved for clinical use in 1992 and displayed an expanded antifungal spectrum that included the problematic molds such as *Aspergillus* species. However, the drug presented extreme challenges in formulation; oral dosage forms proved unreliable due to highly variable adsorption and the IV preparation was eventually withdrawn from use.

Despite their improved antifungal effects the triazoles, like the imidazoles, are associated with potential safety and tolerability issues. These include nausea, vomiting, diarrhea, hepatic toxicity, and QTc prolongation.[30] Drug–drug interactions are also a significant problem due to cross inhibition of a variety of the human CYP450-dependent enzymes.[31]

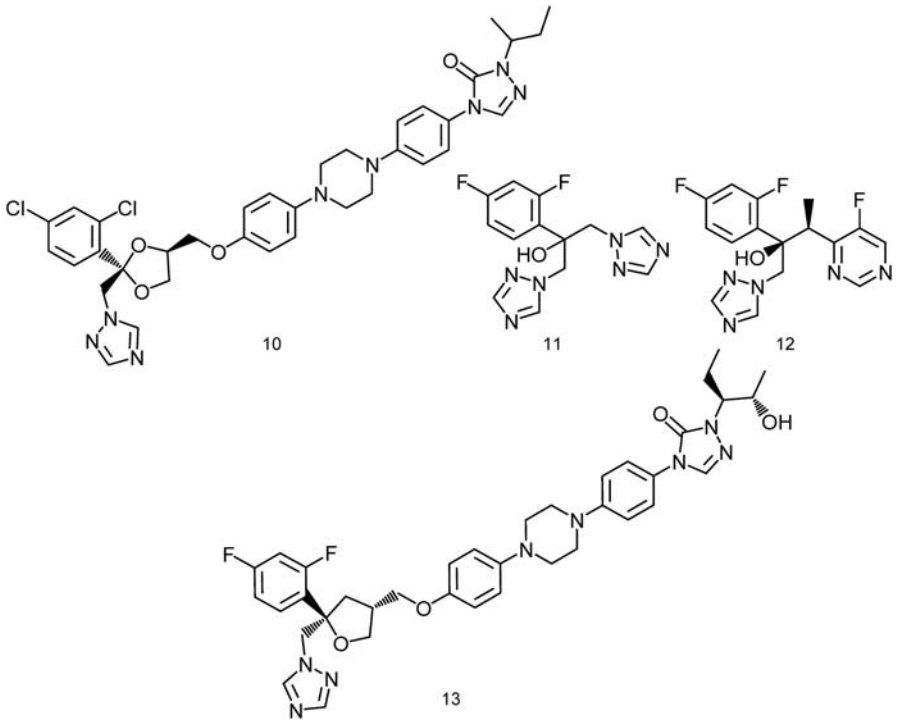

Fig. 5 **10**, Itraconazole; **11**, fluconazole; **12**, voriconazole; and **13**, posaconazole.

The second-generation triazoles, voriconazole (**12**) and posaconazole (**13**) were approved for clinical use in 2002 and 2006, respectively. These demonstrated improved antifungal spectrum, potency, and toxicity profiles over the first-generation azoles. With a 70% 12 week survival rate compared to 57% for the AmB control population,[32] voriconazole rapidly became the gold standard therapy for invasive aspergillosis but its use is associated with significant drug–drug interactions, hypervariable pharmacokinetics, and visual disturbances. Posaconazole has been shown to be effective against *Candida* spp., *Aspergillus* spp., *Cryptococcus* spp., *Zygomycetes* spp., and *Fusarium* spp. infections, with reduced inhibition of cytochrome *c*-dependent enzymes resulting in less pronounced drug–drug interactions.

The most recent triazole azole compounds to be developed are ravuconazole (**14**), albaconazole (**16**), isavuconazole (**17**), and its prodrug isavuconazonium (**18**) (Fig. 6).

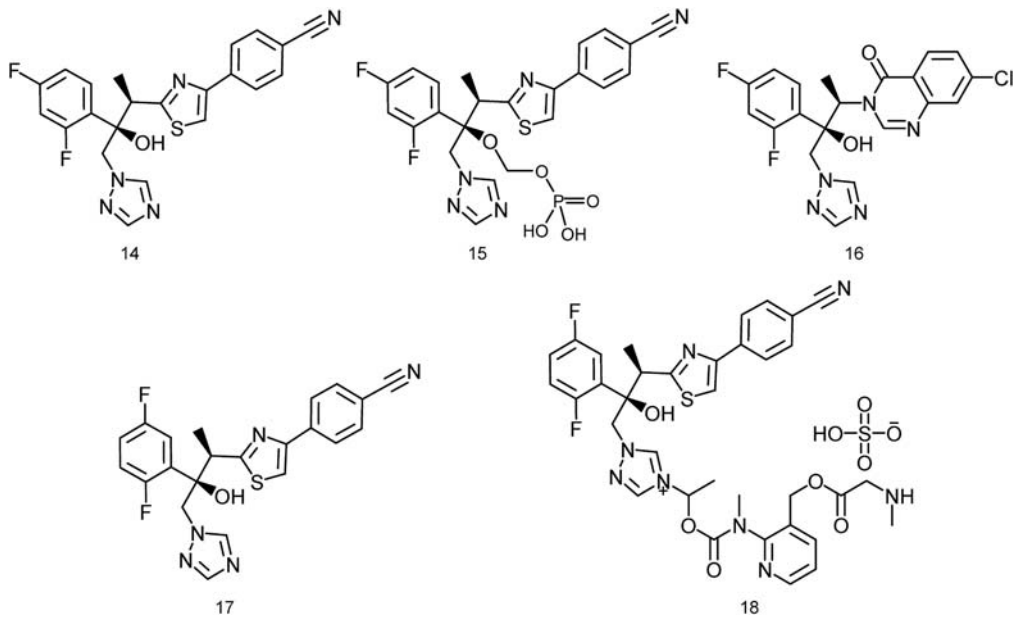

Fig. 6 **14**, Ravuconazole; **15**, BMS-379224; **16**, albaconazole; **17**, isavuconazole; and **18**, isavuconazonium.

Isavuconazonium was granted approval by the US FDA in 2015 for the treatment of invasive aspergillosis and mucormycosis. Isavuconazonium sulfate is a water-soluble prodrug of isavuconazole that is rapidly cleaved by plasma esterases upon either IV or oral administration. This is advantageous because the IV formulations for both voriconazole and posaconazole contain sulfobutyl cyclodextrins, which are implicated in nephrotoxicity. In comparison to voriconazole, isavuconazole displays a significantly lower rate of drug-related adverse events, but while drug–drug interactions are also reduced, they remain significant. Other side effects such as nausea, vomiting, and diarrhea are also common, but the visual disturbances, hallucinations, and photosensitivity witnessed with voriconazole have not been observed. The antifungal activity of isavuconazole against *Candida* spp. and some of the most common *Aspergillus* spp. is generally comparable with voriconazole and posaconazole.[33] As is common with other azoles,[34] isavuconazole suffers from a similar increase in minimum inhibitory concentration (MIC) with azole-resistant organisms through a variety of resistance mechanisms.[35]

Ravuconazole (**14**) is currently in clinical trials and is an isomer of isavuconazole. Ravuconazole is an oral agent while the phosphonooxymethyl ether derivative BMS-379224 (**15**), a much more soluble prodrug,[36] is in development for IV use. Ravuconazole displays an antifungal spectrum similar to voriconazole but with limited activity against *Fusarium* spp., *Scedosporium* spp., and *Zygomycetes* spp.[37–39]

Albaconazole (**16B**) is also in clinical trials and displays >80% bioavailability, good oral pharmacokinetics, and an antifungal spectrum that includes *Scedosporium prolificans*,[40] which is otherwise difficult to treat. Interestingly albaconazole also displays an encouraging safety profile relative to other members of the class. Albaconazole is currently in trials for onychomycosis and *Candida vulvovaginitis* and displays promising results, although natural resistance has been observed.[37,38]

5.22.2.4 Allylamines

The allylamines naftifine (**19**) and terbinafine (**20**) (Fig. 7) form a class of antifungal agents that act via inhibition of ergosterol synthesis at the level of squalene epoxidase, with minimal effects on mammalian cholesterol synthesis. The subsequent accumulation of squalene within the fungal cell leads to an increase in cell permeability, with disruption of intracellular organization and eventually cell death. The allylamines are fungicidal against dermatophytes and have fungistatic activity against *Candida* spp. Naftifine is the original member of the class and is efficacious when administered topically against superficial dermatomycoses.[41] Terbinafine can be utilized both topically and orally to treat fungal infections of skin, nails, and hair and is the drug of choice for dermatophyte onchomycosis.[42]

5.22.2.5 Echinocandins

The echinocandins are semisynthetic lipopeptides derived from the fermentation broths of fungi that are cyclic hexapeptides with N-linked acyl lipid side chains. Caspofungin (**21**), micafungin (**22**), and anidulafungin (**23**) are derivatives of lipopeptides from *Glarea lozoyensis*, *Coleophoma empedra*, and *A. nidulans*, respectively (Fig. 8).

The echinocandins elicit an antifungal effect by inhibition of the synthesis of 1,3-β-D-glucan, an essential component of the fungal cell wall. 1,3-β-D-glucan is particularly prominent in the cell wall of *Candida* and *Aspergillus* species but is not present in mammalian cells, and therefore the echinocandins avoid direct human cell toxicity. They are fungicidal against *Candida* species, including those known to be intrinsically resistant to azoles and AmB, but are fungistatic against *Aspergillus* species.[43,44] Lacking oral bioavailability, all three echinocandins are administered by IV infusion. Central nervous system tissue penetration is minimal, but the echinocandins distribute extensively into other major tissues such as lung, liver, and spleen. The class is generally well tolerated, with mild adverse effects that include local phlebitis, fever, abnormal liver function tests, and haemolysis.[45] The echinocandins demonstrate an additive to synergistic effect with triazoles when used in combination therapy for the treatment of *A. fumigatus*.[46]

The development of resistance to echinocandins has been reported to arise due to the selection of either stable mutational or reversible physiological alterations.[47]

5.22.3 Notable Others

5.22.3.1 Nikkomycin Z

Nikkomycin Z (**24**) is a uridine-based secondary metabolite of *Streptomyces tendae* initially isolated in the mid-1970s and subsequently shown to inhibit the activity of fungal chitin synthase (Fig. 9). The polysaccharide chitin is an important structural

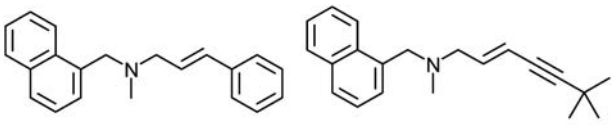

19 20

Fig. 7 **19**, Naftifine and **20**, terbinafine.

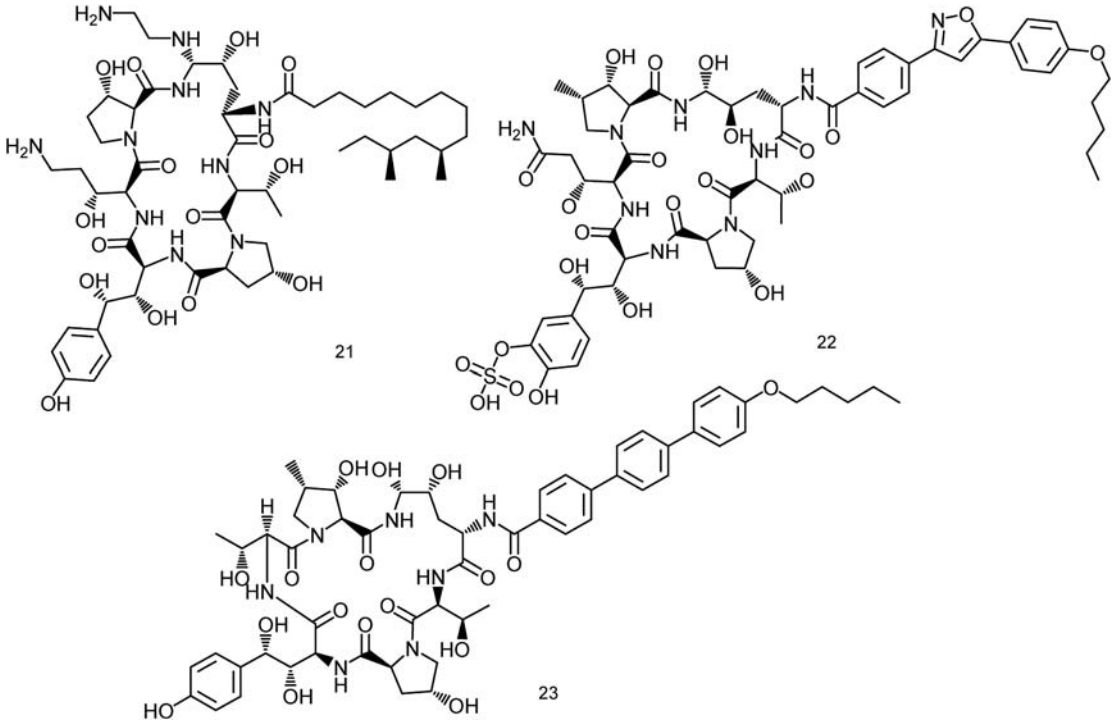

Fig. 8 **21**, Caspofungin; **22**, micafungin; and **23**, anidulafungin.

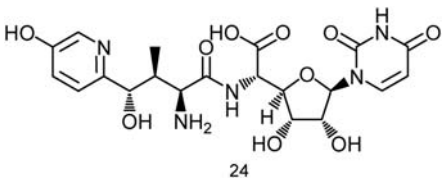

Fig. 9 **24**, Nikkomycin Z.

component of the cell wall of many fungi. Originally identified in an agrochemical fungicide program, no commercial products were developed and Nikkomycin Z became a research tool. In the late 1990s it was discovered that Nikkomycin Z had good in vivo activity against *Coccidiodes immitis*, the causative agent of Valley Fever, an endemic fungal infection occurring in Arizona. Nikkomycin Z is now under clinical development for the treatment of coccidioidomycosis[48] and has entered Phase II clinical trials. The agent is also active against other endemic fungal pathogens such as *Histoplasma capsulatum* and *Blastomyces dermatidis*. Nikkomycin displays acceptable oral bioavailability and is well tolerated with no adverse effects with doses up to 2000 mg.

5.22.3.2 Tavaborole

Tavaborole (**25**, Fig. 10) is a low molecular weight benzoxaborole derivative that is the first of its class and exploits a novel mode of action: inhibition of aminoacyl-transfer ribonucleic acid synthetase prevents fungal protein synthesis, leading to inhibition of cell growth and ultimately to cell death. Tavaborole was approved for the topical treatment of onychomycosis of the toe nail in July 2014 and has shown a favorable safety and efficacy profile.[49]

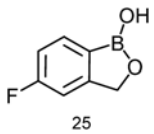

Fig. 10 **25**, Tavaborole.

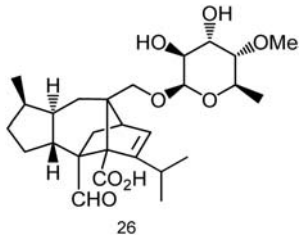

26

Fig. 11 **26**, Sordarin.

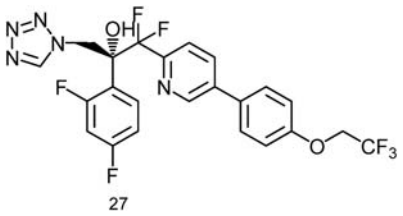

27

Fig. 12 **27**, VT-1161.

5.22.3.3 Sordarins

The sordarins are a family of compounds that have a tetracyclic diterpene glycoside substructure (Fig. 11). Unlike other antifungals that target the integrity of the fungal cell wall, the sordarins act by the inhibition of fungal protein synthesis through the inhibition of elongation factor 2.[50] With good activity against *Candida albicans* and a number of other prevalent pathogenic fungi, sordarin (**26**) and its derivatives are interesting class for future antifungal development.

5.22.4 New Antifungals in Clinical Development

5.22.4.1 VT-1161

VT-1161 (**27**, Fig. 12) is an example of a metalloenzyme inhibitor consisting of a core scaffold coupled to a metal binding group (MBG) designed to interact with the metal ion intrinsic to the target enzyme. The potency of metalloenzyme inhibitors relates to the affinity of the MBG for the metal and is a function of the electronic forces in the immediate environment. While the potency can therefore be tuned by altering the affinity of the MBG for the metal, overly strong interactions can lead to nonspecific inhibition.

Previously this principle has been well exemplified with the azoles, discussed earlier.[51] In the first-generation azoles the 1-imidazole moiety served as a high affinity MBG that was often associated with off-target side effects. In the triazole-containing second-generation azoles, the affinity of the MBG was reduced and the drugs were better tolerated, although drug–drug interactions and liver toxicity remained significant clinical issues.[52]

VT-1161 was derived from a structure-guided effort specifically targeting MBGs with lower affinity for the CYP51 iron complex. Viamet Pharmaceuticals hypothesized that the off-target effects of both imidazole and triazole antifungals were due to high affinity MBG interactions. An antifungal drug discovery program was devised to identify MBGs with reduced or differential metal affinity between human and fungal CYP51. A series of MBGs were selected in silico and ranked for their predicted affinity to the CYP51 heme–iron complex. Initially a 1-tetrazole MBG was identified as of high interest and from this a number of additional targets were modeled and tested using in vitro activity against *C. albicans* and CYP3A4 assays as primary screens.

Docking studies of the 1-tetrazole MBGs in CYP51 suggested that conserved tyrosine 118 residue could be exploited through π-stacking interactions. A series of electron-deficient 2,5-disubstituted pyridines were designed to exploit this possibility. Through these modifications, analogs were discovered with significant improvements in in vitro potency and good oral efficacy in murine models of invasive candidiasis.[52] Following further rounds of modeling and synthesis, further improvements in potency were achieved by incorporating H-bond interactions with Ser378, ultimately leading to the identification of the trifluoroethyl ether-containing analog VT-1161.

VT-1161 has high affinity for the *C. albicans* CYP51 (ERG11) with a dissociation constant K_d of $\leq$39 nm. Conversely, it did not inhibit the human CYP51 at concentrations up to 50 μM, demonstrating a 2000-fold selectivity index.[53]

VT-1161 has activity against *Candida* spp. (including azole-resistant *C. albicans* and *C. glabrata*), *Coccidiodes* spp. and dermatophytes.[54–56]

IC_{50} values against the common CYP enzymes CYP2C9, CYP2C19, and CYP3A4 are up to 10-fold higher for VT-1161 than for voriconazole, highlighting the reduced affinity for human enzymes.[53]

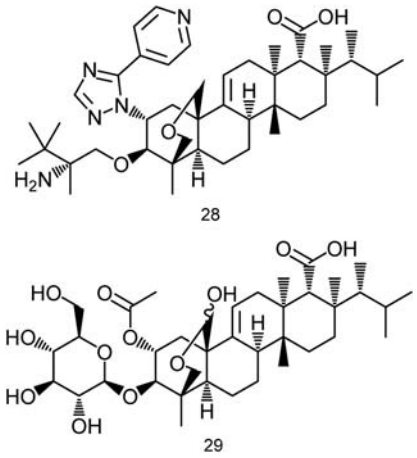

Fig. 13 **28**, SCY-078 and **29**, enfumafungin.

Recently VT-1161 has been reported to be active against the protozoan pathogen *Trypanosoma cruzi* with CYP51 dissociation constants in the region of 24 nM, and reductions in parasitemia in a mouse model of infection with a drug-resistant strain have been demonstrated.[57]

5.22.4.2 SCY-078

SCY-078 (**28**, Fig. 13) was discovered from a multiyear collaboration between Merck & Co and Scynexis. The project was focussed on the discovery and development of orally bioavailable glucan synthase inhibitors, following Merck's earlier success with the approval of the parenteral echinocandin caspofungin.

Initial chemistry was based around the work of Onishi et al.[58] who had previously identified a group of acidic triterpene compounds from a natural product antifungal screen. One of these hits, a triterpenoid glycoside named enfumafungin (**29**) had improved pharmacokinetic properties and comparable in vitro antifungal activity to caspofungin.

The semisynthetic derivatization of enfumafungin targeted improving in vivo activity and bioavailability. Considerable synthetic effort established the key structural features associated with antifungal activity, with the glycosidic ether moiety playing an essential role.[59] Replacement with an amino ether moiety and installation of the 1,2,4-triazole heterocycle at the C2 position provided significant improvement in oral bioavailability without loss of antifungal activity.[60]The resulting optimized compound was MK3118, which was renamed SCY-078 after the compound was in-licensed by Scynexis.

The spectrum of activity of SCY-078 is similar to that of the echinocandins, with potent in vitro activity across a broad range of clinical *Aspergillus* and *Candida* spp. MIC_{90} values are reported to be lower than caspofungin for SCY-078 against *C. albicans*, *C. glabrata*, and *C. parapsilosis* but higher for *C. krusei*.[61–63] Potency against a range of clinical *Aspergillus* species is significantly lower for SCY-078 than for the echinocandins with MIC_{90} values in the range 0.12–0.25 $\mu g\,mL^{-1}$ versus 0.03–0.06 $\mu g\,mL^{-1}$ for caspofungin.[61]

Mutations in the fungal glucan synthase gene (FKS) are known to cause reduced susceptibility to the echinocandins, with a corresponding reduction in clinical effectiveness.[64] SCY-078 shows enhanced activity against *C. albicans* and *C. glabrata* isolates with known FKS mutations and so represents an alternative clinical option when FKS-resistant species are identified.[65]

5.22.4.3 CD101

CD101 (**30**, Fig. 14) is a derivative of the echinocandin anidulafungin with an improved stability profile, allowing its use as a topical agent. Trials for VVC and invasive *C. albicans* are ongoing.

CD101 represents the first echinocandin candidate identified from a program aimed at developing molecules with alternate dosing routes and more flexible administration. The research was undertaken at Seachaid Pharmaceuticals, which focussed specifically on modifications of pneumocandin B, caspofungin, and anidulafungin. CD101 incorporates a modified cyclic peptide bearing a quaternized choline ether derivative. The result is an echinocandin with unique chemical and biological properties that include physical and chemical stability, high solubility, enhanced spectrum of activity and potency, extended plasma half-life, and improved safety margins.[66]

CD 101 has very favorable preclinical characteristics with minimal interaction with recombinant CYP enzymes, and no notable effects on liver enzymes. No macroscopic effects were seen in the liver following 14 day IV administration, nor were there any effects on hematology, coagulation, or urinalysis.[67,68] A notable feature is the prolonged plasma half-life, which was increased 5–10-fold in representative toxicological species over the other marketed echinocandins (Table 1). In humans, the half-life is in excess of 80 h, leading to the possibility of once weekly IV dosing.[66–68]

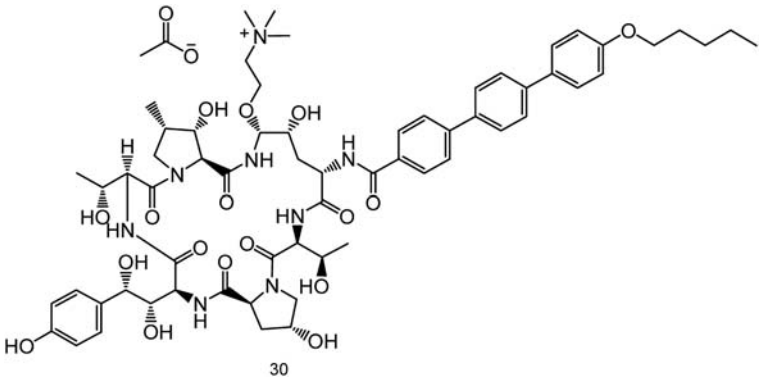

Fig. 14 **30**, CD101.

Table 1 Half-life of prior echinocandins and CD101 **30** in various species

	Half life (h)			
Species	*Caspofungin*	*Micafungin*	*Anidulafungin*	*CD101*
Rat	6–7	5	18–22	30
Dog	NA	NA	12–16	53
Monkey	5–6	NA	8	40
Chimpanzee	5–8	NA	30	81
Man	9–11	10–17	24–26	>80

CD0101 retains an antifungal spectrum similar to the existing echinocandins, with potent activity across *Candida* species comparable to anidulafungin and superior to micafungin and caspofungin.[69–71]

Phase II trials exploring the utility of CD101 (**30**), dosed IV, for the treatment of candidemia are currently being initiated, following the successful completion of Phase I studies in which no adverse effects or clinical signs were observed. CD101 is also being developed as a topical treatment for VVC.

5.22.4.4 F901318

F901318 (**31**, Fig. 15) is a pyrrole glyoxylamide derivative that is the first member of the novel orotomide class of antifungals. Discovered by classical whole cell phenotypic screening, the series was optimized iteratively with antifungal activity and pharmacokinetics driving further improvements. F901318 acts by inhibition of the fungal dihydroorotate dehydrogenase (PyrE), which catalyzes the oxidation of dihydroorotate to orotate in the de novo synthesis of pyrimidines and as such is essential for cell growth.[72] F901318 displays potent activity against clinically relevant *Aspergillus* spp. and an extended spectrum against other intrinsically resistant molds[73,74] including azole-resistant aspergilli.[74] No activity is seen against *Candida* spp., *Cryptococcus*, or the *Mucorales*.

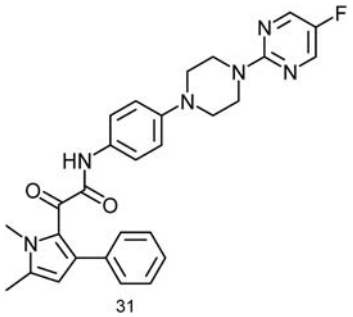

Fig. 15 **31**, F901318.

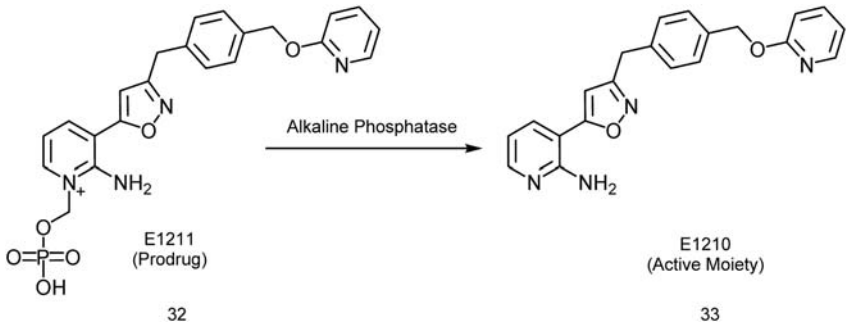

Fig. 16 **32**, E1211 and **33**, E1210.

F901318 demonstrated excellent survival rates in lethal immunosuppressed murine models of invasive aspergillosis with 100% survival at doses of 10 mg kg^{-1} dosed three times daily,[75] administered either IV or orally. The drug was well tolerated in Phase I IV studies and is currently progressing to Phase II.

5.22.4.5 E1210

E1210 (**33**, Fig. 16) was developed from an initial screening hit, 1-(4-butylbenzyl)isoquinoline, that was shown to act by the inhibition of glycosylphosphatidylinositol (GPI) anchored proteins. Further chemical optimization led to the development of the isoxazole E1210 and its corresponding phosphate prodrug E1211 (**32**).[76]

GPI anchored proteins are significant components of the cell walls of eukaryotic microorganisms, including fungi. GPI anchored cell wall proteins play a vital role in cell wall structural architecture and regeneration and are implicated in host cell adhesion.[77] E1210 specifically prevents GPI protein maturation through the inhibition of inositol acyltransferase (GWT1). The reduction in acylated inositol produces defects in the fungal cell leading to the inhibition of hyphal elongation and reduced adherence to biological substrates. The inhibition of GWT1 appears to be specific to fungi, and E1210 exhibits broad spectrum activity against yeast and filamentous fungal pathogens.

In vitro activity has been demonstrated against a range of clinically significant *Candida* species including both azole-resistant and echinocandin-resistant strains. For the majority of *Candida* species tested ($n = 154$) the MIC ranges were tightly clustered in the range 0.008–0.06 μg mL^{-1}. One species, *C. krusei*, had significantly raised MIC levels (2 to >32 μg mL^{-1}) compared to other isolates tested.[78] A lesser level of activity against aspergilli was also demonstrated. The MICs for the key species *A. fumigatus*, *A. flavus*, *A. terreus*, and *A. niger* ranged from 0.016 to 0.13 μg mL^{-1}. *Fusarium* and *Scedosporium* are genera of fungi against which current antifungals are commonly ineffective, but E1210 is highly active against the dominant pathogens in these genera including *Fusarium solani* (0.015–0.12 μg mL^{-1}) and *Scedosporium prolificans* (0.03–0.25 μg mL^{-1}).

In vivo, E1210 proved effective in treating invasive fungal infections in immunocompromised murine models infected with *Candida*, *Aspergillus*, and *Fusarium*.[76] Oral administration of E1210 twice daily at 12.5 mg kg^{-1} resulted in 89% survival in a model of disseminated candidiasis. In a lethal murine model of pulmonary aspergillosis, E1210 (**33**) at 25 mg kg^{-1} was shown to result in 100% protection. The oral bioavailability of E1210 (**33**) in these models was calculated at 57.5% and the drug was well tolerated at doses up to 300 mg kg^{-1}, with adaptive hepatocellular hypertrophy cited as the main toxicity signal.

Following out-licensing, E1210 is being developed by Amplyx Pharmaceuticals in the form of the prodrug E1211, named APX1211, presumably to increase solubility for the purposes of enhancing oral bioavailability.

5.22.4.6 VL-2397

VL-2397 (**35**, Fig. 17) (formerly ASP2397) is a novel IV antifungal agent currently in Phase I development. The compound was initially identified from a natural product library using whole cell screening aimed at finding novel molecules with antiaspergillus activity. The compound is structurally related to the cyclic hexapeptide siderophore ferrichrome (**34**) and was isolated from an environmental isolate of the fungus *Acremonium*.

The antifungal spectrum of VL-2397 includes both filamentous fungi and yeasts but the agent cannot be considered truly broad spectrum due to significant species gaps. For example, in vitro activity has been demonstrated against clinical aspergilli including *A. fumigatus*, *A. terreus*, and *A. flavus* with MIC values in the range 0.06–16 μg mL^{-1}, but the MIC against *A. niger* is >16 μg mL^{-1}. Similarly activity is reported against *C. glabrata* (MIC < 2 μg mL^{-1}) but other clinically significant *Candida* spp. including *C. albicans* have considerably reduced susceptibility (MIC > 16 μg mL^{-1}). *A. fumigatus* strains with the G54E and M220K CYP51A mutations were resistant to VL-2397 (**35**).[79,80] The limited breadth of activity across *Aspergillus* species may prove to be a limitation clinically, as precise species diagnosis is rarely available at the start of antifungal therapy. Interestingly in the presence of human serum the MIC activity range for *Aspergillus* spp. is increased for some species.

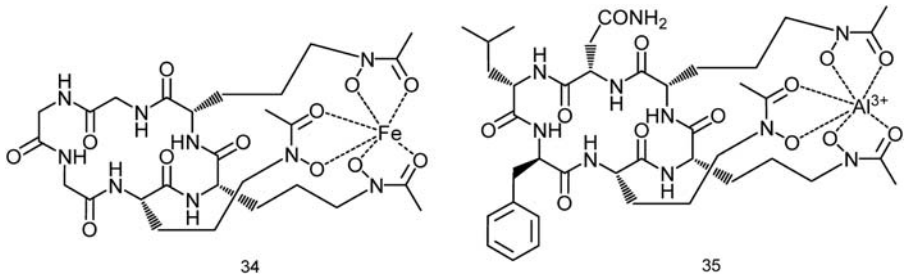

Fig. 17 **34**, Ferrichrome and **35**, VL-2397.

The antifungal activity of VL-2397 is rapid and results in the arrest of hyphal elongation in germinated conidia. VL-2397 is fungicidal with a two Log_{10} reduction in fungal organ burden observed in murine infection model werethe exposure was four times the MIC after 48 h. Uptake studies have shown that VL-2397 is actively transported by the aspergillus siderophore transporter SIT1 and that it accumulates within hyphae. UV mutant strains that are resistant to VL-2397 can be restored to sensitivity by the addition of extra chromosomal copies of SIT1. Conversely, mutation in the SIT1 transporter confers resistance. Thus uptake phenomenon alone is insufficient for an antifungal effect, suggesting an alternate intracellular target exists.

VL-2397 showed excellent survival benefit at doses of 4 and 8 mg kg^{-1} twice daily in both azole susceptible and azole refractory murine models of invasive aspergillosis. Survival correlated with lung tissue burden reductions of 1–2 log_{10} and reductions in lung inflammation and necrosis. At a dose of 8 mg kg^{-1} BID, VL-2397 demonstrated superior survival over other existing antifungals in a delayed treatment mode. The compound also showed no antagonistic effect when dosed with posaconazole in combination therapy studies.[79,80]

5.22.5 Summary

Systemic antifungal drug discovery and development has historically lagged behind that of antibacterials. Numerically, the number of systemic antifungal infections is low and would rank as an orphan disease indication for all species causing disease, and in the last century mortality rates from invasive candidiasis and invasive aspergillosis infections approached 80%.

The turn of the 21st century saw the introduction of third-generation azoles such as voriconazole and posaconazole which transformed treatment for invasive aspergillosis, reducing mortality rates considerably. Similarly, the introduction of the echinocandins provided an effective alternative treatment for invasive candidiasis, again reducing mortality. These two classes of agents along with AmB remain the totality of the antifungal armamentarium for systemic fungal infections. The emergence of global resistance within the aspergilli, increasing year on year, has cast doubt on the future of the azoles as a frontline therapy. Similarly changes in the epidemiology and the emergence of echinocandin resistance have led to reduced effectiveness of current agents for the treatment of candidiasis. Given that only three classes of antifungals are used to treat these diseases, new agents with alternate mechanisms are desperately needed.

Antifungal drug research and development has entered a new era with multiple new compounds in clinical development. Several target known mechanisms, for example, VT-1161, SCY-078, and CD101, and these agents may overcome the resistance issues seen with current agents. Other compounds in development are new chemical classes and act via completely new mechanisms. By inhibiting new cellular targets, F901318, APX001, and VL-2397 have the potential to make a bigger therapeutic impact, particularly against infections where current agents are of little use.

References

1. Brown, G. D.; et al. Hidden Killers: Human Fungal Infections. *Sci. Transl. Med.* **2012,** *4* (165).
2. Havlickova, B.; Czaika, V. A.; Friedrich, M. Epidemiological Trends in Skin Mycoses Worldwide. *Mycoses* **2009,** *52* (1), 95.
3. Sobel, J. D. Vulvovaginal candidosis. *Lancet* **2007,** *9* (369), 9577.
4. Mikulska, M.; Del Bono, V.; Ratto, S.; Viscoli, C. Occurrence, Presentation and Treatment of Candidemia. *Expert Rev. Clin. Immunol.* **2012,** *8* (8), 755–765.
5. Dagenais, T. R.; Keller, N. P. Pathogenesis of *Aspergillus fumigatus* in Invasive Aspergillosis. *Clin. Microbiol. Rev.* **2009,** *22* (3), 447–465.
6. Maertens, J. A.; et al. Isavuconazole Versus Voriconazole for Primary Treatment of Invasive Mould Disease Caused by *Aspergillus* and Other Filamentous Fungi (SECURE): A Phase 3, Randomised-Controlled, Non-Inferiority Trial. *Lancet* **2016,** *387* (10020), 760–769.
7. Verweij, P. E.; et al. International Expert Opinion on the Management of Infection Caused by Azole-Resistant *Aspergillus fumigatus*. *Drug Resist. Updat.* **2015,** *21–22,* 30–40.
8. Park, B. J.; et al. Estimation of the Current Global Burden of Cryptococcal Meningitis Among Persons Living With HIV/AIDS. *AIDS* **2009,** *23,* 525–530.
9. Perfect, J. R.; Bicanic, T. Cryptococcosis Diagnosis and Treatment: What Do We Know Now. *Fungal Genet. Biol.* **2015,** *78,* 49–54.
10. Engelthaler, D. M.; Hicks, N. D.; Gillece, J. D.; Roe, C. C.; Schupp, J. M.; Driebe, E. M.; Gilgado, F.; Carriconde, F.; Trilles, L.; Firacative, C.; Ngamskulrungroj, P.; Castañeda, E.; Lazera, M. D. S.; Melhem, M. S. C.; Pérez-Bercoff, Å.; Huttley, G.; Sorrell, T. C.; Voelz, K.; May, R. C.; Fisher, M. C.; Thompson, G. R., III; Lockhart, S. R.; Keim, P.; Meyer, W. *Cryptococcus gattii* in North American Pacific Northwest: Whole-Population Genome Analysis Provides Insights Into Species Evolution and Dispersal. *MBio* **2014,** *5* (4), e01464-14.

11. Caffrey, P.; et al. Amphotericin Biosynthesis in *Streptomyces nodosus*: Deductions From Analysis of Polyketide Synthase and Late Genes. *Chem. Biol.* **2001,** *8* (7), 713–723.
12. Baginski, M.; Czub, J. Amphotericin B and Its New Derivatives—Mode of Action. *Curr. Drug Metab.* **2009,** *10* (5), 459–469.
13. Laniado-Laborin, R.; Cabrales-Vargas, M. N. Amphotericin B: Side Effects and Toxicity. *Rev. Iberoam. Micol.* **2009,** *26* (4), 223–227.
14. Barrett, J. P.; Vardulaki, K. A.; Conlon, C. A systematic Review of the Antifungal Effectiveness and Tolerability of Amphotericin B Formulations. *Clin. Ther.* **2003,** *25* (5), 1295–1320.
15. Ellis, D. Amphotericin B: Spectrum and Resistance. *J. Antimicrob. Chemother.* **2002,** *49* (Suppl. 1), 7–10.
16. Heidelberger, C.; et al. Fluorinated Pyrimidines. A New Class of Tumor Inhibitory Compounds. *Nature* **1957,** *179,* 663–666.
17. Tassel, D.; Madoff, M. A. Treatment of *Candida sepsis* and *Cryptococcus meningitis* With 5-Fluorocytosine. A New Antifungal Agent. *JAMA* **1968,** *206* (4), 830–832.
18. Polak, A.; Scholer, H. J. Mode of Action of 5 Fluorocytosine and Mechanisms of Resistance. *Chemotherapy* **1975,** *21* (3–4), 113–130.
19. Vermes, A.; Guchelaar, H. J.; Dankert, J. Flucytosine: A Review of Its Pharmacology, Clinical Indications, Pharmacokinetics, Toxicity and Drug Interactions. *J. Antimicrob. Chemother.* **2000,** *46,* 171–179.
20. Waldorf, A. R.; Polak, A. Mechanism of Action of 5-Fluorocytosine. *Antimicrob. Agents Chemother.* **1983,** *23* (1), 79–85.
21. Hope, W. W.; Tabernero, L.; Denning, D. W.; Anderson, M. J. Molecular Mechanisms of Primary Resistance to Flucytosine in *Candida albicans*. *Antimicrob. Agents Chemother.* **2004,** *48* (11), 4377–4386.
22. Perfect, J. R.; Dismukes, W. E.; Dromer, F.; et al. Clinical Practice Guildelines for the Management of Cryptociccal Disease: 2010 Update by the Infectious Disease Society of America. *Clin. Infect. Dis.* **2010,** *50* (3), 291–322.
23. Maertens, J. A. History of the Development of Azole Derivatives. *Clin. Microbiol. Infect.* **2004,** *10,* 1–10.
24. Ghannoum, M. A.; Rice, L. B. Antifungal Agents: Mode of Action, Mechanisms of Resistance, and Correlation of These Mechanisms With Bacterial Resistance. *Clin. Microbiol. Rev.* **1999,** *12* (4), 501–517.
25. Sheehan, D. J.; Hitchcock, C. A.; Sibley, C. M. Current and Emerging Azole Antifungal Agents. *Clin. Microbiol. Rev.* **1999,** *12* (1), 40–79.
26. Gupta, A. K.; Daigle, D.; Foley, K. A. Drug safety Assessment of Oral Formulations of Ketoconazole. *Expert Opin. Drug Saf.* **2015,** *14* (2), 325–334.
27. Sugar, A. M.; et al. Pharmacology and Toxicity of High-Dose Ketoconazole. *Antimicrob. Agents Chemother.* **1987,** *31* (12), 1874–1878.
28. US Food and Drug Administration, 2016. [Online] Available at: http://www.fda.gov/Drugs/DrugSafety/ucm362415.htm.
29. Rotta, I.; Otuki, M. F.; Sanches, A. C.; Correr, C. J. Efficacy of Topical Antifungal Drugs in Different Dermatomycoses: A Systematic Review With Meta-Analysis. *Rev. Assoc. Med. Bras.* **2012,** *58* (3), 308–318.
30. Cronin, S.; Chandrasekar, P. H. Safety of Triazole Antifungal Drugs in Patients With Cancer. *J. Antimicrob. Chemother.* **2010,** *65* (3), 410–416.
31. Bruggemann, R. J.; Alffenaar, J. W.; Blijlevens, N. M.; et al. Clinical Relevance of the Pharmacokinetic Interactions of Azole Antifungal Drugs With Other Coadministered Agents. *Clin. Infect. Dis.* **2009,** *48* (10), 1441–1458.
32. Herbrecht, R.; Denning, D. W.; Patterson, T. F.; Bennett, J. E.; Greene, R. E.; Oestmann, J. W.; Kern, W. V.; Marr, K. A.; Ribaud, P.; Lortholary, O.; Sylvester, R.; Rubin, R. H.; Wingard, J. R.; Stark, P.; Durand, C.; Caillot, D.; Thiel, E.; Chandrasekar, P. H.; Hodges, M. R.; Schlamm, H. T.; Troke, P. F.; de Pauw, B.; Invasive Fungal Infections Group of the European Organisation for Research and Treatment of Cancer and the Global Aspergillus Study Group. Voriconazole Versus Amphotericin B for Primary Therapy of Invasive Aspergillosis. *N. Engl. J. Med.* **2002,** *347,* 408–415.
33. Miceli, M. H.; Kauffman, C. A. Isavuconazole: A New Broad-Spectrum Triazole Antifungal Agent. *Clin. Infect. Dis.* **2015,** *61* (10), 1558–1565.
34. Kanafani, Z. A.; Perfect, J. R. Resistance to Antifungal Agents: Mechanisms and Clinical Impact. *Clin. Infect. Dis.* **2008,** *46* (1), 120–128.
35. Sanglard, D.; Coste, A. T. Activity of Isavuconazole and Other Azoles Against Candida Clinical Isolates and Yeast Model Systems With Known Azole Resistance Mechanisms. *Antimicrob. Agents Chemother.* **2015,** *60* (1), 229–238.
36. Ueda, Y.; et al. Phosphonooxymethyl Prodrugs of the Broad Spectrum Antifungal Azole, Ravuconazole: Synthesis and Biological Properties. *Bioorg. Med. Chem. Lett.* **2003,** *13* (21), 3669–3672.
37. Allen, D.; Wilson, D.; Drew, R.; Perfect, J. Azole Antifungals: 35 Years of Invasive Fungal Infection Management. *Expert Rev. Anti Infect. Ther.* **2015,** *13* (6), 787–798.
38. Pasqualotto, A. C.; Denning, D. W. New and Emerging Treatments for Fungal Infections. *J. Antimicrob. Chemother.* **2008,** *61* (1), i19–i30.
39. Thompson, G. R.; Wiederhold, N. P. Isavuconazole: A Comprehensive Review of Spectrum of Activity of a New Triazole. *Mycopathologia* **2010,** *170* (5), 291–313.
40. Capilla, J.; Ortoneda, M.; Pastor, F. J.; Guarro, J. In Vitro Antifungal Activities of the New Triazole UR-9825 Against Clinically Important Filamentous Fungi. *Antimicrob. Agents Chemother.* **2001,** *45* (9), 2635–2637.
41. Gupta, A. K.; Ryder, J. E.; Cooper, E. A. Naftifine: A Review. *J. Cutan. Med. Surg.* **2008,** *12* (2), 51–58.
42. Darkes, M. J.; Scott, L. J.; Goa, K. L. Terbinafine: A Review of Its Use in Onychomycosis in Adults. *Am. J. Clin. Dermatol.* **2003,** *4* (1), 39–65.
43. Aguilar-Zapata, D.; Petraitiene, R.; Petraitis, V. Echinocandins: The Expanding Antifungal Armamentarium. *Clin. Infect. Dis.* **2015,** *61* (6), S604–S611.
44. Eschenauer, G.; DePestel, D. D.; Carver, P. L. Comparison of Echinocandin Antifungals. *Ther. Clin. Risk Manag.* **2007,** *3* (1), 71–97.
45. Denning, D. W. Echinocandin Antifungal Drugs. *Lancet* **2003,** *362* (9390), 1142–1151.
46. Chen, S. C.; Slavin, M. A.; Sorrell, T. C. Echinocandin Antifungal Drugs in Fungal Infections. *Drugs* **2011,** *71* (1), 11–41.
47. Walker, L. A.; Gow, N. A.; Munro, C. A. Fungal Echinocandin Resistance. *Fungal Genet. Biol.* **2010,** *47* (2), 117–126.
48. Nix, D. E.; Swezey, R. R.; Hector, R.; Galgiani, J. N. Pharmacokinetics of Nikkomycin Z After Single Rising Oral Doses. *Antimicrob. Agents Chemother.* **2009,** *53* (6), 2517–2521.
49. Markham, A. Tavaborole: First Global Approval. *Drugs* **2014,** *74* (13), 1555–1558.
50. Liang, H. Sordarin, an Antifungal Agent With a Unique Mode of Action. *Beilstein J. Org. Chem.* **2008,** *4* (31).
51. Podust, L. M.; Poulos, T. L.; Waterman, M. R. Crystal Structure of Cytochrome P450 14-alpha-Sterol Demethylase (CYP51) From *Mycobacterium tuberculosis* in Complex With Azole Inhibitors. *Proc. Natl. Acad. Sci.* **2001,** *96* (6), 3068–3073.
52. Hoekstra, W. J.; et al. Design and Optimization of Highly-Selective Fungal CYP51 Inhibitors. *Bioorg. Med. Chem. Lett.* **2014,** *24* (15), 3455–3458.
53. Warrilow, A. G.; et al. The Clinical Candidate VT-1161 Is a Highly Potent Inhibitor of *Candida albicans* CYP51 but Fails to Bind the Human Enzyme. *Antimicrob. Agents Chemother.* **2014,** *58* (12), 7121–7127.
54. Garvey, E. P.; et al. VT-1161 Dosed Once Daily or Once Weekly Exhibits Potent Efficacy in Treatment of Dermatophytosis in a Guinea Pig Model. *Antimicrob. Agents Chemother.* **2015,** *59* (4), 1992–1997.
55. Garvey, E. P.; et al. Efficacy of the Clinical Agent VT-1161 Against Fluconazole-Sensitive and -Resistant *Candida albicans* in a Murine Model of Vaginal Candidiasis. *Antimicrob. Agents Chemother.* **2015,** *59* (9), 5563–5573.
56. Shubitz, L. F.; et al. Evaluation of VT-1161 for Treatment of Coccidioidomycosis in Murine Infection Models. *Antimicrob. Agents Chemother.* **2015,** *59* (12), 7249–7254.
57. Hoekstra, W. J.; et al. Clinical Candidate VT-1161's Antiparasitic Effect In Vitro, Activity in a Murine Model of Chagas Disease, and Structural Characterization in Complex With the Target Enzyme CYP51 From *Trypanosoma cruzi*. *Antimicrob. Agents Chemother.* **2015,** *60* (2), 1058–1066.
58. Onishi, J.; Meinz, M.; Thompson, J.; Curotto, J.; Dreikorn, S.; Rosenbach, M.; Douglas, C.; Abruzzo, G.; Flattery, A.; Kong, L.; Cabello, A.; Vicente, F.; Pelaez, F.; Diez, M. T.; Martin, I.; Bills, G.; Giacobbe, R.; Dombrowski, A.; Schwartz, R.; Morris, S.; Harris, G.; Tsipouras, A.; Wilson, K.; Kurtz, M. B. Discovery of Novel Antifungal (1,3)-β-D-Glucan Synthase Inhibitors. *Antimicrob. Agents Chemother.* **2000,** *44* (2), 368–377.
59. Heasley, B. H.; et al. Synthesis and Biological Evaluation of Antifungal Derivatives of Enfumafungin as Orally Bioavailable Inhibitors of β-1,3-Glucan Synthase. *Bioorg. Med. Chem. Lett.* **2012,** *22,* 6811–6816.
60. Apgar, J.; et al. Novel Orally Active Inhibitors of β-1,3-Glucan Synthesis Derived From Enfumafungin. *Bioorg. Med. Chem. Lett.* **2015,** *25* (15), 5813–5818.

61. Lamoth, F.; Alexander, B. D. Antifungal Activities of SCY-078 (MK-3118) and Standard Antifungal Agents Against Clinical Non-Aspergillus Mold Isolates. *Antimicrob. Agents Chemother.* **2015,** *59* (1), 4308–4311.
62. Pfaller, M. A.; Messer, S. A.; Motyl, M. R.; Jones, R. N.; Castanheira, M. Activity of MK-3118, a New Oral Glucan Synthase Inhibitor, Tested Against *Candida* spp. by Two International Methods (CLSI and EUCAST). *J. Antimicrob. Chemother.* **2013,** *68* (4), 858–863.
63. Pfaller, M. A.; et al. In Vitro Activity of a New Oral Glucan Synthase Inhibitor (MK-3118) Tested Against *Aspergillus* spp. by CLSI and EUCAST Broth Microdilution Methods. *Antimicrob. Agents Chemother.* **2013,** *57,* 1065–1068.
64. Perlin, D. S. Echinocandin Resistance in Candida. *Clin. Infect. Dis.* **2015,** *61* (6), 612–617.
65. Jiménez-Ortigosa, C.; Paderu, P.; Motyl, M. R.; Perlin, D. S. Enfumafungin Derivative MK-3118 Shows Increased in vitro Potency Against Clinical Echinocandin-Resistant *Candida* Species and *Aspergillus* Species Isolates. *Antimicrob. Agents Chemother.* **2014,** *58* (2), 1248–1251.
66. James, K.; et al. *Structure–Activity Relationship of a Series of Echinocandins and the Discovery of CD101, a Highly Stable and Soluble, Once-Weekly Novel Echinocandin;* ICAAC: Washington, DC, 2015. F-750.
67. Ong, V.; et al. *Preclinical Evaluation Shows CD101, a Novel Echinocandin, Is Highly Stable;* ICAAC: Washington, DC, 2015. A-015.
68. Ong, V.; Hough, G.; Schlosser, M.; Bartizal, K.; Balkovec, J.; James, K.; Krishnan, R. *Preclinical Evaluation Shows CD101, a Novel Echinocandin, Is Highly Stable With No Hepatotoxicity in Rats;* ICAAC: Washington, DC, 2015. A-015.
69. Castanheira, M.; et al. *Activity of a Novel Echinocandin CD101 IV Tested Against Most Common* Candida *and* Aspergillus *Species, Including Echinocandin- and Azole-Resistant Strains;* ICAAC: Washington, DC, 2014. M-1082.
70. Hall, D.; Bonifas, R.; Shinabarger, D. L.; Pillar, L. M. *Evaluation of the In Vitro Activity of CD101, a Novel Echinocandin, and Comparators Against Recent Clinical Isolates of* Candida *spp;* ICAAC: Washington, DC, 2015. M-850.
71. Hall, D.; Shinabarger, D. L.; Pillar, C. M. *Evaluation of the Fungicidal Activity of CD101, a Novel Echinocandin, and Comparators Against Recent Clinical Isolates of Candida spp;* ICAAC: Washington, DC, 2015. M-852.
72. Oliver, J.; et al. *F901318, a Novel Antifungal Agent From the Orotomide Class: Discovery and Mechanism of Action;* ICAAC: San Diego, CA, 2015. F749.
73. Fothergill, A.; Wiederhold, N.; Sibley, G.; Kennedy, A.; Oliver, J.; Birch, M.; Law, D. *Spectrum of Activity of F901318, the First Agent from the New Orotomide Class of Antifungals;* ICCAC: San Diego CA, 2015. F756.
74. Beckmann, N.; et al. *Activity of F901318, a member of the new orotomide class of antifungal agents, against clinical* Aspergillus *isolates from the UK and Austria;* ICAAC: San Diego, CA, 2015.
75. Law, D.; et al. *In Vivo Efficacy of Orally Dosed F901318, in a Murine Model of Disseminated Aspergillosis;* ICAAC: San Diego, CA, 2015, 759.
76. Hata, K.; et al. Efficacy of Oral E1210, a New Broad-Spectrum Antifungal With a Novel Mechanism of Action, in Murine Models of Candidiasis, Aspergillosis, and Fusariosis. *Antimicrob. Agents Chemother.* **2011,** *55* (10), 4543–4551.
77. Richard, M. L.; Plaine, A. Comprehensive Analysis of Glycosylphosphatidylinositol-Anchored Proteins in *Candida albicans. Eukaryot. Cell* **2007,** *6* (2), 119–133.
78. Miyazaki, M.; et al. In Vitro Activity of E1210, a Novel Antifungal, Against Clinically Important Yeasts and Molds. *Antimicrob. Agents Chemother.* **2011,** *55* (10), 4652–4658.
79. Nakamura, I.; et al. *ASP2397: A Novel Natural Product With Potent Fungicidal Activity Against* Aspergillus *spp. (2);* ICAAC: Washington, DC, 2014. F1591.
80. Nakamura, I.; Ohsumi, K.; Yoshikawa, K.; Kanasaki, R.; Masaki, T.; Takase, S.; Hashimoto, M.; Fujie, A.; Nakai, T. Washington, DC, 2014; F1590.

5.23 Antiparasitic Agents

RT Jacobs, Anacor Pharmaceuticals, Palo Alto, CA, United States

© 2017 Elsevier Ltd. All rights reserved.

5.23.1	**Introduction**	717
5.23.2	**Protozoans**	718
5.23.2.1	Apicomplexans	718
5.23.2.1.1	Plasmodium	718
5.23.2.1.2	Toxoplasma	722
5.23.2.1.3	Cryptosporidia	723
5.23.2.2	Kinetoplastids	724
5.23.2.2.1	Leishmania	725
5.23.2.2.2	Trypanosoma cruzi	729
5.23.2.2.3	Trypanosoma brucei	731
5.23.2.3	Amoebas: *Entamoeba* and *Giardia* Species	736
5.23.3	**Helminths**	737
5.23.3.1	Nematodes	737
5.23.3.1.1	Soil-transmitted helminths	737
5.23.3.1.2	Filarial worms	737
5.23.3.2	Trematodes: *Schistosoma* and *Fasciola*	738
5.23.4	**Summary and Conclusions**	739
References		741
Relevant Websites		750

5.23.1 Introduction

Parasitic infections are estimated to lead to over 2 million deaths per year and account for close to 200 million disability-adjusted life years.[1] Though endemic in all countries and regions of the world, parasitic infections are disproportionately problematic in regions of poverty, where they have been associated with limiting rates of economic development. While a great diversity of organisms are known to be responsible for parasitic infections, it is generally appreciated that monocellular protozoans and multicellular helminths compose the majority of species of interest. In the protozoan class, several classes dominate the landscape of public attention—apicomplexans such as *Plasmodium falciparum* and *Cryptosporidium parvum* as causative agents of malaria and diarrhea, respectively; kinetoplastids such as *Trypanosoma cruzi* and *Leishmania donovani* as causative agents of Chagas disease and visceral leishmaniasis, respectively; and amoebas such as *Giardia lamblia*, also a causative agent of diarrhea. A great diversity of helminth infections have been documented and can be grouped into those caused by roundworms (nematodes)—flatworms (trematodes) or tapeworms (cestodes). Given the diversity of helminths that are known to infect humans, it is not surprising that the organs targeted by and consequences of such infections are also quite diverse, ranging from gastrointestinal infections leading to discomfort and diarrhea to infections of the central nervous system (CNS) leading to neurological damage and death.

Routes of infection by parasites, whether protozoan or helminth, are also quite varied, ranging from transmission by insect vectors, to ingestion from contaminated food or water supplies, to infection through mucosal surfaces or open wounds. In addition, some parasitic infections can be passed from mothers to their unborn children through placental blood transfer or from individual to individual via transfusion of infected blood.

Medicinal chemistry strategies to discover new treatments for parasitic infections are similarly diverse, with several recent developments in both societal perspective and science impacting the nature of work in this area. From the social perspective, increased public awareness of the plight of people in underdeveloped parts of the world to be disproportionately affected by parasitic infections has prompted the establishment of a geographically and financially broad range of philanthropic organizations that provide funds for drug discovery projects to address these classically "neglected" diseases.[2] Similarly, governments across North America, Europe, and Asia have expanded funding of work in support of drug discovery for diseases of the developing world, and product development partnerships (PDPs) such as Medicines for Malaria Venture (MMV), the Drugs for Neglected Diseases Initiative (DNDI) and the Global Alliance for TB Drug Development have emerged as mechanisms for coordination of efforts across the globe to ensure efficient utilization of the limited funds available for these diseases.

Scientifically, advances in the ability to determine the sequence of the entire complement of genetic information in a rapid and cost-effective manner have allowed for identification of biochemical targets for a number of parasitic organisms. Increases in speed of sequencing, coupled with advanced bioinformatic approaches for comparison of drug-resistant mutant parasites, for example, have increased the ability of drug discovery teams to deconvolute results from phenotypic screening of compound libraries to identify the molecular target of known and potential drugs, thus providing new approaches to design of selective antiparasitics. These

advances, in conjunction with renewed interest in utilization of natural products and biodiversity, have provided drug discovery teams with previously unexplored classes of molecules for optimization. Another trend in the discovery of new antiparasitic drugs is the growing emphasis on repurposing existing drugs from other human disease targets for these infections. This interest is, in part, due to the increased understanding of potential biochemical targets for antiparasitics as a consequence of the genetic sequencing efforts described in the preceding text, but is also a consequence of the perception that progression of these drugs to clinical trials may be quicker and less costly than *de novo* design of new chemical entities.

Taken together, these changes in public perception and scientific capacity bode well for the future discovery and development of new antiparasitics. The future does indeed look bright for addressing the significant unmet medical need in this area. This article will highlight some of the more recent approaches and advances for both protozoan and helminth infections.

5.23.2 Protozoans

5.23.2.1 Apicomplexans

The apicomplexan phylum of protozoa is characterized by the presence of an organelle (the apicoplast) that is likely derived from an endosymbiotic relationship between the parasite and a bacterium and/or algae in the ancient past.[3] As the apicoplast is unique to the parasite, it has been considered to be a potential target for drugs that could have potent antiparasitic activity while exhibiting minimal effects on the mammalian host.[4] Of the apicomplexans, *Plasmodium* species are the most extensively characterized and addressed by drug discovery efforts, as they are the causative agents of malaria, which is responsible for approximately 500,000 deaths per year.[5]

Toxoplasma gondii is also a widely distributed apicomplexan parasite with significant impact on both humans and animals. In the United States alone, it has been estimated that over 1 million people are infected with this parasite each year.[6] While otherwise healthy people exhibit minimal symptoms when infected with *T. gondii*, immunocompromised individuals can suffer from significant neurological impairment[7] and ocular disease.[6,8] In addition, pregnant women infected with *T. gondii* are at risk for miscarriage and can pass the infection to their unborn child.[9]

Like *Toxoplasma*, the apicomplexan parasite *Cryptosporidium parvum* is widely prevalent across the globe and results in persistent diarrhea in children and immunocompromised patients[10] and is the second leading cause of death due to diarrhea in children.[11] In addition to the acute consequences of diarrhea, infection with *Cryptosporidium* in children has been associated with impaired cognitive function and reduced growth rates.[12]

Treatment options for individuals infected with these parasites are often limited, and most treatments suffer from suboptimal efficacy and toxicity profiles. In the case of malaria, resistance to existing treatments has become a major challenge in many parts of the world.[13] For toxoplasmosis and cryptosporidiosis, very few new drugs have been discovered or developed due to the lack of financial incentives and commercial market potential. Therefore, treatment of these diseases is addressed through the use of older agents.[14]

5.23.2.1.1 Plasmodium

Significant advances in the treatment of malaria have occurred over the past decade, though emergence of resistance to even the newest treatment options continues to be a significant and emerging problem.[13,15] For example, the development and use of artemisinins (**Fig. 1**), semisynthetic drugs derived from a natural product from the plant *Artemisia annua*,[16] were widely viewed as a large step forward in the early 2000s, but by 2006, it was clear that monotherapy with these drugs was resulting in emergence of resistance, and the WHO actively promoted development of combination therapy approaches.[17]

In response to this need, several artemisinin combination therapies have been developed and are currently available to patients as summarized in **Table 1** and **Figs. 1** and **2**.

Even with these combination therapies, resistance continues to develop, and additional new chemical entities are required to provide long-term treatment options.[23] Fortunately, several new strategies, through both exploration of novel mechanisms of action and repurposing of existing drugs, provide promise for continued expansion of the armamentarium of antimalarials.

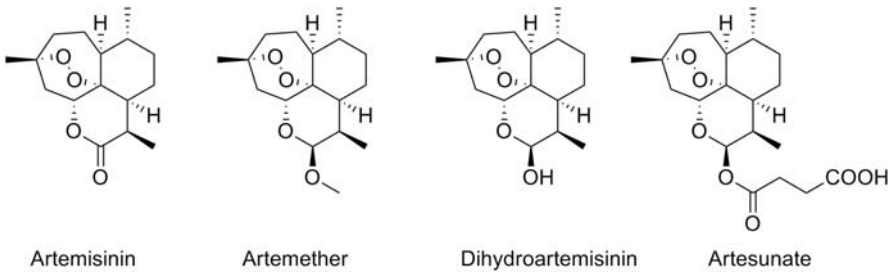

Fig. 1 Artemisinins used to treat malaria.

Table 1 Artemisinin combination therapies approved for treatment of malaria

Product	*Artemisinin component*	*Partner drug*	*Approval date*	*Partners*	*References*
Coartem	Artemether	Lumefantrine	2001/2009	Novartis, MMV	18
ASAQ Winthrop	Artesunate	Amodiaquine	2007	Sanofi, MMV, DNDI	19
Eurartesim	Dihydroartemisinin	Piperaquine	2011	Sigma-Tau, MMV	20
Pyramax	Artesunate	Pyronaridine	2012	Shin Poong, Iowa, MMV	21
ASMQ	Artesunate	Mefloquine	2012	Farmanguinos, DNDI	22

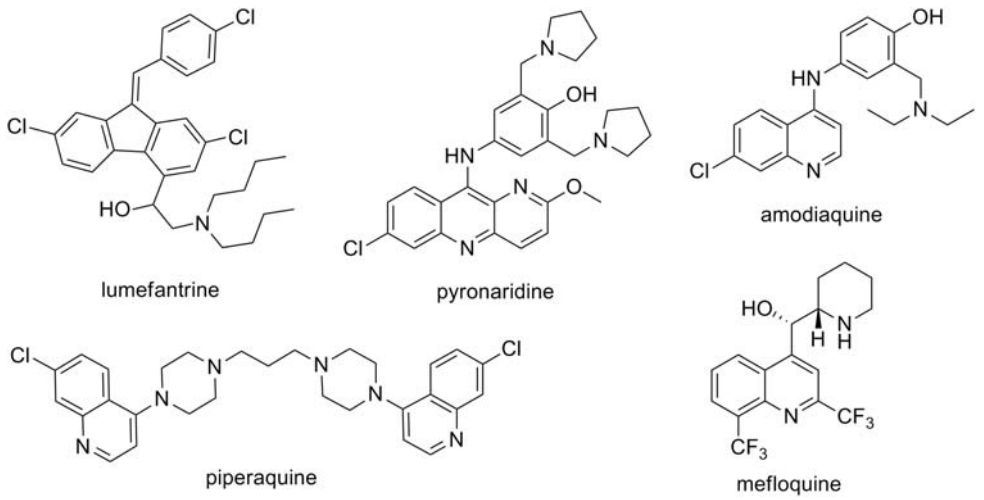

Fig. 2 Molecules used in combination with artemisinins for treatment of malaria.

5.23.2.1.1.1 Synthetic peroxides

Building on the success of artemisinins, which are semisynthetic molecules based on a natural product core containing an endoperoxide, a multinational drug discovery team—including medicinal chemists at the University of Nebraska—began exploration of fully synthetic endoperoxides as potential antimalarials. Early work in the dispirotrioxolanes focused on very lipophilic analogs that contained a sterically demanding adamantane core to provide highly potent compounds with modest pharmacokinetic properties (Fig. 3).[24] Attempts to reduce lipophilicity and increase oral bioavailability while maintaining good antimalarial potency were generally successful, with piperidines,[25] aminomethylcyclohexanes,[26] and aminoalkylcarboxamides[27] all demonstrating improved "drug-like" properties relative to the original leads. The first compound from this class that was progressed to clinical trials was

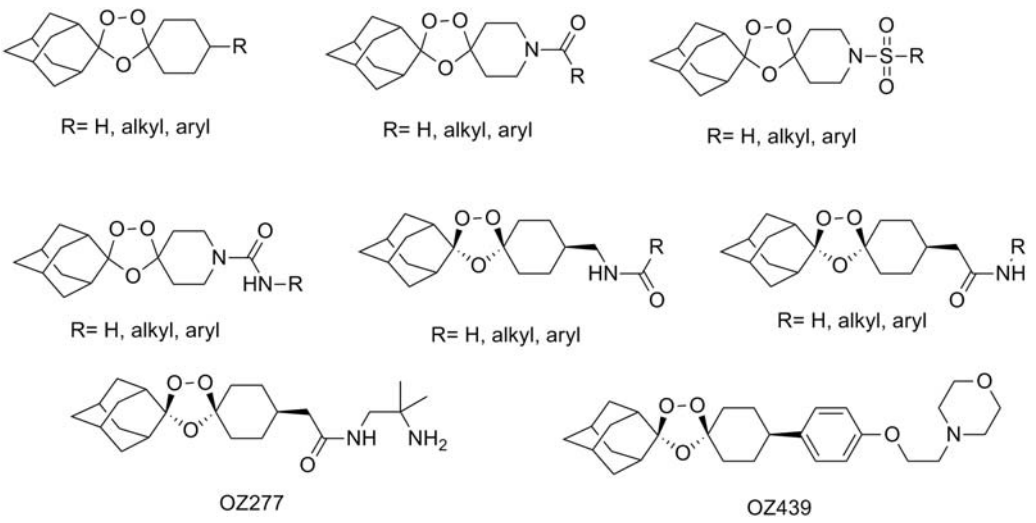

Fig. 3 Synthetic trioxolane peroxides for malaria.

OZ277, which exhibited excellent potency, bioavailability, and safety in preclinical models.[28] After successful completion of phase I trials, OZ277 was evaluated in patients, where it was found to have a threefold lower exposure compared with that seen in healthy volunteers, a difference that was attributed to instability of OZ277 due to high levels of free iron in the blood of infected patients.[29] Consequently, efficacy as a monotherapy was not as high as anticipated, which prompted further evaluation of OZ277 as a combination therapy with the known antimalarial piperaquine.[30] In parallel, further exploration of the dispirotrioxolanes identified the morpholine analog OZ439, which demonstrated improved pharmacokinetics in both animal models and human volunteers.[31] With this improved exposure, OZ439 has been evaluated in an open label phase IIa trial in patients infected with uncomplicated *P. falciparum* or *P. vivax* malaria, where it demonstrated significant parasite reduction rates and a favorable safety profile.[32] Further human clinical trials are under way to establish its potential as a single-dose cure for malaria.[33]

5.23.2.1.1.2 Spiroindolones

Through whole-cell phenotypic screening, a series of spiroindolones was discovered by a team at the Novartis Institute for Tropical Diseases as having activity against cultured intraerythrocytic *P. falciparum*. Initially synthesized as a mixture of isomers, it was quickly determined that the antimalarial activity was found in only the 1*R*,3*S* diastereomer (**Fig. 4**).[34] The result of the initial SAR exploration of this series, which focused on improvements in physicochemical and pharmacokinetic properties, was the identification of NITD609.[35] Subsequently renamed KAE609 (or cipargamin), this compound was progressed to clinical trials in human volunteers, where it was shown to exhibit approximately dose-proportional pharmacokinetics following single or multiple doses.[36] In a phase IIa study in patients infected with either *P. falciparum* or *P. vivax*, KAE609 was found to rapidly clear parasitemia following administration of 30 mg kg^{-1} for 3 days.[37] Evidence has been presented for the cation ATPase PfATP4 as the likely biochemical target for KAE609, offering the potential for discovery of additional chemical scaffolds as antimalarials.[38]

5.23.2.1.1.3 Imidazolopiperazines and imidazolopyrazines

A second series of compounds to emerge from large-scale screening efforts at Novartis were the imdazolopiperazines (**Fig. 5**). The initial leads from the HTS,[39] which contained metabolically sensitive functionality on the imidazolopiperazine core including a 3,4-methylenedioxoaniline, exhibited good *in vitro* potency but poor oral bioavailability.[40] Modification of the substituents at C(2), N(3), and N(7) of the imidazolopiperazine core afforded analogs with improved metabolic stability, good oral exposure, and *in vivo* efficacy in a *P. berghei* mouse model, but micromolar affinity for the hERG channel was perceived as a liability. This liability

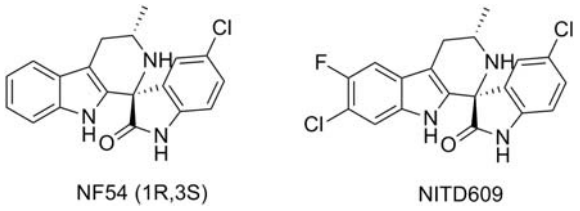

Fig. 4 Spiroindolones for treatment of malaria.

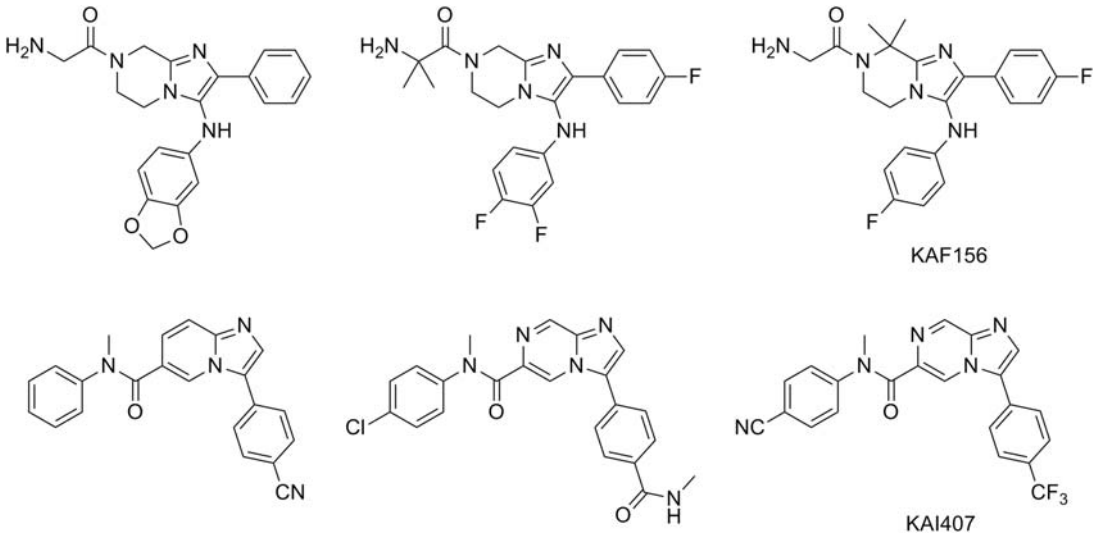

Fig. 5 Imidazolopiperazines and imidazolopyrazines identified by Novartis HTS.

was overcome through introduction of methyl groups at C(8) of the core, which also improved potency and oral exposure.[41] From these efforts, the clinical candidate KAF156 has been identified; this compound has demonstrated potent *in vivo* efficacy as well as activity against multiple stages of the *P. falciparum* life cycle.[42] Initial studies on parasites selected for resistance to KAF156 have suggested a novel protein target for this compound, designated PfCARL, though further work remains to confirm the exact role of this protein in the mechanism of action of KAF156.[42]

From the same HTS effort, a structurally similar series of imidazopyridines was identified (Fig. 5) that were of modest potency against blood stage parasites but were found to have activity against liver stage parasites.[43] Optimization of this class through variation of the C(3) aryl and C(5) amide substituents, accompanied by "scaffold hopping" to the imidazolopyrazine core, provided compounds with good physicochemical and pharmacokinetic properties and *in vivo* activity against the liver stage of the malaria parasite.[44] Selection of parasites resistant to one of the leads in this series, KAI407, has resulted in the identification of phosphatidylinositol-4-OH kinase (PI(4)K), a lipid kinase, as a likely target of this class of compounds.[45]

5.23.2.1.1.4 Benzoxaboroles

A new class of boron-containing agents, the benzoxaboroles, has demonstrated considerable utility as antiparasitics (vide infra), including activity against malaria. From a phenotypic whole-cell screen, a series of 7-carboxyethylbenzoxaboroles was identified as having submicromolar activity against *P. falciparum*.[46] Early SAR suggested that a carboxylic acid or acid isostere was required for activity, as amides, ketones, and esters were essentially inactive. Continued exploration of the series demonstrated that the boron-containing heterocycle was essential for activity, and minor modification of the substituents improved potency.[47] In addition to this series, the Anacor group has recently reported exploration of a series of 6-(hetero)aryloxybenzoxaboroles (Fig. 6) as antimalarials.[48] In the latter series, the parent carboxylic acids as well as esters and amides were found to be potent *in vitro*, with several compounds demonstrating good pharmacokinetic profiles and *in vivo* efficacy following oral administration.[48] To date, no definitive data on the biochemical target(s) of these boron-containing compounds have been reported.

5.23.2.1.1.5 Quinoline carboxamides

Screening of a kinase scaffold library against *P. falciparum* by scientists at the University of Dundee identified a 2,6-disubstituted quinolone carboxamide (Fig. 7) as a lead antimalarial. Optimization of this lead through modification of the amide substituent and incorporation of a solubilizing group on the C(2) aryl group led to the identification of DDD107498, which has been progressed to preclinical status.[49] Generation of drug-resistant parasites, followed by genomic sequencing studies identified *P. falciparum* translation elongation factor 2, which is essential for protein synthesis in the parasite as a potential target of this class.

Taken together, these efforts from a broad range of academic and industrial laboratories demonstrate the value of phenotypic screening coupled with genetics-based target identification to discover new scaffolds and mechanisms of action for treatment of malaria. Extension of these strategies to other parasitic diseases is ongoing.

5.23.2.1.1.6 Dihydroorotate dehydrogenase inhibitors

In contrast to the structural classes described in the preceding text that were initially identified from phenotypic screens, another strategy that has also been successful in identification of antimalarial leads has been to target specific essential enzymes in the *P. falciparum* life cycle. One such example is dihydroorotate dehydrogenase (DHODH), the rate-limiting enzyme in the pyrimidine biosynthesis pathway.[50] As the malaria parasite cannot salvage pyrimidine bases or nucleosides from the environment, *de novo*

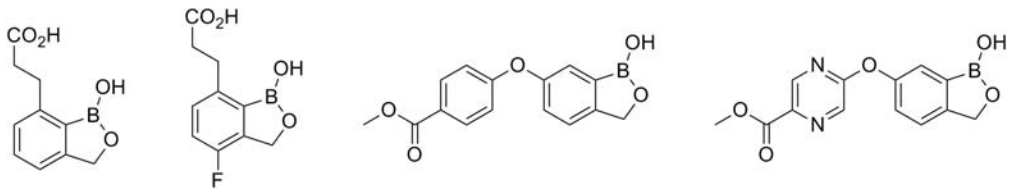

Fig. 6 Benzoxaboroles for malaria.

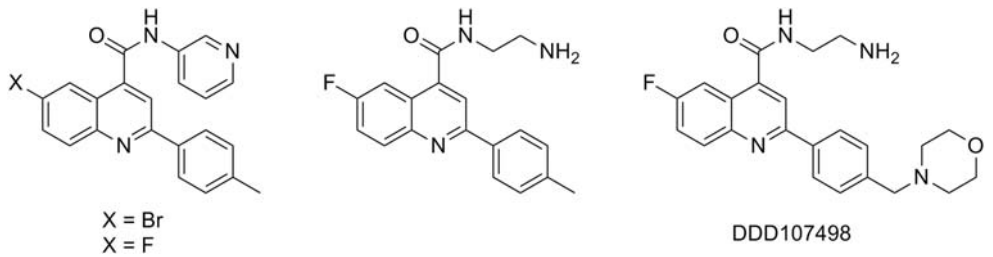

Fig. 7 Dundee quinolone carboxamide antimalarials.

biosynthesis is essential, and inhibition of DHODH has been shown to be an effective approach to killing the parasite. Following cloning and expression of *P. falciparum* DHODH, high-throughput screening of a chemical library identified hundreds of starting points for lead optimization.[51] Early hits from this screen were compromised by poor activity in whole-cell assays, but a series of triazolopyrimidines was found to address this limitation.[52] Initial optimization focused on improvement of metabolic stability and identified the 4-trifluoromethylphenyl analog DSM74 (**Fig. 8**) as an attractive lead that exhibited good pharmacokinetics and *in vivo* efficacy in a mouse model of malaria.[53] Further optimization of this lead resulted in the identification of DSM265, which has been found to have low plasma clearance and a long half-life in preclinical species, as well as an attractive profile in preclinical safety studies.[54] DSM265 has progressed to phase I clinical trials.

5.23.2.1.2 Toxoplasma

5.23.2.1.2.1 Repurposing of antimalarial and anticancer drug candidates

Among foodborne parasitic pathogens, *T. gondii* is estimated to affect the largest number of patients and cause the largest number of hospitalizations and deaths annually in the United States.[55] Given the taxonomic similarity to *Plasmodium*, it is not surprising that compounds demonstrated to have antimalarial activity have been explored for toxoplasmosis. For example, workers in Cameroon have recently reported screening of the MMV Malaria Box[56] in an *in vitro* phenotypic assay and identified a number of hits including the piperidine acetamide shown in **Fig. 9**.[57] In another example of repurposing of a *P. falciparum*-active compound for use against *Toxoplasma* infections, the spiroindolone NITD609 was found to be a cidal inhibitor of *T. gondii* in both *in vitro* and *in vivo* models.[58]

Quinolines, and in particular aminoquinolines, have been well described as antimalarials. Screening of a number of aminoquinolines originally prepared as potential anticancer agents has identified a number of analogs as potential starting points with nanomolar activity against *T. gondii*.[59] Another anticancer agent, gefitinib, has also shown weak activity against *T. gondii* and has been suggested as a repurposing candidate.[60]

A final repurposing approach for *T. gondii* activity has focused on the FDA-approved rheumatoid arthritis drug auranofin.[61] This compound, a complex of gold, has been demonstrated to reduce growth of the parasite both *in vitro* and *in vivo*. While the biochemical target of auranofin in *T. gondii* has not been rigorously established, it is likely that it acts through inhibition of thioredoxin reductase, as this has been shown in a leukemia cell line[62] and *Schistosoma mansoni*,[63] as has inhibition of the related glutathione reductase in *Leishmania infantum*.[64]

5.23.2.1.2.2 Kinase inhibitors

With the availability of genome sequences for a variety of apicomplexan parasites, including *T. gondii*, classes of protein targets with utility for drug discovery across other areas have been a popular focus of efforts in this field. One such class is kinases, which have shown great promise in diverse therapeutic areas and provide opportunities for treatment of toxoplasmosis.[65] A particular kinase

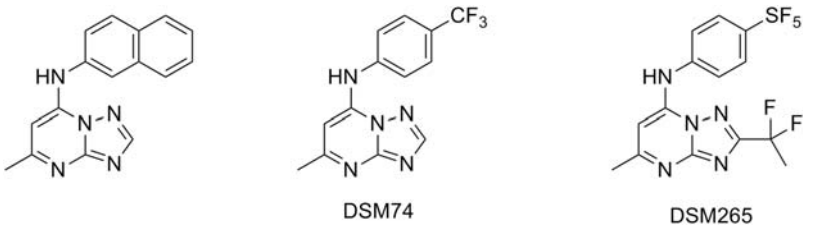

Fig. 8 Triazolopyrimidine DHODH inhibitors.

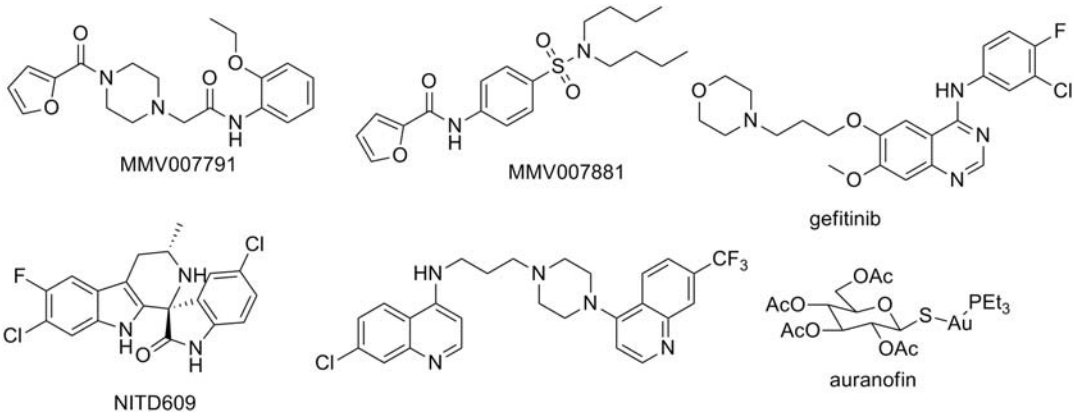

Fig. 9 Lead compounds active against *T. gondii*.

that has yielded promising leads for the latter is the *T. gondii* calcium-dependent protein kinase 1 (TgCDPK1).[66] Careful analysis of the crystal structure of TgCDPK1 revealed that a small but significant difference between this kinase and representative mammalian kinases of the same class provided an opportunity for design of parasite-specific inhibitors.[67] Based in part on early work on pyrazolopyrimidine scaffolds identified as inhibitors of Src-family kinases,[68] a series of potent and selective inhibitors of TgCDPK1 (and the related enzyme from *C. parvum*; see section "Kinase inhibitors"), depicted in **Fig. 10**, were identified and termed "bumped-kinase inhibitors."[69] Optimization of this series of pyrazolopyrimidines has led to the advanced lead BKI1294, which has efficacy following oral administration in a murine model of toxoplasmosis.[70] A second series of benzoylbenzimidazoles has also been described as inhibitors of TgCDPK1 (**Fig. 10**).[71]

5.23.2.1.3 Cryptosporidia

In comparison with the aforementioned apicomplexan parasites, drug discovery efforts for cryptosporidiosis have been less well developed, with only a small number of advanced leads and repurposing candidates having been identified. Recently, a cell-based HTS assay for *C. parvum* has been developed and used to screen both a library of FDA-approved drugs[72] and the open-access Malaria Box.[73] From the FDA-approved drug library, a particularly interesting outcome was identification of a number of approved HMG-CoA reductase (HMGR) inhibitors (**Fig. 11**) that exhibited low micromolar activity against *C. parvum*.[72] Bioinformatic analysis of the *C. parvum* genome suggested that it was unlikely that the HMGR inhibitors were directly inhibiting parasite growth, but were inhibiting production of isopentenyl pyrophosphate (IPP) in the mammalian host cell, which is an essential nutrient for the parasite. This hypothesis was supported by biochemical studies that showed that the parasites could be protected by addition of IPP to the growth medium.[72] Screening of the malaria box library identified several potential starting points for lead optimization, the most explored of which was a series of quinolinols (**Fig. 11**) that exhibited submicromolar potency.[73]

5.23.2.1.3.1 Kinase inhibitors

As *C. parvum* and *T. gondii* are phylogenetically closely related, it should not be surprising that targets identified in one parasite would be attractive in the other. Such is the case with the calcium-dependent protein kinase inhibitors such as BKI1294 discussed

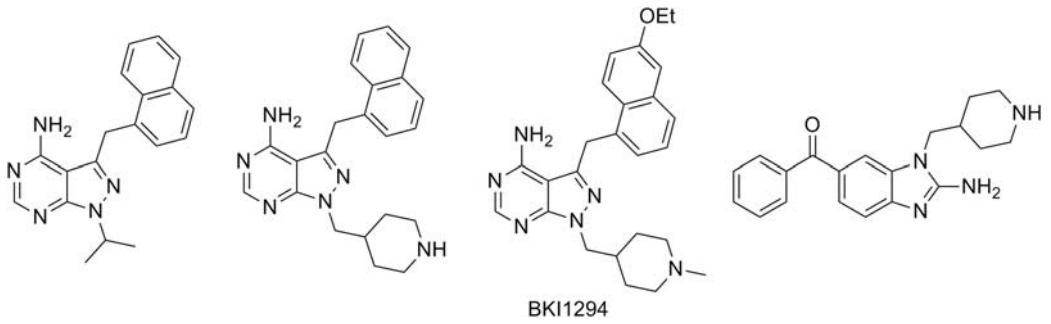

Fig. 10 Inhibitors of TgCDPK1 for treatment of toxoplasmosis.

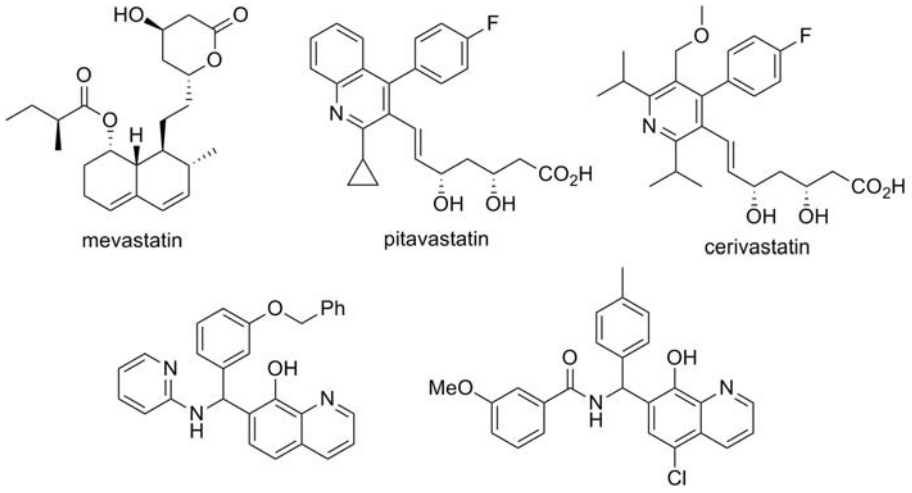

Fig. 11 Leads identified from repurposing screening for *Cryptosporidium*.

in section "Kinase inhibitors" for *Toxoplasma*, which have also been shown to be efficacious in a mouse model of cryptosporidiosis.[74]

5.23.2.1.3.2 Inosine-5′-monophosphate dehydrogenase inhibitors

One biochemical target that has provided multiple starting points for development of drug candidates for cryptosporidiosis is inosine-5′-monophosphate dehydrogenase.[75] This enzyme, which is important to the parasite's ability to generate guanine nucleotides, was identified as a potential target, cloned, expressed, and used in high-throughput screens of over 100,000 compounds to identify several hundred hits.[76] Based on this outcome, hit-to-lead and lead optimization projects focused on ureas,[77] benzimidazoles,[78] benzoxazoles,[79] phthalazinones,[80] and benzopyranopyrazoles[81] have been reported (**Fig. 12**). These efforts have been aided by X-ray crystallography of several compounds complexed in the active site of *Cp*IMPDH,[81,82] and several compounds from these series have demonstrated oral activity in a mouse model of cryptosporidiosis, validating IMPDH as a target for this disease.[83]

5.23.2.2 Kinetoplastids

The kinetoplastids are a diverse class of flagellated unicellular parasites characterized by the presence of several unique and conserved structural organelles including the kinetoplast and glycosome.[84] The kinetoplast is a network of mitochondrial DNA; transcription of kinetoplast genes, RNA editing, and maintenance of the catenated DNA network are unique to this class of parasites.[85] The glycosome is an unusual peroxisome-like organelle that localizes the seven enzymes of the glycolytic pathway, the sole source of ATP and energy in kinetoplastids.[86] As a consequence of the presence of these unique organelles and pathways, drugs targeting biochemical targets associated with them have become attractive targets for drug discovery.[84]

The most widely distributed kinetoplastid order is *Leishmania*, which infect individuals in subtropical climates around the globe, including Asia, the Middle East, Africa, southern Europe, and Central and South America.[87] Diseases caused by *Leishmania* species range from relatively mild and ultimately self-resolving cutaneous leishmaniasis, to disfiguring mucocutaneous leishmaniasis, to the potentially fatal visceral leishmaniasis. Since 2005, cutaneous leishmaniasis has been identified as a problem for military forces participating in conflicts in Afghanistan and Iraq.[88] Mucocutaneous leishmaniasis is widely distributed in both southern Europe and the Americas and represents a significant health problem, particularly in children.[89] The most serious disease caused by *Leishmania* parasites, visceral leishmaniasis, is most prevalent in India and Eastern Africa, and significant mortality continues to be an issue in these areas.[90]

Chagas disease, caused by the parasite *T. cruzi*, is widely distributed across Central and South America and is considered the leading infectious cause of cardiomyopathy and death due to parasitic infection in the Western Hemisphere.[91] It is estimated that over 7 million individuals are infected with *T. cruzi* parasites, and over 100 million are at risk.[92] With continued global warming, northward expansion of *T. cruzi* infections into the United States has been observed.[93] A particular challenge of Chagas disease is that the acute symptoms are relatively minor, such that the majority of patients are undiagnosed for decades; only 30% of chronically infected individuals will develop cardiovascular disease.[94]

The final major genus of kinetoplastid parasites important in human disease is the multiple *Trypanosoma brucei* subspecies responsible for human African trypanosomiasis (HAT) or African sleeping sickness. Although epidemiologically the least widespread of the kinetoplastids, infections by *T. brucei* are particularly problematic as they are inevitably fatal if untreated. Distributed across sub-Saharan Africa, it is estimated that only 50,000–70,000 individuals are infected with *T. brucei*, though it is likely that actual incidence is somewhat higher due to the difficulty in reaching disease-endemic areas and reluctance of individuals to be screened.[92] Like Chagas disease, individuals acutely infected with *T. brucei* (stage 1 disease) experience only mild, nonspecific symptoms (e.g., fever, headache, and muscle aches), which makes diagnosis difficult.[95] It is only upon migration of the parasites across the blood–brain barrier and progression to stage 2 disease that the hallmark symptoms of HAT such as sleep disturbances,

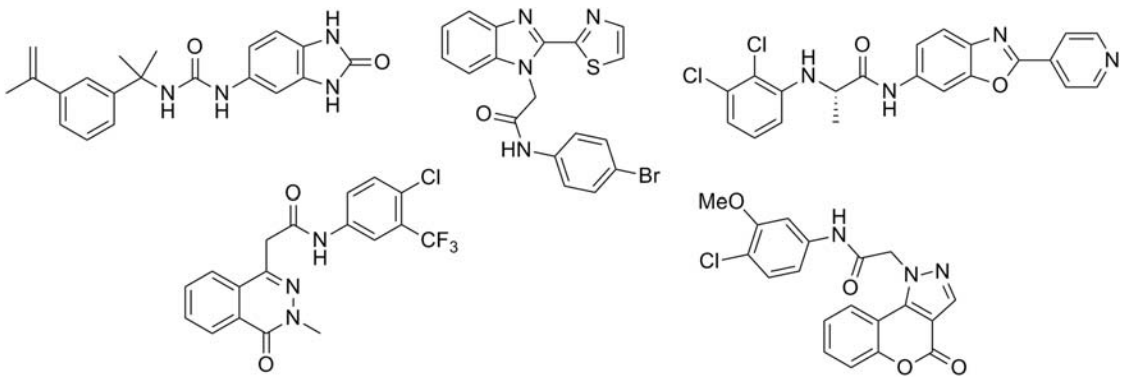

Fig. 12 Inhibitors of IMPDH for *Cryptosporidium*.

hallucinations, and sensory disorders emerge. Confirmation of stage 2 HAT requires collection of cerebrospinal fluid by way of a lumbar puncture, a procedure that is challenging to perform in the field.[96]

Drugs available to treat the kinetoplastid diseases are relatively old and are summarized in Table 2 and Fig. 13. Significant toxicities are known for most of these drugs, and emergence of resistance has been reported for many.[97]

As with other parasitic diseases, drug discovery efforts for the kinetoplastid diseases have benefited over the past decade from increased funding from philanthropic organizations such as the Bill & Melinda Gates Foundation and the Wellcome Trust[2] and have focused on either unique biochemical targets in the parasites or repurposing of approved or clinically relevant therapeutics.

5.23.2.2.1 Leishmania

Although the *Leishmania* parasites are closely related from a taxonomic perspective, the range of disease caused by individual species of *Leishmania* is quite varied, ranging from relatively mild and self-curing cutaneous leishmaniases to more severe disfiguring mucocutaneous leishmaniases and potentially fatal visceral leishmaniases.[98] It is beyond the scope of this article to discuss the similarities and differences between the various manifestations of leishmaniasis, but these differences have substantial impact on the drug discovery strategies employed for each disease. Depending on the specific parasite targeted, programs may need to focus on physicochemical properties to enable development of specific formulations or routes of administration or on identification of compounds that balance efficacy across a wide range of *Leishmania* strains.[87a]

5.23.2.2.1.1 Diamidines and arylimidamides

Based on the well-known antileishmanial agent pentamidine, efforts to discover improved diamidines have been a key area of exploration in the past decade.[99] In a series of papers in the early 2000s, Boykin and coworkers described numerous variations of the diamidines, with modifications of the linker between the two amidine moieties providing a central theme for modulation of both DNA binding affinity and physicochemical properties, as summarized in Fig. 14.[100]

One of the key limitations of the diamidines, which were examined for not only their activity against *Leishmania* spp. but also *T. cruzi* and *T. brucei*, centered on their poor pharmacokinetic profiles, attributable to the dicationic nature of the molecules. This limitation prompted several avenues of exploration, including preparation and evaluation of prodrugs[101] and less basic reversed diamidines designated arylimidamides.[102] Emerging from the arylimidamide effort were the advanced leads DB745 and DB766 (Fig. 15), which demonstrated potent antileishmanial activity, moderate oral bioavailability, and efficacy in animal models of leishmaniasis.[103] Further optimization of the arylimidamide class to improve pharmacokinetic properties afforded additional advanced leads such as DB1852 and DB1960. Unfortunately, repeat-dose toxicology studies have suggested that adverse effects on the host will limit the utility of these compounds.[104]

Table 2 Available drugs for treatment of kinetoplastid diseases[97]

	Decade introduced	*Route of administration*	*Uses and limitations*
Leishmaniasis (visceral and cutaneous)			
Sodium stibogluconate	1950s	Intramuscular, intravenous	Variable efficacy and emergence of resistance
Meglumine antimoniate	1950s	Intramuscular, intravenous	Variable efficacy and emergence of resistance
Amphotericin B	1980s	Intravenous	Effective in areas where resistance has emerged. Expense of lipid formulations limits use
Miltefosine	1980s	Oral	Effective in areas where resistance has emerged. Potentially teratogenic
Paromomycin	2000s	Intramuscular	Variable efficacy
Chagas disease			
Nifurtimox	1960s	Oral	Requires 60–120 days treatment. GI, dermatologic, and neurological toxicity
Benznidazole	1970s	Oral	Requires 40–80 days treatment. GI, dermatologic, and neurological toxicity
Human African trypanosomiasis			
Suramin	1910s	Intramuscular	First-line therapy for stage 1 *T. rhodesiense*, not effective in stage 2. Emergence of resistance
Pentamidine	1930s	Intramuscular	First-line therapy for stage 1 *T. gambiense*, not effective in stage 2. Emergence of resistance
Melarsoprol	1940s	Intravenous	First-line therapy for stage 2 HAT. Significant toxicity. Painful injection
Eflornithine	1970s	Intravenous	Emerging first-line therapy for stage 2 HAT. Requires 14 days of infusions (4 day^{-1}). Can be combined with nifurtimox (oral) to reduce course of treatment to 10 days

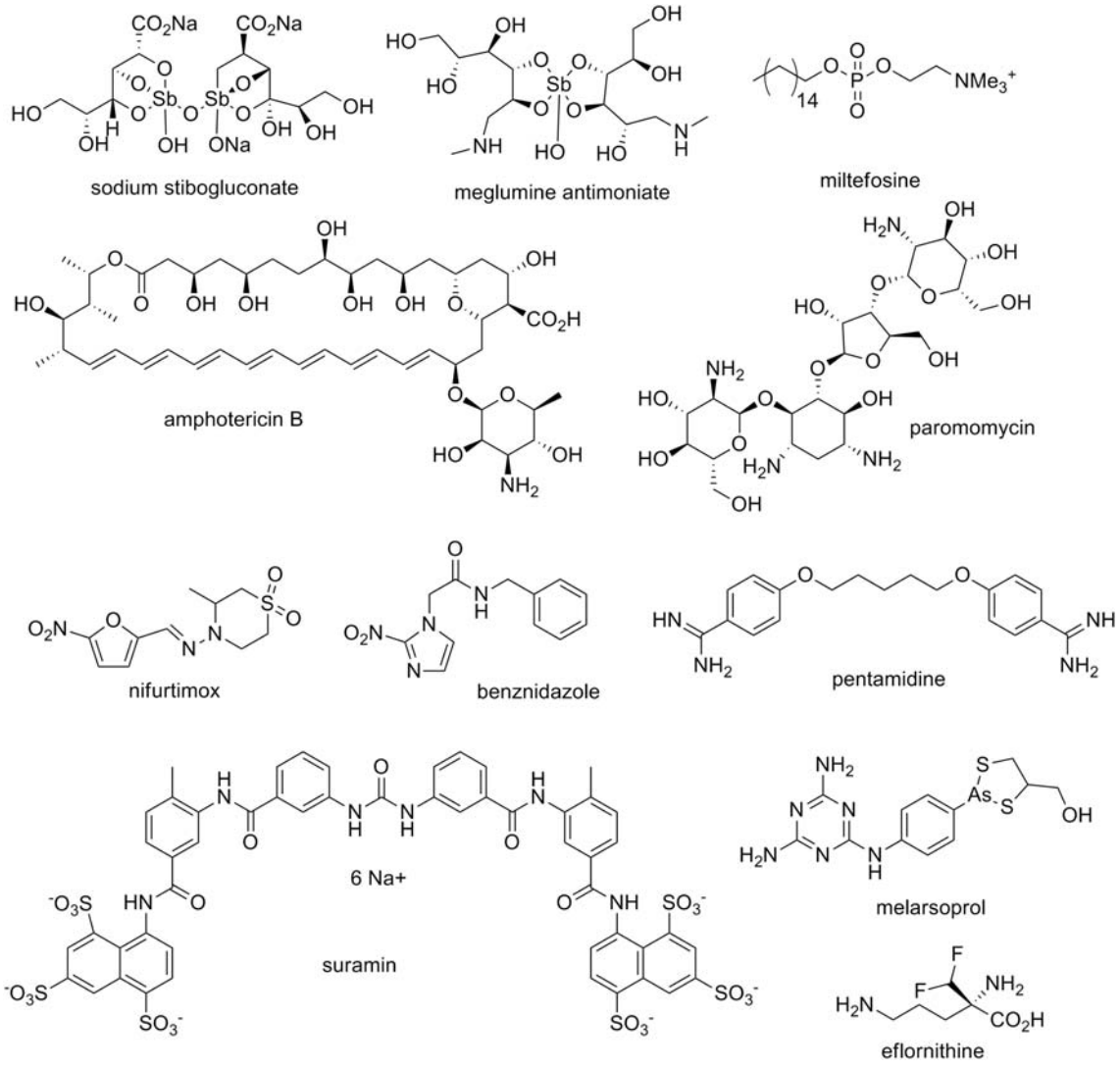

Fig. 13 Current treatments for kinetoplastid infections.

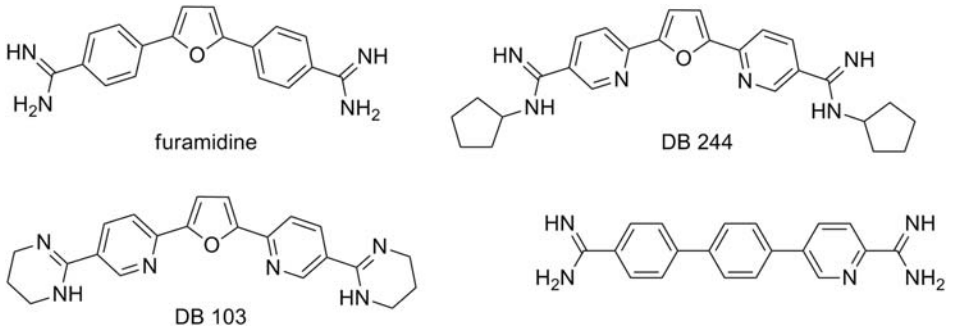

Fig. 14 Diamidines evaluated for antileishmanial activity.

5.23.2.2.1.2 Cdc2-related kinase 3 inhibitors

As in other parasites, inhibition of cell cycle kinase targets provides an attractive approach to development of antileishmanial drugs, provided one can obtain sufficient selectivity for disruption of the parasite life cycle relative to effects on the mammalian host. One such target is the Cdc2-related kinase 3 (CRK3), originally identified as a potential target in the late 1990s[105] and demonstrated to

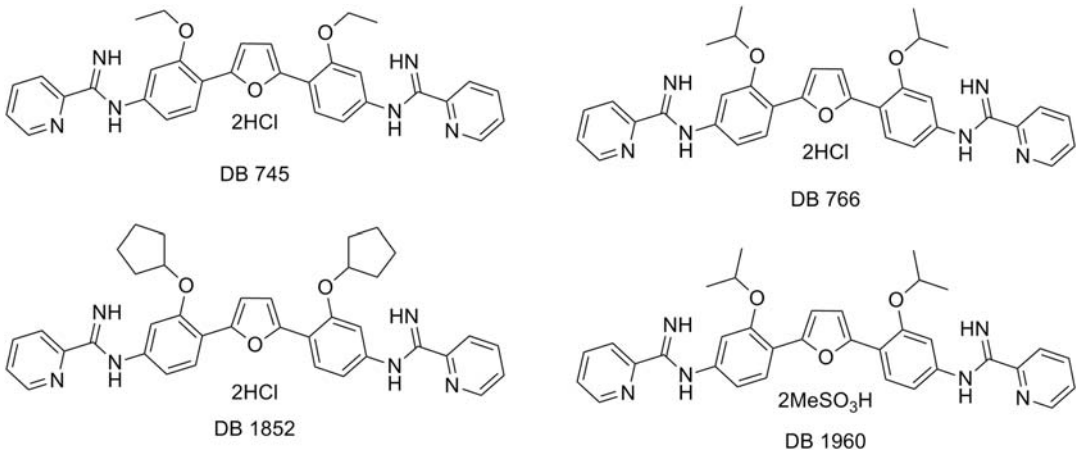

Fig. 15 Arylimidamides for visceral leishmaniasis.

be essential to growth of *Leishmania* spp. in the early 2000s.[106] More recently, screening of several kinase inhibitor libraries afforded a number of hits for initiation of medicinal chemistry programs, as summarized in Fig. 16.[107]

To date, none of these series have progressed to delivery of a preclinical candidate, despite some optimization to provide very potent and selective inhibitors of CRK3. It has been suggested that this failure indicates that CRK3 is not essential for parasite proliferation, despite the early genetic data that suggested this to be the case.[107c] This outcome highlights one of the major challenges for antiparasitic drug discovery—the all-too-frequent disconnect between biochemical potency and lack of cellular activity, which has caused many in the field to discount the value of target-based screening approaches in favor of phenotypic cell-based screening.

5.23.2.2.1.3 Inhibitors of dihydrofolate reductase–thymidylate synthase

Inhibition of inhibitors of dihydrofolate reductase–thymidylate synthase (DHFR–TS) has long been a potentially attractive target for design of antileishmanial drug candidates.[108] Early studies of 2,4-diaminopyrimidines and 2,4-diaminoquinazolines (Fig. 17) as inhibitors of leishmanial DHFR–TS identified a number of potent enzyme inhibitors, but activity in parasite proliferation assays

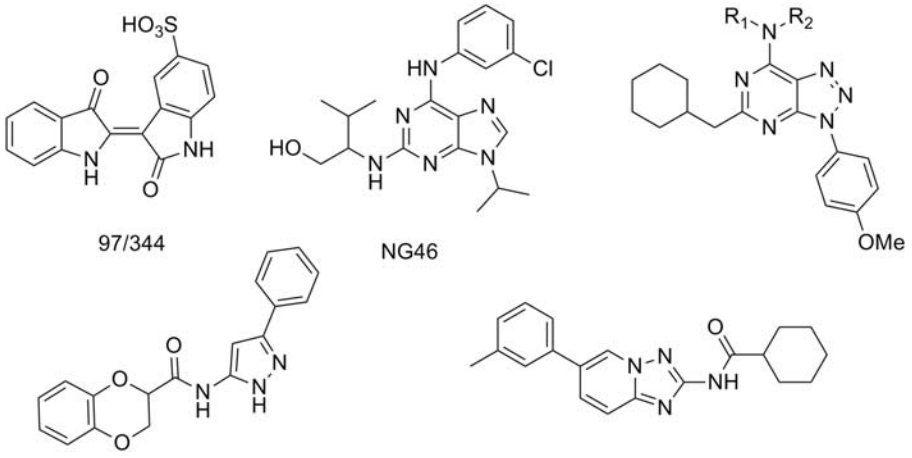

Fig. 16 CRK3 inhibitors as antileishmanials.

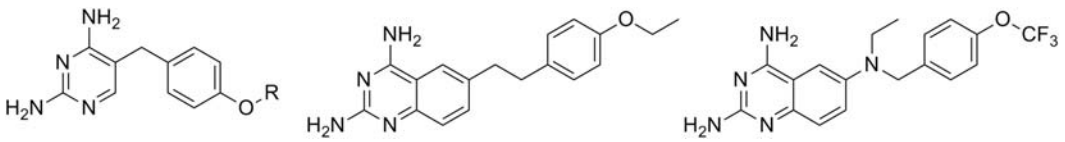

Fig. 17 Dihydrofolate reductase–thymidylate synthase inhibitors as antileishmanials.

was suboptimal, presumably due to poor physicochemical properties.[109] More recently, a related series of quinazolines with an aminoethyl linker has been shown to inhibit growth of *L. mexicana* promastigotes at low micromolar concentrations.[110]

5.23.2.2.1.4 Hits from phenotypic screening

As described in the preceding text, the difficulty of obtaining compounds that are active in whole-cell assays starting from biochemical targets has prompted greater dependence on use of phenotypic assays as primary screens for identification of lead series. Several classes of molecules have been identified in the past several years utilizing *L. donovani* and *L. infantum* parasites hosted in macrophages. Among these are series of aminothiazoles,[111] *N*(2),*N*(4) disubstituted quinazolines,[112] substituted quinolines,[113] and aminopyrazole carboxamides[114] (**Fig. 18**). The aminothiazoles exhibited very good *in vitro* potency, but were challenged by poor metabolic stability and pharmacokinetics.[111] In the quinazoline series, optimized analogs demonstrated good physicochemical and pharmacokinetic properties, but demonstrated only modest efficacy in a mouse model of visceral leishmaniasis due to toxicity at higher doses.[112b] In the quinoline series, an optimized analog was identified, which was efficacious in a hamster model following oral dosing.[113b] Further exploration of this series focused on minimizing the CYP1A2 inhibition of the lead candidate, but did not provide additional compounds with sufficient *in vivo* efficacy to be considered further.[113a] The most successful lead series identified from these screening efforts was the aminopyrazole series, which achieved good exposure following oral dosing, resulting in over 90% reduction of parasite load in hamsters following 5 days of dosing at 40 mg $kg^{-1}day^{-1}$.[114]

Taken together, these observations provide support for the continued use of phenotypic assays for identification of leads, as this approach overcomes the translation of activity in a biochemical assay to activity in a whole-cell assay.

5.23.2.2.1.5 Repurposing of approved and clinically evaluated drugs

Repurposing of approved drugs for use in treatment of leishmaniasis has been a popular approach over the last several years. As described earlier, the attractiveness of this approach is the perception that approval of these drugs for a new indication will be faster and less costly than for new chemical entities.

The rheumatoid arthritis drug auranofin (see **Fig. 7**), a gold (I) complex, was shown to inhibit trypanothione reductase derived from *L. infantum*, as well as to have antiproliferative effects on the promastigote stage of this strain.[64] In a more recent study, auranofin has been demonstrated to have significant *in vitro* and *in vivo* activity against several *Leishmania* strains, most notably *L. major* and *L. amazonensis*, which are important causative strains for cutaneous disease.[115] In addition to auranofin itself, an additional 39 gold(I) complexes were evaluated, with several demonstrating improved potency and selectivity relative to host cells. Cell biology studies suggested that auranofin caused apoptosis in *Leishmania* parasites via an undefined mechanism that induced caspase 3/7-like activity and DNA fragmentation.

Screening of a number of commercially available protein kinase inhibitors in several *Leishmania* strains identified sorafenib, sunitinib, and lapatinib (**Fig. 19**) as having micromolar-level activity *in vitro*.[116] Subsequent evaluation of these compounds in an *in vivo* model of visceral leishmaniasis revealed only modest efficacy. Independently, Pollastri and coworkers also identified lapatinib as having potent activity against *T. brucei* and pursued a lead optimization program on this class (vide infra).[117] The same group also identified the Aurora kinase inhibitor hesperadin as a potential repurposing candidate for leishmaniasis and other kinetoplastid diseases.[118]

The serotonin receptor antagonist ketanserin (**Fig. 19**) was also found to have modest activity against *L. donovani* promastigotes and amastigotes (in THP-1 cells) while exhibiting little cytotoxicity to the THP-1 cells.[119] The antileishmanial activity of ketanserin was attributed to its interaction with HMGR in the parasite, supported by enzyme inhibition studies and weaker activity in HMGR-overexpressing parasites. The tricyclic antidepressant mianserin was also evaluated and shown to be antileishmanial via the same mechanism.[120] Work from the same group has also demonstrated activity for the HMGR inhibitors atorvastatin, simvastatin, and mevastatin (**Fig. 11**).[121] Further characterization of the effect of mevastatin on sterol metabolism in *L. donovani* revealed significant and dose-dependent reduction of ergosterol levels and accumulation of lipid bodies in the parasites that impacted parasite viability.[121b]

Though not a primary focus for leishmaniasis applications, nitroheterocyclic compounds have been found to be efficacious against the other kinetoplastids (vide infra). Consequently, evaluation of nitroheterocycles as potential antileishmanials has been reported. For example, the advanced clinical candidate fexinidazole has been evaluated in preclinical studies, where it

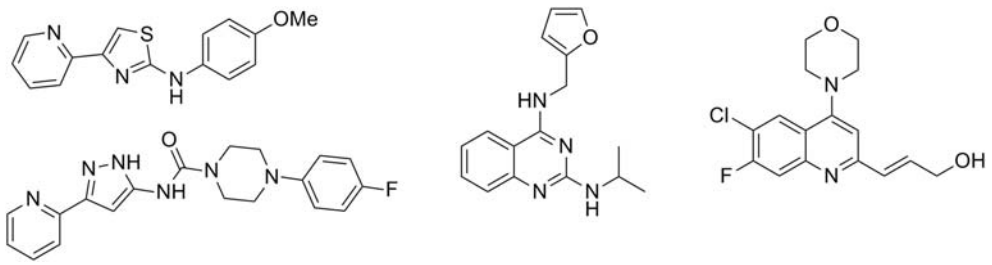

Fig. 18 Antileishmanial leads from phenotypic screening.

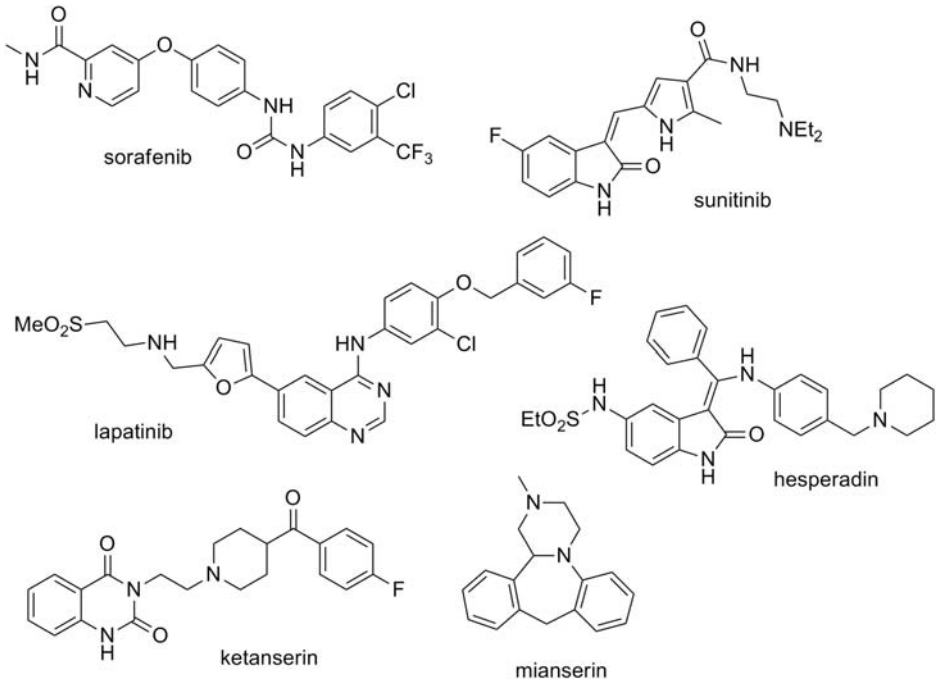

Fig. 19 Repurposed approved drugs identified as potential starting points for antileishmanials.

demonstrated efficacy equivalent to miltefosine in a mouse model of visceral leishmaniasis.[122] In a similar repurposing strategy, it has been reported that a single enantiomer of the antitubercular clinical candidate PA-824 has an attractive *in vitro* and *in vivo* profile with potential for oral administration.[123]

5.23.2.2.2 Trypanosoma cruzi

As described in section "Kinetoplastids," infection of individuals with *T. cruzi* results in development of Chagas disease, a chronic condition that ultimately leads to gastrointestinal and cardiac problems decades after initial infection.[124] Though described as a single disease, the genetic diversity of *T. cruzi* complicates treatment of Chagas patients, resulting in highly variable efficacy for existing drugs and facile development of resistance in the infected population.[125] The importance of identifying drug candidates and biochemical targets that will provide broad efficacy across the diversity of *T. cruzi* strains encountered in the field has been highlighted in the past several years through the failure of several clinical candidates from the azole class of ergosterol biosynthesis inhibitors.[126] In addition to the view that exposure to these clinical candidates was insufficient to effect cure in all individuals, the variability in strain susceptibility has been put forth as contributory to the negative outcome.[127] These failures are in sharp contrast to clinical experience with the nitroimidazoles benznidazole and nifurtimox, which have been the standard of care for Chagas disease for decades, though a recent trial of benznidazole has suggested that, while parasitemia is significantly reduced in patients treated with this drug, beneficial effects on cardiac function are not significant.[128] As a consequence of these observations, drug discovery efforts in the past several years have moved away from identification of additional candidates that act on the CYP51 enzyme to more diverse and novel mechanisms of action, with phenotypic screening of compound libraries in newly developed and validated *in vitro* and *in vivo* assays taking a prominent role.[129]

5.23.2.2.2.1 Ergosterol biosynthesis (CYP51) inhibitors

In spite of the recent failure of both posaconazole and ravuconazole to demonstrate meaningful efficacy in clinical trials,[126] several new inhibitors of CYP51 (VFV and VNI) have been reported (**Fig. 20**).[130] The strategies supporting the proposals for progression of these newer compounds to preclinical studies are centered on (a) utilization of crystallographic data to optimize both potency and selectivity for the *T. cruzi* enzyme[130a,c] and (b) modulation of physicochemical and pharmacokinetic properties to improve exposure and tissue distribution.[130b–d]

5.23.2.2.2.2 Nitroheterocycles

The clinical utility of benznidazole and nifurtimox for treatment of Chagas disease continues to provide enthusiasm for exploration of new nitro-substituted heterocycles, despite the potential genotoxicity exhibited by many members of this broad structural motif.[131] One of the most advanced clinical candidates from this class that is being explored for utility in both Chagas disease and HAT, fexinidazole, has been thoroughly profiled in a range of assays predictive of genotoxicity potential, and it has been concluded that it presents minimal risk to patients.[132] Several groups have reported a range of five-membered nitro-substituted

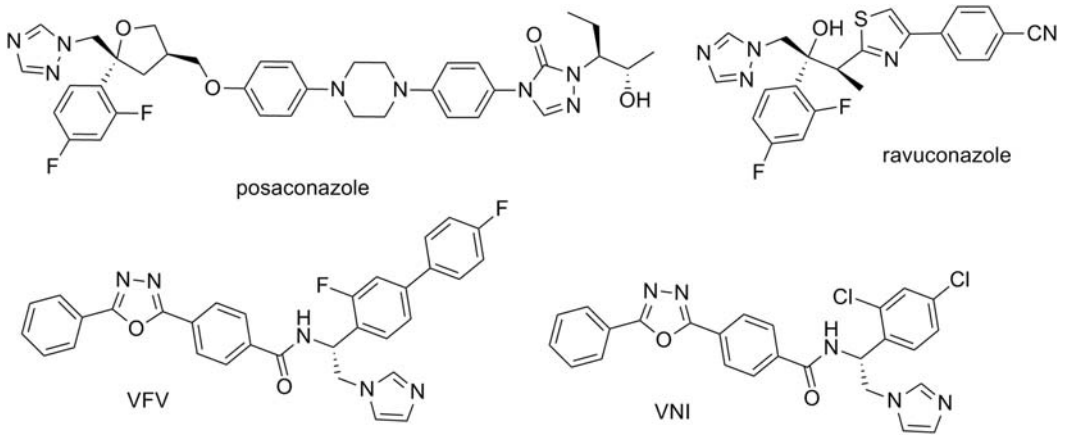

Fig. 20 CYP51 inhibitors evaluated for Chagas disease.

heterocycles (Fig. 21) over the past several years with variable potency against *T. cruzi* and focused on improvement of physicochemical and pharmacokinetic properties to achieve better *in vivo* efficacy.[133] Based in part on the observation that the combination of benznidazole and posaconazole in an acute murine infection model of Chagas disease provided superior efficacy to either agent alone,[134] Papadopoulou and coworkers synthesized and evaluated a series of 3-nitrotriazoles structurally related to fluconazole in an effort to generate bifunctional drug candidates.[135] While several analogs demonstrated good *in vitro* potency against *T. cruzi* and inhibition of the TcCYP51 enzyme, little evidence for synergism was observed in an *in vivo* efficacy experiment.

5.23.2.2.2.3 Lipophilic amines: Inhibitors of squalene synthase

In another example of repurposing an antibacterial clinical candidate for use as an antiparasitic, it has recently been reported that the antitubercular drug SQ109 (Fig. 22) holds promise for treatment of Chagas disease.[136] Originally discovered from screening of a combinatorial library of lipophilic 1,2-ethylenediamine analogs[137] and shown to have acceptable pharmacokinetics in mice,[138] SQ109 was progressed to clinical trials for tuberculosis.[139] The antitubercular mechanism of action of SQ109 was proposed to involve inhibition of a transporter important for cell wall biosynthesis,[140] with subsequent studies supporting multiple modes of action, including uncoupling of pH gradients and membrane potentials[141] and inhibition of dehydrosqualene synthase.[142] Earlier work from several laboratories had shown that lipophilic amines, such as quinuclidines, inhibit *T. cruzi* squalene synthase, though none have progressed to preclinical status.[143]

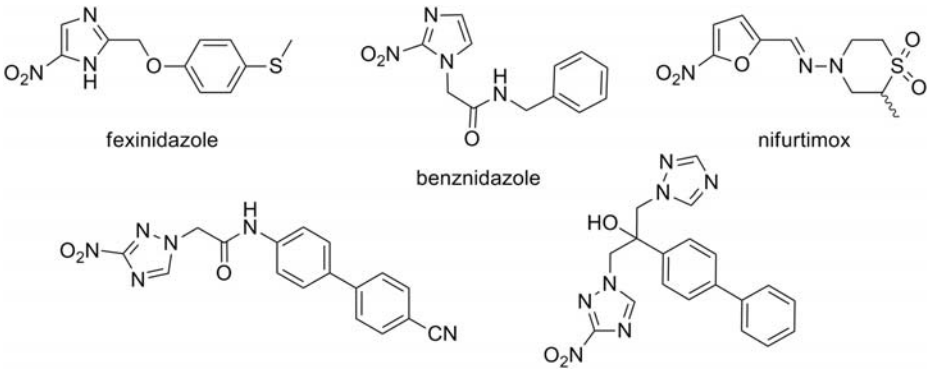

Fig. 21 Nitro-substituted heterocycles for Chagas disease.

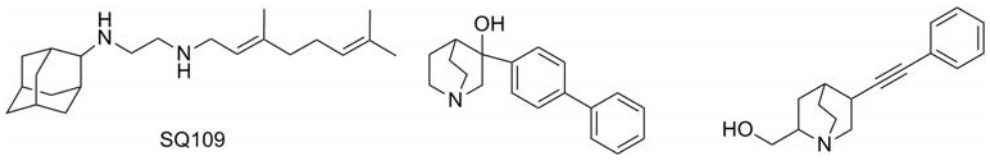

Fig. 22 Lipophilic amines explored as treatments for Chagas disease.

5.23.2.2.3 Trypanosoma brucei

The final kinetoplastid parasite to be considered is *T. brucei*, the causative agent of human African sleeping sickness. Though similar to the *Leishmania* spp. and *T. cruzi* parasites discussed in the preceding text, the site of *T. brucei* infection poses the added challenge to drug discovery of requiring molecules with the ability to cross the blood–brain barrier for robust and durable *in vivo* efficacy. This challenge has proved to be significant, as several of the biochemical targets pursued for other kinetoplastids (e.g., kinases) require structural features such as multiple hydrogen bond donor/acceptor pairs in drug candidates to achieve high potency and selectivity, and these limit CNS penetration. For example, while a subset of *T. brucei* mitogen-activated protein kinases was found to be the target(s) of a series of diaminopyrimidines, their utility as candidates for treatment of HAT was limited due to poor CNS permeability.[144] Similar limitations have been observed for other targets and series as highlighted in the following sections. In some cases, this has resulted in "repurposing" of lead series to either *Leishmania* or *T. cruzi*. A strong trend in HAT discovery over the past several years has been an increasing appreciation of the interplay between pharmacokinetics and pharmacodynamics. As with other protozoan parasites, many hit series have been identified by phenotypic screening from a variety of compound library sources.[145] This approach has been particularly attractive for *T. brucei*, as the parasite is free-living and not dependent on maintenance in a host mammalian cell, rendering it the most easily cultured of the kinetoplastids. Consequently, it is anticipated that repurposing of *T. brucei* hits to the other kinetoplastids and apicomplexans will be a feature of future work, highlighting the importance of cross collaboration between research groups in these areas.

5.23.2.2.3.1 Diamidines

Described earlier as potential candidates for treatment of leishmaniasis, the diamidines related to the clinically effective stage 1 sleeping sickness drug pentamidine have continued to receive attention from the drug discovery community. Most notably, DB289, a methoxyamidine prodrug of the diamidine DB75 (**Fig. 23**), was progressed to clinical trials for stage 1 sleeping sickness following an extensive lead optimization and preclinical development program.[146] Though early clinical experience with DB289 was quite encouraging, longer duration treatment of patients resulted in liver and kidney toxicities that ultimately led to discontinuation of its development.[147]

Continued optimization of the diamidine series, with a focus on identification of analogs with superior pharmacokinetics, CNS penetration, and safety, has resulted in the progression of several aza analogs of DB289, including DB829,[148] DB844,[149] and 28DAP10[150] to preclinical evaluation for both stage 1 and stage 2 sleeping sickness.

While these compounds have been extensively characterized in a variety of *in vitro* and *in vivo* models, there is no evidence that any have progressed to clinical trials.

5.23.2.2.3.2 Trypanosomal phosphodiesterase inhibitors

Another class of targets that have garnered attention for treatment of HAT are the phosphodiesterases (PDEs), in particular TbrPDEB1 and TbrPDEB2.[151] These enzymes have been shown to be essential for control of cyclic adenosine monophosphate levels in the parasite, and disruption of their function by RNAi results in parasite death.[151a,b] Early efforts in the discovery of TbrPDEB1 inhibitors looked to repurpose inhibitors of the human PDE4 enzyme, resulting in the exploration of a number of potential leads (**Fig. 24**). In particular, two series of compounds, the first based on a phthalazinone[151b] and the second on a pyrazolinone core,[152] were identified from a proprietary PDE-focused screening library. Unfortunately, elaboration of these leads to provide parasite-selective inhibitors has proved difficult. In order to address this limitation, a virtual screening approach using a crystal structure of TbrPDEB1 has been pursued, resulting in the identification of additional scaffolds for optimization.[153]

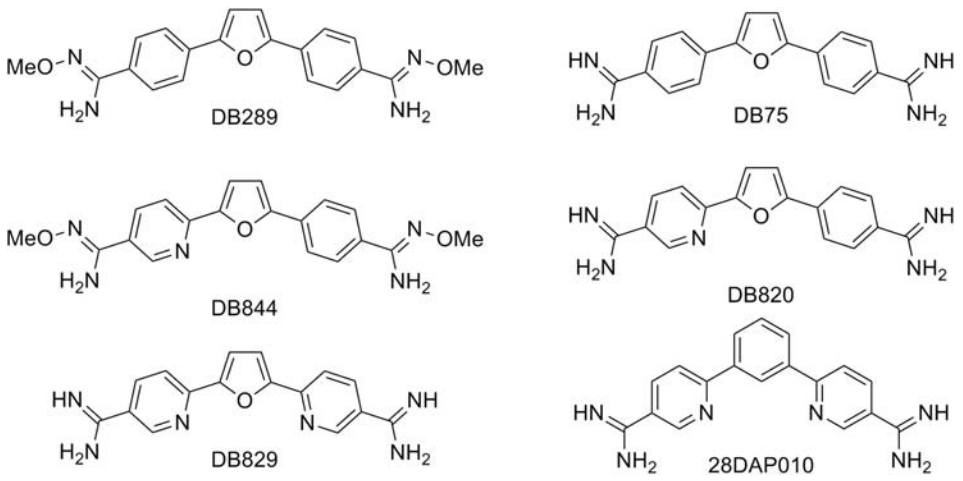

Fig. 23 Diamidines for human African trypanosomiasis.

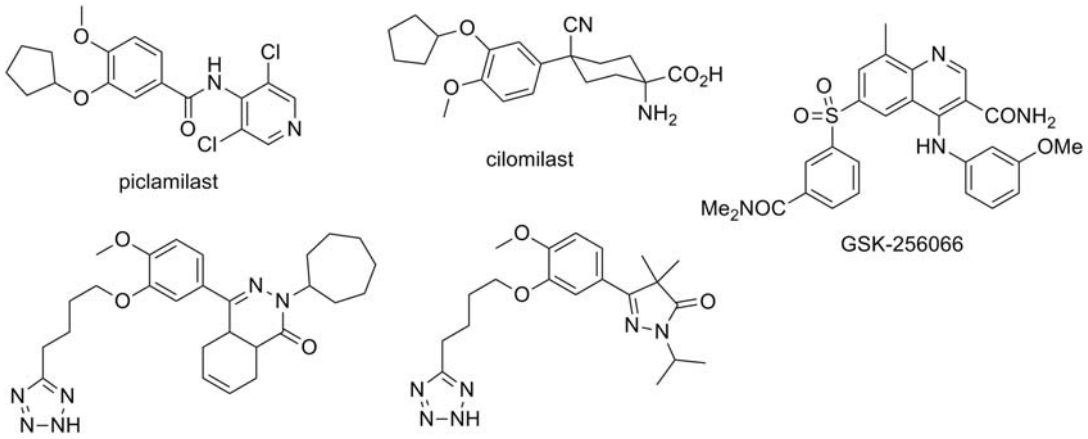

Fig. 24 Inhibitors of TbPDE4B1.

Concurrent with these efforts, consideration of additional human PDE4 inhibitors prompted exploration of a series of catechol diethers based on piclamilast.[154] Work focused on modification of the dichloropyridine region of this molecule proved unsuccessful, with only weak activity for TbPDEB1 observed.[155] Somewhat more success has been reported for modification of the hPDE4 inhibitor cilomilast, with identification of an analog with submicromolar activity against TbPDEB1 and modest activity in a whole-cell assay.[156] Most recently, an effort focused on the 4-aminoquinoline class represented by GSK-256066 has been reported with similar outcomes.[157] Synthesis and characterization of over 40 analogs of this lead identified a number of compounds with single-digit micromolar activity for both the TbPDEB1 and TbPDEB2 enzymes, but these compounds retained nanomolar affinity for the hPDE4 enzyme, limiting their utility.[157] These studies highlight the challenge of repurposing existing human therapeutics for neglected diseases, suggesting that the initial enthusiasm exhibited by the industry for "quick wins" using this approach may need to be reevaluated.

5.23.2.2.3.3 Benzoxaboroles

From a phenotypic whole-cell screen of compounds against *T. brucei*, a series of 6-substituted benzoxaboroles were identified as leads for treatment of HAT as outlined in **Fig. 25**.[158] From this initial work, it was demonstrated that thioethers, sulfoxides, sulfones, and amides were all submicromolar actives *in vitro*, and the 4-chlorophenylsulfoxide was shown to be active in an *in vivo* model.[159] Initial optimization of the series focused on 6-carboxamides and identified SCYX-6759 as an advanced lead with good *in vitro* potency, acceptable pharmacokinetics, and oral activity in models of HAT.[160] While SCYX-6759 was robustly active in a stage 1 HAT model, the pharmacokinetics of this compound in the brain were insufficient to warrant progression to preclinical status, which prompted further optimization focused on increasing brain exposure. These efforts led to the discovery of the clinical candidate SCYX-7158,[161] which has recently completed a phase I clinical trial where it demonstrated very good pharmacokinetics and safety in human volunteers.[162]

5.23.2.2.3.4 Aminoacyl tRNA synthetase inhibitors

Aminoacyl tRNA synthetases (aaRSs) are essential to *T. brucei* (and other parasites) for protein synthesis; hence, inhibition of individual enzymes in this class has been postulated to provide attractive targets for drugs, especially if one were to design compounds selective for the parasite enzyme(s). Of the 24 aaRSs encoded by the *T. brucei* genome, 16 have been shown to be essential for parasite survival by either RNAi or chemical methods.[163] While some enzymes such as isoleucyl-RS and histidyl-RS have been explored

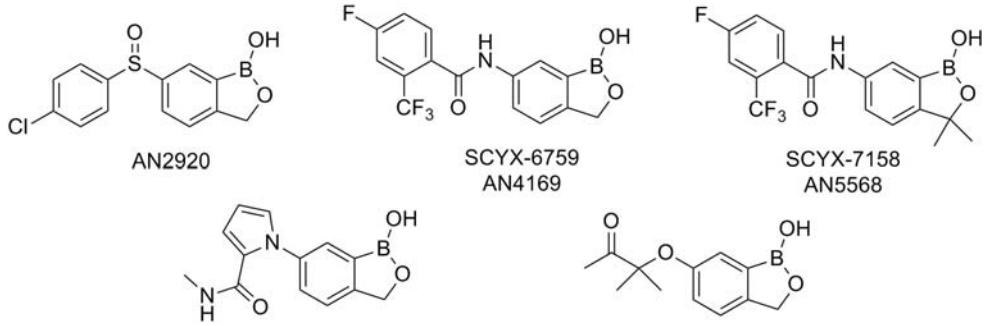

Fig. 25 Benzoxaboroles for HAT.

only for substrate-based inhibitors,[164] others such as methionyl-RS and leucyl-RS have yielded more diverse scaffolds as leads for drug discovery (Fig. 26).[165]

In the case of the methionyl-RS, a series of diaryl diamines have been explored, with numerous examples exhibiting nanomolar potency in whole-cell *T. brucei* assays and no effect on mammalian cells.[165a] The most potent compound from this series was found to be efficacious in a murine model, but poor pharmacokinetics and permeability into the CNS precluded further development. To address these issues, the 4-quinolone moiety in early compounds was replaced by a urea, affording compounds with good oral pharmacokinetics, including CNS exposure.[165b] Further understanding of the structural features in both the quinolone and urea series has been gleaned through extensive cocrystallization of inhibitors from both classes with *T. brucei* methionyl-RS.[165c] Most recently, screening of a large library of compounds, coupled with counterscreening in a human methionyl-RS functional assay to reject nonselective compounds, has identified additional chemical scaffolds for optimization including a series of indoles.[165d]

For leucyl-RS, attempts to capitalize on the known benzoxaborole scaffold known to interact with the editing domain of fungal[166] and bacterial[167] enzymes afforded a series of weakly active analogs (Fig. 25).[165e] Screening of a small library of compounds in a *T. brucei* leucyl-RS aminoacylation assay identified a series *N*-sulfamoylthioureas.[165f] Lastly, virtual screening of a database of commercially available compounds led to exploration of a series of pyrrolinones, also providing weakly active leads for further optimization.[168] These efforts suggest that identification of high-potency compounds for this enzyme may be challenging.

5.23.2.2.3.5 *N*-Myristoyltransferase inhibitors

Posttranslational modification of proteins is an essential cellular function for modulation of biochemical pathways, directing proteins to specific subcellular organelles and identifying proteins to be degraded. One modification, effected by the enzyme *N*-myristoyltransferase (NMT), is myristoylation—a process that has been shown to be essential in kinetoplastids through RNA interference studies[169] and that has been postulated to play an important role in the life cycle of protozoan parasites including *T. brucei*, *Leishmania* spp., and *P. falciparum*. Early explorations repurposing fungal NMT inhibitors further validated this target for both *T. brucei* and *L. major*, but these compounds were insufficiently potent to progress to *in vivo* studies.[170]

In 2010, workers at the Dundee Drug Discovery Unit reported the identification of a potent TbNMT inhibitor, DDD64558 (Fig. 27), from screening of a diversity-based library and conducted early hit-to-lead work to identify DDD85646 as a lead compound with modest oral pharmacokinetics and efficacy in a murine model of HAT.[171] Further optimization of this lead focused on reduction of polar surface area improved the CNS permeability of the series to afford the brain-penetrant compound DDD100097 with some efficacy in a stage 2 HAT model.[172] Additional lead series based on thiazolidinone and benzomorpholinone scaffolds from the initial screen and optimization of these series to further improve potential for CNS permeability and full efficacy in HAT have also been reported.[173]

In part, based on these observations, renewed interest in NMT inhibitors as leads for treatment of both malaria and leishmaniasis has been observed, as these diseases do not require CNS penetration for efficacy. As in the *T. brucei* program, hits for *L. donovani*, *P. falciparum*, and *P. vivax* NMT were identified from screening of diversity libraries (Fig. 28).[174] Concurrently, optimization of known fungal and *T. brucei* NMT inhibitors was undertaken in conjunction with X-ray crystallography to identify a series of benzofuran-based *P. falciparum* NMT inhibitors.[175]

Taken together, these efforts highlight the potential for application of leads and biochemical targets across parasites, with medicinal chemical optimization specific to each to efficiently target the relevant specific compartment or tissue.

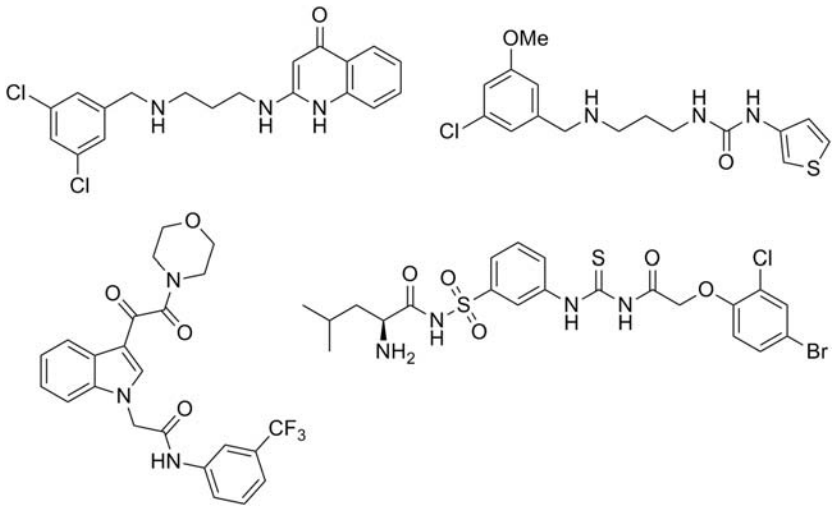

Fig. 26 Inhibitors of aminoacyl tRNA synthetases for HAT.

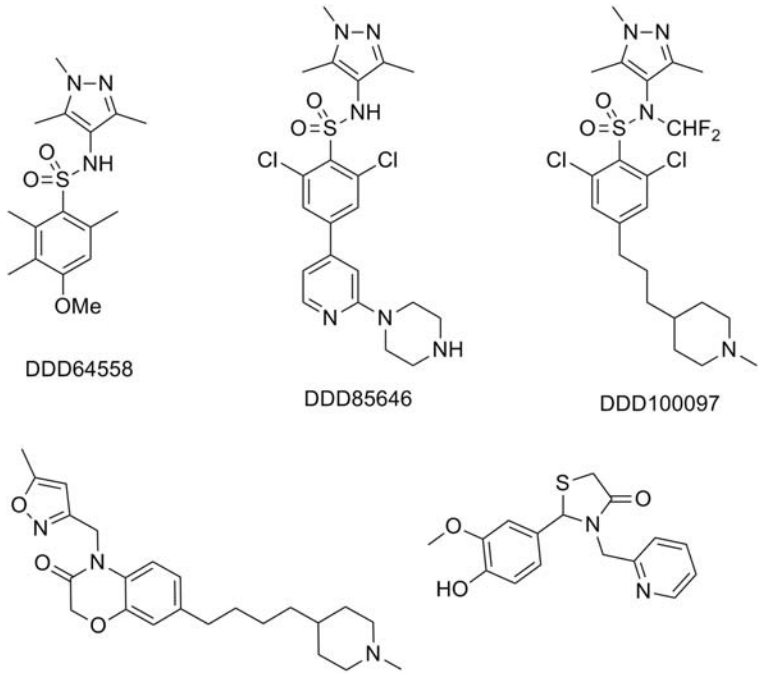

Fig. 27 Inhibitors of *T. brucei N*-myristoyltransferase.

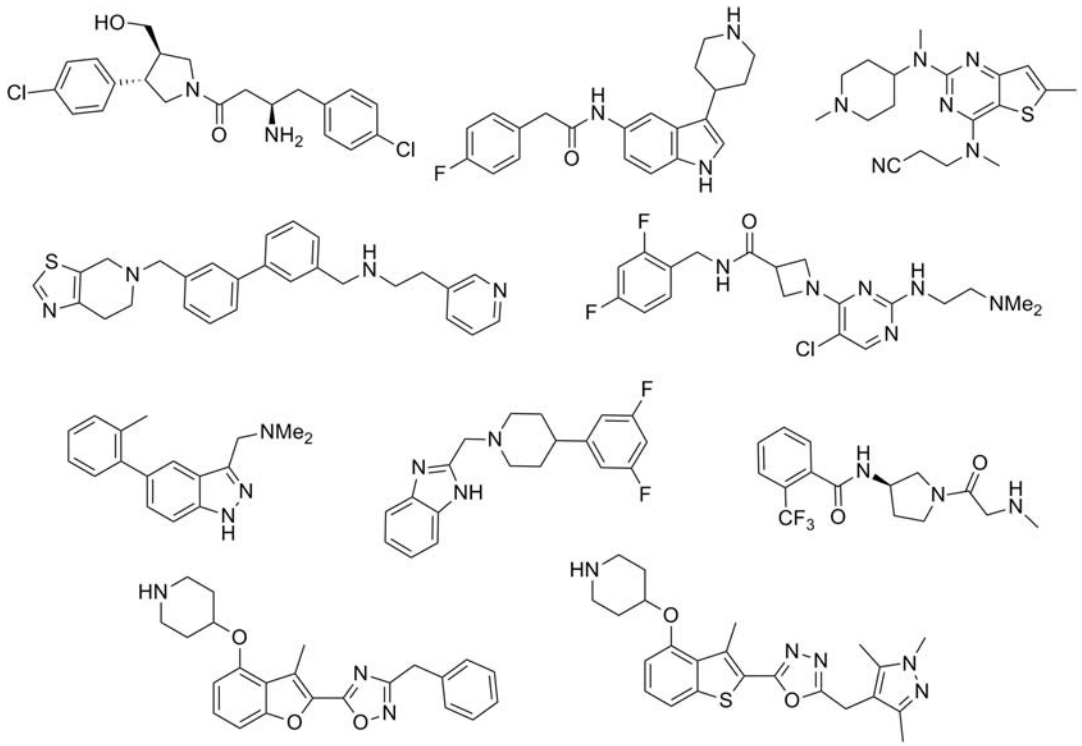

Fig. 28 Inhibitors of *P. falciparum* and *L. donovani N*-myristoyltransferase.

5.23.2.2.3.6 Hit identification from phenotypic screening

As with the other kinetoplastids, the ability to screen large compound libraries against cultured *T. brucei* has been used to advantage to identify numerous classes of hits for optimization. Both diversity-oriented and biochemically targeted libraries have been evaluated, and numerous hit series have been identified (**Fig. 29**). One class of molecules, a series of 2-phenyloxazolopyridine amides, was identified and pursued independently by two groups, one from the Monash University and the second from the University of Washington.[176] Both screening efforts used diversity libraries assembled from commercial sources and identified the same hit, mining their databases for similar compounds to establish early SAR trends. Based on these, both groups initiated hit-to-lead synthetic chemistry campaigns focused on modification of three regions—the amide moiety, the aryl spacer, and the heterocyclic core. The most advanced lead from these studies is a pyrrolidine amide of an imidazopyridine core, which demonstrated an attractive *in vitro* and *in vivo* pharmacokinetic profile and was efficacious in a murine model of HAT.[176b]

Additional hits from the Monash University team have also been reported, including *N*-sulfonyl-tetrahydroquinolines,[177] pyridyl benzamides,[178] and arylpyrazine carboxamides.[179] The latter is the most advanced of these series affording a lead compound with low nanomolar activity against *T. brucei* and good physicochemical and modest *in vitro* pharmacokinetic properties.[179] One feature of this series that has been highlighted is its similarity to known kinase inhibitors, suggesting the potential for scaffold hopping.

The potential attractiveness of known kinase inhibitors and scaffolds as starting points for drug discovery projects for *T. brucei* has also been highlighted by the outcome of high-throughput phenotypic screens of kinase-focused libraries at GSK/Northeastern University, the University of Dundee, and Institut Pasteur Korea.[145,180] In the GSK/NEU screen, over one hundred hits representing over fifty structural classes were identified with submicromolar potency and evidence for cidality.[180a] The pharmacokinetic profiles of several representative compounds were evaluated, and one (NEU-1053) was progressed to an *in vivo* efficacy study. From the Dundee effort, a series of imidazopyrazinones was identified; preliminary hit-to-lead work, including scaffold hopping to a pyrazolopyridine core, was reported. Taken together, these studies suggest that a considerable diversity of kinase-directed scaffolds offer opportunities for continued exploration of novel chemical space and mechanistic approaches.

Screening of a protease-focused library at Dundee afforded a series of indoline carboxamides, which were progressed to hit-to-lead studies, resulting in the identification of several analogs that exhibited cures in a murine stage 1 HAT model and partial cures in a stage 2 model.[181] Lastly, groups at St. Jude Children's Research Hospital and the Eskitis Institute have independently reported screening and evaluation of small libraries of histone deacetylase inhibitors (HDACs).[182]

As can be seen from the preceding paragraphs, numerous opportunities exist for development of new drug candidates to treat HAT should more advanced clinical candidates fail to deliver the promise held in current trials. Finally, the potential to repurpose hits from *T. brucei* screens to other kinetoplastid and apicomplexan parasites exists, and will likely be the focus of future work in this area.

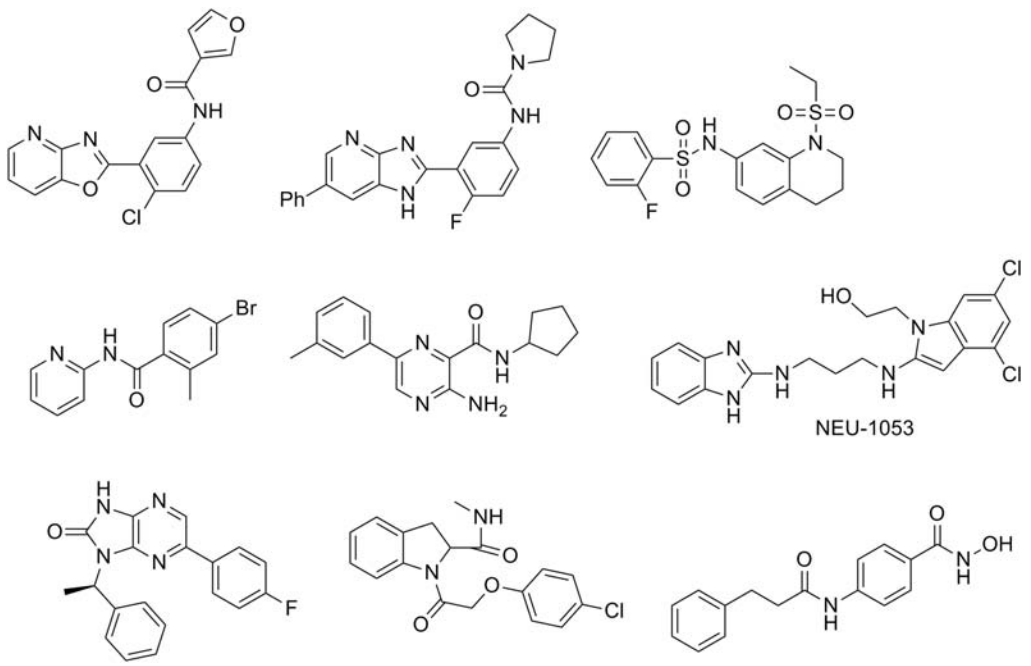

Fig. 29 Phenotypic screening hits for *T. brucei*.

5.23.2.3 Amoebas: *Entamoeba* and *Giardia* Species

Amoebiasis caused by the parasite *Entamoeba histolytica* is estimated to cause over 100,000 deaths per year, making it the second most deadly parasitic infection behind malaria.[183] Most infections with *E. histolytica* are confined to the intestine, resulting in diarrhea, but a proportion migrate to the liver, where abscesses can develop and lead to death.[183a] The current standard of care for *E. histolytica* infections is metronidazole, a nitroheterocyclic drug that is compromised by significant side effects including neurotoxicity[184] and carcinogenicity.[185] Despite these limitations, relatively little drug discovery has been conducted on this disease. This paucity of research is in part due to the difficulty of developing a high-throughput screen for this anaerobic parasite. The challenge is evident in efforts from the Castillo lab repurposing of benzimidazoles, benzotriazoles, and related heterocycles (**Fig. 30**) known to be active against nematodes and protozoa.[186] In these studies, a small number of compounds were selected based on comparison with known antiparasitics and by computational screening of large databases. A similar strategy for identification of inhibitors of heat shock protein 90 for *E. histolytica* activity[187] based on a high-throughput screen in *P. falciparum*[188] has also been reported. Additional efforts to identify starting points via *in silico* methods (e.g., docking to homology models of key protein targets) have been reported for inhibition of *E. histolytica* hexokinase 1.[189] Several series of compounds with antiamoebic properties have been reported as leads including pyrazolo[3,4-d]pyrimidines, pyrazolines, and bis-pyrimidines.[190]

Despite the challenges posed by screening an anaerobic pathogen, the outcome of two screens has been reported. In the first, screening of a library of FDA-approved and commercially available compounds identified the gold complex auranofin (vide supra; **Fig. 9**) as a potential lead for *E. histolytica*.[191] More recently, repurposing of the 400-member open-access Malaria Box identified two leads (**Fig. 30**) for *E. histolytica*.[57] Further optimization and development of these newly identified leads offer promise for future treatment of this amoebiasis.

Like *E. histolytica*, infection of individuals with *Giardia* parasites results in acute life-threatening diarrheal disease, particularly in children.[192] Repeated infection with *Giardia* has been associated with reduced growth rates of children and "failure to thrive" in many parts of the developing world. Treatments for giardiasis include metronidazole and related nitroheterocycles, and emergence of resistance to these drugs has been reported.[193] Unfortunately, very little new medicinal chemistry projects have been initiated against *Giardia*, with most leads arising from cross screening of compounds designed for other parasites such as *E. histolytica* and *L. donovani*. Similar repurposing screens to those described in the preceding text have identified a small number of compounds that inhibited growth of *G. lamblia* including the gold complex auranofin (**Fig. 9**).[191] It was shown that auranofin was active against metronidazole-resistant strains, inhibited the giardial thioredoxin oxidoreductase, and was active in several rodent models of giardiasis.[194]

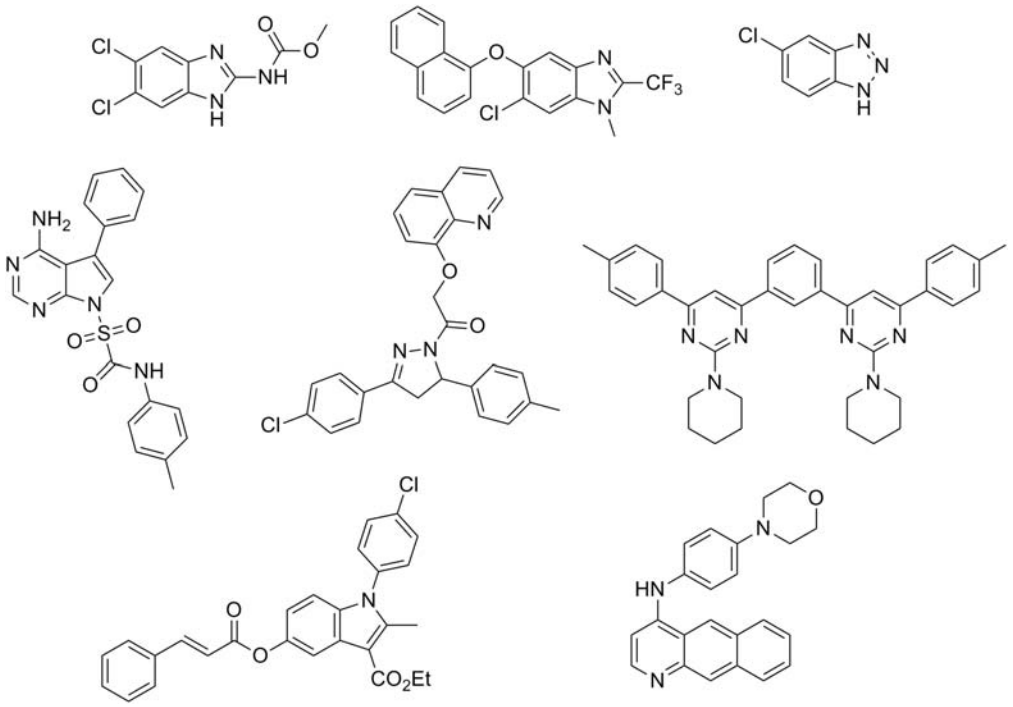

Fig. 30 Leads for treatment of amoebiasis caused by *E. histolytica*.

5.23.3 Helminths

In comparison with protozoans, drug discovery efforts aimed at elimination of helminth infections have been markedly less well developed. Multiple reasons account for this difference, including the existence of relatively effective broad-spectrum anthelmintics such as ivermectin and albendazole, the absence of robust high-throughput screening methodologies, and the much greater complexity and diversity of helminth biology.

5.23.3.1 Nematodes

5.23.3.1.1 Soil-transmitted helminths

Intestinal infections caused by helminths that spend a portion of their life cycle in the soil are widespread across the world and cause significant morbidity and mortality.[195] In fact, it is generally accepted that soil-transmitted helminth infections carry the highest burden of all neglected tropical diseases excluding malaria.[1] While some infections are relatively benign (i.e., *E. vermicularis* (pinworm)), others such as those caused by *A. duodenale* and *N. americanus* (hookworm) can result in significant anemia,[196] stunted growth,[197] and impaired cognitive ability[198] in children.

Despite these impacts, very little drug discovery and development have occurred over the past 10 years, indicative of the effectiveness of existing treatments. The well-known drugs albendazole, mebendazole, pyrantel pamoate, and levamisole (**Fig. 31**) continue to be the mainstay treatments for these diseases, with mass drug administration (MDA) programs having been very effective across the globe.[199]

5.23.3.1.2 Filarial worms

Infections by tissue-dwelling filarial worms such as *Wuchereria bancrofti*, *Brugia malayi*, *Onchocerca volvulus*, and *Dracunculus medinensis* are common across South America, Africa, and Asia. Diseases caused these infections (lymphatic filariasis, river blindness, and Guinea worm, respectively) are of substantial concern, particularly in sub-Saharan Africa.[200] Considerable effort has been expended on elimination of these parasites through a variety of means, including transmission blocking through improved sanitation[201] and MDA.[202]

Individuals who are bitten by mosquitoes carrying the larval stages of *W. bancrofti* or *B. malayi* will develop lymphatic filariasis (LF), where the larvae develop into adult worms in the lymphatic tissues. Long-term infection results in development of lymphedema, predominantly in the legs, ankles, and feet, commonly referred to as elephantiasis. This results in significant loss of mobility due to the swelling, rendering the individual unable to lead a normal productive life. Similarly, onchocerciasis develops in patients bitten by the black fly of the genus *Similium*, which host the larval stages of *O. volvulus*. This parasitic worm develops in subcutaneous nodules, with microfilaria migrating to the eyes of the patient, where they die and cause inflammation. Chronic inflammation caused by *O. volvulus* microfilaria in the eye ultimately leads to blindness.[200]

Current treatment of LF is accomplished through MDA programs utilizing albendazole, ivermectin, and diethylcarbamazine (**Fig. 32**).[203] These programs are targeted at reducing transmission by killing microfilaria in infected people, as the drugs do not kill the adult worm. Similarly, MDA programs with ivermectin have been employed for treatment of onchocerciasis. While this approach has been very successful in many countries and regions, several limitations have prompted continued exploration of new drug candidates to treat this disease. More specifically, the fact that the current drugs only kill the microfilaria and not the adult worms requires yearly retreatment for 4–6 years, and coinfection of patients with related filarial worm species, most significantly *Loa loa*, precludes use of ivermectin due to risk of serious side effects caused by rapid concomitant death of the *L. loa* worms.[204] Consequently, current drug discovery programs are focused on discovery of macrofilaricidal compounds that do not quickly kill microfilaria.

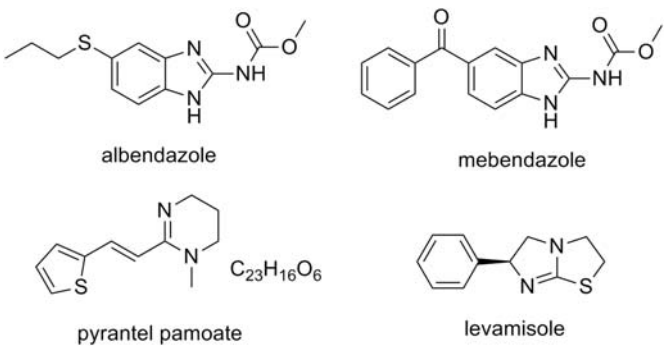

Fig. 31 Current drugs for treatment of soil-transmitted helminth infections.

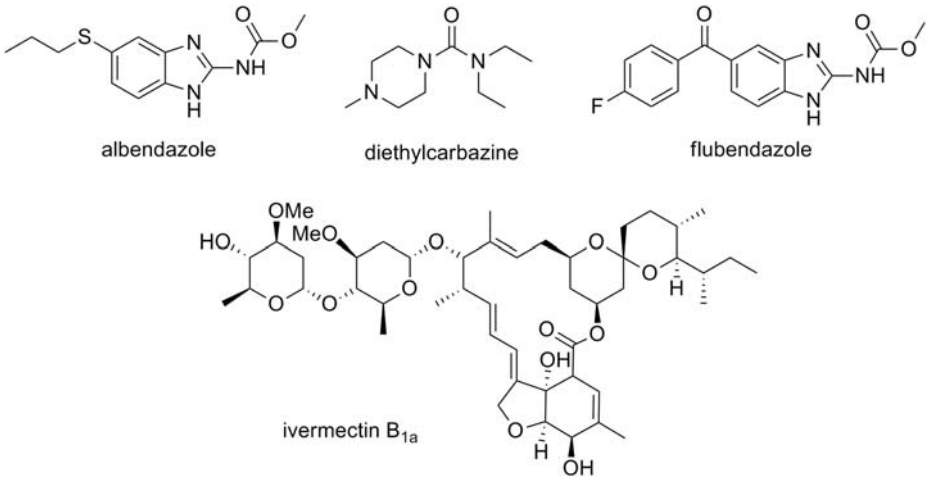

Fig. 32 Current treatments for lymphatic filariasis and onchocerciasis.

5.23.3.1.2.1 *Direct-acting macrofilaricides*

Consequently, the focus of drug discovery efforts for LF and onchocerciasis has been on discovery of macrofilaricidal agents that can cure patients with short courses of treatment (e.g., $<$14–28 days) and can be used in regions where coinfection with *L. loa* is possible. Described earlier in this article, a repurposed drug that has shown promising efficacy in animal models of LF is the gold complex auranofin (**Fig. 9**).[205] Auranofin was found to kill *B. malayi* worms at micromolar concentrations *in vitro* and affected up to 91% reduction of worm burden in an *in vivo* study in gerbils.[205] Mechanism of action studies supported the premise that auranofin inhibits the thioredoxin reductase enzyme, analogous to its mechanism in other parasites.[205]

In another repurposing project, the potential for the tubulin polymerization inhibitor flubendazole (**Fig. 32**) to be reformulated to improve oral bioavailability has been explored as a means to treat LF and onchocerciasis in Africa.[206] Of some concern to this approach, however, is the known embryotoxicity of flubendazole, which may preclude use in children and women of childbearing potential.[207] In addition, flubendazole and one of its metabolites have been shown to be aneugenic in an *in vivo* micronucleus test, although it has been argued that the risk posed to patients treated for a short period of time as required for anthelmintic efficacy is low.[208]

A third example of repurposing applied to discovery of anthelmintic drugs for LF and onchocerciasis is work reported on the development of NMT inhibitors.[209] The sequences of NMT enzymes of *B. malayi*, *O. volvulus*, and other filarial worms were compared with the homologous enzymes in other parasites and humans. The *B. malayi* enzyme was expressed in *E. coli* and used to screen several leads identified in a kinetoplastid NMT project (**Fig. 27**), where nanomolar activity was demonstrated. Finally, two lead compounds DDD85646 and DDD100870 were found to reduce motility of male and female *B. malayi* adults in culture.[209]

5.23.3.1.2.2 *Anti-*Wolbachia *compounds*

One of the unique features of the filarial worms that cause LF and onchocerciasis is the presence of an endosymbiotic bacterium, *Wolbachia*.[210] It has been known for quite some time that antibacterial drugs such as doxycycline that kill the *Wolbachia* present in worms are effective as antifilarials, as the growth of *Wolbachia*-depleted worms is inhibited, embryogenesis in female worms is interrupted, and the overall life span of the worms is significantly reduced.[211] One of the particularly attractive features of an anti-*Wolbachia* approach is that the eyeworm *L. loa* does not harbor the endosymbiont and, as such, is not affected by antibacterials.[210c] This "selectivity" is particularly important, as concurrent killing of both *O. volvulus* and *L. loa* has been associated with serious adverse events in the field.[212] Although effective, use of doxycycline (or minocycline) in disease-endemic areas is complicated by the need to treat patients for long periods (4–6 weeks).

As with direct-acting macrofilaricides, a significant effort has been applied to repurposing of approved drugs as anti-*Wolbachia* agents.[213] This effort has been facilitated by the development of high-throughput screens utilizing either *A. albopictus*[214]- or *D. melanogaster*[215]-derived cell lines infected with *Wolbachia*, which have allowed screening of thousands of known drugs as well as novel compound libraries.[216] Perhaps not surprisingly, a large percentage of the hits from screening known drugs were antibiotics, including representatives from the tetracycline, fluoroquinolone, and rifamycin classes (**Fig. 33**).[213] Very recently, a number of macrolides derived from tylosin have been reported as having significant anti-*Wolbachia* activity and have been evaluated in preclinical models of LF and onchocerciasis.[217]

5.23.3.2 Trematodes: *Schistosoma* and *Fasciola*

The trematodes are parasitic flatworms that are widely distributed geographically and infect both animals and humans. The two most important trematodes of relevance to human health are *Schistosoma* spp. and *Fasciola* spp., which infect the gastrointestinal

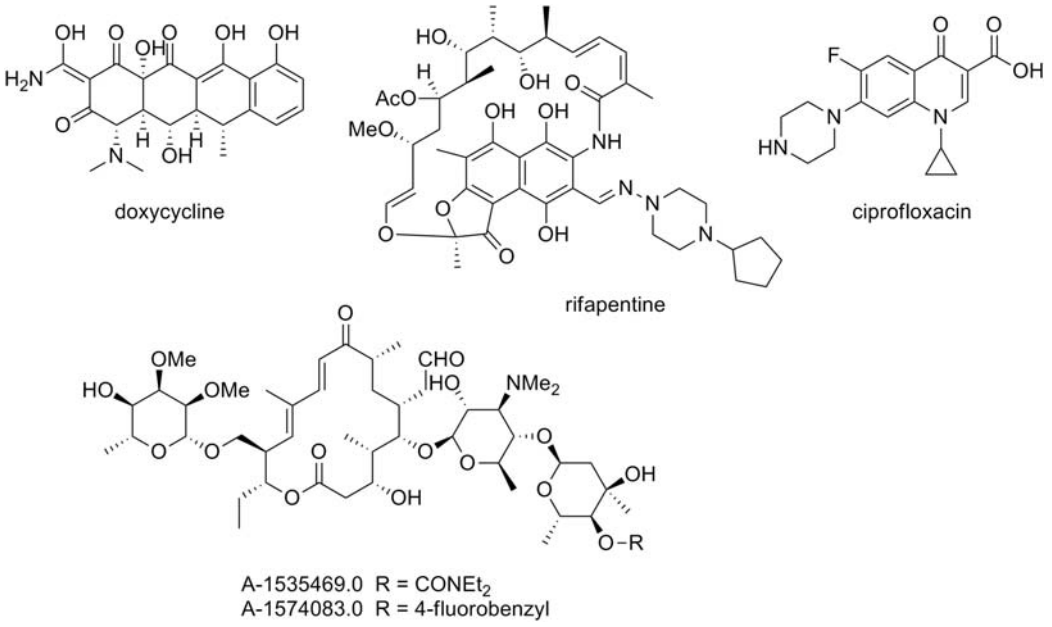

Fig. 33 Compounds active against *Wolbachia* spp. with potential as anthelmintics.

tract and liver, respectively. Infections are propagated by consumption of untreated drinking water, as these parasites are hosted in snails that are present in lakes and rivers around the globe. It has been estimated that over 265 million individuals are infected with *Schistosoma*, with over 280,000 deaths annually.[218] Epidemiological data for *Fasciola* infection in humans are less readily available, but a 2005 estimate suggested that over 90 million individuals are at risk.[219]

Despite the significant impact of *Schistosoma* infections on human health, the only drug used to treat schistosomiasis is praziquantel.[220] While generally effective, concerns over emergence of resistance continue to grow due to the reliance on a single drug. Numerous efforts have emerged to discover new drugs to treat schistosomiasis, primarily focused on development and application of high-throughput screens against the larval stage of *Schistosoma*, the schistosomula, which can be isolated from snails in culture.[221] Using these screening methods, a number of chemotypes have been identified from both commercial and proprietary compound libraries, representatives of which are depicted in **Fig. 34**.[221a,222]

Based on these hits, several early hit-to-lead or lead optimization projects have emerged and focused on a diaryl urea from the MMV Malaria Box[223] and synthetic peroxides previously studied as antimalarials (**Fig. 3**).[224] The synthetic peroxides have also been found to be effective against *F. hepatica*.[225]

In addition to phenotypic screening, a limited number of biochemical targets have been evaluated as sources of new chemotypes for treatment of schistosomiasis. One such example is the class I *S. mansoni* histone deacetylase 8.[226] This work has been facilitated by the availability of recombinant enzyme and X-ray crystallography of lead compounds bound to the enzyme active site.[227] Preliminary optimization of a series of hydroxamic acids afforded a lead with nanomolar affinity for the enzyme and activity against the schistosomula (**Fig. 35**).[228] More recently, the same researchers have characterized and developed a screening assay to identify leads from the class III HDAC, *S. mansoni* sirtuin 1.[229]

A third biochemical target that has been examined as a source for antischistosomal leads is polo-like kinase 1 (PLK1). Following validation of the target for development of schistosomula by RNAi, screening of known human PLK1 inhibitors identified a series of benzimidazole thiophenes (**Fig. 35**) as leads for this enzyme.[230]

5.23.4 Summary and Conclusions

In the past decade, considerable effort has been expended on the discovery and development of new drug candidates for the treatment of a wide range of parasitic infections. Much of this work has been facilitated by collaborative efforts between governments, philanthropic organizations, and PDPs that aim to close the gap that exists between economic incentive and unmet medical need. In particular, the Bill and Melinda Gates Foundation has committed to eradication of the top 10 parasitic diseases by 2020 and has provided considerable resources, both financial and organizational, to achieve this goal. Clinical candidates for both protozoan (malaria, HAT, and Chagas disease) and helminth (onchocerciasis) have recently been identified, with lead optimization programs focused on leishmaniasis, amoebiasis, and schistosomiasis progressing toward preclinical candidates. Continued engagement of the partners identified in the preceding text is critical to the long-term success of discovery and development efforts in this area. One of the main areas of focus in the past few years has been to repurpose approved drugs and clinical

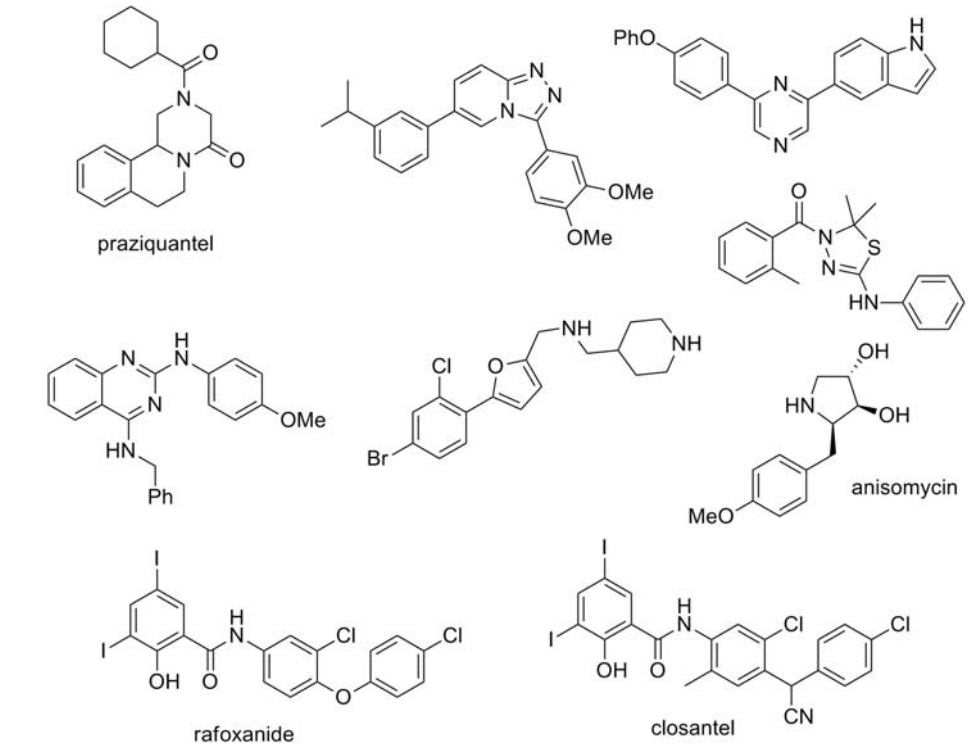

Fig. 34 Representative antischistosomal hits from screening of commercial libraries.

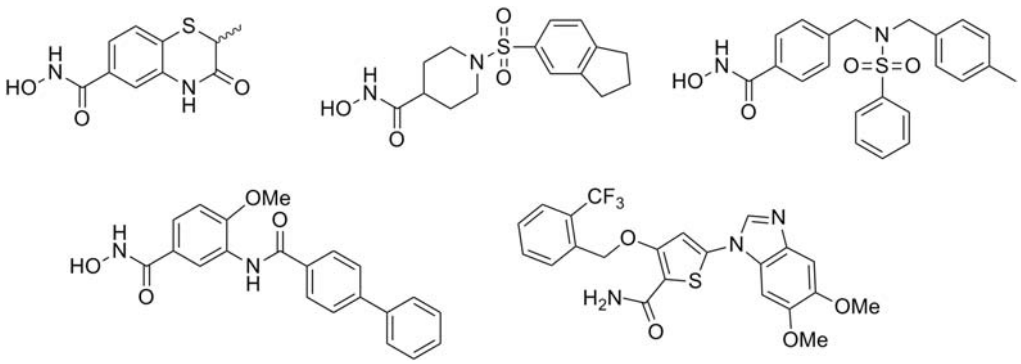

Fig. 35 Leads from target-based screening for antischistosomal compounds.

candidates from other diseases for use in parasitic infections, an approach that has been facilitated by a significantly increased understanding of the biochemistry of the target organisms. While this approach has offered some quick wins (e.g., ivermectin and fexinidazole) in providing useful treatments for some diseases, there remains a need for new chemical entities that are designed to kill parasites by those biochemistries that are unique to the parasite. These scientific strategies, coupled with creative approaches for funding of discovery and development projects for what are often diseases of the developing world, offer hope for continued progress in this field.

See also: 8.20. Case History: AN5568 (SCYX-7158). 8.21. KAE609 (Cipargamin): Discovery of Spiroindolone Antimalarials. 8.22. Medicinal Chemistry Case History: Discovery of the Dihydroorate Dehydrogenase Inhibitor DSM265 as an Antimalarial Drug Candidate.

References

1. Murray, C. J.; Vos, T.; Lozano, R.; Naghavi, M.; Flaxman, A. D.; Michaud, C.; Ezzati, M.; Shibuya, K.; Salomon, J. A.; Abdalla, S.; Aboyans, V.; Abraham, J.; Ackerman, I.; Aggarwal, R.; Ahn, S. Y.; Ali, M. K.; Alvarado, M.; Anderson, H. R.; Anderson, L. M.; Andrews, K. G.; Atkinson, C.; Baddour, L. M.; Bahalim, A. N.; Barker-Collo, S.; Barrero, L. H.; Bartels, D. H.; Basanez, M. G.; Baxter, A.; Bell, M. L.; Benjamin, E. J.; Bennett, D.; Bernabe, E.; Bhalla, K.; Bhandari, B.; Bikbov, B.; Bin Abdulhak, A.; Birbeck, G.; Black, J. A.; Blencowe, H.; Blore, J. D.; Blyth, F.; Bolliger, I.; Bonaventure, A.; Boufous, S.; Bourne, R.; Boussinesq, M.; Braithwaite, T.; Brayne, C.; Bridgett, L.; Brooker, S.; Brooks, P.; Brugha, T. S.; Bryan-Hancock, C.; Bucello, C.; Buchbinder, R.; Buckle, G.; Budke, C. M.; Burch, M.; Burney, P.; Burstein, R.; Calabria, B.; Campbell, B.; Canter, C. E.; Carabin, H.; Carapetis, J.; Carmona, L.; Cella, C.; Charlson, F.; Chen, H.; Cheng, A. T.; Chou, D.; Chugh, S. S.; Coffeng, L. E.; Colan, S. D.; Colquhoun, S.; Colson, K. E.; Condon, J.; Connor, M. D.; Cooper, L. T.; Corriere, M.; Cortinovis, M.; de Vaccaro, K. C.; Couser, W.; Cowie, B. C.; Criqui, M. H.; Cross, M.; Dabhadkar, K. C.; Dahiya, M.; Dahodwala, N.; Damsere-Derry, J.; Danaei, G.; Davis, A.; De Leo, D.; Degenhardt, L.; Dellavalle, R.; Delossantos, A.; Denenberg, J.; Derrett, S.; Des Jarlais, D. C.; Dharmaratne, S. D.; Dherani, M.; Diaz-Torne, C.; Dolk, H.; Dorsey, E. R.; Driscoll, T.; Duber, H.; Ebel, B.; Edmond, K.; Elbaz, A.; Ali, S. E.; Erskine, H.; Erwin, P. J.; Espindola, P.; Ewoigbokhan, S. E.; Farzadfar, F.; Feigin, V.; Felson, D. T.; Ferrari, A.; Ferri, C. P.; Fevre, E. M.; Finucane, M. M.; Flaxman, S.; Flood, L.; Foreman, K.; Forouzanfar, M. H.; Fowkes, F. G.; Fransen, M.; Freeman, M. K.; Gabbe, B. J.; Gabriel, S. E.; Gakidou, E.; Ganatra, H. A.; Garcia, B.; Gaspari, F.; Gillum, R. F.; Gmel, G.; Gonzalez-Medina, D.; Gosselin, R.; Grainger, R.; Grant, B.; Groeger, J.; Guillemin, F.; Gunnell, D.; Gupta, R.; Haagsma, J.; Hagan, H.; Halasa, Y. A.; Hall, W.; Haring, D.; Haro, J. M.; Harrison, J. E.; Havmoeller, R.; Hay, R. J.; Higashi, H.; Hill, C.; Hoen, B.; Hoffman, H.; Hotez, P. J.; Hoy, D.; Huang, J. J.; Ibeanusi, S. E.; Jacobsen, K. H.; James, S. L.; Jarvis, D.; Jasrasaria, R.; Jayaraman, S.; Johns, N.; Jonas, J. B.; Karthikeyan, G.; Kassebaum, N.; Kawakami, N.; Keren, A.; Khoo, J. P.; King, C. H.; Knowlton, L. M.; Kobusingye, O.; Koranteng, A.; Krishnamurthi, R.; Laden, F.; Lalloo, R.; Laslett, L. L.; Lathlean, T.; Leasher, J. L.; Lee, Y. Y.; Leigh, J.; Levinson, D.; Lim, S. S.; Limb, E.; Lin, J. K.; Lipnick, M.; Lipshultz, S. E.; Liu, W.; Loane, M.; Ohno, S. L.; Lyons, R.; Mabweijano, J.; MacIntyre, M. F.; Malekzadeh, R.; Mallinger, L.; Manivannan, S.; Marcenes, W.; March, L.; Margolis, D. J.; Marks, G. B.; Marks, R.; Matsumori, A.; Matzopoulos, R.; Mayosi, B. M.; McAnulty, J. H.; McDermott, M. M.; McGill, N.; McGrath, J.; Medina-Mora, M. E.; Meltzer, M.; Mensah, G. A.; Merriman, T. R.; Meyer, A. C.; Miglioli, V.; Miller, M.; Miller, T. R.; Mitchell, P. B.; Mock, C.; Mocumbi, A. O.; Moffitt, T. E.; Mokdad, A. A.; Monasta, L.; Montico, M.; Moradi-Lakeh, M.; Moran, A.; Morawska, L.; Mori, R.; Murdoch, M. E.; Mwaniki, M. K.; Naidoo, K.; Nair, M. N.; Naldi, L.; Narayan, K. M.; Nelson, P. K.; Nelson, R. G.; Nevitt, M. C.; Newton, C. R.; Nolte, S.; Norman, P.; Norman, R.; O'Donnell, M.; O'Hanlon, S.; Olives, C.; Omer, S. B.; Ortblad, K.; Osborne, R.; Ozgediz, D.; Page, A.; Pahari, B.; Pandian, J. D.; Rivero, A. P.; Patten, S. B.; Pearce, N.; Padilla, R. P.; Perez-Ruiz, F.; Perico, N.; Pesudovs, K.; Phillips, D.; Phillips, M. R.; Pierce, K.; Pion, S.; Polanczyk, G. V.; Polinder, S.; Pope, C. A., Iii; Popova, S.; Porrini, E.; Pourmalek, F.; Prince, M.; Pullan, R. L.; Ramaiah, K. D.; Ranganathan, D.; Razavi, H.; Regan, M.; Rehm, J. T.; Rein, D. B.; Remuzzi, G.; Richardson, K.; Rivara, F. P.; Roberts, T.; Robinson, C.; De Leon, F. R.; Ronfani, L.; Room, R.; Rosenfeld, L. C.; Rushton, L.; Sacco, R. L.; Saha, S.; Sampson, U.; Sanchez-Riera, L.; Sanman, E.; Schwebel, D. C.; Scott, J. G.; Segui-Gomez, M.; Shahraz, S.; Shepard, D. S.; Shin, H.; Shivakoti, R.; Singh, D.; Singh, G. M.; Singh, J. A.; Singleton, J.; Sleet, D. A.; Sliwa, K.; Smith, E.; Smith, J. L.; Stapelberg, N. J.; Steer, A.; Steiner, T.; Stolk, W. A.; Stovner, L. J.; Sudfeld, C.; Syed, S.; Tamburlini, G.; Tavakkoli, M.; Taylor, H. R.; Taylor, J. A.; Taylor, W. J.; Thomas, B.; Thomson, W. M.; Thurston, G. D.; Tleyjeh, I. M.; Tonelli, M.; Towbin, J. A.; Truelsen, T.; Tsilimbaris, M. K.; Ubeda, C.; Undurraga, E. A.; van der Werf, M. J.; van Os, J.; Vavilala, M. S.; Venketasubramanian, N.; Wang, M.; Wang, W.; Watt, K.; Weatherall, D. J.; Weinstock, M. A.; Weintraub, R.; Weisskopf, M. G.; Weissman, M. M.; White, R. A.; Whiteford, H.; Wiebe, N.; Wiersma, S. T.; Wilkinson, J. D.; Williams, H. C.; Williams, S. R.; Witt, E.; Wolfe, F.; Woolf, A. D.; Wulf, S.; Yeh, P. H.; Zaidi, A. K.; Zheng, Z. J.; Zonies, D.; Lopez, A. D.; AlMazroa, M. A.; Memish, Z. A. Disability-Adjusted Life Years (DALYs) For 291 Diseases and Injuries in 21 Regions, 1990–2010: A Systematic Analysis for the Global Burden of Disease Study 2010. *Lancet* **2012,** *380* (9859), 2197–2223.
2. Bost, F.; Jacobs, R. T.; Kowalczyk, P. Informatics for Neglected Diseases Collaborations. *Curr. Opin. Drug Discov. Devel.* **2010,** *13* (3), 286–296.
3. Maréchal, E.; Cesbron-Delauw, M.-F. The Apicoplast: A New Member of the Plastid Family. *Trends Plant Sci.* **2001,** *6* (5), 200–205.
4. (a) McFadden, G. I.; Roos, D. S. Apicomplexan Plastids As Drug Targets. *Trends Microbiol.* **1999,** *7* (8), 328–333; (b) Ralph, S. A.; D'Ombrain, M. C.; McFadden, G. I. The Apicoplast As an Antimalarial Drug Target. *Drug Resist. Updat.* **2001,** *4* (3), 145–151; (c) Dahl, E. L.; Rosenthal, P. J. Apicoplast Translation, Transcription and Genome Replication: Targets for Antimalarial Antibiotics. *Trends Parasitol.* **2008,** *24* (6), 279–284.
5. World Malaria Report. 2015. http://www.who.int/malaria/publications/world-malaria-report-2015/report/en/.
6. Jones, J. L.; Holland, G. N. Annual Burden of Ocular Toxoplasmosis in the United States. *Am. J. Trop. Med. Hyg.* **2010,** *82* (3), 464–465.
7. (a) Dannemann, B.; McCutchan, J. A.; Israelski, D.; Antoniskis, D.; Leport, C.; Luft, B.; Nussbaum, J.; Clumeck, N.; Morlat, P.; Chiu, J.; Vilde, J.-L.; Orellana, M.; Feigal, D.; Bartok, A.; Heseltine, P.; Leedom, J.; Remington, J. Treatment of Toxoplasmic Encephalitis in Patients With AIDSA Randomized Trial Comparing Pyrimethamine Plus Clindamycin to Pyrimethamine Plus Sulfadiazine. *Ann. Intern. Med.* **1992,** *116* (1), 33–43; (b) Demar, M.; Hommel, D.; Djossou, F.; Peneau, C.; Boukhari, R.; Louvel, D.; Bourbigot, A. M.; Nasser, V.; Ajzenberg, D.; Darde, M. L.; Carme, B. Acute Toxoplasmoses in Immunocompetent Patients Hospitalized in an Intensive Care Unit in French Guiana. *Clin. Microbiol. Infect.* **2012,** *18* (7), E221–E231.
8. Gilbert, R. E.; Freeman, K.; Lago, E. G.; Bahia-Oliveira, L. M. G.; Tan, H. K.; Wallon, M.; Buffolano, W.; Stanford, M. R.; Petersen, E.; for The European Multicentre Study on Congenital, T.. Ocular Sequelae of Congenital Toxoplasmosis in Brazil Compared With Europe. *PLoS Negl. Trop. Dis.* **2008,** *2* (8), e277.
9. (a) Halsby, K.; Guy, E.; Said, B.; Francis, J.; O'Connor, C.; Kirkbride, H.; Morgan, D. Enhanced Surveillance for Toxoplasmosis in England and Wales, 2008–2012. *Epidemiol. Infect.* **2014,** *142* (8), 1653–1660; (b) Nogareda, F.; Le Strat, Y.; Villena, I.; De Valk, H.; Goulet, V. Incidence and Prevalence of *Toxoplasma gondii* Infection in Women in France, 1980–2020: Model-Based Estimation. *Epidemiol. Infect.* **2014,** *142* (08), 1661–1670.
10. Chen, X.-M.; Keithly, J. S.; Paya, C. V.; LaRusso, N. F. Cryptosporidiosis. *N. Engl. J. Med.* **2002,** *346* (22), 1723–1731.
11. Kotloff, K. L.; Blackwelder, W. C.; Nasrin, D.; Nataro, J. P.; Farag, T. H.; van Eijk, A.; Adegbola, R. A.; Alonso, P. L.; Breiman, R. F.; Golam Faruque, A. S.; Saha, D.; Sow, S. O.; Sur, D.; Zaidi, A. K. M.; Biswas, K.; Panchalingam, S.; Clemens, J. D.; Cohen, D.; Glass, R. I.; Mintz, E. D.; Sommerfelt, H.; Levine, M. M. The Global Enteric Multicenter Study (GEMS) of Diarrheal Disease in Infants and Young Children in Developing Countries: Epidemiologic and Clinical Methods of the Case/Control Study. *Clin. Infect. Dis.* **2012,** *55* (Suppl. 4), S232–S245.
12. Guerrant, D. I.; Moore, S. R.; Lima, A. A.; Patrick, P. D.; Schorling, J. B.; Guerrant, R. L. Association of Early Childhood Diarrhea and Cryptosporidiosis With Impaired Physical Fitness and Cognitive Function Four-Seven Years Later in a Poor Urban Community in Northeast Brazil. *Am. J. Trop. Med. Hyg.* **1999,** *61* (5), 707–713.
13. Anthony, M. P.; Burrows, J. N.; Duparc, S.; Moehrle, J. J.; Wells, T. N. The Global Pipeline of New Medicines for the Control and Elimination of Malaria. *Malar. J.* **2012,** *11,* 316.
14. World Health Organization. WHO Global Health Estimates Technical Paper WHO/HIS/HIS/GHE/2013.4. WHO methods and data sources for global burden of disease estimates 2000–2011. http://www.who.int/healthinfo/global_burden_disease/estimates/en/index2.html.
15. Wells, T. N. C.; van Huijsduijnen, R. H.; Van Voorhis, W. C. Malaria Medicines: A Glass Half Full? *Nat. Rev. Drug Discov.* **2015,** *14* (6), 424–442.
16. Tu, Y. Y.; Ni, M. Y.; Zhong, Y. R.; Li, L. N.; Cui, S. L.; Zhang, M. Q.; Wang, X. Z.; Liang, X. T. Studies on the Constituents of *Artemisia annua* L. (Author's Transl). *Yao Xue Xue Bao* **1981,** *16* (5), 366–370.

17. (a). WHO briefing on malaria treatment guidelines and artemisinin monotherapies. http://www.who.int/malaria/publications/atoz/meeting_briefing19april/en/. (b) Hawkes, M.; Conroy, A. L.; Kain, K. C. Spread of Artemisinin Resistance in Malaria. *N. Engl. J. Med.* **2014,** *371* (20), 1944–1945; (c) Ashley, E. A.; Dhorda, M.; Fairhurst, R. M.; Amaratunga, C.; Lim, P.; Suon, S.; Sreng, S.; Anderson, J. M.; Mao, S.; Sam, B.; Sopha, C.; Chuor, C. M.; Nguon, C.; Sovannaroth, S.; Pukrittayakamee, S.; Jittamala, P.; Chotivanich, K.; Chutasmit, K.; Suchatsoonthorn, C.; Runcharoen, R.; Hien, T. T.; Thuy-Nhien, N. T.; Thanh, N. V.; Phu, N. H.; Htut, Y.; Han, K. T.; Aye, K. H.; Mokuolu, O. A.; Olaosebikan, R. R.; Folaranmi, O. O.; Mayxay, M.; Khanthavong, M.; Hongvanthong, B.; Newton, P. N.; Onyamboko, M. A.; Fanello, C. I.; Tshefu, A. K.; Mishra, N.; Valecha, N.; Phyo, A. P.; Nosten, F.; Yi, P.; Tripura, R.; Borrmann, S.; Bashraheil, M.; Peshu, J.; Faiz, M. A.; Ghose, A.; Hossain, M. A.; Samad, R.; Rahman, M. R.; Hasan, M. M.; Islam, A.; Miotto, O.; Amato, R.; MacInnis, B.; Stalker, J.; Kwiatkowski, D. P.; Bozdech, Z.; Jeeyapant, A.; Cheah, P. Y.; Sakulthaew, T.; Chalk, J.; Intharabut, B.; Silamut, K.; Lee, S. J.; Vihokhern, B.; Kunasol, C.; Imwong, M.; Tarning, J.; Taylor, W. J.; Yeung, S.; Woodrow, C. J.; Flegg, J. A.; Das, D.; Smith, J.; Venkatesan, M.; Plowe, C. V.; Stepniewska, K.; Guerin, P. J.; Dondorp, A. M.; Day, N. P.; White, N. J. Tracking Resistance to Artemisinin, C., Spread of Artemisinin Resistance in *Plasmodium falciparum* Malaria. *N. Engl. J. Med.* **2014,** *371* (5), 411–423.
18. (a) Mulenga, M.; VangGeertruyden, J. P.; Mwananyanda, L.; Chalwe, V.; Moerman, F.; Chilengi, R.; Van Overmeir, C.; Dujardin, J. C.; D'Alessandro, U. Safety and Efficacy of Lumefantrine-Artemether (Coartem) for the Treatment of Uncomplicated *Plasmodium falciparum* Malaria in Zambian Adults. *Malar. J.* **2006,** *5,* 73; (b) Fanello, C. I.; Karema, C.; van Doren, W.; Van Overmeir, C.; Ngamije, D.; D'Alessandro, U. A Randomised Trial to Assess the Safety and Efficacy of Artemether-Lumefantrine (Coartem) for the Treatment of Uncomplicated *Plasmodium falciparum* Malaria in Rwanda. *Trans. R. Soc. Trop. Med. Hyg.* **2007,** *101* (4), 344–350.
19. (a) Sirima, S. B.; Gansane, A. Artesunate-Amodiaquine for the Treatment of Uncomplicated Malaria. *Expert Opin. Investig. Drugs* **2007,** *16* (7), 1079–1085; (b) Ndiaye, J. L.; Randrianarivelojosia, M.; Sagara, I.; Brasseur, P.; Ndiaye, I.; Faye, B.; Randrianasolo, L.; Ratsimbasoa, A.; Forlemu, D.; Moor, V. A.; Traore, A.; Dicko, Y.; Dara, N.; Lameyre, V.; Diallo, M.; Djimde, A.; Same-Ekobo, A.; Gaye, O. Randomized, Multicentre Assessment of the Efficacy and Safety of ASAQ—A Fixed-Dose Artesunate-Amodiaquine Combination Therapy in the Treatment of Uncomplicated *Plasmodium falciparum* Malaria. *Malar. J.* **2009,** *8,* 125; (c) Zwang, J.; Olliaro, P.; Barennes, H.; Bonnet, M.; Brasseur, P.; Bukirwa, H.; Cohuet, S.; D'Alessandro, U.; Djimde, A.; Karema, C.; Guthmann, J. P.; Hamour, S.; Ndiaye, J. L.; Martensson, A.; Rwagacondo, C.; Sagara, I.; Same-Ekobo, A.; Sirima, S. B.; van den Broek, I.; Yeka, A.; Taylor, W. R.; Dorsey, G.; Randrianarivelojosia, M. Efficacy of Artesunate-Amodiaquine for Treating Uncomplicated Falciparum Malaria in Sub-Saharan Africa: A Multi-Centre Analysis. *Malar. J.* **2009,** *8,* 203.
20. (a) Myint, H. Y.; Ashley, E. A.; Day, N. P.; Nosten, F.; White, N. J. Efficacy and Safety of Dihydroartemisinin-Piperaquine. *Trans. R. Soc. Trop. Med. Hyg.* **2007,** *101* (9), 858–866; (b) Zwang, J.; Ashley, E. A.; Karema, C.; D'Alessandro, U.; Smithuis, F.; Dorsey, G.; Janssens, B.; Mayxay, M.; Newton, P.; Singhasivanon, P.; Stepniewska, K.; White, N. J.; Nosten, F. Safety and Efficacy of Dihydroartemisinin-Piperaquine in Falciparum Malaria: A Prospective Multi-Centre Individual Patient Data Analysis. *PLoS One* **2009,** *4* (7), e6358.
21. (a) Nosten, F. H. Pyronaridine-Artesunate for Uncomplicated Falciparum Malaria. *Lancet* **2010,** *375* (9724), 1413–1414; (b) Kurth, F.; Belard, S.; Basra, A.; Ramharter, M. Pyronaridine-Artesunate Combination Therapy for the Treatment of Malaria. *Curr. Opin. Infect. Dis.* **2011,** *24* (6), 564–569; (c) Duparc, S.; Borghini-Fuhrer, I.; Craft, C. J.; Arbe-Barnes, S.; Miller, R. M.; Shin, C. S.; Fleckenstein, L. Safety and Efficacy of Pyronaridine-Artesunate in Uncomplicated Acute Malaria: An Integrated Analysis of Individual Patient Data From Six Randomized Clinical Trials. *Malar. J.* **2013,** *12,* 70.
22. (a) Faye, B.; Ndiaye, J. L.; Tine, R.; Sylla, K.; Gueye, A.; Lo, A. C.; Gaye, O. A Randomized Trial of Artesunate Mefloquine Versus Artemether Lumefantrine for the Treatment of Uncomplicated *Plasmodium falciparum* malaria in Senegalese Children. *Am. J. Trop. Med. Hyg.* **2010,** *82* (1), 140–144; (b) Bouyou-Akotet, M. K.; Ramharter, M.; Ngoungou, E. B.; Mamfoumbi, M. M.; Mihindou, M. P.; Missinou, M. A.; Kurth, F.; Belard, S.; Agnandji, S. T.; Issifou, S.; Heidecker, J. L.; Trapp, S.; Kremsner, P. G.; Kombila, M. Efficacy and Safety of a New Pediatric Artesunate-Mefloquine Drug Formulation for the Treatment of Uncomplicated Falciparum Malaria in Gabon. *Wien. Klin. Wochenschr.* **2010,** *122* (5–6), 173–178; (c) Agomo, P. U.; Meremikwu, M. M.; Watila, I. M.; Omalu, I. J.; Odey, F. A.; Oguche, S.; Ezeiru, V. I.; Aina, O. O. Efficacy, Safety and Tolerability of Artesunate-Mefloquine in the Treatment of Uncomplicated *Plasmodium falciparum* Malaria in Four Geographic Zones of Nigeria. *Malar. J.* **2008,** *7,* 172; (d) Massougbodji, A.; Kone, M.; Kinde-Gazard, D.; Same-Ekobo, A.; Cambon, N.; Mueller, E. A. A Randomized, Double-Blind Study on the Efficacy and Safety of a Practical Three-Day Regimen With Artesunate and Mefloquine for the Treatment of Uncomplicated *Plasmodium falciparum* Malaria in Africa. *Trans. R. Soc. Trop. Med. Hyg.* **2002,** *96* (6), 655–659.
23. (a) Leang, R.; Taylor, W. R.; Bouth, D. M.; Song, L.; Tarning, J.; Char, M. C.; Kim, S.; Witkowski, B.; Duru, V.; Domergue, A.; Khim, N.; Ringwald, P.; Menard, D. Evidence of Falciparum Malaria Multidrug Resistance to Artemisinin and Piperaquine in Western Cambodia: Dihydroartemisinin-Piperaquine Open-Label Multicenter Clinical Assessment. *Antimicrob. Agents Chemother.* **2015,** *59,* 4719–4726; (b) Djimde, A. A.; Makanga, M.; Kuhen, K.; Hamed, K. The Emerging Threat of Artemisinin Resistance in Malaria: Focus on Artemether-Lumefantrine. *Expert Rev. Anti Infect. Ther.* **2015,** *13,* 1031–1045; (c) Taylor, S. M.; Juliano, J. J. Artemisinin Combination Therapies and Malaria Parasite Drug Resistance: The Game Is Afoot. *J. Infect. Dis.* **2014,** *210* (3), 335–337.
24. Dong, Y.; Chollet, J.; Matile, H.; Charman, S. A.; Chiu, F. C.; Charman, W. N.; Scorneaux, B.; Urwyler, H.; Santo Tomas, J.; Scheurer, C.; Snyder, C.; Dorn, A.; Wang, X.; Karle, J. M.; Tang, Y.; Wittlin, S.; Brun, R.; Vennerstrom, J. L. Spiro and Dispiro-1,2,4-trioxolanes As Antimalarial Peroxides: Charting a Workable Structure-Activity Relationship Using Simple Prototypes. *J. Med. Chem.* **2005,** *48* (15), 4953–4961.
25. Padmanilayam, M.; Scorneaux, B.; Dong, Y.; Chollet, J.; Matile, H.; Charman, S. A.; Creek, D. J.; Charman, W. N.; Tomas, J. S.; Scheurer, C.; Wittlin, S.; Brun, R.; Vennerstrom, J. L. Antimalarial Activity of *N*-Alkyl amine, Carboxamide, Sulfonamide, and Urea Derivatives of a Dispiro-1,2,4-trioxolane Piperidine. *Bioorg. Med. Chem. Lett.* **2006,** *16* (21), 5542–5545.
26. Tang, Y.; Dong, Y.; Wittlin, S.; Charman, S. A.; Chollet, J.; Chiu, F. C.; Charman, W. N.; Matile, H.; Urwyler, H.; Dorn, A.; Bajpai, S.; Wang, X.; Padmanilayam, M.; Karle, J. M.; Brun, R.; Vennerstrom, J. L. Weak Base Dispiro-1,2,4-trioxolanes: Potent Antimalarial Ozonides. *Bioorg. Med. Chem. Lett.* **2007,** *17* (5), 1260–1265.
27. Dong, Y.; Wittlin, S.; Sriraghavan, K.; Chollet, J.; Charman, S. A.; Charman, W. N.; Scheurer, C.; Urwyler, H.; Santo Tomas, J.; Snyder, C.; Creek, D. J.; Morizzi, J.; Koltun, M.; Matile, H.; Wang, X.; Padmanilayam, M.; Tang, Y.; Dorn, A.; Brun, R.; Vennerstrom, J. L. The Structure-Activity Relationship of the Antimalarial Ozonide Arterolane (OZ277). *J. Med. Chem.* **2010,** *53* (1), 481–491.
28. Vennerstrom, J. L.; Arbe-Barnes, S.; Brun, R.; Charman, S. A.; Chiu, F. C.; Chollet, J.; Dong, Y.; Dorn, A.; Hunziker, D.; Matile, H.; McIntosh, K.; Padmanilayam, M.; Santo Tomas, J.; Scheurer, C.; Scorneaux, B.; Tang, Y.; Urwyler, H.; Wittlin, S.; Charman, W. N. Identification of an Antimalarial Synthetic Trioxolane Drug Development Candidate. *Nature* **2004,** *430* (7002), 900–904.
29. Olliaro, P.; Wells, T. N. The Global Portfolio of New Antimalarial Medicines Under Development. *Clin. Pharmacol. Ther.* **2009,** *85* (6), 584–595.
30. Patil, C.; Katare, S.; Baig, M.; Doifode, S. Fixed Dose Combination of Arterolane and Piperaquine: A Newer Prospect in Antimalarial Therapy. *Ann. Med. Health Sci. Res.* **2014,** *4* (4), 466–471.
31. (a) Charman, S. A.; Arbe-Barnes, S.; Bathurst, I. C.; Brun, R.; Campbell, M.; Charman, W. N.; Chiu, F. C.; Chollet, J.; Craft, J. C.; Creek, D. J.; Dong, Y.; Matile, H.; Maurer, M.; Morizzi, J.; Nguyen, T.; Papastogiannidis, P.; Scheurer, C.; Shackleford, D. M.; Sriraghavan, K.; Stingelin, L.; Tang, Y.; Urwyler, H.; Wang, X.; White, K. L.; Wittlin, S.; Zhou, L.; Vennerstrom, J. L. Synthetic Ozonide Drug Candidate OZ439 Offers New Hope for a Single-Dose Cure of Uncomplicated Malaria. *Proc. Natl. Acad. Sci. U. S. A.* **2011,** *108* (11), 4400–4405; (b) Moehrle, J. J.; Duparc, S.; Siethoff, C.; van Giersbergen, P. L.; Craft, J. C.; Arbe-Barnes, S.; Charman, S. A.; Gutierrez, M.; Wittlin, S.; Vennerstrom, J. L. First-in-Man Safety and Pharmacokinetics of Synthetic Ozonide OZ439 Demonstrates an Improved Exposure Profile Relative to Other Peroxide Antimalarials. *Br. J. Clin. Pharmacol.* **2013,** *75* (2), 524–537; (c) Wang, X.; Dong, Y.; Wittlin, S.; Charman, S. A.; Chiu, F. C.; Chollet, J.; Katneni, K.; Mannila, J.; Morizzi, J.; Ryan, E.; Scheurer, C.; Steuten, J.; Santo Tomas, J.; Snyder, C.; Vennerstrom, J. L. Comparative Antimalarial Activities and ADME Profiles of Ozonides (1,2,4-Trioxolanes) OZ277, OZ439, and Their 1,2-Dioxolane, 1,2,4-Trioxane, and 1,2,4,5-Tetraoxane Isosteres. *J. Med. Chem.* **2013,** *56* (6), 2547–2555.
32. Phyo, A. P.; Jittamala, P.; Nosten, F. H.; Pukrittayakamee, S.; Imwong, M.; White, N. J.; Duparc, S.; Macintyre, F.; Baker, M.; Mohrle, J. J. Antimalarial Activity of Artefenomel (Oz439), a Novel Synthetic Antimalarial Endoperoxide, in Patients With *Plasmodium falciparum* and *Plasmodium vivax* Malaria: An Open-Label Phase 2 Trial. *Lancet Infect. Dis.* **2016,** *16* (1), 61–69.
33. Phase IIb Study to Investigate the Efficacy of OZ439 and Piperaquine Phosphate Co-Administered to Adults and Children With Uncomplicated *Plasmodium falciparum*. https://clinicaltrials.gov/ct2/show/NCT02083380.

34. Yeung, B. K.; Zou, B.; Rottmann, M.; Lakshminarayana, S. B.; Ang, S. H.; Leong, S. Y.; Tan, J.; Wong, J.; Keller-Maerki, S.; Fischli, C.; Goh, A.; Schmitt, E. K.; Krastel, P.; Francotte, E.; Kuhen, K.; Plouffe, D.; Henson, K.; Wagner, T.; Winzeler, E. A.; Petersen, F.; Brun, R.; Dartois, V.; Diagana, T. T.; Keller, T. H. Spirotetrahydro Beta-Carbolines (Spiroindolones): A New Class of Potent and Orally Efficacious Compounds for the Treatment of Malaria. *J. Med. Chem.* **2010,** *53* (14), 5155–5164.
35. Rottmann, M.; McNamara, C.; Yeung, B. K.; Lee, M. C.; Zou, B.; Russell, B.; Seitz, P.; Plouffe, D. M.; Dharia, N. V.; Tan, J.; Cohen, S. B.; Spencer, K. R.; Gonzalez-Paez, G. E.; Lakshminarayana, S. B.; Goh, A.; Suwanarusk, R.; Jegla, T.; Schmitt, E. K.; Beck, H. P.; Brun, R.; Nosten, F.; Renia, L.; Dartois, V.; Keller, T. H.; Fidock, D. A.; Winzeler, E. A.; Diagana, T. T. Spiroindolones, a Potent Compound Class for the Treatment of Malaria. *Science* **2010,** *329* (5996), 1175–1180.
36. Leong, F. J.; Li, R.; Jain, J. P.; Lefevre, G.; Magnusson, B.; Diagana, T. T.; Pertel, P. A First-in-Human Randomized, Double-Blind, Placebo-Controlled, Single- and Multiple-Ascending Oral Dose Study of Novel Antimalarial Spiroindolone KAE609 (Cipargamin) to Assess Its Safety, Tolerability, and Pharmacokinetics in Healthy Adult Volunteers. *Antimicrob. Agents Chemother.* **2014,** *58* (10), 6209–6214.
37. White, N. J.; Pukrittayakamee, S.; Phyo, A. P.; Rueangweerayut, R.; Nosten, F.; Jittamala, P.; Jeeyapant, A.; Jain, J. P.; Lefevre, G.; Li, R.; Magnusson, B.; Diagana, T. T.; Leong, F. J. Spiroindolone KAE609 for Falciparum and Vivax Malaria. *N. Engl. J. Med.* **2014,** *371* (5), 403–410.
38. (a) Spillman, N. J.; Kirk, K. The Malaria Parasite Cation ATPase PfATP4 and Its Role in the Mechanism of Action of a New Arsenal of Antimalarial Drugs. *Int. J. Parasitol. Drugs Drug Resist.* **2015,** *5* (3), 149–162; (b) Turner, H. Spiroindolone NITD609 Is a Novel Antimalarial Drug That Targets the P-Type ATPase PfATP4. *Future Med. Chem.* **2016,** *8,* 227–238.
39. Plouffe, D.; Brinker, A.; McNamara, C.; Henson, K.; Kato, N.; Kuhen, K.; Nagle, A.; Adrian, F.; Matzen, J. T.; Anderson, P.; Nam, T. G.; Gray, N. S.; Chatterjee, A.; Janes, J.; Yan, S. F.; Trager, R.; Caldwell, J. S.; Schultz, P. G.; Zhou, Y.; Winzeler, E. A. In Silico Activity Profiling Reveals the Mechanism of Action of Antimalarials Discovered in a High-Throughput Screen. *Proc. Natl. Acad. Sci. U. S. A.* **2008,** *105* (26), 9059–9064.
40. Wu, T.; Nagle, A.; Kuhen, K.; Gagaring, K.; Borboa, R.; Francek, C.; Chen, Z.; Plouffe, D.; Goh, A.; Lakshminarayana, S. B.; Wu, J.; Ang, H. Q.; Zeng, P.; Kang, M. L.; Tan, W.; Tan, M.; Ye, N.; Lin, X.; Caldwell, C.; Ek, J.; Skolnik, S.; Liu, F.; Wang, J.; Chang, J.; Li, C.; Hollenbeck, T.; Tuntland, T.; Isbell, J.; Fischli, C.; Brun, R.; Rottmann, M.; Dartois, V.; Keller, T.; Diagana, T.; Winzeler, E.; Glynne, R.; Tully, D. C.; Chatterjee, A. K. Imidazolopiperazines: Hit to Lead Optimization of New Antimalarial Agents. *J. Med. Chem.* **2011,** *54* (14), 5116–5130.
41. Nagle, A.; Wu, T.; Kuhen, K.; Gagaring, K.; Borboa, R.; Francek, C.; Chen, Z.; Plouffe, D.; Lin, X.; Caldwell, C.; Ek, J.; Skolnik, S.; Liu, F.; Wang, J.; Chang, J.; Li, C.; Liu, B.; Hollenbeck, T.; Tuntland, T.; Isbell, J.; Chuan, T.; Alper, P. B.; Fischli, C.; Brun, R.; Lakshminarayana, S. B.; Rottmann, M.; Diagana, T. T.; Winzeler, E. A.; Glynne, R.; Tully, D. C.; Chatterjee, A. K. Imidazolopiperazines: Lead Optimization of the Second-Generation Antimalarial Agents. *J. Med. Chem.* **2012,** *55* (9), 4244–4273.
42. Kuhen, K. L.; Chatterjee, A. K.; Rottmann, M.; Gagaring, K.; Borboa, R.; Buenviaje, J.; Chen, Z.; Francek, C.; Wu, T.; Nagle, A.; Barnes, S. W.; Plouffe, D.; Lee, M. C.; Fidock, D. A.; Graumans, W.; van de Vegte-Bolmer, M.; van Gemert, G. J.; Wirjanata, G.; Sebayang, B.; Marfurt, J.; Russell, B.; Suwanarusk, R.; Price, R. N.; Nosten, F.; Tungtaeng, A.; Gettayacamin, M.; Sattabongkot, J.; Taylor, J.; Walker, J. R.; Tully, D.; Patra, K. P.; Flannery, E. L.; Vinetz, J. M.; Renia, L.; Sauerwein, R. W.; Winzeler, E. A.; Glynne, R. J.; Diagana, T. T. KAF156 is an Antimalarial Clinical Candidate With Potential for Use in Prophylaxis, Treatment, and Prevention of Disease Transmission. *Antimicrob. Agents Chemother.* **2014,** *58* (9), 5060–5067.
43. Zou, B.; Nagle, A.; Chatterjee, A. K.; Leong, S. Y.; Tan, L. J.; Sim, W. L.; Mishra, P.; Guntapalli, P.; Tully, D. C.; Lakshminarayana, S. B.; Lim, C. S.; Tan, Y. C.; Abas, S. N.; Bodenreider, C.; Kuhen, K. L.; Gagaring, K.; Borboa, R.; Chang, J.; Li, C.; Hollenbeck, T.; Tuntland, T.; Zeeman, A. M.; Kocken, C. H.; McNamara, C.; Kato, N.; Winzeler, E. A.; Yeung, B. K.; Diagana, T. T.; Smith, P. W.; Roland, J. Lead Optimization of Imidazopyrazines: A New Class of Antimalarial With Activity on Plasmodium Liver Stages. *ACS Med. Chem. Lett.* **2014,** *5* (8), 947–950.
44. Zeeman, A. M.; van Amsterdam, S. M.; McNamara, C. W.; Voorberg-van der Wel, A.; Klooster, E. J.; van den Berg, A.; Remarque, E. J.; Plouffe, D. M.; van Gemert, G. J.; Luty, A.; Sauerwein, R.; Gagaring, K.; Borboa, R.; Chen, Z.; Kuhen, K.; Glynne, R. J.; Chatterjee, A. K.; Nagle, A.; Roland, J.; Winzeler, E. A.; Leroy, D.; Campo, B.; Diagana, T. T.; Yeung, B. K.; Thomas, A. W.; Kocken, C. H. KAI407, a Potent Non-8-Aminoquinoline Compound That Kills *Plasmodium cynomolgi* Early Dormant Liver Stage Parasites In Vitro. *Antimicrob. Agents Chemother.* **2014,** *58* (3), 1586–1595.
45. McNamara, C. W.; Lee, M. C.; Lim, C. S.; Lim, S. H.; Roland, J.; Nagle, A.; Simon, O.; Yeung, B. K.; Chatterjee, A. K.; McCormack, S. L.; Manary, M. J.; Zeeman, A. M.; Dechering, K. J.; Kumar, T. R.; Henrich, P. P.; Gagaring, K.; Ibanez, M.; Kato, N.; Kuhen, K. L.; Fischli, C.; Rottmann, M.; Plouffe, D. M.; Bursulaya, B.; Meister, S.; Rameh, L.; Trappe, J.; Haasen, D.; Timmerman, M.; Sauerwein, R. W.; Suwanarusk, R.; Russell, B.; Renia, L.; Nosten, F.; Tully, D. C.; Kocken, C. H.; Glynne, R. J.; Bodenreider, C.; Fidock, D. A.; Diagana, T. T.; Winzeler, E. A. Targeting Plasmodium PI(4)K to Eliminate Malaria. *Nature* **2013,** *504* (7479), 248–253.
46. Zhang, Y. K.; Plattner, J. J.; Freund, Y. R.; Easom, E. E.; Zhou, Y.; Gut, J.; Rosenthal, P. J.; Waterson, D.; Gamo, F. J.; Angulo-Barturen, I.; Ge, M.; Li, Z.; Li, L.; Jian, Y.; Cui, H.; Wang, H.; Yang, J. Synthesis and Structure-Activity Relationships of Novel Benzoxaboroles As a New Class of Antimalarial Agents. *Bioorg. Med. Chem. Lett.* **2011,** *21* (2), 644–651.
47. Zhang, Y. K.; Plattner, J. J.; Freund, Y. R.; Easom, E. E.; Zhou, Y.; Ye, L.; Zhou, H.; Waterson, D.; Gamo, F. J.; Sanz, L. M.; Ge, M.; Li, Z.; Li, L.; Wang, H.; Cui, H. Benzoxaborole Antimalarial Agents. Part 2: Discovery of Fluoro-Substituted 7-(2-Carboxyethyl)-1,3-dihydro-1-hydroxy-2,1-benzoxaboroles. *Bioorg. Med. Chem. Lett.* **2012,** *22* (3), 1299–1307.
48. Zhang, Y.-K.; Plattner, J. J.; Easom, E. E.; Jacobs, R. T.; Guo, D.; Sanders, V.; Freund, Y. R.; Campo, B.; Rosenthal, P. J.; Bu, W.; Gamo, F.-J.; Sanz, L. M.; Ge, M.; Li, L.; Ding, J.; Yang, Y. Benzoxaborole Antimalarial Agents. Part 4. Discovery of Potent 6-(2-(Alkoxycarbonyl)pyrazinyl-5-oxy)-1,3-dihydro-1-hydroxy-2,1-benzoxaboroles. *J. Med. Chem.* **2015,** *58* (13), 5344–5354.
49. Baragana, B.; Hallyburton, I.; Lee, M. C. S.; Norcross, N. R.; Grimaldi, R.; Otto, T. D.; Proto, W. R.; Blagborough, A. M.; Meister, S.; Wirjanata, G.; Ruecker, A.; Upton, L. M.; Abraham, T. S.; Almeida, M. J.; Pradhan, A.; Porzelle, A.; Martinez, M. S.; Bolscher, J. M.; Woodland, A.; Norval, S.; Zuccotto, F.; Thomas, J.; Simeons, F.; Stojanovski, L.; Osuna-Cabello, M.; Brock, P. M.; Churcher, T. S.; Sala, K. A.; Zakutansky, S. E.; Jimenez-Diaz, M. B.; Sanz, L. M.; Riley, J.; Basak, R.; Campbell, M.; Avery, V. M.; Sauerwein, R. W.; Dechering, K. J.; Noviyanti, R.; Campo, B.; Frearson, J. A.; Angulo-Barturen, I.; Ferrer-Bazaga, S.; Gamo, F. J.; Wyatt, P. G.; Leroy, D.; Siegl, P.; Delves, M. J.; Kyle, D. E.; Wittlin, S.; Marfurt, J.; Price, R. N.; Sinden, R. E.; Winzeler, E. A.; Charman, S. A.; Bebrevska, L.; Gray, D. W.; Campbell, S.; Fairlamb, A. H.; Willis, P. A.; Rayner, J. C.; Fidock, D. A.; Read, K. D.; Gilbert, I. H. A Novel Multiple-Stage Antimalarial Agent That Inhibits Protein Synthesis. *Nature* **2015,** *522* (7556), 315–320.
50. Reyes, P.; Rathod, P. K.; Sanchez, D. J.; Mrema, J. E. K.; Rieckmann, K. H.; Heidrich, H.-G. Enzymes of Purine and Pyrimidine Metabolism From the Human Malaria Parasite, *Plasmodium falciparum. Mol. Biochem. Parasitol.* **1982,** *5* (5), 275–290.
51. Baldwin, J.; Michnoff, C. H.; Malmquist, N. A.; White, J.; Roth, M. G.; Rathod, P. K.; Phillips, M. A. High-Throughput Screening for Potent and Selective Inhibitors of *Plasmodium falciparum* Dihydroorotate Dehydrogenase. *J. Biol. Chem.* **2005,** *280* (23), 21847–21853.
52. Phillips, M. A.; Gujjar, R.; Malmquist, N. A.; White, J.; El Mazouni, F.; Baldwin, J.; Rathod, P. K. Triazolopyrimidine-Based Dihydroorotate Dehydrogenase Inhibitors With Potent and Selective Activity Against the Malaria Parasite *Plasmodium falciparum. J. Med. Chem.* **2008,** *51* (12), 3649–3653.
53. Gujjar, R.; Marwaha, A.; El Mazouni, F.; White, J.; White, K. L.; Creason, S.; Shackleford, D. M.; Baldwin, J.; Charman, W. N.; Buckner, F. S.; Charman, S.; Rathod, P. K.; Phillips, M. A. Identification of a Metabolically Stable Triazolopyrimidine-Based Dihydroorotate Dehydrogenase Inhibitor With Antimalarial Activity in Mice. *J. Med. Chem.* **2009,** *52* (7), 1864–1872.
54. Phillips, M. A.; Lotharius, J.; Marsh, K.; White, J.; Dayan, A.; White, K. L.; Njoroge, J. W.; El Mazouni, F.; Lao, Y.; Kokkonda, S.; Tomchick, D. R.; Deng, X.; Laird, T.; Bhatia, S. N.; March, S.; Ng, C. L.; Fidock, D. A.; Wittlin, S.; Lafuente-Monasterio, M.; Benito, F. J.; Alonso, L. M.; Martinez, M. S.; Jimenez-Diaz, M. B.; Bazaga, S. F.; Angulo-Barturen, I.; Haselden, J. N.; Louttit, J.; Cui, Y.; Sridhar, A.; Zeeman, A. M.; Kocken, C.; Sauerwein, R.; Dechering, K.; Avery, V. M.; Duffy, S.; Delves, M.; Sinden, R.; Ruecker, A.; Wickham, K. S.; Rochford, R.; Gahagen, J.; Iyer, L.; Riccio, E.; Mirsalis, J.; Bathhurst, I.; Rueckle, T.; Ding, X.; Campo, B.; Leroy, D.; Rogers, M. J.; Rathod, P. K.; Burrows, J. N.; Charman, S. A. A Long-Duration Dihydroorotate Dehydrogenase Inhibitor (DSM265) for Prevention and Treatment of Malaria. *Sci. Transl. Med.* **2015,** *7* (296), 296ra111.
55. Elaine, S.; Robert, M. H.; Frederick, J. A.; Robert, V. T.; Marc-Alain, W.; Sharon, L. R.; Jeffery, L. J.; Patricia, M. G. Foodborne Illness Acquired in the United States—Major Pathogens. *Emerg. Infect. Dis. J.* **2011,** *17* (1), 7.

56. Spangenberg, T.; Burrows, J. N.; Kowalczyk, P.; McDonald, S.; Wells, T. N.; Willis, P. The Open Access Malaria Box: A Drug Discovery Catalyst for Neglected Diseases. *PLoS One* **2013,** *8* (6), e62906.
57. Boyom, F. F.; Fokou, P. V.; Tchokouaha, L. R.; Spangenberg, T.; Mfopa, A. N.; Kouipou, R. M.; Mbouna, C. J.; Donfack, V. F.; Zollo, P. H. Repurposing the Open Access Malaria Box to Discover Potent Inhibitors of *Toxoplasma gondii* and *Entamoeba histolytica*. *Antimicrob. Agents Chemother.* **2014,** *58* (10), 5848–5854.
58. Zhou, Y.; Fomovska, A.; Muench, S.; Lai, B. S.; Mui, E.; McLeod, R. Spiroindolone That Inhibits PfATPase4 Is a Potent, Cidal Inhibitor of *Toxoplasma gondii* Tachyzoites in vitro and In Vivo. *Antimicrob. Agents Chemother.* **2014,** *58* (3), 1789–1792.
59. Kadri, D.; Crater, A. K.; Lee, H.; Solomon, V. R.; Ananvoranich, S. The Potential of Quinoline Derivatives for the Treatment of *Toxoplasma gondii* Infection. *Exp. Parasitol.* **2014,** *145,* 135–144.
60. Yang, Z.; Ahn, H. J.; Nam, H. W. Gefitinib Inhibits the Growth of *Toxoplasma gondii* in HeLa Cells. *Korean J. Parasitol.* **2014,** *52* (4), 439–441.
61. Andrade, R. M.; Chaparro, J. D.; Capparelli, E.; Reed, S. L. Auranofin Is Highly Efficacious Against *Toxoplasma gondii* in vitro and in an in vivo Experimental Model of Acute Toxoplasmosis. *PLoS Negl. Trop. Dis.* **2014,** *8* (7), e2973.
62. Liu, J. J.; Liu, Q.; Wei, H. L.; Yi, J.; Zhao, H. S.; Gao, L. P. Inhibition of Thioredoxin Reductase by Auranofin Induces Apoptosis in Adriamycin-Resistant Human K562 Chronic Myeloid Leukemia Cells. *Pharmazie* **2011,** *66* (6), 440–444.
63. Caroli, A.; Simeoni, S.; Lepore, R.; Tramontano, A.; Via, A. Investigation of a Potential Mechanism for the Inhibition of SmTGR by Auranofin and Its Implications for *Plasmodium falciparum* Inhibition. *Biochem. Biophys. Res. Commun.* **2012,** *417* (1), 576–581.
64. Ilari, A.; Baiocco, P.; Messori, L.; Fiorillo, A.; Boffi, A.; Gramiccia, M.; Di Muccio, T.; Colotti, G. A Gold-Containing Drug Against Parasitic Polyamine Metabolism: The X-ray Structure of Trypanothione Reductase From *Leishmania infantum* in Complex With Auranofin Reveals a Dual Mechanism of Enzyme Inhibition. *Amino Acids* **2012,** *42* (2–3), 803–811.
65. Wei, F.; Wang, W.; Liu, Q. Protein Kinases of *Toxoplasma gondii*: Functions and Drug Targets. *Parasitol. Res.* **2013,** *112* (6), 2121–2129.
66. (a) Billker, O.; Lourido, S.; Sibley, L. D. Calcium-Dependent Signaling and Kinases in Apicomplexan Parasites. *Cell Host Microbe* **2009,** *5* (6), 612–622; (b) Lourido, S.; Shuman, J.; Zhang, C.; Shokat, K. M.; Hui, R.; Sibley, L. D. Calcium-Dependent Protein Kinase 1 Is an Essential Regulator of Exocytosis in *Toxoplasma*. *Nature* **2010,** *465* (7296), 359–362; (c) Ojo, K. K.; Larson, E. T.; Keyloun, K. R.; Castaneda, L. J.; Derocher, A. E.; Inampudi, K. K.; Kim, J. E.; Arakaki, T. L.; Murphy, R. C.; Zhang, L.; Napuli, A. J.; Maly, D. J.; Verlinde, C. L.; Buckner, F. S.; Parsons, M.; Hol, W. G.; Merritt, E. A.; Van Voorhis, W. C. *Toxoplasma gondii* Calcium-Dependent Protein Kinase 1 Is a Target for Selective Kinase Inhibitors. *Nat. Struct. Mol. Biol.* **2010,** *17* (5), 602–607.
67. Wernimont, A. K.; Artz, J. D.; Finerty, P., Jr.; Lin, Y. H.; Amani, M.; Allali-Hassani, A.; Senisterra, G.; Vedadi, M.; Tempel, W.; Mackenzie, F.; Chau, I.; Lourido, S.; Sibley, L. D.; Hui, R. Structures of Apicomplexan Calcium-Dependent Protein Kinases Reveal Mechanism of Activation by Calcium. *Nat. Struct. Mol. Biol.* **2010,** *17* (5), 596–601.
68. Bishop, A. C.; Kung, C.-Y.; Shah, K.; Witucki, L.; Shokat, K. M.; Liu, Y. Generation of Monospecific Nanomolar Tyrosine Kinase Inhibitors via a Chemical Genetic Approach. *J. Am. Chem. Soc.* **1999,** *121* (4), 627–631.
69. (a) Murphy, R. C.; Ojo, K. K.; Larson, E. T.; Castellanos-Gonzalez, A.; Perera, B. G.; Keyloun, K. R.; Kim, J. E.; Bhandari, J. G.; Muller, N. R.; Verlinde, C. L.; White, A. C., Jr.; Merritt, E. A.; Van Voorhis, W. C.; Maly, D. J. Discovery of Potent and Selective Inhibitors of Calcium-Dependent Protein Kinase 1 (CDPK1) From *C. parvum* and *T. gondii*. *ACS Med. Chem. Lett.* **2010,** *1* (7), 331–335; (b) Larson, E. T.; Ojo, K. K.; Murphy, R. C.; Johnson, S. M.; Zhang, Z.; Kim, J. E.; Leibly, D. J.; Fox, A. M. W.; Reid, M. C.; Dale, E. J.; Perera, B. G. K.; Kim, J.; Hewitt, S. N.; Hol, W. G. J.; Verlinde, C. L. M. J.; Fan, E.; Van Voorhis, W. C.; Maly, D. J.; Merritt, E. A. Multiple Determinants for Selective Inhibition of Apicomplexan Calcium-Dependent Protein Kinase CDPK1. *J. Med. Chem.* **2012,** *55* (6), 2803–2810.
70. Doggett, J. S.; Ojo, K. K.; Fan, E.; Maly, D. J.; Van Voorhis, W. C. Bumped Kinase Inhibitor 1294 Treats Established *Toxoplasma gondii* Infection. *Antimicrob. Agents Chemother.* **2014,** *58* (6), 3547–3549.
71. Zhang, Z.; Ojo, K. K.; Johnson, S. M.; Larson, E. T.; He, P.; Geiger, J. A.; Castellanos-Gonzalez, A.; White, A. C., Jr.; Parsons, M.; Merritt, E. A.; Maly, D. J.; Verlinde, C. L.; Van Voorhis, W. C.; Fan, E. Benzoylbenzimidazole-Based Selective Inhibitors Targeting *Cryptosporidium parvum* and *Toxoplasma gondii* Calcium-Dependent Protein Kinase-1. *Bioorg. Med. Chem. Lett.* **2012,** *22* (16), 5264–5267.
72. Bessoff, K.; Sateriale, A.; Lee, K. K.; Huston, C. D. Drug Repurposing Screen Reveals FDA-Approved Inhibitors of Human HMG-CoA Reductase and Isoprenoid Synthesis That Block *Cryptosporidium parvum* Growth. *Antimicrob. Agents Chemother.* **2013,** *57* (4), 1804–1814.
73. Bessoff, K.; Spangenberg, T.; Foderaro, J. E.; Jumani, R. S.; Ward, G. E.; Huston, C. D. Identification of *Cryptosporidium parvum* Active Chemical Series by Repurposing the Open Access Malaria Box. *Antimicrob. Agents Chemother.* **2014,** *58* (5), 2731–2739.
74. Castellanos-Gonzalez, A.; White, A. C., Jr.; Ojo, K. K.; Vidadala, R. S.; Zhang, Z.; Reid, M. C.; Fox, A. M.; Keyloun, K. R.; Rivas, K.; Irani, A.; Dann, S. M.; Fan, E.; Maly, D. J.; Van Voorhis, W. C. A Novel Calcium-Dependent Protein Kinase Inhibitor As a Lead Compound for Treating Cryptosporidiosis. *J. Infect. Dis.* **2013,** *208* (8), 1342–1348.
75. Umejiego, N. N.; Li, C.; Riera, T.; Hedstrom, L.; Striepen, B. *Cryptosporidium parvum* IMP Dehydrogenase: Identification of Functional, Structural, and Dynamic Properties That Can Be Exploited for Drug Design. *J. Biol. Chem.* **2004,** *279* (39), 40320–40327.
76. Umejiego, N. N.; Gollapalli, D.; Sharling, L.; Volftsun, A.; Lu, J.; Benjamin, N. N.; Stroupe, A. H.; Riera, T. V.; Striepen, B.; Hedstrom, L. Targeting a Prokaryotic Protein in a Eukaryotic Pathogen: Identification of Lead Compounds Against Cryptosporidiosis. *Chem. Biol.* **2008,** *15* (1), 70–77.
77. Gorla, S. K.; Kavitha, M.; Zhang, M.; Liu, X.; Sharling, L.; Gollapalli, D. R.; Striepen, B.; Hedstrom, L.; Cuny, G. D. Selective and Potent Urea Inhibitors of *Cryptosporidium parvum* Inosine 5'-Monophosphate Dehydrogenase. *J. Med. Chem.* **2012,** *55* (17), 7759–7771.
78. Kirubakaran, S.; Gorla, S. K.; Sharling, L.; Zhang, M.; Liu, X.; Ray, S. S.; Macpherson, I. S.; Striepen, B.; Hedstrom, L.; Cuny, G. D. Structure-Activity Relationship Study of Selective Benzimidazole-Based Inhibitors of *Cryptosporidium parvum* IMPDH. *Bioorg. Med. Chem. Lett.* **2012,** *22* (5), 1985–1988.
79. Gorla, S. K.; Kavitha, M.; Zhang, M.; Chin, J. E.; Liu, X.; Striepen, B.; Makowska-Grzyska, M.; Kim, Y.; Joachimiak, A.; Hedstrom, L.; Cuny, G. D. Optimization of Benzoxazole-Based Inhibitors of *Cryptosporidium parvum* Inosine 5'-Monophosphate Dehydrogenase. *J. Med. Chem.* **2013,** *56* (10), 4028–4043.
80. Johnson, C. R.; Gorla, S. K.; Kavitha, M.; Zhang, M.; Liu, X.; Striepen, B.; Mead, J. R.; Cuny, G. D.; Hedstrom, L. Phthalazinone Inhibitors of Inosine-5'-Monophosphate Dehydrogenase From *Cryptosporidium parvum*. *Bioorg. Med. Chem. Lett.* **2013,** *23* (4), 1004–1007.
81. Sun, Z.; Khan, J.; Makowska-Grzyska, M.; Zhang, M.; Cho, J. H.; Suebsuwong, C.; Vo, P.; Gollapalli, D. R.; Kim, Y.; Joachimiak, A.; Hedstrom, L.; Cuny, G. D. Synthesis, in vitro Evaluation and Cocrystal Structure of 4-Oxo-[1]benzopyrano[4,3-c]pyrazole *Cryptosporidium parvum* Inosine 5'-Monophosphate Dehydrogenase (CpIMPDH) Inhibitors. *J. Med. Chem.* **2014,** *57* (24), 10544–10550.
82. Kim, Y.; Makowska-Grzyska, M.; Gorla, S. K.; Gollapalli, D. R.; Cuny, G. D.; Joachimiak, A.; Hedstrom, L. Structure of Cryptosporidium IMP Dehydrogenase Bound to an Inhibitor With in vivo Antiparasitic Activity. *Acta Crystallogr. F Struct. Biol. Commun.* **2015,** *71* (Pt 5), 531–538.
83. Gorla, S. K.; McNair, N. N.; Yang, G.; Gao, S.; Hu, M.; Jala, V. R.; Haribabu, B.; Striepen, B.; Cuny, G. D.; Mead, J. R.; Hedstrom, L. Validation of IMP Dehydrogenase Inhibitors in a Mouse Model of Cryptosporidiosis. *Antimicrob. Agents Chemother.* **2014,** *58* (3), 1603–1614.
84. Barrett, M. P.; Burchmore, R. J. S.; Stich, A.; Lazzari, J. O.; Frasch, A. C.; Cazzulo, J. J.; Krishna, S. The Trypanosomiases. *Lancet* **2003,** *362* (9394), 1469–1480.
85. Shapiro, T. A.; Englund, P. T. The Structure and Replication of Kinetoplast DNA. *Annu. Rev. Microbiol.* **1995,** *49,* 117–143.
86. Lakhdar-Ghazal, F.; Blonski, C.; Willson, M.; Michels, P.; Perie, J. Glycolysis and Proteases As Targets for the Design of New Anti-Trypanosome Drugs. *Curr. Top. Med. Chem.* **2002,** *2* (5), 439–456.
87. (a) Elfari, M.; Schnur, L. F.; Strelkova, M. V.; Eisenberger, C. L.; Jacobson, R. L.; Greenblatt, C. L.; Presber, W.; Schonian, G. Genetic and Biological Diversity Among Populations of *Leishmania major* From Central Asia, the Middle East and Africa. *Microbes Infect.* **2005,** *7* (1), 93–103; (b) Campos-Ponce, M.; Ponce, C.; Ponce, E.; Maingon, R. D. Leishmania Chagasi/Infantum: Further Investigations in Leishmania Tropisms in Atypical Cutaneous and Visceral Leishmaniasis Foci in Central America. *Exp. Parasitol.* **2005,** *109* (4), 209–219; (c) Maia, C.; Cardoso, L. Spread of *Leishmania infantum* in Europe With Dog Travelling. *Vet. Parasitol.* **2015,** *213* (1–2), 2–11; (d) Pratlong, F.; Lami, P.; Ravel, C.; Balard, Y.; Dereure, J.; Serres, G.; Baidouri, F. E.; Dedet, J. P. Geographical Distribution and Epidemiological Features of Old World *Leishmania infantum* and *Leishmania donovani* Foci, Based on the Isoenzyme Analysis of 2277 Strains. *Parasitology* **2013,** *140* (4), 423–434.

88. (a) Centers for Disease Control and Prevention (CDC). Prevention, Cutaneous Leishmaniasis in U.S. Military Personnel—Southwest/Central Asia, 2002–2003. *MMWR Morb. Mortal. Wkly. Rep.* **2003,** *52* (42), 1009–1012; (b) van Thiel, P. P.; Leenstra, T.; de Vries, H. J.; van der Sluis, A.; van Gool, T.; Krull, A. C.; van Vugt, M.; de Vries, P. J.; Zeegelaar, J. E.; Bart, A.; van der Meide, W. F.; Schallig, H. D.; Faber, W. R.; Kager, P. A. Cutaneous Leishmaniasis (*Leishmania major* Infection) in Dutch Troops Deployed in Northern Afghanistan: Epidemiology, Clinical Aspects, and Treatment. *Am. J. Trop. Med. Hyg.* **2010,** *83* (6), 1295–1300.
89. Marra, F.; Chiappetta, M. C.; Vincenti, V. Ear, Nose and Throat Manifestations of Mucocutaneous Leishmaniasis: A Literature Review. *Acta Biomed.* **2014,** *85* (1), 3–7.
90. (a) Das, P.; Samuels, S.; Desjeux, P.; Mittal, A.; Topno, R.; Siddiqui, N. A.; Sur, D.; Pandey, A.; Sarnoff, R. Annual Incidence of Visceral Leishmaniasis in an Endemic Area of Bihar, India. *Trop. Med. Int. Health* **2010,** *15* (Suppl. 2), 4–11; (b) Chappuis, F.; Alirol, E.; Worku, D. T.; Mueller, Y.; Ritmeijer, K. High Mortality Among Older Patients Treated With Pentavalent Antimonials for Visceral Leishmaniasis in East Africa and Rationale for Switch to Liposomal Amphotericin B. *Antimicrob. Agents Chemother.* **2011,** *55* (1), 455–456.
91. Hotez, P. J.; Molyneux, D. H.; Fenwick, A.; Kumaresan, J.; Sachs, S. E.; Sachs, J. D.; Savioli, L. Control of Neglected Tropical Diseases. *N. Engl. J. Med.* **2007,** *357* (10), 1018–1027.
92. World Health Organization. WHO Technical Report 975. Research Priorities for Chagas Disease, Human African Trypanosomiasis and Leishmaniasis. http://www.who/int/tdr/publications/research_priorities/en/.
93. (a) Kuehn, B. M. Putting Chagas Disease on the US Radar Screen. *JAMA* **2015,** *313* (12), 1195–1197; (b) Montgomery, S. P.; Starr, M. C.; Cantey, P. T.; Edwards, M. S.; Meymandi, S. K. Neglected Parasitic Infections in the United States: Chagas Disease. *Am. J. Trop. Med. Hyg.* **2014,** *90* (5), 814–818.
94. Coura, J. R.; Castro, S. L. D. A Critical Review on Chagas Disease Chemotherapy. *Mem. Inst. Oswaldo Cruz* **2002,** *97*, 3–24.
95. Sternberg, J. M. Human African Trypanosomiasis: Clinical Presentation and Immune Response. *Parasite Immunol.* **2004,** *26* (11–12), 469–476.
96. World Health Organization. WHO Technical Report 881. Control and surveillance of African trypanosomiasis: report of a WHO Expert Committee. http://www.who.int/csr/resources/publications/CSR_ISR_2000_1tryps/en/.
97. Croft, S. L. Drugs for Kinetoplastid Diseases—Current Situation and Challenges. In *Neglected Diseases and Drug Discovery;* Palmer, M. J., Wells, T. N. C., Eds.; Royal Society of Chemistry: London, UK, World Health Organization, 2012; pp 134–158.
98. Croft, S. L.; Olliaro, P. Leishmaniasis Chemotherapy—Challenges and Opportunities. *Clin. Microbiol. Infect.* **2011,** *17* (10), 1478–1483.
99. (a) Werbovetz, K. Diamidines as Antitrypanosomal, Antileishmanial and Antimalarial Agents. *Curr. Opin. Investig. Drugs* **2006,** *7* (2), 147–157; (b) Soeiro, M. N.; De Souza, E. M.; Stephens, C. E.; Boykin, D. W. Aromatic Diamidines As Antiparasitic Agents. *Expert Opin. Investig. Drugs* **2005,** *14* (8), 957–972.
100. (a) Gonzalez, J. L.; Stephens, C. E.; Wenzler, T.; Brun, R.; Tanious, F. A.; Wilson, W. D.; Barszcz, T.; Werbovetz, K. A.; Boykin, D. W. Synthesis and Antiparasitic Evaluation of Bis-2,5-[4-guanidinophenyl]thiophenes. *Eur. J. Med. Chem.* **2007,** *42* (4), 552–557; (b) Rosypal, A. C.; Werbovetz, K. A.; Salem, M.; Stephens, C. E.; Kumar, A.; Boykin, D. W.; Hall, J. E.; Tidwell, R. R. Inhibition by Dications of in vitro Growth of *Leishmania major* and *Leishmania tropica*: Causative Agents of Old World Cutaneous Leishmaniasis. *J. Parasitol.* **2008,** *94* (3), 743–749; (c) Hu, L.; Arafa, R. K.; Ismail, M. A.; Wenzler, T.; Brun, R.; Munde, M.; Wilson, W. D.; Nzimiro, S.; Samyesudhas, S.; Werbovetz, K. A.; Boykin, D. W. Azaterphenyl Diamidines As Antileishmanial Agents. *Bioorg. Med. Chem. Lett.* **2008,** *18* (1), 247–251; (d) Soeiro, M. N.; Werbovetz, K.; Boykin, D. W.; Wilson, W. D.; Wang, M. Z.; Hemphill, A. Novel Amidines and Analogues As Promising Agents Against Intracellular Parasites: A Systematic Review. *Parasitology* **2013,** *140* (8), 929–951.
101. (a) Midgley, I.; Fitzpatrick, K.; Taylor, L. M.; Houchen, T. L.; Henderson, S. J.; Wright, S. J.; Cybulski, Z. R.; John, B. A.; McBurney, A.; Boykin, D. W.; Trendler, K. L. Pharmacokinetics and Metabolism of the Prodrug DB289 (2,5-Bis[4-(*N*-methoxyamidino)phenyl]furan monomaleate) in Rat and Monkey and Its Conversion to the Antiprotozoal/Antifungal Drug DB75 (2,5-Bis(4-guanylphenyl)furan dihydrochloride). *Drug Metab. Dispos.* **2007,** *35* (6), 955–967; (b) Thuita, J. K.; Karanja, S. M.; Wenzler, T.; Mdachi, R. E.; Ngotho, J. M.; Kagira, J. M.; Tidwell, R.; Brun, R. Efficacy of the Diamidine DB75 and Its Prodrug DB289, Against Murine Models of Human African Trypanosomiasis. *Acta Trop.* **2008,** *108* (1), 6–10.
102. (a) Stephens, C. E.; Brun, R.; Salem, M. M.; Werbovetz, K. A.; Tanious, F.; Wilson, W. D.; Boykin, D. W. The Activity of Diguanidino and 'Reversed' Diamidino 2,5-diarylfurans Versus *Trypanosoma cruzi* and *Leishmania donovani*. *Bioorg. Med. Chem. Lett.* **2003,** *13* (12), 2065–2069; (b) Collar, C. J.; Zhu, X.; Werbovetz, K.; Boykin, D. W.; Wilson, W. D. Molecular Factors Governing Inhibition of Arylimidamides Against *Leishmania*: Conservative Computational Modeling to Improve Chemotherapies. *Bioorg. Med. Chem.* **2011,** *19* (15), 4552–4561; (c) Reid, C. S.; Farahat, A. A.; Zhu, X.; Pandharkar, T.; Boykin, D. W.; Werbovetz, K. A. Antileishmanial Bis-arylimidamides: DB766 Analogs Modified in the Linker Region and Bis-Arylimidamide Structure-Activity Relationships. *Bioorg. Med. Chem. Lett.* **2012,** *22* (22), 6806–6810; (d) Liu, Z. Y.; Wenzler, T.; Brun, R.; Zhu, X.; Boykin, D. W. Synthesis and Antiparasitic Activity of New Bis-Arylimidamides: DB766 Analogs Modified in the Terminal Groups. *Eur. J. Med. Chem.* **2014,** *83,* 167–173.
103. Wang, M. Z.; Zhu, X.; Srivastava, A.; Liu, Q.; Sweat, J. M.; Pandharkar, T.; Stephens, C. E.; Riccio, E.; Parman, T.; Munde, M.; Mandal, S.; Madhubala, R.; Tidwell, R. R.; Wilson, W. D.; Boykin, D. W.; Hall, J. E.; Kyle, D. E.; Werbovetz, K. A. Novel Arylimidamides for Treatment of Visceral Leishmaniasis. *Antimicrob. Agents Chemother.* **2010,** *54* (6), 2507–2516.
104. Zhu, X.; Liu, Q.; Yang, S.; Parman, T.; Green, C. E.; Mirsalis, J. C.; de Nazare Correia Soeiro, M.; Mello de Souza, E.; da Silva, C. F.; da Gama Jaen Batista, D.; Stephens, C. E.; Banerjee, M.; Farahat, A. A.; Munde, M.; Wilson, W. D.; Boykin, D. W.; Wang, M. Z.; Werbovetz, K. A. Evaluation of Arylimidamides DB1955 and DB1960 as Candidates Against Visceral Leishmaniasis and Chagas' Disease: in vivo Efficacy, Acute Toxicity, Pharmacokinetics, and Toxicology Studies. *Antimicrob. Agents Chemother.* **2012,** *56* (7), 3690–3699.
105. (a) Wang, Y.; Dimitrov, K.; Garrity, L. K.; Sazer, S.; Beverley, S. M. Stage-Specific Activity of the *Leishmania major* CRK3 Kinase and Functional Rescue of a *Schizosaccharomyces pombe* cdc2 Mutant. *Mol. Biochem. Parasitol.* **1998,** *96* (1–2), 139–150; (b) Grant, K. M.; Hassan, P.; Anderson, J. S.; Mottram, J. C. The crk3 Gene of *Leishmania mexicana* Encodes a Stage-Regulated cdc2-Related Histone H1 Kinase That Associates With p12. *J. Biol. Chem.* **1998,** *273* (17), 10153–10159.
106. Hassan, P.; Fergusson, D.; Grant, K. M.; Mottram, J. C. The CRK3 Protein Kinase Is Essential for Cell Cycle Progression of *Leishmania mexicana*. *Mol. Biochem. Parasitol.* **2001,** *113* (2), 189–198.
107. (a) Grant, K. M.; Dunion, M. H.; Yardley, V.; Skaltsounis, A. L.; Marko, D.; Eisenbrand, G.; Croft, S. L.; Meijer, L.; Mottram, J. C. Inhibitors of *Leishmania mexicana* CRK3 Cyclin-Dependent Kinase: Chemical Library Screen and Antileishmanial Activity. *Antimicrob. Agents Chemother.* **2004,** *48* (8), 3033–3042; (b) Walker, R. G.; Thomson, G.; Malone, K.; Nowicki, M. W.; Brown, E.; Blake, D. G.; Turner, N. J.; Walkinshaw, M. D.; Grant, K. M.; Mottram, J. C. High Throughput Screens Yield Small Molecule Inhibitors of Leishmania CRK3:CYC6 Cyclin-Dependent Kinase. *PLoS Negl. Trop. Dis.* **2011,** *5* (4), e1033; (c) Cleghorn, L. A.; Woodland, A.; Collie, I. T.; Torrie, L. S.; Norcross, N.; Luksch, T.; Mpamhanga, C.; Walker, R. G.; Mottram, J. C.; Brenk, R.; Frearson, J. A.; Gilbert, I. H.; Wyatt, P. G. Identification of Inhibitors of the Leishmania cdc2-Related Protein Kinase CRK3. *ChemMedChem* **2011,** *6* (12), 2214–2224.
108. Nare, B.; Hardy, L. W.; Beverley, S. M. The Roles of Pteridine Reductase 1 and Dihydrofolate Reductase-Thymidylate Synthase in Pteridine Metabolism in the Protozoan Parasite *Leishmania major*. *J. Biol. Chem.* **1997,** *272* (21), 13883–13891.
109. (a) Khabnadideh, S.; Pez, D.; Musso, A.; Brun, R.; Perez, L. M.; Gonzalez-Pacanowska, D.; Gilbert, I. H. Design, Synthesis and Evaluation of 2,4-Diaminoquinazolines As Inhibitors of Trypanosomal and Leishmanial Dihydrofolate Reductase. *Bioorg. Med. Chem.* **2005,** *13* (7), 2637–2649; (b) Pez, D.; Leal, I.; Zuccotto, F.; Boussard, C.; Brun, R.; Croft, S. L.; Yardley, V.; Ruiz Perez, L. M.; Gonzalez Pacanowska, D.; Gilbert, I. H. 2,4-Diaminopyrimidines as Inhibitors of Leishmanial and Trypanosomal Dihydrofolate Reductase. *Bioorg. Med. Chem.* **2003,** *11* (22), 4693–4711.
110. Mendoza-Martinez, C.; Correa-Basurto, J.; Nieto-Meneses, R.; Marquez-Navarro, A.; Aguilar-Suarez, R.; Montero-Cortes, M. D.; Nogueda-Torres, B.; Suarez-Contreras, E.; Galindo-Sevilla, N.; Rojas-Rojas, A.; Rodriguez-Lezama, A.; Hernandez-Luis, F. Design, Synthesis and Biological Evaluation of Quinazoline Derivatives as Anti-Trypanosomatid and Anti-Plasmodial Agents. *Eur. J. Med. Chem.* **2015,** *96,* 296–307.
111. Bhuniya, D.; Mukkavilli, R.; Shivahare, R.; Launay, D.; Dere, R. T.; Deshpande, A.; Verma, A.; Vishwakarma, P.; Moger, M.; Pradhan, A.; Pati, H.; Gopinath, V. S.; Gupta, S.; Puri, S. K.; Martin, D. Aminothiazoles: Hit to Lead Development to Identify Antileishmanial Agents. *Eur. J. Med. Chem.* **2015,** *102,* 582–593.

112. (a) Van Horn, K. S.; Zhu, X.; Pandharkar, T.; Yang, S.; Vesely, B.; Vanaerschot, M.; Dujardin, J. C.; Rijal, S.; Kyle, D. E.; Wang, M. Z.; Werbovetz, K. A.; Manetsch, R. Antileishmanial Activity of a Series of *N*(2),*N*(4)-Disubstituted Quinazoline-2,4-diamines. *J. Med. Chem.* **2014,** *57* (12), 5141–5156; (b) Zhu, X.; Van Horn, K. S.; Barber, M. M.; Yang, S.; Wang, M. Z.; Manetsch, R.; Werbovetz, K. A. SAR Refinement of Antileishmanial *N*(2),*N*(4)-Disubstituted Quinazoline-2,4-diamines. *Bioorg. Med. Chem.* **2015,** *23* (16), 5182–5189.
113. (a) Gopinath, V. S.; Rao, M.; Shivahare, R.; Vishwakarma, P.; Ghose, S.; Pradhan, A.; Hindupur, R.; Sarma, K. D.; Gupta, S.; Puri, S. K.; Launay, D.; Martin, D. Design, Synthesis, ADME Characterization and Antileishmanial Evaluation of Novel Substituted Quinoline Analogs. *Bioorg. Med. Chem. Lett.* **2014,** *24* (9), 2046–2052; (b) Gopinath, V. S.; Pinjari, J.; Dere, R. T.; Verma, A.; Vishwakarma, P.; Shivahare, R.; Moger, M.; Kumar Goud, P. S.; Ramanathan, V.; Bose, P.; Rao, M. V.; Gupta, S.; Puri, S. K.; Launay, D.; Martin, D. Design, Synthesis and Biological Evaluation of 2-Substituted Quinolines As Potential Antileishmanial Agents. *Eur. J. Med. Chem.* **2013,** *69,* 527–536.
114. Mowbray, C. E.; Braillard, S.; Speed, W.; Glossop, P. A.; Whitlock, G. A.; Gibson, K. R.; Mills, J. E. J.; Brown, A. D.; Gardner, J. M. F.; Cao, Y.; Hua, W.; Morgans, G. L.; Feijens, P.-B.; Matheeussen, A.; Maes, L. J. Novel Amino-Pyrazole Ureas With Potent in vitro and in vivo Antileishmanial Activity. *J. Med. Chem.* **2015,** *58* (24), 9615–9624.
115. Sharlow, E. R.; Leimgruber, S.; Murray, S.; Lira, A.; Sciotti, R. J.; Hickman, M.; Hudson, T.; Leed, S.; Caridha, D.; Barrios, A. M.; Close, D.; Grogl, M.; Lazo, J. S. Auranofin is an Apoptosis-Simulating Agent With in vitro and in vivo Anti-Leishmanial Activity. *ACS Chem. Biol.* **2014,** *9* (3), 663–672.
116. Sanderson, L.; Yardley, V.; Croft, S. L. Activity of Anti-Cancer Protein Kinase Inhibitors Against *Leishmania* spp. *J. Antimicrob. Chemother.* **2014,** *69* (7), 1888–1891.
117. Patel, G.; Karver, C. E.; Behera, R.; Guyett, P. J.; Sullenberger, C.; Edwards, P.; Roncal, N. E.; Mensa-Wilmot, K.; Pollastri, M. P. Kinase Scaffold Repurposing for Neglected Disease Drug Discovery: Discovery of an Efficacious, Lapatinib-Derived Lead Compound for Trypanosomiasis. *J. Med. Chem.* **2013,** *56* (10), 3820–3832.
118. Patel, G.; Roncal, N. E.; Lee, P. J.; Leed, S. E.; Erath, J.; Rodriguez, A.; Sciotti, R. J.; Pollastri, M. P. Repurposing Human Aurora Kinase Inhibitors As Leads for Anti-Protozoan Drug Discovery. *Medchemcomm* **2014,** *5* (5), 655–658.
119. Singh, S.; Dinesh, N.; Kaur, P. K.; Shamiulla, B. Ketanserin, an Antidepressant, Exerts Its Antileishmanial Action via Inhibition of 3-Hydroxy-3-methylglutaryl Coenzyme A Reductase (HMGR) Enzyme of *Leishmania donovani*. *Parasitol. Res.* **2014,** *113* (6), 2161–2168.
120. Dinesh, N.; Kaur, P. K.; Swamy, K. K.; Singh, S. Mianserin, an Antidepressant Kills *Leishmania donovani* by Depleting Ergosterol Levels. *Exp. Parasitol.* **2014,** *144,* 84–90.
121. (a) Dinesh, N.; Pallerla, D. S. R.; Kaur, P. K.; Kishore Babu, N.; Singh, S. Exploring *Leishmania donovani* 3-Hydroxy-3-methylglutaryl Coenzyme A Reductase (HMGR) as a Potential Drug Target by Biochemical, Biophysical and Inhibition Studies. *Microb. Pathog.* **2014,** *66,* 14–23; (b) Dinesh, N.; Soumya, N.; Singh, S. Antileishmanial Effect of Mevastatin Is Due to Interference With Sterol Metabolism. *Parasitol. Res.* **2015,** *114* (10), 3873–3883.
122. Wyllie, S.; Patterson, S.; Stojanovski, L.; Simeons, F. R.; Norval, S.; Kime, R.; Read, K. D.; Fairlamb, A. H. The Anti-Trypanosome Drug Fexinidazole Shows Potential for Treating Visceral Leishmaniasis. *Sci. Transl. Med.* **2012,** *4* (119), 119re1.
123. Patterson, S.; Wyllie, S.; Stojanovski, L.; Perry, M. R.; Simeons, F. R.; Norval, S.; Osuna-Cabello, M.; De Rycker, M.; Read, K. D.; Fairlamb, A. H. The R Enantiomer of the Antitubercular Drug PA-824 As a Potential Oral Treatment for Visceral Leishmaniasis. *Antimicrob. Agents Chemother.* **2013,** *57* (10), 4699–4706.
124. (a) Rassi, A., Jr.; Rassi, A.; Marin-Neto, J. A. Chagas Disease. *Lancet* **2010,** *375* (9723), 1388–1402; (b) Bern, C. Chagas' Disease. *N. Engl. J. Med.* **2015,** *373* (5), 456–466.
125. Zingales, B.; Miles, M. A.; Moraes, C. B.; Luquetti, A.; Guhl, F.; Schijman, A. G.; Ribeiro, I. Drug Discovery for Chagas Disease Should Consider *Trypanosoma cruzi* Strain Diversity. *Mem. Inst. Oswaldo Cruz* **2014,** *109,* 828–833.
126. (a) Molina, I.; Salvador, F.; Sanchez-Montalva, A. Posaconazole Versus Benznidazole for Chronic Chagas' Disease. *N. Engl. J. Med.* **2014,** *371* (10), 966; (b) Urbina, J. A. Recent Clinical Trials for the Etiological Treatment of Chronic Chagas Disease: Advances, Challenges and Perspectives. *J. Eukaryot. Microbiol.* **2015,** *62* (1), 149–156; (c) Torrico, F. E1224-Results of Proof-of-Concept Clinical Trial in Patients With Chronic Indeterminate Chagas Disease. 62nd Annual Meeting of the American Society of Tropical Medicine and Hygiene**;** American Society for Tropical Medicine and Hygiene: Washington, D.C, 2013; (d) Molina, I.; Salvador, F.; Sanchez-Montalva, A. The Use of Posaconazole Against Chagas Disease. *Curr. Opin. Infect. Dis.* **2015,** *28* (5), 397–407.
127. (a) Moraes, C. B.; Giardini, M. A.; Kim, H.; Franco, C. H.; Araujo-Junior, A. M.; Schenkman, S.; Chatelain, E.; Freitas-Junior, L. H. Nitroheterocyclic Compounds Are More Efficacious Than CYP51 Inhibitors Against *Trypanosoma cruzi*: Implications for Chagas Disease Drug Discovery and Development. *Sci. Rep.* **2014,** *4,* 4703; (b) Francisco, A. F.; Lewis, M. D.; Jayawardhana, S.; Taylor, M. C.; Chatelain, E.; Kelly, J. M. Limited Ability of Posaconazole to Cure Both Acute and Chronic *Trypanosoma cruzi* Infections Revealed by Highly Sensitive in vivo Imaging. *Antimicrob. Agents Chemother.* **2015,** *59* (8), 4653–4661.
128. Morillo, C. A.; Marin-Neto, J. A.; Avezum, A.; Sosa-Estani, S.; Rassi, A., Jr.; Rosas, F.; Villena, E.; Quiroz, R.; Bonilla, R.; Britto, C.; Guhl, F.; Velazquez, E.; Bonilla, L.; Meeks, B.; Rao-Melacini, P.; Pogue, J.; Mattos, A.; Lazdins, J.; Rassi, A.; Connolly, S. J.; Yusuf, S.; Investigators, B. Randomized Trial of Benznidazole for Chronic Chagas' Cardiomyopathy. *N. Engl. J. Med.* **2015,** *373* (14), 1295–1306.
129. (a) Canavaci, A. M.; Bustamante, J. M.; Padilla, A. M.; Perez Brandan, C. M.; Simpson, L. J.; Xu, D.; Boehlke, C. L.; Tarleton, R. L. In Vitro and in vivo High-Throughput Assays for the Testing of Anti-*Trypanosoma cruzi* Compounds. *PLoS Negl. Trop. Dis.* **2010,** *4* (7), e740; (b) Bustamante, J. M.; Tarleton, R. L. Methodological Advances in Drug Discovery for Chagas Disease. *Expert Opin. Drug Discov.* **2011,** *6* (6), 653–661; (c) Alonso-Padilla, J.; Rodriguez, A. High Throughput Screening for Anti-*Trypanosoma cruzi* Drug Discovery. *PLoS Negl. Trop. Dis.* **2014,** *8* (12), e3259; (d) Urbina, J. A.; McKerrow, J. H. Drug Susceptibility of Genetically Engineered *Trypanosoma cruzi* Strains and Sterile Cure in Animal Models as a Criterion for Potential Clinical Efficacy of Anti-*T. cruzi* Drugs. *Antimicrob. Agents Chemother.* **2015,** *59* (12), 7923–7924; (e) Riley, J.; Brand, S.; Voice, M.; Caballero, I.; Calvo, D.; Read, K. D. Development of a Fluorescence-Based *Trypanosoma cruzi* CYP51 Inhibition Assay for Effective Compound Triaging in Drug Discovery Programmes for Chagas Disease. *PLoS Negl. Trop. Dis.* **2015,** *9* (9), e0004014.
130. (a) Lepesheva, G. I.; Hargrove, T. Y.; Anderson, S.; Kleshchenko, Y.; Furtak, V.; Wawrzak, Z.; Villalta, F.; Waterman, M. R. Structural Insights Into Inhibition of Sterol 14Alpha-demethylase in the Human Pathogen *Trypanosoma cruzi*. *J. Biol. Chem.* **2010,** *285* (33), 25582–25590; (b) Villalta, F.; Dobish, M. C.; Nde, P. N.; Kleshchenko, Y. Y.; Hargrove, T. Y.; Johnson, C. A.; Waterman, M. R.; Johnston, J. N.; Lepesheva, G. I. VNI Cures Acute and Chronic Experimental Chagas Disease. *J. Infect. Dis.* **2013,** *208* (3), 504–511; (c) Hoekstra, W. J.; Hargrove, T. Y.; Wawrzak, Z.; Batista, D. D.; da Silva, C. F.; Nefertiti, A. S.; Rachakonda, G.; Schotzinger, R. J.; Villalta, F.; Soeiro, M. N.; Lepesheva, G. I. Antiparasitic Effect In Vitro, Activity in a Murine Model of Chagas Disease, and Structural Characterization in Complex With the Target Enzyme CYP51 From *Trypanosoma cruzi* of the Potent Clinical Candidate VT-1161. *Antimicrob. Agents Chemother.* **2016,** *60,* 1058–1066; (d) Lepesheva, G. I.; Hargrove, T. Y.; Rachakonda, G.; Wawrzak, Z.; Pomel, S.; Cojean, S.; Nde, P. N.; Nes, W. D.; Locuson, C. W.; Calcutt, M. W.; Waterman, M. R.; Daniels, J. S.; Loiseau, P. M.; Villalta, F. VFV as a New Effective CYP51 Structure-Derived Drug Candidate for Chagas Disease and Visceral Leishmaniasis. *J. Infect. Dis.* **2015,** *212* (9), 1439–1448.
131. (a) Buschini, A.; Giordani, F.; de Albuquerque, C. N.; Pellacani, C.; Pelosi, G.; Rossi, C.; Zucchi, T. M.; Poli, P. Trypanocidal Nitroimidazole Derivatives: Relationships Among Chemical Structure and Genotoxic Activity. *Biochem. Pharmacol.* **2007,** *73* (10), 1537–1547; (b) Buschini, A.; Ferrarini, L.; Franzoni, S.; Galati, S.; Lazzaretti, M.; Mussi, F.; Northfleet de Albuquerque, C.; Maria Araujo Domingues Zucchi, T.; Poli, P. Genotoxicity Revaluation of Three Commercial Nitroheterocyclic Drugs: Nifurtimox, Benznidazole, and Metronidazole. *J. Parasitol. Res.* **2009,** *2009,* 463575.
132. Tweats, D.; Bourdin Trunz, B.; Torreele, E. Genotoxicity Profile of Fexinidazole—A Drug Candidate in Clinical Development for Human African Trypanomiasis (Sleeping Sickness). *Mutagenesis* **2012,** *27* (5), 523–532.
133. (a) Papadopoulou, M. V.; Bloomer, W. D.; Rosenzweig, H. S.; O'Shea, I. P.; Wilkinson, S. R.; Kaiser, M.; Chatelain, E.; Ioset, J. R. Discovery of Potent Nitrotriazole-Based Antitrypanosomal Agents: in vitro and in vivo Evaluation. *Bioorg. Med. Chem.* **2015,** *23* (19), 6467–6476; (b) Papadopoulou, M. V.; Bloomer, W. D.; Rosenzweig, H. S.; O'Shea, I. P.; Wilkinson, S. R.; Kaiser, M. 3-Nitrotriazole-Based Piperazides As Potent Antitrypanosomal Agents. *Eur. J. Med. Chem.* **2015,** *103,* 325–334; (c) de Andrade, P.; Galo, O. A.; Carvalho, M. R.; Lopes, C. D.; Carneiro, Z. A.; Sesti-Costa, R.; de Melo, E. B.; Silva, J. S.; Carvalho, I. 1,2,3-Triazole-Based Analogue of Benznidazole Displays Remarkable Activity Against *Trypanosoma cruzi*. *Bioorg. Med. Chem.* **2015,** *23* (21), 6815–6826; (d) Papadopoulou, M. V.; Bloomer, W. D.; Rosenzweig, H. S.; Kaiser, M.; Chatelain, E.; Ioset, J. R. Novel 3-Nitro-1H-1,2,4-triazole-Based Piperazines and 2-Amino-1,3-benzothiazoles as Antichagasic Agents. *Bioorg. Med. Chem.* **2013,** *21* (21), 6600–6607; (e) Papadopoulou, M. V.; Bloomer, W. D.; Rosenzweig, H. S.; Chatelain, E.; Kaiser, M.; Wilkinson, S. R.; McKenzie, C.; Ioset, J. R. Novel 3-Nitro-1H-1,2,4-triazole-Based Amides and Sulfonamides As Potential Antitrypanosomal Agents. *J. Med. Chem.* **2012,** *55* (11), 5554–5565.

134. Diniz Lde, F.; Urbina, J. A.; de Andrade, I. M.; Mazzeti, A. L.; Martins, T. A.; Caldas, I. S.; Talvani, A.; Ribeiro, I.; Bahia, M. T. Benznidazole and Posaconazole in Experimental Chagas Disease: Positive Interaction in Concomitant and Sequential Treatments. *PLoS Negl. Trop. Dis.* **2013,** *7* (8), e2367.
135. Papadopoulou, M. V.; Bloomer, W. D.; Lepesheva, G. I.; Rosenzweig, H. S.; Kaiser, M.; Aguilera-Venegas, B.; Wilkinson, S. R.; Chatelain, E.; Ioset, J. R. Novel 3-Nitrotriazole-Based Amides and Carbinols As Bifunctional Antichagasic Agents. *J. Med. Chem.* **2015,** *58* (3), 1307–1319.
136. Veiga-Santos, P.; Li, K.; Lameira, L.; de Carvalho, T. M.; Huang, G.; Galizzi, M.; Shang, N.; Li, Q.; Gonzalez-Pacanowska, D.; Hernandez-Rodriguez, V.; Benaim, G.; Guo, R. T.; Urbina, J. A.; Docampo, R.; de Souza, W.; Oldfield, E. SQ109, a New Drug Lead for Chagas Disease. *Antimicrob. Agents Chemother.* **2015,** *59* (4), 1950–1961.
137. Protopopova, M.; Hanrahan, C.; Nikonenko, B.; Samala, R.; Chen, P.; Gearhart, J.; Einck, L.; Nacy, C. A. Identification of a New Antitubercular Drug Candidate, SQ109, From a Combinatorial Library of 1,2-Ethylenediamines. *J. Antimicrob. Chemother.* **2005,** *56* (5), 968–974.
138. Jia, L.; Tomaszewski, J. E.; Hanrahan, C.; Coward, L.; Noker, P.; Gorman, G.; Nikonenko, B.; Protopopova, M. Pharmacodynamics and Pharmacokinetics of SQ109, a New Diamine-Based Antitubercular Drug. *Br. J. Pharmacol.* **2005,** *144* (1), 80–87.
139. Zumla, A.; Nahid, P.; Cole, S. T. Advances in the Development of New Tuberculosis Drugs and Treatment Regimens. *Nat. Rev. Drug Discov.* **2013,** *12* (5), 388–404.
140. Sacksteder, K. A.; Protopopova, M.; Barry, C. E., III; Andries, K.; Nacy, C. A. Discovery and Development of SQ109: A New Antitubercular Drug With a Novel Mechanism of Action. *Future Microbiol.* **2012,** *7* (7), 823–837.
141. Li, K.; Schurig-Briccio, L. A.; Feng, X.; Upadhyay, A.; Pujari, V.; Lechartier, B.; Fontes, F. L.; Yang, H.; Rao, G.; Zhu, W.; Gulati, A.; No, J. H.; Cintra, G.; Bogue, S.; Liu, Y. L.; Molohon, K.; Orlean, P.; Mitchell, D. A.; Freitas-Junior, L.; Ren, F.; Sun, H.; Jiang, T.; Li, Y.; Guo, R. T.; Cole, S. T.; Gennis, R. B.; Crick, D. C.; Oldfield, E. Multitarget Drug Discovery for Tuberculosis and Other Infectious Diseases. *J. Med. Chem.* **2014,** *57* (7), 3126–3139.
142. Lin, F. Y.; Liu, C. I.; Liu, Y. L.; Zhang, Y.; Wang, K.; Jeng, W. Y.; Ko, T. P.; Cao, R.; Wang, A. H.; Oldfield, E. Mechanism of Action and Inhibition of Dehydrosqualene Synthase. *Proc. Natl. Acad. Sci. U. S. A.* **2010,** *107* (50), 21337–21342.
143. (a) Orenes Lorente, S.; Gomez, R.; Jimenez, C.; Cammerer, S.; Yardley, V.; de Luca-Fradley, K.; Croft, S. L.; Ruiz Perez, L. M.; Urbina, J.; Gonzalez Pacanowska, D.; Gilbert, I. H. Biphenylquinuclidines As Inhibitors of Squalene Synthase and Growth of Parasitic Protozoa. *Bioorg. Med. Chem.* **2005,** *13* (10), 3519–3529; (b) Cammerer, S. B.; Jimenez, C.; Jones, S.; Gros, L.; Lorente, S. O.; Rodrigues, C.; Rodrigues, J. C.; Caldera, A.; Ruiz Perez, L. M.; da Souza, W.; Kaiser, M.; Brun, R.; Urbina, J. A.; Gonzalez Pacanowska, D.; Gilbert, I. H. Quinuclidine Derivatives As Potential Antiparasitics. *Antimicrob. Agents Chemother.* **2007,** *51* (11), 4049–4061; (c) Sealey-Cardona, M.; Cammerer, S.; Jones, S.; Ruiz-Perez, L. M.; Brun, R.; Gilbert, I. H.; Urbina, J. A.; Gonzalez-Pacanowska, D. Kinetic Characterization of Squalene Synthase From *Trypanosoma cruzi*: Selective Inhibition by Quinuclidine Derivatives. *Antimicrob. Agents Chemother.* **2007,** *51* (6), 2123–2129.
144. Mercer, L.; Bowling, T.; Perales, J.; Freeman, J.; Nguyen, T.; Bacchi, C.; Yarlett, N.; Don, R.; Jacobs, R.; Nare, B. 2,4-Diaminopyrimidines as Potent Inhibitors of *Trypanosoma brucei* and Identification of Molecular Targets by a Chemical Proteomics Approach. *PLoS Negl. Trop. Dis.* **2011,** *5* (2), e956.
145. Faria, J.; Moraes, C. B.; Song, R.; Pascoalino, B. S.; Lee, N.; Siqueira-Neto, J. L.; Cruz, D. J.; Parkinson, T.; Ioset, J. R.; Cordeiro-da-Silva, A.; Freitas-Junior, L. H. Drug Discovery for Human African Trypanosomiasis: Identification of Novel Scaffolds by the Newly Developed HTS SYBR Green Assay for *Trypanosoma brucei*. *J. Biomol. Screen.* **2015,** *20* (1), 70–81.
146. Burri, C. Chemotherapy Against Human African Trypanosomiasis: Is There a Road to Success? *Parasitology* **2010,** *137* (14), 1987–1994.
147. Paine, M. F.; Wang, M. Z.; Generaux, C. N.; Boykin, D. W.; Wilson, W. D.; De Koning, H. P.; Olson, C. A.; Pohlig, G.; Burri, C.; Brun, R.; Murilla, G. A.; Thuita, J. K.; Barrett, M. P.; Tidwell, R. R. Diamidines for Human African Trypanosomiasis. *Curr. Opin. Investig. Drugs* **2010,** *11* (8), 876–883.
148. Wenzler, T.; Yang, S.; Braissant, O.; Boykin, D. W.; Brun, R.; Wang, M. Z. Pharmacokinetics, *Trypanosoma brucei* Gambiense Efficacy, and Time of Drug Action of DB829, a Preclinical Candidate for Treatment of Second-Stage Human African Trypanosomiasis. *Antimicrob. Agents Chemother.* **2013,** *57* (11), 5330–5343.
149. Thuita, J. K.; Wang, M. Z.; Kagira, J. M.; Denton, C. L.; Paine, M. F.; Mdachi, R. E.; Murilla, G. A.; Ching, S.; Boykin, D. W.; Tidwell, R. R.; Hall, J. E.; Brun, R. Pharmacology of DB844, an Orally Active Aza Analogue of Pafuramidine, in a Monkey Model of Second Stage Human African Trypanosomiasis. *PLoS Negl. Trop. Dis.* **2012,** *6* (7), e1734.
150. Wenzler, T.; Yang, S.; Patrick, D. A.; Braissant, O.; Ismail, M. A.; Tidwell, R. R.; Boykin, D. W.; Wang, M. Z.; Brun, R. In Vitro and in vivo Evaluation of 28DAP010, a Novel Diamidine for Treatment of Second-Stage African Sleeping Sickness. *Antimicrob. Agents Chemother.* **2014,** *58* (8), 4452–4463.
151. (a) Oberholzer, M.; Marti, G.; Baresic, M.; Kunz, S.; Hemphill, A.; Seebeck, T. The *Trypanosoma brucei* cAMP Phosphodiesterases TbrPDEB1 and TbrPDEB2: Flagellar Enzymes That Are Essential for Parasite Virulence. *FASEB J.* **2007,** *21* (3), 720–731; (b) de Koning, H. P.; Gould, M. K.; Sterk, G. J.; Tenor, H.; Kunz, S.; Luginbuehl, E.; Seebeck, T. Pharmacological Calidation of *Trypanosoma brucei* Phosphodiesterases As Novel Drug Targets. *J. Infect. Dis.* **2012,** *206* (2), 229–237; (c) Seebeck, T.; Sterk, G. J.; Ke, H. Phosphodiesterase Inhibitors As a New Generation of Antiprotozoan Drugs: Exploiting the Benefit of Enzymes That Are Highly Conserved Between Host and Parasite. *Future Med. Chem.* **2011,** *3* (10), 1289–1306; (d) Shakur, Y.; de Koning, H. P.; Ke, H.; Kambayashi, J.; Seebeck, T. Therapeutic Potential of Phosphodiesterase Inhibitors in Parasitic Diseases. *Handb. Exp. Pharmacol.* **2011,** *204,* 487–510.
152. Orrling, K. M.; Jansen, C.; Vu, X. L.; Balmer, V.; Bregy, P.; Shanmugham, A.; England, P.; Bailey, D.; Cos, P.; Maes, L.; Adams, E.; van den Bogaart, E.; Chatelain, E.; Ioset, J. R.; van de Stolpe, A.; Zorg, S.; Veerman, J.; Seebeck, T.; Sterk, G. J.; de Esch, I. J.; Leurs, R. Catechol Pyrazolinones As Trypanocidals: Fragment-Based Design, Synthesis, and Pharmacological Evaluation of Nanomolar Inhibitors of Trypanosomal Phosphodiesterase B1. *J. Med. Chem.* **2012,** *55* (20), 8745–8756.
153. Jansen, C.; Wang, H.; Kooistra, A. J.; de Graaf, C.; Orrling, K. M.; Tenor, H.; Seebeck, T.; Bailey, D.; de Esch, I. J.; Ke, H.; Leurs, R. Discovery of Novel *Trypanosoma brucei* Phosphodiesterase B1 Inhibitors by Virtual Screening Against the Unliganded TbrPDEB1 Crystal Structure. *J. Med. Chem.* **2013,** *56* (5), 2087–2096.
154. Bland, N. D.; Wang, C.; Tallman, C.; Gustafson, A. E.; Wang, Z.; Ashton, T. D.; Ochiana, S. O.; McAllister, G.; Cotter, K.; Fang, A. P.; Gechijian, L.; Garceau, N.; Gangurde, R.; Ortenberg, R.; Ondrechen, M. J.; Campbell, R. K.; Pollastri, M. P. Pharmacological Validation of *Trypanosoma brucei* Phosphodiesterases B1 and B2 as Druggable Targets for African Sleeping Sickness. *J. Med. Chem.* **2011,** *54* (23), 8188–8194.
155. Woodring, J. L.; Bland, N. D.; Ochiana, S. O.; Campbell, R. K.; Pollastri, M. P. Synthesis and Assessment of Catechol Diether Compounds As Inhibitors of Trypanosomal Phosphodiesterase B1 (TbrPDEB1). *Bioorg. Med. Chem. Lett.* **2013,** *23* (21), 5971–5974.
156. Amata, E.; Bland, N. D.; Hoyt, C. T.; Settimo, L.; Campbell, R. K.; Pollastri, M. P. Repurposing Human PDE4 Inhibitors for Neglected Tropical Diseases: Design, Synthesis and Evaluation of Cilomilast Analogues As *Trypanosoma brucei* PDEB1 Inhibitors. *Bioorg. Med. Chem. Lett.* **2014,** *24* (17), 4084–4089.
157. Ochiana, S. O.; Bland, N. D.; Settimo, L.; Campbell, R. K.; Pollastri, M. P. Repurposing Human PDE4 Inhibitors for Neglected Tropical Diseases. Evaluation of Analogs of the Human PDE4 Inhibitor GSK-256066 As Inhibitors of PDEB1 of *Trypanosoma brucei*. *Chem. Biol. Drug Des.* **2015,** *85* (5), 549–564.
158. Jacobs, R. T.; Plattner, J. J.; Nare, B.; Wring, S. A.; Chen, D.; Freund, Y.; Gaukel, E. G.; Orr, M. D.; Perales, J. B.; Jenks, M.; Noe, R. A.; Sligar, J. M.; Zhang, Y. K.; Bacchi, C. J.; Yarlett, N.; Don, R. Benzoxaboroles: A New Class of Potential Drugs for Human African Trypanosomiasis. *Future Med. Chem.* **2011,** *3* (10), 1259–1278.
159. Ding, D.; Zhao, Y.; Meng, Q.; Xie, D.; Nare, B.; Chen, D.; Bacchi, C. J.; Yarlett, N.; Zhang, Y. K.; Hernandez, V.; Xia, Y.; Freund, Y.; Abdulla, M.; Ang, K. H.; Ratnam, J.; McKerrow, J. H.; Jacobs, R. T.; Zhou, H.; Plattner, J. J. Discovery of Novel Benzoxaborole-Based Potent Antitrypanosomal Agents. *ACS Med. Chem. Lett.* **2010,** *1* (4), 165–169.
160. Nare, B.; Wring, S.; Bacchi, C.; Beaudet, B.; Bowling, T.; Brun, R.; Chen, D.; Ding, C.; Freund, Y.; Gaukel, E.; Hussain, A.; Jarnagin, K.; Jenks, M.; Kaiser, M.; Mercer, L.; Mejia, E.; Noe, A.; Orr, M.; Parham, R.; Plattner, J.; Randolph, R.; Rattendi, D.; Rewerts, C.; Sligar, J.; Yarlett, N.; Don, R.; Jacobs, R. Discovery of Novel Orally Bioavailable Oxaborole 6-Carboxamides That Demonstrate Cure in a Murine Model of Late-Stage Central Nervous System African Trypanosomiasis. *Antimicrob. Agents Chemother.* **2010,** *54* (10), 4379–4388.
161. Jacobs, R. T.; Nare, B.; Wring, S. A.; Orr, M. D.; Chen, D.; Sligar, J. M.; Jenks, M. X.; Noe, R. A.; Bowling, T. S.; Mercer, L. T.; Rewerts, C.; Gaukel, E.; Owens, J.; Parham, R.; Randolph, R.; Beaudet, B.; Bacchi, C. J.; Yarlett, N.; Plattner, J. J.; Freund, Y.; Ding, C.; Akama, T.; Zhang, Y. K.; Brun, R.; Kaiser, M.; Scandale, I.; Don, R. SCYX-7158, an Orally-Active Benzoxaborole for the Treatment of Stage 2 Human African Trypanosomiasis. *PLoS Negl. Trop. Dis.* **2011,** *5* (6), e1151.
162. Tarral, A. Human African Trypanosomiasis: First in Man Clinical Trial of a New Medicinal Product, the SCYX-7158. https://clinicaltrials.gov/ct2/show/NCT01533961?term=SCYX-7158&rank=1.

163. Kalidas, S.; Cestari, I.; Monnerat, S.; Li, Q.; Regmi, S.; Hasle, N.; Labaied, M.; Parsons, M.; Stuart, K.; Phillips, M. A. Genetic Validation of Aminoacyl-tRNA Synthetases as Drug Targets in *Trypanosoma brucei*. *Eukaryot. Cell* **2014,** *13* (4), 504–516.
164. (a) Cestari, I.; Stuart, K. Inhibition of Isoleucyl-tRNA Synthetase As a Potential Treatment for Human African Trypanosomiasis. *J. Biol. Chem.* **2013,** *288* (20), 14256–14263; (b) Merritt, E. A.; Arakaki, T. L.; Gillespie, J. R.; Larson, E. T.; Kelley, A.; Mueller, N.; Napuli, A. J.; Kim, J.; Zhang, L.; Verlinde, C. L.; Fan, E.; Zucker, F.; Buckner, F. S.; van Voorhis, W. C.; Hol, W. G. Crystal Structures of Trypanosomal Histidyl-tRNA Synthetase Illuminate Differences Between Eukaryotic and Prokaryotic Homologs. *J. Mol. Biol.* **2010,** *397* (2), 481–494.
165. (a) Shibata, S.; Gillespie, J. R.; Kelley, A. M.; Napuli, A. J.; Zhang, Z.; Kovzun, K. V.; Pefley, R. M.; Lam, J.; Zucker, F. H.; Van Voorhis, W. C.; Merritt, E. A.; Hol, W. G.; Verlinde, C. L.; Fan, E.; Buckner, F. S. Selective Inhibitors of Methionyl-tRNA Synthetase Have Potent Activity Against *Trypanosoma brucei* Infection in Mice. *Antimicrob. Agents Chemother.* **2011,** *55* (5), 1982–1989; (b) Shibata, S.; Gillespie, J. R.; Ranade, R. M.; Koh, C. Y.; Kim, J. E.; Laydbak, J. U.; Zucker, F. H.; Hol, W. G.; Verlinde, C. L.; Buckner, F. S.; Fan, E. Urea-Based Inhibitors of *Trypanosoma brucei* Methionyl-tRNA Synthetase: Selectivity and in vivo Characterization. *J. Med. Chem.* **2012,** *55* (14), 6342–6351; (c) Koh, C. Y.; Kim, J. E.; Wetzel, A. B.; de van der Schueren, W. J.; Shibata, S.; Ranade, R. M.; Liu, J.; Zhang, Z.; Gillespie, J. R.; Buckner, F. S.; Verlinde, C. L.; Fan, E.; Hol, W. G. Structures of *Trypanosoma brucei* Methionyl-tRNA Synthetase With Urea-Based Inhibitors Provide Guidance for Drug Design Against Sleeping Sickness. *PLoS Negl. Trop. Dis.* **2014,** *8* (4), e2775; (d) Pedro-Rosa, L.; Buckner, F. S.; Ranade, R. M.; Eberhart, C.; Madoux, F.; Gillespie, J. R.; Koh, C. Y.; Brown, S.; Lohse, J.; Verlinde, C. L.; Fan, E.; Bannister, T.; Scampavia, L.; Hol, W. G.; Spicer, T.; Hodder, P. Identification of Potent Inhibitors of the *Trypanosoma brucei* Methionyl-tRNA Synthetase via High-Throughput Orthogonal Screening. *J. Biomol. Screen.* **2015,** *20* (1), 122–130; (e) Ding, D.; Meng, Q.; Gao, G.; Zhao, Y.; Wang, Q.; Nare, B.; Jacobs, R.; Rock, F.; Alley, M. R.; Plattner, J. J.; Chen, G.; Li, D.; Zhou, H. Design, Synthesis, and Structure-Activity Relationship of *Trypanosoma brucei* Leucyl-tRNA Synthetase Inhibitors As Antitrypanosomal Agents. *J. Med. Chem.* **2011,** *54* (5), 1276–1287; (f) Zhang, F.; Du, J.; Wang, Q.; Hu, Q.; Zhang, J.; Ding, D.; Zhao, Y.; Yang, F.; Wang, E.; Zhou, H. Discovery of *N*-(4-Sulfamoylphenyl)thioureas as *Trypanosoma brucei* Leucyl-tRNA Synthetase Inhibitors. *Org. Biomol. Chem.* **2013,** *11* (32), 5310–5324.
166. Rock, F. L.; Mao, W.; Yaremchuk, A.; Tukalo, M.; Crepin, T.; Zhou, H.; Zhang, Y. K.; Hernandez, V.; Akama, T.; Baker, S. J.; Plattner, J. J.; Shapiro, L.; Martinis, S. A.; Benkovic, S. J.; Cusack, S.; Alley, M. R. An Antifungal Agent Inhibits an Aminoacyl-tRNA Synthetase by Trapping tRNA in the Editing Site. *Science* **2007,** *316* (5832), 1759–1761.
167. Hernandez, V.; Crepin, T.; Palencia, A.; Cusack, S.; Akama, T.; Baker, S. J.; Bu, W.; Feng, L.; Freund, Y. R.; Liu, L.; Meewan, M.; Mohan, M.; Mao, W.; Rock, F. L.; Sexton, H.; Sheoran, A.; Zhang, Y.; Zhang, Y. K.; Zhou, Y.; Nieman, J. A.; Anugula, M. R.; Keramane el, M.; Savariraj, K.; Reddy, D. S.; Sharma, R.; Subedi, R.; Singh, R.; O'Leary, A.; Simon, N. L.; De Marsh, P. L.; Mushtaq, S.; Warner, M.; Livermore, D. M.; Alley, M. R.; Plattner, J. J. Discovery of a Novel Class of Boron-Based Antibacterials With Activity Against Gram-Negative Bacteria. *Antimicrob. Agents Chemother.* **2013,** *57* (3), 1394–1403.
168. Zhao, Y.; Wang, Q.; Meng, Q.; Ding, D.; Yang, H.; Gao, G.; Li, D.; Zhu, W.; Zhou, H. Identification of *Trypanosoma brucei* Leucyl-tRNA Synthetase Inhibitors by Pharmacophore- and Docking-Based Virtual Screening and Synthesis. *Bioorg. Med. Chem.* **2012,** *20* (3), 1240–1250.
169. (a) Price, H. P.; Menon, M. R.; Panethymitaki, C.; Goulding, D.; McKean, P. G.; Smith, D. F. Myristoyl-CoA:Protein *N*-Myristoyltransferase, an Essential Enzyme and Potential Drug Target in Kinetoplastid Parasites. *J. Biol. Chem.* **2003,** *278* (9), 7206–7214; (b) Bowyer, P. W.; Tate, E. W.; Leatherbarrow, R. J.; Holder, A. A.; Smith, D. F.; Brown, K. A. *N*-Myristoyltransferase: A Prospective Drug Target for Protozoan Parasites. *ChemMedChem* **2008,** *3* (3), 402–408; (c) Tate, E. W.; Bell, A. S.; Rackham, M. D.; Wright, M. H. N-Myristoyltransferase As a Potential Drug Target in Malaria and Leishmaniasis. *Parasitology* **2014,** *141* (Special Issue 01), 37–49.
170. Panethymitaki, C.; Bowyer, P. W.; Price, H. P.; Leatherbarrow, R. J.; Brown, K. A.; Smith, D. F. Characterization and Selective Inhibition of Myristoyl-CoA:Protein *N*-Myristoyltransferase From *Trypanosoma brucei* and *Leishmania major*. *Biochem. J.* **2006,** *396* (2), 277–285.
171. (a) Frearson, J. A.; Brand, S.; McElroy, S. P.; Cleghorn, L. A.; Smid, O.; Stojanovski, L.; Price, H. P.; Guther, M. L.; Torrie, L. S.; Robinson, D. A.; Hallyburton, I.; Mpamhanga, C. P.; Brannigan, J. A.; Wilkinson, A. J.; Hodgkinson, M.; Hui, R.; Qiu, W.; Raimi, O. G.; van Aalten, D. M.; Brenk, R.; Gilbert, I. H.; Read, K. D.; Fairlamb, A. H.; Ferguson, M. A.; Smith, D. F.; Wyatt, P. G. *N*-Myristoyltransferase Inhibitors As New Leads to Treat Sleeping Sickness. *Nature* **2010,** *464* (7289), 728–732; (b) Brand, S.; Cleghorn, L. A.; McElroy, S. P.; Robinson, D. A.; Smith, V. C.; Hallyburton, I.; Harrison, J. R.; Norcross, N. R.; Spinks, D.; Bayliss, T.; Norval, S.; Stojanovski, L.; Torrie, L. S.; Frearson, J. A.; Brenk, R.; Fairlamb, A. H.; Ferguson, M. A.; Read, K. D.; Wyatt, P. G.; Gilbert, I. H. Discovery of a Novel Class of Orally Active Trypanocidal *N*-Myristoyltransferase Inhibitors. *J. Med. Chem.* **2012,** *55* (1), 140–152.
172. Brand, S.; Norcross, N. R.; Thompson, S.; Harrison, J. R.; Smith, V. C.; Robinson, D. A.; Torrie, L. S.; McElroy, S. P.; Hallyburton, I.; Norval, S.; Scullion, P.; Stojanovski, L.; Simeons, F. R.; van Aalten, D.; Frearson, J. A.; Brenk, R.; Fairlamb, A. H.; Ferguson, M. A.; Wyatt, P. G.; Gilbert, I. H.; Read, K. D. Lead Optimization of a Pyrazole Sulfonamide Series of *Trypanosoma brucei N*-Myristoyltransferase Inhibitors: Identification and Evaluation of CNS Penetrant Compounds as Potential Treatments for Stage 2 Human African Trypanosomiasis. *J. Med. Chem.* **2014,** *57* (23), 9855–9869.
173. Spinks, D.; Smith, V.; Thompson, S.; Robinson, D. A.; Luksch, T.; Smith, A.; Torrie, L. S.; McElroy, S.; Stojanovski, L.; Norval, S.; Collie, I. T.; Hallyburton, I.; Rao, B.; Brand, S.; Brenk, R.; Frearson, J. A.; Read, K. D.; Wyatt, P. G.; Gilbert, I. H. Development of Small-Molecule *Trypanosoma brucei N*-Myristoyltransferase Inhibitors: Discovery and Optimisation of a Novel Binding Mode. *ChemMedChem* **2015,** *10* (11), 1821–1836.
174. (a) Bell, A. S.; Mills, J. E.; Williams, G. P.; Brannigan, J. A.; Wilkinson, A. J.; Parkinson, T.; Leatherbarrow, R. J.; Tate, E. W.; Holder, A. A.; Smith, D. F. Selective Inhibitors of Protozoan Protein *N*-Myristoyltransferases as Starting Points for Tropical Disease Medicinal Chemistry Programs. *PLoS Negl. Trop. Dis.* **2012,** *6* (4), e1625; (b) Goncalves, V.; Brannigan, J. A.; Whalley, D.; Ansell, K. H.; Saxty, B.; Holder, A. A.; Wilkinson, A. J.; Tate, E. W.; Leatherbarrow, R. J. Discovery of *Plasmodium vivax N*-Myristoyltransferase Inhibitors: Screening, Synthesis, and Structural Characterization of Their Binding Mode. *J. Med. Chem.* **2012,** *55* (7), 3578–3582.
175. (a) Yu, Z.; Brannigan, J. A.; Moss, D. K.; Brzozowski, A. M.; Wilkinson, A. J.; Holder, A. A.; Tate, E. W.; Leatherbarrow, R. J. Design and Synthesis of Inhibitors of *Plasmodium falciparum N*-Myristoyltransferase, a Promising Target for Antimalarial Drug Discovery. *J. Med. Chem.* **2012,** *55* (20), 8879–8890; (b) Rackham, M. D.; Brannigan, J. A.; Moss, D. K.; Yu, Z.; Wilkinson, A. J.; Holder, A. A.; Tate, E. W.; Leatherbarrow, R. J. Discovery of Novel and Ligand-Efficient Inhibitors of *Plasmodium falciparum* and *Plasmodium vivax N*-Myristoyltransferase. *J. Med. Chem.* **2013,** *56* (1), 371–375; (c) Rackham, M. D.; Brannigan, J. A.; Rangachari, K.; Meister, S.; Wilkinson, A. J.; Holder, A. A.; Leatherbarrow, R. J.; Tate, E. W. Design and Synthesis of High Affinity Inhibitors of *Plasmodium falciparum* and *Plasmodium vivax N*-Myristoyltransferases Directed by Ligand Efficiency Dependent Lipophilicity (LELP). *J. Med. Chem.* **2014,** *57* (6), 2773–2788.
176. (a) Ferrins, L.; Rahmani, R.; Sykes, M. L.; Jones, A. J.; Avery, V. M.; Teston, E.; Almohaywi, B.; Yin, J.; Smith, J.; Hyland, C.; White, K. L.; Ryan, E.; Campbell, M.; Charman, S. A.; Kaiser, M.; Baell, J. B. 3-(Oxazolo[4,5-b]pyridin-2-yl)anilides as a Novel Class of Potent Inhibitors for the Kinetoplastid *Trypanosoma brucei*, the Causative Agent for Human African Trypanosomiasis. *Eur. J. Med. Chem.* **2013,** *66,* 450–465; (b) Tatipaka, H. B.; Gillespie, J. R.; Chatterjee, A. K.; Norcross, N. R.; Hulverson, M. A.; Ranade, R. M.; Nagendar, P.; Creason, S. A.; McQueen, J.; Duster, N. A.; Nagle, A.; Supek, F.; Molteni, V.; Wenzler, T.; Brun, R.; Glynne, R.; Buckner, F. S.; Gelb, M. H. Substituted 2-Phenylimidazopyridines: A New Class of Drug Leads for Human African Trypanosomiasis. *J. Med. Chem.* **2014,** *57* (3), 828–835.
177. Rashad, A. A.; Jones, A. J.; Avery, V. M.; Baell, J.; Keller, P. A. Facile Synthesis and Preliminary Structure-Activity Analysis of New Sulfonamides Against *Trypanosoma brucei*. *ACS Med. Chem. Lett.* **2014,** *5* (5), 496–500.
178. Ferrins, L.; Gazdik, M.; Rahmani, R.; Varghese, S.; Sykes, M. L.; Jones, A. J.; Avery, V. M.; White, K. L.; Ryan, E.; Charman, S. A.; Kaiser, M.; Bergstrom, C. A.; Baell, J. B. Pyridyl Benzamides as a Novel Class of Potent Inhibitors for the Kinetoplastid *Trypanosoma brucei*. *J. Med. Chem.* **2014,** *57* (15), 6393–6402.
179. Rahmani, R.; Ban, K.; Jones, A. J.; Ferrins, L.; Ganame, D.; Sykes, M. L.; Avery, V. M.; White, K. L.; Ryan, E.; Kaiser, M.; Charman, S. A.; Baell, J. B. 6-Arylpyrazine-2-carboxamides: A New Core for *Trypanosoma brucei* Inhibitors. *J. Med. Chem.* **2015,** *58* (17), 6753–6765.
180. (a) Diaz, R.; Luengo-Arratta, S. A.; Seixas, J. D.; Amata, E.; Devine, W.; Cordon-Obras, C.; Rojas-Barros, D. I.; Jimenez, E.; Ortega, F.; Crouch, S.; Colmenarejo, G.; Fiandor, J. M.; Martin, J. J.; Berlanga, M.; Gonzalez, S.; Manzano, P.; Navarro, M.; Pollastri, M. P. Identification and Characterization of Hundreds of Potent and Selective Inhibitors of *Trypanosoma brucei* Growth From a Kinase-Targeted Library Screening Campaign. *PLoS Negl. Trop. Dis.* **2014,** *8* (10), e3253; (b) Woodland, A.; Thompson, S.; Cleghorn, L. A.; Norcross, N.; De Rycker, M.; Grimaldi, R.; Hallyburton, I.; Rao, B.; Norval, S.; Stojanovski, L.; Brun, R.; Kaiser, M.; Frearson, J. A.; Gray, D. W.; Wyatt, P. G.; Read, K. D.; Gilbert, I. H. Discovery of Inhibitors of *Trypanosoma brucei* by Phenotypic Screening of a Focused Protein Kinase Library. *ChemMedChem* **2015,** *10* (11), 1809–1820.

181. Cleghorn, L. A.; Albrecht, S.; Stojanovski, L.; Simeons, F. R.; Norval, S.; Kime, R.; Collie, I. T.; De Rycker, M.; Campbell, L.; Hallyburton, I.; Frearson, J. A.; Wyatt, P. G.; Read, K. D.; Gilbert, I. H. Discovery of Indoline-2-carboxamide Derivatives as a New Class of Brain-Penetrant Inhibitors of *Trypanosoma brucei*. *J. Med. Chem.* **2015,** *58* (19), 7695–7706.
182. (a) Carrillo, A. K.; Guiguemde, W. A.; Guy, R. K. Evaluation of Histone Deacetylase Inhibitors (HDACi) as Therapeutic Leads for Human African Trypanosomiasis (HAT). *Bioorg. Med. Chem.* **2015,** *23* (16), 5151–5155; (b) Engel, J. A.; Jones, A. J.; Avery, V. M.; Sumanadasa, S. D.; Ng, S. S.; Fairlie, D. P.; Adams, T. S.; Andrews, K. T. Profiling the Anti-Protozoal Activity of Anti-Cancer HDAC Inhibitors Against *Plasmodium* and *Trypanosoma* Parasites. *Int. J. Parasitol. Drugs Drug Resist.* **2015,** *5* (3), 117–126.
183. (a) Stanley, S. L., Jr. Amoebiasis. *Lancet* **2003,** *361* (9362), 1025–1034; (b) WHO WHO/PAHO/UNESCO Report: A Consultation With Experts on Amoebiasis; Mexico City, Mexico, January 28, 1997, pp. 13–14.
184. Kuriyama, A.; Jackson, J. L.; Doi, A.; Kamiya, T. Metronidazole-Induced Central Nervous System Toxicity: A Systematic Review. *Clin. Neuropharmacol.* **2011,** *34* (6), 241–247.
185. Bendesky, A.; Menendez, D.; Ostrosky-Wegman, P. Is Metronidazole Carcinogenic? *Mutat. Res.* **2002,** *511* (2), 133–144.
186. (a) Valdez, J.; Cedillo, R.; Hernández-Campos, A.; Yépez, L.; Hernández-Luis, F.; Navarrete-Vázquez, G.; Tapia, A.; Cortés, R.; Hernández, M.; Castillo, R. Synthesis and Antiparasitic Activity of 1H-Benzimidazole Derivatives. *Bioorg. Med. Chem. Lett.* **2002,** *12* (16), 2221–2224; (b) Hernández-Luis, F.; Hernández-Campos, A.; Castillo, R.; Navarrete-Vázquez, G.; Soria-Arteche, O.; Hernández-Hernández, M.; Yépez-Mulia, L. Synthesis and Biological Activity of 2-(Trifluoromethyl)-1H-benzimidazole Derivatives Against Some Protozoa and *Trichinella spiralis*. *Eur. J. Med. Chem.* **2010,** *45* (7), 3135–3141; (c) Lopez-Vallejo, F.; Castillo, R.; Yepez-Mulia, L.; Medina-Franco, J. L. Benzotriazoles and Indazoles Are Scaffolds With Biological Activity Against *Entamoeba histolytica*. *J. Biomol. Screen.* **2011,** *16* (8), 862–868.
187. Shahinas, D.; Debnath, A.; Benedict, C.; McKerrow, J. H.; Pillai, D. R. Heat Shock Protein 90 Inhibitors Repurposed Against *Entamoeba histolytica*. *Front. Microbiol.* **2015,** *6,* 368.
188. Shahinas, D.; Liang, M.; Datti, A.; Pillai, D. R. A Repurposing Strategy Identifies Novel Synergistic Inhibitors of *Plasmodium falciparum* Heat Shock Protein 90. *J. Med. Chem.* **2010,** *53* (9), 3552–3557.
189. Saucedo-Mendiola, M. L.; Salas-Pacheco, J. M.; Najera, H.; Rojo-Dominguez, A.; Yepez-Mulia, L.; Avitia-Dominguez, C.; Tellez-Valencia, A. Discovery of *Entamoeba histolytica* Hexokinase 1 Inhibitors Through Homology Modeling and Virtual Screening. *J. Enzyme Inhib. Med. Chem.* **2014,** *29* (3), 325–332.
190. (a) Hayat, F.; Salahuddin, A.; Azam, A. Synthesis, Characterization, Antiamoebic Activity and Cytotoxicity of New Pyrazolo[3, 4-d]pyrimidine-6-one Derivatives. *J. Enzyme Inhib. Med. Chem.* **2011,** *26* (4), 472–479; (b) Parveen, H.; Hayat, F.; Mukhtar, S.; Salahuddin, A.; Khan, A.; Islam, F.; Azam, A. Synthesis, Characterization and Biological Evaluation of Novel 2,4,6-Trisubstituted Bis-Pyrimidine Derivatives. *Eur. J. Med. Chem.* **2011,** *46* (9), 4669–4675.
191. Debnath, A.; Parsonage, D.; Andrade, R. M.; He, C.; Cobo, E. R.; Hirata, K.; Chen, S.; Garcia-Rivera, G.; Orozco, E.; Martinez, M. B.; Gunatilleke, S. S.; Barrios, A. M.; Arkin, M. R.; Poole, L. B.; McKerrow, J. H.; Reed, S. L. A High-Throughput Drug Screen for *Entamoeba histolytica* Identifies a New Lead and Target. *Nat. Med.* **2012,** *18* (6), 956–960.
192. Savioli, L.; Smith, H.; Thompson, A. Giardia and Cryptosporidium Join the 'Neglected Diseases Initiative'. *Trends Parasitol.* **2006,** *22* (5), 203–208.
193. Tian, H. F.; Chen, B.; Wen, J. F. Giardiasis, Drug Resistance, and New Target Discovery. *Infect. Disord. Drug Targets* **2010,** *10* (4), 295–302.
194. Tejman-Yarden, N.; Miyamoto, Y.; Leitsch, D.; Santini, J.; Debnath, A.; Gut, J.; McKerrow, J. H.; Reed, S. L.; Eckmann, L. A Reprofiled Drug, Auranofin, Is Effective Against Metronidazole-Resistant *Giardia lamblia*. *Antimicrob. Agents Chemother.* **2013,** *57* (5), 2029–2035.
195. (a) Pullan, R. L.; Brooker, S. J. The Global Limits and Population at Risk of Soil-Transmitted Helminth Infections in 2010. *Parasit. Vectors* **2012,** *5,* 81; (b) Brooker, S.; Hotez, P. J.; Bundy, D. A. P. Soil-Transmitted Helminths (Geohelminths). In *Manson's Tropical Diseases;* Farrar, J., Hotez, P. J., Junghanss, T., Kang, G., Lalloo, D., White, N. J., Eds.; 23rd ed; Elsevier Saunders: Philadelphia, PA, 2014; pp 766–794.
196. Smith, J. L.; Brooker, S. Impact of Hookworm Infection and Deworming on Anaemia in Non-Pregnant Populations: A Systematic Review. *Trop. Med. Int. Health* **2010,** *15* (7), 776–795.
197. Stephenson, L. S.; Latham, M. C.; Adams, E. J.; Kinoti, S. N.; Pertet, A. Physical Fitness, Growth and Appetite of Kenyan School Boys With Hookworm, *Trichuris trichiura* and *Ascaris lumbricoides* Infections Are Improved Four Months After a Single Dose of Albendazole. *J. Nutr.* **1993,** *123* (6), 1036–1046.
198. Jardim-Botelho, A.; Raff, S.; Rodrigues Rde, A.; Hoffman, H. J.; Diemert, D. J.; Correa-Oliveira, R.; Bethony, J. M.; Gazzinelli, M. F. Hookworm, *Ascaris lumbricoides* Infection and Polyparasitism Associated With Poor Cognitive Performance in Brazilian Schoolchildren. *Trop. Med. Int. Health* **2008,** *13* (8), 994–1004.
199. Vercruysse, J.; Levecke, B.; Prichard, R. Human Soil-Transmitted Helminths: Implications of Mass Drug Administration. *Curr. Opin. Infect. Dis.* **2012,** *25* (6), 703–708.
200. Simonsen, P. E.; Fischer, P. U.; Hoerauf, A.; Weil, G. J. The Filariases. In *Manson's Tropical Diseases;* Farrar, J., Hotez, P. J., Junghanss, T., Kang, G., Lalloo, D., White, N. J., Eds.; 23rd ed; Elsevier Saunders: Philadelphia, PA, 2014; pp 737–765.
201. Ruiz-Tiben, E.; Hopkins, D. R. Dracunculiasis (Guinea Worm Disease) Eradication. *Adv. Parasitol.* **2006,** *61,* 275–309.
202. (a) Simonsen, P. E.; Derua, Y. A.; Kisinza, W. N.; Magesa, S. M.; Malecela, M. N.; Pedersen, E. M. Lymphatic Filariasis Control in Tanzania: Effect of Six Rounds of Mass Drug Administration With Ivermectin and Albendazole on Infection and Transmission. *BMC Infect. Dis.* **2013,** *13,* 335; (b) Simonsen, P. E.; Pedersen, E. M.; Rwegoshora, R. T.; Malecela, M. N.; Derua, Y. A.; Magesa, S. M. Lymphatic Filariasis Control in Tanzania: Effect of Repeated Mass Drug Administration With Ivermectin and Albendazole on Infection and Transmission. *PLoS Negl. Trop. Dis.* **2010,** *4* (6), e696.
203. Ichimori, K.; King, J. D.; Engels, D.; Yajima, A.; Mikhailov, A.; Lammie, P.; Ottesen, E. A. Global Programme to Eliminate Lymphatic Filariasis: The Processes Underlying Programme Success. *PLoS Negl. Trop. Dis.* **2014,** *8* (12), e3328.
204. Kamgno, J.; Pion, S. D.; Tejiokem, M. C.; Twum-Danso, N. A.; Thylefors, B.; Boussinesq, M. Randomized, Controlled, Double-Blind Trial With Ivermectin on *Loa loa* Microfilaraemia: Efficacy of a Low Dose (Approximately 25 microg/kg) Versus Current Standard Dose (150 microg/kg). *Trans. R. Soc. Trop. Med. Hyg.* **2007,** *101* (8), 777–785.
205. Bulman, C. A.; Bidlow, C. M.; Lustigman, S.; Cho-Ngwa, F.; Williams, D.; Rascon, A. A., Jr.; Tricoche, N.; Samje, M.; Bell, A.; Suzuki, B.; Lim, K. C.; Supakorndej, N.; Supakorndej, P.; Wolfe, A. R.; Knudsen, G. M.; Chen, S.; Wilson, C.; Ang, K. H.; Arkin, M.; Gut, J.; Franklin, C.; Marcellino, C.; McKerrow, J. H.; Debnath, A.; Sakanari, J. A. Repurposing Auranofin As a Lead Candidate for Treatment of Lymphatic Filariasis and Onchocerciasis. *PLoS Negl. Trop. Dis.* **2015,** *9* (2), e0003534.
206. (a) Ceballos, L.; Mackenzie, C.; Geary, T.; Alvarez, L.; Lanusse, C. Exploring the Potential of Flubendazole in Filariasis Control: Evaluation of the Systemic Exposure for Different Pharmaceutical Preparations. *PLoS Negl. Trop. Dis.* **2014,** *8* (5), e2838; (b) Mackenzie, C. D.; Geary, T. G. Flubendazole: A Candidate Macrofilaricide for Lymphatic Filariasis and Onchocerciasis Field Programs. *Expert Rev. Anti Infect. Ther.* **2011,** *9* (5), 497–501.
207. (a) Longo, M.; Zanoncelli, S.; Messina, M.; Scandale, I.; Mackenzie, C.; Geary, T.; Marsh, K.; Lindley, D.; Mazue, G. In Vivo Preliminary Investigations of the Effects of the Benzimidazole Anthelmintic Drug Flubendazole on Rat Embryos and Fetuses. *Reprod. Toxicol.* **2014,** *49,* 33–42; (b) Longo, M.; Zanoncelli, S.; Colombo, P. A.; Harhay, M. O.; Scandale, I.; Mackenzie, C.; Geary, T.; Madrill, N.; Mazue, G. Effects of the Benzimidazole Anthelmintic Drug Flubendazole on Rat Embryos In Vitro. *Reprod. Toxicol.* **2013,** *36,* 78–87.
208. Tweats, D. J.; Johnson, G. E.; Scandale, I.; Whitwell, J.; Evans, D. B. Genotoxicity of Flubendazole and Its Metabolites in vitro and the Impact of a New Formulation on in vivo Aneugenicity. *Mutagenesis* **2016,** *31,* 309–321.
209. Galvin, B. D.; Li, Z.; Villemaine, E.; Poole, C. B.; Chapman, M. S.; Pollastri, M. P.; Wyatt, P. G.; Carlow, C. K. A Target Repurposing Approach Identifies *N*-Myristoyltransferase as a New Candidate Drug Target in Filarial Nematodes. *PLoS Negl. Trop. Dis.* **2014,** *8* (9), e3145.
210. (a) Taylor, M. J.; Hoerauf, A.; Townson, S.; Slatko, B. E.; Ward, S. A. Anti-*Wolbachia* Drug Discovery and Development: Safe Macrofilaricides for Onchocerciasis and Lymphatic Filariasis. *Parasitology* **2014,** *141* (1), 119–127; (b) Slatko, B. E.; Taylor, M. J.; Foster, J. M. The *Wolbachia* Endosymbiont as an Anti-Filarial Nematode Target. *Symbiosis* **2010,** *51* (1), 55–65; (c) Taylor, M. J.; Hoerauf, A.; Bockarie, M. Lymphatic Filariasis and Onchocerciasis. *Lancet* **2010,** *376* (9747), 1175–1185.

211. (a) Rao, R. U.; Huang, Y.; Abubucker, S.; Heinz, M.; Crosby, S. D.; Mitreva, M.; Weil, G. J. Effects of Doxycycline on Gene Expression in *Wolbachia* and *Brugia malayi* Adult Female Worms In Vivo. *J. Biomed. Sci.* **2012,** *19,* 21; (b) Hoerauf, A.; Specht, S.; Buttner, M.; Pfarr, K.; Mand, S.; Fimmers, R.; Marfo-Debrekyei, Y.; Konadu, P.; Debrah, A. Y.; Bandi, C.; Brattig, N.; Albers, A.; Larbi, J.; Batsa, L.; Taylor, M. J.; Adjei, O.; Buttner, D. W. *Wolbachia* Endobacteria Depletion by Doxycycline as Antifilarial Therapy Has Macrofilaricidal Activity in Onchocerciasis: A Randomized Placebo-Controlled Study. *Med. Microbiol. Immunol.* **2008,** *197* (3), 295–311.
212. Gardon, J.; Gardon-Wendel, N.; Demanga, N.; Kamgno, J.; Chippaux, J. P.; Boussinesq, M. Serious Reactions After Mass Treatment of Onchocerciasis With Ivermectin in an Area Endemic for *Loa loa* Infection. *Lancet* **1997,** *350* (9070), 18–22.
213. Johnston, K. L.; Ford, L.; Umareddy, I.; Townson, S.; Specht, S.; Pfarr, K.; Hoerauf, A.; Altmeyer, R.; Taylor, M. J. Repurposing of Approved Drugs From the Human Pharmacopoeia to Target *Wolbachia* Endosymbionts of Onchocerciasis and Lymphatic Filariasis. *Int. J. Parasitol. Drugs Drug Resist.* **2014,** *4* (3), 278–286.
214. Clare, R. H.; Cook, D. A.; Johnston, K. L.; Ford, L.; Ward, S. A.; Taylor, M. J. Development and Validation of a High-Throughput Anti-*Wolbachia* Whole-Cell Screen: A Route to Macrofilaricidal Drugs Against Onchocerciasis and Lymphatic Filariasis. *J. Biomol. Screen.* **2015,** *20* (1), 64–69.
215. Serbus, L. R.; Landmann, F.; Bray, W. M.; White, P. M.; Ruybal, J.; Lokey, R. S.; Debec, A.; Sullivan, W. A Cell-Based Screen Reveals That the Albendazole Metabolite, Albendazole Sulfone, Targets *Wolbachia*. *PLoS Pathog.* **2012,** *8* (9), e1002922.
216. A-WOL; Anti-*Wolbachia* Consortium. http://www.a-wol.com.
217. (a) von Geldern, T.; Johnston, K.; Clare, R.; Marsh, K.; Ma, J.; Stolarik, D.; Morton, H.; Ford, L.; Turner, J.; Specht, S.; Hoerauf, A.; Ward, S.; Kempf, D.; Taylor, M. Tylosin Analogs As Anti-Filarial Agents, Part A: Medicinal Chemistry Optimization and Candidate Selection. 64th Annual Meeting of the American Society for Tropical Medicine and Hygiene, Philadelphia, PA, 2015; (b) Turner, J. D.; Ford, L.; Tyrer, H.; Sjoberg, J.; Gamble, J.; Cook, D.; von Geldern, T.; Marsh, K.; Wanji, S.; Ward, S.; Taylor, M. J. Tylosin Analogs As Anti-Filarial Agents, Part B: Pre-Clinical Evaluation in Rodent Models of Lymphatic Filariasis and Onchocerciasis. 64th Annual Meeting of the American Society of Tropical Medicine and Hygiene, Philadelphia, PA, 2015.
218. World Health Organization. Schistosomiasis: Number of People Treated Worldwide in 2013. *Wkly. Epidemiol. Rec.* **2015,** *90* (5), 25–32.
219. Keiser, J.; Utzinger, J. Emerging Foodborne Trematodiasis. *Emerg. Infect. Dis.* **2005,** *11* (10), 1507–1514.
220. (a) Doenhoff, M. J.; Hagan, P.; Cioli, D.; Southgate, V.; Pica-Mattoccia, L.; Botros, S.; Coles, G.; Tchuem Tchuente, L. A.; Mbaye, A.; Engels, D. Praziquantel: Its Use in Control of Schistosomiasis in Sub-Saharan Africa and Current Research Needs. *Parasitology* **2009,** *136* (13), 1825–1835; (b) Doenhoff, M. J.; Cioli, D.; Utzinger, J. Praziquantel: Mechanisms of Action, Resistance and New Derivatives for Schistosomiasis. *Curr. Opin. Infect. Dis.* **2008,** *21* (6), 659–667.
221. (a) Mansour, N. R.; Paveley, R.; Gardner, J. M.; Bell, A. S.; Parkinson, T.; Bickle, Q. High Throughput Screening Identifies Novel Lead Compounds With Activity Against Larval, Juvenile and Adult *Schistosoma mansoni*. *PLoS Negl. Trop. Dis.* **2016,** *10* (4), e0004659; (b) Lalli, C.; Guidi, A.; Gennari, N.; Altamura, S.; Bresciani, A.; Ruberti, G. Development and Validation of a Luminescence-Based, Medium-Throughput Assay for Drug Screening in *Schistosoma mansoni*. *PLoS Negl. Trop. Dis.* **2015,** *9* (1), e0003484.
222. (a) Ingram-Sieber, K.; Cowan, N.; Panic, G.; Vargas, M.; Mansour, N. R.; Bickle, Q. D.; Wells, T. N.; Spangenberg, T.; Keiser, J. Orally Active Antischistosomal Early Leads Identified From the Open Access Malaria Box. *PLoS Negl. Trop. Dis.* **2014,** *8* (1), e2610; (b) Abdulla, M. H.; Ruelas, D. S.; Wolff, B.; Snedecor, J.; Lim, K. C.; Xu, F.; Renslo, A. R.; Williams, J.; McKerrow, J. H.; Caffrey, C. R. Drug Discovery for Schistosomiasis: Hit and Lead Compounds Identified in a Library of Known Drugs by Medium-Throughput Phenotypic Screening. *PLoS Negl. Trop. Dis.* **2009,** *3* (7), e478.
223. Cowan, N.; Datwyler, P.; Ernst, B.; Wang, C.; Vennerstrom, J. L.; Spangenberg, T.; Keiser, J. Activities of *N,N'*-Diarylurea MMV665852 Analogs Against *Schistosoma mansoni*. *Antimicrob. Agents Chemother.* **2015,** *59* (4), 1935–1941.
224. (a) Xue, J.; Wang, X.; Dong, Y.; Vennerstrom, J. L.; Xiao, S. H. Effect of Ozonide OZ418 Against *Schistosoma japonicum* Harbored in Mice. *Parasitol. Res.* **2014,** *113* (9), 3259–3266; (b) Keiser, J.; Ingram, K.; Vargas, M.; Chollet, J.; Wang, X.; Dong, Y.; Vennerstrom, J. L. In Vivo Activity of Aryl Ozonides Against *Schistosoma* Species. *Antimicrob. Agents Chemother.* **2012,** *56* (2), 1090–1092.
225. (a) Meister, I.; Duthaler, U.; Huwyler, J.; Rinaldi, L.; Bosco, A.; Cringoli, G.; Keiser, J. Efficacy and Pharmacokinetics of OZ78 and MT04 Against a Natural Infection With *Fasciola hepatica* in Sheep. *Vet. Parasitol.* **2013,** *198* (1–2), 102–110; (b) Wang, X.; Zhao, Q.; Vargas, M.; Dong, Y.; Sriraghavan, K.; Keiser, J.; Vennerstrom, J. L. The Activity of Dispiro Peroxides Against *Fasciola hepatica*. *Bioorg. Med. Chem. Lett.* **2011,** *21* (18), 5320–5323; (c) Kirchhofer, C.; Vargas, M.; Braissant, O.; Dong, Y.; Wang, X.; Vennerstrom, J. L.; Keiser, J. Activity of OZ78 Analogues Against *Fasciola hepatica* and *Echinostoma caproni*. *Acta Trop.* **2011,** *118* (1), 56–62.
226. Kannan, S.; Melesina, J.; Hauser, A. T.; Chakrabarti, A.; Heimburg, T.; Schmidtkunz, K.; Walter, A.; Marek, M.; Pierce, R. J.; Romier, C.; Jung, M.; Sippl, W. Discovery of Inhibitors of *Schistosoma mansoni* HDAC8 by Combining Homology Modeling, Virtual Screening, and in vitro Validation. *J. Chem. Inf. Model.* **2014,** *54* (10), 3005–3019.
227. (a) Stolfa, D. A.; Marek, M.; Lancelot, J.; Hauser, A. T.; Walter, A.; Leproult, E.; Melesina, J.; Rumpf, T.; Wurtz, J. M.; Cavarelli, J.; Sippl, W.; Pierce, R. J.; Romier, C.; Jung, M. Molecular Basis for the Antiparasitic Activity of a Mercaptoacetamide Derivative That Inhibits Histone Deacetylase 8 (HDAC8) From the Human Pathogen *Schistosoma mansoni*. *J. Mol. Biol.* **2014,** *426* (20), 3442–3453; (b) Marek, M.; Kannan, S.; Hauser, A. T.; Moraes Mourao, M.; Caby, S.; Cura, V.; Stolfa, D. A.; Schmidtkunz, K.; Lancelot, J.; Andrade, L.; Renaud, J. P.; Oliveira, G.; Sippl, W.; Jung, M.; Cavarelli, J.; Pierce, R. J.; Romier, C. Structural Basis for the Inhibition of Histone Deacetylase 8 (Hdac8), a Key Epigenetic Player in the Blood Fluke *Schistosoma mansoni*. *PLoS Pathog.* **2013,** *9* (9), e1003645.
228. Heimburg, T.; Chakrabarti, A.; Lancelot, J.; Marek, M.; Melesina, J.; Hauser, A. T.; Shaik, T. B.; Duclaud, S.; Robaa, D.; Erdmann, F.; Schmidt, M.; Romier, C.; Pierce, R. J.; Jung, M.; Sippl, W. Structure-Based Design and Synthesis of Novel Inhibitors Targeting HDAC8 from *Schistosoma mansoni* for the Treatment of Schistosomiasis. *J. Med. Chem.* **2016,** *59* (6), 2423–2435.
229. (a) Schiedel, M.; Marek, M.; Lancelot, J.; Karaman, B.; Almlof, I.; Schultz, J.; Sippl, W.; Pierce, R. J.; Romier, C.; Jung, M. Fluorescence-Based Screening Assays for the NAD(+)-Dependent Histone Deacetylase smSirt2 From *Schistosoma mansoni*. *J. Biomol. Screen.* **2015,** *20* (1), 112–121; (b) Lancelot, J.; Caby, S.; Dubois-Abdesselem, F.; Vanderstraete, M.; Trolet, J.; Oliveira, G.; Bracher, F.; Jung, M.; Pierce, R. J. *Schistosoma mansoni* Sirtuins: Characterization and Potential as Chemotherapeutic Targets. *PLoS Negl. Trop. Dis.* **2013,** *7* (9), e2428.
230. Long, T.; Neitz, R. J.; Beasley, R.; Kalyanaraman, C.; Suzuki, B. M.; Jacobson, M. P.; Dissous, C.; McKerrow, J. H.; Drewry, D. H.; Zuercher, W. J.; Singh, R.; Caffrey, C. R. Structure-Bioactivity Relationship for Benzimidazole Thiophene Inhibitors of Polo-Like Kinase 1 (PLK1), a Potential Drug Target in *Schistosoma mansoni*. *PLoS Negl. Trop. Dis.* **2016,** *10* (1), e0004356.

Relevant Websites

www.gatesfoundation.org—The Bill & Melinda Gates Foundation is guided by the belief that every life has equal value, with funding and coordination of drug discovery projects in neglected diseases as part of its global health program.

www.wellcome.ac.uk—The Wellcome Trust is an independent global charitable foundation dedicated to improving health.

www.dndi.org—The Drugs for Neglected Diseases Initiative is a collaborative, patients' needs-driven, nonprofit drug research and development organization that is developing new treatments for neglected diseases.

www.mmv.org—The Medicines for Malaria Venture is a product development partnership (PDP) that is focused on discovery and development of new, effective, and affordable antimalarial drugs.

www.eupathdb.org—The Eukaryotic Pathogen Database Resources website is the portal to websites containing genomics information for apicomplexans, kinetoplastids, amoebas, and other pathogenic parasites.

www.wormbase.org—WormBase is a website dedicated to the exploration and understanding of nematode biology.

COMPREHENSIVE MEDICINAL CHEMISTRY III

This page intentionally left blank

COMPREHENSIVE MEDICINAL CHEMISTRY III

EDITORS-IN-CHIEF

Samuel Chackalamannil
Rutgers University, Piscataway, NJ, United States

David Rotella
Montclair State University, Montclair, NJ, United States

Simon E. Ward
University of Sussex, Brighton, United Kingdom

VOLUME 6

BIOLOGICS MEDICINE

VOLUME EDITOR

Ved Srivastava
Intarcia Therapeutics, Durham, NC, United States

ELSEVIER

Elsevier
Radarweg 29, PO Box 211, 1000 AE Amsterdam, The Netherlands
The Boulevard, Langford Lane, Kidlington, Oxford OX5 1GB, United Kingdom
50 Hampshire Street, 5th Floor, Cambridge, MA 02139, United States

Copyright © 2017 Elsevier Ltd. All rights reserved

No part of this publication may be reproduced or transmitted in any form or by any means, electronic or mechanical, including photocopying, recording, or any information storage and retrieval system, without permission in writing from the publisher. Details on how to seek permission, further information about the Publisher's permissions policies and our arrangements with organizations such as the Copyright Clearance Center and the Copyright Licensing Agency, can be found at our website: www.elsevier.com/permissions.

This book and the individual contributions contained in it are protected under copyright by the Publisher (other than as may be noted herein).

Notices
Knowledge and best practice in this field are constantly changing. As new research and experience broaden our understanding, changes in research methods, professional practices, or medical treatment may become necessary.

Practitioners and researchers may always rely on their own experience and knowledge in evaluating and using any information, methods, compounds, or experiments described herein. In using such information or methods they should be mindful of their own safety and the safety of others, including parties for whom they have a professional responsibility.

To the fullest extent of the law, neither the Publisher nor the authors, contributors, or editors, assume any liability for any injury and/or damage to persons or property as a matter of products liability, negligence or otherwise, or from any use or operation of any methods, products, instructions, or ideas contained in the material herein.

Library of Congress Cataloging-in-Publication Data
A catalog record for this book is available from the Library of Congress

British Library Cataloguing-in-Publication Data
A catalogue record for this book is available from the British Library

ISBN 978-0-12-803200-8

For information on all publications visit our website at
http://store.elsevier.com

Working together
to grow libraries in
developing countries
www.elsevier.com • www.bookaid.org

Publisher: Oliver Walter
Acquisition Editor: Rachel Gerlis
Content Project Manager: Gemma Tomalin
Associate Content Project Manager: Marise Willis
Designer: Mark Rogers

Printed and bound in the United Kingdom

PREFACE

Previous editions of *Comprehensive Medicinal Chemistry*, published in 1990 and 2006, provided an integrated reference source that encompassed all major aspects of drug discovery research. The third edition follows this tradition and considerably expands its scope and content.

The trailblazing scientific discoveries of the 21st century have brought new opportunities for drug discovery research. The discipline of medicinal chemistry continues to evolve as it adapts to these new opportunities and strives to solve new challenges. Covered in the new edition are not only the breakthrough therapies of the past decade in cancer, hepatitis C, heart failure, dyslipidemia, cystic fibrosis, multiple sclerosis, HIV, etc., but also extensive discussion of new business models in drug discovery research, shifting industry demographics, emerging technologies, *in silico* drug discovery tools, experimental ADME and toxicology, and biologics medicine. The tone of this edition is prospective in which contributors identify outstanding issues and paths forward in their area of expertise. The aim is to provide drug discovery scientists in industry, government, academia, and research organizations with a contemporary global perspective on the field that includes a look ahead in selected areas.

The eight individual volumes fulfill these objectives and include extensive discussion of biomolecular therapeutics, drug targeting and delivery, development of chemical biology tools, data collection and analysis, *in silico* models as predictors for biological properties, identification/validation of new targets, approaches to quantify target engagement, new methods for synthesis of drug candidates such as green chemistry, development of novel scaffolds for drug discovery, and the role of regulatory agencies in drug discovery.

The individual volume editors have done an outstanding job to identify topics and contributors to meet these goals and we thank them for their hardwork and diligence. In volume 1, Ana Martinez and Carmen Gil recruited an international group of contributors who provide chapters on the emerging role of organizations other than traditional pharmaceutical companies in drug discovery, the evolving science of chemical biology, and new organic chemistry contributions to the discipline. In volume 2, Helmut Buschmann, Norbert Handler, and Andrea Wolkerstorfer have accomplished a seemingly impossible task and attracted world-leading experts across the wide field of drug discovery enabling technologies, covering contemporary thinking in a wide range of key disciplines that enable modern medicinal chemistry and drug discovery and development. The computational enabling technologies are the focus of volume 3, in which Andy Davis and Colin Edge have assembled chapters covering both ligand-based and protein structure–based advances as well as exciting new methodologies and case studies exploiting these. Alan Wilson identified experts in the fields of pharmacokinetics and toxicology who describe a wide range of contemporary advances in prediction and analysis of pharmaceutical properties and drug safety in volume 4. In volume 5, Ian Collins, Louis Lombardo, and Will Watkins have assembled leading experts to discuss high impact drug discovery accomplishments over the past decade in cancer chemotherapeutics, immunology and inflammation, and infectious diseases therapeutic areas. Ved Srivastava edited volume 6 on biologic medicines, a significant and rapidly evolving area where medicinal chemistry plays an important role. The chapters in this volume provide timely information on not only protein-based drugs, such as monoclonal antibodies and therapeutic proteins, but also peptides and nucleic acid–based therapeutics. Volume 7, edited by Adrian Hall, Santhosh Neelamkavil, and Rob Jones, presents a detailed account of the major advances in CNS, metabolic, and cardiovascular fields over the past decade and the promising new opportunities. Joerg Holenz edited volume 8 that presents case histories of successful drug discovery and strategic differentiation that have resulted in commercialized drugs and candidates in advanced clinical trials.

We are truly grateful to the publishing team at Elsevier that includes Gemma Tomalin, Rachel Gerlis, Marise Willis, and Sean Simms for their assistance and support throughout the process. With their expertise, this project became what we believe is a noteworthy and valuable resource for the discipline of medicinal chemistry. We look forward to the response and feedback of our colleagues who will use this information in their own work.

Samuel Chackalamannil, David P. Rotella, and Simon E. Ward

EDITORS-IN-CHIEF: BIOGRAPHIES

Dr. Samuel Chackalamannil

Dr. Chackalamannil obtained his PhD in chemistry from Yale University in 1984 and subsequently worked in drug discovery research at Schering-Plough Corporation and Merck Research Laboratories, where he was a distinguished fellow when he left in 2011. Since then, he has been teaching at Ernest Mario School of Pharmacy, Rutgers University, New Jersey.

Dr. Chackalamannil has significant accomplishments in the discovery of new medicines. He led the discovery of vorapaxar (Zontivity®), an FDA-approved antiplatelet drug for the prevention of heart attack and stroke. His group also discovered a PDE-5 inhibitor clinical candidate dasantafil and an adenosine A2a antagonist clinical candidate for the treatment of Parkinson's disease. Altogether, he was responsible for the discovery of nine development candidates in cardiovascular, central nervous system, and metabolic disease areas.

Dr. Chackalamannil is a coinventor of 62 allowed US patents and numerous patent applications worldwide. He has published 81 peer-reviewed articles and has coauthored a book. He has also given numerous lectures at international meetings and academic institutions.

Dr. Chackalamannil is a two-time recipient of the Thomas Alva Edison Award for Emerging Technology Patent and a two-time recipient of the Presidential Award for Discovery at Schering-Plough Research Institute. He has chaired several sessions at American Chemical Society national meetings and Gordon Research Conference on Medicinal Chemistry and was an organizer for Chemistry as a Life Science Symposium.

Dr. David Rotella

Dr. Rotella earned a PhD in medicinal chemistry from The Ohio State University and carried out postdoctoral research in organic chemistry at Penn State University. He joined the faculty at Montclair State University in July 2011 as the Margaret and Herman Sokol Professor of medicinal chemistry after a successful career in the pharmaceutical industry. He is an expert in the discovery and optimization of small molecule drug candidates for use in metabolic, cardiovascular, cancer, and central nervous system diseases. His current research is focused on discovering new lead compounds for use in parasitic and central nervous system diseases. He has coedited the seventh edition of *Burger's Medicinal Chemistry* and is a senior editor for the Royal Society of Chemistry's Drug Discovery book series. He has authored over 40 peer-reviewed articles, is an inventor on 8 issued US patents, and has contributed 10 book chapters.

Simon E. Ward

Simon Ward has an MA in natural sciences and PhD in synthetic organic chemistry from Cambridge University, UK. He has a wide-ranging experience of drug discovery in both large and small companies (GlaxoSmithKline, Knoll Pharmaceuticals, Vernalis, Chiroscience, BioCrea) and specialist experience of discovering and developing drugs for central nervous system indications. He has led multidisciplinary project teams and medicinal chemistry groups from target identification through to early clinical studies, delivering multiple clinical development candidates across indications. He is a fellow of the Royal Society of Chemistry. He is currently a professor of medicinal chemistry at the University of Sussex, UK, and the director of the Sussex Drug Discovery Centre, which he established within the University of Sussex in 2010.

This page intentionally left blank

CONTRIBUTORS TO VOLUME 6

K L Ackley
Nitto Denko Avecia, Cincinnati, OH, United States

V Aduda
Nitto Denko Avecia, Cincinnati, OH, United States

J-M Ahn
University of Texas at Dallas, Richardson, TX, United States

R Ajina
Georgetown University School of Medicine, Washington, DC, United States

D AlDeghaither
Georgetown University School of Medicine, Washington, DC, United States

T Bekaii-Saab
Mayo Clinic, Phoenix, AZ, United States

H Cramer
WAVE Life Sciences, Ltd., Cambridge, MA, United States

M Culler
Ipsen Bioscience, Inc, Cambridge, MA, United States

J Z Dong
Neon Therapeutics, Cambridge, MA, United States

B Gorovits
Pfizer, Andover, MA, United States

S-p Han
Beckman Research Institute of City of Hope, Duarte, CA, United States

J Hill
Ipsen Bioscience, Inc, Cambridge, MA, United States

K R Ito
Osaka University, Osaka, Japan

S Jablonski
Georgetown University School of Medicine, Washington, DC, United States

K Kassees
University of Texas at Dallas, Richardson, TX, United States

P T P Kaumaya
The Comprehensive Cancer Center, The Ohio State Wexner Medical Center, Department of Ob/Gyn, Columbus, OH, United States

S Kim
Ipsen Bioscience, Inc, Cambridge, MA, United States

T-K Lee
University of Texas at Dallas, Richardson, TX, United States

B Manandhar
University of Texas at Dallas, Richardson, TX, United States

C Norman
KBI Biopharma Inc., Durham, NC, United States

S Obika
Osaka University, Osaka, Japan

L Otvos, Jr.
OLPE, LLC, Audubon, PA, United States

E Paredes
Nitto Denko Avecia, Cincinnati, OH, United States

R Pillutla
Bristol-Myers Squibb, Princeton, NJ, United States

M P Ramprasad
aTyr Pharma, San Diego, CA, United States

J J Rossi
Beckman Research Institute of City of Hope, Duarte, CA, United States

L J Scherer
Beckman Research Institute of City of Hope, Duarte, CA, United States

A A Shukla
KBI Biopharma Inc., Durham, NC, United States

M L Smythe
Protagonist Therapeutics Inc, St Lucia, QLD, Australia; and The Institute for Molecular Bioscience, The University of Queensland, St Lucia, QLD, Australia

M Takahashi
Beckman Research Institute of City of Hope, Duarte, CA, United States

N Tsomaia
Ipsen Bioscience, Inc, Cambridge, MA, United States

L M Weiner
Georgetown University School of Medicine, Washington, DC, United States

L Wolfe
KBI Biopharma Inc., Durham, NC, United States

S Yoon
Beckman Research Institute of City of Hope, Duarte, CA, United States

A M Yousif
University of Texas at Dallas, Richardson, TX, United States

CONTENTS OF VOLUME 6

Preface *v*

Editors-in-Chief: Biographies *vii*

Contributors to Volume 6 *ix*

Editorial Board *xiii*

Introduction *xv*

6.01 Peptide-Based Cancer Vaccines and Therapeutics for Solid Tumors Overexpressing HER-1, HER-2, HER-3, VEGF and IGF-1R 1
P T P Kaumaya and T Bekaii-Saab

6.02 Cancer Immunotherapy 32
R Ajina, D AlDeghaither, S Jablonski, and L M Weiner

6.03 Strategy and Tactics for Designing Analogs: Biochemical Characterization of the Large Molecules 66
J-M Ahn, K Kassees, T-K Lee, B Manandhar, and A M Yousif

6.04 Chimeric Somatostatin—Dopamine Compounds (Dopastatins) for the Treatment of Neuroendocrine Disease 116
J Hill, S Kim, N Tsomaia, J Z Dong, and M Culler

6.05 Basic Principles of Formulation for Biotherapeutics: Approaches to Alternative Drug Delivery 131
L Otvos, Jr.

6.06 Orally Delivered Peptides for Treatment of Inflammatory Bowel Disease 157
M L Smythe

6.07 Evolution of mAb Downstream Process Platforms 171
A A Shukla, L Wolfe, and C Norman

6.08 Emerging Bioanalytical Methods for the Bioanalysis of Biotherapeutics 180
B Gorovits and R Pillutla

6.09 Analytical and Formulation Development Road Map for Protein Therapeutics 198
M P Ramprasad

6.10 Recent Advances in Medicinal Chemistry of Antisense Oligonucleotides 216
K R Ito and S Obika

6.11 Manufacturing of Oligonucleotides 233
E Paredes, V Aduda, K L Ackley, and H Cramer

6.12 Current Progress and Future Prospects in Nucleic Acid Based Therapeutics 280
M Takahashi, S-p Han, L J Scherer, S Yoon, and J J Rossi

EDITORIAL BOARD

EDITORS-IN-CHIEF

Samuel Chackalamannil
Rutgers University, Piscataway, NJ, United States

David Rotella
Montclair State University, Montclair, NJ, United States

Simon E. Ward
University of Sussex, Brighton, United Kingdom

VOLUME 1
GENERAL PERSPECTIVE - THE FUTURE OF DRUG DISCOVERY

VOLUME EDITORS

Ana Martinez
Centro de Investigaciones Biologicas-CSIC, Madrid, Spain

Carmen Gil
Centro de Investigaciones Biologicas-CSIC, Madrid, Spain

VOLUME 2
DRUG DISCOVERY TECHNOLOGIES

VOLUME EDITORS

Helmut Buschmann
Savira Pharmaceuticals GmbH, Vienna, Austria

Norbert Handler
Savira Pharmaceuticals GmbH, Vienna, Austria

Andrea Wolkerstorfer
Baxalta Innovations GmbH — Now part of Shire, Vienna, Austria

VOLUME 3
IN SILICO DRUG DISCOVERY TOOLS

VOLUME EDITORS

Andrew M. Davis
AstraZeneca R&D Gothenburg, Gothenburg, Sweden

Colin Edge
GlaxoSmithKline Medicines Research Centre, Stevenage, United Kingdom

VOLUME 4
EXPERIMENTAL ADME AND TOXICOLOGY

VOLUME EDITOR

Alan G. E. Wilson
Lexicon Pharmaceuticals, The Woodlands, TX, United States

VOLUME 5
CANCER, IMMUNOLOGY AND INFLAMMATION, AND INFECTIOUS DISEASE

VOLUME EDITORS

Ian Collins
The Institute of Cancer Research, London, United Kingdom

William Watkins
Gilead Sciences, Foster City, CA, United States

Louis J. Lombardo
Bristol-Myers Squibb Research and Development, Princeton, NJ, United States

VOLUME 6
BIOLOGICS MEDICINE

VOLUME EDITOR

Ved Srivastava
Intarcia Therapeutics, Durham, NC, United States

VOLUME 7
CNS, PAIN, METABOLIC SYNDROME, CARDIOVASCULAR, TISSUE FIBROSIS AND URINARY INCONTINENCE

VOLUME EDITORS

Adrian Hall
UCB BioPharma SPRL, Brussels, Belgium

Santhosh Neelamkavil
Merck Research Laboratories, Kenilworth, NJ, United States

Rob Jones
BlackThorn Therapeutics, San Francisco, CA, United States

VOLUME 8
CASE HISTORIES IN RECENT DRUG DISCOVERY

VOLUME EDITOR

Joerg Holenz
R&D Neurosciences TAU, GSK, PA, United States

INTRODUCTION

Biopharmaceuticals are now becoming an innovative strategy for developing new therapeutic agents. The field of biologics medicine is expanding into new areas of molecular diversity, which comprises polypeptides, oligonucleotides (DNA, siRNA, microRNA), antibodies (monoclonal and conjugated antibodies), and PNA (peptide nucleic acid) structures. The aim of introducing biologics medicine to the *Comprehensive Medicinal Chemistry* series is to present an overview of different large molecule drug modalities and the innovative science and challenges involved in developing biologics-based medicine. Biopharmaceuticals are in an earlier stage of development relative to small molecules, but the field is progressing exponentially. Advances in the basic science and application of technologies related to DNA/RNA heteroduplex oligonucleotide, antisense oligonucleotide (ASO) mRNA/protein, and transformative heterodimeric IgG bispecific antibodies including clinical evaluation of drug candidates in the field are accelerating.

During the last four decades, peptide therapeutics progress has grown exponentially. There are more than a thousand peptide molecules currently being studied for therapeutic indications in a variety of disease areas such as cancer, infectious disease, metabolic diseases, CNS, and numerous others. Several molecule types including linear and cyclic peptides, peptide mimetics, peptide conjugates are currently being developed in different dosage forms including parental, buccal, inhalation, or oral. There are some challenges that still need to be overcome such as target validation, understanding the intracellular targets, cost-effectiveness, and patient-friendly noninvasive delivery. Recently approved peptide-based drugs such as GLP-1 agonists (Trulicity™ and Tanzeum™) for diabetes are great examples of clinical successes of peptide−protein/antibody hybrid technologies.

Protein-based biologics are advancing rapidly as exemplified by the progress of a number of candidates in clinical trials and with the approval of several first-in-class therapies such as a CD38 monoclonal antibody (Darzalex™) for multiple myeloma, an IL-5 antagonist monoclonal antibody (Nucala™) for asthma, a bispecific mab-CD19-CD3 (Blincyto™) for leukemia, and a vaccine for meningitis B (Trumenba™). However, the challenges and risk mitigation strategies with large biomolecules such as immunogenicity, multidomain binding protein interactions, formulation, and manufacturing and assessing appropriate drug delivery alternatives need to be clearly understood.

In this volume, we have focused on four themes—vaccine therapies, peptide therapeutics, antibody/protein-based therapeutics, and oligonucleotides (RNA-based medicine). The first two chapters describe contributions on the current status and future direction of peptide vaccines and cancer immunotherapy, followed by chapters on peptide therapeutics covering the general strategy and tactics for designing peptide analogs with specific examples of peptide drug candidates including clinical studies for neuroendocrine diseases. This is followed by describing basic formulation principles and various approaches for alternatives to parental biologic drug delivery, which include an example of an orally active peptide for the treatment of gastric disorders.

Subsequent chapters cover the cutting-edge science for recombinant antibody development and manufacturing processes, current- and next-generation platforms, emerging novel bioanalytical methods for biological molecule characterization, and a formulation development roadmap for protein therapeutics.

The final section covers the medicinal chemistry and the downstream process of oligonucleotide-based medicine, drug discovery of ASO mRNA/protein, the current and future prospects of RNA-based therapeutics, and an extensive description of the process for manufacturing oligonucleotide-based molecules.

I would like to thank all the authors who contributed to this volume of comprehensive medicinal chemistry. I highly appreciate all their hardwork in writing the chapter and sharing their expertise with a broad spectrum of readers. Thanks to Elsevier project team members especially Gemma Tomalin and Editors-in-Chief Prof. David P. Rotella and Prof. Samuel Chackalamannil for continued support and advice in editing this volume.

VED Srivastava, PhD
Intarcia Therapeutics
Research Triangle Park, NC 27990

PERMISSION ACKNOWLEDGMENTS

The following material is reproduced with kind permission of Taylor & Francis

Scheme 2 Cellular Imaging in Drug Discovery: Biomolecular Imaging and Informatics (HCS, HCA, HCI)
Figure 2 Past Present Future
Figure 5 Past Present Future
Figure 6 Past Present Future
www.taylorandfrancisgroup.com

The following material is reproduced with kind permission of Oxford University press

Table 1 Targeting G-quadruplex Nucleic Acids for Cancer Therapy
Table 2 Targeting G-quadruplex Nucleic Acids for Cancer Therapy
Figure 1 Protein Structure Prediction and Homology Modelling
www.oup.com

The following material is reproduced with kind permission of American Association for the Advancement of Science

Figure 3b,c Cellular Imaging in Drug Discovery: Biomolecular Imaging and Informatics (HCS, HCA, HCI)
www.aaas.org

The following material is reproduced with kind permission of Nature Publishing Group

Table 4 Use of Stem Cells in Toxicology
Table 6 Use of Stem Cells in Toxicology
Figure 17 Strategy and Tactics for Designing Analogs; Biochemical Characterization of the Large Molecules
Figure 30 Strategy and Tactics for Designing Analogs; Biochemical Characterization of the Large Molecules
Figure 2 Cellular Imaging in Drug Discovery: Biomolecular Imaging and Informatics (HCS, HCA, HCI)
Figure 3a Cellular Imaging in Drug Discovery: Biomolecular Imaging and Informatics (HCS, HCA, HCI)
Figure 4 Cellular Imaging in Drug Discovery: Biomolecular Imaging and Informatics (HCS, HCA, HCI)
Figure 5a Cellular Imaging in Drug Discovery: Biomolecular Imaging and Informatics (HCS, HCA, HCI)
Figure 9a Cellular Imaging in Drug Discovery: Biomolecular Imaging and Informatics (HCS, HCA, HCI)
Figure 20 Epigenetics: Novel Therapeutics Targeting Epigenetics
Figure 1 UCB5857
Figure 6 Empirical and Physics Based Calculations of Physical Properties
Figure 4 Progress and Challenges in the Development if PET Ligands to Aid CNS Drug Discovery
http://www.nature.com

6.01 Peptide-Based Cancer Vaccines and Therapeutics for Solid Tumors Overexpressing HER-1, HER-2, HER-3, VEGF and IGF-1R

PTP Kaumaya, The Comprehensive Cancer Center, The Ohio State Wexner Medical Center, Department of Ob/Gyn, Columbus, OH, United States
T Bekaii-Saab, Mayo Clinic, Phoenix, AZ, United States

© 2017 Elsevier Ltd. All rights reserved.

6.01.1 Introduction 2
6.01.1.1 Immunotherapy 2
6.01.1.1.1 Active immunotherapy 2
6.01.1.1.2 mAb therapies 3
6.01.1.1.3 Disadvantages of antibody immunotherapy 3
6.01.1.1.4 Small-molecule TKIs 3
6.01.1.1.5 Peptide-based cancer vaccines 3
6.01.1.1.6 Vaccine studies are focused on a cellular immune response 3
6.01.1.1.7 Rational design of B-cell peptide vaccines 4
6.01.1.1.8 Chimeric peptides incorporating "promiscuous" T-cell epitopes 4
6.01.1.1.9 Enhancing immunogenicity of peptide vaccines 4
6.01.1.1.10 Peptide therapeutics 5
6.01.2 High-Value Cancer Targets Overexpressing RTK'S 5
6.01.2.1 Breast Cancer 5
6.01.2.2 Gastric Carcinoma 6
6.01.2.3 Human Colorectal Cancer 6
6.01.2.4 Pancreatic Cancer 6
6.01.3 Targeted Therapies With RTK'S 7
6.01.3.1 Human Epidermal Growth Factor Receptors and Cancer 7
6.01.3.1.1 Structure and signaling of HER proteins 7
6.01.3.1.2 HER-2 and cancer 8
6.01.3.1.3 HER-1 (EGFR) and cancer 8
6.01.3.1.4 HER-3 and cancer 8
6.01.3.1.5 IGF-1R and cancer 9
6.01.3.1.6 Angiogenesis and cancer: VEGF 9
6.01.4 Peptide Immunotherapeutic Approaches 9
6.01.4.1 Peptide Vaccine Versus Peptide Therapeutics 9
6.01.4.1.1 Significance of peptide vaccine approaches 10
6.01.4.1.2 Significance of peptide mimic approaches 10
6.01.4.1.3 Overall strategy 11
6.01.4.1.4 Road map for the design of an effective peptide vaccine versus a peptide mimic strategy 12
6.01.5 Targeted Therapies Against HER-2 13
6.01.5.1 Humanized mAbs and Small-Molecule Inhibitors 13
6.01.5.1.1 Development of trastuzumab and treatment 13
6.01.5.1.2 Clinical trials of trastuzumab 13
6.01.5.1.3 Side effects of trastuzumab treatments 14
6.01.5.1.4 Possible mechanisms of action and resistance to trastuzumab 14
6.01.5.1.5 Trastuzumab-DM1 15
6.01.5.1.6 Pertuzumab: HER-2 dimerization inhibitor 15
6.01.6 Rationale for Developing HER-2 Vaccines 15
6.01.6.1 Numerous X-Ray Crystallographic Structural Studies Reveal How the HER Family Initiates Signal Transduction 15
6.01.6.1.1 Structural studies with HER-2 and trastuzumab 15
6.01.6.1.2 Structural studies with HER-2 and pertuzumab 16
6.01.6.1.3 Rationale for conformational HER-2 epitopes 16
6.01.6.1.4 Design and evaluation of novel pertuzumab-binding conformational B-cell epitopes 17
6.01.6.1.5 Design and evaluation of novel trastuzumab/Herceptin-binding conformational B-cell epitopes 17
6.01.7 VEGF Peptide Strategies 18
6.01.7.1 VEGF Peptide Mimics 18
6.01.7.1.1 Design and synthesis of VEGF peptide mimics 18
6.01.7.1.2 Combination therapy targeting both HER-2 and VEGF in cancer 19

6.01.8	**Crucial Peptides Targeting HER-1, HER-3, and IGF-1R Have Been Identified and Fully Characterized Biochemically and Immunologically**	20
6.01.8.1	Extensive Cross talk Among ErbB/HER Receptors	20
6.01.8.1.1	HER-1	20
6.01.8.1.2	HER-3	20
6.01.8.1.3	IGF-1R	22
6.01.9	**Conclusions and Future Outlook**	23
References		23

6.01.1 Introduction

Traditional chemotherapy and radiotherapy regimens are often associated *with significant toxicities and severe debilitating side effects, limited by a narrow therapeutic* index and frequently acquired resistance toxicity.[1,2] Over the past two decades, the paradigm for cancer treatment has evolved to selective, mechanism-based targeted therapies (monoclonal antibodies, mAbs) and tyrosine kinase inhibitors (TKIs) that block the growth and spread of cancer with fewer side effects than nonspecific chemotherapies (reviewed in Kaumaya[3]). The market for mAb therapeutics currently stands at more than $60B annually. Receptor tyrosine kinases (RTKs) transduce growth-promoting signals that drive the development and progression of many types of cancer.[4] The most aggressive RTKs are the epidermal growth factor receptors (ErbB), which include EGFR (HER-1), HER-2, HER-3, and HER-4; vascular endothelial growth factor receptor (VEGFR)[5]; and insulin growth factor receptor (IGFR)[6] have been prime targets for developing a plethora of FDA-approved RTK inhibitors.[7] Targeted therapies with HER-2 (trastuzumab, pertuzumab, lapatinib) and EGFR (cetuximab, gefitinib, erlotinib) have markedly improved survival in the adjuvant setting but still demonstrate significant toxicities, intrinsic or acquired resistance, and the majority of patients finally succumb to their disease. Thus, novel approaches and other treatment options are urgently needed (reviewed by Kaumaya[3]) to overcome these difficulties.

The greatest potential significance of our peptide strategy is twofold: (1) It combines multiple mechanisms of action by activating both B- and T-cell functions and promoting immunological clearance; (2) it is also a targeted approach aimed at inhibiting molecular signaling pathways that are crucial for tumor growth and maintenance. The major attraction of the peptide vaccine approach is the potential for a sustained antitumor effect related to immunological memory that protects against relapsing tumors, obviating the requirement for multiple infusions of humanized mAbs or small-molecule inhibitors and overcoming escape mechanisms.

Our studies have made major contributions to the existing fields of cancer immunology, drug development, and mechanisms of cancer pharmacology by (1) developing new immune-based approaches to combat receptor kinase-driven cancers and (2) understanding and overcoming clinically relevant mechanisms of resistance to currently used HER-2-directed agents. To promote a rational, systematic development of combination therapies in multivariate ways, next-generation combination therapies can be constructed with a clear understanding of how mechanisms of resistance to multidrug regimens differ from single agent resistance. Active immunotherapy with conformational B-cell epitopes affords the possibility of generating an enduring immune response, eliciting protein-reactive high-affinity antipeptide antibodies. In addition, immunologic memory is elicited with an active approach; the longevity of the immune response could prevent the reemergence of the tumor. Additional benefits of the peptide vaccine approach include the ease and rapid synthesis, safety, lack of toxicity, and cost-effectiveness.

6.01.1.1 Immunotherapy

Recent advances in immunology and tumor biology have opened new avenues for the clinical testing of rationally designed vaccination strategies against cancer. Innovative and rationale strategies are needed to enhance the immunogenicity of inherently weak immunogenic self-antigens such as HER-2. Active, specific immunotherapy for cancer holds great potential of providing an approach for treating cancers, which have not been controlled by conventional therapy, with very little or no associated toxicity. Active immunotherapy offers many advantages, including tumor specificity and the activation of immune responses against antigens that are selectively expressed by tumor cells. As a result, nonspecific toxicity to normal tissues is reduced and antitumor responses are more durable and adaptable to cancer control at different stages of disease, including early-stage disease and disease with low tumor burdens.

6.01.1.1.1 Active immunotherapy

Vaccines have been used in both preclinical and clinical studies including peptide, DNA, whole-cell, dendritic cell, and adoptive therapy. HER-2 vaccines have been designed that use whole-cell expressing tumor antigens,[8] proteins,[9] DNA,[10] and B-cell epitope peptides[11] as sources of antigen. Many cancer immunotherapeutic strategies are designed to activate specific cytotoxic T-cells (CTLs) which play a major role in tumor rejection, and there are numerous reviews on this subject.[12] Preexisting CD4 T-cell and antibody-mediated immunity against HER-2 have been described in patients with HER-2+ breast cancer providing further rationale for

active-specific immunotherapy strategies to augment the anti-HER-2 immune response.[13] Most of the immunotherapies targeting the HER-2 oncoprotein have focused on T-cell epitopes, and several studies have produced notable results indicating that vaccinated patients can develop immunity to HER-2 peptides and native protein.[14] Recent clinical trial results using a HER-2 CTL epitope showed an increase in disease-free survival in vaccinated HER-2/neu-expressing breast cancer patients (85.7%) compared to the control group (59.8%).[15] However, the effectiveness of a CTL vaccine for clinical use is limited to patients who express the appropriate HLA haplotype.

6.01.1.1.2 mAb therapies

mAb therapies have been successful and generated new interest in the contribution of humoral effector molecules. There has been a number of mAbs developed that target solid tumors. These targets include cell-surface proteins and antigens involved in tumor-associated vasculature that support tumor growth. Trastuzumab, a humanized mAb specific for HER-2, is active in combination with chemotherapy in patients with breast cancer overexpressing HER-2. A mAb targeting CD20 (IDEC-C2B8, Rituximab/Rituxan) is approved for use in B cell non-Hodgkin's lymphoma and is among the most effective mAb therapies.[16] Cetuximab (Erbitux) and panitumumab (Vectibix) both target EGFR and are approved for treatment by the FDA to treat colorectal cancer. Both these anti-EGFR mAbs block ligand–receptor interactions. VEGF (vascular endothelial growth factor) and its receptors (Flt-1 and KDR) have been implicated in promoting solid tumor growth and metastasis by stimulating tumor-associated angiogenesis. Bevacizumab (Avastin) is a recombinant humanized IgG1 mAb that is approved for treatment of the lung and colorectal cancers. Bevacizumab binds VEGF and prevents the interaction of VEGF with its receptors on the surface of endothelial cells.

6.01.1.1.3 Disadvantages of antibody immunotherapy

Humanized mAb's approved for treatment of several cancers is fraught with a number of concerns exist. Treatment is expensive and has a limited duration of action, necessitating repeated administrations of the mAb.[17] The half-life of IgG administered intravenously can range from 5 to 21 days. Thus, repeated treatments with trastuzumab are necessary; patients typically receive the mAb every week to 3 weeks. The repeated treatment with trastuzumab raises the cost of passive immunotherapy with this mAb to ~$150,000 USD a year. Additionally, patients are constantly infused with a large quantity of trastuzumab, which contributes to the cardiotoxicity associated with trastuzumab treatment.

6.01.1.1.4 Small-molecule TKIs

Another therapeutic approach is the use of small-molecule TKIs that inhibit the specific catalytic activity of HER kinases by interfering with the binding of ATP. This area of study was revolutionized by the discovery of modified quinazoline compounds as highly specific and potent inhibitors of EGFR.[18,19] The clinical success of the ABL-kinase inhibitor imatinib mesylate (Gleevec; Novartis) in the treatment of ABL-driven leukemia[20] raised hopes that drugs targeting HER kinases implicated in other types of cancers would be similarly efficacious. However, TKIs lack the singular target specificity of antibodies.

Various strategies involving TKIs have been developed to target EGFR and/or its family members, and these are in a range of stages for clinical testing. Nearly all of these agents are ATP analogs and inhibit kinase activity by binding the ATP pocket of the catalytic domain.[21] Gefitinib (Iressa; AstraZeneca) and erlotinib (Tarceva; OSI Pharmaceuticals, Genentech), which bind to the ATP binding site of the intrinsic tyrosine kinase domain of EGFR, received fast-track approval by the US FDA in 2003 and 2004, respectively, for patients with advanced NSCLC who had failed to respond to conventional chemotherapy. In addition, lapatinib (Tykerb; GlaxoSmithKline), a dual inhibitor of EGFR and HER-2 kinases, is being investigated in phase II and III trials in combination with chemotherapy and/or hormonotherapy. In cell-based assays these orally bioavailable ErbB family TKIs are effective at inhibiting both EGFR and HER-2, and EGFR and HER-2 phosphorylation. Despite this success, TKIs have shown very limited clinical activity, marked by modest delays in tumor progression. Although gefitinib received fast-track approval in 2003, the conditions of the approval were restricted in 2004 because of negative results of the phase III Iressa Survival Evaluation in Lung Cancer (ISEL) trial.[22] Gefitinib is not presently clinically available in the United States.

6.01.1.1.5 Peptide-based cancer vaccines

Vaccination has been one of the most successful clinical interventions for the prevention of human diseases. Vaccines have contributed to the eradication of smallpox, an extremely contagious and deadly disease. The occurrence of other diseases such as polio, measles, mumps, rubella, chickenpox, and typhoid has decreased significantly as a result of vaccination. Despite a large body of work, there is still no effective cancer vaccine. This, in large part, is due to the immune system's weak and ineffective response to cancer, whereas the immune system responds efficiently to bacteria, viruses, and other agents. It has long been thought because of tolerance to self, tumor-associated antigens are not antigenic because they are self-antigens. This is an argument against active immunotherapy. However, it has been proposed that this issue can be circumvented using subdominant epitopes with a synthetic peptide vaccine.[14a] Peptide vaccines can be broadly characterized into two groups: cellular (T cell) and humoral (B cell) vaccines.

6.01.1.1.6 Vaccine studies are focused on a cellular immune response

T-cell epitopes are used exclusively due to the fact that when presented in the context of MHC Class I, the resulting activated CTLs can become activated and lyse transformed tumor or infected cells. This response is thought to be the most prominent mechanism utilized by the immune system to control viral replication and kill transformed tumor cells. However, the humoral arm could play a critical role in the generation of an antitumor response. The successful clinical usage of passively infused mAbs points to the

effectiveness of the humoral arm of the immune system. B-cell epitope vaccines are designed to induce a protective humoral response. This response includes creation of antibody-producing plasma cells as well as immunologic memory. B-cell epitopes have been used in a variety of vaccines. Peptides have the potential to be safe, noninfective, well-defined, and stable vaccines. Several factors need to be considered in formulating an effective peptide vaccine; these factors include inclusion of a universal T-helper epitope and the necessity to mimic the structure of the parent antigen to generate high-affinity Abs.

6.01.1.1.7 Rational design of B-cell peptide vaccines

In the design of a synthetic peptide vaccine, it is necessary that the B-cell epitope be presented along with an appropriate helper T-cell epitope. The interaction between B cells and T cells recognizing the same antigen is essential for B-cell proliferation and differentiation and the generation of high-affinity antibodies that are of the IgG isotype. For sequences shorter than 15 residues, peptides are traditionally coupled to a larger carrier protein such as keyhole limpet hemocyanin (KLH) or bovine serum albumin (BSA). This approach can be problematic for several reasons including epitope suppression by the carrier protein and poorly defined constructs due to lack of control during the chemical coupling reaction. Several alternatives have been described to produce conformationally stable peptides.

6.01.1.1.8 Chimeric peptides incorporating "promiscuous" T-cell epitopes

The ideal vaccine should be composed of appropriate tumor antigen B-cell epitopes or CTL epitopes, and a universally immunogenic T-helper epitope. Another alternative involves B- and T-cell epitopes constructed in a colinear fashion. This has limited usage when the T-helper epitope is recognized by one or a few MHC class II alleles. Thus the identification of "universal" or "promiscuous" T-helper epitopes that bind multiple MHC haplotypes is necessary in the design of an optimum vaccine. Universal T-helper epitopes from tetanus toxoid (TT) and measles virus fusion (MVF) protein have been identified.[23] B-cell epitopes are synthesized as chimeric constructs with MVF promiscuous T_H epitope,[11a,c] thus proving the utility of a chimeric vaccine construct incorporating B and T_H epitopes in a collinear fashion. The most important consideration in the successful design of a peptide vaccine is that the B-cell epitope must be covalently linked to the "helper" T-cell epitope at either the N- or C-terminus (**Fig. 1**). The size of the B-cell epitope should minimally be ~18 amino acid residues (~900 Å^2) the size of antigen:antibody binding region to ensure the peptide propensity to adopt a defined structure, The helper T-cell should ideally be a "promiscuous" epitope (~18 residues) and the linker (~4 residues), and the final construct should consist between 40 and 60 amino acid residues. Traditionally, peptide sequences are coupled to a larger carrier protein such as BSA, TT, or KLH to induce immunogenicity. This approach is fraught with difficulties as the resulting conjugate is subject to processing by the immune cells and the resulting B-cell epitope may not represent the exact epitope identity or configuration resulting in low-affinity antibodies.

6.01.1.1.9 Enhancing immunogenicity of peptide vaccines

In addition the peptide vaccine must be formulated with an adjuvant or cytokines. Adjuvants are usually defined as compounds that increase and/or moderate the intrinsic immunogenicity of an antigen.[16] Different types of receptors on antigen-presenting cells (APCs) can be targeted by adjuvants. Oil-in-water emulsion adjuvants are thought to be linked to the depot for the antigen at the site of vaccination recruiting APC's such as macrophages and B cells. Muramyl dipeptides are a ubiquitous constituent of bacterial cell walls and are recognized by APCs such as macrophages. The muramyl dipeptide synthetic compound *N*-acetyl-glucosamine-3 yl-acetyl L-alanyl-D-isoglutamine when emulsified in ISA720 (SEPPIC) can be used as an adjuvant to activate APCs and has been used extensively in our laboratory with success. Oil-in-water emulsion adjuvants are thought to be linked to the depot effect as well. Tiny drops of antigen are surrounded by oil, trapping the antigen. As a result the antigen is released slowly over a prolonged period, destruction of the antigen is delayed, and an individual's exposure to the antigen is lengthened. Montanide ISA 720 is one such emulsion approved for human usage and is used in the Phase I Clinical Trial.

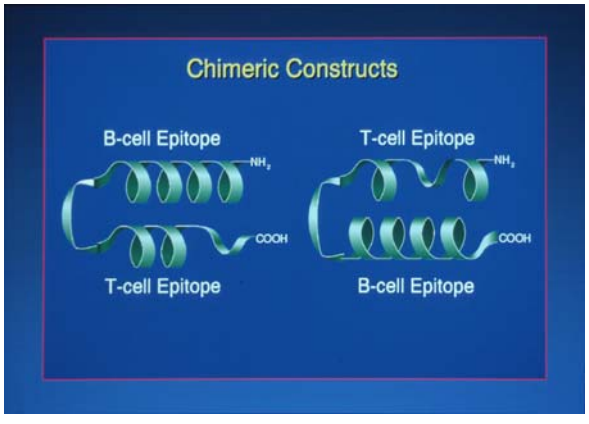

Fig. 1 Chimeric peptides incorporating B- and T-cell epitopes.

6.01.1.1.10 Peptide therapeutics

A relatively newer class of targeted therapeutic drugs is emerging in cancer drug development, and these drugs are called peptide therapeutics. Peptides are short sequences of amino acids that can be produced biosynthetically, via natural or recombinant microbial fermentations, or chemically, through mechanisms such as solution-based or solid-phase peptide synthesis. The concept of using peptides as therapeutics has been historically disregarded, mainly due to peptide stability, susceptibility to degradation, size (>5000 Da), and consequent limitations in methods of delivery (low oral bioavailability). In recent years, however, the development of peptides as drugs is attracting increasing attention from the pharmaceutical industry, especially as the technologies for peptide development and manufacturing continue to mature. New synthetic strategies to improve productivity and reduce metabolism of peptides, along with alternative routes of administration, have been developed in recent years, and a large number of peptide-based drugs are now being marketed.[17] As of 2010, there were ~60 therapeutic peptides on the market, 150 in clinical phases and 400 in advance preclinical stages. Peptide drugs are now being universally marketed, and more than 100 pharmaceutical and biotech companies are now active in the peptide field. Of the products now approved, about 30 peptide drugs are currently marketed in the United States, and 17% are used in the cancer clinical setting.[24] The peptide therapeutics foundation anticipates that pharmaceutical and biotechnology industries will continue to focus on these versatile molecules because of the increased acceptance of injected drugs on the market, the availability of new formulation and delivery technologies, and the relatively high approval success rates.

Development of peptide therapeutics has the potential of overcoming some of the obstacles observed with mAbs and TKIs. Currently, one of the greatest strengths of peptides as potential therapies lies in the powerful new approaches for discovering and screening new drug candidates. In theory, peptide-based drugs have given oncologists an opportunity to expand the repertoire of "druggable proteins." As mentioned before, mAbs and TKIs are limited to the number of candidates they can effectively target; mAbs are too large and complex for entry into the cell, while small-molecule inhibitors are limited to proteins with well-defined small binding pockets. Peptides are also small enough to penetrate the cell membrane, and they can be rationally designed to target almost any protein of interest.[25] Peptides now have a broad range of potential clinical benefits against numerous protein targets, with applications in some of the most prevalent disease categories.[26] These molecules are rationally designed to mimic the binding region between two or more proteins involved in various disease states. A perfect peptide agent is designed rationally and has the ability to reach, bind, and antagonize the function of a target protein with high selectivity and affinity.[27] Their small size and specific binding properties make peptides ideal candidates for physiologically disrupting on-target functional protein–protein complexes. Peptide-therapeutics may consequently aide in the reduction of current therapeutic problems, such as off-target side effects and the requirement of high-dosage treatment.

6.01.2 High-Value Cancer Targets Overexpressing RTK'S

The crucial tenet of our research program requires the identification of important therapeutic targets that drives cancer metastasis though mechanisms of resistance, the rapid development of effective peptide antagonists directed against these RTK targets, and the efficient testing of these agents in relevant animal models of human cancer. We have focused on Breast and GI cancers: (1) metastatic gastric or gastroesophageal (GE) junction adenocarcinoma, (2) colorectal, and (3) pancreatic cancers.

6.01.2.1 Breast Cancer

Breast cancer is a heterogeneous group of diseases consisting of multiple subtypes.[28] In 2016, it is estimated by the American Cancer Society that 249,260 people will be diagnosed with breast cancer and 40,890 people will die as the consequence of this disease. HER-2 overexpressing breast cancer represents about 20–30% of all breast cancer cases.[29] Breast cancers that show amplification and overexpression of the *HER-2* gene represent about 20% of metastatic cases.[29a] HER-2 overexpression is associated with aggressive growth and poor clinical outcomes.[30] Despite the success of trastuzumab, ~70% of patients develop resistance to monotherapy within 1 year (acquired resistance),[31] and ~35% do not respond at all (de novo resistance).[32] Since 2007, three new HER-2-targeted therapies (lapatinib, pertuzumab, and T-DM1) have been approved, but even the latest iteration, kadcyla (T-DM1), demonstrates resistance *suggesting that the current approved drugs remain ineffective in the long term*. Cross talk and compensatory signaling networks limit the activity of most targeted therapies, including HER-2-targeted agents. Multiple mechanisms of trastuzumab resistance have been proposed. The mechanisms through which trastuzumab blocks tumor growth include reduced downstream signaling, inhibition of angiogenesis, and increased immune activity, primarily antibody-dependent cellular cytotoxicity (ADCC).[31]

Increased expression of the insulin-like growth factor-1 receptor (IGF-1R) also reduces the growth inhibitory activity of trastuzumab.[33] Among patients with HER-2-overexpressing breast cancer, high IGF-1R expression and activation correlate with worse response to preoperative trastuzumab and chemotherapy[34] and reduced progression-free survival.[35] Others and we have reported the formation of a unique receptor complex containing IGF-1R and HER-2 in resistant cells. This complex facilitates cross talk from IGF-1R to HER-2, resulting in sustained HER-2 phosphorylation in resistant cells.[36] HER-3 has also been shown to be involved in acquired resistance to HER2-targeted therapies and other inhibitors that directly or indirectly antagonize PI3K signaling.[37] HER-2 antibody trastuzumab has been shown to be mediated by increased HER-3 signaling in part due to heterodimerization of HER-2 and HER-3 which is critical for the growth and progression of HER-2 positive breast cancers,[3,38] or HER-2 and IG-1R and in part through the formation of heterotrimers involving HER-2, HER-3, and IGF-1R.[36b]

6.01.2.2 Gastric Carcinoma

Gastric carcinoma is a substantial health care problem worldwide, with over 900,000 new diagnoses and 700,000 deaths worldwide annually, making it the second leading cause of cancer mortality in the world.[39] In 2016, it is estimated that 16,910 men and women will be diagnosed with esophageal cancer and 15,690 people (92%) will die as the consequence of this disease.[40] (http://www.cancer.org). Esophageal adenocarcinoma (EAC) has a very high fatality rate and is one of the fastest rising cancers worldwide. In the past, patients with advanced or metastatic gastric or gastroesophageal junction cancer have had few treatment options and generally poor survival rates. HER-2 is overexpressed in gastric (21%) or gastroesophageal junction cancers (33%), in association with an increased risk of metastasis, decreased survival,[21] and increased tumor invasion[41]; this correlation between HER-2 overexpression and poor prognostic markers established HER-2 as a potential therapeutic target. Trastuzumab has been approved for patients with HER-2-positive metastatic gastric adenocarcinoma in combination with chemotherapy.[42] Trastuzumab (Herceptin Genentech/Roche) has been shown to improve the survival of patients with advanced gastric cancer.[43] Trastuzumab resistance is a major clinical problem to be resolved in patients with HER-2-positive gastric cancers. Using HER-2-amplified cell lines, Kim et al.[44] demonstrated that secondary oncogenic events could confer resistance to HER-2-directed therapies. Several studies have reported the overexpression of HER-1 (EGFR) and HER-2 in esophageal cancers with extremely high rates in esophageal adenocarcinoma when compared to squamous cell carcinomas of the esophagus[45]; inhibition of these receptor kinases is now widely considered as a therapeutic strategy in the treatment of these cancers.[46] HER-1 overexpression is correlated with poor prognosis in EAC[47] makes it an attractive target for drug therapy. Several studies have reported the dual overexpression of HER-1 and HER-2 in EAC[45]; thus, there is a potential clinical benefit in cotargeting HER-1 and HER-2 in EAC.[48] HER-1 and HER-2 targeted inhibitors are widely considered a potential therapeutic strategy in the treatment of EAC.[46] Novel therapeutic targets are urgently needed because the inadequate improvement in the cure rate of about 10% realized by adjunctive treatments to surgery is unacceptable as >50% patients with localized gastric cancer succumb to their disease.[49] Additionally, the HER-2-targeted hmAb pertuzumab (Perjeta) has had significant clinical success in the treatment of breast cancer when combined with trastuzumab[50]; similar dual-targeting clinical trials are under way for esophageal cancer (NCT02120911).

6.01.2.3 Human Colorectal Cancer

Human colorectal cancer (CRC) is one of the most common malignancies and remains largely incurable. Colorectal cancer is the third most common malignancy in men and the second most common in women worldwide accounting for 8% of global cancer deaths. In 2016, it is estimated that 95,270 men and women will be diagnosed with colon cancer, and 49,190 people will die as the consequence of this disease. HER-1 and HER-2 are highly implicated in colorectal cancers,[51] and cetuximab, a blocking anti-EGFR mAb, is effective in combination with chemotherapy or as single agent for the treatment of patients with KRAS wild-type metastatic colorectal cancer.[52,53] After an initial response, secondary resistance invariably ensues, thereby limiting the clinical benefit of this drug[54] leading to treatment failure. An extensive effort has been made to understand cancer cell resistance mechanism(s) to EGFR inhibitors.[1] A rationally designed combination of trastuzumab and lapatinib was effective in HER-2+ mCRC (ORR 34%, Control of Disease 78%, TTP 5.5 months). HER-2+ mCRC patients were primarily resistant to cetuximab or panitumumab, supporting the use of HERACLES dual therapy in anti-EGFR-naive patients (presented as ASCO, Annual 2015). In developed countries, colorectal cancer (CRC) is the third most common malignancy, but it is the second most frequent cause of cancer-related death. Clinicians are still faced with numerous challenges in the treatment of this disease, and future approaches which target the molecular features of the disorder will be critical for success in this disease setting. HER-1 and HER-2 are highly implicated in colorectal cancers,[51] and cetuximab, a blocking anti-EGFR mAb, is effective in combination with chemotherapy or as single agent for the treatment of patients with KRAS wild-type metastatic colorectal cancer.[53,55] After an initial response, secondary resistance invariably ensues, thereby limiting the clinical benefit of this drug[38d] leading to treatment failure. An extensive effort has been made to understand cancer cell resistance mechanism(s) to EGFR inhibitors.[5f] A rationally designed combination of trastuzumab and lapatinib was effective in HER-2+ mCRC (ORR 34%, Control of Disease 78%, TTP 5.5 months). HER2+ mCRC patients were primarily resistant to cetuximab or panitumumab, supporting the use of HERACLES dual therapy in anti-EGFR-naive patients (presented at ASCO, Annual 2015).

6.01.2.4 Pancreatic Cancer

An estimated 46,420 new cases of pancreatic cancer (PC) are expected to occur in the United States during 2016 with an estimated 39,590 deaths. Several studies demonstrate that HER-1 overexpression correlates with poor prognosis and increased metastasis of PCs.[56] Several recent studies also show that HER-3 is frequently upregulated in cancers with HER-1 (EGFR) overexpression. HER-3 signaling has been shown to be a major driver of resistance to IGF-1R-targeted agents. It is clear that innovative approaches are needed for the prevention and treatment of PC.[57] IGF-1R has also been implicated in the growth and development of multiple tumor types[58] and is expressed in 50–60% of pancreatic cancers.[59] The IGF-1R:IGF-1 pathway is implicated in the development of resistance to anticancer drugs[6a,60] in pancreatic cancer.[61] HER-1 is implicated in aggressive pancreatic cancers with poor patient outcome[62] and decreases overall survival.[63] Increased expression of IGF-1R increases the expression of HER-1 and results in the formation of IGF-1R/HER-1 dimers.[64] There is considerable evidence of cross talk between HER-1 and IGF-1R in pancreatic cancer cells.[65]

6.01.3 Targeted Therapies With RTK'S

6.01.3.1 Human Epidermal Growth Factor Receptors and Cancer

The human epidermal growth factor receptor (HER) family consists of four homologous members: HER-1 (EGFR), HER-2, HER-3, and HER-4.[66] In response to a ligand, these RTKs can form homodimers or heterodimers and initiate intracellular signaling. The HER family of proteins form part of a complex signaling cascade that modulate cell proliferation, survival, and adhesion.[67] These HER receptors are also involved in tumorigenesis when their signaling functions are inefficiently regulated.[66,67]

The signaling pathways of HER family members, VEGF and IGF-1R and the current drugs that target these oncoproteins in cancer, are shown in Fig. 2. HER-2 can heterodimerize with any of the ligand-activated HER receptors (HER-1, HER-3, or HER-4), and this association leads to intracellular signaling via two major pathways, the MAPK pathway and the PI3K pathway, leading to proliferation, cell survival, metastasis, and angiogenesis. On the other hand, VEGF can bind to its main receptor, VEGFR-2 (KDR), and this binding causes intracellular phosphorylation of the receptor, thereby stimulating the PI3K pathway and stimulating angiogenesis. The signaling pathways can be targeted extracellularly using humanized mAbs, such as trastuzumab and pertuzumab (HER-2), cetuximab (EGF receptor), bevacizumab (Avastin) (VEGF), and cixutumumab (IGF-1R) which can prevent ligand binding and activation of the receptors or can directly block binding of an activated receptor to another. At the intracellular level, small-molecule inhibitors, such as sunitinib (VEGF), lapatinib (HER-1 and HER-2), and erlotinib (HER-2), can disrupt the phosphorylation sites and directly prevent activation of the PI3K or MAPK pathways. P, phosphate; VEGFR, VEGF receptor.

6.01.3.1.1 Structure and signaling of HER proteins

All four HER receptors (EGFR, HER-2, HER-3, and HER-4) share extracellular domains (composed of four subdomains, two of which are disulfide-rich) with high structural homology, a single transmembrane spanning helix, and a cytoplasmic portion that contains a conserved but not equally functional tyrosine kinase domain flanked by a carboxy-terminal tail with autophosphorylation sites. The extracellular region consists of ~620 amino acids arranged into four subdomains, called L1 (I), S1 (II), L2 (III), and (IV).[68] Despite their structural homology, the HER family members differ with respect to preferred ligands, affinity for ligands, tyrosine kinase activity, and rate of cellular downregulation.[69] All HER ligands have in common an EGF-like domain of ~60 amino acids including six cysteine residues that interact covalently to form three loops.[70] HER ligands can be divided into three groups.[71]

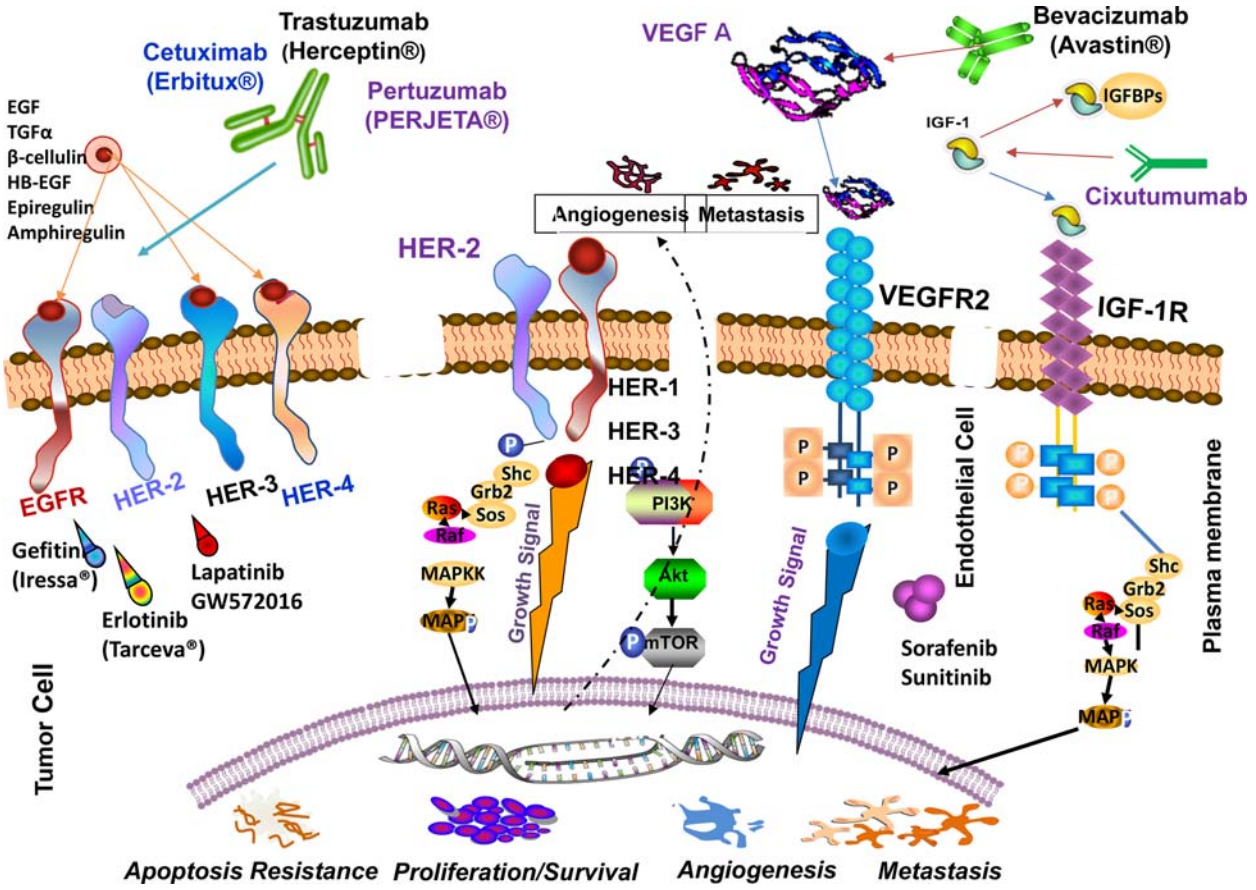

Fig. 2 Signal transduction pathways drive cancer metastasis.

The first group specifically binds EGFR, including EGF, amphiregulin (AR), and TGF-α. The second group exhibits dual specificity for EGFR and HER-4 including betacellulin, heparin-binding EGF, and epiregulin.[4a] The third group is composed of the neuregulins (NRG, also called heregulins, HRG) and includes two subgroups based on their ability to bind HER-3 and HER-4 or only HER-4. In particular, HER-2 has no known ligand-binding activity, while HER-3 lacks intrinsic kinase activity.[66b,c,67,72] Ligand binding to the extracellular domain initiates a conformational rearrangement that allows for dimerization (pairing). Specifically, ligands bind to domains I and III and cause a conformational change. Domain II becomes exposed, and the receptor can then undergo dimerization.[73] Receptor dimerization is an essential requirement for HER function and for the signaling activity of these receptors.[68a] Only EGFR and HER-4 are completely functional in terms of ligand binding and kinase activity. HER-2 appears to lack a high-affinity ligand,[74] and HER-3 has impaired kinase activity,[75] relying on the kinase activation of its heterodimerization partners for activation.

HER-2 plays a major coordinating role in this network, since each receptor with a specific ligand seems to prefer HER-2 as its heterodimeric partner.[76] HER-2-containing heterodimers potently amplify signaling because HER-2 reduces the rate of ligand dissociation, allowing strong and prolonged activation of downstream signaling pathways.[77] The most significant intracellular pathways activated by the HER receptors are those involving the phosphatidylinositol-3-kinase (PI3K) and mitogen-activated protein kinase (MAPK).[78] In normal cells activation of the HER family initiates a rich network of signaling pathways that control normal cell growth, differentiation, motility, and adhesion in several cell lineages.[79] The formation of heterodimers and the resulting activation are temporally and spatially controlled in normal cells and tissues.[80]

6.01.3.1.2 HER-2 and cancer

HER-2 is an attractive therapeutic target in cancers for several reasons. The amount of HER-2 expressed on cancer cells is much higher than in normal adult tissues,[81] potentially reducing the toxicity of HER-2 targeting drugs. Tumors with a high expression of HER-2 often show homogenous, intense IHC staining,[82] signifying that HER-2 targeted therapy would target most cancer cells in a given patient. Additionally, HER-2 overexpression is found in both the primary and metastatic sites,[83] suggesting that HER-2-targeted therapy may be effective in all disease sites. Increased wild-type HER-2 expression levels causes dysregulation of the HER network in tumor cells, providing both growth and survival advantages for the tumor.[84] Slamon et al. demonstrated that HER-2 amplification is a significant predictor of both overall survivor and time to relapse in the breast cancer patients and overexpression of HER-2 occurs in 20–30% of invasive breast cancers.[29]

Breast cancers can have up to 25–50 copies of the HER-2 gene and up to 100-fold increase in HER-2 protein expression resulting in up to 2 million receptors expressed at the tumor cell surface.[85] FDA-approved tests for determining HER-2 status include immunohistochemistry (IHC) for protein overexpression using the Herceptest KIT (Dako) or gene amplification by fluorescent in situ hybridization (FISH). HER-2 overexpression has been defined by IHC as being highest (reported as 3+) when receptor levels near 2 million, or medium intensity (2+) when receptor levels are around 500,000. Normal levels of membrane-bound HER-2 are ~20,000–50,000 per cell.[31] Breast cancers overexpressing HER-2 have biological characteristics that differentiate them from other types of breast cancers including resistance to certain hormonal agents, increased sensitivity to certain cytotoxic chemotherapeutic agents, and increased propensity to metastasize to the brain.[86] Additionally, HER-2 overexpression and amplification are seen in subsets of gastric, esophageal, endometrial, uterine, ovarian, and lung cancers.[45d,87]

6.01.3.1.3 HER-1 (EGFR) and cancer

HER-1 (EGFR) is central to human tumorigenesis, and deregulation of this receptor is mainly due to increased expression[88] and mutations in different domains of the receptor.[89] EGFR is overexpressed in most epithelial cancers including breast/triple negative breast cancer (TNBC (14–90%),[90] nonsmall cell lung (NSCLC) lung (40–80%),[91] head and neck (80–100%), colorectal (25–77%), and other cancers). HER-1 overexpression in tumors is responsible for aggressiveness, poor prognosis, decreased survival, poor response to therapy, and development of resistance.[92] HER-1 forms heterodimers with other HER family members like HER-2, HER-3, and HER-4 resulting in aggressive forms of cancer with lower survival rates.[93] The development of antibodies targeting HER-1 is mainly dependent on structural studies that help outline the details of the receptors and other conformational changes affecting its activation and downstream signaling. HER-1 signaling is highly dependent on ligand binding which is a key factor in releasing the dimerization arm of the receptors,[94] and this explains why many of the anti-HER-1 antibodies are directed toward the ligand-binding region. Cetuximab, a humanized mAb, binds HER-1 and prevents ligand binding and is FDA approved for the treatment of metastatic colorectal cancers with high EGFR expression.[95] However, the emergence of resistance to cetuximab has led to the proposal that other mechanisms exist that are independent of ligand binding, and this has led to the development of other antibodies with key epitopes that are different from cetuximab. For instance, activation of other HER family receptors may help in the stabilization of HER-1 even in the absence of ligand binding.[96] These studies simply illustrate that multiple HER-1 targeting strategies can be employed in targeting EGFR signaling mechanisms in cancer, and this may avoid resistance and additively or synergistically inhibit tumor growth.

6.01.3.1.4 HER-3 and cancer

HER-3, the third member of the HER family, is a single membrane-spanning receptor that exerts its function through heterodimerization with other HER family receptors. HER-3, like the other members of the HER family, consists of an extracellular domain, a transmembrane domain, and an intracellular domain. HER-3 overexpression is commonly seen in various malignancies such as breast cancer; colorectal carcinoma; squamous cell carcinoma of the head and neck; and gastric, ovarian, prostate, and bladder

cancers. Subdomain II also contains the dimerization loop required for dimer formation. Unlike HER-1 and HER-2, it cannot form a homodimer and lacks the intracellular kinase activity. Unliganded receptor adopts a confirmation that inhibits dimerization. Binding of neuregulin to the ligand-binding subdomains (I and III) induces a conformational change in ErbB3 that causes the protrusion of the dimerization loop in subdomain II, activating the protein for dimerization. Activation of HER3-containing heterodimers leads to HER-3 phosphorylation and subsequent activation of signaling pathways. It was previously considered not to contain tyrosine kinase activity and catalytic activity, and the intracellular region of HER-3 could not bind ATP and be autophosphorylated. Thus, the clinical value of HER-3 was ignored. Currently, biochemical analysis has confirmed that the kinase domain of HER-3 is a specific allosteric activator; it acts as a functional activator to activate the recipient kinase (HER-1, HER-2, HER-4). With the in-depth knowledge of its structure and function, studies on the relationship of HER-3 and human tumors are rapidly increasing. HER-3 is closely related to tumorigenesis, progression, and metastasis. HER-3 also has the highest binding affinity for phosphoinositol 3-kinase (PI3K) when compared to all other HER proteins. As a result, HER3 serves as a key activator in downstream signaling of PI3K, which ultimately leads to apoptosis resistance in a wide range of cancers.[97] HER-3 is involved in resistance to targeted therapy and may serve as a new therapeutic target. The expression of HER-3 helps predict prognosis and treatment efficacy. HER-3 has become a focus of concern in the HER family and has gained significant attention in the search for cancer treatment.

6.01.3.1.5 IGF-1R and cancer

The insulin-like growth factor receptor (IGFR) has been implicated in the growth and development of several malignancies.[58] IGF-1R belongs to the insulin receptor (IR) family that includes the IR (a homodimer), IGF-1R (a homodimer), IGF-1R/IR (hybrid, heterodimeric receptors), and the mannose-6-phosphate receptor (also known as IGF-2R). The main signaling pathway implicated in cancer is the IGF-1R:IGF-1 pathway which supports the growth of many different types. This pathway does not only contribute to tumorigenesis but is highly implicated in the development of resistance to other anticancer drugs that are available in the clinic.[6a,60] The IGF-1:IGF-1R pathway has been shown to play critical roles in many cancers including lung,[98] breast,[99] pancreas,[61] colorectal,[100] prostate,[101] and head and neck[102] cancers. Apart from the HER family receptors, the insulin-like growth factor has emerged as a key regulator of tumorigenesis in colorectal cancer.[103] Expression of IGF-IR and its ligands are therefore considered as potential prognostic and predictive markers in colorectal cancer.[104] Downregulation of IGF-1R dependent pathways have also been shown to sensitize colorectal cancer cells to apoptosis mediating agents indicating that IGF-1R may play a role in resistance development in colorectal cancer cells signaling.[105] Recent studies have even implicated IGF-1R-dependent pathways as a cause of resistance to cetuximab-based therapies in colorectal cancer,[18] and this indicates that a combined approach targeting the HER family receptor and IGF-IR will effectively target colorectal cancer cells and shutdown alternative signaling pathways.

6.01.3.1.6 Angiogenesis and cancer: VEGF

Angiogenesis, or formation of new blood vessels, is crucial to cancer tumor growth. Tumor growth, progression, and metastasis are critically influenced by the production of the proangiogenic factor vascular endothelial factor (VEGF). Virtually all solid tumors are neovascularized by the time they are detected. However, there is a prevascular phase during early tumor development where few or no tumor cells are angiogenic, and expansion of the tumor is restricted to a few millimeters. When enough tumor cells become angiogenic, the tumor can expand progressively and shed metastatic cells. This "angiogenic switch" has recently been documented in several forms of cancer.[19] One of the most proangiogenic factors known today is vascular endothelial growth factor, or VEGF.[5g] VEGF expression is increased in many different types of cancer, and most tumor cells secrete VEGF.[20] It is also thought that VEGF is a key promoter of metastasis.[22] VEGF is a 34–42 kDa, homodimeric, heparin binding, disulfide-bonded glycoprotein that has several isoforms arising from splice variants.[5d,g,20,106] VEGF has three known tyrosine kinase receptors: Flt-1 (VEGF-R1), KDR (VEGF-R2, Flk-1), and Flt-4 (VEGF-R3). VEGF-R1 has a higher affinity for VEGF, but it has been shown that VEGF-R2 is the biologically relevant receptor. Therefore, VEGF and its receptors VEGFR-1 and VEGFR-2 are prime targets for antiangiogenic intervention which is thought to be one of the most promising approaches in cancer therapy. Overexpression of VEGF also occurs in many different types of cancer, and thus VEGF and its receptors VEGFR1 and VEGFR2 are considered as prime targets for antiangiogenic intervention.[5h–j] Most importantly, overexpression of HER-2 is associated with increased expression of VEGF at both the RNA and protein level in breast cancer cells, and a positive association between HER-2 and VEGF expression in breast cancer patients has been identified.[5i] Specialized cancer treatments with antiangiogenic agents approved by the FDA include mAb, bevacizumab (Avastin) or small TKIs, SU11248 (sunitinib), and BAY 43-9006 (sorafenib).[107] Although the clinical application of these drugs in cancer therapy is promising, drug resistance development and long-term side effects like hypertension and endothelium dysfunction remain a concern.[108]

6.01.4 Peptide Immunotherapeutic Approaches

6.01.4.1 Peptide Vaccine Versus Peptide Therapeutics

These are two fundamentally different approaches that also exhibit different mechanisms of action. The only commonality is that both approaches utilize the same functional B-cell epitope as the main ingredient in the vaccine or in the therapeutic peptide. Fig. 3 depicts the difference between the two approaches.

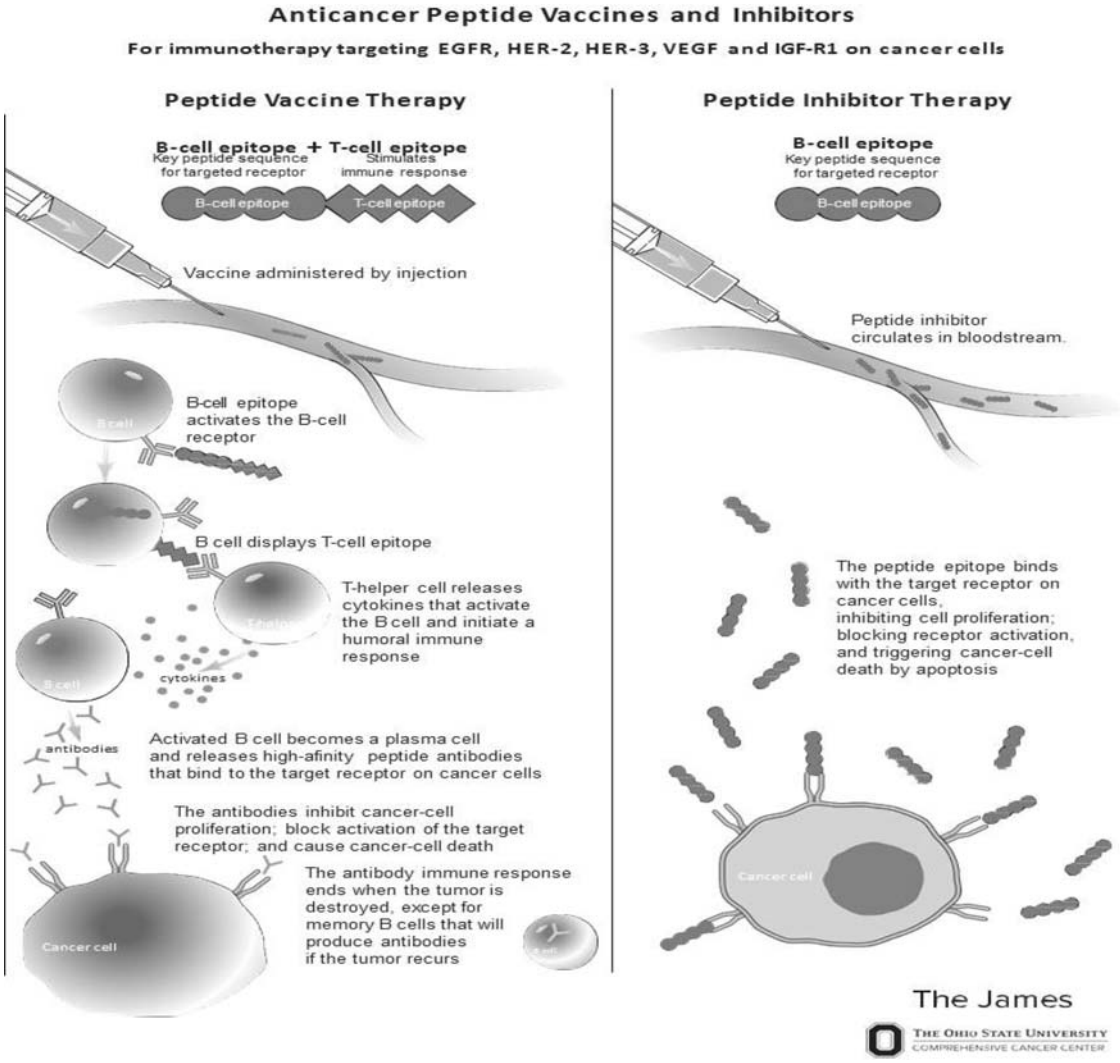

Fig. 3 Peptide vaccine versus peptide therapeutics.

6.01.4.1.1 Significance of peptide vaccine approaches

The greatest potential significance of our proposed strategy is twofold. (1) It combines multiple mechanisms of action by activating both B- and T-cell functions and promoting immunological clearance. (2) It is also a targeted approach aimed at inhibiting molecular signaling pathways that are crucial for tumor growth and maintenance. The major attraction of the peptide vaccine approach is the potential for a sustained antitumor effect related to immunological memory that protects against relapsing tumors, obviating the requirement for multiple infusions of humanized mAbs and overcoming escape mechanisms. Active immunotherapy offers many advantages, including tumor specificity and the activation of immune responses against antigens that are selectively expressed by tumor cells. As a result, nonspecific toxicity to normal tissues is reduced and antitumor responses are more durable and adaptable to cancer control at different stages of disease, including early-stage disease and disease with low tumor burdens. Additional benefits of the peptide vaccine approach include the ease and rapid synthesis, safety, lack of toxicity, and cost-effectiveness.

6.01.4.1.2 Significance of peptide mimic approaches

The significance of the peptide approach versus receptor-targeted mAbs and small molecules is that rationally designed peptide mimics represent a viable therapeutic strategy for blocking aberrant molecular signaling pathways with high affinity, high specificity, strong potency, and improved safety profiles.[27] There are several advantages of peptide therapeutics over mAbs and small molecules: (1) peptides will not accumulate in specific organs such as the kidney and liver, minimizing potential toxic side effects; (2) the tight structural relationship between the constructed peptide and the physiologically active parent molecules from which it is derived minimizes side effects; and (3) peptides help reduce current therapeutic problems, such as off-target side effects, requirements for high-dose regimens, and minimal drug–drug interactions. Generally, peptides are not directly linked to severe side effects since

they are composed of naturally occurring amino acids that are metabolically tolerable. In contrast, small molecules can build up in various organs, ultimately leading to severe toxic side effects.

Peptides are small protein-like chains of amino acids, and a peptide mimic is a peptide or a peptide-like molecule that intends to mimic one portion of the entire protein which is usually a binding or active site of an enzyme.[109] Peptides are easily synthesized, optimized, chemically stable, easily deliverable, and amenable to site-specific modification to target and kill cancer cells[110] with minimal toxicity. Peptide mimics offer the benefits of being water soluble, nonimmunogenic, and the ability to easily cross tissue barriers.[111] The main goal is to maintain the conformational space and orientation of the bioactive surface while retaining sufficient flexibility to bind cooperatively with a given receptor.[112]

Importantly, the simplicity of producing clinical grade peptides allows for rapid translation into phase I/II trials in humans patients. The disadvantages of peptide drugs are mainly related to their in vivo instability including short half-life and low bioavailability, susceptibility to proteases, formulation, and manufacturing challenges. New synthetic strategies to improve productivity and reduce metabolism of peptides, along with alternative routes of administration, have been developed in recent years, and a large number of peptide-based drugs are now being marketed.[17] There are ~60 therapeutic peptides on the market, 150 in clinical phases, and 400 in advance preclinical stages. Among the products that are approved, about 30 peptide drugs are currently marketed in the United States, and 17% are used to treat cancer.[24] One of the major drawbacks of using peptides as therapy is their high susceptibility to proteosomal degradation.[113] This obstacle can be overcome with the use of pseudo and modified peptides. The retro-inverso modification is the reversal of the peptide backbone by inverting the amino acid sequence, as well as reversal of the amino acid chirality by utilizing D-amino acids (**Fig. 4**). The resulting product is a topographical equivalent of the parent peptide with the amino side chain in similar orientation. Because retro-inverso peptides are synthesized with D-amino acids and proteases usually recognize L-amino acids, they should be resistant to proteosomal degradation and therefore will increase the bioavailability of the peptidomimetic therapeutic in vivo.[113,114]

6.01.4.1.3 Overall strategy

Innovative immune-based therapies that target receptor kinases have the potential to achieve long-term control in several tumor types without causing the numerous toxicities associated with most FDA-approved anticancer combination regimens. We have tested our model outlined in **Fig. 5** in multiple disease types. We have addressed several crucial issues in developing epitope-driven peptide vaccines over the past two decades by developing innovative anticancer strategies.[66b,115] Our strategy as outlined in **Fig. 1** consists of several steps: (1) initial prediction of B-cell epitopes is based on multiple computerized antigenicity/immunogenicity algorithms.[116] This represents a critical component in the overall process. (2) B-cell linear epitopes are refined through mutagenesis studies, and epitopes are modeled based on the three-dimensional native antigen structure and antigen:antibody complex if available. The unique B-cell epitope peptides are engineered to recapitulate the exquisite native structure of the tumor antigen.[117] This is a crucial prerequisite to developing high-affinity antibodies given that B-cell epitopes can be both linear (contiguous amino acid sequence) and conformational (discontinuous in the primary sequence but close in proximity of the folded 3D structure). (3) The chimeric vaccine is designed to include a "promiscuous" T-cell epitope[118] for a universal vaccine for an outbred population that can bypass haplotype-restricted immune responses; (4) highly efficacious native-like antipeptide–antibodies are then elicited in animals[11a,b,119] from the immunogen emulsified with an adjuvant in a squalene–arlacel oil–water ISA720 vehicle; (5) stable peptide mimics are designed as retro-inverso analogs that can block receptor:ligand interactions;[114b,120] (6) both antibodies and peptide mimics are used in a series of in vitro assays in different human cell lines to evaluate their efficacy. By corroborating the data, we are able to reduce the numbers of lead candidates to a minimum. (7) Combinations of the best performing epitopes are assessed in combination with human cell lines to determine synergy/additivity; (8) in vitro testing of potential combinations is then performed in different tumor cell lines using NOD/SCID mice as a surrogate animal model to simulate human cancers and evaluate the effects of peptide antibodies elicited in response to the vaccine epitopes. We can then finalize the potential candidates; (9) evaluate the effects of peptide mimics/antibodies elicited in response to finalize the potential candidates; (10) test efficacy in transgenics or appropriate animal model; (11) finally, conduct human clinical trials[121] to assess safety and toxicity.

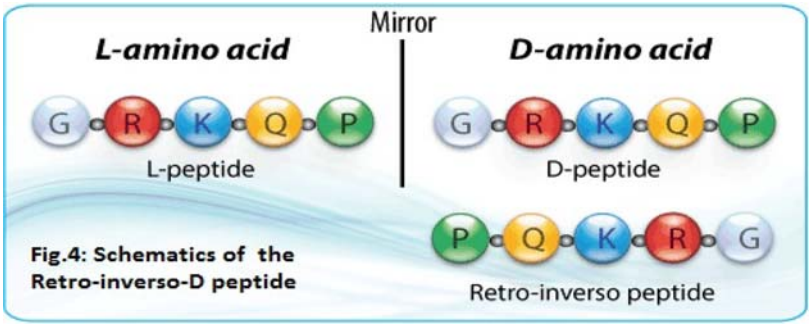

Fig. 4 Schematics of the retro-inverso-D peptide.

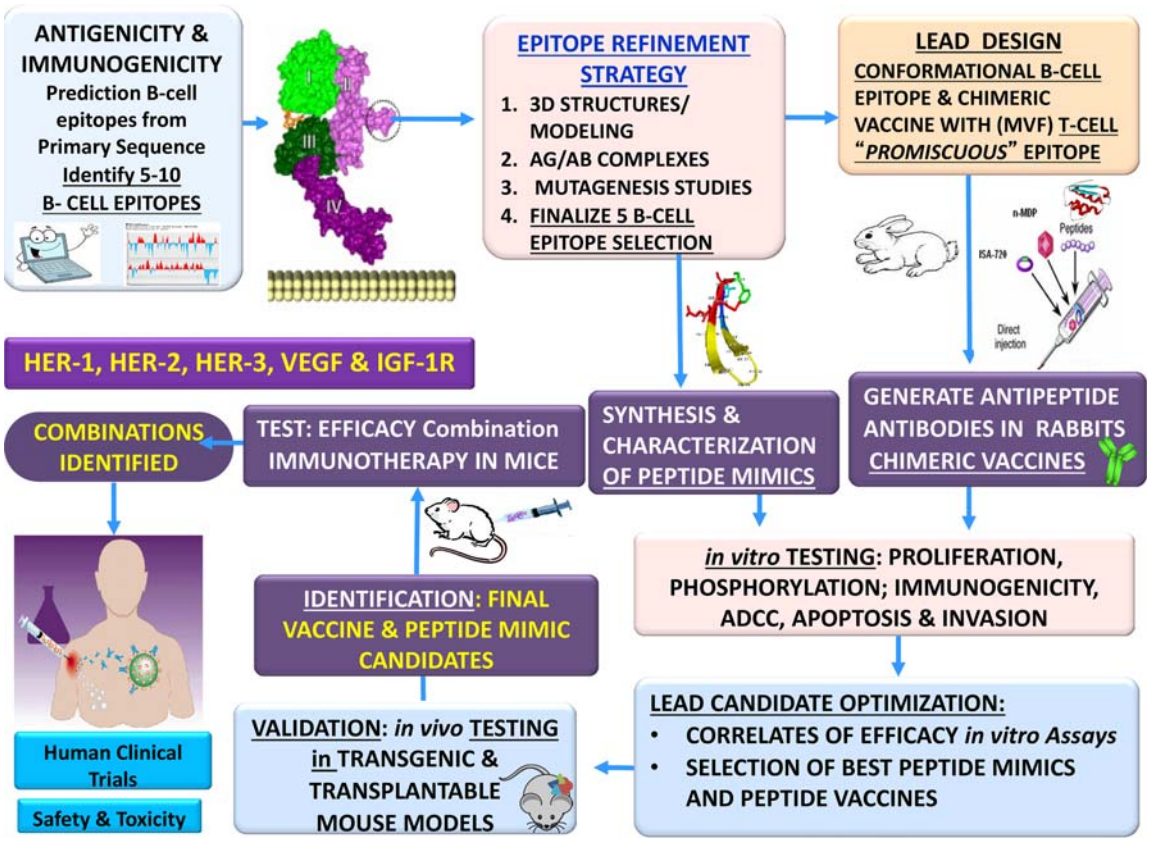

Fig. 5 Overall strategy of peptide approaches.

6.01.4.1.4 Road map for the design of an effective peptide vaccine versus a peptide mimic strategy

Our oncoimmunology approach is based on targeting signaling networks that are potential drivers of resistance and tumor progression while eliciting durable immune responses. Given the lack of preclinical models (transgenic or syngeneic animal model) to reliably predict clinical activity of vaccine constructs (active immunization) that target multiple tumor types concurrently, we have instead utilized a *surrogate and indirect model* in which rabbit antibodies elicited by the vaccine are used to test the efficacy of the vaccine *in transplantable mouse models challenged with human tumor cell lines*. Our peptide mimics serve a similar purpose, to corroborate the effects of the antibodies in transplantable mouse models as their mode of action is similar by preventing the heterodimerization of RTK. This allows us to have increased confidence in validating the vaccine epitopes. The peptide mimics could be a therapeutic approach by itself.

Fig. 6 outlines our road map of designing peptide vaccines and peptide mimics and their mode of action toward the same goal of tumor destruction by several mechanisms. *Pathway A* involves the *design of chimeric peptides*[117a,c] *comprising the conformational B-cell epitope and incorporating a "promiscuous" T-cell epitope*.[118] The vaccine is emulsified with an adjuvant (nor-MDP) in a vehicle (ISA 720; squalene/arlacel) (**C**) and used for vaccination. When relevant transgenic mice (MMTV/neu) or a syngeneic model (**D1**) is available for assessing vaccine efficacy, these mice are immunized sc with the chimeric peptide vaccine and tumor growth/reduction is monitored over time.[11a,c,119] Rabbits are used as a surrogate model (**D2**) to develop high-affinity antipeptide antibodies which can be used to treat transplantable mouse models (NOD/SCID) (**E1**) after tumor challenge. Tumor growth is then monitored over time as we have described.[122] *Pathway B* involves *the design of conformational B-cell-peptide mimics* with enhanced proteolytic stability.[4-b,120a,122b] Because a T-cell epitope is not included, the peptide lacks immunogenicity, thus the peptide mimic treatment does not elicit antibody production. The peptide mimics are dissolved in PBS and are injected in mice by *iv* treatment (**E2**) at the time of tumor challenge with repeated weakly treatment until control mice develop large tumors. This strategy allows us to corroborate effectiveness of antibody treatment versus peptide treatment,[123] allowing us to prioritize peptide constructs for testing in (1) transgenic mouse models (**F**) and (2) human clinical trials (**G**).[121] Both the vaccine and peptide mimic approach can induce tumor cell death by a variety of antitumor cellular mechanisms (e.g., ADCC (only Ab)), inhibition of proliferation or phosphorylation, and apoptosis. The mode of action for active immunization: The conformational peptide epitope binds the B-cell receptor, and the measles virus MVF "promiscuous" T-cell epitope binds MHC class II and does not require antigen processing,[118,124] preserving the native structure of the vaccine construct. On the other hand, the mechanism of action for the peptide mimic is direct binding of the B-cell peptide mimic to the receptor, preventing heterodimerization.

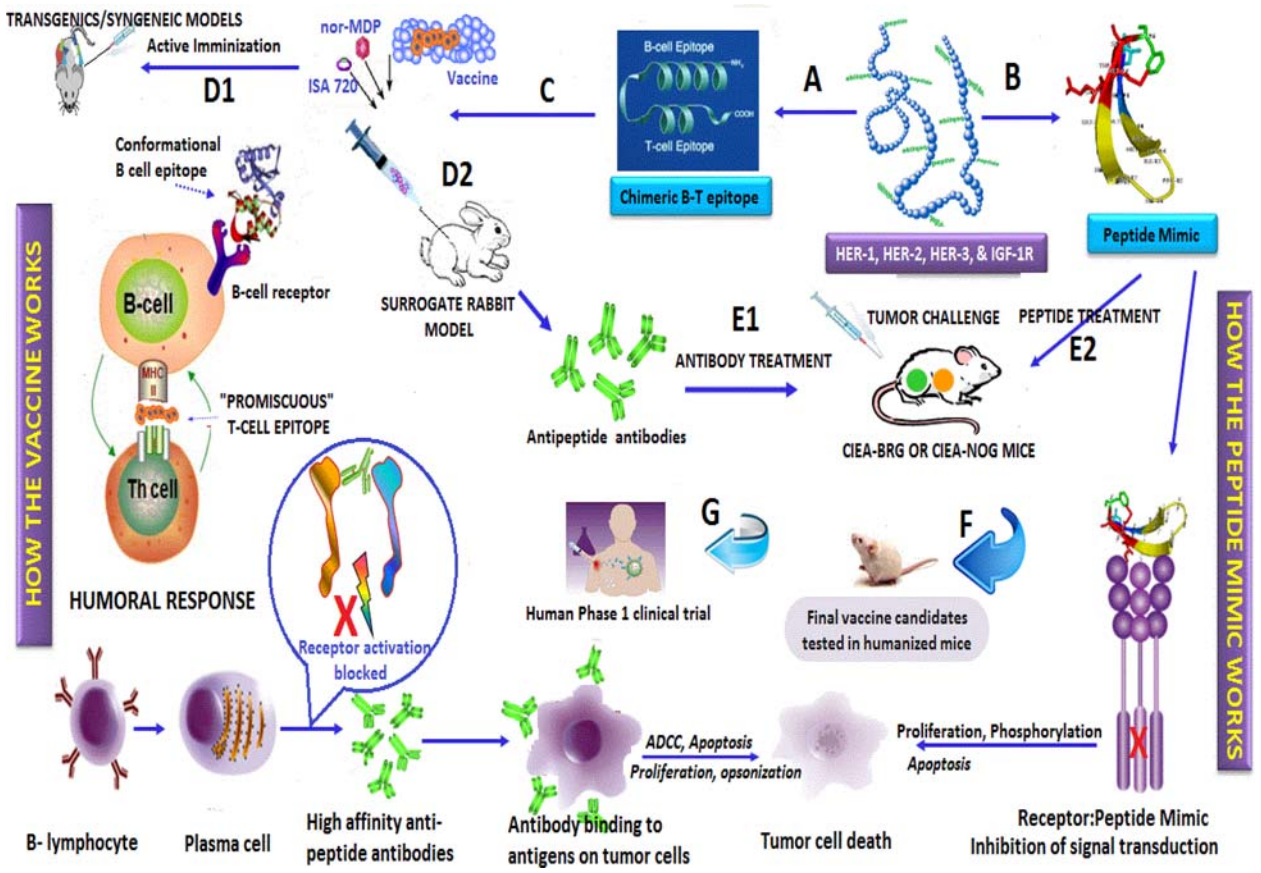

Fig. 6 Road map for combined peptide strategies.

6.01.5 Targeted Therapies Against HER-2

6.01.5.1 Humanized mAbs and Small-Molecule Inhibitors

Over the last decade, many drugs have been developed to target the HER family members especially HER-1 and HER-2, and some of these drugs have gained FDA approval, while others are still being evaluated in clinical trials.[125] Most of the FDA-approved targeting HER-1 (cetuximab, erlotinib, and gefitinib) and HER-2 (trastuzumab, pertuzumab, and lapatinib) have significant toxicities with unacceptable safety profiles in most patients.[126]

6.01.5.1.1 Development of trastuzumab and treatment

Since HER-2 is a membrane-bound receptor, exposed to the extracellular matrix, development of mAb's could bind the ECD of HER-2 and interfere with signal transduction and thus inhibit tumorigenic HER-2 function.[127] Over 100 mAbs directed against the ECD of HER-2 have been generated. Dependent upon epitope specificity, the interaction of HER-2 and anti-HER-2 antibodies (Abs) resulted in no effect, inhibition, or stimulation of tumor growth.[128] One of these anti-HER-2 mAb was developed for clinical testing, initially identified as mouse mAb 4D5. 4D5 was created by the fusion of a mouse myeloma cell line with splenocytes from BALB/c mice immunized NIH 3T3 cells stably transfected with HER-2.[7a,129] 4D5 was selected from a panel of mouse anti-HER-2 Abs at Genentech Inc. because it inhibited the growth of breast tumor cell lines overexpressing HER-2 in both anchorage-dependent and independent assays in vitro and inhibited tumor growth in mouse models.[7a,130] To avoid human antimouse antibody responses, mouse mAb 4D5 was humanized.[131] The IgG1 isotype is favored due to its ability to support effector functions such as ADCC and CDC.[132] Trastuzumab proved to be more efficient than its murine counterpart 4D5 in mediating ADCC.[131,133] Additional preclinical studies demonstrated trastuzumab's ability to reduce cell culture antiproliferative activity and antitumor efficacy in mouse xenograft studies.[133b,134]

6.01.5.1.2 Clinical trials of trastuzumab

Trastuzumab tested as a single agent in HER-2 overexpressing metastatic breast cancer demonstrated response rates of 12–34% for a median duration of 9 months.[135] The most beneficial clinical use of trastuzumab has been in combination with a variety of cytotoxic chemotherapies.[127] Trastuzumab added to multiple chemotherapy treatments significantly increases their antitumor

efficacy.[136] Trastuzumab's largest impact has been in the treatment of patients with potentially curable early-stage breast cancer.[127] The addition of trastuzumab to chemotherapy regimens to early-stage HER-2 overexpressing breast cancer patients, who receive chemotherapy after surgical resection, significantly prolongs disease-free survival and reduces the chance of recurrence.[137] As a result of these studies, trastuzumab has recently been approved in combination with doxorubicin, cyclophosphamide, and paclitaxel in adjuvant treatment for early-stage breast cancer after primary therapy.[138] The clinical activity of trastuzumab is limited to HER-2 overexpressing tumors, and trastuzumab has no significant activity against breast cancers without HER-2 overexpression.[135c,139]

6.01.5.1.3 Side effects of trastuzumab treatments

Despite the impressive clinical results with trastuzumab, there are side effects associated with this mAb including cardiotoxicity. Initial clinical trials revealed trastuzumab had significant cardiotoxicity, with the incidence of cardiac dysfunction ranging from 4% to 7%.[140] Subsequent randomized clinical trials demonstrated significant trastuzumab-associated cardiotoxicity, with 5–17% increase in left ventricular ejection fraction, a measure of the pumping ability of the heart, and 1–3% increase in congestive heart failure.[141] The mechanism of trastuzumab-induced cardiac dysfunction is not fully understood.[142] HER-2 may aid in the repair of cardiac myocyte injury. Thus, the use of trastuzumab and the loss of HER-2-dependent cardiac myocyte survival pathways could make patients more vulnerable to cardiac damage.[143]

Fevers and chills are the most common side effects that patients experience after receiving trastuzumab. The fever and chills are sometimes accompanied by rigors (uncontrollable shaking). Fevers, chills, and rigors respond well to simple medical treatments. Other side effects experienced by patients receiving trastuzumab include rash, shortness of breath, low blood pressure, nausea/vomiting, pain, headache, dizziness, and asthenia (weakness). All of these side effects occurred most commonly either during the first dose of trastuzumab and not very frequently thereafter. The use of Herceptin may be associated with damage to the heart muscle and an associated decrease in heart function and symptoms of congestive heart failure. These symptoms include fatigue and difficulty breathing. Heart failure has occurred in about 4% of patients who have received trastuzumab alone. Most patients treated with trastuzumab have been treated previously with a class of drugs called anthracyclines that can sometimes injure the heart. The chance of heart failure may be lower in patients who have not received anthracyclines. The risk of heart problems with trastuzumab may be greater in patients receiving higher total amounts of trastuzumab, in patients with a previous history of heart disease, and in patients who have received X-ray therapy to the chest. This condition may be reversible with medication, but persistent severe heart failure may be possible. Some patients have a very slight decrease in heart function, while others have actually died of heart failure. Heart failure may only show up many months after trastuzumab treatments have been stopped. Allergic reactions (rash, itching, difficulty breathing, or even shock) may be seen following treatment with Herceptin as with any foreign protein, but these are uncommon. Lowered numbers of red blood cells and/or white blood cells may occur following treatment with trastuzumab (about 1% of the time). Diarrhea was seen in about 25% of patients receiving Trastuzumab alone. Because one of these epitopes correspond to trastuzumab, it is possible that similar reactions may occur in the patients. Therefore, cardiac status will be determined using history and physical, vital signs, troponin levels, EKG, and MUGA scan results. Our experience with similar epitopes in our previous trial showed none of the signs described earlier.

6.01.5.1.4 Possible mechanisms of action and resistance to trastuzumab

Many studies have attempted to decipher the molecular mechanisms underlying the clinical activity of trastuzumab. Early studies supported trastuzumab-mediated endocytosis and degradation of the HER-2 receptor,[144] with consequent inhibition of the downstream PI3K and MAPK signaling pathways. However, other studies have shown trastuzumab does not downregulate HER-2.[145] Austin et al., using immunofluorescence and quantitative immunoelectron microscopy, demonstrated that trastuzumab binds and internalizes with surface HER-2 but reappears with HER-2 at the cell surface, only accompanying HER-2 passively along its normal endocytic recycling route.[145a] Trastuzumab binding to HER-2 inhibits the proteolytic cleavage and shedding of HER-2 by matrix metalloproteases.[146] This could be a part of the antitumor properties of trastuzumab since truncated HER-2 is associated with increased kinase activity and increased transforming efficiency,[147] although many HER-2 overexpressing breast cancers do not have significant truncation of HER-2.[127] Trastuzumab is unable to inhibit HER-2 from dimerizing with other members of the HER family including EGFR and HER-3.[148]

While the effect of trastuzumab on the function of its direct target HER-2 remains to be identified, numerous studies have described the effects of trastuzumab on downstream signaling pathways. Cells treated with trastuzumab undergo arrest during the G1 phase of the cell cycle modulated by the induction of p27, with a concurrent reduction in proliferation.[149] Overexpression of HER-2 in tumors is associated with increased angiogenesis and expression of vascular endothelial growth factor (VEGF).[150] Trastuzumab exhibits certain antiangiogenic properties. Trastuzumab treatment on HER-2 overexpressing breast cancers reduces tumor volume and decreases microvessel density in vivo.[151] Trastuzumab may block PI3K signaling via disrupting the interaction between HER-2 and Src tyrosine kinase, leading to the inactivation of Src with subsequent activation of the PI3K inhibitor PTEN.[152]

In light of recent data indicating that trastuzumab does not downregulate cell-surface HER-2, there is a renewed interest in another possible mechanism of action of trastuzumab, its ability to induce an immune response via its Fc domain. Trastuzumab is highly efficient at activating ADCC in vitro.[131,153] Natural killer (NK) cells, a major immune cell type involved in ADCC, express the Fc-γ receptor III, to which the Fc domain of trastuzumab binds, activating NK-mediated cell lysis. Xenograft studies with mice bearing HER-2 overexpressing tumors displayed a tumor regression rate of 96% when treated with trastuzumab. Mice lacking the Fc receptor showed only 29% tumor growth inhibition when treated with trastuzumab.[134b] This model provides convincing evidence that the antitumor activity of trastuzumab is mediated through immunological targeting mechanisms.[127]

6.01.5.1.5 Trastuzumab-DM1

Trastuzumab-DM1 (T-DM1; Genentech/Roche, South San Francisco, California) is a novel chemistry-driven conjugated HER-2 mAb in which the trastuzumab is conjugated with a fungal toxin DM1 (maytansine).[154] The purpose of developing this compound is to overcome trastuzumab resistance and boost the efficacy of this targeted strategy. Maytansine is an antimicrotubule agent that inhibits the assembly of cellular microtubules. In vitro studies showed that the cytotoxicity of maytansine is over 1000 times that of any other chemotherapeutic agent.[155] In trastuzumab-DM1, trastuzumab mainly works as a carrier that delivers DM1 to the tumor cells labeled with HER-2. Trastuzumab-DM1's mechanism of action is independent of functional HER-2 signaling but only requires a high expression level of HER-2 on the cellular surface. Therefore, trastuzumab-DM1 can successfully overcome several trastuzumab resistance mechanisms related to HER-2 downstream signaling, such as PI3K mutation and PTEN downregulation.

6.01.5.1.6 Pertuzumab: HER-2 dimerization inhibitor

Pertuzumab (Omnitarg; Genentech/Roche, South San Francisco, California) is a humanized mAb that targets the extracellular domain of HER-2. From the panel of anti-HER-2 mAbs developed at Genentech Inc., the mAb 2C4 was also selected for further characterization. Compared with mAb 4D5, 2C4 has diminished antiproliferative activity in vitro with the HER-2 overexpressing cell line SKBR3.[7a] Agus et al. showed that 2C4 but not trastuzumab is able to block the association of HER-2 and HER-3 in breast cancer cell lines,[148a] indicating 2C4 has properties distinct from trastuzumab. Additionally it was reported that 2C4 inhibited heregulin-mediated HER-2 phosphorylation and MAPK and Akt activation in breast cancer cells not overexpressing HER-2.[148a] In vivo preclinical xenograft studies have demonstrated 2C4 has activity on breast, ovarian, and prostate tumors including tumors without HER-2 overexpression.[148a,156] 2C4 has been humanized to be used for human clinical usage,[157] and the resulting humanized mAb is called pertuzumab (Omnitarg). Limited data have been presented on 2C4 or pertuzumab's ability to inhibit cell signaling pathways since these mAbs are not yet accessible to the wider scientific community.[127] Phase I studies of pertuzumab revealed the agent was well tolerated with side effects of fatigue, nausea, and vomiting.[158] A number of phase II trials have been conducted in breast, nonsmall cell lung cancer (NSCLC),[159] ovarian,[160] and prostate[161] cancers. Clinical responses were seen in a Phase II trial of ovarian cancer patients, with an overall response rate of 4.3%.[160] Pertuzumab has shown synergy with trastuzumab in vitro,[162] and a phase II trial is investigating the effect of a combination of pertuzumab and trastuzumab in HER-2 overexpressing breast cancer.[163] The effects of pertuzumab on HER-2 expressing cancers await additional preclinical and clinical studies.

6.01.6 Rationale for Developing HER-2 Vaccines

6.01.6.1 Numerous X-Ray Crystallographic Structural Studies Reveal How the HER Family Initiates Signal Transduction

There are many crystal structure determination of the HER receptors alone or in combination with either antibodies or their ligand. These studies have provided us with accurate identification of the binding regions for rational design.

6.01.6.1.1 Structural studies with HER-2 and trastuzumab

Two independent groups published crystal structures of the extracellular region of HER-2.[164] HER-2 adopts an open conformation that resembles the ligand-activated state of EGFR. The contact between domains II and IV, observed in ligand-less EGFR and HER-3, is absent in HER-2, instead an interaction between domains I and III is seen. This structure of HER-2 is similar to a ligand-activated state, showing HER-2 poised to dimerize with other HER receptors in the absence of direct ligand binding and explains the inability of HER-2 to bind any known ligands.

The structure of soluble HER-2-trastuzumab Fab complex reveals that trastuzumab binds on the C-terminal side of domain IV of the HER-2 ECD (Fig. 7). The trastuzumab-HER-2 interaction buries 1350 Å^2 of the HER-2 surface. Three loops are observed to make contact with trastuzumab. Loop 1 contains residues 579–583 and loop 3 contains residues 615–625, and these loops are composed

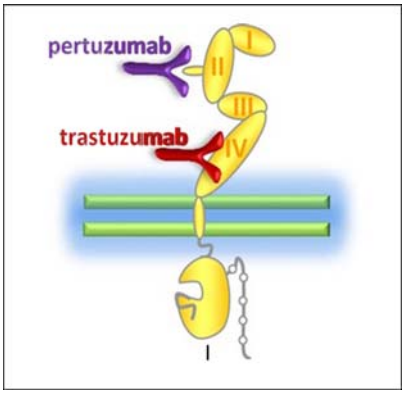

Fig. 7 HER-2-binding sites.

of primarily electrostatic interactions with trastuzumab. Loop 2 comprises residues 592–595, and this loop makes primarily hydrophobic contacts with trastuzumab. The specific details of the contact region between HER-2 and trastuzumab may allow for the design of possible small peptides or peptide analogues.

6.01.6.1.2 Structural studies with HER-2 and pertuzumab

The crystal structure of the HER-2 ECD bound to pertuzumab reveals this mAb binds a different epitope than trastuzumab, found at the center of domain II, near the junction of domains I, II, and II[165] (Fig. 7). The contact buries 1210 Å^2 on the HER-2 side of the interface. The interface between HER-2 and pertuzumab is mostly polar, with few hydrophobic or charged residues in the interface. Domain II in HER-2 and EGFR is highly conserved, and this is the same region involved in EGFR dimerization. This region overlaps with pertuzumab binding, indicating that pertuzumab binds at the HER-2 dimerization interface. This structure provides a model in which pertuzumab sterically interferes with HER-2 dimerizing with other members of the HER family and thereby interrupts the growth signals mediated by HER-2 ligand-activated heterodimers. However, the structure and function analysis demonstrated that pertuzumab binds to a quite distinct site of the HER-2 extracellular part from that of trastuzumab and is considered to serve as a HERs dimerization inhibitor. Receptor dimerization can occur between two different EGFR family members (heterodimerization) or between two symmetric EGFR receptors (homodimerization).

6.01.6.1.3 Rationale for conformational HER-2 epitopes

To induce functional cross-reactive immune responses, it appears essential that peptide design takes into account conformational correctness.[166] One approach to achieve molecular mimicry to the parent protein is through constricting the peptide by cyclization. Linear peptides are very flexible and can adopt an assortment of conformations in solution, but only a few of these conformations are responsible for their immunoreactivity. Cyclic peptides can cause favored spatial arrangements that reproduce the bioactive conformation resulting in superior binding and immunological properties. There are several extensive reviews on the cyclization of peptides.[167] Disulfide bridges are important evolutionarily conserved structural motifs found in many biologically important peptides and proteins including hormones, growth factors, and immunogloblins. Artificial introduction of disulfide bonds into designed peptide vaccines is performed with the goal to improve the cross-reactivity of the elicited antibodies to the native protein and thus enhanced activity of the vaccine. Regioselective pairing of disulfides can occur by controlled chemistries involving orthogonally removable Cys protecting groups. The utility of peptide cyclization with the incorporation of the two native disulfide bonds of the 626–649 sequence of HER-2 has been shown by our group previously.[11b]

The structures of the HER-2-trastuzumab complex and the HER-2-pertuzumab complex (Figs. 8A and 9A) have led to new insights into the mechanistic and biological activities of HER-2 antibodies as well as the process of ligand-induced receptor dimerization which in turn has empowered us to rationally design more effective HER-2 conformational epitopes with potentially increased efficacy for preventing and inhibiting tumor growth. To date no conformational peptides have been designed and tested based on the crystal structure of the HER-2 ECD in complex with the trastuzumab or the pertuzumab Fab fragments, hence these studies are novel.

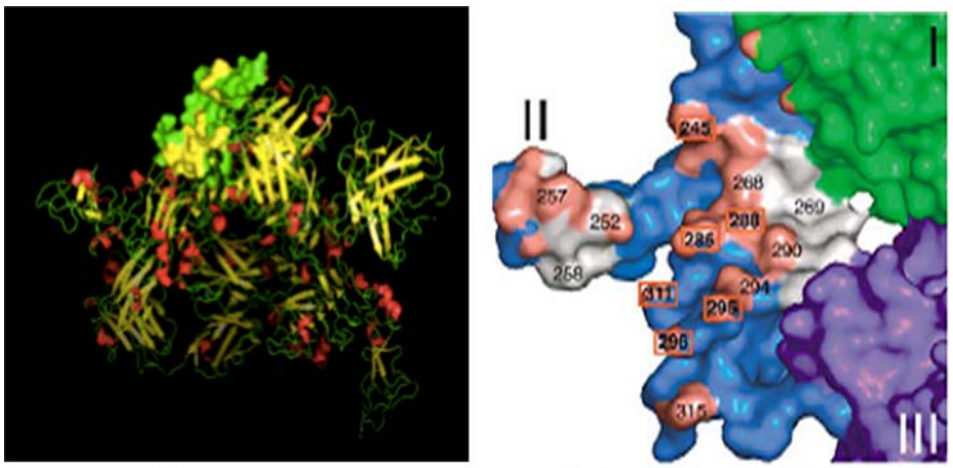

Fig. 8 Crystal structure of HER-2 pertuzumab-binding site. (A) X-ray structure pertuzumab and HER-2 complex and (B) engineered pertuzumab epitope 266–297.

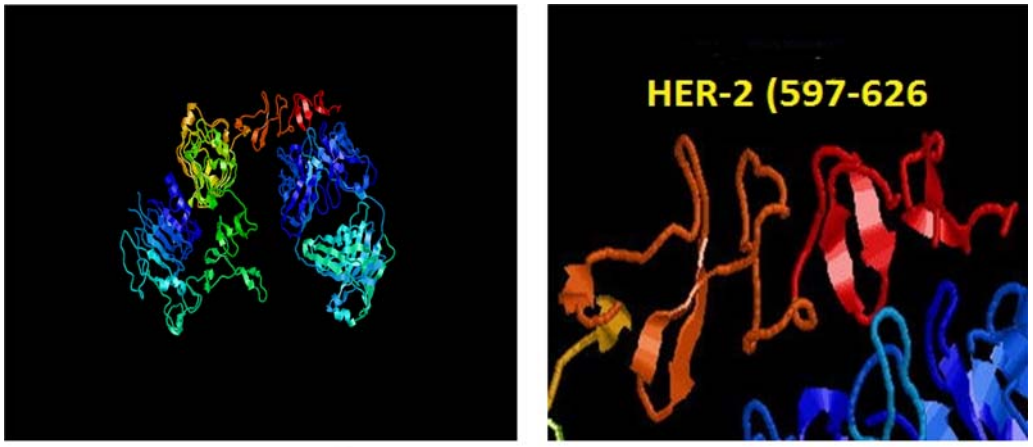

Fig. 9 (A) X-ray structure Herceptin/trastuzumab and HER-2 complex and (B) engineered trastuzumab epitope 597–626.

6.01.6.1.4 Design and evaluation of novel pertuzumab-binding conformational B-cell epitopes

The crystal structure of pertuzumab bound to the ECD of HER-2/neu[91] elucidated the details of interacting region of residues 266–333 (Fig. 8B). We examined three different sequences, 266–296, 298–333, and 315–333, to determine the best minimal conformational epitope for effective B-cell immunization. We report on the activity of several constructs containing complex, differential disulfide pairings as well as their linear counterparts in order to mimic the pertuzumab-binding conformational region.

The immunogenicity of each cyclized (Cyc) and noncyclized (NC) constructs were determined in both mice and rabbits, eliciting a high affinity, high titer antibody responses. The antibodies recognized the native HER-2/neu receptor. Additionally, only three of the six putative constructs 266–296(CYC), 266–296(NC), and 315–333(CYC) were able to mediate ADCC and reduce phosphorylation of the HER-2/neu tyrosine kinase domain. Epitope 266–296 was able to suppress cellular proliferation in heregulin (HRG)-stimulated MCF-7 cells. Our results show that these pertuzumab-like epitope constructs had statistically reduced tumor onset in both transplantable tumor models (FVB/n and Balb/c) and significant reduction in tumor development in two transgenic mouse tumor models (Balb-neuT and VEGF$^{+/-}$Neu2-5$^{+/-}$). These studies demonstrate that both the linear (NC) and conformational (CYC) peptide vaccines corresponding to residues 266–296 of the dimerization region of HER-2/neu are able to elicit an immune response with antitumor capabilities, resulting in a peptide vaccine that will be able to mimic the effects of pertuzumab in vivo without the harmful side effects associated with mAb therapy.

6.01.6.1.5 Design and evaluation of novel trastuzumab/Herceptin-binding conformational B-cell epitopes

The three-dimensional structure of human HER-2 in complex with Herceptin (Fig. 9A) revealed that the antigen-binding region of HER-2 spans residues 563–626 that comprises an extensive disulfide bonding pattern.[89,90] In order to minimally dissect the interacting-binding region of HER-2, we have designed four synthetic peptides with different levels of conformational flexibility. The interacting loops in subdomain IV comprise residues in loop 1: 579–583 (two disulfide pairings between C563 and C576, and between C567 and C584), loop 2: 592–595 (cysteine disulfide pairing between C587 and C596), and loop 3: 615–625 (cysteine disulfide between C600 and C623). Chimeric peptides incorporating the MVF "promiscuous" T-cell epitope via a four-residue linker sequence were successfully synthesized, purified, and characterized. All conformationally restricted peptides were recognized by trastuzumab, with 563–598 and 597–626 showing higher reactivity. All peptide sequences prevented the function of trastuzumab inhibiting tumor cell proliferation. All epitopes were immunogenic in FVB/N mice with antibodies against 597–626 and 613–626 recognizing HER-2. The 597–626 epitope was immunogenic in outbred rabbits eliciting antibodies which recognized HER-2 at the HER-2/trastuzumab interface, inhibited proliferation of HER-2-expressing breast cancer cells in vitro, and caused their ADCC. Moreover, immunization with the 597–626 epitope significantly reduced tumor burden in transgenic BALB-*neu*T mice. These results suggest that the peptide B-cell immunogen is appropriate as a vaccine for HER-2-overexpressing cancers since the resulting antibodies show analogous biological properties to trastuzumab. We conclude the HER-2 597–626 sequence is a potential vaccine candidate that could be translated to the clinic. One epitope, 597–626, was pursued for additional studies based on its ability to be recognized by trastuzumab and the ability of antibodies elicited against the peptide to bind HER-2 at the same site as trastuzumab. Antibodies against the 597–626 construct were able to mediate both direct and indirect mechanisms of antitumor activity against HER-2 in vitro. Additionally, the 597–626 peptide vaccine was able to impede the autochthonous tumor formation in BALB-*neu*T transgenic mice.

6.01.7 VEGF Peptide Strategies

Most solid tumors cannot grow beyond a few millimeters without the angiogenic switch being turned on[168] making angiogenesis inhibition a attractive therapeutic strategy for targeting tumors. The most well-known proangiogenic factor today is VEGF,[5g] and its overexpression is reported in many different types of cancers.[19,169]

There are many potentially beneficial combinations applicable in cancer immunotherapy ranging from antibodies to growth factors with small TKI molecules to CTL vaccines with inhibition of regulatory T cells with or without radiation and/or chemotherapy. HER-2 and VEGF represent validated targets for several tumor types, and inhibitors of these growth factors have become key therapies to improve antitumor efficacy. Because of the interdependence between these growth factors, concurrent inhibition of these multiple pathways might result in significantly better therapeutic outcomes.

6.01.7.1 VEGF Peptide Mimics

Unlike other growth receptors that only trigger mitogen pathways, VEGF signaling via VEGFR-2 activates pathways leading to survival, three-dimensional tube organization and vascular permeability.[170] VEGF:VEGFR-2 interaction is therefore very important for angiogenesis, and blocking this interaction is the most attractive model in the development of antiangiogenic drugs.[171]

Our strategy to develop angiogenic inhibitors involves the synthesis of conformational peptides that can mimic the VEGF-binding region to VEGFR-2 which will inhibit angiogenesis by competing with VEGF for binding to its receptor.

6.01.7.1.1 Design and synthesis of VEGF peptide mimics

The interface between VEGF and VEGFR-2 has been mapped by alanine scanning, which showed that the binding site is localized at the loop between β5 and β6.[172] This loop is within the region containing the biologically activity site (also called "hot spot") in the VEGF protein, which includes monoclonal epitope binding (Avastin, G-6, and B20-4) and VEGF receptor binding. Both Muller et al.,[173] who analyzed the contact residues on both sides of the interface of the complex between VEGF and the Fab fragment of a humanized antibody, and Zilberberg et al.[174] analysis of the VEGF sequence interacting with VEGF receptor-2 have concluded that residues spanning sequence 79–93 are important. Thus, we selected the VEGF sequence 102–122 (detailed in Fig. 10) to design our VEGF peptide mimic; this region corresponds to sequence 76–96 in the VEGF crystal structure and includes the entire loop region between β5 and β6.[175]

Our strategy for creating the conformational cyclic peptide VEGF-P3 (CYC) which displays an antiparallel β-sheet (Fig. 10) was to introduce two artificial cysteine residues between residues Gln79 and Gly92, and also between residues Ile80 and Glu93. The

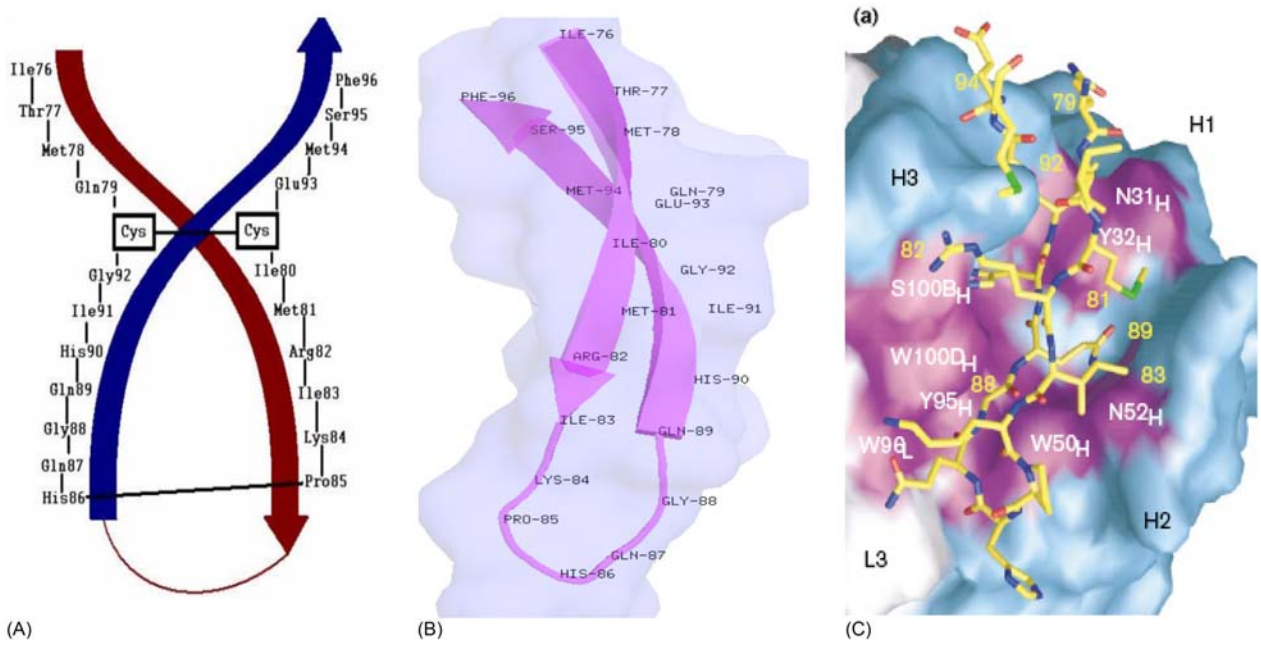

Fig. 10 Schematics of VEGF Peptide mimics. (A) Illustrates the engineered VEGF peptide mimic with two artificial cysteine residues inserted to form a cyclized antiparallel β-structure. The complex peptide is synthesized from Phe96 to Glu93 followed by CYS, and the synthesis continues with Ile80 through Gly92. The other CYS is placed between Gly92 and Gly79 and ends with Ile76. (B) The antiparallel β-sheet structure of VEGF 76–96 connected by loop residues 83–89. (C) The structure of VEGF shows the critical amino acid residues that are involved in binding of VEGF to its receptor VEGFR2.

VEGF-P3 (CYC) was synthesized with cysteines at position 80 and 92 to allow cyclization to yield a peptide mimicking its native conformation that of an antiparallel β-sheet contained within a loop structure. The VEGF-P3 noncyclized peptide after synthesis, cleavage, and HPLC purification was oxidized using iodine and characterized by mass spectrometer. The VEGF-RI-P4 peptide mimic required the use of D-amino acids to yield the retro-inverso (RI) peptidomimetic[176] resulting in a more stable peptide than its L-amino-acid counterpart that would exhibit similar activity and with higher bioavailability. The VEGF mimic peptides were evaluated as inhibitors in several assays where VEGF-dependent signaling pathways are observed. The engineered cyclic VEGF mimic peptide (VEGF-P3(CYC)) shows the highest inhibitory effects in several angiogenic in vitro assays compared to unstructured peptides. We also demonstrate that this VEGF mimic peptide significantly delays tumor growth in a transgenic mouse model ($VEGF^{-/+}$/$Neu2\text{-}5^{-/+}$), in which the acceleration of spontaneous tumor burden is due to overexpression of VEGF. These results indicate that the structure-based design is important to the development of this peptidomimetic and to its antiangiogenic effects. The VEGF-P3(CYC) is the best peptide candidate for the development of a peptidomimetic angiogenic inhibitor.

6.01.7.1.2 Combination therapy targeting both HER-2 and VEGF in cancer

The overexpression of HER-2 is associated with increased expression of VEGF at both the RNA and protein level in human breast cancer cells.[150] In addition, exposure of HER-2 overexpressing cells to trastuzumab significantly decreases VEGF expression.[151a] Taken together these data suggest that VEGF is a downstream target of the HER-2 signaling pathway. A positive association between HER-2 and VEGF expression in breast cancer patients has been identified.[177] A two-pronged approach to target cancer cells by coimmunizing with defined tumor-associated antigens and angiogenesis-associated antigens has been shown to have synergistic effects.[178] Combination treatment with defined tumor- and angiogenesis-associated antigens is well known to produce synergistic effects.[179] Combining antiangiogenic therapies with other direct anticancer agents has been shown to be beneficial in various malignancies.[180] Because of the potential synergy between therapy with HER-2 inhibitors and antiangiogenic therapy with VEGF inhibitors in vitro and in vivo, we evaluated the effects of combination treatment.

From our previous studies, the peptide epitope HER-2-266–296 was shown to produce the best antitumor effects both in vitro and in vivo. We therefore decided to combine this novel HER-2 peptide mimic with our antiangiogenic VEGF peptide mimic with these two peptides.

As shown in Fig. 11, antibodies elicited by immunization with MVF-HER-2 (266–296) vaccine bind to domain II of HER-2 and similarly anti-MVF-HER-2 (597–626) binds domain IV of HER-2 providing dual inhibition of homo/heterodimerization and consequently downstream signaling shutting down the PI3K and MAK kinase pathways, thereby preventing cancer growth and metastasis. On the other hand VEGF peptide mimics P3 and P4 are designed to directly block VEGF binding to VEGFR2 and inhibit intracellular phosphorylation of the tyrosine kinase domain which reduces angiogenesis.

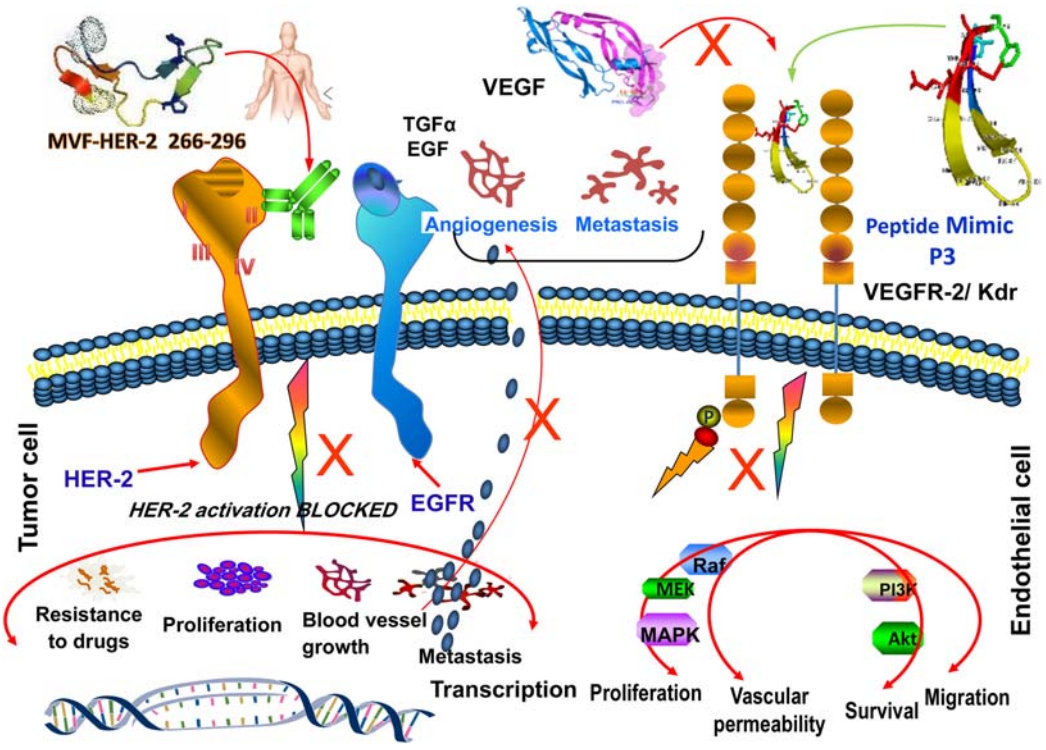

Fig. 11 Combination of HER-2 vaccines and VEGF peptide mimics.

6.01.8 Crucial Peptides Targeting HER-1, HER-3, and IGF-1R Have Been Identified and Fully Characterized Biochemically and Immunologically

6.01.8.1 Extensive Cross talk Among ErbB/HER Receptors

Extensive cross talk among ErbB/HER receptors suggests that blocking signaling from more than one family member may be essential to effectively treat cancer and limit drug resistance. Recently, we have extended our portfolio of RTK inhibitors by identifying crucial and novel peptides targeting HER-1(HER-1),[52] HER-3,[181] and IGF-1R.[38d,182]

6.01.8.1.1 HER-1

The crystal structure of the complex between EGF and EGFR and analysis of the contact residues on both sides of the interface have been well analyzed,[183] while the structural basis for the inhibition of EGFR by cetuximab has also been studied.[95] Results from these two separate studies showed residues critical for cetuximab binding are also important for EGF binding, which indicates that the neutralizing effect of cetuximab binding results from disrupting EGF:EGF receptor interaction. Several residues are important for EGF binding and with the aid of these crystallographic studies and computer-aided analysis; we have selected peptide epitopes that include these key residues for ligand binding as potential candidates for our vaccine and therapeutic approach. Several residues are important for EGF binding and with the aid of these crystallographic studies and computer-aided analysis; we have selected peptide epitopes that include these key residues for ligand binding as potential candidates for our vaccine and therapeutic approach (see **Table 1** and **Fig. 12**).

In this study, we selected three critical epitopes of EGFR (347–374, 382–410, and 418–435) that are all involved in ligand binding and by active immunization in rabbits; we have generated sequence-specific antipeptide antibodies to the EGFR ligand-binding domain. We then evaluated the in vitro antitumor effects of the antibodies and the peptide mimics (B-cell epitope alone) in different signaling assays like cellular proliferation, apoptosis induction, EGFR dephosphorylation, inhibition of signaling pathways, and ADCC. The peptide vaccines were highly immunogenic in both mice and rabbits, and the antibodies elicited were able to specifically recognize the native EGFR receptor as shown by their reactivity in MDA-MB-468 TNBC cells and A549 lung cancer cells in flow cytometry and their binding to recombinant human EGFR in ELISA. The peptide mimics and antipeptide antibodies to all three epitopes inhibited cancer cell growth, prevented EGFR-specific phosphorylation, downregulated EGFR-signaling pathways, caused increased apoptosis, and ADCC in EGFR expressing cells. In mouse model studies, two of the vaccine epitope were able to delay tumor growth in a met-1 transplantable breast cancer model. The antipeptide antibodies also prevented tumor growth in SCID mice that were inoculated with A549 lung cancer cells. Immunohistochemical analysis also showed significant reductions in microvascular density and actively dividing cells in the tumor sections after treatment in the FVB/n breast cancer model. The 382–410 and 418–435 B-cell epitopes were the best candidate both as a vaccine and peptide mimic because it caused significant inhibition in the two mouse models. Our results show that this novel EGFR B-cell epitopes has great potentials to be used as a vaccine or treatment option for EGFR-expressing cancers.

6.01.8.1.2 HER-3

HER-3 is frequently upmodulated in cancers with EGFR or HER-2 overexpression, and HER-3 may provide a route for resistance to agents that target EGFR or HER-2. Currently, therapeutic mAbs such as AMG 888 and MM-121 specifically target HER-3 and are currently being evaluated in clinical trials. Unlike HER-2, HER-3 lacks the ability to form homodimers. As a result, HER-3 signaling is entirely dependent on heterodimerization.[184] Interestingly, the heterodimer of HER-2/HER-3 constitutes the most potent receptor with respect to strength of interaction, ligand-induced tyrosine phosphorylation, and downstream signaling.[5k,120a] It forms a high-affinity heregulin receptor with kinase activity.[185] In addition, the HER-2/HER-3 heterodimer was found to mediate the most mitogenic signal in vitro.[184b,186] It also induced cellular transformation of a mouse fibroblast cell line that expressed nontransforming levels of HER.[184b,186c] The combination of HER-2 and HER-3 receptors may be critical in breast cancer growth and progression, and HER-3 may be a necessary partner for the oncogenic activity of HER-2.[67] HER3 may also provide a route for resistance to agents that target EGFR or HER.[187] Recent evidence suggests that HER-3 contributes to escape from therapeutic suppression by several TKIs in breast cancer.[187a,d,e] In fact, HER-3 expression or signaling is associated with resistance to: HER2 inhibitors in HER2-amplified breast cancers,[187e] EGFR inhibitors in lung cancers,[188] pertuzumab resistance in ovarian cancers,[189] antiestrogen therapies in ER-

Table 1 Identity and sequences of HER-1 peptides

Peptide designation	*Amino acid sequence of HER-1 peptides*
MVF-HER-1-347–374	*KLLSLIKGVIVHRLEGVELGPSL*ILPVAFRGDSFTHTPPLDPQELDILKTV-*CONH2*
HER-1 347–374	*Ac*-ILPVAFRGDSFTHTPPLDPQELDILKTV-CONH2
MVF-HER-1-382–410	*KLLSLIKGVIVHRLEGVEGPSL*LIQAWPENRTDLHAFENLEIIRGRTKQHG-CONH2
HER-1 382–410	Ac-LIQAWPENRTDLHAFENLEIIRGRTKQHG-CONH2
MVF-HER-1-418–435	*KLLSLIKGVIVHRLEGVEGPSL*SLNITSLGLRSLKEISDG-CONH2
HER-1 418–435	Ac-SLNITSLGLRSLKEISDG-CONH2

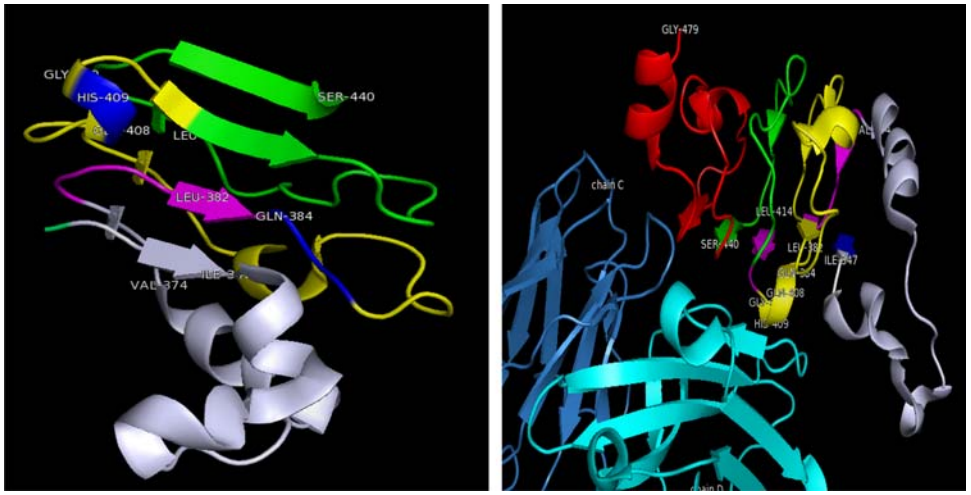

Fig. 12 HER-1 epitopes.

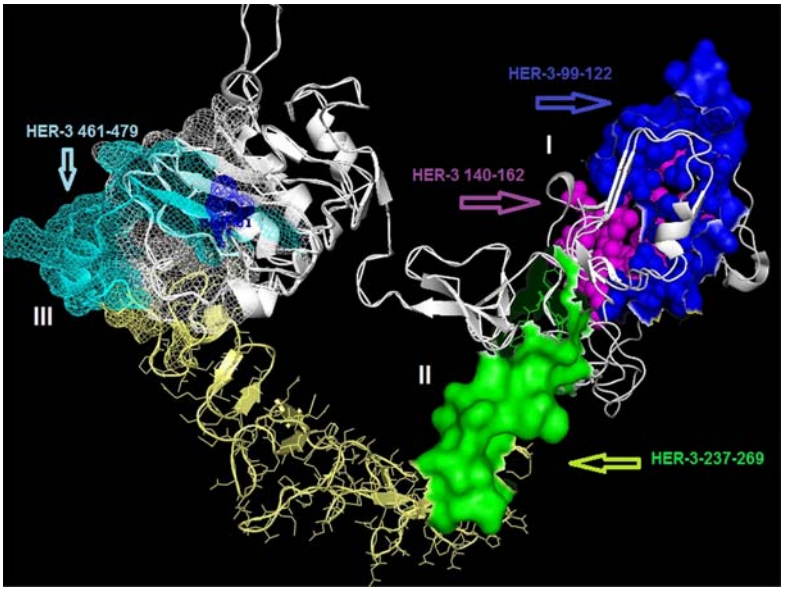

Fig. 13 The crystal structure of the HER-3 extracellular domain (pdb 1M6B). The location of the four HER-3 ECD epitopes is shown to be surface oriented. HER-3 99–122 (blue spheres), HER-3 140–162 (pink spheres), HER-3 237–269 (green surface), and HER-3 461–479 (blue mesh).

positive breast cancers,[189,190] EGFR inhibitors in head and neck cancer,[191] and hormone resistance in prostate cancers.[192] As a result, treatments using HER-3 peptide mimics and antipeptide antibodies can provide maximal benefit.

We have used several computer-generated algorithms to predict potential immunogenic amino acid sequences in domains II and III (involved in dimerization and ligand binding, respectively) of the HER-3 extracellular domain (Fig. 13). The methods used predict antigenic determinants in a protein that have a high chance of producing protein-reactive antipeptide antibodies (B-cell epitopes). Ten profiles were essentially used to predict HER-3 sequences that are hydrophilic or exposed on the surface of a protein. Hydropathy profiles were calculated using the scale of Kyte and Doolittle.[205] Hydrophilicity profiles were generated using the programs Hopp and Woods,[206] Parker,[207] and Fraga.[208] The Janin[209] and Novotny[210] scales were used to predict regions of HER-3 accessibility. Protruding portions of a protein were calculated by Hopp Acrophilicity and Bulk scales.[211] The Welling et al.,[212] Antigenicity profile was used to predict amino acids in antigenic regions. The crystal structure of the complex between D11 and HER3, with analysis of the contact residues of the HER3:D11 interface, was published by Schaefer et al. The residues critical for D11 binding are also important for HRG binding; therefore D11 has the ability to block the HRG:HER3 interaction. Several residues are important for D11 binding, and we have selected a peptide that includes these key residues, HER-3 461–479. We identified and evaluated novel HER-3 peptide epitopes (Table 2) encompassing residues 99–122, 140–162, 237–269, and 461–479 of the HER-3 extracellular domain as putative B-cell epitopes for active immunotherapy against HER-3 positive cancers. The HER-3

Table 2 Indentity and sequences of HER-3 peptides

Peptide designation	*Amino acid sequence of HER-3 peptides*
MVF-HER-3(237–269)	*KLLSLIKGVIVHRLEGVE*-GPSL-VPRCPQPLVYNKLTFQLEPNPHTKYQYGGVCVA-OH
HER-3 (237–269)	Ac-VPRCPQPLVYNKLTFQLEPNPHTKYQYGGVCVA-OH
MVF-HER-3 (461–479)	*KLLSLIKGVIVHRLEGVE*-GPSL-ERLDIKHNRPRRDCVAEGK-NH_2
HER-3 (461–479)	Ac-ERLDIKHNRPRRDCVAEGK-NH_2
HER-3 (99–122)	Ac-FVMLNYNTNSSHALRQLRLTQLTE-NH_2
HER-3 (140–162)	Ac-DTIDWRDIVRDRDAEIVVKDNGR-NH_2

237–269 epitope overlapped with sequences found in all 10 of the prediction algorithms, and the second epitope HER-3 461–479 was found in 9/10 of the hydrophilic profiles. We showed that the HER-3 vaccine antibodies and HER-3 peptide mimics induced antitumor responses: inhibition of cancer cell proliferation, inhibition of receptor phosphorylation, induction of apoptosis, and ADCC. Two of the HER-3 epitopes 237–269 (domain II) and 461–479 (domain III) significantly inhibited growth of xenografts originating from both pancreatic (BxPC3) and breast (JIMT-1) cancers.

6.01.8.1.3 IGF-1R

IGF-1R has evolved as a particularly important target in cancers that have developed resistance to EGFR/HER-1- and HER-2-targeted therapies. IGF-1R overexpression[33] and/or cross talk to HER-2 contribute to the development of trastuzumab resistance.[36c,193] In fact, IGF-1R overexpression and increased signaling have been reported in cell lines and clinical samples derived from trastuzumab-resistant breast cancers.[194] Similarly, cross talk between IGF-1R and EGFR/HER-1[195,196] is associated with the development of resistance to EGFR/HER-1 inhibition.[197] Targeting the IGF:IGF-1R axis with innovative peptide inhibitors and vaccine antibodies represents a promising therapeutic strategy to overcome drug resistance and to provide new avenues for individualized and combination strategies.

We have identified four sequences that are derived from the IGF-IR ligand-binding domain. The four peptide mimics (**Fig. 14**) are IGF-IR-6–33, IGF-IR-56–81, IGF-IR-234–252, and IGF-IR-306–341, and the sequences of the peptides are shown in **Table 3**. These epitopes were designed based on the ligand-binding site of the receptor using crystallographic structures, mutagenesis studies, and models of the complex between the receptor–ligand interactions.[198]

In this study, we designed, synthesized, and characterized several B-cell epitopes from the IGF-1:IGF-1R axis. The chimeric peptide epitopes were highly immunogenic in outbred rabbits, eliciting high levels of peptide vaccine antibodies. The IGF-1R peptide antibodies and peptide mimics inhibited cell proliferation, receptor phosphorylation, induced apoptosis, and ADCC

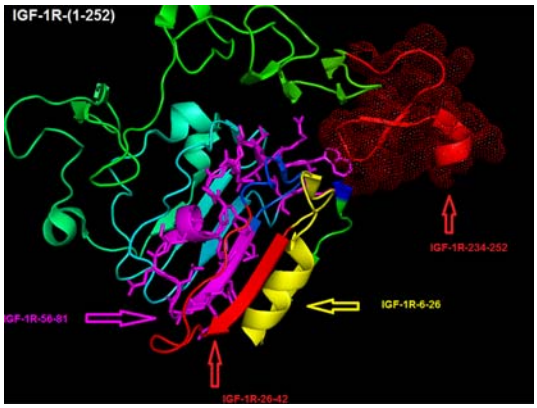

Fig. 14 The three-dimensional crystal structure of IGF-1R extracellular domains 1 and 2. The four predicted IGF-1R peptide epitopes are clearly shown. IGF-1R 6–26 is an α-helix shown in yellow stabilized by the 26–42 sequence is a β-sheet shown in red, and sequence 56–81 is shown in pink with the side chains shown and includes a β-sheet and a turn. The IGF-1R 234–252 includes two antiparallel beta β-strands and a turn and is also shown in red.

Table 3 Identity and sequences of IGF-1R peptides

Peptide designation	*Amino acid sequence of IGF-1R peptides*
IGF-IR-(56–81)	*AC*-LLFRVAGLESLGDLFPNLTVIRGWKL-*CONH2*
IGF-IR-(234–251)	*Ac*-CPPNTYRFEGWRCVDRDFC-*CONH2*
MVF-IGF-IR-(56–81)	*MVF*-LLFRVAGLESLGDLFPNLTVIRGWKL-*COOH*
MVF-IGF-IR-(234–251)	*MVF*-CPPNTYRFEGWRCVDRDFC-*COOH*

and significantly inhibited tumor growth in the BxPC-3 pancreatic and JIMT-1 breast transplantable models of cancer. Our results showed that the 56–81 and 233–251 peptides and antibodies are potential therapeutic and vaccine candidates for the treatment of IGF-1R-expressing cancers, including those that are resistant to the HER-2-targeted antibody, trastuzumab.

6.01.9 Conclusions and Future Outlook

Extensive cross talk among ErbB/HER receptors suggests that blocking signaling from more than one family member may be essential to effectively treat cancer and limit drug resistance. There is a desperate need for new anticancer agents that are less toxic and more effective. Therapies that block the extensive cross talk between RTKs are more likely to overcome drug resistance, including in particular, the signaling networks consisting of IGF-1R, EGFR/HER-1, HER-2, VEGF, and HER-3 play major roles in trastuzumab resistance.[33,36b,c,199] Our studies have made major contributions to the existing fields of cancer immunology, drug development, and mechanisms of cancer pharmacology by (1) developing new immune-based approaches to combat receptor kinase-driven cancers and (2) understanding and overcoming clinically relevant mechanisms of resistance to currently used HER-2-directed agents. To promote a rational, systematic development of combination therapies in multivariate ways, next-generation combination therapies can be constructed with a clear understanding of how mechanisms of resistance to multidrug regimens differ from single agent resistance. We have established the underlying mechanisms that drive the advantages of combination therapies with independent mechanisms of action, and design methods to determine drug targets for combination regimen that effectuates long-term tumor control and destruction.

Due to our prior successes, our next step is to create innovative combinations of B-cell vaccines against multiple RTKs (reviewed in Kaumaya et al.[3]). We hypothesized that this new strategy will synergistically activate host immunity, achieve durable responses with little toxicity, and overcome drug resistance. In order to solve the existing toxicity and resistance problems in immunotherapy, we have expanded our portfolio of already established vaccines to RTK-directed agents (HER-1, HER-2, and VEGF) by identifying novel HER-3 and IGF-1R peptide vaccines and peptide mimics.[38d,200] We have targeted cross talk from insulin-like growth factor-1 receptor (IGF-1R)[6] and HER-3[3,201] to HER-2 to overcome sustained HER-2 signaling and resistance from HER-2-targeted therapies. Ultimately, our goal is to identify the most biologically effective combinations of HER-1, HER-2, HER-3, and/or IGF-1R peptide vaccines to selectively inhibit multiple receptors and signaling pathways to block the extensive receptor cross talk that drives the biology and resistance of HER-2-overexpressing cancers. This strategy holds the promise of achieving durable cures for multiple types of cancers (breast, TNBC, pancreatic, colon, and esophageal cancers) and can be translated to human clinical trials. We have demonstrated efficacy in reducing tumor growth in different xenograft models in multiple cancer indications. We have shown superior synergistic antitumor effects in vitro and in vivo by combining HER-2 and VEGF peptide vaccines/mimics.[202,203] Additionally, we have characterized potential combinations of therapies targeted against HER-3 or IGF-1R with those against HER-2 and HER-1 resulting in highly synergistic in vitro antitumor responses in several tumor types. Rationally designed peptide therapeutics[204] could also represent a novel class of anticancer agents that specifically target cancer cells with lower toxicity to normal tissues, high specificity, and significant biological activity. The combination of different vaccine and therapeutic strategies to target specific molecular pathways that are dysregulated in tumors may create clinical breakthroughs for safe and efficacious cancer cures.

See also: 2.10. Overview of Drug Polypharmacology and Multitargeted Molecular Design. 5.01. Cancer Biology and the Principles of Targeted Cancer Drug Discovery.

References

1. Kaumaya, P. T. Bridging Oncology and Immunology: Expanding Horizons With Innovative Peptide Vaccines and Peptidomimetics. *Immunotherapy* **2013,** *5* (11), 1159–1163.
2. (a) Vanneman, M.; Dranoff, G. Combining Immunotherapy and Targeted Therapies in Cancer Treatment. *Nat. Rev. Cancer* **2012,** *12* (4), 237–251; (b) Galmarini, D.; Galmarini, C. M.; Galmarini, F. C. Cancer Chemotherapy: A Critical Analysis of Its 60 Years of History. *Crit. Rev. Oncol. Hematol.* **2012,** *84* (2), 181–199.
3. Kaumaya, P. T. P. A Paradigm Shift: Cancer Therapy With Peptide-Based B-Cell Epitopes and Peptide Immunotherapeutics Targeting Multiple Solid Tumor Types: Emerging Concepts and Validation of Combination Immunotherapy. *Hum. Vaccin. Immunother.* **2015,** *11* (6), 1368–1386.
4. (a) Yarden, Y.; Sliwkowski, M. X. Untangling the ErbB Signalling Network. *Nat. Rev. Mol. Cell Biol.* **2001,** *2* (2), 127–137; (b) Vicari, D.; Foy, K. C.; Liotta, E. M.; Kaumaya, P. T. Engineered Conformation-Dependent VEGF Peptide Mimics Are Effective in Inhibiting VEGF Signaling Pathways. *J. Biol. Chem.* **2011,** *286* (15), 13612–13625; (c) Foy, K. C.; Miller, M. J.; Moldovan, N.; Bozanovic, T.; Carson, W. E., 3rd; Kaumaya, P. T. Immunotherapy With HER-2 and VEGF Peptide Mimics Plus Metronomic Paclitaxel Causes Superior Antineoplastic Effects in Transplantable and Transgenic Mouse Models of Human Breast Cancer. *Oncoimmunology* **2012,** *1* (7), 1004–1016.
5. (a) Baselga, J.; Arteaga, C. L. Critical Update and Emerging Trends in Epidermal Growth Factor Receptor Targeting in Cancer. *J. Clin. Oncol.* **2005,** *23* (11), 2445–2459; (b) Baselga, J. Targeting Tyrosine Kinases in Cancer: The Second Wave. *Science* **2006,** *312* (5777), 1175–1178; (c) Jain, R. K.; Duda, D. G.; Clark, J. W.; Loeffler, J. S. Lessons From Phase III Clinical Trials on Anti-VEGF Therapy for Cancer. *Nat. Clin. Pract. Oncol.* **2006,** *3* (1), 24–40; (d) Houck, K. A.; Ferrara, N.; Winer, J.; Cachianes, G.; Li, B.; Leung, D. W. The Vascular Endothelial Growth Factor Family: Identification of a Fourth Molecular Species and Characterization of Alternative Splicing OF RNA. *Mol. Endocrinol.* **1991,** *5* (12), 1806–1814; (e) Cobleigh, M. A.; Langmuir, V. K.; Sledge, G. W.; Miller, K. D.; Haney, L.; Novotny, W. F.; Reimann, J. D.; Vassel, A. A Phase I/II Dose-Escalation Trial of Bevacizumab in Previously Treated Metastatic Breast Cancer. *Semin. Oncol.* **2003,** *30* (5 Suppl. 16), 117–124; (f) Hynes, N. E.; Lane, H. A. ERBB Receptors and Cancer: The Complexity of Targeted Inhibitors. *Nat. Rev. Cancer* **2005,** *5* (5), 341–354; (g) Hoeben, A.; Landuyt, B.; Highley, M. S.; Wildiers, H.; Van Oosterom, A. T.; De Bruijn, E. A. Vascular Endothelial Growth Factor and Angiogenesis. *Pharmacol. Rev.* **2004,** *56* (4), 549–580; (h) Zhu, Z.; Witte, L. Inhibition of Tumor Growth and Metastasis by Targeting Tumor-Associated Angiogenesis With Antagonists to the Receptors of Vascular Endothelial Growth Factor. *Invest. New Drugs* **1999,** *17* (3), 195–212; (i) Oshima, R. G.; Lesperance, J.; Munoz, V.; Hebbard, L.; Ranscht, B.; Sharan, N.; Muller, W. J.; Hauser, C. A.; Cardiff, R. D. Angiogenic Acceleration of Neu Induced Mammary Tumor Progression and Metastasis. *Cancer Res.* **2004,** *64* (1), 169–179; (j) Folkman, J. Tumor Angiogenesis: Therapeutic Implications. *N. Engl. J. Med.* **1971,** *285* (21), 1182–1186; (k) Baselga, J.; Swain, S. M. Novel Anticancer Targets: Revisiting ERBB2 and Discovering ERBB3. *Nat. Rev. Cancer* **2009,** *9* (7), 463–475.

6. (a) Pollak, M. N.; Schernhammer, E. S.; Hankinson, S. E. Insulin-Like Growth Factors and Neoplasia. *Nat. Rev. Cancer* **2004,** *4* (7), 505–518; (b) Pollak, M. N. Insulin-Like Growth Factors and Neoplasia. *Novartis Found. Symp.* **2004,** *262,* 84–98. discussion 98–107, 265–268.
7. (a) Hudziak, R. M.; Lewis, G. D.; Winget, M.; Fendly, B. M.; Shepard, H. M.; Ullrich, A. p185HER2 Monoclonal Antibody Has Antiproliferative Effects In Vitro and Sensitizes Human Breast Tumor Cells to Tumor Necrosis Factor. *Mol. Cell. Biol.* **1989,** *9* (3), 1165–1172; (b) Shepard, H. M.; Lewis, G. D.; Sarup, J. C.; Fendly, B. M.; Maneval, D.; Mordenti, J.; Figari, I.; Kotts, C. E.; Palladino, M. A., Jr.; Ullrich, A.; et al. Monoclonal Antibody Therapy of Human Cancer: Taking the HER2 Protooncogene to the Clinic. *J. Clin. Immunol.* **1991,** *11* (3), 117–127; (c) Ryan, A. J.; Wedge, S. R. ZD6474—A Novel Inhibitor of VEGFR and EGFR Tyrosine Kinase Activity. *Br. J. Cancer* **2005,** *92* (Suppl. 1), S6–S13.
8. (a) Reilly, R. T.; Gottlieb, M. B.; Ercolini, A. M.; Machiels, J. P.; Kane, C. E.; Okoye, F. I.; Muller, W. J.; Dixon, K. H.; Jaffee, E. M. HER-2/neu Is a Tumor Rejection Target in Tolerized HER-2/neu Transgenic Mice. *Cancer Res.* **2000,** *60* (13), 3569–3576; (b) Nanni, P.; Nicoletti, G.; De Giovanni, C.; Landuzzi, L.; Di Carlo, E.; Cavallo, F.; Pupa, S. M.; Rossi, I.; Colombo, M. P.; Ricci, C.; Astolfi, A.; Musiani, P.; Forni, G.; Lollini, P. L. Combined Allogeneic Tumor Cell Vaccination and Systemic Interleukin 12 Prevents Mammary Carcinogenesis in HER-2/neu Transgenic Mice. *J. Exp. Med.* **2001,** *194* (9), 1195–1205; (c) Cefai, D.; Morrison, B. W.; Sckell, A.; Favre, L.; Balli, M.; Leunig, M.; Gimmi, C. D. Targeting HER-2/neu for Active-Specific Immunotherapy in a Mouse Model of Spontaneous Breast Cancer. *Int. J. Cancer* **1999,** *83* (3), 393–400.
9. Dela Cruz, J. S.; Lau, S. Y.; Ramirez, E. M.; De Giovanni, C.; Forni, G.; Morrison, S. L.; Penichet, M. L. Protein Vaccination With the HER2/neu Extracellular Domain Plus Anti-HER2/neu Antibody-Cytokine Fusion Proteins Induces a Protective Anti-HER2/neu Immune Response in Mice. *Vaccine* **2003,** *21* (13–14), 1317–1326.
10. (a) Amici, A.; Venanzi, F. M.; Concetti, A. Genetic Immunization Against neu/erbB2 Transgenic Breast Cancer. *Cancer Immunol. Immunother.* **1998,** *47* (4), 183–190; (b) Piechocki, M. P.; Pilon, S. A.; Wei, W. Z. Complementary Antitumor Immunity Induced by Plasmid DNA Encoding Secreted and Cytoplasmic Human ErbB-2. *J. Immunol.* **2001,** *167* (6), 3367–3374; (c) Pupa, S. M.; Invernizzi, A. M.; Forti, S.; Di Carlo, E.; Musiani, P.; Nanni, P.; Lollini, P. L.; Meazza, R.; Ferrini, S.; Menard, S. Prevention of Spontaneous neu-Expressing Mammary Tumor Development in Mice Transgenic for Rat Proto-neu by DNA Vaccination. *Gene Ther.* **2001,** *8* (1), 75–79.
11. (a) Dakappagari, N. K.; Pyles, J.; Parihar, R.; Carson, W. E.; Young, D. C.; Kaumaya, P. T. A Chimeric Multi-Human Epidermal Growth Factor Receptor-2 B Cell Epitope Peptide Vaccine Mediates Superior Antitumor Responses. *J. Immunol.* **2003,** *170* (8), 4242–4253; (b) Dakappagari, N. K.; Lute, K. D.; Rawale, S.; Steele, J. T.; Allen, S. D.; Phillips, G.; Reilly, R. T.; Kaumaya, P. T. Conformational HER-2/neu B-Cell Epitope Peptide Vaccine Designed to Incorporate Two Native Disulfide Bonds Enhances Tumor Cell Binding and Antitumor Activities. *J. Biol. Chem.* **2005,** *280* (1), 54–63; (c) Dakappagari, N. K.; Douglas, D. B.; Triozzi, P. L.; Stevens, V. C.; Kaumaya, P. T. Prevention of Mammary Tumors With a Chimeric HER-2 B-Cell Epitope Peptide Vaccine. *Cancer Res.* **2000,** *60* (14), 3782–3789; (d) Jasinska, J.; Wagner, S.; Radauer, C.; Sedivy, R.; Brodowicz, T.; Wiltschke, C.; Breiteneder, H.; Pehamberger, H.; Scheiner, O.; Wiedermann, U.; Zielinski, C. C. Inhibition of Tumor Cell Growth by Antibodies Induced After Vaccination With Peptides Derived From the Extracellular Domain of Her-2/neu. *Int. J. Cancer* **2003,** *107* (6), 976–983.
12. (a) Weber, J. Peptide Vaccines for Cancer. *Cancer Invest.* **2002,** *20* (2), 208–221; (b) Buteau, C.; Markovic, S. N.; Celis, E. Challenges in the Development of Effective Peptide Vaccines for Cancer. *Mayo Clin. Proc.* **2002,** *77* (4), 339–349; (c) Lazoura, E.; Apostolopoulos, V. Rational Peptide-Based Vaccine Design for Cancer Immunotherapeutic Applications. *Curr. Med. Chem.* **2005,** *12* (6), 629–639.
13. Disis, M. L.; Calenoff, E.; McLaughlin, G.; Murphy, A. E.; Chen, W.; Groner, B.; Jeschke, M.; Lydon, N.; McGlynn, E.; Livingston, R. B.; et al. Existent T-Cell and Antibody Immunity to HER-2/neu Protein in Patients With Breast Cancer. *Cancer Res.* **1994,** *54* (1), 16–20.
14. (a) Disis, M. L.; Gralow, J. R.; Bernhard, H.; Hand, S. L.; Rubin, W. D.; Cheever, M. A. Peptide-Based, but Not Whole Protein, Vaccines Elicit Immunity to HER-2/neu, Oncogenic Self-Protein. *J. Immunol.* **1996,** *156* (9), 3151–3158; (b) Disis, M. L.; Grabstein, K. H.; Sleath, P. R.; Cheever, M. A. Generation of Immunity to the HER-2/neu Oncogenic Protein in Patients With Breast and Ovarian Cancer Using a Peptide-Based Vaccine. *Clin. Cancer Res.* **1999,** *5* (6), 1289–1297; (c) Disis, M. L.; Gooley, T. A.; Rinn, K.; Davis, D.; Piepkorn, M.; Cheever, M. A.; Knutson, K. L.; Schiffman, K. Generation of T-Cell Immunity to the HER-2/neu Protein After Active Immunization With HER-2/neu Peptide-Based Vaccines. *J. Clin. Oncol.* **2002,** *20* (11), 2624–2632.
15. Peoples, G. E.; Gurney, J. M.; Hueman, M. T.; Woll, M. M.; Ryan, G. B.; Storrer, C. E.; Fisher, C.; Shriver, C. D.; Ioannides, C. G.; Ponniah, S. Clinical Trial Results of a HER2/neu (E75) Vaccine to Prevent Recurrence in High-Risk Breast Cancer Patients. *J. Clin. Oncol.* **2005,** *23* (30), 7536–7545.
16. Guy, B. The Perfect Mix: Recent Progress in Adjuvant Research. *Nat. Rev. Microbiol.* **2007,** *5* (7), 505–517.
17. Vlieghe, P.; Lisowski, V.; Martinez, J.; Khrestchatisky, M. Synthetic Therapeutic Peptides: Science and Market. *Drug Discov. Today* **2010,** *15* (1–2), 40–56.
18. Inno, A.; Di Salvatore, M.; Cenci, T.; Martini, M.; Orlandi, A.; Strippoli, A.; Ferrara, A. M.; Bagala, C.; Cassano, A.; Larocca, L. M.; Barone, C. Is There a Role for IGF1R and c-MET Pathways in Resistance to Cetuximab in Metastatic Colorectal Cancer? *Clin. Colorectal Cancer* **2011,** *10* (4), 325–332.
19. Hanahan, D.; Folkman, J. Patterns and Emerging Mechanisms of the Angiogenic Switch During Tumorigenesis. *Cell* **1996,** *86* (3), 353–364.
20. Ferrara, N. Vascular Endothelial Growth Factor as a Target for Anticancer Therapy. *Oncologist* **2004,** *9* (Suppl. 1), 2–10.
21. Ross, J. S.; McKenna, B. J. The HER-2/neu Oncogene in Tumors of the Gastrointestinal Tract. *Cancer Invest.* **2001,** *19* (5), 554–568.
22. Saito, H.; Tsujitani, S.; Ikeguchi, M.; Maeta, M.; Kaibara, N. Relationship Between the Expression of Vascular Endothelial Growth Factor and the Density of Dendritic Cells in Gastric Adenocarcinoma Tissue. *Br. J. Cancer* **1998,** *78* (12), 1573–1577.
23. (a) Partidos, C. D.; Steward, M. W. Prediction and Identification of a T Cell Epitope in the Fusion Protein of Measles Virus Immunodominant in Mice and Humans. *J. Gen. Virol.* **1990,** *71* (Pt 9), 2099–2105; (b) Paniana-Bordignon, P.; Tan, A.; Termijtelen, A.; Demotz, S.; Corradin, G.; Lanzavecchia, A. Universally Immunogenic T Cell Epitopes: Promiscuous Binding to Human MHC Class II and Promiscuous Recognition by T Cells. *Eur. J. Immunol.* **1989,** *19,* 2237.
24. Reichert, J. *Development Trends for Peptide Therapeutics*. http://www.peptidetherapeutics.org/PTF_Summary, 2008 (accessed 2008).
25. Qiu, X. Q.; Wang, H.; Cai, B.; Wang, L. L.; Yue, S. T. Small Antibody Mimetics Comprising Two Complementarity-Determining Regions and a Framework Region for Tumor Targeting. *Nat. Biotechnol.* **2007,** *25* (8), 921–929.
26. Latham, P. W. Therapeutic Peptides Revisited. *Nat. Biotechnol.* **1999,** *17* (8), 755–757.
27. Ahrens, V. M.; Bellmann-Sickert, K.; Beck-Sickinger, A. G. Peptides and Peptide Conjugates: Therapeutics on the Upward Path. *Future Med. Chem.* **2012,** *4* (12), 1567–1586.
28. Perou, C. M.; Sorlie, T.; Eisen, M. B.; van de Rijn, M.; Jeffrey, S. S.; Rees, C. A.; Pollack, J. R.; Ross, D. T.; Johnsen, H.; Akslen, L. A.; Fluge, O.; Pergamenschikov, A.; Williams, C.; Zhu, S. X.; Lonning, P. E.; Borresen-Dale, A. L.; Brown, P. O.; Botstein, D. Molecular Portraits of Human Breast Tumours. *Nature* **2000,** *406* (6797), 747–752.
29. (a) Slamon, D. J.; Clark, G. M.; Wong, S. G.; Levin, W. J.; Ullrich, A.; McGuire, W. L. Human Breast Cancer: Correlation of Relapse and Survival With Amplification of the HER-2/neu Oncogene. *Science* **1987,** *235* (4785), 177–182; (b) Slamon, D. J.; Godolphin, W.; Jones, L. A.; Holt, J. A.; Wong, S. G.; Keith, D. E.; Levin, W. J.; Stuart, S. G.; Udove, J.; Ullrich, A.; Press, M. F. Studies of the HER-2/neu Proto-Oncogene in Human Breast and Ovarian Cancer. *Science* **1989,** *244* (4905), 707–712.
30. Slamon, D. J. Proto-Oncogenes and Human Cancers. *N. Engl. J. Med.* **1987,** *317* (15), 955–957.
31. Nahta, R.; Yu, D.; Hung, M. C.; Hortobagyi, G. N.; Esteva, F. J. Mechanisms of Disease: Understanding Resistance to HER2-Targeted Therapy in Human Breast Cancer. *Nat. Clin. Pract. Oncol.* **2006,** *3* (5), 269–280.
32. Garrett, J. T.; Arteaga, C. L. Resistance to HER2-Directed Antibodies and Tyrosine Kinase Inhibitors: Mechanisms and Clinical Implications. *Cancer Biol. Ther.* **2011,** *11* (9), 793–800.
33. Lu, Y.; Zi, X.; Zhao, Y.; Mascarenhas, D.; Pollak, M. Insulin-Like Growth Factor-I Receptor Signaling and Resistance to Trastuzumab (Herceptin). *J. Natl. Cancer Inst.* **2001,** *93* (24), 1852–1857.
34. Harris, L. N.; You, F.; Schnitt, S. J.; Witkiewicz, A.; Lu, X.; Sgroi, D.; Ryan, P. D.; Come, S. E.; Burstein, H. J.; Lesnikoski, B. A.; Kamma, M.; Friedman, P. N.; Gelman, R.; Iglehart, J. D.; Winer, E. P. Predictors of Resistance to Preoperative Trastuzumab and Vinorelbine for HER2-Positive Early Breast Cancer. *Clin. Cancer Res.* **2007,** *13* (4), 1198–1207.
35. Gallardo, A.; Lerma, E.; Escuin, D.; Tibau, A.; Munoz, J.; Ojeda, B.; Barnadas, A.; Adrover, E.; Sanchez-Tejada, L.; Giner, D.; Ortiz-Martinez, F.; Peiro, G. Increased Signalling of EGFR and IGF1R, and Deregulation of PTEN/PI3K/Akt Pathway Are Related With Trastuzumab Resistance in HER2 Breast Carcinomas. *Br. J. Cancer* **2012,** *106* (8), 1367–1373.

36. (a) Chakraborty, A. K.; Liang, K.; DiGiovanna, M. P. Co-Targeting Insulin-Like Growth Factor I Receptor and HER2: Dramatic Effects of HER2 Inhibitors on Nonoverexpressing Breast Cancer. *Cancer Res.* **2008,** *68* (5), 1538–1545; (b) Huang, X.; Gao, L.; Wang, S.; McManaman, J. L.; Thor, A. D.; Yang, X.; Esteva, F. J.; Liu, B. Heterotrimerization of the Growth Factor Receptors erbB2, erbB3, and Insulin-Like Growth Factor-i Receptor in Breast Cancer Cells Resistant to Herceptin. *Cancer Res.* **2010,** *70* (3), 1204–1214; (c) Nahta, R.; Yuan, L. X.; Zhang, B.; Kobayashi, R.; Esteva, F. J. Insulin-Like Growth Factor-I Receptor/Human Epidermal Growth Factor Receptor 2 Heterodimerization Contributes to Trastuzumab Resistance of Breast Cancer Cells. *Cancer Res.* **2005,** *65* (23), 11118–11128.
37. (a) Amin, D. N.; Sergina, N.; Ahuja, D.; McMahon, M.; Blair, J. A.; Wang, D.; Hann, B.; Koch, K. M.; Shokat, K. M.; Moasser, M. M. Resiliency and Vulnerability in the HER2-HER3 Tumorigenic Driver. *Sci. Transl. Med.* **2010,** *2* (16), 16ra7; (b) Serra, V.; Scaltriti, M.; Prudkin, L.; Eichhorn, P. J.; Ibrahim, Y. H.; Chandarlapaty, S.; Markman, B.; Rodriguez, O.; Guzman, M.; Rodriguez, S.; Gili, M.; Russillo, M.; Parra, J. L.; Singh, S.; Arribas, J.; Rosen, N.; Baselga, J. PI3K Inhibition Results in Enhanced HER Signaling and Acquired ERK Dependency in HER2-Overexpressing Breast Cancer. *Oncogene* **2011,** *30* (22), 2547–2557.
38. (a) Liu, B.; Ordonez-Ercan, D.; Fan, Z.; Edgerton, S. M.; Yang, X.; Thor, A. D. Downregulation of erbB3 Abrogates erbB2-Mediated Tamoxifen Resistance in Breast Cancer Cells. *Int. J. Cancer* **2007,** *120* (9), 1874–1882; (b) Yen, L.; Benlimame, N.; Nie, Z. R.; Xiao, D.; Wang, T.; Al Moustafa, A. E.; Esumi, H.; Milanini, J.; Hynes, N. E.; Pages, G.; Alaoui-Jamali, M. A. Differential Regulation of Tumor Angiogenesis by Distinct ErbB Homo- and Heterodimers. *Mol. Biol. Cell* **2002,** *13* (11), 4029–4044; (c) Rajkumar, T.; Stamp, G. W.; Hughes, C. M.; Gullick, W. J. c-erbB3 Protein Expression in Ovarian Cancer. *Clin. Mol. Pathol.* **1996,** *49* (4), M199–M202; (d) Sanabria-Figueroa, E.; Donnelly, S. M.; Foy, K. C.; Buss, M. C.; Castellino, R. C.; Paplomata, E.; Taliaferro-Smith, L.; Kaumaya, P. T.; Nahta, R. Insulin-Like Growth Factor-1 Receptor Signaling Increases the Invasive Potential of Human Epidermal Growth Factor Receptor 2-Overexpressing Breast Cancer Cells via Src-Focal Adhesion Kinase and Forkhead Box Protein M1. *Mol. Pharmacol.* **2015,** *87* (2), 150–161.
39. Power, D. G.; Reynolds, J. V. Localized Adenocarcinoma of the Esophagogastric Junction—Is There a Standard of Care? *Cancer Treat. Rev.* **2010,** *36* (5), 400–409.
40. Cunningham, D.; Starling, N.; Rao, S.; Iveson, T.; Nicolson, M.; Coxon, F.; Middleton, G.; Daniel, F.; Oates, J.; Norman, A. R. Capecitabine and Oxaliplatin for Advanced Esophagogastric Cancer. *N. Engl. J. Med.* **2008,** *358* (1), 36–46.
41. Rossi, E.; Grisanti, S.; Villanacci, V.; Della Casa, D.; Cengia, P.; Missale, G.; Minelli, L.; Buglione, M.; Cestari, R.; Bassotti, G. HER-2 Overexpression/Amplification in Barrett's Oesophagus Predicts Early Transition From Dysplasia to Adenocarcinoma: A Clinico-Pathologic Study. *J. Cell. Mol. Med.* **2009,** *13* (9B), 3826–3833.
42. Okines, A. F.; Cunningham, D. Trastuzumab: A Novel Standard Option for Patients With HER-2-Positive Advanced Gastric or Gastro-Oesophageal Junction Cancer. *Therap. Adv. Gastroenterol.* **2012,** *5* (5), 301–318.
43. Bang, Y. J.; Van Cutsem, E.; Feyereislova, A.; Chung, H. C.; Shen, L.; Sawaki, A.; Lordick, F.; Ohtsu, A.; Omuro, Y.; Satoh, T.; Aprile, G.; Kulikov, E.; Hill, J.; Lehle, M.; Ruschoff, J.; Kang, Y. K.; To, G. A. T. I. Trastuzumab in Combination With Chemotherapy Versus Chemotherapy Alone for Treatment of HER2-Positive Advanced Gastric or Gastro-Oesophageal Junction Cancer (ToGA): A Phase 3, Open-Label, Randomised Controlled Trial. *Lancet* **2010,** *376* (9742), 687–697.
44. Kim, J.; Fox, C.; Peng, S.; Pusung, M.; Pectasides, E.; Matthee, E.; Hong, Y. S.; Do, I. G.; Jang, J.; Thorner, A. R.; Van Hummelen, P.; Rustgi, A. K.; Wong, K. K.; Zhou, Z.; Tang, P.; Kim, K. M.; Lee, J.; Bass, A. J. Preexisting Oncogenic Events Impact Trastuzumab Sensitivity in ERBB2-Amplified Gastroesophageal Adenocarcinoma. *J. Clin. Invest.* **2014,** *124* (12), 5145–5158.
45. (a) Friess, H.; Fukuda, A.; Tang, W. H.; Eichenberger, A.; Furlan, N.; Zimmermann, A.; Korc, M.; Buchler, M. W. Concomitant Analysis of the Epidermal Growth Factor Receptor Family in Esophageal Cancer: Overexpression of Epidermal Growth Factor Receptor mRNA but Not of c-erbB-2 and c-erbB-3. *World J. Surg.* **1999,** *23* (10), 1010–1018; (b) Walch, A.; Specht, K.; Bink, K.; Zitzelsberger, H.; Braselmann, H.; Bauer, M.; Aubele, M.; Stein, H.; Siewert, J. R.; Hofler, H.; Werner, M. Her-2/neu Gene Amplification, Elevated mRNA Expression, and Protein Overexpression in the Metaplasia-Dysplasia-Adenocarcinoma Sequence of Barrett's Esophagus. *Lab. Invest.* **2001,** *81* (6), 791–801; (c) Geddert, H.; Zeriouh, M.; Wolter, M.; Heise, J. W.; Gabbert, H. E.; Sarbia, M. Gene Amplification and Protein Overexpression of c-erb-b2 in Barrett Carcinoma and Its Precursor Lesions. *Am. J. Clin. Pathol.* **2002,** *118* (1), 60–66; (d) Mimura, K.; Kono, K.; Hanawa, M.; Mitsui, F.; Sugai, H.; Miyagawa, N.; Ooi, A.; Fujii, H. Frequencies of HER-2/neu Expression and Gene Amplification in Patients With Oesophageal Squamous Cell Carcinoma. *Br. J. Cancer* **2005,** *92* (7), 1253–1260.
46. Ayyappan, S.; Prabhakar, D.; Sharma, N. Epidermal Growth Factor Receptor (EGFR)-Targeted Therapies in Esophagogastric Cancer. *Anticancer Res.* **2013,** *33* (10), 4139–4155.
47. Bosset, J. F.; Gignoux, M.; Triboulet, J. P.; Tiret, E.; Mantion, G.; Elias, D.; Lozach, P.; Ollier, J. C.; Pavy, J. J.; Mercier, M.; Sahmoud, T. Chemoradiotherapy Followed by Surgery Compared With Surgery Alone in Squamous-Cell Cancer of the Esophagus. *N. Engl. J. Med.* **1997,** *337* (3), 161–167.
48. (a) Tanner, M.; Hollmen, M.; Junttila, T. T.; Kapanen, A. I.; Tommola, S.; Soini, Y.; Helin, H.; Salo, J.; Joensuu, H.; Sihvo, E.; Elenius, K.; Isola, J. Amplification of HER-2 in Gastric Carcinoma: Association With Topoisomerase IIalpha Gene Amplification, Intestinal Type, Poor Prognosis and Sensitivity to Trastuzumab. *Ann. Oncol.* **2005,** *16* (2), 273–278; (b) Marx, A. H.; Tharun, L.; Muth, J.; Dancau, A. M.; Simon, R.; Yekebas, E.; Kaifi, J. T.; Mirlacher, M.; Brummendorf, T. H.; Bokemeyer, C.; Izbicki, J. R.; Sauter, G. HER-2 Amplification Is Highly Homogenous in Gastric Cancer. *Hum. Pathol.* **2009,** *40* (6), 769–777.
49. Elimova, E.; Shiozaki, H.; Wadhwa, R.; Sudo, K.; Chen, Q.; Estrella, J. S.; Blum, M. A.; Badgwell, B.; Das, P.; Song, S.; Ajani, J. A. Medical Management of Gastric Cancer: A 2014 Update. *World J. Gastroenterol.* **2014,** *20* (38), 13637–13647.
50. Swain, S. M.; Kim, S. B.; Cortes, J.; Ro, J.; Semiglazov, V.; Campone, M.; Ciruelos, E.; Ferrero, J. M.; Schneeweiss, A.; Knott, A.; Clark, E.; Ross, G.; Benyunes, M. C.; Baselga, J. Pertuzumab, Trastuzumab, and Docetaxel for HER2-Positive Metastatic Breast Cancer (CLEOPATRA Study): Overall Survival Results From a Randomised, Double-Blind, Placebo-Controlled, Phase 3 Study. *Lancet Oncol.* **2013,** *14* (6), 461–471.
51. (a) Radinsky, R.; Risin, S.; Fan, D.; Dong, Z.; Bielenberg, D.; Bucana, C. D.; Fidler, I. J. Level and Function of Epidermal Growth Factor Receptor Predict the Metastatic Potential of Human Colon Carcinoma Cells. *Clin. Cancer Res.* **1995,** *1* (1), 19–31; (b) Kluftinger, A. M.; Robinson, B. W.; Quenville, N. F.; Finley, R. J.; Davis, N. L. Correlation of Epidermal Growth Factor Receptor and c-erbB2 Oncogene Product to Known Prognostic Indicators of Colorectal Cancer. *Surg. Oncol.* **1992,** *1* (1), 97–105.
52. Foy, K. C.; Wygle, R. M.; Miller, M. J.; Overholser, J. P.; Bekaii-Saab, T.; Kaumaya, P. T. Peptide Vaccines and Peptidomimetics of EGFR (HER-1) Ligand Binding Domain Inhibit Cancer Cell Growth in vitro and In Vivo. *J. Immunol.* **2013,** *191* (1), 217–227.
53. Ciardiello, F.; De Vita, F.; Orditura, M.; Comunale, D.; Galizia, G. Cetuximab in the Treatment of Colorectal Cancer. *Future Oncol.* **2005,** *1* (2), 173–181.
54. Foy, K. C.; Miller, M. J.; Moldovan, N.; Carson, W. E.; Kaumaya, P. P. Correction to: Foy KC, Miller MJ, Moldovan N, Carson III WE, Kaumaya PTP. Combined Vaccination With HER-2 Peptide Followed by Therapy With VEGF Peptide Mimics Exerts Effective Anti-Tumor and Anti-Angiogenic Effects In Vitro and In Vivo. Oncolmmunology 2012; 1:1048–1060. *Oncoimmunology* **2013,** *2* (1), e23914.
55. Overholser, J.; Ambegaokar, K. H.; Eze, S. M.; Sanabria-Figueroa, E.; Nahta, R.; Bekaii-Saab, T.; Kaumaya, P. T. Anti-Tumor Effects of Peptide Therapeutic and Peptide Vaccine Antibody Co-Targeting HER-1 and HER-2 in Esophageal Cancer (EC) and HER-1 and IGF-1R in Triple-Negative Breast Cancer (TNBC). *Vaccines* **2015,** *3* (3), 519–543.
56. Friess, H.; Kleeff, J.; Korc, M.; Buchler, M. W. Molecular Aspects of Pancreatic Cancer and Future Perspectives. *Dig. Surg.* **1999,** *16* (4), 281–290.
57. Lowery, M. A.; O'Reilly, E. M. New Approaches to the Treatment of Pancreatic Cancer: From Tumor-Directed Therapy to Immunotherapy. *BioDrugs* **2011,** *25* (4), 207–216.
58. Yakar, S.; Leroith, D.; Brodt, P. The Role of the Growth Hormone/Insulin-Like Growth Factor Axis in Tumor Growth and Progression: Lessons From Animal Models. *Cytokine Growth Factor Rev.* **2005,** *16* (4–5), 407–420.
59. (a) Stoeltzing, O.; Liu, W.; Reinmuth, N.; Fan, F.; Parikh, A. A.; Bucana, C. D.; Evans, D. B.; Semenza, G. L.; Ellis, L. M. Regulation of Hypoxia-Inducible Factor-1Alpha, Vascular Endothelial Growth Factor, and Angiogenesis by an Insulin-Like Growth Factor-I Receptor Autocrine Loop in Human Pancreatic Cancer. *Am. J. Pathol.* **2003,** *163* (3), 1001–1011; (b) Ishiwata, T.; Bergmann, U.; Kornmann, M.; Lopez, M.; Beger, H. G.; Korc, M. Altered Expression of Insulin-Like Growth Factor II Receptor in Human Pancreatic Cancer. *Pancreas* **1997,** *15* (4), 367–373.
60. Adams, T. E.; Epa, V. C.; Garrett, T. P.; Ward, C. W. Structure and Function of the Type 1 Insulin-Like Growth Factor Receptor. *Cell. Mol. Life Sci.* **2000,** *57* (7), 1050–1093.
61. Bergmann, U.; Funatomi, H.; Yokoyama, M.; Beger, H. G.; Korc, M. Insulin-Like Growth Factor I Overexpression in Human Pancreatic Cancer: Evidence for Autocrine and Paracrine Roles. *Cancer Res.* **1995,** *55* (10), 2007–2011.
62. (a) Jemal, A.; Siegel, R.; Xu, J.; Ward, E. Cancer Statistics, 2010. *CA Cancer J. Clin.* **2010,** *60* (5), 277–300; (b) Cartwright, T.; Richards, D. A.; Boehm, K. A. Cancer of the Pancreas: Are We Making Progress? A Review of Studies in the US Oncology Research Network. *Cancer Control* **2008,** *15* (4), 308–313.

63. (a) Valsecchi, M. E.; McDonald, M.; Brody, J. R.; Hyslop, T.; Freydin, B.; Yeo, C. J.; Solomides, C.; Peiper, S. C.; Witkiewicz, A. K. Epidermal Growth Factor Receptor and Insulinlike Growth Factor 1 Receptor Expression Predict Poor Survival in Pancreatic Ductal Adenocarcinoma. *Cancer* **2012,** *118* (14), 3484–3493; (b) Dong, M.; Nio, Y.; Guo, K. J.; Tamura, K.; Tian, Y. L.; Dong, Y. T. Epidermal Growth Factor and Its Receptor as Prognostic Indicators in Chinese Patients With Pancreatic Cancer. *Anticancer Res.* **1998,** *18* (6B), 4613–4619; (c) Sherwood, E. R.; Van Dongen, J. L.; Wood, C. G.; Liao, S.; Kozlowski, J. M.; Lee, C. Epidermal Growth Factor Receptor Activation in Androgen-Independent but Not Androgen-Stimulated Growth of Human Prostatic Carcinoma Cells. *Br. J. Cancer* **1998,** *77* (6), 855–861.
64. (a) Morgillo, F.; Woo, J. K.; Kim, E. S.; Hong, W. K.; Lee, H. Y. Heterodimerization of Insulin-Like Growth Factor Receptor/Epidermal Growth Factor Receptor and Induction of Survivin Expression Counteract the Antitumor Action of Erlotinib. *Cancer Res.* **2006,** *66* (20), 10100–10111; (b) Kuribayashi, A.; Kataoka, K.; Kurabayashi, T.; Miura, M. Evidence That Basal Activity, but Not Transactivation, of the Epidermal Growth Factor Receptor Tyrosine Kinase Is Required for Insulin-Like Growth Factor I-Induced Activation of Extracellular Signal-Regulated Kinase in Oral Carcinoma Cells. *Endocrinology* **2004,** *145* (11), 4976–4984.
65. Guix, M.; Faber, A. C.; Wang, S. E.; Olivares, M. G.; Song, Y.; Qu, S.; Rinehart, C.; Seidel, B.; Yee, D.; Arteaga, C. L.; Engelman, J. A. Acquired Resistance to EGFR Tyrosine Kinase Inhibitors in Cancer Cells Is Mediated by Loss of IGF-Binding Proteins. *J. Clin. Invest.* **2008,** *118* (7), 2609–2619.
66. (a) Ueno, Y.; Sakurai, H.; Tsunoda, S.; Choo, M. K.; Matsuo, M.; Koizumi, K.; Saiki, I. Heregulin-Induced Activation of ErbB3 by EGFR Tyrosine Kinase Activity Promotes Tumor Growth and Metastasis in Melanoma Cells. *Int. J. Cancer* **2008,** *123* (2), 340–347; (b) Kaumaya, P. T. P. HER-2/neu Cancer Vaccines: Present Status and Future Prospects. *Int. J. Pept. Res. Ther.* **2006,** *12* (1), 65–77; (c) Koutras, A. K.; Fountzilas, G.; Kalogeras, K. T.; Starakis, I.; Iconomou, G.; Kalofonos, H. P. The Upgraded Role of HER3 and HER4 Receptors in Breast Cancer. *Crit. Rev. Oncol. Hematol.* **2010,** *74* (2), 73–78.
67. Croce, C. M.; Iorio, M. V.; Casalini, P.; Piovan, C.; Di Leva, G.; Merlo, A.; Triulzi, T.; Menard, S.; Tagliabue, E. microRNA-205 Regulates HER3 in Human Breast Cancer. *Cancer Res.* **2009,** *69* (6), 2195–2200.
68. (a) Baselga, J.; Swain, S. M. Novel Anticancer Targets: Revisiting ERBB2 and Discovering ERBB3. *Nat. Rev. Cancer* **2009,** *9* (7), 463–475; (b) Leahy, D. J.; Cho, H. S. Structure of the Extracellular Region of HER3 Reveals an Interdomain Tether. *Science* **2002,** *297* (5585), 1330–1333.
69. Srinivasan, R.; Leverton, K. E.; Sheldon, H.; Hurst, H. C.; Sarraf, C.; Gullick, W. J. Intracellular Expression of the Truncated Extracellular Domain of c-erbB-3/HER3. *Cell. Signal.* **2001,** *13* (5), 321–330.
70. Barbacci, E. G.; Guarino, B. C.; Stroh, J. G.; Singleton, D. H.; Rosnack, K. J.; Moyer, J. D.; Andrews, G. C. The Structural Basis for the Specificity of Epidermal Growth Factor and Heregulin Binding. *J. Biol. Chem.* **1995,** *270* (16), 9585–9589.
71. Casalini, P.; Iorio, M. V.; Galmozzi, E.; Menard, S. Role of HER Receptors Family in Development and Differentiation. *J. Cell. Physiol.* **2004,** *200* (3), 343–350.
72. Eisenberg, D.; Landgraf, R. Heregulin Reverses the Oligomerization of HER3. *Biochemistry* **2000,** *39* (29), 8503–8511.
73. Radhakrishnan, R.; Shi, F. M.; Telesco, S. E.; Liu, Y. T.; Lemmon, M. A. ErbB3/HER3 Intracellular Domain Is Competent to Bind ATP and Catalyze Autophosphorylation. *Proc. Natl. Acad. Sci. U. S. A.* **2010,** *107* (17), 7692–7697.
74. Klapper, L. N.; Glathe, S.; Vaisman, N.; Hynes, N. E.; Andrews, G. C.; Sela, M.; Yarden, Y. The ErbB-2/HER2 Oncoprotein of Human Carcinomas May Function Solely as a Shared Coreceptor for Multiple Stroma-Derived Growth Factors. *Proc. Natl. Acad. Sci. U. S. A.* **1999,** *96* (9), 4995–5000.
75. Guy, P. M.; Platko, J. V.; Cantley, L. C.; Cerione, R. A.; Carraway, K. L., 3rd. Insect Cell-Expressed p180erbB3 Possesses an Impaired Tyrosine Kinase Activity. *Proc. Natl. Acad. Sci. U. S. A.* **1994,** *91* (17), 8132–8136.
76. (a) Tzahar, E.; Waterman, H.; Chen, X.; Levkowitz, G.; Karunagaran, D.; Lavi, S.; Ratzkin, B. J.; Yarden, Y. A Hierarchical Network of Interreceptor Interactions Determines Signal Transduction by Neu Differentiation Factor/Neuregulin and Epidermal Growth Factor. *Mol. Cell. Biol.* **1996,** *16* (10), 5276–5287; (b) Graus_Porta, D.; Beerli, R. R.; Daly, J. M.; Hynes, N. E. ErbB-2, the Preferred Heterodimerization Partner of All ErbB Receptors, Is a Mediator of Lateral Signaling. *EMBO J.* **1997,** *16* (7), 1647–1655.
77. (a) Beerli, R. R.; Graus-Porta, D.; Woods-Cook, K.; Chen, X.; Yarden, Y.; Hynes, N. E. Neu Differentiation Factor Activation of ErbB-3 and ErbB-4 Is Cell Specific and Displays a Differential Requirement for ErbB-2. *Mol. Cell. Biol.* **1995,** *15* (12), 6496–6505; (b) Graus-Porta, D.; Beerli, R. R.; Hynes, N. E. Single-Chain Antibody-Mediated Intracellular Retention of ErbB-2 Impairs Neu Differentiation Factor and Epidermal Growth Factor Signaling. *Mol. Cell. Biol.* **1995,** *15* (3), 1182–1191.
78. Olayioye, M. A.; Neve, R. M.; Lane, H. A.; Hynes, N. E. The ErbB Signaling Network: Receptor Heterodimerization in Development and Cancer. *EMBO J.* **2000,** *19* (13), 3159–3167.
79. (a) Gassmann, M.; Casagranda, F.; Orioli, D.; Simon, H.; Lai, C.; Klein, R.; Lemke, G. Aberrant Neural and Cardiac Development in Mice Lacking the ErbB4 Neuregulin Receptor. *Nature* **1995,** *378* (6555), 390–394; (b) Meyer, D.; Birchmeier, C. Multiple Essential Functions of Neuregulin in Development. *Nature* **1995,** *378* (6555), 386–390; (c) Threadgill, D. W.; Dlugosz, A. A.; Hansen, L. A.; Tennenbaum, T.; Lichti, U.; Yee, D.; LaMantia, C.; Mourton, T.; Herrup, K.; Harris, R. C.; et al. Targeted Disruption of Mouse EGF Receptor: Effect of Genetic Background on Mutant Phenotype. *Science* **1995,** *269* (5221), 230–234.
80. Menard, S.; Pupa, S. M.; Campiglio, M.; Tagliabue, E. Biologic and Therapeutic Role of HER2 in Cancer. *Oncogene* **2003,** *22* (42), 6570–6578.
81. Press, M. F.; Cordon-Cardo, C.; Slamon, D. J. Expression of the HER-2/neu Proto-Oncogene in Normal Human Adult and Fetal Tissues. *Oncogene* **1990,** *5* (7), 953–962.
82. Paik, S.; Hazan, R.; Fisher, E. R.; Sass, R. E.; Fisher, B.; Redmond, C.; Schlessinger, J.; Lippman, M. E.; King, C. R. Pathologic Findings From the National Surgical Adjuvant Breast and Bowel Project: Prognostic Significance of erbB-2 Protein Overexpression in Primary Breast Cancer. *J. Clin. Oncol.* **1990,** *8* (1), 103–112.
83. Niehans, G. A.; Singleton, T. P.; Dykoski, D.; Kiang, D. T. Stability of HER-2/neu Expression Over Time and at Multiple Metastatic Sites. *J. Natl. Cancer Inst.* **1993,** *85* (15), 1230–1235.
84. (a) Pierce, J. H.; Arnstein, P.; DiMarco, E.; Artrip, J.; Kraus, M. H.; Lonardo, F.; Di Fiore, P. P.; Aaronson, S. A. Oncogenic Potential of erbB-2 in Human Mammary Epithelial Cells. *Oncogene* **1991,** *6* (7), 1189–1194; (b) Liu, Y.; el-Ashry, D.; Chen, D.; Ding, I. Y.; Kern, F. G. MCF-7 Breast Cancer Cells Overexpressing Transfected c-erbB-2 Have an In Vitro Growth Advantage in Estrogen-Depleted Conditions and Reduced Estrogen-Dependence and Tamoxifen-Sensitivity In Vivo. *Breast Cancer Res. Treat.* **1995,** *34* (2), 97–117.
85. (a) Venter, D. J.; Tuzi, N. L.; Kumar, S.; Gullick, W. J. Overexpression of the c-erbB-2 Oncoprotein in Human Breast Carcinomas: Immunohistological Assessment Correlates With Gene Amplification. *Lancet* **1987,** *2* (8550), 69–72; (b) Kallioniemi, O. P.; Kallioniemi, A.; Kurisu, W.; Thor, A.; Chen, L. C.; Smith, H. S.; Waldman, F. M.; Pinkel, D.; Gray, J. W. ERBB2 Amplification in Breast Cancer Analyzed by Fluorescence In Situ Hybridization. *Proc. Natl. Acad. Sci. U. S. A.* **1992,** *89* (12), 5321–5325; (c) Lohrisch, C.; Piccart, M. An Overview of HER2. *Semin. Oncol.* **2001,** *28* (6 Suppl. 18), 3–11.
86. Gabos, Z.; Sinha, R.; Hanson, J.; Chauhan, N.; Hugh, J.; Mackey, J. R.; Abdulkarim, B. Prognostic Significance of Human Epidermal Growth Factor Receptor Positivity for the Development of Brain Metastasis After Newly Diagnosed Breast Cancer. *J. Clin. Oncol.* **2006,** *24* (36), 5658–5663.
87. (a) Morrison, C.; Zanagnolo, V.; Ramirez, N.; Cohn, D. E.; Kelbick, N.; Copeland, L.; Maxwell, G. L.; Fowler, J. M. HER-2 Is an Independent Prognostic Factor in Endometrial Cancer: Association With Outcome in a Large Cohort of Surgically Staged Patients. *J. Clin. Oncol.* **2006,** *24* (15), 2376–2385; (b) Yano, T.; Doi, T.; Ohtsu, A.; Boku, N.; Hashizume, K.; Nakanishi, M.; Ochiai, A. Comparison of HER2 Gene Amplification Assessed by Fluorescence In Situ Hybridization and HER2 Protein Expression Assessed by Immunohistochemistry in Gastric Cancer. *Oncol. Rep.* **2006,** *15* (1), 65–71; (c) Cirisano, F. D.; Karlan, B. Y. The Role of the HER-2/neu Oncogene in Gynecologic Cancers. *J. Soc. Gynecol. Investig.* **1996,** *3* (3), 99–105; (d) Berchuck, A.; Rodriguez, G.; Kinney, R. B.; Soper, J. T.; Dodge, R. K.; Clarke-Pearson, D. L.; Bast, R. C., Jr. Over-expression of HER-2/neu in Endometrial Cancer Is Associated With Advanced Stage Disease. *Am. J. Obstet. Gynecol.* **1991,** *164* (1 Pt 1), 15–21; (e) Kern, J. A.; Schwartz, D. A.; Nordberg, J. E.; Weiner, D. B.; Greene, M. I.; Torney, L.; Robinson, R. A. p185neu Expression in Human Lung Adenocarcinomas Predicts Shortened Survival. *Cancer Res.* **1990,** *50* (16), 5184–5187.
88. Arteaga, C. L. Overview of Epidermal Growth Factor Receptor Biology and Its Role as a Therapeutic Target in Human Neoplasia. *Semin. Oncol.* **2002,** *29* (5 Suppl. 14), 3–9.
89. Boerner, J. L.; Danielsen, A.; Maihle, N. J. Ligand-Independent Oncogenic Signaling by the Epidermal Growth Factor Receptor: v-ErbB as a Paradigm. *Exp. Cell Res.* **2003,** *284* (1), 111–121.
90. (a) Gluz, O.; Liedtke, C.; Gottschalk, N.; Pusztai, L.; Nitz, U.; Harbeck, N. Triple-Negative Breast Cancer—Current Status and Future Directions. *Ann. Oncol.* **2009,** *20* (12), 1913–1927; (b) Pintens, S.; Neven, P.; Drijkoningen, M.; Van Belle, V.; Moerman, P.; Christiaens, M. R.; Smeets, A.; Wildiers, H.; Vanden Bempt, I. Triple Negative Breast Cancer: A Study From the Point of View of Basal CK5/6 and HER-1. *J. Clin. Pathol.* **2009,** *62* (7), 624–628.

91. Hirsch, F. R.; Varella-Garcia, M.; Bunn, P. A., Jr.; Di Maria, M. V.; Veve, R.; Bremmes, R. M.; Baron, A. E.; Zeng, C.; Franklin, W. A. Epidermal Growth Factor Receptor in Non-Small-Cell Lung Carcinomas: Correlation Between Gene Copy Number and Protein Expression and Impact on Prognosis. *J. Clin. Oncol.* **2003,** *21* (20), 3798–3807.
92. Herschkowitz, J. I.; Lubet, R. Mouse Models of Triple Negative [Basal-Like/Claudin Low] Breast Cancer. *Breast Dis.* **2010,** *32* (1–2), 63–71.
93. Brabender, J.; Danenberg, K. D.; Metzger, R.; Schneider, P. M.; Park, J.; Salonga, D.; Holscher, A. H.; Danenberg, P. V. Epidermal Growth Factor Receptor and HER2-neu mRNA Expression in Non-Small Cell Lung Cancer Is Correlated With Survival. *Clin. Cancer Res.* **2001,** *7* (7), 1850–1855.
94. Ferguson, K. M.; Berger, M. B.; Mendrola, J. M.; Cho, H. S.; Leahy, D. J.; Lemmon, M. A. EGF Activates Its Receptor by Removing Interactions That Autoinhibit Ectodomain Dimerization. *Mol. Cell* **2003,** *11* (2), 507–517.
95. Li, S.; Schmitz, K. R.; Jeffrey, P. D.; Wiltzius, J. J.; Kussie, P.; Ferguson, K. M. Structural Basis for Inhibition of the Epidermal Growth Factor Receptor by Cetuximab. *Cancer Cell* **2005,** *7* (4), 301–311.
96. Sawano, A.; Takayama, S.; Matsuda, M.; Miyawaki, A. Lateral Propagation of EGF Signaling After Local Stimulation Is Dependent on Receptor Density. *Dev. Cell* **2002,** *3* (2), 245–257.
97. (a) Engelman, J. A.; Schoeberl, B.; Faber, A. C.; Li, D. N.; Liang, M. C.; Crosby, K.; Onsum, M.; Burenkova, O.; Pace, E.; Walton, Z.; Nie, L.; Fulgham, A.; Song, Y.; Nielsen, U. B.; Wong, K. K. An ErbB3 Antibody, MM-121, Is Active in Cancers With Ligand-Dependent Activation. *Cancer Res.* **2010,** *70* (6), 2485–2494; (b) Hynes, N. E.; Holbro, T.; Beerli, R. R.; Maurer, F.; Koziczak, M.; Barbas, C. F. The ErbB2/ErbB3 Heterodimer Functions as an Oncogenic Unit: ErbB2 Requires ErbB3 to Drive Breast Tumor Cell Proliferation. *Proc. Natl. Acad. Sci. U. S. A.* **2003,** *100* (15), 8933–8938; (c) Sithanandam, G.; Anderson, L. M. The ERBB3 Receptor in Cancer and Cancer Gene Therapy. *Cancer Gene Ther.* **2008,** *15* (7), 413–448; (d) Tzahar, E.; Waterman, H.; Chen, X. M.; Levkowitz, G.; Karunagaran, D.; Lavi, S.; Ratzkin, B. J.; Yarden, Y. A Hierarchical Network of Interreceptor Interactions Determines Signal Transduction by neu Differentiation Factor/Neuregulin and Epidermal Growth Factor. *Mol. Cell. Biol.* **1996,** *16* (10), 5276–5287.
98. Yu, H.; Spitz, M. R.; Mistry, J.; Gu, J.; Hong, W. K.; Wu, X. Plasma Levels of Insulin-Like Growth Factor-I and Lung Cancer Risk: A Case–Control Analysis. *J. Natl. Cancer Inst.* **1999,** *91* (2), 151–156.
99. Hankinson, S. E.; Willett, W. C.; Colditz, G. A.; Hunter, D. J.; Michaud, D. S.; Deroo, B.; Rosner, B.; Speizer, F. E.; Pollak, M. Circulating Concentrations of Insulin-Like Growth Factor-I and Risk of Breast Cancer. *Lancet* **1998,** *351* (9113), 1393–1396.
100. Ma, J.; Pollak, M. N.; Giovannucci, E.; Chan, J. M.; Tao, Y.; Hennekens, C. H.; Stampfer, M. J. Prospective Study of Colorectal Cancer Risk in Men and Plasma Levels of Insulin-Like Growth Factor (IGF)-I and IGF-Binding Protein-3. *J. Natl. Cancer Inst.* **1999,** *91* (7), 620–625.
101. Chan, J. M.; Stampfer, M. J.; Giovannucci, E.; Gann, P. H.; Ma, J.; Wilkinson, P.; Hennekens, C. H.; Pollak, M. Plasma Insulin-Like Growth Factor-I and Prostate Cancer Risk: A Prospective Study. *Science* **1998,** *279* (5350), 563–566.
102. Wu, X.; Zhao, H.; Do, K. A.; Johnson, M. M.; Dong, Q.; Hong, W. K.; Spitz, M. R. Serum Levels of Insulin Growth Factor (IGF-I) and IGF-Binding Protein Predict Risk of Second Primary Tumors in Patients With Head and Neck Cancer. *Clin. Cancer Res.* **2004,** *10* (12 Pt 1), 3988–3995.
103. (a) Freier, S.; Weiss, O.; Eran, M.; Flyvbjerg, A.; Dahan, R.; Nephesh, I.; Safra, T.; Shiloni, E.; Raz, I. Expression of the Insulin-Like Growth Factors and Their Receptors in Adenocarcinoma of the Colon. *Gut* **1999,** *44* (5), 704–708; (b) Lahm, H.; Suardet, L.; Laurent, P. L.; Fischer, J. R.; Ceyhan, A.; Givel, J. C.; Odartchenko, N. Growth Regulation and Co-stimulation of Human Colorectal Cancer Cell Lines by Insulin-Like Growth Factor I, II and Transforming Growth Factor Alpha. *Br. J. Cancer* **1992,** *65* (3), 341–346.
104. Peters, G.; Gongoll, S.; Langner, C.; Mengel, M.; Piso, P.; Klempnauer, J.; Ruschoff, J.; Kreipe, H.; von Wasielewski, R. IGF-1R, IGF-1 and IGF-2 Expression as Potential Prognostic and Predictive Markers in Colorectal-Cancer. *Virchows Arch.* **2003,** *443* (2), 139–145.
105. Pennarun, B.; Kleibeuker, J. H.; Oenema, T.; Stegehuis, J. H.; de Vries, E. G.; de Jong, S. Inhibition of IGF-1R-Dependent PI3K Activation Sensitizes Colon Cancer Cells Specifically to DR5-Mediated Apoptosis but Not to rhTRAIL. *Anal. Cell. Pathol. (Amst.)* **2010,** *33* (5), 229–244.
106. (a) Tischer, E.; Mitchell, R.; Hartman, T.; Silva, M.; Gospodarowicz, D.; Fiddes, J. C.; Abraham, J. A. The Human Gene for Vascular Endothelial Growth Factor. Multiple Protein Forms Are Encoded Through Alternative Exon Splicing. *J. Biol. Chem.* **1991,** *266* (18), 11947–11954; (b) Ferrara, N.; Henzel, W. J. Pituitary Follicular Cells Secrete a Novel Heparin-Binding Growth Factor Specific for Vascular Endothelial Cells. *Biochem. Biophys. Res. Commun.* **1989,** *161* (2), 851–858.
107. (a) Ferrara, N.; Hillan, K. J.; Novotny, W. Bevacizumab (Avastin), A Humanized Anti-VEGF Monoclonal Antibody for Cancer Therapy. *Biochem. Biophys. Res. Commun.* **2005,** *333* (2), 328–335; (b) Sebolt-Leopold, J. S.; English, J. M. Mechanisms of Drug Inhibition of Signalling Molecules. *Nature* **2006,** *441* (7092), 457–462; (c) Dancey, J. E.; Chen, H. X. Strategies for Optimizing Combinations of Molecularly Targeted Anticancer Agents. *Nat. Rev. Drug Discov.* **2006,** *5* (8), 649–659.
108. Morabito, A.; De Maio, E.; Di Maio, M.; Normanno, N.; Perrone, F. Tyrosine Kinase Inhibitors of Vascular Endothelial Growth Factor Receptors in Clinical Trials: Current Status and Future Directions. *Oncologist* **2006,** *11* (7), 753–764.
109. Mizejewski, G. J. Peptides as Receptor Ligand Drugs and Their Relationship to G-Coupled Signal Transduction. *Expert Opin. Investig. Drugs* **2001,** *10* (6), 1063–1073.
110. Boohaker, R. J.; Lee, M. W.; Vishnubhotla, P.; Perez, J. M.; Khaled, A. R. The Use of Therapeutic Peptides to Target and to Kill Cancer Cells. *Curr. Med. Chem.* **2012,** *19* (22), 3794–3804.
111. Taylor, E. M.; Otero, D. A.; Banks, W. A.; O'Brien, J. S. Retro-Inverso Prosaptide Peptides Retain Bioactivity, Are Stable In Vivo, and Are Blood–Brain Barrier Permeable. *J. Pharmacol. Exp. Ther.* **2000,** *295* (1), 190–194.
112. Hruby, V. J. Conformational and Topographical Considerations in the Design of Biologically Active Peptides. *Biopolymers* **1993,** *33* (7), 1073–1082.
113. Fischer, P. M. The Design, Synthesis and Application of Stereochemical and Directional Peptide Isomers: A Critical Review. *Curr. Protein Pept. Sci.* **2003,** *4* (5), 339–356.
114. (a) Fletcher, M. D.; Campbell, M. M. Partially Modified Retro-Inverso Peptides: Development, Synthesis, and Conformational Behavior. *Chem. Rev.* **1998,** *98* (2), 763–796; (b) Allen, S. D.; Rawale, S. V.; Whitacre, C. C.; Kaumaya, P. T. Therapeutic Peptidomimetic Strategies for Autoimmune Diseases: Costimulation Blockade. *J. Pept. Res.* **2005,** *65* (6), 591–604.
115. (a) Sundaram, R.; Dakappagari, N. K.; Kaumaya, P. T. P. Synthetic Peptides as Cancer Vaccines. *Biopolymers* **2002,** *66* (3), 200–216; (b) Lynch, M. P.; Kaumaya, P. T. P. Advances in HTLV-1 Peptide Vaccines and Therapeutics. *Curr. Protein Pept. Sci.* **2006,** *7* (2), 137–145; (c) Steele, J. T.; Allen, S. D.; Kaumaya, P. T. P. Cancer Immunotherapy With Rationally Designed Synthetic Peptides. In *Handbook of Biologically Active Peptides;* Kastin, A. J., Ed.; Academic Press, Elsevier, 2006; pp 491–498; (d) Foy, K. C.; Vicari, D.; Kaumaya, P. T. P. Therapeutic Peptides Targeting HER-2/neu and VEGF Signaling Pathways in Breast Cancer. In *Handbook of Biologically Active Peptides;* Kastin, A. J., Ed., 2nd ed.; Academic Press, Elsevier, 2013; pp 612–616; (e) Miller, M. J.; Foy, K. C.; Kaumaya, P. T. P. Cancer Immunotherapy: Present Status, Future Perspective, and a New Paradigm of Peptide Immunotherapeutics. *Discov. Med.* **2013,** *15* (82), 166–176.
116. (a) Kaumaya, P. T.; Conrad, S. F.; DiGeorge, A. M.; Lairmore, M. D. Glycosylation-Dependent Peptide Antigenic Determinants of env gp46 HTLV-1. *Leukemia* **1995,** *9* (Suppl. 1), S133–S138; (b) Singh, H.; Ansari, H. R.; Raghava, G. P. Improved Method for Linear B-Cell Epitope Prediction Using Antigen's Primary Sequence. *PLoS ONE* **2013,** *8* (5), e62216.
117. (a) Kaumaya, P. T.; VanBuskirk, A. M.; Goldberg, E.; Pierce, S. K. Design and Immunological Properties of Topographic Immunogenic Determinants of a Protein Antigen (LDH-C4) as Vaccines. *J. Biol. Chem.* **1992,** *267* (9), 6338–6346; (b) Kaumaya, P. T.; Berndt, K. D.; Heidorn, D. B.; Trewhella, J.; Kezdy, F. J.; Goldberg, E. Synthesis and Biophysical Characterization of Engineered Topographic Immunogenic Determinants With Alpha Alpha Topology. *Biochemistry* **1990,** *29* (1), 13–23; (c) Kaumaya, P. T.; Kobs-Conrad, S.; Seo, Y. H.; Lee, H.; VanBuskirk, A. M.; Feng, N.; Sheridan, J. F.; Stevens, V. Peptide Vaccines Incorporating a 'Promiscuous' T-Cell Epitope Bypass Certain Haplotype Restricted Immune Responses and Provide Broad Spectrum Immunogenicity. *J. Mol. Recognit.* **1993,** *6* (2), 81–94.
118. Srinivasan, M.; Domanico, S. Z.; Kaumaya, P. T.; Pierce, S. K. Peptides of 23 Residues or Greater Are Required to Stimulate a High Affinity Class II-Restricted T Cell Response. *Eur. J. Immunol.* **1993,** *23* (5), 1011–1016.
119. (a) Allen, S. D.; Garrett, J. T.; Rawale, S. V.; Jones, A. L.; Phillips, G.; Forni, G.; Morris, J. C.; Oshima, R. G.; Kaumaya, P. T. Peptide Vaccines of the HER-2/neu Dimerization Loop Are Effective in Inhibiting Mammary Tumor Growth In Vivo. *J. Immunol.* **2007,** *179* (1), 472–482; (b) Garrett, J. T.; Rawale, S.; Allen, S. D.; Phillips, G.; Forni, G.; Morris, J. C.; Kaumaya, P. T. Novel Engineered Trastuzumab Conformational Epitopes Demonstrate In Vitro and In Vivo Antitumor Properties Against HER-2/neu. *J. Immunol.* **2007,** *178* (11), 7120–7131.

120. (a) Srinivasan, M.; Wardrop, R. M.; Gienapp, I. E.; Stuckman, S. S.; Whitacre, C. C.; Kaumaya, P. T. A Retro-Inverso Peptide Mimic of CD28 Encompassing the MYPPPY Motif Adopts a Polyproline Type II Helix and Inhibits Encephalitogenic T Cells In Vitro. *J. Immunol.* **2001,** *167* (1), 578–585; (b) Srinivasan, M.; Gienapp, I. E.; Stuckman, S. S.; Rogers, C. J.; Jewell, S. D.; Kaumaya, P. T.; Whitacre, C. C. Suppression of Experimental Autoimmune Encephalomyelitis Using Peptide Mimics of CD28. *J. Immunol.* **2002,** *169* (4), 2180–2188.
121. Kaumaya, P. T.; Foy, K. C.; Garrett, J.; Rawale, S. V.; Vicari, D.; Thurmond, J. M.; Lamb, T.; Mani, A.; Kane, Y.; Balint, C. R.; Chalupa, D.; Otterson, G. A.; Shapiro, C. L.; Fowler, J. M.; Grever, M. R.; Bekaii-Saab, T. S.; Carson, W. E., 3rd. Phase I Active Immunotherapy With Combination of Two Chimeric, Human Epidermal Growth Factor Receptor 2, B-Cell Epitopes Fused to a Promiscuous T-Cell Epitope in Patients With Metastatic and/or Recurrent Solid Tumors. *J. Clin. Oncol.* **2009,** *27* (31), 5270–5277.
122. (a) Ying, J. E.; Zhu, L. M.; Liu, B. X. Developments in Metastatic Pancreatic Cancer: Is Gemcitabine Still the Standard? *World J. Gastroenterol.* **2012,** *18* (8), 736–745; (b) Rossidis, G.; Arroyo, M. R.; Abbitt, P. L.; Grobmyer, S. R.; Hochwald, S. N. Malignant Transformation of a Pancreatic Serous Cystadenoma. *Am. Surg.* **2012,** *78* (2), 260–263.
123. Miller, M. J.; Foy, K. C.; Kaumaya, P. T. Cancer Immunotherapy: Present Status, Future Perspective, and a New Paradigm of Peptide Immunotherapeutics. *Discov. Med.* **2013,** *15* (82), 166–176.
124. Smolenski, L. A.; Kaumaya, P.; Atassi, M. Z.; Pierce, S. K. Characteristics of Peptides Which Compete for Presented Antigen-Binding Sites on Antigen-Presenting Cells. *Eur. J. Immunol.* **1990,** *20* (5), 953–960.
125. (a) Johnston, J. B.; Navaratnam, S.; Pitz, M. W.; Maniate, J. M.; Wiechec, E.; Baust, H.; Gingerich, J.; Skliris, G. P.; Murphy, L. C.; Los, M. Targeting the EGFR Pathway for Cancer Therapy. *Curr. Med. Chem.* **2006,** *13* (29), 3483–3492; (b) Howe, L. R.; Brown, P. H. Targeting the HER/EGFR/ErbB Family to Prevent Breast Cancer. *Cancer Prev. Res. (Phila.)* **2011,** *4* (8), 1149–1157.
126. Grothey, A. Recognizing and Managing Toxicities of Molecular Targeted Therapies for Colorectal Cancer. *Oncology (Williston Park)* **2006,** *20* (14 Suppl. 10), 21–28.
127. Moasser, M. M. Targeting the Function of the HER2 Oncogene in Human Cancer Therapeutics. *Oncogene* **2007,** *26* (46), 6577–6592.
128. Yip, Y. L.; Smith, G.; Koch, J.; Dubel, S.; Ward, R. L. Identification of Epitope Regions Recognized by Tumor Inhibitory and Stimulatory Anti-ErbB-2 Monoclonal Antibodies: Implications for Vaccine Design. *J. Immunol.* **2001,** *166* (8), 5271–5278.
129. Fendly, B. M.; Winget, M.; Hudziak, R. M.; Lipari, M. T.; Napier, M. A.; Ullrich, A. Characterization of Murine Monoclonal Antibodies Reactive to Either the Human Epidermal Growth Factor Receptor or HER2/neu Gene Product. *Cancer Res.* **1990,** *50* (5), 1550–1558.
130. Shepard, H. M.; Lewis, G. D.; Sarup, J. C.; Fendly, B. M.; Maneval, D.; Mordenti, J.; Figari, I.; Kotts, C. E.; Palladino, M. A., Jr.; Ullrich, A.; et al. Monoclonal Antibody Therapy of Human Cancer: Taking the HER2 Protooncogene to the Clinic. *J. Clin. Immunol.* **1991,** *11* (3), 117–127.
131. Carter, P.; Presta, L.; Gorman, C. M.; Ridgway, J. B.; Henner, D.; Wong, W. L.; Rowland, A. M.; Kotts, C.; Carver, M. E.; Shepard, H. M. Humanization of an Anti-p185HER2 Antibody for Human Cancer Therapy. *Proc. Natl. Acad. Sci. U. S. A.* **1992,** *89* (10), 4285–4289.
132. Carter, P. J. Potent Antibody Therapeutics by Design. *Nat. Rev. Immunol.* **2006,** *6* (5), 343–357.
133. (a) Lewis, G. D.; Figari, I.; Fendly, B.; Wong, W. L.; Carter, P.; Gorman, C.; Shepard, H. M. Differential Responses of Human Tumor Cell Lines to Anti-p185HER2 Monoclonal Antibodies. *Cancer Immunol. Immunother.* **1993,** *37* (4), 255–263; (b) Tokuda, Y.; Ohnishi, Y.; Shimamura, K.; Iwasawa, M.; Yoshimura, M.; Ueyama, Y.; Tamaoki, N.; Tajima, T.; Mitomi, T. In Vitro and In Vivo Anti-Tumour Effects of a Humanised Monoclonal Antibody Against c-erbB-2 Product. *Br. J. Cancer* **1996,** *73* (11), 1362–1365.
134. (a) Baselga, J.; Norton, L.; Albanell, J.; Kim, Y. M.; Mendelsohn, J. Recombinant Humanized Anti-HER2 Antibody (Herceptin) Enhances the Antitumor Activity of Paclitaxel and Doxorubicin Against HER2/neu Overexpressing Human Breast Cancer Xenografts. *Cancer Res.* **1998,** *58* (13), 2825–2831; (b) Clynes, R. A.; Towers, T. L.; Presta, L. G.; Ravetch, J. V. Inhibitory Fc Receptors Modulate in vivo Cytoxicity Against Tumor Targets. *Nat. Med.* **2000,** *6* (4), 443–446.
135. (a) Baselga, J.; Tripathy, D.; Mendelsohn, J.; Baughman, S.; Benz, C. C.; Dantis, L.; Sklarin, N. T.; Seidman, A. D.; Hudis, C. A.; Moore, J.; Rosen, P. P.; Twaddell, T.; Henderson, I. C.; Norton, L. Phase II Study of Weekly Intravenous Recombinant Humanized Anti-p185HER2 Monoclonal Antibody in Patients With HER2/neu-Overexpressing Metastatic Breast Cancer (See Comments) *J. Clin. Oncol.* **1996,** *14* (3), 737–744; (b) Cobleigh, M. A.; Vogel, C. L.; Tripathy, D.; Robert, N. J.; Scholl, S.; Fehrenbacher, L.; Wolter, J. M.; Paton, V.; Shak, S.; Lieberman, G.; Slamon, D. J. Multinational Study of the Efficacy and Safety of Humanized Anti-HER2 Monoclonal Antibody in Women Who Have HER2-Overexpressing Metastatic Breast Cancer That Has Progressed After Chemotherapy for Metastatic Disease. *J. Clin. Oncol.* **1999,** *17* (9), 2639–2648; (c) Vogel, C. L.; Cobleigh, M. A.; Tripathy, D.; Gutheil, J. C.; Harris, L. N.; Fehrenbacher, L.; Slamon, D. J.; Murphy, M.; Novotny, W. F.; Burchmore, M.; Shak, S.; Stewart, S. J.; Press, M. Efficacy and Safety of Trastuzumab as a Single Agent in First-Line Treatment of HER2-Overexpressing Metastatic Breast Cancer. *J. Clin. Oncol.* **2002,** *20* (3), 719–726.
136. (a) Slamon, D. J.; Leyland-Jones, B.; Shak, S.; Fuchs, H.; Paton, V.; Bajamonde, A.; Fleming, T.; Eiermann, W.; Wolter, J.; Pegram, M.; Baselga, J.; Norton, L. Use of Chemotherapy Plus a Monoclonal Antibody Against HER2 for Metastatic Breast Cancer That Overexpresses HER2. *N. Engl. J. Med.* **2001,** *344* (11), 783–792; (b) Marty, M.; Cognetti, F.; Maraninchi, D.; Snyder, R.; Mauriac, L.; Tubiana-Hulin, M.; Chan, S.; Grimes, D.; Anton, A.; Lluch, A.; Kennedy, J.; O'Byrne, K.; Conte, P.; Green, M.; Ward, C.; Mayne, K.; Extra, J. M. Randomized Phase II Trial of the Efficacy and Safety of Trastuzumab Combined With Docetaxel in Patients With Human Epidermal Growth Factor Receptor 2-Positive Metastatic Breast Cancer Administered as First-Line Treatment: The M77001 Study Group. *J. Clin. Oncol.* **2005,** *23* (19), 4265–4274.
137. (a) Piccart-Gebhart, M. J.; Procter, M.; Leyland-Jones, B.; Goldhirsch, A.; Untch, M.; Smith, I.; Gianni, L.; Baselga, J.; Bell, R.; Jackisch, C.; Cameron, D.; Dowsett, M.; Barrios, C. H.; Steger, G.; Huang, C. S.; Andersson, M.; Inbar, M.; Lichinitser, M.; Lang, I.; Nitz, U.; Iwata, H.; Thomssen, C.; Lohrisch, C.; Suter, T. M.; Ruschoff, J.; Suto, T.; Greatorex, V.; Ward, C.; Straehle, C.; McFadden, E.; Dolci, M. S.; Gelber, R. D.; Herceptin Adjuvant Trial Study Team. Trastuzumab After Adjuvant Chemotherapy in HER2-Positive Breast Cancer. *N. Engl. J. Med.* **2005,** *353* (16), 1659–1672; (b) Romond, E. H.; Perez, E. A.; Bryant, J.; Suman, V. J.; Geyer, C. E., Jr.; Davidson, N. E.; Tan-Chiu, E.; Martino, S.; Paik, S.; Kaufman, P. A.; Swain, S. M.; Pisansky, T. M.; Fehrenbacher, L.; Kutteh, L. A.; Vogel, V. G.; Visscher, D. W.; Yothers, G.; Jenkins, R. B.; Brown, A. M.; Dakhil, S. R.; Mamounas, E. P.; Lingle, W. L.; Klein, P. M.; Ingle, J. N.; Wolmark, N. Trastuzumab plus adjuvant chemotherapy for operable HER2-positive breast cancer. *N. Engl. J. Med.* **2005,** *353* (16), 1673–1684.
138. FDA Expands Us of Herceptin for Early-Stage Breast Cancer. *Mayo Clin. Womens Healthsource* **2007,** *11* (6), 3.
139. Mass, R. D.; Press, M. F.; Anderson, S.; Cobleigh, M. A.; Vogel, C. L.; Dybdal, N.; Leiberman, G.; Slamon, D. J. Evaluation of Clinical Outcomes According to HER2 Detection by Fluorescence In Situ Hybridization in Women With Metastatic Breast Cancer Treated With Trastuzumab. *Clin. Breast Cancer* **2005,** *6* (3), 240–246.
140. Seidman, A.; Hudis, C.; Pierri, M. K.; Shak, S.; Paton, V.; Ashby, M.; Murphy, M.; Stewart, S. J.; Keefe, D. Cardiac Dysfunction in the Trastuzumab Clinical Trials Experience. *J. Clin. Oncol.* **2002,** *20* (5), 1215–1221.
141. Tan-Chiu, E.; Yothers, G.; Romond, E.; Geyer, C. E., Jr.; Ewer, M.; Keefe, D.; Shannon, R. P.; Swain, S. M.; Brown, A.; Fehrenbacher, L.; Vogel, V. G.; Seay, T. E.; Rastogi, P.; Mamounas, E. P.; Wolmark, N.; Bryant, J. Assessment of Cardiac Dysfunction in a Randomized Trial Comparing Doxorubicin and Cyclophosphamide Followed by Paclitaxel, With or Without Trastuzumab as Adjuvant Therapy in Node-Positive, Human Epidermal Growth Factor Receptor 2-Overexpressing Breast Cancer: NSABP B-31. *J. Clin. Oncol.* **2005,** *23* (31), 7811–7819.
142. Force, T.; Krause, D. S.; Van Etten, R. A. Molecular Mechanisms of Cardiotoxicity of Tyrosine Kinase Inhibition. *Nat. Rev. Cancer* **2007,** *7* (5), 332–344.
143. Pegram, M.; Ngo, D. Application and Potential Limitations of Animal Models Utilized in the Development of Trastuzumab (Herceptin): A Case Study. *Adv. Drug Deliv. Rev.* **2006,** *58* (5–6), 723–734.
144. (a) Cuello, M.; Ettenberg, S. A.; Clark, A. S.; Keane, M. M.; Posner, R. H.; Nau, M. M.; Dennis, P. A.; Lipkowitz, S. Down-Regulation of the erbB-2 Receptor by Trastuzumab (Herceptin) Enhances Tumor Necrosis Factor-Related Apoptosis-Inducing Ligand-Mediated Apoptosis in Breast and Ovarian Cancer Cell Lines That Overexpress erbB-2. *Cancer Res.* **2001,** *61* (12), 4892–4900; (b) Citri, A.; Alroy, I.; Lavi, S.; Rubin, C.; Xu, W.; Grammatikakis, N.; Patterson, C.; Neckers, L.; Fry, D. W.; Yarden, Y. Drug-Induced Ubiquitylation and Degradation of ErbB Receptor Tyrosine Kinases: Implications for Cancer Therapy. *EMBO J.* **2002,** *21* (10), 2407–2417; (c) Lee, S.; Yang, W.; Lan, K. H.; Sellappan, S.; Klos, K.; Hortobagyi, G.; Hung, M. C.; Yu, D. Enhanced Sensitization to Taxol-Induced Apoptosis by Herceptin Pretreatment in ErbB2-Overexpressing Breast Cancer Cells. *Cancer Res.* **2002,** *62* (20), 5703–5710.
145. (a) Austin, C. D.; De Maziere, A. M.; Pisacane, P. I.; van Dijk, S. M.; Eigenbrot, C.; Sliwkowski, M. X.; Klumperman, J.; Scheller, R. H. Endocytosis and Sorting of ErbB2 and the Site of Action of Cancer Therapeutics Trastuzumab and Geldanamycin. *Mol. Biol. Cell* **2004,** *15* (12), 5268–5282; (b) Longva, K. E.; Pedersen, N. M.; Haslekas, C.; Stang, E.; Madshus, I. H. Herceptin-Induced Inhibition of ErbB2 Signaling Involves Reduced Phosphorylation of Akt but Not Endocytic Down-Regulation of ErbB2. *Int. J. Cancer* **2005,** *116* (3), 359–367.

146. (a) Molina, M. A.; Codony-Servat, J.; Albanell, J.; Rojo, F.; Arribas, J.; Baselga, J. Trastuzumab (Herceptin), a Humanized Anti-Her2 Receptor Monoclonal Antibody, Inhibits Basal and Activated Her2 Ectodomain Cleavage in Breast Cancer Cells. *Cancer Res.* **2001,** *61* (12), 4744–4749; (b) Liu, P. C.; Liu, X.; Li, Y.; Covington, M.; Wynn, R.; Huber, R.; Hillman, M.; Yang, G.; Ellis, D.; Marando, C.; Katiyar, K.; Bradley, J.; Abremski, K.; Stow, M.; Rupar, M.; Zhuo, J.; Li, Y. L.; Lin, Q.; Burns, D.; Xu, M.; Zhang, C.; Qian, D. Q.; He, C.; Sharief, V.; Weng, L.; Agrios, C.; Shi, E.; Metcalf, B.; Newton, R.; Friedman, S.; Yao, W.; Scherle, P.; Hollis, G.; Burn, T. C. Identification of ADAM10 as a Major Source of HER2 Ectodomain Sheddase Activity in HER2 Overexpressing Breast Cancer Cells. *Cancer Biol. Ther.* **2006,** *5* (6), 657–664.
147. (a) Segatto, O.; King, C. R.; Pierce, J. H.; Di Fiore, P. P.; Aaronson, S. A. Different Structural Alterations Upregulate in vitro Tyrosine Kinase Activity and Transforming Potency of the erbB-2 Gene. *Mol. Cell. Biol.* **1988,** *8* (12), 5570–5574; (b) Molina, M. A.; Saez, R.; Ramsey, E. E.; Garcia-Barchino, M. J.; Rojo, F.; Evans, A. J.; Albanell, J.; Keenan, E. J.; Lluch, A.; Garcia-Conde, J.; Baselga, J.; Clinton, G. M. NH(2)-Terminal Truncated HER-2 Protein but Not Full-Length Receptor Is Associated With Nodal Metastasis in Human Breast Cancer. *Clin. Cancer Res.* **2002,** *8* (2), 347–353.
148. (a) Agus, D. B.; Akita, R. W.; Fox, W. D.; Lewis, G. D.; Higgins, B.; Pisacane, P. I.; Lofgren, J. A.; Tindell, C.; Evans, D. P.; Maiese, K.; Scher, H. I.; Sliwkowski, M. X. Targeting Ligand-Activated ErbB2 Signaling Inhibits Breast and Prostate Tumor Growth. *Cancer Cell* **2002,** *2* (2), 127–137; (b) Diermeier, S.; Horvath, G.; Knuechel-Clarke, R.; Hofstaedter, F.; Szollosi, J.; Brockhoff, G. Epidermal Growth Factor Receptor Coexpression Modulates Susceptibility to Herceptin in HER2/neu Overexpressing Breast Cancer Cells via Specific erbB-Receptor Interaction and Activation. *Exp. Cell Res.* **2005,** *304* (2), 604–619.
149. (a) Sliwkowski, M. X.; Lofgren, J. A.; Lewis, G. D.; Hotaling, T. E.; Fendly, B. M.; Fox, J. A. Nonclinical Studies Addressing the Mechanism of Action of Trastuzumab (Herceptin). *Semin. Oncol.* **1999,** *26* (4 Suppl. 12), 60–70; (b) Lane, H. A.; Beuvink, I.; Motoyama, A. B.; Daly, J. M.; Neve, R. M.; Hynes, N. E. ErbB2 Potentiates Breast Tumor Proliferation Through Modulation of p27(Kip1)-Cdk2 Complex Formation: Receptor Overexpression Does Not Determine Growth Dependency. *Mol. Cell. Biol.* **2000,** *20* (9), 3210–3223; (c) Marches, R.; Uhr, J. W. Enhancement of the p27Kip1-Mediated Antiproliferative Effect of Trastuzumab (Herceptin) on HER2-Overexpressing Tumor Cells. *Int. J. Cancer* **2004,** *112* (3), 492–501.
150. Yen, L.; You, X. L.; Al Moustafa, A. E.; Batist, G.; Hynes, N. E.; Mader, S.; Meloche, S.; Alaoui-Jamali, M. A. Heregulin Selectively Upregulates Vascular Endothelial Growth Factor Secretion in Cancer Cells and Stimulates Angiogenesis. *Oncogene* **2000,** *19* (31), 3460–3469.
151. (a) Izumi, Y.; Xu, L.; di Tomaso, E.; Fukumura, D.; Jain, R. K. Tumour Biology: Herceptin Acts as an Anti-Angiogenic Cocktail. *Nature* **2002,** *416* (6878), 279–280; (b) Klos, K. S.; Zhou, X.; Lee, S.; Zhang, L.; Yang, W.; Nagata, Y.; Yu, D. Combined Trastuzumab and Paclitaxel Treatment Better Inhibits ErbB-2-Mediated Angiogenesis in Breast Carcinoma Through a More Effective Inhibition of Akt Than Either Treatment Alone. *Cancer* **2003,** *98* (7), 1377–1385.
152. Nagata, Y.; Lan, K. H.; Zhou, X.; Tan, M.; Esteva, F. J.; Sahin, A. A.; Klos, K. S.; Li, P.; Monia, B. P.; Nguyen, N. T.; Hortobagyi, G. N.; Hung, M. C.; Yu, D. PTEN Activation Contributes to Tumor Inhibition by Trastuzumab, and Loss of PTEN Predicts Trastuzumab Resistance in Patients. *Cancer Cell* **2004,** *6* (2), 117–127.
153. Carson, W. E.; Parihar, R.; Lindemann, M. J.; Personeni, N.; Dierksheide, J.; Meropol, N. J.; Baselga, J.; Caligiuri, M. A. Interleukin-2 Enhances the Natural Killer Cell Response to Herceptin-Coated Her2/neu-Positive Breast Cancer Cells. *Eur. J. Immunol.* **2001,** *31* (10), 3016–3025.
154. Lewis Phillips, G. D.; Li, G.; Dugger, D. L.; Crocker, L. M.; Parsons, K. L.; Mai, E.; Blattler, W. A.; Lambert, J. M.; Chari, R. V.; Lutz, R. J.; Wong, W. L.; Jacobson, F. S.; Koeppen, H.; Schwall, R. H.; Kenkare-Mitra, S. R.; Spencer, S. D.; Sliwkowski, M. X. Targeting HER2-Positive Breast Cancer With Trastuzumab-DM1, an Antibody-Cytotoxic Drug Conjugate. *Cancer Res.* **2008,** *68* (22), 9280–9290.
155. Chari, R. V. Targeted Cancer Therapy: Conferring Specificity to Cytotoxic Drugs. *Acc. Chem. Res.* **2008,** *41* (1), 98–107.
156. Takai, N.; Jain, A.; Kawamata, N.; Popoviciu, L. M.; Said, J. W.; Whittaker, S.; Miyakawa, I.; Agus, D. B.; Koeffler, H. P. 2C4, a Monoclonal Antibody Against HER2, Disrupts the HER Kinase Signaling Pathway and Inhibits Ovarian Carcinoma Cell Growth. *Cancer* **2005,** *104* (12), 2701–2708.
157. Adams, C. W.; Allison, D. E.; Flagella, K.; Presta, L.; Clarke, J.; Dybdal, N.; McKeever, K.; Sliwkowski, M. X. Humanization of a Recombinant Monoclonal Antibody to Produce a Therapeutic HER Dimerization Inhibitor, Pertuzumab. *Cancer Immunol. Immunother.* **2006,** *55* (6), 717–727.
158. Agus, D. B.; Gordon, M. S.; Taylor, C.; Natale, R. B.; Karlan, B.; Mendelson, D. S.; Press, M. F.; Allison, D. E.; Sliwkowski, M. X.; Lieberman, G.; Kelsey, S. M.; Fyfe, G. Phase I Clinical Study of Pertuzumab, a Novel HER Dimerization Inhibitor, in Patients With Advanced Cancer. *J. Clin. Oncol.* **2005,** *23* (11), 2534–2543.
159. Heymach, J. V.; Nilsson, M.; Blumenschein, G.; Papadimitrakopoulou, V.; Herbst, R. Epidermal Growth Factor Receptor Inhibitors in Development for the Treatment of Non-Small Cell Lung Cancer. *Clin. Cancer Res.* **2006,** *12* (14 Pt 2), 4441s–4445s.
160. Gordon, M. S.; Matei, D.; Aghajanian, C.; Matulonis, U. A.; Brewer, M.; Fleming, G. F.; Hainsworth, J. D.; Garcia, A. A.; Pegram, M. D.; Schilder, R. J.; Cohn, D. E.; Roman, L.; Derynck, M. K.; Ng, K.; Lyons, B.; Allison, D. E.; Eberhard, D. A.; Pham, T. Q.; Dere, R. C.; Karlan, B. Y. Clinical Activity of Pertuzumab (rhuMAb 2C4), a HER Dimerization Inhibitor, in Advanced Ovarian Cancer: Potential Predictive Relationship With Tumor HER2 Activation Status. *J. Clin. Oncol.* **2006,** *24* (26), 4324–4332.
161. Agus, D. B.; Sweeney, C. J.; Morris, M. J.; Mendelson, D. S.; McNeel, D. G.; Ahmann, F. R.; Wang, J.; Derynck, M. K.; Ng, K.; Lyons, B.; Allison, D. E.; Kattan, M. W.; Scher, H. I. Efficacy and Safety of Single-Agent Pertuzumab (rhuMAb 2C4), a Human Epidermal Growth Factor Receptor Dimerization Inhibitor, in Castration-Resistant Prostate Cancer After Progression From Taxane-Based Therapy. *J. Clin. Oncol.* **2007,** *25* (6), 675–681.
162. Nahta, R.; Hung, M. C.; Esteva, F. J. The HER-2-Targeting Antibodies Trastuzumab and Pertuzumab Synergistically Inhibit the Survival of Breast Cancer Cells. *Cancer Res.* **2004,** *64* (7), 2343–2346.
163. Walshe, J. M.; Denduluri, N.; Berman, A. W.; Rosing, D. R.; Swain, S. M. A Phase II Trial With Trastuzumab and Pertuzumab in Patients With HER2-Overexpressed Locally Advanced and Metastatic Breast Cancer. *Clin. Breast Cancer* **2006,** *6* (6), 535–539.
164. (a) Cho, H. S.; Mason, K.; Ramyar, K. X.; Stanley, A. M.; Gabelli, S. B.; Denney, D. W., Jr.; Leahy, D. J. Structure of the Extracellular Region of HER2 Alone and in Complex With the Herceptin Fab. *Nature* **2003,** *421* (6924), 756–760; (b) Garrett, T. P.; McKern, N. M.; Lou, M.; Elleman, T. C.; Adams, T. E.; Lovrecz, G. O.; Kofler, M.; Jorissen, R. N.; Nice, E. C.; Burgess, A. W.; Ward, C. W. The Crystal Structure of a Truncated ErbB2 Ectodomain Reveals an Active Conformation, Poised to Interact With Other ErbB Receptors. *Mol. Cell* **2003,** *11* (2), 495–505.
165. Franklin, M. C.; Carey, K. D.; Vajdos, F. F.; Leahy, D. J.; de Vos, A. M.; Sliwkowski, M. X. Insights into ErbB Signaling From the Structure of the ErbB2-Pertuzumab Complex. *Cancer Cell* **2004,** *5* (4), 317–328.
166. Arnon, R.; Van Regenmortel, M. H. Structural Basis of Antigenic Specificity and Design of New Vaccines. *FASEB J.* **1992,** *6* (14), 3265–3274.
167. (a) Davies, J. S. The Cyclization of Peptides and Depsipeptides. *J. Pept. Sci.* **2003,** *9* (8), 471–501; (b) Katsara, M.; Tselios, T.; Deraos, S.; Deraos, G.; Matsoukas, M. T.; Lazoura, E.; Matsoukas, J.; Apostolopoulos, V. Round and Round We Go: Cyclic Peptides in Disease. *Curr. Med. Chem.* **2006,** *13* (19), 2221–2232.
168. Soffer, S. Z.; Moore, J. T.; Kim, E.; Huang, J.; Yokoi, A.; Manley, C.; O'Toole, K.; Stolar, C.; Middlesworth, W.; Yamashiro, D. J.; Kandel, J. J. Combination Antiangiogenic Therapy: Increased Efficacy in a Murine Model of Wilms Tumor. *J. Pediatr. Surg.* **2001,** *36* (8), 1177–1181.
169. Hanahan, D.; Christofori, G.; Naik, P.; Arbeit, J. Transgenic Mouse Models of Tumour Angiogenesis: The Angiogenic Switch, Its Molecular Controls, and Prospects for Preclinical Therapeutic Models. *Eur. J. Cancer* **1996,** *32A* (14), 2386–2393.
170. Nagy, J. A.; Benjamin, L.; Zeng, H.; Dvorak, A. M.; Dvorak, H. F. Vascular Permeability, Vascular Hyperpermeability and Angiogenesis. *Angiogenesis* **2008,** *11* (2), 109–119.
171. Gasparini, G.; Longo, R.; Toi, M.; Ferrara, N. Angiogenic Inhibitors: A New Therapeutic Strategy in Oncology. *Nat. Clin. Pract. Oncol.* **2005,** *2* (11), 562–577.
172. Keyt, B. A.; Nguyen, H. V.; Berleau, L. T.; Duarte, C. M.; Park, J.; Chen, H.; Ferrara, N. Identification of Vascular Endothelial Growth Factor Determinants for Binding KDR and FLT-1 Receptors. Generation of Receptor-Selective VEGF Variants by Site-Directed Mutagenesis. *J. Biol. Chem.* **1996,** *271* (10), 5638–5646.
173. (a) Muller, Y. A.; Li, B.; Christinger, H. W.; Wells, J. A.; Cunningham, B. C.; de Vos, A. M. Vascular Endothelial Growth Factor: Crystal Structure and Functional Mapping of the Kinase Domain Receptor Binding Site. *Proc. Natl. Acad. Sci. U. S. A.* **1997,** *94* (14), 7192–7197; (b) Muller, Y. A.; Chen, Y.; Christinger, H. W.; Li, B.; Cunningham, B. C.; Lowman, H. B.; de Vos, A. M. VEGF and the Fab Fragment of a Humanized Neutralizing Antibody: Crystal Structure of the Complex at 2.4 Å Resolution and Mutational Analysis of the Interface. *Structure* **1998,** *6* (9), 1153–1167.
174. Zilberberg, L.; Shinkaruk, S.; Lequin, O.; Rousseau, B.; Hagedorn, M.; Costa, F.; Caronzolo, D.; Balke, M.; Canron, X.; Convert, O.; Lain, G.; Gionnet, K.; Goncalves, M.; Bayle, M.; Bello, L.; Chassaing, G.; Deleris, G.; Bikfalvi, A. Structure and Inhibitory Effects on Angiogenesis and Tumor Development of a New Vascular Endothelial Growth Inhibitor. *J. Biol. Chem.* **2003,** *278* (37), 35564–35573.

175. Muller, Y. A.; Christinger, H. W.; Keyt, B. A.; de Vos, A. M. The Crystal Structure of Vascular Endothelial Growth Factor (VEGF) Refined to 1.93 Å Resolution: Multiple Copy Flexibility and Receptor Binding. *Structure* **1997,** *5* (10), 1325–1338.
176. (a) Goodman, M.; Ro, S.; Yamazaki, T.; Spencer, J. R.; Toy, A.; Huang, Z.; He, Y.; Reisine, T. Topochemical Design of Bioactive Peptides and Peptidomimetics. *Bioorg. Khim.* **1992,** *18* (10–11), 1375–1393; (b) Chorev, M.; Goodman, M. Recent Developments in Retro Peptides and Proteins—An Ongoing Topochemical Exploration. *Trends Biotechnol.* **1995,** *13* (10), 438–445; (c) Chorev, M. The Partial Retro-Inverso Modification: A Road Traveled Together. *Biopolymers* **2005,** *80* (2–3), 67–84.
177. Konecny, G. E.; Meng, Y. G.; Untch, M.; Wang, H. J.; Bauerfeind, I.; Epstein, M.; Stieber, P.; Vernes, J. M.; Gutierrez, J.; Hong, K.; Beryt, M.; Hepp, H.; Slamon, D. J.; Pegram, M. D. Association Between HER-2/neu and Vascular Endothelial Growth Factor Expression Predicts Clinical Outcome in Primary Breast Cancer Patients. *Clin. Cancer Res.* **2004,** *10* (5), 1706–1716.
178. (a) Sun, X.; Kanwar, J. R.; Leung, E.; Lehnert, K.; Wang, D.; Krissansen, G. W. Angiostatin Enhances B7.1-Mediated Cancer Immunotherapy Independently of Effects on Vascular Endothelial Growth Factor Expression. *Cancer Gene Ther.* **2001,** *8* (10), 719–727; (b) Kuo, C. J.; Farnebo, F.; Yu, E. Y.; Christofferson, R.; Swearingen, R. A.; Carter, R.; von Recum, H. A.; Yuan, J.; Kamihara, J.; Flynn, E.; D'Amato, R.; Folkman, J.; Mulligan, R. C. Comparative Evaluation of the Antitumor Activity of Antiangiogenic Proteins Delivered by Gene Transfer. *Proc. Natl. Acad. Sci. U. S. A.* **2001,** *98* (8), 4605–4610; (c) Nair, S.; Boczkowski, D.; Moeller, B.; Dewhirst, M.; Vieweg, J.; Gilboa, E. Synergy Between Tumor Immunotherapy and Antiangiogenic Therapy. *Blood* **2003,** *102* (3), 964–971.
179. Grunstein, J.; Roberts, W. G.; Mathieu-Costello, O.; Hanahan, D.; Johnson, R. S. Tumor-Derived Expression of Vascular Endothelial Growth Factor Is a Critical Factor in Tumor Expansion and Vascular Function. *Cancer Res.* **1999,** *59* (7), 1592–1598.
180. Schneider, B. P.; Wang, M.; Radovich, M.; Sledge, G. W.; Badve, S.; Thor, A.; Flockhart, D. A.; Hancock, B.; Davidson, N.; Gralow, J.; Dickler, M.; Perez, E. A.; Cobleigh, M.; Shenkier, T.; Edgerton, S.; Miller, K. D. Association of Vascular Endothelial Growth Factor and Vascular Endothelial Growth Factor Receptor-2 Genetic Polymorphisms With Outcome in a Trial of Paclitaxel Compared With Paclitaxel Plus Bevacizumab in Advanced Breast Cancer: ECOG 2100. *J. Clin. Oncol.* **2008,** *26* (28), 4672–4678.
181. Miller, M. J.; Foy, K. C.; Overholser, J. P.; Nahta, R.; Kaumaya, P. T. P. HER-3 Peptide Vaccines/Mimics: Combined Therapy With IGF-1R, HER-2, and HER-1 Peptides Induces Synergistic Antitumor Effects Against Breast and Pancreatic Cancer Cells. *Oncoimmunology* **2014,** *3* (11), e956012.
182. Foy, K. C.; Miller, M. J.; Overholser, J.; Donnelly, S. M.; Nahta, R.; Kaumaya, P. T. P. IGF-1R Peptide Vaccines/Mimics Inhibit the Growth of BxPC3 and JIMT-1 Cancer Cells and Exhibit Synergistic Antitumor Effects With HER-1 and HER-2 Peptides. *Oncoimmunology* **2014,** *3* (11), e956005.
183. Burgess, A. W.; Cho, H. S.; Eigenbrot, C.; Ferguson, K. M.; Garrett, T. P.; Leahy, D. J.; Lemmon, M. A.; Sliwkowski, M. X.; Ward, C. W.; Yokoyama, S. An Open-and-Shut Case? Recent Insights Into the Activation of EGF/ErbB Receptors. *Mol. Cell* **2003,** *12* (3), 541–552.
184. (a) Brennan, P. J.; Kumagai, T.; Berezov, A.; Murali, R.; Greene, M. I. HER2/Neu: Mechanisms of Dimerization/Oligomerization. *Oncogene* **2002,** *21* (2), 328; (b) Stern, D. F. ERBB3/HER3 and ERBB2/HER2 Duet in Mammary Development and Breast Cancer. *J. Mammary Gland Biol. Neoplasia* **2008,** *13* (2), 215–223.
185. Landgraf, R.; Eisenberg, D. Heregulin Reverses the Oligomerization of HER3. *Biochemistry* **2000,** *39* (29), 8503–8511.
186. (a) Lee-Hoeflich, S. T.; Crocker, L.; Yao, E.; Pham, T.; Munroe, X.; Hoeflich, K. P.; Sliwkowski, M. X.; Stern, H. M. A Central Role for HER3 in HER2-Amplified Breast Cancer: Implications for Targeted Therapy. *Cancer Res.* **2008,** *68* (14), 5878–5887; (b) Pinkas-Kramarski, R.; Soussan, L.; Waterman, H.; Levkowitz, G.; Alroy, I.; Klapper, L.; Lavi, S.; Seger, R.; Ratzkin, B. J.; Sela, M.; Yarden, Y. Diversification of Neu Differentiation Factor and Epidermal Growth Factor Signaling by Combinatorial Receptor Interactions. *EMBO J.* **1996,** *15* (10), 2452–2467; (c) Alimandi, M.; Romano, A.; Curia, M. C.; Muraro, R.; Fedi, P.; Aaronson, S. A.; Di Fiore, P. P.; Kraus, M. H. Cooperative Signaling of ErbB3 and ErbB2 in Neoplastic Transformation and Human Mammary Carcinomas. *Oncogene* **1995,** *10* (9), 1813–1821.
187. (a) Liu, B. L.; Ordonez-Ercan, D.; Fan, Z. Y.; Edgerton, S. M.; Yang, X. H.; Thor, A. D. Downregulation of erbB3 Abrogates erbB2-Mediated Tamoxifen Resistance in Breast Cancer Cells. *Int. J. Cancer* **2007,** *120* (9), 1874–1882; (b) Alaoui-Jamali, M. A.; Yen, L.; Benlimame, N.; Nie, Z. R.; Xiao, D. Z.; Wang, T. Q.; Al Moustafa, A. E.; Esumi, H.; Milanini, J.; Hynes, N. E.; Pages, G. Differential Regulation of Tumor Angiogenesis by Distinct ErbB Homo- and Heterodimers. *Mol. Biol. Cell* **2002,** *13* (11), 4029–4044; (c) Rajkumar, T.; Stamp, G. W. H.; Pandha, H. S.; Waxman, J.; Gullick, W. J. Expression of the Type 1 Tyrosine Kinase Growth Factor Receptors EGF Receptor, c-erbB2 and c-erbB3 in Bladder Cancer. *J. Pathol.* **1996,** *179* (4), 381–385; (d) Moasser, M. M.; Sergina, N. V. The HER Family and Cancer: Emerging Molecular Mechanisms and Therapeutic Targets. *Trends Mol. Med.* **2007,** *13* (12), 527–534; (e) Moasser, M. M.; Sergina, N. V.; Rausch, M.; Wang, D. H.; Blair, J.; Hann, B.; Shokat, K. M. Escape From HER-Family Tyrosine Kinase Inhibitor Therapy by the Kinase-Inactive HER3. *Nature* **2007,** *445* (7126), 437–441.
188. Engelman, J. A.; Zejnullahu, K.; Mitsudomi, T.; Song, Y.; Hyland, C.; Park, J. O.; Lindeman, N.; Gale, C. M.; Zhao, X.; Christensen, J.; Kosaka, T.; Holmes, A. J.; Rogers, A. M.; Cappuzzo, F.; Mok, T.; Lee, C.; Johnson, B. E.; Cantley, L. C.; Janne, P. A. MET Amplification Leads to Gefitinib Resistance in Lung Cancer by Activating ERBB3 Signaling. *Science* **2007,** *316* (5827), 1039–1043.
189. Amler, L.; Makhija, S.; Januario, T.; Lin, C. Y.; Derynck, M.; Birkner, M.; Matulonis, U.; Strauss, A.; Sliwkowski, M.; Paton, V. Downregulation of HER3: A Potential Surrogate for Activation of HER2 Through Heterodimerization may Predict Clinical Benefit in Ovarian Cancer From Pertuzumab, a HER Dimerization Inhibiting Antibody. *Mol. Cancer Ther.* **2007,** *6* (12), 3572s.
190. (a) Jordan, V. C.; Osipo, C.; Meeke, K.; Cheng, D.; Weichel, A.; Bertucci, A.; Liu, H. Role for HER2/neu and HER3 in Fulvestrant-Resistant Breast Cancer. *Int. J. Oncol.* **2007,** *30* (2), 509–520; (b) Lykkesfeldt, A. E.; Frogne, T.; Benjaminsen, R. V.; Sonne-Hansen, K.; Sorensen, B. S.; Nexo, E.; Laenkholm, A. V.; Rasmussen, L. M.; Riese, D. J.; de Cremoux, P.; Stenvang, J. Activation of ErbB3, EGFR and Erk Is Essential for Growth of Human Breast Cancer Cell Lines With Acquired Resistance to Fulvestrant. *Breast Cancer Res. Treat.* **2009,** *114* (2), 263–275; (c) Arteaga, C. L.; Miller, T. W.; Perez-Torres, M.; Narasanna, A.; Guix, M.; Stal, O.; Perez-Tenorio, G.; Gonzalez-Angulo, A. M.; Hennessy, B. T.; Mills, G. B.; Kennedy, J. P.; Lindsley, C. W. Loss of Phosphatase and Tensin Homologue Deleted on Chromosome 10 Engages ErbB3 and Insulin-Like Growth Factor-I Receptor Signaling to Promote Antiestrogen Resistance in Breast Cancer. *Cancer Res.* **2009,** *69* (10), 4192–4201.
191. Elenius, K.; Erjala, K.; Sundvall, M.; Junttila, T. T.; Zhang, N.; Savisalo, M.; Mali, P.; Kulmaia, J.; Pulkkinen, J.; Grenman, R. Signaling via ErbB2 and ErbB3 Associates With Resistance and Epidermal Growth Factor Receptor (EGFR) Amplification With Sensitivity to EGFR Inhibitor Gefitinib in Head and Neck Squamous Cell Carcinoma Cells. *Clin. Cancer Res.* **2006,** *12* (13), 4103–4111.
192. Hamburger, A. W.; Zhang, Y. X.; Linn, D.; Liu, Z. Q.; Melamed, J.; Tavora, F.; Young, C. Y.; Burger, A. M. EBP1, an ErbB3-Binding Cancer and Implicated in Protein, Is Decreased in Prostate Hormone Resistance. *Mol. Cancer Ther.* **2008,** *7* (10), 3176–3186.
193. (a) Balana, M. E.; Labriola, L.; Salatino, M.; Movsichoff, F.; Peters, G.; Charreau, E. H.; Elizalde, P. V. Activation of ErbB-2 via a Hierarchical Interaction Between ErbB-2 and Type I Insulin-Like Growth Factor Receptor in Mammary Tumor Cells. *Oncogene* **2001,** *20* (1), 34–47; (b) Camirand, A.; Lu, Y.; Pollak, M. Co-Targeting HER2/ErbB2 and Insulin-Like Growth Factor-1 Receptors Causes Synergistic Inhibition of Growth in HER2-Overexpressing Breast Cancer Cells. *Med. Sci. Monit.* **2002,** *8* (12), BR521–BR526.
194. Nahta, R. Deciphering the Role of Insulin-Like Growth Factor-I Receptor in Trastuzumab Resistance. *Chemother. Res. Pract.* **2012,** *2012,* 648965.
195. Jin, Q.; Esteva, F. J. Cross-Talk Between the ErbB/HER Family and the Type I Insulin-Like Growth Factor Receptor Signaling Pathway in Breast Cancer. *J. Mammary Gland Biol. Neoplasia* **2008,** *13* (4), 485–498.
196. Baserga, R.; Peruzzi, F.; Reiss, K. The IGF-1 Receptor in Cancer Biology. *Int. J. Cancer* **2003,** *107* (6), 873–877.
197. Zahorowska, B.; Crowe, P. J.; Yang, J. L. Combined Therapies for Cancer: A Review of EGFR-Targeted Monotherapy and Combination Treatment With Other Drugs. *J. Cancer Res. Clin. Oncol.* **2009,** *135* (9), 1137–1148.
198. Epa, V. C.; Ward, C. W. Model for the Complex Between the Insulin-Like Growth Factor I and Its Receptor: Towards Designing Antagonists for the IGF-1 Receptor. *Protein Eng. Des. Sel.* **2006,** *19* (8), 377–384.
199. (a) Dua, R.; Zhang, J.; Nhonthachit, P.; Penuel, E.; Petropoulos, C.; Parry, G. EGFR Over-Expression and Activation in High HER2, ER Negative Breast Cancer Cell Line Induces Trastuzumab Resistance. *Breast Cancer Res. Treat.* **2010,** *122* (3), 685–697; (b) Junttila, T. T.; Akita, R. W.; Parsons, K.; Fields, C.; Lewis Phillips, G. D.; Friedman, L. S.; Sampath, D.; Sliwkowski, M. X. Ligand-Independent HER2/HER3/PI3K Complex Is Disrupted by Trastuzumab and Is Effectively Inhibited by the PI3K Inhibitor GDC-0941. *Cancer Cell* **2009,** *15* (5), 429–440; (c) Ritter, C. A.; Perez-Torres, M.; Rinehart, C.; Guix, M.; Dugger, T.; Engelman, J. A.; Arteaga, C. L. Human Breast Cancer Cells Selected for Resistance to Trastuzumab in vivo Overexpress Epidermal Growth Factor Receptor and ErbB Ligands and Remain Dependent on the ErbB Receptor Network. *Clin. Cancer Res.* **2007,** *13* (16), 4909–4919.

200. (a) Miller, M. J.; Foy, K. C.; Overholser, J. P.; Nahta, R.; Kaumaya, P. T. HER-3 Peptide Vaccines/Mimics: Combined Therapy With IGF-1R, HER-2, and HER-1 Peptides Induces Synergistic Antitumor Effects Against Breast and Pancreatic Cancer Cells. *Oncoimmunology* **2014,** *3* (11), e956012; (b) Foy, K. C.; Miller, M. J.; Overholser, J.; Donnelly, S. M.; Nahta, R.; Kaumaya, P. T. IGF-1R Peptide Vaccines/Mimics Inhibit the Growth of BxPC3 and JIMT-1 Cancer Cells and Exhibit Synergistic Antitumor Effects With HER-1 and HER-2 Peptides. *Oncoimmunology* **2014,** *3* (11), e956005.
201. Cook, N.; Frese, K. K.; Bapiro, T. E.; Jacobetz, M. A.; Gopinathan, A.; Miller, J. L.; Rao, S. S.; Demuth, T.; Howat, W. J.; Jodrell, D. I.; Tuveson, D. A. Gamma Secretase Inhibition Promotes Hypoxic Necrosis in Mouse Pancreatic Ductal Adenocarcinoma. *J. Exp. Med.* **2012,** *209* (3), 437–444.
202. Foy, K. C.; Liu, Z.; Phillips, G.; Miller, M.; Kaumaya, P. T. Combination Treatment With HER-2 and VEGF Peptide Mimics Induces Potent Anti-Tumor and Anti-Angiogenic Responses in vitro and In Vivo. *J. Biol. Chem.* **2011,** *286* (15), 13626–13637.
203. Foy, K. C.; Miller, M. J.; Moldovan, N.; Carson, W. E.; Kaumaya, P. T. P. Combined Vaccination With HER-2 Peptide Followed by Therapy With VEGF Peptide Mimics Exerts Effective Anti-Tumor and Anti-Angiogenic Effects In Vitro and In Vivo. *Oncoimmunology* **2012,** *1* (7), 1048–1060.
204. (a) Kaumaya, P. T. Could Precision-Engineered Peptide Epitopes/Vaccines Be the Key to a Cancer Cure? *Future Oncol.* **2011,** *7* (7), 807–810; (b) Kaumaya, P. T.; Foy, K. C. Peptide Vaccines and Targeting HER and VEGF Proteins may Offer a Potentially New Paradigm in Cancer Immunotherapy. *Future Oncol.* **2012,** *8* (8), 961–987.
205. Kyte, J.; Dolittle, R. F. A Simple Method for Displaying the Hydropathic Character of a Protein. *J. Mol. Biol.* **1982,** *157* (1), 105–132.
206. Hopp, T. P.; Woods, K. R. Prediction of Protein Antigenic Determinants from Amino Acid Sequences. *Proc. Natl. Acad. Sci. USA* **1981,** *78,* 3824–3828.
207. Parker, J. M.; Guo, D.; Hodges, R. S. New Hydrophilicity Scale Derived from High-performance Liquid Chromatography Peptide Retention Data: Correlation of Predicted Surface Residues with Antigenicity and X-ray-Derived Accessible Sites. *Biochemistry* **1986,** *25* (19), 5425–5432.
208. Fraga, S. Theoretical Prediction of Protein Antigenic Determinants from Amino Acids. *Can. J. Chem* **1982,** *60,* 2606.
209. Janin, J. Surface and Inside Volumes in Globular Proteins. *Nature* **1979,** *277* (5696), 491–492.
210. Novotny, J.; Handschumacher, M.; Haber, E.; Bruccoleri, R. E.; Carlson, W. B.; Fanning, D. W.; Smith, J. A.; Rose, G. D. Antigenic Determinants in Proteins Coincide with Surface Regions Accessible to Large Probes (Antibody Domains). *Proc. Natl. Acad. Sci. USA* **1986,** *83,* 226–230.
211. Hopp, T. Prediction of Protein Surfaces and Interaction Sites from Amino Acid Sequences. In *Synthetic Peptides in Biology and Medicine;* Alitalo, K., Partanen, P., Vaheri, A., Eds.; 1985; pp 3–12.
212. Welling, G. W.; Weijer, W. J.; van der Zee, R.; Welling-Wester, S. Prediction of Sequential Antigenic Regions in Proteins. *FEBS Lett* **1985,** *188* (2), 215–218.

6.02 Cancer Immunotherapy

R Ajina, D AlDeghaither, S Jablonski, and LM Weiner, Georgetown University School of Medicine, Washington, DC, United States

© 2017 Elsevier Ltd. All rights reserved.

6.02.1	**Cancer and the Immune System**	32
6.02.1.1	The Immune System Is Crucial for Survival	32
6.02.1.2	Components of the Immune System	33
6.02.1.2.1	Innate immunity	33
6.02.1.2.2	Adaptive immunity	33
6.02.1.2.3	Phagocytosis	34
6.02.1.2.4	Antigen presentation	34
6.02.1.2.5	T-cell activation	34
6.02.1.2.6	B-cell activation	34
6.02.1.2.7	Antibodies	34
6.02.1.2.8	Cytokines	35
6.02.1.2.9	Complement	35
6.02.1.3	Cancer Immunity	35
6.02.1.3.1	Cancer cells can overwhelm the host immune system	35
6.02.1.3.2	Cancers can hide from the host immune system	35
6.02.1.3.3	Cancers can subvert the immune system	36
6.02.1.3.4	Cancers can erect shields to deflect the immune system	36
6.02.1.3.5	Cancer cells can acquire resistance to immune cell killing	37
6.02.1.3.6	Cancer cells can defend against T-cell frontal assaults	37
6.02.2	**Cancer Immunotherapy**	37
6.02.2.1	The Principle of Cancer Immunotherapy	37
6.02.2.2	Limitations of Conventional Cancer Treatments	37
6.02.2.3	History of Cancer Immunotherapy	38
6.02.2.4	Cancer Immunoediting	39
6.02.2.5	Types of Cancer Immunotherapy	39
6.02.2.5.1	Monoclonal antibodies	39
6.02.2.5.2	Cellular cancer immunotherapy	46
6.02.2.5.3	Cancer vaccines	48
6.02.2.5.4	Cytokines	49
6.02.2.6	Targets for Cancer Immunotherapy	50
6.02.2.6.1	Targeting cancer cells	50
6.02.2.6.2	Targeting the tumor microenvironment	53
6.02.2.6.3	Targeting immune cells	55
6.02.2.7	Future Directions	57
References		58

6.02.1 Cancer and the Immune System

Since President Richard Nixon declared war on cancer in 1971, real progress has been made to improve cancer prevention, early detection, and treatment.[1,2] This effort has led to a decrease in the mortality rates for most cancers, including lung, breast, colon, and prostate.[3] Nevertheless, the war on cancer has not been won, and much work remains to be done.[1] In the United States, cancer is the second most common cause of death, exceeded only by heart disease.[4] It is estimated that ~1.6 million cases are diagnosed and about 585,720 cancer patients die from this disease yearly, in the United States.[5] It is expected that over the next 14 years, cancer will surpass heart disease and become the leading cause of death.[6]

Typically, host immunity can detect and destroy cancer cells through an immune surveillance mechanism.[7] However, some malignant cells have the capacity to adapt to immune selection pressures, thereby avoiding immune-mediated destruction.[8] To restore and enhance the immune system's ability to fight cancer, it is important to first understand the link between cancer and immunity.

6.02.1.1 The Immune System Is Crucial for Survival

The immune system is composed of diverse organs, tissues, cells, and soluble molecules. All these components work together, in a highly organized manner, to protect individuals from external and internal dangers.[9] In fact, humans are exposed to millions of

potential pathogens every day.[10] To protect the body from these dangerous invaders, the immune system identifies the pathogens, eliminates them, and creates a memory response to prevent future infection.[9] Moreover, although the human body is home to billions of microbiota,[11] this system can differentiate between harmful and beneficial microorganisms. Additionally, in a human body with 37.2 trillion cells,[12] billions of cells experience mutations every day.[10] Some of these mutations can transform normal cells into cancerous cells.[13] Fortunately, the human body has efficient anticancer defense mechanisms, including tumor immune surveillance.[14] This process allows the immune system to recognize and destroy cancerous and/or precancerous cells leaving normal cells intact.[7]

6.02.1.2 Components of the Immune System

6.02.1.2.1 Innate immunity

The immune system is typically divided into two main categories: innate and adaptive. The innate immune system is so named because it is present at birth. It involves physical and chemical barriers and cellular and humoral components. Innate immunity has readily available recognition properties that are not specifically directed against a particular organism or target. For example, skin prevents the entry of pathogens, mucus in the respiratory tract traps dirt and dangerous molecules, and tears and saliva have antibacterial enzymes that work like antibiotics. When these barriers fail, humoral and cellular components orchestrate an effective response against the invader. An invading pathogen then activates the complement system and stimulates cytokine production, which can recruit innate killer cells. These cells include granulocytes (basophils, eosinophils, and neutrophils), mast cells, macrophages, dendritic cells (DCs), and natural killer (NK) cells (Fig. 1).[9] Whether or not the innate immune response eliminates the danger, it may trigger an adaptive immune response through now well-understood mechanisms.[15]

6.02.1.2.2 Adaptive immunity

The adaptive immune response is also called the acquired immune response because it is acquired after the exposure to foreign antigens. It involves T and B lymphocytes and their secretory molecules (Fig. 1). B cells and T cells can recognize specific structures, called epitopes, on antigens that elicit immune responses. Primary lymphoid organs, including bone marrow and the thymus, produce the primary repertoire of B and T lymphocytes. These cells remain naive and inactive, until they interact with antigens

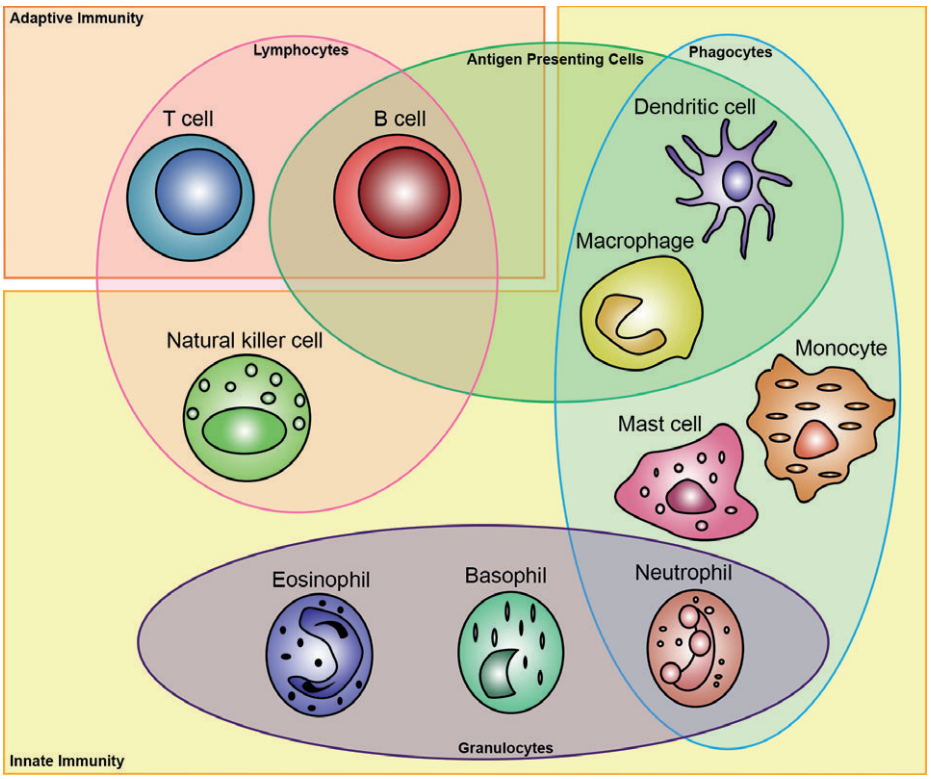

Fig. 1 Cells of the immune system. The immune system has two major functional components: innate and adaptive. Cellular components involved in the innate immune response include natural killer cells, granulocytes (neutrophils, basophils, and eosinophils), macrophages, and dendritic cells. Some of these cell populations function as professional antigen-presenting cells, as do B lymphocytes. Innate immunity thus has direct antiinfection and antitumor properties and also presents antigens to cells of the adaptive immune system, which is composed of B lymphocytes and T lymphocytes.

in secondary lymphoid tissues, such as lymph nodes, tonsils, spleen, Peyer's patches, and mucosa-associated lymphoid tissue. Following activation of naive T cells and B cells, they differentiate into effector cells and memory cells. Although B and T lymphocytes have some similarities, they differ in many aspects. First, B cells are produced by the bone marrow, whereas T cells originate in the bone marrow, but then they move to the thymus to complete their maturation. Second, the B-cell receptor (BCR) is composed of a membrane-bound immunoglobulin molecule bound to a signal transduction moiety (CD79). Immunoglobulins can also be synthesized in secreted forms by activated B cells or plasma cells. Thus, B lymphocytes can interact with free and membrane-bound antigens. Also, they recognize both linear (i.e., peptide sequences) and conformational epitopes with exquisite specificity and high affinity. In contrast, the T-cell receptors (TCR) are located on the surface of T lymphocytes. They can only recognize short peptide fragments bound to major histocompatibility complex proteins (MHCs) on antigen-presenting cells (APCs).[9] Of note, although it has been known for decades that only adaptive immune cells have immunologic memory, recent studies have shown that innate immune cells can also remember previously encountered antigens.[16]

6.02.1.2.3 Phagocytosis

Phagocytosis is a process mediated by a specialized group of innate immune cells called phagocytes, including neutrophils, monocytes, macrophages, DC, and mast cells. During phagocytosis, phagocytes engulf solid particles, larger than 0.5 μm in diameter, such as bacteria and dead tissue cells. After internalization, these particles are confined to intracellular vesicles called phagosomes, which then fuse with endosomes or lysosomes forming phagolysosomes. These vesicles contain enzymes and toxic peroxides that are able to break down the engulfed particles. Besides clearance and neutralization, macrophages and dendritic cells, which function also as APCs, are important in processing and presenting the phagocytosed antigens to T cells. Additionally, phagocytosis is typically accompanied by the production of inflammatory cytokines, which can recruit innate immune cells to the site of infection and, ultimately, determine the nature of the adaptive immune response.[17]

6.02.1.2.4 Antigen presentation

All nucleated cells have the ability to process and present antigens via MHC class I (MHC I), which can activate cytotoxic $CD8^+$ T cells. Therefore, all mammalian cells, except red blood cells (RBCs), are considered as nonprofessional APCs. By contrast, professional APCs, including DCs, macrophages, and B lymphocytes, are highly specialized cells. They can process and present an antigen together with MHC I or MHC class II (MHC II) on their surfaces. Thereby, this Ag–MHC complex can stimulate helper $CD4^+$ T cells or cytotoxic $CD8^+$ T cells, respectively.[9] It should be noted that although antigen presentation is required for T-cell activation, this process does not initiate an immune response in and of itself.[1]

6.02.1.2.5 T-cell activation

There are two signals required for the activation of naive T cells. The first signal is called "signal 1" or "recognition signal." It involves the specific recognition of an Ag–MHC complex by TCR in the context with CD4 or CD8 coreceptors. The second signal is called "signal 2" or "costimulatory signal." It is provided through the binding of APC-based B7.1 or B7.2 molecules to CD28 on T cells. By delivering only signal 1, the antigen would not be recognized by TCR, leading to T-cell deletion or rendering them unresponsive (anergic). In contrast, T cells that receive the second signal only cannot recognize the specific peptide and thereby may remain naive. In other words, to activate a T cell, it has to get stimulated by an APC through both signal 1 and signal 2, and receiving one of the signals only is not sufficient. Once they are activated, T lymphocytes can proliferate and differentiate into effector cells, such as cytotoxic and helper T cells, or memory T cells.[9]

On the other hand, because there are severe adverse effects of immune system overstimulation, this process has to be tightly regulated. Hence, activated T cells are typically turned off once they have done their jobs and before they develop chronic inflammation and tissue damage. In fact, deactivating T cells is very important to maintain self-tolerance and prevent autoimmunity. There are many strategies employed by the immune system to reduce the activity of effector T cells. This includes (1) induction of immunomodulatory cytokines, such as interleukin 10 (IL-10) and transforming growth factor beta (TGF-β); (2) stimulation of immunosuppressive cells, such as regulatory T (T-reg) cells; and (3) upregulation of immune checkpoints, including anticytotoxic T lymphocyte-associated antigen 4 (CTLA-4), and antiprogrammed death 1 (PD-1).[1,18]

6.02.1.2.6 B-cell activation

Mature B cells released from the bone marrow remain inactive in peripheral tissues until they interact with an antigen. As mentioned earlier, the B cell is one of the three professional APCs.[9] Thus, engagement of a BCR with an antigen initiates a cascade of intracellular signaling, leading to the internalization of the antigen, processing, and presentation on an MHC II molecule to $CD4^+$ T cells.[19] The activated T cells can then provide a second activation signal to the B cell, resulting in B-cell proliferation and differentiation into a plasma cell, the antibody-producing cell, or memory B cell.[20]

6.02.1.2.7 Antibodies

Antibodies are the major components of the humoral immune response. Each antibody interacts with the specific antigen that induced B-cell activation and immunoglobulin production.[20] Antibodies can eliminate immunogenic molecules and manipulate cell biology through several mechanisms, for example, antibody-dependent cellular cytotoxicity (ADCC), complement-dependent cytotoxicity (CDC), cell signaling disruption, antibody-dependent cellular phagocytosis (ADCP), agglutination, and

neutralization.[21] Nowadays, antibody-based drugs have become one of the most important therapeutics for cancer.[22,23] Further details will be discussed later in this article.

6.02.1.2.8 Cytokines

The term cytokine encompasses a large and diverse family of regulatory molecules.[24] They are low-molecular-weight bioactive proteins[25] that are used as a common chemical language for communication within and between cells.[26] They play a major role in regulating cellular proliferation, survival, differentiation, activation, migration, and death. Depending on many factors, such as cytokine concentrations, cytokine receptor expression, type of secretory cells, and the activation state of surrounding cells, they can mediate either local or systemic effects. Also, they can induce antitumor or protumor immune responses.[27]

6.02.1.2.9 Complement

The complement system is a proteolytic cascade made up of a large number of distinct proteins that interact with one another. Besides recruiting immune cells to the problem area, the complement proteins can promote the destruction of free pathogens in the circulation via agglutination reaction. They tag their targets in a process called opsonization, allowing the immune system to recognize and eliminate the danger. Also, they can cause target cell lysis through the formation of a membrane attack complex (MAC).[20]

6.02.1.3 Cancer Immunity

There are many escape routes that cancer cells can employ to overcome an antitumor immune response, for example, overwhelming, hiding from, subverting, shielding from, outlasting, and defending against the host immune response. However, these cells only do what is advantageous for their growth and survival. They do not use all the immune escape strategies, and they do not use any one arbitrarily.[1] Also, the selected strategies are not fixed, but are constantly changing.[28,29] Accordingly, to restore the immune system's ability to eliminate the cancer, we need to understand the immune escape mechanisms and determine which ones are dominantly employed in a particular patient.

6.02.1.3.1 Cancer cells can overwhelm the host immune system

Lymphoma and leukemia are cancers that start in leukocytes located in the lymph nodes and in the blood, respectively. Transformation of immune cells, such as T and B lymphocytes, into malignant cells promotes ineffective regulation of immunologic recognition and function, leading to ineffective anticancer immune responses.[30] Moreover, some rapidly proliferating malignancies might create a rapidly expanding tumor burden that overwhelms the kinetics and amplitude of available immune defense mechanisms.[1] To restore host immunity against cancer cells, autologous or allogeneic T cells can be infused into patients. In some situations, T cells genetically modified to react against an accessible tumor-related antigen, that is, chimeric antigen receptor (CAR) T cells, have shown remarkable antitumor properties.[31] T-cell immunotherapy involves the use of T cells that replace ineffective host immunity with cells bearing potent effector functions against tumor antigens.[32] However, if a cancer cell population employs other escape mechanisms that suppress T-cell activation, homing, or function, T-cell therapy alone would not be sufficient to restore a patient's immunity and to eradicate malignant cells. Thus, immunotherapy combinations might be needed.[33]

6.02.1.3.2 Cancers can hide from the host immune system

Malignant cells can avoid immune detection by either hiding their antigens or hiding themselves physically. For example, cancer cells might reduce antigen presentation so that T cells are blind to their presence.[33] In support of this hypothesis is the fact that many types of malignancies can lose up to 90% of normal MHC I expression.[34] Also, loss of members of the antigen-processing machinery (APM), such as the transporter associated with antigen processing (TAP), the endoplasmic reticulum aminopeptidase associated with antigen processing (eraap in mice and erap1 and erap2 in humans), and tapasin, was shown to correlate with poor cancer prognosis. These molecules are responsible for antigen translocation into the endoplasmic reticulum (ER), final trimming, and editing of the peptide before loading on MHC I.[35] Many oncogenes that are highly expressed in aggressive malignancies can interfere with antigen presentation and promote the outgrowth of MHC I-deficient tumor types. For example, it has been suggested that HER2 oncogene expression is inversely correlated with MHC I and TAP. To emphasize this, the level of surface MHC I on HER2+ breast carcinoma cell lines was evaluated after HER2 silencing by siRNA. This experiment showed significant increase in MHC I expression after HER2 knockdown. Moreover, it was reported that HER2 overexpression may induce defects in APM components. Consequently, it is suggested that HER2 has an important role in protecting cancer cells from immune system-mediated destruction.[36] Another strategy that tumors employ to reduce antigen presentation is by downregulating target antigen expression.[37] Poor tumor antigenicity stimulates a weak, slow, and nondestructive anticancer immune response. This phenotype, which is also called immunoediting, allows tumor cells to escape from immune-mediated rejection and promote cancer progression.[38]

The most important immune cells that can kill cancers directly are cytotoxic T lymphocytes (CTLs) and NK cells.[39] Interestingly, these cells perform complementary roles; CTLs lyse tumors expressing antigens on MHC I, and NK cells lyse cells lacking MHC I on their surface.[40] This shows how the immune system carefully orchestrates the elimination of abnormal cells. The question of how cancer cells elude these seemingly complementary lines of defense has not yet been fully elucidated. One possible explanation is that NK cell-mediated immunosurveillance is not sufficient to eliminate cancer cells. It is argued that in most cases immune cell infiltrates contain many more T cells than NK cells.[35] Another explanation is that MHC I can act as tumor suppressor molecule.

Thus, its downregulation promotes tumor progression that outweighs the antitumor effects of NK cells. In fact, it has been reported that in human melanoma cells, MHC I regulates cell cycle gene expression, invasion, cellular proliferation, and intrinsic oncogenic capacity.[41] Another possible interpretation is that tumor cells can overcome the absence of MHC I molecules by expressing inhibitory ligands, such as the nonclassical MHC I human leukocyte antigens G (HLA-G) and E (HLA-E). Nevertheless, the evidence supporting this hypothesis of the "replacement model" is not very strong. Indeed, HLA-E can stimulate both inhibition and activation of antigen presentation, and its presence can be associated with good and bad prognosis. Also, HLA-E expression may not be restricted to MHC I-deficient tumors.[35]

In addition, malignant cells can be physically sequestered from immune recognition and destruction through three different mechanisms. For example, some malignancies such as pancreatic adenocarcinoma may develop within dense collagenous stroma in the tumor microenvironment (TME).[42,43] The fibrotic TME in pancreatic cancers, which are generally associated with poor prognosis and high mortality rates, serves as a physical and functional barrier between the pancreatic tumor and immune cells, potentially allowing cancer cells to avoid immune surveillance.[44] Second, malignant cells growing in immune-privileged sites, such as the brain or the eye, cannot be detected by host immunity. Finally, cancer cells that fail to migrate to lymph nodes, where antigens can be presented to adaptive immune cells, might escape from immune recognition.[42]

6.02.1.3.3 Cancers can subvert the immune system

Under the influence of cellular transformation, cancer cells, immune cells, and stromal cells secrete immune-inhibitory cytokines, such as IL-10, IL-6, and TGF-β.[26] Simultaneously, cancer cells stimulate the local induction of immunosuppressive cells, including T-reg cells, myeloid-derived suppressor cells (MDSCs), tumor-associated fibroblasts (TAFs), "type 2" macrophages, and DCs. As a consequence, malignant cells become able to escape from cancer immune surveillance.[1] Not surprisingly, many clinical trials have aimed to restore the immune-activating microenvironment by neutralizing the suppressive cytokines[26] and/or targeting the cellular components of the immunosuppressive TME.[45–47]

Furthermore, cancer cells can subvert antitumor host immunity by promoting hypoxia and manipulating cellular metabolism.[48] An example of metabolism-mediated immune escape strategy used by cancer cells is the modulation of the tryptophan (TRP) to kynurenine (KYN) metabolic pathway. In this pathway, tumor cells or myeloid cells express high levels of indoleamine 2,3-dioxygenase 1 (IDO1), which is the first and rate-limiting enzyme in the degradation of TRP. Subsequently, when T cells are starved for TRP, they cannot divide and thus cannot respond to the activation signals. Therefore, it is suggested that targeting IDO1 or the other key components of this pathway, such as general control nondepressible 2 (GCN2) and TRP-2,3-dioxygenase 2 (TDO), may reverse cancer-associated immunosuppression.[49] To test this hypothesis, many clinical trials have been launched to evaluate the safety and efficacy of IDO1-targeting interventions in cancer patients.[50] In line with that, it is hypothesized that adding IDO1 inhibitors to immune checkpoint inhibitors may improve patients' outcomes.[51] To examine this idea, mouse syngeneic tumor models were utilized to demonstrate that treatment with the combination of an IDO1 inhibitor and anti-PD-L1 antibody improved antitumor immunity and efficacy compared with the mice treated with anti-PD-L1 alone.[52]

Another mechanism of metabolism-mediated immune escape in cancer is hypoxia-driven immunosuppression. Under conditions of low oxygen supply, cancer cells tend to change their metabolic phenotypes to enhance their survival and progression. Also, hypoxia can modulate the function of the surrounding immune cells and vascular cells to further promote tumorigenesis and cancer immune evasion.[53] The master regulators of hypoxia are the transcription factors hypoxia-inducible factors (HIFs).[54] They are stimulated in response to limited O_2 supply[55] and can be stabilized via upregulation of glycolysis. Interestingly, it has been shown that HIF transcription factors can mediate immunosuppression through multiple mechanisms. For example, HIF-1a can stimulate expansion of MDSCs and promote their differentiation toward tumor-associated macrophages (TAMs). Also, hypoxia can enhance T-cell differentiation toward the tumor-promoting T-helper 2 (T_H2) phenotype and away from the antitumor T_H1 phenotype.[53] This concept was supported by various preclinical studies in animal models with HIF-1a deletions or knockdown. These studies revealed that the HIF-1a-deficient CTLs and helper T cells can produce more pro-inflammatory cytokines, such as IFN-γ, compared with HIF-1a-expressing control T cells, confirming the role of HIF-1a in T-cell suppression.[56] Based on this observation, it was hypothesized that because innate and adaptive immune cells are modified under poor oxygen supply, targeting tumor hypoxia in combination with immunotherapies might improve cancer treatments.[57]

6.02.1.3.4 Cancers can erect shields to deflect the immune system

Another mechanism that cancers employ to elude the immune system is shedding cancer-related antigens into the circulation and/or surrounding microenvironment, and thus, T cells may be accordingly diverted.[1] In fact, circulating tumor-associated antigens can be ingested and presented by a specific type of APC, liver sinusoidal endothelial cells (LSECs). The recognition of the peptide–MHC complex on LSEC by antigen-specific $CD8^+$ T cells can lead to the production of functionally incapacitated cytotoxic T cells. These cells are neither able to produce cytokines nor able to directly kill antigen-expressing tumor cells.[58,59] Interestingly, this feature has been reported in various cancer types, including carcinoembryonic antigen (CEA) in colorectal carcinoma (CRC),[60] cancer antigen-125 (CA125) in ovarian cancer,[61] HER2/neu in breast cancer,[62] and prostate-specific antigen (PSA) in prostate cancer.[63] Nevertheless, although antigen shedding might contribute to tumor immune escape, it can improve the efficiency for the delivery of cancer antibody-based therapeutics.[64]

6.02.1.3.5 Cancer cells can acquire resistance to immune cell killing

CTLs and NK cells mediate their cytotoxic functions by activating either the death receptor pathway or the granule exocytosis pathway. In the death receptor pathway, death ligands on tumor-specific CTLs or NK cells engage their receptors, such as Fas ligand (FasL/CD95L/APO1L), or the TNF-related apoptosis-inducing ligand (TRAIL/Apo2L) on the target cell surface.[42] Then, the receptor–ligand interaction induces the extrinsic cascades to initiate apoptosis, which causes target cell death.[53] It has been shown that cancer cells can develop resistance to immune cell killing by modulating the death receptor pathway.[42] In fact, in human CRC patients, loss of Fas expression and/or function is associated with enhanced metastatic potential of colon carcinoma cells. It is suggested that Fas-deficient tumor cells preexist in the primary colon cancers. Then, under immune-selective pressure, these Fas-resistant cell populations emerge and influence cancer metastatic capability. Supporting evidence comes from the observation that, in FasL knockout mice, the increase in spontaneous tumor metastasis is associated with a deficiency of the Fas-mediated apoptosis.[65]

However, it must be stressed that within the context of cancer development, the decrease in Fas expression and function acts only as an "enhancer" and not as an "initiator."[65] Moreover, although directly targeting FasL and using Fas receptor agonists were hoped to be useful for cancer therapy, these treatments resulted in severe toxicities that have precluded their systemic use.[66] TRAIL-R1 and TRAIL-R2, deletions, mutations, and downregulation of these receptors have been reported in many types of cancer, including head and neck cancer and nonsmall cell lung cancers. As expected, these alterations can impair tumor immunosurveillance by NK and T cells, promoting cancer immune evasion and progression.[42] To elucidate the role of TRAIL ligand–receptor signaling in tumor development, different mouse models were utilized. Preclinical studies showed that neutralization of TRAIL in tumor mouse models promotes tumor development and may also enhance tumor metastasis in perforin-deficient mice.[67] Unlike Fas/FasL targeting therapies, TRAIL receptor agonists (TRAs) should more selectively trigger apoptosis in cancer cells. This strategy has demonstrated robust antitumor activity in many preclinical studies.[68]

Furthermore, NK cell and CTL-mediated lysis by cytotoxic granules plays a critical role in adaptive immunity against cancer cells.[69] In the granule exocytosis pathway, the pore-forming protein, perforin, secreted by activated immune cells, promotes granzyme delivery to the target cell cytosol. After entry, the granzymes cleave their intracellular substrates, inducing membrane damage and target cell swelling and lysis.[51,53] Interestingly, it has been reported by many groups that perforin-deficient mice and humans are more susceptible to cancer.[70]

6.02.1.3.6 Cancer cells can defend against T-cell frontal assaults

Besides the suppression effects of immune-modulatory cytokines and immunosuppressive cells, cancer cells can upregulate immune checkpoints to further defend against effector T cells.[18,71] As mentioned earlier, immune checkpoint pathways are critical to avoiding autoimmunity and immune system overstimulation. However, during malignancy, these pathways are commonly co-opted by cancer cells, leading to suppression of antitumor immunity.[18,1] Targeting immune checkpoints, such as CD28/CTLA4 and PD-1/PD-L1 pathways, has been shown to have significant clinical efficacy in many types of cancer.[72–75] Indeed, these immunotherapies are able to restore antitumor immunity and mediate very prolonged tumor regressions, allowing them to receive great attention.[76]

In addition, tumor cells may defend against T cells by utilizing the FasL/Fas pathway. Activated lymphocytes typically express Fas receptors. Therefore, it is hypothesized that high expression of Fas on the surface of cancer cells enables them to kill tumor-infiltrating lymphocytes (TILs). Although it is still controversial, it was reported that malignant cells can induce apoptosis of Fas-sensitive lymphocytes in vitro. Also, FasL expression has shown to be associated with increased apoptosis of tumor-infiltrating effector cells in vivo. These results suggest that increased expression of FasL on the cancer cell surface might be considered as a tumor escape mechanism.[77] Notably, besides immune checkpoints and FasL, cancer cells can overexpress many other ligands for negative regulatory receptors on T cells, such as CD200 and receptor-binding cancer antigen expressed on SiSo cells-1 (RCAS1).[78]

6.02.2 Cancer Immunotherapy

6.02.2.1 The Principle of Cancer Immunotherapy

It is well established that the immune system can identify cancer cells and destroy them in a process called immunosurveillance.[7] However, it also has the ability to edit cancer cells and induce their immune evasion.[8] Therefore, cancer immunotherapies are designed to cure cancer by enhancing the cancer immunosurveillance activity and/or restoring antitumor host immunity.

6.02.2.2 Limitations of Conventional Cancer Treatments

The traditional types of cancer treatments are surgery, chemotherapy, radiation therapy, and targeted therapy. Surgery is the oldest discipline among these oncological treatments. It has been thought that Leonidas of Alexandria was the first to describe an oncologically adequate surgical procedure.[79] In the 1st century AD, he removed breast cancerous cells with adjacent healthy cells by alternately cutting and cauterizing the tissue with hot irons.[80] Nowadays, surgery remains the most effective single modality in cancer treatment.[79] Nonetheless, curative surgery is limited to localized tumors.[81,82] Moreover, in many cases, surgery alone may not be sufficient to decrease the chance of metastasis[83] or tumor recurrence.[84–86]

After the use of surgery in cancer treatment, radiation therapy was implemented to treat localized malignant tumors that were not surgically removed. The field of radiation oncology was born a few years after the discovery of X-rays in 1895 by Wilhelm

Conrad Röntgen.[87] The principle of radiation therapy is to use a very high dosage of radiation to damage cancer cells. Then, DNA damage can lead to the death of cancer cells and tumor shrinkage.[88] Despite the fact that radiation therapy is used to treat about half of all solid tumors, it has limitations. For example, it can cause early and late toxicity and have a negative impact on quality of life in patients.[89] Also, radiation therapy is primarily a local modality.[90]

Later, it was found that chemotherapy could be used to treat cancers that could not be removed by surgery or destroyed by radiation. During the Second World War, the US military sent pathologists to conduct autopsies from soldiers affected by mustard gas, a chemical agent that was used in the war, to uncover the mechanism of its toxicity. Unexpectedly, pathologists found that affected individuals had profoundly low levels of white blood cells with shrinkage of lymph nodes. This finding encouraged the US Department of Defense (DOD) to study the potential therapeutic applications of mustard gas. DOD recruited two pharmacologists from the Yale School of Medicine, Louis Goodman and Alfred Gilman. The hypothesis was that if mustard gas could destroy normal white blood cells, it might be able to destroy cancer cells, too. When the preclinical animal experiments supported the hypothesis, a patient with non-Hodgkin's lymphoma was treated with nitrogen mustard. This chemotherapy showed great impact on the patient's health; however, the effect only lasted for a few weeks.[91] Mechanistic studies showed that the chemotherapy disrupted the DNA of replicating malignant cells. In addition, chemotherapy can damage the DNA of normal, actively replicating cells, such as cells in the bone marrow and in the digestive system, and hair follicles. Therefore, chemotherapy not only can be effective but also has significant toxicities.[92]

In the late 1990s, with the advance in molecular biology techniques, scientists identified many molecules in/on cancer cells that can enhance malignant cell proliferation and survival.[93] Thus, new therapies have been developed to more selectivity target malignant cells. As a result, targeted therapies are predicted to kill cancer cells with less toxicity[94] and fewer or different off-target effects compared with chemotherapy and radiation therapy.[95] Nevertheless, cancer cells have shown to be highly resilient drug targets, since resistance frequently emerges to all[96] but a handful of targeted therapies, such as BCR-ABL inhibitors in chronic myelogenous leukemia (CML).[1]

Today, immunotherapy has been added as an important modality of cancer therapy, supplementing and in some cases replacing the need for traditional modalities such as chemotherapy.[97,98]

6.02.2.3 History of Cancer Immunotherapy

In the early 1890s, Dr. William B. Coley noticed that some cancer patients with acute bacterial infections had spontaneous tumor regressions. Based on this observation, he injected a patient with an inoperable soft tissue sarcoma with Coley's toxins,[99] which was composed of a mixture of live *Streptococcus*, *Serratia marcescens*, *Staphylococcus*, and *Escherichia coli* bacteria.[100] Interestingly, the tumor in that patient underwent extensive necrosis, and the patient remained disease-free until he died of heart disease 33 years later.[101] Nevertheless, at that time, there was an increasing emphasis on X-ray and radium treatment and, subsequently, chemotherapy.[100] By contrast, Coley's work was not reproducible and most cases treated with his method ended in failure and death.[102,103] Therefore, the field of cancer immunology was neglected for many years.

In 1909, Paul Ehrlich, a Nobel Prize winner, also predicted a role for immunity in protecting against tumors.[104] He suggested that cancer would occur if the immune system did not suppress the growth of continuously arising cancer.[105] Although the idea of host-protective role of immunity against cancer was compelling, it had to wait for the maturation of the developing field of immunology.[37] In the late 1950s, Macfarlane Burnet from Australia and Lewis Thomas proposed the concept of immunologic surveillance of cancer. They speculated that lymphocytes play a major role in protecting against tumor development.[106] The concept was difficult to validate due to the lack of appropriate animal models and good experimental designs.[37]

Although Coley's toxins did not have significant antitumor efficacy, many groups of cancer immunologists still believed in the concept of antitumor immunity. Therefore, to understand the interaction between immunity and cancer, they used Bacillus Calmette–Guérin (BCG) vaccine. This vaccine was made of a live attenuated strain of *Mycobacterium bovis*, which was expected to stimulate a local inflammatory response with the infiltration of granulocytes, macrophages, and lymphocytes that collectively can kill cancer cells.[107] In the 1950s, BCG was shown to have antineoplastic qualities in mice.[108] However, in the 1970s, this therapy was shown to be ineffective in treating human cancers, and thus, it was discarded.[107]

The effort was continued until 1974 when Osias Stutman published his report in *Science*. Stutman used athymic CBA/H strain nude mice, which lack an adaptive immune system, as a model to test the hypothesis. He argued that if this hypothesis was correct, these immunodeficient mice would have an increased incidence of tumors induced by 3-methylcholanthrene (MCA), a chemical carcinogen, compared with wild-type (WT) mice. The results suggested otherwise.[37] Two years later, in 1976, Alvaro Morales reported that the BCG treatment could reduce bladder tumor recurrence remarkably.[109] However, Stutman's conclusion was very convincing, and controlled trials in advanced bladder cancer failed to support Morales' results. Consequently, the claim that host immunity was capable of detecting and destroying cancer cells could not be supported.

About two decades after the apparent death of the immune surveillance hypothesis, a major shift occurred in the field of cancer immunology. Scientists realized that there are caveats to Stutman's conclusions: (1) The CBA/H nude mouse model that he used in his experiments may have been highly sensitive to MCA-induced tumor formation; (2) these nude mice have detectable levels of functional T cells, NK cells, and other innate effector lymphocytes. Thus, they are not completely immunodeficient and so they could possess some degree of immunosurveillance capacity; (3) another supporting piece of evidence came when scientists used a different titer of MCA to induce tumors in nude and SCID mice on a BALB/c background.[37] It was clear that nude and SCID mice were more susceptible to tumor formation than WT mice; and (4) additional studies showed that perforin −/− mice and

recombination-activating gene 2 (RAG2 −/−) mice have a greater sensitivity to MCA-induced tumors compared with their WT counterparts.[37,110] Furthermore, it proved possible to improve the BCG therapeutic response. Morales reported that a minimum of 3 weeks of treatment was necessary, and the vaccine had to be given intradermally.[109] Subsequent studies showed that BCG vaccination can lead to statistically significant reduction in tumor growth and risk of bladder cancer recurrence. As a consequence of these encouraging findings, in 1990, BCG was the first FDA-approved immunotherapy to treat certain types of bladder cancer.[107] A few years later, in 1995 and 1998, interferon alpha-2 (IFN-α 2) and interleukin 2 (IL-2), respectively, received FDA approval, as well.[111]

6.02.2.4 Cancer Immunoediting

As a result of these discoveries, resistance to the immunosurveillance theory weakened.[110] Nevertheless, scientists did not have answers for many important questions. For example, why do cancers occur in immunocompetent individuals[37]? Do cancers result from a failure of "immunosurveillance"? These questions remained unanswered until the cancer immunoediting concept was evolved. In late 1990s, Robert Schreiber proposed that the immune system not only is capable of identifying and destroying developing cancer but also can manipulate cancer cells and enhance their malignancy. His proposal was based on a series of seminal experiments demonstrating this phenomenon. To do these experiments, a cohort of sex-, stage-, and strain-matched WT mice and immune-deficient RAG2 −/− mice on a pure 129/SvEv background were used.[8] RAG2 −/− mice carry a germ-line mutation in which a large portion of the RAG-2 coding region is deleted. This gene encodes a protein that is important for V(D)J recombination during B- and T-cell maturation. Hence, homozygous mutants are viable, but have very immature lymphoid cells, and thus, they are considered as completely immune-deficient.[112] In these experiments, both WT and RAG2 −/− mice developed malignant sarcomas after treatment with MCA, the same powerful carcinogen that Stutman used. Not surprisingly, RAG2 −/− mice that did not have adaptive immunity exposed to MCA developed tumors more rapidly and in a higher number than the WT mice. Thereafter, cells were inoculated into naive WT and Rag2 −/− mice. This experiment showed that regardless of the immune status of the recipient mice, if the tumor originally grew in WT mice, in the presence of an intact immune system, it could always form progressively growing tumors. Similarly, if the tumor was originally generated in and explanted into immune-deficient mice, it could rapidly grow and form cancers. However, when the tumors were originally generated in immune-deficient mice and explanted into WT mice, 50% of tumors were rejected spontaneously. The suggested explanation of this phenomenon was that the tumors that originally grew in WT mice had already undergone attack and "editing" by the intact host immune system. They found that these cancer cells displayed a reduced level of immunogenicity, making them less recognizable by the immune system. In contrast, tumors that grew first in the absence of immune selection pressure were unedited. Hence, they were highly immunogenic and still could be recognized and killed by the mice with intact immune systems.[8]

Finally, it must be stressed that when tumors were isolated from WT or RAG-2 −/− mice and transplanted into RAG-2 −/− recipients, they all grew at the same rate. This observation confirmed that these tumors consisted of transformed cancer cells, and there were no inherent growth differences between tumors. As a result, the rejection only happened because there was no immune editing, suggesting that the immune system exerts both host-protective and tumor-sculpting effects on developing tumors.[8] Later studies revealed that the effect of the immune system on cancer cells depends on many factors, including the stage and nature of transforming events and the type and activity of immune-infiltrating cells.[113]

Subsequent work has provided a mechanistic framework for the concept of immune editing. Schreiber and colleagues characterized this process as consisting of three phases: *elimination*, *equilibrium*, and *escape*. First, the immune system is usually successful in eliminating developing tumors bearing strong antigens (*elimination*), though resistant cells may remain. Then, in the *equilibrium* phase, cancer cells display low levels of immunogenicity or develop immune defense mechanisms, creating in effect a smoldering truce with the immune system. Also, during this phase, the natural selection of tumor variants may occur over a period of many years, allowing cancer cells to move into the *escape* phase. In that process, these resistant cells change their antigen profile and acquire additional mutations. Therefore, they gain the ability to escape from immune attack, proliferate, and metastasize.[114]

6.02.2.5 Types of Cancer Immunotherapy

Cancer immunotherapy encompasses many treatment modalities, including monoclonal antibodies, cellular therapies, cancer vaccines, and cytokines. Although these treatments have different mechanisms of action, they all aim to enhance the body's immune system to fight the enemy cancer within.

6.02.2.5.1 Monoclonal antibodies

Monoclonal antibody-based treatments have emerged as important therapeutics for both hematologic malignancies and solid tumors[22] (**Table 1**). Before discussing monoclonal antibody-based cancer therapeutics in detail, we provide an overview of the antibody types, structures, biological effector functions, and mechanisms of action.

6.02.2.5.1.1 Definitions

Antibodies are glycoproteins belonging to the immunoglobulin (Ig) superfamily. They bind to native (unaltered and unprocessed) membrane-bound or soluble antigens. Under appropriate conditions, antigen–antibody interaction can induce immune response to eliminate the target. The antigen sequence that is recognized by antibodies is called the *epitope*, which consists of hydrophilic sequences of 6–7 amino acids. On the other hand, the antigen-binding site of an antibody, which can recognize and bind

Table 1 FDA-approved antibodies for the treatment of cancer

Target		*Generic name (trade name)*	*Conjugation*	*Origin*	*Isotype (conjugate)*	*Cancer(s) treated*	*Initial approval*
Cancer cells	CD20	Rituximab (Rituxan)[115,116]	Unconjugated	Chimeric	IgG1	Chronic lymphocytic leukemia, non-Hodgkin's lymphoma	1997
		Ibritumomab tiuxetan (Zevalin)[117]	RIT	Murine	IgG1 (^{90}Y)	Non-Hodgkin's lymphoma	2002
		Ofatumumab (Arzerra)[118,119]	Unconjugated	Human (XenoMouse)	IgG1	Chronic lymphocytic leukemia	2009
		Obinutuzumab (Gazyva)[120,121]	Unconjugated	Humanized	IgG1	Chronic lymphocytic leukemia, non-Hodgkin's lymphoma	2013
	CD19	Blinatumomab (Blincyto)[122]		BiTE		Acute lymphocytic leukemia	2014
	CD30	Brentuximab vedotin (Adcetris)[123]	ADC	Chimeric	IgG1 (MMAE)	Hodgkin's lymphoma, systemic anaplastic large cell lymphoma	2011
	CD38	Daratumumab (Darzalex)[124]	Unconjugated	Human	IgG1	Multiple myeloma	2015
	HER2 (ErbB2)	Trastuzumab (Herceptin)[125,126]	Unconjugated	Humanized	IgG1	Breast, gastric cancers	1998
		Pertuzumab (Perjeta)[127]	Unconjugated	Humanized	IgG1	Breast cancer	2012
		Ado-trastuzumab emtansine (Kadcyla)[128]	ADC	Humanized	IgG1 (DM1)	Breast cancer	2013
	EGFR (ErbB1)	Cetuximab (Erbitux)[129–132]	Unconjugated	Chimeric	IgG1	Colorectal, squamous head/neck, lung cancers	2004
		Panitumumab (Vectibix)[133]	Unconjugated	Human	IgG2	Colorectal cancer	2006
		Necitumumab (Portrazza)[132,134]	Unconjugated	Humanized	IgG1	Squamous nonsmall cell lung cancer	2015
	SLAMF7	Elotuzumab (EMPLICITI)[135]	Unconjugated	Humanized	IgG1	Multiple myeloma	2015
	GD2	Dinutuximab (Unituxin)[136,137]	Unconjugated	Chimeric	IgG1	Neuroblastoma	2015
Microenvironment	VEGF	Bevacizumab (Avastin)[138–141]	Unconjugated	Humanized	IgG1	Colorectal, nonsmall cell lung, ovarian, fallopian tube, peritoneal, cervical cancers, glioblastoma, renal carcinoma	2004
		Ziv-aflibercept (Zaltrap)[142]	Unconjugated	Humanized	IgG1	Colorectal cancer	2012
	VEGFR2	Ramucirumab (Cyramza)[143–145]	Unconjugated	Humanized	IgG1	Gastric, gastroesophageal junction adenocarcinoma, colorectal, nonsmall cell lung cancers	2014
	RANKL	Denosumab (Xgeva)[146]	Unconjugated	Human	IgG2	Breast cancer	2013
Immune cells	CTLA-4 (CD152)	Ipilimumab (Yervoy)[72]	Unconjugated	Humanized	IgG1	Melanoma	2011
		Tremelimumab[147]	Unconjugated	Humanized	IgG2	Malignant mesothelioma	2015
	PD-1	Nivolumab (Opdivo)[73,148–150]	Unconjugated	Human	IgG4	Melanoma, squamous nonsmall cell lung cancer, renal cell carcinoma	2014
		Pembrolizumab (Keytruda)[151,152]	Unconjugated	Humanized	IgG4	Melanoma, nonsmall cell lung cancer	2015

specifically to a single epitope, is called the *paratope*. Typically, each immunogenic molecule is heterogeneous, meaning that it has multiple different epitopes.[9] Each of these epitopes can stimulate one plasma cell clone to produce specifically binding antibodies. That said, antibodies secreted from a single B clone are referred to as *monoclonal antibodies*, whereas the ones produced from multiple B-cell clones within the body are referred to as *polyclonal antibodies*.[153]

6.02.2.5.1.2 Antibody types

Based on the structural differences in the constant region of the heavy chain, antibodies are divided into five classes: IgM, IgD, IgG, IgE, and IgA.[9] Immunoglobulin M (IgM) antibodies present as either a membrane-bound form expressed on B cells or a secreted

form (sIgM) found in the blood. sIgM has a pentavalent structure; it has ten antigen-binding sites. Hence, it can form strong interactions with its binding partners. Also, IgM is typically synthesized early during an immune response.[154] Immunoglobulin G (IgG) antibodies emerge subsequently.[9] IgG is the most abundant immunoglobulin type, accounting for ~75% of the total serum Ig proteins in a healthy individual.[155] There are four IgG isotypes (IgG1, IgG2, IgG3, and IgG4), which are named in order of decreasing abundance.[156] Each of these subclasses has structurally and/or functionally distinct constant domains.[155] Membrane-bound immunoglobulin D (IgD) antibodies are coexpressed with IgM on the surface of naive B cells. However, the biological significance of IgD has remained obscure since its discovery in 1965. Recent studies suggested that this class of Ig is important in enhancing mucosal immunity of the upper respiratory tract.[157] However, immunoglobulin A (IgA) antibodies have the most critical roles in mucosal immunity. Finally, immunoglobulin E (IgE) antibodies play a fundamental role in mediating allergic reactions.[1] The most typical antibody type used for cancer therapeutics is typically of the IgG class[22]; therefore, this section focuses mainly on IgG immunoglobulins.

6.02.2.5.1.3 Antibody structure

Although IgG antibodies are the smallest antibodies, they are still considered large molecules, having a molecular weight of ~150 kDa. As indicated in Fig. 2, each IgG molecule has a dimeric structure; it is composed of two identical heavy and light chains arranged in a Y shape. Also, IgG antibodies have two antigen-binding fragments (Fabs) and one constant fragment (Fc). The former, which is represented by the two arms of the Y, includes two heavy- and light-chain heterodimers.[20] Fab also is subdivided into hypervariable (HV) and framework (FR) regions. The HV regions of each heavy and light chain combine to form the antigen-binding sites, which are called complementarity-determining regions (CDRs).[158] Whereas the Fc part, which is represented by the tail of the Y, includes the heavy-chain dimers derived from the second and third constant domains.[9] Through the Fc region, antibodies interact with other molecules and cells to exhibit antibody effector functions.[159]

6.02.2.5.1.4 History of monoclonal antibody-based cancer therapeutics

In 1975, César Milstein and Georges J.F. Köhler developed the hybridoma technology, which involved the fusion of a plasma cell with a myeloma cancer cell.[160] Under specific conditions, using these hybrid cells, which were then called hybridomas, they were able to produce monoclonal antibodies against tumor cell surface antigens.[161] Because this technology had a great impact on modern biological and clinical research, in 1984, Kohler and Milstein received the Nobel Prize for Medicine and Physiology.[162]

6.02.2.5.1.5 Types of monoclonal antibody-based cancer therapeutics

6.02.2.5.1.5.1 Murine monoclonal antibodies

Monoclonal antibodies were initially developed from mice and thus had significant drawbacks: (1) They were immunogenic in humans,[22] (2) mouse monoclonal antibodies have relatively weak binding affinity for the human Fc receptors (therefore, they have shorter half-life compared with human IgG), and (3) they mediate weak antibody-dependent cellular cytotoxicity (ADCC) and complement-dependent cytotoxicity (CDC), resulting in minimum biological effects.[163] Not surprisingly, only two murine monoclonal antibodies have been approved for clinical use: ibritumomab tiuxetan (Zevalin)[117] and tositumomab (Bexxar)[164]; both of these agents consist of anti-CD20 antibodies that deliver radioactive particles to CD20-expressing lymphomas. Neither agent has emerged as a major treatment option for the management of these types of neoplasms.

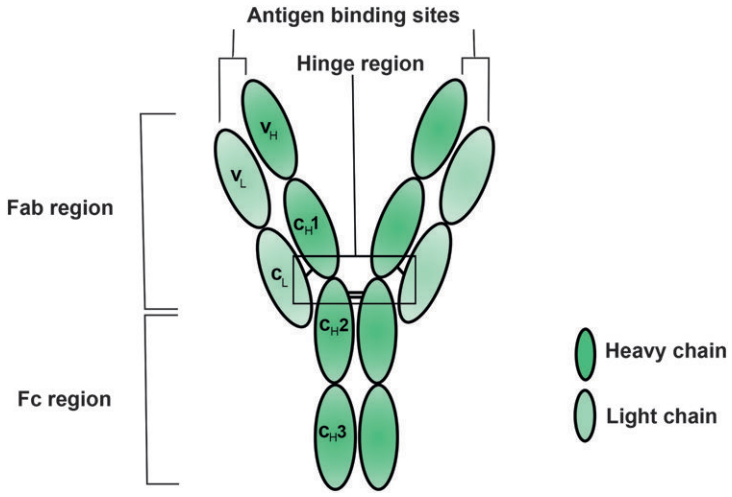

Fig. 2 Structure of an immunoglobulin G (IgG) molecule. The IgG molecule is a dimer composed of two heavy chains and two light chains. The heavy chains dimerize to form the Fc domain, which serves as an immune recruiting signal, whereas heavy-chain to light-chain dimers form the Fab domain that is responsible for the antibody binding to its target antigen.

6.02.2.5.1.5.2 Chimeric murine–human monoclonal antibodies

In an attempt to overcome the drawbacks of mouse monoclonal antibodies and still retain antigen specificity, genetic engineering was applied to generate chimeric mouse–human antibodies. This technique allowed for the production of monoclonal antibodies that are ~65% human. The entire antigen-specific variable domains are usually encoded by mouse genes, whereas the constant regions are from human genes (Fig. 3).[163] Currently, at least three FDA-approved chimeric antibodies are used as cancer immunotherapies: rituximab (Rituxan),[115,116] brentuximab vedotin (Adcetris),[123] and cetuximab (Erbitux).[129–132] Although chimeric monoclonal antibodies have shown highly encouraging results in these and other diseases, they may induce hypersensitivity and serum sickness, and altered pharmacokinetic profiles (i.e., rapid systemic clearance) may reduce the efficacy of the antibody project.[163] As a result, there remained an urgent need to improve monoclonal antibody technology.

6.02.2.5.1.5.3 Humanized monoclonal antibodies

Later advances in antibody engineering allowed for the synthesis of humanized monoclonal antibodies. To humanize an antibody, only the hypervariable regions from murine origin are grafted onto the human antibody framework and constant regions (Fig. 3). These molecules have high similarity to human antibodies; they are ~95% human.[165] The majority of FDA-approved monoclonal antibodies for the treatment of cancer belong to this category, for example, the HER2-targeting antibody trastuzumab (Herceptin), which is the first humanized monoclonal antibody to be approved for therapeutic use,[125,126] and elotuzumab (EMPLICITI), which is the most recently approved cancer monoclonal antibody drug.[135]

6.02.2.5.1.5.4 Fully human monoclonal antibodies

To further reduce antibody immunogenicity, fully human monoclonal antibodies have been generated (Fig. 3). Today, three human monoclonal antibodies are licensed to treat malignancies: ofatumumab (Arzerra),[118] panitumumab (Vectibix),[133] and denosumab (Xgeva).[146] Antibodies that belong to this category have been synthesized by phage display libraries or transgenic mouse technologies over the last 25 years.[166] However, their production still involves a labor- and cost-intensive multistep process.[167] For instance, the transgenic mouse methodology requires the creation of a specific mouse strain.[168] The phage display technique requires counting of transducing units and sequencing the phage DNA from each individual colony or plaque.[167]

6.02.2.5.1.5.5 Conjugated monoclonal antibodies (immunoconjugates)

Immunoconjugates are antibodies conjugated to a therapeutic agent, via a linker. The antibody, through its Fab region, binds specifically to its target on the surface of malignant cells. The linker attaches the effector molecule to the antibody and releases it at the target site to kill cancer cells or the surrounding TME.[169] According to the type of the cytotoxic agent, conjugated monoclonal antibodies can be divided into four groups.

6.02.2.5.1.5.5.1 Antibody–drug conjugates. To overcome some limitations of conventional chemotherapies, which usually damage healthy tissues and may cause multiple severe adverse reactions, antibody–drug conjugates (ADCs) have been developed. This type of immunotherapy utilizes monoclonal antibodies that bind to cancer antigens with high specificity. Therefore, they can deliver a highly potent cytotoxic agent to the target site, leaving normal cells intact.[170] Brentuximab vedotin[123] and trastuzumab emtansine[128] are the only two licensed ADCs by the FDA. They are approved for the treatment of certain lymphomas and certain breast cancers, respectively.

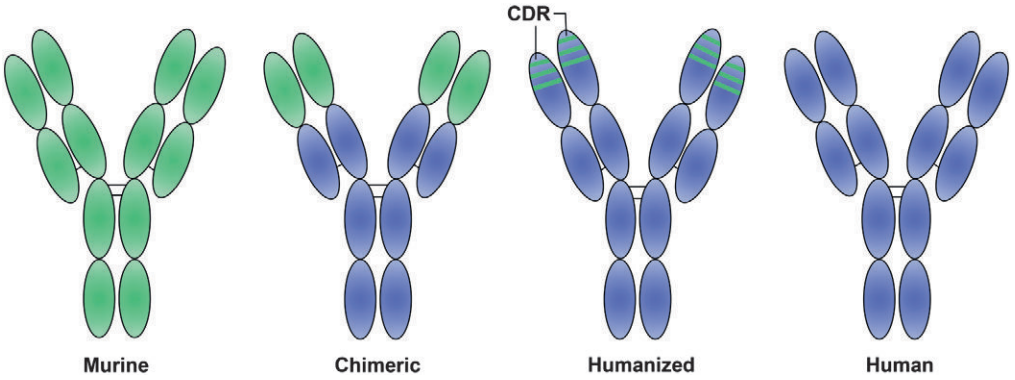

Fig. 3 Types of monoclonal antibodies. Hybridoma technology initially was employed to generate murine monoclonal antibodies. Cloning of mouse variable genes into human constant-region genes by genetic engineering generates chimeric antibodies. The insertion of mouse complementarity-determining regions (CDRs) onto human constant and variable domain frameworks generates humanized antibodies. Fully human antibodies can be generated by the use of purely in vitro antibody engineering techniques, by immunizing human IgG transgenic mice or by employing human hybridomas.

6.02.2.5.1.5.5.2 Radioimmunoconjugates. Radioimmunoconjugates (RICs) are generated by linking an antibody to a radioactive isotope, allowing the delivery of higher doses of radiation therapy to the target site. Therefore, while RIC treatments are expected to increase the therapeutic efficacy of radiation therapy, they can decrease the potential risk of radiation off-target effects.[171] Ibritumomab tiuxetan (Zevalin)[117] and tositumomab (Bexxar)[164] have been the only FDA-approved radioimmunoconjugates. Tositumomab has been discontinued by the manufacturer due to infrequent practitioner use, attributed in part to the complicated nature of its administration.[165]

6.02.2.5.1.5.5.3 Immunocytokine conjugates. It is well accepted that cytokine treatments for cancer can result in durable responses. However, some cancer patients treated with cytokines experienced severe side effects.[26] Therefore, it was hypothesized that delivering the cytokines directly to the target site at high doses will cause less toxicity and exert powerful antitumor effects.[172] To test this hypothesis, some cytokines that stimulate antitumor responses, such as IL-2, interleukin 12 (IL-12), and tumor necrosis factor-α (TNF-α), were conjugated to immunoglobulin antibodies.[173] These immunocytokine conjugates (ICs) are still under clinical investigation.[174]

6.02.2.5.1.5.5.4 Immunotoxins. Immunotoxins are obtained by conjugating catalytic toxins with monoclonal antibodies. Catalytic toxins are typically derived from bacteria (e.g., *Pseudomonas* exotoxin) or plants (e.g., ricin).[175] Although there is no FDA-approved immunotoxin yet, several drugs have been evaluated in clinical trials and demonstrate promising properties.[176]

6.02.2.5.1.5.6 Fab-engineered monoclonal antibodies and antibody-like molecules

As mentioned earlier, the Fab domain is the portion of the antibody responsible for antigen recognition and binding. Indeed, in mouse xenograft models, only between 10% and 30% of injected dose of targeting IgG antibodies can be retained by the tumors. More importantly, in humans, due to the larger vascular and extravascular volume of distribution, this portion can reduce to $<0.1\%$.[177–179] To overcome this challenge, it was first hypothesized that generating antibody variants with very high affinity may improve selective tumor delivery and prolong tumor retention,[180] overcoming a "binding site barrier."[181] However, surprisingly, these modified antibodies had modest therapeutic effects.[169] These findings allowed for the generation of another hypothesis, namely, that very high-affinity interactions between antibodies and tumor antigens may impair the penetration of monoclonal antibodies from the vasculature to the tumors; this proved to be true.[182] Moreover, it was found that antibodies with high binding affinity can be rapidly internalized and degraded.[183] Also, they can bind to shed tumor antigens in the circulation, resulting in their diversion from the tumors.[184] Collectively, these observations suggest that modifying the affinity between antibodies and their target antigens requires careful consideration of consequences for selective tumor targeting.[169]

Another strategy employed to improve antibody therapeutic benefit was to generate smaller fragments, such as Fab and their recombinantly engineered counterparts.[169] The hypothesis was that the large size of IgG antibodies impedes their extravasation and thus impairs their tumor penetration properties. Accordingly, generating smaller fragments might help overcome this problem.[179] Also, these fragments can be cleared more rapidly from the body, improving their selectivity against their targets.[185] However, subsequent studies showed that quantitative delivery of these smaller molecules may be required for high efficacy.[169]

Recombinant protein engineering has allowed the design of monovalent single-chain Fv (scFv) fragments, which are composed of the variable domains (V_H and V_L) or even intact IgG molecules to bind to multiple targets, for example, bispecific monoclonal antibodies engineered to recognize two targets and trispecific antibodies engineered to recognize three targets. The typical goal of dual engagement is to bring the target, mainly tumor antigen such as EGFR, EpCAM, or CD19, in a close proximity to activated effector cells such as T lymphocytes, to elicit immune-mediated killing.[165] Other bispecific formats can simultaneously engage distinct tumor antigens or epitopes on the same antigen. Examples of bispecific antibody-based molecules include the BiTE (bispecific T-cell engager),[122] DART (dual-affinity retargeting),[186] and TandAb (tetravalent tandem antibody) structures.[187] BLINCYTO (blinatumomab) is the first BiTE immunotherapy to be approved by the FDA. It engages CD3 and CD19 and was approved in 2014 for the treatment of patients with Philadelphia chromosome-negative (Ph−) relapsed or refractory B-cell precursor acute lymphoblastic leukemia (ALL).[122]

6.02.2.5.1.5.7 Fc-engineered monoclonal antibodies

When an antibody interacts with an antigen through the Fab domain, the Fc region of the same antibody stimulates immune cells to attack the bound antigen. The Fc domain mediates effector activities by binding to Fc gamma receptors (FcγRs) expressed on effector cells. There are several known types of FcγRs that are divided into two main groups: activating receptors, including FcγRI (CD64), FcγRIIA (CD32A), FcγRIIC (CD32C), FcγRIIIA (CD16A), FcγRIIIB (CD16B), and FcγRIV (in mice), and an inhibitory receptor FcγRIIB (CD32B).[165,188]

In most cases, the therapeutic significance of the Fc domain relies on its ability to induce antitumor responses and to remain stable over a long period of time.[165] In fact, one of the main antitumor mechanisms of action mediated by IgG is ADCC. This process is frequently mediated by NK cells, which rely on FcγRIIIa. Thus, the binding affinity between the antibody's Fc domain and FcγRIIIa is very critical. Nevertheless, it was reported that 80% of the White population has a phenylalanine, instead of valine, in position 158 of FcγRIIIa, which represents a low-affinity variant of the receptor. Also, IgG affinity for FcγRIIIa can be highly influenced by posttranslational modifications of the Fc domain. The glycosylation of the two conserved asparagine (Asn) residues in each of the Ch2 domains of the Fc region can change antibody structure and function dramatically. For example, the presence of fucose residues on Asn297 was shown to reduce the affinity of IgG to FcγRIIIa, leading to a reduction in ADCC efficiency. While

it is currently infeasible to modify human genes in vivo, it is relatively easy to produce therapeutic antibodies with defucosylated Fc regions. Interestingly enough, it is assumed that defucosylated antibodies have higher affinity for FcγRIIIa/b, making them more efficient anticancer drugs. To generate these antibodies, new cell lines were developed by deleting the *FUT8* gene coding for the enzyme α-1,6-fucosyltransferase or overexpressing a recombinant β-1,4-N-acetylglucosaminyltransferase III in CHO cells.[189] An example of an anticancer therapeutic that utilizes the principle of Fc region defucosylation is obinutuzumab (GAZYVA).[190]

IgG antibodies also bind to the neonatal Fc receptor (FcRn). FcRns are structurally distinct from FcγRs; each receptor is a heterodimer composed of an MHC class I-like heavy chain and a b_2 microglobulin (b_2m) light chain. FcRns bind to IgG antibodies and albumin in a pH-dependent manner in which the affinity between FcRn and IgG is inversely related to the pH level. FcRns are found in an acidic endosomal compartment within endothelial cells and circulating monocytes. These cells can internalize IgG antibodies by endocytosis, allowing for IgG–FcRn interaction with high affinity at low pH (<6.5). Then, this complex is carried back to the cell surface where it is exposed to the physiological pH (7.4). This process decreases the affinity between the two molecules, leading to the dissociation of the IgG antibodies from the FcRns. Therefore, FcRn is able to recycle IgG back into circulation, protect it from transcytotic lysosomal catabolism, and thus extend its serum half-life from 1 day to several weeks.[191] To demonstrate this property, FcRn knockout mice were utilized. It was reported that, in these mice, the catabolism rate for IgG accelerated up to 10 times compared with WT control animals.[192] Moreover, several studies demonstrated that FcRn can contribute to antibody-mediated antigen presentation.[191] Accordingly, to determine if this is clinically relevant, scientists have manipulated IgG Fc domains by mutagenesis to increase their affinity for FcRn at acidic pH. To date, a noncancer treatment, motavizumab-YTE, which is an Fc-modified monoclonal antibody that targets respiratory syncytial virus (RSV), has finished a phase I clinical trial.[193] However, there is no approved cancer therapy that utilizes this principle.

6.02.2.5.1.6 Antibody mechanisms of action

The mechanisms of tumor cell killing by IgG antibody can be summarized as follows (**Fig. 4**).

6.02.2.5.1.6.1 Perturbation of signaling pathways

In order for cells to function and survive, they must communicate with each other and with their external environment through signaling molecules. Cells need to communicate to maintain protein synthesis, proliferation, differentiation, maturation, motility, and polarity under tight control. During tumor initiation and progression, malignant cells acquire a number of genetic and epigenetic alterations that favor their uncontrolled growth and immortalization.[194] One of the main antitumor activities of antibodies is the disruption of key components in cancer signaling pathways that are involved in the maintenance of the malignant phenotype.[22] Blocking of relevant ligand–receptor binding can be accomplished by using either neutralizing antibodies directed against the receptor or the ligand. Other antibodies might therapeutically function as signaling agonists.

6.02.2.5.1.6.2 Delivery of cytotoxic agents

As mentioned earlier in this section, monoclonal antibodies can be used for cancer therapy to deliver therapeutic agents to the site of tumor. Conjugated cytotoxic drugs, radiolabeled isotopes, toxins, and cytokines can kill target cells with higher specificity, improved efficiency, and less toxicity.[169]

6.02.2.5.1.6.3 Stimulation of tumor-specific immune responses

Antibodies can trigger innate immunity using three different mechanisms: ADCC, CDC, and ADCP. Also, following the induction of innate immunity, antibodies can stimulate adaptive immune responses.

6.02.2.5.1.6.3.1 Antibody-dependent cellular cytotoxicity. ADCC is an important mechanism by which monoclonal antibodies are able to elicit killing of antibody-coated target cells. Through Fab antigen-specific binding, the Fc portion serves as an immune recruiting signal. It binds to its receptors (FcRs) on the surface of effector cells such as NK cells, neutrophils, γδ T cells, DCs, and macrophages. Then, the Fc–FcR cross-linking results in the formation of an immune synapse leading to direct tumor cell lysis through the release of perforins and granzymes.[22,195] The interaction between Fc and its receptor is not always stimulatory to the effector cell, but it can also be inhibitory, depending on which FcR is engaged.[165] A positive killing signal in macrophages, neutrophils, NK cells, and DCs is facilitated by both FcγRI and FcγRIIIa.[195] This concept has been supported and mechanistically dissected through the use of FcγRI, FcγRIIIa, and FcγRIIB knockout mice.[196] While NK cells are considered to be important ADCC effector cells, macrophages and dendritic cells can mediate ADCC, as well.[197] More importantly, the significance of FcγR interactions has been observed in the clinic, where a correlation was found between FcγR polymorphism and the efficacy of therapeutic antibodies, including rituximab in lymphoma, cetuximab in metastatic colorectal cancer, and trastuzumab in HER2/neu-positive metastatic breast cancer.[198–201]

6.02.2.5.1.6.3.2 Complement-dependent cytotoxicity. Complement can trigger activation of immune responses against cancer cells in different ways. Therapeutic and natural antibodies are generated to target specific antigens expressed on the surface of cancer cells. Upon the engagement of multiple antibodies to their targets on a cancer cell, the C1 complex can attach to the antibody Fc domain and thereby activate the classical complement pathway. The serine protease C1 complex can cleave other complement components C4 and C2, leading to the formation of C3 convertase (C4b2a). This enzyme can then convert C3 into C3a and C3b. The former is an anaphylatoxin that recruits immune effector cells to the site of complement activation, whereas C3b incorporates into C3

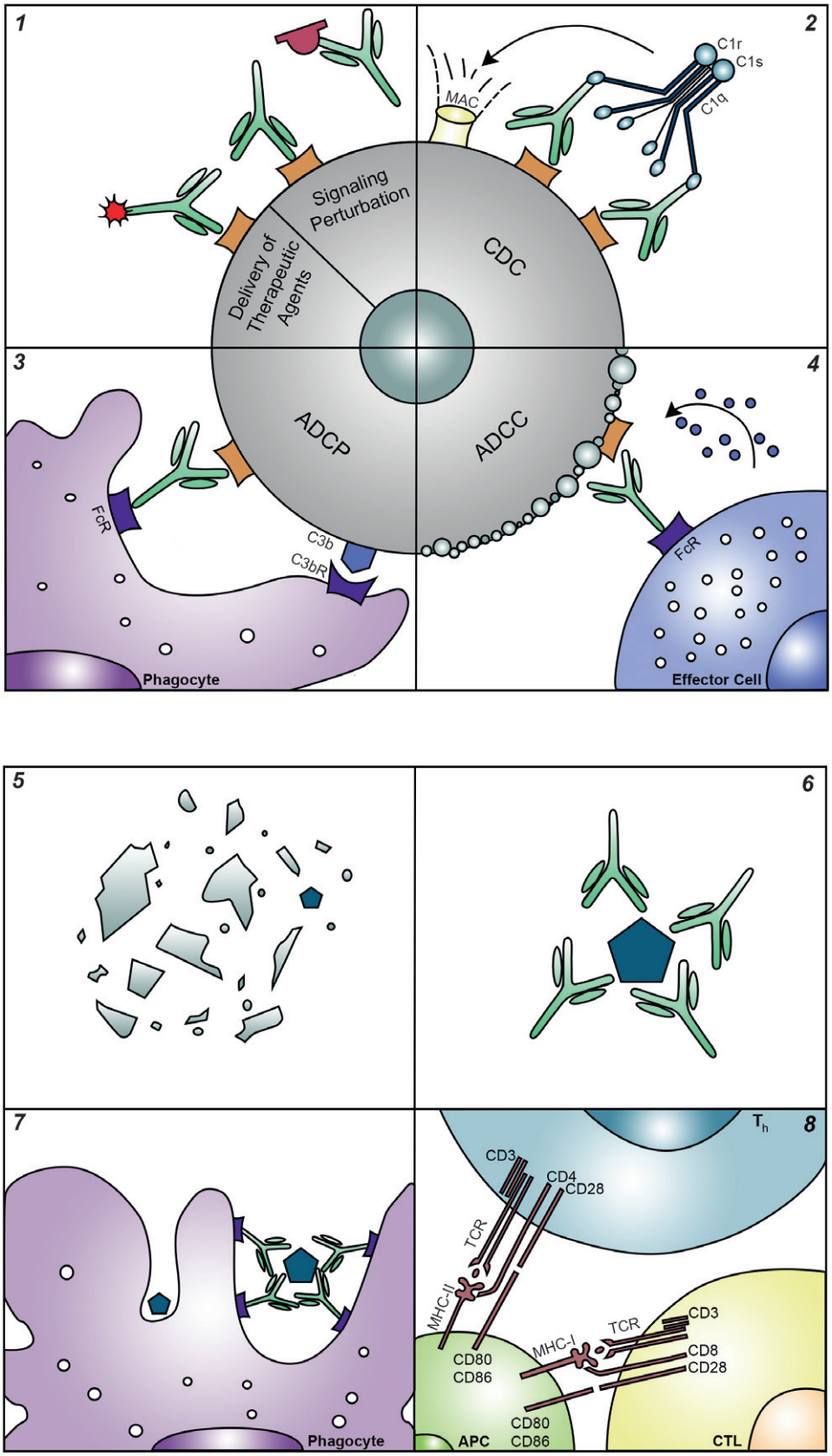

Fig. 4 Mechanisms of action of antibody-based immunotherapy in cancer. Mechanisms of action of antibodies in cancer therapy are diverse and represent the versatility of antibody-based approaches. Here, different strategies of antibody-mediated antitumor immunity are depicted. (1) Perturbation of signaling pathways: monoclonal antibodies can block ligand–receptor binding by targeting either the receptor or the ligand. Delivery of cytotoxic agents: also, monoclonal antibodies can deliver cytotoxic agents to targeted cells. (2) Stimulation of complement-dependent cytotoxicity (CDC): antibodies can cause target cell lysis through the formation of the membrane attack complex (MAC). (3) Stimulation of antibody-dependent cellular cytotoxicity (ADCC): the Fc portion of monoclonal antibodies can engage immune effector cells including NK cells, macrophages, and dendritic cells through FcRs, which can lead to target cell fragmentation. (4) Stimulation of antibody-dependent cellular phagocytosis (ADCP): opsonized cancer cells can engage to phagocytes, which can lead to target cell phagocytosis. (5) CDC, ADCC, and ADCP can lead to target cell fragmentation and release of tumor antigens. (6) Opsonization of released tumor antigens. (7) Phagocytosis of opsonized tumor antigens. (8) Induction of adaptive immunity: internalized tumor particles and phagocytized antigens can be processed and presented via MHC class I and MHC class II, which can activate $CD8^+$ and $CD4^+$ T cells, respectively.

convertase, activating other proteins in the pathway. Finally, this can lead to the formation of the membrane attack complex (MAC) and the production of a stronger anaphylatoxin, C5a. MAC, a transmembrane channel that works as a pore in the target cell surface, can disrupt cellular homeostasis, leading to cancer cell death and fragmentation. As a result, this process is called complement-dependent cytotoxicity (CDC). Moreover, C3b can trigger the formation of additional MAC channels by activating the alternative complement pathway. Accordingly, the complement system can influence the efficacy of some cancer therapeutic monoclonal antibodies.[202]

There is a large amount of evidence supporting CDC as a major mechanism of rituximab antitumor activity.[202] For example, lymphoma syngeneic knockout animals completely lacking C1q ($C1qa^{-/-}$) are capable of mediating ADCC. However, in these mice, the antitumor effect of rituximab therapy was abrogated. Therefore, it was concluded that C1q is required for rituximab to exert therapeutic benefit.[203] Further evidence has emerged for the relationship between CDC and rituximab therapeutic effects. It was reported that in follicular lymphoma patients, polymorphisms in the *C1qA* gene influence the efficacy of rituximab.[204] However, it must be stressed that the precise antitumor mechanism of action for rituximab is multifactorial. Further, although many chronic lymphocytic leukemia (CLL) patients have been successfully treated with this antibody, CLL cells express low levels of CD20, making them less susceptible to CDC.[205] Therefore, while the complement cascade is required for optimal rituximab treatment effect, there are other mechanisms of action that can be important. Additionally, ofatumumab is a human monoclonal antibody that targets a distinct epitope of CD20.[206] It binds to C1q with higher avidity and thus induces greater CDC compared with rituximab, which may explain why ofatumumab is able to destroy rituximab-resistant large B-cell lymphoma cell lines and demonstrates clinical efficacy.[207]

6.02.2.5.1.6.3.3 Antibody-dependent cellular phagocytosis. Another important function of C3b is the opsonization of target cells and molecules. C3b deposition on cancer cells allows their engagement to phagocytes that express C3b receptors (C3bR) on their surface.[202] Because phagocytes express FcyRs on their surface, too, they can also bind to cancer cells that are tagged by antibodies. Both mechanisms of opsonization allow phagocytes to recognize, engulf, and destroy cancer cells.[208]

6.02.2.5.1.6.3.4 Induction of adaptive immunity. Antibody-targeted cytotoxicity initiated by CDC, ADCC, and ADCP can generate tumor cell fragments and release tumor antigens. Therefore, the cell lysis products can be taken up by professional APCs, such as DCs, either directly by phagocytosis or after opsonization and internalization via specific receptor-mediated processes.[209] Then, these antigens can be processed and presented via MHC I and MHC II. Antigen–MHC II complexes can prime $CD4^+$ T-cell responses that are important in stimulating humoral immunity and activating cell-mediated immune activity.[210] While extracellular antigen presentation by MHC II is relatively simple, subsequent antigen cross-presentation via MHC I is very complex and incompletely understood.[209] After the internalization of exogenous antigens by professional APCs, they transfer from the lumen of endocytic compartments to the cytosol. Therefore, the antigens get degraded and loaded onto MHC I molecules by peptide exchange.[211] This process is called antigen cross-presentation, and it has many potentially advantageous features. First, it allows therapeutic antibodies, which are generated against a specific antigen on cancer cells, to induce adaptive immunity that may extend beyond the targeted antigen. Secondly, typically, antibodies can only interact with extracellular antigens. However, cross-presentation allows them to induce immune responses against intracellular antigens, which are thought to be inaccessible to antibody therapies. Thirdly, antigen cross-presentation activates helper $CD4^+$ and CTL $CD8^+$ T cells, enabling immunologic memory directed against the presented antigens. Thus, this process may provide long-term immunity and prevent tumor recurrence.[210] In fact, many lines of evidence support this hypothesis. For instance, clinical response to rituximab usually needs about 6 weeks after initiation of treatment. This lag time is consistent with an adaptive immune mechanism of action.[156,159,212]

6.02.2.5.2 Cellular cancer immunotherapy

6.02.2.5.2.1 T cell-based cancer immunotherapy

The crucial role of tumor-infiltrating lymphocytes (TILs) in cancer treatment was first emphasized in the 1960s. Using murine tumor models, it was shown that the transfer of syngeneic lymphocytes that had been previously sensitized to tumor antigens can result in modest growth inhibition of small established tumors.[213] Another interesting study was published about a decade later, in 1979. It was reported that the relative relapse rate in leukemia patients who underwent allogeneic bone marrow transplantation and developed graft-versus-host disease was 2.5 times less than in patients without this complication. This result suggested that donor-derived T cells can target and eliminate leukemic cells, emphasizing that T-cell transfer may elicit antitumor immunity.[214,215] Meanwhile, in 1976, IL-2 was first identified by Morgan et al.[216] Experiments showed that IL-2 induces in vitro growth of antigen-stimulated T cells, leaving their effector functions intact,[213] and thus, it was described as "T-cell growth factor."[216] In 1982, studies demonstrated that the adoptive transfer of syngeneic murine lymphocytes isolated from the spleen and expanded with IL-2, also called lymphokine-activated killer (LAK) cells, can cure mice with disseminated FBL-3 lymphoma.[213] A few years later, in 1986, it was shown that lymphocytes found within neoplastic lesions (TILs) expanded with IL-2 were 50–100 times more effective in their therapeutic potency than LAK cells, when transferred to mice bearing micrometastases. More importantly, these cells could mediate regression of established lung and liver tumors in murine models.[217] In addition, a subsequent study determined that TILs isolated from resected melanomas can be expanded in vitro, generating a sufficient number of cells that are capable of selectively recognizing autologous tumors. This new approach allowed the induction of clinical trials to evaluate the antitumor therapeutic efficacy of expanded TILs in treating patients with metastatic melanoma.[213] However, although some patients with metastatic melanoma and renal cell carcinoma experienced remarkable, curative clinical responses following high-dose IL-2 therapy, with or without

infusions of autologous LAK cells or TIL, the results for most patients treated on these clinical trials were disappointing. The infused lymphocytes were unable to persist in the circulation and they disappeared within days after transfusion. This short-term response to the adoptive transfer approach limited the applicability of this treatment for more than a decade.[213,218] In 2002, a new discovery was made that dramatically changed the effectiveness of tumor-infiltrating lymphocyte (TIL) therapy.[213] It was shown that lymphodepletion produced by chemotherapy with or without radiation immediately before TIL transfusion increased rates of cancer regression.[213,218] Indeed, the transferred antitumor lymphocytes accounted for up to 80% of $CD8^+$ T cells in patients' circulation a month after transfer. The exact mechanism as to how lymphodepletion improves the effectiveness of TIL therapy is complex and remains to be determined.[213]

Tumor-reactive TILs are usually generated by first resecting the tumor specimen and digesting it into a single-cell suspension or multiple tumor fragments. Then, individual cells are grown in the presence of IL-2, resulting in pure cultures of tumor-specific lymphocytes within 2–3 weeks. Following the confirmation of their reactivity against tumors, they can be rapidly expanded for about 5–6 weeks, generating 10^{11} lymphocytes that can be infused back into patients who have received a lymphodepleting preparative regimen.[213,218] Interestingly, in patients with metastatic melanoma, adoptive cell therapy using autologous TILs can induce complete durable regression beyond 5 years, suggesting that these patients are cured. The overall response rates and complete response rates for this disease were around 50% and 20%, respectively. Notably, responses were seen in all visceral sites including the brain.[218]

Despite the fact that adoptive transfer of autologous TILs could show improved patient outcomes in melanoma, this therapeutic strategy has some limitations. First, it seems that this treatment approach may not be applicable to malignancies other than melanoma. In fact, the reasons behind this phenomenon are not fully understood. A possible explanation is that melanoma tumors have high frequency of immunogenic mutations, which can enhance antitumor T-cell responses. However, it should be noted that other highly mutated tumors, such as lung cancer, have not consistently shown significant therapeutic response rates to autologous TIL therapy.[213,218] Secondly, the antigens recognized by transferred lymphocytes have to be cancer-specific and not expressed on essential normal cells. Thirdly, to isolate infiltrating lymphocytes within the neoplastic lesions, the patient has to provide a surgical resection. Also, this patient has to be able to tolerate the lymphodepletion and IL-2-based treatments. Further, generated TILs have to be expanded ex vivo without loss of their antitumor cytotoxicity. This has to be done in specialized laboratories that have highly trained personnel. While these laboratory procedures may require several weeks, the patient may not be able to wait for this long because of rapid disease progression. Finally, cancer cells can suppress the function of transferred TILs by employing various escape mechanisms, such as upregulating immune checkpoints.[218]

New approaches have been developed in order to broaden the application of T cell-based therapy to treat other types of malignancy. These strategies involve the generation of genetically modified peripheral blood T cells to express either conventional alpha–beta TCRs or CARs. The genetic modifications can be achieved by using virus vectors (retroviruses or lentiviruses) or a transposon system (Sleeping Beauty). Then, transfected cells can be expanded and transferred into patients following their treatment with lymphodepleting agents.[213]

TCR T cells are peripheral blood T lymphocytes redirected by the integration of genes encoding TCRs targeting specific tumor-associated antigens. There are at least two main advantages of TCR T-cell therapy. First, surgical resection of the tumor is not needed to obtain the cells, improving the feasibility of this treatment. Also, TCR can recognize intracellular tumor antigens displaying target peptides in the context of self-MHC, overcoming a limitation of CAR T-cell therapy. On the other hand, a major limitation of TCR therapy is the difficulty in identifying tumor antigens that are not expressed by normal cells.[213] In fact, since 2006, TCR T cells have been used in clinical trials to target antigens expressed by normal tissues. Therefore, as expected, these trials were accompanied by on- or off-target toxicity, limiting the therapeutic efficacy of TCR therapy. For example, melanoma differentiation antigens (MDAs), such as melanoma antigen recognized by T cells 1 (MART1) and glycoprotein 100 (gp100), are normally expressed by melanocytes found in the skin, retina, and inner ear. Thus, patients treated with MART1 and gp100 TCR cells experienced skin rash, uveitis, and hearing loss. Another example is CEA antigen, which is expressed on normal epithelial cells throughout the gastrointestinal tract. TCR cells targeting CEA resulted in dose-limiting severe colitis. Similarly, targeting melanoma-associated antigen 3 (MAGE-A3), which is expressed in the central nervous system, by TCR was associated with neurological toxicity. Moreover, MAGE-A3-specific TCRs unexpectedly recognized a cardiac peptide antigen called titin, leading to off-target interaction and fatal cardiac toxicity. By contrast, NY-ESO-1 is an antigen that is usually detected in tumors but not in normal tissues. Hence, NY-ESO-1-specific TCR cells have appeared to be relatively safe.[218] Another limitation of this therapy is that transferred T cells only recognize the relevant Ag-derived peptide–MHC complex. Because MHC I molecules are commonly downregulated upon cellular transformation, these tumors may escape T cell-induced antitumor immune responses. Finally, TCR therapy can only be administered to MHC-compatible patients.[213]

To overcome some of these obstacles, CAR therapy has been developed. First-generation CAR T cells were constructed by fusing an scFv fragment to T-cell intracellular signaling domains, targeting tumor antigens displayed on the tumor cell surface. Second- and third-generation CARs include intracellular domains of one or multiple costimulatory molecules, such as CD28, OX40, and 4-1BB.[218] One major advantage of this treatment approach is that CARs on genetically modified T cells are similar to cell surface immunoglobulin antibodies on B cells. So, they do not depend on antigen processing and presentation. As a result, they can target tumors that have impaired antigen presentation capacity or downregulated HLA class I molecules. Finally, similar to TCRs, peripheral blood T lymphocytes are used to generate the CAR T cells, and thus, surgical tumor resection is unnecessary.[213] In 2010, T lymphocytes genetically engineered to express CARs were tested in a clinical trial for the first time. CAR T cells against CD19 mediated regression in advanced B-cell lymphoma.[219] Many trials have been conducted subsequently, evaluating the clinical utility of

CAR T cells targeting different tumor-associated antigens, including HER2 for colorectal cancer, folate receptor-a (FRA) for ovarian cancer, and carbonic anhydrase IX (CAIX) for renal cell carcinoma. Unfortunately, to date, the clinical results have demonstrated that CARs have low efficacy in solid tumor and significant toxicities, though it is hoped that continued development of this approach will overcome obstacles to widening the scope of therapeutic indications for this exciting new treatment modality. One promising example is the use of GD2-targeting CAR T cells to treat neuroblastoma.[218]

In conclusion, T cell-based therapy requires continued intensive study to lay the groundwork for major improvements in toxicity, applicability, and clinical efficacy. Also, compared with off-the-shelf monoclonal antibodies that can be applied across tumor types, adoptive T-cell therapy is personalized for each patient. Therefore, it is more expensive, labor-intensive, and time-consuming. However, it has some unique features that allow this treatment to be clinically useful. For example, administered T cells have high-avidity recognition against tumor antigens. Secondly, T cells can proliferate in the circulation and maintain their antitumor effector functions after transfer. Hence, they can be considered as "living drugs." Finally, while immunodepletion before transfusion is important to achieve a desirable number of circulating antitumor T cells for at least 1 month, it may also eliminate suppressor cells, such as T-reg and MDSCs, providing a favorable microenvironment tumor-directed T-cell function.[213]

6.02.2.5.2.2 NK cell-based cancer immunotherapy

NK cells are a type of lymphocytes that are distinct from T and B lymphocytes and are characterized by the following properties: (1) NK cells are components of the innate immunity. Therefore, they kill their target cells without prior immunization and they lack antigen specificity, (2) they are larger in size, and (3) they contain cytotoxic cytoplasmic granules, such as perforins and granzymes.[220]

NK cells express activating receptors, including the natural cytotoxicity receptors (NCRs), and inhibitory receptors, including killer cell immunoglobulin-like receptors (KIRs). The inhibitory receptors bind to MHC I molecules and thereby inhibit NK cell activation. Because MHC I is expressed on almost all cell types, the interaction between these two surface molecules prevents NK cell killing of normal cells. However, under stress conditions, target cells, such as transformed cells or virus-infected cells, downregulate MHC I molecules, leaving the inhibitory receptor inactive and thus activating NK cells (missing-self-recognition). On the other hand, activating receptors can activate NK cell-mediated killing once they bind to pathogen-encoded molecules (nonself-recognition) or self-expressed proteins that are upregulated by transformed or infected cells (stress-induced self-recognition). Typically, there are multiple NK cell activation and inhibitory receptors on a given NK cell. Therefore, whether NK cells will kill the target cell or not depends on the balance between the inhibitory and activating signals.[220]

NK cells can induce killing of malignant cells directly and indirectly. As mentioned previously, direct tumor elimination by NK cells can be achieved by activating either the death receptor pathway or the granule exocytosis pathway. Another mechanism of direct NK-mediated cytotoxicity includes the release of effector molecules, such as IFN-γ and nitric oxide (NO), and ADCC. Additionally, NK cells can induce tumor cell lysis indirectly by releasing various cytokines, chemokines, and growth factors. Accumulating evidence in both mice and humans emphasizes the role of NK cells in tumor clearance. For example, an 11-year follow-up study of cancer patients indicated that the cancer risk was associated with low NK-like cytotoxicity. Moreover, it was shown that in patients with colorectal carcinoma, gastric carcinoma, and squamous cell lung cancer, NK cell infiltration into the tumor is considered as a positive prognostic marker.[220]

Cancer cells can employ many strategies to evade NK cell attack and diminish their cytotoxic activity. One mechanism is by upregulating MHC I expression, which results in a stronger inhibitory signal to NK cells. Another escape mechanism is decreasing the number and activity of NK cells. A supporting observation is that in AML, NCR expression is often impaired.[221] Also, impaired ADCC activity has been reported in various malignancies, including head and neck, breast, gastric, esophageal, cervical, and urological cancers, as well as leukemia and myeloma.[222,223]

Consequently, NK cells may become good therapeutic targets for cancer treatment.[220] Besides their role in mediating ADCC in therapeutic antibody treatments against malignant cells, cellular-based strategies have shown good therapeutic impact on cancer treatment. The first attempt was to test the antitumor effect of autologous NK cell adoptive transfer. Strikingly, although this treatment approach can result in high levels of circulating NK cells, it failed to mediate tumor regression.[224] Then, an alternative strategy was to use allogeneic NK cell adoptive transfer. This strategy, which is based on selecting mismatched donors with specific criteria, has been more successful for treatment of leukemia and solid cancers and has been considered as a safe therapy with minimal toxicity. To further improve NK cell-based immunotherapy, strategies using adoptively transferred genetically modified NK cells have been tested. For example, NK cells with altered cytokine expression, activating receptor overexpression, and inhibitory receptor downregulation have been used. This therapeutic approach has been shown to increase the cytotoxic capacity, proliferative rate, survival ability, and in vivo antitumor activity of transferred NK cells. NK cells with chimeric tumor antigen-specific receptors have been generated and examined for adoptive transfer. Chimeric receptors against HER2/neu, CEA, CD33, CD20, and CD19 showed increased specific cytotoxicity both in vitro and in vivo. However, these immunotherapies are still under development.[220]

6.02.2.5.3 Cancer vaccines

Cancer vaccines fall into two main categories: prophylactic vaccines and therapeutic vaccines.[225]

6.02.2.5.3.1 Prophylactic cancer vaccines

The principle of preventive cancer vaccination is to prime the immune system and create an antigen-specific memory to prevent future infections. Thereby, when exposure occurs, the immune system would be ready to eliminate the antigen quickly and

effectively and thus precludes disease occurrence. Currently, there are two prophylactic infectious targets for which there are FDA-approved vaccines: hepatitis B virus (HBV) and human papilloma virus (HPV).[226] Hepatocellular carcinoma is the second most common cause of death from cancer worldwide,[227] and chronic HBV infection is associated with 50–75% of all cases.[226] Likewise, cervical cancer is the most common cause of cancer-related deaths in women,[228] and high-risk HPV serotypes directly cause most cervical cancers and are also associated with other genital, oropharyngeal, and anal cancers. HBV and HPV vaccines that prevent infection have reduced the risk of liver and cervical cancers, respectively, making them clinically very useful. Nevertheless, it must be noted that once a person gets infected, prophylactic vaccines cannot prevent cancer from developing.[226]

6.02.2.5.3.2 Therapeutic cancer vaccines

These vaccines aim to treat established tumors by stimulating the host anticancer immune response.[225] Various approaches for therapeutic cancer vaccination have been studied in preclinical and clinical settings, including vaccination with tumor cells, cancer-related peptides, proteins, and DNA molecules, as well as DC vaccination.[229] However, except for sipuleucel-T (Provenge), all therapeutic vaccines tested for cancer treatment have been unsuccessful in inducing tumor regression and improving survival to the extent that they can be approved for use by regulatory authorities. It is believed that the major reasons behind this failure are the potent immunosuppressive effect of the TME,[226] the downregulation of MHC molecules on the surfaces of malignant cells, and the low immunogenicity of tumor antigens that have been selected as vaccine targets.[230] Moreover, many therapeutic vaccines have limited efficacy because they promote immune destruction of normal cells bearing the antigen of interest. However, this is not a problem with the prophylactic vaccines because they induce immune responses against antigens of the oncogenic viruses, which are not expressed by normal human cells.[226]

6.02.2.5.4 Cytokines

Cytokines mediate their biological effects by first binding to common and shared receptors. These receptors can be grouped into seven families: type I and type II cytokine receptors, immunoglobulin superfamily receptors, tumor necrosis factor (TNF) receptors, G protein-coupled receptors, TGF-β receptors, and IL-17 receptors. The major cytokines involved in cancer immunotherapy are the interferons, IL-2 and its related cytokines (IL-7, IL-15, and IL-21), IL-6, granulocyte macrophage colony-stimulating factor (GM-CSF), IL-10, and TGF-β. All these cytokines, except TGF-β, bind to either type I or type II receptors. The engagement of the cytokines to these receptors activates the Janus kinase–signal transducer and activator of transcription (JAK–STAT) signaling pathway,[26] which regulates the transcription of a wide range of genes that are involved in many physiological processes.[231]

6.02.2.5.4.1 The roles of cytokines in cancer treatment

IFN-α was the first approved immunotherapy for adjuvant therapy of high-risk melanoma.[232] IL-2 was the first immunotherapy used for the effective treatment of metastatic cancer. In the 1980s, it was shown that the intravenous administration of high doses of recombinant human IL-2 can cause tumor regression in mice, and it was shown subsequently to have curative potential in some patients with metastatic melanoma and renal cell carcinoma.[233,234] The cytokine-based approaches for cancer treatment can be divided as the following:

6.02.2.5.4.1.1 Administration of cytokines that exhibit antitumor activity

To date, two cytokines have received FDA approval for cancer treatment: (1) IL-2, which was approved for treating renal cell carcinoma and metastatic melanoma in 1992 and 1998, respectively,[235] and (2) IFN-α, which achieved FDA approval in 1995 for the adjuvant treatment of patients with advanced melanoma.[236] IFN-α was also approved for use in hairy cell leukemia (HCL) in 1986; however, because of its low therapeutic efficacy in HCL, it has been superseded by more effective therapies.[237] Notably, although IL-2 and IFN-α have been used in the clinic for more than two decades, significant challenges still exist. It is very difficult to achieve meaningful antitumor responses using these cytokines without also causing treatment-limiting toxicities.[26]

6.02.2.5.4.1.2 Neutralization of immunosuppressive cytokines

Besides the cytokines that exhibit immunostimulatory properties, there is another group of cytokines that have immune-suppressive activity, such as TGF-β, IL-10, IL-4, and IL-13. Although many treatments targeting the immunosuppressive cytokines have been considered and developed, none of them have demonstrated sufficient anticancer activity to warrant FDA approval. It is likely that the underlying barrier to the utility of these approaches is their pleiotropism, meaning that some cytokines act on many different cell types and have diverse and/or opposing effects. This is further complicated by the redundancy of cytokine signaling, meaning that multiple cytokines can mediate the same functional effects. Another challenge is that TGF-β and few other cytokines have dual functions, as they may induce both immune activation and immune suppression, depending on the stage of the disease and the context of their use.[26]

6.02.2.5.4.1.3 Improving the efficacy of adoptive T-cell therapy

As mentioned in the preceding text, adoptive T-cell therapy involves isolating a patient's T lymphocytes, expanding them ex vivo, followed by reinfusion of these cells into the patient. During the ex vivo generation of antitumor T cells, IL-2 and IL-2-related growth factors can be used to stimulate the growth of T cells and maintain their cytotoxic activity. Besides the addition of cytokines ex vivo, the administration of low-dose IL-2 to the patient following T-cell infusions has become a standard component of adoptive cellular

therapy. IL-2 can prolong the survival of the adoptively transferred cells and thus can improve the chances of a favorable clinical outcome.[26]

6.02.2.5.4.1.4 Improving the efficacy of cancer vaccination

In an attempt to improve DC vaccination, different mixtures of cytokines can be used during various steps of this procedure. For example, IL-4 and GM-CSF can be used to elicit DC from peripheral blood monocytes obtained by leukapheresis. Also, TNF-α and IL-1β can be used to enhance the maturation of isolated DCs to potent APCs. In addition to the ex vivo cytokine treatment, GM-CSF can also be used to activate DCs by infusing this molecule within the vaccine. The "built-in" GM-CSF strategy was employed in the development of sipuleucel-T prostate cancer vaccine, improving its efficacy and allowing for its FDA approval.[26]

6.02.2.5.4.2 Strategies for cytokine delivery

In the 1980s, when cytokines first were tested in clinical trials, they were administered directly into the patients. However, due to the treatment-limiting toxicities and severe adverse effects of systemic cytokine administration, many alternative strategies have been developed. This includes (1) immunocytokine conjugates, also called cytokine–antibody fusion molecules; (2) recombinant viruses, for example, attenuated oncolytic herpes simplex virus type 1 encoding GM-CSF, which can selectively replicate in tumor cells; (3) cell engineering approaches, which involve the infusion of GM-CSF into allogeneic irradiated whole-cell tumor vaccines; and (4) cytokine PEGylation. Conjugation of the polymer polyethylene glycol (PEG) to the cytokine has been shown to decrease its clearance from plasma and increase its in vivo half-life significantly.[26]

6.02.2.6 Targets for Cancer Immunotherapy

Immunotherapies can be developed to target cancer cells, to manipulate the TME, or to enhance antitumor host immunity.

6.02.2.6.1 Targeting cancer cells

Tumor antigens may serve as good targets for cancer immunotherapy. They can be divided into two main categories: tumor-specific antigens (TSAs; neoantigens) and tumor-associated antigens (TAAs), which include overexpressed self-proteins, tissue-specific differentiation antigens, and cancer testis (oncofetal) antigens.

6.02.2.6.1.1 Targeting tissue-specific differentiation antigens

These antigens are shared between tumors and the normal tissue of origin, such as CD20 and CD19, which are expressed by both normal and cancer B cells.[238]

6.02.2.6.1.1.1 CD20

CD20 is a transmembrane protein expressed on B cells. Early experiments suggested that it was important in the regulation of human B-cell activation, proliferation, and Ca^{2+} transport. However, CD20-deficient ($CD20^{-/-}$) mice appeared normal.[239] Hence, the exact biological function of CD20 and its physiological ligand remain to be fully defined.[240] Regardless of the uncertainty in the biological role of this antigen, it is a good target for cancer immunotherapy. This is because (1) it is expressed specifically on B cells, but not found on other normal cells; (2) it is not expressed on the first stage of B-cell development, but only on pre-B cells and mature B lymphocytes[241]; and (3) it can be detected in more than 95% of malignant B cells.[242]

Today, there are four clinically available anti-CD20 monoclonal antibodies, and several more are being investigated. Rituximab was the first monoclonal antibody licensed for therapeutic use.[243] It was discovered in 1991, entered human phase I trials in 1993, and was approved for use in adults with CD20-positive B-cell lymphoma in 1997.[244] It is a mouse–human chimeric monoclonal antibody against CD20, consisting of human IgG1 constant region with mouse variable regions.[245] Therefore, it can selectively bind to CD20 on B cells while inducing cell-mediated effector functions to destroy the target cells.

A few years later, in 2002, ibritumomab tiuxetan was licensed for the treatment of non-Hodgkin's lymphoma.[117] Also, it was the first radioimmunotherapy approved for the treatment of cancer. It consists of an anti-CD20 murine IgG1 monoclonal antibody ibritumomab, linked to the radiolabeled isotope yttrium-90.[244] The monoclonal antibody portion of ibritumomab tiuxetan binds to CD20 specifically on the surface of malignant cells. When such cells are exposed to radiation, it destroys all the CD20-positive B cells and the immediately surrounding CD20-negative malignant cells. However, due to the "cross fire" effect, normal cells that are not targeted by the antibody also can be damaged by the radiation. Notably, radioimmunotherapies are predicted to be more successful in treating B-cell lymphomas, but may have limited translational success in solid tumors. In contrast to solid tumor targets, CD20 is a good radioimmunotherapy target because malignant B cells have high inherent radiation sensitivity and vascularity.[246] By contrast, solid tumor cells are typically less radiosensitive, and radioimmunoconjugates have comparatively limited initial penetration into solid tumors.[169]

Since the approval of rituximab in 1997, many efforts have aimed to improve its efficacy. This has involved the exploration of resistance mechanisms, pharmacokinetic parameters, and the evaluation of subcutaneous route.[247] While rituximab has proved to be an important and effective therapy for many patients, there remains room to improve response rates and the duration of clinical benefit. Therefore, a new-generation anti-CD20 monoclonal antibody has been generated that may provide advantages over rituximab. One of the potential limitations of rituximab was that it is a chimeric monoclonal antibody that might be immunogenic in some cases. Accordingly, humanized and fully human antibodies have been developed. These second-generation drugs include

ocrelizumab, veltuzumab, and ofatumumab.[245] Ofatumumab is the only approved fully human anti-CD20 monoclonal antibody, binds to CD20 with higher avidity, possesses higher ADCC activity, and binds to C1q complement protein with higher avidity and thus stimulates greater CDC.[159,248] Clinical trials have supported the potential relevance of these preclinical data. Ofatumumab is useful for the therapy of refractory CLL patients, leading to its approval in 2009. Ocrelizumab and veltuzumab are humanized antibodies and are still under investigation.[119]

Furthermore, to improve the affinity of anti-CD20 antibodies, especially in patients who have a low-affinity version of the Fc receptor, third-generation antibodies were synthesized. These are humanized monoclonal antibodies that are modified in the Fc region. Obinutuzumab (GAZYVA) is the first FDA-approved glycoengineered antibody-based therapy.[120,121,249] In vitro experiments indicated that the Fc alterations enhanced immune effector cell activities including ADCC, ADCP, and direct nonapoptotic cell death, whereas it reduced CDC,[190] which may not be an obligatory requirement for improved clinical efficacy.[250] This drug has led to significant clinical improvement over first-generation anti-CD20 immunotherapy with rituximab in a phase III trial in CLL, leading to its approval in 2013.[190]

Besides targeting CD20 antigen by monoclonal antibodies, CD20-specific CARs have been tested in a pilot clinical trial. T cells containing CARs with CD28 and 4-1BB costimulatory domains were transferred to three patients after cyclophosphamide lymphodepletion. Two patients, who participated in this trial without evaluable disease, remained progression-free for 12 and 24 months. The third patient had an objective partial remission and relapsed at 12 months.[251]

6.02.2.6.1.1.2 CD19

CD19 is a transmembrane protein that is specifically expressed in normal and neoplastic B cells. It serves as an attractive target for immunotherapy for many reasons: (1) It is expressed on most B-cell malignancies; (2) it is expressed in the B-cell lineage at an early stage, even before the expression of CD20; (3) it internalizes efficiently in lymphoma tumor models[252]; and (4) it is possibly involved in the development of B-cell cancers. For example, several studies reported that CD19 can upregulate the expression and phosphorylation of c-Myc,[253] which is a proto-oncogene that is found mutated and/or overexpressed in many malignancies.[254] Accordingly, CD19 may be considered as a poor prognostic factor in human lymphomas.[253]

These facts, therefore, provided a stimulus to target CD19 for the treatment of B-cell leukemia and lymphoma. Many methods have been tested in preclinical experiments and clinical trials. Early attempts, in the 1990s, focused on utilizing conjugates of anti-CD19 antibodies and cytotoxic agents, such as ricin A chain, pokeweed antiviral protein, and the plant-derived ribosome-inactivating protein saporin. The aim of these drugs was to eliminate cells expressing CD19 directly. However, because of design limitations of the conjugated molecules, and low efficacies of antimurine antibodies, these treatments were not successful.[253]

An example of approved next-generation anti-CD19 therapies is the bispecific T-cell engager (BiTE) antibodies, blinatumomab (BLINCYTO). This agent has demonstrated striking activity in patients with advanced, CD19-expressing leukemias.[255] Additional antibody-based therapeutics targeting CD19 include the fucosylated, humanized antibodies Medi-551 and MDX-1342. These drugs exhibit high affinity to FcγRIIIA. Further, CAR–CD19-specific T-cell therapy is currently being studied in many clinical trials and with very promising results. These CARs are genetically modified T cells that are composed of extracellular recognition sequences, CARs, designed to engage CD19 on target cells, with T-cell intracellular signaling components, resulting in enhanced T-cell responses against CD19-positive cells.[253]

6.02.2.6.1.1.3 CD30

CD30 is a transmembrane protein that is expressed in normal activated T cells, B cells, NK cells, and malignant cells. Currently, the molecular function of CD30 in human physiology is still unclear. However, it has been suggested that CD30-mediated signaling plays an important role in regulating the development of both effector and memory $CD4^+$ cells. In 2011, the FDA granted accelerated approval to brentuximab vedotin for the treatment of certain patients with Hodgkin's lymphoma or systemic anaplastic large cell lymphoma (ALCL). Brentuximab vedotin is an antibody–drug conjugate (ADC). It is composed of anti-CD30 mouse–human chimeric IgG1 monoclonal antibody. Each antibody carries an average of four monomethyl auristatin E (MMAE) groups, via a protease-sensitive dipeptide linker. Upon the ligation of the monoclonal antibody portion of brentuximab vedotin with CD30 on the surface of cancer cells, the molecule is internalized via endocytosis. Then, the dipeptide linker gets cleaved, allowing for the release of the MMAE, a potent antimicrotubule drug that binds to tubulin and disrupts the microtubule network within the cell, leading to induction of cell cycle arrest and apoptosis. Consequently, this ADC has three advantages. It can discriminate between normal and cancer cells and thus has lower in vivo toxicity. MMAE conjugated with the monoclonal antibody remains relatively stable in the circulation; therefore, it has a higher cytotoxicity. Finally, if a small fraction of MMAE is released into the TME, it might kill surrounding untargeted CD30-expressing malignant cells as well as nonmalignant cells that have protumor effects. These observations were supported by clinical trials that have demonstrated brentuximab vedotin's durable antitumor activity with a manageable safety profile in patients with Hodgkin's lymphoma and ALCL.[256]

6.02.2.6.1.2 Targeting overexpressed self-proteins

During the course of tumor progression, malignant cells may increase the expression of normal proteins that possess proliferation- or survival-promoting function.[257] Examples of self-proteins that are commonly overexpressed in various types of malignancies are two members of the ErbB family receptors: epidermal growth factor receptor (EGFR/HER1/ErbB1) and human epidermal growth factor receptor 2 (HER2/ErbB2).

6.02.2.6.1.2.1 Epidermal growth factor receptor

Overexpression of EGFR has been reported in many patients with early-stage epithelial tumors, including lung, HNSCC, colon, pancreatic, brain, and breast. Therefore, it was hypothesized that this receptor plays a critical role in cancer initiation and progression. Intensive research over the past three decades has shown that EGFR engages a very complex signaling network. The receptor consists of an extracellular ligand-binding domain, transmembrane domain, juxtamembrane nuclear localization signal (NLS), tyrosine kinase domain, and tyrosine-rich C-terminal tail. EGFR receptor–ligand interaction induces conformational changes in the receptor that stimulates its dimerization with another EGFR molecule (homodimerization) or with other activated HER family members (heterodimerization). Upon dimerization, receptors' intrinsic tyrosine kinase domains get activated, inducing phosphorylation of tyrosine residues on C-terminal tails. Then, activated EGFR activates several signaling pathways, such as RAS/MAPK, PI(3)K-Akt, PLC-PKC, and Jak-STAT.[258] These EGFR-mediated downstream signaling cascades have been strongly implicated in tumor growth and progression.[259] Accordingly, EGFR has been one of the most targeted receptors in the field of oncology.[258]

In 2004, the FDA allowed for accelerated approval of cetuximab (Erbitux) for the treatment of metastatic colorectal cancer. This accelerated approval was based on the tumor response rates in phase II trials. Cetuximab is a mouse–human chimeric monoclonal antibody that binds specifically to the extracellular domain of EGFR. It blocks binding of ligands to this receptor and thus inhibits downstream signaling.[259] Also, it has been shown that cetuximab may establish antitumor response via ADCC and CDC.[134] Seven years after the initial approval of cetuximab, FDA expanded its approval for patients with head and neck squamous cell carcinoma (HNSCC).[260] Because this antibody mediates its function through its binding to EGFR, the association between EGFR expression levels and cetuximab clinical outcome has been widely studied. For example, the FLEX trial reported that advanced nonsmall cell lung cancer (NSCLC) patients who have tumors with elevated levels of EGFR expression would have survival benefit from the addition of cetuximab to first-line chemotherapy. Thus, in some groups of patients, EGFR expression is considered a tumor-predictive biomarker.[261]

Panitumumab is another anti-EGFR monoclonal antibody that was approved by the FDA in 2006.[133] Like cetuximab, it blocks ligand–receptor interactions, but differs from cetuximab in several ways. For example, it is a fully human antibody and so induces allergic reactions in fewer than 1% of treated patients. Second, it belongs to the class of IgG2 immunoglobulin antibodies, meaning that it has no or limited ability to induce ADCC. Finally, while the half-life of cetuximab in the plasma is up to 1 week, it reaches 2 weeks for panitumumab, presumably because it is a fully human antibody. Thus, it can be administered less frequently, adding to patient convenience.[262] To directly compare the efficacy and toxicity of both agents, the phase III ASPECCT (A Study of Panitumumab Efficacy and Safety Compared to Cetuximab) study was conducted. In this study, 999 chemotherapy-refractory metastatic colorectal cancer patients with *KRAS* exon 2 wild-type tumors were recruited. This trial showed that panitumumab is noninferior to cetuximab. Also, they reported that these agents provide similar overall survival benefit and toxicity profiles in this population.[263]

Recently, in 2015, necitumumab (PORTRAZZA), a new anti-EGFR monoclonal antibody, received FDA approval for the treatment of metastatic NSCLC. It is mechanistically similar to cetuximab as both of them belong to the IgG1 subclass. However, because necitumumab is a fully human antibody, fewer adverse immune reactions are expected to occur.[264] Additionally, matuzumab, a humanized anti-EGFR monoclonal IgG1 antibody, is currently being tested in clinical trials.[265] Finally, it is worthy to note that there are many approved small-molecule inhibitors that can also target EGFR, such as gefitinib, erlotinib, lapatinib, icotinib hydrochloride, and afatinib. This category of cancer drugs is beyond the scope of this review and it has been comprehensively covered elsewhere.[266–269]

6.02.2.6.1.2.2 Human epidermal growth factor receptor 2

Similar to EGFR, HER2 receptor can be activated through homodimerization or heterodimerization with members of the ErbB family, leading to phosphorylation of tyrosine residues on C-terminal tails and activation. Thereby, receptor phosphorylation activates downstream signaling molecules, which promote oncogenic transformation and tumorigenesis. However, HER2 is different than the other receptors of the ErbB family in that it has no known high-affinity ligand.[270] Notably, overexpression of HER2 has been reported in a variety of cancer types, including carcinomas of the breast, bladder, and pancreas; nonsmall cell lung cancer (NSCLC); and ovary, endometrium, colon, kidney, head and neck, stomach, esophagus, and prostate cancers.[271] In some cases, most notably in breast and gastric cancers, this overexpression is caused by gene amplification.[272] Based on this observation, HER2 has become an attractive and important target for cancer therapy. In fact, several antibody-based therapeutics and small-molecule inhibitors targeting HER2 have received FDA approval, and many others are currently being tested in clinical studies or preclinical experiments.[125–128]

Trastuzumab (Herceptin) is a humanized monoclonal antibody that targets the HER2 extracellular domain. This drug is approved by the FDA for the treatment of HER2-overexpressing early-stage and metastatic breast cancer and HER2-overexpressing metastatic gastric cancer.[273] The precise mechanism of action for trastuzumab is not fully elucidated. However, several mechanisms have been proposed, including blocking the downstream signaling pathways involved in cancer initiation and progression, enhancing HER2 internalization and degradation, inhibiting extracellular domain proteolysis, promoting cell cycle arrest and apoptosis, stimulating immune destruction by mediating ADCC, and inhibiting DNA repair and angiogenesis.[274]

Not surprisingly, trastuzumab, in combination with chemotherapy, improves response rates, disease-free survival, and overall survival in HER2-positive breast cancer and gastric cancer patients. However, in the case of metastatic breast cancers, most patients develop disease progression within 12 months, and about 15% of early-stage HER2-positive breast cancer patients relapse after trastuzumab-based adjuvant chemotherapy.[274] Therefore, several attempts have been made to improve HER2-targeted therapies. In 2012, the second anti-HER2 antibody, pertuzumab (Perjeta), was licensed to treat metastatic HER2-positive breast cancer in

combination with trastuzumab and a taxane in the first-line setting.[275–277] Pertuzumab is a humanized IgG1 monoclonal antibody that targets an epitope of the extracellular domain of HER2 that is distinct from that that binds to trastuzumab. Similar to trastuzumab, pertuzumab blocks receptor dimerization and prevents activation of downstream signaling pathways.[274]

To further improve the therapeutic efficacy of HER2-targeted treatments, an anti-HER2 monoclonal antibody was conjugated to a cytotoxic antimicrotubule agent (DM1) to create trastuzumab emtansine (T-DM1; Kadcyla). While trastuzumab can mediate its antitumor effect, DM1 acts as a highly potent cytotoxic agent.[274] Interestingly, further studies supported the hypothesis that T-DM1 has greater activity than trastuzumab with high selectivity for HER2-positive cells.[278,279] As a result, T-DM1 achieved FDA approval for the treatment of patients with breast cancer in 2013.[128]

6.02.2.6.1.3 Targeting cancer testis antigens

This group of antigens is normally only expressed in germ cells; however, because they have oncogenic functions, including support of growth, survival, and metastasis, they are frequently activated in malignancies. Cancer testis antigens (CTs) frequently are cancer-specific, immunogenic, and commonly expressed in various types of cancer, making them promising candidate targets for cancer treatment.[280]

In general, the two approaches that have been applied to target CTs are cancer vaccination and adoptive T-cell therapy. To date, many CTs that have been targeted by immunotherapies, such as MAGE, GAGE, SSX, CT45, and NY-ESO-1, and many clinical trials have been conducted to test the therapeutic benefit of this approach. Indeed, at least 35 clinical studies have been performed that solely target NY-ESO-1. Although there is no CT antigen-based immunotherapy that has received FDA approval, some DNA methyltransferase (DNMT) inhibitors, which have been licensed for the treatment of hematologic malignancies, have shown to upregulate the expression of CT antigens on the surface of cancer cells. Hence, it has been hypothesized that DNMT inhibitors may trigger immune responses against tumor-expressed CTs.[280] Support for this hypothesis comes from the observation that combined treatment with azacitidine, a DNMT inhibitor, and sodium valproate has been associated with induction of MAGE-specific T-cell responses in AML and myeloid dysplastic syndrome patients. These findings suggest that combining DNMT inhibitors with CT antigen-based immunotherapy may induce CT antigen expression, allowing for the induction of potent antitumor immunity.[281]

6.02.2.6.1.4 Targeting tumor-specific antigens

This type of antigen is specifically expressed by tumors and not present in normal cells. They represent either oncogenic viral proteins or mutant antigens. During tumorigenesis, cancer cells acquire mutations that are important for their transformation (driver mutations). Also, as a result of genetic instability, these cells can acquire random mutations that may not provide a growth advantage (passenger mutations). Virtually, all cancers contain somatic mutations, and many of these mutations encode for TSAs that can be recognized by $CD8^+$ T cells, resulting in antitumor immune responses. Since these mutant antigens are new to the immune system, they are named neoantigens. It has been claimed that targeting neoantigens has certain advantages over targeting TAAs. For example, TSAs are nonself-proteins and thus are unlikely to induce immunologic tolerance. TAAs are frequently poorly immunogenic and may exhibit lower affinity to TCRs compared with TSAs. Accordingly, there is increasing interest in TSAs as potential targets for immune recognition and destruction.[257]

Early experiments indicated that it is possible to find TSAs and utilize them clinically to treat cancer. However, using conventional antigen-cloning approaches, this process is time-consuming and poorly adaptable to patient care. In 2012, two groups proposed distinct strategies that utilize genomics and bioinformatics approaches to identify tumor-specific mutant proteins. Both approaches employed a combination of next-generation sequencing, *in silico* epitope prediction, and immunologic approaches to identify and validate neoantigens in murine models (B16-F10 melanoma and MCA-induced sarcoma). Interestingly, the two independent studies determined that the proposed strategies could shorten the time frame needed to identify TSAs to only a few weeks. In the following year, this work was extended to human cancers.

The framework of personalized TSA-based cancer immunotherapy is first to compare the genome of tumor and normal tissues by whole-exome sequencing and RNA-Seq, allowing for the identification of nonsynonymous somatic mutations that are specifically expressed in the tumor but not in the normal cells. The next step is to predict the MHC epitopes that the T cells can recognize. The list of candidate antigens can then be used to treat cancer patients either by generating neoantigen vaccines or by transfusing mutant neoantigen-specific autologous T cells.[257]

Meanwhile, studies showed that checkpoint inhibitors may facilitate the expansion of preexisting T cells specific for tumor neoantigens in human melanoma patients. Therefore, it was suggested that the combination of checkpoint blockade immunotherapy with personalized cancer vaccines, or individualized adoptive cell therapies, may show increased therapeutic impact. It is argued that they would at least enhance many aspects of antitumor immunity.[257] Such concepts merit further investigation.

6.02.2.6.2 Targeting the tumor microenvironment

Tumors are complex tissues composed of cancer cells; various types of stromal cells, including endothelial cells; fibroblasts and immune cells; and extracellular matrix. Recent studies have shown that the TME plays an important role in both malignant tumor progression and treatment response.[282]

6.02.2.6.2.1 Targeting the tumor vasculature

Angiogenesis is defined as the formation of new blood vessels from preexisting vessels and circulating endothelial precursors.[283] The link between tumor growth and angiogenesis was first proposed more than a century ago. Thereafter, in 1927, a study showed that

the vascular architecture varied in several murine tumors, suggesting that the tumor environment can highly influence the growth and morphology of surrounding blood vessels.[284] About a decade later, in 1939, it was hypothesized that cancer cells can promote angiogenesis by the secretion of blood vessel growth-stimulating factor, which was then associated with rapid growth of transplanted tumors.[285] Today, it is well established that while proliferating cancer cells stimulate angiogenesis, new blood vessels supply tumors with oxygen and nutrients, allowing tumors not only to survive but also to progress and metastasize.[284]

Vascular endothelial growth factor A (VEGF-A) is a major regulator of normal and abnormal angiogenesis.[285] When tumors and surrounding stromal cells secrete VEGF-A, it binds to its receptors, VEGFR-1 and VEGFR-2, or its coreceptors, neuropilin 1 (NRP1) and NRP2. This ligand binding leads to receptor dimerization and phosphorylation, activating multiple downstream signaling pathways, which can promote the survival and proliferation of endothelial cells and enhance filopodial extension, chemotaxis, and ECM degradation, leading to increased angiogenesis and vascular permeability.[284]

In addition, accumulating evidence suggests that VEGF not only has an important role in tumor angiogenesis but also may induce immune suppression via different mechanisms.[286] For example, VEGF secreted in the TME may act as a strong negative modulator of DC function.[287] In fact, tumor-bearing mice treated with anti-VEGF antibody showed significant increases in the number and function of DCs in draining lymph nodes and spleens.[288,289] More importantly, treating lung, breast, and colorectal carcinoma patients with anti-VEGF antibody led to improved DC development and increased DC populations in the peripheral blood.[290,291] Also, VEGF can induce immune suppression by inhibiting T-cell development and promoting the expression of PD-1 and other inhibitory checkpoints, which can lead to T-cell exhaustion.[292] Supportive evidence came from studies that have shown that blocking VEGF or its receptors can enhance T-cell antitumor immunity.[293] Moreover, VEGF may promote the expansion of immunosuppressive cells, such as MDSCs and T-regs.[291,294] In line with these findings, blocking the VEGF signaling pathway in breast cancer animal models resulted in increased maturation of DCs and inhibited infiltration of immune-suppressive cells.[295]

Not surprisingly, VEGF-A–VEGFR signaling pathway has become an attractive target for cancer therapy. In fact, different strategies have been employed to target VEGF-A and its receptors directly, using antibody-based therapies, tyrosine kinase inhibitors (TKIs), and soluble VEGFR/VEGFR hybrids. Also, many other approaches have been developed to target the components of this signaling pathway indirectly, such as chemotherapy and targeted therapies against tumor antigens or against other components of the TMEs.[296] In this section, we will focus on bevacizumab (Avastin), ziv-aflibercept (Zaltrap), and ramucirumab (Cyramza) as they are relevant to cancer immunotherapies.

Bevacizumab (Avastin) was the first antiangiogenic drug approved for cancer therapy.[36,138,139,141] It is a humanized IgG1 monoclonal antibody against human VEGF-A. It neutralizes VEGF after its secretion from tumor cells and thus inhibits VEGF-A binding to its receptors. Hence, this treatment is expected to cause a regression of existing tumor blood vessels, reduction in the formation of new blood vessels, and normalization of surviving vessels. Thereby, it can limit the blood supply to tumor tissues and enhance the delivery of anticancer treatments.[297] Additionally, a recent study indicated that although bevacizumab is a human antibody and it does not recognize mouse VEGF-A, it could suppress angiogenesis in three different animal models through its binding to FcγRI (CD64) and c-Cbl, impairing macrophage migration.[298]

In addition, because the new tumor vessels within or surrounding the neoplastic lesions are usually structurally abnormal and leaky, they can increase interstitial pressure and hence restrict the delivery of cytotoxic agents. Therefore, it was hypothesized that bevacizumab may have a synergistic therapeutic effect when combined with chemotherapy. Thereafter, many clinical trials supported these hypotheses, leading to the first FDA approval of bevacizumab in 2004 for the treatment of patients with colorectal cancer. Then, over the following years, this approval was expanded to other cancers, including NSCLC, renal cell carcinomas, and glioblastoma. However, the significant benefit from the addition of bevacizumab was not seen in all malignancies, such as in metastatic HER2-negative breast cancer and prostatic and pancreatic cancers.[297] Moreover, ziv-aflibercept (Zaltrap) was also generated to target VEGF-A besides other members of the VEGF family, including VEGF-B and PlGF. It is a soluble recombinant fusion protein composed of the second Ig domain to VEGFR-1 and the third Ig domain of VEGFR-2 to the Fc section of human IgG1.[299] It binds to VEGF ligands with high affinity, preventing them from engaging to their receptors, and it was approved to treat colorectal cancer in 2012.[142]

Furthermore, given the fact that VEGFR2 is the main mediator of VEGF-A biological effects, many drugs have been developed to target this molecule, including ramucirumab (IMC-1121B). This concept is supported by the observation that VEGFR-2 −/− knockout mice cannot survive due to defective development of blood islands, endothelial cells, and hematopoietic cells. Ramucirumab is a fully humanized monoclonal IgG1 antibody that prevents VEGF ligand binding to the receptor through neutralizing VEGFR-2. It received its initial FDA approval in 2014 for the treatment of patients with advanced or metastatic gastric cancer or gastroesophageal junction (GEJ) carcinoma who had previously failed first-line chemotherapy.[297] Today, it is also approved for colorectal and nonsmall cell lung cancers[143–145].

6.02.2.6.2.2 Targeting the extracellular matrix

An example of a cancer therapeutic antibody that targets a specific soluble ligand is denosumab (Xgeva). It is an anti-RANKL human monoclonal antibody that was approved in 2013 by the FDA for the treatment of bone metastases in breast cancer patients,[300] the most frequent site of metastasis among these patients.[301] Interestingly, it was discovered that bone-disseminated breast cancer cells can modulate bone environments. These malignant cells were shown to stimulate osteoblasts to overexpress the receptor activator of nuclear factor-kB ligand (RANKL). The ligation of RANKL molecules to their receptors on the surface of osteoclast precursors can increase maturation, activity, and life span of osteoclasts. Then, osteoclasts, through the secretion of growth factors and cytokines, can promote tumor progression and metastasis, suggesting that RANKL pathway plays a major role in tumorigenesis and

metastasis.[300] Also, RANK ligand–receptor interaction can increase the risk of cancer-related bone diseases.[302] Therefore, denosumab and other RANKL antagonists, such as bisphosphonates, may exert potent antitumor effects. Interestingly, studies have shown that fibroblasts, T and B lymphocytes, and DCs within the TME can express high levels of RANKL. Indeed, the role of RANKL/RANK signaling in immunity is very important. It regulates lymph node development, lymphocyte differentiation, dendritic cell survival, T-cell activation, and immune tolerance. Not surprisingly, in addition to the osteoclast-dependent effects of RANKL/RANK signaling on tumorigenesis, some studies have suggested that this pathway can manipulate antitumor host immunity. For example, it may have direct effects on DC survival and T-cell proliferation and function. However, DC and monocytes in RANKL and RANK knockout (KO) mice develop normally and exhibit intact function. Therefore, further investigation is needed.[303–305]

6.02.2.6.3 Targeting immune cells

6.02.2.6.3.1 Targeting T lymphocytes

During tumorigenesis, T lymphocytes may migrate toward the TME, where they exhibit a significant effect on cancer development. Although this effect can range from protumor to antitumor responses, for many malignancies, including melanoma, renal cell cancer, colon cancer, ovarian cancer, and some subtypes of breast cancer, the presence of cytotoxic $CD8^+$ lymphocytes is associated with favorable outcomes.[32,306] Infiltrated T lymphocytes within the tumor are mainly of $CD8^+$ and $CD4^+$ subtypes. While $CD8^+$ can induce tumor cell lysis directly,[42] $CD4^+$ can promote tumor rejection by activating other immune cells, such as $CD8^+$ T cells and B cells, and secreting various types of cytokines and chemokines. However, upon cellular transformation, malignant cells can manipulate the function of immune cells, including T lymphocytes, to evade immune destruction. Therefore, to restore or enhance the immune system's ability to fight cancer, different immunotherapies have been developed to generate, educate, and/or enhance T-cell activity directed against tumor antigens.

Tumor-infiltrating T cells have distinctive properties. They can kill cancer cells directly and indirectly. They can mediate tumor rejection through various mechanisms. Also, as they are components of the adaptive immunity, they are able recognize tumor antigens specifically, and then later, they may create immunologic memory against these antigens.[257] As a result, T cells have been receiving increasing attention as a therapeutic target for cancer treatment. Cancer immunotherapies that target T cells can induce either antigen-specific or nonantigen-specific T-cell responses. Indeed, immune checkpoint inhibitors, such as anti-CTLA-4 and anti-PD1/PDL1, and cytokines, such as IL-2, have emerged as the most effective immunotherapies that can broadly activate the immune system to focus T cell-mediated antigen-specific, antitumor immune responses.

CTLA-4 (CD152) is a molecule expressed on activated T cells. It binds B7 molecules with a high avidity, outcompeting the activating effects of CD28 binding to B7 and thus attenuating T-cell proliferation and activation. Therefore, CTLA-4 defines a class of inhibitory or immune checkpoint molecules on T cells.[307] Several CTLA-4 antagonistic antibodies have been developed and evaluated in clinical trials. Currently, two of them have received FDA approval, ipilimumab (Yervoy) and tremelimumab.[72,147] After decades of intensive research and development, ipilimumab was shown to improve treatment outcomes in advanced melanoma. Treatment improved overall survival (OS), induced some durable responses, and may be curative in some patients. This IgG1 fully human monoclonal antibody targets CTLA-4 on T cells to reverse the inhibitory signal and allow B7 molecules to stimulate T cells through CD28.[308] However, additional mechanisms of action have been identified. For example, CTLA-4 is expressed within tumors to a higher extent on T-reg cells than on effector T cells. Therefore, similar to many other monoclonal antibodies, the FcγR of anti-CTLA-4 can result in elimination of T-reg cells by mediating ADCC, leaving effector T cells intact.[309] Moreover, it was identified that CTLA-4 signaling can induce IDO production in APCs and subsequently inhibit T-cell proliferation.[310] Also, CTLA-4 interaction with B7 molecules on APCs stimulates their internalization and thus prevents their binding to CD28.[311]

PD1 is another inhibitory molecule on T cells. While PD1 is expressed on the surfaces of activated T cells, its ligand (PD-L1) is expressed by malignant cells and APCs. When PD-L1 engages PD-1, it interrupts the signaling of CD28 in the cytoplasm of T cells, resulting in "exhausted" and ineffective T cells.[73,312] The expression level and kinetics of PD-1 depend on the strength and kinetics of T-cell activation, which also depend on the amount and source of the target antigen.[313] To date, two anti-PD-1-targeting antibodies are approved by the FDA: nivolumab (Opdivo) in 2014[73,312] and pembrolizumab (Keytruda) in 2015.[151,152] Both of these immunotherapies are approved for the treatment of patients with melanoma and squamous nonsmall cell lung cancer; moreover, nivolumab (Opdivo) is also approved for renal cell carcinoma.

Many other immune checkpoints are utilized by cancer cells to modulate antitumor immune responses. These ligand–receptor interactions can deliver either costimulatory signals or inhibitory signals. In fact, the favorable treatment outcomes of CTLA-4 and PD1/PDL1 antagonists have provided a stimulus for many groups to intensely search for new targets. Today, many new agents are under clinical evaluation, targeting immune checkpoints such as OX40, GITR, TIM-3, and LAG-3.[18]

Another strategy that has been employed to promote T-cell activity without targeting a specific tumor antigen is through the use of IL-2. In 1986, it was reported that the direct administration of high doses of recombinant human IL-2, even without adoptive transfusion of autologous TIL, can cause tumor regression in mice.[217] Driven by these encouraging results, clinical trials of recombinant IL-2 in patients with metastatic cancer were initiated. Interestingly, this treatment approach could result in complete durable tumor regressions in some patients with metastatic melanoma,[314] allowing for its approval in the 1990s.[315] IL-2 mediates its physiological functions by promoting the proliferation and activation of T cells, B cells, and NK cells, resulting in improved antitumor immunity. Nevertheless, since IL-2 can also promote T-reg cell activity, it may act as regulatory cytokine, rather than a purely stimulatory T-cell growth factor.[26]

In addition to the induction of nonspecific T-cell activation, novel treatments that stimulate antigen-specific T-cell responses have also received considerable attention. This includes T cell-based therapies, bispecific/trispecific antibodies, and immunotherapies that can enhance DC-mediated T-cell activation.

6.02.2.6.3.2 Targeting dendritic cells

DCs are bone marrow-derived cells that are found in all tissues in the body. Typically, inactive DCs exhibit high antigen-capture activity and binding capacity, allowing them to sense for a wide range of danger signals efficiently.[316] The main types of antigen receptors expressed on DCs are mannose receptor (MR), DC-SIGN, scavenger receptor (SR), DEC-205, and Toll-like receptors (TLRs).[317] Each of these receptors can bind to specific types of antigens. Also, each antigen receptor interaction can activate DCs through distinct molecular pathways and thus induce various types of immune cell responses.[316] DCs play a central role in the priming of $CD4^+$ and $CD8^+$ T cells.[318] Detection of an antigen by DCs triggers its internalization, processing, and presentation on MHC molecules. When lymph node-resident DCs detect an antigen directly in the lymph node, they present the antigen to naive T cells. This interaction may result in T-cell priming, proliferation, and clonal expansion. Subsequently, when inactive DCs in peripheral tissues capture the same antigen, they migrate to the lymph node, where they meet with the already activated antigen-specific T cells, promoting the generation of effector T cells. Hence, DCs act as a bridge between innate and adaptive immunity. Additionally, DCs can regulate humoral immunity through the interaction with B cells directly or indirectly, by stimulating the expansion and differentiation of $CD4^+$ helper T cells. Besides the regulation of adaptive immune cells, DCs can also regulate the cells of the innate immune system, such as NK cells and mast cells.[316]

In the context of cancer, DCs play a major role in initiating antitumor responses. For instance, the interaction between DCs and dying tumor cells triggers at least three different signals, including "find me," "eat me," and "do not eat me" signals. First, apoptotic cancer cells secrete soluble mediators, such as lipid lysophosphatidylcholine (LPC), sphingosine-1-phosphate (S1P), chemokine (C-X3-C motif) ligand 1 (CX3CL1), and the nucleotides ATP and UTP, that recruit DCs and other phagocytes to the site of tumor ("find me" signals). The second step is the exposure of several membrane-bound molecules on the surface of dying tumor cells, including phosphatidylserine, $\alpha v\beta 5$ integrin, and CD36. These molecules tag the target cells and thus promote their recognition and engulfment by phagocytes ("eat me" signals). Additional "eat me" signals are opsonizing antibodies, including therapeutic antibodies and antibody-like molecules, and complement components. Upon the binding of these molecules to tumor antigens, DCs can recognize cancer cells, through the FcyRs and complement receptors, respectively, leading to tumor cell eradication (ADCP).[316,319]

Malignant cells can employ a variety of strategies to impair the anticancer properties of DCs and thus enhance tumor growth and progression. This includes upregulating the "do not eat me" signals, switching the differentiation of monocytes to macrophages rather than DCs, inhibiting DC maturation through the secretion of IL-10 and other immunosuppressive cytokines, preventing efficient antigen processing and presentation to T cells, and stimulating the production of protumor DCs, which indirectly favor tumor growth.[316] Accordingly, research efforts have targeted DCs in order to restore and enhance host immunity against cancer.

One approach is to inhibit the "do not eat me" signals or inhibit the inhibitors of phagocytosis, such as CD47. These molecules can downregulate the phagocytosis of cancer cells, allowing them to escape from immune destruction. CD47 on target cells can bind to SIRPα on macrophages, DCs, and other myeloid cells. This ligand–receptor interaction triggers prophagocytic inhibitory signals and prevents proper cytoskeleton rearrangements that are necessary for phagocytosis.[320] Interestingly, various types of solid tumors, such as ovarian cancer, bladder cancer, breast cancer, and leiomyosarcoma, as well as hematopoietic malignancies, including AML, tend to induce high levels of CD47 expression on their cell surfaces.[208] These observations provided the rationale to target the CD47-SIRPa axis for cancer therapy. Several in vivo studies have supported this hypothesis.[321,322] For example, human B-cell non-Hodgkin's lymphoma-engrafted mice treated with anti-CD47 antibodies showed reduced lymphoma burden and improved survival. Also, using the same model, it was reported that the addition of CD47 blockade to rituximab treatment led to elimination of lymphoma and cure. Driven by the encouraging results, a humanized anti-CD47 antibody (Hu5F9-G4) was developed and is in clinical development for patients with AML and solid tumors.[322]

Another strategy is to induce DC antitumor activity by autologous DC vaccination. To deliver this vaccine, DCs are first isolated from cancer patients and cultured ex vivo with tumor antigens, resulting in DC activation. Then, activated DCs are reinfused back into the patients. This therapy was proposed to increase tumor antigen presentation to T cells, thereby enhancing host immunity against the tumor and inducing immunologic memory to reduce the chance of cancer recurrence.[316] However, this approach has not yet routinely induced strong T-cell responses that can completely eliminate established tumors.[323] To enhance the efficacy of DC vaccination, key regulators have been modified in DCs. These strategies include overexpression of costimulatory molecules, such as CD80, CD54, and CD58, and tumor-associated antigens, such as CEA.[324] To date, sipuleucel-T is the only DC vaccine that has achieved FDA approval. It was shown to modestly improve overall survival in prostate cancer, without meaningful decreases in symptoms or tumor measures, leading to its approval in 2010.[325,326]

Another strategy to enhance the interaction between DCs and T cells is by using agonistic monoclonal antibodies that target cell surface molecules, such as CD40. The rationale for the use of this immunotherapy for cancer treatment is that the engagement of CD40 on APCs with its ligand CD154 (CD40L) on activated CD4 + T cells can enhance the expression of MHC and costimulatory molecules, leading to improved T-cell priming and differentiation. Also, this receptor–ligand binding can promote the secretion of pro-inflammatory cytokines, which may indirectly activate NK cells. Moreover, CD40 ligation can promote apoptosis and reduce

proliferation, causing tumor regression. Based on these findings, anti-CD40 agonistic antibodies that mimic the function of CD40L were developed and are currently being tested in clinical trials.[327,328] Importantly, monoclonal antibody-based immunotherapies are expected to overcome some challenges of the autologous DC vaccination, including time and money efficiency, and the risk of ex vivo cellular activation and expansion.[329]

6.02.2.7 Future Directions

Immunotherapeutics have been shown to be successful in making cancer a controllable and curable disease in an increasing number of malignancies, but many challenges remain. Resistance is a major obstacle to successful cancer immunotherapy, and it can be divided into three main types: intrinsic resistance, naturally acquired resistance, and treatment-induced acquired resistance. In general, the effectiveness of the immunotherapeutic approach relies on the competence of the host's immune system and the level of tumor immunogenicity. Therefore, it is difficult to treat patients who have systemic immune failure, such as HIV and transplantation patients, and elderly people. A possible solution for these individuals is to transfer activated tumor-specific T cells that can restore the antitumor host immunity using autologous or allogeneic adoptive T-cell therapy. Moreover, even when there are a sufficient number of competent T lymphocytes, tumors that do not contain potent immunogens may not be recognized by the T cells. To overcome this challenge, DNA-damaging agents, such as chemotherapy and radiation therapy, can be used in combination with immunotherapies. This therapeutic strategy is hoped to increase the number of mutations, leading ultimately to more immunogenic tumors and improved patient outcomes.[330]

In addition to systemic immune failure, local immune dysfunction can also be seen in many cancer patients. A noninflammatory TME may result in impaired immune cell recruitment to the site of neoplastic lesions. Also, an immunosuppressive TME can influence the activity of TILs, rendering them unable to induce antitumor immune responses. For these cases, targeting components of the TME might help to restore the immune system's ability to eradicate the cancer.[330]

Besides intrinsic resistance, naturally acquired resistance frequently occurs in cancer. For example, under immune selection pressure, cancer cells can evade immune destruction by continuously selecting cancer cell populations that are less immunogenic, have impaired antigen processing and presentation capacity,[330] or have mutations that may give the cells a growth advantage. For example, primary resistance to the anti-EGFR antibodies cetuximab and panitumumab has been reported in colorectal cancer patients with activating KRAS mutations.[159] Another escape strategy commonly employed by malignant cells is the upregulation of immune checkpoint proteins. These escape mechanisms may result in failure of many immunotherapies. To reverse this acquired resistance, combination therapy of immune checkpoint inhibitors with standard cancer treatments or cell-based immunotherapies may be necessary.[330]

There is an urgent need to identify biomarkers that can assist in selecting the patients who are likely to respond, as well as biomarkers that can help to select the right treatment with the right dosing schedule. These findings will not only make the therapy more effective, and safer, but also decrease the cost and allow the treatments to be more easily available for more cancer patients.[331–333]

With regard to personalized cancer immunotherapies, although it is predicted that therapeutically targeting TSAs can make cancer treatment more specific, more effective, and safer, this approach may have limited translational success. One issue is that it is not very clear if personalized immunotherapy might lead to any autoimmune consequences. Also, it may not be possible to complete the development of the treatment within a clinically relevant time frame. Moreover, it involves the use of sequencing technologies, and thus, it may create many logistical challenges, for example, how to prioritize potential tumor-specific antigens for selection as therapy targets and how to achieve highly accurate sequencing results. Because of the complexity of these issues, many cancer patients may have limited or no access to personalized immunotherapy until these issues have been successfully addressed.[334]

Therapeutic cancer vaccines may have improved efficacy when administered earlier during the disease course, perhaps because cancer patients have lower tumor burdens and more intact immune systems capable of eliciting stronger immune responses against tumors.[335]

Cancer immunotherapy-related toxicities are different depending on the type of administered treatment.[336] The associated symptoms can range from very mild, such as itching and inflammation, to severe disease and even death.[337] Cytokine therapy, including high-dose IL-2 treatment, is typically associated with nonspecific T-cell reactivity.[336] The most common side effect of IL-2 therapy is capillary leak syndrome, which is potentially life-threatening.[338] However, a recent study reported a retrospective analysis of the outcomes of 500 patients with metastatic renal cell carcinoma or melanoma treated with high-dose IL-2. In this analysis, IL-2-mediated toxicities were reversible and the incidence of fatal toxicity was $<1\%$.[339] In contrast, other immunotherapies, including vaccines, CAR and TCR cellular therapies, and checkpoint inhibitors, may activate T cells more specifically, causing specific organ damage.[336] Some cancer therapeutic antibodies such as rituximab and alemtuzumab have significant risks for infusion reactions (over 50% each). However, these reactions are mostly mild. Only $\sim 0.3\%$ of treated patients can have serious reactions.[337]

Immunotherapy is changing the paradigm for cancer treatment. Indeed, its ability to prolong tumor regression and cure cancer with mostly manageable side effects challenges prior dogmas and creates new directions for cancer therapy. Moreover, many novel, promising immunotherapeutics are being currently evaluated in clinical trials. Future prospects for this exciting field have never been brighter.

See also: 5.01. Cancer Biology and the Principles of Targeted Cancer Drug Discovery. 5.11. Cancer Immunotherapy—An Emerging Field that Bridges Oncology and Immunology Research.

References

1. Weiner, L. M. Cancer Immunology for the Clinician. *Clin. Adv. Hematol. Oncol.* **2015,** *13* (5), 299–306.
2. Tiwari, A. K.; Roy, H. K. Progress Against Cancer (1971–2011): How Far Have We Come? *J. Intern. Med.* **2012,** *271* (4), 392–399.
3. Siegel, R. L.; Miller, K. D.; Jemal, A. Cancer Statistics, 2016. *CA Cancer J. Clin.* **2016,** *66* (1), 7–30.
4. Kufe, D. W.; Frei, E. *Cancer Medicine 6;* B.C. Decker: Hamilton (ON), 2003.
5. Siegel, R.; Ma, J.; Zou, Z.; Jemal, A. Cancer Statistics, 2014. *CA Cancer J. Clin.* **2014,** *64* (1), 9–29.
6. American Society of Clinical Oncology. The State of Cancer Care in America, 2014: A Report by the American Society of Clinical Oncology. *J. Oncol. Pract.* **2014,** *10* (2), 119–142.
7. Prehn, R. T. Immunosurveillance, Regeneration and Oncogenesis. *Prog. Exp. Tumor Res.* **1971,** *14,* 1–24.
8. Shankaran, V.; Ikeda, H.; Bruce, A. T.; White, J. M.; Swanson, P. E.; Old, L. J.; Schreiber, R. D. IFNgamma and lymphocytes prevent primary tumour development and shape tumour immunogenicity. *Nature* **2001,** *410* (6832), 1107–1111.
9. Murphy, K. *Janeway's Immunobiology;* Garland Publishing: New York (NY), 2014.
10. Alberts, B.; Johnson, A.; Lewis, J.; Walter, P.; Raff, M.; Roberts, K. *Molecular Biology of the Cell,* 4th ed.; Garland Science: New York (NY), 2002.
11. Karlsson, F.; Tremaroli, V.; Nielsen, J.; Bäckhed, F. Assessing the Human Gut Microbiota in Metabolic Diseases. *Diabetes* **2013,** *62* (10), 3341–3349.
12. Bianconi, E.; Piovesan, A.; Facchin, F.; Beraudi, A.; Casadei, R.; Frabetti, F.; Vitale, L.; Pelleri, M. C.; Tassani, S.; Piva, F.; et al. An Estimation of the Number of Cells in the Human Body. *Ann. Hum. Biol.* **2013,** *40* (6), 463–471.
13. Boland, C. R.; Ricciardiello, L. How Many Mutations Does It Take to Make a Tumor? *PNAS* **1999,** *96* (26), 14675–14677.
14. Pikor, L. A.; Bell, J. C.; Diallo, J.-S. Oncolytic Viruses: Exploiting Cancer's Deal with the Devil. *Trends Cancer* **2015,** *1* (4), 266–277.
15. Iwasaki, A.; Medzhitov, R. Control of Adaptive Immunity by the Innate Immune System. *Nat. Immunol.* **2015,** *16* (4), 343–353.
16. Netea, M. G. Training Innate Immunity: The Changing Concept of Immunological Memory in Innate Host Defence. *Eur. J. Clin. Investig.* **2013,** *43* (8), 881–884.
17. Moretti, J.; Blander, J. M. Insights into Phagocytosis-Coupled Activation of Pattern Recognition Receptors and Inflammasomes. *Curr. Opin. Immunol.* **2014,** *26,* 100–110.
18. Pardoll, D. M. The Blockade of Immune Checkpoints in Cancer Immunotherapy. *Nat. Rev. Cancer* **2012,** *12* (4), 252–264.
19. Treanor, B. B-Cell Receptor: From Resting State to Activate. *Immunology* **2012,** *136* (1), 21–27.
20. Janeway, C. A., Jr; Travers, P.; Walport, M.; et al. Immunobiology. In *The Immune System in Health and Disease, 5th edition;* Garland Science: New York (NY), 2001.
21. Forthal, D. N. Functions of Antibodies. *Microbiol. Spectr.* **2014,** *2* (4), 1.
22. Weiner, L. M.; Surana, R.; Wang, S. Monoclonal Antibodies: Versatile Platforms for Cancer Immunotherapy. *Nat. Rev. Immunol.* **2010,** *10* (5), 317–327.
23. Scott, A. M.; Wolchok, J. D.; Old, L. J. Antibody Therapy of Cancer. *Nat. Rev. Cancer* **2012,** *12* (4), 278–287.
24. Zaleska, M.; Olszewski, W. L.; Durlik, M.; Miller, N. E. Signaling Proteins Are Represented in Tissue Fluid/Lymph From Soft Tissues of Normal Human Legs at Concentrations Different From Serum. *Lymphat. Res. Biol.* **2013,** *11* (4), 203–210.
25. Stenken, J. A.; Poschenrieder, A. J. Bioanalytical Chemistry of Cytokines—A Review. *Anal. Chim. Acta* **2015,** *853,* 95–115.
26. Lee, S.; Margolin, K. Cytokines in Cancer Immunotherapy. *Cancers* **2011,** *3* (4), 3856–3893.
27. Landskron, G.; De la Fuente, M.; Thuwajit, P.; Thuwajit, C.; Hermoso, M. A. Chronic Inflammation and Cytokines in the Tumor Microenvironment. *J. Immunol. Res.* **2014,** *2014* (2), 149185, 19.
28. Dunn, G. P.; Old, L. J.; Schreiber, R. D. The Immunobiology of Cancer Immunosurveillance and Immunoediting. *Immunity* **2004,** *21* (2), 137–148.
29. Smyth, M. J.; Dunn, G. P.; Schreiber, R. D. Cancer Immunosurveillance and Immunoediting: The Roles of Immunity in Suppressing Tumor Development and Shaping Tumor Immunogenicity. In *Cancer Immunotherapy*; *Advances in ImmunologyAdvances in Immunology*; Elsevier, 2006, vol. 90; pp 1–50. https://www.ncbi.nlm.nih.gov/pubmed/16730260.
30. Ramsay, A. G.; Gribben, J. G. Immune Dysfunction in Chronic Lymphocytic Leukemia T Cells and Lenalidomide as an Immunomodulatory Drug. *Haematologica* **2009,** *94* (9), 1198–1202.
31. Maude, S. L.; Frey, N.; Shaw, P. A.; Aplenc, R.; Barrett, D. M.; Bunin, N. J.; Chew, A.; Gonzalez, V. E.; Zheng, Z.; Lacey, S. F.; et al. Chimeric Antigen Receptor T Cells for Sustained Remissions in Leukemia. *N. Engl. J. Med.* **2014,** *371* (16), 1507–1517. http://dx.doi.org/10.1056/NEJMoa1407222.
32. Gajewski, T. F.; Schreiber, H.; Fu, Y.-X. Innate and Adaptive Immune Cells in the Tumor Microenvironment. *Nat. Immunol.* **2013,** *14* (10), 1014–1022.
33. Biragyn, A.; Longo, D. L. Neoplastic "Black Ops": Cancer's Subversive Tactics in Overcoming Host Defenses. *Semin. Cancer Biol.* **2012,** *22* (1), 50–59.
34. Aptsiauri, N.; García-Lora, A. M.; Garrido, F. *'Hard' and 'Soft' Loss of MHC Class I Expression in Cancer Cells. Tumor Immunology and Immunotherapy;* Oxford University Press: USA, 2014.
35. Fruci, D.; Benevolo, M.; Cifaldi, L.; Lorenzi, S.; Monaco Lo, E.; Tremante, E.; Giacomini, P. Major Histocompatibility Complex Class I and Tumour Immuno-Evasion: How to Fool T Cells and Natural Killer Cells at One Time. *Curr. Oncol.* **2012,** *19* (1), 39–41.
36. Poschke, I.; Mougiakakos, D.; Kiessling, R. Camouflage and Sabotage: Tumor Escape From the Immune System. *Cancer Immunol. Immunother.* **2011,** *60* (8), 1161–1171.
37. Dunn, G. P.; Bruce, A. T.; Ikeda, H.; Old, L. J.; Schreiber, R. D. Cancer Immunoediting: From Immunosurveillance to Tumor Escape. *Nat. Immunol.* **2002,** *3* (11), 991–998.
38. Blankenstein, T.; Coulie, P. G.; Gilboa, E.; Jaffee, E. M. The Determinants of Tumour Immunogenicity. *Nat. Rev. Cancer* **2012,** *12* (4), 307–313.
39. Jenkins, M. R.; Rudd-Schmidt, J. A.; Lopez, J. A. Failed CTL/NK Cell Killing and Cytokine Hypersecretion Are Directly Linked Through Prolonged Synapse Time. *J. Exp. Med.* **2015,** *212* (3), 307–317.
40. Topham, N. J.; Hewitt, E. W. Natural Killer Cell Cytotoxicity: How Do They Pull the Trigger? *Immunology* **2009,** *128* (1), 7–15.
41. Garrido, C.; Paco, L.; Romero, I.; Berruguilla, E.; Stefansky, J.; Collado, A.; Algarra, I.; Garrido, F.; Garcia-Lora, A. M. MHC Class I Molecules Act as Tumor Suppressor Genes Regulating the Cell Cycle Gene Expression, Invasion and Intrinsic Tumorigenicity of Melanoma Cells. *Carcinogenesis* **2012,** *33* (3), 687–693.
42. Igney, F. H.; Krammer, P. H. Immune Escape of Tumors: Apoptosis Resistance and Tumor Counterattack. *J. Leukoc. Biol.* **2002,** *71* (6), 907–920.
43. Bartholin, L. *Pancreatic Cancer and the Tumor Microenvironment: Mesenchyme's Role in Pancreatic Carcinogenesis;* Transworld Research Network: Trivandrum (India), 2012.
44. Hamada, S.; Masamune, A.; Shimosegawa, T. Alteration of Pancreatic Cancer Cell Functions by Tumor-Stromal Cell Interaction. *Front. Physiol.* **2013,** *4,* 318.
45. Wesolowski, R.; Markowitz, J.; Carson, W. E. Myeloid Derived Suppressor Cells—A New Therapeutic Target in the Treatment of Cancer. *J. Immunother. Cancer* **2013,** *1,* 10.
46. König, M.; Rharbaoui, F.; Aigner, S.; Dälken, B.; Schüttrumpf, J. Tregalizumab—A Monoclonal Antibody to Target Regulatory T Cells. *Front. Immunol.* **2016,** *7* (5), 1151.
47. Byrne, W. L.; Mills, K. H. G; Lederer, J. A.; O'Sullivan, G. C. Targeting Regulatory T Cells in Cancer. *Cancer Res.* **2011,** *71* (22), 6915–6920.
48. Masson, N.; Ratcliffe, P. J. Hypoxia Signaling Pathways in Cancer Metabolism: The Importance of Co-Selecting Interconnected Physiological Pathways. *Cancer Metab.* **2014,** *2* (1), 3.
49. Platten, M.; von Knebel Doeberitz, N.; Oezen, I.; Wick, W.; Ochs, K. Cancer Immunotherapy by Targeting IDO1/TDO and Their Downstream Effectors. *Front. Immunol.* **2014,** *5,* 673.

50. Vacchelli, E.; Aranda, F.; Eggermont, A.; Sautès-Fridman, C.; Tartour, E.; Kennedy, E. P.; Platten, M.; Zitvogel, L.; Kroemer, G.; Galluzzi, L. Trial Watch: IDO Inhibitors in Cancer Therapy. *Oncoimmunology* **2014,** *3* (10), e957994.
51. Bellone, M.; Calcinotto, A. Ways to Enhance Lymphocyte Trafficking Into Tumors and Fitness of Tumor Infiltrating Lymphocytes. *Front. Oncol.* **2013,** *3,* 231.
52. Spahn, J.; Peng, J.; Lorenzana, E.; Kan, D.; Hunsaker, T.; Segal, E.; Mautino, M.; Brincks, E.; Pirzkall, A.; Kelley, S.; et al. Improved Anti-Tumor Immunity and Efficacy Upon Combination of the IDO1 Inhibitor GDC-0919 with Anti-PD-L1 Blockade Versus Anti-PD-L1 Alone in Preclinical Tumor Models. *J. Immunother. Cancer* **2015,** *3* (Suppl. 2), 303.
53. Kareva, I.; Hahnfeldt, P. The Emerging "Hallmarks" of Metabolic Reprogramming and Immune Evasion: Distinct or Linked? *Cancer Res.* **2013,** *73* (9), 2737–2742.
54. Kaur, B.; Khwaja, F. W.; Severson, E. A.; Matheny, S. L.; Brat, D. J.; Van Meir, E. G. Hypoxia and the Hypoxia-Inducible-Factor Pathway in Glioma Growth and Angiogenesis. *Neuro-Oncology* **2005,** *7* (2), 134–153.
55. Cavadas, M. A.; Nguyen, L. K.; Cheong, A. Hypoxia-Inducible Factor (HIF) Network: Insights From Mathematical Models. *Cell Commun. Signal.* **2013,** *11* (1), 42.
56. Lukashev, D.; Klebanov, B.; Kojima, H.; Grinberg, A.; Ohta, A.; Berenfeld, L.; Wenger, R. H.; Ohta, A.; Sitkovsky, M. Cutting Edge: Hypoxia-Inducible Factor 1alpha and Its Activation-Inducible Short Isoform I.1 Negatively Regulate Functions of CD4+ and CD8+ T Lymphocytes. *J. Immunol.* **2006,** *177* (8), 4962–4965.
57. Palazón, A.; Aragonés, J.; Morales-Kastresana, A.; de Landázuri, M. O.; Melero, I. Molecular Pathways: Hypoxia Response in Immune Cells Fighting or Promoting Cancer. *Clin. Cancer Res.* **2012,** *18* (5), 1207–1213.
58. Höchst, B.; Diehl, L. Antigen Shedding Into the Circulation Contributes to Tumor Immune Escape. *Oncoimmunology* **2012,** *1* (9), 1620–1622.
59. Höchst, B.; Schildberg, F. A.; Böttcher, J.; Metzger, C.; Huss, S.; Türler, A.; Overhaus, M.; Knoblich, A.; Schneider, B.; Pantelis, D.; et al. Liver Sinusoidal Endothelial Cells Contribute to CD8T Cell Tolerance Toward Circulating Carcinoembryonic Antigen in Mice. *Hepatology* **2012,** *56* (5), 1924–1933.
60. Goldstein, M. J.; Mitchell, E. P. Carcinoembryonic Antigen in the Staging and Follow-Up of Patients with Colorectal Cancer. *Cancer Investig.* **2009,** *23* (4), 338–351.
61. Marth, C.; Egle, D.; Auer, D.; Rössler, J.; Zeimet, A. G.; Vergote, I.; Daxenbichler, G. Modulation of CA-125 Tumor Marker Shedding in Ovarian Cancer Cells by Erlotinib or Cetuximab. *Gynecol. Oncol.* **2007,** *105* (3), 716–721.
62. Tsé, C.; Gauchez, A.-S.; Jacot, W.; Lamy, P.-J. HER2 Shedding and Serum HER2 Extracellular Domain: Biology and Clinical Utility in Breast Cancer. *Cancer Treat. Rev.* **2012,** *38* (2), 133–142.
63. Alix-Panabières, C.; Rebillard, X.; Brouillet, J.-P.; Barbotte, E.; Iborra, F.; Segui, B.; Maudelonde, T.; Jolivet-Reynaud, C.; Vendrell, J.-P. Detection of Circulating Prostate-Specific Antigen-Secreting Cells in Prostate Cancer Patients. *Clin. Chem.* **2005,** *51* (8), 1538–1541.
64. Pak, Y.; Zhang, Y.; Pastan, I.; Lee, B. Antigen Shedding May Improve Efficiencies for Delivery of Antibody-Based Anticancer Agents in Solid Tumors. *Cancer Res.* **2012,** *72* (13), 3143–3152.
65. Liu, K. Role of Apoptosis Resistance in Immune Evasion and Metastasis of Colorectal Cancer. *World J. Gastrointest. Oncol.* **2010,** *2* (11), 399–406.
66. Peter, M. E.; Hadji, A.; Murmann, A. E.; Brockway, S.; Putzbach, W.; Pattanayak, A.; Ceppi, P. The Role of CD95 and CD95 Ligand in Cancer. *Cell Death Differ.* **2015,** *22* (4), 549–559.
67. Smyth, M. J.; Takeda, K.; Hayakawa, Y.; Peschon, J. J.; van den Brink, M. R. M; Yagita, H. Nature's TRAIL—On a Path to Cancer Immunotherapy. *Immunity* **2003,** *18* (1), 1–6.
68. Lemke, J.; von Karstedt, S.; Zinngrebe, J.; Walczak, H. Getting TRAIL Back on Track for Cancer Therapy. *Cell Death Differ.* **2014,** *21* (9), 1350–1364.
69. Lee, H. C.; Wondimu, A.; Liu, Y.; Ma, J. S. Y; Radoja, S.; Ladisch, S. Ganglioside Inhibition of CD8+ T Cell Cytotoxicity: Interference with Lytic Granule Trafficking and Exocytosis. *J. Immunol.* **2012,** *189* (7), 3521–3527.
70. Voskoboinik, I.; Whisstock, J. C.; Trapani, J. A. Perforin and Granzymes: Function, Dysfunction and Human Pathology. *Nat. Rev. Immunol.* **2015,** *15* (6), 388–400.
71. Herbst, R. S.; Soria, J.-C.; Kowanetz, M.; Fine, G. D.; Hamid, O.; Gordon, M. S.; Sosman, J. A.; McDermott, D. F.; Powderly, J. D.; Gettinger, S. N.; et al. Predictive Correlates of Response to the Anti-PD-L1 Antibody MPDL3280A in Cancer Patients. *Nature* **2014,** *515* (7528), 563–567.
72. Hodi, F. S.; O'Day, S. J.; McDermott, D. F.; Weber, R. W.; Sosman, J. A.; Haanen, J. B.; Gonzalez, R.; Robert, C.; Schadendorf, D.; Hassel, J. C.; et al. Improved Survival with Ipilimumab in Patients with Metastatic Melanoma. *N. Engl. J. Med.* **2010,** *363* (8), 711–723. http://dx.doi.org/10.1056/NEJMoa1003466 2010.
73. Topalian, S. L.; Hodi, F. S.; Brahmer, J. R.; Gettinger, S. N.; Smith, D. C.; McDermott, D. F.; Powderly, J. D.; Carvajal, R. D.; Sosman, J. A.; Atkins, M. B.; et al. Safety, Activity, and Immune Correlates of Anti-PD-1 Antibody in Cancer. *N. Engl. J. Med.* **2012,** *366* (26), 2443–2454. http://dx.doi.org/10.1056/NEJMoa1200690 2012.
74. Hamid, O.; Robert, C.; Daud, A.; Hodi, F. S.; Hwu, W.-J.; Kefford, R.; Wolchok, J. D.; Hersey, P.; Joseph, R. W.; Weber, J. S.; et al. Safety and Tumor Responses with Lambrolizumab (Anti–PD-1) in Melanoma. *N. Engl. J. Med.* **2013,** *369* (2), 134–144. http://dx.doi.org/10.1056/NEJMoa1305133.
75. Powles, T.; Eder, J. P.; Fine, G. D.; Braiteh, F. S.; Loriot, Y.; Cruz, C.; Bellmunt, J.; Burris, H. A.; Petrylak, D. P.; Teng, S.-L.; et al. MPDL3280A (Anti-PD-L1) Treatment Leads to Clinical Activity in Metastatic Bladder Cancer. *Nature* **2014,** *515* (7528), 558–562.
76. Mellman, I.; Coukos, G.; Dranoff, G. Cancer Immunotherapy Comes of Age. *Nature* **2011,** *480* (7378), 480–489.
77. Houston, A.; Waldron-Lynch, F. D.; Bennett, M. W.; Roche, D.; O'Sullivan, G. C.; Shanahan, F.; O'Connell, J. Fas Ligand Expressed in Colon Cancer Is Not Associated with Increased Apoptosis of Tumor Cells In Vivo. *Int. J. Cancer* **2003,** *107* (2), 209–214.
78. Randazzo, M.; Terness, P.; Opelz, G.; Kleist, C. Active-Specific Immunotherapy of Human Cancers with the Heat Shock Protein Gp96-Revisited. *Int. J. Cancer* **2012,** *130* (10), 2219–2231.
79. Wyld, L.; Audisio, R. A.; Poston, G. J. The Evolution of Cancer Surgery and Future Perspectives. *Nat. Rev. Clin. Oncol.* **2015,** *12* (2), 115–124.
80. Papavramidou, N.; Papavramidis, T.; Demetriou, T. Ancient Greek and Greco-Roman Methods in Modern Surgical Treatment of Cancer. *Ann. Surg. Oncol.* **2010,** *17* (3), 665–667.
81. Joensuu, H.; Hohenberger, P.; Corless, C. L. Gastrointestinal Stromal Tumour. *Lancet* **2013,** *382* (9896), 973–983.
82. Riall, T. S.; Lillemoe, K. D. Underutilization of Surgical Resection in Patients with Localized Pancreatic Cancer. *Ann. Surg.* **2007,** *246* (2), 181–182.
83. Demicheli, R.; Retsky, M. W.; Hrushesky, W. J. M.; Baum, M.; Gukas, I. D. The Effects of Surgery on Tumor Growth: A Century of Investigations. *Ann. Oncol.* **2008,** *19* (11), 1821–1828.
84. Walker, A. S.; Johnson, E. K.; Maykel, J. A.; Stojadinovic, A.; Nissan, A.; Brucher, B.; Champagne, B. J.; Steele, S. R. Future Directions for the Early Detection of Colorectal Cancer Recurrence. *J. Cancer* **2014,** *5* (4), 272–280.
85. Räsänen, M.; Carpelan-Holmström, M.; Mustonen, H.; Renkonen-Sinisalo, L.; Lepistö, A. Pattern of Rectal Cancer Recurrence After Curative Surgery. *Int. J. Colorectal Dis.* **2015,** *30* (6), 775–785.
86. Park, C.; Lee, I. J.; Jang, S. H.; Lee, J. W. Factors Affecting Tumor Recurrence After Curative Surgery for NSCLC: Impacts of Lymphovascular Invasion on Early Tumor Recurrence. *J. Thorac. Dis.* **2014,** *6* (10), 1420–1428.
87. Kułakowski, A. The Contribution of Marie Skłodowska-Curie to the Development of Modern Oncology. *Anal. Bioanal. Chem.* **2011,** *400* (6), 1583–1586.
88. Baskar, R.; Lee, K. A.; Yeo, R.; Yeoh, K.-W. Cancer and Radiation Therapy: Current Advances and Future Directions. *Int. J. Med. Sci.* **2012,** *9* (3), 193–199.
89. Bentzen, S. M. Preventing or Reducing Late Side Effects of Radiation Therapy: Radiobiology Meets Molecular Pathology. *Nat. Rev. Cancer* **2006,** *6* (9), 702–713.
90. Formenti, S. C.; Demaria, S. Systemic Effects of Local Radiotherapy. *Lancet Oncol.* **2009,** *10* (7), 718–726.
91. Spain, P. D.; Kadan-Lottick, N. Observations of Unprecedented Remissions Following Novel Treatment for Acute Leukemia in Children in 1948. *J. R. Soc. Med.* **2012,** *105* (4), 177–181.
92. Pérez-Herrero, E.; Fernández-Medarde, A. Advanced Targeted Therapies in Cancer: Drug Nanocarriers, The Future of Chemotherapy. *Eur. J. Pharm. Biopharm.* **2015,** *93,* 52–79.
93. Arruebo, M.; Vilaboa, N.; Sáez-Gutierrez, B.; Lambea, J.; Tres, A.; Valladares, M.; González-Fernández, Á. Assessment of the Evolution of Cancer Treatment Therapies. *Cancers* **2011,** *3* (3), 3279–3330.

94. DeAngelis, C. Side Effects Related to Systemic Cancer Treatment: Are We Changing the Promethean Experience with Molecularly Targeted Therapies. *Curr. Oncol.* **2008,** *15* (4), 198–199.
95. Padma, V. V. An Overview of Targeted Cancer Therapy. *BioMedicine* **2015,** *5* (4), 19.
96. Zahreddine, H.; Borden, K. L. Mechanisms and Insights Into Drug Resistance in Cancer. *Front. Pharmacol.* **2013,** *4,* 28.
97. West, H. Nivolumab as First Line Monotherapy for Advanced Non-Small Cell Lung Cancer: Could We Replace First Line Chemotherapy with Immunotherapy? *Transl. Lung Cancer Res.* **2014,** *3* (6), 400–402.
98. Gururajan, M.; Posadas, E. M.; Chung, L. W. K. Future Perspectives of Prostate Cancer Therapy. *Transl. Androl. Urol.* **2012,** *1* (1), 19–32.
99. Hoption Cann, S. A.; van Netten, J. P.; van Netten, C. Dr William Coley and Tumour Regression: A Place in History or in the Future. *Postgrad. Med. J.* **2003,** *79,* 672–680.
100. Říhová, B.; Šťastný, M. History of Immuno-Therapy From Coley Toxins to Check-Points of the Immune Reaction. *Klin. Onkol.* **2015,** *28* (Suppl. 4), 4S8–4S14.
101. Kienle, G. S. Fever in Cancer Treatment: Coley's Therapy and Epidemiologic Observations. *Glob. Adv. Health Med.* **2012,** *1* (1), 92–100. http://dx.doi.org/10.7453/gahmj.2012.1.1.016.
102. D'Angelo, S. P.; Tap, W. D.; Schwartz, G. K.; Carvajal, R. D. Sarcoma Immunotherapy: Past Approaches and Future Directions. *Sarcoma* **2014,** *2014* (10), 391967, 13.
103. Narkia, M. *Coley'S Toxins/Issel'S Fever Therapy,* 1996. http://cancerguide.org/coley.html.
104. Ehrlich, P. *Ueber Den Jetzigen Stand Der Karzinomforschung. Vortrag Gehalten Vor Den Studenten Der Amsterdamer Universitaet, Vereinigung Fuer Wissenschaftliche …*; Beitraege zur Experimentellen Pathologie und …, 1909.
105. Kaplan, D. H.; Shankaran, V.; Dighe, A. S.; Stockert, E.; Aguet, M.; Old, L. J.; Schreiber, R. D. Demonstration of an Interferon Gamma-Dependent Tumor Surveillance System in Immunocompetent Mice. *PNAS* **1998,** *95* (13), 7556–7561.
106. Corthay, A. Does the Immune System Naturally Protect Against Cancer? *Front. Immunol.* **2014,** *5,* 197.
107. Gandhi, N. M.; Morales, A.; Lamm, D. L. Bacillus Calmette-Guérin Immunotherapy for Genitourinary Cancer. *BJU Int.* **2013,** *112* (3), 288–297.
108. Fuge, O.; Vasdev, N.; Allchorne, P.; Green, J. S. Immunotherapy for Bladder Cancer. *Res. Rep. Urol.* **2015,** *7,* 65–79.
109. Morales, A.; Eidinger, D.; Bruce, A. W. Intracavitary Bacillus Calmette-Guerin in the Treatment of Superficial Bladder Tumors. *J. Urol.* **1976,** *116* (2), 180–183.
110. Manjili, M. H. Revisiting Cancer Immunoediting by Understanding Cancer Immune Complexity. *J. Pathol.* **2011,** *224* (1), 5–9.
111. Jiang, T.; Zhou, C. The Past, Present and Future of Immunotherapy Against Tumor. *Transl. Lung Cancer Res.* **2015,** *4* (3), 253–264.
112. Shinkai, Y.; Rathbun, G.; Lam, K. P.; Oltz, E. M.; Stewart, V.; Mendelsohn, M.; Charron, J.; Datta, M.; Young, F.; Stall, A. M.; et al. RAG-2-Deficient Mice Lack Mature Lymphocytes Owing to Inability to Initiate v(D)J Rearrangement. *Cell* **1992,** *68* (5), 855–867.
113. Mittal, D.; Gubin, M. M.; Schreiber, R. D.; Smyth, M. J. New Insights Into Cancer Immunoediting and Its Three Component Phases—Elimination, Equilibrium and Escape. *Curr. Opin. Immunol.* **2014,** *27,* 16–25.
114. Dunn, G. P.; Old, L. J.; Schreiber, R. D. The Three Es of Cancer Immunoediting. *Annu. Rev. Immunol.* **2004,** *22* (1), 329–360.
115. Maloney, D. G.; Grillo-López, A. J.; White, C. A.; Bodkin, D.; Schilder, R. J.; Neidhart, J. A.; Janakiraman, N.; Foon, K. A.; Liles, T.-M.; Dallaire, B. K.; et al. IDEC-C2B8 (Rituximab) Anti-CD20 Monoclonal Antibody Therapy in Patients with Relapsed Low-Grade Non-Hodgkin's Lymphoma. *Blood* **1997,** *90* (6), 2188–2195.
116. Jaglowski, S. M.; Byrd, J. C. Rituximab in Chronic Lymphocytic Leukemia. *Semin. Hematol.* **2010,** *47* (2), 156–169.
117. Witzig, T. E.; Flinn, I. W.; Gordon, L. I.; Emmanouilides, C.; Czuczman, M. S.; Saleh, M. N.; Cripe, L.; Wiseman, G.; Olejnik, T.; Multani, P. S.; et al. Treatment with Ibritumomab Tiuxetan Radioimmunotherapy in Patients with Rituximab-Refractory Follicular Non-Hodgkin's Lymphoma. *J. Clin. Oncol.* **2002,** *20* (15), 3262–3269.
118. Coiffier, B.; Losic, N.; Rønn, B. B.; Lepretre, S.; Pedersen, L. M.; Gadeberg, O.; Frederiksen, H.; van Oers, M. H. J; Wooldridge, J.; Kloczko, J.; et al. Pharmacokinetics and Pharmacokinetic/Pharmacodynamic Associations of Ofatumumab, a Human Monoclonal CD20 Antibody, in Patients with Relapsed or Refractory Chronic Lymphocytic Leukaemia: A Phase 1–2 Study. *Br. J. Haematol.* **2010,** *150* (1), 58–71.
119. Coiffier, B.; Lepretre, S.; Pedersen, L. M.; Gadeberg, O.; Fredriksen, H.; van Oers, M. H. J; Wooldridge, J.; Kloczko, J.; Holowiecki, J.; Hellmann, A.; et al. Safety and Efficacy of Ofatumumab, a Fully Human Monoclonal Anti-CD20 Antibody, in Patients with Relapsed or Refractory B-Cell Chronic Lymphocytic Leukemia: A Phase 1–2 Study. *Blood* **2008,** *111* (3), 1094–1100.
120. Cartron, G.; de Guibert, S.; Dilhuydy, M.-S.; Morschhauser, F.; Leblond, V.; Dupuis, J.; Mahe, B.; Bouabdallah, R.; Lei, G.; Wenger, M.; et al. Obinutuzumab (GA101) in Relapsed/Refractory Chronic Lymphocytic Leukemia: Final Data From the Phase 1/2 GAUGUIN Study. *Blood* **2014,** *124* (14), 2196–2202.
121. Sehn, L. H.; Chua, N. S.; Mayer, J.; Dueck, G. S.; Trněny, M.; Bouabdallah, K.; Fowler, N. H.; Delwail, V.; Press, O. W.; Salles, G. A.; et al. GADOLIN: Primary Results From a Phase III Study of Obinutuzumab Plus Bendamustine Compared with Bendamustine Alone in Patients with Rituximab-Refractory Indolent Non-Hodgkin Lymphoma. *J. Clin. Oncol.* **2015,** *33* (15 Suppl.), LBA8502. ASCO Meeting Abstracts.
122. Przepiorka, D.; Ko, C.-W.; Deisseroth, A.; Yancey, C. L.; Candau-Chacon, R.; Chiu, H.-J.; Gehrke, B. J.; Gomez-Broughton, C.; Kane, R. C.; Kirshner, S.; et al. FDA Approval: Blinatumomab. *Clin. Cancer Res.* **2015,** *21* (18), 4035–4039.
123. Vaklavas, C.; Forero-Torres, A. Safety and Efficacy of Brentuximab Vedotin in Patients with Hodgkin Lymphoma or Systemic Anaplastic Large Cell Lymphoma. *Ther. Adv. Hematol.* **2012,** *3* (4), 209–225.
124. Donk, N. W. C. J.; Janmaat, M. L.; Mutis, T.; Lammerts van Bueren, J. J.; Ahmadi, T.; Sasser, A. K.; Lokhorst, H. M.; Parren, P. W. H. I. Monoclonal Antibodies Targeting CD38 in Hematological Malignancies and Beyond. *Immunol. Rev.* **2016,** *270* (1), 95–112.
125. Slamon, D. J.; Leyland-Jones, B.; Shak, S.; Fuchs, H.; Paton, V.; Bajamonde, A.; Fleming, T.; Eiermann, W.; Wolter, J.; Pegram, M.; et al. Use of Chemotherapy Plus a Monoclonal Antibody Against HER2 for Metastatic Breast Cancer That Overexpresses HER2. *N. Engl. J. Med.* **2001,** *344* (11), 783–792. http://dx.doi.org/10.1056/NEJM200103153441101.
126. Bang, Y.-J.; Van Cutsem, E.; Feyereislova, A.; Chung, H. C.; Shen, L.; Sawaki, A.; Lordick, F.; Ohtsu, A.; Omuro, Y.; Satoh, T.; et al. Trastuzumab in Combination with Chemotherapy Versus Chemotherapy Alone for Treatment of HER2-Positive Advanced Gastric or Gastro-Oesophageal Junction Cancer (ToGA): A Phase 3, Open-Label, Randomised Controlled Trial. *The Lancet* **2010,** *376* (9742), 687–697.
127. Blumenthal, G. M.; Scher, N. S.; Cortazar, P.; Chattopadhyay, S.; Tang, S.; Song, P.; Liu, Q.; Ringgold, K.; Pilaro, A. M.; Tilley, A.; et al. First FDA Approval of Dual Anti-HER2 Regimen: Pertuzumab in Combination with Trastuzumab and Docetaxel for HER2-Positive Metastatic Breast Cancer. *Clin. Cancer Res.* **2013,** *19* (18), 4911–4916.
128. Amiri-Kordestani, L.; Blumenthal, G. M.; Xu, Q. C.; Zhang, L.; Tang, S. W.; Ha, L.; Weinberg, W. C.; Chi, B.; Candau-Chacon, R.; Hughes, P.; et al. FDA Approval: Ado-Trastuzumab Emtansine for the Treatment of Patients with HER2-Positive Metastatic Breast Cancer. *Clin. Cancer Res.* **2014,** *20* (17), 4436–4441.
129. Bokemeyer, C.; Bondarenko, I.; Makhson, A.; Hartmann, J. T.; Aparicio, J.; de Braud, F.; Donea, S.; Ludwig, H.; Schuch, G.; Stroh, C.; et al. Fluorouracil, Leucovorin, and Oxaliplatin with and without Cetuximab in the First-Line Treatment of Metastatic Colorectal Cancer. *J. Clin. Oncol.* **2009,** *27* (5), 663–671.
130. Vermorken, J. B.; Mesia, R.; Rivera, F.; Remenar, E.; Kawecki, A.; Rottey, S.; Erfan, J.; Zabolotnyy, D.; Kienzer, H.-R.; Cupissol, D.; et al. Platinum-Based Chemotherapy Plus Cetuximab in Head and Neck Cancer. *N. Engl. J. Med.* **2009,** *359* (11), 1116–1127. http://dx.doi.org/10.1056/NEJMoa0802656.
131. Bonner, J. A.; Harari, P. M.; Giralt, J.; Cohen, R. B.; Jones, C. U.; Sur, R. K.; Raben, D.; Baselga, J.; Spencer, S. A.; Zhu, J.; et al. Radiotherapy Plus Cetuximab for Locoregionally Advanced Head and Neck Cancer: 5-Year Survival Data From a Phase 3 Randomised Trial, and Relation Between Cetuximab-Induced Rash and Survival. *Lancet Oncol.* **2010,** *11* (1), 21–28.
132. Pirker, R.; Pereira, J. R.; Szczesna, A.; von Pawel, J.; Krzakowski, M.; Ramlau, R.; Vynnychenko, I.; Park, K.; Yu, C. T.; Ganul, V.; et al. Cetuximab Plus Chemotherapy in Patients with Advanced Non-Small-Cell Lung Cancer (FLEX): An Open-Label Randomised Phase III Trial. *The Lancet* **2009,** *373* (9674), 1525–1531.
133. Van Cutsem, E.; Peeters, M.; Siena, S.; Humblet, Y.; Hendlisz, A.; Neyns, B.; Canon, J.-L.; Van Laethem, J.-L.; Maurel, J.; Richardson, G.; et al. Open-Label Phase III Trial of Panitumumab Plus Best Supportive Care Compared with Best Supportive Care Alone in Patients with Chemotherapy-Refractory Metastatic Colorectal Cancer. *J. Clin. Oncol.* **2007,** *25* (13), 1658–1664.
134. Pirker, R. Epidermal Growth Factor Receptor-Directed Monoclonal Antibodies in Nonsmall Cell Lung Cancer: An Update. *Curr. Opin. Oncol.* **2015,** *27* (2), 87–93.

135. Palumbo, A.; Sonneveld, P. Preclinical and Clinical Evaluation of Elotuzumab, a SLAMF7-Targeted Humanized Monoclonal Antibody in Development for Multiple Myeloma. *Expert. Rev. Hematol.* **2015,** *8* (4), 481–491.
136. Ozkaynak, M. F.; Gilman, A. L.; Yu, A. L.; London, W. B.; Sondel, P. M.; Smith, M. A.; Seeger, R.; Reynolds, C. P.; Maris, J. M.; Park, J. R. A Comprehensive Safety Trial of Chimeric Antibody 14.18 (ch14.18) with GM-CSF, IL-2, and Isotretinoin in High-Risk Neuroblastoma Patients Following Myeloablative Therapy: A Children's Oncology Group Study. *J. Clin. Oncol.* **2014,** *32:5s* (suppl; abstr 10044). ASCO Meeting Abstracts.
137. Desai, A. V.; Fox, E.; Smith, L. M.; Lim, A. P.; Maris, J. M.; Balis, F. M. Pharmacokinetics of the Chimeric Anti-GD2 Antibody, ch14.18, in Children with High-Risk Neuroblastoma. *Cancer Chemother. Pharmacol.* **2014,** *74* (5), 1047–1055.
138. Hochster, H. S.; Hart, L. L.; Ramanathan, R. K.; Childs, B. H.; Hainsworth, J. D.; Cohn, A. L.; Wong, L.; Fehrenbacher, L.; Abubakr, Y.; Saif, M. W.; et al. Safety and Efficacy of Oxaliplatin and Fluoropyrimidine Regimens with or Without Bevacizumab as First-Line Treatment of Metastatic Colorectal Cancer: Results of the TREE Study. *J. Clin. Oncol.* **2008,** *26* (21), 3523–3529.
139. Vredenburgh, J. J.; Desjardins, A.; Herndon, J. E.; Dowell, J. M.; Reardon, D. A.; Quinn, J. A.; Rich, J. N.; Sathornsumetee, S.; Gururangan, S.; Wagner, M.; et al. Phase II Trial of Bevacizumab and Irinotecan in Recurrent Malignant Glioma. *Clin. Cancer Res.* **2007,** *13* (4), 1253–1259.
140. Oza, A. M.; Cook, A. D.; Pfisterer, J.; Embleton, A.; Ledermann, J. A.; Pujade-Lauraine, E.; Kristensen, G.; Carey, M. S.; Beale, P.; Cervantes, A.; et al. Standard Chemotherapy with or Without Bevacizumab for Women with Newly Diagnosed Ovarian Cancer (ICON7): Overall Survival Results of a Phase 3 Randomised Trial. *Lancet Oncol.* **2015,** *16* (8), 928–936.
141. Escudier, B.; Bellmunt, J.; Négrier, S.; Bajetta, E.; Melichar, B.; Bracarda, S.; Ravaud, A.; Golding, S.; Jethwa, S.; Sneller, V. Phase III Trial of Bevacizumab Plus Interferon Alfa-2a in Patients with Metastatic Renal Cell Carcinoma (AVOREN): Final Analysis of Overall Survival. *J. Clin. Oncol.* **2010,** *28* (13), 2144–2150.
142. Anuj Patel, W. S. Ziv-Aflibercept in Metastatic Colorectal Cancer. *Biologics* **2014,** *8,* 13–25.
143. Fala, L. Cyramza (Ramucirumab) Approved for the Treatment of Advanced Gastric Cancer and Metastatic Non-Small-Cell Lung Cancer. *Am. Health Drug Benefits* **2015,** *8* (Spec Feature), 49–53.
144. Larkins, E.; Scepura, B.; Blumenthal, G. M.; Bloomquist, E.; Tang, S.; Biable, M.; Kluetz, P.; Keegan, P.; Pazdur, R. U. S. Food and Drug Administration Approval Summary: Ramucirumab for the Treatment of Metastatic Non-Small Cell Lung Cancer Following Disease Progression On or After Platinum-Based Chemotherapy. *Oncologist* **2015,** *20* (11), 1320–1325.
145. Gambardella, V.; Tarazona, N.; Cejalvo, J. M.; Roselló, S.; Cervantes, A. Clinical Pharmacokinetics and Pharmacodynamics of Ramucirumab in the Treatment of Colorectal Cancer. *Expert Opin. Drug Metab. Toxicol.* **2016,** *12* (4), 449–456.
146. Sohn, W.; Simiens, M. A.; Jaeger, K.; Hutton, S.; Jang, G. The Pharmacokinetics and Pharmacodynamics of Denosumab in Patients with Advanced Solid Tumours and Bone Metastases: A Systematic Review. *Br. J. Clin. Pharmacol.* **2014,** *78* (3), 477–487.
147. Calabrò, L.; Morra, A.; Fonsatti, E.; Cutaia, O.; Fazio, C.; Annesi, D.; Lenoci, M.; Amato, G.; Danielli, R.; Altomonte, M.; et al. Efficacy and Safety of an Intensified Schedule of Tremelimumab for Chemotherapy-Resistant Malignant Mesothelioma: An Open-Label, Single-Arm, Phase 2 Study. *Lancet Respir. Med.* **2015,** *3* (4), 301–309.
148. Wolchok, J. D.; Kluger, H.; Callahan, M. K.; Postow, M. A.; Rizvi, N. A.; Lesokhin, A. M.; Segal, N. H.; Ariyan, C. E.; Gordon, R.-A.; Reed, K.; et al. Nivolumab Plus Ipilimumab in Advanced Melanoma. *N. Engl. J. Med.* **2013,** *369* (2), 122–133.
149. Brahmer, J.; Reckamp, K. L.; Baas, P.; Crinò, L.; Eberhardt, W. E. E; Poddubskaya, E.; Antonia, S.; Pluzanski, A.; Vokes, E. E.; Holgado, E.; et al. Nivolumab Versus Docetaxel in Advanced Squamous-Cell Non-Small-Cell Lung Cancer. *N. Engl. J. Med.* **2015,** *373* (2), 123–135.
150. Motzer, R. J.; Escudier, B.; McDermott, D. F.; George, S.; Hammers, H. J.; Srinivas, S.; Tykodi, S. S.; Sosman, J. A.; Procopio, G.; Plimack, E. R.; et al. Nivolumab Versus Everolimus in Advanced Renal-Cell Carcinoma. *N. Engl. J. Med.* **2015,** *373* (19), 1803–1813.
151. Ribas, A.; Puzanov, I.; Dummer, R.; Schadendorf, D.; Hamid, O.; Robert, C.; Hodi, F. S.; Schachter, J.; Pavlick, A. C.; Lewis, K. D.; et al. Pembrolizumab Versus Investigator-Choice Chemotherapy for Ipilimumab-Refractory Melanoma (KEYNOTE-002): A Randomised, Controlled, Phase 2 Trial. *Lancet Oncol.* **2015,** *16* (8), 908–918.
152. Garon, E. B.; Rizvi, N. A.; Hui, R.; Leighl, N.; Balmanoukian, A. S.; Eder, J. P.; Patnaik, A.; Aggarwal, C.; Gubens, M.; Horn, L.; et al. Pembrolizumab for the Treatment of Non-Small-Cell Lung Cancer. *N. Engl. J. Med.* **2015,** *372* (21), 2018–2028.
153. Leenaars, M.; Hendriksen, C. F. M. Critical Steps in the Production of Polyclonal and Monoclonal Antibodies: Evaluation and Recommendations. *ILAR J.* **2005,** *46* (3), 269–279.
154. Ehrenstein, M. R.; Notley, C. A. The Importance of Natural IgM: Scavenger, Protector and Regulator. *Nat. Rev. Immunol.* **2010,** *10* (11), 778–786.
155. Koro, C.; Bielecka, E.; Dahl-Knudsen, A.; Enghild, J. J.; Scavenius, C.; Brun, J. G.; Binder, V.; Hellvard, A.; Bergum, B.; Jonsson, R.; et al. Carbamylation of Immunoglobulin Abrogates Activation of the Classical Complement Pathway. *Eur. J. Immunol.* **2014,** *44* (11), 3403–3412.
156. Vidarsson, G.; Dekkers, G.; Rispens, T. IgG Subclasses and Allotypes: From Structure to Effector Functions. *Front. Immunol.* **2014,** *5* (16), 520.
157. Chen, K.; Cerutti, A. New Insights Into the Enigma of Immunoglobulin D. *Immunol. Rev.* **2010,** *237* (1), 160–179.
158. Chailyan, A.; Marcatili, P.; Tramontano, A. The Association of Heavy and Light Chain Variable Domains in Antibodies: Implications for Antigen Specificity. *FEBS J.* **2011,** *278* (16), 2858–2866.
159. Shuptrine, C. W.; Surana, R.; Weiner, L. M. Monoclonal Antibodies for the Treatment of Cancer. *Semin. Cancer Biol.* **2012,** *22* (1), 3–13.
160. Köhler, G.; Milstein, C. Continuous Cultures of Fused Cells Secreting Antibody of Predefined Specificity. *Nature* **1975,** *256* (5517), 495–497.
161. Pasqualini, R.; Arap, W. Hybridoma-Free Generation of Monoclonal Antibodies. *PNAS* **2004,** *101* (1), 257–259.
162. Kaartinen, M. *The 1984 Nobel Prize in Medicine (Cesar Milstein, George Köhler, Niels Jerne)*; Lääketieteen Nobelin palkinnot vuonna 1984; Duodecim; lääketieteellinen aikakauskirja, 1984; Vol. 100, pp 1573–1578.
163. Buss, N. A.; Henderson, S. J.; McFarlane, M.; Shenton, J. M.; de Haan, L. Monoclonal Antibody Therapeutics: History and Future. *Curr. Opin. Pharmacol.* **2012,** *12* (5), 615–622.
164. Kaminski, M. S.; Zelenetz, A. D.; Press, O. W.; Saleh, M.; Leonard, J.; Fehrenbacher, L.; Lister, T. A.; Stagg, R. J.; Tidmarsh, G. F.; Kroll, S.; et al. Pivotal Study of Iodine I 131 Tositumomab for Chemotherapy-Refractory Low-Grade or Transformed Low-Grade B-Cell Non-Hodgkin's Lymphomas. *J. Clin. Oncol.* **2001,** *19* (19), 3918–3928.
165. AlDeghaither, D.; Smaglo, B. G.; Weiner, L. M. Beyond Peptides and mAbs—Current Status and Future Perspectives for Biotherapeutics with Novel Constructs. *J. Clin. Pharmacol.* **2015,** *55* (S3), S4–S20.
166. Brüggemann, M.; Osborn, M. J.; Ma, B.; Hayre, J.; Avis, S.; Lundstrom, B.; Buelow, R. Human Antibody Production in Transgenic Animals. *Arch. Immunol. Ther. Exp. (Warsz.)* **2015,** *63* (2), 101–108.
167. Dias-Neto, E.; Nunes, D. N.; Giordano, R. J.; Sun, J.; Botz, G. H.; Yang, K.; Setubal, J. C.; Pasqualini, R.; Arap, W. Next-Generation Phage Display: Integrating and Comparing Available Molecular Tools to Enable Cost-Effective High-Throughput Analysis. *PLoS ONE* **2009,** *4* (12), e8338.
168. Kumar, T. R.; Larson, M.; Wang, H.; McDermott, J.; Bronshteyn, I. Transgenic Mouse Technology: Principles and Methods. *Mol. Biol.* **2009,** *590,* 335–362. Chapter 22.
169. Smaglo, B. G.; AlDeghaither, D.; Weiner, L. M. The Development of Immunoconjugates for Targeted Cancer Therapy. *Nat. Rev. Clin. Oncol.* **2014,** *11* (11), 637–648.
170. Bouchard, H.; Viskov, C.; Garcia-Echeverria, C. Antibody–Drug Conjugates—A New Wave of Cancer Drugs. *Bioorg. Med. Chem. Lett.* **2014,** *24* (23), 5357–5363.
171. Burtner, C. R.; Chandrasekaran, D.; Santos, E. B.; Beard, B. C.; Adair, J. E.; Hamlin, D. K.; Wilbur, D. S.; Sandmaier, B. M.; Kiem, H.-P. (211)Astatine-Conjugated Monoclonal CD45 Antibody-Based Nonmyeloablative Conditioning for Stem Cell Gene Therapy. *Hum. Gene Ther.* **2015,** *26* (6), 399–406.
172. Wang, T.; Somasundaram, R.; Herlyn, M. Combination Therapy of Immunocytokines with Ipilimumab: A Cure for Melanoma? *J. Invest. Dermatol.* **2013,** *133* (3), 595–596.
173. Schwager, K.; Hemmerle, T.; Aebischer, D.; Neri, D. The Immunocytokine L19-IL2 Eradicates Cancer When Used in Combination with CTLA-4 Blockade or with L19-TNF. *J. Invest. Dermatol.* **2013,** *133* (3), 751–758.
174. Danielli, R.; Patuzzo, R.; Di Giacomo, A. M.; Gallino, G.; Maurichi, A.; Di Florio, A.; Cutaia, O.; Lazzeri, A.; Fazio, C.; Miracco, C.; et al. Intralesional Administration of L19-IL2/L19-TNF in Stage III or Stage IVM1a Melanoma Patients: Results of a Phase II Study. *Cancer Immunol. Immunother.* **2015,** *64* (8), 999–1009.

175. Pastan, I.; Hassan, R.; FitzGerald, D. J.; Kreitman, R. J. Immunotoxin Treatment of Cancer. *Annu. Rev. Med.* **2007,** *58* (1), 221–237.
176. Kreitman, R. J.; Pastan, I. Immunoconjugates in the Management of Hairy Cell Leukemia. *Best Pract. Res. Clin. Haematol.* **2015,** *28* (4), 236–245.
177. Siegel, J. A.; Pawlyk, D. A.; Lee, R. E.; Sasso, N. L.; Horowitz, J. A.; Sharkey, R. M.; Goldenberg, D. M. Tumor, Red Marrow, and Organ Dosimetry for 131I-Labeled Anti-Carcinoembryonic Antigen Monoclonal Antibody. *Cancer Res.* **1990,** *50* (3 Suppl.), 1039s–1042s.
178. Buchsbaum, D. J. Experimental Approaches to Increase Radiolabeled Antibody Localization in Tumors. *Cancer Res.* **1995,** *55* (23 Suppl.), 5729s–5732s.
179. Goldenberg, D. M.; Sharkey, R. M. Novel Radiolabeled Antibody Conjugates. *Oncogene* **2007,** *26* (25), 3734–3744.
180. Adams, G. P.; Schier, R.; Marshall, K.; Wolf, E. J.; McCall, A. M.; Marks, J. D.; Weiner, L. M. Increased Affinity Leads to Improved Selective Tumor Delivery of Single-Chain Fv Antibodies. *Cancer Res.* **1998,** *58* (3), 485–490.
181. Saga, T.; Neumann, R. D.; Heya, T.; Sato, J.; Kinuya, S.; Le, N.; Paik, C. H.; Weinstein, J. N. Targeting Cancer Micrometastases with Monoclonal Antibodies: A Binding-Site Barrier. *PNAS* **1995,** *92* (19), 8999–9003.
182. Adams, G. P.; Schier, R.; McCall, A. M.; Simmons, H. H.; Horak, E. M.; Alpaugh, R. K.; Marks, J. D.; Weiner, L. M. High Affinity Restricts the Localization and Tumor Penetration of Single-Chain Fv Antibody Molecules. *Cancer Res.* **2001,** *61* (12), 4750–4755.
183. Rudnick, S. I.; Lou, J.; Shaller, C. C.; Tang, Y.; Klein-Szanto, A. J. P.; Weiner, L. M.; Marks, J. D.; Adams, G. P. Influence of Affinity and Antigen Internalization on the Uptake and Penetration of Anti-HER2 Antibodies in Solid Tumors. *Cancer Res.* **2011,** *71* (6), 2250–2259.
184. Zhang, Y.; Pastan, I. High Shed Antigen Levels Within Tumors: An Additional Barrier to Immunoconjugate Therapy. *Clin. Cancer Res.* **2008,** *14* (24), 7981–7986.
185. Covell, D. G.; Barbet, J.; Holton, O. D.; Black, C. D.; Parker, R. J.; Weinstein, J. N. Pharmacokinetics of Monoclonal Immunoglobulin G1, F(Ab′)2, and Fab′ in Mice. *Cancer Res.* **1986,** *46* (8), 3969–3978.
186. Moore, P. A.; Zhang, W.; Rainey, G. J.; Burke, S.; Li, H.; Huang, L.; Gorlatov, S.; Veri, M. C.; Aggarwal, S.; Yang, Y.; et al. Application of Dual Affinity Retargeting Molecules to Achieve Optimal Redirected T-Cell Killing of B-Cell Lymphoma. *Blood* **2011,** *117* (17), 4542–4551.
187. Reusch, U.; Burkhardt, C.; Fucek, I.; Le Gall, F.; Le Gall, M.; Hoffmann, K.; Knackmuss, S. H. J; Kiprijanov, S.; Little, M.; Zhukovsky, E. A. A Novel Tetravalent Bispecific TandAb (CD30/CD16A) Efficiently Recruits NK Cells for the Lysis of CD30+ Tumor Cells. *MAbs* **2014,** *6* (3), 728–739.
188. Bruhns, P. Properties of Mouse and Human IgG Receptors and Their Contribution to Disease Models. *Blood* **2012,** *119* (24), 5640–5649.
189. Chames, P.; Van Regenmortel, M.; Weiss, E.; Baty, D. Therapeutic Antibodies: Successes, Limitations and Hopes for the Future. *Br. J. Pharmacol.* **2009,** *157* (2), 220–233.
190. Illidge, T.; Klein, C.; Sehn, L. H.; Davies, A.; Salles, G.; Cartron, G. Obinutuzumab in Hematologic Malignancies: Lessons Learned to Date. *Cancer Treat. Rev.* **2015,** *41* (9), 784–792.
191. Roopenian, D. C.; Akilesh, S. FcRn: The Neonatal Fc Receptor Comes of Age. *Nat. Rev. Immunol.* **2007,** *7* (9), 715–725.
192. Kane, S. V.; Acquah, L. A. Placental Transport of Immunoglobulins: A Clinical Review for Gastroenterologists Who Prescribe Therapeutic Monoclonal Antibodies to Women During Conception and Pregnancy. *Am. J. Gastroenterol.* **2009,** *104* (1), 228–233.
193. Robbie, G. J.; Criste, R.; Dall'acqua, W. F.; Jensen, K.; Patel, N. K.; Losonsky, G. A.; Griffin, M. P. A Novel Investigational Fc-Modified Humanized Monoclonal Antibody, Motavizumab-YTE, Has An Extended Half-Life in Healthy Adults. *Antimicrob. Agents Chemother.* **2013,** *57* (12), 6147–6153.
194. Martin, G. S. Cell Signaling and Cancer. *Cancer Cell* **2003,** *4* (3), 167–174.
195. Kohrt, H. E.; Houot, R.; Marabelle, A.; Cho, H. J.; Osman, K.; Goldstein, M.; Levy, R.; Brody, J. Combination Strategies to Enhance Antitumor ADCC. *Immunotherapy* **2012,** *4* (5), 511–527.
196. Clynes, R. A.; Towers, T. L.; Presta, L. G.; Ravetch, J. V. Inhibitory Fc Receptors Modulate In Vivo Cytotoxicity Against Tumor Targets. *Nat. Med.* **2000,** *6* (4), 443–446.
197. Ferris, R. L.; Jaffee, E. M.; Ferrone, S. Tumor Antigen-Targeted, Monoclonal Antibody-Based Immunotherapy: Clinical Response, Cellular Immunity, and Immunoescape. *J. Clin. Oncol.* **2010,** *28* (28), 4390–4399.
198. Di Fiore, F.; Sesboüé, R.; Michel, P.; Sabourin, J. C.; Frebourg, T. Molecular Determinants of Anti-EGFR Sensitivity and Resistance in Metastatic Colorectal Cancer. *Br. J. Cancer* **2010,** *103* (12), 1765–1772.
199. Musolino, A.; Naldi, N.; Bortesi, B.; Pezzuolo, D.; Capelletti, M.; Missale, G.; Laccabue, D.; Zerbini, A.; Camisa, R.; Bisagni, G.; et al. Immunoglobulin G Fragment C Receptor Polymorphisms and Clinical Efficacy of Trastuzumab-Based Therapy in Patients with HER-2/Neu-Positive Metastatic Breast Cancer. *J. Clin. Oncol.* **2008,** *26* (11), 1789–1796.
200. Cartron, G.; Dacheux, L.; Salles, G.; Solal-Celigny, P.; Bardos, P.; Colombat, P.; Watier, H. Therapeutic Activity of Humanized Anti-CD20 Monoclonal Antibody and Polymorphism in IgG Fc Receptor FcgammaRIIIa Gene. *Blood* **2002,** *99* (3), 754–758.
201. Zhang, W.; Gordon, M.; Schultheis, A. M.; Yang, D. Y.; Nagashima, F.; Azuma, M.; Chang, H.-M.; Borucka, E.; Lurje, G.; Sherrod, A. E.; et al. FCGR2A and FCGR3A Polymorphisms Associated with Clinical Outcome of Epidermal Growth Factor Receptor Expressing Metastatic Colorectal Cancer Patients Treated with Single-Agent Cetuximab. *J. Clin. Oncol.* **2007,** *25* (24), 3712–3718.
202. Rogers, L. M.; Veeramani, S.; Weiner, G. J. Complement in Monoclonal Antibody Therapy of Cancer. *Immunol. Res.* **2014,** *59* (1–3), 203–210.
203. Di Gaetano, N.; Cittera, E.; Nota, R.; Vecchi, A.; Grieco, V.; Scanziani, E.; Botto, M.; Introna, M.; Golay, J. Complement Activation Determines the Therapeutic Activity of Rituximab In Vivo. *J. Immunol.* **2003,** *171* (3), 1581–1587.
204. Racila, E.; Link, B. K.; Weng, W.-K.; Witzig, T. E.; Ansell, S.; Maurer, M. J.; Huang, J.; Dahle, C.; Halwani, A.; Levy, R.; et al. A Polymorphism in the Complement Component C1qA Correlates with Prolonged Response Following Rituximab Therapy of Follicular Lymphoma. *Clin. Cancer Res.* **2008,** *14* (20), 6697–6703.
205. Jaglowski, S. M.; Alinari, L.; Lapalombella, R.; Muthusamy, N.; Byrd, J. C. The Clinical Application of Monoclonal Antibodies in Chronic Lymphocytic Leukemia. *Blood* **2010,** *116* (19), 3705–3714.
206. Teeling, J. L.; Mackus, W. J. M.; Wiegman, L. J. J. M.; van den Brakel, J. H. N; Beers, S. A.; French, R. R.; van Meerten, T.; Ebeling, S.; Vink, T.; Slootstra, J. W.; et al. The Biological Activity of Human CD20 Monoclonal Antibodies is Linked to Unique Epitopes on CD20. *J. Immunol.* **2006,** *177* (1), 362–371.
207. Cheson, B. D. Ofatumumab, A Novel Anti-CD20 Monoclonal Antibody for the Treatment of B-Cell Malignancies. *J. Clin. Oncol.* **2010,** *28* (21), 3525–3530.
208. Weiskopf, K.; Weissman, I. L. Macrophages are Critical Effectors of Antibody Therapies for Cancer. *MAbs* **2015,** *7* (2), 303–310.
209. Fehres, C. M.; Unger, W. W. J.; Garcia-Vallejo, J. J.; van Kooyk, Y. Understanding the Biology of Antigen Cross-Presentation for the Design of Vaccines Against Cancer. *Front. Immunol.* **2014,** *5* (Suppl. 1), 149.
210. Weiner, L. M.; Murray, J. C.; Shuptrine, C. W. Antibody-Based Immunotherapy of Cancer. *Cell* **2012,** *148* (6), 1081–1084.
211. Segura, E.; Amigorena, S. Cross-Presentation in Mouse and Human Dendritic Cells. *Adv. Immunol.* **2015,** *127,* 1–31.
212. Hainsworth, J. D.; Litchy, S.; Burris, H. A.; Scullin, D. C.; Corso, S. W.; Yardley, D. A.; Morrissey, L.; Greco, F. A. Rituximab as First-Line and Maintenance Therapy for Patients with Indolent Non-Hodgkin's Lymphoma. *J. Clin. Oncol.* **2002,** *20* (20), 4261–4267.
213. Rosenberg, S. A.; Restifo, N. P. Adoptive Cell Transfer as Personalized Immunotherapy for Human Cancer. *Science* **2015,** *348* (6230), 62–68.
214. Stromnes, I. M.; Schmitt, T. M.; Chapuis, A. G.; Hingorani, S. R.; Greenberg, P. D. Re-adapting T Cells for Cancer Therapy: From Mouse Models to Clinical Trials. *Immunol. Rev.* **2014,** *257* (1), 145–164.
215. Weiden, P. L.; Flournoy, N.; Thomas, E. D.; Prentice, R.; Fefer, A.; Buckner, C. D.; Storb, R. Antileukemic Effect of Graft-Versus-Host Disease in Human Recipients of Allogeneic-Marrow Grafts. *N. Engl. J. Med.* **1979,** *300* (19), 1068–1073.
216. Morgan, D. A.; Ruscetti, F. W.; Gallo, R. Selective in Vitro Growth of T Lymphocytes From Normal Human Bone Marrows. *Science* **1976,** *193* (4257), 1007–1008.
217. Rosenberg, S. A.; Spiess, P.; Lafreniere, R. A New Approach to the Adoptive Immunotherapy of Cancer with Tumor-Infiltrating Lymphocytes. *Science* **1986,** *233* (4770), 1318–1321.
218. Houot, R.; Schultz, L. M.; Marabelle, A.; Kohrt, H. T-Cell-Based Immunotherapy: Adoptive Cell Transfer and Checkpoint Inhibition. *Cancer Immunol. Res.* **2015,** *3* (10), 1115–1122.
219. Rosenberg, S. A.; Kochenderfer, J. N. Personalized Cell Transfer Immunotherapy for B-Cell Malignancies and Solid Cancers. *Mol. Ther.* **2011,** *19* (11), 1928–1930.

220. Cheng, M.; Chen, Y.; Xiao, W.; Sun, R.; Tian, Z. NK Cell-Based Immunotherapy for Malignant Diseases. *Cell. Mol. Immunol.* **2013,** *10* (3), 230–252.
221. Waldhauer, I.; Steinle, A. NK Cells and Cancer Immunosurveillance. *Oncogene* **2008,** *27* (45), 5932–5943.
222. Yoshida, R.; Tazawa, H.; Hashimoto, Y.; Yano, S.; Onishi, T.; Sasaki, T.; Shirakawa, Y.; Kishimoto, H.; Uno, F.; Nishizaki, M.; et al. Mechanism of Resistance to Trastuzumab and Molecular Sensitization via ADCC Activation by Exogenous Expression of HER2-Extracellular Domain in Human Cancer Cells. *Cancer Immunol. Immunother.* **2012,** *61* (11), 1905–1916.
223. Kono, K.; Takahashi, A.; Ichihara, F.; Sugai, H.; Fujii, H.; Matsumoto, Y. Impaired Antibody-Dependent Cellular Cytotoxicity Mediated by Herceptin in Patients with Gastric Cancer. *Cancer Res.* **2002,** *62* (20), 5813–5817.
224. Parkhurst, M. R.; Riley, J. P.; Dudley, M. E.; Rosenberg, S. A. Adoptive Transfer of Autologous Natural Killer Cells Leads to High Levels of Circulating Natural Killer Cells but Does Not Mediate Tumor Regression. *Clin. Cancer Res.* **2011,** *17* (19), 6287–6297.
225. Chambers, C. V. Cancer Vaccines. *Prim. Care* **2011,** *38* (4), 703–715. viii–ix.
226. Weiner, L. M.; Surana, R.; Murray, J. Vaccine Prevention of Cancer: Can Endogenous Antigens Be Targeted? *Cancer Prev. Res. (Phila.)* **2010,** *3* (4), 410–415.
227. Au, J. S.; Frenette, C. T. Management of Hepatocellular Carcinoma: Current Status and Future Directions. *Gut Liver* **2015,** *9* (4), 437–448.
228. Lowy, D. R.; Schiller, J. T. Reducing HPV-Associated Cancer Globally. *Cancer Prev. Res. (Phila.)* **2012,** *5* (1), 18–23.
229. Butterfield, L. H. Cancer Vaccines. *BMJ* **2015,** *350,* h988.
230. Bodey, B.; Siegel, S. E.; Kaiser, H. E. Failure of Cancer Vaccines: The Significant Limitations of This Approach to Immunotherapy. *Anticancer Res.* **2000,** *20* (4), 2665–2676.
231. Silver-Morse, L.; Li, W. X. JAK-STAT in Heterochromatin and Genome Stability. *JAKSTAT* **2013,** *2* (3), e26090.
232. Kirkwood, J. M.; Ibrahim, J. G.; Sondak, V. K. High-and Low-Dose Interferon Alfa-2b in High-Risk Melanoma: First Analysis of Intergroup Trial E1690/S9111/C9190. *J. Clin. Oncol.* **2000,** *18,* 2444–2458.
233. Rosenberg, S. A.; Mulé, J. J.; Spiess, P. J.; Reichert, C. M.; Schwarz, S. L. Regression of Established Pulmonary Metastases and Subcutaneous Tumor Mediated by the Systemic Administration of High-Dose Recombinant Interleukin 2. *J. Exp. Med.* **1985,** *161* (5), 1169–1188.
234. Atkins, M. B.; Lotze, M. T.; Dutcher, J. P.; Fisher, R. I.; Weiss, G.; Margolin, K.; Abrams, J.; Sznol, M.; Parkinson, D.; Hawkins, M.; et al. High-Dose Recombinant Interleukin 2 Therapy for Patients with Metastatic Melanoma: Analysis of 270 Patients Treated Between 1985 and 1993. *J. Clin. Oncol.* **1999,** *17* (7), 2105–2116.
235. Rosenberg, S. A. Cancer Immunotherapy Comes of Age. *Nat. Clin. Pract. Oncol.* **2005,** *2* (3), 115.
236. Herndon, T. M.; Demko, S. G.; Jiang, X.; He, K.; Gootenberg, J. E.; Cohen, M. H.; Keegan, P.; Pazdur, R. U. S. Food and Drug Administration Approval: Peginterferon-Alfa-2b for the Adjuvant Treatment of Patients with Melanoma. *Oncologist* **2012,** *17* (10), 1323–1328.
237. Jonasch, E.; Haluska, F. G. Interferon in Oncological Practice: Review of Interferon Biology, Clinical Applications, and Toxicities. *Oncologist* **2001,** *6* (1), 34–55.
238. Buonaguro, L.; Petrizzo, A.; Tornesello, M. L.; Buonaguro, F. M. Translating Tumor Antigens Into Cancer Vaccines. *Clin. Vaccine Immunol.* **2011,** *18* (1), 23–34.
239. Smith, M. R. Rituximab (Monoclonal Anti-CD20 Antibody): Mechanisms of Action and Resistance. *Oncogene* **2003,** *22* (47), 7359–7368.
240. Boross, P.; Leusen, J. H. W. Mechanisms of Action of CD20 Antibodies. *Am. J. Cancer Res.* **2012,** *2* (6), 676–690.
241. Rehnberg, M.; Amu, S.; Tarkowski, A.; Bokarewa, M. I.; Brisslert, M. Short- and Long-Term Effects of Anti-CD20 Treatment on B Cell Ontogeny in Bone Marrow of Patients with Rheumatoid Arthritis. *Arthritis Res. Ther.* **2009,** *11* (4), R123.
242. Davis, T. A.; Czerwinski, D. K.; Levy, R. Therapy of B-Cell Lymphoma with Anti-CD20 Antibodies Can Result in the Loss of CD20 Antigen Expression. *Clin. Cancer Res.* **1999,** *5* (3), 611–615.
243. Levene, A. P.; Singh, G.; Palmieri, C. Therapeutic Monoclonal Antibodies in Oncology. *J. R. Soc. Med.* **2005,** *98* (4), 146–152.
244. Grillo-López, A. J. Rituximab: An Insider's Historical Perspective. *Semin. Oncol.* **2000,** *27* (6 Suppl. 12), 9–16.
245. Oflazoglu, E.; Audoly, L. P. Evolution of Anti-CD20 Monoclonal Antibody Therapeutics in Oncology. *MAbs* **2010,** *2* (1), 14–19.
246. Micallef, I. N. M. Ongoing Trials with Yttrium 90-Labeled Ibritumomab Tiuxetan in Patients with Non-Hodgkin's Lymphoma. *Clin Lymphoma* **2004,** *5* (Suppl. 1), S27–S32.
247. Feugier, P. A Review of Rituximab, the First Anti-CD20 Monoclonal Antibody Used in the Treatment of B Non-Hodgkin's Lymphomas. *Future Oncol.* **2015,** *11* (9), 1327–1342.
248. Rezvani, A. R.; Maloney, D. G. Rituximab Resistance. *Best Pract. Res. Clin. Haematol.* **2011,** *24* (2), 203–216.
249. Shah, A. New Developments in the Treatment of Chronic Lymphocytic Leukemia: Role of Obinutuzumab. *Ther. Clin. Risk Manag.* **2015,** *11,* 1113–1122.
250. Uchida, J.; Lee, Y.; Hasegawa, M.; Liang, Y.; Bradney, A.; Oliver, J. A.; Bowen, K.; Steeber, D. A.; Haas, K. M.; Poe, J. C.; et al. Mouse CD20 Expression and Function. *Int. Immunol.* **2004,** *16* (1), 119–129.
251. Till, B. G.; Jensen, M. C.; Wang, J.; Qian, X.; Gopal, A. K.; Maloney, D. G.; Lindgren, C. G.; Lin, Y.; Pagel, J. M.; Budde, L. E.; et al. CD20-Specific Adoptive Immunotherapy for Lymphoma Using a Chimeric Antigen Receptor with Both CD28 and 4-1BB Domains: Pilot Clinical Trial Results. *Blood* **2012,** *119* (17), 3940–3950.
252. Raufi, A.; Ebrahim, A. S.; Al-Katib, A. Targeting CD19 in B-Cell Lymphoma: Emerging Role of SAR3419. *Cancer Manag. Res.* **2013,** *5,* 225–233.
253. Katz, B.-Z.; Herishanu, Y. Therapeutic Targeting of CD19 in Hematological Malignancies: Past, Present, Future and Beyond. *Leuk. Lymphoma* **2014,** *55* (5), 999–1006.
254. Hoffman, B.; Liebermann, D. A. Apoptotic Signaling by C-MYC. *Oncogene* **2008,** *27* (50), 6462–6472.
255. Sanford, M. Blinatumomab: First Global Approval. *Drugs* **2015,** *75* (3), 321–327.
256. van de Donk, N. W. C. J.; Dhimolea, E. Brentuximab Vedotin. *MAbs* **2012,** *4* (4), 458–465.
257. Gubin, M. M.; Artyomov, M. N.; Mardis, E. R.; Schreiber, R. D. Tumor Neoantigens: Building a Framework for Personalized Cancer Immunotherapy. *J. Clin. Invest.* **2015,** *125* (9), 3413–3421.
258. Brand, T. M.; Iida, M.; Luthar, N.; Starr, M. M.; Huppert, E. J.; Wheeler, D. L. Nuclear EGFR as a Molecular Target in Cancer. *Radiother. Oncol.* **2013,** *108* (3), 370–377.
259. Graham, J.; Muhsin, M.; Kirkpatrick, P. Cetuximab. *Nat. Rev. Drug Discov.* **2004,** *3* (7), 549–550.
260. Kabolizadeh, P.; Kubicek, G. J.; Heron, D. E.; Ferris, R. L.; Gibson, M. K. The Role of Cetuximab in the Management of Head and Neck Cancers. *Expert Opin. Biol. Ther.* **2012,** *12* (4), 517–528.
261. Pirker, R.; Pereira, J. R.; von Pawel, J.; Krzakowski, M.; Ramlau, R.; Park, K.; de Marinis, F.; Eberhardt, W. E.; Paz-Ares, L.; Störkel, S.; et al. EGFR Expression as a Predictor of Survival for First-Line Chemotherapy Plus Cetuximab in Patients with Advanced Non-Small-Cell Lung Cancer: Analysis of Data From the Phase 3 FLEX Study. *Lancet Oncol.* **2012,** *13* (1), 33–42.
262. Krawczyk, P. A.; Kowalski, D. M. Genetic and Immune Factors Underlying the Efficacy of Cetuximab and Panitumumab in the Treatment of Patients with Metastatic Colorectal Cancer. *Contemp. Oncol. (Pozn.)* **2014,** *18* (1), 7–16.
263. Price, T. J.; Peeters, M.; Kim, T. W.; Li, J.; Cascinu, S.; Ruff, P.; Suresh, A. S.; Thomas, A.; Tjulandin, S.; Zhang, K.; et al. Panitumumab Versus Cetuximab in Patients with Chemotherapy-Refractory Wild-Type KRAS Exon 2 Metastatic Colorectal Cancer (ASPECCT): A Randomised, Multicentre, Open-Label, Non-Inferiority Phase 3 Study. *Lancet Oncol.* **2014,** *15* (6), 569–579.
264. Cohen, R. B. Current Challenges and Clinical Investigations of Epidermal Growth Factor Receptor (EGFR)- and ErbB Family-Targeted Agents in the Treatment of Head and Neck Squamous Cell Carcinoma (HNSCC). *Cancer Treat. Rev.* **2014,** *40* (4), 567–577.
265. Binder, D.; Hegenbarth, K. Emerging Options for the Management of Non-Small Cell Lung Cancer. *Clin. Med. Insights Oncol.* **2013,** *7* (7), 221–234.
266. Ellis, P. M.; Coakley, N.; Feld, R.; Kuruvilla, S.; Ung, Y. C. Use of the Epidermal Growth Factor Receptor Inhibitors Gefitinib, Erlotinib, Afatinib, Dacomitinib, and Icotinib in the Treatment of Non-Small-Cell Lung Cancer: A Systematic Review. *Curr. Oncol.* **2015,** *22* (3), e183–e215.
267. Liang, W.; Wu, X.; Fang, W.; Zhao, Y.; Yang, Y.; Hu, Z.; Xue, C.; Zhang, J.; Zhang, J.; Ma, Y.; et al. Network Meta-Analysis of Erlotinib, Gefitinib, Afatinib and Icotinib in Patients with Advanced Non-Small-Cell Lung Cancer Harboring EGFR Mutations. *PLoS ONE* **2014,** *9* (2), e85245.
268. Lee, C.-C.; Shiao, H.-Y.; Wang, W.-C.; Hsieh, H.-P. Small-Molecule EGFR Tyrosine Kinase Inhibitors for the Treatment of Cancer. *Expert Opin. Investig. Drugs* **2014,** *23* (10), 1333–1348.
269. Hojjat-Farsangi, M. Small-Molecule Inhibitors of the Receptor Tyrosine Kinases: Promising Tools for Targeted Cancer Therapies. *Int. J. Mol. Sci.* **2014,** *15* (8), 13768–13801.

270. Yarden, Y. Biology of HER2 and Its Importance in Breast Cancer. *Oncology* **2001,** *61* (Suppl. 2), 1–13.
271. Scholl, S.; Beuzeboc, P.; Pouillart, P. Targeting HER2 in Other Tumor Types. *Ann. Oncol.* **2001,** *12* (Suppl. 1), S81–S87.
272. Boku, N. HER2-Positive Gastric Cancer. *Gastric Cancer* **2014,** *17* (1), 1–12.
273. Kulhari, H.; Pooja, D.; Rompicharla, S. V. K.; Sistla, R.; Adams, D. J. Biomedical Applications of Trastuzumab: As a Therapeutic Agent and a Targeting Ligand. *Med. Res. Rev.* **2015,** *35* (4), 849–876.
274. Tolaney, S. New HER2-Positive Targeting Agents in Clinical Practice. *Curr. Oncol. Rep.* **2014,** *16* (1), 359.
275. Baselga, J.; Cortés, J.; Kim, S.-B.; Im, S.-A.; Hegg, R.; Im, Y.-H.; Roman, L.; Pedrini, J. L.; Pienkowski, T.; Knott, A.; et al. Pertuzumab Plus Trastuzumab Plus Docetaxel for Metastatic Breast Cancer. *N. Engl. J. Med.* **2012,** *366* (2), 109–119. http://dx.doi.org/10.1056/NEJMoa1113216.
276. Dao, B. D.; Ho, H.; Quintal, L. N. Combination Pertuzumab, Trastuzumab, and Taxane for Metastatic Breast Cancer After First Progression: A Single Institution's Experience. *J. Oncol. Pharm. Pract.* **2016,** *22* (2), 261–264.
277. Swain, S. M.; Kim, S.-B.; Cortés, J.; Ro, J.; Semiglazov, V.; Campone, M.; Ciruelos, E.; Ferrero, J.-M.; Schneeweiss, A.; Knott, A.; et al. Overall Survival Benefit with Pertuzumab, Trastuzumab, and Docetaxel for HER2-Positive Metastatic Breast Cancer in CLEOPATRA, A Randomised Phase 3 Study. *Lancet Oncol.* **2013,** *14* (6), 461–471.
278. Chung, A.; Cui, X.; Audeh, W.; Giuliano, A. Current Status of Anti–Human Epidermal Growth Factor Receptor 2 Therapies: Predicting and Overcoming Herceptin Resistance. *Clin. Breast Cancer* **2013,** *13* (4), 223–232.
279. Lewis Phillips, G. D.; Li, G.; Dugger, D. L.; Crocker, L. M.; Parsons, K. L.; Mai, E.; Blättler, W. A.; Lambert, J. M.; Chari, R. V. J.; Lutz, R. J.; et al. Targeting HER2-Positive Breast Cancer with Trastuzumab-DM1, An Antibody-Cytotoxic Drug Conjugate. *Cancer Res.* **2008,** *68* (22), 9280–9290.
280. Gjerstorff, M. F.; Andersen, M. H.; Ditzel, H. J. Oncogenic Cancer/Testis Antigens: Prime Candidates for Immunotherapy. *Oncotarget* **2015,** *6* (18), 15772–15787.
281. Goodyear, O.; Agathanggelou, A.; Novitzky-Basso, I.; Siddique, S.; McSkeane, T.; Ryan, G.; Vyas, P.; Cavenagh, J.; Stankovic, T.; Moss, P.; et al. Induction of a CD8+ T-Cell Response to the MAGE Cancer Testis Antigen by Combined Treatment with Azacitidine and Sodium Valproate in Patients with Acute Myeloid Leukemia and Myelodysplasia. *Blood* **2010,** *116* (11), 1908–1918.
282. Klemm, F.; Joyce, J. A. Microenvironmental Regulation of Therapeutic Response in Cancer. *Trends Cell Biol.* **2015,** *25* (4), 198–213.
283. Hillen, F.; Griffioen, A. W. Tumour Vascularization: Sprouting Angiogenesis and Beyond. *Cancer Metastasis Rev.* **2007,** *26* (3–4), 489–502.
284. Ferrara, N. VEGF and the Quest for Tumour Angiogenesis Factors. *Nat. Rev. Cancer* **2002,** *2* (10), 795–803.
285. Ribatti, D.; Vacca, A.; Dammacco, F. The Role of the Vascular Phase in Solid Tumor Growth: A Historical Review. *Neoplasia* **1999,** *1* (4), 293–302.
286. Ellis, L. M.; Hicklin, D. J. VEGF-Targeted Therapy: Mechanisms of Anti-Tumour Activity. *Nat. Rev. Cancer* **2008,** *8* (8), 579–591.
287. Gabrilovich, D. I.; Chen, H. L.; Girgis, K. R.; Cunningham, H. T.; Meny, G. M.; Nadaf, S.; Kavanaugh, D.; Carbone, D. P. Production of Vascular Endothelial Growth Factor by Human Tumors Inhibits the Functional Maturation of Dendritic Cells. *Nat. Med.* **1996,** *2* (10), 1096–1103.
288. Gabrilovich, D.; Ishida, T.; Oyama, T.; Ran, S.; Kravtsov, V.; Nadaf, S.; Carbone, D. P. Vascular Endothelial Growth Factor Inhibits the Development of Dendritic Cells and Dramatically Affects the Differentiation of Multiple Hematopoietic Lineages In Vivo. *Blood* **1998,** *92* (11), 4150–4166.
289. Gabrilovich, D. I.; Ishida, T.; Nadaf, S.; Ohm, J. E.; Carbone, D. P. Antibodies to Vascular Endothelial Growth Factor Enhance the Efficacy of Cancer Immunotherapy by Improving Endogenous Dendritic Cell Function. *Clin. Cancer Res.* **1999,** *5* (10), 2963–2970.
290. Osada, T.; Chong, G.; Tansik, R.; Hong, T.; Spector, N.; Kumar, R.; Hurwitz, H. I.; Dev, I.; Nixon, A. B.; Lyerly, H. K.; et al. The Effect of Anti-VEGF Therapy on Immature Myeloid Cell and Dendritic Cells in Cancer Patients. *Cancer Immunol. Immunother.* **2008,** *57* (8), 1115–1124.
291. Xu, M. M.; Pu, Y.; Zhang, Y.; Fu, Y.-X. The Role of Adaptive Immunity in the Efficacy of Targeted Cancer Therapies. *Trends Immunol.* **2016,** *37* (2), 141–153.
292. Voron, T.; Colussi, O.; Marcheteau, E.; Pernot, S.; Nizard, M.; Pointet, A. L.; Latreche, S.; Bergaya, S.; Benhamouda, N.; Tanchot, C.; Stockmann, C.; Combe, P.; Berger, A.; Zinzindohoue, F.; Yagita, H.; Tartour, E.; Taieb, J.; Terme, M. VEGF—A Modulates Expression of Inhibitory Checkpoints on CD8+ T Cells in Tumors. *J. Exp. Med.* **2015,** *212,* 139–148.
293. Gabrilovich, D. I.; Hurwitz, A. A. In *Tumor-Induced Immune Suppression;* Gabrilovich, D. I., Hurwitz, A. A., Eds.; Springer Science & Business Media: New York, NY, 2014.
294. Alfaro, C.; Suarez, N.; Gonzalez, A.; Solano, S.; Erro, L.; Dubrot, J.; Palazon, A.; Hervas-Stubbs, S.; Gurpide, A.; Lopez-Picazo, J. M.; et al. Influence of Bevacizumab, Sunitinib and Sorafenib as Single Agents or in Combination on the Inhibitory Effects of VEGF on Human Dendritic Cell Differentiation From Monocytes. *Br. J. Cancer* **2009,** *100* (7), 1111–1119.
295. Roland, C. L.; Lynn, K. D.; Toombs, J. E.; Dineen, S. P.; Udugamasooriya, D. G.; Brekken, R. A. Cytokine Levels Correlate with Immune Cell Infiltration After Anti-VEGF Therapy in Preclinical Mouse Models of Breast Cancer. *PLoS ONE* **2009,** *4* (11), e7669.
296. El-Kenawi, A. E.; El-Remessy, A. B. Angiogenesis Inhibitors in Cancer Therapy: Mechanistic Perspective on Classification and Treatment Rationales. *Br. J. Pharmacol.* **2013,** *170* (4), 712–729.
297. Ferrara, N.; Adamis, A. P. Ten Years of Anti-Vascular Endothelial Growth Factor Therapy. *Nat. Rev. Drug Discov.* **2016,** *15* (6), 385–403.
298. Bogdanovich, S.; Kim, Y.; Mizutani, T.; Yasuma, R.; Tudisco, L.; Cicatiello, V.; Bastos-Carvalho, A.; Kerur, N.; Hirano, Y.; Baffi, J. Z.; et al. Human IgG1 Antibodies Suppress Angiogenesis in a Target-Independent Manner. *Signal Transduct. Target Ther.* **2016,** *1,* 15001.
299. Rodriguez, M. Ziv-Aflibercept Use in Metastatic Colorectal Cancer. *J. Adv. Pract. Oncol.* **2013,** *4* (5), 348–352.
300. Yoneda, T.; Tanaka, S.; Hata, K. Role of RANKL/RANK in Primary and Secondary Breast Cancer. *World J. Orthop.* **2013,** *4* (4), 178–185.
301. Ahn, S. G.; Lee, H. M.; Cho, S.-H.; Lee, S. A.; Hwang, S. H.; Jeong, J.; Lee, H.-D. Prognostic Factors for Patients with Bone-Only Metastasis in Breast Cancer. *Yonsei Med. J.* **2013,** *54* (5), 1168–1177.
302. Kohli, S. S.; Kohli, V. S. Role of RANKL-RANK/Osteoprotegerin Molecular Complex in Bone Remodeling and Its Immunopathologic Implications. *Indian J. Endocrinol. Metab.* **2011,** *15* (3), 175–181.
303. Cheng, M. L.; Fong, L. Effects of RANKL-Targeted Therapy in Immunity and Cancer. *Front. Oncol.* **2014,** *3,* 29.
304. Yoshida, H.; Kong, Y.-Y. OPGL Is a Key Regulator of Osteoclastogenesis, Lymphocyte Development and Lymph-Node Organogenesis. *Nature* **1999,** *397* (6717), 315–323.
305. Dougall, W. C.; Glaccum, M.; Charrier, K.; Rohrbach, K.; Brasel, K.; De Smedt, T.; Daro, E.; Smith, J.; Tometsko, M. E.; Maliszewski, C. R.; et al. RANK is Essential for Osteoclast and Lymph Node Development. *Genes Dev.* **1999,** *13* (18), 2412–2424.
306. Galon, J.; Costes, A.; Sanchez-Cabo, F.; Kirilovsky, A.; Mlecnik, B.; Lagorce-Pagès, C.; Tosolini, M.; Camus, M.; Berger, A.; Wind, P.; et al. Type, Density, and Location of Immune Cells Within Human Colorectal Tumors Predict Clinical Outcome. *Science* **2006,** *313* (5795), 1960–1964.
307. Krummel, M. F.; Allison, J. P. CD28 and CTLA-4 Have Opposing Effects on the Response of T Cells to Stimulation. *J. Exp. Med.* **1995,** *182* (2), 459–465.
308. Camacho, L. H. CTLA-4 Blockade with Ipilimumab: Biology, Safety, Efficacy, and Future Considerations. *Cancer Med.* **2015,** *4* (5), 661–672.
309. Simpson, T. R.; Li, F.; Montalvo-Ortiz, W.; Sepulveda, M. A.; Bergerhoff, K.; Arce, F.; Roddie, C.; Henry, J. Y.; Yagita, H.; Wolchok, J. D.; et al. Fc-Dependent Depletion of Tumor-Infiltrating Regulatory T Cells Co-Defines the Efficacy of Anti-CTLA-4 Therapy Against Melanoma. *J. Exp. Med.* **2013,** *210* (9), 1695–1710.
310. Fallarino, F.; Grohmann, U.; Hwang, K. W.; Orabona, C.; Vacca, C.; Bianchi, R.; Belladonna, M. L.; Fioretti, M. C.; Alegre, M.-L.; Puccetti, P. Modulation of Tryptophan Catabolism by Regulatory T Cells. *Nat. Immunol.* **2003,** *4* (12), 1206–1212.
311. Berg, M.; Zavazava, N. Regulation of CD28 Expression on CD8+ T Cells by CTLA-4. *J. Leukoc. Biol.* **2008,** *83* (4), 853–863.
312. Topalian, S. L.; Drake, C. G.; Pardoll, D. M. Targeting the PD-1/B7-H1(PD-L1) Pathway to Activate Anti-Tumor Immunity. *Curr. Opin. Immunol.* **2012,** *24* (2), 207–212.
313. Okazaki, T.; Chikuma, S.; Iwai, Y.; Fagarasan, S.; Honjo, T. A Rheostat for Immune Responses: The Unique Properties of PD-1 and Their Advantages for Clinical Application. *Nat. Immunol.* **2013,** *14* (12), 1212–1218.
314. Lotze, M. T.; Frana, L. W.; Sharrow, S. O.; Robb, R. J.; Rosenberg, S. A. In Vivo Administration of Purified Human Interleukin 2. I. Half-Life and Immunologic Effects of the Jurkat Cell Line-Derived Interleukin 2. *J. Immunol.* **1985,** *134* (1), 157–166.
315. Rosenberg, S. A. IL-2: The First Effective Immunotherapy for Human Cancer. *J. Immunol.* **2014,** *192* (12), 5451–5458.

316. Palucka, K.; Banchereau, J. Cancer Immunotherapy via Dendritic Cells. *Nat. Rev. Cancer* **2012,** *12* (4), 265–277.
317. Apostolopoulos, V.; Thalhammer, T.; Tzakos, A. G.; Stojanovska, L. Targeting Antigens to Dendritic Cell Receptors for Vaccine Development. *J. Drug Deliv.* **2013,** *2013* (4), 1–22.
318. Beacock-Sharp, H.; Donachie, A. M.; Robson, N. C.; Mowat, A. M. A Role for Dendritic Cells in the Priming of Antigen-Specific CD4+ and CD8+ T Lymphocytes by Immune-Stimulating Complexes In Vivo. *Int. Immunol.* **2003,** *15* (6), 711–720.
319. Ravichandran, K. S. Find-Me and Eat-Me Signals in Apoptotic Cell Clearance: Progress and Conundrums. *J. Exp. Med.* **2010,** *207* (9), 1807–1817.
320. Chao, M. P.; Weissman, I. L.; Majeti, R. The CD47–SIRPα Pathway in Cancer Immune Evasion and Potential Therapeutic Implications. *Curr. Opin. Immunol.* **2012,** *24* (2), 225–232.
321. Vonderheide, R. H. CD47 Blockade as Another Immune Checkpoint Therapy for Cancer. *Nat. Med.* **2015,** *21* (10), 1122–1123.
322. Liu, C.-Y.; Wang, L.; Guo, W.; Yu, C.-F.; Zhang, F.; Wang, W.-B.; Li, M.; Gao, K. Development of a Novel Reporter Gene Method for Determination of ADCC Potency of Anti-CD20 Monoclonal Antibody. *Yao Xue Xue Bao* **2015,** *50* (1), 94–98.
323. Song, X.-T.; Kabler, K. E.; Shen, L.; Rollins, L.; Huang, X. F.; Chen, S.-Y. A20 is an Antigen Presentation Attenuator, and Its Inhibition Overcomes Regulatory T Cell-Mediated Suppression. *Nat. Med.* **2008,** *14* (3), 258–265.
324. Turnis, M. E.; Rooney, C. M. Enhancement of Dendritic Cells as Vaccines for Cancer. *Immunotherapy* **2010,** *2* (6), 847–862. http://dx.doi.org/10.2217/imt.10.56 2010.
325. Anassi, E.; Ndefo, U. A. Sipuleucel-T (Provenge) Injection: The First Immunotherapy Agent (Vaccine) for Hormone-Refractory Prostate Cancer. *Pharm Ther* **2011,** *36* (4), 197–202.
326. Julie, N.; Graff, E. D. C. Sipuleucel-T in the Treatment of Prostate Cancer: An Evidence-Based Review of Its Place in Therapy. *Core Evid.* **2015,** *10,* 1–10.
327. Vonderheide, R. H.; Bajor, D. L.; Winograd, R.; Evans, R. A.; Bayne, L. J.; Beatty, G. L. CD40 Immunotherapy for Pancreatic Cancer. *Cancer Immunol. Immunother.* **2013,** *62* (5), 949–954.
328. Bajor, D. L.; Xu, X.; Torigian, D. A.; Mick, R.; Garcia, L. R.; Richman, L. P.; Desmarais, C.; Nathanson, K. L.; Schuchter, L. M.; Kalos, M.; et al. Immune Activation and a 9-Year Ongoing Complete Remission Following CD40 Antibody Therapy and Metastasectomy in a Patient with Metastatic Melanoma. *Cancer Immunol. Res.* **2014,** *2* (11), 1051–1058.
329. Goyvaerts, C.; Breckpot, K.; Goyvaerts, C. Pros and Cons of Antigen-Presenting Cell Targeted Tumor Vaccines. *J. Immunol. Res.* **2015,** *2015* (3), 1–18.
330. Kelderman, S.; Schumacher, T. N. M.; Haanen, J. B. A. G. Acquired and Intrinsic Resistance in Cancer Immunotherapy. *Mol. Oncol.* **2014,** *8* (6), 1132–1139.
331. Juergens, R. A.; Zukotynski, K. A.; Singnurkar, A.; Snider, D. P.; Valliant, J. F.; Gulenchyn, K. Y. Imaging Biomarkers in Immunotherapy. *Biomark. Cancer* **2016,** *8* (Suppl. 2), 1–13.
332. Schumacher, T. N.; Kesmir, C.; van Buuren, M. M. Biomarkers in Cancer Immunotherapy. *Cancer Cell* **2015,** *27* (1), 12–14.
333. Ascierto, P. A.; Munn, D. H.; Palucka, A. K. Highlights and Summary of the 28th Annual Meeting of the Society for Immunotherapy of Cancer. *J. Immunother. Cancer* **2014,** *2,* 15.
334. Schumacher, T. N.; Schreiber, R. D. Neoantigens in Cancer Immunotherapy. *Science* **2015,** *348* (6230), 69–74.
335. Gulley, J. L.; Madan, R. A.; Schlom, J. Impact of Tumour Volume on the Potential Efficacy of Therapeutic Vaccines. *Curr. Oncol.* **2011,** *18* (3), 150–157.
336. Weber, J. S.; Yang, J. C.; Atkins, M. B. Toxicities of Immunotherapy for the Practitioner. *J. Clin. Oncol.* **2015,** *33* (18), 2092–2099.
337. Guan, M.; Zhou, Y.-P.; Sun, J.-L.; Chen, S.-C. Adverse Events of Monoclonal Antibodies Used for Cancer Therapy. *BioMed Res. Int.* **2015,** *2015* (2), 428169, 13.
338. Medin, J.; Fowler, D. In *Experimental and Applied Immunotherapy;* Medin, J., Fowler, D., Eds.; Springer Science & Business Media: Totowa, NJ, 2010.
339. Payne, R.; Glenn, L.; Hoen, H.; Richards, B.; Smith, J. W.; Lufkin, R.; Crocenzi, T. S.; Urba, W. J.; Curti, B. D. Durable Responses and Reversible Toxicity of High-Dose Interleukin-2 Treatment of Melanoma and Renal Cancer in a Community Hospital Biotherapy Program. *J. Immunother. Cancer* **2014,** *2* (1), 13.

6.03 Strategy and Tactics for Designing Analogs: Biochemical Characterization of the Large Molecules[☆]

J-M Ahn, K Kassees, T-K Lee, B Manandhar, and AM Yousif, University of Texas at Dallas, Richardson, TX, United States

© 2017 Elsevier Ltd. All rights reserved.

6.03.1	**Minimum Active Sequence**	68
6.03.1.1	Cholecystokinin	68
6.03.1.2	Melanin-Concentrating Hormone	68
6.03.1.3	P-Selectin	68
6.03.1.4	Annexin A1	69
6.03.1.5	Eptifibatide	69
6.03.1.6	Enfuvirtide	69
6.03.1.7	Octreotide	69
6.03.1.8	Teriparatide	69
6.03.1.9	Sermorelin	69
6.03.1.10	Glucagon-Like Peptide-1	69
6.03.2	**Modifications at the Termini and Side Chains**	70
6.03.2.1	N-Acetylation	70
6.03.2.2	*N*-Pyroglutamate Formation	70
6.03.2.3	C-Amidation	71
6.03.2.4	PEGylation	71
6.03.2.5	Lipidation	72
6.03.2.6	Glycosylation	75
6.03.3	**Amino Acid Modification**	77
6.03.3.1	D-Amino Acids	77
6.03.3.1.1	Desmopressin	77
6.03.3.1.2	Octreotide	78
6.03.3.1.3	Bivalirudin	78
6.03.3.1.4	Icatibant	78
6.03.3.1.5	GnRH analogs	78
6.03.3.2	N-Methylation	78
6.03.3.3	C^{α}-Tetrasubstitution	81
6.03.3.4	β-Amino Acids	81
6.03.4	**Peptide Bond Replacements and Pseudopeptides**	82
6.03.4.1	Reduced Bond (CH_2NH)	83
6.03.4.2	Methylene Thioether (CH_2S)	83
6.03.4.3	Methylene Ether (CH_2O)	84
6.03.4.4	Alkylidene (CH═CH)	84
6.03.4.5	Endothiopeptide (CSNH)	84
6.03.4.6	Depsipeptide (CO_2)	84
6.03.4.7	Thioester (COS)	84
6.03.4.8	Ketomethylene ($COCH_2$)	84
6.03.4.9	Phosphonamide (PO_2RN)	84
6.03.4.10	Azapeptide (CONHNR)	85
6.03.4.11	Azasulfurylpeptide (AsF, $CONHNRSO_2$)	85
6.03.4.12	Retro-Inverso (RI, NHCO)	85
6.03.5	**Macrocyclic Peptides**	88
6.03.5.1	Tyrocidine A	89
6.03.5.2	Cyclosporine A	89
6.03.5.3	Colistin A	89
6.03.5.4	PMX53 (3D53)	91
6.03.5.5	Octreotide (Sandostatin)	92
6.03.5.6	Conopeptides	92
6.03.5.7	Linaclotide	93

[☆]The names of the authors are listed in alphabetical order.

6.03.5.8 Cyclic Melanocortin Analogs 94
6.03.5.9 Cyclic Opioid Peptides 95
6.03.6 Stabilization of Secondary Structures 95
6.03.6.1 Stabilized β-Turns 95
6.03.6.2 Stabilized β-Sheets 97
6.03.6.3 Stabilized α-Helices 98
6.03.7 Combinatorial Peptide Libraries 104
6.03.7.1 Spatially Addressable Parallel Synthesis 105
6.03.7.2 Split and Mix Synthesis 106
6.03.7.3 Phage Display Library 106
References 108

Abbreviations

Aβ Amyloid-β peptide
ACTH Adrenocorticotropic hormone
Aib 2-Aminoisobutyric acid
Alloc Allyloxycarbonyl
BBB Blood–brain barrier
Bcl-2 B-cell lymphoma 2
Bcl-w Bcl-2-like protein 2
Bcl-xL B-cell lymphoma-extra large
BH Bcl-2 homology
Bim Bcl-2-interacting mediator of cell death
BIV Bovine immunodeficiency virus
Boc *t*-Butyloxycarbonyl
BOP (Benzotriazol-1-yloxy)tris(dimethylamino)phosphonium hexafluorophosphate
C5a Complement fragment 5a
Cba 3-Cyclobutylalanine
CBP CREB-binding protein
CCK Cholecystokinin
CD Circular dichroism
cGMP Cyclic guanosine monophosphate
CH1 Cysteine/histidine-rich domain-1
Cha 3-Cyclohexylalanine
CNS Central nervous system
CRF Corticotropin-releasing factor
C-TAD C-Terminal transactivation domain
Dab 2,4-Diaminobutyric acid
DBU 1,8-Diazabicyclo[5.4.0]undec-7-ene
DCC *N*,*N*′-Dicyclohexylcarbodiimide
DFMO α-Difluoromethylornithine
DIC *N*,*N*′-Diisopropylcarbodiimide
DIEA *N*,*N*-Diisopropylethylamine
DMF *N*,*N*-Dimethylformamide
DMSO Dimethyl sulfoxide
DNA Deoxyribonucleic acid
DPPA Diphenylphosphoryl azide
DPP-IV Dipeptidyl peptidase-IV
FDA Food and Drug Administration
Fmoc 9-Fluorenylmethyloxcarbonyl
FP Fluorescence polarization
GBM Glioblastoma multiforme
GCC Guanylate cyclase C
GHRF Growth hormone-releasing factor
GLP-1 Glucagon-like peptide-1
GnRH Gonadotropin-releasing hormone
Hao Hydrazine, 5-amino-2-methoxybenzoic acid, and oxalic acid
HBS Hydrogen bond surrogate
HDM2 Human double minute 2 homologue
HDMX Human double minute X
hIAPP Human islet amyloid polypeptide
HIF-1 Hypoxia-inducible factor-1
HIV Human immunodeficiency virus
HOBt 1-Hydroxybenzotriazole
HR-C Heptad repeat C
HRE Hypoxia response element
hαSyn Human α-synuclein
hβ2M Human β2-microglobulin
JBD JNK-binding motif
JIP-1/IB1 JNK-interacting protein-1/islet-brain 1
JNK c-Jun N-terminal kinase
LAA Lipoamino acid
LHRH Luteinizing hormone-releasing hormone
LPSs Lipopolysaccharides
MAS Minimum active sequence
MCH Melanin-concentrating hormone
Mcl-1 Myeloid cell leukemia sequence 1
MCR Melanocortin receptor
MDM2 Murine double minute 2
MeBmt (2S,3R,4R,6E)-3-Hydroxy-4-methyl-2-methylamino-6-octenoic acid
MSH Melanocyte-stimulating hormone
nAChR Nicotine acetylcholine receptor
NBS *N*-Bromosuccinimide
NCL Native chemical ligation
NMM *N*-Methylmorpholine
NMR Nuclear magnetic resonance
NVOC 6-Nitroveratryloxycarbonyl
PAM Phenylacetamidomethyl
PEG Polyethylene glycol
PEGA Poly(ethylene glycol) dimethylacrylamide

PET Positron emission tomography
PPI Protein–protein interaction
Puma p53-upregulated modulator of apoptosis
REAL Reversible aqueous lipidation
RI Retro-inverso
RNA Ribonucleic acid
RSV Respiratory syncytial virus
SPPS Solid-phase peptide synthesis
SPR Surface plasmon resonance
TAR Transactivator response element
TE Thioesterase
TFA Trifluoroacetic acid
TFE Trifluoroethanol
Tic 1,2,3,4-Tetrahydroisoquinoline-3-carboxylic acid
TIS Triisopropylsilane
VEGF Vascular endothelial growth factor

6.03.1 Minimum Active Sequence

A minimum active sequence (MAS) is defined as the shortest amino acid sequence that can be derived from an endogenous peptide without compromise of potency or binding affinity to its native target. Conventionally, after discovery of a biologically active peptide or protein, key amino acid residues that contribute to bioactivity must first be identified. Alanine scanning and D-amino acid substitution are often carried out to identify any such residues of significance. Once essential amino acids are located, the truncation process can begin while maintaining important residues (i.e., pharmacophores) within the sequence of truncated peptides. This process removes "biologically redundant" amino acid residues that contribute little to the molecular recognition of the full-length peptide or protein.[1] The identification of an MAS via truncation is typically carried out by stepwise deletion of amino acids at either terminus or both termini.

Endogenous peptides in initial stages are often too lengthy to be effectively synthesized in a high yield, and truncation is a logical step for transformation of peptides to a manageable size. This not only facilitates efficient synthesis but also subsequently enables comprehensive structure–activity studies, both of which may accelerate drug development processes. There are a plethora of truncation studies reported to date, and **Table 1** highlights several peptide therapeutics that are already approved by the Food and Drug Administration (FDA).

6.03.1.1 Cholecystokinin

Cholecystokinin (CCK) is a peptide hormone primarily responsible for stimulating the digestion of fat and protein and inducing satiety. Several biologically active forms of CCK have been identified, such as CCK58, CCK33, CCK22, and CCK8. The most prevalent is the C-terminal octapeptide CCK8 [CCK(26–33)] that is widely distributed throughout both the peripheral and central nervous systems (CNS). The truncated octapeptide was previously thought to be the MAS of CCK, showing nanomolar affinity and efficacy on the two CCK receptor subtypes (CCK-A and CCK-B/gastrin receptor). However, the C-terminal tetrapeptide CCK(30–33) was found to have comparable activity,[2] and it has since been established as the MAS required for nanomolar affinity in the brain, while the sulfated octapeptide [sulfated CCK(26–33)] is the MAS for nanomolar affinity on the pancreatic tissue.

6.03.1.2 Melanin-Concentrating Hormone

Truncation studies of the heptadecapeptide melanin-concentrating hormone (MCH) have determined an MAS comprising only eleven residues.[3] Systematic deletion from the C-terminus was found to be acceptable up to the residue at position 16, resulting in MCH(5–15) that is equipotent to the full-length peptide. However, another deletion of Trp at position 15 significantly provoked the potency (>10-fold decrease).

6.03.1.3 P-Selectin

P-selectin is a 140-kDa integral membrane glycoprotein. In order to identify the active core region in the lectin domain, deletions from both the N- and C-termini were carried out. Two sequences, residues 36–49 and 41–50, were found to be the MAS and showed substantial inhibitory activity of selectin-dependent leukocyte adhesion.[4]

Table 1 Selected examples of truncated peptide therapeutics approved by the FDA

Peptide/protein	*Trade name*	*Manufacturer*	*Parent peptide/protein*	*Original size*	*MAS size*
Enfuvirtide	Fuzeon	Roche	HIV-1 envelope protein gp41	345-mer	36-mer
Eptifibatide	Integrilin	Millennium	Disintegrin protein	73-mer	7-mer
Octreotide	Sandostatin	Novartis	Somatostatin	14/28-mer	8-mer
Teriparatide	Forteo	Eli Lilly	Human parathyroid hormone	84-mer	34-mer
Sermorelin	Geref	Serono	Human growth hormone-releasing hormone	44-mer	29-mer

6.03.1.4 Annexin A1

Derived from the N-terminal region of a 37 kDa glucocorticoid-regulated protein and previously referred to as lipocortin 1, annexin A1 (acetyl 2–26) was identified as the MAS for anti-inflammatory activity.[5] The truncated N-acetylated peptide that contains 25 amino acids (residues 2–26) showed a similar efficacy to that of the native protein.[6]

6.03.1.5 Eptifibatide

Eptifibatide (Integrilin, Millennium Pharmaceuticals) is an FDA-approved glycoprotein IIb/IIIa antagonist for anticoagulant activity. It is a platelet aggregation inhibitor indicated for patients with acute coronary syndrome and those undergoing percutaneous coronary intervention. This antagonist is a cyclic heptapeptide derived from Cys-rich snake venom that is a 73-amino acid-containing disintegrin protein. Truncation of the long peptide to a short loop, in addition to other modifications like guanylation at Lys side chain and deamination at the N-terminus, resulted in a highly potent therapeutic peptide.[7]

6.03.1.6 Enfuvirtide

A milestone achievement of truncation is the enfuvirtide (DP-178) peptide, formally known as T-20. It is marketed by Roche under the trade name Fuzeon and was approved by the FDA in 2003 as the first human immunodeficiency virus (HIV) fusion inhibitor, forming a new class of antiretroviral drugs. Enfuvirtide is a 36-amino acid-containing peptide of which sequence corresponds to the residues 638–673 of HIV-1_{LAI} isolate.[8] This peptide binds to glycoprotein 41 (gp41) of HIV type 1 (HIV-1) that is involved in the fusion of the virus with the membrane of the CD4+ host cell.[9] It prevents the viral entry by closing the entry pore for the viral capsid.

6.03.1.7 Octreotide

Octreotide is an FDA-approved peptide drug marketed under the brand name Sandostatin by Novartis Pharmaceuticals. It is an octapeptide somatostatin analog and is primarily employed for treating growth hormone-producing tumors and pituitary tumors.[10] It is also used as a radiopharmaceutical. An indium-111-labeled octreotide (octreoscan) is used to noninvasively image tumors expressing the somatostatin receptor.

Octreotide differs from examples described in the preceding text because truncation has not only achieved the MAS but also improved the half-life. Somatostatin inhibits the release of numerous hormones that include glucagon, insulin, secretin, and growth hormone. However, its therapeutic use is highly compromised due to its short half-life of about 2 min.[11] Search for a long-acting somatostatin analog led to the octapeptide that contains the essential pharmacophore Phe^7-Trp^8-Lys^9-Thr^{10} with substitution of D-Trp at position 8 and is constrained by a disulfide linkage.[12]

6.03.1.8 Teriparatide

Teriparatide is a recombinant form of N-terminally truncated and 34-amino acid-containing human parathyroid hormone (1–34). It is marketed by Eli Lilly under the brand name Forteo. It is prescribed as an anabolic agent indicated for use in postmenopausal women with osteoporosis.[13] The parent human parathyroid hormone is an 84-amino acid-containing peptide synthesized and secreted by the parathyroid glands. The truncated N-terminal fragment (residues 1–34) exhibits comparable biological activity and pharmacological profile with its parent peptide in stimulating bone formation.[14] It acts on the kidneys, intestine, and bone to regulate plasma calcium homeostasis by increasing intracellular calcium.

6.03.1.9 Sermorelin

Sermorelin is an analog of growth hormone-releasing hormone (GHRH) primarily used for diagnostic purposes. It is a 29-amino acid-containing fragment of endogenous human GHRH, also represented as GHRH (1–29). Sermorelin is the shortest fully functional synthetic fragment of GHRH.[15] It was marketed under the trade name of Geref by Serono Laboratories, but the FDA recently listed it as a "discontinued drug product."

6.03.1.10 Glucagon-Like Peptide-1

Glucagon-like peptide-1 (GLP-1) is a 30-amino acid incretin produced by the intestinal L cells. It plays an important physiological role in glucose homeostasis primarily by stimulating insulin secretion from pancreatic β cells as a response to food intake.[16] While many truncated peptides of GLP-1 failed to offer biological activity, Mapelli and coworkers reported on the discovery of an 11-mer GLP-1 analog that comprises an N-terminal nonapeptide connected to a substituted C-terminal biphenylalanine dipeptide.[17] It was found to be a full agonist to the GLP-1 receptor and also showed improved half-life over that of the full-length peptide.

6.03.2 Modifications at the Termini and Side Chains

Peptides carry a number of polar functional groups, such as ammonium groups at the N-terminus and Lys side chain; carboxylate groups at the C-terminus and the side chains of Asp and Glu; thiol groups of Cys; hydroxyl groups from Ser, Thr, and Tyr; and guanidine groups from Arg. These hydrophilic functional groups in peptides are often modified to improve affinity to their targets, to enhance metabolic stability, and to gain new physicochemical and biological properties.

6.03.2.1 N-Acetylation

N-terminal acetylation is the most common form of N-terminal modification and places an acetyl group at the amino end of a peptide. It is one of the most common posttranslational covalent modifications of proteins and is catalyzed by a set of N-terminal acetyltransferases that transfer an acetyl group from acetyl coenzyme A to the α-amino group of the first amino acid residue.[18] The α-melanocyte-stimulating hormone (α-MSH) is an example of a naturally acetylated peptide. Synthetically, acetylation can be made by using acetic anhydride at the end of peptide synthesis.

Acetylation removes a positive charge from the N-terminus and decreases the net charge of a peptide, which may change the solubility profile. It can enhance proteolytic stability of peptides in addition to improving biological activity.[19] The removal of the positive charge at the N-terminus may help synthetic peptides mimic endogenous proteins more closely, in particular when the sequence of a peptide is derived from the segments in a protein. Acetylation has also been found to enhance cell permeability and intestinal absorption of peptides. In addition, acetylation has been used as an important tool for MS/MS sequencing of peptides and proteins.[20]

This N-terminal capping strategy has been widely used in peptide drug development. N-acetylation of a somatostatin analog was found to improve the half-life significantly from 3 min of the natural peptide to approximately 400 min.[21] An N-acetylated pentapeptide thymopoietin analog demonstrated similar metabolic protection, showing no detectable degradation, whereas the native peptide had a half-life of approximately 1 min.[22] Enfuvirtide and gonadotropin-releasing hormone (GnRH) analogs including abarelix acetate, cetrorelix acetate, degarelix acetate, and ganirelix acetate are FDA-approved N-acetylated peptide therapeutics (Table 2). N-Acetylated cyclic pentapeptide ADH-1 (Exherin), developed by Adherex Technologies for inhibiting N-cadherin to disrupt tumor vasculature, is currently undergoing phase II clinical trials.[24]

6.03.2.2 *N*-Pyroglutamate Formation

Discovered in the late 1880s, pyroglutamate (pE), also known as pyrrolidone carboxylate or 5-oxoproline, is a cyclic amino acid formed as a result of dehydration of glutamate.[25] Catalyzed by glutaminyl cyclases (QCs), the N-terminal α-amino group of either Glu or Gln cyclizes to form a lactam bond during posttranslational modification (Fig. 1).[26] There are numerous examples of N-terminal pE-containing peptides and proteins originated from plants and animals (Table 3).[23]

In addition to Gln, Glu at the N-terminus can undergo spontaneous cyclization for irreversible formation of a pE at elevated temperature or under an acidic condition.[27] Whereas the conversion of Glu to a pE occurs more slowly than Gln, it has been observed to take place near a physiological condition.[27a] On the other hand, an *N*-pyroglutamate can be chemically synthesized by condensing the carboxylic acid side chain of an N-terminal Glu with its N^{α}-amine by using a coupling reagent, which results in the formation of a lactam bond.

Gastrin-17, neurotensin, thyrotropin-releasing hormone (TRH), GnRH, and fibronectin are examples of pE-containing peptides of human origin.[26] The pE moiety is often found to be important for exerting biological functions of the peptides. The pE of thyrotropin-releasing factor is involved in receptor recognition.[28] On the other hand, pE-containing peptides have been found to cause an altered effect over their non-pE-containing counterparts. For example, a pE helix B surface peptide derived from erythropoietin (EPO) was found to have a cardioprotective action against ischemic myocardial damage similar to EPO, but lacked the undesirable parallel activation of erythropoiesis and thrombogenesis that occurs with EPO.[29] pE is also found to provide stability

Table 2 Selected examples of FDA-approved N-acetylated peptide therapeutics[23]

Peptide	*Trade name*	*Manufacturer*
Enfuvirtide	Fuzeon	Roche
Abarelix	Plenaxis	Praecis Pharmaceuticals, Speciality European Pharma
Cetrorelix	Cetrotide	AEterna Zentaris, Merck Serono
Degarelix	Degarelix acetate, Firmagon	Ferring Pharmaceuticals, Astellas Pharma
Ganirelix	Antagon, Ganirelix acetate injection, Orgalutran	Organon
ADH-1	Exherin	Adherex Technologies
Afamelanotide or melanotan-1	Scenesse	Clinuvel Pharmaceuticals
Spaglumat magnesium/sodium	Rhinaaxia Wa, Naaxia	Laboratoires Théa
Thymalfasin	Zadaxin	SciClone Pharmaceuticals International

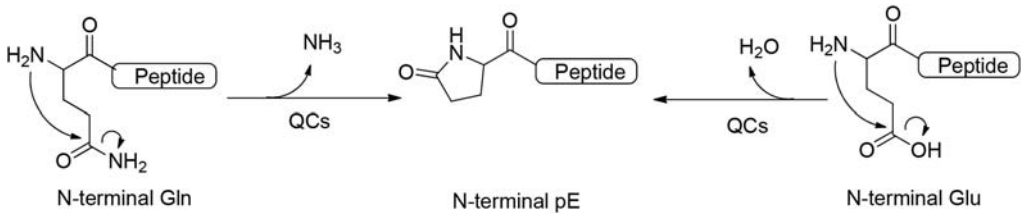

Fig. 1 Mechanism of pyroglutamate formation from Gln and Glu catalyzed by glutaminyl cyclases (QCs).

Table 3 Selected examples of FDA-approved peptide therapeutics containing pyroglutamate[23]

Peptide	*Trade name*	*Manufacturer*
Ceruletide	Takus, Tymtran	Pharmacia and Upjohn, Farmitalia Carlo Erba
Buserelin	Bigonist, Suprefact	Sanofi-Aventis
Gonadorelin	Factrel, Kryptocur, Lutrelef, Lutrepulse, Relefact, Stimu LH	Baxter Healthcare, Ferring Pharmaceuticals, Sanofi-Aventis, Wyeth Pharmaceuticals
Goserelin	Zoladex	AstraZeneca
Histrelin	Supprelin, Supprelin LA, Vantas	Endo Pharmaceuticals, Roberts Pharmaceutical, Shire Pharmaceuticals
Leuprorelin	Eligard, Enantone, Lucrin Depot, Lupron, Lupron Depot, Prostap, Viadur	Abbott, Alza, Astellas Pharma, Bayer, Bedford Labs, Genzyme, Johnson & Johnson, QLT, Sanofi-Aventis, Takeda, Teva, Wyeth
Nafarelin	Synarel, Synrelina	Pfizer, Searle
Triptorelin	Decapeptyl, Diphereline, Gonapeptyl, Pamorelin, Trelstar Depot, Trelstar LA	Debiopharm, Ferring Pharmaceuticals, Beaufour Ipsen Pharma, Watson Laboratories
Protirelin or Thyroliberin	Thypinone, Thyrel TRH, Stimu TSH	Abbott, Ferring Pharmaceuticals

against N-terminal degradation by aminopeptidases as demonstrated with GnRH[30] and monocyte chemotactic protein-2.[31] It is interesting to note that N-pE analogs of GnRH act as agonists in combination with other modifications, while N-acetylated analogs are found to be antagonists.

6.03.2.3 C-Amidation

The formation of a carboxamide at the last amino acid in the sequence of a peptide is one of the most common and important posttranslational modifications. More than the half of all biologically active peptides and proteins are α-amidated at the C-terminus, and the C-amidation appears to be essential for their full biological activity.[32] It is catalyzed by a bifunctional enzyme, peptidylglycine α-amidating monooxygenase (PAM). Calcitonin, oxytocin, and vasopressin are examples of C-amidated endogenous peptides.

C-terminal amidation of a peptide produces effects similar to those of N-acetylation. These include a change in net charge, which alters the solubility profile. It can also improve proteolytic stability by evasion from carboxypeptidases, as observed in peptides like endomorphon-1. While a carboxylate group may be converted to an ester to prevent degradation by carboxypeptidases, esters are susceptible to numerous esterases, and C-amidation therefore offers a more effective alternative. C-terminal amidation increased the in vivo half-life of Met-enkephalin from seconds to nearly an hour, along with other modifications.[33]

6.03.2.4 PEGylation

Covalent attachment of one or more polyethylene glycol (PEG) chains to a peptide or protein is called PEGylation. Compared with other N- and C-terminal modifications that may naturally occur (e.g., N-acetylation, N-pyroglutamylation, and C-amidation), PEGylation is strictly a synthetic modification. As it is nontoxic, nonimmunogenic, nonantigenic, and highly soluble in aqueous media, PEG appears to be the most biologically compatible polymer and is approved by the FDA for internal use.

PEGylation is primarily used to overcome disadvantageous physicochemical properties of biomolecules like peptides and proteins. It prolongs circulation half-life in the body, which requires less frequent administration and ultimately leads to better patient compliance. PEGylation also increases the aqueous solubility of peptides and enhances resistance to proteases and metabolic enzymes. Reduction of immunogenicity of conjugated biomolecules is another attribute of PEGylation, which may be significant for using peptides of nonhuman origin. PEG also frequently serves as a spacer or linker. A bifunctional PEG spacer can connect a peptide to another molecule. Since the first instance of PEGylation of albumin and catalase in the late 1970s by Davis and

Abuchowski,[34] a number of chemical and enzymatic methods have been developed for conjugating PEG, including site-specific modification.

Pegademase bovine was the first PEGylated protein drug approved by the FDA in 1990. It is marketed by Enzon Pharmaceuticals under the brand name Adagen for the treatment of X-linked severe combined immunodeficiency syndrome as an alternative to bone marrow transplantation and enzyme replacement by gene therapy. Since then, a number of PEGylated peptide and protein drugs have entered the market (**Table 4**).

One of the unfortunate consequences of PEGylation may be a loss of biological activity. However, this loss can be compensated by a prolonged circulation time resulting from increased stability, which gives a higher hydrodynamic volume.[36] For example, 40 kDa branched PEG-conjugated antiviral protein PEG-interferon-α-2a has only 7% of the antiviral activity of the unmodified protein[37]; however, the PEGylated conjugate showed higher in vivo efficacy for the treatment of hepatitis C compared with the unmodified form by virtue of its improved pharmacokinetics.

The most important properties to consider for PEGylation are the size and structure of the PEG chain and the site of attachment on a peptide. Since PEG is a synthetic polymer, it is polydisperse, and a batchwise variation in the number of monomers is inevitable, which in turn yields a Gaussian distribution of the molecular weight.[36] Thus, conjugation of such a polydisperse polymer may lead to a population of drug conjugates that have slightly different physicochemical and pharmacokinetic properties dependent on the size of the PEG chain. The size of PEG is important since proper clearance from the body depends largely on this factor. It is usually excreted in urine and feces. However, if the molecular weight is too large, it may accumulate in the liver.

Peptides and proteins are typically sensitive to modification. In addition, chemical reactions used to make a modification should be mild enough not to denature or inactivate such delicate biomolecules. The site of modification and the type of chemical reactions for the conjugation should be carefully considered for PEGylation of peptides and proteins. While the imidazole group of His, carboxylic group of Glu/Asp, hydroxyl group of Ser/Tyr, and even the carboxamide side chain of Gln have been reported for the conjugation,[35] PEGylation is typically carried out at the side chains of either Lys or Cys (**Fig. 2**).

The amino groups of the Lys side chain and the N-terminus are the most exploited sites for PEGylation. The conjugation is carried out by either alkylation or acylation. While alkylation does not alter the total charge of a protein, acylation forms a neutral amide bond that removes a positive charge. The change in the surface charge may play a role in target interaction. Examples of reactive functional groups to amines for PEGylation are shown in **Fig. 2A**. Trichlorotriazine and aldehyde yield a conjugated product that maintains the positive charge after PEGylation.[34b,38] Attachment of PEG to an amine via an activated carboxylic acid like *N*-hydroxysuccinimide ester forms an amide bond.[39] Similarly, carbonate-activated PEGs like *p*-nitrophenyl chloroformate, succinimidyl carbonate, and benzotriazole create a stable urethane linkage.[40]

The thiol group of Cys is an outstanding nucleophile for site-specific modifications. PEG conjugation via a stable thioether linkage can be conveniently produced with PEG-derivatized maleimide, vinyl sulfone, or iodoacetyl groups.[41] Since the prevalence of Cys is lower than that of Lys, the thiol-mediated conjugation can be more site-specific. An ortho-pyridyl disulfide-derivatized PEG can make a reversible disulfide bond with Cys of peptides, which can be reduced to release the native proteins under a mild condition.[42] A thiol-ene reaction has also been attempted to conjugate a copolymer of di(ethylene glycol) methyl ether methacrylate and allyl methacrylate to α-keratin via hetero-Michael addition.[43]

In addition to amino and mercapto groups, the hydroxyl groups of Ser, Thr, and Tyr have been employed for PEGylation. While modification at Ser and Thr usually requires reaction conditions that are too harsh for proteins, an enzymatic approach has been successfully applied for site-directed PEGylation by using glycosyltransferases to attach PEG to O-glycans.[44] Tyr of Leu-enkephalin and salmon calcitonin were conjugated with diazonium salt-terminated linear monomethoxy poly(ethylene glycol)s (mPEGs) and poly(mPEG) methacrylate.[45] While the acyl-His bond is not stable, PEG conjugation to the imidazole group of His in interferon-α-2b has been reported to produce a prodrug that slowly releases the protein.[46] In addition, azide–alkyne cycloaddition (also known as "click chemistry") has also been used to make PEGylated peptides.[47]

6.03.2.5 Lipidation

Conjugation of a fatty acid is referred to as lipidation, and it increases lipophilicity of conjugated peptides and proteins. Lipidation is one of the most commonly encountered posttranslational modifications that modulates hydrophobicity, secondary structures,

Table 4 Selected examples of FDA-approved PEGylated peptide/protein therapeutics[35]

Peptide/protein	*Trade name*	*Manufacturer*	*PEG size (kDa)*
Pegademase	Adagen	Enzon	5
Pegaspargase	Oncaspar	Enzon	5
Pegfilgrastim	Neulasta	Amgen	20
Peginterferon-α-2b	PegIntron	Schering-Plough, Enzon	12
Peginterferon-α-2a	Pegasys	Hoffmann-La Roche	40
Pegvisomant	Somavert	Pfizer	5
PEG-EPO	Mircera	Roche	40
Certolizumab pegol	Cimzia	Nektar, UCB Pharma	40

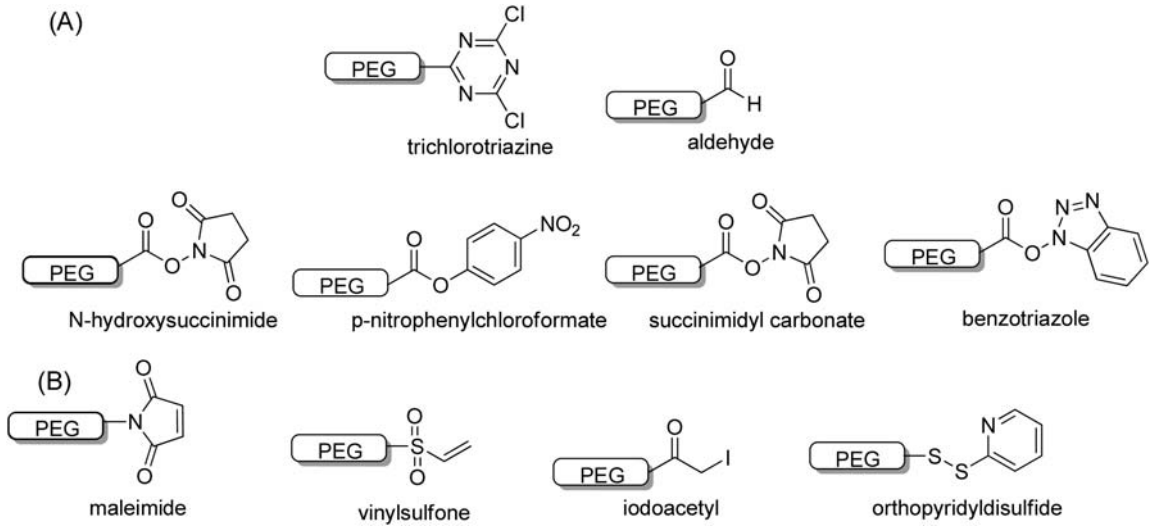

Fig. 2 PEG-derivatized functional groups reactive toward (A) an amine and (B) a thiol.

and self-assembling propensities. Lipidated peptides can also offer enhanced metabolic stability, membrane permeability, bioavailability, and pharmacokinetic and pharmacodynamic properties.[48] Moreover, it increases plasma stability and decreases renal clearance of peptides, which leads to a long circulation half-life. GLP-1 analog liraglutide (Victoza), insulin detemir (Levemir), and antibiotics like daptomycin and polymyxin B are examples of lipidated peptide therapeutics approved by the FDA (Table 5).

Marketed as Victoza by Novo Nordisk, liraglutide is a GLP-1 analog prepared by attaching a C16 fatty acid to an amino side chain of Lys via a γ-glutamyl spacer. The conjugation of the fatty acid increased the plasma half-life from 1.2 to 13 h after subcutaneous injection.[49] Similarly, tesamorelin, an analog of human growth-releasing factor hGRF(1–44)NH_2, has a *trans*-3-hexenoyl moiety conjugated to Tyr that resulted in resistance against dipeptidyl peptidase-IV (DPP-IV) degradation.[50]

Besides increasing plasma stability, lipidation has also been utilized as a strategy to improve absorption by passive diffusion. Peptide drugs, in particular hydrophilic ones, are lipidated to enhance membrane permeability. For example, a naturally occurring dipeptide thymic immunomodulator that has high hydrophilic character and low permeability was conjugated to 2-aminododecanoic acid to improve oral absorption.[51]

The chain length of a lipid moiety is an important parameter that needs to be considered for lipidation since the length may have a strong impact on the bioactivity of lipidated peptides.[48] However, an increase in the chain length most likely leads to a decrease in aqueous solubility. A longer chain fatty acid conjugate of Phe-Asp-Cys-amide was found to be more effective than its shorter chain counterpart in inhibition of melittin-induced hemolysis.[52] On the other hand, a longer lipid chain connected to an enkephalin analog unfortunately led to a decrease in biological activity despite improved cell permeability from its increase in length.[53]

The site and chemical reaction for lipidation also need to be carefully considered. Modification of peptides and proteins with lipids can be carried out by similar reactions used for PEGylation. Amines of the N-terminus and the lysine side chain are the most exploited lipid modification sites. N-terminal myristoylation and palmitoylation are common peptide lipidation strategies. For example, palmitoyl lipidation at the N-terminus of the α-helix 2 fragment of STAT3 showed an enhanced inhibition of breast cancer cell growth.[54] The significance of the site of lipidation is made clear with the example of the lipidated analog of cecropin A–melittin hybrid peptide, CA(1–7)M(2–9). Acylation with saturated linear fatty acids at Lys^7 showed drastically decreased leishmanicidal activities, whereas acylation at Lys^1 to either the α- or ε-amino group increased the activity up to 3 times against promastigotes and up to 15 times against amastigotes.[55]

Among many lysine lipidations, insulin detemir (Levemir), a long-acting human insulin analog, is probably one of the most well-demonstrated examples (Fig. 3).[56] Marketed by Novo Nordisk, Levemir is an insulin analog with a myristic acid conjugated

Table 5 Selected examples of FDA-approved lipidated peptide/protein therapeutics

Peptide/protein	*Trade name*	*Manufacturer*	*Type of lipid*
Insulin detemir	Levemir	Novo Nordisk	Fatty acid (C14)
Liraglutide	Victoza, Saxenda	Novo Nordisk	Fatty acid (C16)
Daptomycin	Cubicin	Cubist Pharmaceuticals	Fatty acid (C10)
Tesamorelin	Egrifta	Theratechnologies	Fatty acid (C6)
Teicoplanin	Targocid	Sanofi-Aventis	Fatty acid (mixture)
Insulin degludec	Tresiba	Novo Nordisk	Acidic fatty acid (C16)

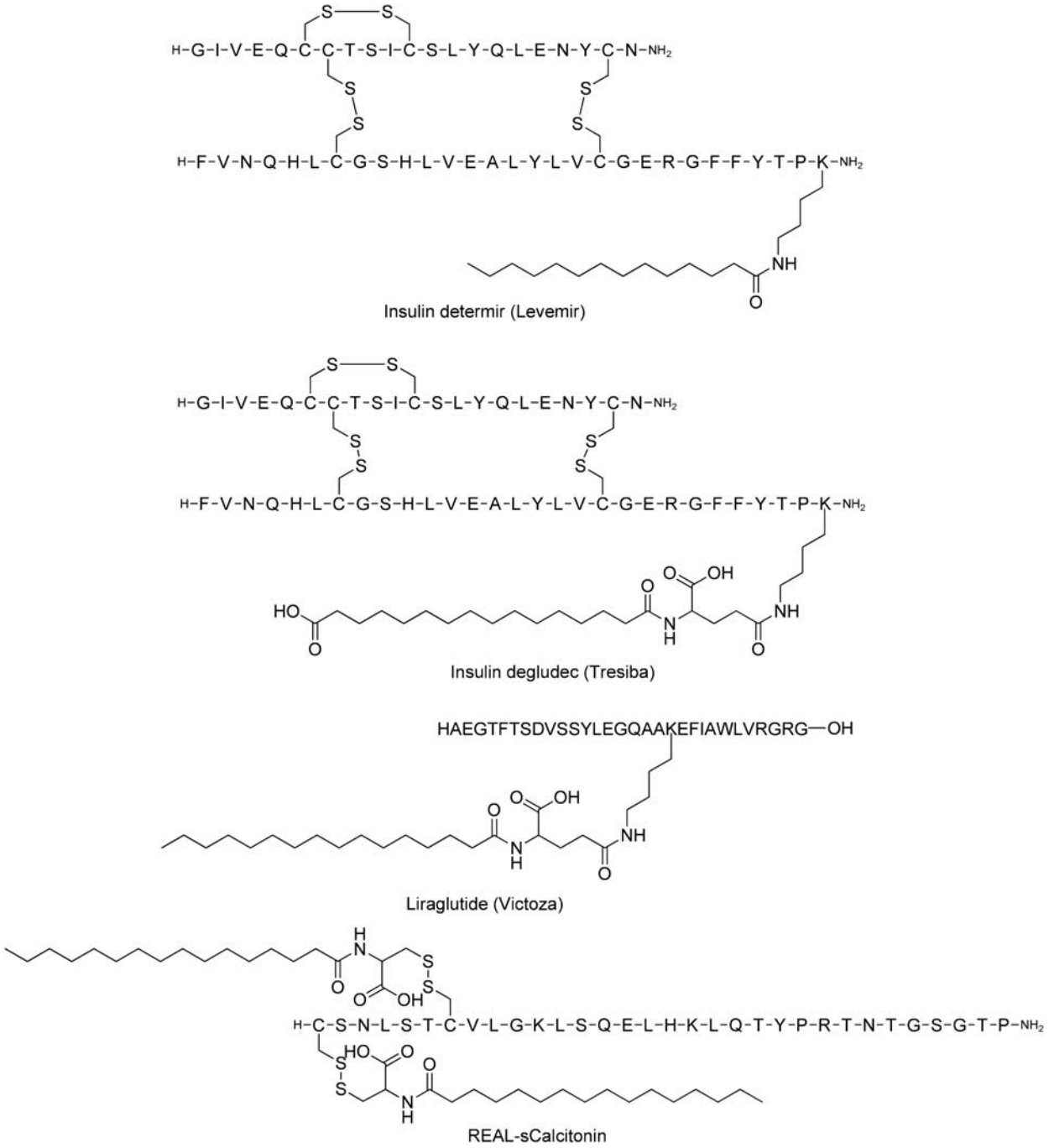

Fig. 3 Structures of lipidated peptides.

to the ε-amino group of Lys[29] of the B chain without Thr[30]. It showed outstanding serum binding affinity and a blood glucose-lowering effect for longer duration, up to 24 h.[56,57] An additional milestone example is liraglutide, another FDA-approved peptide drug lipidated at the ε-amino group of Lys of GLP-1.

The thiol group of Cys, if present, is an easily accessible site for lipidation of peptides and proteins. One of the widely used methods for Cys lipidation is called reversible aqueous lipidation (REAL) technology that involves the lipidation of peptides via a disulfide bond formation reaction between (*N*-palmitoyl cysteinyl)-2-pyridyl disulfide and the thiol group of Cys.[58] DiC_{16}-desmopressin lipidated with the REAL technology showed fourfold longer antidiuretic activity compared with the unmodified desmopressin.[59] Similarly, salmon calcitonin was also successfully lipidated with *N*-palmitoyl cysteinyl 2-pyridyl disulfide.[60] The reversibly lipidized peptides exhibited not only improved pharmacokinetic and pharmacodynamic behaviors but also

enhanced oral bioavailability. Lipids conjugated via labile linkages can be cleaved to release native biomolecules under a suitable condition.[61] Such a prodrug strategy has the advantage of enhancing the pharmacological characteristics of a parent peptide without decreasing its activity and selectivity.[62]

Lipidation can also be accomplished by introduction of unnatural lipoamino acids (LAAs).[63] Toth's group reported an amino acid-based oligopeptide system that combines the structural features of lipids and amino acids. Lipidation of ryanodine receptor agonist with LAA improved Ca^{2+} release activity and permeability across caco-2 cells without disrupting the α-helical structure-bearing critical residues.[64] In addition, a carboxylic fatty acid has been used for lipidation. Acylation with a dicarboxylic acid changes the positively charged amine into a negatively charged carboxylate. Insulin degludec, marketed by Novo Nordisk under the brand name Tresiba, is one of the successful examples of lipidation, and it was recently approved by the FDA in 2015.[65] It is an extremely long-acting insulin, and the hexadecandioyl fatty diacid is conjugated via a γ-glutamic acid spacer to the ε-amino group of Lys^{B29} of the B chain lacking Thr^{B30}.

6.03.2.6 Glycosylation

Glycosylation is the covalent attachment of oligosaccharide moieties to peptides or proteins and is considered the most complex posttranslational modification.[66] Glycopeptides and glycoproteins are important components of biochemical processes, and they play significant roles in cell growth regulation, immune response, binding of pathogens, cancer cell metastasis, and inflammation. Glycans on proteins may also play a role in protein folding and stabilization of tertiary structure.[67] Since the conjugated sugar moieties can be very large and bulky, it can either facilitate or inhibit protein–protein interactions (PPIs). In addition, glycosylation increases the aqueous solubility of biomolecules.

There are a number of natural and synthetic glycopeptides and glycoproteins used as therapeutics. For example, glycopeptide antibiotics have been instrumental in the fight against infectious diseases.[68] Vancomycin was approved in 1958 by the FDA to treat penicillin-resistant staphylococci, and lipoglycopeptide analogs of vancomycin, such as telavancin and dalbavancin, have been developed to tackle increasing cases of resistance.[68] In addition, glycoconjugate vaccines comprising a fully synthetic capsular polysaccharide antigen of *Haemophilus influenzae* type b (Hib) have been developed.[69]

A variety of functional groups can be used to form a glycosidic bond, and different types of linkages are often found within a single molecule. In 1961, Johansen and coworkers first reported on glycosylation in ovalbumin via a GlcNAc-β-Asn linkage.[70] For glycosylation, several factors must be considered, such as the site of glycosylation, the type of glycan composition, and the length, size, and structure of the glycan. There are mainly five different types of glycosidic linkages found in nature (**Fig. 4**): N-linked (bound to the amino group of an amino acid, usually Asn), O-linked (bound to the hydroxyl group of Ser, Thr, or Tyr), glypiation (linked to a phospholipid), C-linked (linked to the indole ring of Trp), and phosphoglycosylation (bound to Ser via a phosphodiester bond).[71] Thirteen monosaccharides and 8 amino acids have been identified that participate in glycosidic bond formation to date.[71]

Glycosylation still remains a less explored field for peptide therapeutic development. In recent years, however, there has been a growing interest in the development of new methods for linking sugars to peptides. Synthesis of a glycopeptide/glycoprotein requires robust chemical methods from both carbohydrate and peptide fields since it involves the formation of the integral glycan–amino acid bond.[72] Glycopeptides are chemically synthesized mainly by two different strategies: linear assembly and convergent assembly. Linear assembly uses glycoamino acid building blocks. Glycoamino acids are synthesized separately and later assembled together by using solid-phase peptide synthesis (SPPS) protocol.[73] Protected glycoamino acids are now commercially available, ready for coupling onto a growing peptide on polymer support. However, extensive protection and deprotection steps

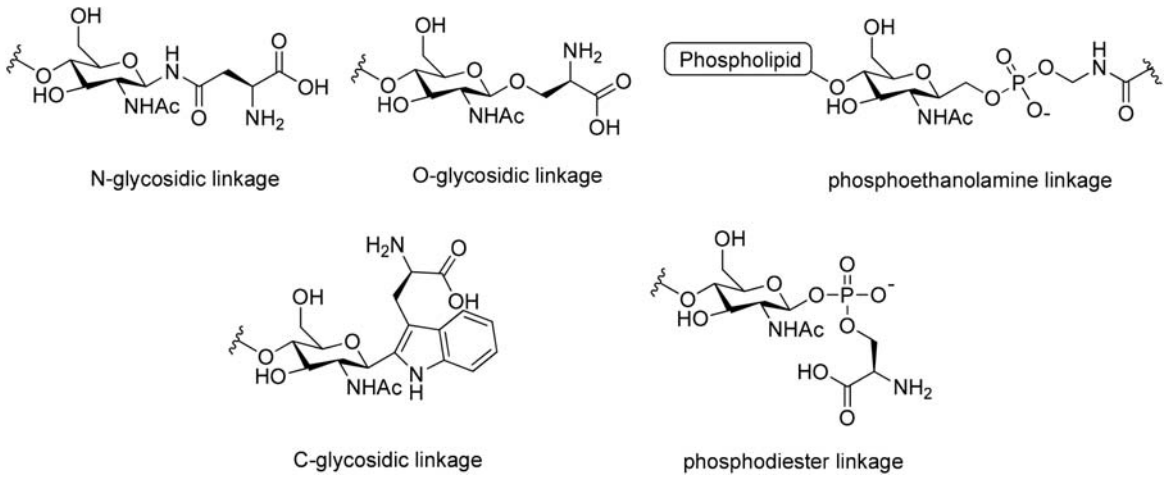

Fig. 4 Structures of glycosidic linkages.

of both the carbohydrate moieties and amino acids, along with the limitation on the length of peptides that can be synthesized with acceptable purity, may compromise effective production of glycosylated biomolecules, especially glycoproteins. In convergent assembly, a peptide chain and glycan residues are synthesized separately, and glycosylation can be carried out later on a specific side-chain residue of the peptide.[72] Direct convergent peptide glycosylation often produces a lower yield, but has been used to couple glucosamine to carboxylates of peptides.[74]

A number of chemical strategies have been developed for the synthesis of natural glycosidic linkages (Fig. 5). A reaction of either protected or deprotected glucosamine with protected Asp is the most commonly used route for N-linked glycosylation.[75] Staudinger ligation strategy was also developed to conjugate glycosyl azides to carboxylates or their derivatives of peptides in the presence of PPh_3.[76] On the other hand, O-linked glycosidic linkages are formed most commonly on the hydroxyl group of Ser or Thr by using standard glycosyl donors. Field and coworkers reported the synthesis of 1,2-trans disaccharides in high yields by activating

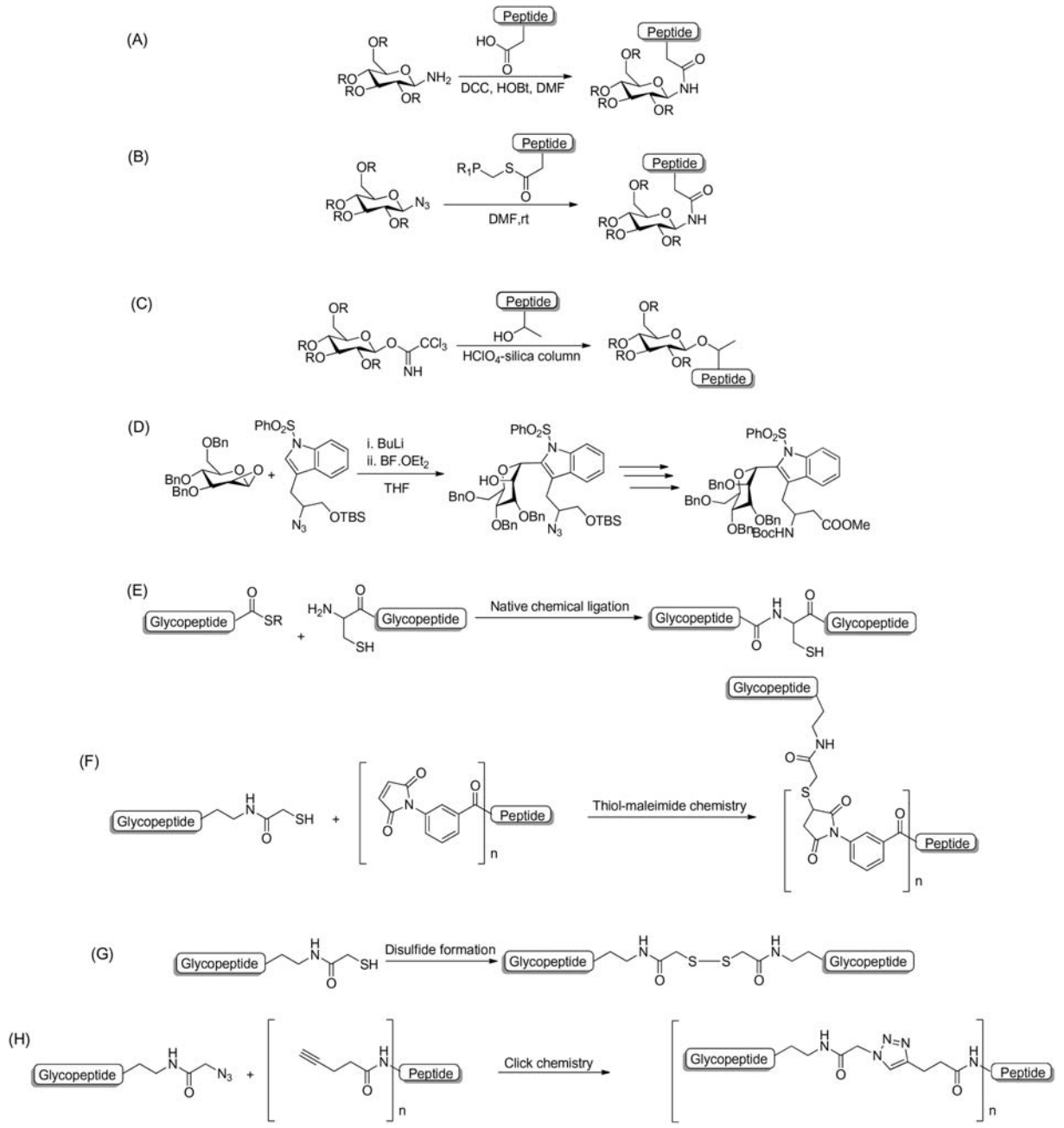

Fig. 5 Synthetic strategies for the preparation of glycopeptides. (A) N-linked, (B) N-linked via Staudinger reaction, (C) O-linked, (D) C-linked, (E) via native chemical ligation, (F) via thiol–maleimide chemistry, (G) via disulfide formation, and (H) via azide–alkyne cycloaddition reaction ("click chemistry").

ester-protected glycosyl trichloroacetimidate donors with perchloric acid immobilized on silica.[77] For C-linked glycosidic bond formation between Trp and mannose moieties, Ito and coworkers carried out ring opening of a benzyl-protected 1,2-anhydro-mannose with a lithiated indole derivative. After a series of functional group conversion and deprotection steps, glycoamino acids were synthesized as building blocks for peptide elongation.

Chemical glycosylation methods are not limited to the production of natural glycoproteins. Neoglycoproteins that bear unnatural glycosidic linkages can be synthesized by using reactive side-chain functional groups like the amine and thiol of Lys and Cys, respectively.[78] One of the most widely used and robust convergent synthetic strategies is native chemical ligation (NCL). Diptericin is an antibacterial glycopeptide that contains 82 amino acids and 2 O-linked glycosylation sites, and its total synthesis was accomplished by NCL.[79] Glycosylation has also been carried out with site-selective Cys ligation utilizing thiol–maleimide chemistry.[80] Cu-catalyzed azide–alkyne cycloaddition (often referred as "click chemistry") is another robust bioconjugation method, making triazole-linked glycopeptides. This method has been used to synthesize simple glycoconjugates,[81] multiglycan peptides,[80] and carbohydrate-conjugated peptide libraries.[82]

6.03.3 Amino Acid Modification

Peptides are easily degradable biomolecules, and this becomes one of the major hurdles for developing peptide therapeutics.[83] Proteases and metabolic enzymes lower half-life and bioavailability, which returns suboptimal pharmacokinetic profiles. In order to tackle these issues, numerous strategies have been devised, and this section summarizes amino acid modifications, such as D-amino acid substitution, N-methylation, C^{α}-tetrasubstitution, and β-amino acid substitution.

6.03.3.1 D-Amino Acids

Peptides and proteins are primarily composed of natural amino acids that have L-configuration. Natural peptides containing D-amino acids, however rare, do exist and are the results of posttranslational modification of L-amino acids. More than 30 examples of such D-amino acid-containing peptides have been isolated from a variety of species including frogs, snails, crustaceans, spiders, and mammals.[84] Since the unnatural configuration of D-amino acids is not recognized by proteases, substitution with D-amino acids can increase metabolic stability significantly. In addition, the D-configuration allows peptides to access different conformational spaces over their natural L-amino acid counterparts, which may impose local conformational constraints and lead to stabilization of unique structures.

The most common purpose for the incorporation of D-amino acids in synthetic peptides is to provide enhanced proteolytic stability. This is well demonstrated by the works of Tugyi and coworkers on an MUC2 peptide that contains the PTGTQ epitope of an MUC2 protein backbone-specific monoclonal antibody.[85] The N- and C-terminal flanking regions were replaced by up to three D-amino acids. The epitope function of the resulting peptides was found to be uncompromised by these D-amino acid substitutions (e.g., tpTPTGTQtpt). Extending the peptide chain with D-amino acids only to the N-terminus (tPTPTGTQTPT and tptPTGTQTPT) increased the stability, but failed to protect completely from degradation. On the other hand, adding both flanks with D-amino acids successfully offered complete protection.

[GLP-1(7–36)-NH_2] is a 30-amino acid-containing incretin and highly susceptible to degradation by DPP-IV at the penultimate peptide bond between Ala^8 and Glu^9. The resulting metabolite, GLP-1(9–36)-NH_2, is found to have 100-fold lower binding affinity to its receptor (GLP-1R) and negligible agonist activity (>10,000-fold decrease) compared with the intact peptide.[86] The cleavage of the dipeptide by DPP-IV was successfully inhibited by the substitution of Ala^8 with D-Ala with nearly no loss of biological activity.[87]

Although incorporation of D-amino acids is mostly linked to proteolytic stability, this modification has also proved valuable for enhancement of biological activity by the stabilization of a β-turn conformation as demonstrated in many peptides including α-MSH. Substitution of Phe^7 with D-Phe in α-MSH produced a potent analog by stabilizing a β-turn structure required for receptor interaction.[88] It has been found that cyclic pentapeptides with one D-amino acid placed at the $i+1$ position prefer to adopt a β-turn conformation (type II′).[89] This preference was exampled by cyclic pentapeptides of thymopoietin.[90] In addition, the cyclic RGD pentapeptide cilengitide, c[RGDf(N-Me)V], demonstrated substantially increased potency as compared with its linear peptide after introduction of D-Phe, in combination with N-methylation of Val. It is currently in phase III clinical trial for the treatment of glioblastomas.[89] Similarly, substitution of L-Pro^4 with D-Pro in β-casomorphin-(5) and β-casomorphin-(4) amide resulted in high binding affinity and selectivity to μ-opioid receptor.[91] Conversely, some naturally occurring peptides with D-amino acids have been found to lose their biological activity when substituted with L-amino acids.[92]

6.03.3.1.1 Desmopressin

One of the first examples of peptide therapeutics is desmopressin. It is an analog of vasopressin containing a desaminocysteine residue at position 1 along with D-Arg substitution for Arg at position 8.[93] The resulting vasopressin analog is orally active even at a dose 1/75th of natural lysine vasopressin, mainly due to its enhanced permeability across intestinal epithelia and proteolytic stability.[94]

6.03.3.1.2 Octreotide

Octreotide is a somatostatin analog and marketed under the brand name Sandostatin by Novartis. Before the cyclic octapeptide octreotide was developed, a potent somatostatin analog was designed with D-Trp at position 8, which increased its potency by eight-fold.[21] Conformational and structure–activity studies showed a β-turn (type II′) stabilized by the introduction of the D-Trp residue that accounts for the improvement in potency. This substitution with D-Trp was carried forward to the design of octreotide.

6.03.3.1.3 Bivalirudin

Bivalirudin, marketed as Angiomax by the Medicines Company, is a 20-amino acid-containing peptide derived from an anticoagulant protein found in the saliva of the medicinal leech, *Hirudo medicinalis*. It is a potent, highly specific, and reversible inhibitor of thrombin. D-Phe is placed at the N-terminus to provide resistance to proteolytic cleavage, resulting in an increased circulation half-life.

6.03.3.1.4 Icatibant

Icatibant is a potent, specific, and reversible antagonist to the bradykinin B2 receptor. It was approved by the FDA in 2011 for the treatment of hereditary angioedema and is marketed by Jerini under the trade name Firazyr. Icatibant is a synthetic decapeptide with structural similarity to native 9-mer bradykinin, but bearing heavy modifications with five unnatural amino acids including two D-amino acids, D-Arg^{1} and D-Tic^{8}.[95]

6.03.3.1.5 GnRH analogs

Analogs of GnRH are additional examples of D-amino acid substitution for modulating peptide conformation.[23b] Native GnRH is a 10-amino acid-containing peptide with N-terminal pyroglutamation and C-terminal amidation. As GnRH binds to its pituitary receptor with a β-turn conformation formed at Gly^{6}, a series of GnRH analogs with substitution at position 6 with various D-amino acids was synthesized (Table 6).[23b]

6.03.3.2 N-Methylation

Methylation is one of the most prevalent and simplest posttranslational modifications found in peptides and proteins. Methyltransferases are responsible for the modifications at various functional groups, including carboxylates; the sulfhydryl and thioether side chain of Cys and Met, respectively; and the nitrogen of the N$^{\alpha}$-amine group of amino acids and the side chains of Lys, Arg, His, Asn, and Gln. Among these, N-methylation is the most common and has a great impact on overall physical and chemical properties of peptides and proteins. Nature has several fine examples of N-methylated cyclic peptides (e.g., cyclosporine and omphalotin, a powerful immunosuppressant[96] and a nematicide,[97] respectively) and linear peptides (e.g., hemiasterlin, a cytotoxic peptide[98]), shown in Fig. 6.

N-Methylation is a useful tool for restricting phi and psi angles in the peptide backbone.[99] This structure-constraining strategy has been widely used to understand backbone conformations and ultimately applied to modulate the biological activity and selectivity of peptides. Proline is frequently found to induce β-turn structures and well known to have *cis*-peptide bonds.[100] Since N-methylation influences the *cis*–*trans* equilibrium of the peptide bond by inducing steric hindrance, it has been studied as a replacement for Pro.[100] One advantage of this substitution is the capability to place a side-chain functional group that is not present in Pro.

Table 6 Selected examples of D-amino acid-containing peptide therapeutics approved by the FDA[23]

Peptide	*Trade name (manufacturer)*	*Modification*	*FDA approval*
Desmopressin	DDAV (Sanofi-Aventis), Stimate (CSL Behring), Minirin (Ferring)	D-Arg^{8}	1984, 1994, 2002
Octreotide	Sandostatin (Novartis)	D-Trp^{8}	1988
Bivalirudin	Angiomax (Medicines Co.)	D-Phe^{1}	2000
Icatibant	Firazyr (Jerini)	D-Arg^{1}, D-Tic^{8}	2011
GnRH analogs			
Abarelix	Plenaxis (Praecis)	D-Asp^{6}	2003
Buserelin	Suprefact (Sanofi-Aventis)	D-Ser(tBu)^{6}	
Cetrorelix	Cetrotide (EMD Serono/Asta Medica)	D-Citrulline^{6}	1997
Deslorelin	Suprelorin (Peptech)	D-Trp^{6}	
Ganirelix	Antagon (Organon)	D-Diethylhomo-Arg^{6}	1999
Goserelin	Zoladex (AstraZeneca)	D-Ser(tBu)^{6}	1989
Leuprolide	Lupron (Takeda/Abbott), Viadur (Johnson & Johnson), Eligard (Sanofi-Aventis)	D-Leu^{6}	1985, 2000, 2002
Nafarelin	Synarel (Pfizer)	D-Napthyl-Ala^{6}	1990
Triptorelin	Decapeptyl, Trelstar (Watson Laboratories)	D-Trp^{6}	2001

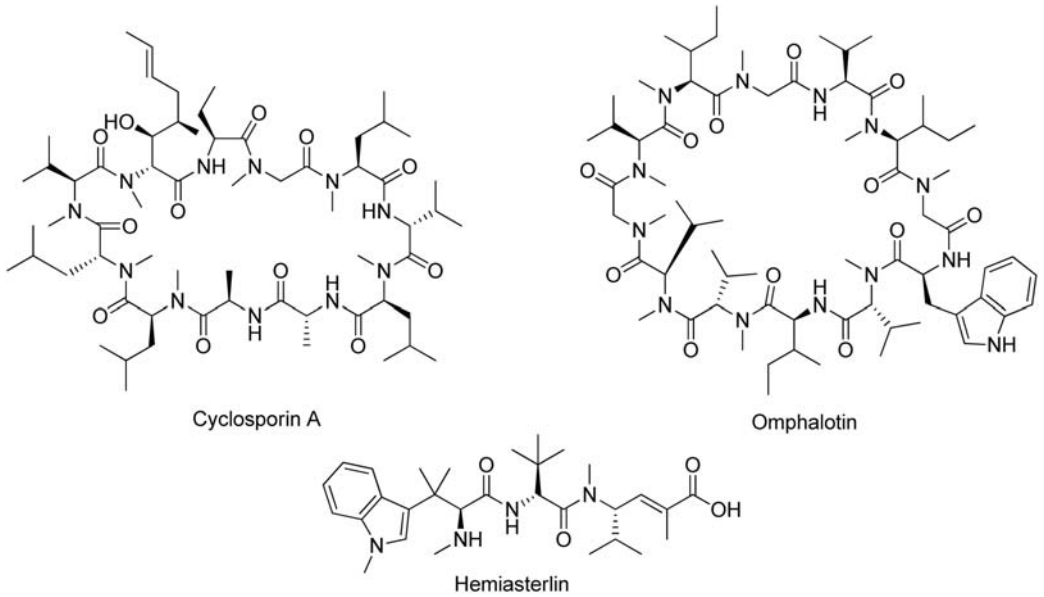

Fig. 6 Naturally occurring N-methylated cyclic and linear peptides.

Increased selectivity resulting from N-methylation is well demonstrated by cyclic RGD peptide integrin ligands.[101] N-Methylation of solvent-exposed amide bonds resulted in significant enhancement of selectivity to integrin receptor subtypes due to reduced backbone flexibility. N-Methylation also modulates the properties of a peptide by reducing the number of amide protons that play a role in forming hydrogen bonds. This property has been exploited to avoid aggregation of peptides into β sheets. For example, N-methylation of islet amyloid polypeptide at two sites resulted in a nonamyloidogenic analog.[102] It also raises hydrophobicity of peptides, which may promote membrane permeability, although the exact mechanism of enhanced permeability is not fully elucidated.[103]

N-Methylation also promotes resistance to proteolytic cleavage. For example, DhHP-6, a microperoxidase mimetic peptide that scavenges reactive oxygen species, was subjected to site-specific multiple N-methylation.[104] It was found that tri-N-methylation of DhHP-6 could significantly increase intestinal flux, which resulted in up to threefold enhanced intestinal permeability. In addition, N-methylation at a particular residue like Glu led to prolonged resistance against proteolytic degradation, resulting in up to a 140-fold longer half-life. All these features of N-methylation summate to ultimately improve bioavailability, and N-methylation has been reported in many peptides. Examples include TRH, opioid peptides, somatostatin, luteinizing hormone-releasing hormone (LHRH), bombesin, bradykinin, CCK, angiotensin II, endothelin, insulin, neurotensin, tachykinin, RGD peptides, C5a anaphylatoxin, pseudopeptides for MHC-II, β-amyloid, corticotropin-releasing factor, and growth hormone-releasing factor. Some of these peptides are currently under various stages of clinical trials, while others are already on the market (**Table 7**).[99]

N-Methylation, in particular mono-N-methylation, has been utilized in numerous peptides.[105] There are two main synthetic routes for preparing N-methylated peptides, and one involves the use of presynthesized N-methylated amino acids as building blocks for peptide synthesis. A variety of N-methylated amino acids, although expensive, are now commercially available. On the other hand, synthesis of N-methylated amino acids and derivatives is well established, including direct N^{α}-methylation of N^{α}-protected amino acids or amino acid esters and 5-oxazolidinone formation and reduction (**Fig. 7**).[106] Several other methods have been also reported, such as reductive amination, Mitsunobu reaction, and Diels–Alder and subsequent retro-Diels–Alder reactions.[99,106] Biron and coworkers reported an efficient synthetic procedure of N-methylated amino acids that does not require laborious purification steps.[106] N^{α}-Methyl-N^{α}-(*o*-nitrobenzenesulfonyl)-α-amino acids (N-Me-oNBS amino acids) are compatible with Fmoc SPPS protocols and can be prepared by N-alkylation of an N^{α}-arylsulfonylamino ester. The oNBS protecting group can be selectively removed with mercaptoethanol and 1,8-diazabicyclo[5.4.0]undec-7-ene (DBU) during SPPS.

Table 7 Selected examples of N-methylated peptide therapeutics

Peptide/protein	*Trade name*	*Manufacturer*	*N-Methylation*
Cyclosporine	Sandimmune, Neoral, Restasis, Gengraf	Novartis, Allegran, Abbott	Multiple N-Me
Abarelix	Plenaxis	Praecis	N-Me-Tyr
Plitidepsin	Aplidin	PharmaMar	Di-N-Me
Cilengitide	Cilengitide (phase III)	Merck KGaA	N-Me-Val

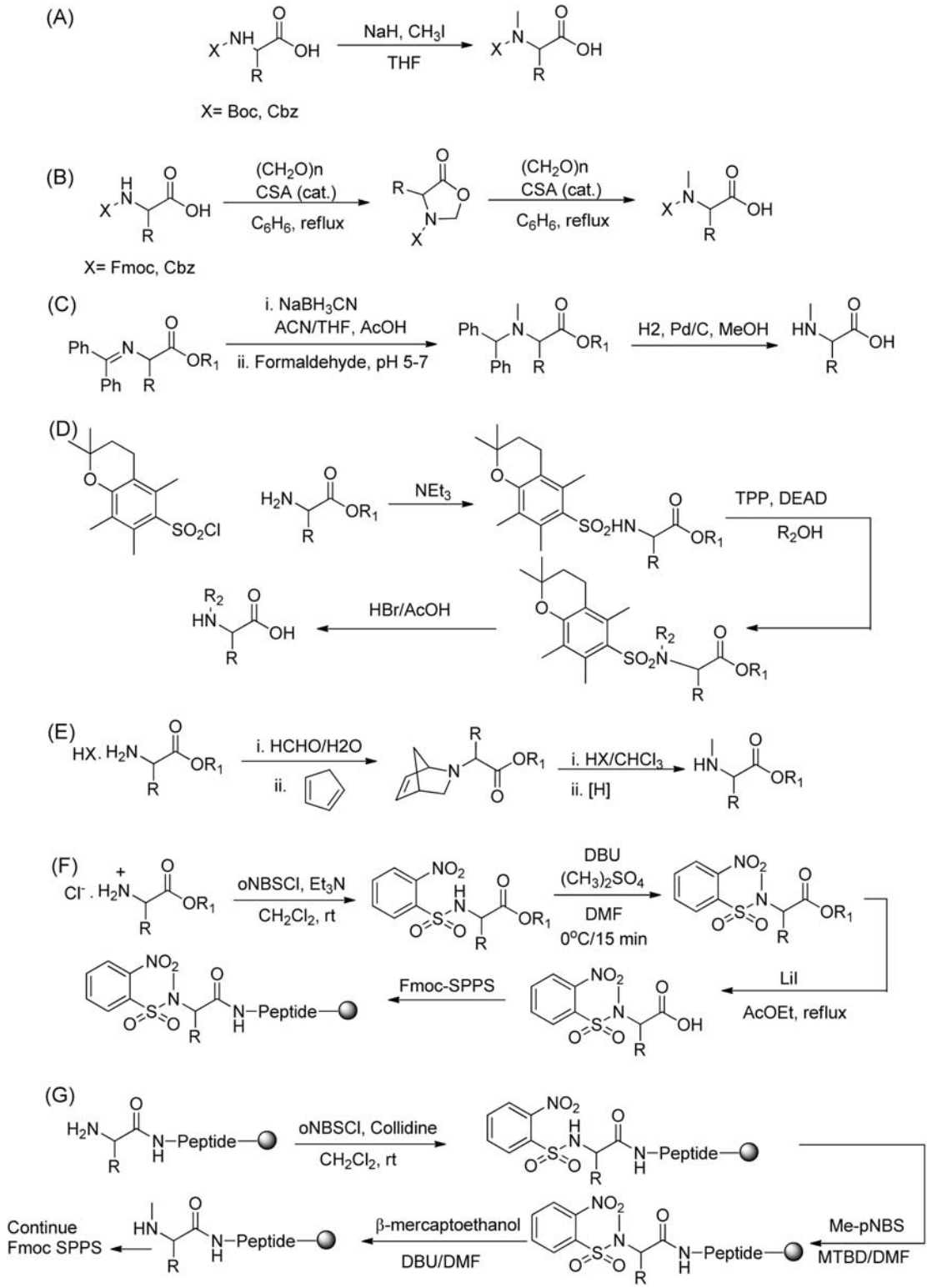

Fig. 7 N-Methylation reactions of amino acids and peptides.[106–108] (A) Direct N-methylation, (B) 5-oxazolidinone method, (C) reductive amination, (D) Mitsunobu reaction, (E) Diels–Alder and subsequent retro-Diels–Alder reactions, (F) oNBS protecting group strategy, (G) oNBS strategy on solid phase.

The second route for N-methylation involves site-specific N-methylation on a resin-bound peptide after the peptide is fully assembled in solid phase.[107] This method also involves an oNBS protecting group for site-specific methylation reactions. An activated amino group of a peptide bound on resin is methylated either via a nucleophilic substitution reaction with dimethyl sulfate and DBU[109] or via a Mitsunobu reaction.[110]

6.03.3.3 C^{α}-Tetrasubstitution

Noncoded and unnatural amino acids are frequently used in structure–activity studies of peptides to investigate and optimize their conformation and interaction with biological targets. In particular, α,α-disubstituted α-amino acids, also known as C^{α}-tetrasubstituted amino acids or quaternary amino acids, have gained tremendous attention lately.[111] While natural α-amino acids have only one side chain stemming from the α-carbon, α,α-disubstituted α-amino acids have two side chains attached to it (Fig. 8). Aminoisobutyric acid (Aib) is an example of a simple quaternary amino acid, and it is a strong helix inducer that forms 3_{10}-helices on oligomerization.

Quaternary amino acids are found in the structures of many drugs. For example, α-difluoromethylornithine,[112] eflornithine as common name, is on the WHO model list of essential medicines for the treatment of facial hirsutism and African trypanosomiasis (sleeping sickness). It is marketed by Sanofi-Aventis under the brand name Ornidyl. Similarly, methyldopa (L-α-methyl-3,4-dihydroxyphenylalanine) is an indirect-acting α-adrenergic antagonist psychoactive agent.[113] It is marketed under the brand names of Aldomet, Aldoril, and Dopamet by Aspen Pharmacare, Merck, and Novartis, respectively, for the treatment of hypertension and gestational hypertension. There are also naturally occurring peptaibol peptides that contain Aib. Alamethicin is a peptide antibiotic containing 8 Aib residues distributed throughout the sequence of 20 natural and unnatural amino acids.[114] Lantibiotics, a class of antibiotics often used as veterinary antibiotics and food preservatives, also possess Aib.[115]

Like D-amino acid substitution and N-methylation, one of the main advantages of quaternary amino acids is introduction of local conformational constraints that may induce more global structural changes. Incorporation of Aib or other related C^{α}-tetrasubstituted amino acids can create a folding nucleus for helix formation. The type of helix formed by Aib has been found to depend on the prevalence of Aib in the peptide sequence.[116] It was observed that 3_{10}-helices are favored when more than 40% of the sequence are Aib, while α-helices are preferred when the Aib content in the sequence is less than 40%. As unnatural amino acids, they offer proteolytic resistance and may increase selectivity and affinity to target proteins. For instance, mono- or di-Aib substitution of D-Ala^2 and/or Phe^3, critical N-terminal residues of amphibian skin opioid deltorpin C, exhibited high δ-opioid receptor affinity and up to ninefold greater selectivity than the parent peptide.[117] Substitution with Aib also resulted in inhibition of human islet amyloid polypeptide amyloid fibril formation.[118]

6.03.3.4 β-Amino Acids

While naturally occurring α-amino acids have both amino and carboxylic acid groups bonded to the same α-carbon center (C^{α}), β-amino acids have the amino group connected to the β-carbon (C^{β}). The major difference between β-peptides and their natural α-counterparts is the addition of a methylene group to the peptide backbone. There are two types of β-amino acids, β^2-amino acids and β^3-amino acids (Fig. 9A). A β-amino acid with its side chain attached to the α-carbon is called a β^2-amino acid. If the side chain is bonded to the β-carbon, it is called a β^3-amino acid. Peptides made up of β^2-amino acids are referred as β^2-peptides, and β^3-peptides consist of β^3-amino acids.

β-Peptides are similar to α-peptides in many ways. Both contain amide bonds capable of forming and stabilizing intra- and intermolecular hydrogen bonds.[119] β-Peptides adopt diverse secondary structures, such as helices, sheets, and turns, contradictory to earlier speculation that the additional carbon–carbon bond in the backbone may cause chaotic increase in their structures.[120] More diverse structures like 10/12-, 12-, and 14-helices are indeed observed.[121] This suggests that β-amino acids can offer structural diversity and exert unique and significant biological functions unsatisfied by α-amino acids alone.[122]

Among many β-amino acids occurring in natural products, β-alanine is the most prevalent. It is an essential amino acid component of pantothenic acid in coenzyme A and carnosine in muscle tissue. β-Amino acids are found in cyclic nonribosomal peptides and their polyketide hybrids that include microcystin-LR, iturin A, guineamide A, and dolastin D.[122] Some of the most common biologically active natural products that contain β-amino acids are the anticancer agent taxol, the infamously addictive drug cocaine, and the antibiotics, penicillin V and nocardicin A. While β-amino acid building blocks are commercially available for the synthesis of β-peptides, a number of synthetic methods have been developed, including Arndt–Eistert homologation of N-protected α-amino acids.[123]

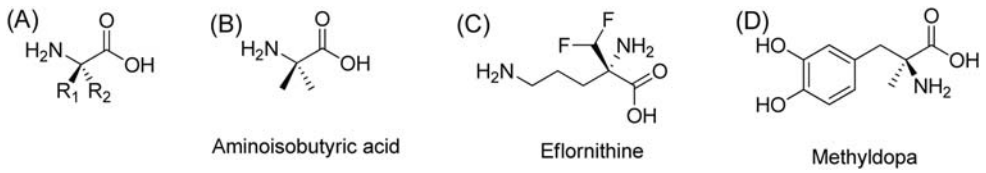

Fig. 8 Structures of (A) C^{α}-tetrasubstituted amino acid, (B) aminoisobutyric acid (Aib), (C) eflornithine, and (D) methyldopa.

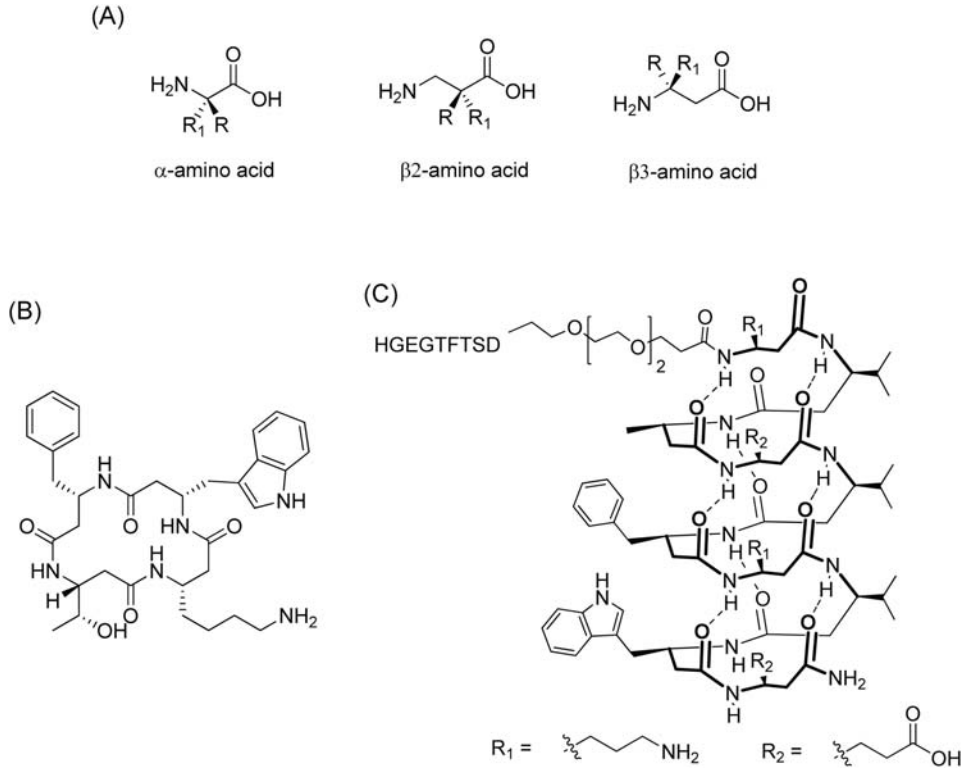

Fig. 9 Structures of (A) α-, β^2-, and β^3-amino acids, (B), β-peptide analog of octreotide, and (C) β^3-peptide analog of GLP-1.

Although biologically active peptides are dominated by α-peptides, β-peptides have been of interest since as early as the 1920s.[120] The major advantage of β-peptides over the α-form is that β-peptides are stable to proteolytic degradation in vitro and in vivo. This has encouraged the incorporation of β-amino acids to achieve increased resistance to enzymatic degradation, while maintaining the structure and function of natural peptides. Seebach and coworkers conducted one of the simplest yet most successful comparisons of their structural and enzymatic stability by using a β-hexapeptide [H-(β-HVal-β-HAla-β-HLeu)$_2$-OH] and its natural α-counterpart [H-(Val-Ala-Leu)$_2$-OH].[123] Surprisingly, β-peptide helices are more stable than those present in α-peptides. In addition, the β-peptide was resistant to cleavage by pepsin at pH 2 for at least 60 h, whereas the corresponding α-hexapeptide was degraded almost instantaneously.

Besides the structural and metabolic stability, β-peptides have been examined on their capability of interacting with proteins. For example, a β^3-decapeptide was designed based on the HIV gp41 C-terminal WWI epitope and it was found to inhibit gp41 six-helix bundle formation.[124] It was also demonstrated that short β-peptide 14-helices can inhibit an intramolecular PPI in vivo. β-Peptide analogs of the cyclic α-octapeptide octreotide have been investigated to improve the biological properties (**Fig. 9B**), and it is interesting that a β-peptide analog, although in a micromolar range, showed affinity to five human somatostatin receptors.[125] Likewise, a β^3-peptide analog of GLP-1 was developed by Schepartz and coworkers.[126] The analog is made of nine α-amino acids at the N-terminus of exendin-4 and a 14-helix β^3-peptide at the C-terminus, connected together with a short PEG chain (**Fig. 9C**). Despite a weak potency, this analog can interact with and activate the GLP-1 receptor. While the natural GLP-1 is highly susceptible to proteolytic degradation, the β^3-peptide analog showed significantly enhanced in vivo stability.

In addition to homogenous β-peptides, mixed α/β-peptides have also been investigated. A cyclic tetrapeptide c[Ser(OtBu)-β-Ala-Gly-β-Asp(OMe)] forms a 14-membered ring with alternating α- and β-amino acids, and it was found to make a tubelike assembly by virtue of stacks of intermolecular hydrogen bonds.[127] Similarly, Clark and coworkers developed a new class of self-assembling transmembrane ion channels in phospholipid bilayers based on cyclic β^3-peptides.[128] It is interesting that the conformation adopted by an α/β-peptide can be controlled by the pattern of β-amino acids in the backbone and other molecular parameters like the side-chain topology and solvent.[129] Alternating α- and β-amino acids in the sequence prevents the resulting α/β-peptides from being recognized by proteolytic enzymes, enhancing enzyme stability.[130]

6.03.4 Peptide Bond Replacements and Pseudopeptides

All the peptide modifications described earlier (e.g., peptide truncation; N-acetylation and pyroglutamylation; conjugation of PEG, oligosaccharide, and lipid; and substitution with D-, *N*-methyl, and β-amino acids) have one thing in common: the native amide

bond. The outcome of these modifications is still a peptide. On the other hand, a new class of molecules known as pseudopeptides, also referred to as amide bond surrogates, arises when the amide bond is replaced by other functional groups, altering the backbone structure of peptides (Fig. 10). The nomenclature used for such a replacement is known as a "psi bracket," indicating the type of chemical structure incorporated.[131] For example, an Ala-Gly pseudopeptide with a CH_2CH_2 backbone is denoted as Alaψ[CH_2CH_2]Gly. The advantage of pseudopeptides is complete resistance to proteolytic degradation of the amide bond. This advantage, however, comes with a heavy toll for conformation, flexibility, and hydrophobicity.

6.03.4.1 Reduced Bond (CH_2NH)

Reduced peptide bond ψ[CH_2NH] is one of the simplest peptide bond replacement strategies, and it offers free rotation around the C═N bond (ω angle).[132] This change helps to determine the significance of a carbonyl group or specific amide bond in peptides. It introduces a basic functional group (i.e., amino group) that can be protonated and increase the hydrophilicity.[131] It has been widely used in the design of metabolically stable analogs of natural peptides.[132] For example, an amide bond surrogate ψ[CH_2NH] between Tyr^1 and Gly^2 of Met-enkephalin improved the potency by twofold compared with the unmodified peptide, in combination with a methioninol replacing Met at the C-terminus.[133] On the other hand, replacement of the same amide bond with a hydrocarbon analog (CH_2CH_2) led to a significant decrease in activity compared with its reduced bonded analog. Similarly, replacement of the natural amide bond between Leu^{10} and Leu^{11} of an octapeptide analog (residues 6–13) of equine angiotensinogen with the reduced bond surrogate CH_2NH significantly increased binding affinity and resistance to the cleavage by renin.[134]

6.03.4.2 Methylene Thioether (CH_2S)

Methylene thioether ψ[CH_2S] replacement is another reduced bond surrogate. It increases the lipophilicity and may be advantageous for membrane permeability; however, it may lead to a loss of potency by virtue of its high flexibility.[131] For example, ψ[CH_2S] replacement between Gly^6 and Leu^7 in an LHRH agonist resulted in a loss of activity, while the same replacement between

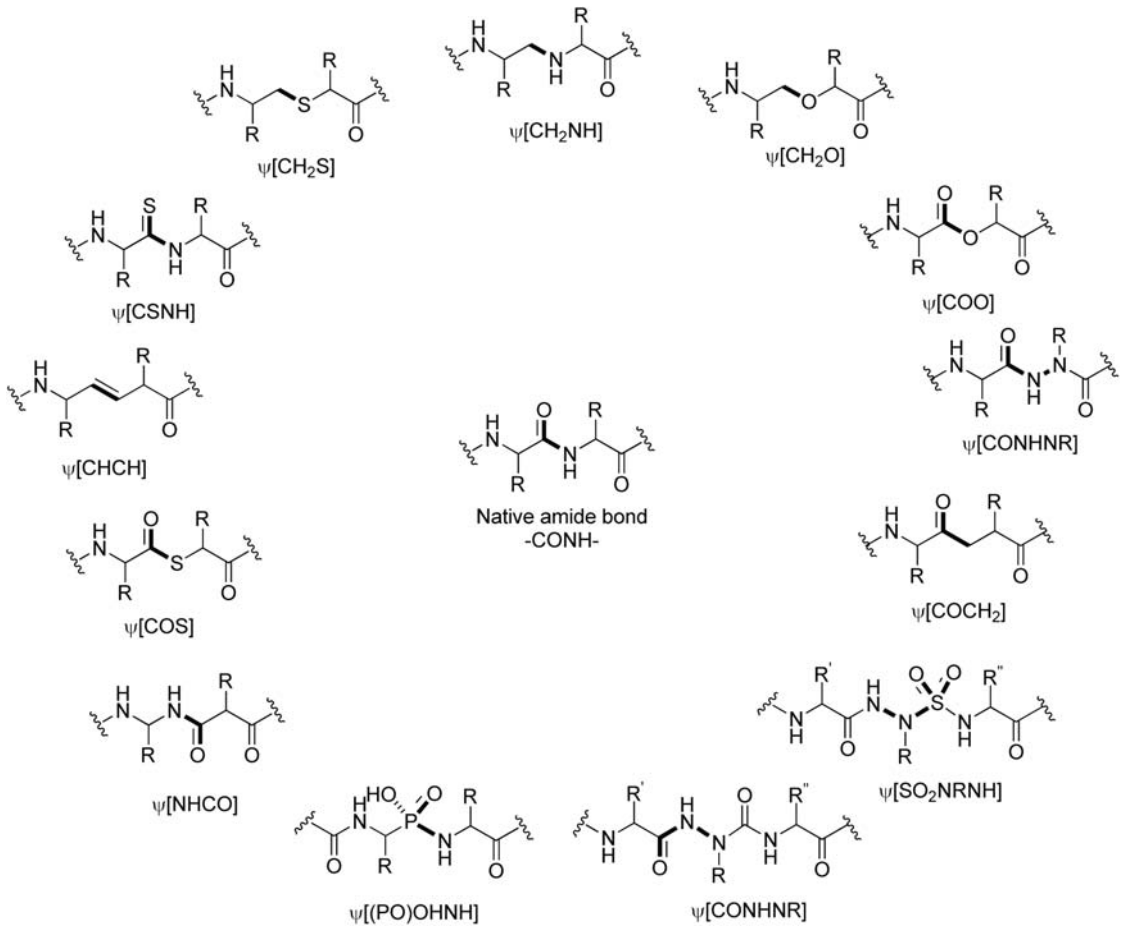

Fig. 10 Structures of amide bond surrogates.

Tyr^5-Gly^6 and Pro^9-Gly^{10} retained about 2% and 10% of the original activity, respectively.[135] In the case of antagonist analogs, the N- and C-terminal modification retained substantial LHRH and FSH inhibitory activity, while the modification at the amide bond between positions 6–7 was not tolerated.

6.03.4.3 Methylene Ether (CH_2O)

Methylene ether ψ[CH_2O] pseudopeptides are very similar to methylene thioester analogs with respect to their conformation and lipophilicity. This reduced backbone consists of an oxygen atom instead of the amino group that participates in the amide bond formation in natural peptide linkage.

6.03.4.4 Alkylidene (CH═CH)

Preservation of the stereochemistry imparted by the natural amide bond may be of importance when choosing a suitable surrogate. An alkylidene ψ[CH═CH] surrogate can be the best replacement for mimicking the planarity and rigidity of an amide bond.[131] In addition, the distance between the two α-carbons (C^{α}═C^{α}) is also found to be equal to that of natural dipeptides. An example of such a modification is the N-terminal amide bond replacement of Leu^5-enkephalin analogs by a *trans*-double bond.[136] The ψ[CH═CH] pseudopeptide replaced at Tyr^1-Gly^2 retained comparable activity with that of its parent peptide.

6.03.4.5 Endothiopeptide (CSNH)

A thioamide group is isosteric to the amide bond. Instead of a carbonyl, a thioamide has a thiocarbonyl group. Replacement with a thioamide bond ψ[CSNH] retains the bond length and angle within 0.01 Å and 0.5° compared with the natural amide bond.[137] Conversion of an amide carbonyl to a thiocarbonyl has become relatively easy with the development of a thionation reagent called Lawesson's reagent.[138] Endothiopeptides containing a thioamide in their backbones cannot form a strong hydrogen bond with it, and this may reveal critical information on the importance of a particular amide bond.[139]

6.03.4.6 Depsipeptide (CO_2)

In depsipeptides, one or more of the amide bonds are replaced with an ester bond ψ[CO_2]. There are a number of depsipeptides in nature, especially cyclic depsipeptides such as anticancer agent romidepsin, antibiotic agent etamycin, and anti-HIV agents papuamides A and B. Synthesis of depsipeptides is relatively easier compared with other pseudopeptides. Depsipeptides are synthesized with α-hydroxy acids as building blocks that can be prepared from α-amino acids.[140] Modification of the amide bond to an ester increases the lipophilicity that may subsequently increase cell permeability. Depsipeptides have been also used to determine the importance of hydrogen bonds that are formed by amide bonds in natural peptides.

6.03.4.7 Thioester (COS)

Thioester ψ[COS] modification on the peptide backbone is not widely used, because enzymes that hydrolyze the native amide bond can also cleave thioester bonds at an approximately equal rate of proteolytic degradation. Like depsipeptides, thioester backbones are relatively easy to be synthesized compared with other pseudopeptides, by condensation between an α-amino acid and an α-mercapto acid.

6.03.4.8 Ketomethylene ($COCH_2$)

A ketomethylene ψ[$COCH_2$] surrogate consists of a ketone functional group and a methylene moiety substituting for the amino group of an amide bond. It is highly resistant to degradation by proteases, but lacks the rigidity of the native amide bond. Since the ketomethylene group cannot serve as a hydrogen bond donor, its exchange of an amide bond may cause a substantial impact on the overall structure of peptides. Two ketomethylene analogs of substance P were synthesized by incorporating the ketomethylene surrogate ψ[$COCH_2$] between Phe^8 and Gly^9, and a hexameric pseudopeptide was found to be a full agonist and contracted isolated guinea pig ileum with 70% potency of the parent peptide.[141] It also acts as a potent inhibitor of substance P-degrading peptidase.

6.03.4.9 Phosphonamide (PO_2RN)

Enzyme inhibitors have been designed by replacing a scissile amide bond with an isostere that mimics the tetrahedral transition state of enzyme-catalyzed amide bond hydrolysis. The tetrahedral phosphorus atom in an α-aminophosphonamide or α-aminophosphonamidate ψ[PO_2RN] offers this geometry and leads to strong inhibition of proteases.[142] Cyclophilins are peptidylprolyl isomerases (PPIases) that catalyze the *cis–trans* interconversion of the aminoacyl-prolyl amide bond.[143] PPIases play a critical role in protein folding, replication of HIV-1 virions in host CD4 + T-cells, and other biological processes like cellular multiplication and communication.[144] As a cytosolic member of the human cyclophilin subfamily, hCyp-18 is also the main receptor of the

undecapeptide cyclosporine, implicated in immunosuppression.[145] Damage and coworkers made a phosphonamide analog containing a Glyψ(PO_2RN)Pro surrogate (R═H or alkyl group) as a selective transition-state analog inhibitor of cyclophilin, and this pseudopeptide was found to be a micromolar inhibitor of hCyp-18 (Fig. 11B).[147]

6.03.4.10 Azapeptide (CONHNR)

Bearing semicarbazides, azapeptides are created by substituting the α-carbon atom of an α-amino acid with a nitrogen atom. This connects the side chain of an α-amino acid to the achiral nitrogen center instead of the chiral α-carbon. Experimental and theoretical studies have demonstrated that aza-amino acids in peptides have characteristic structural preferences.[148] The dihedral angles (ϕ and ψ) of aza-amino acids favor 90° ± 30° and 0° ± 30° and 90° ± 30° and 180° ± 30°, which promote and stabilize β-turn and polyproline II structures, respectively, when placed at the $i+2$ position.[148]

As β-turn conformations are recognized by numerous proteins, such as the cluster of differentiation 36 (CD36) class B scavenger receptor, integrins, and the prostaglandin $F_{2\alpha}$ receptor (FP), azapeptides have been designed to target such proteins. Hexarelin is a β-turn adopting hexapeptide ligand to the CD36 receptor, and two azapeptides were developed to stabilize the β-turn structure (Fig. 12A).[149] They exhibited comparable affinities (2.4 and 1.3 μM) with that of hexarelin (2.3 μM). Cyclic RGD pentapeptides, such as peptide 1 and cilengitide (Fig. 12B), adopt a β-turn conformation and exhibit subnanomolar activity with high selectivity for the $\alpha_v\beta_3$ integrin receptor.[150] Aza-scanning is substitution of an aza-amino acid for each α-amino acid residue in the sequence of a peptide,[151] and aza-scanning of cyclic RGD pentapeptide antagonists discovered an aza-Gly-containing analog that retained nanomolar activity to the $\alpha_v\beta_3$ integrin receptor.[151]

The prostaglandin FP plays a crucial role in regulating uterine activity for human labor and parturition. In search of novel tocolytic agents, azapeptides have been developed and showed strong potency in lowering the strength and duration of both PGF2α-induced and spontaneous myometrium contractions.[152] Azapeptides were designed to mimic a potent ligand to FP, PDC113.824, and were found to adopt a β-turn structure (type I and II′)[152b] and showed significant tocolytic activity in delaying preterm labor in a mouse model (Fig. 12C).[152a]

6.03.4.11 Azasulfurylpeptide (AsF, CONHNRSO$_2$)

AsFs are peptidomimetics possessing an amino acid residue of which the α-carbon and the carbonyl have been replaced with a nitrogen atom and a sulfonyl group, respectively, to form an *N*-aminosulfamide group. The tetrahedral sulfur in the *N*-aminosulfamide moiety favors an ω-torsional angle of ±90° and ϕ-torsional angle of ±60° and ±100°, instead of *cis*- and *trans*-amide configurations at 0° and ±180°, respectively. Because of these preferred dihedral angles, AsFs are found to adopt a γ-turn conformation and show higher stability to enzyme degradation.[153] An AsF was designed with an azasulfurylphenylalanine moiety to mimic the tetrahedral transition-state geometry and was found to be a micromolar inhibitor of HIV-1 proteinase (Fig. 13). Human urotensin $II^{(4-11)}$ (*h*UII) is a vasoconstrictor peptide and has been suggested to adopt a γ-turn conformation that is stabilized by a disulfide bridge and intramolecular hydrogen bonds between Trp^7 and Tyr^9.[154] Cyclic AsFs of *h*UII were synthesized to investigate the role of backbone structure on their biological activity.[154]

6.03.4.12 Retro-Inverso (RI, NHCO)

RI peptides are linear peptides of which the amino acid sequence is reversed and the α-carbon chirality of the amino acid residues is inverted from L to D (Fig. 14). This isosteric modification maintains the side-chain topology identical to the parent peptide in an

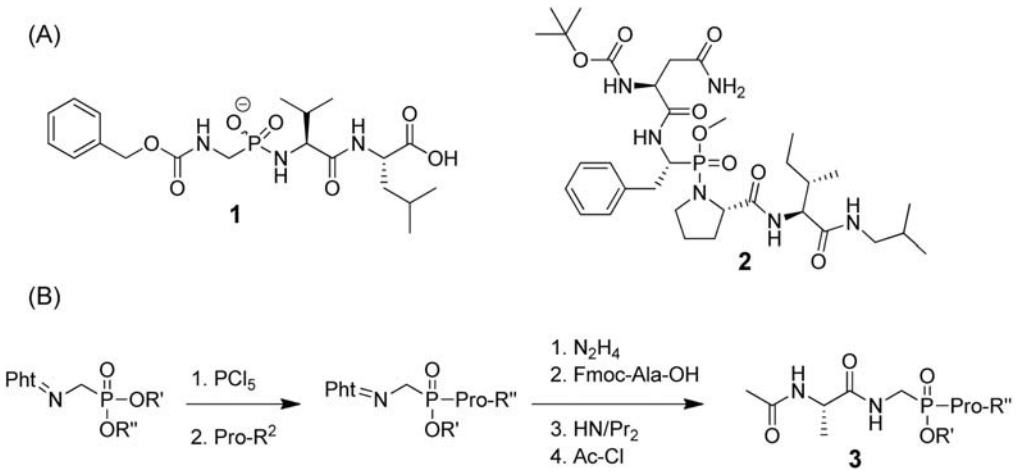

Fig. 11 (A) Structures of a phosphonamide inhibitor of thermolysin (1)[146] and a phosphonamidate inhibitor of HIV-1 proteinase (2)[142] and (B) synthesis of a phosphonamide inhibitor of hCyp-18 (3).[147]

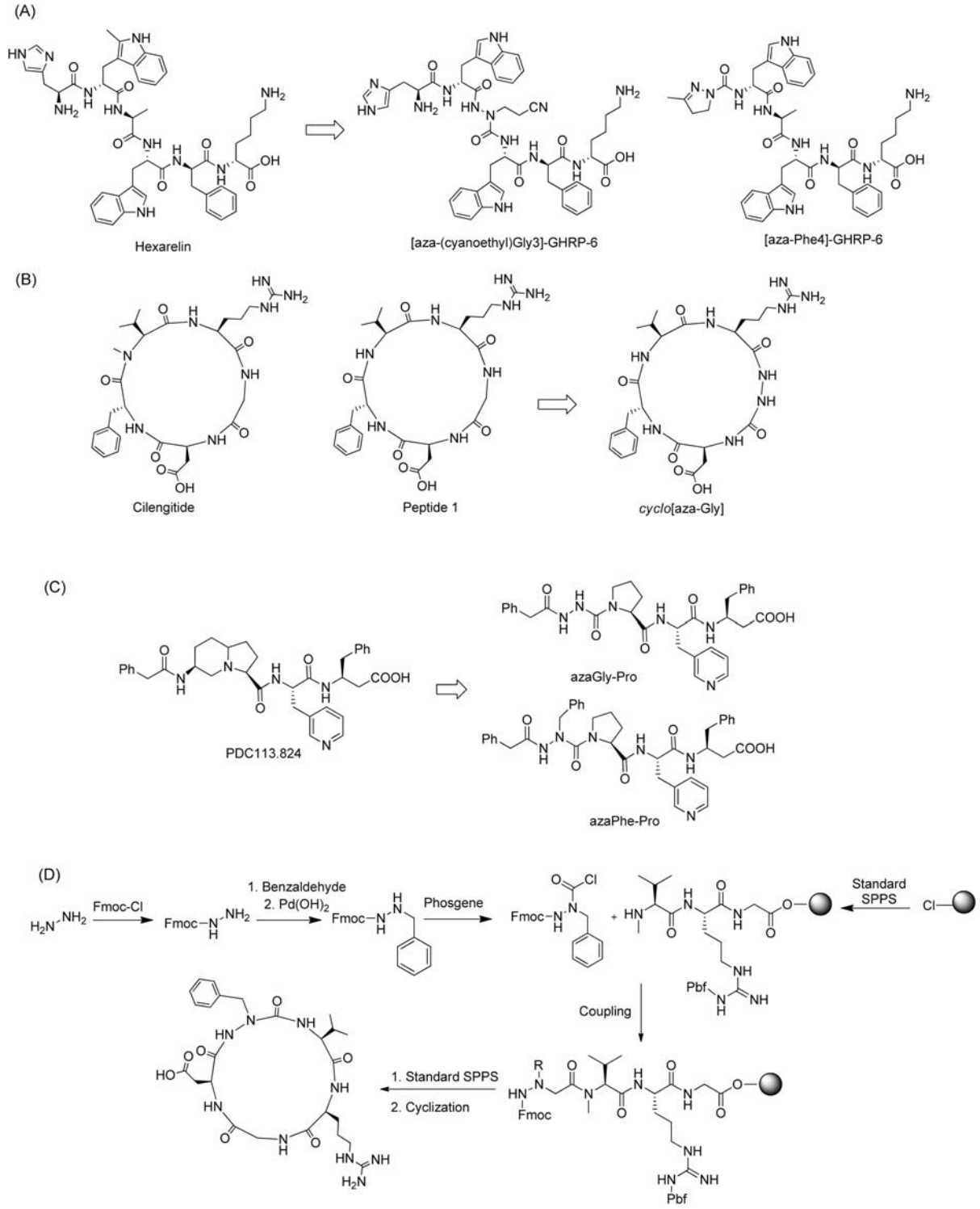

Fig. 12 Structures of azapeptides: (A) hexarelin, (B) cyclic RGD pentapeptides, and (C) PDC113.824 and (D) the synthesis of a cyclic RGD azapentapeptide.

extended conformation.[155] RI peptides are an attractive alternative to natural peptides as pharmaceuticals due to their high metabolic stability with retention of the majority of pharmacophores and potentially comparable biological activity. Thus, RI peptides have been widely employed for the study of PPIs through the design of peptidomimetics that emulate the shape of peptide epitopes and interfaces of PPIs.[156]

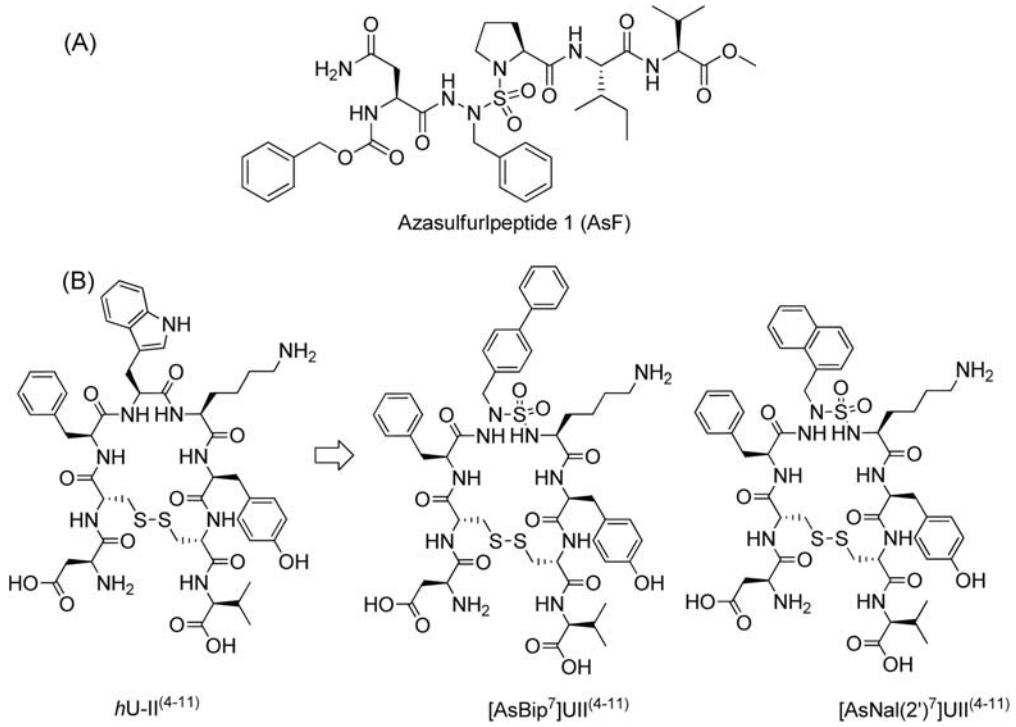

Fig. 13 Structures of azasulfurylpeptides targeting (A) HIV-1 proteinase and (B) human urotensin II receptor.

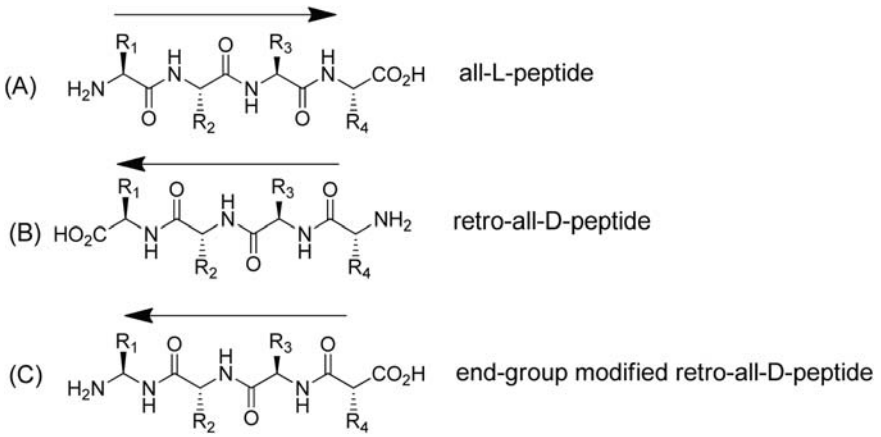

Fig. 14 Structures of retro-inverso peptides: (A) L-peptide, (B) retro-inverso peptide, (C) end group-modified retro-inverso peptide containing a gem-diaminoalkyl residue at R_1 and a malonyl residue at R_4.

Chorev[155] and coworkers synthesized partially modified RI analogs of enkephalin (Fig. 15A and B), in which two consecutive peptide bonds were reversed by introduction of gem-diamino and D-amino acids.[157] The formyl group at the C-terminus reproduces the electronic and steric characteristics of a carboxamide. The RI peptides 15A and 15B are three times as potent as their corresponding natural enkephalins 15C and 15D, respectively. Notably, the RI peptides 15A and 15B also displayed an activity profile similar to that of β-endorphin inducing catatonia in rats that lasted 3 h following intracisternal injection, indicating that the RI linkage can protect the peptides from enzymatic degradation.[157]

Schorderet and coworkers developed a cell-permeable and protease-resistant peptide inhibitor to selectively block the access of c-Jun NH_2-terminal kinase (JNK) to c-Jun.[158] The RI peptide D-JNKI-1, also known as XG-102, comprises a 10-amino acid-containing HIV transcriptional activator (Tat) (48–57) delivery sequence and a 20-residue long JNK-binding motif (JBD20) of JNK-interacting protein-1/islet-brain 1 with two Pro residues inserted as a spacer between the Tat and JBD20 peptides to allow maximal flexibility (Fig. 16). The use of all-D-retro-inverso form (D-JNKI-1) brought in remarkable stability against proteolytic degradation and extended its half-life in vivo. D-JNKI-1 showed inhibitory activity against JNK (IC_{50} ~20 μM), whereas 1 μM of D-JNKI-1 is

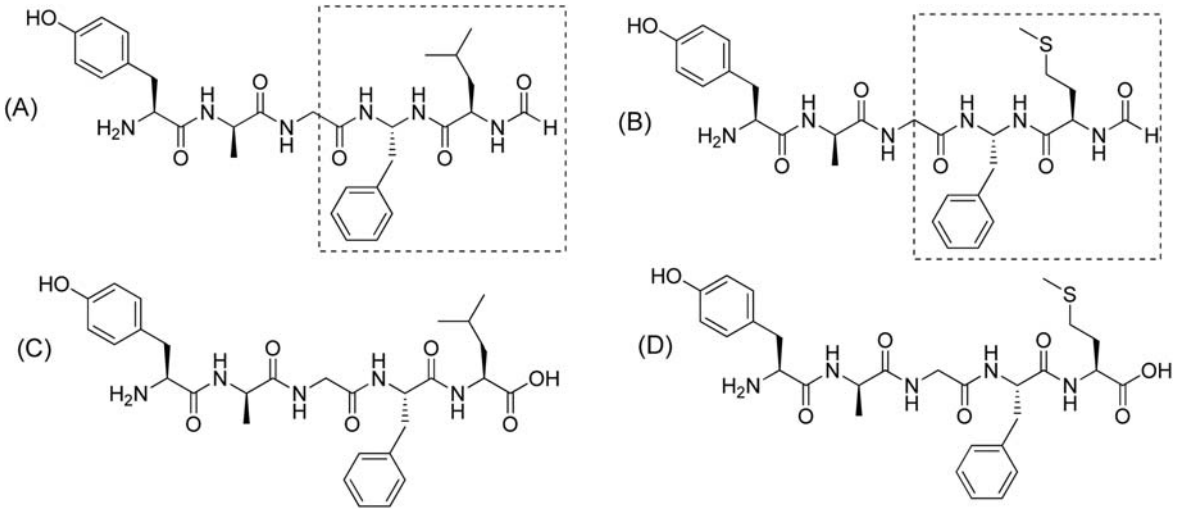

Fig. 15 Partially modified retro-inverso analogs of enkephalins (A and B) and corresponding natural enkephalins (C and D).

D-JNKI-1	tdqsrpvqpflnlttprkpr-pp-rrrqrrkkrG
HIV-1 Tat (48-57)	GRKKRRQRRR
JBD20	RPKRPTTLNLFPQVPRSQDT
^{L}CDX	FKESWREARGTRIERG
^{D}CDX	greirtgraerwsekf

Fig. 16 Sequences of D-JNKI-1 and ^{D}CDX. *Lowercase letters* denote D-amino acids.

sufficient for preventing pancreatic β cells from interleukin-1β-induced apoptosis by 50%.[158] D-JNKI-1 was examined for its neuroprotective effect in an ischemic stroke model in rodents.[159] D-JNKI-1 was expected to block neuronal apoptosis induced by excitotoxicity during cerebral ischemia. This cell-penetrating RI peptide showed powerful protection (>90%), even when D-JNKI-1 was administered 6–12 h after the onset of ischemia. This study indicates that neuronal death can be blocked even 6–12 h after the onset of stroke and established a proof of principle for the JNK pathway as a target for therapeutic intervention.[159]

To overcome enzymatic barriers in the blood–brain barrier (BBB) as well as in circulating blood, Lu and coworkers developed an RI peptide ligand to nicotine acetylcholine receptors (nAChRs)[160] based on a 16-amino acid-containing peptide ^{L}CDX that was derived from the loop II region of the snake neurotoxin candoxin (Fig. 16).[161] BBB mainly consists of brain endothelial cells connected by tight junctions and protects the brain from toxic molecules in the bloodstream while supplying essential nutrients to the brain. However, BBB becomes a hurdle to drugs and drug delivery systems for the treatment of CNS diseases.[162] nAChRs are highly expressed in brain capillary endothelial cells, and they have been known to promote BBB crossing to deliver various therapeutic agents to the brain.[161]

^{D}CDX, an RI analog of ^{L}CDX, showed fivefold higher binding affinity ($IC_{50}=84.5$ nM) as compared with the parent L-peptide ^{L}CDX ($IC_{50}=441.6$ nM). In addition, ^{D}CDX was found to be exceptionally stable in lysosomal homogenate and serum after 4 h incubation, while ^{L}CDX underwent fast degradation. ^{D}CDX demonstrated significantly higher transcytosis efficiency in an in vitro BBB monolayer as compared with ^{L}CDX. In vivo studies showed that ^{D}CDX mediates brain-targeted drug delivery of doxorubicin-loaded liposomes when conjugated to the surface of PEGylated liposomes and significantly prolongs the survival time of intracranial human glioblastoma multiforme-bearing nude mice.

6.03.5 Macrocyclic Peptides

Functions of proteins depend on properly formed three-dimensional structures that are organized by highly ordered folding of polypeptide backbones.[163] Small yet structurally defined regions are frequently responsible for biological activity of proteins; thus, they are of high interest for development of new therapeutic candidates. However, such short peptide segments, typically containing less

than 15 amino acid residues, have several limitations for therapeutic application. Short peptides often lose their well-defined structures or adopt less organized conformations in solution when taken out of proteins, which results in loss of binding affinity to their targets. In addition, short peptides are prone to proteolytic degradation, especially in an extended conformation,[164] and have difficulty in penetrating cellular membranes.[165] These drawbacks severely compromise the use of short peptides as therapeutics. Cyclization has been recognized as an efficient means to restrict peptide conformational flexibility and promote protein-like bioactive conformations.[166] Cyclic peptides often exhibit enhanced potency, proteolytic stability, membrane permeability, and bioavailability, all of which strongly improve drug-like properties.[131,167]

6.03.5.1 Tyrocidine A

Tyrocidine A is a cyclic decapeptide isolated from *Bacillus brevis*, showing bactericidal activity against a broad spectrum of Gram-positive organisms.[168] It forms an amphipathic β-sheet structure in which the hydrophobic face is oriented toward the membrane interior, while the hydrophilic surface is presented to the aqueous phase.[169] The cyclic peptide binds to bacterial membranes and disrupts structural integrity, resulting in bacterial cell death.[170] Walsh and coworkers employed a chemoenzymatic approach to achieve macrocyclization of tyrocidine A in which isolated thioesterase domains catalyzed the cyclization of linear peptides that were immobilized on a solid-phase support with a biomimetic linker (**Fig. 17**). They constructed a library of cyclic peptides containing natural and unnatural amino acids at the D-Phe^4 position. Two analogs, A02 and F10, displayed broad-spectrum activity against Gram-positive and Gram-negative microorganisms and reduced hemolytic effects related to the tyrocidine A.[171]

6.03.5.2 Cyclosporine A

Cyclosporine A is an immunosuppressant indicated for preventing organ rejection in transplantation surgery. It is a highly N-methylated, macrocyclic, 11-amino acid-containing peptide isolated from the fungus *Tolypocladium inflatum* (*Beauveria nivea*).[172] This macrocyclic peptide consists of seven N-methylated amino acids and four hydrogen-bonded amide protons, and it displays drug-like properties, such as cell membrane permeability, proteolytic stability, and oral bioavailability.[173] Wenger synthesized cyclosporine A by first coupling two short peptides (tetra- and heptapeptides shown in **Fig. 18A**), which contained the unusual amino acid (2S,3R,4R,6E)-3-hydroxy-4-methyl-2-methylamino-6-octenoic acid, followed by cyclizing the linear undecapeptide with (benzotriazol-1-yloxy)tris(dimethylamino)phosphonium hexafluorophosphate (BOP).[174]

Danishefsky and coworkers utilized an isonitrile coupling reaction to synthesize cyclosporine A (**Fig. 18B**). In the isonitrile-mediated amide bond formation, a thioacid was treated with an isonitrile to provide a putative formimidate (thio)carboxylate mixed anhydride that was intercepted by an amine, generating a dipeptide. The isonitrile coupling method was used to elongate the peptide and cyclize the linear undecapeptide.[175]

6.03.5.3 Colistin A

Colistin (polymyxin E) is a polymyxin antibiotic produced by the soil bacterium *Bacillus polymyxa*.[176] It was approved in the late 1950s for the treatment of acute and chronic infections caused by certain sensitive strains of Gram-negative bacteria. After

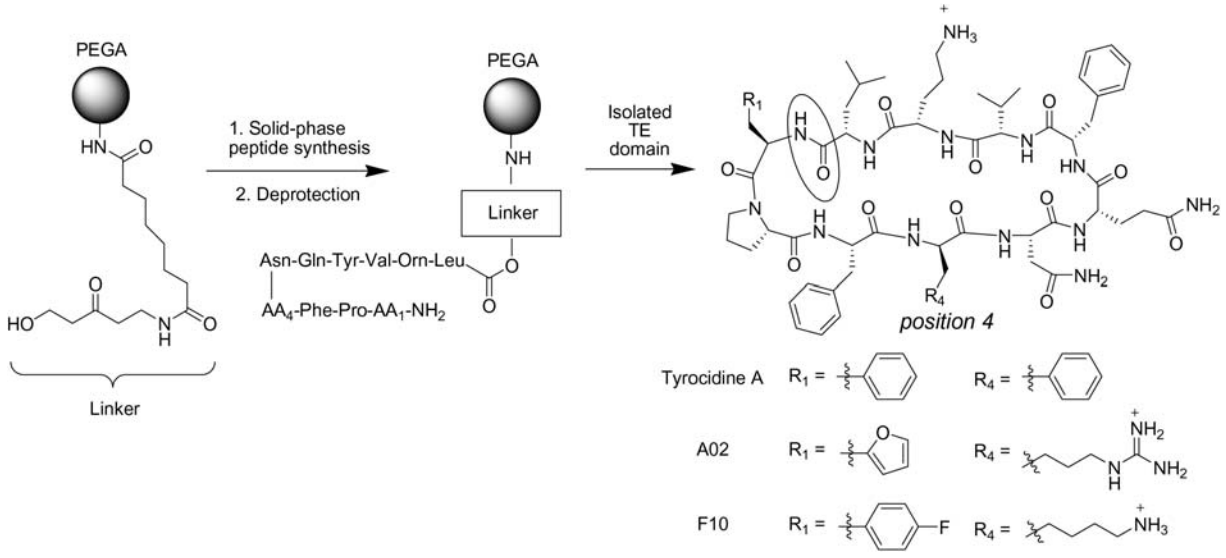

Fig. 17 Biomimetic macrocycle synthesis of tyrocidine A and its analogs.

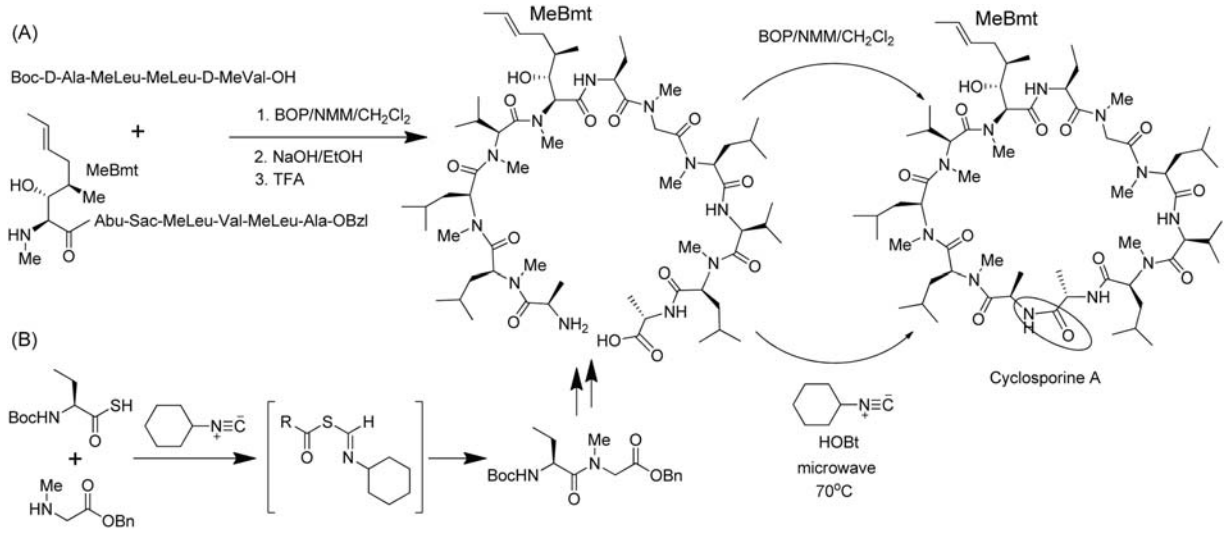

Fig. 18 Synthesis of cyclosporine A.

introduction in clinical practice, the use of colistin gradually declined because of its nephrotoxicity. However, with antibacterial resistance on the rise, colistin was recently reintroduced to treat severe, multidrug-resistant Gram-negative bacterial infections.[177]

Colistin is a mixture of cyclic polypeptides colistin A and B that are acylated by (*S*)-6-methyloctanoic acid and (*S*)-6-methylheptanoic acid, respectively. The hydrophobic (N-terminal fatty acyl chain and a D-Leu-Leu) and hydrophilic (three or four cationic amino acids) regions of colistins create amphiphilic surfaces that enable detergent-like interactions with bacterial membranes and bactericidal action. Colistin interacts with the lipid A of lipopolysaccharides (LPSs) on the outer membrane of Gram-negative bacteria and displaces the calcium and magnesium bridges that stabilize the LPS. Subsequently, colistin permeabilizes the bacterial outer membrane and disrupts the integrity of the inner membrane, ultimately causing cell death.[178] Kline and coworkers reported a synthetic procedure using Fmoc/tBu SPPS protocols and Alloc protection for Dab[4] (Fig. 19). The partially protected peptide, prepared on 2-chlorotrityl resin, underwent a cyclization reaction, followed by full deprotection to afford colistin.[179]

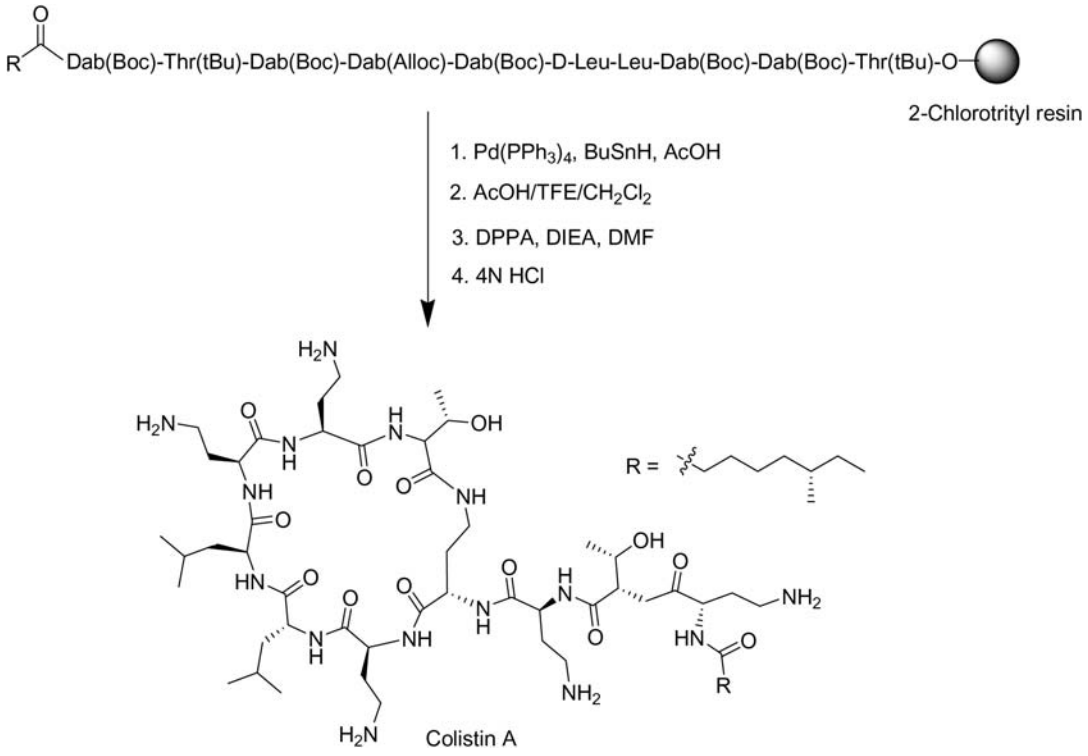

Fig. 19 Solid-phase synthesis of colistin A.

6.03.5.4 PMX53 (3D53)

Complement fragment (C)5a is a 74-amino acid-containing pro-inflammatory polypeptide produced during activation of the complement cascade of serum proteins in response to stimuli, such as infectious organisms (e.g., bacteria, viruses, and parasites) and tissue damaged by physical, chemical, or neoplastic insults.[180] C5a regulates many types of cells, including human immune cells, by binding to a specific receptor on the cell surface, triggering cellular immune responses, and releasing numerous inflammatory mediators.[181] However, overexpression or underregulation of C5a is implicated in several diseases like rheumatoid arthritis, adult respiratory distress syndrome, ischemia/reperfusion injury, and sepsis.[182]

In an effort to combat the effects of C5a in disease development, Fairlie and coworkers developed a C5a antagonist by mimicking the C-terminus of C5a responsible for binding to and activating the C5a receptor. Based on the structure of a truncated hexapeptide,[183] PMX53 was derived to stabilize a putative turn structure. PMX53 features a pentapeptide macrocycle formed by a lactam linkage between Orn^2 and Arg^6.[184] It showed potent full antagonism ($IC_{50} = 20$ nM) and oral activity at 0.3–10 mg kg^{-1} doses in rodent models of inflammatory and other diseases and is currently under clinical trials.[182]

PMX53 was prepared by cyclizing the linear peptide in solution that was synthesized on PAM resin using Boc chemistry (Fig. 20A).[184] In a convergent approach, two tripeptide fragments, Ac-Phe-Orn-(Boc)-Pro-OH and H-D-Cha-Trp(For)-Arg-OEt, were coupled to form a linear hexapeptide that, after deprotection, was cyclized in solution with BOP, affording PMX53 (Fig. 20B).[185]

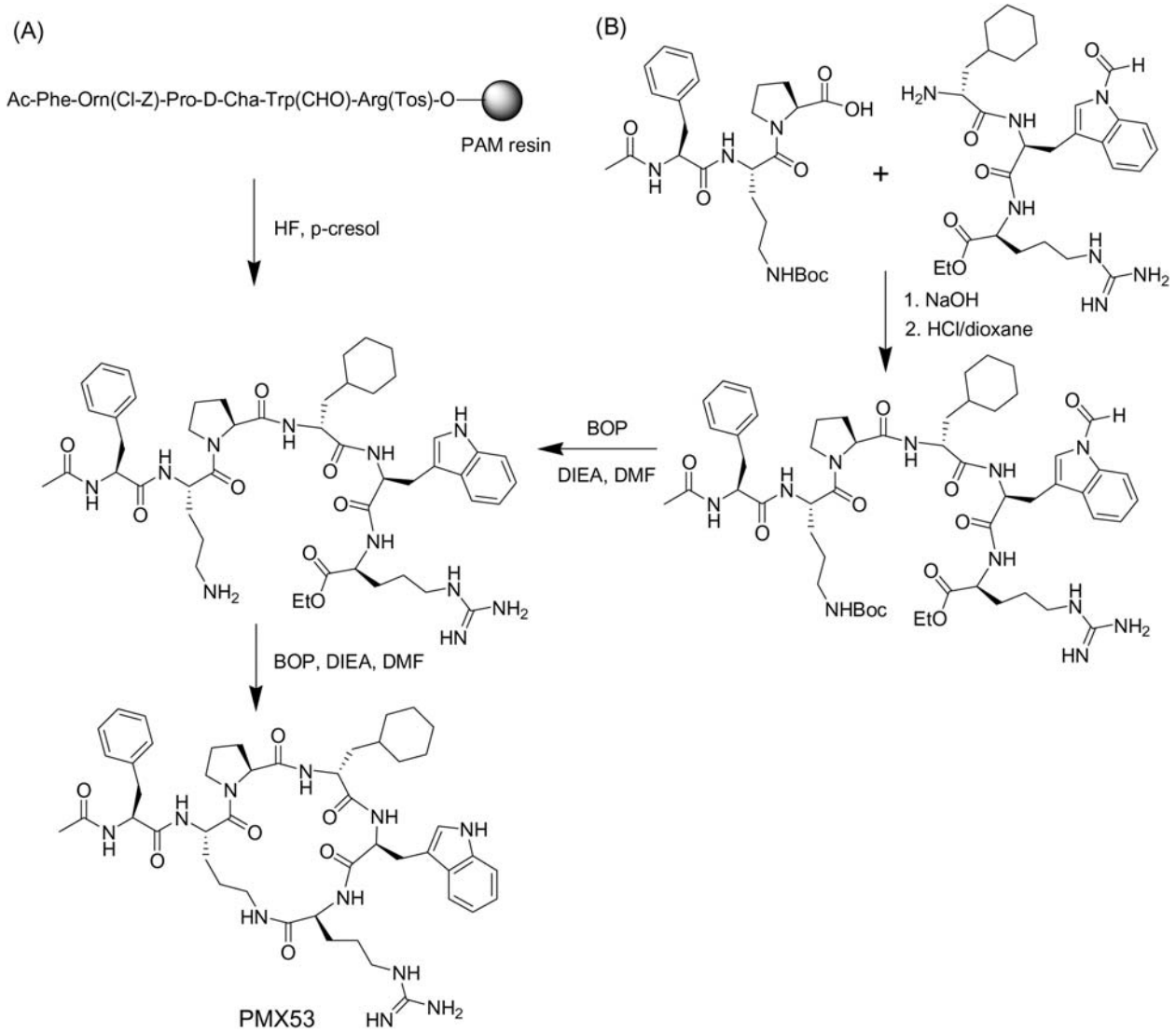

Fig. 20 Synthesis of PMX53. (A) Solid-phase synthesis of a linear peptide intermediate and subsequent solution-phase cyclization. (B) A convergent approach to prepare the linear peptide precursor.

6.03.5.5 Octreotide (Sandostatin)

Somatostatin (Fig. 21), a cyclic tetradecapeptide, has been isolated from ovine hypothalamus. It inhibits the release of numerous peptide hormones including glucagon, insulin, secretin, and growth hormone. Somatostatin has been employed in the treatment of acute gastrointestinal disorders, but its therapeutic use is limited by the short in vivo half-life of 1–2 min.[186]

Octreotide, a synthetic octapeptide analog of somatostatin, was developed to mimic the pharmacology of somatostatin (Fig. 21). The pharmacophore of somatostatin, Phe^7-Trp^8-Lys^9-Thr^{10}, was conformationally restricted by a disulfide linkage between two Cys residues, and D-Phe and D-Trp at positions 1 and 4, respectively, were introduced to improve druggability by enhancing proteolytic stability and potency. Together with the disulfide cross-link, D-Trp^4 was found to stabilize a β-turn structure (type II′) in the pharmacophore.[187] The carboxylic acid at the C-terminus was reduced to an alcohol to further increase stability against enzymatic degradation. Octreotide was found to be more potent than the native hormone in inhibiting the secretion of growth hormone both in vitro and in vivo.[188] It is successfully used in the treatment of neuroendocrine disorders, such as acromegaly and gastroenteropancreatic neuroendocrine tumors.[189] It was prepared in solution on the semi-industrial scale by using the 4 + 2 + 2 strategy, followed by deprotection and oxidative cyclization (Fig. 22).[190]

6.03.5.6 Conopeptides

Conopeptides are a group of neurotoxic peptides expressed in the venom duct of cone snails (Conoidea, *Conus*). These are highly structured peptides of which sequences comprise 10–30 amino acids with one or more disulfide bonds. Conotoxins have been the subject of pharmacological interest because of their high potency and selectivity for a broad range of cellular targets.[191] For example,

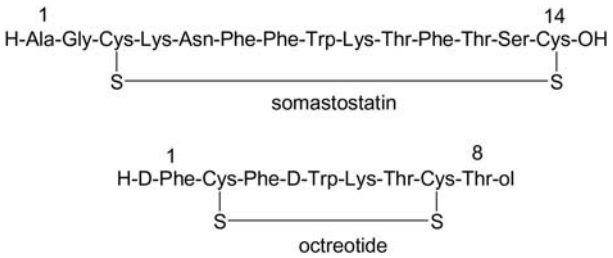

Fig. 21 Structures of somatostatin and octreotide.

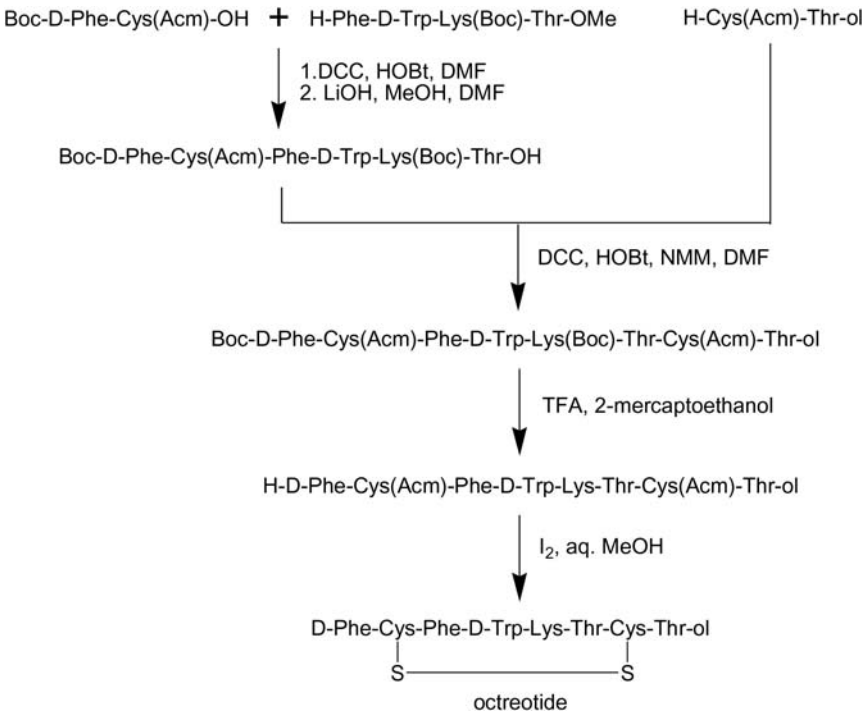

Fig. 22 Synthesis of octreotide.

conopeptide MVIIA, marketed as ziconotide by Prialt, is a synthetic equivalent of a conopeptide form *Conus magus*, and it selectively blocks Cav2.2 N-type voltage-gated calcium channels[192] It is approved by the FDA for treating severe chronic pain.

Conopeptides can be synthesized by following standard SPPS protocols; however, forming the correct disulfide linkages is a challenging task. Several methods have been developed for regioselective formation of multiple disulfide bonds after the construction of a linear peptide on solid support, and these methods include oxidation (S–S formation), reduction (S–S breakage), and isomerization (S–S rearrangement) reactions.[193] A common regioselective in-solution disulfide bond formation utilizes a variety of thiol-protecting groups, such as triphenylmethyl (S-Trt), acetamidomethyl (S-Acm), *t*-butyl (S-tBu), and *p*-methylbenzyl (S-Meb) groups. Typically, a peptide is cleaved from solid support with all S-protecting groups intact except for S-Trt (**Fig. 23**). The first disulfide bond is formed by air oxidation between the free Cys residues.[194] The second disulfide bond is generally formed by treatment with iodine. The S-Meb protecting group appears to be more stable than the S-tBu group at room temperature under trifluoroacetic acid,[195] which allows selective formation of the third disulfide bridge. The fourth disulfide bond is finally formed by increasing the reaction temperature from 25°C to 65°C.

6.03.5.7 Linaclotide

Linaclotide was approved by the FDA for the treatment of chronic idiopathic constipation and irritable bowel syndrome with constipation in adults.[196] It is a synthetic peptide analog of diarrheagenic bacterial enterotoxins and endogenous hormones guanylin

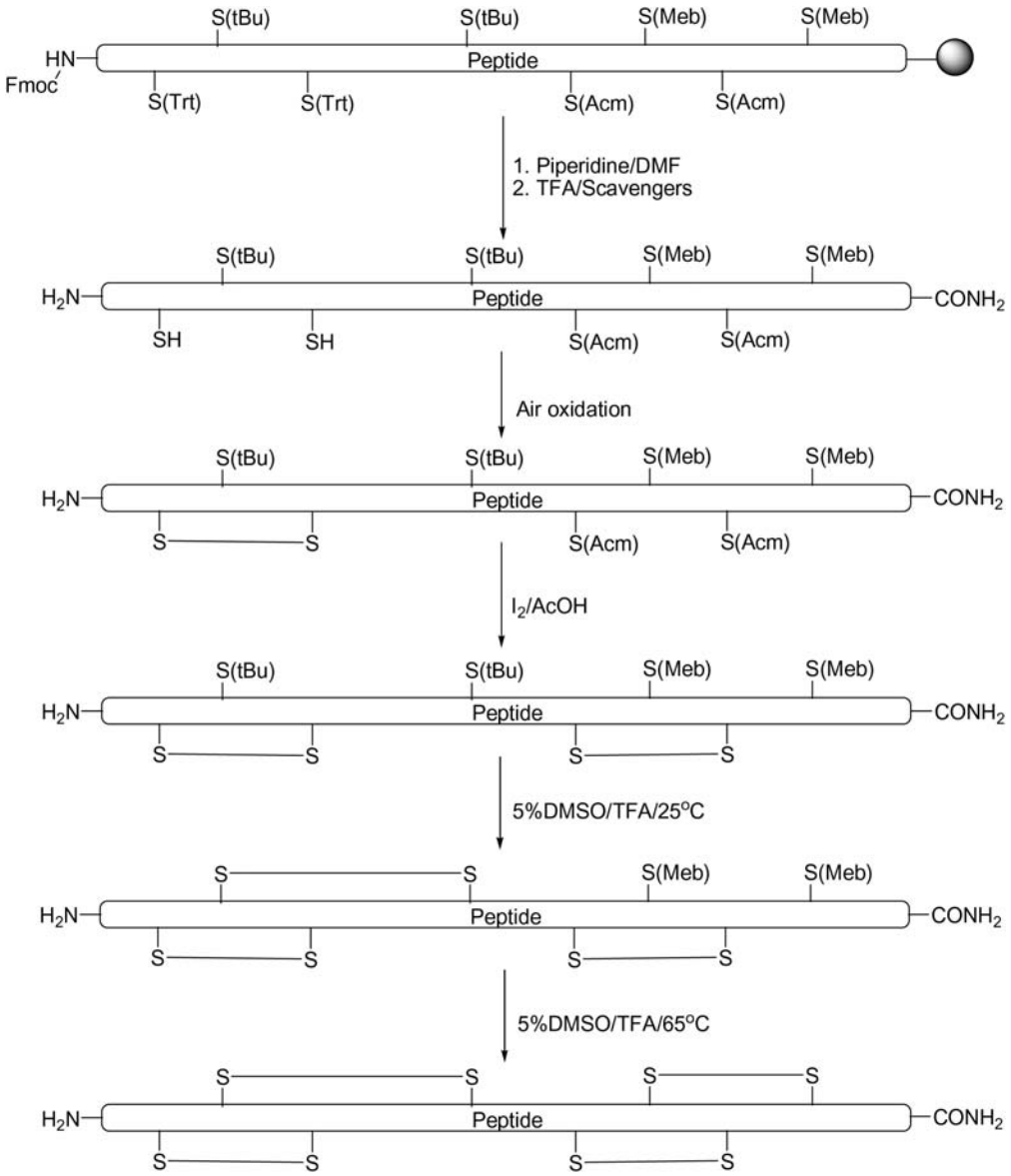

Fig. 23 Synthesis of conopeptides with multiple disulfide bridges.

and uroguanylin, which act as a potent guanylate cyclase C (GCC) receptor agonist. On intestinal epithelial surfaces, linaclotide binds to and activates the GCC receptor, which subsequently stimulates the production of cyclic guanosine monophosphate. This in turn increases intestinal motility and fluid secretion and ultimately reduces abdominal pain.[197] Linaclotide is an orally available 14-residue long peptide that features three intramolecular disulfide bonds between C1–C6, C2–C10, and C5–C13. These structures improve resistance to proteolytic degradation in the gastrointestinal tract.[198]

Albericio and coworkers synthesized linaclotide by using a random disulfide bond formation strategy.[199] A linear peptide containing six Cys residues was prepared in solid phase and cyclized in solution. A disulfide bond analysis by using a modified method developed by Wu and Watson[200] confirmed that the correct pairing of Cys residues was achieved, indicating that the linear peptide can fold naturally to the right conformation (Fig. 24).

6.03.5.8 Cyclic Melanocortin Analogs

Melanocortin receptors are seven transmembrane-spanning G protein-coupled receptors that increase the intracellular cAMP level upon ligand binding, and five receptor subtypes (MC1R–MC5R) have been identified to date.[193,201] The endogenous melanocortin peptides are α-, β-, and γ-melanocyte-stimulating hormones and adrenocorticotropic hormone and have a conserved tetrapeptide sequence (His-Phe-Arg-Trp) that is found to be essential for receptor interaction.[202] Extensive structure–activity relationship studies have been carried out for the tetrapeptide pharmacophore and flanking regions of α-MSH. Phe^7, after examination by gas chromatography, was identified as a predominantly racemized residue, and this discovery led to the design of a highly potent and prolonged acting α-MSH analog, NDP-MSH, with D-Phe at position 7 (Table 8).[203]

Both α-MSH and NDP-MSH adopt a folded conformation that places the aromatic residues [i.e., His^6, Phe^7 (or D-Phe^7), and Trp^9] on the same side in a β-turn structure. This places the hydrophilic residues (Glu^5, Arg^8, and Lys^{11}) on the opposite face and brings Glu^5 and Lys^{11} in close proximity. To stabilize the turn conformation around the pharmacophore, a lactam bridge between Asp^5 and Lys^{11} was created, resulting in a small cyclic analog, melanotan II (MTII in Table 8).[204] Interestingly, substitution

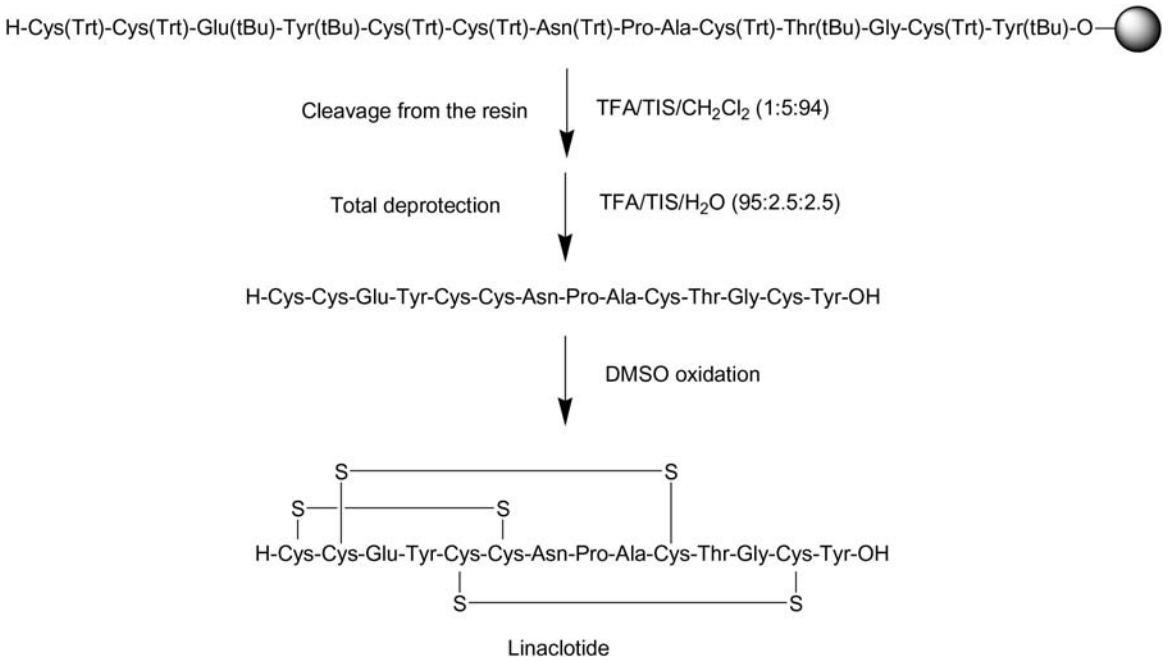

Fig. 24 Synthesis of linaclotide.

Table 8 Sequences of melanocortin peptides

Ligand	*Sequence*
α-MSH	Ac-Ser-Tyr-Ser-**Met**-Glu-His-**Phe**-Arg-Trp-Gly-Lys-Pro-Val-NH_2
NDP-MSH	Ac-Ser-Tyr-Ser-**Nle**-Glu-His-**DPhe**-Arg-Trp-Gly-Lys-Pro-Val-NH_2
MTII	Ac-**Nle**-*c*[Asp-His-**DPhe**-Arg-Trp-Gly-Lys]-NH_2
SHU9119	Ac-**Nle**-*c*[Asp-His-**DNal(2′)**-Arg-Trp-Gly-Lys]-NH_2

of D-Phe at position 7 with a bulky aromatic amino acid like D-Nal(2′) converted the potent agonist into a strong antagonist SHU9119 to MC3R and MC4R.[205]

6.03.5.9 Cyclic Opioid Peptides

Endogenous opioid pentapeptides (i.e., [Met^5]- and [Leu^5]-enkephalin) bind to several subtypes of opioid receptors, such as μ-, δ-, and k-opioid receptors.[206] To achieve selectivity to a receptor subtype, conformationally constrained analogs were synthesized utilizing a disulfide linkage between D-Cys^2 and D/L-Cys^5.[207] A cyclized peptide, c[D-Cys^2,D-Cys^5]enkephalin, was found to be twice as potent as c[D-Cys^2,L-Cys^5]enkephalin and 73 times as potent as [Met^5]enkephalin. The cyclic peptide c[D-Cys^2,D-Cys^5]enkephalin showed a moderate preference for the μ-opioid receptor over the δ-subtype and was found to be more resistant to enzymatic degradation than [Met^5]enkephalin.[207]

Mosberg and coworkers continued the search for selective enkephalin analogs and introduced a germinal disubstituted penicillamine (Pen) at position 2 along with the disulfide bridge between residues 2 and 5.[208] The resulting peptides, c[D-Pen^2,L-Cys^5]- and c[D-Pen^2,D-Cys^5]-enkephalinamide, showed a high δ-opioid receptor specificity. In addition, a carboxylate at the C-terminus was found to increase the selectivity to the δ-subtype.[209] A more constrained analog was further designed by the introduction of two Pen residues at positions 2 and 5, and the resulting peptide c[D-Pen^2,D-Pen^5]-enkephalin (DPDPE) showed an order of magnitude improvement for selectivity to the δ-opioid receptor (**Fig. 25**).[210] Conformational analysis by nuclear magnetic resonance (NMR) and molecular modeling suggested a type IV β-turn and transannular interactions of the aromatic side chains of Tyr^1 and Phe^4 with the β,β-dimethyl groups of D-Pen^2.[211]

6.03.6 Stabilization of Secondary Structures

Peptides can be folded to a variety of conformations, and several key structures have been commonly observed, such as α-helix, β-sheet, and reverse turns. These secondary structures are important for the topography of peptides and proteins, playing a role in target recognition. However, due to the entropy effect, short peptides have difficulty in retaining such organized conformations by themselves, resulting in a loss of biological activity. Thus, stabilization of protein secondary structures has been practiced to improve peptide leads.

6.03.6.1 Stabilized β-Turns

β-Turns are one of the most common structural motifs in proteins and change the direction of the peptide backbone by nearly 180°, allowing the peptide chain to fold back onto itself.[212] A β-turn is defined by four consecutive amino acids and has a characteristic of the distance between two α-carbons of residues i and $i+3$ being less than 7.0 Å (**Fig. 26**). β-Turn structures can be further classified to various types according to the backbone torsional angles (ϕ_{i+1}, ψ_{i+1}, ϕ_{i+2}, and ψ_{i+2}) in residues $i+1$ and $i+2$. Type I and II β-turns are the most common, and they are stabilized by a backbone hydrogen bond between the CO of residue i and the NH of residue $i+3$.[212c,213] Type I and II β-turns are different mainly in the orientation of the amide bond between the residues $i+1$ and $i+2$ on the plane of the β-turn. Type I′ and II′ β-turns are mirror images of the backbone conformations of type I and type II, respectively.

Statistical analysis revealed that Pro and Gly residues are favored in β-turns presumably due to the cyclic structure of Pro and the flexibility of Gly.[214] Hydrophilic amino acids, such as Asn and Asp, also have a high propensity for a β-turn formation mainly owing to their placement on solvent-exposed surfaces of globular proteins. In addition to their role in protein folding,[215] β-turns can also serve as recognition motifs of PPIs.[216]

One method for stabilizing a β-turn structure is to create a disulfide bridge between side chains. By employing this strategy, Hruby and coworkers designed conformationally restricted μ-opioid receptor antagonists based on a somatostatin template.[217] Although somatostatin binds weakly to opioid receptors, its analog octreotide was found to bind to the μ-opioid receptor with

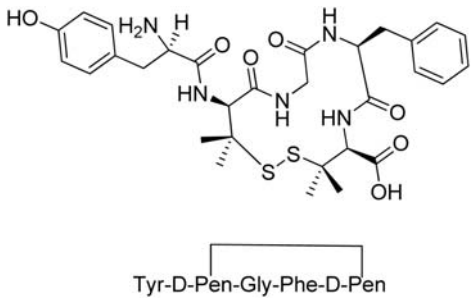

Fig. 25 Structure of c[D-Pen^2,D-Pen^5]-enkephalin (DPDPE).

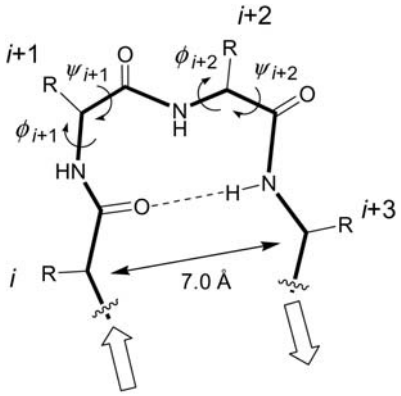

	ϕ_{i+1}	ψ_{i+1}	ϕ_{i+2}	ψ_{i+2}
type I	-60	-30	-90	0
type I'	-60	120	80	0
type II	60	30	90	0
type II'	60	-120	-80	0

Fig. 26 The structure and classification of β-turns.

an IC_{50} value of 38 nM.[218] This observation led them to convert somatostatin to an opioid ligand.[217] To develop a selective μ-opioid receptor antagonist with little or no somatostatin-like biological activity, they used the tetrapeptide somatostatin sequence (Phe-D-Trp-Lys-Thr) as a β-turn adopting template. A series of conformationally restricted somatostatin analogs were synthesized with disulfide bridges, and a leading compound CTP exhibited a high affinity to the μ-opioid receptor (IC_{50} = 3.7 nM), 7000 times more potent than somatostatin (**Table 9** and **Fig. 27**). CTP showed approximately 200-fold increased selectivity to the μ-opioid receptor over the δ-subtype. Conformational analysis by NMR showed that CTP possesses a well-defined type II′ β-turn at the core tetrapeptide motif with a hydrogen bond between Tyr^3 and Thr^6.[220]

To lower affinity to the somatostatin receptor, Lys^5 of CTP was replaced with Orn, and the resulting peptide CTOP showed significantly improved specificity to the μ-opioid receptor over the somatostatin receptor (**Table 9** and **Fig. 27**).[221] In addition to the cyclization via the disulfide bridge, D-Phe^1 was substituted with D-Tic to offer a topographical constraint in a χ conformational space on the side chain of residue 1, and the resulting peptide TCTOP showed further enhanced receptor selectivity.[222]

Another approach to induce and stabilize a β-turn structure is the dipeptide D-Pro-L-Pro that was found to adopt a stable type II′ β-turn[223] and facilitate the nucleation of β-hairpins.[224] A β-hairpin structure is composed of two consecutive hydrogen-bonded antiparallel β-strands connected by a loop region that typically comprises 1–5 amino acid residues.[225] β-Turns are the most abundant structures in the loop segment with a preference of types I′ and II′.[226] β-Hairpins are a key motif in antiparallel β-sheets,[227] and they are widely found in a variety of proteins including IgG antibodies,[228] cytokine receptors,[229] growth factors,[230] integrins,[231] and viral proteins.[232] In addition, naturally occurring bioactive cyclic antimicrobial peptides (e.g., protegrins, polyphemusins, and tachyplesin), gramicidin S, and tyrocidine are known to adopt β-hairpin structures.[233]

The β-hairpin-stabilizing template D-Pro-L-Pro was designed to stabilize β-hairpin structures of the L3 loop region of the anti-hemagglutinin antibody HC19. The loop mimetic 1 was created by transplanting the loop from the immunoglobulin framework onto a D-Pro-L-Pro template (**Fig. 28**). NMR studies showed that the mimetic adopts a β-hairpin conformation and aromatic stacking between the side chains of Trp residues located on opposite sides of the hairpin, which are essentially identical to those in the antibody crystal structure.[234]

Robinson and coworkers utilized the D-Pro-L-Pro template to design inhibitors of the Tat protein–transactivation response element (TAR) interaction in bovine immunodeficiency virus (BIV). They prepared mimetics containing 12 amino acid loops by transplanting the key residues of Tat for binding to TAR (Thr^{72}-Ile^{79}) onto the D-Pro-L-Pro template.[235] One of these mimetics,

Table 9 Selective μ-opioid receptor antagonists designed on a somatostatin template[219]

Biding affinity (IC_{50}, nM)			
Compound	*μ opioid*	*δ opioid*	*Somatostatin*
Somatostatin	27,000	16,400	6
CTP	3.7	8400	690
CTOP	2.8	13,500	24,330
TCTOP	1.4	16,000	20,400

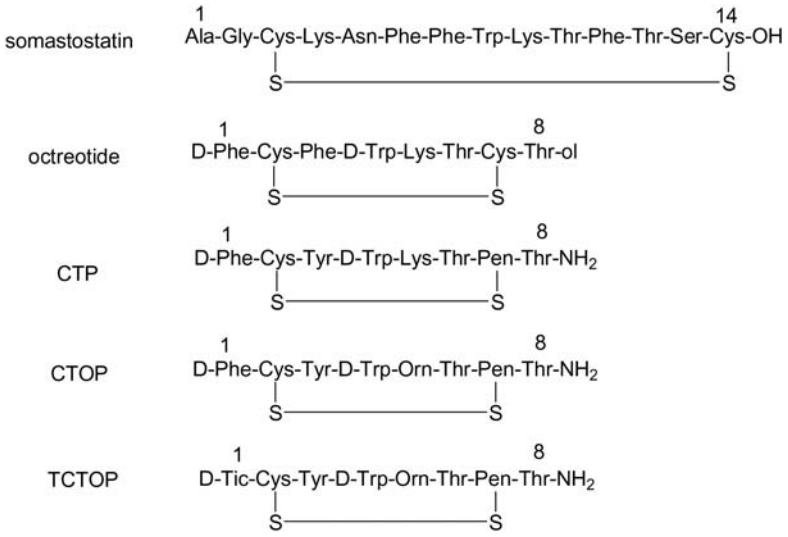

Fig. 27 Selective μ-opioid receptor antagonists.

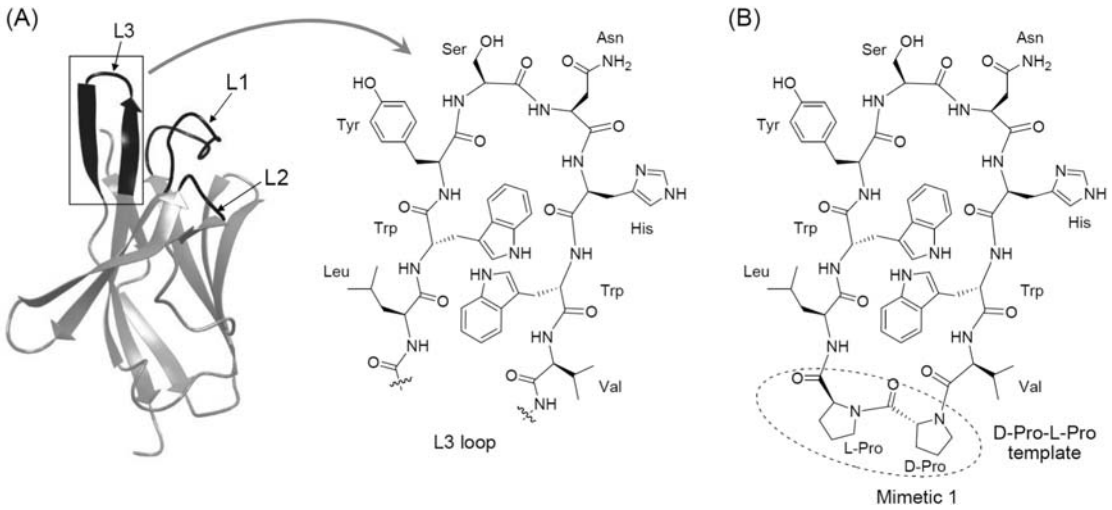

Fig. 28 Structures of (A) β-hairpin of the L3 loop of the anti-influenza hemagglutinin antibody HC19 and (B) a β-hairpin mimetic 1 created with D-Pro-L-Pro template.

BIV-2, was found to bind to TAR RNA with a K_d value of 150 nM, comparable with that of the wild-type BIV Tat (65–81) peptide ($K_d = 50$ nM).[235] An NMR study showed that BIV-2 adopts a β-hairpin conformation and binds to TAR RNA with an orientation opposite to what is observed in the Tat protein.[236] Based on the structure of the mimetic–TAR RNA complex, they modified the sequence and found that L-22 binds to TAR RNA with a 10-fold increase in activity, compared with BIV-2 (Fig. 29).[237]

β-Hairpin mimetics were employed as a scaffold to preorganize the side chains of the i, $i+4$, and $i+7$ positions of an α-helical peptide, representing one helical face.[238] Inhibitors were developed to disrupt p53–HDM2 interaction by mounting the critical residues, such as Phe^{19}, Trp^{23}, and Leu^{26} in an amphipathic α-helical p53 peptide onto the D-Pro-L-Pro dipeptide template. Based on molecular modeling, Phe^{19}, Trp^{23}, and Leu^{26} of the p53 peptide were incorporated into the positions 1, 3, and 4 of the mimetics, respectively. Although mimetic 2 showed a weak binding affinity ($IC_{50} = 125$ μM), further optimization led to mimetic 8 that contains a 6-chlorotryptophan[239] at position 3, showing a 900-fold increase in affinity for human double minute 2 (HDM2) ($IC_{50} = 140$ nM) (Fig. 29). A crystal structure of the mimetic 8 in complex with HDM2 confirmed that it adopts a β-hairpin conformation, and the side chains of Phe, 6-ClTrp, and Leu occupy the hydrophobic pocket on the surface of HDM2.[240]

6.03.6.2 Stabilized β-Sheets

Amyloid fibrils are insoluble protein aggregates, and their formation may cause a variety of human degenerative disorders including Alzheimer's disease, Parkinson's disease, Huntington's disease, prion disease, and type II diabetes, each of which is associated with

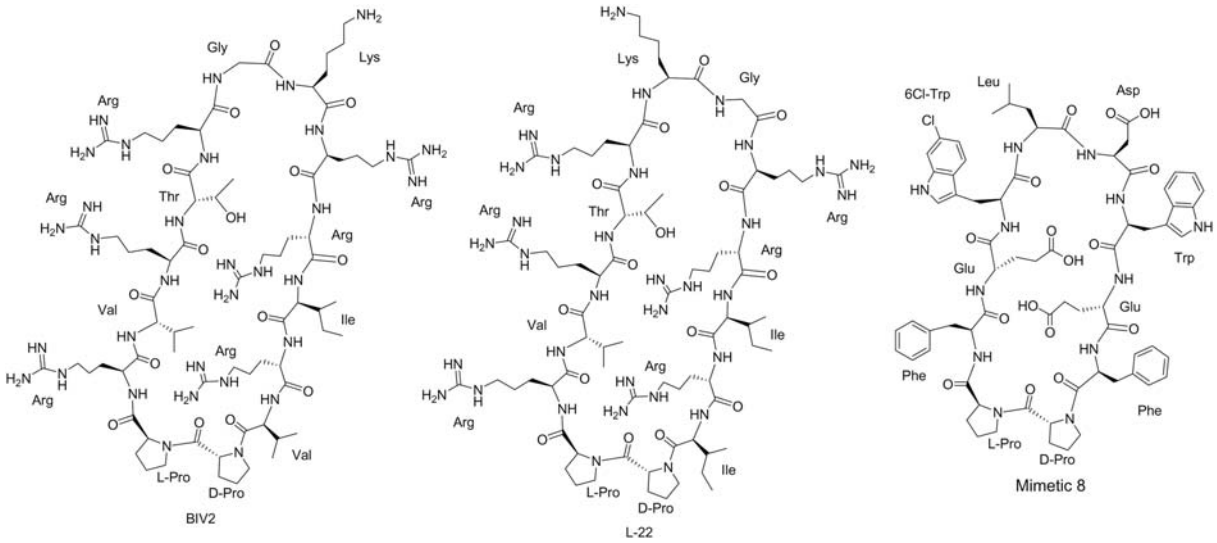

Fig. 29 Structures of β-hairpin peptidomimetics: BIV2, L-22, and mimetic 8.

a specific peptide or protein.[241] For example, β-amyloid protein, α-synuclein, and islet amyloid peptide are related to Alzheimer's disease, Parkinson's disease, and type II diabetes, respectively.[242] Despite the differences in amino acid sequences, native structures, and physiological activities, amyloidogenic peptides and proteins share a characteristic cross-β-sheet structure in which adjacent β-sheets are held together tightly by zipper-like side-chain interactions with a network of hydrogen bonds running parallel to the fibril axis.[243]

Nowick and coworkers have developed macrocyclic β-sheet mimics as a platform to display amyloidogenic peptides from various amyloid proteins.[244] The β-sheet mimics comprise a heptapeptide β-strand (the upper strand, R_1–R_7), one Hao template (hydrazine, 5-amino-2-methoxybenzoic acid, and oxalic acid), and four additional amino acids (the lower strand, R_8–R_{11}) and two δ-linked Orn turns (**Fig. 30**). The Hao template was designed to facilitate β-sheet dimer formation with the upper strand and to prevent the opposite side of the lower strand from making higher oligomers, as demonstrated by X-ray crystallography.[245]

The mimics 1a, 1m, and 1o (**Fig. 30**) possess amyloidogenic heptapeptide sequences derived from amyloid-β peptide (Aβ), human β_2-microglobulin, and human α-synuclein, respectively, and delayed aggregation of their parent proteins.[246] In particular, the mimic 1a blocked $A\beta_{40}$ and $A\beta_{42}$ aggregation by 430% and 600%, respectively, up to 20 μM Aβ peptides, and reduced the toxicity of $A\beta_{40}$ and $A\beta_{42}$ in PC-12 pheochromocytoma cells.

6.03.6.3 Stabilized α-Helices

PPIs are frequently controlled by well-ordered secondary structures like α-helices, regulating essential biological processes including enzyme activity, protein synthesis, transcription, DNA binding, immune response, and signal transduction.[247] Thus, α-helices found

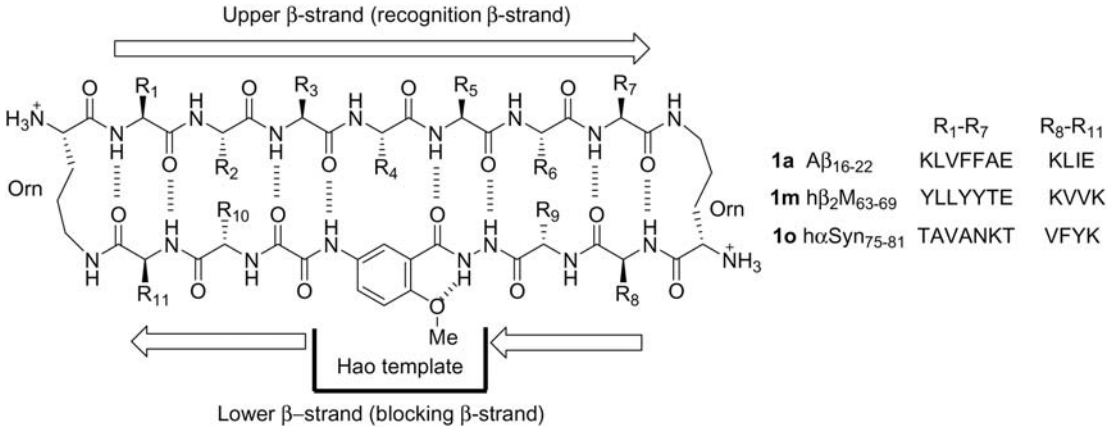

Fig. 30 Structure of β-sheet mimic Hao and its stabilization of β-strands.

at the interfaces of PPIs have been recognized as attractive targets to intervene for treating diverse human diseases including cancer, neurological disorder, and viral infection.[247a,248] However, short peptides (typically <15-mer in size) derived from such helical segments in proteins have several limitations. Short peptides often lose their well-defined structures or fail to adopt organized conformations like α-helices in solution when taken out of the proteins, resulting in decreased binding affinity to their targets.[249] In addition, short peptides are susceptible to proteolytic degradation, especially when they are in an extended conformation, and have difficulty in penetrating cellular membranes.[164,250] These drawbacks severely compromise effective use of short peptides as PPI modulators. To overcome these limitations, a variety of methods have been developed for stabilizing helical structures that not only retain high binding affinity but also provide resistance to proteolysis and even cell permeability.

Cross-linking the side chains of appropriately spaced residues is well known to stabilize α-helices, and a variety of cross-linking methods have been developed (**Fig. 31**).[251] Among them, formation of a lactam bridge offers a convenient means for introducing conformational constraints into a peptide structure.[252] An amide linkage can be created between amine- and carboxylic acid-bearing amino acid residues that are located at the i and $i+3$, i and $i+4$, or i and $i+7$ positions in the peptide sequence and has demonstrated its capability of stabilizing α-helices (**Fig. 31A**).[253] To investigate the effect of the length and orientation of a lactam bridge on helicity, Lys or Orn and Asp or Glu were placed at the positions i and $i+4$ (i.e., positions 1 and 5), respectively, in a cyclic pentapeptide. This study showed that a lactam bridge between Lys at the position i and Asp at the position $i+4$ was superior to others for stabilizing α-helicity, independent of concentration, TFE, denaturants, and proteases.[253] A variety of orthogonal protecting groups for amines and carboxylic acids have been developed, allowing facile synthesis of mono- and bis-lactam-bridged peptides in solid phase.[254]

Schultz and coworkers reported that an intramolecular disulfide bond between D- and L-2-amino-6-mercaptohexanoic acid placed at the i and $i+7$ positions stabilized a short α-helical peptide.[255] The resulting disulfide-containing cyclic peptides displayed an enhanced helicity compared with the linear counterpart. In addition, the disulfide linkage between D-Cys at the i position and Cys at the $i+3$ position also increased the helicity (**Fig. 31B**).[256]

Another cross-linking method is making a nonnative carbon–carbon bond (often referred as "hydrocarbon stapling") that may increase resistance to proteolysis over that observed with lactam and disulfide bridges. The Grubbs group reported the hydrocarbon stapling via a ring-closing metathesis reaction with O-allyl-protected Ser residues located on adjacent helical turns.[257] As an alternative hydrocarbon stapling approach, Verdine and coworkers devised an all-hydrocarbon cross-linking system in which the cross-link is created between two amino acids bearing olefinic side chains placed at the i and $i+4/i+7$ positions, followed by an olefin metathesis reaction (**Fig. 31C**). Hydrocarbon-stapled peptides show not only enhanced and stabilized helical structures but also increased membrane permeability, presumably resulting from the lipophilic nature of the cross-link.[258]

The Ghadiri and Hopkins groups exploited the affinity of a transition metal ion to ligands for the stabilization of α-helical peptides. Peptides carrying His and Cys residues at the i and $i+4$ positions interact with a transition metal ion like Ca^{2+} and Ni^{2+} and form a bidentate metal complex, which fixes the peptide in an α-helical conformation (**Fig. 31D**).[259] Oppositely charged residues on the same side of an α-helical peptide can also stabilize a helical conformation by making a salt bridge. This ion pair system of Glu at the i position and Lys at the $i+4$ position has been employed to increase the helicity of peptides (**Fig. 31E**).[260]

Alleman and coworkers developed a photocontrollable system that manipulates peptide conformations by irradiation of light.[261] An azobenzene cross-link placed between two Cys residues undergoes *cis–trans* isomerization upon irradiation in a reversible manner, switching the structure of a peptide between α-helix and random coil (**Fig. 31F**).

Glucagon is a 29-amino acid-containing peptide hormone secreted by the α cells of pancreatic islets. It plays a critical role in glucose homeostasis by stimulating gluconeogenesis and glycogenolysis in hepatocytes and lipolysis in adipocytes during the hypoglycemic state. Thus, glucagon receptor antagonists may be of interest in the treatment of diabetes mellitus.[262] Hruby and coworkers utilized a salt bridge to increase the α-helicity of glucagon.[263] Two Lys and a Glu were introduced in the sequence of glucagon to create a salt bridge for the stabilization of the α-helical structure at the C-terminal region of the peptide (**Fig. 32**). The resulting [$Lys^{17,18}$, Glu^{21}]glucagon displayed an increased binding affinity and receptor activation potency (five- to sevenfold increase).

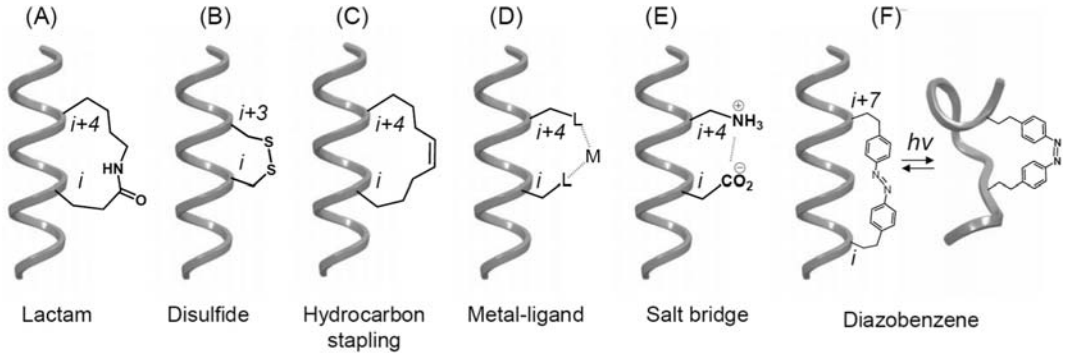

Fig. 31 Selected examples of side chain-cross-linked α-helical peptides.

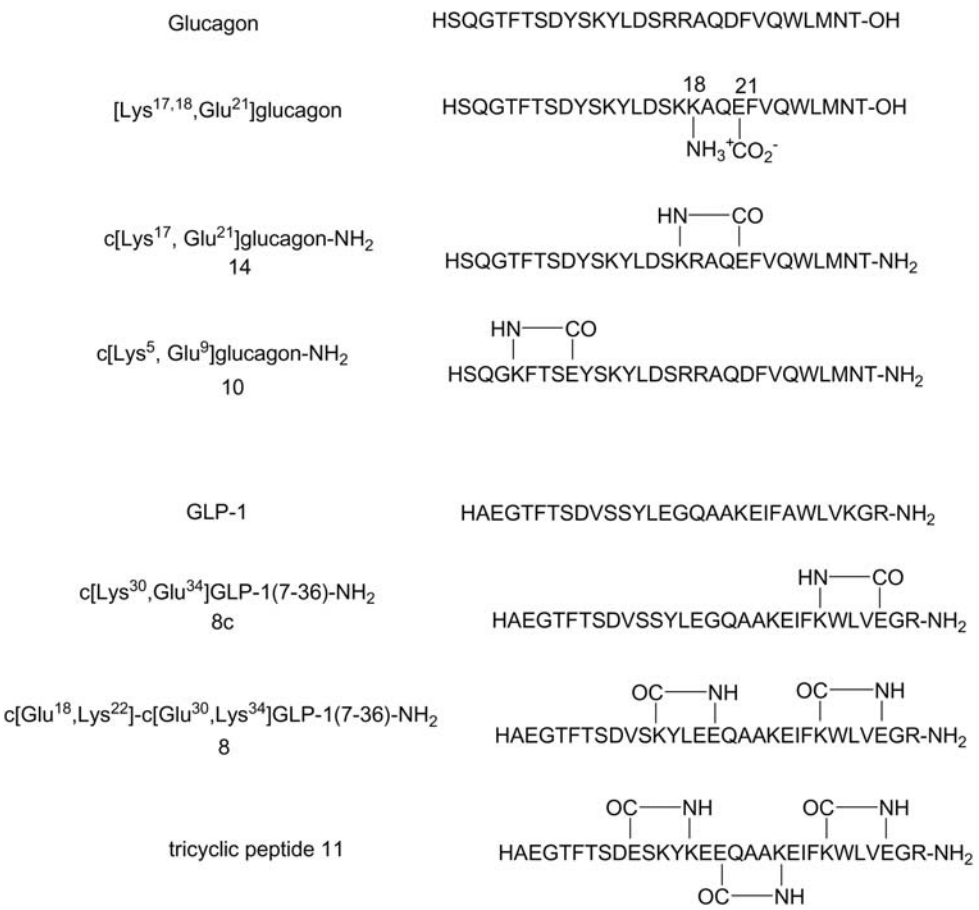

Fig. 32 Structures of glucagon and GLP-1 analogs.

The increased potency appears to be caused by a significantly increased α-helical content as determined by circular dichroism (CD) spectroscopy and X-ray crystallography.

Ahn and coworkers developed a positional cyclization scanning approach to determine the presence and location of secondary structures in the bioactive conformation of glucagon.[264] Positional cyclization scanning consists of a series of structure–activity relationship studies with conformationally restricted peptides to interrogate the structural requirement for optimal receptor recognition. Conformational restrictions were surveyed in the sequence of glucagon with a disulfide bridge between two Cys at the i and $i+5$ positions for stabilization of a turn conformation and a lactam bridge between Lys at the i position and Glu at the $i+4$ position for fixation of a helical structure. Based on the binding affinity changes and the locations of the conformational restrictions, they reached a model of two helical segments in the N- and C-terminal regions, connected by a short and nonhelical segment. Some of the lactam-bridged glucagon analogs were found to have an enormous increase in binding affinity (six- to eightfold increase) and receptor-stimulating potency (up to 21-fold increase).

GLP-1 is a 30-amino acid-containing incretin, and its primary role is regulating postprandial insulin release. It also induces pancreatic β-cell differentiation and proliferation, inhibits apoptosis of the β cells, blocks glucagon secretion, decelerates gastric emptying, reduces appetite, and induces satiety. All of these regulatory functions have made this peptide an attractive therapeutic for treating diabetes.[265] To elucidate the receptor-bound conformation of GLP-1, Ahn and coworkers prepared a series of conformationally constrained GLP-1 analogs by introducing a lactam bridge between Lys at the i position and Glu at the $i+4$ position at various locations in the GLP-1 sequence (**Fig. 32**).[266]

This study identified two lactam bridges that significantly stabilize two helical segments at the N- and C-terminal regions of the peptide. Based on those results, they designed and synthesized bicyclic and tricyclic GLP-1 analogs by placing multiple lactam bridges together to simultaneously stabilize both α-helical segments in the N- and C-terminal regions of the peptide.[267] These highly constrained GLP-1 analogs showed not only outstanding conformational stability, which increased binding affinity and receptor activating potency (two- to fourfold increase), but also remarkable metabolic stability against enzymatic degradation. The most potent bicyclic GLP-1 analog, [D-Ala^8]-c[Glu^{18},Lys^{22}]-c[Glu^{30},Lys^{34}]GLP-1(7–36)-NH_2, has been under evaluation for its utility in pancreatic β-cell imaging with PET modality.[16,268]

A 13-residue-containing peptide 2, derived from respiratory syncytial virus (RSV) fusion protein, was constrained with two back-to-back lactam bridges to fix it in an α-helical conformation (**Fig. 33**).[269] The resulting bicyclic peptide 1 was found to be highly

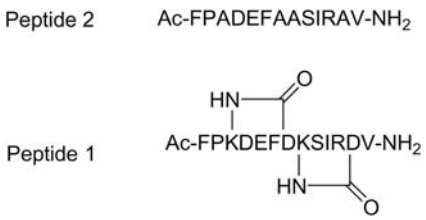

Fig. 33 RSV fusion inhibitor stabilized by two lactam bridges.

α-helical in water, determined by CD and NMR spectroscopy, correctly positioning crucial binding residues (F488, I491, and V493) on the same helical face and the lactam bridges on a noninteracting face of the helix. This compound showed potent activity in both a recombinant fusion assay and an RSV antiviral assay (IC_{50} value of 25 and 36 nM, respectively). In contrast, the linear peptide 2 had no α-helical structure in water and showed no antiviral activity up to 10 μM. The potency of the bicyclic peptide 1 for inhibiting RSV fusion ($IC_{50}=25$ nM) also contrasts starkly with the potency for the full-length heptad repeat C peptide ($IC_{50}=2900$ nM) in a cell fusion assay.[270]

HDM2 and human double minute X (HDMX) induce tumorigenesis by inhibiting the tumor suppressor p53.[271] HDM2 acts as a ubiquitin ligase that directly binds to p53, leading to proteasomal degradation of p53.[272] Although HDMX binds to p53 at the same site as HDM2, HDMX inhibits p53 transactivation by sequestering it into inactive complexes due to its lack of ubiquitin ligase activity.[273] Thus, inhibition of HDM2 can be compromised by overexpression of HDMX, and blocking both proteins appears to be key for restoring p53 activity in a number of cancers.[274]

Verdine and coworkers applied the hydrocarbon stapling strategy for creating peptide-based HDM2 inhibitors that exhibit high affinity for HDM2 and readily enter cells.[275] A panel of stapled peptides was designed based on the p53-derived 15-mer peptide by installing an all-hydrocarbon staple between the residues at the *i* and *i*+7 positions (**Fig. 34**). Fluorescence polarization (FP) assays with HDM2 identified a stapled p53 peptide (SAH-p53-4) as a potent inhibitor with a K_d value of 0.92 nM, which is nearly three orders of magnitude greater than that of the wild-type p53(14–29) peptide ($K_d=410$ nM). However, SAH-p53-4 was unable to penetrate the cell membrane.

To adjust the ionized state of the peptide, SAH-p53-4 was modified by replacing Asp and Glu with Asn and Gln, respectively, and by substituting Leu and Lys to Gln and Arg, respectively, as previously reported to participate in p53 nuclear export (L14Q)[276] and ubiquitylation (K24R).[277] The resulting stapled peptide (SAH-p53-8) efficiently penetrated cells and showed high binding affinity to HDM2 with a K_d value of 55 nM (**Fig. 34**). Furthermore, SAH-p53-8 exhibited dose-dependent inhibition of SJSA-1 cells with an EC_{50} value of 8.8 μM and triggered caspase-3 activation with an EC_{50} value of 5.8 μM, demonstrating that SAH-p53-8 inhibited cell

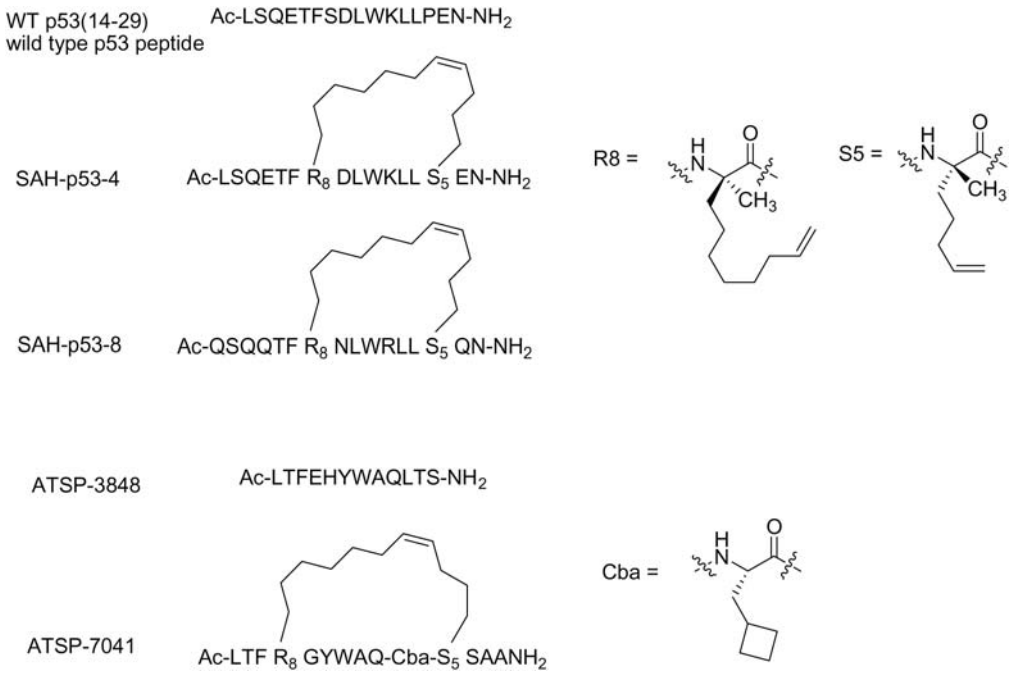

Fig. 34 Hydrocarbon-stapled p53 peptides.

viability by activating apoptosis in HDM2-overexpressing SJSA-1 cells.[275] The crystal structure of the SAH-p53-8/MDM2 complex revealed that the interaction of the stapled peptide to the protein is similar to that of the native p53 peptide. In addition, the staple appears to make hydrophobic contacts with the rim of the MDM2 binding site, enhancing the binding affinity.[278]

Sawyer and coworkers developed a potent and selective dual inhibitor of MDM2 and MDMX, ATSP-7041 (Fig. 34), which effectively activates the p53 pathway in tumors both in vitro and in vivo.[279] A series of stapled peptides was synthesized by placing a hydrocarbon staple between Glu^{20} and Thr^{27} of a phage display-derived peptide, ATSP-3848. In addition to the conventional molecular recognition elements (e.g., Phe^{19}, Trp^{23}, and Leu^{26}), the stapled peptides in the study feature Tyr^{22}, which was identified as another key amino acid. The stapled peptides were further modified to enhance solubility and target binding. Substitution of His^{21} and Leu^{26} with Glu and 3-cyclobutylalanine, respectively, and C-terminal extension with Ala-Ala created a potent dual inhibitor of MDM2 and MDMX, ATSP-7041. FP assays showed that ATSP-7041 has strong binding affinity to both MDM2 ($K_i = 0.9$ nM) and MDMX ($K_i = 7$ nM). A crystal structure of MDMX complexed with ATSP-7041 revealed that the stapled peptide binds to the p53 binding site of MDMX in an identical manner to that of the wild-type p53 peptide. In addition, the staple moiety also associates with MDMX, highlighting the potential of the hydrocarbon staple to further enhance molecular recognition. ATSP-7041 induced reactivation of the main p53 cellular functions, such as cell-cycle arrest and apoptosis, and also suppressed growth of cancer cells that overexpress MDM2 (SJSA-1 cells) or MDMX (MCF-7 cells). Furthermore, ATSP-7041 suppressed tumor growth in human xenograft models and possesses favorable pharmacokinetic and tissue distribution properties.[279]

The α-helix is structurally stabilized by a network of hydrogen bonds formed between the carbonyl of the residue at the *i* position and the amide proton of the residue at the $i+4$ position. To initiate the folding process for a helix, three consecutive amino acid residues need to adopt a helical orientation, which is an entropically unfavorable step.[280] Thus, helix-inducing templates can promote helix formation and prevent fraying of the ends by fixing the orientation of the first three residues of a peptide in an α-helical conformation. Kemp and coworkers developed an N-terminal template 3 that is capable of enforcing α-helix formation (Fig. 35). The pyrrolidine ring and thiamethylene bridge of template 3 constrain its pi and psi angles to the ideal helix value, which makes template 3 assume a helix nucleating conformation.[281]

Another approach for constraining to induce an α-helical structure is introduction of a cross-link that mimics the hydrogen bond between the carbonyl and amide proton of two residues at the *i* and $i+4$ positions, respectively. The Satterthwait group designed a hydrazone link to replace a hydrogen bond in an α-helix (Fig. 35).[282] Arora and coworkers further elaborated the covalent mimic and utilized a chemically stable carbon–carbon bond that can be prepared by a ring-closing metathesis reaction between olefin-bearing residues at the *i* and $i+4$ positions (Fig. 35).[283] The resulting hydrogen bond surrogate (HBS) approach stabilizes α-helical conformation in short peptide sequences (e.g., 7–12-residue long peptides).

Hypoxia-inducible factor-1 (HIF-1) is a transcriptional factor that plays a crucial role in adaptive responses of tumor cells to changes in oxygen level. Under hypoxic conditions, HIF-1 activates transcription of HIF-1 target genes (e.g., vascular endothelial growth factor) that regulate a variety of biological processes including angiogenesis, cell proliferation and survival, glucose metabolism, and migration. The elevated level of HIF-1 has been correlated to tumor progression and angiogenesis, making the HIF-1 pathway an attractive target for cancer therapeutics.[284] The HIF-1α subunit forms a heterodimer with its β-subunit and binds to the hypoxia response element. HIF-1α triggers transcription of target genes by recruiting transcriptional coactivator proteins including CBP/p300. The C-terminal transactivation domain (C-TAD) of HIF-1α forms three short helices (helix 1, G784-D788; helix2, D799-A804; and helix 3, E817-Q824) and wraps around the cysteine/histidine-rich domain-1 (CH1) of p300.[285]

Arora and coworkers developed HBS1 peptide based on the helix 3. For synthetic efficiency, Leu^{819} was replaced with Ala in HBS1 (Fig. 36). Tryptophan fluorescence binding assay showed that HBS1 binds to p300 CH1 with a K_d of 690 nM. Peptide 3, an unconstrained analog of HBS1, binds to the CH1 domain with a K_d of 6060 nM, indicating that stabilization of the α-helical conformation in such a short peptide can offer a significant increase (ninefold) in binding affinity. FP assay with the p300 CH1 domain and fluorescein-labeled HIF-1α C-TAD peptide (residues 786–826) demonstrated that HBS1 disrupted the complex

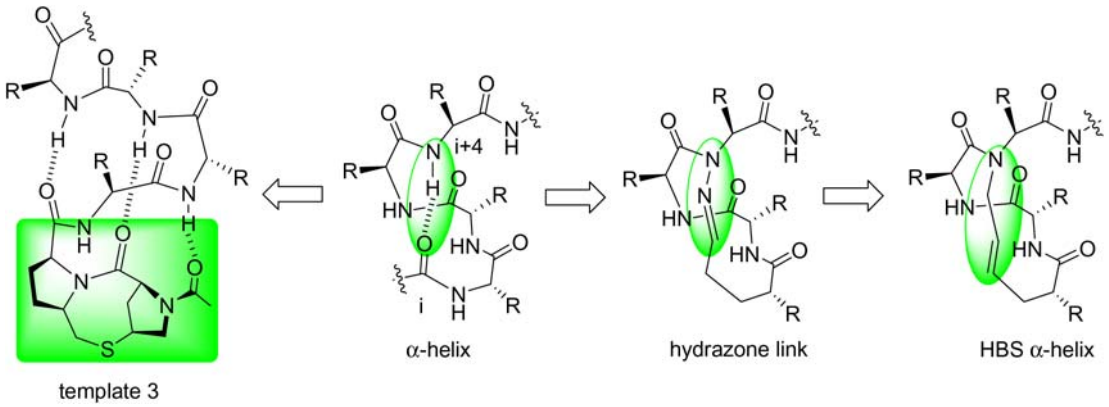

Fig. 35 Structure of helix-inducing templates.

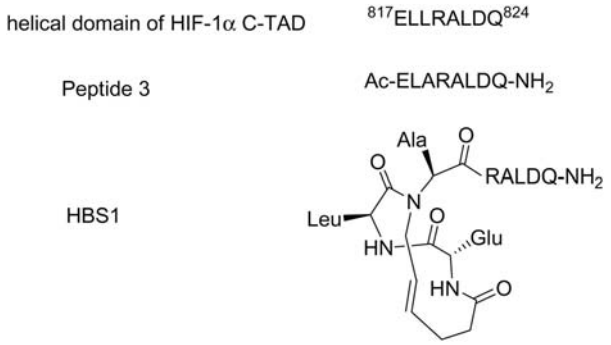

Fig. 36 Structures of HBS-HIF-1α peptide.

with a K_i value of 3.5 μM, while the linear peptide 3 did not inhibit the complex formation. Gene expression profiling with oligonucleotide microarrays revealed that HBS1 effectively inhibited the transcription of hypoxia-inducible genes with relatively minimal perturbation of nontargeted signaling pathways. Furthermore, HBS1 successfully suppressed tumor growth in a mouse tumor xenograft model.[286]

β-Amino acids differ from α-amino acids in that they have an additional carbon atom in the backbone, and β-peptides can form well-defined three-dimensional structures. β^3-Peptides generally have a high propensity to form a 14-helix that is stabilized by 14-membered rings resulting from a hydrogen bond between an amide proton on the residue *i* and a carbonyl on the residue $i+2$. While the α-helix has 3.6 residues in a single turn, the 14-helix makes a turn with approximately every 3 residues (**Fig. 37**).[287] β-Peptides have advantages over their α-amino acid counterparts, such as enhanced conformational and proteolytic stability. In addition to homogeneous β-peptides containing exclusively β-amino acids, heterogeneous α/β-peptides have both α- and β-amino acids and are also capable of adopting diverse helical conformations.[288]

Schepartz and coworkers used the β-peptide 14-helix as a scaffold for mimicking the projection of the three hydrophobic side chains (i.e., Phe^{19}, Trp^{23}, and Leu^{26}) from the α-helical segment of p53 (**Fig. 38**).[289] For these three key residues, β^3-homoleucine, β^3-homotryptophan, and β^3-homophenylalanine were incorporated at positions 3, 6, and 9, respectively, of deca-β-peptides and were expected to form one face of a 14-helix. The 14-helix was also stabilized with a salt bridge between the side chains of β^3-homoornithine and β^3-homoglutamic acid placed on a solvent-exposed surface of the helix. The 14-helix structure in β53-1 was confirmed by CD and NMR spectroscopy. A fluorescein conjugate of β53-1 was found to bind HDM2 with a K_d value of 292 nM, while p53 peptide showed a K_d value of 72.5 nM.[289] Substitution of a 3-trifluoromethylphenylalanine for Trp^{23} increased binding affinity to HDM2 ($K_d = 28.2$ nM).[290]

In spite of their strong affinity to HDM2, β-peptides are typically not cell-permeable, which limits their utility as potential therapeutics. Thus, Schepartz and coworkers introduced either a diether or hydrocarbon bridge between the residues at the *i* and $i+3$ positions in order to increase cellular uptake (**Fig. 38**). β-Peptides containing a diether (47OS) or hydrocarbon linkage (47CS)

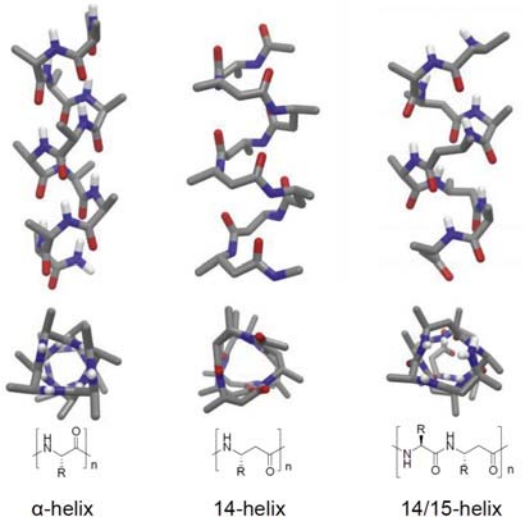

Fig. 37 Structures of α-helix, 14-helix, and 14/15-helix formed by α-peptide, β-peptide, and mixed α/β-peptide, respectively.

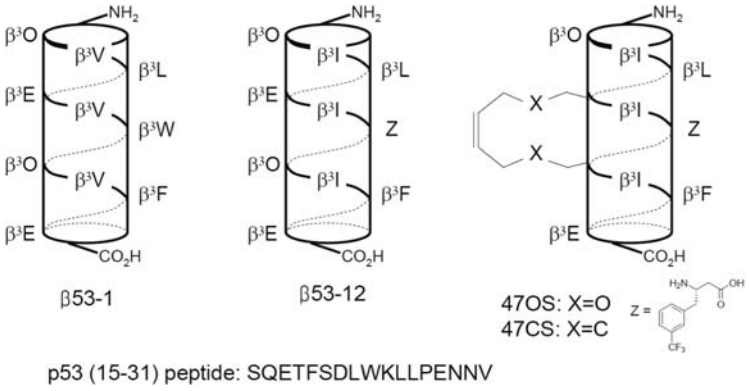

Fig. 38 Structures of p53 β-peptides.

between positions 4 and 7 bind to HDM2 with K_d values of 53.9 and 94.1 nM, respectively, comparable with the native p53 peptide, and these stapled β-peptides showed significant cell uptake.[291]

Although β-peptides have the capability to form 12- or 14-helices, their binding affinity to Bcl-xL proteins was found to be very weak ($IC_{50} > 500$ μM), presumably because the backbone of β-peptides does not precisely reproduce the side-chain projection pattern of an α-helix. Gellman and coworkers developed an alternative approach of partial replacement of the α-amino acid residues in a helical peptide sequence with analogous β-amino acids to retain the recognition properties of the original α-helix.[292] A variety of α/β-peptide homologues in ααβααβ, ααβ, and αααβ repeat patterns were evaluated on their ability to inhibit antiapoptotic Bcl-2 proteins. They synthesized a series of α/β-peptides in the ααβααβ pattern to represent the BH3 domain of Puma that binds promiscuously to antiapoptotic Bcl-2 family members (Fig. 39). Among them, α/β-peptide 4 showed the highest binding affinity with a K_i value of less than 1 nM to Bcl-xL and a K_i value of 150 nM to Mcl-1 in FP assays. In addition, α/β-peptide 4 showed significantly improved resistance against degradation by proteinase K and pronase, compared with the Puma BH3 α-peptide.[293] The crystal structure of the α/β-peptide bound to Bcl-xL showed that the α/β-peptide accurately mimics the four key side chains, organizing the same hydrophobic surface as the native BH3 domain does. It also forms an ion pair between Asp^{14} of the peptide and Arg of Bcl-xL that is conserved in all of the anti- and proapoptotic Bcl-2 protein complexes.[294]

In addition, ααβααβ, ααβ, and αααβ repeat patterns were examined in the context of mimicking the helical BH3 domain of Bim (Fig. 39). Surface plasmon resonance experiments suggested that αααβ-peptide 7 is superior to the other α/β-peptides (e.g., ααβααβ- and ααβ-peptide) in reproducing the binding profile of the Bim BH3 domain. α/β-Peptide 7 showed comparable affinity on Bcl-2, Bcl-w, Bcl-xL, and Mcl-1 with those of the Bim BH3 peptide with IC_{50} values of 5.2, 7.5, 7.5, and 2.4 nM, respectively. The crystal structure of α/β-peptide 4c complexed with Bcl-xL revealed that four hydrophobic side chains of α/β-peptide 4c (Ile^3, Leu^7, β^3-$hIle^{10}$, and β^3-$hPhe^{14}$) dock into the BH3-binding pockets of Bcl-xL. α/β-Peptide 7 was examined on wild-type mouse embryonic fibroblast (MEF) that is protected from apoptosis because of overexpressed Mcl-1 and Bcl-xL, to determine the peptide's capability to initiate apoptosis signaling, and it was observed to induce cytochrome *c* release in wild-type MEF extracts.[295]

6.03.7 Combinatorial Peptide Libraries

Peptide libraries are a valuable research tool to identify biologically active compounds for chemical biology and drug discovery, and these libraries can be generated by either chemical or biological approaches. A number of combinatorial methods have been

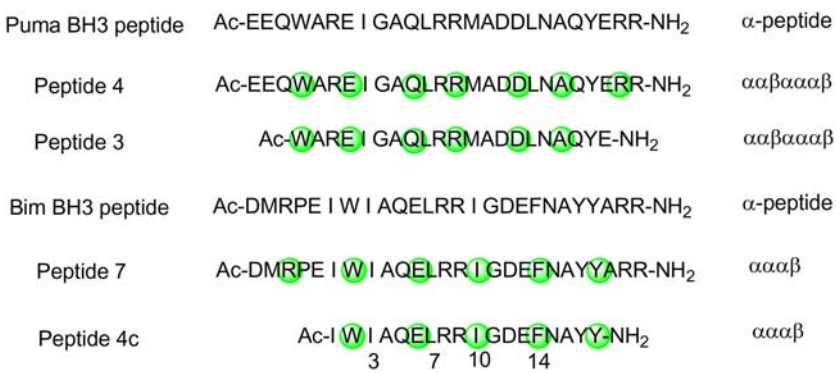

Fig. 39 Primary sequences of BH3 peptides derived from Puma and Bim and their α/β-peptide analogs. β^3-Amino acids are highlighted in *green*.

developed for the production of peptide libraries, allowing high-throughput synthesis and screening to facilitate rapid drug discovery. These synthetic methods include parallel synthesis, split–mix synthesis, and peptide microarray.[296]

6.03.7.1 Spatially Addressable Parallel Synthesis

In a parallel synthesis method, individual peptides are synthesized in separate reaction vessels, and this defines the sequence of a peptide based on the location of a particular reaction vessel. Geysen and coworkers reported the first combinatorial peptide library prepared with a multipin technology (Fig. 40A).[297] In this method, individual peptides were chemically synthesized on polyacrylic acid-grafted polyethylene pins that were arrayed in a 96-well microtiter plate. Each well in the plate served as a distinct reaction vessel. Pin loading levels are relatively low (approximately 50 nmol pin^{-1}) compared with standard solid supports.

Houghten and coworkers introduced a tea-bag method for multiple peptide synthesis (Fig. 40B).[298] In this method, peptide synthesis occurs on polymer beads that are sealed inside labeled and porous polypropylene packets. Amino acid couplings are carried out by immersing each packet in a solution of an activated amino acid. By using this method, a 248-membered peptide library of 13-residue long peptides was constructed in the quantity of 10–20 mg for each peptide.

With SPOT synthesis protocol, a peptide library can be produced in a stepwise manner on a flat surface like functionalized cellulose membrane by following standard SPPS procedures (Fig. 41).[299] A solution containing an activated amino acid is dispensed on the membrane, and the resulting circular spots serve as independent microreactors. The dispensed volume determines the spot size that defines the number and quantity of peptides that can be assembled on the membrane. A completed peptide library can be either screened directly while bound to the membrane or released from the membrane for subsequent solution-phase bioassays. Although the density of peptide libraries from SPOT synthesis is relatively low (approximately 20 spots cm^{-2}) compared with photolithographic methods (vide infra), SPOT synthesis offers several advantages for building peptide libraries, such as ease of experimental procedures, inexpensive equipment, and highly flexible library formats.

Fodor and coworkers first described light-directed, spatially addressable peptide array synthesis by combining solid-phase chemistry with lithography techniques (Fig. 42).[300] In this method, a photolabile group [e.g., 6-nitroveratryloxycarbonyl (NVOC)] is used for protecting the α-amino groups of amino acids. The photolabile group on a glass substrate is removed in a spatially defined manner by illuminating specific regions through a lithographic mask. Subsequently, the released amino groups in the exposed

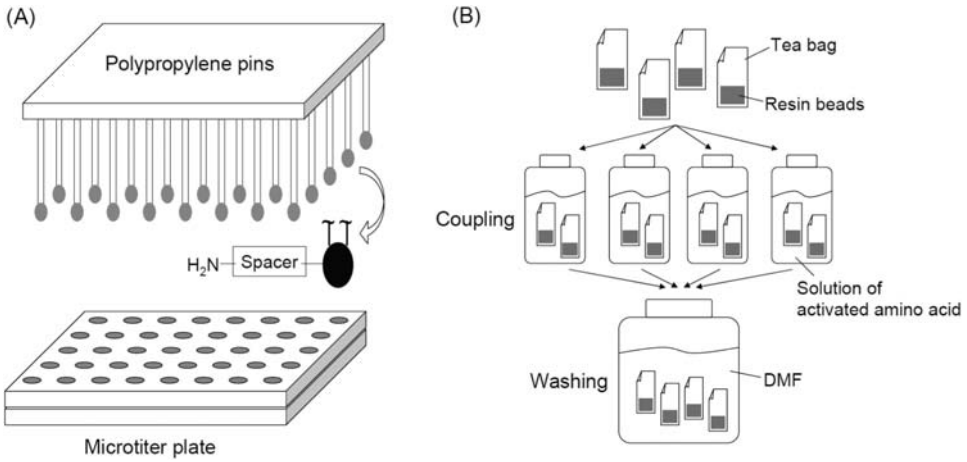

Fig. 40 Spatially addressable parallel peptide libraries. (A) Multipin and (B) tea-bag methods.

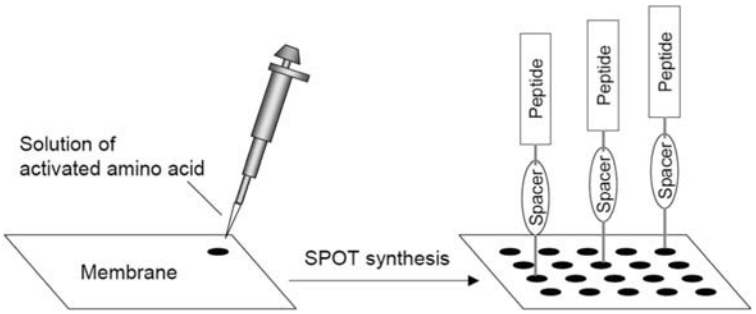

Fig. 41 SPOT synthesis of peptide libraries.

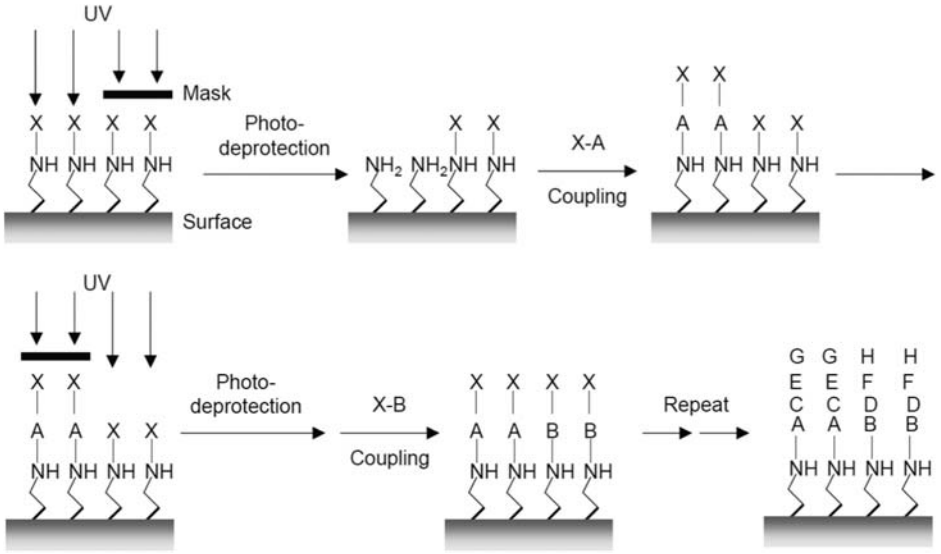

Fig. 42 Light-directed, spatially addressable peptide array synthesis.

sectors are coupled to an NVOC-protected amino acid. By repeating the selective photodeprotection and coupling cycles, they prepared a peptide array consisting of 40,000 compounds cm^{-2} with a $50 \times 50\ \mu m^2$ mask.

6.03.7.2 Split and Mix Synthesis

Hruby and coworkers reported a split and mix synthesis strategy for the construction of libraries with equimolar mixtures of peptides.[301] In this method, resin beads are split into multiple, equally sized portions in separate reaction vessels for coupling individual amino acids separately. All resin portions are then combined and mixed thoroughly. By repeating the procedure for 3 coupling steps with 3 amino acids, a combinatorial library of 27 peptides, for instance, can be readily prepared (**Fig. 43**). The library size increases with the number of coupling steps and amino acids. A pentapeptide library with 20 natural amino acids would contain 3,200,000 different peptides. Alternatively, a large peptide library can be prepared by coupling mixtures of all amino acids in one reaction vessel. To compensate for the difference in coupling rates of each amino acid, the ratio of amino acids in the coupling mixture can be corrected by adjusting their relative concentrations.[302]

Since this split and mix method produces mixture-based libraries, a deconvolution process is required to identify active molecules in the mixture of peptides. There are two main deconvolution approaches, an iterative process[303] and positional scanning.[304] Using the iterative deconvolution approach, a set of sublibraries are prepared in a manner such that each separate sublibrary has a defined amino acid at position 1 with a combination of all amino acids at the remaining positions 2–6 (**Fig. 44A**). Screening the sublibrary determines the most effective amino acid at the defined position (e.g., Asp in **Fig. 44A**). With the best amino acid fixed at position 1, another sublibrary containing a defined amino acid at the next position is prepared and screened to determine the best amino acid residue at position 2. Repeating this procedure for all of the positions, a complete sequence of the final peptide can be identified.

In the positional scanning approach, separate positional libraries are produced, each of which contains a defined amino acid at one position and a combination of all amino acids at the others (**Fig. 44B**). All sublibraries are then examined to determine the most effective amino acid at each position. Final peptide sequences are reconstructed by placing the amino acid that shows the best results at each position.

6.03.7.3 Phage Display Library

In the phage display technique, foreign DNA fragments are inserted into the encoding gene for a bacteriophage (phage) coat protein for inducing the phage to express peptides on its surface without affecting virus infectivity.[305] Filamentous phage M13 is the most widely used for peptide display due to its high capacity for replication and ability to accommodate large pieces of foreign DNA. Peptides are expressed as fusions to the N-terminus of pIII proteins of M13 phage (**Fig. 45**). The phage display is easy to grow and amplify through infection to the bacteria host *E. coli*, which generates a diversity of 10^8–10^{10} different peptide sequences. The sequences of biologically active peptides identified from phage display libraries can be easily determined by DNA sequencing.

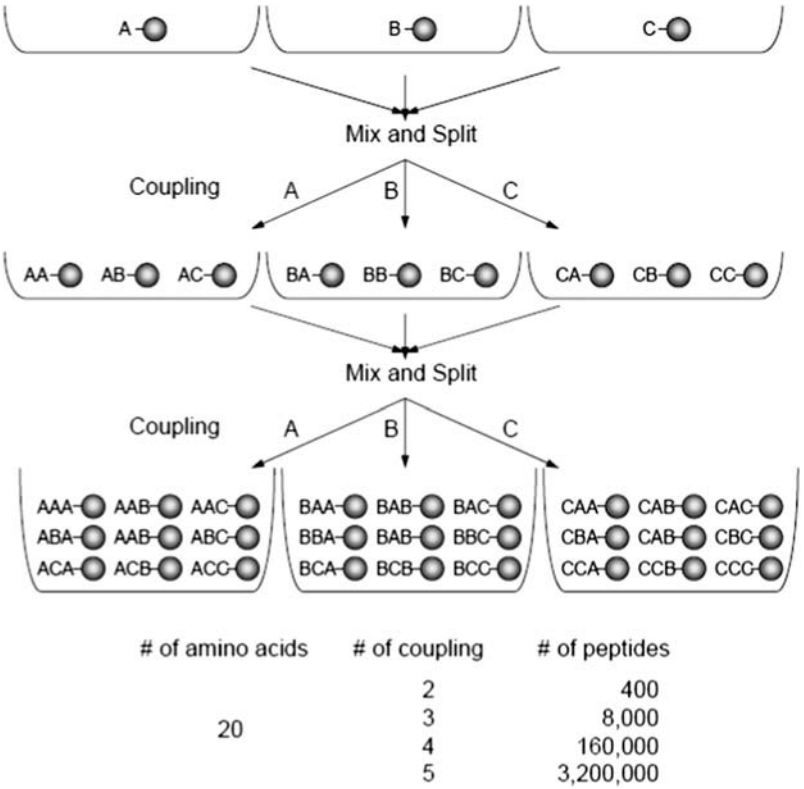

# of amino acids	# of coupling	# of peptides
20	2	400
	3	8,000
	4	160,000
	5	3,200,000

Fig. 43 Split and mix method for the synthesis of peptide library.

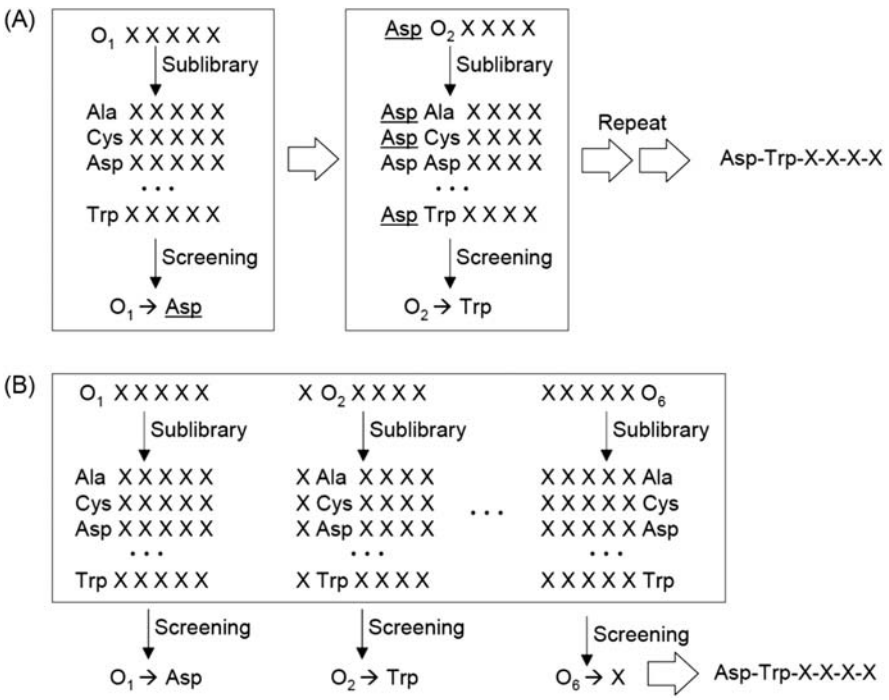

Fig. 44 (A) Iterative and (B) positional scanning deconvolution approaches.

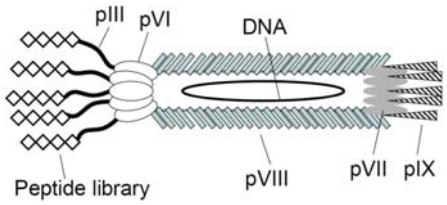

Fig. 45 M13 bacteriophage particle for phage display library.

See also: 1.11. Future of Medicinal Chemistry: Next-Generation Therapeutics. 7.12. GLP-1 Receptor Agonists for the Treatment of Diabetes and Obesity.

References

1. Horwell, D. C.; Pritchard, M. C.; Raphy, J. Design of Non-Peptide Agonists and Antagonists for Neuropeptide Receptors. In *Advances in Amino Acid Mimetics and Peptidomimetics,* Abell, A., Ed.; Vol. 2, JAI Press Inc: Stamford, Connecticut, 1999; pp 166–188.
2. Horwell, D. C.; Beeby, A.; Clark, C. R.; Hughes, J. Synthesis and Binding Affinities of Analogs of Cholecystokinin-(30–33) as Probes for Central Nervous System Cholecystokinin Receptors. *J. Med. Chem.* **1987,** *30* (4), 729–732.
3. Castrucci, A. M. D. L.; Lebl, M.; Hruby, V. J.; Matsunaga, T. O.; Hadley, M. E. Melanin Concentrating Hormone (MCH): The Message Sequence. *Life Sci.* **1989,** *45* (13), 1141–1148.
4. Kruszynski, M.; Nakada, M. T.; Tam, S. H.; Taylor, A. H.; Fieles, W. E.; Heavner, G. A. Determination of the Core Sequence of an Antagonist of Selectin-Dependent Leukocyte Adhesion and Correlation of Its Structure With Molecular Modeling Studies. *Arch. Biochem. Biophys.* **1996,** *331* (1), 23–30.
5. Cirino, G.; Cicala, C.; Sorrentino, L.; Ciliberto, G.; Arpaia, G.; Perretti, M.; Flower, R. J. Anti-Inflammatory Actions of an N-Terminal Peptide From Human Lipocortin 1. *Br. J. Pharmacol.* **1993,** *108* (3), 573–574.
6. Perretti, M.; Ahluwalia, A.; Harris, J. G.; Goulding, N. J.; Flower, R. J. Lipocortin-1 Fragments Inhibit Neutrophil Accumulation and Neutrophil-Dependent Edema in the Mouse. A Qualitative Comparison With an Anti-CD11b Monoclonal Antibody. *J. Immunol.* **1993,** *151* (8), 4306–4314.
7. Scarborough, R. M.; Naughton, M. A.; Teng, W.; Rose, J. W.; Phillips, D. R.; Nannizzi, L.; Arfsten, A.; Campbell, A. M.; Charo, I. F. Design of Potent and Specific Integrin Antagonists. Peptide Antagonists With High Specificity for Glycoprotein IIb-IIIa. *J. Biol. Chem.* **1993,** *268* (2), 1066–1073.
8. Wild, C.; Greenwell, T.; Matthews, T. A Synthetic Peptide From HIV-1 gp41 Is a Potent Inhibitor of Virus-Mediated Cell-Cell Fusion. *AIDS Res. Hum. Retroviruses* **1993,** *9* (11), 1051–1053.
9. Greenberg, M. L.; Cammack, N. Resistance to Enfuvirtide, the First HIV Fusion Inhibitor. *J. Antimicrob. Chemother.* **2004,** *54* (2), 333–340.
10. Bauer, W.; Briner, U.; Doepfner, W.; Haller, R.; Huguenin, R.; Marbach, P.; Petcher, T. J.; Pless, J. SMS 201–995: A Very Potent and Selective Octapeptide Analogue of Somatostatin With Prolonged Action. *Life Sci.* **1982,** *31* (11), 1133–1140.
11. Reichlin, S. Somatostatin. *N. Engl. J. Med.* **1983,** *309* (24), 1495–1501.
12. Rivier, J.; Brown, M.; Vale, W. D-Trp8-Somatostatin: An Analog of Somatostatin More Potent Than the Native Molecule. *Biochem. Biophys. Res. Commun.* **1975,** *65* (2), 746–751.
13. (a) Riek, A. E.; Towler, D. A. The Pharmacological Management of Osteoporosis. *Mo. Med.* **2011,** *108* (2), 118–123; (b) Saag, K. G.; Shane, E.; Boonen, S.; Marín, F.; Donley, D. W.; Taylor, K. A.; Dalsky, G. P.; Marcus, R. Teriparatide or Alendronate in Glucocorticoid-Induced Osteoporosis. *N. Engl. J. Med.* **2007,** *357* (20), 2028–2039.
14. Mosekilde, L.; Sogaard, C. H.; Danielsen, C. C.; Torring, O.; Nilsson, M. H. L. The Anabolic Effects of Human Parathyroid Hormone (hPTH) on Rat Vertebral Body Mass Are also Reflected in the Quality of Bone, Assessed by Biomechanical Testing: A Comparison Study Between hPTH-(1–34) and hPTH-(1–84). *Endocrinology* **1991,** *129* (1), 421–428.
15. Prakash, A.; Goa, K. Sermorelin: A Review of Its Use in the Diagnosis and Treatment of Children With Idiopathic Growth Hormone Deficiency. *Biodrugs* **1999,** *12* (2), 139–157.
16. Manandhar, B.; Ahn, J.-M. Glucagon-Like Peptide-1 (GLP-1) Analogs: Recent Advances, New Possibilities, and Therapeutic Implications. *J. Med. Chem.* **2015,** *58* (3), 1020–1037.
17. Mapelli, C.; Natarajan, S. I.; Meyer, J.-P.; Bastos, M. M.; Bernatowicz, M. S.; Lee, V. G.; Pluscec, J.; Riexinger, D. J.; Sieber-McMaster, E. S.; Constantine, K. L.; Smith-Monroy, C. A.; Golla, R.; Ma, Z.; Longhi, D. A.; Shi, D.; Xin, L.; Taylor, J. R.; Koplowitz, B.; Chi, C. L.; Khanna, A.; Robinson, G. W.; Seethala, R.; Antal-Zimanyi, I. A.; Stoffel, R. H.; Han, S.; Whaley, J. M.; Huang, C. S.; Krupinski, J.; Ewing, W. R. Eleven Amino Acid Glucagon-Like Peptide-1 Receptor Agonists With Antidiabetic Activity. *J. Med. Chem.* **2009,** *52* (23), 7788–7799.
18. Starheim, K. K.; Gevaert, K.; Arnesen, T. Protein N-Terminal Acetyltransferases: When the Start Matters. *Trends Biochem. Sci.* **2012,** *37* (4), 152–161.
19. Arnesen, T. Towards a Functional Understanding of Protein N-Terminal Acetylation. *PLoS Biol.* **2011,** *9* (5), e1001074.
20. Mikami, T.; Takao, T.; Yanagi, K.; Nakazawa, H. N(α) Selective Acetylation of Peptides. *Mass Spectrom.* **2012,** *1* (2), A0010.
21. Benuck, M.; Marks, N. Differences in the Degradation of Hypothalamic Releasing Factors by Rat and Human Serum. *Life Sci.* **1976,** *19* (8), 1271–1276.
22. Heavner, G. A.; Kroon, D. J.; Audhya, T.; Goldstein, G. Biologically Active Analogs of Thymopentin With Enhanced Enzymatic Stability. *Peptides* **1986,** *7* (6), 1015–1019.
23. (a) Vlieghe, P.; Lisowski, V.; Martinez, J.; Khrestchatisky, M. Synthetic Therapeutic Peptides: Science and Market. *Drug Discov. Today* **2010,** *15* (1–2), 40–56; (b) Gracia, S. R.; Gaus, K.; Sewald, N. Synthesis of Chemically Modified Bioactive Peptides: Recent Advances, Challenges and Developments for Medicinal Chemistry. *Future Med. Chem.* **2009,** *1* (7), 1289–1310.
24. Williams, E.; Williams, G.; Gour, B. J.; Blaschuk, O. W.; Doherty, P. A Novel Family of Cyclic Peptide Antagonists Suggests That N-Cadherin Specificity Is Determined by Amino Acids That Flank the HAV Motif. *J. Biol. Chem.* **2000,** *275* (6), 4007–4012.
25. Haitinger, L. Vorläufige Mittheilung über Glutaminsäure und Pyrrol. *Monatsh. Chem. Verw. Tl.* **1882,** *3* (1), 228–229.
26. Schilling, S.; Wasternack, C.; Demuth, H.-U. Glutaminyl Cyclases From Animals and Plants: A Case of Functionally Convergent Protein Evolution. *Biol. Chem.* **2008,** *389* (8), 983–991.
27. (a) Liu, Y. D.; Goetze, A. M.; Bass, R. B.; Flynn, G. C. N-Terminal Glutamate to Pyroglutamate Conversion in vivo for Human IgG2 Antibodies. *J. Biol. Chem.* **2011,** *286* (13), 11211–11217; (b) Yu, L.; Vizel, A.; Huff, M. B.; Young, M.; Remmele, R. L., Jr.; He, B. Investigation of N-Terminal Glutamate Cyclization of Recombinant Monoclonal Antibody in Formulation Development. *J. Pharm. Biomed. Anal.* **2006,** *42* (4), 455–463.
28. Goren, H. J.; Bauce, L. G.; Vale, W. Forces and Structural Limitations of Binding of Thyrotrophin-Releasing Factor to the Thyrotrophin-Releasing Receptor: The Pyroglutamic Acid Moiety. *Mol. Pharmacol.* **1977,** *13* (4), 606–614.

29. Ahmet, I.; Tae, H.-J.; Juhaszova, M.; Riordon, D. R.; Boheler, K. R.; Sollott, S. J.; Brines, M.; Cerami, A.; Lakatta, E. G.; Talan, M. I. A Small Nonerythropoietic Helix B Surface Peptide Based Upon Erythropoietin Structure Is Cardioprotective Against Ischemic Myocardial Damage. *Mol. Med.* **2011,** *17* (3–4), 194–200.
30. Morty, R. E.; Bulau, P.; Pelle, R.; Wilk, S.; Abe, K. Pyroglutamyl Peptidase Type I From *Trypanosoma brucei*: A New Virulence Factor From African Trypanosomes That De-Blocks Regulatory Peptides in the Plasma of Infected Hosts. *Biochem. J.* **2006,** *394* (Pt 3), 635–645.
31. Van Coillie, E.; Proost, P.; Van Aelst, I.; Struyf, S.; Polfliet, M.; De Meester, I.; Harvey, D. J.; Van Damme, J.; Opdenakker, G. Functional Comparison of Two Human Monocyte Chemotactic Protein-2 Isoforms, Role of the Amino-Terminal Pyroglutamic Acid and Processing by CD26/Dipeptidyl Peptidase IV. *Biochemistry* **1998,** *37* (36), 12672–12680.
32. Kim, K.-H.; Seong, B. Peptide Amidation: Production of Peptide Hormones In Vivo and In Vitro. *Biotechnol. Bioprocess Eng.* **2001,** *6* (4), 244–251.
33. Gesellchen, P. D.; Santerre, R. F. Synthesis of Peptides and Proteins by Chemical and Biotechnological Means. In *Peptide and Protein Drug Delivery;* Lee, V. H., Ed.; Marcel Dekker, Inc: New York, 1991; p 91.
34. (a) Abuchowski, A.; McCoy, J. R.; Palczuk, N. C.; van Es, T.; Davis, F. F. Effect of Covalent Attachment of Polyethylene Glycol on Immunogenicity and Circulating Life of Bovine Liver Catalase. *J. Biol. Chem.* **1977,** *252* (11), 3582–3586; (b) Abuchowski, A.; van Es, T.; Palczuk, N. C.; Davis, F. F. Alteration of Immunological Properties of Bovine Serum Albumin by Covalent Attachment of Polyethylene Glycol. *J. Biol. Chem.* **1977,** *252* (11), 3578–3581.
35. Veronese, F. M.; Mero, A. The Impact of PEGylation on Biological Therapies. *Biodrugs* **2008,** *22* (5), 315.
36. Veronese, F. M.; Pasut, G. PEGylation, Successful Approach to Drug Delivery. *Drug Discov. Today* **2005,** *10* (21), 1451–1458.
37. Bailon, P.; Palleroni, A.; Schaffer, C. A.; Spence, C. L.; Fung, W. J.; Porter, J. E.; Ehrlich, G. K.; Pan, W.; Xu, Z. X.; Modi, M. W.; Farid, A.; Berthold, W.; Graves, M. Rational Design of a Potent, Long-Lasting Form of Interferon: A 40 kDa Branched Polyethylene Glycol-Conjugated Interferon Alpha-2a for the Treatment of Hepatitis C. *Bioconjug. Chem.* **2001,** *12* (2), 195–202.
38. Harris, J. M.; Sedaghat-Herati, M. R. Preparation and Use of Polyethylene Glycol Propionaldehyde. U.S. Patent 5,252,714 A, 1993.
39. Kozlowski, A.; Milton Harris, J. Improvements in Protein PEGylation: Pegylated Interferons for Treatment of Hepatitis C. *J. Control. Release* **2001,** *72* (1–3), 217–224.
40. Miron, T.; Wilchek, M. A Simplified Method for the Preparation of Succinimidyl Carbonate Polyethylene Glycol for Coupling to Proteins. *Bioconj. Chem.* **1993,** *4* (6), 568–569.
41. Heredia, K. L.; Maynard, H. D. Synthesis of Protein-Polymer Conjugates. *Org. Biomol. Chem.* **2007,** *5* (1), 45–53.
42. Woghiren, C.; Sharma, B.; Stein, S. Protected Thiol-Polyethylene Glycol: A New Activated Polymer for Reversible Protein Modification. *Bioconj. Chem.* **1993,** *4* (5), 314–318.
43. Slavin, S.; Khoshdel, E.; Haddleton, D. M. Biological Surface Modification by 'Thiol-Ene' Addition of Polymers Synthesised by Catalytic Chain Transfer Polymerisation (CCTP). *Polym. Chem.* **2012,** *3* (6), 1461–1466.
44. DeFrees, S.; Wang, Z. G.; Xing, R.; Scott, A. E.; Wang, J.; Zopf, D.; Gouty, D. L.; Sjoberg, E. R.; Panneerselvam, K.; Brinkman-Van der Linden, E. C.; Bayer, R. J.; Tarp, M. A.; Clausen, H. GlycoPEGylation of Recombinant Therapeutic Proteins Produced in *Escherichia coli*. *Glycobiology* **2006,** *16* (9), 833–843.
45. Jones, M. W.; Mantovani, G.; Blindauer, C. A.; Ryan, S. M.; Wang, X.; Brayden, D. J.; Haddleton, D. M. Direct Peptide Bioconjugation/PEGylation at Tyrosine With Linear and Branched Polymeric Diazonium Salts. *J. Am. Chem. Soc.* **2012,** *134* (17), 7406–7413.
46. Lee, S.; McNemar, C. Substantially Pure Histidine-Linked Protein Polymer Conjugates. U.S. Patent 5,985,263 A, 1999.
47. Lutz, J.-F.; Börner, H. G.; Weichenhan, K. Combining ATRP and "Click" Chemistry: A Promising Platform Toward Functional Biocompatible Polymers and Polymer Bioconjugates. *Macromolecules* **2006,** *39* (19), 6376–6383.
48. Zhang, L.; Bulaj, G. Converting Peptides Into Drug Leads by Lipidation. *Curr. Med. Chem.* **2012,** *19* (11), 1602–1618.
49. Knudsen, L. B.; Nielsen, P. F.; Huusfeldt, P. O.; Johansen, N. L.; Madsen, K.; Pedersen, F. Z.; Thogersen, H.; Wilken, M.; Agerso, H. Potent Derivatives of Glucagon-Like Peptide-1 With Pharmacokinetic Properties Suitable for Once Daily Administration. *J. Med. Chem.* **2000,** *43* (9), 1664–1669.
50. Ferdinandi, E. S.; Brazeau, P.; High, K.; Procter, B.; Fennell, S.; Dubreuil, P. Non-Clinical Pharmacology and Safety Evaluation of TH9507, a Human Growth Hormone-Releasing Factor Analogue. *Basic Clin. Pharmacol. Toxicol.* **2007,** *100* (1), 49–58.
51. Bergeon, J. A.; Chan, Y. N.; Charles, B. G.; Toth, I. Oral Absorption Enhancement of Dipeptide L-Glu-L-Trp-OH by Lipid and Glycosyl Conjugation. *Biopolymers* **2008,** *90* (5), 633–643.
52. Rivett, D.; Hewish, D.; Kirkpatrick, A.; Werkmeister, J. Inhibition of Membrane-Active Peptides by Fatty Acid–Peptide Hybrids. *J. Protein Chem.* **1999,** *18* (3), 291–295.
53. (a) Uchiyama, T.; Kotani, A.; Tatsumi, H.; Kishida, T.; Okamoto, A.; Okada, N.; Murakami, M.; Fujita, T.; Fujiwara, Y.; Kiso, Y.; Muranishi, S.; Yamamoto, A. Development of Novel Lipophilic Derivatives of DADLE (Leucine Enkephalin Analogue): Intestinal Permeability Characteristics of DADLE Derivatives in Rats. *Pharm. Res.* **2000,** *17* (12), 1461–1467; (b) Kellam, B.; Drouillat, B.; Dekany, G.; Starr, M. S.; Toth, I. Synthesis and in vitro Evaluation of Lipoamino Acid and Carbohydrate-Modified Enkephalins as Potential Antinociceptive Agents. *Int. J. Pharm.* **1998,** *161* (1), 55–64.
54. Timofeeva, O. A.; Gaponenko, V.; Lockett, S. J.; Tarasov, S. G.; Jiang, S.; Michejda, C. J.; Perantoni, A. O.; Tarasova, N. I. Rationally Designed Inhibitors Identify STAT3 N-Domain as a Promising Anticancer Drug Target. *ACS Chem. Biol.* **2007,** *2* (12), 799–809.
55. Chicharro, C.; Granata, C.; Lozano, R.; Andreu, D.; Rivas, L. N-Terminal Fatty Acid Substitution Increases the Leishmanicidal Activity of CA(1–7)M(2–9), a Cecropin-Melittin Hybrid Peptide. *Antimicrob. Agents Chemother.* **2001,** *45* (9), 2441–2449.
56. Asada, H.; Douen, T.; Mizokoshi, Y.; Fujita, T.; Murakami, M.; Yamamoto, A.; Muranishi, S. Stability of Acyl Derivatives of Insulin in the Small Intestine: Relative Importance of Insulin Association Characteristics in Aqueous Solution. *Pharm. Res.* **1994,** *11* (8), 1115–1120.
57. (a) Kurtzhals, P.; Havelund, S.; Jonassen, I.; Kiehr, B.; Larsen, U. D.; Ribel, U.; Markussen, J. Albumin Binding of Insulins Acylated With Fatty Acids: Characterization of the Ligand-Protein Interaction and Correlation Between Binding Affinity and Timing of the Insulin Effect In Vivo. *Biochem. J.* **1995,** *312* (Pt 3), 725–731; (b) Hermansen, K.; Davies, M.; Derezinski, T.; Martinez Ravn, G.; Clauson, P.; Home, P. A 26-Week, Randomized, Parallel, Treat-to-Target Trial Comparing Insulin Detemir With NPH Insulin as Add-On Therapy to Oral Glucose-Lowering Drugs in Insulin-Naïve People With Type 2 Diabetes. *Diabetes Care* **2006,** *29* (6), 1269–1274.
58. Ekrami, H. M.; Kennedy, A. R.; Shen, W. C. Water-Soluble Fatty Acid Derivatives as Acylating Agents for Reversible Lipidization of Polypeptides. *FEBS Lett.* **1995,** *371* (3), 283–286.
59. Wang, J.; Shen, D.; Shen, W. C. Preparation, Purification, and Characterization of a Reversibly Lipidized Desmopressin With Potentiated Anti-Diuretic Activity. *Pharm. Res.* **1999,** *16* (11), 1674–1679.
60. Wang, J.; Chow, D.; Heiati, H.; Shen, W.-C. Reversible Lipidization for the Oral Delivery of Salmon Calcitonin. *J. Control. Release* **2003,** *88* (3), 369–380.
61. Blanchfield, J. T.; Lew, R. A.; Smith, A. I.; Toth, I. The Stability of Lipidic Analogues of GnRH in Plasma and Kidney Preparations: The Stereoselective Release of the Parent Peptide. *Bioorg. Med. Chem. Lett.* **2005,** *15* (6), 1609–1612.
62. Goodwin, D.; Simerska, P.; Toth, I. Peptides as Therapeutics With Enhanced Bioactivity. *Curr. Med. Chem.* **2012,** *19* (26), 4451–4461.
63. Toth, I. A Novel Chemical Approach to Drug Delivery: Lipidic Amino Acid Conjugates. *J. Drug Target.* **1994,** *2* (3), 217–239.
64. Dulhunty, A. F.; Cengia, L.; Young, J.; Pace, S. M.; Harvey, P. J.; Lamb, G. D.; Chan, Y. N.; Wimmer, N.; Toth, I.; Casarotto, M. G. Functional Implications of Modifying RyR-Activating Peptides for Membrane Permeability. *Br. J. Pharmacol.* **2005,** *144* (6), 743–754.
65. FDA Approves Two New Drug Treatments for Diabetes Mellitus. http://www.fda.gov/NewsEvents/Newsroom/PressAnnouncements/ucm464321.htm (accessed 13 December 2015).
66. Spiro, R. G. Glycoproteins. In *Advances in Protein Chemistry*, Anfinsen, C. B., Edsall, J. T., Eds.; Vol. 27, Academic Press: New York, 1973; pp 349–467.
67. Imperiali, B.; O'Connor, S. E. Effect of N-Linked Glycosylation on Glycopeptide and Glycoprotein Structure. *Curr. Opin. Chem. Biol.* **1999,** *3* (6), 643–649.
68. Butler, M. S.; Hansford, K. A.; Blaskovich, M. A. T.; Halai, R.; Cooper, M. A. Glycopeptide Antibiotics: Back to the Future. *J. Antibiot.* **2014,** *67* (9), 631–644.
69. Dagan, R.; Poolman, J.; Siegrist, C.-A. Glycoconjugate Vaccines and Immune Interference: A Review. *Vaccine* **2010,** *28* (34), 5513–5523.
70. Johansen, P. G.; Marshall, R. D.; Neuberger, A. Carbohydrates in Protein. 3. The Preparation and Some of the Properties of a Glycopeptide From Hen's-Egg Albumin. *Biochem. J.* **1961,** *78* (3), 518–527.
71. Spiro, R. G. Protein Glycosylation: Nature, Distribution, Enzymatic Formation, and Disease Implications of Glycopeptide Bonds. *Glycobiology* **2002,** *12* (4), 43r–56r.

72. Gamblin, D. P.; Scanlan, E. M.; Davis, B. G. Glycoprotein Synthesis: An Update. *Chem. Rev.* **2009,** *109* (1), 131–163.
73. (a) Shao, N.; Xue, J.; Guo, Z. Chemical Synthesis of CD52 Glycopeptides Containing the Acid-Labile Fucosyl Linkage. *J. Org. Chem.* **2003,** *68* (23), 9003–9011; (b) Yamamoto, N.; Takayanagi, A.; Yoshino, A.; Sakakibara, T.; Kajihara, Y. An Approach for a Synthesis of Asparagine-Linked Sialylglycopeptides Having Intact and Homogeneous Complex-Type Undecadisialyloligosaccharides. *Chemistry (Easton)* **2007,** *13* (2), 613–625.
74. Anisfeld, S. T.; Lansbury, P. T. A Convergent Approach to the Chemical Synthesis of Asparagine-Linked Glycopeptides. *J. Org. Chem.* **1990,** *55* (21), 5560–5562.
75. Deras, I. L.; Takegawa, K.; Kondo, A.; Kato, I.; Lee, Y. C. Synthesis of a High-Mannose-Type Glycopeptide Analog Containing a Glucose-Asparagine Linkage. *Bioorg. Med. Chem. Lett.* **1998,** *8* (13), 1763–1766.
76. Inazu, T.; Kobayashi, K. A New Simple Method for the Synthesis of Nα-Fmoc-Nβ-Glycosylated-L-Asparagine Derivatives. *Synlett* **1993,** *1993* (11), 869–870.
77. Mukhopadhyay, B.; Maurer, S. V.; Rudolph, N.; van Well, R. M.; Russell, D. A.; Field, R. A. From Solution Phase to "On-Column" Chemistry: Trichloroacetimidate-Based Glycosylation Promoted by Perchloric Acid−Silica. *J. Org. Chem.* **2005,** *70* (22), 9059–9062.
78. Bill, R. M.; Flitsch, S. L. Chemical and Biological Approaches to Glycoprotein Synthesis. *Chem. Biol.* **1996,** *3* (3), 145–149.
79. Shin, Y.; Winans, K. A.; Backes, B. J.; Kent, S. B. H.; Ellman, J. A.; Bertozzi, C. R. Fmoc-Based Synthesis of Peptide-αThioesters: Application to the Total Chemical Synthesis of a Glycoprotein by Native Chemical Ligation. *J. Am. Chem. Soc.* **1999,** *121* (50), 11684–11689.
80. Wan, Q.; Chen, J.; Chen, G.; Danishefsky, S. J. A Potentially Valuable Advance in the Synthesis of Carbohydrate-Based Anticancer Vaccines Through Extended Cycloaddition Chemistry. *J. Org. Chem.* **2006,** *71* (21), 8244–8249.
81. van Kasteren, S. I.; Kramer, H. B.; Jensen, H. H.; Campbell, S. J.; Kirkpatrick, J.; Oldham, N. J.; Anthony, D. C.; Davis, B. G. Expanding the Diversity of Chemical Protein Modification Allows Post-Translational Mimicry. *Nature* **2007,** *446* (7139), 1105–1109.
82. Lin, H.; Walsh, C. T. A Chemoenzymatic Approach to Glycopeptide Antibiotics. *J. Am. Chem. Soc.* **2004,** *126* (43), 13998–14003.
83. Zhu, L.; Tamvakopoulos, C.; Xie, D.; Dragovic, J.; Shen, X.; Fenyk-Melody, J. E.; Schmidt, K.; Bagchi, A.; Griffin, P. R.; Thornberry, N. A.; Sinha Roy, R. The Role of Dipeptidyl Peptidase IV in the Cleavage of Glucagon Family Peptides: in vivo Metabolism of Pituitary Adenylate Cyclase Activating Polypeptide-(1–38). *J. Biol. Chem.* **2003,** *278* (25), 22418–22423.
84. Bai, L.; Sheeley, S.; Sweedler, J. V. Analysis of Endogenous D-Amino Acid-Containing Peptides in Metazoa. *Bioanal. Rev.* **2009,** *1* (1), 7–24.
85. Tugyi, R.; Uray, K.; Iván, D.; Fellinger, E.; Perkins, A.; Hudecz, F. Partial D-Amino Acid Substitution: Improved Enzymatic Stability and Preserved Ab Recognition of a MUC2 Epitope Peptide. *Proc. Natl. Acad. Sci. U. S. A.* **2005,** *102* (2), 413–418.
86. (a) Mentlein, R.; Gallwitz, B.; Schmidt, W. E. Dipeptidyl-Peptidase IV Hydrolyses Gastric Inhibitory Polypeptide, Glucagon-Like Peptide-1(7–36)amide, Peptide Histidine Methionine and Is Responsible for Their Degradation in Human Serum. *Eur. J. Biochem.* **1993,** *214* (3), 829–835; (b) Montrose-Rafizadeh, C.; Yang, H.; Rodgers, B. D.; Beday, A.; Pritchette, L. A.; Eng, J. High Potency Antagonists of the Pancreatic Glucagon-Like Peptide-1 Receptor. *J. Biol. Chem.* **1997,** *272* (34), 21201–21206.
87. Sarrauste de Menthiere, C.; Chavanieu, A.; Grassy, G.; Dalle, S.; Salazar, G.; Kervran, A.; Pfeiffer, B.; Renard, P.; Delagrange, P.; Manechez, D.; Bakes, D.; Ktorza, A.; Calas, B. Structural Requirements of the N-Terminal Region of GLP-1-[7–37]-NH2 for Receptor Interaction and cAMP Production. *Eur. J. Med. Chem.* **2004,** *39* (6), 473–480.
88. Sawyer, T. K.; Sanfilippo, P. J.; Hruby, V. J.; Engel, M. H.; Heward, C. B.; Burnett, J. B.; Hadley, M. E. 4-Norleucine, 7-D-Phenylalanine-Alpha-Melanocyte-Stimulating Hormone: A Highly Potent Alpha-Melanotropin With Ultralong Biological Activity. *Proc. Natl. Acad. Sci. U. S. A.* **1980,** *77* (10), 5754–5758.
89. Mas-Moruno, C.; Rechenmacher, F.; Kessler, H. Cilengitide: The First Anti-Angiogenic Small Molecule Drug Candidate. Design, Synthesis and Clinical Evaluation. *Anticancer Agents Med. Chem.* **2010,** *10* (10), 753–768.
90. Kessler, H.; Kutscher, B.; Klein, A. Peptidkonformationen, 39. NMR-Studien zur Konformation von Cyclopentapeptidanalogen des Thymopoietins. *Liebigs Ann. Chem.* **1986,** *1986* (5), 893–913.
91. Liebmann, C.; Szücs, M.; Neubert, K.; Hartrodt, B.; Arold, H.; Barth, A. Opiate Receptor Binding Affinities of Some D-Amino Acid Substituted β-Casomorphin Analogs. *Peptides* **1986,** *7* (2), 195–199.
92. Kuwada, M.; Teramoto, T.; Kumagaye, K. Y.; Nakajima, K.; Watanabe, T.; Kawai, T.; Kawakami, Y.; Niidome, T.; Sawada, K.; Nishizawa, Y.; et al. Omega-Agatoxin-TK Containing D-Serine at Position 46, but Not Synthetic Omega-[L-Ser46]agatoxin-TK, Exerts Blockade of P-Type Calcium Channels in Cerebellar Purkinje Neurons. *Mol. Pharmacol.* **1994,** *46* (4), 587–593.
93. Zaoral, M.; Kolc, J.; Sorm, F. Amino acids and Peptides. LXXI. Synthesis of 1-Deamino-8-D-γ-aminobutyrine-vasopressin, 1-Deamino-8-D-lysine-vasopressin, and 1-Deamino-8-D-arginine-vasopressin. *Czech. Chem. Commun.* **1967,** *32* (3), 1250–1257.
94. (a) Rado, J. P.; Marosi, J.; Szende, L.; Borbely, L.; Tako, J.; Fischer, J. The Antidiuretic Action of 1-Deamino-8-D-arginine vasopressin (DDAVP) in Man. *Int. J. Clin. Pharmacol. Biopharm.* **1976,** *13* (3), 199–209; (b) Vilhardt, H.; Lundin, S. In Vitro Intestinal Transport of Vasopressin and Its Analogues. *Acta Physiol. Scand.* **1986,** *126* (4), 601–607.
95. CHMP assessment report for Firazyr. http://www.ema.europa.eu/docs/en_GB/document_library/EPAR_-_Public_assessment_report/human/000899/WC500022970.pdf.
96. Stahelin, H. F. The History of Cyclosporin A (Sandimmune) Revisited: Another Point of View. *Experientia* **1996,** *52* (1), 5–13.
97. Sterner, O.; Etzel, W.; Mayer, A.; Anke, H. Omphalotin, a New Cyclic Peptide With Potent Nematicidal Activity From *Omphalotus olearius* II. Isolation and Structure Determination. *Nat. Prod. Lett.* **1997,** *10* (1), 33–38.
98. Talpir, R.; Benayahu, Y.; Kashman, Y.; Pannell, L.; Schleyer, M. Hemiasterlin and Geodiamolide TA; Two New Cytotoxic Peptides From the Marine Sponge *Hemiasterella minor* (Kirkpatrick). *Tetrahedron Lett.* **1994,** *35* (25), 4453–4456.
99. Sagan, S.; Karoyan, P.; Lequin, O.; Chassaing, G.; Lavielle, S. N- and C Alpha-Methylation in Biologically Active Peptides: Synthesis, Structural and Functional Aspects. *Curr. Med. Chem.* **2004,** *11* (21), 2799–2822.
100. Laufer, B.; Chatterjee, J.; Frank, A. O.; Kessler, H. Can N-Methylated Amino Acids Serve as Substitutes for Prolines in Conformational Design of Cyclic Pentapeptides? *J. Pept. Sci.* **2009,** *15* (3), 141–146.
101. Chatterjee, J.; Ovadia, O.; Zahn, G.; Marinelli, L.; Hoffman, A.; Gilon, C.; Kessler, H. Multiple N-Methylation by a Designed Approach Enhances Receptor Selectivity. *J. Med. Chem.* **2007,** *50* (24), 5878–5881.
102. Velkova, A.; Tatarek-Nossol, M.; Andreetto, E.; Kapurniotu, A. Exploiting Cross-Amyloid Interactions to Inhibit Protein Aggregation but Not Function: Nanomolar Affinity Inhibition of Insulin Aggregation by an IAPP Mimic. *Angew. Chem. Int. Ed.* **2008,** *47* (37), 7114–7118.
103. Ovadia, O.; Greenberg, S.; Chatterjee, J.; Laufer, B.; Opperer, F.; Kessler, H.; Gilon, C.; Hoffman, A. The Effect of Multiple N-Methylation on Intestinal Permeability of Cyclic Hexapeptides. *Mol. Pharm.* **2011,** *8* (2), 479–487.
104. Dong, Q. G.; Zhang, Y.; Wang, M. S.; Feng, J.; Zhang, H. H.; Wu, Y. G.; Gu, T. J.; Yu, X. H.; Jiang, C. L.; Chen, Y.; Li, W.; Kong, W. Improvement of Enzymatic Stability and Intestinal Permeability of Deuterohemin-Peptide Conjugates by Specific Multi-Site N-Methylation. *Amino Acids* **2012,** *43* (6), 2431–2441.
105. Chatterjee, J.; Gilon, C.; Hoffman, A.; Kessler, H. N-Methylation of Peptides: A New Perspective in Medicinal Chemistry. *Acc. Chem. Res.* **2008,** *41* (10), 1331–1342.
106. Biron, E.; Kessler, H. Convenient Synthesis of N-Methylamino Acids Compatible With Fmoc Solid-Phase Peptide Synthesis. *J. Org. Chem.* **2005,** *70* (13), 5183–5189.
107. Miller, S. C.; Scanlan, T. S. Site-Selective N-Methylation of Peptides on Solid Support. *J. Am. Chem. Soc.* **1997,** *119* (9), 2301–2302.
108. (a) Chruma, J. J.; Sames, D.; Polt, R. General Method for the Synthesis of *N*-Methyl Amino Acids and *N*-Alkyl Amino Esters From O'Donnell's Schiff Bases. *Tetrahedron Lett.* **1997,** *38* (29), 5085–5086; (b) Wiśniewski, K.; Kołodziejczyk, A. S. Pmc-Protected Amino Acid Esters as Substrates in *N*-Alkylamino Acid Synthesis. *Tetrahedron Lett.* **1997,** *38* (3), 483–486; (c) Grieco, P. A.; Bahsas, A. Immonium Ion Based Synthetic Methodology: A Novel Method for the N-Methylation of Dipeptides and Amino Acid Derivatives via Retro Aza Diels-Alder Reactions. *J. Org. Chem.* **1987,** *52* (26), 5746–5749.
109. Biron, E.; Chatterjee, J.; Kessler, H. Optimized Selective N-Methylation of Peptides on Solid Support. *J. Pept. Sci.* **2006,** *12* (3), 213–219.
110. Reichwein, J. F.; Liskamp, R. M. J. Site-Specific N-Alkylation of Peptides on the Solid Phase. *Tetrahedron Lett.* **1998,** *39* (10), 1243–1246.
111. Vogt, H.; Brase, S. Recent Approaches Towards the Asymmetric Synthesis of [Small Alpha],[Small Alpha]-Disubstituted [Small Alpha]-Amino Acids. *Org. Biomol. Chem.* **2007,** *5* (3), 406–430.

112. Bey, P.; Gerhart, F.; Van Dorsselaer, V.; Danzin, C. Alpha-(Fluoromethyl)dehydroornithine and Alpha-(Fluoromethyl)dehydroputrescine Analogues as Irreversible Inhibitors of Ornithine Decarboxylase. *J. Med. Chem.* **1983,** *26* (11), 1551–1556.
113. Stein, G. A.; Bronner, H. A.; Pfister, K. α-Methyl α-Amino Acids. II.1 Derivatives of DL-Phenylalanine. *J. Am. Chem. Soc.* **1955,** *77* (3), 700–703.
114. Leitgeb, B.; Szekeres, A.; Manczinger, L.; Vágvölgyi, C.; Kredics, L. The History of Alamethicin: A Review of the Most Extensively Studied Peptaibol. *Chem. Biodivers.* **2007,** *4* (6), 1027–1051.
115. van Kraaij, C.; de Vos, W. M.; Siezen, R. J.; Kuipers, O. P. Lantibiotics: Biosynthesis, Mode of Action and Applications. *Nat. Prod. Rep.* **1999,** *16* (5), 575–587.
116. Karle, I. L.; Balaram, P. Structural Characteristics of Alpha-Helical Peptide Molecules Containing Aib Residues. *Biochemistry* **1990,** *29* (29), 6747–6756.
117. Bryant, S. D.; Guerrini, R.; Salvadori, S.; Bianchi, C.; Tomatis, R.; Attila, M.; Lazarus, L. H. Helix-Inducing α-Aminoisobutyric Acid in Opioid Mimetic Deltorphin C Analogues. *J. Med. Chem.* **1997,** *40* (16), 2579–2587.
118. Gilead, S.; Gazit, E. Inhibition of Amyloid Fibril Formation by Peptide Analogues Modified With α-Aminoisobutyric Acid. *Angew. Chem. Int. Ed.* **2004,** *43* (31), 4041–4044.
119. Cheng, R. P.; Gellman, S. H.; DeGrado, W. F. β-Peptides: From Structure to Function. *Chem. Rev.* **2001,** *101* (10), 3219–3232.
120. Seebach, D.; Beck, A. K.; Bierbaum, D. J. The World of β- and γ-Peptides Comprised of Homologated Proteinogenic Amino Acids and Other Components. *Chem. Biodivers.* **2004,** *1* (8), 1111–1239.
121. Martinek, T. A.; Fulop, F. Peptidic Foldamers: Ramping up Diversity. *Chem. Soc. Rev.* **2012,** *41* (2), 687–702.
122. Kudo, F.; Miyanaga, A.; Eguchi, T. Biosynthesis of Natural Products Containing [Small Beta]-Amino Acids. *Nat. Prod. Rep.* **2014,** *31* (8), 1056–1073.
123. Seebach, D.; Overhand, M.; Kühnle, F. N. M.; Martinoni, B.; Oberer, L.; Hommel, U.; Widmer, H. β-Peptides: Synthesis by Arndt-Eistert Homologation With Concomitant Peptide Coupling. Structure Determination by NMR and CD Spectroscopy and by X-ray Crystallography. Helical Secondary Structure of a β-Hexapeptide in Solution and Its Stability Towards Pepsin. *Helv. Chim. Acta* **1996,** *79* (4), 913–941.
124. Stephens, O. M.; Kim, S.; Welch, B. D.; Hodsdon, M. E.; Kay, M. S.; Schepartz, A. Inhibiting HIV Fusion With a Beta-Peptide Foldamer. *J. Am. Chem. Soc.* **2005,** *127* (38), 13126–13127.
125. Gademann, K.; Ernst, M.; Hoyer, D.; Seebach, D. Synthesis and Biological Evaluation of a Cyclo-β-Tetrapeptide as a Somatostatin Analogue. *Angew. Chem. Int. Ed.* **1999,** *38* (9), 1223–1226.
126. Denton, E. V.; Craig, C. J.; Pongratz, R. L.; Appelbaum, J. S.; Doerner, A. E.; Narayanan, A.; Shulman, G. I.; Cline, G. W.; Schepartz, A. A β-Peptide Agonist of the GLP-1 Receptor, a Class B GPCR. *Org. Lett.* **2013,** *15* (20), 5318–5321.
127. Karle, I. L.; Handa, B. K.; Hassall, C. H. The Conformation of the Cyclic Tetrapeptide L-Ser(O-t-Bu)-[beta]-Ala-Gly-L-[beta]-Asp(OMe) Containing a 14-Membered Ring. *Acta Crystallogr. Sect. B* **1975,** *31* (2), 555–560.
128. Clark, T. D.; Buehler, L. K.; Ghadiri, M. R. Self-Assembling Cyclic Beta-3-Peptide Nanotubes as Artificial Transmembrane Ion Channels. *J. Am. Chem. Soc.* **1998,** *120,* 651–656.
129. Mándity, I. M.; Wéber, E.; Martinek, T. A.; Olajos, G.; Tóth, G. K.; Vass, E.; Fülöp, F. Design of Peptidic Foldamer Helices: A Stereochemical Patterning Approach. *Angew. Chem. Int. Ed.* **2009,** *48* (12), 2171–2175.
130. Hook, D. F.; Bindschadler, P.; Mahajan, Y. R.; Sebesta, R.; Kast, P.; Seebach, D. The Proteolytic Stability of 'Designed' Beta-Peptides Containing Alpha-Peptide-Bond Mimics and of Mixed Alpha, Beta-Peptides: Application to the Construction of MHC-Binding Peptides. *Chem. Biodivers.* **2005,** *2* (5), 591–632.
131. Adessi, C.; Soto, C. Converting a Peptide Into a Drug: Strategies to Improve Stability and Bioavailability. *Curr. Med. Chem.* **2002,** *9* (9), 963–978.
132. Santagada, V.; Frecentese, F.; Fiorino, F.; Cirillo, D.; Perissutti, E.; Severino, B.; Terracciano, S.; Caliendo, G. A Valuable Synthesis of Reduced Peptide Bond by Microwave Irradiation. *QSAR Comb. Sci.* **2004,** *23* (10), 899–901.
133. Hudson, D.; Sharpe, R.; Szelke, M. Methionine Enkephalin and Isosteric Analogues. *Int. J. Pept. Protein Res.* **1980,** *15* (2), 122–129.
134. Szelke, M.; Leckie, B. J.; Tree, M.; Brown, A.; Grant, J.; Hallett, A.; Hughes, M.; Jones, D. M.; Lever, A. F. H-77: A Potent New Renin Inhibitor. In Vitro and In Vivo Studies. *Hypertension* **1982,** *4* (3 Pt 2), 59–69.
135. Spatola, A. F.; Agarwal, N. S.; Bettag, A. L.; Yankeelov, J. A., Jr.; Bowers, C. Y.; Vale, W. W. Synthesis and Biological Activities of Pseudopeptide Analogues of LH-RH: Agonists and Antagonists. *Biochem. Biophys. Res. Commun.* **1980,** *97* (3), 1014–1023.
136. Hann, M. M.; Sammes, P. G.; Kennewell, P. D.; Taylor, J. B. On Double Bond Isosteres of the Peptide Bond; an Enkephalin Analogue. *J. Chem. Soc., Chem. Commun.* **1980,** *5,* 234–235.
137. La Cour, T. F. M.; Hansen, H. A. S.; Clausen, K. I. M.; Lawesson, S. O. The Geometry of the Thiopeptide Unit. *Int. J. Pept. Protein Res.* **1983,** *22* (4), 509–512.
138. Clausen, K.; Thorsen, M.; Lawesson, S. O. Studies on Amino Acids and Peptides—I: Synthesis of *N*-Benzyloxycarbonylendo-Thiodipeptide Esters. *Tetrahedron* **1981,** *37* (21), 3635–3639.
139. Kajtár, M.; Hollósi, M.; Kajtár, J.; Majer, Z.; Kövér, K. E. Chiroptical Properties and Solution Conformations of Protected Endothiodipeptide Esters. *Tetrahedron* **1986,** *42* (14), 3931–3942.
140. Winitz, M.; Bloch-Frankenthal, L.; Izumiya, N.; Birnbaum, S. M.; Baker, C. G.; Greenstein, J. P. Studies on Diastereoisomeric α-Amino Acids and Corresponding α-Hydroxy Acids. VII. Influence of β-Configuration on Enzymic Susceptibility. *J. Am. Chem. Soc.* **1956,** *78* (11), 2423–2430.
141. Ewenson, A.; Laufer, R.; Chorev, M.; Selinger, Z.; Gilon, C. Ketomethylene Pseudopeptide Analogs of Substance P: Synthesis and Biological Activity. *J. Med. Chem.* **1986,** *29* (2), 295–299.
142. Camp, N. P.; Perrey, D. A.; Kinchington, D.; Hawkins, P. C. D.; Gani, D. Synthesis of Peptide Analogues Containing Phosphonamidate Methyl Ester Functionality: HIV-1 Proteinase Inhibitors Possessing Unique Cell Uptake Properties. *Biorg. Med. Chem.* **1995,** *3* (3), 297–312.
143. Helekar, S. A.; Patrick, J. Peptidyl Prolyl Cis-Trans Isomerase Activity of Cyclophilin A in Functional Homo-Oligomeric Receptor Expression. *Proc. Natl. Acad. Sci.* **1997,** *94* (10), 5432–5437.
144. Hamilton, G. S.; Steiner, J. P. Immunophilins: Beyond Immunosuppression. *J. Med. Chem.* **1998,** *41* (26), 5119–5143.
145. Steinkasserer, A.; Harrison, R.; Billich, A.; Hammerschmid, F.; Werner, G.; Wolff, B.; Peichl, P.; Palfi, G.; Schnitzel, W.; Mlynar, E. Mode of Action of SDZ NIM 811, a Nonimmunosuppressive Cyclosporin A Analog With Activity Against Human Immunodeficiency Virus Type 1 (HIV-1): Interference With Early and Late Events in HIV-1 Replication. *J. Virol.* **1995,** *69* (2), 814–824.
146. Bartlett, P. A.; Marlowe, C. K. Phosphonamidates as Transition-State Analog Inhibitors of Thermolysin. *Biochemistry* **1983,** *22* (20), 4618–4624.
147. Demange, L.; Moutiez, M.; Dugave, C. Synthesis and Evaluation of Glyψ(PO2R-N)Pro-Containing Pseudopeptides as Novel Inhibitors of the Human Cyclophilin hCyp-18. *J. Med. Chem.* **2002,** *45* (18), 3928–3933.
148. AndrÉ, F.; Boussard, G. U. Y.; Bayeul, D.; Didierjean, C.; Aubry, A.; Marraud, M. Aza-Peptides II. X-ray Structures of Aza-Alanine and Aza-Asparagine-Containing Peptides. *J. Pept. Res.* **1997,** *49* (6), 556–562.
149. Sabatino, D.; Proulx, C.; Pohankova, P.; Ong, H.; Lubell, W. D. Structure–Activity Relationships of GHRP-6 Azapeptide Ligands of the CD36 Scavenger Receptor by Solid-Phase Submonomer Azapeptide Synthesis. *J. Am. Chem. Soc.* **2011,** *133* (32), 12493–12506.
150. Laufer, B.; Frank, A. O.; Chatterjee, J.; Neubauer, T.; Mas-Moruno, C.; Kummerlöwe, G.; Kessler, H. The Impact of Amino Acid Side Chain Mutations in Conformational Design of Peptides and Proteins. *Chem. Eur. J.* **2010,** *16* (18), 5385–5390.
151. Spiegel, J.; Mas-Moruno, C.; Kessler, H.; Lubell, W. D. Cyclic Aza-Peptide Integrin Ligand Synthesis and Biological Activity. *J. Org. Chem.* **2012,** *77* (12), 5271–5278.
152. (a) Boukanoun, M. K.; Hou, X.; Nikolajev, L.; Ratni, S.; Olson, D.; Claing, A.; Laporte, S. A.; Chemtob, S.; Lubell, W. D. Investigation of the Active Turn Geometry for the Labour Delaying Activity of Indolizidinone and Azapeptide Modulators of the Prostaglandin F2[Small Alpha] Receptor. *Org. Biomol. Chem.* **2015,** *13* (28), 7750–7761; (b) Bourguet, C. B.; Goupil, E.; Tassy, D.; Hou, X.; Thouin, E.; Polyak, F.; Hébert, T. E.; Claing, A.; Laporte, S. A.; Chemtob, S.; Lubell, W. D. Targeting the Prostaglandin F2α Receptor for Preventing Preterm Labor With Azapeptide Tocolytics. *J. Med. Chem.* **2011,** *54* (17), 6085–6097.

153. (a) Cheeseright, T. J.; Daenke, S.; Elmore, D. T.; Jones, J. H. Azasulfonamidopeptides as Peptide Bond Hydrolysis Transition State Analogues. Part 2. Potential HIV-1 Proteinase Inhibitor. *J. Chem. Soc., Perkin Trans.* **1994,** *1* (14), 1953–1955; (b) Turcotte, S.; Lubell, W. D. Crystal Structure Analyses of Azasulfuryltripeptides Reveal Potential for γ-Turn Mimicry†. *Pept. Sci.* **2015,** *104* (5), 622–628.
154. Merlino, F.; Yousif, A. M.; Billard, É.; Dufour-Gallant, J.; Turcotte, S.; Grieco, P.; Chatenet, D.; Lubell, W. D. Urotensin II(4–11) Azasulfuryl Peptides: Synthesis and Biological Activity. *J. Med. Chem.* **2016,** *59* (10), 4740–4752.
155. Chorev, M.; Goodman, M. A Dozen Years of Retro-Inverso Peptidomimetics. *Acc. Chem. Res.* **1993,** *26* (5), 266–273.
156. (a) Fletcher, M. D.; Campbell, M. M. Partially Modified Retro-Inverso Peptides: Development, Synthesis, and Conformational Behavior. *Chem. Rev.* **1998,** *98* (2), 763–796; (b) Chorev, M. The Partial Retro-Inverso Modification: A Road Traveled Together. *Biopolymers* **2005,** *80* (2–3), 67–84.
157. Chorev, M.; Shavitz, R.; Goodman, M.; Minick, S.; Guillemin, R. Partially Modified Retro-Inverso-Enkephalinamides: Topochemical Long-Acting Analogs In Vitro and In Vivo. *Science* **1979,** *204* (4398), 1210–1212.
158. Bonny, C.; Oberson, A.; Negri, S.; Sauser, C.; Schorderet, D. F. Cell-Permeable Peptide Inhibitors of JNK: Novel Blockers of Beta-Cell Death. *Diabetes* **2001,** *50* (1), 77–82.
159. (a) Borsello, T.; Clarke, P. G.; Hirt, L.; Vercelli, A.; Repici, M.; Schorderet, D. F.; Bogousslavsky, J.; Bonny, C. A Peptide Inhibitor of c-Jun N-Terminal Kinase Protects Against Excitotoxicity and Cerebral Ischemia. *Nat. Med.* **2003,** *9* (9), 1180–1186; (b) Hirt, L.; Badaut, J.; Thevenet, J.; Granziera, C.; Regli, L.; Maurer, F.; Bonny, C.; Bogousslavsky, J. D-JNKI1, a Cell-Penetrating c-Jun-N-Terminal Kinase Inhibitor, Protects Against Cell Death in Severe Cerebral Ischemia. *Stroke* **2004,** *35* (7), 1738–1743.
160. Wei, X.; Zhan, C.; Shen, Q.; Fu, W.; Xie, C.; Gao, J.; Peng, C.; Zheng, P.; Lu, W. Back Cover: A D-Peptide Ligand of Nicotine Acetylcholine Receptors for Brain-Targeted Drug Delivery (Angew. Chem. Int. Ed. 10/2015). *Angew. Chem. Int. Ed.* **2015,** *54* (10), 3152.
161. Zhan, C.; Li, B.; Hu, L.; Wei, X.; Feng, L.; Fu, W.; Lu, W. Micelle-Based Brain-Targeted Drug Delivery Enabled by a Nicotine Acetylcholine Receptor Ligand. *Angew. Chem. Int. Ed.* **2011,** *50* (24), 5482–5485.
162. Wei, X.; Chen, X.; Ying, M.; Lu, W. Brain Tumor-Targeted Drug Delivery Strategies. *Acta Pharm. Sin. B* **2014,** *4* (3), 193–201.
163. (a) Stites, W. E. Protein Interactions: Interface Structure, Binding Thermodynamics, and Mutational Analysis. *Chem. Rev.* **1997,** *97* (5), 1233–1250; (b) Perkins, J. R.; Diboun, I.; Dessailly, B. H.; Lees, J. G.; Orengo, C. Transient Protein-Protein Interactions: Structural, Functional, and Network Properties. *Structure* **2010,** *18* (10), 1233–1243.
164. Tyndall, J. D.; Nall, T.; Fairlie, D. P. Proteases Universally Recognize Beta Strands in Their Active Sites. *Chem. Rev.* **2005,** *105* (3), 973–999.
165. Sood, A.; Panchagnula, R. Peroral Route: An Opportunity for Protein and Peptide Drug Delivery. *Chem. Rev.* **2001,** *101* (11), 3275–3303.
166. (a) Hill, T. A.; Shepherd, N. E.; Diness, F.; Fairlie, D. P. Constraining Cyclic Peptides to Mimic Protein Structure Motifs. *Angew. Chem. Int. Ed. Engl.* **2014,** *53* (48), 13020–13041; (b) Marsault, E.; Peterson, M. L. Macrocycles Are Great Cycles: Applications, Opportunities, and Challenges of Synthetic Macrocycles in Drug Discovery. *J. Med. Chem.* **2011,** *54* (7), 1961–2004.
167. (a) Gilon, C.; Halle, D.; Chorev, M.; Selinger, Z.; Byk, G. Backbone Cyclization: A New Method for Conferring Conformational Constraint on Peptides. *Biopolymers* **1991,** *31* (6), 745–750; (b) Burton, P. S.; Conradi, R. A.; Ho, N. F.; Hilgers, A. R.; Borchardt, R. T. How Structural Features Influence the Biomembrane Permeability of Peptides. *J. Pharm. Sci.* **1996,** *85* (12), 1336–1340; (c) McGeary, R. P.; Fairlie, D. P. Macrocyclic Peptidomimetics: Potential for Drug Development. *Curr. Opin. Drug Discov. Devel.* **1998,** *1* (2), 208–217.
168. Ruttenberg, M. A.; Mach, B. Studies on Amino Acid Substitution in the Biosynthesis of the Antibiotic Polypeptide Tyrocidine. *Biochemistry* **1966,** *5* (9), 2864–2869.
169. Loll, P. J.; Upton, E. C.; Nahoum, V.; Economou, N. J.; Cocklin, S. The High Resolution Structure of Tyrocidine A Reveals an Amphipathic Dimer. *Biochim. Biophys. Acta* **2014,** *1838* (5), 1199–1207.
170. Shai, Y. Mode of Action of Membrane Active Antimicrobial Peptides. *Biopolymers* **2002,** *66* (4), 236–248.
171. Kohli, R. M.; Walsh, C. T.; Burkart, M. D. Biomimetic Synthesis and Optimization of Cyclic Peptide Antibiotics. *Nature* **2002,** *418* (6898), 658–661.
172. Faulds, D.; Goa, K. L.; Benfield, P. Cyclosporin. A Review of Its Pharmacodynamic and Pharmacokinetic Properties, and Therapeutic Use in Immunoregulatory Disorders. *Drugs* **1993,** *45* (6), 953–1040.
173. Holt, D. W.; Mueller, E. A.; Kovarik, J. M.; van Bree, J. B.; Kutz, K. The Pharmacokinetics of Sandimmun Neoral: A New Oral Formulation of Cyclosporine. *Transplant. Proc.* **1994,** *26* (5), 2935–2939.
174. Wenger, R. M. Synthesis of Cyclosporine. Total Syntheses of 'Cyclosporin A' and 'Cyclosporin H', Two Fungal Metabolites Isolated From the Species *Tolypocladium inflatum* GAMS. *Helv. Chim. Acta* **1984,** *67* (2), 502–525.
175. Wu, X.; Stockdill, J. L.; Wang, P.; Danishefsky, S. J. Total Synthesis of Cyclosporine: Access to N-Methylated Peptides via Isonitrile Coupling Reactions. *J. Am. Chem. Soc.* **2010,** *132* (12), 4098–4100.
176. Koyama, Y.; Kurosasa, A.; Tsuchiya, A.; Takakuta, K. A New Antibiotic 'Colistin' Produced by Spore-Forming Soil Bacteria. *J. Antibiot. (Tokyo)* **1950,** *3,* 457–458.
177. Li, J.; Nation, R. L.; Milne, R. W.; Turnidge, J. D.; Coulthard, K. Evaluation of Colistin as an Agent Against Multi-Resistant Gram-Negative Bacteria. *Int. J. Antimicrob. Agents* **2005,** *25* (1), 11–25.
178. Velkov, T.; Thompson, P. E.; Nation, R. L.; Li, J. Structure–Activity Relationships of Polymyxin Antibiotics. *J. Med. Chem.* **2010,** *53* (5), 1898–1916.
179. Kline, T.; Holub, D.; Therrien, J.; Leung, T.; Ryckman, D. Synthesis and Characterization of the Colistin Peptide Polymyxin E1 and Related Antimicrobial Peptides. *J. Pept. Res.* **2001,** *57* (3), 175–187.
180. Dunkelberger, J. R.; Song, W. C. Complement and Its Role in Innate and Adaptive Immune Responses. *Cell Res.* **2010,** *20* (1), 34–50.
181. Makrides, S. C. Therapeutic Inhibition of the Complement System. *Pharmacol. Rev.* **1998,** *50* (1), 59–87.
182. Monk, P. N.; Scola, A. M.; Madala, P.; Fairlie, D. P. Function, Structure and Therapeutic Potential of Complement C5a Receptors. *Br. J. Pharmacol.* **2007,** *152* (4), 429–448.
183. Wong, A. K.; Finch, A. M.; Pierens, G. K.; Craik, D. J.; Taylor, S. M.; Fairlie, D. P. Small Molecular Probes for G-Protein-Coupled C5a Receptors: Conformationally Constrained Antagonists Derived From the C Terminus of the Human Plasma Protein C5a. *J. Med. Chem.* **1998,** *41* (18), 3417–3425.
184. Finch, A. M.; Wong, A. K.; Paczkowski, N. J.; Wadi, S. K.; Craik, D. J.; Fairlie, D. P.; Taylor, S. M. Low-Molecular-Weight Peptidic and Cyclic Antagonists of the Receptor for the Complement Factor C5a. *J. Med. Chem.* **1999,** *42* (11), 1965–1974.
185. Reid, R. C.; Abbenante, G.; Taylor, S. M.; Fairlie, D. P. A Convergent Solution-Phase Synthesis of the Macrocycle Ac-Phe-[Orn-Pro-D-Cha-Trp-Arg], a Potent New Antiinflammatory Drug. *J. Org. Chem.* **2003,** *68* (11), 4464–4471.
186. Reichlin, S. Somatostatin (Second of Two Parts). *N. Engl. J. Med.* **1983,** *309* (25), 1556–1563.
187. (a) Pohl, E.; Heine, A.; Sheldrick, G. M.; Dauter, Z.; Wilson, K. S.; Kallen, J.; Huber, W.; Pfaffli, P. J. Structure of Octreotide, a Somatostatin Analogue. *Acta Crystallogr. D Biol. Crystallogr.* **1995,** *51* (Pt 1), 48–59; (b) Hernández, B.; Coïc, Y.-M.; Kruglik, S. G.; Carelli, C.; Cohen, R.; Ghomi, M. Octreotide Used for Probing the Type-II′ β-Turn CD and Raman Markers. *J. Phys. Chem. B* **2012,** *116* (31), 9337–9345.
188. Bauer, W.; Briner, U.; Doepfner, W.; Haller, R.; Huguenin, R.; Marbach, P.; Petcher, T. J. Pless, SMS 201–995: A Very Potent and Selective Octapeptide Analogue of Somatostatin With Prolonged Action. *Life Sci.* **1982,** *31* (11), 1133–1140.
189. Anthony, L.; Freda, P. U. From Somatostatin to Octreotide LAR: Evolution of a Somatostatin Analogue. *Curr. Med. Res. Opin.* **2009,** *25* (12), 2989–2999.
190. Balaev, A. N.; Osipov, V. N.; Okhmanovich, K. A.; Reshetnikov, E. V.; Fedorov, A. E. A New Liquid-Phase Method for the Synthesis of Octreotide. *Pharm. Chem. J.* **2013,** *47* (7), 378–381.
191. Endean, R.; Gyr, P.; Surridge, J. The Pharmacological Actions on Guinea-Pig Ileum of Crude Venoms From the Marine Gastropods *Conus striatus* and *Conus magus*. *Toxicon* **1977,** *15* (4), 327–337.
192. Terlau, H.; Olivera, B. M. Conus Venoms: A Rich Source of Novel Ion Channel-Targeted Peptides. *Physiol. Rev.* **2004,** *84* (1), 41–68.
193. Arolas, J. L.; Aviles, F. X.; Chang, J.-Y.; Ventura, S. Folding of Small Disulfide-Rich Proteins: Clarifying the Puzzle. *Trends Biochem. Sci.* **2006,** *31* (5), 292–301.
194. Atherton, E.; Sheppard, R. C.; Ward, P. Peptide Synthesis. Part 7. Solid-Phase Synthesis of Conotoxin G1. *J. Chem. Soc., Perkin Trans.* **1985,** *1,* 2065–2073.

195. Cuthbertson, A.; Indrevoll, B. A Method for the One-Pot Regioselective Formation of the Two Disulfide Bonds of α-Conotoxin SI. *Tetrahedron Lett.* **2000,** *41* (19), 3661–3663.
196. Dolgin, E. Drug Pipeline Is Flush With New Options for Chronic Constipation. *Nat. Med.* **2012,** *18* (9), 1308–1309.
197. Pitari, G. M. Pharmacology and Clinical Potential of Guanylyl Cyclase C Agonists in the Treatment of Ulcerative Colitis. *Drug Des. Devel. Ther.* **2013,** *7*, 351–360.
198. Harris, L. A.; Crowell, M. D. Linaclotide, a New Direction in the Treatment of Irritable Bowel Syndrome and Chronic Constipation. *Curr. Opin. Mol. Ther.* **2007,** *9* (4), 403–410.
199. Gongora-Benitez, M.; Tulla-Puche, J.; Paradis-Bas, M.; Werbitzky, O.; Giraud, M.; Albericio, F. Optimized Fmoc Solid-Phase Synthesis of the Cysteine-Rich Peptide Linaclotide. *Biopolymers* **2011,** *96* (1), 69–80.
200. Wu, J.; Watson, J. T. Assignment of Disulfide Bonds in Proteins by Chemical Cleavage and Peptide Mapping by Mass Spectrometry. *Methods Mol. Biol.* **2002,** *194,* 1–22.
201. (a) Chhajlani, V.; Wikberg, J. E. S. Molecular Cloning and Expression of the Human Melanocyte Stimulating Hormone Receptor cDNA. *FEBS Lett.* **1992,** *309* (3), 417–420; (b) Mountjoy, K. G.; Robbins, L. S.; Mortrud, M. T.; Cone, R. D. The Cloning of a Family of Genes That Encode the Melanocortin Receptors. *Science* **1992,** *257* (5074), 1248–1251.
202. Eipper, B. A.; Mains, R. E. Structure and Biosynthesis of Pro-Adrenocorticotropin/Endorphin and Related Peptides. *Endocr. Rev.* **1980,** *1* (1), 1–27.
203. Li, C. H.; Hemmasi, B. Adrenocorticotropin. 40. Synthesis of a Protected Nonapeptide and of a Biogically Active Nonadecapeptide Related to Adrenocorticotropic Hormone. [5-Glutamine]adrenocorticotropin-(1–19). *J. Med. Chem.* **1972,** *15* (3), 217–219.
204. Al-Obeidi, F.; Castrucci, A. M. D. L.; Hadley, M. E.; Hruby, V. J. Potent and Prolonged-Acting Cyclic Lactam Analogs of Alpha-Melanotropin: Design Based on Molecular Dynamics. *J. Med. Chem.* **1989,** *32* (12), 2555–2561.
205. Hruby, V. J.; Lu, D.; Sharma, S. D.; Castrucci, A. L.; Kesterson, R. A.; Al-Obeidi, F. A.; Hadley, M. E.; Cone, R. D. Cyclic Lactam Alpha-Melanotropin Analogs of Ac-Nle4-Cyclo [Asp5, D-Phe7, Lys10]-Alpha-Melanocyte-Stimulating Hormone-(4–10)-NH2 With Bulky Aromatic Amino Acids at Position 7 Show High Antagonist Potency and Selectivity at Specific Melanocortin Receptors. *J. Med. Chem.* **1995,** *38* (18), 3454–3461.
206. (a) Wolozin, B. L.; Pasternak, G. W. Classification of Multiple Morphine and Enkephalin Binding Sites in the Central Nervous System. *Proc. Natl. Acad. Sci.* **1981,** *78* (10), 6181–6185; (b) Lord, J. A. H.; Waterfield, A. A.; Hughes, J.; Kosterlitz, H. W. Endogenous Opioid Peptides: Multiple Agonists and Receptors. *Nature* **1977,** *267* (5611), 495–499.
207. Schiller, P. W.; Eggimann, B.; DiMaio, J.; Lemieux, C.; Nguyen, T. M. D. Cyclic Enkephalin Analogs Containing a Cystine Bridge. *Biochem. Biophys. Res. Commun.* **1981,** *101* (2), 337–343.
208. Mosberg, H. I.; Hurst, R.; Hruby, V. J.; Galligan, J. J.; Burks, T. F.; Gee, K.; Yamamura, H. I. [D-Pen2, L-cys5]enkephalinamide and [D-Pen2, D-cys5]enkephalinamide, Conformationally Constrained Cyclic Enkephalinamide Analogs With Delta Receptor Specificity. *Biochem. Biophys. Res. Commun.* **1982,** *106* (2), 506–512.
209. Mosberg, H. I.; Hurst, R.; Hruby, V. J.; Galligan, J. J.; Burks, T. F.; Gee, K.; Yamamura, H. I. Conformationally Constrained Cyclic Enkephalin Analogs With Pronounced Delta Opioid Receptor Agonist Selectivity. *Life Sci.* **1983,** *32* (22), 2565–2569.
210. (a) Mosberg, H. I.; Hurst, R.; Hruby, V. J.; Gee, K.; Yamamura, H. I.; Galligan, J. J.; Burks, T. F. Bis-Penicillamine Enkephalins Possess Highly Improved Specificity Toward Delta Opioid Receptors. *Proc. Natl. Acad. Sci.* **1983,** *80* (19), 5871–5874; (b) Mosberg, H. I.; Hurst, R.; Hruby, V. J.; Gee, K.; Akiyama, K.; Yamamura, H. I.; Galligan, J. J.; Burks, T. F. Cyclic Penicillamine Containing Enkephalin Analogs Display Profound Delta Receptor Selectivities. *Life Sci.* **1983,** *33* (Suppl. 1), 447–450.
211. Hruby, V. J.; Kao, L. F.; Pettitt, B. M.; Karplus, M. The Conformational Properties of the Delta Opioid Peptide [Cyclic] [D-pen2, D-pen5]enkephalin in Aqueous Solution Determined by NMR and Energy Minimization Calculations. *J. Am. Chem. Soc.* **1988,** *110* (11), 3351–3359.
212. (a) Venkatachalam, C. M. Stereochemical Criteria for Polypeptides and Proteins. V. Conformation of a System of Three Linked Peptide Units. *Biopolymers* **1968,** *6* (10), 1425–1436; (b) Lewis, P. N.; Momany, F. A.; Scheraga, H. A. Chain Reversals in Proteins. *Biochim. Biophys. Acta* **1973,** *303* (2), 211–229; (c) Chou, P. Y.; Fasman, G. D. β-Turns in Proteins. *J. Mol. Biol.* **1977,** *115* (2), 135–175.
213. Chou, K. C. Prediction of Tight Turns and Their Types in Proteins. *Anal. Biochem.* **2000,** *286* (1), 1–16.
214. Hutchinson, E. G.; Thornton, J. M. A Revised Set of Potentials for Beta-Turn Formation in Proteins. *Protein Sci.* **1994,** *3* (12), 2207–2216.
215. Marcelino, A. M.; Gierasch, L. M. Roles of Beta-Turns in Protein Folding: From Peptide Models to Protein Engineering. *Biopolymers* **2008,** *89* (5), 380–391.
216. Ruiz-Gomez, G.; Tyndall, J. D.; Pfeiffer, B.; Abbenante, G.; Fairlie, D. P. Update 1 of: Over One Hundred Peptide-Activated G Protein-Coupled Receptors Recognize Ligands With Turn Structure. *Chem. Rev.* **2010,** *110* (4), Pr1-41.
217. Pelton, J. T.; Gulya, K.; Hruby, V. J.; Duckles, S. P.; Yamamura, H. I. Conformationally Restricted Analogs of Somatostatin With High Mu-Opiate Receptor Specificity. *Proc. Natl. Acad. Sci. U. S. A.* **1985,** *82* (1), 236–239.
218. Maurer, R.; Gaehwiler, B. H.; Buescher, H. H.; Hill, R. C.; Roemer, D. Opiate Antagonistic Properties of an Octapeptide Somatostatin Analog. *Proc. Natl. Acad. Sci.* **1982,** *79* (15), 4815–4817.
219. Hruby, V. J.; Agnes, R. S. Conformation-Activity Relationships of Opioid Peptides With Selective Activities at Opioid Receptors. *Biopolymers* **1999,** *51* (6), 391–410.
220. Sugg, E. E.; Tourwe, D.; Kazmierski, W.; Hruby, V. J.; Van Binst, G. Proton n.m.r. Investigation of Conformational Influence of Penicillamine Residues on the Disulfide Ring System of Opioid Receptor Selective Somatostatin Derivatives. *Int. J. Pept. Protein Res.* **1988,** *31* (2), 192–200.
221. Pelton, J. T.; Kazmierski, W.; Gulya, K.; Yamamura, H. I.; Hruby, V. J. Design and Synthesis of Conformationally Constrained Somatostatin Analogues With High Potency and Specificity for mu Opioid Receptors. *J. Med. Chem.* **1986,** *29* (11), 2370–2375.
222. Kazmierski, W.; Wire, W. S.; Lui, G. K.; Knapp, R. J.; Shook, J. E.; Burks, T. F.; Yamamura, H. I.; Hruby, V. J. Design and Synthesis of Somatostatin Analogues With Topographical Properties That Lead to Highly Potent and Specific mu Opioid Receptor Antagonists With Greatly Reduced Binding at Somatostatin Receptors. *J. Med. Chem.* **1988,** *31* (11), 2170–2177.
223. Nair, C. M.; Vijayan, M.; Venkatachalapathi, Y. V.; Balaram, P. X-Ray Crystal Structure of Pivaloyl-D-Pro-L-Pro-L-Ala-*N*-methylamide; Observation of a Consecutive [Small Beta]-Turn Conformation. *J. Chem. Soc., Chem. Commun.* **1979,** *24,* 1183–1184.
224. Bean, J. W.; Kopple, K. D.; Peishoff, C. E. Conformational Analysis of Cyclic Hexapeptides Containing the D-Pro-L-Pro Sequence to Fix Beta-Turn Positions. *J. Am. Chem. Soc.* **1992,** *114* (13), 5328–5334.
225. Sibanda, B. L.; Blundell, T. L.; Thornton, J. M. Conformation of Beta-Hairpins in Protein Structures. A Systematic Classification With Applications to Modelling by Homology, Electron Density Fitting and Protein Engineering. *J. Mol. Biol.* **1989,** *206* (4), 759–777.
226. Sibanda, B. L.; Thornton, J. M. [Beta]-Hairpin Families in Globular Proteins. *Nature* **1985,** *316* (6024), 170–174.
227. Rotondi, K. S.; Gierasch, L. M. Natural Polypeptide Scaffolds: Beta-Sheets, Beta-Turns, and Beta-Hairpins. *Biopolymers* **2006,** *84* (1), 13–22.
228. Chothia, C.; Lesk, A. M.; Tramontano, A.; Levitt, M.; Smith-Gill, S. J.; Air, G.; Sheriff, S.; Padlan, E. A.; Davies, D.; Tulip, W. R.; et al. Conformations of Immunoglobulin Hypervariable Regions. *Nature* **1989,** *342* (6252), 877–883.
229. Walter, M. R.; Windsor, W. T.; Nagabhushan, T. L.; Lundell, D. J.; Lunn, C. A.; Zauodny, P. J.; Narula, S. K. Crystal Structure of a Complex Between Interferon-[Gamma] and Its Soluble High-Affinity Receptor. *Nature* **1995,** *376* (6537), 230–235.
230. Oefner, C.; D'Arcy, A.; Winkler, F. K.; Eggimann, B.; Hosang, M. Crystal Structure of Human Platelet-Derived Growth Factor BB. *EMBO J.* **1992,** *11* (11), 3921–3926.
231. Xiong, J. P.; Stehle, T.; Zhang, R.; Joachimiak, A.; Frech, M.; Goodman, S. L.; Arnaout, M. A. Crystal Structure of the Extracellular Segment of Integrin Alpha Vbeta3 in Complex With an Arg-Gly-Asp Ligand. *Science* **2002,** *296* (5565), 151–155.
232. Kielian, M.; Rey, F. A. Virus Membrane-Fusion Proteins: More Than One Way to Make a Hairpin. *Nat. Rev. Microbiol.* **2006,** *4* (1), 67–76.
233. Robinson, J. A. Beta-Hairpin Peptidomimetics: Design, Structures and Biological Activities. *Acc. Chem. Res.* **2008,** *41* (10), 1278–1288.
234. Favre, M.; Moehle, K.; Jiang, L.; Pfeiffer, B.; Robinson, J. A. Structural Mimicry of Canonical Conformations in Antibody Hypervariable Loops Using Cyclic Peptides Containing a Heterochiral Diproline Template. *J. Am. Chem. Soc.* **1999,** *121* (12), 2679–2685.
235. Athanassiou, Z.; Dias, R. L.; Moehle, K.; Dobson, N.; Varani, G.; Robinson, J. A. Structural Mimicry of Retroviral tat Proteins by Constrained Beta-Hairpin Peptidomimetics: Ligands With High Affinity and Selectivity for Viral TAR RNA Regulatory Elements. *J. Am. Chem. Soc.* **2004,** *126* (22), 6906–6913.

236. Leeper, T. C.; Athanassiou, Z.; Dias, R. L.; Robinson, J. A.; Varani, G. TAR RNA Recognition by a Cyclic Peptidomimetic of Tat Protein. *Biochemistry* **2005,** *44* (37), 12362–12372.
237. Athanassiou, Z.; Patora, K.; Dias, R. L.; Moehle, K.; Robinson, J. A.; Varani, G. Structure-Guided Peptidomimetic Design Leads to Nanomolar Beta-Hairpin Inhibitors of the Tat-TAR Interaction of Bovine Immunodeficiency Virus. *Biochemistry* **2007,** *46* (3), 741–751.
238. Fasan, R.; Dias, R. L.; Moehle, K.; Zerbe, O.; Vrijbloed, J. W.; Obrecht, D.; Robinson, J. A. Using a Beta-Hairpin to Mimic an Alpha-Helix: Cyclic Peptidomimetic Inhibitors of the p53-HDM2 Protein-Protein Interaction. *Angew. Chem. Int. Ed. Engl.* **2004,** *43* (16), 2109–2112.
239. Garcia-Echeverria, C.; Chene, P.; Blommers, M. J.; Furet, P. Discovery of Potent Antagonists of the Interaction Between Human Double Minute 2 and Tumor Suppressor p53. *J. Med. Chem.* **2000,** *43* (17), 3205–3208.
240. Fasan, R.; Dias, R. L.; Moehle, K.; Zerbe, O.; Obrecht, D.; Mittl, P. R.; Grutter, M. G.; Robinson, J. A. Structure-Activity Studies in a Family of Beta-Hairpin Protein Epitope Mimetic Inhibitors of the p53-HDM2 Protein-Protein Interaction. *Chembiochem* **2006,** *7* (3), 515–526.
241. Aguzzi, A.; O'Connor, T. Protein Aggregation Diseases: Pathogenicity and Therapeutic Perspectives. *Nat. Rev. Drug Discov.* **2010,** *9* (3), 237–248.
242. Knowles, T. P. J.; Vendruscolo, M.; Dobson, C. M. The Amyloid State and Its Association With Protein Misfolding Diseases. *Nat. Rev. Mol. Cell Biol.* **2014,** *15* (6), 384–396.
243. Greenwald, J.; Riek, R. Biology of Amyloid: Structure, Function, and Regulation. *Structure* **2010,** *18* (10), 1244–1260.
244. Nowick, J. S. Exploring β-Sheet Structure and Interactions With Chemical Model Systems. *Acc. Chem. Res.* **2008,** *41* (10), 1319–1330.
245. Khakshoor, O.; Lin, A. J.; Korman, T. P.; Sawaya, M. R.; Tsai, S. C.; Eisenberg, D.; Nowick, J. S. X-Ray Crystallographic Structure of an Artificial Beta-Sheet Dimer. *J. Am. Chem. Soc.* **2010,** *132* (33), 11622–11628.
246. Cheng, P.-N.; Liu, C.; Zhao, M.; Eisenberg, D.; Nowick, J. S. Amyloid β-Sheet Mimics That Antagonize Protein Aggregation and Reduce Amyloid Toxicity. *Nat. Chem.* **2012,** *4* (11), 927–933.
247. (a) Peczuh, M. W.; Hamilton, A. D. Peptide and Protein Recognition by Designed Molecules. *Chem. Rev.* **2000,** *100* (7), 2479–2494; (b) Mohan, A.; Oldfield, C. J.; Radivojac, P.; Vacic, V.; Cortese, M. S.; Dunker, A. K.; Uversky, V. N. Analysis of Molecular Recognition Features (MoRFs). *J. Mol. Biol.* **2006,** *362* (5), 1043–1059; (c) Kohn, W. D.; Mant, C. T.; Hodges, R. S. α-Helical Protein Assembly Motifs. *J. Biol. Chem.* **1997,** *272* (5), 2583–2586; (d) Jochim, A. L.; Arora, P. S. Assessment of Helical Interfaces in Protein-Protein Interactions. *Mol. Biosyst.* **2009,** *5* (9), 924–926; (e) Bullock, B. N.; Jochim, A. L.; Arora, P. S. Assessing Helical Protein Interfaces for Inhibitor Design. *J. Am. Chem. Soc.* **2011,** *133* (36), 14220–14223.
248. Davis, J. M.; Tsou, L. K.; Hamilton, A. D. Synthetic Non-Peptide Mimetics of Alpha-Helices. *Chem. Soc. Rev.* **2007,** *36* (2), 326–334.
249. (a) Schneider, J. P.; Kelly, J. W. Templates That Induce Alpha-Helical, Beta-Sheet, and Loop Conformations. *Chem. Rev.* **1995,** *95* (6), 2169–2187; (b) Doig, A. J. Recent Advances in Helix-Coil Theory. *Biophys. Chem.* **2002,** *101–102,* 281–293.
250. Walensky, L. D.; Kung, A. L.; Escher, I.; Malia, T. J.; Barbuto, S.; Wright, R. D.; Wagner, G.; Verdine, G. L.; Korsmeyer, S. J. Activation of Apoptosis In Vivo by a Hydrocarbon-Stapled BH3 Helix. *Science* **2004,** *305* (5689), 1466–1470.
251. Andrews, M. J. I.; Tabor, A. B. Forming Stable Helical Peptides Using Natural and Artificial Amino Acids. *Tetrahedron* **1999,** *55* (40), 11711–11743.
252. Felix, A. M.; Heimer, E. P.; Wang, C. T.; Lambros, T. J.; Fournier, A.; Mowles, T. F.; Maines, S.; Campbell, R. M.; Wegrzynski, B. B.; Toome, V.; et al. Synthesis, Biological Activity and Conformational Analysis of Cyclic GRF Analogs. *Int. J. Pept. Protein Res.* **1988,** *32* (6), 441–454.
253. Shepherd, N. E.; Hoang, H. N.; Abbenante, G.; Fairlie, D. P. Single Turn Peptide Alpha Helices With Exceptional Stability in Water. *J. Am. Chem. Soc.* **2005,** *127* (9), 2974–2983.
254. Taylor, J. W. The Synthesis and Study of Side-Chain Lactam-Bridged Peptides. *Biopolymers* **2002,** *66* (1), 49–75.
255. Jackson, D. Y.; Prudent, J. R.; Baldwin, E. P.; Schultz, P. G. A Mutagenesis Study of a Catalytic Antibody. *Proc. Natl. Acad. Sci. U. S. A.* **1991,** *88* (1), 58–62.
256. Galande, A. K.; Bramlett, K. S.; Trent, J. O.; Burris, T. P.; Wittliff, J. L.; Spatola, A. F. Potent Inhibitors of LXXLL-Based Protein-Protein Interactions. *Chembiochem* **2005,** *6* (11), 1991–1998.
257. Blackwell, H. E.; Grubbs, R. H. Highly Efficient Synthesis of Covalently Cross-Linked Peptide Helices by Ring-Closing Metathesis. *Angew. Chem. Int. Ed.* **1998,** *37* (23), 3281–3284.
258. (a) Schafmeister, C. E.; Po, J.; Verdine, G. L. An All-Hydrocarbon Cross-Linking System for Enhancing the Helicity and Metabolic Stability of Peptides. *J. Am. Chem. Soc.* **2000,** *122* (24), 5891–5892; (b) Walensky, L. D.; Bird, G. H. Hydrocarbon-Stapled Peptides: Principles, Practice, and Progress. *J. Med. Chem.* **2014,** *57* (15), 6275–6288.
259. (a) Ghadiri, M. R.; Choi, C. Secondary Structure Nucleation in Peptides. Transition Metal Ion Stabilized Alpha-Helices. *J. Am. Chem. Soc.* **1990,** *112* (4), 1630–1632; (b) Ruan, F.; Chen, Y.; Hopkins, P. B. Metal Ion-Enhanced Helicity in Synthetic Peptides Containing Unnatural, Metal-Ligating Residues. *J. Am. Chem. Soc.* **1990,** *112* (25), 9403–9404.
260. Marqusee, S.; Baldwin, R. L. Helix Stabilization by Glu-…Lys+ Salt Bridges in Short Peptides of De Novo Design. *Proc. Natl. Acad. Sci. U. S. A.* **1987,** *84* (24), 8898–8902.
261. Woolley, G. A. Photocontrolling Peptide Alpha Helices. *Acc. Chem. Res.* **2005,** *38* (6), 486–493.
262. Jiang, G.; Zhang, B. B. Glucagon and Regulation of Glucose Metabolism. *Am. J. Physiol. Endocrinol. Metab.* **2003,** *284* (4), E671–E678.
263. Krstenansky, J. L.; Trivedi, D.; Johnson, D.; Hruby, V. J. Conformational Considerations in the Design of a Glucagon Analog With Increased Receptor Binding and Adenylate Cyclase Potencies. *J. Am. Chem. Soc.* **1986,** *108* (7), 1696–1698.
264. Ahn, J. M.; Gitu, P. M.; Medeiros, M.; Swift, J. R.; Trivedi, D.; Hruby, V. J. A New Approach to Search for the Bioactive Conformation of Glucagon: Positional Cyclization Scanning. *J. Med. Chem.* **2001,** *44* (19), 3109–3116.
265. Holst, J. J.; Deacon, C. F.; Vilsboll, T.; Krarup, T.; Madsbad, S. Glucagon-Like Peptide-1, Glucose Homeostasis and Diabetes. *Trends Mol. Med.* **2008,** *14* (4), 161–168.
266. Murage, E. N.; Schroeder, J. C.; Beinborn, M.; Ahn, J. M. Search for Alpha-Helical Propensity in the Receptor-Bound Conformation of Glucagon-Like Peptide-1. *Bioorg. Med. Chem.* **2008,** *16* (23), 10106–10112.
267. Murage, E. N.; Gao, G.; Bisello, A.; Ahn, J. M. Development of Potent Glucagon-Like Peptide-1 Agonists With High Enzyme Stability via Introduction of Multiple Lactam Bridges. *J. Med. Chem.* **2010,** *53* (17), 6412–6420.
268. Manandhar, B.; Lo, S.-T.; Murage, E.; Lin, M.; Sun, X.; Ahn, J.-M. Targeting GLP-1R for Non-Invasive Assessment of Pancreatic Beta-Cell Mass. In Lebl, M., EdPeptides Across the Pacific: Proceedings of the 23rd American Peptide Symposium; American Peptide Society: San Diego, CA, 2013; pp 172–173.
269. McLellan, J. S.; Ray, W. C.; Peeples, M. E. Structure and Function of Respiratory Syncytial Virus Surface Glycoproteins. *Curr. Top. Microbiol. Immunol.* **2013,** *372,* 83–104.
270. Shepherd, N. E.; Hoang, H. N.; Desai, V. S.; Letouze, E.; Young, P. R.; Fairlie, D. P. Modular Alpha-Helical Mimetics With Antiviral Activity Against Respiratory Syncitial Virus. *J. Am. Chem. Soc.* **2006,** *128* (40), 13284–13289.
271. Wade, M.; Li, Y. C.; Wahl, G. M. MDM2, MDMX and p53 in Oncogenesis and Cancer Therapy. *Nat. Rev. Cancer* **2013,** *13* (2), 83–96.
272. Tao, W.; Levine, A. J. Nucleocytoplasmic Shuttling of Oncoprotein Hdm2 is Required for Hdm2-Mediated Degradation of p53. *Proc. Natl. Acad. Sci. U. S. A.* **1999,** *96* (6), 3077–3080.
273. Marine, J. C.; Dyer, M. A.; Jochemsen, A. G. MDMX: From Bench to Bedside. *J. Cell Sci.* **2007,** *120* (Pt 3), 371–378.
274. Hu, B.; Gilkes, D. M.; Chen, J. Efficient p53 Activation and Apoptosis by Simultaneous Disruption of Binding to MDM2 and MDMX. *Cancer Res.* **2007,** *67* (18), 8810–8817.
275. Bernal, F.; Tyler, A. F.; Korsmeyer, S. J.; Walensky, L. D.; Verdine, G. L. Reactivation of the p53 Tumor Suppressor Pathway by a Stapled p53 Peptide. *J. Am. Chem. Soc.* **2007,** *129* (9), 2456–2457.
276. Zhang, Y.; Xiong, Y. A p53 Amino-Terminal Nuclear Export Signal Inhibited by DNA Damage-Induced Phosphorylation. *Science* **2001,** *292* (5523), 1910–1915.
277. Li, M.; Brooks, C. L.; Wu-Baer, F.; Chen, D.; Baer, R.; Gu, W. Mono- Versus Polyubiquitination: Differential Control of p53 Fate by Mdm2. *Science* **2003,** *302* (5652), 1972–1975.
278. Baek, S.; Kutchukian, P. S.; Verdine, G. L.; Huber, R.; Holak, T. A.; Lee, K. W.; Popowicz, G. M. Structure of the Stapled p53 Peptide Bound to Mdm2. *J. Am. Chem. Soc.* **2012,** *134* (1), 103–106.

279. Chang, Y. S.; Graves, B.; Guerlavais, V.; Tovar, C.; Packman, K.; To, K. H.; Olson, K. A.; Kesavan, K.; Gangurde, P.; Mukherjee, A.; Baker, T.; Darlak, K.; Elkin, C.; Filipovic, Z.; Qureshi, F. Z.; Cai, H.; Berry, P.; Feyfant, E.; Shi, X. E.; Horstick, J.; Annis, D. A.; Manning, A. M.; Fotouhi, N.; Nash, H.; Vassilev, L. T.; Sawyer, T. K. Stapled Alpha-Helical Peptide Drug Development: A Potent Dual Inhibitor of MDM2 and MDMX for p53-Dependent Cancer Therapy. *Proc. Natl. Acad. Sci. U. S. A.* **2013,** *110* (36), E3445–E3454.
280. Zimm, B. H.; Bragg, J. K. Theory of the Phase Transition Between Helix and Random Coil in Polypeptide Chains. *J. Chem. Phys.* **1959,** *31* (2), 526–535.
281. Kemp, D. S.; Curran, T. P.; Boyd, J. G.; Allen, T. J. Studies of N-Terminal Templates for Alpha-Helix Formation. Synthesis and Conformational Analysis of Peptide Conjugates of (2S,5S,8S,11S)-1-Acetyl-1,4-diaza-3-keto-5-carboxy-10-thiatricyclo[2.8.1.04,8]tridecane (Ac-Hel1-OH). *J. Org. Chem.* **1991,** *56* (23), 6683–6697.
282. Cabezas, E.; Satterthwait, A. C. The Hydrogen Bond Mimic Approach: Solid-Phase Synthesis of a Peptide Stabilized as an α-Helix With a Hydrazone Link. *J. Am. Chem. Soc.* **1999,** *121* (16), 3862–3875.
283. (a) Chapman, R. N.; Dimartino, G.; Arora, P. S. A Highly Stable Short Alpha-Helix Constrained by a Main-Chain Hydrogen-Bond Surrogate. *J. Am. Chem. Soc.* **2004,** *126* (39), 12252–12253; (b) Patgiri, A.; Jochim, A. L.; Arora, P. S. A Hydrogen Bond Surrogate Approach for Stabilization of Short Peptide Sequences in Alpha-Helical Conformation. *Acc. Chem. Res.* **2008,** *41* (10), 1289–1300.
284. Poon, E.; Harris, A. L.; Ashcroft, M. Targeting the Hypoxia-Inducible Factor (HIF) Pathway in Cancer. *Expert Rev. Mol. Med.* **2009,** *11,* e26.
285. Dames, S. A.; Martinez-Yamout, M.; De Guzman, R. N.; Dyson, H. J.; Wright, P. E. Structural Basis for Hif-1 Alpha/CBP Recognition in the Cellular Hypoxic Response. *Proc. Natl. Acad. Sci. U. S. A.* **2002,** *99* (8), 5271–5276.
286. Kushal, S.; Lao, B. B.; Henchey, L. K.; Dubey, R.; Mesallati, H.; Traaseth, N. J.; Olenyuk, B. Z.; Arora, P. S. Protein Domain Mimetics as in vivo Modulators of Hypoxia-Inducible Factor Signaling. *Proc. Natl. Acad. Sci. U. S. A.* **2013,** *110* (39), 15602–15607.
287. Cheng, R. P.; Gellman, S. H.; DeGrado, W. F. Beta-Peptides: From Structure to Function. *Chem. Rev.* **2001,** *101* (10), 3219–3232.
288. Horne, W. S.; Gellman, S. H. Foldamers With Heterogeneous Backbones. *Acc. Chem. Res.* **2008,** *41* (10), 1399–1408.
289. Kritzer, J. A.; Lear, J. D.; Hodsdon, M. E.; Schepartz, A. Helical Beta-Peptide Inhibitors of the p53-hDM2 Interaction. *J. Am. Chem. Soc.* **2004,** *126* (31), 9468–9469.
290. Parks, D. J.; Lafrance, L. V.; Calvo, R. R.; Milkiewicz, K. L.; Gupta, V.; Lattanze, J.; Ramachandren, K.; Carver, T. E.; Petrella, E. C.; Cummings, M. D.; Maguire, D.; Grasberger, B. L.; Lu, T. 1,4-Benzodiazepine-2,5-diones as Small Molecule Antagonists of the HDM2-p53 Interaction: Discovery and SAR. *Bioorg. Med. Chem. Lett.* **2005,** *15* (3), 765–770.
291. Bautista, A. D.; Appelbaum, J. S.; Craig, C. J.; Michel, J.; Schepartz, A. Bridged Beta(3)-Peptide Inhibitors of p53-hDM2 Complexation: Correlation Between Affinity and Cell Permeability. *J. Am. Chem. Soc.* **2010,** *132* (9), 2904–2906.
292. Sadowsky, J. D.; Schmitt, M. A.; Lee, H. S.; Umezawa, N.; Wang, S.; Tomita, Y.; Gellman, S. H. Chimeric (Alpha/Beta + Alpha)-Peptide Ligands for the BH3-Recognition Cleft of Bcl-XL: Critical Role of the Molecular Scaffold in Protein Surface Recognition. *J. Am. Chem. Soc.* **2005,** *127* (34), 11966–11968.
293. Horne, W. S.; Boersma, M. D.; Windsor, M. A.; Gellman, S. H. Sequence-Based Design of Alpha/Beta-Peptide Foldamers That Mimic BH3 Domains. *Angew. Chem. Int. Ed. Engl.* **2008,** *47* (15), 2853–2856.
294. Lee, E. F.; Smith, B. J.; Horne, W. S.; Mayer, K. N.; Evangelista, M.; Colman, P. M.; Gellman, S. H.; Fairlie, W. D. Structural Basis of Bcl-xL Recognition by a BH3-Mimetic Alpha/Beta-Peptide Generated by Sequence-Based Design. *Chembiochem* **2011,** *12* (13), 2025–2032.
295. Boersma, M. D.; Haase, H. S.; Peterson-Kaufman, K. J.; Lee, E. F.; Clarke, O. B.; Colman, P. M.; Smith, B. J.; Horne, W. S.; Fairlie, W. D.; Gellman, S. H. Evaluation of Diverse Alpha/Beta-Backbone Patterns for Functional Alpha-Helix Mimicry: Analogues of the Bim BH3 Domain. *J. Am. Chem. Soc.* **2012,** *134* (1), 315–323.
296. Falciani, C.; Lozzi, L.; Pini, A.; Bracci, L. Bioactive Peptides From Libraries. *Chem. Biol.* **2005,** *12* (4), 417–426.
297. Geysen, H. M.; Meloen, R. H.; Barteling, S. J. Use of Peptide Synthesis to Probe Viral Antigens for Epitopes to a Resolution of a Single Amino Acid. *Proc. Natl. Acad. Sci. U. S. A.* **1984,** *81* (13), 3998–4002.
298. Houghten, R. A. General Method for the Rapid Solid-Phase Synthesis of Large Numbers of Peptides: Specificity of Antigen-Antibody Interaction at the Level of Individual Amino Acids. *Proc. Natl. Acad. Sci. U. S. A.* **1985,** *82* (15), 5131–5135.
299. Frank, R. Spot-Synthesis: An Easy Technique for the Positionally Addressable, Parallel Chemical Synthesis on a Membrane Support. *Tetrahedron* **1992,** *48* (42), 9217–9232.
300. Fodor, S. P.; Read, J. L.; Pirrung, M. C.; Stryer, L.; Lu, A. T.; Solas, D. Light-Directed, Spatially Addressable Parallel Chemical Synthesis. *Science* **1991,** *251* (4995), 767–773.
301. Lam, K. S.; Salmon, S. E.; Hersh, E. M.; Hruby, V. J.; Kazmierski, W. M.; Knapp, R. J. A New Type of Synthetic Peptide Library for Identifying Ligand-Binding Activity. *Nature* **1991,** *354* (6348), 82–84.
302. Ostresh, J. M.; Winkle, J. H.; Hamashin, V. T.; Houghten, R. A. Peptide Libraries: Determination of Relative Reaction Rates of Protected Amino Acids in Competitive Couplings. *Biopolymers* **1994,** *34* (12), 1681–1689.
303. Houghten, R. A.; Pinilla, C.; Blondelle, S. E.; Appel, J. R.; Dooley, C. T.; Cuervo, J. H. Generation and Use of Synthetic Peptide Combinatorial Libraries for Basic Research and Drug Discovery. *Nature* **1991,** *354* (6348), 84–86.
304. Pinilla, C.; Appel, J. R.; Blanc, P.; Houghten, R. A. Rapid Identification of High Affinity Peptide Ligands Using Positional Scanning Synthetic Peptide Combinatorial Libraries. *Biotechniques* **1992,** *13* (6), 901–905.
305. Smith, G. P. Filamentous Fusion Phage: Novel Expression Vectors That Display Cloned Antigens on the Virion Surface. *Science* **1985,** *228* (4705), 1315–1317.

6.04 Chimeric Somatostatin–Dopamine Compounds (Dopastatins) for the Treatment of Neuroendocrine Disease

J Hill, S Kim*, and N Tsomaia, Ipsen Bioscience, Inc, Cambridge, MA, United States
JZ Dong*, Neon Therapeutics, Cambridge, MA, United States
M Culler, Ipsen Bioscience, Inc, Cambridge, MA, United States

© 2017 Elsevier Ltd. All rights reserved.

6.04.1	**Introduction**	116
6.04.2	**Somatostatin**	117
6.04.2.1	Lanreotide (Somatuline®) and Octreotide (Sandostatin®)	117
6.04.2.2	Mechanism of Action	117
6.04.2.3	Initial Design: Selection of the SST Agonist Peptide Fragment	119
6.04.2.4	Initial Design: Selection of the DA Receptor Agonist Fragments	120
6.04.2.5	Dopastatin Synthesis and Structure–Activity Relationship	122
6.04.3	**Profiling of BIM-23A760**	124
6.04.3.1	BIM-23A760 Phase 1 Clinical Studies	125
6.04.3.2	BIM-23A760 Phase 2a and b Clinical Studies	126
6.04.3.3	BIM-23A760 Metabolite Analysis	126
6.04.4	**Second-Generation Dopastatin Design Concepts**	127
6.04.5	**Second-Generation Design and Discovery of Lead Compound BIM-065**	128
6.04.6	**Second-Generation Dopastatin: Current Status**	129
References		129
Relevant Websites		130

Abbreviations

D2R Dopamine receptor type 2
DA Dopamine agonists
Dop1 Dopamine fragments with N-6 methyl group
Dop2 Dopamine fragments with N-6 propyl group
GH Growth hormone
IGF1 Insulin-like growth factor 1
PK Pharmacokinetics
PRL Prolactin
SC Subcutaneous
SST Somatostatin
SSTR2 Type 2 somatostatin receptor
SSTR5 Type 5 somatostatin receptor

6.04.1 Introduction

The development of somatostatin–dopamine chimeric compounds began with the search for more effective therapies for acromegaly. Acromegaly, which is caused by chronic, excess growth hormone (GH) secretion, is nearly always due to a benign tumor of the somatotroph cells of the pituitary gland. GH is one of the main factors responsible for regulation of growth and metabolism. Its production and release are normally tightly regulated through the dual action of two factors originating in the hypothalamic region of the brain: which stimulates the release of GH, and somatostatin (SST), which inhibits GH secretion. GH acts by binding to and activating specific receptors in the liver which results in the production and release of insulin-like growth factor 1 (IGF1), which is the primary effector of GH action. In addition to inducing growth and metabolic actions, circulating levels of IGF1 feedback to act on both the hypothalamus and the pituitary, to suppress GH secretion. When a somatotroph tumor (somatotropinoma) develops, GH secretion escapes the normal regulatory mechanisms and is secreted in excess, resulting in excess production of IGF1. When a somatotroph tumor occurs prior to the closure of the epiphyseal plates at the time of puberty, the excess GH and IGF1 production induces excess growth that can result in gigantism. Following puberty, and closure of the epiphyseal plates, excess GH and IGF1 induce growth of the soft tissues with resulting in physical changes in appearance, significant morbidity, and potentially, mortality.

*IPSEN employees

6.04.2 Somatostatin

SST was first isolated from hypothalamic extracts in 1973, based on the suppression of GH secretion from cultured rat anterior pituitary cells.[1] The ability of SST to suppress GH is the basis for the development of several therapeutic SST analogs that retain the GH-suppressing property of natural SST, but have greatly enhanced metabolic stability and circulating half-lives. SST analogs are the most widely used medical therapy for controlling GH secretion in acromegaly; however, they are only fully effective in normalizing GH and IGF1 in approximately 35% of patients,[2] as illustrated in Fig. 1.

6.04.2.1 Lanreotide (Somatuline®) and Octreotide (Sandostatin®)

Part of the explanation as to why the current SST analogs are not more effective is due to the lack of information available for SST receptors (SSTRs) at the time of their development. The currently used analogs, lanreotide (Somatuline®) and octreotide (Sandostatin®) (Fig. 2), were developed prior to the elucidation of the SSTRs, and were optimized on the basis of minimizing the recognized ability of SST to suppress insulin, while maximizing the suppression of GH in rat models.[3–6] With the discovery of five distinct SSTRs, it was found that the type 2 SSTR (SSTR2) is the primary receptor responsible for suppressing GH secretion in the rat.[7] Consequently, both lanreotide and octreotide are highly potent at SSTR2 (Table 1).

6.04.2.2 Mechanism of Action

Later studies, utilizing human pituitary cells, revealed that in humans, unlike rats, both SSTR2 and SSTR5 suppress GH secretion,[7] and that activation of both receptors results in significantly greater suppression of GH than either alone.[10] Recognizing that natural SST has the ability to activate all five of the SSTRs, the combined activation of SSTR2 and SSTR5 is likely the mechanism by which GH secretion is normally suppressed in humans. This finding further suggests that one of the key factors responsible for the rather low percentage of acromegalic patients that are fully normalized by the currently available SST analogs is the need for greater activation of SSTR5, in combination with the ability to effectively activate SSTR2.

The concept that potent activation of both SSTR2 and 5 induces greater efficacy in suppressing GH than activation of SSTR2 alone is further substantiated by studies in cultured, human GH-secreting tumor cells using a potent, bi-selective activator of both the SSTR2 and 5 receptors, BIM-23244. Tumor cells were collected from acromegalic patients classified as either fully or only partially controlled clinically by the current SST analog, octreotide, and placed into culture. When tested in the cell cultures, octreotide induced a dose-related suppression of GH from the cells collected from fully responsive patients, but was only partially effective in suppressing GH from cells collected from partially responsive patients. In contrast, the SSTR2 and 5 bi-selective analog, BIM-23244, induced a full dose-related suppression of GH secretion in the cells from both populations, confirming greater efficacy from combined activation of both SSTR2 and 5.[11]

Unfortunately, additional studies into the pancreatic actions of the SSTRs revealed that, while activation of the SSTR2 indirectly suppresses insulin by suppressing glucagon secretion from the alpha cells, which still allows a normal insulin response to glucose, the activation of SSTR5 directly suppresses insulin secretion from the beta cells and does not allow the pancreas to respond to normal stimuli, resulting in the development of hyperglycemia.[12,13] Thus, therapeutic analogs with potent SSTR5 activity are

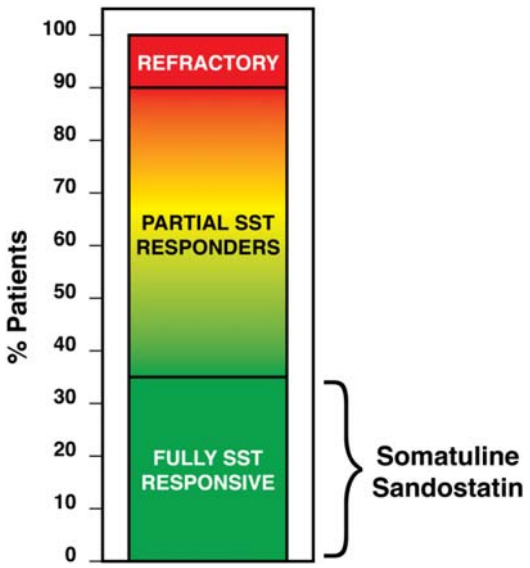

Fig. 1 Spectrum of acromegalic patients.

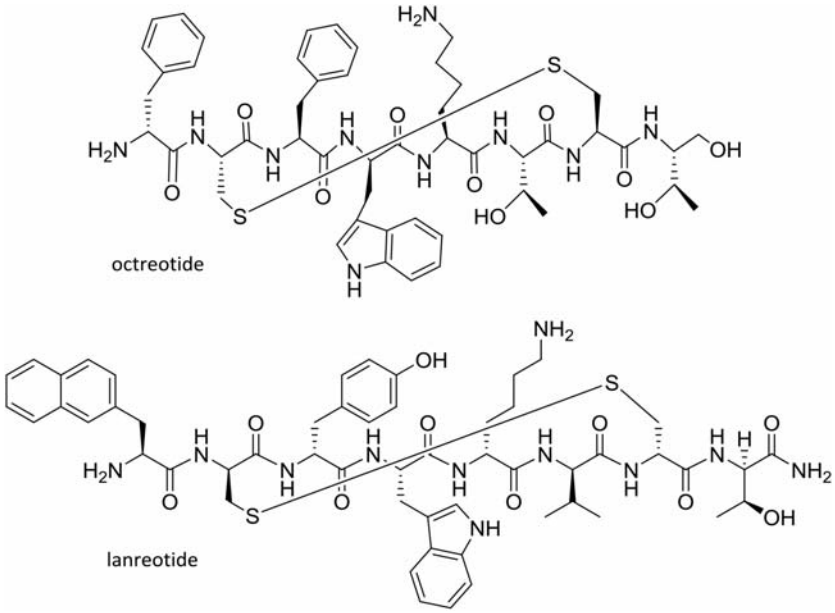

Fig. 2 Structures of octreotide and lanreotide.

Table 1 Human somatostatin receptor binding affinities of selected peptides (nM)

Compound	*SSTR1*	*SSTR2*	*SSTR3*	*SSTR4*	*SSTR5*
Somatostatin 14[a]	2.0	0.3	1.2	2.0	1.4
Lanreotide[b]	>1000	0.75	97.9	>1000	5.21
Octreotide[c]	576	0.43	37.7	>1000	9.24
BIM-23015[c]	>1000	0.85	>1000	>1000	7.74
BIM-23023[b]	>1000	0.43	86.9	>1000	4.18
BIM-23190[b]	>1000	0.35	215	>1000	11.1
BIM-23197[b]	>1000	0.19	26.8	>1000	9.81

[a]Data from Culler.[8]
[b]Data from Gillespie.[9]
[c]IPSEN historical data.

potentially problematic for chronic use. Understanding that the currently used clinical analogs of SST were optimized on the basis of separating GH- and insulin-suppressing activity, explains the greater potency at SSTR2 versus SSTR5, and, consequently, at least in part explains the reason for their inability to normalize GH and IGF1 in a greater percentage of acromegalic patients. While combined, potent activation of both SSTR2 and 5 proved to be problematic, it did establish the concept that activation of multiple receptors could offer enhanced therapeutic options for acromegaly, as well as other target diseases.

Building on the concept of targeting multiple receptors to achieve greater efficacy, observations reported in the clinical literature indicated that treatment of acromegalic patients with a combination of SST and dopamine (DA) agonists results in greater control of GH than the use of either agent alone.[14–17] DA, which is the natural suppressor of prolactin (PRL) secretion, stimulates GH secretion in normal individuals; however, in acromegalic subjects, DA suppresses GH.[18] These clinical observations lead to the idea of combining structural elements of both SST and DA into a single, chimeric compound that would retain the ability to interact with both receptors. Once prototype chimeric compounds had been obtained, studies in cultured primary human GH-secreting adenoma cells were used to compare the GH-suppressing activity of the chimera versus individual SST and DA analogs, both alone and in combination. In this system, both the individual SST and DA analogs produced dose-related suppression of GH secretion; however, in contrast to the clinical literature, when tested at the cellular level, the combination of SST and DA agonists produced no greater suppression of GH than the SST agonist. In sharp contrast to the results with combined individual SST and DA analogs, the addition of the dual SST and DA chimeric compound induced significantly superior potency and efficacy in suppressing GH.[19,20] In addition, the chimeric compounds were significantly more potent than individual DA analogs in suppressing PRL secretion from culture-mixed GH- and PRL-secreting adenomas.[19,20]

While the actual mechanism for the superior activity of the chimeric compound versus combined individual agonists remains unknown, an intriguing possibility has presented itself with the observation that SST and DA receptors interact to form heterodimers that, once activated, induce greater effect than the monomeric receptors.[21,22] While it is unlikely that the chimeric SST–DA

compounds physically induce heterodimer formation, it is possible that they stabilize the receptor interactions that occur spontaneously, and, in doing so, produce greater activation of transduction mechanisms and, consequently, greater efficacy in suppressing GH. This possibility remains to be fully elucidated.

Finally, acromegalic tumors are not alone in being affected by both SST and DA. Other potential indications include ACTH-secreting corticotroph tumors that cause Cushing's disease; prolactinomas, that in most cases are highly sensitive to the suppressive actions of DA, but in a portion of cases are resistant; nonfunctioning-pituitary adenomas that are largely derived from the gonadotroph cells, and are so-called because they secrete nothing of biological consequence but pose a threat from unabated growth; and the gastroenteropancreatic neuroendocrine tumors (GEP-NETs) of the GI tract. Additional study will be required to determine if the enhanced interactions observed between SST and DA receptors in acromegalic tumors, and induced by the chimeric SST–DA compounds, also occurs in other cell types, and offers the potential for treatment by this novel class of compounds.

6.04.2.3 Initial Design: Selection of the SST Agonist Peptide Fragment

We initiated our designs for the chimeric molecules by selecting peptide fragments targeting SSTR2 from our extensive library of somatostatin-like peptides. These peptide analogs were produced at IPSEN during the development of lanreotide primarily as selective dual SSTR2 and SSTR5 agonists. All peptides with potent, selective SSTR2 agonist activity that were structurally similar to octreotide and lanreotide were selected for initial evaluation. Binding activity across all five of the human SSTR subtypes was then assessed relative to somatostatin, lanreotide and octreotide (Table 1). In general, these compounds had excellent activity for SSTR2 with approximately 10-fold less activity on SSTR5, poor activity on SSTR3, and little to no activity on SSTR1 and 4.

We focused our attention on the peptides BIM-23190 and BIM-23197 (Fig. 3), which besides having a desirable selectivity profile against the SSTRs, had also been evaluated for their pharmacokinetic properties in rats.[9] BIM-23190 and BIM-23197 demonstrated improved plasma stability with terminal half-lives of 3.76 and 3.26 h, respectively, when compared with lanreotide, which is

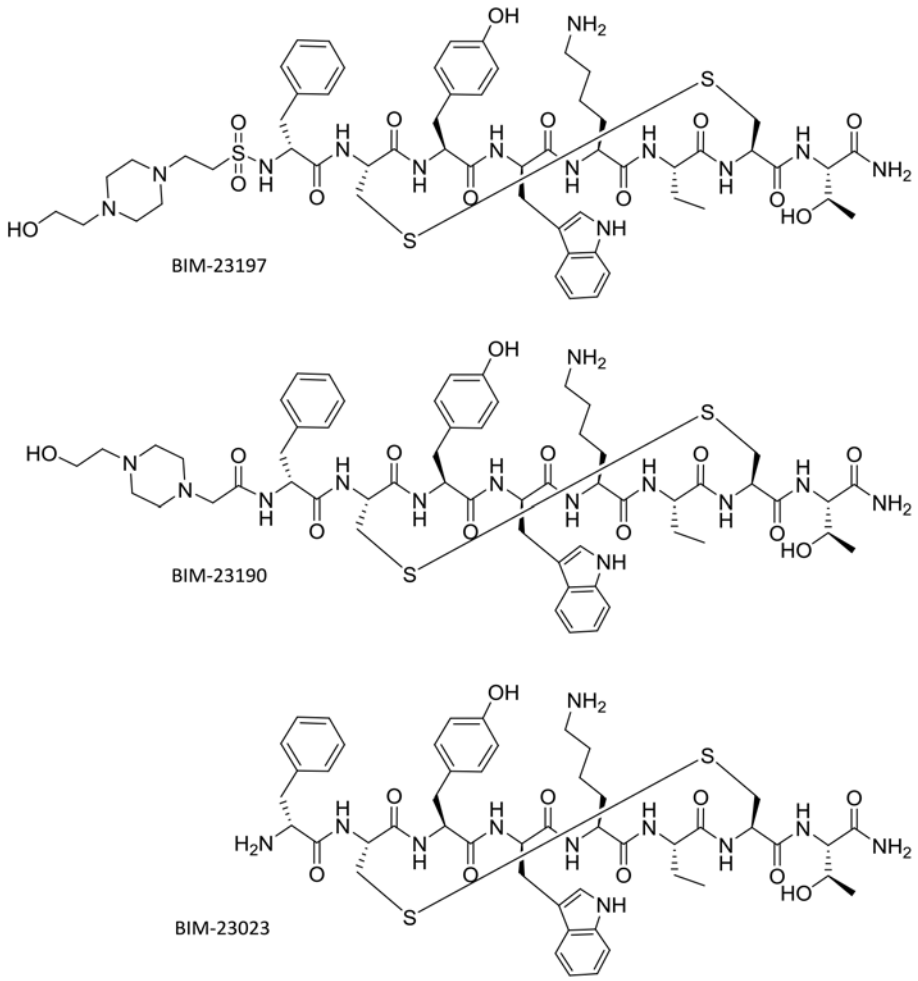

Fig. 3 Chemical structures of selected SST peptide analogs.

rapidly metabolized within 1 h. They also had desirable tissue distribution profiles, with a preference for adrenal, pituitary, and pancreatic tissues that closely correlates with the abundance of SSTR2 mRNA seen in these tissues.[9]

Peptides BIM-23190 and BIM-23197 were also interesting from a structural point of view as they differ from lanreotide primarily in the groups attached at the N-terminal amino acid. The addition of these groups did not seem to have an effect on the overall selectivity or the level of binding to the SSTRs, but did significantly increase the in vivo terminal half-lives. These data suggested that using the N-terminal region of these peptides as an attachment point for different groups, like a DA agonist, would be a good place to start. Potentially with these type of modifications, it might be possible to maintain the good receptor binding profile and beneficial effects on PK and tissue distribution seen with molecules like BIM-23190 and 23197. The parent peptide of both BIM-23190 and 23197 analogs was the same peptide BIM-23023, which then became our scaffold of choice for the preparation of the first chimeric dual agonists or dopastatins.

6.04.2.4 Initial Design: Selection of the DA Receptor Agonist Fragments

At the beginning of the dopastatin project, IPSEN did not have any molecules in its compound repository that were specifically designed to target DA receptors. Therefore, we conducted a comprehensive search of the literature for existing DA receptor subtype 2 (D2R) agonists. The search focused on small molecules in order to keep the molecular weight of the final compound as low as possible and not counteract the desirable physical properties associated with the peptide. Four potential candidates seemed reasonable: pergolide, cabergoline, terguride, and bromocriptine (**Fig. 4**). From this list, bromocriptine, a semisynthetic analog of ergocryptine,[23] was eliminated because of its complicated structure (polycyclic tripeptide group) and instability in vivo.[24] This left only three compounds as potential starting points for the DA fragment that would be attached to the peptide.

Examination of the three remaining structures showed that they only differ in the substitutions at the N-6 and C-8 positions. None of them, unfortunately, had obvious attachment points for coupling to a peptide, or were available in large enough quantities to allow for easy chemical modification. Therefore, development of a synthetic route to these fragments that was both flexible and scalable became a high priority for the project. Fortunately, starting from the readily available lysergol, a synthetic route (**Scheme 1**) which was suitable for producing analogs of all three parent molecules, was able to be developed.[25] Selective reduction of the protected lysergol ring junction double bond produced the desired "core scaffold" with the correct stereochemistry. Subsequent removal of the N-6 methyl group with ACE-Cl then allowed easy substitution with other groups, such as the propyl chain found in pergolide. One of the key features needed in the DA fragments was a good attachment point to link to the peptide. In that regard, further modification at the C-8 position of the "core scaffold" via displacement of the mesylate from intermediate 2 with 2-thioacetate and hydrolysis, yielded an acid group suitable for coupling to the N-terminal amine of the peptide (**Scheme 1**). In particular, the DA fragments with the N-6 methyl or propyl groups shown in **Scheme 1**, named "Dop1" and "Dop2," respectively, were used extensively throughout the program. By using similar chemistry, we were able to make a variety of DA fragments suitable for coupling to the peptide. To be sure that the modifications we had made to the fragments were not going to adversely affect their ability to bind the D2R receptor, we tested most of the fragments for their D2R affinity prior to coupling (**Table 2**). Those fragments that retained activity were then coupled to the peptide fragments to make the first dopastatins.[25]

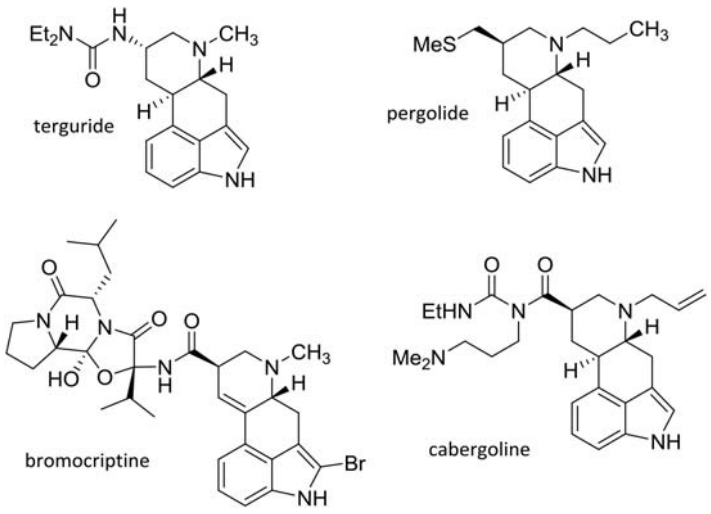

Fig. 4 Chemical structures of dopamine agonists.

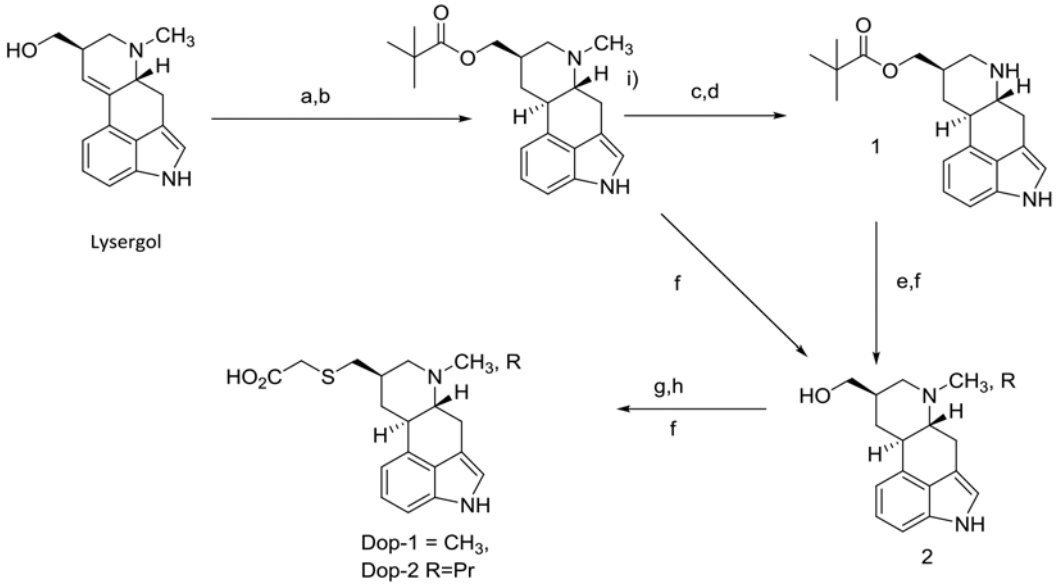

a) Piv-Cl/DMAP/Pyr, b) H_2/10% Pd-C/DMF-Pyr (10:1) 60°C, c) $Cl_3COCOCl$/DCE/$KHCO_3$ reflux, d) Zn dust/AcOH, e) R-I/K_2CO_3/DMF, f) 2M NaOH/MeOH, g) MsCl/Pyr, h) K_2CO_3/$HSCH_2CO_2Et$

Scheme 1 Synthesis of Dop1- and Dop2-type fragments.

Table 2 Dopamine receptor binding affinity of various fragments (nM)

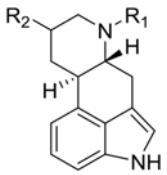

Dopamine fragment	R_1	R_2	*D2R*[a]
BIM-53061	Me	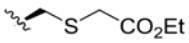	293
BIM-53097	Pr	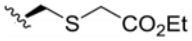	80
BIM-53306	Me	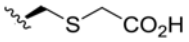	NT
BIM-53307	Pr	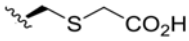	433
BIM-53320	Me	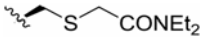	58
BIM-53309	Pr	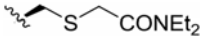	44
BIM-53301	Allyl	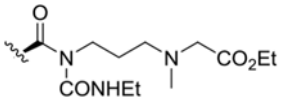	36
BIM-53302	Allyl	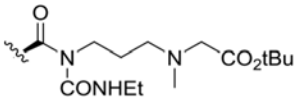	15
BIM-53315	Me	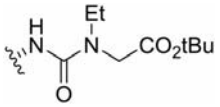	42
BIM-53316	Me	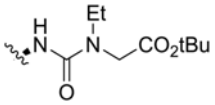	898

NT = Not tested.
[a]IPSEN historical data.

6.04.2.5 Dopastatin Synthesis and Structure–Activity Relationship

The synthesis of the chimeric compounds began with the solid-phase peptide synthesis on Rink® resin of the peptide fragment using standard Fmoc chemistry. Cyclization to form the disulfide bridge, followed by coupling to the DA fragment, deprotection, and purification by reverse-phase HPLC, produced the desired chimeric dopastatin molecules. For example, BIM-53097 (Dop2) was coupled to Boc-BIM-23023 to create dopastatin analog BIM-23A387 (Scheme 2).

A library of dopastatin analogs was produced in this manner by coupling a variety of DA fragments to the terminal amino group of the peptides. The DA and SSTR binding affinities were then evaluated using radioligand binding assays with membranes from transfected CHO-K1 cells expressing the appropriate receptor subtype. From the library of dopastatin molecules, several structure–activity relationship trends became apparent. As exemplified by the compounds derived from the BIM-23023 peptide (Table 3), the pergolide-based DA fragments, such as those used for BIM-23A370 and BIM23A387, gave the best overall affinity at both the D2R and SSTR2 receptors. Additionally, compounds with propyl groups at N-6 had higher D2R affinity than their methyl counterparts. Following these observations, most of the subsequent optimization focused on compounds which retained these modifications.

The type and length of the linkers used for the coupling of the DA fragment to the peptide were also extensively studied. Various Aepa and/or Doc linkers (Table 4) were used to test the effects of length, rigidity, and polarity with both Dop1- and Dop2-type fragments. The reason for choosing Aepa as the linker was the following. First, the N-termini of both lanreotide and octreotide are positively charged (free amines), and Aepa, which has two free amines, would maintain or increase this positive charge. Second, both peptides BIM-23190 and BIM-23197 with excellent SSTR2 binding affinity and in vivo PK properties contain similar groups to Aepa at their N-termini (Fig. 3), which we would like to mimic. The Doc linker was selected because of its good hydrophilic properties and structural flexibility that would allow the DA fragment to find its best binding conformation. Having a linear ethylene oxide unit, Doc also allows the distance between the peptide and DA moieties to be extended slightly further than with Aepa, which might help facilitate the simultaneous interaction with both the D2R and SSTR2 binding sites. To further explore if the length of the linker would have a positive impact on binding, we also used the double linkers Doc–Doc or Aepa–Aepa. In general, the binding affinity data showed that the Doc linker consistently outperformed the positively charged Aepa (see BIM-23A732 vs. BIM-23A730 and BIM-23A756 vs. BIM-23A745) (Table 4). Interestingly, the length of the linker turned out to be the more critical parameter. Compounds with double spacers had lower affinity than those with only a single spacer, and the no linker or directly attached DA compounds like BIM-23A370 and BIM-23A387 had significantly higher affinity. Again, the N-6 propyl Dop2 compounds consistently outperformed the N-6 methyl Dop1 analogs.

From the binding data, the best compound, BIM-23A387, was chosen as a lead candidate for further biological evaluation. The ability of BIM-23A387 to suppress GH and PRL secretion was assessed in cell cultures prepared from human GH-secreting pituitary adenomas collected at surgery from acromegalic patients. BIM-23A387 was compared to its parent SST peptide analog, BIM-23023, and the D2R agonist, BIM-53097 (Dop2), both of which had comparable activities as BIM-23A387 at their respective receptors.[19]

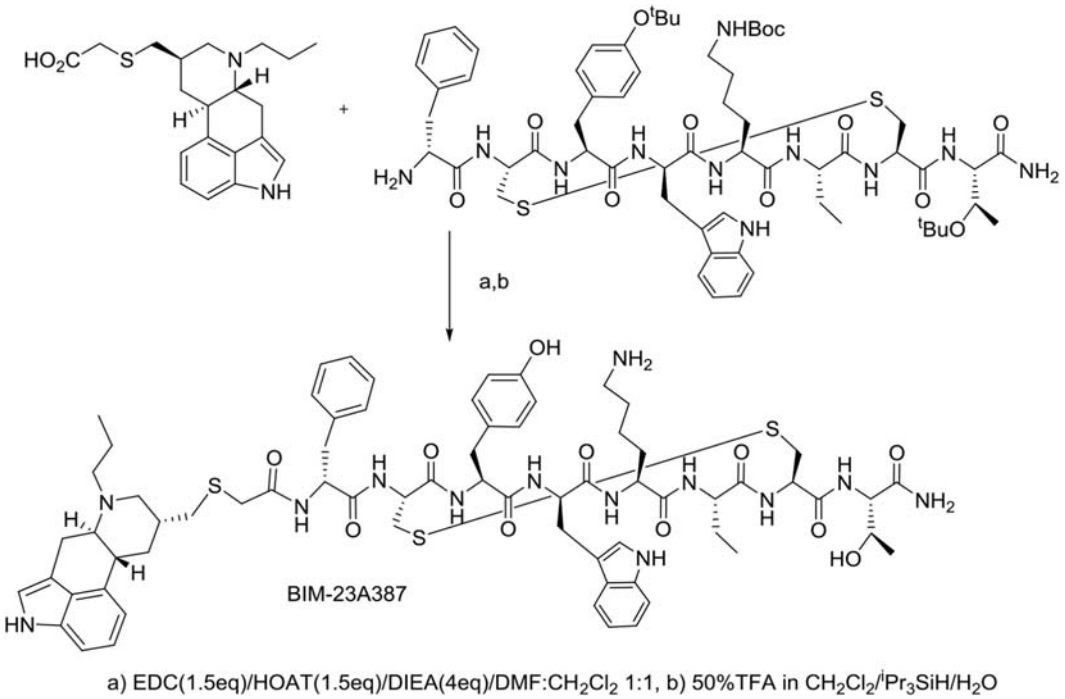

Scheme 2 Synthesis of dopastatin analog BIM-23A387.

Table 3 Binding affinity of dopastatins derived from peptide BIM-23023 (nM)

Dopastatin	*Dopamine fragment*	*D2R*	*SSTR1*	*SSTR2*	*SSTR3*	*SSTR4*	*SSTR5*
BIM-23A755	53301 N6-H	193	345	0.2	267	≥1000	NT
BIM-23A754	53301 N6-Pr	65	509	0.5	798	≥1000	NT
BIM-23A370	53306 (Dop1)	31	826	0.1	75	≥1000	≥1000
BIM-23A387	53097 (Dop2)	22	691	0.1	72	≥1000	23

NT = Not tested.

Table 4 Binding affinity (nM) of linker-spaced dopastatins derived from peptide BIM-23023

BIM #	*Dopamine fragment*	*Linker*	*D2R*	*hSSTR2*
BIM-23A732	Dop1	Doc	255	0.21
BIM-23A730	Dop1	Aepa	292	0.38
BIM-23A739	Dop1	Doc–Doc	277	0.34
BIM-23A370	Dop1	–	31.2	0.1
BIM-23A756	Dop2	Doc	86	0.1
BIM-23A745	Dop2	Aepa	142	0.34
BIM-23A728	Dop2	Aepa–Aepa	328	1.74
BIM-23A387	Dop2	–	22.1	0.1

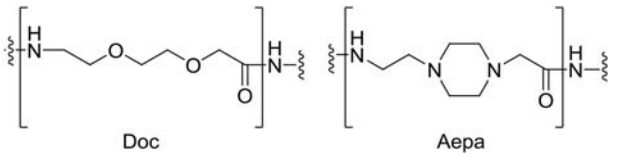

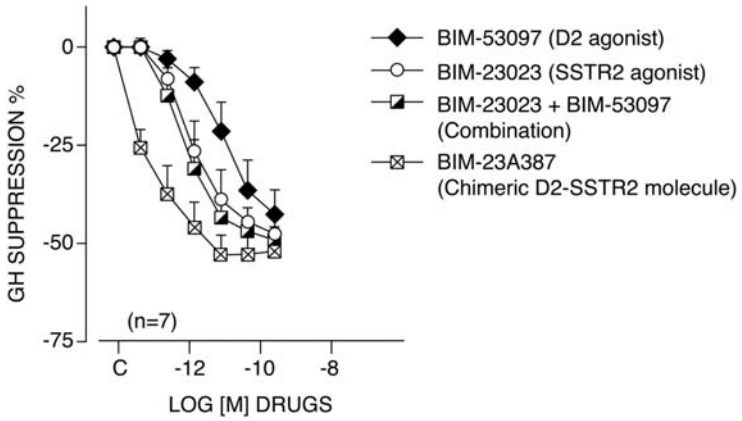

Fig. 5 Dose responses of GH suppression by D2R agonist BIM-53097, SSTR2 agonist BIM-23023, the combination of both compounds, and BIM-23A387 in seven octreotide-sensitive adenomas.[19]

While BIM-23A387 showed similar maximal inhibition of GH release as the combination of the two individual SST and DA analogs, the mean EC_{50} for suppressing GH secretion was 50-fold lower than for the individual agonists, either tested individually or combined (Fig. 5).

Similar data for BIM-23A387 was obtained with tumors collected from individuals that, clinically, were only partially responsive to octreotide; however, significantly greater maximal suppression of GH was obtained with the dopastatin analog versus the combination of the two individual agents. In addition, a mean 73% ± 6% inhibition of PRL secretion from mixed GH- and PRL-secreting tumors further demonstrated the superior activity of BIM-23A387. For all the samples, real-time PCR quantitative analysis was performed on the tumor fragments to confirm the expression of D2R and SSTR2 receptors.

Following the success of BIM-23A387, we decided to investigate the optimal ratio of DA fragments relative to the peptide to try and further increase D2R activity. In order to increase the number of DA fragments in the final molecule, it was necessary to increase the number of linker sites on the peptide. This was done by using lysine as a terminal amino acid, in addition to, or as a replacement for, the terminal D-phenylalanine.

Table 5 Binding affinity of dopastatins with varying dopamine fragments (nM)

BIM #	*Dopamine fragment*	*Peptide modification*	*D2R*	*SSTR2*
BIM-23A387	Dop2	23,023	22.1	0.1
BIM-23A766	2xDop2	23,023 + Lys	17.6	0.2
BIM-23A757	2xDop2	23,023 + Lys-Phe	8.6	0.5
BIM-23A760	2xDop2	23,023 + D-Lys-Phe	15	0.03

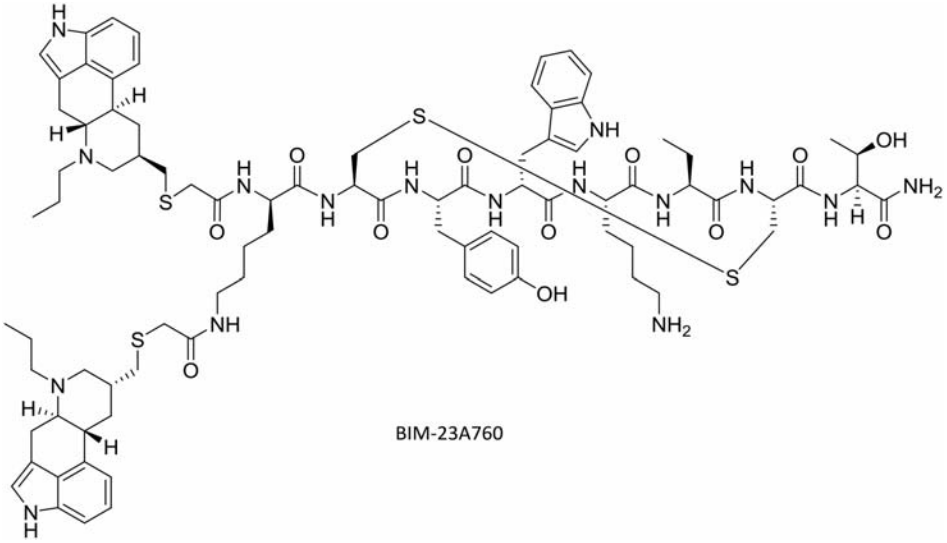

Fig. 6 Structure of BIM-23A760.

Table 6 Receptor binding profile of BIM-23A760 (nM)

	SSTR1	*SSTR2*	*SSTR3*	*SSTR4*	*SSTR5*	*D2R*
BIM-23A760	843	0.03	160	>1000	42	15

Addition of a lysine bearing two Dop2 fragments to the peptide resulted in the compound BIM-23A766 with minor improvement in DR2 binding (Table 5). When the terminal phenylalanine was replaced with lysine, as in BIM-23A757, the affinity at the D2R did increase but at the expense of affinity at the SSTR2 receptor. In order to more closely mimic the D-phenylalanine present in the parent peptide and enhance the enzymatic stability of the linker, the lysine was replaced by its D-isomer resulting in compound BIM-23A760. Impressively, a dramatic improvement was seen on the SSTR2 binding without any loss to the DR2 affinity. Compound BIM-23A760 turned out to be the best SSTR2 binder we had achieved to date and became the lead molecule for the program selected for preclinical development.

BIM-23A760 (Fig. 6) was fully profiled against all of the SSTRs (Table 6) and demonstrated excellent selectivity for the SSTR2. With good primary affinity, we were particularly keen to see if this would translate into improved cellular and in vivo activity.

BIM-23A760 was studied in a comprehensive set of experiments focused on the suppression of GH and PRL in 18 human GH adenomas that were only partially responsive to octreotide or lanreotide. It was compared with octreotide, BIM-23A387, and a number of other dopastatin analogs.[20] BIM-23A760 demonstrated significantly superior suppression of GH, both in terms of potency and maximal suppression, as compared with the individual SST and DA analogs, both alone and in combination, as well as compared with the original dopastatin prototype, BIM-23A387. With these in vitro results in hand we began to profile BIM-23A760 in vivo.

6.04.3 Profiling of BIM-23A760

After initial in vitro evaluation, BIM-23A760 was tested in several animal models, including normal cynomolgus monkeys.[26] A single, subcutaneous (SC) injection of 1 nM to 1 μM kg^{-1} produced a significant, dose-related suppression of GH from 15 min to 48 h postinjection. There was a similar dose-related effect on PRL and dose-related suppression of IGF-1 at 24 h postinjection.

Significantly, no effect was observed on insulin secretion or circulating glucose at any time or dose of BIM-23A760 during the study.[27] These results suggested that BIM-23A760, may be an effective therapy for a larger percentage of acromegalic patients than currently available with pure SST and dopmaine agonists, with no untoward effects on either insulin secretion or glycemic control.

BIM-23A760 was subsequently advanced into clinical development primarily based on the following criteria:

- High affinity and selectivity for the DA and SSTRs.
- Greatly enhanced potency and efficacy in suppressing GH secretion from cultured human acromegalic tumors, as compared with SST and DA analogs, both alone and in combination.
- Efficacy in multiple in vivo animal models.
- Excellent safety results, no clinical toxicity signs seen in animal studies and no effect on insulin secretion or glycemic control.

6.04.3.1 BIM-23A760 Phase 1 Clinical Studies

Phase 1 PK studies with single SC bolus injections of BIM-23A760 in healthy subjects demonstrated dose proportionality (Fig. 7) and an extended half-life. Pharmacodynamic effects on PRL levels showed significant suppression for prolonged periods of time >8 days with doses >1 mg with no significant side effects[28] (Fig. 8). Doses of 1 and 4 mg were subsequently selected for further evaluation during Phase 2 studies.

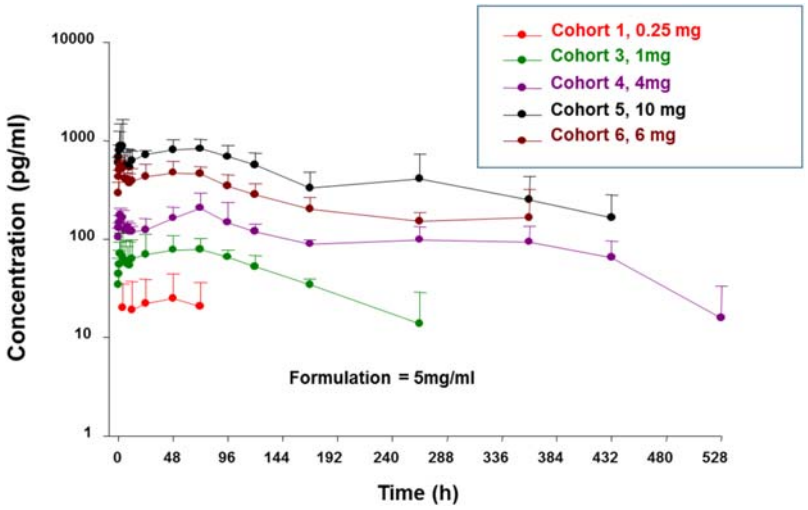

Fig. 7 Phase 1 pharmacokinetics of BIM-23A760 from single subcutaneous bolus injections in healthy subjects.

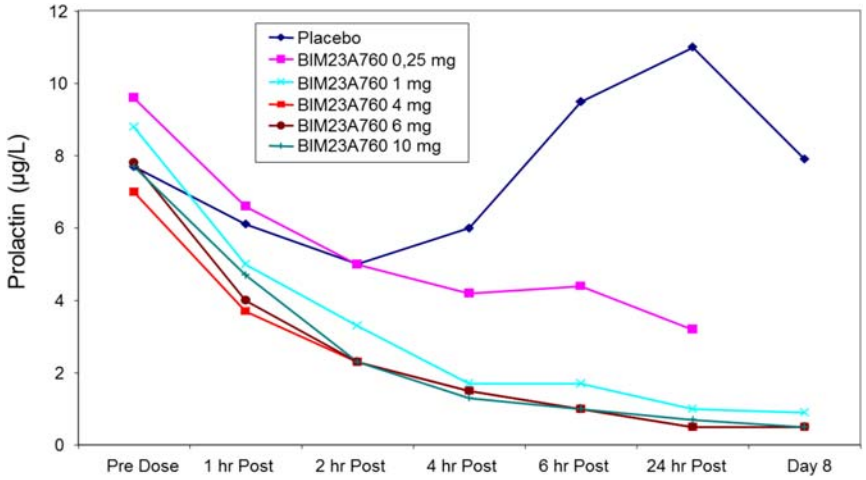

Fig. 8 Phase 1 PRL pharmacodynamic effects of BIM-23A760 from single SC bolus injections in healthy subjects.

6.04.3.2 BIM-23A760 Phase 2a and b Clinical Studies

The initial Phase 2a study on BIM-23A760 in acromegalic patients demonstrated that a single SC dose resulted in a significant and prolonged, dose-related suppression of circulating GH levels[29] (Fig. 9).

Unexpectedly, however, during the Phase 2b Tulipia study, NCT00994214, examining chronic, repeat dosing of BIM-23A760 in acromegalic patients, the suppressive effect on circulating GH levels diminished over time, while PRL levels remained profoundly suppressed. Without the ability to be effective when dosed over an extended period of time, BIM-23A760 was withdrawn from further clinical studies.

In order to determine the cause for the lack of sustained effect upon GH levels, the clinical blood samples were examined to determine the concentration of BIM-23A760, and were analyzed for major metabolites.

6.04.3.3 BIM-23A760 Metabolite Analysis

The follow-up study of the clinical blood samples revealed that BIM-23A760 produced a metabolite that was present in high concentrations and that accumulated rapidly with continued administration (Fig. 10). The metabolite consisted of the terminal lysine amino acid coupled to both of the DA fragments (Fig. 11). The affinity of the BIM-23A760 metabolite at the D2R receptor was compared to that of BIM-23A760 and found to be similar (Table 7). Strikingly, however, the metabolite turned out to be >200-fold more potent at activating the D2R receptor than its parent BIM-23A760, with an EC_{50} of 0.005 nM. The metabolite also demonstrated significantly lower plasma protein binding than BIM-23A760, indicating that it might be more readily available for binding

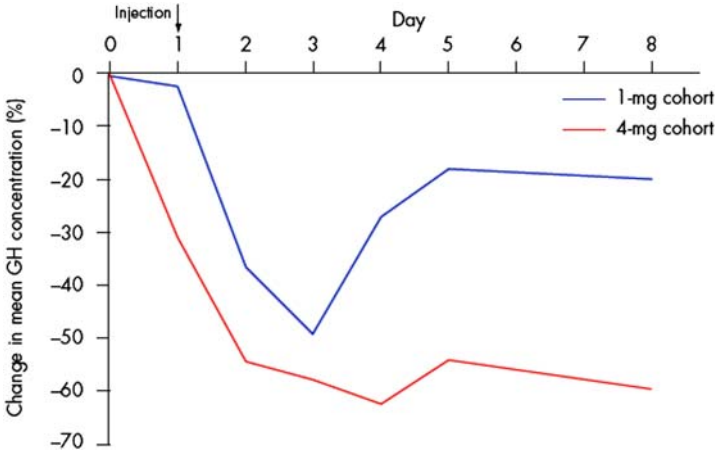

Fig. 9 Phase 2a study of GH levels in acromegalic patients from single SC bolus injection of BIM-23A760.

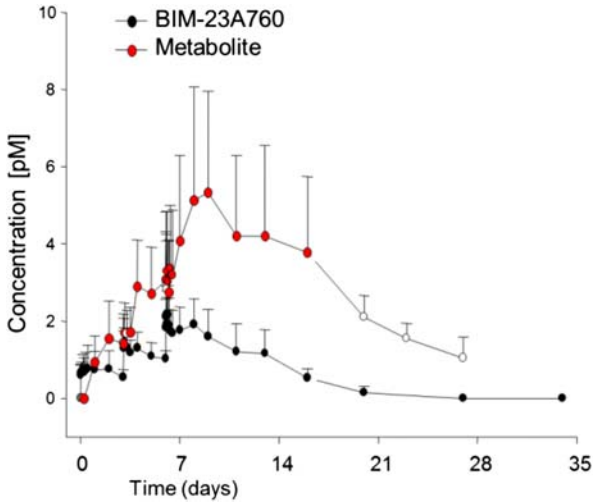

Fig. 10 PK of BIM23A760 and its major metabolite in human subjects.

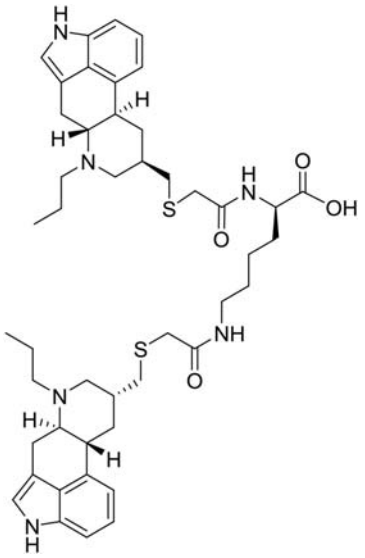

Fig. 11 Structure of the major metabolite of BIM-23A760.

Table 7 Comparison of the receptor activity of BIM-23A760 and its major metabolite (nM)

	D2R	
Compound	*Binding (K_i)*	*cAMP (EC_{50})*
BIM-23A760	4.5	1.1
Metabolite	7.8	0.005

to the receptor than BIM-23A760. With increased availability and superior potency at the D2R receptor, the metabolite may effectively outcompete BIM-23A760, reducing its ability to act as a dual-receptor agonist, and its synergistic effect. The observed accumulation of the metabolite over time would likely exacerbate this problem. Based on these findings, a theory was proposed that the observed loss of BIM-23A760 clinical efficacy with chronic administration might be due to the accumulating metabolite competing with BIM-23A760 for the DA receptor.

6.04.4 Second-Generation Dopastatin Design Concepts

Although BIM-23A760 was stopped in Phase 2 clinical development for lack of continued efficacy, the concept of a chimeric dual SST-DA agonist as a treatment for acromegaly still remained valid. We, therefore, chose to redesign the dopastatin molecules and create a second-generation compound to overcome the limitations associated with BIM-23A760.

Coincidentally, as the clinical development of BIM-23A760 was being stopped, pergolide, the marketed DA analog that formed the basis of the DA fragment for most of the dopastatins, was also withdrawn from the US market for human use (FDA advisory). Published studies earlier in 2003 and 2004 had revealed a link between the drug and increased rates of heart disease and cardiac fibrosis.[30] The cause of these effects seemed to be associated with significant agonist activity at the serotonin 2B receptor (5HT2B). Similar effects were observed with several other ergoline compounds such as cabergoline.[31] Interestingly, while pergolide acts as a full 5HT2B agonist, lisuride, a structurally similar compound exhibits no agonist activity at the 5HT2B receptor, and had not been linked to any adverse cardiac side effects.[31] In 2008, scientists from the University of Berlin characterized a number of pergolide derivatives in order to identify the molecular fingerprint that might be responsible for its adverse cardiac effects. Specifically, eight derivatives were tested with varying substitutions at positions N-6 and C-8 (Fig. 12). The data showed that the 5HT2B activity was almost completely attenuated when the N-6 propyl group was switched to a methyl group, while changes at the C-8 position showed little effect. Following this information, we chose to focus only on the N-6 methylated compounds for incorporation into our second-generation compound designs to minimize the chance for 5HT2B activity.

Another critical factor for the second-generation compound design centered around metabolism. With a major interfering metabolite possibly leading to the failure of BIM-23A760 in the clinic, producing compounds that minimized metabolite

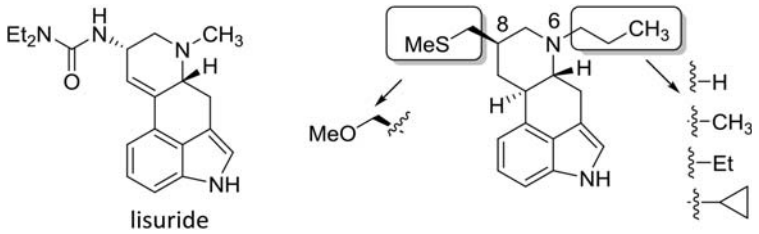

Fig. 12 Lisuride and pergolide analogs studied for 5HT2B receptor activity.

formation, or that produced metabolites with minimal capacity to interfere at the receptors, was a high priority. To assess our second-generation compounds, we also developed a new screening paradigm incorporating the following criteria:

- Increasing metabolic stability by fivefold relative to BIM-23A760, with no active metabolite that can interfere with the parent compound.
- Maintain efficacy at suppressing GH activity ≥ BIM-23A760.
- Decrease protein binding fivefold compared to BIM-23A760.
- Improve selectivity for DA receptors by reducing activity on 5HT2B receptor threefold compared to BIM-23A760.

With specific criteria established for the development of a second-generation compound, the program was taken back into research focused on delivering compounds against these parameters.

6.04.5 Second-Generation Design and Discovery of Lead Compound BIM-065

In order to minimize the formation of metabolites containing DA fragments, the peptide scaffold and the linker of the first-generation compounds were completely redesigned. Unlike the first-generation compounds, such as BIM-23A760, the linker was designed without a readily cleavable amide bond. The cyclic disulfide was also removed and replaced by cyclizing the peptide from its C-terminus to a sidechain residue. We also chose to eliminate any amino acid residues that would extend beyond the cyclic system to avoid additional enzymatic degradation. Incorporation of nonnatural amino acids also allowed for fine-tuning of the physical properties, particularly solubility. A series of high-affinity selective compounds were made, resulting with the selection of BIM-065 as a lead candidate. BIM-065 was directly compared to the first-generation lead compound BIM-23A760 for activity at the SST and DA receptors (Table 8).

BIM-065 demonstrated up to 16-fold greater SSTR2 agonist activity and similar selectivity versus SSTR5, compared to BIM-23A760. The excellent selectivity of BIM-065 for SSTR2 over SSTR5 continued to minimize adverse effects due to changing insulin levels. BIM-065 is threefold less active at the 5-HT2b receptor than BIM-23A760, and it is only a partial agonist, which greatly reduces the chance for any associated cardiovascular effects. In primary human tissue cultures of GH-secreting adenoma cells, BIM-065 demonstrates a clear dose-dependent suppression of GH secretion with an EC_{50} of 0.5 pM, and a maximal inhibition of GH release of 61%, demonstrating that the potency and efficacy of BIM-065 in suppressing GH secretion is superior to that of BIM-23A760 (Table 9).

Table 8 Receptor activation profile for lead compound BIM-065

	SSTR2 *EC_{50} nM* *(%E_{max})*		*SSTR5* *EC_{50} nM* *(%E_{max})*		*D2R* *EC_{50} nM* *(%E_{max})*		*5-HT2b* *EC_{50} nM* *(%E_{max})*
Compound	*Ca^{2+}*	*cAMP*	*Ca^{2+}*	*cAMP*	*Ca^{2+}*	*cAMP*	*Ca^{2+}*
BIM-23A760	10.8	32.3	397.1 (63%)	105.9	16.7	1.1	31.2
BIM-065	2.2	2.2	388.6 (63%)	49.7	5.0	2.1	104.1 (55%)

Table 9 GH inhibition by dopastatins, BIM-23A760 and BIM-065

EC_{50} (pM)		*GH inhibition (%)*	
BIM-065	*BIM-23A760*	*BIM-065*	*BIM-23A760*
0.5	2.5	61	41

Table 10 Comparison of the first- and second-generation dopastatins and their primary metabolites

	D2R			5HT2B		
	Binding	Ca^{2+}	cAMP	Binding	Ca^{2+}	
Compound	K_i (nM)	EC_{50} (nM)	EC_{50} (nM)	K_i (nM)	EC_{50} (nM)	$\%E_{max}$
BIM-23A760	4.4	16.7	1.1	1.4	31.2	92.1
760 metabolite	7.8	4.4	0.005	13.6	36.2	103.4
BIM-065	27.2	5.0	2.1	74.9	104.1	55.0
065 metabolite	490.8	836.8	21.8	>1000	>1000	68.4

In addition to improved potency and efficacy, BIM-065 has much better physicochemical properties than BIM-23A760. It is freely soluble at pH 5.5 ($\geq$113 mg mL^{-1}), with lower plasma protein binding, and an unbound fraction of ~7–12% as compared with ~0.5–0.7% for BIM-23A760. More importantly, its overall metabolic stability is greatly improved. In S9 fractions, BIM-065 has a half-life of greater than 180 min versus only 10 min for BIM-23A760. Despite these significant improvements, when BIM-065 was tested in vivo it still produced a significant metabolite. Because of the issues seen with the first-generation metabolite, we were extremely concerned about profiling the activity of the metabolite on the D2R and 5HT2B receptors, as well as its effects on GH secretion. We were pleased to find that the profile of the BIM-065 metabolite was significantly different than both BIM-065 and the metabolite of BIM-23A760 (Table 10).

The D2R and 5HT2B binding and activity of the BIM-056 metabolite are significantly less than the parent compound, BIM-065. The metabolite was also tested in rats with multiple doses up to 10,000 times greater than BIM-065 with no significant adverse events or accumulation after 5 days dosing. Most importantly, the ability of the metabolite to interfere with the effect of BIM-065 on GH secretion was tested in cultured pituitary adenomas that were partially responsive to octreotide. Increasing concentrations of the metabolite up to 10,000-fold excess were unable to alter the effect of BIM-065 on GH release tested at both the EC_{50} and EC_{80} effective concentrations.

6.04.6 Second-Generation Dopastatin: Current Status

With an improved biochemical and physicochemical profile, BIM-065 is able to overcome the major obstacle of producing an interfering metabolite that is believed to have resulted in the failure of the first-generation compound, BIM-23A760. BIM-065 has subsequently advanced through its preclinical evaluation and is currently completing Phase 1 clinical studies. Subsequent trials will help to validate BIM-065, as well as the overall dopastatin approach of a chimeric dual D2R and SSTR2 agonist, for the treatment of acromegaly, and indeed other potential indications that may be amenable to treatment through combined activation of SST and DA receptors.

See also: 1.11. Future of Medicinal Chemistry: Next-Generation Therapeutics.

References

1. Brazeau, P. F.; Vale, W.; Burgus, R.; Ling, N.; Butcher, M.; Rivier, J.; Guillemin, R. Hypothalamic Polypeptide That Inhibits the Secretion of Immunoreactive Pituitary Growth Hormone. *Science* **1973,** *179* (4068), 77–79.
2. Caron, P. J.; Bevan, J. S.; Petersenn, S.; Flanagan, D.; Tabarin, A.; Prévost, G.; Maisonobe, P.; Clermont, A. Tumor Shrinkage With Lanreotide Autogel 120 mg as Primary Therapy in Acromegaly: Results of a Prospective Multicenter Clinical Trial. *J. Clin. Endocrinol. Metab.* **2014,** *99* (4), 1282–1290.
3. Brown, M.; Rivier, J.; Vale, W. Somatostatin: Analogs With Selected Biological Activities. *Science* **1977,** *196,* 1467–1469.
4. Coy, D. H.; Meyers, C.; Arimura, A.; Schally, A. V.; Redding, T. W. Observations on the Growth Hormone, Insulin, and Glucagon Release-Inhibiting Activities of Somatostatin Analogues. *Metabolism* **1978,** *27,* 1407–1410.
5. Bauer, W.; Briner, U.; Doepfner, W.; Haller, R.; Huguenin, R.; Marbach, P.; Petcher, T. J.; Pless, E. A Very Potent and Selective Octapeptide Analogue of Somatostatin With Prolonged Action. *Life Sci.* **1982,** *31,* 1133–1140.
6. Heiman, M. L.; Murphy, W. A.; Coy, D. H. Differential Binding of Somatostatin Agonists to Somatostatin Receptors in Brain and Adenohypophysis. *Neuroendocrinology* **1987,** *45,* 429–436.
7. Coy, D. H.; Murphy, W. A.; Raynor, K.; Reisine, T. The New Pharmacology of Somatostatin and Its Multiple Receptors. *J. Pediatr. Endocrinol.* **1993,** *6,* 205–209.
8. Culler, M. D. Somatostatin-Dopamine Chimeras: A Novel Approach to Treatment of Neuroendocrine Tumors. *Horm. Metab. Res.* **2011,** *43,* 854–857.
9. Gillespie, T. J.; Erenberg, A.; Kim, S.; Dong, J.; Taylor, J. E.; Hau, V.; Davis, T. P. Novel Somatostatin Analogs for the Treatment of Acromegaly and Cancer Exhibit Improved In Vivo Stability and Distribution. *J. Pharmacol. Exp. Ther.* **1998,** *285,* 95–104.
10. Shimon, I.; Yan, X.; Taylor, J. E.; Weiss, M. H.; Culler, M. D.; Melmed, S. Somatostatin Receptor (SSTR) Subtype-Selective Analogues Differentially Suppress In Vitro Growth Hormone and Prolactin in Human Pituitary Adenomas. Novel Potential Therapy for Functional Pituitary Tumors. *J. Clin. Invest.* **1997,** *100,* 2386–2392.
11. Saveanu, A.; Gunz, G.; Dufour, H.; Caron, P.; Fina, F.; Ouafik, L.; Culler, M. D.; Moreau, J. P.; Enjalbert, A.; Jaquet, P. Bim-23244, a Somatostatin Receptor Subtype 2- and 5-Selective Analog With Enhanced Efficacy in Suppressing Growth Hormone (GH) From Octreotide-Resistant Human GH-Secreting Adenomas. *J. Clin. Endocrinol. Metab.* **2001,** *86,* 140–145.

12. Zambre, Y.; Ling, Z.; Chen, M. C.; Hou, X.; Woon, C. W.; Culler, M.; Taylor, J. E.; Coy, D. H.; Van Schravendijk, C.; Schuit, F.; Pipeleers, D. G.; Eizirik, D. L. Inhibition of Human Pancreatic Islet Insulin Release by Receptor-Selective Somatostatin Analogs Directed to Somatostatin Receptor Subtype 5. *Biochem. Pharmacol.* **1999,** *57,* 1159–1164.
13. Orskov, H.; Moller, N.; Schmitz, O. Study of Two Somatostatin Receptor (SSTR) Subtype Specific Analogues in Healthy Male Subjects. Proceedings of the 81st Annual Meeting of the Endocrine Society, San Diego, CA, USA, OR44-44.
14. Flogstad, A. K.; Halse, J.; Grass, P.; Abisch, E.; Djøseland, O.; Kutz, K.; Bodd, E.; Jervell, J. A Comparison of Octreotide, Bromocriptine, or a Combination of Both Drugs in Acromegaly. *J. Clin. Endocrinol. Metab.* **1994,** *79,* 461–465.
15. Li, J. K.; Chow, C. C.; Yeung, V. T.; Mak, T. W.; Ko, G. T.; Swaminathan, R.; Chan, J. C.; Cockram, C. S. Treatment of Chinese Acromegaly With a Combination of Bromocriptine and Octreotide. *Aust. N. Z. J. Med.* **2000,** *30,* 457–461.
16. Marzullo, P.; Ferone, D.; Di Somma, C.; Pivonello, R.; Filippella, M.; Lombardi, G.; Colao, A. Efficacy of Combined Treatment With Lanreotide and Cabergoline in Selected Therapy-Resistant Acromegalic Patients. *Pituitary* **1998,** *1,* 115–120.
17. Minniti, G.; Jaffrain-Rea, M. L.; Baldelli, R.; Ferretti, E.; Caracciolo, B.; Bultrini, A.; Gulino, A.; Tamburrano, G. Acute Effects of Octreotide, Cabergoline and a Combination of Both Drugs on GH Secretion in Acromegalic Patients. *Clin. Ter.* **1997,** *148,* 601–607.
18. Camanni, F.; Massara, F.; Belforte, L.; Molinatti, G. M. Changes in Plasma Growth Hormone Levels in Normal and Acromegalic Subjects Following Administration of 2-Bromo-Alpha-Ergocryptine. *J. Clin. Endocrinol. Metab.* **1975,** *40,* 363–366.
19. Saveanu, A.; Lavaque, E.; Gunz, G.; Barlier, A.; Kim, S.; Taylor, J. E.; Culler, M. D.; Enjalbert, A.; Jaquet, P. Demonstration of Enhanced Potency of a Chimeric Somatostatin-Dopamine Molecule, BIM-23A387, in Suppressing Growth Hormone and Prolactin Secretion from Human Pituitary Somatotroph Adenoma Cells. *J. Clin. Endocrinol. Metab.* **2002,** *87,* 5545–5552.
20. Jaquet, P.; Gunz, G.; Saveanu, A.; Dufour, H.; Taylor, J.; Dong, J.; Kim, S.; Moreau, J. P.; Enjalbert, A.; Culler, M. D. Efficacy of Chimeric Molecules Directed Towards Multiple Somatostatin and Dopamine Receptors on Inhibition of GH and Prolactin Secretion from GH-Secreting Pituitary Adenomas Classified as Partially Responsive to Somatostatin Analog Therapy. *Eur. J. Endocrinol.* **2005,** *153,* 135–141.
21. Rocheville, M.; Lange, D. C.; Kumar, U.; Patel, S. C.; Patel, R. C.; Patel, Y. C. Receptors for Dopamine and Somatostatin: Formation of Hetero-Oligomers With Enhanced Functional Activity. *Science* **2000,** *288,* 154–157.
22. Baragli, A.; Kumar, U.; Patel, R. C. Heterooligomerization of Dopamine (D2R) and Somatostatin Receptors (SSTR2) in CHO-K1 Cells and Cortical Cultured Neurons. Proceedings of the 85th Annual Meeting of the Endocrine Society (Abstract P2-669).
23. Fluckiger, E., Troxler, F., and Hofmann, A. 2-Bromo-Alpha-Ergocryptine as a Lactation Inhibitor. US Patents US3752888 A, 1973.
24. Schran, H. F.; Tse, F. L. S.; Bhuta, S. I. Pharmacokinetics and Pharmacodynamics of Bromocriptine in the Rat. *Biopharm. Drug Dispos.* **1985,** *6,* 301–311.
25. Dong, Z. X., Culler, M. D., and Shen, Y. Somatostatin-Dopamine Chimeric Analogs. US Patents US8822442 B2, 2014.
26. Culler, M.; Dong, J.; Taylor, J. The Somatostatin-Dopamine Chimeric Molecule, BIM-23A760, is Highly Efficacious in Suppressing GH in Normal, Cynomolgus Monkeys (Macaca Fascicularis). In Proceedings of the 88th Annual Meeting of the Endocrine Society, Philadelphia, PA, USA, Abstract O9–6; 2006.
27. Culler, M.; Dong, J.; Taylor, J. The Somatostatin-Dopamine Chimeric Molecule, BIM-23A760, Does not Induce the Insulin/Glycemic Effects Observed With Individual Somatostatin or Dopamine Agonists in Cynomolgus Monkeys (Macaca Fascicularis). In Proceedings of the 12th Meeting of the European Neuroendocrine Association, Athens, Greece, 2006.
28. Froehlich, J.; Ramis, J.; Lesage, C.; Obach, R. Safety, Pharmacokinetics (PK) and Pharmacodynamics (PD) After Subcutaneous (s. c.) Administration (adm) of BIM23A760, a Chimeric Compound Combining Dopaminergic Agonist and Somatostatin Analogue, in Healthy Male Volunteers. In 91 st Annual Meeting of the Endocrine Society, Washington, DC Abstract P3-685, 2009.
29. Lesage, C.; Seymour, C.; Urbanavicius, V.; Beckers, A.; Kazanavicius, G.; Colao, A. A Phase II Exploratory Study of BIM23A760 in Acromegalic Patients: Preliminary Results of Safety and Effi Cacy After a Single-Dose Administration. In 91 st Annual Meeting of the Endocrine Society, Washington, DC, 2009.
30. Van Camp, G.; Flamez, A.; Cosyns, B.; Weytjens, C.; Muyldermans, L.; Van Zandijcke, M.; De Sutter, J.; Santens, P.; Decoodt, P.; Moerman, C.; Schoors, D. Treatment of Parkinson's Disease With Pergolide and Relation to Restrictive Valvular Heart Disease. *Lancet* **2004,** *363,* 1179–1183.
31. Jähnichen, S.; Horowski, R.; Pertz, H. H. Pergolide and Cabergoline But not Lisuride Exhibit Agonist Efficacy at Serotonin 5-HT2B Receptors. *Institut für Pharmazie;* Freie Universität Berlin: 14195 Berlin, Germany, 2004.

Relevant Websites

32. List 5–10 websites related to the topic of your chapter, using top-level website addresses and a short title/description of the website.
33. http://web.archive.org/web/20070408111551/http://www.fda.gov/cder/drug/advisory/pergolide.htm–FDA Public Health Advisory: Pergolide (marketed as Permax).
34. https://www.tga.gov.au/publication-issue/australian-adverse-drug-reactions-bulletin-vol-23-no-4 –Australian Adverse Drug Reactions Bulletin, Vol. 23, No. 4, August 2004.
35. http://userpage.fu-berlin.de/~hpertz/Presentation001.pdf. https://clinicaltrials.gov/ct2/show/NCT00994214–Jähnichen S., Horowski R. & Pertz H.H. Pergolide and Cabergoline But not Lisuride Exhibit Agonist Efficacy at Serotonin 5-HT2B Receptors.

6.05 Basic Principles of Formulation for Biotherapeutics: Approaches to Alternative Drug Delivery

L Otvos, Jr., OLPE, LLC, Audubon, PA, United States

© 2017 Elsevier Ltd. All rights reserved.

6.05.1	**Introduction**	131
6.05.2	**Basic Formulation Principles**	132
6.05.2.1	Solution Behavior of Nucleic Acids	132
6.05.2.2	Solution Behavior of Proteins and Peptides	132
6.05.2.3	Freezing and Lyophilization	133
6.05.2.4	Excipients Added to Solution Formulations	134
6.05.3	**Biodistribution of Peptides and Small Proteins**	135
6.05.3.1	Reasons of Low Oral Bioavailability of Polypeptides	135
6.05.3.2	BBB Penetration and Renal Clearance	135
6.05.4	**Penetration Enhancers**	136
6.05.4.1	Basic Principles	136
6.05.4.2	Active Transport	136
6.05.4.2.1	Carbohydrates	136
6.05.4.3	Passive Transport	138
6.05.4.3.1	Cationic antimicrobial peptides as drug delivery vehicles	138
6.05.4.4	Particle Delivery	138
6.05.4.4.1	Nanoparticles as modern drug delivery systems	139
6.05.4.5	Competing Peptide Drug Delivery Technologies	140
6.05.4.6	Microspheres and Lipids in Protein Drug Delivery	140
6.05.4.7	Additional Paracellular Transport-Enhancing Additives	141
6.05.4.7.1	Amino acid- and peptide-based transporters	141
6.05.5	**Improving In Vivo Circulation Time**	142
6.05.5.1	Pegylation	143
6.05.5.1.1	Proteins	143
6.05.5.1.2	Carbohydrates and nucleic acids	144
6.05.5.2	Conjugation to Fc Antibody Fragments	144
6.05.5.3	Albumin-Binding	145
6.05.5.4	Hyperglycosylation and Lipidation of Large Proteins	146
6.05.6	**Alternative Administration Routes**	146
6.05.6.1	Intranasal	147
6.05.6.2	Pulmonary, Transdermal, Buccal, Rectal, and Vaginal	147
6.05.7	**Convenient Subcutaneous and Intramuscular Delivery Devices**	148
6.05.8	**Implantable Devices for Subcutaneous Drug Delivery**	148
References		149

6.05.1 Introduction

Biologic-based drugs are difficult to administer to patients in their native form. Proper formulation ensures the safety and efficacy of the active pharmaceutical ingredient (API) at the time of dosing and for extended periods of time in storage. The easiest storage of orally available drugs is in the tablet or capsule forms they are administered to patients. However, most biological drugs, such as peptides, proteins, and nucleic acids, are unstable and/or fail to be absorbed during enteric administration. The Lipinski's rule of five placed biological drug APIs into the unwanted second-grade pharmaceutical category.[1] The requirements for less than 500 Da molecular weight (MW), low hydrophilicity, less than five hydrogen-bond donors, and 10 acceptors all precluded biologics from being considered as desirable drugs for medicinal chemists. It was just very recently when it became clear that peptides/proteins outperform small molecules at the phase II → phase III transition stage (except for oncology applications) with 29% for small molecules and 42% for the biological drug candidates.[2] Although new delivery technologies widen the way peptide/protein APIs are stored, still, the most common forms are lyophilized powders or aqueous solutions in vials or other closed containers. Thus, the first tier of biological drug formulation is to make sure the solution structures are stable and deliverable, and their administration poses no danger to the patients.

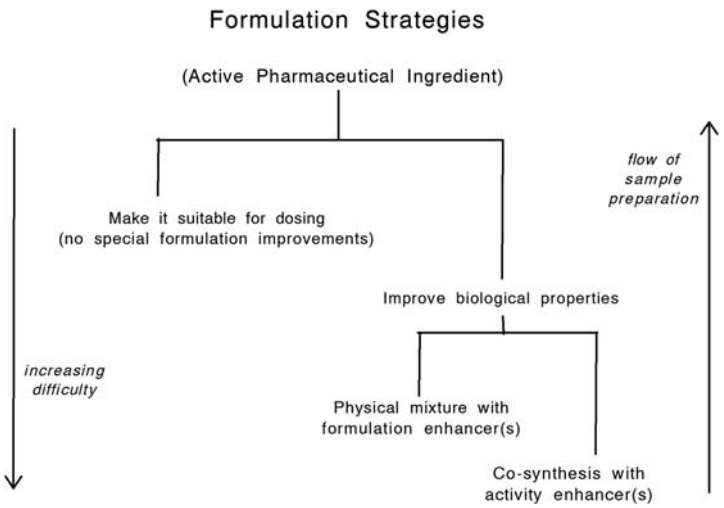

Fig. 1 Levels of formulation complexity for peptide and protein drugs.

The second tier of formulation returns to the drawbacks of peptide and protein drugs frequently cited, that is, proteolytic instability, low levels of oral activity and poor blood–brain barrier (BBB) penetration, disconnect between pharmacokinetic and pharmacodynamics parameters, and rapid renal and sometimes hepatic clearance.[3] To overcome these potentially troubling properties, biological dugs are either physically mixed or covalently linked to absorption enhancers, sequence and structure stabilizers, or agents aiming to delay the elimination time (Fig. 1).

Either with or without activity enhancers, various devices used for quick and efficient mucosal, subcutaneous, or intramuscular administration of any drug are optimized for peptide and protein API delivery.

6.05.2 Basic Formulation Principles

6.05.2.1 Solution Behavior of Nucleic Acids

The focus of this article is peptide and protein drugs that not only have proved clear therapeutical value by now but also for which significant medicinal chemistry efforts are devoted. Nevertheless, nucleic acids as drugs cannot be ignored, although gene therapy is still in its infancy in terms of clinical significance and treatment preference among all drug classes.[4] DNA-based drugs include plasmids and aptamers, and oligonucleotides are used as antisense and antigene applications. RNAs are also applied as aptamers and antisense treatment options, in addition to more contemporary variations such as small interfering and microRNAs.

Upon direct injection into skeletal and heart muscle, purified plasmid DNA is able to express recombinant genes.[5,6] The injection cocktails contain circular or linear nucleic acids dissolved in phosphate-buffered saline alone or in aqueous buffers supplemented with hypoxanthine, thymidine, sodium pyruvate, L-glutamine, trace elements, and growth factors. Alternatively, the DNA is dissolved in 5–20% sucrose prior injection by using a narrow needle.[7] Interestingly, naked plasmid DNA provides better gene transduction results than DNA complexes. Inflammation-inducing chemicals introduced during sample purification, including EDTA, endotoxins, and ethidium bromide, have to be removed from the solution to be administered. The efficacy of naked DNA delivery to tissues can be increased if physical force is applied, most notably pressure or high-frequency, low-voltage electric pulses.[8,9] Purely synthetic vectors seem to be safer than nucleic acids produced by viruses although at the same time they are also less efficacious.[10]

DNA is sensitive to hydrolytic degradation with significantly lower half-lives in room temperature than at colder environments.[11] This argues for storage as a lyophilized form especially as freezing, the first step of the lyophilization protocol, is the second safest storage form of synthetically made DNA therapeutics.

6.05.2.2 Solution Behavior of Proteins and Peptides

The basic formulation strategies of biopolyamides are regulated by the solution behavior of proteins and peptides. The regularly used distinction between peptides and proteins is still unclear and does not really apply to here. If we consider peptides as any native or backbone-modified polyamide that can be made on a contemporary peptide synthesizer, then the limit in size (approximately 100 residues) exceeds the arbitrary cutoff of 50 amino acids originally setup by the US Food and Drug Administration (FDA).[12] New FDA definition of peptides places the limit of amino acids to 40 residues although retains the 100 residue limit for entirely synthetic polyamides. More important, however, is how these molecules change some of their properties upon storage.

Proteins in solution can undergo a series of physical and biochemical alterations. For the sake of this discussion, we have to disregard enzymatic degradation or isomerization induced by catalysts included in the formulation. While this requirement seems

plausible for pharmaceutical grade preparations, other protein[13] or enzyme[14] contaminants are not unheard of in protein batches undergoing less thorough cleaning steps. The two main chemical modifications of protein formulations are deamidation and oxidation[15] in addition to biochemical alterations such as aggregation and denaturation or more generally conformational changes.[16] Other factors that may modify the physical characteristics of proteins in solution are pH, osmolality (ionic strength), temperature, and buffer composition.[17]

The main source of deamidation is the hydrolysis of asparagine and glutamine residues into aspartic acids and glutamic acids, respectively.[18] The reaction mechanism proceeds through cyclic imide intermediates without influence of time or temperature, suggesting a pathway without any direct side-chain hydrolysis.[19] One of the best known examples is insulin in which AsnB3 is deamidated in neutral and AsnA21 in acidic conditions. Similar reaction can also be observed for peptides such as exenatide. Conjugative degradation of model short aspartyl peptides was observed in aqueous solutions, and the reaction mechanism was suggested to be an alternative route to irreversible denaturation of proteins.[20] Similarly, isomerization of aspartic acid bonds at positions 1 and 7 into isoaspartates at the amyloid Aβ peptide results in the formation of extended structure, which can lead to aggregation in Alzheimer's disease.[21] As shown by using smaller peptides, a diisomerized Aβ fragment exhibits increased stability toward serum peptidases compared with the unmodified or single isoaspartic acid-containing peptides, suggesting yet another possible mechanism of enrichment of isomerized Aβ in the affected brains. Finally, isomerized Aβ fragments are more immunogenic than those having regular aspartic acid side-chain structures. While peptides are in general unable to induce antibody production in animals, if it does happen, immunogenicity of modified peptides and especially proteins is detrimental for potential therapeutic use. Other nonenzymatic chemical modifications of proteins include the loss of carbohydrate side chains or reduction of disulfide bonds together with formation of nonnative Cys–Cys bridges.

Aggregation is the assembly of protein chains to higher MW, even sometimes visible or subvisible particles.[16] For most cases, conformational changes leading to extended structures precede macromolecular aggregation, and thus, it is important to maintain the thermodynamic and structural stability of proteins in liquid environment. Some of the aggregates formed upon storage are/can be reversed before administration to patients, although, in these cases, emerged toxicity issues should be studied very diligently. When aggregation is not reversible, visible precipitates form that are similar to a priori insoluble protein deposits. In our experience, addition of various adiponectin protein preparations to cells induces a wide range of biological responses (or lack thereof),[22] and this phenomenon was explained as the varying aggregation state of commercial adiponectin preparations from monomers through trimers to hexamers.[23] In addition to the β-pleated sheet-forming potential (or related to that), the extreme hydrophobicity of adiponectin protein and its C-terminal, active domain, prevents pharmaceutical development at the research scale and is expected to raise even larger problems when the larger polyamide preparations are ready for vialing and clinical development.[24] In this regard, active site peptides are significantly easier to handle and optimize for maximal therapeutic effects.[25]

In addition to aggregation initiated by thermodynamic instability of monomers, physical stress can also induce aggregation of protein therapeutics. From these, the most studied processes are thermally induced and mechanically induced aggregation, where the former category can be expanded with aggregation taking place during freeze-drying cycles.

Exposure to hydroxyl radicals leads aggregation to the last most studied protein modification, that is, oxidation. Hydroxyl radicals in solution, but not exposure to superoxides, can produce covalently bound protein aggregates together with extensive changes in net electric charge.[26] Tryptophan is lost, and bityrosine biphenol appears during hydroxyl radical exposure. Residual metals can initiate oxidative degradation in proteins, even when tight controls with stringent specification on the amount of metal impurities are implemented.[27] Redox-active transition metals influence the processing and/or storage of biological pharmaceuticals and are capable of generating radicals by redox reactions with organic and inorganic substrates and molecular oxygen.[28] The major mechanisms of oxygen activation by metal ions are Fenton/Haber–Weiss reaction and autoxidation.[27] The substrates are molecular oxygen, superoxide, and hydrogen peroxide. Organic solvents or photochemical reactions involving some excipients can also induce oxidative damage in protein therapeutics.

6.05.2.3 Freezing and Lyophilization

To avoid the problems related to physical and biochemical changes of proteins and peptides in aqueous solutions, freezing and lyophilization are the preferred method for long-term storage of these polyamides. Freezing of peptides and proteins is certainly a useful procedure to avoid deterioration of the products by significantly slowing down or completely stopping of kinetically controlled processes. However, repeated freeze–thaw cycles have their own dangers for protein quality and biological activity. While slow freezing (at a freezing rate about $1^{\circ}C\ min^{-1}$) and fast thawing (at a thawing rate $> 10^{\circ}C\ min^{-1}$) protocols yield higher activity recovery, fast freezing with slow thawing results in more severe damage to proteins.[29] This phenomenon is probably due to surface-induced denaturation during the freezing and thawing process. The freezing damage of proteins and aqueous solutions can be reduced by optimally selecting the type of storage buffer type and its composition.

Protein chemistry laboratories recommend adding 5% glycerol or sucrose or various salts to sufficiently stabilize a protein to freezing in liquid nitrogen. Many enzymes that are stable at high concentrations appear to be unstable when used or stored after dilution. The reason of this observation is likely adsorption to the wall of the containers used for storage. In this case, siliconizing the containers or adding low concentrations of surfactants or auxiliary proteins can eliminate the loss of protein activity. If the right solution is found for freezing, the main difficulty is securing stringent cold chain conditions for storage, shipping, and distribution.[16]

During freeze-drying, most of the solvents used for purification, usually water, are removed under mild conditions under reduced pressure. The basic principle of lyophilization is sublimation, an endothermic phase transition that produces gas (in our case water vapor) directly from a solid state (ice for proteins). Lyophilization proceeds through three steps, that is, freezing and primary and secondary drying in industrial conditions. In laboratory environment, the two drying stages are usually combined. After freezing the aqueous solutions well below 0°C, at research scale down to −20°C to −40°C, at industrial scale to −10°C, primary drying is initiated by introducing vacuum in the drying chamber/container.[30] The internal pressure is reduced below the saturated vapor pressure of ice at the frozen product temperature providing a driving force for sublimation. At research scale, the container under vacuum is immediately placed to ambient temperature. In large-scale lyophilizers, when the frozen bulk water is removed at low temperature, the temperature is raised to ambient values or above, to evaporate the bound water remaining in the product. The cycle is completed when the desired residual moisture level is achieved.

Depending upon the design and quality of the apparatus, the strength of the vacuum applied and the temperature of the frozen cake, lyophilized peptides always contain 20–30% (w/w) residual solvent, usually water, and sometimes solvents remaining from the reversed-phase liquid chromatography steps such as trifluoroacetic acid and acetonitrile. First, it is imperative to repeat the lyophilization cycle from diluted acetic acid to remove all trifluoroacetate liquid and counterions that can significantly change animal responses (cells are usually not sensitive to low concentration of organic counterions). Second, the actual peptide concentration of the lyophilized samples has to be quantitatively identified. In our experience, amino acid analysis is not suitable for that purpose. We calibrated high performance liquid chromatography (HPLC) columns used for nothing else than this purpose with marketed peptide drugs of known peptide content and run the samples through this column before testing in any biological system.[21]

For pharmaceutical proteins, excipients are added to the freeze-drying mixture to avoid the production of unwanted side products or eliminate potentially harmful conditions.[30] These may include buffers (tris, histidine, or citrate) to prevent acidification during freezing; specific ligands or pH conditions to ensure the thermodynamic stability of the protein; carbohydrates, most preferably trehalose or sucrose, to inhibit protein unfolding and provide a glassy matrix, perhaps a bulking agent (e.g., mannitol, glycine, or hydroxyethyl starch); and finally nonionic surfactants to reduce protein aggregation.

6.05.2.4 Excipients Added to Solution Formulations

When the protein or peptide has to be formulated in solution, generally regarded as safe agent excipients are added to prevent the potential physical and biochemical modifications and to ensure safe and efficacious dosing in humans, in veterinary applications, or in experimental animals. It is important to emphasize that one set of excipients that are useful for one protein may be detrimental to others; the optimal solution composition has to be identified for each molecule, administration route and duration, and packaging consideration.[31] Each excipient works with a different mode of action by weakening undesired or strengthening stabilizing forces. The following list gives a first look into the potential additives in liquid formulation of proteins:

- Reducing surface tension
  - (i) *Surfactants*: Polysorbates Tween 20 or Tween 80[32,33] below 0.5% (preventing the proteins to reach the air–liquid or liquid–surface interfaces or agitation-induced aggregation), polyoxyethylene glycol dodecyl ether Brij 35, sodium dodecyl sulfate, and poloxamers Pluronic F-68 and F-127. Protein pharmaceuticals applied to include human growth hormone and hemoglobin.
  - (ii) *Ancillary protein*: Human serum albumin prevents adsorption due to high interfacial activity but needs to be used with appropriate formulation pH and ionic-strength additives.[34]
  - (iii) *Polysaccharides*: Dextran or polyethylene glycol is able to protect against surface adsorption[35,36] and used for albumin, myoglobin, and β-galactosidase.
- Preserving protein/peptide integrity
  - (i) *Reducing and chelating agents*: Ascorbic acid and sulfurous acid salts (up to 1%) are the most popular antioxidants in the food and pharmaceutical industries.[37] When used together with heavy metals, the use of ascorbic acid needs chelating agents.[38] Monothioglycerol as antioxidant helps to maintain the stability of oxytetracyclin but not that of a gastrin derivative.[39,40] Additional chelating agents are citric acid and thioglycolic acid.[41]
  - (ii) *Bacterial growth prevention*: These agents are not true antimicrobials in the sense of medical therapy against bacterial infections. Rather, they simply are organic compounds that prevent bacterial growth in the protein formulation. Some of the most frequently used are phenol, metacresol, benzyl alcohol, parabens, and thimerosal (the latter for vaccines).
  - (iii) *Amino acids*: Histidine, arginine, lysine, aspartic acid, glutamic acid, and glycine.[42] While these excipients were suggested to stabilize proteins by a variety of mechanisms,[43] it is intriguing that except glycine, they all contain positively or negatively charged side chains. These can either directly increase solubility of the large polypeptide or provide charged environment eliminating ionic agents that induce aggregation.
- Adjusting the ionic environment
  - (i) *pH stabilizers*: Buffers in mM concentrations provide optimal solubility and stability of the formulation while maintaining an acceptable environment for drug administration to the patient or experimental animal population.[44] The buffers are

regular pH-adjusting systems used in everyday laboratory practice such as phosphate, bicarbonate, sulfate, nitrate, acetate, and pyruvate. Sometimes, they function as chelating agents. Acidification can be prevented by addition of extra Mg^{2+} or Zn^{2+} salts.

(ii) *Solution tonicity*: In parenteral drug administration, isotonic behavior of the solutions prevents irritation, pain, and tissue damage at the site of inoculation. The isotonic environment is reached by addition of electrolytes (NaCl), glycerol, and/or dextrose.[45]

6.05.3 Biodistribution of Peptides and Small Proteins

6.05.3.1 Reasons of Low Oral Bioavailability of Polypeptides

The intestinal epithelium represents a major barrier through which molecules can be absorbed. The phospholipid bilayer of the plasma membrane of epithelial cells is considered the major factor restricting the free movement of substances from the lumen to the bloodstream through the transcellular pathway.[46] While hydrophobic and small molecules can penetrate this system, the enterocyte membrane is almost impermeable to large hydrophilic biopolymers such as peptides and proteins.[47]

6.05.3.2 BBB Penetration and Renal Clearance

In addition to the intestinal epithelium, proteins cannot enter certain biological barriers restricting their use in diseases developing outside the brain or the urinary tract. The BBB is normally impermeable to proteins in order to prevent circulating biopolymers to enter the central nervous system (CNS)[48] with the largest substance found to cross the BBB being a chemoattractant with a MW of 7800 Da.[49] The glomerular barrier is slightly more forgiving, yet the largest protein showing well-measurable sieving coefficient is myoglobin[50] with an MW of still less than 18,000 Da. In contrast, peptide-based drugs match everything protein therapeutics can offer but do not suffer from size or manufacturing capacity limitations.[51] In fact, as peptide drugs not only pass through the kidneys but also downright undergo renal clearance, kidney-targeting peptide drugs can be concentrated at the desired site of action. For example, one of our antibacterial peptides was inactive in systemic infection but was very efficacious in an *Escherichia coli* urinary tract infection model.[52] Peptides are concentrated in the kidneys as soon as 30 min after administration, with full renal clearance in a couple of hours (**Fig. 2**).

Contemporary oncology treatment modalities target cancer-specific cell surface receptors and frequently employ monoclonal antibodies (mAb) as effector molecules. While this strategy works against many tumor types, the limitations to cross the BBB and enter the kidneys prevent targeted biological therapy to brain or kidney cancers. This leaves us only with bevacizumab (Avastin) to treat metastatic renal cell carcinoma.[54] Likewise, currently, there is no "standard of care" for recurrent malignant glioma, but most frequently patients are treated with a combination of bevacizumab (preventing angiogenesis) and alkylating agents or topoisomerase inhibitors.[55] As with other alkylating agents, temozolomide treatment can be considered only as a palliative care and carries serious toxicity concerns.[56] Clearly, kidney and brain cancer patients would enormously benefit from a targeted biological therapy that promises to be highly efficacious, nontoxic, and widely available. Penetration enhancers across the BBB and peptide drugs targeting the urinary tract could do just that.

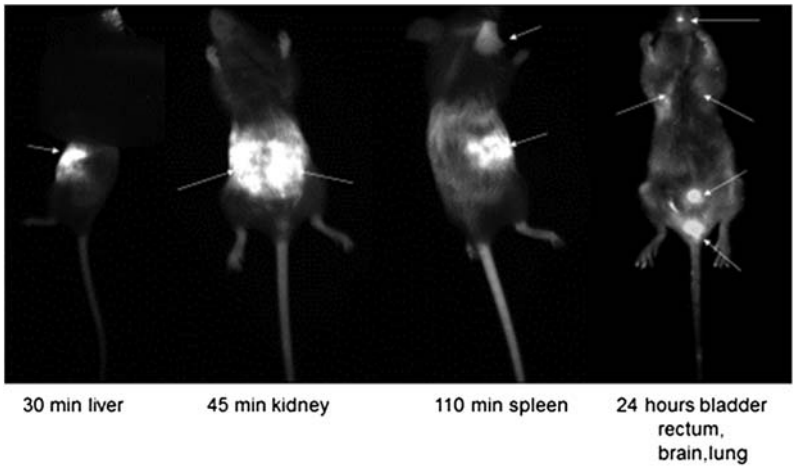

Fig. 2 Biodistribution of the leptin receptor agonist peptide E1Free[53] conjugated to a near infrared dye. Thirty μg-labeled peptide was administered intraperitoneally to mice. In addition to the organs containing the peptide, at the 45 and 110 min pictures, the injection site can also be seen.

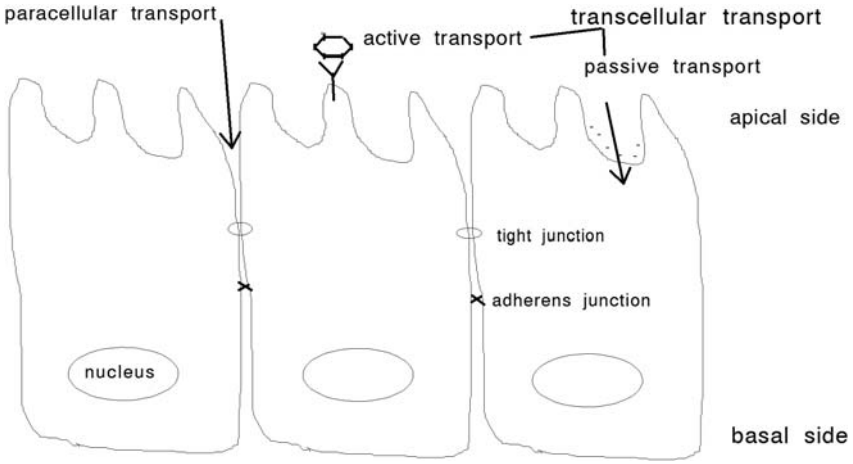

Fig. 3 Summary of the transepithelial intestinal pathways: active transport, transcellular passive transport, and paracellular transport.

6.05.4 Penetration Enhancers

6.05.4.1 Basic Principles

Due to the low bioavailability of peptides and proteins and the fast renal clearance of polyamides below 40–60 kD in size, strategies have to be developed that apply the principle of the "Trojan horse": the peptides have to be smuggled into the cells and tissues by using carrier systems that are compatible with epithelial cell entry.[57]

Potential avenues to solve the problem. As we know it today, there are three potential ways of delivering peptides into cells and across the intestinal epithelial layer (Fig. 3). In some cases, it is enough if the penetration/absorption/targeting enhancers just physically mixed with the peptide and protein drugs. However, in most cases, cosynthesis or postpreparation covalent coupling provides the best and desired results.

6.05.4.2 Active Transport

By using the active transport mechanism of the cells, we can target cell surface receptors that recognize and internalize specific molecules. These include carbohydrate receptors, lipoprotein receptors, transferring receptors, and receptors involved in cell adhesion. The carrier bioconjugates explored so far for this purpose include antibodies, carbohydrates, viral proteins, and some molecules of endogenous origin.[58]

6.05.4.2.1 Carbohydrates

From the active peptide delivery agents, carbohydrate-mediated transport has received the most attention. The reason for this is probably the simplicity of both the synthesis of glycopeptides and the interpretation of the in vitro biochemical and in vivo efficacy results. Appropriately protected and activated glycoamino acid monomers, suitable for automated solid-phase peptide synthesis, are widely available from a number of commercial sources. Glycobiology, as an ever-emerging specialty, provides ample biological background for glycopeptide applications.

6.05.4.2.1.1 Examples of mannose-mediated active transport

It was shown that mannosylation of proteins can facilitate their entry to the cells via the mannose-binding protein.[59] The mannose receptor is highly expressed on the surface of cells, especially dendritic cells, and accordingly, numerous advantages were taken of this mechanism to deliver pharmaceutical agents into cells, ranging from targeted gene transfer,[60] to lymphoscintigraphy by receptor-mediated delivery of a nonparticulate imaging agent,[61] to modulation of pathogenic T-cell reactivity by altered peptide ligands.[62] In this last case, a 100- to 1000-fold lower concentration of a bis-mannosylated peptide was sufficient for complete blocking of the proliferative T-cell response against the agonist peptide compared with the nonmannosylated analog.[62] Around the millennium, we proposed that entry of subunit peptide vaccine candidates into antigen-presenting cells can be facilitated by coupling mannose to synthetic peptide antigens in terminal positions, where the mannose does not interfere with MHC-binding or TcR recognition and prepared a prototype peptide vaccine for this purpose.[63] Although mannosylation appears to improve the antigenic properties of the peptide construct, it has a less favorable effect on the immunogenic properties. Similarly to our results, mannosylation neither enhanced nor impaired the protective effect of peptide vaccination in a reproducible fashion.[64] This may be due to the presence of soluble mannose-binding protein in the serum that scavenges the mannosylated antigens for degradation by the liver before the antigen reaches the specialized antigen-presenting cells. In

addition, macrophages, which are poor stimulators of naive T cells, may compete with the professional antigen-presenting dendritic cells for peptide immunogens.

6.05.4.2.1.2 Bioavailability and in vivo efficacy of glycosylated peptides

A pioneering example for improving the oral bioavailability of a peptide drug by glycosylation was published in 1993, when somatostatin analogs were prepared using the Amadori reaction. Coupling a maltose (α-D-Glc(1–4)-1-deoxy-D-Fru) to the N-terminal of the octapeptide (D)Phe-Cys-Phe-(D)Trp-Lys-Thr-Cys-Throl resulted in about 10-fold increased oral bioavailability while maintaining the selectivity and duration of action of the original peptide.[65] In healthy male volunteers, both 1 and 5 mg kg^{-1} day^{-1} oral doses (over a 14 day period) of the glycopeptide led to the suppression of the fasting level and postprandial release of gastrointestinal and pancreatic hormones.[66] Native glycoproteins carry asparagine-, serine-, or threonine-linked carbohydrates attached *via* true glycosidic bonds. With the advent of high-throughput solid-phase peptide synthesis, glycoamino acid building blocks are readily available in an affordable price, thus ensuing research focused on "real" glycopeptides. When the serine residue located in midchain position in an analog of the antidiuretic drug vasopressin Cys-(D)Tyr-Phe-Ser-Asn-Cys-Pro-Arg-Gly was replaced with a serine carrying a β-D-galactosyl moiety, a significant increase in intraintestinal absorption was observed in rats.[67] The peptide plasma concentration was elevated from 0.4 ng mL^{-1} (unglycosylated peptide) to as high as 2.5 ng mL^{-1} (glycopeptide) 60 min after 100 μg intraintestinal dosing. While the delivery across the intestinal epithelium was improved in this case, the glycopeptide exhibited a decreased level of receptor binding, as indicated by the decrease of the in vitro antidiuretic activity from 810 to 0.31 IU $\mu mole^{-1}$, underlining the importance of the carbohydrate positioning in the peptide sequence.

Replacement of the 20 proteinogenic amino acid residues with modified versions at terminal positions reduces the ability of exopeptidases to digest peptide-based drugs. If sugar is incorporated to these positions, glycosylation serves as both a stability enhancer and a delivery module. Glycosylation of C-terminal serine or threonine in enkephalin analogs improves both stability of the peptide drugs and their penetration across the BBB.[68] After intravenous administration, nine Tyr-(D)Thr-Gly-Phe-Leu-xxx enkephalin glycopeptides produced full antinociceptive effects ranging from 2.2 μmole kg^{-1} IV A50 (95% CI) for the peptide-containing C-terminal D-Gal-α(1 → 6)-D-Glc-coupled serine to 22 μmole kg^{-1} IV A50 (95% CI) for a glycopeptide that contains β-Glc moiety attached to D-threonine.[69] Disaccharide-containing derivatives exhibited potencies that equaled or exceeded that of morphine, but the use of a longer carbohydrate chain (e.g., maltobiose to maltotriose 6.8–10.9 μmole kg^{-1} IV A50 (95% CI)) or more than one monosaccharide in the glycopeptide (e.g., Ser(β-Glc)-Ser(β-Glc) at 140 μmole kg^{-1} IV A50 (95% CI)) diminished the activity figures. While sugar incorporation generally slightly reduced the ability of the enkephalin glycopeptides to bind their receptors, the monosaccharide composition itself or orientation of the anomeric carbon to the peptide side chain had little effect.

We designed 12–14 amino acid long glycopeptides corresponding to the third leptin receptor-binding domain of leptin protein carrying β-*O*-serine- and α-*O*-threonine-linked glucose and *N*-acetyl-galactosamine moieties very close to the N-terminal.[53,70] The representative of the first-generation glycopeptide, Tyr(I_2)-Serβ(Glc)-Thr-Glu-Val-Val-Ala-Leu-Ser-Arg-Leu-Dap(Ac), bound to isolated leptin receptor on solid-phase assays and activated ERK-1/2 signaling in leptin receptor-positive MCF-7 breast cancer cells at 100–500 nM concentrations. In mouse models, the glycopeptides penetrate the BBB more efficiently than unglycosylated leptin protein itself, and this improved BBB penetration results in improved hypothalamic actions, such as appetite control. When added intraperitoneally, the second-generation leptin glycopeptide Tyr(I_2)-Ser-Thrα(GalNAc)-Glu-Val-Val-Ala-Leu-Ser-Arg-Aca reduces weight gain in mice fed with high-fat peanut diet in a dose-dependent manner. Obese mice lost weight, corresponding to a net 6.5% total body weight loss, while similar mice treated with leptin protein did not. In mice undergoing leptin glycopeptide treatment, several obesity-related pathologies (i.e., abnormal metabolic profile and liver histology as well as infertility) were normalized, while unglycosylated leptin protein therapy could not show similar positive treatment outcomes. The studies provide further support to the notion that class I hexose transporters (involved in BBB delivery) do not significantly discriminate between glucose and galactose moieties.[71]

The earlier studies addressed either intestinal drug absorption or BBB penetration. In a more recent report, both of these desired functions are improved by sugar attachment to endomorphin-1, an opioid tetrapeptide with the sequence Tyr-Pro-Trp-Phe.[72] Lactose was attached to the N-terminal through a succinamic ester spacer between the peptide and the carbohydrate and using an N-linked glycosidic bond. Once again, glycosylation improved the metabolic stability and membrane permeability of the peptide, although reduced the μ-opioid receptor-binding affinity from pM concentrations to 15 nM. Significantly, at a single oral dose of 10 μmole kg^{-1}, the plasma concentration elevated from zero to 20 μM in 60 min. The glycopeptide produced a dose-dependent pain relief after oral administration in rats with a paw withdrawal threshold of eight when given at 16 μmol kg^{-1}. These results provide clear evidence that the glycosylated opioid analog was not only adsorbed in the intestinal epithelium but also penetrated into the brain. The oral efficacy of the glycopeptide was comparable with that of morphine. It needs to be mentioned that 1-3β-galactose-containing moieties should be avoided because these are quickly neutralized by the antigalactose antibody, which is the most abundant antibody in humans.

These examples show that incorporation of mono- or disaccharides into terminal or near-terminal positions of peptide drugs improves not only the metabolic stability but also the ability of the peptides to cross biological layers that are otherwise impermeant to unmodified peptide drug leads. In general, glycosylation was repeatedly found to only slightly alter the conformation of the peptides, if it made any change in the peptide structure at all,[73] and therefore, the receptor-binding parameters are not expected to be significantly modulated. Many peptide API manufacturers offer small- and large-scale production of glycosylated peptides.

6.05.4.3 Passive Transport

Passive transport can utilize the abundant negative charges of the cell surface. Endocytosis in this case is initiated by binding of polycationic substances to these negative charges. While generally receptor-mediated uptake is characterized by K_d values in the low nanomolar range and maximum binding capacities of less than 1 pmol mg^{-1} membrane protein, the absorptive-mediated uptake features micromolar saturation constants and several nmol mg^{-1} binding capacities.[74] Enzymatic treatments revealed that the anionic microdomains on the luminal side of endothelial capillaries consist of negatively charged glycoproteins with sialic acid residues, while the abluminal anionic-binding sites contain heparan sulfates.[75] Cationic peptides not only bind to cellular surfaces but also indeed undergo an enhanced cellular uptake. In vitro and in vivo studies with a dynorphin analog and an analog of adrenocorticotropic hormone show pharmacokinetic characteristics of the brain typical for absorptive-mediated transcytosis.[76,77] In vivo, approximately 15% of cationized bovine serum albumin taken up was transcytosed into postcapillary extracellular space. Actually, cationized rat serum albumin accumulated very well after intravenous bolus injection in the kidney and the brain, less significantly in the liver, and not at all in the myocardium and the lungs.[78]

6.05.4.3.1 Cationic antimicrobial peptides as drug delivery vehicles

The potential to deliver drug leads through the anionic surfaces of cells is well represented by the proline-rich native antibacterial peptide family, originally isolated from insects.[79] Similar to other antimicrobial peptides,[80] the proline-rich peptides are also rich in cationic residues, arginine, lysine, and histidine. Cationic peptides, just like cationized proteins, are generally able to interact electrostatically with the negatively charged bacterial phospholipids and then insert into the model membranes of planar bilayers or liposomes.[81,82] Although these processes often involve formation of channels or pores, alternative mechanisms were also suggested. According to these, the peptides either cooperatively destroy the membrane barrier without channel formation[83] or just create brief disruptions in permeability.[84] It is clear that permeabilization of the cytoplasmic membrane to destroy the membrane potential is not lethal per se.[85] This is especially true for peptides that are rich not only in positively charged residues but also in prolines.[86] For example, it was argued that one of the insect-derived peptides, apidaecin, or its mammalian analog PR-39 enters bacterial cells without any disruption of the membrane structure and consecutively meets their intracellular target biopolymer.[87,88]

The special role of proline residues was best documented on buforin II, an antimicrobial peptide acting on bacterial DNA and RNA.[89] Confocal fluorescence microscopic studies show that buforin II accumulates in the cytoplasm.[90] When the key proline is replaced with leucine, the preferred amino acid residue in antibacterial peptides with amphipathic alpha-helix structure,[91] the ability of the peptide to accumulate intracellularly is decreased, and therefore, the antibacterial activity is reduced. The peptides with bacteria-specific target proteins are not expected to be toxic to host cells and organisms, and indeed, we showed that two of the proline-rich peptide family members, pyrrhocoricin and drosocin, lack toxicity to mammalian cells and healthy mice up to 100 mg kg^{-1},[92,93] the highest dose studied. Pyrrhocoricin and some of its derivatives enter not only bacteria but also mammalian cells (macrophages). Native pyrrhocoricin penetrates the susceptible organism *E. coli* very efficiently and the nonsusceptible bacterium *Staphylococcus aureus* to a significant degree.[94] The antibacterial peptide also enters human monocyte-derived dendritic cells. A chimera made of a pyrrhocoricin dimer and two copies of a shorter (nine residues) class I major histocompatibility complex epitope successfully entered bacterial and mammalian cells. The chimera when tested for its immunologic properties activated human dendritic cells significantly more strongly than any of the two independent fragments alone yet lacked mammalian cell toxicity. These results confirm the utility of designed cationic antibacterial peptide analogs for delivery of peptidic cargo across cell membranes in general and their potential as carriers for epitope-based vaccines in particular.

Generally speaking, peptides penetrate into bacteria easier than they do into mammalian cells. The interaction of most peptides with eukaryotic membranes is inhibited by the lack of negatively charged lipids on the surface of such cells, by the rather low membrane potential across the plasma membrane and by the presence of cholesterol, in contrast to bacterial membranes that are abundant of anionic surface phospholipids, have high transmembrane potential, and lack cholesterol.[95] However, peptides with strong membrane-disintegrating activity may overcome these gaps. For example, cecropin, another antibacterial peptide of insect origin, is deadly to mice at a 100 mg kg^{-1} dose.[96] Even less clearly, membrane-active peptides, like PR-39, can penetrate eukaryotes; this peptide rapidly enters human microvascular endothelial cells.[97] These peptides become toxic if they stay attached to the membrane and destroy the eukaryotes. However, if they only cross the membrane to inhibit a bacteria-specific intracellular target, they can selectively kill obligate or facultative intracellular pathogens, and more generally, they can be used to deliver foreign pharmacophores into mammalian cells and hence improve the delivery of nonantimicrobial drug leads.

6.05.4.4 Particle Delivery

Delivery by using nano- or microparticles involves the uptake of biodegradable polymers by the M cells of the Peyer's patches. Particles currently used for oral delivery fall into two classes: (a) nanoparticles, ranging in size from 10 to 1000 nm and (b) microparticles ranging from 1 μm to 1 mm.[98] In general, the smaller the particle, the better the peptide drug is absorbed, due to the difficulty to engulf larger particles and improved hydrophobic/hydrophilic ratio.

Insulin can be encapsulated very efficiently in oil-containing poly(isobutyl cyanoacrylate) nanocapsules, and these nanocapsules show unexpected biological activity after intragastric administration.[99] Salmon calcitonin is a highly water-soluble basic peptide, consisting of 32 amino acid residues. Calcitonin absorption via the gastrointestinal tract is significantly enhanced after

incorporation into nanoparticles.[100] In earlier approaches, nanoparticles were usually made by grafting the peptide drugs to the terminal positions of hydrophobic vinyl monomers.

In contrast, microparticles are almost exclusively made from copolymers of lactic acid and glycolic acid (PLG). The composition and the viscosity strongly influence the release kinetics of PLG microspheres. In our hands, a 50:50 PLG microsphere releases peptide immunogens in a 1-week period.[101] The successful drug delivery by the PLG microspheres was documented by oral immunization with *Bordetella pertussis* fimbriae proteins.[102] When mice were immunized with 10 μg proteins orally, the resulting response was comparable with administering equivalent amounts of the immunogens absorbed onto Alhydrogel or administered intraperitoneally. Exenatide is formulated into 0.06 mm diameter microspheres of PLG that hydrate in situ and form amalgam.[103] The peptide is released in multiple stages, from $<1\%$ in the first few hours to as long as 2 weeks. This formulation is currently in the market with the commercial name Bydureon against type 2 diabetes.

In our experience, immunization of mice with 31D, a T-cell epitopic peptide entrapped in PLG microspheres, improved the antibody response compared with naked antigen, but did not reach the level of antibody production when the peptide was administered in complete Freund's adjuvant. In spite of some initial success, we did not find the PLG microspheres useful for the delivery of synthetic peptides or oligonucleotides on the long run.

6.05.4.4.1 Nanoparticles as modern drug delivery systems

Contemporary particle delivery focuses on nanostructures as vehicles. Uptake of nanostructures has been reported to be 15–250 times greater than that of microparticles in the 1–10 μm range.[104] Nanostructures not only are able to protect drugs from the degradation in the gastrointestinal tract but also allow delivery of drugs into many tissues of the body. Importantly, by bypassing the liver, biological drugs encapsulated in nanoparticles escape first-pass metabolism. Nanometer-size structures are easily taken up by cells and penetrate tissues.

Plasmid DNA-encoding cytokine genes, including mIL-12 and mIFN-gamma, show enhanced antitumor activity and improved survival time in mice compared with naked pmIL-12 when incorporated into 100 nm size poly[alpha-(4-aminobutyl)-L-glycolic acid (PAGA) particles.[105,106] Cholesterol conjugates of linear polyethylenimine, an effective nonviral gene carrier, 250 nm in size, induce protein expression levels higher than the gene product alone without any significant loss in cell viability. The differences in rates of transfection of the lipid/pDNA complexes in Renca cells are partly due to conformational changes upon interaction with the plasma membrane.[107] The preferred nonviral gene delivery vectors are polycation/DNA complexes formed between cationic polymers and DNA through electrostatic interactions.[108] Nanoparticles made from polyamidoamine–polylysine graft copolymers appear to be promising gene vectors with low cytotoxicity, high transfection efficiency, and advantageous serum stability parameters.[109] Inoculation of a dendrimeric version of these nanostructures complexed with the pVEGF165 gene into balloon-injured rabbit carotid arteries results in inhibition of restenosis by increasing VEGF165 expression in vessels.[110] Dendrimers appear to be nonimmunogenic and exhibit the highest efficiency of transfection among other nonviral structures without the drawback characteristic for viral systems.[111] However, the consensus is that further studies are required before the dendrimer/DNA complexes can be used in human gene therapy.

Liposomes are spherical vesicles in which the aqueous compartment is enclosed by a mixed hydrophilic/hydrophobic molecule layer. These structures greatly vary in their composition, size, or surface charge characteristics and used frequently as drug, vaccine, or nonpharmaceutical formulations as carriers. A nanosize multifunctional liposome, containing a magnetic resonance imaging probe, and paclitaxel and the targeting peptide c(RGDyk) overcame the insolubility of paclitaxel and improved drug delivery efficiency to the tumor.[112] Modification of the c(RGDyk) peptide part significantly enhanced the cytotoxicity of the drug in A549 tumor cells. Isolated mouse retinas were treated with liposomes encapsulating either recoverin, an endogenous protein involved in visual phototransduction, or antibodies against it. The contents of intravitreally injected liposomes encapsulating either rhodamine B or recoverin were released in higher amount in the photoreceptor layer than in the other regions of the retina.[113] Remarkably, the released protein functioned in accordance with the current model of phototransduction. From the vaccine field, iontophoresis of antigen peptide-loaded nanogels results in the accumulation of gp100 peptide in the epidermis and subsequent increase in the number of Langerhans cells.[114] As a consequence, tumor growth is significantly suppressed by iontophoresis of the antigen peptide-loaded nanogels, and these structures can represent an effective transdermal delivery system for anticancer vaccination. It needs to be added that liposomes can be made from a great variety of ingredients and protocols making these a very heterogeneous group of nanostructures.

Microemulsions are also generally below 100 nm in size, but for these, the physical properties and the thermodynamic stability of the complexes are the dominant factors.[115] They are composed of two phases of two immiscible liquids that are mixed together and stabilized with surfactants (a main and potentially a cosurfactant). Just like their larger (and unstable) brothers, the emulsions, microemulsions can be prepared either oil-in-water or water-in-oil. Perhaps even more than dendrimers, microemulsions require more studies to exclude some of the observed drawbacks and guarantee their potential for use in clinic,[116] primarily because of phase inversion and the use of toxic alcohols used in the early preparations.[103] When a paclitaxel-containing microemulsion was spiked with penetratin (see section "**Competing Peptide Drug Delivery Technologies**"), a large increase in transepidermal water loss (twofold) was observed suggesting that penetratin addition increases the barrier-disrupting and penetration-enhancing effects of microemulsions.[117] The ratio Δcutaneous/Δtransdermal delivery was the highest among all the formulations studied, suggesting its potential for drug localization within cutaneous tumor lesions. When studying the optimal preparation protocol of these drug delivery systems, a water-in-oil microemulsion was loaded with model bovine serum albumin and cytochrome *c*.[118] In the next step, this phase was dispersed in water resulting in microemulsion formation with a size of approximately

620 nm. The nanostructured particles were able to control the release of the water-soluble proteins freeing only < 10–15% protein in a day.

Nanoparticles are solid colloidal particles that can be made from various macromolecules in which therapeutic drugs can be adsorbed, entrapped, or covalently attached. Nanoparticles are remarkably stable systems, yet they allow controlled release of the hydrophilic biopolymer cargo. Their advantages over larger structures include their ability to pass through small capillary vessels due to their very small volume and increased serum stability by avoiding phagocyte clearance and their ability to penetrate not only tissue gaps to reach distinct organs but also cells themselves. Remarkably, nanoparticles can promote mucosal uptake of incorporated peptides.[119] Incorporation into nanostructural carriers can improve the efficacy of antimicrobial peptides possibly through controlled release properties.[120] Lactic acid, glycolic acid, cellulose acetate, and vinyl alcohol polymers can be used for the preparation of antimicrobial compound-impregnated dressings by electrospinning.[121] Electrospinning is a simple, economical, and thus frequently used technique during which small highly cationic biopolymers concentrate on the surface of the biomaterials allowing controlled but fast release upon contact with moist wound surfaces.[122] For example, electrospun nanofibers deliver LL-37, a cathelicidin peptide, consistently while still maintaining its antimicrobial functions.[123]

In a report receiving much attention, nisin-containing electrospun nanofiber wound dressings significantly reduce *S. aureus* load in a mouse skin abrasion/infection model.[124] We incorporated a 20-mer-modified antimicrobial peptide, called APO monomer, into polyvinyl alcohol nanofibers and polymerized the complex into a solid patch dressing.[125] Mice were subjected to skin excision after which some wounds were infected with a near-lethal dose of multidrug-resistant *Acinetobacter baumannii* strain. When the wounds were subjected to histopathology after 3 days of single patch treatment, APO monomer-containing dressings improved wound appearance and accelerated wound healing. The wound sizes and bacterial loads were statistically significantly reduced compared with similar treatment with colistin, the leading similarly polyamide-based treatment option to Gram-negative infections. Significant to this book article, the nanofiber carrier had more pronounced in vivo efficacy compared with intramuscular administration of the same peptide drug, by using only one-tenth of the API. Considering an average wartime cutaneous abrasion size of $< 20\ cm^2$[126] and even less in the civilian population, antibacterial peptide-impregnated nanofiber wound patches can be developed as effective and economical treatment modalities to skin infections in burn and blast injuries on the streets and in military environments.

6.05.4.5 Competing Peptide Drug Delivery Technologies

The delta sleep-inducing peptide, Trp-Ala-Gly-Gly-Asp-Ala-Ser-Gly-Glu, was reported to be able to permeate biological barriers, although it does not cross the gastrointestinal epithelium-mimicking Caco-2 cell layer system.[127] Other cell-penetrating protein-derived peptides include penetratin (Arg-Gln-Ile-Lys-Ile-Trp-Phe-Gln-Asn-Arg-Arg-Met-Lys-Trp-Lys-Lys), signal sequence-based peptides exhibiting highly hydrophobic α-helical structures, and Ly-Arg-Lys-Lys-Arg-Arg-Gln-Arg-Arg-Arg-Pro-Pro-Gln, corresponding to the 48–60 fragment of the Tat protein from the human immunodeficiency virus 1.[128–131] Synthetic analogs are transportan, the amphiphilic model peptide made of oligomers of Lys-Leu-Ala-Leu, and a Tat analog made of β-amino acid residues.[132] Additional cell-penetrating peptides come from virus proteins, leucine zipper proteins, and yeast transcription factor.[133] Except for the helical signal sequence-based peptides, the common structural characteristic of these protein fragments and synthetic constructs is the abundance of positively charged residues, arginine and lysine, making these peptides often capable of binding to not only negatively charged membrane surfaces but also nucleic acids (compared with buforin II). In fact, hepta- or octaarginine appears to be the best carrier for translocation of cargo into cells.[134] However, increasingly efficient cell penetration is often accompanied by destruction of the cell membrane and hence toxicity.[135] Remarkably, most of these cell-penetrating peptides lack proline residues known to break helices. Indeed, the earlier listed cell-permeating peptides are also helical in membrane environments.[132] When multiple proline-containing drug delivery vehicles are used, the lack of helix formation is expected preventing toxicity to the host.

6.05.4.6 Microspheres and Lipids in Protein Drug Delivery

While microparticle- and lipid-mediated delivery of proteins was partially discussed in previous sections describing the general passive drug delivery technologies dealing mostly with peptides, a separate chapter is justified due to the increased chemical sensitivity of proteins and such making the preparation and applications of the complexes increasingly troublesome. For example, proteins can undergo a series of undesired structural changes upon incorporation into PLG microspheres, including deamidation, thiol-catalyzed disulfide exchange, and conformational modifications.[136] Exactly, this is the reason why coadditives are regularly explored to dampen the erosion processes occurring in PLG polymers.[137]

A typical cargo of PLG microspheres is insulin that lies at the border between peptides and proteins.[138] Biodegradable PLG–polyethylene glycol (PEG; see in the succeeding text) graft copolymer formulations sustain insulin delivery and cartilage repair by chondrocyte cell delivery. With one injection of the insulin formulation, the blood glucose levels were controlled for 5–16 days depending upon the polymer composition.[139] The cartilage defect was also repaired using chondrocyte suspension in the thermogelling PLG/PEG microspheres compared with control. PLG microspheres containing recombinant human epidermal growth factor were prepared using a solvent evaporation method based on multiple water-in-oil-in-water emulsions.[140] After a single subcutaneous dosing, blood concentration of the protein was maintained for 9–11 days culminating in superior gastric ulcer healing effects compared with twice a day subcutaneous administration of the growth factor dissolved in saline solution.

Staying with insulin but moving to lipidic formulations, oral administration of insulin entrapped to various liposomal forms consisting mixtures of dipalmitoyl phosphatidylcholine and dipalmitoyl phosphatidylethanol induces hyperinsulinemia in rats resulting in the decrease of blood glucose concentration.[141] A dose of 2 mg kg^{-1} of liposome-entrapped CuZn superoxide dismutase administered intraperitoneally to Mongolian gerbils increases the endogenous enzyme activity in normal brain tissue and, when given at the late stages of ischemia, counteracts both the ischemic reduction of endogenous superoxide dismutase and the elevated peroxidation level of mitochondrial membranes.[142] While encapsulation of another enzyme, L-asparaginase, into microsize liposomes decreases the circulation time of the enzyme, incorporation into small nanosize liposomes prolongs it by almost tenfold.[143] The survival time of animals bearing asparaginase-dependent tumors is doubled after treatment with selected liposomal formulations compared with treatment using the free enzyme. Factor VIII (FVIII) is a multidomain protein that prevents hemophilia A, a bleeding disorder, but upon exogenous FVIII administration to patients, inhibitory antibodies are generated.[144] When a complex with *O*-phospho-serine (the head group of phosphatidylserine) was administered in mice, the conjugate retained FVIII's in vivo activity in hemophilia suggesting that the FVIII–lipid mimic complex may be beneficial to increase the physical stability and reduce immunogenicity of the recombinant protein preparations.[145]

6.05.4.7 Additional Paracellular Transport-Enhancing Additives

Paracellular transport of larger molecules takes advantage of the tight junctions between epithelial cells[146] by using permeation enhancers[147] to allow the penetration of biopolymers exceeding 11 Å radii that otherwise would be retained at the apical side.[57] For efficient protein delivery, the tight junctions have to be opened only transiently as the free flow of toxins and other biological pathogens can result in dire consequences.[148]

Tight junctions are regulated by Ca ions, and thus, Ca^{2+} chelators, such as ethylenediaminetetraacetate, can open the gap between epithelial cells and promote biopolymer transport.[149] In normal calcium concentrations, paracellular transport enhancers 2.5 mM ethylene glycol-bis(beta-aminoethyl ether)-*N*,*N*,*N*′,*N*′-tetraacetic acid, 1.5% w/v trimethyl chitosan chloride, and 0.2 mM palmitoyl carnitine chloride increased the transport of 1–10 mM clodronate in human intestinal epithelial Caco-2 cell cultures by 190 (130)-, 20 (70)-, and 10 (35)-fold, respectively.[150] Along these lines, the intracellular enzyme activity and cell monolayer permeability of anionic (sodium dodecyl sulfate and sodium dioctyl sulfosuccinate) and nonionic (polysorbate 80 and polyoxyl 40 hydrogenated castor oil) synthetic surfactants were studied in monolayers of Caco-2 cells grown on microporous polycarbonate filters.[151] All surfactants, especially the anionic ones, demonstrate concentration-dependent effects on intracellular enzyme activities, cell permeability, and morphology. Hydrophilic marker molecules appear to permeate epithelial monolayers through different pathways. Bile acids sodium taurocholate, sodium taurodeoxycholate, and sodium taurodihydrofusidate function in a highly similar manner, as much as in another study, the bile salt sodium taurodeoxycholate was a more effective enhancer than the more polar sodium taurocholate.[152] Enhancement of the permeability marker phenol red transport was reversed within 2 h after treatment suggesting that surfactant-induced acute intestinal wall damage can be rapidly repaired.

An early report suggested that salicylate ion on rat small intestinal brush-border membrane vesicles can promote drug absorption based on increases in plasma membrane permeability through actions on plasma membrane proteins rather than directly interacting with membrane lipids.[153] Indeed, uptake of insulin into human red blood cells is significantly enhanced by the presence of salicylate and 5-methoxysalicylate in the assay medium.[154] The mechanism of permeation enhancer action depends on an affinity to the protein fraction in the erythrocyte membrane. Medium-chain fatty acids induce rapid increase in epithelial permeability as studied on the hydrophilic marker molecule sodium fluorescein.[155] Enzyme inhibition experiments suggest that the effects on epithelial permeability are mediated through phospholipase C-dependent inositol triphosphate/diacylglycerol pathways. Mechanistically, the increase of calcium levels is considered to induce the contraction of calmodulin-dependent actin microfilament, followed by dilatation of the paracellular route.[156] For both medium-chain fatty acids (caproic, caprylic, and capric acids) and their acylglycerols (mono-, di-, and triacylglycerols), the transport-enhancing effects are correlated with the reduction in surface tension and with a surface energy-lowering coefficient.[157] In order to promote drug absorption, acylcarnitines must surpass a 10 carbon unit chain length to effectively partition into the membrane and have to perturb the lipid order beyond a threshold value of 15–20%.[158] The membrane-perturbing capacity may serve as an indicator of the absorption-enhancing potential of unrelated aliphatic-type compounds. While palmitoyl carnitine has the properties of many commonly used biochemical detergents, palmitoyl coenzyme A produces neither leakage nor solubilization of phosphatidylcholine bilayers forming large unilamellar vesicles.[159]

6.05.4.7.1 Amino acid- and peptide-based transporters

N-acylated, non-α-amino acids were used to demonstrate the oral delivery of heparin in vivo in rats and primates.[160] *N*-(8-(2-hydroxybenzoyl)-amino) caprylate is one of a series of drug delivery agents (Eligen transporters) that interact weakly and noncovalently with insulin, increasing its lipophilicity and thereby its ability to cross the gastrointestinal epithelium.[161] Although these amino acid derivatives are expected to act through the paracellular pathway, confocal microscopy and immunocytochemistry indicate that insulin is rather transported transcellularly without detectable alteration of the tight junctions between adjacent cells. In preclinical and phase I clinical trials, oral dosing with Eligen insulin led to a rapid elevation of plasma insulin and subsequent decrease in plasma glucose levels.[162] In addition, the activity was stronger, and the onset was more rapid with the formulated insulin than with injected insulin. Using the same drug delivery technology, after the first oral dose, salmon calcitonin evoked dose-dependent decreases in serum type I collagen (−60.8% to −81.8% from baseline) compared with placebo.[163] The first clinical trial indicated that the Eligen technology-based oral formulation of calcitonin can potentially be used as safe and effective treatment for

postmenopausal bone loss. In addition to its pronounced effect on bone resorption, this novel oral salmon calcitonin formulation may also reduce cartilage degradation.[164] However, in later clinical trials, the present formulation of oral salmon calcitonin did not provide reproducible clinical benefits in patients with symptomatic knee osteoarthritis.[165]

The combination of *N*-acylated amino acids and the proteins and peptides to be delivered forms an insoluble complex at low pH preventing degradation before being dissolved in the upper part of the small intestine that exhibits higher pH values.[166] By using human growth hormone as a drug to be transported, it was shown that the permeation enhancer has specificity for a particular protein and the enhancer and the peptide/protein drug must be in solution together to be effective.[167] Pretreating the tissue with the *N*-acyl-amino acid transporter and then adding the protein do not increase tissue permeability. These penetration enhancers and/or the human growth hormone does not induce cell damage, at least up to 1 h, and the damage seen after 2 h is also significantly lower than with other known transport enhancers.[168] Indeed, clinical adverse effects are related to the bioactive drug rather than to the carrier.[163] It is worth noting that when *N*-(8-(2-hydroxy-5-chloro-benzoyl)-amino) caprylate was administered together with human parathyroid hormone, the peptide cargo disappeared from the blood faster after oral than after subcutaneous administration.[169] Doses of 2.5–5 mg of oral parathyroid hormone resulted in exposure levels closest to 20 μg subcutaneous teriparatide without an increase of adverse effects in healthy postmenopausal women.

The zonula occludens toxin, secreted by cholera pathogen *Vibrio cholerae*[170], is a close relative of the human zonulin protein that modulates the permeability of tight junctions between cells in the wall of the digestive tract.[171] The C-terminal region of zonula occludens toxin contains an octapeptide Gly-Gly-Val-Leu-Val-Gln-Pro-Gly that is responsible for the binding to a specific receptor in intestinal cell membranes and inducing reversible opening of tight junctions between cells and allows paracellular permeability in a nontoxic manner.[172] Zonula occludens toxin at 4.0 μg mL^{-1} concentration statistically significantly enhances delivery of sucrose, inulin, and doxorubicin in bovine brain microvessel endothelial cells suggesting the utility of this transport enhancer to increase the brain permeability of CNS-active drugs, including anticancer agents.[173] Plasma concentration of cyclosporine A is significantly increased over a range of 1.55–2.50-fold at 10–40 mg kg^{-1} intraduodenal dose of the hexapeptide Phe-Cys-Ile-Gly-Arg-Leu.[174] This synthetic peptide represents the shortest sequence that retains the zonula occludens toxin permeating effect on intercellular tight junctions. A bioadhesive agent, carrageenan, improves the permeation-enhancing effect of the hexapeptide by 2.5-fold as documented by pharmacokinetic measurements after coadministration of ritonavir, the toxin peptide and carrageenan.[175] While the transport peptide itself is instable in neutral to basic pH and with increasing reaction time, coadditives 5% dextrose and a 1% mixture of the constituent arginine, cysteine, and glycine amino acids significantly improve the stability parameters at pH 7.4 for at least 6 h.[176] Functionally, the hexapeptide reversibly reduces the transepithelial electric resistance and increases Lucifer yellow permeability in Caco-2 cell monolayers in vitro and elevates the pharmacokinetic parameters of calcitonin by 5.2-fold.[177]

E-cadherin is a calcium-dependent cell–cell adhesion molecule that plays pivotal roles in epithelial cell behavior and tissue formation being present in all epithelial barriers including in brain endothelial cells.[178] E-cadherin is important for establishing and maintaining apicobasal polarity and for the formation of tight junctions.[179] In bovine brain microvessel endothelial cells, Leu-Arg-Ala-His-Ala-Val-Asp-Val-Asn-Gly, a decapeptide generated from the EC-1 domain of N-cadherin, modulates a distinct Ca^{2+}-dependent cell adhesion mechanism suggesting a possibility of creating channels for paracellular drug delivery across the BBB.[180] An N-terminally acetylated hexapeptide Ala-Asp-Thr-Pro-Pro-Val derived from the EC-1 bulge region of E-cadherin improves mannitol transport 3–5-fold when administered from either the apical or the basolateral side or from both sides simultaneously in Madin–Darby canine kidney cell monolayers.[181] Another acetylated E-cadherin hexapeptide Ser-His-Ala-Val-Ser-Ser was found to enhance the permeation of mannitol and daunomycin through the BBB in a rat brain perfusion model and exhibit a synergistic effect in enhancing the BBB permeation of daunomycin.[182] Synthetic peptides corresponding to the two putative extracellular domains of the tight junction integral membrane protein occludin reversibly disrupt the transepithelial permeability barrier at concentrations of <5 μM.[183] Other occludin-derived peptides were able to impair junction resealing when 0.5–1.5 mg mL^{-1} peptides were included in the apical bathing fluid.[184]

Additional peptides derived from the *Clostridium perfringens* enterotoxin or selected by phage display can reversibly increase paracellular transport and enhance drug delivery and such have a potential to be used as pharmaceutical excipients to improve drug delivery across epithelial barriers and the BBB.[185] The *C. perfringens* toxins act on claudins, a multigene family proteins that constitute tight junction strands.[186] Upon incubation of the carboxy-terminal fragment of the *C. perfringens* toxin and cells expressing claudins, reconstituted tight junction strands gradually disintegrate and disappear from their cell surface. Nasal immunization with the enterotoxin fused with the pneumococcal surface protein A, an important antigen for the induction of protective immunity against *Streptococcus pneumoniae* infection, induces protein antigen-specific antibodies in the serum and bronchoalveolar lavage fluid indicating that the *C. perfringens* toxin is an efficient vaccine delivery system.[187]

6.05.5 Improving In Vivo Circulation Time

In addition to potential immunogenicity issues, the major criticism toward biotherapeutics concerns their short half-life in vivo.[188] This is especially troublesome for peptides and small proteins (below 30–40 kDa in size) that are rapidly eliminated through the kidneys suggesting that the best utilization of peptide drugs is in fact against diseases of the urinary tract where these therapeutics concentrate.[189,190] Even if serum stability of peptide drugs can be improved by incorporating nonnatural amino acid residues,[191] the disconnect between pharmacokinetics and pharmacodynamics due to fast renal clearance while still activating or deactivating

receptors or other target biopolymers poses serious regulatory hurdles.[192] Smart modifications in peptide backbone and side-chain composition can overcome short plasma half-life, but because these do not directly involve formulation strategies, these are not detailed here, and the reader is referred to specialty reports.[193,194] The three major strategies to improve in vivo circulation time reviewed here are equally applicable to both proteins and peptides and come directly from biotherapeutics formulation studies. In addition to pegylation and albumin, and Fc conjugation, further examples will be provided for the formulation enhancement of protein therapeutics by hyperglycosylation and lipidation.

6.05.5.1 Pegylation

6.05.5.1.1 Proteins

Incorporation of PEG moieties (pegylation) to proteins was originally introduced to enable protection from destruction during drug delivery.[195] Indeed, PEG attachment reduces the renal clearance rate of polyamides.[196] However, it quickly turned out that PEG addition provides numerous pharmacological benefits to protein therapeutics. Pegylation of β-glucosidase from sweet almonds and α-galactosidase from green coffee beans results in alterations of the catalytic properties of the enzymes exhibiting increased K_m and decreased V_{max} values.[197] Additionally, PEG-modified adenosine deaminase loses its immunogenicity in mice following multiple intravenous injections providing additional justification for protein pegylation strategies.[198] Early pegylation synthetic protocols used various chemistries to couple activated PEG moieties to side-chain amino ε-amino and the N-terminal α-amino groups on the surface of proteins.[199] The uncontrolled and multiple modifications of lysines provided an assembly of PEG isomer mixtures with different molecular masses.[200] It was subsequently recognized that pegylation can produce a decrease in the in vitro activity of proteins[201] and can influence the binding affinity of therapeutic proteins to cellular receptors resulting in changes in the bioactivity of peptides and proteins.[202] Additionally, large amounts of diol contaminants present in methoxy-PEG derivatives form irreversible aggregates with proteins.[203] Site-specific pegylation has been shown to avoid ubiquitous PEG incorporation, associated heterogeneity in the conjugates,[204,205] and expectedly interference with single target or ligand-binding sites. SsoPox, an enzyme derived from *Sulfolobus solfataricus*, hydrolyzes and inactivates a variety of organophosphate compounds. Mono-N-terminal pegylation of SsoPox with PEG propionaldehyde results in improvement in the thermostability and protease resistance of the enzyme as measured by a functional assay.[206] Additional potentially controlled PEG conjugation chemistries include the use of heterobifunctional and branched PEG derivatives[207] and enzymatic PEG incorporation into less frequently occurring residues in proteins or residues distant from the active sites.[208,209]

As expected from the increased molecular size, pegylation brings about an extended circulation time in vivo due to reduced renal clearance rate together with increased protease stability.[210] In vitro, interferon α-2a decorated with a branched 40 kDa PEG moiety (attached to single lysines) lost 93% of the original activity, but in vivo, it is severalfold more efficacious than naked interferon α-2a.[211] The markedly improved pharmacological profile can be explained by a 70-fold increase in serum half-life and a 50-fold increase in mean plasma residence time concomitant with sustained serum concentrations. Proper selection of the PEG structure can preserve even the in vitro activities. A trimer-structured, 43 kDa PEG conjugated to interferon α-2a by forming an amide bond retained comparable in vitro bioactivities to the native protein while exhibiting slow absorption and markedly reduced clearance in rats, thereby increasing the biological half-life by about 40-fold relative to naked interferon α-2a.[212] Returning to the kidney elimination profiles, pegylated proteins are highly hydrated, and thus, their hydrodynamic radii are in fact 5–10-fold higher than it could be expected based on purely their molecular size.[213,214] This increased aqueous package not only decreases the glomerular filtration rate but also concomitantly improves solubility.[215] However, the increased hydrophilicity may prevent full-body biodistribution, as it was shown on a 5 kDa linear PLG conjugate of uricase, which appears to reach the lowest distribution levels in all examined organs when compared with other polymeric conjugates of uricase of approximately the same size.[216] Uricase carrying a branched PEG moiety behaved better.

Branched PEG-containing enzymes exhibit increased temperature stability and widened pH stability, as well as greater stability to proteolytic digestion compared with linear PEG-containing analogs.[217] Pegylated granulocyte-colony stimulating factor forms soluble aggregates and such avoids precipitation.[218] The stability increase toward aggregation is largely independent from the size of the attached PEG unit. Apparently, steric hindrance by PEG influences aggregation rate, while aqueous solubility is mediated by polar PEG groups on the aggregate surface. While these findings look very attractive at first sight, others reported that conjugation to thiol-reactive PEGs enhances the tendency of granulocyte-colony stimulating factor to aggregate.[219] Aggregation in this case does not involve changes in the secondary structure of the protein because circular dichroism spectra remained unchanged upon PEG incorporation. In general, polydispersity, a natural property of synthetic polymers, over 20 kDa makes PEG-conjugated proteins prone to aggregation.[220] Currently, additional problems are reported with pegylated proteins,[221,222] for example, unexpected immune reactions upon intravenous administration of pegylated liposomes or other particles, and by extension supposedly of any pegylated protein and DNA.[223] Indeed, induction of anti-PEG immunoglobulins when formulated in liposomes was detected resulting in losing their long-circulating characteristic when they repeatedly administrated to the same animals.[224] From a clinical standpoint, PEG interferon can induce pulmonary toxicity that is rare, but fatality can occur.[225] Upon pegylated interferon-α and ribavirin therapy for chronic hepatitis C, ischemic colitis was diagnosed without clear pathogenesis but potential involvement in immunoregulatory, vasospastic, and procoagulant mechanisms.[226]

Having said this, pegylated biotherapeutics made enormous impact on medicine starting with the approval of pegadamase (pegylated bovine adenosine deaminase for the treatment of severe combined immunodeficiency disease) in 1990.[227] Pegylated asparaginase was administered to 24 patients undergoing bone marrow transplantation for acute lymphoblastic leukemia as a consolidation

therapy.[228] Although of these eight remained in remission, the authors could not recommend the drug as a single-agent, postbone marrow transplant chemotherapy. In spite of the observed side effect during hepatitis C treatment, PEG interferon in combination with ribavirin is shown to be very efficacious in reducing hepatitis C viral load and maintaining effective sustained viral suppression in patients.[229] In short-term clinical studies mostly on pretreated, acromegalic patients with pegvisomant, a pegylated growth hormone antagonist, insulin-like growth factor 1 levels were normalized in the majority of cases.[230] Certolizumab pegol is a pegylated humanized Fab′ fragment of an antitumor necrosis factor-α mAb demonstrating high neutralizing potency.[231] In phase III clinical trials, subcutaneous certolizumab pegol administration at 400 mg once every 4 weeks is effective as induction and maintenance therapy in patients with moderate to severe Crohn's disease. Finally, once-monthly peginesatide (a synthetic, pegylated, peptide-based erythropoiesis-stimulating agent) resulted in some decrease in mean hemoglobin levels in individuals on hemodialysis.[232] Although 79% of the patients experienced adverse events, the majority of these were mild or moderate in severity.

6.05.5.1.2 Carbohydrates and nucleic acids

Carbohydrates can be considered biotherapeutics, although their drug properties are distinct from those of proteins and nucleic acids and, thus, are not heavily discussed in this book chapter. However, pegylation efforts are abundant on both the stand-alone sugar structures and the carbohydrate parts of glycoproteins, and a brief introduction of these complexes appears to be justified here.

Just like for nonglycosylated proteins, covalent attachment of PEG moieties to the carbohydrate region of glycoproteins has been mainly used to enhance the pharmacokinetic properties of the polyamide.[233] Glycopegylation is focused on sialic acid-containing proteins with native or enzymatically linked glycan conjugated to the peptide backbone. The PEG adducts can be either enzymatically introduced after sialic acid removal and Sia-PEG retransfer to the uncovered terminal Gal units of the linked glycan[234] or chemically on an *O*- or *N*-linked glycan of a newly created sugar.[235] The in vivo potency and efficacy of intravenous FVIII conjugated with a 40 kDa PEG were no different than before pegylation.[236] Nevertheless, the PEG-containing glycoprotein had a longer duration of effect in FVIII-deficient mouse models with approximately a twofold prolonged half-life in mice, rabbits, and cynomolgus monkeys. From sialic acid-pegylated thyroid-stimulating hormone analogs, a 40 kDa monopegylated conjugate exhibited a 3.5-fold longer duration of action than the naked hormone in rats, as a fivefold lower affinity was more than compensated by a 23-fold extension of circulation half-life.[237] From stand-alone short carbohydrates, several unprotected carbohydrate units of mannose, fucose, or lactose have been incorporated into the surface of pegylated dendritic polymers.[238] The larger dendrimer variants exhibit increased capacity to aggregate lectins. From longer polysaccharides, a natural graminan-type 5 kDa fructan demonstrated a 47-fold increased elimination half-life compared with the nonpegylated parent analog while preserving 74% of the bioactivity of the carbohydrate.[239] Lactobionic acid bearing galactose was coupled with chitosan for liver specificity, and PEG was grafted to the sugar to increase stability in water and enhance cell permeability.[240] Indeed, the PEG–carbohydrate conjugate forms complex with DNA, and pegylation appears to increase the stability of the DNA/carbohydrate complex.

This leads us to pegylation of nucleic acids. Currently, intensive efforts are devoted to overcome the adverse effects of serum protein binding of nucleic acid therapeutics with lipid- and polymer-based systems that efficiently transfer nucleic acids in the presence of serum leading the pack.[241] Pegylated components sterically shield the delivery vehicles from blood constituents[242] as amphiphilic polyacrylamide and polyvinylpyrrolidone modified with long-chain fatty acyl groups are able to incorporate into the liposomal membrane and, similar to PEG, prolong liposome circulation in vivo. The protective efficacy of modified polymers decreases with increased MW of the polymeric structures.[243] Pegylation in general has a clear benefit to circulation time although it is also known to interfere with trafficking involved in intracellular delivery and render nucleic acid vectors more susceptible to agitation-induced damage during processing.[244] After cellular uptake, nonpegylated liposomes efficiently escape from endosomes and release phosphodiester oligonucleotides (PO-ONs) in the cytoplasm ensuing rapid degradation in the intracellular environment.[245] In contrast, pegylated liposomes fail to protect PO-ONs they carry, leading to rapid degradation of the PO-ONs in the endosomal compartment. In addition, the PEG chains inhibit endosomal escape of the degraded oligonucleotides explaining why pegylated liposomes fail to establish an antisense effect. Other studies have reported that pegylation significantly lowers the cellular interaction and uptake of the lipid nanoparticles, resulting in reduced biological activity. Pegylation-induced weakening of the electrostatic binding of cationic liposome–DNA nanoparticles to cells has been considered a possible cause for reduced gene delivery efficacy of sterically stabilized nanoparticles.[246]

From the positive side, sense strand pegylation increased the silencing potency of an α-chemokine receptor siRNA, which had modest activity in its wild-type form.[247] Apparently, PEG chains at the 3′ terminus of both strands of siRNA are well tolerated by the RNAi effector. In another study, pegylation improves the receptor-mediated transfection efficiency of peptide-targeted, self-assembling, anionic nanocomplexes.[248] Pegylation of a multifunctional envelope-type nanodevice composed of a pH-sensitive cationic lipid results in the increase in the accumulation of siRNA in tumor tissue by 240-fold.[249] Administration of siRNA at $3\,mg\,kg^{-1}$ in the complex resulted in 50% reduction in the target gene mRNA and protein. Using a photocleavable PEG moiety, the antisense activity can be regulated with high spatial and temporal resolution, allowing precise regulation of gene expression in biological systems.[250]

6.05.5.2 Conjugation to Fc Antibody Fragments

In the human placenta, the Fc receptor for IgG, FcRn, mediates transport of IgG across epithelial barriers by transcytosis.[251] Transepithelial transport by FcRn explains how humoral immunity transfers from mother to infant. The absorptive epithelial cells that

line the intestine continue to express FcRn in adult life,[252] and as expected, cells in culture expressing FcRn exhibit FcRn-dependent transcytosis of IgG in both directions in vitro.[253] In a fusion protein, consisting of erythropoietin (Epo) and the Fc fragment of murine IgG1, while the Epo part binds to erythroid progenitor cells in the bone marrow and promotes proliferation of the red cell lineage, the Fc fragment binds specifically to FcRn.[251] The Fc fragment promotes transepithelial transport in vivo, measured by reticulocytosis 4 days after administration of the fusion protein to mucosal surfaces. As the transport of IgG across epithelial barriers by FcRn does not depend on transepithelial pH gradients established at epithelial surfaces,[254] it was proposed that FcRn can function as a transporter for proteins containing Fc at any mucosal surface that expresses FcRn.

To exploit this technology in drug development, Fc fusion monomers were prepared with both recombinant FVIII and factor IX.[255] Preclinical and clinical data demonstrate improved pharmacokinetics for both factors. Importantly, in phase I/IIa studies, the two factor proteins showed 1.5–1.7-fold and 3.0–4.0-fold longer elimination half-lives, respectively. Phase III clinical trials verified a clear advantage for patients treated on prophylaxis versus those treated on demand with both Fc fusion proteins without basically any side effect.[256] Only a single injection of the factor IX construct at a median dose of 91 IU kg^{-1} was required in 86% of surgeries to maintain hemostasis during the procedure.

In other types of constructs, Fc fragments harboring a single C-terminal selenocysteine residue (Fc-Sec) are directed against a variety of targets by changing the peptide to which they are conjugated.[257] When a targeting and additional cytotoxic warheads were attached by cycloaddition reactions of tetrazine or azide-containing linker, the Fc-Sec proteins were successfully targeting folate receptor-expressing tumor cells. Other chemistries are also explored to attach Fc to protein and peptide drug candidates. The active peptide fragment of a bicyclic peptide antagonist was fused to an Fc, and the peptide was subsequently cyclized by chemically reacting its three cysteine residues with tris(bromomethyl)benzene.[258] After optimization of the linker and the Fc fragment arrangements, the bicyclic peptide was fully functional with K_i of 76 nM and exhibited an extended half-life of 1.5 days in mice. Even biomimetic carbonate-hydroxyapatite nanocrystals appear to be suitable substrates to produce nanoparticles, which can be functionalized with full antibodies and Fc fragments for efficient targeted drug delivery to tumors.[259] While upon binding of antibody to antigen and Fc receptor none of the conjugates exhibit altered antigen affinity, observed changes in thermostability require consideration for the choice of conjugation chemistry, depending on the actual molecular model and particular application of the conjugate.[260] Dulaglutide, marketed by Eli Lilly, is a long-acting glucagon-like peptide 1 analog (residues 7–37) for the treatment of type 2 diabetes.[261] Dulaglutide consists of the peptide drug covalently linked to an Fc fragment of human IgG4, thereby protecting it from inactivation by dipeptidyl peptidase-4. Indeed, pharmacokinetic studies demonstrated a half-life in humans of up to 90 h, making dulaglutide an ideal candidate for once-weekly dosing.

Protein conjugates to antibodies and Fc fusion proteins seem likely to represent extensively engineered biotherapeutic drugs in the future aimed to improve their performance with enhanced effector functions or extended half-life.[262] Two older concepts for improving antibodies, namely, antibody-drug conjugates and bispecific antibodies, have advanced to clinical success stage. Applying the technology to DNA, anti-CD3 chemically self-assembled antibody nanorings with valencies ranging from two to eight could be employed not only for radionuclide or small-molecule drug but also even for potentially oligonucleotide delivery to T cells without the negative effect of activation of the mAb parts, as has been observed for other antibody conjugated nanoparticles.[263] In a specific application of the concept, two bioorthogonal, enzyme-mediated reactions were used in combination with oxime ligation and self-assembly based on peptide nucleic acid (PNA)–DNA base pairing to couple a synthetic PNA oligomer to the C-terminal of the Fc dimer upon sequence-specific sortase A-mediated transpeptidation.[264] Hybridization of the resulting Fc-PNA conjugate with a tailored DNA aptamer that binds the cancer-related hepatocyte growth factor receptor led to a hybrid construct, which showed strong and specific binding to the target and was readily internalized by target-overexpressing cells.

6.05.5.3 Albumin-Binding

In addition to immunoglobulins, the Fc receptor also binds albumin with high affinity only at a low pH ($pH < 6.5$) in acidic endosomes, preventing its degradation *via* the lysosomal pathway and returning it to the extracellular space (pH 7.4).[265] Human serum albumin is synthesized by the liver and remains in the circulation for weeks (half-life is 19 days).[266] Albumin is able to bind both endogenous substances such as long-chain fatty acids, steroids, and exogenous compounds and drugs, such as warfarin, ibuprofen, chlorpromazine, and naproxen.[267] In addition to the blood, the protein is prevalent in the skin, gut, muscle, and other fluids and secretions[266] significantly increasing the residence time of the substances it binds to.[268] Because solid tumors commonly possess an immature, highly permeable vasculature,[269] retention of albumin was observed in various solid tumors including sarcoma and ovarian carcinoma.[270] The potential of albumin as a protein drug delivery vehicle came after recognizing that it binds a number of endogenous proteins including albondin, its putative receptor,[271] and the market approval of nab-paclitaxel, the paclitaxel-loaded albumin nanoparticle.[272] The paclitaxel–albumin conjugate has a better therapeutic index than paclitaxel alone.[273]

Insulin detemir, an insulin analog in which myristic acid is bound to LysB29, is quickly absorbed after which it binds to albumin in the blood through its fatty acid at position B29.[274] The half-life of the insulin detemir is 5–7 h after subcutaneous administration to type 1 diabetes patients.[275] Ongoing clinical trials employ albumin-antibody fusion proteins for treating HER2/neu positive breast cancer and an antidiabetic glucagon-like peptide-1 agonist analog bound to recombinant human albumin.[276] From the nucleic acid portfolio, introduction of human serum albumin preserves the capacity of branched polyethylenimine to complex with siRNA and protects it against extracellular endonucleases while affording significantly improved internalization and silencing efficiency in endothelial and metastatic breast cancer epithelial cells.[277] Albiglutide is a yet another glucagon-like peptide-1 7–36 analog, this time coupled to recombinant human albumin.[278] This formulation is approved in adults for the treatment of type 2

diabetes mellitus. After once-weekly subcutaneous administration, albiglutide is absorbed through the lymphatic circulation and reaches maximum concentrations in a few days while maintaining exposures for 4–5 weeks. Remarkably, no clinically relevant adverse drug interactions have been observed.

6.05.5.4 Hyperglycosylation and Lipidation of Large Proteins

Earlier, it was discussed how addition of carbohydrate groups can improve the pharmacological properties of peptide drugs. This concept is here extended to hyperglycosylation of protein therapeutics. Polysialic acid is an endogenous carbohydrate moiety and, similarly to PEG, strongly hydrophilic and can be attached to the side-chain amino group of Lys through reductive amination.[279] During polysialylation, proteins are decorated with the naturally occurring, biodegradable α(2-8)-linked polysialic acid. As opposed to PEG that in principle can induce immune reactions to the host upon prolonged accumulation in the body, polysialylated proteins can be engineered to stay nonimmunogenic throughout the therapy course.[279,280] When an L-asparaginase was coupled covalently to colominic acid, a low-molecular-mass polysialic acid, the construct retained the enzymatic activity of the native enzyme.[281] While the hyperglycosylated asparaginase constructs exhibited resistance to proteolysis, most of the native enzyme was inactivated under the same conditions in mouse plasma. In vivo, intravenously administered glycoconjugate exhibited a significant increase in the half-life compared with the native enzyme.

A hyperglycosylated form of Epo is approved in the United States. This analog exhibits a threefold longer half-life than Epo itself and thus can be dosed once a week compared with the weekly three injections of naked Epo.[138] In another model, polysialylation generally increased the blood half-life of a therapeutic antibody Fab fragment resulting in higher tumor uptake in a human tumor xenograft mouse model.[282] One Fab-carbohydrate conjugate had over a fivefold increase in blood exposure approaching the bioavailability of a whole IgG. Likewise, chemical polysialylation can increase the half-life of an antiplacental alkaline and anticarcinoembryonic antigen single-chain Fv by 3.4–4.9-fold, resulting in a 10.6–15.2-fold increase in blood exposure.[283]

Lipid-based drug delivery encompasses not only the microemulsion and regular emulsions and solid–lipid nanoparticles discussed earlier but also liposomes, lipid implants, inverse lipid micelles, and lipid microtubules and cylinders.[284] The activity of small-sized PEG–liposomes-containing superoxide dismutase was compared with that of the same enzyme entrapped in stearylamine liposomes upon intravenous injection in an arthritic rat model.[285] Both lipidic structures showed a superior therapeutic activity compared with the naked enzyme, with PEG–liposomes inducing stronger anti-inflammatory effects than the stearylamine-type liposome formulation.

Experiments in hemophilic and nonhemophilic mice indicate that the circulation time and clotting efficacy of exogenous FVIII are significantly enhanced in PEG–liposome formulation suggesting the feasibility of using pegylated liposomal FVIII to extend the duration of hemostatic efficacy in the treatment of hemophilia A.[286] This protein delivery system seems to be universal as similar formulation of G-CSF extended its circulation time and results in higher G-CSF levels several hours after both subcutaneous and intravenous injection in mice.[287] The pegylated liposomal G-CSF had significantly improved efficacy in the mobilization of hematopoietic stem cells from the bone marrow to the peripheral blood. A series of phase I and phase II clinical trials were conducted to assess the safety and potential activity of liposomal drugs, using anthracyclines as example, in the management of both solid and hematologic tumors.[288] These studies confirmed that liposomal drug formulation is well tolerated, and in fact, the activity spectrum of the drugs can be expanded in lipidic structures. Further clinical studies of liposomal drug therapy are in progress to fully establish their safety, efficacy, and dosing in the treatment of various diseases.

6.05.6 Alternative Administration Routes

While the focus of this book chapter is to introduce the potential excipients, additives, and conjugation partners for biotherapeutics, enhancement of in vivo biological activities can be achieved by merely moving from direct intravenous, subcutaneous, or intramuscular (infrequently intracerebral vein) injections to alternative drug administration modes. Especially so as these delivery techniques often require their own excipient and additive formulations.

Although the distinction from noninvasive administration modes is somewhat artificial, subcutaneous or other long-releasing protein depot systems are considered a separate group of invasive administration methods.[289] In 2004, the FDA approved a 45 mg 6-month depot leuprorelin for the palliative treatment of locally advanced or metastatic prostate cancer.[290] Sustained release of leuprorelin from PLG microspheres as a six-monthly 30 mg peptide dosage was tested for efficacy and clinical safety in a recent European multicenter prospective trial.[291] A 12-month subcutaneous implant was briefly available for clinical use after approval by the FDA in 2000 for treatment of metastatic prostate cancer.[292] Although the implantable leuprolide delivery system was found to provide effective suppression of testosterone in patients with advanced prostate cancer,[293] the drug did not gain popularity and was eventually discontinued by the manufacturer.[290] In an interesting extension, bifunctional peptides that can simultaneously bind to a growth factor and an implantable biomaterial can be used to control the delivery and release of growth factors at the site of implantation as it was shown on a chimeric peptide consisting of a bone morphogenetic protein active site and collagen fragment.[294] Proteins can be used as implantable biomaterials themselves. Based in vitro and in vivo investigations in dogs that had demonstrated cellular ingrowth and tissue regeneration through a collagen scaffold, a feasibility clinical trial was conducted on nine patients.[295] The protein-based biomaterial scaffold was found to be implantable and to be safe over the 3-year period.

A unique family of devices made of silk proteins provides functional biomaterials with built-in optical signal and contrast enhancement without adverse biological effects and ultimately degrades to regenerate native tissue.[296]

6.05.6.1 Intranasal

The nasal tissue is highly permeable and is situated in an extensively vascularized environment while providing only limited proteolytic activity; consequently, intranasal administration is a highly viable option for protein and peptide drug delivery.[297] The predominant proteolytic enzyme is aminopeptidase,[298] whose activity can be easily downregulated by acylating the amino termini of the biotherapeutics.[193] The absorption of peptide drugs can be further improved by using enzyme inhibitors as absorption enhancers. A new class of alkylsaccharide transmucosal delivery enhancement agents overcomes the principal limitations preventing broad acceptance of intranasal administration for biotherapeutics such as poor transmucosal absorption and damage to the nasal mucosa.[299] Intranasal delivery of a modified leptin fragment (targeting the MC4 receptor[300]) is feasible and has significant effects on regulating body weight gain, food and water intake, serum glucose, insulin sensitivity, and bone formation in mice lacking endogenous leptin production.[301] The comparative absorption of intranasally administered insulin relative to subcutaneous insulin is 12.0% (dominant nostril) or 15.4% (nondominant nostril) over a 2 h period.[302] Sneezer patients and those with moderately blocked nostrils experienced lower adsorption rates.

Nasal delivery avoids the hepatic first-pass effect highly accelerating drug delivery, although the enzymatic barrier of the nasal mucosa creates a pseudo-first-pass effect. Agents that enter the olfactory receptor cells by endocytotic or pinocytotic mechanisms can take advantage of the olfactory nerve pathway and thus be transported by intracellular axonal transport to the olfactory bulb.[303] The olfactory nerve is directly connected to the olfactory tract and the olfactory bulb, making possible for drugs to reach the CNS without the control of the BBB.[304]

In patients of type 1 diabetes, peak serum levels of intranasally administered insulin were generally attained in 15–20 min and remained elevated for approximately 1 h.[305] Mean peak insulin levels were dose-dependent, and glucose waned 1.5–2 h postinsulin dosing. A total of 1255 postmenopausal women with established osteoporosis received 200 IU salmon calcitonin nasal spray or placebo after which the risk of new vertebral fractures was evaluated.[306] The intranasally administered peptide significantly reduced the fracture risk of by 33% along with a 12% decrease in bone turnover. Plasma levels of desmopressin administered as a nasal spray to patients were two- to threefold higher than those measured after instilling the peptide as nasal drops with similar increases in FVIII activity.[307] Patients suffering from mild hemophilia A, von Willebrand's disease, or platelet disorders self-administered the nasal desmopressin spray and experienced decreased blood loss and shortened duration of epistaxis, menorrhagia, tissue bleeding, and bleeding in connection with minor surgery or tooth extraction.[308] The efficacy of intranasally administered nafarelin, a gonadotropin-releasing hormone agonist, was compared with that of oral danazol in 213 patients with laparoscopically confirmed endometriosis.[309] The mean laparoscopic scores decreased at the same level, indicating that nasal nafarelin is an effective agent for treating endometriosis and other than hypoestrogenism has only few side effects. In contrast, chronic nasal treatment of patients suffering from prostate cancer with luteinizing hormone-releasing hormone reduces basal serum testosterone concentration levels, but not as much as subcutaneous administration of the same drug does.[310]

6.05.6.2 Pulmonary, Transdermal, Buccal, Rectal, and Vaginal

While intranasal formulation of peptide and protein drug receives the most attention and is considered the most viable alternative to intravenous or subcutaneous drug administration, some other delivery methods are also investigated.

There potential advantages of administering biotherapeutics to the lung as an aerosol include a rapid onset of action, high local concentration by delivery directly to the airways, and needle-free systemic delivery of drugs with poor oral bioavailability.[311] Several studies showed that a dose of 1.0–1.5 $U kg^{-1}$ body weight human regular insulin aerosol controlled fasting glucose levels and postprandial glucose levels although this dose posed an early limitation to this route of administration, since it was approximately 10 times the dose given subcutaneously.[312,313] Although a pulmonary insulin preparation was approved by the FDA in 2006 and others were in late clinical trials soon thereafter, all were discontinued due to transient safety issues, predominantly the increased level of appearance of increased insulin-binding antibodies, coughing, and reduction in diffusing capacity, compared with injected insulin.[34] Second generation of insulin inhalers completed clinical trials and waiting for market approval.[314] In our hands, while an antimicrobial peptide appears to be effective against *Klebsiella pneumoniae* lung infection when administrated pulmonary, it is also more toxic than an intramuscular dosage form.[315] Regarding to nucleic acid therapies, clinical trials with aerosolized gene vectors documented low levels of gene transfer concomitant with lung inflammation and induced humoral and cellular immune responses, shortcomings that have not been overcome.[316]

Transdermal delivery of large and hydrophilic drugs requires the partial disruption of the stratum corneum and as such more belong to the invasive drug-dosing category than to the group of alternative administration technologies. Having said that, microneedles and thermal ablation are rapidly progressing through clinical trials for delivery of macromolecules such as insulin and parathyroid hormone[317] and may become soon successful alternative formulation strategies with minimal discomfort. Theoretically, the buccal mucosa offers advantages over the oral route making it attractive for the delivery of peptides and proteins; however, the buccal mucosa still exhibits permeability-limiting properties, and therefore, for the delivery of macromolecules, the use of chemical penetration enhancers, physical methods, particulate systems, and mucoadhesive formulations is the norm and with promises for

Fig. 4 The market is saturated with miniature needles for type A insulin delivery pen devices. They offer soft, comfortable daily self-injections.

the future rather than current times.[318] This statement appears to apply also for vaginal and rectal administration for biotherapeutics not to mention low patient compliance with these formulation routes.[319,320]

6.05.7 Convenient Subcutaneous and Intramuscular Delivery Devices

Even if subcutaneous or intramuscular administration of peptide or protein drugs is needed, currently, the market is saturated with personalized, reusable, and virtually painless transdermal or intranasal medical devices.[321] For example, electronic autoinjectors are available for first-line therapies against multiple sclerosis.[322] The device features adjustable injection settings and an electronic dosing log during subcutaneous administration of interferon ß-1a. The second major use of autoinjectors is the chronic delivery of mAbs in rheumatoid arthritis. The pharmacokinetic properties and tolerability of subcutaneous administration of golimumab by autoinjector or by a standard needle and syringe are comparable.[323] Modeling the self-administration process, high level of patient acceptance was observed for self-injection with the autoinjector among patients with rheumatoid arthritis.[324] In particular, patients with severe hand disability were able to successfully comply with device instructions.

More than 2 billion pen injectors and multidose syringes are used each year by patients who need frequent injections against diabetes and with growth hormones, which often require weighed dosages or dose titration.[325,326] Miniature needles (punching a bladder at the end of prefilled multidose pens) help avoid needle phobia and reduce the risk of needlestick injury in many self-administered daily dosed drugs such as insulin or the glucagon-like peptide analogs. In addition to painless self-administration drug dosing, multidose pens and cartridges offer a softer impact on the environment and easier disposal (Fig. 4).

6.05.8 Implantable Devices for Subcutaneous Drug Delivery

The initial scientific (as opposed to market) success of leuprolide implants initiated further investigations in continuous subcutaneous delivery of drugs. One such novel subcutaneous delivery system is composed of three technologies: osmotic minipumps, minipump placement technology, and high-temperature therapeutic stabilization processes.[327] In a 6-month extension to a randomized, 24-week phase II study in subjects with type 2 diabetes, ITCA 650 implants induced sustained glycemic control, as measured by reducing HbA1c levels, and sustainable weight loss with only mild and transient adverse effects.[328] If approved, ITCA 650 will represent the first once- or twice-yearly injection-free exenatide therapy. Such devices offer significant advantages over existing drug delivery technologies in the future. At the time of completing this article, the FDA approved Probuphine, the first buprenorphine implant that uses a polymer matrix sustained-release technology[329] for the maintenance treatment of opioid dependence.

See also: 4.01. Role of Predictive ADME/PK in Drug Discovery, Safety Assessment, and Clinical Development.

References

1. Lipinski, C. A.; Lombardo, F.; Dominy, B. W.; Feeney, P. J. Experimental and Computational Approaches to Estimate Solubility and Permeability in Drug Discovery and Development Settings. *Adv. Drug Deliv. Rev.* **2001,** *46,* 3–26.
2. Hay, M.; Thomas, D. W.; Craighead, L.; Economides, C.; Rosenthal, J. Clinical Development Success Rates for Investigational Drugs. *Nat. Biotechnol.* **2014,** *32,* 40–51.
3. Otvos, L., Jr.; Wade, J. D. Current Challenges in Peptide-Based Drug Discovery. *Front. Chem.* **2014,** *2,* 62.
4. Pushpendra, S.; Arvind, P.; Anil, B. Nucleic Acids as Therapeutics. In *Nucleic Acids Sequences to Molecular Medicine;* Erdmann, V. A., Barciszewski, J., Eds.; Springer-Verlag: Berlin, 2012; pp 19–45.
5. Wolff, J. A.; Malone, R. W.; Williams, P.; Chong, W.; Acsadi, G.; Jani, A.; Felgner, P. L. Direct Gene Transfer Into Mouse Muscle In Vivo. *Science* **1990,** *247* (4949 Pt 1), 1465–1468.
6. Acsadi, G.; Jiao, S. S.; Jani, A.; Duke, D.; Williams, P.; Chong, W.; Wolff, J. A. Direct Gene Transfer and Expression Into Rat Heart In Vivo. *New Biol.* **1991,** *3,* 71–81.
7. Leiden, G. M.; Barr, E. In Vivo Gene Transfer Into the Heart. In *Gene Therapeutics: Methods and Applications of Direct Gene Transfer;* Wolff, J. A., Ed.; Birkhauser: Boston, MA, 1994; pp 363–381.
8. Mann, M. J.; Gibbons, G. H.; Hutchinson, H. Pressure-Mediated Oligonucleotide Transfection of Rat and Human Cardiovascular Tissues. *Proc. Natl. Acad. Sci. U. S. A.* **1999,** *96,* 6411–6416.
9. Rizzuto, G.; Cappelletti, M.; Maione, D. Efficient and Regulated Erythropoietin Production by Naked DNA Injection and Muscle Electroporation. *Proc. Natl. Acad. Sci. U. S. A.* **1999,** *96,* 6417–6422.
10. Anchordoguy, T. J.; Armstrong, T. K.; Molina, M. D. C.; Allison, S. D.; Zhang, Y.; Patel, M. M.; Lentz, Y. K.; Koe, G. S. Physical Stabilization of Plasmid DNA-Based Therapeutics During Freezing and Drying. In *Lyophilization of Biopharmaceuticals;* Constantino, H. R., Pikal, M. J., Eds.; American Association of Pharmaceutical Scientists: Arlington, VA, 2004; pp 605–642.
11. Scott, C. Formulation Development. *BioProcess Intern.* **2006**, (Suppl), 42–56.
12. Carton, J. M.; Strohl, W. R. Protein Therapeutics (Introduction to Biopharmaceuticals). In *Biological and Small Molecule Drug Research and Development;* Ganelin, R., Jefferts, R., Roberts, S., Eds.; Academic Press: Waltham, MA, 2013; pp 127–159.
13. Mackichan, J. J. Influence of Protein Binding and Use of Unbound (Free) Drug Concentrations. In *Applied Pharmacokinetics and Pharmacodynamics;* Burton, M. E., Shaw, L. M., Schentag, J. J., Evans, W. E., Eds.; Lippincott, Williams & Wilkins: Philadelphia, PA, 2006; pp 82–120.
14. Flurkey, A.; Cooksey, J.; Reddy, A.; Spoonmore, K.; Rescigno, A.; Inlow, J.; Flurkey, W. H. Enzyme, Protein, Carbohydrate, and Phenolic Contaminants in Commercial Tyrosinase Preparations: Potential Problems Affecting Tyrosinase Activity and Inhibition Studies. *J. Agric. Food Chem.* **2008,** *56,* 4760–4768.
15. Wright, J. Overview of Protein Formulation and Delivery. In *Protein Formulation and Delivery;* McNally, E. J., Ed.; Marcel Dekker, Inc: New York, 2000; pp 1–5.
16. Arora, P.; Gandhi, R.; Kelly, T. Overview of Drug Product Development for Protein Therapeutics: Present Strategies and Future Perspectives. *Am. Pharm. Rev.* **2011,** 1–5.
17. Cleland, J. L.; Powell, M. F.; Shire, S. J. The Development of Stable Protein Formulations: A Close Look at Protein Aggregation, Deamidation, and Oxidation. *Crit. Rev. Therapeutic Drug Carrier Syst.* **1993,** *10,* 307–377.
18. Bischoff, R.; Kolbe, H. V. J. Deamidation of Asparagine and Glutamine Residues in Proteins and Peptides: Structural Determinants and Analytical Methodology. *J. Chromatogr. B* **1994,** *662,* 261–278.
19. Brange, J.; Langkjaer, L.; Havelund, S.; Volund, A. Chemical Stability of Insulin. 1. Hydrolytic Degradation During Storage of Pharmaceutical Preparations. *Pharm. Res.* **1992,** *6,* 715–726.
20. Schon, I.; Nyeki, O. Unprecedented Transformation of Aspartyl Peptides by Conjugative Degradation. *J. Chem. Soc., Chem. Commun.* **1994,** 393–394.
21. Szendrei, G. I.; Fabian, H.; Mantsch, H. H.; Lovas, S.; Nyéki, O.; Schön, I.; Otvos, L., Jr. Aspartate-Bond Isomerization Affects the Major Conformations of Synthetic Peptides. *Eur. J. Biochem.* **1994,** *226,* 917–924.
22. Otvos, L., Jr.; Knappe, D.; Hoffmann, R.; Kovalszky, I.; Olah, J.; Hewitson, T. D.; Stawikowska, R.; Stawikowski, M.; Cudic, P.; Lin, F.; Wade, J. D.; Surmacz, E.; Lovas, S. Development of Second Generation Peptides Modulating Cellular Adiponectin Receptor Responses. *Front. Chem.* **2014,** *2,* 93.
23. Wijesekara, N.; Krishnamurthy, M.; Bhattacharjee, A.; Suhail, A.; Sweeney, G.; Wheeler, M. B. Adiponectin-Induced ERK and Akt Phosphorylation Protects Against Pancreatic β-Cell Apoptosis and Increases Insulin Gene Expression and Secretion. *J. Biol. Chem.* **2010,** *285,* 33623–33631.
24. Otvos, L., Jr.; Haspinger, E.; La Russa, F.; Maspero, F.; Graziano, P.; Kovalszky, I.; Lovas, S.; Nama, K.; Hoffmann, R.; Knappe, D.; Cassone, M.; Wade, J.; Surmacz, E. Design and Development of a Peptide-Based Adiponectin Receptor Agonist for Cancer Treatment. *BMC Biotechnol.* **2011,** *11,* 90.
25. Otvos, L., Jr.; Kovalszky, I.; Olah, J.; Coroniti, R.; Knappe, D.; Nollmann, F. I.; Hoffmann, R.; Wade, J. D.; Lovas, S.; Surmacz, E. Optimization of Adiponectin-Derived Peptides for Inhibition of Cancer Cell Growth and Signaling. *Biopolymers* **2015,** *104,* 156–166.
26. Davies, K. J. Protein Damage and Degradation by Oxygen Radicals. I. General Aspects. *J. Biol. Chem.* **1987,** *262,* 9895–9901.
27. Sadineni, V.; Chandrasekharan, S.; Nassar, M. N. Implications of Trace Levels of Redox-Active Metals in Drug-Product Formulation. *BioPharm. Int.* **2014,** *27,* 4.
28. Hovorka, S. W.; Hong, J.; Cleland, J. L.; Schoneich, C. Metal-Catalyzed Oxidation of Human Growth Hormone: Modulation by Solvent-Induced Changes of Protein Conformation. *J. Pharm. Sci.* **2001,** *90,* 58–69.
29. Cao, E.; Chen, Y.; Cui, Z.; Foster, P. R. Effect of Freezing and Thawing Rates on Denaturation of Proteins in Aqueous Solutions. *Biotechnol. Bioeng.* **2003,** *82,* 684–690.
30. Carpenter, J. F.; Chang, B. S.; Garzon-Rodriguez, W.; Randolph, T. W. Rationale Design of Stable Lyophilized Protein Formulations: Theory and Practice. In *Rationale Design of Stable Protein Formulations – Theory and Practice;* Carpenter, F., Manning, M. C., Eds.; Kluwer Academic/Plenum publishers: New York, 2002; pp 109–133.
31. Jorgensen, L.; Hostrup, S.; Moeller, E. H.; Grohganz, H. Recent Trends in Stabilising Peptides and Proteins in Pharmaceutical Formulation – Considerations in the Choice of Excipients. *Expert Opin. Drug Deliv.* **2009,** *6,* 1219–1230.
32. Kerwin, B. A.; Heller, M. C.; Levin, S. H.; Randolph, T. W. Effects of Tween 80 and Sucrose on Acute Short-Term Stability and Long-Term Storage at −20°C of a Recombinant Hemoglobin. *J. Pharm. Sci.* **1998,** *87,* 1062–1068.
33. Chou, D. K.; Krishnamurthy, R.; Randolph, T. W.; Carpenter, J. F.; Manning, M. C. Effects of Tween 20 and Tween 80 on the Stability of Albutropin During Agitation. *J. Pharm. Sci.* **2005,** *94,* 1368–1381.
34. Hawe, A.; Friess, W. Formulation Development for Hydrophobic Therapeutic Proteins. *Pharm. Dev. Technol.* **2007,** *12,* 223–237.
35. Yuan, W.; Geng, Y.; Wu, F.; Liu, Y.; Guo, M.; Zhao, H.; Jin, T. Preparation of Polysaccharide Glassy Microparticles With Stabilization of Proteins. *Int. J. Pharm.* **2009,** *366,* 154–159.
36. Chi, E. Excipients and their effects on the quality of biologics. *AAPS* **2015**.
37. Pramanick, S.; Singodia, D.; Chandel, V. Excipient Selection in Parenteral Formulation Development. *Pharma Times* **2013,** *45,* 65–77.
38. Li, S.; Nguyen, T. H.; Schoneich, C.; Borchardt, R. T. Aggregation and Precipitation of Human Relaxin Induced by Metal-Catalyzed Oxidation. *Biochemistry* **1995,** *34,* 5762–5772.
39. Sosabowski, J. K.; Lee, M.; Dekker, B. A.; Simmons, B. P.; Singh, S.; Beresford, H.; Hagan, S. A.; McKenzie, A. J.; Mather, S. J.; Watson, S. A. Formulation Development and Manufacturing of a Gastrin/CCK-2 Receptor Targeting Peptide as an Intermediate Drug Product for a Clinical Imaging Study. *Eur. J. Pharm. Sci.* **2007,** *31,* 102–111.

40. Delepee, R.; Maume, D.; Le Bizec, B.; Pouliquen, H. Preliminary Assays to Elucidate the Structure of Oxytetracycline's Degradation Products in Sediments Determination of Natural Tetracyclines by High-Performance Liquid Chromatography-Fast Atom Bombardment Mass Spectrometry. *J. Chromatogr. B Biomed. Sci. Appl.* **2000,** *748,* 369–381.
41. Wang, W. Instability, Stabilization, and Formulation of Liquid Protein Pharmaceuticals. *Int. J. Pharm.* **1999,** *185,* 129–188.
42. Parkins, D. A.; Lashmar, U. T. The Formulation of Biopharmaceutical Products. *Pharm. Sci. Technol. Today* **2000,** *3,* 129–137.
43. Preformulation and Formulation of Therapeutic Peptides and Proteins. In *Therapeutic Peptides and Proteins;* Banga, A. K., Ed.; CRC Press: Boca Raton, FL, 2015; pp 97–147.
44. Katayama, D. S.; Nayar, R.; Chou, D. K.; Valente, J. J.; Cooper, J.; Henry, C. S.; Van der Velde, D. G.; Villarete, L.; Liu, C. P.; Manning, M. C. Effect of Buffer Species on the Thermally Induced Aggregation of Interferon-τ. *J. Pharm. Sci.* **2006,** *95,* 1212–1226.
45. Avis, K. E. Parenteral Preparations. In *Remington's Pharmaceutical Sciences;* Martin, E. W., Ed.; Mack Publishing Co.: Easton, PA, 1965; pp 498–524.
46. Wong, A.; Toth, I. Lipid, Sugar and Lipopolysaccharide Based Delivery Systems. *Curr. Med. Chem.* **2001,** *8,* 1123–1136.
47. Kompella, U. B.; Lee, V. H. Delivery Systems for Penetration Enhancement of Peptide and Protein Drugs: Design Considerations. *Adv. Drug Deliv. Rev.* **2001,** *46,* 211–245.
48. Banks, W. A. Characteristics of Compounds That Cross the Blood–Brain Barrier. *BMC Neurol.* **2009,** *9* (Suppl. 1), S3.
49. Pan, W.; Kastin, A. J. Changing the Chemokine Gradient: CINC1 Crosses the Blood–Brain Barrier. *J. Neuroimmunol.* **2001,** *115,* 64–70.
50. Haralddson, B.; Nystrom, J.; Deen, V. M. Properties of the Glomerular Barrier and Mechanisms of Proteinuria. *Physiol. Rev.* **2008,** *88,* 451–487.
51. Loffet, A. Peptides as Drugs: Is There a Market? *J. Pept. Sci.* **2002,** *8,* 1–7.
52. Cudic, M.; Lockatell, C. V.; Johnson, D. E.; Otvos, L., Jr. In Vitro and In Vivo Activity of an Antibacterial Peptide Analog Against Uropathogens. *Peptides* **2003,** *24,* 807–820.
53. Otvos, L., Jr.; Terrasi, M.; Cascio, S.; Cassone, M.; Abbadessa, G.; di Pascali, F.; Scolaro, L.; Knappe, D.; Stawikowski, M.; Cudic, P.; Wade, J. D.; Hoffmann, R.; Surmacz, E. Development of a Pharmacologically Improved Peptide Agonist of the Leptin Receptor. *Biochim. Biophys. Acta* **2008,** *1783,* 1745–1754.
54. Wright, I.; Kapoor, A. Current Systemic Management of Metastatic Renal Cell Carcinoma – First Line and Second Line Therapy. *Curr. Opin. Support. Palliat. Care* **2011,** *5,* 211–221.
55. Gil, M. J.; de Las Penas, R.; Reynes, G.; Balana, C.; Perez-Segura, P.; Garcia-Velasco, A.; Mesia, C.; Gallego, O.; Fernandez-Chacon, C.; Martínez-García, M.; Herrero, A.; Andres, R.; Benavides, M.; Quintanar, T.; Perez-Martin, X. Bevacizumab Plus Irinotecan in Recurrent Malignant Glioma Shows High Overall Survival in a Multicenter Retrospective Pooled Series of the Spanish Neuro-Oncology Research Group (GEINO). *Anticancer Drugs* **2012,** *23,* 659–665.
56. Chamberlain, M. C. Temozolomide: Therapeutic Limitations in the Treatment of Adult High-Grade Glioma. *Expert Rev. Neurother.* **2010,** *10,* 1537–1544.
57. Fasano, A. Innovative Strategies for the Oral Delivery of Drugs and Peptides. *Trends Biotechnol.* **1998,** *16,* 152–157.
58. Vyas, S. P.; Singh, A.; Sihorkar, V. Ligand-Receptor-Mediated Drug Delivery: An Emerging Paradigm in Cellular Drug Targeting. *Crit. Rev. Ther. Drug Carrier Syst.* **2001,** *18,* 1–76.
59. Sallusto, F.; Cella, M.; Danieli, C.; Lanzavecchia, A. Dendritic Cells Use Macropinocytosis and the Mannose Receptor to Concentrate Macromolecules in the Major Histocompatibility Complex Class II Compartment: Downregulation by Cytokines and Bacterial Products. *J. Exp. Med.* **1995,** *182,* 389–400.
60. Diebold, S.; Kursa, M.; Wagner, E.; Cotton, M.; Zenke, M. Mannose Polyethylenimine Conjugates for Targeted DNA Delivery Into Dendritic Cells. *J. Biol. Chem.* **1999,** *274,* 19087–19094.
61. Vera, D. R.; Wisner, E. R.; Stadalnik, R. C. Sentinel Node Imaging via a Nonparticulate Receptor-Binding Radiotracer. *J. Nucl. Med.* **1997,** *38,* 530–535.
62. Agnes, M. C.; Tan, A.; Jordens, R.; Geluk, A.; Roep, B. O.; Ottenhoff, T.; Drijfhout, J. W.; Koning, F. Strongly Increased Efficiency of Altered Peptide Ligands by Mannosylation. *Int. Immunol.* **1998,** *10,* 1299–1304.
63. Kragol, G.; Otvos, L., Jr. Orthogonal Solid-Phase Synthesis of Tetramannosylated Peptide Constructs Carrying Three Independent Branched Epitopes. *Tetrahedron* **2001,** *57,* 957–966.
64. van Bergen, J.; Ossendorp, F.; Jordens, R.; Mommaas, A. M.; Drijfhout, J. W.; Koning, F. Get Into the Groove! Targeting Antigens to MHC Class II. *Immunol. Rev.* **1999,** *127,* 87–96.
65. Albert, R.; Marbach, P.; Bauer, W.; Briner, U.; Fricker, G.; Bruns, C.; Pless, J. SDZ CO 611: A Highly Potent Glycated Analog of Somatostatin With Improved Oral Activity. *Life Sci.* **1993,** *53,* 517–525.
66. Nelson-Piercy, C.; Hammond, P. J.; Gwilliam, M. E.; Khandan-Nia, N.; Myers, M. J.; Ghatei, M. A.; Bloom, S. R. Effect of a New Oral Somatostatin Analog (SDZ CO 611) on Gastric Emptying, Mouth to Cecum Transit Time, and Pancreatic and Gut Hormone Release in Normal Male Subjects. *J. Clin. Endocrinol. Metab.* **1994,** *78,* 329–336.
67. Kilhberg, J.; Ahman, J.; Walse, B.; Drakenberg, T.; Nilsson, A.; Söderberg-Ahlm, C.; Bengtsson, B.; Olsson, H. Glycosylated Peptide Hormones: Pharmacological Properties and Conformational Studies of Analogues of (1-Desamino, 8-D-Arginine) Vasopressin. *J. Med. Chem.* **1995,** *38,* 161–169.
68. Egleton, R. D.; Davis, T. P. Development of Neuropeptide Drugs That Cross the Blood–Brain Barrier. *J. Am. Soc. Exp. NeuroTher.* **2005,** *2,* 44–53.
69. Elmagbari, N. O.; Egleton, R. D.; Palian, M. M.; Lowery, J. J.; Schmid, W. R.; Davis, P.; Navratilova, E.; Dhanasekaran, M.; Keyari, C. M.; Yamamura, H. I.; Porreca, F.; Hruby, V. J.; Polt, R.; Bilsky, E. J. Antinociceptive Structure-Activity Studies With Enkephalin-Based Opioid Glycopeptides. *J. Pharmacol. Exp. Ther.* **2004,** *311,* 290–297.
70. Kovalszky, I.; Surmacz, E.; Scolaro, L.; Cassone, M.; Ferla, R.; Sztodola, A.; Olah, J.; Hatfield, M. P.; Lovas, S.; Otvos, L., Jr. Leptin-Based Glycopeptide Induces Weight Loss and Simultaneously Restores Fertility in Animal Models. *Diabetes Obes. Metab.* **2010,** *12,* 393–402.
71. Manolescu, A. R.; Witkowska, K.; Kinnaird, A.; Cessford, T.; Cheeseman, C. Facilitated Hexose Transporters: New Perspectives on Form and Function. *Physiology* **2007,** *22,* 234–240.
72. Varamini, P.; Mansfeld, F. M.; Blanchfield, J. T.; Wyse, B. D.; Smith, M. T.; Toth, I. Synthesis and Biological Evaluation of an Orally Active Glycosylated Endomorphin-1. *J. Med. Chem.* **2012,** *55,* 5859–5867.
73. McManus, A. M.; Otvos, L., Jr.; Hoffmann, R.; Craik, D. J. Conformational Studies by NMR of the Antimicrobial Peptide, Drosocin, and Its Non-Glycosylated Derivative: Effects of Glycosylation on Solution Conformation. *Biochemistry* **1999,** *38,* 705–714.
74. Bickel, U.; Yoshikawa, T.; Partridge, W. M. Delivery of Peptides and Proteins Through the Blood–Brain Barrier. *Adv. Drug Deliv. Rev.* **2001,** *4,* 247–279.
75. Vorbrodt, A. W. Ultracytochemical Characterization of Anionic Sites in the Wall of Brain Capillaries. *J. Neurocytol.* **1989,** *18,* 359–368.
76. Terasaki, T.; Deguchi, Y.; Sato, H.; Hirai, K.; Tsuji, A. In Vivo Transport of a Dynorphin-Like Analgesic Peptide, E-2078, Through the Blood–Brain Barrier: An Application of Brain Microdialysis. *Pharm. Res.* **1991,** *8,* 815–820.
77. Shimura, T.; Tabata, S.; Ohnishi, T.; Terasaki, T.; Tsuji, A. Transport Mechanism of a New Behaviorally Highly Potent Adrenocorticotropic Hormone (ACTH) Analog, Ebiratide, Through the Blood–Brain Barrier. *J. Pharmacol. Exp. Ther.* **1991,** *258,* 459–465.
78. Pardridge, W. M.; Triguero, D.; Buciak, J. L.; Yang, J. Evaluation of Cationized Rat Albumin as a Potential Blood–Brain Barrier Drug Transport Vector. *J. Pharmacol. Exp. Ther.* **1990,** *255,* 893–899.
79. Otvos, L., Jr. Antibacterial Peptides Isolated From Insects. *J. Pept. Sci.* **2000,** *6,* 497–511.
80. Wu, M.; Maier, E.; Benz, R.; Hancock, R. E. W. Mechanism of Interaction of Different Classes of Cationic Antimicrobial Peptides With Planar Bilayers and With the Cytoplasmic Membrane of *Escherichia coli. Biochemistry* **1999,** *38,* 7235–7242.
81. Christensen, B.; Fink, J.; Merrifield, R. B.; Mauzerall, D. Channel-Forming Properties of Cecropins and Related Model Compounds Incorporated Into Planar Lipid Membranes. *Proc. Natl. Acad. Sci. U. S. A.* **1988,** *85,* 5072–5076.
82. Lehrer, R. I.; Barton, A.; Daher, K. A.; Harwig, S. S. L.; Ganz, T.; Selsted, M. E. Monocyte-Chemotactic Activity of Defensins From Human Neutrophils. *J. Clin. Invest.* **1989,** *84,* 553–561.
83. Shai, Y. Molecular Recognition Between Membrane-Spanning Polypeptides. *Trends Biochem. Sci.* **1985,** *20,* 460–464.
84. Matsuzaki, K.; Mitani, Y.; Akada, K. Y.; Murase, O.; Yoneyama, S.; Zasloff, M.; Miyajima, K. Mechanism of Synergism Between Antimicrobial Peptides Magainin 2 and PGLa. *Biochemistry* **1998,** *37,* 15144–15153.

85. Friedrich, C. L.; Moyles, D.; Beveridge, T. J.; Hancock, R. E. Antibacterial Action of Structurally Diverse Cationic Peptides on Gram-Positive Bacteria. *Antimicrob. Agents Chemother.* **2000,** *44,* 2086–2092.
86. Cudic, M.; Otvos, L., Jr. Intracellular Targets of Antibacterial Peptides. *Curr. Drug Targets* **2002,** *3,* 101–106.
87. Gallo, R. L.; Huttner, K. M. Antimicrobial Peptides: An Emerging Concept in Cutaneous Biology. *J. Invest. Dermatol.* **1998,** *111,* 739–743.
88. Castle, M.; Nazarian, A.; Yi, S. S.; Tempst, P. Lethal Effects of Apidaecin on *Escherichia coli* Involve Sequential Molecular Interactions With Diverse Targets. *J. Biol. Chem.* **1999,** *274,* 32555–32564.
89. Park, C. B.; Kim, H. S.; Kim, S. C. Mechanism of Action of the Antimicrobial Peptide Buforin II: Buforin II Kills Microorganisms by Penetrating the Cell Membrane and Inhibiting Cellular Functions. *Biochem. Biophys. Res. Commun.* **1998,** *244,* 253–257.
90. Park, C. B.; Yi, K.; Matsuzaki, K.; Kim, M. S.; Kim, S. C. Structure-Activity Analysis of Buforin II, a Histone H2A-Derived Antimicrobial Peptide: The Proline Hinge Is Responsible for the Cell-Penetrating Ability of Buforin II. *Proc. Natl. Acad. Sci. U. S. A.* **2000,** *97,* 8245–8250.
91. Oren, Z.; Hong, J.; Shai, Y. A Repertoire of Novel Antibacterial Diastereomeric Peptides With Selective Cytolytic Activity. *J. Biol. Chem.* **1997,** *272,* 14643–14649.
92. Hoffmann, R.; Bulet, P.; Urge, L.; Otvos, L., Jr. Range of Activity and Metabolic Stability of Synthetic Antibacterial Glycopeptides From Insects. *Biochim. Biophys. Acta* **1999,** *1426,* 459–467.
93. Otvos, L., Jr.; Bokonyi, K.; Varga, I.; Otvos, B. I.; Hoffmann, R.; Ertl, H. C. J.; Wade, J. D.; McManus, A. M.; Craik, D. J.; Bulet, P. Insect Peptides With Improved Protease-Resistance Protect Mice Against Bacterial Infection. *Protein Sci.* **2000,** *9,* 742–749.
94. Otvos, L., Jr.; Cudic, M.; Chua, B. Y.; Deliyannis, G.; Jackson, D. C. An Insect Antibacterial Peptide-Based Drug Delivery System. *Mol. Pharm.* **2004,** *1,* 220–232.
95. Hancock, R. E.; Lehrer, R. Cationic Peptides: A New Source of Antibiotics. *Trends Biotechnol.* **1998,** *16,* 82–88.
96. Moore, A. J.; Devine, D. A.; Bibby, M. C. Preliminary Experimental Anticancer Activity of Cecropins. *Pept. Res.* **1994,** *7,* 265–269.
97. Chan, Y.; Gallo, R. L. PR-39, a Syndecan-Inducing Antimicrobial Peptide, Binds and Affects p130Cas. *J. Biol. Chem.* **1998,** *273,* 28978–28985.
98. Tan, M. L.; Choong, P. F.; Dass, C. R. Recent Developments in Liposomes, Microparticles and Nanoparticles for Protein and Peptide Drug Delivery. *Peptides* **2010,** *31,* 184–193.
99. Aboubakar, M.; Puisieux, F.; Couvreu, P.; Vauthier, C. Physicochemical Characterization of Insulin-Loaded Poly(isobutylcyano acrylate) Nanocapsules Obtained by Interfacial Polymerization. *Int. J. Pharm.* **1999,** *183,* 63–66.
100. Sakuma, S.; Hayashi, M.; Akashi, M. Design of Nanoparticles Composed of Graft Copolymers for Oral Peptide Delivery. *Adv. Drug Deliv. Rev.* **2001,** *47,* 21–37.
101. Ertl, H. C. J.; Varga, I.; Xiang, Z. Q.; Kaiser, K.; Stephens, L.; Otvos, L., Jr. Poly(DL-lactide-*co*-glycolide) Microspheres as Carriers for Peptide Vaccines. *Vaccine* **1996,** *14,* 879–885.
102. Jones, D. H.; McBride, B. W.; Hornton, C.; O'Hagan, D. T.; Robinson, A.; Farrar, G. H. Orally Administered Microencapsulated *Bordetella pertussis* Fimbriae Protect Mice From *B. pertussis* Respiratory Infection. *Infect. Immun.* **1996,** *64,* 489–494.
103. DeYoung, M. B.; MacConell, L.; Sarin, V.; Trautmann, M.; Herbert, P. Encapsulation of Exenatide in Poly-(D, L-lactide-*co*-glycolide) Microspheres Produced an Investigational Long-Acting Once-Weekly Formulation for Type 2 Diabetes. *Diabetes Technol. Ther.* **2011,** *13,* 1145–1154.
104. Emeye, M. O.; Obidike, I. C.; Akpabio, E. I.; Ofoefule, S. I. Nanotechnology in Drug Delivery. In *Recent Advances in Novel Drug Carrier Systems;* Sezer, A. D., Ed.; InTech: India, 2012; pp 69–106.
105. Maheshwari, A.; Mahato, R. I.; McGregor, J.; Han, S.; Samlowski, W. E.; Park, J. S.; Kim, S. W. Soluble Biodegradable Polymer-Based Cytokine Gene Delivery for Cancer Treatment. *Mol. Ther.* **2000,** *2,* 121–130.
106. Maheshwari, A.; Han, S.; Mahato, R. I.; Kim, S. W. Biodegradable Polymer-Based Interleukin-12 Gene Delivery: Role of Induced Cytokines, Tumor Infiltrating Cells and Nitric Oxide in Anti-Tumor Activity. *Gene Ther.* **2002,** *9,* 1075–1084.
107. Furgeson, D. Y.; Chan, W. S.; Yockman, J. W.; Kim, S. W. Modified Linear Polyethylenimine-Cholesterol Conjugates for DNA Complexation. *Bioconjug. Chem.* **2003,** *14,* 840–847.
108. Sun, X.; Zhang, N. Cationic Polymer Optimization for Efficient Gene Delivery. *Mini Rev. Med. Chem.* **2010,** *10,* 108–125.
109. Pan, S.; Wang, C.; Zeng, X.; Wen, Y.; Wu, H.; Feng, M. Short Multi-Armed Polylysine-Graft-Polyamidoamine Copolymer as Efficient Gene Vectors. *Int. J. Pharm.* **2011,** *420,* 206–215.
110. Zeng, X.; Pan, S.; Li, J.; Wang, C.; Wen, Y.; Wu, H.; Wang, C.; Wu, C.; Feng, M. A Novel Dendrimer Based on Poly (L-Glutamic Acid) Derivatives as an Efficient and Biocompatible Gene Delivery Vector. *Nanotechnology* **2011,** *22,* 375102.
111. Shcharbin, D.; Shakhbazau, A.; Bryszewska, M. Poly(amidoamine) Dendrimer Complexes as a Platform for Gene Delivery. *Expert Opin. Drug Deliv.* **2013,** *10,* 1687–1698.
112. Ren, L.; Chen, S.; Li, H.; Zhang, Z.; Ye, C.; Liu, M.; Zhou, X. MRI-Visible Liposome Nanovehicles for Potential Tumor-Targeted Delivery of Multimodal Therapies. *Nanoscale* **2015,** *7,* 12843–12850.
113. Asteriti, S.; Dal Cortivo, G.; Pontelli, V.; Cangiano, L.; Buffelli, M.; Dell'Orco, D. Effective Delivery of Recombinant Proteins to Rod Photoreceptors via Lipid Nanovesicles. *Biochem. Biophys. Res. Commun.* **2015,** *461,* 665–670.
114. Toyoda, M.; Hama, S.; Ikeda, Y.; Nagasaki, Y.; Kogure, K. Anti-Cancer Vaccination by Transdermal Delivery of Antigen Peptide-Loaded Nanogels via Iontophoresis. *Int. J. Pharm.* **2015,** *483,* 110–114.
115. Majuru, S.; Oyewumi, M. O. Nanotechnology in Drug Development and Life Cycle Management. In *Nanotechnology in Drug Development;* de Villiers, M. M., Aramwit, P., Kwon, G. S., Eds.; Springer: New York, 2009; pp 597–619.
116. Silva, A. C.; Lopes, C. M.; Lobo, J. M.; Amaral, M. H. Delivery Systems for Biopharmaceuticals. Part II: Liposomes, Micelles, Microemulsions and Dendrimers. *Curr. Pharm. Biotechnol.* **2015,** *16,* 955–965.
117. Pepe, D.; McCall, M.; Zheng, H.; Lopes, L. B. Protein Transduction Domain-Containing Microemulsions as Cutaneous Delivery Systems for an Anticancer Agent. *J. Pharm. Sci.* **2013,** *102,* 1476–1487.
118. Chemelli, A.; Maurer, M.; Geier, R.; Glatter, O. Optimized Loading and Sustained Release of Hydrophilic Proteins From Internally Nanostructured Particles. *Langmuir* **2012,** *28,* 16788–16797.
119. Jung, T.; Kamm, W.; Breitenbach, A.; Kaiserling, E.; Xiao, J. X.; Kissel, T. Biodegradable Nanoparticles for Oral Delivery of Peptides: Is There a Role for Polymers to Affect Mucosal Uptake? *Eur. J. Pharm. Biopharm.* **2000,** *50,* 147–160.
120. Sobczak, M.; Debek, C.; Oledzka, E.; Kozlowski, R. Polymeric Systems of Antimicrobial Peptides – Strategies and Potential Applications. *Molecules* **2013,** *18,* 14122–14137.
121. Gao, Y.; Truong, B.; Zhu, Y.; Kyratzys, I. L. Electrospun Antibacterial Nanofibers: Production, Activity and In Vivo Applications. *J. Appl. Polym. Sci.* **2014,** *131,* 40797.
122. Liu, X.; Lin, T.; Gao, Y.; Xu, Z.; Huang, C.; Yao, G.; Jiang, L.; Tang, Y.; Wang, X. Antimicrobial Electrospun Nanofibers of Cellulose Acetate and Polyester Urethane Composite for Wound Dressing. *J. Biomed. Mater. Res. B Appl. Biomater.* **2012,** *100B,* 1556.
123. Gatti, J. W.; Smithgall, M. C.; Paranjape, S. M.; Rolfes, R. J.; Paranjape, M. Using Electrospun Poly(ethylene-oxide) Nanofibers for Improved Retention and Efficacy of Bacteriolytic Antibiotics. *Biomed. Microdevices* **2013,** *15,* 887–893.
124. Heunis, T. D.; Smith, C.; Dicks, L. M. Evaluation of a Nisin-Eluting Nanofiber Scaffold to Treat *Staphylococcus aureus*-Induced Skin Infections in Mice. *Antimicrob. Agents Chemother.* **2013,** *57,* 3928–3935.
125. Sebe, I.; Ostorhazi, E.; Fekete, A.; Kovacs, K. N.; Zelko, R.; Kovalszky, I.; Li, W.; Wade, J. D.; Szabo, D.; Otvos, L., Jr. Polyvinyl Alcohol Nanofiber Formulation of the Designer Antimicrobial Peptide APO Sterilizes *Acinetobacter baumannii*-Infected Skin Wounds in Mice. *Amino Acids* **2016,** *48,* 203–211.
126. Delorme, E. *War Surgery (English Translation H. Meric);* H.K. Lewis: London, 1915.
127. Augustijns, P. F.; Borchardt, R. T. Transport and Metabolism of δ Sleep-Inducing Peptide in Cultured Human Intestinal Epithelial Cell Monolayers. *Drug Metab. Dispos.* **1995,** *23,* 1372–1378.

128. Lindgren, M.; Hallbrink, M.; Prochiantz, A.; Langel, U. Cell-Penetrating Peptides. *Trends Pharacol. Sci.* **2000,** *21,* 99–103.
129. Derossi, D.; Chassaing, G.; Prochiantz, A. Trojan Peptides: The Penetratin System for Intracellular Delivery. *Trends Cell Biol.* **1998,** *8,* 84–87.
130. Suzuki, T.; Futaki, S.; Niwa, M.; Tanaka, S.; Ueda, K.; Sugiura, Y. Possible Existence of Common Internalization Among Arginine-Rich Peptides. *J. Biol. Chem.* **2002,** *277,* 2437–2443.
131. Magzoub, M.; Kilk, K.; Eriksson, G.; Langel, U.; Graslund, A. Interaction and Structure of Cell Penetrating Peptides in the Presence of Phospholipid Vesicles. *Biochim. Biophys. Acta* **2001,** *1512,* 77–89.
132. Umezawa, N.; Gelman, M. A.; Haigis, M. C.; Raines, R. T.; Gellmann, S. H. Translocation of a β-Peptide Across Cell Membranes. *J. Am. Chem. Soc.* **2002,** *124,* 368–369.
133. Futaki, S.; Suzuki, T.; Ohashi, W.; Yagami, T.; Tanaka, S.; Ueda, K.; Sugiura, Y. Arginine-Rich Peptides: An Abundant Source of Membrane-Permeable Peptides Having Potential as Carriers for Intracellular Protein Delivery. *J. Biol. Chem.* **2001,** *276,* 5836–5840.
134. Rothbard, J. B.; Garlington, S.; Lin, Q.; Kirschberg, T.; Kreider, E.; Grane, P. L.; Wender, P. A.; Khavari, P. A. Conjugation of Arginine Oligomers to Cyclosporin A Facilitates Topical Delivery and Inhibition of Inflammation. *Nat. Med.* **2000,** *6,* 1253–1257.
135. Hallbrink, M.; Floren, A.; Elmquist, A.; Pooga, M.; Bartfai, T.; Langel, U. Cargo Delivery Kinetics of Cell-Penetrating Peptides. *Biochim. Biophys. Acta* **2001,** *1515,* 101–109.
136. Cleland, J. L. Development of Stable Formulations for PLGA/PLA Microsphere Vaccines. *Res. Immunol.* **1998,** *149,* 45–47.
137. Choi, S.-W.; Kim, J.-H. Design of Surface-Modified Poly(D, L-lactide-coglycolide) Nanoparticles for Targeted Drug Delivery to Bone. *J. Control. Release* **2007,** *122,* 24–30.
138. Pisal, D. S.; Kosloski, M. P.; Balu-Iyer, S. V. Delivery of Therapeutic Proteins. *J. Pharm. Sci.* **2010,** *99,* 2557–2575.
139. Jeong, B.; Lee, K. M.; Gutowska, A.; An, Y. H. Thermogelling Biodegradable Copolymer Aqueous Solutions for Injectable Protein Delivery and Tissue Engineering. *Biomacromolecules* **2002,** *3,* 865–868.
140. Han, K.; Lee, K. D.; Gao, Z. G.; Park, J. S. Preparation and Evaluation of Poly(L-lactic acid) Microspheres Containing rhEGF for Chronic Gastric Ulcer Healing. *J. Control. Release* **2001,** *75,* 259–269.
141. Kisel, M. A.; Kulik, L. N.; Tsybovsky, I. S.; Vlasov, A. P.; Vorobyov, M. S.; Kholodova, E. A.; Zabarovskaya, Z. V. Liposomes With Phosphatidylethanol as a Carrier for Oral Delivery of Insulin: Studies in the Rat. *Int. J. Pharm.* **2001,** *216,* 105–114.
142. Stanimirovic, D. B.; Markovic, M.; Micic, D. V.; Spatz, M.; Mrsulja, B. B. Liposome-Entrapped Superoxide Dismutase Reduces Ischemia/Reperfusion 'Oxidative Stress' in Gerbil Brain. *Neurochem. Res.* **1994,** *19,* 1473–1478.
143. Gaspar, M. M.; Perez-Soler, R.; Cruz, M. E. Biological Characterization of L-Asparaginase Liposomal Formulations. *Cancer Chemother. Pharmacol.* **1996,** *38,* 373–377.
144. Astermark, J. FVIII Inhibitors: Pathogenesis and Avoidance. *Blood* **2015,** *125,* 2045–2051.
145. Purohit, V. S.; Ramani, K.; Sarkar, R.; Kazazian, H. H., Jr.; Balasubramanian, S. V. Lower Inhibitor Development in Hemophilia A Mice Following Administration of Recombinant Factor VIII-O-phospho-L-serine Complex. *J. Biol. Chem.* **2005,** *280,* 17593–17600.
146. Morishita, M.; Khafagy, E.-S.; Shofner, J. P.; Peppas, N. A. Oral Delivery Systems. In *Biodrug Delivery Systems: Fundamentals, Applications and Clinical Development;* Morishita, M., Park, K., Eds.; CRC Press: Boca Raton, FL, 2010; pp 172–186.
147. Salamat-Miller, N.; Johnston, T. P. Current Strategies Used to Enhance the Paracellular Transport of Therapeutic Polypeptides Across the Intestinal Epithelium. *Int. J. Pharm.* **2005,** *294,* 201–216.
148. Bernkop-Schnurch, A.; Kast, C. E.; Guggi, D. Permeation Enhancing Polymers in Oral Delivery of Hydrophilic Macromolecules: Thiomer/GSH Systems. *J. Control. Release* **2003,** *93,* 95–103.
149. Kan, K. S.; Coleman, R. The Calcium Ionophore A23187 Increases the Tight-Junctional Permeability in Rat Liver. *Biochem. J.* **1988,** *256,* 1039–1041.
150. Raima, J.; Tormalehto, S.; Yritys, K.; Junginger, H. E.; Monkkonen, J. Effects of Various Absorption Enhancers on Transport of Clodronate Through Caco-2 Cells. *Int. J. Pharm.* **2003,** *261,* 129–136.
151. Anderberg, E. K.; Nystrom, C.; Artursson, P. Epithelial Transport of Drugs in Cell Culture. VII: Effects of Pharmaceutical Surfactant Excipients and Bile Acids on Transepithelial Permeability in Monolayers of Human Intestinal Epithelial (Caco-2) Cells. *J. Pharm. Sci.* **1992,** *81,* 879–887.
152. Swenson, E. S.; Milisen, W. B.; Curatolo, W. Intestinal Permeability Enhancement: Efficacy, Acute Local Toxicity, and Reversibility. *Pharm. Res.* **1994,** *11,* 1132–1142.
153. Kajii, H.; Horie, T.; Hayashi, M.; Awazu, S. Effects of Salicylic Acid on the Permeability of the Plasma Membrane of the Small Intestine of the Rat: A Fluorescence Spectroscopic Approach to Elucidate the Mechanism of Promoted Drug Absorption. *J. Pharm. Sci.* **1986,** *75,* 475–478.
154. Nishihata, T.; Higuchi, T.; Kamada, A. Salicylate-Promoted Permeation of Cefoxitin, Insulin and Phenylalanine Across Red Cell Membrane. Possible Mechanism. *Life Sci.* **1984,** *34,* 437–445.
155. Lindmark, T.; Kimura, Y.; Artursson, P. Absorption Enhancement Through Intracellular Regulation of Tight Junction Permeability by Medium Chain Fatty Acids in Caco-2 Cells. *J. Pharmacol. Exp. Ther.* **1998,** *284,* 362–369.
156. Tomita, M.; Hayashi, M.; Awazu, S. Absorption-Enhancing Mechanism of Sodium Caprate and Decanoylcarnitine in Caco-2 Cells. *J. Pharmacol. Exp. Ther.* **1995,** *272,* 739–743.
157. Shima, M.; Yohdoh, K.; Yamaguchi, M.; Kimura, Y.; Adachi, S.; Matsuno, R. Effects of Medium-Chain Fatty Acids and Their Acylglycerols on the Transport of Penicillin V Across Caco-2 Cell Monolayers. *Biosci. Biotechnol. Biochem.* **1997,** *61,* 1150–1155.
158. LeCluyse, E. L.; Appel, L. E.; Sutton, S. C. Relationship Between Drug Absorption Enhancing Activity and Membrane Perturbing Effects of Acylcarnitines. *Pharm. Res.* **1991,** *8,* 84–87.
159. Requero, M. A.; Goñi, F. M.; Alonso, A. The Membrane-Perturbing Properties of Palmitoyl-Coenzyme A and Palmitoylcarnitine. A Comparative Study. *Biochemistry* **1995,** *34,* 10400–10405.
160. Leone-Bay, A.; Paton, D. R.; Variano, B.; Leipold, H.; Rivera, T.; Miura-Fraboni, J.; Baughman, R. A.; Santiago, N. Acylated Non-Alpha-Amino Acids as Novel Agents for the Oral Delivery of Heparin Sodium, USP. *J. Control. Release* **1998,** *50,* 41–49.
161. Malkov, D.; Angelo, R.; Wang, H. Z.; Flanders, E.; Tang, H.; Gomez-Orellana, I. Oral Delivery of Insulin With the Eligen Technology: Mechanistic Studies. *Curr. Drug Deliv.* **2005,** *2,* 191–197.
162. Hoffman, A.; Qadri, B. Eligen Insulin — A System for the Oral Delivery of Insulin for Diabetes. *IDrugs* **2008,** *11,* 433–441.
163. Tanko, L. B.; Bagger, Y. Z.; Alexandersen, P.; Devogelaer, J. P.; Reginster, J. Y.; Chick, R.; Olson, M.; Benmammar, H.; Mindeholm, L.; Azria, M.; Christiansen, C. Safety and Efficacy of a Novel Salmon Calcitonin (sCT) Technology-Based Oral Formulation in Healthy Postmenopausal Women: Acute and 3-Month Effects on Biomarkers of Bone Turnover. *J. Bone Miner. Res.* **2004,** *19,* 1531–1538.
164. Bagger, Y. Z.; Tanko, L. B.; Alexandersen, P.; Karsdal, M. A.; Olson, M.; Mindeholm, L.; Azria, M.; Christiansen, C. Oral Salmon Calcitonin Induced Suppression of Urinary Collagen Type II Degradation in Postmenopausal Women: A New Potential Treatment of Osteoarthritis. *Bone* **2005,** *37,* 425–430.
165. Karsdal, M. A.; Byrjalsen, I.; Alexandersen, P.; Bihlet, A.; Andersen, J. R.; Riis, B. J.; Bay-Jensen, A. C.; Christiansen, C. Treatment of Symptomatic Knee Osteoarthritis With Oral Salmon Calcitonin: Results From Two Phase 3 Trials. *Osteoarthritis Cartilage* **2015,** *23,* 532–543.
166. Karsdal, M. A.; Riis, B. J.; Mehta, N.; Stern, W.; Arbit, E.; Christiansen, C.; Henriksen, K. Lessons Learned From the Clinical Development of Oral Peptides. *Br. J. Clin. Pharmacol.* **2015,** *79,* 720–732.
167. Mlynek, G. M.; Calvo, L. J.; Robinson, J. R. Carrier-Enhanced Human Growth Hormone Absorption Across Isolated Rabbit Intestinal Tissue. *Int. J. Pharm.* **2000,** *197,* 13–21.
168. Wu, S. J.; Robinson, J. R. Transcellular and Lipophilic Complex-Enhanced Intestinal Absorption of Human Growth Hormone. *Pharm. Res.* **1999,** *16,* 1266–1272.
169. Hammerle, S. P.; Mindeholm, L.; Launonen, A.; Kiese, B.; Loeffler, R.; Harfst, E.; Azria, M.; Arnold, M.; John, M. R. The Single Dose Pharmacokinetic Profile of a Novel Oral Human Parathyroid Hormone Formulation in Healthy Postmenopausal Women. *Bone* **2012,** *50,* 965–973.
170. Daugherty, A. L.; Mrsny, R. J. Regulation of the Intestinal Epithelial Paracellular Barrier. *Pharm. Sci. Technol. Today* **1999,** *2,* 281–287.
171. Vanuytsel, T.; Vermeire, S.; Cleynen, I. The Role of Haptoglobin and Its Related Protein, Zonulin, in Inflammatory Bowel Disease. *Tissue Barriers* **2013,** *1,* e27321.

172. Di Pierro, M.; Lu, R.; Uzzau, S.; Wang, W.; Margaretten, K.; Pazzani, C.; Maimone, F.; Fasano, A. Zonula Occludens Toxin Structure-Function Analysis. Identification of the Fragment Biologically Active on Tight Junctions and of the Zonulin Receptor Binding Domain. *J. Biol. Chem.* **2001,** *276,* 19160–19165.
173. Karyekar, C. S.; Fasano, A.; Raje, S.; Lu, R.; Dowling, T. C.; Eddington, N. D. Zonula Occludens Toxin Increases the Permeability of Molecular Weight Markers and Chemotherapeutic Agents Across the Bovine Brain Microvessel Endothelial Cells. *J. Pharm. Sci.* **2003,** *92,* 414–423.
174. Song, K. H.; Fasano, A.; Eddington, N. D. Effect of the Six-Mer Synthetic Peptide (AT1002) Fragment of Zonula Occludens Toxin on the Intestinal Absorption of Cyclosporin A. *Int. J. Pharm.* **2008,** *351,* 8–14.
175. Song, K. H.; Eddington, N. D. The Impact of AT1002 on the Delivery of Ritonavir in the Presence of Bioadhesive Polymer, Carrageenan. *Arch. Pharm. Res.* **2012,** *35,* 937–943.
176. Song, K. H.; Eddington, N. D. The Influence of Stabilizer and Bioadhesive Polymer on the Permeation-Enhancing Effect of AT1002 in the Nasal Delivery of a Paracellular Marker. *Arch. Pharm. Res.* **2012,** *35,* 359–366.
177. Gopalakrishnan, S.; Pandey, N.; Tamiz, A. P.; Vere, J.; Carrasco, R.; Somerville, R.; Tripathi, A.; Ginski, M.; Paterson, B. M.; Alkan, S. S. Mechanism of Action of ZOT-Derived Peptide AT-1002, a Tight Junction Regulator and Absorption Enhancer. *Int. J. Pharm.* **2009,** *365,* 121–130.
178. van Roy, F.; Berx, G. The Cell-Cell Adhesion Molecule E-Cadherin. *Cell. Mol. Life Sci.* **2008,** *65,* 3756–3788.
179. Halbleib, J. M.; Nelson, W. J. Cadherins in Development: Cell Adhesion, Sorting, and Tissue Morphogenesis. *Genes Dev.* **2006,** *20,* 3199–3214.
180. Pal, D.; Audus, K. L.; Siahaan, T. J. Modulation of Cellular Adhesion in Bovine Brain Microvessel Endothelial Cells by a Decapeptide. *Brain Res.* **1997,** *747,* 103–113.
181. Sinaga, E.; Jois, S. D.; Avery, M.; Makagiansar, I. T.; Tambunan, U. S.; Audus, K. L.; Siahaan, T. J. Increasing Paracellular Porosity by E-Cadherin Peptides: Discovery of Bulge and Groove Regions in the EC1-Domain of E-Cadherin. *Pharm. Res.* **2002,** *19,* 1170–1179.
182. Kiptoo, P.; Sinaga, E.; Calcagno, A. M.; Zhao, H.; Kobayashi, N.; Tambunan, U. S.; Siahaan, T. J. Enhancement of Drug Absorption Through the Blood-Brain Barrier and Inhibition of Intercellular Tight Junction Resealing by E-Cadherin Peptides. *Mol. Pharm.* **2011,** *8,* 239–249.
183. Wong, V.; Gumbiner, B. A Synthetic Peptide Corresponding to the Extracellular Domain of Occludin Perturbs the Tight Junction Permeability Barrier. *J. Cell Biol.* **1997,** *136,* 399–409.
184. Lacaz-Vieira, F.; Jaeger, M. M.; Farshori, P.; Kachar, B. Small Synthetic Peptides Homologous to Segments of the First External Loop of Occludin Impair Tight Junction Resealing. *J. Membr. Biol.* **1999,** *168,* 289–297.
185. Deli, M. A. Potential Use of Tight Junction Modulators to Reversibly Open Membranous Barriers and Improve Drug Delivery. *Biochim. Biophys. Acta* **2009,** *1788,* 892–910.
186. Sonoda, N.; Furuse, M.; Sasaki, H.; Yonemura, S.; Katahira, J.; Horiguchi, Y.; Tsukita, S. *Clostridium perfringens* Enterotoxin Fragment Removes Specific Claudins From Tight Junction Strands: Evidence for Direct Involvement of Claudins in Tight Junction Barrier. *J. Cell Biol.* **1999,** *147,* 195–204.
187. Suzuki, H.; Watari, A.; Hashimoto, E.; Yonemitsu, M.; Kiyono, H.; Yagi, K.; Kondoh, M.; Kunisawa, J. C-Terminal *Clostridium perfringens* Enterotoxin-Mediated Antigen Delivery for Nasal Pneumococcal Vaccine. *PLoS One* **2015,** *10,* e0126352.
188. Veronese, F. M.; Pasut, G. PEGylation: Posttranslational Bioengineering of Protein Biotherapeutics. *Drug Discov. Today Technol.* **2008,** *5,* e57–e64.
189. Klootwijk, W.; Sleddens-Linkels, E.; de Boer, R.; Jansen, C. A.; Autar, R.; de Herder, W. W.; Boevé, E. R.; Visser, T. J.; de Greef, W. J. Renal Clearance of the Thyrotropin-Releasing Hormone-Like Peptide Pyroglutamyl-Glutamyl-Prolineamide in Humans. *J. Clin. Endocrinol. Metab.* **1997,** *82,* 3068–3073.
190. Haversen, L. A.; Engberg, I.; Baltzer, L.; Dolphin, G.; Hanson, L. A.; Mattsby-Baltzer, I. Human Lactoferricin and Peptides Derived From a Surface-Exposed Helical Region Reduce Experimental *Escherichia coli* Urinary Tract Infection in Mice. *Infect. Immun.* **2000,** *68,* 5816–5823.
191. Otvos, L., Jr.; Cappelletto, B.; Varga, I.; Wade, J. D.; Xiang, Z. Q.; Kaiser, K.; Stephens, L. J.; Ertl, H. C. J. The Effects of Post-Translational Side-Chain Modifications on the Stimulatory Activity, Serum Stability and Conformation of Synthetic Peptides Carrying T Helper Cell Epitopes. *Biochim. Biophys. Acta* **1996,** *1313,* 11–19.
192. Otvos, L., Jr.; Vetter, S. W.; Koladia, M.; Knappe, D.; Schmidt, R.; Ostorhazi, E.; Kovalszky, I.; Bionda, N.; Cudic, P.; Surmacz, E.; Wade, J. D.; Hoffmann, R. The Designer Leptin Antagonist Peptide Allo-aca Compensates for Short Serum Half-Life With Very Tight Binding to the Receptor. *Amino Acids* **2014,** *46,* 873–882.
193. Otvos, L., Jr. Peptide-Based Drug Design: Here and Now. *Methods Mol. Biol.* **2008,** *494,* 1–8.
194. Rodriguez, M. C.; Cudic, M. Optimization of Physicochemical and Pharmacological Properties of Peptide Drugs by Glycosylation. *Methods Mol. Biol.* **2013,** *1081,* 107–136.
195. Davis, F. F.; Abuchowski, A.; van Es, T.; Palczuk, N. C.; Chen, R.; Savoca, K.; Wieder, K. Enzyme-Polyethylene Glycol Adducts: Modified Enzymes With Unique Properties. In *Enzyme Engineering;* Broun, G. B., Manecke, G., Wingard L. B. Jr., Eds.; Plenum Press: New York, 1978; pp 169–173.
196. Yowell, S. L.; Blackwell, S. Novel Effects With Polyethylene Glycol Modified Pharmaceuticals. *Cancer Treat Rev.* **2002,** *28* (Suppl A), 3–6.
197. Wieder, K. J.; Davis, F. F. Enzyme Therapy: II. Effect of Covalent Attachment of Polyethylene Glycol on Biochemical Parameters and Immunological Determinants of β-Glucosidase and α-Galactosidase. *J. Appl. Biochem.* **1983,** *5,* 337–347.
198. Davis, S.; Abuchowski, A.; Park, Y. K.; Davis, F. F. Alteration of the Circulating Life and Antigenic Properties of Bovine Adenosine Deaminase in Mice by Attachment of Polyethylene Glycol. *Clin. Exp. Immunol.* **1981,** *46,* 649–652.
199. Roberts, M. J.; Harris, J. M. Attachment of Degradable Poly(ethylene glycol) to Proteins Has the Potential to Increase Therapeutic Efficacy. *J. Pharm. Sci.* **1998,** *87,* 1440–1445.
200. Zalipsky, S. Chemistry of Polyethylene Glycol Conjugates With Biologically Active Molecules. *Adv. Drug Deliv. Rev.* **1995,** *16,* 157–182.
201. Harris, J. M.; Chess, R. B. Effect of Pegylation on Pharmaceuticals. *Nat. Rev. Drug Discov.* **2003,** *2,* 214–221.
202. Harris, J. M.; Martin, N. E.; Modi, M. Pegylation: A Novel Process for Modifying Pharmacokinetics. *Clin. Pharmacokinet.* **2011,** *40,* 539–551.
203. Jain, A.; Jain, S. K. PEGylation: An Approach for Drug Delivery. A Review. *Crit. Rev. Ther. Drug Carrier Syst.* **2008,** *25,* 403–447.
204. Roberts, M. J.; Bentley, M. D.; Harris, J. M. Chemistry for Peptide and Protein PEGylation. *Adv. Drug Deliv. Rev.* **2012,** *64,* 116–127.
205. Kinstler, O.; Molineux, G.; Treuheit, M.; Ladd, D.; Gegg, C. Mono-N-Terminal Poly(Ethylene Glycol)-Protein Conjugates. *Adv. Drug Deliv. Rev.* **2002,** *54,* 477–485.
206. Parikh, H.; Bajaj, P.; Tripathy, R. K.; Pande, A. H. Improving Properties of Recombinant SsoPox by Site-Specific Pegylation. *Protein Pept. Lett.* **2015,** *22* (12), 1098–1103.
207. Vugmeyster, Y.; Entrican, C. A.; Joyce, A. P.; Lawrence-Henderson, R. F.; Leary, B. A.; Mahoney, C. S.; Patel, H. K.; Raso, S. W.; Olland, S. H.; Hegen, M.; Xu, X. Pharmacokinetic, Biodistribution, and Biophysical Profiles of TNF Nanobodies Conjugated to Linear or Branched Poly(Ethylene Glycol). *Bioconjug. Chem.* **2012,** *23,* 1452–1462.
208. Sato, H. Enzymatic Procedure for Site-Specific Pegylation of Proteins. *Adv. Drug Deliv. Rev.* **2002,** *54,* 487–504.
209. Veronese, F. M.; Pasut, G. PEGylation, Successful Approach to Drug Delivery. *Drug Discov. Today* **2005,** *10,* 1451–1458.
210. Bailon, P.; Berthold, W. Polyethylene Glycol-conjugated Pharmaceutical Proteins. *Pharm. Sci. Technol. Today* **1998,** *1,* 352–356.
211. Bailon, P.; Palleroni, A.; Schaffer, C. A.; Spence, C. L.; Fung, W. J.; Porter, J. E.; Ehrlich, G. K.; Pan, W.; Xu, Z. X.; Modi, M. W.; Farid, A.; Berthold, W.; Graves, M. Rational Design of a Potent, Long-Lasting Form of Interferon: A 40 kDa Branched Polyethylene Glycol-Conjugated Interferon α-2a for the Treatment of Hepatitis C. *Bioconjug. Chem.* **2001,** *12,* 195–202.
212. Jo, Y. W.; Youn, Y. S.; Lee, S. H.; Kim, B. M.; Kang, S. H.; Yoo, M.; Choi, E. C.; Lee, K. C. Long-Acting Interferon-α 2a Modified With a Trimer-Structured Polyethylene Glycol: Preparation, In Vitro Bioactivity, In Vivo Stability and Pharmacokinetics. *Int. J. Pharm.* **2006,** *309,* 87–93.
213. Knauf, M. J.; Bell, D. P.; Hirtzer, P.; Luo, Z. P.; Young, J. D.; Katre, N. V. Relationship of Effective Molecular Size to Systemic Clearance in Rats of Recombinant Interleukin-2 Chemically Modified With Water-Soluble Polymers. *J. Biol. Chem.* **1988,** *263,* 15064–15070.
214. Bhat, R.; Timasheff, S. N. Steric Exclusion Is the Principal Source of the Preferential Hydration of Proteins in the Presence of Polyethylene Glycols. *Protein Sci.* **1992,** *1,* 1133–1143.
215. Caliceti, P.; Veronese, F. M. Pharmacokinetic and Biodistribution Properties of Poly(Ethylene Glycol)-Protein Conjugates. *Adv. Drug Deliv. Rev.* **2003,** *55,* 1261–1277.
216. Caliceti, P.; Schiavon, O.; Veronese, F. M. Biopharmaceutical Properties of Uricase Conjugated to Neutral and Amphiphilic Polymers. *Bioconjug. Chem.* **1999,** *10,* 638–646.
217. Monfardini, C.; Schiavon, O.; Caliceti, P.; Morpurgo, M.; Harris, J. M.; Veronese, F. M. A Branched Monomethoxypoly(Ethylene Glycol) for Protein Modification. *Bioconjug. Chem.* **1995,** *6,* 62–69.

218. Rajan, R. S.; Li, T.; Aras, M.; Sloey, C.; Sutherland, W.; Arai, H.; Briddell, R.; Kinstler, O.; Lueras, A. M.; Zhang, Y.; Yeghnazar, H.; Treuheit, M.; Brems, D. N. Modulation of Protein Aggregation by Polyethylene Glycol Conjugation: GCSF as a Case Study. *Protein Sci.* **2006,** *15,* 1063–1075.
219. Veronese, F. M.; Mero, A.; Caboi, F.; Sergi, M.; Marongiu, C.; Pasut, G. Site-Specific Pegylation of G-CSF by Reversible Denaturation. *Bioconjug. Chem.* **2007,** *18,* 1824–1830.
220. Veronese, F. M. Peptide and Protein PEGylation: A Review of Problems and Solutions. *Biomaterials* **2001,** *22,* 405–417.
221. Pelegri-O'Day, E. M.; Lin, E. W.; Maynard, H. D. Therapeutic Protein-Polymer Conjugates: Advancing Beyond PEGylation. *J. Am. Chem. Soc.* **2014,** *136,* 14323–14332.
222. Zhang, F.; Liu, M. R.; Wan, H. T. Discussion About Several Potential Drawbacks of PEGylated Therapeutic Proteins. *Biol. Pharm. Bull.* **2014,** *37,* 335–339.
223. Ishida, T.; Ichihara, M.; Wang, X.; Yamamoto, K.; Kimura, J.; Majima, E.; Kiwada, H. Injection of PEGylated Liposomes in Rats Elicits PEG-Specific IgM, Which Is Responsible for Rapid Elimination of a Second Dose of PEGylated Liposomes. *J. Control. Release* **2006,** *112,* 15–25.
224. Wang, X.; Ishida, T.; Kiwada, H. Anti-PEG IgM Elicited by Injection of Liposomes Is Involved in the Enhanced Blood Clearance of a Subsequent Dose of PEGylated Liposomes. *J. Control. Release* **2007,** *119,* 236–244.
225. Hegade, V. S.; Sood, R.; Saralaya, D.; Moreea, S. Pulmonary Complications of Treatment With Pegylated Interferon for Hepatitis C Infection-Two Case Reports. *Ann. Hepatol.* **2013,** *12,* 629–633.
226. Leung, Y.; Urbanski, S. J.; Schindel, L.; Myers, R. P. Ischemic Colitis During Pegylated Interferon-α and Ribavirin Therapy for Chronic Hepatitis C. *Can. J. Gastroenterol.* **2006,** *20,* 661–663.
227. Baldo, B. A. Enzymes Approved for Human Therapy: Indications, Mechanisms and Adverse Effects. *BioDrugs* **2015,** *29,* 31–55.
228. Graham, M. L.; Asselin, B. L.; Herndon, J. E., 2nd; Casey, J. R.; Chaffee, S.; Ciocci, G. H.; Daeschner, C. W.; Davis, A. R.; Gold, S.; Halperin, E. C.; Laughlin, M. J.; Martin, P. L.; Olson, J. F.; Kurtzberg, J. Toxicity, Pharmacology and Feasibility of Administration of PEG-L-Asparaginase as Consolidation Therapy in Patients Undergoing Bone Marrow Transplantation for Acute Lymphoblastic Leukemia. *Bone Marrow Transplant.* **1998,** *21,* 879–885.
229. Wang, Y. S.; Youngster, S.; Grace, M.; Bausch, J.; Bordens, R.; Wyss, D. F. Structural and Biological Characterization of Pegylated Recombinant Interferon α-2b and Its Therapeutic Implications. *Adv. Drug Deliv. Rev.* **2002,** *54,* 547–570.
230. Roelfsema, F.; Biermasz, N. R.; Pereira, A. M.; Romijn, J. Nanomedicines in the Treatment of Acromegaly: Focus on Pegvisomant. *Int. J. Nanomed.* **2006,** *1,* 385–398.
231. Blick, S. K. A.; Curran, M. P. Certolizumab Pegol. *BioDrugs* **2007,** *21,* 195–201.
232. Fishbane, S.; Roger, S. D.; Martin, E.; Runyan, G.; O'Neil, J.; Qiu, P.; Locatelli, F. Peginesatide for Maintenance Treatment of Anemia in Hemodialysis and Nondialysis Patients Previously Treated With Darbepoetin-α. *Clin. J. Am. Soc. Nephrol.* **2013,** *8,* 538–545.
233. Giorgi, M. E.; Agusti, R.; de Lederkremer, R. M. Carbohydrate PEGylation, an Approach to Improve Pharmacological Potency. *Beilstein J. Org. Chem.* **2014,** *10,* 1433–1444.
234. Ostergaard, H.; Bjelke, J. R.; Hansen, L.; Petersen, L. C.; Pedersen, A. A.; Elm, T.; Møller, F.; Hermit, M. B.; Holm, P. K.; Krogh, T. N.; Petersen, J. M.; Ezban, M.; Sorensen, B. B.; Andersen, M. D.; Agerso, H.; Ahmadian, H.; Balling, K. W.; Christiansen, M. L.; Knobe, K.; Nichols, T. C.; Bjorn, S. E.; Tranholm, M. Prolonged Half-Life and Preserved Enzymatic Properties of Factor IX Selectively PEGylated on Native N-Glycans in the Activation Peptide. *Blood* **2011,** *118,* 2333–2341.
235. Youn, Y. S.; Na, D. H.; Yoo, S. D.; Song, S. C.; Lee, K. C. Carbohydrate-Specifically Polyethylene Glycol-Modified Ricin A-Chain With Improved Therapeutic Potential. *Int. J. Biochem. Cell Biol.* **2005,** *37,* 1525–1533.
236. Stennicke, H. R.; Kjalke, M.; Karpf, D. M.; Balling, K. W.; Johansen, P. B.; Elm, T.; Ovlisen, K.; Möller, F.; Holmberg, H. L.; Gudme, C. N.; Persson, E.; Hilden, I.; Pelzer, H.; Rahbek-Nielsen, H.; Jespersgaard, C.; Bogsnes, A.; Pedersen, A. A.; Kristensen, A. K.; Peschke, B.; Kappers, W.; Rode, F.; Thim, L.; Tranholm, M.; Ezban, M.; Olsen, E. H.; Bjorn, S. E. A Novel B-Domain O-GlycoPEGylated FVIII (N8-GP) Demonstrates Full Efficacy and Prolonged Effect in Hemophilic Mice Models. *Blood* **2013,** *121,* 2108–2116.
237. Park, A.; Honey, D. M.; Hou, L.; Bird, J. J.; Zarazinski, C.; Searles, M.; Braithwaite, C.; Kingsbury, J. S.; Kyazike, J.; Culm-Merdek, K.; Greene, B.; Stefano, J. E.; Qiu, H.; McPherson, J. M.; Pan, C. Q. Carbohydrate-Mediated Polyethylene Glycol Conjugation of TSH Improves Its Pharmacological Properties. *Endocrinology* **2013,** *154,* 1373–1383.
238. Fernandez-Megia, E.; Correa, J.; Riguera, R. "Clickable" PEG-Dendritic Block Copolymers. *Biomacromolecules* **2006,** *7,* 3104–3111.
239. Lin, X.; Wang, S.; Jiang, Y.; Wang, Z. J.; Sun, G. L.; Xu, D. S.; Feng, Y.; Shen, L. Poly(Ethylene Glycol)-Radix Ophiopogonis Polysaccharide Conjugates: Preparation, Characterization, Pharmacokinetics and In Vitro Bioactivity. *Eur. J. Pharm. Biopharm.* **2010,** *76,* 230–237.
240. Park, I. K.; Kim, T. H.; Park, Y. H.; Shin, B. A.; Choi, E. S.; Chowdhury, E. H.; Akaike, T.; Cho, C. S. Galactosylated Chitosan-Graft-Poly(Ethylene Glycol) as Hepatocyte-Targeting DNA Carrier. *J. Control. Release* **2001,** *76,* 349–362.
241. Xu, L.; Anchordoquy, T. Drug Delivery Trends in Clinical Trials and Translational Medicine: Challenges and Opportunities in the Delivery of Nucleic Acid-Based Therapeutics. *J. Pharm. Sci.* **2011,** *100,* 38–52.
242. Torchilin, V. P.; Omelyanenko, V. G.; Papisov, M. I.; Bogdanov, A. A., Jr.; Trubetskoy, V. S.; Herron, J. N.; Gentry, C. A. Poly(Ethylene Glycol) on the Liposome Surface: On the Mechanism of Polymer-Coated Liposome Longevity. *Biochim. Biophys. Acta* **1994,** *1195,* 11–20.
243. Torchilin, V. P.; Shtilman, M. I.; Trubetskoy, V. S.; Whiteman, K.; Milstein, A. M. Amphiphilic Vinyl Polymers Effectively Prolong Liposome Circulation Time In Vivo. *Biochim. Biophys. Acta* **1994,** *1195,* 181–184.
244. Harvie, P.; Wong, F. M.; Bally, M. B. Use of Poly(Ethylene Glycol)-Lipid Conjugates to Regulate the Surface Attributes and Transfection Activity of Lipid-DNA Particles. *J. Pharm. Sci.* **2000,** *89,* 652–663.
245. Remaut, K.; Lucas, B.; Braeckmans, K.; Demeester, J.; De Smedt, S. C. Pegylation of Liposomes Favours the Endosomal Degradation of the Delivered Phosphodiester Oligonucleotides. *J. Control. Release* **2007,** *117,* 256–266.
246. Majzoub, R. N.; Chan, C. L.; Ewert, K. K.; Silva, B. F.; Liang, K. S.; Jacovetty, E. L.; Carragher, B.; Potter, C. S.; Safinya, C. R. Uptake and Transfection Efficiency of PEGylated Cationic Liposome-DNA Complexes With and Without RGD-Tagging. *Biomaterials* **2014,** *35,* 4996–5005.
247. Gaziova, Z.; Baumann, V.; Winkler, A. M.; Winkler, J. Chemically Defined Polyethylene Glycol siRNA Conjugates With Enhanced Gene Silencing Effect. *Bioorg. Med. Chem.* **2014,** *22,* 2320–2326.
248. Tagalakis, A. D.; Kenny, G. D.; Bienemann, A. S.; McCarthy, D.; Munye, M. M.; Taylor, H.; Wyatt, M. J.; Lythgoe, M. F.; White, E. A.; Hart, S. L. PEGylation Improves the Receptor-Mediated Transfection Efficiency of Peptide-Targeted, Self-Assembling, Anionic Nanocomplexes. *J. Control. Release* **2014,** *174,* 177–187.
249. Sakura, Y.; Hatakeyama, H.; Sato, Y.; Hyodo, M.; Akita, H.; Harashima, H. Gene Silencing via RNAi and siRNA Quantification in Tumor Tissue Using MEND, a Liposomal siRNA Delivery System. *Mol. Ther.* **2013,** *21,* 1195–1203.
250. Govan, J. M.; McIver, A. L.; Deiters, A. Stabilization and Photochemical Regulation of Antisense Agents Through PEGylation. *Bioconjug. Chem.* **2011,** *22,* 2136–2142.
251. Spiekermann, G. M.; Finn, P. W.; Ward, E. S.; Dumont, J.; Dickinson, B. L.; Blumberg, R. S.; Lencer, W. I. Receptor-Mediated Immunoglobulin G Transport Across Mucosal Barriers in Adult Life: Functional Expression of FcRn in the Mammalian Lung. *J. Exp. Med.* **2002,** *196,* 303–310.
252. Israel, E. J.; Taylor, S.; Wu, Z.; Mizoguchi, E.; Blumberg, R. S.; Bhan, A.; Simister, N. E. Expression of the Neonatal Fc Receptor, FcRn, on Human Intestinal Epithelial Cells. *Immunology* **1997,** *92,* 69–74.
253. Dickinson, B. L.; Badizadegan, K.; Wu, Z.; Ahouse, J. C.; Zhu, X.; Simister, N. E.; Blumberg, R. S.; Lencer, W. I. Bidirectional FcRn-Dependent IgG Transport in a Polarized Human Intestinal Epithelial Cell Line. *J. Clin. Invest.* **1999,** *104,* 903–911.
254. Ghetie, V.; Ward, E. S. Multiple Roles for the Major Histocompatibility Complex Class I-Related Receptor FcRn. *Annu. Rev. Immunol.* **2000,** *18,* 739–766.
255. Mancuso, M. E.; Mannucci, P. M. Fc-Fusion Technology and Recombinant FVIII and FIX in the Management of the Hemophilias. *Drug Des. Devel. Ther.* **2014,** *8,* 365–371.
256. Powell, J. S.; Pasi, K. J.; Ragni, M. V.; Ozelo, M. C.; Valentino, L. A.; Mahlangu, J. N.; Josephson, N. C.; Perry, D.; Manco-Johnson, M. J.; Apte, S.; Baker, R. I.; Chan, G. C.; Novitzky, N.; Wong, R. S.; Krassova, S.; Allen, G.; Jiang, H.; Innes, A.; Li, S.; Cristiano, L. M.; Goyal, J.; Sommer, J. M.; Dumont, J. A.; Nugent, K.; Vigliani, G.; Brennan, A.; Luk, A.; Pierce, G. F. Phase 3 Study of Recombinant Factor IX Fc Fusion Protein in Hemophilia B. *N. Engl. J. Med.* **2013,** *369,* 2313–2323.

257. Thomas, J. D.; Cui, H.; North, P. J.; Hofer, T.; Rader, C.; Burke, T. R., Jr. Application of Strain-Promoted Azide-Alkyne Cycloaddition and Tetrazine Ligation to Targeted Fc-Drug Conjugates. *Bioconjug. Chem.* **2012,** *23,* 2007–2013.
258. Angelini, A.; Diderich, P.; Morales-Sanfrutos, J.; Thurnheer, S.; Hacker, D.; Menin, L.; Heinis, C. Chemical Macrocyclization of Peptides Fused to Antibody Fc Fragments. *Bioconjug. Chem.* **2012,** *23,* 1856–1863.
259. Iafisco, M.; Varoni, E.; Di Foggia, M.; Pietronave, S.; Fini, M.; Roveri, N.; Rimondini, L.; Prat, M. Conjugation of Hydroxyapatite Nanocrystals With Human Immunoglobulin G for Nanomedical Applications. *Colloids Surf. B Biointerfaces* **2012,** *90,* 1–7.
260. Acchione, M.; Kwon, H.; Jochheim, C. M.; Atkins, W. M. Impact of Linker and Conjugation Chemistry on Antigen Binding, Fc Receptor Binding and Thermal Stability of Model Antibody-Drug Conjugates. *MAbs* **2012,** *4,* 362–372.
261. Jimenez-Solem, E.; Rasmussen, M. H.; Christensen, M.; Knop, F. K. Dulaglutide, a Long-Acting GLP-1 Analog Fused With an Fc Antibody Fragment for the Potential Treatment of Type 2 Diabetes. *Curr. Opin. Mol. Ther.* **2010,** *12,* 790–797.
262. Carter, P. J. Introduction to Current and Future Protein Therapeutics: A Protein Engineering Perspective. *Exp. Cell Res.* **2011,** *317,* 1261–1269.
263. Li, Q.; So, C. R.; Fegan, A.; Cody, V.; Sarikaya, M.; Vallera, D. A.; Wagner, C. R. Chemically Self-Assembled Antibody Nanorings (CSANs): Design and Characterization of an Anti-CD3 IgM Biomimetic. *J. Am. Chem. Soc.* **2010,** *132,* 17247–17257.
264. Dickgiesser, S.; Rasche, N.; Nasu, D.; Middel, S.; Hörner, S.; Avrutina, O.; Diederichsen, U.; Kolmar, H. Self-Assembled Hybrid Aptamer-Fc Conjugates for Targeted Delivery: A Modular Chemoenzymatic Approach. *ACS Chem. Biol.* **2015,** *10,* 2158–2165.
265. Anderson, C. L.; Chaudhury, C.; Kim, J.; Bronson, C. L.; Wani, M. A.; Mohanty, S. Perspective—FcRn Transports Albumin: Relevance to Immunology and Medicine. *Trends Immunol.* **2006,** *27,* 343–348.
266. Peters, T. *All About Albumin: Biochemistry, Genetics and Medical Applications;* Academic Press Limited: San Diego, CA, 1996.
267. Merlot, A. M.; Kalinowski, D. S.; Richardson, D. R. Unraveling the Mysteries of Serum Albumin-More Than Just a Serum Protein. *Front. Physiol.* **2014,** *5,* 299.
268. Kragh-Hansen, U. Molecular Aspects of Ligand Binding to Serum Albumin. *Pharmacol. Rev.* **1981,** *33,* 17–53.
269. Carmeliet, P.; Jain, R. K. Angiogenesis in Cancer and Other Diseases. *Nature* **2000,** *407,* 249–257.
270. Andersson, C.; Iresjo, B. M.; Lundholm, K. Identification of Tissue Sites for Increased Albumin Degradation in Sarcoma-Bearing Mice. *J. Surg. Res.* **1991,** *50,* 156–162.
271. Tiruppathi, C.; Finnegan, A.; Malik, A. B.. Isolation and Characterization of a Cell Surface Albumin-Binding Protein From Vascular Endothelial Cells. *Proc. Natl. Acad. Sci. USA* **1996,** *93,* 250–254.
272. Kudlowitz, D.; Muggia, F. Nanoparticle Albumin-Bound Paclitaxel (Nab-Paclitaxel): Extending Its Indications. *Expert Opin. Drug Saf.* **2014,** *13,* 681–685.
273. Socinski, M. A.; Bondarenko, I.; Karaseva, N. A.; Makhson, A. M.; Vynnychenko, I.; Okamoto, I.; Hon, J. K.; Hirsh, V.; Bhar, P.; Zhang, H.; Iglesias, J. L.; Renschler, M. F. Weekly Nab-Paclitaxel in Combination With Carboplatin Versus Solvent-Based Paclitaxel Plus Carboplatin as First-Line Therapy in Patients With Advanced Non-Small-Cell Lung Cancer: Final Results of a Phase III Trial. *J. Clin. Oncol.* **2012,** *30,* 2055–2062.
274. Sethi, A.; Sher, M.; Akram, M. R.; Karim, S.; Khiljee, S.; Sajjad, A.; Shah, S. N.; Murtaza, G. Albumin as a Drug Delivery and Diagnostic Tool and Its Market Approved Products. *Acta Pol. Pharm.* **2013,** *70,* 597–600.
275. Morales, J. Defining the Role of Insulin Detemir in Basal Insulin Therapy. *Drugs* **2007,** *67,* 2557–2584.
276. Elsadek, B.; Kratz, F. Impact of Albumin on Drug Delivery — New Applications on the Horizon. *J. Control. Release* **2012,** *157,* 4–28.
277. Nicolì, E.; Syga, M. I.; Bosetti, M.; Shastri, V. P. Enhanced Gene Silencing Through Human Serum Albumin-Mediated Delivery of Polyethylenimine-siRNA Polyplexes. *PLoS One* **2015,** *10,* e0122581.
278. Young, M. A.; Wald, J. A.; Matthews, J. E.; Scott, R.; Hodge, R. J.; Zhi, H.; Reinhardt, R. R. Clinical Pharmacology of Albiglutide, a GLP-1 Receptor Agonist. *Postgrad. Med.* **2014,** *126,* 84–97.
279. Gregoriadis, G.; Jain, S.; Papaioannou, I.; Laing, P. Improving the Therapeutic Efficacy of Peptides and Proteins: A Role for Polysialic Acids. *Int. J. Pharm.* **2005,** *300,* 125–130.
280. Mazmanian, S. K.; Liu, C. H.; Tzianabos, A. O.; Kasper, D. L. An Immunomodulatory Molecule of Symbiotic Bacteria Directs Maturation of the Host Immune System. *Cell* **2005,** *122,* 107–118.
281. Fernandes, A. I.; Gregoriadis, G. Polysialylated Asparaginase: Preparation, Activity and Pharmacokinetics. *Biochim. Biophys. Acta* **1997,** *1341,* 26–34.
282. Constantinou, A.; Epenetos, A. A.; Hreczuk-Hirst, D.; Jain, S.; Deonarain, M. P. Modulation of Antibody Pharmacokinetics by Chemical Polysialylation. *Bioconjug. Chem.* **2008,** *19,* 643–650.
283. Constantinou, A.; Epenetos, A. A.; Hreczuk-Hirst, D.; Jain, S.; Wright, M.; Chester, K. A.; Deonarain, M. P. Site-Specific Polysialylation of an Antitumor Single-Chain Fv Fragment. *Bioconjug. Chem.* **2009,** *20,* 924–931.
284. Porter, C. J.; Wasan, K. M.; Constantinides, P. Lipid-Based Systems for the Enhanced Delivery of Poorly Water Soluble Drugs. *Adv. Drug Deliv. Rev.* **2008,** *60,* 615–616.
285. Luisa Corvo, M.; Jorge, J. C.; van't Hof, R.; Cruz, M. E.; Crommelin, D. J.; Storm, G. Superoxide Dismutase Entrapped in Long-Circulating Liposomes: Formulation Design and Therapeutic Activity in Rat Adjuvant Arthritis. *Biochim. Biophys. Acta* **2002,** *1564,* 227–236.
286. Baru, M.; Carmel-Goren, L.; Barenholz, Y.; Dayan, I.; Ostropolets, S.; Slepoy, I.; Gvirtzer, N.; Fukson, V.; Spira, J. Factor VIII Efficient and Specific Non-Covalent Binding to PEGylated Liposomes Enables Prolongation of its Circulation Time and Haemostatic Efficacy. *Thromb. Haemost.* **2005,** *93,* 1061–1068.
287. Yatuv, R.; Carmel-Goren, L.; Dayan, I.; Robinson, M.; Baru, M. Binding of Proteins to PEGylated Liposomes and Improvement of G-CSF Efficacy in Mobilization of Hematopoietic Stem Cells. *J. Control. Release* **2009,** *135,* 44–50.
288. Alberts, D. S.; Muggia, F. M.; Carmichael, J.; Winer, E. P.; Jahanzeb, M.; Venook, A. P.; Skubitz, K. M.; Rivera, E.; Sparano, J. A.; DiBella, N. J.; Stewart, S. J.; Kavanagh, J. J.; Gabizon, A. A. Efficacy and Safety of Liposomal Anthracyclines in Phase I/II Clinical Trials. *Semin. Oncol.* **2004,** *31* (6 Suppl. 13), 53–90.
289. Cleland, J. L.; Langer, R. Formulation and Delivery of Proteins and Peptides. In *Formulation and Delivery of Proteins and Peptides;* Cleland, J. L., Langer, R., Eds.; American Chemical Society: Washington, DC, 1994; pp 1–19.
290. Sethi, R.; Sanfilippo, N. Six-Month Depot Formulation of Leuprorelin Acetate in the Treatment of Prostate Cancer. *Clin. Interv. Aging* **2009,** *4,* 259–267.
291. Periti, P.; Mazzei, T.; Mini, E. Clinical Pharmacokinetics of Depot Leuprorelin. *Clin. Pharmacokinet.* **2002,** *41,* 485–504.
292. Fowler, J. E.; Flanagan, M.; Gleason, D. M.; Klimberg, I. W.; Gottesman, J. E.; Sharifi, R. Evaluation of an Implant That Delivers Leuprolide for 1 Year for the Palliative Treatment of Prostate Cancer. *Urology* **2000,** *55,* 639–642.
293. Fowler, J. E., Jr.; Gottesman, J. E.; Reid, C. F.; Andriole, G. L., Jr.; Soloway, M. S. Safety and Efficacy of an Implantable Leuprolide Delivery System in Patients With Advanced Prostate Cancer. *J. Urol.* **2000,** *164,* 730–734.
294. Hamilton, P. T.; Jansen, M. S.; Ganesan, S.; Benson, R. E.; Hyde-Deruyscher, R.; Beyer, W. F.; Gile, J. C.; Nair, S. A.; Hodges, J. A.; Gron, H. Improved Bone Morphogenetic Protein-2 Retention in an Injectable Collagen Matrix Using Bifunctional Peptides. *PLoS One* **2013,** *8,* e70715.
295. Stone, K. R.; Steadman, J. R.; Rodkey, W. G.; Li, S. T. Regeneration of Meniscal Cartilage With Use of a Collagen Scaffold. Analysis of Preliminary Data. *J. Bone Joint Surg. Am.* **1997,** *79,* 1770–7177.
296. Tao, H.; Kainerstorfer, J. M.; Siebert, S. M.; Pritchard, E. M.; Sassaroli, A.; Panilaitis, B. J.; Brenckle, M. A.; Amsden, J. J.; Levitt, J.; Fantini, S.; Kaplan, D. L.; Omenetto, F. G. Implantable, Multifunctional, Bioresorbable Optics. *Proc. Natl. Acad. Sci. U. S. A.* **2012,** *109,* 19584–19589.
297. Rahbek, U. L.; Hubalek, F.; Bjerregaard, S. Peptide and Protein Drug Delivery Systems for Nonparenteral Routes of Administration. In *Pharmaceutical Formulation Development of Peptides and Proteins;* Hovgaard, L., Frokjaer, S., Van de Weert, M., Eds.; CRC Press: Boca Raton, FL, 2013; pp 270–296.
298. Sarkar, M. A. Drug Metabolism in the Nasal Mucosa. *Pharm. Res.* **1992,** *9,* 1–9.
299. Maggio, E. T.; Pillion, D. J. High Efficiency Intranasal Drug Delivery Using Intravail® Alkylsaccharide Absorption Enhancers. *Drug Deliv. Transl. Res.* **2013,** *3,* 16–25.
300. Grasso, P.; Lee, D. W.; Leinung, M. C. Leptin-Related Peptides. US Patent 7,208,572; 2007.

301. Waldrop, M. A.; Leinung, M. C.; Lee, D. W.; Grasso, P. Intranasal Delivery of Mouse [D-Leu-4]-OB3, a Synthetic Peptide Amide With Leptin-Like Activity, Improves Energy Balance, Glycaemic Control, Insulin Sensitivity and Bone Formation in Leptin-Resistant C57BLK/6-m db/db Mice. *Diabetes Obes. Metab.* **2010,** *12,* 871–875.
302. Leary, A. C.; Dowling, M.; Cussen, K.; O'Brien, J.; Stote, R. M. Pharmacokinetics and Pharmacodynamics of Intranasal Insulin Spray (Nasulin) Administered to Healthy Male Volunteers: Influence of the Nasal Cycle. *J. Diabetes Sci. Technol.* **2008,** *2,* 1054–1060.
303. Illum, L. Transport of Drugs From the Nasal Cavity to the Central Nervous System. *Eur. J. Pharm. Sci.* **2000,** *11,* 1–18.
304. Yi, X.; Manickam, D. S.; Brynskikh, A.; Kabanov, A. V. Agile Delivery of Protein Therapeutics to CNS. *J. Control. Release* **2014,** *190,* 637–663.
305. Leary, A. C.; Stote, R. M.; Cussen, K.; O'Brien, J.; Leary, W. P.; Buckley, B. Pharmacokinetics and Pharmacodynamics of Intranasal Insulin Administered to Patients With Type 1 Diabetes: A Preliminary Study. *Diabetes Technol. Ther.* **2006,** *8,* 81–88.
306. Chesnut, C. H., 3rd; Silverman, S.; Andriano, K.; Genant, H.; Gimona, A.; Harris, S.; Kiel, D.; LeBoff, M.; Maricic, M.; Miller, P.; Moniz, C.; Peacock, M.; Richardson, P.; Watts, N.; Baylink, D. A Randomized Trial of Nasal Spray Salmon Calcitonin in Postmenopausal Women With Established Osteoporosis: The Prevent Recurrence of Osteoporotic Fractures Study. *Am. J. Med.* **2000,** *109,* 267–276.
307. Harris, A. S.; Nilsson, I. M.; Wagner, Z.-G.; Alkner, U. Intranasal Administration of Peptides: Nasal Deposition, Biological Response, and Absorption of Desmopressin. *J. Pharm. Sci.* **1986,** *75,* 1085–1088.
308. Lethagen, S.; Tennvall, G. R. Self-Treatment With Desmopressin Intranasal Spray in Patients With Bleeding Disorders: Effect on Bleeding Symptoms and Socioeconomic Factors. *Ann. Hematol.* **1993,** *66,* 257–260.
309. Henzl, M. R.; Corson, S. L.; Moghissi, K.; Buttram, V. C.; Berqvist, C.; Jacobson, J. Administration of Nasal Nafarelin as Compared With Oral Danazol for Endometriosis. A Multicenter Double-Blind Comparative Clinical Trial. *N. Engl. J. Med.* **1988,** *318,* 485–489.
310. Faure, N.; Labrie, F.; Lemay, A.; Belanger, A.; Gourdeau, Y.; Laroche, B.; Robert, G. Inhibition of Serum Androgen Levels by Chronic Intranasal and Subcutaneous Administration of a Potent Luteinizing Hormone-Releasing Hormone (LH-RH) Agonist in Adult Men. *Fertil. Steril.* **1982,** *37,* 416–424.
311. Laube, B. L. The Expanding Role of Aerosols in Systemic Drug Delivery, Gene Therapy and Vaccination: An Update. *Transl. Respir. Med.* **2014,** *2,* 3.
312. Laube, B. L.; Georgopoulos, A.; Adams, G. K., 3rd. Preliminary Study of the Efficacy of Insulin Aerosol Delivered by Oral Inhalation in Diabetic Subjects. *JAMA* **1993,** *269,* 2106–2109.
313. Skyler, J. S.; Cefalu, W. T.; Kourides, I. A.; Landschulz, W. H.; Balagtas, C. C.; Cheng, S. L.; Gelfand, R. A. Efficacy of Inhaled Human Insulin in Type 1 Diabetes Mellitus: A Randomized Proof-of-Concept Study. *Lancet* **2001,** *357,* 331–335.
314. Rosenstock, J.; Lorber, D. L.; Gnudi, L.; Howard, C. P.; Bilheimer, D. W.; Chang, P. C.; Petrucci, R. E.; Boss, A. H.; Richardson, P. C. Prandial Inhaled Insulin Plus Basal Insulin Glargine Versus Twice Daily Biaspart Insulin for Type 2 Diabetes: A Multicentre Randomised Trial. *Lancet* **2010,** *375,* 2244–2253.
315. Ostorhazi, E.; Holub, M. C.; Rozgonyi, F.; Harmos, F.; Cassone, M.; Wade, J. D.; Otvos, L., Jr. Broad-Spectrum Antimicrobial Efficacy of Peptide A3-APO in Mouse Models of Multidrug-Resistant Wound and Lung Infections Cannot Be Explained by In Vitro Activity Against the Pathogens Involved. *Int. J. Antimicrob. Agents* **2011,** *37,* 480–484.
316. Griesenbach, U.; Alton, E. W. Progress in Gene and Cell Therapy for Cystic Fibrosis Lung Disease. *Curr. Pharm. Des.* **2012,** *18,* 642–662.
317. Prausnitz, M. R.; Langer, R. Transdermal Drug Delivery. *Nat. Biotechnol.* **2008,** *26,* 1261–1268.
318. Caon, T.; Jin, L.; Simoes, C. M.; Norton, R. S.; Nicolazzo, J. A. Enhancing the Buccal Mucosal Delivery of Peptide and Protein Therapeutics. *Pharm. Res.* **2015,** *32,* 1–21.
319. Richardson, J. L.; Illum, L. (D) Routes of Delivery: Case Studies: (8) The Vaginal Route of Peptide and Protein Drug Delivery. *Adv. Drug Deliv. Rev.* **1992,** *8,* 341–366.
320. Bruno, B. J.; Miller, G. D.; Lim, C. S. Basics and Recent Advances in Peptide and Protein Drug Delivery. *Ther. Deliv.* **2013,** *4,* 1443–1467.
321. Otvos, L., Jr. Peptide-Based Drug Discovery and Development. Common Misconceptions. *Pharmaceut. Outsourcing* **2014,** *15,* 40–43.
322. Lugaresi, A. RebiSmart™ (Version 1.5) Device for Multiple Sclerosis Treatment Delivery and Adherence. *Expert Opin. Drug Deliv.* **2013,** *10,* 273–283.
323. Xu, Z.; Marciniak, S. J., Jr.; Frederick, B.; Kim, L.; Zhuang, Y.; Davis, H. M.; Zhou, H. Pharmacokinetic Bridging Approach for Developing Biologics-Delivery Devices: A Case Study With a Golimumab Autoinjector. *Clin. Ther.* **2015,** *37,* 427–438.
324. Schwarzenbach, F.; Dao Trong, M.; Grange, L.; Laurent, P. E.; Abry, H.; Cotton, J.; Granger, C. Results of a Human Factors Experiment of the Usability and Patient Acceptance of a New Autoinjector in Patients With Rheumatoid Arthritis. *Patient Prefer Adher.* **2014,** *8,* 199–209.
325. Wong, M.; Abdulnabi, R.; Carey, M. A.; Fu, H. A Randomized, Cross-Over Comparison of Preference Between Two Reusable Insulin Pen Devices in Pen-Naïve Adults With Diabetes. *Curr. Med. Res. Opin.* **2013,** *29,* 465–473.
326. Kappelgaard, A. M.; Mikkelsen, S.; Knudsen, T. K.; Fuchs, G. S. Patient Preference for a New Growth Hormone Injection Device: Results of an Open-Label Study in Japanese Pediatric Patients. *J. Pediatr. Endocrinol. Metab.* **2011,** *24,* 489–496.
327. Mullard, A. Once-Yearly Device Takes on Daily and Weekly Diabetes Drugs. *Nat. Biotechnol.* **2014,** *32,* 1178.
328. Henry, R. R.; Rosenstock, J.; Logan, D.; Alessi, T.; Luskey, K.; Baron, M. A. Continuous Subcutaneous Delivery of Exenatide via ITCA 650 Leads to Sustained Glycemic Control and Weight Loss for 48 Weeks in Metformin-Treated Subjects With Type 2 Diabetes. *J. Diabetes Complications* **2014,** *28,* 393–398.
329. White, J.; Bell, J.; Saunders, J. B.; Williamson, P.; Makowska, M.; Farquharson, A.; Beebe, K. L. Open-Label Dose-Finding Trial of Buprenorphine Implants (Probuphine) for Treatment of Heroin Dependence. *Drug Alcohol Depend.* **2009,** *103,* 37–43.

6.06 Orally Delivered Peptides for Treatment of Inflammatory Bowel Disease

ML Smythe, Protagonist Therapeutics Inc, St Lucia, QLD, Australia; and The Institute for Molecular Bioscience, The University of Queensland, St Lucia, QLD, Australia

© 2017 Elsevier Ltd. All rights reserved.

6.06.1	**Inflammatory Bowel Disease**	157
6.06.1.1	The Pathological Manifestations of IBD	158
6.06.1.2	Summary	158
6.06.2	**Constrained and Stable Peptides**	159
6.06.2.1	Disulfide-Rich Peptides	159
6.06.2.2	Examples of DRPs	159
6.06.2.3	Summary	161
6.06.3	**Protease Stability for Peptides**	162
6.06.4	**Redox Stability**	162
6.06.5	**Stability to Microbes**	163
6.06.6	**Permeability**	163
6.06.6.1	Permeability at the Epithelial Surface	164
6.06.6.2	Transporters on Intestinal Epithelial Cells	164
6.06.6.3	Absorption in the GI Tract	164
6.06.7	**Impact of Food**	165
6.06.8	**Orally Delivered and Targeted Agents for Treatment of IBD**	165
6.06.9	**Conclusion**	165
Acknowledgments		166
References		166

6.06.1 Inflammatory Bowel Disease

Inflammatory bowel disease (IBD), which encompasses ulcerative colitis (UC) and Crohn's disease (CD), is a chronic disease that causes inflammation, abdominal pain, diarrhea, and weight loss, as well as fatigue and anemia in severe cases. IBD has an onset in early adulthood and a lifelong impact; this disease poses a significant economic burden to society with annual estimated direct costs of $US 5.9 billion[1,2] and an increasing worldwide incidence.[3,4]

CD may involve any part of the gastrointestinal (GI) tract, but typically affects the distal end of the small intestine (ileum) and the proximal end of the large intestine (colon), while UC is restricted to the colon. CD may affect all layers of the intestine, resulting in deep ulcers that penetrate the bowel wall and lead to abscesses in the abdomen and fistulas that connect the bowel to other organs. UC affects only the mucosa of the colon and is more evenly distributed. A cure is desperately needed for IBD; however, the underpinning etiology is unknown. IBD is considered a heterogenous disease, triggered by a balance between a patient's genetic susceptibility, environmental triggers, immune system, and the intestinal microflora.[5] Increased intestinal permeability ("leaky gut") has been implicated as a pathogenic factor for >20 years.[6] This increased intestinal permeability may lead to microbial antigen exposure, which in turn initiates disease; alternatively, a compromised immune defense caused by genetic defects may lead to abnormal bacterial exposure to the mucosal immune system, resulting in inflammation and leaky gut.

The early onset of IBD, along with its persistent and chronic nature, emphasizes the need for safe and efficacious therapies. Treatment regimens are constantly evolving (e.g., step-up or step-down therapy) but may involve combinations of aminosalicylates, antibiotics, corticosteroids, immunosuppressives, and targeted biologics.[7] Each of these agents has specific side effect limitations. The current clinical approach for treating IBD involves the initial treatment of patients with the mildest form of drug therapy, with subsequent escalation to less-safe drugs in nonresponding patients. Injected biologics target particular proteins that have proven defective, deficient, or excessive in people with IBD. However, injection results in ablation of the same pathway in both healthy and diseased tissues for extended periods, leading to exaggerated pharmacology.[8] Such biologics are used as the last step prior to surgery. The development of anti-Tumor Necrosis Factor-α (anti-TNF) therapies, such as infliximab, adalimumab, and certolizumab pegol, has significantly improved the quality of life of many patients with IBD, but only a third of these patients remain in remission after 1 year, and the need of surgery remains high in patients receiving anti-TNF therapy.[3] Side effects associated with TNF blockers include lymphoma, infections, congestive heart failure, demyelinating disease, a lupus-like syndrome, induction of auto-antibodies, injection site reactions, and additional systemic side effects.[9] Many patients become intolerant to anti-TNF treatment[10]; switching from one agent to another is an established, though not ideal, treatment approach.[11]

6.06.1.1 The Pathological Manifestations of IBD

The pathological manifestations of IBD are localized primarily in the GI tract, though extraintestinal manifestations may be found in most other organs.[12,13] Analysis of the inflamed mucosa from patients with UC and CD has revealed an increased expression of certain proinflammatory cytokines such as IL-1, IL-6, IL-8, IL-23, and TNF-α.[14–17] Fecal TNF has been shown to be a useful marker of disease activity, suggesting enhanced local expression.[18] In mice, mucosally produced TNF has been shown to be sufficient to induce disease, indicating that targeted intestinal blockade of gut-derived TNF would be efficacious.[19] In humans treated with an anti-TNF drug, ~73% of patients with active disease had higher levels of the drug in serum than in tissue, compared to ~33% of patients in remission. The tissue:serum ratio of anti-TNF drug was highest in uninflamed areas and lowest in severely inflamed areas, suggesting that patients with high serum anti-TNF levels have active disease because tissue levels of anti-TNF are insufficient to neutralize local TNF production.[20]

The anti-TNF antibodies infliximab and adalimumab have been injected locally (adjacent to fistulas),[21,22] and infliximab has been administered topically by rectal instillation.[23] In each study, significant efficacy was apparent with local topical delivery, suggesting not only the ability to infiltrate through mucosal barriers but also that local activity is sufficient to treat disease. Similarly, treatment in a chemically induced rat model of colitis with an avian polyclonal anti-TNF antibody (administered orally twice daily for 5 days) ameliorated all disease parameters, whether treatment was initiated before or after the onset of disease.[24] The antibody was found to be localized in the lamina propria, and hence could penetrate inflamed regions of the colon. The orally administered antibody had very low systemic concentrations, and the antibody was not active when delivered IV at these concentrations, suggesting that oral efficacy reflected local tissue concentrations and not systemic exposure. A polyclonal collection of anti-TNF antibodies derived from bovine colostrum was also orally administered to several mouse models of IBD[25] and was effective in treating murine IBD. The antibody was observed in colonic tissue by immunohistochemistry, was thought to be intact, and exhibited minimal systemic absorption.

The localized nature of IBD is supported by the therapeutic effect of aminosalicylates; the efficacy of this class has been correlated with the drug concentration in intestinal mucosa,[26] while systemic drug concentrations may be indicative of adverse events.[27] Numerous studies on the topical/rectal delivery of aminosalicylates and steroids have shown improved efficacy with limited side effects when compared with systemic delivery.[28]

6.06.1.2 Summary

In summary, the major pathological manifestations and sites of target action in IBD appear limited to intestinal tissue. Therefore, an ideal therapeutic would be delivered orally and act from the luminal side (thereby achieving high drug concentrations locally in the diseased mucosa and enhancing efficacy), with limited systemic bioavailability (to reduce the potential for systemically driven adverse effects) (Fig. 1). The extent of gut targeting required to treat disease will be highly dependent on the specific target and the required site of target engagement. Indeed, the required drug levels in the gut can range from no GI tissue absorption for "soluble" targets within the lumen, to a degree of penetration to access membrane-bound targets on the luminal side of the apical membrane, to significant permeability to access targets in the lamina propria or on the basolateral side of the membrane. Given the important roles of cytokines in both inducing and protecting intestinal inflammation, it is not surprising that numerous protein–protein interaction targets are under clinical investigation, including IL-1β, IL-5, IL-13, IL-18, IL-22, and IL-23. Small molecule (SM) approaches are also being pursued, with a predominant focus on inhibiting cytokine-mediated effects by targeting intracellular downstream signaling targets, but these lack the selectivity of blocking specific cytokine-mediated signaling. There is, therefore, significant opportunity to develop orally delivered and targeted drugs that block key cytokine signaling.

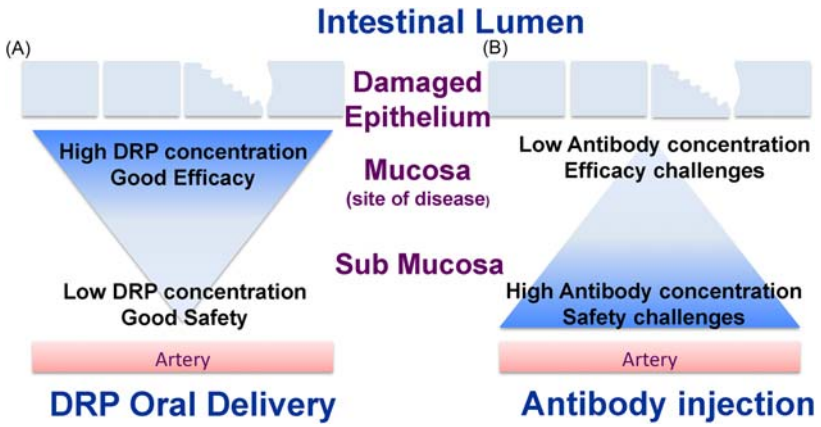

Fig. 1 (A) The oral delivery of constrained peptides will result in high concentrations of drug in the diseased tissue (mucosa) and lower systemic concentrations. (B) In contrast, injected antibodies result in high concentrations systemically and lower concentrations in diseased tissues.

6.06.2 Constrained and Stable Peptides

To achieve oral delivery of targeted drugs, compounds must be orally stable, able to reach and then penetrate the diseased GI tract to achieve high concentrations in the lamina propria, and able to bind the large flat macromolecular surfaces that underpin cytokine-based signaling. The spectrum of available drugs consists primarily of SMs that target deep binding pockets to inhibit enzyme function and macromolecular antibodies to bind and block signaling of large macromolecular protein complexes. SMs can be orally delivered but are unlikely to modulate cytokine (protein–protein interaction) targets, while monoclonal antibodies are able to block cytokine targets but are unlikely to be orally stable and delivered. Peptide-based drugs have gathered momentum as a class of therapeutics, but linear peptides are not generally orally stable. Constrained peptides and macrocycles may offer unique advantages for the treatment of IBD.

6.06.2.1 Disulfide-Rich Peptides

One class of constrained peptides are disulfide-rich peptides (DRPs).[29] DRPs are ideal scaffolds for drug development and have favorable features for diverse clinical applications. These constrained peptides possess disulfide-strained cores that impart extraordinary chemical and biological stability characteristics, along with sequence flexibility that allows the introduction of novel functionalities. DRPs permit the engineering of a large surface footprint in a spatially controlled manner to modulate protein–protein interaction targets.[30–33] DRPs are found throughout nature and have evolved SM-like properties and remarkable chemical stability. It has been shown that some DRPs can be boiled, incubated at 65°C, or exposed to 1 N HCl or 1 N NaOH without a loss of structural or functional integrity.[34] Avimers, a DRP subclass, are derived from human A domains and exhibit stability during incubation for 2 weeks at temperatures between 50°C and −80°C.[35]

Many DRPs are found in protease-rich environments and have evolved stability characteristics that overcome limitations that have plagued the development of peptide-based drugs (**Table 1** and **Fig. 2**). For instance, defensins are a well-characterized family of antimicrobial DRPs[36] that are expressed by epithelial cells throughout the small intestine and colon; notably, these tissues are predominant sites for manifestation of IBD.[37] Trefoil peptides have been shown to be stable for up to 6 days in the stomach contents of rats and for more than 24 h in components of the small intestine of humans[38]; such peptides are excreted intact in the urine when administered parenterally. Due to their stability characteristics and small size, several DRPs have been tested for permeability. For example, conotoxins modified with lipidic amino acids were shown to have improved permeability in Caco-2 assays,[39] and a series of cyclic cysteine knots were shown to have good permeability through rat intestine.[40,41]

6.06.2.2 Examples of DRPs

As a consequence of these characteristics, several DRPs have been evaluated in various disease models of IBD. For example, the trefoil family (TFF) of DRPs comprises TFF1, TFF2, and TFF3, all of which may play essential roles in epithelial restitution and repair within the GI tract. These TFFs have been studied in numerous rodent models of disease, including ethanol-induced gastric injury,[42] indomethacin-induced gastric injury,[42] burn-induced gastric injury,[43] aspirin-induced gastric injury,[44] chemical (Dextran sodium sulfate (DSS) and 2,4,6-Trinitrobezenesulfonic acid (TNBS)) models,[45,46] mitomycin C models,[46] and ischemic reperfusion injury in weaning rats.[47] Depending on the specific model, distinct DRPs showed superior efficacy when administered either orally[45,46] or parenterally.

Kalata is a cyclic DRP that is found in the African plant *Oldenlandia affinis* and was identified as the orally active ingredient in an herbal tea that is drunk by women of the Lula tribe during childbirth. The compound is thermally stable and orally active.[48] Kalata has been used as the base scaffold to engineer new functions onto a peptide while maintaining the oral characteristics. For example, Tam and coworkers used molecular grafting of bioactive peptides onto the kalata B1 framework to develop an orally active bradykinin B1 receptor antagonist for the treatment of inflammatory pain.[49] Other DRPs have been engineered with new activity and oral delivery; for instance, an α-conotoxin Vc1.1 analog has shown potential for treating neuropathic pain when delivered orally.[50] In both of these cases,[49,50] the authors reported oral activity but did not provide systemic bioavailability. Oxytocin analogs incorporating disulfide-bond isosteres were efficacious when delivered orally, but it was suggested the actions of these analogs were predominantly topical (i.e., localized to the gut wall).[51] As extensively reviewed by Craik et al.,[52] there have been numerous cases of engineering DRPs with new functions. Discontinuous surfaces have been engineered[31] onto DRPs resulting in potent and selective cytokine antagonists.[30] A select set of DRP structures that function or are found in the GI tract are shown in **Fig. 2**.

In the context of clinical data, linaclotide (Linzess) is a once-daily orally administered drug for treatment of irritable bowel syndrome with constipation (IBS-C). The compound is a DRP agonist of guanylate cyclase 2C (GC-C); the compound acts locally within the lumen of the GI tract and is minimally bioavailable. Linaclotide was derived from a heat-stable enterotoxin, which is found in the GI tract. In Phase 1 human trials, 3–5% of the oral linaclotide dose was excreted in feces as a pharmacologically active peptide (linaclotide plus a deleted C-terminal Tyr analog MM-419447), demonstrating that orally administered active peptides are available to stimulate GC-C throughout the GI tract. Nonetheless, ex vivo studies showed that linaclotide is rapidly proteolysed in intestinal fluids from mice, rats, and humans under reducing conditions.[53] Plecanatide and dolcanatide, derivatives of a naturally occurring GI DRP hormone (uroguanylin), have been identified for the treatment of several GI disorders. Both compounds are delivered orally; plecanatide is in registration for chronic idiopathic constipation, while dolcanatide is in Phase 2 trials for opioid-induced constipation and Phase 1 trials for UC. Plecanatide is completely degraded in simulated intestinal fluid (SIF) within

Table 1 Sequences and disulfide-bond patterns of select marketed, clinical, or preclinical disulfide-rich peptides that have been delivered orally

Linaclotide	Marketed for treatment of IBS-C. Derivative of an enterotoxin found in GI tract	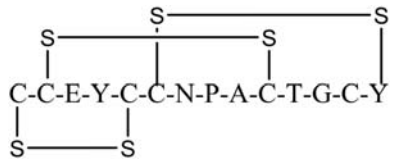
Plecanatide	In the clinic for chronic idiopathic constipation. Is a derivative of uroguanylin	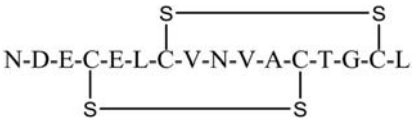
Dolcanatide	In the clinic for opioid-induced constipation. Is a derivative of uroguanylin	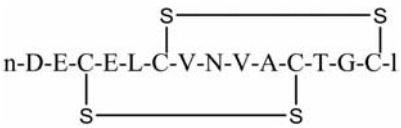
cVC1.1	Preclinical. α-conotoxin derivative for treatment of pain	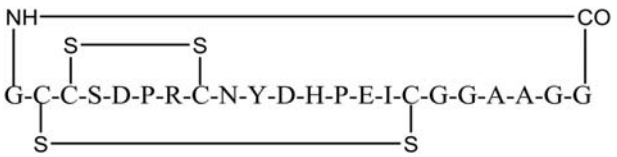
Kalata	Orally delivered uterotonic agent. Used as base scaffold	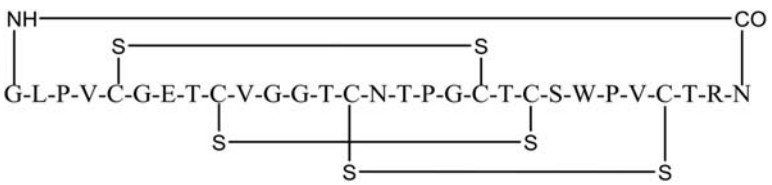
MII	Preclinical, orally bioavailable	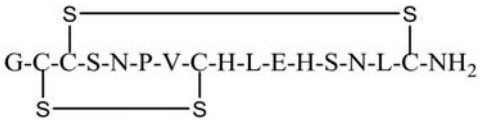

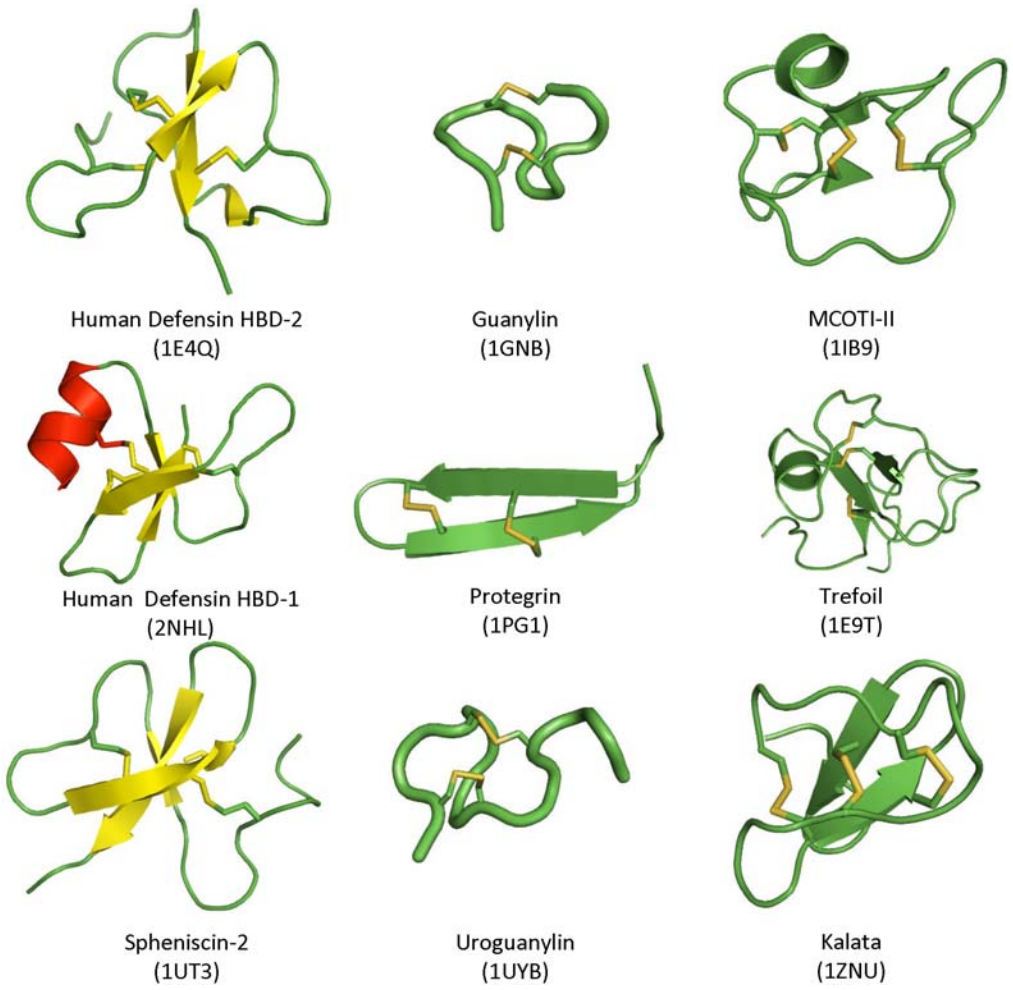

Fig. 2 Diverse series of experimental structures of disulfide-rich peptides that have been found or function orally. This includes human defensin, guanylin, uroguanylin, and trefoil that are found in the GI tract of humans, Sphensiscin-2 found in GI tract of penguins, kalata an active ingredient in orally ingested tea, and protegrin that has been orally delivered in human clinical trials.

2 h to form an active metabolite. Dolcanatide is more stable, losing 20% of its biological activity after 24 h incubation in SIF.[54] Desmopressin, another DRP, is relatively stable in the GI tract.[55] Although this compound exhibits low bioavailability (~0.1%), desmopressin possesses high potency and is efficacious when orally delivered. In clinical trials, DRPs of the TFF class have been employed for treatment of the oral cavity, specifically as a mouth rinse formulation of human TFF1 (a *Lactococcus lactis*-induction of secreted human TFF1)[56] and as an oral spray for the prevention of oral mucositis.[57] Formulation strategies for oral delivery of peptides typically involve enteric coating and formulation with protease inhibitors and permeation enhancers.[58] A variety of peptides[58] (e.g., salmon calcitonin, GLP2, GLP1, PYY-(3–36), insulin, parathyroid hormone, and octreotide) have been formulated for oral delivery and are currently marketed or in different stages of clinical development.

6.06.2.3 Summary

In conclusion, there are numerous examples of orally stable DRPs that can be categorized as follows: (1) found and function naturally in the GI tract (e.g., enterotoxin precursors to linaclotide); (2) orally stable characteristics following ingestion (e.g., kalata B1); (3) stable DRP scaffolds with oral bioavailability and/or activity (e.g., conotoxin analog CV1.1); (4) formulated for oral delivery (e.g., calcitonin, insulin).

To be an effective treatment for IBD, an orally delivered DRP must attain appropriate free-drug exposure in diseased mucosal tissue (target site of action) at levels that exceed pharmacological potency over the desired period of time. To achieve this goal, numerous chemical stability constraints need to be overcome. The molecule must be stable to various pHs that range from strongly acidic in the stomach (pH 1.5–1.9), trending toward basic in the small intestine (pH ~7.5), and then weakly acidic in the colon (pH 5–7).[59] Thus, compounds must remain stable and may need to maintain potent biological activity over a broad pH range. There are also various

metabolic and physical barriers that DRPs must overcome to be orally active. A key component of the GI stability hurdle is the required duration of stability. For effective topical delivery, DRPs must be stable during their transit through the various GI compartments.[60] The total transit times in healthy volunteers range from 5.1 to 58.3 h (median 27.4 h).[61] The transit time in the colon is significantly longer and more variable than that in the intestine, with a reported range of 6–48 h.[62] The small intestine transit time, where the proteolytic hurdle is thought to be highest, has been reported to range from 0.5 to 9.5 h, with a mean of ~3 h.[62] The motility and transit in the colon is highly influenced by defecation time in healthy patients. Patients with IBD have been reported to have accelerated intestinal transit times.[63–65] This is relevant given a reported increase in GI absorption of desmopressin with pretreatment of loperamide, presumably due to lowering GI motility.[66]

6.06.3 Protease Stability for Peptides

Protease stability is vitally important for orally delivered peptide-based drug candidates. Compared to other organs, the GI tract contains the highest levels of proteases.[67] Protease metabolism in the GI tract can occur by luminally secreted enzymes (pepsin, trypsin, chymotrypsin, elastase, and carboxypeptidase A/B secreted from the pancreas), by brush border membrane-bound enzymes (various carboxypeptidases, endopeptidases, and aminopeptidases), or by protease secretion by bacteria on the luminal side or by immune and mesenchymal cells in the lamina propria. It is estimated that 40 different proteases are encountered in the GI tract of humans[68] and that the lumen incorporates gram quantities of proteases secreted from the pancreas.[69] Compared to brush border enzymes, the luminally secreted proteases were found to be 16- and 40-fold more effective at metabolizing insulin as a substrate in rats and guinea pigs, respectively.[70,71] The regulated production of proteases is key to intestinal homeostasis; altering this process can lead to gut inflammation and destruction, a key pathological feature of IBD. A fourfold increase in trypsin-like activity has been reported in UC patients,[72] and matrix metalloproteases have been implicated in IBD pathogenesis.[73,74] Increased concentrations of proteases have been found in the feces of patients with IBD.[72,75–78] It is reasonable to assume that in a diseased state, the proteolytic hurdle may be elevated for orally administered DRP therapeutics.

While it is widely reported that the colon is an environment with relatively reduced proteolytic activity,[79] it may still present a significant metabolic hurdle to orally delivered peptide-based drugs. Macfarlane et al. observed that stool from a patient who had undergone a pancreatectomy, and who therefore lacked pancreatic proteases, had proteolytic activity comparable to that of the stool of healthy individuals.[80] Such proteolytic activity is assumed to be derived from enteric microbes,[80,81] which are known to produce an array of aspartic, cysteine, metallo, and serine proteases.[75] The dominant proteolytic bacteria types in the human colon are reported as streptococci, *Bacteroides* spp., and *Clostridium* spp.[82,83] Hence, simply formulating DRPs to reach the colon may be inadequate, as a degree of intrinsic protease stability may still be required.

Proteases typically cleave peptide substrates in extended or elongated conformations.[84] DRPs are tightly knotted globular structures and are considered resistant to proteolysis.[52] However, the GI tract is a reducing environment, likely reducing disulfides to yield linear peptides that would be suitable elongated substrates for numerous proteases.

6.06.4 Redox Stability

Disulfide-bond formation is a reversible process with numerous biological functions, including stabilization of protein fold, enzyme catalysis, and protection against oxidative damage.[85] The ability to form and break a disulfide-bond depends on the disulfide bond stability, the environmental redox state, and the nature of the oxidant and reductant.

The reducing environment in the GI tract is a balance between the glutathione/glutathione disulfide (GSH/GSSG), cysteine/cystine (Cys/CySS), and reduced and oxidized thioredoxin (Trx/TrxSS) redox systems that ensure redox homeostasis.[86] The redox environment supports the gut microflora, aids nutrient absorption, counteracts oxidant-induced epithelial injury, and regulates intestinal cell transformation and apoptosis.[87]

Under these reducing conditions, DRPs may be unstable as a result of thiol/disulfide exchange, yielding linear analogs that would be susceptible to proteolysis. The redox stability of disulfide bonds in proteins can vary over an enormous range.[88] Proteins with the thioredoxin fold have active sites comprising a shared Cys1-Xaa2-Yaa3-Cys4 motif, in which the two cysteines are reversibly disulfide bonded. Despite the structural similarities of these proteins, the redox potential of the disulfide bond can vary by at least 7 kcal mol^{-1}, a 10^5-fold difference in equilibrium constant. The modulation of the redox potential of the disulfide bonds may be due to sequence differences within the conserved fold, in particular the ionization properties of active site residues.[89] These sequence effects also have been observed in the redox stability of DRPs. The high redox stability of octreotide toward GSH was explained by the presence of a Phe residue on each side of the Cys.[90,91] The higher degradation of oxytocin compared to vasotocin was explained by the Arg for Leu change at residue 8, which destabilizes the disulfide bond (due to the presence of the positively charged Arg stabilizing the dithiol).[91,92] Therefore sequence can have a significant impact on redox stability, which bodes well for the design of redox-stable DRP analogs. The redox hurdle may be lower in IBD patients, as both GSH levels and c-glutamylcysteine synthetase enzyme activity (required for GSH synthesis) are decreased in inflamed intestinal mucosa.[93] If necessary, numerous disulfide-bond isosteres can be used to eliminate or reduce redox liabilities.[94]

6.06.5 Stability to Microbes

The concentration of bacteria in the large intestine ranges from 10^{10} to 10^{12} CFU mL^{-1},[95] leading to the suggestion that the GI microflora has the ability to act as an organ with a metabolic potential equal to or greater than that of the liver.[96] Certainly the microbiota is capable of undertaking a large number of chemical transformations,[97] but these organisms also comprise significant proteolytic activity, as described earlier. The presence of GI microflora has implications for DRP-based therapies, as evidenced by the TFF of DRPs (TFF1, TFF2, and TFF3) that are remarkably stable, yet are reportedly broken down in the colon by the action of bacterial proteins.[38]

6.06.6 Permeability

Given adequate stability during GI transit, several physical barriers need to be surmounted prior to drug permeation at the epithelial surface. These include dissolution from semisolid luminal contents, diffusion through viscous mucus layers, and finally transit through an unstirred water layer prior to reaching the epithelial wall.

The stomach has a relatively thick mucus layer, while the intestine has a relatively thin, loose, and unattached mucus layer that harbors high concentrations of antibacterial peptides and proteins.[98] Bacterial exposure is minimized by flushing, which involves coordinated liquid and mucus secretion with intense motor activity; in rats, these processes have been reported to yield mucus turnover times of 40–270 min.[99] In contrast, the colon has a thick, two-layered mucus coating, the inner layer of which is impenetrable to bacteria and has a turnover time of about 1 h in mice.[98] Mucus undergoes some changes in IBD. In CD, the mucus is thicker than commonly observed, whereas in UC patients, the mucus layer is thin.[100,101] The mucins themselves also may undergo changes, including variations in protein length and glycosylation in IBD patients.[102] Underlying the mucus layer and protruding from the apical surface is the glycocalyx, or unstirred layer, which is a glycoprotein–polysaccharide layer that forms another barrier. The viscous nature of the mucus layer, estimated to be 1000- to 10,000-fold higher than water at low shear rates,[103] and its high turnover rate impedes access to the epithelial surface.

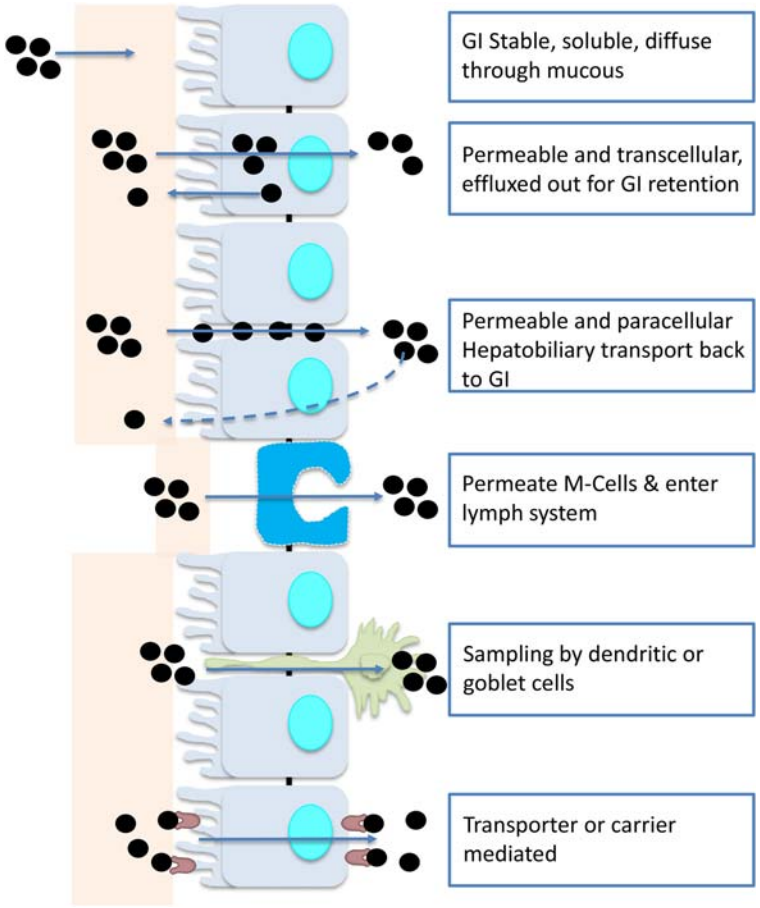

Fig. 3 Select examples of various mechanisms of permeating GI tissue with a focus on GI retention.

6.06.6.1 Permeability at the Epithelial Surface

Having reached the membrane, molecules may enter tissue via various pathways (Fig. 3), including the paracellular route (which involves diffusion between the aqueous pores at tight junctions between intestinal enterocytes), transcellular diffusion across the lipid cell membrane, and/or the involvement of membrane transporters. The paracellular route classically is thought to be used by small soluble compounds that can squeeze between adjoining cells. However, 14 synthetic peptides labeled with an amino acid fluorophore were found to cross the membrane using the paracellular route.[104] For transcellular absorption, compounds need to have the right physiochemical balance between solubility (to be exposed to and interact with the membrane) and hydrophobicity (to penetrate the membrane). The constrained peptide-like derivative cyclosporine is thought to permeate by transcellular mechanisms, specifically involving a conformational change, resulting in the formation of internal hydrogen bonds and exposure of a hydrophobic surface that facilitates membrane absorption and transcellular diffusion.[105] Cyclosporine, valinomycin, and gramicidin D[106] are known to be substrates for efflux transporters, such as *P*-glycoprotein, which decrease intracellular accumulation and ultimately transcellular diffusion across the intestinal epithelium.

6.06.6.2 Transporters on Intestinal Epithelial Cells

Various transporters have been identified on intestinal epithelial cells, including amino and oligopeptide transporters, bile transporters, vitamin transporters, carbohydrate transporters, monocarboxylic acid transporters, and phosphate transporters.[107] Covalent conjugation of carrier molecules to peptides has been used to exploit such transporters.[108] In some cases, such transporters are used to achieve retention or restriction to the GI tract. For example, with lumen or apical targets and permeable compounds, absorption followed by efflux can enhance GI retention and target exposure within the lumen.[109,110] For permeable compounds and targets in the GI tissue, the bile excretion pathway can be exploited due to the excretion of the drug from the liver back to the GI tract where it can be reabsorbed.[109,110]

Once compounds have penetrated the membrane surface, they may be exposed to another series of metabolic enzymes, such as CYP450. While human intestine comprises less P450 than the liver, these enzymes are strategically positioned (concentrated in the villus tips) to maximize exposure to intestinal contents.[111] Inflamed tissues exhibit increased mucosal metabolism and accumulate increased numbers of lymphocytes and neutrophils (which express P450s); therefore, such enzymes may significantly affect local drug delivery. For example, cyclosporine is orally bioavailable but is metabolized by P450s in intestinal membranes, an event that reduces cyclosporine's oral bioavailability.[112,113]

Patients with active CD have shown downregulation or redistribution of the tight junction-sealing proteins such as occludin, claudin-5, and claudin-8.[114] Genome-wide association studies of IBD patients have also revealed several susceptibility genes linked to barrier integrity.[115] The permeability of high-molecular-weight compounds is expected to be enhanced in diseased patients.[116] Indeed, PEG4000 is absorbed to higher levels in CD patients than in healthy patients.[117–119] Similarly, bacteria-derived antigens are known to leak across the gut wall in diseased patients, and systemic antibodies to these antigens are used as biomarkers indicative of more severe disease.[120] Asymptomatic first-degree relatives of CD patients[121–123] have increased intestinal permeability and are at greater risk of developing the disease.[124–126] Furthermore, increased intestinal permeability in patients in clinical remission predicts an elevated risk of early relapse.[118,127–131] The intestinal permeability of IBD patients is more broadly affected in GI tissues and is not restricted to areas of epithelial injury.[114] This enhanced permeability bodes well for the delivery of high-molecular-weight compounds to diseased mucosal tissues after oral administration. However, the bulk of clinical permeability studies have used various combinations of low-molecular-weight and soluble sugars; thus, while a substantial body of data supports a barrier defect in IBD, the impact of this defect on the absorption of high-molecular-weight compounds is not as well defined.

6.06.6.3 Absorption in the GI Tract

As peptides transit the GI tract, there will be regional differences in the thickness of mucus, pH, surface area, exposure time, membrane permeability, and dissolution capacity; all of these parameters will affect absorption. The total surface area of the small intestine has been reported as 2×10^6 cm^2, of which 200–2000 cm^2 (0.01–0.1%) comprise water-filled pores.[132] M cells, which comprise 1% (20,000 cm^2) of the intestinal surface, are more exposed and have a high transit capacity.[133] The colon has a much smaller surface area (30 cm^2), longer residence time, lower proteolytic barrier, and larger microbial metabolic hurdle; however, the nature of the large intestinal contents and the lack of fluid result in dissolution challenges. The lower parts of the GI tract (jejunum and ileum) have lower trans-epithelial electrical resistance and hence leakier paracellular tight junctions,[134,135] which are considered the major sites of drug absorption. It is also important to note that the colon and intestine are not uniform, with a magnetic resonance imaging study suggesting that the small intestine in the fasted state contained 319 mL of water as a series of 12-mL pockets, while in the fed state it harbored 156 mL total as a series of 4-mL pockets.[136] In the colon, the fluid volume is in the range of 1–44 mL, with an average pocket volume of 13 mL.[136] This characteristic could be leveraged to provide localized high-concentration pockets of drug candidates; the resulting concentration gradients might help to drive drug uptake, enabling the delivery from the lumen to the underlying lymphoid tissues.[137–139] Similarly, absorption through Peyer's patches has been explored as a potential route for uptake of orally administered protein and peptide drugs.[140,141] Goblet cells have been reported to sample and internalize relatively large-molecular-weight compounds (BSA and 10-kDa dextran) from the lumen and then transfer such molecules to dendritic cells.[142]

6.06.7 Impact of Food

Food is known to affect the GI environment by modulating gastric pH, changing GI viscosity, and altering the frequency of gastric emptying; food also serves as a matrix for drug adsorption. Food may have minimal effects on the absorption of soluble and permeable compounds, while having large effects on the absorption of insoluble and permeable compounds by virtue of increased GI secretions and biliary solubilization of compounds.[143] Food has been reported to have drastic effects on the oral bioavailability of calcitonin[144] and desmopressin,[66] with conflicting reports regarding the impact on cyclosporine absorption.[145,146]

6.06.8 Orally Delivered and Targeted Agents for Treatment of IBD

There are now several clinical and preclinical examples of orally delivered and targeted constrained peptides to treat IBD. Protagonist therapeutics has described PTG-100, a constrained peptide that is currently in Phase 1 clinical trials. PTG-100 binds to α4β7 and is effectively an oral equivalent of the marketed antibody Entyvio (vedolizumab). PTG-100 has been reported to be a potent and selective antagonist of α4β7, is orally stable, and GI restricted with little or no systemic bioavailability. Daily oral dosing has shown efficacy in DSS-treated mice, and high blood receptor occupancy in cynomologous monkeys.[147,148] Another constrained peptide developed by Protagonist is PTG-200 which is a potent and selective IL-23 receptor antagonist, orally stable with 40% of dose recovered in rat feces, and GI restricted, with minimal systemic exposure. The compound shows efficacy in a TNBS-induced colitis model in rats.[149] With respect to orally administered antibodies and biologics, several different strategies are emerging. PRX-106 is a nonabsorbable orally administered BT-2 plant cell that expresses etanercept and has shown efficacy in weight loss and improved bowel histology in mice.[150] This is in spite of etanercept being ineffective in treatment of CD.[151] Similarly, *L. lactis* has been engineered to express murine-TNF-neutralizing nanobodies; oral administration of the resulting bacterium reduced inflammation in DSS mice.[152] Avaxia recently described an orally administered, milk-derived, polyclonal anti-TNF antibody; in a Phase 1 study, this mixture showed efficacy trends when administered to moderate to severe UC patients at 3.5 g day^{-1}. Other orally delivered SM approaches that are in development include Janus kinase inhibitors (peficitinib, tofacitinib, filgotinib), an immunomodulatory drug (laquinimod), an α4 antagonist (AJM-300), agonists of sphingosine phosphate receptors (ozanimod, amiselimod, and APD334), and an antisense therapy (GED-0301) targeting SMAD7.

Over time, patients may develop neutralizing antibodies to the TNF antagonist drugs, resulting in rapid clearance and patients must be switched to other TNF antagonists.[153] Constrained peptides are expected to have lower immunogenicity[154,155] as they are protease-resistant, making it difficult to present linear epitopes to T-cells, have small size and less epitope density compared to other biologics, lack a hydrophobic core (a key requirement for T-cell recognition[156]), and are orally delivered with low systemic concentrations. Therefore, orally delivered constrained peptides have the potential to achieve longer term remission for patients when compared with systemic biologics.

6.06.9 Conclusion

IBD is characterized by localized inflammation of intestinal tissues and is ideally suited for therapeutic management using orally delivered agents that result in high drug concentrations at the target site of action along with minimal systemic concentrations. Systemically delivered biologics, specifically the anti-TNFs, have revolutionized the treatment of IBD, but surgery is still required in 70–80% of the treated patients.[157] Systemic immunosuppression, immunological side effects, and intolerance are associated with anti-TNF therapy. Compliance issues with anti-TNF antibodies in IBD treatment have been reported to occur in 25% of patients, but can reach as high as 60%.[158–160] Noncompliant patients have a greater need for hospitalization, which increases healthcare costs. Up to 80% of patients would prefer oral treatment alone.[161] Hence a targeted orally delivered therapy approach with equivalent efficacy and enhanced safety may benefit patients through longer remission and better compliance, which would have significant impact on patient quality of life and healthcare costs.

Constrained peptides provide a unique chemical modality for the oral treatment of IBD. They have a proven capacity to modulate the large, flat, discontinuous surfaces that are characteristic of the clinically validated cytokine-based targets in IBD, in combination with favorable chemical and biological stability.[30] These properties are augmented by the clinical features of IBD itself, primarily the reduced integrity of tight junctions, the impact on the intestinal barrier, and the localized nature of the disease. However, orally delivered peptides must be sufficiently stable to transit the GI tract, exhibit maximum solubility for rapid dissolution, and have the required size and physicochemistry to transit the mucus and glycocalyx layers to reach the epithelial surface. Once there, these peptides must possess the required physicochemical and conformational properties to either squeeze through paracellular junctions or to interact with and ultimately permeate the membrane without being effluxed or metabolized. Alternatively, interaction with a transporter or carrier can facilitate membrane crossing to provide access to the appropriate target site, at a suitable concentration, and duration of time to achieve a pharmacological effect.

Despite all these challenges, there is accumulating preclinical evidence that constrained peptides have the required physiochemical characteristics to transit the entire GI tract and provide the concentrations of free drug at the target site of action that exceed pharmacological potency over the desired time frame. There are numerous in vitro, ex vivo, and in vivo systems that can be used to profile candidates for the stability and permeability features needed to render agents orally active. However, the intestinal

physiology (e.g., proteolytic enzymes, bile salts, motility, pH profile, and permeability) can differ between animal models and human systems. These distinctions are exemplified by the differing proteolytic stabilities of trefoil peptides in rat and human intestinal fluids,[38] or the differing permeation of Dextran 4000 in various species.[162] Animal models of disease have played a key role in understanding inflammatory processes that affect disease, but CD and UC are highly heterogenous diseases, and the translational record of such animal models has been questioned.[163,164] Such species differences have been and will continue to be challenging in the preclinical evaluation and optimization of orally delivered candidates and translation to clinical settings.

Pursuing a GI-restricted strategy provides an effective means of achieving high local concentrations of drug at the desired site of action while minimizing concentrations in other regions that could lead to unwanted side effects by minimizing off-target effects or on-target effects in healthy tissue. Targeted agents currently include injectable antibodies that modulate macromolecular cytokine or integrin targets. Constrained peptides would appear to be ideal for blocking such targets, as they are capable of binding and blocking large macromolecular proteins with the potential of being orally stable and orally delivered. There are orally delivered and marketed peptide-based drug and several clinical and preclinical examples for treating GI diseases. Such a GI-targeting strategy using constrained peptides would also have broader therapeutic applications due to the increasing realization that the gut and associated microbiota may play a role in many diseases, including systemic diseases, due to its endocrine role and communication with CNS in addition to absorbing nutrients and minerals. With respect to IBD, dampening the immune response locally in the GI tract may lead to localized safety consequences, for example increased GI infection, which would need to be monitored. With several preclinical and early clinical examples of orally delivered and targeted constrained peptides in development for treatment of IBD, the next few years will be pivotal in the evaluation of such a GI strategy to provide a safe and convenient treatment paradigm for patients.

Acknowledgments

I would like to acknowledge the many colleagues, collaborators, and investors of Protagonist who have helped to contribute to the concepts outlined in this article.

See also: 2.03. Multiobjective Optimization of Biological and Physical Properties in Drug Discovery.

References

1. Kappelman, M. D.; Rifas-Shiman, S. L.; Porter, C. Q.; Ollendorf, D. A.; Sandler, R. S.; Galanko, J. A.; Finkelstein, J. A. Direct Health Care Costs of Crohn's Disease and Ulcerative Colitis in US Children and Adults. *Gastroenterology* **2008,** *135,* 1907.
2. Peng Yu, A.; Cabanilla, L.; Qiong Wu, E.; Mulani, P.; Chao, J. The Costs of Crohn's Disease in the United States and Other Western Countries: A Systematic Review. *Curr. Med. Res. Opin.* **2008,** *24,* 319.
3. Loftus, E., Jr.; Schoenfeld, P.; Sandborn, W. The Epidemiology and Natural History of Crohn's Disease in Population-Based Patient Cohorts from North America: A Systematic Review. *Aliment. Pharmacol. Ther.* **2002,** *16,* 51.
4. Loftus, E., Jr. Clinical Epidemiology of Inflammatory Bowel Disease: Incidence, Prevalence, and Environmental Influences. *Gastroenterology* **2004,** *126,* 1504.
5. Sartor, R. B. Mechanisms of Disease: Pathogenesis of Crohn's Disease and Ulcerative Colitis. *Nat. Clin. Pract. Gastroenterol. Hepatol.* **2006,** *3,* 390.
6. Antoni, L.; Nuding, S.; Wehkamp, J.; Stange, E. F. Intestinal Barrier in Inflammatory Bowel Disease. *World J. Gastroenterol.* **2014,** *20,* 1165.
7. Kuhbacher, T.; Folsch, U. R. Practical Guidelines for the Treatment of Inflammatory Bowel Disease. *World J. Gastroenterol.* **2007,** *13,* 1149.
8. Sathish, J. G.; Sethu, S.; Bielsky, M. C.; de Haan, L.; French, N. S.; Govindappa, K.; Green, J.; Griffiths, C. E.; Holgate, S.; Jones, D.; Kimber, I.; Moggs, J.; Naisbitt, D. J.; Pirmohamed, M.; Reichmann, G.; Sims, J.; Subramanyam, M.; Todd, M. D.; Van Der Laan, J. W.; Weaver, R. J.; Park, B. K. Challenges and Approaches for the Development of Safer Immunomodulatory Biologics. *Nat. Rev. Drug Discov.* **2013,** *12,* 306.
9. Scheinfeld, N. A. Comprehensive Review and Evaluation of the Side Effects of the Tumor Necrosis Factor Alpha Blockers Etanercept, Infliximab and Adalimumab. *J. Dermatolog. Treat.* **2004,** *15,* 280.
10. Gisbert, J.; Panes, J. Loss of Response and Requirement of Infliximab Dose Intensification in Crohn's Disease: A Review. *Am. J. Gastroentrol.* **2009,** *104,* 760.
11. de Silva, P. S.; Nguyen, D. D.; Sauk, J.; Korzenik, J.; Yajnik, V.; Ananthakrishnan, A. N. Long-Term Outcome of a Third Anti-TNF Monoclonal Antibody After the Failure of Two Prior Anti-TNFs in Inflammatory Bowel Disease. *Aliment. Pharmacol. Ther.* **2012,** *36,* 459.
12. Levine, J. S.; Burakoff, R. Extraintestinal Manifestations of Inflammatory Bowel Disease. *Gastroenterol. Hepatol.* **2011,** *7,* 235.
13. Card, T. R.; Langan, S. M.; Chu, T. P. Extra-Gastrointestinal Manifestations of Inflammatory Bowel Disease May Be Less Common Than Previously Reported. *Dig. Dis. Sci.* **2016;** http://dx.doi.org/10.1007/s10620-016-4195-1. PMID: 27193564.
14. Liu, Z.; Yadav, P. K.; Xu, X.; Su, J.; Chen, C.; Tang, M.; Lin, H.; Yu, J.; Qian, J.; Yang, P. C.; Wang, X. The Increased Expression of IL-23 in Inflammatory Bowel Disease Promotes Intraepithelial and Lamina Propria Lymphocyte Inflammatory Responses and Cytotoxicity. *J. Leukoc. Biol.* **2011,** *89,* 597.
15. Sartor, R. B. Cytokines in Intestinal Inflammation: Pathophysiological and Clinical Considerations. *Gastroenterology* **1994,** *106,* 533.
16. Fiocchi, C. Inflammatory Bowel Disease: Etiology and Pathogenesis. *Gastroenterology* **1998,** *115,* 182.
17. Papadakis, K. A.; Targan, S. R. Role of Cytokines in the Pathogenesis of Inflammatory Bowel Disease. *Annu. Rev. Med.* **2000,** *51,* 289.
18. Braegger, C. P.; Nicholls, S.; Murch, S. H.; Stephens, S.; MacDonald, T. T. Tumour Necrosis Factor Alpha in Stool as a Marker of Intestinal Inflammation. *Lancet* **1992,** *339,* 89.
19. Bamias, G.; Dahman, M. I.; Arseneau, K. O.; Guanzon, M.; Gruska, D.; Pizarro, T. T.; Cominelli, F. Intestinal-Specific TNFalpha Overexpression Induces Crohn's-Like Ileitis in Mice. *PLoS One* **2013,** *8,* e72594.
20. Yarur, A. J.; Jain, A.; Sussman, D. A.; Quintero, M. A.; Princen, F.; Kirkland, R.; Deshpande, A. R.; Singh, S.; Abreu, M. T. The Association of Tissue Anti-TNF Drug Levels With Serological and Endoscopic Disease Activity in Inflammatory Bowel Disease: The ATLAS Study. *Gut* **2016,** *65,* 249.
21. Poggioli, G.; Laureti, S.; Pierangeli, F.; Rizzello, F.; Ugolini, F.; Gionchetti, P.; Campieri, M. Local Injection of Infliximab for the Treatment of Perianal Crohn's Disease. *Dis. Colon Rectum* **2005,** *48,* 768.

22. Poggioli, G.; Laureti, S.; Pierangeli, F.; Bazzi, P.; Coscia, M.; Gentilini, L.; Gionchetti, P.; Rizzello, F. Local Injection of Adalimumab for Perianal Crohn's Disease: Better Than Infliximab? *Inflamm. Bowel Dis.* **2010,** *16,* 1631.
23. Molnar, T.; Farkas, K.; Nagy, F.; Nemeth, I.; Wittmann, T. Topically Administered Infliximab Can Work in Ulcerative Proctitis Despite the Ineffectiveness of Intravenous Induction Therapy. *Am. J. Gastroenterol.* **2009,** *104,* 1857.
24. Worledge, K. L.; Godiska, R.; Barrett, T. A.; Kink, J. A. Oral Administration of Avian Tumor Necrosis Factor Antibodies Effectively Treats Experimental Colitis in Rats. *Dig. Dis. Sci.* **2000,** *45,* 2298.
25. Bhol, K. C.; Tracey, D. E.; Lemos, B. R.; Lyng, G. D.; Erlich, E. C.; Keane, D. M.; Quesenberry, M. S.; Holdorf, A. D.; Schlehuber, L. D.; Clark, S. A.; Fox, B. S. AVX-470: A Novel Oral Anti-TNF Antibody With Therapeutic Potential in Inflammatory Bowel Disease. *Inflamm. Bowel Dis.* **2013,** *19,* 2273.
26. Frieri, G.; Giacomelli, R.; Pimpo, M.; Palumbo, G.; Passacantando, A.; Pantaleoni, G.; Caprilli, R. Mucosal 5-Aminosalicylic Acid Concentration Inversely Correlates With Severity of Colonic Inflammation in Patients With Ulcerative Colitis. *Gut* **2000,** *47,* 410.
27. Rhodes, J. M.; Robinson, R.; Beales, I.; Pugh, S.; Dickinson, R.; Dronfield, M.; Speirs, C. J.; Wilkinson, P.; Wilkinson, S. P. Clinical Trial: Oral Prednisolone Metasulfobenzoate (Predocol) vs. Oral Prednisolone for Active Ulcerative Colitis. *Aliment. Pharmacol. Ther.* **2008,** *27,* 228.
28. Frei, P.; Biedermann, L.; Manser, C. N.; Wilk, M.; Manz, M.; Vavricka, S. R.; Rogler, G. Topical Therapies in Inflammatory Bowel Disease. *Digestion* **2012,** *86* (Suppl. 1), 36.
29. Hartig, G. R. S.; Tran, T. T.; Smythe, M. L. Intramolecular Disulphide Bond Arrangements in Nonhomologous Proteins. *Protein Sci.* **2005,** *14,* 474.
30. Ranganath, S.; Bhandari, A.; Avitahl-Curtis, N.; McMahon, J.; Wachtel, D.; Zhang, J.; Leitheiser, C.; Bernier, S. G.; Liu, G.; Tran, T. T.; Celino, H.; Tobin, J.; Jung, J.; Zhao, H.; Glen, K. E.; Graul, C.; Griffin, A.; Schairer, W. C.; Higgins, C.; Reza, T. L.; Mowe, E.; Rivers, S.; Scott, S.; Monreal, A.; Shea, C.; Bourne, G.; Coons, C.; Smith, A.; Tang, K.; Mandyam, R. A.; Masferrer, J.; Liu, D.; Patel, D. V.; Fretzen, A.; Murphy, C. A.; Milne, G. T.; Smythe, M. L.; Carlson, K. E. Discovery and Characterization of a Potent Interleukin-6 Binding Peptide With Neutralizing Activity In Vivo. *PLoS One* **2015,** *10,* e0141330.
31. Smythe, M. L.; Dooley, M. J.; Andrews, P. R. The University of Queensland, Protein Engineering. WO 00/23474. 2000 Apr 27.
32. Barkan, D. T., Cheng, X. L., Celino, H., Tran, T. T., Bhandari, A., Craik, C. S., Sali, A., Smythe, M. L., Clustering of disulfide-rich peptides provides scaffolds for hit discovery by phage display: application to interleukin-23 (submitted for publication).
33. Moore, S. J.; Cochran, J. R. Engineering Knottins as Novel Binding Agents. *Methods Enzymol.* **2012,** *503,* 223.
34. Kolmar, H. Biological Diversity and Therapeutic Potential of Natural and Engineered Cystine Knot Microproteins. *Curr. Opin. Pharmacol.* **2009,** *9,* 1.
35. Silverman, J.; Lu, Q.; Bakker, A.; To, W.; Duguay, A.; Alba, B. M.; Smith, R.; Rivas, A.; Li, P.; Le, H.; Whitehorn, E.; Moore, K. W.; Swimmer, C.; Perlroth, V.; Vogt, M.; Kolkman, J.; Stemmer, W. P. C. Multivalent Avimer Proteins Evolved by Exon Shuffling of a Family of Human Receptor Domains. *Nat. Biotechnol.* **2005,** *23,* 1556.
36. Cunliffe, R. N. α-Defensins in the Gastrointestinal Tract. *Mol. Immunol.* **2003,** *40,* 463.
37. O'Neil, D.; Porter, M.; Elewaut, D.; Anderson, G.; Eckmann, L.; Ganz, T.; Kagnoff, M. Expression and Regulation of the Human β-Defensins hBD-1 and hBD-2 in Intestinal Epithelium. *J. Immunol.* **1999,** *163,* 6718.
38. Kjellev, S.; Vestergaard, E. M.; Nexø, E.; Thygesen, P.; Eghøj, M. S.; Jeppesen, P. B.; Thim, L.; Pedersen, N. B.; Poulsen, S. S. Pharmacokinetics of Trefoil Peptides and Their Stability in Gastrointestinal Contents. *Peptides* **2007,** *28,* 1197.
39. Blanchfield, J. T.; Dutton, J. L.; Hogg, R. C.; Gallagher, O. P.; Craik, D. J.; Jones, A.; Adams, D. J.; Lewis, R. J.; Alewood, P. F.; Toth, I. Synthesis, Structural Elucidation, In Vitro Biological Activity, Toxicity, and Caco-2 Cell Permability of Lipophilic Analogues of α-Conotoxin MII. *J. Med. Chem.* **2003,** *46,* 1266.
40. Werle, M.; Kafedjiiski, K.; Kolmar, H.; Bernkop-Schnurch, A. Evaluation and Improvement of the Properties of the Novel Cystine-Knot Microprotein McoEeTI for Oral Administration. *Int. J. Pharm.* **2007,** *332,* 72.
41. Werle, M.; Schmitz, T.; Huang, H.-L.; Wentzel, A.; Kolmar, H.; Bernkop-Schnurch, A. The Potential of Cystine-Knot Microproteins as Novel Pharmacophoric Scaffolds in Oral Peptide Drug Delivery. *J. Drug Target.* **2006,** *14,* 137.
42. Babyatsky, M. W.; deBeaumont, M.; Thim, L.; Podolsky, D. K. Oral Trefoil Peptides Protect Against Ethanol- and Indomethacin-Induced Gastric Injury in Rats. *Gastroenterology* **1996,** *110,* 489.
43. Sun, Y.; Wu, W.; Zhang, Y.; Lv, S.; Wang, L.; Wang, S.; Peng, X. Stability Analysis of Recombinant Human TFF2 and Its Therapeutic Effect on Burn-Induced Gastric Injury in Mice. *Burns* **2009,** *35,* 869.
44. Cook, G. A.; Thim, L.; Yeomans, N. D.; Giraud, A. S. Oral Human Spasmolytic Polypeptide Protects Against Aspirin-Induced Gastric Injury in Rats. *J. Gastroenterol. Hepatol.* **1998,** *13,* 363.
45. Li, J.; Zhou, R.; He, W. C.; Xia, B. Effects of Recombinant Human Intestinal Trefoil Factor on Trinitrobenzene Sulphonic Acid Induced Colitis in Rats. *Mol. Biol. Rep.* **2011,** *38,* 4787.
46. Poulsen, S. S.; Kissow, H.; Hare, K.; Hartmann, B.; Thim, L. Luminal and Parenteral TFF2 and TFF3 Dimer and Monomer in Two Models of Experimental Colitis in the Rat. *Regul. Pept.* **2005,** *126,* 163.
47. Carrasco, R.; Pera, M.; May, F. E. B.; Westley, B. R.; Martinez, A.; Morales, L. Trefoil Factor Family Peptide 3 Prevents the Development and Promotes Healing of Ischemia-Reperfusion Injury in Weanling Rats. *J. Pediatr. Surg.* **2004,** *39,* 1693.
48. Colgrave, M. L.; Jones, A.; Craik, D. J. Peptide Quantification by Matrix-Assisted Laser Desorption Ionisation Time-of-Flight Mass Spectrometry: Investigations of the Cyclotide Kalata B1 in Biological Fluids. *J. Chromatogr. A* **2005,** *1091,* 187.
49. Wong, C. T.; Rowlands, D. K.; Wong, C. H.; Lo, T. W.; Nguyen, G. K.; Li, H. Y.; Tam, J. P. Orally Active Peptidic Bradykinin B1 Receptor Antagonists Engineered From a Cyclotide Scaffold for Inflammatory Pain Treatment. *Angew. Chem.* **2012,** *51,* 5620.
50. Clark, R. J.; Jensen, J.; Nevin, S. T.; Callaghan, B. P.; Adams, D. J.; Craik, D. J. The Engineering of an Orally Active Conotoxin for the Treatment of Neuropathic Pain. *Angew. Chem. Int. Ed. Engl.* **2010,** *49,* 6545.
51. de Araujo, A. D.; Mobli, M.; Castro, J.; Harrington, A. M.; Vetter, I.; Dekan, Z.; Muttenthaler, M.; Wan, J.; Lewis, R. J.; King, G. F.; Brierley, S. M.; Alewood, P. F. Selenoether Oxytocin Analogues Have Analgesic Properties in a Mouse Model of Chronic Abdominal Pain. *Nat. Commun.* **2014,** *5,* 3165.
52. Northfield, S. E.; Wang, C. K.; Schroeder, C. I.; Durek, T.; Kan, M. W.; Swedberg, J. E.; Craik, D. J. Disulfide-Rich Macrocyclic Peptides as Templates in Drug Design. *Eur. J. Med. Chem.* **2014,** *77,* 248.
53. Busby, R. W.; Kessler, M. M.; Bartolini, W. P.; Bryant, A. P.; Hannig, G.; Higgins, C. S.; Solinga, R. M.; Tobin, J. V.; Wakefield, J. D.; Kurtz, C. B.; Currie, M. G. Pharmacologic Properties, Metabolism, and Disposition of Linaclotide, a Novel Therapeutic Peptide Approved for the Treatment of Irritable Bowel Syndrome With Constipation and Chronic Idiopathic Constipation. *J. Pharmacol. Exp. Ther.* **2013,** *344,* 196.
54. Shailubhai, K.; Synergy Pharmaceuticals, I., Ed.; 2015. WO/2015/054500 2015. Apr 16.
55. Lundin, S.; Bengtsson, H. I.; Folkesson, H. G.; Westrom, B. R. Degradation of [Mercaptopropionic acid1, D-arginine8]-Vasopressin (dDAVP) in Pancreatic Juice and Intestinal Mucosa Homogenate. *Pharmacol. Toxicol.* **1989,** *65,* 92.
56. Caluwaerts, S.; Vandenbroucke, K.; Steidler, L.; Neirynck, S.; Vanhoenacker, P.; Corveleyn, S.; Watkins, B.; Sonis, S.; Coulie, B.; Rottiers, P. AG013, a Mouth Rinse Formulation of *Lactococcus lactis* Secreting Human Trefoil Factor 1, Provides a Safe and Efficacious Therapeutic Tool for Treating Oral Mucositis. *Oral Oncol.* **2010,** *46,* 564.
57. Peterson, D. E.; Barker, N. P.; Akhmadullina, L. I.; Rodionova, I.; Sherman, N. Z.; Davidenko, I. S.; Rakovskaya, G. N.; Gotovkin, E. A.; Shinkarev, S. A.; Kopp, M. V.; Kulikov, E. P.; Moiseyenko, V. M.; Gertner, J. M.; Firsov, I.; Tuleneva, T.; Yarosh, A.; Woon, C.-W. Phase II, Randomized, Double-Blind, Placebo-Controlled Study of Recombinant Human Intestinal Trefoil Factor Oral Spray for Prevention of Oral Mucositis in Patients With Colorectal Cancer Who Are Receiving Fluorouracil-Based Chemotherapy. *J. Clin. Oncol.* **2009,** *27,* 4333.
58. Aguirre, T. A.; Teijeiro-Osorio, D.; Rosa, M.; Coulter, I. S.; Alonso, M. J.; Brayden, D. J. Current Status of Selected Oral Peptide Technologies in Advanced Preclinical Development and in Clinical Trials. *Adv. Drug Deliv. Rev.* **2016**. in press.

59. Nugent, S. G.; Kumar, D.; Rampton, D. S.; Evans, D. F. Intestinal Luminal pH in Inflammatory Bowel Disease: Possible Determinants and Implications for Therapy With Aminosalicylates and Other Drugs. *Gut* **2001,** *48,* 571.
60. McConnell, E. L.; Fadda, H. M.; Basit, A. W. Gut Instincts: Explorations in Intestinal Physiology and Drug Delivery. *Int. J. Pharm.* **2008,** *364,* 213.
61. John, V. A.; Shotton, P. A.; Moppert, J.; Theobald, W. Gastrointestinal Transit of Oros Drug Delivery Systems in Healthy Volunteers: A Short Report. *Br. J. Clin. Pharmacol.* **1985,** *19* (Suppl. 2), 203S.
62. Coupe, A. J.; Davis, S. S.; Wilding, I. R. Variation in Gastrointestinal Transit of Pharmaceutical Dosage Forms in Healthy Subjects. *Pharm. Res.* **1991,** *8,* 360.
63. Vassallo, M.; Camilleri, M.; Phillip, S. F.; Brown, M. L.; Chapman, N. J.; Thomforde, G. M. Transit Through the Proximal Colon Influences Stool Weight in the Irritable Bowel Syndrome. *Gastroenterology* **1992,** *102,* 102.
64. De Schepper, H. U.; De Man, J. G.; Moreels, T. G.; Pelckmans, P. A.; De Winter, B. Y. Review Article: Gastrointestinal Sensory and Motor Disturbances in Inflammatory Bowel Disease—Clinical Relevance and Pathophysiological Mechanisms. *Aliment. Pharmacol. Ther.* **2008,** *27,* 621.
65. Hebden, J. M.; Blackshaw, P. E.; Perkins, A. C.; Wilson, C. G.; Spiller, R. C. Limited Exposure of the Healthy Distal Colon to Orally-Dosed Formulation is Further Exaggerated in Active Left-Sided Ulcerative Colitis. *Aliment. Pharmacol. Ther.* **2000,** *14,* 155.
66. Callreus, T.; Lundahl, J.; Hoglund, P.; Bengtsson, P. Changes in Gastrointestinal Motility Influence the Absorption of Desmopressin. *Eur. J. Clin. Pharmacol.* **1999,** *55,* 305.
67. Antalis, T. M.; Shea-Donohue, T.; Vogel, S. N.; Sears, C.; Fasano, A. Mechanisms of Disease: Protease Functions in Intestinal Mucosal Pathobiology. *Nat. Clin. Pract. Gastroenterol. Hepatol.* **2007,** *4,* 393.
68. Woodley, J. F. Enzymatic Barriers for GI Peptide and Protein Delivery. *Crit. Rev. Ther. Drug Carrier Syst.* **1994,** *11,* 61.
69. Vlieghe, P.; Lisowski, V.; Martinez, J.; Khrestchatisky, M. Synthetic Therapeutic Peptides: Science and Market. *Drug Discov. Today* **2010,** *15,* 40.
70. Bernkop-Schnurch, A. The Use of Inhibitory Agents to Overcome the Enzymatic Barrier to Perorally Administered Therapeutic Peptides and Proteins. *J. Control. Release* **1998,** *52,* 1.
71. Ikesue, K.; Kopeckova, P.; Kopecek, J. Degradation of Proteins by Guinea Pig Intestinal Enzymes. *Int. J. Pharm.* **1993,** *95,* 171.
72. Roka, R.; Demaude, J.; Cenac, N.; Ferrier, L.; Salvador-Cartier, C.; Garcia-Villar, R.; Fioramonti, J.; Bueno, L. Colonic Luminal Proteases Activate Colonocyte Proteinase-Activated Receptor-2 and Regulate Paracellular Permeability in Mice. *Neurogastroenterol. Motil.* **2007,** *19,* 57.
73. Baugh, M. D.; Perry, M. J.; Hollander, A. P.; Davies, D. R.; Cross, S. S.; Lobo, A. J.; Taylor, C. J.; Evans, G. S. Matrix Metalloproteinase Levels Are Elevated in Inflammatory Bowel Disease. *Gastroenterology* **1999,** *117,* 814.
74. Pedersen, G.; Saermark, T.; Kirkegaard, T.; Brynskov, J. Spontaneous and Cytokine Induced Expression and Activity of Matrix Metalloproteinases in Human Colonic Epithelium. *Clin. Exp. Immunol.* **2009,** *155,* 257.
75. Carroll, I. M.; Maharshak, N. Enteric Bacterial Proteases in Inflammatory Bowel Disease-Pathophysiology and Clinical Implications. *World J. Gastroenterol.* **2013,** *19,* 7531.
76. Bustos, D.; Negri, G.; De Paula, J. A.; Di Carlo, M.; Yapur, V.; Facente, A.; De Paula, A. Colonic Proteinases: Increased Activity in Patients With Ulcerative Colitis. *Medicina* **1998,** *58,* 262.
77. Ruseler-van Embden, J. G.; van Lieshout, L. M. Increased Proteolysis and Leucine Aminopeptidase Activity in Faeces of Patients With Crohn's Disease. *Digestion* **1988,** *40,* 33.
78. Steck, N.; Mueller, K.; Schemann, M.; Haller, D. Republished: Bacterial Proteases in IBD and IBS. *Postgrad. Med. J.* **2013,** *89,* 25.
79. Maroni, A.; Zema, L.; Del Curto, M. D.; Foppoli, A.; Gazzaniga, A. Oral Colon Delivery of Insulin With the Aid of Functional Adjuvants. *Adv. Drug Deliv. Rev.* **2012,** *64,* 540.
80. Macfarlane, G. T.; Allison, C.; Gibson, S. A.; Cummings, J. H. Contribution of the Microflora to Proteolysis in the Human Large Intestine. *J. Appl. Bacteriol.* **1988,** *64,* 37.
81. Gibson, S. A.; McFarlan, C.; Hay, S.; MacFarlane, G. T. Significance of Microflora in Proteolysis in the Colon. *Appl. Environ. Microbiol.* **1989,** *55,* 679.
82. Macfarlane, G. T.; Cummings, J. H.; Allison, C. Protein Degradation by Human Intestinal Bacteria. *J. Gen. Microbiol.* **1986,** *132,* 1647.
83. Nyangale, E. P.; Mottram, D. S.; Gibson, G. R. Gut Microbial Activity, Implications for Health and Disease: The Potential Role of Metabolite Analysis. *J. Proteome Res.* **2012,** *11,* 5573.
84. Madala, P. K.; Tyndall, J. D.; Nall, T.; Fairlie, D. P. Update 1 of: Proteases Universally Recognize Beta Strands in Their Active Sites. *Chem. Rev.* **2010,** *110,* PR1.
85. Go, Y. M.; Jones, D. P. The Redox Proteome. *J. Biol. Chem.* **2013,** *288,* 26512.
86. Circu, M. L.; Aw, T. Y. Intestinal Redox Biology and Oxidative Stress. *Semin. Cell Dev. Biol.* **2012,** *23,* 729.
87. Circu, M. L.; Aw, T. Y. Redox Biology of the Intestine. *Free Radic. Res.* **2011,** *45,* 1245.
88. Gilbert, H. F. Thiol/Disulfide Exchange Equilibria and Disulfide Bond Stability. *Methods Enzymol.* **1995,** *251,* 8.
89. Kortemme, T.; Darby, N. J.; Creighton, T. E. Electrostatic Interactions in the Active Site of the N-Terminal Thioredoxin-Like Domain of Protein Disulfide Isomerase. *Biochemistry* **1996,** *35,* 14503.
90. Snyder, G. H.; Cennerazzo, M. J.; Karalis, A. J.; Field, D. Electrostatic Influence of Local Cysteine Environments on Disulfide Exchange Kinetics. *Biochemistry* **1981,** *20,* 6509.
91. Huck, C.; Pezzei, V.; Schmitz, T.; Bonn, G.; Bernkop-Schnurch, A. Oral Peptide Delivery: Are There Remarkable Effects on Drugs Through Sulfhydryl Conjugation? *J. Drug Target.* **2006,** *14,* 117.
92. Lappi, A. K.; Lensink, M. F.; Alanen, H. I.; Salo, K. E.; Lobell, M.; Juffer, A. H.; Ruddock, L. W. A Conserved Arginine Plays a Role in the Catalytic Cycle of the Protein Disulphide Isomerases. *J. Mol. Biol.* **2004,** *335,* 283.
93. Biasi, F.; Leonarduzzi, G.; Oteiza, P. I.; Poli, G. Inflammatory Bowel Disease: Mechanisms, Redox Considerations, and Therapeutic Targets. *Antioxid. Redox Signal.* **2013,** *19,* 1711–1747.
94. Kowalczyk, R.; Harris, P. W.; Brimble, M. A.; Callon, K. E.; Watson, M.; Cornish, J. Synthesis and Evaluation of Disulfide Bond Mimetics of Amylin-(1–8) as Agents to Treat Osteoporosis. *Bioorg. Med. Chem.* **2012,** *20,* 2661.
95. Blaut, M.; Clavel, T. Metabolic Diversity of the Intestinal Microbiota: Implications for Health and Disease. *J. Nutr.* **2007,** *137,* 751S.
96. Scheline, R. R. Metabolism of Foreign Compounds by Gastrointestinal Microorganisms. *Pharmacol. Rev.* **1973,** *25,* 451.
97. Sousa, T.; Paterson, R.; Moore, V.; Carlsson, A.; Abrahamsson, B.; Basit, A. W. The Gastrointestinal Microbiota as a Site for the Biotransformation of Drugs. *Int. J. Pharm.* **2008,** *363,* 1.
98. Johansson, M. E.; Sjovall, H.; Hansson, G. C. The Gastrointestinal Mucus System in Health and Disease. *Nat. Rev. Gastroenterol. Hepatol.* **2013,** *10,* 352.
99. Lehr, C. M.; Poelma, F. G. J.; Junginger, H. E.; Tukker, J. J. An Estimate of Turnover Time of Intestinal Mucus Gel Layer in the Rat In Situ Loop. *Int. J. Pharm.* **1991,** *70,* 235.
100. Pullan, R. D.; Thomas, G. A.; Rhodes, M.; Newcombe, R. G.; Williams, G. T.; Allen, A.; Rhodes, J. Thickness of Adherent Mucus Gel on Colonic Mucosa in Humans and Its Relevance to Colitis. *Gut* **1994,** *35,* 353.
101. Rankin, B. J.; Srivastava, E. D.; Record, C. O.; Pearson, J. P.; Allen, A. Patients With Ulcerative Colitis Have Reduced Mucin Polymer Content in the Adherent Colonic Mucus gel. *Biochem. Soc. Trans.* **1995,** *23,* 104S.
102. Corfield, A. P.; Carroll, D.; Myerscough, N.; Probert, C. S. Mucins in the Gastrointestinal Tract in Health and Disease. *Front. Biosci.* **2001,** *6,* D1321.
103. Lai, S. K.; Wang, Y. Y.; Hanes, J. Mucus-Penetrating Nanoparticles for Drug and Gene Delivery to Mucosal Tissues. *Adv. Drug Deliv. Rev.* **2009,** *61,* 158.
104. Dodoo, A. N.; Bansal, S.; Barlow, D. J.; Bennet, F. C.; Hider, R. C.; Lansley, A. B.; Lawrence, M. J.; Marriott, C. Systematic Investigations of the Influence of Molecular Structure on the Transport of Peptides Across Cultured Alveolar Cell Monolayers. *Pharm. Res.* **2000,** *17,* 7.
105. Alex, A.; Millan, D. S.; Perez, M.; Wakenhut, F.; Whitlock, G. A. Intramolecular Hydrogen Bonding to Improve Membrane Permeability and Absorption in Beyond Rule of Five Chemical Space. *Med. Chem. Commun.* **2011,** *2,* 669.
106. Eytan, G. D.; Borgnia, M. J.; Regev, R.; Assaraf, Y. G. Transport of Polypeptide Ionophores into Proteoliposomes Reconstituted With Rat Liver P-Glycoprotein. *J. Biol. Chem.* **1994,** *269,* 26058.

107. Li, X. Y.; Yu, M. R.; Fan, W. W.; Gan, Y.; Hovgaard, L.; Yang, M. S. Orally Active-Targeted Drug Delivery Systems for Proteins and Peptides. *Expert Opin. Drug Deliv.* **2014,** *11,* 1435.
108. Al-Hilal, T. A.; Alam, F.; Byun, Y. Oral Drug Delivery Systems Using Chemical Conjugates or Physical Complexes. *Adv. Drug Deliv. Rev.* **2013,** *65,* 845.
109. Fyfe, M. C. Non-Systemic Intestine-Targeted Drugs. *Prog. Med. Chem.* **2016,** *55,* 1.
110. Filipski, K. J.; Varma, M. V.; El-Kattan, A. F.; Ambler, C. M.; Ruggeri, R. B.; Goosen, T. C.; Cameron, K. O. Intestinal Targeting of Drugs: Rational Design Approaches and Challenges. *Curr. Top. Med. Chem.* **2013,** *13,* 776.
111. Kaminsky, L. S.; Fasco, M. J. Small Intestinal Cytochromes P450. *Crit. Rev. Toxicol.* **1991,** *21,* 407.
112. Fahr, A. Cyclosporin Clinical Pharmacokinetics. *Clin. Pharmacokinet.* **1993,** *24,* 472.
113. Tjia, J. F.; Webber, I. R.; Back, D. J. Cyclosporin Metabolism by the Gastrointestinal Mucosa. *Br. J. Clin. Pharmacol.* **1991,** *31,* 344.
114. Teshima, C. W.; Dieleman, L. A.; Meddings, J. B. Abnormal Intestinal Permeability in Crohn's Disease Pathogenesis. *Ann. N. Y. Acad. Sci.* **2012,** *1258,* 159.
115. Fries, W.; Belvedere, A.; Vetrano, S. Sealing the Broken Barrier in IBD: Intestinal Permeability, Epithelial Cells and Junctions. *Curr. Drug Targets* **2013,** *14,* 1460.
116. Hollander, D.; Vadheim, C. M.; Brettholz, E.; Petersen, G. M.; Delahunty, T.; Rotter, J. I. Increased Intestinal Permeability in Patients With Crohn's Disease and Their Relatives. A Possible Etiologic Factor. *Ann. Intern. Med.* **1986,** *105,* 883.
117. Koch, S.; Nusrat, A.; Parkos, C. A.; D'Amato, M.; Rioux, J. D. In *Molecular Genetics of Inflammatory Bowel Disease;* Springer Science + Business Media: New York, NY, 2013; p 265.
118. Kiesslich, R.; Duckworth, C. A.; Moussata, D.; Gloeckner, A.; Lim, L. G.; Goetz, M.; Pritchard, D. M.; Galle, P. R.; Neurath, M. F.; Watson, A. J. Local Barrier Dysfunction Identified by Confocal Laser Endomicroscopy Predicts Relapse in Inflammatory Bowel Disease. *Gut* **2012,** *61,* 1146.
119. Parlesak, A.; Bode, J.; Bode, C. Parallel Determination of Gut Permeability in Man With *M*, 400, *M*, 1500, *M*, 4000 and *M*, 10000 Polyethylene Glycol. *Eur. J. Clin. Chem. Clin. Biochem.* **1994,** *32,* 813.
120. Ferrante, M.; Henckaerts, L.; Joossens, M.; Pierik, M.; Joossens, S.; Dotan, N.; Norman, G. L.; Altstock, R. T.; Van Steen, K.; Rutgeerts, P.; Van Assche, G.; Vermeire, S. New Serological Markers in Inflammatory Bowel Disease Are Associated With Complicated Disease Behaviour. *Gut* **2007,** *56,* 1394.
121. Orholm, M.; Munkholm, P.; Langholz, E.; Nielsen, O. H.; Sorensen, T. I.; Binder, V. Familial Occurrence of Inflammatory Bowel Disease. *N. Engl. J. Med.* **1991,** *324,* 84.
122. Binder, V.; Orholm, M. Familial Occurrence and Inheritance Studies in Inflammatory Bowel Disease. *Neth. J. Med.* **1996,** *48,* 53.
123. Monsen, U.; Bernell, O.; Johansson, C.; Hellers, G. Prevalence of Inflammatory Bowel Disease Among Relatives of Patients With Crohn's Disease. *Scand. J. Gastroenterol.* **1991,** *26,* 302.
124. May, G. R.; Sutherland, L. R.; Meddings, J. B. Is Small Intestinal Permeability Really Increased in Relatives of Patients With Crohn's Disease? *Gastroenterology* **1993,** *104,* 1627.
125. Peeters, M.; Geypens, B.; Claus, D.; Nevens, H.; Ghoos, Y.; Verbeke, G.; Baert, F.; Vermeire, S.; Vlietinck, R.; Rutgeerts, P. Clustering of Increased Small Intestinal Permeability in Families With Crohn's Disease. *Gastroenterology* **1997,** *113,* 802.
126. Fries, W.; Renda, M. C.; Lo Presti, M. A.; Raso, A.; Orlando, A.; Oliva, L.; Giofre, M. R.; Maggio, A.; Mattaliano, A.; Macaluso, A.; Cottone, M. Intestinal Permeability and Genetic Determinants in Patients, First-Degree Relatives, and Controls in a High-Incidence Area of Crohn's Disease in Southern Italy. *Am. J. Gastroenterol.* **2005,** *100,* 2730.
127. Wyatt, J.; Vogelsang, H.; Hubl, W.; Waldhoer, T.; Lochs, H. Intestinal Permeability and the Prediction of Relapse in Crohn's Disease. *Lancet* **1993,** *341,* 1437.
128. Hilsden, R. J.; Meddings, J. B.; Hardin, J.; Gall, D. G.; Sutherland, L. R. Intestinal Permeability and Postheparin Plasma Diamine Oxidase Activity in the Prediction of Crohn's Disease Relapse. *Inflamm. Bowel Dis.* **1999,** *5,* 85.
129. D'Inca, R.; Di Leo, V.; Corrao, G.; Martines, D.; D'Odorico, A.; Mestriner, C.; Venturi, C.; Longo, G.; Sturniolo, G. C. Intestinal Permeability Test as a Predictor of Clinical Course in Crohn's Disease. *Am. J. Gastroenterol.* **1999,** *94,* 2956.
130. Arnott, I. D.; Kingstone, K.; Ghosh, S. Abnormal Intestinal Permeability Predicts Relapse in Inactive Crohn Disease. *Scand. J. Gastroenterol.* **2000,** *35,* 1163.
131. Tibble, J. A.; Sigthorsson, G.; Bridger, S.; Fagerhol, M. K.; Bjarnason, I. Surrogate Markers of Intestinal Inflammation Are Predictive of Relapse in Patients With Inflammatory Bowel Disease. *Gastroenterology* **2000,** *119,* 15.
132. Renukuntla, J.; Vadlapudi, A. D.; Patel, A.; Boddu, S. H.; Mitra, A. K. Approaches for Enhancing Oral Bioavailability of Peptides and Proteins. *Int. J. Pharm.* **2013,** *447,* 75.
133. Sahu, K. K.; Minz, S.; Kaurav, M.; Pandey, R. S. Proteins and Peptides: The Need to Improve Them as Promising Therapeutics for Ulcerative Colitis. *Artif. Cells Nanomed. Biotechnol.* **2016,** *44,* 642.
134. Deli, M. A. Potential Use of Tight Junction Modulators to Reversibly Open Membranous Barriers and Improve Drug Delivery. *Biochim. Biophys. Acta* **2009,** *1788,* 892.
135. Ward, P. D.; Tippin, T. K.; Thakker, D. R. Enhancing Paracellular Permeability by Modulating Epithelial Tight Junctions. *Pharm. Sci. Technol. Today* **2000,** *3,* 346.
136. Schiller, C.; Frohlich, C. P.; Giessmann, T.; Siegmund, W.; Monnikes, H.; Hosten, N.; Weitschies, W. Intestinal Fluid Volumes and Transit of Dosage Forms as Assessed by Magnetic Resonance Imaging. *Aliment. Pharmacol. Ther.* **2005,** *22,* 971.
137. Kraehenbuhl, J. P.; Neutra, M. R. Epithelial M Cells: Differentiation and Function. *Annu. Rev. Cell Dev. Biol.* **2000,** *16,* 301.
138. Yun, Y.; Cho, Y. W.; Park, K. Nanoparticles for Oral Delivery: Targeted Nanoparticles With Peptidic Ligands for Oral Protein Delivery. *Adv. Drug Deliv. Rev.* **2013,** *65,* 822.
139. Buda, A.; Sands, C.; Jepson, M. A. Use of Fluorescence Imaging to Investigate the Structure and Function of Intestinal M Cells. *Adv. Drug Deliv. Rev.* **2005,** *57,* 123.
140. Mahato, R. I.; Narang, A. S.; Thoma, L.; Miller, D. D. Emerging Trends in Oral Delivery of Peptide and Protein Drugs. *Crit. Rev. Ther. Drug Carrier Syst.* **2003,** *20,* 153.
141. Shakweh, M.; Ponchel, G.; Fattal, E. Particle Uptake by Peyer's Patches: A Pathway for Drug and Vaccine Delivery. *Expert Opin. Drug Deliv.* **2004,** *1,* 141.
142. McDole, J. R.; Wheeler, L. W.; McDonald, K. G.; Wang, B.; Konjufca, V.; Knoop, K. A.; Newberry, R. D.; Miller, M. J. Goblet Cells Deliver Luminal Antigen to CD103 + Dendritic Cells in the Small Intestine. *Nature* **2012,** *483,* 345.
143. Martinez, M. N.; Amidon, G. L. A Mechanistic Approach to Understanding the Factors Affecting Drug Absorption: A Review of Fundamentals. *J. Clin. Pharmacol.* **2002,** *42,* 620.
144. Karsdal, M. A.; Henriksen, K.; Bay-Jensen, A. C.; Molloy, B.; Arnold, M.; John, M. R.; Byrjalsen, I.; Azria, M.; Riis, B. J.; Qvist, P.; Christiansen, C. Lessons Learned From the Development of Oral Calcitonin: The First Tablet Formulation of a Protein in Phase III Clinical Trials. *J. Clin. Pharmacol.* **2011,** *51,* 460.
145. Friman, S.; Backman, L. A New Microemulsion Formulation of Cyclosporin: Pharmacokinetic and Clinical Features. *Clin. Pharmacokinet.* **1996,** *30,* 181.
146. Browne, B. J.; Jordan, S.; Welsh, M. S.; Van Buren, C.; Kahan, B. D. Diet and Cyclosporin A—Pharmacokinetic Comparison Between Neoral and Sandimmune Gelatin Capsules. *Transplant. Proc.* **1994,** *26,* 2959.
147. Mattheakis, L.; Bhandari, A.; Bai, L.; Zemede, G.; Tran, V.; Spencer, N.; Celino, H.; Frederick, B.; Xu, C.; Dias, J.; Annamalai, T.; Habtezion, A.; Patel, D.; Liu, D. Advances in IBD—Crohn's & Colitis Foundation's Clinical & Research Conference.
148. Mattheakis, L.; Bhandari, A.; Bai, L.; Zemede, G.; Tran, V.; Celino, H.; Frederick, B.; Zhao, L.; Dogra, M.; Lister, H.; Tovera, J.; Shah, S.; Annamalai, T.; Patel, D.; Liu, D. Crohn's & Colitis Foundation's Clinical & Research Conference.
149. Cheng, X.; Bhandari, A.; Bourne, G.; Frederick, B.; Zhang, J.; McMahon, J.; Scott, S.; Celino, H.; Zemede, G.; Spencer, N.; Tran, V.; Dogra, M.; Dias, J.; Bai, L.; Annamalai, T.; Smythe, M.; Mattheakis, L.; Patel, D.; Liu, D. ICMI, 2015, Berlin, Germany.
150. Shaaltiel, Y.; Ya'acov, A. B.; Shabat, Y.; Zolotarov, L.; Gingis-Velitski, S.; Almon, E.; Aviezer, D.; Ilan, Y. Tu2029 a Novel Method for Anti-TNF Based-Oral Immunotherapy: Oral Administration of a Plant Cell-Expressed Recombinant Anti-TNF Fusion Protein for Treating of Crohn's Disease. *Gastroenterology* **2014,** *146,* S-901.
151. Sandborn, W. J.; Hanauer, S. B.; Katz, S.; Safdi, M.; Wolf, D. G.; Baerg, R. D.; Tremaine, W. J.; Johnson, T.; Diehl, N. N.; Zinsmeister, A. R. Etanercept for Active Crohn's Disease: A Randomized, Double-Blind, Placebo-Controlled Trial. *Gastroenterology* **2001,** *121,* 1088.
152. Vandenbroucke, K.; de Haard, H.; Beirnaert, E.; Dreier, T.; Lauwereys, M.; Huyck, L.; Van Huysse, J.; Demetter, P.; Steidler, L.; Remaut, E.; Cuvelier, C.; Rottiers, P. Orally Administered *L. lactis* Secreting an Anti-TNF Nanobody Demonstrate Efficacy in Chronic Colitis. *Mucosal Immunol.* **2010,** *3,* 49.

153. Bartelds, G. M.; Krieckaert, C. L.; Nurmohamed, M. T.; van Schouwenburg, P. A.; Lems, W. F.; Twisk, J. W.; Dijkmans, B. A.; Aarden, L.; Wolbink, G. J. Development of Antidrug Antibodies Against Adalimumab and Association With Disease Activity and Treatment Failure During Long-Term Follow-up. *JAMA* **2011,** *305,* 1460.
154. Craik, D. J.; Clark, R. J.; Daly, N. L. Potential Therapeutic Applications of the Cyclotides and Related Cystine Knot Mini-Proteins. *Expert Opin. Investig. Drugs* **2007,** *16,* 595.
155. Maillere, B. J.; Mourier, G.; Herve, M.; Cotton, J.; Leroy, S.; Menez, A. Immunogenicity of a Disulfide-Containing Neurotoxin: Presentation to T-Cells Requires a Reduction Step. *Toxicon* **1995,** *33,* 475.
156. Rammensee, H.-G. Chemistry of Peptides Associated With MHC Class I and Class II Molecules. *Curr. Opin. Immunol.* **1995,** *7,* 85.
157. de Buck van Overstraeten, A.; Wolthuis, A.; D'Hoore, A. Surgery for Crohn's Disease in the Era of Biologicals: A Reduced Need or Delayed Verdict? *World J. Gastroenterol.* **2012,** *18,* 3828.
158. Lopez, A.; Billioud, V.; Peyrin-Biroulet, C.; Peyrin-Biroulet, L. Adherence to Anti-TNF Therapy in Inflammatory Bowel Diseases: A Systematic Review. *Inflamm. Bowel Dis.* **2013,** *19,* 1528.
159. Kane, S. V.; Cohen, R. D.; Aikens, J. E.; Hanauer, S. B. Prevalence of Nonadherence With Maintenance Mesalamine in Quiescent Ulcerative Colitis. *Am. J. Gastroenterol.* **2001,** *96,* 2929.
160. Kane, S. V.; Chao, J.; Mulani, P. M. Adherence to Infliximab Maintenance Therapy and Health Care Utilization and Costs by Crohn's Disease Patients. *Adv. Ther.* **2009,** *26,* 936.
161. Moody, G. A.; Eaden, J. A.; Helyes, Z.; Mayberry, J. F. Oral or Rectal Administration of Drugs in IBD? *Aliment. Pharmacol. Ther.* **1997,** *11,* 999.
162. Nejdfors, P.; Ekelund, M.; Jeppsson, B.; Westrom, B. R. Mucosal In Vitro Permeability in the Intestinal Tract of the Pig, the Rat, and Man: Species- and Region-Related Differences. *Scand. J. Gastroenterol.* **2000,** *35,* 501.
163. Koboziev, I.; Karlsson, F.; Zhang, S.; Grisham, M. B. Pharmacological Intervention Studies Using Mouse Models of the Inflammatory Bowel Diseases: Translating Preclinical Data into New Drug Therapies. *Inflamm. Bowel Dis.* **2011,** *17,* 1229.
164. Auer, K.; Trachter, R.; Van den Bogaerde, J.; Bassaganya-Riera, J.; Sorrentino, D. Translational Research and Efficacy of Biologics in Crohn's Disease: A Cautionary Tale. *Expert Rev. Clin. Immunol.* **2014,** *10,* 219.

6.07 Evolution of mAb Downstream Process Platforms

AA Shukla, L Wolfe, and C Norman, KBI Biopharma Inc., Durham, NC, United States

© 2017 Elsevier Ltd. All rights reserved.

6.07.1	**Introduction to mAb Platform Processes**	171
6.07.2	**Current and Evolving Downstream Process Platforms for mAbs**	172
6.07.2.1	Drivers for mAb Platform Evolution	172
6.07.2.2	Recent Downstream Platforms for mAbs	172
6.07.2.3	A Broadly Applicable mAb Downstream Platform	174
6.07.3	**New Technologies Impacting mAb Downstream Processing**	175
6.07.4	**Next-Generation Antibody Constructs Impacting the Process Platform**	176
6.07.5	**Conclusions**	178
References		178

6.07.1 Introduction to mAb Platform Processes

Monoclonal antibodies (mAbs) are the most successful class of biopharmaceuticals today. More than 50 mAbs have been approved and sales of mAbs are expected to cross $125 billion by 2020.[1] The ability to bind to specific targets with high specificity and affinity and the ease of developing human or humanized sequences to a target have been behind the explosive growth of this class of pharmaceutical products. The last 20 years have seen the rapid growth of this class of therapeutics with over 300 mAbs in clinical development today. Today mAbs are approved for a wide range of indications covering oncology,[2] autoimmune disorders, and rare disease indications.

While the ability to target cell surface targets with great specificity has been behind the rise of mAbs,[3] one must not lose sight of the development of process platform technologies that have enabled rapid production of mAbs for clinical trials as well as at commercial scale. The ease and speed of producing mAbs has enabled rapid entry of these product candidates into clinical trials and the scalability and robustness of these processes has hugely facilitated large-scale commercial supply.

Development of a manufacturing process for a protein requires the consideration of many different factors, including removal of impurities, robustness, scalability, and ready availability of raw materials for large-scale production. Consideration has to be given not only to the scale needed for early clinical supply, but also the ability of the process to support long-term supply needs and scales. As a result, utilizing well-established unit operations is a key aspect of developing manufacturing processes. The aspects of robustness, scalability, and reproducibility mean that manufacturing processes often look quite different from those that can be employed in the laboratory for purifying small quantities of proteins. Process development can be a time-consuming activity and require significant amounts of experimentation. As a result, when possible the industry has gravitated toward platform approaches.

A platform approach has distinct advantages from a business standpoint. Speed to clinic is often a key determinant of a company's success. mAb platforms have enabled progression from gene to Investigational New Drug (IND) in less than a year, which is a significant improvement over molecules that require involved development efforts that can extend up to 2 years. This reduced experimentation also implies a reduction in the cost of the development effort. The predictability of a process platform enables organizations such as manufacturing and quality control to adopt a templated set of documents which also reduces the time and resources spent on production and release testing.

mAb therapeutics particularly lend themselves toward the application of platform approaches. Use of a well-developed mammalian cell culture expression system enables development of stable cell lines in a very rapid and templated fashion for mAbs. Several expression vectors have been optimized specifically for mAb production.[4,5] Robust fed-batch cell culture processes have been developed for mAbs. Several of these have been scaled to large-scale production and characterized extensively giving a good idea of the operating parameters that influence these processes.[6,7] Cell line development and upstream cell culture processes lend themselves to a templated approach very well. However, for most proteins the greatest area of divergence comes in the form of the downstream purification process that has to be customized for each protein based on its properties as well as that of key impurities. The Fc region of mAbs binds very specifically to immobilized Protein A which is a cell wall component of *Staphylococcus aureus*. Protein A affinity chromatography has been shown to be widely applicable for mAbs and can achieve >95% purity with very little development on this mode of chromatography.[8] The chief challenge after Protein A chromatography is to remove residual host cell protein (HCP) impurities, high molecular weight (HMW) aggregate, DNA, and have the capability of removing adventitious viruses.

A number of downstream process platforms for mAbs have been developed at leading biopharmaceutical companies.[9–13] The ability to use a generic approach across molecules and starting from a template decrease the amount of experimentation needed compared with a protein that cannot enable the inclusion of an affinity step in the downstream process. These downstream process platforms have successfully enabled the progression of a large number of mAb products into the clinic and commercial space.

6.07.2 Current and Evolving Downstream Process Platforms for mAbs

6.07.2.1 Drivers for mAb Platform Evolution

This section describes several downstream process schemes that have been developed at leading biopharmaceutical companies and successfully employed for mAb manufacturing at large scale. Several aspects are in common across these process schemes. mAbs are extracellularly secreted into the cell culture medium during mammalian cell culture. Harvest and recovery schemes typically utilize centrifugation followed by depth filtration and a series of membrane filters.[14,15] At smaller scales, centrifugation may be dispensed with and a series of depth filters with the coarser pore size filters first may often be utilized. The platform process almost always commences with Protein A chromatographic capture.[16] In some cases, selective washes can be built into the Protein A step operation to further enhance HCP clearance.[17] Non-Protein A schemes have been developed and employed for large-scale manufacturing[18] as for any therapeutic protein but have not caught on given the absence of a generic approach and issues with process robustness. The process will also include two dedicated orthogonal viral clearance steps as per International Committee on Harmonization (ICH) guidelines. Low pH viral inactivation and viral filtration through a parvoviral grade filter are widely employed for mAbs.[19] The low pH incubation step is typically placed immediately after Protein A chromatography since the Protein A column elutes in a low pH buffer. Following Protein A chromatography and viral inactivation, one or two polishing chromatographic steps are employed to clear HMW aggregate,[20] HCPs,[21] DNA, and to provide viral clearance potential. Chief differences among platform approaches lie in the nature of the polishing chromatographic steps. Given the high titer cell culture processes that are increasingly common in industry today (5–10 g L^{-1}), there is a significant need for high column loadings on polishing chromatographic steps.

Each company ends up customizing its mAb downstream platform approach based upon its own expression system and cell culture process as well as the mAb type and subclass they predominantly employ in discovery research. The primary criterion is that the platform approach needs to be robust and applicable across a wide range of IgG molecules without significant modification. Another key criterion is the ability of the platform to fit in the manufacturing schedule and minimize the amount of time spent in downstream processing for any one batch. As a result, another key driver is the loading capacity that is possible for any of the polishing steps.

6.07.2.2 Recent Downstream Platforms for mAbs

Amgen was one of the first companies to disclose its approach to a downstream process platform.[9] A completely templated approach was shown not to be possible, but a small number of development experiments should lead to answers about process parameters that need to be customized.[10] Examples of such process parameters include examples such as the Protein A elution pH and the choice of polishing chromatographic steps depending on the chief set of impurities that need clearance. **Fig. 1** shows the platform downstream scheme in use at Amgen at the time. The polishing steps typically employed were cation-exchange chromatography (CEX) in a bind and elute mode followed by either hydrophobic interaction chromatography (HIC) in a flow-through mode if HMW aggregates needed to be cleared or anion-exchange chromatography (AEX) in a flow-through mode if only HCP

Fig. 1 Platform approach to mAb downstream processing at Amgen.

clearance was needed. In a few cases, hydroxyapatite was employed if specific product-related impurities needed to be removed. In situations in which adequate HCP and HMW clearance were obtained after the first polishing CEX step, anion-exchange membrane chromatography was employed to provide for another step with viral clearance potential.[22]

Another leading company to develop a pipeline of mAbs using a platform approach was Genentech.[13,23,24] Genentech historically employed CEX and AEX as part of its downstream platform (Fig. 2). The trend appeared to initially be to utilize CEX in a bind and elute mode as the first polishing step followed by AEX in a flow-through mode of operation. mAbs usually have a basic p*I* and hence bind tightly to CEX resins and tend to flow-through readily on AEX resins. The CEX step clears both HMW and HCP. The AEX step, however, is noted to require a low load conductivity in order to successfully remove HCPs. This can lead to a bottleneck during plant operation due to the need for large volume in-process hold tanks to hold the AEX load. The possible use of mixed-mode Captoadhere resin in place of more typical AEX resins is mentioned to help reduce the need for significant dilution.

One of the key drawbacks of using AEX is that it only provides clearance for HCPs and not for HMW aggregates. This particular drawback has been mitigated by the development of an AEX step operated in a weak partitioning mode[25] in which the product actually has some measure of retention on the resin. In this mode of operation, the AEX step has actually been shown to be capable of reducing HMW content in addition to HCP species. Mechanistically, we speculate that interactions with the somewhat hydrophobic parts of the resin backbone set in at very low conductivities, enabling some degree of HMW removal to occur.

Both of these schemes suffer from the drawback of requiring significant dilution of the load material for the AEX step. In addition, CEX and AEX alone are often unable to provide adequate HMW clearance. HMW levels can vary for mAbs, but levels of $>5\%$ HMW aggregate after Protein A chromatography are not that uncommon. Such levels often require recourse to a HIC step as has been mentioned earlier.[9] Another innovative approach has been to operate the HIC step under highly overloaded conditions (>200 g L^{-1}) under no salt conditions.[26] This approach entails the use of a highly hydrophobic HIC resin with no additional kosmotropic salt added to the load. pH conditions of the load are modulated to enable HMW removal under these extreme overloaded conditions. The use of such an ultra-high capacity step enables the processing of large production quantities of mAbs and is used as part of the mAb platform at Biogen (Fig. 3) in combination with a flow-through AEX step. The ability to load the polishing steps at very high loads enables a reduction in column cycling and decreases the duration of floor time taken for a batch.

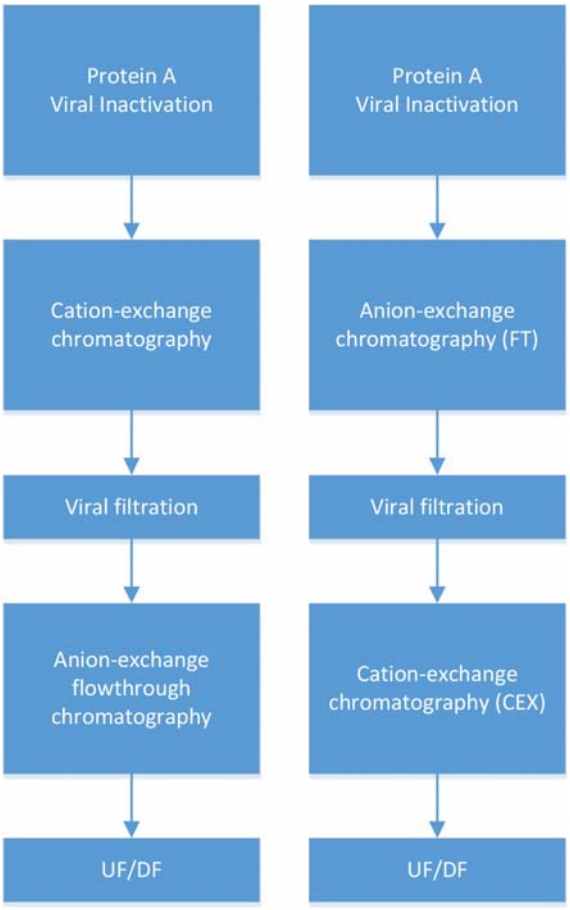

Fig. 2 Genentech mAb downstream process platform.

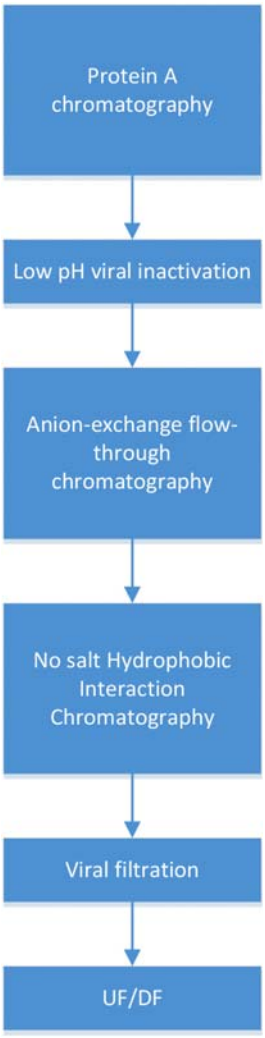

Fig. 3 Platform mAb downstream process at Biogen.

A similar flow-through only polishing scheme has been discussed by Millipore-Sigma.[27] In this proposed format, CEX would be operated under highly overloaded conditions during the loading step. When operated in this fashion, CEX has the ability to clear some level of HCPs. It is again speculated by us that this occurs due to weak hydrophobic interactions with the chromatographic backbone. This polishing step is then combined with AEX flow-through to complete the sequence.

Contract development and manufacturing (CDMO) requires the ability to incorporate many different cell lines and cell culture processes into the downstream platform approach. This places significant challenges on the downstream platform scheme since both HCP and HMW reduction are simultaneously required. These simultaneous demands on the downstream mAb platform are illustrated in Fig. 4.

6.07.2.3 A Broadly Applicable mAb Downstream Platform

CEX and AEX in their traditional flavors do not fulfill this need. A key modification made in this regard has been the use of multimodal chromatography as part of the mAb downstream platform. Multimodal chromatography involves the incorporation of a hydrophobic moiety into the ligands structure for either AEX or CEX.[28] The increased hydrophobicity of the chromatographic resin now enable improved clearance of HMW on both CEX and AEX modes which are arguably most suited for mAb processing. In addition, both these modes of chromatography are also capable of HCP and DNA clearance as well. mAbs do differ in terms of their own hydrophobicity. As a result, the platform downstream process for mAbs at KBI is defined as AEX (with resin hydrophobicity that can vary from Q Sepharose FF or Capto Q to Fractogel SO3 to multimodal chromatographic resins such as Captoadhere and Nuvia cPrime). This modulation of hydrophobicity enables optimal conditions to be tailored for each mAb. Similarly, the CEX bind and elute step is also operated on a range of hydrophobicities ranging from mild to moderate depending on the resin selected.

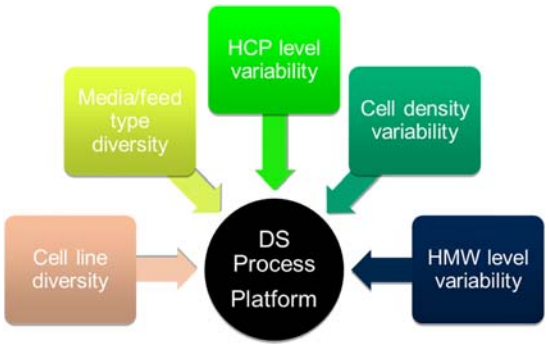

Fig. 4 Range of factors considered in determining KBI Biopharma's platform approach.

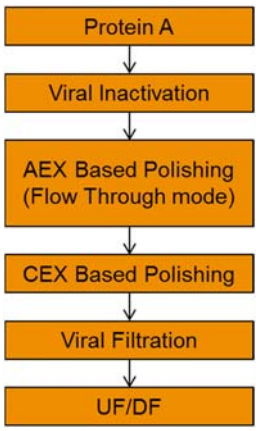

Fig. 5 KBI Biopharma's approach to mAb downstream processing for FIH manufacturing.

While this approach does entail some degree of experimental work, a preferred approach using multimodal chromatography for both AEX and CEX is employed as the primary platform with recourse to less hydrophobic stationary phases should the mAb require it. This approach is illustrated in Fig. 5 and has been useful in terms of its breadth of covering a wide range of mAb constructs, cell lines, and cell culture processes at KBI.

Fig. 6 shows the clearance profiles for HMW aggregates and HCPs through this platform process for a number of mAbs. As can be seen from the figure, HMW aggregate levels of $<1\%$ and low HCP levels <50 ppm are always observed using this platform. The ability to cover a wide range of mAb constructs is a key, especially for a CDMO organization such as KBI.

6.07.3 New Technologies Impacting mAb Downstream Processing

Traditional chromatography is batch process. Steps start from column sanitization, equilibration, and loading through to washes, elution, strip, and column regeneration and storage. A batch operation is limited in terms of its throughput and productivity. First of all chromatographic columns can only be operated at a maximum diameter of 2 m owing to flow distribution limitations. Current resins can only be packed to a maximum of 30 cm bed height (20 cm typically) owing to pressure drop limitations. This inherently limits the amount of product that can be processed per cycle. When multiple cycles are required, product intermediate needs to be held for a longer duration of time. Product holds also end up using valuable tank volume in manufacturing facilities which are also limited. Continuous chromatographic separations can turn this batch operation into a continuous or semicontinuous process[29] as shown in Fig. 7. Combined with a continuous upstream perfusion cell culture process, this can alter the current paradigm of how biopharmaceutical production processes are designed.[30,31] Continuous chromatographic separation can be conducted using one of many formats. Periodic counter current chromatography is one of the formats (from GE Healthcare) and utilizes multiple columns that are continuously operated in different phases of the operation cycle.[32] Other formats include multicolumn countercurrent solvent gradient purification that enables recycling of the front and tail ends of the peaks to boost yield as well as purity via the ContiChrom system from ChromaCon and the BioSMB technology from Tarpon Biosystems (now part of Pall Corporation).

Another means of boosting productivity is to move from chromatographic operations to nonchromatographic separations. Various systems such as selective precipitation schemes using polymers and aqueous two-phase separations (ATPS) can be utilized

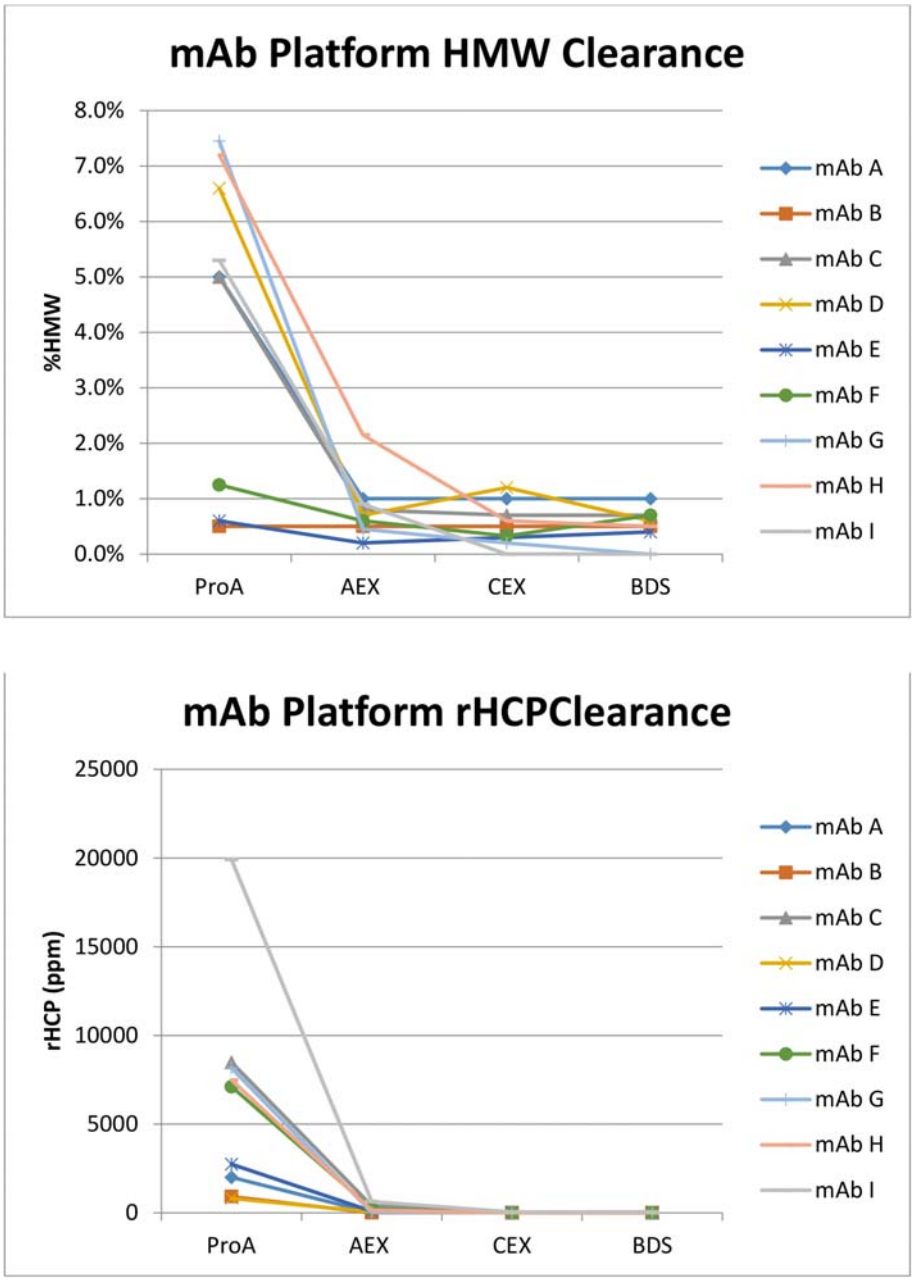

Fig. 6 Performance of the KBI Biopharma platform DSP approach for several mAbs. (A) HMW clearance and (B) HCP clearance.

to capture the entire bioreactor batch in one operation rather than relying on multiple chromatographic cycles. A variety of polymers have been utilized for mAb precipitation including polyanionic polymers to precipitate the product[33] and caprylic acid precipitation of HCP impurities.[34] ATPS rely upon the creation of two separate phases in solution by mixing a polymer and salt or two polymers with each other. Examples include poly-ethylene glycol (PEG)-salt and dextran-PEG ATPS.[35] Both of these separation technologies have interesting possibilities and can significantly raise the bar on throughput that is currently possible from manufacturing facilities. However, both areas need further development to establish themselves as scalable technology that can be applied without significant development for a wide range of mAbs.

6.07.4 Next-Generation Antibody Constructs Impacting the Process Platform

The other major factor that leads to evolution of the platform approach is the specific mAb-like construct that is being developed as a potential therapeutic. The biotechnology industry is rapidly moving beyond conventional mAbs into a variety of constructs

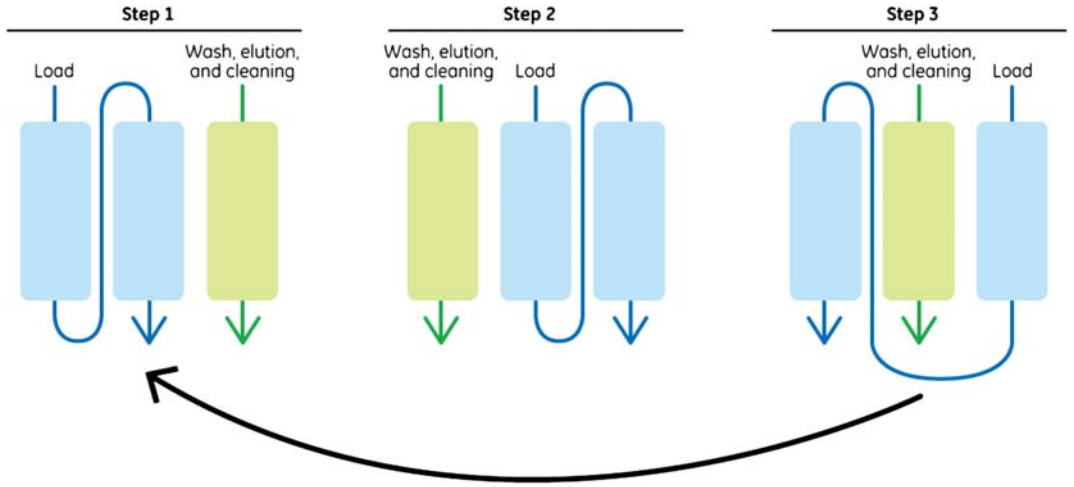

Fig. 7 Principle of continuous chromatography.

including Fc fusion proteins, bispecific antibodies (bsAbs), and antibody-fusion proteins. Each of these new constructs requires modifications of the original mAb platform process to enable their production.

Fc fusion proteins are created by joining the coding sequence for the Fc region of a mAb to the coding sequence for another protein.[36] The Fc region offers several advantages as a fusion partner. Many biologically active peptides and proteins have a short serum half-life reflecting their rapid clearance through the kidneys. The Fc region can bind to the neonatal Fc receptor to extend the half-life of antibodies, and the same benefits are conferred on fusion partners.[37] Seven Fc fusion proteins are commercially available as approved biopharmaceuticals and at least two of them (Enbrel and Orencia) have already achieved blockbuster status with sales of over US$ 1 billion per year. The original platform for mAbs at Amgen included the purification of Fc fusion proteins.[9] However, several key downstream differences do exist for Fc fusion proteins, including the possibility of susceptibility to proteolytic cleavage and the possibility of higher HMW aggregate levels being present than regular mAbs. A typical mAb downstream platform approach usually is effective, with possible adjustments to the polishing steps to account for stability of the molecule and effective HMW clearance.

bsAbs are designed proteins capable of simultaneously binding and neutralizing two different antigens (ligands, cell receptor, or cytokines) or two distinct epitopes on the same antigen.[38] As a result of this property, bsAbs can serve as mediators in redirecting immune effectors and cytotoxic agents like T-cells to tumors or to infecting organisms such as bacteria. The fact that two arms of the mAb are different leads to several processing challenges that are unique to bsAbs. For example, if the two halves of the mAb are expressed separately, a downstream process that requires disassembly of the two halves followed by reassembly to form the heterodimeric species will have to be conducted.[39] In addition to the recombination steps, even if the formation of homodimeric species is discouraged (by use of a knob-in-hole methodology or a similar technology that encourages heterodimer formation), small quantities of the homodimers will form and will have to be removed by downstream processing. As a result, this format of bsAbs requires a more complex downstream process.

However, use of a common light chain along with the knob-in-hole technology (KiH) enables the formation of a bsAb in cell culture expression.[40] Homodimer formation is discouraged due to the KiH construct. The small quantities of homodimer that are formed can be removed if the sequences selected for those have a biochemical difference. This can be done even in the absence of a common light chain. For example, in the XmAb technology from Xencor, the homodimer and heterodimer have a small difference in charge in their engineered Fc regions that enables their separation on CEX. The other purpose of the engineering approach is the enhance effector function of the bSAb.[41]

An antibody–drug conjugate (ADC) is a mAb conjugated with a cytotoxic agent via a linker with the primary aim of treating cancer.[42] ADCs can be produced in a downstream process identically to conventional mAbs except for a chemical conjugation step at the end of the downstream process. This is typically followed by ultrafiltration/diafiltration (UF/DF) to remove the conjugating chemicals. The chief difference from mAbs is the requirement for more stringent containment and personnel protection due to the toxic nature of the conjugate.

Other next-generation mAb constructs include peptide fusions to mAbs at either the C or N termini to further enhance the ability to bind to more than one target at a time. Examples include anticalins fused to a mAb structure.[43] A whole range of other therapeutic options exist as shown in Fig. 8, including engineered scFvs, diabodies, and tribodies and Fab conjugates in the form of dimers or trimers.[44] Each of these therapeutic modalities can lead to the development of platform process approaches if they become prevalent as a therapeutic modality.

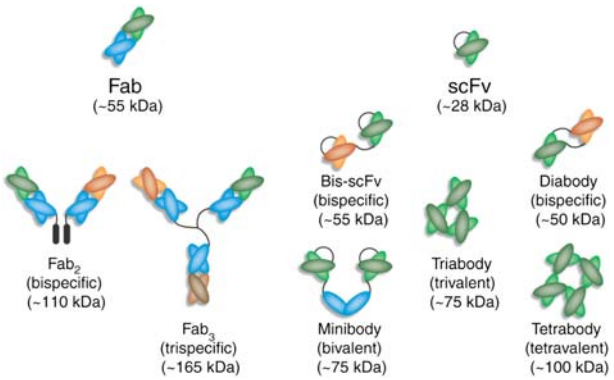

Fig. 8 Possible next-generation antibody formats.

6.07.5 Conclusions

This article has discussed the need for a platform approach for mAbs and its utility in accelerating the progression of many different therapeutics toward the clinic and market. The use of a platform approach has enabled many biopharmaceutical companies to successfully progress mAbs from gene to IND in a year or less. Based upon their internal antibody construct, cell line, and cell culture process, each biopharmaceutical organization has developed its favorite platform approach. Latest trends include the use of multimodal chromatography as part of the process platform and the use of two high loading polishing steps in a flow-through mode of operation. These modifications have enabled even broader applicability of the mAb platform as well as are meaningfully addressing the throughput bottleneck in downstream processing.

As cell culture productivity continues to advance, other alternative formats to help improve the productivity of the downstream process are being advanced. These include the operation of the Protein A chromatographic step in a continuous mode rather than a batch format. Continuous processing could conceivably be extended for the entire downstream process in the future. Nonchromatographic separation steps using precipitation or ATPS are another possible future direction for mAb downstream processing.

More radical alterations of the mAb downstream process platform are being undertaken for next-generation mAb products such as bsAbs and antibody fragments. The next decade will see further evolution of the mAb downstream process platform based on the drivers of productivity and new molecule formats.

References

1. Ecker, S. D.; Jones, D.; Levine, H. The Therapeutic Monoclonal Antibody Market. *mAbs* **2015,** *7* (1), 9–14.
2. Sliwkowski, M.; Mellman, I. Antibody Therapeutics in Cancer. *Science* **2013,** *341,* 1192–1198.
3. Reichert, J. Metrics for Antibody Therapeutics Development. *mAbs* **2010,** *2* (6), 695–700.
4. Chusainow, J.; Yang, Y.; Yeoh, J.; Toh, P.; Asvadi, P.; Wong, P.; Yap, M. A Study of mAb Producing CHO Cell Lines—What Makes a Stable High Producer. *Biotechnol. Bioeng.* **2009,** *102,* 1182–1196.
5. Andersen, D.; Reilly, D. Production Technologies for mAbs and Their Fragments. *Curr. Opin. Biotechnol.* **2004,** *15,* 456–462.
6. Racher, A.; Birch, J. Antibody Production. *Adv. Drug Deliv. Rev.* **2006,** *58,* 671–685.
7. Li, F.; Vijayasankaran, N.; Shen, A.; Kiss, R.; Amanullah, A. Cell Culture Processes for mAb Production. *mAbs* **2010,** *2* (5), 466–479.
8. Gagnon, P. *Purification Tools for mAbs;* Validated Biosystems: Tucson, AZ, 1995.
9. Shukla, A.; Hubbard, B.; Tressel, T.; Guhan, S.; Low, D. Downstream Processing of Monoclonal Antibodies—Application of Platform Approaches. *J. Chromatogr. B* **2007,** *848,* 28–39.
10. Shukla, A.; Thommes, J. Advances in Large-Scale Production of Monoclonal Antibodies and Related Proteins. *Trends Biotechnol.* **2010,** *28* (5), 253–261.
11. Rathore, A.; Godavarti, R.; Kumar, V.; Tugcu, N. Evolution of the mAb Purification Platform. *Biopharm* **2013,** *26* (11), 1–7.
12. Chon, J.; Zarbis-Papastoitsis, G. Advances in the Production and Downstream Processing of Antibodies. *New Biotechnol.* **2011,** *28* (5), 458–463.
13. Kelley, B. Industrialization of mAb Production Technology: The Bioprocessing Industry at a Cross-Roads. *mAbs* **2009,** *1* (5), 443–452.
14. Kandula, S.; Babu, S.; Jin, M.; Shukla, A. Design of a Filter Train for Precipitate Removal in Monoclonal Antibody Downstream Processing. *Biotechnol. Appl. Biochem.* **2009,** *54,* 149–155.
15. Shukla, A.; Kandula, J. Harvest & Recovery of Monoclonal Antibodies from Large-Scale Mammalian Cell Culture. *Biopharm* **2008,** *21* (5), 34–45.
16. Liu, Z.; Mostafa, S.; Shukla, A. A Comparison of Protein A Chromatographic Stationary Phases: Performance Characteristics for Monoclonal Antibody Purification. *Biotechnol. Appl. Biochem.* **2015,** *62* (1), 37–47.
17. Shukla, A.; Hinckley, P. Host Cell Protein Clearance During Protein A Chromatography–Development of an Improved Column Wash Step. *Biotechnol. Prog.* **2008,** *24,* 1115–1121.
18. Arunakumari, A.; Wang, J.; Ferreira, G. Improved Downstream Process Design for Human mAb Production. *Biopharm Intl* **2007**, (Suppl.), 36–40. Supplement February.
19. Shukla, A.; Aranha, H. Viral Clearance for Biopharmaceutical Downstream Processes. *Pharm. Bioprocess.* **2015,** *3* (2), 127–138.
20. Vazquez-Rey, M.; Lang, D. Aggregates in mAb Manufacturing Processes. *Biotechnol. Bioeng.* **2011,** *108,* 1494–1508.
21. Shukla, A.; Jiang, C.; Ma, J.; Rubacha, M.; Flansburg, L.; Lee, S. Demonstration of Robust Host Cell Protein Clearance in Biopharmaceutical Downstream Processes. *Biotechnol. Prog.* **2008,** *24,* 615–622.
22. Zhou, J.; Tressel, T. Basic Concepts in Q Membrane Chromatography for mAb Production. *Biotechnol. Prog.* **2006,** *22* (2), 341–349.

23. Kelley, B. Very Large-Scale mAb Purification: The Case for Conventional Unit Operations. *Biotechnol. Prog.* **2007,** *23,* 995–1008.
24. Trexler-Schmidt, M.; Sze-Khoo, S.; Cothran, A.; Thai, B.; Sargis, S.; Lebreton, B.; Kelley, B.; Blank, G. Purification Strategies to Purify 5 g/L of mAbs. *Biopharm Intl* **2011,** 8–15. Supplement March.
25. Kelley, B.; Tobler, S.; Brown, P.; Coffman, J.; Godavarti, R.; Iskra, T.; Switzer, M.; Vunnum, S. Weak Partitioning Chromatography for AEX Purification of mAbs. *Biotechnol. Bioeng.* **2008,** *101* (3), 553–566.
26. Ghose, S.; Tao, Y.; Conley, L.; Cecchini, D. Purification of mAbs by HIC Under No Salt Conditions. *mAbs* **2013,** *5* (5), 795–800.
27. Phillips, M. Next Generation mAb Platforms. ACS National Meeting, March 13–17, San Diego.
28. Wolfe, L.; Barringer, C.; Mostafa, S.; Shukla, A. Multimodal Chromatography: Characterization of Protein Binding and Selectivity Enhancement Through Mobile Phase Modulators. *J. Chromatogr. A* **2014,** *1340,* 151–156.
29. Konstantinov, K.; Cooney, C. White Paper on Continuous Bioprocessing: May 20–21, 2014 Continuous Manufacturing Symposium. *J. Pharm. Sci.* **2015,** *104* (3), 813–820.
30. Croughan, M.; Konstantinov, K.; Cooney, C. The Future of Industrial Bioprocessing—Batch or Continuous? *Biotechnol. Bioeng.* **2015,** *112* (4), 648–651.
31. Zydney, A. Perspectives on Integrated Continuous Bioprocessing—Opportunities and Challenges. *Curr. Opin. Chem. Eng.* **2015,** *10,* 8–13.
32. Warikoo, V.; et al. Integrated Continuous Production of Recombinant Therapeutic Proteins. *Biotechnol. Bioeng.* **2012,** *109,* 3018–3029.
33. McDonald, P.; Victa, C.; Franklin-Carter, J.; Fahrner, R. Selective Antibody Precipitation Using Polyelectrolytes: A Novel Approach to the Purification of mAbs. *Biotechnol. Bioeng.* **2009,** *102* (4), 1141–1151.
34. Brodsky, Y.; Zhang, C.; Yigzaw, Y.; Vedantham, G. Caprylic Acid Precipitation Method for Impurity Reduction: An Alternative to Traditional Chromatography for mAb Purification. *Biotechnol. Bioeng.* **2012,** *109* (10), 2589–2598.
35. Azevedo, A.; Rosa, P.; Ferreira, I.; Aires-Barros, R. Chromatography-Free Recovery of Biopharmaceuticals Through Aqueous two Phase Processing. *Trends Biotechnol.* **2009,** *27* (4), 240–247.
36. Beck, A.; Reichert, J. Therapeutic Fc-Fusion Proteins and Peptides as Successful Alternatives to Antibodies. *mAbs* **2011,** *3* (5), 415–416.
37. Roopenian, D. C.; Akilesh, S. FcRn: The Neonatal Fc Receptor Comes of Age. *Nat. Rev. Immunol.* **2007,** *7* (9), 715–725.
38. Kontermann, R. Dual Targeting Strategies With Bispecific Antibodies. *mAbs* **2012,** *4* (2), 182–197.
39. Ladiwala, A.; Kaleas, K.; Giese, G.; Mehta, A.; Persson, J.; Dowd, C.; Butler, M.; Lester, P. Evolution of a Standard Downstream Purification Process for Knob-in-Hole bsAbs. Recovery of Biological Products XVII, Bermuda, 19–24 June.
40. Merchant, M.; Zhu, Z.; Yuan, J.; Goddard, A.; Adams, C.; Presta, L.; Carter, P. An Efficient Route to Human Bispecific IgG. *Nat. Biotechnol.* **1998,** *16,* 677–681.
41. Zalevsky, J.; Leung, I.; Karki, S.; Chu, S.; Zhukovsky, E.; Desjarlais, J.; Carmichael, D.; Lawrence, C. The Effect of Fc Engineering on an Anti CD19 Antibody. *Blood* **2009,** *113,* 3735–3743.
42. Zolot, R.; Basu, S.; et al. Antibody–Drug Conjugates. *Nat. Rev. Drug Discov.* **2013,** *12,* 259–260.
43. Schelhuber, S.; Skerra, A. Anticalins as an Alternative to Antibody Technology. *Expert. Opin. Biol. Ther.* **2005,** *5* (11), 1453–1462.
44. Hudson, P.; Souriau, C. Engineered Antibodies. *Nat. Med.* **2003,** *9* (1), 129–134.

6.08 Emerging Bioanalytical Methods for the Bioanalysis of Biotherapeutics

B Gorovits, Pfizer, Andover, MA, United States
R Pillutla, Bristol-Myers Squibb, Princeton, NJ, United States

© 2017 Elsevier Ltd. All rights reserved.

6.08.1	**Differentiating Aspects of Bioanalysis of Biotherapeutics**	180
6.08.1.1	Ligand Binding Assay	181
6.08.1.2	Anti-drug Antibody	181
6.08.2	**Basics of LBAs**	181
6.08.2.1	LBA Assay Types	182
6.08.2.1.1	Variety of analytes measured by LBA	183
6.08.2.1.2	Critical value of assay reagents and controls	184
6.08.2.1.3	Significance and the nature of matrix interferences in LBA protocols	185
6.08.2.1.4	LBA method development and qualification requirements	188
6.08.3	**LBA Technology Platforms—Past, Present, and Future**	190
6.08.3.1	ECL Assays	190
6.08.3.1.1	Pros and cons/considerations	191
6.08.3.2	Gyrolab	191
6.08.3.2.1	Pros and cons/considerations	191
6.08.3.3	Biacore	191
6.08.3.3.1	Pros and cons/considerations	191
6.08.3.4	ForteBio	192
6.08.3.4.1	Pros and cons/considerations	192
6.08.3.5	Luminex	192
6.08.3.5.1	Pros and cons/considerations	192
6.08.3.6	Acoustic Membrane Microparticle Technology on the ViBE Platform (Bioscale)	192
6.08.3.6.1	Pros and cons/considerations	193
6.08.3.7	SIMOA (Quanterix)	193
6.08.3.7.1	Pros and cons/considerations	193
6.08.3.8	Singulex Erenna	193
6.08.3.8.1	Pros and cons/considerations	193
6.08.3.9	Maverick (Genalyte)	193
6.08.3.9.1	Pros and cons/considerations	194
6.08.3.10	Imperacer Immuno-Polymerase Chain Reaction (PCR) (Chimera Biotech)	194
6.08.3.10.1	Pros and cons/considerations	194
6.08.3.11	SQI Diagnostics	194
6.08.3.11.1	Pros and cons/considerations	194
6.08.4	**Evolving Landscape of LBA Technologies and Regulatory Expectations**	194
References		195

6.08.1 Differentiating Aspects of Bioanalysis of Biotherapeutics

Todays' spectrum of biotherapeutic modalities is highly diverse, including recombinant versions of endogenous human proteins, full length and fragments of monoclonal antibodies, protein conjugates including antibody drug conjugates (ADCs), fusion proteins including immunoglobulin Fc fusions, various types of novel scaffolds, synthetic peptides, and oligonucleotides. The high complexity of protein structure and relatively large molecular size of a typical biotherapeutic results in a very common and expected degree of heterogeneity. Although a high degree of primary sequence and structural integrity is expected, the final product will contain a mixture of multiple isoforms varying based on the site of posttranslational modification (e.g., glycosylation), charge and size. The exact degree of heterogeneity will depend on the nature and type of biotherapeutic. In some cases, for example for ADCs, heterogeneity is a direct result of the manufacturing procedure (e.g., conjugation chemistry) and may be controlled.[1,2] In other cases, for example, for monoclonal antibody-based compounds, sequence heterogeneity may be a minor factor. Depending on the type of heterogeneity, biotherapeutic variants could have different pharmacokinetic (PK), pharmacodynamics (PD), or immunogenic properties. Such variants may also be variably detected in bioanalytical methods used to evaluate drug exposure and efficacy.

6.08.1.1 Ligand Binding Assay

Most biotherapeutics are either directly homologous to an endogenous protein or are designed to bind to an endogenous protein component, whether in circulation (humoral) or on a cell surface. Assays can be designed to assess total or target free versus target bound drug concentrations. It is important to understand that administration of a biotherapeutic may directly impact homeostasis through a positive or a negative feedback mechanism, for example, by increased expression or accumulation of drug target, increased expression of the cell surface target, etc. Depending on the bioanalytical assay strategy, induced changes in turn may have an impact on concentration of the measured moiety of the drug, for example, when a target free drug is detected. High homology of biotherapeutic to an endogenous protein presents additional challenge when attempting to determine exposure to the drug in the presence of endogenous protein homologue. This is a common issue for enzyme replacement therapy compounds and resembles analytical challenges experienced when developing protein biomarker (BM) assays. Lastly, typical ligand binding assay (LBA) protocols rarely include sample pretreatment steps. Components of a highly complex biological matrix often present an analytical challenge due to the ability to bind to assay components and reagents. Understanding all of these and other biological considerations are critical to designing the bioanalytical strategy for a biotherapeutic. Some of the topics related to the drug concentration analysis outlined above will be discussed in more detail later in this article.

6.08.1.2 Anti-drug Antibody

In addition to a typical drug concentration analysis (PK), biotherapeutics are expected to be evaluated for the ability to induce an immune response. All biotherapeutics have the potential to trigger an immune response that can result in the production of drug-specific antibodies (anti-drug antibody, ADA) with different specificities. While the production of an anti-drug immune response may have no clinical impact in some cases, it may also lead to a reduction or complete loss of exposure (PK), an impact on pharmacological activity (efficacy impact) or in some cases result in a serious clinical sequelae (safety impact). It is therefore important to conduct a careful risk evaluation and perform ongoing monitoring of immunogenicity potential of biotherapeutics by applying sensitive and specific methods allowing detection and where needed appropriate characterization of immune response to the drug. Generation and characteristics of ADAs is typically expected to be evaluated in nonclinical and clinical studies although the exact goals of ADA evaluation at various phases of drug development are vastly different. Human nature of protein sequences and structure elements of majority of biotherapeutics makes them foreign in nonhuman species resulting in an expected and frequently observed robust immune response. Therefore, for a typical biotherapeutic, immunogenicity in a nonclinical setting is expected and not predictive of immunogenicity potential in a human study. However, an understanding of ADA development in a nonclinical study may facilitate in interpretation of drug PK, efficacy, and toxicity. Information obtained during nonclinical evaluation may therefore be useful for the overall immunogenicity risk assessment of a biotherapeutic. Immunogenicity risk evaluation is commonly viewed as an ongoing process that starts as early as identification of the drug candidate or even at the point of identifying drug modality type. Immunogenicity risk factors include product, patient, and treatment-specific characteristics. Product related factors are the nature of the drug primary sequence, homology to an endogenous protein, presence of contaminants, and drug aggregates, etc.[3] Patients' immune status, frequency, duration and route of drug administration, and drug formulation details are other important factors to be considered. Immunogenicity predictive capabilities and tools are still under development, including in silico evaluation methodologies.[4] Most typically, immunogenicity during clinical development phase includes detection and characterization techniques aiming to detect drug-specific ADAs as well as antibodies able to neutralize drug mode of action (MOA), also called neutralizing antibody (NAb). NAb specificity as well as other drug domain specificities are frequently viewed as an important element of immunogenicity evaluation in the clinic.

ADA response may comprise of various isotype of immunoglobulins including IgM, IgG, and IgEs. ADAs are relatively large proteins (e.g., IgGs are 150 kDa proteins) and may bind multivalent drug molecules simultaneously (e.g., IgM may bind up to 10 drug molecules). Therefore, ADAs may form various size immune complexes with the circulating drug which could potentially lead to an impact on the drug PK. Such immune complexes may be cleared from the system by various endogenous mechanisms, for example high-order immune complexes are taken up and destroyed by macrophages.[5] Induction of ADA and formation of immune complexes therefore has the potential to affect overall drug PK profile. The exact nature of the impact often depends on the drug molecular weight and initial drug clearance characteristics. While for large protein therapeutics with a slow clearance, immune complex formation may lead to an accelerated PK, the opposite could be expected for small peptide-based drugs.[6] In addition to a direct impact on drug PK profile, ADAs may impact bioanalytical methods used to determine drug concentration. Structural complexity of biotherapeutics frequently results in a direct interconnection between analytical protocols used to evaluate their PK and immunogenicity characteristics. ADA may directly interfere in PK assays by binding and forming immune complex with the drug in circulation and therefore blocking it from interaction with the PK assay reagents. In reverse, residual drug is expected to impact ADA detecting assays. When designing bioanalytical strategy, it is important to understand if and how the ADA may impact PK and PD measurements and vice versa. A totality of data, including PK and ADA information, should be considered to understand the true reason for the abnormal PK profile.[6]

6.08.2 Basics of LBAs

Historically and driven by the typically large molecular weight of biotherapeutics as well as high specificity requirements, bioanalysis of biologic compounds has been largely based on various types of LBA protocols. Although other analytical platforms exist

(e.g., direct activity measurement for enzyme-based therapeutics[7] and most recently LCMS applications),[8,9] LBA remains the most commonly applied platform.

LBA procedures can be defined as methods that rely on specific interactions between analyte and its cognate receptor or a specific antibody reagent. Therefore, they are based on high affinity binding to confer the requisite specificity and sensitivity to measure analyte of interest. Typically, specific reagents are required to generate a highly selective assay including monoclonal ADA and recombinant versions of drug target. In the simplest format, the analyte of interest is captured on a solid surface via a capture molecule (an antibody or ligand) and this complex is detected by the binding of a detector molecule (again an antibody or ligand) that generates a signal. Various assay set ups exist based on broad range of analytical platforms, read out technologies, and reagent types. Various LBA analytical platforms have been developed based on the type of the final read out protocol. For example, the most common LBA method is an enzyme-linked immuno-sorbent assay (ELISA) test that is based on a chromogenic, luminescent, or fluorescent read out approach. Other read out technologies include electrochemiluminescence (ECL), radioactivity detection (radioactive immunoprecipitation assay, RIA), fluorescence, time delayed fluorescence, and more. Other systems are based on physical measurements that avoid the need for reagent labeling, for example surface plasmon resonance (SPR)-based technologies. Various technology platforms that are in use and/or emerging are discussed later in this article.

The high flexibility of the LBA approach allows for various assay formats including competitive, solid and solution phase, direct binding, sandwich, and bridge and other formats. The exact choice of LBA assay format is highly dependent on the nature of the analyte in question, type of the assay matrix, required assay sensitivity, specificity, and other expected assay characteristics. Often, assay format reflects modality and MOA of the drug. For example, monoclonal antibody-based compounds are highly homologous to the endogenous human immunoglobulins but can be specifically detected in a LBA method by using drug molecular target or an anti-idiotypic antibody reagent.

6.08.2.1 LBA Assay Types

The following bioanalytical measurements are typically expected to be performed for a biotherapeutic in support of nonclinical and clinical studies:

- Drug concentration assays:
  - Quantitative measurement of drug concentrations in biological matrices designed to enable PK analysis of drug exposure in vivo. PK assays are applied during typical toxicology and clinical evaluations, including comparability studies. PK assays provide critical PK information required to establish accurate and quantitative drug exposure values, including drug area under the curve and clearance. High-quality PK assays are critical when predicting drug efficacious dose, enabling dose projection, or comparing drug product lots. An appropriate LBA protocol should be established and applied during study support to report most relevant drug analyte. This specific topic is discussed later in the article. The majority of biotherapeutic compounds that are approved or currently in development either comprise of a fully wild type human germline sequence or are highly homologous to a human protein analog. Examples include enzyme replacement therapy compounds which are to a large degree identical to a wild type protein. Monoclonal antibodies as biotherapeutic compounds are either fully human or contain limited nonhuman sequence (e.g., humanized mAbs). The specificity parameter of a biotherapeutic PK assay is therefore highly critical. Common PK assay formats are shown in **Table 1**. Due to dynamic equilibrium and saturable nature of binding between assay reagents and analyte in question, LBA methods produce a nonlinear assay response curve against analyte concentration. Most often, LBA protocols produce sigmoidal curves that are best fit using four or five parameter logistic fitting algorithms (4PL or 5PL).[10]
- Immunogenicity assessment assays:
  - ADA detection assays—designed to evaluate immune response to a biotherapeutic drug. In response to administration of a biotherapeutic, a polyclonal ADA response with various immunoglobulin isotypes should be expected. It is a regulatory expectation that ADA assays are capable of detecting all possible ADA isotypes specific to various epitopes found on the drug molecule. The semiquantitative nature of ADA assays is a critical characteristic to understand. Each ADA response is unique producing a distinct collection of anti-drug antibodies with specific range of isotypes, epitope specificities, and binding (Kd)

Table 1 Typical LBA assay formats (see also **Fig. 1**)

Assay format	*Required reagents*	*Applications*
Sandwich PK	Anti-drug antibody, drug target	Most commonly used set up for PK evaluations. Examples include mAb, ERT, and other large biotherapeutic modalities
Bridge PK	Labeled drug target	A variation of sandwich PK assay format. Applicable when analyzing for a Free mAb drug concentration
Competitive PK	Anti-drug antibody	A popular PK LBA assay set up for low MW biotherapeutics, for example, peptides
Direct binding ADA	Labeled anti-drug antibody reagent	An alternative ADA assay format
Bridge-based ADA	Labeled drug reagents	Most commonly used to analyze ADA presence

characteristics. It is therefore not possible to produce a drug-specific reference ADA material to generate assay standards and Quality Control (QC) samples. In a typical ADA assay, results are reported as titer or similar data format. The semiquantitative nature of reported values makes comparison of results obtained for a given biotherapeutic in different studies or between products challenging.

- NAb characterization assays are designed to establish neutralizing specificity of ADAs. NAb specificity can be identified as the ability to block or hinder drug MOA. Various formats of NAb assays can be roughly divided into cell-based and noncell-based protocols. The noncell-based assays are frequently designed as plate based and therefore can be viewed as a LBA protocol. The choice between cell- and noncell-based NAb assay format is driven by several factors; primary among these is the drug MOA.[11] NAb characterization is most relevant during clinical evaluations and typically expected by regulatory agencies at specific stages of clinical development. The nonclinical NAb characterization of ADA response is typically limited and conducted only if can inform on the potential safety or efficacy implications in the clinic.

– BM analysis is a common expectation during drug development including development of biotherapeutics. BM analysis will not be reviewed in this article as it has been described in detail elsewhere.[12]

6.08.2.1.1 Variety of analytes measured by LBA

Depending on the drug type, nature of the drug target, and other biological parameters, circulating drug can be presented in various forms, including free, bound (fully or partially complexed with the target), and total (free + bound). The mass action law provides a relationship between various drug analyte forms given that all system parameters are known, including drug target binding characteristics, soluble target concentration, and impact of microenvironment. Similarly, based on the mass action law, one should expect that any sample preparation (e.g., extraction), dilution, other sample manipulation procedures as well as assay incubation conditions will have an impact on the balance between the drug forms present in the sample. Details of the assay set up, nature of reagents used, and any sample pretreatment applied will define the exact nature of the drug form/analyte quantified in the method.

Free drug analyte can be defined as the active drug fraction that is not bound to either the target or drug-specific ADA, particularly NAbs. In cases when more than one target binding site is available on the drug molecule (e.g., mAb-based biotherapeutic), a partially free drug modality is also possible. Free drug analyte can be detected in an assay that is based on the ability of drug to bind its target. Because drug: target and drug: ADA interactions are dynamic and governed by the mass action law, the in vitro determined free drug concentration may not directly reflect the real in vivo situation. For example, sample dilutions are frequently used to avoid significant matrix interferences and to make sure that drug concentration falls within the assay range of quantitation. At the same time, sample dilution will perturb drug: target dynamic equilibrium and affect final reported free drug concentration. Prolonged assay incubation times and assay reagent concentrations also have a potential to influence final free drug assay outcome.[13]

Bound (or complexed) drug analyte represents drug bound to the target or to a drug-specific ADA/NAb. Bound drug also represents concentration of the drug target complex. Similar to the free drug analyte, assay conditions may impact the final reported concentration in the bound drug assay as the drug—target interaction is typically reversible and not covalent.

A total drug analyte can be defined as inclusive of all subfractions and analytes (e.g., free, bound, and partially free/bound). Depending on the drug type and assay set up and characteristics, total drug analyte can also include products of partial drug degradation in vivo. A significant degradation of a drug will likely completely negate assay ability to detect the remaining fragment. An appropriately designed total drug assay may require a sample pretreatment step in order to remove any interfering factors, including drug bound ADA or other binding proteins found in the assay matrix. Total drug assay may be considered when drug MOA and safety are not well understood or include all drug forms (i.e., free and bound). An example of a total drug assay can be a PK assay designed to detect a human mAb-based compound in a nonhuman matrix and utilizing generic anti-human IgG framework reagents. This assay may still be impacted by the presence of ADA and may require a pretreatment, for example, an acid dissociation step.[14]

In addition to a direct blocking of biotherapeutic binding sites by the drug target or ADA, primary sequence, secondary, tertiary, and higher order structural integrity are critical to maintain activity level of a biotherapeutic. Any small or large modifications to the protein sequence or structure, including posttranslational modifications, small or large sequence degradation in vivo may change final compound activity. Understanding whether the measured analyte is free from the target or ADA may not be in some cases equal to a measurement of an active drug component.[15] An assay measuring active drug concentration would need to reflect the drug MOA which may or may not be accomplished using LBA-based platform. For example, if the drug MOA is primarily based on binding to a soluble target, one can design a LBA method to determine active drug concentration. If on the other hand drug MOA includes activation of a cellular target, cell killing, or an enzyme activity, other analytical platforms would require to be considered to determine active drug concentrations.

Biologics consisting of small molecular weight toxin or synthetic polymers conjugated to protein component represent a growing category of biotherapeutics, including monoclonal antibodies conjugated to a cytotoxic drug (ADCs), polyethylene glycol conjugated proteins, and more. For these and similar categories of biologics more than one analyte may be required to fully describe compound PK. For example, for ADCs, it is not uncommon to consider up to four analytes, particularly during early clinical evaluations,[16] including drug conjugated antibody analyte, total antibody (includes conjugated and unconjugated antibody), antibody conjugated and unconjugated toxin analytes. Only some analytes are tested by LBA protocols while others require application of LCMS methods. Bioanalysis of ADCs represents a growing link between analytical platforms previously exclusively applied for large versus small MW molecules. Critically, application of LCMS for the analysis of large Molecular Weight (MW) analytes has

significantly grown based on the ADC compound example.[17] LCMS protocols used to determine large MW analytes frequently start with an affinity capture (AC) step which is highly similar to a typical LBA procedure. After proteins are partially or completely separated from other components of biological matrix, they are digested to produce unique peptide motifs which are detected by an LCMS application.[17] These AC LCMS protocols can therefore be viewed as an extension of the LBA technique in general but with a highly specific LCMS read out.

6.08.2.1.2 Critical value of assay reagents and controls

The exact nature of the analyte detected in a LBA method as well as the assay sensitivity, accuracy, and reproducibility are highly dependent on the type and specificity of the capture and detection reagents. Assay reagents are among the most critical components of the analytical system with a high impact on the final quality of the assay. Most typical reagents used in LBA protocols include polyclonal and monoclonal antibodies specific to the intended analyte, recombinant drug target, and various types of conjugates allowing to generate the final assay read out signal.[18,19] Other reagent types have been gaining momentum in recent years, including F(ab)2 based and aptamers.[20] Both promise a shorter production time, improved in vitro selection process, and significantly reduced resupply cycle time.

Lack of a sample pretreatment step in typical LBA protocol often leads to a potential interference caused by components of the sample matrix. A reagent's ability to specifically and with a high binding affinity recognize assay analyte is of highest importance. Understanding a reagent's specificity toward drug and its products of degradation could be critical in order to fully appreciate final assay specificity. For example, assays used to measure conjugated antibody analyte in support of ADCs may be sensitive to the number of small molecule toxin moieties conjugated on the antibody, also called drug to antibody ratio. Such ratio is known to change during ADC circulation in vivo, generating products of deconjugation with a lower ratio value. The ability of an assay to detect ADC components with various toxins to antibody ratios will to a large degree depend on the type of reagents used in the assay.[17]

The assay specificity characteristics should be viewed in the context of the biological matrix. For example, an anti-human IgG reagent should be specifically recognizing human mAb-based drug in a nonhuman biological matrix. Assays designed to detect human IgG in nonhuman matrix can be applied to a broad range of human mAB-based compounds and because of this it is sometimes referred to as "generic" assays. These are commonly applied during early discovery phase of drug development. Human IgG reporting generic assays are expected to report a total drug analyte concentration. The switch to an anti-drug-specific antibody reagent based assay is often made later in development and particularly important when developing clinical analytical protocols. A change from a generic anti-human IgG-based assay to a drug-specific reagent based protocol may result in a change in the nature of the analyte detected in the method. For example a change from a total to free drug analyte may occur with further implications for PK data interpretation and extrapolation. The change in the assay reagents may therefore impact overall drug PK data interpretation.

Generation of critical reagents that demonstrate appropriate quality and specificity is often a lengthy process that is highly dependent on the type of required material (**Table 2**). Early review of bioanalytical strategy including the need for required reagents is therefore highly beneficial. For example, during early discovery phase, teams are encouraged to discuss preferred analyte type to be measured and therefore assay set up and reagents needed so the material becomes available by the time clinical assay development is initiated. Relatively early initiation of specific reagents is often viewed as a business risk due to potential project attrition. Yet, it is critical to appreciate the importance of timely access to high-quality reagents to avoid suboptimal assay quality or unnecessary delays in project advancement.

Most assay reagents are produced by various types of biological processes, including in vivo (e.g., polyclonal antibody) or by cell expression (e.g., monoclonal antibody). A certain degree of lot-to-lot variability should therefore be expected and needs to be factored in as a component of reagent life cycle management strategy. For example, polyclonal antibody reagents which may be used during early development phase are difficult to reproduce due to the inherent variability of animal immune response and a potential change of ADA characteristics in a given animal as the immune response continues to mature. A change in a critical reagent lot should be carefully assessed for a potential impact on the LBA method performance, including assay accuracy, precision,

Table 2 LBA reagents characteristics and types

Reagent type	*Time to acquire*	*Characteristics*
Monoclonal anti-drug antibody	6–9 months	High single epitope specificity, high affinity
Polyclonal anti-drug antibody	3–6 months	Multiple epitope specificity, can be high affinity
Molecular drug target	Several months depending on complexity of the molecule	Generally high affinity based on the drug MOA
Generic anti-human IgG reagent	Commonly commercially available	Anti-framework specificity not compatible with human matrix
Aptamers	Potentially <3 months	Potentially high affinity binding. Limited experience across industry
F(ab)2	Potentially <3 months	Potentially high affinity binding. Limited experience across industry

and lower limit of quantification. A successful reagent life cycle strategy should account for a long term, often multiyear support needs including several assay transfers between various analytical labs.

Assay reagents are expected to be appropriately characterized, for example, by determining purity and concentration of the active component. Although routine monitoring of reagent stability is not generally required, assay performance is expected to decline if the activity of any of the assay reagents deteriorates.[18]

6.08.2.1.3 Significance and the nature of matrix interferences in LBA protocols

LBA-based protocols are expected to deliver sensitive, accurate, and precise analyte measurement with high selectivity and specificity. LBA assay performance is expected to be significantly challenged by the complexity of assay biological matrix. Potential interfering factors vary based on the matrix type (e.g., serum, plasma, or urine) but also due to distinct variations specific to disease and patient conditions. Assay interferences related to the presence of endogenous proteins, lipids, peptides, and other matrix components may negatively impact assay performance and therefore result in reporting of inaccurate drug concentration value or an incorrect ADA score.

Many assay interfering factors are matrix components that are present at various abundance levels and capable of binding to assay analyte or reagents with various affinity (**Table 3**). In other cases, presence of drug-specific interfering factors may be expected based on the drug MOA. The exact nature of interference also depends on the set up of the method and type of reagents used. For example, polyreactive (heterophilic) antibodies, rheumatoid factors (RFs), and human anti-animal antibodies (e.g., human anti-mouse antibody (HAMA)) may interfere in PK assays utilizing mouse or other nonhuman scaffold capture reagent (**Fig. 1A–C**). RF interference may lead to either under- or overreporting in PK assays. Performance of bridge format ADA assay is known to be impacted in the presence of multimeric drug target, RFs, or other drug binding proteins often causing false ADA positive sample score. Drug-specific antibodies (ADAs) either present in patients before treatment (pre-existing antibodies) or induced as a result of drug treatment, can also be viewed as highly specific interfering factors. These have been discussed earlier in the present article.

In certain cases impact of potential interference could be predicted based on an understanding of the drug biology and MOA. For example, presence of circulating drug target may impact ADA assay performance as the multimeric target can bind and bridge assay reagents similar to a multivalent ADA protein. A circulating endogenous drug target receptor may interfere in the drug PK assay by binding and blocking target assay reagent. Such potential interferences are typically evaluated early in the assay development phase by testing recovery of quality controls in the presence of endogenously added recombinant versions of known interferants or testing several individual study relevant samples from the disease population with varying levels of interferant in the presence and without the drug.

In other cases, unknown matrix interference may be observed which is typically investigated by analysis of individual matrix samples to determine relative drug recovery (observed vs. expected drug concentrations). It is critical to assess assay performance using individual drug naïve samples versus pooled matrix preparations as in the latter the relative impact of interference may be diluted. Biological matrix composition may also depend on the disease condition. For example, higher than normal amounts of RF are expected to be present in rheumatoid arthritis patient sera versus that for normal population. If study population is expected to include obese patients, an impact of lipemic matrix preparation on the assay may be considered.[21]

Various strategies have been suggested to mitigate matrix interference and improve LBA method performance. Matrix interferences may be removed or blocked via a sample pretreatment step or by applying a particular blocking agent. Both strategies rely on careful evaluation of the nature of interfering matrix component. For example, human anti-animal antibody interference can

Table 3 Common assay interfering factors

Interference type	*Definition*	*Possible cause*	*Potential assay impact*
Rheumatoid factor (RF)	Human antibodies most commonly binding to the Fc fragment of human IgG, other specificities have been described. RFs are most typically IgM isotype immunoglobulins	Disease type or unknown	PK—often leads to over recovery ADA—false positive score
Heterophilic antibody	Natural antibodies or auto-antibodies polyreactive to heterogeneous antigens	Natural Ab diversity Exposure to food antigens, animals, or animal-based proteins	Typically results in false recovery. Impacts varies on the assay type
Human anti-animal antibody (HAAA)	High affinity antibodies specific to a known animal antigen. Examples: human anti-mouse (HAMA) or human anti-bovine IgG (HABIA) antibodies	Exposure to animal proteins	Typically results in false recovery
Soluble drug target	Drug molecular target found in circulation	Drug MOA based	PK—may block drug binding to the assay reagent causing underrecovery ADA—may cause false positive reporting due to multimeric target impact on bridge ADA assay format

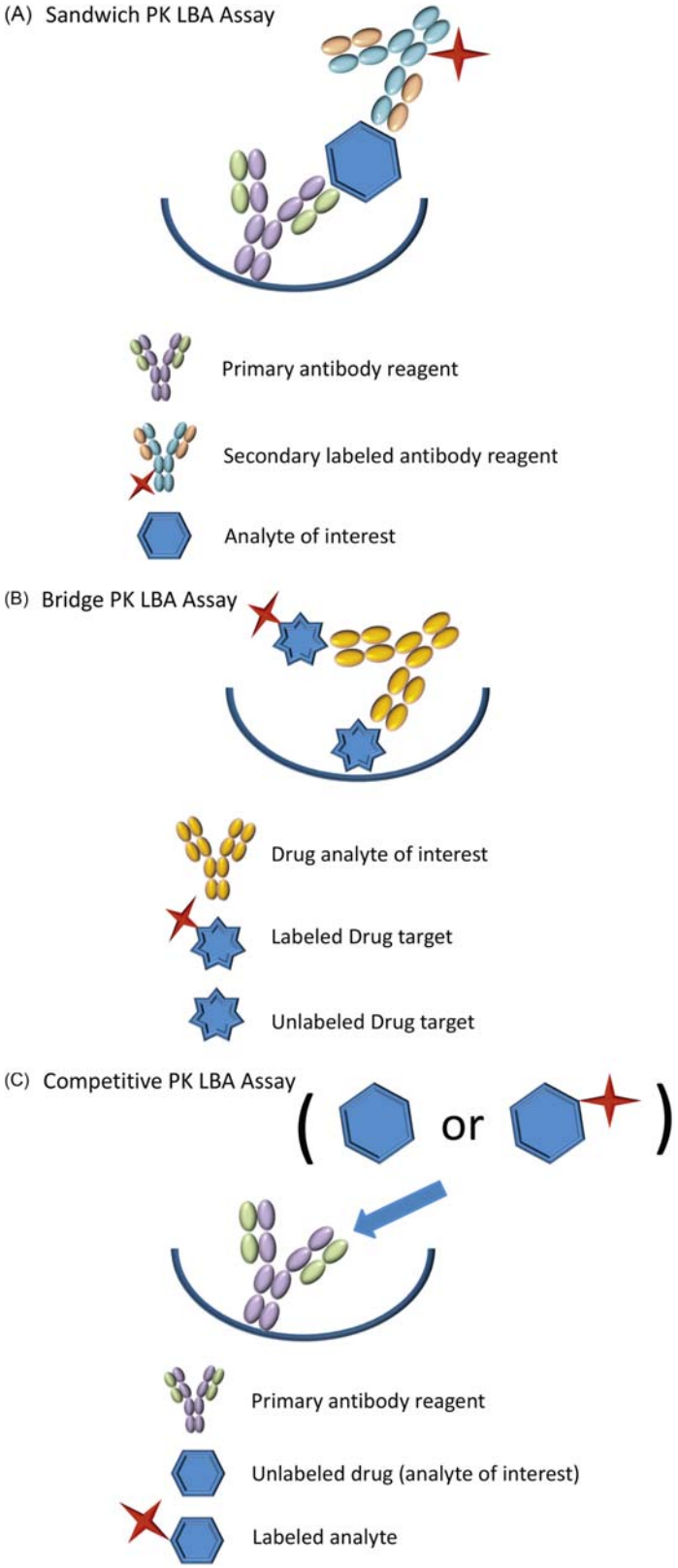

Fig. 1 Typical ligand binding assay set up and reagents. (A) Sandwich PK LBA assay. (B) Bridge PK LBA assay. (C) Competitive PK LBA assay. (D) Direct binding ADA assay. (E) Bridge ADA assay.

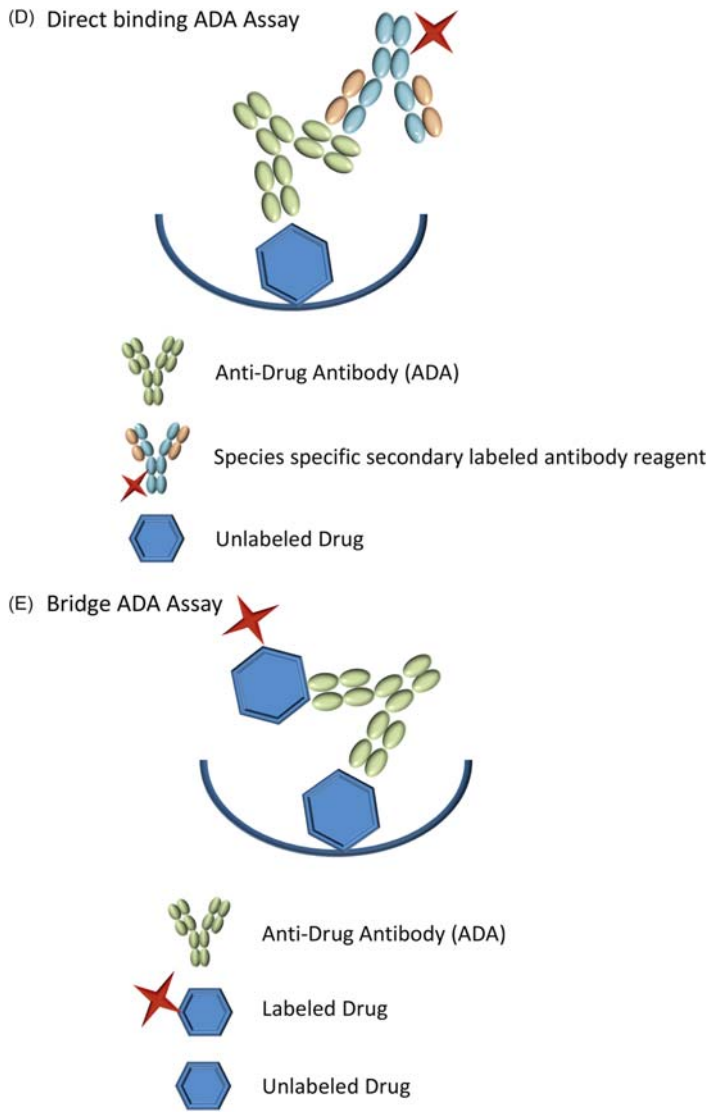

Fig. 1 (*continued*).

be addressed by including serum or immunoglobulins from respective species as one of the assay buffer components. As an example, HAMA interference can be addressed by including normal mouse serum or mouse immunoglobulins. In some cases, a known interference can be removed in a sample pretreatment step. For example, assay interference due to the presence of multimeric drug target can be mitigated by an immunoprecipitation step that removes target from the sample or by blocking drug target from binding to the drug reagent via an unrelated anti-target antibody.[22] RF could be removed from the sample by incubating with an aggregated preparation of human IgG or by using various commercially available RF binding reagents. Other drug-specific methods have also been described.

Initially observed matrix interferences may require a significant change to the assay set up or the type of reagents used. For example, use of a F(ab′)2 was shown to be beneficial versus a full length IgG reagent when mitigating RF impact.[23] Another common approach to reduce matrix interference is to apply high sample dilution. Because interfering components are generally expected to have low affinity to the assay components, high dilution factors will favor high affinity interactions between assay reagents and the analyte. High minimal required sample dilution factors can be helpful but should be expected to impact assay limits of quantitation.

In all cases, in addition to neutralization of an interfering factor, sample pretreatment step may negatively impact overall analyte recovery. For example, RF blocking reagents may also bind and remove a mAb-based drug thereby impacting assay reported results. Removing the Fc fragment from ADA assay reagent may result in an incomplete reporting of anti-drug immune responses as the immunogenicity response to the entire drug molecule is expected.[24]

It is important to note that AC LCMS applications used for analysis of biotherapeutics may be similarly impacted by low affinity binding matrix components based on the nature of the initial AC step.

6.08.2.1.4 LBA method development and qualification requirements

6.08.2.1.4.1 PK assay development and qualification

Similar to other analytical methods, LBA protocols undergo initial development phase followed by qualification or, where required, a formal validation phase. Typical steps taken during LBA PK method development phase are:

- Identification of assay analyte is a critical step generally requiring a consultation with a PK PD project lead.
- Definition of assay format and assay reagents—these are tightly connected with the analyte type but can also be driven by the availability of specific reagents and other assay components (Fig. 1A–C).
- Selection of the biological matrix may be dictated by available PK–PD modeling data, analyte stability and distribution information, impact of various matrix additives (e.g., protease inhibitors, anti-coagulates) on the analyte stability, and assay performance.
- Establishing assay minimal required dilution is a step directly relevant to the matrix interference observed in the assay, expected assay sensitivity, and analytical platform chosen for the method.
- Assay specificity and selectivity characteristics are generally assessed using individual matrix samples tested as neat or spiked with a known potential interfering substance, for example RF or drug target. Assay selectivity and specificity characteristics are tightly linked with the assay format and/or assay reagents type. Use of individual disease or study related matrix material is preferred to appropriately reflect potential matrix effects on the assay.
- Due to nonlinearity of signal response in a typical LBA method, an appropriate fitting algorithm (e.g., 4PL vs. 5PL fit) is established to achieve better assay reproducibility across assay range of quantification.
- Range of assay standard calibrators is established.
- Assay quality control including lower and upper limit of detection samples are evaluated to determine assay range of quantification, precision, and accuracy parameters. Precision and accuracy evaluation is expected to be conducted using separately prepared quality control samples (e.g., prepared at the low limit of quantification, LLOQ). Use of calibration standards in order to evaluate assay range of quantification and assay precision, accuracy/characteristics should be avoided.
- Typically dynamic range of LBA method is narrow leading to a required sample dilution during routine sample analysis. LBA methods are therefore evaluated for the assay dilution linearity by testing a high-concentration QC sample mimicking a study C_{max} concentration.

As a result of above evaluations, assay conditions may require an adjustment or a sample pretreatment step can be a necessity. For example, if a significant under- or overrecovery is observed in a relevant disease matrix, the choice of assay reagents may be re-examined.

If PK assays are expected to be used in support of a regulated study, an additional assay validation step is required. A well-established set of parameters listed below is typically evaluated as described in several regulatory guideline documents as well as in the industry white paper publications.[25–27]

- Assay range of quantification, including concentrations of assay standards used to generate calibration curve. Typically at least six nonzero standards are expected within the range of assay quantification. Additional standards may be included as anchor points outside the range of the assay in order to improve curve fitting algorithm
- Assay precision and accuracy characteristics, including tests conducted at the assay LLOQ; low, mid, and high QC levels and at the assay ULOQ level
- Assay specificity and selectivity characteristics are confirmed using final assay conditions by testing study relevant disease individual drug naïve matrix samples spiked at various QC concentrations
- Stability of the assay analyte is assessed in the assay matrix under conditions relevant to study sample testing environment, for example, −20°C/−70°C (a long-term stability, exact choice of conditions depends on the study set up), room temperature and freeze/thaw cycles
- Confirm assay dilutional linearity under the final assay conditions
- Confirm assay robustness and ruggedness if applicable

6.08.2.1.4.2 ADA assay development and qualification

ADA assays are performed to determine presence of drug-specific immunoglobulins in study samples. General ideas behind ADA assay development and qualification/validation have been carefully described in several regulatory and industry guideline documents and white papers.[28–30] Most commonly, a tier-based approach to testing for immunogenicity induction is applied which involves initial screening for putative ADA positive samples followed by specificity test to confirm drug-specific binding. Additional tests may be conducted to produce final reportable titer value as well as to characterize ADA response for the neutralizing anti-drug specificity (NAb). An example of a testing flow chart is shown in Fig. 2. During initial sample testing, screening assays are applied to distinguish between ADA positive and ADA negative samples by comparing to the screening assay cutpoint value. Samples that generate assay signal at or above assay cutpoint are defined as positive and samples that generate assay signal below cutpoint value

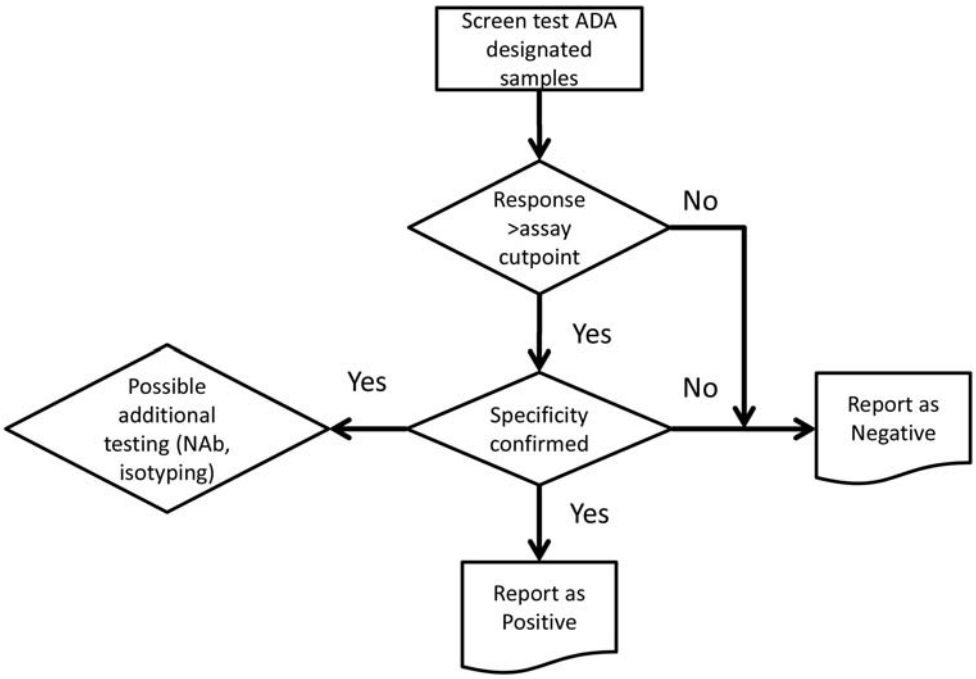

Fig. 2 Example of ADA testing flow chart.

are defined as negative. Screening assay cutpoint is commonly statistically defined as the 95th percentile of the signal distribution generated by analysis of a collection of drug naïve study relevant individual samples.[28]

Subsequent confirmatory test is often based on the ability of unlabeled drug added to sample to inhibit assay signal by blocking ADA binding to the assay reagents. The reduction in the assay signal (% inhibition) is used to determine whether ADA binding is drug specific. Similar to the screening assay, sample specific % inhibition value is compared to the confirmatory assay cutoff value that was established during assay validation phase based on analysis of drug naïve study relevant individual matrix samples. Sample is defined as ADA positive and drug specific if the percent inhibition value is at or above the confirmatory assay cutoff value. If sample produces % inhibition below confirmatory cutoff, it is defined as nonspecific to the drug. Similar to the screen assay cutpoint, confirmatory cutoff value is statistically defined as a 99th (or 99.9th) percentile of the distribution obtained by analysis of drug naïve study relevant individual samples.

Various ADA screening assay formats and analytical platforms are available with the final assay type driven by the specific nature of biotherapeutic and species type. A direct binding format (**Fig. 1D**) may be applied when detecting immune response to a human biotherapeutic in animal studies. The same may be evaluated for a human matrix based assay but developers should be aware of a potentially high background signal due to a high concentration of endogenous human immunoglobulins. A bridging assay format (**Fig. 1E**) provides appropriately specific and sensitive methods and addresses many of the matrix interference related issues. Bridge assay format is commonly applied when detecting immune responses in clinical studies. This allows one to address species specificity as the same assay reagents can be applied in both nonclinical and clinical matrices. Various types of platforms are used in the ADA detecting protocols including methods with chromogenic (ELISA), ECL, luminescence, and radioactivity (RIA) detection. Label-free platforms are also applied (e.g., SPR).

Due to the diversity of a typical ADA response (polyclonality, variations of isotypes and affinities of response found in particular sample), it is not possible to generate a true ADA assay reference material. Positive (PC) and negative (NC) controls are applied to monitor assay performance based on the specific PC and NC performance characteristics that are established during assay validation phase. Assay PCs are typically monoclonal or polyclonal drug-specific nonhuman antibodies obtained by hyperimmunizing laboratory animals, for example mice, rabbits, or monkeys. Assay NC is typically prepared using drug naïve study specific matrix. Assay sensitivity is one of the parameters assessed during assay development based on PC material performance. Although as stated above PC does not appropriately represent incurred study sample, it is a regulatory expectation to ensure that an ADA method should detect at least 250 and 500 ng mL^{-1} of PC material in clinical and nonclinical assays, respectively.

Based on the typical assay set up, ADA protocols are known to be impacted by the presence of residual drug in the sample. ADA assay drug tolerance, or ability to detect ADA in the presence of unlabeled drug, is a critical characteristic of a method. It can be evaluated based on the performance of the assay PC material although direct application of the drug tolerance value toward incurred study sample analysis is discouraged. Various methods have been developed to improve ADA assay drug tolerance parameter including assay method modification and use of sample pretreatment.[31,32]

Typical steps applied during ADA method development phase are listed below:

- Assay reagents identification, including generation and selection of the assay PC
- Identification of the NC and assay matrix
- Selection of the assay analytical platform and format, generation of other assay reagents (e.g., detection reagent)
- Evaluation of assay buffer, reagent conjugation conditions, matrix starting dilution, and incubation times with the goal to minimize irrelevant nonspecific binding but retain assay ability to detect drug-specific ADA
- Evaluation of assay sensitivity and drug tolerance with respect to PC
- Selection of confirmatory assay conditions, including unlabeled drug concentration added to the sample

Similar to PK assays, ADA protocols expected to be used in support of regulated studies require additional assay validation steps. A set of parameters listed below is typically evaluated as described in several regulatory guideline documents as well as in the industry White paper publications.[24,28–30]

- Screening assay cutpoint and confirmatory cutoff values. The same set of data generated using analysis of individual matrix samples allows to understand potential sources of interference
- Assay precision, robustness, and sensitivity are evaluated based on the performance of the assay PC material
- Acceptance criteria for PC and NC materials are established

Similar steps and parameters are typically assessed during NAb assay development and validation.[11,33]

6.08.3 LBA Technology Platforms—Past, Present, and Future

Rosalyn Yalow won the Nobel Prize for Medicine in 1977 for the development of radio-immunoassays of peptide hormones. The technique was introduced as a way to measure insulin levels in plasma and was based on the finding that insulin-binding antibodies are present in the serum of patients treated with insulin.[34,35] This revolutionized the field of clinical chemistry, because it was the first time one was able to measure hormone levels in blood using an in vitro method. Changes to the mode of capture and/or detection can enhance the sensitivity of detection and/or linear range of the assay. Radioimmunoassays use isotope labeled detectors that significantly enhance the sensitivity of the assays. However, nonisotopic methods that do not require the analyst to be exposed to harmful radiolabeled reagents have taken the place of radiometric assays.

LBA technologies have evolved considerably over the years from the birth of radio-immunoassays in 1959 by Berson and Yalow to present day assay systems with a myriad of highly sensitive, nonradiometric methods. In an ELISA, the detector is coupled to an enzyme such as horse radish peroxidase (HRP) or alkaline phosphatase. Upon addition of the corresponding substrate, the substrate is converted to a colored product. The amount of color produced is proportional to the amount of complex captured and therefore provides a means of quantitation of the analyte. Such LBAs are referred to as colorimetric ELISAs. Traditionally, bioanalytical labs have relied on colorimetric ELISAs for the PK determination of biotherapeutics and these have become the gold standard for LBAs. ELISAs continue to be the workhorse of the ligand binding bioanalytical lab and offer several advantages such as ease of execution, nonproprietary reagents, and instruments that are readily available in most bioanalytical and clinical labs. However, colorimetric ELISAs are often limited in the range and sometimes sensitivity of the assay. In addition, they often require multiple washes between steps and when performed manually without automation can be rather tedious. Changing the substrate in an ELISA to a chemiluminescent substrate can enhance the range and sensitivity of the assay even with the same reagents. Technology advances have given birth to many new LBA platforms over the years, several of which have gained wide use in bioanalysis. Some of these technologies are described later, along with some considerations regarding advantages and disadvantages. More information can be found in several recent review publications describing next generation LBA platforms and read out technologies.[36–39]

6.08.3.1 ECL Assays

The application of electrogenerated chemiluminescence or ECL to LBAs began in early 1990s.[40–42] ECL immunoassays may be described as an ELISA with modified capture surfaces and a different readout. The ECL immunoassay platform can be implemented in various formats similar to ELISAs such as sandwich, competitive, or bridging assays.[43] Capture antibodies may be passively coated or biotinylated and captured on streptavidin-coated plates. The basic principle of ECL is the generation of a species at an electrode surface when a voltage is applied, which then undergo chemical electron-transfer reactions to form excited states that generate light. In ECL immunoassays, the detector molecule (e.g., detector antibody) is labeled with an electrochemiluminescent label. Ruthenium bipyridyl derivative [$Ru(bpy)_3^{2+}$] is the most commonly used label coupled with tripropylamine (TPA) as the co-reactant. Immune complexes are captured on the surface of an electrode and voltage is applied to the electrode in the presence of the co-reactant (TPA). Electrical stimulation triggers the reaction of ruthenium bipyridyl with TPA resulting in the emission of light followed by subsequent regeneration of the $Ru(bpy)_3^{2+}$ species which can then cycle multiple times through the reaction for signal amplification. The proposed mechanism of the reaction has been described in detail by Blackburn et al.[41] Instrumentation for ECL immunoassays requires a reaction vessel, a means to conduct electric current and a way to measure the emitted light. ORIGEN-1 was the first commercially available ECL instrument from Igen International Inc. (later BioVeris Corp. and now owned by Roche Diagnostics Corp.) that uses magnetic beads to bind immune complexes, which are then captured on a platinum electrode

which conducts electric current when voltage is applied. The resulting light signal is measured by a photomultiplier tube. This technology platform found widespread use in several bioanalytical labs in the early to mid-2000s. However, this is no longer available as a standalone analyzer for bioanalytical labs and a plate-based system from Meso Scale Discovery (MSD), LLC has become the ECL platform of choice in the bioanalytical lab. This system uses disposable microtiter plates with the electrodes integrated into the bottom of the plates and the signal captured using a cooled CCD (charge coupled device) camera.

6.08.3.1.1 Pros and cons/considerations

- ECL immunoassays have the advantage of being highly sensitive with a wide dynamic range when compared with the ELISA counterpart. These assays are also less susceptible to matrix interferences.
- The MSD system also offers multiplexing capabilities—with multiple capture spots per well, allowing the simultaneous capture and detection of up to 10 analytes per well. Some recent advances allow the user to create custom multiplexed assays in the lab which is an added benefit.
- Ruthenylation is via NHS-ester linkage (similar to biotinylation and takes place through –NH side chains. When labeling detector molecules, particularly if the detector is a small protein one should pay attention to the number and location of lysines in the molecule to ensure that labeling does not render the molecule inert in the binding reaction.
- Bridging across multiple batches of labeled reagents can be tricky with validated assays. Therefore, one should characterize the conjugates thoroughly to obtain information on average number of labels/molecule, species distribution, etc.
- Potential for cross-talk between wells when a high signal sample is next to a low signal sample.

6.08.3.2 Gyrolab

The Gyrolab platform from Gyros AB combines microfluidic technology and fluorescent detection in a fully automated system. The technology is based on the proprietary compact disks (CD) engineered with microstructures and highly reproducible nanoliter microfluidics.[44,45] Each CD contains 12 segments, each comprised of 8 microstructures. Each microstructure contains a sample delivery channel, a column packed with streptavidin beads, a common reagent channel, and hydrophobic barriers to gate and control the flow of liquids when the CD is subjected to different rotational speeds. The instrument contains two carousels—one for microtiter plates that contain samples and reagents, the other for CDs. Delivery of liquids is by a robotic arm that injects excess volumes. The overflow volumes are removed by an initial low speed spin, followed by a higher speed spin that allows the liquid to overcome the hydrophobic barriers. Assay formats are similar to ELISA with a biotinylated capture antibody that is captured on the streptavidin columns and an Alexa-fluor-labeled detection antibody.

6.08.3.2.1 Pros and cons/considerations

- Small sample and reagent volumes, significantly lower than ELISA or ECL even with the dead volume and overflow volumes taken into consideration
- Wide dynamic range, low background, high signal, reduced matrix effects (lower than ELISA and ECL)
- Fully automated system with higher throughput
- Dynamic range can be extended by using CDs of different capacities (20 nL, 200 nL, and 1000 nL). For example, going from a Bioaffy 200 CD to a 20 nL, can increase the ULOQ, whereas the 1000 nL CD can increase the sensitivity (or lower the LLOQ) of the assay
- CDs are expensive

6.08.3.3 Biacore

This is the first label-free technology for the detection and measurement of biomolecular interactions that is based on SPR.[46] The SPR phenomenon occurs when polarized light, under conditions of total internal reflection, strikes an electrically conducting gold layer at the interface between media of different refractive indices: the glass of a sensor surface (high refractive index) and a buffer (low refractive index). When molecules are immobilized on a sensor surface there is a change in refractive index that changes the angle at which reduced intensity polarized light is reflected. This change in angle is proportional to the mass of bound material. The Biacore systems comprise surface chemistry, flow systems, and optical detection methods that generate profiles of binding and dissociation in real time enabling determination of specificity, affinity, kinetic behavior, and sample concentration. This technology has been available since 1990 and came into use in bioanalytical labs in early 2000s, particularly in the characterization of binding interactions and subsequently also used in detection of ADAs.[47,48]

6.08.3.3.1 Pros and cons/considerations

- Provides all the advantages of label-free technologies such as no labeling of reagents or analyte needed. Secondly, removes the risk of affecting protein: protein interactions between the analyte and reagents due to masking of binding sites
- Low throughput on the Biacore X100 (max 15 samples) but increased throughput on the newer T100 (384 samples)
- Sensor chips are expensive and analysts need some training on the platform

6.08.3.4 ForteBio

ForteBio is based on an optical principle called biolayer interferometry which is also a label-free technology for measuring biomolecular interactions.[49] In this system, the interference pattern of white light reflected from two surfaces is analyzed—a layer of immobilized protein on the biosensor tip and an internal reference layer. The ligand is immobilized on the biosensor tip and binding of the ligand to analyte in solution causes a change in optical thickness resulting in a wavelength shift that is proportional to the number of molecules bound to the sensor tip. In the Octet system from ForteBio, the tip of a fiber optic probe is coated with ligand and acts as the biosensor. That tip is then dipped into the sample containing analyte in a microtiter plate. This also earned the technology the name Dip-and-Read ELISA or ELISA-on-a-stick. The assay is read by shining white light down the length of the fiber. Interference between light reflecting off-the reference and immobilized surfaces of the tip creates a distinctive pattern of light returning up the fiber. As molecules bind to the immobilized sensor surface, the interference pattern changes proportional to the amount of analyte bound to the tip. This allows the technology to be used for quantitation of analyte as well as for kinetic measurements. In the bioanalytical lab this technology has gained utility in screening and characterization of reagents.

6.08.3.4.1 Pros and cons/considerations

- The biosensor detector surface is brought to the sample and does not use any microfluidics
- Nondestructive method for detection of analyte
- Minimizes matrix and other interferences since detection occurs at the biosensor tip. This allows the system to be used to screen hybridoma supernatants, cell culture samples, and complex matrices with minimal sample pretreatment
- No labeling of capture or detector reagents required which has a twofold advantage. Firstly, no labeling of reagents or analyte needed. Secondly, removes the risk of affecting protein: protein interactions between the analyte and reagents due to masking of binding sites

6.08.3.5 Luminex

This is probably one of the oldest multiplexing technologies in LBAs and has been in use since 2000.[50,51] It utilizes microsphere beads that are dyed with red and infrared fluorophores of varying intensities. By coating each type of microsphere with a different capture reagent, multiple analytes can be captured simultaneously from the sample and differentially measured based on the intensity of each dye by a flow cytometer. Theoretically, the Luminex system can detect up to 100 different analytes in various matrices such as serum, plasma, cell culture supernatants, and even in tears.[52] This technology has been used particularly in the detection and/or quantitation of multiple BMs from clinical samples allowing researchers to establish correlations with disease indication or treatment outcomes. For example, an assay to detect multiple different pro-inflammatory cytokines was developed on the Luminex platform from the same sample volume that would allow the detection of one cytokine using a traditional ELISA in juvenile idiopathic arthritis where sample volumes from pediatric population are limiting.[53]

6.08.3.5.1 Pros and cons/considerations

- Minimum sample volume of 25–50 μL is required which could be limiting in some cases. However, since multiple analytes can be measured with the same sample volume that would translate to reduced sample volume requirements overall
- Several multiplex kits are available in the market that can be quickly implemented
- For custom assay development, initial effort is required with labeling of individual reagents and establishing little or no cross-reactivity with other analytes in the multiplex
- Range of detection for each analyte cannot be optimized as the assay measures multiple analytes at the same time. For instance, at a given sample dilution while one analyte may be above the limit of detection, another analyte may require lower dilution
- Data acquisition, analysis, and representation is very complex with multiple analytes and increases as the number of analytes in the assay increases

6.08.3.6 Acoustic Membrane Microparticle Technology on the ViBE Platform (Bioscale)

This technology available from BioScale utilizes a nonoptical detection system which determines analyte concentration by measuring changes in the oscillating frequency of a vibrating biosensor membrane made from piezoelectric material. In this system, the capture reagent is on magnetic microparticles and the detection reagent is tagged with a fluorescent label such as fluorescein. Immune complexes are formed in solution and captured by flowing the solution over the membrane, where a magnetic field drives the magnetic beads to the surface of the biosensor. Immune complexes are captured by anti-fluorescein antibodies on the membrane surface. When the magnetic field is removed, only the bound complexes remain while unbound components are washed away. The signal measured in this system is the change in vibrational frequency which is proportional to the mass of magnetic bead complexes that remain bound to the biosensor. Upon completion, the surface of the sensor is regenerated and returned to baseline frequency for another round of analysis. Over the past few years there have been reports in literature of the application of this technology platform to various bioanalytical assays such as BMs, PK, and ADA.[54–57]

6.08.3.6.1 Pros and cons/considerations

- Low interference from matrix and other components; demonstrated utility across several different matrices such as serum, plasma, urine, ascites, tissue extracts, and cell culture supernatants
- Highly sensitive due to amplification of the signal
- Walk-away ability on the ViBE instrument for this technology. However due to limited deck capacity, the throughput is not very high (two to three microtiter plates at a time) despite the automated platform
- Bioscale provides labeling kits for custom assay development as well as off-the-shelf kits for cell signaling, cytokines, and endocrines

6.08.3.7 SIMOA (Quanterix)

This is a proprietary ultra-sensitive technology available from Quanterix and stands for single molecule array (SIMOA). The technology is based on detection of single molecules in femtoliter-sized wells, where immune complexes captured on paramagnetic beads are isolated and sealed in the presence of enzyme substrate. The sealing step confines the fluorescent product of the enzyme–substrate reaction to femtoliter volumes to generate high local concentrations of the fluorescent product, and the fluorescence generated by a single enzyme can be detected on an uncooled CCD camera using a white light excitation source. This is an ultra-sensitive technology that has application particularly in the detection of BMs that may be present in very low levels. Sensitivity of 30 fg mL^{-1} for detection of prostate-specific antigen and 10 fg mL^{-1} for tumor necrosis factor alpha have been reported.[58]

6.08.3.7.1 Pros and cons/considerations

- Ultra-sensitive technology that has begun to gain use particularly in the detection of BMs that may be present in very low levels.
- The platform uses the same reagents as a traditional ELISA to form immune complexes and uses significantly less reagents.
- Ability to multiplex—this platform has been successfully used to detect multiple analytes.[59]
- Data acquisition is a fast process because the final signal acquisition is done on a planar array with standard imaging.
- Fully automated platform where the instrument can perform sample dilution, mixing, washing, incubation, and data acquisition steps.

6.08.3.8 Singulex Erenna

Single molecule counting technology by Singulex is another ultra-sensitive immunoassay system where the first step is similar to a traditional ELISA and involves the formation of an immune complex using capture and detection reagents.[60,61] The immune complexes are then eluted using a modified elution step such that the complex is broken apart and the eluate is drawn into the Erenna system capillary tube which contains a very small interrogation space that is illuminated by a laser. Single fluorescently labeled molecules are detected as they generate flashes of light when they pass through the interrogation space. Fluorescence events are digitally counted by photon detectors. The technology is highly sensitive and limit of quantitation in the fg mL^{-1} range have been reported for measurement of various cytokines in serum[62] and in the pg mL^{-1} range for oligomers of Aβ in Spinal Cerebral Fluid (SCF).[63] Similar to the SIMOA system, the high sensitivity of this immunoassay platform has found application in the quantitation of BMs, particularly those that are present in very low levels and cannot be detected by traditional methods.

6.08.3.8.1 Pros and cons/considerations

- Highly sensitive assay with the ability to measure low pg mL^{-1} and even fg mL^{-1} concentrations of analyte
- Flexibility of bead- or plate-based assays in 96- or 384-well format
- Although pg mL^{-1} sensitivity has been reported for plate-based assay format, this may potentially produce lower sensitivity assays versus that for bead-based format methods[64]
- Method involves several washing, spinning, and plate transfer steps which can increase variability[62] and the system does not offer any automation, although off-line automation may be done
- Relatively low throughput as sampling occurs one well at a time and up to 1 min per well read time
- Cannot be used for multiplexing and carryover can be an issue

6.08.3.9 Maverick (Genalyte)

Technology utilizes a proprietary multiplex detection system based on silicon photonics that utilizes ring resonance to measure binding of molecules to sensors on a miniature silicon chip.[65] Silicon photonic devices comprised of 128 micro-fabricated rings are arrayed on a single disposable chip in a pattern of four per analyte resulting in 32 clusters. The Maverick system detects changes in resonance wavelength as molecules bind to the surface of the sensor for real-time measurement of ligand binding. Calibrators establish concentration-dependent spectral shifts that can be used for quantitation of analyte in unknown samples. Samples

prepared in 96 well plates are loaded into the instrument where an automated fluidics system draws 2–5 μL of sample into the specific array, followed by presentation of the array to the detection system. It can be used as a label-free technology or enhanced using enzyme conjugates (such as Streptavidin conjugated to horse radish peroxidase (SA-HRP)).

6.08.3.9.1 Pros and cons/considerations

- System is a walk away once preparatory steps are completed
- Uses low sample volume
- Multiplexing capability
- Useful for BM measurements
- Limited use to-date for other applications in the bioanalytical lab

6.08.3.10 Imperacer Immuno-Polymerase Chain Reaction (PCR) (Chimera Biotech)

As the name indicates, this technology combines LBA with the signal amplification power of quantitative PCR (qPCR) read out.[39,66] Analyte is captured using an antibody, while the detector antibody is conjugated to DNA instead of an enzyme as in a traditional ELISA. Detection is by amplification of the DNA via qPCR. This technology is proprietary and available from Chimera Biotech. The amplification power of PCR provides the method with high sensitivity which has been applied for the measurement of several BMs such as those for neurodegenerative disorders in the periphery rather than brain tissue or cerebrospinal fluid, microsampling for metabolic BMs, and quantitating cytokines at <1 pg mL^{-1} range. In addition to BM measurements, Imperacer has also been applied in PK measurements and ADA detection in immunogenicity assays.

6.08.3.10.1 Pros and cons/considerations

- High sensitivity due to amplification of signal by PCR; but amplification of nonspecific signals can lead to high background, therefore it is important to use reagents with high specificity
- Nonspecific interactions can be reduced by diluting samples, while still obtaining sufficient sensitivity

6.08.3.11 SQI Diagnostics

This is a dual-layer multiplexing technology with the ability to multiplex at both capture and detection levels.[67] Each well in the microtiter plate contains a grid of 16×13 spots that can be printed with different capture antibodies. Upon binding of analyte from sample, a mixture of detection antibodies that are differentially labeled are added. Detection is by a multiwavelength scanner that allows the simultaneous detection of multiple fluorescent labels. The platform is integrated into a fully automated system that can automate all steps from pipetting, washing, and drying of plates, to reading on the multiwavelength fluorescent microarray scanner and data analysis. The technology has application in immunogenicity testing for isotyping and epitope mapping in one step.

6.08.3.11.1 Pros and cons/considerations

- The large number of spots per well allow inclusion of six to seven replicates for each capture reagent
- Plates have to be printed with capture reagents—this can become costly and rate limiting
- Fully automated system with walk away ability
- Data analysis can be complex due to the amount of data that is generated from each plate

The above list of technologies is by no means exhaustive, but provides a brief overview of some of the available technologies that are available for use in the bioanalytical lab. The choice of platform will depend on many factors such as flexibility of the platform, sample volume requirements, throughput needs, ease of assay development, availability of the platform, 21 CFR Part 11 compliance requirements,[68] costs of instrument and/or consumables, reagent labeling requirements, sensitivity, and multiplexing needs to name just a few. A comparison of some of these technologies with respect to sensitivity, multiplexing, throughput, and real-time measurement was published by the Emerging Technologies working group within the Ligand Binding Assay Bioanalytical Focus Group of the AAPS Biotec section.[36–39] As technologies continue to evolve at a rapid pace, several improvements to the technology, its interface with other systems (such as Laboratory Information Management System (LIMS)' systems) or compliance with the 21 CFR Part 11 may have improved since the time of publication of these review articles.

6.08.4 Evolving Landscape of LBA Technologies and Regulatory Expectations

Advanced LBA technologies are moving away from historical plate-based approaches. Improved robustness and ability to continuously run higher number of samples in some of the new technologies allows for a larger run batch leading to potential need to include more than a single set of standards and QCs with additional QCs placed throughout the run batch. Questions regarding

overall number and positioning of the assay QCs through the run batch will need to be addressed in interactions with regulatory agencies. High precision of some of the new generation LBA technologies also calls into question the need for replicate analysis of QCs and unknown samples. While sample testing in duplicates or even triplicates has been a staple for many years, an active discussion regarding potential use of single replicate testing has been recently initiated.

In addition to advancements within the LBA field, there has been a significant progress in merging traditional LCMS and ligand binding technologies. Hybrid AC LCMS protocols have been developed and reported for a variety of endogenous proteins and biotherapeutics, for example, ADCs[17,69–71] offering specificity and sensitivity obtained through the initial AC step combined with analyte specificity obtained via the use of LCMS methodology.

As pointed out earlier in this article, the landscape of LBA technologies continues to evolve. This is in part promoted by evolution of biotherapeutic modalities which now include various types of alternative scaffold proteins, bi-specific antibodies, ADCs, and nucleotide-based biologics. Often, complexity of the drug structure is tightly associated with a high degree of complexity of the drug MOA. Multifaceted and frequently multistep MOA presents additional requirements to the type of analyte to be measured in the assay, sensitivity and selectivity of the method, requirement to handle smaller sample volume, and need for a broad assay dynamic range. Many of the new generation LBA technologies are designed to address some of these considerations, but new challenges abound. With the rapid pace of advancement in science and technology, and the need for personalized medicine, one can envision a future where drug concentration and other bioanalytical measurements become a routine test that can be run within minutes in a doctor's office or clinic with a tiny finger prick.

See also: 4.01. Role of Predictive ADME/PK in Drug Discovery, Safety Assessment, and Clinical Development.

References

1. Carter, P. J.; Senter, P. D. Antibody-Drug Conjugates for Cancer Therapy. *Cancer J.* **2008,** *14* (3), 154–169.
2. Rosenberg, A. S. Immunogenicity of Biological Therapeutics: A Hierarchy of Concerns. *Dev. Biol.* **2003,** *112,* 15–21.
3. Mire-Sluis, A. R.; Barrett, Y. C.; Devanarayan, V.; Koren, E.; Liu, H.; Maia, M.; et al. Recommendations for the Design and Optimization of Immunoassays Used in the Detection of Host Antibodies Against Biotechnology Products. *J. Immunol. Methods* **2004,** *289* (1–2), 1–16. http://dx.doi.org/10.1016/j.jim.2004.06.002.
4. Koren, E.; De Groot, A. S.; Jawa, V.; Beck, K. D.; Boone, T.; Rivera, D.; et al. Clinical Validation of the "In Silico" Prediction of Immunogenicity of a Human Recombinant Therapeutic Protein. *Clin. Immunol.* **2007,** *124* (1), 26–32. http://dx.doi.org/10.1016/j.clim.2007.03.544.
5. Rojas, J. R.; Taylor, R. P.; Cunningham, M. R.; Rutkoski, T. J.; Vennarini, J.; Jang, H.; et al. Formation, Distribution, and Elimination of Infliximab and Anti-infliximab Immune Complexes in Cynomolgus Monkeys. *J. Pharmacol. Exp. Ther.* **2005,** *313* (2), 578–585. http://dx.doi.org/10.1124/jpet.104.079277.
6. Sailstad, J. M.; Amaravadi, L.; Clements-Egan, A.; Gorovits, B.; Myler, H. A.; Pillutla, R. C.; et al. A White Paper—Consensus and Recommendations of a Global Harmonization Team on Assessing the Impact of Immunogenicity on Pharmacokinetic Measurements. *AAPS J.* **2014,** *16* (3), 488–498. http://dx.doi.org/10.1208/s12248-014-9582-y.
7. Lee, K.; Jin, X.; Zhang, K.; Copertino, L.; Andrews, L.; Baker-Malcolm, J.; et al. A Biochemical and Pharmacological Comparison of Enzyme Replacement Therapies for the Glycolipid Storage Disorder Fabry Disease. *Glycobiology* **2003,** *13* (4), 305–313. http://dx.doi.org/10.1093/glycob/cwg034.
8. Stevenson, L.; Garofolo, F.; DeSilva, B.; Dumont, I.; Martinez, S.; Rocci, M.; et al. 2013 White Paper on Recent Issues in Bioanalysis: 'Hybrid'—the Best of LBA and LCMS. *Bioanalysis* **2013,** *5* (23), 2903–2918. http://dx.doi.org/10.4155/bio.13.238.
9. Jenkins, R.; Duggan, J. X.; Aubry, A. F.; Zeng, J.; Lee, J. W.; Cojocaru, L.; et al. Recommendations for Validation of LC-MS/MS Bioanalytical Methods for Protein Biotherapeutics. *AAPS J.* **2015,** *17* (1), 1–16. http://dx.doi.org/10.1208/s12248-014-9685-5.
10. Findlay, J. W.; Dillard, R. F. Appropriate Calibration Curve Fitting in Ligand Binding Assays. *AAPS J.* **2007,** *9* (2), E260–E267. http://dx.doi.org/10.1208/aapsj0902029.
11. Gupta, S.; Indelicato, S. R.; Jethwa, V.; Kawabata, T.; Kelley, M.; Mire-Sluis, A. R.; et al. Recommendations for the Design, Optimization, and Qualification of Cell-Based Assays Used for the Detection of Neutralizing Antibody Responses Elicited to Biological Therapeutics. *J. Immunol. Methods* **2007,** *321* (1–2), 1–18.
12. DePrimo, S. E. Comprehensive Medicinal Chemistry II. *Drug Discov. Technol.* **2007,** *3,* 69–85. http://dx.doi.org/10.1016/B0-08-045044-X/00076-6. http://www.sciencedirect.com/science/article/pii/B008045044X000766.
13. Lee, J. W.; Kelley, M.; King, L. E.; Yang, J.; Salimi-Moosavi, H.; Tang, M. T.; et al. Bioanalytical Approaches to Quantify "Total" and "Free" Therapeutic Antibodies and Their Targets: Technical Challenges and PK/PD Applications Over the Course of Drug Development. *AAPS J.* **2011,** *13* (1), 99–110. http://dx.doi.org/10.1208/s12248-011-9251-3.
14. Kelley, M.; Ahene, A. B.; Gorovits, B.; Kamerud, J.; King, L. E.; McIntosh, T.; et al. Theoretical Considerations and Practical Approaches to Address the Effect of Anti-drug Antibody (ADA) on Quantification of Biotherapeutics in Circulation. *AAPS J.* **2013,** *15* (3), 646–658. http://dx.doi.org/10.1208/s12248-013-9468-4.
15. Heinrich, J.; Staack, R. F.; Stubenrauch, K. G.; Papadimitriou, A. Proposal for a Harmonized Descriptive Analyte Nomenclature for Quantitative Large-Molecule Bioanalysis. *Bioanalysis* **2015,** *7* (24), 3057–3062. http://dx.doi.org/10.4155/bio.15.218.
16. Gorovits, B.; Alley, S. C.; Bilic, S.; Booth, B.; Kaur, S.; Oldfield, P.; et al. Bioanalysis of Antibody-Drug Conjugates: American Association of Pharmaceutical Scientists Antibody-Drug Conjugate Working Group Position Paper. *Bioanalysis* **2013,** *5* (9), 997–1006. http://dx.doi.org/10.4155/bio.13.38.
17. Kaur, S.; Xu, K.; Saad, O. M.; Dere, R. C.; Carrasco-Triguero, M. Bioanalytical Assay Strategies for the Development of Antibody Drug Conjugate Biotherapeutics. *Bioanalysis* **2013,** *5* (2), 201–226. http://dx.doi.org/10.4155/bio.12.299.
18. O'Hara, D. M.; Theobald, V.; Egan, A. C.; Usansky, J.; Krishna, M.; TerWee, J.; et al. Ligand Binding Assays in the 21st Century Laboratory: Recommendations for Characterization and Supply of Critical Reagents. *AAPS J.* **2012,** *14* (2), 316–328. http://dx.doi.org/10.1208/s12248-012-9334-9.
19. Rup, B.; O'Hara, D. Critical Ligand Binding Reagent Preparation/Selection: When Specificity Depends on Reagents. *AAPS J.* **2007,** *9* (2), E148–E155. http://dx.doi.org/10.1208/aapsj0902016.
20. Porschewski, P.; Grattinger, M. A.; Klenzke, K.; Erpenbach, A.; Blind, M. R.; Schafer, F. Using Aptamers as Capture Reagents in Bead-Based Assay Systems for Diagnostics and Hit Identification. *J. Biomol. Screen.* **2006,** *11* (7), 773–781. http://dx.doi.org/10.1177/1087057106292138.
21. Stevenson, L.; Kelley, M.; Gorovits, B.; Kingsley, C.; Myler, H.; Österlund, K.; et al. Consensus and Recommendations of the L2 Global Harmonization Team, Large Molecule Specific Assay Operation for Pharmacokinetic Ligand Binding Assays. *AAPS J.* **2013,** *16,* 83. http://dx.doi.org/10.1208/s12248-013-9542-y.
22. Gorovits, B.; McNally, J.; Fiorotti, C.; Leung, S. Protein-Based Matrix Interferences in Ligand-Binding Assays. *Bioanalysis* **2014,** *6* (8), 1131–1140. http://dx.doi.org/10.4155/bio.14.56.
23. Rispens, T.; de Vrieze, H.; de Groot, E.; Wouters, D.; Stapel, S.; Wolbink, G. J.; et al. Antibodies to Constant Domains of Therapeutic Monoclonal Antibodies: Anti-hinge Antibodies in Immunogenicity Testing. *J. Immunol. Methods* **2012,** *375* (1–2), 93–99. http://dx.doi.org/10.1016/j.jim.2011.09.011.

24. Committee for Medicinal Products for Human Use C. Guideline on Immunogenicity Assessment of Biotechnology Derived Therapeutic Proteins; Doc Ref EMEA/CHMP/BMWP/14327/2006; 2007.
25. DeSilva, B.; Smith, W.; Weiner, R.; Kelley, M.; Smolec, J.; Lee, B.; et al. Recommendations for the Bioanalytical Method Validation of Ligand-Binding Assays to Support Pharmacokinetic Assessments of Macromolecules. *Pharm. Res.* **2003,** *20* (11), 1885–1900.
26. FDA. Guidance for Industry: Bioanalytical Method Validation; [Docket No. 98D–1195]; Federal Register 66; 2001; pp 28526–28527.
27. European Medicines Agency E. Guideline on Bioanalytical Method Validation 2011; Available from. http://www.ema.europa.eu/docs/en_GB/document_library/Scientific_guideline/2011/08/WC500109686.pdf.
28. Shankar, G.; Devanarayan, V.; Amaravadi, L.; Barrett, Y. C.; Bowsher, R.; Finco-Kent, D.; et al. Recommendations for the Validation of Immunoassays Used for Detection of Host Antibodies Against Biotechnology Products. *J. Pharm. Biomed. Anal.* **2008,** *48* (5), 1267–1281. http://dx.doi.org/10.1016/j.jpba.2008.09.020.
29. FDA. Guidance for Industry Immunogenicity Assessment for Therapeutic Protein Products; Draft Guidance; 2013.
30. FDA. Draft Guideline; Guidance for Industry Assay Development for Immunogenicity Testing of Therapeutic Proteins; 2009.
31. Bourdage, J. S.; Cook, C. A.; Farrington, D. L.; Chain, J. S.; Konrad, R. J. An Affinity Capture Elution (ACE) Assay for Detection of Anti-Drug Antibody to Monoclonal Antibody Therapeutics in the Presence of High Levels of Drug. *J. Immunol. Methods* **2007,** *327* (1–2), 10–17.
32. Mikulskis, A.; Yeung, D.; Subramanyam, M.; Amaravadi, L. Solution ELISA as a Platform of Choice for Development of Robust, Drug Tolerant Immunogenicity Assays in Support of Drug Development. *J. Immunol. Methods* **2011,** *365* (1–2), 38–49. http://dx.doi.org/10.1016/j.jim.2010.11.011.
33. Gupta, S.; Devanarayan, V.; Finco, D.; Gunn, G. R., 3rd.; Kirshner, S.; Richards, S.; et al. Recommendations for the Validation of Cell-Based Assays Used for the Detection of Neutralizing Antibody Immune Responses Elicited Against Biological Therapeutics. *J. Pharm. Biomed. Anal.* **2011,** *55* (5), 878–888. http://dx.doi.org/10.1016/j.jpba.2011.03.038.
34. Berson, S. A.; Yalow, R. S. Quantitative Aspects of the Reaction Between Insulin and Insulin-Binding Antibody. *J. Clin. Invest.* **1959,** *38* (11), 1996–2016.
35. Wu, A. H. A Selected History and Future of Immunoassay Development and Applications in Clinical Chemistry. *Clin. Chim. Acta* **2006,** *369* (2), 119–124. http://dx.doi.org/10.1016/j.cca.2006.02.045.
36. Fraser, S.; Cameron, M.; O'Connor, E.; Schwickart, M.; Tanen, M.; Ware, M. Next Generation Ligand Binding Assays—Review of Emerging Real-Time Measurement Technologies. *AAPS J.* **2014,** *16* (5), 914–924. http://dx.doi.org/10.1208/s12248-014-9643-2.
37. Mora, J.; Chunyk, A. G.; Dysinger, M.; Purushothama, S.; Ricks, C.; Österlund, K.; et al. Next Generation Ligand Binding Assays—Review of Emerging Technologies' Capabilities to Enhance Throughput and Multiplexing. *AAPS J.* **2014,** *16* (6), 1175–1184. http://dx.doi.org/10.1208/s12248-014-9660-1.
38. Spriggs, F. P.; Zhong, Z. D.; Safavi, A.; Jani, D.; Dontha, N.; Kant, A.; et al. Ligand Binding Assays in the 21st Century Laboratory: Platforms. *AAPS J.* **2012,** *14* (1), 113–118.
39. Fischer, S. K.; Joyce, A.; Spengler, M.; Yang, T.-Y.; Zhuang, Y.; Fjording, M. S.; et al. Emerging Technologies to Increase Ligand Binding Assay Sensitivity. *AAPS J.* **2014,** *17* (1), 93–101. http://dx.doi.org/10.1208/s12248-014-9682-8.
40. Deaver, D. R. A New Non-Isotopic Detection System for Immunoassays. *Nature* **1995,** *377* (6551), 758–760. http://dx.doi.org/10.1038/377758a0.
41. Blackburn, G. F.; Shah, H. P.; Kenten, J. H.; Leland, J.; Kamin, R. A.; Link, J.; et al. Electrochemiluminescence Detection for Development of Immunoassays and DNA Probe Assays for Clinical Diagnostics. *Clin. Chem.* **1991,** *37* (9), 1534–1539.
42. Rhyne, P. W.; Wong, O. T.; Zhang, Y. J.; Weiner, R. S. Electrochemiluminescence in Bioanalysis. *Bioanalysis* **2009,** *1* (5), 919–935. http://dx.doi.org/10.4155/bio.09.80.
43. Zhang, Q.-Y.; Chen, H.; Lin, Z.; Lin, J.-M. Comparison of Chemiluminescence Enzyme Immunoassay Based on Magnetic Microparticles With Traditional Colorimetric ELISA for the Detection of Serum α-Fetoprotein. *J. Pharm. Anal.* **2012,** *2* (2), 130–135. http://dx.doi.org/10.1016/j.jpha.2011.10.001.
44. Given, A. M.; Whalen, P. M.; O'Brien, P. J.; Ray, C. A. Development and Validation of an Alpha Fetoprotein Immunoassay Using Gyros Technology. *J. Pharm. Biomed. Anal.* **2012,** *64–65,* 8–15. http://dx.doi.org/10.1016/j.jpba.2012.02.001.
45. Mora, J. R.; Obenauer-Kutner, L.; Vimal Patel, V. Application of the Gyrolab Platform to Ligand-Binding Assays: A User's Perspective. *Bioanalysis* **2010,** *2* (10), 1711–1715. http://dx.doi.org/10.4155/bio.10.122.
46. Fivash, M.; Towler, E. M.; Fisher, R. J. BIAcore for Macromolecular Interaction. *Curr. Opin. Biotechnol.* **1998,** *9* (1), 97–101.
47. Mytych, D. T.; La, S.; Barger, T.; Ferbas, J.; Swanson, S. J. The Development and Validation of a Sensitive, Dual-Flow Cell, SPR-Based Biosensor Immunoassay for the Detection, Semi-Quantitation, and Characterization of Antibodies to Darbepoetin Alfa and Epoetin Alfa in Human Serum. *J. Pharm. Biomed. Anal.* **2009,** *49* (2), 415–426. http://dx.doi.org/10.1016/j.jpba.2008.11.028.
48. Jason-Moller, L.; Murphy, M.; Bruno, J. Overview of Biacore Systems and Their Applications. Chapter 19: Unit 19.3. In *Current Protocols in Protein Science;* Coligan, J. E.; et al., Eds.; 2006; http://dx.doi.org/10.1002/0471140864.ps1913s45.
49. Do, T.; Ho, F.; Heidecker, B.; Witte, K.; Chang, L.; Lerner, L. A Rapid Method for Determining Dynamic Binding Capacity of Resins for the Purification of Proteins. *Protein Expr. Purif.* **2008,** *60* (2), 147–150. http://dx.doi.org/10.1016/j.pep.2008.04.009.
50. Britze, A.; Palmfeldt, J.; Gregersen, N.; Ovesen, T. 44-Plex Cytokine Profile of Cholesteatoma. *Acta Otolaryngol.* **2014,** *134* (1), 41–50. http://dx.doi.org/10.3109/00016489.2013.844360.
51. Vignali, D. A. Multiplexed Particle-Based Flow Cytometric Assays. *J. Immunol. Methods* **2000,** *243* (1–2), 243–255.
52. Le Guezennec, X.; Quah, J.; Tong, L.; Kim, N. Human Tear Analysis With Miniaturized Multiplex Cytokine Assay on "Wall-Less" 96-Well Plate. *Mol. Vis.* **2015,** *21,* 1151–1161.
53. de Jager, W.; te Velthuis, H.; Prakken, B. J.; Kuis, W.; Rijkers, G. T. Simultaneous Detection of 15 Human Cytokines in a Single Sample of Stimulated Peripheral Blood Mononuclear Cells. *Clin. Diagn. Lab. Immunol.* **2003,** *10* (1), 133–139.
54. Yan, Z. H.; Madison, L. L.; Burkhardt, A.; Yu, J.; Tayber, O.; Li, Z.; et al. Analysis of Two Pharmacodynamic Biomarkers Using Acoustic Micro Magnetic Particles on the ViBE Bioanalyzer. *Anal. Biochem.* **2011,** *410* (1), 13–18. http://dx.doi.org/10.1016/j.ab.2010.11.012.
55. Jalali-Yazdi, F.; Corbin, J. M.; Takahashi, T. T.; Roberts, R. W. Robust, Quantitative Analysis of Proteins Using Peptide Immunoreagents, In Vitro Translation, and an Ultra-sensitive Acoustic Resonant Sensor. *Anal. Chem.* **2014,** *86* (10), 4715–4722. http://dx.doi.org/10.1021/ac500084d.
56. Chilewski, S. D.; Dickerson, W. M.; Mora, J. R.; Saab, A.; Alderman, E. M. Evaluation of Acoustic Membrane Microparticle (AMMP) Technology for a Sensitive Ligand Binding Assay to Support Pharmacokinetic Determinations of a Biotherapeutic. *AAPS J.* **2014,** *16* (6), 1366–1371. http://dx.doi.org/10.1208/s12248-014-9659-7.
57. Dong, H.; Mora, J. R.; Brockus, C.; Chilewski, S. D.; Dodge, R.; Merrifield, C.; et al. Development of a Generic Anti-PEG Antibody Assay Using BioScale's Acoustic Membrane Microparticle Technology. *AAPS J.* **2015,** *17* (6), 1511–1516. http://dx.doi.org/10.1208/s12248-015-9799-4.
58. Rissin, D. M.; Kan, C. W.; Campbell, T. G.; Howes, S. C.; Fournier, D. R.; Song, L.; et al. Single-Molecule Enzyme-Linked Immunosorbent Assay Detects Serum Proteins at Subfemtomolar Concentrations. *Nat. Biotechnol.* **2010,** *28* (6), 595–599. http://dx.doi.org/10.1038/nbt.1641.
59. Rivnak, A. J.; Rissin, D. M.; Kan, C. W.; Song, L.; Fishburn, M. W.; Piech, T.; et al. A Fully-Automated, Six-Plex Single Molecule Immunoassay for Measuring Cytokines in Blood. *J. Immunol. Methods* **2015,** *424,* 20–27. http://dx.doi.org/10.1016/j.jim.2015.04.017.
60. St Ledger, K.; Agee, S. J.; Kasaian, M. T.; Forlow, S. B.; Durn, B. L.; Minyard, J.; et al. Analytical Validation of a Highly Sensitive Microparticle-Based Immunoassay for the Quantitation of IL-13 in Human Serum Using the Erenna Immunoassay System. *J. Immunol. Methods* **2009,** *350* (1–2), 161–170. http://dx.doi.org/10.1016/j.jim.2009.08.012.
61. Marjot, J.; Liebetrau, C.; Goodson, R. J.; Kaier, T.; Weber, E.; Heseltine, P.; et al. The Development and Application of a High-Sensitivity Immunoassay for Cardiac Myosin-Binding Protein C. *Transl. Res.* **2015;** http://dx.doi.org/10.1016/j.trsl.2015.11.008.
62. Shukla, R.; Santoro, J.; Bender, F. C.; Laterza, O. F. Quantitative Determination of Human Interleukin 22 (IL-22) in Serum Using Singulex-Erenna(R) Technology. *J. Immunol. Methods* **2013,** *390* (1–2), 30–34. http://dx.doi.org/10.1016/j.jim.2013.01.002.
63. Yang, T.; O'Malley, T. T.; Kanmert, D.; Jerecic, J.; Zieske, L. R.; Zetterberg, H.; et al. A Highly Sensitive Novel Immunoassay Specifically Detects Low Levels of Soluble Abeta Oligomers in Human Cerebrospinal Fluid. *Alzheimers Res. Ther.* **2015,** *7* (1), 14. http://dx.doi.org/10.1186/s13195-015-0100-y.

64. Esparza, T. J.; Zhao, H.; Cirrito, J. R.; Cairns, N. J.; Bateman, R. J.; Holtzman, D. M.; et al. Amyloid-Beta Oligomerization in Alzheimer Dementia Versus High-Pathology Controls. *Ann. Neurol.* **2013,** *73* (1), 104–119. http://dx.doi.org/10.1002/ana.23748.
65. Valera, E.; Shia, W. W.; Bailey, R. C. Development and Validation of an Immunosensor for Monocyte Chemotactic Protein 1 Using a Silicon Photonic Microring Resonator Biosensing Platform. *Clin. Biochem.* **2016,** *49* (1), 121–126. http://dx.doi.org/10.1016/j.clinbiochem.2015.09.001.
66. Adler, M.; Schulz, S.; Fischer, R.; Niemeyer, C. M. Detection of Rotavirus From Stool Samples Using a Standardized Immuno-PCR ("Imperacer") Method With End-Point and Real-Time Detection. *Biochem. Biophys. Res. Commun.* **2005,** *333* (4), 1289–1294. http://dx.doi.org/10.1016/j.bbrc.2005.06.027.
67. Lea, P.; Keystone, E.; Mudumba, S.; Kahama, A.; Ding, S. F.; Hansen, J.; et al. Advantages of Multiplex Proteomics in Clinical Immunology: The Case of Rheumatoid Arthritis: Novel IgXPLEX: Planar Microarray Diagnosis. *Clin. Rev. Allergy Immunol.* **2011,** *41* (1), 20–35. http://dx.doi.org/10.1007/s12016-009-8189-z.
68. FDA. Guidance for Industry Part 11, Electronic Records; Electronic Signatures—Scope and Application; US Department of Health and Human Services Food and Drug Administration; 2003.
69. Xu, K.; Liu, L.; Saad, O. M.; Baudys, J.; Williams, L.; Leipold, D.; et al. Characterization of Intact Antibody-Drug Conjugates From Plasma/Serum In Vivo by Affinity Capture Capillary Liquid Chromatography-Mass Spectrometry. *Anal. Biochem.* **2011,** *412* (1), 56–66.
70. Liu, A.; Kozhich, A.; Passmore, D.; Gu, H.; Wong, R.; Zambito, F.; et al. Quantitative Bioanalysis of Antibody-Conjugated Payload in Monkey Plasma Using a Hybrid Immuno-Capture LC-MS/MS Approach: Assay Development, Validation, and a Case Study. *J. Chromatogr. B Anal. Technol. Biomed. Life Sci.* **2015,** *1002,* 54–62. http://dx.doi.org/10.1016/j.jchromb.2015.08.007.
71. Neubert, H.; Muirhead, D.; Kabir, M.; Grace, C.; Cleton, A.; Arends, R. Sequential Protein and Peptide Immunoaffinity Capture for Mass Spectrometry-Based Quantification of Total Human Beta-Nerve Growth Factor. *Anal. Chem.* **2013,** *85* (3), 1719–1726. http://dx.doi.org/10.1021/ac303031q.

6.09 Analytical and Formulation Development Road Map for Protein Therapeutics

MP Ramprasad, aTyr Pharma, San Diego, CA, United States

© 2017 Elsevier Ltd. All rights reserved.

6.09.1	**Introduction**	198
6.09.1.1	Analytical	198
6.09.1.2	Formulation	199
6.09.1.3	Early Product Development	199
6.09.1.4	Major Pitfalls in CMC	199
6.09.1.5	The Target Product Profile	200
6.09.2	**Analytical Method Development**	200
6.09.2.1	General Principles Analytical Method Development	200
6.09.2.2	HPLC and UPLC Method Development	202
6.09.3	**Potency Assay Development**	202
6.09.4	**Method Qualification and Validation**	204
6.09.5	**Specification**	204
6.09.6	**Reference Standard**	205
6.09.7	**Biochemical and Biophysical Characterization and Comparability**	206
6.09.7.1	Comparability	206
6.09.8	**Formulation Development**	208
6.09.9	**Preformulation and Forced Degradation**	208
6.09.10	**Formulation Optimization**	209
6.09.11	**Lyophilized Drug Product Development**	211
6.09.12	**Stability Studies and Expiration Dating**	212
6.09.12.1	Clinical In-Use Stability Studies	214
6.09.12.2	Extractable and Leachable Studies	214
6.09.13	**Conclusions**	215
References		215
Relevant Websites		215

6.09.1 Introduction

Analytical and formulation development (AFD) is a key function within chemistry, manufacturing, and controls (CMC) of drug development programs responsible for the evaluation and establishment of consistent product quality and stability. AFD is integral to process development, optimization and manufacturing, and release and characterization of drug substance (DS) and drug product (DP) for use in nonclinical and clinical studies during development, and plays a vital role in manufacturing and commercial supply of therapeutics. The *process is the product*, which means that the manufacturing process including upstream protein expression, the downstream protein purification and formulation, and the analytical and characterization methods used to characterize and optimize the process, together defines the product quality and the stability of the DS and DP. Process knowledge is heavily dependent on accurate and precise measuring techniques used to test and examine the quality of drug components, raw materials, and finished products. The two functions in AFD are also highly interwoven and interdependent and, in many small- to mid-size organizations, constitute a single functional unit, typically part of process/pharmaceutical sciences (Fig. 1).

6.09.1.1 Analytical

Analytical methods including biochemical and biophysical characterization methods are required to evaluate and screen formulations and their stability; while a reasonably stable formulation along with forced-degraded formulations are required to develop, optimize, and qualify the analytical methods. Analytical methods and characterization also are very important not only as in-process tools but also to troubleshoot the DS and DP process, to identify root cause, and to establish corrective and preventative action (CAPA) to mitigate future problems during manufacturing and assessment of product quality and stability. In addition, analytical methods play a significant role in comparability studies at different phases of product development from nonclinical to postapproval of DP as the process, scale, and manufacturing site changes occur.

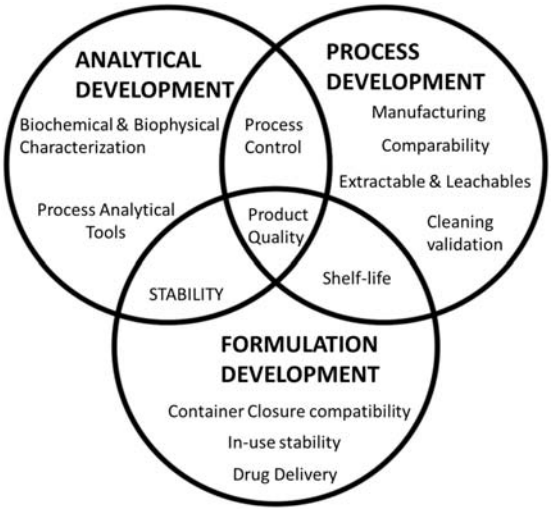

Fig. 1 Interdependence of manufacturing process development and AFD.

6.09.1.2 Formulation

Formulation development not only is involved in developing a stable formulation for a given dosage form but also during life cycle management and typically entails developing additional dosage forms, product presentations, and various drug delivery modes representing different routes of administration.[1] Further, formulation development also encompasses material compatibility, in-use, and long-term stability studies to evaluate and ensure that the DS and DP are adequately stable during different phases of clinical development and as a commercial product. Furthermore, the various dosage forms and complex drug delivery systems, together with combination drugs and devices, significantly expand the scope of this exciting field that enables patient-friendly drug treatments, often times throughout the lifetime.

6.09.1.3 Early Product Development

During the discovery phase of the projects, in start-ups, typically the chemistry/medicinal chemistry and biology groups gain an early understanding of the physicochemical and biological properties of the early hits and lead molecules of new molecular entities. For the development teams (process and CMC teams) that come in later, it is important to establish a rapport and good collaboration with the early research teams to get a comprehensive picture of the structural and functional requirements of the advancing therapeutic candidates. Small-scale expression of the recombinant protein and purification is typically performed by the research groups whose main focus is on establishing the biological activity using in vitro and in vivo assays that form the basis of potency assays and efficacy animal models.

The product development (AFD) scientists can contribute to the project initially by evaluating the in-use stability of the early protein buffered solutions and by a preliminary gauge of the degradation pathways of the upcoming leads, which allows for recommended storage and precautions to be taken during preparation of dosing solutions and sample preparation for in vitro studies. As the discovery phase of the project matures into identifying and optimizing new lead molecules for development, the internal technology transfer from discovery to development teams is the foundation of process and product development that involves developing a well-thought-out strategy and plan for early protein production, analytical, and formulation development. Execution of the development plan in an organized, systematic, and timely manner is critical to meeting the business milestones that is crucial to the investors and shareholders. When performed concurrently, it generally takes 9–12 months to complete AFD work for phase 1 and 2 clinical development, including method qualification, and obtain accelerated and preliminary real-time stability data with the lead formulation.

6.09.1.4 Major Pitfalls in CMC

Some of the major pitfalls[2] in the analytical and formulation development plan are outlined in the **Table 1**. A well-thought-out road map, active project management, establishment of quality systems, and constant project monitoring are crucial to avoid these pitfalls and for successful product development. Strong and experienced leadership and talented personnel with appropriate training experience, motivation, and project ownership, together with corporate and fiscal commitment to dedicated CMC activities, are central to achieving the goals and milestones. The importance of active communication, self-awareness, peer-review, and cross functional collaboration with internal teams and external contract service providers (CSP) cannot be overemphasized.

Table 1 Pitfalls in analytical and formulation development impacting CMC development

1	Not well-thought-out development strategy
2	No pre-IND meeting to obtain agency feedback on CMC issues or consultation with SMEs
3	Not spending sufficient time on development, method transfer/establishment and qualification of robust analytical methods, and development of a robust and stable formulation
4	Setting the specification too tight early in development leads to failed batches
5	Not considering composition of approved DP and determining allowable ranges of generally regarded as safe (GRAS) excipients and researching list and concentration range of FDA inactive ingredients in approved products
6	Not spending sufficient time on investigating OOS and OOT to understand root cause
7	Not employing sufficient resources, utilizing appropriate project management tools, and working collaboratively with QC, RA, and QA to set development strategy and resolve issues
8	Not spending sufficient time and stringency with data integrity and documentation review; and active communication, supervision, and ensuring compliance of GLP and cGMP procedures
9	Wrong choice of CRO/CMO for analytical and formulation development and insufficient real-time and accelerated stability studies

6.09.1.5 The Target Product Profile

At the core of product development is the target product profile (TPP). The TPP is a strategic development tool and usually a living reference document for the most current information on the intended product characteristics and use.[3] The benefit of using the TPP in R&D is that it provides a clear and tangible vision and focus and gives the core team a glimpse of what could be a real product with the goal of improving patient health. In the early phase of development, the TPP typically involves developing a list of product description, mechanism of action, pharmacology, potential indication(s), and a description of the primary and secondary clinical endpoints that are required to evaluate the value proposition of the drug to overcome unmet medical needs. For the development scientist, the TPP is the framework to plan and develop appropriate manufacturing process, the analytical and physicochemical characterization tool box, and a robust and stable formulation required for the intended route of drug delivery during the early phases of development. The TPP is a dynamic summary that changes as knowledge of the drug increases. It is recommended that the TPP be updated regularly to reflect new information about the drug and changes in the clinical development program. Further, regulatory guidance documents from the FDA, ICH, WHO, and other agencies provide a compass to develop a road map to investigational drugs and licensing application for commercialization.

6.09.2 Analytical Method Development

In the very early phase of development, not many analytical methods are required to support discovery research: mainly strength (protein concentration), an identity assay, a purity assay, and an activity assay suffice the lead to hit generation phase. These four assays are generally sufficient for also optimizing protein engineering and selection of lead candidates in concert with pharmacokinetic and efficacy evaluation. However, it is advisable to quickly also develop additional purity assays and characterize the post-translational modifications (PTM) using forced-degradation studies early during development to enable an understanding of the stability of the molecule and determine if additional protein engineering can be employed to replace any potential hot spots in the sequence based on knowledge of the product-specific degradation pathways.

Typically, IND-enabling analytical method development[4] originates after nomination of the lead new molecular entity (NME) for development. Analytical method development generally involves developing distinct product-specific methods and verification of the compendial methods that are required to assess strength, identity, safety, purity, and quality (SISPQ) of the DS and DP. The available regulatory guidance documents and summary basis of approval (SBA) dossiers for approved products are helpful in constructing a plan toward meeting the requirement for IND/IMPD submission; however, they do not offer a comprehensive summary in a single document that allows a step-by-step work flow and detailed planning and development of timelines around various drug development activities. The general chapters in the United States Pharmacopeia (USP) shown in **Table 2** provide guidance on analytical procedures, transfer of methods, and handling of compendial procedures for intended use.[5] Further, it is important to understand the requirements for different phases of clinical development and eventual commercialized drug. For example, validated analytical methods are not necessarily required during product and process development activities or when used in characterization studies. Nevertheless, analytical methods should be scientifically sound (e.g., specific, sensitive, and accurate) and provide results that are reliable during early-phase development. There should be assurance of proper equipment function for laboratory experiments. Procedures for analytical method and equipment maintenance, documentation practices, and calibration practices supporting process development efforts should be documented and described.

6.09.2.1 General Principles Analytical Method Development

General principles and platform approaches to analytical method development can be implemented based on the extensive experience and published literature from hundreds of biologic drugs that have been approved and are in various stages of clinical

Table 2 General USP chapters

USP chapter	*Analytical procedure description*
⟨1058⟩	Analytical Instrument Qualification
<621>	Chromatography
<1010>	Analytical Data – Interpretation and Treatment
<1032>	Design and Development of Biological Assays
<1033>	Biological Assay Validation
<1224>	Transfer of Analytical Procedures
<1225>	Validation of Compendial Procedures
<1226>	Verification of Compendial Procedures

development. Table 3 shows a representative list of analytical methods and intended purpose required to release batches of DS and DP after GMP manufacturing for clinical investigation.[4] For lyophilized DPs, additional assays include cake appearance, reconstitution time, and moisture content by Karl Fischer analysis.

Compendial methods, published as general chapters, by various agencies such as USP, EP, and JP, include less complex methods that have been validated in large-scale collaborative studies and can be implemented in a QC lab after brief verification under condition of use, to demonstrate compliance to the published compendia. These methods do not typically require validation and include general physicochemical properties of the DS/DP formulation such as visual appearance, pH, osmolality, extraction volume or container content, and microbiological testing (endotoxin, bioburden, sterility, viruses, and mycoplasma) and process residuals related to ensuring safety, namely, host cell protein (HCP), residual DNA, and residual protein A. These methods are generally available at contract manufacturing organizations (CMO) and contract research organizations (CRO) dealing with release and stability testing of DS and DP. While these methods do not need validation, the role of the sponsor companies is to ensure that proper SOPs are followed by the contracted QC laboratories while implementing these methods, and the analytical results are consistent between laboratories. Depending on the formulation and the chosen method, some amount of time will need to be invested in overcoming any challenges associated with interference (inhibition/enhancement) of endotoxin measurement. The prime advantage of the chromogenic kinetic method over the conventional gel-clot method is the ability to quantify the endotoxins in the sample. The gel-clot method, on the other hand, may be subjective especially in borderline cases where the gel formed may be viscous/semisolid.

In the initial phases of clinical development through phase 2 studies, it is typical to employ platform commercial HCP assays that offer a broad menu of well-validated, robust generic kits to quantify the majority of the host cell protein contaminants derived from the host expression system. These kits typically involve ELISA-based immunoassay using a mixture of polyclonal antibodies to detect and quantify the HCPs from the cell proteome. The use of these kits in the early development phases is common and sometimes can also be justified for commercial products after demonstration of HCP coverage and sensitivity. Although the ELISA-based HCP kits are used as the industry gold standard, there are limitations of these generic kits, especially in relation to the sensitivity of the method to detect less abundant HCPs and identify contaminant proteins representing all host strains. Later phases of process development typically requires development of a process-specific HCP assay that is representative and may be unique to a given upstream and or downstream process, involving design and enrichment of certain impurities.[6] The suitability of use of the commercial kits in later clinical phases will need to be justified on a case-by-case basis with adequate scientific justification of the impurity coverage of the assay. Recently, LC-MS/MS approaches are rapidly being developed to significantly increase the sensitivity. However, the very high sensitivity of the mass spectrometry may prove to be overly sensitive to detect every single HCP at levels that may not

Table 3 cGMP batch release assays for drug substance and drug product

Characteristic	*Release methods*	*DS*	*DP*
General characteristics	Visual appearance including color, clarity, and particles pH, osmolality	✓	✓
Strength	Protein concentration	✓	✓
Potency	Enzymatic, ligand-binding assay, ELISA, cell-based, in vivo animal assay (one or more of these assays)	✓	✓
Identity	Western blotting, IEF/icIEF, peptide mapping	✓	✓
Safety	Endotoxin, bioburden, sterility, mycoplasma, viruses, TEM for retroviruses	✓	–
Safety	Endotoxin, sterility	–	✓
Purity	SDS-PAGE, CE-SDS, SE-HPLC, IEX-HPLC, RP-HPLC or HIC-HPLC	✓	✓
Impurities	HCP, residual DNA, residual protein A, antifoam agents, residual antibiotics, residual flocculants, residual solvents	✓	–
Particulate matter	Subvisible particulate matter by light obscuration	–	✓
Container content	Extractable volume	–	✓

Table 4 Key ICH guidelines for biotechnological/biological product characterization

ICH guidance documents	*Scope of the guidance*
Q2(R1)	Validation of Analytical Procedures
Q3A (R2)	Impurities in New Drug Substances
Q3B (R2)	Impurities in New Drug Products
Q3C (R5)	Impurities: Guidelines for Residual Solvents
Q3D	Guidelines for Elemental Impurities
Q5E	Comparability of Biotechnological/Biological Products Subject to Changes in their Manufacturing Process
Q6B	Specifications: Test Procedures and Acceptance Criteria for Biotechnological/Biological Products

impact the safety of the product. Appropriate guidelines and validation of these newly advancing tools have to be established before adaptation to release products.

Most of the time in analytical method development is dedicated to developing product-specific identity, purity/impurity assays, and potency assay. Protein concentration measurement is usually performed by UV spectroscopy using the Beer–Lambert principle. The theoretical molar absorption coefficient at 280 nm (aromatic residues) derived from the theoretical protein sequence based on the refined Gill and von Hippel equation.[7] At later stages of drug development, the experimental extinction coefficient is determined using amino acid quantitation of highly recoverable amino acids although generally to only confirm the value. Gel-based methods for identity and purity analysis are well described in the literature (Bio-Rad and Life Technologies application notes) and are the initial workhorse methods during the research phase and transition to early development. In the last decade, the capillary electrophoretic methods of denaturing electrophoresis and imaged capillary isoelectric focusing (CE-SDS and icIEF) have been routinely applied to get better quantitation of the well-resolved impurities and oligosaccharide analysis (CE-LIF). Much of the method development around these methods involves optimizing sample preparation, including stabilizers, and treatment conditions; selection of appropriate stationary phase; and improving resolution.[8]

Some of the ICH guidance documents that are relevant to analytical method validation, specifications, and characterization of impurities in DS and DP are listed in **Table 4**.

6.09.2.2 HPLC and UPLC Method Development

HPLC and UPLC method development is at the core of purity/impurity methods and some in-process methods including titer assay, some identity assays, refolding efficiency, peptide mapping, and LC-MS-based characterization methods. The advancement of sophisticated equipment, including sensitive detectors, the availability of a host of different modes of separation, and user-friendly integration and data analysis and reporting software tools, has made this fast-paced separations field extremely efficient for control of product quality and establishing process control and characterization of comparability of manufacturing changes during the life cycle of product development. Traditionally, size exclusion, reversed phase, and ion-exchange HPLC-based methods have been used as orthogonal approaches to identifying, characterizing, and controlling the levels of high and low molecular weight, hydrophobic/polar impurities, and charge-based heterogeneity, respectively. Additional modes of LC-based separations including normal phase and mixed-mode HILIC, HIC, HPAEC, and analytical protein A have been utilized for extended characterization and analysis of glycosylation. Method development with the LC-based separations[9] involves choice of the mode and column packing dimension, selection and optimization of the mobile phase solvent(s) and modifiers, the gradients, and experimental conditions to obtain efficient and robust methods. Software applications and USP column performance criteria such as plates, resolution, peak area recovery, and tailing allow efficient tools to be applied to monitor and standardize the method. Further, with the experience gained and published literature on a variety of nonglycosylated polypeptides and proteins and innumerable monoclonal antibodies, a platform-based initial assessment of method development allows for a much faster and easier path to method optimization. **Fig. 2** shows the various steps in HPLC method development and optimization before method qualification, and **Table 5** shows a few of the common HPLC columns and methods used in DS and DP release of both Mab and non-Mab proteins.

6.09.3 Potency Assay Development

The potency assay is a critical quality attribute from the very beginning of process development and hence needs to be carefully strategized. Typically, an in vitro activity assay is developed by the discovery team early in the project as the principal assay read out to assess the functional capability of the therapeutic, to screen hits and variants, and to select the lead candidates from protein engineering that are advanced for further product development and quality attributes (PK, PD, toxicity, process development, and stability assessment). The preliminary assay format may be representative of the chosen target(s) in regard to the mechanism of action (MOA) involving binding/inhibition or may simply reflect an activity relating to a region of the molecule to demonstrate conformational integrity (proper protein folding). It is important to note that with Mabs where the target is generally defined by

Fig. 2 HPLC method development process and work flow.

Table 5 Some common HPLC methods, purpose, and starting method parameters

Method	*Purpose*	*Example method parameters*
SE-HPLC (size exclusion)	Separation of molecules is by size and shape. The chromatographic elution time is typically characteristic for a particular molecule. The purpose of SE-HPLC analysis is to assess the protein aggregation, dissociation of oligomers, and fragmentation	Tosoh SW3000 4.6 mm × 30 cm, 4 μm 0.2 M sodium phosphate, 0.1 M NaCl, pH 7.0; isocratic; 0.3 mL/min Sample diluted to 1 mg/mL in formulation buffer A280 detection
RP-HPLC (reversed phase)	Separation is based on hydrophobicity of the proteins and variants. The chromatographic elution time is typically characteristic for a particular molecule. The purpose of this method is to assess degradants and variants such as oxidation, disulfide forms, and amino acid misincorporation. The RP-HPLC method can also be used to determine expression titers in harvest samples	Zorbax 300 SB-C3 2.1 mm × 15 cm, 5 μm Acetonitrile/water 0–90% gradient with 0.1% TFA; 0.3–0.4 mL/min Sample diluted to 1 mg/mL in starting mobile phase A214 detection
IEX-HPLC (ion exchange)	Separation is by charge primarily through electrostatic interactions between amino acid side chains and the opposite surface charge of the ion-exchange resin. The purpose of IEX-HPLC analysis is to assess charge variants such as acetylation, methylation, sialylation, proteolytic cleavage, carboxylation, and deamidation	ProPac WCX-10 4.0 mm × 25 cm, 5 μm 0.02 M sodium phosphate, 0.0–0.8 M NaCl gradient, pH 6.0–7.0; 0.5 mL/min Sample diluted to 1–2 mg/mL in formulation buffer A280 detection
NP-HPLC (normal phase)	Determine N-linked oligosaccharide profile of glycoproteins such as Mab after deglycosylation using PNGase and glycan derivatization using 2-aminobenzoic acid (2AA). Separation is based on size, linkage, and structure, using high-to-low concentration acetonitrile	Tosoh TSKgel Amide-80 4.6 mm × 5 cm, 3 μm Acetonitrile/water 100–0.2% gradient with 0.2% TEA and acetic acid; 0.3–0.4 mL/min Remove deglycosylated protein after PNGase and 2AA by SPE; reconstitute dried extract in acetonitrile FLD detection, Ex 355 nm/Em 420 nm

the antigen-binding Fab region, the actual efficacy of the therapeutic in vivo may involve other regions of the molecule (such as the Fc for effector functions involving complement-dependent or antibody-dependent cytotoxicity). Further, while the primary efficacy end points for a chosen indication are generally chosen based on the in vitro activity, the actual MOA in vivo may not necessarily depend on such activity and could be more complex. This is just one of the many challenges sponsor companies face during product development.[10]

The main desired characteristics of a potency assay include representative biological activity that is quantitative and can be used in batch release; property that is stability-indicating and can measure significant loss of potency (preferably >10–15%), and assay consistency with controlled variability. It is typical to explore more than one potency assay initially. These may be concurrent and may represent orthogonal functions of the protein in vitro that may or may not have a direct correlation with the MOA in vivo. These surrogate assays are very useful to gaining an initial assessment of functional activity and typically accelerate the path to batch release and IND-enabling data package. As experience is gained in clinical development and further in-depth experiments are carried out to truly understand the MOA, the regulatory agencies expect development and validation of a meaningful cell-based potency assay at the time of licensure (BLA). Ideally, if there is good correlation between in vitro potency assay and in vivo efficacy, this really helps to define the therapeutic dose and frequency.

Some additional challenges and considerations while developing potency assays are controlling high assay variability (broad specification initially and tighten later), and establishing stability-indicating properties of the assay (using forced-degradation studies).

6.09.4 Method Qualification and Validation

The AFD team is usually responsible for prequalification of the product-specific analytical methods to demonstrate that they are fit for use. Prequalification generally involves assessment of precision (repeatability and variability expressed as % coefficient of variance), accuracy, and where they are intended to be quantitative methods, assessment of linearity, and LOD/LOQ. This subset of validation parameters (accuracy, repeatability and intermediate precision, reproducibility, linearity and range, specificity/selectivity, and robustness) are not evaluated in-depth during the initial R&D phase. However, it is highly advisable to perform some initial assessment of these parameters to achieve some consistency of the methods before venturing to transfer them to a CMO or CRO for method qualification. Qualification and validation terms are interchangeably and loosely used during development, without a full understanding of the differences. Qualification establishes that the assay design is confirmed as being capable of producing reproducible results suitable for the specified purpose, and typically involves evaluation of all validation parameters except robustness. **Table 6** describes the various validation parameters that are required for the different types of analytical methods. During validation, the assay is tested against specific acceptance criteria set in advance to verify that the performance characteristics of the method are suitable and reliable for the intended application. Robustness is generally determined during phase 3 clinical development at the time of method validation, whereas the earlier phases of development only require methods to be qualified for batch release and stability studies.[11] The design of qualification/validation protocols for the individual test methods have to be described and approved by QA, and the successful completion of such studies have to be documented in detailed qualification/validation reports including a summary of the acceptance criteria.

6.09.5 Specification

Once the methods are optimized and qualified, they can be routinely used to analyze samples from the downstream process purification steps to assess the purity and impurity profiles and gain an understanding of the step yields and purity at each unit operation during manufacturing. Initial acceptance criteria around the SISPQ attributes of the purified DS are set based on the process performance and generally targeting >90–95% purity by SE-HPLC, 75–85% by IEX-HPLC, and around 85–90% by RP/HIC-HPLC. As process improvements and optimization are performed (including final formulation selection), one can start to slowly tighten the specification, after some initial assessment of the formulation stability under storage and accelerated stability conditions (ICH Q6B). **Table 7** shows an example of DS and DP specification with release tests

Table 6 Qualification and validation parameters for different classes of analytical methods

Parameter	*Strength*	*Identity*	*Safety*	*Potency*	*Purity*
Accuracy	+	−	+	+	+
Linearity	+	−	+	+	+
Range	+	−	+	+	+
Specificity	+	+	+	+	+
Precision	+	+	+	+	+
Robustness	−	+	−	+	+

Table 7 Example drug substance and drug product specification for early-phase development

Analytical test	*Acceptance criteria*	*Drug substance/drug product*
Appearance	Clear to opalescent Colorless to slightly yellow solution Essentially free of visible particles/some particles may be observed	DS and DP
pH	pH x.x ± 0.3	DS and DP
Osmolality	300 ± 100 mOsmol/kg	DP, DS (optional)
Western Blot	Comparable to reference standard with an apparent MW of ~xx kDa for major band	DS and DP
SDS-PAGE	Comparable to reference standard with an apparent MW of ~xx kDa for major band	DS and DP
Peptide Map by HPLC	Comparable to reference standard	DS
A280 protein concentration	x.x ± 10% mg/mL	DS and DP
RP-HPLC	≥90.0% Main peak purity ≤10.0% Impurity	DS and DP
IEX-HPLC	≥80.0% Main peak purity ≤20.0% Total impurities ≤x.x% Any single impurity	DS and DP
SE-HPLC	≥95.0% Main peak purity ≤3.0% HMW ≤2.0% LMW	DS and DP
Residual DNA	≤0.1 ng/mg protein	DS
Residual HCP	≤100 ng/mg protein	DS
Residual endotoxin	≤1.0 EU/mL	DS and DP
Bioburden	TYMC and TAMC ≤ 10 CFU/10 mL	DS
Potency	x.x± 25% Units/mg	DS and DP
Sterility	No growth detected	DP
Particulate matter by light obscuration	≤600 particles/container for ≥25 μm particle size ≤6000 particles/container ≥10 μm particle size	DP
Extraction volume	x.x± 10% mL	DP

and acceptance criteria. It is important to consider the process capability, the requirements from WHO and regulatory guidance documents for the safety assays (including results from pilot PK and toxicity studies), and the overall stability of the protein and formulation while setting specification for phase 1 and 2 clinical development[12] Setting the specification too tight without adequate manufacturing experience and statistical analysis of process performance/robustness in regard to product purity and control of analytical method variability can lead to failing batches and financial and timeline consequences.

6.09.6 Reference Standard

With the methods qualified and specification defined, GMP batches of DS and DP can be released. Typically, batch release also requires an analytical reference standard[13] that has been derived from a representative manufacturing scale. The reference standard (RS) is qualified using a set of batch release assays defining product strength, identity, purity, and quality. Further, the RS is characterized using a comprehensive set of biochemical and biophysical characterization assays (described in the next section) to compile the primary, secondary, tertiary, and higher-order structure of the protein, along with posttranslational modifications (PTMs) and potency characteristics. This defines a framework of well-characterized RS that is stored under the most stable frozen condition (≤−80°C) to allow maximum shelf life and comparison to new lots of DS and DP that may undergo further process and manufacturing scale changes during the different phases of clinical development. Generally, the first RS is produced from an earlier prototype process development and is referred to as interim reference standard (IRS). Later, as the process is optimized for GMP manufacturing, a primary reference standard is derived from an engineering manufacturing-scale lot or the first GMP lot and aliquoted (1000s) in small containers for single use. The ICHQ7 guidance recommends a two-tier RS system through the development cycle. Essentially, what this means is that a primary RS is produced from a lot representative of the clinical trial material and is qualified. Subsequently, other working secondary reference standard may be used prepared from additional lots representative of the clinical trial material in order to save the primary RS and extend its use as long as possible. It is recommended to not change the primary reference standard as much as possible since it requires extensive testing and characterization to qualify against the original primary RS. If a new primary reference standard needs to be established due to significant manufacturing changes, qualification and appropriate bridging studies should be performed to migrate to using the new reference standard.

6.09.7 Biochemical and Biophysical Characterization and Comparability

The biochemical and biophysical characterization methods are the essence of a comprehensive understanding of the new molecular entity or therapeutic protein. While the purity methods and batch release data provide reasonable assurance that the drug meets the SISPQ requirements, it is the characterization methods that provide a broader picture about the structure of the molecule that allows a comprehensive description of the unique 1-D (protein sequence) to 3-D structural signature of the protein. Consequently, there is a regulatory requirement to perform detailed characterization of the protein and report the methods and the data in the IND package. The common characterization methods used,[14] the principle, and the intended purpose are shown in **Table 8**. Typically, not all of these characterization methods are available in a single laboratory, and it is quite common to utilize several different laboratories to complete the overall characterization.

Major advances in instrumentation, affordability, and standardized procedures have allowed routine use of LC–MS and LC–MS/MS methods to gain an in-depth characterization of the product-related impurities and heterogeneity[15] and help identify very-low-abundance impurities such as misincorporated amino acids and certain rare PTMs such as acetylation, methylation, and some unique clipped protein species. In combination with fraction collection of well-resolved impurity peaks by analytical and semipreparative HPLC columns, and if needed using 2-D LC approaches, it is possible to identify and characterize trace amount of impurities (0.5–1% of the main HPLC peak). LC-based peptide mapping fingerprints have become very common to use as routine identity methods that now replace the traditional Western blotting method. Generally, two identity methods are preferred, although with peptide mapping, it allows a very unique protein sequence signature that is highly specific to the protein of interest. LC–MS/MS methods are also becoming very popular in the identification of trace amounts of HCP due to the very high sensitivity, and the industry is moving toward complementing the ELISA-based HCP methods with mass spectrometry methods to better characterize and understand the risk with certain HCPs.

Certain methods such as analytical ultracentrifugation (AUC) are not readily available, and there are only a few established laboratories that perform this testing routinely, and one needs to plan and get the samples in the queue to enable a finished IND package. AUC is the gold standard for characterization of high-molecular-weight soluble aggregates by sedimentation velocity centrifugation and is the reference method to qualify the workhorse SE-HPLC method. Although very sensitive to detection of HMW > 0.1–0.2% (LOQ of the method), for high-concentration protein formulations, the samples have to be diluted in the formulation buffer, and hence the reversible aggregates are harder to quantify by AUC.

6.09.7.1 Comparability

Manufacturing changes are inherent and typically occur throughout process development. The drivers for these changes are generally optimization of the process to obtain higher yields and purity (including cell strain and upstream fermentation and downstream purification scale changes for larger supply of clinical trial material). The changes include manufacturing site changes associated with this, optimization of the downstream purification process to enhance purity and improve cost of goods for a commercial process, formulation changes including container/closure modifications to enhance stability and shelf life and change in storage temperature, and alternate dosage forms and DP presentations. Accordingly, the aim of the comparability studies is to evaluate the impact of these singular or multiple changes on the SISPQ of the DS and DP and gain an in-depth understanding of the differences between the pre-change and post-change product. The objectives and considerations of selection and interpretation of the battery of characterization tests to be performed to demonstrate equivalence of the product biologically, immunochemically, and pharmacologically, using highly sensitive analytical methods, are laid out in the ICH Q5E guidance.

Depending on the stage of clinical development and the extent of changes, the expectation from the regulatory agencies and the work load will increase, and the specific comparability protocols needs to be tailored, preferably with input from the FDA. During the earlier stages of manufacturing changes, it is common to conduct a precomparability assessment involving preliminary comparison of product quality attributes including biophysical comparison of representative batches of GMP DS from prechange and a batch of representative DS from the scaled-up post-change manufacturing process. This allows building confidence in the comparability between the process changes and performing characterization of any new or increased impurities using HPLC peak enrichment approaches. Side-by-side analysis of pre- and post-change batches are important to minimize minor differences of analytical results from day-to-day and system/analyst variability. The precomparability study is followed by GMP manufacturing using the new process and a more formal comparability assessment using both DS and DP batches from the old and new process.

Further, side-by-side forced-degradation and accelerated stability studies are instrumental in demonstrating comparability of the pre- and post-change product under stress conditions, which may be able to tease out the differences better than under nonstress studies. It is important to remember that comparability does not mean the product is identical but that "they are highly similar and the knowledge gained from comparability studies are sufficiently predictive to ensure any differences in quality attributes have no adverse impact upon safety or efficacy of the drug product." The selection and number of batches to be used for the comparability studies are important considerations and depending on the extent of changes involved (especially upstream in the manufacturing process) may warrant PK and PD studies in animals, and in some cases, perhaps, clinical PK and efficacy would be required as well.[16] Further, the breadth and stringency of analytical methods and biological studies required to demonstrate comparability of pre- and postchange commercially marketed products and to develop biosimilar products are indeed much higher.

Table 8 Common biochemical and biophysical characterization methods and description

Characterization method	*Principle*	*Purpose/output parameters*
Intact mass by electrospray ionization-time of flight mass spectrometry (ESI-TOF)	It is a high-throughput analytical method to determine molecular weights with high accuracy and high resolution. The main purpose of intact mass measurements is to ensure protein identity and to assess degradants and posttranslational modifications	Accurate mass under denaturing condition Disulfide status Qualitative assessment of minor and low abundance variants and degradants based on mass
Amino acid Analysis (AAA)	The protein is hydrolyzed by acid hydrolysis at 110°C, followed by precolumn derivatization using o-phthalaldehyde and 9-fluorenylmethyl chloroformate and separation on RP-HPLC with fluorescence detection	Amino acid composition Extinction Coefficient
Peptide mapping by LC-MS/MS	Proteins are digested using 1–3 different proteases such as trypsin, Lys-C, and Glu-C, and the peptides are separated by LC and/or LC-MS/MS methods	Fingerprint of all peptides from digest with distinct retention times Protein sequence coverage based on intact MS Disulfide mapping, PTM analysis, variants. and impurity characterization
Imaged capillary isoelectric focusing (icIEF)	icIEF separation is conducted by focusing isoforms in an ampholytic pH gradient through an applied electric field using capillary electrophoresis, followed by continuous UV detection of the whole capillary High resolution, efficiency, speed, reproducibility, and enhanced quantitation are the advantages over conventional CE	Isoelectric point Charge heterogeneity
High-pH anion-exchange chromatography with pulsed amperometric detection (HPAEC-PAD)	LC-based separation of negatively charged molecules is performed at very high pH with detection of nonderivitized and nonchromogenic glycans achieved through amperometric detection	Separation, identity, and quantitation of glycans, glycopeptides, monosaccharides, and sialic acid
Circular Dichroism (CD)	CD measures differences in absorbance between left and right circularly polarized light and hence asymmetrical properties of the chromophores, such as tryptophan, tyrosine, phenylalanine, disulfide, and peptide. Near UV CD determines the tertiary structure due to asymmetrical environments of tryptophan, tyrosine, phenylalanine, and disulfide. Far UV CD determines the secondary structure due to asymmetrical environments of peptide	Molar elipticity profile vs wavelength; spectral maxima and minima in the aromatic AA region for near UV, and at 210/222 nm for far UV CD spectra Secondary structural analysis and estimation of alpha helix, beta pleat, and rand coil structures
Differential scanning calorimetry (DSC)	DSC is a thermodynamic tool measuring the heat energy uptake that occurs in a protein sample with a regulated increase in temperature. Changes in the heat capacity result from the disruption of forces that stabilize the native protein structure. The thermal transition temperature ™ represents the midpoint of native and unfolded protein and is indicative of any conformational change	# of transitions and transition temperature (Tm) T onset of unfolding
SEC with multiangle light scattering (SEC-MALS)	The intensity of the radiated light depends on the magnitude of the dipole induced in the macromolecule detected by a refractive index detector and provides a measure of the molecular weight and hydrodynamic radius	Mw, weight averaged molar mass of each peak z-averaged mean square radius
Analytical ultracentrifugation (AUC)	Sedimentation velocity, measured in an analytical ultracentrifuge, is an absolute and gold standard method for obtaining information about the protein size, aggregation, association, and conformation. It is based on the principle of differential sedimentation velocity of varying sizes and conformation of proteins	Sedimentation coefficient (Svedberg) % purity based on size distribution

(Continued)

Table 8 Common biochemical and biophysical characterization methods and description—cont'd

Characterization method	*Principle*	*Purpose/output parameters*
Dynamic Light Scattering (DLS)	DLS measures the light scattering associated with Brownian motion and relates the intensity of scattering to the size of the particles defined by the Rayleigh approximation. Larger particles have slower motion and higher light scattering than smaller particles, and the intensity is proportional to the sixth power of hydrodynamic diameter	Particle size distribution, 1 nm–1 μm % polydispersity Z-average diameter in nm Diameter of individual particle populations
Micro flow Imaging (MFI)	MFI combines the direct imaging capabilities of digital microscopy with the precise control of microfluidics. Images of the sample are captured as it passes through the flow cell's sensing and analyzed by applying various filters to create a database of particle count, size, transparency, and morphology	Particle #/mL Particle size distribution 1–100 μm and statistics High-resolution images of particles showing morphology

6.09.8 Formulation Development

The formulation of an injectable protein DS or DP consists of the API, excipients including buffer, tonicity agent, and stabilizers, and the container/closure system. Additionally, in the case of advanced formulations such as sustained-release formulations, one or more constituents representing the delivery platform formulation or a medical device is also included. Further, for combination products, more than one API may be included along with constituent formulation matrix. The goal of formulation development is to ensure that a formulation when packaged in a specific container will remain within its physical, chemical, microbiological, therapeutic, and toxicological specifications until the assigned expiration date based on stability studies.[17] Additionally, the formulation development should strive to minimize the amount of impurities during storage and handling to mitigate safety/immunogenicity issues, demonstrate compatibility with components and stability during administration, evaluate dosage forms that are patient-friendly, and explore enhanced drug delivery approaches using various routes of administration to improve PK and PD parameters. The stages in formulation development include preformulation and forced-degradation studies, formulation optimization, and commercial formulation development. The various activities associated with these phases of formulation development are summarized in **Table 9**.

6.09.9 Preformulation and Forced Degradation

Since the major goal of formulation development is to assess the stability of the molecule, it is important to demonstrate the stability-indicating properties of the analytical methods and characterization methods in the toolbox used to assess formulation performance. Generally, since the protein to be formulated is obtained from either the discovery or downstream process development group, these personnel may have some understanding of the in-use stability of the protein under normal handling conditions (e.g., solubility, turbidity, activity, and some assessment of protein aggregation by SDS-PAGE and SE-HPLC). The formulation scientist should engage in discussions early during development with these groups and learn about the molecule behavior. An in-depth assessment of protein stability is accomplished by first mapping out the potential hot spots in the protein sequence from the protein sequence such as oxidation, deamidation, and proteolysis. Next, working with the analytical development scientists, a comprehensive forced-degradation study[18] is performed to evaluate and quantify the changes at various stress conditions including appropriate control conditions. The data from the forced-degradation study can then be compiled to generate a stress map that provides a quick reference tool to plan the formulation studies aimed at minimizing product degradation. An example of such a stress map is shown in **Fig. 3**. A simple depiction of the susceptibility (to various stresses) and severity (quantitation of impurities) of degradation using a three-color code provides a snapshot of the allowable boundaries during downstream purification, formulation, and the most stability-indicating methods to use in the toolbox for stability assessment and comparability.

It is important to know that during the early development, only small amounts of protein may be available for formulation work. Further, there is a lot of pressure from the preclinical group to quickly provide a "reasonably stable" formulation for pilot toxicity and PK/efficacy studies. So, good planning and collaboration are crucial at this stage to ensure there is sufficient protein available for analytical and formulation development while supporting the preclinical development at the same time and setting realistic expectations. The typical order of preformulation screening (**Table 10**) involves a range of buffers covering pH ranges generally between 4 and 8, with or without any tonicity modifiers; followed by screening of stabilizing excipients such as sodium chloride, sucrose, sorbitol (as stabilizers and tonicity modifiers); solubility assessment at a range of protein concentration without and

Table 9 Formulation development stages and key activities

Formulation stage	*Activities and points to consider*
Preformulation and forced degradation	Understanding physicochemical properties of API(s) Developing stability-indicating methods Estimating product's stability by forced-degradation study Dosage form (liquid, frozen, and lyophilized) and storage temperature decision based on stability and trend analysis Formulation parameters – Buffer – pH – Salt/sugars as tonicity modifiers and bulking agents – Cofactors – API concentration and solubility – Stabilizers (cryoprotectants, lyoprotectants, surfactants, antioxidants, chelators, preservatives, etc.)
Formulation optimization	Maximizing the stability of the API using DOE Evaluate various dosage forms, reconstitution, single- vs. multi-dose forms Dose range and frequency for clinical indication(s); fixed dose vs. variable dose Route of delivery, self-administration, patient's delivery capability, container/packaging, delivery devices Expiration target to cover the clinical trial duration and evaluation of allowable stability excursions Selection of API and excipient(s) sources and alternate vendors Container/closure compatibility and in-use (bed side) stability of clinical dose in infusion bags, lines, and rate of infusion
Commercial formulation development	Commercially feasible formulation that meets the TPP The final formulation should maintain the SISPQ attributes of the drug during all the shipping, handling, and uses specified on the label Commercial storage at Depots, labeling, cold-chain supply and distribution considerations Real-time stability with optimized manufacturing process lasting 1–2 years or more, with expiration target of $\geq$2 years Develop clinical experience with commercial formulation in pivotal clinical trials Container closure and delivery device/technology evaluation (e.g., pens, prefilled syringes, and depot formulations)

with different surfactants and concentrations of surfactants; and finally screening of additional stabilizers to minimize specific degradation pathways (aggregation, oxidation, deamidation, and proteolysis).

Early preformulation work does not need to be performed at high protein concentrations. At this stage, the intended indications and efficacious doses are also not known; so, it is difficult to target specific API concentration in the formulation. For early clinical development, an API concentration is chosen based on efficacy in animal models and the dosing range planned for toxicological studies. After gaining clinical experience from phase 2 safety and efficacy studies, further adjustments in the formulation protein concentration can be made, if necessary, along with evaluation of different fill volumes and presentations of DP to meet the specific patient indications.

For most proteins, it is common to initially develop a frozen liquid formulation for preclinical studies and phase 1/2 clinical trials. The intent is to stage the work and cut costs on in-depth formulation optimization for late stage and commercial formulation development. Also, at this early stage, without a full understanding of the formulation stability under shipping and handling conditions, it is convenient to ship materials between CMO, fill finish, clinical sites, and storage depot sites when the DP vials are frozen. However, it is prudent to evaluate the stability of the early prototype formulation under refrigerated storage condition for an extended period of time (1–2 years) to determine if the same formulation can be used later for a commercial formulation. If certain specific degradation products and higher content of these are observed, adjustments can be made to mitigate the instability (e.g., increasing antioxidants and/or combination with chelators). Additionally, a stability-data-driven decision can be made on committing to a liquid or lyophilized formulation for further development and optimization.

6.09.10 Formulation Optimization

After gaining reasonable experience with the phase 1 and early phase 2 formulation in clinical development, one can use the knowledge to fine-tune the strength, formulation stability, and dosage form to develop a commercial formulation that has extended shelf life and desired product quality and presentation attributes. The changes can vary and include increased protein concentration and fill volume, better buffering capacity, and finer adjustments of pH and excipient concentrations for most optimal formulation stability using design of experiments (DOE).

Stress Conditions	ANALYTICAL TOOLS										
	Visual	A280	A340	Non-Reduced SDS-PAGE	Reduced SDS-PAGE	SE-HPLC	IEX-HPLC	DLS	DSC	Intact mass	
Stability indication	Insoluble aggregates	Strength	Turbidity/ aggregates	Soluble covalent aggregates, fragmentation		Soluble Aggregation	Deamidation; fragmentation	Soluble Aggregates, particle size	Thermal stability, Tm	Chemical modification	Fragmentation
40°C; 1, 2 wk	No Change	No Change	No Change	No Change	No Change	HMW increase from 1% to 4%	No significant change	No change	No Change	No change	No change
pH 3, RT; 1-3d	No Change	No Change	No Change	Additional HMW & LMW bands detected	Additional LMW bands detected	Loss of main peak	No change	Slight increase in diameter	Drop in Tm by >10°C	No Change	fragmentation
pH 9, RT; 1-3d	No Change	No Change	No Change	No Change	No Change	HMW increase from 1% to 2%	Slight increase in acidic species, no change in fragmentation	No change	No Change	No change	No change
0.1% H_2O_2, RT 2hr	No Change	No Change	No Change	No Change	No Change	No change	No change	No change	No Change	Met Oxidation	No change
FZ/THAW -80°C/RT; 5,-10 Cycles	No Change	No Change	No Change	No Change	No Change	No Change	No change	Slight increase in diameter	No Change	No change	No change
Agitation RT 300RPM 1-3d	No Change	No Change	No Change	No change	No change	No Change	No change	No change	No Change	No change	No change

Fig. 3 Example forced-degradation stress map. Red, significant change; *yellow*, noticeable changes; *green*, no change.

Table 10 Formulation excipient categories and common excipient ranges

Excipient category	*Most common excipients*	*Typical ranges*
Buffers (pH 4–8)	Acetate, succinate, citrate, histidine, phosphate, tris	10–25 mM
Tonicity modifiers/cryoprotectants	Sucrose, sodium chloride, trehalose, sorbitol, and combinations	50–300 mM targeting ~300 mOsmol/kg
Bulking agents/lyoprotectants	Sucrose, trehalose, mannitol, glycine	3–5%
Stabilizers		
● Aggregation mitigator	Arginine, histidine	>0.2 M
● Antioxidants	Methionine, EDTA	1–10 mM
● Surfactants	Polysorbate 20 or 80	0.001–0.1%
● Cofactors	Zn, Ca, Mg	Low mM
● Preservative	*m*-Cresol, methylparaben, phenols	0.2–0.5%

Traditional, formulation development focuses on changing one factor at a time. This approach is based on varying one independent factor while keeping other independent factors constant. This approach intrinsically cannot detect interactions between factors and is very time consuming. In contrast, DOE takes into account all input variables simultaneously, systematically, and efficiently. Each single input variable and multivariable interaction can be evaluated, and their effect(s) on each response variable can be identified. The main steps involved in DOE studies[19] are the following:

1. Define the objective.
2. Define experimental factors (buffer type, pH, stabilizer(s), and concentration).
3. Select the design (full factorial, fractional factorial, center point, mixture design, etc.) and run the experiment, typically under accelerated stability conditions to tease out the differences between formulations.
4. Perform statistical analysis including ANOVA and interpret the significant factors that impact product stability using the software generated *p* values, *F* ratio, and desirability factor.

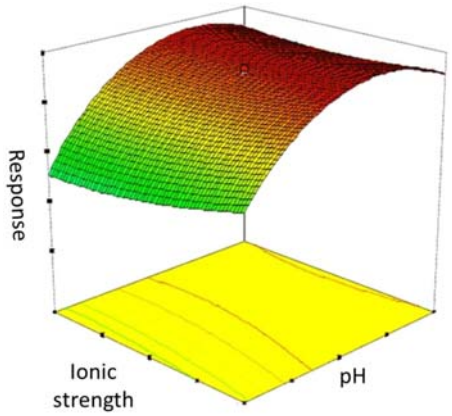

Fig. 4 Response surface DOE showing impact of varying ionic strength and pH on measured response.

5. Choose a model and fit the data to determine correlation. This is then followed by fine-tuning and confirming the statistical model.

A 3-D plot showing the effect of pH and ionic strength to maximize the optimal formulation parameters is shown in Fig. 4. Using a response surface DOE study, the impact of the individual factors affecting the purity and stability of the formulation can be assessed under various stress conditions, and optimal ranges of these parameters can be adapted during the manufacturing process to establish the final most optimal formulation. In the example shown in the figure, both higher pH and ionic strength have a positive impact on the desired response, and a combination of midrange of pH and ionic strength seems to yield the highest desirability.

DOE studies are especially very helpful when the effect of many factors to optimize the formulation needs to be studied. For example, to develop combination DPs involving more than one API/DS, several excipients and stabilizers that are important for rendering the stability to the individual API formulations will need to be tested in combination, and the type and concentrations of these components will need to be balanced using DOE experiments.

6.09.11 Lyophilized Drug Product Development

If the API is inherently unstable (e.g., most antibody–drug conjugates and proteolytic enzymes), then effort is focused on developing a lyophilized formulation early during development. It generally takes additional time to screen several excipients and develop an optimized lyophilization cycle, as well as develop additional methods to characterize, evaluate a reconstitution procedure, and establish in-use stability of the reconstituted product. The different steps involved in the development of a lyophilized formulation[20] are summarized in the succeeding text:

1. Screen combination of lyoprotectants (bulking agents such as mannitol and glycine) and cryoprotectants (sucrose and trehalose) and other stabilizers that are compatible in the liquid DS formulation prior to lyophilization.
2. Preliminary assessment of "lyophilizability" using a conservative lyophilization cycle in a pilot lyophilizer.
3. Determining Tg'/collapse temperature of liquid formulation to enable choice of shelf temperature below this temperature to prevent collapse of the DP freeze concentrate and evolving cake.
4. Cycle optimization including temperature ramp and annealing during freezing (if required), primary and secondary drying steps. Assessment of requirement of N_2 versus argon gas overlay and headspace measurement.
5. Long-term stability and characterization including Tg analysis of the dried lyophilized formulation for appropriate storage condition (refrigerated or room temperature) of lyophilized product. Accelerated stability assessment utilizing cake appearance, reconstitution time, moisture content, and product-specific stability-indicating purity/impurity methods.
6. Effect of high osmolality and development of a reconstitution strategy for high-concentration protein formulations.
7. Tech transfer of optimized lyophilization cycle to CMO for production scale lyophilizer, applying appropriate geometric calculations and freeze/dry parameters, and fine-tuning.

Fig. 5 shows an illustration of the lyophilization cycle in the upper panel involving the following steps:

(a) Freezing of the liquid DS (ice crystal growth and solidification of the amorphous or crystalline cryoprotectant/bulking agent that may also need an annealing step)
(b) Primary drying under vacuum where the majority of the water is removed by sublimation
(c) Secondary drying at elevated temperature to remove the adsorbed water vapor
(d) Back filling of the chamber with N_2 gas and stoppering of the vials

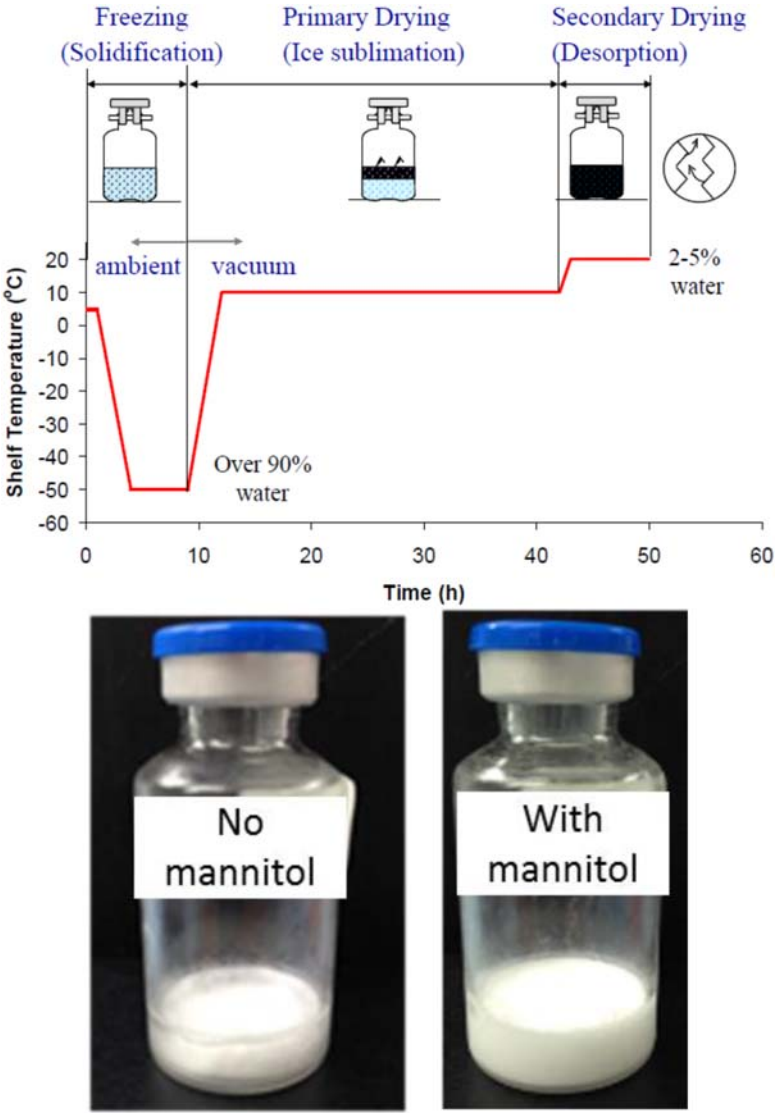

Fig. 5 Lyophilization process (with permission from Samir Sane, Genentech) and cake appearance of formulation without (microcollapsed cake) and with bulking agent (elegant cake).

Typical cycle times involve about 2–3 days for most protein formulations. Cycle times can vary depending on whether an annealing step is required due to the need to include bulking agents such as mannitol and how much water can be tolerated in the final formulation. Cycle optimization can be significantly accelerated and enhanced in some pilot lyophilizers such as LyoStar II using the SMART computerized system. The SMART technology constantly monitors the product temperature using thermal probes and, with a data feedback loop, controls the shelf temperature under a constant vacuum during the primary drying phase in the cycle to minimize cycle times in a single run. Further, secondary drying times can be monitored by using a sample thief to retrieve vials during the run to perform moisture analysis. Formulations that contain some sodium chloride can significantly benefit by the inclusion of mannitol that yields elegant cakes that are more stable and resistant to micro collapse (Fig. 5, lower panel).

For the intended purpose of covering general formulation strategies for biologics, it is not possible to discuss development of specialized formulations such a very high-protein-concentration formulations for certain Mabs and the design and use of sustained-release formulations, drug delivery, and drug/device combinations.[1]

6.09.12 Stability Studies and Expiration Dating

Early preformulation, forced-degradation, and accelerated stability studies provide a comprehensive assessment of the robustness of the formulation and allow a best guess of the long-term stability of the protein formulation. For small molecule and even some

Table 11 ICH stability guidance documents

ICH guidance	*Scope*	*Description*
Q1A	Stability testing of new drug substance and products	General guidance on stability studies involving selection of batches, stress conditions for accelerated testing, long-term testing, testing frequency, acceptance criteria, and evaluation of results
Q1B	Photostability	Photostability guidance covering testing of DS and DP, including controls, in primary and secondary packaging and the final marketing packaging, involving visible and UV light together (option 1) or preferable separately (option 2), and the work flow path
Q1D	Bracketing and matrix design	General principles for reduced stability testing and provides examples of bracketing and matrixing designs
Q1E	Evaluation of stability data	This document extends the main guideline by explaining possible situations where extrapolation of retest periods/shelf lives beyond the real-time data may be appropriate. Furthermore, it provides examples of statistical approaches to stability-data analysis
Q5C	Stability testing of biotechnological/ biological products	This document augments the stability guideline Q1A and deals with the particular aspects of stability test procedures needed to take account of the special characteristics of products in which the active components are typically proteins and/or polypeptides

short peptide APIs, the degradation pathways can be linear with increasing temperature and allow prediction of long-term stability by Arrhenius transformation and extrapolation of shelf life. However, for large proteins, it is generally very difficult to predict the stability of the formulation due to multiple degradation pathways that do not trend linearly in Arrhenius plots and in some cases plateau after some time under accelerated conditions. Hence, real-time stability studies are required to obtain realistic shelf life assessment. Table 11 summarizes the various ICH guidance documents describing the conduct of the stability studies, and Table 12 shows an example of the storage conditions for long-term and accelerated stability study along with the testing frequency.

For the long-term and accelerated stability studies, appropriate stability-indicating methods should be chosen from the panel of release assays including potency assay, to determine the qualitative and quantitative changes during storage. It is important to use qualified stability chambers and qualified assays for this purpose to minimize the assay variability and truly determine the impact of storage conditions on the product. Stability studies are performed using QA-approved stability protocols and are typically performed by QC personnel that are trained in the staging, monitoring, and administration of the analytical methods. The protocol should clearly specify the batch to be used, the container/closure used, configuration of vial staging (upright, sideways, or inverted), the conditions and time points, number of retain containers, and the analytical testing panel. Further, documentation, reporting, trending, and handling of any deviations, out-of-specification (OOS), and out-of-trend (OOT) results should also be captured in the protocol and investigated if there are atypical results.

In addition to the storage condition and accelerated stability studies on both DS and DP, bulk freeze/thaw study on DS that is representative of the container scale used for long-term cold-chain storage and photostability studies on the DP in its primary packaging and secondary packaging should be performed. It is also important to plan appropriate and timely audits of the QC and GMP stability labs, as well as any third-party analytical CRO, and depot storage/labeling service organizations that would be engaged in the storage, shipment, and conduct of stability studies. The Q1E guidance describes how the stability data are evaluated and trended to conservatively project shelf life of the product based on real-time and long-term stability data. While projections can be used as a general guide, stability commitment to continue the studies has to be made to accumulate real-time stability data to compare against the projected expiration date. In the early phases of development, it is typical to have retests performed at regular intervals as part of the stability study and to extend the expiration dating based on the results.

Process development typically involves hold-time stability studies to be performed during the downstream purification steps. In addition to these handling conditions, at later stages of development, appropriate storage, shipping, and distribution stability studies have to be performed to be compliant with USP<1079> good storage and distribution practices. After a comprehensive map of stability study data is obtained, one can use this database of stability knowledge to determine any excursions that may occur through the life cycle of the product lot.[21]

An example of how this can be used to determine impactful events (such as a temperature excursion at a certain elevated temperature) outside of the tested stability studies is shown in Fig. 6. In this example, the excursion at 32°C after 1 week would be questionable in regard to the use of the DP outside of the tested time intervals.

Table 12 Key stability conditions and testing frequency for a refrigerated drug product

	Interval (months)								
Storage conditions	0	1M	3M	6M	9M	12M	18M	24M	36M
2–8°C (Long-term)	X	X	X	X	X	X	X	X	X
25°C/65%RH (Accelerated)		X	X	X					

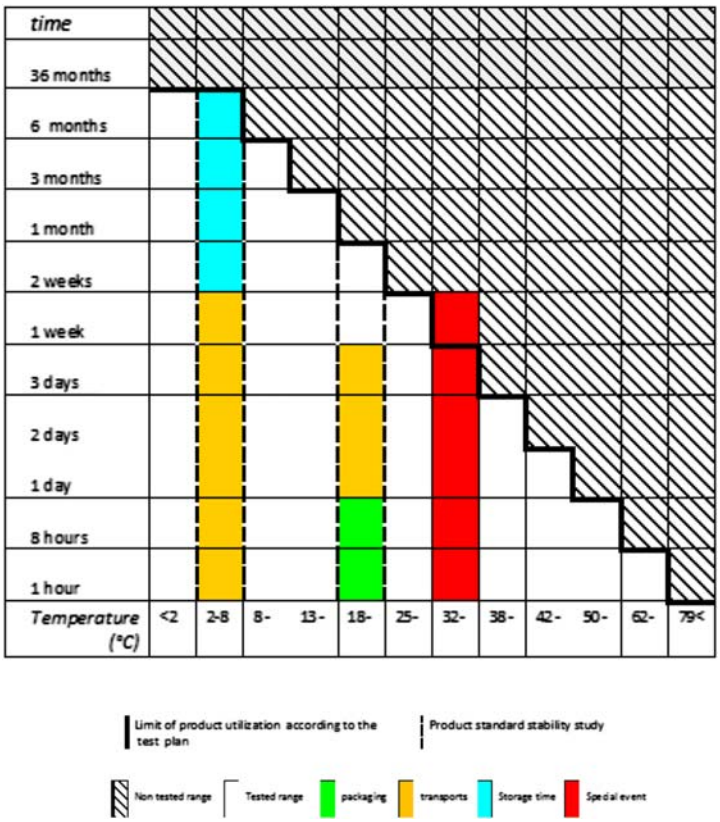

Fig. 6 Depiction of how the stability knowledge can be used to determine impact of excursion with permission from Claude Ammann.[21]

6.09.12.1 Clinical In-Use Stability Studies

In addition to the stability studies of DS and DP in their storage containers, clinical in-use stability studies should be performed to evaluate and establish guidelines of handling during drug dose solution preparation and administration to patients in the pharmacy manual. Intravenous infusion is a common route of delivery for therapeutic monoclonal antibody drug products and many are administered as a continuous infusion at room temperature upon dilution into a carrier solution, usually 0.9% sodium chloride and in some cases 5% dextrose. Compatibility of the diluted DP in infusion bags with contact materials such as polyvinylchloride (PVC) and polyolefin (PO), as well as associated infusion lines, syringes, and needles should all be considered and evaluated in an in-use study. Further, stability testing of lyophilized DPs after reconstitution or dilution, if applicable, should be conducted to provide information for the labeling on the preparation, storage condition, and in-use period of the reconstituted or diluted product. ICH Q1A(R2) and USP<795> pharmaceutical compounding guidelines recommend that this testing be performed on the reconstituted or diluted product through the proposed in-use period, typically up to 24 or 48 h.[22]

6.09.12.2 Extractable and Leachable Studies

During later stages of development, extractable and leachable studies[23] should also be performed with product contact materials that are used during various unit operations of manufacturing, to determine the type and level of impurities that may impact safety of the DP (USP<1663> and USP<1664>). Extractables represent chemicals that are extracted from a product contact material when exposed to a solvent under exaggerated conditions of time and temperature; and leachables are substances that migrate from the containers and closures in to the formulation under accelerated storage conditions. These compounds are generally additives in the container/closure and product contact process materials and include elastomers, fillers, antioxidants, lubricants, stabilizers, and coloring agents. Sources of leachables include storage containers, delivery devices such as syringes, IV bags and tubing, manufacturing equipment, and potentially secondary packaging components as well. These compounds may potentially interact with DP or excipients and cause inactivation and conformational changes of posttranslational modifications that may impact safety and potency of the DP. The extractable and leachable studies are usually performed after the process is optimized. For the earlier clinical development phases, generally, obtaining a list of extractable (LOE) substances from the various vendors of materials is sufficient for assessment of a worst-case scenario. A risk-based assessment on the toxicity of these components in relation to the

drug dose administered is needed to develop and validate analytical methods specific for these contaminants that allow establishment of safety thresholds and assurance.

6.09.13 Conclusions

Overall, analytical and formulation development of biologics play a prominent and significant role in manufacturing, release of batches, and stability of the DS and DP. There is considerable amount of overlap and interdisciplinary activities within process sciences and AFD. Efficient strategy, planning, organization, and highly disciplined and GMP-compliant execution of development, qualification, and routine testing are necessary to build quality by design (QbD) into the manufacturing process and the DP throughout its life cycle.

See also: 8.01. Medicinal Chemistry Case History: Osimertinib (AZD9291).

References

1. Skalko-Basnet, N. The Role of Delivery Systems in Improved Therapy. *Biologics* **2014,** *8,* 107–114.
2. Markovic, I. Chemistry, Manufacturing and Control Issues in Production of Therapeutic Biologic Protein Products. FDA presentation.
3. Guidance for Industry and Review Staff: Target Product Profile—A Strategic Development Process Tool. U.S. Department of Health and Human Services Food and Drug Administration Center for Drug Evaluation and Research (CDER), March, 2007.
4. Shintani, H. Development of Test Method for Pharmaceutical and Biopharmaceutical Products. *Pharmaceut. Anal. Acta* **2013,** *4,* 258, 1–14.
5. United States Pharmacopeial Convention: General Methods, General Chapters and Biotechnology Methods, USP 39 NF-34, May 2016.
6. Wang, F.; Richardson, D.; Shameem, M. Host-Cell Protein Measurement and Control. *BioPharm Int.* **2015,** *28* (6), 32–38.
7. Maity, H.; Wei, A.; Chen, E.; Haidar, J. N.; Srivastava, A.; Goldstein, J. Comparison of Predicted Extinction Coefficients of Monoclonal Antibodies With Experimental Values as Measured by the Edelhoch Method. *Int. J. Biol. Macromol.* **2015,** *77,* 260–265.
8. Michels, D. A.; Salas-Solano, O.; Felten, C. Imaged Capillary Isoelectric Focusing for Charge-Variant Analysis of Biopharmaceuticals. *BioProcess Int.* **2011,** *9* (10), 48–54.
9. *HPLC of Peptides and Proteins in Methods in Molecular Biology Series*; Aguilar, M.-I., Ed.; Humana Press, 2004; Vol. 251.
10. Rieder, N.; Gazzano-Santoro, H.; Schenerman, M.; Strause, R.; Fuchs, C.; Mire-Sluis, A.; McLeod, L. D. The Roles of Bioactivity Assays in Lot Release and Stability Testing. *BioProcess Int.* **2010,** *8,* 33–42.
11. Chan, C. C. Analytical Method Validation: Principles and Practices. In *Pharmaceutical Manufacturing Handbook: Regulations and Quality; Gad, S. C., Ed.; Wiley Interscience;* 2008; pp 727–742.
12. Noonan, P. Setting Specifications and Expiry Dates. In *The Challenge of CMC Regulatory Compliance for Biopharmaceuticals and Other Biologics; Geigert, J., Ed.; Springer;* 2013; pp 257–290.
13. Mire-Sluis, A.; Ritter, N.; Cherney, B.; Schmalzing, D.; Blümel, M. Reference Standards for Therapeutic Proteins. *BioProcess Int.* **2014,** *12* (3), 26–36.
14. Federici, M.; Lubiniecki, A.; Manikwar, P.; Volkin, D. B. Analytical Lessons Learned From Selected Therapeutic Protein Drug Comparability Studies. *Biologicals* **2013,** *41* (3), 131–147.
15. Mo, J.; Tymiak, A. A.; Chen, G. Mass Spectrometric Characterization in Protein Therapeutics Discovery. In *Characterization of Protein Therapeutics Using Mass Spectrometry;* Chen, G., Ed.; 2013. Springer.
16. Putnam, W. S.; Prabhu, S.; Zheng, Y.; Subramanyam, M.; Wang, Y.-M. C. Pharmacokinetic, Pharmacodynamics and Immunogenicity Comparability Assessment Strategies for Monoclonal Antibodies. *Trends Biotechnol.* **2010,** *28,* 509–516.
17. Nail, S.; Akers, M. Formulation Development of Protein Dosage Forms. In *Development and Manufacture of Protein Pharmaceuticals;* Nail, S., Akers, M., Eds.; 2002; pp 47–114. Springer.
18. Chan, C. P. Forced Degradation Studies: Current Trends and Future Perspectives for Protein-Based Therapeutics. *Expert Rev. Proteomics* **2016,** *13,* 1–8.
19. Grillo, A. O.; Perkins, M.; Kane, M.; Penn, N. Characterizing the Formulation Design Space. *BioPharm Int.* **2010,** *23* (3), 30–39.
20. Nail, S.; Jiang, S.; Chongprasert, S.; Knopp, S. A. Fundamentals of Freeze-Drying. In *Development and Manufacture of Protein Pharmaceuticals;* Nail, S., Akers, M., Eds.; 2002; pp 281–353. Springer.
21. Ammann, C. Stability Studies Needed to Define the Handling and Transport Conditions of Sensitive Pharmaceutical or Biotechnological Products. *AAPS PharmSciTech* **2011,** *12* (4), 1264–1275.
22. Sreedhara, A.; Glover, Z. K.; Piros, N.; Xiao, N.; Patel, A.; Kabakoff, B. Stability of IgG1 Monoclonal Antibodies in Intravenous Infusion Bags Under Clinical In-Use Conditions. *J. Pharm. Sci.* **2012,** *101* (1), 21–30.
23. Wakankar, A. A.; Wang, Y. J.; Canova-Davis, E.; Ma, S.; Schmalzing, D.; Grieco, J.; Milby, T.; Reynolds, T.; Mazzarella, K.; Hoff, E.; Gomez, S.; Martin-Moe, S. On developing a Process for Conducting Extractable-Leachable Assessment of Components Used for Storage of Biopharmaceuticals. *J. Pharm. Sci.* **2010,** *99* (5), 2209–2218.

Relevant Websites

http://www.ich.org/products/guidelines/quality/article/quality-guidelines.html.
http://www.usp.org/usp-nf.
http://www.fda.gov/BiologicsBloodVaccines/GuidanceComplianceRegulatoryInformation/Guidances/General/ucm217665.htm.
https://www.agilent.com/cs/library/eseminars/Public/Method%20Development%20for%20Peptides%20and%20Proteins.pdf.

6.10 Recent Advances in Medicinal Chemistry of Antisense Oligonucleotides

KR Ito and S Obika, Osaka University, Osaka, Japan

© 2017 Elsevier Ltd. All rights reserved.

6.10.1	**Introduction to the Medicinal Chemistry of Antisense Oligonucleotides**	216
6.10.1.1	What Are Antisense Oligonucleotides?	216
6.10.1.2	Chemical and Medicinal Chemistry Properties of ASOs	217
6.10.2	**Improvement in Nuclease Resistance**	218
6.10.2.1	Backbone Modifications	218
6.10.2.2	Sugar Modifications	219
6.10.2.2.1	Ring size	219
6.10.2.2.2	Bulkiness of the substituent on the bridging moiety	219
6.10.3	**Improvement in Target-Binding Affinity and Potency**	220
6.10.3.1	Sugar Modifications and Bridged Nucleic Acids (BNAs)	220
6.10.3.1.1	LNA, alkyl LNAs, and their isomers	220
6.10.3.1.2	Replacement of oxygen with carbon	221
6.10.3.1.3	Introduction of heteroatoms into the bridge	222
6.10.3.1.4	Introduction of cation into the bridge	223
6.10.3.1.5	Control of torsion angles	223
6.10.3.1.6	Summary	224
6.10.3.2	Number and/or Mode of Introduction of Sugar Modifications	225
6.10.3.2.1	Gapmers	225
6.10.3.2.2	Too high an affinity drastically decreases potency	225
6.10.3.3	Backbone Modifications	226
6.10.4	**ADME**	226
6.10.4.1	Sugar Modifications	226
6.10.4.2	Length of the ASOs	227
6.10.5	**Target Specificity, Hybridization-Dependent Off-Target Effects, and Safety**	227
6.10.5.1	Overview of the Safety of ASOs	227
6.10.5.1.1	Class effects of phosphorothioated ASOs	227
6.10.5.1.2	Target specificity and hepatotoxicity	228
6.10.5.2	Medicinal Chemistry Approaches to Improving Safety Profiles	228
6.10.5.2.1	Sequence design	228
6.10.5.2.2	Nucleobase modifications	229
6.10.5.2.3	Gap design	229
6.10.6	**Conclusion**	230
References		230

6.10.1 Introduction to the Medicinal Chemistry of Antisense Oligonucleotides

6.10.1.1 What Are Antisense Oligonucleotides?

Oligonucleotide-based drugs are a new class of therapeutics undergoing clinical trials worldwide to assess their ability to target severe diseases and diseases with no current means of treatment.[1–4] This article will provide an overview of the medicinal chemistry of antisense oligonucleotides (ASOs), a family of intensively investigated and evolving oligonucleotide-based drugs. ASOs are single-stranded oligonucleotides whose sequences are complementary to the intended target RNAs. The target RNA can be of any type, including mRNA, pre-mRNA, and microRNA.[2] ASOs can change the splicing pattern of target pre-mRNA by steric blocking of the spliceosome or inhibit the function of the target RNA. The function of the target RNA can be inhibited by two major mechanisms. One is steric blockage, the approach used by anti-microRNA ASOs, and the other is cleavage of the target RNA with RNase H1, which recognizes DNA/RNA heteroduplexes and exclusively cleaves the RNA strand (**Fig. 1**). Two ASO drugs, fomivirsen sodium and mipomersen sodium, have been approved by the FDA to date. Fomivirsen sodium targets the transcripts of the major immediate early region 2 (IE2) of human cytomegalovirus (HCMV) and is indicated for the local treatment of HCMV retinitis, whereas mipomersen sodium targets apoB mRNA and is indicated for patients with homozygous familial hypercholesterolemia as an adjunct to lipid-lowering medications and diet.[5,6]

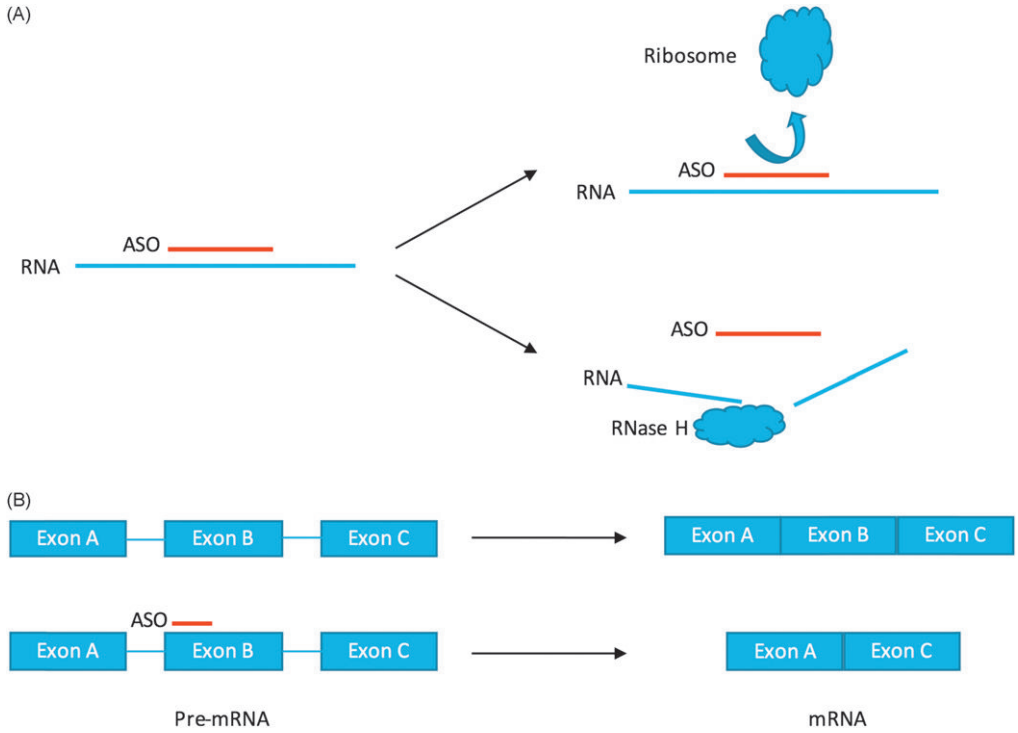

Fig. 1 Mechanisms of action of ASOs. Steric-blocking ASO (A, *upper*), RNase H-recruiting ASO (A, *lower*), and splice-switching ASO (B).

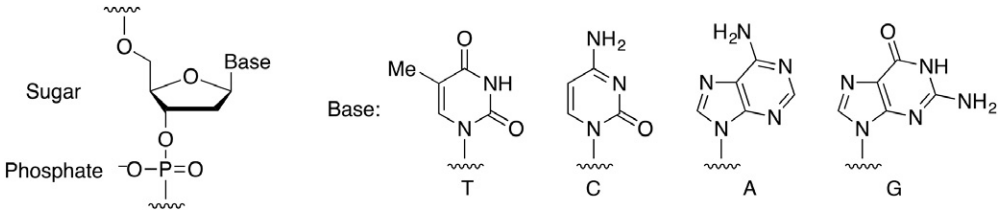

Fig. 2 Chemical structure of DNA.

6.10.1.2 Chemical and Medicinal Chemistry Properties of ASOs

Oligonucleotides are chemically composed of three units: nucleobases, sugars, and phosphodiester backbone (Fig. 2). Each unit comprises many heteroatoms and hydrogen-bonding donors and acceptors. The phosphodiester backbone is strongly acidic, and thus, ASOs are typically synthesized as the sodium salt. ASOs are highly hydrophilic and ionic in nature, and their oral bioavailability is generally very low,[7] thus limiting the route of administration to subcutaneous, intravenous, or local administration (such as intrathecal or intravitreous injection).[4]

A large body of information is accumulated during the discovery process of small-molecule drugs, such as molecular size, lipophilicity, shape, hydrogen-bonding properties, and polarity, and these characteristics are correlated to solubility, membrane permeability, metabolic stability, receptor promiscuity, in vivo toxicity, and chemical stability.[8–10] ASOs are chemically synthesized and are highly chemically modified, so they share some common features with small-molecule drugs. However, due to their unique physicochemical properties and mechanism of action and their unusual drug metabolism, the medicinal chemistry approach taken with ASOs is also rather different from that of small-molecule drugs (Table 1).

Medicinal chemistry studies of ASOs have focused on overcoming the shortcomings of natural DNA and/or RNA oligonucleotides as therapeutics, namely, (i) extreme lability toward nucleases, which makes their in vivo half-lives very short; (ii) limited binding affinity toward the target RNA; and (iii) the lack of ability to distribute to the target organ and/or tissue, thus requiring appropriate drug delivery technologies.

There are two major medicinal chemistry approaches for ASOs, as described in detail in the succeeding text. One is to develop an optimal chemical unit for oligonucleotides, which is what we call "unit chemistry". Examples include the development of a new nucleoside monomer or a new analog for the phosphodiester linkage. The other approach is to choose the best combination of unit chemistries and to optimize the total molecular properties of ASOs such as length, lipophilicity, gap size (required to support

Table 1 Properties of small-molecule drugs and antisense oligonucleotides

	Small-molecule drugs	*Antisense oligonucleotides*
Manufacturing	Chemical	Chemical
Medicinal chemistry	Applicable	Applicable
Molecular weight	~500	~5000
Electric charges	0~±2	Polyanion
Mechanism of action	Bind to protein (3-D structure-specific)	Bind to RNA (sequence-specific)
Root of administration	Oral (if appropriate)	Injection (low oral bioavailability)

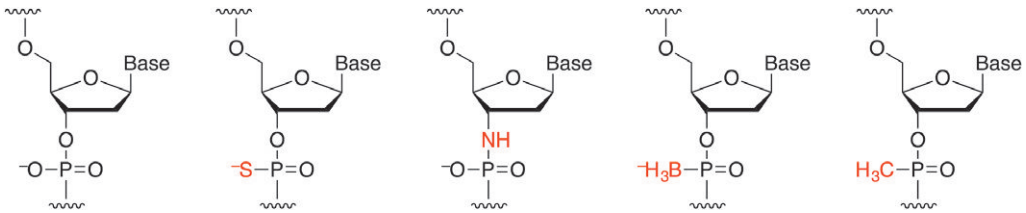

Fig. 3 Examples of phosphate backbone modifications.[18]

an RNase H1-based mechanism of action), and target-binding affinity. These two approaches together have recently significantly improved the stability and potency of ASOs in vivo, but at the same time, new problems have become apparent. For example, some ASOs that recruit RNase H1 activity due to high-affinity modifications (such as locked nucleic acid (LNA)) may cause hepatotoxicity[11–15] and induce significant knockdown of nontargeted RNA; this is called hybridization-dependent off-target effects.[15–17] In light of these recent findings, background information and recent developments toward high-affinity modifications will be discussed in this article, in conjunction with a discussion of the chemical approaches well combined with such high-affinity modifications. The two medicinal chemistry approaches used to develop ASOs will be reviewed from multiple viewpoints, including nuclease resistance, target-binding affinity and potency, absorption, distribution, metabolism and excretion (ADME), target specificity, and safety.

6.10.2 Improvement in Nuclease Resistance

6.10.2.1 Backbone Modifications

Natural oligonucleotides are rapidly degraded in vivo due to the hydrolysis of phosphodiester linkages by nucleases. Consequently, one of the first examples of the chemical modification of ASOs was of the phosphodiester backbone[18] (Fig. 3). The most successful modification of the many reported to date is the replacement of a nonbridging oxygen with sulfur.[19–21] This modification is called a phosphorothioate, and it dramatically improves the stability of ASOs in vitro and in vivo.[21,22] In addition to high nuclease resistance, plasma proteins bind rapidly to phosphorothioated ASOs, enabling the ASOs to escape renal filtration, and thus distribute to the targeted tissues and enter the target cells.[22,23] Another backbone modification found in candidate ASOs in clinical development is the phosphorodiamidate linkage in morpholino oligonucleotides (Fig. 4). This modification provides almost complete nuclease resistance, but in contrast to phosphorothioated ASOs, the plasma protein binding rate of morpholino oligonucleotides is low, limiting their pharmacokinetic profiles.[22] Thus, most ASOs in clinical use or in clinical development are phosphorothioates.

The replacement of one of the two nonbridging oxygen atoms by sulfur introduces chirality at the phosphorous atom of phosphorothioated ASOs (Fig. 5). Most phosphorothioated ASOs currently in clinical use are mixtures of all the possible diastereomers originating from the phosphorothioate linkage (2^{n-1} diastereomers).[24] The chirality of phosphorothioate affects resistance toward hydrolysis by nucleases and other properties of ASOs, as we discuss later in this article.

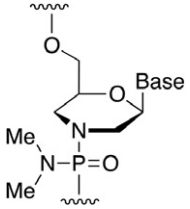

Fig. 4 Chemical structure of morpholino oligonucleotide.

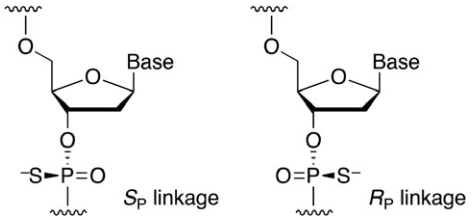

Fig. 5 Stereochemistry of phosphorothioate.

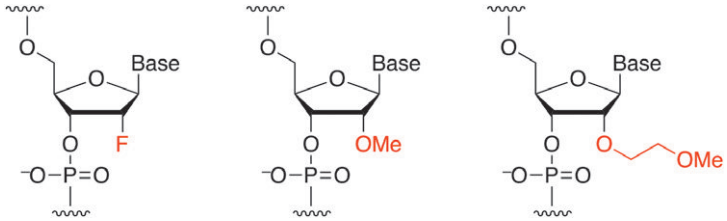

Fig. 6 Examples of 2′ modifications.[25]

6.10.2.2 Sugar Modifications

Another approach for resisting nuclease degradation is to modify the sugar units of oligonucleotides. Most oligonucleotides containing nucleosides with modified sugars exhibit higher nuclease resistance than oligonucleotides composed of natural nucleosides.[25]

The most traditional sugar modification is the introduction of a substituent at the 2′-position, for example, 2′-F, 2′-OMe, or one of the best known 2′-modified nucleoside, 2′-*O*-methoxyethyl (MOE) (Fig. 6). Generally, larger substituents provide higher nuclease resistance.[25] On the other hand, sugar modifications greatly affect target-binding affinity, with larger substituents in particular often decreasing affinity, yet both nuclease resistance and target-binding affinity should be high to achieve good in vivo efficacy. 2′-*O*-MOE achieves this, and this modification is present in the FDA-approved ASO mipomersen sodium, the first approved systemic ASO to enter the world market.[6,26–28]

A newer type of sugar modification is found in bridged nucleic acids (BNAs). BNAs have a bicyclic sugar moiety, and the sugar is locked into the $C_{3'}$-*endo* conformation[29–32] (Fig. 7); consequently, BNAs exhibit extremely high target RNA-binding affinity and also show significantly higher nuclease resistance compared with natural oligonucleotides.[30] Based on BNAs reported to date, a larger ring size or the introduction of additional substituents on the bridging moiety results in higher nuclease resistance. Examples of BNAs exhibiting these characteristics are provided next.

6.10.2.2.1 Ring size

ENA and PrNA are analogs of LNA in which the methylene bridge of LNA (a five-membered ring) is enhanced to ethylene (a six-membered ring) and propylene (a seven-membered ring), respectively[33,34] (Fig. 8). The nuclease resistance of ENA and PrNA toward 3′ exonuclease (snake venom phosphodiesterase) was tested. Under conditions where oligonucleotide containing a LNA was completely degraded within a few minutes, the half-life of oligonucleotides containing a single ENA residue was ~15 min, while approximately 70% of oligonucleotides with a single PrNA residue remained intact even after 90 min of incubation.

6.10.2.2.2 Bulkiness of the substituent on the bridging moiety

*scp*BNA has a cyclopropane ring at the 6′-position of LNA[35] (Fig. 9). The effect of this additional substituent on resistance toward 3′ exonuclease (snake venom phosphodiesterase) was evaluated. Under conditions where the natural oligonucleotide and oligonucleotides with a single LNA residue were digested in 5 and 20 min, respectively, over 50% of oligonucleotides with a scpBNA residue remained intact after 80 min.

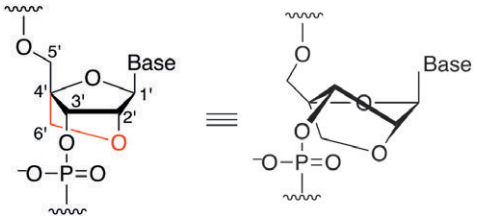

Fig. 7 Chemical structure and conformation of LNA.

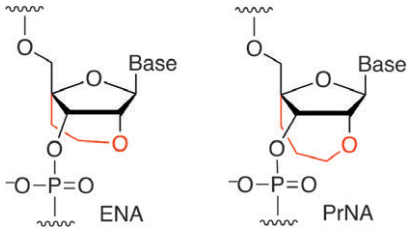

Fig. 8 Chemical structures of ENA and PrNA.

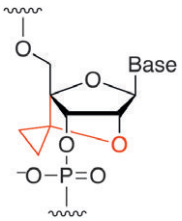

Fig. 9 Chemical structure of scpBNA.

6.10.3 Improvement in Target-Binding Affinity and Potency

Poor target-binding affinity of ASOs will likely limit their potency, so it is clear that improving target-binding affinity is essential for achieving highly potent ASOs.

Target-binding affinity is affected by many factors. For example, sequence context affects target-binding affinity because it defines the total number of hydrogen bonds and stacking interactions of the ASO–RNA duplex. Thus, longer ASOs or ASOs with higher G/C content tend to exhibit stronger in vitro target-binding affinity.

Although stronger target-binding affinity is generally considered advantageous, we recently obtained evidence that extraordinarily high affinity markedly decreases in vitro and in vivo potency for reasons that may depend on the mode of action of the ASO, as discussed later. These observations indicate that target-binding affinity is one parameter affecting potency, but optimization of all the molecular attributes is important to realizing a good lead ASO. Although improved target-binding affinity has provided highly potent ASOs, in vitro affinity as assessed by T_m is just one of the important parameters affecting the utility of ASOs.

6.10.3.1 Sugar Modifications and Bridged Nucleic Acids (BNAs)

Sugar modification impacts the target-binding affinity of ASOs, likely by affecting the sugar conformation. For example, introduction of an electron-withdrawing substituent at the 2′-position of DNA such as 2′-F, 2′-OMe, or 2′-*O*-MOE favors the $C_{3'}$-*endo* conformation due to the gauche effect. This RNA-type sugar conformation improves the affinity of the ASO toward the target RNA.[1,25]

A significant improvement in the target-binding affinity was achieved in 1997 when our group first reported the synthesis of 2′,4′-BNA, also known as LNA.[29–32] LNA has a 2′-*O*,4′-*C*-methylene bridge, and the sugar is locked into the $C_{3'}$-*endo* conformation (Fig. 7). Introduction of the 2′-*O*,4′-*C*-methylene bridge dramatically increases the hybridization affinity of ASO toward the target RNA. Swayze et al. compared the potency of ASOs containing LNA with those containing 2′-*O*-MOE[11] and showed that the LNA modification radically increased the binding affinity, resulting in about five times higher in vivo antisense potency.

This finding by Swayze and coworkers stimulated significant effort to develop analogs of LNA. In the succeeding text, we discuss LNA and its analogs (BNAs), because they are the most important sugar modifications found in current ASOs.

6.10.3.1.1 LNA, alkyl LNAs, and their isomers

6.10.3.1.1.1 LNA

LNA was the first nucleoside analog synthesized with its sugar locked into the $C_{3'}$-*endo* conformation. This analog exhibits significantly increased target-binding affinity (ΔT_m/modification = approximately +5°C compared with natural DNA).[30–32]

6.10.3.1.1.2 Ring-expanded LNAs

As mentioned earlier, ENA and PrNA are homologues of LNA in which the five-membered methylene bridge of LNA is enhanced to ethylene (a six-membered ring) and propylene (a seven-membered ring), respectively (Fig. 8). Compared with LNA, ENA exhibits slightly decreased target-binding affinity (ΔT_m/modification = approximately +3.5°C compared with natural DNA),[33,34] whereas PrNA shows decreased target-binding affinity that is similar to that of natural DNA

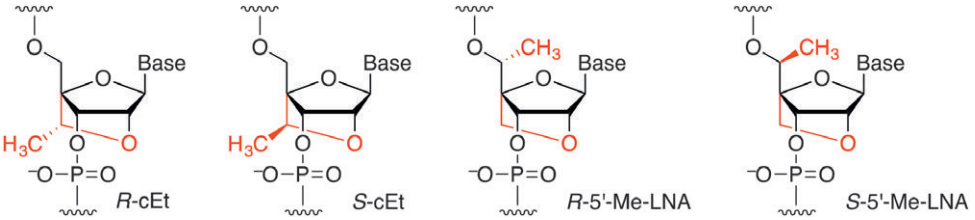

Fig. 10 Chemical structures of cEts and 5′-Me-LNAs.

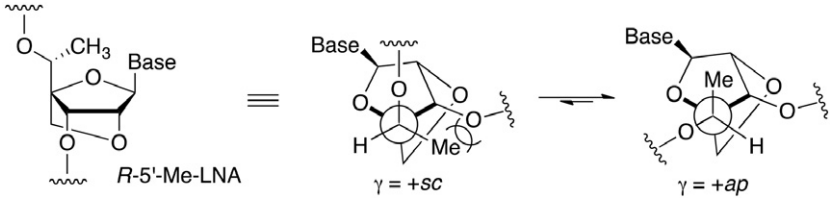

Fig. 11 Conformational change induced by *R*-5′-Me group.

(ΔT_m/modification = approximately $-0.5°C$).[33,34] The lack of increased binding affinity of PrNA is likely due to steric hindrance caused by the large ring.

6.10.3.1.1.3 Alkyl LNAs

cEt, 5′-Me-LNA, and scpBNA are five-membered ring BNAs (Figs. 9 and 10). cEt and 5′-Me-LNA are isomers of ENA and have a methyl group on the bridging carbon (6′-position) or 5′ carbon of LNA, respectively. scpBNA has a cyclopropane ring at the 6′-position. Except for *R*-5′-Me-LNA, these additional modifications to LNA had minimum effect on target-binding affinity; thus, their ΔT_m/modification values were comparable to that of LNA.[35–37] The 5′-Me group of *R*-5′-Me-LNA is believed to induce an unfavorable change in the γ torsion angle due to steric repulsion, leading to a lower binding affinity (ΔT_m/modification ≈ 5°C for *S*-5′-Me-LNA, cEt, scpBNA, and LNA, $\approx -1 \sim +3°C$)[37] (Fig. 11).

6.10.3.1.1.4 Antisense potency of ASOs containing LNA, alkyl LNAs, or their isomers

The higher binding affinity of LNA compared with that achieved by conventional modifications, for example, 2′-*O*-MOE, significantly increased in vitro and in vivo antisense efficacy. The ED_{50} values in the mouse liver of ASOs targeting TNFRSF1A-associated via death domain (TRADD) mRNA were as low as 2 mg kg^{-1} for LNA ASOs and approximately 9 mg kg^{-1} for MOE ASOs.[11] Furthermore, although the target-binding affinities of ASOs containing *R*-cEt or *S*-cEt were similar, in vitro and in vivo antisense efficacies were significantly stronger for ASOs containing *S*-cEt.[36]

Despite the target-binding affinities of LNA analogs being comparable to that of LNA, ASOs with LNA typically exhibit lower in vivo ED_{50} values than do ASOs containing LNA analogs.[36,37]

Modification with LNA seems effective also for antisense-mediated modulation of pre-mRNA splicing. Designed appropriately, 15-mer ASOs containing LNA induced significant amount of exon-skipped mRNA, while ASOs with 2′-OMe-RNA showed exon-skipping activity no higher than no treatment control under the same conditions in vitro.[38]

6.10.3.1.2 Replacement of oxygen with carbon

CarbaLNA and methylene-cLNA are two examples of LNA analogs in which the bridging oxygen in LNA is replaced with carbon (Fig. 12).

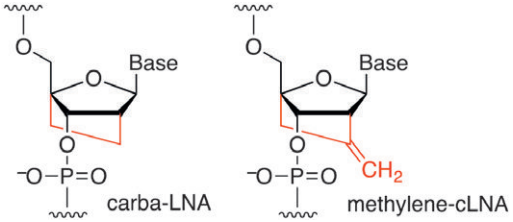

Fig. 12 Chemical structures of carbaLNA and methylene-cLNA.

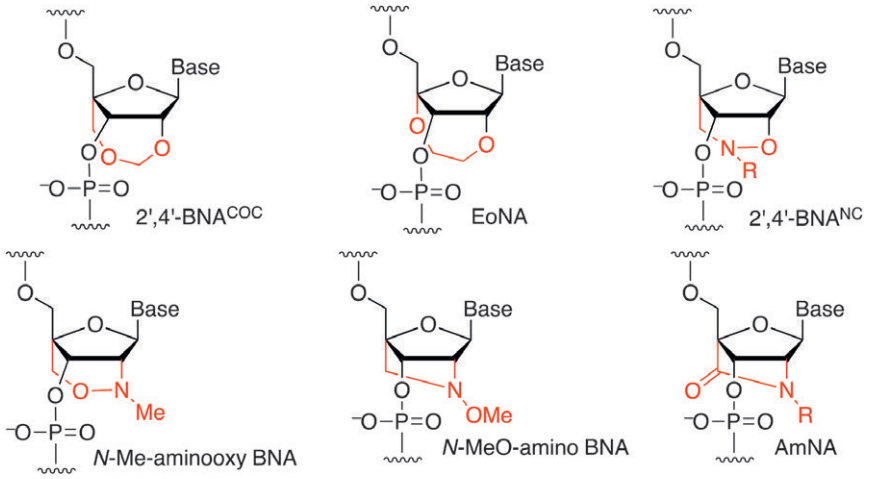

Fig. 13 Chemical structures of 2′,4′-BNA^{COC}, EoNA, 2′,4′-BNA^{NC} and its isomers, and AmNA.

A methylene linkage replaces this oxygen in carbaLNA; this modification slightly attenuates the target-binding affinity compared with LNA (ΔT_m/modification = approximately +3.6°C for carbaLNA vs. +4.5°C for LNA).[39]

In methylene-cLNA, an exomethylene replaces the bridging oxygen. Oligonucleotides with this modification exhibit similar or slightly improved target-binding affinity compared with oligonucleotides with LNA (ΔT_m/modification = approximately +4.8°C to +7.1°C for methylene-cLNA vs. +4.5°C to +6.1°C for LNA).[40]

The crystal structure of methylene-cLNA indicates that the edge of the exomethylene can form a hydrogen bond. Hydration of the duplex is believed to be important for its thermal stability. Therefore, the ability of methylene-cLNA to form a hydrogen bond and the inability of carbaLNA to hydrogen bond may explain their increased and decreased target-binding affinity compared with LNA, respectively.[40]

The in vitro and in vivo antisense potencies of 14-mers and 18-mers of methylene-cLNA ASOs and LNA ASOs targeting mouse *PTEN* mRNA were compared. 14-Mer LNA ASO showed the lowest in vitro IC_{50} and in vivo ED_{50} values (2.8 μM and 3.5 mg kg^{-1}, respectively) of the analogs tested, while the 14-mer methylene-cLNA showed only slightly lower antisense potency (IC_{50} and ED_{50} values of 3.9 μM and 4.9 mg kg^{-1}, respectively). Methylene-cLNA may therefore be considered to be a bioisostere of LNA.[40]

6.10.3.1.3 Introduction of heteroatoms into the bridge

The hydration of the duplex is very important, and thus, the effects of introducing heteroatoms into the bridge structure are of great interest. In the succeeding text, we describe several examples of BNAs containing multiple heteroatoms in the bridge structure (Fig. 13).

6.10.3.1.3.1 2′,4′-BNA^{COC}

2′,4′-BNA^{COC} contains a methylenoxymethylene bridge structure[41,42] and can be considered as an analog of PrNA, with an oxygen atom replacing one methylene linkage. The target RNA-binding affinity of 2′,4′-BNA^{COC} is higher than that of PrNA (ΔT_m/modification = approximately +1°C to 2°C for 2′,4′-BNA^{COC} and approximately −0.5°C for PrNA).[34,41,42] Recently, our group succeeded in replacing the C4′ methylene linkage of PrNA with an oxygen atom (EoNA). EoNA is an isomer of 2′,4′-BNA^{COC} and exhibits higher target-binding affinity than 2′,4′-BNA^{COC} toward some target sequences (ΔT_m/modification = approximately +1°C to 3.6°C).[43]

6.10.3.1.3.2 2′,4′-BNA^{NC}

2′,4′-BNA^{NC} is an analog of ENA in which a methylene linkage is replaced with a nitrogen atom.[44,45] Substituents on the nitrogen atom affect target-binding affinity, as discussed earlier in the section on nuclease resistance. The smaller the substituent, the higher the target-binding affinity (ΔT_m/modification = approximately +5.3°C to 6.3°C for 2′,4′-BNA^{NC} (NH), +4.7°C to +6.0°C for 2′,4′-BNA^{NC} (NMe), +4.7°C to 5.5°C for 2′,4′-BNA^{NC} (NBn), and +5.0°C to +7.0°C for LNA).[45] Although no data for direct comparison are available, the ΔT_m/modification of ASOs containing 2′,4′-BNA^{NC} appears to be typically higher than that of ENA.

There are several reports on the antisense efficacy of ASOs containing 2′,4′-BNA^{NC}.[46–48]

Prakash et al. tested the antisense efficacy of ASOs containing LNA, 2′,4′-BNA^{NC} (NMe or NH), or isomers of 2′,4′-BNA^{NC} (NMe) in mice.[46] Among the isomers of 2′,4′-BNA^{NC}, the ASO containing the original 2′,4′-BNA^{NC} (NMe) showed the highest target-binding affinity and in vitro and in vivo antisense potency (ED_{50} = 6 mg kg^{-1}). While ASO containing LNA showed the least ED_{50} value (3 mg kg^{-1}) accompanied with elevation of alanine aminotransferase (ALT), elevation of ALT was not observed for ASO with 2′,4′-BNA^{NC} even at the highest dose tested (14.8 mg kg^{-1}). Surprisingly, 2′,4′-BNA^{NC} (NH) exhibited quite similar target-binding affinity and in vitro IC_{50} value to 2′,4′-BNA^{NC} (NMe), but ASO containing 2′,4′-BNA^{NC} (NH) was inactive in vivo

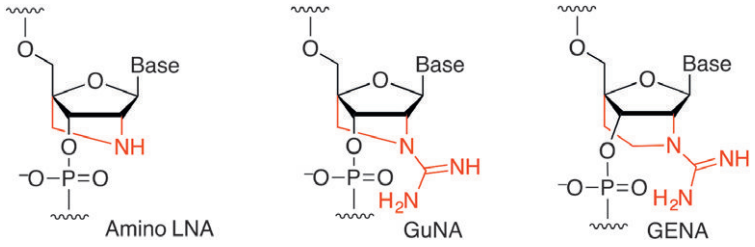

Fig. 14 Chemical structures of amino LNA, GuNA, and GENA.

($ED_{50} > 37$ mg kg^{-1}). The authors confirmed that ASOs with 2′,4′-BNA^{NC} (NH) was absent in the liver even after the highest dose of administration. This is indicating that the presence or absence of the methyl group changes the PK profile dynamically.

6.10.3.1.3.3 AmNA

AmNA is an amido-bridged BNA. The amide moiety in AmNA is hindered, so AmNA (NH) is unstable in the basic conditions generally used for the deprotection of ASOs during synthesis.[49]

Similar to 2′,4′-BNA^{NC}, the smaller the substituent on the nitrogen atom, the higher the target-binding affinity (ΔT_m/modification = approximately +7°C for NMe, +3°C for N*i*-Pr, and +4°C for NBn).[50]

ASO containing LNA reduced liver apoC-III mRNA by 45%, whereas ASOs containing AmNA achieved a knockdown of 40% (AmNA (NMe)) or 30% (AmNA (N*i*-Pr)), and ASO containing AmNA(NBn) showed no knockdown ability.

As discussed earlier, the introduction of heteroatoms into the bridge sometimes improves the target-binding affinity and resistance toward nucleases. However, there are no reports of these analogs exhibiting superior in vivo activity compared with ASOs containing LNA, indicating that antisense potency is defined by more than just in vitro target-binding affinity and nuclease resistance.

6.10.3.1.4 Introduction of cation into the bridge

The interaction of ASO and target mRNA is the hybridization of two polyanionic molecules, so one approach to improve the target-binding affinity of ASOs has been to introduce cations into the oligonucleotide. The introduction of an amine or guanidine into the bridge may improve the binding affinity of such modified ASOs compared with other BNAs due to partial cancelation of the negative charge (Fig. 14).

6.10.3.1.4.1 Amino LNA

Amino LNA has an amino group instead of the bridging ether moiety of LNA.[51] The amino group should act as a cationic center and offer an attachment point for conjugation with other molecules.

However, the introduction of this basic moiety had no effect on target-binding affinity compared with LNA (ΔT_m/modification = approximately +7.3°C for LNA and +6.3°C for amino LNA (NH)).[51]

6.10.3.1.4.2 GuNA and GENA

A BNA containing the basic guanidino-group (GuNA) has also been developed.[52] Our report of a five-membered ring GuNA was rapidly followed by a publication describing a six-membered GuNA, named GENA.[53]

The guanidine group is far more basic than an amine, and the positive charge should be much more stable over a wide pH range.

The target-binding affinity of oligonucleotides with GuNA was compared with that of LNA. In a comparison of oligonucleotides containing five modifications, the ΔT_m/modification of GuNA exceeded that of LNA (ΔT_m/modification = approximately +8.8°C for GuNA and +5.6°C for LNA).[52]

In contrast, the target-binding affinities of oligonucleotides containing GENA were the same as that of natural DNA.[53]

GuNA exhibited increased target-binding affinity due to both the incorporation of cation into the bridge and the conformational locking. To our knowledge, GuNA is the first analog to show substantially increased target-binding affinity compared with LNA.

Given that amino LNA did not exhibit the increased target-binding affinity demonstrated by GuNA and that GENA likewise showed no affinity gain due to the bridged structure, the introduction of cation appears to significantly enhance target-binding affinity only when the spatial configuration of the cation is appropriate.

6.10.3.1.5 Control of torsion angles

High target-binding affinity of BNA analogs is explained by the sugar conformational property strictly locked to $C_{3'}$-*endo*. Paralleled to this approach, attempts to control the torsion angle of sugar phosphate backbone have been made. Appropriate preorganization of torsion angles defining the structure of ASO should contribute to higher target-binding affinity (Fig. 15).

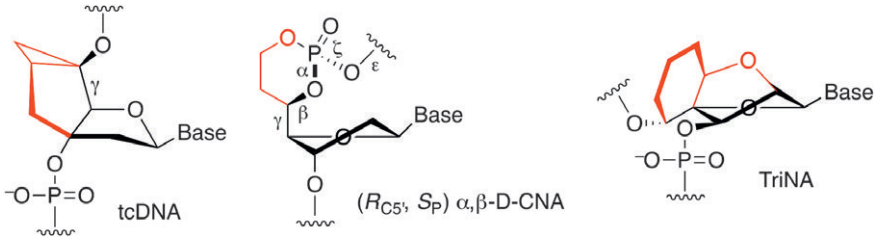

Fig. 15 Chemical structures of tcDNA, α,β-D-CNA, and TriNA.

6.10.3.1.5.1 tcDNA

Leumann et al. prepared tricyclo-DNA to control the γ torsion angle within +*ac* range.[54,55] The γ torsion angle of tcDNA is controlled by linking the C3′ and C5′ carbons of DNA via ethylene bridge and annelated cyclopropane ring. Although γ torsion angle in natural DNA–DNA and RNA–RNA duplexes is within +*sc*, target-binding affinity of this analog increased a little bit compared with natural DNA (ΔT_m/modification = approximately +1°C).[54,55]

6.10.3.1.5.2 CNA

In the same context with the approach taken by Leumann et al., Vigroux and Escudier et al. developed nucleoside analogs locking the phosphate backbone torsion angles, which is called constrained nucleic acids (CNAs).[56–58] α,β-D-CNA has a dioxaphosphorinane ring locking the α and β dihedral angles, which are locked at the canonical (*gauche*(−) and *trans*) conformation, as in A- and B-form duplexes, or the noncanonical (*gauche*(+) and *trans*) conformation depending on the stereochemistry (($R_{C5'}$ and S_P) or ($S_{C5'}$ and R_P), respectively). Expectedly, the target-binding affinity was higher for the oligonucleotides containing α,β-D-CNA controlling the α and β dihedral angles into canonical orientations (ΔT_m/modification ≈ +3°C for α,β-D-CNA locking into canonical orientation and +6°C for LNA while α,β-D-CNA locking into noncanonical orientation destabilized the thermal stability of duplex).[56,57]

6.10.3.1.5.3 TriNA

As described earlier, the locking of the sugar and torsion angle into an appropriate conformation succeeded in improving the target-binding affinity. Hanessian and Seth et al. tried to combine these modifications into one nucleoside analog by making another bridge on the α-L-LNA scaffold (TriNA).[59] As the α-L-LNA skeleton is quite similar to LNA, target-binding affinity of oligonucleotides containing α-L-LNA is comparable to those with LNA[60,61] (Fig. 16). The additional bridge introduced on TriNA was expected to restrict rotation around γ dihedral angle of α-L-LNA.

Target-binding affinity of oligonucleotides containing TriNA was compared with those with LNA or α-L-LNA, and it was shown that TriNA is comparable or superior to LNA and α-L-LNA depending on the sequences introduced (ΔT_m/modification = approximately +4.7°C to 8.3°C for TriNA and +4.5°C to 6.3°C for LNA and α-L-LNA).[59]

6.10.3.1.6 Summary

ASOs containing LNA exhibit higher antisense in vivo efficacy than more traditional chemical modifications, such as 2′-*O*-MOE. This observation supports a trend in the medicinal chemistry of ASOs to develop a nucleoside unit that enhances target-binding affinity. To date, many BNA analogs have been developed, and most show both improved resistance toward degradation by nucleases and increased target-binding affinity compared with natural oligonucleotides, but the in vivo and clinical efficacy data are very

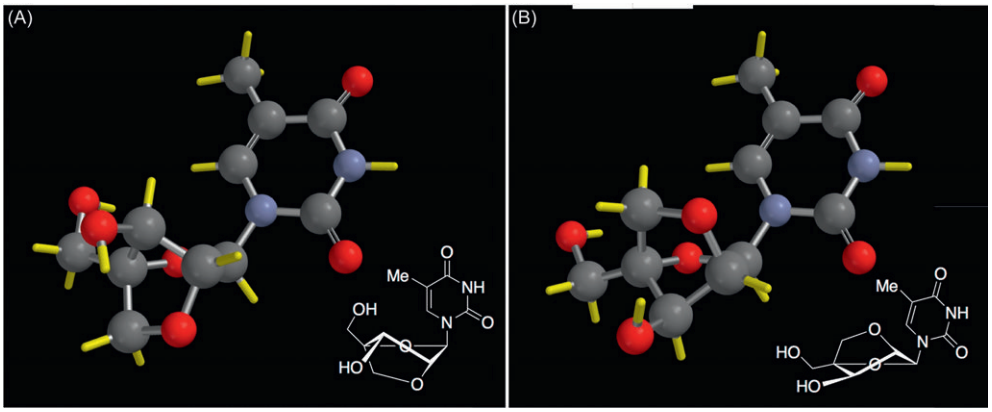

Fig. 16 Structures of LNA-T and α-L-LNA-T.

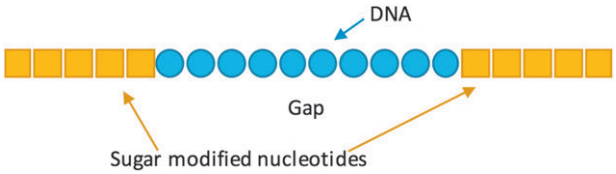

Fig. 17 Schematic image of gapmer (5-10-5).

incomplete for BNA analogs other than LNA and cEt. Thus, a better understanding of the key factors required for highly potent ASOs must await detailed in vivo and clinical data of promising BNA analogs.

6.10.3.2 Number and/or Mode of Introduction of Sugar Modifications

How a chemical modification is used is as important as which chemical modification is used. Further to our discussion of several sugar modifications, here, we discuss strategies for the design of potent ASOs with sugar modifications, focusing on the number of modifications.

6.10.3.2.1 Gapmers

It is essential for ASOs to maintain RNase H1-recruiting activity. RNase H1 recognizes DNA/RNA heteroduplexes and cleaves the RNA strand.[62] Many of the sugar modifications discussed earlier are RNA derivatives, thus making the ASOs RNA-like; consequently, ASOs fully modified with BNAs, 2′-*O*-MOE, or most other sugar modifications do not recruit RNase H1.[11,25,63–65]

Lima et al. studied thoroughly the design of ASOs modified with 2′-*O*-MOE and the RNase H1 cleavage mechanism toward these derivatives.[64,65] They clearly showed that partial modification of ASO with 2′-*O*-MOE, leaving large regions of unmodified DNA, allows RNase H1 to access the ASO/RNA duplex and cleave the RNA. The report by Lima and coworkers suggests the following guidelines for the design of efficacious ASOs:

(1) The introduction of sugar modifications inhibits the cleavage reaction of RNase H1 at both 5′ and 3′ sides of the modifications. Therefore, it is strongly recommended that the sugar modifications be introduced at the ends of the sequence.
(2) Sugar modifications inhibit the reaction of RNase H1, so the number of these modifications should be minimized.
(3) The number of modifications introduced should be the minimum required to obtain the required target-binding affinity.

These guidelines have likely influenced the sequence design of 5-10-5, known as gapmer, which contains five 2′-*O*-MOE nucleotides at each end of the sequence and 10 deoxyribonucleotides between these clusters of 2′-*O*-MOEs. This design motif is common in 2′-*O*-MOE ASOs (Fig. 17).

The concept behind gapmer also works well in LNA. Swaize et al. constructed 20-mer ASOs and reported that LNA exhibited higher antisense potency than 2′-*O*-MOE in a 2-16-2 modification pattern.[11] The number of modifications required for high antisense potency was smaller for LNA than for 2′-*O*-MOE, reflecting its higher target-binding affinity.

6.10.3.2.2 Too high an affinity drastically decreases potency

Koch et al. reported that shorter LNA ASOs work more efficaciously.[66] They showed that 12-, 13-, and 14-mer ASOs with LNA modification patterns of 2-8-2, 2-8-3, and 3-8-3, respectively, exhibit higher antisense activity both in vitro and in vivo than longer ASOs. For example, the in vitro IC_{50}s of expression of apoB mRNA were 0.2–0.4 nM for the 12- to 14-mers and 2.7 and 5.0 nM for the 16-mer and 20-mer, respectively. The longer ASOs were anticipated to show decreased in vivo distribution to the target tissue, but the concentration time profiles of 12-mer and 16-mer LNA ASOs in the murine liver were similar. Taken together with the finding that the target-binding affinity of 12-mer LNA ASO is weaker than that of 16-mer LNA ASO ($T_m = 53°C$ for 12-mer and 63°C for 16-mer), there appears to be an optimal target-binding affinity earlier, which the ASO exhibits dramatically decreased potency. We also demonstrated the importance of "optimum T_m" using 2′,4′-BNA^{NC} ASOs. Intriguingly, ASOs bearing different sugar modifications exhibited similar optimum T_ms (60–65°C) and in vitro potency.[47] Thus, the relevance of "optimum T_m" is not unique to LNA.

The optimum T_m observed in ASOs bearing high-affinity modifications is likely due to the mechanism of action. In the RNase H1 recruitment of ASOs, immediate release of ASO from the cleaved target RNA is essential in order for the enzyme to enter the next cleavage reaction cycle. Our group demonstrated experimentally that the turnover of ASOs is inhibited when the target-binding affinity of the ASO is too high and that the in vivo potency of the ASOs is affected by their turnover ability.[67] Independently, a group from Santaris Pharma analyzed kinetic models, potency, and affinity and showed that the turnover ability of ASOs might be related to their in vivo potency.[68] It is therefore important to consider the effect of sequence length and number of modifications in an ASO on the turnover ability of the ASO, in addition to the criteria discussed earlier.

Splicing-switching ASOs with LNA modifications showed that the apparent favored binding affinity ($T_m = 80–90°C$) was higher than that of RNase H1 recruiting ASOs ($T_m = 60–65°C$), but further increase in affinity impaired exon-skipping potency.[38] It is possible that ASOs with higher affinity with impaired skipping potency form higher-ordered structures form stem-loops and/or homodimerize or homopolymerize.

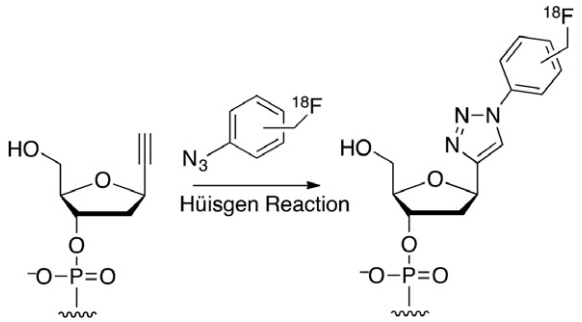

Fig. 18 Labeling of oligonucleotides for PET imaging.

6.10.3.3 Backbone Modifications

As discussed earlier, ASOs are inactive in vivo in the absence of backbone modification, so ASOs are typically fully modified with phosphorothioates, although this generally reduces target-binding affinity (ΔT_m/modification = approximately −0.6 to −0.3°C compared with the phosphodiester linkage).[24]

The target-binding affinity of phosphorothioated ASOs is also affected by the chirality of the phosphorothioate (Fig. 5).

Wan et al. prepared ASOs, with and without control of the chirality of the phosphorothioate linkages in the gap regions. ASOs with all R_P chirality in the gap showed higher target-binding affinity than those with all S_P (ΔT_m/modification = approximately +0.2°C and −0.2°C to −0.5°C, respectively, compared with stereo-random phosphorothioate linkages).[24] The antisense potency of these ASOs was tested in vitro, and R_P ASOs were confirmed to show higher potency than S_P ASOs. However, in vivo tests showed that the antisense potency in the mouse liver of R_P and S_P ASOs was similar and that stereo-random ASOs showed the highest potency.[24] At the same time, the amount of intact ASO in the liver tissue was shown to be very low for R_P ASO. Thus, the higher antisense potency of R_P observed in vitro appears to be canceled out by its weaker antinuclease resistance in vivo.

6.10.4 ADME

The medicinal chemistry of ASOs must take into account their ADME, but the main focus to date has been improving the distribution and enhancing the resistance of ASOs toward metabolism and particularly nuclease resistance, as discussed earlier.

The distribution of ASOs to the target tissue is a critical factor for maximizing efficacy and minimizing adverse effects. Systemically administered naked phosphorothioated ASOs tend to distribute mainly to the kidneys and liver. Suzuki, Watanabe et al., and our group developed a method for ^{18}F-radiolabeling of ASOs utilizing Hüisgen reaction to monitor ADME time profile of ASOs in vivo by positron emission tomography[69,70] (Fig. 18). The ADME profile of ASOs modified with or without phosphorothioate (PS) and/or LNA (ASO-PO-DNA, ASO-PO-LNA, ASO-PS-DNA, and ASO-PS-LNA) was assessed in rats. ASOs without PS modification (ASO-PO-DNA and ASO-PO-LNA) rapidly passed through the liver and kidneys and moved to the renal medulla, bladder, and intestine. On the other hand, ASOs modified with PS (ASO-PS-DNA and ASO-PS-LNA) accumulated in the kidneys and liver.[70] As discussed previously, phosphorothioate modification alters not only the nuclease resistance but also the plasma protein binding pattern. This would be the reason why ADME profile was profoundly affected by backbone chemistry, although the nuclease resistance of ASO-PO-LNA was considered significantly higher than that of ASO-PO-DNA.

To alter or improve the specificity of the distribution profile, many conjugate and/or nanoparticle drug delivery system approaches have been investigated.[71–76] For example, the conjugation of ASOs with GalNAc results in improved distribution specificity toward hepatocytes.[73–75]

On the other hand, here, we introduce two examples of medicinal chemistry approaches to altering the ADME, in particular the distribution of ASOs.

6.10.4.1 Sugar Modifications

The distribution and potency of ASOs were altered by tuning the hydrophobicity of the ASO by chemical modification. AmNA was used as a scaffold because tuning could be accomplished by altering the alkyl substituent on the bridging amide moiety (Fig. 13). The hydrogen was substituted with methyl, isopropyl, or benzyl groups, and the hydrophobicity of the oligonucleotides increased. The in vivo behavior of AmNA-ASOs respectively modified with (NMe), (N*i*-Pr), or (NBn) was evaluated. The hepatic distribution of the more hydrophobic ASOs with AmNA (N*i*-Pr) and AmNA (NBn) was higher than that of AmNA (NMe)[50] (Fig. 13).

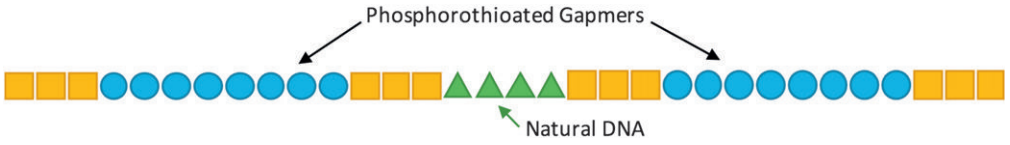

Fig. 19 Schematic image of multimer.

6.10.4.2 Length of the ASOs

Phosphorothioated ASOs are believed to be distributed in vivo by multiple proteins. The phosphorothioated backbone increases the binding rate of ASOs to plasma proteins, but shorter phosphorothioated ASOs show a lower plasma protein binding rate (e.g., ~95% for a 20-mer ASO vs. ~80% for a 13-mer).[77] Since protein binding likely affects the efficiency of distribution to the targeted tissue, longer ASOs with phosphorothioate modifications may be more potent ASOs. However, as discussed earlier, longer ASOs generally show higher target-binding affinity, and the optimal length is typically 12- to 16-mers for ASOs modified with LNA. Krieg et al. linked two 15-mer phosphorothioated ASO gapmers (multimer) modified with LNA via a linker comprising natural nucleotides so that the linker would be cleaved by endonucleases after distribution to the target tissue (Fig. 19). Dosing mice with the same amount of monomer or homodimer ASO (10 mg kg^{-1} and twice a week) demonstrated that the homodimer exhibits much higher antisense potency than its monomer.[78]

6.10.5 Target Specificity, Hybridization-Dependent Off-Target Effects, and Safety

6.10.5.1 Overview of the Safety of ASOs

Target specificity is an important factor strongly related to the safety of a drug and sometimes defines the safety margin of the drug. The effects arising from the contact of the drug molecule with any other molecules than the target molecule are considered an off-target effect. The off-target effects of ASOs are generally classified into two groups: hybridization-dependent off-target effects and nonhybridization-dependent off-target effects.[22,79] Hybridization-dependent off-target effects are defined as nontargeted effects caused by the hybridization of ASOs with other nucleic acids in vivo.

6.10.5.1.1 Class effects of phosphorothioated ASOs

The administration of a high dose of ASO can give rise to off-target effects (known as "class effects") such as prolongation of activated partial thromboplastin time (aPTT) and nonhybridization-dependent off-target effects such as the activation of complement, thrombocytopenia, and immunostimulation.[22,79] These effects can limit the maximum dose in clinical use.

6.10.5.1.1.1 Prolongation of aPTT

Administration of phosphorothioated antisense oligodeoxyribonucleotide molecule targeting human intercellular adhesion molecule-1 mRNA prolonged plasma clotting times in both monkey and human studies.[80] Thorough studies by Sheehan and Lan revealed that the ASO inhibited the calcium-dependent portion of the intrinsic pathway.[80] The authors demonstrated that the sense and randomized sequences of the phosphorothioated oligonucleotides exhibit the same profile on the inhibition of the clotting reaction, whereas an oligonucleotide with the same sequence as the ASO but without phosphorothioate modifications showed no inhibitory activity. Thus, the prolongation of aPTT in monkey and human likely arises from the phosphorothioate backbone and not the sequence. The prolongation of aPTT is plasma concentration-dependent, and thus, clinically controlling the peak concentration may help prevent hemorrhagic adverse events.

6.10.5.1.1.2 Immunostimulation, activation of complement, and thrombocytopenia

Phosphorothioated ASOs appear to be immunostimulatory in nature, and many reports indicate that ASOs act as pro-inflammatory compounds. Common inflammatory reactions observed after the administration of ASOs are injection site reaction, flu-like symptoms, and activation of complement.[22,79] Although correlations with these adverse events are unclear, thrombocytopenia is observed in clinical trials of phosphorothioated ASOs.[81]

The causes of pro-inflammatory effects by phosphorothioated ASOs remain under investigation, but several pathways are believed to play important roles. For example, ASOs mainly composed of DNA and especially sequences containing the CpG motif may stimulate toll-like receptor 9 (TLR9) and induce inflammatory reactions.[22,79]

Maybe independently from the TLR-mediated reaction, the activation of complement occurs with phosphorothioated ASOs. Phosphorothioated ASOs are known to activate the complement cascade alternative pathway. Henry et al. reported that ASOs may bind and interfere with factor H, an important factor in this alternative pathway.[82–84] The authors compared the complement activation profiles of ASOs with different chemical modifications and found that the introduction of a 2′-*O*-MOE and/or phosphodiester linkage in place of a phosphorothioate linkage reduces complement activation in monkey serum.[82–84]

While the activation of complement is clearly observed in monkeys, the sensitivity of activation by ASOs appears to depend on the species. Therefore, the clinical relevance of the activation reaction is difficult to predict from nonclinical data. Moreover,

although it was considered independent reactions, recently, it has been reported that the TLR9 pathway and complement activation pathway may interact with each other.[85] Further investigations are therefore needed to understand and control such adverse reactions.

6.10.5.1.2 Target specificity and hepatotoxicity

As the chemical sophistication of ASOs increases and their antisense effect are optimized, the dose of ASO required to achieve the desired antisense effect will likely decrease dramatically. In addition, the trend in the medicinal chemistry of ASOs to use shorter oligonucleotides should worsen target specificity because shorter oligonucleotides theoretically may have larger number of target RNAs that have perfect match with the ASOs. Thus, ASOs must exhibit satisfactory target specificity, as otherwise dose-limiting toxicity could change from nonhybridization-dependent off-target effects to hybridization-dependent off-target effects, which are much more related to the mode of action of ASOs.

There are many reports of hepatotoxicity induced by ASOs with high-affinity modifications such as LNA.[11–15]

Hepatotoxicity induced by ASOs with LNA can be lethal, depending on the ASO and the dose administered.[11–15] Hepatotoxicity is well characterized in rodents and easily detected by monitoring changes in serum enzymes such as ALT. An elevated serum ALT level is usually observed several days after subcutaneous or intravenous injection of ASO into mice.

Liver damage may be due to nonhybridization-dependent off-target effects and/or hybridization off-target effects, and the severity of the hepatotoxicity of ASOs with the same sequence reportedly varies significantly depending on the chemistry introduced. For example, the replacement of LNA in hepatotoxic ASO with other high-affinity modifications such as cEt or 2′,4′-BNA^{NC} was shown to reduce toxicity without significantly affecting the on-target effect,[36,46] suggesting that a nonhybridization-dependent process contributes to the onset of the toxicity to some extent. In this context, Burdick et al. reported that some highly hepatotoxic ASOs with LNA were more likely to bind to hepatocellular proteins in vitro than nontoxic ASOs with the same modification patterns as the toxic ASOs.

On the other hand, recent reports have supported the hypothesis that hepatotoxicity induced by ASOs with high-affinity modifications is due to hybridization-dependent off-target effects. For example, Kamola et al. reported that ASOs containing chemical modifications that increase target-binding affinity, such as LNA, showed significant hybridization-dependent off-target effects in vitro.[17] In addition, Burel et al. reported that hybridization-dependent off-target effects also occur in vivo and are the cause of hepatotoxicity induced by ASOs containing high-affinity chemical modifications.[15] The authors also confirmed that hepatotoxicity is caused by ASOs containing either cEt or LNA modifications. The authors showed only experimental data from mice, but adverse effects related to hepatotoxicity or elevated serum ALT levels are also reported in clinical trials of ASOs containing high-affinity modifications.[86,87] Therefore, the hepatotoxicity of ASOs is apparently not unique to rodents.

6.10.5.2 Medicinal Chemistry Approaches to Improving Safety Profiles

In addition to the toxic effects of ASOs discussed earlier, acute tubular necrosis and injection site reactions can be the cause of decreasing the dose or discontinuing treatment.[88,89] It is unclear whether these off-target effects are hybridization-dependent or nonhybridization-dependent, but improved target specificity appears crucial for the evolution of ASOs as a promising therapeutic approach.

Minimizing potential off-target effects through sequence design requires choosing a sequence with a minimum number of potential off-target RNAs.[90] Moreover, sequence design and optimizing the combination of chemical modifications may help select a safer ASO candidate with regard to nonhybridization-dependent off-target effects. The escape of ASOs with phosphorothioated modifications from TLR9 may illustrate a structure–activity relationship related to nonhybridization-dependent off-target effects. TLR9 recognizes single-stranded nonmethylated DNA, prompting investigation of the effects of chemical modification of the sugars and nucleobases of ASOs. Vollmer et al. evaluated the effects of replacing the deoxyribonucleoside unit with LNA monomer and demonstrated that partial replacement decreased the immunomodulation property of phosphorothioated ASOs.[91] In addition, the authors showed that modification of the CpG unit by LNA was sufficient to strongly decrease TLR9-mediated signaling. The CpG unit is an important factor for the recognition of ASOs by TLR9; consequently, nucleobase modification of the CpG unit is a powerful approach. Furthermore, chemical modifications on the Hoogsteen side of a nucleobase should not affect Watson–Crick base-pairing ability, and therefore, this approach is also attractive (Fig. 20). Uhlmann et al. demonstrated that replacing the cytosine or guanine of CpG by 5-methylcytosine or 7-deazaguanine resulted in an 81% or 69% reduction in maximum human TLR9 activation, respectively.[92,93]

Further examples of medicinal chemistry approaches contributing to the safety of ASOs are provided in the succeeding text.

6.10.5.2.1 Sequence design

The sequences of ASOs as potential candidates for drug development are generally selected through in vitro and in vivo screening. The screening strategy depends on the developmental strategy and general knowledge of the developer and has led to the sequence design of safer ASOs.

6.10.5.2.1.1 Toxic motif of ASOs

Lindow et al. developed a random forest classifier in which oligonucleotides are regarded as being composed of dinucleotide units. The authors trained the statistical model using highly hepatotoxic and nontoxic LNA ASOs to predict the toxicity of the ASOs.[12]

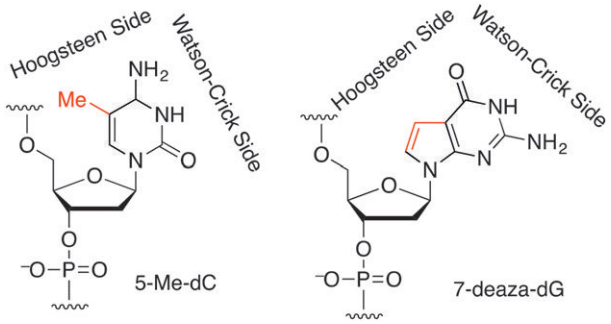

Fig. 20 Chemical structures of 5-Me-dC and 7-deaza-dG.

Hollingshead et al. similarly analyzed statistically and experientially the available hepatotoxicity data of LNA ASOs in mice and found that toxic LNA ASOs are more likely to contain TCC and TGC motifs in their sequences.[13] These studies do not explain why dinucleotide and/or trinucleotide units of ASO affect the hepatotoxicity profiles of ASOs but may nonetheless shed light on how to minimize the potential risk of hepatotoxicity.

6.10.5.2.2 Nucleobase modifications

High-affinity chemical modifications, typified by LNA, generally do not destroy sequence selectivity but do increase binding affinity. It has been reported that the potency of hybridization-dependent off-target effects is highly correlated with the binding affinity of ASO for the target sequence,[17] suggesting that improving the hybridization selectivity between the on-target sequence and off-target sequence would improve the specificity of the antisense effect.

The most stable mismatch is generally the G-T wobble base pair,[94] so off-target RNAs that hybridize with ASOs containing G-T mismatches may show affinity comparable to the intended on-target RNA. 2-Thiothymidine has a thiocarbonyl moiety in place of the 2-carbonyl moiety, and this modification weakens the hydrogen bond in the G-T wobble base pair[95] (Fig. 21). Østergaard et al. tested the utility of 2-thiothymidine for improving the selectivity of the antisense effect between the on-target RNA and an off-target RNA by introducing G-T mismatches. They confirmed that the ASO with 2-thiothymidine shows a larger difference in target-binding affinity between on-target and off-target RNAs than does the ASO with natural thymidine ($\Delta T_m = 2.2°C$ for thymidine and 4.9°C for 2-thiotymidine), but the improvement in in vitro antisense selectivity was small compared with the difference in target-binding affinity (IC_{50} selectivity, 17.6-fold for thymidine and 23.4-fold for 2-thiothymidine).[96] Importantly, they also tested the effects of this nucleobase modification at different positions in the ASO and found that introduction of the nucleobase modification in the gap region sometimes improved the selectivity of the antisense effects between on-target and off-target RNA by affecting the cleavage pattern of RNase H1, independent of affinity.[96] This observation suggests that medicinal chemistry approaches may alter the spectrum or specificity of antisense effects.

6.10.5.2.3 Gap design

Even if the ASO hybridizes to off-target RNAs, no hybridization-dependent off-target effects should occur unless RNase H1 cleaves the RNA. Thus, repression of the cleavage of off-target RNA by RNase H1 is a reasonable approach for improving the specificity of RNase H1-dependent ASOs. As discussed earlier, gap design is one widely used approach.

In 2013, Seth et al. reported that shortening the gap length of ASOs bearing *S*-cEt and 2′-*O*-MOE modifications from nine nucleotides to seven dramatically improved the in vitro antisense selectivity between on-target and single mismatch-containing off-target RNA (IC_{50} selectivity, 6.9-fold for ASO with a 9 nt gap and as high as >133-fold for ASO with a 7 nt gap).[97]

Koizumi et al. had already reported this approach applying into ENA gapmer ASO in 2007. The authors realized the importance of antisense specificity, because they found that the target mRNA was cleaved by RNase H not only at the target site but also at nontarget sites. The nontarget cleavage sites were attributed to partial base pairing between the mRNA and the ENA gapmer.[16]

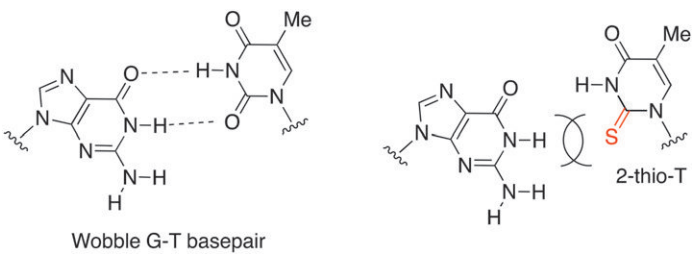

Fig. 21 Wobble G-T base pair and 2-thio-T.

Shortening the gap size of the ENA gapmer significantly reduced cleavage of the target mRNA at nontarget sites, suggesting that this approach could minimize hybridization-dependent off-target effects.

Too small a gap size greatly decreases antisense potency, and therefore, the gap size should be optimized to balance the acceptable risk for potential off-target effects and the anticipated pharmacological effect.

6.10.6 Conclusion

Advances in the unit chemistry of ASOs and our understanding of the design of ASOs have led to dramatically improved nuclease resistance in vivo and in antisense potency. In parallel with the medicinal chemistry approach, DDS has also resulted in exciting advances in antisense technology. For example, ASOs conjugated with GalNAc exhibit remarkable antisense potency in the liver. We now have the ability to design increasing potent ASOs.

Increases in the potency of ASOs have highlighted the need to balance potency and safety, whereas increased potency has mainly been achieved through sugar and backbone modifications; improved safety of ASOs appears to rely on nucleobase modifications feature.

Medicinal chemistry has made major contributions to the advance of antisense technology, but the medicinal chemistry of ASOs may play a decisive role in overcoming the remaining challenges of this therapeutic technology.

See also: 2.01. Drug Discovery Technologies: Current and Future Trends.

References

1. Yamamoto, T.; Nakatani, M.; Narukawa, K.; Obika, S. Antisense Drug Discovery and Development. *Future Med. Chem.* **2011,** *3,* 339–365.
2. McClorey, G.; Wood, M. J. An Overview of the Clinical Application of Antisense Oligonucleotides for RNA-Targeting Therapies. *Curr. Opin. Pharmacol.* **2015,** *24,* 52–58.
3. Marafini, I.; Fusco, D. D.; Calabrese, E.; Sedda, S.; Pallone, F.; Monteleone, G. Antisense Approach to Inflammatory Bowel Disease: Prospects and Challenges. *Drugs* **2015,** *75,* 723–730.
4. Jirka, S.; Aartsma-Rus, A. An Update on RNA-Targeting Therapies for Neuromuscular Disorders. *Curr. Opin. Neurol.* **2015,** *28,* 515–521.
5. Prescribing Information of Vitravene™ Injection (Fomivirsen Sodium Intravitreal Injectable) Approved by the FDA.
6. Prescribing Information of Kynamro® (Mipomerse Sodium) Injection Approved by the FDA.
7. Tillman, L. G.; Geary, R. S.; Hardee, G. E. Oral Delivery of Antisense Oligonucleotides in Man. *J. Pharm. Sci.* **2008,** *97,* 225–236.
8. Lipinski, C. A.; Lombardo, F.; Dominy, B. W.; Feeney, P. J. Experimental and Computational Approaches to Estimate Solubility and Permeability in Drug Discovery and Development Settings. *Adv. Drug Deliv. Rev.* **2001,** *46,* 3–26.
9. Lesson, P. D.; Springthorpe, B. The Influence of Drug-Like Concepts on Decision-Making in Medicinal Chemistry. *Nat. Rev. Drug Discov.* **2007,** *6,* 881–890.
10. Hopkins, A. L.; Keserü, G. M.; Leeson, P. D.; Rees, D. C.; Reynolds, C. H. The Role of Ligand Efficiency Metrics in Drug Discovery. *Nat. Rev. Drug Discov.* **2014,** *13,* 105–121.
11. Swayze, E. E.; Siwkowski, A. M.; Wancewicz, E. V.; Migawa, M. T.; Wyrzykiewicz, T. Z.; Hung, G.; Monia, B. P.; Bennett, C. F. Antisense Oligonucleotides Containing Locked Nucleic Acid Improve Potency but Cause Significant Hepatotoxicity in Animals. *Nucleic Acids Res.* **2007,** *35,* 687–700.
12. Hagedorn, P. H.; Yakimov, V.; Ottosen, S.; Kmmler, S.; Nielsen, N. F.; Høg, A. M.; Hedtjärn, M.; Meldgaard, M.; Møller, M. R.; Ørum, H.; Koch, T.; Lindow, M. Hepatotoxic Potential of Therapeutic Oligonucleotides can be Predicted From Their Sequence and Modification Pattern. *Nucleic Acid Ther.* **2013,** *23,* 302–310.
13. Burdick, A. D.; Sciabola, S.; Mantena, S. R.; Hollingshead, B. D.; Stanton, R.; Warneke, J. A.; Zeng, M.; Martsen, E.; Medvedev, A.; Makarov, S. S.; Reed, L. A.; Davis, J. W., II; Whiteley, L. O. Sequence Motifs Associated With Hepatotoxicity of Locked Nucleic Acid—Modified Antisense Oligonucleotides. *Nucleic Acids Res.* **2014,** *42,* 4882–4891.
14. Kakiuchi-Kiyota, S.; Koza-Taylor, P. H.; Mantena, S. R.; Nelms, L. F.; Enayetallah, A. E.; Hoolingshead, B. D.; Burdick, A. D.; Reed, L. A.; Warneke, J. A.; Whiteley, L. O.; Ryan, A. M.; Mathialagan, N. Comparison of Hepatic Transcription Profiles of Locked Ribonucleic Acid Antisense Oligonucleotides: Evidence of Distinct Pathways Contributing to Non-Target Mediated Toxicity in Mice. *Toxicol. Sci.* **2014,** *138,* 234–248.
15. Burel, S. A.; Hart, C. E.; Cauntay, P.; Hsiao, J.; Machemer, T.; Katz, M.; Watt, A.; Bui, H.; Younis, H.; Sabripour, M.; Freier, S. M.; Hung, G.; Dan, A.; Prakash, T. P.; Seth, P. P.; Swayze, E. E.; Bennett, C. F.; Crooke, S. T.; Henry, S. P. Hepatotoxicity of High Affinity Gapmer Antisense Oligonucleotides is Mediated by RNase H1 Dependent Promiscuous Reduction of Very Long Pre-mRNA Transcripts. *Nucleic Acids Res.* **2015,** *44,* 2093–2109.
16. Takagi-Sato, M.; Tokuhiro, S.; Kawaida, R.; Koizumi, M. Fine-Tuning of ENA® Gapmers as Antisense Oligonucleotides for Sequence-Specific Inhibition. *Oligonucleotides* **2007,** *17,* 291–301.
17. Kamola, P. J.; Kitson, J. D.; Turner, G.; Maratou, K.; Eriksson, S.; Panjwani, A.; Warnock, L. C.; Douillar Guilloux, G. A.; Moores, K.; Koppe, E. L.; Wixted, W. E.; Wilson, P. A.; Gooderham, N. J.; Gant, T. W.; Clark, K. L.; Hughes, S. A.; Edbrooke, M. R.; Parry, J. D. In Silico and In Vitro Evaluation of Exonic and Intronic Off-Target Effects Form a Critical Element of Therapeutic ASO Gapmer Optimization. *Nucleic Acids Res.* **2015,** *43,* 8638–8650.
18. Micklefield, J. Backbone Modification of Nucleic Acids: Synthesis, Structure and Therapeutic Applications. *Curr. Med. Chem.* **2001,** *8,* 1157–1179.
19. Clercq, E.; Eckstein, F.; Sternbach, H.; Mrigan, T. C. The Antiviral Activity of Thiophosphate-Substituted Polyribonucleotides In Vitro and In Vivo. *Virology* **1970,** *42,* 421–428.
20. Stec, W. J.; Zon, G.; Egan, W.; Stec, B. Automated Solid-Phase Synthesis, Separation, and Stereochemistry of Phosphorothioate Analogues of Oligodeoxyribonucleotides. *J. Am. Chem. Soc.* **1984,** *106,* 6077–6079.
21. Matsukura, M.; Shinozuka, K.; Zon, G.; Mitsuya, H.; Reitz, M.; Cohen, J. S.; Broder, S. Phosphorothioate Analogs of Oligodeoxynucleotides: Inhibitors of Replication and Cytopathic Effects of Human Immunodeficiency Virus. *Proc. Natl. Acad. Sci. U. S. A.* **1987,** *84,* 7706–7710.
22. Levin, A. A.; Henry, S. P. Toxicology of Oligonucleotide Therapeutics and Understanding the Relevance of the Toxicities. In *Preclinical Safety Evaluation of Biopharmaceuticals: A Science-Based Approach to Facilitating Clinical Trials;* Cavagnaro, J. A., Ed.; John Wiley & Sons, Inc: Hoboken, NJ, USA, 2008; pp 537–574.
23. Miller, C. M.; Donner, A. J.; Blank, E. E.; Egger, A. W.; Kellar, B. M.; Østergaard, M. E.; Seth, P. P.; Harris, E. N. Stabilin-1 and Stabilin-2 are Specific Receptors for the Cellular Internalization of Phosphorothioate-Modified Antisense Oligonucleotides (ASOs) in the Liver. *Nucleic Acids Res.* **2016,** *44,* 2782–2794.
24. Wan, W. B.; Migawa, M. T.; Vasquez, G.; Murray, H. M.; Nichols, J. G.; Gaus, H.; Berdeja, A.; Lee, S.; Hart, C. E.; Lima, W. F.; Swayze, E. E.; Seth, P. P. Synthesis, Biophysical Properties and Biological Activity of Second Generation Antisense Oligonucleotides Containing Chiral Phosphorothioate Linkages. *Nucleic Acids Res.* **2014,** *42,* 13456–13468.
25. Prakash, T. P. An Overview of Sugar-Modified Oligonucleotides for Antisense Therapeutics. *Chem. Biodivers.* **2011,** *8,* 1616–1641.
26. Martin, P. Ein neuer Zugang zu 2′-*O*-Alkylribonucleosiden und Eigenschaften deren Oligonucleotide. *Helv. Chim. Acta* **1995,** *78,* 486–504.

27. Graham, M. J.; Lee, R. G.; Bell, T. A., III; Fu, W.; Mullick, A. E.; Alexander, V. J.; Singleton, W.; Viney, N.; Geary, R.; Su, J.; Baker, B. F.; Burkey, J.; Crooke, S. T.; Crooke, R. M. Antisense Oligonucleotide Inhibition of Apolipoprotein C-III Reduces Plasma Triglycerides in Rodents, Nonhuman Primates, and Humans. *Circ. Res.* **2013,** *112,* 1479–1490.
28. Chiriboga, C. A.; Swoboda, K. J.; Darras, B. T.; Iannaccone, S. T.; Montes, J.; De Vivo, D. C.; Norris, D. A.; Bennett, C. F.; Bishop, K. M. Results From a Phase 1 Study of Nusinersen (ISIS-SMN$_{Rx}$) in Children With Spinal Muscular Atrophy. *Neurology* **2016,** *86,* 890–897.
29. Obika, S.; Nanbu, D.; Hari, Y.; Morio, K.; In, Y.; Ishida, T.; Imanishi, T. Synthesis of 2′-*O*,4′-*C*-Methyleneuridine and -Cytidine. Novel Bicyclic Nucleosides Having a Fixed $C_{3'}$-*endo* Sugar Puckering. *Tetrahedron Lett.* **1997,** *38,* 8735–8738.
30. Singh, S. K.; Nielsen, P.; Koshkin, A. A.; Wengel, J. LNA (Locked Nucleic Acids): Synthesis and High-Affinity Nucleic Acid Recognition. *Chem. Commun.* **1998,** 455–456.
31. Obika, S.; Nanbu, D.; Hari, Y.; Andoh, J.; Morio, K.; Doi, T.; Imanishi, T. Stability and Structural Features of the Duplexes Containing Nucleoside Analogues With a Fixed N-Type Conformation, 2′-*O*,4′-*C*-Methyleneribonucleosides. *Tetrahedron Lett.* **1998,** *39,* 5401–5404.
32. Koshkin, A. A.; Singh, S. K.; Nielsen, P.; Rajwanshi, V. K.; Kumar, R.; Meldgaard, M.; Olsen, C. E.; Wengel, J. LNA (Locked Nucleic Acids): Synthesis of the Adenine, Cytosine, Guanine, 5-Methylcytosine, Thymine and Uracil Bicyclonucleoside Monomers, Oligomerisation, and Unprecedented Nucleic Acid Recognition. *Tetrahedron* **1998,** *54,* 3607–3630.
33. Morita, K.; Hasegawa, C.; Kaneko, M.; Tsutsumi, S.; Sone, J.; Ishikawa, T.; Imanishi, T.; Koizumi, M. 2′-*O*,4′-*C*-Ethylene-Bridged Nucleic Acids (ENA): Highly Nuclease-Resistant and Thermodynamically Stable Oligonucleotides for Antisense Drug. *Bioorg. Med. Chem. Lett.* **2002,** *12,* 73–76.
34. Morita, K.; Takagi, M.; Hasegawa, C.; Kaneko, M.; Tsutsumi, S.; Sone, J.; Ishikawa, T.; Imanishi, T.; Koizumi, M. Synthesis and Properties of 2′-*O*,4′-*C*-Ethylene-Bridged Nucleic Acids (ENA) as Effective Antisense Oligonucleotides. *Bioorg. Med. Chem.* **2003,** *11,* 2211–2226.
35. Yamaguchi, T.; Horiba, M.; Obika, S. Synthesis and Properties of 2′-*O*,4′-*C*-Spirocyclopropylene Bridged Nucleic Acid (scpBNA), an Analogue of 2′,4′-BNA/LNA Bearing a Cyclopropane Ring. *Chem. Commun.* **2015,** *51,* 9737–9740.
36. Seth, P. P.; Siwkowski, A.; Allerson, C. R.; Vasquez, G.; Lee, S.; Prakash, T. P.; Wancewicz, E. V.; Witchell, D.; Swayze, E. E. Short Antisense Oligonucleotides With Novel 2′-4′ Conformationally Restricted Nucleoside Analogues Show Improved Potency Without Increased Toxicity in Animals. *J. Med. Chem.* **2009,** *52,* 10–13.
37. Seth, P. P.; Allerson, C. R.; Siwkowski, A.; Vasquez, G.; Berdeja, A.; Migawa, M. T.; Gaus, H.; Prakash, T. P.; Bhat, B.; Swayze, E. E. Configuration of the 5′-Methyl Group Modulates the Biophysical and Biological Properties of Locked Nucleic Acid (LNA) Oligonucleotides. *J. Med. Chem.* **2010,** *53,* 8309–8318.
38. Shimo, T.; Tachibana, K.; Saito, K.; Yoshida, T.; Tomita, E.; Waki, R.; Yamamoto, T.; Doi, T.; Inoue, T.; Kawakami, J.; Obika, S. Design and Evaluation of Locked Nucleic Acid-Based Splice-Switching Oligonucleotides In Vitro. *Nucleic Acids Res.* **2014,** *42,* 8174–8187.
39. Xu, J.; Dupouy, C.; Chattopadhyaya, J. Synthesis of Conformationally Locked Carba-LNAs Through Intramolecular Free-Radical Addition to C═N. Electrostatic and Steric Implication of the Carba-LNA Substituents in the Modified Oligos for Nuclease and Thermodynamic Stabilities. *J. Org. Chem.* **2009,** *74,* 6534–6554.
40. Seth, P. P.; Allerson, C. R.; Berdeja, A.; Siwkowski, A.; Pallan, P. S.; Gaus, H.; Prakash, T. P.; Watt, A. T.; Egli, M.; Swayze, E. E. An Exocyclic Methylene Group Acts as a Bioisostere of the 2′-Oxygen Atom in LNA. *J. Am. Chem. Soc.* **2010,** *132,* 14942–14950.
41. Hari, Y.; Obika, S.; Ohnishi, R.; Eguchi, K.; Osaki, T.; Ohishi, H.; Imanishi, T. Synthesis and Properties of 2′-*O*,4′-*C*-Methyleneoxymethylene Bridged Nucleic Acid. *Bioorg. Med. Chem.* **2006,** *14,* 1029–1038.
42. Mitsuoka, Y.; Kodama, T.; Ohnishi, R.; Hari, Y.; Imanishi, T.; Obika, S. A Bridged Nucleic Acid, 2′,4′-BNA^{COC}: Synthesis of Fully Modified Oligonucleotides Bearing Thymine, 5-Methylcytosine, Adenine and Guanine 2′,4′-BNA^{COC} Monomers and RNA-Selective Nucleic-Acid Recognition. *Nucleic Acids Res.* **2009,** *37,* 1225–1238.
43. Hari, Y.; Morikawa, T.; Osawa, T.; Obika, S. Synthesis and Properties of 2′-*O*,4′-*C*-Ethyleneoxy Bridged 5-Methyluridine. *Org. Lett.* **2013,** *15,* 3702–3705.
44. Miyashita, K.; Rahman, S. M. A.; Seki, S.; Obika, S.; Imanishi, T. N-Methyl Substituted 2′,4′-BNA^{NC}: A Highly Nuclease-Resistant Nucleic Acid Analogue With High-Affinity RNA Selective Hybridization. *Chem. Commun.* **2007,** 3765–3767.
45. Rahman, S. M. A.; Seki, S.; Obika, S.; Yoshikawa, H.; Miyashita, K.; Imanishi, T. Design, Synthesis, and Properties of 2′,4′-BNA^{NC}: A Bridged Nucleic Acid Analogue. *J. Am. Chem. Soc.* **2008,** *130,* 4886–4896.
46. Prakash, T. P.; Siwkowski, A.; Allerson, C. R.; Migawa, M. T.; Lee, S.; Gaus, H. J.; Black, C.; Seth, P. P.; Swayze, E. E.; Bhat, B. Antisense Oligonucleotides Containing Conformationally Constrained 2′,4′-(N-Methoxy)aminomethylene and 2′,4′-Aminooxymethylene and 2′-*O*,4′-*C*-Aminomethylene Bridged Nucleoside Analogues Show Improved Potency in Animal Models. *J. Med. Chem.* **2010,** *53,* 1636–1650.
47. Yamamoto, T.; Yasuhara, H.; Wada, F.; Harada-Shiba, M.; Imanishi, T.; Obika, S. Superior Silencing by 2′,4′-BNA^{NC}-Based Short Antisense Oligonucleotides Compared to 2′,4′-BNA/LNA-Based Apolipoprotein B Antisense Inhibitors. *J. Nucleic Acids* **2012,** *2012,* 707323.
48. Yamamoto, T.; Harada-Shiba, M.; Nakatani, M.; Wada, S.; Yasuhara, H.; Narukawa, K.; Sasaki, K.; Shibata, M.; Torigoe, H.; Yamaoka, T.; Imanishi, T.; Obika, S. Cholesterol-Lowering Action of BNA-Based Antisense Oligonucleotides Targeting PCSK9 in Atherogenic Diet-Induced Hypercholesterolemic Mice. *Mol. Ther. Nucleic Acids* **2012,** *1,* e22.
49. Yahara, A.; Shrestha, A. R.; Yamamoto, T.; Hari, Y.; Osawa, T.; Yamaguchi, M.; Nishida, M.; Kodama, T.; Obika, S. Amido-Bridged Nucleic Acids (AmNAs): Synthesis, Duplex Stability, Nuclease Resistance, and In Vitro Antisense Potency. *ChemBioChem* **2012,** *13,* 2513–2516.
50. Yamamoto, T.; Yahara, A.; Waki, R.; Yasuhara, H.; Wada, F.; Harada-Shiba, M.; Obika, S. Amido-Bridged Nucleic Acids With Small Hydrophobic Residues Enhance Hepatic Tropism of Antisense Oligonucleotides In Vivo. *Org. Biomol. Chem.* **2015,** *13,* 3757–3765.
51. Singh, S. K.; Kumar, R.; Wengel, J. Synthesis of 2′-Amino-LNA: A Novel Conformationally Restricted High-Affinity Oligonucleotide Analogue With a Handle. *J. Org. Chem.* **1998,** *63,* 10035–10039.
52. Shrestha, A. R.; Kotobuki, Y.; Hari, Y.; Obika, S. Guanidine Bridged Nucleic Acid (GuNA): An Effect of a Cationic Bridged Nucleic Acid on DNA Binding Affinity. *Chem. Commun.* **2014,** *50,* 575–577.
53. Barman, J.; Gurav, D.; Oommen, O. P.; Varghese, O. P. 2′-*N*-Guanidino,4′-*C*-Ethylene Bridged Thymidine (GENA-T) Modified Oligonucleotide Exhibits Triplex Formation With Excellent Enzymatic Stability. *RSC Adv.* **2015,** *5,* 12257–12260.
54. Steffens, R.; Leumann, C. J. Tricyclo-DNA: A Phosphodiester-Backbone Based DNA Analog Exhibiting Strong Complementary Base-Pairing Properties. *J. Am. Chem. Soc.* **1997,** *119,* 11548–11549.
55. Steffens, R.; Leumann, C. J. Synthesis and Thermodynamic and Biophysical Properties of Tricyclo-DNA. *J. Am. Chem. Soc.* **1999,** *121,* 3249–3255.
56. Dupouy, C.; Iché-Tarrat, N.; Durrier, M.; Rodriguez, F.; Escudier, J.; Vigroux, A. Watson–Crick Base-Pairing Properties of Nucleic Acid Analogues With Stereocontrolled α and β Torsion Angles (α,β-D-CNAs). *Angew. Chem. Int. Ed.* **2006,** *45,* 3623–3627.
57. Boissonnet, A.; Dupouy, C.; Millard, P.; Durrieu, M.; Tarrat, N.; Escudier, J. α,β-D-CNA Featuring Canonical and Noncanonical α/β Torsional Angles Behaviours Within Oligonucleotides. *New J. Chem.* **2011,** *35,* 1528–1533.
58. Dupouy, C.; Lavedan, P.; Escudier, J. Synthesis and Structure of Dinucleotides With *S*-Type Sugar Puckering and Noncanonical ε and ζ Torsion Angle Combination (ν2,ε,ζ-D-CNA). *Eur. J. Org. Chem.* **2008,** *2008,* 1285–1294.
59. Hanessian, S.; Schroeder, B. R.; Giacometti, R. D.; Merner, B. L.; Østergaard, M.; Swayze, E. E.; Seth, P. P. Structure-Based Design of a Highly Constrained Nucleic Acid Analogue: Improved Duplex Stabilization by Restricting Sugar Pucker and Torsion Angle γ. *Angew. Chem. Int. Ed.* **2012,** *51,* 11242–11245.
60. Rajwanshi, V. K.; Håkansson, A. E.; Sørensen, M. D.; Pitsch, S.; Singh, S. K.; Kumar, R.; Nielsen, P.; Wengel, J. The Eight Stereoisomers of LNA (Locked Nucleic Acid): A Remarkable Family of Strong RNA Binding Molecules. *Angew. Chem. Int. Ed.* **2000,** *39,* 1656–1659.
61. Sørensen, M. D.; Kværnø, L.; Bryld, T.; Håkansson, A. E.; Verbeure, B.; Herdewijn, P.; Wengel, J. r-L-ribo-Configured Locked Nucleic Acid (r-L-LNA): Synthesis and Properties. *J. Am. Chem. Soc.* **2002,** *124,* 2164–2176.
62. Nowotny, M.; Cerritelli, S. M.; Ghirlando, R.; Gaidamakov, S. A.; Crouch, R. J.; Yang, W. Specific Recognition of RNA/DNA Hybrid and Enhancement of Human RNase H1 Activity by HBD. *EMBO J.* **2008,** *27,* 1172–1181.
63. Shibahara, S.; Mukai, S.; Nishihara, T.; Inoue, H.; Ohtsuka, E.; Morisawa, H. Site-Directed Cleavage of RNA. *Nucleic Acids Res.* **1987,** *15,* 4403–4415.

64. Lima, W. F.; Rose, J. B.; Nichols, J. G.; Wu, H.; Migawa, M. T.; Wyrzykiewicz, T. K.; Vasquez, G.; Swayze, E. E.; Crooke, S. T. The Positional Influence of the Helical Geometry of the Heteroduplex Substrate on Human RNase H1 Catalysis. *Mol. Pharmacol.* **2007,** *71,* 73–82.
65. Lima, W. F.; Rose, J. B.; Nichols, J. G.; Wu, H.; Migawa, M. T.; Wyrzykiewicz, T. K.; Siwkowski, A. M.; Crooke, S. T. Human RNase H1 Discriminates Between Subtle Variations in the Structure of the Heteroduplex Substrate. *Mol. Pharmacol.* **2007,** *71,* 83–91.
66. Straarup, E. M.; Fisker, N.; Hedtjärn, M.; Lindholm, M. W.; Rosenbohm, C.; Aarup, V.; Hansen, H. F.; Ørum, H.; Hansen, J. B. R; Koch, T. Short Locked Nucleic Acid Antisense Oligonucleotides Potently Reduce Apolipoprotein B mRNA and Serum Cholesterol in Mice and Non-Human Primates. *Nucleic Acids Res.* **2010,** *38,* 7100–7111.
67. Yamamoto, T.; Fujii, N.; Yasuhara, H.; Wada, S.; Wada, F.; Shigesada, N.; Harada-Shiba, M.; Obika, S. Evaluation of Multiple-Turnover Capability of Locked Nucleic Acid Antisense Oligonucleotides in Cell-Free RNase H-Mediated Antisense Reaction and in Mice. *Nucleic Acids Ther.* **2014,** *24,* 283–290.
68. Pedersen, L.; Hagedorn, P. H.; Lindholm, M. W.; Lindow, M. A Kinetic Model Explains Why Shorter and Less Affine Enzyme-Recruiting Oligonucleotides can be More Potent. *Mol. Ther. Nucleic Acids* **2014,** *3,* e149.
69. Kuboyama, T.; Nakahara, M.; Yoshino, M.; Cui, Y.; Sako, T.; Wada, Y.; Imanishi, T.; Obika, S.; Watanabe, Y.; Suzuki, M.; Doi, H. Stoichiometry-Focused ^{18}F-Labeling of Alkyne-Substituted Oligodeoxynucleotides Using Azido([^{18}F]Fluoromethyl)Benzenes by Cu-Catalyzed Huisgen Reaction. *Bioorg. Med. Chem.* **2011,** *19,* 249–255.
70. Mukai, H.; Ozaki, D.; Cui, Y.; Kuboyama, T.; Yamato-Nagata, H.; Onoe, K.; Takahashi, M.; Wada, Y.; Imanishi, T.; Kodama, T.; Obika, S.; Suzuki, M.; Doi, H.; Watanabe, Y. Quantitative Evaluation of the Improvement in the Pharmacokinetics of a Nucleic Acid Drug Delivery System by Dynamic PET Imaging With ^{18}F-Incorporated Oligodeoxynucleotides. *J. Control. Release* **2014,** *180,* 92–99.
71. Nishina, T.; Numata, J.; Nishina, K.; Yoshida-Tanaka, K.; Nitta, K.; Piao, W.; Iwata, R.; Ito, S.; Kuwahara, H.; Wada, T.; Mizusawa, H.; Yokota, T. Chimeric Antisense Oligonucleotide Conjugated to α-Tocopherol. *Mol. Ther. Nucleic Acids* **2015,** *4,* e220.
72. Nishina, K.; Piao, W.; Yoshida-Tanaka, K.; Sujino, Y.; Nishina, T.; Yamamoto, T.; Nitta, K.; Yoshioka, K.; Kuwahara, H.; Yasuhara, H.; Baba, T.; Ono, F.; Miyata, K.; Miyake, K.; Seth, P. P.; Low, A.; Yoshida, M.; Bennett, C. F.; Kataoka, K.; Mizusawa, H.; Obika, S.; Yokota, T. DNA/RNA Heteroduplex Oligonucleotide for Highly Efficient Gene Silencing. *Nat. Commun.* **2015,** *6,* 7969.
73. Prakash, T. P.; Graham, M. J.; Yu, J.; Carty, R.; Low, A.; Chppell, A.; Schmidt, K.; Zhao, C.; Aghajan, M.; Murray, H. F.; Riney, S.; Booten, S. L.; Murray, S. F.; Gaus, H.; Crosby, J.; Lima, W. F.; Guo, S.; Monia, B. P.; Swayze, E. E.; Seth, P. P. Targeted Delivery of Antisense Oligonucleotides to Hepatocytes Using Triantennary *N*-Acetylgalactosamine Improves Potency 10-Fold in Mice. *Nucleic Acids Res.* **2014,** *42,* 8796–8807.
74. Østergaard, M. E.; Yu, J.; Kinberger, G. A.; Wan, W. B.; Migawa, M. T.; Vasquez, G.; Schmidt, K.; Gaus, H. J.; Murray, H. M.; Low, A.; Swayze, E. E.; Prakash, T. P.; Seth, P. P. Efficient Synthesis and Biological Evaluation of 5′-GalNAc Conjugated Antisense Oligonucleotides. *Bioconjugate Chem.* **2015,** *26,* 1451–1455.
75. Yamamoto, T.; Sawamura, M.; Wada, F.; Harada-Shiba, M.; Obika, S. Serial Incorporation of a Monovalent GalNAc Phosphoramidite Unit Into Hepatocyte-Targeting Antisense Oligonucleotides. *Bioorg. Med. Chem.* **2016,** *24,* 26–32.
76. Juliano, R. L. The Delivery of Therapeutic Oligonucleotides. *Nucleic Acids Res.* **2016,** *44,* 6518–6548.
77. Watanabe, T. A.; Geary, R. S.; Levin, A. A. Plasma Protein Binding of an Antisense Oligonucleotide Targeting Human ICAM-1 (ISIS 2302). *Oligonucleotides* **2006,** *16,* 169–180.
78. Subramanian, R. R.; Wysk, M. A.; Ogilvie, K. M.; Bhat, A.; Kuang, B.; Rockel, T. D.; Weber, M.; Uhlmann, E.; Krieg, A. M. Enhancing Antisense Efficacy With Multimers and Multi-Targeting Oligonucleotides (MTOs) Using Cleavable Linkers. *Nucleic Acids Res.* **2015,** *43,* 9123–9132.
79. Frazier, K. S. Antisense Oligonucleotide Therapies: The Promise and the Challenges From a Toxicologic Pathologist's Perspective. *Toxicol. Pathol.* **2015,** *43,* 78–89.
80. Sheehan, J. P.; Lan, H. Phosphorothioate Oligonucleotides Inhibit the Intrinsic Tenase Complex. *Blood* **1998,** *92,* 1617–1625.
81. Jason, T. L. H.; Koropatnick, J.; Berg, R. W. Toxicology of Antisense Therapeutics. *Toxicol. Appl. Pharmacol.* **2004,** *201,* 66–83.
82. Henry, S. P.; Giclas, P. C.; Leeds, J.; Pangburn, M.; Auletta, C.; Levin, A. A.; Kornbrust, D. J. Activation of the Alternative Pathway of Complement by a Phosphorothioate Oligonucleotide: Potential Mechanism of Action. *J. Pharmacol. Exp. Ther.* **1997,** *281,* 810–816.
83. Henry, S. P.; Beattie, G.; Yeh, G.; Chappel, A.; Giclas, P.; Mortari, A.; Jagels, M. A.; Kornbrust, D. J.; Levin, A. A. Complement Activation is Responsible for Acute Toxicities in Rhesus Monkeys Treated With a Phosphorothioate Oligodeoxynucleotide. *Int. Immunopharmacol.* **2002,** *2,* 1657–1666.
84. Henry, S. P.; Jagels, M. A.; Hugli, T. E.; Manalili, S.; Geary, R. S.; Giclas, P. C.; Levin, A. A. Mechanism of Alternative Complement Pathway Dysregulation by a Phosphorothioate Oligonucleotide in Monkey and Human Serum. *Nucleic Acid Ther.* **2014,** *24,* 326–335.
85. Mangsbo, S. M.; Sanchez, J.; Anger, K.; Lambris, J. D.; Ekdahl, K. N.; Loskog, A. S.; Nilsson, B.; Tötterman, T. H. Complement Activation by CpG in a Human Whole Blood 1 Loop System: Mechanisms and Immunomodulatory Effects. *J. Immunol.* **2009,** *183,* 6724–6732.
86. Bianchini, D.; Omlin, A.; Pezaro, C.; Lorente, D.; Ferraldeschi, R.; Mukherji, D.; Crespo, M.; Figueiredo, I.; Miranda, S.; Riisnaes, R.; Zivi, A.; Buchbinder, A.; Rathkopf, D. E.; Attard, G.; Scher, H. I.; Bono, J.; Danila, D. C. First-in-Human Phase I Study of EZN-4176, a Locked Nucleic Acid Antisense Oligonucleotide to Exon 4 of the Androgen Receptor mRNA in Patients With Castration-Resistant Prostate Cancer. *Br. J. Cancer* **2013,** *109,* 2579–2586.
87. Hong, D.; Kurzrock, R.; Kim, Y.; Woessner, R.; Younes, A.; Nemunaitis, J.; Fowler, N.; Zhou, T.; Sxhmidt, J.; Jo, M.; Lee, S. J.; Yamashita, M.; Hughes, S. G.; Fayad, L.; Piha-Paul, S.; Nadella, M. V. P.; Mohseni, M.; Lawson, D.; Reimer, C.; Blakey, D. C.; Xiao, X.; Hsu, J.; Revenko, A.; Monia, B. P.; MacLeod, A. R. AZD9150, a Next-Generation Antisense Oligonucleotide Inhibitor of *STAT3* With Early Evidence of Clinical Activity in Lymphoma and Lung Cancer. *Sci. Transl. Med.* **2015,** *7,* 314ra185.
88. Wong, E.; Gldberg, T. Mipomersen (Kynamro): A Novel Antisense Oligonucleotide Inhibitor for the Management of Homozygous Familial Hypercholesterolemia. *P.T.* **2014,** *39,* 119–122.
89. Poelgeest, E. P.; Hodges, M. R.; Moerland, M.; Tessier, Y.; Levin, A. A.; Persson, R.; Lindholm, M. W.; Erichsen, K. D.; Ørum, H.; Cohen, A. F.; Burggraaf, J. Antisense-Mediated Reduction of Proprotein Convertase Subtilisin/Kexin Type 9 (PCSK9): A First-in-Human Randomized, Placebo-Controlled Trial. *Br. J. Clin. Pharmacol.* **2015,** *80,* 1350–1361.
90. Lindow, M.; Vornlocher, H.; Riley, D.; Kornbrust, D. J.; Burchard, J.; Whiteley, L. O.; Kamens, J.; Thompson, J. D.; Nochur, S.; Younis, H.; Bartz, S.; Parry, J.; Ferrari, N.; Henry, S. P.; Levin, A. A. Assessing Unintended Hybridization-Induced Biological Effects of Oligonucleotides. *Nat. Biotechnol.* **2012,** *30,* 920–923.
91. Vollmer, J.; Jepsen, J. S.; Uhlman, E.; Schetter, C.; Jurk, M.; Wader, T.; Wüllner, M.; Krieg, A. M. Modulation of CpG Oligodeoxynucleotide-Mediated Immune Stimulation by Locked Nucleic Acid (LNA). *Oligonucleotides* **2004,** *14,* 23–31.
92. Sheela, F.; Driller, H. Alternating d(G-C)$_3$ and d(C-G)$_3$ Hexanucleotides Containing 7-Deaza-2′-Deoxyguanosine or 8-aza-7-Deaza-2′-Deoxyguanosine in Place of dG. *Nucleic Acids Res.* **1989,** *17,* 901–910.
93. Jurk, M.; Kritzler, A.; Debelak, H.; Vollmer, J.; Krieg, A. M.; Uhlmann, E. Structure–Activity Relationship Studies on the Immune Stimulatory Effects of Base-Modified CpG Toll-Like Receptor 9 Agonists. *ChemMedChem* **2006,** *1,* 1007–1014.
94. Sugimoto, N.; Nakano, M.; Nakano, S. Thermodynamics–Structure Relationship of Single Mismatches in RNA/DNA Duplexes. *Biochemistry* **2000,** *39,* 11270–11281.
95. Testa, S. M.; Dsney, M. D.; Truner, D. H.; Kierzek, R. Thermodynamics of RNA–RNA Duplexes with 2- or 4-Thiouridines: Implications for Antisense Design and Targeting a Group I Intron. *Biochemistry* **1999,** *38,* 16655–16662.
96. Østergaard, M. E.; Kumar, P.; Nichols, J.; Watt, A.; Sharma, P. K.; Nielsen, P.; Seth, P. P. Allele-Selective Inhibition of Mutant Huntingtin with 2-Thio- and C5-Triazolylphenyl-Deoxythymidine-Modified Antisense Oligonucleotides. *Nucleic Acid Ther.* **2015,** *25,* 266–274.
97. Østergaard, M. E.; Southwell, A. L.; Kordasiewicz, H.; Watt, A. T.; Skotte, N. H.; Doty, C. N.; Vaid, K.; Villanueva, E. B.; Swayze, E. E.; Bennett, C. F.; Hayden, M. R.; Seth, P. P. Rational Design of Antisense Oligonucleotides Targeting Single Nucleotide Polymorphisms for Potent and Allele Selective Suppression of Mutant Huntingtin in the CNS. *Nucleic Acids Res.* **2013,** *41,* 9634–9650.

6.11 Manufacturing of Oligonucleotides

E Paredes, V Aduda, and KL Ackley, Nitto Denko Avecia, Cincinnati, OH, US
H Cramer, WAVE Life Sciences, Ltd., Cambridge, MA, US

© 2017 Elsevier Ltd. All rights reserved.

Dedicated to Nanda Sinha, a great mentor and chemist, who passed away in 2016.

6.11.1	**Introduction**	234
6.11.2	**Classes of Therapeutic Oligonucleotides**	234
6.11.3	**Most Common Chemical Modifications in Therapeutic Oligonucleotides**	235
6.11.3.1	Modification of the Internucleotide Linkage	235
6.11.3.2	Modifications of the Sugar	237
6.11.3.3	Modification of the Heterocyclic Base	238
6.11.4	**Historical Perspective of Oligonucleotide Synthesis**	238
6.11.5	**Raw Material-Related Impurities**	239
6.11.5.1	Phosphoramidite-Related Impurities	239
6.11.5.2	Nonreactive and Noncritical Impurities	240
6.11.5.3	Reactive but Noncritical Impurities	240
6.11.5.4	Reactive and Critical Impurities	240
6.11.6	**Solid Supports**	241
6.11.6.1	Nucleoside-Loaded Supports	242
6.11.7	**Formation of Branchmers**	244
6.11.7.1	Generation of $n-1$ (PS)/$n-1$ (PO) Impurities	244
6.11.8	**Universal Supports**	245
6.11.9	**Reagent-Related Impurities**	247
6.11.9.1	Detritylation Reagent	247
6.11.9.2	Activator	247
6.11.9.3	Thiolation/Oxidation	247
6.11.9.4	Capping Reagent	248
6.11.10	**Research-Scale Manufacture of Oligonucleotides**	248
6.11.10.1	Oligonucleotide Solid-Phase Synthesis Cycle	249
6.11.10.2	Oligonucleotide Cleavage and Deprotection	252
6.11.10.3	Oligonucleotide Purification	253
6.11.10.4	Oligonucleotide Isolation	257
6.11.11	**Manufacturing Process and Equipment for Oligonucleotide Used as Therapeutics**	258
6.11.11.1	Oligonucleotide Synthesis Equipment	258
6.11.11.2	Oligonucleotide Cleavage and Deprotection Equipment	258
6.11.11.3	Oligonucleotide Chromatography Equipment	259
6.11.11.4	Oligonucleotide Ultrafiltration & Diafiltration Equipment	260
6.11.11.5	Oligonucleotide Lyophilization Process and Equipment	261
6.11.12	**Small-Scale Modeling for Oligonucleotide Manufacturing**	261
6.11.13	**Analytic Tools to Support Oligonucleotide Manufacturing**	265
6.11.13.1	Commonly Used HPLC Techniques for the Analysis of Oligonucleotides	265
6.11.14	**Regulatory Aspects of Oligonucleotides**	268
6.11.14.1	Setting Specifications	269
6.11.14.1.1	Assay	270
6.11.14.2	Characterization of Oligonucleotides	270
6.11.15	**Summary**	271
6.11.16	**Outlook**	272
Acknowledgments		272
References		272
Relevant Websites		279

6.11.1 Introduction

The concept of using synthetic oligonucleotides (ONs) to control gene expression dates back to the late 1970s, when Zamecnik and Stephenson first demonstrated targeted gene silencing using a short synthetic ON.[1] These pioneering studies were the beginning of a new targeted gene silencing approach termed antisense. Thereby, a synthetic ON complementary to a target mRNA is introduced into cells with the intent to block gene expression through either translational inhibition or enzymatic cleavage of the mRNA target.

Over the years, scientists realized that ONs can have many other modes of action besides Watson–Crick type base pairing with the targeted RNA. Two of the three ON therapeutics approved as of today are working by an antisense mechanism; the other, Macugen, is an aptamer and works through its three-dimensional structure by binding to the 165 isoform of antivascular endothelial growth factor (VEGF), a protein that plays a critical role in angiogenesis.

While only three ON therapeutics have been approved by the FDA as of today, there are many more in late-stage clinical trials. Several more ON drugs are expected to be entering the market over the next couple of years. ON-based therapeutics are poised to become the third therapeutic platform besides small molecule and peptide drugs. Vitravene (Fomivirsen) was the first antisense therapeutic, which made it to the market and was approved by the FDA in 1998.[2] It is used for the treatment of cytomegalovirus retinitis (CMV) in immunocompromised patients and is injected intraocularly. Macugen (Pegaptanib) was approved in 2004 and is also injected into the eye. It is a pegylated aptamer-targeting VEGF and is used for the treatment of neovascular (wet) age-related macular degeneration (AMD).[3] Mipomersen (Kynamro) was approved in 2013 and is used to treat homozygous familial hypercholesterolemia (HoFH).[4] It is targeting apolipoprotein B (apoB) (see **Table 12** in Regulatory Aspects of Oligonucleotides section).

6.11.2 Classes of Therapeutic Oligonucleotides

Most therapeutic ONs currently in clinical trials belong to the following classes: antisense, aptamers, immune stimulatory, decoys, or RNA interference (including small interfering RNA (siRNA), microRNA, and short hairpin RNA (shRNA)).[5]

Antisense therapeutics act by binding to and then cleaving the target RNA in order to interfere with translation and prevent the synthesis of disease-causing proteins. Second-generation antisense ONs are characterized by modifications of the 2′-hydroxyl group of the ribose, usually 2′-*O*-methyl (OMe), 2′-*O*-methoxyethyl, 2′-fluoro or 2′-4′-bridged analogs. Toxicity of these ONs is reduced and target affinity is increased compared with first-generation antisense ONs; however, these modifications prevent the activation of RNase H. This shortcoming can be circumvented by the design of gapmers, which are composed of blocks of modified nucleotides in the termini separated by a central gap of deoxyribonucleotides that induce RNase H cleavage of the target RNA. Second-generation antisense ONs are often further stabilized by the introduction of phosphorothioate groups into the backbone.[6]

A substantial proportion of diseases is caused by missplicing of the pre-mRNA. Antisense ONs are increasingly applied for splicing correction.[7] These ONs are not aimed at cleaving the target RNA; rather, they prevent incorrect splicing or redirect splicing. No stretch of deoxyribonucleotide bases is required for splice switching ONs as for RNA-cleaving antisense.

Early on, it was realized that many antisense ONs were unexpectedly immune stimulatory. The immune stimulatory effect was based on the number and location of CpG motifs in the ON.[8] Later Toll-like receptor 9 (TLR9) was identified as the mediator of the immune stimulatory effect of CpG oligodeoxyribonucleotides.[9] TLR9 recognizes ONs containing unmethylated CpG dinucleotides, which are common in most bacteria and DNA viruses but not in vertebrate DNA. The interaction with this foreign ON and TLR9 leads to immune stimulation. The phosphorothioate modification is an essential element in immune stimulatory ONs.[10] These beneficial effects of CpG ONs provide the basis for improved vaccines and immunotherapeutic for cancer, allergic, and infectious diseases, which are being pursued in a variety of ongoing clinical trials.

Aptamers constitute a special group of ONs whose effect and target affinity lie in their ability to form 3D structures that enable them to recognize and bind strongly to both small and large molecules. In contrast to other classes of ON therapeutics, aptamers interact with and bind to their targets through structural recognition, a process similar to that of an antigen–antibody interaction. However, due to their small size and intrinsic ON properties, aptamers offer several advantages over protein antibodies in both their clinical applicability and a less challenging synthesis process. Aptamers typically act as ligands for proteins, often receptors, in either the intra- or extracellular environment, allowing the aptamer to affect the functionality of downstream effectors.

ON aptamers are being identified and optimized through a process called SELEX (Systematic Evolutions of Ligands by Exponential Enrichment).[11] Thereby, a diverse starting library goes through iterative rounds of selection for binding to the target protein, followed by partitioning and amplification of binding clones. These tools were essential for developing most of the therapeutic aptamers, which are in the clinic today.[5,12] Apart from therapeutic applications where the aptamer is the drug, aptamers have also been used for targeted delivery of ONs. For this purpose, an aptamer capable of entering the target cell through receptor-mediated endocytosis is connected to a therapeutic ON by direct conjugation or containing the functionalized aptamer on the surface of the formulation.

Double-stranded oligodeoxynucleotides are examples of decoy ONs. They are designed to prevent transcription factor binding competitively to the promoter region of targeted genes, thus inhibiting transcription. Decoy ONs targeting NF-ĸB have shown therapeutic effects for several indications in various animal models[13] and in the clinic.[14] Decoy ONs were also applied to the inhibition of signal transduction and transcription factors (STAT).[15]

In 1998, double-stranded RNAs were discovered to be the silencing effectors to regulate gene functions in *Caenorhabditis elegans*.[16] Shortly thereafter, similar phenomena were found also in plants,[17] which uncovered the new world of RNA interference

(RNAi) and heralded a revolution in RNA regulation. RNAi is defined as a mechanism of specific posttranscriptional gene silencing mediated by small RNAs, including endogenous microRNA (miRNA) and exogenous small interfering RNA (siRNA) or short hairpin RNA (shRNA).[18] Double-stranded small RNAs incorporate into the RNA-induced silencing complex (RISC), suppressing the gene expression by either degrading mRNA or blocking mRNA translation.[19] All of these three modes of RNA interference, miRNA, siRNA and shRNA, are being pursued as therapeutics.[20]

Small interfering RNA (siRNA) therapeutics are usually 21 nucleotides long, double-stranded RNAs with a two-base overhang. However, not all siRNAs are created equal; some are blunt ended and not all are 21 bases long. Most siRNAs are chemically modified,[21] with an antisense active strand (or guide strand) that is complementary to a sequence in the target mRNA. siRNAs are taken up by RISC, which ejects the sense or passenger strand, leaving the antisense strand to bind to the target mRNA and mediate its sequence-specific cleavage by the RISC RNase Argonaute 2. This is an efficient catalytic process because after the cleaved mRNA is released, the guide-strand-bound RISC binds to another mRNA and starts a new round of cleavage.[22] A recent review from Wittrup and Lieberman discusses the current state of siRNA therapeutics in the clinic.[23]

microRNA (miRNA or miR) plays essential functions during embryogenesis and tissue development and during cell differentiation, proliferation, and survival.[24] Unlike siRNAs and shRNA, miRNAs are only partially complementary to their target mRNAs' 3′-untranslated region (UTR), regulating their targets via all four Ago proteins (AGO1–4).[25] A perfect match is not a necessity for miRNA to function; thus, the change in the expression of a single miRNA may affect hundreds of different genes.[26]

miRNA mimics and anti-miRs (antogomiRs or miRNA antagonists) represent the two major approaches, which are being developed as microRNA therapeutic agents.[27] miRNA mimics the function of endogenous microRNAs. They represent miRNA replacement therapy that aims to restore the expression of tumor-suppressive miRNAs. Anti-miRs are used to inhibit oncomiRs, tumor suppressor miRs, and metastamiRs when disease results from an overexpression of the miRNA.

Anti-miR-type microRNA therapeutics predominantly function via a steric blockage, in which miRNA function is inhibited by strong hybridization to block RISC loading. Anti-miRs may be designed to trigger miRNA cleavage by RNase H as well, but this has been less common thus far.[72,195] A typical anti-miR therapeutic is a perfect complement to the miRNA target. microRNA therapeutics are single stranded, mostly fairly short, chemically modified oligoribonucleotides to enhance nuclease stability and target-binding affinity.

shRNAs have been developed as therapeutics as well. shRNAs are processed by Dicer and then incorporated into RISC, followed by the same cytoplasmic RNAi process as in siRNA.[196] Other related technologies have recently garnered a lot of attention like mRNA therapeutics and CRISPR CAS9.

6.11.3 Most Common Chemical Modifications in Therapeutic Oligonucleotides

The development of ON for the different therapeutics areas has all shown this class of therapeutics to be highly potent and effective in in vitro cell assays. However, translation from the bench to the clinic has been hampered by significant challenges arising from poor in vivo stability, ineffective uptake into targeted cells, and off-target effects including immunostimulation. Early on it was realized that native DNA and RNA structures had to be chemically modified in order to make them suitable as therapeutics. Chemical modifications were introduced to alter the stability of ONs, increase their affinity toward the target, facilitate cellular uptake, and enhance their bioavailability in vivo (**Fig. 1**). Chemical modifications of nucleic acids can be classified into three categories: modification of the (1) internucleotide linkage, (2) the sugar, and (3) the heterocyclic nucleobase. Besides direct modification of the nucleic acid, conjugation represents another very effective way to improve intracellular delivery or in vivo pharmacokinetics and biodistribution of ONs.[28] Modifications discussed here will focus on alterations frequently seen in therapeutic ONs, currently pursued in clinical trials, and by no means are meant to be exhaustive. For further reading please see recent review article from Deleavey and Damha.[29]

6.11.3.1 Modification of the Internucleotide Linkage

The internucleotide phosphodiester linkages of DNA and RNA are negatively charged at physiological pH and can be readily cleaved by endo- and exonucleases found in serum and within mammalian cells. Chemical modifications of these bonds have been extensively studied, and several chemical strategies have proved very successful for improving nuclease resistance, some of which are still compatible with an RNase H-mediated mRNA cleavage mechanism, and a few impart additional beneficial characteristics to ONs. This review will focus only on the backbone modifications with clinical applications.

One of the most common backbone modification is the phosphorothioate modification, where the oxygen in the phosphodiester bond is replaced by sulfur.[30] The chemical synthesis of the phosphorothioate ONs results in a roughly 1:1 mixture of the two diastereoisomers (R and S). As this results during each phosphorothioate coupling, all phosphorothioate-modified ONs currently in the clinic are a complex mixture of diastereoisomers. However, a stereocontrolled synthesis was achieved first by Stec and coworkers,[31] and more recently an improved synthetic route was introduced by Wade and coworkers[32] and later refined by others,[33] making stereoselective phosphorothioate ON synthesis achievable for the first time at scales suitable for the development of therapeutics.

Initially, phosphorothioates were introduced into the antisense methodology because of the nuclease resistance of the phosphorothioate linkage in comparison with that of the phosphate linkage. However, as experimental data accumulated, it was detected that this chemical modification also facilitates cellular uptake and bioavailability in vivo. This backbone modification

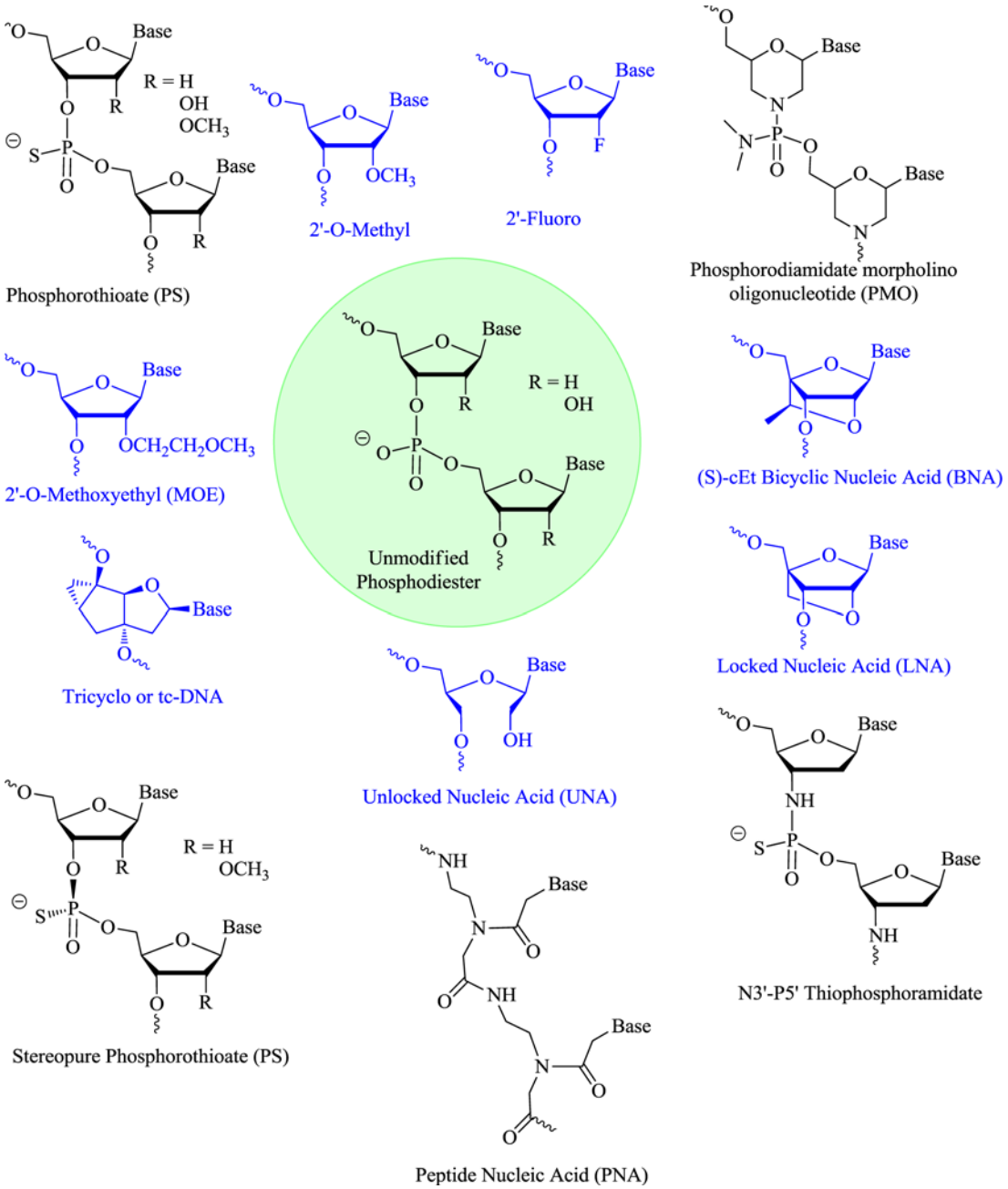

Fig. 1 Most common chemical modifications used in therapeutic oligonucleotides. *Blue color* indicates sugar modification; *black color* backbone modification. The circle in the middle indicates unmodified natural RNA and DNA.

is present in a large proportion of the ONs in various phases of clinical trials. Additionally, both antisense ONs approved by the US Food and Drug Administration are fully phosphorothioated (Table 12).

Peptide nucleic acids (PNAs) are a radically different class of ON analogs that contain a peptide replacement for the sugar phosphate backbone, yet maintain the ability to Watson–Crick base pair with complementary RNA and DNA.[34] PNAs have a neutral charge backbone composed of *N*-(2-aminoethyl)glycine, exhibit significant nuclease and protease resistance[35] and bind to its complimentary target with higher affinity than DNA or RNA.[36] PNAs do not activate RNase H and can act via a translational inhibition mechanism,[37] in siRNA overhangs,[38] and in numerous other biological pathways including splice-switching activities.[39] Despite their uncharged nature, PNAs do not readily cross cell membranes. These limitations have been addressed by the conjugation of PNA to short peptides,[40] which also helps increasing solubility. The short peptides employed were also able to improve tissue distribution. However, both pharmacokinetic and potency hurdles remain for PNA ON drugs, and concerns remain as to whether the modification is too stable in tissues.[37]

In the N3′–P5′ phosphoramidate modification, the 3′-OH group of the internucleotide bond is replaced with a 3′-amine functionality.[41] N3′–P5′ phosphoramidate modifications adopt a North sugar conformation, making them suitable mimics for RNA substitution.[42] As a result, N3′–P5′ phosphoramidate containing ONs lack the ability to activate RNase H-mediated cleavage,[43] but feature good binding affinity for target sequences and high nuclease resistance. Introduction of sulfur in place of one of the nonbridging oxygen atoms does not alter the RNA-binding properties of these compounds.[44] A palmitoyl-conjugated thiophosphoramidate-modified ON, Imetelstat, has shown promise as an anti-telomerase agent.[45]

Phosphorodiamidate morpholino ONs (PMOs) have an uncharged backbone, where the furanose ring has been replaced with a morpholine ring and a phosphorodiamidate linkage is connecting the morpholine nitrogen atom with the 5′-hydroxyl group. Because of the phosphorodiamidate linkage, morpholino ONs are neutral. These modifications are similar in affinity to DNA–DNA duplexes and are nuclease stable. PMOs can have similar or even improved binding affinity for target strands,[46] and can be used as translational inhibitors and anti-miRNAs.[37] Although PMOs lack the ability to trigger RNase H, they have proved resistant to nuclease degradation[47] and show promise for modulating splicing and translation arrest.[48]

Therapeutic ONs are often also conjugated with biologically relevant moieties.[49] ON conjugates have demonstrated increased circulation times, improved cellular uptake and endosomal release, and targeted tissue uptake and cellular localization. The following types of conjugates have been investigated in clinical trials: lipids including cholesterol,[50] small molecules (in particular in combination with aptamers),[51] PEG (polyethylene glycol),[52] nucleic acids (see aptamers), peptides,[53] and carbohydrates in particular GalNAc.[54] For further reading, several recent review articles are available on ON conjugates and their biological activity and synthetic strategies.[28b,49,55]

6.11.3.2 Modifications of the Sugar

Modifications to the ribose provide a remarkable level of control over the sugar conformation in the nucleotide, which determines the ON's binding affinity toward its complementary strand and duplex structure. Sugar puckering can be altered through gauche and anomeric effects of the neighboring hydroxyl groups or via steric restraints.[56] Most nucleotide sugars and analogs adopt conformations characterized as either "North" (C 3′-endo and C 2′-exo), or "South" (C 2′-endo and C 3′-exo). In the B-form, most prevalent in double-stranded DNA, riboses adopt the "South" conformation, whereas in the A-form, most prevalent in double-stranded RNA, riboses adopt the "North" conformation.

The 2′-*O*-methyl (2′-*O*-Me) nucleoside analog is one of the most widely used modification in ON therapeutics. Compared with a DNA strand, incorporation of 2′-*O*-Me units within ONs increases binding affinity for RNA complements[57] and increases nuclease stability.[58] 2′-*O*-Me ribose prefers a North sugar conformation[59] and forms A-form duplexes.[59b] The 2′-*O*-Me modification has been widely applied in antisense ON research, especially when incorporated in the so-called "gapmer" ON constructs. 2′-*O*-Me modified ONs are in many clinical trials[60] and can be found in the first FDA-approved aptamer, Macugen.[61] These analogs are also well suited for siRNA modification. Indeed, 2′-*O*-Me units are well tolerated in siRNAs,[23,27a] although this modification is not tolerated at every location of the RNA duplex, particularly the guiding strand.[62] 2′-*O*-Me modifications have been shown to reduce immunostimulatory properties of siRNAs.[63]

The 2′-*O*-MOE (2′-*O*-(2-methoxyethyl)) modification has been used in several therapeutic candidates undergoing clinical trials.[37] Like with 2′-*O*-Me, the 2′-*O*-MOE modification increases target-binding affinity (2°C per insert)[64] and improves nuclease stability.[64a] 2′-*O*-MOE modifications adopt a North sugar conformation.[37,64a] 2′-*O*-MOE groups have been successfully applied to antisense ON using the aforementioned gapmer design and in siRNA, especially in the passenger strand.[65] One of the approved antisense therapeutics, Mipomersen, is a second-generation antisense ON containing phosphorothioate linkages and 2′-*O*-MOE sugars.[4a]

The 2′-fluoro modification is another popular chemical modification particularly for siRNA. 2′-fluoro, like 2′-*O*-Me, is an RNA mimic, preferentially adopting a North sugar pucker,[66] at least partly due to the strong gauche effect imparted by the 2′-fluorine. Much like 2′-*O*-Me, 2′-fluoro increases binding affinity for target RNA sequences (2–3°C per insert versus DNA) [37,64b,67]. 2′-Fluoro modification is very well tolerated in siRNA, in both the guide and the passenger strands [62b,68]. The 2′-fluoro substitution has allowed for the complete elimination of RNAs from siRNAs without compromising incorporation into RISC, thereby providing duplexes with increased stability and potency that still act via activation of the RNAi pathway.[69] Like 2′-*O*-Me, 2′-fluoro modifications can also be found in the FDA-approved aptamer, Macugen.[61]

Locked nucleic acid (LNA) or 2′,4′-bicyclic nucleic acid (2′,4′-BNA) is a chemically modified RNA analog where a methylene bridge is forming a covalent linkage between the 2′-OH and the C-4′ of the sugar.[70] These nucleoside analogs are essentially locked in a North sugar conformation that closely mimics the A-form prevalent in RNA, which effectively preorganizes LNA for RNA binding.[70,71] LNA shows the highest duplex stability effects of all chemical modifications, with stabilizations of 5–6°C per insert.[70a] As a result, LNAs have proved very useful in anti-miRNA,[72] antisense ON,[71] and siRNA applications [62b,73]. The strong binding properties of LNA make them particularly useful in anti-miRNA applications, where short sequences can be necessary for miRNA specificity. LNAs were found to be excellent antisense ON modifications when used in gapmer constructs.[74] LNA modifications are also compatible with siRNA chemistry requirements.[73] LNA modifications show improved nuclease resistance[74] and can reduce siRNA immunostimulatory response.[63]

Other bicyclic nucleic acids (BNAs) have been introduced over the years.[65] A BNA analog, which has been successfully applied to generation 2.5 therapeutic antisense ONs, is (S)-cEt BNA, where (S)-cEt BNAs are mixed into the 2′-*O*-MOE flanks of a MOE gapmer. (S)-cEt and LNA show similar Tm and in vitro and in vivo activities. However, (S)-cEt BNA ONs showed an improved toxicity profile

relative to LNA ONs. These data suggest that (S)-cEt BNA has the potential to improve the therapeutic index of antisense drugs.[65] Bicyclo[3.1.0]hexane-based nucleoside analogs (2p-deoxy-methanocarba nucleosides [MC]) adopt a North sugar conformation, enhance thermal stability of duplexes, and enhance siRNA serum stability.[75] Another conformationally constrained nucleoside analog, tricyclo-DNA (tc-DNA), has shown promise in early development.[76] It is based on a tricyclic rather than bicyclic ring system. tc-DNA shows enhanced binding affinity to RNA, does not activate RNase H, and is stable to nucleases.[76]

Contrasting the rigid nature of LNA, the highly flexible unlocked nucleic acid (UNA) (or "seconucleoside") modification is also being developed for application in ON therapeutics. UNA, missing the covalent C2′–C3′ bond of a ribose sugar, is not conformationally restrained and can be used to influence ON flexibility.[77] UNA can reduce duplex T_m up to 5–10°C per insert[77,78] but still facilitates antisense strand selection into the RISC complex. UNA modifications placed into the seed region of a siRNA guide strand can significantly reduce off-target effects.[79]

6.11.3.3 Modification of the Heterocyclic Base

Chemically modified nucleobases have also found application in ON analog development. Although perhaps less common than sugar and backbone modifications, modified nucleobases are numerous and can be used to affect thermal stability,[80] reduce immunostimulation, and affect siRNA off-target effects.[81]

Modification of the heterocycle has focused mainly on increasing binding affinity for complementary nucleic acids.[80,82] This may be accomplished through increasing stacking interactions or by increasing the strength of the Watson–Crick base pairs. The 5-bromo- and 5-iodo-uracil substitutes of uracil, and 2,6-diaminopurine in place of adenine have been used to achieve increased duplex stability by increasing the strength of the Watson–Crick hydrogen bonding while maintaining and improving native base pairing recognition.[62b,68,83]

The C5 position has been a common place for chemical manipulation on pyrimidine heterocycles because substitution at this position increases affinity without affecting the ability to serve as an RNase H substrate. Substituting the C5 hydrogen of deoxycytidine with a methyl group improves the T_m of the DNA–RNA duplex by approximately 0.5°C per substitution[84] owing to enhanced base stacking on the 5′-side nucleobase. C-5 propynyl pyrimidine base modifications also increase duplex thermal stability and are compatible with RNase-H-mediated gene silencing but have shown some associated toxicity.[37,85]

6.11.4 Historical Perspective of Oligonucleotide Synthesis

In the beginning of the 20th century, biochemists realized that DNA played an important role as biomolecule in the living cell. Initially, a major emphasis was taken to determine its structure, which was accomplished by Watson and Crick in 1953.[86] Subsequently, in 1955, Michelson and Todd[87] reported the first synthesis of a dinucleotide with proper 3′–5′ orientation. The challenges in the synthesis of DNA were selective protection and deprotection of various reactive moieties present in deoxyribonucleosides. These challenges were successfully resolved by Khorana and his group,[88] who introduced various protecting groups (trityl groups for primary hydroxyl and benzoyl, and isobutyryl for exocyclic amines) in the 1950s and 1960s and also reported the first synthesis of sequence-defined oligodeoxynucleotide.[89] Interestingly, most of these protecting groups are still in use today. The chemical strategy used was termed phosphate diester, as after condensation a phosphate diester was formed. In spite of some of the early shortcomings, this strategy was successfully utilized for the assembly of a synthetic gene.[90]

In the 1960s and 1970s, Letsinger and his team introduced a new synthesis strategy termed phosphate triester methodology, which addressed some of the shortcomings of the phosphate diester approach.[91] The phosphate triester approach was further improved through the introduction of better coupling agents by several groups, in particular Reese,[92] Narang,[93] and Cramer.[94] The introduction of solid-phase synthesis by Letsinger and coworkers[91] simplified ON synthesis to the point of having them readily available to support research in molecular biology, recombinant technology, and genetic engineering.

Newer applications, especially exploration of synthetic ONs for therapeutic and diagnostic purposes, started to emerge in the 1970s and 1980s after Zamecnik and Stephenson[1b] reported the inhibition of Rous sarcoma viral ribonucleic acid (RNA) translation and viral replication in cells. These investigations provided impetus for the development of novel synthesis strategies based on P(III) chemistry.[95] Caruthers[96] in the United States and Köster[97] in Germany, respectively, introduced methyl-phosphoramidite and β-cyanoethyl-phosphoramidite chemistries. During the same time period, Garegg et al.[98] from Sweden and Fröhler et al.[99] from the United States introduced a synthetic approach based on H-phosphonate chemistry originally adapted to diribonucleoside synthesis by Todd et al.[100]

Along with oligodeoxynucleotide chemistry advances, strategies for synthesis of oligoribonucleotides were also independently developed by two groups (Reese in United Kingdom[92] and Ogilvie in Canada[101]). The chemistry developed by Ogilvie utilized *t*-butyldimethylsilyl protection for the 2′-hydroxyl group, whereas Reese's group applied tetrahydropyran and variants. The 2′-*O*-*t*-butyldimethylsilyl group is still the preferred protecting group for oligoribonucleotide manufacturing today. Several review articles are discussing the different chemical approaches used for making synthetic ONs.[102] At present, the β-cyanoethyl-phosphoramidite chemistry is predominantly used in solid support-based ON synthesis. The specific synthesis cycle and steps involved are presented later in this report (**Fig. 2**).

The impurities present in ONs depend on the synthesis methods utilized during their preparation. The chain elongation step in the phosphate diester approach used during the early days of ON synthesis is very slow and results in branching of the chain as the

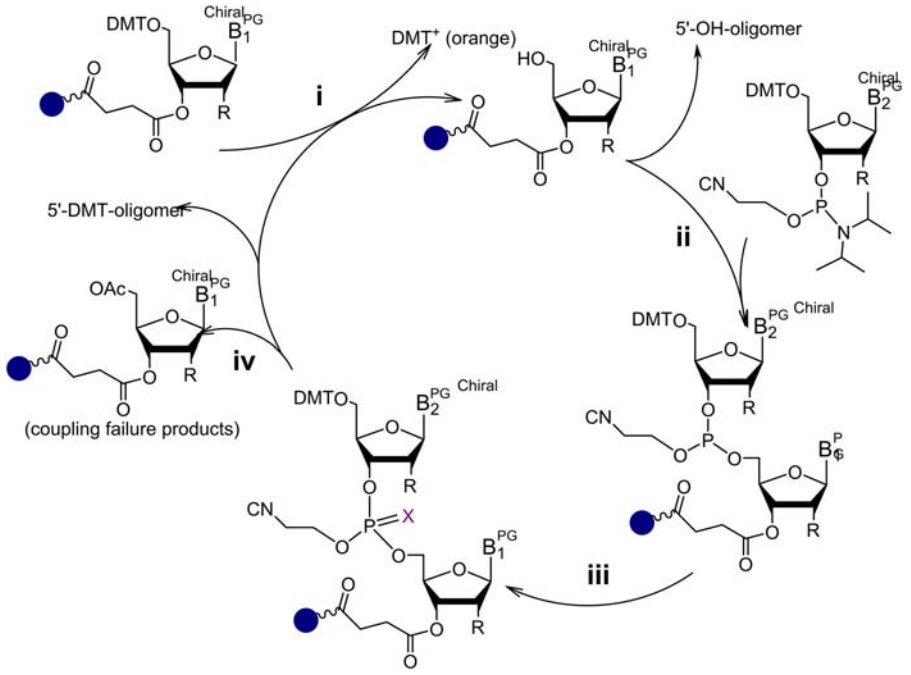

Fig. 2 Solid-phase synthesis cycle for oligonucleotide synthesis.

resulting phosphate diester is exposed to activation and condensation. Subsequently, the phosphate triester approach was developed, where the chain elongation step is much faster and the coupling reaction proceeds without the need for activating agents. The phosphate triester formed is not exposed to further activation, thereby mitigating the formation of branched impurities. However, branching or modification can still occur at the heterocyclic bases especially at the unprotected O-6 position of guanine and the O-4 position of thymine/uracil. Impurities can further result from strand cleavage during the removal of the phosphate protecting groups.

The introduction of the microprocessor in the 1980s allowed automation of ON synthesis. Two synthetic approaches based on phosphoramidite and H-phosphonate chemistries were predominantly adapted for automated synthesis. During early stages of automation, instrument-related impurities such as deletion of monomers or double additions were observed. H-phosphonate-related impurities were based on unwanted capping taking place with the activating reagent pivaloyl chloride or adamantanoyl chloride present during chain elongation resulting in failure sequences. This article will mainly cover impurities introduced when using the phosphoramidite approach since it is being used predominantly today.

6.11.5 Raw Material-Related Impurities

6.11.5.1 Phosphoramidite-Related Impurities

All nucleosides used in the synthesis of therapeutic ONs today are sourced exclusively from man-made synthetic sources and must be certified to be BSE- and TSE-(transmissible spongiform encephalopathy) free. Nucleosides' reactive sites need to be selectively protected before converting them to phosphoramidites. The protection of the 5′-hydroxyl (and the 2′-hydroxyl group in RNA) and all exocyclic amino groups is necessary to minimize side reactions during ON synthesis.

Phosphoramidite impurities are predominantly introduced through the following three sources:

(1) The introduction of nucleoside protecting groups
(2) The quality of synthetic nucleosides (α-anomeric and 3′-substituted impurities)
(3) The quality of the phosphitylating reagent

These impurities may influence the overall quality of ONs as these impurities can be reactive and critical. Based on their reactivity and criticality, impurities are divided into three categories[103]:

(1) Nonreactive and noncritical
(2) Reactive but noncritical
(3) Reactive and critical

For a recent in-depth discussion on this topic, please refer to a recent review article on this topic and the references therein.[104]

6.11.5.2 Nonreactive and Noncritical Impurities

This class of impurities is made up of nonphosphorylated nucleosides and hydrolyzed or oxidized phosphite species. These impurities do not interfere with the synthesis of ONs. Impurities can be either nucleoside-based or phosphitylating reagent-based and are mostly formed during the phosphitylation of the protected nucleoside (PNS) to make the phosphoramidites. Fig. 3 shows the conversion of a PNS to a phosphoramidites and what type of impurities can be formed during this reaction.

6.11.5.3 Reactive but Noncritical Impurities

Reactive but noncritical phosphoramidite impurities are generated from nucleoside impurities with partially modified N, 5′-O or 2′-O (RNA)-protecting groups. These phosphoramidite impurities will also incorporate into the ON chain but will be removed together with the standard protecting groups without impacting the quality of the synthesized ON.

The most commonly used 5′-hydroxyl protecting group is the dimethyltrityl (DMT) group. Impurities are reactive modified trityl chlorides (composed of methoxy, methyl trityl, or monochlorodimethoxytrityl) and nonreactive dimethoxytritanol. Another type of reactive protecting group impurities is those associated with exocyclic amine protection of the nucleoside base. In place of standard protecting groups (Bz on C and A, and iBu on G), chlorobenzoyl protecting groups on cytosine, adenine and *n*-butyryl on guanosine are the most common impurities. Fig. 4 marks the places where impurities can be seen in the phosphoramidites.

6.11.5.4 Reactive and Critical Impurities

Sources of reactive and critical impurities are the following:

(1) Preparation of the unprotected nucleoside
(2) Protection of the 2′, 3′ and 5′-hydroxyl groups of the sugar
(3) Protection of the exocyclic amino group of the base
(4) Originate from reactive impurities in the phosphitylating reagent

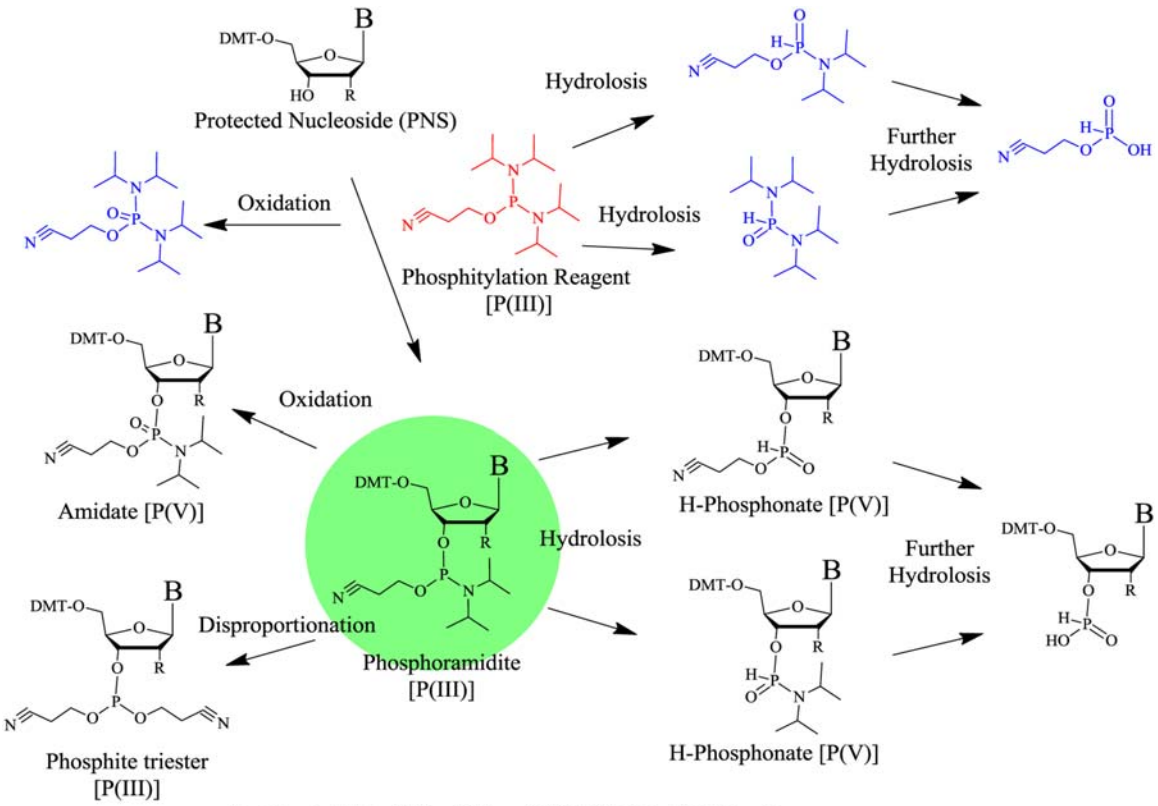

Fig. 3 Nonreactive and noncritical impurities and how they being created during the making of the phosphoramidite. Centered with *green* background shows the phosphoramidite. Structures in *blue* are degradation products from the phosphitylation reagent. Phosphitylating reagent in red if not fully removed would be a reactive and critical impurity.

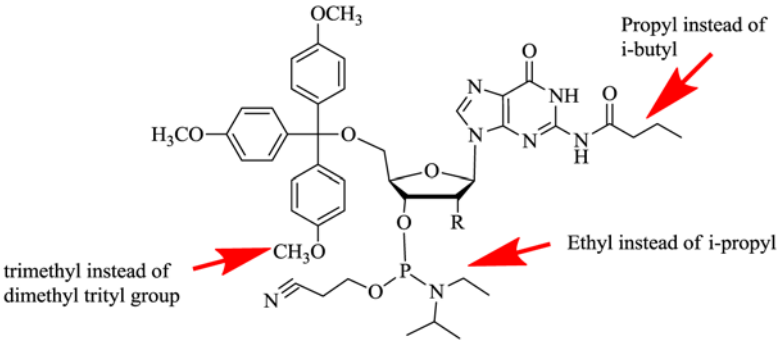

Fig. 4 Example of reactive but noncritical impurities created by impurities in the protecting groups.

Incorporation of these reactive impurities has significant impact on the quality or nature of the ON synthesized. Hence, control of the impurities is of utmost importance. Examples for reactive and critical impurities resulting from impurities in nucleoside-phosphoramidites are given in Fig. 5. Structure **1** in Fig. 5 is α-isomer, structure **2** 3′-phosphoramidite, and structure **3** 5′-phosphoramidite. The 3′-phosphoramidite is a common impurity of all RNA-type phosphoramidites, in particular with TBDMSi-protection. Any isomeric impurities are difficult to detect since they have the same mass and also similar retention time during HPLC analysis and similar chemical field in the ^{31}P-NMR. However, the quality of the nucleosides and phosphitylating reagent has greatly improved over the years, and today, only small levels of most impurities are detected in amidites used in ON manufacturing for therapeutic applications.

Impurity **4** in Fig. 5 results from an impurity in the phosphitylation reagent. The iso-propyl group is not being removed during standard cleavage and deprotection conditions and will form an impurity in the final ON having a mass of +42 Da. Impurities **5** and **6** are being formed when introducing the protecting groups to the nucleosides. The DMT-group in impurity **5** will be removed during detritylation step of the synthesis and then is available during the next coupling reaction to react with the incoming amidite to form branchmers. The same fate will have impurity **6**, the formation of branchmers.

As mentioned earlier, impurity **2** is a common impurity found in 2′-modified sugars and will form a 2′, 5′- instead of a 3′, 5′-linkage. Since these impurities are phosphoramidite manufacturing process related, their complete elimination is unlikely but they can be monitored and controlled using proper analytic methods and appropriate specifications for the phosphoramidites. HPLC-MS analysis is an important tool for the accurate identification of impurities impacting the quality of ONs. ^{1}H NMR and RP-HPLC have been used for identification of nucleoside-phosphoramidites. ^{31}P NMR and RP-HPLC can be effectively used for controlling reactive impurities in phosphoramidites. An example for a phosphoramidite analyzed by HPLC and ^{31}P NMR is illustrated in Figs. 6 and 7. The HPLC analysis (Fig. 6) shows two noncritical impurities and one critical impurity. The noncritical impurities are the hydrolyzed phosphoramidites and a double DMT-protected nucleoside, 5′,3′-*O*-Di-DMT-2′-*O*-Me adenosine. The critical impurity is the phosphoramidite with an additional DMT group in the base. The ^{31}P NMR does not show the double DMT-protected nucleoside, since this impurity does not contain any phosphorous. However, only ^{31}P NMR will detect impurities resulting from the phosphitylation reagent since it does not have a chromophore and is therefore not UV active.

6.11.6 Solid Supports

The solid supports used in ON synthesis also present a potential source of impurities, and a good understanding of the different types of supports and processing conditions is important to reduce the impurity burden in the final product. Traditionally, silica-based controlled pore glass (CPG) was almost exclusively used in phosphoramidite-based solid-phase ON synthesis. CPG supports could be manufactured with predefined pore sizes and space required for a growing ON chain. They are nonswelling and inert to the solvents and reagents used during ON synthesis. Typically, in ONs synthesis, a CPG support with a pore size of 500 Å is used for ONs up to a length of 30 bases and a pore diameter of 1000 Å for up to 50 bases.[105] The lengths of therapeutic ONs are generally under 50 bases long; hence, CPG support with 500 Å or 1000 Å pore size satisfies this need. Disadvantages of glass supports, however, include the instability toward basic conditions used during cleavage and deprotection and low loading capacity, which can lead to formation of impurities.

To mitigate CPG's disadvantages, highly cross-linked polystyrene[106] and methacrylate[107] supports were developed. These initially developed supports have low loadings and are still in use for small-scale ON synthesis.[108] Later, high-loaded macroporous polystyrene supports with loadings of 200 μmol nucleoside per gram of support were developed by Pharmacia Biotech (now part of GE Healthcare). Another high-loading solid support, NittoPhase, originally developed in collaboration with ISIS Pharmaceuticals is being sold by Nitto Denko. Latest developments have led to a support called NittoPhase HL with loadings of 400 μmol nucleoside per gram. Other high-loaded supports have been developed or are in development. ISIS Pharmaceuticals has developed a new polystyrene-based high-loaded support (350 μmol/g), which recently was made available commercially by GE Healthcare

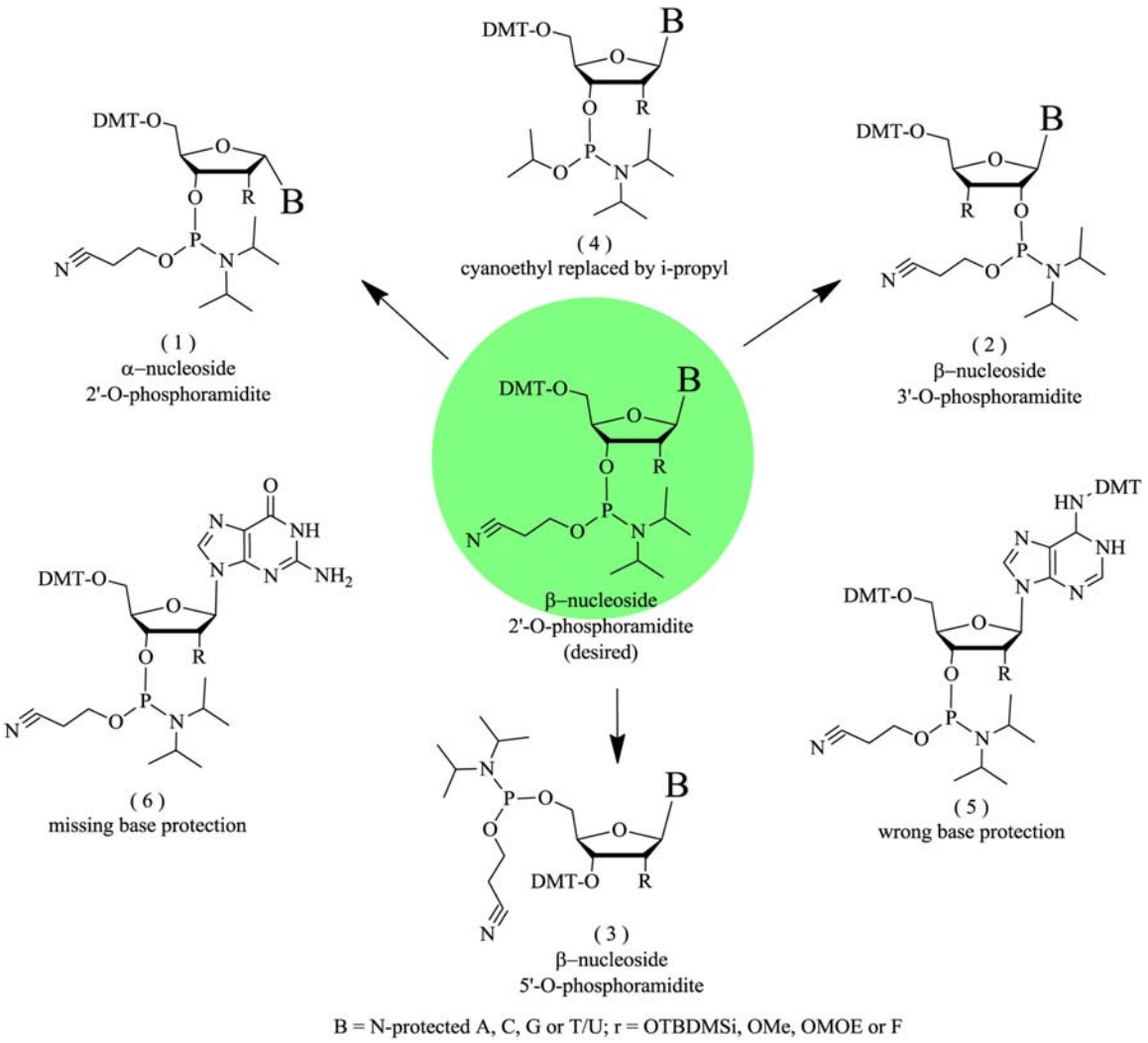

Fig. 5 Example for reactive and critical impurities in nucleoside-phosphoramidites. The structure in the green circle shows the desired phosphoramidite. Structure 1 is the α-isomer, structure 2 the 3′-phosphoramidite and structure 3 the 5′-phosphoramidite. Impurity 4 results from an impurity in the phosphitylation reagent. Impurities 5 and 6 are being formed when introducing the protecting groups to the nucleosides.

under the name Primer Support 5G. The different chemistries used for the development of solid supports utilized in ON synthesis are summarized in Fig. 8.

6.11.6.1 Nucleoside-Loaded Supports

Traditionally, a nucleoside succinate is allowed to react with an amino- or hydroxyl-functionalized support to create a nucleoside-loaded support.[109] The succinate linkage thus created between solid support and nucleoside is stable to conditions and reagents used during solid-phase synthesis. At the end of the synthesis, during basic cleavage and deprotection conditions, the succinate linkage is hydrolyzed, releasing the ON chain from the support. Other more base-labile linkers have been developed such as oxalate[110] and Q-linker,[111] but the succinate linkage is the most widely used one in large-scale synthesis. The stable succinate linkage allows selective removal of cyanoethyl phosphate protecting groups without releasing the ON from the support using on-column base washing. This inhibits acrylonitrile adduct formation of the heterocyclic bases, in particular thymine.[112]

CPG supports require a spacer in between the nucleoside succinate and the functional group of the support to ensure good coupling efficiencies. Thereby, the amino- or glyceryl-functionalized CPG support is derivatized with a long-chain alkyl amine (LCAA)[113] (see Fig. 8) or other similar linkers as described by Sirna Therapeutics[114] or others[105a] before attaching the nucleoside succinate. With polystyrene supports, functional (amino or hydroxyl) groups are reacted directly with the nucleoside succinate, and no additional linker is required.

The coupling of a nucleoside-3′-*O*-succinate to the support can be performed with 2,2′-dithiobis(5-nitropyridine) (DTNP) and dimethylaminopyridine (DMAP) followed by addition of triphenylphosphine (TPP) and LCAA-CPG.[115] Alternatively, the

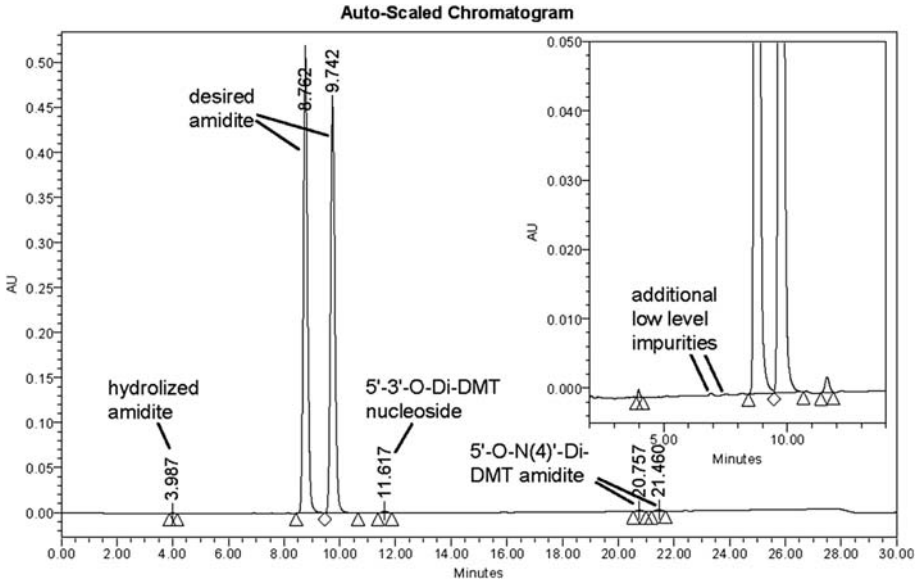

Fig. 6 2′-*O*-Methyl-A phosphoramidite analyzed by HPLC (purity of 99.3%).

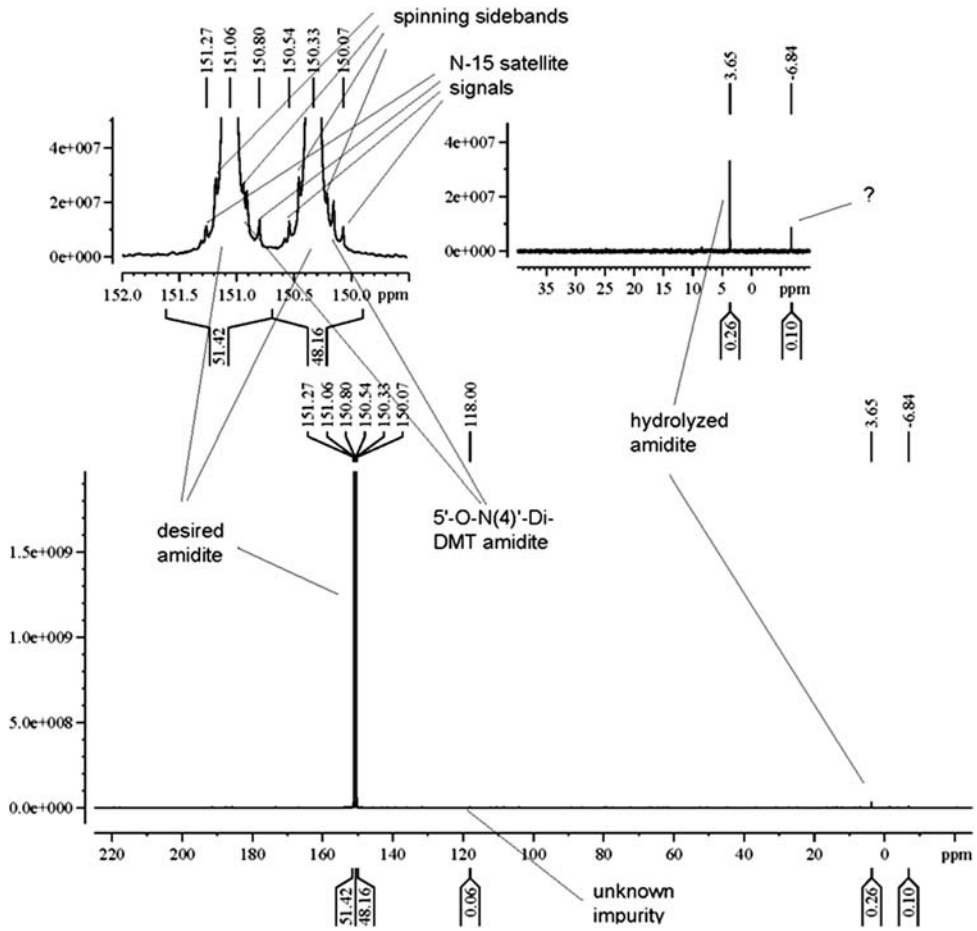

Fig. 7 2′-*O*-Methyl-A phosphoramidite analyzed by ^{31}P-NMR (purity of 99.5%).

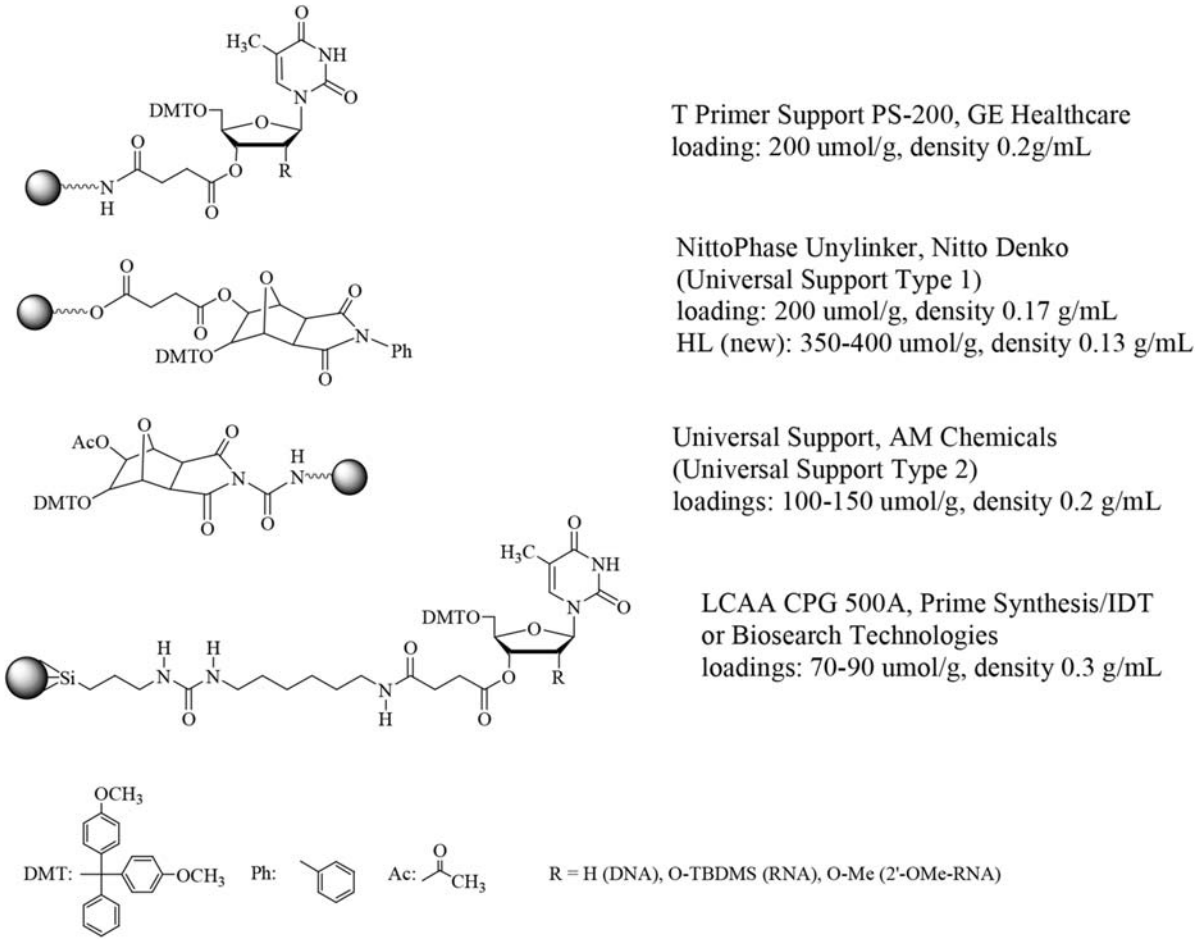

Fig. 8 Common types of supports used in solid-phase oligonucleotide synthesis.

nucleoside-3′-*O*-succinate can be attached to LCAA-CPG using a variety of phosphonium or uronium coupling agents or soluble carbodiimides, namely, diisopropylcarbodiimide[116] and DMAP.[117]

6.11.7 Formation of Branchmers

During manufacture or storage of nucleoside-loaded support, the loss of protecting groups of the heterocyclic base can lead to impurities, called branchmers, in particular for cytidine (C) and adenine (A) nucleoside-loaded supports. Free or unprotected exocyclic amino groups, when exposed to the coupling conditions, will also react with the incoming phosphoramidite resulting in branching and eventually leading to a species having almost twice the molecular weight ($2n-1$).[118] In RNA synthesis, acidic triethylamine trihydrogen fluoride (TEA-3HF) is commonly used for the removal of the 2′-O silyl protecting group. This acidic reagent reacts during desilylation with the amidate group between the exocyclic amino and the first nucleoside after the branching point, cleaving the chain and resulting in the formation of a $n-1$ from the 3′-end carrying a 3′-phosphate group.[119] A capping step prior to the start of the synthesis would limit any free exocyclic amino moiety and thereby prevent 3′-terminal branching. However, any free 5′-hydroxyl group created by the loss of the dimethoxytrityl (DMT) group would be capped as well, resulting in yield losses.

6.11.7.1 Generation of $n-1$ (PS)/$n-1$ (PO) Impurities

$n-1$ impurities containing a 3′-terminal PS/PO group are formed when any unprotected functional group left on the support is able to react with a nucleoside-phosphoramidite. When using a nucleoside-loaded support, this would lead to an ON missing the 3′-base, (called $n-1$) from the 3′-end, since the 3′-nucleoside is part of the support. The $n-1$ would be connected to the support via a phosphodiester (PO, oxidation) or phosphorothioate bond (PS, sulfurization). The cleavage of such a bond will typically result in an $n-1$ impurity having a 3′-terminal phosphate or 3′-terminal phosphorothioate (3′-TPT).[120]

These impurities cannot easily be removed, and therefore, it is important that all functional groups remaining on the support are capped. Amino or hydroxyl groups of polystyrene supports usually react well with regular capping reagents. However, unreacted surface silanol groups of CPG are more difficult to cap and cannot be blocked with standard capping reagents. Silanol groups can be classified as "free" or "associated."[121] The associated form consists of two adjacent silanols with hydrogen bound to each other (vicinal) or a silanol with two hydroxyls located on the same atom (geminal). Associated silanols are reactive to trimethylchlorosilane (TMCS), while free silanols are more reactive toward hexamethyldisilazane (HMDS).[122] Repetitious silanization (monolayer conditions) or single silanization followed by a dual silanol capping treatment with TMCS and HMDS, can provide complete coverage of all silanol groups. The $n-1$ impurity from the 3′-end used to be a common side product in ON synthesis using CPG supports, because of the difficulties in capping free silanols. As standard capping reagents are unable to block free silanols, alternative means of capping using phosphorylation reagents such as diethoxy *N*,*N*-diisopropyl (DDP)[123] or bis-2-cyanoethyl-*N*,*N*-diisopropyl phosphoramidite followed by oxidation[124] have been suggested.

The loss of capping of the support can also occur during storage. Capping loss during storage or incompletely capped support will have the same result, 3′-($n-1$) impurities in the final ON. These 3′-($n-1$) impurities often contain a 3′-terminal thiophosphate or phosphate group. A capping step prior to the first synthesis cycle would prevent $n-1$ (3′-end) formation. While a simple capping step using acetic anhydride would efficiently cap free exocyclic amino groups of the heterocyclic base as mentioned earlier, it would be ineffective in capping free silanol groups of the CPG support. Also, any 5′-*O*-DMT-group lost during storage would be capped as well resulting in diminished yields.

$n-1$ impurities with 3′-terminal PS/PO are also formed when acid-labile nucleosides are loaded onto the solid support. For example, deoxyadenosine and, to a lesser extent, deoxyguanosine supports are prone to depurination at prolonged acid treatments during synthesis resulting in $n-1$ impurity.[125] The amount of N-glycosidic-bond cleavage is highly dependent on the nature of the base-protecting group. Classical protecting groups like benzoyl for adenosine and isobutyryl for guanosine are more sensitive to depurination than fast deprotecting groups such as alkyl formamidine or phenoxyacetyl and p-substituted phenoxyacetyl groups, with formamidine being the least sensitive. Linking adenosine via the exocyclic amino group to the support has been suggested to minimize the $n-1$ impurity.[125a] Then, an adenine loss due to depurination would result in the loss of the ON chain during synthesis; hence, no depurinated impurity would remain in the product.

6.11.8 Universal Supports

Solid supports without preloaded nucleosides are termed Universal support. These supports have several advantages over nucleoside-loaded supports. They do not suffer from the loss of base-protecting groups during storage or preparation. The formation of branchmers, depurinated species, $n-1$ with 3′-terminal PS/PO as described for nucleoside-loaded supports, can be avoided. Additionally, same universal support can be used for oligodeoxynucleotide and oligoribonucleotide synthesis. Many different universal supports have been developed over the years.[126] Today, the most widely used universal supports are UnyLinker[127] (**Fig. 8**) and Universal A-Support[128] (**Fig. 10**). UnyLinker was developed by Guzaev et al.,[127a] and its use was further refined by Ravikumar et al.[127b]

Two different variants of UnyLinker are available. The UnyLinker bicyclic ring system can be connected to the support either via the nitrogen of the maleimide group (type I) or through one of the hydroxyl groups of the diol (type II) (**Fig. 8**). The ON chain grows on the other hydroxyl groups of the diol. In the case of the type II support, the nitrogen of the maleimide group is typically protected by a phenyl group.[127b] Glen Research also offers a methyl-protected derivative called UnySupport[129] for high-throughput ON synthesis. During cleavage and deprotection (C&D), the vicinal hydroxyl group, protected during the synthesis by an acetyl group (type I) or connected to the support via a succinate (type II), is liberated and attacks the phosphodiester (oxidation)/phosphorothioate (sulfurization) group leading to the elimination of the 3′-OH ON.[127b] Incomplete cleavage of type II UnyLinker can lead to an impurity where the 3′-end of the ON is still attached to the UnyLinker via a phosphodiester/phosphorothioate group (**Fig. 9**). The majority of bicyclic impurity created during ammonia cleavage conditions has an additional mass of 261 (PO) or 277 Da (PS). If methylamine is used for cleavage of the support, the mass difference is 275 (PO) and 291 (PS). The bicyclic impurity represented in **Fig. 9** can further react with NH_4OH or NH_2Me, respectively, and open up the succinimide ring. This type of impurity can be avoided with the type II UnyLinker, in which the nitrogen of the maleimide group is connected to the support via a stable amide bond.[130] Incomplete cleavage of this type of UnyLinker would only lead to some yield loss; however, extending the cleavage and deprotection time would minimize any loss in yield.

The hydroxyl group of the diol system required for ON growth is typically protected with a DMT-group. As a secondary hydroxyl group, it is less reactive and more sterically hindered than the 5′-hydroxyl group of a sugar. Hence, its removal requires a longer exposure time to detritylation reagent, dichloroacetic acid (DCA), during detritylation. Once the trityl group has been removed, the resultant secondary hydroxyl moiety reacts more slowly to the incoming phosphoramidite. Both of these phenomena can lead to the formation of $n-1$ from the 3′-end, a common impurity found when using UnyLinker. However, these problems can be mitigated by extending the first detritylation step (or using 10% DCA solution) and extending the first coupling time.

The Universal A-Support was developed by Azhayev et al. and is available on both polystyrene and CPG supports [128] (**Fig. 10**). The cleavage and 3′-dephosphorylation reaction are facilitated by a solution of 4 M anhydrous ammonia in methanol. The labile dichloroacetyl group is cleaved prior to the β-elimination of the cyanoethyl protection group of the phosphate moiety. This is followed by the rapid intramolecular nucleophilic attack on the phosphotriester function by the hydroxyl group. This

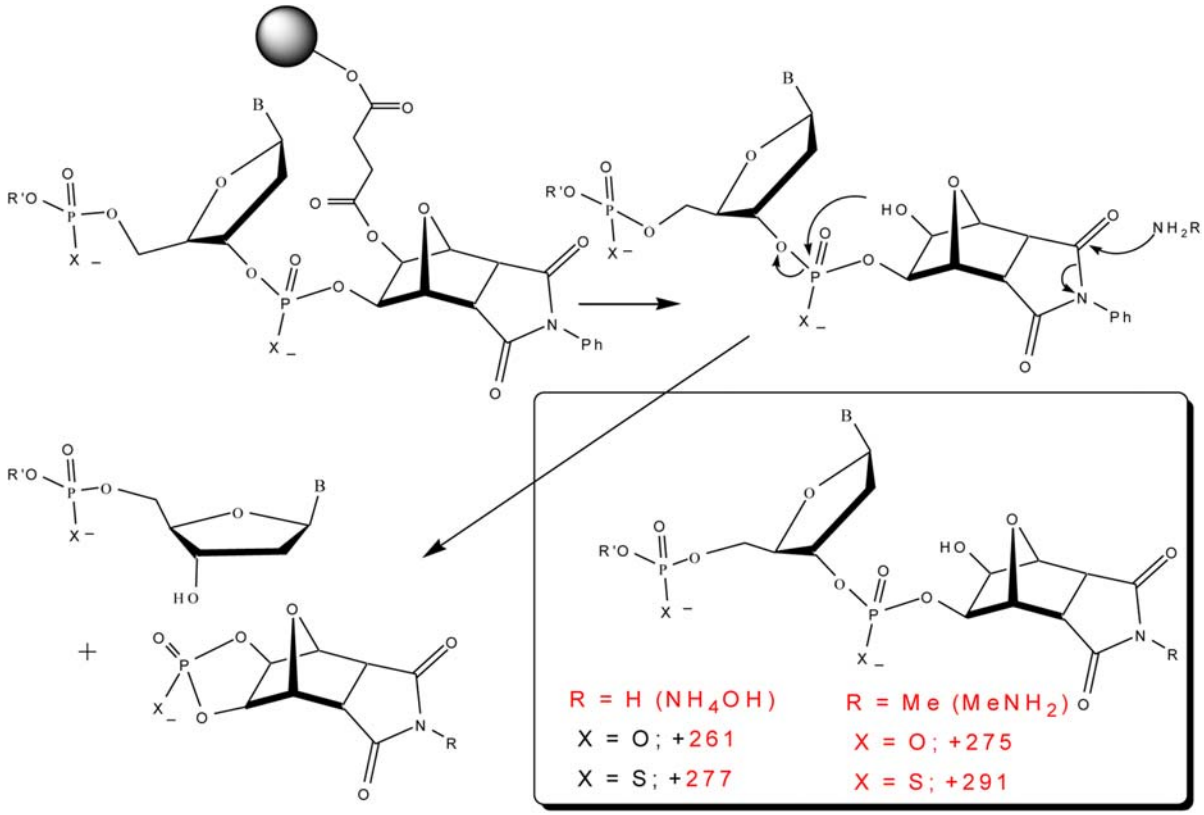

Fig. 9 Proposed mechanism for formation of bicyclic impurity.

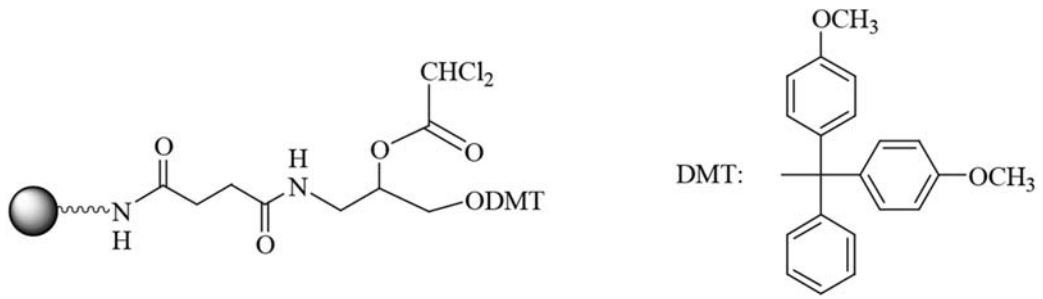

Fig. 10 Structure of Universal A-Support.

reaction is additionally assisted by the neighboring amide function. For a quantitative release of the ON from the support, it is critical that the dichloroacetyl group is cleaved prior to the cyanoethyl phosphate protecting group closest to the spacer of the support. Once the cyanoethyl group is cleaved, the hydroxyl group is not able to attack the phosphorus since it now represents a negatively charged phosphodiester function and the ON remains attached to the support. It therefore is important to use mildly basic conditions for the initial selective removal of the dichloroacetyl group. Universal A-Support is therefore not compatible with the base wash (e.g., DEA (diethylamine) wash) typically performed in large-scale ON manufacturing for the release of the phosphate protecting groups before initiating cleavage and deprotection, in order to minimize the formation of the CNET impurity.

After removing the solid support, further deprotection procedures typically employ addition of aqueous ammonium hydroxide to the solution of ON in methanolic ammonia and overnight heating at 55°C. A more easily accessible Universal A-Support was recently introduced where the succinylamido-linked support is replaced by a urea-linked support.[131]

6.11.9 Reagent-Related Impurities

6.11.9.1 Detritylation Reagent

Traditionally dilute solutions of trichloroacetic acid (TCA, pK_a 0.8) or dichloroacetic acid (DCA, p*K*a 1.5) in dichloromethane (DCM) were used as detritylation reagent for ON synthesis.[125b,132] Later, it was recognized that a high concentration of a weak acid (15% DCA in DCM) is more effective at driving detritylation toward completion than either a low concentration of a weak acid (3% DCA in DCM) or a low concentration of a strong acid such as 3% TCA.[132a] The high volatility (boiling point 40°C) of DCM and its high toxicity and carcinogenicity pose a health hazard for personnel and the environment in large-scale manufacturing of ONs. As a consequence in large-scale synthesis, DCM has been replaced with toluene, without compromising yield or quality of the synthesized ON.[133] Again, the amount of DCA in toluene appeared to be more effective at higher concentrations.[134] However, 3% DCA in toluene is still widely used in the industry as higher concentration of DCA may be more corrosive to the synthesizer and its components, which are typically made of stainless steel.

Increased exposure of ONs to acids leads to depurination, and therefore, the acid contact time needs to be controlled. The detritylation reaction is complex[125b,132] and the amount of acid needed depends on the type of support used and increases with the ON chain length and is therefore not constant. The trityl cation generated during detritylation has an intense yellow/orange color, and it has been used to determine the end point of the detritylation reaction using spectrophotometric methods. Using this approach, the acid contact time can be minimized/controlled without affecting trityl removal. Incomplete removal of trityl can lead to the formation of $n-1$ impurities. Commercial DCA has been found to contain trace amounts of chloral (trichloroacetaldehyde), which can react with free 5′-hydroxyl groups during the detritylation reaction resulting into an adduct with an added mass of 147 Da.[135]

6.11.9.2 Activator

No impurities are known to result from impurities present in the activator solutions. Activators work through an acidic-based mechanism involving nucleophilic attack. Activators work as an acidic catalyst, thus not only making the dialkyl amino group a better leaving group[136] but also replacing the amino group before reacting with the 5′-terminal hydroxyl.[137]

6.11.9.3 Thiolation/Oxidation

After coupling, the P(III) triester linkage formed is unstable toward acidic reagent and is therefore converted to a stable P(V) triester linkage before further chain elongation. The most prevalent oxidation reagent used in ON synthesis is a water-containing iodine solution. The composition of the oxidation reagent used in large-scale manufacturing is typically 50 mM iodine in 90% pyridine and 10% water.[138] Concentrations of iodine used in ON synthesis may vary from 20 to 100 mM, and oxidation reagent for small-scale synthesizers typically includes THF[97a] as a solvent. Sometimes, lutidine is used in place of pyridine.[139] THF is not compatible with some of the components of the pumps and valves of large-scale ON synthesizers prohibiting the use of THF in large-scale synthesis. Lower concentrations of iodine are used for oxidation in the case of sensitive base or backbone modifications. However, some modifications have been found to be unstable to oxidation with iodine-containing solutions, regardless of iodine concentration. Also, in phosphodiester (PO), phosphorothioate (PS) gapmer iodine tends to convert some of the PS bonds into the more chemically stable PO bonds resulting into an ON with a mass of 16 Da less than the desired product.

As the coupling step in ON synthesis is very moisture-sensitive, a nonaqueous oxidation reagent would be preferred to maintain a water-free environment during each step of the synthesis cycle. Low water iodine mixtures have been suggested for the synthesis of methylphosphonates to avoid side-product formation.[140] One nonaqueous oxidizer that has been used for both DNA and RNA synthesis is *t*-butyl hydroperoxide.[141] Peroxides, however, are unstable compounds and not suited for large-scale manufacturing. A very mild oxidation reagent useful for the synthesis of modified ONs has been recommended, which is 0.1–0.5 M (1S)-(+)-(10-camphorsulfonyl) oxaziridine (CSO) in anhydrous acetonitrile.[142] Recently several other nonaqueous and non-iodine oxidation reagents have been described.[124,143] Besides the disadvantages mentioned, iodine remains the oxidation reagent of choice for ON synthesis as other nonaqueous reagents are either expensive or unstable and therefore not suited and/or economical for large-scale synthesis.

During ON synthesis by the phosphoramidite approach, a phosphorothioate is introduced by oxidizing the phosphite triester using a sulfur transfer reagent. The first described sulfur reagent was elemental sulfur.[144] However, elemental sulfur is difficult to keep fully dissolved and is therefore not suitable for automated synthesizers. With phosphorothioate ONs being one of the most important modifications, a large number of efficient sulfurizing reagents have been developed over the years. These include tetraethylthiuram disulfide (TETD),[145] bis(*O*,*O*-diisopropoxy phosphinothioyl) disulfide (Stec's reagent),[146] 3*H*-1,2-benzodithiol-3-one-1,1,-dioxide (Beaucage reagent),[147] phenylacetyl disulfide (PADS),[148] 3-ethoxy-1,2,4-dithiazoline-5-one (EDITH),[149] 1,2-dithiazole-5-thione (xanthane hydride or ADTT),[150] 3-((dimethylamino-methylidene)amino)-3*H*-1,2,4-dithiazole-3-thione (DDTT),[151] dimethylthiuram disulfide (DTD),[152] 3-phenyl-1,2,4-dithiazoline-5-one (PolyOrg Sulfa or POS),[153] and various sulfonic acid derivatives.[154]

Initially, TETD was the most prevalent sulfurization agent. Later, TETD was replaced by Beaucage reagent due to TETD's slow reactivity in particular for RNA synthesis. While Beaucage reagent was more efficient with faster reaction kinetics, it was not very suitable for large-scale applications due to its limited stability in solution and also due to formation of phosphate diester impurity

during thiolation. PADS and xanthane hydride were found to be inexpensive, efficient, and fast-reacting sulfurizing reagents. Therefore, these two sulfurizing reagents prevail in large-scale manufacturing today. Reagents like DDTT and POS offer better stability and/or solubility and are currently being used in small-scale synthesis.

6.11.9.4 Capping Reagent

The capping reaction is a key step in ON synthesis and serves in preventing unwanted chain elongation. Hence, control of the capping conditions is vital to limit impurity levels. Acetic anhydride is the most common capping reagent. Historically, it was used as a mixture with 2,6-lutidine, tetrahydrofuran (THF), and 4-*N*,*N*-dimethylamino pyridine (DMAP), which acts as an acetylation catalyst.[97a] Recent studies[155] have shown that DMAP converts dG and dG-containing oligomers into fluorescent derivatives and in the presence of ammonium hydroxide converts further to 2,6-diaminopurine deoxyribonucleoside (2,6-DAP), a potentially mutagenic nucleoside analog. *N*-Methylimidazole (NMI) has been suggested as an alternative to DMAP, which does not undergo the same side reactions.[155] Today, NMI has replaced DMAP as capping catalyst in routine ON synthesis.

The protection of guanosine by the phenoxyacetyl group precludes the use of acetic anhydride as the capping agent. An exchange reaction occurs between the guanine phenoxyacetyl group and the acetyl group of acetic anhydride during the capping reaction. This impurity is quite stable toward standard cleavage and deprotection and can be detected by HPLC-MS and results in a mass of +42 Da. To avoid formation of this adduct, acetic anhydride can be replaced by phenoxyacetic anhydride[156] or trimethylacetic anhydride.[157] A similar adduct formation was observed for isobutyryl-protected guanosine when using acetic anhydride as capping reagent. Isobutyric anhydride was suggested to replace acetic anhydride for capping.[158]

During synthesis of phosphorothioate ONs, capping needs to be performed after sulfurization. If this reaction occurs after capping, higher levels of the phosphodiester impurity can be observed.[145] For phosphodiester ON synthesis, capping may be performed before or after oxidation.

Acetic anhydride cannot be combined with the acetylation catalyst prior to capping. Therefore, two capping reagents (Cap A and Cap B) are delivered during the synthesis from two different bottle positions, which are being mixed inline. One of the capping reagents contains NMI (or DMAP) and the other contains acetic anhydride. In addition, one of either reagent contains a base, either pyridine or lutidine. THF has been replaced with acetonitrile (ACN) in large-scale synthesis. However, neither NMI nor acetic anhydride is stable in combination with base in the presence of ACN. Therefore, in large-scale synthesis, three capping reagents are used: Cap A, containing 20% NMI in acetonitrile; Cap B1, containing 40% acetic anhydride in acetonitrile; and Cap B2, containing 60% lutidine in acetonitrile. Typically, Cap B1 and Cap B2 are mixed together prior to use.

Capping efficiency is another important factor and if uncontrolled can lead to low yields and increased impurity levels. The efficiency of capping is dependent on the nature and amount of the activating agent, for example, NMI or DMAP[159] in the capping mixture (**Table 1**). DMAP appears to be more effective as a capping activator relative to NMI, though it has fallen out of favor due to its tendency to lead to guanosine modifications (vide supra). To overcome these, Glen Research has introduced a phosphoramidite-based capping reagent called UniCap (**Fig. 11**), which is also well suited for H-phosphonate chemistry.

The activating agent, NMI, has been shown to contain low levels of trimethylhexahydrotriazine, which can react with nucleotides to form a +85 Da impurity.[33] The mechanism of formation of this impurity is thought to involve a Mannich-type reaction between the enolate anion of acetic anhydride and the imine formed from trimethylhexahydrotriazine (**Fig. 12**).

As discussed, capping based on derivatives of acetic anhydride appears to be more complicated and gives rise to more impurities than would be expected. Therefore, capping using a terminating phosphoramidite like UniCap (**Fig. 11**) was suggested not only for the capping of the support[123,124] but also for capping after each coupling step.[159]

6.11.10 Research-Scale Manufacture of Oligonucleotides

The overall manufacture of ONs can be generally broken down into four steps: solid-phase synthesis, cleavage and deprotection (C&D), chromatographic purification, and downstream isolation. As mentioned earlier, the laboratory-scale synthesis of ONs is commonly achieved through the widely accepted phosphoramidite approach in the solid phase.[96,97,160] During solid-phase synthesis, phosphoramidite monomers are reacted sequentially onto a solid support in efforts to generate the full-length ON desired. The manufacture of an ON carrying 20 residues generally requires about ~80 iterative reactions. Following synthesis, the C&D step releases the ON from the solid support and removes the requisite synthesis protecting groups. This step is generally

Table 1 Comparison of capping mixtures (Glen Research)

Synthesizer	*Cap A solution*	*Cap B solution*	*Capping efficiency (%)*
Expedite	THF/Ac_2O (9:1)	10% NMI/THF/Py (8:1)	90.5 ± 1.9
ABI 394	THF/Pyr/Ac_2O (8:1:1)	10% NMI/THF	88.8 ± 2.5
ABI 394	THF/Lut/Ac_2O (8:1:1)	10% NMI/THF	89.1 ± 2.0
ABI 394	THF/Lut/Ac_2O (8:1:1)	16% NMI/THF	96.6 ± 1.4
ABI 394	THF/Lut/Ac_2O (8:1:1)	6.5% DMAP/THF	99.4 ± 0.3
All	UniCap	NA	98.6 ± 0.4

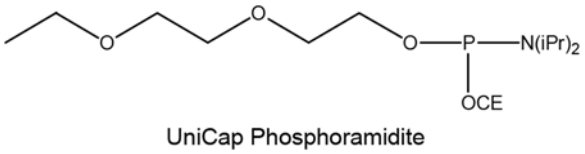

UniCap Phosphoramidite

Fig. 11 Structure of phosphoramidite capping reagent, UniCap.

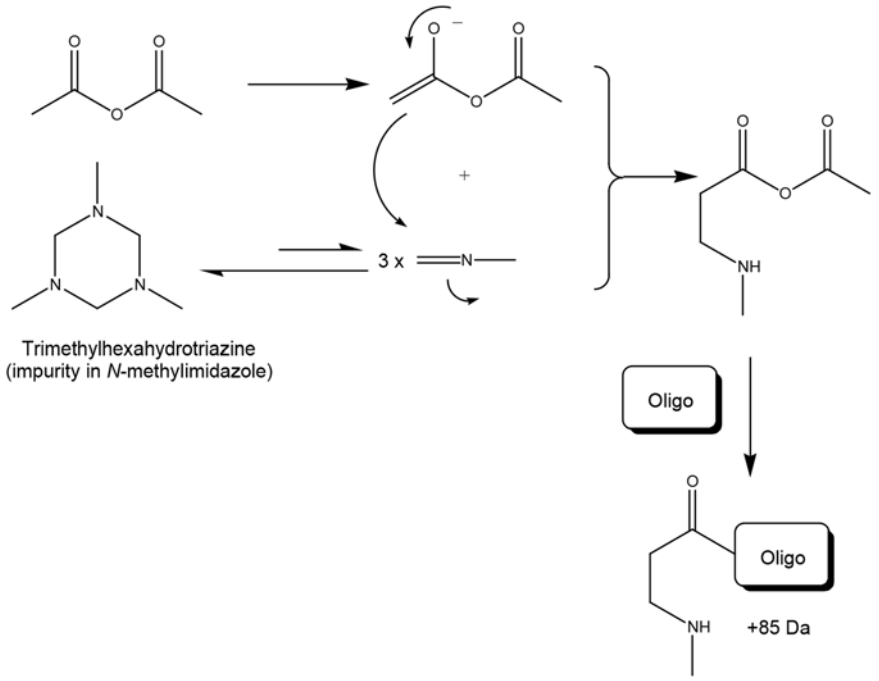

Trimethylhexahydrotriazine
(impurity in *N*-methylimidazole)

Fig. 12 Postulated mechanism for the generation of NMI-based +85 Da impurity. According to ISIS talk (Andy McPherson, Tides 2014) the adduct sits on N(3) of T: $CH_2N(CH_3)C(O)CH_3$.

performed in batch mode where the entirety of the solid support manufactured is reacted with deprotection solutions in a reactor. The crude material generated is then purified generally using chromatographic purification to isolate full-length ONs from their related impurities. Finally, isolation through desalting and further lyophilization yields pure ON solid material.

6.11.10.1 Oligonucleotide Solid-Phase Synthesis Cycle

The solid-phase synthesis cycle for the manufacture of ONs can be generally performed in four iterative steps (Fig. 2). Initially, a solid support carrying the first nucleosidic residue is placed on a solid support housing to ensure the requisite anhydrous conditions. As discussed, there are alternative supports for ON manufacturing, most notably the UnyLinker support, which can be used. Their use is similar to base-loaded supports for synthesis but poses challenges during C&D as discussed later in this review. In either case, the support is then treated with 3–10% DCA in either DCM or toluene (i in Fig. 2) to remove the most commonly used DMT-protecting group. The newly released hydroxyl group is then free to react in the subsequent step with the next desired residue in the ON sequence. The next residue is added as a phosphoramidite monomer that is mixed with an activator (to facilitate the reaction) just prior to its addition to the solid support (ii in Fig. 2). Commonly, activators such as tetrazole, 5-ethylthio tetrazole, 4,5-dicyanoimidazole, and benzylthiotetrazole are used. The newly formed phosphotriester (P^{III}) is not sufficiently stable for the remainder of the synthesis and thus is generally oxidized (iii in Fig. 2) to a phosphate triester (P^{V}) using an aqueous iodine solution in either pyridine or pyridine/tetrahydrofuran mixture (X = O in Fig. 2). If a phosphorothioate is desired (X = S in Fig. 2), incubation with a solution of phenoxyaceticdisulfide (PADS) in acetonitrile or xanthane hydride (XH) in pyridine is commonly used to yield the desired P–S bond. Before restarting the next cycle, nonreacted species are terminated by the use of either acetic anhydride or isobutyric anhydride in the presence of NMI in acetonitrile (iv in Fig. 2). This re-masks the nonreacted hydroxyl to prevent further growth in the subsequent coupling cycles. Repeating the four steps (detritylation, coupling, oxidation, and capping) iteratively can generate ONs in the $1–100^{+}$ range.

The fastidious process of solid-phase ON synthesis can be simplified by the use of solid-phase synthesizers that are available from several manufacturers (Table 2). The use of these synthesizers has allowed for the fast synthesis of ONs where a 20-mer

Table 2 Commercially available oligonucleotide synthesizer models

Synthesizer	*Throughput*	*Manufacturer*	*Support housing type*	*System pump type*	*Reagent ports*	*Amidite ports*	*Number column ports*	*Synthesis scale (μmol)*	*Monitoring capabilities*	*Pros*	*Cons*
12-column	Medium	Polygen GmbH	Slider block	Piston pumps	3	8	10	0.001–5	UV	No pre-packed columns required. Simple maintenance due to design. Low amidite consumption	Fastidious support loading and unloading. Sliders need to be maintained well to avoid leakage
96-column Workstation	High				6	6	96	1–5			
ABI 392	Low	Applied Biosystems	Luer Column	Ar gas	8	8	4	0.04–15	None	Stand alone. Fast cycle time. Options for automatic amidite dilution and online cleavage	Closed Frame. Limited monitoring. Product discontinued with limited access to parts and support
ABI 394/3400	Low				8	5 or 8	2 or 4		Trityl (optional)		
Expedite 8905/ 8909	Low	Perceptive Expedite			6 or 8	5 or 9	2	0.050–15	Trityl (optional)	Fast cycle time	
ABI/Biolytic 3900	Medium	Biolytic Lab Performance	Pipette-Tip		11	14	4 × 12	0.04–1	None	Open Frame. Low amidite consumption	Limited monitoring. Requires Ar chamber purge and blanket
Dr. Oligo 48	Medium				11	18	4 × 12		UV		
Dr. Oligo 192/ 768	High		Open plastic column		11	23	192/768	0.001–2			
Dr. Oligo 768	High							0.04–1			
Mermade 4	Low	Bioautomation			9	10	4	0.020–5		Semi-Open frame. Low amidite consumption	Limited monitoring. Requires Ar chamber purge and blanket. Reagent ports clog easily
Mermade12	Medium				9	20	12	0.020–200			
Mermade 192X	Low				9	30	192	0.020–5			
AKTA OP10/ 100	Low	GE Healthcare	Closed ss and glass columns	Piston pumps	12	12	7	1–9000	UV (3λ in parallel), Conductivity, Pressure, Flowrate	Closed system amenable to CIP. Allows for reagent recirculation. UNICORN software allows for thorough synthesis data analysis. Very precise amidite and reagent delivery	Requires larger synthesis scale. Large dead volumes

DNA strand can be synthesized in ~4–5 h. The choice of synthesizer is generally dictated by the level of throughput desired. Table 2 presents instruments with low (1–4 concurrent syntheses), medium (5–50^{+} concurrent syntheses), and high (96–768^{+} concurrent syntheses) throughput. The second consideration is the type of chemistry required, which generally dictates the number of amidite or reagent ports necessary. Generally, the preparation of ON primer DNAs only requires a few ports, while the synthesis of heavily derivatized API candidates would require more available ports. The commercially available synthesizers range between 5 and 30 amidite ports and between 3 and 12 reagent ports. The third consideration is synthesis scale range. The different available synthesizers can fall in one of the four general categories: small research scale (0.001–2 μmol), medium research scale (0.020–5 μmol), large research scale (0.050–15 μmol), and lab-scale manufacturing/modeling scale (1–9000 μmol). Although a synthesizer can be selected based solely on the above categories, an additional consideration must be evaluated. Generally, small-scale synthesizers have limited monitoring capabilities if any (i.e., only UV or conductivity), while larger scale synthesizers have multiple monitoring capabilities. Although generating DNA primers might not require diligent monitoring of the synthesis, API candidate synthesis and small-scale modeling prior to large-scale manufacture require diligent monitoring in efforts to optimize the synthesis cycle and prevent the formation of unwanted impurities.

Although the solid-phase synthesis of ONs can generate materials of high purity, there are several major impurities that can be formed if improper cycle conditions are used. A comprehensive review by Cramer et al. summarizes ON impurity formation in detail.[161] The impurities mentioned range from simple termination sequences ($n-1$, $n-2$, $n-3$, etc…) due to process inefficiencies to complex adducts. Given that process inefficiency impurities warrant their own review and most are broadly understood, this review will focus on impurities that can be affected by improper small-scale modeling and improper instrument setups, which are discussed later in this review. Depuration generally occurs in acidic conditions such as during detritylation where the glycosidic bond connecting the sugar and the nucleosidic base is broken.[162] This process generally affects purines, which carry an imino group at position 7 of the nucleosidic base. Nucleosidic base loss generates what is called an abasic site (Fig. 13). These abasic sites are known to be generally unstable and quickly breakdown resulting in ON-strand breakage. Thus, depurination not only results in an abasic site but also can lead to increased levels of failure sequences.

Another common impurity that carried over to the final ON arises from incomplete oxidation/sulfurization where the P^{III} center is not oxidized/sulfurized to the P^{v} center during the oxidation/thiolation step. As this center is sufficiently stable during capping conditions, the impurity carries over to the following detritylation step. During detritylation, release of the DMT^{+} cation and subsequent attack by the P^{III} center can result in a DMT-phosphate formation[162c,163] (Fig. 14). The formed DMT-phosphonate impurity generally elutes long after the full-length product (FLP) by reversed phase chromatography and could carry over to the final API if purified by other means.

A very common impurity generated during deprotection is the formation of a cyanoethyl (CNEt) adduct.[112,164] This impurity is generated when the CNEt phosphate protecting group is released by the C&D reagent as acrylonitrile. This highly reactive molecule is known to add to the N^{3}-position of thymidine (Fig. 15). To prevent the formation of this impurity, generally, an amine wash is

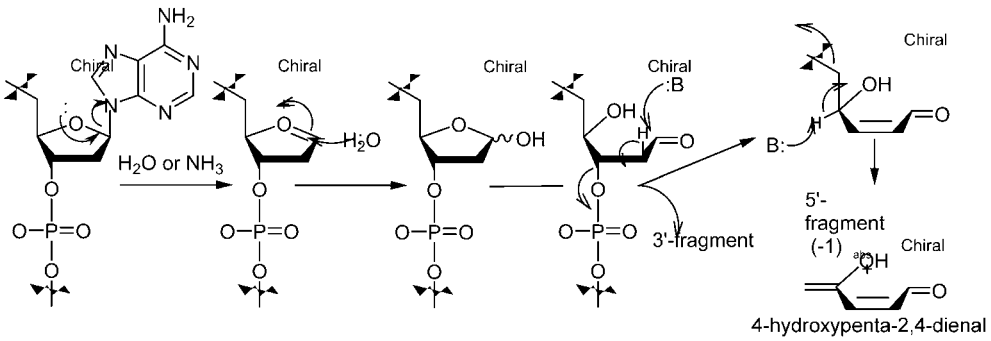

Fig. 13 Depurination of deoxyadenosine followed by strand cleavage via postulated β-elimination

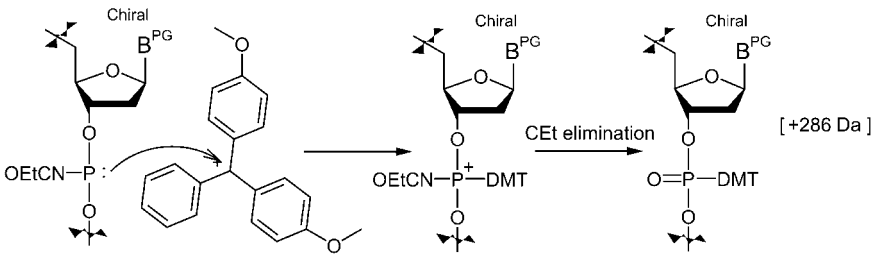

Fig. 14 Postulated mechanism of the DMT-phosphonate formation following inefficient oxidation/sulfurization.

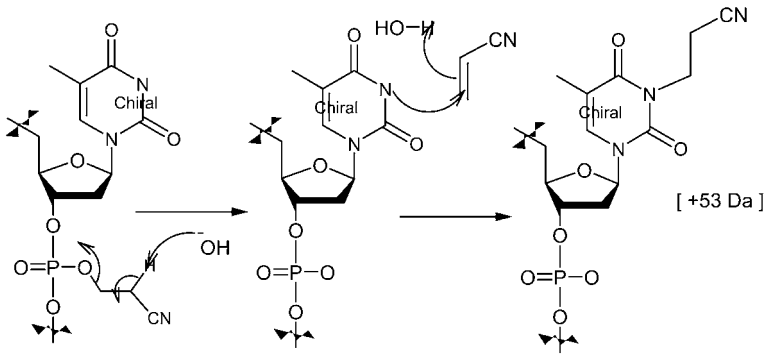

Fig. 15 Postulated mechanism of the formation of the CNEt adduct.

performed at the end of synthesis and prior to the C&D to selectively remove the phosphate protecting groups, while the ON is still attached to the solid support. The physical separation of phases is generally sufficient to prevent the adduct formation.

However, a second impurity can be formed during C&D due to the final amine wash around the phosphorous center. As the final amine wash releases acrylonitrile, P–S-containing residues are particularly susceptible where the CNEt is known to add to the sulfur in the phosphorothioate moiety. Further, this impurity is postulated to be susceptible to nucleophilic attack by a hydroxide, which can be resolved by the release of 3-mercaptopropanenitrile and conversion of the phosphorothioate to a canonical phosphate[165] (Fig. 16).

6.11.10.2 Oligonucleotide Cleavage and Deprotection

ON C&D, as mentioned before, releases the ON from the solid support used during synthesis and removes requisite synthesis protecting groups (Fig. 17). This process is generally carried out in batch mode where the entirety of the solid support manufactured is incubated with C&D reagents. Following deprotection, the spent ON support is filtered and the crude solution recovered.

As mentioned earlier, the reagent choice for C&D has historically favored amine bases, which are routinely used for deprotection (Table 3). Specific reagent choice in this step of manufacture is heavily dictated by the modifications present in the ON. Although DNA primers are amenable to practically any deprotection reagent, certain sensitive modifications require mild conditions. As a general guidance, the C&D conditions to be used are dictated by the most sensitive residue in an ON. Of note, these sensitive modifications often place requirements on the other residues' protecting groups, that is, "fast"-deprotection groups in the case of mild deprotection reagents.

In the case of RNA manufacture, an additional reaction is required to yield the naive RNA. Although, there are alternative technologies developed for 2′-protection;[166] most generally, the 2′-OH of the naive ON is masked with a 2′-*O*-*tert*-butyldimethylsilyl protecting group for synthesis[92,101,102,160a,160c] (Table 4). This protecting group is base stable and thus survives C&D. Therefore, the second step, dubbed desilylation, removes the silyl protecting group. This is generally achieved by the addition of a fluoride reagent in either acidic media or anhydrous conditions to prevent ON degradation. With the use of acidic TEA·3HF reagent, the intermediate ON is not readily soluble in water once the internucleotide phosphates are protonated; therefore, the use of DMSO or similar cosolvents is essential for complete deprotection.

There are several general C&D-related impurities that can be obtained when using improper C&D conditions. As with synthesis, the review by Cramer et al. also summarizes ON impurity formation during C&D in detail.[161] For the purposes of this review, only those impurities that can be affected by improper small-scale modeling and improper instrument setups, which are discussed later in this review, will be reevaluated. As depicted in Fig. 13, depurination can occur with the use of C&D reagents. However, an

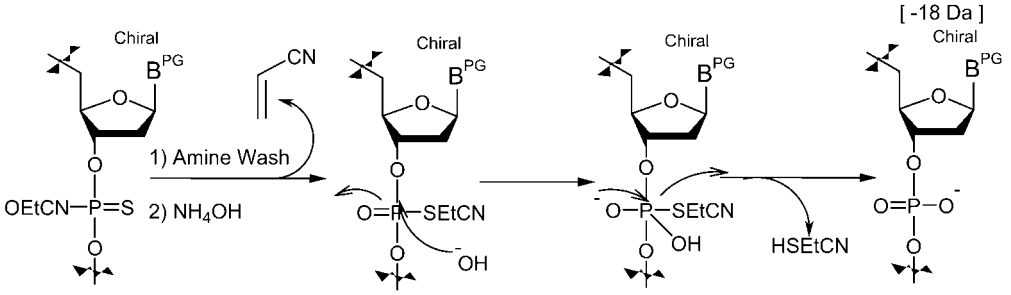

Fig. 16 Proposed mechanism for the loss of sulfur during C&D.

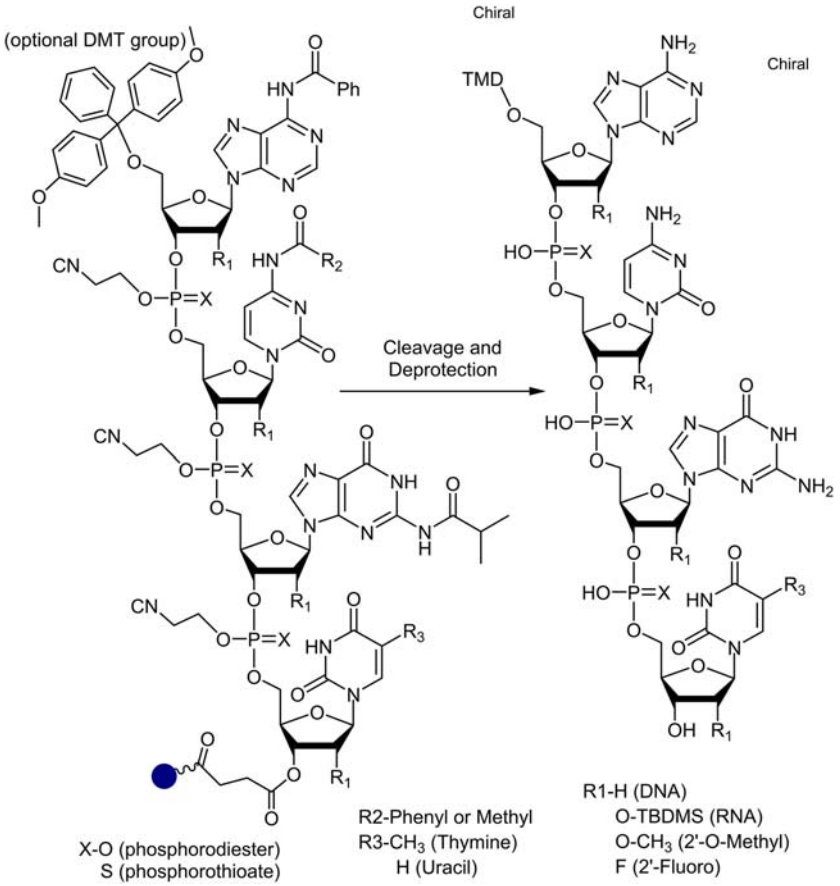

Fig. 17 Oligonucleotide C&D.

additional depyrimidination is prevalent when using ammonia reagents, particularly AMA. The partial and complete loss of the thymidine and uracil moieties due to ammonia can yield a partial ("urea" form) or complete abasic site[167] (**Fig. 18**).

An additional impurity generated from the use of AMA is the transamination of cytidine when a benzoyl protecting group is used for the nucleobase[168] (**Fig. 19**). However, the use of the acetyl protection was found to not lead to the impurity.

Some 2′-modifications, like in the case of RNA or 2′-F, are particularly susceptible to degradation. It is widely known that RNA ONs, carrying a naive 2′-OH, are susceptible to internucleotide strand breakage in the presence of base. Abstraction of the 2′-OH proton by a neighboring base leads to the SN2 attack to the internucleotide phosphate, which through a trigonal bipyramidal intermediate releases the neighboring 5′-OH resulting in strand breakage[169] (**Fig. 20**).

For 2′-F ONs, although strand cleavage is not possible as the 2′-fluoride is not a good nucleophile, an alternative reaction is possible in the case of pyrimidines. The attack of exocyclic electrons to the pyrimidine ring causes a rearrangement of the electron cloud, which can lead to nucleophilic attack on the 2′-position. As the fluoride is a good leaving group, the residue readily adopts the 2′-anhydro configuration. Further, hydrolysis of this structure is known to generate the arabinose final impurity[170] (**Fig. 21**).

6.11.10.3 Oligonucleotide Purification

The purification of ON crude solutions is generally achieved by chromatographic methods.[171] An intermediate desalting operation can be performed prior to purification by simple ON precipitation or by using commercially available desalting solid supports or filtration membranes (discussed later in this report). The choice of chromatographic type and its associated setups heavily relies on the expected ON use. Although ON primers require little to no purification, therapeutic ONs require extensive chromatographic purification to ensure that a high-quality API is manufactured. **Table 5** summarizes the most widely used modes available for ON purification. As the sheer number of electrophoresis boxes and HPLC equipment available to carry out laboratory-scale purification warrants its own report, this review will only focus on the choice of purification support. The use of gel electrophoresis to purify ONs dates back to their applications in biochemistry.[172] As such, the use of agarose and polyacrylamide gels provides a straightforward approach to purifications based mostly on rough size discrimination. Although this is generally acceptable for ON primers and other simple applications, this approach is not generally acceptable for API manufacturing. Taking advantage

Table 3 C&D reagents

Reagent choice	*Incubation temperature (°C)*	*Incubation time (h)*	*Special considerations*	*Additional comments*
Ammonium hydroxide	r.t.—65	2–16	Lower temperature and shorter time should be considered in combination with Pac-A, iPr-Pac-G, Ac-C monomers for base sensitive modifications such as Cyanine Dye derivatives, and BHQ quenchers	
NH_4OH/EtOH (3:1)	Similar to Ammonium Hydroxide		Similar to ammonium hydroxide, recommended for C&D with polymer-based solid supports	
AMA-Ammonium hydroxide:Methylamine (1:1)	r.t.—55	0.2–3	Fast deprotection conditions that require use of Ac-C monomer. Bz-C or Bz-5Me-C monomer would lead to increased amount of N4 transamination by product	Not recommended for most fluorescein analogs. Generates an impurity that does not exhibit absorbance in the visible region
Methylamine	r.t.—35	0.2–3	Fast deprotection conditions. Generates significant levels of N4 transamidation with Bz-C or Bz-5Me-C monomer	
EMAM-Ethanolic AMA	Similar to AMA		Similar to AMA but optimal for long RNA oligos	
Ammonia or Methylamine gas	variable	1	Requires specialty equipment	
0.05 M K_2CO_3 in MeOH	r.t.		Need Pac-A, iPr-Pac-G, Ac-C monomers, (Pac2O) capping reagent. Recommended for oligos with base sensitive modifications	
0.4 M NaOH in MeOH/H_2O (4:1)	80	~0.2	Recommended for Acridines or Carboxylates containing oligo	Generates sodium salt. Can be performed without pressure issues
t-butylamine/MeOH/H_2O (1:1:2)	55	17–20	Recommended for TAMRA derivatives	
t-butylamine/H_2O (1:3)	60	6		
30–50% Ethylene diamine in EtOH	25	0.5–1	Recommended for P-ethyl derivatives	Generates a low level of ethyl loss

of the internucleotide phosphate, anion-exchanged and ion-paired reversed-phase chromatographic purifications on HPLC equipment are widely used for the purification of ON APIs.

The use of the anion exchange technique[171a,171d,171g,173] (particularly with Q Sepharose and TSK Gel resins) ensures that fine separation between ONs and their closely related $n-1$, $n-2\cdots$ and $n+1$, $n+2\cdots$ sequences, and even PO impurities for phosphorothioates are discriminated. Additionally, as the elution is generally performed with sodium salts, the process in turn ensures that synthesis- and C&D-related counterions are removed, and the purified ON is isolated in its desired sodium form. On the other hand, the use of IP-RP approaches ensures that not only charge-based residues but also charge-neutral lipophilic impurities are

Table 4 Desilylation conditions

2′-protecting group	*Reagent choice*	*Incubation temperature (°C)*	*Incubation time (h)*	*Additional comments*
Tertbutyldimethylsilyl (TBDMS or TBS)	TBAF in THF	r.t.	9–17	Requires anhydrous conditions, useful for triphosphate containing oligomer
	TEA-3HF	40–60	2–3	
Triisopropylsilyloxymethyl (TOM)	TBAF in THF	r.t.	9	No degradation expected after 50 h
	TEA-3HF	65	2–3	
Ethylene glycol monoacetate orthoester (ACE)	100mM AcOH:TEMED pH 3.8	60	1	Requires specialty synthesis conditions
Pivaloyloxymethyl (PiVOM)	Ammonium hydroxide	r.t.	3	Requires evaporation to facilitate formaldehyde loss and can form a formaldehyde adduct to G residues
ortho-nitrobenzoyl (*o*-NBz) and derivatives	λ at 280–350 nm	r.t.	1–3	Requires specialty equipment
Thionocarbamate (TC)	Neat Ethylenediamine	r.t.	2	High Amidite cost due to patent protection

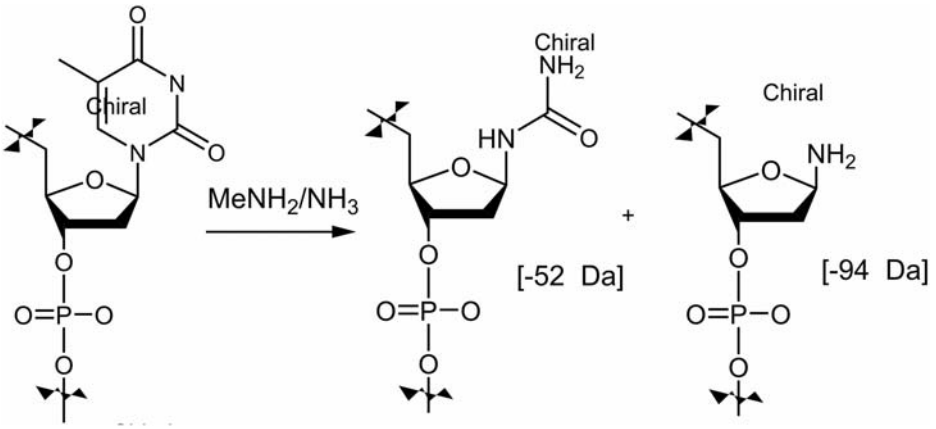

Fig. 18 Partial and complete depyrimidination of thymidine.

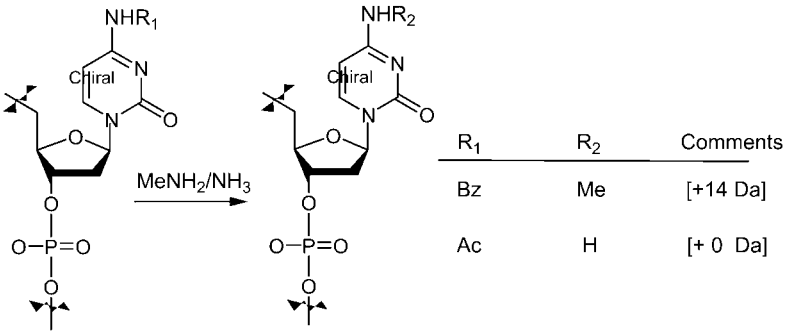

Fig. 19 Transamination of N-Bz cytidine.

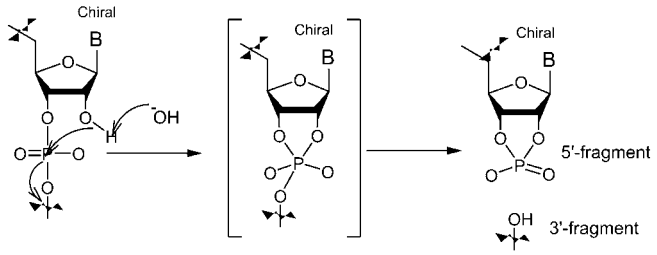

Fig. 20 RNA internucleotide strand breakage in base.

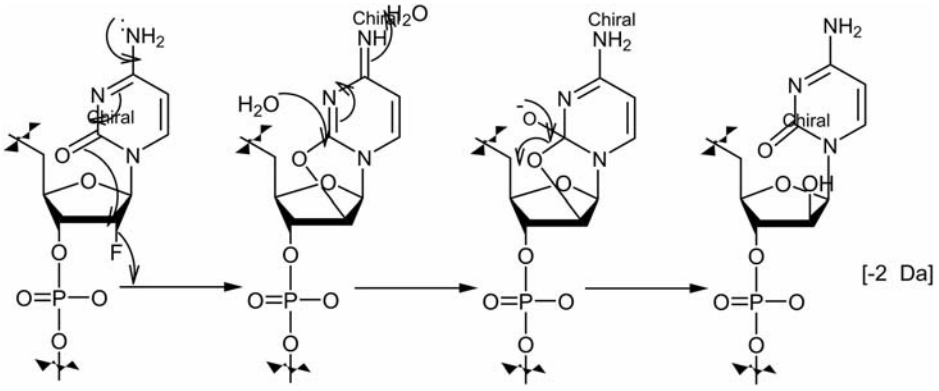

Fig. 21 Defluorination of cytidine.

Table 5 Chromatographic purification of oligonucleotides

Purification type	*Oligo Crude requirements*	*Eluent system required*	*Oligo counterion after purification*	*Name*	*Manufacturer*	*Solid support type*	*Particle size, um*	*Pressure rating, psi*	*Exchange ligand*	*Comments*
Electrophoresis	Aqueous buffer	TBE buffer with Urea	Mixed	PAGE or Agarose GE	Various	Cross-linked acrylamide or agarose	N/A	Low	Matrix	Urea usage not amenable to therapeutic use
Anion Exchange	Low crude conductivity	Sodium Phosphate buffer/ Sodium Hydroxide with NaBr/NaCl	Sodium form	Q Sepharose FF	GE Healthcare	Cross-linked Agarose	45–165	30	Quaternary Ammonium	General application capture resin with good recoveries and yield
				Q Sepharose HP	GE Healthcare	Cross-linked Agarose	34	40	Quaternary Ammonium	
				Source 30Q/15Q	GE Healthcare	Polystyrene divenylbenzene	30/15	300	Quaternary Ammonium	High loading polishing resin with near quantitative recovery
				TSK Gel SuperQ-5PW	Tosoh Bioscience	Polymethacrylate	30/20	300	Quaternary Ammonium	Medium loading polishing resin with strong anion exchange characteristics
				TOYOPearl GigaCap	Tosoh Bioscience	Polymethacrylate	35	40	Quaternary Ammonium	
				Oligo-WAX	Phenomenex	High-purity Silica	10	–	Quaternary Ammonium	Ammonia ligand deprotonates at pH 9
Reversed Phase	Low organic content	TEAAc with ACN/EtOH	TEA	Oligo-RP	Phenomenex	Silica Organic Composite	10	–	C18	
				Triart C18	YMC America	Silica Organic Composite	10–20	–	C18	
				Source 30/15 RPC	GE Healthcare	Polystyrene divinylbenzene	30/15	300	Matrix surface	Good loading and recovery
				Oligo R3	Thermo Scientific	Cross-linked poly-divinylbenzene	30	300	C18	Loading and recovery are generally low
				Amberchrom XT30/ 20	Dow Chemicals	Polystyrene divenylbenzene	30/20	300	C4	
				TSK gel Phenyl-5PW	Tosoh Bioscience	Polymethacrylate	10 to 20	300	Phenyl	
				PRP-C18	Hamilton Company	Polystyrene divenylbenzene	10	>1000	C18	
Multimodal Phase	Low organic/ Low conductivity	AEX or RP buffers	Variable	CaptoAdhereImpress	GE Healthcare	Highly cross-linked Agarose	75	40	N-benzyl-n-methyl ethanolamine	
				Zeosphere DRP, attraction/ repulsion	Zeochem	Silica	10	–	C18/8/4 and quaternary ammonium	

discriminated.[174] However, as IP-RP chromatography requires the use of a counterion, generally triethylamine, an additional salt-exchange step is required to yield the purified ON in its sodium form. Further, the purification power of both techniques can be harnessed in the use of anion-exchange resins, which at their core carry slightly lipophilic matrices (Source 15Q). This is currently a trend where now fully multimodal purification resins are being developed for finer purification discriminatory potential.

Alternative considerations for purification resin choice are reusability, safe pH range, operational backpressure, purification loading, and recovery. Resin reusability plays a big part of fixed purification systems that would handle heavy purification schedule workloads. This factor is mostly determined by the resin type and attachment chemistry. Although attachment chemistries are generally proprietary, polymeric supports like styrene and methacrylate are generally accepted as more reusable when compared with silica supports. Safe pH range is a consideration when strict GLP practices are in place, which require heavy cleaning schedules, for which the trend generally follows reusability. Operational back pressure is generally a consideration in semiprep HPLC systems that can have prohibitive pressure limits. For this consideration, smaller-sized beads are generally observed to exhibit higher operating pressures. Further, disparate choice of purification support nature to selected eluents (i.e., aqueous buffers on silica-based resins) also exhibits high operational back pressure. However, for all laboratory-scale purifications, operational backpressure is seldom an issue. Purification loading and recovery are an important consideration when dealing with high-throughput applications. Generally, IP-RP resins have lower loading limits and generally exhibit lower recoveries than their anion-exchange counterparts. Given all the considerations, purification resin choice is highly sequenced and application-dependent with additional considerations like available equipment setups playing an important part in the final decision.

6.11.10.4 Oligonucleotide Isolation

Following purification or if purification was not performed, following C&D, downstream isolation is performed by simple ON precipitation or by using commercially available desalting solid supports or filtration membranes (**Table 6**). The choice of approach heavily depends on the manufacturing scale and the expected application. By far, the most widely used isolation method in research-scale applications is the use of precipitation using sodium salts (generally acetate) and alcohols (generally ethanol for DNA and isopropanol for RNA sequences). The use of this approach in research scale is generally straightforward and does not require significant equipment investment. However, the conditions need to be optimized in order to maximize yield and to avoid the coprecipitation of salt in the final product. For this, the conditions are significantly varied with ON type, length, and concentration. A more elegant approach at research scale is the use of desalting columns. For this, generally, three approaches are used. For the first approach, the use of reversed-phase media (Pierce™ columns from Thermo or SepPak® columns from Waters) allows for the desalting of ONs by adhering them to a C18 or similar lipophilic media with the use of an ion-pair reagent (generally triethylamine—TEA). Following binding, a water rinse is performed to effectively desalt the ON bound on the support. Final elution is performed with a volatile organic solvent (generally acetonitrile), which then is removed through lyophilization. However, through this approach, the TEA salt of the ON is obtained. For the second approach, a cation-exchange resin is used to trap the counterion salt itself, while the unbound ON flows through in the effectively desalted water (PD 10 or NAP 25 columns from GE). This approach yields an ON of whatever salt state was loaded onto the column. These two approaches can be performed in a matter of minutes with minimal equipment investment but require the use of disposable specialty columns. The third approach uses a spin filter, which is used to concentrate a particular sample using an appropriately sized filter (Ambicon® filters from Millipore). Repeated water additions and concentrations can lower the effective salt concentration significantly. This approach is time-consuming and generally does not result in good recoveries. A similar but more optimized method for ON isolation and one more adapted to API manufacturing is the use of tangential flow filtration (TFF). This approach also employs an appropriately sized filter membrane (membranes available from Pall or Millipore) but now uses a pump to circulate the sample through the TFF setup making the process more efficient (**Fig. 22**). For TFF, a sample placed in a feed vessel is fed against the membrane holder, which houses an appropriately sized membrane filter. Given a feed pressure higher than the osmotic pressure of the solution, the salt solution passes through the membrane's pores, while the ON is diverted back to the feed vessel. As the solution concentrates,

Table 6 Oligonucleotide downstream isolation

Method	*Ease*	*Specialty equipment requirements*	*Manufacturer*	*Scale*	*Isolated ON form*	*General application*
Precipitation	+++	Centrifuge	N/A	Varies	Na form (excess NaOAc salt)	General lab and some API manufacturing
RP desalting columns	+	C18 SepPak® or similar columns and centrifuge	Waters	Research	TEA form	General lab application
Salt-exchange columns	++	Nap-25®or similar columns and centrifuge/HPLC	GE Healthcare	Research	Same salt form as loaded	
Spin filters	+	Ambicon® or similar columns and centrifuge	EMD Millipore	Research		
Tangential flow filtration	+	T-series® membranes and TFF set up	Pall	Larger scale API manufacturing		API manufacturing

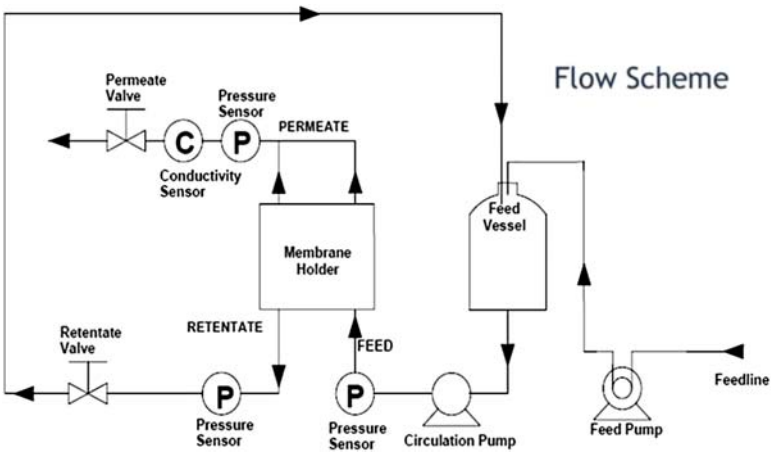

Fig. 22 Tangential flow filtration schematic.

concerted addition of purified water effectively desalts the solution. The main drawback of this approach is the requirement of a large solution volume due to the system void volume.

Following desalting, the ON either isolated or reconstituted in purified water can be used directly for its intended application or isolated as powder through lyophilization. The choice of lyophilization equipment is generally based on the size of batch needed to be processed as a single batch. As this is not generally prohibitive in research scale, further considerations on lyophilization equipment choice are discussed later in this report.

6.11.11 Manufacturing Process and Equipment for Oligonucleotide Used as Therapeutics

The increase in demand for pharmaceutical-grade ON quantities has been accompanied by the development and innovation of cost-effective manufacturing technologies. As discussed earlier, ON synthesis quality has been improved by using raw materials with the highest purity specifications possible. At the same time, yields and throughput have been increased by the introduction of high-loaded polymer supports like NittoPhase™. Therapeutic oligo manufacturers have also developed and optimized technologies that allow them to access ONs with a wide variety of chemistries. However, the manufacture of ONs in the 50 g to kilo scale and beyond is still not trivial.

As has been discussed in Research-scale manufacture of oligonucleotides section above, the ON-manufacturing process consists of five to six major steps depending on the type of oligo being manufactured. Of these, the synthesis step is the most complex and requires the use of sophisticated equipment with their associated control software. The key steps for large-scale ON manufacturing are shown in Fig. 23. During manufacture, each of these steps uses specifically designed equipment with associated in-process controls (IPC) to ensure batch reliability and ON quality.

6.11.11.1 Oligonucleotide Synthesis Equipment

Table 2 delineates the commercially available ON synthesizers that are routinely used for research scale/grade synthesis. Among equipment manufacturers, only GE has synthesis skids from the μmol scale (ÄKTA oligopilot 10/100) to 5 mole (OligoProcess) scale. OligoProcess and Oligo Process Industrial systems are generally custom-built and can be tailored to meet the end user's needs. As such, each individual system is customizable to operate within a dynamic range of ~10, that is a system with a maximum scale of 1000 mmol has a lower end of 100 mmol and so on. The advantage of GE systems is that they all employ the same "flow-through column" technology and are controlled by the versatile UNICORN software. This allows for seamless scale up from the ÄKTA oligopilot plus. For mid-scale production runs (10–50 mmol), GE has the OP400 system which bridges the gap between the ÄKTA instrument and the OligoProcess equipment.

There are other players in the large-scale ONs equipment like LEWA and ASAHI KASEI. These companies have traditionally occupied the chromatography and downstream processing space but are capable of building custom synthesizers by using their existing pump and valve technologies. Such custom jobs are normally done in collaboration with the end users.

6.11.11.2 Oligonucleotide Cleavage and Deprotection Equipment

Oligo deprotection involves three steps: removal of the CNET protecting group from the phosphate backbone, cleavage of the oligo chain from the support, and base deprotection. Depending on the C&D reagents and the type of oligo being processed, the phosphate deprotection may be performed during the synthesis step. However, irrespective of the reagents and conditions being

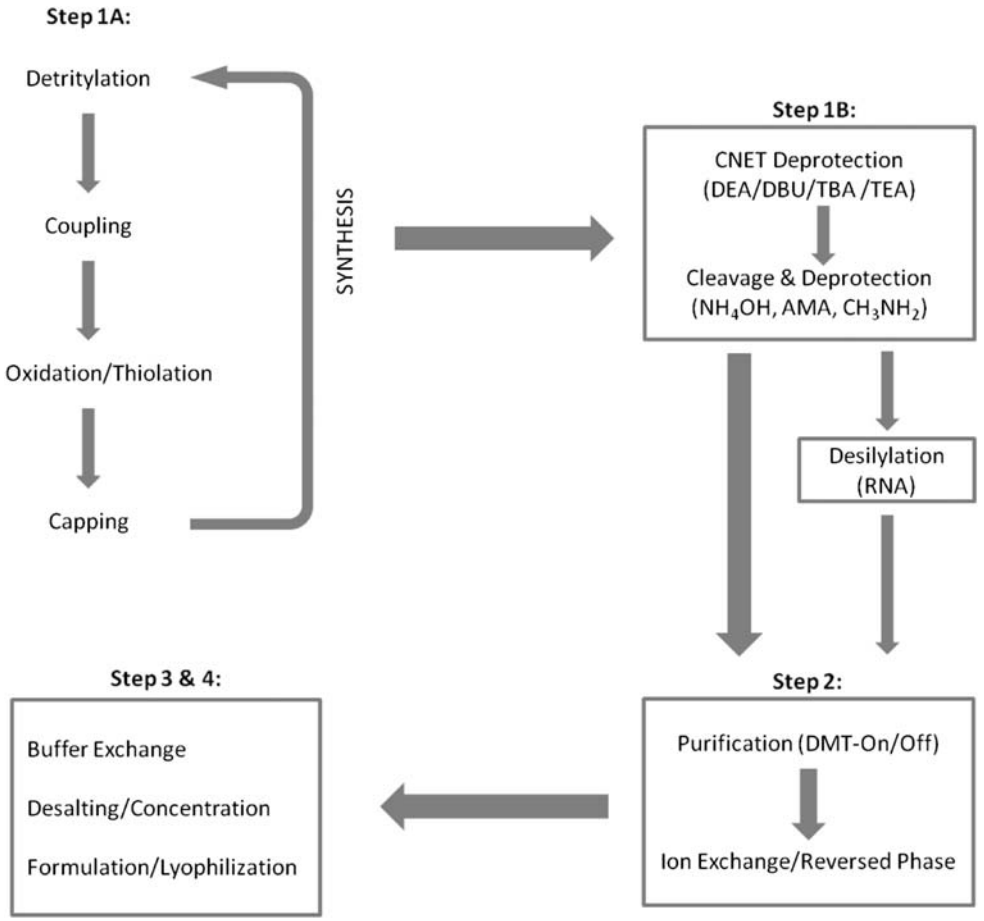

Fig. 23 Oligonucleotides manufacturing process steps.

used (Table 3), the C&D step involves soaking the oligo-bound support in the reagent and shaking the mixture using temperature-controlled orbital shakers. When using reagents that can build pressure like ammonia, it is recommended to use shakers with either heating blocks or water bath. The process also requires the use of custom-built reaction vessels that can handle the C&D conditions.

For certain production applications, the batch size might require larger than commercially available shakers, and even if available, such a process may not be performed safely. In such instances, an on-column cleavage and deprotection strategy can be used. In this strategy, the oligo-bound support is not unpacked from the column housing following synthesis. A customized heated reservoir/reactor and pump system is used to deliver the C&D reagents into the column. The solution is then recirculated until the process is complete. The solution containing the deprotected ON is then recovered and further processed as desired. Fig. 24 shows an on-column cleavage and deprotection schematic.

For RNAs, the 2′-OTBDMS group must also be removed (desilylation) prior to further processing. This is typically achieved by treating the already deprotected solution from the C&D step with a fluoride source as described in Table 4. These reactions are carried out in jacketed reactors with overhead mechanical stirrers. As this step involves heating, cooling, and tight pH control, the system used must have both an efficient heat transfer and mixing capability for scalable and reproducible operations. Fig. 25 shows typical jacketed reactor systems with heater/chillers for different scale desylilations.

6.11.11.3 Oligonucleotide Chromatography Equipment

Unlike ON synthesis that requires highly specialized equipment, which may not be readily available especially at large scales, chromatography systems are more accessible since these systems have wider applications ranging from biopharmaceuticals to small molecules. The key to efficient therapeutic-grade ON purifications therefore lies mostly on the stationary phase, eluent, and conditions used. Equally important is the purification column and column packing strategy employed. Nonetheless, for purification equipment designed for ONs, GE is among the industry leaders with the ÄKTA purification platforms, which complement their synthesizers. Just like in synthesis, GE provides skids from the research-scale (ÄKTA purifier/pure) to large-volume manufacturing (BioProcess/ÄKTAprocess). The ÄKTApurifier and BioProcess have been discontinued and replaced with AKTApure and ÄKTAprocess, respectively. The ÄKTAprocess can deliver flow rates up to 2000 L/h, whereas the UNICORN software makes processes

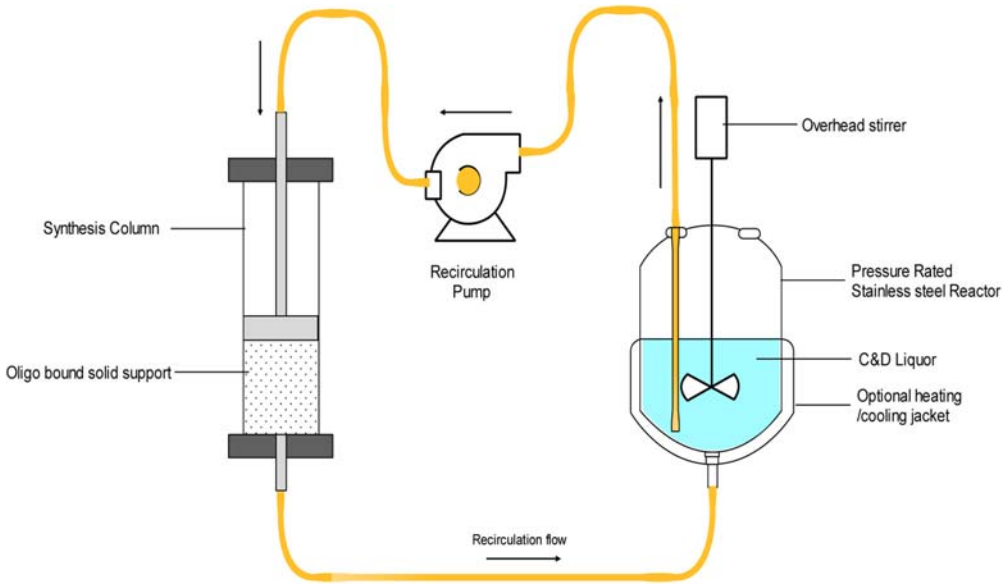

Fig. 24 On-column cleavage and deprotection schematic.

Fig. 25 Typical jacketed reactor systems with heater/chillers for different scale desylilations.

developed on GE's purification platforms easy to scale up and transfer; the systems suffer from their both pressure and low temperature ratings and are not amenable for processes, which require high pressure and sufficient denaturing temperature conditions. Similarly to the equipment, GE's purification columns are generally designed for low-pressure applications at temperatures below 40°C.

For high pressure and temperature purification equipment, ASAHI KASEI, LEWA, and Novasep are among the major players. For purification columns, Load & Lock stainless columns (Agilent and Agar Machining) have high-pressure dynamic axial compression (DAC) packing, which provides improved bed stability and higher loading. They can also be jacketed for use at higher temperatures.

6.11.11.4 Oligonucleotide Ultrafiltration & Diafiltration Equipment

As discussed in the Research-scale manufacture of oligonucleotides section above, the UF/DF approach used depends on the manufacturing scale and the expected application. For 500-μmol scales and above, a tangential flow filtration system (TFF), as shown in Fig. 22 and described in the section therein, is recommended. TFF systems are the easiest to set up and are readily amenable to scale up. All that is needed is membrane holder, two pumps, pressure gauges, tubing with fittings, and a sample reservoir. The ease of setting these up allows the end user a lot of flexibility. Membrane holders and accessories can be obtained from key manufacturers like EMD Millipore, PALL, or Sartorius.

However, for those in need of fully automated systems, GE's ÄKTAcrossflow is available for small-scale applications. The attendant UNICORN software allows for instant in-process control (IPC) and process log. For pilot and manufacturing-scale applications, GE's UniFlux system is available in sizes of 10, 30, 120, and 400 LPM. Fully automated large-scale TFF skids like

the Allegro series are also available from PALL. Not to be left behind, EMD Millipore also recently launched the fully automated Mobius® FlexReady Solution. A versatile system, this machine can be switched from a TFF to chromatography skid with minimum component changes. There are several other manufacturers of TFF systems for applications beyond ON purification and desalting.

6.11.11.5 Oligonucleotide Lyophilization Process and Equipment

Since the pH of double-distilled water is about 5.5, ONs in aqueous solutions will slowly undergo acid-catalyzed depurination over time. At the same time, there is a considerable risk of contamination from microorganisms, which might lead to degradation. Therefore, for long-term storage and easier handling, purified ONs are typically lyophilized (freeze-dried) to powder in the final manufacturing step. As briefly discussed earlier in this report, during the TFF step of large-scale manufacture, the desalted ON API is concentrated to a predetermined concentration. This concentration, usually a range, is a controlled process parameter to ensure that upon lyophilization, a product with a consistent morphology is obtained.

Lyophilization is performed using a freezer dryer, which is a machine consisting of a sample chamber, a condenser, and a vacuum pump. The ON API is frozen and lyophilized to obtain the final product in powder form via sublimation. Common benchtop freeze dryers are manufactured by Labconco, while pilot and production freeze dryers include VirTis Genesis and Hull.

There are four main steps in the lyophilization process, namely, sample preparation, freezing, primary drying, and secondary drying. In the sample preparation step, the desalted ON API solution is filtered through a 0.2-μm filter to remove bioburden and in-process particulates from the drug product. The filtered solution is then transferred into vials for small-scale batches or into freeze-drying trays or containers. These containers, like Gore LyoGuard® trays, are specially made with optimal volume capacity and fitted with membranes that allow for water removal without product spills or contamination.

The container or tray with the product is then placed inside the sample chamber shelf and frozen, usually at -40°C. The rate of freezing depends on the temperature of the shelf, the amount of product in each tray, and the height of the solution in each tray. These factors alongside the concentration of the ON will in turn impact the drying rate and the morphology of the product obtained. It is therefore critical that these factors be put into consideration when developing the lyophilization recipe. During this step, the frozen water exists in the product solution in two forms:

(a) Water free (unbound) from the ON solid
(b) Water trapped within the solid product

After the freezing step, the primary drying step kicks in. In this step, the condenser temperature is lowered to a temperature much lower than that of the lyophilization chamber, usually less than -70°C. The chamber pressure is then lowered by pulling the vacuum. These sets of conditions result in a phase change from solid to gas, that is the free water frozen water sublimes to vapor, which is then instantaneously trapped in the -70°C condenser and turned back to ice. Since the sublimation process is accompanied by a decrease in product temperature, the chamber shelves are heated to keep the resultant product cake at constant temperature. It is typical to monitor both the shelf and the product temperatures during this process. When both temperatures reach equilibrium, it is an indication that the primary drying step is complete.

After the completion of the primary drying step, no "free water" is left in the product. But the trapped water is still within the solid product. Since this water is more difficult to remove, the shelf temperature is increased gradually, usually to $25 \pm 5^{\circ}$C at the same or lower pressures used for primary drying.

6.11.12 Small-Scale Modeling for Oligonucleotide Manufacturing

The precarious relationship between production-scale manufacturing and small-scale modeling approaches requires diligent scrutiny. Lowered yield, changes in impurity profile, and process deviations are among the most common critical scale-up issues that are attributed to improper small-scale models. Therefore, any work to ensure reliable scale-up manufactures needs to focus around critical processing steps and establish scalable operating parameters. This section will cover several case studies where appropriate small-scale models were developed, some after painfully gained scale-up experience, to ensure reliable manufactures. The case studies discussed will include at least a single parameter from each of the ON-manufacturing steps.

One of the most complex manufacturing operations to model given the sheer number of critical operating parameters is solid-phase synthesis. Although each step during synthesis has a scalable critical parameter worth discussion, this review will focus on the most critical and one of the easiest parameters to model during synthesis process development work: synthesis support bed height. This parameter is critical as it bridges the relationship between scalable process flow rates and reagent contact time. The experience discussed is based mainly on a case study centered on the relationship between bed height and detritylation-dependent depurination.

For the study, the synthesis of a fully phosphorothioated 18-mer oligodeoxynucleotide was performed at three different bed heights keeping all other parameters constant (Table 7). As mentioned earlier, performing the syntheses in this manner would lead to a positively linear relationship between bed height and reagent contact time. Although for most reagents, this is generally not an issue, extending the contact time of the detritylation reagent with oligodeoxynucleotides, which are sensitive to acid-based depurination and further strand cleavage during C&D, would lead to lower FLP purity (Fig. 26). The first three experiments in the

Table 7 Influence of synthesis bed height on depurination[175]

Scale (mmol)	*Bed height (cm)*	*Column volume (mL)*	*Detroit flow rate, cm/h (mL/min)*	*Detroit flow rate (CV/min)*	*FLP purity (%)*
0.25	2	6.3	400 (21)	3.3	87
1.69	4.5	43.8	400 (65)	1.5	83
3.37	9	87.5	400 (65)	0.7	78
0.25	2	6.3	200 (10)	1.6	83
0.25	2	6.3	65 (3.5)	0.6	77

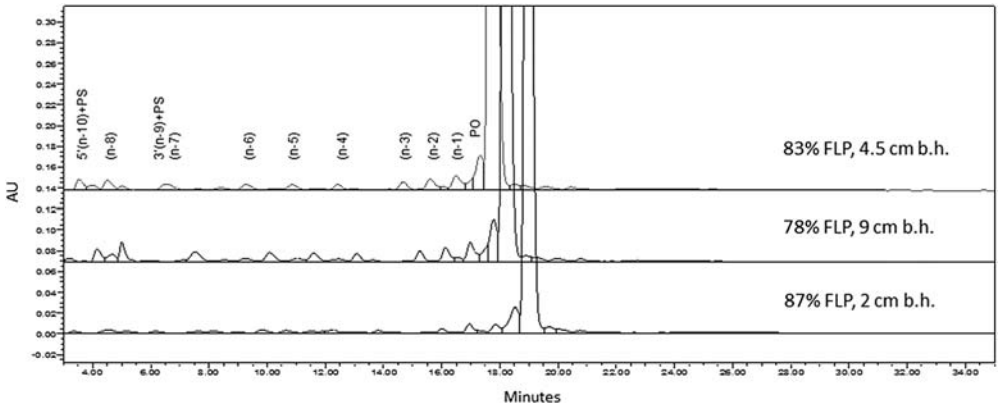

Fig. 26 Influence of synthesis bed height on depurination. Acid-induced depurination of an 18-mer PS DNA followed by strand breakage during C&D leads to lowered FLP content in the crude at higher bed heights.[175]

experimental set demonstrate this fact where the synthesis at 9-cm bed height results in higher levels of prepeak impurities as compared with the synthesis at 2-cm bed height. To demonstrate that this is generally not attributed to other reagents' contact time and is mainly due to detritylation-dependent depurination during extended detritylation contact times, performing an additional two syntheses at the short 2-cm bed height but using reagent flow rates for detritylation reagent that mimic the higher bed height also causes the crude material quality to drop. Therefore, the relationship between reagent flow rates and synthesis support housing proportions needs to be scrutinized on the basis of critical reagent contact times to ensure reliable scale-up manufactures.

As C&D processes are generally performed in basic media at elevated temperatures, the most critical and challenging parameter to model during process development work is heat transfer. Although a solution in a small vessel might reach the desired internal temperature in a fraction of an hour, larger vessels require significant more heat to be transferred to reach the optimal internal deprotection temperatures. As this process is heavily influenced by vessel proportions, materials of construction, and even heating element characteristics, developing a small-scale model for C&D is deceptively simple. In some instances, after determining ramp-up rates, simply adjusting incubation time at large scale is sufficient to ensure reliable manufactures. However, as ramp-up rates for larger scales are generally harder to determine and as the large-scale equipment is significantly different from lab-scale heating elements, the process can be challenging. This process is complicated further in the case of oligoribonucleotides. In addition to C&D considerations, following ON removal from the solid support and base deprotection, the removal of the requisite 2′-OH protecting groups needs to be carried out in an acidic media with an organic cosolvent. As the reaction pH is being adjusted from ~11 to ~5, a large exothermic reaction needs to be controlled. Additionally, as both the 2′-protected ON and the several reagent byproducts precipitate during this transition, precise heat control is critical to ensure reliable manufactures. Therefore, diligent alignment of heating/cooling capabilities needs to be established. In the next case study, a set of three C&D reactions are presented (Fig. 27). In the first experiment, the crude material for a 24-mer ON conjugate with 2′-OH, 2′-OMe, and 2′-F modifications that underwent C&D using an appropriate heating scale-down model is presented (PD model in Fig. 27). Attempting a similar reaction at manufacturing scale using equipment setup with nonmodel heating/cooling characteristics generates a significantly lower quality crude material. As the heat generated is uncontrolled and the ramp-up/down rates are slower, significant ON damage is evident from the impurity profile (nonmodel heating in Fig. 27). Finally, ensuring that the heating/cooling capabilities of the large-scale equipment are in line with the small-scale model ensures a reliable manufacture.

Another process operation where large-scale equipment is easily misaligned is ON purification. For this process operation, myriad parameters need to be taken into account to ensure a successful manufacture. Although column packing methodologies, column conditioning, incoming crude matrix, loading/elution flow rates, eluent preparation, operating backpressure, among others, are important to a successful purification, one of the most challenging parameters to align is purification temperature. Given that heat transfer differs widely between scales and equipment setups and that temperature might even vary within the equipment

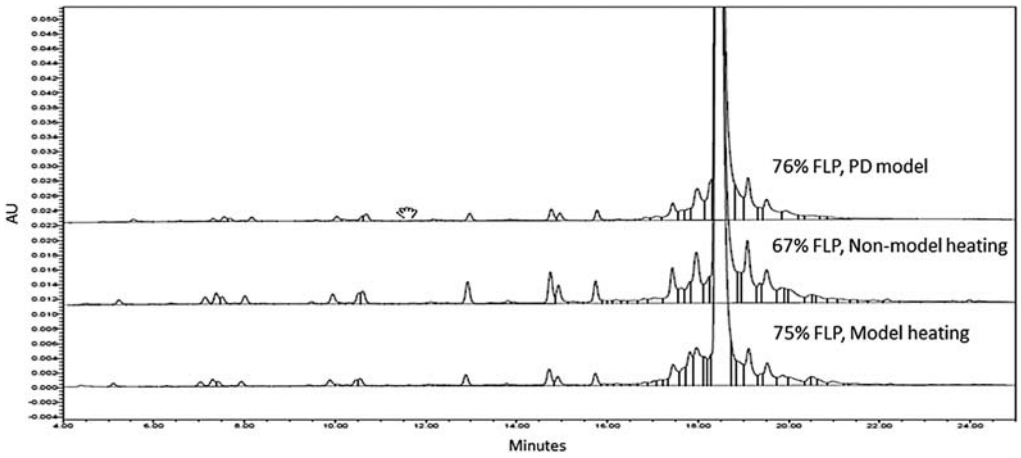

Fig. 27 Influence of C&D heat transfer on crude quality.

itself (between eluent tanks, pump system, eluent heaters, column inlet, column outlet, and even fractionation temperature), it is critical to ensure that not only the purification temperature wherever measured but also the actual heating and cooling rates at every step are being modeled. The following case study presents the heated purification of a 21-mer RNA mix-mer conjugate. From Table 8, it is clear that high temperature is necessary to denature the RNA during purification. Any attempts at purifying this material at temperatures lower than 30°C resulted in low-quality fractions. However, there is a balance between denaturation for purification and heat-generated degradation. For this material, it was found that purification at 40–50°C resulted in high quality fractions. However, further addition of 5°C of heat resulted in lower quality fractions again mostly due to degradation. Further, it was found that the time spent at temperature within the heating elements before interaction with the column was also critical, thus implicating ramp-up rates. Overall, tight temperature control and maintaining heat transfer rates during purification among other critical parameters are critical for a smooth scale up of heated purifications.

As mentioned earlier in this report, the most widely accepted choice for ON isolation following purification at manufacturing scales is TFF or diafiltration (Fig. 22). In this process, a solution is fed against an appropriately sized membrane to remove the purification salts and other byproducts. Additionally, this process allows for the concentration of the purified material to ensure that the subsequent lyophilization step is simplified. As such, diligent modeling of ON concentration throughout the diafiltration process and control of the system physical parameters such as transmembrane pressure (TMP), membrane flux, and diafiltration volumes fed need to be controlled. For this, the most straightforward approach at developing a predictive small-scale model is to build a proportionally scaled version of the large-scale TFF system. As the large-scale batch sizes are generally proportionally larger than their respective system void volumes, developing small-scale models for TFF generally requires the use of custom-built pumps, vessels, tubing, and even sensors that will both minimize void volumes and be able to operate within the large-scale operating conditions. Table 9 summarizes parameters for a standard TFF operation with particular focus on critical scalable parameters to ensure reliable TFF operations.

The generally last step in the manufacturing process is the isolation of ON API powder through lyophilization (Fig. 28). As discussed earlier, a desalted ON solution is shelf frozen in an appropriate tray inside the lyophilizer equipment (denoted freezing in Fig. 28). Once the solutions are frozen, strong vacuum is applied to the chamber to begin the process of lyophilization. Once the system reaches strong vacuum, to aid the process of water sublimation, slight heat is applied gradually to the frozen trays (denoted shelf heating in Fig. 28). Through the primary drying process, as lower amounts of water are being removed and heat is still being

Table 8 RNA purifications are highly sensitive to purification temperature

Scale (mmol)	~0.6			
Crude purity	~80%			
Column diameter (cm)	2.5			
Bed height (cm)	30			
Column volume (mL)	152			
Purification temperature (°C)	30	40	50	55
Loading mg/mL media	~25			
Flow rate (cm/h)	200			
Eluent A	Sodium phosphate with ACN cosolvent			
Eluent B	Eluent A + 1M NaBr			
Highest fraction purity	87	90	92	87

Table 9 Critical parameters for accurate desalting small-scale modeling[175]

Parameters	*Small-scale model—5 mmol*	*Full scale batch—250 mmol*
Membrane area (m^2)	0.1	5
Initial concentration (mg/mL)	2	2
Initial solution volume (L)	10	500
Total g	20	1000
Pump flow rate (L/min)	0.8	40
TMP	3.0 ± 0.5 bar	3.0 ± 0.5 bar
Permeate flow rate (mL/min)	60	3000
Flux in LMH ($L/m^2/h$)	36	36
Target Concentration Before Diafiltration (mg/mL)	40	40
Volume before diafiltration (L)	0.5	25
Concentration factor (CF)	20	20
Diafiltration volume (DV)	15 ± 3	15 ± 3
Final volume (before rinse) (L)	0.25	12.5
Final concentration (before rinse) (mg/mL)	79	79
Final concentration factor	40	40
Final volume (after rinse) (L)	0.28	14
Final concentration (after rinse) (mg/mL)	71	71

supplied to the product shelves, the observed tray temperature slowly rises to the desired set point until it equilibrates to the system (plateau in Fig. 28). To remove strongly associated water molecules (secondary drying in Fig. 28), stronger vacuum is applied, and the instrument set temperature is set to ambient. As one can imagine, the process as described is such highly dependent on equipment capabilities and sample volume that the process of small-scale modeling seems prohibitive. However, a simple solution is available. As the lyophilization rates are system-dependent but the evaporation from one tray is expectedly independent from another at a particular equipment load, a model where a single tray (*red arrows* in Fig. 28) carries ON material while the remainder of the trays that would form part of the manufacturing scale are filled with water provides a simple and reliable small-scale model for that lyophilization equipment. This approach ensures that the capabilities of the particular system to be used in the manufacture are taken into consideration while minimizing the cost of the development study.

Overall, diligent scrutiny and control over scalable parameters and diligent manufacturing equipment modeling provide a route for reliable large-scale manufactures. Careful attention to system proportions, void volumes, heat transfer, equipment loading, and sample concentration, among other critical operating parameters, ensures that any process development activities are useful in predicting large-scale manufactures. Through this responsible process, development approach, batch reliability and ON quality can be maximized and maintained.

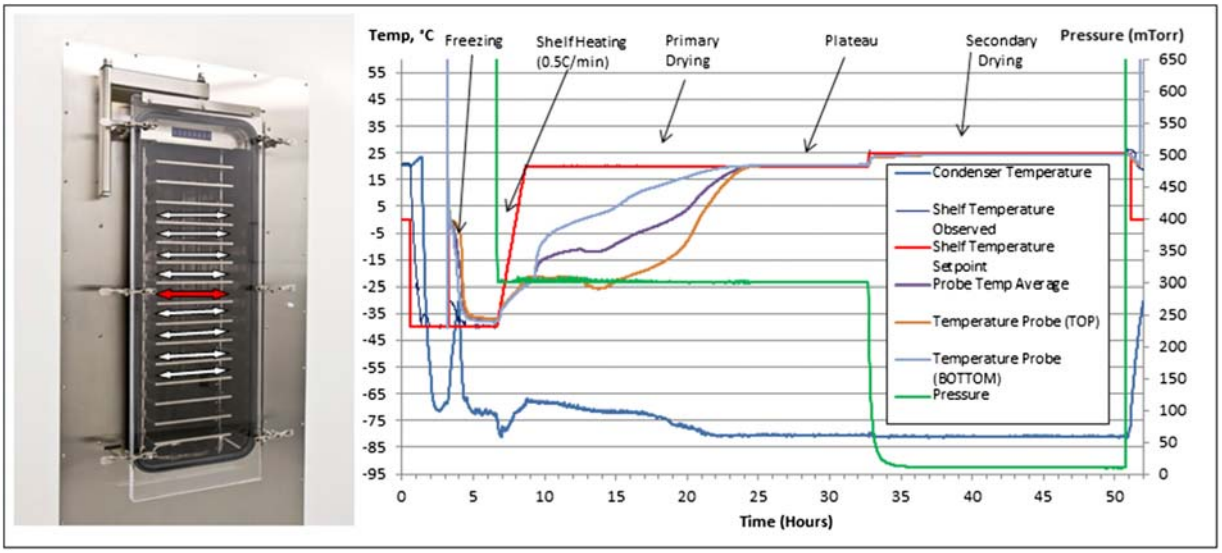

Fig. 28 Lyophilization small-scale modeling considerations.[175]

6.11.13 Analytic Tools to Support Oligonucleotide Manufacturing

Analysis of ONs can be a challenge due to their size and the structural similarity of their process-related impurities. Analytic techniques such as NMR, FT-IR, Raman spectroscopy, and total molecular weight by mass spectrometry are, by themselves, not suitable for ONs. Purity analysis of ONs can also be challenging, and HPLC, one of the most common techniques for measuring the purity of small-molecule drugs, has not always been adequate for measuring purity of ONs. Just a few decades ago, HPLC methods did not provide sufficient resolution of ONs and their process-related impurities. Alternative techniques such as denaturing polyacrylamide gel electrophoresis (PAGE) and capillary gel electrophoreses (CGE) had to be employed, but these techniques did not always have the attributes needed for routine QC testing. Fortunately, recent advances in analytic instrumentation and chromatographic packing materials provide today's analysts with an array of analytic methods that are suitable for establishing identity and measuring purity of synthetic ONs. The method(s) selected will depend upon the structure of the ON and the intended purpose of the test. Method characteristics such as analysis time, sensitivity, specificity, robustness, test complexity, and availability of instrumentation must also be considered.

Table 10 shows the methods that are most commonly used to analyze ONs manufactured for therapeutic use. The two most important analytic techniques used to support ON manufacturing are HPLC and mass spectrometry. HPLC methods such as reversed-phase ion pair, anion exchange, and size exclusion provide critical information about the purity of the ONs. Mass spectrometric methods such as MALDI-ToF, ESI-MS, and tandem mass spectrometry can all provide critical structural information. The combination of HPLC with mass spectrometric detection provides a third powerful technique. For this reason, the role of HPLC with mass spectrometric detection in the analysis of ONs will be discussed in its own section separate from HPLC and from mass spectrometry.

6.11.13.1 Commonly Used HPLC Techniques for the Analysis of Oligonucleotides

Reversed-phase ion-pair chromatography utilizes a hydrophobic stationary phase and a mobile phase containing an ion-pair reagent, which is typically an alkylated amine added at low concentration. Although the name of the technique suggests that the separation mechanism is driven by the electrostatic formation of an ion pair between the negatively charged ON and the positively charged alkyl amine, the actual separation mechanism is more complex. The amine's alkyl chains can bind with the lipophilic stationary phase leaving the cationic portion of the molecule exposed to analytes migrating through the column. The retention time of negatively charged analytes increases as a result of the electrostatic interaction with the modified stationary phase.[178] Commonly used ion-pair reagents include triethylammonium acetate, hexylammonium acetate, tetrabutyl ammonium acetate, and triethyl amine with hexafluoroisopropanol. Hexafluoroisopropanol is not considered an ion-pair reagent, but it has been shown to enhance separations.[179] The ion-pair reagent selected depends upon the needed selectivity and whether or not compatibility with mass spectrometric detection is required. The longer the ON, the more difficult it is to resolve the full-length product from process-related impurities due to their very small differences in hydrophobicities. The incorporation of phosphorothioate modifications results in the formation of a mixture of diastereomers that can also lead to peak broadening and further diminish resolution. In spite of these limitations, ion-pair chromatography is an important analytic technique for analysis of in-process samples and API. The technique's utility has been further enhanced by improvements in commercially available stationary phases.

Most separations are carried out on silica-based sorbents. Column manufacturers have significantly improved these packing materials through increased cross-linking, introduction of polar functional groups, and use of hybrid phases with silica coated onto a solid core. These new stationary phases operate at wide pH ranges, have good mechanical stability, and are available in particle sizes as low as 2 μm. Smaller sorbent particle sizes not only lead to increased plate counts but also require an HPLC system capable of operating reliably at backpressures as high as 1000 bar. Because of the high-molecular weight of ONs, mass transfer through the pores of the stationary phase can be slow and lead to peak broadening, but these effects can be minimized through the use of sorbents with a solid core coated with silica. A more detailed discussion of these topics and a comprehensive review of ion-pair separations for ONs was written by Cramer et al.[180]

Anion-exchange chromatography is widely used in the analysis of ONs.[181] Anion-exchange methods tend to be robust and well suited for in-process control or final product testing. The anionic ON interacts with the cationic functional groups on the stationary phase. Neutral and weak anions elute first followed by strongly charged molecules. Gradient separations are achieved by increasing the ionic strength of the mobile phase over time until all species of interest have eluted. Stationary phases usually consist of pellicular resin with a quaternary amine-functional group. Some column manufacturers produce anion-exchange columns that are designed exclusively for the separation of ONs. Anion-exchange columns are stable at pH as high as 12.5 and temperatures as high as 85 degrees centigrade making them excellent for use in separations involving ON single strands that are prone to forming strong secondary structures or duplexes that one wishes to analyze in the denatured state. Anion-exchange chromatography was shown to be capable of separating a full-length phosphorothioate ON from mono- and diphosphodiester species.[182] Like ion-pair chromatography, anion-exchange chromatography may not be capable of resolving all process-related impurities and degradation products from the full-length product, so drug sponsors may choose to utilize both chromatographic techniques to measure impurities and characterize their ON.

Size-exclusion chromatography (SEC) can be utilized to separate single strands from duplex and to separate single strand from their corresponding polymer conjugates. Molecules are separated based upon their size. Molecules too large to diffuse into the pores of the stationary phase elute first, and smaller molecules that are capable of diffusing through the stationary phase are retained

Table 10 Commonly used analytic techniques for analysis of oligonucleotides

Purpose	*Analytic technique*	*Application*
Confirmation of identity	Mass spectrometry (single mass analyzer)	ESI-MS and MALDI-ToF are commonly used to measure total molecular weight. For research-grade ONs, this test is typically accepted for establishing identity since the probability of synthesizing an incorrect, isobaric sequence is low. Total molecular weight alone is not sufficient for establishing identity of an ON used in clinical applications. The correct order of nucleotides must be established through another technique. ONs can be enzymatically digested to form a series of fragments that may then be analyzed by MALDI-ToF to confirm the correct sequence of nucleotides is present
	Tandem mass spectrometry	Tandem mass spectrometers generate ions *in situ*, and the ions pass through two or more stages of analysis. An electrospray ionization source coupled to a single-quadrupole mass analyzer followed by a time of flight mass analyzer is an example of a tandem mass spectrometer commonly used to analyze ONs. Tandem mass spectrometry is useful for analyzing an ON's sequence and confirming identity. Enzymatic digestion of the sample prior to analysis is not necessary since fragmentation is performed in the gaseous phase. Complete sequence coverage cannot be obtained for some longer sequences (typically longer than 30 nucleotides) and some chemically modified sequences. In instances where 100% sequence coverage is not obtained, additional techniques may be used to positively establish identity for ONs for therapeutic use
	UV spectroscopy for measurement of duplex melting temperature (T_m)	The melting temperature, or T_m, is the temperature at which half the population of complementary single strands exist in the duplex state and half exist in the denatured state. The T_m is a characteristic of the nucleotide sequence and thus can be used as an identity test. UV spectroscopy is the most common method for measuring T_m, although alternative techniques such as differential scanning calorimetry and circular dichroism may also be used. Annealed single strands in the duplex form have lower UV absorbance than single strands that are denatured. A duplex solution can be placed in the cell of a UV-Vis spectrophotometer with heating/cooling capabilities. As the temperature of the UV cell is increased, the duplex structure is disturbed and begins to denature. During the denaturing process, the corresponding increase in UV absorbance at 260 nm is measured, and the T_m can then be determined[176]
	^{31}P NMR	Unmodified ONs contain phosphate diester linkages with a ^{31}P NMR signal between 0 and 1 ppm. Many ONs are synthesized to have some or all of the nonbridging oxygen atoms of the phosphate diesters replaced by sulfur atoms to enhance their chemical stability. The resulting PS bonds yield a ^{31}P NMR signal between 50 and 60 ppm. ^{31}P NMR can measure the ratio of the PO to PS bonds in an ON making it suitable for confirming the correct molecular backbone is present. Other identity tests should be used in combination with ^{31}P NMR because this technique cannot demonstrate that the sequence of nucleotides is correct. ^{31}P NMR may also be used as a purity/impurity test to quantitate the amount of PO impurity in certain phosphorothioate ONs. A comparison of ^{31}P NMR and LC-MS for measurement of PO impurity has been studied and was shown to be in good agreement.[177] Anion-exchange chromatography may also be used to measure PO impurities as well
	Elemental spectroscopy (flame atomic absorption spectroscopy (FAA), inductively coupled plasma optical emission spectroscopy (ICP-OES), inductively coupled plasma mass spectrometry (ICP-MS))	Any of these techniques are capable of confirming identity of the counterion and determining the quantity of counterion present. Nearly all therapeutic ONs are produced as sodium salts. Testing for sodium serves to both establish the identity of the salt form present and confirm the purity of the ON. Many ONs are purified using anion-exchange chromatography with buffers containing sodium salts. Confirming that sodium levels are within preestablished ranges proves that purification buffer salts were removed from the ON prior to lyophilization. ONs intended for therapeutic use should also be tested for heavy metals. Frequently, ICP-MS can be used to analyze the counterion and confirm heavy metals are below the required acceptance criteria. Sodium counterion is usually present at 5–7% by weight, whereas heavy metal acceptance criteria are usually in the low ppm range. Multiple sample preparations typically must be made if ICP-MS is the technique selected for measuring both sodium and heavy metals in order to stay within the linear dynamic range of the instrument
	Ion chromatography	Ion chromatography with conductivity detection may be used to quantify the counterion and confirm its identity based upon retention time. Ion chromatography can also be a useful technique for testing for residual reagents used during manufacturing such as buffer salts and sodium acetate
	Sodium ion selective electrode	Sodium ion selective electrodes (ISE) may also be used to quantify the sodium counterion. ISE is attractive due to its low cost, ease of use, and short analysis times. These attributes make ISE an attractive technique for in-process testing and analysis of nonclinical samples, but techniques such as ICP-OES and ICP-MS are typically favored for analysis of the final drug substance

Table 10 Commonly used analytic techniques for analysis of oligonucleotides—cont'd

Purpose	*Analytic technique*	*Application*
	HPLC	HPLC retention time compared with a reference standard is a commonly used identity test for small-molecule drugs, but HPLC retention time is not a sufficient identity test for ONs due to the structural similarity of process-related impurities and degradation products. If a specification is established to determine identity based upon HPLC retention time, additional more specific analytic techniques such as sequencing by tandem mass spectrometry and Tm should also be used to confirm identity
Purity and assay	UV–vis spectroscopy (260 nm)	UV spectroscopy is used to quantify the amount of ON present through simple application of Beer's Law. A theoretical calculation of the molar extinction coefficient can be made if the ON sequence is known. UV spectroscopy is used during manufacturing to quantify the amount of ON present so that yield may be determined after a manufacturing step. UV spectroscopy is frequently used to measure total ON content in the final lyophilized ON
	HPLC—single strands	Anion-exchange chromatography with UV detection and reversed-phase ion-pair chromatography with UV or UV-MS detection are the two most common methods for measuring single-strand purity. If a well-characterized reference standard is available, then these techniques may also be utilized to perform an assay analysis
	HPLC—duplex	Size-exclusion chromatography, nondenaturing anion-exchange chromatography with UV detection, and nondenaturing reversed-phase ion-pair chromatography with UV or UV-MS detection are the most common methods for measuring duplex purity. If a well-characterized reference standard is available, then these techniques may also be utilized to perform an assay analysis
Other QC Tests	Bacterial endotoxins	Limulus Amebocyte lysate (LAL) test is commonly used
	Microbial testing	Testing should be conducted in accordance with the appropriate compendial methods
	Karl Fischer coulometry	This technique is used to determine the amount of water present in the ON. Oven attachments are frequently used to avoid direct introduction of the ON into the coulometric cell
	Gas chromatography with flame ionization detection (FID) or electron capture detection (ECD)	Residual solvents from the manufacturing process can be quantified with this method
	ICP-MS	ICP-MS is now widely used to test for heavy metals and any other elements that may be a residual from the manufacturing process. For example, silicon may be an element of interest if the manufacturing process contains a purification step utilizing silica-based chromatography packing

longer. Stationary phases most commonly used include chemically bonded porous silica gel and hydrophilic polymeric resins. Silica-based columns are typically used for separations of duplexes and single strands because of their ability to separate molecules ranging from 7 to 15 kDa. Polymeric resins may be a better choice when separating larger analytes such as pegylated ONs and high-molecular-weight multiplexes.[183] SEC may be used as an in-process control test to monitor the annealing process and determine when sufficient quantities of each single strand have been combined. Some ONs are conjugated to other molecules, such as polyethylene glycol (PEG), that are polydisperse. For these polydisperse conjugates, SEC may be used to determine the polydispersity index (PDI), which is a measure of the distribution of molecular weights of a polymer.[184]

Mass spectrometry can be used to measure an ON's molecular weight and determine its nucleotide sequence. The two most commonly used instruments for determining molecular weight are the matrix-assisted laser desorption ionization time of flight mass spectrometer (MALDI-ToF) and the electrospray ionization single-quadrupole mass spectrometer (ESI-MS). The MALDI-ToF has the advantage of generating and separating singly charged ions, which makes interpretation of mass spectra simpler. ESI-MS generates multiply charged ions that are separated based on their mass-to-charge ratios (m/z), and although this can make the mass spectra more difficult to interpret, it allows ONs with molecular weights above the upper mass limit of the spectrometer to still be analyzed. Deconvolution software must be used to transform the m/z data into the final mass spectrum. Both techniques are hindered by the formation of cationic adducts (usually Na^+ and K^+) that reduce sensitivity, so care must be taken that samples and reagents are free of interfering salts. Fountain et al. utilized HPLC desalting prior to ESI-MS analysis and developed a high-throughput method capable of analyzing one sample every 1.5 min with an average mass accuracy of 80 ppm.[185]

Confirming the correct nucleotide sequence is performed using one of two methods. The first involves enzymatic digestion of the ON to form a series of nucleotide fragments. Enzymes that digest from the 5′ direction to the 3′ direction may be used. The mixture of fragments is analyzed by MALDI-ToF, and the series of masses can be used to generate a sequence ladder that confirms the correct order of nucleotides. Since MALDI-ToF generates and separates singly charged ions, the mixture of fragments can be analyzed without prior separation. ESI-MS is not capable of separating such a complex mixture since each fragment would produce multiple ions having different mass-to-charge ratios making the spectra too complex to decipher. Tandem mass spectrometry is another option for determining an ON sequence. Fragments are produced in the gas phase. The ON backbone can be cleaved in four

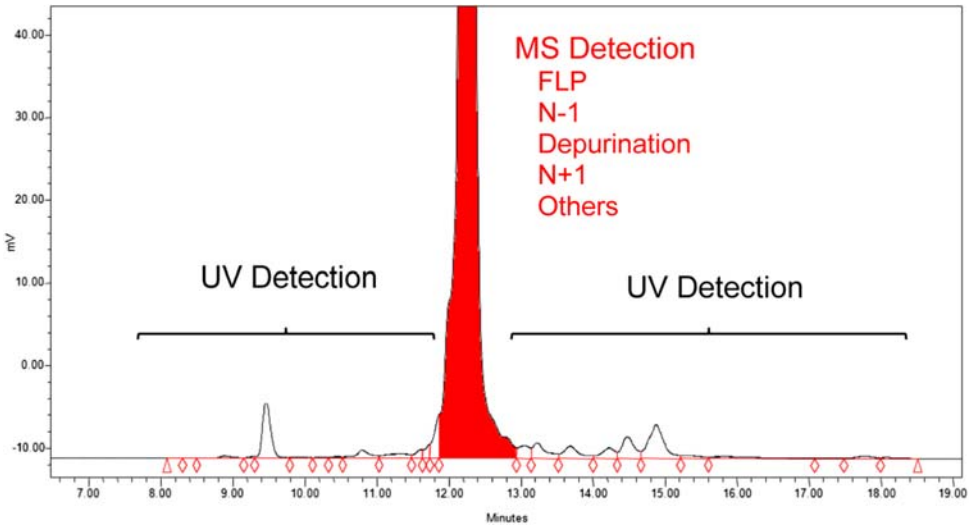

Fig. 29 Impurities quantified by UV detection and MS detection.[177]

possible positions across the diester bridge, namely, the two P–O bonds and two phosphoester bonds.[186] Nomenclature proposed by McLuckey et al. is widely accepted and typically used when reporting MS/MS sequencing data.[187] The lack of commercially available software can make data analysis tedious especially if one is attempting to perform de novo sequencing. MS/MS sequencing is most commonly used to confirm a known sequence, so the analyst has an indication of the fragments to expect.

Ion-pair chromatographic separation coupled with UV and mass spectrometric detection (LC-MS) is a very powerful tool for identifying and quantifying ONs and their related substances. Ideally, one would optimize the chromatographic separation so that as many species as possible could be quantified by UV detection and identified by LC-MS characterization. Only those species that cannot be resolved would be quantified by mass spectrometry. Given recent development in UPLC technologies, the separation capabilities of analytic methods have improved drastically. Well-developed UPLC methods (as demonstrated in Fig. 26) are providing the means to analyze most closely related impurities via UV quantitation, which significantly reduces analysis time. However, for impurities that do not separate well from the main peak, LC-MS is still capable of providing both structural and purity data and allows for quantification of such analytes. Mass spectrometry quantitation requires that individual ions be extracted from the total ion chromatogram (TIC) in order to quantify individual species, so processing of data tends to be more cumbersome than processing of UV data. Fig. 29 shows a UV chromatogram from an LC-MS separation and the species that are quantified by UV and those that are quantified by MS. Analysts should take care that the ion-pair reagents used are volatile and do not suppress ionization.

6.11.14 Regulatory Aspects of Oligonucleotides

ONs are an emerging therapeutic class, and no formal regulatory guidelines specifically addressing chemistry, manufacturing, and control aspects (CMC) of ONs have been published. Table 11 shows the only ON therapeutics approved by the US FDA.

In 1993, when the therapeutic ON field was in its infancy, representatives from the FDA published guidance in the scientific literature rather than in the form of a guidance document.[188] Subsequent guidance from regulatory agencies has come in the form of presentations made at industry conferences.[188,189] Consultants and industry experts have also published guidance based upon their experiences with regulatory agencies.[190]

Table 11 Oligonucleotide therapeutics approved by the US FDA

Drug name	*Approval year*	*Indication*	*Manufacturer at time of approval*
Vitravene™ (Fomivirsen Sodium)	1998	Cytomegalovirus	Isis Pharmaceuticals, Inc.
MACUGEN® (Pegaptanib Sodium)	2007	Neovascular (wet) age-related macular degeneration	Co-developed by Eyetech Pharmaceuticals, Inc., and Pfizer Inc.
KYNAMRO® (Mipomersen Sodium)	2013	Homozygous familial hypercholesterolemia (HoFH)	Genzyme (a Sanofi company)

Information from US FDA Website.

Therapeutic ONs are produced via a synthetic chemical process that utilizes chemically derived starting materials. ONs are frequently referred to in the industry as *big small molecules*. They are regulated as new chemical entities (NCEs), typically being reviewed by FDA's Center for Drug Evaluation and Research (CDER) unless the ON is a vaccine component or an element of a combination product.

Most ICH guidelines applicable to small molecule drug development are applicable to ONs. ICHQ3A(R2) (Impurities in New Drug Substances) and ICHQ6A (Specifications: Test Procedures and Acceptance Criteria for New Drug Substances and New Drug Products: Chemical Substances) specifically state that ONs are excluded from the scope of the documents, but the spirit of these documents still applies even if some specific details such as the impurity thresholds in ICHQ3A(R2) do not. The size and chemical structure of therapeutic ONs are such that special consideration must be given when setting specifications, developing an assay, and characterizing the ON. Therefore, only these three unique aspects will be discussed further here.

6.11.14.1 Setting Specifications

Specifications consist of two elements, the analytic method to be used and the corresponding acceptance criteria. Acceptance criteria should be established based upon patient safety considerations, but process capabilities and analytic method capabilities should also be considered. Acceptance criteria are meaningless if the analytic methods used are not capable of measuring within the targeted range. Furthermore, either a process that cannot consistently produce material meeting specification should be redesigned or the specification should be examined to determine what acceptance criteria are achievable with available manufacturing technology and within product's safety profile.

Identity of the ON must be established through a combination of tests. Tandem mass spectrometry may be capable of confirming the correct nucleotide sequence, but even in this case, an additional test is required to confirm the counterion present. For ONs that cannot be fully sequenced, a combination of identity tests may be applied such as T_m, total molecular weight by mass spectrometry, and HPLC retention time to confirm identity. Each of the three tests is not specific enough to independently establish identity, but identity may be confirmed when the tests are viewed as a group. Identity of individual single strands should be established prior to formation of a duplex, and additional identity tests should be conducted on the duplex to confirm that the correct single strands were annealed during production. Identity of ONs conjugated after solid-phase synthesis should be established prior to the conjugation reaction, and then, additional identification tests should be performed on the conjugate. Table 10 shows the tests commonly used to establish identity of ON products. The tests selected will depend upon the molecule's structure and the capabilities of the analytic method. Identity tests must demonstrate suitable specificity in order to unequivocally establish identity of the ON.

Purity is assessed by one or more techniques capable of separating ONs by their chain length. Process-related impurities and degradation products are structurally similar to the full-length ON making it difficult to analytically resolve these species. A single chromatographic technique may not be capable of resolving all species of interest. Orthogonal methods such as anion-exchange chromatography and ion-pair chromatography may be used when it is not possible to resolve all impurities with a single method. Alternatively, a single chromatographic method with orthogonal detectors (LC-UV-MS) may be used.

Tracking and reporting of ON impurities can be difficult because a single chromatographic peak may represent a mixture of impurities. For example, the $n-1$ impurity does not represent a single failure sequence but rather a group of failure sequences, all having one less nucleotide than the target sequence. The deleted nucleotide may be at any position in the chain. In addition, low-level impurities may not be baseline-resolved from one another, and small peaks may merge with one another from run to run only to reappear later. Development of a robust method and establishment of appropriate system suitability controls help to minimize these issues, but they cannot be eliminated entirely. Automated integration methods do not always work well with ONs due to the lack of baseline resolution for some low-level impurities. One approach is to integrate and report these low-level impurities as groups to help minimize variability from run to run and allow for better tracking and control of impurities. Quality control test methods involving chromatographic separation should also contain explicit instructions for integration to avoid variability from analyst to analyst.

Small-molecule drugs are routinely produced with purities in excess of 98%, but typical purities for therapeutic ONs may range from 85% to 95% as measured by HPLC. The achievable purity depends upon the ON's length, the characteristics of the sequence, and the chemical modifications incorporated into the molecule. Drug sponsors are encouraged to adopt state-of-the-art analytic methods even if doing so results in lowered measured purities. ICH Q3A(R2) provides dose-dependent thresholds for reporting, identifying, and qualifying impurities in small-molecule drugs, but these thresholds are not appropriate for ONs. The current view of most regulators is that the drug sponsor must develop and support the thresholds used for a particular ON based upon toxicology data and sound scientific principles. Nevertheless, the lack of general guidance can be daunting to those new to the field, and having some knowledge of thresholds typically used in the industry is useful. Table 12 shows the thresholds proposed by

Table 12 Thresholds for therapeutic oligonucleotides proposed by McArdle

Reporting	0.20%
Identification	0.50%
Qualification	1.50%

McArdle[191] for therapeutic ONs. These thresholds are not binding, and what is achievable may vary depending upon the specific ON. The thresholds presented in Table 12 are consistent with the thresholds used by many ON drug sponsors.

Purity specifications should be established for duplexes and the single strands that form the duplex. Chromatographic methods do not have sufficient resolution to separate imperfect duplexes, so having purity specifications for individual single strands is critical to ensure the resulting duplex has the necessary purity. A nondenaturing chromatographic method is used to determine the amount of duplex and single strands present. The duplex purity specification is based upon the amount of total duplex present. Some drug sponsors establish a specification to define the identity and maximum allowable quantity of excess single strand in the final duplex product.

The approach taken when setting purity specifications for ON conjugates is dependent upon the method of conjugation and the nature of the conjugate. A single purity specification may be established if the conjugation is performed during the solid-phase synthesis and the unconjugated ON is never isolated. If the conjugation is conducted after the solid-phase synthesis, then a purity specification is typically established for the unconjugated ON and the conjugated ON.

Most therapeutic ONs are produced as lyophilized powders. A specification for water content is frequently established to ensure that the lyophilization process is under control. Acceptance criteria as high as 15% are common due to the hygroscopic nature of ONs. Some chemically modified ONs may be more prone to degradation in the presence of water, and more stringent specifications may be established for these molecules. If lower water content is required, then special precautions must be made during lyophilization and packaging to ensure a dry environment that will prevent the ON from adsorbing atmospheric moisture.

A bioassay is not required for most ONs when identity, purity, and potency can be suitably established with other analytic methods. Aptamers are a particular class of ONs that require a specific three-dimensional conformation in order to exhibit their characteristic biological activity. For this reason, a bioassay is frequently included in the specifications for aptamers but not for most other ONs. The necessary three-dimensional structure is highly dependent upon the sample matrix, so bioassay may be part of the drug product specifications rather than the drug substance specifications. Perhaps after a suitable body of data has been generated to demonstrate that aptamers with the correct identity and purity in a given sample matrix will always assume the correct three-dimensional structure, then bioassay might be eliminated from product specifications. Some bioassays have high-method variability making them difficult QC tests to implement and validate. Nevertheless, the body of data to support elimination of bioassay is not currently available, and hence an aptamer bioassay is typically expected by regulatory agencies.

Other specifications such as bacterial endotoxin, bioburden, residual solvents, and heavy metals are established using the same methodology applied to other small molecule drugs, and the reader is directed to consult the relevant regulatory guidance documents if further information is required.

6.11.14.1.1 Assay

In the early phases of drug development, a quantitative assay against a high-purity reference standard is typically not needed. The UV absorbance of a solution prepared with a known weight of ON may be measured, and a theoretically derived extinction coefficient can be used to determine the total ON content. Multiplying the total ON content by the percentage of full-length product obtained using an analytic method capable of separating by chain length can provide an assay value suitable for the early stages of development.

During the later stages of development, a well characterized, high-purity reference standard should be prepared for use in a weight-based assay. A chromatographic method with UV and/or MS detection is typically used. The hygroscopic and electrostatic nature of ONs makes it difficult to weigh small quantities of sample and introduces a source of variability into the assay. Aliquots of reference standard may be stored as aqueous solutions to minimize these effects to speed preparation of calibration curve standards. Some methods specify that samples must be prepared in a dry box to avoid the adsorption of atmospheric humidity. Other methods specify that sample be allowed to equilibrate to atmospheric humidity before the sample is analyzed. This technique is referred to as conditioned moisture.[192] Assay methods should clearly define how the reference standard and the sample are to be stored and prepared to ensure the accuracy of the results obtained. The method should also clearly state what corrections the analyst should make for water, residual solvents, excess counterion (e.g., Na^+), and any other impurities.

6.11.14.2 Characterization of Oligonucleotides

Table 10 lists tests that are commonly performed as part of routine QC testing. Additional characterization testing is typically performed on one or more batches, usually a reference standard, in order to establish the ON structure and physicochemical properties. The following analytic tests are frequently used to characterize ONs:

- *NMR*—ONs yield complex ^1H and ^{13}C NMR spectra, but NMR can still be a valuable tool in the characterization and structure elucidation of ONs. 2D NOESY and 2D TOCSY/COSY can be used to identify base pairs and show connectivity in duplexes. ^1H and ^{13}C NMR experiments are typically included in characterization testing used to support regulatory filings. A summary of the NMR experiments that can be performed to characterize ONs has been described elsewhere.[193]
- *Base composition analysis*—Samples are enzymatically degraded into their constituent bases. The bases are quantified to demonstrate that they are in the correct stoichiometric ratio. This is a useful technique especially when 100% sequence coverage cannot be obtained by mass spectrometric sequencing methods.

- *UV-vis spectroscopy*—A wavelength scan should be obtained that shows the λ_{max} and λ_{min}. Novel chemical modifications may cause the actual extinction coefficient to differ from the theoretical value, so an experimentally derived extinction coefficient should be obtained.
- *X-ray powder diffraction (XRPD)*—Used to show that the ON is an amorphous solid.
- *FT-IR*—Spectra should further confirm structure.
- *Dynamic vapor sorption*—Measures the adsorption of atmospheric moisture over time.
- *Circular dichroism*—Useful for measuring conformational properties of ONs in solution.
- *Solubility*—A range of common solvents should be tested.

Forced degradation studies performed per ICH guidelines are also necessary to ascertain if analytic methods are stability indication. These studies also elucidate degradation pathways and produce degradation products that can be further characterized. For duplexes and conjugates, forced degradation studies may be performed on the individual single strands and the final duplex or conjugate.

Most ONs in clinical development are being produced by contract manufacturing organizations (CMO), so some comments about the roles and responsibilities of drug sponsors and CMOs are appropriate. The relationship between the drug sponsor and the CMO should be viewed as a potential long-term partnership, so proper diligence should be performed in the CMO evaluation and selection phase. A drug sponsor should select a CMO after careful review of the CMO's capabilities and technical expertise. Consideration should be given to the CMO's ability to support drug manufacturing through clinical development, process validation, and commercialization. A thorough quality audit should be performed at the CMO prior to manufacturing of clinical materials, and a quality agreement should be established, so roles and responsibilities are clearly defined prior to manufacturing. The CMO may provide guidance on setting specifications based upon knowledge of the capabilities of the manufacturing processes and the analytic methods to be used. However, the drug sponsor is ultimately responsible for ensuring that appropriate specifications are established based upon toxicological studies, final dosage form, route of administration, and anticipated dose. The information of the CMO is to provide the drug sponsor regarding analytic methods and raw materials, and the manufacturing process should be clearly defined in a business contract. Some information might be proprietary to the CMO, and restrictions upon how this information can be shared and used may exist. Clear communication by both sides throughout the drug's development is crucial to the overall success of the program.

The scope of work to be conducted by the CMO should be carefully planned and realistic timelines established. Although standard methodology is used to synthesize most ONs, individual sequences may have unique properties that require further sequence-specific optimization of standard methods. In 2011, a survey was conducted of people working at biopharmaceutical CMOs. Respondents were asked about the most common mistakes made by clients. Ninety-two percent responded that clients do not build in sufficient time for their project, and clients want to contain cost by doing limited development runs but still expect successful full scale manufacturing.[194]

6.11.15 Summary

Synthetic ONs have been explored for therapeutic and diagnostic purposes for more than two decades. These efforts have presently culminated into FDA approving two drug products. Many ONs (c.100) are currently undergoing clinical trials and are at various stages of investigations. The drug development requires, apart from successful clinical trials, understanding of the quality of drug substance/drug product and proper characterization of any impurities it may contain. In this article, we have tried to describe the potential sources and measures that can be taken to control these impurities. In solid-phase ON synthesis, based on phosphoramidite chemistry, sources of impurities have been subdivided into three categories: building block-related (nucleoside-phosphoramidites), synthesis reagent-related (solid supports and ancillary reagents), and process-related impurities (side reactions during synthesis).

The structure of nucleoside-phosphoramidite related impurities has been provided for clear understandings. Of the three types of impurities present in nucleoside-phosphoramidite, only reactive and critical components are incorporated in ON synthesis and contribute to impurities in the drug substance. The nature of these potential impurities has been elucidated as far as possible. Impurities in synthesis reagents including various solid supports have been described. Potential impurities generated in the ON due to impurities found in reagents and solid supports have been illustrated, and means to alleviate and control these impurities have been suggested.

The lab-scale manufacture of ONs including critical equipment, raw material, and process options has been described in detail. ON impurities originating from the synthesis process (detritylation, coupling, capping, oxidation, or sulfurization, release of the ON from the support, and removal of protecting groups) have been explained, and possible mechanisms to their formation have been provided. Further, large-scale manufacturing equipment considerations have been summarized. Additionally, small-scale modeling approaches to develop each of the manufacturing process operations for large-scale manufacture have been described. The discussion is focused around how scalable parameters affect ON quality.

Additionally, the related analytic tools that are involved in the development of processes and used to analyze ONs are also summarized in full detail. Finally, clinical development considerations based on regulatory guidance for ON programs have been described.

6.11.16 Outlook

Over the past two decades, concurrent to ON-based therapeutic investigations, significant developments have been made in the characterization and manufacture of ONs. Analytic techniques such as strong anion-exchange HPLC, matrix-assisted light desorption ionization-time of flight (MALDI-TOF) MS, IP-RP-HPLC, HPLC-MS, UPLC, and MS/MS have been instrumental in identifying and characterizing various impurities. Impurities detected and identified in nucleoside-phosphoramidites and synthesis reagents provide a means for controlling quality of ONs. Similarly, optimizations of the manufacturing process and developments in large-scale manufacturing equipment have ensured that manufacturing technology can support the rapidly expanding ON field and maturing ON-based API pipelines. Further, strict modeling and in-process optimization minimize impurities and ensure robust manufacturing processes, thereby building confidence in the quality of ON drugs manufactured. These advancements pave the way for future ON clinical applications.

Acknowledgments

We thank Gary Burt from Avecia for providing 31P-NMR, HPLC, and mass data of phosphoramidites released by the QC Department of Avecia.

References

1. (a) Stephenson, M. L.; Zamecnik, P. C. Inhibition of Rous sarcoma viral RNA Translation by a Specific Oligodeoxyribonucleotide. *Proc. Natl. Acad. Sci. U. S. A.* **1978,** *75* (1), 285–288; (b) Zamecnik, P. C.; Stephenson, M. L. Inhibition of Rous sarcoma Virus Replication and Cell Transformation by a Specific Oligodeoxynucleotide. *Proc. Natl. Acad. Sci. U. S. A.* **1978,** *75* (1), 280–284.
2. (a) Piascik, P. Fomiversen Sodium Approved to Treat CMV Retinitis. *J. Am. Pharm. Assoc. (Wash.)* **1999,** *39* (1), 84–85; (b) Perry, C. M.; Balfour, J. A. Fomivirsen. *Drugs* **1999,** *57* (3), 375–380. discussion 381.
3. (a) Pegaptanib Sodium (Macugen) for Macular Degeneration. *Med. Lett. Drugs Ther.* **2005,** *47* (1212), 55–56; (b) Hussain, R. M.; Harris, A.; Siesky, B.; Yung, C. W.; Ehrlich, R.; Prall, R. The Effect of Pegaptanib (Macugen((R))) Injection on Retinal and Retrobulbar Blood Flow in Retinal Ischaemic Diseases. *Acta Ophthalmol.* **2015,** *93* (5), e399–e400.
4. (a) Hair, P.; Cameron, F.; McKeage, K. Mipomersen Sodium: First Global Approval. *Drugs* **2013,** *73* (5), 487–493; (b) Raal, F. J.; Santos, R. D.; Blom, D. J.; Marais, A. D.; Charng, M. J.; Cromwell, W. C.; Lachmann, R. H.; Gaudet, D.; Tan, J. L.; Chasan-Taber, S.; Tribble, D. L.; Flaim, J. D.; Crooke, S. T. Mipomersen, an Apolipoprotein B Synthesis Inhibitor, for Lowering of LDL Cholesterol Concentrations in Patients With Homozygous Familial Hypercholesterolaemia: A Randomised, Double-Blind, Placebo-Controlled Trial. *Lancet* **2010,** *375* (9719), 998–1006.
5. Lundin, K. E.; Gissberg, O.; Smith, C. I. Oligonucleotide Therapies: The Past and the Present. *Hum. Gene Ther.* **2015,** *26* (8), 475–485.
6. Eckstein, F. Phosphorothioates, Essential Components of Therapeutic Oligonucleotides. *Nucleic Acid Ther.* **2014,** *24* (6), 374–387.
7. (a) Aartsma-Rus, A. Antisense-Mediated Exon Skipping: Networking to Meet Opportunities and to Overcome Challenges. *Nucleic Acid Ther.* **2014,** *24* (1), 1–3; (b) Disterer, P.; Kryczka, A.; Liu, Y.; Badi, Y. E.; Wong, J. J.; Owen, J. S.; Khoo, B. Development of Therapeutic Splice-Switching Oligonucleotides. *Hum. Gene Ther.* **2014,** *25* (7), 587–598; (c) Kole, R.; Krainer, A. R.; Altman, S. RNA Therapeutics: Beyond RNA Interference and Antisense Oligonucleotides. *Nat. Rev. Drug Discov.* **2012,** *11* (2), 125–140.
8. Krieg, A. M.; Yi, A. K.; Matson, S.; Waldschmidt, T. J.; Bishop, G. A.; Teasdale, R.; Koretzky, G. A.; Klinman, D. M. CpG Motifs in Bacterial DNA Trigger Direct B-Cell Activation. *Nature* **1995,** *374* (6522), 546–549.
9. Hemmi, H.; Takeuchi, O.; Kawai, T.; Kaisho, T.; Sato, S.; Sanjo, H.; Matsumoto, M.; Hoshino, K.; Wagner, H.; Takeda, K.; Akira, S. A Toll-Like Receptor Recognizes Bacterial DNA. *Nature* **2000,** *408* (6813), 740–745.
10. (a) Kandimalla, E. R.; Bhagat, L.; Wang, D.; Yu, D.; Sullivan, T.; La Monica, N.; Agrawal, S. Design, Synthesis and Biological Evaluation of Novel Antagonist Compounds of Toll-Like Receptors 7, 8 and 9. *Nucleic Acids Res.* **2013,** *41* (6), 3947–3961; (b) Krieg, A. M. CpG Still Rocks! Update on an Accidental Drug. *Nucleic Acid Ther.* **2012,** *22* (2), 77–89.
11. (a) Tuerk, C.; Gold, L. Systematic Evolution of Ligands by Exponential Enrichment: RNA Ligands to Bacteriophage T4 DNA Polymerase. *Science* **1990,** *249* (4968), 505–510; (b) Ellington, A. D.; Szostak, J. W. In Vitro Selection of RNA Molecules That Bind Specific Ligands. *Nature* **1990,** *346* (6287), 818–822.
12. (a) Zhou, J.; Rossi, J. J. Cell-Type-Specific, Aptamer-Functionalized Agents for Targeted Disease Therapy. *Mol. Ther. Nucleic Acids* **2014,** *3*, e169; (b) Keefe, A. D.; Pai, S.; Ellington, A. Aptamers as Therapeutics. *Nat. Rev. Drug Discov.* **2010,** *9* (7), 537–550; (c) Hoellenriegel, J.; Zboralski, D.; Maasch, C.; Rosin, N. Y.; Wierda, W. G.; Keating, M. J.; Kruschinski, A.; Burger, J. A. The Spiegelmer NOX-A12, a Novel CXCL12 Inhibitor, Interferes With Chronic Lymphocytic Leukemia Cell Motility and Causes Chemosensitization. *Blood* **2014,** *123* (7), 1032–1039; (d) Bouchard, P. R.; Hutabarat, R. M.; Thompson, K. M. Discovery and Development of Therapeutic Aptamers. *Annu. Rev. Pharmacol. Toxicol.* **2010,** *50,* 237–257.
13. (a) Ozaki, K.; Makino, H.; Aoki, M.; Miyake, T.; Yasumasa, N.; Osako, M. K.; Nakagami, H.; Rakugi, H.; Morishita, R. Therapeutic Effect of Ribbon-Type Nuclear Factor-KappaB Decoy Oligonucleotides in a Rat Model of Inflammatory Bowel Disease. *Curr. Gene Ther.* **2012,** *12* (6), 484–492; (b) D'Acquisto, F.; Ialenti, A.; Ianaro, A.; Di Vaio, R.; Carnuccio, R. Local Administration of Transcription Factor Decoy Oligonucleotides to Nuclear Factor-KappaB Prevents Carrageenin-Induced Inflammation in Rat Hind Paw. *Gene Ther.* **2000,** *7* (20), 1731–1737; (c) De Stefano, D.; De Rosa, G.; Carnuccio, R. NFkappaB Decoy Oligonucleotides. *Curr. Opin. Mol. Ther.* **2010,** *12* (2), 203–213; (d) Dajee, M.; Muchamuel, T.; Schryver, B.; Oo, A.; Alleman-Sposeto, J.; De Vry, C. G.; Prasad, S.; Ruhrmund, D.; Shyamsundar, R.; Mutnick, D.; Mai, K.; Le, T.; Parham, C.; Zhang, J.; Komuves, L.; Colby, T.; Hudak, S.; McEvoy, L. M.; Ehrhardt, R. O. Blockade of Experimental Atopic Dermatitis via Topical NF-kappaB Decoy Oligonucleotide. *J. Invest. Dermatol.* **2006,** *126* (8), 1792–1803; (e) Nakamura, H.; Aoki, M.; Tamai, K.; Oishi, M.; Ogihara, T.; Kaneda, Y.; Morishita, R. Prevention and Regression of Atopic Dermatitis by Ointment Containing NF-kB Decoy Oligodeoxynucleotides in NC/Nga Atopic Mouse Model. *Gene Ther.* **2002,** *9* (18), 1221–1229.
14. (a) Suzuki, J.; Tezuka, D.; Morishita, R.; Isobe, M. An Initial Case of Suppressed Restenosis With Nuclear Factor-Kappa B Decoy Transfection After Percutaneous Coronary Intervention. *J. Gene Med.* **2009,** *11* (1), 89–91; (b) Egashira, K.; Suzuki, J.; Ito, H.; Aoki, M.; Isobe, M.; Morishita, R. Long-Term Follow up of Initial Clinical Cases With NF-KappaB Decoy Oligodeoxynucleotide Transfection at the Site of Coronary Stenting. *J. Gene Med.* **2008,** *10* (7), 805–809.
15. (a) Igawa, K.; Satoh, T.; Yokozeki, H. A Therapeutic Effect of STAT6 Decoy Oligodeoxynucleotide Ointment in Atopic Dermatitis: A Pilot Study in Adults. *Br. J. Dermatol.* **2009,** *160* (5), 1124–1126; (b) Stadlbauer, T. H.; Wagner, A. H.; Holschermann, H.; Fiedel, S.; Fingerhuth, H.; Tillmanns, H.; Bohle, R. M.; Hecker, M. AP-1 and STAT-1 Decoy Oligodeoxynucleotides Attenuate Transplant Vasculopathy in Rat Cardiac Allografts. *Cardiovasc. Res.* **2008,** *79* (4), 698–705.
16. Fire, A.; Xu, S.; Montgomery, M. K.; Kostas, S. A.; Driver, S. E.; Mello, C. C. Potent and Specific Genetic Interference by Double-Stranded RNA in *Caenorhabditis elegans*. *Nature* **1998,** *391* (6669), 806–811.
17. Hamilton, A. J.; Baulcombe, D. C. A Species of Small Antisense RNA in Posttranscriptional Gene Silencing in Plants. *Science* **1999,** *286* (5441), 950–952.

18. Wang, Z.; Rao, D. D.; Senzer, N.; Nemunaitis, J. RNA Interference and Cancer Therapy. *Pharm. Res.* **2011,** *28* (12), 2983–2995.
19. (a) Martinez, J.; Patkaniowska, A.; Urlaub, H.; Luhrmann, R.; Tuschl, T. Single-Stranded Antisense siRNAs Guide Target RNA Cleavage in RNAi. *Cell* **2002,** *110* (5), 563–574; (b) Zamore, P. D.; Tuschl, T.; Sharp, P. A.; Bartel, D. P. RNAi: Double-Stranded RNA Directs the ATP-Dependent Cleavage of mRNA at 21 to 23 Nucleotide Intervals. *Cell* **2000,** *101* (1), 25–33.
20. Deng, Y.; Wang, C. C.; Choy, K. W.; Du, Q.; Chen, J.; Wang, Q.; Li, L.; Chung, T. K.; Tang, T. Therapeutic Potentials of Gene Silencing by RNA Interference: Principles, Challenges, and New Strategies. *Gene* **2014,** *538* (2), 217–227.
21. Watts, J. K.; Yu, D.; Charisse, K.; Montaillier, C.; Potier, P.; Manoharan, M.; Corey, D. R. Effect of Chemical Modifications on Modulation of Gene Expression by Duplex Antigene RNAs That Are Complementary to Non-coding Transcripts at Gene Promoters. *Nucleic Acids Res.* **2010,** *38* (15), 5242–5259.
22. (a) Elbashir, S. M.; Harborth, J.; Lendeckel, W.; Yalcin, A.; Weber, K.; Tuschl, T. Duplexes of 21-Nucleotide RNAs Mediate RNA Interference in Cultured Mammalian Cells. *Nature* **2001,** *411* (6836), 494–498; (b) Robb, G. B.; Brown, K. M.; Khurana, J.; Rana, T. M. Specific and Potent RNAi in the Nucleus of Human Cells. *Nat. Struct. Mol. Biol.* **2005,** *12* (2), 133–137.
23. Wittrup, A.; Lieberman, J. Knocking Down Disease: A Progress Report on siRNA Therapeutics. *Nat. Rev. Genet.* **2015,** *16* (9), 543–552.
24. Ling, H.; Fabbri, M.; Calin, G. A. MicroRNAs and Other Non-coding RNAs as Targets for Anticancer Drug Development. *Nat. Rev. Drug Discov.* **2013,** *12* (11), 847–865.
25. John, B.; Enright, A. J.; Aravin, A.; Tuschl, T.; Sander, C.; Marks, D. S. Human MicroRNA Targets. *PLoS Biol.* **2004,** *2* (11), e363.
26. Aagaard, L.; Rossi, J. J. RNAi Therapeutics: Principles, Prospects and Challenges. *Adv. Drug Deliv. Rev.* **2007,** *59* (2-3), 75–86.
27. (a) Li, Z.; Rana, T. M. Therapeutic Targeting of microRNAs: Current Status and Future Challenges. *Nat. Rev. Drug Discov.* **2014,** *13* (8), 622–638; (b) Taylor, M. A.; Schiemann, W. P. Therapeutic Opportunities for Targeting microRNAs in Cancer. *Mol. Cell Ther.* **2014,** *2* (30), 1–13; (c) Tutar, L.; Tutar, E.; Ozgur, A.; Tutar, Y. Therapeutic Targeting of microRNAs in Cancer: Future Perspectives. *Drug Dev. Res.* **2015,** *76* (7), 382–388.
28. (a) Singh, Y.; Murat, P.; Defrancq, E. Recent Developments in Oligonucleotide Conjugation. *Chem. Soc. Rev.* **2010,** *39* (6), 2054–2070; (b) Juliano, R. L.; Ming, X.; Nakagawa, O. The Chemistry and Biology of Oligonucleotide Conjugates. *Acc. Chem. Res.* **2012,** *45* (7), 1067–1076; (c) Marlin, F.; Simon, P.; Saison-Behmoaras, T.; Giovannangeli, C. Delivery of Oligonucleotides and Analogues: The Oligonucleotide Conjugate-Based Approach. *Chembiochem* **2010,** *11* (11), 1493–1500.
29. Deleavey, G. F.; Damha, M. J. Designing Chemically Modified Oligonucleotides for Targeted Gene Silencing. *Chem. Biol.* **2012,** *19* (8), 937–954.
30. Eckstein, F. Nucleoside Phosphorothioates. *J. Am. Chem. Soc.* **1966,** *88,* 4292–4294.
31. (a) Guga, P.; Stec, W. J. Synthesis of Phosphorothioate Oligonucleotides With Stereodefined Phosphorothioate Linkages. *Curr. Protoc. Nucleic Acid Chem.* **2003**. Chapter 4, Unit 4 17; (b) Yang, X. B.; Sierzchala, A.; Misiura, K.; Niewiarowski, W.; Sochacki, M.; Stec, W. J.; Wieczorek, M. W. The First Stereocontrolled Solid-Phase Synthesis of Di-, Tri-, and Tetra[adenosine (2',5') phosphorothioate]s. *J. Org. Chem.* **1998,** *63* (20), 7097–7100; (c) Stec, W. J.; Karwowski, B.; Boczkowska, M.; Guga, P.; Koziolkiewicz, M.; Sochacki, M.; Wieczorek, M. W.; Blaszczyk, J. Deoxyribonucleoside 3'-O-(2-thio- and 2-oxo-"spiro"-4,4-Pentamethylene-1,2,3-Oxathiaphospholane)s: Monomers for Stereocontrolled Synthesis of Oligo(Deoxyribonucleoside Phosphorothioate)s and Chimeric PS/PO Oligonucleotides. *J. Am. Chem. Soc.* **1998,** *120,* 7156–7167.
32. (a) Oka, N.; Kondo, T.; Fujiwara, S.; Maizuru, Y.; Wada, T. Stereocontrolled Synthesis of Oligoribonucleoside Phosphorothioates by an Oxazaphospholidine Approach. *Org. Lett.* **2009,** *11* (4), 967–970; (b) Oka, N.; Yamamoto, M.; Sato, T.; Wada, T. Solid-Phase Synthesis of Stereoregular Oligodeoxyribonucleoside Phosphorothioates Using Bicyclic Oxazaphospholidine Derivatives as Monomer Units. *J. Am. Chem. Soc.* **2008,** *130* (47), 16031–16037.
33. Meena, M.; Butler, D.; Iwamoto, N.; Svrzikapa, N.; Verdine, G. L.; Zlatev, I. Chiral Design. WO2015107425, 2015.
34. Egholm, M.; Buchardt, O.; Christensen, L.; Behrens, C.; Freier, S. M.; Driver, D. A.; Berg, R. H.; Kim, S. K.; Norden, B.; Nielsen, P. E. PNA Hybridizes to Complementary Oligonucleotides Obeying the Watson-Crick Hydrogen-Bonding Rules. *Nature* **1993,** *365* (6446), 566–568.
35. Demidov, V. V.; Potaman, V. N.; Frank-Kamenetskii, M. D.; Egholm, M.; Buchard, O.; Sonnichsen, S. H.; Nielsen, P. E. Stability of Peptide Nucleic Acids in Human Serum and Cellular Extracts. *Biochem. Pharmacol.* **1994,** *48* (6), 1310–1313.
36. Uhlmann, E. Peptide Nucleic Acids (PNA) and PNA-DNA Chimeras: From High Binding Affinity Towards Biological Function. *Biol. Chem.* **1998,** *379* (8/9), 1045–1052.
37. Bennett, C. F.; Swayze, E. E. RNA Targeting Therapeutics: Molecular Mechanisms of Antisense Oligonucleotides as a Therapeutic Platform. *Annu. Rev. Pharmacol. Toxicol.* **2010,** *50,* 259–293.
38. Potenza, N.; Moggio, L.; Milano, G.; Salvatore, V.; Di Blasio, B.; Russo, A.; Messere, A. RNA Interference in Mammalia Cells by RNA-3'-PNA Chimeras. *Int. J. Mol. Sci.* **2008,** *9* (3), 299–315.
39. Nielsen, P. E. Peptide Nucleic Acids (PNA) in Chemical Biology and Drug Discovery. *Chem. Biodivers.* **2010,** *7* (4), 786–804.
40. (a) Abes, S.; Turner, J. J.; Ivanova, G. D.; Owen, D.; Williams, D.; Arzumanov, A.; Clair, P.; Gait, M. J.; Lebleu, B. Efficient Splicing Correction by PNA Conjugation to an R6-Penetratin Delivery Peptide. *Nucleic Acids Res.* **2007,** *35* (13), 4495–4502; (b) Wancewicz, E. V.; Maier, M. A.; Siwkowski, A. M.; Albertshofer, K.; Winger, T. M.; Berdeja, A.; Gaus, H.; Vickers, T. A.; Bennett, C. F.; Monia, B. P.; Griffey, R. H.; Nulf, C. J.; Hu, J.; Corey, D. R.; Swayze, E. E.; Kinberger, G. A. Peptide Nucleic Acids Conjugated to Short Basic Peptides Show Improved Pharmacokinetics and Antisense Activity in Adipose Tissue. *J. Med. Chem.* **2010,** *53* (10), 3919–3926.
41. Gryaznov, S. M.; Lloyd, D. H.; Chen, J. K.; Schultz, R. G.; DeDionisio, L. A.; Ratmeyer, L.; Wilson, W. D. Oligonucleotide N3'−>P5' Phosphoramidates. *Proc. Natl. Acad. Sci. U. S. A.* **1995,** *92* (13), 5798–5802.
42. Gryaznov, S. M. Oligonucleotide n3'−>p5' Phosphoramidates and Thio-Phoshoramidates as Potential Therapeutic Agents. *Chem. Biodivers.* **2010,** *7* (3), 477–493.
43. Heidenreich, O.; Gryaznov, S.; Nerenberg, M. RNase H-Independent Antisense Activity of Oligonucleotide N3'−>P5' Phosphoramidates. *Nucleic Acids Res.* **1997,** *25* (4), 776–780.
44. Pongracz, K.; Gryaznov, S. M. alpha-Oligodeoxyribonucleotide N3'−>P5' Phosphoramidates: Synthesis and Duplex Formation. *Nucleic Acids Res.* **1998,** *26* (4), 1099–1106.
45. (a) Chiappori, A. A.; Kolevska, T.; Spigel, D. R.; Hager, S.; Rarick, M.; Gadgeel, S.; Blais, N.; Von Pawel, J.; Hart, L.; Reck, M.; Bassett, E.; Burington, B.; Schiller, J. H. A Randomized Phase II Study of the Telomerase Inhibitor Imetelstat as Maintenance Therapy for Advanced Non-Small-Cell Lung Cancer. *Ann. Oncol.* **2015,** *26* (2), 354–362; (b) Koziel, J. E.; Herbert, B. S. The Telomerase Inhibitor Imetelstat Alone, and in Combination With Trastuzumab, Decreases the Cancer Stem Cell Population and Self-Renewal of HER2+ Breast Cancer Cells. *Breast Cancer Res. Treat.* **2015,** *149* (3), 607–618; (c) Tefferi, A.; Lasho, T. L.; Begna, K. H.; Patnaik, M. M.; Zblewski, D. L.; Finke, C. M.; Laborde, R. R.; Wassie, E.; Schimek, L.; Hanson, C. A.; Gangat, N.; Wang, X.; Pardanani, A. A Pilot Study of the Telomerase Inhibitor Imetelstat for Myelofibrosis. *N. Engl. J. Med.* **2015,** *373* (10), 908–919; (d) Bjorn, M. E.; Nielsen, C. H.; Hasselbalch, H. C. Telomerase Inhibitor Imetelstat in Essential Thrombocythemia and Myelofibrosis. *N. Engl. J. Med.* **2015,** *373* (26), 2579–2580; (e) Baerlocher, G. M.; Oppliger Leibundgut, E.; Ottmann, O. G.; Spitzer, G.; Odenike, O.; McDevitt, M. A.; Roth, A.; Daskalakis, M.; Burington, B.; Stuart, M.; Snyder, D. S. Telomerase Inhibitor Imetelstat in Patients With Essential Thrombocythemia. *N. Engl. J. Med.* **2015,** *373* (10), 920–928.
46. (a) Summerton, J. Morpholino Antisense Oligomers: The Case for an RNase H-Independent Structural Type. *Biochim. Biophys. Acta* **1999,** *1489* (1), 141; (b) Du, L.; Gatti, R. A. Potential Therapeutic Applications of Antisense Morpholino Oligonucleotides in Modulation of Splicing in Primary Immunodeficiency Diseases. *J. Immunol. Methods* **2011,** *365* (1-2), 1–7.
47. Summerton, J.; Weller, D. Morpholino Antisense Oligomers: Design, Preparation, and Properties. *Antisense Nucleic Acid Drug Dev.* **1997,** *7* (3), 187–195.
48. (a) Arechavala-Gomeza, V.; Anthony, K.; Morgan, J.; Muntoni, F. Antisense Oligonucleotide-Mediated Exon Skipping for Duchenne Muscular Dystrophy: Progress and Challenges. *Curr. Gene Ther.* **2012,** *12* (3), 152–160; (b) Mendell, J. R.; Rodino-Klapac, L. R.; Sahenk, Z.; Roush, K.; Bird, L.; Lowes, L. P.; Alfano, L.; Gomez, A. M.; Lewis, S.; Kota, J.; Malik, V.; Shontz, K.; Walker, C. M.; Flanigan, K. M.; Corridore, M.; Kean, J. R.; Allen, H. D.; Shilling, C.; Melia, K. R.; Sazani, P.; Saoud, J. B.; Kaye, E. M.; Eteplirsen Study, G. Eteplirsen for the Treatment of Duchenne Muscular Dystrophy. *Ann. Neurol.* **2013,** *74* (5), 637–647; (c) Mendell, J. R.; Goemans, N.; Lowes, L. P.; Alfano, L. N.; Berry, K.; Shao, J.; Kaye, E. M.; Mercuri, E.; Eteplirsen Study Group and Telethon Foundation DMD Italian Network. Longitudinal Effect of Eteplirsen vs. Historical Control on Ambulation in DMD. *Ann. Neurol.* **2016,** *79,* 257–271.
49. Ming, X.; Laing, B. Bioconjugates for Targeted Delivery of Therapeutic Oligonucleotides. *Adv. Drug Deliv. Rev.* **2015,** *87,* 81–89.

50. (a) Patwa, A.; Gissot, A.; Bestel, I.; Barthelemy, P. Hybrid Lipid Oligonucleotide Conjugates: Synthesis, Self-Assemblies and Biomedical Applications. *Chem. Soc. Rev.* **2011,** *40* (12), 5844–5854; (b) Lorenz, C.; Hadwiger, P.; John, M.; Vornlocher, H. P.; Unverzagt, C. Steroid and Lipid Conjugates of siRNAs to Enhance Cellular Uptake and Gene Silencing in Liver Cells. *Bioorg. Med. Chem. Lett.* **2004,** *14* (19), 4975–4977.
51. Sun, H.; Zhu, X.; Lu, P. Y.; Rosato, R. R.; Tan, W.; Zu, Y. Oligonucleotide Aptamers: New Tools for Targeted Cancer Therapy. *Mol. Ther. Nucleic Acids* **2014,** *3*.
52. Bailon, P.; Won, C. Y. PEG-Modified Biopharmaceuticals. *Expert Opin. Drug Deliv.* **2009,** *6* (1), 1–16.
53. Coursindel, T.; Jarver, P.; Gait, M. J. Peptide-Based in vivo Delivery Agents for Oligonucleotides and siRNA. *Nucleic Acid Ther.* **2012,** *22* (2), 71–76.
54. (a) Nair, J. K.; Willoughby, J. L.; Chan, A.; Charisse, K.; Alam, M. R.; Wang, Q.; Hoekstra, M.; Kandasamy, P.; Kel'in, A. V.; Milstein, S.; Taneja, N.; O'Shea, J.; Shaikh, S.; Zhang, L.; van der Sluis, R. J.; Jung, M. E.; Akinc, A.; Hutabarat, R.; Kuchimanchi, S.; Fitzgerald, K.; Zimmermann, T.; van Berkel, T. J.; Maier, M. A.; Rajeev, K. G.; Manoharan, M. Multivalent N-Acetylgalactosamine-Conjugated siRNA Localizes in Hepatocytes and Elicits Robust RNAi-Mediated Gene Silencing. *J. Am. Chem. Soc.* **2014,** *136* (49), 16958–16961; (b) Matsuda, S.; Keiser, K.; Nair, J. K.; Charisse, K.; Manoharan, R. M.; Kretschmer, P.; Peng, C. G.; V Kel'in, A.; Kandasamy, P.; Willoughby, J. L.; Liebow, A.; Querbes, W.; Yucius, K.; Nguyen, T.; Milstein, S.; Maier, M. A.; Rajeev, K. G.; Manoharan, M. siRNA Conjugates Carrying Sequentially Assembled Trivalent N-Acetylgalactosamine Linked Through Nucleosides Elicit Robust Gene Silencing In Vivo in Hepatocytes. *ACS Chem. Biol.* **2015,** *10* (5), 1181–1187; (c) Prakash, T. P.; Graham, M. J.; Yu, J.; Carty, R.; Low, A.; Chappell, A.; Schmidt, K.; Zhao, C.; Aghajan, M.; Murray, H. F.; Riney, S.; Booten, S. L.; Murray, S. F.; Gaus, H.; Crosby, J.; Lima, W. F.; Guo, S.; Monia, B. P.; Swayze, E. E.; Seth, P. P. Targeted Delivery of Antisense Oligonucleotides to Hepatocytes Using Triantennary N-Acetyl Galactosamine Improves Potency 10-fold in Mice. *Nucleic Acids Res.* **2014,** *42* (13), 8796–8807; (d) Prakash, T. P.; Brad Wan, W.; Low, A.; Yu, J.; Chappell, A. E.; Gaus, H.; Kinberger, G. A.; Ostergaard, M. E.; Migawa, M. T.; Swayze, E. E.; Seth, P. P. Solid-Phase Synthesis of 5'-Triantennary N-Acetylgalactosamine Conjugated Antisense Oligonucleotides Using Phosphoramidite Chemistry. *Bioorg. Med. Chem. Lett.* **2015,** *25* (19), 4127–4130; (e) Yamamoto, T.; Sawamura, M.; Wada, F.; Harada-Shiba, M.; Obika, S. Serial Incorporation of a Monovalent GalNAc Phosphoramidite Unit Into Hepatocyte-Targeting Antisense Oligonucleotides. *Bioorg. Med. Chem.* **2016,** *24* (1), 26–32.
55. (a) Manoharan, M. Oligonucleotide Conjugates as Potential Antisense Drugs With Improved Uptake, Biodistribution, Targeted Delivery, and Mechanism of Action. *Antisense Nucleic Acid Drug Dev.* **2002,** *12* (2), 103–128; (b) Lonnberg, H. Solid-Phase Synthesis of Oligonucleotide Conjugates Useful for Delivery and Targeting of Potential Nucleic Acid Therapeutics. *Bioconjug. Chem.* **2009,** *20* (6), 1065–1094.
56. (a) Altona, C.; Sundaralingam, M. Conformational Analysis of the Sugar Ring in Nucleosides and Nucleotides. A New Description Using the Concept of Pseudorotation. *J. Am. Chem. Soc.* **1972,** *94* (23), 8205–8212; (b) Blackburn, G. M.; Gait, M. G.; Loakes, D. *Nucleic Acids in Chemistry and Biology;* IRL Press at Oxford University Press: Oxford, England, New York, 2006; pp. 13–76.
57. Majlessi, M.; Nelson, N. C.; Becker, M. M. Advantages of 2'-O-Methyl Oligoribonucleotide Probes for Detecting RNA Targets. *Nucleic Acids Res.* **1998,** *26* (9), 2224–2229.
58. Rettig, G. R.; Behlke, M. A. Progress Toward In Vivo Use of siRNAs-II. *Mol. Ther.* **2012,** *20* (3), 483–512.
59. (a) Kawai, G.; Yamamoto, Y.; Kamimura, T.; Masegi, T.; Sekine, M.; Hata, T.; Iimori, T.; Watanabe, T.; Miyazawa, T.; Yokoyama, S. Conformational Rigidity of Specific Pyrimidine Residues in tRNA Arises From Posttranscriptional Modifications That Enhance Steric Interaction Between the Base and the 2'-Hydroxyl Group. *Biochemistry* **1992,** *31* (4), 1040–1046; (b) Nishizaki, T.; Iwai, S.; Ohtsuka, E.; Nakamura, H. Solution Structure of an RNA.2'-O-Methylated RNA Hybrid Duplex Containing an RNA.DNA Hybrid Segment at the Center. *Biochemistry* **1997,** *36* (9), 2577–2585.
60. (a) Sharma, V. K.; Sharma, R. K.; Singh, S. K. Antisense Oligonucleotides: Modifications and Clinical Trials. *Med. Chem. Commun.* **2014,** *5,* 1454–1471; (b) Sharma, V. K.; Watts, J. K. Oligonucleotide Therapeutics: Chemistry, Delivery and Clinical Progress. *Future Med. Chem.* **2015,** *7* (16), 2221–2242.
61. Ng, E. W.; Shima, D. T.; Calias, P.; Cunningham, E. T., Jr.; Guyer, D. R.; Adamis, A. P. Pegaptanib, a Targeted Anti-VEGF Aptamer for Ocular Vascular Disease. *Nat. Rev. Drug Discov.* **2006,** *5* (2), 123–132.
62. (a) Czauderna, F.; Fechtner, M.; Dames, S.; Aygun, H.; Klippel, A.; Pronk, G. J.; Giese, K.; Kaufmann, J. Structural Variations and Stabilising Modifications of Synthetic siRNAs in Mammalian Cells. *Nucleic Acids Res.* **2003,** *31* (11), 2705–2716; (b) Deleavey, G. F.; Watts, J. K.; Damha, M. J. Chemical Modification of siRNA. *Curr. Protoc. Nucleic Acid Chem.* **2009**. Chapter 16, Unit 16 3.
63. Whitehead, K. A.; Dahlman, J. E.; Langer, R. S.; Anderson, D. G. Silencing or Stimulation? siRNA Delivery and the Immune System. *Annu. Rev. Chem. Biomol. Eng.* **2011,** *2,* 77–96.
64. (a) Manoharan, M. 2'-Carbohydrate Modifications in Antisense Oligonucleotide Therapy: Importance of Conformation, Configuration and Conjugation. *Biochim. Biophys. Acta* **1999,** *1489* (1), 117; (b) Viazovkina, E.; Mangos, M. M.; Elzagheid, M. I.; Damha, M. J. Solid-Phase Synthesis of 2'-deoxy-2'-fluoro- beta-D-Oligoarabinonucleotides (2'F-ANA) and Their Phosphorothioate Derivatives. *Curr. Protoc. Nucleic Acid Chem.* **2002**. Chapter 4, Unit 4 15.
65. Prakash, T. P. An Overview of Sugar-Modified Oligonucleotides for Antisense Therapeutics. *Chem. Biodivers.* **2011,** *8* (9), 1616–1641.
66. Ikeda, H.; Fernandez, R.; Wilk, A.; Barchi, J. J., Jr.; Huang, X.; Marquez, V. E. The Effect of Two Antipodal Fluorine-Induced Sugar Puckers on the Conformation and Stability of the Dickerson-Drew Dodecamer Duplex [d(CGCGAATTCGCG)]2. *Nucleic Acids Res.* **1998,** *26* (9), 2237–2244.
67. Kawasaki, A. M.; Casper, M. D.; Freier, S. M.; Lesnik, E. A.; Zounes, M. C.; Cummins, L. L.; Gonzalez, C.; Cook, P. D. Uniformly Modified 2'-deoxy-2'-fluoro Phosphorothioate Oligonucleotides as Nuclease-Resistant Antisense Compounds With High Affinity and Specificity for RNA Targets. *J. Med. Chem.* **1993,** *36* (7), 831–841.
68. Watts, J. K.; Deleavey, G. F.; Damha, M. J. Chemically Modified siRNA: Tools and Applications. *Drug Discov. Today* **2008,** *13* (19-20), 842–855.
69. Allerson, C. R.; Sioufi, N.; Jarres, R.; Prakash, T. P.; Naik, N.; Berdeja, A.; Wanders, L.; Griffey, R. H.; Swayze, E. E.; Bhat, B. Fully 2'-Modified Oligonucleotide Duplexes With Improved In Vitro Potency and Stability Compared to Unmodified Small Interfering RNA. *J. Med. Chem.* **2005,** *48* (4), 901–904.
70. (a) Koshkin, A. A.; Singh, S. K.; Nielsen, P.; Rajwanshi, V. K.; Kumar, R.; Meldgaard, M.; Olsen, C. E.; Wengel, J. LNA (Locked Nucleic Acids): Synthesis of the Adenine, Cytosine, Guanine, 5-Methylcytosine, Thymine and Uracil Bicyclonucleoside Monomers, Oligomerisation, and Unprecedented Nucleic Acid Recognition. *Tetrahedron* **1998,** *54,* 3607–3630; (b) Obika, S.; Nanbu, D.; Hari, Y.; Andoh, J.; Morio, K.; Doi, T.; Imanishi, T. Stability and Structural Features of the Duplexes Containing Nucleoside Analogues With a Fixed N-Type Conformation, 2'-O,4'-C-Methyleneribonucleosides. *Tetrahedron Lett.* **1998,** *39* (23), 5401–5404.
71. Braasch, D. A.; Corey, D. R. Locked Nucleic Acid (LNA): Fine-Tuning the Recognition of DNA and RNA. *Chem. Biol.* **2001,** *8* (1), 1–7.
72. Lennox, K. A.; Behlke, M. A. Chemical Modification and Design of Anti-miRNA Oligonucleotides. *Gene Ther.* **2011,** *18* (12), 1111–1120. http://dx.doi.org/10.1038/gt.2011.100.
73. (a) Braasch, D. A.; Jensen, S.; Liu, Y.; Kaur, K.; Arar, K.; White, M. A.; Corey, D. R. RNA Interference in Mammalian Cells by Chemically-Modified RNA. *Biochemistry* **2003,** *42* (26), 7967–7975; (b) Elmen, J.; Thonberg, H.; Ljungberg, K.; Frieden, M.; Westergaard, M.; Xu, Y.; Wahren, B.; Liang, Z.; Orum, H.; Koch, T.; Wahlestedt, C. Locked Nucleic Acid (LNA) Mediated Improvements in siRNA Stability and Functionality. *Nucleic Acids Res.* **2005,** *33* (1), 439–447; (c) Hornung, V.; Guenthner-Biller, M.; Bourquin, C.; Ablasser, A.; Schlee, M.; Uematsu, S.; Noronha, A.; Manoharan, M.; Akira, S.; de Fougerolles, A.; Endres, S.; Hartmann, G. Sequence-Specific Potent Induction of IFN-Alpha by Short Interfering RNA in Plasmacytoid Dendritic Cells Through TLR7. *Nat. Med.* **2005,** *11* (3), 263–270; (d) Bramsen, J. B.; Laursen, M. B.; Damgaard, C. K.; Lena, S. W.; Babu, B. R.; Wengel, J.; Kjems, J. Improved Silencing Properties Using Small Internally Segmented Interfering RNAs. *Nucleic Acids Res.* **2007,** *35* (17), 5886–5897; (e) Mook, O. R.; Baas, F.; de Wissel, M. B.; Fluiter, K. Evaluation of Locked Nucleic Acid-Modified Small Interfering RNA In Vitro and In Vivo. *Mol. Cancer Ther.* **2007,** *6* (3), 833–843.
74. Wahlestedt, C.; Salmi, P.; Good, L.; Kela, J.; Johnsson, T.; Hokfelt, T.; Broberger, C.; Porreca, F.; Lai, J.; Ren, K.; Ossipov, M.; Koshkin, A.; Jakobsen, N.; Skouv, J.; Oerum, H.; Jacobsen, M. H.; Wengel, J. Potent and Nontoxic Antisense Oligonucleotides Containing Locked Nucleic Acids. *Proc. Natl. Acad. Sci. U. S. A.* **2000,** *97* (10), 5633–5638.
75. (a) Marquez, V. E.; Siddiqui, M. A.; Ezzitouni, A.; Russ, P.; Wang, J.; Wagner, R. W.; Matteucci, M. D. Nucleosides With a Twist. Can Fixed Forms of Sugar Ring Pucker Influence Biological Activity in Nucleosides and Oligonucleotides? *J. Med. Chem.* **1996,** *39* (19), 3739–3747; (b) Terrazas, M.; Ocampo, S. M.; Perales, J. C.; Marquez, V. E.; Eritja, R. Effect of North Bicyclo[3.1.0]hexane 2'-Deoxy-Pseudosugars on RNA Interference: A Novel Class of siRNA Modification. *Chembiochem* **2011,** *12* (7), 1056–1065.
76. (a) Renneberg, D.; Bouliong, E.; Reber, U.; Schumperli, D.; Leumann, C. J. Antisense Properties of Tricyclo-DNA. *Nucleic Acids Res.* **2002,** *30* (13), 2751–2757; (b) Ittig, D.; Luisier, S.; Weiler, J.; Schumperli, D.; Leumann, C. J. Improving Gene Silencing of siRNAs via Tricyclo-DNA Modification. *Artif. DNA PNA XNA* **2010,** *1* (1), 9–16.

77. Mangos, M. M.; Min, K. L.; Viazovkina, E.; Galarneau, A.; Elzagheid, M. I.; Parniak, M. A.; Damha, M. J. Efficient RNase H-Directed Cleavage of RNA Promoted by Antisense DNA or 2'F-ANA Constructs Containing Acyclic Nucleotide Inserts. *J. Am. Chem. Soc.* **2003,** *125* (3), 654–661.
78. Campbell, M. A.; Wengel, J. Locked vs. Unlocked Nucleic Acids (LNA vs. UNA): Contrasting Structures Work Towards Common Therapeutic Goals. *Chem. Soc. Rev.* **2011,** *40* (12), 5680–5689.
79. Vaish, N.; Chen, F.; Seth, S.; Fosnaugh, K.; Liu, Y.; Adami, R.; Brown, T.; Chen, Y.; Harvie, P.; Johns, R.; Severson, G.; Granger, B.; Charmley, P.; Houston, M.; Templin, M. V.; Polisky, B. Improved Specificity of Gene Silencing by siRNAs Containing Unlocked Nucleobase Analogs. *Nucleic Acids Res.* **2011,** *39* (5), 1823–1832.
80. Herdewijn, P. Heterocyclic Modifications of Oligonucleotides and Antisense Technology. *Antisense Nucleic Acid Drug Dev.* **2000,** *10* (4), 297–310.
81. Peacock, H.; Kannan, A.; Beal, P. A.; Burrows, C. J. Chemical Modification of siRNA Bases to Probe and Enhance RNA Interference. *J. Org. Chem.* **2011,** *76* (18), 7295–7300.
82. (a) Sanghvi, Y. S.; Hoke, G. D.; Freier, S. M.; Zounes, M. C.; Gonzalez, C.; Cummins, L.; Sasmor, H.; Cook, P. D. Antisense Oligodeoxynucleotides: Synthesis, Biophysical and Biological Evaluation of Oligodeoxynucleotides Containing Modified Pyrimidines. *Nucleic Acids Res.* **1993,** *21* (14), 3197–3203; (b) Revenkar, G. R.; Rao, T. S. DNA With Altered Bases. In *Comprehensive Natural Products Chemistry: DNA and Aspects of Molecular Biology;* Kool, E. T., Ed.; Pergamon Press: Oxford, 1999; pp 313–339.
83. Chiu, Y. L.; Rana, T. M. siRNA Function in RNAi: A Chemical Modification Analysis. *RNA* **2003,** *9* (9), 1034–1048.
84. Freier, S. M.; Altmann, K. H. The Ups and Downs of Nucleic Acid Duplex Stability: Structure-Stability Studies on Chemically-Modified DNA:RNA Duplexes. *Nucleic Acids Res.* **1997,** *25* (22), 4429–4443.
85. Shen, L.; Siwkowski, A.; Wancewicz, E. V.; Lesnik, E.; Butler, M.; Witchell, D.; Vasquez, G.; Ross, B.; Acevedo, O.; Inamati, G.; Sasmor, H.; Manoharan, M.; Monia, B. P. Evaluation of C-5 Propynyl Pyrimidine-Containing Oligonucleotides In Vitro and In Vivo. *Antisense Nucleic Acid Drug Dev.* **2003,** *13* (3), 129–142.
86. Watson, J. D.; Crick, F. H. Molecular Structure of Nucleic Acids; a Structure for Deoxyribose Nucleic Acid. *Nature* **1953,** *171* (4356), 737–738.
87. Michelson, A. M.; Todd, A. R. Nucleotides Part XXXII. Synthesis of a Dithymidine Dinucleotide Containing a 3′: 5′-Internucleotidic Linkage. *J. Chem. Soc.* **1955,** 2632–2638.
88. Schaller, H.; Weimann, G.; Lerch, B.; Khorana, H. G. Studies on Polynucleotides. XXIV.1 The Stepwise Synthesis of Specific Deoxyribopolynucleotides (4).2 Protected Derivatives of Deoxyribonucleosides and New Syntheses of Deoxyribonucleoside-3″ Phosphates. *J. Am. Chem. Soc.* **1963,** *85,* 3821–3827.
89. (a) Gilham, P. T.; Khorana, H. G. Studies on Polynucleotides. I. A New and General Method for the Chemical Synthesis of the C5″-C3″ Internucleotidic Linkage. Syntheses of Deoxyribo-dinucleotides. *J. Am. Chem. Soc.* **1958,** *80,* 6212–6222; (b) Khorana, H. G. *Some Recent Developments in the Chemistry of Phosphate Esters of Biological Interest;* John Wiley: London, 1961.
90. Khorana, H. G. Total Synthesis of a Gene. *Science* **1979,** *203* (4381), 614–625.
91. Letsinger, R. L.; Mahadevan, V. Oligonucleotide Synthesis on a Polymer Support. *J. Am. Chem. Soc.* **1965,** *87,* 3526–3527.
92. Reese, C. B. The Chemical Synthesis of Oligo- and Poly-nucleotides by the Phosphotriester Approach. *Tetrahedron* **1978,** *34,* 3143–3179.
93. (a) Itakura, K.; Bahl, C. P.; Katagiri, N.; Michiniewicz, J.; Wightman, R. H.; Narang, S. A. A Modified Triester Method for the Synthesis of Deoxyribopolynucleotides. *Can. J. Chem.* **1973,** *51,* 3649–3651; (b) Itakura, K.; Katagiri, N.; Bahl, C. P.; Wightman, R. H.; Narang, S. A. Improved Triester Approach for the Synthesis of Pentadecathymidylic Acid. *J. Am. Chem. Soc.* **1975,** *97* (25), 7327–7332; (c) Narang, S. A. DNA Synthesis. *Tetrahedron* **1983,** *39,* 3–22.
94. Catlin, J. C.; Cramer, F. Deoxy Oligonucleotide Synthesis via the Triester Method. *J. Org. Chem.* **1973,** *38* (2), 245–250.
95. Letsinger, R. L.; Lunsford, W. B. Synthesis of Thymidine Oligonucleotides by Phosphite Triester Intermediates. *J. Am. Chem. Soc.* **1976,** *98* (12), 3655–3661.
96. (a) Beaucage, S. L.; Caruthers, M. H. Deoxynucleoside Phosphoramidites—A New Class of Key Intermediates for Deoxypolynucleotide Synthesis. *Tetrahedron Lett.* **1981,** *22,* 1859–1862; (b) McBride, L. J.; Caruthers, M. H. An Investigation of Several Deoxynucleoside Phosphoramidites Useful for Synthesizing Deoxyoligonucleotides. *Tetrahedron Lett.* **1983,** *24,* 245–248.
97. (a) Sinha, N. D.; Biernat, J.; McManus, J.; Koster, H. Polymer Support Oligonucleotide Synthesis XVIII: Use of Beta-Cyanoethyl-N, N-Dialkylamino-/N-Morpholino Phosphoramidite of Deoxynucleosides for the Synthesis of DNA Fragments Simplifying Deprotection and Isolation of the Final Product. *Nucleic Acids Res.* **1984,** *12* (11), 4539–4557; (b) Sinha, N. D.; Biernat, J.; Koster, H. β-Cyanoethyl N, N-Dialkylamino/N-Morpholinomonochloro Phosphoamidites, New Phosphitylating Agents Facilitating Ease of Deprotection and Work-up of Synthesized Oligonucleotides. *Tetrahedron Lett.* **1983,** *24,* 5843–5846.
98. Garegg, P. J.; Regberg, T.; Stawinski, J.; Stromberg, R. Nucleoside Hydrogenphosphonates in Oligonucleotide Synthesis. *Chem. Scripta* **1986,** *26,* 59–62.
99. Froehler, B. C.; Ng, P. G.; Matteucci, M. D. Synthesis of DNA via Deoxynucleoside H-Phosphonate Intermediates. *Nucleic Acids Res.* **1986,** *14* (13), 5399–5407.
100. Hall, R. H.; Todd, A.; Webb, R. F. Nucleotides. Part XLI. Mixed Anhydrides as Intermediates in the Synthesis of Dinucleoside Phosphates. *J. Chem. Soc.* **1957,** 3291–3296.
101. Ogilvie, K. K.; Sadana, K. L.; Thompson, E. A.; Quilliam, M. A.; Westmore, J. B. The Use of Silyl Groups in Protecting the Hydroxyl Functions of Ribonucleosides. *Tetrahedron Lett.* **1974,** *15,* 2861–2863.
102. (a) Engels, J. W.; Uhlmann, E. Gene Synthesis. *Angew. Chem. Int. Ed. Engl.* **1989,** *28,* 716–734; (b) Engels, J. W.; Sprunkel, B.; Uhlmann, E. DNA Synthesis. In *Biotechnology,* vol. 2, Rehm, H. J., Reed, G., Pühler, A., Stadler, P., Eds.; 2nd ed.; VCH: Weinheim, 1993; pp 317–369; (c) Beaucage, S.; Iyer, R. P. Advances in the Synthesis of Oligonucleotides by the Phosphoramidite Approach. *Tetrahedron* **1992,** *48,* 2223–2311.
103. (a) Sanghvi, Y. S. A status Update of Modified Oligonucleotides for Chemotherapeutics Applications. *Curr. Protoc. Nucleic Acid Chem.* **2011**. Chapter 4, Unit 4 1 1-22; (b) He, K.; Hasan, A. *Classification and Characterization of Impurities in Phosphoramidites Used in Making Therapeutic Oligonucleotides: Risk Mitigation Strategies for Entering Clinical Phases;* Thermo Fisher Scientific: Milwaukee, WI, 2009. Tech Note MK0010D01.
104. Cramer, H.; Finn, K. J.; Sinha, N. D. Oligonucleotide Impurities and Their Origin. In *Analysis of Oligonucleotides and Their Related Substances;* Elder, D., Okafo, G., Webb, M., Eds.; ILM Publications: London, 2013; pp 21–100.
105. (a) Katzhendler, J.; Cohen, S.; Rahamim, E.; Weisz, M.; Ringel, I.; Deutsch, J. The Effect of Spacer, Linkage and Solid Support on the Synthesis of Oligonucleotides. *Tetrahedron* **1989,** *45,* 2777–2792; (b) Kozlov, I. A.; Dang, M.; Sikes, K.; Kotseroglou, T.; Barker, D. L.; Zhao, C. Significant Improvement of Quality for Long Oligonucleotides by Using Controlled Pore Glass With Large Pores. *Nucleosides Nucleotides Nucleic Acids* **2005,** *24* (5-7), 1037–1041.
106. (a) Vu, H.; McCollum, C.; Lotys, C.; Andrus, A. New Reagents and Solid Support for Automated Oligonucleotide Synthesis. *Nucleic Acids Symp. Ser.* **1990,** *22,* 63–64; (b) McCollum, C.; Andrus, A. An Optimized Polystyrene Support for Rapid, Efficient Oligonucleotide Synthesis. *Tetrahedron Lett.* **1991,** *32,* 4069–4072.
107. Reddy, M. P.; Michael, M. A.; Farooqui, F.; Girgis, S. New and Efficient Solid Support for the Synthesis of Nucleic Acids. *Tetrahedron Lett.* **1994,** *35,* 5771–5774.
108. (a) Pon, R. T. Solid-Phase Supports for Oligonucleotide Synthesis. *Methods Mol. Biol.* **1993,** *20,* 465–496; (b) Pon, R. T. Solid-Phase Supports for Oligonucleotide Synthesis. *Curr. Protoc. Nucleic Acid Chem.* **2001**. Chapter 3, Unit 3.1.
109. Yip, K. F.; Tsou, K. C. A New Polymer-Support Method for the Synthesis of Ribooligonucleotide. *J. Am. Chem. Soc.* **1971,** *93,* 3272–3276.
110. Alul, R. H.; Singman, C. N.; Zhang, G. R.; Letsinger, R. L. Oxalyl-CPG: A Labile Support for Synthesis of Sensitive Oligonucleotide Derivatives. *Nucleic Acids Res.* **1991,** *19* (7), 1527–1532.
111. (a) Pon, R. T.; Yu, S. Hydroquinone-O, O'-Diacetic Acid ('Q-Linker') as a Replacement for Succinyl and Oxalyl Linker Arms in Solid Phase Oligonucleotide Synthesis. *Nucleic Acids Res.* **1997,** *25* (18), 3629–3635; (b) Pon, R. T.; Yu, S. Hydroquinone-O, O'-Diacetic Acid as a More Labile Replacement for Succinc Acid Linkers in Solid-Phase Oligonucleotide Synthesis. *Tetrahedron Lett.* **1997,** *38* (19), 3327–3330.
112. Capaldi, D. C.; Gaus, H.; Krotz, A. H.; Arnold, J.; Carty, R. L.; Moore, M. N.; Scozzari, A. N.; Lowery, K.; Cole, D. L.; Ravikumar, V. T. Synthesis of High-Quality Antisense Drugs. Addition of Acrylonitrile to Phosphorothioate Oligonucleotides: Adduct Characterization and Avoidance. *Org. Process Res. Dev.* **2003,** *7* (6), 832–838.
113. Gough, G. R.; Brunden, M. J.; Gilham, P. T. 2′(3′)-O-Benzoyluridine 5′ Linked to Glass: An All-Purpose Support for Solid Phase Synthesis of Oligodeoxyribonucleotides. *Tetrahedron Lett.* **1983,** *24* (48), 5321–5324.
114. Vargeese, C.; Wang, W. Methods and Reagents for Oligonucleotide Synthesis. U.S. Patent 7,205,399, April 17, 2007.
115. Kumar, P.; Sharma, A. K.; Sharma, P.; Garg, B. S.; Gupta, K. C. Express Protocol for Functionalization of Polymer Supports for Oligonucleotide Synthesis. *Nucleos. Nucleot.* **1996,** *15,* 879–888.

116. Bhongle, N. N.; Tang, J. Y. A Convenient and Practical Method for Derivatization of Solid Supports for Nucleic Acid Synthesis. *Synth. Commun.* **1995,** *25,* 3671–3679.
117. (a) Pon, R. T.; Yu, S. Rapid Automated Derivatization of Solid-Phase Supports for Oligonueleotide Synthesis Using Uronium or Phosphonium Coupling Reagents. *Tetrahedron Lett.* **1997,** *38,* 3331–3334; (b) Pon, R. T.; Yu, S.; Sanghvi, Y. S. Rapid Esterification of Nucleosides to Solid-Phase Supports for Oligonucleotide Synthesis Using Uronium and Phosphonium Coupling Reagents. *Bioconjug. Chem.* **1999,** *10* (6), 1051–1057.
118. Kurata, C.; Bradley, K.; Gaus, H.; Luu, N.; Cedillo, I.; Ravikumar, V. T.; Van Sooy, K.; McArdle, J. V.; Capaldi, D. C. Characterization of High Molecular Weight Impurities in Synthetic Phosphorothioate Oligonucleotides. *Bioorg. Med. Chem. Lett.* **2006,** *16* (3), 607–614.
119. Cazenave, C.; Bathany, K.; Rayner, B. Formation of N-Branched Oligonucleotides as By-Products in Solid-Phase Oligonucleotide Synthesis. *Oligonucleotides* **2006,** *16* (2), 181–185.
120. Ravikumar, V. T.; Capaldi, D. C.; Lima, W. F.; Lesnik, E.; Turney, B.; Cole, D. L. Antisense Phosphorothioate Oligodeoxyribonucleotide Targeted Against ICAM-1: Synthetic and Biological Characterization of a Process-Related Impurity Formed During Oligonucleotide Synthesis. *Bioorg. Med. Chem.* **2003,** *11* (21), 4673–4679.
121. Holik, M.; Matejkova, B. Determination of Hydroxyl Groups and Water Content In Silica by Nuclear Magnetic Resonance Spectroscopy. *J. Chromatogr.* **1981,** *213,* 33–39.
122. Snyder, I. R. *Principles of Adsorption Chromatography;* M. Dekker: New York, 1968.
123. Yu, D.; Tang, J.-Y.; Iyer, R. P.; Agrawal, S. Diethoxy N, N-diisopropyl Phosphoramidite as an Improved Capping Reagent in the Synthesis of Oligonucleotides Using Phosphoramidite Chemistry. *Tetrahedron Lett.* **1994,** *35,* 8565–8568.
124. Cvetovich, R. J. Hydrogen Peroxide Oxidation of Phosphite Triesters in Oligonucleotide Syntheses. *Org. Process Res. Dev.* **2010,** *14,* 295–297.
125. (a) Ravikumar, V. T.; Kumar, R. K.; Capaldi, D. C.; Turney, B.; Rentel, C.; Cole, D. L. Antisense Phosphorothioate Oligodeoxyribonucleotide Targeted Against ICAM-1: Use of I-Linker to Eliminate 3'-Terminal Phosphorothioate Monoester Formation. *Org. Process Res. Dev.* **2003,** *7,* 259–266; (b) Septak, M. Kinetic Studies on Depurination and Detritylation of CPG-Bound Intermediates During Oligonucleotide Synthesis. *Nucleic Acids Res.* **1996,** *24* (15), 3053–3058; (c) Suzuki, T.; Ohsumi, S.; Makino, K. Mechanistic Studies on Depurination and Apurinic Site Chain Breakage in Oligodeoxyribonucleotides. *Nucleic Acids Res.* **1994,** *22* (23), 4997–5003.
126. (a) Nelson, P. S.; Muthini, S.; Vierra, M.; Acosta, L.; Smith, T. H. Rainbow Universal CPG: A Versatile Solid Support for Oligonucleotide Synthesis. *Biotechniques* **1997,** *22* (4), 752–756; (b) Lyttle, M. H.; Dick, D. J.; Hudson, D.; Cook, R. M. A Phosphate Bound Universal Linker for DNA Synthesis. *Nucleos. Nucleot.* **1999,** *18,* 1809–1824; (c) Schcuer-Larsen, C.; Rosenbohm, C.; Jøgensen, T. J. D.; Wengel, J. Introduction of a Universal Solid Support for Oligonucleotide Synthesis. *Nucleos. Nucleot.* **1997,** *16,* 67–80; (d) Scott, S.; Hardy, P.; Sheppard, R. C.; McLean, M. J. A Universal Support for Oligonucleotide Synthesis. In Epton, R., EdInnovations and Perspectives in Solid Phase Synthesis, 3rd International Symposium; Mayflower Worldwide, 1994; pp 115–124; (e) Kumar, P.; Dhawan, G.; Chandra, R.; Gupta, K. C. Polyamine-Assisted Rapid and Clean Cleavage of Oligonucleotides From cis-Diol Bearing Universal Support. *Nucleic Acids Res.* **2002,** *30* (23), e130; (f) Kumar, P.; Mahajan, S.; Gupta, K. C. Universal Reusable Polymer Support for Oligonucleotide Synthesis. *J. Org. Chem.* **2004,** *69* (19), 6482–6485; (g) Anderson, E.; Brown, T.; Picken, D. Novel Photocleavable Universal Support for Oligonucleotide Synthesis. *Nucleosides Nucleotides Nucleic Acids* **2003,** *22* (5-8), 1403–1406; (h) Anderson, K. M.; Jaquinod, L.; Jensen, M. A.; Ngo, N.; Davis, R. W. A Novel Catechol-Based Universal Support for Oligonucleotide Synthesis. *J. Org. Chem.* **2007,** *72* (26), 9875–9880; (i) Morvan, F.; Meyer, A.; Vasseur, J. J. A Universal and Recyclable Solid Support for Oligonucleotide Synthesis. *Curr. Protoc. Nucleic Acid Chem.* **2007**. Chapter 3, Unit 3.16.
127. (a) Guzaev, A. P.; Manoharan, M. A Conformationally Preorganized Universal Solid Support for Efficient Oligonucleotide Synthesis. *J. Am. Chem. Soc.* **2003,** *125* (9), 2380–2381; (b) Ravikumar, V. T.; Kumar, R. K.; Olsen, P.; Moor, M. N.; Carty, R. L.; Andrade, M.; Gorman, D.; Zhu, X.; Cedillo, I.; Wang, Z.; Mendez, L.; Scozzari, A. N.; Aguirre, G.; Somanathan, R.; Bernees, S. UnyLinker: An Efficient and Scaleable Synthesis of Oligonucleotides Utilizing a Universal Linker Molecule: A Novel Approach To Enhance the Purity of Drugs. *Org. Process Res. Dev.* **2008,** *12,* 399–410.
128. (a) Azhayev, A. V. A New Universal Solid Support for Oligonucleotide Synthesis. *Tetrahedron* **1999,** *55* (3), 787; (b) Azhayev, A. V.; Antopolsky, M. L. Amide Group Assisted 3'-Dephosphorylation of Oligonucleotides Synthesized on Universal A-Supports. *Tetrahedron* **2001,** *57,* 4977–4986; (c) Azhayev, A. V.; Antopolsky, M. L.; Tennilä, T. M. L.; Mackie, H.; Randolph, J. B. A Comparative Study of Commercially Available Universal Supports. *Genet. Eng. News* **2005,** *25* (5).
129. Glen Research Corporation. *High Load Glen UnySupport*. The Glen Report; Glen Research Corporation: Sterling, VA, 2009. Vol. 21, No. 1, p. 14.
130. Guzaev, A. P., Guidelines for Selection and Use of Universal Solid Supports. AM Chemicals, Oceanside, CA, Vol. Version 1.6. **2005**.
131. (a) Glen Research Corporation. *Improving Universal Support II for Oligonucleotide Synthesis*. The Glen Report; Glen Research Corporation: Sterling, VA, 2008. Vol. 20, No. 1, pp. 14–15; (b) Yagodkin, A.; Azhayev, A. Carbamoylation of Amines, Thiophenols, Mercaptanes and Phenols Employing Organic Azides. U.S. Patent 2,010,093,981, 2010.
132. (a) Paul, C. H.; Royappa, A. T. Acid Binding and Detritylation During Oligonucleotide Synthesis. *Nucleic Acids Res.* **1996,** *24* (15), 3048–3052; (b) Caruthers, M. H.; Barone, A. D.; Beaucage, S. L.; Dodds, D. R.; Fisher, E. F.; McBride, L. J.; Matteucci, M.; Stabinsky, Z.; Tang, J. Y. Chemical Synthesis of Deoxyoligonucleotides by the Phosphoramidite Method. *Methods Enzymol.* **1987,** *154,* 287–313; (c) Atkinson, T.; Smith, M. Solid-Phase Synthesis of Oligodeoxyribonucleotides by the Phosphotriester Method. In *Oligonucleotide Synthesis: A Practical Approach;* Gait, M. J., Ed.; IRL Press: Oxford/Washington DC, 1984.
133. (a) Krotz, A. H.; Carty, R. L.; Moore, M. N.; Scozzari, A. N.; Cole, D. L.; Ravikumar, V. T. Synthesis of Antisense Oligonucleotides Using Environmentally Friendly and Safe Deprotection Procedures. *Green Chem.* **1999,** *1,* 277–281; (b) Krotz, A. H.; Carty, R. L.; Scozzari, A. N.; Cole, D. L.; Ravikumar, V. T. Large-Scale Synthesis of Antisense Oligonucleotides without Chlorinated Solvents. *Org. Process Res. Dev.* **2000,** *4,* 190–193; (c) Krotz, A. H.; Cole, D. L.; Ravikumar, V. T. Synthesis of an Antisense Oligonucleotide Targeted Against C-Raf Kinase: Efficient Oligonucleotide Synthesis Without Chlorinated Solvents. *Bioorg. Med. Chem.* **1999,** *7* (3), 435–439.
134. Cheruvallath, Z. S.; Carty, R. L.; Andrade, M.; Moore, M. N.; Song, Q.; Rentel, C.; Cole, D. L.; Ravikumar, V. T. Efficient Synthesis of Antisense Phosphorothioate Oligonucleotides: Evaluation of Dichloroacetic Acid at Higher Concentration to Reduce Cycle Time. *Org. Process Res. Dev.* **2003,** *7,* 917–920.
135. Gaus, H.; Olsen, P.; Sooy, K. V.; Rentel, C.; Turney, B.; Walker, K. L.; McArdle, J. V.; Capaldi, D. C. Trichloroacetaldehyde Modified Oligonucleotides. *Bioorg. Med. Chem. Lett.* **2005,** *15* (18), 4118–4124.
136. Nurminen, E. J.; Mattinen, J. K.; Lönnberg, H. Protonation of Phosphoramidites. The Effect on Nucleophilic Displacement. *J. Chem. Soc. Perkin Trans.* **2000,** *2,* 2238–2240.
137. (a) Dahl, B. H.; Nielsen, J.; Dahl, O. Mechanistic Studies on the Phosphoramidite Coupling Reaction in Oligonucleotide Synthesis. I. Evidence for Nucleophilic Catalysis by Tetrazole and Rate Variations With the Phosphorus Substituents. *Nucleic Acids Res.* **1987,** *15* (4), 1729–1743; (b) Berner, S.; Muhlegger, K.; Seliger, H. Studies on the Role of Tetrazole in the Activation of Phosphoramidites. *Nucleic Acids Res.* **1989,** *17* (3), 853–864; (c) Nurminen, E. J.; Mattinen, J. K.; Lönnberg, H. Kinetics and Mechanism of Tetrazole-Catalyzed Phosphoramidite Alcoholysis. *J. Chem. Soc. Perkin Trans.* **1998,** *2,* 1621–1628.
138. Beaucage, S. L.; Caruthers, M. H. Synthetic Strategies and Parameters Involved in the Synthesis of Oligodeoxyribonucleotides According to the Phosphoramidite Method. *Curr. Protoc. Nucleic Acid Chem.* **2001**. Chapter 3, Unit 3.3.
139. Dorman, M. A.; Noble, S. A.; McBride, L. J.; Caruthers, M. H. Synthesis of Oligodeoxynucleotides and Oligodeoxynucleotide Analogs Using Phosphoramidite Intermediates. *Tetrahedron* **1984,** *40,* 95–102.
140. Hogrefe, R. I.; Reynolds, M. A.; Vaghefi, M. M.; Young, K. M.; Riley, T. A.; Klem, R. E.; Arnold, L. J., Jr. An Improved Method for the Synthesis and Deprotection of Methylphosphonate Oligonucleotides. In *Protocols for Oligonucleotides and Analogs: Synthesis and Properties,* vol. 20, Agrawal, S., Ed.; Humana Press: Totowa, NJ, 1993.
141. (a) Hayakawa, Y.; Uchiyama, M.; Noyori, R. Nonaqueous Oxidation of Nucleoside Phosphites to the Phosphates. *Tetrahedron Lett.* **1986,** *27,* 4191–4194; (b) Sproat, B.; Colonna, F.; Mullah, B.; Tsou, D.; Andrus, A.; Hampel, A.; Vinayak, R. An Efficient Method for the Isolation and Purification of Oligoribonucleotides. *Nucleos. Nucleot.* **1995,** *14,* 255–273.
142. (a) Glen Research Corporation. *Non-Aqueous Oxidation with 10-Camphorsulfonyl-Oxaziridine*. The Glen Report; Glen Research Corporation: Sterling, VA, 1996. Vol. 9, No. 1, pp. 8–9; (b) Ugi, I.; Jacob, P.; Landgraf, B.; Rupp, C.; Lemmen, P.; Verfuerth, U. Phosphite Oxidation and the Preparation of Five-Membered Cyclic Phosphorylating Reagents via the Phosphites. *Nucleos. Nucleot.* **1988,** *7,* 605–608; (c) Dellinger, D. J.; Sheehan, D. M.; Christensen, N. K.; Lindberg, J. G.; Caruthers, M. H. Solid-Phase Chemical Synthesis of Phosphonoacetate and Thiophosphonoacetate Oligodeoxynucleotides. *J. Am. Chem. Soc.* **2003,** *125* (4), 940–950; (d) Manoharan, M.; Lu, Y.; Casper, M. D.; Ju, G. Allyl Group as a Protecting Group for Internucleotide Phosphate and Thiophosphate Linkages in Oligonucleotide Synthesis: Facile Oxidation and Deprotection Conditions. *Org. Lett.* **2000,** *2,* 243–246.

143. (a) Sierzchala, A. B..; Dellinger, D. J.; Betley, J. R.; Wyrzykiewicz, T. K.; Yamada, C. M.; Caruthers, M. H. Solid-Phase Oligodeoxynucleotide Synthesis: A Two-Step Cycle Using Peroxy Anion Deprotection. *J. Am. Chem. Soc.* **2003,** *125* (44), 13427–13441; (b) Uzagare, M. C.; Padiya, K. J.; Salunkhe, M. M.; Sanghvi, Y. S. NBS–DMSO as a Nonaqueous Nonbasic Oxidation Reagent for the Synthesis of Oligonucleotides. *Bioorg. Med. Chem. Lett.* **2003,** *13,* 3537–3540; (c) Kataoka, M.; Hattori, A.; Okino, S.; Hyodo, M.; Asano, M.; Kawai, R.; Hayakawa, Y. Ethyl(methyl)dioxirane as an Efficient Reagent for the Oxidation of Nucleoside Phosphites Into Phosphates Under Nonbasic Anhydrous Conditions. *Org. Lett.* **2001,** *3,* 815–818; (d) Saneyoshi, H.; Miyata, K.; Seio, K.; Sekine, M. 1,1-Dihydroperoxycyclododecane as a New, Crystalline Non-hygroscopic Oxidizer for the Chemical Synthesis of Oligodeoxyribonucleotides. *Tetrahedron Lett.* **2006,** *47,* 8945–8947.
144. Burgers, P. M. J.; Eckstein, F. Synthesis of Dinucleoside Monophosphorothioates via Addition of Sulphur to Phosphite Triesters. *Tetrahedron Lett.* **1978,** *19,* 3835–3838.
145. Vu, H.; Hirschbein, B. L. Internucleotide Phosphite Sulfurization With Tetraethylthiuram Disulfide. Phosphorothioate Oligonucleotide Synthesis via Phosphoramidite Chemistry. *Tetrahedron Lett.* **1991,** *32,* 3005–3008.
146. Stec, W. J.; Uznanski, B.; Wilk, A.; Hirschbein, B. L.; Fearon, K. L.; Bergot, B. J. Bis(O, O-diisopropoxy phosphinothioyl) Disulfide—A Highly Efficient Sulfurizing Reagent for Cost-Effective Synthesis of oligo(nucleoside phosphorothioate)s. *Tetrahedron Lett.* **1993,** *34,* 5317–5320.
147. Iyer, R. P.; Phillips, L. R.; Egan, W.; Regan, J. B.; Beaucage, S. L. The Automated Synthesis of Sulfur-Containing Oligodeoxyribonucleotides Using 3H-1,2-benzodithiol-3-one 1,1-dioxide as a Sulfur-Transfer Reagent. *J. Org. Chem.* **1990,** *55,* 4693–4699.
148. (a) Krotz, A. H.; Gorman, D.; Mataruse, P.; Foster, C.; Godbout, J. D.; Coffin, C. C.; Scozzari, A. N. Phosphorothioate Oligonucleotides With Low Phosphate Diester Content: Greater Than 99.9% Sulfurization Efficiency With "Aged" Solutions of Phenylacetyl Disulfide (PADS). *Org. Process Res. Dev.* **2004,** *8,* 852–858; (b) Cheruvallath, Z. S.; Carty, R. L.; Moore, M. N.; Capaldi, D. C.; Krotz, A. H.; Wheeler, P. D.; Turney, B. J.; Craig, S. R.; Gaus, H. J.; Scozzari, A. N.; Cole, D. L.; Ravikumar, V. T. Synthesis of Antisense Oligonucleotides: Replacement of 3H-1,2-Benzodithiol-3-one 1,1-Dioxide (Beaucage Reagent) With Phenylacetyl Disulfide (PADS) as Efficient Sulfurization Reagent: From Bench to Bulk Manufacture of Active Pharmaceutical Ingredient. *Org. Process Res. Dev.* **2000,** *4,* 199–204; (c) Roelen, H. C. P. F.; Kamer, P. C. J.; van den Elst, H.; van der Marel, G. A.; van Boom, J. H. A Study on the Use of Phenylacetyl Disulfide in the Solid-Phase Synthesis of Oligodeoxynucleoside Phosphorothioates. *Recl. Trav. Chim. Pays-Bas* **1991,** *110,* 325–331.
149. (a) Ma, M. Y.; Dignam, J. C.; Fong, G. W.; Li, L.; Gray, S. H.; Jacob-Samuel, B.; George, S. T. Evaluation of 3-Ethoxy-1,2,4-Dithiazoline-5-one (EDITH) as a New Sulfurizing Reagent in Combination With Labile Exocyclic Amino Protecting Groups for Solid-Phase Oligonucleotide Synthesis. *Nucleic Acids Res.* **1997,** *25* (18), 3590–3593; (b) Xu, Q.; Barany, G.; Hammer, R. P.; Musier-Forsyth, K. Efficient Introduction of Phosphorothioates Into RNA Oligonucleotides by 3-ethoxy-1,2,4-dithiazoline-5-one (EDITH). *Nucleic Acids Res.* **1996,** *24* (18), 3643–3644; (c) Xu, Q.; Musier-Forsyth, K.; Hammer, R. P.; Barany, G. Use of 1,2,4-Dithiazolidine-3,5-Dione (DtsNH) and 3-Ethoxy-1,2,4-Dithiazoline-5-one (EDITH) for Synthesis of Phosphorothioate-Containing Oligodeoxyribonucleotides. *Nucleic Acids Res.* **1996,** *24* (9), 1602–1607.
150. (a) Tang, J.-Y.; Han, Y.; Tang, J. X.; Zhang, Z. Large-Scale Synthesis of Oligonucleotide Phosphorothioates Using 3-Amino-1,2,4-dithiazole-5-thione as an Efficient Sulfur-Transfer Reagent. *Org. Process Res. Dev.* **2000,** *4,* 194–198; (b) Hanusek, J.; Russell, M. A.; Laws, A. P.; Jansa, P.; Atherton, J. H.; Fettes, K.; Page, M. I. Mechanism of the Sulfurisation of Phosphines and Phosphites Using 3-Amino-1,2,4-Dithiazole-5-Thione (Xanthane Hydride). *Org. Biomol. Chem.* **2007,** *5* (3), 478–484; (c) Han, Y.; Tang, J.; Zhang, Z.; Tang, J.-Y. *Sulfur Transfer Reagents for Oligonucleotide Synthesis,* 2000.
151. (a) Guzaev, A. P. *Sulfur Transfer Reagents for Oligonucleotide Synthesis,* 2010; (b) Guzaev, A. P. Reactivity of 3H-1,2,4-Dithiazole-3-Thiones and 3H-1,2-Dithiole-3-Thiones as Sulfurizing Agents for Oligonucleotide Synthesis. *Tetrahedron Lett.* **2011,** *52,* 434–437.
152. (a) Wang, Z.; Song, Q.; Sanghvi, Y. S. Dimethylthiarum Disulfide: New Sulfur Transfer Reagent in Phosphorothioates Oligonucleotide Synthesis. *Methods Mol. Biol.* **2005,** *288,* 51–64; (b) Song, Q.; Wang, Z.; Sanghvi, Y. S. A Short, Novel, and Cheaper Procedure for Oligonucleotide Synthesis Using Automated Solid Phase Synthesizer. *Nucleosides Nucleotides Nucleic Acids* **2003,** *22* (5-8), 629–633.
153. Roy, S. K.; Tang, J.-Y. *Sulfurizing Reagent: 3-Aryl-1,2,4-Dithiazoline-5-Ones,* 2002.
154. Efimov, V. A.; Kalinkina, A. L.; Chakhmakhcheva, O. G.; Hill, T. S.; Jayaraman, K. New Efficient Sulfurizing Reagents for the Preparation of Oligodeoxyribonucleotide Phosphorothioate Analogues. *Nucleic Acids Res.* **1995,** *23* (20), 4029–4033.
155. Eadie, J. S.; Davidson, D. S. Guanine Modification During Chemical DNA Synthesis. *Nucleic Acids Res.* **1987,** *15* (20), 8333–8349.
156. Chaix, C.; Molko, D.; Teoule, R. The Use of Labile Base Protecting Groups in Oligoribonucleotide Synthesis. *Tetrahedron Lett.* **1989,** *30,* 71–74.
157. Zhu, Q.; Delaney, M. O.; Greenberg, M. M. Observation and Elimination of N-Acetylation of Oligonucleotides Prepared Using Fast-Deprotecting Phosphoramidites and Ultra-Mild Deprotection. *Bioorg. Med. Chem. Lett.* **2001,** *11* (9), 1105–1107.
158. (a) Sinha, N.; Kuchimanchi, S. N.; Miranda, G.; Shaikh, S. Manufacture of Therapeutic Oligonucleotides: Development of New Reagents and Processes. *Indian J. Chem.* **2006,** *45B,* 2297–2304; (b) Sinha, N. D.; Michaud, D. P. Recent Developments in the Chemistry, Analysis and Control for the Manufacture of Therapeutic-Grade Synthetic Oligonucleotides. *Curr. Opin. Drug Discov. Devel.* **2007,** *10* (6), 807–818.
159. Glen Research Corporation. *UniCap Phosphoramidite, An Alternative to Acetic Anhydride Capping.* The Glen Report; Glen Research Corporation: Sterling, VA, 2004. Vol. 17, No. 1, pp. 14–15.
160. (a) Marshall, W. S.; Kaiser, R. J. Recent Advances in the High-Speed Solid Phase Synthesis of RNA. *Curr. Opin. Chem. Biol.* **2004,** *8* (3), 222–229; (b) Reese, C. B. The Chemical Synthesis of Oligo- and Poly-nucleotides: A Personal Commentary. *Tetrahedron* **2002,** *58* (44), 8893–8920; (c) Muller, S.; Wolf, J.; Ivanov, S. A. Current Strategies for the Synthesis of RNA. *Curr. Org. Synth.* **2004,** *1,* 293–307.
161. Cramer, H.; Finn, K. J.; Sinha, N. D. Oligonucleotide Impurities and Their Origin. In *Analytical Characterization and Separation of Oligonucleotides and Their Impurities;* Okafo, G., Webb, M., Elder, D., Eds.; ILM Publications, a trading division of International Labmate Limited, 2012; pp 21–100.
162. (a) Horn, T.; Urdea, M. S. Solid Supported Hydrolysis of Apurinic Sites in Synthetic Oligonucleotides for Rapid and Efficient Purification on Reverse-Phase Cartridges. *Nucleic Acids Res.* **1988,** *16* (24), 11559–11571; (b) Efcavitch, J. W.; Heiner, C. Depurination as a Yield Decreasing Mechanism in Oligodeoxynucleotide Synthesis. *Nucleos. Nucleot.* **1985,** *4,* 267; (c) Glen Research Corporation. *Technical Brief—Synthesis of Long Oligonucleotides.* The Glen Report; Glen Research Corporation: Sterling, VA, 2009. Vol. 21, No. 2, p. 14.
163. Capaldi, D. C.; Gaus, H. J.; Carty, R. L.; Moore, M. N.; Turney, B. J.; Decottignies, S. D.; McArdle, J. V.; Scozzari, A. N.; Ravikumar, V. T.; Krotz, A. H. Formation of 4,4'-Dimethoxytrityl-C-Phosphonate Oligonucleotides. *Bioorg. Med. Chem. Lett.* **2004,** *14* (18), 4683–4690.
164. Eritja, R.; Robles, J.; Avino, A.; Albericio, F.; Pedroso, E. A Synthetic Procedure for the Preparation of Oligonucleotides without Using Ammonia and Its Application for the Synthesis of Oligonucleotides Containing O-4-Alkyl Thymidines. *Tetrahedron* **1992,** *48,* 4171–4182.
165. (a) Kodra, J. T.; Kehler, J.; Dahl, O. Stability of Oligodeoxynucleoside Phosphorodithioates and Phosphorothioates in Aqueous Ammonia. *Nucleic Acids Res.* **1995,** *23* (16), 3349–3350; (b) Reese, C. B.; Song, Q. Avoidance of Sulfur Loss During Ammonia Treatment of Oligonucleotide Phosphorothioates. *Nucleic Acids Res.* **1997,** *25* (14), 2943–2944; (c) Turney, B. J.; Cheruvallath, Z. S.; Andrade, M.; Cole, D. L.; Ravikumar, V. T. Stability of Phosphorothioate Oligonucleotides in Aqueous Ammonia in Presence of Stainless Steel. *Nucleos. Nucleot.* **1999,** *18* (1), 89–93.
166. (a) Weiss, P. A. *TOM-Protecting-Group—A Major Improvement in RNA Synthesis;* Glen Research: Sterling, VA, 1998. Vol. 11, No. 2; (b) Scaringe, S. A.; Wincott, F. E.; Caruthers, M. H. Novel RNA Synthesis Method Using 5'-O-Silyl-2'-O-orthoester Protecting Groups. *J. Am. Chem. Soc.* **1998,** *120* (45), 11820–11821; (c) Lavergne, T.; Janin, M.; Dupouy, C.; Vasseur, J.-J.; Debart, F. Chemical Synthesis of RNA with Base-Labile 2′-O-(Pivaloyloxymethyl)-Protected Ribonucleoside Phosphoramidites. In *Current Protocols in Nucleic Acid Chemistry;* John Wiley & Sons, Inc, 2001; (d) Stutz, A.; Pitsch, S. Automated RNA-Synthesis With Photocleavable Sugar and Nucleobase Protecting Groups. *Synlett* **1999,** *1999* (Suppl. 1), 930–934; (e) Dellinger, D. J.; Timár, Z.; Myerson, J.; Sierzchala, A. B.; Turner, J.; Ferreira, F.; Kupihár, Z.; Dellinger, G.; Hill, K. W.; Powell, J. A.; Sampson, J. R.; Caruthers, M. H. Streamlined Process for the Chemical Synthesis of RNA Using 2′-O-Thionocarbamate-Protected Nucleoside Phosphoramidites in the Solid Phase. *J. Am. Chem. Soc.* **2011,** *133* (30), 11540–11556; (f) Semenyuk, A.; Földesi, A.; Johansson, T.; Estmer-Nilsson, C.; Blomgren, P.; Brännvall, M.; Kirsebom, L. A.; Kwiatkowski, M. Synthesis of RNA Using 2'-O-DTM Protection. *J. Am. Chem. Soc.* **2006,** *128* (38), 12356–12357.
167. Hill, K. W. Understanding Oligonucleotide Production: Identification of Process-Related Impurities. *DIA 1st Oligonucleotide-based Therapeutics Conference, Washington, DC.*

168. (a) Reddy, M. P.; Hanna, N. B.; Farooqui, F. Fast Cleavage and Deprotection of Oligonucleotides. *Tetrahedron Lett.* **1994,** *35,* 4311–4314; (b) Reddy, M. P.; Hanna, N. B.; Farooqui, F. Elimination of Transamination Side Product by the Use of dCAc Methylphosphonamidite in the Synthesis of Oligonucleoside Methylphosphonates. *Tetrahedron Lett.* **1996,** *37,* 8691–8694.
169. Oivanen, M.; Kuusela, S.; Lonnberg, H. Kinetics and Mechanisms for the Cleavage and Isomerization of the Phosphodiester Bonds of RNA by Bronsted Acids and Bases. *Chem. Rev.* **1998,** *98* (3), 961–990.
170. (a) Calvitt, C. J.; Levin, D. S.; Shepperd, B. T.; Gruenloh, C. J. Chemistry at the 2' Position of Constituent Nucleotides Controls Degradation Pathways of Highly Modified Oligonucleotide Molecules. *Oligonucleotides* **2010,** *20* (5), 239–251; (b) Krug, A.; Oretskaya, T. S.; Volkov, E. M.; Cech, D.; Shabarova, Z. A.; Rosenthal, A. The Behaviour of 2′-Deoxy-2′-Fluorouridine Incorporated into Oligonucleotides by the Phosphoramidite Approach. *Nucleos. Nucleot.* **1989,** *8,* 1473–1483; (c) Doerr, I. L.; Fox, J. J. Nucleosides. XXXIX. 2'-Deoxy-2'-Fluorocytidine, 1-.beta.-D-Arabinofuranosyl-2-Amino-1,4(2H)-4-Iminopyrimidine, and Related Derivatives. *J. Org. Chem.* **1967,** *32,* 1462–1471; (d) Seiffert, S.; Debelak, H.; Hadwiger, P.; Jahn-Hofmann, K.; Roehl, I.; Vornlocher, H. P.; Noll, B. Characterization of Side Reactions During the Annealing of Small Interfering RNAs. *Anal. Biochem.* **2011,** *414* (1), 47–57.
171. (a) Noll, B.; Seiffert, S.; Hertel, F.; Debelak, H.; Hadwiger, P.; Vornlocher, H. P.; Roehl, I. Purification of Small Interfering RNA Using Nondenaturing Anion-Exchange Chromatography. *Nucleic Acid Ther.* **2011,** *21,* 383–393. XXX; (b) Gjerde, D. T.; Hoang, L.; Hornby, D. *RNA Purification and Analysis: Sample Preparation, Extraction, Chromatography;* Wiley-VCH: Weinheim, 2009. p. xi, p. 195; (c) Vargeese, C. Deprotection and Purification of Oligonucleotides and Their Derivatives. U.S. Patent 6,989,442, 2006
(d) Shanagar, J. Purification of a Synthetic Oligonucleotide by Anion Exchange Chromatography: Method Optimisation and Scale-up. *J. Biochem. Biophys. Methods* **2005,** *64* (3), 216–225; (e) Deshmukh, R. R.; Eriksson, K. O.; Moore, P.; Cole, D. L.; Sanghvi, Y. S. A Case Study: Oligonucleotide Purification From Gram to Hundred Gram Scale. *Nucleosides Nucleotides Nucleic Acids* **2001,** *20* (4–7), 567–576; (f) Andrus, A.; Kuimelis, R. G. Overview of Purification and Analysis of Synthetic Nucleic Acids. *Curr. Protoc. Nucleic Acid Chem.* **2001**. Chapter 10, Unit 10.3; (g) Deshmukh, R. R.; Cole, D. L.; Sanghvi, Y. S. Purification of Antisense Oligonucleotides. *Methods Enzymol.* **2000,** *313,* 203–226; (h) Wincott, F.; DiRenzo, A.; Shaffer, C.; Grimm, S.; Tracz, D.; Workman, C.; Sweedler, D.; Gonzalez, C.; Scaringe, S.; Usman, N. Synthesis, Deprotection, Analysis and Purification of RNA and Ribozymes. *Nucleic Acids Res.* **1995,** *23* (14), 2677–2684.
172. (a) Lilley, D. M. J. Analysis of Branched Nucleic Acid Structure Using Comparative Gel Electrophoresis. *Q. Rev. Biophys.* **2008,** *41* (1), 1–39; (b) Dinther, F. H. M. V.; Bally, R. W.; Sommeren, T. P. V. Evaluation of Three Commercially Available Capillary (gel)electrophoresis Kits for Single Stranded DNA Oligonucleotide Analysis. *J. Chromatogr. A* **1998,** *817,* 273–279; (c) Srivatsa, G. S.; Batt, M.; Schuette, J.; Carlson, R. H.; Fitchett, J.; Lee, C.; Cole, D. L. Quantitative Capillary Gel Electrophoresis Assay of Phosphorothioate Oligonucleotides in Pharmaceutical Formulations. *J. Chromatogr. A* **1994,** *680,* 469–477; (d) Paulus, A.; Gassmann, E.; Field, M. J. Calibration of Polyacrylamide Gel Columns for the Separation of Oligonucleotides by Capillary Electrophoresis. *Electrophoresis* **1990,** *11* (9), 702–708.
173. (a) Bergot, B. J.; Egan, W. Separation of Synthetic Phosphorothioate Oligodeoxynucleotides From Their Oxygenated (Phosphodiester) Defect Species by Strong-Anion-Exchange High-Performance Liquid Chromatography. *J. Chromatogr. A* **1992,** *599,* 35–42; (b) Deshmukh, R. R.; Miller, J. E.; De Leon, P.; Leich, W. E., II; Cole, D. L.; Sanghvi, Y. S. Process Development for Purification of Therapeutic Antisense Oligonucleotides by Anion-Exchange Chromatography. *Org. Process Res. Dev.* **2000,** *4,* 205–213; (c) Metelev, V.; Agrawal, S. Ion-Exchange High-Performance Liquid Chromatography Analysis of Oligodeoxyribonucleotide Phosphorothioates. *Anal. Biochem.* **1992,** *200* (2), 342–346; (d) Banerjee, A.; Bose, H. S.; Roy, K. B. Fast and Simple Anion-Exchange Chromatography for Large-Scale Purification of Self-Complementary Oligonucleotides. *Biotechniques* **1991,** *11* (5), 650–656; (e) Cohn, W. E. The Anion-Exchange Separation of Ribonucleotides. *J. Am. Chem. Soc.* **1950,** *72,* 1471–1478.
174. (a) Cramer, H.; Finn, K. J.; Herzberg, E. Purity Analysis and Impurities Determination by Reversed-Phase HPLC. In *Handbook of Analysis of Oligonucleotides and Related Products;* Bonilla, J., Srivatsa, G. S., Eds.; CRC Press: Boca Raton, FL, 2011; pp 1–46; (b) McCarthy, S. M.; Gilar, M.; Gebler, J. Reversed-Phase Ion-Pair Liquid Chromatography Analysis and Purification of Small Interfering RNA. *Anal. Biochem.* **2009,** *390* (2), 181–188; (c) Lei, B.; Li, S.; Xi, L.; Li, J.; Liu, H.; Yao, X. Novel Approaches for Retention Time Prediction of Oligonucleotides in Ion-Pair Reversed-Phase High-Performance Liquid Chromatography. *J. Chromatogr. A* **2009,** *1216* (20), 4434–4439; (d) McCarthy, S. M.; Warren, W. J.; Dubey, A.; Gilar, M. Ion-Pairing Systems for Reversed-Phase Chromatoraphy Separation of Oligonucleotides. TIDES Conference, Las Vegas, NV; (e) Kirkland, J. J. Development of Some Stationary Phases for Reversed-Phase High-Performance Liquid Chromatography. *J. Chromatogr. A* **2004,** *1060* (1–2), 9–21; (f) Azarani, A.; Hecker, K. H. RNA Analysis by Ion-Pair Reversed-Phase High Performance Liquid Chromatography. *Nucleic Acids Res.* **2001,** *29* (2), E7.
175. Cramer, H. Development of Small Scale Models to Predict Large Scale Manufacturing Results. EuroTIDES, Berlin.
176. Zhu, H.; Srivatsa, G. S. Tm Analysis of Oligonucleotides. In *Handbook of Analysis of Oligonucleotides and Related Products;* Bonilla, J. V., Srivatsa, G. S., Eds.; CRC Press, 2011; p 511.
177. Huber, E. W. Advantages and Disadvantages Related to Use of Quantitative LC/MS Methods for Routine QC Testing. US Tides Conference, Boston.
178. Cecchi, T. Ion Pairing Chromatography. *Crit. Rev. Anal. Chem.* **2008,** *38,* 161–231.
179. Gilar, M.; Kenneth, F. J.; Budman, Y.; Holyoke, J. L.; Davoudi, H.; Gebler, J. C. Characterization of Therapeutic Oligonucleotides Using Liquid Chromatography With On-Line Mass Spectrometry Detection. *Oligonucleotides* **2003,** *13,* 229–243.
180. Cramer, H.; Finn, K. J.; Herzberg, E. Purity Analysis and Impurities Determination by Reversed-Phase High-Performance Liquid Chromatography. In *Handbook of Analysis of Oligonucleotides and Related Products;* Bonilla, J. V., Srivatsa, G. S., Eds.; CRC Press, 2011; p 511.
181. Thayer, J.; Murugaiah, V.; Wu, Y. Purity Analysis and Impurities Determination by AEX-HPLC. In *Handbook of Analysis of Oligonucleotides and Related Products;* Bonilla, J. V., Srivatsa, G. S., Eds.; CRC Press, 2011; p 511.
182. Srivatsa, G. S.; Klopchin, P.; Batt, M.; Feldman, M.; Carlson, R. H.; Cole, D. L. Selectivity of Anion Exchange Chromatography and Capillary Gel Electrophoresis for the Analysis of Phosphorothioate Oligonucleotides. *J. Pharm. Biomed. Anal.* **1997,** *16,* 619–630.
183. Chan, M. F.; Roymoulik, I. Purity Analysis and Molecular Weight Determination by Size Exclusion HPLC. In *Handbook of Analysis of Oligonucleotides and Related Products;* Bonilla, J. V., Srivatsa, G. S., Eds.; CRC Press, 2011; p 511.
184. Capaldi, D.; Ackley, K.; Brooks, D.; Carmody, J.; Draper, K.; Kambhampati, R. V. B.; Kretschmer, M.; Levin, D.; McArdle, J.; Noll, B.; Raghavachari, R.; Roymoulik, I.; Sharma, B. P. B.; Thürmer, R.; Wincott, F. Quality Aspects of Oligonucleotide Drug Development: Specifications for Active Pharmaceutical Ingredients. *Drug Inform. J.* **2012,** *46* (5), 611–626.
185. Kenneth, F. J.; Gilar, M.; Gebler, J. C. Electrospray Ionization Mass Spectrometric Analysis of Nucleic Acids Using High-Throughput On-Line Desalting. *Rapid Commun. Mass Spectrom.* **2004,** *18,* 1295–1302.
186. Smith, M. Characterisation of a Modified Oligonucleotide Together With Its Synthetic Impurities Using Accurate Mass Measurements. *Rapid Commun. Mass Spectrom.* **2011,** *25,* 511–525.
187. McLuckey, S. A. Habibi-Goudarzi, Ion-Trap Tandem Mass-Spectrometry Applied to Small Multiply-Charged Oligonucleotides With a Modified Base. *J. Am. Soc. Mass Spectrom.* **1994,** *5,* 740–747.
188. Kambhampati, R. V. B. Points to Consider for the Submission of Chemistry, Manufacturing, and Controls (CMC) Information in Oligonucleotide Based Therapeutic Drug Applications. DIA Industry and Health Authority Conference on Oligonucleotide-based Therapeutics, Bethesda, MD.
189. Thürmer, R. Special Issues in Regulating Oligonucleotides (CMC). Asia Tides, Tokyo; (b) Ståhlbom, A. Regulatory Expectations for the Quality of Oligonucleotide Products in the EU. EuroTides Conference, Berlin.
190. (a) Crooke, S. T. Commentary: Regulatory Issues Affecting Oligonucleotides. *Antisense Res. Dev.* **1993,** *3,* 301–306; (b) Srivatsa, G. S.; Chan, M. F. Analysis of Therapeutic Oligonucleotides—Meeting Regulatory Expectations for Drug Quality. *Chim. Oggi Chem. Today* **2010,** *28* (6), 22–24; (c) Srivatsa, G. S. Regulatory Considerations for the Development of Oligonucleotide Therapeutics. In *Handbook of Analysis of Oligonucleotides and Related Products;* Bonilla, J. V., Srivatsa, G. S., Eds.; CRC Press, 2011; p 511.
191. McArdle, J. V. Thresholds. DIA 3rd Oligonucleotide-based Therapeutics Conference Bethesda, MD.
192. Michaud, D. P. Oligonucleotide Assay and Potency. In *Handbook of Analysis of Oligonucleotides and Related Products;* Bonilla, J. V., Srivatsa, G. S., Eds.; CRC Press, 2011; p 511.

193. DeRider, M. L.; Brooks, D.; Burt, G. Structure Determination by NMR. In *Handbook of Analysis of Oligonucleotides and Related Products;* Bonilla, J. V., Srivatsa, G. S., Eds.; CRC Press, 2011; p 511.
194. Langer, E. *Survey: The Client-Contractor Relationship;* BioPharm International, 2011.
195. Abu Lila, A. S.; Kato, C.; Fukushima, M.; Huang, C. L.; Wada, H.; Ishida, T. Downregulation of thymidylate synthase by RNAi molecules enhances the antitumor effect of pemetrexed in an orthotopic malignant mesothelioma xenograft mouse model. *Int. J. Oncol.* **2016**.
196. Yu, J. Y.; DeRuiter, S. L.; Turner, D. L. RNA interference by expression of short-interfering RNAs and hairpin RNAs in mammalian cells. *Proc. Natl. Acad. Sci. USA* **2002,** *99* (9), 6047–6052.

Relevant Websites

www.Avecia.com—Nitto Avecia—World leader in Pre-clinical to Clinical manufacture of Oligonucleotides.
www.GElifesciences.com—GE Healthcare-Leader in Large-Scale Oligonucleotide Equipment Manufacture.
http://www.ich.org/home.html—ICH-Council for Harmonization of Technical Requirements for Pharmaceuticals for Human Use.

6.12 Current Progress and Future Prospects in Nucleic Acid Based Therapeutics

M Takahashi, S-p Han, LJ Scherer, S Yoon, and JJ Rossi, Beckman Research Institute of City of Hope, Duarte, CA, United States

© 2017 Elsevier Ltd. All rights reserved.

6.12.1	**Introduction**	280
6.12.2	**Synthetic Therapeutic Oligonucleotides**	281
6.12.2.1	Antisense Oligonucleotides (ASOs)	281
6.12.2.1.1	Chemical modification	281
6.12.2.1.2	Pharmacokinetic properties of ASOs	284
6.12.2.1.3	ASOs in clinical development	284
6.12.2.1.4	Challenges and future perspectives	286
6.12.2.2	RNA Interference (RNAi)	286
6.12.2.2.1	Cytoplasmic RNAi processing	287
6.12.2.2.2	Transcriptional silencing and activation	290
6.12.2.2.3	Types of synthetic RNAi substrates	290
6.12.2.2.4	Focus areas for improving potency and safety	292
6.12.2.2.5	Effective delivery	293
6.12.2.2.6	Potential therapeutic applications of RNAi	293
6.12.2.2.7	RNAi in clinical development	293
6.12.2.2.8	Challenges and future perspectives	295
6.12.2.3	Aptamers	295
6.12.2.3.1	Chemical modifications	295
6.12.2.3.2	Potential therapeutic applications of aptamers	296
6.12.2.3.3	Aptamers in clinical development	298
6.12.2.3.4	Challenges and future perspectives	299
6.12.3	**Biochemically Produced RNAs**	299
6.12.3.1	RNAi Triggers	299
6.12.3.1.1	Pri-miRNA mimics	299
6.12.3.1.2	shRNA triggers	301
6.12.3.1.3	Ago2shRNAs	301
6.12.3.1.4	Biochemically produced RNAi in clinical development	302
6.12.3.1.5	Challenges and future perspectives	302
6.12.3.2	CRISPR/Cas9	303
6.12.3.2.1	Potential therapeutic applications of CRISPR/Cas9	303
6.12.3.2.2	Challenges and future perspectives	305
6.12.4	**Conclusions**	306
References		306

6.12.1 Introduction

The emergence of nucleic acid based therapeutics dates back to 1978 when Zamecnik and Stephanson first reported inhibition of viral replication using short oligonucleotides that bind complementary viral RNA targets.[1] The discovery of these functional DNAs, aka "antisense oligonucleotides (ASOs)" along with the progress in solid phase DNA synthesis technology opened a new era of therapeutic drug discovery as nucleic acid–based therapeutics have been recognized as potential alternatives to conventional small molecule based drugs. Shortly after the report of first ASOs, catalytic function was discovered in protozoan and bacterial RNAs by a Czechian group.[2] This breakthrough discovery made over 30 years ago uncovered regulatory function of RNAs in cells and sparked wide spread researches on biological functions of RNAs. In 1993, the first microRNA, lin-4 was discovered by two groups.[3] Over the past two decades, numerous miRNAs have been identified in a variety of organisms including humans. It has been also shown that miRNA dysregulation is associated with a number of diseases.[4] Another important RNA function was reported in 1998 by Fire et al. who discovered RNA interference as antiviral immune system in the nematode *Caenorhabditis elegans*.[5] Shortly thereafter, synthetic short exogenous double-stranded RNAs, or siRNAs were introduced into mammalian cells and achieved sequence-specific gene silencing.[6] Since then, siRNA has been widely accepted not only as a research tool but also as a potential therapeutic intervention. Other classes of functional RNAs being considered for development as therapeutics include, riboswitches,[7] PIWI interacting RNAs[8] and CRISPR/Cas9 system.[9] Interestingly, whole human genome sequencing and studies of human transcriptomes

revealed that 98% of human genome which was previously thought to be nonfunctional "junk" DNA is actually transcribed into RNA[10]; these long noncoding RNAs[4b] have potential regulatory functions and thus are potential targets for medical intervention These series of discoveries shed light on significant roles of RNA in cells, and at the same time, also gave rise to the idea of utilizing these functional RNAs as therapeutics.

Rapid progress in sequencing technology has uncovered a number of disease-related genes that are "undruggable" by conventional pharmaceuticals. Mechanisms of action of most nucleic acid based drugs are based on Watson-Crick base pairing with target DNA/RNA in sequence-specific manner. Thus, nucleic acid based drugs can in theory, target virtually any nucleic acid gene products including these undruggable targets. In addition, it has been shown that some single-stranded nucleic acids, so-called aptamers can interact with proteins, nucleic acids, and small molecules. Often regarded as "chemical antibodies," aptamers can be engineered to complex with multiple different proteins and small molecules by forming specific secondary or tertiary structures for molecular interactions.[11] Given these attractive features, the functional nucleic acids have gained escalated attention by academic and industry researchers from all over the world and extensive research has been performed for the purpose of developing new classes of therapeutics. ASOs have made the most significant advances as therapeutics. Two ASO based drugs have been approved by the United States Food and Drug Administration (FDA) and many clinical studies are ongoing for a variety of diseases.[12] This remarkable progress was made possible by chemical modifications that stabilize ASOs and improve their functions as well as bioavailability in biological fluid.[13]

Technological knowledge and skills developed during early researches on ASOs and ribozymes made a significant contribution to the rapid progress of emerging RNAi-based drug development. Despite tremendous effort and billions of dollars invested over the past two decades, the development of RNAi-based drugs has been facing serious challenges because of their unfavorable physiological nature for intracellular delivery.[14] However, recent clinical studies of RNAi-based drugs showed potential benefit and promising therapeutic efficacy which could potentially lead to approval in near future.

In parallel to the works on ASOs and siRNAs, aptamer development has been taking place since 1990s. Aptamers are obtained by a multiround selection process called "Systematic Evolution of Ligands by EXponential enrichment" (SELEX).[15] Due to their monoclonal antibody-like properties, aptamers are potentially useful as therapeutic agents for multiple diseases. They are also being explored for various other applications such as diagnostics, biosensors, imaging, biomarker discovery, and targeted drug delivery. One aptamer therapeutic is currently commercially available and many are in clinical trials.

Recently, the CRISPR/Cas9 system has emerged as an important new genome engineering approach that has been quickly adopted by laboratories around the world.[9] This powerful and highly specific genome editing technology can target, edit, or modify genomic DNA in a variety of cells and organisms including humans. Interestingly, in the CRISPR/Cas9 system, RNA molecules play critical roles in determining target specificity. A clinical trial of one application of the system will soon be opened. We will briefly overview this highly promising RNA-guided technology below.

This chapter is divided into two broad categories; (1) synthetic therapeutic oligonucleotides and (2) biochemically produced therapeutic RNAs. We will discuss the current advances and potential challenges in the development of nucleic acid therapeutics along with mechanisms of action and some examples for applications. The challenges in developing nucleic acid based therapeutics include their extremely unstable nature in biological fluid, poor PK properties, and potential activation of innate immunity. In addition, intracellular delivery remains the major obstacle in application of nucleic acid therapeutics. We will address how scientists approach these challenges.

6.12.2 Synthetic Therapeutic Oligonucleotides

6.12.2.1 Antisense Oligonucleotides (ASOs)

The basic concept underlying ASO technology is very simple: antagonizing cellular RNA molecules via Watson-Click base pairing. Unlike small molecule and antibody based drugs, most of which target proteins, the most common target of ASOs are messenger RNA (mRNA). An ASO recognizes and binds the complementary sequence in the target mRNA, thus inhibiting translation. However, ASO targets are not limited to mRNA which also include viral genomic RNA, pre-mRNA, miRNA, and other noncoding RNA categories. For example, the pioneering work by Zemecnik and Stephanson demonstrated inhibition of viral replication in chick embryo fibroblast tissue cultures infected with Rous sarcoma virus (RSV) using 13-nucleotide (nt) long DNA, ultimately called an "antisense oligonucleotides," that was complementary to the reiterated terminal sequence of RSV 35S RNA.[1b]

Typical ASOs are short, synthetic single-stranded DNA molecules (~15–25-nt long) that bind complementary sequences in target RNA molecules which are subsequently degraded by various cellular mechanisms.[13] Certain ASOs sterically block the access of cellular machinery to target RNA, resulting in translation or splicing inhibition.[16] This steric-blocking strategy can also be useful for repairing defective RNA or for splicing modulation. Of the target cleavage mechanisms, the RNase H-dependent cleavage is well studied and the best understood antisense mechanism.[17] This requires recruitment of RNase H enzyme that recognizes DNA–RNA hybrid, cutting the RNA component. As different mechanisms lead to different outcomes, ASO design depends on the intended use.

6.12.2.1.1 Chemical modification

Single-stranded DNAs and RNAs are extremely instable in body fluids as well as extracellular environments. Unmodified or naked ASOs can be quickly degraded by circulating nucleases in a body. Moreover, their poor intracellular uptake, pharmacokinetic (PK) and pharmacodynamic (PD) properties, and potential activation of innate immunity are also major obstacles to their use as

therapeutics. Thus, scientists have devoted substantial effort over the past 30 years to developing numerous chemical modifications that confer drug-like properties to ASOs. These modifications have been introduced to phosphate backbone, sugar moiety, and/or bases of ASOs.[18] The earliest and most widely used chemical modification is the phosphorothioate (PS) backbone modification (first-generation modification, Fig. 1), wherein one of the nonbinding oxygen atoms in the phosphodiester (PO) backbone on the natural DNA and RNA molecules is substituted by a sulfur atom.[19] The sulfur substitution in the ASO backbone creates a chiral center at the phosphorus atom, leading to a Sp or Rp diastereomer at each chiral center during synthesis resulting in a $2^{(n-1)}$ diastereo mixture of *n*-mer PS-ASOs. Generally, the Sp configuration provides higher nuclease resistance to ASOs compared to Rp, whereas Rp-ASOs show higher binding affinity than Sp-ASOs. Thus, the overall mixture has a higher nuclease resistance but lower binding affinity (about $-0.8°C$ per linkage) compared to its corresponding unmodified PO-ASO.[20] The PS modification shows high solubility and is also one of the few modifications that supports RNase H activity. Increased protein affinity is also a notable feature of the PS modification[21] and high plasma protein binding enhances circulation time while reducing elimination of PS-ASOs by renal excretion. In addition, it may also contribute to tissue distribution and cellular uptake.[22] Despite continuous controversies regarding various side effects, the PS modification is currently used as one of the essential parts of therapeutic ASOs. A major milestone in ASO development was achieved in 1998 when fomivirsen (Vitravene), developed by Ionis Pharmaceuticals (formerly ISIS Pharmaceuticals),[23] became the first FDA approved ASO therapeutic for the treatment of cytomegalovirus (CMV) retinitis in AIDS patients. This 21-nt PS-ASO targets CMV mRNA, inhibiting production of the IE2 protein that is essential for viral replication. Intraocular injection of fomivirsen at 330 μg dose every other week as induction and monthly as maintenance thereafter significantly delayed disease progression in patients (~90 days). This limited local injection eliminated systemic exposure, avoiding potential systemic side effects. However, the common side effects reported in clinical trials were increased intraocular pressure and mild to moderate intraocular inflammation.[24] Since the emergence of other highly active drugs for CMV retinitis and highly active antiretroviral therapy, the number of CMV retinitis patients has significantly dropped. Due to poor demand, fomiversen has been withdrawn from market.

Modifications on the 2′-position of the sugar moiety have provided enhanced drug-like properties to ASOs. Such 2′-substituents include 2′-*O*-methyl (2′-OMe) and 2′-*O*-methoxyethyl (2′-MOE) (Fig. 1). Sugar pucker of these 2′-*O*-alkyl modified ASOs, causes

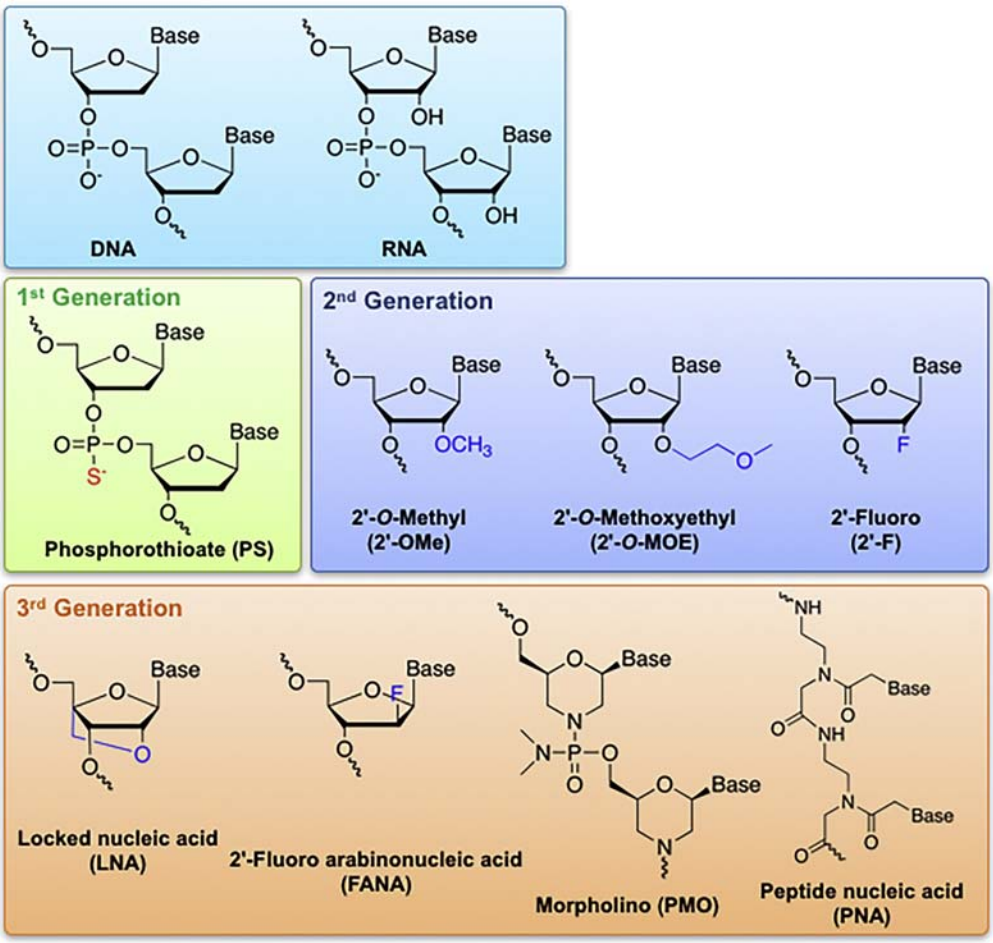

Fig. 1 Chemical modifications of oligonucleotides.

these so-called second-generation ASOs to adopt an energy favorable *C3′-endo* conformation in the furanose pseudorotation cycle, thus increasing binding affinity to RNA.[25] Substitution to these bulky alkoxy groups has also shown to dramatically improve nuclease resistance. 2′-OMe is one of most well characterized nucleic acid analogues. 2′-OMe modification increases T_m by about 1.7°C per modification against its complementary RNA compared to its corresponding unmodified DNA. The advantage of the 2′-OMe modification is that it is a naturally occurring posttranscriptional RNA modification in cells (e.g., tRNA, mRNA cap); therefore, 2′-OMe modified ASOs generally do not activate the innate immune response. 2′-MOE modification is currently the most intensely studied and most advanced in therapeutic ASO development. 2′-MOE modification also offers high binding affinity to its complementary RNA (+2°C per modification) and enhanced nuclease resistance.[25] X-ray crystallography analysis of 2′-MOE modified oligonucleotides revealed a unique structural feature of this nucleoside analogue.[26] Multiple gauche effects around the 2′-MOE substituent locks the sugar pucker in the *C3′*-endo conformation, and that in turn traps water molecules in the ethylene chain of 2′-MOE, assisted by the adjacent phosphate residue. This supports extensive hydration of the molecule and the increased nuclease resistance. Despite their therapeutically favorable properties, these second generation chemistries lack the capacity of recruiting RNase H for target RNA cleavage. Although these modifications are quite useful for steric blocking, there is some limitation in modification patterns for ASOs for RNase H-dependent cleavage. Introduction of gapmer design, where a central DNA region is flanked by several 2′-modified residues, has greatly minimized this limitation. This design allows RNase H recruitment to the central DNA region, whereas the 2′-modified ends stabilize duplex and protect the ASO from nuclease degradation. Many of the second-generation ASOs have been tested or are currently being tested in clinical trials. A 2′-MOE-PS ASO, Mipomersen (KINAMRO, Ionis Pharmaceuticals) has been approved by FDA in 2013 for treatment of homozygous familial hypercholesterolemia.[27] Details will be discussed below.

The third-generation ASOs have been developed to further enhance target affinity and specificity, nuclease resistance, and pharmacokinetics. Among these modifications are peptide nucleic acids (PNAs), 2′,4′-bicyclic nucleic acid (BNA) or locked nucleic acid (LNA), phosphorodiamidate morpholino oligomers (PMOs), and 2′-fluoro-arabinonucleic acids (FANA) (**Fig. 1**).

Unlike other nucleic acid analogues, PNAs have a pseudopeptide backbone in place of phosphodiester backbone which still maintains the ability to Watson-Crick base pair through nucleobases attached to the peptide backbone via methylene carbonyl linkage.[28] PNAs are noncharged nucleotide analogues that show high binding affinity to both DNA and RNA, nuclease/peptidase resistance, and target specificity.[29] PNA based ASOs are mainly used for steric blocking purpose as they are unavailable for the RNase H dependent cleavage mechanism. It is also known that PNA can form PNA/DNA triplex or double duplexes with double-double stranded DNA, as such PNA can elicit antigene activity. Despite these interesting features, they have problems related to solubility and cell-membrane penetration. These have been addressed by the use of charged peptides in the backbone, conjugation of short peptides[30] or cell-penetrating peptides.[31] Substantial studies have been done to assess efficacy of PNA-ASOs in vitro as well as in vivo. Although delivery and pharmacokinetic properties of PNA remain to be solved, recent studies of splice modulating PNAs targeting dystrophin mRNA for treatment of Duchenne muscular dystrophy (DMD) demonstrated promising therapeutic efficacy of PNAs in mice models.[32]

LNA is also one of well known nucleic acid analogues. LNA structure is characterized by a methylene bridge connecting the 2′-oxygen and the 4′-carbon atoms in the sugar moiety, which locks the sugar pucker in *C3′-endo* conformation resulting in a significant increase of binding affinity to complementary RNA.[33] Single LNA substitution raises T_m of duplexes by 2–8°C compared to the corresponding unmodified duplexes.[34] Like the second generation modifications, LNA modifications offer high nuclease resistance, but are not capable of recruiting RNase H, unless the gapmer design is used. Several LNA modified ASOs have already been tested in clinical trials. Among these, a microRNA-122 inhibitor, Miravirsen (Roche, formerly Santaris Pharma),[35] is the first and currently the most advanced antimicroRNA LNA-ASO, (phase I and phase II) which will be discussed later in this section. Although LNA modification related toxicity is reported in some cases,[36] LNA modified ASOs still hold promise and potency in clinical development.

Another unique but potential chemical modification is PMO. This modified analogue consists of a morpholine ring in place of the furanose, and a neutral phosphorodiamidate backbone between the nitrogen atom of the morpholine ring and the hydroxy group of next residue.[37] The binding affinity of PMO to its complementary RNA is only slightly higher than DNA but it is highly sequence specific and extremely stable against nuclease degradation.[38] In contrast to PNA, which is also a noncharged analogue, PMO shows excellent water solubility. This is probably because the nucleobases of PMOs are well stacked in aqueous solution whereas PNA shows poor stacking of the bases.[38] Because of its lack of RNase H activation ability, PMO is primarily used in steric blocking mechanisms or translation arrest. Some PMOs have showed great promise in preclinical and clinical studies. Eteplirsen (Sarepta Therapeutics), a PMO designed to skip exon 51 of dystrophin mRNA in DMD patients is currently one of the most successful therapeutic ASOs and has shown encouraging outcome in clinical studies.[39]

While many 2′-modified analogues show RNA-like properties, FANA is considered to be a DNA mimic in terms of its structure. The fluorine atom which is placed on the β position (top-face) of the nucleoside franose ring of FANA has a significant influence on nucleoside conformation and stability. Because of the high electronegativity and small steric effect of the fluorine atom, FANA adopts a more DNA-like β-type helix conformation,[40] not through the DNA-like *C2′-endo* conformation, but through *O4′-endo* conformation.[41] Interestingly, unlike other sugar modified analogues, studies have shown that FANA can elicit RNase H mediated cleavage probably due to its DNA-like conformation, relatively high conformational flexibility, and lower steric hindrance.[42] FANA modification also increases melting temperature of duplexes and offers high nuclease resistance.[43] Various FANA modified ASOs with PS or PO backbones against clinically relevant targets have been tested in vitro as well as in vivo. For example, FANA modified ASOs that target different isoforms of phosphodiesterase type IV (PDE4) to treat chronic obstructive pulmonary disease showed dose-dependent inhibition of target mRNAs in cells.[44] Treatment of mice with combined PDE-FANA-ASOs exhibited significant

protection from the smoke-induced inflammation. Compared to existing PDE inhibitors, the ASOs showed more potent and broader antiinflammatory effects. Another interesting feature of FANA has been revealed in a recent study showing that FANA modified ASOs with PS backbone were compatible with gymnotic delivery and were as effective at gene expression as corresponding LNA modified oligonucleotides.[45] These unique characteristics of FANA could be great advantages in future clinical development.

6.12.2.1.2 Pharmacokinetic properties of ASOs

Due to their large size, multiple negative charges and hydrophilic nature, oligonucleotides naturally lack drug-like properties that follow Lipinski's rule of five stating that pharmacologically active drugs have molecular weight of less than 500 Da and high lipophilicity. Moreover, as mentioned above, unmodified oligonucleotides are extremely susceptible to serum nucleases resulting in degradation. Chemical modifications can improve not only physical properties but also PK properties of ASOs. PK and biodistribution of the first- and second-generation ASOs have been intensely studied both in preclinical and clinical studies. Most ASOs that have been developed for the purpose of therapeutic use contain PS modifications known to facilitate plasma protein binding, thus enhancing tissue bioavailability. It has been reported that more than 85% of administered ASOs are bound to plasma proteins such as albumin.[46] Additional modifications on the 2′ position improve binding affinity to target RNA and significantly increase tissue and serum stability. When administered by intravenous (IV) infusion or subcutaneous (SC) injection, these second-generation ASOs go into systemic circulation and are rapidly distributed into various tissues (minutes to hours) with high bioavailability (>90%).[22,47] In contrast, uncharged ASOs such as PNA and PMO and unmodified ASOs have less binding affinity to plasma proteins, resulting in inefficient tissue bioavailability and rapid renal excretion.[48] To elicit the desired pharmacological effect, ASOs must cross plasma membrane to reach their targets in the nucleus or cytoplasm. Protein bound ASOs are taken into cells via nonproductive pathway resulting in accumulation of lysosomes or functional uptake where ASOs gain access to target RNAs. A study showed that the functional uptake is dependent on a clathrin-associated adopter protein, AP2M1 but by a clathrin- and caveolin-independent process.[49] Once ASOs enter cells, they exhibit a long half-life of generally 2–4 weeks. The main intracellular metabolic pathway of the second-generation ASOs is nuclease degradation. After tissue absorption, the ASOs are slowly degraded by nucleases and eliminated via excretion in urine. Reported PK properties of the second-generation ASOs are generally similar and independent of sequence but rather depend on chemical modifications, making it easy to predict clinical PK properties that facilitate rapid drug development.

6.12.2.1.3 ASOs in clinical development

Despite early failures in clinical trials and relatively slow initial progress, numerous ASOs are currently being tested in clinical trials against various diseases (listed in **Table 1**). Many of these have shown promising pharmacological effects and properties, which will soon be tested in advanced phase clinical trials. Until now, two ASOs have been approved by the US FDA. Although the first ASO drug, fomivirsen has been retracted from market, newly approved mipomersen is actively being used for treatment of patients. Here, we discuss clinical trial progress and result of some potential ASO therapeutic candidates.

6.12.2.1.3.1 ASO mipomersen (KYNAMRO)—2′-MOE-PS modified gapmer

Mipomersen (KYNAMRO, Ionis Pharmaceuticals) is a 2′-MOE and PS modified ASO gapmer that binds to apolipoprotein B100 (ApoB100) mRNA resulting in inhibition of ApoB100 protein synthesis via RNase H mediated cleavage mechanism in the liver.[50] The drug was approved by the US FDA in 2012 with an orphan drug status for treating patients with homozygous familial hypercholesterolemia (HoFH).[27] HoFH is a rare genetic disorder with two mutant alleles at the *LDLR*, *APOB*, *PCSK9*, or *LDLRAP1* gene locus. The HoFH patients have very high level of plasma low-density lipoprotein cholesterol (LDL-c) (untreated, >13 mmol L^{-1} (>500 mg dL^{-1}); treated, ≥8 mmol L^{-1} (≥300 mg dL^{-1})) and high risk for cardiovascular disease. In a phase III study, a weekly subcutaneous injection of 200 mg mipomersen for 26 weeks reduced LDL-c level by 25% compared with placebo (3.3%).[27] Significant reductions in levels of apoB (27%) and lipoprotein (a) (31%) and no change in high-density lipoprotein cholesterol (HDL-c) were also observed. Adverse events observed in mipomersen treated patients include injection site reactions, flu-like symptoms, elevated alanine aminotransferase, and increased liver fat. Mirapomersen has also been tested in heterozygous FH patients. With the same treatment regimen, the phase III study in patients with severe HeFH met a primary efficacy endpoint, a significant reduction in LDL-c, which was similar to that observed in the phase III study in HoFH patients.[51] Long-term efficacy and safety of mipomersen has been examined in open-label extended dosing study in patients with FH taking maximally tolerated lipid-lowering therapy.[52] The patients received a weekly subcutaneous injection of 200 mg mipomersen for up to 104 weeks. The mean decrease in LCL-c was ~28%. Mean reductions in apoB and lipoprotein (a) levels were ~30% and ~17%, respectively. Common adverse events included injection site reactions and flu-like symptoms. Despite the treatment efficacy, mipomersen was not approved by the European Union due to concerns regarding potential liver toxicity.

6.12.2.1.3.2 IONIS-TTR_{Rx}—2′-MOE-PS modified gapmer ASO

Transthyretin (TTR) amyloidosis is a rare but fatal genetic disease which is caused by a mutation of TTR gene. The disease is characterized by deposition of abnormal forms of TTR amyloid in various tissues and organs including heart and peripheral nerves. Patients with FAP experience ongoing debilitating nerve damage throughout their body resulting in organ failure and loss of motor functions. IONIS-TTR_{Rx} (IONIS Pharmaceuticals) is a second-generation 2′-MOE and PS modified ASO gapmer that targets the TTR mRNA, leading to reductions in both mutant and wild-type TTR protein. In an open-label phase II study in patients with TTR amyloid cardiomyopathy, a weekly injection of IONIS-TTR_{Rx} for 12 months decreased left ventricular mass by 1.9% from baseline

Table 1 ASOs in clinical trials or marketed

Intervention	*Company*	*Target*	*Indication*	*Phase*	*Status*	*Clinical trial ID*
Mipomersen (KYNAMRO)	Ionis	ApoB100	Familial hypercholesterolemia		Approved	
Alicaforsen	Ionis	ICAM-1	Crohn's disease	III	Active	NCT00048295
				III	Completed	NCT00048113
			Ulcerative colitis	II	Completed	NCT00063830
				II	Completed	NCT00063414
IONIS-TTR Rx	Ionis	TTR	Familial amyloid polyneuropathy	III	Active	NCT01737398
Volanesorsen	Ionis	ApoCIII	Familial chylomicronemia syndrome Lipoprotein lipase deficiency Hyperlipoproteinemia type 1	III	Recruiting	NCT02658175
Apatorsen	OncoGenex	Hsp27	Castration resistant prostate cancer	II	Completed	NCT01120470
			Bladder cancer	II	Active	NCT01780545
			Squamous cell lung cancer	II	Recruiting	NCT02423590
			Neoplasms	I	Completed	NCT00487786
BP1001	Bio-Path	Grb2	Acute myeloid leukemia	II	Recruiting	NCT02781883
			Recurrent adult acute myeloid leukemia Acute lymphoblastic leukemia Myelodysplastic syndrome Ph1 positive chronic myeloid leukemia	I	Active	NCT01159028
Custirsen	OncoGenex	clusterin	Breast cancer	II	Completed	NCT00258375
			Prostate cancer	II	Recruiting	NCT00138918
			Multiple cancer	I	Completed	NCT00471432
ISIS-FGFR4Rx	Ionis	FGFR4	Obesity	II	Enrolling	NCT02476019
ISIS-FXIRx	Ionis	Factor XI	Venous thromboembolism	II	Completed	NCT01713361
ISIS-GCCRRx	Ionis	GCGR	Type 2 diabetes mellitus	II	Completed	NCT01968265
ISIS-PTP1BRx	Ionis	PTP-1B	Type 2 diabetes mellitus	II	Completed	NCT01918865
ISIS-DMPKRx	Ionis	DMPK	Myotonic dystrophy type 1	I/II	Recruiting	NCT02312011
IONIS-HTTRx	Ionis	HTT	Huntington's disease	I/II	Recruiting	NCT02519036
IONIS-STAT3Rx	Ionis	STAT3	Advanced cancers	I/II	Active	NCT01563302
IONIS-AR-2.5Rx	Ionis	AR	Advanced solid tumors with AR pathway	I	Completed	NCT02144051
IONIS-STAT3-2.5Rx	Ionis	STAT3	Advanced adult hepatocellular carcinoma Hepatocellular carcinoma metastatic	I	Completed	NCT01839604
IONIS APO(a)-LRx	Ionis	Apo(a)	Elevated lipoprotein(a) [Lp(a)]	I	Completed	NCT02414594
ISIS SOD1Rx	Ionis	SOD1	Familial amyotrophic lateral sclerosis	I	Completed	NCT01041222
			Amyotrophic lateral sclerosis	I	Recruiting	NCT02623699
AVI-7100	Sarepta	M1, M2	Influenza	I	Completed	NCT01747148
Miravirsen	Santaris/Roche	miR-122	Hepatitis C	II	Active	NCT01727934
				II	Active	NCT02031133
				II	Completed	NCT01200420
Drisapersen	BioMarin/GSK	DMD exon 51	Duchenne muscular dystrophy (DMD)	III	Enrolling	NCT02636686
				III	Completed	NCT01254019
Eteplisen	Sarepta	DMD exon 51	Duchenne muscular dystrophy (DMD)		Approved	
SRP-4045	Sarepta	DMD exon 45	Duchenne muscular dystrophy (DMD)	I/II	Active	NCT02530905
SRP-4053	Sarepta	DMD exon 53	Duchenne muscular dystrophy (DMD)	I/II	Recruiting	NCT02310906
DS-5141b	Daiichi Sankyo	DMD exon 45	Duchenne muscular dystrophy (DMD)	I/II	Recruiting	NCT02667483
NS-065/NCNP-01	Nippon Shinyaku	DMD exon 53	Duchenne muscular dystrophy (DMD)	I	Active	NCT02081625

Listed clinical studies are found in clinicaltrials.gov. Most advanced clinical studies for each ASO are listed.

as measured by MRI.[53] A phase III study is being conducted with a weekly injection of 300 mg IONIS-TTRRX to measure efficacy and safety of the drug in patients with familial amyloid polyneuropathy.

6.12.2.1.3.3 Eteplirsen—Exon skipping PMO

DMD is a genetic disorder caused by a mutation of the dystrophin gene at locus Xp21 (X chromosome). A variety of specific mutations can cause translational frameshifts and thus abrogates dystrophin protein synthesis. Dystrophin protein connects actin filaments to the plasma membrane of muscle fiber. The absence of distrophin protein causes progressive loss of mobility and death. The disease affects one in 3500–5000 boys worldwide and the symptoms usually appear at a very young age (2–3 years old).[54] Eteplirsen is a PMO based ASO that targets exon 51 in the dystrophin pre-mRNA. Upon binding eteplirsen, exon 51 is skipped and excised during the pre-mRNA splicing, restoring the downstream reading frame of dystrophin in some mutations. It has been reported that exon 51 skipping is applicable to the largest group of DMD patients (13%). In a recently reported phase IIB study where DMD patients were continually treated with a weekly intravenous injection of eteplirsen (30 or 50 mg kg^{-1}) or placebo for

over 3 years, eteplirsen-treated patients showed a statistically significant advantage in 6-min walk test (6MWT) at 36 months.[39] The most common adverse events seen in eteplirsen-treated patients include headaches, procedural pain and proteinuria, but none of them was serious. In September 2016, Eteplirsen received an accelerated approval from the US FDA. Other PMO ASOs designed to skip other exones are also under development. Among these, SRP-4053 and SRP-4045 have also entered phase 3 clinical trial.

6.12.2.1.3.4 Miravirsen—LNA modified ASO for microRNA inhibition

Miravirsen is the first antimiRNA ASO that entered clinical trials. Miravirsen is a 15-nt LNA-PS modified ASO for treatment of hepatitis C virus (HCV) infection that targets miR-122, a highly abundant miRNA expressed in the liver that regulates HCV replication.[35] A Phase IIa study was conducted to examine long-term efficacy and safety of miravirsen in patients with chronic HCV genotype 1 infection.[55] Five weekly subcutaneous injections of miravirsen at doses of 3, 5, or 7 mg kg^{-1} resulted in dose-dependent and prolonged reduction in HCV RNA levels. In the following 14 weeks after treatment, no virus was detected in total of 5 out of 27 treated patients. In the subsequent long-term safety and efficacy study, one patient showed a prolonged undetectable HCV RNA period until 29 weeks. No serious adverse affects or mutations in miR-122 binding site of HCV RNA were observed among the treated patients.[55]

6.12.2.1.4 Challenges and future perspectives

While significant advantages have been made in ASO so far, clinical progress is limited by a number of challenges. These include, but are not limited to, cytotoxicity, off-target effects, and efficient delivery. Among these, efficient delivery of ASOs to target tissues and organs is the primary challenge for many ASOs being tested in clinical trials. Systemically administered ASOs broadly distribute in various organs. Given that liver is one of the organs that exhibit the highest concentration of systemically administered ASOs, ASOs targeting liver diseases, for example mipomersen, are currently the most advanced and successful in clinical development. Besides systemic administrations (SC and IV), various routes of ASO administrations have been tested including intradermal and intraocular delivery. Although ASOs do not cross the blood–brain barrier, intrathecal delivery has been used as an alternative route to deliver ASOs to the central nervous system (CNS) to treat neurodegenerative diseases. For example, IONIS-$SOD1_{Rx}$, a second-generation ASO designed to target superoxide dismutase 1 (SOD1) to treat familial amyotrophic lateral sclerosis (ALS), was tested in phase I clinical trial by intrathecal administration using an external pump over 11·5 h at increasing doses.[56] Widespread delivery of the ASO to the CNS was observed. The conjugation of a specific delivery ligand is another strategy to facilitate target cell specific uptake of ASOs. Triantennary *N*-acetyl galactosamine (GalNac), a ligand for the hepatocyte-specific asialoglycoprotein receptor, for instance, has been tested in clinical trials as an excellent delivery platform of siRNAs that target multiple hepatocellular targets.[57] Conjugation of GalNac has also shown to improve potency of ASOs approximately 10-fold for gene silencing and enhance duration of pharmacological effect in mouse liver.[58]

It has been almost 40 years since the first report of ASO. Only two ASO therapeutics have reached the market so far. Compared to other classes of therapeutic agents, ASOs have unique mechanism of action and physical and pharmaceutical properties, thus holding a great potential for becoming first-in-class drugs for undruggable molecular targets with other classes of therapeutics (e.g., small molecules and monoclonal antibodies). Considering recent significant improvement in technologies including chemistries, delivery strategies, and cost efficient synthesis, PK properties of ASOs have significantly improved and many ASOs being tested in clinical and preclinical trials exhibit drug-like properties. Indeed, a number of ASOs are being tested in advanced stages of clinical trials (phase II and phase III), suggesting that ASOs therapeutics will become cutting-edge treatment approach of various diseases in not-too-distant future.

6.12.2.2 RNA Interference (RNAi)

RNA interference[59] is a nearly ubiquitous pathway in multicellular organisms used for cellular immunity and developmental regulation that employs small microRNAs (miRNAs) for specificity. In mammals, miRNAs[60] regulate many aspects of development and are expressed in nearly all cells. MiRNA biogenesis[61] starts in the nucleus, where long primary miRNAs transcripts (pri-miRNAs) containing partially mismatched RNA duplexes are initially cleaved by the Microprocessor complex.[62] Microprocessor is a heterotrimeric complex consisting of one molecule of the RNase III protein Drosha and two molecules of the cofactor DGCR8. Drosha measures 11 bp from the pri-miRNA single stranded RNA-double stranded RNA (ssRNA-dsRNA) junction at the base of the pri-microRNA to excise the ~70 nt pre-miRNA hairpin. DGCR8 provides efficiency and precision to the excision.[63] The resulting pre-miRNAs are exported to the cytoplasm,[64] where they are recognized and further processed by the Dicer[65] enzyme to produce 22 nt RNA duplexes. Subsequently one strand of the cleavage product is inserted into an Argonaute[66] protein by the RISC loading complex (RLC)[67] to become the guide strand for a mature RNA induced silencing complex (RISC) (**Fig. 2**).[68]

RISC uses efficient mechanisms to scan cytoplasmic mRNAs for sequences complementary to the guide strand.[69] Matching mRNAs are inhibited from translation, and destabilized, or degraded via catalytic means (**Table 2**).[70]

Several factors make RNAi a highly attractive mechanism for therapeutic applications.[71] Among these factors: (1) it allows prolonged and efficient inhibition and degradation of mRNAs and other targeted RNA transcripts; (2) the sequence based targeting mechanism allows inhibition of targets that are not druggable by small molecules; (3) the ability to inhibit different targets by changing the guide sequence makes RNAi a platform technology that could simplify drug development for disparate targets.

Over the past decade, a number of groups have developed synthetic RNAi triggers that utilize the cytoplasmic portions of the RNAi loading pathway to assemble RISC using synthetic guide strands. We will discuss the elements of this pathway that are

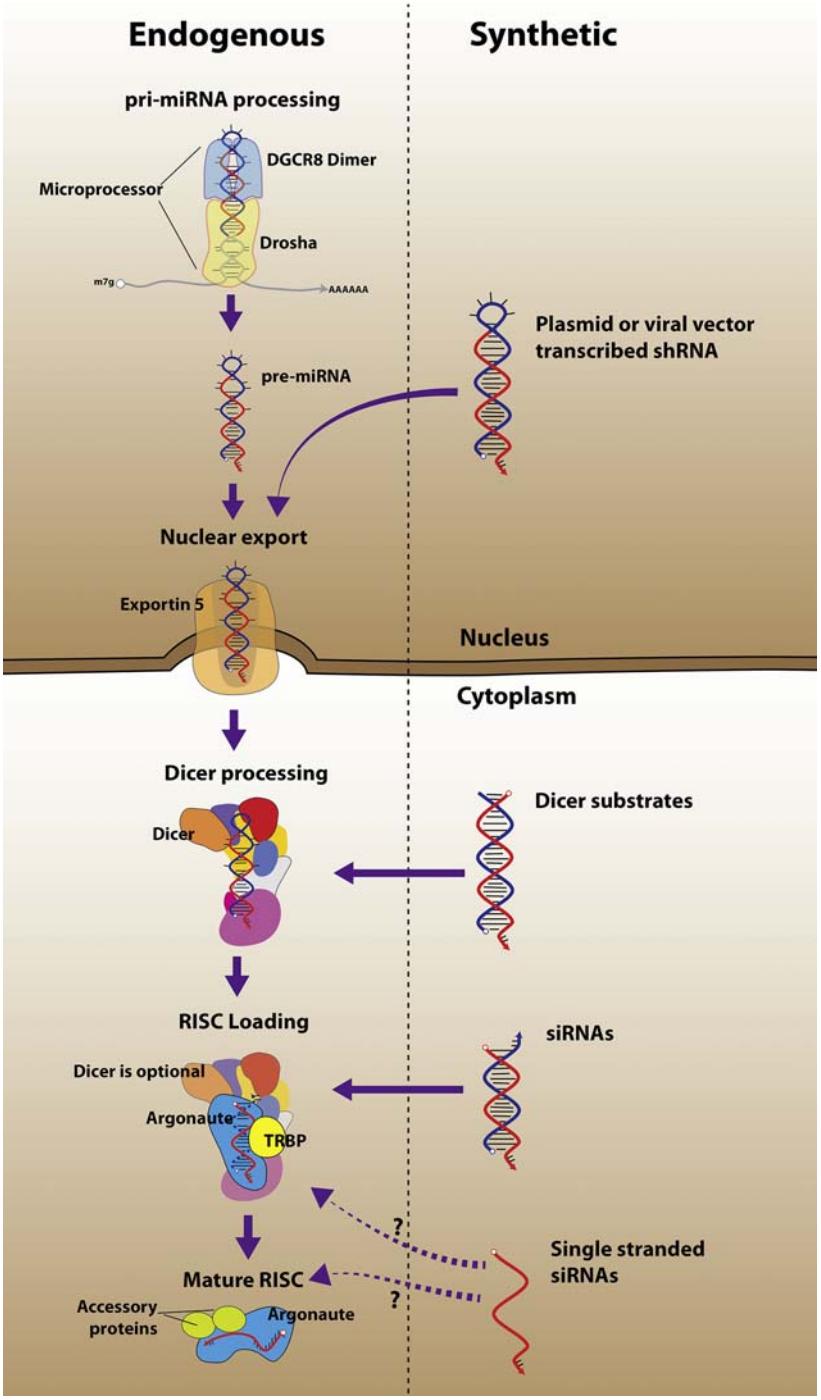

Fig. 2 Select steps in the biogenesis of mammalian microRNAs and points of entry into the pathways for select synthetic RNAi triggers. For single stranded RNA, it is unclear at this point how the chemically modified strands actually enter RISC, although Dicer cleavage is not involved.

important for their functioning, review the major variants of these substrates, summarize the important technical issues, and survey the current state of clinical development (Fig. 2).

6.12.2.2.1 Cytoplasmic RNAi processing

To understand how synthetic RNAi triggers function, it is illustrative to look at the functioning of the cytoplasmic portion of the mammalian RNAi pathway (Fig. 2).[61b] Mammalian pre-miRNA[64,72] are usually ~70 bp or longer RNA hairpins with a number of mismatches in the stem. The 5′ and 3′ termini of the hairpins result from cleavage of pri-miRNAs by the Microprocessor complex.[62c] Ideally, this produces a Dicer substrate with a blunt 5′ terminus bearing a terminal phosphate, and a 3′ two-base overhang.[73]

Table 2 RNAi in clinical trials

Intervention	*Company*	*Target*	*Condition*	*Phase*	*Status*	*Clinical trial ID*
Patisiran (ALN-TTR02)	Alnylam	TTR	Amyloidosis	III	Enrolling	NCT02510261
			TTR-mediated amyloidosis	III	Active	NCT01960348
			Amyloidosis, hereditary Amyloid neuropathies, familial Familial amyloid polyneuropathies Amyloid neuropathies Amyloidosis, hereditary, transthyretin-related			
Revusiran (ALN-TTRSC02)	Alnylam	TTR	Familial amyloidotic cardiomyopathy (FAC) Amyloidosis, hereditary Amyloid neuropathies, familial Amyloid neuropathies Amyloidosis, hereditary, transthyretin-related Familial transthyretin cardiac amyloidosis	III	Active	NCT02319005
			Transthyretin (TTR)-mediated amyloidosis Familial amyloidotic polyneuropathy (FAP) ATTR amyloidosis Familial amyloid neuropathies	II	Active	NCT02595983
			TTR-mediated amyloidosis	II	Active	NCT02292186
			ATTR amyloidosis	I	Recruiting	NCT02797847
QPI-1002	Quark	p53	Delayed graft function	III	Recruiting	NCT02610296
			Acute kidney injury	II	Recruiting	NCT02610283
QPI-1007	Quark	Caspase 2	Nonarteritic anterior ischemic optic neuropathy	II\III	Recruiting	NCT02341560
			Glaucoma, angle-closure, primary, acute	II	Completed	NCT01965106
ARC-520	Arrowhead	HBV	Hepatitis B	II	Recruiting	NCT02604212
				II	Recruiting	NCT02604199
				II	Recruiting	NCT02577029
				II	Recruiting	NCT02452528
				II	Recruiting	NCT02065336
				II	Recruiting	NCT02738008
Bamosiran	Sylentis	ADRB2	Open angle glaucoma	II	Completed	NCT02250612
			Ocular hypertension	II	Completed	NCT01739244
PF-04523655	Quark	RTP801	Choroidal neovascularization Diabetic retinopathy Diabetic macular edema	II	Completed	NCT01445899
RXI-109	Rxi	sd-rxRNA against CTGF	Keloid	II	Completed	NCT02079168
			Hypertrophic scar	II	Completed	NCT02030275
			Hypertrophic scar	II	Recruiting	NCT02246465
			Age-related macular degeneration Subfoveal choroidal neovascularization Subretinal scarring Subretinal fibrosis	I\II	Recruiting	NCT02599064
SYL1001	Sylentis	TRPV1	Ocular pain Dry eye syndrome	II	Completed	NCT02455999
TKM-HBV	Arbutus	HBV	Hepatitis B, chronic	II	Recruiting	NCT02631096
ALN-AAT	Alnylam	α-1 antitrypsin	Antitrypsin deficiency liver disease	I/II	Active	NCT02503683
ALN-CC5	Alnylam	C5	Paroxysmal nocturnal hemoglobinuria (PNH)	I/II	Active	NCT02352493
ALN-GO1	Alnylam	Glycolate oxidase	Primary hyperoxaluria type 1 (PH1)	I/II	Recruiting	NCT02706886
ALN-HBV	Alnylam	HBV transcript	Hepatitis B	I/II	Recruiting	NCT02826018
Atu027	Silence Therapeutics	PKN3	Carcinoma, pancreatic ductal	I\II	Completed	NCT01808638
DCR-MYC	Dicerna	MYC	Hepatocellular carcinoma	I\II	Recruiting	NCT02314052
Fitusiran (ALN-AT3SC)	Alnylam	Antithrombin	Hemophilia A Hemophilia B	I/II	Recruiting	NCT02554773
QPI-1002 (I5NP)	Quark	p53	Delayed graft function Other complication of kidney transplant	I\II	Completed	NCT00802347

Table 2 RNAi in clinical trials—cont'd

Intervention	*Company*	*Target*	*Condition*	*Phase*	*Status*	*Clinical trial ID*
TKM-PLK1	Arbutus	PLK1	Hepatocellular carcinoma	I|II	Completed	NCT02191878
(TKM-080301)			Cancer	I|II	Completed	NCT01262235
			Neuroendocrine tumors			
			Adrenocortical carcinoma			
ALN-AS1	Alnylam	ALAS1	Acute intermittent porphyria	I	Recruiting	NCT02452372
ALN-PCSSC	Alnylam	PCSK9	Hypercholesterolemia	I	Completed	NCT02314442
ARC-521	Arrowhead	HBV genome	Hepatitis B	I	Recruiting	NCT02797522
ARC-AAT	Arrowhead	Mutant α-1 antitrypsin	Alpha-1 antitrypsin deficiency	I	Recruiting	NCT02363946
DCR-PH1	Dicerna	Glycolate oxidase	Primary hyperoxaluria type 1	I	Recruiting	NCT02795325
QPI-1007	Quark	p53	Optic atrophy	I	Completed	NCT01064505
			Nonarteritic anterior ischemic optic neuropathy			
MRG-201	miRagen	mir-29b mimic	Limited scleroderma	I	Recruiting	NCT02603224
			Localized scleroderma			
			Diffuse scleroderma			
MRX34	Mirna	mir-34 mimic	Primary liver cancer	I	Recruiting	NCT01829971
			SCLC			
			Lymphoma			
			Melanoma			
			Multiple myeloma			
			Renal cell carcinoma			
			NSCLC			
MTL-CEBPA	Mina Alpha	saRNA activating CEBPA	Hepatocellular carcinoma	I	Recruiting	NCT02716012

Listed clinical studies are found in clinicaltrials.gov. Most advanced clinical studies for each RNAi therapeutic are listed.

Dicer[74] is the enzyme that processes pre-miRNAs in the cytoplasm. Human Dicer is a ~82 KD protein consisting of PAZ, dsRBD, Ribonuclease III, and helicase domains. The PAZ domain binds to the 5′ phosphate and 3′ overhang of the pre-miRNA, anchoring the hairpin in place while the dsRBD domain interacts with the stem to further stabilize binding.[74] This places the RNAse III domain at fixed distance from the PAZ domain binding site, resulting in cleavage of the opposing sides of the hairpin at the 19 and 21 bps from the terminus, producing a 19 bp duplex with a 5′ phosphate and 2 nt 3′ overhangs on both ends.[74] (The functioning of the helicase domain on Dicer is not completely understood, but it appears to increase the rate of processing for mismatched RNA hairpins at the expense of slower kinetics for perfectly matched duplexes.[75] In addition, there is some evidence for relatively large scale conformational changes in the Dicer-pre-miRNA complex during Dicer processing[76].)

6.12.2.2.1.1 Strand selection

After Dicer cleavage, a RISC loading complex (RLC)[67,77] forms around the RNA duplex, and one strand is loaded by an Argonaute protein while the opposing strand is removed. Guide strand selection[78] is known to favor incorporation of the strand whose 5′ terminus is at the weaker base-paired end (the last ~6 bp) of the RNA duplex.[78a,79] Thus, RNA duplexes with the same number of G–C base-pairs at either end tend to result in an ~50% probability for loading either strand, while those with a markedly more AU rich terminus tend to favor loading of the strand with the AU rich 5′ end.

6.12.2.2.1.2 RISC structure and function

While mature RISC can have multiple associated proteins, the most basic element is an Argonaute protein with bound guide strand. The crystal structure of human Ago2 with bound guide strand has been reported.[68,80] The 5′ terminal phosphate of the guide strand is held in Ago2's PAZ domain. Bases 2–8 are arranged in an alpha-helical configuration by numerous protein-RNA contacts, leading to a distinctive domain that favors rapid base-pairing.[68,80] Corresponding to this structural picture, functional assays of Ago2 activity show that the guide strand is divided into domains with distinct functions,[81] with the seed region being most important for target recognition. Experiments further show that preorganization of the seed region bases increases speed of target site recognition and stability of base-pairing[69a] and surveys of miRNA binding sites show a preeminent importance for base-pair matches in the seed region.[82] In addition to preorganization of the guide strand, Ago2 apparently executes a dynamic search process where a three dimensional diffusional search for mRNA targets is followed by one-dimensional diffusion along the mRNA to find the cognate target site.[69b] Together, these mechanisms allow RISC to efficiently and correctly recognize small (~7 base) target sites on large mRNAs.[69c]

6.12.2.2.1.3 Target inhibition

Endogenous miRNAs usually have targets sites in the 3′ UTR of multiple mRNAs (although there are also sites in open reading frames).[82] Each target site is usually complementary to the seed region of the guide strand, but not complementary to the entire guide strand. When miRNAs are attached to a target mRNA, protein cofactors destabilize binding of mRNA bound protective proteins, resulting in an increased rate of mRNA degradation.[70a] There is also evidence for direct inhibition of protein translation, although this is believed to be a less important mechanism.[70a]

In contrast to endogenous miRNAs, most synthetic RNAi substrates utilize guide strands with full length complementarity to target sites in either the 3′ UTR or the protein coding region[83] which typically are referred to as small interfering RNAs or siRNAs. Full length base-pairing allows Ago2 to directly cleave target RNA transcripts between the 11th and 12th base-pair (counting from the 5′ of the guide strand) via its integral slicer activity.[81,84] However, Ago2 is the only human Ago with slicer activity and there is currently no know method to direct guide strand distribution specifically to Ago2. Past studies on the distribution of miRNA guide strand between different human Argonautes seem to indicate an even distribution for most miRNAs.[85]

6.12.2.2.2 Transcriptional silencing and activation

In addition to inhibiting or degrading mRNAs and other target transcripts in the cytoplasm, small RNA is known to induce transcriptional silencing in yeast, plants and other organisms.[86] The extent to which this effect occurs in humans is currently under investigation.[87] Also, a number of investigators have reported small activating RNAs[88] that can stimulate gene expression by targeting certain promoter regions. Although there is currently not a clear understanding of the mechanisms by which transcriptional activation occur, small activating RNAs may become an important class of RNAi therapeutics.

6.12.2.2.3 Types of synthetic RNAi substrates

Synthetic RNAi substrates are RNAi triggers that are produced exogenously via chemical synthesis and then transfected into target cells (Fig. 3).

A major difference between synthetic duplex RNAi triggers and endogenous miRNAs is that the synthetic triggers are usually completely base-paired, whereas endogenous miRNAs have mismatches that can affect passenger strand sequence, Dicer processing, and RISC loading. Thus, even when a synthetic RNAi trigger has identical intended guide sequence as a natural miRNA, it could still have considerable functional differences.

There are two main types of synthetic RNAi triggers:

- Dicer substrates have duplex regions that are longer than 19 bp, and enter the RNAi loading pathway via cleavage by Dicer followed by RISC loading.
- Non-Dicer substrates have duplexes that are 17–19 bp, and enter the RNAi pathway without Dicer cleavage.

Currently, both types of RNAi triggers are under active development for clinical applications. Here, we survey some representative variants.

Small interfering RNA (siRNA) are 19 bp RNA duplexes with two base 3′ overhangs on either end.[89] They are not cleaved by Dicer and do not require Dicer for RISC loading. siRNAs are one of the first and most widely used synthetic RNAi triggers, with advantages such as low synthesis cost due to the short component strands, mature technology development, high potency, and good stability resulting from extensive incorporation of chemical modifications in some variants.[83a] They are widely available from commercial sources and a number of siRNA based therapeutics are under clinical or preclinical development (Fig. 3).

Short-hairpin RNA (shRNA) are RNA hairpins that are efficiently processed by Dicer. The hairpins usually have 19–29 bp duplexes, at least 4 nt in the terminal loop, and a siRNA like blunt end geometry.[90] These substrates are more difficult to synthesize chemically due to the length of the strand and are thus most often produced via in vitro transcription systems. Clinical applications of shRNAs usually involve delivery of bacteria that excrete shRNAs[91] or viral vectors that produce expressed shRNAs in transduced cells,[92] and will be discussed elsewhere in this chapter.

Dicer substrate siRNA (DsiRNA) are 23–28 bp RNA duplexes that are cleaved by Dicer.[93] The duplex termini are asymmetric. The putative guide strand has an siRNA like two base 3′ overhang. The 3′ of the putative passenger strand is blunt ended with the last two bases being DNA.

In direct comparisons with canonical siRNAs with identical guide strand sequences, DsiRNAs exhibited more efficient RISC loading, better persistence of the guide strand, and better loading selectivity for the guide strand.[94] These combined effects lead to significantly improved RNAi performance.

DsiRNAs are compatible with stabilizing 2′-F and 2′-O-methyl chemical modifications[95] and can use delivery methods similar to those for siRNAs. They are sold commercially for scientific research and are under preclinical and clinical development by Dicerna Pharmaceuticals for therapeutic applications.

Synthetic small hairpin RNAs (sshRNA) are small hairpin RNAs with 19 bp or shorter RNA duplexes.[96] They are not processed by Dicer. Instead, they are incorporated into RISC via one of two pathways, depending on the position of the guide strand.[96b]

If the guide sequence is at the 5′ terminus of the sshRNA, then the strand is directly loaded into Argonaute. The passenger side of the sshRNA is then either cleaved by Ago2's slicer activity or decoupled from base-pairing with the guide strand side by the Ago. (Compare with AgoshRNAs below.) If the guide sequence is at the 3′ terminus of the sshRNA, then the terminal loop of the strand needs to be cleaved by endonucleases such as RNAse A. The resulting duplex then enters RISC much like a regular siRNA. sshRNAs are currently under preclinical development for treatment of Hepatitis delta virus and wound healing applications.

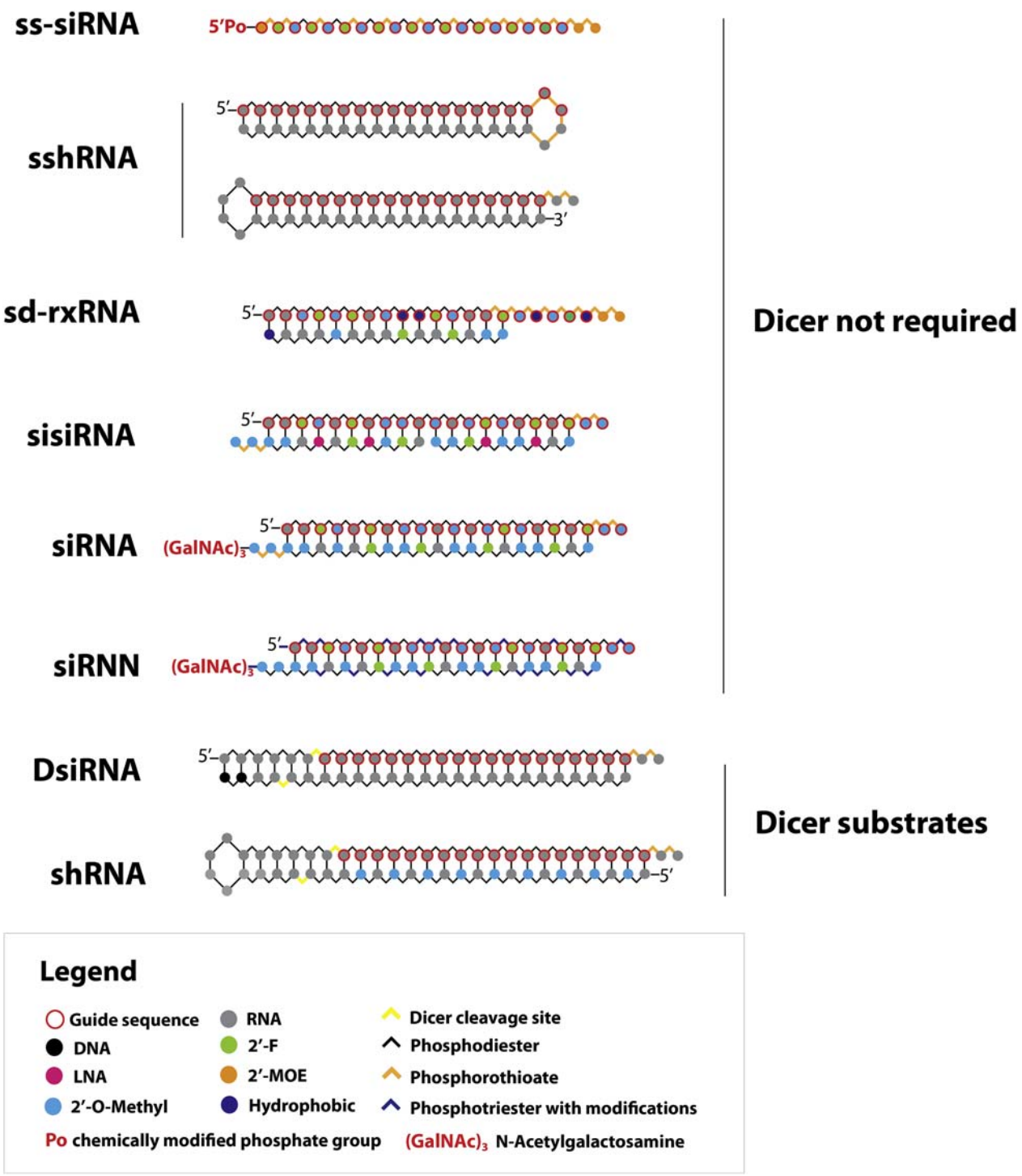

Fig. 3 Select synthetic RNAi triggers and typical patterns of chemical modification for therapeutic applications. RNAi triggers are frequently modified with 2′-F and 2′-OMe bases to enhance in vivo stability and safety. Additional modifications, such as hydrophobic moieties, can impart additional function such as enhanced cell entry. In general, a therapeutic RNAi trigger will undergo a number of rounds of development to find optimal modification patterns for in vivo potency and safety.

Short-interfering ribonucleic neutrals (siRNN) are a new variety of RNAi trigger developed by the Dowdy group at UCSD.[97] siRNNs are ribonucleic duplexes with neutral phosphor-triester backbone linkages instead of negatively charged phosphor diester backbone. The neutral backbone linkage allows easier cell entry and facilitates conjugation of additional targeting or endosome disrupting ligands. Inside the cytosol, enzymatic processing converts the phosphor triesters into phospho diester linkages that are

compatible with the RNAi pathway. Thus, this allows a synthetic RNAi trigger to have favorable self-delivering properties without compromising RNAi efficiency. siRNNs have been licensed to Solstice Biologics for further development.

Single stranded siRNAs (ss-siRNA) are under development by Ionis Pharmaceuticals and collaborators.[98] The key motivation for developing single stranded RNAi agents is that phosphorothioate modified single stranded oligonucleotides can have significant systemic tissue distribution and can enter cells via gymnosis. As such, a potent single stranded siRNA could have significant advantages in ease of delivery, and simplicity of formulation (and by extension regulatory approval).

However, in order to enter RISC, single stranded oligonucleotides have to utilize extensive chemical modifications to be significantly resistant to exonuclease and endonuclease degradation without having these modifications compromise the ability of the oligo to interact with Argonaute and act as a guide strand.

Recently, Ionis Pharmaceuticals and collaborators published results showing that extensively chemically modified, partially phosphorothioated single stranded oligonucleotides can enter RISC to guide RNAi silencing.[98a] Although the best achieved activity was still $\sim 10\times$ less efficient compared to a double-stranded siRNA, ss-siRNAs may become an important new class of RNAi triggers with further improvements in RNAi efficiency.

6.12.2.2.4 Focus areas for improving potency and safety

Clinical application of synthetic RNAi triggers requires careful optimization of sequence and composition to improve potency and safety. Important considerations include

1. Avoiding passenger strand activity.
2. Avoiding nonspecific toxicity.
3. Enhancing construct stability
4. Identifying effective target sites.

Passenger strand RISC loading is a significant concern for RNAi drugs because the passenger strand could direct RNAi activity towards unintended targets, resulting in toxic side effects. A number of solutions have been devised to address this problem via sequence design,[83b,99] structural motifs,[93,100] or chemical modifications.[101] One example is small internally segmented siRNAs (sisiRNA).[102] These are novel siRNA variants in which the passenger strand is divided into two 10–12 nt segments that are too short to be loaded into RISC. To thermodynamically stabilize the small duplexes, locked nucleic acid modifications[103] are used.

As an alternative to changing the structural characteristics, it is also possible to use chemical modifications. Snead et al. reported that modification of the 5′ of the siRNA passenger strand with an unlocked nucleic acid[104] eliminates passenger strand loading.

Avoiding nonspecific toxicity. In addition to spurious passenger strand activity, nonspecific toxicity can arise from immunogenic responses to RNA duplexes.[105] There are now well established routes for avoiding immunogenic toxicity.[106] First, RNA duplexes should be kept to a minimal possible length as immunogenic activation by PKR and other sensors for RNA duplexes are length dependent. Secondly, judicious incorporation of 2′-OMe and other chemical modifications in RNA duplexes can reduce immunogenicity. Thirdly, preclinical testing for oligonucleotide based therapeutics need to utilize primates in order to adequately assess toxicity in humans.[107]

In addition to immunogenic toxicity, phosphorothioate[108] modified oligonucleotides and LNA[109] modified oligonucleotides are known to have nonspecific toxicity in animals. Clinical development strategies include minimization of the use of such modifications, avoidance of certain problematic motifs for LNAs, and iterative refinement and testing, which will be a theme in general for all of the issues involving clinical development.

Enhancing construct stability. Achieving potent therapeutic effects require construct stability against disassembly or degradation during in vivo delivery. A number of potent and safe chemical modifications have been developed for therapeutic oligonucleotides and a subset of these is compatible with RNAi triggers.[83a,99,110]

The effects and compatibility of chemical modifications in RNAi triggers is often position dependent. For example, long contiguous stretches of 2′-OMe or 2′-fluoro (2′-F) on the guide strand and at the Dicer cleavage sites of DsiRNAs significantly inhibited RNAi activity, but alternating patterns of 2′-OMe modifications on the passenger strand enhanced nuclease resistance without significantly compromising RNAi efficiency.[110]

In general, it is reasonable to expect that chemical modifications that do not inhibit Dicer processing or eliminate favorable contacts between the guide strand and Argonaute can lead to effective RNAi activity. Indeed, McRae and colleagues recently published crystal structures of chemically modified guide strands with human Ago2,[111] showing position dependent effects of different chemical modifications. Recent clinical experiences indicate that careful application of chemical modifications can result in safe and potent RNAi triggers.

Identifying effective target sites. There is a significant body of work on the rational design of siRNAs for clinical applications.[83b,112] Basic target site considerations should take into account the conservation of the site across pertinent transcript variants, possible homologies with other genes that could cause off-target effects, the local predicted secondary structure, the asymmetry of the cognate guide strand for biasing strand loading. However, due to the unpredictable nature of secondary and tertiary structure in long RNA transcripts, the effects of protein binding and translation, and the incomplete understanding of how these issues affect RISC binding, and the vast complexity of the transcriptome and mammalian cells in general, target site selection will require extensive experimental evaluation of potential targets.[107]

6.12.2.2.5 Effective delivery

Delivery is a major challenge in RNAi therapeutics because synthetic RNAi triggers are hydrophilic macromolecules that cannot cross the cell membrane and are subject to rapid clearance by both the kidneys and the reticuloendothelial system. Delivery methods must allow RNAi triggers to safely cross multiple physiological barriers for effective distribution to target tissues, uptake by target cells and escape into the cytosol.[113] Generally, 10 mg kg^{-1} dosing levels are considered an upper limit for clinical applications, and <1 mg kg^{-1} levels are preferred. Current methods under development include:

- Polymeric nanoparticles[114]
- Liposomes and lipid nanoparticles[115]
- Antibody conjugated delivery[116]
- Aptamer conjugated delivery[117]
- Polymeric materials[118]
- Conjugation of molecular ligands[119]
- Backbone modified siRNAs[97b]
- Spherical nucleic acids[120]
- DNA and RNA nanostructures[121]

6.12.2.2.6 Potential therapeutic applications of RNAi

6.12.2.2.6.1 Nanolayered siRNA delivery for wound healing

The Hammond lab at MIT has been developing electrostatically assembled coatings that incorporate siRNA for sutures[122] and dressings.[123] A substrate material, such as nylon, is first coated with alternating layers of positively charged polymer and negatively charged dextran sulfate, then positively charged chitosan and negatively charged siRNA are added layer by layer, resulting in μg cm^{-2} loading levels. At the site of application, siRNAs are shed together with chitosan, resulting in effective delivery.

In an animal study, a dressing coated with an siRNA targeting matrix metalloproteinase 9 (MMP9) was able to inhibit MMP9 expression and increase wound healing at model wound sites in mice. The mean level of MMP9 activity was decreased by ~50% at the 2 week time point, and there was significantly better wound closure.[123]

6.12.2.2.6.2 Tat/rev DsiRNA with gp120 aptamer for HIV treatment

GP120 is a glycoprotein expressed on the surface of HIV-1 and associated with HIV infected cells. The Rossi lab at City of Hope has developed a 2′-F substituted gp120 RNA aptamer for inhibition of HIV-1 activity and delivery of siRNA to HIV infected cells.[124] The aptamer binds gp120 at 50–100 nM K_d, and are internalized in gp160 expressing HIV infected cells.

Subsequent work utilized this aptamer to delivery anti-tat/rev DsiRNAs to HIV-1 infected mice.[117,125] The tat/rev siRNA was conjugated to chemically synthesized gp-120 aptamers via either a polycarbon linker[125] or a polycarbon linker conjugated 2′-OMe RNA duplex adapter region.[117] In the first study,[125] treatment of mice 3 weeks after HIV infection with weekly treatments of 0.38 mg kg^{-1} of aptamer-conjugated DsiRNA resulted in reduction of viral load to undetectable levels by week 5 or week 8, with viral rebound after end of treatment. In contrast, treatment with siRNA alone gave no detectable benefit.

In the second study,[117] utilization of the RNA adapter allowed multiplexed delivery of three different anti-HIV siRNAs. Weekly injections of this cocktail at ~0.4 mg kg^{-1} levels (0.25 nmol total of the three DsiRNAs) resulted in an ~100× to 1000× reduction in plasma viral RNA after 5 weeks of treatment (9.5 weeks post infection). A second independent experiment using biweekly injections at 22.5 weeks after treatment resulted in elimination of detectable viral RNA from plasma.

6.12.2.2.6.3 Tat/rev DsiRNA with PAMAM dendrimers for HIV treatment

Poly(amidoamine) (PAMAM) dendrimers are well defined branching polymers with exact molecular weight, size, and composition that is controlled by the dendrimer generation. At pH ≤ 7.4, terminal amine groups in the dendrimer at the surface of dendrivers are protonated, giving it high cationic charge suitable for electrostatic association with RNAi triggers. At endosomal pH (~5), the interior tertiary amines of PAMAM dendrimers become also protonated, leading to endosomal disruption and release of RNAi triggers.

Zhou and collaborators[126] loaded G_5 PAMAM with anti-HIV DsiRNA, resulting in 100 nm nanoparticles. These were tested in an HIV-1 infected humanized mouse model via weekly intravenous injection of 0.15 mg kg^{-1}-DsiRNA (combination of anti-tat/rev, anti-CD4, anti-TNPO3). This resulted in suppression of plasma viral RNA by ~1000×, with treatment effects persisting for 3 weeks posttreatment. Retreatment at 24.5 weeks post infection using biweekly injections of DsiRNA-dendrimer conjugates resulted in suppression of viral loads to undetectable levels.

6.12.2.2.7 RNAi in clinical development

6.12.2.2.7.1 ALN-TTR02 (Patisiran), siRNA—lipid nanoparticle

Transthyretin amyloidosis (ATTR) is a rare, fatal, and inherited neurodegenerative disease driven by deposition of liver produced transthyretin (TTR) amyloids in the peripheral nervous system and the heart.[127] Alnylam identified at potent siRNA targeted against the 3′ UTR of transthyretin and encapsulated this siRNA in two generations of lipid nanoparticles[115](ALN-TTR01 and ALN-TTR02) for delivery to hepatocytes.

In a phase I clinical trial, both ALN-TTR01 and ALN-TTR02 demonstrated reduction of circulating transthyretin. 0.15–0.3 mg kg^{-1} doses of ALN-TTR02 achieved maximum reduction of 82.3–86.8% circulating transthyretin at approximately

1 week after single dose administration, and the reduction level ranged from 56.6% to 67.1% after 28 days. The single dose infusion was well tolerated, with mild to moderate reactions observed in 7.7% of participants receiving ALN-TTR02.

A subsequent phase II open label study on ALN-TTR02 (renamed Patisiran)[128] on 27 patients showed >80% sustained serum reduction of transthyretin over the course of 2 years with intravenous injection at 0.3 mg kg^{-1} every 3 weeks, and the drug was well tolerated. Clinical data supported the hypothesis that TTR knockdown has the potential to halt progression of neuropathy.

A phase III clinical trial has been initiated.[129]

6.12.2.2.7.2 ALN-TTRSC (Revusiran), chemically modified siRNA with tri-GalNAc ligand

Revusiran[130] is Alnylam's second candidate against ATTR. Unlike patisiran, revusiran is formulated as a chemically modified siRNA with a conjugated GalNAc ligand that targets the siRNAs to asialoglycoprotein receptors on the surface of hepatocytes.[119] Compared with earlier LNP formulations, GalNAc-conjugated siRNAs are simpler to produce, have well defined, uniform molecular composition, and allow highly efficient delivery to the liver via subcutaneous injections at <10 mg kg^{-1} dosage levels.[119]

In a phase I study on healthy volunteers,[131] revusiran achieved >80% knockdown of serum TTR for up to 50 days on single 5 and 10 mg kg^{-1} subcutaneous injections with mild, rapidly resolved side effects, and a phase II study has begun.[130b]

Alnylam continues to refine the potency of its GalNAc conjugated siRNAs. Extensive lead optimization using proprietary stabilization chemistries in conjunction targeted at enzymatic cleavage sites identified from metabolic profiling resulted in >10× improvements in potency. ALN-AT3, an siRNAs targeted at antithrombin, achieved sustained ~50% knockdown of antithrombin in nonhuman primates via 0.5 mg kg^{-1} weekly dosing followed by 0.125 mg weekly dosing.[132] In October 2016, following reports of cases new onset or worsening peripheral neuropathy in patients taking Revusiran, and findings by an independent data monitoring committee of unfavorable benefit-risk profile in the Phase III ENDEAVOR trial, Alnylam annouced that it was discontinuing the development of revusiran. The company noted that the decision does not affect its other clinical programs.[133]

6.12.2.2.7.3 CALAA-01, RRM2 siRNA—cyclodextrin nanoparticle with transferrin targeting ligand

CALAA-01 was a nanoparticle delivered siRNA for treatment of human solid tumors. The system combined a PEG protected, transferrin (Tf) conjugated cyclodextrin nanoparticle[134] with an siRNA against ribonucleotide reductase subunit 2 (RRM2), a target that was previously shown to be active against solid tumors.

The particles were formulated as a two vial system. One vial contained the cyclodextrin polymer (CDP), adamantine-PEG and adamantine-PEG-Transferrin. A second vial contained the siRNA. When the two vials were combined, the components self-assembled to form ~70 nm diameter nanoparticles.

The nanoparticles were designed to accumulate in tumors via the enhanced permeability and retention effect,[135] achieve preferential endocytosis by cancer cells via Tf ligands, and escape the endosome when imidazoles in the CDP were protonated around pH 6.[134]

A phase I clinical trial was the first to demonstrate evidence of RNAi in target tissues via systemic administration of nanoparticles.[136] CALAA-01 was administered to three patients with metastatic melanoma at doses of 18, 24, and 30 mg m^{-2} siRNA. Biopsy samples from the three patients showed reduction of RRM2 mRNA ranging from 32% to 77% up to 1 month post administration.

However, a subsequent phase Ia and Ib clinical trial involving 24 patients showed dose limiting toxicities in five patients at higher doses of 18–27 mg m^{-2} in the absence of any objective responses to the medication. The study was not able to trace the source of the toxicity but it was likely from components of the nanoparticle, possibly the Tf, but possibly exacerbated by inclusion of the siRNA.[114]

A problem that may have affected the efficacy was the low serum half-life of siRNAs of ~30 min. This was likely due to disassembly of the electrostatically assembled particles at the kidney glomerular basement membrane,[137] which caused the particle formulation to be ineffective at achieving long circulation times for the siRNA.

6.12.2.2.7.4 DCR-MYC, MYC DsiRNA—lipid nanoparticle

DCR-MYC is a Dicer substrate siRNA targeted against the MYC oncogene that is delivered using Dicerna's proprietary EnCore lipid nanoparticle delivery platform.[138]

A phase 1, multicenter, dose escalation trial was initiated in Apr. 2014. Thirty-seven patients with solid tumors or hematological malignancies have been treated in nine dose cohorts ranging from 0.1 to 1.25 mg kg^{-1} once weekly for 2 weeks, followed by a 1 week break.

In a recent press release,[139] Dicerna reported that the medication has been well tolerated. Antitumor activity has been observed in two of three patients with advanced, treatment refractory low-to-intermediate grade pancreatic neuroendocrine tumors (PNET). One patient had a 34% reduction in tumor size. A second patient achieved a complete metabolic response based on F-18 fluorodeoxyglucose positron emission tomography (FDG-PET) imaging. The patient had a 12 month drug holiday before recurrence, at which time the patient was treated again with DCR-MYC and again achieved complete metabolic response while demonstrating a 28.6% reduction in tumor size.

Based on these results, Dicerna began an expansion of the trial focused on enrolling patients with low to intermediate grade PNET who have demonstrated disease progression after treatment with standard therapies.

6.12.2.2.7.5 ARC-520, anti-HBV siRNA with dynamic polyconjugate excipient

ARC-520[107] is a combination of two chemically modified, cholesterol conjugated siRNAs targeting hepatitis B viral transcripts and a coinjected dynamic polyconjugate[118] polymer excipient. The siRNAs are targeted at hepatocytes via the cholesterol group while the Dynamic Polyconjugate (DPC) excipient assists in endosomal escape via pH activated unmasking of membrane disrupting constituent groups.

Arrowhead Pharmaceuticals underwent an extensive clinical development process to formulate ARC-520. It began by identifying conserved sequences that were cross-reactive with >90% of HBV genomes, then cross-screened these sequences to eliminate spurious matches with human mRNA. This resulted in identification of ~140 sequences which were used to generate siRNAs for in vitro testing.

Four lead siRNAs were chosen. 2′-F and 2′-O-methyl modifications were added to increase nuclease resistances and decrease immunogenicity. A phosphorothioate backbone medication was added between the 3′ terminal overhang nucleotides, and a cholesterol group was added for liver targeting.

The lead candidates were transfected in mouse models of chronic hepatitis B together with a DPC excipient (NAG-MLP) and all achieved 10× to 1000× knockdown of hepatitis B surface antigen after a single intravenous injection at 3 or 6 mg kg^{-1} dosage levels (equal doses of siRNA and NAG-MLP), with >10× knockdown lasting approximately 1 month after a single injection. In contrast, no knockdown was observed when siRNAs were injected without NAG-MLP. After further testing, ARC-520 was formulated using two of the lead siRNAs (99.64% coverage of all known HBV genomes) together with NAG-MLP. ARC-502 was tested in a chimpanzee that was chronically infected with HBV, achieving >80% reduction in HBV markers at 3 mg kg^{-1} dosage levels.

A phase I clinical trial showed that ARC-520 was well tolerated in healthy human volunteers at up to 2 mg kg^{-1} intravenous administration, with no severe adverse reactions. Preliminary results from a phase IIa, randomized, double-blind, placebo controlled study showed that single intravenous doses of ARC-520 was well tolerated at up to 3 mg kg^{-1} and resulted in dose-dependent reduction of serum Hepatitis B surface markers. A 50% reduction was observed at 2 mg kg^{-1} dosage levels, with statistically significant reductions seen up to 43–57 days.[107]

6.12.2.2.8 Challenges and future perspectives

With the recent spate of exciting clinical results for patisiran, revusiran, and other hepatocyte-targeted, chemically modified RNAi therapeutics, the regulatory approval of the first RNAi drugs maybe imminent. This is the culmination of 15 years of improvements in the design, stability, safety, and delivery of synthetic RNAi triggers.

There are now a burgeoning number of hepatocyte targeted RNAi drugs under clinical investigation due to the availability of safe and efficient methods for delivery of RNAi triggers to the liver, but it remains challenging to achieve effective delivery to other tissues. Although a number of exciting technologies for systemic delivery are under development, and indications of clinical success in some solid tumors, the field will likely need new ideas or novel combinations of technologies to solve complex challenges involved in tissue distribution, cell selective uptake, and endosomal escape. Prior clinical experiences indicate that delivery methods must balance pharmacokinetics, targeting selectivity and safety, with complexity in manufacturing and regulatory approval. Pharmacokinetics and targeting selectivity could favor nanoparticle formulations, but safety and complexity tends to favor molecularly well-defined molecular constructs. Going forward, the field may have to weigh these issues carefully for different tissue types, and may have to design constructs that combine the best features of nanoparticles and molecular constructs while assimilating new clinical knowledge such as the tendency of electrostatic assemblies to disassemble in the human kidney.[137]

Despite these challenges, there is every reason to believe that the synthetic RNAi field will continue to advance at a rapid pace and provide exciting new therapeutic options for difficult to treat medical conditions.

6.12.2.3 Aptamers

Aptamers are structured nucleic acid ligands that are naturally found or artificially designed to inhibit a wide variety of targets including proteins, cultured cells, and whole organisms[140] via a technology called SELEX. As they hold their three-dimensional structures by well-defined complementary nucleic acid sequences,[15a,141] aptamer structures are stable even when exposed to biologically induced reducing conditions. For therapeutic molecules, they offer significant advantages over antibodies: high specificity, better structural stability, lower toxicity, and lower immunogenicity.[142] Moreover, the affinity and specificity of aptamers is comparable to, or even greater than, the affinity and specificity of antibodies.[142] Another advantage over antibodies is that aptamers can be fine-tuned and their size reduced after selection through the chemical synthesis.

6.12.2.3.1 Chemical modifications

SELEX allows the incorporation of modified nucleotides so that aptamers can be generated that are highly nuclease-resistant and it is applicable for clinical trials. 2′-OMe and 2′-F pyrimidines are the most commonly employed modified RNA aptamers. As described previously, the 2′-OMe modified RNAs have been widely described as being able to evade innate immune recognition. Lee et al. discovered that RNAs containing 2′-F pyrimidines differentially controlled the activation of pattern recognition receptors (PRRs).[143] They found that the activity of RNAs that stimulate Toll-like receptors (TLR) 3 and 7 was abrogated by employing the incorporation of 2′-F pyrimidines. They also reported that RNAs containing 2′-OMe pyrimidines and triphosphates at 5′ end

completely abolished the induction of cell death and cytokine expression in the cells. It suggests that 2′-F and 2′-OMe modifications can be used to reduce adverse and off-target effects of therapeutic aptamers development.

6.12.2.3.2 Potential therapeutic applications of aptamers

6.12.2.3.2.1 Antagonistic aptamers

Some viruses naturally express short and structured regulatory RNAs (aptamers) that bind and antagonize cellular proteins. These aptamers demonstrated therapeutic applications; an example is HIV-derived stem–loop TAR regulatory RNA that represses the viral protein Tat and inhibits HIV replication.[144] Here we discuss the antagonistic aptamer for therapeutics.

Anti-PD-1 antibodies have now been approved for the treatment of melanoma. As antibody mimics, DNA aptamers against the murine extracellular domain of PD-1 have been developed.[145] Anti-PD1 aptamer blocks the PD-1:PD-L1 interaction and functionally inhibits the PD-L1-mediated suppression of IL-2 secretion in primary T-cells. A PEGylated form of anti-PD1 aptamer retains the ability to block the PD-1:PD-L1 interaction, and significantly suppresses the growth of PD-L1 positive colon carcinoma cells in vivo with a potency equivalent to an antagonistic anti-PD-1 antibody. Importantly, the anti-PD-1 DNA aptamer treatment is not associated with off-target TLR-9-related immune responses.

Cancer metastasis is a major cause of death in various cancers. However, metastatic cancers are yet to be treated with current therapeutics. An RNA aptamer inhibiting the enzymatic activity of prostate-specific membrane antigen (PSMA) has been developed in a preclinical model system.[146] Treatment of prostatic cancer cells with the aptamer resulted in reduced cell migration/invasion in culture and metastatic disease in vivo. Pharmacokinetic and biodistribution studies in vivo confirmed target specificity and absence of nonspecific on/off-target effects.

The surface glycoprotein hemagglutinin (HA) of influenza virus is responsible for viral attachment to sialic acid-containing host cell receptors and facilitates the initial stage of viral infection. An RNA aptamer which is specific to the glycosylated receptor-binding domain of the HA protein (gHA1) has been isolated.[147] The anti-HA aptamer specifically binds to the target protein and suppressed viral attachment to host cells by neutralizing the receptor-binding site of influenza virus HA. Consequently, it inhibits viral infection in host cells. These results indicate that RNA aptamers can be used as a neutralizing antiviral reagent against virus through appropriate therapeutic formulation.

Fibroblast growth factor 2 (FGF2) plays a crucial role in bone remodeling and disease progression. A number of anti-FGF2 monoclonal antibodies (mAbs) have previously been developed to neutralize various activities of FGF2. No anti-FGF2 mAbs have entered clinical trials; however, development of a specific RNA aptamer for human FGF2 has made considerable progress in both in vitro as well as in vivo characterization.[148] The anti-FGF2 aptamer blocks binding of FGF2 to each of its four cellular receptors, inhibits cells proliferation, and restores osteoblast differentiation. The PEGylated form of anti-FGF2 aptamer effectively blocks the bone disruption in mouse and rat models of arthritis and osteoporosis. It also shows that treatment with the anti-FGF2 aptamer exerts a strong analgesic effect, equivalent to morphine, in a mouse model of bone cancer pain. These findings support the dual therapeutic action of the anti-FGF2 aptamer in bone diseases and pain, providing a novel promising approach to the treatment of bone diseases.

The effect of autoantibodies on G-protein coupled receptors is a generally accepted cause for the pathogenesis of a number of diseases, especially in the heart and vascular system. Among these, dilated cardiomyopathy (DCM) is the most intensively investigated pathological situation. Autoantibodies against the β_1-adrenoceptor and the muscarinic M_2-receptor have been found in high percentage of investigated patients in DCM. Immunoadsorption for autoantibody removal has shown a long-term beneficial therapeutic effect. As an alternative, a neutralizing aptamer of autoantibodies against G-protein-coupled receptors has been discovered.[149] The binding and neutralizing effect has been investigated using a bioassay of spontaneously beating neonatal rat cardiomyocytes and enzyme-linked immunosorbent assay (ELISA). It demonstrated broad spectrum neutralization of pathogenic autoantibodies against G-protein-coupled receptors and removal of serum autoantibodies. This data suggests that the aptamer against G-protein coupled receptors might be an appropriate therapeutic candidate in G-protein-coupled receptor autoantibody induced diseases.

6.12.2.3.2.2 Agnostic aptamers

Conventionally, most aptamers are developed to antagonize target function for therapeutic applications. Agnostic aptamers are the contrary concept of antagonistic aptamers. Their function is to activate the function of targets. The new concept of agonistic aptamers has been developed mainly as immunomodulators. The targets of developed agonistic aptamers include 4-1BB, OX-40, CD28, and CD40 for immunological modulation in cancer immunotherapy.[150] In these studies, a monomeric aptamer acts singly as an antagonist, but interestingly, with dimerization converts into an agonistic aptamer that activates immune cells, because receptor signaling requires the ligand-induced oligomerization. Agonistic aptamers have been developed as an alternative to antibody based therapeutics, which can cause severe side effects. Systemic administration of immunomodulatory antibodies has been associated with autoimmune pathologies, conceivably reflecting also the activation of resident autoreactive T-cells. In clinical trials, the antibodies also showed high toxicity. Immunomodulatory aptamers are less toxic and immunogenic options. Also, it is noteworthy that the agonistic immunomodulatory aptamers are as effective as antibodies in in vivo assays.

Agonistic aptamers have also been developed for neurodegenerative disorders and metabolic diseases. Agonistic aptamers against the neurotrophin receptor TrkB selectively activates TrkB in an in vivo model of neurodegenerative disease.[151] The study showed neuroprotective effects of the aptamers in cultured cortical neurons and activation of TrkB upon infusion into the hippocampus in mice; systemic administration of the agonistic TrkB aptamers potentiated kainic acid-induced seizure development.

In metabolic disease, an agonistic aptamer against the insulin receptor promotes glucose uptake through preferential stimulation of Y1150 phosphorylation, both in vitro and in vivo.[152] Even though the insulin agonistic aptamer stimulates autophosphorylation, similar to insulin, it not only binds to an allosteric site distinct from the insulin binding site, but also preferentially induces Y1150 phosphorylation in the IR kinase domain.

6.12.2.3.2.3 Aptamer-targeted oligonucleotide therapeutics

The therapeutic oligonucleotides have remarkable potential for treating human diseases. However, difficulties in specific delivery of nucleic acid based therapeutics to target organs still remain a major impediment in clinical application. Aptamers have emerged as effective delivery vehicles for therapeutic oligonucleotides, including siRNAs, saRNA, miRNAs, anti-miRs, and ASOs. Cell-internalizing aptamers have demonstrated the ability to deliver therapeutic oligonucleotides to target cells. The first aptamer-targeted siRNA drug, designed to target a cytotoxic, cancer-specific siRNA to prostate cancer cells, was described in 2006.[153] Since then, many groups have expanded on this approach to develop aptamer-siRNA chimeras with the ability to specifically target different diseases. These studies highlight the flexibility and broad clinical potential of the aptamer-siRNA chimera platform. By changing the aptamer, the aptamer-siRNA chimera redirects delivery of the applicable RNAi-based therapy to many diseases, including cancer and infectious diseases. This approach is rapidly expanding, as target cell specific delivery, aptamer-siRNA chimera technology has been applied to target molecules such as Her2, PSMA, BAFF-R, gp120, TLR9, MUC1, Nucleolin, CD4, CD8, EpCAM, CCR5, and pancreatic cancer markers.[154]

It is worth noting that a different approach to constructing chimeras that covalently links the aptamer to a cytotoxic siRNA, has been applied against STAT3 transcripts in lymphoma[155] or to deliver small activating RNA to C/EBPα in pancreatic cancer.[154c] Even though outstanding preclinical studies have demonstrated the potential of exploiting aptamers as delivery cargo for RNAi-based therapeutics, the aptamer-based delivery of oligonucleotides have yet to be evaluated in clinical trials.

6.12.2.3.2.4 Delivery of chemotherapeutics

Aptamer mediated delivery of therapeutics is very powerful for targeted therapeutics. Aptamers selected to cell surface membrane components provide an important route for targeted chemotherapeutics. Here, we discuss aptamer drug conjugates for targeted therapeutics. Poor efficacy and off-target systemic toxicity are major problems associated with current chemotherapeutics to treat cancer. Potentially efficacious drugs which would otherwise have limited use in clinical settings due to general toxicity are good candidates for aptamer-targeted delivery.

Epirubicin (Epi), an anthracycline drug, is limited in clinical use because of its cardiotoxicity. Specific delivery of epirubicin has employed polyvalant aptamers, MUC1 and nucleolin (AS1411) aptamers.[156] Epirubicin binds preferably to sequences containing CG. The AS1411 aptamer and its complimentary strand have poly G/C double-stranded areas and MUC1 as a targeting aptamer. The Epi-aptamer conjugate significantly enhances the cellular uptake of Epi and increases its cytotoxicity in target cells (MCF7) as compared with nontargeted cells (CHO).

Cisplatin is a platinum-based chemotherapy drug that is used to treat a variety of cancers. However, its responsiveness is less than 15%, when it is given alone. To improve the efficacy and tolerability of cisplatin, EGFR-targeted albumin-cisplatin nanoparticles (NPs) have been constructed.[157] The cisplatin NPs have been conjugated with EGFR aptamer, which internalized to HeLa cells specifically by receptor mediated endocytosis. The EGFR aptamer functionalized NPs enhance in vitro antitumor effects and markedly improve its tolerability and in vivo efficacy when compared with free cisplatin and other single treatments. Furthermore, reduced systemic and nephrotoxicity was also observed in vivo.

Doxorubicin (DOX) is a widely used chemotherapeutic agent but exhibits cardiotoxicity as a serious adverse side effect in cancer patients. F binds preferably to CG sequences. The MUC1 aptamer can be combined with a DNA tetrahedron (Td) that carries doxorubicin (Dox) within its DNA structure. The complex thus formed (Apt-Td) preferentially binds toMUC1-positive MCF-7 breast cancer cells, similar to the MUC1 aptamer alone. Each Apt-Td complex carries approximately 25 Dox molecules. Moreover, Aptamer-Td selectively delivers Dox into MUC1-positive breast cancer cells but reduces Dox uptake by the MUC1-negative control cells. Dox-loaded Apt-Td induces a significantly higher cytotoxicity to the MUC1-positive cancer cells versus the MUC1-negative control cells.

Gemcitabine (GEM), a nucleoside analogue, is used as the first line of chemotherapy. However, it possesses some drawbacks, such as poor biological half-life resulting from rapid metabolism and the induction of resistance, leading to its restricted therapeutic potential. To increase the efficacy of gemcitabine, GEM-loaded nucleolin aptamer (AS1411) surface-decorated polyethylene glycol-poly nanopolymersome (Apt-GEM-NP) was constructed to target nucleolin-overexpressing nonsmall cell lung cancer (NSCLC).[158] The Apt-GEM-NP exhibited sustained release of drug in physiological conditions and greatly improved the chemotherapeutic efficiency. It clearly showed an enhanced cell proliferation inhibitory effect of AS1411-conjugated NP NSCLC. The great advantages of targeted delivery of anticancer drugs by aptamers are much reduced side effects and improved therapeutic efficacy.

6.12.2.3.2.5 Theragnostics

Theragnostics is a treatment strategy that combines therapeutics with diagnostics. It associates both a diagnostic test and targeted drug therapy, including molecular imaging to develop efficient new targeted therapies.

As molecular imaging and theragnostic tools, aptamers are considered to be promising next-generation ligands. Aptamers are synthetic nucleic acids that can be held together with complementary sequences by base-pair hybridization. Using these characteristics, the complementary oligonucleotide (cODN) hybridization-based aptamer conjugation platform was developed to use

aptamers as the molecular imaging agent.[159] The ^{18}F prelabeled cODN was hybridized with a matched sequence containing nucleolin (AS1411) aptamer. The cODN platform-hybridized aptamers exhibited good serum stability and specific binding affinity towards target cancer cells both in vitro and in vivo. In small-animal PET-CT scan and image analysis, ^{18}F-hybridized aptamers (^{18}F-hybridized AS1411) showed target cancer cell specific localization comparing scrambled aptamer. However, high uptake was observed in the kidneys, intestines, and liver for both in biodistribution.

The human Matrix MetalloProtease-9 (hMMP-9), a marker of malignant tumor, is overexpressed in tumors where it contributes to tumor metastasis. Fully nuclease-resistant hMMP-9 aptamers have been developed as probes for imaging tumors.[160] The hMMP9 aptamer was labeled with S-acetylmercaptoacetyltriglycine (MAG) and DOTA. Tumor uptake was significantly higher for 111In-DOTA-aptamer than for the 111In-DOTA-control oligonucleotide. In a biodistribution study, following IV injection of 111In-DOTA-aptamer, high levels of radioactivity were observed in kidneys and bladder but digestive tract uptake was very limited.

Protein tyrosine kinase-7 (PTK7), a member of receptor tyrosine kinase superfamily initially identified as colon carcinoma kinase-4, is highly expressed in various human malignancies. Its expression is correlated with aggressive biologic behaviors such as increased cell proliferation, invasiveness, and migration. A 41-oligonucleotide DNA aptamer that targets PTK7 was labeled with ^{18}F[161] and evaluated in vivo. In vivo PET imaging clearly visualized specific accumulation of ^{18}F-aptamer in tumor-bearing mice. In biodistribution studies, the labeled aptamer was rapidly cleared from the blood through the kidneys and bladder.

These results consistently showed aptamer-mediated theragnostics are rapidly cleared, but more importantly, strong tumor homing and tumor specific accumulation, suggesting that the aptamer-based platform offers great potential as molecular imaging agents.

6.12.2.3.3 Aptamers in clinical development

Since the first aptamer drug (Macugen) was approved by the FDA, a number of aptamer-based drugs have been developed and reached advanced clinical trials (Table 3). For example, Pegnivacogin, a 2′-F RNA aptamer against coagulation factor IXa coupled to an 40 kDa branched molecule of methoxypoly ethylene glycol (mPEG) to increase half-life in plasma, has finished a phase IIb clinical study by Regado. Unfortunately, acute coronary syndrome and allergic reactions occurred within minutes of a first dose in 3 of 640 patients.[162] Two events met criteria for anaphylaxis and one event a dermal reactions; each event is serious and life-threatening; this lead to early termination of the trial. A broader investigation of these three events, found no other serious allergic reactions to pegnivacogin. In addition, there was no evidence that pegnivacogin caused an inflammatory response, histamine release, or complement activation. However, an association between high levels of antibody to polyethylene glycol (PEG) and the first exposure allergic reactions was identified in more than half of the patients.

Currently, PEGylation of recombinant proteins and antibodies is become the golden standard of the technology due to increased solubility, stability, masking humoral and cellular immunogenicity, protease protection, controlled release, reduced absorption, and reduced injection volume.[163] Since the approval of PEG-adenosine deaminase for severe combined immunodeficiency syndrome in 1990s, at least 12 therapeutic PEGylated agents, including three blockbusters have been approved, with several more in development.[164] In contrast to the accepted general assumption that polyethylene glycol (PEG) is nonimmunogenic and nonantigenic, animal studies clearly showed that some other PEGylated agents can elicit antibody formation against PEG (anti-PEG). In the clinical trials by Regado, it also clearly showed that preexisting antipolyethylene glycol antibody induce severe allergic reactions.

Table 3 Aptamers in clinical trials or marketed

Intervention	*Company*	*Target*	*Indication*	*Phase*	*Status*	*Clinical trial ID*
Macugen	Eyetech/Pfizer	VEGF	Age-related macular degeneration		Approved	
Fovista	Ophthotech	PDGF	Age-related macular degeneration	III	Recruiting	NCT01944839
				III	Recruiting	NCT01940887
				III	Active	NCT01940900
Zimura	Ophthotech	C5	Geographic atrophy Macular degeneration	II/III	Recruiting	NCT02686658
			Idiopathic polypoidal choroidal vasculopathy	II	Completed	NCT02397954
REG1	Regado	Factor Ixa	Coronary artery disease	II	Completed	NCT00715455
				II	Completed	NCT00932100
ARC1779	Archemix	vWF	Purpura, thrombotic thrombocytopenic Von Willebrand disease type-2b	II	Completed	NCT00632242
NOX-A12	NOXXON	CXCL12	Chronic lymphocytic leukemia	II	Active	NCT01486797
			Multiple myeloma	II	Completed	NCT01521533
NOX-H94	NOXXON	Hepcidin	Anemia of chronic disease	II	Completed	NCT01691040
NOX-E36	NOXXON	MCP-1/CCL2	Type 2 diabetes mellitus Albuminuria	II	Completed	NCT01547897

Listed clinical studies are found in clinicaltrials.gov. Most advanced clinical studies for each aptamer are listed.

6.12.2.3.4 Challenges and future perspectives

As a therapeutic molecule, aptamers have been utilized in a variety of fields. Even though aptamers have very attractive features of low immunogenicity and high specificity, the main drawback with the use of aptamers therapeutics is rapid clearance in vivo. The major challenge of aptamer-based therapeutics thus remains longer lasting pharmacokinetics in systemic application. To increase retention time and serum stability in vivo, PEGylation of aptamers has been widely utilized to improve pharmacokinetics. Unfortunately, PEGylation has induced severe allergic reactions which are associated with preexisting antibodies to PEG in clinical trials[162]; however, aptamers have demonstrated efficacy in clinical trials. Alternative formulations to PEGylation need to be developed for aptamer-based therapies. Capping the 3′ and 5′ ends of aptamers, or incorporating modified nucleotides to generate highly nuclease-resistance aptamers during the SELEX are promising avenues of exploration. Currently, to incorporate modified nucleotides, sugar modified nucleotides such as 2′-F or 2′-amino (2′-NH_2) groups on the pyrimidine residues are available for enzymatic synthesis. Inclusion of other modified nucleotides will require the development of new enzymes.

6.12.3 Biochemically Produced RNAs

While synthetic small nucleic acid therapeutics have a variety of potential medical applications, some diseases and conditions may benefit from long-term gene therapy regimens. Engineering disease-susceptible cells to express small RNA therapeutics can fill this need. For instance, the development of an HIV-resistant T cell population using gene therapy remains an important aspect of research geared to developing an HIV cure.[165] The challenges of HIV-1 treatment are based on the high viral mutation rate resulting in the rapid production of escape mutants, coupled with the difficulties in eradication of latently infected cells.[166] Consequently, most anti-HIV gene therapeutic strategies employ a combinatorial approach. These include multiple RNA and/or protein modalities and targeting different stages of the viral replication cycle as well as endogenous cellular proteins. This topic has been covered in depth in other reviews,[167] but for our purposes HIV-1 gene therapy can serve to illustrate general principles in the application of small RNA therapeutic designs.

A number of factors are considered when choosing the most appropriately expressed small RNA modality for a given application. The most crucial include the type of small RNA therapeutic, the expression format or platform, the promoter type, and the ultimate delivery method. These are highly interrelated issues and decisions on the best approach are dependent on the context of the biology of the disease.

U1 interference, ribozymes, aptamers, and RNA interference triggers are some of the major categories of self-contained small RNA therapeutics (in contrast to CRISPR-based strategies, which depend on Cas9 protein a well, see below and **Fig. 5**). The development of therapeutic U1 interference is still in a relatively early stage, but shows promise.[168] RNA enzymes or ribozymes, have been a major focus of RNA therapeutics. Ribozymes have the theoretical advantage of multiple turnover kinetics. Also, as they do not depend on any known cellular pathways, ribozymes are less likely to interfere with critical endogenous processes. However, this latter characteristic also underlies much of the difficulties in developing ribozymes that work efficiently in vivo, where the absence of a protein machinery to enhance ribozyme/target association and compensate for target site inaccessibility compromises target binding and catalysis. As a consequence, ribozyme research has shifted somewhat away from therapeutic applications; nonetheless, progress continues towards a better understanding of ribozyme catalysis[169] which may prove the basis for next generation ribozyme therapeutics.

This discussion will therefore be devoted to recent research that informs the design of expressed RNAi triggers. Our goal is to introduce the reader to different expression platforms and the factors to consider in developing applications of expressed small RNA therapeutics. Additional information and viewpoints can be found in recent reviews.[170]

6.12.3.1 RNAi Triggers

RNAi-based gene therapy strategies may employ either siRNAs (that are fully complementary to the target) or microRNA triggers (see above and **Fig. 2**) of RNA interference. The former is more commonly used for expressed therapeutics as siRNAs typically mediate higher levels of mRNA knockdown through Ago2 cleavage. Both types of triggers can be expressed in contexts or formats that require both Drosha and Dicer, either complex alone, or neither to process the trigger. We will discuss the various formats of expressed RNAi triggers in order of their processing requirements, with an emphasis on more recent research.

6.12.3.1.1 Pri-miRNA mimics

Shortly after the discovery of microRNA genes,[171] the Cullen group showed that it was possible to reprogram human pri-miR30 by replacing the mature miR30 region with sequences complementary to alternate mRNA targets, generating so-called pri-miRNA mimics. However, initial replacement strategies remain unreliable, generating low-potency RNAi triggers,[172] which can still be a problem.[173] Nonetheless, a number of laboratories successfully developed microRNA mimics, based on endogenous single or clustered pri-microRNAs. This approach has markedly improved with greater understanding of the miRNA biogenesis pathway and the features that distinguish effective pri-microRNA substrates.

Several pri-miRNA structural characteristics required for efficient processing emerged from early comparative studies of endogenous pri-microRNAs coupled with mutational analysis. These delineated the basic structural features of the pri-microRNA stem/loop and surrounding context. First, the pri-microRNA stem consists of approximately three helical turns (with some bulges and small loops)

and has a preference for at least 8 bp at the base of the stem.[174] In addition, the cleavage site at position 11 must be double stranded, i.e., not be in a bulge or loop.[175] Also, the flanking regions of the stem/loop are largely single stranded or nonstructured[176] as is the apical loop of at least 10 nt.[174]

Some sequence biases also became apparent.[177] There is also a strong preference for uridine at the 5′ end (5′U) of the mature microRNA.[178] Argonaute loading of the mature miRNA favors loading the 5′ end of the strand of the mature miRNA with the weaker pairing. In the pri-miRNA, for instance, this corresponds to bases 14–16 when the 5′, or 5p side of the hairpin will ultimately become the guide strand; this region should also be fully base-paired.[179] In contrast, a 5′ guanosine on the mature microRNA is disfavored.[178c,180]

The general structural features of pri-microRNAs are well-conserved in the animal kingdom; however, while necessary, they are not sufficient. For instance, *C. elegans* pri-miRs are inefficiently processed in human cells. Based on this observation, the Bartel group devised a high-throughput process to determine structural and sequence motifs that characterize efficient substrates (refer to summary in **Fig. 4**). They constructed large pri-miRNA variant pools of the basal stem (below the Drosha cleavage site) and flanking regions of four human pri-miRNAs and conducted in vitro cleavage reactions in microprocessor lysates. Purified cleaved variants were deep sequenced and analyzed for enriched structural and sequence motifs. Potential candidates were validated independently in microprocessor assays.[181] Two important structural features emerged: an 11 bp (one helical turn) basal stem, flanked by at least nine unstructured nucleotides. However strong primary sequence preferences were also revealed: first, a U/G at positions $-1/+1$ straddling the basal 5′ flanking sequence/stem transition (conserved in many chordate pri-miRNAs); second an apical UGU motif at the 5′ stem/loop transition; and third, a CNNC motif, typically 17–18 nt downstream of the Drosha cleavage site. The SRp20 protein, thought to be involved in splicing regulation, mRNA export and translation initiation, binds the CNNC motif and enhances processing.

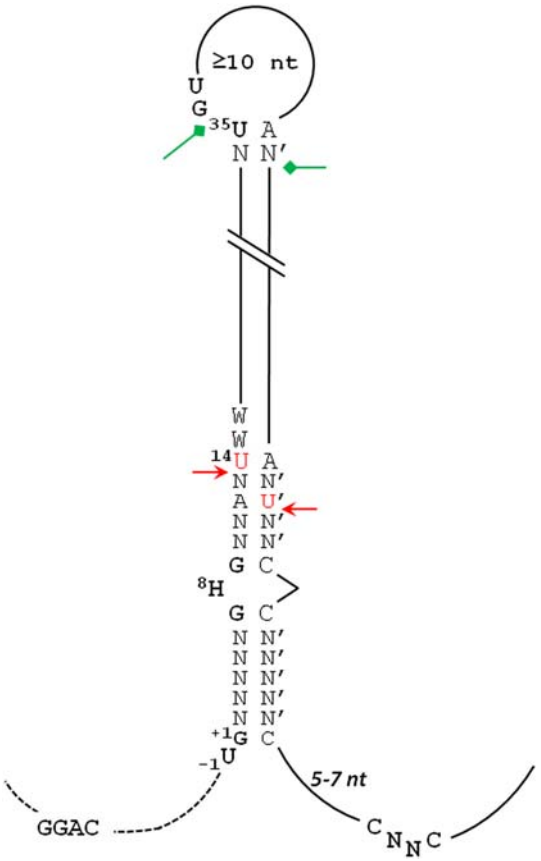

Fig. 4 Pri-miRNA scaffold motifs. Numbering convention is after Fang and Bartel.[182] The stem is fully base paired starting at $+1$, except for base 8. Note that the upper portion is not to scale *(discontinuity marks)*. Shown with optimal basal region of 11 bp below 5′ DROSHA cleavage site, and 24 bp apical region for total stem length of 35 bp. The flanking regions for at least 10 nt on either side and the loop are unstructured. *Red arrows*, microprocessor cleavage sites; *red bases* preferred by DROSHA. *Green arrows*, Dicer cleavage sites. Sequence motifs implicated in enhancing microprocessor activity are shown in *bold*. Motifs in the stem: UG at $-1/+1$; GHG at 7–9; apical UGU. UWW sequence preferred at the end of the guide strand for best siRNA strand selectivity, here shown for the 5p arm. Flanking motifs: METTL3 motif GGAC, variable position likely within 100 nt of the stem; CNNC motif, 16–18 nucleotides downstream of the 3′ DROSHA cleavage site or 5–7 nt from the base of the stem. H, any nucleotide except G; W, either U or A.

Subsequently, the Bartel group performed the complementary analysis on the entire stem region of three pri-miRNAs, using a sophisticated sliding window randomization procedure.[182] Their methodology varied not only the sequence but also generated all possible bulge sequences of 0 (none) 1, and 2 nucleotides. There was strong selection for a narrow window of stem length: 35 ± 1 bp, subsequently confirmed by other researchers.[173] Note that Drosha processing of the pri-miRNA with this stem length generates a pre-miRNA with two helical turns, the preferred length for Dicer processing.[183] In addition, there was a clear preference for stem pairing (both Watson-Crick and noncanonical wobbles) over nonpairing, particularly at the base and the apical three base pairs (33–35), with one exception; position 8. Moreover, this unpaired base is part of a larger sequence motif, GHG (where H is any nucleotide except G) for basal stem nucleotides 7–9.

With these new motifs, the authors were able to successfully implement de novo design of artificial pri-miRNAs favoring 5p selection. All were processed more efficiently than a miR-1 standard in vitro and in vivo. Though initial designs contained fully complementary stems (with the exception of base 8), up to 4 wobble bp and 3 single bp mismatches were as efficiently processed as their fully paired counterparts. This is fortunate, as some wobbles and/or mismatches are likely to enhance genomic stability and facilitate cloning. Also encouraging, from a design viewpoint, is that removal of a single motif had only minor detrimental effects.

Research continues to reveal additional sequence motifs that aid pri-miRNA processing.[173,184] For instance a METTL3 (Methyltransferase-like 3) motif within pri-miRNA flanking regions at various positions is associated with enhanced processing.[173,185] Active areas of interest include the tolerance of pri-miRNA scaffolds to omissions of motifs, the effects of flanking sequences, and the interplay between scaffold and exogenous sequences.[173,180b,182]

As with synthetic siRNAs, off-target effects are a major concern, but additional mechanisms come into play with expressed RNAi triggers. A single pri-miRNA can produce a group of related mature miRNA variants or isomiRs, which are due in part to pri-miRNA cleavage at multiple sites. Endogenous pri-miRNAs vary widely in their propensity to generate isomiRs, which can function to fine-tune regulatory networks.[186] 3′-Terminal miRNA heterogeneity is common; 5′ heterogeneity is less frequent, but more consequential as it changes in the seed sequence of the mature miRNA. Both types of heterogeneity can affect strand selectivity. For these reasons, isomiR production is generally undesirable for designed miRNA mimics. IsomiRs can be due to imprecise microprocessor processing, Dicer processing, or both. Interpreting the contributions of each effect to determine design rules presents challenges. Happily, efficiency and precision determinants can overlap, as when optimized substrate stem length results in both high efficiency and precision,[182,187] but maximal precision may sometimes require compromised efficiency.[180b]

One approach determined pri-miRNA features contributing to processing precision by analyzing sequences surrounding cleavage sites in cellular pri-miRNAs that are homogenously processed, relative to those producing isomiRs.[188] Precision pri-miRS show preferences in the 5′ arm Drosha cut site for a $+14$ position for U over and above the known Ago loading bias[189]. There is also a preference against G in the same position. Dicer also prefers cutting after a uridine on the 5′ arm, while Drosha and Dicer are both biased against cutting before a guanine. Other intriguing observations reveal that the endogenous pri-miRNA scaffolds influence mimic processing efficiency and precision, while structural features within the exogenous sequences affect precision.[173,177,180b]

Liu et al.[190] have begun studies on the possibility of regulating individual endogenous pri-miRNAs with conventional small molecule therapeutics. To identify targets for drug development, they analyzed human pri-miRNAs to see if it was possible to identify unique small structural motifs such as stem bulges, internal loops, and apical loops. They zeroed in on the regions of Drosha and Dicer processing sites, hypothesizing that drug binding to these areas would be more likely to have an effect on miRNA production, and were able to generate a database of motifs specific to individual pri-miRNAs. Ultimately, these motifs also could potentially be incorporated into microRNA mimic scaffolds to regulate expression.

6.12.3.1.2 shRNA triggers

One of the earliest and most extensively used forms of expressed RNAi trigger, as well as the simplest, is the hairpin or shRNA (sometimes referred to as a pre-miRNA), which bypasses Drosha processing. After transcription shRNAs are directly exported to the cytoplasm via exportin 5. There, Dicer cleaves the shRNA into the mature siRNA (**Fig. 3**). ShRNA design is covered elsewhere in detail.[170b,191] Online tools are available to assist shRNA design, and there are a number of commercial vectors that facilitate cloning and expression of shRNAs.

Typically, shRNAs are designed with fully complementary 21–23 base pairs stems using Watson-Crick base pairing, although wobble pairing may be used to optimize thermodynamic properties for optimal strand selection bias in the siRNA product. As discussed above, Dicer cleavage precision is governed by a number of factors. A helpful general guide is the loop-counting rule, which states that Dicer cleaves precisely two nucleotides away from a single-stranded apical loop or internal bulge.[183b]

6.12.3.1.3 Ago2shRNAs

An intriguing approach was recently developed that utilizes Drosha but bypasses Dicer processing. This methodology is based on observations of the unusual processing pathway of the highly conserved miR-451. Processing of pri- to the pre-miR-451 occurs using canonical Drosha processing; however, the resulting pre-miR-451 has an atypically short stem that makes it a poor Dicer substrate.[192] Instead, pre-miR-451 is cleaved by Ago2 to generate a 30 nt guide strand that is subsequently trimmed by Poly(A)-Specific Ribonuclease (PARN).[193] Human pri-miR-451 can be reprogrammed to silence other RNA targets using a standard microRNA mimic approach, maintaining the contexts of the parental pri- and pre-miR-451 precursors.[192a]

A logical extension of this approach is to use the pre-miR-451 structure to design shRNAs that bypass both DROSHA and Dicer processing. These are referred to as AgoshRNAs to emphasize their dependence on Ago2 cleavage and to distinguish them from standard Dicer-dependent shRNAs.[194] AgoshRNA and standard shRNA designs differ in important ways. Typical shRNAs use

a passenger-loop-guide sequence order and have a 21–23 bp stem which is processed by Dicer at two staggered cleavage sites to yield a double-stranded siRNA. In contrast, AgoshRNAs use a guide-loop-passenger format with an optimal stem of 18 bp[193,195] which Ago2 cleaves only once approximately half-way into the 3′ side of the stem, ultimately yielding only one stable single-stranded guide sequence. Ago2 cleavage of tested precursors is precise, but sensitive to mispairing at the cleavage site.[193] With small, 3–5 nt apical loops, this yields a 5′ product containing the guide sequence of about 30–33 nt (depending on the exact size of the loop) and a 3′ product too short to program RISC, theoretically eliminating passenger strand off-target effects.

6.12.3.1.4 Biochemically produced RNAi in clinical development

Gene therapy for HIV-1 continues to be explored due to the persistence of latent HIV-1 reservoirs and the propensity to evolve resistance to conventional drug therapies, which also have considerable side effects. The current approach is to create a resistant immune system by introducing vectors carrying anti-HIV-1 gene therapeutics into hematopoetic stem cells ex vivo followed by reintroduction into the patient.[167a,196] Lentiviral and adeno-associated virus (AAV) vectors are commonly employed to delivery expressed RNA therapeutics with the former the vector of choice for HIV-1 therapeutic applications. Both in silico analyses[197] and empirical results indicate that a minimum of three gene therapeutic HIV-1 antivirals are required to control HIV-1 replication; consequently, multiplexing or combinatorial approaches are common in HIV-1 gene therapy.

As an example, we have developed a lentiviral vector expressing three anti-HIV-1 therapeutic cassettes: a U6-*tat*/*rev* shRNA, a U6 TAR aptamer decoy (in a U16 backbone), and a CCR5 ribozyme under the adenovirus VA promoter. A phase 0 safety and feasibility clinical trial showed that introduction of this vector into hematopoietic stem cells ex vivo, as part of an autologous bone marrow transplant for treatment of AIDS-related lymphoma, was well tolerated in four patients.[198] We then developed a next generation lentiviral therapeutic that expresses three anti-HIV RNAs using the endogenous miR-106b microRNA cluster within an intron of the MCM7 (minichromosome maintenance complex component-7) gene as a platform.[199] The MCM7 cluster was expressed using the constitutive CMV Pol II promoter. Various combinations of miRNA mimics, ribozymes and aptamers mediated efficient knockdown. Moreover, it was possible to add a fourth shRNA directed against the CCR5 HIV-1 cellular coreceptor, expressed from a $tRNA^{Ser}$ promoter, within the cluster. We achieved effective inhibition with this system despite production of much lower amounts of RNAi triggers from the miRNA mimics compared to U6-expressed counterparts.[200] Moreover, the MCM7 platform is compact enough to permit addition of independent expression cassettes in lentiviral vectors; for instance, a U6-aptamer for interaction with abundant substrates. Other anti-HIV combinatorial approaches in development also include anti-HIV proteins.[201] It is clear that the diversity of RNA therapeutic modalities, expression platforms and promoters comprise an impressive set of tools that can be used to treat a number of diseases and conditions.

6.12.3.1.5 Challenges and future perspectives

The exact choice of RNAi trigger format ultimately depends on factors unique to the ultimate therapeutic application, but we mention some general considerations here. The first is ease of design, where shRNA/pre-miR and AgoshRNAs have a clear advantage over pri-miRNA mimics. There is a large body of work addressing construction of traditional shRNAs, while AgoshRNAs are a relatively new technology.

The second major issue relates to toxicity. A common cause of toxicity with both synthetic and expressed RNA triggers are off-target effects due to shared complementarity between the intended target and other cellular RNAs. Best practices to avoid this problem include verifying the phenotype of knockdown with two different RNA triggers whenever possible. Another is poor selectivity of the guide strand (passenger strand effects). We note that passenger strand effects are minimized with AgoshRNA triggers as the 3′ product of cleavage is too small to enter the RNAi pathway.

Problems more common to expressed RNAi triggers include poor processing precision, creating multiple guide strands, and increasing the likelihood of off-target effects; in this regard, pri-miRNA mimics are more difficult to design than shRNAs. Off-target effects tend to increase with expression level as well. Deep sequencing to analyze expressed small RNA products in the cell type of interest is very useful for optimizing expressed therapeutic triggers.

Toxicity can also arise from saturation of the RNAi pathway components, resulting in perturbation of endogenous microRNA production or function. Levels of RNAi pathway proteins can differ widely in different tissues and disease states; the use of the appropriate trigger format can bypass limiting components. The level of trigger expression is also a factor, particularly when multiple siRNAs are required, and can depend on the intrinsic nature of the trigger in conjunction with the promoter (see below).[202] Typically the highest amount of trigger expression is mediated with U6 or H1 promoters of shRNAs. At the other end of the range are Drosha-dependent miRNA mimics under Pol II promoters. It is worth noting that AgoshRNAs produce lower amounts of guide than their cognate shRNAs, even when using Pol III promoters.[195b]

One example of saturation toxicity was reported in which a U6-shRNA therapeutic expressed in mouse liver was fatal. Use of the H1 promoter, which has about half the expression level of U6, was tolerated.[203] Further investigation revealed that when exogenous shRNAs are expressed above a threshold of 12% of total murine liver microRNAs, the resulting fatalities are directly associated with loss of a single isoform of miR-122.[204]

The human promoters of snRNAs U6 and H1 are used extensively to express small RNA therapeutics. Unlike RNA polymerase II promoters, which drive transcripts including extraneous sequences that can interfere with the structure and function of small RNA therapeutics, U6 and H1 promoters utilize RNA polymerase III (Pol III). Pol III promoters have a well-defined start site, and a small, poly U termination signal encoded by a run of at least five thymidines.[205] These features are critical for correct processing of both AgoshRNAs and Dicer-dependent shRNAs/pre-miRNAs, as both enzymes measure from the 5′ end of the transcript, which must

initiate with a G for U6, and preferably a purine for H1. Moreover, these promoters are relatively small allowing them to be easily multiplexed in vectors with size limitations. U6 and H1 mediate very high levels of basal expression (although H1 less than U6), an asset when expressing aptamers which have a stoichiometric mode of action, but a potential disadvantage for RNAi triggers. We developed tRNA promoters that express RNAi triggers as a pre-tRNA-shRNA chimeras, which are processed by endogenous tRNAseZ to release the shRNA moieties. This promoter system produces shRNAs with 5′ terminal mono-phosphates, rather than the 5′ triphosphates found on U6 and H1 transcripts, which at high levels have been linked to activation of cellular immunity. Moreover, we developed tRNA promoter variants that produce lower levels of siRNA triggers than the wild-type tRNA, a possible aid in avoiding toxicity due to overexpression.[206]

Another downside of Pol III promoters is that conditional expression is limited to tetracycline responsive versions of U6 and H1; these are useful for research purposes, but are not likely to be used in actual therapeutic applications.[207] Either constitutive or regulated Pol II promoters can be used to express pri-miRNA mimics, although the resulting cassettes are larger when using Pol III promoters, and other design factors need to be considered.

6.12.3.2 CRISPR/Cas9

The clustered, regularly interspaced, short repeat (CRISPR and CRISPR associated protein system (aka CRISPR/Cas system)) was originally discovered as an adoptive immune system in bacteria against foreign genes.[208] Following the demonstration in 2012, where the CRISPR/Cas9 system was shown to be an RNA-guided DNA endonuclease that uses the RNA to direct a double-stranded break (DSB) of target DNA,[209] CRISPR/Cas9 system has emerged as the most attractive and promising gene-editing tool to transform biology. Among three CRISPR/Cas systems (I, II and III),[210] the type II system has been most commonly used in biological applications because it relies on a single multifunctional protein, Cas9, whereas other types consist of multiple protein complex.[211] In bacteria, the CRISPR system incorporates invading foreign DNA into the CRISPR array encoded in the host genome.[212] The CRISPR arrays are then transcribed into CRISPR RNAs (crRNAs) bearing sequences from the invading DNA (protospacer) and part of CRISPR repeat sequences. The crRNAs hybridize with the transactivating CRISPR RNA (tracrRNA), and the resulting complexes are associated with the Cas9 nuclease (**Fig. 5**). The protospacer sequences guide the crRNA-tracrRNA:Cas9 complex to cause DSBs of the invading DNA that harbors complementary sequences to the protospacer sequence. This sequence recognition system is somewhat restricted by the protospacer adjacent motif (PAM) sequence, a three consecutive nucleotide sequence that must exist adjacent to the 20-nt target sequence. While the original CRISPR/Cas9 complex consists of three components, the simple two-component system which consists of Cas9 and a single guide RNA (sgRNA) is currently most widely adopted. The sgRNA is a fusion of crRNA and tracrRNA (**Fig. 5**), thus playing both roles in the DSB process.[209] An attractive feature of this system is that unlike other genome engineering technology such as zinc-finger nucleases (ZFNs) and transcription activator like effector nucleases (TALENs), which require considerable protein engineering for each target, the CRISPR/Cas9 system only requires a change in protospacer sequence of the sgRNA for each target. There are at least two DSB repairing pathways catalyzed by cellular machinery: nonhomologous end joining (NHEJ) and homology-directed repair (HDR) (**Fig. 5**). NJEJ is the most active and rapid repair pathway that gives various length of insertion or deletion in the DSB site. This random repairing results in translational disruption of reading frame by creating deletions, insertions, or frameshift mutations. On the other hand, HDR can be used to introduce specific nucleotides or sequences by homologous sequence based recombination on the target site. While the efficiency of HDR is generally low ($<10\%$) and usually taken over by NHEJ pathway, it gives precise editing of genomic sequences (**Fig. 5**).[213]

6.12.3.2.1 Potential therapeutic applications of CRISPR/Cas9

This simple but powerful platform of genome editing has rapidly spread and become widely adopted by many researchers. The development of this technology is breathtakingly fast and a number of applications have been reported over the past few years. Nowadays, the use of CRISPR/Cas9 system is available not only for genome editing but also for gene expression regulation, epigenetic modulation, and genome imaging. Exploring therapeutics based on this technology has also been in progress. These include, for example, correction of defective genetic mutations, immunotherapy for cancers, and treating infectious diseases by targeting virus or blocking infectious pathways. Here we will discuss some examples of potential therapeutic applications of CRISPR/Cas9 technology.

As described above, frameshift mutations in the dystrophin gene (*Dmd*) impair myofiber integrity, resulting in functional deterioration of muscle in DMD. Correction of the gene mutation using CRISPR/Cas9 system has been attempted by several groups. Long et al. designed a sgRNA to target a mutation site in dmd exon 23 and a HDR oligonucleotide template, which were injected with Cas9 mRNA to zygotes from mdx DMD model mice that carry a nonsense mutation in exon 23 of *Dmd* gene which disrupts dystrophin expression.[214] The genome editing produced genetically mosaic mice containing 2–100% correction of the *Dmd* gene. In vivo gene correction of Dmd gene was performed separately by three different groups around the same time.[215] In these studies, components of gene editing, including Cas9 and gRNAs that were designed to target exon 23 of the Dmd gene, were systemically delivered using AAV to mxd mice. Deletion of exon 23 by CRISPR/Cas9 mediated genome editing restored dystrophin protein expression in cardiac muscle and skeletal myofibers, enhancing muscle function. These studies indicated that CRISPR/Cas9 mediated genome editing was a potential therapy to treat DMD.

Viral infections have also been shown as potential targets of CRISPR/Cas9 system. Several groups have demonstrated potential use of CRISPR/Cas9 system in targeting viral infections such as human immunodeficiency virus-1 (HIV-1),[216] hepatitis B,[217] Epstein–Barr virus,[218] and human papillomavirus.[219] The most advanced therapeutic genome editing to date is ex vivo ZFN

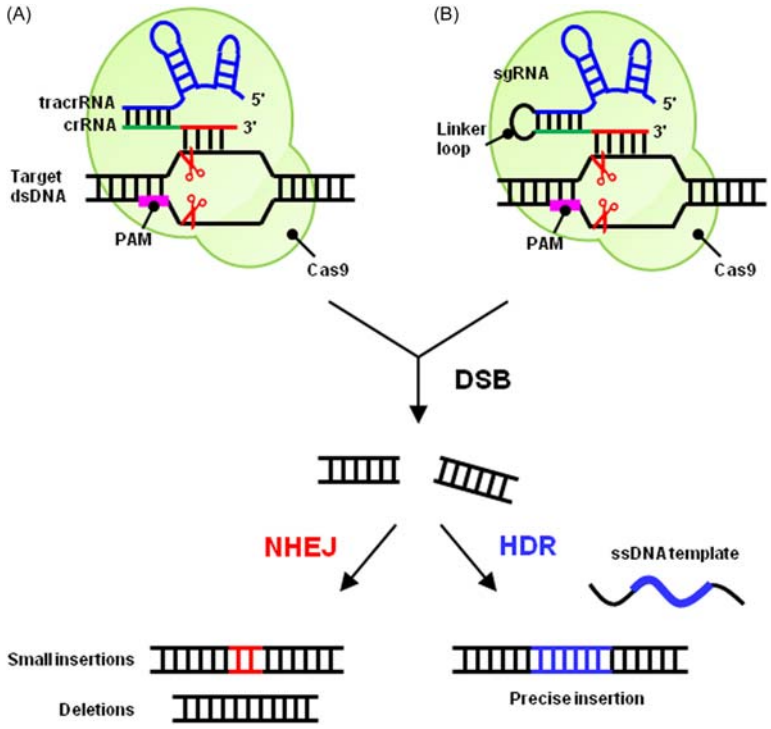

Fig. 5 Schematic of CRISPR/Cas9 mediated genome editing. (A) Naturally occurring CRISPR/Cas9 complex consisting of a pair of crRNA and tracrRNA, and the Cas9 nuclease. (B) Engineered CRISPR/Cas9 complex consisting of single guide RNA which mimics both crRNA and tracrRNA with Cas9 nuclease. These complexes recognize target DNA that is complementary to the 20 nt from 5′ end of sgRNA lying next to a PAM sequence, and cause double-strand breaks (DSBs), which can be repaired by endogenous DNA repair machinery; nonhomologous end joining (NHEJ) or homology-directed repair (HDR). NHEJ repair DSBs generating small insertions or deletions, while HDR introduces desired sequence insertion by recombination of the DSB locus with single-stranded DNA templates.

mediated gene modification of CCR5 gene to prevent HIV-1 infection. The cell surface chemokine receptor CCR5 is the macrophage-tropic HIV-1 coreceptor, which dominates in early stages of HIV-1 infection. Inhibition of CCR5 could lead to disruption of viral entry to host cells. Autologous T-cells, modified by CCR5-ZFN and expanded ex vivo, are being tested in a series of clinical trials in HIV-1 positive patients. Encouraged by this successful example with ZFNs, several CRISPR/Cas9 mediated genome editing approaches against CCR5 have also been developed and tested in various cell types including CD4 + T cells,[216a,d] CD34 + HSCs,[216c] and iPSCs.[216b] For example, Wang et al. used lentiviral vectors expressing Cas9 and CCR5 sgRNAs which were subjected to a single round transduction into HIV-1 susceptible human CD4+ cells.[216a] High frequencies of CCR5 gene disruption was observed without measurable detection of potential off-target modification of the genomic site containing highly homologous sequences to the CCR5 sgRNAs. Since CCR5 gene is highly homologous to CCR2 gene,[216c] when targeting CCR5 with CRISPR/Cas9 system, one should carefully design sgRNAs to avoid potential off-target events. Directly targeting viral genes is also one of potential anti-viral genome editing strategies. Complete excision of the integrated HIV-1 proviral DNA fragment using CRISPR/Cas9 was achieved by targeting the U3 region of HIV-1 long terminal repeat flanking the viral genome.[216e,f] These studies demonstrated the potency of the CRISPR/Cas9 system for preventing viral infection/replication as well as eradication of viral latency which is a major hurdle for achieving a sterilizing HIV cure.

In recent years, T-cell immunotherapy has been gaining widespread attention for its great promise in cancer treatment. In particular, one technology with the most potential is the use of modified T cells that express synthetic receptors known as chimeric antigen receptors, or CARs that recognize cancer-specific cell surface antigens.[220] Such CAR T-cells have shown their potency in treating B-cell lymphoma by targeting cell surface CD19.[221] However, the binding of checkpoint inhibitors on cancer cell surface to PD-1 receptors on T cells blocks antitumor function of T-cells and induce apoptosis and exhaustion. Su et al. successfully demonstrated the gene knockout of PD-1 using CRISPR/Cas9 system in human primary CD4+ T-cells.[222] The disruption of PD-1 expression enhanced cytotoxicity of the T-cells against PD-1 ligand, or PD-L1 expressing M14 melanoma cells. Thus, knockout of checkpoint inhibitors may be a critical strategy to facilitate T-cell immunotherapy for cancer treatment.

Applications of CRISPR/Cas9 technology are not limited to genome editing. Another potential use of the technology involves regulation of gene expression using catalytically inactive "dead Cas9 (dCas9)." A dCas9/sgRNA complex can bind target genomic DNA thereby sterically inhibiting binding or elongation of RNA polymerase. The technology is now known as CRISPR interference (CRISPRi).[223] In a proof-of-concept study by Gilbert et al., transcriptional silencing efficiency of CRISPRi was successfully improved by fusing dCas9 to a repressive chromatin modifier domain, KRAB (Krüppel-associated box) domain of Kox1, which

achieved 5–15-fold repression of target gene expression whereas an unfused dCas9 showed only ~2-fold repression.[223] Specificity of CRISPRi was assessed by using high-throughput screening.[224] The authors found that maximum repression can be achieved when targeting a window of DNA from −50 to +100 bp relative to the transcription starting site. The analysis also showed that CRISPRi activity is highly sensitive to mismatches between the sgRNA and target DNA, suggesting properly designed CRISPRi systems are highly specific.

The dCas9 protein fused to transcription activators such as VP64 (a tetramer of the minimal VP16 domain), p65 (RelA), and p300 has been shown to upregulate transcription in mammalian cells.[225] This approach is known as CRISPR activation (CRISPRa). For example, Saayman et al. demonstrated sgRNA-guided dCas9-VP64 system targeted atLTR promoter region of HIV-1 induced potent transcriptional activation of latent HIV-1 infection in human T cells.[226] Similarly, Limsirichai et al. demonstrated activation of latent HIV-1 expression by two distinct CRISPRa systems.[227] Compared to dCas9-VP64, more robust transcriptional activation was observed when using the synergistic activation mediator (SAM) complex which consists of dCas9-VP64 and an accessory trans-activation domain designed to recruit a complementary suite of transcription and chromatin remodeling factors. Together, CRISPRi and CRISPRa have been shown as powerful tools for systematically manipulating transcription of endogenous genes in human cells. The use of CRISPRi and CRISPRa for gene regulation may offer an alternative to RNAi or RNAa for therapeutics as well as a tool for better understanding gene function.

6.12.3.2.2 Challenges and future perspectives

While CRISPR/Cas9 system has been showing its power and potency of genome editing, a number of challenges still remain to be solved including efficiency, specificity, and delivery of the genome editing components. Several groups have addressed off-target activities of Cas9.[228] Studies showed that mismatches at the 5′ end of target sequences are generally tolerated while mismatches at the 3′-end are not, suggesting that the 3′ terminal sequence is crucial for sgRNA recognition of the target. Pattanayak et al. performed off-target profiling of CRISPR/Cas9 mediated DSB using in vitro selection and high-throughput sequencing. Preselected DNA libraries which contain $>10^{12}$ potential off-target sequences were treated with Cas9/sgRNA complexes of interest which were then subjected to high-throughput sequencing.[228c] The sequencing analysis revealed that a shorter, less-active guide RNA is more specific than a longer, more-active guide RNA. They also found that higher concentrations of Cas9/sgRNA complex can decrease DNA-cleaving specificity, and that potential off-target sites that contain four mutations relative to the on-target site can be modified. A number of approaches to improve the specificity of CRISPR/Cas9 system have been proposed by many researchers. Computational algorithms may be useful to predict proper sgRNA sequences. Indeed, several groups have developed algorithmic tools that help to design sequences of sgRNA with minimized off-target effect. It could also be avoided by delivering purified recombinant Cas9 protein and guide RNA complex[229] or truncation of sgRNAs to reduce binding affinity.[230]

An engineered Cas9 protein that cleaves one strand of the target DNA, known as Cas9 nickase has also been shown to increase specificity.[231] Cas9 nickase contains a point mutation at either the RuvC1 or HNH-like nuclease domain that disrupts cleavage function at either complementary or noncomplementary DNA target strands. Using a pair of Cas9 nickases that require independent binding to target DNA, can generate highly site specific DSB, compared to Cas9 mediated DSB that requires binding at only one site. The Cas9 nickase has also been shown as an useful tool to introduce site specific HDR.

The efficient delivery of CRISPR/Cas9 to the targeted cells is another great challenge.[232] Possible delivery approaches include AAV, adenovirus, lentiviruses, and nonviral physical methods. Due to its low immunogenicity, AAV is currently most widely used for in vivo delivery of CRISPR/Cas9 gene. However, the use of AAV is somewhat limited because of the small packaging capacity of the virus (about 4.9 kb). The size of SpCas9 cDNA is about 4.2 kb long which leaves only 0.7 kb for other regulatory elements necessary for gene expression. Thus, sgRNAs (~100 bp) are usually delivered in separate AAV particles. Recently smaller Cas9 orthologs such as *Staphylococcus aureus* Cas9 which is ~1 kb smaller than SpCas9 have been established which may allow "all-in-one" AAV vectors. Adenovirus and lentivirus have larger packaging capacities that permit inclusion of all CRISPR/Cas9 components. The use of adenovirus is limited because of its serious immunogenicity. Lentiviral vectors, which are based in HIV-1, have LTRs that facilitate host genome integration. However, as CRISPR/Cas9 gene editing requires transient expression of the Cas9 nuclease to limit off-target events, the use of integrase-defective lentiviruses (IDLV) is preferable. Potent nonviral delivery methods for systemic delivery of CRISPR/Cas9 have also been demonstrated. Yin et al. combined lipid nanoparticle-mediated delivery of Cas9 mRNA, AAVs encoding a sgRNA, and induced repair of fumarylacetoacetate hydrolase (Fah) splicing mutations in adult mice.[233]

Furthermore, little is known about the immunogenicity of bacteria originated Cas9 protein in humans so far. Potential toxicity caused by the immunogenicity of the Cas9 protein should be addressed before its application in clinical trials.

Finally, along with its development, this cost-effective and easy-to-use genome editing technology raises ethical concerns that need to be addressed. For example, any genomic changes in the human germline can be potentially passed down to future generations, introducing those changes into the human population. Rules and a regulatory framework that address human germline genome editing should be established in a timely manner in order to avoid inhibiting research and development.

Since the initial discovery that Cas9 is an RNA-programmable DNA endonuclease was published in 2012, an explosive increase in the number of research publications has been seen in PubMed using a keyword "CRISPR": 282 papers in 2013, 606 in 2014, and 1251 in 2015. Recently a research team at the University of Pennsylvania has received permission from US National Institutes of Health (NIH) panel for the first study that proposes using CRISPR/Cas9 genome editing technology in humans to treat cancer. The study proposal is a phase I trial of autologous CAR-T cells expressing NY-ESO-1 TCR in which TCR and PD-1 gene expression is eliminated by genome editing. If approved by the FDA, it will be the first-in-human trial of CRISPR/Cas9 technology. Despite

a number of challenges that remain to be addressed, significant progress has already been made in CRISPR/Cas9 technology and these advances will undoubtedly lead this technology toward understanding and treating a variety of human diseases.

6.12.4 Conclusions

Since the first nucleic acid based drug, fomivirsen, was approved for clinical use more than one and half decades ago, only two agents, macugen and mipomersen have reached the market. Major challenges in therapeutic development that most nucleic acid based therapeutics face include delivery methods, target specificity, effectiveness, immunogenicity, toxicity, and cost of synthesis. These challenges have been addressed by a number of studies and achieved significant improvement. For example, stability and immunogenicity of nucleic acids can be improved by chemical modifications. In addition, some chemical modifications, especially the PS modification, offer drug-like PK/PD properties. Therefore, the majority of currently clinically tested nucleic acid therapeutics are chemically modified. On top of these challenges, targeted delivery remains the major hurdle in clinical development of nucleic acid based therapeutics. The issue has been addressed by developing delivery tools including lipid nano particles, conjugation of target cell-specific ligands and cell-specific aptamers, some of which have already shown clinical significance in advanced phase clinical studies. Gaining a better understanding of the function of targets, PK/PD properties, and functional pathway of the agents will facilitate approaches to improve these challenges, thus enhance clinical development of nucleic acid based therapeutics.

Along with the emergence of CRISPR/Cas9 system, a new nucleic acid based technology, nucleic acid based therapeutics become more important and attractive. One of the advantages of nucleic acid based therapeutics is that, in theory, they can target virtually any genes. Thus, many of nucleic acid based therapeutics currently being tested in clinical trials target rare but life-threatening severe diseases that are difficult to treat by current small molecule based drugs or monoclonal antibodies. Thus, we believe that some of these nucleic acid based therapeutics will soon become available for treatment of those diseases.

See also: 2.10. Overview of Drug Polypharmacology and Multitargeted Molecular Design.

References

1. (a) Stephenson, M. L.; Zamecnik, P. C. Inhibition of Rous Sarcoma Viral RNA Translation by a Specific Oligodeoxyribonucleotide. *Proc. Natl. Acad. Sci. U. S. A.* **1978,** *75* (1), 285–288; (b) Zamecnik, P. C.; Stephenson, M. L. Inhibition of Rous Sarcoma Virus Replication and Cell Transformation by a Specific Oligodeoxynucleotide. *Proc. Natl. Acad. Sci. U. S. A.* **1978,** *75* (1), 280–284.
2. Kruger, K.; Grabowski, P. J.; Zaug, A. J.; Sands, J.; Gottschling, D. E.; Cech, T. R. Self-Splicing RNA: Autoexcision and Autocyclization of the Ribosomal RNA Intervening Sequence of Tetrahymena. *Cell* **1982,** *31* (1), 147–157.
3. (a) Lee, R. C.; Feinbaum, R. L.; Ambros, V. The *C. elegans* Heterochronic Gene lin-4 Encodes Small RNAs With Antisense Complementarity to lin-14. *Cell* **1993,** *75* (5), 843–854; (b) Wightman, B.; Ha, I.; Ruvkun, G. Posttranscriptional Regulation of the Heterochronic Gene lin-14 by lin-4 Mediates Temporal Pattern Formation in *C. elegans*. *Cell* **1993,** *75* (5), 855–862.
4. (a) Davalos, A.; Suarez, Y. MiRNA-Based Therapy: From Bench to Bedside. *Pharmacol. Res.* **2013,** *75,* 1–2; (b) Ling, H.; Fabbri, M.; Calin, G. A. MicroRNAs and Other Non-Coding RNAs as Targets for Anticancer Drug Development. *Nat. Rev. Drug Discov.* **2013,** *12* (11), 847–865.
5. Fire, A.; Xu, S.; Montgomery, M. K.; Kostas, S. A.; Driver, S. E.; Mello, C. C. Potent and Specific Genetic Interference by Double-Stranded RNA in *Caenorhabditis elegans*. *Nature* **1998,** *391* (6669), 806–811.
6. Elbashir, S. M.; Harborth, J.; Lendeckel, W.; Yalcin, A.; Weber, K.; Tuschl, T. Duplexes of 21-Nucleotide RNAs Mediate RNA Interference in Cultured Mammalian Cells. *Nature* **2001,** *411* (6836), 494–498.
7. Breaker, R. R. Complex Riboswitches. *Science* **2008,** *319* (5871), 1795–1797.
8. Kim, V. N. Small RNAs Just Got Bigger: Piwi-Interacting RNAs (piRNAs) in Mammalian Testes. *Genes Dev.* **2006,** *20* (15), 1993–1997.
9. Doudna, J. A.; Charpentier, E. Genome Editing. The New Frontier of Genome Engineering With CRISPR-Cas9. *Science* **2014,** *346* (6213), 1258096.
10. (a) Elgar, G.; Vavouri, T. Tuning in to the Signals: Noncoding Sequence Conservation in Vertebrate Genomes. *Trends Genet.* **2008,** *24* (7), 344–352; (b) Yang, J. X.; Rastetter, R. H.; Wilhelm, D. Non-Coding RNAs: An Introduction. *Adv. Exp. Med. Biol.* **2016,** *886,* 13–32.
11. Rozenblum, G. T.; Lopez, V. G.; Vitullo, A. D.; Radrizzani, M. Aptamers: Current Challenges and Future Prospects. *Expert Opin. Drug Discovery* **2016,** *11* (2), 127–135.
12. Gogtay, N. J.; Sridharan, K. Therapeutic Nucleic Acids: Current Clinical Status. *Br. J. Clin. Pharmacol.* **2016,** *82,* 659–672.
13. Bennett, C. F.; Swayze, E. E. RNA Targeting Therapeutics: Molecular Mechanisms of Antisense Oligonucleotides as a Therapeutic Platform. *Annu. Rev. Pharmacol. Toxicol.* **2010,** *50,* 259–293.
14. Wittrup, A.; Lieberman, J. Knocking Down Disease: A Progress Report on siRNA Therapeutics. *Nat. Rev. Genet.* **2015,** *16* (9), 543–552.
15. (a) Ellington, A. D.; Szostak, J. W. In Vitro Selection of RNA Molecules That Bind Specific Ligands. *Nature* **1990,** *346* (6287), 818–822; (b) Tuerk, C.; Gold, L. Systematic Evolution of Ligands by Exponential Enrichment: RNA Ligands to Bacteriophage T4 DNA Polymerase. *Science* **1990,** *249* (4968), 505–510.
16. Kole, R.; Krainer, A. R.; Altman, S. RNA Therapeutics: Beyond RNA Interference and Antisense Oligonucleotides. *Nat. Rev. Drug Discov.* **2012,** *11* (2), 125–140.
17. (a) Lima, W. F.; Rose, J. B.; Nichols, J. G.; Wu, H.; Migawa, M. T.; Wyrzykiewicz, T. K.; Siwkowski, A. M.; Crooke, S. T. Human RNase H1 Discriminates Between Subtle Variations in the Structure of the Heteroduplex Substrate. *Mol. Pharmacol.* **2007,** *71* (1), 83–91; (b) Lima, W. F.; Rose, J. B.; Nichols, J. G.; Wu, H.; Migawa, M. T.; Wyrzykiewicz, T. K.; Vasquez, G.; Swayze, E. E.; Crooke, S. T. The Positional Influence of the Helical Geometry of the Heteroduplex Substrate on Human RNase H1 Catalysis. *Mol. Pharmacol.* **2007,** *71* (1), 73–82.
18. Yamamoto, T.; Nakatani, M.; Narukawa, K.; Obika, S. Antisense Drug Discovery and Development. *Future Med. Chem.* **2011,** *3* (3), 339–365.
19. Eckstein, F. Phosphorothioates, Essential Components of Therapeutic Oligonucleotides. *Nucleic Acid Ther.* **2014,** *24* (6), 374–387.
20. Koziolkiewicz, M.; Krakowiak, A.; Kwinkowski, M.; Boczkowska, M.; Stec, W. J. Stereodifferentiation—The Effect of P Chirality of Oligo(Nucleoside Phosphorothioates) on the Activity of Bacterial RNase H. *Nucleic Acids Res.* **1995,** *23* (24), 5000–5005.
21. Beltinger, C.; Saragovi, H. U.; Smith, R. M.; LeSauteur, L.; Shah, N.; DeDionisio, L.; Christensen, L.; Raible, A.; Jarett, L.; Gewirtz, A. M. Binding, Uptake, and Intracellular Trafficking of Phosphorothioate-Modified Oligodeoxynucleotides. *J. Clin. Invest.* **1995,** *95* (4), 1814–1823.

22. Geary, R. S.; Norris, D.; Yu, R.; Bennett, C. F. Pharmacokinetics, Biodistribution and Cell Uptake of Antisense Oligonucleotides. *Adv. Drug Deliv. Rev.* **2015,** *87,* 46–51.
23. Roehr, B. Fomivirsen Approved for CMV Retinitis. *J. Int. Assoc. Physicians AIDS Care* **1998,** *4* (10), 14–16.
24. Jabs, D. A.; Griffiths, P. D. Fomivirsen for the Treatment of Cytomegalovirus Retinitis. *Am J. Ophthalmol.* **2002,** *133* (4), 552–556.
25. Manoharan, M. 2′-Carbohydrate Modifications in Antisense Oligonucleotide Therapy: Importance of Conformation, Configuration and Conjugation. *Biochim. Biophys. Acta* **1999,** *1489* (1), 117–130.
26. Teplova, M.; Minasov, G.; Tereshko, V.; Inamati, G. B.; Cook, P. D.; Manoharan, M.; Egli, M. Crystal Structure and Improved Antisense Properties of 2′-O-(2-Methoxyethyl)-RNA. *Nat. Struct. Biol.* **1999,** *6* (6), 535–539.
27. Raal, F. J.; Santos, R. D.; Blom, D. J.; Marais, A. D.; Charng, M. J.; Cromwell, W. C.; Lachmann, R. H.; Gaudet, D.; Tan, J. L.; Chasan-Taber, S.; Tribble, D. L.; Flaim, J. D.; Crooke, S. T. Mipomersen, an Apolipoprotein B Synthesis Inhibitor, for Lowering of LDL Cholesterol Concentrations in Patients With Homozygous Familial Hypercholesterolaemia: A Randomised, Double-Blind, Placebo-Controlled Trial. *Lancet* **2010,** *375* (9719), 998–1006.
28. Nielsen, P. E.; Haaima, G.; Lohse, A.; Buchardt, O. Peptide Nucleic Acids (PNAs) Containing Thymine Monomers Derived from Chiral Amino Acids: Hybridization and Solubility Properties of D-Lysine PNA. *Angew. Chem. Int. Ed. Engl.* **1996,** *35,* 1939–1941.
29. Nielsen, P. E. Peptide Nucleic Acids (PNA) in Chemical Biology and Drug Discovery. *Chem. Biodivers.* **2010,** *7* (4), 786–804.
30. Wancewicz, E. V.; Maier, M. A.; Siwkowski, A. M.; Albertshofer, K.; Winger, T. M.; Berdeja, A.; Gaus, H.; Vickers, T. A.; Bennett, C. F.; Monia, B. P.; Griffey, R. H.; Nulf, C. J.; Hu, J.; Corey, D. R.; Swayze, E. E.; Kinberger, G. A. Peptide Nucleic Acids Conjugated to Short Basic Peptides Show Improved Pharmacokinetics and Antisense Activity in Adipose Tissue. *J. Med. Chem.* **2010,** *53* (10), 3919–3926.
31. Mae, M.; Langel, U. Cell-Penetrating Peptides as Vectors for Peptide, Protein and Oligonucleotide Delivery. *Curr. Opin. Pharmacol.* **2006,** *6* (5), 509–514.
32. (a) Brolin, C.; Shiraishi, T.; Hojman, P.; Krag, T. O.; Nielsen, P. E.; Gehl, J. Electroporation Enhanced Effect of Dystrophin Splice Switching PNA Oligomers in Normal and Dystrophic Muscle. *Mol. Ther.–Nucleic Acids* **2015,** *4*, e267; (b) Gao, X.; Shen, X.; Dong, X.; Ran, N.; Han, G.; Cao, L.; Gu, B.; Yin, H. Peptide Nucleic Acid Promotes Systemic Dystrophin Expression and Functional Rescue in Dystrophin-Deficient mdx Mice. *Mol. Ther.–Nucleic Acids* **2015,** *4*, e255.
33. (a) Obika, S.; Nanbu, D.; Hari, Y.; Morio, K.; In, Y.; Ishida, T.; Imanishi, T. Synthesis of 2′-O,4′-C-Methyleneuridine and -Cytidine: Novel Bicyclic Nucleosides Having a Fixed C3′-Endo Sugar Puckering. *Tetrahedron Lett.* **1997,** *38,* 8735–8738; (b) Koshkin, A. A.; Singh, S. K.; Nielsen, P.; Rajwanshi, V. K.; Kumar, V.; Meldgaard, M.; Olsen, C. E.; Wengel, J. LNA (Locked Nucleic Acids): Synthesis of the Adenine, Cytosine, Guanine, 5-Methylcytosine, Thymine and Uracil Bicyclonucleoside Monomers, Oligomerisation, and Unprecedented Nucleic Acid Recognition. *Tetrahedron* **1998,** *54,* 3607–3630.
34. Lundin, K. E.; Hojland, T.; Hansen, B. R.; Persson, R.; Bramsen, J. B.; Kjems, J.; Koch, T.; Wengel, J.; Smith, C. I. Biological Activity and Biotechnological Aspects of Locked Nucleic Acids. *Adv. Genet.* **2013,** *82,* 47–107.
35. Baek, J.; Kang, S.; Min, H. MicroRNA-Targeting Therapeutics for Hepatitis C. *Arch. Pharm. Res.* **2014,** *37* (3), 299–305.
36. (a) Burdick, A. D.; Sciabola, S.; Mantena, S. R.; Hollingshead, B. D.; Stanton, R.; Warneke, J. A.; Zeng, M.; Martsen, E.; Medvedev, A.; Makarov, S. S.; Reed, L. A.; Davis, J. W., 2nd; Whiteley, L. O. Sequence Motifs Associated With Hepatotoxicity of Locked Nucleic Acid-Modified Antisense Oligonucleotides. *Nucleic Acids Res.* **2014,** *42* (8), 4882–4891; (b) Burel, S. A.; Hart, C. E.; Cauntay, P.; Hsiao, J.; Machemer, T.; Katz, M.; Watt, A.; Bui, H. H.; Younis, H.; Sabripour, M.; Freier, S. M.; Hung, G.; Dan, A.; Prakash, T. P.; Seth, P. P.; Swayze, E. E.; Bennett, C. F.; Crooke, S. T.; Henry, S. P. Hepatotoxicity of High Affinity Gapmer Antisense Oligonucleotides is Mediated by RNase H1 Dependent Promiscuous Reduction of Very Long Pre-mRNA Transcripts. *Nucleic Acids Res.* **2016,** *44* (5), 2093–2109.
37. Stirchak, E. P.; Summerton, J. E.; Weller, D. D. Uncharged Stereoregular Nucleic Acid Analogs: 2. Morpholino Nucleoside Oligomers With Carbamate Internucleoside Linkages. *Nucleic Acids Res.* **1989,** *17* (15), 6129–6141.
38. Summerton, J.; Weller, D. Morpholino Antisense Oligomers: Design, Preparation, and Properties. *Antisense Nucleic Acid Drug Dev.* **1997,** *7* (3), 187–195.
39. Mendell, J. R.; Goemans, N.; Lowes, L. P.; Alfano, L. N.; Berry, K.; Shao, J.; Kaye, E. M.; Mercuri, E.; Eteplirsen Study Group and Telethon Foundation DMD Italian Network. Longitudinal Effect of Eteplirsen Versus Historical Control on Ambulation in Duchenne Muscular Dystrophy. *Ann. Neurol.* **2016,** *79* (2), 257–271.
40. Wilds, C. J.; Damha, M. J. 2′-Deoxy-2′-fluoro-beta-D-arabinonucleosides and Oligonucleotides (2′F-ANA): Synthesis and Physicochemical Studies. *Nucleic Acids Res.* **2000,** *28* (18), 3625–3635.
41. (a) Trempe, J. F.; Wilds, C. J.; Denisov, A. Y.; Pon, R. T.; Damha, M. J.; Gehring, K. NMR Solution Structure of an Oligonucleotide Hairpin With a 2′F-ANA/RNA Stem: Implications for RNase H Specificity Toward DNA/RNA Hybrid Duplexes. *J. Am. Chem. Soc.* **2001,** *123* (21), 4896–4903; (b) Denisov, A. Y.; Noronha, A. M.; Wilds, C. J.; Trempe, J. F.; Pon, R. T.; Gehring, K.; Damha, M. J. Solution Structure of an Arabinonucleic Acid (ANA)/RNA Duplex in a Chimeric Hairpin: Comparison With 2′-Fluoro-ANA/RNA and DNA/RNA Hybrids. *Nucleic Acids Res.* **2001,** *29* (21), 4284–4293.
42. Damha, M. J.; Wilds, C. J.; Noronha, A.; Brukner, I.; Borkow, G.; Arion, D.; Parniak, M. A. Hybrids of RNA and Arabinonucleic Acids (ANA and 2′F-ANA) Are Substrates of Ribonuclease H. *J. Am. Chem. Soc.* **1998,** *120,* 12976–12977.
43. Noronha, A. M.; Wilds, C. J.; Lok, C. N.; Viazovkina, K.; Arion, D.; Parniak, M. A.; Damha, M. J. Synthesis and Biophysical Properties of Arabinonucleic Acids (ANA): Circular Dichroic Spectra, Melting Temperatures, and Ribonuclease H Susceptibility of ANA.RNA Hybrid Duplexes. *Biochemistry* **2000,** *39* (24), 7050–7062.
44. Fortin, M.; D'Anjou, H.; Higgins, M. E.; Gougeon, J.; Aube, P.; Moktefi, K.; Mouissi, S.; Seguin, S.; Seguin, R.; Renzi, P. M.; Paquet, L.; Ferrari, N. A Multi-Target Antisense Approach Against PDE4 and PDE7 Reduces Smoke-Induced Lung Inflammation in Mice. *Respir. Res.* **2009,** *10,* 39.
45. Lebedeva, I.; Benimetskaya, L.; Stein, C. A.; Vilenchik, M. Cellular Delivery of Antisense Oligonucleotides. *Eur. J. Pharm. Biopharm.* **2000,** *50* (1), 101–119.
46. Yu, R. Z.; Kim, T. W.; Hong, A.; Watanabe, T. A.; Gaus, H. J.; Geary, R. S. Cross-Species Pharmacokinetic Comparison from Mouse to man of a Second-Generation Antisense Oligonucleotide, ISIS 301012, Targeting Human Apolipoprotein B-100. *Drug Metab. Dispos.* **2007,** *35* (3), 460–468.
47. Yu, R. Z.; Grundy, J. S.; Geary, R. S. Clinical Pharmacokinetics of Second Generation Antisense Oligonucleotides. *Expert Opin. Drug Metab. Toxicol.* **2013,** *9* (2), 169–182.
48. (a) McMahon, B. M.; Mays, D.; Lipsky, J.; Stewart, J. A.; Fauq, A.; Richelson, E. Pharmacokinetics and Tissue Distribution of a Peptide Nucleic Acid After Intravenous Administration. *Antisense Nucleic Acid Drug Dev.* **2002,** *12* (2), 65–70; (b) Amantana, A.; Iversen, P. L. Pharmacokinetics and Biodistribution of Phosphorodiamidate Morpholino Antisense Oligomers. *Curr. Opin. Pharmacol.* **2005,** *5* (5), 550–555.
49. Koller, E.; Vincent, T. M.; Chappell, A.; De, S.; Manoharan, M.; Bennett, C. F. Mechanisms of Single-Stranded Phosphorothioate Modified Antisense Oligonucleotide Accumulation in Hepatocytes. *Nucleic Acids Res.* **2011,** *39* (11), 4795–4807.
50. (a) Crooke, R. M.; Graham, M. J.; Lemonidis, K. M.; Whipple, C. P.; Koo, S.; Perera, R. J. An Apolipoprotein B Antisense Oligonucleotide Lowers LDL Cholesterol in Hyperlipidemic Mice Without Causing Hepatic Steatosis. *J. Lipid Res.* **2005,** *46* (5), 872–884; (b) Kastelein, J. J.; Wedel, M. K.; Baker, B. F.; Su, J.; Bradley, J. D.; Yu, R. Z.; Chuang, E.; Graham, M. J.; Crooke, R. M. Potent Reduction of Apolipoprotein B and Low-Density Lipoprotein Cholesterol by Short-Term Administration of an Antisense Inhibitor of Apolipoprotein B. *Circulation* **2006,** *114* (16), 1729–1735.
51. Stein, E. A.; Dufour, R.; Gagne, C.; Gaudet, D.; East, C.; Donovan, J. M.; Chin, W.; Tribble, D. L.; McGowan, M. Apolipoprotein B Synthesis Inhibition With Mipomersen in Heterozygous Familial Hypercholesterolemia: Results of a Randomized, Double-Blind, Placebo-Controlled Trial to Assess Efficacy and Safety as Add-on Therapy in Patients With Coronary Artery Disease. *Circulation* **2012,** *126* (19), 2283–2292.
52. Santos, R. D.; Duell, P. B.; East, C.; Guyton, J. R.; Moriarty, P. M.; Chin, W.; Mittleman, R. S. Long-Term Efficacy and Safety of Mipomersen in Patients With Familial Hypercholesterolaemia: 2-Year Interim Results of an Open-Label Extension. *Eur. Heart J.* **2015,** *36* (9), 566–575.
53. IONIS Pharmaceuticals, Inc. Press Release. http://ir.ionispharma.com/phoenix.zhtml?c=222170&p=irol-newsArticle&ID=2105651.
54. Muntoni, F.; Torelli, S.; Ferlini, A. Dystrophin and Mutations: One Gene, Several Proteins, Multiple Phenotypes. *Lancet Neurol.* **2003,** *2* (12), 731–740.
55. van der Ree, M. H.; van der Meer, A. J.; de Bruijne, J.; Maan, R.; van Vliet, A.; Welzel, T. M.; Zeuzem, S.; Lawitz, E. J.; Rodriguez-Torres, M.; Kupcova, V.; Wiercinska-Drapalo, A.; Hodges, M. R.; Janssen, H. L.; Reesink, H. W. Long-Term Safety and Efficacy of MicroRNA-Targeted Therapy in Chronic Hepatitis C Patients. *Antivir. Res.* **2014,** *111,* 53–59.

56. Miller, T. M.; Pestronk, A.; David, W.; Rothstein, J.; Simpson, E.; Appel, S. H.; Andres, P. L.; Mahoney, K.; Allred, P.; Alexander, K.; Ostrow, L. W.; Schoenfeld, D.; Macklin, E. A.; Norris, D. A.; Manousakis, G.; Crisp, M.; Smith, R.; Bennett, C. F.; Bishop, K. M.; Cudkowicz, M. E. An Antisense Oligonucleotide Against SOD1 Delivered Intrathecally for Patients With SOD1 Familial Amyotrophic Lateral Sclerosis: A Phase 1, Randomised, First-in-Man Study. *Lancet Neurol.* **2013,** *12* (5), 435–442.
57. Kanasty, R.; Dorkin, J. R.; Vegas, A.; Anderson, D. Delivery Materials for siRNA Therapeutics. *Nat. Mater.* **2013,** *12* (11), 967–977.
58. Prakash, T. P.; Graham, M. J.; Yu, J.; Carty, R.; Low, A.; Chappell, A.; Schmidt, K.; Zhao, C.; Aghajan, M.; Murray, H. F.; Riney, S.; Booten, S. L.; Murray, S. F.; Gaus, H.; Crosby, J.; Lima, W. F.; Guo, S.; Monia, B. P.; Swayze, E. E.; Seth, P. P. Targeted Delivery of Antisense Oligonucleotides to Hepatocytes Using Triantennary *N*-Acetyl Galactosamine Improves Potency 10-Fold in Mice. *Nucleic Acids Res.* **2014,** *42* (13), 8796–8807.
59. Fire, A.; Xu, S.; Montgomery, M. K.; Kostas, S. A.; Driver, S. E.; Mello, C. C. Potent and Specific Genetic Interference by Double-Stranded RNA in *Caenorhabditis elegans*. *Nature* **1998,** *391* (6669), 806–811.
60. Lau, N. C.; Lim, L. P.; Weinstein, E. G.; Bartel, D. P. An Abundant Class of Tiny RNAs With Probable Regulatory Roles in *Caenorhabditis elegans*. *Science* **2001,** *294* (5543), 858–862.
61. (a) Tomari, Y.; Zamore, P. D. Perspective: Machines for RNAi. *Genes Dev.* **2005,** *19* (5), 517–529; (b) Ha, M.; Kim, V. N. Regulation of MicroRNA Biogenesis. *Nat. Rev. Mol. Cell Biol.* **2014,** *15* (8), 509–524.
62. (a) Lee, Y.; Ahn, C.; Han, J.; Choi, H.; Kim, J.; Yim, J.; Lee, J.; Provost, P.; Radmark, O.; Kim, S.; Kim, V. N. The Nuclear RNase III Drosha Initiates MicroRNA Processing. *Nature* **2003,** *425* (6956), 415–419; (b) Han, J.; Lee, Y.; Yeom, K.-H.; Nam, J.-W.; Heo, I.; Rhee, J.-K.; Sohn, S. Y.; Cho, Y.; Zhang, B.-T.; Kim, V. N. Molecular Basis for the Recognition of Primary microRNAs by the Drosha-DGCR8 Complex. *Cell* **2006,** *125* (5), 887–901; (c) Gregory, R. I.; Yan, K.-p.; Amuthan, G.; Chendrimada, T.; Doratotaj, B.; Cooch, N.; Shiekhattar, R. The Microprocessor Complex Mediates the Genesis of microRNAs. *Nature* **2004,** *432* (7014), 235–240.
63. Nguyen, T. A.; Jo, M. H.; Choi, Y. G.; Park, J.; Kwon, S. C.; Hohng, S.; Kim, V. N.; Woo, J. S. Functional Anatomy of the Human Microprocessor. *Cell* **2015,** *161* (6), 1374–1387.
64. Zeng, Y. Structural Requirements for Pre-microRNA Binding and Nuclear Export by Exportin 5. *Nucleic Acids Res.* **2004,** *32* (16), 4776.
65. Hutvágner, G.; McLachlan, J.; Pasquinelli, A. E.; Bálint, É.; Tuschl, T.; Zamore, P. D. Cellular Function for the RNA-Interference Enzyme Dicer in the Maturation of the *let-7* Small Temporal RNA. *Science* **2001,** *293* (5531), 834–838.
66. Hutvagner, G.; Simard, M. J. Argonaute Proteins: Key Players in RNA Silencing. *Nat. Rev. Mol. Cell Biol.* **2008,** *9* (1), 22–32.
67. MacRae, I. J.; Ma, E.; Zhou, M.; Robinson, C. V.; Doudna, J. A. In Vitro Reconstitution of the Human RISC-Loading Complex. *Proc. Natl. Acad. Sci.* **2008,** *105* (2), 512–517.
68. (a) Elkayam, E.; Kuhn, C.-D.; Tocilj, A.; Haase, A. D.; Greene, E. M.; Hannon, G. J.; Joshua-Tor, L. The Structure of Human Argonaute-2 in Complex with miR-20a. *Cell* **2012,** *150* (1), 100–110; (b) Schirle, N. T.; MacRae, I. J. The Crystal Structure of Human Argonaute2. *Science* **2012,** *336* (6084), 1037–1040.
69. (a) Salomon, W. E.; Jolly, S. M.; Moore, M. J.; Zamore, P. D.; Serebrov, V. Single-Molecule Imaging Reveals That Argonaute Reshapes the Binding Properties of Its Nucleic Acid Guides. *Cell* **2015,** *162* (1), 84–95; (b) Chandradoss, S. D.; Schirle, N. T.; Szczepaniak, M.; MacRae, I. J.; Joo, C. A Dynamic Search Process Underlies MicroRNA Targeting. *Cell* **2015,** *162* (1), 96–107; (c) Klein, M.; Chandradoss, S. D.; Depken, M.; Joo, C. Why Argonaute is Needed to Make microRNA Target Search Fast and Reliable. *Semin. Cell Dev. Biol.* **2016**. in press.
70. (a) Huntzinger, E.; Izaurralde, E. Gene Silencing by microRNAs: Contributions of Translational Repression and mRNA Decay. *Nat. Rev. Genet.* **2011,** *12* (2), 99–110; (b) Wilson, R. C.; Doudna, J. A. Molecular Mechanisms of RNA Interference. *Annu. Rev. Biophys.* **2013,** *42* (1), 217–239.
71. Castanotto, D.; Rossi, J. J. The Promises and Pitfalls of RNA-Interference-Based Therapeutics. *Nature* **2009,** *457* (7228), 426–433.
72. Lund, E.; Güttinger, S.; Calado, A.; Dahlberg, J. E.; Kutay, U. Nuclear Export of MicroRNA Precursors. *Science* **2004,** *303* (5654), 95–98.
73. MacRae, I. J.; Zhou, K.; Doudna, J. A. Structural Determinants of RNA Recognition and Cleavage by Dicer. *Nat. Struct. Mol. Biol.* **2007,** *14* (10), 934–940.
74. MacRae, I. J.; Zhou, K.; Li, F.; Repic, A.; Brooks, A. N.; Cande, W. Z.; Adams, P. D.; Doudna, J. A. Structural Basis for Double-Stranded RNA Processing by Dicer. *Science* **2006,** *311* (5758), 195–198.
75. Soifer, H. S.; Sano, M.; Sakurai, K.; Chomchan, P.; Sætrom, P.; Sherman, M. A.; Collingwood, M. A.; Behlke, M. A.; Rossi, J. J. A Role for the Dicer Helicase Domain in the Processing of Thermodynamically Unstable Hairpin RNAs. *Nucleic Acids Res.* **2008,** *36* (20), 6511–6522.
76. Taylor, D. W.; Ma, E.; Shigematsu, H.; Cianfrocco, M. A.; Noland, C. L.; Nagayama, K.; Nogales, E.; Doudna, J. A.; Wang, H.-W. Substrate-Specific Structural Rearrangements of Human Dicer. *Nat. Struct. Mol. Biol.* **2013,** *20* (6), 662–670.
77. Wang, H.-W.; Noland, C.; Siridechadilok, B.; Taylor, D. W.; Ma, E.; Felderer, K.; Doudna, J. A.; Nogales, E. Structural Insights Into RNA Processing by the Human RISC-Loading Complex. *Nat. Struct. Mol. Biol.* **2009,** *16* (11), 1148–1153.
78. (a) Tomari, Y.; Matranga, C.; Haley, B.; Martinez, N.; Zamore, P. D. A Protein Sensor for siRNA Asymmetry. *Science* **2004,** *306* (5700), 1377–1380; (b) Noland, C. L.; Ma, E.; Doudna, J. A. siRNA Repositioning for Guide Strand Selection by Human Dicer Complexes. *Mol. Cell* **2011,** *43* (1), 110–121.
79. (a) Khvorova, A.; Reynolds, A.; Jayasena, S. D. Functional siRNAs and miRNAs Exhibit Strand Bias. *Cell* **2003,** *115* (2), 209–216; (b) Schwarz, D. S.; Hutvagner, G.; Du, T.; Xu, Z.; Aronin, N.; Zamore, P. D. Asymmetry in the Assembly of the RNAi Enzyme Complex. *Cell* **2003,** *115* (2), 199–208.
80. Schirle, N. T.; Sheu-Gruttadauria, J.; MacRae, I. J. Structural Basis for microRNA Targeting. *Science* **2014,** *346* (6209), 608–613.
81. Wee, L. M.; Flores-Jasso, C. F.; Salomon, W. E.; Zamore, P. D. Argonaute Divides Its RNA Guide into Domains With Distinct Functions and RNA-Binding Properties. *Cell* **2012,** *151* (5), 1055–1067.
82. Lewis, B. P.; Burge, C. B.; Bartel, D. P. Conserved Seed Pairing, Often Flanked by Adenosines, Indicates That Thousands of Human Genes are MicroRNA Targets. *Cell* **2005,** *120* (1), 15–20.
83. (a) Bramsen, J. B.; Laursen, M. B.; Nielsen, A. F.; Hansen, T. B.; Bus, C.; Langkjær, N.; Babu, B. R.; Højland, T.; Abramov, M.; Van Aerschot, A.; Odadzic, D.; Smicius, R.; Haas, J.; Andree, C.; Barman, J.; Wenska, M.; Srivastava, P.; Zhou, C.; Honcharenko, D.; Hess, S.; Müller, E.; Bobkov, G. V.; Mikhailov, S. N.; Fava, E.; Meyer, T. F.; Chattopadhyaya, J.; Zerial, M.; Engels, J. W.; Herdewijn, P.; Wengel, J.; Kjems, J. A Large-Scale Chemical Modification Screen Identifies Design Rules to Generate siRNAs With High Activity, High Stability and Low Toxicity. *Nucleic Acids Res.* **2009,** *37* (9), 2867–2881; (b) Reynolds, A.; Leake, D.; Boese, Q.; Scaringe, S.; Marshall, W. S.; Khvorova, A. Rational siRNA Design for RNA Interference. *Nat. Biotechnol.* **2004,** *22* (3), 326–330.
84. Song, J.-J.; Smith, S. K.; Hannon, G. J.; Joshua-Tor, L. Crystal Structure of Argonaute and Its Implications for RISC Slicer Activity. *Science* **2004,** *305* (5689), 1434–1437.
85. Burroughs, A. M.; Ando, Y.; de Hoon, M. L.; Tomaru, Y.; Suzuki, H.; Hayashizaki, Y.; Daub, C. O. Deep-Sequencing of Human Argonaute-Associated Small RNAs Provides Insight Into miRNA Sorting and Reveals Argonaute Association With RNA Fragments of Diverse Origin. *RNA Biol.* **2011,** *8* (1), 158–177.
86. Holoch, D.; Moazed, D. RNA-Mediated Epigenetic Regulation of Gene Expression. *Nat. Rev. Genet.* **2015,** *16* (2), 71–84.
87. (a) Weinberg, M. S.; Morris, K. V. Transcriptional Gene Silencing in Humans. *Nucleic Acids Res.* **2016,** *44* (14), 6505–6517; (b) Salmanidis, M.; Pillman, K.; Goodall, G.; Bracken, C. Direct Transcriptional Regulation by Nuclear microRNAs. *Int. J. Biochem. Cell Biol.* **2014,** *54,* 304–311.
88. (a) Mao, Q.; Li, Y.; Zheng, X.; Yang, K.; Shen, H.; Qin, J.; Bai, Y.; Kong, D.; Jia, X.; Xie, L. Up-regulation of E-cadherin by Small Activating RNA Inhibits Cell Invasion and Migration in 5637 Human Bladder Cancer Cells. *Biochem. Biophys. Res. Commun.* **2008,** *375* (4), 566–570; (b) Portnoy, V.; Lin, S. H. S.; Li, K. H.; Burlingame, A.; Hu, Z.-H.; Li, H.; Li, L.-C. saRNA-Guided Ago2 Targets the RITA Complex to Promoters to Stimulate Transcription. *Cell Res.* **2016,** *26* (3), 320–335; (c) Janowski, B. A.; Younger, S. T.; Hardy, D. B.; Ram, R.; Huffman, K. E.; Corey, D. R. Activating Gene Expression in Mammalian Cells With Promoter-Targeted Duplex RNAs. *Nat. Chem. Biol.* **2007,** *3* (3), 166–173; (d) Li, L.-C.; Okino, S. T.; Zhao, H.; Pookot, D.; Place, R. F.; Urakami, S.; Enokida, H.; Dahiya, R. Small dsRNAs Induce Transcriptional Activation in Human Cells. *Proc. Natl. Acad. Sci.* **2006,** *103* (46), 17337–17342.
89. Elbashir, S. M.; Lendeckel, W.; Tuschl, T. RNA Interference is Mediated by 21- and 22-Nucleotide RNAs. *Genes Dev.* **2001,** *15* (2), 188–200.
90. (a) Paddison, P. J.; Caudy, A. A.; Bernstein, E.; Hannon, G. J.; Conklin, D. S. Short Hairpin RNAs (shRNAs) Induce Sequence-Specific Silencing in Mammalian Cells. *Genes Dev.* **2002,** *16* (8), 948–958; (b) Dykxhoorn, D. M.; Novina, C. D.; Sharp, P. A. Killing the Messenger: Short RNAs That Silence Gene Expression. *Nat. Rev. Mol. Cell Biol.* **2003,** *4* (6), 457–467.

91. Xiang, S.; Fruehauf, J.; Li, C. J. Short Hairpin RNA-Expressing Bacteria Elicit RNA Interference in Mammals. *Nat. Biotechnol.* **2006,** *24* (6), 697–702.
92. Scherer, L. J.; Frank, R.; Rossi, J. J. Optimization and Characterization of tRNA-shRNA Expression Constructs. *Nucleic Acids Res.* **2007,** *35* (8), 2620–2628.
93. Kim, D.-H.; Behlke, M. A.; Rose, S. D.; Chang, M.-S.; Choi, S.; Rossi, J. J. Synthetic dsRNA Dicer Substrates Enhance RNAi Potency and Efficacy. *Nat. Biotechnol.* **2005,** *23* (2), 222–226.
94. Snead, N. M.; Wu, X.; Li, A.; Cui, Q.; Sakurai, K.; Burnett, J. C.; Rossi, J. J. Molecular Basis for Improved Gene Silencing by Dicer Substrate Interfering RNA Compared With Other siRNA Variants. *Nucleic Acids Res.* **2013,** *41* (12), 6209–6221.
95. Collingwood, M.; Collingwood, S.; Rose, L.; Huang, C.; Hillier, M.; Amarzguioui, M.; Wiiger, H.; Soifer, J.; Rossi, M. Behlke, Chemical Modification Patterns Compatible With High Potency Dicer-Substrate Small Interfering RNAs. *Oligonucleotides* **2008,** *18* (2), 187–200.
96. (a) Ge, Q.; Dallas, A.; Ilves, H.; Shorenstein, J.; Behlke, M. A.; Johnston, B. H. Effects of Chemical Modification on the Potency, Serum Stability, and Immunostimulatory Properties of Short shRNAs. *RNA* **2010,** *16* (1), 118–130; (b) Ge, Q.; Ilves, H.; Dallas, A.; Kumar, P.; Shorenstein, J.; Kazakov, S. A.; Johnston, B. H. Minimal-Length Short Hairpin RNAs: The Relationship of Structure and RNAi Activity. *RNA* **2010,** *16* (1), 106–117.
97. (a) Meade, B. R.; Gogoi, K.; Hamil, A. S.; Palm-Apergi, C.; Berg, A.v.d; Hagopian, J. C.; Springer, A. D.; Eguchi, A.; Kacsinta, A. D.; Dowdy, C. F.; Presente, A.; Lonn, P.; Kaulich, M.; Yoshioka, N.; Gros, E.; Cui, X.-S.; Dowdy, S. F. Efficient Delivery of RNAi Prodrugs Containing Reversible Charge-Neutralizing Phosphotriester Backbone Modifications. *Nat. Biotechnol.* **2014,** *32* (12), 1256–1261; (b) Hamil, A. S.; Dowdy, S. F. Synthesis and Conjugation of Small Interfering Ribonucleic Neutral SiRNNs. In *SiRNA Delivery Methods: Methods and Protocols;* Shum, K., Rossi, J., Eds.; Springer: New York, NY, 2016; pp 1–9.
98. (a) Lima, W. F.; Prakash, T. P.; Murray, H. M.; Kinberger, G. A.; Li, W.; Chappell, A. E.; Li, C. S.; Murray, S. F.; Gaus, H.; Seth, P. P.; Swayze, E. E.; Crooke, S. T. Single-Stranded siRNAs Activate RNAi in Animals. *Cell* **2012,** *150* (5), 883–894; (b) Davidson, B. L.; Monteys, A. M. Singles Engage the RNA Interference Pathway. *Cell* **2012,** *150* (5), 873–875.
99. Judge, A. D.; Bola, G.; Lee, A. C. H.; MacLachlan, I. Design of Noninflammatory Synthetic siRNA Mediating Potent Gene Silencing In Vivo. *Mol. Ther.* **2006,** *13* (3), 494–505.
100. Rose, S. D. Functional Polarity is Introduced by Dicer Processing of Short Substrate RNAs. *Nucleic Acids Res.* **2005,** *33* (13), 4140.
101. Snead, N. M.; Escamilla-Powers, J. R.; Rossi, J. J.; McCaffrey, A. P. 5′ Unlocked Nucleic Acid Modification Improves siRNA Targeting. *Mol. Ther.–Nucleic Acids* **2013,** *2*, e103.
102. Bramsen, J. B.; Laursen, M. B.; Damgaard, C. K.; Lena, S. W.; Ravindra Babu, B.; Wengel, J.; Kjems, J. Improved Silencing Properties Using Small Internally Segmented Interfering RNAs. *Nucleic Acids Res.* **2007,** *35* (17), 5886–5897.
103. Vester, B.; Wengel, J. LNA (Locked Nucleic Acid): High-Affinity Targeting of Complementary RNA and DNA. *Biochemistry* **2004,** *43* (42), 13233–13241.
104. Langkjær, N.; Pasternak, A.; Wengel, J. UNA (Unlocked Nucleic Acid): A Flexible RNA Mimic That Allows Engineering of Nucleic Acid Duplex Stability. *Bioorg. Med. Chem.* **2009,** *17* (15), 5420–5425.
105. Judge, A. D.; Sood, V.; Shaw, J. R.; Fang, D.; McClintock, K.; MacLachlan, I. Sequence-Dependent Stimulation of the Mammalian Innate Immune Response by Synthetic siRNA. *Nat. Biotechnol.* **2005,** *23* (4), 457–462.
106. (a) Jackson, A. L.; Linsley, P. S. Recognizing and Avoiding siRNA off-Target Effects for Target Identification and Therapeutic Application. *Nat. Rev. Drug Discov.* **2010,** *9* (1), 57–67; (b) Judge, A. D. Design of Noninflammatory Synthetic siRNA Mediating Potent Gene Silencing In Vivo. *Mol. Ther.* **2006,** *13* (3), 494.
107. Gish, R. G.; Yuen, M.-F.; Chan, H. L. Y; Given, B. D.; Lai, C.-L.; Locarnini, S. A.; Lau, J. Y. N; Wooddell, C. I.; Schluep, T.; Lewis, D. L. Synthetic RNAi Triggers and Their use in Chronic Hepatitis B Therapies With Curative Intent. *Antivir. Res.* **2015,** *121,* 97–108.
108. Levin, A. A. A Review of Issues in the Pharmacokinetics and Toxicology of Phosphorothioate Antisense Oligonucleotides. *Biochim. Biophys. Acta Gene Struct. Expr.* **1999,** *1489* (1), 69–84.
109. (a) Burel, S. A.; Hart, C. E.; Cauntay, P.; Hsiao, J.; Machemer, T.; Katz, M.; Watt, A.; Bui, H.-h.; Younis, H.; Sabripour, M.; Freier, S. M.; Hung, G.; Dan, A.; Prakash, T. P.; Seth, P. P.; Swayze, E. E.; Bennett, C. F.; Crooke, S. T.; Henry, S. P. Hepatotoxicity of High Affinity Gapmer Antisense Oligonucleotides is Mediated by RNase H1 Dependent Promiscuous Reduction of Very Long Pre-mRNA Transcripts. *Nucleic Acids Res.* **2016,** *44* (5), 2093–2109; (b) Kasuya, T.; Hori, S.-i.; Watanabe, A.; Nakajima, M.; Gahara, Y.; Rokushima, M.; Yanagimoto, T.; Kugimiya, A. Ribonuclease H1-Dependent Hepatotoxicity Caused by Locked Nucleic Acid-Modified Gapmer Antisense Oligonucleotides. *Sci. Rep.* **2016,** *6,* 30377.
110. Collingwood, M. A. Chemical Modification Patterns Compatible With High Potency Dicer-Substrate Small Interfering RNAs. *Oligonucleotides* **2008,** *18* (2), 187.
111. Schirle, N. T.; Kinberger, G. A.; Murray, H. F.; Lima, W. F.; Prakash, T. P.; MacRae, I. J. Structural Analysis of Human Argonaute-2 Bound to a Modified siRNA Guide. *J. Am. Chem. Soc.* **2016,** *138* (28), 8694–8697.
112. (a) Boudreau, R. L.; Spengler, R. M.; Davidson, B. L. Rational Design of Therapeutic siRNAs: Minimizing Off-Targeting Potential to Improve the Safety of RNAi Therapy for Huntington's Disease. *Mol. Ther.* **2011**; (b) Matveeva, O.; Nechipurenko, Y.; Rossi, L.; Moore, B.; Sætrom, P.; Ogurtsov, A. Y.; Atkins, J. F.; Shabalina, S. A. Comparison of Approaches for Rational siRNA Design Leading to a new Efficient and Transparent Method. *Nucleic Acids Res.* **2007,** *35* (8), e63; (c) Liu, Q.; Zhou, H.; Zhu, R.; Xu, Y.; Cao, Z. Reconsideration of in Silico siRNA Design From a Perspective of Heterogeneous Data Integration: Problems and Solutions. *Brief. Bioinform.* **2014,** *15* (2), 292–305.
113. Haussecker, D. Current Issues of RNAi Therapeutics Delivery and Development. *J. Control. Release* **2014,** *195,* 49–54.
114. Zuckerman, J. E.; Gritli, I.; Tolcher, A.; Heidel, J. D.; Lim, D.; Morgan, R.; Chmielowski, B.; Ribas, A.; Davis, M. E.; Yen, Y. Correlating Animal and Human Phase Ia/Ib Clinical Data With CALAA-01, a Targeted, Polymer-Based Nanoparticle Containing siRNA. *Proc. Natl. Acad. Sci.* **2014,** *111* (31), 11449–11454.
115. Jayaraman, M.; Ansell, S. M.; Mui, B. L.; Tam, Y. K.; Chen, J.; Du, X.; Butler, D.; Eltepu, L.; Matsuda, S.; Narayanannair, J. K.; Rajeev, K. G.; Hafez, I. M.; Akinc, A.; Maier, M. A.; Tracy, M. A.; Cullis, P. R.; Madden, T. D.; Manoharan, M.; Hope, M. J. Maximizing the Potency of siRNA Lipid Nanoparticles for Hepatic Gene Silencing In Vivo. *Angew. Chem. Int. Ed.* **2012,** *51* (34), 8529–8533.
116. Song, E.; Zhu, P.; Lee, S.-K.; Chowdhury, D.; Kussman, S.; Dykxhoorn, D. M.; Feng, Y.; Palliser, D.; Weiner, D. B.; Shankar, P.; Marasco, W. A.; Lieberman, J. Antibody Mediated In Vivo Delivery of Small Interfering RNAs via Cell-Surface Receptors. *Nat. Biotechnol.* **2005,** *23* (6), 709–717.
117. Zhou, J.; Neff, C. P.; Swiderski, P.; Li, H.; Smith, D. D.; Aboellail, T.; Remling-Mulder, L.; Akkina, R.; Rossi, J. J. Functional in vivo Delivery of Multiplexed Anti-HIV-1 siRNAs via a Chemically Synthesized Aptamer With a Sticky Bridge. *Mol. Ther.* **2013,** *21* (1), 192–200.
118. Rozema, D. B.; Lewis, D. L.; Wakefield, D. H.; Wong, S. C.; Klein, J. J.; Roesch, P. L.; Bertin, S. L.; Reppen, T. W.; Chu, Q.; Blokhin, A. V.; Hagstrom, J. E.; Wolff, J. A. Dynamic PolyConjugates for Targeted in vivo Delivery of siRNA to Hepatocytes. *Proc. Natl. Acad. Sci.* **2007,** *104* (32), 12982–12987.
119. Nair, J. K.; Willoughby, J. L. S.; Chan, A.; Charisse, K.; Alam, M. R.; Wang, Q.; Hoekstra, M.; Kandasamy, P.; Kel'in, A. V.; Milstein, S.; Taneja, N.; O'Shea, J.; Shaikh, S.; Zhang, L.; van der Sluis, R. J.; Jung, M. E.; Akinc, A.; Hutabarat, R.; Kuchimanchi, S.; Fitzgerald, K.; Zimmermann, T.; van Berkel, T. J. C.; Maier, M. A.; Rajeev, K. G.; Manoharan, M. Multivalent N-Acetylgalactosamine-Conjugated siRNA Localizes in Hepatocytes and Elicits Robust RNAi-Mediated Gene Silencing. *J. Am. Chem. Soc.* **2014,** *136* (49), 16958–16961.
120. Cutler, J. I.; Auyeung, E.; Mirkin, C. A. Spherical Nucleic Acids. *J. Am. Chem. Soc.* **2012,** *134* (3), 1376–1391.
121. (a) Guo, P. The Emerging Field of RNA Nanotechnology. *Nat. Nanotechnol.* **2010,** *5* (12), 833–842; (b) Chao, J.; Liu, H.; Su, S.; Wang, L.; Huang, W.; Fan, C. Structural DNA Nanotechnology for Intelligent Drug Delivery. *Small* **2014,** *10* (22), 4626–4635.
122. Castleberry, S. A.; Golberg, A.; Sharkh, M. A.; Khan, S.; Almquist, B. D.; Austen, W. G., Jr.; Yarmush, M. L.; Hammond, P. T. Nanolayered siRNA Delivery Platforms for Local Silencing of CTGF Reduce Cutaneous Scar Contraction in Third-Degree Burns. *Biomaterials* **2016,** *95,* 22–34.
123. Castleberry, S. A.; Almquist, B. D.; Li, W.; Reis, T.; Chow, J.; Mayner, S.; Hammond, P. T. Self-Assembled Wound Dressings Silence MMP-9 and Improve Diabetic Wound Healing In Vivo. *Adv. Mater.* **2016,** *28* (9), 1809–1817.
124. Zhou, J.; Swiderski, P.; Li, H.; Zhang, J.; Neff, C. P.; Akkina, R.; Rossi, J. J. Selection, Characterization and Application of New RNA HIV gp 120 Aptamers for Facile Delivery of Dicer Substrate siRNAs Into HIV Infected Cells. *Nucleic Acids Res.* **2009,** *37* (9), 3094–3109.

125. Neff, C. P.; Zhou, J.; Remling, L.; Kuruvilla, J.; Zhang, J.; Li, H.; Smith, D. D.; Swiderski, P.; Rossi, J. J.; Akkina, R. An Aptamer-siRNA Chimera Suppresses HIV-1 Viral Loads and Protects From Helper CD4+ T Cell Decline in Humanized Mice. *Sci. Transl. Med.* **2011,** *3* (66), 66ra6.
126. Zhou, J.; Neff, C. P.; Liu, X.; Zhang, J.; Li, H.; Smith, D. D.; Swiderski, P.; Aboellail, T.; Huang, Y.; Du, Q.; Liang, Z.; Peng, L.; Akkina, R.; Rossi, J. J. Systemic Administration of Combinatorial dsiRNAs via Nanoparticles Efficiently Suppresses HIV-1 Infection in Humanized Mice. *Mol. Ther.* **2011,** *19* (12), 2228–2238.
127. Coelho, T.; Adams, D.; Silva, A.; Lozeron, P.; Hawkins, P. N.; Mant, T.; Perez, J.; Chiesa, J.; Warrington, S.; Tranter, E.; Munisamy, M.; Falzone, R.; Harrop, J.; Cehelsky, J.; Bettencourt, B. R.; Geissler, M.; Butler, J. S.; Sehgal, A.; Meyers, R. E.; Chen, Q.; Borland, T.; Hutabarat, R. M.; Clausen, V. A.; Alvarez, R.; Fitzgerald, K.; Gamba-Vitalo, C.; Nochur, S. V.; Vaishnaw, A. K.; Sah, D. W. Y.; Gollob, J. A.; Suhr, O. B. Safety and Efficacy of RNAi Therapy for Transthyretin Amyloidosis. *N. Engl. J. Med.* **2013,** *369* (9), 819–829.
128. Adams, D.; Coelho, T.; Conceicao, I.; Waddington-Cruz, M.; Schmidt, H.; Buades, J.; Campistol, J.; Pouget, J.; Berk, J.; Falzone, R.; White, L.; Bettencourt, B.; Cehelsky, J.; Nochur, S.; Vaishnaw, A.; Gruis, K.; Gollob, J.; Suhr, O. Phase 2 Open-Label Extension Study (OLE) of Patisiran, an Investigational RNAi Therapeutic for Familial Amyloid Polyneuropathy (FAP) (S38.003). *Neurology* **2016,** *86* (16 Suppl.).
129. Donoghue, D. J.; Rothenberg, E.; Hopkins, N.; Baltimore, D.; Sharp, P. A. Heteroduplex Analysis of the Nonhomology Region Between Moloney MuLV and the Dual Host Range Derivative HIX Virus. *Cell* **1978,** *14* (4), 959–970.
130. (a) Butler, J. S.; Chan, A.; Costelha, S.; Fishman, S.; Willoughby, J. L. S.; Borland, T. D.; Milstein, S.; Foster, D. J.; Gonçalves, P.; Chen, Q.; Qin, J.; Bettencourt, B. R.; Sah, D. W.; Alvarez, R.; Rajeev, K. G.; Manoharan, M.; Fitzgerald, K.; Meyers, R. E.; Nochur, S. V.; Saraiva, M. J.; Zimmermann, T. S. Preclinical Evaluation of RNAi as a Treatment for Transthyretin-Mediated Amyloidosis. *Amyloid* **2016,** *23* (2), 109–118; (b) Gillmore, J. D.; Falk, R. H.; Maurer, M. S.; Hanna, M.; Karsten, V.; Vest, J.; Gollob, J.; Hawkins, P. N. Phase 2, Open-Label Extension (OLE) Study of Revusiran, an Investigational RNAi Therapeutic for the Treatment of Patients With Transthyretin Cardiac Amyloidosis. *Orphanet J. Rare Dis.* **2015,** *10* (1), 1–2.
131. Manoharan, M. *TIDES 2014: GalNAc-siRNA With Enhanced Stabilzation Chemistry: ESC-GalNAc-siRNA*. http://www.alnylam.com/web/assets/ALNY-ESC-GalNAc-siRNA-TIDES-May2014-Capella.pdf, 2014 (accessed 20.08.16).
132. Sehgal, A.; Barros, S.; Ivanciu, L.; Cooley, B.; Qin, J.; Racie, T.; Hettinger, J.; Carioto, M.; Jiang, Y.; Brodsky, J.; Prabhala, H.; Zhang, X.; Attarwala, H.; Hutabarat, R.; Foster, D.; Milstein, S.; Charisse, K.; Kuchimanchi, S.; Maier, M. A.; Nechev, L.; Kandasamy, P.; Kel'in, A. V.; Nair, J. K.; Rajeev, K. G.; Manoharan, M.; Meyers, R.; Sorensen, B.; Simon, A. R.; Dargaud, Y.; Negrier, C.; Camire, R. M.; Akinc, A. An RNAi Therapeutic Targeting Antithrombin to Rebalance the Coagulation System and Promote Hemostasis in Hemophilia. *Nat. Med.* **2015,** *21* (5), 492–497.
133. Alnylam Pharmaceuticals Discontinues Revusiran Development, Oct 5, 2016, http://investors.alnylam.com/releasedetail.cfm?ReleaseID=992320.
134. Davis, M. E. The First Targeted Delivery of siRNA in Humans via a Self-Assembling, Cyclodextrin Polymer-Based Nanoparticle: From Concept to Clinic. *Mol. Pharm.* **2009,** *6* (3), 659–668.
135. Iyer, A. K.; Khaled, G.; Fang, J.; Maeda, H. Exploiting the Enhanced Permeability and Retention Effect for Tumor Targeting. *Drug Discov. Today* **2006,** *11* (17–18), 812–818.
136. Davis, M. E.; Zuckerman, J. E.; Choi, C. H. J.; Seligson, D.; Tolcher, A.; Alabi, C. A.; Yen, Y.; Heidel, J. D.; Ribas, A. Evidence of RNAi in Humans From Systemically Administered siRNA via Targeted Nanoparticles. *Nature* **2010,** *464* (7291), 1067–1070.
137. Zuckerman, J. E.; Choi, C. H. J.; Han, H.; Davis, M. E. Polycation-siRNA Nanoparticles can Disassemble at the Kidney Glomerular Basement Membrane. *Proc. Natl. Acad. Sci.* **2012,** *109* (8), 3137–3142.
138. DCR-MYC and the MYC Oncogene. http://dicerna.com/pipeline/genetic-oncology/dcr-myc-and-the-myc-oncogene/ (accessed 21.08.16).
139. Dicerna Updates Progress on the Development of DCR-MYC for the Treatment of Solid Tumors. http://investors.dicerna.com/releasedetail.cfm?ReleaseID=947838 (accessed 21.08.16).
140. (a) Ulrich, H.; Magdesian, M. H.; Alves, M. J.; Colli, W. In Vitro Selection of RNA Aptamers That Bind to Cell Adhesion Receptors of Trypanosoma Cruzi and Inhibit Cell Invasion. *J. Biol. Chem.* **2002,** *277* (23), 20756–20762; (b) Wang, J.; Jiang, H.; Liu, F. In Vitro Selection of Novel RNA Ligands That Bind Human Cytomegalovirus and Block Viral Infection. *RNA* **2000,** *6* (4), 571–583; (c) Blank, M.; Weinschenk, T.; Priemer, M.; Schluesener, H. Systematic Evolution of a DNA Aptamer Binding to rat Brain Tumor Microvessels. Selective Targeting of Endothelial Regulatory Protein Pigpen. *J. Biol. Chem.* **2001,** *276* (19), 16464–16468; (d) Daniels, D. A.; Chen, H.; Hicke, B. J.; Swiderek, K. M.; Gold, L. A Tenascin-C Aptamer Identified by Tumor Cell SELEX: Systematic Evolution of Ligands by Exponential Enrichment. *Proc. Natl. Acad. Sci. U. S. A.* **2003,** *100* (26), 15416–15421; (e) Hicke, B. J.; Marion, C.; Chang, Y. F.; Gould, T.; Lynott, C. K.; Parma, D.; Schmidt, P. G.; Warren, S. Tenascin-C Aptamers are Generated Using Tumor Cells and Purified Protein. *J. Biol. Chem.* **2001,** *276* (52), 48644–48654; (f) Wilson, D. S.; Szostak, J. W. In Vitro Selection of Functional Nucleic Acids. *Annu. Rev. Biochem.* **1999,** *68,* 611–647.
141. Tuerk, C. Using the SELEX Combinatorial Chemistry Process to Find High Affinity Nucleic Acid Ligands to Target Molecules. *Methods Mol. Biol.* **1997,** *67,* 219–230.
142. Que-Gewirth, N. S.; Sullenger, B. A. Gene Therapy Progress and Prospects: RNA Aptamers. *Gene Ther.* **2007,** *14* (4), 283–291.
143. Lee, Y.; Urban, J. H.; Xu, L.; Sullenger, B. A.; Lee, J. 2′Fluoro Modification Differentially Modulates the Ability of RNAs to Activate Pattern Recognition Receptors. *Nucleic Acid Ther.* **2016,** *26* (3), 173–182.
144. Sullenger, B. A.; Gallardo, H. F.; Ungers, G. E.; Gilboa, E. Overexpression of TAR Sequences Renders Cells Resistant to Human Immunodeficiency Virus Replication. *Cell* **1990,** *63* (3), 601–608.
145. Prodeus, A.; Abdul-Wahid, A.; Fischer, N. W.; Huang, E. H.; Cydzik, M.; Gariepy, J. Targeting the PD-1/PD-L1 Immune Evasion Axis With DNA Aptamers as a Novel Therapeutic Strategy for the Treatment of Disseminated Cancers. *Mol. Ther.–Nucleic Acids* **2015,** *4,* e237.
146. Dassie, J. P.; Hernandez, L. I.; Thomas, G. S.; Long, M. E.; Rockey, W. M.; Howell, C. A.; Chen, Y.; Hernandez, F. J.; Liu, X. Y.; Wilson, M. E.; Allen, L. A.; Vaena, D. A.; Meyerholz, D. K.; Giangrande, P. H. Targeted Inhibition of Prostate Cancer Metastases With an RNA Aptamer to Prostate-Specific Membrane Antigen. *Mol. Ther.* **2014,** *22* (11), 1910–1922.
147. Kwon, H. M.; Lee, K. H.; Han, B. W.; Han, M. R.; Kim, D. H.; Kim, D. E. An RNA Aptamer That Specifically Binds to the Glycosylated Hemagglutinin of Avian Influenza Virus and Suppresses Viral Infection in Cells. *PLoS One* **2014,** *9* (5), e97574. in press.
148. Jin, L.; Nonaka, Y.; Miyakawa, S.; Fujiwara, M.; Nakamura, Y. Dual Therapeutic Action of a Neutralizing Anti-FGF2 Aptamer in Bone Disease and Bone Cancer Pain. *Mol. Ther.* **2016**.
149. Wallukat, G.; Muller, J.; Haberland, A.; Berg, S.; Schulz, A.; Freyse, E. J.; Vetter, R.; Salzsieder, E.; Kreutz, R.; Schimke, I. Aptamer BC007 for Neutralization of Pathogenic Autoantibodies Directed Against G-Protein Coupled Receptors: A Vision of Future Treatment of Patients With Cardiomyopathies and Positivity for Those Autoantibodies. *Atherosclerosis* **2016,** *244,* 44–47.
150. (a) Gilboa, E.; McNamara, J., 2nd; Pastor, F. Use of Oligonucleotide Aptamer Ligands to Modulate the Function of Immune Receptors. *Clin. Cancer Res.* **2013,** *19* (5), 1054–1062; (b) Pastor, F.; Soldevilla, M. M.; Villanueva, H.; Kolonias, D.; Inoges, S.; de Cerio, A. L.; Kandzia, R.; Klimyuk, V.; Gleba, Y.; Gilboa, E.; Bendandi, M. CD28 Aptamers as Powerful Immune Response Modulators. *Mol. Ther.–Nucleic Acids* **2013,** *2,* e98; (c) Soldevilla, M. M.; Villanueva, H.; Bendandi, M.; Inoges, S.; Lopez-Diaz de Cerio, A.; Pastor, F. 2-Fluoro-RNA Oligonucleotide CD40 Targeted Aptamers for the Control of B Lymphoma and Bone-Marrow Aplasia. *Biomaterials* **2015,** *67,* 274–285.
151. Huang, Y. Z.; Hernandez, F. J.; Gu, B.; Stockdale, K. R.; Nanapaneni, K.; Scheetz, T. E.; Behlke, M. A.; Peek, A. S.; Bair, T.; Giangrande, P. H.; McNamara, J. O., 2nd. RNA Aptamer-Based Functional Ligands of the Neurotrophin Receptor, TrkB. *Mol. Pharmacol.* **2012,** *82* (4), 623–635.
152. Yunn, N. O.; Koh, A.; Han, S.; Lim, J. H.; Park, S.; Lee, J.; Kim, E.; Jang, S. K.; Berggren, P. O.; Ryu, S. H. Agonistic Aptamer to the Insulin Receptor Leads to Biased Signaling and Functional Selectivity Through Allosteric Modulation. *Nucleic Acids Res.* **2015,** *43* (16), 7688–7701.
153. McNamara, J. O., 2nd; Andrechek, E. R.; Wang, Y.; Viles, K. D.; Rempel, R. E.; Gilboa, E.; Sullenger, B. A.; Giangrande, P. H. Cell Type-Specific Delivery of siRNAs With Aptamer-siRNA Chimeras. *Nat. Biotechnol.* **2006,** *24* (8), 1005–1015.

154. (a) Dassie, J. P.; Giangrande, P. H. Current Progress on Aptamer-Targeted Oligonucleotide Therapeutics. *Ther. Deliv.* **2013,** *4* (12), 1527--1546; (b) Zhou, J.; Satheesan, S.; Li, H.; Weinberg, M. S.; Morris, K. V.; Burnett, J. C.; Rossi, J. J. Cell-Specific RNA Aptamer Against Human CCR5 Specifically Targets HIV-1 Susceptible Cells and Inhibits HIV-1 Infectivity. *Chem. Biol.* **2015,** *22* (3), 379–390; (c) Yoon, S.; Huang, K. W.; Reebye, V.; Mintz, P.; Tien, Y. W.; Lai, H. S.; Saetrom, P.; Reccia, I.; Swiderski, P.; Armstrong, B.; Jozwiak, A.; Spalding, D.; Jiao, L.; Habib, N.; Rossi, J. J. Targeted Delivery of C/EBPalpha -saRNA by Pancreatic Ductal Adenocarcinoma (PDAC)-Specific RNA Aptamers Inhibits Tumor Growth In Vivo. *Mol. Ther.* **2016**; (d) Subramanian, N.; Kanwar, J. R.; Kanwar, R. K.; Sreemanthula, J.; Biswas, J.; Khetan, V.; Krishnakumar, S. EpCAM Aptamer-siRNA Chimera Targets and Regress Epithelial Cancer. *PLoS One* **2015,** *10* (7), e0132407; (e) Gilboa-Geffen, A.; Hamar, P.; Le, M. T.; Wheeler, L. A.; Trifonova, R.; Petrocca, F.; Wittrup, A.; Lieberman, J. Gene Knockdown by EpCAM Aptamer-siRNA Chimeras Suppresses Epithelial Breast Cancers and Their Tumor-Initiating Cells. *Mol. Cancer Ther.* **2015,** *14* (10), 2279–2291.
155. Zhou, J.; Tiemann, K.; Chomchan, P.; Alluin, J.; Swiderski, P.; Burnett, J.; Zhang, X.; Forman, S.; Chen, R.; Rossi, J. Dual Functional BAFF Receptor Aptamers Inhibit Ligand-Induced Proliferation and Deliver siRNAs to NHL Cells. *Nucleic Acids Res.* **2013,** *41* (7), 4266–4283.
156. Yazdian-Robati, R.; Ramezani, M.; Jalalian, S. H.; Abnous, K.; Taghdisi, S. M. Targeted Delivery of Epirubicin to Cancer Cells by Polyvalent Aptamer System In Vitro and In Vivo. *Pharm. Res.* **2016,** *33* (9), 2289–2297.
157. Chen, Y.; Wang, J.; Wang, J.; Wang, L.; Tan, X.; Tu, K.; Tong, X.; Qi, L. Aptamer Functionalized Cisplatin-Albumin Nanoparticles for Targeted Delivery to Epidermal Growth Factor Receptor Positive Cervical Cancer. *J. Biomed. Nanotechnol.* **2016,** *12* (4), 656–666.
158. Alibolandi, M.; Ramezani, M.; Abnous, K.; Hadizadeh, F. AS1411 Aptamer-Decorated Biodegradable Polyethylene Glycol-Poly(lactic-co-glycolic acid) Nanopolymersomes for the Targeted Delivery of Gemcitabine to Non-Small Cell Lung Cancer In Vitro. *J. Pharm. Sci.* **2016,** *105* (5), 1741–1750.
159. Park, J. Y.; Lee, T. S.; Song, I. H.; Cho, Y. L.; Chae, J. R.; Yun, M.; Kang, H.; Lee, J. H.; Lim, J. H.; Cho, W. G.; Kang, W. J. Hybridization-Based Aptamer Labeling Using Complementary Oligonucleotide Platform for PET and Optical Imaging. *Biomaterials* **2016,** *100,* 143–151.
160. Kryza, D.; Debordeaux, F.; Azema, L.; Hassan, A.; Paurelle, O.; Schulz, J.; Savona-Baron, C.; Charignon, E.; Bonazza, P.; Taleb, J.; Fernandez, P.; Janier, M.; Toulme, J. J. Ex Vivo and In Vivo Imaging and Biodistribution of Aptamers Targeting the Human Matrix MetalloProtease-9 in Melanomas. *PLoS One* **2016,** *11* (2), e0149387.
161. Jacobson, O.; Weiss, I. D.; Wang, L.; Wang, Z.; Yang, X.; Dewhurst, A.; Ma, Y.; Zhu, G.; Niu, G.; Kiesewetter, D. O.; Vasdev, N.; Liang, S. H.; Chen, X. 18F-Labeled Single-Stranded DNA Aptamer for PET Imaging of Protein Tyrosine Kinase-7 Expression. *J. Nucl. Med.* **2015,** *56* (11), 1780–1785.
162. Ganson, N. J.; Povsic, T. J.; Sullenger, B. A.; Alexander, J. H.; Zelenkofske, S. L.; Sailstad, J. M.; Rusconi, C. P.; Hershfield, M. S. Pre-existing Anti-polyethylene Glycol Antibody Linked to First-Exposure Allergic Reactions to Pegnivacogin, a PEGylated RNA Aptamer. *J. Allergy Clin. Immunol.* **2016,** *137* (5), 1610–1613. e7.
163. Chen, C.; Constantinou, A.; Deonarain, M. Modulating Antibody Pharmacokinetics Using Hydrophilic Polymers. *Expert Opin. Drug Deliv.* **2011,** *8* (9), 1221–1236.
164. Garay, R. P.; El-Gewely, R.; Armstrong, J. K.; Garratty, G.; Richette, P. Antibodies Against Polyethylene Glycol in Healthy Subjects and in Patients Treated With PEG-Conjugated Agents. *Expert Opin. Drug Deliv.* **2012,** *9* (11), 1319–1323.
165. Deeks, S. G.; Lewin, S. R.; Ross, A. L.; Ananworanich, J.; Benkirane, M.; Cannon, P.; Chomont, N.; Douek, D.; Lifson, J. D.; Lo, Y. R.; Kuritzkes, D.; Margolis, D.; Mellors, J.; Persaud, D.; Tucker, J. D.; Barre-Sinoussi, F.; ; International A.I.D.S. Society Towards a. Cure Working Group.; Alter, G.; Auerbach, J.; Autran, B.; Barouch, D. H.; Behrens, G.; Cavazzana, M.; Chen, Z.; Cohen, E. A.; Corbelli, G. M.; Eholie, S.; Eyal, N.; Fidler, S.; Garcia, L.; Grossman, C.; Henderson, G.; Henrich, T. J.; Jefferys, R.; Kiem, H. P.; McCune, J.; Moodley, K.; Newman, P. A.; Nijhuis, M.; Nsubuga, M. S.; Ott, M.; Palmer, S.; Richman, D.; Saez-Cirion, A.; Sharp, M.; Siliciano, J.; Silvestri, G.; Singh, J.; Spire, B.; Taylor, J.; Tolstrup, M.; Valente, S.; van Lunzen, J.; Walensky, R.; Wilson, I.; Zack, J. International AIDS Society Global Scientific Strategy: Towards an HIV Cure 2016. *Nat. Med.* **2016,** *22* (8), 839–850.
166. (a) Churchill, M. J.; Deeks, S. G.; Margolis, D. M.; Siliciano, R. F.; Swanstrom, R. HIV Reservoirs: What, Where and How to Target Them. *Nat. Rev. Microbiol.* **2016,** *14* (1), 55–60; (b) Margolis, D. M.; Garcia, J. V.; Hazuda, D. J.; Haynes, B. F. Latency Reversal and Viral Clearance to Cure HIV-1. *Science* **2016,** *353* (6297).
167. (a) Bobbin, M. L.; Burnett, J. C.; Rossi, J. J. RNA Interference Approaches for Treatment of HIV-1 Infection. *Genome Med.* **2015,** *7* (1), 50; (b) Burnett, J. C.; Zaia, J. A.; Rossi, J. J. Creating Genetic Resistance to HIV. *Curr. Opin. Immunol.* **2012,** *24* (5), 625–632; (c) DiGiusto, D. L. Stem Cell Gene Therapy for HIV: Strategies to Inhibit Viral Entry and Replication. *Curr. HIV/AIDS Rep.* **2015,** *12* (1), 79–87.
168. Blazquez, L.; Fortes, P. U1 Interference (U1i) for Antiviral Approaches. *Adv. Exp. Med. Biol.* **2015,** *848,* 51–69.
169. (a) Scarborough, R. J.; Gatignol, A. HIV and Ribozymes. *Adv. Exp. Med. Biol.* **2015,** *848,* 97–116; (b) Yang, Z.; Reeves, M.; Ye, J.; Trang, P.; Zhu, L.; Sheng, J.; Wang, Y.; Zen, K.; Wu, J.; Liu, F. RNase P Ribozymes Inhibit the Replication of Human Cytomegalovirus by Targeting Essential Viral Capsid Proteins. *Viruses* **2015,** *7* (7), 3345–3360; (c) Zhai, H.; Chen, Q. J.; Gao, X. M.; Ma, Y. T.; Chen, B. D.; Yu, Z. X.; Li, X. M.; Liu, F.; Xiang, Y.; Xie, J.; Yang, Y. N. Inhibition of the NF-kappaB Pathway by R65 Ribozyme Gene via Adeno-Associated Virus Serotype 9 Ameliorated Oxidized LDL Induced Human Umbilical Vein Endothelial Cell Injury. *Int. J. Clin. Exp. Pathol.* **2015,** *8* (9), 9912–9921.
170. (a) Sioud, M. RNA Interference: Mechanisms, Technical Challenges, and Therapeutic Opportunities. *Methods Mol. Biol.* **2015,** *1218,* 1–15; (b) Bofill-De Ros, X.; Gu, S. Guidelines for the Optimal Design of miRNA-Based shRNAs. *Methods* **2016,** *103,* 157–166.
171. (a) Lagos-Quintana, M.; Rauhut, R.; Lendeckel, W.; Tuschl, T. Identification of Novel Genes Coding for Small Expressed RNAs. *Science* **2001,** *294* (5543), 853–858; (b) Lau, N. C.; Lim, L. P.; Weinstein, E. G.; Bartel, D. P. An Abundant Class of Tiny RNAs With Probable Regulatory Roles in *Caenorhabditis elegans*. *Science* **2001,** *294* (5543), 858–862; (c) Lee, R. C.; Ambros, V. An Extensive Class of Small RNAs in *Caenorhabditis elegans*. *Science* **2001,** *294* (5543), 862–864.
172. Zeng, Y.; Wagner, E. J.; Cullen, B. R. Both Natural and Designed Micro RNAs can Inhibit the Expression of Cognate mRNAs When Expressed in Human Cells. *Mol. Cell* **2002,** *9* (6), 1327–1333.
173. van den Berg, F. T.; Rossi, J. J.; Arbuthnot, P.; Weinberg, M. S. Design of Effective Primary MicroRNA Mimics With Different Basal Stem Conformations. *Mol. Ther.–Nucleic Acids* **2016,** *5*, e278.
174. Zeng, Y.; Yi, R.; Cullen, B. R. Recognition and Cleavage of Primary microRNA Precursors by the Nuclear Processing Enzyme Drosha. *EMBO J.* **2005,** *24* (1), 138–148.
175. Lee, Y.; Ahn, C.; Han, J.; Choi, H.; Kim, J.; Yim, J.; Lee, J.; Provost, P.; Radmark, O.; Kim, S.; Kim, V. N. The Nuclear RNase III Drosha Initiates microRNA Processing. *Nature* **2003,** *425* (6956), 415–419.
176. (a) Zeng, Y.; Cullen, B. R. Efficient Processing of Primary microRNA Hairpins by Drosha Requires Flanking Nonstructured RNA Sequences. *J. Biol. Chem.* **2005,** *280* (30), 27595–27603; (b) Han, J.; Lee, Y.; Yeom, K. H.; Nam, J. W.; Heo, I.; Rhee, J. K.; Sohn, S. Y.; Cho, Y.; Zhang, B. T.; Kim, V. N. Molecular Basis for the Recognition of Primary microRNAs by the Drosha-DGCR8 Complex. *Cell* **2006,** *125* (5), 887–901.
177. Fellmann, C.; Hoffmann, T.; Sridhar, V.; Hopfgartner, B.; Muhar, M.; Roth, M.; Lai, D. Y.; Barbosa, I. A.; Kwon, J. S.; Guan, Y.; Sinha, N.; Zuber, J. An Optimized microRNA Backbone for Effective Single-Copy RNAi. *Cell Rep.* **2013,** *5* (6), 1704–1713.
178. (a) Frank, F.; Fabian, M. R.; Stepinski, J.; Jemielity, J.; Darzynkiewicz, E.; Sonenberg, N.; Nagar, B. Structural Analysis of 5′-mRNA-cap Interactions With the Human AGO2 MID Domain. *EMBO Rep.* **2011,** *12* (5), 415–420; (b) Seitz, H.; Tushir, J. S.; Zamore, P. D. A 5′-Uridine Amplifies miRNA/miRNA* Asymmetry in Drosophila by Promoting RNA-Induced Silencing Complex Formation. *Silence* **2011,** *2,* 4; (c) Humphreys, D. T.; Hynes, C. J.; Patel, H. R.; Wei, G. H.; Cannon, L.; Fatkin, D.; Suter, C. M.; Clancy, J. L.; Preiss, T. Complexity of Murine Cardiomyocyte miRNA Biogenesis, Sequence Variant Expression and Function. *PLoS One* **2012,** *7* (2), e30933.
179. Winter, J.; Diederichs, S. Argonaute Proteins Regulate microRNA Stability: Increased microRNA Abundance by Argonaute Proteins is due to microRNA Stabilization. *RNA Biol.* **2011,** *8* (6), 1149–1157.
180. (a) Warf, M. B.; Johnson, W. E.; Bass, B. L. Improved Annotation of *C. elegans* microRNAs by Deep Sequencing Reveals Structures Associated With Processing by Drosha and Dicer. *RNA* **2011,** *17* (4), 563–577; (b) Galka-Marciniak, P.; Olejniczak, M.; Starega-Roslan, J.; Szczesniak, M. W.; Makalowska, I.; Krzyzosiak, W. J. siRNA Release from Pri-miRNA Scaffolds is Controlled by the Sequence and Structure of RNA. *Biochim. Biophys. Acta* **2016,** *1859* (4), 639–649; (c) Starega-Roslan, J.; Koscianska, E.; Kozlowski, P.; Krzyzosiak, W. J. The Role of the Precursor Structure in the Biogenesis of microRNA. *Cell. Mol. Life Sci.* **2011,** *68* (17), 2859–2871.
181. Auyeung, V. C.; Ulitsky, I.; McGeary, S. E.; Bartel, D. P. Beyond Secondary Structure: Primary-Sequence Determinants License Pri-miRNA Hairpins for Processing. *Cell* **2013,** *152* (4), 844–858.
182. Fang, W.; Bartel, D. P. The Menu of Features that Define Primary MicroRNAs and Enable De Novo Design of MicroRNA Genes. *Mol. Cell* **2015,** *60* (1), 131–145.

183. (a) Macrae, I. J.; Zhou, K.; Li, F.; Repic, A.; Brooks, A. N.; Cande, W. Z.; Adams, P. D.; Doudna, J. A. Structural Basis for Double-Stranded RNA Processing by Dicer. *Science* **2006,** *311* (5758), 195–198; (b) Gu, S.; Jin, L.; Zhang, Y.; Huang, Y.; Zhang, F.; Valdmanis, P. N.; Kay, M. A. The Loop Position of shRNAs and Pre-miRNAs is Critical for the Accuracy of Dicer Processing In Vivo. *Cell* **2012,** *151* (4), 900–911.
184. Watanabe, C.; Cuellar, T. L.; Haley, B. Quantitative Evaluation of First, Second, and Third Generation Hairpin Systems Reveals the Limit of Mammalian Vector-Based RNAi. *RNA Biol.* **2016,** *13* (1), 25–33.
185. Alarcon, C. R.; Lee, H.; Goodarzi, H.; Halberg, N.; Tavazoie, S. F. N6-Methyladenosine Marks Primary microRNAs for Processing. *Nature* **2015,** *519* (7544), 482–485.
186. (a) Tan, G. C.; Chan, E.; Molnar, A.; Sarkar, R.; Alexieva, D.; Isa, I. M.; Robinson, S.; Zhang, S.; Ellis, P.; Langford, C. F.; Guillot, P. V.; Chandrashekran, A.; Fisk, N. M.; Castellano, L.; Meister, G.; Winston, R. M.; Cui, W.; Baulcombe, D.; Dibb, N. J. 5′ isomiR Variation is of Functional and Evolutionary Importance. *Nucleic Acids Res.* **2014,** *42* (14), 9424–9435; (b) Vickers, K. C.; Sethupathy, P.; Baran-Gale, J.; Remaley, A. T. Complexity of microRNA Function and the Role of isomiRs in Lipid Homeostasis. *J. Lipid Res.* **2013,** *54* (5), 1182–1191.
187. Ma, H.; Wu, Y.; Choi, J. G.; Wu, H. Lower and Upper Stem-Single-Stranded RNA Junctions Together Determine the Drosha Cleavage Site. *Proc. Natl. Acad. Sci. U. S. A.* **2013,** *110* (51), 20687–20692.
188. (a) Starega-Roslan, J.; Witkos, T. M.; Galka-Marciniak, P.; Krzyzosiak, W. J. Sequence Features of Drosha and Dicer Cleavage Sites Affect the Complexity of isomiRs. *Int. J. Mol. Sci.* **2015,** *16* (4), 8110–8127; (b) Starega-Roslan, J.; Krol, J.; Koscianska, E.; Kozlowski, P.; Szlachcic, W. J.; Sobczak, K.; Krzyzosiak, W. J. Structural Basis of microRNA Length Variety. *Nucleic Acids Res.* **2011,** *39* (1), 257–268.
189. Frank, F.; Sonenberg, N.; Nagar, B. Structural Basis for 5′-Nucleotide Base-Specific Recognition of Guide RNA by Human AGO2. *Nature* **2010,** *465* (7299), 818–822.
190. Liu, B.; Childs-Disney, J. L.; Znosko, B. M.; Wang, D.; Fallahi, M.; Gallo, S. M.; Disney, M. D. Analysis of Secondary Structural Elements in Human microRNA Hairpin Precursors. *BMC Bioinf.* **2016,** *17,* 112.
191. Moore, C. B.; Guthrie, E. H.; Huang, M. T.; Taxman, D. J. Short Hairpin RNA (shRNA): Design, Delivery, and Assessment of Gene Knockdown. *Methods Mol. Biol.* **2010,** *629,* 141–158.
192. (a) Yang, J. S.; Maurin, T.; Robine, N.; Rasmussen, K. D.; Jeffrey, K. L.; Chandwani, R.; Papapetrou, E. P.; Sadelain, M.; O'Carroll, D.; Lai, E. C. Conserved Vertebrate mir-451 Provides a Platform for Dicer-Independent, Ago2-Mediated microRNA Biogenesis. *Proc. Natl. Acad. Sci. U. S. A.* **2010,** *107* (34), 15163–15168; (b) Cheloufi, S.; Dos Santos, C. O.; Chong, M. M.; Hannon, G. J. A Dicer-Independent miRNA Biogenesis Pathway That Requires Ago Catalysis. *Nature* **2010,** *465* (7298), 584–589; (c) Cifuentes, D.; Xue, H.; Taylor, D. W.; Patnode, H.; Mishima, Y.; Cheloufi, S.; Ma, E.; Mane, S.; Hannon, G. J.; Lawson, N. D.; Wolfe, S. A.; Giraldez, A. J. A Novel miRNA Processing Pathway Independent of Dicer Requires Argonaute2 Catalytic Activity. *Science* **2010,** *328* (5986), 1694–1698.
193. Liu, Y. P.; Karg, M.; Harwig, A.; Herrera-Carrillo, E.; Jongejan, A.; van Kampen, A.; Berkhout, B. Mechanistic Insights on the Dicer-Independent AGO2-Mediated Processing of AgoshRNAs. *RNA Biol.* **2015,** *12* (1), 92–100.
194. Miyoshi, K.; Miyoshi, T.; Siomi, H. Many Ways to Generate microRNA-Like Small RNAs: Non-Canonical Pathways for microRNA Production. *Mol. Genet. Genomics* **2010,** *284* (2), 95–103.
195. (a) Liu, Y. P.; Schopman, N. C.; Berkhout, B. Dicer-Independent Processing of Short Hairpin RNAs. *Nucleic Acids Res.* **2013,** *41* (6), 3723–3733; (b) Liu, Y. P.; Karg, M.; Herrera-Carrillo, E.; Berkhout, B. Towards Antiviral shRNAs Based on the AgoshRNA Design. *PLoS One* **2015,** *10* (6), e0128618.
196. Herrera-Carrillo, E.; Berkhout, B. Bone Marrow Gene Therapy for HIV/AIDS. *Viruses* **2015,** *7* (7), 3910–3936.
197. Scherer, L. J.; Rossi, J. J. Ex Vivo Gene Therapy for HIV-1 Treatment. *Hum. Mol. Genet.* **2011,** *20* (R1), R100–R107.
198. DiGiusto, D. L.; Krishnan, A.; Li, L.; Li, H.; Li, S.; Rao, A.; Mi, S.; Yam, P.; Stinson, S.; Kalos, M.; Alvarnas, J.; Lacey, S. F.; Yee, J. K.; Li, M.; Couture, L.; Hsu, D.; Forman, S. J.; Rossi, J. J.; Zaia, J. A. RNA-Based Gene Therapy for HIV With Lentiviral Vector-Modified CD34(+) Cells in Patients Undergoing Transplantation for AIDS-Related Lymphoma. *Sci. Transl. Med.* **2010,** *2* (36), 36ra43.
199. Aagaard, L. A.; Zhang, J.; von Eije, K. J.; Li, H.; Saetrom, P.; Amarzguioui, M.; Rossi, J. J. Engineering and Optimization of the miR-106b Cluster for Ectopic Expression of Multiplexed Anti-HIV RNAs. *Gene Ther.* **2008,** *15* (23), 1536–1549.
200. (a) Chung, J.; Scherer, L.; Gu, A.; Gardner, A.; Torres-Coronado, M.; Epps, E.; Digiusto, D. L.; Rossi, J. J. Optimized Lentiviral Vectors for HIV Gene Therapy: Multiplexed Expression of Small RNAs and Inclusion of MGMT Drug Resistance Gene. *Mol. Ther.* **2014**; (b) Chung, J.; Zhang, J.; Li, H.; Ouellet, D. L.; DiGiusto, D. L.; Rossi, J. J. Endogenous MCM7 microRNA Cluster as a Novel Platform to Multiplex Small Interfering and Nucleolar RNAs for Combinational HIV-1 Gene Therapy. *Hum. Gene Ther.* **2012,** *23* (11), 1200–1208.
201. (a) Barclay, S. L.; Yang, Y.; Zhang, S.; Fong, R.; Barraza, A.; Nolta, J. A.; Torbett, B. E.; Abedi, M.; Bauer, G.; Anderson, J. S. Safety and Efficacy of a tCD25 Preselective Combination Anti-HIV Lentiviral Vector in Human Hematopoietic Stem and Progenitor Cells. *Stem Cells* **2015,** *33* (3), 870–879; (b) Burke, B. P.; Levin, B. R.; Zhang, J.; Sahakyan, A.; Boyer, J.; Carroll, M. V.; Colon, J. C.; Keech, N.; Rezek, V.; Bristol, G.; Eggers, E.; Cortado, R.; Boyd, M. P.; Impey, H.; Shimizu, S.; Lowe, E. L.; Ringpis, G. E.; Kim, S. G.; Vatakis, D. N.; Breton, L. R.; Bartlett, J. S.; Chen, I. S.; Kitchen, S. G.; An, D. S.; Symonds, G. P. Engineering Cellular Resistance to HIV-1 Infection In Vivo Using a Dual Therapeutic Lentiviral Vector. *Mol. Ther.–Nucleic Acids* **2015,** *4*, e236; (c) Jung, U.; Urak, K.; Veillette, M.; Nepveu-Traversy, M. E.; Pham, Q. T.; Hamel, S.; Rossi, J. J.; Berthoux, L. Preclinical Assessment of Mutant Human TRIM5alpha as an Anti-HIV-1 Transgene. *Hum. Gene Ther.* **2015,** *26* (10), 664–679; (d) Pernet, O.; Yadav, S. S.; An, D. S. Stem Cell-Based Therapies for HIV/AIDS. *Adv. Drug Deliv. Rev.* **2016,** *103,* 187–201.
202. Boudreau, R. L.; Martins, I.; Davidson, B. L. Artificial microRNAs as siRNA Shuttles: Improved Safety as Compared to shRNAs In Vitro and In Vivo. *Mol. Ther.* **2009,** *17* (1), 169–175.
203. Grimm, D.; Streetz, K. L.; Jopling, C. L.; Storm, T. A.; Pandey, K.; Davis, C. R.; Marion, P.; Salazar, F.; Kay, M. A. Fatality in Mice due to Oversaturation of Cellular microRNA/Short Hairpin RNA Pathways. *Nature* **2006,** *441* (7092), 537–541.
204. Valdmanis, P. N.; Gu, S.; Chu, K.; Jin, L.; Zhang, F.; Munding, E. M.; Zhang, Y.; Huang, Y.; Kutay, H.; Ghoshal, K.; Lisowski, L.; Kay, M. A. RNA Interference-Induced Hepatotoxicity Results From Loss of the First Synthesized Isoform of microRNA-122 in Mice. *Nat. Med.* **2016,** *22* (5), 557–562.
205. Orioli, A.; Pascali, C.; Pagano, A.; Teichmann, M.; Dieci, G. RNA Polymerase III Transcription Control Elements: Themes and Variations. *Gene* **2012,** *493* (2), 185–194.
206. Scherer, L. J.; Frank, R.; Rossi, J. J. Optimization and Characterization of tRNA-shRNA Expression Constructs. *Nucleic Acids Res.* **2007,** *35* (8), 2620–2628.
207. (a) Aagaard, L.; Amarzguioui, M.; Sun, G.; Santos, L. C.; Ehsani, A.; Prydz, H.; Rossi, J. J. A Facile Lentiviral Vector System for Expression of Doxycycline-Inducible shRNAs: Knockdown of the Pre-miRNA Processing Enzyme Drosha. *Mol. Ther.* **2007,** *15* (5), 938–945; (b) Sigl, R.; Ploner, C.; Shivalingaiah, G.; Kofler, R.; Geley, S. Development of a Multipurpose GATEWAY-Based Lentiviral Tetracycline-Regulated Conditional RNAi System (GLTR). *PLoS One* **2014,** *9* (5), e97764.
208. Ishino, Y.; Shinagawa, H.; Makino, K.; Amemura, M.; Nakata, A. Nucleotide Sequence of the iap Gene, Responsible for Alkaline Phosphatase Isozyme Conversion in *Escherichia coli*, and Identification of the Gene Product. *J. Bacteriol.* **1987,** *169* (12), 5429–5433.
209. Jinek, M.; Chylinski, K.; Fonfara, I.; Hauer, M.; Doudna, J. A.; Charpentier, E. A Programmable Dual-RNA-Guided DNA Endonuclease in Adaptive Bacterial Immunity. *Science* **2012,** *337* (6096), 816–821.
210. Makarova, K. S.; Haft, D. H.; Barrangou, R.; Brouns, S. J.; Charpentier, E.; Horvath, P.; Moineau, S.; Mojica, F. J.; Wolf, Y. I.; Yakunin, A. F.; van der Oost, J.; Koonin, E. V. Evolution and Classification of the CRISPR-Cas Systems. *Nat. Rev. Microbiol.* **2011,** *9* (6), 467–477.
211. Gasiunas, G.; Barrangou, R.; Horvath, P.; Siksnys, V. Cas9-crRNA Ribonucleoprotein Complex Mediates Specific DNA Cleavage for Adaptive Immunity in Bacteria. *Proc. Natl. Acad. Sci. U. S. A.* **2012,** *109* (39), E2579–E2586.
212. Sander, J. D.; Joung, J. K. CRISPR-Cas Systems for Editing, Regulating and Targeting Genomes. *Nat. Biotechnol.* **2014,** *32* (4), 347–355.
213. Xiong, X.; Chen, M.; Lim, W. A.; Zhao, D.; Qi, L. S. CRISPR/Cas9 for Human Genome Engineering and Disease Research. *Annu. Rev. Genomics Hum. Genet.* **2016,** *17,* 131–154.
214. Long, C.; McAnally, J. R.; Shelton, J. M.; Mireault, A. A.; Bassel-Duby, R.; Olson, E. N. Prevention of Muscular Dystrophy in Mice by CRISPR/Cas9-Mediated Editing of Germline DNA. *Science* **2014,** *345* (6201), 1184–1188.

215. (a) Long, C.; Amoasii, L.; Mireault, A. A.; McAnally, J. R.; Li, H.; Sanchez-Ortiz, E.; Bhattacharyya, S.; Shelton, J. M.; Bassel-Duby, R.; Olson, E. N. Postnatal Genome Editing Partially Restores Dystrophin Expression in a Mouse Model of Muscular Dystrophy. *Science* **2016,** *351* (6271), 400–403; (b) Nelson, C. E.; Hakim, C. H.; Ousterout, D. G.; Thakore, P. I.; Moreb, E. A.; Castellanos Rivera, R. M.; Madhavan, S.; Pan, X.; Ran, F. A.; Yan, W. X.; Asokan, A.; Zhang, F.; Duan, D.; Gersbach, C. A. In Vivo Genome Editing Improves Muscle Function in a Mouse Model of Duchenne Muscular Dystrophy. *Science* **2016,** *351* (6271), 403–407; (c) Tabebordbar, M.; Zhu, K.; Cheng, J. K.; Chew, W. L.; Widrick, J. J.; Yan, W. X.; Maesner, C.; Wu, E. Y.; Xiao, R.; Ran, F. A.; Cong, L.; Zhang, F.; Vandenberghe, L. H.; Church, G. M.; Wagers, A. J. In Vivo Gene Editing in Dystrophic Mouse Muscle and Muscle Stem Cells. *Science* **2016,** *351* (6271), 407–411.
216. (a) Wang, W.; Ye, C.; Liu, J.; Zhang, D.; Kimata, J. T.; Zhou, P. CCR5 Gene Disruption via Lentiviral Vectors Expressing Cas9 and Single Guided RNA Renders Cells Resistant to HIV-1 Infection. *PLoS One* **2014,** *9* (12), e115987; (b) Ye, L.; Wang, J.; Beyer, A. I.; Teque, F.; Cradick, T. J.; Qi, Z.; Chang, J. C.; Bao, G.; Muench, M. O.; Yu, J.; Levy, J. A.; Kan, Y. W. Seamless Modification of Wild-Type Induced Pluripotent Stem Cells to the Natural CCR5Delta32 Mutation Confers Resistance to HIV Infection. *Proc. Natl. Acad. Sci. U. S. A.* **2014,** *111* (26), 9591–9596; (c) Mandal, P. K.; Ferreira, L. M.; Collins, R.; Meissner, T. B.; Boutwell, C. L.; Friesen, M.; Vrbanac, V.; Garrison, B. S.; Stortchevoi, A.; Bryder, D.; Musunuru, K.; Brand, H.; Tager, A. M.; Allen, T. M.; Talkowski, M. E.; Rossi, D. J.; Cowan, C. A. Efficient Ablation of Genes in Human Hematopoietic Stem and Effector Cells Using CRISPR/Cas9. *Cell Stem Cell* **2014,** *15* (5), 643–652; (d) Li, C.; Guan, X.; Du, T.; Jin, W.; Wu, B.; Liu, Y.; Wang, P.; Hu, B.; Griffin, G. E.; Shattock, R. J.; Hu, Q. Inhibition of HIV-1 Infection of Primary CD4 + T-Cells by Gene Editing of CCR5 Using Adenovirus-Delivered CRISPR/Cas9. *J. Gen. Virol.* **2015,** *96* (8), 2381–2393; (e) Ebina, H.; Misawa, N.; Kanemura, Y.; Koyanagi, Y. Harnessing the CRISPR/Cas9 System to Disrupt Latent HIV-1 Provirus. *Sci. Rep.* **2013,** *3,* 2510; (f) Hu, W.; Kaminski, R.; Yang, F.; Zhang, Y.; Cosentino, L.; Li, F.; Luo, B.; Alvarez-Carbonell, D.; Garcia-Mesa, Y.; Karn, J.; Mo, X.; Khalili, K. RNA-Directed Gene Editing Specifically Eradicates Latent and Prevents new HIV-1 Infection. *Proc. Natl. Acad. Sci. U. S. A.* **2014,** *111* (31), 11461–11466.
217. (a) Kennedy, E. M.; Bassit, L. C.; Mueller, H.; Kornepati, A. V.; Bogerd, H. P.; Nie, T.; Chatterjee, P.; Javanbakht, H.; Schinazi, R. F.; Cullen, B. R. Suppression of Hepatitis B Virus DNA Accumulation in Chronically Infected Cells Using a Bacterial CRISPR/Cas RNA-Guided DNA Endonuclease. *Virology* **2015,** *476,* 196–205; (b) Lin, S. R.; Yang, H. C.; Kuo, Y. T.; Liu, C. J.; Yang, T. Y.; Sung, K. C.; Lin, Y. Y.; Wang, H. Y.; Wang, C. C.; Shen, Y. C.; Wu, F. Y.; Kao, J. H.; Chen, D. S.; Chen, P. J. The CRISPR/Cas9 System Facilitates Clearance of the Intrahepatic HBV Templates In Vivo. *Mol. Ther.–Nucleic Acids* **2014,** *3*, e186.
218. Wang, J.; Quake, S. R. RNA-Guided Endonuclease Provides a Therapeutic Strategy to Cure Latent Herpesviridae Infection. *Proc. Natl. Acad. Sci. U. S. A.* **2014,** *111* (36), 13157–13162.
219. (a) Kennedy, E. M.; Kornepati, A. V.; Goldstein, M.; Bogerd, H. P.; Poling, B. C.; Whisnant, A. W.; Kastan, M. B.; Cullen, B. R. Inactivation of the Human Papillomavirus E6 or E7 Gene in Cervical Carcinoma Cells by Using a Bacterial CRISPR/Cas RNA-Guided Endonuclease. *J. Virol.* **2014,** *88* (20), 11965–11972; (b) Zhen, S.; Hua, L.; Takahashi, Y.; Narita, S.; Liu, Y. H.; Li, Y. In Vitro and In Vivo Growth Suppression of Human Papillomavirus 16-Positive Cervical Cancer Cells by CRISPR/Cas9. *Biochem. Biophys. Res. Commun.* **2014,** *450* (4), 1422–1426; (c) Liu, Y. C.; Cai, Z. M.; Zhang, X. J. Reprogrammed CRISPR-Cas9 Targeting the Conserved Regions of HPV6/11 E7 Genes Inhibits Proliferation and Induces Apoptosis in E7-Transformed Keratinocytes. *Asian J. Androl.* **2016,** *18* (3), 475–479.
220. Jackson, H. J.; Rafiq, S.; Brentjens, R. J. Driving CAR T-Cells Forward. *Nat. Rev. Clin. Oncol.* **2016,** *13* (6), 370–383.
221. Park, J. H.; Geyer, M. B.; Brentjens, R. J. CD19-Targeted CAR T-Cell Therapeutics for Hematologic Malignancies: Interpreting Clinical Outcomes to Date. *Blood* **2016,** *127* (26), 3312–3320.
222. Su, S.; Hu, B.; Shao, J.; Shen, B.; Du, J.; Du, Y.; Zhou, J.; Yu, L.; Zhang, L.; Chen, F.; Sha, H.; Cheng, L.; Meng, F.; Zou, Z.; Huang, X.; Liu, B. CRISPR-Cas9 Mediated Efficient PD-1 Disruption on Human Primary T Cells from Cancer Patients. *Sci. Rep.* **2016,** *6,* 20070.
223. Gilbert, L. A.; Larson, M. H.; Morsut, L.; Liu, Z.; Brar, G. A.; Torres, S. E.; Stern-Ginossar, N.; Brandman, O.; Whitehead, E. H.; Doudna, J. A.; Lim, W. A.; Weissman, J. S.; Qi, L. S. CRISPR-Mediated Modular RNA-Guided Regulation of Transcription in Eukaryotes. *Cell* **2013,** *154* (2), 442–451.
224. Gilbert, L. A.; Horlbeck, M. A.; Adamson, B.; Villalta, J. E.; Chen, Y.; Whitehead, E. H.; Guimaraes, C.; Panning, B.; Ploegh, H. L.; Bassik, M. C.; Qi, L. S.; Kampmann, M.; Weissman, J. S. Genome-Scale CRISPR-Mediated Control of Gene Repression and Activation. *Cell* **2014,** *159* (3), 647–661.
225. Didovyk, A.; Borek, B.; Tsimring, L.; Hasty, J. Transcriptional Regulation With CRISPR-Cas9: Principles, Advances, and Applications. *Curr. Opin. Biotechnol.* **2016,** *40,* 177–184.
226. Saayman, S. M.; Lazar, D. C.; Scott, T. A.; Hart, J. R.; Takahashi, M.; Burnett, J. C.; Planelles, V.; Morris, K. V.; Weinberg, M. S. Potent and Targeted Activation of Latent HIV-1 Using the CRISPR/dCas9 Activator Complex. *Mol. Ther.* **2016,** *24* (3), 488–498.
227. Limsirichai, P.; Gaj, T.; Schaffer, D. V. CRISPR-Mediated Activation of Latent HIV-1 Expression. *Mol. Ther.* **2016,** *24* (3), 499–507.
228. (a) Fu, Y.; Foden, J. A.; Khayter, C.; Maeder, M. L.; Reyon, D.; Joung, J. K.; Sander, J. D. High-Frequency off-Target Mutagenesis Induced by CRISPR-Cas Nucleases in Human Cells. *Nat. Biotechnol.* **2013,** *31* (9), 822–826; (b) Hsu, P. D.; Scott, D. A.; Weinstein, J. A.; Ran, F. A.; Konermann, S.; Agarwala, V.; Li, Y.; Fine, E. J.; Wu, X.; Shalem, O.; Cradick, T. J.; Marraffini, L. A.; Bao, G.; Zhang, F. DNA Targeting Specificity of RNA-Guided Cas9 Nucleases. *Nat. Biotechnol.* **2013,** *31* (9), 827–832; (c) Pattanayak, V.; Lin, S.; Guilinger, J. P.; Ma, E.; Doudna, J. A.; Liu, D. R. High-Throughput Profiling of off-Target DNA Cleavage Reveals RNA-Programmed Cas9 Nuclease Specificity. *Nat. Biotechnol.* **2013,** *31* (9), 839–843.
229. Kim, S.; Kim, D.; Cho, S. W.; Kim, J.; Kim, J. S. Highly Efficient RNA-Guided Genome Editing in Human Cells via Delivery of Purified Cas9 Ribonucleoproteins. *Genome Res.* **2014,** *24* (6), 1012–1019.
230. Fu, Y.; Sander, J. D.; Reyon, D.; Cascio, V. M.; Joung, J. K. Improving CRISPR-Cas Nuclease Specificity Using Truncated Guide RNAs. *Nat. Biotechnol.* **2014,** *32* (3), 279–284.
231. (a) Mali, P.; Aach, J.; Stranges, P. B.; Esvelt, K. M.; Moosburner, M.; Kosuri, S.; Yang, L.; Church, G. M. CAS9 Transcriptional Activators for Target Specificity Screening and Paired Nickases for Cooperative Genome Engineering. *Nat. Biotechnol.* **2013,** *31* (9), 833–838; (b) Cho, S. W.; Kim, S.; Kim, Y.; Kweon, J.; Kim, H. S.; Bae, S.; Kim, J. S. Analysis of Off-Target Effects of CRISPR/Cas-Derived RNA-Guided Endonucleases and Nickases. *Genome Res.* **2014,** *24* (1), 132–141.
232. Schmidt, F.; Grimm, D. CRISPR Genome Engineering and Viral Gene Delivery: A Case of Mutual Attraction. *Biotechnol. J.* **2015,** *10* (2), 258–272.
233. Yin, H.; Song, C. Q.; Dorkin, J. R.; Zhu, L. J.; Li, Y.; Wu, Q.; Park, A.; Yang, J.; Suresh, S.; Bizhanova, A.; Gupta, A.; Bolukbasi, M. F.; Walsh, S.; Bogorad, R. L.; Gao, G.; Weng, Z.; Dong, Y.; Kotelianskiy, V.; Wolfe, S. A.; Langer, R.; Xue, W.; Anderson, D. G. Therapeutic Genome Editing by Combined Viral and Non-Viral Delivery of CRISPR System Components In Vivo. *Nat. Biotechnol.* **2016,** *34* (3), 328–333.

This page intentionally left blank

COMPREHENSIVE MEDICINAL CHEMISTRY III

This page intentionally left blank

COMPREHENSIVE MEDICINAL CHEMISTRY III

EDITORS-IN-CHIEF

Samuel Chackalamannil
Rutgers University, Piscataway, NJ, United States

David Rotella
Montclair State University, Montclair, NJ, United States

Simon E. Ward
University of Sussex, Brighton, United Kingdom

VOLUME 7

CNS, PAIN, METABOLIC SYNDROME, CARDIOVASCULAR, TISSUE FIBROSIS AND URINARY INCONTINENCE

VOLUME EDITORS

Adrian Hall
UCB BioPharma SPRL, Brussels, Belgium

Santhosh Neelamkavil
Merck Research Laboratories, Kenilworth, NJ, United States

Rob Jones
BlackThorn Therapeutics, San Francisco, CA, United States

ELSEVIER

Elsevier
Radarweg 29, PO Box 211, 1000 AE Amsterdam, The Netherlands
The Boulevard, Langford Lane, Kidlington, Oxford OX5 1GB, United Kingdom
50 Hampshire Street, 5th Floor, Cambridge, MA 02139, United States

Copyright © 2017 Elsevier Ltd. All rights reserved

No part of this publication may be reproduced or transmitted in any form or by any means, electronic or mechanical, including photocopying, recording, or any information storage and retrieval system, without permission in writing from the publisher. Details on how to seek permission, further information about the Publisher's permissions policies and our arrangements with organizations such as the Copyright Clearance Center and the Copyright Licensing Agency, can be found at our website: www.elsevier.com/permissions.

This book and the individual contributions contained in it are protected under copyright by the Publisher (other than as may be noted herein).

Notices
Knowledge and best practice in this field are constantly changing. As new research and experience broaden our understanding, changes in research methods, professional practices, or medical treatment may become necessary.

Practitioners and researchers may always rely on their own experience and knowledge in evaluating and using any information, methods, compounds, or experiments described herein. In using such information or methods they should be mindful of their own safety and the safety of others, including parties for whom they have a professional responsibility.

To the fullest extent of the law, neither the Publisher nor the authors, contributors, or editors, assume any liability for any injury and/or damage to persons or property as a matter of products liability, negligence or otherwise, or from any use or operation of any methods, products, instructions, or ideas contained in the material herein.

Library of Congress Cataloging-in-Publication Data
A catalog record for this book is available from the Library of Congress

British Library Cataloguing-in-Publication Data
A catalogue record for this book is available from the British Library

ISBN 978-0-12-803200-8

For information on all publications visit our website at
http://store.elsevier.com

Working together
to grow libraries in
developing countries
www.elsevier.com • www.bookaid.org

Publisher: Oliver Walter
Acquisition Editor: Rachel Gerlis
Content Project Manager: Gemma Tomalin
Associate Content Project Manager: Marise Willis
Designer: Mark Rogers

Printed and bound in the United Kingdom

PREFACE

Previous editions of *Comprehensive Medicinal Chemistry*, published in 1990 and 2006, provided an integrated reference source that encompassed all major aspects of drug discovery research. The third edition follows this tradition and considerably expands its scope and content.

The trailblazing scientific discoveries of the 21st century have brought new opportunities for drug discovery research. The discipline of medicinal chemistry continues to evolve as it adapts to these new opportunities and strives to solve new challenges. Covered in the new edition are not only the breakthrough therapies of the past decade in cancer, hepatitis C, heart failure, dyslipidemia, cystic fibrosis, multiple sclerosis, HIV, etc., but also extensive discussion of new business models in drug discovery research, shifting industry demographics, emerging technologies, *in silico* drug discovery tools, experimental ADME and toxicology, and biologics medicine. The tone of this edition is prospective in which contributors identify outstanding issues and paths forward in their area of expertise. The aim is to provide drug discovery scientists in industry, government, academia, and research organizations with a contemporary global perspective on the field that includes a look ahead in selected areas.

The eight individual volumes fulfill these objectives and include extensive discussion of biomolecular therapeutics, drug targeting and delivery, development of chemical biology tools, data collection and analysis, *in silico* models as predictors for biological properties, identification/validation of new targets, approaches to quantify target engagement, new methods for synthesis of drug candidates such as green chemistry, development of novel scaffolds for drug discovery, and the role of regulatory agencies in drug discovery.

The individual volume editors have done an outstanding job to identify topics and contributors to meet these goals and we thank them for their hardwork and diligence. In volume 1, Ana Martinez and Carmen Gil recruited an international group of contributors who provide chapters on the emerging role of organizations other than traditional pharmaceutical companies in drug discovery, the evolving science of chemical biology, and new organic chemistry contributions to the discipline. In volume 2, Helmut Buschmann, Norbert Handler, and Andrea Wolkerstorfer have accomplished a seemingly impossible task and attracted world-leading experts across the wide field of drug discovery enabling technologies, covering contemporary thinking in a wide range of key disciplines that enable modern medicinal chemistry and drug discovery and development. The computational enabling technologies are the focus of volume 3, in which Andy Davis and Colin Edge have assembled chapters covering both ligand-based and protein structure–based advances as well as exciting new methodologies and case studies exploiting these. Alan Wilson identified experts in the fields of pharmacokinetics and toxicology who describe a wide range of contemporary advances in prediction and analysis of pharmaceutical properties and drug safety in volume 4. In volume 5, Ian Collins, Louis Lombardo, and Will Watkins have assembled leading experts to discuss high impact drug discovery accomplishments over the past decade in cancer chemotherapeutics, immunology and inflammation, and infectious diseases therapeutic areas. Ved Srivastava edited volume 6 on biologic medicines, a significant and rapidly evolving area where medicinal chemistry plays an important role. The chapters in this volume provide timely information on not only protein-based drugs, such as monoclonal antibodies and therapeutic proteins, but also peptides and nucleic acid–based therapeutics. Volume 7, edited by Adrian Hall, Santhosh Neelamkavil, and Rob Jones, presents a detailed account of the major advances in CNS, metabolic, and cardiovascular fields over the past decade and the promising new opportunities. Joerg Holenz edited volume 8 that presents case histories of successful drug discovery and strategic differentiation that have resulted in commercialized drugs and candidates in advanced clinical trials.

We are truly grateful to the publishing team at Elsevier that includes Gemma Tomalin, Rachel Gerlis, Marise Willis, and Sean Simms for their assistance and support throughout the process. With their expertise, this project became what we believe is a noteworthy and valuable resource for the discipline of medicinal chemistry. We look forward to the response and feedback of our colleagues who will use this information in their own work.

Samuel Chackalamannil, David P. Rotella, and Simon E. Ward

EDITORS-IN-CHIEF: BIOGRAPHIES

Dr. Samuel Chackalamannil

Dr. Chackalamannil obtained his PhD in chemistry from Yale University in 1984 and subsequently worked in drug discovery research at Schering-Plough Corporation and Merck Research Laboratories, where he was a distinguished fellow when he left in 2011. Since then, he has been teaching at Ernest Mario School of Pharmacy, Rutgers University, New Jersey.

Dr. Chackalamannil has significant accomplishments in the discovery of new medicines. He led the discovery of vorapaxar (Zontivity®), an FDA-approved antiplatelet drug for the prevention of heart attack and stroke. His group also discovered a PDE-5 inhibitor clinical candidate dasantafil and an adenosine A2a antagonist clinical candidate for the treatment of Parkinson's disease. Altogether, he was responsible for the discovery of nine development candidates in cardiovascular, central nervous system, and metabolic disease areas.

Dr. Chackalamannil is a coinventor of 62 allowed US patents and numerous patent applications worldwide. He has published 81 peer-reviewed articles and has coauthored a book. He has also given numerous lectures at international meetings and academic institutions.

Dr. Chackalamannil is a two-time recipient of the Thomas Alva Edison Award for Emerging Technology Patent and a two-time recipient of the Presidential Award for Discovery at Schering-Plough Research Institute. He has chaired several sessions at American Chemical Society national meetings and Gordon Research Conference on Medicinal Chemistry and was an organizer for Chemistry as a Life Science Symposium.

Dr. David Rotella

Dr. Rotella earned a PhD in medicinal chemistry from The Ohio State University and carried out postdoctoral research in organic chemistry at Penn State University. He joined the faculty at Montclair State University in July 2011 as the Margaret and Herman Sokol Professor of medicinal chemistry after a successful career in the pharmaceutical industry. He is an expert in the discovery and optimization of small molecule drug candidates for use in metabolic, cardiovascular, cancer, and central nervous system diseases. His current research is focused on discovering new lead compounds for use in parasitic and central nervous system diseases. He has coedited the seventh edition of *Burger's Medicinal Chemistry* and is a senior editor for the Royal Society of Chemistry's Drug Discovery book series. He has authored over 40 peer-reviewed articles, is an inventor on 8 issued US patents, and has contributed 10 book chapters.

Simon E. Ward

Simon Ward has an MA in natural sciences and PhD in synthetic organic chemistry from Cambridge University, UK. He has a wide-ranging experience of drug discovery in both large and small companies (GlaxoSmithKline, Knoll Pharmaceuticals, Vernalis, Chiroscience, BioCrea) and specialist experience of discovering and developing drugs for central nervous system indications. He has led multidisciplinary project teams and medicinal chemistry groups from target identification through to early clinical studies, delivering multiple clinical development candidates across indications. He is a fellow of the Royal Society of Chemistry. He is currently a professor of medicinal chemistry at the University of Sussex, UK, and the director of the Sussex Drug Discovery Centre, which he established within the University of Sussex in 2010.

This page intentionally left blank

CONTRIBUTORS TO VOLUME 7

G Bebernitz
Novartis Institutes for Biomedical Research, Cambridge, MA, United States

I M Bell
Merck & Co., Inc., West Point, PA, United States

P Beswick
Sussex Drug Discovery Centre, University of Sussex, Brighton, United Kingdom

Paul Beswick
University of Sussex, Brighton, United Kingdom

T Biftu
Merck Research Laboratories, Kenilworth, NJ, United States

E Caroff
Actelion Pharmaceuticals Ltd, Allschwil, Switzerland

P Carrington
Merck Research Laboratories, Kenilworth, NJ, United States

A L Catapano
University of Milan and IRCCS Multimedica, Milano, Italy

K Chen
Innovative Medicines and Early Development, Astrazeneca, Shanghai, People's Republic of China

P Costet
Merck Research Laboratories, Kenilworth, NJ, United States

G M Dubowchik
Bristol-Myers Squibb Co., Wallingford, CT, United States

S D Edmondson
Merck Research Laboratories, Kenilworth, NJ, United States

G M P Giblin
Convergence Pharmaceuticals Limited, a Biogen Company, Cambridge, United Kingdom

H J M Gijsen
Janssen Research & Development, Janssen Pharmaceutica NV, Beerse, Belgium

P W Glunz
Bristol-Myers Squibb Company, Princeton, NJ, United States

A Hall
UCB Pharma, Braine l'Alleud, Belgium

A Hall
UCB, Braine l'Alleud, Belgium

M Halleck
Merck Research Laboratories, Kenilworth, NJ, United States

J Hannestad
Denali Therapeutics, South San Francisco, CA, United States

M Hoek
Merck Research Laboratories, Kenilworth, NJ, United States

Y Huang
Merck Research Laboratories, Kenilworth, NJ, United States

J E Imbriglio
Merck Research Laboratories, Kenilworth, NJ, United States

Y Kazuta
Medicine Creation, Neurology Business Group, Eisai Co., Ltd., Tsukuba-shi, Ibaraki, Japan

J Kehler
H. Lundbeck A/S, Valby, Denmark

T Kurokawa
Medicine Creation, Neurology Business Group, Eisai Co., Ltd., Tsukuba-shi, Ibaraki, Japan

M A Letavic
Janssen Research & Development, L.L.C., San Diego, CA, United States

J J Lynch, Jr.
Merck Research Laboratories, West Point, PA, United States

L Ma
Merck Research Laboratories, Kenilworth, NJ, United States

D T MacPherson
Convergence Pharmaceuticals Limited, a Biogen Company, Cambridge, United Kingdom

J Mercier
UCB Biopharma, Braine-L'Alleud, Belgium

EA Meyer
Actelion Pharmaceuticals Ltd, Allschwil, Switzerland

W Michael Seganish
Merck Research Laboratories, Kenilworth, NJ, United States

G D Norata
University of Milan and IRCCS Multimedica, Milano, Italy

A Palani
Merck Research Laboratories, Kenilworth, NJ, United States

S Pinto
Merck Research Laboratories, Kenilworth, NJ, United States

A Pirillo
E. Bassini Hospital, Cinisello Balsamo, Italy

L Provins
UCB Biopharma, Braine-L'Alleud, Belgium

M L Quan
Bristol-Myers Squibb Company, Princeton, NJ, United States

Tristan Reuillon
University of Sussex, Brighton, United Kingdom

M A Riederer
Actelion Pharmaceuticals Ltd, Allschwil, Switzerland

B T Shireman
Janssen Research & Development, L.L.C., San Diego, CA, United States

R SinhaRoy
Janssen Pharmaceuticals, Inc., Raritan, NJ, United States

J M Smallheer
Bristol-Myers Squibb Company, Princeton, NJ, United States

S Sorota
Merck Research Laboratories, Kenilworth, NJ, United States

H Tsui
Innovative Medicines and Early Development, Astrazeneca, Shanghai, People's Republic of China

A I Velter
Janssen Pharmaceutica NV, Beerse, Belgium

Simon E Ward
University of Sussex, Brighton, United Kingdom

T Watanabe
Medicine Creation, Neurology Business Group, Eisai Co., Ltd., Tsukuba-shi, Ibaraki, Japan

D R Witty
Convergence Pharmaceuticals Limited, a Biogen Company, Cambridge, United Kingdom

Q Zeng
Innovative Medicines and Early Development, Astrazeneca, Shanghai, People's Republic of China

X Zhang
Innovative Medicines and Early Development, Astrazeneca, Shanghai, People's Republic of China

Y-Y Zhou
Merck Research Laboratories, Kenilworth, NJ, United States

CONTENTS OF VOLUME 7

Preface *v*

Editors-in-Chief: Biographies *vii*

Contributors to Volume 7 *ix*

Editorial Board *xiii*

An Introduction to the CNS Section of Volume 7: Recent Approvals and Advances in CNS Drug Discovery *xv*

7.01 Recent Advances and Future Directions in the Treatment of Epilepsy 1
T Kurokawa, Y Kazuta, and T Watanabe

7.02 Progress and Challenges in the Development of PET Ligands to Aid CNS Drug Discovery 20
J Mercier, L Provins, and J Hannestad

7.03 Progress in the Discovery of Ca Channel Blockers for the Treatment of Pain 65
P Beswick

7.04 Sodium Channel Blockers for the Treatment of Pain 131
D R Witty, D T MacPherson, and G M P Giblin

7.05 CGRP Receptor Antagonists for the Treatment of Migraine 176
G M Dubowchik and I M Bell

7.06 Orexin Receptor Antagonists 225
B T Shireman and M A Letavic

7.07 Targeting γ-Secretase for the Treatment of Alzheimer's Disease 280
A Hall and A I Velter

7.08 Targeting β-Secretase (BACE) for the Treatment of Alzheimer's Disease 326
A Hall and H J M Gijsen

7.09 Targeting Phosphodiesterases in the CNS 384
J Kehler

7.10 Inhibiting Kinases in the CNS 408
H Tsui, Q Zeng, K Chen, and X Zhang

7.11 Modulating AMPA Receptors for the Treatment of CNS Disorders 447
Tristan Reuillon, Simon E Ward, and Paul Beswick

7.12 GLP-1 Receptor Agonists for the Treatment of Diabetes and Obesity 481
A Palani, Y-Y Zhou, M Halleck, and P Carrington

7.13 Sodium–Glucose Cotransporters 491
G Bebernitz

7.14 DPP-4 Inhibitors 512
T Biftu and R SinhaRoy

7.15 Advances in Antiplatelet Agents 556
E A Meyer, E Caroff, and M A Riederer

7.16 Advances in Anticoagulants 600
M L Quan, P W Glunz, and J M Smallheer

7.17 Treatments for Heart Failure 628
W Michael Seganish, J J Lynch, Jr. and S Sorota

7.18 Advances in Hypercholesterolemia 663
A Pirillo, G D Norata, and A L Catapano

7.19 Drug Discovery in Tissue Fibrosis 694
S Pinto, M Hoek, Y Huang, P Costet, L Ma, and J E Imbriglio

7.20 β_3-AR Agonists for the Treatment of Overactive Bladder 714
S D Edmondson

EDITORIAL BOARD

EDITORS-IN-CHIEF

Samuel Chackalamannil
Rutgers University, Piscataway, NJ, United States

David Rotella
Montclair State University, Montclair, NJ, United States

Simon E. Ward
University of Sussex, Brighton, United Kingdom

VOLUME 1
GENERAL PERSPECTIVE - THE FUTURE OF DRUG DISCOVERY

VOLUME EDITORS

Ana Martinez
Centro de Investigaciones Biologicas-CSIC, Madrid, Spain

Carmen Gil
Centro de Investigaciones Biologicas-CSIC, Madrid, Spain

VOLUME 2
DRUG DISCOVERY TECHNOLOGIES

VOLUME EDITORS

Helmut Buschmann
Savira Pharmaceuticals GmbH, Vienna, Austria

Norbert Handler
Savira Pharmaceuticals GmbH, Vienna, Austria

Andrea Wolkerstorfer
Baxalta Innovations GmbH — Now part of Shire, Vienna, Austria

VOLUME 3
IN SILICO DRUG DISCOVERY TOOLS

VOLUME EDITORS

Andrew M. Davis
AstraZeneca R&D Gothenburg, Gothenburg, Sweden

Colin Edge
GlaxoSmithKline Medicines Research Centre, Stevenage, United Kingdom

VOLUME 4
EXPERIMENTAL ADME AND TOXICOLOGY

VOLUME EDITOR

Alan G. E. Wilson
Lexicon Pharmaceuticals, The Woodlands, TX, United States

VOLUME 5
CANCER, IMMUNOLOGY AND INFLAMMATION, AND INFECTIOUS DISEASE

VOLUME EDITORS

Ian Collins
The Institute of Cancer Research, London, United Kingdom

William Watkins
Gilead Sciences, Foster City, CA, United States

Louis J. Lombardo
Bristol-Myers Squibb Research and Development, Princeton, NJ, United States

VOLUME 6
BIOLOGICS MEDICINE

VOLUME EDITOR

Ved Srivastava
Intarcia Therapeutics, Durham, NC, United States

VOLUME 7
CNS, PAIN, METABOLIC SYNDROME, CARDIOVASCULAR, TISSUE FIBROSIS AND URINARY INCONTINENCE

VOLUME EDITORS

Adrian Hall
UCB BioPharma SPRL, Brussels, Belgium

Santhosh Neelamkavil
Merck Research Laboratories, Kenilworth, NJ, United States

Rob Jones
BlackThorn Therapeutics, San Francisco, CA, United States

VOLUME 8
CASE HISTORIES IN RECENT DRUG DISCOVERY

VOLUME EDITOR

Joerg Holenz
R&D Neurosciences TAU, GSK, PA, United States

An Introduction to the CNS Section of Volume 7: Recent Approvals and Advances in CNS Drug Discovery

Adrian Hall, UCB, Chemin du Foriest, Braine l'Alleud, Belgium

© 2017 Elsevier Ltd. All rights reserved.

The current CNS section of *Comprehensive Medicinal Chemistry III* aims to cover some of the most prominent areas of CNS research in the last decade. These include disease areas such as epilepsy (Chapter 7.01. Recent Advances and Future Directions in the Treatment of Epilepsy), molecular targets that have received major research effort, e.g., CGRP antagonists (Chapter 7.05. CGRP Antagonists for the Treatment of Migraine), AMPA modulators (Chapter 7.11. Modulating AMPA Receptors for the Treatment of CNS Disorders), γ-secretase modulators (Chapter 7.07. Targeting Gamma Secretase for the Treatment of Alzheimer's Disease), β-secretase/BACE inhibitors (Chapter 7.08. Targeting β-Secretase (BACE) for the Treatment of Alzheimer's Disease), target classes that have received significant and sustained research interest, e.g., PDE inhibitors (Chapter 7.02. Progress and Challenges in the Development if PET Ligands to Aid CNS Drug Discovery), voltage-gated calcium channel blockers (Chapter 7.03. Progress in the Discovery of the Ca Channel Blockers for the Treatment of Pain), voltage-gated sodium channel blockers (Chapter 7.04. Sodium Channel Blockers for the Treatment of Pain), and kinase inhibitors for CNS indications (Chapter 7.10. Inhibiting Kinases in the CNS). In addition, one of the major challenges in CNS drug discovery is the incorporation of biomarkers. To this end, the use of positron emission tomography (PET) is one of the major technologies that is employed to show target engagement or track temporal functional or biomarker changes and greatly enables CNS drug discovery. Thus, a chapter on the progress and challenges in PET discovery (Chapter 7.02. Progress and Challenges in the Development if PET Ligands to Aid CNS Drug Discovery) is a must. Each chapter has been written by experts with deep knowledge of the area, and the authors have been sourced from around the globe (Belgium, China, Denmark, Japan, the United Kingdom, and the United States) and include those from both industry and academia.

CNS drug is often highlighted to have a high rate of attrition, and several companies[1] such as GSK,[2] AZ,[3] BMS,[4,5] and Novartis[6] have reduced or halted neuroscience research in recent years. However, many companies and academic research groups are focused on oncology, which actually has the highest rate of attrition of all disease areas, in terms of likelihood of approval from PhI or probability of PhIII success.[7] Furthermore, while huge advances have been made in the oncology field, many of the newly approved medicines do not offer a cure, but a period of remission, which although can provide a huge improvement for patients there is still room for improvement.

In addition to highlighting some of the areas that are discussed in this section, the introduction also offers an opportunity to review the approvals of CNS drugs over the last decade or so since the publication of the last edition of *Comprehensive Medicinal Chemistry*, to assess the productivity and ingenuity of research in the area. Furthermore, it is possible to look back at the trials and tribulations in the field and see what we can learn from the failures and to highlight the prospective medicines that could impact the lives of many patients.

Although seemingly easy, it is first important to clarify the definition of a CNS drug. For instance, a CNS drug could be labeled as such as it is administered to treat a disease, which is generally associated with a CNS or neurodegenerative disease. However, some CNS diseases can have peripheral components, or the symptoms can be treated by a peripherally active agent. Also, there are not always data to demonstrate that the drug in question penetrates the CNS or acts there. Hence, for the purposes of this overview, a CNS drug is classified as one for which the site of action is believed to be in the CNS, and not one which is simply used to treat a neurological disease.

To this end, information was collected on CNS drug approvals that were launched in any country by year, i.e., not just FDA approvals, from 2005 to 2016 and is summarized in **Table 1**. The information was gathered from Annual Reports in Medicinal Chemistry and Medicinal Chemistry Reviews from the American Chemical Society.[8–18]

As highlighted in **Table 1** and **Fig. 1**, CNS research has provided a steady stream of new drug approvals over this period of time, ranging from two to six per year. It can sometimes be difficult to discern whether a compound represents a new mechanism of action, as for some compounds this is not always clearly defined, or multiple pharmacologies may contribute to its efficacy. For example, over the years there have been many antipsychotic NCEs, which vary to some degree in the aminergic GPCRs they interact with, for example, paliperidone (2007), lurasidone (2010), vilazodone (2011), aripiprazole lauroxil (2015), brexpiprazole (2015), cariprazine (2015), **Table 2**. However, compounds such as flibanserin (2015), which also bears an arylpiperazine moiety, similar to the antipsychotics, has been noted as a first-in-class compound by the FDA as its pharmacology is attributed to $5HT_{1A}$ and D_4 partial agonism in combination with $5HT_{2A}$ antagonism. There are also several compounds, such as lisdexamfetamine (2007), desvenlafaxine (2008), dapoxetine (2009), and vilazodone (2011), which inhibit, to different extents, the aminergic transporters, serotonin (SERT), norepinephrine/noradrenaline (NET), and dopamine (DAT).

Although there have been many compounds with similar pharmacologies, it is noteworthy that multiple first-in-class compounds have been launched in recent years, including ramelteon, an $MT_{1/2}$ agonist for insomnia; ziconotide, an N-type Ca^{2+} channel blocker for pain; rimonabant, a CB_1 antagonist for obesity (now withdrawn); varenicline, an $\alpha_4\beta_2$ agonist for smoking

Table 1 Listing of number of approvals in any country by year

Year	*NMEs*	*NCEs*	*CNS*
2005	24	21	4
2006	27	21	3
2007	20	19	3
2008	24	20	4
2009	28	23	5
2010	24	21	3
2011	26	21	3
2012	30	27	2
2013	27	25	2
2014	47	37	4
2015	38	29	6

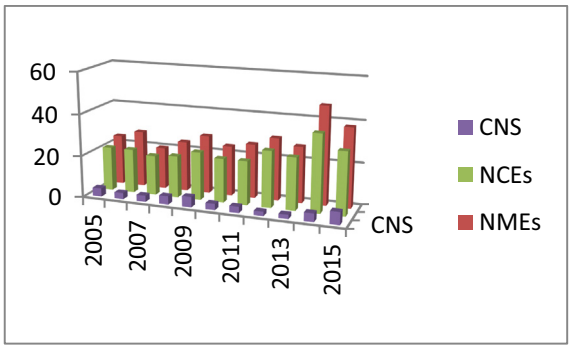

Figure 1 Depiction of the number of CNS drug approvals by year versus the number of NCE and NME approvals.

cessation; fosaprepitant (the first of three NK_1 antagonists to be launched) for emesis; fingolimod, an $S1P_1$ agonist for MS; retigabine, a KCNQ2–5 (K_v7.2–7.5) PAM/channel opener for epilepsy (soon to be withdrawn)[20]; lorcaserin, a $5HT_{2C}$ agonist for obesity; perampanel, an AMPA antagonist for epilepsy; istradefylline, an adenosine A_{2A} antagonist for PD; alectinib, an ALK inhibitor for non–small-cell lung cancer (NSCLC) and associated leptomeningeal metastases; and suvorexant, an $OX_{1/2}$ antagonist for sleep disorders. This steady flow of exciting new medicines highlights that CNS research is still very much alive and can still deliver a huge impact for many patients in the future.

Despite the highlights mentioned above, there have been a number of areas of disappointment in CNS drug discovery in recent years, which highlights the challenges on the field. In terms of Alzheimer's disease, there have been a number of notable failures. Firstly, the γ-secretase inhibitor field (GSIs), where many companies had invested significant resource, and several, such as Lilly with semagacestat and BMS with avagacestat (BMS-708163), progressed compounds to late-stage clinical trials. Compounds from this class failed to impact cognitive decline, actually worsening cognition and having mechanism-based side effects. For example, semagacestat worsened cognition[21] and was associated with increased adverse events such as skin cancers and infections.[22] Avagacestat achieved only 10–15% reductions in CSF amyloid levels, did not impact cognition and produced GI effects[23] as well as basal cell carcinoma (BCC) and squamous cell carcinoma (SCC).[24] Following closely behind, with the promise of overcoming mechanistic side effects were the γ-secretase modulators (GSMs), reviewed in this section (Chapter 7.07. Targeting Gamma Secretase for the Treatment of Alzheimer's Disease). Early compounds such as Flurizan were the subject of much hype,[25] despite the failure to show an effect on amyloid biomarkers.[26] The failure of Flurizan was predicted by many, based on its extremely weak GSM activity, its low CNS penetration and its lack of effect on amyloid levels.[27] Despite significant effort by a range of groups, it appears that none of the more recent GSMs have progressed beyond PhI clinical trials, see Chapter 7.07. Targeting Gamma Secretase for the Treatment of Alzheimer's Disease. This appears to be due to a combination of weak activity and side effects. Hence, it appears that progressing compounds beyond PhI represents a considerable challenge, which may be insurmountable.

In addition to disease-modifying approaches, the field of cognitive enhancers or palliative AD therapeutics has experienced significant attrition. Notable areas include H_3 antagonists, where most pharmaceutical companies had invested research efforts, GSK, with GSK189254[28] and GSK239512,[29,30] and Merck, with MK-0249,[31] were early leaders in the field. However, despite much promise, no improvements in cognition were recorded. Despite this, one of the first H_3 antagonists, pitolisant (Wakix®)[32]

Table 2 List of CNS drug approvals by year, including disease treated, MoA, structure, and name

Year of launch	*Name*	*Structure*	*MoA*	*Use*	*Note*
2005	Eszopiclone (Lunesta™)	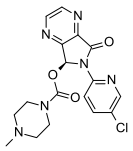	$GABA_A$ PAM	Hypnotic	Single enantiomer of zopiclone
2005	Ramelteon (Rozerem™)	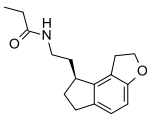	$MT_{1/2}$ agonist	Insomnia	
2005	Rasagiline (Azilect™)	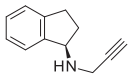	MAO-B inhibitor	Parkinson's disease	
2005	Ziconotide (Prialt™)	Peptide	N-type Ca^{2+} channel blocker	Severe chronic pain	Intrathecal administration
2006	Rimonabant (Acomplia™)	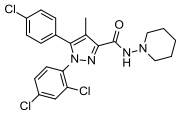	CB_1 antagonist	Obesity	Withdrawn
2006	Rotigotine (Neupro™)	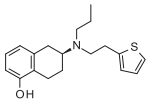	D_2 agonist with D_1 and D_3 agonism, D_4 and D_5 partial agonist	Parkinson's disease	Administered via patch
2006	Varenicline (Chantix™)	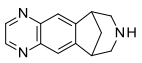	$\alpha_4\beta_2$ nAChR agonist	Smoking cessation	
2007	Lisdexamfetamine (Vyvanse™)	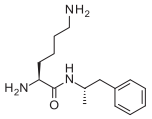	Elevates extracellular dopamine levels via various mechanisms including DAT inhibition	ADHD	L-lysine prodrug of D-amphetamine
2007	Paliperidone (Invega™)	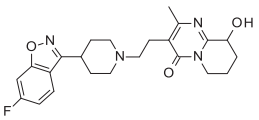	D2, $5HT_{2A}$ antagonist, with affinity for other aminergic receptors such as D_3, $5HT_7$, $5HT_{1D}$, H_1, α_{1A}, α_{2A}, α_{2C}, α_{2B}, and $5HT_{2C}$	Antipsychotic	Metabolite of risperidone
2007	Rufinamide (Inovelon™)	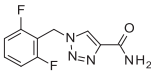	Unknown, thought to be Na channel blocker (prolongation of inactive state)	Anticonvulsant/ Lennox–Gastaut syndrome	
2008	Blonanserin (Lonasen™)	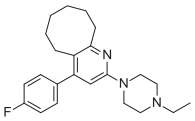	D2, $5HT_{2A}$ antagonist with affinity for other aminergic receptors such as $5HT_6$ and D_3	Antipsychotic	

(Continued)

Table 2 List of CNS drug approvals by year, including disease treated, MoA, structure, and name—cont'd

Year of launch	*Name*	*Structure*	*MoA*	*Use*	*Note*
2008	Desvenlafaxine (Pristiq™)	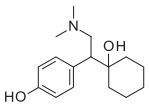	SNRI (SERT, NET inhibitor)	Antidepressant	Metabolite of venlafaxine
2008	Fosaprepitant (Emend™)	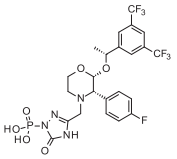	NK_1 antagonist	Antiemetic	Phosphate prodrug
2008	Lacosamide (Vimpat™)	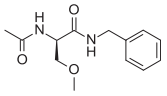	Unknown, potentially via enhancing slow inactivation of voltage-gated Na channels or via CRMP-2	Anticonvulsant	
2009	Armodafinil (Nuvigil™)	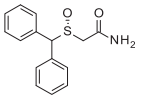	Unknown. Potentially via α1 agonism or DAT inhibition.	Treatment of excessive daytime sleepiness	Single enantiomer of modafinil
2009	Asenapine (Saphris™)	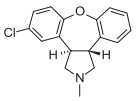	D2, $5HT_{2A}$ antagonist, with similar or higher affinity for $5HT_{2C}$, $5HT_{2A}$, $5HT_{2B}$, $5HT_{7}$, $5HT_{6}$, α_{2B}, D_3, and affinity for other aminergic receptors such as $5HT_{1A}$, $5HT_{1B}$, $5HT_5$, D_1, D_4, H_1, H_2, α_{2A}, α_{2C}, α_1	Antipsychotic	
2009	Dapoxetine (Priligy™)	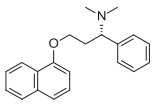	SERT inhibitor (short acting)	Premature ejaculation	
2009	Eslicarbazepine (Zebinix™)	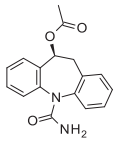	Voltage-gated Na channel blocker	Antiepileptic	Acetate prodrug of 10-hydroxycarbazepine (carbazepine metabolite)
2009	Tapentadol (Nucynta™)	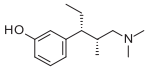	μ-Opioid (MOR) agonist and NET inhibitor	Pain	
2010	Dalfampridine (Ampyra™)		K channel blocker	Multiple sclerosis	
2010	Fingolimod (Gilenya™)	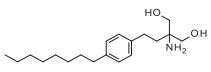	$S1P_1$ agonist	Multiple sclerosis	

Table 2 List of CNS drug approvals by year, including disease treated, MoA, structure, and name—cont'd

Year of launch	*Name*	*Structure*	*MoA*	*Use*	*Note*
2010	Lurasidone (Latuda™)	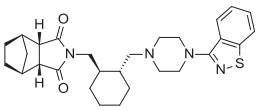	D_2, $5HT_{2A}$, $5HT_7$ antagonist, $5HT_{1A}$ partial agonist with weaker activity at α_{2C} and α_{2A}	Antipsychotic	
2011	Gabapentin enacarbil (Horizant™)	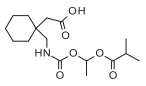	Modulator of N-type Ca^{2+} channel α_2-δ subunit	Restless leg syndrome	Prodrug of gabapentin
2011	Retigabine (Trobalt™, Potiga™)	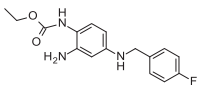	KCNQ2-5 (K_v7.2–7.5) PAM/opener	Anticonvulsant	
2011	Vilazodone (Viibryd™)	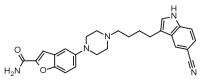	SERT inhibitor and $5HT_{1A}$ partial agonist	Antidepressant	
2012	Lorcaserin (Belviq™)	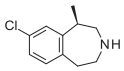	$5HT_{2C}$ agonist, with antagonism of $5TH_{2A}$ & $5HT_{2B}$	Obesity	
2012	Perampanel (Fycompa™)	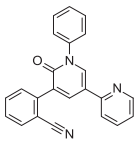	AMPA antagonist	Anticonvulsant	
2013	Istradefylline (Nouriast™)	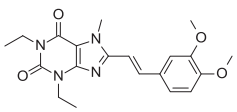	A_{2A} antagonist	Parkinson's disease	
2013	Vortioxetine (Brintellix™)	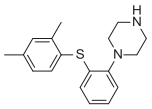	SERT inhibitor, $5HT_{1A}$ and $5HT_{1B}$ partial agonist, and $5HT_3$ and $5HT_7$ antagonist with weaker affinity for $5HT_{1D}$ and NET	Antidepressant	
2014	Alectinib (Alecensa™)	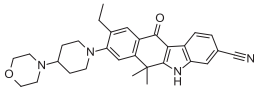	ALK inhibitor	Non–small-cell lung cancer	Demonstrated to penetrate the brain effectively treat leptomeningeal metastases.[19]
2014	Netupitant (Akynzeo™)	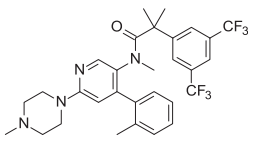	NK_1 antagonist	Emesis	

(Continued)

Table 2 List of CNS drug approvals by year, including disease treated, MoA, structure, and name—cont'd

Year of launch	*Name*	*Structure*	*MoA*	*Use*	*Note*
2014	Suvorexant (Belsomra™)	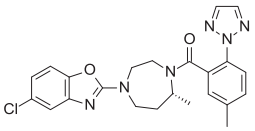	Orexin $OX_{1/2}$ antagonist	Sleep disorders	
2014	Tasimelteon (Hetlioz™)	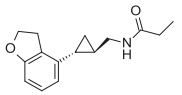	$MT_{1/2}$ agonist	Sleep disorders	
2015	Aripiprazole lauroxil (Aristada™)	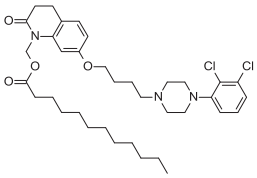	D_2, D_3, $5HT_{1A}$ partial agonist, $5HT_{2A}$ antagonist, with affinity for $5HT_{2B}$, $5HT_7$	Antipsychotic	Prodrug
2015	Brexpiprazole (Rexulti™)	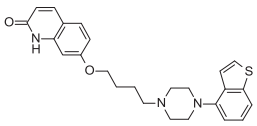	D_2 partial agonist/ antagonist, D_3, $5HT_{1A}$ partial agonist, $5HT_{2A}$ antagonist, with affinity for $5HT_{2B}$, $5HT_7$, α_{1B}, α_{2C}, α_{1A}, H_1, and weak partial agonism at $5HT_{2C}$	Antidepressant, antipsychotic	
2015	Cariprazine (Vraylar™)	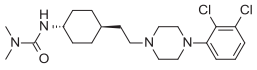	D_3, D_2 antagonist/partial agonist, $5HT_{1A}$ partial agonist $5HT_{2A}$ and $5HT_{2B}$ antagonist with affinity for H_1, $5HT_7$, $5HT_{2C}$, α_{1A}, α_{1D}, σ_1	Antipsychotic	
2015	Flibanserin (Addyi™)	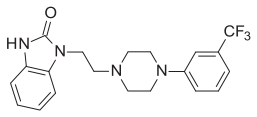	$5HT_{1A}$ partial agonist, $5HT_{2A}$ antagonist and D_4 weak partial agonist	Female sexual dysfunction	
2015	Rolapitant (Varubi™)	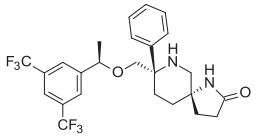	NK_1 antagonist	Emesis	
2015	Safinamide (Xadago™)	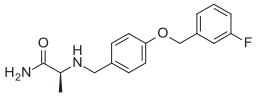	MAO-B inhibitor and Na and Ca channel activity	Parkinson's disease	

2011 does not include Tafamidis (Vyndaqel™), transthyretin (TTR) stabilizer for the treatment of neurodegeneration. 2012 does not include Teriflunomide (Aubagio), dihydroorotate dehydrogenase (DHODH) inhibitor for the treatment of multiple sclerosis, MoA believed to be dampening of immune system via lymphocytes. 2013 does not include dimethyl fumarate (Tecfidera™), thought to be an Nrf2 pathway activator, for the treatment of multiple sclerosis. 2013 does not include ^{18}F-flutemetamol (Vizamyl™) for the diagnosis of AD, Aβ PET ligand.

DAT, dopamine transporter; *MOR*, μ opioid receptor; *NAT*, noradrenaline transporter; *NET*, norepinephrine transporter; *SERT*, serotonin transporter; *SSRI*, selective serotonin reuptake inhibitor.

was recently granted marketing access approval (MAA) in the EU for the treatment of narcolepsy.[33] While this is very positive news, the initial hope of improving cognition was not realized and the return on investment is significantly lower than initially anticipated. $5HT_6$ antagonists have also received a lot of attention, with many companies progressing compounds to clinical trials. Despite promise, early compounds such as SB-742457 from GSK failed to offer sufficient benefit for GSK to progress the compound to PhIII trials. This compound, now known as intepirdine (RVT-101), has recently been acquired by Axovant and is currently undergoing PhIII trials in mild-to-moderate AD.[34] Despite showing promising effects in a PhII 24-week trial in moderate AD when given on top of donepezil,[35] Lu AE58054 from Lundbeck, now known as idalopirdine, initial results from the first (STARSHINE) of three PhIII clinical trials have failed to show efficacy.[36] However, two further PhIII trials (STARBEAM and STARBRIGHT) are ongoing.[36] Another aminergic target for cognitive enhancement, $5HT_4$ agonism/partial agonism also met with disappointment. In addition to enhancing cognition this target was also proposed to modulate amyloid levels,[37,38] although the latter effect appears very weak.[39] Compounds, such as PF-04995724, failed to deliver the anticipated clinical efficacy. Pfizer also experienced further set back when they licensed the mixed aminergic antagonist (including $5HT_7$ and $5HT_6$),[40] dimebon (latrepirdine) showed initial promise in a PhII trial where it apparently improved cognition,[41] only to fail to recapitulate the data in subsequent trials.[42,43] The α7 nicotinic acetyl choline receptor (nAChR) has been the subject of considerable interest due to its potential role in cognition.[44] Thus, many groups have invested resources into the identification of α7 agonists and positive allosteric modulators (PAMs). Disappointingly, two of the most advanced compounds, TC-5619[45] developed by Targacept in conjunction with AZ, and EVP-6124 (encenicline)[46] from EnVivo/Forum, yielded disappointing results,[47] despite initial promise.[48]

Finally, the centrally active CB_1 antagonist rimonabant showed great promise with the demonstration of efficacy in terms of weight loss. Many other companies had also invested effort into what appeared to a very attractive mechanism, and further clinical development compounds were identified, such as Otenabant (Pfizer) and Taranabant (Merck), only for mechanism-based psychiatric side effects, such as depression and anxiety, to lead to the withdrawal of rimonabant.

There was also disappointment with GlyT1 inhibitors, where RG1678 (bitopertin) showed initial promise in proof of concept trials,[49] but failed to reproduce the data in subsequent trials.[50,51]

Negative allosteric modulation (NAM) of the metabotropic glutamate receptor, mGlu5, has received significant medicinal chemistry research over the years.[52,53] There have been numerous development compounds identified and progressed to clinical studies, with dose selection aided by PET studies. However, despite these efforts, the trials have failed to yield positive data, with prominent compounds such as Basimglurant (RO4917523/RG7090)[54,55] and Mavoglurant (AFQ056)[56] failing proof of concept studies in PD,[57,58] depression,[59] fragile X syndrome,[60,61] and other indications.[62]

Thus there have been many notable failures. However, looking back some compounds were perhaps advanced more in hope than on data. For example, early GSIs and GSMs did not clearly demonstrate modulation of amyloid levels in the clinic. In terms of cognition enhancers, perhaps target validation could have been better and it is clear that relying on animal models of cognition is not a viable strategy. As a number of projects did employ PET imaging, it at least permits the mechanism of action to be disproven. However, the major factor for the attrition of most of the mechanisms can be attributed to target validation, hence improving the link between target and disease, ideally via genetics, should be an area of focus going forward.

Despite these numerous disappointments, there have also been numerous major successes as can be seen from the steady stream of drugs reaching the marketplace in the last decade, **Table 2**, including many first-in-class drugs, as listed above. In addition to therapeutic drugs, there have been significant advances in the PET field, as discussed by Mercier and Provins in Chapter 7.02. Progress and Challenges in the Development if PET Ligands to Aid CNS Drug Discovery. This chapter highlights the utility of PET to enhance the success rate of CNS drug discovery and highlights the progress in identifying PET ligands for different biological target classes. The chapter also highlights the fact that PET ligands have not only been used to measure target engagement in the CNS, but there are several examples of PET ligands being used for patient diagnosis/stratification and also in longitudinal studies to measure disease progression, for example, amyloid PET ligands such as PiB, etc. Although lagging somewhat behind, there have been significant recent advances in the tau PET ligand area and this may be an area for future review.

There are also several major areas for hope in the field of CNS research. Notable areas are AD, where BACE inhibitors (reviewed in Chapter 7.08. Targeting β-Secretase (BACE) for the Treatment of Alzheimer's Disease) have made exceptional progress and demonstrated pronounced reductions in CNS amyloid levels. BACE inhibitors from a number of companies are now in late-stage clinical trials and offer the potential to test the amyloid hypothesis in AD. Hall and Gijsen review the fruit of a sustained industry-wide assault on BACE, which is now poised to test the amyloid hypothesis after many years. In a similar vein, Hall and Velter review GSMs (Chapter 7.07. Targeting Gamma Secretase for the Treatment of Alzheimer's Disease), which at one point appeared to be a more promising approach than BACE inhibition to tackle amyloid. Despite significant effort, few compounds have reached clinical trials, apparently hampered by target and compound toxicologies, and those that have reached clinical trials appear to display moderate efficacy at best.

In Chapter 7.05. CGRP Antagonists for the Treatment of Migraine, Dubowchik and Bell chart the progress and status of CGRP antagonists for the treatment of migraine. The mechanism holds great potential due to its novel mechanism, which would block the CGRP-mediated vasodilation, instead of actively inducing vasoconstriction as the triptans, which are $5HT_{1B/1D}$ agonists. Due to the potential advantage, CGRP antagonism promised to allow a prophylactic migraine treatment, which sparked huge interest from the pharmaceutical industry. Despite many years of sustained research and the fact that four compounds have demonstrated clinical efficacy, no CGRP antagonist has yet been launched. The chapter highlights the numerous challenges that researchers have

overcome to identify potent, orally bioavailable antagonists for this family B GPCR. Despite overcoming these challenges, other issues have been encountered, such as elevation of liver enzymes, which have hampered development and perhaps tampered the potential to deliver a prophylactic treatment. Perhaps based on this, Merck recently agreed to license their CGRP programme to Allergan.[63] Hopefully deals like this will ultimately lead to the approval of a CGRP antagonist.

Antagonism of central orexin receptors has been of interest due to their potential role in sleep, addiction, stress, and anxiety. In Chapter 7.06. Orexin Receptor Antagonists for the Treatment of Sleep, Shireman and Letavic review the substantial body of work that has been conducted to identify antagonists for the OX1 and OX2 GPCRs. Several companies have committed effort to this field, and despite rapid early progress and positive clinical data, compound-specific issues were encountered, which prevented further development. Merck have identified numerous development candidates, and their effort has recently been rewarded with the approval of Suvorexant in 2014, **Table 2**. In addition, the area has recently seen some licensing activity with Janssen collaborating on the development of their clinical compound JNJ-42847922 (now also known as MIN-202) to Minerva[64] and Eisai entering a worldwide collaboration on E2006/Lemborexant to Purdue Pharma.[65] Deals such as these may conceivably facilitate future orexin antagonist approvals.

In Chapter 7.09. Targeting phophodiesterases in the CNS, Kehler summarizes the phosphodiesterase (PDE) research in the CNS field. This area has seen sustained research on several family members, with some research groups, e.g., Pfizer actually employing a platform approach to the area. Family members are discussed in turn with reference made to selectivity and structural biology as well as clinical development candidates. Despite much promise, there has been some disappointment within this class, including the PDE9 inhibitor PF-4447943, which failed to improve cognition despite showing target engagement in CSF. Despite this, other research groups are actively pursuing PDE9 inhibitors, although the main area of interest remains PDE10.

Epilepsy is the only specific disease area covered in this section as there has been a diverse array of drug discovery approaches, and in some cases the molecular pharmacology of drugs has not always been elucidated with certainty. Thus in the epilepsy chapter, Kurokawa et al. provide an overview of antiepileptic drugs (AEDs) before covering the approaches employed to identify new compounds and targets. They then comment on some of the more recent AED approvals and next-generation therapeutics in development, then conclude with some recent advances.

Reuillon et al. cover AMPA receptor modulators (Chapter 7.11. Modulating AMPA Receptors for the Treatment of CNS Disorders), focusing on PAMs and highlighting development compounds from several groups. The chapter also comments on notable advances in the antagonist field, namely the advancement to late-stage trails of several antagonists and the approval of perampanel for epilepsy. In addition, some very recent and new advances in targeting TARPs, AMPA regulatory proteins that have selective regional brain distribution, and therefore offers the potential to identify compounds that can antagonize the AMPA receptor without inducing the undesirable side effects is also discussed.

The two chapters in this section that cover the sodium (Witty et al., Chapter 7.04. Sodium Channel Blockers for the Treatment of Pain) and calcium (Beswick, Chapter 7.03. Progress in the Discovery of the Ca Channel Blockers for the Treatment of Pain) ion channels review huge bodies of work. Approaches to both targets face similar challenges in navigating subtype selectivity, measuring target engagement, and also the potential that more than one subtype may contribute to efficacy. In this respect the authors do a fantastic job to cover a huge amount of literature and succinctly while highlighting the numerous clinical development compounds that have been identified by multiple groups.

While it was initially thought of as infeasible to identify and develop CNS penetrant kinase inhibitors due to the molecular properties of ATP-competitive inhibitors, the field has progressed significantly in recent years and has made excellent progress, initially in the oncology field, e.g., alectinib (currently approved for NSCLC) and AZD3759, but also now for a range of CNS diseases, as reviewed in Chapter 7.10. Inhibiting kinases in the CNS.

Inevitably not all areas of CNS research are reviewed in this section. Some promising areas have not been reviewed as they are still too early, or the approaches are somewhat fragmented. For example, there has been a significant and ongoing effort to tackle tau in AD; however, the approaches have been desperate, tackling posttranslational modifications (mainly phosphorylation) and aggregation. Similarly, while there is research targeting α-synuclein, there is insufficient for a comprehensive review article.

References

1. http://www.wsj.com/articles/SB10001424052748704474804576222463927753954.
2. http://www.independent.co.uk/news/business/news/gsk-scales-back-workforce-in-neuroscience-research-1890077.html.
3. http://www.telegraph.co.uk/business/2016/04/29/astrazeneca-embarks-on-cost-cutting-drive-as-it-sharpens-focus-o/.
4. https://www.bms.com/news/features/2013/Pages/Bristol-MyersSquibbEvolvesRDStrategy.aspx.
5. http://blogs.sciencemag.org/pipeline/archives/2013/11/08/exiting_two_therapeutic_areas.
6. http://blogs.sciencemag.org/pipeline/archives/2011/12/06/novartis_no_more_neuroscience.
7. Clinical Development Success Rates 2006–2015. https://www.bio.org/sites/default/files/Clinical%20Development%20Success%20Rates%202006-2015%20-%20BIO,%20Biomedtracker,%20Amplion%202016.pdf.
8. Hegde, S.; Schmidt, M. To Market, to Market–2005. *Ann. Rep. Med. Chem.* **2006,** *41*, 439–477.
9. Hegde, S.; Schmidt, M. To Market, to Market–2006. *Ann. Rep. Med. Chem.* **2007,** *42*, 505–554.
10. Hegde, S.; Schmidt, M. To Market, to Market–2007. *Ann. Rep. Med. Chem.* **2008,** *43*, 455–497.
11. Hegde, S.; Schmidt, M. To Market, to Market–2008. *Ann. Rep. Med. Chem.* **2009,** *44*, 577–632.

12. Hegde, S.; Schmidt, M. To Market, to Market–2009. *Ann. Rep. Med. Chem.* **2010,** *45,* 467–537.
13. Bronson, J.; Dhar, M.; Ewing, W.; Lonberg, N. To Market, to Market–2010. *Ann. Rep. Med. Chem.* **2011,** *46,* 433–502.
14. Bronson, J.; Dhar, M.; Ewing, W.; Lonberg, N. To Market, to Market–2011. *Ann. Rep. Med. Chem.* **2012,** *47,* 499–569.
15. Bronson, J.; Black, A.; Dhar, T. G. M.; Ellsworth, B. A.; Merritt, J. R. To Market, to Market–2012. *Ann. Rep. Med. Chem.* **2013,** *48,* 471–546.
16. Bronson, J.; Black, A.; Dhar, M.; Ellsworth, B. A.; Merritt, J. R. To Market, to Market–2013. *Ann. Rep. Med. Chem.* **2014,** *49,* 437–508.
17. Bronson, J.; Peese, K.; Black, A.; Dhar, M.; Pascine, A.; Ellsworth, B. A.; Merritt, J. R. To Market, to Market–2014. *Med. Chem. Rev.* **2015,** *50,* 461–576.
18. Bronson, J.; Black, A.; Dhar, M.; Ellsworth, B. A.; Merritt, J. R. To Market, to Market–2015. *Med. Chem. Rev.* **2016,** *51,* 439–540.
19. Gainor, J. F.; Sherman, C. A.; Willoughby, K.; Logan, J.; Kennedy, E.; Brastianos, P. K.; Chi, A. S.; Shaw, A. T. Alectinib Salvages CNS Relapses in ALK-Positive Lung Cancer Patients Previously Treated with Crizotinib and Ceritinib. *J. Thorac. Oncol.* **2015,** *10,* 232–236.
20. https://www.epilepsysociety.org.uk/news/epilepsy-drug-trobalt-retigabine-to-be-discontinued-14-09-2016.
21. Lilly Press Release 17th August 2010. https://investor.lilly.com/releasedetail.cfm?releaseid=499794.
22. Doody, R. S.; Raman, R.; Farlow, M.; Iwatsubo, T.; Vellas, B.; Joffe, S.; Kieburtz, K.; He, F.; Sun, X.; Thomas, R. G.; Aisen, P. S. Alzheimer's Disease Cooperative Study Steering Committee; Siemers, E.; Sethuraman, G.; Mohs, R.; Semagacestat Study Group. A Phase 3 Trial of Semagacestat for Treatment of Alzheimer's Disease. *N. Engl. J. Med.* **2013,** *369,* 341–350.
23. Coric, V.; Salloway, S.; van Dyck, C.; Kerselaers, W.; Kaplita, S.; Curtis, C.; Ross, J.; Richter, R. W.; Andreasen, N.; Brody, M.; Sharma, S. K.; Cedarbaum, J. M.; Berman, R. A Phase II Study of the Gamma-Secretase Inhibitor Avagacestat (BMS-708163) in Predementia Alzheimer's Disease. P1-343 *Alzheimer's Dementia* **July 2013,** *9* (4), P283. Supplement.
24. Preston, J.; Berman, R.; Kaplita, S.; Gandhi, K. K.; Lipschitz, A.; Tiller, J.; Yogendran, L.; Hodson, D. S.; Coric, V. Safety and Tolerability of Avagacestat (BMS-708163) in People with Predementia Alzheimer's Disease: Association with Nonmelonoma Skin Cancer. P1-340 *Alzheimer's Dementia* **July 2013,** *9* (4), P282–P283. Supplement.
25. Wilcock, G. K.; Black, S. E.; Hendrix, S. B.; Zavitz, K. H.; Swabb, E. A.; Laughlin, M. A. Eficacy and Safety of Tarenflurbil in Mild to Moderate Alzheimer's Disease: a Randomized Phase II Trial. *Lancet Neurol.* **2008,** *7,* 483–493.
26. Galasko, D. R.; Graff-Radford, N.; May, S.; Hendrix, S.; Cottrell, B. A.; Sagi, S. A.; Mather, G.; Laughlin, M.; Zavitz, K. H.; Swabb, E.; Golde, T. E.; Murphy, M. P.; Koo, E. H. Safety, Tolerability, Pharmacokinetics, and Abeta Levels after Short-term Administration of R-flurbiprofen in Healthy Elderly Individuals. *Alzheimer Dis. Assoc. Disord.* **2007,** *21* (4), 292–299.
27. Green, R. C.; Schneider, L. S.; Amato, D. A.; Beelen, A. P.; Wilcock, G.; Swabb, E. A.; Zavitz, K. H. Effect of Tarenflurbil on Cognitive Decline and Activities of Daily Living in Patients with Mild Alzheimer Disease. *JAMA* **2009,** *302,* 2557–2564.
28. Medhurst, A. D.; Atkins, A. R.; Beresford, I. J.; Brackenborough, K.; Briggs, M. A.; Calver, A. R.; Cilia, J.; Cluderay, J. E.; Crook, B.; Davis, J. B.; Davis, R. K.; Davis, R. P.; Dawson, L. A.; Foley, A. G.; Gartlon, J.; Gonzalez, M. I.; Heslop, T.; Hirst, W. D.; Jennings, C.; Jones, D. N.; Lacroix, L. P.; Martyn, A.; Ociepka, S.; Ray, A.; Regan, C. M.; Roberts, J. C.; Schogger, J.; Southam, E.; Stean, T. O.; Trail, B. K.; Upton, N.; Wadsworth, G.; Wald, J. A.; White, T.; Witherington, J.; Woolley, M. L.; Worby, A.; Wilson, D. M. GSK189254, a Novel H3 Receptor Antagonist that Binds to Histamine H3 Receptors in Alzheimer's Disease Brain and Improves Cognitive Performance in Preclinical Models. *J. Pharmacol. Exp. Ther.* **2007,** *321* (3), 1032–1045.
29. Nathan, P. J.; Boardley, R.; Scott, N.; Berges, A.; Maruff, P.; Sivananthan, T.; Upton, N.; Lowy, M. T.; Nestor, P. J.; Lai, R. The Safety, Tolerability, Pharmacokinetics and Cognitive Effects of GSK239512, a Selective Histamine H Receptor Antagonist in Patients with Mild to Moderate Alzheimer's Disease: a Preliminary Investigation. *Curr. Alzheimer Res.* **2013,** *10* (3), 240–251.
30. Jarskog, L. F.; Lowy, M. T.; Grove, R. A.; Keefe, R. S.; Horrigan, J. P.; Ball, M. P.; Breier, A.; Buchanan, R. W.; Carter, C. S.; Csernansky, J. G.; Goff, D. C.; Green, M. F.; Kantrowitz, J. T.; Keshavan, M. S.; Laurelle, M.; Lieberman, J. A.; Marder, S. R.; Maruff, P.; McMahon, R. P.; Seidman, L. J.; Peykamian, M. A. A Phase II Study of a Histamine H Receptor Antagonist GSK239512 for Cognitive Impairment in Stable Schizophrenia Subjects on Antipsychotic Therapy. *Schizophr. Res.* **2015,** *164,* 136–142.
31. F Egan, M.; Zhao, X.; Gottwald, R.; Harper-Mozley, L.; Zhang, Y.; Snavely, D.; Lines, C.; Michelson, D. Randomized Crossover Study of the Histamine H3 Inverse Agonist MK-0249 for the Treatment of Cognitive Impairment in Patients with Schizophrenia. *Schizophr. Res.* **2013,** *146,* 224–230.
32. Syed, Y. Y. Pitolisant: First Global Approval. *Drugs* **2016,** *76,* 1313–1318.
33. http://www.ema.europa.eu/docs/en_GB/document_library/EPAR_-_Summary_for_the_public/human/002616/WC500204748.pdf.
34. Information Taken From Axovant Website on PhIII (MINDSET) Trial http://axovant.com/pipeline/intepirdine-rvt-101/.
35. Lundbeck Press Release 16th July 2013. http://investor.lundbeck.com/releasedetail.cfm?releaseid=777646.
36. Lundbeck Press Release 22nd September 2016. http://investor.lundbeck.com/releasedetail.cfm?ReleaseID=990541.
37. Lezoualc'h, F.; Robert, S. J. The Serotonin 5-HT4 Receptor and the Amyloid Precursor Protein Processing. *Exp. Gerontol.* **2003,** *38,* 159–166.
38. Shen, F.; Smith, J. A. M.; Chang, R.; Bourdet, D. L.; Tsuruda, P. R.; Obedencio, G. P.; Beattie, D. T. 5-HT_4 Receptor Agonist Mediated Enhancement of Cognitive Function in Vivo and Amyloid Precursor Protein Processing in Vitro: A Pharmacodynamics and Pharmacokinetic Assessment. *Neuropharmacology* **2011,** *61,* 69–79.
39. Duvvuri, S.; Nicholas, T.; Leurent, C.; Raunig, D.; Plotka, A.; Schwam, E.; Grimwood, S.; Rowinski, C.; Rapp, T. L. Modulation of Soluble APPα in Brain by PF-04995274, a 5HT4 Partial Agonist, Following Single Oral Doses in Healthy Human Volunteers: Study Design and PK-pd Analysis. *Alzheimer's Dementia* **2012,** *8* (4), P288–P289. Supplement.
40. Okun, I.; Tkachenko, S. E.; Khvat, A.; Mitkin, O.; Kazey, V.; Ivachtchenko, A. V. From Anti-allergic to Anti-Alzheimer's: Molecular Pharmacology of Dimebon. *Curr. Alzheimer Res.* **2010,** *7* (2), 97–112.
41. Doody, R. S.; Gavrilova, S. I.; Sano, M.; Thomas, R. G.; Aisen, P. S.; Bachurin, S. O.; Seely, L.; Hung, D. Effect of Dimebon on Cognition, Activities of Daily Living, Behaviour, and Global Function in Patients with Mild-to-Moderate Alzheimer's Disease: a Randomised, Double-Blind, Placebo-Controlled Study. *Lancet* **2008,** *372,* 207–215.
42. Jones, R. W. Dimebon Disappointment. *Alzheimer's Res. Ther.* **2010,** *2,* 25.
43. Bezprozvanny, I. The Rise and Fall of Dimebon. *Drug News Perspect.* **2010,** *23* (8), 518–523.
44. Lightfoot, A. P.; Kew, J. N. C.; Skidmore, J. α7 Nicotinic Acetylcholine Receptor Agonists and Positive Allosteric Modulators. *Prog. Med. Chem.* **2008,** *46,* 131–171.
45. Walling, D.; Marder, S. R.; Kane, J.; Fleischhacker, W. W.; Keefe, R. S. E.; Hosford, D. A.; Dvergsten, C.; Segreti, A. C.; Beaver, J. S.; Toler, S. M.; Jett, J. E.; Dunbar, G. C. Phase 2 Trial of an Alpha-7 Nicotinic Receptor Agonist (TC-5619) in Negative and Cognitive Symptoms of Schizophrenia. *Schizophr. Bull.* **2016,** *42,* 335–343.
46. Prickaerts, J.; van Goethem, N. P.; Chesworth, R.; Shapiro, G.; Boess, F. G.; Methfessel, C.; Reneerkens, O. A. H.; Flood, D. G.; Hilt, D.; Gawryl, M.; Bertrand, S.; Bertrand, D.; König, G. EVP-6124, a Novel and Selective 7 Nicotinic Acetylcholine Receptor Partial Agonist, Improves Memory Performance by Potentiating the Acetylcholine Response of 7 Nicotinic Acetylcholine Receptors. *Neuropharmacology* **2012,** *62,* 1099–1110.
47. Information of the Status of EVP-6124 (encenicline) Taken From Alzforum Website 24th October 2016. http://www.alzforum.org/therapeutics/encenicline. http://www.alzforum.org/news/research-news/rare-severe-side-effects-sideline-some-phase-3-encenicline-trials.
48. Lieberman, J. A.; Dunbar, G.; Segreti, A. C.; Girgis, R. R.; Seoane, F.; Beaver, J. S.; Duan, N.; Hosford, D. A. A Randomized Exploratory Trial of an Alpha-7 Nicotinic Receptor Agonist (TC-5619) for Cognitive Enhancement in Schizophrenia. *Neuropyschopharmacology* **2013,** *38,* 968–975.
49. Umbricht, D.; Alberati, D.; Martin-Facklam, M.; Borroni, E.; Youssef, E. A.; Ostland, M.; Wallace, T. L.; Knoflach, F.; Dorflinger, E.; Wettstein, J. G.; Bausch, A.; Garibaldi, G.; Santarelli, L. Effect of Bitopertin, a Glycine Reuptake Inhibitor, on Negative Symptoms of Schizophrenia a Randomized, Double-blind, Proof-of-concept Study. *JAMA Psychiatry* **2014,** *71* (6), 637–646.
50. Roche Press Release 21st January 2014. Roche Provides Update on the First Two of Six Phase III Studies of Bitopertin in Schizophrenia. http://www.roche.com/media/store/releases/med-cor-2014-01-21.htm.

51. Bugarski-Kirola, D.; Wang, A.; Abi-Saab, D.; Blättler, T. A Phase II/III Trial of Bitopertin Monotherapy Compared with Placebo in Patients with an Acute Exacerbation of Schizophrenia – Results from the CandleLyte Study. *Eur. Neuropsychopharmacol.* **2014,** *24,* 1024–1036.
52. Rocher, J. P.; Bonnet, B.; Boléa, C.; Lütjens, R.; Le Poul, E.; Poli, S.; Epping-Jordan, M.; Bessis, A. S.; Ludwig, B.; Mutel, V. mGluR5 Negative Allosteric Modulators Overview: a Medicinal Chemistry Approach towards a Series of Novel Therapeutic Agents. *Curr. Top. Med. Chem.* **2011,** *11* (6), 680–695.
53. Célanire, S.; Duvey, G.; Poli, S.; Rocher, J. P. mGluR2 Activators and MGluR5 Blockers Advancing in the Clinic for Major CNS Disorders. *Ann. Rep. Med. Chem.* **2012,** *47,* 71–88.
54. Jaeschke, G.; Kolczewski, S.; Spooren, W.; Vieira, E.; Bitter-Stoll, N.; Boissin, P.; Borroni, E.; Büttelmann, B.; Ceccarelli, S.; Clemann, N.; David, B.; Funk, C.; Guba, W.; Harrison, A.; Hartung, T.; Honer, M.; Huwyler, J.; Kuratli, M.; Niederhauser, U.; Pähler, A.; Peters, J.-U.; Petersen, A.; Prinssen, E.; Ricci, A.; Rueher, D.; Rueher, M.; Schneider, M.; Spurr, P.; Stoll, T.; Tännler, D.; Wichmann, J.; Porter, R. H.; Wettstein, J. G.; Lindemann, L. Metabotropic Glutamate Receptor 5 Negative Allosteric Modulators: Discovery of 2-chloro-4-[1-(4-fluorophenyl)-2,5-dimethyl-1H-imidazol-4-ylethynyl]pyridine (Basimglurant, RO4917523), a Promising Novel Medicine for Psychiatric Diseases. *J. Med. Chem.* **2015,** *58,* 1358–1371.
55. Lindemann, L.; Porter, R. H.; Scharf, S. H.; Kuennecke, B.; Bruns, A.; von Kienlin, M.; Harrison, A. C.; Paehler, A.; Funk, C.; Gloge, A.; Schneider, M.; Parrott, N. J.; Polonchuk, L.; Niederhauser, U.; Morairty, S. R.; Kilduff, T. S.; Vieira, E.; Kolczewski, S.; Wichmann, J.; Hartung, T.; Honer, M.; Borroni, E.; Moreau, J.-L.; Prinssen, E.; Spooren, W.; Wettstein, J. G.; Jaeschke, G. Pharmacology of Basimglurant (RO4917523, RG7090), a Unique Metabotropic Glutamate Receptor 5 Negative Allosteric Modulator in Clinical Development for Depression. *J. Pharmacol. Exp. Ther.* **2015,** *353* (1), 213–233.
56. Vranesic, I.; Ofner, S.; Flor, P. J.; Bilbe, G.; Bouhelal, R.; Enz, A.; Desrayaud, S.; McAllister, K.; Kuhn, R.; Gasparini, F. AFQ056/mavoglurant, a Novel Clinically Effective MGluR5 Antagonist: Identification, SAR and Pharmacological Characterization. *Bioorg. Med. Chem.* **2014,** *22,* 5790–5803.
57. Kumar, R.; Hauser, R. A.; Mostillo, J.; Dronamraju, N.; Graf, A.; Merschhemke, M.; Kenney, C. Mavoglurant (AFQ056) in Combination with Increased Levodopa Dosages in Parkinson's Disease Patients. *Int. J. Neurosci.* **2016,** *126* (1), 20–24.
58. Petrov, D.; Pedros, I.; de Lemos, M. L.; Pallàs, M.; Canudas, A. M.; Lazarowski, A.; Beas-Zarate, C.; Auladell, C.; Folch, J.; Camins, A. Mavoglurant as a Treatment for Parkinson's Disease. *Expert Opin. Investig. Drugs* **2014,** *23* (8), 1165–1179.
59. Quiroz, J. A.; Tamburri, P.; Deptula, D.; Banken, L.; Beyer, U.; Rabbia, M.; Parkar, N.; Fontoura, P.; Santarelli, L. Efficacy and Safety of Basimglurant as Adjunctive Therapy for Major Depression: A Randomized Clinical Trial. *JAMA Psychiatry* **2016,** *73* (7), 675–684.
60. Berry-Kravis, E.; Des Portes, V.; Hagerman, R.; Jacquemont, S.; Charles, P.; Visootsak, J.; Brinkman, M.; Rerat, K.; Koumaras, B.; Zhu, L.; Barth, G. M.; Jaecklin, T.; Apostol, G.; von Raison, F. Mavoglurant in Fragile X Syndrome: Results of Two Randomized, Double-Blind, Placebo-controlled Trials. *Sci. Trans. Med.* **2016,** *8* (321), 321ra5.
61. National Fragile X Foundation Press Release 24th April 2014. https://fragilex.org/2014/research/news-reports-and-commentaries/novartis-announces-results-of-mavoglurant-mglur5-afq056-clinical-trials-and-the-conclusion-of-the-long-term-extension-study/and Fraxa Release 24th April 2014 http://www.fraxa.org/novartis-discontinues-development-mavoglurant-afq056-fragile-x-syndrome/.
62. Reilmann, R.; Rouzade-Dominguez, M. L.; Saft, C.; Süssmuth, S. D.; Priller, J.; Rosser, A.; Rickards, H.; Schöls, L.; Pezous, N.; Gasparini, F.; Johns, D.; Landwehrmeyer, G. B.; Gomez-Mancilla, B. A Randomized, Placebo-Controlled Trial of AFQ056 for the Treatment of Chorea in Huntington's Disease. *Mov. Disord.* **2015,** *30* (3), 427–431.
63. Allergan Press Release 7th July 2015. http://www.allergan.com/news/news/thomson-reuters/allergan-enters-into-licensing-agreement-with-merc.
64. J&J Press Release 19th June 2014. https://www.jnj.com/media-center/press-releases/johnson-johnson-innovation-catalyzes-new-and-exciting-science-and-technology-in-pharmaceutical-medical-device-diagnostic-and-consumer-healthcare-spaces. Minerva Press Release 21st January 2015. http://ir.minervaneurosciences.com/releasedetail.cfm?releaseid=892355.
65. Purdue Pharma Press Release 31st August 2015. http://www.purduepharma.com/news-media/2015/08/eisai-and-purdue-pharma-enter-worldwide-collaboration-to-develop-and-commercialize-lemborexant/.

PERMISSION ACKNOWLEDGMENTS

The following material is reproduced with kind permission of Taylor & Francis

Scheme 2 Cellular Imaging in Drug Discovery: Biomolecular Imaging and Informatics (HCS, HCA, HCI)
Figure 2 Past Present Future
Figure 5 Past Present Future
Figure 6 Past Present Future
www.taylorandfrancisgroup.com

The following material is reproduced with kind permission of Oxford University press

Table 1 Targeting G-quadruplex Nucleic Acids for Cancer Therapy
Table 2 Targeting G-quadruplex Nucleic Acids for Cancer Therapy
Figure 1 Protein Structure Prediction and Homology Modelling
www.oup.com

The following material is reproduced with kind permission of American Association for the Advancement of Science

Figure 3b,c Cellular Imaging in Drug Discovery: Biomolecular Imaging and Informatics (HCS, HCA, HCI)
www.aaas.org

The following material is reproduced with kind permission of Nature Publishing Group

Table 4 Use of Stem Cells in Toxicology
Table 6 Use of Stem Cells in Toxicology
Figure 17 Strategy and Tactics for Designing Analogs; Biochemical Characterization of the Large Molecules
Figure 30 Strategy and Tactics for Designing Analogs; Biochemical Characterization of the Large Molecules
Figure 2 Cellular Imaging in Drug Discovery: Biomolecular Imaging and Informatics (HCS, HCA, HCI)
Figure 3a Cellular Imaging in Drug Discovery: Biomolecular Imaging and Informatics (HCS, HCA, HCI)
Figure 4 Cellular Imaging in Drug Discovery: Biomolecular Imaging and Informatics (HCS, HCA, HCI)
Figure 5a Cellular Imaging in Drug Discovery: Biomolecular Imaging and Informatics (HCS, HCA, HCI)
Figure 9a Cellular Imaging in Drug Discovery: Biomolecular Imaging and Informatics (HCS, HCA, HCI)
Figure 20 Epigenetics: Novel Therapeutics Targeting Epigenetics
Figure 1 UCB5857
Figure 6 Empirical and Physics Based Calculations of Physical Properties
Figure 4 Progress and Challenges in the Development if PET Ligands to Aid CNS Drug Discovery
http://www.nature.com

7.01 Recent Advances and Future Directions in the Treatment of Epilepsy

T Kurokawa, Y Kazuta, and T Watanabe, Medicine Creation, Neurology Business Group, Eisai Co., Ltd., Tsukuba-shi, Ibaraki, Japan

© 2017 Elsevier Ltd. All rights reserved.

7.01.1	**Introduction**	1
7.01.1.1	General Introduction to Epilepsy	1
7.01.1.2	Classification of Epilepsy	2
7.01.1.3	Management of Epilepsy	2
7.01.2	**Anti-Epileptic Drugs**	2
7.01.2.1	First-Generation AEDs (–1970s)	2
7.01.2.2	Second-Generation AEDs (1980s–1990s)	3
7.01.2.3	Third-Generation AEDs (2000s)	3
7.01.3	**Preclinical Strategies for the Development of AEDs**	3
7.01.3.1	Overview of Common Preclinical Strategies	3
7.01.3.1.1	Random in vivo phenotypic screening	3
7.01.3.1.2	Structural modification of a known antiepileptic	7
7.01.3.1.3	Hypothesis-driven, target-based approach	8
7.01.3.2	Development of Levetiracetam, Brivaracetam, and Seletracetam	8
7.01.3.2.1	Levetiracetam	8
7.01.3.2.2	Development of second-generation compounds of levetiracetam	9
7.01.3.2.3	Summary	9
7.01.3.3	Development of Carbamazepine, Oxcarbazepine, and Eslicarbazepine Acetate	10
7.01.3.3.1	Carbamazepine	10
7.01.3.3.2	Oxcarbazepine	10
7.01.3.3.3	Eslicarbazepine acetate	11
7.01.3.4	Development of Perampanel	11
7.01.3.4.1	Background	11
7.01.3.4.2	Discovery of perampanel, a novel non-competitive AMPA receptor antagonist	12
7.01.3.4.3	Preclinical profile of perampanel	14
7.01.4	**Future Perspectives**	14
7.01.4.1	Overview	14
7.01.4.2	Next-Generation AEDs Currently Undergoing Clinical Development	15
7.01.4.3	Recent Advances in AED Development	15
7.01.4.3.1	Animal models and random phenotypic in vivo screening	15
7.01.4.3.2	Potential drug targets for AEDs	16
7.01.5	**Conclusion**	17
References		17
Relevant Websites		19

7.01.1 Introduction

7.01.1.1 General Introduction to Epilepsy

Epilepsy is a common neurological condition in the world. The estimated median prevalence of active epilepsy is 4.9 out of 1000 people in developed countries and 12.7 out of 1000 people in rural areas of developing countries.[1] Epilepsy is one of the oldest recognized conditions. The first description of an epileptic seizure was written in 2000 BC in the Akkadian language, which was spoken in the ancient region of Mesopotamia.[2] The word "epilepsy" is derived from the Greek verb, *epilambanem*, which means "to take hold of" or "to seize."

Epilepsy is simply defined as the predisposition to generate recurrent seizures. Epileptic seizures are sudden, brief episodes of involuntary body movement, and are also accompanied by loss of consciousness depending on the type of epilepsy. Epileptic seizures result from abnormal electrical discharges within the brain; therefore, depending on the part of the brain where the electrical discharges originate, these seizures can vary from an instantaneous lapse of attention or series of muscle spasms to more severe, prolonged convulsions. A single seizure does not necessarily indicate that someone has epilepsy, and up to 10% of all people experience one unproven seizure in their lifetime.[3] The International League Against Epilepsy currently defines epilepsy as a disease of the brain defined by any of the following conditions: (1) at least two unprovoked seizures occurring greater than 24 h apart; (2) one unprovoked seizure and a probability of further seizures similar to the general recurrence risk after two unprovoked seizures, occurring over the next 10 years; or (3) diagnosis of an epilepsy syndrome.[4]

7.01.1.2 Classification of Epilepsy

With advance in the diagnosis of epilepsy and genetic biotechnology, the classification of epilepsies has been revised several times. The modern epilepsy classification was first introduced in 1970 by the International League Against Epilepsy, and it was revised in 1981 to include the relationship between seizure type and electroencephalogram finding.[5] In 1989, it was again revised to provide a classification of epilepsies and epileptic syndromes that took account of seizure type and etiology.[6] Although a number of risk factors for the development of epilepsy, such as age, head injury, stroke, central nervous system infections, and developmental and genetic factors,[7] have been identified, the causes for more than 50% of cases of epilepsy remain unknown due to the heterogeneous nature of the condition.[8] Therefore, the classification does not cover the full spectrum of epileptic conditions; however, it is helpful for providing a clinical overview of the condition. Recently, the International League Against Epilepsy recommended an update to the classification, introducing new terms and concepts; they recommended replacing the etiologic categories of *idiopathic*, *symptomatic*, and *cryptogenic* with categories of *genetic*, *structural-metabolic*, and *unknown*.[9] The general classification of epilepsy is shown in Fig. 1.

7.01.1.3 Management of Epilepsy

Despite advances in surgical procedures for treating epilepsy, pharmacotherapy remains the primary therapeutic means of management. In the past three decades, more than 20 antiepileptic drugs (AEDs) have been developed and approved. The successful management of epilepsy relies on accurate diagnosis and the proper selection and utilization of pharmacotherapy. Approximately 70% of patients with newly diagnosed epilepsy remain seizure-free after starting on the currently available AEDs.[10] However, since these medications fail to control seizures in 30% of patients, there remains a considerable medical need for more efficacious drugs for the management of epilepsy.

7.01.2 Anti-Epileptic Drugs[11,12]

7.01.2.1 First-Generation AEDs (— 1970s)

Potassium bromide was the first effective AED to be popularized when, in 1857, Sir Charles Locock commented in the *Lancet* on his use of potassium bromide in 15 cases of "hysterical epilepsy" in young women.[13] Since then and until the early 1970s, AEDs were generally developed only after a chance discovery that a compound had anti-convulsant properties. One well-known example of a drug developed using this approach is the still commonly used medication phenobarbital, which was serendipitously found to have anti-convulsant properties by Alfred Hauptmann in 1912.

Epilepsy is a result of excessive abnormal activity of the cortical neurons in the brain, and the current pharmacological era of AED therapy began with the discovery of the antiepileptic effects of anesthetics and hypnotics. In 1937, Tracy Putnam and Houston

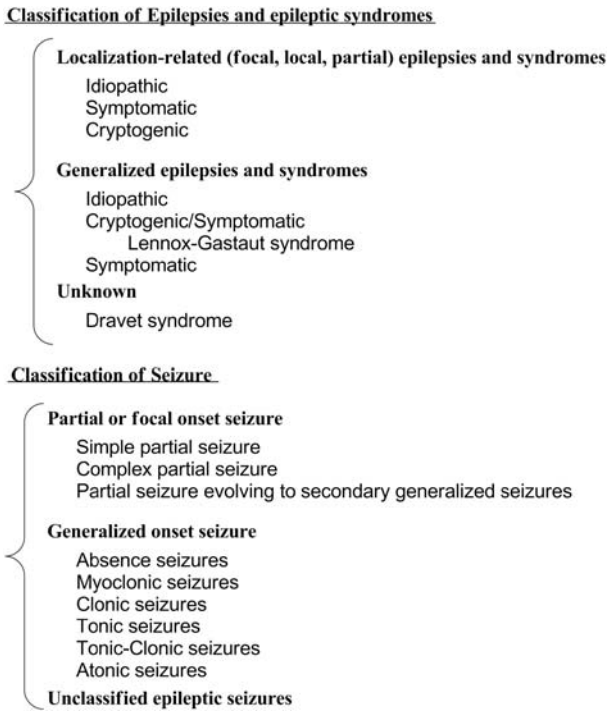

Fig. 1 General classification of epilepsy.

Merritt discovered the strong anti-convulsant properties of phenytoin in electroshock-induced seizure animal models, making phenytoin the first AED discovered by means of animal experimentation. The next AEDs to be developed were primidone, ethosuximide, the benzodiazepines, carbamazepine, and valproic acid. Although the anti-convulsant properties of valproic acid, which remains a first-line choice for the prevention of generalized seizures, was discovered serendipitously, carbamazepine, which is also still a widely used first-line AED, was developed empirically. Current clinically approved AEDs are summarized in Table 1 and Fig. 2.

7.01.2.2 Second-Generation AEDs (1980s–1990s)

At the end of the 1970s, large AED screening programs such as the Anticonvulsant Screening Program (ASP) of the National Institute of Neurological Disorders and Stroke (NINDS) of the US National Institutes of Health (NIH) began screening new chemical entities to encourage and facilitate the discovery and development of new therapeutic agents for the symptomatic treatment of epilepsy. By using a random screening approach with simple rodent models of seizures such as the maximal electroshock (MES) and pentylenetetrazole (PTZ)-induced seizure models, these programs identified many promising lead compounds. Although these animal models of acute seizures do not fully reflect the "true epilepsy" that occurs in epileptic brains, they are technically simple to perform and permit high throughput, and by the end of the 20th century this approach had afforded a range of novel AEDs, including lamotrigine, gabapentin, and topiramate. Although these AEDs have good efficacy and a broad spectrum of activities against different types of seizure, they also have strong central nervous system side effects such as sedation and motor impairment because they act mainly via Na^+ channel blockade and gamma-aminobutyric acid (GABA) potentiation. Therefore, although random screening using simple models of acute seizures is suitable for obtaining broad-spectrum AEDs, it might not be suitable for obtaining AEDs that are effective against drug-refractory seizures or that can prevent or modify the condition. Although many promising novel AEDs were discovered during this period, it was also realized that the broad-spectrum approach would need to be adjusted if drugs with efficacy against drug-resistant seizures were to be developed.

7.01.2.3 Third-Generation AEDs (2000s)

Since 2000, a number of novel AEDs identified by using chronic seizure animal models such as kindling and GAERS, or non-conventional acute seizure models such as 6 Hz model, in tandem with older animal models of acute seizures, have started to be launched. Through this kind of approach, several promising anti-epileptic drug candidates for the treatment of drug-resistant epilepsy were identified. In addition, some AEDs with different mechanisms of actions from conventional ones such as Na^+ channel blockade, GABA potentiation or Ca^{2+} channel blockade, have been placed on the market, like levetiracetam with SV2A binding, retigabine with K^+ channel activator or perampanel with AMPA antagonist. And also in clinical, several novel AEDs have shown highly efficacy, such as stiripentol in Dravet syndrome, vigabatrin in West syndrome, and rufinamide in Lennox–Gastaut syndrome. It may be argued that broad spectrum concept is not suitable to identify AEDs with higher efficacy in refractory epilepsy. Since many epilepsy patients have suffered from pharmacoresistant epilepsy, AED research has shifted from a broad-spectrum approach to a more target-based approach with prevention and modification of epilepsy as the targets for the next generation of AEDs.

7.01.3 Preclinical Strategies for the Development of AEDs

7.01.3.1 Overview of Common Preclinical Strategies

Historically, AEDs have been developed using one of three preclinical strategies: (1) random in vivo phenotypic screening; (2) structural modification of a known antiepileptic; or (3) hypothesis-driven, target-based approach.[12] Since each approach has its own pros and cons (see Table 3), it is likely that the development of the next generation of AEDs will require complementary hybridization of these approaches.

7.01.3.1.1 Random in vivo phenotypic screening

Until recently, most AED development programs followed a random phenotypic screening approach using animal models of seizures. This approach has afforded a range of useful lead compounds and has contributed greatly to the development of many of the clinically effective AEDs currently available. The screening campaign of the US NIH is one such example of this approach, and this program was instrumental in the development of several currently available AEDs (eg, felbamate [Felbatol]; topiramate [Topamax]; lacosamide [Vimpat]; retigabine [Potiga]; and rufinamide [Banzel, Inovelon]).[14]

Rodent models of seizures are the most commonly used means of screening for compounds with antiepileptic activity (Table 2). In these models, susceptibility to generate seizures is induced via electrical or chemical stimuli or genetic modification. Several experimental models have been developed for the various epilepsies and epileptic syndromes, including pharmacoresistant epilepsy, and each model offers, to some extent, a means of differentiating an exploratory AED from existing AEDs. Therefore, historically, the development of novel animal models of seizures is closely related to the discovery of new AEDs.

The success of random in vivo phenotypic screening can be attributed to the translatability of the animal models in the clinical development of AEDs. Animal models with a similarly high predictive value do not exist for other central nervous system disorders, such as bipolar disorder and migraine.[15] Further advantages of using animal models are that they are sensitive to the anticonvulsant

Table 1 Current clinically approved antiepileptic drugs[12]

Antiepileptic drug	*Year of approval*[a]	*Mechanism of action*	*Approved indications*	*Marketing company*
Potassium bromide	1857	GABA potentiation(hypothesized mechanism of action)	Primary generalized tonic–clonic seizures, myoclonic seizures	Dow
Phenobarbital	1912	GABA potentiation	Partial and generalized convulsive seizures, status epileptus, sedation, anxiety disorders, sleep disorders	Bayer
Phenytoin	1938	Na^+ channel blockade	Partial and generalized convulsive seizures, focal seizures, status epilepticus, trigeminal neuralgia	Parke-Davis/Pfizer
Trimethadione	1946	T-type Ca^{2+} channel blockade	Absence seizures	Abbott
Primidone	1954	GABA potentiation	Partial onset seizures, primary generalized tonic–clonic seizures, focal seizures, myoclonic seizures	Imperial Chemical Industries
Ethosuximide	1958	T-type Ca^{2+} channel blockade	Absence seizures	Parke-Davis/Pfizer
Diazepam	1963	GABA potentiation (GABA A receptor benzodiazepine site)	Convulsive disorders, status epilepticus, anxiety disorder, alcohol withdrawal	Roche
Carbamazepine	1964	Na^+ channel blockade	Partial onset seizures, primary generalized tonic–clonic seizures, trigeminal neuralgia, bipolar disorder	Novartis
Valproic acid	1967	Multiple (GABA potentiation, Na^+ channel blockade, T-type Ca^{2+} channel blockade or NMDA receptor inhibition, etc.)	Partial onset seizures, absence seizures, migraine prophylaxis, bipolar disorder	Sanofi/Abbott
Clonazepam	1968	GABA potentiation (GABA A receptor benzodiazepine site)	Lennox–Gastaut syndrome, akinetic seizures, mycolonic seizures, absence seizures, panic disorders	Roche
Clobazam	1975	GABA potentiation (GABA A receptor benzodiazepine site)	Adjunctive therapy for Lennox–Gastaut syndrome, anxiety disorders	Hoechst Roussel/Lundbeck/Sanofi
Progabide	1985	GABA potentiation	Primary generalized tonic–clonic seizures, Lennox–Gastaut syndrome, mycolonic seizures, muscle hypertonia	Synthelado
Vigabatrin	1989	GABA potentiation (GABA aminotransferase inhibition)	Infantile spasms, adjunctive therapy for refractory complex partial seizures	Sanofi/Lundbeck
Lamotrigine	1990	Na^+ channel blockade, glutamate transporter inhibition	Partial onset seizures, adjunctive therapy for primary generalized tonic–clonic seizures and Lennox–Gastaut syndrome, bipolar disorder	GlaxoSmithKline
Oxcarbazepine	1990	Na^+ channel blockade	Partial onset seizures	Novartis
Felbamate	1993	Multiple (GABA potentiation, Na^+ channel blockade, Ca^{2+} channel blockade or NMDA receptor inhibition, etc.)	Partial onset seizures, adjunctive therapy for Lennox–Gastaut syndrome	Carter-Wallance/MedPointe Pharmaceuticals
Gabapentin	1993	Ca^{2+} channel blockade ($\alpha 2\delta$ subunit)	Partial onset seizures, postherpetic neuralgia	Parke-Davis/Pfizer
Topiramate	1995	Multiple (GABA potentiation, Na^+ channel blockade, Ca^{2+} channel blockade, AMPA receptor inhibition, kainate receptor inhibition or carbonic anhydrate II inhibition, etc.)	Partial onset seizures, primary generalized tonic–clonic seizures, adjunctive therapy for Lennox–Gastaut syndrome	Janssen/Johnson & Johnson
Tiagabine	1996	GABA potentiation (GABA reuptake inhibition)	Adjunctive therapy for partial onset seizures	Novo Nordisk

Levetiracetam	2000	SV2A modulation, high-voltage-activated N-type Ca^{2+} channel blockade	Partial onset seizures, myoclonic seizures, primary generalized tonic–clonic seizures	UCB Pharma
Zonisamide	2000	Na^{+} channel blockade, T-type Ca^{2+} channel blockade	Partial seizures	Elan
Stiripentol	2002	GABA potentiation (GABA aminotransferase inhibition, GABA reuptake inhibition), Na^{+} channel blockade, lactate dehydrogenase inhibition	Dravet syndrome	Biocodex
Pregabalin	2004	Ca^{2+} channel blockade ($\alpha 2\delta$ subunit), L-type Ca^{2+} channel blockade	Adjunctive therapy for partial onset seizures, neuropathic pain, anxiety disorder, fibromyalgia	Pfizer
Rufinamide	2004	Na^{+} channel blockade	Adjunctive therapy for Lennox–Gastaut syndrome	Eisai
Lacosamide	2008	Enhanced slow inactivation of voltage-gated Na^{+} channels, NMDA receptor antagonism (glycine site)	Partial onset seizures	UCB Pharma
Eslicarbazepine acetate	2009	Na^{+} channel blockade	Partial onset seizures	Bial/Eisai
Retigabine	2011	K^{+} channel activation, GABA aminotransferase inhibition	Adjunctive therapy for partial onset seizures	GlaxoSmithKline
Perampanel	2012	AMPA receptor antagonism	Adjunctive therapy for partial onset seizures and primary generalized tonic–clonic seizures	Eisai

[a]Year in which the drug was first approved or marketed in the United States or Europe.

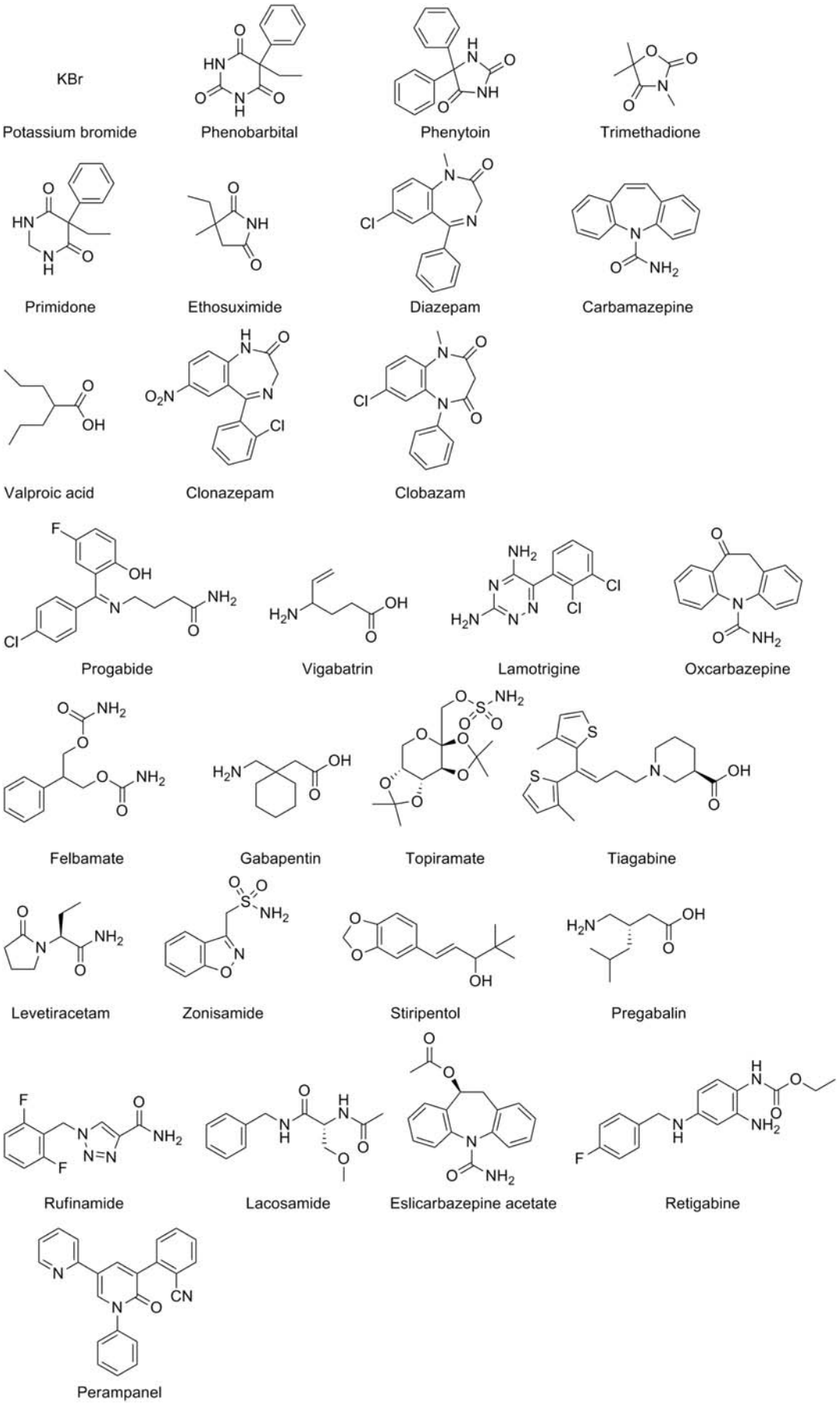

Fig. 2 Structures of the clinically approved antiepileptic drugs shown in **Table 1**.

Table 2 Representative animal models of seizures[12,16–18]

Seizure model	*Seizure modelled*	*Description*
Acute seizure models		
Maximal electroshock (MES)	Generalized tonic–clonic seizure	In the MES test, rodents receive a brief (0.2 s) 50- or 60-Hz electrical stimulus to induce maximal seizures of their hind limbs, with tonic extension as the endpoint of the test. This test is a gold standard for the early detection of anticonvulsant activity
Subcutaneous pentylenetetrazole (scPTZ)	Absence or myoclonic seizure	In the scPTZ test, a convulsive dose of PTZ is subcutaneously administered and rodents are observed, usually for 30 min, for the occurrence of a threshold seizure. This test is a gold standard for the early detection of anticonvulsant activity
6 Hz psychomotor	Therapy-resistant epilepsy (depending on current intensity)	Electrical stimulation via low-frequency (6 Hz) rectangular pulses of 0.2-ms duration is delivered through corneal electrodes for a total of 3 s to induce seizures that are reminiscent of the psychomotor seizures occurring in human limbic epilepsy. At high currents (eg, 44 mA), most antiepileptic drugs loose efficacy, suggesting that this may be a useful model of therapy-resistant limbic seizures
Audiogenic seizure	Generalized seizures	High-frequency sound is used to induce seizures in the rodent. This model has high sensitivity for detecting anticonvulsant effects. Regardless of mechanism of action, most current antiepileptic drugs show an effect in this model
Chronic seizure models		
Kindling	Partial seizures	Chronic model that is currently used by most antiepileptic drug discovery programs and is thought to adequately predict anticonvulsant activity against partial seizures in the clinic. Repeated application of electrical stimuli via a depth electrode in the limbic system (amygdala or hippocampus) of rats induces seizures that are permanently enhanced in severity and duration. Modified kindling models, such as the phenytoin-resistant kindled rat and the lamotrigine-resistant kindled rat, have been developed as pharmacoresistant epilepsy models. The corneal kindled mouse model is a simple modified kindling model that enables high-throughput screening
GAERS (genetic absence epileptic rat from Strasbourg)	Generalized absence seizures	GAERS is a genetic model of generalized absence seizures. All GAERS rats develop spike-wave electrographic seizures. A homozygous, missense, single mutation in the gene encoding Cav3.2 T-type Ca^{2+} channel has been reported in the GAERS rat
Others		
Status epilepticus	Status epilepticus	Status epilepticus is a life-threatening condition in humans that is characterized by continuous seizure or multiple seizures with loss of consciousness. Experimental rodent models represent the continuous seizure state, which can be induced by kainic acid, pilocarpine, lithium-pilocarpine, or electrical stimulation

Table 3 Pros and cons of common approaches to the preclinical development of antiepileptic drugs

Preclinical approach	*Pros*	*Cons*
Random in vivo phenotypic screening	Direct detection of in vivo efficacy Novel mechanisms of action found serendipiously	Difficult to understand structure-activity relationship Labor-intensive screening Identification of mechanism of action
Structural modification of a known antiepileptic	Clear starting point for medicinal chemistry Established assay system	Differentiation from previously developed antiepileptic drugs
Hypothesis-driven, target-based approach	Clear rationale Compound optimization	Drug target validation

effects of a compound regardless of its mechanism of action, and this offers the opportunity to find compounds with novel mechanisms of action. On the other hand, this approach more often than not yields lead compounds with multiple or unclear mechanisms of action, which generally makes it difficult to develop the compound into a marketable drug.

7.01.3.1.2 Structural modification of a known antiepileptic

New drug discovery from analogs of known drugs is a widely used approach in medicinal chemistry. Without exception in AED development, more than 10 new AEDs that are structural analogs of existing AEDs have been developed, and most have advantageous profiles in term of pharmacokinetics, toxicity, tolerability, and reduced potential for drug interactions compared with their parent compound. These AEDs are regarded as second-generation compounds to former AEDs such as carbamazepine. An advantage of this approach over in vivo phenotypic screening lies in compound optimization. Furthermore, this would enable a less costly operation because there is no need to establish an assay or seed-finding campaign, if the differentiation strategy is established.

7.01.3.1.3 Hypothesis-driven, target-based approach

Few AEDs have been developed by means of hypothesis-driven, target-based strategies targeted at mechanisms of action related to seizure generation such as imbalances in GABAergic inhibition/glutamatergic excitation. Although the heterogeneous nature of epilepsy makes this approach difficult, advances in our understanding of the mechanisms of epilepsy have supported drug discovery via hypothesis-driven strategies. Hypothesis-driven, target-based drug development has advantages over in vivo phenotypic screening in terms of compound optimization; however, in hypothesis-driven, target-based drug development it is often difficult to validate the biological target.

7.01.3.2 Development of Levetiracetam, Brivaracetam, and Seletracetam[19–22]

Levetiracetam and its analogs, carbamazepine and its analogs, and perampanel are examples of AEDs that were developed by means of the three preclinical development approaches of (1) random in vivo phenotypic screening; (2) structural modification of a known antiepileptic; and (3) hypothesis-driven, target-based approach.

7.01.3.2.1 Levetiracetam

Levetiracetam was originally synthesized as a structural analog of the nootropic piracetam (2-oxo-1-pyrrolidine acetamide), which itself is used clinically to enhance the seizure protection conferred by carbamazepine in epileptic patients.[23] Nootropic drugs, which are used clinically as cognition-enhancing agents in the elderly, have shown anti-convulsant effects in models of various seizures; however, by themselves they have only weak anti-convulsant effects.[24–26] The antiepileptic properties of levetiracetam were identified by means of random in vivo phenotypic screening using a mouse model of audiogenic seizures. Discovery of levetiracetam and its related compounds is shown in Fig. 3.

Photo-affinity labeling studies using [^{3}H]ucb 30889, a radioactive ligand of levetiracetam, have shown that the target protein of levetiracetam is synaptic vesicle protein SV2 isoform A, which is present in all neurons.[27,28] SV2A is the most widely distributed isoform of SV2 that is ubiquitously expressed in the brain and in edocrine cells. SV2A is thought to be involved in neuronal excitability, neurotransmitter exocytosis, and vesicle fusion modulation.[28–34] In animal models of epilepsy, there was a strong correlation between the binding affinities for SV2A of levetiracetam and its close analogs and the anti-seizure activities of these compounds.[28] However, the precise mechanism of how the binding of levetiracetam to SV2A is involved in its anti-seizure effects is not yet fully understood. There are reports that levetiracetam selectively inhibits high-voltage-activated N-type Ca^{2+} channels[35–37] or presynptic voltage-dependent Ca^{2+} channels,[38] and SV2A binding may be a key component of this Ca^{2+} channel blockade.

Levetiracetam has a unique anti-seizure profile compared to first-generation AEDs. It does not have efficacy in the MES and PTZ-induced seizure models, but it does have substantial antiepileptic effects in absence seizure and kindling models with a very high safety margin (Table 4).[21,39,40] Levetiracetam is currently indicated for the treatment of partial onset seizures, myoclonic seizures, and primary generalized tonic–clonic seizures.

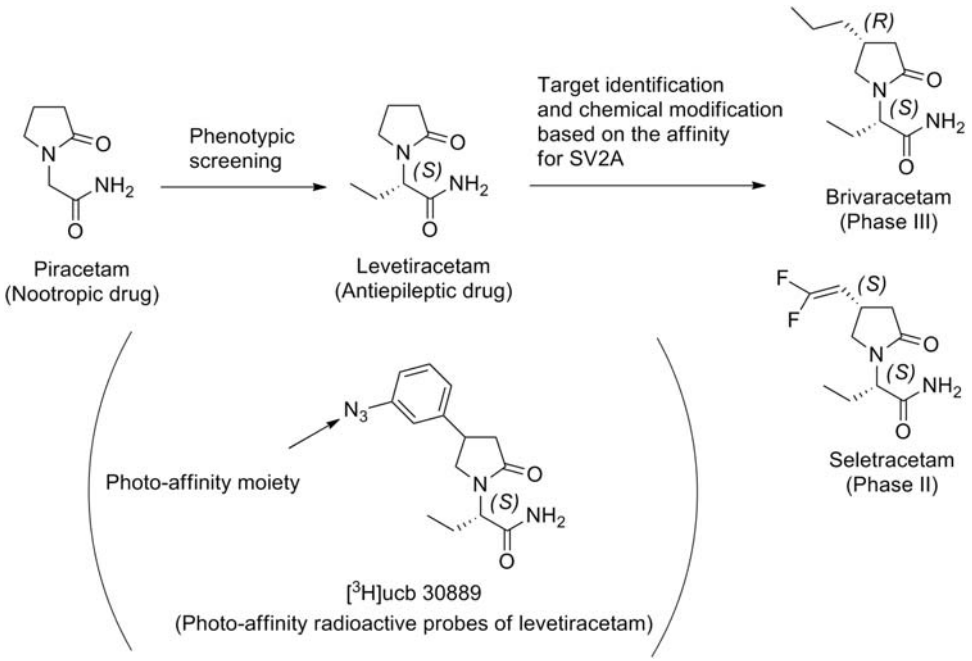

Fig. 3 Discovery of levetiracetam and its related compounds.

Table 4 In vivo activities of levetiracetam, brivaracetam, and selectracetam[19]

Model	*Levetiracetam*	*Brivaracetam*	*Seletracetam*
Binding affinity for SV2A (pIC_{50})	6.1	7.1	7.1
Mouse MES	ineffective	113 (i.p.)	ineffective
Mouse PTZ (s.c.)	ineffective	30 (i.p.)	ineffective
Mouse 6 Hz (44 mA)	19.4 (i.p.)	4.4 (i.p.)	–
Rat GEARS	>170 (i.p.)	67.9 (i.p.)	0.15 (i.p.)
Mouse corneal kindling	7.3 (i.p.)	1.2 (i.p.)	0.31 (i.p.)
Protective index (mouse corneal kindling[a], TD_{50}/ED_{50})	148	46	1048

[a]Protective index is the ratio of TD_{50} (rotarod test) to ED_{50} (seizure protection) in corneal kindled mice.

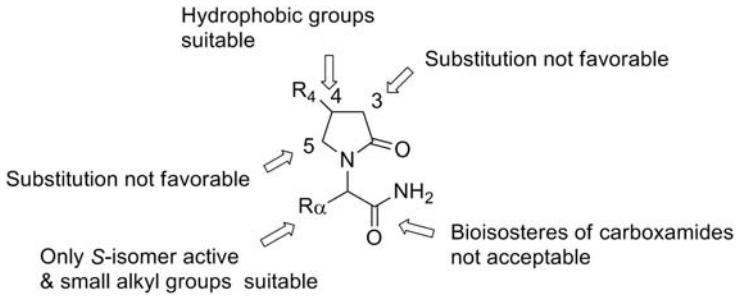

Fig. 4 Structure–activity relationship of levetiracetam and its analogs based on binding affinity.

7.01.3.2.2 Development of second-generation compounds of levetiracetam

Structure–activity relationship studies of levetiracetam were systematically conducted to identify analogs with higher binding affinities for SV2A than levetiracetam.[22] During this screening, compounds were tested both in a binding assay with [^{3}H]ucb 30889 and in a mouse model of audiogenic seizures, and the binding affinity for SV2A and anti-seizure effect of the compounds were found to be well correlated.[28] The structure–activity relationships of analogs of 2-oxopyrrolidine acetamide based on their affinity for SV2A is summarized in Fig. 4.

The carboxamide moiety of levetiracetam was found to be play an important role in the binding affinity, and other bioisosteres of carboxamide, such as carboxylic acid, ethyl ester, thioamide, and amidine, were not acceptable. Substitution of various side chains at the α-position of the carboxamide of levetiracetam was also examined; however, none of the compounds examined exceeded levetiracetam in terms of SV2A binding affinity. The *S*-enantiomers of side-chain analogs had higher binding affinity than the *R*-enantiomers. Although substitution at the 3- and/or 5-position of the 2-pyrrolidine ring did not produce compounds with improved binding affinity, the addition of hydrophobic groups at the 4-position did. Through the exploration of substitution at the 4-position, brivaracetam (propyl moiety at the 4-position of levetiracetam) and seletracetam (2,2-difluorovinyl moiety at the 4-position of levetiracetam) were discovered as second-generation antiepileptics of levetiracetam.

Brivaracetam has 10-fold higher binding affinity for SV2A and superior efficacy than levetiracetam in various animal models of epilepsy.[41,42] Unlike levetiracetam, brivaracetam has anti-seizure effects in the MES and PTZ-induced seizure models, possibly due to its inhibition of voltage-dependent Na^+ channels.[43] Brivaracetam has a linear pharmacokinetic profile in humans, 100% oral bioavailability, and dose-dependent efficacy. Four phase III trials have been completed, and several long-term, open-label, follow-up trials of brivaracetam as adjunctive treatment are on-going.[44]

Seletracetam also has 10-fold higher binding affinity for SV2A and greater in vivo efficacy in many animal models than levetiracetam. In particular, it has a higher protective index (1048) than has levetiracetam in corneal kindled mice.[45] Unlike brivaracetam, selectracetam does not decrease MES and PTZ-induced seizures in mice because it has no effect on voltage-dependent Na^+ channels.[46] The phase II clinical trials of seletracetam seem to be on hold.

7.01.3.2.3 Summary

The successful development of brivaracetam and selectacetam shows a viable approach for the development of next-generation antiepileptic drugs. Brivaracetam and selectacetam were discovered through target-based in vitro high-throughput screening developed after the mechanism of action of levetiracetam had been identified. A large proportion of antiepileptic compounds have been discovered via phenotypic screening, and further elucidation of their mechanisms of action might be a shortcut to producing next-generation compounds with superior efficacy compared with the parent compounds. Compounds obtained by chemical structural modification do not necessary have the exact same pharmacological, toxicological, and pharmacokinetic profiles as the parent compound. Small changes in the chemical structure of a molecule can cause marked changes in compound's potency, range of anti-convulsant activities, or safety margin, and brivaracetam and selectacetam are examples where this has been harnessed to provide improved AEDs.

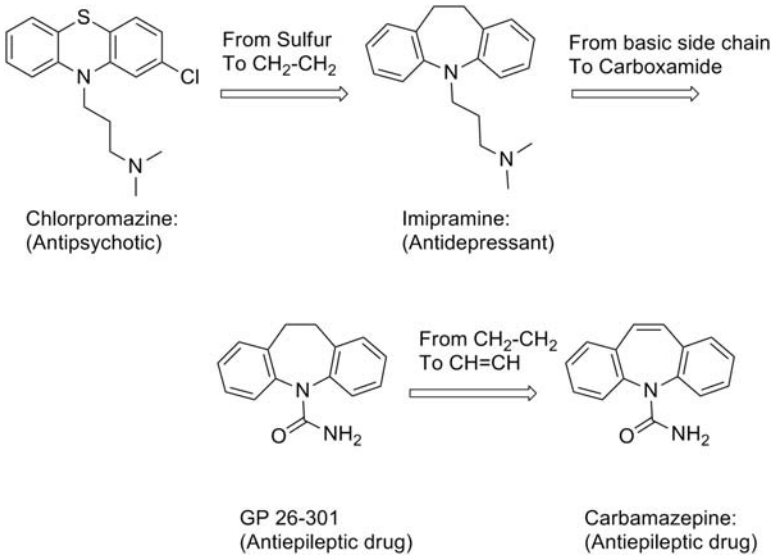

Fig. 5 Discovery of carbamazepine.

7.01.3.3 Development of Carbamazepine, Oxcarbazepine, and Eslicarbazepine Acetate

7.01.3.3.1 Carbamazepine

The antiepileptic effects of carbamazepine derivatives were discovered by chance in the 1950s when tricyclic derivatives of the antipsychotic chlorpromazine were synthesized.[47] One of these tricyclic derivatives, imipramine, in which the sulfur in the central moiety of chlorpromazine is replaced with CH_2–CH_2, was discovered to have antidepressant rather than antipsychotic effects. Next, GP 26–301, in which the basic side chain of imipramine is substituted for a carbamoyl group, was found to have potent anticonvulsant activity in an MES model. Further optimization by replacing CH_2–CH_2 in the central moiety of GP 26–301 with CH=CH produced the anticonvulsant carbamazepine (Fig. 5).

Carbamazepine is currently one of the most widely used first-line AEDs for the prevention of partial and generalized tonic–clonic seizures, but it is ineffective against absence or myoclonic seizures. Carbamazepine is also used to treat neuropathic pain and some psychiatric disorders. Although carbamazepine has multiple targets, it is widely accepted that the main mechanism of action is inhibition of voltage-gated sodium channels.[47,48]

The most frequently observed adverse effects associated with carbamazepine are dizziness, drowsiness, unsteadiness, nausea, and vomiting, which generally occur at the start of therapy. These neurotoxic adverse effects are dose-related and reversible in most patients. Idiosyncratic reactions in the hemopoietic system, skin, liver, and cardiovascular system have been also reported.[49] The mechanisms of toxicity are unclear; however, 10,11-epoxide, an active metabolite of carbamazepine, is likely responsible for at least some of the adverse effects (Fig. 6).[50] Moreover, it is well known that carbamazepine and 10,11-epoxide are potent inducers of CYP3A4; therefore, carbamazepine has high potential for interacting with other drugs.

7.01.3.3.2 Oxcarbazepine

Since carbamazepine is not effective in several types of patients and is associated with several adverse effects, a number of derivatives were synthesized and examined preclinically with the hope of finding a compound with an improved efficacy and safety profile. Of these derivatives, oxcarbazepine had the most promising profile and was selected for further development.[51] In preclinical and clinical studies, oxcarbazepine was shown to have anticonvulsant efficacy comparable to that of carbamazepine.

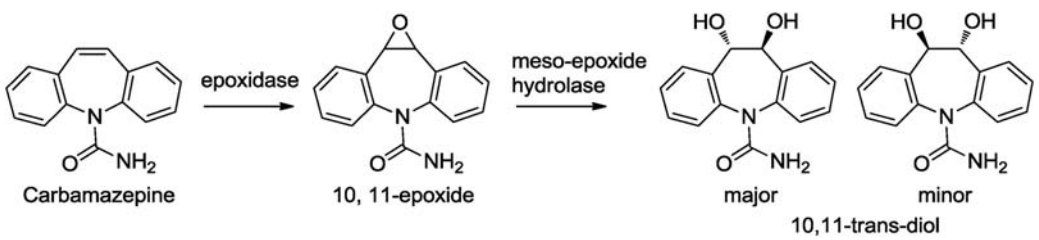

Fig. 6 Metabolism of carbamazepine.

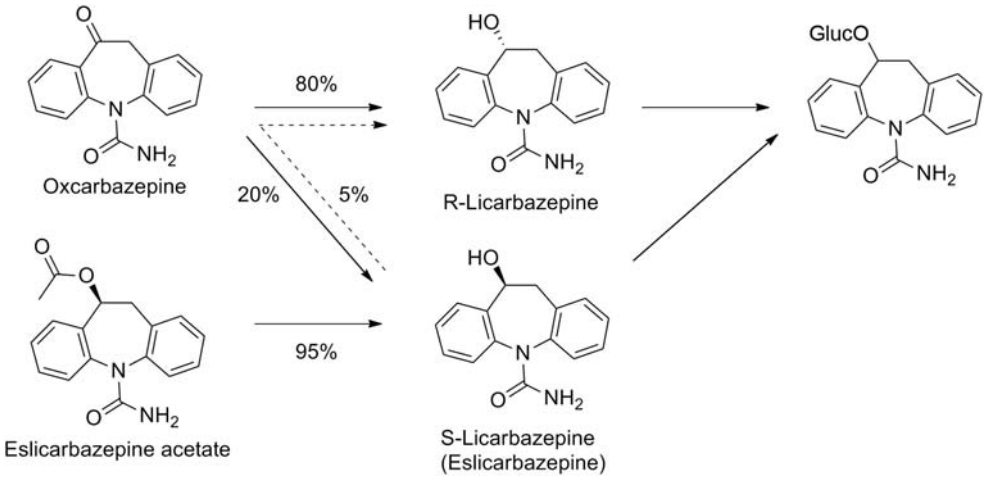

Fig. 7 Metabolism of oxcarbazepine and eslicarbazepine acetate.

The adverse effect profiles of oxcarbazepine and carbamazepine are also similar, although the adverse effects associated with oxcarbazepine are less frequent and less severe than those associated with carbamazepine.[52] In addition, there is no auto-induction of CYP mediated metabolism, and there are fewer interactions of oxcarbazepine with other drugs compared with carbamazepine. The major difference between oxcarbazepine and carbamazepine is in their metabolism. Oxcarbazepine has a 10-ketone group, and is almost completely metabolized to the biologically active compound licarbazepine in humans (Fig. 7).[53] Licarbazepine has an (*S*)/(*R*) ratio of approximately 80/20.[11] Licarbazepine is then conjugated to a glucuronide and excreted by the kidneys. Unlike carbamazepine, oxcarbazepine is not oxidatively metabolized to 10,11-epoxide, which is probably one reason why oxcarbazepine is associated with fewer allergic reactions, less enzyme induction, and fewer side effects. Oxcarbazepine is currently indicated as monotherapy or adjunctive therapy for the treatment of partial onset seizures in adults and children.

7.01.3.3.3 Eslicarbazepine acetate

Since oxcarbazepine is an achiral prodrug that is metabolically transformed into a mixture of two active enantiomers, its corresponding esters are also potential prodrugs. A number of esters of licarbazepine were synthesized and tested in a MES model using gastric tube administration,[54] and from these esters, eslicarbazepine acetate was found to be as potent anticonvulsant as carbamazepine, and more potent than both oxcarbazepine and (*R*)-licarbazepine acetate (Table 5). Interestingly, in another MES model using intraperitoneal administration, eslicarbazepine acetate was nearly threefold more potent than eslicarbazepine and had a wider protective index.[54]

In humans, eslicarbazepine acetate is metabolized mainly to (*S*)-licarbazepine. Less than 5% of (*S*)-licarbazepine is then converted to (*R*)-licarbazepine via oxidation to oxcarbazepine (Fig. 7).[11,55] As a result, the area under the curve for (*S*)-licarbazepine is 16% greater than that for the equivalent dose of oxcarbazepine. Indeed, patients in a phase III clinical trial who were treated with carbamazepine benefited in reduction in seizure frequency from the addition of concomitant eslicarbazepine acetate. In addition, eslicarbazepine acetate significantly improved quality of life during long-term (1-year), open-label studies conducted after the phase III studies.[56] Eslicarbazepine is currently approved as adjunctive therapy in adults with partial-onset seizures with or without secondary generalization.

7.01.3.4 Development of Perampanel[57–59]

7.01.3.4.1 Background

Glutamate is an excitatory neurotransmitter in the human brain that has principal roles in a variety of physiological functions. Glutamate receptors are classified based on their mode of signal transduction as either metabotropic glutamate receptors or ionotropic glutamate receptors. Metabotropic glutamate receptors are coupled with G-protein and they modulate synaptic transmission

Table 5 In vivo activity of carbamazepine, oxcarbazepine, (*R*)-licarbazepine acetate, and eslicarbazepine acetate[54]

Parameter	*Carbamazepine*	*Oxcarbazepine*	*(R)-licarbazepine acetate*	*Eslicarbazepine acetate*
T_{max} (h)	2	2	8	2
Rat maximal electroshock seizure model ED_{50} (mg/kg)	5.4 ± 0.8	10 ± 1.9	10.9 ± 2.3	4.7 ± 0.9
Rotarod TD_{50} (mg/kg)	251 ± 9.8	>1000	>1000	358.7 ± 17.2
Protective index (TD_{50}/ED_{50})	46.5	>100	>91.7	76.3

via a second messenger. Ionotropic glutamate receptors possess a ligand-gated ion channel and therefore mediate fast synaptic transmissions. Ionotropic glutamate receptors are further differentiated into three types by the appearance of their selective antagonists (ie, α-amino-3-hydroxy-5-methyl-4-isoxazolepropanoic acid—AMPA; kainite, and *N*-methyl-D-aspartic acid—NMDA). Since abnormal increases in glutamate concentration in the brain trigger seizure activity,[60] epilepsy and some epileptic syndromes are thought to be linked to over-activity of ionotropic glutamate receptors, and the AMPA ionotropic glutamate receptors is most critical for the generation of epileptic discharges.[61] Furthermore, the AMPA receptor is a crucial mediator of seizure propagation.[62] Thus, antagonism of the AMPA receptor is a promising target for AED development. Representative AMPA receptor antagonists are shown in Fig. 8.[63,64]

The first selective AMPA receptor antagonists were quinoxalinedione derivatives such as NBQX; however, this series of compounds has poor blood–brain barrier penetration and poor solubility under neutral conditions. A polar moiety was introduced in an attempt to improve the compound's solubility; however, this resulted in less blood–brain barrier penetration. Other competitive AMPA receptor antagonists, fanapanel and tezampanel, have not yet advanced to clinical trial. Selurampanel, a quinazolinedione sulfonamide, is being tested in a phase II study for the treatment of epilepsy, migraine, and tinnitus.

The exploration of novel AMPA receptor antagonists has now expanded to include a variety of non-competitive antagonists. These compounds have the functional advantage that they exert their antagonist activity even when the level of glutamate is elevated. The 2,3-benzodiazepine-type compounds, which include talampanel, drove early research into AMPA antagonism. Talampanel demonstrated modest in vitro inhibitory efficacy but better in vivo efficacy, indicating blood–brain barrier penetration. However, it was also found to have a short-half life.[19] Talampanel was assessed in clinical trials for the treatment of various disease conditions, including epilepsy and amyotrophic lateral sclerosis, but it is yet to reach the market. Therefore, perampanel is the first selective AMPA receptor antagonist that was approved for the treatment of epilepsy.

7.01.3.4.2 Discovery of perampanel, a novel non-competitive AMPA receptor antagonist

To identify a starting compound for medicinal chemistry, two high-throughput screening campaigns were conducted using a rat cortical neuron AMPA-induced cell-death assay and a tritium-labeled AMPA binding assay to detect compounds with competitive AMPA receptor antagonist activity. Hit compounds were further screened by using an AMPA-induced Ca^{2+} influx assay to evaluate inhibitory potency and exclude false-positives. Through these assays, 2,4-diphenyl-4*H*-[1,3,4]oxadiazin-5-one, which is a commercially available compound, was selected for further development (AMPA-induced Ca^{2+} influx assay, $IC_{50} = 9.17$ μM; Fig. 9). The selection of this compound was based not only on its potential for chemical modification but also on its structural uniqueness compared with previously reported AMPA antagonists.[57]

The initial structure–activity relationship study for 2,4-diphenyl-4*H*-[1,3,4]oxadiazin-5-one focused on replacement of the two side-chains attached to the central oxadiazinone core. Introduction of an aliphatic substituent such as a benzyl or cyclohexyl group instead of the phenyl group resulted in a marked decrease in receptor inhibitory activity, indicating that conjugated aromaticity is necessary for AMPA inhibitory activity in oxadiazinone derivatives.[57] Next, the central ring structure was altered to try and produce a compound with improved AMPA receptor inhibitory activity and metabolic stability. Keeping the carbonyl group and the two phenyl substituents on the central ring structure, several chemical modifications were examined (Fig. 9). Introduction of diazinone ($IC_{50} = 28.10$ μM) or converting the central core to a pyridone derivative ($IC_{50} = 69.54$ μM, 57.72 μM) diminished but still

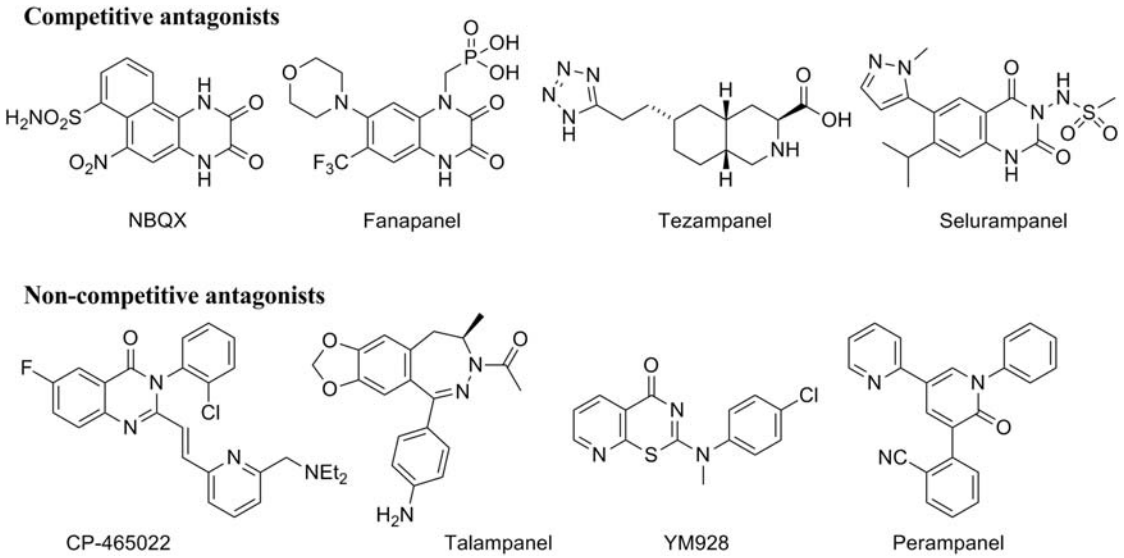

Fig. 8 AMPA (α-amino-3-hydroxy-5-methyl-4-isoxazolepropanoic acid) antagonists.

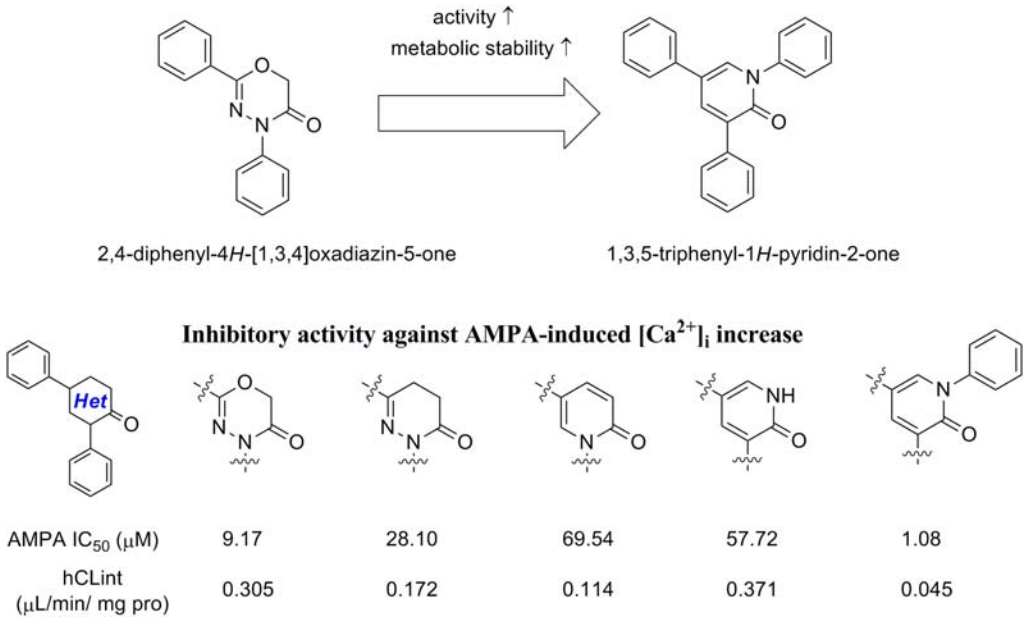

Fig. 9 Exploration of the central oxadiazinone core of 2,4-diphenyl-4*H*-[1,3,4]oxadiazin-5-one.

maintained in vitro inhibitory activity of the compound. A comparison of the two pyridone isomers suggested that acidic hydrogen affected metabolic stability in humans, and the presence of acidic hydrogen is also known to generally hamper blood–brain barrier penetration. Therefore, addition of one more phenyl group to the pyridone central core to mask the acidic hydrogen produced 1,3,5-triphenyl-1*H*-pyridin-2-one, which showed dramatically improved AMPA inhibitory activity ($IC_{50} = 1.08$ μM) and intrinsic clearance in humans in a microsome stability assay. The identification of 1,3,5-triphenyl-1*H*-pyridin-2-one was a major milestone in the drug discovery history of perampanel.

Next, a systematic series of structure–activity relationship studies using the 1,3,5-triphenyl-1*H*-pyridin-2-one template were conducted by focusing on optimization of the individual aromatic rings located at the 1, 3, and 5-positions of the central pyridone ring (Fig. 10). At the 5-position, 2-pyridine was found to be the optimal substituent in terms of receptor inhibitory activity.

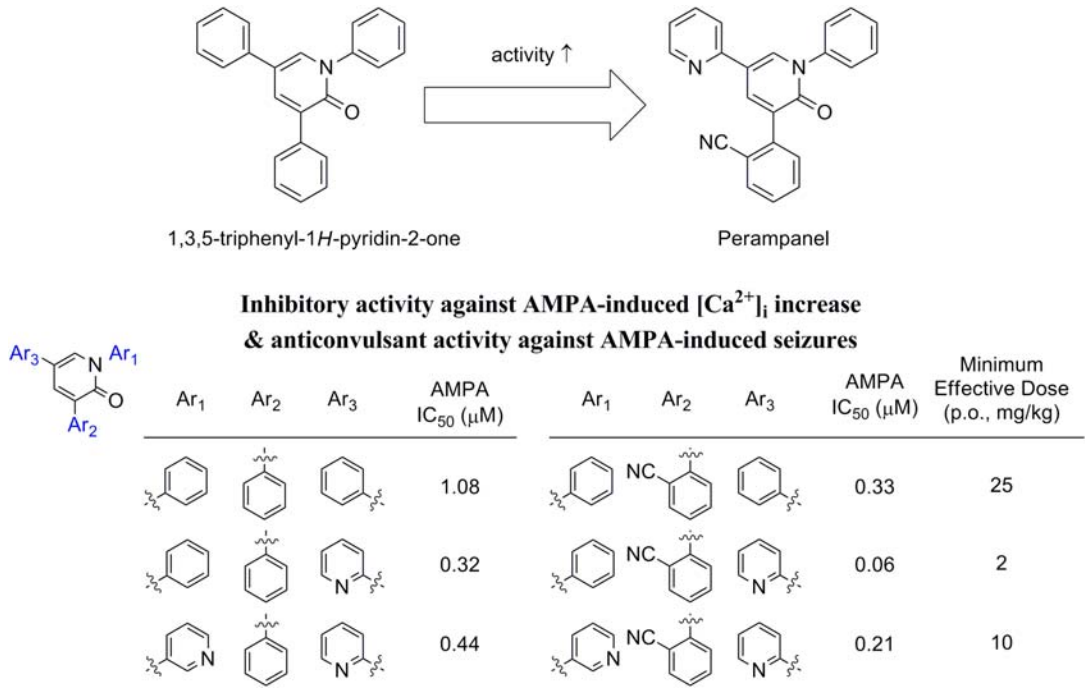

Fig. 10 Optimization of the individual aromatic rings of 1,3,5-triphenyl-1*H*-pyridin-2-one.

The replacement of phenyl with 2-pyridyl improved the receptor inhibitory activity at the submicromolar level. Substitutions at the 3-position were also found to increase receptor inhibitory activity. 2-cyanophenyl was the most active, by comparison with the compounds with a cyano moiety at the *ortho*, *meta*, or *para* positions. The effects of cyano, halogen (F or Cl), alkyl, or alkoxy substituents at the *ortho* position were also examined. A cyano substitution was found to have the greatest impact on receptor inhibitory activity.[57] Both the electron-withdrawing properties and the bulkiness of a cyano substituent on the phenyl group, which induces a twist angle between the central pyridone core and the 3-aryl ring, were found to be essential for improving receptor inhibitory activity. At the 1-position, a wide range of substituents produced AMPA receptor inhibitory activity, but the optimization indicated that nonsubstituted phenyl produced the best activity in vitro.

The most potent compounds from the structure–activity relationship studies were further evaluated in vivo using a mouse AMPA-induced seizure model (**Fig. 10**) and the data indicated that 2-(2-oxo-1-phenyl-5-pyridin-2-yl-1,2-dihydropyridin-3-yl) benzonitrile (perampanel) was the most promising compound, leading to its selection for clinical development.

7.01.3.4.3 Preclinical profile of perampanel

Perampanel is a novel pyridone derivative that has extremely high receptor inhibitory activity in vitro and in vivo ($IC_{50} = 60$ nM in an AMPA-induced Ca^{2+} influx assay; minimum effective dose = 2 mg/kg, per os in an AMPA-induced seizure model) and a favorable pharmacokinetic profile for clinical use in that it has good metabolic stability in humans (intrinsic clearance = 0.009 μL/min/mg protein) and good blood–brain barrier penetration (cerebrospinal fluid-to-unbound plasma concentration ratio in mice = 1.14).[57] A binding assay[58] indicated that perampanel binds at a similar binding site on the AMPA receptor as other non-competitive AMPA antagonists. Furthermore, perampanel is highly selective for the AMPA receptor against 63 physiologically relevant enzymes, ion channels, and neurotransmitter transporters, including NMDA and kainate receptors.[57]

The in vivo potency of perampanel was confirmed in several animal models of seizures. Perampanel demonstrated antiseizure activity in both the MES and subcutaneous PTZ (scPTZ) models of acute seizures (MES test, $ED_{50} = 1.6$ mg/kg p.o.; scPTZ test, $ED_{50} = 0.94$ mg/kg p.o.).[58] These ED_{50} values are much lower than those for carbamazepine ($ED_{50} = 21$ mg/kg p.o. and > 100 mg/kg p.o., respectively) and sodium valproate ($ED_{50} = 460$ mg/kg p.o. and 350 mg/kg p.o., respectively). In addition, perampanel prevents 6-Hz seizure (at 44 mA) ($ED_{50} = 2.8$ mg/kg, p.o.).[59]

Perampanel was proven to be efficacious in a rat amygdala kindling model of chronic seizures.[58] However, it was inactive at doses of 1, 3, and 10 mg/kg p.o. in a GAERS (Generic Absence Epilepsy Rat from Strasbourg) model.[58] A similar trend has been observed with other non-competitive AMPA receptor antagonists.[65]

In a lithium–pilocarpine rat model of status epilepticus, 8 mg/kg of perampanel administered intravenously prevented further seizures when administered at 10, 30, or 60 min after seizure onset, and its efficacy was observed in all individual animals tested.[59] In contrast, 20 mg/kg diazepam administered intravenously terminated the seizure only when administered at 10 min after seizure onset in some of the animals tested.

The effect of co-administration of perampanel with other AEDs was also examined in animal models of seizures.[59] Enhanced seizure protection was observed in the 6-Hz seizure test with combinations of perampanel with carbamazepine, phenytoin, or valproic acid. In a rat amygdala kindling model, at least additive and in some cases a synergistic effect, was observed when perampanel was combined with levetiracetam, lamotorigine, carbamazepine, or valproic acid.

In a phase III study,[66–70] adjunctive perampanel reduced the frequencies of primary generalized tonic–clonic seizures as well as the one of partial-onset seizures, compared with placebo. Consequently, perampanel is now approved for the treatment of partial-onset seizure in over 45 countries, including European Union, United States, and Canada, and in 2015 the indications were expanded in the United States and European Union to include primary generalized tonic–clonic seizures.

7.01.4 Future Perspectives

7.01.4.1 Overview

Many AEDs have been developed since the first reported use of potassium bromide, and more than 20 AEDs are currently available. However, approximately 30% of patients with epilepsy still suffer from recurrent seizures.[10] Adverse events such as dizziness, somnolence, and fatigue are also still frequently reported.[71] Although some of the more recently launched AEDs have improved efficacy and safety profiles, more efficacious and better-tolerated AEDs are needed.

The AEDs currently available have been developed primarily for their effects in suppressing epileptic seizures, that is, they have been developed as anti-seizure drugs. A target for developing AEDs would be shifted to next stage. A drugs that prevent progression to epilepsy once a patient develops or is exposed to a risk factor, that is, drugs that are antiepileptogenic, may become a game-changer in epilepsy treatment.

Epileptic disorders have a heterogeneous pathological background, and pharmacoresistance can arise from multifactorial causes such as reduction of drug-target sensitivity and overexpression of multidrug transporters in the epileptic brain.[72] Therefore, the heterogeneous nature of epilepsy makes it difficult to treat. Further study of the genetic basis of epilepsy and of its etiologies, as well as of the mechanisms involved in AED resistance and the development to epileptic condition, will be indispensable in the development of next-generation AEDs.

7.01.4.2 Next-Generation AEDs Currently Undergoing Clinical Development

Some of the AEDs currently undergoing clinical investigation have novel chemical structures and mechanisms of action. Selected next-generation AEDs are summarized in Table 6 and Fig. 11.

Ganaxolone is a synthetic analog of the endogenous neurosteroid allopregnanolone, a metabolite of progesterone, that is currently undergoing phase III clinical trials in adults with partial seizures. YKP-3089 is an orally active small compound currently undergoing phase II clinical trials. YKP-3089 selectively inhibits the inactivated state of Na^+ channels and preferentially blocks persistent sodium current. It also increases inhibitory synaptic transmission by modulating presynaptic GABA release.[44] Naluzotan is a 5-hydroxytrytamine 1A receptor agonist currently undergoing phase II clinical trials for the treatment of epilepsy. 4-Chlorokynurenine is an NMDA gycine B receptor antagonist currently undergoing phase II clinical trials for the treatment of major depressive disorder and phase I clinical trials for the treatment of epilepsy, Parkinson's disease, and neuropathic pain. Tonabersat is a neuronal gap junction modulator currently undergoing phase I clinical development for the treatment of epilepsy.

7.01.4.3 Recent Advances in AED Development

7.01.4.3.1 Animal models and random phenotypic in vivo screening

Animal models of seizures have made a crucial contribution to the development of effective AEDs. Along with advances in genomics, certain genetic mutations that result in the development of epileptic disorders have been elucidated. These findings have led to new genetic variant-induced seizure models that are expected to more accurately reflect epilepsy in humans.[11] For example, changes in Na^+ channel pharmacosensitivity are associated with downregulation of the β1 and β2 subunits of Na^+ channels. Therefore, a transgenic model with a mutation in the β1 subunit gene (SCNB1) would potentially be one tool to tackle phamacoresistant epilepsy. As for antieplileptogenic drug, its discovery would require the adequate experimental models and also the diagnosis method for developing epileptic condition.

The basis of phenotypic screening for AED discovery is the exposure of the central nervous system to a series of test compounds. Along with the development of chemoinformatics, some favorable property to blood–brain barrier penetration have been proposed.[73] Various strategies to access biologically relevant areas in chemical space have been developed (eg, diversity-oriented synthesis, biology-oriented synthesis). These methodologies should help us to construct an adequate central nervous system-oriented library of compounds. Novel animal models and advances in medicinal chemistry will support AED discovery.

Table 6 Selected antiepileptic drugs currently undergoing clinical development

Antiepileptic drug	*Development phase*[a]	*Hypothesized mechanism of action*	*Targeted condition*	*Developing company*
Ganaxolone	Phase III	GABA A receptor modulation	Epilepsy, fragile X syndrome, anxiety, post-traumatic stress disorder	CoCensys, Marinus Pharmaceuticals
YKP-3089 (structure not disclosed)	Phase II	Selective blockade of the inactivated state of Na^+ channels and facilitation of presynaptic GABA release	Epilepsy	SK Biopharmaceuticals
Naluzotan	Phase II	5-HT1A receptor agonism, signal transduction modulation	Epilepsy	Epi Pharmaceuticals, Proximagen
4-Chlorokynurenine	Phase I	NMDA glycine B receptor antagonism, signal transduction modulation	Epilepsy, major depressive disorder, Parkinson's disease, neuropathic pain	VistaGen/Sanofi
Tonabersat	Phase I	Gap junction modulation	Epilepsy	Upsher–Smith, Proximagen

[a]Highest clinical study phase for epilepsy.

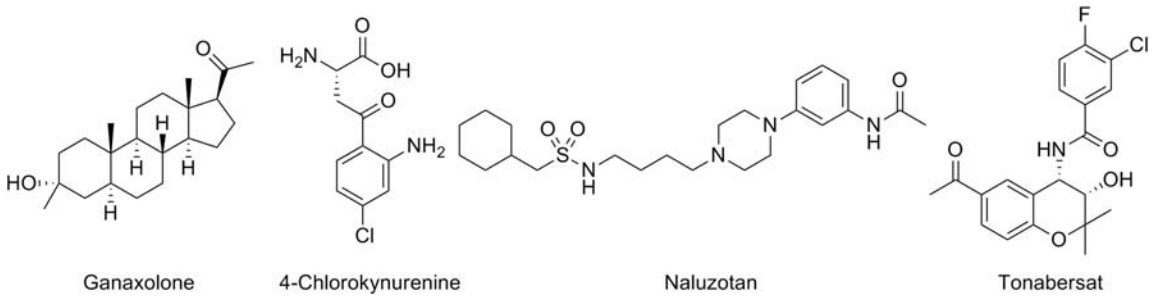

Fig. 11 Structures of the antiepileptic drugs currently undergoing clinical development shown in Table 6.

7.01.4.3.2 Potential drug targets for AEDs[12]

The majority of AEDs have been developed preclinically by means of in vivo phenotypic screening using animal models of seizures, which has meant that the mechanisms of action have only been identified after the compound was found to have antiepileptic effects. However, recent advances in our understanding of the cellular and molecular events involved in epilepsy has led to a shift towards hypothesis-driven, target-based approaches for the development of more efficacious and better-tolerated AEDs and antiepileptogenic drugs. In particular, systems biology incorporating functional genomics, transcriptomics, proteomics, epigenetics, and metabolomics, coupled with high-throughput technologies, is a powerful tool for identifying the causal pathways of ictogenesis and epileptogenesis, which can then be used to define new candidate targets.[74] Many existing AEDs exert their anti-seizure effects via voltage-gated sodium channel blockade and GABA potentiation, and reduced sensitivity of these targets is thought to be involved in the development of AED-resistant chronic epilepsy in humans and other species.[72,75] Therefore, novel AEDs acting through molecular targets that are not desensitized in the epileptic condition could offer promise for future AED discovery. Potential targets include inflammatory pathways, cation–chloride co-transporters, monoaminergic systems, and genetic and epigenetic targets.

7.01.4.3.2.1 Inflammatory pathways

Evidence indicating the strong involvement of inflammatory pathways in both ictogenesis and epileptogenesis is being rapidly accumulated.[76–78] Clinical evidence suggests that steroids and other anti-inflammatory drugs have anti-convulsant effects in some drug-resistant epilepsy syndromes.[77] Many preclinical studies have shown that interleukin-1β, toll-like receptor 4, and very late antigen-4 (also known as α4β1 integrin) have key roles in the inflammatory pathways involved in icogenesis and epileptogenesis. Belnacasan (Fig. 12), an interleukin-1β-converting enzyme, reduces acute and pharmacoresistant chronic seizures in mice.[79] It was examined in phase II clinical trials for the treatment of partial epilepsy; however, these clinical studies were stopped due to a business-related decision.[80] Toll-like receptor 4 is a key factor involved in innate immunity. The activation of interleukin-1 receptor/toll-like receptor signaling in neurons and glia (microglia and astrocytes) is considered to be a crucial step in the inflammatory brain response following seizures and epileptogenic brain insults.[81] Toll-like receptor 4 antagonists are reported to delay seizure precipitation and reduce acute and chronic seizure activity in rodents.[82]

7.01.4.3.2.2 Cation–chloride co-transporters

The shift from inhibitory to excitatory GABA-mediated transmission in neurons may contribute to the chronic hyperexcitability of epileptic neurons. This shift is attributed to the alternation in the intracellular chloride concentration caused by dramatic changes in expression of cation–chloride co-transporters such as bumetanide-sensitive sodium-potassium-chloride co-transporter 1 (NKCC1; also known as SLC12A2) and electroneutral potassium chloride co-transporter 2 (KCC2; also known as SLC12A5).[83] Therefore, these cation–chloride co-transporters could be a potential target for the treatment of refractory epilepsy and epileptogenesis. The NKCC1 inhibitor bumetanide (Fig. 12) is reported to block neonatal seizures in rodents.[84]

7.01.4.3.2.3 Monoaminergic systems

Patients with epilepsy suffer not only from seizures but also from considerable cognitive impairment and psychiatric comorbidities.[85] The monoaminergic system is heavily involved in psychiatric diseases such as anxiety, depression, bipolar disorders, and sleep disorders, but it also contributes to the regulation of the seizure threshold as well.[86–88] Therefore, molecules engaged in serotonergic, noradrenergic, or dopaminergic neurotransmission may be suitable targets for novel epilepsy treatments that attenuate the neurological comorbidities associated with epilepsy as well as control the generation of seizures. Naluzotan (Fig. 11), a selective 5-hydroxytryptamine 1A receptor agonist, is currently undergoing phase II clinical studies for the treatment of epilepsy. Approaches targeting a single mechanism that is involved in both seizures and the associated neurological comorbidities may be a promising means of discovering novel AEDs.

7.01.4.3.2.4 Genetic and epigenetic targets

In models of acquired epilepsy, gene expression appears to change in a time-dependent manner, and various events that occur simultaneously may be closely linked to epileptogenesis. Therefore, attractive novel targets for antiepileptogenesis could be found in the genetic and epigenetic alternations found in epilepsy.[89]

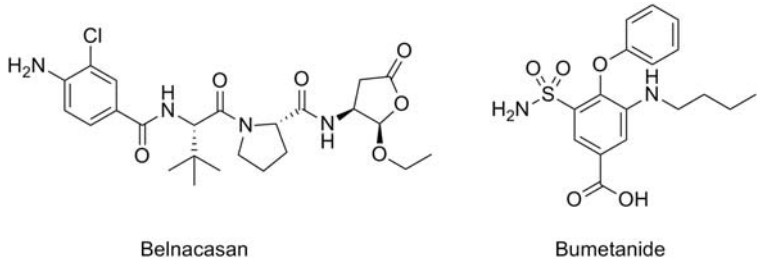

Fig. 12 Chemical structures of belnacasan and bumetanide.

7.01.5 Conclusion

Many patients with epilepsy still experience uncontrollable epileptic seizures despite the range of currently available AEDs, indicating that there are treatment targets that remain unidentified. Further elucidation of the molecular and genetic basis of the various seizure types and mechanisms of epileptogenesis will produce new avenues for the discovery of novel drug targets, which will lead to the development of novel epilepsy therapies. A target-based approach is the most direct means of obtaining more efficacious and better-tolerated AEDs and antiepileptogenetic drugs. However, despite recent technological innovations in this area and advances in our understanding of the cellular and molecular events leading to epilepsy, this approach remains difficult. One of the reasons for this is the complex intertwining of the many factors and molecules that are involved in the epileptic condition. Therefore, to move towards the ultimate goal in epilepsy treatment, which is a "permanent cure," we must utilize the full range of approaches to preclinical development that are available to us.

References

1. Ngugi, A. K.; Bottomley, C.; Kleinschmidt, I.; Sander, J. W.; Newton, C. R. Estimation of the Burden of Active and Life-Time Epilepsy: A Meta-Analytic Approach. *Epilepsia* **2010,** *51* (5), 883–890.
2. Magiorkinis, E.; Sidiropoulou, K.; Diamantis, A. Hallmarks in the History of Epilepsy: Epilepsy in Antiquity. *Epilepsy Behav.* **2010,** *17* (1), 103–108.
3. World Health Organization. Epilepsy. http://www.who.int/mediacentre/factsheets/fs999/en/.
4. Fisher, R. S.; Acevedo, C.; Arzimanoglou, A.; Bogacz, A.; Cross, J. H.; Elger, C. E.; Engel, J., Jr.; Forsgren, L.; French, J. A.; Glynn, M.; Hesdorffer, D. C.; Lee, B. I.; Mathern, G. W.; Moshé, S. L.; Perucca, E.; Scheffer, I. E.; Tomson, T.; Watanabe, M.; Wiebe, S. A Practical Clinical Definition of Epilepsy. *Epilepsia* **2014,** *55* (4), 475–482.
5. From the Commission on Classification and Terminology of the International League Against Epilepsy, Proposal for Revised Clinical and Electroencephalographic Classification of Epileptic Seizures. *Epilepsia* **1981,** *22,* 489–501.
6. Commission on Classification and Terminology of the International League Against Epilepsy. Proposal for Revised Classification of Epilepsies and Epileptic Syndromes. *Epilepsia* **1989,** *30* (4), 389–399.
7. Duncan, J. S.; Sander, J. W.; Sisodiya, S. M.; Walker, M. C. Adult Epilepsy. *Lancet* **2006,** *367* (9516), 1087–1100.
8. Banerjee, P. N.; Hauser, W. A. Incidence and Prevalence. In *Epilepsy: A Comprehensive Text Book,* Vol. 1, Engel J. Jr., Pedley, T. A., Eds.; Lippincott Williams & Wilkins: Philadelphia, 2008; pp 45–56, 2nd ed.
9. Berg, A. T.; Scheffer, I. E. New Concepts in Classification of the Epilepsies: Entering the 21st Century. *Epilepsia* **2011,** *52* (6), 1058–1062.
10. Brodie, M. J.; Barry, S. J. E.; Bamagous, G. A.; Norrie, J. D.; Kwan, P. Patterns of Treatment Response in Newly Diagnosed Epilepsy. *Neurology* **2012,** *78,* 1548–1554.
11. Bialer, M.; White, H. S. Key Factors in the Discovery and Development of New Antiepileptic Drugs. *Nat. Rev. Drug Discov.* **2010,** *9,* 68–82.
12. Löscher, W.; Klitgaard, H.; Twyman, R.; Schmidt, D. New Avenues for Anti-Epileptic Drug Discovery and Development. *Nat. Rev. Drug Discov.* **2013,** *12,* 757–776.
13. Eadie, M. J. Sir Charles Locock and Porassium Bromide. *J. R. Coll. Physicians Edinb.* **2012,** *42* (3), 274–279.
14. Stables, J.P.; Kupferberg, H.J. The NIH Anticonvulsant Drug Development. (ADD) Program: Preclinical Anticonvulsant Screening Project. http://www.ninds.nih.gov/research/asp/addadd_review.pdf.
15. Perucca, E.; French, J.; Bialer, M. Development of New Antiepileptic Drugs: Challenges, Incentives, and Recent Advances. *Lancet Neurol.* **2007,** *6* (9), 793–804.
16. Löscher, W. Critical Review of Current Animal Models of Seizures and Epilepsy Used in the Discovery and Development of New Antiepileptic Drugs. *Seizure* **2011,** *20,* 359–368.
17. Powell, K. L.; Cain, S. M.; Ng, C.; Sirdesai, S.; David, L. S.; Kyi, M.; Garcia, E.; Tyson, J. R.; Reid, C. A.; Bahlo, M.; Foote, S. J.; Snutch, T. P.; O'Brien, T. J. A $Ca_v3.2$ T-Type Calcium Channel Point Mutation Has Splice-Variant-Specific Effects on Function and Segreates With Seizure Expression in a Polygenic Rat Model of Absence Epilepsy. *J. Neurosci.* **2009,** *29* (2), 371–380.
18. Barton, M. E.; Klein, B. D.; Wolf, H. H.; White, H. S. Pharmacological Characterization of the 6 Hz Psychomotor Seizure Model of Partial Epilepsy. *Epilepsy Res.* **2001,** *47* (3), 217–227.
19. Mittapalli, G. K.; Roberts, E. Structure Activity Relationships of Novel Antiepileptic Drugs. *Curr. Med. Chem.* **2014,** *21* (6), 722–754.
20. Gower, A. J.; Noyer, M.; Verloes, R.; Gobert, J.; Wulfert, E. ucb L059, a Novel Anti-Convulsant Drug: Pharmacological Profile in Animals. *Eur. J. Pharmacol.* **1992,** *222,* 193–203.
21. Löscher, W.; Honack, D. Profile of ucb L059, a Novel Anticonvulsant Drug, in Models of Partial and Generalized Epilepsy in Mice and Rats. *Eur. J. Pharmacol.* **1993,** *232,* 147–158.
22. Kenda, B. M.; Matagne, A. C.; Talaga, P. E.; Pasau, P. M.; Differding, E.; Lallemand, B. I.; Frycia, A. M.; Moureau, F. G.; Klitgaard, H. V.; Gillard, M. R.; Fuks, B.; Michel, P. Discovery of 4-Substituted Pyrrolidone Butanamides as New Agents With Significant Antiepileptic Activity. *J. Med. Chem.* **2004,** *47,* 530–549.
23. Chaudhry, H. R.; Najam, N.; De Mahieu, C.; Raza, A.; Ahmad, B. Clinical Use of Piracetam in Epileptic Patients. *Epilepsia* **1991,** *32* (Suppl. 1), 100.
24. Schmit, J. Comparative Studies on the Anticonvulsant Effectiveness of Nootropic Drugs in Kindled Rats. *Biomed. Biochim. Acta* **1990,** *49,* 413–419.
25. Fisher, W.; Kittner, H.; Schubert, S. Effectiveness of Piracetam, Meclofenoxate and Vinpocetine in Different Seizure Tests on the Mouse. *Pharmazie* **1991,** *46,* 359–360.
26. Keller, G. Anticonvulsant Effects of Piracetam, Meclofenoxate and Vinpocetine on Acute and Kindled Pentyenetetrazole (PTZ) Induced Seizure. *Naunyn-Schmiedeberg's. Arch. Pharmacol.* **1991,** *343* (Suppl 1), R112.
27. Fuks, B.; Gillard, M.; Michel, P.; Lynch, B.; Vertongen, P.; Leprince, P.; Klitgaard, H.; Chatelain, P. Localization and Photoaffinity Labelling of the Levetiracetam Binding Site in Rat Brain and Certain Cell Lines. *Eur. J. Pharmacol.* **2003,** *478,* 11–19.
28. Lynch, B. A.; Lambeng, N.; Nocka, K.; Kensel-Hammes, P.; Bajjalieh, S. M.; Matagne, A.; Fuks, B. The Synaptic Vesicle Protein SV2A is the Binding Site for the Antiepileptic Drug Levetiracetam. *Proc. Natl. Acad. Sci. U. S. A.* **2004,** *101,* 9861–9866.
29. Reigada, D.; Díez-Pérez, I.; Gorostiza, P.; Verdaguer, A.; Gómez de Aranda, I.; Pineda, O.; Vilarrasa, J.; Marsal, J.; Blasi, J.; Aleu, J.; Solsona, C. Control of Neurotransmitter Release by an Internal Gel Matrix in Synaptic Vesicles. *Proc. Natl. Acad. Sci. U. S. A.* **2003,** *100,* 3485–3490.
30. Janz, R.; Goda, Y.; Geppert, M.; Missler, M.; Südhof, T. C. SV2A and SV2B Function as Redundant Ca^{2+} Regulators in Neurotransmitter Release. *Neuron* **1999,** *24,* 1003–1016.
31. Xu, T.; Bajjalieh, S. M. SV2A Modulates the Size of the Readily Releasable Pool of Secretory Vesicles. *Nat. Cell Biol.* **2001,** *3,* 691–698.
32. Schivell, A. E.; Batchelor, R. H.; Bajjalieh, S. M. Isoform-Specific, Calcium-Regulated Interaction of the Synaptic Vesicle Proteins SV2 and Synaptotagmin. *J. Biol. Chem.* **1996,** *271* (44), 27770–27775.
33. Pyle, R. A.; Schivell, A. E.; Hidaka, H.; Bajjalieh, S. M. Phosphorylation of Synaptic Vesicle Protein 2 Modulates Binding to Synaptotagmin. *J. Biol. Chem.* **2000,** *275* (22), 17195–17200.
34. Bajjalieh, S. M.; Frantz, G. D.; Weimann, J. M.; McConnell, S. K.; Scheller, R. H. Differential Expression of Synaptic Vesicle Protein 2 (SV2) Isoforms. *J. Neurosci.* **1994,** *14* (9), 5223–5235.

35. Pisani, A.; Bonsi, P.; Martella, G.; De Persis, C.; Costa, C.; Pisani, F.; Bernardi, G.; Carabresi, P. Intracelluar Calcium Increase in Epileptiform Activity: Modulation by Levetiracetam and Lamotrigine. *Epilepsia* **2004,** *45* (7), 719–728.
36. Lukyanetz, E. A.; Shkryl, V. M.; Kostyuk, P. G. Selective Blockade of N-Type Calsium Channels by Levetiracetam. *Epilepsia* **2002,** *43* (1), 9–18.
37. Niespodziany, I.; Klitgaard, H.; Margineanu, D. G. Levetiracetam Inhibits the High-Voltage-Activated Ca^{2+} Current in Pyramidal Neurones of Rat Hippocampal Slices. *Neurosci. Lett.* **2001,** *306* (1–2), 5–8.
38. Vogl, C.; Mochida, S.; Wolff, C.; Whalley, B. J.; Stephens, G. J. The Synaptic Vesicle Glycoprotein 2A Ligand Levetiracetam Inhibits Presynaptic Ca^{2+} Channels Through an Intracelluar Pathway. *Mol. Pharmacol.* **2012,** *82* (2), 199–208.
39. Klitgaard, H.; Matagne, A.; Gobert, J.; Wulfert, E. Evidence for a Unique Profile of Levetiracetam in Rodent Models of Seizures and Epilepsy. *Eur. J. Pharmacol.* **1998,** *353* (2–3), 191–206.
40. Löscher, W.; Honack, D.; Rundfeldt, C. Antiepileptogenic Effects of the Novel Anticonvulsant Levetiracetam (ucb L059) in the Kindling Model of Temporal Lobe Epilepsy. *J. Pharmacol. Exp. Ther.* **1998,** *284* (2), 474–479.
41. Matagne, A.; Margineanu, D. G.; Kenda, B.; Micheal, P.; Klitgaard, H. Anti-Convulsive and Anti-Epileptic Properties of Brivaracetam (ucb 34714), a High-Affinity Ligand for the Synaptic Vesicle Protein, SV2A. *Br. J. Pharmacol.* **2008,** *154* (8), 1662–1671.
42. Gillard, M.; Fuks, B.; Leclercq, K.; Matagne, A. Binding Characteristics of Brivaracetam, a Selective, High-Affinity SV2A Ligand in Rat, Mouse and Human Brain: Relationship to Anti-Convulsant Properties. *Eur. J. Pharmacol.* **2011,** *664* (1–3), 36–44.
43. Zona, C.; Pieri, M.; Carunchio, I.; Curcio, L.; Klitgaard, H.; Margineanu, D. G. Brivaracetam (ucb 34714) Inhibits Na^{+} Current in Rat Cortical Neurons in Culture. *Epilepsy Res.* **2010,** *88* (1), 46–54.
44. Bialer, M.; Johannessen, S. I.; Levy, R. H.; Perucca, E.; Tomson, T.; White, H. S. Progress Report on New Antiepileptic Drugs: A Summary of the Twelfth Eilat Conference (EILAT XII). *Epilepsy Res.* **2015,** *111,* 85–141.
45. Matagne, A.; Margineanu, D. G.; Potschka, H.; Löscher, W.; Michel, P.; Kenda, B.; Klitgaard, H. Profile of the New Pyrrolidone Derivative Seletracetam (ucb 44212) in Animal Models of Epilepsy. *Eur. J. Pharmacol.* **2009,** *614* (1–3), 30–37.
46. Pisani, A.; Bonsi, P.; Martella, G.; Cuomo, D.; Klitgaard, H.; Margineanu, D. G. Seletracetam (ucb 44212), a New Pyrrolidone Derivative, Inhibits High-Voltage-Activated Ca^{2+} Currents and Intracellular $[Ca^{2+}]$ Increase in Rat Cortical Neurons In Vitro. *Epilepsia* **2005,** *46* (Suppl. 8), 119–120.
47. Fertig, E. J.; Mattson, R. H. Carbamazepine. In *Epilepsy: A Comprehensive Text Book,* Vol. 2, Engel J. Jr., Pedley, T. A., Eds.; Lippincott Williams & Wilkins: Philadelphia, 2008; pp 1543–1555, 2nd ed.
48. Ambrósio, A. F.; Soares-da-Silva, P.; Carvalho, C. M.; Carvalho, A. P. Mechanisms of Action of Carbamazepine and Its Derivatives, Oxcarbazepine, BIA 2–093, and BIA 2–024. *Neurochem. Res.* **2002,** *27* (1/2), 121–130.
49. Uetrecht, J.; Naisbitt, D. J. Idiosyncratic Adverse Drug Reactions: Current Concepts. *Pharmacol. Rev.* **2013,** *65,* 779–808.
50. Bu, H.-Z.; Kang, P.; Deese, A. J.; Zhao, P.; Pool, W. F. Human in vitro Glutathionyl and Protein Adducts of Carbamazepine-10,11-Epoxide, a Stable and Pharmacologically Active Metabolite of Carbamazepine. *Drug Metab. Dispos.* **2005,** *33* (12), 1920–1924.
51. Schmutz, M.; Brugger, F.; Gentsch, C.; McLean, M. J.; Olpe, H. R. Oxcarbazepine: Preclinical Anticonvulsant Profile and Putative Mechanisms of Action. *Epilepsia* **1994,** *35* (Suppl. 5), S47–S50.
52. Shorvon, S. Oxcarbazepine: A Review. *Seizure* **2000,** *9,* 75–79.
53. Schwabe, S. Oxcarbazepine: Clinical Development Program. *Epilepsia* **1994,** *35* (Suppl. 5), S51–S53.
54. Benes, J.; Parada, A.; Figueiredo, A. A.; Alves, P. C.; Freitas, A. P.; Learmonth, D. A.; Cunha, R. A.; Garrett, J.; Soares-da-Silva, P. Anticonvulsant and Sodium Channel-Blocking Properties of Novel 10,11-Dihydro-5*H*-dibenz[*b*,*f*]azepine-5-carboxamide Derivatives. *J. Med. Chem.* **1999,** *42* (14), 2582–2587.
55. Singh, R. P.; Asconapé, J. J. A Review of Eslicarbazepine Acetate for the AdjunctiveTreatment of Partial-Onset Epilepsy. *J. Cent. Nerv. Syst. Dis.* **2011,** *3,* 179–187.
56. Halász, P.; Cramer, J. A.; Hodoba, D.; Członkowska, A.; Guekht, A.; Maia, J.; Elger, C.; Almeida, L.; Soares-da-Silva, P. Long-Term Efficacy and Safety of Eslicarbazepine Acetate: Results of a 1-year Open-Label Extension Study in Partial-Onset Seizures in Adults With Epilepsy. *Epilepsia* **2010,** *51* (10), 1963–1969.
57. Hibi, S.; Ueno, K.; Nagato, S.; Kawano, K.; Ito, K.; Norimine, Y.; Takenake, O.; Hanada, T.; Yonaga, M. Discovery of 2-(2-Oxo-1-phenyl-5-pyridin-2-yl-1,2-dihydropyridin-3-yl) benzonitrile (Perampanel): A Novel, Noncompetitive α-Amino-3-hydroxyl-5-methyl-4-isoxazolepropanoic Acid (AMPA) Receptor Antagonist. *J. Med. Chem.* **2012,** *55* (23), 10584–10600.
58. Hanada, T.; Hashizume, Y.; Tokuhara, N.; Takenaka, O.; Kohmura, N.; Ogasawara, A.; Hatakeyama, S.; Ohgoh, M.; Ueno, M.; Nishizawa, Y. Perampanel: A Novel, Orally Active, Noncompetitive AMPA-Receptor Antagonist That Reduces Seizure Activity in Rodent Models of Epilepsy. *Epilepsia* **2011,** *52* (7), 1331–1340.
59. Hanada, T. The Discovery and Development of Perampanel for the Treatment of Epilepsy. *Expert Opin. Drug Discovery* **2014,** *9* (4), 449–458.
60. Takagaki, G. The Dawn of Excitatory Amino Acid Research in Japan. The Pioneering Work by Professor Takashi Hayashi. *Neurochem. Int.* **1996,** *29* (3), 225–229.
61. Rogawski, M. A. AMPA Receptors as a Molecular Target in Epilepsy Therapy. *Acta Neurol. Scand.* **2013,** *127* (Suppl.197), 9–18.
62. Tortorella, A.; Halonen, T.; Sahibzada, N.; Gale, K. A Crucial Role of the α-Amino-3-hydroxy-5-methylisoxazole-4-propionic Acid Subtype of Glutamate Receptors in Piriform and Perirhinal Cortex for the Initiation and Propagation of Limbic Motor Seizures. *J. Pharmacol. Exp. Ther.* **1997,** *280* (3), 1401–1405.
63. Faught, E. BGG492 (Selurampanel), an AMPA/Kainite Receptor Antagonist Drug for Epilepsy. *Expert Opin. Investig. Drugs* **2014,** *23* (1), 107–113.
64. Inami, H.; Shishikura, J.; Yasunaga, T.; Ohno, K.; Yamashita, H.; Kato, K.; Sakamoto, S. Synthesis, Structure-Axtivity Relationships, and Anticonvulsant Activities of 2-Amino-*4H*-pyrido[3,2-e][1,3]thiazin-4-one Derivatives as Orally Active AMPA Receptor Antagonists. *Bioorg. Med. Chem.* **2015,** *23* (8), 1788–1799.
65. Jakus, R.; Graf, M.; Ando, R. D.; Balogh, B.; Gacsalyi, I.; Levay, G.; Kantor, S.; Bagdy, G. Effect of Two Noncompetitive AMPA Recepotor Antagonists GYKI 52466 and GYKI 53405 on Vigilance, Behavior and Spike-Wave Discharges in a Genetic Rat Model of Absence Epilepsy. *Brain Res.* **2004,** *1008* (2), 236–244.
66. French, J. A.; Krauss, G. L.; Wechsler, R. T.; Wang, W.-F.; DiVentura, B.; Brandt, C.; Trinka, E.; O'Brien, T. J.; Laurenza, A.; Patten, A.; Bibbiani, F. Perampanel for Tonic-Clonic Seizures in Idiopathic Generalized Epilepsy: A Randomized Trial. *Neurology* **2015,** *85* (11), 950–957.
67. French, J. A.; Krauss, G. L.; Biton, V.; Squillacote, D.; Yang, H.; Laurenza, A.; Kumar, D.; Rogawski, M. A. Adjunctive Perampanel for Refractory Partial-Onset Seizures: Randomized Phase III Study 304. *Neuorolgy* **2012,** *79* (6), 589–596.
68. French, J. A.; Krauss, G. L.; Steinhoff, B. J.; Squillacote, D.; Yang, H.; Kumar, D.; Laurenza, A. Evaluation of Adjunctive Perampanel in Patients With Refractory Partial-Onset Seizures: Results of Randomized Global Phase III Study 305. *Epilepsia* **2013,** *54* (1), 117–125.
69. Krauss, G. L.; Serratosa, J. M.; Villanueva, V.; Endziniene, M.; Hong, Z.; French, J.; Yang, H.; Squillacote, D.; Edwards, H. B.; Zhu, J.; Laurenza, A. Randomized Phase III Study 306: Adjunctive Perampanel for Refractory Partial-Onset Seizures. *Neuorolgy* **2012,** *78* (18), 1408–1415.
70. Steinhoff, B. J.; Ben-Menachem, E.; Ryvlin, P.; Shorvon, S.; Kramer, L.; Satlin, A.; Squillacote, D.; Yang, H.; Zhu, J.; Laurenza, A. Efficacy and Safety of Adjunctive Perampanel for the Treatment of Refractory Partial Seizures: A Pooled Analysis of Three Phase III Studies. *Epilepsia* **2013,** *54* (8), 1481–1489.
71. St. Louis, E. K. Minimizing AED Adverse Effects: Improving Quality of Life in the Interictal State in Epilepsy Care. *Curr. Neuropharmacol.* **2009,** *7* (2), 106–114.
72. Schmidt, D.; Löscher, W. Drug Resistance in Epilepsy: Putative Neurobiologic and Clinical Mechanisms. *Epilepsia* **2005,** *46* (6), 858–877.
73. Wager, T. T.; Chandrasekaran, R. Y.; Hou, X.; Troutman, M. D.; Verhoest, P. R.; Villalobos, A.; Will, Y. Defining Desirable Central Nervous System Drug Space Through the Alignment of Molecular Properties, In Vitro ADME, and Safety Attributes. *ACS Chem. Neurosci.* **2010,** *1* (6), 420–434.
74. Loeb, J. A. Identifying Targets for Preventing Epilepsy Using Systems Biology. *Neurosci. Lett.* **2011,** *497* (3), 205–212.
75. Remy, S.; Beck, H. Molecular and Cellular Mechanisms of Pharmacoresistance in Epilepsy. *Brain* **2006,** *129* (1), 18–35.
76. Vezzani, A.; Balosso, S.; Ravizza, T. The Role of Cytokines in the Pathophysiology of Epilepsy. *Brain Behav. Immun.* **2008,** *22,* 797–803.
77. Vezzani, A.; French, J.; Bartfai, T.; Baram, T. Z. The Role of Inflammation in Epilepsy. *Nat. Rev. Neurol.* **2011,** *7,* 31–40.

78. Vezzani, A.; Friedman, A.; Dingledine, R. J. The Role of Inflammation in Epileptogenesis. *Neuropharmacology* **2013,** *69,* 16–24.
79. Maroso, M.; Balosso, S.; Ravizza, T.; Iori, V.; Wright, C. I.; French, J.; Vezzani, A. Interleukin-1 Beta Biosynthesis Inhibition Reduces Acute Seizures and Drug Resistant Chronic Epileptic Activity in Mice. *Neurotherapeutics* **2011,** *8,* 304–315.
80. Bialer, M.; Johannessen, S. I.; Levy, R. H.; Perucca, E.; Tomson, T.; White, H. S. Progress Report on New Antiepileptic Drugs: A Summary of the Eleventh Eilat Conference (EILAT XI). *Epilepsy Res.* **2013,** *103,* 2–30.
81. Vezzani, A.; Maroso, M.; Balosso, S.; Sanchez, M. A.; Bartfai, T. IL-1 Receptor/Toll-Like Receptor Signaling in Infection, Inflammation, Stress and Neurodegeneration Couples Hyperexcitability and Seizures. *Brain Behav. Immun.* **2011,** *25,* 1281–1289.
82. Maroso, M.; Balosso, S.; Ravizza, T.; Liu, J.; Aronica, E.; Iyer, A. M.; Rossetti, C.; Molteni, M.; Casalgrandi, M.; Manfredi, A. A.; Bianchi, M. E.; Vezzani, A. Toll-Like Receptor 4 and High-Mobility Group Box-1 are Involved in Ictogenesis and Can Be Targeted to Reduce Seizures. *Nat. Med.* **2010,** *16* (4), 413–420.
83. Löscher, W.; Puskarjov, M.; Kaila, K. Cation-Chloride Cotransporters NKCC1 and KCC2 as Potential Targets for Novel Antiepileptic and Epileptogenic Treatments. *Neuropharmacology* **2013,** *69,* 62–74.
84. Dzhala, V. I.; Talos, D. M.; Sdrulla, D. A.; Brumback, A. C.; Mathews, G. C.; Benke, T. A.; Delpire, E.; Jensen, E.; Staley, K. J. NKCC1 Transporter Facilitates Seizures in the Developing Brain. *Nat. Med.* **2005,** *11* (11), 1205–1213.
85. Tellez-Zenteno, J. F.; Patten, S. B.; Jette, N.; Williams, J.; Wiebe, S. Psychiatric Comorbidity in Epilepsy: A Population-Based Analysis. *Epilepsia* **2007,** *48,* 2336–2344.
86. Kanner, A. M. Can Neurobiological Pathogenic Mechanisms of Depression Facilitate the Development of Seizure Disorders? *Lancet Neurol.* **2012,** *11,* 1093–1102.
87. Rocha, L.; Alonso-Vanegas, M.; Villeda-Hernandez, J.; Mujica, M.; Cisneros-Franco, J. M.; Lopez-Gomez, M.; Zavala-Tecuapetla, C.; Frias-Soria, C. L.; Segovia-Vila, J.; Borsodi, A. Dopamine Abnormalities in the Neocortex of Patients With Temporal Lobe Epilepsy. *Neurobiol. Dis.* **2012,** *45,* 499–507.
88. Szot, P. Common Factors Among Alzheimer's Disease, Parkinsoin's Disease, and Epilepsy: Possible Role of the Noradrenergic Nerve System. *Epilepsia* **2012,** *53* (Suppl.1), 61–66.
89. Lukasiuk, K.; Dabrowski, M.; Adach, A.; Pitkanen, A. Epileptogenesis-Related Genes Revisited. *Prog. Brain Res.* **2006,** *158,* 223–241.

Relevant Websites

http://www.ilae.org/—International League Against Epilepsy.
http://www.ninds.nih.gov/—National Institute of Neurological Disorders and Stroke.
http://www.ninds.nih.gov/research/asp/index.htm#PANAChE—Anticonvulsant Screening Program.
http://square.umin.ac.jp/jes/en/—The Japan Epilepsy Society.
http://www.who.int/topics/epilepsy/en/—World Health Organization: Epilepsy.

7.02 Progress and Challenges in the Development of PET Ligands to Aid CNS Drug Discovery

J Mercier* **and L Provins***, UCB Biopharma, Braine-L'Alleud, Belgium
J Hannestad, Denali Therapeutics, South San Francisco, CA, United States

© 2017 Elsevier Ltd. All rights reserved.

7.02.1	**Introduction**	20
7.02.1.1	What Is PET Imaging	20
7.02.1.2	How PET Imaging Can Aid CNS Drug Discovery	21
7.02.2	**Recent PET Imaging Tracers in Neurosciences**	22
7.02.2.1	Introduction	22
7.02.2.2	PET Tracers Targeting G Protein-Coupled Receptors	22
7.02.2.2.1	Tracers in clinical use	23
7.02.2.2.2	Recent developments	23
7.02.2.3	PET Tracers Targeting Enzymes	33
7.02.2.3.1	Tracers in clinical use	33
7.02.2.3.2	Recent developments	33
7.02.2.4	PET Tracers Targeting Ion Channels	37
7.02.2.4.1	Tracers in clinical use	37
7.02.2.4.2	Recent developments	37
7.02.2.5	PET Tracers Targeting Transporters	39
7.02.2.5.1	Tracers in clinical use	40
7.02.2.5.2	Recent developments	40
7.02.2.6	PET Tracers Targeting Aggregated Proteins	44
7.02.2.6.1	Tracers in clinical use	44
7.02.2.6.2	Recent developments	44
7.02.2.6.3	Future developments	47
7.02.3	**Some Present and Future Challenges of PET Imaging**	47
7.02.3.1	Improved Radiosynthesis Methods	47
7.02.3.2	Immuno-PET in Neurosciences	48
7.02.3.3	Neuroinflammation Imaging Beyond Translocator Protein	49
7.02.3.3.1	Selected PET tracers under investigation	49
7.02.3.3.2	Recent developments	49
7.02.3.3.3	Possible future developments	53
7.02.3.4	Reimbursement of Approved Diagnostic PET Agents	53
7.02.4	**Concluding Remarks**	54
References		54

7.02.1 Introduction

7.02.1.1 What Is PET Imaging

Positron emission tomography (PET) is a quantitative molecular imaging technology based on radiotracers. Those are labeled with short-lived positron-emitting isotopes of atoms commonly available in small-molecule drug candidates, typically ^{11}C and ^{18}F. The short half-life of these positron-emitting isotopes (respectively, 20 and 110 min) and their specific decay into coincident and highly tissue-penetrant γ-rays allows relatively noninvasive in vivo imaging with good spatial resolution and very high sensitivity. PET radiotracers can therefore provide quantitation of biochemical processes within a living human being, including within the central nervous system (CNS) (Fig. 1).

These characteristics confer to PET imaging the potential to assess neurological processes in healthy human subjects and those in various disease states. When combined with the increasing availability of μPET cameras allowing performing preclinical studies in small animals, PET imaging becomes a powerful translational tool to support drug discovery.

*These authors contributed equally to the work.

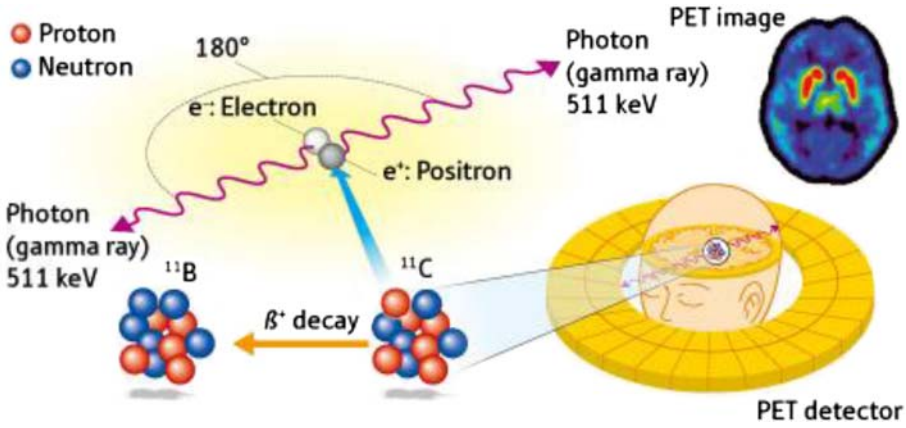

Fig. 1 Ref. 1: Coincident γ-rays detection affords PET its high sensitivity and spatial resolution. Suzuki, M. Molecular imaging that will bring about a revolution in diagnosis and drug discovery: How Positron Emission Tomography Works. http://www.rikenresearch.riken.jp/eng/frontline/5656.

7.02.1.2 How PET Imaging Can Aid CNS Drug Discovery

Despite many efforts over the last 15 years to decrease the attrition in drug development, there is still less than a 10% chance that a drug entering clinical trials will reach the market. Attrition is the highest for oncology and CNS drug development, in particular with novel targets with limited understanding of the biology.[2] In order to reduce drug attrition in clinical trials and to continue to attract investment, the pharmaceutical industry must develop reliable translational evaluation tools that will enable faster and better decisions.[3]

Due to the inaccessibility of the brain in living humans, the development of translational tools to support CNS drug discovery has to rely on noninvasive techniques like in vivo imaging. Over the last years, a few imaging technologies have been increasingly used to support drug discovery. They include the use of radioisotope-based techniques, mainly PET and to a lesser extent single-photon emission computed tomography (SPECT), magnetic resonance imaging (MRI), and more particularly functional MRI.[4]

Among the radioisotope-based imaging techniques that can aid CNS drug discovery, PET is particularly well suited as it relies on the incorporation of radioisotopes that are already present in most small-molecule drug candidates. It can provide quantitative information to support the decision-making process at different stages of preclinical and clinical drug development (**Fig. 2**).[5,6]

First, PET imaging can provide brain PK information in living subjects. Through the direct radiolabeling of a drug candidate, information regarding the blood–brain barrier (BBB) penetration in both healthy and diseased subjects can be obtained. Taking advantage of the microdosing concept, such studies can even be performed while the drug candidate is still at a preclinical development stage, providing a quick read-out before the first administration in humans at pharmacological doses. However, this straightforward approach raises first a radiochemistry challenge. Indeed, the direct labeling of a drug candidate may be synthetically challenging, and the development of new labeling methodologies to expand the radiochemist's toolbox would be very beneficial to this approach. This challenge will be briefly addressed in the concluding remarks of this article.

Secondly, the development of a validated PET ligand for the protein targeted by the drug development program provides the opportunity to assess, through blocking studies, the target occupancy of a drug candidate. These studies provide critical information such as the relationship between target occupancy and administered dose as well as the target occupancy kinetics. When obtained in phase I of clinical development, such information is decision-making to select the most appropriate dose range and regimen for

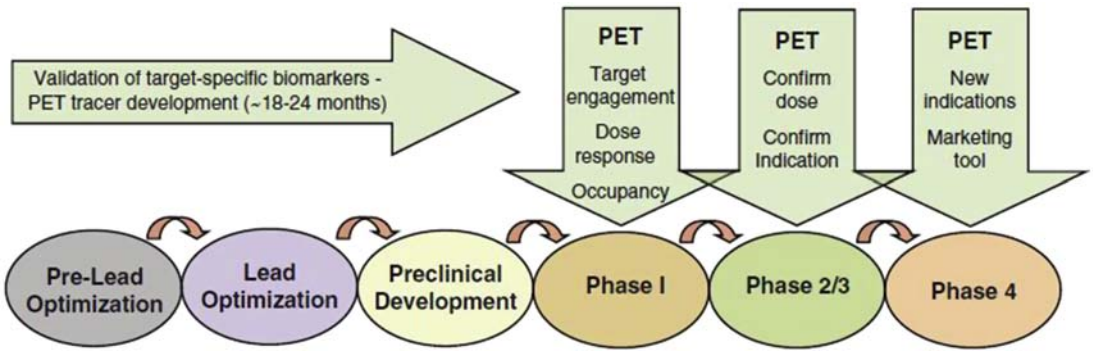

Fig. 2 Potential impact of PET imaging in the drug discovery process. Adapted from Grachev, I. D.; Hargreaves, R. J. Integrative Processes: Neuroscience Clinical Imaging Biomarkers. In *Imaging in CNS Drug Discovery and Development: Implications for Disease and Therapy*; Springer Science+-Business Media, LLC, 2010; pp 363–379.

phase II POC studies. As discussed in the next section, the design, synthesis, and validation of a tracer for a specific target is a challenging journey and may take several years. This is the major challenge of this approach.

Thirdly, PET imaging studies can also be performed with known physiology or pathophysiology biomarkers labeled with a positron emitter. Such studies can provide some insight into the mechanism of action of a drug candidate and can allow patient stratification, monitoring of disease progression, or be used for proof of pharmacology or as objective endpoints in phase II POC. The identification and validation of such pharmacodynamic imaging biomarkers is still an unmet need for most drug development programs in neurological diseases. However, they could drastically speed-up the clinical development by providing surrogate molecular endpoints of behavioral changes for POC studies.

This article will provide an overview of the available PET tracers for clinical studies and of the recent advances in the identification of novel PET tracers for specific protein targets in neurosciences. It is not intended to be an exhaustive review of all PET tracers available but will rather focus on targets that have either been recently investigated in clinical trials or been addressed preclinically for the first time. This article will also discuss some of the current and future challenges and limits to develop new PET tracers and will eventually suggest future areas of interest in the field.

7.02.2 Recent PET Imaging Tracers in Neurosciences

7.02.2.1 Introduction

Designing PET tracers requires the targeting of compounds with specific properties that are not necessarily aligned with the properties of drug candidates. Many reviews[7–10] have discussed the ideal properties of a tracer for brain imaging and these can be summarized as follows:

- high affinity (usually expressed as $B_{max}/K_D > 10$) and specificity to achieve sufficient signal (bound specifically at the target) to background (nonspecifically bound) ratio;
- moderate log P ($1.5 < \log P < 3$) in order to highly penetrate the BBB without resulting in excessive nonspecific binding (NSB);
- moderate to high clearance from a reference tissue of the target of interest;
- no brain-penetrant radiolabeled metabolite to ensure that the measured radioactivity represents only the amount of parent tracer in the tissue of interest;
- not a P-gP substrate;
- late-stage incorporation of a suitable radionuclide (typically ^{11}C or ^{18}F);
- high-specific activity to stay in tracer conditions, especially for targets with low densities;
- simple automated synthetic procedure, compliant with the good manufacturing practices, for reliable production in clinical use.

Although these properties do not necessarily align with the ones of drug candidates, the multiparameter optimization (MPO) challenge to design a good PET imaging tracer is conceptually very similar to developing a new drug. Therefore, medicinal chemists and PET imaging scientists have made several attempts to develop metrics, indices, and models[11] aimed at predicting the probability of success of a molecule to become a suitable tracer. Considering that NSB is a frequent cause of failure for candidate PET tracers, most of these approaches are actually aimed at better predicting the NSB risk. Zhang et al. analyzed 62 successful PET ligands and proposed a CNS PET MPO score based on both in silico and experimental physicochemical design parameters predictive of reduced NSB risk.[9] Alternatively, other groups have reported various computational[12] or experimental methods, mostly relying on surrogate measurements of the lipophilicity and of the interaction of the candidate tracer molecule with artificial membrane systems.[8,13,14]

Due to these challenging requirements, many compounds produced by the pharmaceutical industry in the last decade for multiple target proteins did not translate into numerous new imaging agents in clinical use. Indeed, only about 40 have been successfully developed for imaging in humans.[10,15] The next sections will briefly review these successful tracers according to their target class and discuss the most recent developments and areas of interest.

7.02.2.2 PET Tracers Targeting G Protein-Coupled Receptors

About 30% of marketed drugs are targeting G Protein-Coupled receptors (GPCRs). These are involved in numerous pathophysiological processes, including in the CNS. Neuroreceptors such as dopaminergic or serotoninergic receptors were historically the targets of choice for the development of the first PET tracers for CNS use. One might have thought a couple of years ago that GPCRs were drug targets of the past. However, recent scientific and technological breakthroughs simply demonstrated the contrary.

In the last 5 years, the crystallization of transmembrane proteins has started to become a routine drug discovery tool, as demonstrated by the dramatic increase in the number of GPCRs structures solved in the last 2 years. The emergence and development of novel areas of interest in drug design such as allosterism, other complex ligand–receptor interactions, the importance of residence time, or the number of receptors of physiological importance still to be deorphanized have also contributed to a sort of "rebirth" of the target class, as illustrated by an exponential growth in the number of papers, reviews, conferences, and new drug candidates targeting GPCRs.

As a consequence, the development of PET tracers targeting GPCRs is still of critical importance. Various challenges such as the design of tracers that bind allosterically to the receptors, the development of agonist tracers, or simply the identification of PET ligands of novel orphan receptors remain a hot topic that will be discussed in this section.

7.02.2.2.1 Tracers in clinical use

See Table 1.

7.02.2.2.2 Recent developments

7.02.2.2.2.1 Dopaminergic receptors[25,26,60,61]

7.02.2.2.2.1.1 D1 receptors (Table 1, Scheme 1)

D1 receptors play an important role in several pathologies such as schizophrenia, cognitive disorders, and Parkinson's disease (PD). [^{11}C]NNC112 and [^{11}C]SCH23390 have been available for decades and have become valuable tools to investigate and understand those diseases in vivo. These are still currently widely used in clinical studies.[23,24,62–64]

Both tracers were developed as selective D1 orthosteric antagonists but suffer from a relative lack of D1 specific binding due to high affinity for the 5HT2A receptor.[65] Other closely related and more selective ligands, such as [^{11}C]SCH39166 and [^{11}C]NNC756, were developed but their evaluation was plagued by low specificity or tracer kinetics issues. Given the renewed interest for noncatechol selective D1 orthosteric agonists or allosteric modulators,[66,67] there is a strong need for selective D1 radiotracers for human use either to support the development of drug candidates or to delineate D1 receptor roles in pathologies of interest.

7.02.2.2.2.1.2 D2/D3 receptors (Table 1, Scheme 2)

D2 and D3 receptors are involved in numerous neurological or neuropsychiatric disorders such as PD, schizophrenia, anxiety, or drug addiction. The first PET tracers that were developed, [^{11}C]Raclopride, [^{11}C]FLB 457, and [^{18}F]Fallypride, are D2/D3

Table 1 CNS radiotracers used in human studies for GPGRs

Molecular target	*^{11}C-labeled ligand*	*^{18}F-labeled ligand*	*Selected references*
Adenosine A1		[^{18}F]CPFPX	16,17
Adenosine A2A	[^{11}C]SCH442416	[^{18}F]MNI-444	18,19
CB1	[^{11}C]MePPEP	[^{18}F]FEMMEP-d2	20,21
	[^{11}C]OMAR	[^{18}F]MK-9470	
	[^{11}C]SD5024		
CB2	[^{11}C]GW842166		22
D1	[^{11}C]NNC 112		23,24
	[^{11}C]SCH 23390		
D2/D3	[^{11}C]Raclopride	[^{18}F]Fallypride	25,26
	[^{11}C]FLB 457		
	[^{11}C]MNPA (agonist)		
	[^{11}C](+)PHNO (agonist)		
	[^{11}C]NPA (agonist)		
H1	[^{11}C]Doxepin		27,28
H3	[^{11}C]GSK189254	[^{18}F]FMH3	29–31
	[^{11}C]MK8278		
	[^{11}C]TASP457		
5-HT1A	[carbonyl-^{11}C]WAY	[^{18}F]FCWAY	32–35
	[carbonyl-^{11}C]DWAY	[^{18}F]MefWAY	
	[^{11}C]CUMI (agonist)	[^{18}F]MPPF	
5-HT1B	[^{11}C]AZ10419369		36–38
	[^{11}C]P943		
5-HT2A	[^{11}C]MDL 1000907	[^{18}F]Altanserin	39,40
		[^{18}F]Altanserin-d2	
5-HT4	[^{11}C]SB-207145		41
5-HT6	[^{11}C]GSK-215083		42
M1	[^{11}C]GSK1034702 (PAM)		43
mGluR1	[^{11}C]ITMM	[^{18}F]FIMX	44,45
mGluR5	[^{11}C]SP 203	[^{18}F]SP 203	46–48
	[^{11}C]ABP688	[^{18}F]F-FPEB	
	[^{11}C]AZD9272		
NK1		[^{18}F]SPA-RQ	49–51
		[^{18}F]MK-0999 ([^{18}F]FE-SPA-RQ)	
NOP	[^{11}C]NOP-1A		52
Opiate (KOR)	[^{11}C]GR 103545		53
Opiate (DOR)	[^{11}C]Methylnaltrindole		54,55
Opiate (MOR)	[^{11}C]Diprenorphine	[^{18}F]Fluoroethyl-diprenorphine	54–57
	[^{11}C]Carfentanil (agonist)		
Sigma	[^{11}C]SA4503		58,59

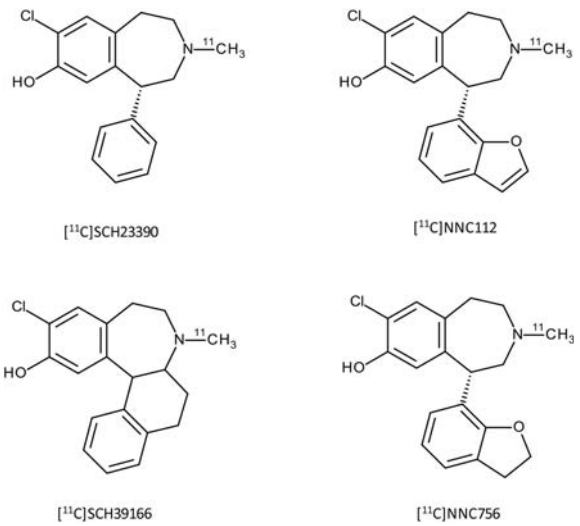

Scheme 1 Selected D1 receptor PET tracers.

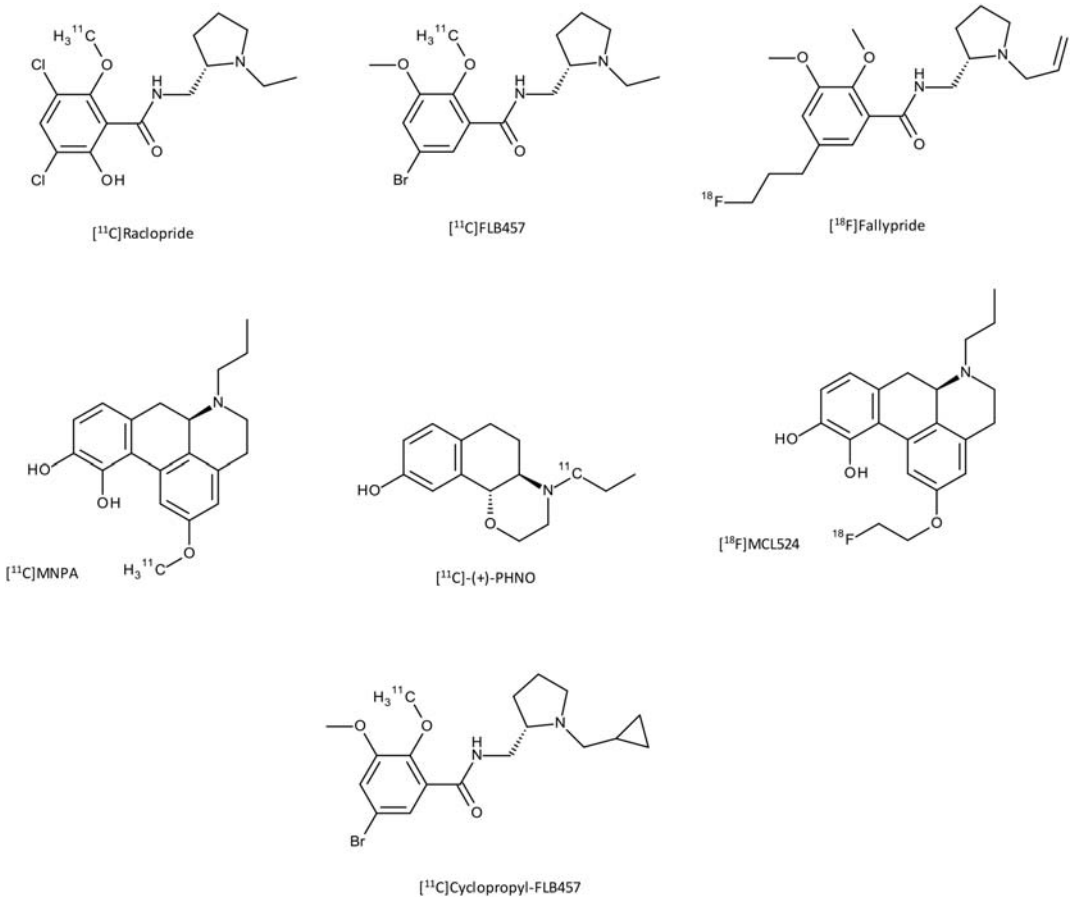

Scheme 2 Selected D2/3 receptor PET tracers.

nonselective antagonists. Limitations to their use are due to their lack of preference for high-affinity G-protein-coupled states of the receptors, therefore rendering them less suited for the imaging of synaptic neurotransmission. This has been overcome by the development of agonist tracers such as [^{11}C]MNPA, [^{11}C]NPA, or [^{11}C](+)PHNO which display higher affinities for receptor G-protein complexes allowing to study or diagnose disorders linked to the relative abundance of these receptor states.

Recent developments are focused on the discovery of [^{18}F]-labeled agonist tracers which could potentially offer several advantages thanks to the longer-lived [^{18}F] compared to [^{11}C]. [^{18}F]MCL-524[68] was recently identified and validated in cynomolgus monkeys. It displays high affinity for the D2 receptor in its high-affinity state, favorable specific D2/D3 binding, and suitable kinetic properties. It has not been reported to be used in humans yet. Other [^{18}F] D2/D3 potential tracers have also been recently reported but still suffer from suboptimal properties, in particular nonspecific binding.[69]

Over the last couple of years, there has been a considerable interest in the development of selective D2 or D3 receptor ligands, and in the differentiation of their respective functional roles in humans. In particular, the more restricted localization and distribution of D3 receptors in brain areas such as nucleus accumbens suggests a specific role in drug abuse pathologies or as a potential target for antipsychotics with reduced side effects, such as extrapyramidal motor symptoms, compared with D2 antagonists. Most available radiotracers are nonselective D2/D3 antagonists or agonists and cannot distinguish between those two receptors in humans. It has nevertheless been recently demonstrated that [^{11}C](+)PHNO preferentially binds to the D3 receptor subtype in vivo with about 20-fold selectivity. Several studies in healthy volunteers or Parkinson's patients have suggested the suitability of [^{11}C](+)PHNO as a D3-preferring probe in humans despite a suboptimal brain distribution in D3-specific areas.[70–73] Several groups have also reported efforts toward the identification of suitable selective [^{18}F]-labeled tracers,[74,75] but none of the potential radiotracers are suitable yet for brain imaging, mainly due to high nonspecific binding, despite subnanomolar affinities and promising selectivity for dopamine and serotonin receptor subtypes.

Selective D2 radiotracers are also of high interest. Promising high-affinity ligands, such as [^{11}C]Cyclopropyl-FLB 457, for the selective imaging D2 receptors in extrastriatal low-density regions in cynomolgus monkey brains or in postmortem human autoradiography have been reported.[76] [^{11}C]Cyclopropyl-FLB 457 is characterized by picomolar D2 in vitro affinity, about 100-fold selectivity versus D3 receptor, high-specific binding in low-density D2 regions, and high brain uptake in monkeys.

7.02.2.2.2.1.3 D4 receptors (**Scheme 3**)

D4 is the third subtype of the D2-like family of receptors. Despite having been cloned in 1991, its pathophysiological functions, localization, and brain distribution remain unclear and matter of controversy. A D4-selective radiotracer would therefore allow a better understanding of the role of D4 in living brains. There have been several attempts to develop [^{11}C] or [^{18}F]-labeled D4 PET ligands but none of them have proved to be successful as of today. Considerable challenges have been reported over the past few years and are associated with the difficulty to combine very high affinity for the D4 receptor, which is characterized by a low B_{max} value, high selectivity for other dopamine receptor subtypes, and low nonspecific binding.[77–80]

7.02.2.2.2.2 Histaminergic receptors

PET ligands for the selective brain imaging of histamine receptors subtypes have been recently reviewed.[81] PET radiotracers have been developed for human use in the case of H1 and H3 receptors.

7.02.2.2.2.2.1 H1 receptors (**Table 1**, **Scheme 4**)

[^{11}C]Pyrilamine and [^{11}C]Doxepin have been developed as selective H1R radiotracers and extensively used to study H1R binding in vivo in several species including humans. [^{11}C]-Doxepin is the most widely used and the most suitable ligand because of a higher metabolic stability and higher contrast in brain images. Numerous studies were performed in humans in order to investigate cognitive and sedative side effects of H1 antagonists and have demonstrated a correlation of sleepiness with brain receptor occupancies. [^{11}C]Doxepin is still used today as part of the evaluation of H1 receptor occupancy of novel drug candidates.[28]

7.02.2.2.2.2.2 H3 receptors (**Table 1**, **Scheme 5**)

Several selective H3R radiotracers have been developed over the last decade, mainly to support the numerous drug candidates that have progressed toward clinical development and proof-of-concept studies.

[^{11}C]GSK189254[29] and [^{11}C]MK8278[30] were developed and used in humans to measure H3R occupancy of several H3 inverse agonist drug candidates developed for the treatment of cognitive or sleep disorders, in particular GSK189254,[29] GSK239512,[82] AZD5213,[83] MK0249, and MK3134. However, it has been reported that [^{11}C]GSK189254 suffers from a very low K_D and slow kinetics in the brain, in particular in high density regions such as the striatum of globus pallidus, limiting the precision of PET quantification, while [^{11}C]MK8278 displayed large test–retest variability.

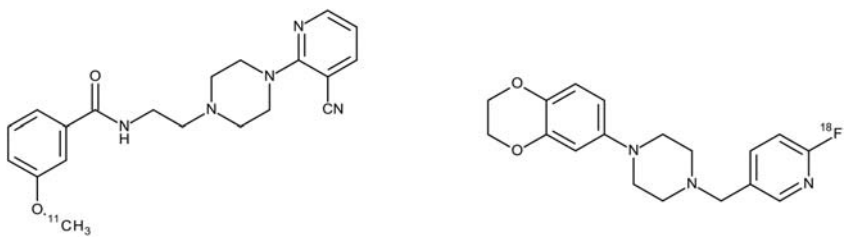

Scheme 3 Selected D4 receptor PET tracers.

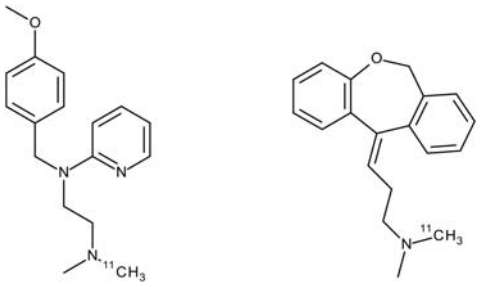

Scheme 4 Selected H1 receptor PET tracers.

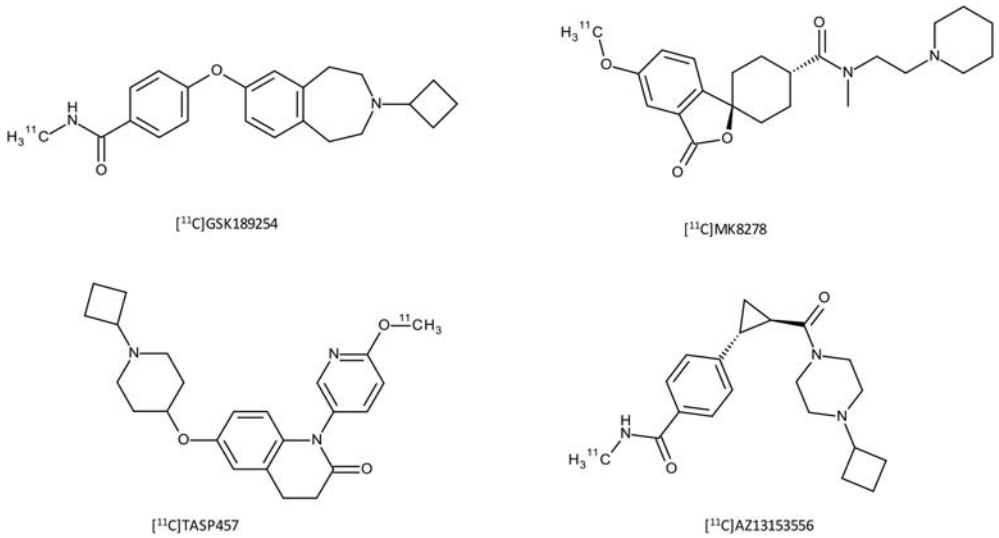

Scheme 5 Selected H3 receptor PET tracers.

More recently, several groups have reported efforts to overcome the limitations of the available ligands for human use. In particular, [^{11}C]TASP457 was identified as a suitable ligand with faster kinetics than [^{11}C]GSK189254 and higher brain penetration than [^{11}C]MK8278. Promising human data have been obtained, demonstrating that [^{11}C]TASP457 is suitable for the investigation of H3 receptor density in human.[84,85] Similarly, [^{11}C]AZ13153556 was also recently reported to display improved preclinical properties, in particular lower affinity in vitro in rat and nonhuman primate tissue homogenates and in autoradiography using brain sections from rats and human as well as in vivo through PET measurements in mice and nonhuman primates. Faster kinetics in a head-to-head comparison study with [^{11}C]GSK189254 were also confirmed, offering some potential for improved properties in human.[86] [^{18}F]FMH3 was also tested in humans as the first [^{18}F]-labeled H3 PET tracer.[31]

*7.02.2.2.2.3 H4 receptors (**Scheme 6**)*

The development of selective H4R radiotracers is still in its infancy with few reports of [^{11}C] radiolabeled analogs of the prototypical antagonists JNJ7777120[87] and VUF10558.[88] The field is nevertheless evolving thanks to the identification of other selective high-affinity ligands as potential starting points for the discovery of PET ligands.[81]

7.02.2.2.2.3 Muscarinic receptors[89]

*7.02.2.2.2.3.1 M1 receptors (**Table 1**, **Scheme 7**)*

Among the five muscarinic acetylcholine receptor (mACh-R) subtypes, M1 is the most prevalent in the central nervous system. It is mainly localized in forebrain regions such as the basal ganglia, hippocampus, and cortical areas and is thought to play a role in cognition and motor control. Initial tracers such as [^{11}C]-MPB or [^{11}C]QNB are unselective muscarinic antagonists displaying slow kinetics. These tracers are unable to distinguish between muscarinic receptor subtypes and, as antagonists, between high- and low-affinity states of the receptors.

[^{11}C]AF150(S) was discovered and designed from cevimeline (AF102B), a rigidified analog of acetylcholine acting as an orthosteric agonist. It displays modest M1 functional selectivity versus the peripherally restricted M3 receptor subtype and is selective over

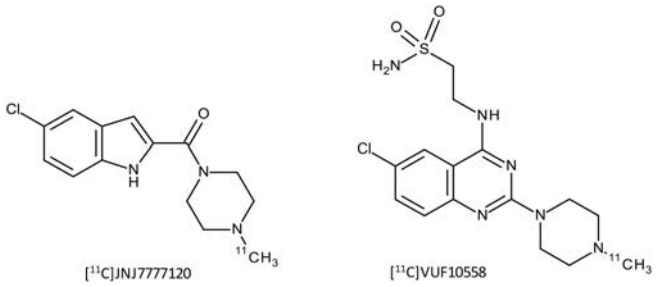

Scheme 6 Selected H4 receptor PET tracers.

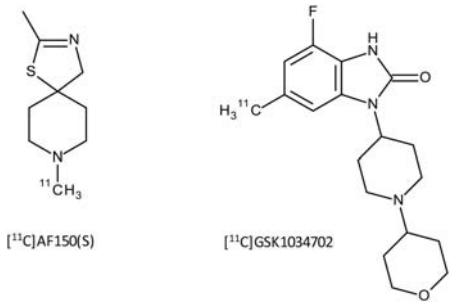

Scheme 7 Selected M1 receptor PET tracers.

M2, M4, and M5 subtypes. [^{11}C]AF150(S) displays rapid and high brain uptake in rats and binding in M1-R rich brain areas was demonstrated with autoradiography. Its potential for human use remains to be demonstrated.[90,91] The only selective M1-R radiotracer tested in humans is [^{11}C]GSK1034702 which is obtained by direct labeling of GSK1034702, a novel M1 positive allosteric modulator (PAM), and was used to quantify the brain penetration of its drug candidate analog in order to derisk its progression into clinical trials. Thus, PET scans were performed in baboons and healthy human volunteers. Good brain uptake was demonstrated as well as BBB passage mainly through passive diffusion or active influx.[43]

7.02.2.2.2.4 Serotoninergic receptors[92]

*7.02.2.2.2.4.1 5HT1A receptors (**Table 1**, **Scheme 8**)*

Several [^{11}C] and [^{18}F] selective 5HT1A antagonist radioligands have been developed over the last decade. Some of them are being used in human subjects but still suffer from [^{11}C]-driven short half-life ([^{11}C]WAY100635 and analogs), high level of in vivo defluorination ([^{18}F]FCWAY), or P-gp efflux ([^{18}F]-MPPF, [^{18}F]FCWAY).[32] Defluorination might be circumvented through concomitant use of disulfiram (1,1′,1″,1‴-[disulfanediylbis(carbonothioylnitrilo)]tetraethane) but its potential neurotoxicity hampers a more widespread use. Current trends are therefore focused on the identification of suitable [^{18}F] tracers which are better able to resist defluorination, such as [^{18}F]Mefway.[35,93] One selective 5HT1A agonist, [^{11}C]CUMI-101, selectively binds to the G-protein coupled state of the 5HT1A receptor and has been developed. It is available for human use.[33,94,95] Its [^{18}F]-labeled analog has been reported as [^{18}F]FECUMI-101.[96]

*7.02.2.2.2.4.2 5HT2 receptors (**Table 1**, **Scheme 9**)*

5HT2 receptors have three subtypes 5HT2A, 2B, and 2C, of which the 5HT2A is the most abundant receptor in the human brain. Several antagonist radioligands are available but none of them is able to discriminate between high- and low-affinity binding states. Current efforts therefore focus on the discovery of 5HT2A agonist tracers such as [^{18}F]FECIMBI-36 allowing the quantification of binding to G-protein bound forms.[97]

*7.02.2.2.2.4.3 5HT4 receptors (**Table 1**, **Scheme 10**)*

High densities of 5HT4R are detected in several brain regions (basal ganglia, limbic structures) and are potentially involved in several pathologies such as depression, ADHD, obesity/anorexia and possibly Alzheimer's disease (AD), and Huntington disease. Selective antagonist radiotracers have been developed and [^{11}C]SB207145 has been evaluated in human volunteers.[41,98] Current research efforts mainly focus on the identification of either suitable [^{18}F]-based tracers or selective agonist radioligands such as [^{18}F]MNI698[99] or [^{11}C]-Prucalopride,[100] respectively, but none of them has yet been evaluated in human.

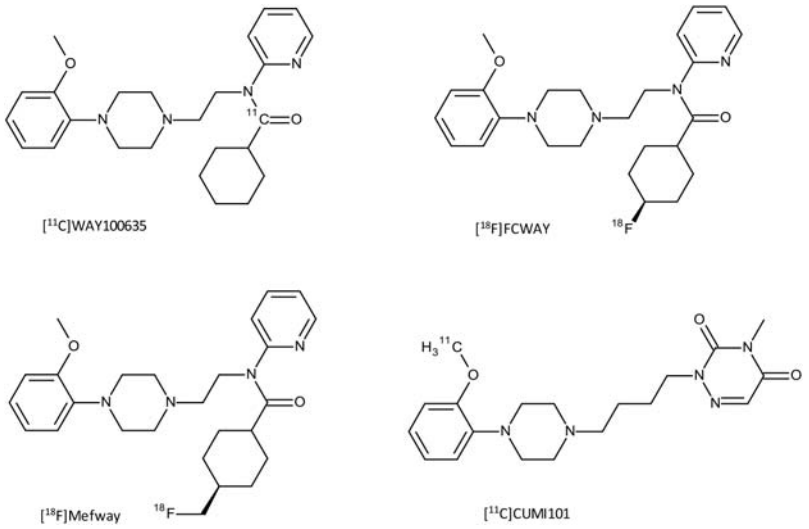

Scheme 8 Selected 5HT1A receptor PET tracers.

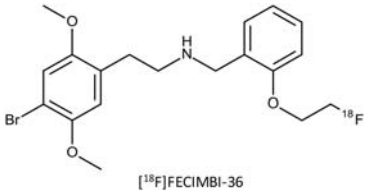

Scheme 9 Selected 5HT2 receptor PET tracers.

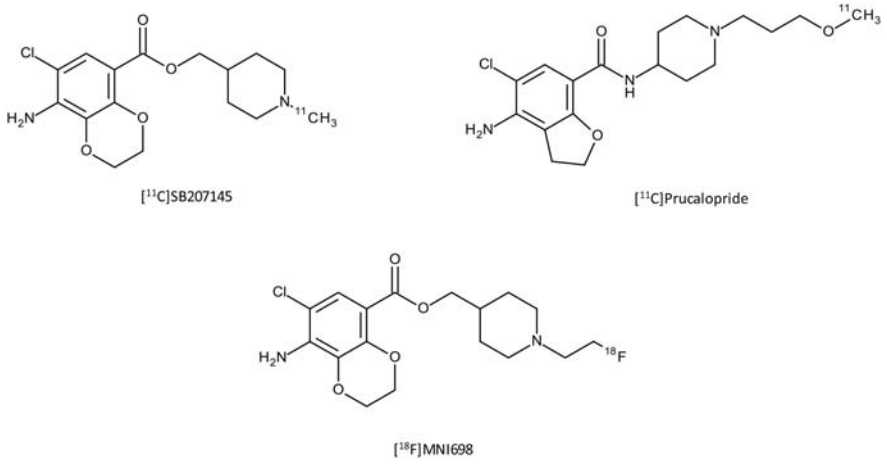

Scheme 10 Selected 5HT4 receptor PET tracers.

*7.02.2.2.2.4.4 5HT6 receptors (**Table 1**, **Scheme 11**)*

5HT6 receptor antagonists are currently in clinical development for the symptomatic treatment of cognitive disorders associated with AD. [^{11}C]GSK215083, however, characterized by a modest approximately fivefold 5HT6/5HT2A selectivity, has recently been evaluated in human subjects in order to better understand the mechanism of action of the 5HT6/5HT2A antagonist SB742457, currently in phase II. The PET studies aimed to delineate its receptor occupancies and the respective contribution of each target in the cognitive enhancing properties of the candidate at the active doses.

Data obtained with [^{11}C]GSK215083 support its use as a suitable 5HT6 imaging marker in human. Saturation of 5HT6 receptors at all doses of SB742457 and a dose-dependent engagement of 5HT2A receptors were observed, suggesting that the blockade of both targets was required to ensure therapeutic efficacy in patients.[42]

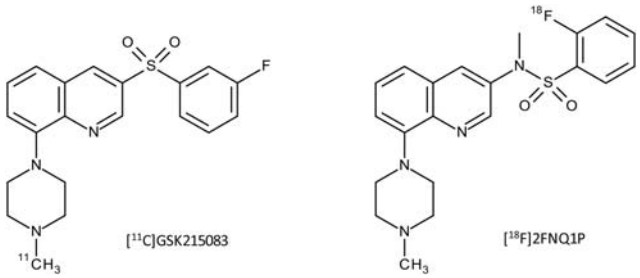

Scheme 11 Selected 5HT6 receptor PET tracers.

More selective [^{18}F]-5HT6 radiotracers are also currently being developed but none of them has yet reached clinical trials.[101] [^{18}F]2FNQ1P was recently discovered and evaluated in rats, cats, and macaques and displays encouraging results in terms of specific in vivo 5HT6 binding.[102]

*7.02.2.2.2.4.5 5HT7 receptors (**Scheme 12**)*

5HT7 selective PET imaging probes have not demonstrated applicability in human yet. Several groups have reported their design efforts as well as some biological characterization.[103,104] The most promising selective radioligand so far is [^{11}C]Cimbi-717 characterized by a specific binding in accordance with 5-HT7R distribution, adequate tracer kinetics, and a dose-dependent decline in cerebral binding after receptor blockade by the widely used prototypical selective 5HT7 antagonist SB-269970.[105]

7.02.2.2.2.5 Metabotropic glutamate receptors[106]

Metabotropic glutamate receptors are classified into three groups: group I (mGLUR1 and mGLUR5), group II (mGLUR2 and mGLUR3), and group III (mGLUR4, mGLUR6, mGLUR7, and mGLUR8). Attempts have been made to develop PET ligands for several receptors, covering all three groups.

*7.02.2.2.2.5.1 mGLU1 receptors (**Table 1**, **Scheme 13**)*

mGLU1 receptors belong to group I, together with mGLUR5 which is closely related both structurally and functionally but very distinct in terms of brain distribution. mGLUR1 is highly expressed in the cerebellum and implicated in anxiety, mood disorders, stroke, PD, Huntington disease, pain, and schizophrenia.

Selective mGLUR1 radioligands have been reported, and as of today, two of them have been validated in human: [^{11}C]ITMM[44,45] and [^{18}F]FIMX.[107,108] The former is, however, characterized by slow kinetics and moderate brain uptake. Dosimetry of [^{18}F]FIMX limits its use to a low number of daily radioligand injections in humans. The development of the [^{11}C] analog was initiated to overcome this limitation and to allow multiple scans per day in the same subject. The overall properties observed in monkeys suggest superiority to [^{11}C]ITMM and a similar profile compared to its [^{18}F]-labeled analog.[109]

*7.02.2.2.2.5.2 mGLU2 receptors (**Scheme 14**)*

mGLU2 receptors belong to group II and are mainly expressed on presynaptic terminals. mGLU2 stimulation with orthosteric agonists or PAMs reduces excessive synaptic glutamate levels and is therefore a very attractive target to treat positive and negative symptoms in schizophrenia patients.[110] The concept has been validated in patients with LY2140023, an orthosteric dual mGLUR2/3 agonist.[111] Current efforts focus on the discovery and development of PAMs with improved selectivity, a lower tendency to receptor desensitization and only acting "on-demand," in presence of the endogenous glutamate. There are few reports disclosing selective mGLUR2 tracers based upon PAMs.[112] One major challenge is the ability to radiolabel potent and selective cold PAMs to image their specific allosteric binding site. Promising [^{11}C]-labeled PET candidates based on a series of 1,2,4-triazolo[4,3a]pyridine PAMs with adequate potency and selectivity, brain penetration, and biodistribution have been reported.[113] Modulation of mGLUR2

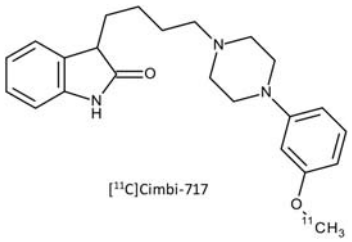

Scheme 12 Selected 5HT7 receptor PET tracers.

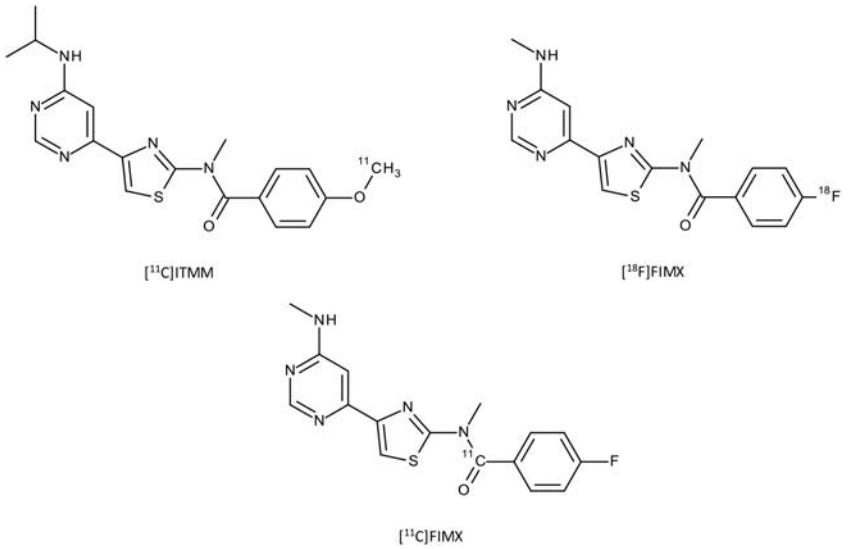

Scheme 13 Selected mGLU1 receptor PET tracers.

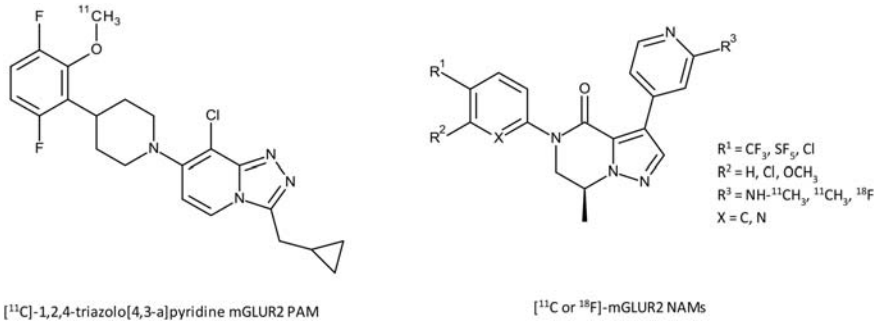

Scheme 14 Selected mGLU2 receptor PET tracers.

with orthosteric antagonists or negative allosteric modulators offers promise in the treatment of mood and cognitive disorders or autism. [^{18}F] and [^{11}C]-labeled compounds have recently been disclosed.[114]

*7.02.2.2.2.5.3 mGLU4 receptors (**Scheme 15**)*

mGLU4 receptors belong to group III and are mainly expressed presynaptically in the striatum, hippocampus, thalamus, and cerebellum. Their activation with either orthosteric agonists or PAMs could have potential benefits in neurological disorders such as PD.[115,116] Numerous mGLUR4 PAMs have been reported triggering the need for the identification of suitable selective radiotracers[117–119] with adequate properties in rats but no PET ligand was found suitable yet for clinical studies.

*7.02.2.2.2.5.4 mGLU5 receptors (**Table 1**, **Scheme 16**)*

mGLU5 receptors (group I) are highly expressed in cerebrum and involved in several neuropsychiatric, neurodevelopmental, and neurological disorders among which Fragile X or Down's syndrome, schizophrenia, PD, Pick's disease, psychosis, or AD are the most recognized. Reviews summarizing state-of-the-art knowledge around mGLUR5 and the development of selective radioligands have been published.[120,121] mGLUR5 is an attractive target for drug development and neuroimaging and provides an interesting mean to study and understand the pathophysiology of multiple glutamate-related CNS disorders, to measure mGLUR5 receptor occupancy of drug candidates, and to aid dose selection. Selective tracers have been developed and tested in humans. [^{11}C]ABP688,[46,122] [^{18}F]FPEB,[47] and [^{18}F]SP203[123] are the most widely used and are characterized by suitable tracer kinetics and dosimetry but test–retest studies have been reported to be poorly reproducible for [^{11}C]ABP688.[124] Individual differences due to glutathione trapping of the alkyne moiety might explain the variability. Nonalkyne tracers such as [^{11}C]AZD9272,[48] which have been evaluated in human volunteers, have been disclosed. In addition, further lead optimization has allowed the identification of tetrazole ligands with promising properties including reliable test–retest studies.[124] Promising [^{18}F]-labeled tracers such as [^{18}F]PSS232[125] have also been reported but display significant defluorination in vivo. All of the PET tracers reported to date behave as mGLUR5 negative allosteric modulators, thus no studies have reported the development of mGLUR5 PAM tracers.

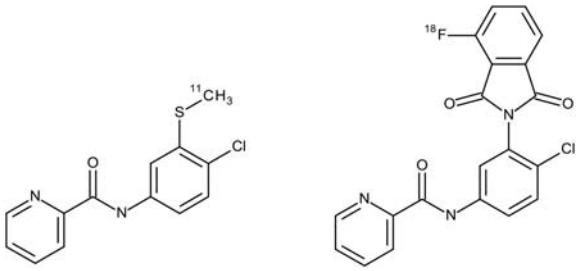

Scheme 15 Selected mGLU4 receptor PET tracers.

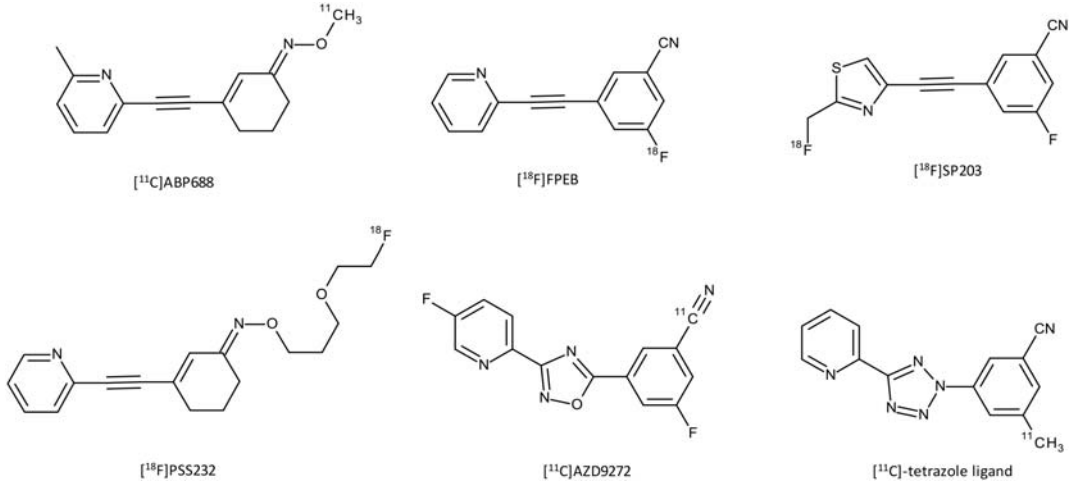

Scheme 16 Selected mGLU5 receptor PET tracers.

7.02.2.2.2.6 Adenosine receptors

An exhaustive overview of adenosine receptor PET tracers was published in 2007.[126] PET tracers for human use are only available for A1 and A2a receptor subtypes.[127]

*7.02.2.2.2.6.1 A2a receptors (**Table 1**, **Scheme 17**)*

Initial xanthine-based [^{11}C] tracers were characterized by a low signal-to-noise ratio, high level of nonspecific binding, and multiple and undefined binding sites, causing retention of radioactivity. Nonxanthine ligands usually display superior properties and [^{11}C] SCH442416 was the first nonxanthine PET tracer suitable for A2a receptor mapping.[18] Direct [^{11}C]-labeling of preladenant, a drug candidate recently terminated in phase III due to lack of differentiation, has also been reported but has only been evaluated in rats.[128] More recently, several research efforts have focused on the development of longer half-life [^{18}F]-based selective A2a radiotracers,[129] which potentially offer better regional distribution (striatum vs. cerebellum) and higher brain uptake than [^{11}C] SCH442416, as well as lower nonspecific binding. Similarly, [^{18}F]MNI444 was recently characterized in humans based upon preliminary evaluation in nonhuman primates.[19,130] A study in human volunteers demonstrated its suitability as an imaging A2a radiotracer in human brain thanks to superior kinetic properties and brain distribution, consistent with A2a densities, and allowing cerebellum as a reference region.

7.02.2.2.2.7 Cannabinoid receptors

*7.02.2.2.2.7.1 Cannabinoid type 2 (CB2) receptors (**Table 1**, **Scheme 18**)*

While CB1 PET tracers are well known and used in clinical development for the imaging of CB1 receptors in several pathologies such as substance abuse disorders or obesity,[21] selective CB2 radiotracers are still in their early days. CB2 receptors, while mainly expressed in immune cells, are also present in the brain, though at lower expression levels, and constitute a promising target for AD[131] or amyotrophic lateral sclerosis (ALS).[132] Numerous publications have reported the discovery of [^{11}C] or [^{18}F]-labeled PET tracers over the last 5 years, such as those shown in **Scheme 18**, and one clinical study has recently been reported with [^{11}C]GW842166.[22,133,134]

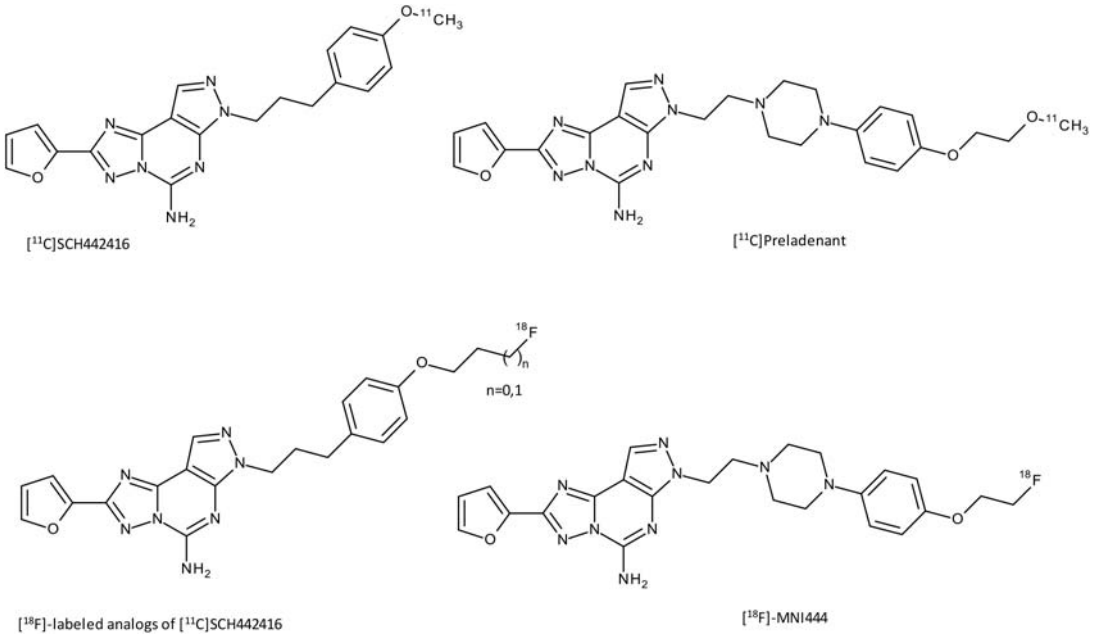

Scheme 17 Selected A2a receptor PET tracers.

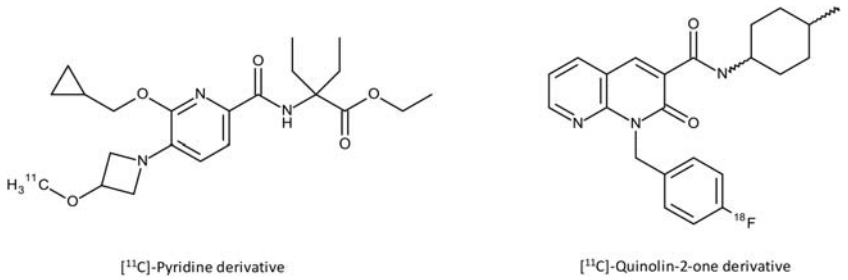

Scheme 18 Selected CB2 receptor PET tracers.

7.02.2.2.2.8 Other receptors

*7.02.2.2.2.8.1 Oxytocin receptor (**Scheme 19**)*

The oxytocin receptors (OXTR or OTR) are neuroendocrine receptors involved in modulating human social behaviors and relationships including cognition in psychiatric or neurological disorders. Neuroimaging of OXTR is of growing importance and could allow the in vivo quantification and precise localization of the receptors in the brain. Only a few papers have reported attempts to identify suitable tracers. [^{18}F] and [^{11}C]-labeled compounds such as [^{18}F]ALS-I-41 or labeled derivatives of WAY-162720 have been identified but none of them was able to display adequate brain penetrance although studies in marmoset have shown that some compounds do seem to cross the BBB, however further investigations are needed to ensure signal specificity.[135–137]

*7.02.2.2.2.8.2 Sigma-1 receptors (**Table 1**, **Scheme 20**)*

Although sigma-1 receptors are not GPCRs but are rather unique integral membrane chaperone proteins with no homology to other receptors, it was felt important to mention them given their important role in several neuropsychiatric and neurodegenerative diseases. Indeed, sigma-1 agonists have shown efficacy in animal models of AD, depression, and schizophrenia, while antagonists display some potential as antinociceptive agents. [^{11}C]SA4503 is the first and only sigma-1 radiotracer approved and evaluated in humans[58,59] and used to quantify sigma-1 receptor density. It displays a widespread distribution in all brain regions of healthy subjects but decreased distribution in brain areas of early AD patients, demonstrating a reduced cerebral and cerebellar sigma-1 receptor density in the early stage of the disease. The absence of a reference region, sigma-1 receptor being expressed in all brain areas, renders its use rather complex for early AD diagnosis, given the need for arterial blood sampling. Although interesting results have been obtained with [^{11}C]SA4503, several groups have recently reported their efforts in the design of [^{18}F]-labeled tracers with longer half-life compared to [^{11}C]-derivatives and displaying better selectivities versus sigma-2 receptor and the vesicular acetylcholine transporter. The testing of a [^{18}F]-fluorobutyl spirocyclic derivative[138] or of [^{18}F]-TZ3108[139] in rats or nonhuman primates has

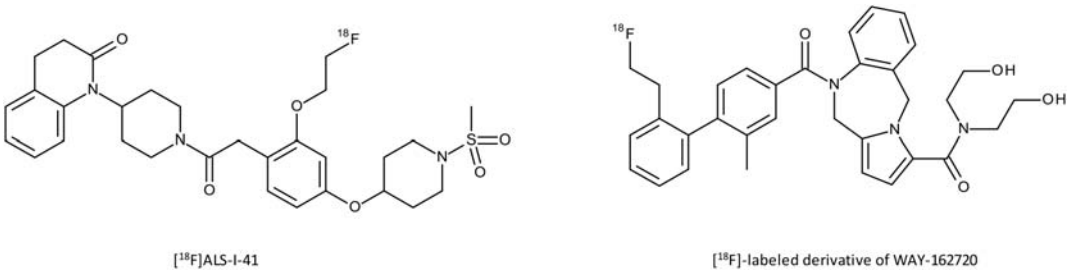

Scheme 19 Selected OXT receptor PET tracers.

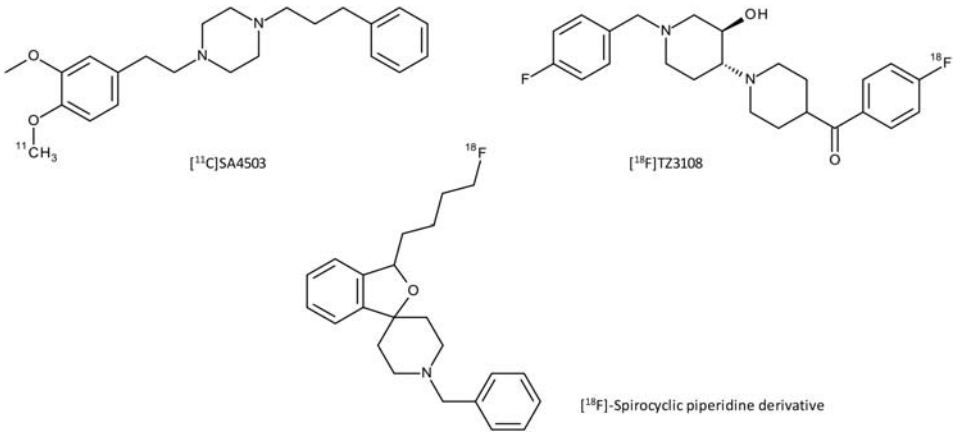

Scheme 20 Selected sigma-1 receptor PET tracers.

shown promising profiles, characterized by specific brain uptake, high selectivity, and non-brain-penetrant radiometabolites. However, no further development has been reported.

7.02.2.3 PET Tracers Targeting Enzymes

Although historically focus was placed on the imaging and detection of neuroreceptors such as GPCRs, probing enzymes and enzymatic processes in the brain is of utmost importance. However, the development of PET tracers has proven to be much more challenging than expected since enzymes are often characterized by too low catalytic rate for the production of enzymatic products within the time limits of PET detection. Progress in the discovery of suitable high-affinity inhibitors as potential tracers has permitted scientists to monitor several key processes in the brain such as protein or neurotransmitter synthesis or metabolism, cell proliferation or to study intracellular systems.[140]

The following section will focus on some recent developments in the field, and particularly on the imaging of selected kinases and phosphodiesterase subtypes.

7.02.2.3.1 Tracers in clinical use

See Table 2.

7.02.2.3.2 Recent developments

7.02.2.3.2.1 Phosphodiesterase inhibitors

Phosphodiesterases (PDE) are a class of enzymes which catalyze the hydrolysis of phosphodiester bonds of 3′,5′-cyclic adenosine monophosphate (cAMP) and/or cyclic guanosine monophosphate (cGMP), two key secondary messengers involved in numerous intracellular downstream signaling pathways from GPCRs. About 50 different PDE isoforms have been grouped into 11 subfamilies (PDE1-11) according to their amino acid sequence, kinetic properties, or substrate. PDE4 and PDE7 display cAMP-selectivity, PDE5, 6, and 9 are cGMP-specific, while PDE1, 2, 3, 10, and 11 are able to hydrolyze both types of cyclic nucleotides with similar affinity.[155] The development of selective PDE1-11 inhibitors has been the subject of intense research efforts over the last decades and several suitable PET radiotracers of PDE enzymes have been identified and were recently reviewed.[156] In particular, and given the importance of PDE2,[157] 7, and 10 in several brain diseases, those specific radiotracers will be briefly discussed hereafter.

Table 2 CNS radiotracers used in human studies for enzymes

Molecular target	*^{11}C-labeled ligand*	*^{18}F-labeled ligand*	*Selected references*
AChE	[^{11}C]MP4A		141
Aromatase	[^{11}C]Vorozole		142
DOPA decarboxylase		[^{18}F]F-DOPA [^{18}F]FMT	25,143
FAAH	[^{11}C]CURB		144,145
MAO-A	[^{11}C]Harmine [^{11}C]Clorgyline [^{11}C]Befloxatone		146,147
MAO-B	[^{11}C]Deprenyl-d2		148,149
PDE2A		[^{18}F]-PF05270430	150
PDE4	[^{11}C](R)-Rolipram		151
PDE10A	[^{11}C]IMA107 [^{11}C]MP-10 [^{11}C]Lu AE92686	[^{18}F]MNI659	152–154

*7.02.2.3.2.1.1 PDE2A (**Table 2**, **Scheme 21**)*

PDE2A is mainly expressed in limbic area and basal ganglia. Increased levels of cyclic nucleotides in these regions, through selective PDE2A inhibition, could be of importance for cognitive processes. Only a few reports deal with the identification of selective PDE2A PET ligands. [^{18}F]-Triazine derivatives[158] were recently disclosed but are not suitable for in vivo imaging purposes due to the formation of brain-penetrant radiometabolites accumulating in reference regions such as the cerebellum. Imidazo[5,1f]-[1,2,4] triazines,[159] among which [^{18}F]-PF05270430 was tested in cynomolgus monkeys and recently in humans, were also reported.[150] Consistent with reported PDE2A distribution, high uptake of [^{18}F]-PF05270430 was observed in striatum and low uptake in cerebellum and no defluorination was detected. The signal in striatum was dose-dependently blocked by a reference PDE2A inhibitor. Low-binding potential in humans is nevertheless observed. [1,2,4]Triazolo[4,3a]quinoxalines[160] were also reported in a patent application but are lacking selectivity and also bind to PDE10A with high affinity.

*7.02.2.3.2.1.2 PDE7 (**Scheme 22**)*

PDE7 is, together with PDE4, a cAMP-specific PDE subtype. PDE7 inhibitors might therefore advantageously replace PDE4 inhibitors which are characterized by proemetic properties limiting their clinical use. Beyond the well-known potential in inflammatory and T-cell driven diseases, selective PDE7 inhibitors have been shown to improve motor function and induce some level of

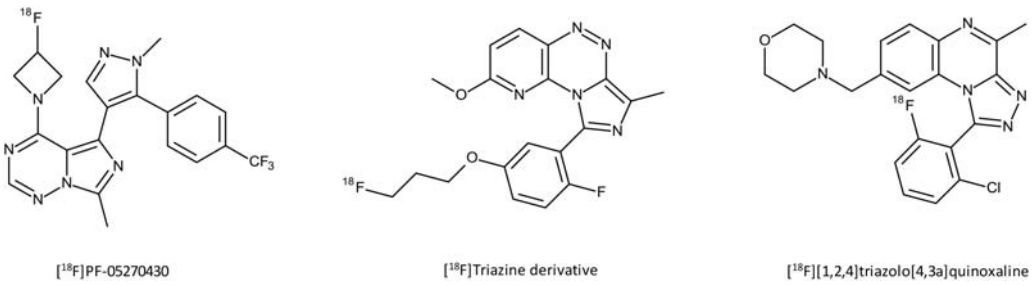

Scheme 21 Selected PDE2 PET tracers.

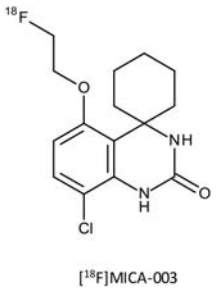

Scheme 22 Selected PDE7 PET tracer.

neuroprotection in animal models of PD.[161] Additional potential benefits in drug or alcohol-addiction disorders have raised the interest in PDE7 and triggered the need to identify a suitable PET tracer in order to quantify PDE7 in the brain, to delineate the role of PDE7 in neurological disorders, and to support the development of selective inhibitors. Only one group has reported the design and synthesis of a [^{18}F]-labeled tracer, [^{18}F]MICA-003, based on a spiroquinazolinone scaffold. Despite favorable kinetics and homogenous distribution in the brain, in vivo evaluation in mice nevertheless indicated the presence of [^{18}F]-fluoroethanol as a major brain-penetrant radiometabolite, therefore impairing PDE7 quantification and further development.[162]

*7.02.2.3.2.1.3 PDE10A (**Table 2**, **Scheme 23**)*

PDE10A is a dual cAMP/cGMP hydrolyzing enzyme which has triggered considerable interest over the last few years thanks to its high expression in the brain and in particular in the striatal medium spiny neurons in conjunction with its relatively low expression in periphery. Selective PDE10A inhibitors could therefore play a major role in several pathophysiologies such as schizophrenia, Huntington's disease, or addiction.[163–166] A high therapeutic potential combined with an optimal target density and restricted distribution in the brain, facilitating strong PET signals, has triggered a lot of interest from pharmaceutical companies and academic groups.

Several PET tracers are currently used in clinical development. Recently, [^{18}F]MNI659 demonstrated that a PDE10A radiotracer could be a useful biomarker of striatal neurodegeneration in patients with early Huntington disease.[152] [^{11}C]IMA107 was also reported to be particularly promising after first-in-human studies based upon direct comparison with [^{11}C]MP10[167,168] in baboons.[153] [^{11}C]IMA107 was recently evaluated in patients with chronic schizophrenia in order to assess PDE10A brain expression in comparison with healthy subjects. Results did not show any significant correlation between [^{11}C]IMA107 binding potential and the severity of the psychotic symptoms and no alteration of PDE10A in schizophrenic patients was found.[154] [^{18}F]AMG580 was discovered by scientists at Amgen and hold promises for human use.[169,170] [^{11}C]MK-8193,[171,172] [^{11}C]T-773,[173,174] [^{11}C]TZ1964B,[175] [^{11}C]Lu AE92686,[176] [^{18}F]JNJ-42259152, and [^{18}F]JNJ-42071965[177–179] were also reported as promising ligands.

7.02.2.3.2.2 Kinase inhibitors

While the development of PET ligands to support the development of kinase inhibitors and to monitor enzymes densities in oncology is a fast-growing field with several clinical studies ongoing, in vivo PET imaging in neurology and neuro-oncology appears much more complex to tackle. In addition to the usual requirements needed for successful PET ligand design, subnano- or

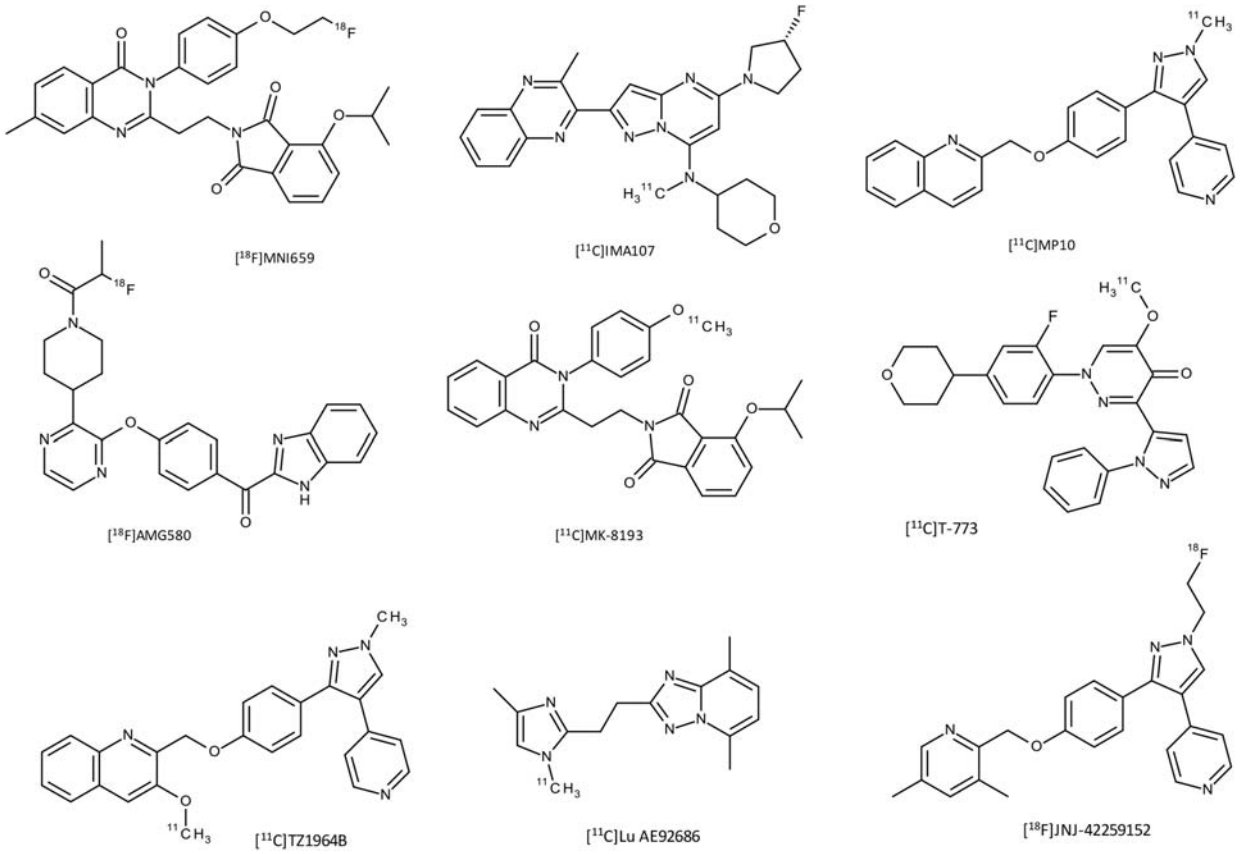

Scheme 23 Selected PDE10 PET tracers.

picomolar affinity for the kinase target is needed, representing a particular challenge in the case of ATP-competitive kinase inhibitors with low $K_{M,ATP}$ values. Furthermore, the use of kinase PET radiotracers beyond tumor imaging or biodistribution studies might be limited and challenging to interpret since most kinase inhibitors lack sufficient selectivity for a large part of the kinome. Brain penetration is another key element to consider, knowing that numerous kinase inhibitors are characterized by suboptimal physicochemical properties such as polar surface area, or lipophilicity and/or interactions with ABC transporters (e.g., P-glycoprotein) which impair BBB penetration and foster nonspecific binding. Finally, huge variations in $K_{M,ATP}$ values between ATP-competitive kinases, differences between Type 1 and Type 2 inhibitors, in terms either of residence time and selectivity or binding mode and interactions with the DFG motif and the associated requirement for polar groups, render the development of PET tracers quite challenging. Advances in the field of kinase imaging have been reviewed recently.[180] Several examples are described, in particular in the case of tyrosine kinase (e.g., Trk inhibitors)[181–183] and serine/threonine kinase inhibitors which are further detailed hereafter.

*7.02.2.3.2.2.1 Glycogen synthase kinase 3 (GSK-3) (**Scheme 24**)*

GSK-3 is a serine/threonine kinase family member. It has two isoforms (α and β) and is involved in glycogen metabolism. Interest in the development of selective GSK-3 inhibitors was triggered by its high abundance in the brain and its implication in the pathogenesis of several neurological and neurodegenerative diseases. It is indeed known to phosphorylate Tau which has been liked to AD and is therefore associated with the progression of tauopathies. There is an important need for suitable in vivo quantification and an early diagnostic tool to allow the measurement of target engagement of novel GSK-3 inhibitors, to help their development.[184] The first reported potential PET tracers, [^{11}C]AR-A014418[185] and [^{11}C]PyrATP-1,[186] were not able to cross the BBB according to autoradiography experiments in rats, despite apparent favorable in vitro properties. Two recent papers have disclosed the identification and preclinical characterization in rodents and nonhuman primates of two promising brain-penetrant ATP-competitive GSK-3 PET tracers, [^{11}C]SB-216763[187] and [^{11}C]PF-367.[188,189] Both display single-digit nanomolar GSK-3 affinity, high selectivity, and uniform brain distribution, consistent with the ubiquitous enzyme distribution throughout all brain areas. However, no human studies have been reported to date.

*7.02.2.3.2.2.2 Rho-kinase (**Scheme 25**)*

Rho-kinase is another serine–threonine protein kinase. In addition to considerable interest in many peripheral disorders, it may also be involved in the pathogenesis of several neurological diseases such as AD, stroke, and ischemia–reperfusion injury. *N*-[^{11}C]methyl-hydroxyfasudil was designed based on hydroxyfasudil, a major active metabolite of fasudil, a known ATP-competitive Rho-kinase inhibitor developed for the treatment of ischemic stroke. It showed widespread distribution but low-level radioactivity in mouse brain. Data in a mouse cold brain injury model suggest that it binds to the active form of Rho-kinase. Insufficient binding affinity and low lipophilicity, hence the low brain penetrance of *N*-[^{11}C]methyl-hydroxyfasudil, impair its use for human purposes and further efforts are required to identify suitable Rho-kinase PET tracers.[190,191]

*7.02.2.3.2.3 Transglutaminase (TG2) inhibitors (**Scheme 26**)*

TG2 is an ubiquitously expressed calcium-dependent transglutaminase. It is involved in the formation of toxic protein aggregates through inter- and intramolecular crosslinking and potentially in several neurodegenerative disorders such as Parkinson's disease,

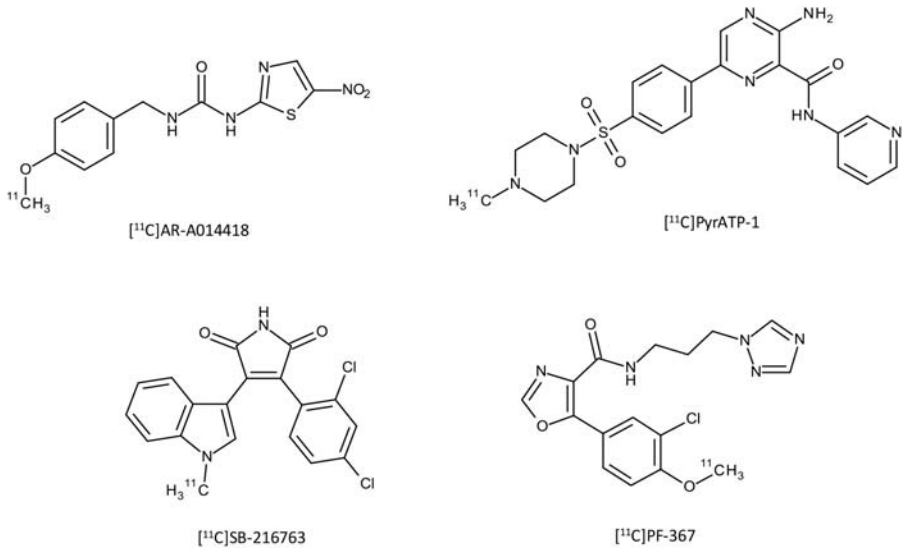

Scheme 24 Selected GSK-3 PET tracers.

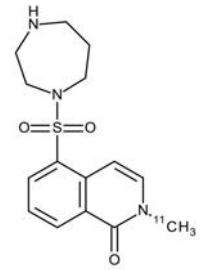

N-[^{11}C]Methyl-hydroxyfasudil

Scheme 25 Selected Rho-kinase PET tracer.

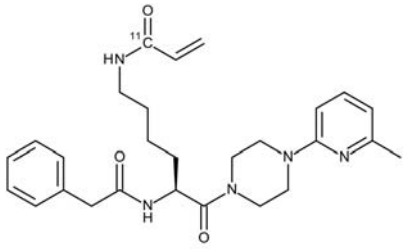

[^{11}C]-TG2 inhibitor

Scheme 26 Selected TG2 PET tracer.

Huntington's disease, and AD.[192,193] The first example of a selective [^{11}C]-radiolabeled TG2 inhibitor was recently reported.[194] However, the brain uptake was nevertheless very low in rats, impairing further CNS use.

7.02.2.4 PET Tracers Targeting Ion Channels

Ion channels are membrane proteins which control the flow of ions through the cell membrane in almost all living species. Despite the fact that a large number of ion channels are known, only a few have been thoroughly studied and even less have seen the development of successful PET tracers for clinical application, namely only the γ-aminobutyric acid–benzodiazepine receptor (GABA-A) and the nicotinic acetylcholine receptor (nAChR), both of which are ligand-gated.[195] Therefore, PET imaging of neuronal ion channel-linked receptors should be a developing area of preclinical and clinical research in the coming years.

The following section will briefly review the most recent clinical application of GABA-A and nAChR PET tracers and will discuss some of the challenges faced to develop a successful PET tracer of a third important class of ion channel receptor, namely the *N*-methyl-D-aspartate (NMDA) receptor. P2X7, another ion channel recently investigated for PET imaging, will be discussed in the neuroinflammation section.

7.02.2.4.1 Tracers in clinical use

See **Table 3**.

7.02.2.4.2 Recent developments

7.02.2.4.2.1 Neuronal nAChR

*7.02.2.4.2.1.1 α4β2-nAChR[197205] (**Table 3**, **Scheme 27**)*

Neuronal nAChRs are involved in many neurological processes and have been implicated in several neurodegenerative diseases, including AD, PD, and multiple system atrophy (MSA), as well as in epilepsy, depression, schizophrenia, and dementia.

Five PET radiotracers, one ^{11}C-labeled, [^{11}C]nicotine, and four ^{18}F-labeled, [^{18}F]2-FA, [^{18}F]6-FA, [^{18}F]Flubatine, and [^{18}F]AZAN have been used for imaging the α4β2 subtype in human. Although an ideal PET ligand for this receptor subtype has not yet been definitively established, [^{18}F]2-FA has been extensively used in recent years for clinical studies in AD, PD, and schizophrenia.[196,206] More recently, two novel α4β2 selective PET tracers, [^{18}F]Flubatine and [^{18}F]AZAN, have been developed and validated in human.[198,199,207] The first data in human suggest that they display very favorable characteristics, including better kinetics than [^{18}F]2-FA, warranting further investigation with these novel tracers. More recently, [^{18}F]Nifene and [^{18}F]Niofene, two analogs of [^{18}F]2-FA, have demonstrated improved kinetics over [^{18}F]2-FA in preclinical studies.[208,209] However, these tracers have not yet been assessed in clinical studies but their improved kinetic profile may bring benefit compared to [^{18}F]2-FA.

Table 3 CNS radiotracers used in human studies for ion channels

Molecular target	*^{11}C-labeled ligand*	*^{18}F-labeled ligand*	*Selected references*
Nicotinic (α4β2)	[^{11}C]nicotine	2-[^{18}F]FA-85380 or [^{18}F]2-FA [^{18}F]6-FA [^{18}F]AZAN [^{18}F]Flubatine	196–199
Nicotinic (α7)	[^{11}C]CHIBA-1001	[^{18}F]ASEM	200–202
GABA-A	[^{11}C]Flumazenil [^{11}C]Ro15-4513	[^{18}F]Flumazenil [^{18}F]Fluoroethylflumazenil	203,204

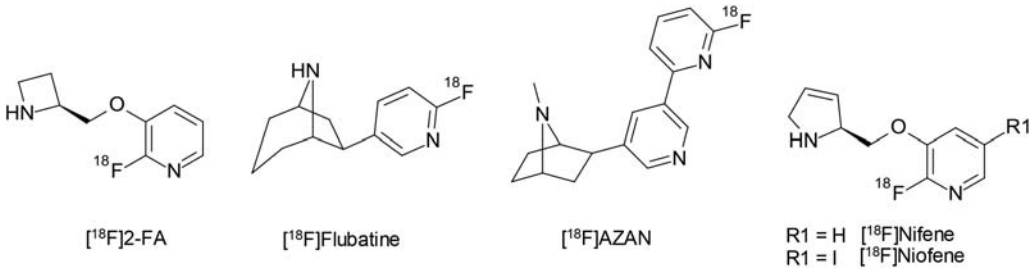

Scheme 27 Representative structures of α4β2 selective PET tracers.

*7.02.2.4.2.1.2 α7-nAChR (**Table 3**, **Scheme 28**)*

Agonists of the α7-nAChR have been developed as potential therapeutic drugs for diseases such as schizophrenia disease and AD. Therefore, an α7-nAChR selective PET tracer to measure receptor occupancy in the living human brain is of high interest for the pharmaceutical industry. Although much effort has been devoted to create specific PET radioligands for the α7-nAChR, only [^{11}C]CHIBA-1001 and [^{18}F]ASEM are currently available for clinical studies.

Although [^{11}C]CHIBA-1001 has a high level of nonspecific binding in the human brain, it has been used to measure the target occupancy of two antagonist drug candidates;[200] however, a novel tracer with lower nonspecific binding would be required for more accurate occupancy measurements. More promising preclinical and clinical human brain imaging data have been reported recently with [^{18}F]ASEM which may be the first highly specific α7-nAChR radioligand available for human PET imaging.[201,202]

*7.02.2.4.2.2 γ-aminobutyric acid A–benzodiazepine receptor (GABA-A—BZR)[203] (**Table 3**, **Scheme 29**)*

GABA-A is a ligand-gated ion channel found on most neurons in the brain. The GABA-A ion channel has been reported to be a potential marker of various pathological conditions, such as PD, Huntington's chorea, AD, and epilepsy. The benzodiazepine binding site is an allosteric modulatory site on the GABA-A ion channel. Many different chemotypes can bind to this allosteric site and this is the binding site of all GABA-A PET tracers used to date. There are six subtypes of the GABA-A ion channel and, except for the tracer [^{11}C]Ro15-4513, which exhibits some selectivity for the α5 subtype, all available other tracers are nonselective.[203]

Currently, the most widely used GABA-A PET tracer is still [^{11}C]Flumazenil, despite its radiolabeling with ^{11}C. In particular, it has been used recently to quantify the GABA-A ion channel in the brain of Fragile X patients.[204] By contrast to Flumazenil which is not selective for the various subtypes of GABA-A, [^{11}C]Ro15-4513 has a higher affinity for the α5 subtype. The first human PET data indicated that [^{11}C]Ro15-4513 can be used to explore the functional role of this subtype in humans.[210,211]

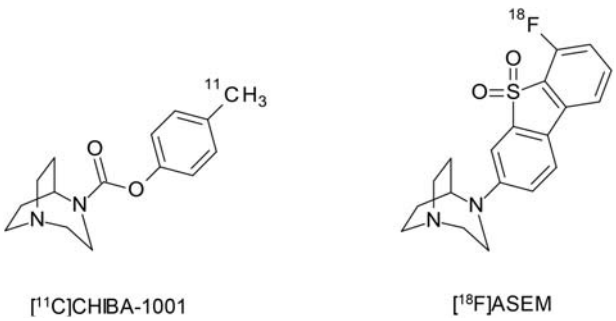

Scheme 28 Structures of the only two α7 tracers used in clinics.

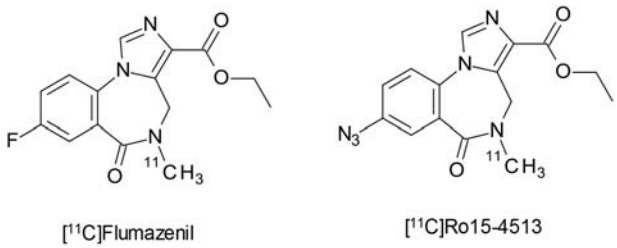

Scheme 29 Structures of some flumazenil-based GABA-A PET tracers used in clinics.

Although [^{11}C]Flumazenil is broadly available for PET studies, its radiolabeling with ^{11}C still requires access to a cyclotron for production of ^{11}C. An ^{18}F-labeled tracer would allow a much broader application. ^{18}F-labeling of Flumazenil itself has long been considered unachievable due to the inactivated aromatic ring to perform an aromatic nucleophilic substitution. Therefore, [^{18}F]Fluoroethylflumazenil has been developed to circumvent the radiochemistry issue. Unfortunately, this tracer has lower affinity and faster metabolism than Flumazenil, which limit its use.[203] As discussed in the section addressing radiosynthesis methods, there have been considerable efforts in the last few years to explore novel F-18 labeling methodologies to broaden the chemical space of substrates that can be radiolabeled. The use of diaryl iodonium salts as labeling precursors has allowed chemists to perform aromatic nucleophilic substitution on unactivated aryl rings. This methodology has been successfully applied to the radiosynthesis of [^{18}F]Flumazenil, thus providing much broader access to this tracer (**Scheme 30**).[212]

7.02.2.4.2.3 NMDA receptor[213]

Among the ionotropic glutamate receptors, the NMDA subtype plays a key role in processes involving excitatory neurotransmission, including learning, memory, and synaptic plasticity. It has been extensively investigated by many research groups in order to develop a suitable PET tracer for human use. Efforts have been mostly devoted to compounds binding to the channel blocker site, also named phencyclidine (PCP) binding site, as well as to the NR2B-specific allosteric site, often named the ifenprodil-binding site. These efforts have been recently reviewed in several papers.[195,213] Unfortunately, to date, no suitable PET tracer for human PET imaging of the NMDA receptor has been identified, thus further improvements are necessary before a satisfactory PET radiotracer is developed. Low brain penetration has been a significant challenge for most tracer candidates developed for the PCP-binding site while lack of selectivity, especially over the sigma-1 receptor, has been a recurrent issue for compounds targeting the ifenprodil-binding site.

7.02.2.5 PET Tracers Targeting Transporters

In the past two decades, due to their implication in a broad range of neurological and neuropsychiatric conditions, transporters of neurotransmitters have been extensively investigated as targets for the developments of PET imaging tracers. In order to develop suitable PET tracers for human use for most of these transporters, several recurrent challenges had to be solved. A prominent challenge has been selectivity and to some extent is still an issue, for example, for dopamine transporter (DAT) tracers. Due to the high affinity required for these PET tracers, achieving a suitable kinetic profile (i.e., achieving equilibrium in timeframe compatible with the half-life of PET radioisotopes) has also been a significant challenge. Finally, as described later, researchers are still struggling to develop an ^{18}F-labeled version of some of the early tracers developed using ^{11}C and further work may still be required to identify suitable ^{18}F tracers for these transporters.

The following section will review the challenges and advances during the last 5 years in order to make available specific ^{18}F-labeled PET tracers of neurotransmitter transporters for broad clinical use.

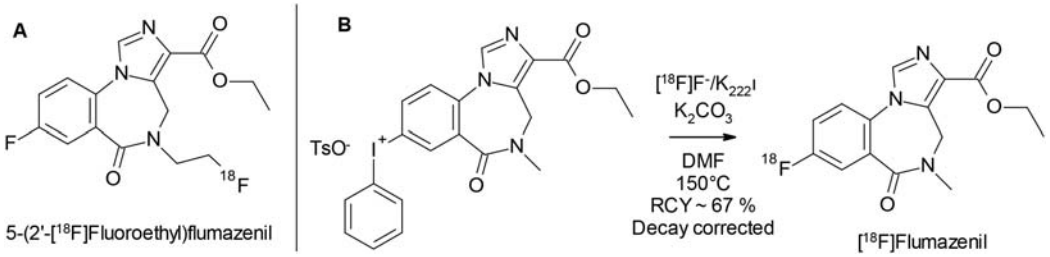

Scheme 30 (A) Structure of [^{18}F]Fluoroethylflumazenil; (B) recent improvement of the synthesis of [^{18}F]Flumazenil.

7.02.2.5.1 Tracers in clinical use

See Table 4.

7.02.2.5.2 Recent developments

7.02.2.5.2.1 Dopamine transporter (DAT) (Table 4, Schemes 31 and 32)

Imaging of the presynaptic DAT has been widely used in PD patients over the last 2 decades and has been mainly performed using SPECT.[233] Although SPECT imaging is slightly less sensitive and provides lower spatial resolution in human than PET imaging, it has the advantage of being much cheaper and uses longer half-life radioisotopes. Indeed, slow equilibration kinetics has been a major property of early imaging tracers such as β-CIT, preventing the use of the shorter half-life PET radioisotopes (typically ^{11}C and ^{18}F) to perform imaging studies at equilibrium. The most widely used SPECT tracer for DAT imaging is [^{123}I]FP- CIT or [^{123}I]Ioflupane, which has been approved by the FDA in 2011 for clinical imaging of DAT and is commercialized under the brand-name DaTscan™.

Besides the slow equilibration kinetics, the lack of selectivity versus the serotonin transporter (SERT) of early DAT tracers has also been a significant issue. The most widely used tracers to date are not selective and SERT binding may be a confounding factor for image analysis outside of the striatum or in patients receiving selective serotonin reuptake inhibitor (SSRI) medication. Therefore, some research groups have developed and validated new tracers during the last decade in order to fix both the slow kinetics and selectivity issues and some of these tracers have been radiolabeled with PET radioisotopes. Among the most characterized new tracers are [^{18}F]FE-PE2I and [^{18}F]FECNT (Scheme 32).

Both tracers have been tested in healthy human volunteers and in PD patients.[214–217] Both compounds have suitable kinetics allowing accurate quantification using a reference tissue model and are both more selective versus SERT. In particular, [^{18}F]FE-PE2I has excellent selectivity in vivo[234] which should allow its use for DAT quantification in both striatum and substantia nigra,[215] by contrast to the current gold standard [^{123}I]Ioflupane which allows only DAT quantification in striatum.

7.02.2.5.2.2 Norepinephrine transporter (Table 4, Schemes 33 and 34)

PET imaging of the norepinephrine transporter (NET) has a wide range of possible applications in neurology and psychiatry, including diseases such as AD, depression, and attention deficit hyperactivity disorder. A few PET tracers have been developed in the last decade based on the reboxetine template. Among these tracers, [^{11}C]MeNER (or [^{11}C]MRB) and [^{18}F]FMeNER-d2 (Scheme 33) have progressed to human studies and allowed the first in vivo quantification of NET in human as well as the first occupancy

Table 4 CNS radiotracers used in human studies for transporters

Molecular target	*^{11}C-labeled ligand*	*^{18}F-labeled ligand*	*Selected references*
DAT	[^{11}C]PE2I [^{11}C]Methylphenidate	[^{18}F]FP-CIT [^{18}F]FE-PE2I [^{18}F]FECNT	214–217
Glycine T1	[^{11}C]GSK 931145 [^{11}C]RO5013853	[^{18}F]MK-6577	218–221
NET	[^{11}C]MeNER/[^{11}C]MRB [^{11}C]MeNET	[^{18}F]FMeNER-d2	222–224
SERT	[^{11}C]DASB [^{11}C]MADAM [^{11}C]AFM [^{11}C]HOMADAM	4-[^{18}F]FADAM	225
SV2A	[^{11}C]UCB-A [^{11}C]UCB-J	[^{18}F]UCB-H	226–229
VMAT2	[^{11}C]MTBZ [^{11}C]DTBZ	[^{18}F]Florbenazine/[^{18}F]AV-133/[^{18}F]FP-DTBZ	230–232

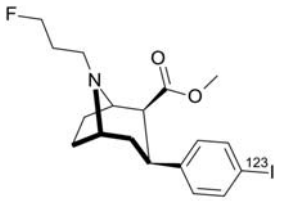

[^{123}I]Ioflupane

Scheme 31 Most widely used DAT SPECT tracer.

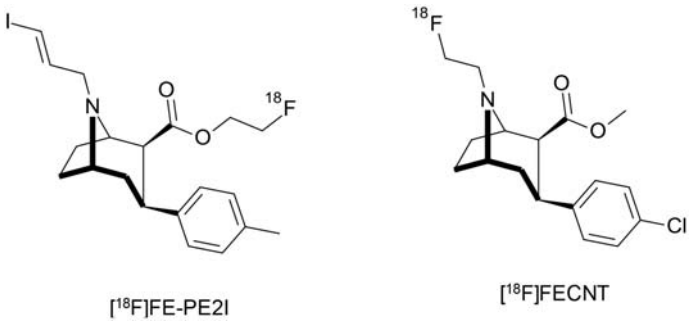

Scheme 32 Most characterized ^{18}F-radiolabeled DAT PET tracers.

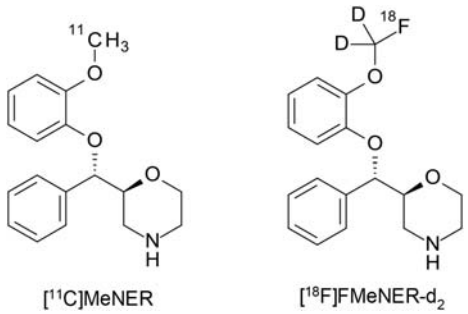

Scheme 33 Reboxetine-based NET PET tracers used in human.

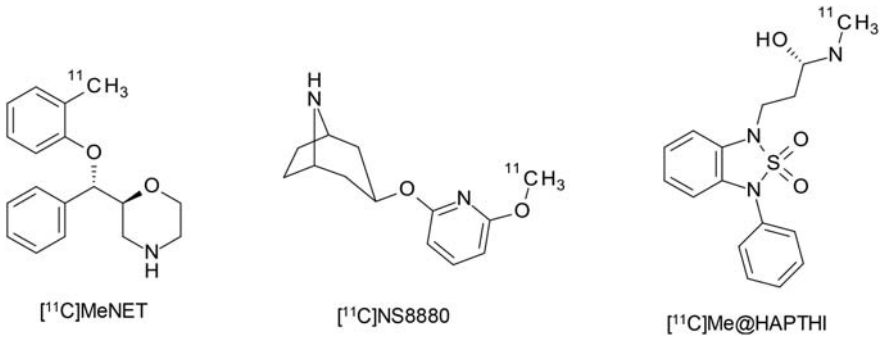

Scheme 34 Novel NET PET tracers.

study with methylphenidate.[222,223] However, these tracers suffer from slow kinetics and a quite low specific-to-non-specific binding ratio which leads to suboptimal imaging properties.

These limitations have triggered additional efforts to identify improved NET PET tracers. A few new candidate molecules [^{11}C]MeNET, [^{11}C]NS8880, and [^{11}C]Me@HAPTHI have been reported recently (**Scheme 34**).

[^{11}C]MeNET is the only one so far to have been tested in humans. It shares the same chemotype as the previous tracers and, although it is reported to have a slightly improved kinetic profile, it has a very similar, low, specific-to-non-specific binding ratio as its previous analogs.[224] By contrast, [^{11}C]NS8880 and [^{11}C]Me@HAPTHI have been developed from novel chemotypes and may therefore bring a different profile. Initial preclinical studies with [^{11}C]NS8880 suggest that it may have an improved kinetic profile but it still has low specific-to-non-specific binding ratio.[235] [^{11}C]Me@HAPTHI has only been characterized in vitro so far and will require more data before any conclusion can be drawn. However, if its pharmacokinetic profile turns out to be suitable, its subnanomolar affinity for NET may eventually lead to an improved specific-to-non-specific binding ratio in vivo.[236]

*7.02.2.5.2.3 Serotonin transporter (SERT) (**Table 4**, **Schemes 35–37**)*

Alterations of the SERT have been implicated mainly in neuropsychiatric disorders such as depression, anxiety, and suicide. SERT is also the target of the SSRI antidepressant drugs. Therefore, SERT PET imaging would enable the measurement of SERT density in these psychiatric disorders[238] and also target occupancy of SSRIs.[239]

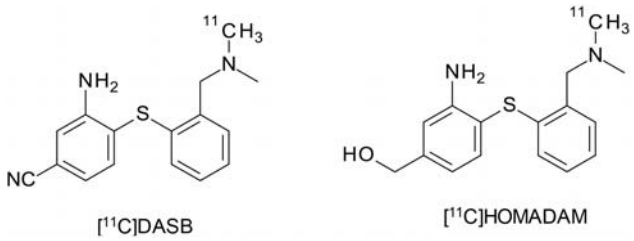

Scheme 35 Most widely used SERT tracer [^{11}C]DASB and its analog [^{11}C]HOMADAM.

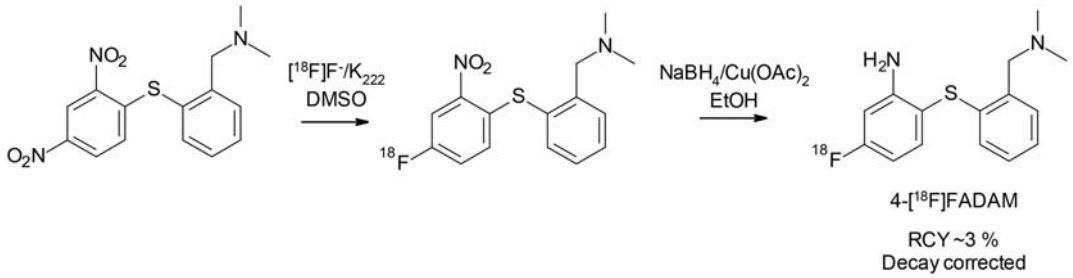

Scheme 36 Low-yield two-step radiosynthesis of 4-[^{18}F]FADAM.

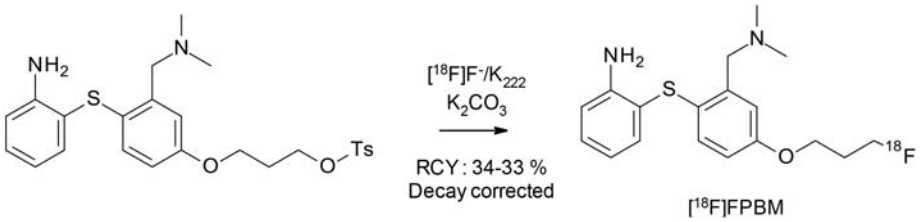

Scheme 37 Efficient radiosynthesis of [^{18}F]FPBM recently reported.[237]

Several successful PET tracers have been developed from the so-called diaryl sulfide chemotype.[225] Among those PET tracers [^{11}C]DASB and [^{11}C]HOMADAM (**Scheme 35**) have been compared in monkey and tested in human and both provide suitable properties to image SERT. The most widely used tracer, [^{11}C]DASB, has excellent selectivity, kinetic profile, and reproducibility allowing accurate quantification. However, its widespread clinical use is limited by the short half-life of its radioisotope.

Therefore, significant efforts have been made more recently to develop an ^{18}F-labeled SERT PET tracer that could facilitate commercial delivery. The only successful ^{18}F-labeled SERT PET tracer reported to date in human is 4-[^{18}F]FADAM.[240] 4-[^{18}F]FADAM showed high-specific binding and a suitable kinetic profile suggesting that it could be used to image SERT in human. However, its radiosynthesis provides very low and unreliable radiochemical yields preventing its widespread clinical use (**Scheme 36**). 4-[^{18}F]FADAM is a typical example of an ^{18}F-labeled PET tracer that would benefit from the development of novel radiolabeling methods as discussed in the section addressing radiosynthesis methods.

[^{18}F]FPBM has been suggested as an alternative ^{18}F-labeled SERT PET tracer and very promising data have been recently reported in cynomolgus monkey, suggesting a high-specific binding and faster kinetics than 4-[^{18}F]FADAM.[237] In addition, an efficient one-step radiosynthesis of [^{18}F]FPBM has been developed that should facilitate its possible translation to human studies (**Scheme 37**).

*7.02.2.5.2.4 Glycine transporter Type 1 (GlyT-1) (**Table 4**, **Scheme 38**)*

The glycine transporter type (GlyT-1) is expressed at glutamatergic synapses throughout the mammalian brain and has therefore been implicated in diseases such as schizophrenia. The current interest by the pharmaceutical industry in developing GlyT-1 inhibitors has led to the demand for a GlyT-1 PET tracer. Such a PET tracer would be useful to support drug development and, in particular, to drive the dose selection for human efficacy studies. Indeed, as efficacy in animal models of schizophrenia has been reported to show an inverted-U shape response dose response curve,[241] adopting a maximum tolerated dose paradigm in a proof-of-concept study may result in GlyT-1 inhibition outside of the efficacious range. Therefore, the support of a suitable PET tracer to measure GlyT-1 occupancy in human and its relationship with the administered dose may be critical for the success of GlyT-1 inhibitors in clinical development.

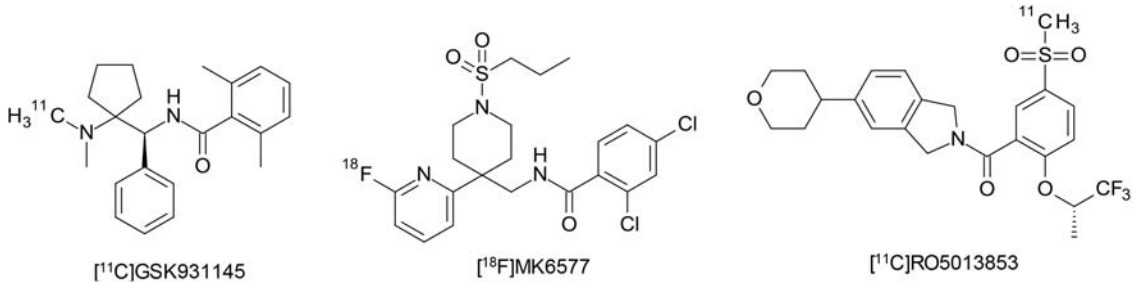

Scheme 38 Structure of the three GlyT-1 PET tracers used in clinical studies.

Three GlyT-1 PET tracers have recently been developed and characterized in human. While they are all reported to be suitable for target occupancy measurements,[218–220] the test–retest variability of [^{11}C]GSK931145 is much higher and precludes its use for measuring interpopulation GlyT1 differences. Both [^{11}C]RO5013853 and [^{18}F]MK6577 provide lower variability. The better profile of [^{18}F]MK6577 has also been confirmed in a head-to-head comparative study between with [^{11}C]GSK931145 in the same monkey.[221]

*7.02.2.5.2.5 Vesicular monoamine transporter type 2 (VMAT2) (**Table 4**, **Scheme 39**)*

The vesicular monoamine transporter type 2 (VMAT2) is involved in the transport of monoamines from cytosol to presynaptic vesicles of monoaminergic neurons. VMAT2 density is linearly correlated with the integrity of the dopaminergic neurons in the substantia nigra.[242] While at the early stage of PD, other imaging modalities such as aromatic L-amino acid decarboxylase (AADC) and DAT imaging can be affected by compensatory mechanisms, it is reported that VMAT2 availability is less affected by compensatory regulation.[243,244] Therefore, VMAT2 PET imaging may be a better biomarker for the quantification of the presynaptic dopaminergic neurons.

[^{11}C]Dihydrotetrabenazine ([^{11}C]DTBZ) has been reported as a suitable PET tracer for the accurate quantification of the nigrostriatal integrity.[245,246] However, the short half-life of ^{11}C prevents its widespread clinical use. Therefore, [^{18}F]-9-fluoropropyl-(1)-dihydrotetrabenzazine ([^{18}F]FP-DTBZ/[^{18}F]florbenazine/[^{18}F]AV-133) has been recently developed to allow a potential broader commercial use. [^{18}F]AV-133 has high affinity and selectivity for VMAT2, and preclinical and human clinical studies have demonstrated its suitability for quantification of VMAT2 density.[230–232] [^{18}F]AV-133 is currently in phase II clinical development as a potential diagnostic biomarker of PD and PD progression.

*7.02.2.5.2.6 Synaptic vesicle proteins 2 (SV2) (**Table 4**, **Scheme 40**)*

The synaptic vesicle glycoprotein 2A (SV2A) is a 12-transmembrane glycoprotein expressed ubiquitously in synaptic vesicles in all brain areas.[247,248] SV2A is critical for synaptic function, but the exact role of SV2A in neurotransmitter release is still unclear. Mice deficient in SV2A develop seizures and die within 3 weeks of birth, indicating the role of SV2A in epilepsy. To this end, SV2A is the molecular target for the antiepileptic drug levetiracetam (LEV).[249,250] In addition, SV2A dysfunction has been implicated in other neurological disorders such as AD.[251,252]

PET imaging can be used to measure changes in the density of a molecular target in various disease conditions. Therefore, PET imaging of SV2A could be used to measure brain levels of SV2A in patients with epilepsy, AD, or other neurological conditions where SV2A may play a role, and potentially as a biomarker of synaptic density in neurodegenerative disorders. PET tracers can also be used to measure a drug's binding to a target, and so PET imaging of SV2A could be used to characterize binding of SV2A-targeting drugs.

Direct radiolabeling of LEV has been reported[253]; however, its low affinity and slow brain penetration hamper its ability to perform well as a PET tracer. Hence, several high-affinity SV2A ligands that penetrate the brain rapidly have been developed over the last years: UCB-A, UCB-H, and UCB-J.[226]

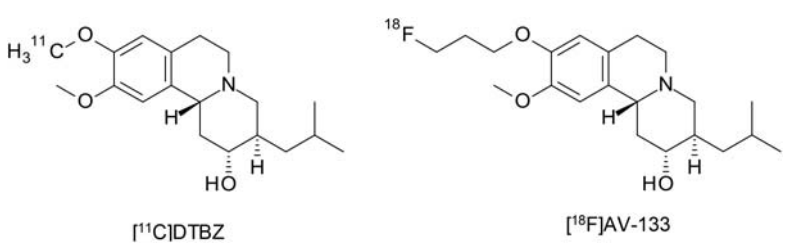

Scheme 39 Structure of the two most widely used VMAT2 PET tracers.

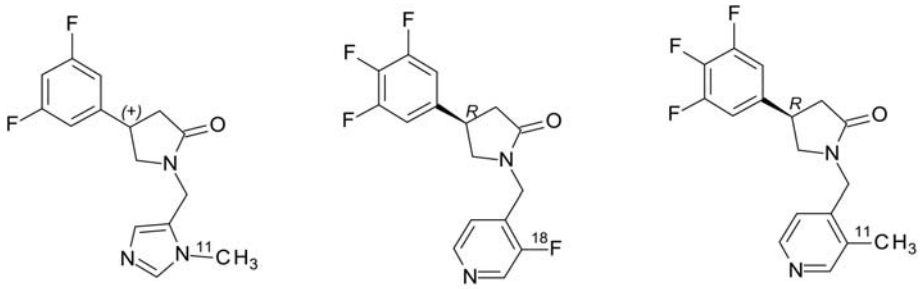

Scheme 40 CNS radiotracers that have developed for the SV2A protein.

UCB-A has been radiolabeled with C-11 and tested in mini-pigs and rhesus monkeys. Although the tracer shows slow kinetics, preclinical data suggest that it can be used to quantify SV2A expression and to study target occupancy.[254] Further testing in human is required to confirm these preclinical data. UCB-H was radiolabeled with F-18 and displayed good kinetics in rats[227] and nonhuman primates, and acceptable dosimetry in humans.[255] However, its multistep radiosynthesis has proven challenging and will require improvement to broaden its use as tracer. Finally, the most recent ligand, [^{11}C]UCB-J, has been reported as the best-in-class SV2A tracer in nonhuman primates.[228] The first-in-human data were recently reported and confirm the excellent behavior of [^{11}C]UCB-J in healthy volunteers[229] as well as its potential to quantify SV2A density in the human brain.

Quantification of synaptic density is typically performed using immunohistochemical approaches with antibodies that target key proteins located in the proximity to the synapse, such as synaptophysin (SYN) which is present in the membrane of presynaptic vesicles.[256] These methods are, however, limited to in vitro experiments and there is still a need for an in vivo synapse quantification technique. PET imaging in combination with a suitable radioligand for SV2A may allow this goal to be achieved. Synaptic vesicle protein-2 (SV2) is present in all vertebrates and located in the presynaptic vesicle membranes, like SYN. SV2 consists of three isoforms SV2A, SV2B, and SV2AC, with SV2A being the only isoform ubiquitously and homogeneously located in synaptic vesicles across the brain.[247] Thus, PET quantification of the SV2A signal may provide an excellent in vivo surrogate measurement of synaptic density. Thus SV2A PET has the potential to find broad application as a biomarker for research, clinical diagnosis, and therapeutic monitoring purposes in neurodegenerative and psychiatric diseases.[229]

By contrast to SV2A, the SV2C isoform has quite limited distribution and is found primarily in regions such as the basal ganglia and the brainstem but is undetectable in the cerebral cortex and the hippocampus.[257] Two recent studies suggest that SV2C could play a role in the pathogenesis of PD and that SV2C expression might be a useful marker to positively impact on personalized prevention and treatment strategies in PD.[258–260] A recent attempt to develop a PET tracer selective for the SV2C isoform [^{18}F]UCB-F was reported in 2013.[261] Despite the fact that the tracer did not work in vivo due to limited brain penetration and rapid metabolism, the close match between the ex vivo autoradiography binding of [^{18}F]UCB-F and the reported distribution of SV2C suggests that further optimization may lead to a selective SV2C PET tracer.

7.02.2.6 PET Tracers Targeting Aggregated Proteins

Abnormally aggregated proteins, such as β-amyloid, hyperphosphorylated tau, and α-synuclein, are now well recognized to play a major role in the pathology of neurodegenerative disorders such as AD, progressive supranuclear palsy and PD, etc. Therefore, over the past 5 years, they have become the hottest targets for developing novel molecular neuroimaging tracers as well as disease-modifying treatments.

7.02.2.6.1 Tracers in clinical use

See **Table 5**.

7.02.2.6.2 Recent developments

*7.02.2.6.2.1 β-amyloid (**Table 5**, **Scheme 41**)*

Early work with [^{11}C]PIB has demonstrated that β-amyloid imaging strongly correlates with the histopathology of β-amyloid deposits.[262] As a consequence, many efforts have been devoted to develop several β-amyloid PET tracers and over the last years, three of which ([^{18}F]Florbetapir, [^{18}F]Flutemetamol, and [^{18}F]Florbetaben) have obtained approval from the US Food and Drug Administration (FDA) to measure the density of β-amyloid plaques in adults with cognitive impairment who are being evaluated for AD and other causes of cognitive decline.

These tracers are used in the evaluation of AD and dementia, only in combination with other diagnostic tests. Indeed, a positive scan does not establish a diagnosis of AD, but simply means that there is a higher amount of amyloid in the brain compared with an

Table 5 CNS radiotracers used in human studies for aggregated proteins

Molecular target	*^{11}C-labeled ligand*	*^{18}F-labeled ligand*	*Selected references*
β-Amyloid	[^{11}C]PIB	[^{18}F]Florbetapir [^{18}F]Flutemetamol [^{18}F]Florbetaben [^{18}F]AZD 4694 [^{18}F]FBM [^{18}F]FDDNP [^{18}F]-SMIBR-W372 [^{18}F]MK3328	262–264
Tau	[^{11}C]PPB3	[^{18}F]AV1451 (T807) [^{18}F]THK523 [^{18}F] THK5351 [^{18}F]GTP-1 [^{18}F]RO6958948	265–269
α-Synuclein	[^{11}C]BF-227	[^{18}F]BF-227	270,271

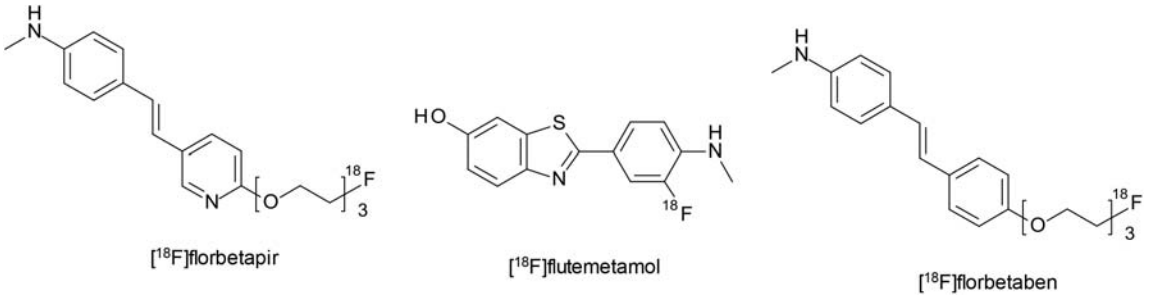

Scheme 41 CNS radiotracers that have used in human studies for aggregated proteins.

age-matched healthy control. A negative scan with these tracers means that there is little or no β-amyloid accumulation in the brain. Consequently, it could be concluded that the cause of the cognitive decline is probably not due to AD, when the β-amyloid PET scan is negative.

Importantly for neuroscience drug discovery, two recent studies have demonstrated that β-amyloid imaging can be applied to enhance patient selection for clinical trials and the monitoring of therapeutic interventions.[263,272] In these two small phase II and phase IB studies with anti-β-amyloid monoclonal antibodies, a positive baseline β-amyloid PET scan was a required entry criterion in order to select appropriate patients. A follow-up scan performed after a few months of treatment demonstrated significant reduction in β-amyloid plaques in the brain of treated patients compared with placebo (**Fig. 3**). These two studies demonstrate the potential of PET imaging to inform the drug development process beyond the historical use of target occupancy assessment. They pave the way for more studies and with novel tracers, therefore enabling better and faster decisions.

*7.02.2.6.2.2 Tau (**Table 5**, **Schemes 42** and **43**)*

More recently, literature evidence has suggested that tau protein aggregates might be more closely related to cognitive decline in AD than β-amyloid deposits.[273–275] Therefore, it is believed that antitau treatments may delay the progression of AD as well as other tau-mediated neurodegenerative diseases. As demonstrated recently, it is expected that tau imaging would promote the establishment of such disease-modifying antitau therapies. This has led to numerous discovery programs aimed at developing a PET tracer that binds selectively to tau aggregates.

Compared with β-amyloid, developing a selective tau tracer is associated with more challenges. First, tau is an intracellular protein, therefore the radiotracer must be able not only to cross the BBB, but also the plasma membrane. Furthermore, due to the heterogeneity of tau (multiple isoforms and posttranslational modifications) in different tauopathies, it is important that the radiotracer can at least bind to both 3R and 4R isoforms in order to be useful to detect tau in several disorders. Another challenge is the secondary β-sheet structure that tau shares with β-amyloid and α-synuclein aggregates. Most tracers reported so far for aggregated proteins are flat, poly-aromatic compounds that are likely to bind to the highly similar core of the β-sheet structure.[276] As a consequence, early tracers such as 2-(1-{6-[(2-[^{18}F]Fluoroethyl)(methyl)amino]-2-naphthyl}ethylidene) malononitrile ([^{18}F]FDDNP) (**Scheme 42**) are reported to bind undistinguishably to β-amyloid and tau aggregates. [^{18}F]FDDNP was proposed as a PET tracer to allow the visualization of tau aggregates in the human brain, but it binds with equal affinities to both senile plaques and neurofibrillary tangles, showing a lack of selectivity for tau over β-amyloid.

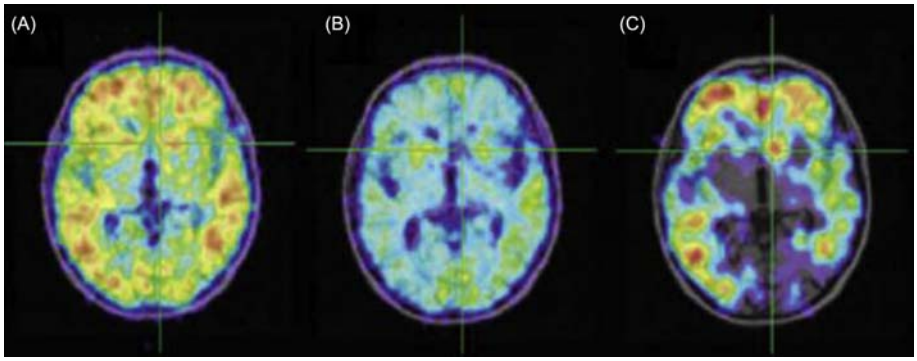

Fig. 3 Overall [^{11}C]PIB SUVR decrease observed in a patient treated with 2 × 200 mg of Gantenerumab. Baseline scan (A), posttreatment scan (B), and difference map (C). Adapted from Ostrowitzki, S.; Deptula, D.; Thurfjell, L.; Barkhof, F.; Bohrmann, B.; Brooks, D. J.; Klunk, W. E.; Ashford, E.; Yoo, K.; Xu, Z.-X.; Loetscher, H.; Santarelli, L. Mechanism of Amyloid Removal in Patients With Alzheimer Disease Treated With Gantenerumab. *Arch. Neurol.* **2012**, *69* (2), 198–207.

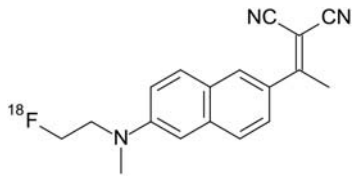

Scheme 42 Chemical structure of the nonselective amyloid tracer [^{18}F]FDDNP.

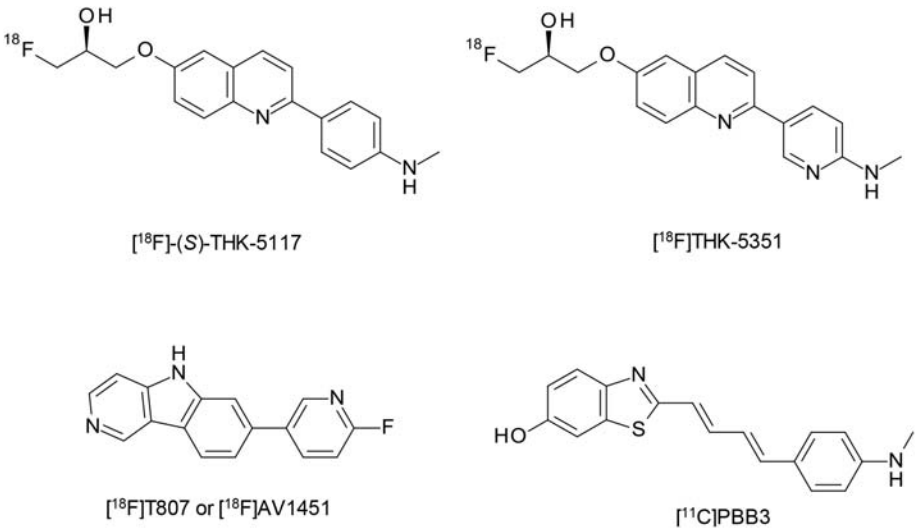

Scheme 43 Chemical structures of the most advanced known selective tau tracer in clinical development.

Many research groups have focused on developing a tau-selective PET tracer and these efforts have been recently reviewed by several authors.[265–268] Several of these novel tracers (**Scheme 43**) have now entered clinical development and are progressing toward larger phase II studies.

Among the first selective radiotracers that have been tested in AD patients is [^{18}F]T807, now known as [^{18}F]AV1451. This tricyclic pyrido-indole derivative was initially selected for its ability to selectively bind to tau over β-amyloid plaques, its rapid uptake and washout, and low off-target binding to other common central nervous system targets.[277] With several clinical studies in AD and other tauopathies successfully completed,[278,279] it is now progressing in phase II clinical development in AD. However, the binding of this tracer to Tau in other tauopathies is still controversial[269] and some possible off-target binding has been reported, such as binding to the monoamine oxidase (MAO) enzymes[280] and to neuromelanin containing neurons.[281]

Taking into consideration these possible limitations of [^{18}F]AV1451, novel tracers like [^{18}F]GTP-1[282] and [^{18}F]RO6958948[283,284] have recently been characterized in human. The chemical structure of these tracers is still unknown, and the reported data, although encouraging, are still very limited. Additional studies will be required to understand whether these novel tracers may bring any significant benefit compared with AV-1451.

7.02.2.6.3 Future developments

Besides β-amyloid and tau, other proteins are known to form aggregates such as α-synuclein, TDP43, or Huntingtin, and have been implicated in neurodegenerative disorders such as PD, ALS and Huntington's diseases, respectively. To date, no selective PET tracers for these proteins have been reported and would be highly desireable in order to support the accurate diagnosis of these diseases as well the development of disease-modifying therapies.

Fostered by the very high unmet need[285,286] and the support of the Michael J. Fox Foundation,[287] the most active area of research is currently the identification of a selective α-synuclein PET tracer. Many research groups are currently investigating the development of such a tracer, however, only limited data have been reported so far.

The most advanced tracer characterized so far is BF227 (**Table 5**, **Scheme 44**). This tracer has been reported to bind to α-synuclein with low nanomolar affinity[270] and has been tested in a clinical study involving patients suffering from MSA.[271] The published data demonstrated higher distribution volumes in the subcortical white matter, globus pallidus, substantia nigra, and other regions of the brain of MSA subjects compared with controls. However, BF227 is not a selective α-synuclein PET tracer and binds to β-amyloid with very high affinity as well. Therefore, these clinical data should be treated with caution as a significant uptake due to binding to β-amyloid may be a confounding factor.

A recent paper reported [^{125}I]SIL23 (**Scheme 45**) as a novel α-synuclein radioligand with moderate affinity.[288] The molecule binds to α-synuclein aggregates in postmortem brain tissue from PD patients. The density of binding sites of SIL23 correlated with the level of aggregated α-synuclein in PD brain tissue and should be high enough to enable in vivo imaging provided a higher affinity ligand than SIL23 can be identified. Furthermore, high nonspecific binding, likely due to the high lipophilicity, appears to be a limiting factor in the use of SIL23 in autoradiography experiments.

Despite this recent progress and the interest from many research groups, no selective α-synuclein PET tracer has been reported yet and it will be a major challenge for the next few years in order to meet the needs and timelines of therapeutic molecules already in clinical development.[289,290]

7.02.3 Some Present and Future Challenges of PET Imaging

7.02.3.1 Improved Radiosynthesis Methods

As described in the introduction section, meeting all the medicinal chemistry requirements that make a PET tracer successful is already very challenging and yet PET radiotracer development suffers the additional burden of a limited scope of molecules for which isotope labeling is possible, particularly with ^{18}F.[291–293]

Well-established ^{18}F fluorination methods, now classified as conventional processes, typically rely on thermal activation or the use of highly reactive reagents (e.g., [^{18}F]F_2) for ^{18}F-C bond construction. These fundamental reactions, for example, S_N2, S_NAr, and S_EAr have transformed PET imaging and enable the routine production of the most commonly used tracers in the clinic. [^{18}F]-Fluorodeoxyglucose (FDG) is currently produced by nucleophilic substitution of a triflate leaving group with ^{18}F-fluoride and ^{18}F-DOPA by electrophilic fluoro-destannylation with [^{18}F]F_2. On the other hand, with the increasing demand for new ^{18}F-labeled molecules to improve diagnosis, to progress personalized medicine, and as a tool to facilitate drug discovery, radiochemists are currently facing

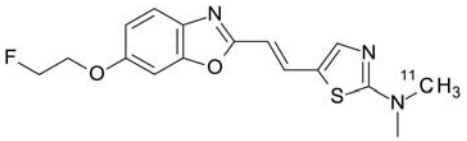

[^{11}C]BF227

Scheme 44 Chemical structure of the nonselective α-synuclein tracer [^{11}C]BF227.

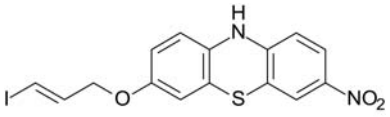

[^{125}I]SIL23

Scheme 45 Chemical structure of the a-synuclein radioligand [^{125}I]SIL23.

the challenge of labeling molecules that are not easily within reach using well-established methods for ^{18}F incorporation. This limitation typically leads researchers to design new radiotracers based on what can be labeled, rather than what should be labeled. Fundamentally new fluorination chemistry that is suitable for ^{18}F-fluorination could expand the accessible chemical space for labeling and open the door to new chemical entities for use in PET research, radiotracer discovery, and ultimately clinical imaging.

A first option to contribute to radiotracer structural diversity is to consider the large number of reactions requiring F^+ reagents for C–F bond formation and to develop these pathways for ^{18}F labeling. This strategy presents numerous challenges, not least the production of ^{18}F-labeled F^+ reagents, produced in high-specific activity (**Scheme 46**). The design of innovative chemistry that could transform ^{18}F fluoride into F^+ reagents is an exciting, but notoriously complex, problem that has met today only with limited success.[294]

A second option is to expand the substrate scope for the conventional S_NAr using ^{18}F fluoride, in particular toward heteroaromatics and electron-rich aromatics. Recent breakthroughs have emerged with metal activation as a new manifold to induce ^{18}F-C bond formation. Since 2010, a range of metals (Ag, Pd, Ir, Ni, Co, Cu, Mn) have been used to induce ^{18}F incorporation on sp2-hybridized carbons (**Scheme 47**).[295–298] This new era opens the door to a myriad of possibilities considering the number of metal-mediated processes one could consider for ^{18}F-labeling.

The majority of the advances in ^{18}F radiochemistry occurred in recent years have not progressed far beyond fundamental research and the path toward clinical use is still not clear. As an unfortunate consequence, it is therefore difficult to measure the value of these new radiofluorination methods and it will probably not be possible for several more years.

7.02.3.2 Immuno-PET in Neurosciences

In the past decade, antibodies have clearly demonstrated their utility as therapeutics.[299] They provide highly selective and effective drugs to treat a variety of diseases such as oncology, immunology, and autoimmunity. The success of antibody therapeutics validates their ability to find and engage their targets in vivo. More recently, triggered by the huge unmet need for therapeutic options for neurodegenerative disorders, the development of immunotherapeutic approaches targeting β-amyloid, tau, and α-synuclein has received considerable attention.[300,301] However, the antibodies targeting neurodegenerative processes will have to enter the brain in order to achieve the adequate engagement of their target. This is of course a considerable challenge to achieve for an antibody, but it is also a similar challenge to measure the target engagement of the antibody within the brain. Thus, it is not surprising that there is a renewed interest in the utility of imaging agents based on antibodies.

The antibodies have the ability to engage their target with nanomolar or picomolar affinity. The large size of antibodies also allows the conjugation with a variety of cargoes bearing suitable functional groups for molecular nuclear imaging applications, without perturbing their innate specificity and affinity. These properties provide a strong foundation to develop highly sensitive imaging agents. Similar to therapeutic antibodies, these immuno-PET tracers will have to cross the BBB in order to be taken up in sufficient quantity to bind to their target protein and provide good imaging contrast. This will represent the most important challenge to overcome in order to apply immune-PET imaging in neurosciences. The second significant challenge of using monoclonal antibodies as molecular templates for developing PET imaging tracers is their slow kinetics of distribution. Due to their large size, molecular weight, and their high hydrophilicity, monoclonal antibodies have very low volume of distribution leading to slow distribution to tissue, not compatible with short half-life emitting radioisotopes.[302] Monoclonal antibodies have therefore mostly been

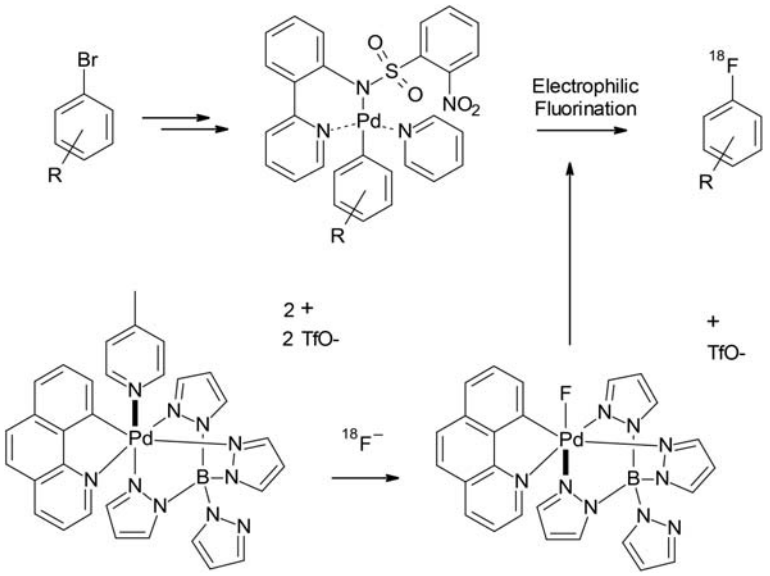

Scheme 46 Pd-mediated electrophilic fluorination starting from ^{18}F fluoride.

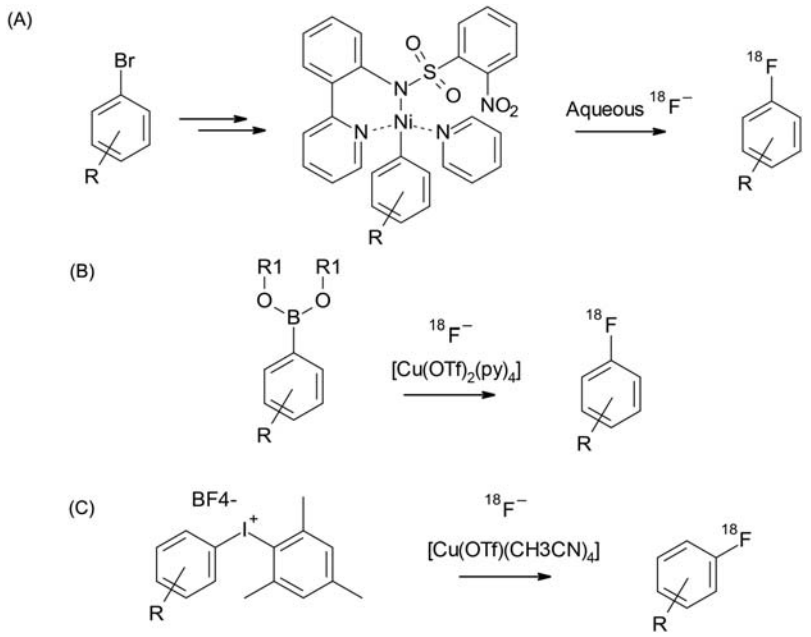

Scheme 47 (A) Ni-mediated S_NAr of electron-rich aromatics; (B) Cu-mediated S_NAr of electron-rich aromatics from boronic derivatives; (C) Cu-mediated S_NAr of electron-rich aromatics from iodonium salts.

radiolabeled using coordinating positron-emitting radiometals with longer decay half-lives such as ^{64}Cu ($T_{1/2}=12.7$ h), ^{86}Y ($T_{1/2}=14.7$ h), and ^{89}Zr ($T_{1/2}=78.5$ h) allowing to measure antibody uptake in the target tissue up to several days postadministration. However, a major drawback of using these radiometals is a drastic increase of the radiation burden incurred by the subjects. According to the US Code of Federal Regulations Title 21 (21CFR361.1), the whole body radiation dose is limited to 30 mSv for single administration and to 50 mSv for total annual commitment. The typical whole body radiation dose for patients receiving 74 MBq ^{89}Zr is about 40 mSv, which is high and clearly limits the field of possible applications.[303]

In order to meet these important challenges, advanced antibody engineering using either antibody fragments, such as scFv or nanobodies, or bi-specific antibodies bearing an epitope allowing receptor-mediated transcytosis may be required to increase the kinetics and the extent of the distribution in tissue. These approaches have been reviewed by Freise and Wu[304] and Schirrmacher et al.,[305] and the first preclinical experiments recently reported are encouraging (Fig. 4).[306–308] Finally, a pretargeted immuno-PET approach using the bioorthogonal reaction between transcyclooctene and tetrazine has also recently been successfully reported to overcome these challenges.[309,310]

7.02.3.3 Neuroinflammation Imaging Beyond Translocator Protein

Interactions between the brain and the immune system, and their role in the pathophysiology of neurologic diseases, are an area of increased interest to drug developers. Genetic, epidemiologic, clinical, postmortem, and animal model data indicate that interactions between the brain and the immune system modulate the pathophysiology of a range of neurological diseases. In order to advance this area of medicine, imaging tools to measure immune activity in the brain of living humans are needed.

This article focuses exclusively on radioisotope-based imaging; however, it is important to point out that magnetic resonance (MR)-based methods to image neuroinflammation are very important. For instance, gadolinium-based MR can detect BBB breakdown, while MR using labeled iron oxide particles is being developed to detect myeloperoxidase activity, free radicals, metalloproteinases, and endothelial adhesion molecules, and to track immune cell entry into the brain.[311,312]

PET with ^{18}F-fluorodeoxyglucose (FDG) can image inflammation (which is characterized by high metabolism) in peripheral tissues that otherwise have low baseline metabolism, for example, atherosclerosis, vasculitis, and rheumatoid arthritis,[313] but FDG cannot be used to detect inflammation in tissues with high baseline metabolism such as the myocardium and the brain.[314]

7.02.3.3.1 Selected PET tracers under investigation

See Table 6.

7.02.3.3.2 Recent developments

*7.02.3.3.2.1 Translocator Protein (**Table 6**, **Scheme 48**)*

Currently, the cornerstone of neuroinflammation PET imaging are tracers that bind to the translocator protein (TSPO), a mitochondrial protein that is upregulated in activated microglia and reactive astrocytes. The first-generation tracer ^{11}C-PK11195 is limited by

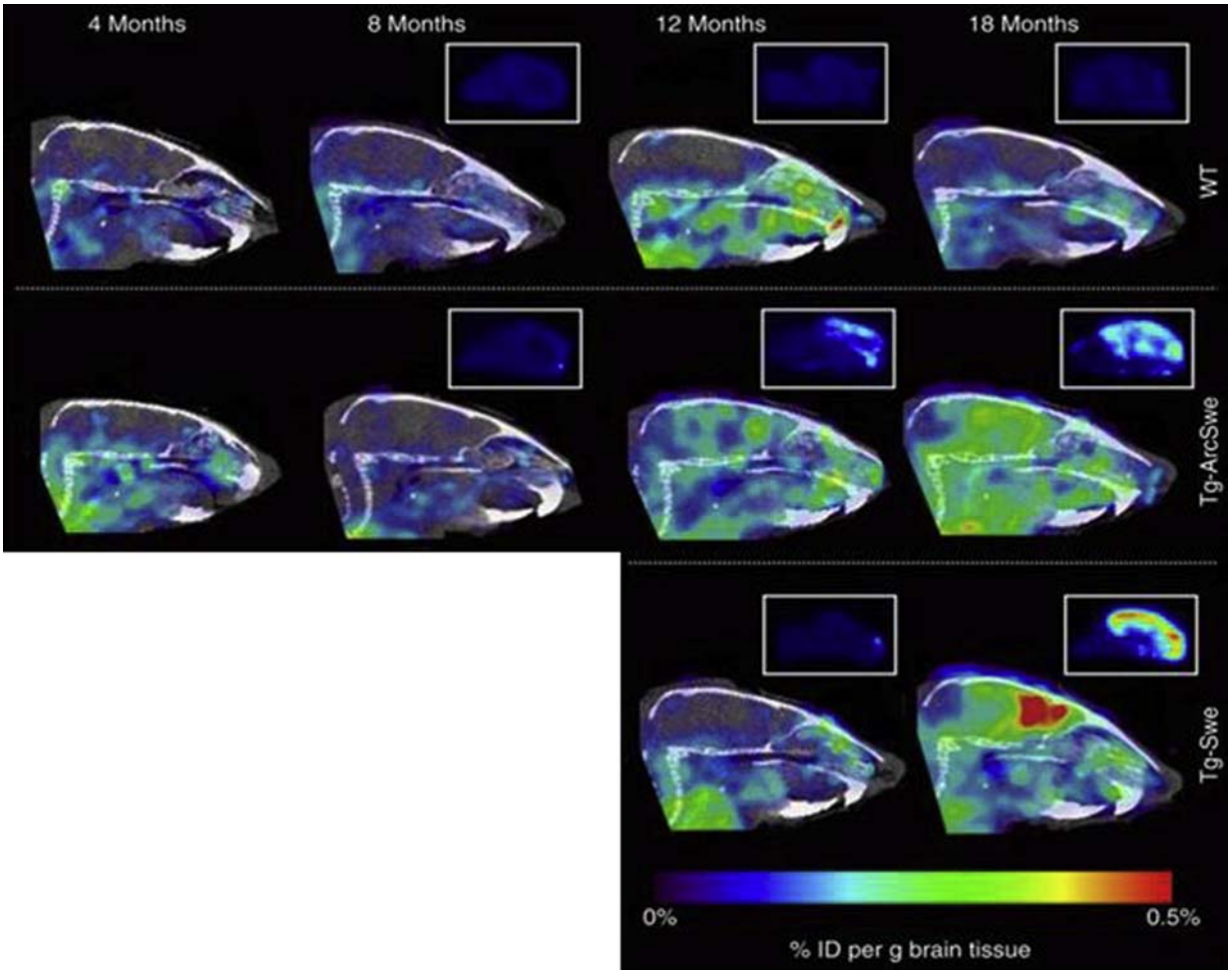

Fig. 4 Comparison of PET images postinjection of [^{124}I]8D3-F(ab0)2-h158 from WT, tg-ArcSwe, and tg-Swe mice of different ages demonstrating progression of Ab pathology.[306] Sehlin, D.; Fang, X.; Cato, L.; Antoni, G.; Lannfelt, L.; Syvänen, S. Antibody-based PET imaging of amyloid beta in mouse models of Alzheimer's disease. *Nat. Commun.* **2016**, *7*, 10759.

Table 6 CNS radiotracers used in human studies for imaging neuroinflammation

Molecular target	*^{11}C-labeled ligand*	*^{18}F-labeled ligand*	*Selected references*
TSPO	[^{11}C](R)-PK 11195 [^{11}C]PBR28 [^{11}C]DAA1106 [^{11}C]DPA-713	[^{18}F]FEPPA [^{18}F]PBR111 [^{18}F]DPA-714	315
MAO-B	[^{11}C]Deprenyl-d2		148,149
CB2	^{11}C-A-836339 ^{11}C-KD2 ^{11}C-RS-016		316,317
COX-2	NA	NA	318
Monoacylglycerol lipase (MAGL)	[^{11}C]SAR127303		319
Arachidonic acid	[^{11}C]-AA	[^{18}F]-FAA	320,321
P2X7	[^{11}C]GSK1482160 [^{11}C]A-740003		322,323
MMPs	(^{123}I)-CGS 27023A (MMP-3)	(^{18}F)-CGS 27023A (MMP-3)	324
Integrin $\alpha 4\beta 1$	^{64}Cu-CB-TE1A1P-PEG4-LLP2A		325
VCAM-1		^{18}F-4V	326
xCT		[^{18}F]FASu	327

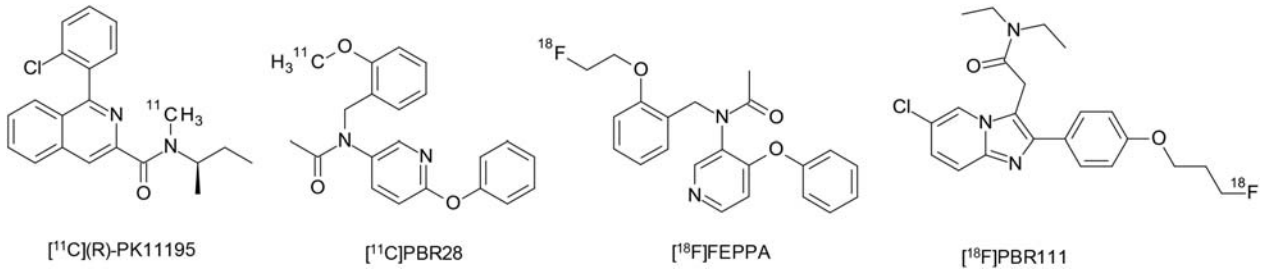

Scheme 48 Selected TSPO radiotracers used in human studies.

a low signal-to-noise ratio, but several second-generation TSPO tracers have been developed and validated in humans in the last decade.[315] These new TSPO tracers have greatly improved sensitivity, but, unlike ^{11}C-PK11195, their affinity for TSPO is modulated by a polymorphism in the TSPO gene.[328] Fortunately, this polymorphism can be easily genotyped and taken into account in the image analysis. It has been suggested that the quantification of TSPO binding may be complicated by the existence of a vascular compartment[329]; however, this idea remains controversial.

The main limitation of TSPO PET imaging is that it does not distinguish between microglia and astrocytes and probably not between various microglial phenotypes (e.g., M1 vs. M2). In other words, TSPO PET imaging is a gross measure of neuroinflammation that does not provide much information about the underlying molecular processes. New tracers that target more specific activities or cellular markers would be beneficial to further our understanding of immune–brain interactions.

*7.02.3.3.2.2 MAO-B (**Table 6**, **Schemes 49** and **50**)*

The monoamine oxidase B enzyme (MAO-B) is located in serotoninergic neurons and on the outer mitochondrial membrane of astrocytes. In particular, it has been reported that MAO-B expression is highly abundant in astrocytes with upregulated activity in sites of neuroinflammation.[330] As a consequence, MAO-B has been suggested as a potential PET imaging biomarker of neuroinflammation in neurodegenerative disorders.

Several PET tracers, both reversible and irreversible binders, have been developed to image MAO-B but only two have been validated in human, that is, [^{11}C]deprenyl and [^{11}C]deprenyl-D2 (**Scheme 49**).[331,332]

Deuteration of [^{11}C]deprenyl is required in order to overcome the issue of blood flow delivery dependence of the tracer in brain areas where MAO-B is highly abundant and thus, to achieve a better quantification of this tracer.[333] Another limitation of deprenyl is the ^{11}C-labeling which hampers its availability for large multisite clinical studies in various patient populations. Consequently, some groups have developed ^{18}F-labeled MAO-B PET tracers (**Scheme 50**).[334,335] Some promising results in nonhuman primates have been reported with [^{18}F]rasagiline-D2, but further studies will be required to achieve validation in humans.[336]

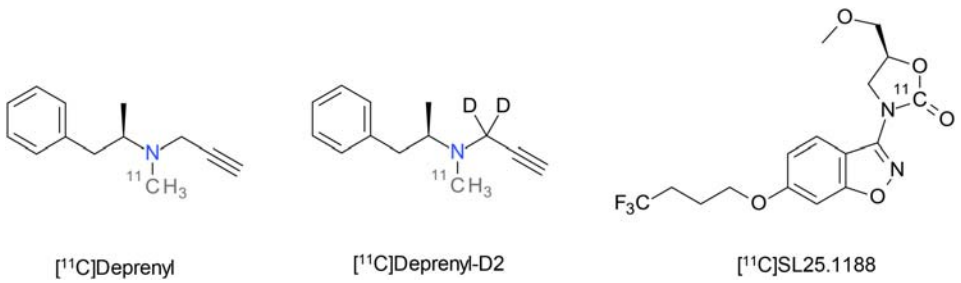

Scheme 49 Selected irreversible (Deprenyl) and reversible (SL25.118) MAO-B PET tracers.

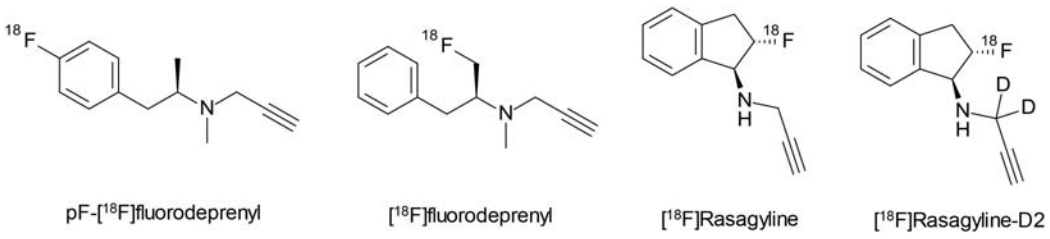

Scheme 50 Selected irreversible ^{18}F-labeled MAO-B PET tracers under investigation.

7.02.3.3.2.3 CB2 (see also Section "Cannabinoid receptors") (Tables 1 and 6)

Cannabinoid Type 2 receptor (CB2) agonists have also been investigated as markers of neuroinflammation, including ^{11}C-A836339[316,337] and ^{11}C-RS-016,[317] which, unlike the older ^{11}C-methoxy-Sch225336,[338] have good brain penetration. CB2 PET appears to be a good marker for microglial activation; however, it has the same main limitation as TSPO, that is, it does not provide much information about the underlying molecular processes.

7.02.3.3.2.4 Arachidonic acid turnover (Table 6, Scheme 51)

Cyclooxygenase-2 (COX-2; aka prostaglandin-endoperoxide synthase 2) converts arachidonic acid (AA) to prostaglandins, which are essential mediators of inflammation. Several PET tracers to measure COX-2 activity have been developed (reviewed by Tietz et al.[318]) over the last years; however, so far none of these tracers has suitable imaging properties to allow in vivo studies of COX-2 activity emphasizing again that developing an imaging tracer does not simply involve the introduction of a radiolabeled isotope into a drug molecule.

The enzyme monoacylglycerol lipase converts 2-arachidonoylglycerol to AA, which provides a further source for prostaglandin E2 synthesis. A suitable PET tracer for monoacylglycerol lipase, ^{11}C-SAR127303, was recently characterized preclinically.[319] PET tracers that measure AA turnover, for example, 1-[^{11}C]-AA[320] and [^{18}F]-FAA[321] may be useful in understanding changes in AA turnover and its role in inflammation.

7.02.3.3.2.5 P2X7 (Table 6, Scheme 52)

P2X7, which is a member of the ATP-gated ion channel family, plays an important role in inflammation[339] and in neurological disorders associated with inflammation such as PD and AD.[340] Recently, three novel PET tracers have been developed for P2X7. No biological data are reported yet on [^{11}C]-GSK1482160[322] and [^{11}C]-A-740003[323] has very low brain uptake, which prevents analyses of their utility. However, [^{11}C]JNJ-54173717 displays favorable characteristics for in vivo evaluation and will be evaluated in a clinical study in a near future.[341]

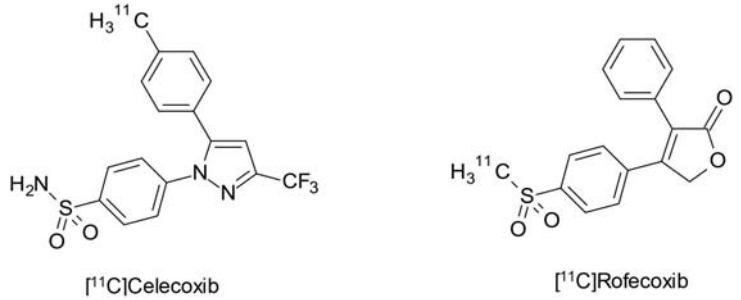

Scheme 51 Examples of COX-2 inhibitors unsuitable for PET imaging.

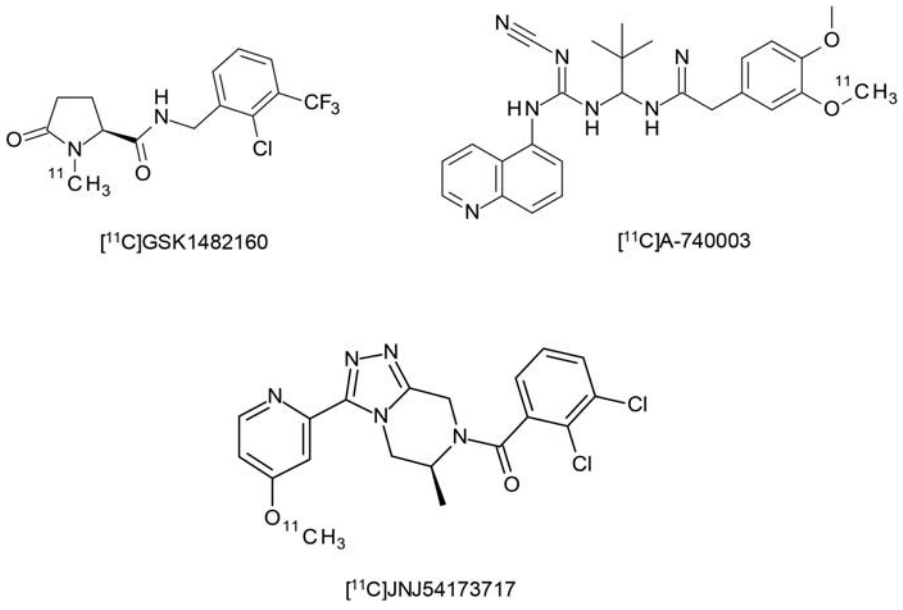

Scheme 52 Recent examples of P2X7 candidate PET tracers.

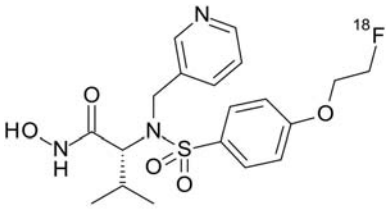

[18F]fluoro-CGS27023A

Scheme 53 Preliminary attempt to develop a MMP-3 PET tracer.

*7.02.3.3.2.6 MMPs (**Table 6**, **Scheme 53**)*

Matrix metalloproteinases (MMPs) are expressed as a result of inflammation or injury and have been implicated in the pathophysiology of AD[342] and stroke.[343] The MMP-3 inhibitor CGS 27023A has been radiolabeled with ^{18}F for PET and ^{123}I for SPECT imaging,[324,344] but this is still exploratory work and no information yet is available about its performance in the human brain.

*7.02.3.3.2.7 VCAM-1 and α4β1 integrin (**Table 6**)*

Vascular cell adhesion molecule 1 (VCAM-1 or CD106) is expressed in endothelial cells in response to cytokines (e.g., TNFα and IL-1β) and mediates adhesion of leukocytes including lymphocytes and monocytes. The leukocyte ligand for VCAM-1 is α4β1 integrin (also known as Very Late Antigen 4). Together with the β2-integrins αLβ2 and αMβ2, α4β1 is an important mediator of leukocyte trafficking, including entry of neutrophils in the brain.[345] PET tracers have been developed both for α4β1 integrin[325] and VCAM-1.[326] Such tracers could provide important information about the recruitment of blood leukocytes during brain diseases; however, as these are peptides, they are unlikely to penetrate the brain.

*7.02.3.3.2.8 Alternate options (**Table 6**, **Scheme 54**)*

PET imaging of oxidative stress may also be possible with ^{18}F-5-fluoro-L-aminosuberic acid ([^{18}F]FASu), which is taken up by the cystine/glutamate transporter xCT. This transporter is upregulated when cells experience oxidative stress[327] because cystine uptake is necessary to maintain levels of glutathione, an essential antioxidant.[346] However, [^{18}F]FASu, like the other reported xCT PET tracers,[327] is an amino acid derivative that does not cross the BBB and therefore imaging neuroinflammation via xCT would require the design of novel, non-amino acid-based, PET tracers.

Activated microglia release β-glucuronidase and the PET tracer [^{18}F]FEAnGA has been developed to measure β-glucuronidase activity. Despite relatively low brain uptake, [^{18}F]FEAnGA was able to detect an increased release of β-glucuronidase in a preclinical model of neuroinflammation.[347] It remains to be seen if this will become an important method of measuring microglial activation.

7.02.3.3.3 Possible future developments

One area that has not been developed is PET tracers to detect microglia activated to an M2 phenotype. Potential M2 markers include arginase-1, interleukin-4 (IL-4), IL-10, and IL-13. Another M2 marker is TGFβ. ^{89}Zr-fresolimumab, a large molecule tracer, has been developed and used to image TGFβ in gliomas,[348] but whether this tracer can cross the BBB in the absence of a glioma is not yet known.

7.02.3.4 Reimbursement of Approved Diagnostic PET Agents

Molecular imaging techniques hold the potential to provide important information to clinicians in order to better understand the onset and time course of many diseases as well as their response to drugs and therapies. They could be used to personalize treatments on a molecular phenotypic basis which could be established at the time of diagnosis and monitored throughout the course of therapy. This is particularly true for diseases that are localized in areas of the body where it is not practical or safe to obtain tissue samples for analysis, such as the brain.[349] Neuroscience is at the dawn of a new era, now focusing mostly on disease-modifying

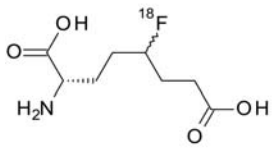

[^{18}F]FASu

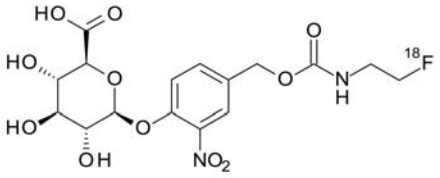

[^{18}F]FEAnGA

Scheme 54 PET tracers for xCT and β-glucuronidase imaging.

approaches to treat neurodegenerative disorders and molecular imaging will be a key technique to allow clinicians and drug researchers to characterize and monitor therapies noninvasively over time.

However, these techniques, in particular PET imaging, are expensive and ensuring the clinical viability of new PET imaging tracers will require not only regulatory approval by the Food and Drug Administration (FDA) or the European Medicines Agency (EMA) but, above all, reimbursement from health insurance carriers and national authorities such as the Center for Medicare and Medicaid Services (CMS) in the United States.[349,350] Indeed, marketing approval does not necessarily lead to insurance coverage as recently exemplified by the recent CMS decision regarding the β-amyloid PET tracers,[351] whereby CMS decided there was insufficient evidence to conclude that PET amyloid imaging is reasonable and necessary for the diagnosis or treatment of patients with dementia or neurodegenerative disease. The need to show improved health outcomes was central in this decision. The CMS decision not to cover amyloid PET imaging agents has been an important disappointment in the nuclear medicine community. However, it gives a signal about the type of evidence that will be required for insurance coverage of future diagnostic radiopharmaceuticals. Clinical studies designed to demonstrate combined diagnostic accuracy and improved health outcomes may be required to obtain both marketing and insurance approval of new radiopharmaceuticals and such clinical studies may only be possible once viable therapeutic options have been discovered.

7.02.4 Concluding Remarks

The development of a novel PET tracer for clinical use is not a trivial process and it may take several years from early research until tracer validation in human. Still, the use of PET imaging to support CNS drug development has tremendously increased in the last decade. Although some targets are still resistant to the development of PET imaging agents, many new tracers have been made available for human use in the recent years as a result of increased collaboration between the pharmaceutical industry and the PET experts. In the case where several tracers are available for the same target or receptor, it is often challenging to identify which one may be the best tracer to use as there are very few head-to-head comparisons reported in the literature. More studies like the one performed by the Yale group with the GlyT-1 tracers [^{11}C]GSK931145 and [^{18}F]MK-6577[221] may be needed in the future to help researchers identify which tracer will best suits their needs.

Undoubtedly, the most active area of research in the last 5 years has been and is still the development of novel PET tracers aimed at imaging the neurodegenerative process. In this context, the identification of molecules binding selectively to the various aggregated proteins involved in neurodegeneration still represents a considerable challenge for the field. However, considering the prohibitive cost of large phase III clinical studies aimed at demonstrating a disease-modifying effect, this challenge has to be met by the PET field in order to support the selection/stratification of patients entering these clinical trials and to monitor the therapeutic intervention over time on an individualized basis.

Finally, development of novel PET tracers is not possible without efficient radiolabeling methodologies. There have been some efforts in recent years to broaden the scope of the existing methods and to develop fundamentally new methods to enlarge the accessible chemical space for radiolabeling. Considering the high MPO challenge that developing a novel PET tracer is, removing radiochemistry from the critical path in order to allow the medicinal chemists to select the best molecules rather than the ones that can be radiolabeled may lead to significant advances in the future.

References

1. Suzuki, M. Molecular Imaging That Will Bring About a Revolution in Diagnosis and Drug Discovery: How Positron Emission Tomography Works. *Riken Res.* **2009,** *5* (6), 13–16.
2. Kola, I.; Landis, J. Can the Pharmaceutical Industry Reduce Attrition Rates? *Nat. Rev. Drug Discov.* **2004,** *3* (8), 711–715.
3. Goetghebeur, P.; Swartz, J. True Alignment of Preclinical and Clinical Research to Enhance Success in CNS Drug Development: A Review of the Current Evidence. *J. Psychopharmacol.* **2016,** *30* (7), 586–594.
4. George, N.; Gean, E.; Nandi, A.; Frolov, B.; Zaidi, E.; Lee, H.; Brašić, J.; Wong, D. Advances in CNS Imaging Agents: Focus on PET and SPECT Tracers in Experimental and Clinical Use. *CNS Drugs* **2015,** *29* (4), 313–330.
5. Grachev, I. D.; Hargreaves, R. J. Integrative Processes: Neuroscience Clinical Imaging Biomarkers. In *Imaging in CNS Drug Discovery and Development: Implications for Disease and Therapy;* Springer Science+Business Media, LLC, New-York, 2010; pp 363–379.
6. Piel, M.; Vernaleken, I.; Rösch, F. Positron Emission Tomography in CNS Drug Discovery and Drug Monitoring. *J. Med. Chem.* **2014,** *57* (22), 9232–9258.
7. Honer, M.; Gobbi, L.; Martarello, L.; Comley, R. A. Radioligand Development for Molecular Imaging of the Central Nervous System With Positron Emission Tomography. *Drug Discov. Today* **2014,** *19* (12), 1936–1944.
8. Auberson, Y.; Briard, E.; Sykes, D.; Reilly, J.; Healy, M. Ligand Specific Efficiency (LSE) Index for PET Tracer Optimization. *ChemMedChem* **2016,** *11,* 1415–1427.
9. Zhang, L.; Villalobos, A.; Beck, E.; Bocan, T.; Chappie, T.; Chen, L.; Grimwood, S.; Heck, S.; Helal, C.; Hou, X.; Humphrey, J.; Lu, J.; Skaddan, M.; McCarthy, T.; Verhoest, P.; Wager, T.; Zasadny, K. Design and Selection Parameters to Accelerate the Discovery of Novel Central Nervous System Positron Emission Tomography (PET) Ligands and Their Application in the Development of a Novel Phosphodiesterase 2A PET Ligand. *J. Med. Chem.* **2013,** *56* (11), 4568–4579.
10. Van de Bittner, G. C.; Ricq, L.; Hooker, J. M. A Philosophy for CNS Radiotracer Design. *Acc. Chem. Res.* **2014,** *47,* 3127–3134.
11. Gunn, R.; Guo, Q.; Salinas, C.; Tziortzi, A.; Searle, G. Advances in Biomathematical Modeling for PET Neuroreceptor Imaging. *Drug Discov. Today Technol.* **2011,** *8* (2–4), e45–e51.
12. Dickson, C.; Gee, A.; Bennacef, I.; Gould, I.; Rosso, L. Further Evaluation of Quantum Chemical Methods for the Prediction of Non-Specific Binding of Positron Emission Tomography Tracers. *Phys. Chem. Chem. Phys.* **2011,** *13* (48), 21552–21557.
13. Jiang, Z.; Reilly, J.; Everatt, B.; Briard, E. A Rapid Vesicle Electrokinetic Chromatography Method for the In Vitro Prediction of Non-Specific Binding for Potential PET Ligands. *J. Pharm. Biomed. Anal.* **2011,** *54* (4), 722–729.

14. Assmus, F.; Seelig, A.; Gobbi, L.; Borroni, E.; Glaentzlin, P.; Fischer, H. Label-Free Assay for the Assessment of Nonspecific Binding of Positron Emission Tomography Tracer Candidates. *Eur. J. Pharm. Sci.* **2015,** *79,* 27–35.
15. National Institute of Mental Health. CNS Radiotracers That Have Been Advanced for Use in Human Studies. http://www.nimh.nih.gov/research-priorities/therapeutics/cns-radiotracer-table.shtml (accessed August 21, 2015).
16. Elmenhorst, D.; Meyer, P. T.; Matusch, A.; Winz, O. H.; Bauer, A. Caffeine Occupancy of Human Cerebral A1 Adenosine Receptors: in vivo Quantification With 18F-CPFPX and PET. *J. Nucl. Med.* **2012,** *53,* 1723–1729.
17. Meyer, P. T.; Elmenhorst, D.; Matusch, A.; Winz, O.; Zilles, K.; Bauer, A. A1 Adenosine Receptor PET Using [18F]CPFPX: Displacement Studies in Humans. *Neuroimage* **2006,** *32,* 1100–1105.
18. Brooks, D. J.; Papapetropoulos, S.; Vandenhende, F.; Tomic, D.; He, P.; Coppell, A.; O'Neill, G. An Open-Label, Positron Emission Tomography Study to Assess Adenosine A2a Brain Receptor Occupancy of Vipadenant (BIIB014) at Steady-State Levels in Healthy Male Volunteers. *Clin. Neuropharmacol.* **2010,** *33,* 55–60.
19. Barret, O.; Hannestad, J.; Vala, C.; Alagille, D.; Tavares, A.; Laruelle, M.; Jennings, D.; Marek, K.; Russell, D.; Seibyl, J.; Tamagnan, G. Characterization in Humans of 18F-MNI-444, a PET Radiotracer for Brain Adenosine 2A Receptors. *J. Nucl. Med.* **2015,** *56,* 586–591.
20. Horti, A. G.; Van Laere, K. Development of Radioligands for In Vivo Imaging of Type 1 Cannabinoid Receptors (CB1) in Humans. *Curr. Pharm. Des.* **2008,** *14,* 3363–3383.
21. Hirvonen, J. In Vivo Imaging of the Cannabinoid CB1 Receptor With Positron Emission Tomography. *Clin. Pharmacol. Ther.* **2015,** *97,* 565–567.
22. An Imaging Study to Investigate the Distribution of GW842166X in the Brain (NCT00511524). https://clinicaltrials.gov/ct2/show/NCT00511524?term=cb2&rank=2.
23. Thompson, J. L.; Rosell, D. R.; Slifstein, M.; Girgis, R. R.; Xu, X.; Ehrlich, Y.; Kegeles, L. S.; Hazlett, E. A.; Abi-Dargham, A.; Siever, L. J. Prefrontal Dopamine D1 Receptors and Working Memory in Schizotypal Personality Disorders: A PET Study With [11C]NNC112. *Psychopharmacology (Berl)* **2014,** *231,* 4231–4240.
24. Abi-Dargham, A.; Xu, X.; Thompson, J. L.; Gil, R.; Kegeles, L. S.; Urban, N. N. R.; Hwang, D.-R.; Laruelle, M.; Slifstein, M. Increased Prefrontal Cortical D1 Receptors in Drug Naïve Patients With Schizophrenia: A PET Study With [11C]NNC112. *J. Psychopharmacol.* **2012,** *26,* 794–805.
25. Elsinga, P. H.; Hatano, K.; Ishiwata, K. PET Tracers for Imaging of the Dopaminergic System. *Curr. Med. Chem.* **2006,** *13,* 2139–2153.
26. Niccolini, F.; Su, P.; Politis, M. Dopamine Receptor Mapping With PET Imaging in Parkinson's Disease. *J. Neurol.* **2014,** *261,* 2251–2263.
27. Tashiro, M.; Mochizuki, H.; Sakurada, Y.; Ishii, K.; Oda, K.; Kimura, Y.; Sasaki, T.; Ishiwata, K.; Yanai, K. Brain Histamine H Receptor Occupancy of Orally Administered Antihistamines Measured by Positron Emission Tomography With (11)C-Doxepin in a Placebo-Controlled Crossover Study Design in Healthy Subjects: A Comparison of Olopatadine and Ketotifen. *Br. J. Clin. Pharmacol.* **2006,** *61,* 16–26.
28. Sato, H.; Ito, C.; Tashiro, M.; Hiraoka, K.; Shibuya, K.; Funaki, Y.; Iwata, R.; Matsuoka, H.; Yanai, K. Histamine H1 Receptor Occupancy by the New-Generation Antidepressants Fluvoxamine and Mirtazapine: A Positro Emission Tomography Study in Healthy Volunteers. *Psychopharmacology (Berl)* **2013,** *230,* 227–234.
29. Ashworth, S.; Rabiner, E. A.; Gunn, R. N.; Plisson, C.; Wilson, A. A.; Comley, R. A.; Lai, R. Y. K.; Gee, A. D.; Laruelle, M.; Cunningham, V. J. Evaluation of 11C-GSK189254 as a Novel Radioligand for the H3 Receptor in Humans Using PET. *J. Nucl. Med.* **2010,** *51,* 1021–1029.
30. Van Laere, K. J.; Sanabria-Bohórquez, S. M.; Mozley, D. P.; Burns, D. H.; Hamill, T. G.; Van Hecken, A.; De Lepeleire, I.; Koole, M.; Bormans, G.; de Hoon, J.; Depré, M.; Cerchio, K.; Plalcza, J.; Han, L.; Renger, J.; Hargreaves, R. J.; Iannone, R. 11C-MK-8278 PET as a Tool for Pharmacodynamic Brain Occupancy of Histamine 3 Receptor Inverse Agonists. *J. Nucl. Med.* **2014,** *55,* 65–72.
31. Tamagnan, G.; Barret, O.; Alagille, D.; Hamill, T.; Baldwin, R.; Koren, A.; Russell, D.; Jennings, D.; Marek, K.; Seibyl, J. First Assessment of [18F]-FMH3 in Human, a Selective Histamine H3 Receptor PET Tracer. *J. Nucl. Med.* **2011,** *52* (Suppl. 1), 394.
32. Liow, J. S.; Zoghbi, S. S.; Hu, S.; Hall, M. D.; Hines, C. S.; Shetty, H. U.; Araneta, M. D.; Page, E. M.; Pike, V. W.; Kreisl, W. C.; Herscovitch, P.; Gottesman, M. M.; Theodore, W. H.; Innis, R. B. 18F-FCWAY, a Serotonin 1A Receptor Radioligand, is a Substrate for Efflux Transport at the Human Blood–Brain Barrier. *Neuroimage* **2016,** *138,* 134–140.
33. Kumar, J. S.; Milak, M. S.; Majo, V. J.; Prabhakaran, J.; Mali, P.; Savenkova, L.; Mann, J. J.; Parsey, R. V. Comparison of High and Low Affinity Serotonin 1A Receptors by PET In Vivo in Nonhuman Primates. *J. Pharmacol. Sci.* **2012,** *120,* 254–257.
34. Takano, H.; Ito, H.; Takahashi, H.; Arakawa, R. O. M.; Kodaka, F.; Otsuka, T.; Kato, M.; Suhara, T. Serotonergic Neurotransmission in the Living Human Brain: A Positron Emission Tomography Study Using [^{11}C]Dasb and [^{11}C]WAY100635 in Young Healthy Men. *Synapse* **2011,** *65,* 624–633.
35. Choi, J. Y.; Lyoo, C. H.; Kim, J. S.; Kim, K. M.; Kang, J. H.; Choi, S.-H.; Kim, J.-J.; Ryu, Y. H. 18F-Mefway PET Imaging of Serotonin 1A Receptors in Humans: A Comparison With 18F-FCWAY. *PLoS One* **2015,** *10.* e0121342.
36. Saricicek, A.; Chen, J.; Planeta, B.; Ruf, B.; Subramanyam, K.; Maloney, K.; Matuskey, D.; Labaree, D.; Desorno, L.; Neumeister, A.; Krystal, J. H.; Gallezot, J. D.; Huang, Y.; Carson, R. E.; Bhagwagar, Z. Test-Retest Reliability of the Novel 5-HT1B Receptor PET Radioligand [11C]P943. *Eur. J. Nucl. Med. Mol. Imaging* **2015,** *42,* 468–477.
37. Nord, M.; Finnema, S. J.; Schain, M.; Halldin, C.; Farde, L. Test-Retest Reliability of [11C]AZ10419369 Binding to 5-HT(1B) Receptors in Human Brain. *Eur. J. Nucl. Med. Mol. Imaging* **2014,** *41,* 301–307.
38. Varrone, A.; Svenningsson, P.; Marklund, P.; Fatouros-Bergmann, H.; Forsberg, A.; Halldin, C.; Nilsson, L. G.; Farde, L. 5-HT1B Receptor Imaging and Cognition: A Positron Emission Tomography Study in Control Subjects and Parkinson's Disease Patients. *Synapse* **2015,** *69,* 365–374.
39. Talbot, P. S.; Slifstein, M.; Hwang, D. R.; Huang, Y.; Scher, A.; Abi-Dargham, A.; Laruelle, M. Extended Characterisation of the Serotonin 2A (5-HT2A) Receptor-Selective PET Radiotracer 11C-MDL100907 in Humans: Quantitative Analysis, Test-Retest Reproducibility, and Vulnerability to Endogenous 5-HT Tone. *Neuroimage* **2012,** *59,* 271–285.
40. Ettrup, A.; Svarer, C.; McMahon, B.; da Cunha-Bang, S.; Lehel, S.; Moller, K.; Dyssegaard, A.; Ganz, M.; Beliveau, V.; Jorgensen, L. M.; Gillings, N.; Knudsen, G. M. Serotonin 2A Receptor Agonist Binding in the Human Brain With [(11)C]Cimbi-36: Test-Retest Reproducibility and Head-to-Head Comparison With the Antagonist [(18)F]Altanserin. *Neuroimage* **2016,** *130,* 167–174.
41. Marner, L.; Gillings, N.; Madsen, K.; Erritzoe, D.; Baaré, W. F.; Svarer, C.; Hasselbalch, S. G.; Knudsen, G. M. Brain Imaging of Serotonin 4 Receptors in Humans With [11C]SB207145-PET. *Neuroimage* **2010,** *50,* 855–861.
42. Parker, C. A.; Rabiner, E. A.; Gunn, R. N.; Searle, G.; Martarello, L.; Comley, R. A.; Davy, M.; Wilson, A. A.; Houle, S.; Mizrahi, R.; Laruelle, M.; Cunningham, V. J. Human Kinetic Modeling of the 5HT6 PET Radioligand 11C-GSK215083 and Its Utility for Determining Occupancy at Both 5HT6 and 5HT2A Receptors by SB742457 as a Potential Therapeutic Mechanism of Action in Alzheimer Disease. *J. Nucl. Med.* **2015,** *56,* 1901–1909.
43. Ridler, K.; Cunningham, V.; Huiban, M.; Martarello, L.; Pampols-Maso, S.; Passchier, J.; Gunn, R. N.; Searle, G.; Abi-Dargham, A.; Slifstein, M.; Watson, J.; Laruelle, M.; Rabiner, E. A. An Evaluation of the Brain Distribution of [11C]GSK1034702, a Muscarinic-1 (M1) Positive Allosteric Modulator in the Living Human Brain Using Positron Emission Tomography. *EJNMMI Res.* **2014,** *4,* 66.
44. Toyahara, J.; Sakata, M.; Oda, K.; Ishii, K.; Ito, K.; Hiura, M.; Fujinaga, M.; Yamasaki, T.; Zhang, M. R.; Ishiwata, K. Initial Human PET Studies of Metabotropic Glutamate Receptor Type 1 Ligand 11C-ITMM. *J. Nucl. Med.* **2013,** *54,* 1302–1307.
45. Yamasaki, T.; Maeda, J.; Fujinaga, M.; Nagai, Y.; Hatori, A.; Yui, J.; Xie, L.; Nengaki, N.; Zhang, M.-R. PET Brain Kinetics Studies of 11C-ITMM and 11C-ITDM, Radioprobes for Metabotropic Glutamate Receptor Type 1, in a Nonhuman Primate. *Am. J. Nucl. Med. Mol. Imaging* **2014,** *4,* 260–269.
46. DuBois, J. M.; Rousset, O. G.; Rowley, J.; Porras-Betancourt, M.; Reader, A. J.; Labbe, A.; Massarweh, G.; Soucy, J.-P.; Rosa-Neto, P.; Kobayashi, E. Characterization of Age/Sex and the Regional Distribution of mGluR5 Availability in the Healthy Human Brain Measured by High-Resolution [11C]ABP688 PET. *Eur. J. Nucl. Med. Mol. Imaging* **2016,** *43,* 152–162.
47. Wong, D. F.; Waterhouse, R.; Kuwabara, H.; Kim, J.; Brasic, J. R.; Chamroonrat, W.; Stabins, M.; Holt, D. P.; Dannals, R. F.; Hamill, T. G.; Mozley, P. D. 18F-FPEB, a PET Radiopharmaceutical for Quantifying Metabotropic Glutamate 5 Receptors: A First-in-Human Study of Radiochemical Safety, Biokinetics, and Radiation Dosimetry. *J. Nucl. Med.* **2013,** *54,* 388–396.
48. Kagedal, M.; Cselényi, Z.; Nyberg, S.; Jönsson, S.; Raboisson, P.; Stenkrona, P.; Hooker, A. C.; Karlsson, M. O. Non-Linear Mixed Effects Modelling of Positron Emission Tomography Data for Simultaneous Estimation of Radioligand Kinetics and Occupancy in Healthy Volunteers. *Neuroimage* **2012,** *61,* 849–856.

49. Van Laere, K.; De Hoon, J.; Bormans, G.; Koole, M.; Derdelinckx, I.; De Lepeleire, I.; Declercq, R.; Sanabria Bohorquez, S. M.; Hamill, T.; Mozley, P. D.; Tatosian, D.; Xie, W.; Liu, Y.; Liu, F.; Zappacosta, P.; Mahon, C.; Butterfield, K. L.; et al. Equivalent Dynamic Human Brain NK1-Receptor Occupancy Following Single-Dose i.v. Fosaprepitant vs. Oral Aprepitant as Assessed by PET Imaging. *Clin. Pharmacol. Ther.* **2012,** *92,* 243–250.
50. Okumura, M.; Arakawa, R.; Ito, H.; Seki, C.; Takahashi, H.; Takano, H.; Haneda, E.; Nakao, R.; Suzuki, H.; Suzuki, K.; Okubo, Y.; Suhara, T. Quantitative Analysis of NK1 Receptor in the Human Brain Using PET With 18F-FE-SPA-RQ. *J. Nucl. Med.* **2008,** *49,* 1749–1755.
51. Hargreaves, R. Imaging Substance P Receptors (NK1) in the Living Human Brain Using Positron Emission Tomography. *J. Clin. Psychiatry* **2002,** *63* (Suppl. 11), 18–24.
52. Lohith, T. G.; Zoghbi, S. S.; Morse, C. L.; Araneta, M. F.; Barth, V. N.; Goebl, N. A.; Tauscher, J. T.; Pike, V. W.; Innis, R. B. Brain and Whole-Body Imaging of Nociceptin/Orphanin FQ Peptide Receptor in Humans Using the PET Ligand 11C-NOP-1A. *J. Nucl. Med.* **2012,** *53,* 385–392.
53. Naganawa, N.; Jacobsen, L. K.; Zheng, M. Q.; Lin, S. F.; Banerjee, A.; Byon, W.; Weinzimmer, D.; Tomasi, G.; Nabulsi, N.; Grimwood, S.; Badura, L. L.; Carson, R. E.; McCarthy, Y. J.; Huang, Y. Evaluation of the Agonist PET Radioligand [^{11}C]GR103545 to Image Kappa Opioid Receptor in Humans: Kinetic Model Selection, Test-Retest Reproducibility and Receptor Occupancy by the Antagonist PF-04455242. *Neuroimage* **2014,** *99,* 69–79.
54. Weerts, E. M.; Wand, G. S.; Kuwabara, H.; Munro, C. A.; Dannals, R. F.; Hilton, J.; Frost, J. J.; McCaul, M. E. Positron Emission Tomography Imaging of mu- and Delta-Opioid Receptor Binding in Alcohol-Dependent and Healthy Control Subjects. *Alcohol. Clin. Exp. Res.* **2011,** *35,* 2162–2173.
55. Madar, I.; Lesser, R. P.; Krauss, G.; Zubieta, J. K.; Lever, J. R.; Kinter, C. M.; Ravert, H. T.; Musachio, J. L.; Mathews, W. B.; Dannals, R. F.; Frost, J. J. Imaging of Delta- and mu-Opioid Receptors in Temporal Lobe Epilepsy by Positron Emission Tomography. *Ann. Neurol.* **1997,** *41,* 358–367.
56. Baier, B.; Bense, S.; Birklein, F.; Buchholz, H. G.; Mischke, A.; Schreckenberger, M.; Dietrich, M. Evidence for Modulation of Opioidergic Activity in Central Vestibular Processing: A [(18)F] Diprenorphine PET Study. *Hum. Brain Mapp.* **2010,** *31,* 550–555.
57. Wey, H. Y.; Catana, C.; Hooker, J. M.; Dougherty, D. D.; Knudsen, G. M.; Wang, D. J.; Chonde, D. B.; Rosen, B. R.; Gollub, R. L.; Kong, J. Simultaneous fMRI-PET of the Opioidergic Pain System in Human Brain. *Neuroimage* **2014,** *2,* 275–282.
58. Toyohara, J.; Sakata, M.; Ishiwata, K. Imaging of Sigma1 Receptors in the Human Brain Using PET and [11C]SA4503. *Cent. Nerv. Syst. Agents Med. Chem.* **2009,** *9,* 190–196.
59. Mishina, M.; Ohyama, M.; Ishii, K.; Kitamura, S.; Kimura, Y.; Oda, K.-I.; Kawamura, K.; Sasaki, T.; Kobayashi, T.; Katayama, Y.; Ishiwata, K. Low Density of Sigma1 Receptors in Early Alzheimer's Disease. *Ann. Nucl. Med.* **2008,** *22,* 151–156.
60. Banerjee, A.; Prante, O. Subtype-Selective Dopamine Receptor Radioligands for PET Imaging: Current Status and Recent Developments. *Curr. Med. Chem.* **2012,** *19,* 3957–3966.
61. Prante, O.; Maschauer, S.; Banerjee, A. Radioligands for the Dopamine Receptor Subtypes. *J. Label. Compd. Radiopharm.* **2013,** *56,* 130–148.
62. Poels, E. M.; Girgis, R. R.; Thompson, J. L.; Slifstein, M.; Abi-Dargham, A. In Vivo Binding of the Dopamine-1 Receptor PET Tracers [11C]NNC112 and [11C]SCH23390: A Comparison Study in Individuals With Schizophrenia. *Psychopharmacology (Berl)* **2013,** *228,* 167–174.
63. Plaven-Sigray, P.; Gustavsson, P.; Farde, L.; Borg, J.; Stenkrona, P.; Nyberg, L.; Bäckman, L.; Cervenka, S. Dopamine D1 Receptor Availability is Related to Social Behavior: A Positron Emission Tomography Study. *Neuroimage* **2014,** *102,* 590–595.
64. Pfizer. A Study to Evaluate D1 Receptor Occupancy (RO) Following Single Dose of PF-06412562 in Healthy Male Volunteers (PET). https://clinicaltrials.gov/ct2/show/NCT02124213?term=pfizer+D1+PET&rank=1; 2014.
65. Ekelund, J.; Slifstein, M.; Narendran, R.; Guillin, O.; Belani, H.; Guo, N.; Hwang, Y.; Hwang, D.; Abi-Dargham, A.; Laruelle, M. In Vivo DA D1 Receptor Selectivity of NNC 112 and SCH 23390. *Mol. Imaging Biol.* **2007,** *9,* 117–125.
66. Lewis, M. A.; Hunihan, L.; Watson, J.; Gentles, R. G.; Hu, S.; Huang, Y.; Bronson, J.; Macor, J. E.; Beno, B. R.; Ferante, M.; Hendricson, A.; Knox, R. J.; Molski, T. F.; Kong, Y.; Cvijic, M. E.; Rockwell, K. L.; Weed, M. R.; Cacace, A. M.; Westphal, R. S.; Alt, A.; Brown, J. M. Discovery of D1 Dopamine Receptor Positive Allosteric Modulators: Characterization of Pharmacology and Identification of Residues that Regulate Species Selectivity. *J. Pharmacol. Exp. Ther.* **2015,** *354,* 340–349.
67. Coe, J. W.; Allen, J. A.; Davoren, J. E.; Dounay, A. B.; Efremov, I. V.; Gray, D. L. F.; Guilmette, E. R.; Harris, A. R.; Helal, C. J.; Henderson, J. L.; Mente, S. R.; Nason, D. M.; O'Neil, S. V.; Subramanyam, C.; Xu, W. Heteroaromatic Compounds and Their Use as Dopamine D1 Ligands. WO2014/072881, 2014.
68. Finnema, S. J.; Stepanov, V.; Nakao, R.; Sromek, A. W.; Zhang, T.; Neumeyer, J. L.; George, S. R.; Seeman, P.; Stabin, M. G.; Jonsson, C.; Farde, L.; Halldin, C. 18F-MCL-524, an 18F-Labeled Dopamine D2 and D3 Receptor Agonist Sensitive to Dopamine: A Preliminary PET Study. *J. Nucl. Med.* **2014,** *55,* 1164–1170.
69. Shalgunov, V.; van Wieringen, J.-P.; Janssen, H. M.; Fransen, P. M.; Dierckx, R. A. J. O.; Michel, M. C.; Booij, J.; Elsinga, P. H. Synthesis and Evaluation in Rats of Dopamine D2/3 Receptor Agonist 18F-AMC20 as a Potential Radioligand for PET. *J. Nucl. Med.* **2015,** *56,* 133–139.
70. Le Foll, B.; Wilson, A. A.; Graff, A.; Boileau, I.; Di Ciano, P. Recent Methods for Measuring Dopamine D3 Receptor Occupancy In Vivo: Importance for Drug Development. *Front. Pharmacol.* **2014,** *5,* 1–12.
71. Payer, D. E.; Guttman, M.; Kish, S. J.; Tong, J.; Adams, J. R.; Rusjan, P.; Houle, S.; Furukawa, Y.; Wilson, A. A.; Boileau, I. D3 Dopamine Receptor-Preferring [11C]PHNO PET Imaging in Parkinson Patients With Dyskinesia. *Neurology* **2016,** *86,* 224–230.
72. Payer, D. E.; Guttman, M.; Kish, S. J.; Tong, J.; Strafella, A.; Zack, M.; Adams, J. R.; Rusjan, P.; Houle, S.; Furukawa, Y.; Wilson, A. A.; Boileau, I. [11C]-(+)-PHNO PET Imaging of Dopamine D2/3 Receptors in Parkinson's Disease With Impulse Control Disorders. *Mov. Disord.* **2015,** *30,* 160–166.
73. Le Foll, B.; Payer, D.; Di Ciano, P.; Guranda, M.; Nakajima, S.; Tong, J.; Mansouri, E.; Wilson, A. A.; Houle, S.; Meyer, J. H.; Graff-Guerrero, A.; Boileau, I. Occupancy of Dopamine D3 and D2 Receptors by Buspirone: A [11C]-(+)-PHNO PET Study in Humans. *Neuropsychopharmacology* **2016,** *41,* 529–537.
74. Hocke, C.; Cumming, P.; Maschauer, S.; Kuwert, T.; Gmeiner, P.; Prante, O. Biodistribution Studies of two 18F-Labeled Pyridinylphenyl Amides as Subtype Selective Radioligands for the Dopamine D3 Receptor. *Nucl. Med. Biol.* **2014,** *41,* 223–228.
75. Nebel, N.; Maschauer, S.; Bartuschat, A. L.; Fehler, S. K.; Hübner, H.; Gmeiner, P.; Kuwert, T.; Heinrich, M. R.; Prante, O.; Hocke, C. Synthesis and Evaluation of Fluoro Substituted Pyridinylcarboxamides and Their Prehylazo Analogues for Potential Dopamine D3 Receptor PET Imaging. *Bioorg. Med. Chem. Lett.* **2014,** *24,* 5399–5403.
76. Airaksinen, A. J.; Nag, S.; Finnema, S. J.; Mukherjee, J.; Chattopadhyay, S.; Gulyas, B.; Farde, L.; Halldin, C. [11C]Cyclopropyl-FLB457: A PET Radioligand for Low Densities of Dopamine D2 Receptors. *Bioorg. Med. Chem.* **2008,** *16,* 6467–6473.
77. Kügler, F.; Sihver, W.; Ermert, J.; Hübner, H.; Gmeiner, P.; Prante, O.; Coenen, H. H. Evaluation of 18F-Labeled Benzodioxine Piperazine-Based Dopamine D4 Receptor Ligands: Lipophilicity as a Determinate on Nonspecific Binding. *J. Med. Chem.* **2011,** *54,* 8343–8352.
78. Lacivita, E.; De Giorgio, P.; Lee, I. T.; Rodeheaver, S. I.; Weiss, B. A.; Fracasso, C.; Caccia, S.; Berardi, F.; Perrone, R.; Zhang, M.-R.; Maeda, J.; Higuchi, M.; Suhara, T.; Schetz, J. A.; Leopoldo, M. Design, Synthesis, Radiolabeling, and In Vivo Evaluation of Carbon-11 Labeled *N*-[2-[4-(3-Cyanopyridin-2-yl)Piperazin-1-yl]Ethyl]-3-Methoxybenzamide, a Potential Positron Emission Tomography Tracer for the Dopamine D4 Receptors. *J. Med. Chem.* **2010,** *53,* 7344–7355.
79. Lacivita, E.; De Giorgio, P.; Colabufo, N. A.; Berardi, F.; Perrone, R.; Niso, M.; Leopoldo, M. Design, Synthesis, Lipophilic Properties, and Binding Affinities of Potential Ligands in Positron Emission Tomography (PET) for Visualization of Brain Dopamine D4 Receptors. *Chem. Biodivers.* **2014,** *11,* 299–309.
80. Leopoldo, M.; Selivanova, S.; Müller, A.; Lacivita, E.; Schetz, J.; Ametamey, S. In Vitro and In Vivo Evaluation of *N*-(2-(4-(3-Cyanopyridin-2-yl)Piperazin-1-yl)Ethyl)-3-[11C]Methoxybenzamide, a Positron Emission Tomography (PET) Radioligand for Dopamine D4 Receptors, in Rodents. *Chem. Biodivers.* **2014,** *11,* 1298–1308.
81. Funke, U.; Vugts, D. J.; Janssen, B.; Spaans, A.; Kruijer, P. S.; Lammertsma, A. A.; Perk, L. R.; Windhorst, A. D. 11C-Labeled and 18F-Labeled PET Ligands for Subtype-Specific Imaging of Histamine Receptors in the Brain. *J. Label. Compd. Radiopharm.* **2013,** *56,* 120–129.
82. Asworth, A.; Berges, A.; Rabiner, E. A.; Wilson, A. A.; Comley, R. A.; Lai, R. Y. K.; Boardley, R.; Searle, G.; Gunn, R. N.; Laruelle, M.; Cunningham, V. J. Unexpected High Affinity of a Novel H3 Receptor Antagonist, GSK239512, In Vivo in Human Brain, Determined Using Poitron Emission Tomography (PET). *Br. J. Pharmacol.* **2014,** *171,* 1241–1249.
83. Jucaite, A.; Takano, A.; Boström, E.; Jostell, K. G.; Stenkrona, P.; Halldin, C.; Segerdahl, M.; Nyberg, S. AZD5213: A Novel Histamine H3 Receptor Antagonist Permitting High Daytime and Low Nocturnal H3 Receptor Occupancy, a PET Study in Human Subjects. *Int. J. Neuropsychopharmacol.* **2013,** *16,* 1231–1239.

84. Kimura, Y.; Seki, C.; Ikoma, Y.; Ichise, M.; Kawamura, K.; Takahata, K.; Moriguchi, S.; Nagashima, T.; Ishii, T.; Kitamura, S.; Niwa, F.; Endo, H.; Yamada, M.; Higuchi, M.; Zhang, M.-R.; Suhara, T. [11C]TASP457, a Novel PET Ligand for Histamine H3 Receptors in Human Brain. *Eur. J. Nucl. Med. Mol. Imaging* **2016,** *43,* 1653–1663.
85. Koga, K.; Maeda, J.; Tokunaga, M.; Hanyu, M.; Kawamura, K.; Ohmichi, M.; Nakamura, T.; Nagai, Y.; Seki, C.; Kimura, Y.; Minamimoto, T.; Zhang, M.-R.; Fukumura, T.; Suhara, T.; Higuchi, M. Development of TASP0410457 (TASP457), a Novel Dihydroquinolinone Derivative as a PET Radioligand for Central Histamine H3 Receptors. *EJNMMI Res.* **2016,** *6,* 11.
86. Schou, M.; Varnäs, K.; Jureus, A.; Ahlgren, C.; Malmquist, J.; Häggkvist, J.; Tari, L.; Wesolowski, S. S.; Throner, S. R.; Brown, D. G.; Nilsson, M.; Johnström, P.; Finnema, S. J.; Nakao, R.; Amini, N.; Takano, A.; Farde, L. Discovery and Preclinical Validation of [11C]AZ13153556, a Novel Probe for the Histamine Type 3 Receptor. *ACS Chem. Neurosci.* **2016,** *7,* 177–184.
87. Jablonowski, J. A.; Grice, C. A.; Chai, W.; Dvorak, C. A.; Venable, J. D.; Kwok, A. K.; Ly, K. S.; Wei, J.; Baker, S. M.; Desai, P. J.; Jiang, W.; Wllson, S. J.; Thurmond, R. L.; Karlsson, L.; Edwards, J. P.; Lovenberg, T. W.; Carruthers, N. I. The First Potent and Selective Non-Imidazole Human Histamine H4 Receptor Antagonists. *J. Med. Chem.* **2003,** *46,* 3957–3960.
88. Smits, R. A.; Adami, M.; Istyastono, E. P.; Zuiderveld, O. P.; van Dam, C. M. E.; de Kanter, F. J. J.; Jongejan, A.; Coruzzi, G.; Leurs, R.; de Esch, I. J. P. Synthesis and QSAR of Quinazoline Sulfonamides as Highly Potent Human Histamine H4 Receptor Inverse Agonists. *J. Med. Chem.* **2010,** *53,* 2390–2400.
89. Tsukada, H.; Nishiyama, S.; Takahashi, K. Imaging of Muscarinic Receptors in the Central Nervous System. In *Muscarinic Receptors: From Structure to Animal Models;* Myslivecek, J., Jakubik, J., Eds.; *Neuromethods, Vol. 107:;* Springer: New York, NY, 2016; pp 181–203. Chapter 10.
90. Buiter, H. J. C.; Leysen, J. E.; Schuit, R. C.; Fisher, A.; Lammertsma, A. A.; Windhorst, A. D. Radiosynthesis and Biological Evaluation of the M1 Muscarinic Acetylcholine Receptor Agonist Ligand [11C]AF150(S). *J. Label. Compd. Radiopharm.* **2012,** *55,* 264–273.
91. Buiter, H. J. C.; Windhorst, A. D.; Huisman, M. C.; Yaqub, M.; Knol, D. L.; Fisher, A.; Lammertsma, A. A.; Leysen, J. E. [11C]AF150(S), an Agonist PET Ligand for M1 Muscarinic Acetylcholine Receptors. *EJNMMI Res.* **2013,** *3,* 19.
92. Dileep Kumar, J. S.; Mann, J. J. PET Tracers for Serotonin Receptors and Their Applications. *Cent. Nerv. Syst. Agents Med. Chem.* **2014,** *14,* 96–112.
93. Hillmer, A. T.; Wooten, D. W.; Bajwa, A. K.; Higgins, A. T.; Lao, P. J.; Betthauser, T. J.; Barnhart, T. E.; Rowley, H. A.; Stone, C. K.; Johnson, S. C.; Mukherjee, J.; Christian, B. T. First-in-Human Evaluation of 18F-Mefway, a PET Radioligand Specific to Serotonin-1A Receptors. *J. Nucl. Med.* **2014,** *55,* 1973–1979.
94. Milak, M. S.; DeLorenzo, C.; Zanderigo, F.; Prabhakaran, J.; Kumar, J. S.; Majo, V. J.; Mann, J. J.; Parsey, R. V. In Vivo Quantification of Human Serotonin 1A Receptor Using 11C-CUMI-101, an Agonist PET Radiotracer. *J. Nucl. Med.* **2010,** *51,* 1892–1900.
95. Hines, C. S.; Liow, J. J.; Zanotti-Fregonara, P.; Hirvonen, J.; Morse, C.; Pike, V. W.; Innis, R. B. Human Biodistribution and Dosimetry of ^{11}C-CUMI-101, an Agonist Radioligand for Serotonin-1a Receptors in Brain. *PLoS One* **2011,** *6.* e25309.
96. Majo, V. J.; Milak, M. S.; Prabhakaran, J.; Mali, P.; Savenkova, L.; Simpson, N. R.; Mann, J. J.; Parsey, R. V.; Kumar, J. S. Synthesis and In Vivo Evaluation of [18F]2-(4-(4-(2-(2-Fluoroethoxy)Phenyl)Piperazin-1-yl)Butyl)-4-Methyl-1,2,4-Triazine-3,5(2H,4H)-Dione ([18F]FECUMI-101) as an Imaging Probe for 5-HT1A Receptor Agonist in Nonhuman Primates. *Bioorg. Med. Chem.* **2013,** *21,* 5598–5604.
97. Prabhakaran, J.; Underwood, M. D.; Kumar, J. S. D.; Simpson, N. R.; Kassir, S. A.; Bakalian, M. J.; Mann, J. J.; Arango, V. Synthesis and In Vitro Evaluation of [18F]FECIMBI-36: A Potential Agonist PET Ligand for 5-HT2A/2C Receptors. *Bioorg. Med. Chem. Lett.* **2015,** *25,* 3933–3936.
98. Gee, A. D.; Martarello, L.; Passchier, J.; Wishart, M.; Parker, C.; Matthews, J.; Comley, R. Synthesis and Evaluation of [11C]SB207145 as the First In Vivo Serotonin 5-HT4 Receptor Radioligand for PET Imaging in Man. *Curr. Radiopharm.* **2008,** *1,* 110–114.
99. Tavares, A. A. S.; Caillé, F.; Barret, O.; Papin, C.; Lee, H.; Morley, T. J.; Fowles, K.; Holden, D.; Seibyl, J. P.; Alagille, D.; Tamagnan, G. In Vivo Evaluation of 18F-MNI698: An 18F-Labeled Radiotracer for Imaging of Serotonin 4 Receptors in Brain. *J. Nucl. Med.* **2014,** *55,* 858–864.
100. Buiter, H. J. C.; Windhorst, A. D.; Huisman, M. C.; De Maeyer, J. H.; Schuurkes, J. A. J.; Lammertsma, A. A.; Leysen, J. E. Radiosynthesis and Preclinical Evaluation of [11C] Prucalopride as a Potential Agonist PET Ligand for the 5-HT4 Receptor. *EJNMMI Res.* **2013,** *3,* 24.
101. Colomb, J.; Becker, G.; Fieux, S.; Zimmer, L.; Billard, T. Syntheses, Radiolabelings, and In Vitro Evaluations of Fluorinated PET Radioligands of 5-HT6 Serotoninergic Receptors. *J. Med. Chem.* **2014,** *57,* 3884–3890.
102. Becker, G.; Colomb, J.; Sgambato-Faure, V.; Tremblay, L.; Billard, T.; Zimmer, L. Preclinical Evaluation of [18F]2FNQ1P as the First Fluorinated Serotonin 5-HT6 Radioligand for PET Imaging. *Eur. J. Nucl. Med. Mol. Imaging* **2015,** *42,* 495–502.
103. Tiwari, A. K.; Yui, J.; Aggarwal, S.; Yamasaki, T.; Xie, L.; Chadha, N.; Zhang, Y.; Fujinaga, M.; Shimoda, Y.; Kumata, K.; Mishra, A. K.; Ogawa, M.; Zhang, M.-R. Design, Synthesis and Biological Evaluation of Small Molecule-Based PET Radioligands for the 5-Hydroxytryptamine 7 Receptor. *RSC Adv.* **2015,** *5,* 19752–19759.
104. Hansen, H. D.; Andersen, V. L.; Lehel, S.; Magnussen, J. H.; Dyssegaard, A.; Stroth, N.; Kristensen, J. L.; Knudsen, G. M.; Herth, M. M. Labeling and Preliminary In Vivo Evaluation of the 5-HT7 Receptor Selective Agonist [11C]E-55888. *Bioorg. Med. Chem. Lett.* **2015,** *25,* 1901–1904.
105. Hansen, H. D.; Herth, M. M.; Ettrup, A.; Andersen, V. L.; Lehel, S.; Dyssegaard, A.; Kristensen, J. L.; Knudsen, G. M. Radiosynthesis and In Vivo Evaluation of Novel Radioligands for PET Imaging of Cerebral 5-HT7 Receptors. *J. Nucl. Med.* **2014,** *55,* 640–646.
106. Majo, V. J.; Prabhakaran, J.; Mann, J. J.; Dileep Kumar, J. S. PET and SPECT Tracers for Glutamate Receptors. *Drug Discov. Today* **2013,** *18,* 173–184.
107. Xu, R.; Zanotti-Fregonara, P.; Zoghbi, S. S.; Gladding, R. L.; Woock, A. E.; Innis, R. B.; Pike, V. W. Synthesis and Evaluation in Monkey of [18F]4-Fluoro-*N*-Methyl-*N*-(4-(6-(Methylamino)Pyrimidin-4-yl)Thiazol-2-yl)Benzamide ([18F]FIMX): A Promising Radioligand for PET Imaging of Brain Metabotropic Glutamate Receptor 1 (mGluR1). *J. Med. Chem.* **2013,** *56,* 9146–9155.
108. Zanotti-Fregonara, P.; Xu, R.; Zoghbi, S. S.; Liow, J. S.; Fujita, M.; Veronese, M.; Gladding, R. L.; Rallis-Frutos, D.; Hong, J.; Pike, V. W.; Innis, R. B. The PET Radioligand 18F-FIMX Images and Quantifies Metabotropic Glutamate Receptor 1 in Proportion to the Regional Density of Its Gene Transcript in Human Brain. *J. Nucl. Med.* **2016,** *57,* 242–247.
109. Hong, J.; Lu, S.; Xu, R.; Liow, J.-S.; Woock, A. E.; Jenko, K. J.; Gladding, R. L.; Zoghbi, S. S.; Innis, R. B.; Pike, V. W. [Carbonyl-11C]4-Fluoro-*N*-Methyl-*N*-(4-(6-(Methylamino)Pyrimidin-4-yl)Thiazol-2-yl)Benzamide ([11C]FIMX) is an Effective Radioligand for PET Imaging of Metabotropic Glutamate Receptor 1 (mGluR1) in Monkey Brain. *Nucl. Med. Biol.* **2015,** *42,* 967–974.
110. Fell, M. J.; McKinzie, D. L.; Monn, J. A.; Svensson, K. A. Group II Metabotropic Glutamate Receptor Agonists and Positive Allosteric Modulators as Novel Treatments for Schizophrenia. *Neuropharmacology* **2012,** *62,* 473–483.
111. Kinon, B. J.; Gomez, J. C. Clinical Development of Pomaglumetad Methionil: A Non-Dopaminergic Treatment for Schizophrenia. *Neuropharmacology* **2013,** *66,* 82–86.
112. Wang, J.-Q.; Zhang, Z.; Kuruppu, D.; Brownell, A.-L. Radiosynthesis of PET Radiotracers as a Prodrug for Imaging Group II Metabotropic Glutamate Receptors In Vivo. *Bioorg. Med. Chem. Lett.* **2012,** *22,* 1958–1962.
113. Andrés, J.-I.; Alcazar, J.; Cid, J. M.; De Angelis, M.; Iturrino, L.; Langlois, X.; Lavreysen, H.; Trabanco, A. A.; Celen, S.; Bormans, G. Synthesis, Evaluation, and Radiolabeling of New Potent Positive Allosteric Modulators of the Metabotropic Glutamate Receptor 2 as Potential Tracers for Positron Emission Tomography Imaging. *J. Med. Chem.* **2012,** *55,* 8685–8699.
114. Van Gool, M.; Andrés-Gil, J.; Alcazar-Vaca, M.; Bormans, G.; Celen, S.; Joost, V. Radiolabelled MGLUR2 PET Ligands. WO2016/087489, 2016.
115. Lindsley, C. W.; Hopkins, C. R. Metabotropic Glutamate Receptor 4 (mGlu4)-Positive Allosteric Modulators for the Treatment of Parkinson's Disease: Historical Perspective and Review of the Patent Literature. *Expert Opin. Ther. Pat.* **2012,** *22,* 461–481.
116. Amalric, M.; Lopez, S.; Goudet, C.; Fisone, G.; Battaglia, G.; Nicoletti, F.; Pin, J. P.; Acher, F. C. Group III and Subtype 4 Metabotropic Glutamate Receptor Agonists: Discovery and Pathophysiological Applications in Parkinson's Disease. *Neuropharmacology* **2013,** *66,* 53–64.
117. Kil, K.-E.; Poutiainen, P.; Zhang, Z.; Zhu, A. K. D.; Prabhakar, S.; Choi, J.-K.; Tannous, B. A.; Brownell, A.-L. Synthesis and Evaluation of *N*-(Methylthiophenyl)Picolinamide Derivatives as PET Radioligands for Metabotropic Glutamate Receptor Subtype 4. *Bioorg. Med. Chem. Lett.* **2016,** *26,* 133–139.

118. Kil, K.-E.; Poutiainen, P.; Zhang, Z.; Zhu, A.; Choi, J.-K.; Jokivarsi, K.; Brownell, A.-L. Radiosynthesis and Evaluation of an 18F-Labeled Positron Emission Tomography (PET) Radioligand for Metabotropic Glutamate Receptor Subtype 4 (mGlu4). *J. Med. Chem.* **2014,** *57,* 9130–9138.
119. Kil, K.-E.; Zhang, Z.; Jokivarsi, K.; Gong, C.; Choi, J.-K.; Kura, S.; Brownell, A.-L. Radiosynthesis of *N*-(4-Chloro-3-[11C]Methoxyphenyl)-2-Picolinamide ([11C]ML128) as a PET Radiotracer for Metabotropic Glutamate Receptor Subtype 4 (mGlu4). *Bioorg. Med. Chem.* **2013,** *21,* 5955–5962.
120. Pillai, R. L. I.; Tipre, D. N. Metabotropic Glutamate Receptor 5—A Promising Target in Drug Development and Neuroimaging. *Eur. J. Nucl. Med. Mol. Imaging* **2016,** *43,* 1151–1170.
121. Li, D.; Shan, H.; Conti, P.; Li, Z. PET Imaging of Metabotropic Glutamate Receptor Subtype 5 (mGluR5). *Am. J. Nucl. Med. Mol. Imaging* **2012,** *2,* 29–32.
122. Zimmer, E. R.; Parent, M. J.; Leuzy, A.; Aliaga, A.; Aliaga, A.; Moquin, L.; Schirrmacher, E. S.; Soucy, J.-P.; Skelin, I.; Gratton, A.; Gauthier, S.; Rosa-Neto, P. Imaging In Vivo Glutamate Fluctuations With [11C]ABP688: A GLT-1 Challenge With Ceftriaxone. *J. Cereb. Blood Flow Metab.* **2015,** *35,* 1169–1174.
123. Brown, A. K.; Kimura, Y.; Zoghbi, S. S.; Siméon, F. G.; Liow, J. S.; Kreisl, W. C.; Taku, A.; Fujita, M.; Pike, V. W.; Innis, R. B. Metabotropic Glutamate Subtype 5 Receptors are Quantified in the Human Brain With a Novel Radioligand for PET. *J. Nucl. Med.* **2008,** *49,* 2042–2048.
124. Shimoda, Y.; Yamasaki, T.; Fujinaga, M.; Ogawa, M.; Kurihara, Y.; Nengaki, N.; Kumata, K.; Yui, J.; Hatori, A.; Xie, L.; Zhang, Y.; Kawamura, K.; Zhang, M.-R. Synthesis and Evaluation of Novel Radioligands Based on 3-[5-(Pyridin-2-yl)-2*H*-Tetrazol-2-yl]Benzonitrile for Positron Emission Tomography Imaging of Metabotropic Glutamate Receptor Subtype 5. *J. Med. Chem.* **2016,** *59,* 3980–3990.
125. Milicevcic Sephton, S.; Müller Herde, A.; Mu, L.; Keller, C.; Rüdisühli, S.; Auberson, Y.; Schibli, R.; Krämer, S. D.; Ametamey, S. Preclinical Evaluation and Test-Retest Studies of [18F]PSS232, a Novel Radioligand for Targeting Metabotropic Glutamate Receptor 5 (mGlu5). *Eur. J. Nucl. Med. Mol. Imaging* **2015,** *42,* 128–137.
126. Ishiwata, K.; Kimura, Y.; de Vries, E. F. J.; Elsinga, P. H. PET Tracers for Mapping Adenosine Receptors as Probes for Diagnosis of CNS Disorders. *Cent. Nerv. Syst. Agents Med. Chem.* **2007,** *7,* 57–77.
127. Khanapur, S.; van Waarde, A.; Ishiwata, K.; Leenders, K. L.; Dierckx, R. A. J. O.; Elsinga, P. H. Adenosine A(2A) Receptors Antagonists as Positron Emission Tomography (PET) Tracers. *Curr. Med. Chem.* **2014,** *21,* 312–328.
128. Zhou, X.; Khanapur, S.; Huizing, A. P.; Zijlma, R.; Schepers, M.; Dierckx, R. A. J. O.; van Waarde, A.; de Vries, E. F. J.; Elsinga, P. H. Synthesis and Preclinical Evaluation of 2-(2-Furanyl)-7-[2-[4-[4-(2-[11C]Methoxyethoxy)Phenyl]-1-Piperazinyl]Ethyl]7*H*-Pyrazolo[4,3-*e*][1,2,4]Triazolo[1,5-*c*]Pyrimidine-5-Amine ([11C]Preladenant) as a PET Tracer for the Imaging of Cerebral Adenosine A2A Rece. *J. Med. Chem.* **2014,** *57,* 9204–9210.
129. Khanapur, S.; Paul, S.; Shah, A.; Vatakuti, S.; Koole, M. J. B.; Zijlma, R.; Dierckx, R. A. J. O.; Luurtsema, G.; Garg, P.; van Waarde, A.; Elsinga, P. H. Development of [18F]-Labeled Pyrazolo[4,3-*e*]-1,2,4- Triazolo[1,5-*c*]Pyrimidine (SCH442416) Analogs for the Imaging of Cerebral Adenosine A2A Receptors With Positron Emission Tomography. *J. Med. Chem.* **2014,** *57,* 6765–6780.
130. Barret, O.; Hannestad, J.; Alagille, D.; Vala, C.; Tavares, A.; Papin, C.; Morley, T.; Fowles, K.; Lee, H.; Seibyl, J.; Tytgat, D.; Laruelle, M.; Tamagnan, G. Adenosine 2A Receptor Occupancy By Tozadenant and Preladenant in Rhesus Monkeys. *J. Nucl. Med.* **2014,** *55,* 1712–1718.
131. Aso, E.; Ferrer, I. CB2 Cannabinoid Receptor as Potential Target Against Alzheimer's Disease. *Front. Neurosci.* **2016,** *10,* 243.
132. Shoemaker, J. L.; Seely, K. A.; Reed, R. L.; Crow, J. P.; Prather, P. L. The CB2 Cannabinoid Agonist AM-1241 Prolongs Survival in a Transgenic Mouse Model of Amyotrophic Lateral Sclerosis When Initiated at Symptom Onset. *J. Neurochem.* **2007,** *101,* 87–98.
133. Slavik, R.; Grether, U.; Müller Herde, A.; Gobbi, L.; Fingerle, J.; Ullmer, C.; Krämer, S. D.; Schibli, R.; Mu, L.; Ametamey, S. M. Discovery of a High Affinity and Selective Pyridine Analog as a Potential Positron Emission Tomography Imaging Agent for Cannabinoid Type 2 Receptor. *J. Med. Chem.* **2015,** *58,* 4266–4277.
134. Saccomanni, G.; Pascali, G.; Carlo, S. D.; Panetta, D.; De Simone, M.; Bertini, S.; Burchielli, S.; Digiacomo, M.; Macchia, M.; Manera, C.; Salvadori, P. A. Design, Synthesis and Preliminary Evaluation of (18)F-Labelled 1,8-Naphthyridin- and Quinolin-2-one-3-Carboxamide Derivatives for PET Imaging of CB2 Cannabinoid Receptor. *Bioorg. Med. Chem. Lett.* **2015,** *25,* 2532–2535.
135. Wenzel, B.; Mollitor, J.; Deuther-Conrad, W.; Dukic-Stefanovic, S.; Kranz, M.; Vraka, C.; Teodoro, R.; Günther, R.; Donat, C. K.; Ludwig, F.-A.; Fischer, S.; Smits, R.; Wadsak, W.; Mitterhauser, M.; Steinbach, J.; Hoepping, A.; Brust, P. Development of a Novel Nonpeptidic 18F-Labeled Radiotracer for In Vivo Imaging of Oxytocin Receptors With Positron Emission Tomography. *J. Med. Chem.* **2016,** *59,* 1800–1817.
136. Smith, A. L.; Freeman, S. M.; Barnhart, T. E.; Abbott, D. H.; Ahlers, E. O.; Kukis, D. L.; Bales, K. L.; Goodman, M. M.; Young, L. J. Initial Investigation of Three Selective and Potent Small Molecule Oxytocin Receptor PET Ligands in New World Monkeys. *Bioorg. Med. Chem. Lett.* **2016,** *26,* 3370–3375.
137. Smith, A. L.; Freeman, S. M.; Voll, R. J.; Young, L. J.; Goodman, M. M. Investigation of an F-18 Oxytocin Receptor Selective Ligand via PET Imaging. *Bioorg. Med. Chem. Lett.* **2013,** *23,* 5415–5420.
138. Maisonial, A.; Maestrup, E. G.; Fischer, S.; Hiller, A.; Scheunemann, M.; Wiese, C.; Schepmann, D.; Steinbach, J.; Deuther-Conrad, W.; Wünsch, B.; Brust, P. A 18F-Labeled Fluorobutyl-Substituted Spirocyclic Piperidine Derivative as a Selective Radioligand for PET Imaging of Sigma1 Receptors. *ChemMedChem* **2011,** *6,* 1401–1410.
139. Jin, H.; Fan, J.; Zhang, X.; Li, J.; Flores, H. P.; Perlmutter, J. S.; Parsons, S. M.; Tu, Z. Radiosynthesis and In Vivo Evaluation of a Novel Sigma1 Selective PET Ligand. *Med. Chem. Commun.* **2014,** *5,* 1669–1677.
140. Holland, J. P.; Cumming, P.; Vasdev, N. PET Radiopharmaceuticals for Probing Enzymes in the Brain. *Am. J. Nucl. Med. Mol. Imaging* **2013,** *3,* 194–216.
141. Kikuchi, T.; Okamura, T.; Zhang, M. R.; Irie, T. PET Probes for Imaging Brain Acetylcholinesterase. *J. Label. Compd. Radiopharm.* **2013,** *56,* 172–179.
142. Biegon, A.; Kim, S. W.; Alexoff, D. L.; Jayne, M.; Carter, P.; Hubbard, B.; King, P.; Logan, J.; Muench, L.; Pareto, D.; Schlyer, D.; Shea, C.; Telang, F.; Wang, G. J.; Xu, Y.; Fowler, J. S. Unique Distribution of Aromatase in the Human Brain: In Vivo Studies With PET and [*N*-Methyl-11C]Vorozole. *Synapse* **2010,** *64,* 801–807.
143. Calabria, F. F.; Calabria, E.; Gangemi, V.; Cascini, G. L. Current Status and Future Challenges of Brain Imaging With (18)F-DOPA PET for Movement Disorders. *Hell. J. Nucl. Med.* **2016,** *19,* 33–41.
144. Boileau, I.; Bloomfield, P. M.; Rusjan, P.; Mizrahi, R.; Mufti, A.; Vitcu, I.; Kish, S. J.; Houle, S.; Wilson, A. A.; Tong, J. Whole-Body Radiation Dosimetry of 11C-Carbonyl-URB694: A PET Tracer for Fatty Acid Amide Hydrolase. *J. Nucl. Med.* **2014,** *55,* 1993–1997.
145. Rusjan, P. M.; Wilson, A. A.; Mizrahi, R.; Boileau, I.; Chavez, S. E.; Lobaugh, N. J.; Kish, S. J.; Houle, S.; Tong, J. Mapping Human Brain Fatty Acid Amide Hydrolase Activity With PET. *J. Cereb. Blood Flow Metab.* **2013,** *33,* 407–414.
146. Sacher, J.; Rabiner, E. A.; Clark, M.; Rusjan, P.; Soliman, A.; Boskovic, R.; Kish, S. J.; Wilson, A. A.; Houle, S.; Meyer, J. H. Dynamic, Adaptive Changes in MAO-A Binding After Alterations in Substrate Availability: An In Vivo [(11)C]-Harmine Positron Emission Tomography Study. *J. Cereb. Blood Flow Metab.* **2012,** *32,* 443–446.
147. Zanotti-Fregonara, P.; Leroy, C.; Rizzo, G.; Roumenov, D.; Trichard, C.; Martinot, J. L.; Bottlaender, M. Imaging of Monoamine Oxidase-A in the Human Brain With [11C] Befloxatone: Quantification Strategies and Correlation With mRNA Transcription Maps. *Nucl. Med. Commun.* **2014,** *35,* 1254–1261.
148. Hirvonen, J.; Kailajärvi, M.; Haltia, T.; Koskimies, S.; Nagren, K.; Virsu, P.; Oikonen, V.; Sipilä, H.; Ruokoniemi, P.; Virtanen, K.; Scheinin, M.; Rinne, J. O. Assessment of MAO-B Occupancy in the Brain With PET and [11C]-L-Deprenyl-D2: A Dose-Finding Study With a Novel MAO-B Inhibitor, EVT 301. *Clin. Pharmacol. Ther.* **2009,** *85,* 506–512.
149. Fowler, J. S.; Logan, J.; Shumay, E.; Alia-Klein, N.; Wang, G. J.; Volkow, N. D. Monoamine Oxidase: Radiotracer Chemistry and Human Studies. *J. Label. Compd. Radiopharm.* **2015,** *58,* 51–64.
150. Chen, L.; Nabulsi, N.; Naganawa, M.; Zasadny, K.; Skaddan, M. B.; Zhang, L.; Najafzadeh, S.; Lin, S. F.; Helal, C. J.; Boyden, T. L.; Chang, C.; Ropchan, J.; Carson, R. E.; Villalobos, A.; Huang, Y. Preclinical Evaluation of 18F-PF-05270430, a Novel PET Radioligand for the Phosphodiesterase 2A Enzyme. *J. Nucl. Med.* **2016,** *57,* 1448–1453.
151. Kenk, M.; Thomas, A.; Lortie, M.; deKemp, R.; Beanlands, R. S.; DaSilva, J. N. PET Measurements of cAMP-Mediated Phosphodiesterase-4 With (R)-[11C]Rolipram. *Curr. Radiopharm.* **2011,** *4,* 44–58.
152. Russell, D. S.; Jennings, D. L.; Barret, O.; Tamagnan, G. D.; Carroll, V. M.; Caillé, F.; Alagille, D.; Morley, T. J.; Papin, C.; Seibyl, J. P.; Marek, K. L. Change in PDE10 Across Early Huntington Disease Assessed by [18F]MNI-659 and PET Imaging. *Neurology* **2016,** *86,* 748–754.
153. Plisson, C.; Weinzimmer, D.; Jakobsen, S.; Natesan, S.; Salinas, C.; Lin, S.-F.; Labaree, D.; Zheng, M.-Q.; Nabulsi, N.; Marques, T. R.; Kapur, S.; Kawanishi, E.; Saijo, T.; Gunn, R. N.; Carson, R. E.; Rabiner, E. A. Phosphodiesterase 10A PET Radioligand Development Program: From Pig to Human. *J. Nucl. Med.* **2014,** *55,* 595–601.

154. Marqués, T. R.; Natesan, S.; Niccolini, F.; Politis, M.; Gunn, R. N.; Searle, G. E.; Howes, O.; Rabiner, E. A.; Kapur, S. Phosphodiesterase 10A in Schizophrenia: A PET Study Using [11C]IMA107. *Am. J. Psychiatry* **2016,** *173,* 714–721.
155. Omori, K.; Kotera, J. Overview of PDEs and Their Regulation. *Circ. Res.* **2007,** *100,* 309–327.
156. Schröder, S.; Wenzel, B.; Deuther-Conrad, W.; Scheunemann, M.; Brust, P. Novel Radioligands for Cyclic Nucleotide Phosphodiesterase Imaging With Positron Emission Tomography: An Update on Developments Since 2012. *Molecules* **2016,** *21,* 650.
157. Zhang, C.; Yu, Y.; Ruan, L.; Wang, C.; Pan, J.; Klabnik, J.; Lueptow, L.; Zhang, H.-T.; O'Donnell, J. M.; Xu, Y. The Roles of Phosphodiesterase 2 in the Central Nervous and Peripheral Systems. *Curr. Pharm. Des.* **2015,** *21,* 274–290.
158. Schröder, S.; Wenzel, B.; Deuther-Conrad, W.; Teodoro, R.; Egerland, U.; Kranz, M.; Scheunemann, M.; Höfgen, N.; Steinbach, J.; Brust, P. Synthesis, 18F-Radiolabelling and Biological Characterization of Novel Fluoroalkylated Triazine Derivatives for In Vivo Imaging of Phosphodiesterase 2A in Brain via Positron Emission Tomography. *Molecules* **2015,** *20,* 9591–9615.
159. Zhang, L.; Villalobos, A.; Beck, E. M.; Bocan, T.; Chappie, T. A.; Chen, L.; Grimwood, S.; Heck, S. D.; Helal, C. J.; Hou, X.; Humphrey, J. M.; Lu, J.; Skaddan, M. B.; McCarthy, T. J.; Verhoest, P. R.; Wager, T. T.; Zasadny, K. Design and Selection Parameters to Accelerate the Discovery of Novel Central Nervous System Positron Emission Tomography (PET) Ligands and Their Application in the Development of a Novel Phosphodiesterase 2A PET Ligand. *J. Med. Chem.* **2013,** *56,* 4568–4579.
160. Andrés, J. I.; Rombouts, F. J. R.; Trabanco, A. A.; Vanhoof, G. C. P.; De Angelis, M.; Buijnsters, P. J. J. A.; Guillemont, J. E. G.; Bormans, G. M. R.; Celen, S. J. L. 1-Aryl-4-Methyl-[1,2,4]Triazolo[4,3-a]Quinoxaline Derivatives. WO2013/000924, 2013.
161. Gil, C.; Campillo, N. E.; Perez, D. I.; Martinez, A. PDE7 Inhibitors as New Drugs for Neurological and Inflammatory Disorders. *Expert Opin. Ther. Pat.* **2008,** *18,* 1127–1139.
162. Thomae, D.; Servaes, S.; Vazquez, N.; wyffels, L.; Dedeurwaerdere, S.; Van der Veken, P.; Joossens, J.; Augustyns, K.; Stroobants, S.; Staelens, S. Synthesis and Preclinical Evaluation of an 18F Labeled PDE7 Inhibitor for PET Neuroimaging. *Nucl. Med. Biol.* **2015,** *42,* 975–981.
163. Kehler, J.; Nielsen, J. PDE10A Inhibitors: Novel Therapeutic Drugs for Schizophrenia. *Curr. Pharm. Des.* **2011,** *17,* 137–150.
164. Chappie, T. A.; Helal, C. J.; Hou, X. Current Landscape of Phosphodiesterase 10A (PDE10A) Inhibition. *J. Med. Chem.* **2012,** *55,* 7299–7331.
165. Wilson, L. S.; Brandon, N. J. Emerging Biology of PDE10A. *Curr. Pharm. Des.* **2015,** *21,* 378–388.
166. Garcia, A. M.; Redondo, M.; Martinez, A.; Gil, C. Phosphodiesterase 10 Inhibitors: New Disease Modifying Drugs for Parkinson's Disease? *Curr. Med. Chem.* **2014,** *21,* 1171–1187.
167. Lin, S.-F.; Labaree, D.; Chen, M.-K.; Holden, D.; Gallezot, J.-D.; Kapinos, M.; Teng, J.-K.; Najafzadeh, S. Further Evaluation of [11C]MP-10 as a Radiotracer for Phosphodiesterase 10A: PET Imaging Study in Rhesus Monkeys and Brain Tissue Metabolite Analysis. *Synapse* **2015,** *69,* 86–95.
168. Plisson, C.; Salinas, C.; Weinzimmer, D.; Labaree, D.; Lin, S.-F.; Ding, Y.-S.; Jakobsen, S.; Smith, P. W.; Eiji, K.; Carson, R. E.; et al. Radiosynthesis and In Vivo Evaluation of [11C]MP-10 as a Positron Emission Tomography Radioligand for Phosphodiesterase 10A. *Nucl. Med. Biol.* **2011,** *38,* 875–884.
169. Hu, E.; Chen, N.; Kunz, R. K.; Hwang, D.-R.; Michelsen, K.; Davis, C.; Ma, J.; Shi, J.; Lester-Zeiner, D.; Hungate, R.; Treanor, J.; Chen, H.; Allen, J. R. Discovery of Phosphodiesterase 10A (PDE10A) PET Tracer AMG 580 to Support Clinical Studies. *ACS Med. Chem. Lett.* **2016,** *7,* 719–723.
170. Chen, H.; Lester-Zeiner, D.; Shi, J.; Miller, S.; Glaus, C.; Hu, E.; Chen, N.; Able, J.; Biorn, C.; Wong, J.; et al. AMG 580: A Novel Small Molecule Phosphodiesterase 10A (PDE10A) Positron Emission Tomography Tracer. *J. Pharmacol. Exp. Ther.* **2015,** *352,* 327–337.
171. Cox, C. D.; Hostetler, E. D.; Flores, B. A.; Evelhoch, J. L.; Fan, H.; Gantert, L.; Holahan, M.; Eng, W.; Joshi, A.; McGaughey, G.; Meng, X.; Purcell, M.; Raheem, I. T.; Riffel, K.; Yan, Y.; Renger, J. J.; Smith, S. M.; Coleman, P. J. Discovery of [11C]MK-8193 as a PET Tracer to Measure Taregt Engagement of Phosphodiesterase 10A (PDE10A) Inhibitors. *Bioorg. Med. Chem. Lett.* **2015,** *25,* 4893–4898.
172. Hostetler, E. D.; Fan, H.; Joshi, A. D.; Zeng, Z.; Eng, W.; Gantert, L.; Holahan, M.; Meng, X.; Miller, P.; O'Malley, S.; et al. Preclinical Characterization of the Phosphodiesterase 10A PET Tracer [11C]MK-8193. *Mol. Imaging Biol.* **2016,** *18,* 579–587.
173. Takano, A.; Stepanov, V.; Gulyas, B.; Nakao, R.; Amini, N.; Miura, S.; Kimura, H.; Taniguchi, T.; Halldin, C. Evaluation of a Novel PDE10A PET Radioligand, [11C]T-773, in Nonhuman Primates: Brain and Whole Body PET and Brain Autoradiography. *Synapse* **2015,** *69,* 345–355.
174. Takano, A.; Stepanov, V.; Nakao, R.; Amini, N.; Gulyás, B.; Kimura, H.; Halldin, C. Brain PET Measurement of PDE10A Occupancy by TAK-063, a New PDE10A Inhibitor, Using [11C]T-773 in Nonhuman Primates. *Synapse* **2016,** *70,* 253–263.
175. Liu, H.; Jin, H.; Yue, X.; Zhang, X.; Yang, H.; Li, J.; Flores, H.; Su, Y.; Perlmutter, J. S.; Tu, Z. Preclinical Evaluation of a Promising C-11 Labeled PET Tracer for Imaging Phosphodiesterase 10A in the Brain of Living Subject. *Neuroimage* **2015,** *121,* 253–262.
176. Kehler, J.; Kilburn, J. P.; Estrada, S.; Christensen, S. R.; Wall, A.; Thibblin, A.; Lubberink, M.; Bundgaard, C. Discovery and Development of 11C-Lu AE92686 as a Radioligand for PET Imaging of Phosphodiesterase10a in the Brain. *J. Nucl. Med.* **2014,** *55,* 1513–1518.
177. Van Laere, K.; Ahmad, R. U.; Hudyana, H.; Dubois, K.; Schmidt, M. E.; Celen, S.; Bormans, G.; Koole, M. Quantification of 18F-JNJ-42259152, a Novel Phosphodiesterase 10A PET Tracer: Kinetic Modeling and Test-Retest Study in Human Brain. *J. Nucl. Med.* **2013,** *54,* 1285–1293.
178. Celen, S.; Koole, M.; Ooms, M.; De Angelis, M.; Sannen, I.; Cornelis, J.; Alcazar, J.; Schmidt, M.; Verbruggen, A.; Langlois, X.; Van Laere, K.; Andrés, J. I.; Bormans, G. Preclinical Evaluation of [18F]JNJ42259152 as a PET Tracer for PDE10A. *Neuroimage* **2013,** *82,* 13–22.
179. Ooms, M.; Celen, S.; Koole, M.; Langlois, X.; Schmidt, M.; de Angelis, M.; Andrés, J. I.; Verbruggen, A.; van Laere, K.; Bormans, G. Synthesis and Biological Evaluation of Carbon-11 and Fluorine-18 Labeled Tracers for In Vivo Visualization of PDE10A. *Nucl. Med. Biol.* **2014,** *41,* 695–704.
180. Bernard-Gauthier, V.; Bailey, J. J.; Berke, S.; Schirrmacher, R. Recent Advances in the Development and Application of Radiolabeled Kinase Inhibitors for PET Imaging. *Molecules* **2015,** *20,* 22200–22207.
181. Bernard-Gauthier, V.; Aliaga, A.; Aliaga, A.; Boudjemeline, M.; Hopewell, R.; Kostikov, A.; Rosa-Neto, P.; Thiel, A.; Schirrmacher, R. Syntheses and Evaluation of Carbon-11- and Fluorine-18-Radiolabeled Pan-Tropomyosin Receptor Kinase (Trk) Inhibitors: Exploration of the 4-Aza-2-Oxindole Scaffold as Trk PET Imaging Agents. *ACS Chem. Neurosci.* **2015,** *6,* 260–276.
182. Bernard-Gauthier, V.; Bailey, J. J.; Aliaga, A.; Kostikov, A.; Rosa-Neto, P.; Wuest, M.; Brodeur, G. M.; Wuest, F.; Schirrmacher, R. Development of Subnanomolar Radiofluorinated (2-Pyrrolidin-1-yl)Imidazo[1,2-*b*]Pyridazine pan-Trk Inhibitors as Candidate PET Imaging Probes. *Med. Chem. Commun.* **2015,** *6,* 2184–2193.
183. Bernard-Gauthier, V.; Boudjemeline, M.; Rosa-Neto, P.; Thiel, A.; Schirrmacher, R. Towards Tropomyosin-Related Kinase B (TrkB) Receptor Ligands for Brain Imaging With PET: Radiosynthesis and Evaluation of 2-(4-[18F]Fluorophenyl)-7,8-Dihydroxy-4*H*-Chromen-4-one and 2-(4-([*N*-Methyl-11C]-Dimethylamino)Phenyl)-7,8-Dihydroxy-4*H*-Chromen-4-one. *Bioorg. Med. Chem.* **2013,** *21,* 7816–7829.
184. Pandey, M. K.; DeGrado, T. R. Glycogen Synthase Kinase-3 (GSK-3)-Targeted Therapy and Imaging. *Theranostics* **2016,** *6,* 571–593.
185. Vasdev, N.; Garcia, A.; Stableford, W. T.; Young, A. B.; Meyer, J. H.; Houle, S.; Wilson, A. A. Synthesis and Ex Vivo Evaluation of Carbon-11 Labelled *N*-(4-Methoxybenzyl)-*N*′-(5-Nitro-1,3-Thiazol-2-yl)-Urea ([11C]AR-A014418): A Radiolabelled Glycogen Synthase Kinase-3β Specific Inhibitor for PET Studies. *Bioorg. Med. Chem. Lett.* **2005,** *15,* 5270–5273.
186. Cole, E. L.; Shao, X.; Sherman, P.; Quesada, C.; Fawaz, M. V.; Desmond, T. J.; Scott, P. J. H. Synthesis and Evaluation of [11C]PyrATP-1, a Novel Radiotracer for PET Imaging of Glycogen Synthase Kinase-3β (GSK-3β). *Nucl. Med. Biol.* **2014,** *41,* 507–512.
187. Li, L.; Shao, X.; Cole, E. L.; Ohnmacht, S. A.; Ferrari, V.; Hong, Y. T.; Williamson, D. J.; Fryer, T. D.; Quesada, C. A.; Sherman, P.; Riss, P. J.; Scott, P. J. H.; Aigbirhio, F. I. Synthesis and Initial In Vivo Studies With [11C]SB-216763: The First Radiolabeled Brain Penetrative Inhibitor of GSK-3. *ACS Med. Chem. Lett.* **2015,** *6,* 548–552.
188. Liang, S.; Chen, J.; Normandin, M.; Collier, T.; Perlis, R.; Holson, E.; Haggarty, S.; El Fakhri, G. K. R.; Vasdev, N. Discovery of [11C]PF-367 for Neuroimaging of Glycogen Synthase Kinase 3. *J. Nucl. Med.* **2015,** *56* (Suppl. 3), 491.
189. Liang, S.; Chen, J.; Normandin, M.; Chang, J.; Chang, G.; Taylor, C.; Trapa, P.; Plummer, M.; Para, K.; Conn, E.; Lopresti-Morrow, L.; Lanyon, L.; Cook, J.; Richter, K.; Nolan, C.; Schachter, J.; Janat, F.; Che, Y.; Shanmugasundaram, V.; Lefker, B.; Enerson, B.; Livni, E.; Wang, L.; Guehl, N.; Patnaik, D.; Wagner, F.; Perlis, R.; Holson, E.; Haggarty, S.; El Fakhri, G.; Kurumbail, R.; Vasdev, N. Discovery of a Highly Selective Glycogen Synthase Kinase-3 Inhibitor (PF-04802367) That Modulates Tau Phosphorylation in the Brain: Translation for PET Neuroimaging. *Angew. Chem. Int. Ed. Engl.* **2016,** *55* (33), 9601–9605.

190. Taniguchi, J.; Seki, C.; Takuwa, H.; Kawaguchi, H.; Ikoma, Y.; Fujinaga, M.; Kanno, I.; Zhang, M.-R.; Kuwabara, S.; Ito, H. Evaluation of Rho-Kinase Activity in Mice Brain Using *N*-[11C]-Methyl-Hydroxyfasudil With Positron Emission Tomography. *Mol. Imaging Biol.* **2014,** *16,* 395–402.
191. Valdivia, A. C.; Mason, S.; Collins, J.; Buckley, K. R.; Coletta, P.; Beanlands, R. S.; DaSilva, J. N. Radiosynthesis of *N*-[11C]-Methyl-Hydroxyfasudil as a New Potential PET Radiotracer for rho-Kinases (ROCKs). *Appl. Radiat. Isot.* **2010,** *68,* 325–328.
192. Grosso, H.; Mouradian, M. M. Transglutaminase 2: Biology, Relevance to Neurodegenerative Diseases and Therapeutic Implications. *Pharmacol. Ther.* **2012,** *133,* 392–410.
193. Ientile, R.; Curro, M.; Caccamo, D. Transglutaminase 2 and Neuroinflammation. *Amino Acids* **2015,** *47,* 19–26.
194. van der Wildt, B.; Wilhelmus, M. M. M.; Bijkerk, J.; Haveman, L. Y. F.; Kooijman, E. J. M.; Schuit, R. C.; Bol, J. G. J. M.; Jongenelen, C. A. M.; Lammertsma, A. A.; Drukarch, B.; Windhorst, A. D. Development of Carbon-11 Labeled Acryl Amides for Selective PET Imaging of Active Tissue Transglutaminase. *Nucl. Med. Biol.* **2016,** *43,* 232–242.
195. Kassenbrock, A.; Vasdev, N.; Liang, S. Selected PET Radioligands for Ion Channel Linked Neuroreceptor Imaging: Focus on GABA, NMDA and nACh Receptors. *Curr. Top. Med. Chem.* **2016,** *16* (16), 1830–1842.
196. Kendziorra, K.; Wolf, H.; Meyer, P.; Barthel, H.; Hesse, S.; Becker, G.; Luthardt, J.; Schildan, A.; Patt, M.; Sorger, D.; Seese, A.; Gertz, H.; Sabri, O. Decreased Cerebral α4β2* Nicotinic Acetylcholine Receptor Availability in Patients With Mild Cognitive Impairment and Alzheimer's Disease Assessed With Positron Emission Tomography. *Eur. J. Nucl. Med. Mol. Imaging* **2011,** *38* (3), 515–525.
197. Horti, A.; Kuwabara, H.; Holt, D.; Dannals, R.; Wong, D. Recent PET Radioligands With Optimal Brain Kinetics for Imaging Nicotinic Acetylcholine Receptors. *J. Label. Compd. Radiopharm.* **2013,** *56* (3–4), 159–166.
198. Wong, D.; Kuwabara, H.; Kim, J.; Brasic, J.; Chamroonrat, W.; Gao, Y.; Valentine, H.; Willis, W.; Mathur, A.; McCaul, M.; Wand, G.; Gean, E.; Dannals, R.; Horti, A. PET Imaging of High-Affinity α4β2 Nicotinic Acetylcholine Receptors in Humans With 18F-AZAN, a Radioligand With Optimal Brain Kinetics. *J. Nucl. Med.* **2013,** *54* (8), 1308–1314.
199. Patt, M.; Becker, G.; Grossmann, U.; Habermann, B.; Schildan, A.; Wilke, S.; Deuther-Conrad, W.; Graef, S.; Fischer, S.; Smits, R.; Hoepping, A.; Wagenknecht, G.; Steinbach, J.; Gertz, H.; Hesse, S.; Schönknecht, P.; Brust, P.; Sabri, O. Evaluation of Metabolism, Plasma Protein Binding and Other Biological Parameters After Administration of (−)-[(18)F]Flubatine in Humans. *Nucl. Med. Biol.* **2014,** *41* (6), 489–494.
200. Ishikawa, M.; Sakata, M.; Toyohara, J.; Oda, K.; Ishii, K.; Wu, J.; Yoshida, T.; Iyo, M.; Ishiwata, K.; Hashimoto, K. Occupancy of α7 Nicotinic Acetylcholine Receptors in the Brain by Tropisetron: A Positron Emission Tomography Study Using [(11)C]CHIBA-1001 in Healthy Human Subjects. *Clin. Psychopharmacol. Neurosci.* **2011,** *9* (3), 111–116.
201. Wong, D.; Kuwabara, H.; Pomper, M.; Holt, D.; Brasic, J.; George, N.; Frolov, B.; Willis, W.; Gao, Y.; Valentine, H.; Nandi, A.; Gapasin, L.; Dannals, R.; Horti, A. Human Brain Imaging of α7 nAChR With [(18)F]ASEM: A New PET Radiotracer for Neuropsychiatry and Determination of Drug Occupancy. *Mol. Imaging Biol.* **2014,** *16* (5), 730–738.
202. Horti, A. Development of [(18)F]ASEM, a Specific Radiotracer for Quantification of the α7-nAChR With Positron-Emission Tomography. *Biochem. Pharmacol.* **2015,** *97* (4), 566–575.
203. Andersson, J.; Halldin, C. PET Radioligands Targeting the Brain GABAA/Benzodiazepine Receptor Complex. *J. Label. Compd. Radiopharm.* **2013,** *56* (3–4), 196–206.
204. D'Hulst, C.; Heulens, I.; Van der Aa, N.; Goffin, K.; Koole, M.; Porke, K.; Van De Velde, M.; Rooms, L.; Van Paesschen, W.; Van Esch, H.; Van Laere, K.; Kooy, R. Positron Emission Tomography (PET) Quantification of GABAA Receptors in the Brain of Fragile X Patients. *PLoS One* **2015,** *10* (7). e0131486.
205. Mo, Y.; Yin, Y.; Li, Y. Neural nAChRs PET Imaging Probes. *Nucl. Med. Commun.* **2014,** *35* (2), 135–143.
206. Brašić, J.; Cascella, N.; Kumar, A.; Zhou, Y.; Hilton, J.; Raymont, V.; Crabb, A.; Guevara, M.; Horti, A.; Wong, D. Positron Emission Tomography Experience With 2-[^{18}F]Fluoro-3-(2(*S*)-Azetidinylmethoxy)Pyridine (2-[^{18}F]FA) in the Living Human Brain of Smokers With Paranoid Schizophrenia. *Synapse* **2012,** *66* (4), 352–368.
207. Smits, R.; Fischer, S.; Hiller, A.; Deuther-Conrad, W.; Wenzel, B.; Patt, M.; Cumming, P.; Steinbach, J.; Sabri, O.; Brust, P.; Hoepping, A. Synthesis and Biological Evaluation of Both Enantiomers of [(18)F]Flubatine, Promising Radiotracers With Fast Kinetics for the Imaging of α4β2-Nicotinic Acetylcholine Receptors. *Bioorg. Med. Chem.* **2014,** *22* (2), 804–812.
208. Hillmer, A.; Wooten, D.; Slesarev, M.; Ahlers, E.; Barnhart, T.; Schneider, M.; Mukherjee, J.; Christian, B. Measuring α4β2* Nicotinic Acetylcholine Receptor Density In Vivo With [(18)F]Nifene PET in the Nonhuman Primate. *J. Cereb. Blood Flow Metab.* **2013,** *33* (11), 1806–1814.
209. Kuruvilla, S.; Hillmer, A.; Wooten, D.; Patel, A.; Christian, B.; Mukherjee, J. Synthesis and Evaluation of 2-(18)F-Fluoro-5-Iodo-3-[2-(*S*)-3,4-Dehydropyrrolinylmethoxy]Pyridine ((18)F-Niofene) as a Potential Imaging Agent for Nicotinic α4β2 Receptors. *Am. J. Nucl. Med. Mol. Imaging* **2014,** *4* (4), 354–364.
210. Lingford-Hughes, A.; Hume, S.; Feeney, A.; Hirani, E.; Osman, S.; Cunningham, V.; Pike, V.; Brooks, D.; Nutt, D. Imaging the GABA-Benzodiazepine Receptor Subtype Containing the Alpha5-Subunit In Vivo With [11C]Ro15 4513 Positron Emission Tomography. *J. Cereb. Blood Flow Metab.* **2002,** *22* (7), 878–889.
211. Stokes, P.; Myers, J.; Kalk, N.; Watson, B.; Erritzoe, D.; Wilson, S.; Cunningham, V.; Riano Barros, D.; Hammers, A.; Turkheimer, F.; Nutt, D.; Lingford-Hughes, A. Acute Increases in Synaptic GABA Detectable in the Living Human Brain: A [^{11}C]Ro15-4513 PET Study. *Neuroimage* **2014,** *99,* 158–465.
212. Moon, B.; Kil, H.; Park, J.; Kim, J.; Park, J.; Chi, D.; Lee, B.; Kim, S. Facile Aromatic Radiofluorination of [18F]Flumazenil From Diaryliodonium Salts With Evaluation of Their Stability and Selectivity. *Org. Biomol. Chem.* **2011,** *9* (24), 8346–8355.
213. Fuchigami, T.; Nakayama, M.; Yoshida, S. Development of PET and SPECT Probes for Glutamate Receptors. *ScientificWorldJournal* **2015,** *2015,* 716514.
214. Sasaki, T.; Ito, H.; Kimura, Y.; Arakawa, R.; Takano, H.; Seki, C.; Kodaka, F.; Fujie, S.; Takahata, K.; Nogami, T.; Suzuki, M.; Fujiwara, H.; Takahashi, H.; Nakao, R.; Fukumura, T.; Varrone, A.; Halldin, C.; Nishikawa, T.; Suhara, T. Quantification of Dopamine Transporter in Human Brain Using PET With 18F-FE-PE2I. *J. Nucl. Med.* **2012,** *53* (7), 1065–1073.
215. Fazio, P.; Svenningsson, P.; Forsberg, A.; Jönsson, E.; Amini, N.; Nakao, R.; Nag, S.; Halldin, C.; Farde, L.; Varrone, A. Quantitative Analysis of ^{18}F-(E)-*N*-(3-Iodoprop-2-Enyl)-2β-Carbofluoroethoxy-3β-(4′-Methyl-Phenyl) Nortropane Binding to the Dopamine Transporter in Parkinson Disease. *J. Nucl. Med.* **2015,** *56* (5), 714–720.
216. Davis, M.; Votaw, J.; Bremner, J.; Byas-Smith, M.; Faber, T.; Voll, R.; Hoffman, J.; Grafton, S.; Kilts, C.; Goodman, M. Initial Human PET Imaging Studies With the Dopamine Transporter Ligand 18F-FECNT. *J. Nucl. Med.* **2003,** *44* (6), 855–861.
217. Nye, J.; Votaw, J.; Bremner, J.; Davis, M.; Voll, R.; Camp, V.; Goodman, M. Quantification of Dopamine Transporter Density With [18F]FECNT PET in Healthy Humans. *Nucl. Med. Biol.* **2014,** *41* (3), 217–222.
218. Gunn, R.; Murthy, V.; Catafau, A.; Searle, G.; Bullich, S.; Slifstein, M.; Ouellet, D.; Zamuner, S.; Herance, R.; Salinas, C.; Pardo-Lozano, R.; Rabiner, E.; Farre, M.; Laruelle, M. Translational Characterization of [11C]GSK931145, a PET Ligand for the Glycine Transporter Type 1. *Synapse* **2011,** *65* (12), 1319–1332.
219. Wong, D.; Ostrowitzki, S.; Zhou, Y.; Raymont, V.; Hofmann, C.; Borroni, E.; Kumar, A.; Parkar, N.; Brašić, J.; Hilton, J.; Dannals, R.; Martin-Facklam, M. Characterization of [11C]RO5013853, a Novel PET Tracer for the Glycine Transporter Type 1 (GlyT1) in Humans. *Neuroimage* **2013,** *75,* 282–290.
220. Joshi, A.; Sanabria-Bohórquez, S.; Bormans, G.; Koole, M.; De Hoon, J.; Van Hecken, A.; Depre, M.; De Lepeleire, I.; Van Laere, K.; Sur, C.; Hamill, T. Characterization of the Novel GlyT1 PET Tracer [18F]MK-6577 in Humans. *Synapse* **2015,** *69* (1), 33–40.
221. Zheng, M.; Lin, S.; Holden, D.; Naganawa, M.; Ropchan, J.; Najafzaden, S.; Kapinos, M.; Tabriz, M.; Carson, R.; Hamill, T.; Huang, Y. Comparative Evaluation of Two Glycine Transporter 1 Radiotracers [11C]GSK931145 and [18F]MK-6577 in Baboons. *Synapse* **2016,** *70* (3), 112–120.
222. Hannestad, J.; Gallezot, J.-D.; Planeta-Wilson, B.; Lin, S.; Williams, W.; van Dyck, C.; Malison, R.; Carson, R.; Ding, Y. Clinically Relevant Doses of Methylphenidate Significantly Occupy Norepinephrine Transporters in Humans In Vivo. *Biol. Psychiatry* **2010,** *68* (9), 854–860.
223. Takano, A.; Gulyás, B.; Varrone, A.; Karlsson, P.; Schou, M.; Airaksinen, A.; Vandenhende, F.; Tauscher, J.; Halldin, C. Imaging the Norepinephrine Transporter With Positron Emission Tomography: Initial Human Studies With (S, S)-[18F]FMeNER-D2. *Eur. J. Nucl. Med. Mol. Imaging* **2008,** *35* (1), 153–157.
224. Adhikarla, V.; Zeng, F.; Votaw, J.; Goodman, M.; Nye, J. Compartmental Modeling of [(11)C]MENET Binding to the Norepinephrine Transporter in the Healthy Human Brain. *Nucl. Med. Biol.* **2016,** *43* (5), 318–323.
225. Stehouwer, J.; Goodman, M. 11-C and 18-F PET Radioligands for the Serotonin Transporter (SERT). *J. Label. Compd. Radiopharm.* **2013,** *56* (3–4), 114–119.

226. Mercier, J.; Archen, L.; Bollu, V.; Carré, S.; Evrard, Y.; Jnoff, E.; Kenda, B.; Lallemand, B.; Michel, P.; Montel, F.; Moureau, F.; Price, N.; Quesnel, Y.; Sauvage, X.; Valade, A.; Provins, L. Discovery of Heterocyclic Nonacetamide Synaptic Vesicle Protein 2A (SV2A) Ligands With Single-Digit Nanomolar Potency: Opening Avenues Towards the First SV2A Positron Emission Tomography (PET) Ligands. *ChemMedChem* **2014,** *9* (4), 693–968.
227. Warnock, G.; Aerts, J.; Bahri, M.-A.; Bretin, F.; Lemaire, C.; Giacomelli, F.; Mievis, F.; Mestdagh, N.; Buchanan, T.; Valade, A.; Mercier, J.; Wood, M.; Gillard, M.; Seret, A.; Luxen, A.; Salmon, E.; Plenevaux, A. Evaluation of 18F-UCB-H as a Novel PET Tracer for Synaptic Vesicle Protein 2A in the Brain. *J. Nucl. Med.* **2014,** *55* (8), 1336–1341.
228. Nabulsi, N.; Mercier, J.; Holden, D.; Carré, S.; Najafzadeh, S.; Vandergeten, M.-C.; Lin, S.-F.; Deo, A.; Price, N.; Wood, M.; Lara-Jaime, T.; Montel, F.; Laruelle, M.; Carson, R.; Hannestad, J.; Huang, Y. Synthesis and Preclinical Evaluation of 11C-UCB-J as a PET Tracer for Imaging the Synaptic Vesicle Glycoprotein 2A in the Brain. *J. Nucl. Med.* **2016,** *57* (5), 777–784.
229. Finnema, S.; Nabulsi, N.; Eid, T.; Detyniecki, K.; Lin, S.; Chen, M.; Dhaher, R.; Matuskey, D.; Baum, E.; Holden, D.; Spencer, D.; Mercier, J.; Hannestad, J.; Huang, Y.; Carson, R. Imaging Synaptic Density in the Living Human Brain. *Sci. Transl. Med.* **2016,** *8* (348), 348ra96.
230. Lin, K.; Weng, Y.; Wey, S.; Hsiao, I.; Lu, C.; Skovronsky, D.; Chang, H.; Kung, M.; Yen, T. Whole-Body Biodistribution and Radiation Dosimetry of 18F-FP-(+)-DTBZ (18F-AV-133): A Novel Vesicular Monoamine Transporter 2 Imaging Agent. *J. Nucl. Med.* **2010,** *51* (9), 1480–1485.
231. Lin, S.; Lin, K.; Hsiao, I.; Hsieh, C.; Lin, W.; Lu, C.; Wey, S.; Yen, T.; Kung, M.; Weng, Y. In Vivo Detection of Monoaminergic Degeneration in Early Parkinson Disease by (18)F-9-Fluoropropyl-(+)-Dihydrotetrabenzazine PET. *J. Nucl. Med.* **2014,** *55* (1), 73–79.
232. Siderowf, A.; Pontecorvo, M.; Shill, H.; Mintun, M.; Arora, A.; Joshi, A.; Lu, M.; Adler, C.; Galasko, D.; Liebsack, C.; Skovronsky, D.; Sabbagh, M. PET Imaging of Amyloid With Florbetapir F 18 and PET Imaging of Dopamine Degeneration With 18F-AV-133 (Florbenazine) in Patients With Alzheimer's Disease and Lewy Body Disorders. *BMC Neurol.* **2014,** *14,* 79.
233. Varrone, A.; Halldin, C. New Developments of Dopaminergic Imaging in Parkinson's Disease. *Q. J. Nucl. Med. Mol. Imaging* **2012,** *56* (1), 68–82.
234. Ziebell, M. Evaluation of the Superselective Radioligand [123I]PE2I for Imaging of the Dopamine Transporter in SPECT. *Dan. Med. Bull.* **2011,** *58* (5), B4279.
235. Vase, K.; Peters, D.; Nielsen, E.; Alstrup, A.; Bender, D. [11C]NS8880, a Promising PET Radiotracer Targeting the Norepinephrine Transporter. *Nucl. Med. Biol.* **2014,** *41* (9), 758–764.
236. Rami-Mark, C.; Berroterán-Infante, N.; Philippe, C.; Foltin, S.; Vraka, C.; Hoepping, A.; Lanzenberger, R.; Hacker, M.; Mitterhauser, M.; Wadsak, W. Radiosynthesis and First Preclinical Evaluation of the Novel Norepinephrine Transporter Pet-Ligand [(11)C]ME@HAPTHI. *EJNMMI Res.* **2015,** *5,* 34.
237. Qiao, H.; Zhang, Y.; Wu, Z.; Zhu, L.; Choi, S.; Ploessl, K.; Kung, H. One-Step Preparation of [(18)F]FPBM for PET Imaging of Serotonin Transporter (SERT) in the Brain. *Nucl. Med. Biol.* **2016,** *43* (8), 470–477.
238. Kim, E.; Howes, O.; Park, J.; Kim, S.; Shin, S.; Kim, B.; Turkheimer, F.; Lee, Y.; Kwon, J. Altered Serotonin Transporter Binding Potential in Patients With Obsessive-Compulsive Disorder Under Escitalopram Treatment: [11C]DASB PET Study. *Psychol. Med.* **2016,** *46* (2), 357–366.
239. Baldinger, P.; Kranz, G.; Haeusler, D.; Savli, M.; Spies, M.; Philippe, C.; Hahn, A.; Höflich, A.; Wadsak, W.; Mitterhauser, M.; Lanzenberger, R.; Kasper, S. Regional Differences in SERT Occupancy After Acute and Prolonged SSRI Intake Investigated by Brain PET. *Neuroimage* **2014,** *88,* 252–262.
240. Huang, W.; Huang, S.; Ho, P.; Ma, K.; Huang, Y.; Yeh, C.; Liu, R.; Cheng, C.; Shiue, C. PET Imaging of the Brain Serotonin Transporters (SERT) With *N,N*-Dimethyl-2-(2-Amino-4-[18F]Fluorophenylthio)Benzylamine (4-[18F]-ADAM) in Humans: A Preliminary Study. *Eur. J. Nucl. Med. Mol. Imaging* **2013,** *40* (1), 115–124.
241. Castner, S.; Murthy, N.; Ridler, K.; Herdon, H.; Roberts, B.; Weinzimmer, D.; Huang, Y.; Zheng, M.; Rabiner, E.; Gunn, R.; Carson, R.; Williams, G.; Laruelle, M. Relationship Between Glycine Transporter 1 Inhibition as Measured With Positron Emission Tomography and Changes in Cognitive Performances in Nonhuman Primates. *Neuropsychopharmacology* **2014,** *39* (12), 2742–2749.
242. Kilbourn, M. In Vivo Radiotracers for Vesicular Neurotransmitter Transporters. *Nucl. Med. Biol.* **1997,** *24* (7), 615–619.
243. Lee, C.; Samii, A.; Sossi, V.; Ruth, T.; Schulzer, M.; Holden, J.; Wudel, J.; Pal, P.; de la Fuente-Fernandez, R.; Calne, D.; Stoessl, A. In Vivo Positron Emission Tomographic Evidence for Compensatory Changes in Presynaptic Dopaminergic Nerve Terminals in Parkinson's Disease. *Ann. Neurol.* **2000,** *47* (4), 493–503.
244. Nandhagopal, R.; Kuramoto, L.; Schulzer, M.; Mak, E.; Cragg, J.; McKenzie, J.; McCormick, S.; Ruth, T.; Sossi, V.; de la Fuente-Fernandez, R.; Stoessl, A. Longitudinal Evolution of Compensatory Changes in Striatal Dopamine Processing in Parkinson's Disease. *Brain* **2011,** *134* (Pt 11), 3290–3298.
245. Koeppe, R.; Frey, K.; Vander Borght, T.; Karlamangla, A.; Jewett, D.; Lee, L.; Kilbourn, M.; Kuhl, D. Kinetic Evaluation of [11C]Dihydrotetrabenazine by Dynamic PET: Measurement of Vesicular Monoamine Transporter. *J. Cereb. Blood Flow Metab.* **1996,** *16* (6), 1288–1299.
246. Martin, W.; Wieler, M.; Stoessl, A.; Schulzer, M. Dihydrotetrabenazine Positron Emission Tomography Imaging in Early, Untreated Parkinson's Disease. *Ann. Neurol.* **2008,** *63* (3), 388–394.
247. Bajjalieh, S. M.; Frantz, G. D.; Weimann, J. M.; McConnell, S. K.; Scheller, R. H. Differential Expression of Synaptic Vesicle Protein 2 (SV2) Isoforms. *J. Neurosci.* **1994,** *14,* 5223–5235.
248. Bajjalieh, S.; Peterson, K.; Shinghal, R.; Scheller, R. SV2, a Brain Synaptic Vesicle Protein Homologous to Bacterial Transporters. *Science* **1992,** *257,* 1271–1273.
249. Gillard, M. Binding Characteristics of Levetiracetam to Synaptic Vesicle Protein 2A (SV2A) in Human Brain and in CHO Cells Expressing the Human Recombinant Protein. *Eur. J. Pharmacol.* **2006,** *536,* 102–108.
250. Kaminski, R.; Gillard, M.; Klitgaard, H. Targeting SV2A for Discovery of Antiepileptic Drugs. In *Jasper's Basic Mechanisms of the Epilepsies,* 4th ed.; Oxford University Press: Bethesda, MD, 2012.
251. Robinson, J.; Molina-Porcel, L.; Corrada, M. Perforant Path Synaptic Loss Correlates With Cognitive Impairment and Alzheimer's Disease in the Oldest-Old. *Brain* **2014,** *137,* 2578–2587.
252. Kaufman, A.; Salazar, S.; Haas, L.; Yang, J.; Kostylev, M.; Jeng, A.; Robinson, S.; Gunther, E.; van Dyck, C.; Nygaard, H.; Strittmatter, S. Fyn Inhibition Rescues Established Memory and Synapse Loss in Alzheimer Mice. *Ann. Neurol.* **2015,** *77* (6), 953–971.
253. Cai, H.; Mangner, T.; Muzik, O.; Wang, M.; Chugani, D.; Chugani, H. Radiosynthesis of [11C]Levetiracetam: A Potential Marker for PET Imaging of SV2A Expression. *ACS Med. Chem. Lett.* **2014,** *5* (10), 1152–1155.
254. Estrada, S.; Lubberink, M.; Thibblin, A.; Sprycha, M.; Buchanan, T.; Mestdagh, N.; Kenda, B.; Mercier, J.; Provins, L.; Gillard, M.; Tytgat, D.; Antoni, G. [11C]UCB-A, a Novel PET Tracer for Synaptic Vesicle Protein 2A. *Nucl. Med. Biol.* **2016,** *43* (6), 325–332.
255. Bretin, F.; Bahri, M.-A.; Bernard, C.; Warnock, G.; Aerts, J.; Mestdagh, N.; Buchanan, T.; Otoul, C.; Koestler, F.; Mievis, F.; Giacomelli, F.; Degueldre, C.; Hustinx, R.; Luxen, A.; Seret, A.; Plenevaux, A.; Salmon, E. Biodistribution and Radiation Dosimetry for the Novel SV2A Radiotracer [(18)F]UCB-H: First-in-Human Study. *Mol. Imaging Biol.* **2015,** *17* (4), 557–564.
256. Buckley, K.; Kelly, R. B. Identification of a Transmembrane Glycoprotein Specific for Secretory Vesicles of Neural and Endocrine Cells. *J. Cell Biol.* **1985,** *100,* 1284–1294.
257. Janz, R.; Südhof, T. SV2C is a Synaptic Vesicle Protein With an Unusually Restricted Localization: Anatomy of a Synaptic Vesicle Protein Family. *Neuroscience* **1999,** *94* (4), 1279–1290.
258. Dardou, D.; Dassesse, D.; Cuvelier, L.; Deprez, T.; De Ryck, M.; Schiffmann, S. Distribution of SV2C mRNA and Protein Expression in the Mouse Brain With a Particular Emphasis on the Basal Ganglia System. *Brain Res.* **2011,** *1367,* 130–145.
259. Dardou, D.; Monlezun, S.; Foerch, P.; Courade, J.-P.; Cuvelier, L.; De Ryck, M.; Schiffmann, S. A Role for Sv2c in Basal Ganglia Functions. *Brain Res.* **2013,** *1507,* 61–73.
260. Hill-Burns, E.; Singh, N.; Ganguly, P.; Hamza, T.; Montimurro, J.; Kay, D.; Yearout, D.; Sheehan, P.; Frodey, K.; McLear, J.; Feany, M.; Hanes, S.; Wolfgang, W.; Zabetian, C.; Factor, S.; Payami, H. A Genetic Basis for the Variable Effect of Smoking/Nicotine on Parkinson's Disease. *Pharmacogenomics J.* **2013,** *13* (6), 530–537.
261. Warnock, G.; Aerts, J.; Mestdagh, N.; Valade, A.; Mercier, J.; Buchanan, T.; Plenevaux, A.; Luxen, A. *Evaluation of a New [18F] Labeled Tracer Targeting Synaptic Vesicle Protein 2C by Ex Vivo Autoradiography and In Vivo PET Study in Rat Brain*. Orbi (Open Repository and Bibliography). http://hdl.handle.net/2268/163938, 2013 (accessed June 27, 2016).
262. Ikonomovic, M. D.; Klunk, W. E. Post-Mortem Correlates of In Vivo PiB-PET Amyloid Imaging in a Typical Case of Alzheimer's Disease. *Brain* **2008,** *131,* 1630–1645.

263. Ostrowitzki, S.; Deptula, D.; Thurfjell, L.; Barkhof, F.; Bohrmann, B.; Brooks, D. J.; Klunk, W. E.; Ashford, E.; Yoo, K.; Xu, Z.-X.; Loetscher, H.; Santarelli, L. Mechanism of Amyloid Removal in Patients With Alzheimer Disease Treated With Gantenerumab. *Arch. Neurol.* **2012,** *69* (2), 198–207.
264. Shoghi-Jadid, K.; Small, G.; Agdeppa, E.; Kepe, V.; Ercoli, L.; Siddarth, P.; Read, S.; Satyamurthy, N.; Petric, A.; Huang, S.; Barrio, J. Localization of Neurofibrillary Tangles and Beta-Amyloid Plaques in the Brains of Living Patients With Alzheimer Disease. *Am. J. Geriatr. Psychiatry* **2002,** *10* (1), 24–35.
265. Ariza, M.; Kolb, H.; Moechars, D.; Rombouts, F.; Andrés, J. Tau Positron Emission Tomography (PET) Imaging: Past, Present, and Future. *J. Med. Chem.* **2015,** *58* (11), 4365–4382.
266. Okamura, N.; Harada, R.; Furukawa, K.; Furumoto, S.; Tago, T.; Yanai, K.; Arai, H.; Kudo, Y. Advances in the Development of Tau PET Radiotracers and Their Clinical Applications. *Ageing Res. Rev.* **2016,** *30,* 107–113.
267. Dani, M.; Brooks, D.; Edison, P. Tau Imaging in Neurodegenerative Diseases. *Eur. J. Nucl. Med. Mol. Imaging* **2016,** *43* (6), 1139–1150.
268. Harada, R.; Okamura, N.; Furumoto, S.; Tago, T.; Yanai, K.; Arai, H.; Kudo, Y. Characteristics of Tau and Its Ligands in PET Imaging. *Biomolecules* **2016,** *6* (1), 7–21.
269. Sander, K.; Lashley, T.; Gami, P.; Gendron, T.; Lythgoe, M.; Rohrer, J.; Schott, J.; Revesz, T.; Fox, N.; Årstad, E. Characterization of tau Positron Emission Tomography Tracer [18F]AV-1451 Binding to Postmortem Tissue in Alzheimer's Disease, Primary Tauopathies, and Other Dementias. *Alzheimers Dement.* **2016,** *12* (11), 1116–1124.
270. Fodero-Tavoletti, M.; Mulligan, R.; Okamura, N.; Furumoto, S.; Rowe, C.; Kudo, Y.; Masters, C.; Cappai, R.; Yanai, K.; Villemagne, V. In Vitro Characterisation of BF227 Binding to Alpha-Synuclein/Lewy Bodies. *Eur. J. Pharmacol.* **2009,** *617* (1–3), 54–58.
271. Kikuchi, A.; Takeda, A.; Okamura, N.; Tashiro, M.; Hasegawa, T.; Furumoto, S.; Kobayashi, M.; Sugeno, N.; Baba, T.; Miki, Y.; Mori, F.; Wakabayashi, K.; Funaki, Y.; Iwata, R.; Takahashi, S.; Fukuda, H.; Arai, H.; Kudo, Y.; Yanai, K.; Itoyama, Y. In Vivo Visualization of Alpha-Synuclein Deposition by Carbon-11-Labelled 2-[2-(2-Dimethylaminothiazol-5-yl)Ethenyl]-6-[2-(Fluoro)Ethoxy]Benzoxazole Positron Emission Tomography in Multiple System Atrophy. *Brain* **2010,** *133* (Pt 6), 1772–1778.
272. Sevigny, J.; Chiao, P.; BussiÒre, T.; Weinreb, P.; Williams, L.; Maier, M.; Dunstan, R.; Salloway, S.; Chen, T.; Ling, Y.; O'Gorman, J.; Qian, F.; Arastu, M.; Li, M.; Chollate, S.; Brennan, M.; Quintero-Monzon, O.; Scannevin, R.; Arnold, H.; Engber, T.; Rhodes, K.; Ferrero, J.; Hang, Y.; Mikulskis, A.; Grimm, J.; Hock, C.; Nitsch, R.; Sandrock, A. The antibody aducanumab reduces Aβ plaques in Alzheimer's disease. *Nature* **2016,** *537* (7618), 50–56.
273. Arriagada, P. V.; Growdon, J. H.; Hedley-Whyte, E. T.; Hyman, B. T. Neurofibrillary Tangles but Not Senile Plaques Parallel Duration and Severity of Alzheimer's Disease. *Neurology* **1992,** *42* (3 Pt 1), 631–639.
274. Maccioni, R. B.; Farías, G.; Morales, I.; Navarrete, L. The Revitalized Tau Hypothesis on Alzheimer's Disease. *Arch. Med. Res.* **2010,** *41* (3), 226–231.
275. Villemagne, V. L.; Furumoto, S.; Fodero-Tavoletti, M.; Harada, R.; Mulligan, R. S.; Kudo, Y.; Masters, C. L.; Yanai, K.; Rowe, C.; Okamura, N. The Challenges of Tau Imaging. *Future Neurol.* **2012,** *7* (4), 409–421.
276. Parikh, N.; Klimov, D. Molecular Mechanisms of Alzheimer's Biomarker FDDNP Binding to Aβ Amyloid Fibril. *J. Phys. Chem. B* **2015,** *119* (35), 11568–11580.
277. Xia, C.; Arteaga, J.; Chen, G.; Gangadharmath, U.; Gomez, L.; Kasi, D.; Lam, C.; Liang, Q.; Liu, C.; Mocharla, V.; Mu, F.; Sinha, A.; Su, H.; Szardenings, A.; Walsh, J.; Wang, E.; Yu, C.; Zhang, W.; Zhao, T.; Kolb, H. [18F]T807, a Novel Tau Positron Emission Tomography Imaging Agent for Alzheimer's Disease. *Alzheimers Dement.* **2013,** *9* (6), 666–676.
278. Chien, D.; Bahri, S.; Szardenings, A.; Walsh, J.; Mu, F.; Su, M.; Shankle, W.; Elizarov, A.; Kolb, H. Early Clinical PET Imaging Results With the Novel PHF-Tau Radioligand [F-18]-T807. *J. Alzheimers Dis.* **2013,** *34* (2), 467–468.
279. Schwarz, A.; Yu, P.; Miller, B.; Shcherbinin, S.; Dickson, J.; Navitsky, M.; Joshi, A.; Devous, M.; Mintun, M. Regional Profiles of the Candidate tau PET Ligand 18F-AV-1451 Recapitulate Key Features of Braak Histopathological Stages. *Brain* **2016,** *139,* 1539–1550.
280. Vermeiren, C.; Mercier, J.; Viot, D.; Mairet-Coello, G.; Hannestad, J.; Courade, J.-P.; Citron, M.; Gillard, M. T807, a Reported Selective Tau Tracer, Binds With Nanomolar Affinity to Monoamine Oxidase a. *Alzheimers Dement.* **2015,** *15* (7 supplement), 283.
281. Marquié, M. N. M.; Vanderburg, C.; Costantino, I.; Bien, E.; Rycyna, L.; Klunk, W.; Mathis, C.; Ikonomovic, M.; Debnath, M.; Vasdev, N.; Dickerson, B.; Gomperts, S.; Growdon, J.; Johnson, K.; Frosch, M.; Hyman, B.; Gómez-Isla, T. Validating Novel Tau Positron Emission Tomography Tracer [F-18]-AV-1451 (T807) on Postmortem Brain Tissue. *Ann. Neurol.* **2015,** *78* (5), 787–800.
282. Bohorquez, S. Quantification, Test-retest and Dosimetry of the Novel Genentech Tau Probe 1, [18F]GTP1. *Human Amyloid Imaging Meeting, Miami*.
283. Wong, D.; Borroni, E.; Kuwabara, H.; George, N.; Rosenberg, P.; Lyketsos, C.; Resnick, S.; Thambisetty, M.; Brasic, J.; Gapasin, L.; Willis, W.; Knust, H.; Guerard, M.; Belli, S.; Muri, D.; Carey, T.; Bedding, A.; Wandel, C.; Hansrod, T.; Honer, M.; Moghekar, A.; Boess, F.; Albert, M.; Shaya, E.; Oh, E.; Ostrowitzki, S.; Dannals, R.; Comley, R. First In-Human PET Study of 3 Novel Tau Radiopharmaceuticals: [11C]RO6924963, [11C]RO6931643, and [18F]RO6958948. *Alzheimers Dement.* **2015,** *11* (7 supplement), P850–P851.
284. Wong, D. Clinical Evaluation of [18F]RO6958948, a New Radioligand for Imaging Tau Pathology in AD. *Human Amyloid Imaging Meeting, Miami*.
285. Vernon, A.; Ballard, C.; Modo, M. Neuroimaging for Lewy Body Disease: Is the In Vivo Molecular Imaging of α-Synuclein Neuropathology Required and Feasible? *Brain Res. Rev.* **2010,** *65* (1), 28–55.
286. Shah, M.; Seibyl, J.; Cartier, A.; Bhatt, R.; Catafau, A. Molecular Imaging Insights Into Neurodegeneration: Focus on α-Synuclein Radiotracers. *J. Nucl. Med.* **2014,** *55* (9), 1397–1400.
287. Alpha-Synuclein Imaging Prize. https://www.michaeljfox.org/research/imaging-prize.html.
288. Bagchi, D.; Yu, L.; Perlmutter, J.; Xu, J.; Mach, R.; Tu, Z.; Kotzbauer, P. Binding of the Radioligand SIL23 to α-Synuclein Fibrils in Parkinson Disease Brain Tissue Establishes Feasibility and Screening Approaches for Developing a Parkinson Disease Imaging Agent. *PLoS One* **2013,** *8* (2). e55031.
289. Phase 1 Study of NPT200-11 in Healthy Subjects (NCT02606682). https://clinicaltrials.gov/ct2/show/study/NCT02606682?view=record.
290. Multiple Ascending Dose Study of PRX002 in Patients With Parkinson's Disease (NCT02157714). https://clinicaltrials.gov/ct2/show/NCT02157714?term=prothena&rank=7.
291. Tredwell, M.; Gouverneur, V. 18F Labeling of Arenes. *Angew. Chem. Int. Ed. Engl.* **2012,** *51* (46), 11426–11437.
292. Brooks, A.; Topczewski, J.; Ichiishi, N.; Sanford, M.; Scott, P. Late-Stage [18F]Fluorination: New Solutions to Old Problems. *Chem. Sci.* **2014,** *5* (12), 4545–4553.
293. Preshlock, S.; Tredwell, M.; Gouverneur, V. (18)F-Labeling of Arenes and Heteroarenes for Applications in Positron Emission Tomography. *Chem. Rev.* **2016,** *116* (2), 719–766.
294. Lee, E.; Kamlet, A.; Powers, D.; Neumann, C.; Boursalian, G.; Furuya, T.; Choi, D.; Hooker, J.; Ritter, T. A Fluoride-Derived Electrophilic Late-Stage Fluorination Reagent for PET Imaging. *Science* **2011,** *334* (6056), 639–642.
295. Lee, E.; Hooker, J.; Ritter, T. Nickel-Mediated Oxidative Fluorination for PET With Aqueous [18F] Fluoride. *J. Am. Chem. Soc.* **2012,** *134* (42), 17456–17458.
296. Tredwell, M.; Preshlock, S.; Taylor, N.; Gruber, S.; Huiban, M.; Passchier, J.; Mercier, J.; Génicot, C.; Gouverneur, V. A General Copper-Mediated Nucleophilic 18F Fluorination of Arenes. *Angew. Chem. Int. Ed. Engl.* **2014,** *53* (30), 7751–7755.
297. Ichiishi, N.; Brooks, A.; Topczewski, J.; Rodnick, M.; Sanford, M.; Scott, P. Copper-Catalyzed [18F]Fluorination of (Mesityl)(Aryl)Iodonium Salts. *Org. Lett.* **2014,** *16* (12), 3224–3227.
298. Preshlock, S.; Calderwood, S.; Verhoog, S.; Tredwell, M.; Huiban, M.; Hienzsch, A.; Gruber, S.; Wilson, T.; Taylor, N.; Cailly, T.; Schedler, M.; Collier, T.; Passchier, J.; Smits, R.; Mollitor, J.; Hoepping, A.; Mueller, M.; Genicot, C.; Mercier, J.; Gouverneur, V. Enhanced Copper-Mediated (18)F-Fluorination of Aryl Boronic Esters Provides Eight Radiotracers for PET Applications. *Chem. Commun. (Camb.)* **2016,** *52* (54), 8361–8364.
299. Scott, A.; Wolchok, J.; Old, L. Antibody Therapy of Cancer. *Nat. Rev. Cancer* **2012,** *12* (4), 278–287.
300. Pedersen, J.; Sigurdsson, E. Tau Immunotherapy for Alzheimer's Disease. *Trends Mol. Med.* **2015,** *21* (6), 394–402.
301. Wisniewski, T.; Goñi, F. Immunotherapeutic Approaches for Alzheimer's Disease. *Neuron* **2015,** *85* (6), 1162–1176.
302. Keizer, R.; Huitema, A.; Schellens, J.; Beijnen, J. Clinical Pharmacokinetics of Therapeutic Monoclonal Antibodies. *Clin. Pharmacokinet.* **2010,** *49* (3), 493–507.
303. Tinianow, J.; Gill, H.; Ogasawara, A.; Flores, J.; Vanderbilt, A.; Luis, E.; Vandlen, R.; Darwish, M.; Junutula, J.; Williams, S.; Marik, J. Site-Specifically 89Zr-Labeled Monoclonal Antibodies for ImmunoPET. *Nucl. Med. Biol.* **2010,** *37* (3), 289–297.

304. Freise, A.; Wu, A. In Vivo Imaging With Antibodies and Engineered Fragments. *Mol. Immunol.* **2015,** *67* (2 Pt A), 142–152.
305. Schirrmacher, R.; Bernard-Gauthier, V.; Reader, A.; Soucy, J.; Schirrmacher, E.; Wängler, B.; Wängler, C. Design of Brain Imaging Agents for Positron Emission Tomography: Do Large Bioconjugates Provide an Opportunity for In Vivo Brain Imaging? *Future Med. Chem.* **2013,** *5* (14), 1621–1634.
306. Sehlin, D.; Fang, X.; Cato, L.; Antoni, G.; Lannfelt, L.; Syvänen, S. Antibody-Based PET Imaging of Amyloid Beta in Mouse Models of Alzheimer's Disease. *Nat. Commun.* **2016,** *7,* 10759.
307. Fissers, J.; Waldron, A.; De Vijlder, T.; Van Broeck, B.; Pemberton, D.; Mercken, M.; Van Der Veken, P.; Joossens, J.; Augustyns, K.; Dedeurwaerdere, S.; Stroobants, S.; Staelens, S.; Wyffels, L. Synthesis and Evaluation of a Zr-89-Labeled Monoclonal Antibody for Immuno-PET Imaging of Amyloid-β Deposition in the Brain. *Mol. Imaging Biol.* **2016,** *18* (4), 598–605.
308. Krishnaswamy, S.; Lin, Y.; Rajamohamedsait, W.; Rajamohamedsait, H.; Krishnamurthy, P.; Sigurdsson, E. Antibody-Derived In Vivo Imaging of Tau Pathology. *J. Neurosci.* **2014,** *34* (50), 16835–16850.
309. Houghton, J.; Zeglis, B.; Abdel-Atti, D.; Sawada, R.; Scholz, W.; Lewis, J. Pretargeted Immuno-PET of Pancreatic Cancer: Overcoming Circulating Antigen and Internalized Antibody to Reduce Radiation Doses. *J. Nucl. Med.* **2016,** *57* (3), 453–459.
310. Altai, M.; Perols, A.; Tsourma, M.; Mitran, B.; Honarvar, H.; Robillard, M.; Rossin, R.; ten Hoeve, W.; Lubberink, M.; Orlova, A.; Karlström, A.; Tolmachev, V. Feasibility of Affibody-Based Bioorthogonal Chemistry-Mediated Radionuclide Pretargeting. *J. Nucl. Med.* **2016,** *57* (3), 431–436.
311. Gauberti, M.; Montagne, A.; Quenault, A.; Vivien, D. Molecular Magnetic Resonance Imaging of Brain-Immune Interactions. *Front. Cell. Neurosci.* **2014,** *27* (8), 389.
312. Pulli, B.; Chen, J. Imaging Neuroinflammation—From Bench to Bedside. *J. Clin. Cell. Immunol.* **2014,** *5,* 226.
313. Buscombe, J. PET Imaging of Inflammation. *Q. J. Nucl. Med. Mol. Imaging* **2014,** *58* (3), 284–289.
314. Tarkin, J.; Joshi, F.; Rudd, J. PET Imaging of Inflammation in Atherosclerosis. *Nat. Rev. Cardiol.* **2014,** *11* (8), 443–457.
315. Vivash, L.; O'Brien, T. Imaging Microglial Activation with TSPO PET: Lighting Up Neurologic Diseases? *J. Nucl. Med.* **2016,** *57* (2), 165–168.
316. Horti, A.; Gao, Y.; Ravert, H.; Finley, P.; Valentine, H.; Wong, D.; Endres, C.; Savonenko, A.; Dannals, R. Synthesis and Biodistribution of [11C]A-836339, a New Potential Radioligand for PET Imaging of Cannabinoid Type 2 Receptors (CB2). *Bioorg. Med. Chem.* **2010,** *18* (14), 5202–5207.
317. Slavik, R.; Herde, A.; Bieri, D.; Weber, M.; Schibli, R.; Krämer, S.; Ametamey, S.; Mu, L. Synthesis, Radiolabeling and Evaluation of Novel 4-oxo-Quinoline Derivatives as PET Tracers for Imaging Cannabinoid Type 2 Receptor. *Eur. J. Med. Chem.* **2015,** *92,* 554–564.
318. Tietz, O.; Marshall, A.; Wuest, M.; Wang, M.; Wuest, F. Radiotracers for Molecular Imaging of Cyclooxygenase-2 (COX-2) Enzyme. *Curr. Med. Chem.* **2013,** *30* (35), 4350–4369.
319. Wang, C.; Placzek, M.; Van de Bittner, G.; Schroeder, F.; Hooker, J. A Novel Radiotracer for Imaging Monoacylglycerol Lipase in the Brain Using Positron Emission Tomography. *ACS Chem. Neurosci.* **2016,** *7* (4), 484–489.
320. Esposito, G.; Giovacchini, G.; Liow, J.; Bhattacharjee, A.; Greenstein, D.; Schapiro, M.; Hallett, M.; Herscovitch, P.; Eckelman, W.; Carson, R.; Rapoport, S. Imaging Neuroinflammation in Alzheimer's Disease With Radiolabeled Arachidonic Acid and PET. *J. Nucl. Med.* **2008,** *49* (9), 1414–1421.
321. Pichika, R.; Taha, A.; Gao, F.; Kotta, K.; Cheon, Y.; Chang, L.; Kiesewetter, D.; Rapoport, S.; Eckelman, W. The Synthesis and In Vivo Pharmacokinetics of Fluorinated Arachidonic Acid: Implications for Imaging Neuroinflammation. *J. Nucl. Med.* **2012,** *53* (9), 1383–1391.
322. Gao, M.; Wang, M.; Green, M.; Hutchins, G.; Zheng, Q. Synthesis of [(11)C]GSK1482160 as a New PET Agent for Targeting P2X(7) Receptor. *Bioorg. Med. Chem. Lett.* **2015,** *25* (9), 1965–1970.
323. Janssen, B.; Vugts, D.; Funke, U.; Spaans, A.; Schuit, R.; Kooijman, E.; Rongen, M.; Perk, L.; Lammertsma, A.; Windhorst, A. Synthesis and Initial Preclinical Evaluation of the P2X7 Receptor Antagonist [^{11}C]A-740003 as a Novel Tracer of Neuroinflammation. *J. Label. Compd. Radiopharm.* **2014,** *57* (8), 509–516.
324. Matusiak, N.; van Waarde, A.; Bischoff, R.; Oltenfreiter, R.; van de Wiele, C.; Dierckx, R.; Elsinga, P. Probes for Non-Invasive Matrix Metalloproteinase-Targeted Imaging With PET and SPECT. *Curr. Pharm. Des.* **2013,** *19* (25), 4647–4672.
325. Beaino, W.; Anderson, C. PET Imaging of Very Late Antigen-4 in Melanoma: Comparison of 68Ga- and 64Cu-Labeled NODAGA and CB-TE1A1P-LLP2A Conjugates. *J. Nucl. Med.* **2014,** *55* (11), 1856–1863.
326. Nahrendorf, M.; Keliher, E.; Panizzi, P.; Zhang, H.; Hembrador, S.; Figueiredo, J.; Aikawa, E.; Kelly, K.; Libby, P.; Weissleder, R. 18F-4V for PET-CT Imaging of VCAM-1 Expression in Atherosclerosis. *JACC Cardiovasc. Imaging* **2009,** *2* (10), 1213–1222.
327. Webster, J.; Morton, C.; Johnson, B.; Yang, H.; Rishel, M.; Lee, B.; Miao, Q.; Pabba, C.; Yapp, D.; Schaffer, P. Functional Imaging of Oxidative Stress With a Novel PET Imaging Agent, 18F-5-Fluoro-L-Aminosuberic Acid. *J. Nucl. Med.* **2014,** *55* (4), 657–664.
328. Owen, D.; Yeo, A.; Gunn, R.; Song, K.; Wadsworth, G.; Lewis, A.; Rhodes, C.; Pulford, D.; Bennacef, I.; Parker, C.; StJean, P.; Cardon, L.; Mooser, V.; Matthews, P.; Rabiner, E.; Rubio, J. An 18-kDa Translocator Protein (TSPO) Polymorphism Explains Differences in Binding Affinity of the PET Radioligand PBR28. *J. Cereb. Blood Flow Metab.* **2012,** *32* (1), 1–5.
329. Turkheimer, F.; Rizzo, G.; Bloomfield, P.; Howes, O.; Zanotti-Fregonara, P.; Bertoldo, A.; Veronese, M. The Methodology of TSPO Imaging With Positron Emission Tomography. *Biochem. Soc. Trans.* **2015,** *43* (4), 586–592.
330. Gulyás, B.; Pavlova, E.; Kása, P.; Gulya, K.; Bakota, L.; Várszegi, S.; Keller, E.; Horváth, M.; Nag, S.; Hermecz, I.; Magyar, K.; Halldin, C. Activated MAO-B in the Brain of Alzheimer Patients, Demonstrated by [11C]-L-Deprenyl Using Whole Hemisphere Autoradiography. *Neurochem. Int.* **2011,** *58* (1), 60–68.
331. Fowler, J.; Logan, J.; Volkow, N.; Wang, G. Translational Neuroimaging: Positron Emission Tomography Studies of Monoamine Oxidase. *Mol. Imaging Biol.* **2005,** *7* (6), 377–387.
332. Vasdev, N.; Sadovski, O.; Moran, M.; Parkes, J.; Meyer, J.; Houle, S.; Wilson, A. Development of New Radiopharmaceuticals for Imaging Monoamine Oxidase B. *Nucl. Med. Biol.* **2011,** *38* (7), 933–943.
333. Fowler, J.; Wang, G.; Logan, J.; Xie, S.; Volkow, N.; MacGregor, R.; Schlyer, D.; Pappas, N.; Alexoff, D.; Patlak, C.; et al. Selective Reduction of Radiotracer Trapping by Deuterium Substitution: Comparison of Carbon-11-L-Deprenyl and Carbon-11-Deprenyl-D2 for MAO B Mapping. *J. Nucl. Med.* **1995,** *36* (7), 1255–1262.
334. Nag, S.; Varrone, A.; Tóth, M.; Thiele, A.; Kettschau, G.; Heinrich, T.; Lehmann, L.; Halldin, C. In Vivo Evaluation in Cynomolgus Monkey Brain and Metabolism of [^{18}F] Fluorodeprenyl: A new MAO-B pet Radioligand. *Synapse* **2012,** *66* (4), 323–330.
335. Nag, S.; Lehmann, L.; Kettschau, G.; Heinrich, T.; Thiele, A.; Varrone, A.; Gulyas, B.; Halldin, C. Synthesis and Evaluation of [^{18}F]Fluororasagiline, a Novel Positron Emission Tomography (PET) Radioligand for Monoamine Oxidase B (MAO-B). *Bioorg. Med. Chem.* **2012,** *20* (9), 3065–3071.
336. Nag, S.; Lehmann, L.; Kettschau, G.; Toth, M.; Heinrich, T.; Thiele, A.; Varrone, A.; Halldin, C. Development of a Novel Fluorine-18 Labeled Deuterated Fluororasagiline ([(18)F] Fluororasagiline-D2) Radioligand for PET Studies of Monoamino Oxidase B (MAO-B). *Bioorg. Med. Chem.* **2013,** *21* (21), 6634–6641.
337. Savonenko, A.; Melnikova, T.; Wang, Y.; Ravert, H.; Gao, Y.; Koppe, I.; Lee, D.; Pletnikova, O.; Cho, E.; Sayyida, N.; Hiatt, A.; Troncoso, J.; Davies, P.; Dannals, R.; Pomper, M.; Horti, A. Cannabinoid CB2 Receptors in a Mouse Model of Aβ Amyloidosis: Immunohistochemical Analysis and Suitability as a PET Biomarker of Neuroinflammation. *PLoS One* **2015,** *10* (6). e0129618.
338. Evens, N.; Bosier, B.; Lavey, B.; Kozlowski, J.; Vermaelen, P.; Baudemprez, L.; Busson, R.; Lambert, D.; Van Laere, K.; Verbruggen, A.; Bormans, G. Labelling and Biological Evaluation of [(11)C]Methoxy-Sch225336: A Radioligand for the Cannabinoid-Type 2 Receptor. *Nucl. Med. Biol.* **2008,** *35* (7), 793–800.
339. Di Virgilio, F. P2X Receptors and Inflammation. *Curr. Med. Chem.* **2015,** *22* (7), 866–877.
340. Sáez-Orellana, F.; Godoy, P.; Silva-Grecchi, T.; Barra, K.; Fuentealba, J. Modulation of the Neuronal Network Activity by P2X Receptors and Their Involvement in Neurological Disorders. *Pharmacol. Res.* **2015,** *101,* 109–115.
341. Ory, D.; Celen, S.; Gijsbers, R.; Van Den Haute, C.; Postnov, A.; Koole, M.; Vandeputte, C.; Andrés, J.; De Angelis, M.; Langlois, X.; Bhattacharya, A.; Schmidt, M.; Alcazar, J.; Vanduffel, W.; Letavic, M.; Van Laere, K.; Verbruggen, A.; Debyser, Z.; Bormans, G. Preclinical Evaluation of a P2X7 Receptor Selective Radiotracer: PET Studies in a Rat Model With Local Overexpression of the Human P2X7 Receptor and in Non-Human Primates. *J. Nucl. Med.* **2016,** *57,* 1436–1441.

342. Wang, X.; Tan, M.; Yu, J.; Tan, L. Matrix Metalloproteinases and Their Multiple Roles in Alzheimer's Disease. *Biomed. Res. Int.* **2014,** *2014,* 908636.
343. Yang, Y.; Rosenberg, G. Matrix Metalloproteinases as Therapeutic Targets for Stroke. *Brain Res.* **1623,** *2015,* 30–38.
344. Wagner, S.; Breyholz, H.; Höltke, C.; Faust, A.; Schober, O.; Schäfers, M.; Kopka, K. A New 18F-Labelled Derivative of the MMP Inhibitor CGS 27023A for PET: Radiosynthesis and Initial Small-Animal PET Studies. *Appl. Radiat. Isot.* **2009,** *67* (4), 606–610.
345. Neumann, J.; Riek-Burchardt, M.; Herz, J.; Doeppner, T.; König, R.; Hütten, H.; Etemire, E.; Männ, L.; Klingberg, A.; Fischer, T.; Görtler, M.; Heinze, H.; Reichardt, P.; Schraven, B.; Hermann, D.; Reymann, K.; Gunzer, M. Very-Late-Antigen-4 (VLA-4)-Mediated Brain Invasion by Neutrophils Leads to Interactions With Microglia, Increased Ischemic Injury and Impaired Behavior in Experimental Stroke. *Acta Neuropathol.* **2015,** *129* (2), 259–277.
346. Bridges, R.; Lutgen, V.; Lobner, D.; Baker, D. Thinking Outside the Cleft to Understand Synaptic Activity: Contribution of the Cystine-Glutamate Antiporter (System xc-) to Normal and Pathological Glutamatergic Signaling. *Pharmacol. Rev.* **2012,** *64* (3), 780–802.
347. Antunes, I.; Doorduin, J.; Haisma, H.; Elsinga, P.; van Waarde, A.; Willemsen, A.; Dierckx, R.; de Vries, E. 18F-FEAnGA for PET of β-Glucuronidase Activity in Neuroinflammation. *J. Nucl. Med.* **2012,** *53* (3), 451–458.
348. den Hollander, M.; Bensch, F.; Glaudemans, A.; Oude Munnink, T.; Enting, R.; den Dunnen, W.; Heesters, M.; Kruyt, F.; Lub-de Hooge, M.; Cees de Groot, J.; Pearlberg, J.; Gietema, J.; de Vries, E.; Walenkamp, A. TGF-β Antibody Uptake in Recurrent High-Grade Glioma Imaged With 89Zr-Fresolimumab PET. *J. Nucl. Med.* **2015,** *56* (9), 1310–1314.
349. Hoffman, J.; Gambhir, S.; Kelloff, G. Regulatory and Reimbursement Challenges for Molecular Imaging. *Radiology* **2007,** *245* (3), 645–660.
350. Herscovitch, P. Regulatory Approval and Insurance Reimbursement: The Final Steps in Clinical Translation of Amyloid Brain Imaging. *Clin. Transl. Imaging* **2015,** *3,* 75–77.
351. Jacques, L.; Syrek Jensen, T.; Rollins, J.; Burton Coachman, B.; Caplan, S.; Hakim, R.; Roche, J.; Hutter, J. *Decision Memo for Beta Amyloid Positron Emission Tomography in Dementia and Neurodegenerative Disease (CAG-00431 N).* CMS.Gov Center for Medicare & Medicaid Services. https://www.cms.gov/medicare-coverage-database/details/nca-decision-memo.aspx?NCAId=265, 2013

7.03 Progress in the Discovery of Ca Channel Blockers for the Treatment of Pain

P Beswick, Sussex Drug Discovery Centre, University of Sussex, Brighton, United Kingdom

© 2017 Elsevier Ltd. All rights reserved.

7.03.1	**Introduction**	65
7.03.2	**Voltage-Gated Calcium Channels—Structure and Function**	66
7.03.2.1	Channel Subtypes	66
7.03.2.2	Channel Structure	66
7.03.2.3	Channel Distribution and Function	66
7.03.3	**Target Validation**	68
7.03.4	**Mechanism of Action**	69
7.03.5	**Inhibitors of Voltage-Gated Calcium Channels**	70
7.03.5.1	Compounds Under Clinical Evaluation	70
7.03.5.1.1	Z160	70
7.03.5.1.2	CNV2197944	70
7.03.5.1.3	ABT-639	71
7.03.5.1.4	Z944	72
7.03.5.1.5	Ethosuximide	72
7.03.5.1.6	Microgabalin	72
7.03.5.2	Cav2.1 Inhibitors	72
7.03.5.2.1	Nomenclature	72
7.03.5.2.2	Target validation	72
7.03.5.2.3	Compounds known to inhibit Cav2.1	73
7.03.5.3	Cav2.2 Inhibitors	75
7.03.5.3.1	Early inhibitors	76
7.03.5.3.2	Small-molecule blockers based on peptide toxin structures	76
7.03.5.3.3	Arylthiazolidinediones	79
7.03.5.3.4	Dihydropyridines	80
7.03.5.3.5	Diarylmethylpiperazines	81
7.03.5.3.6	Sulfones and sulfonamides	89
7.03.5.3.7	Indole-derived structures	96
7.03.5.3.8	Miscellaneous templates	98
7.03.5.4	Cav2.3 Blockers	99
7.03.5.5	Cav3 Blockers	100
7.03.5.5.1	Early molecules	100
7.03.5.5.2	Sulfonamides	100
7.03.5.5.3	Piperidine- and piperazine-based structures	103
7.03.5.5.4	Piperazines and homopiperazines	109
7.03.5.5.5	Pyridyl amides	110
7.03.5.5.6	Quinazoline derivatives	111
7.03.5.5.7	Dihydropyridine derivatives	113
7.03.5.5.8	Indoles	113
7.03.5.5.9	Dihydroquinazolines	113
7.03.5.5.10	Miscellaneous chemotypes disclosed only in the patent literature	114
7.03.5.6	Alpha 2 Delta Ligands	114
7.03.5.6.1	Amino acid-derived structures	114
7.03.5.6.2	Gababutins	118
7.03.5.6.3	Nonamino acid structures	120
7.03.6	**Conclusion**	122
References		123

7.03.1 Introduction

In the last decade there has been a large increase in drug discovery projects focussed on voltage-gated ion channel targets fuelled by a combination of factors including the development of new technologies which allow rapid screening.[1–3] The discovery of highly potent and selective peptide toxins, which have allowed improved target validation both preclinically and in certain cases

clinically[4,5] and through advances in genetics which have provided further target validation. The identification of channelopathies not only serves as excellent target validation but also offers the potential of a personalized medicine approach to the treatment of disease.[6] All of these advances have enabled successful drug discovery programs in the voltage-gated calcium channel field, and there is now a highly selective and efficacious agent in clinical use which acts through inhibition of Cav2.2 channels and is derived from a snail toxin.[7] Additionally a number of small-molecule inhibitors have entered clinical stages of development (Section "Compounds Under Clinical Evaluation") which have added to a class of older drugs, gabapentin and pregabalin, which were previously thought to act via another target but in recent years have been shown to be ligands of voltage-gated calcium channels.

In recent years there have been many excellent reviews covering the medicinal chemistry,[8–13] biology,[14–19] structure,[20,21] patents,[22] and clinical efficacy of calcium channel blockers.[23–26] This article will focus on medicinal chemistry advances in the field over the last 10 years.

Voltage-gated calcium channels are expressed predominantly on nerve and muscle cells, the channels as their name suggests, react to changes in the potential of the cell membrane allowing calcium ions to enter the cells. This results in an increase of the calcium concentration in the cytoplasm initiating a number of key biochemical processes which include hormone secretion, neurotransmitter release, and gene transcription.[27] Due to the key role in facilitating calcium entry into cells the voltage-gated calcium channel family has a rich pharmacology, and for certain channels there is strong disease association and consequently been the focus of drug discovery groups for many years. Recent genetic data[28–31] has both reinforced existing disease association and highlighted new potential therapeutic indications and current interest in this family of proteins is therefore very high. It is important to note that the genetic studies highlight changes in calcium channel function in a number of disorders many of which are not pain indications. For the Medicinal Chemist voltage-gated calcium channels have proved to be highly tractable to small-molecule drug discovery with a number of agents in widespread clinical use and others at various stages of clinical development. Marketed agents are currently used to treat a number of important clinical indications including hypertension, pain, and epilepsy. Disease association studies reported to date highlight the potential in a broad spectrum of disorders. This article will focus only on progress in the area of pain including migraine but will not cover progress in other therapeutic areas.

7.03.2 Voltage-Gated Calcium Channels—Structure and Function

7.03.2.1 Channel Subtypes

Voltage-Gated calcium channels were originally classified in terms of the voltage required to activate them, and two distinct classes were described, namely, low voltage activated (now known as T-type channels) and high voltage activated (L, P/Q-, N-, and R-type channels).[32] Subsequently with the identification of small-molecule ligands the pharmacology was investigated resulting in the further classification of channel subtypes.[33] The first selective pharmacological agents identified were those which targeted the L-type family which was given the name due to the large conductance observed when the channel is open. The discovery of peptide natural products largely derived from cone snail and spider toxins allowed the current classification of the channel family to be established with the identification of peptide ligands which were selective for channel subtypes.[4] Current nomenclature classifies voltage-gated calcium channels according to the subunits which form the pore of the channel of the so-called Cavα1 subunits. Currently 10 distinct channels have been identified. The L-type family comprises four subtypes (Cav1.1–Cav1.4); the T-type family comprises three (Cav3.1–Cav3.3); and for the P/Q (Cav2.1), N- (Cav2.2), and R-type (Cav2.3) families there is currently only one member known.[18] Each Cavα1 subunit is encoded by a distinct gene CACNA1A-S.

7.03.2.2 Channel Structure

All of the channels possess the same general structure,[18,34] each consisting of a pore forming unit (α1) and in some cases combinations of regulatory or auxiliary units (β and α2δ). The α1 unit determines the general functional characteristics of the channel, including pharmacology, voltage dependence, and conductivity; the auxiliary units can play a role in these too and additionally affect other processes such as trafficking. Functional channels are classified according to their α1 subunit of which currently 10 are known, each one being encoded by a distinct CACNA1 gene. Additionally the α2δ subunits are encoded by four distinct genes CACNA2D1-4. To date a number of distinct binding sites for different classes of drugs have been identified both on the α1 subunits and on the α2δ unit.[35–37] For the currently known subtypes each channel has a different expression profile and function which is described in the following section. Specific sites on the channels which bind different classes of drugs have been identified (Fig. 1). Most bind to sites on the α1 subunit although one class of drug has been shown to bind to the α2δ subunit.[37] Voltage-gated calcium channel structures have been known and publically available to medicinal chemists for a number of years but as yet there are no reports of ligands that have been designed using the available structural information. Channel structure has been thoroughly reviewed in recent articles[18,34] and will not be covered in detail in this article.

7.03.2.3 Channel Distribution and Function

Voltage-gated channels are widely distributed throughout the central nervous system and peripheral tissues and play a diverse array of physiological roles (Table 1). Nine of the 10 voltage-gated calcium channels subtypes are highly expressed either in the brain or

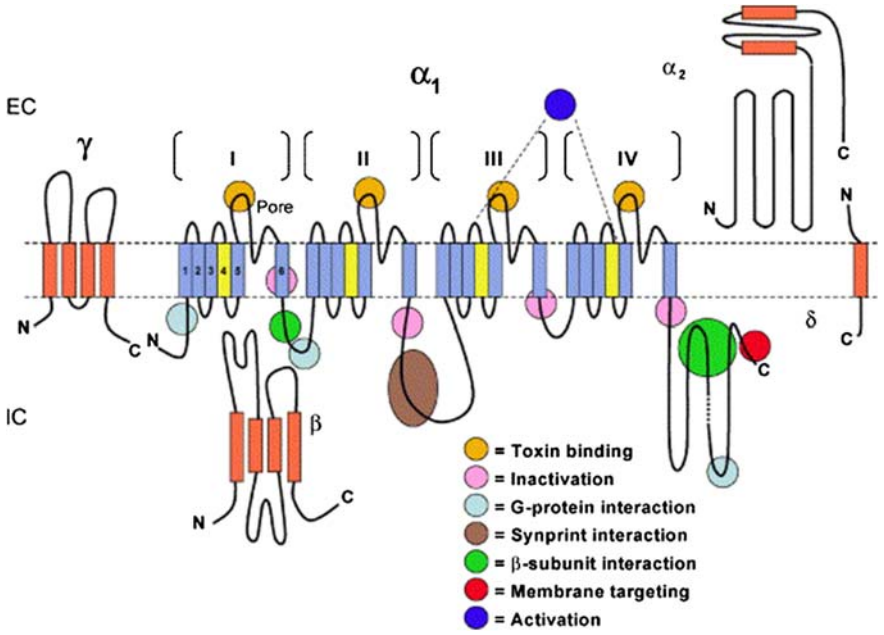

Fig. 1 Structure of voltage-gated calcium channels.

Table 1 Tissue distribution of voltage-gated calcium channels

Channel family	*Channel subtype*	*Gene*	*Tissue distribution*
L type	Cav1.1	CACNA1S	Skeletal muscle (high) Brain (low)
	Cav1.2	CACNA1C	Heart (ventricular muscle), smooth muscle, brain, and secretory cells
	Cav1.3	CACNA1D	Heart (sino atrial node) Ear (inner hair cells)
	Cav1.4	CACNA1F	Retina
P/Q type	Cav2.1	CACNA1A	Brain (high in cerebellum) and presynaptic nerve terminals
N type	Cav2.2	CACNA1B	Central and peripheral nervous system
R type	Cav2.3	CACNA1E	Brain
T type	Cav3.1	CACNA1G	Cardiac muscle, skeletal muscle, and neurons
	Cav3.2	CACNA1H	Cardiac muscle, neurons
	Cav3.3	CACNA1I	Neurons

on the neuronal tissue and with the exception of some members of the L-type family all are involved in sensory processing and are therefore potential targets for the development of new analgesic agents.

P/Q-type channels are best characterized for their role in migraine[31] and less so in other types of pain signaling. P/Q channels are widely expressed on presynaptic nerve terminal in the CNS where they have been shown to regulate neurotransmitter release. Their role in pain signaling associated with migraine comes from studies which provide strong evidence that activation of P/Q channels is a key process in neurotransmitter release, particularly glutamate in cortical and trigeminal neurons during certain migraine attacks.[38] N-type channels are highly expressed on presynaptic nerve terminals, when activated they trigger the release of key neurotransmitters which are well-characterized mediators of pain signaling including calcitonin gene-related peptide (CGRP), substance P and glutamate.[39] It has also been well characterized that opiate analgesics exert their effect on neurotransmitter release through indirectly blocking N-type calcium channel activity on stimulation of presynaptic opiate receptors.[40] R-type channels are perhaps the least well-understood member of the family, particularly regarding how their function is implicated in pain signaling. Their biophysical profile is the closest to that of the T-type family, suggesting a role in neuroexcitability. R-type channels have been shown to be expressed in Dorsal Root Ganglion (DRG) neurons and to control the release of neurotransmitters which strongly implicates them in pain signaling.[41]

T-type channels have very different biophysical characteristics compared to other family members, they are activated at lower voltages which positions them in the ideal range to regulate neuronal excitability which is supported by studies that have implicated them in processes linked to epilepsy. Neuronal excitability is also closely associated with pain signaling particularly in individuals with neuropathic pain conditions. Cav3.2 channels have also been shown to be expressed on primary afferent nerves further supporting the role of T-type channels in pain signaling.[42]

All of the channel subtypes have an associated α2δ subunit. These subunits play a role on modulating channel function. The mechanism of this modulation has been the subject of debate for many years and has only recently been established.[43] The mechanism is discussed in Section "Alpha 2 Delta Ligands."

7.03.3 Target Validation

Voltage-gated calcium channels are perhaps among the most highly validated pain targets. For certain channel subtypes there is either direct clinical target validation or strong genetic association. Table 2 summarizes the clinical and genetic target validation data currently available. For all families, with the exception of L-type channels, strong preclinical target validation packages are published. These have been enabled in many cases by the availability of highly potent and selective channel ligands isolated from animal toxins. It is important to note that the validity of preclinical validation for pain targets has in recent years been called into question largely due to the high failure rate of compounds in clinical trials which had previously demonstrated encouraging data in preclinical models. Table 2 summarizes preclinical target validation data currently available.

The most highly validated channel subtype is Cav2.2 for which there is a peptide channel blocker ziconotide, currently on the market.[7] The success of ziconotide prompted huge interest among the drug discovery community and has resulted in a large number of structurally diverse small-molecule blockers being identified, some of which are currently under clinical investigation.[8] It is also worth noting that opiate analgesics indirectly inhibit Cav2.2 function through stimulation of opiate receptors on presynaptic nerve terminals thus adding strength to the direct target validation data.[40]

Of some concern however is that one small-molecule Cav2.2 blocker Z160 has recently been reported to have failed to show any analgesic efficacy in two phase 2 studies; one in patients with diabetic neuropathy and a second in patients with lumbosacral radiculopathy (LSR)[14] where ziconotide has been reported to show excellent analgesic efficacy in a number of clinical studies.[7] This recent observation potentially asks a question about the exact nature of channel inhibition required for optimal analgesic efficacy, and it will be interesting to see how compounds currently in clinical evaluation perform in similar studies (Section "Compounds Under Clinical Evaluation").

Cav2.1 is strongly implicated in the pathology of migraine in particular a rare condition known as familial hemiplegic migraine 1 (FHM1) which is associated with gain of function mutations of the CACNA1A gene.[44] The genetic evidence is further supported by the fact that a number of drugs which show clinical efficacy in patients with FHM1 such as flunarizine[45] and verapamil[47] also have activity at Cav2.1 channels; however it is important to note that the clinical agents tested are not selective. It has also been shown that the extracts from medicinal plants such as feverfew or butterbur which show efficacy in treating various forms of migraine contain compounds which inhibit the Cav2.1 channel. However similar to the drugs which have demonstrated clinical efficacy, these compounds are not selective.[48] In contrast to the high level of target validation in migraine the same is not true for other pain modalities where validation is limited to preclinical studies.

Cav2.3 remains largely unexplored compared with other voltage-gated channel family members, and any target validation reported is limited to preclinical studies with a selective peptide ligand.

The T-type family has some limited and also confusing human genetic data which has recently been published.[46] A single patient was reported to have a loss of function mutation of the CACNA1H gene which resulted in a phenotype characterized by chronic pain and absence seizures. This observation is in contrast to preclinical knockout studies which result in reduced sensitivity.[49] Before any firm conclusions can be reached it is important to identify further individuals with altered Cav3.2 function. In addition to the genetic data a recent failed clinical study with a small-molecule Cav3.2 blocker ABT-639 failed to produce efficacy.[50,51]

In addition to selective modulation of specific channel subtypes it is important to highlight that agents which bind to the α2δ subunit also show clinical efficacy particularly in neuropathic pain. Gabapentin and pregabalin are both currently marketed for the treatment of neuropathic pain and exert their effect through this site.[52,53]

The genetic and clinical target validation is further supported by preclinical data in rodents which have either been genetically modified or have pain phenotypes modified by treatment with selective tool compounds.[12] The availability of selective tool compounds isolated from animal toxins has enabled many of these studies.[4] The validity of animal pain models has been called into question recently,[54–56] given the poor translation of preclinical data into the clinical setting and given the high level of clinical

Table 2 Clinical and genetic target validation data

Channel family	*Channel subtype*	*Gene*	*Validation*	*Observation*	*Reference*
P/Q type	Cav2.1	CACNA1A	Genetic association	Gain on function mutation linked to Familial Hemiplegic Migraine	44
			Clinical data	Agents with Cav21.1 inhibitory activity have shown clinical efficacy	45
N type	Cav2.2	CACNA1B	Clinical data with Ziconotide	Efficacy demonstrated in multiple pain states including those intractable to opiate therapy	7
T type	Cav3.2	CACNA1H	Genetic association	Single person identified with a CACNA1H mutation leading to a chronic pain phenotype	46

target validation for this target family preclinical data will not be discussed. It should be noted that despite the high level of target validation small molecules which inhibit voltage-gated calcium channel function have recently failed to show efficacy in clinical trials.[14,50,51] Reports of the discovery of these molecules suggest that the compounds were designed with a heavy reliance on animal model data (Sections "Neuromed compounds" and "ABT639 and related compounds"), and no other translational studies were performed. Encouragingly there are recent reports of more recent molecules that have been identified with potentially more robust translational packages which include in vivo electrophysiology studies and measurement of the compounds effect on neurotransmitter release. It will be interesting to follow the progression of these compounds into clinical evaluation.

7.03.4 Mechanism of Action

Peptide blockers such as ziconotide have to be administered intrathecally to avoid severe adverse effects on the cardiovascular system resulting in a dramatic fall in blood pressure,[57] yet small-molecule Cav2.2 blockers developed recently retain the analgesic efficacy of ziconotide in preclinical testing yet do not affect the cardiovascular system. The reason the small molecules have an improved safety profile is that they are so-called state-dependent blockers which are able to spare functions, such as neurotransmitter release, that are required for normal central processing and peripheral sympathetic control of cardiac and smooth muscle function yet block sensory neurons involved in pain processing. The small molecules have a higher affinity for a state of the channel which occurs to a higher degree in situations where cells are operating under nonresting, typically high frequency conditions.[58] Voltage-gated ion channels can exist in a number of different states, and some blockers can exert their action selectively through a single state or a subset of states and such compounds are referred to as state-dependent blockers. Once channels enter the inactivated state, a characteristic interval must pass before the channel can be reactivated. Fig. 2A represents a model of the different states. Voltage-gated calcium channels exist in open and closed (or resting) states and various inactivated states together with various intermediate closed states. It has been suggested that a channel entering an inactivated state is comparable with receptor desensitization, wherein the continued influence of an activating stimulus, in this case depolarizing transmembrane voltage sufficient to cause channel opening, loses its ability to sustain the channel in the open state. The inactivated state is believed to represent a different protein conformation distinct from both the open and closed states.

There are many theories describing how channels can enter inactivated states. One widely accepted model which fits with observations of channels on sensory neurons and the effects of certain drugs is so-called closed state inactivation proposed by Winquist.[58] Channels are able to access an inactivated state through an intermediate closed state (the so-called closed state inactivation or CSI). Intermediate closed states occur at potentials which are below the threshold required for channel opening. This explains the concept of use-dependent block (Fig. 2B), whereby channels which undergo rapid cycling through different intermediate states, for example, when exposed to rapid high frequency stimulations are preferentially blocked compared to those cycling at lower frequencies. This phenomenon explains physiological observation, whereby compounds are able to inhibit calcium channels operating at high frequencies such as those on sensory neurons fitting aberrantly in pain states but have little or no effect on channels functioning under low-frequency conditions such as in the heart.

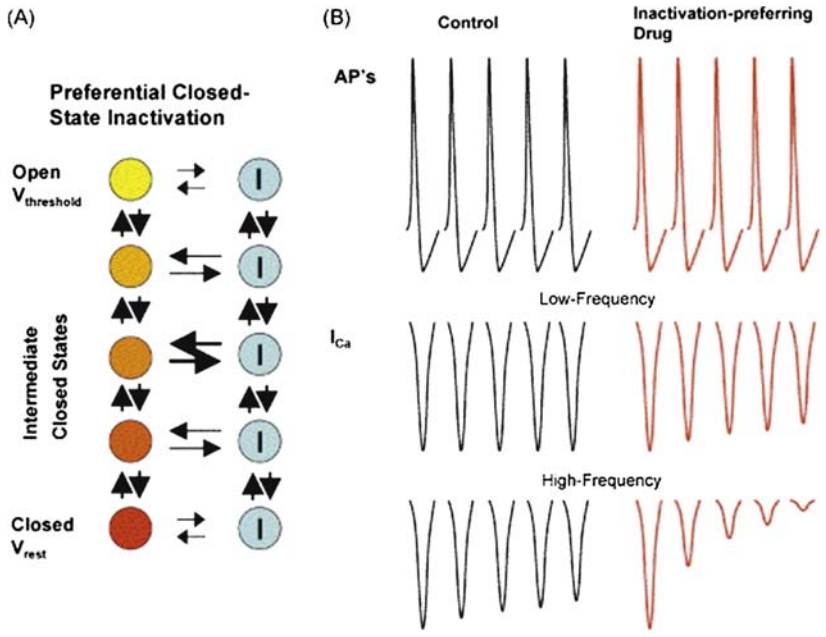

Fig. 2 State-dependent inhibition.

Drugs such as ziconotide, for example, do not selectively bind to a single state of the channel and have different pharmacology to state-dependent blockers which are typically small molecules although state-dependent peptides have been reported.[59] State-dependent inhibition therefore offers an opportunity to achieve a therapeutic window between analgesic effects and target-driven side effects. All drug discovery efforts based on voltage-gated calcium channels have targeted state dependence and have identified molecules with excellent therapeutic indices preclinically and which are safe and well tolerated where tested in humans. However while only a very small number of molecules have been tested, a state-dependent inhibitor of a voltage-gated calcium channel has yet to demonstrate robust clinical efficacy, and it will be interesting to observe the results of clinical studies in the near future to see if the situation changes.

7.03.5 Inhibitors of Voltage-Gated Calcium Channels

The literature is confusing as different authors use different nomenclature when referring to channels and channel subtypes. For clarity and consistency in this article channels will be referred to using the α1 subunit nomenclature, for example, Cav2.1, Cav2.1, etc., with the exception of Section "Alpha 2 Delta Ligands" which covers molecules which act through binding to the α2δ subunit.

There has been an explosion in terms of publications covering voltage-gated calcium channel inhibitors in recent years. This is largely due to advances in technology which have allowed the development of screening assays with sufficient throughput to support drug discovery projects.[1–3] Current technology allows assays to be run to support ongoing chemistry projects and also high-throughput screening campaigns for voltage-gated ion channels. Early drug discovery programs were hampered by the low throughput of conventional electrophysiological techniques and achieved only limited success. Recently through the application of diversity screening techniques a wide variety of molecular scaffolds have been identified which inhibit calcium channels, particularly inhibitors of the Cav2.2 and Cav3 channel families. The majority of compounds covered by patents and journal articles which have published to date cover compounds described as either selective Cav2.2 or Cav3 inhibitors. There has been little if any work in the field of Cav2.1 and Cav2.3 channels. The exact reason for this bias is unclear; it is possible that the Cav2.2 and Cav3 family are more tractable from a small-molecule perspective or linked to the higher level of target validation currently reported for these channels. Additionally there has been some work focussed on the identification of molecules which bind to the α2δ subunit both based around the gabapentin and pregabalin scaffolds and some based on hits identified through screening approaches.

7.03.5.1 Compounds Under Clinical Evaluation

Several compounds have reached clinical trials and are shown in Table 3.

7.03.5.1.1 Z160

The first Cav2.2 inhibitor to enter clinical evaluation was Z160 (1) (previously known as NP118809, NMED 160, and MK6721), most recently developed by Epirus following the merger with Zalicus. The compound was originally identified by Neuromed (Section "Neuromed compounds") and for a brief period jointly developed in partnership with Merck Development was terminated in 2013 after the compound failed to show efficacy in two clinical studies. Z160 did not meet the primary endpoint in either of two phase 2 clinical studies in patients with LSR[60] and postherpetic neuralgia.[61] It is encouraging that in both studies the drug was reported to be well tolerated. No reason has been given to explain the failures, and in a statement on the company website Zalicus commented that they had conducted a review of both studies and adequate exposures had been achieved.

It is important to note that the physical properties of the compound were not optimal for a CNS drug due to very high lipophilicity and caused possible problems during development as indicated by a press release in 2007 after a collaboration between Merck and Neuromed was terminated following a decision to abandon an earlier clinical study due to the compound failing "to demonstrate the ideal pharmaceutical characteristics necessary to advance the compound further into development." The reasons for withdrawal were likely to be due to poor physical properties as evidenced by a patent which presents data showing that the bioavailability can be enhanced by dosing after a high fat meal[62] which is later followed by a number of formulation patents.[63,64]

7.03.5.1.2 CNV2197944

A second Cav2.2 blocker with an unknown structure CNV2197944 being developed by Calchan Pharmaceuticals following its discovery by scientists at GlaxoSmithKline is currently in phase 2 trials. Following the decision by GSK to exit neuroscience focussed research in 2011 the development of a number of pain assets was continued through the formation of a spin-out company; Convergence Pharmaceuticals. Convergence progressed CNV2197944 into phase 1 studies where it was shown to be well tolerated and a have a pharmacokinetic profile suitable for progression [Source Convergence website]. In 2013 Convergence announced the start of two phase 2 studies in two different patient groups, one in patients with PHN[65] and a second in patients with peripheral diabetic neuropathy.[66] Both studies have now completed but as yet no results have been released. Early in 2015 Convergence was acquired by Biogen who continued to work on certain assets which did not include CNV2197944. Currently CNV2197944 is being developed by Calchan pharmaceuticals a second spin-out company formed by former Convergence management. To date no data from any of the human studies with CNV2197944 have been published.

Table 3 Voltage-gated calcium channel inhibitors under clinical evaluation

Compound	*Structure*	*Target channel*	*Status*
Z160	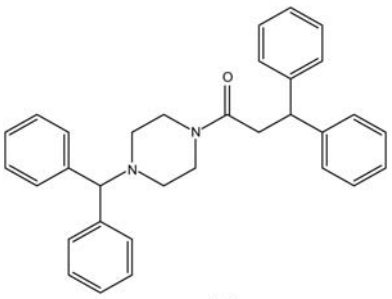 (1)	Cav2.2	Terminated–failed phase 2
CNV2197944	Unknown	Cav2.2	Phase 2
ABT639	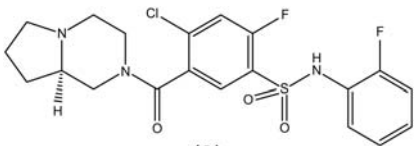 (2)	Cav3	Terminated–failed phase 2
Z944	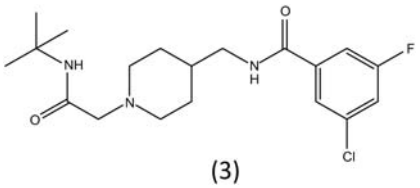 (3)	Ca3	Phase 2
Ethosuximide	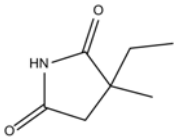 (4)	Cav3	Proof of concept
Microgabalin	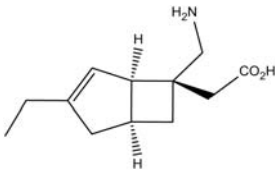 (5)	α2δ	Phase 3

7.03.5.1.3 ABT-639

A similar picture emerges for T-type channels with one compound ABT-639 (2) having recently failed in a clinical study in patients with diabetic neuropathy.[50] In the trial patients were given 100 mg ABT-639 twice daily for a period of 6 weeks. When assessing the mean changes from baseline in patient-recorded pain scores at the end of week 6, there was no significant difference observed for ABT-639 compared with placebo. Pregabalin treatment resulted in a transient improvement in pain compared with placebo, which did not persist throughout the study. In a parallel[51] study which used a technique called microneurography to examine effects on spontaneous C fiber activity, patients were given a 100 mg single dose of ABT-639. Results showed that the drug behaved no differently to placebo although interestingly lidocaine also showed no difference to placebo. In addition it also failed to show an effect in an experimental medicine study which looked at intradermal capsaicin experimental pain model in healthy adults.[67] In a phase 1 study ABT-639 was well tolerated and demonstrated a pharmacokinetic profile supportive of progression.[68] The reason for the failure in the clinical studies is again not clear. ABT-639 is described as being peripherally restricted in preclinical pharmacokinetic studies,[69] and it is possible that a centrally penetrant molecule could have had a better chance of success.

7.03.5.1.4 Z944

Z944 (3) is a selective Cav3 blocker, originally identified by Zalicus scientists. Following the acquisition of Zalicus by Epirus Biopharmaceutical, its development has continued and Epirus are currently evaluating Z944 in a phase 2 study. The compound was safe and well tolerated in a phase 1 study, and in a subsequent phase 1b study Z944 is reported to have shown efficacy in experimental medicine studies of both neuropathic and inflammatory pain.[70] Volunteers were given four administrations of Z944, 20, 40, or 80 mg or placebo every 2 h, and laser-evoked potentials (LEPs) from skin were measured following either topical administration of capsaicin (to model neuropathic pain) or a UV burn (to model inflammatory pain). Z944 reduced peak-to-peak amplitudes of the LEPs and also pain scores from the volunteers determined using a visual analogue scale. Epirus also state that the study results prompted work to look for controlled release formulations for future studies.

Currently there is no other development reported, but with the large volume of patents covering compounds that inhibit Cav2.2 and the T-type family it is reasonable to expect that new compounds will enter early development shortly, indeed there maybe molecules in early development as this information is not often made publically available by companies.

The following sections will describe in detail the structures of known inhibitors of voltage-gated calcium channels that have been published to date together with structure–activity relationships and, where appropriate, pharmacokinetic data and the in vivo efficacy results.

7.03.5.1.5 Ethosuximide

Ethosuximide (4) is an existing drug used to treat epilepsy and is currently under clinical evaluation for its potential to treat neuropathic pain.[71] The compound has been shown to inhibit Cav3 channels; however it also has activity at other targets.[72]

7.03.5.1.6 Mirogabalin

Daiichi Sankyo is developing a compound, mirogabalin (5, DS-5565) which is reported in the patent literature to be a potent α2δ ligand (binding $IC_{50} = 14$ nM). The medicinal chemistry relating to the identification of this compound has not been disclosed, but the company has reported clinical data from two phase 2 studies in patients with diabetic neuropathy which demonstrated positive effects at doses of 15, 20, and 30 mg per day.[73,74] Studies in patients with fibromyalgia on currently ongoing[75] and the company is currently recruiting patients to begin phase 3 studies.

There are other agents which have calcium channel blocking activity which are currently being developed for nonpain indication such as epilepsy and insomnia. As these conditions are beyond the scope of this article the compounds will not be discussed in detail, but ongoing studies will be highlighted in the following sections.

7.03.5.2 Cav2.1 Inhibitors

Currently there are no selective small-molecule inhibitors of Cav2.1 reported, and this is in some ways surprising given the strong genetic association with familial hemiplegic migraine,[31,44] a fact that has been highlighted by several authors who have expressed the need for such a compound.[76,77] The only truly selective Cav2.1 inhibitors that are currently available are peptides such as ω-agatoxin 1VA[78] which has been used for target validation studies.[79] Small-molecule inhibitors are reported but are all nonselective; these are natural products, marketed drugs, or compounds designed as inhibitors of related channels which have showed activity at Cav2.1 (Section "**Compounds known to inhibit Cav2.1**"). It has been suggested that selectivity may not be possible to achieve as that while there is clear evidence that a gain of function mutation of Cav2.1 leads to Familial Hemiplegic Migraine[44] the gain of function is dependent on the particular splice background in which the mutation is present.[80]

7.03.5.2.1 Nomenclature

Cav2.1 channels are also known as P/Q channels, the reason for the nomenclature is historic as P-type current were first identified in Purkinje neurons of the cerebellum and are distinct from Q-type current identified in cerebellar granule neurons, both being characterized by sensitivity to the toxin ω-agatoxin-IVA and are generated by ion channels encoded by the gene CACNA1A.[81] As the exact distinction is unclear, the channels are commonly referred to as P/Q channels. The channels have an expression profile similar to the related Cav2.2 channels, the distinction being that Cav2.1 channels show a greater bias toward neuronal expression in the CNS.[82]

7.03.5.2.2 Target validation

To date a number of mutations of the CACNA1A1 gene which encodes the pore forming unit of the Cav2.1 channel have been identified. Mutations which lead to a gain of function of the channel are associated with migraine, most commonly FHM1,[44] conversely loss of function mutations are associated with Episodic Ataxia type 2.[83] The biochemical and physiological consequences of the mutations have been extensively studied and are consistent with the linkage to a migraine phenotype with both cells and neuronal tissues expressing a channel that has a shift in the voltage required to activate them resulting in enhanced neurotransmitter release and neuroexcitability.[23] Mice expressing a mutant form of the channel associated with FHM possess a phenotype consistent with the disease which can be reversed by treatment with ω-agatoxin 1VA.[84] It is important to consider that loss of function mutations of Cav2.1 has also been identified which are linked to ataxia (Episodic Ataxia type 1), thus suggesting that direct inhibition of the channel would not be appropriate as a treatment for migraine. A state-dependent inhibitor which binds to the inactivated state of the channel however has the potential to restore normal function and provide a safe effective therapy. Preclinical

target validation for Cav2.1 inhibition to be a treatment for migraine in general has also been described.[79] Agatoxin application is able to reverse the hyperexcitibility of the trigeminal nerve in a mouse model of general migraine. Finally as described in the following section certain agents in current clinical use have shown activity in migraine clinical studies. This data should be treated with some caution as none of the agents are selective Cav2.1 blockers.

7.03.5.2.3 Compounds known to inhibit Cav2.1

Currently available agents which have activity at Cav2.1 channels fall into three groups: peptide toxins, existing drugs shown to have Cav2.1 inhibitory activity in addition to activity at other targets, and small molecules which were originally designed as ligands for other targets but have been found to be Cav2.1 inhibitors as part of selectivity screening studies.[76] Reference[76] contains a thorough review of currently known agents which have been shown to interact with Cav2.1 channels and are summarized in the following paragraphs.

There are many toxins that have been reported to be potent blockers of Cav2.1 channels; however most are nonselective. Currently only toxins are reported to be selective, ω-agatoxin-IVA and ω-agatoxin-IVB. Both are reported to have inhibitory activity in the nanomolar range and to produce complete channel block at sub-nanomolar concentrations. ω-Agatoxin-IVA has been shown to bind to the outside of the pore forming α1 subunit where other toxins studied have been demonstrated to bind in the pore itself. It has been suggested that the different binding mode of ω-agatoxin-IVA may explain its selectivity compared to other known peptide inhibitors.

Many known drugs have been reported to have activity at Cav2.1 channels (**Fig. 3**). Virtually all members of the calcium channel blocker class of antihypertensives, including the structurally diverse compounds verapamil (6), diltiazem (7), and amlodipine (8), where tested have activity at Cav2.1. While potency varies from compound to compound this class of drug shows little selectivity across the Cav 1.2, Cav2.1, and Cav2.2 family members; verapamil is reported to inhibit Cav2.1 channels with an IC_{50} of 62 μM, Cav1.2 channels with an IC_{50} of 4 μM and produces full inhibition of Cav2.2 at 40 μM. Amlodipine appears generally more potent and less selective inhibiting Cav2.1 with IC_{50} values ranging from 3 to 11.5 μM, inhibiting Cav1.2 with an IC_{50} ranging from 1.2 to 4.2 μM and Cav2.2 in the range of 0.14–7.9 μM. Interestingly there are several reports of migraine being successfully treated with amlodipine and other drugs of this class[85,86]; however it is difficult to draw any conclusions as to which channel if any is responsible for the beneficial effect. Cav2.1 activity is not limited to the antihypertensive class of compounds. Drugs such as fluspirilene (11), gabapentin (12), isoproterenol (13), lamotrigine (14), and levetiracetam (15) have also demonstrated activity. All of the compounds in **Fig. 4** are reported to inhibit Cav2.1 channels in the micromolar range, but none of the compounds show any significant selectivity for Cav2.1. It is also important to note as highlighted in a recent review[76] that all of the Cav2.1 inhibitory data published on these compounds has been generated in different laboratories often using different protocols and care should be exercised when making comparisons.

Additional nonselective Cav2.1 inhibitors have recently been published by groups engaged in projects focussed on the identification of selective Cav2.2 inhibitors,[76] and examples are shown in **Fig. 4**. The molecules will be described in more detail in Section "**Merck compounds**." As they were not identified through a targeted search for a selective Cav2.1 blocker, little information has been published regarding SAR at Cav2.1 channels or functional activity associated with this activity. Z160 (1) was the first small molecule rationally designed Cav2.1 inhibitor to enter clinical studies. The compound displays some selectivity for Cav2.2 channels (IC_{50} 0.04–0.2 μM) but is still a relatively potent inhibitor of Cav2.1 channels (IC_{50} 0.12–0.65 μM) and Cav1.2 channels (IC_{50} 0.3–0.5 μM). While detailed SAR for activity at Cav2.2 and Cav1.2 channels is reported, little data describing selectivity over Cav2.1 channels has been described. A-1048400 (16) is a related compound identified by Abbott, and it has a similar profile regarding selectivity inhibiting Cav2.1 channels with an IC_{50} of 1.3 μM and Cav2.2 channels with an IC_{50} of 0.8 μM when in the inactivated state and shows some evidence of state dependence inhibiting Cav2.1 and Cav2.2 with IC_{50}s of 16.1 and 4.1 μM, respectively, when in the closed state.

LY393615 (17) was described by the Lilly group and was derived from a high-throughput screening hit which was optimized to be a nonselective agent for the treatment of ischemia. It is reported to block Cav2.1, 2.2, and 2.3 currents with IC_{50} values of 4.1, 19, and 5.2 μM, respectively. In addition to inhibiting calcium channel function the compound is also reported to be a sodium channel blocker.

TROX-1 (18) is a compound identified by the Merck group as part of their Cav2.2 blocker program and was profiled extensively but terminated due to poor selectivity over Cav2.1 and Cav2.3 channels. The compound is described as a nonselective blocker of Cav2 channels, and data is presented in two assay formats TROX-1 having depolarized IC_{50} values of 0.19, 0.29, and 0.28 μM at Cav2.1, 2.2, and 2.3, respectively, in a manual electrophysiology assay and using matched conditions in a calcium influx assay IC_{50} of 1.8, 0.69, and 1.1 μM were observed. Merck reports that the compound was extensively profiled in vivo with no serious adverse effects being observed.

In addition to marketed drugs and compounds identified with Cav2.1 activity, projects focussed on other channel subtypes. A third group of molecules has been published that possess Cav2.1 inhibitory activity, namely, natural products of the petassin (19) family and eudesmol isomers (20) (**Fig. 5**). Of particular interest is that these compounds have been shown to be present in extracts of medicinal plants which have demonstrated clinical efficacy in treating migraine.[87] Both petassin A (19) and α eudesmol (20) have been shown to demonstrate strong use-dependent block of Cav2.1 channels at concentration of 3–10 μM.[87] In summary no selective small-molecule inhibitors of Cav2.1 channels are currently reported; however many structurally diverse compounds do nonselectively inhibit channel function, suggesting that this channel is a chemically tractable target for drug discovery. Given recent genetic findings it is reasonable to expect that selective agents will be reported in the near future.

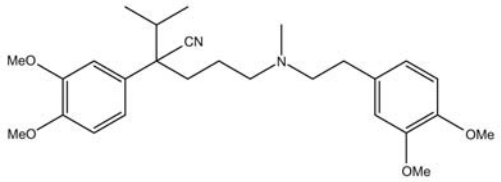

(6)

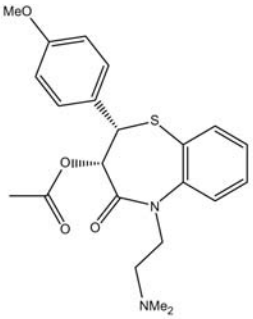

(7)

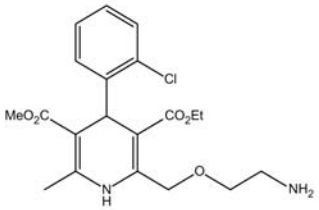

(8)

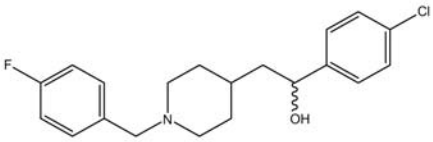

(9)

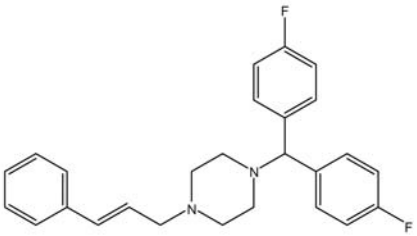

(10)

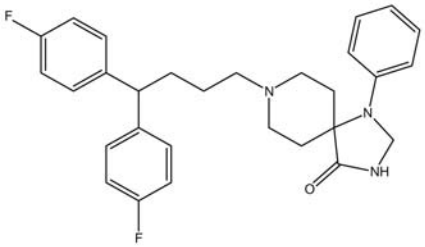

(11)

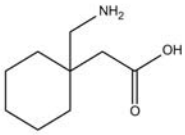

(12)

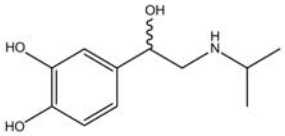

(13)

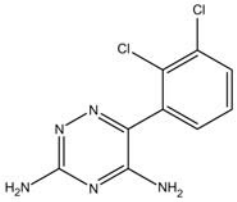

(14)

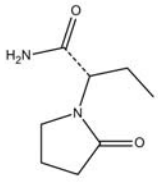

(15)

Fig. 3 Known drugs with inhibitory activity at Cav2.1 channels.

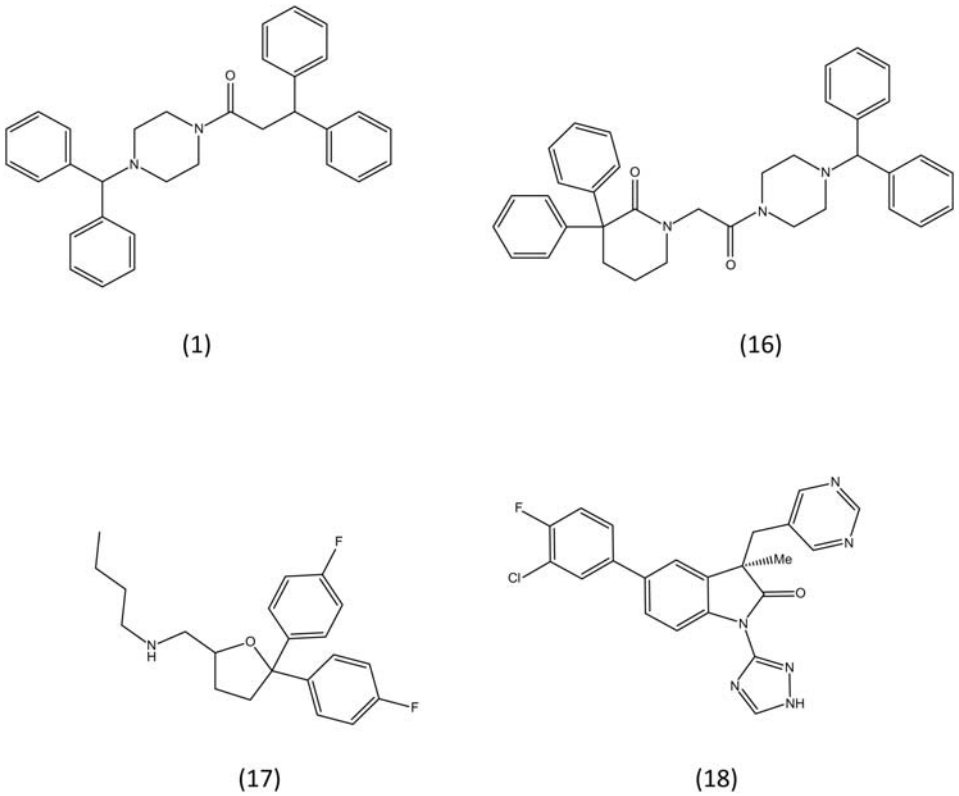

Fig. 4 Other voltage-gated calcium channel blockers with inhibitory activity at Cav2.1 channels.

7.03.5.3 Cav2.2 Inhibitors

In contrast to Cav2.1 there are many reports describing focussed efforts to discover agents which act through inhibition of the Cav2.2 channel. The majority of these highlight pain as the primary indication; however some early work centered on agents to treat ischemia. The reason for the high level of interest can be attributed to the success of ziconotide,[23–25] the selective peptide Cav2.2 inhibitor currently licensed for the treatment of neuropathic pain and which shows excellent clinical efficacy. The ziconotide data makes the Cav2.2 channel a rare and highly sought after clinically validated target and hence the high level of interest which continues today. As described in Section "**Compounds Under Clinical Evaluation**" following the success of the ziconotide small-molecule, state-dependent, Cav2.2 blockers have been identified, some of which have progressed to clinical studies (**Table 3**). Given the large volume of patent filings in the area it can be expected that further agents will enter clinical evaluation in the coming years. The fact that one of the small molecules failed to show clinical efficacy raises an important question as to what is the optimal profile for an efficacious yet safe Cav2.2 blocking agent to treat pain? As previously described ziconotide is efficacious yet has to be administered directly into the spinal cord as systemic delivery leads to severe, mechanism-driven cardiovascular adverse effects. Side effects arise as the peptide blocks all states of the channel and therefore blocks all channel function. State-dependent compounds have since been identified which can be administered systemically without causing the adverse effects seen with ziconotide in clinical studies and also demonstrate preclinical analgesic efficacy in a variety of models, however as yet are still to demonstrate clinical efficacy. The reasons for the failure of Z160 are not yet understood, and these observations prompt the question as to whether the biophysical profile of the compound possibly suboptimal, and if so what profile should a safe and efficacious compound possess? One possible explanation is that in some cases compounds are not screened adequately as they are progressed

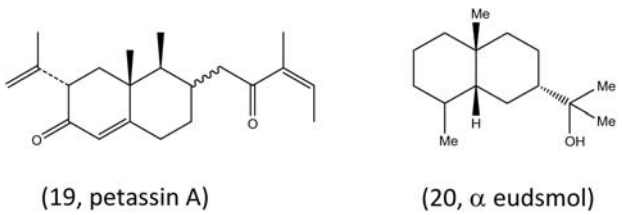

Fig. 5 Natural products from medicinal plants used to treat migraine with inhibitory activity at Cav2.1 channels.

from electrophysiological profiling to pharmacokinetic studies and then once the target profile has been achieved advanced to animal testing. Given the number of recent reports which question the translatability of preclinical pain models more confidence is needed that a compound will be efficacious in clinical testing. Encouragingly workers are starting to do this, the Janssen group recently reported studies with one of their Cav2.2 molecules which showed the compound was able to inhibit neurotransmitter release from spinal cord slices in a similar manner to ziconotide,[88] thus allowing a more in depth comparison and also providing a potential translational biomarker with which to measure target engagement in early clinical studies.

A number of different strategies have been used to identify small-molecule Cav2.2 blockers including structure-based design based on selective peptide ligands, modification of known compounds which nonselectively inhibit Cav2.2 and high-throughput screening. While there are a large number of medicinal chemistry publications which describe in detail the discovery of various Cav2.2 inhibitor templates there are many more novel structures only described in the patent literature publishing very little data, hence like many areas of active medicinal chemistry it is not possible to understand the full picture at any moment in time. An additional complication which makes comparing compound profiles difficult is that frequently different groups use different assay formats or report data in different ways therefore allowing only meaningful comparisons to be made with data from the same laboratory.

7.03.5.3.1 Early inhibitors

Early reports of Cav2.2 inhibitors focused on compounds for the treatment of both pain and ischemia. These have been thoroughly reviewed[89–92] and will only be briefly summarized in this article. Compounds include SB-206284A (21), PD 151307 (23), PD 175069 (24), NS 649 (28), and E2050 (29) and are shown in Fig. 6.

The medicinal chemistry behind the discovery of SB-206284A (21) has not been published, but comparing the right-hand side aryl groups and the relative position of the basic center in each compound one can speculate that they might bind in a similar region of the protein. The biological profile has been published,[93] and the compound inhibits calcium channels in a DRG preparation with an IC_{50} of 5.6 μM. The Parke-Davis group has described the discovery of PD175069 (24) derived from a screening hit PD151307 (23), which was a potent Cav2.2 blocker ($IC_{50}=0.32$ μM, in human IMR32 neuroblastoma cells) but had poor physicochemical properties, in particular poor aqueous solubility and stability.[94] The ester could be replaced with an amide to give as compound with similar activity. Further modification of the urea gave the tertiary amine PD175069 (24). In a subsequent article[95] Parke-Davis described the preparation of conformationaly restrained analogues in which the left-hand acyclic amine is cyclized to form a piperidine with retention of activity. Subsequently Parke-Davis has described a number of other analogs[96–99] together with structurally distinct compounds designed using the structure of conotoxin peptides (see Section "Small-molecule blockers based on peptide toxin structures").

One of the earliest examples of Cav2.2 blockers being described specifically for the treatment of pain is the quinolone (22) which appears in a 2002 patent.[100] The detailed medicinal chemistry behind the discovery of this compound has not been published.

Ono has also described the discovery of amino acid-derived inhibitors arising from screening hits. Compound (25) was a hit chosen for investigation and reported to have $IC_{50}=3.4$ μM (IMR calcium flux assay and $IC_{50}=34$ μM IMR electrophysiology assay) with significant activity at Cav1.2 (selectivity 4.4-fold). The corresponding enantiomer had a similar profile in terms of both potency and selectivity.[101] Encouraged by the profile of (25) it was studied in vivo in the formalin model of analgesia[102] where it showed modest activity after *intrathecal* injection (34% reversal of effect, 3 mmol kg^{-1}). Following a detailed SAR investigation (26) was identified[103] which is a more potent Cav2.2 blocker in the calcium assay ($IC_{50}=0.17$ μM) but with a similar profile in electrophysiology ($IC_{50}=25$ μM) and with slightly improved selectivity over Cav1.2 (12-fold). This compound however failed to demonstrate any analgesic efficacy in two pain models following oral dosing. The lack of efficacy may have been due to poor solubility which is reported by Ono. Further work showed that the left-hand ring of the diphenyl ether group present in (26) could be replaced with a piperidine (27) giving a compound with a similar biological profile ($IC_{50}=0.33$ μM in the IMR calcium assay) and 15-fold selectivity of Cav1.2, but more potent in electrophysiology (76% inhibition at 3 μM, compared with 25% for (26)). Compound (27) was subsequently tested in two pain models where, unlike (26), it showed activity having minimum effective doses of 10 and 30 mg kg^{-1} in the rat formalin and CCI models,[104] respectively, following oral dosing.

No SAR has been published for NS-649 (28), but its synthesis and biological profile have been described.[105] Similarly little has been described relating to the discovery of E2050 (29).

7.03.5.3.2 Small-molecule blockers based on peptide toxin structures

Using the structure of the highly active and selective conotoxin peptides, one of which has demonstrated clinical efficacy is a potentially attractive starting point for small-molecule design; however it is an area which has significant challenges. A number of groups have taken this approach and have identified inhibitors with activities in the low micromolar region. Most of the work published to date has been based on the structures of ω-conotoxin MVIIA and ω-conotoxin GVIA.

The first group to report work in this area was Parke-Davis. They used the ^1H NMR structure of ω-conotoxin MVIIA in combination with the knowledge that key residues, namely, Lys2, Arg10, Leu11, Tyr13, and Arg21 were key for binding to the Cav2.2 channel to design a scaffold in which three of the residues Arg10, Leu11, Tyr13 were incorporated in a spacial orientation close to that observed in the peptide structure. The initial design[106] was not successful giving a compound (30) which showed only 19% inhibition at 10 μM in an IMR32 assay.[107] Further optimization of the scaffold through molecular modeling gave (31) a 2.7 μM inhibitor, a compound which more closely resembles the conformation of the peptide. A subsequent publication[108] describes compounds in which a quinolone moiety is introduced by formation of a ring through cyclization from one of the central

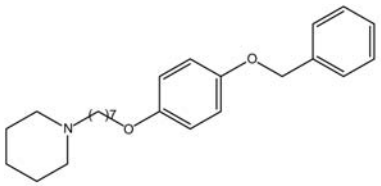

(21,SB-206284A)

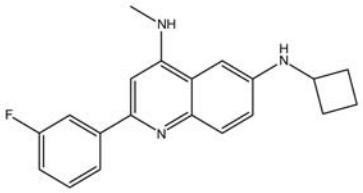

(22)

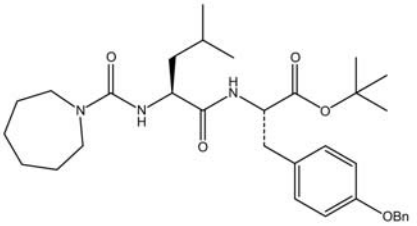

(23, PD 151307)

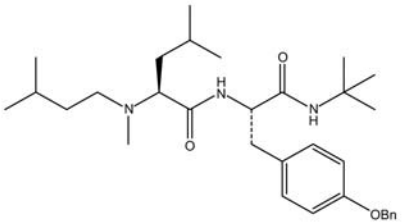

(24, PD 175069)

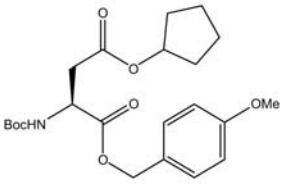

(25)

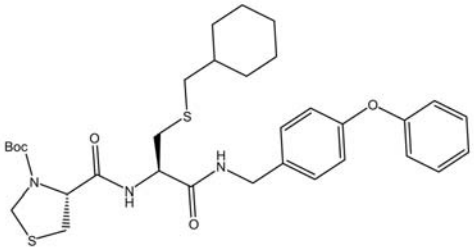

(26)

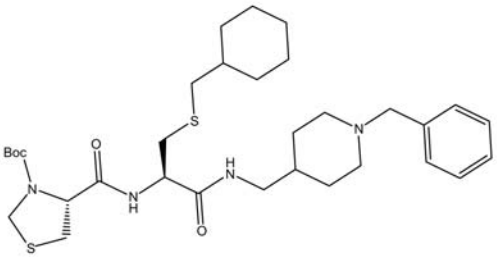

(27)

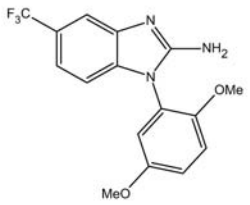

(28, NS 649)

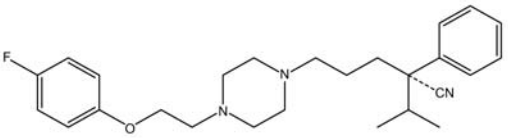

(29, E2050)

Fig. 6 Early reported Cav2.2 blockers.

phenyl rings onto the chain which links the Tyr13 mimetic. No biological data is reported for these latter compounds. The compounds in Fig. 7 are the only ones reported to be designed using ω-conotoxin MVIIA as the template. Most workers have focused on the more selective ω-conotoxin GVIA.

Fig. 8 shows the initial compounds published using this strategy from a group at Monash University. The scaffolds were again designed using a knowledge of the ^{1}H NMR structure of the peptide in combination with the knowledge that Lys2 and Tyr13 residues were crucial for potency and that Arg17, Tyr22, and Lys24 were also needed but were less important. The group decided that three residues should be incorporated into the peptidomimetic and that Lys2 and Tyr13 should be two of them and used computational chemistry to aid the selection of Arg17 as the third. Once the residues were chosen they were combined with a series of scaffolds designed to mimic the natural peptide conformation and hold the key residues in the optimal space to interact with the channel.[109] The benzthiazole (33) and antharanilamide (34) derivatives showed activities of 98 and 68 μM, respectively, when tested in a rat vas deferens assay and with binding affinities in the single figure micromolar range.[110,111] Extensive SAR studies have been reported around these scaffolds[112] which have focused on variation of the groups postulated to mimic Lys 2 and Arg 17. A variety of basic groups are tolerated in combination with various chain lengths; however none of the modifications led to a significant increase in potency. The nature of the Tyr13 mimetic has also been investigated; results showed that the hydroxyl group could be removed with little effect on activity and a slight increase in potency when replaced with a fluorine atom. In addition to investigating the chain length of the linker, the nature of the linkage to the aromatic core was investigated and data demonstrated that the ether linkage in (34) could be effectively replaced by an amide with no effect on potency. Despite very thorough SAR investigation around these scaffolds workers have not been able to achieve submicromolar activity within this series. It was reported that for some compounds there was some evidence of selectivity with (33) being reported to be 30-fold selective over Cav2.2. In

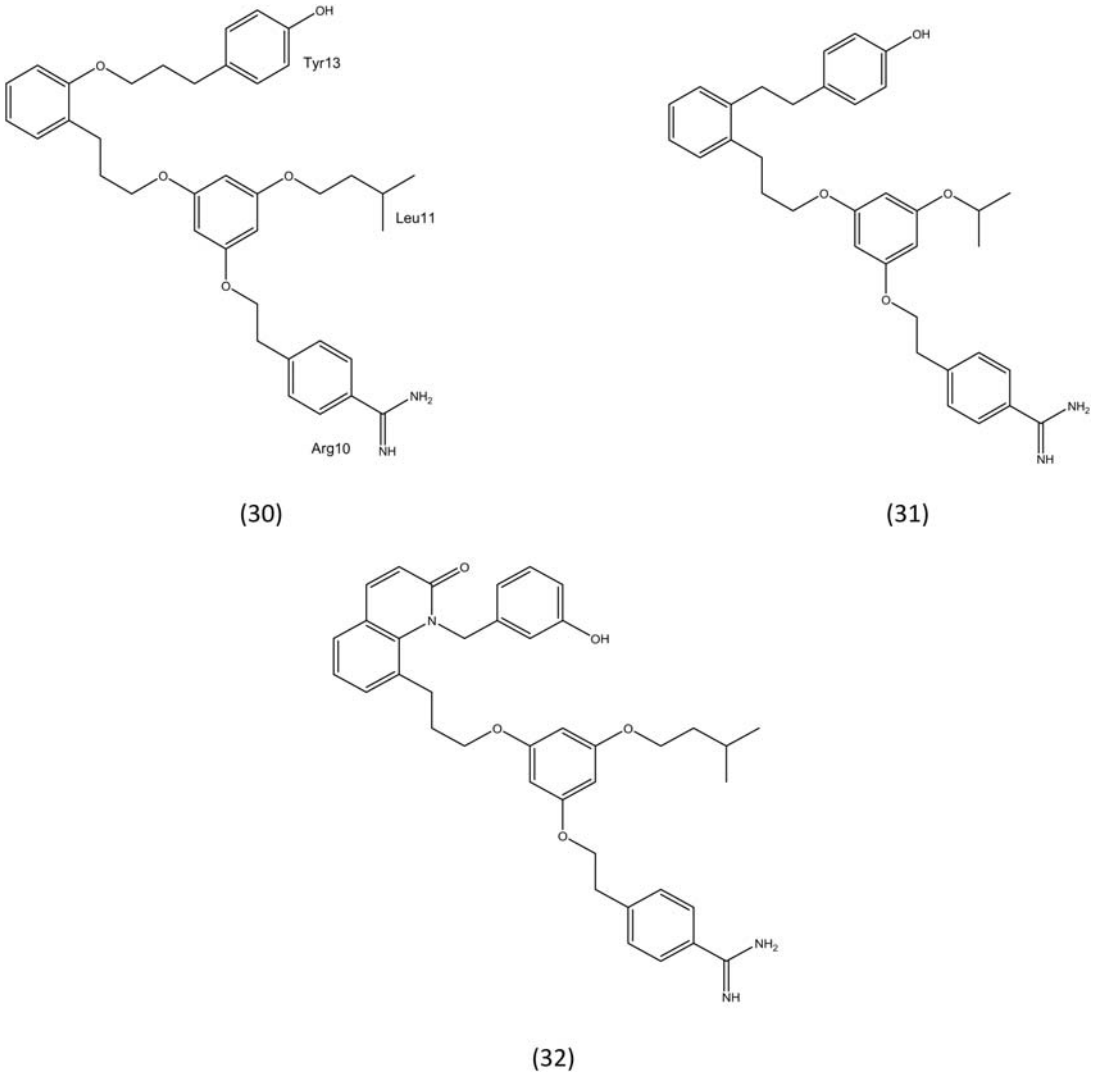

Fig. 7 Peptidomimetics designed from the structure of ω-conotoxin MVIIA.

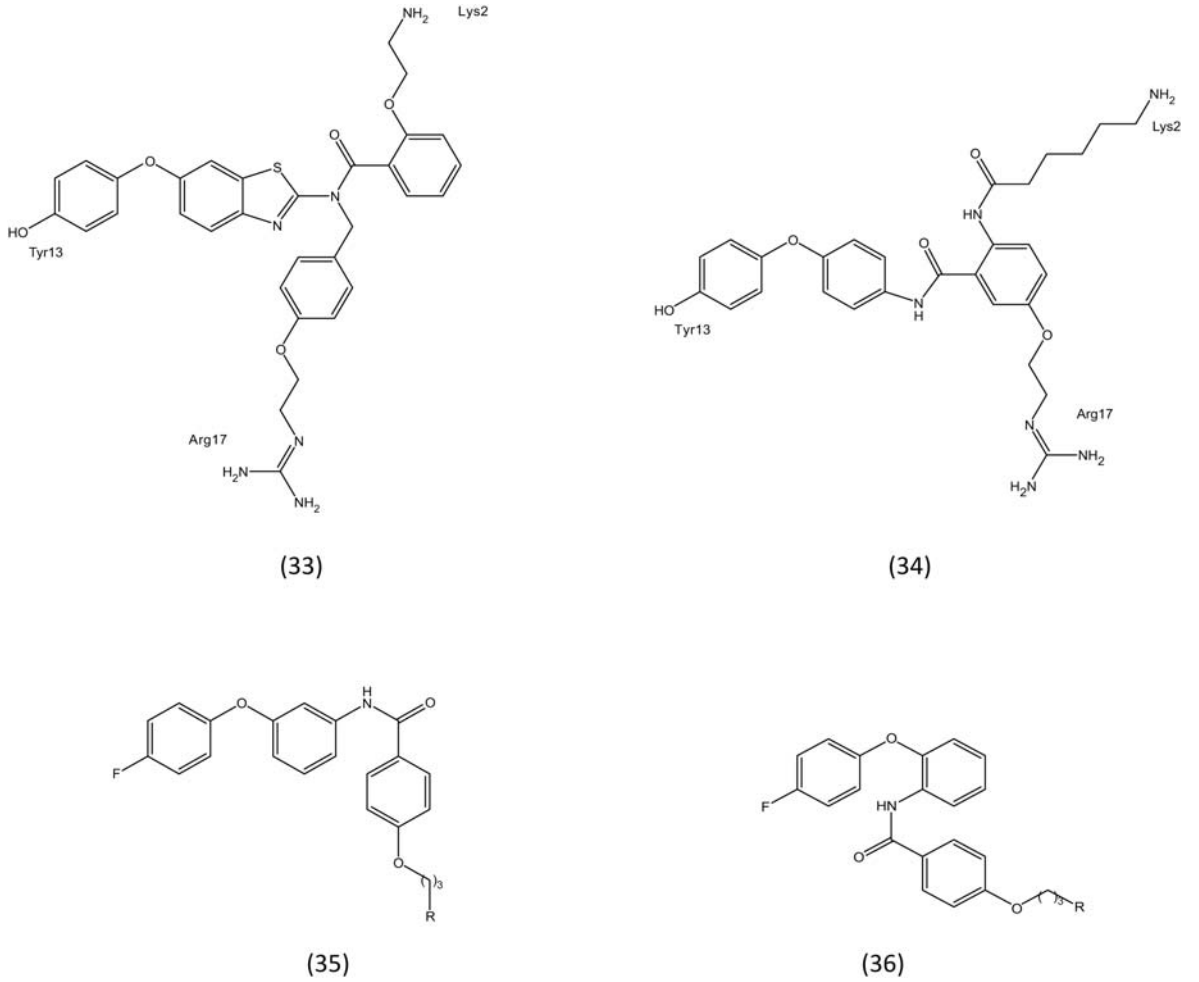

Fig. 8 Peptidomimetics designed from the structure of ω-conotoxin GVIA.

a recent article[113] truncated derivatives were reported (35 and 36) in which one of the side-chain mimetics was deleted with the aim of improving the physical properties. It was found that it was possible to retain activity in these truncated molecules but the nature of the side-chain mimetic which could be deleted was determined by the isomer of the central phenoxy aniline. Deleting either chain in the original para isomeric series resulted in a significant drop in activity ($IC_{50} > 700$ μM in functional assays). Changing to the meta phenoxy anilide (35) removal of the Arg17 mimetic side chain is preferred (R = NH_2 $IC_{50} = 35$ μM, R = guanidine $IC_{50} = 185$ μM) in the ortho series (36) the reverse was found to be the case (R = NH_2 $IC_{50} = 124$ μM, R = guanidine $IC_{50} = 46$ μM).

7.03.5.3.2.1 Hybrid compounds

Recently hybrid molecules have been reported[114] which incorporate common pharmacophoric features of another structurally distinct class of small-molecule Cav2.2 blockers into the phenoxy anilide template (Fig. 9). The authors noted that a number of reported small-molecule Cav2.2 blockers such as Z160 (1) and A-1048400 (16) contain a diphenylmethylpiperazine group and investigated the potential of replacing the phenoxy anilide group in the anilide series (37) with the substituted piperazine. They also highlighted that this should avoid any potential toxicity which may be caused by a phenoxy anilide. Four hybrid compounds were reported which showed activity in both binding and functional assays but was not improved over previous peptidomimentics. The analogues with highest binding affinity were guanidines (R2 = guanidine, R1 = H ($IC_{50} = 12$ μM), F ($IC_{50} = 16$ μM)), where R2 was a primary amine the fluoro derivative was the more potent compound (R1 = F, $IC_{50} = 65$ μM, R1 = H $IC_{50} = 214$ μM). All of the compounds however showed weak activity ($IC_{50} = > 100$ μM) in two functional assay formats.

7.03.5.3.3 Arylthiazolidinediones

7.03.5.3.3.1 Ionix compounds

Ionix has published data on a series of 2-Arylthiazolidinediones in 2007 (Fig. 10).[115] The series was identified through a screening campaign, the original hits identified were (38, $IC_{50} = 1.68$ μM, 5.6-fold selective over Cav1.2 (IMR32 fluorescence-based assay)) and (39, $IC_{50} = 0.66$ μM, 12.8-fold selective over Cav1.2). Preliminary SAR investigation showed that (39) was more amenable

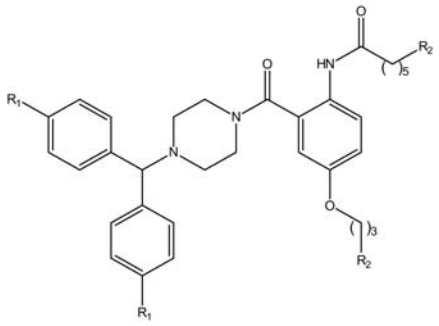

(37)

Fig. 9 Hybrid molecules derived from peptidomimetics and diphenylmethylpiperazine based compounds.

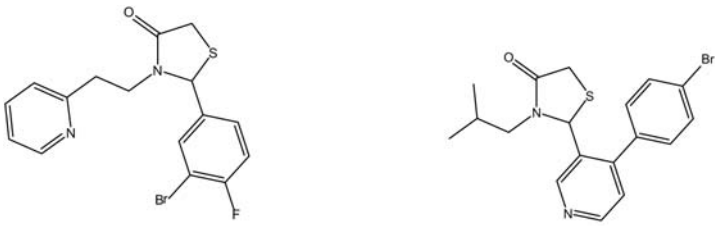

(38) (39)

(40) (41)

Fig. 10 2-Arylthiazolidinedione Cav2.2 blockers.

to modification, and the Ionix group focused on this template. Overall none of the modifications described gave large changes in either potency or selectivity, but a few interesting observations were highlighted. A variety of alkyl replacements for the sec butyl group were tolerated, as was changing the position of the nitrogen in the pyridine ring and the nature of the lipophilic group on the phenyl ring. The pyridyl isomer present in (39) was generally preferred. Separation of the enantiomers produced the largest difference in activity and selectivity as illustrated by compounds (40) and (41), (40) was a relatively weak blocker of Cav2.2 channels ($IC_{50}=4.44\ \mu M$) and nonselective over Cav1.2 (2.9-fold), whereas the enantiomer (41) was more potent ($IC_{50}=0.73\ \mu M$) and showed selectivity over Cav1.2 (31.8-fold). No additional data on these compounds has been reported. The compounds described in the Ionix paper are covered by two patents.[116,117]

7.03.5.3.3.2 Arylthiazolidinediones published in the patent literature

In addition to the publications from Ionix, two patents, a Chinese research institute, published in 2010[118] covering (42) and 2013[119] covering (43) describe series of related molecules (Fig. 11). No data is given in the filings.

7.03.5.3.4 Dihydropyridines

The 1,4-dihydropyridine class of drugs is one of the best characterized class of voltage-gated calcium channel blockers. They exert their antihypertensive action largely through inhibition of Cav1 channels. In recent years a number of these compounds have been shown to have activity at other voltage-gated calcium channels, clinidipine (44), $R=O(CH_2)_2OMe$), for example, is reported to inhibit both Cav1.2 and Cav2.2 channels. Ajinomoto has reported studies around the clinidipine template to enhance selectivity for Cav2.2 (Fig. 12). Studies focused on APJ2708 (44), R = H) which they report to be an equipotent blocker of Cav1.2 and

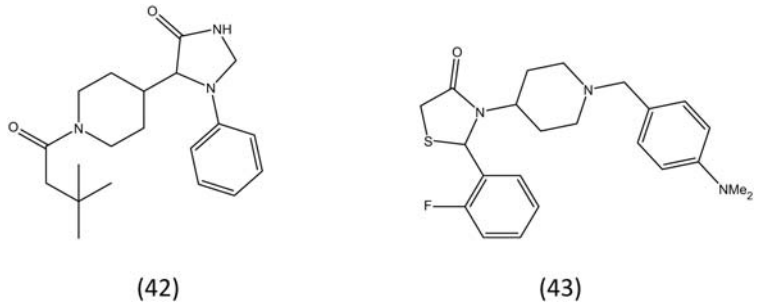

Fig. 11 Arylthiazolidinediones published in the patent literature.

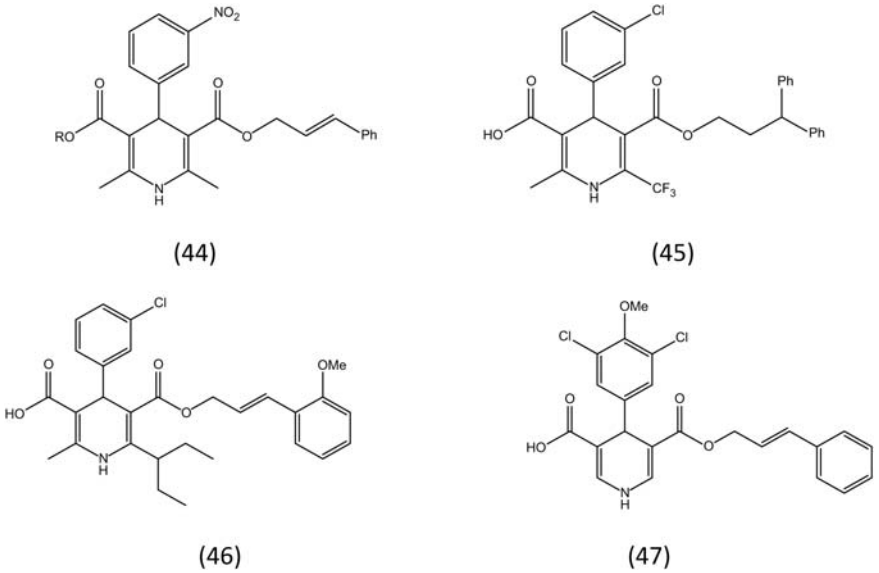

Fig. 12 Dihydropyridines published by Ajinomoto.

Cav2.2. Modulation of the lipophilic side chain produced (45), a compound selective for Cav2.2 channels (Cav2.2 $IC_{50} = 1.7$ μM, Cav2.2 $IC_{50} = 1.8$ μM). The assay formats used are different and have different sensitivities (IMR-32 calcium flux assays to determine Cav2.2 activity and a rat aortic ring (magus) assay for Cav1.2). The IMR-32 assay is reported to be approximately 1000-fold more sensitive than the magus assay, thus confusing data interpretation. Ajinomoto claims that (45) is 1600-fold selective for Cav2.2 over Cav1.2. Compound (45) was progressed to the rat formalin pain model where it demonstrated similar efficacy to clinidipine when dosed orally at 30 mg kg^{-1}. However, (45) was not progressed further due to poor solubility, reported to be 3.5 mg mL^{-1}, with a log *D* reported to be 3.5.[120] Further modification produced (46) a compound with reduced lipophilicity (log $D = 1.29$) and with similar activity and selectivity to (45) (Cav2.2 $IC_{50} = 2.5$ μM, Cav2.2 $IC_{50} = 5.9$ μM), combined with a slight improvement in solubility (10.2 mg mL^{-1}).[121] In a recent article (47) is reported,[122] the (+) isomer of which shows a slight increase in potency compared with previous compounds and improved selectivity (Cav2.2 $IC_{50} = 0.72$ μM, Cav2.2 $IC_{50} = 40$ μM) and when dosed orally at 3 mg kg^{-1} demonstrated similar efficacy to Gabapentin (100 mg kg^{-1}) in the rat formalin model. No patents have published covering these compounds nor has any development been reported.

7.03.5.3.5 Diarylmethylpiperazines

This class of compound is one that has received much attention in recent years and has led to the identification of compounds which have entered clinical evaluation, most notable being Z160 (1). The starting point for work in this area was two known drugs flunarizine (48) and lomerizine (49) (Fig. 13). Both compounds were shown to possess significant Cav2.2 inhibitory activity but were not selective. As both compounds contain a diarylmethylpiperazine group, it was originally suggested that this is a key contributor to the Cav2.2 blocking activity of these molecules.

7.03.5.3.5.1 Early molecules

A number of groups published Cav2.2 blockers containing the diphenylmethyl group, and the first reports came from the Parke-Davis group who reported that (50, Fig. 14) possessed Cav2.2 blocking activity[123]; however the compound is also reported to

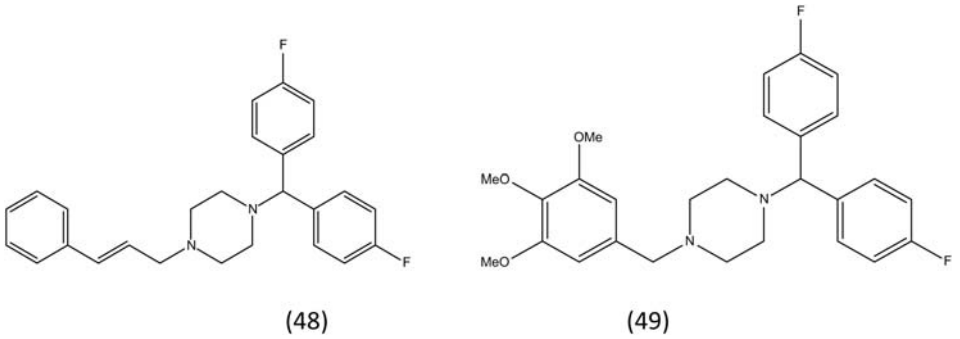

Fig. 13 Flunarizine (48) and Lomerizine (49).

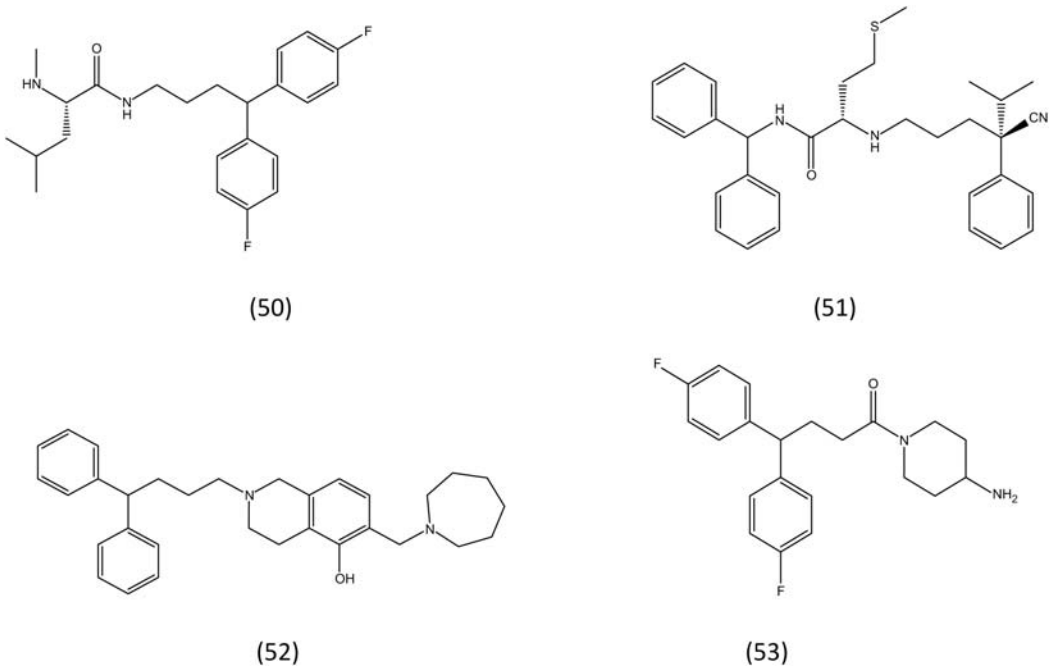

Fig. 14 Prototype Cav2.2 blockers containing a diphenylmethyl group.

be a Cav1.2 blockers as well as having activities at neuronal sodium and potassium channels. In a second article[124] Parke-Davis reported (52) which was a compound resulting from the optimisation of a screening hit that contained the hydroxyl tetrahydroisoquinoline grouping and possessed only weak potency ($IC_{50} = 35$ μM in a IMR32 assay), appending the diphenylmethyl group produced a compound with significantly increased potency ($IC_{50} = 1.1$ μM). Compound (51) appears in an early patent from Lilly,[125] however, is not reported outside the patent literature. The first report of the design of a molecule containing the diphenylmethyl moiety comes from the University of Florence[126] where they describe the discovery of (53), and their interest in designing Cav2.2 blocker came from earlier work focused on Cav1.2 blockers.

7.03.5.3.5.2 Neuromed compounds

Neuromed, who was subsequently known as Zalicus and more recently Epirus, drove the initial work in this area which led to the identification of the clinical candidate Z160 (1) (previously known as NP118809, NMED 160, and MK-6721). The initial working hypothesis was that while the diarylmethylpiperazine group was primarily responsible for the Cav2.2 blocking activity the cinnamyl groups of flunarizine (48) and the benzyl group of lomerizine (49) were contributing to the off target activities in particular Cav1.2 inhibition.[127] In the Neuromed electrophysiology assays neither compound had any selectivity; flunarizine having an estimated IC_{50} of 0.08 and 0.3 μM at Cav2.2 and Cav1.2, respectively, and lomerizine having a similar profile with IC_{50} values of 0.09 and 0.15 μM at Cav2.2 and Cav1.2. Initial investigations focused on compounds in which a second diphenylmethyl group was introduced in place of the substituents postulated to be responsible for the off target activity (Fig. 15). The diphenylmethyl group was attached to the piperazine through a variety of different linkers (54). When the linker was a simple alkyl chain ($X = CH_2$) all of

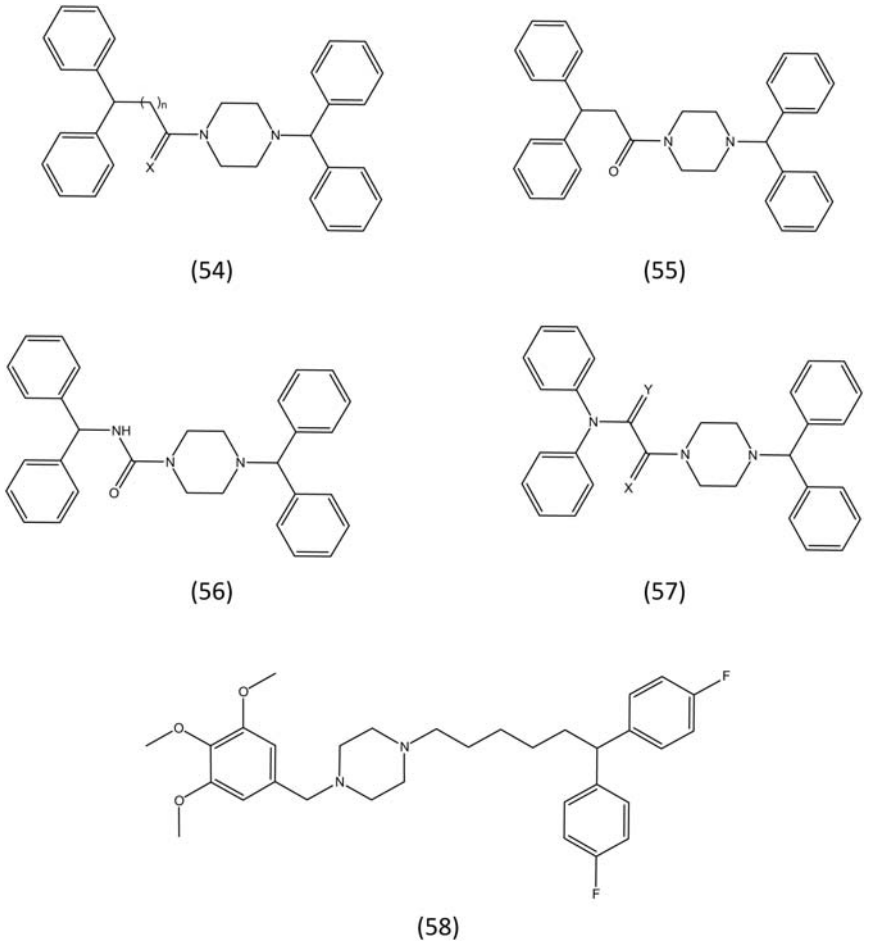

Fig. 15 Compounds reported by Neuromed derived from flunarizine and lomerizine.

the compounds were less active than the known drugs, the most potent compound having an $IC_{50} = 5$ μM ($n = 1$). The introduction of a carbonyl linker (X = O) resulted in an active compound with improved selectivity and interesting SAR. Compound (55) had an $IC_{50} = 0.11$ μM and a selectivity of 111-fold over Cav1.2; however small changes to the length of the linker resulted in significant loss of activity, with only one other compound reported to be active (54, $n = 2$) has an $IC_{50} = 23$ μM. Further investigation of linker modifications showed that nitrogen atoms could be incorporated with retention of potency but a loss in selectivity (56) having an $IC_{50} = 0.15$ μM at Cav2.2 channels but with a reduced selectivity of 12-fold. Moving the nitrogen to the benzylic position (57) resulted in compounds with different activities dependent on the position of the carbonyl group. When the carbonyl group was attached to the piperazine (57; X = O, Y = H_2) a loss in potency was observed Cav2.2 $IC_{50} = 6.6$ μM, with the isomeric compound (57; X = H_2, Y = O) retaining activity. Selectivity was not reported on the latter two compounds. Compound (55) is identified by the authors as NP118809 early in the publication.

In a parallel investigation the effect of increasing the chain length in lomerizine is reported, little SAR is reported but the profile of NP078585 (58) is described, the compound is equipotent with NP118809 but much less selective (12-fold).

The detailed profiles of NP118809 (55) and NP078585 (58) are described. Both molecules showed acceptable pharmacokinetic profiles in the rat. NP078585 was relatively quickly absorbed ($T_{max} = 1$ h), with a good half-life (4.5 h) and an oral bioavailability of 20%. NP118809 was more slowly absorbed ($T_{max} = 2.3$ h) with a half-life of 2.1 h and a bioavailability of 30%.

Both compounds are active in the rat formalin model of neuropathic pain when dosed at 25 mg kg^{-1} (*ip*). When profiled against the hERG channel NP118809 was found to be a weak blocker ($IC_{50} = 7.4$ μM), in contrast NP078585 was a highly potent blocker (98.7% inhibition at 1 μM).

This publication is the first report of NP118809 (Z160) which became the first small-molecule Cav2.2 blocker to enter clinical evaluation. The compound is covered by a number of patents[128,129] including previously described formulation patents, but other than these very little else has been reported on this compound to date.

Two subsequent publications from Neuromed describe further optimisation of NP118809[130] and NP078585.[131] The work on NP118809 focuses on demonstration of additional SAR with a strong emphasis on improving aqueous solubility.[130] Initial studies focused on the investigation of substitution of the benzhydryl group (Fig. 16, 59) focusing on introduction of small lipophilic

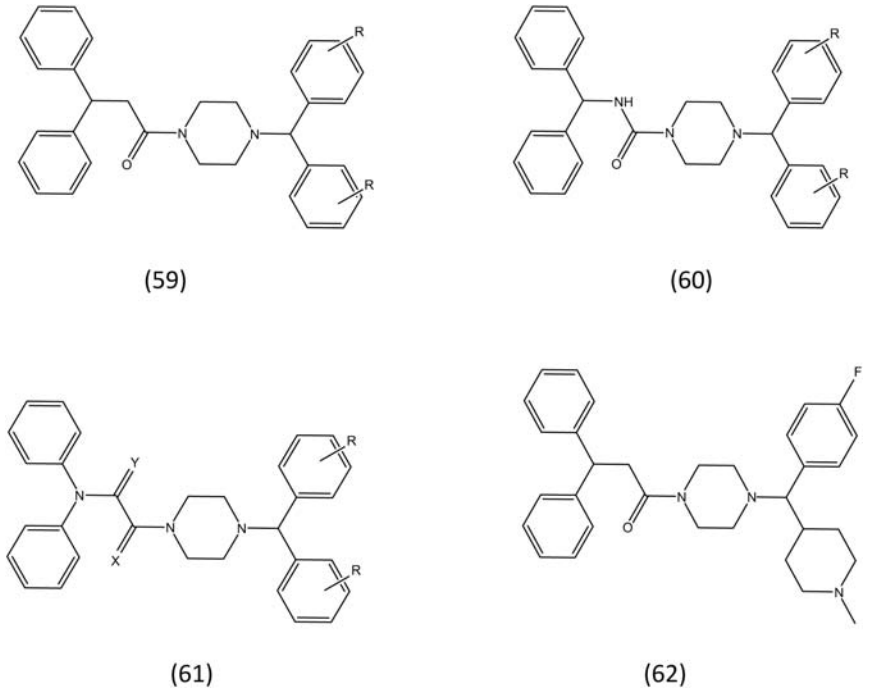

Fig. 16 Compounds prepared by Neuromed during the optimisation of NP118809.

groups which differed in their electronic nature. For mono substitution a wide variety of groups are tolerated with a slight preference for electron withdrawing groups. Optimal potency and selectivity was seen with R = 2-chloro which produced a compound with Cav2.2 $IC_{50} = 0.09$ μM and selectivity > 1000-fold over Cav1.2. A second study investigated the effects of a similar range of lipophilic substituents when introduced into analogues of (60) and (61). The results were similar to those seen with (59) and unsurprisingly all of the analogues had poor aqueous solubility and was never greater than that of NP118809 (0.52 μg mL^{-1}). Replacing one of the aromatic rings of the diphenylmethyl group with a piperidine however did enhance solubility and importantly retain both potency and selectivity. Compound (62) was a potent Cav2.2 blocker ($IC_{50} = 0.1$ μM) with similar selectivity to NP118809 (110-fold) and an aqueous solubility of 72.7 μg mL^{-1}; however when tested in a rat model of neuropathic pain [spinal nerve ligation (SNL) model], it failed to show analgesic efficacy. No pharmacokinetic data on the compound is given, so the reason for lack of efficacy is not clear.

A second publication[131] describes work focused on NP078585, where the focus is on reduction of the hERG inhibition previously reported to be an issue with this compound. Initially the work investigated introducing amide linkers between the side chains and the central piperazine in combination with varying the substituents (R) on the left-hand phenyl ring (63, Fig. 17). This initial work resulted in (64) which had a dramatic improvement in overall profile compared with NP078585, having Cav2.2 $IC_{50} = 0.09$ μM, selectivity of 900-fold over Cav1.2 and hERG $IC_{50} = 9.0$ μM. Trifluormethyl and methyl groups were also investigated as alternatives to tert-butyl but lost potency at Cav2.2. Following the initial success neuromed went on to investigate modifications of the central piperazine ring. Initially they investigated the effect of adding a simple methyl group and found that this was able to increase Cav2.2 potency and selectivity over hERG, but the selectivity profile of the compound was highly dependent on the position and isomeric nature of the methyl group as illustrated by (65) and (66). Both compounds were very potent Cav2.2 blockers ((65) $IC_{50} = 0.01$ μM and (66) $IC_{50} = 0.04$ μM) but had different hERG profiles ((65) $IC_{50} = 0.9$ μM and (66) $IC_{50} = 4.9$ μM).

In addition to substitution of the piperazine ring, replacements were also investigated in the form of 3-amino pyrrolidines (67), and while encouraging profiles were obtained, the compounds were generally inferior to the corresponding piperazines. Compounds (64) and (65) were selected for study in two different pain models. Both showed good efficacy when dosed at 30 mg kg^{-1} (*ip*) in the formalin model and when tested at the same dose but by oral administration in the Chung model of neuropathic pain[132] both (64) and (65) were able to significantly reverse thermal hyperalgesia but only (65) was efficacious at reversing mechanical hyperalgesia. The medicinal chemistry article of this second series is also accompanied by a second publication which focuses on the synthesis on the chiral piperazine derivatives.[133]

The compounds described in Neuromed's publications are covered by a number of patent applications[134–136]; however no development has been reported for Cav2.2 blockers other than Z160.

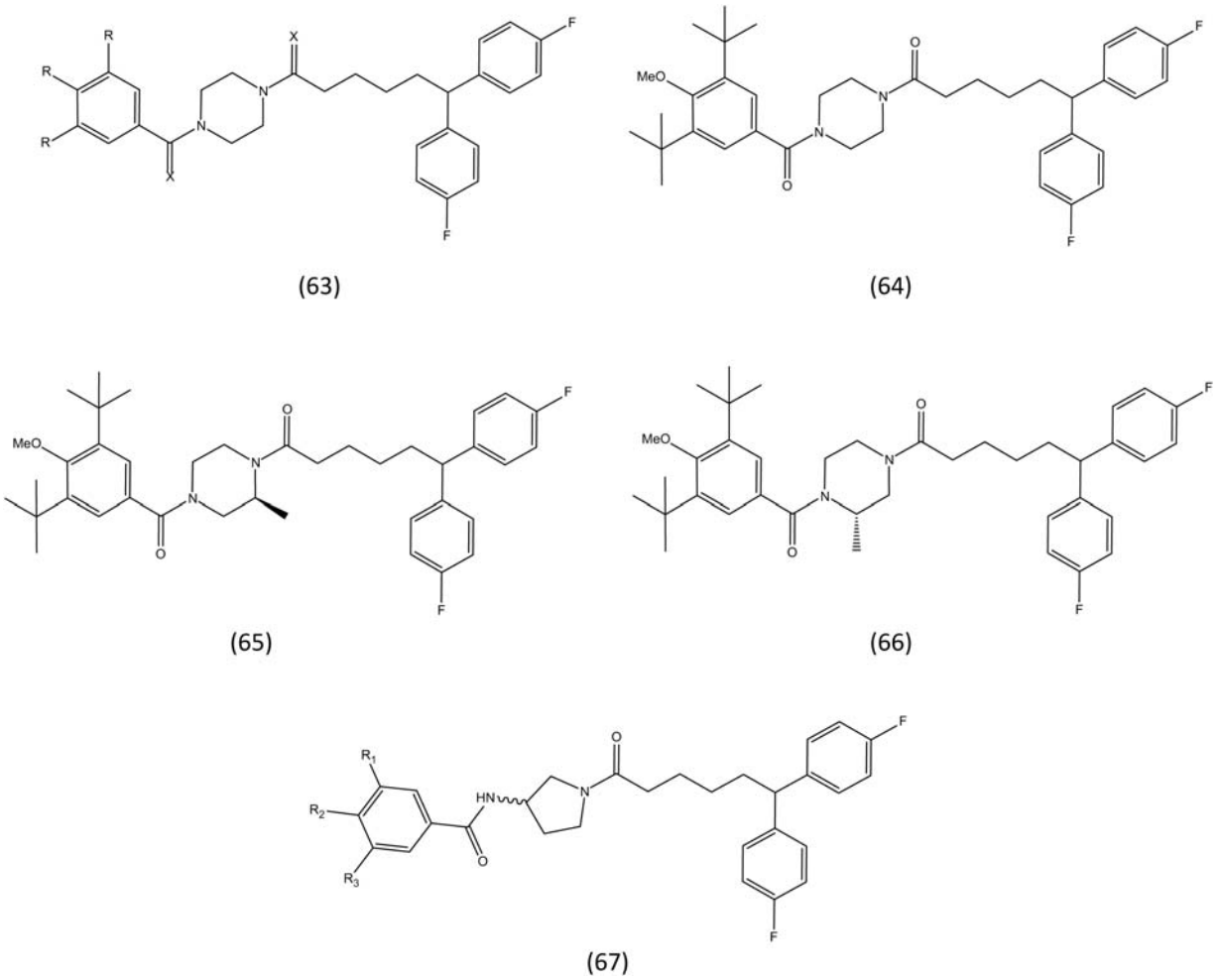

Fig. 17 Compounds prepared by Neuromed during the optimisation of NP078585.

7.03.5.3.5.3 Abbott compounds

Abbott has described the identification of a series of diphenyl lactams in which the diphenylmethyl group is incorporated into the lactam ring[137] (**Fig. 18**). The work led to two advanced compounds A-686085 (69) and A-1048400 (16) whose detailed profiles have been described in a subsequent publication.[138] The series was identified through high-throughput screening with the original hit being trimethoxy compound (68). Comparing the structure of the hit with the compounds published by the Neuromed group led to the proposal that the diphenyl lactam might be acting as an isostere for the diphenylmethylpiperazine. To test their proposal Abbott prepared several small sets of compounds based on the general structure (70). Initially both 5- and 6-membered ring lactams were synthesized and analogues prepared in which a piperazine ring substituted with either a benzhydryl group (70, R = phenyl, D = N) or benzyl group (70, R = H, D = N) was attached through an acetamide linker. The initial set of compounds tested was benzyhydryl derivatives, and all compounds were tested in a FLIPR assay. Promising activity was seen in both 5- and 6-membered lactam analogues with a set of benzhydryl groups which were either unsubstituted or had a halogen (chlorine or fluorine) in the 4 position of each benzene ring. pIC_{50} values ranged from 5.4 to 6.4. Work was quickly stopped as all compounds suffered from poor aqueous solubility (< 25 μM, neutral pH) largely due to the high lipophilicity (cLogP > 6 in most cases). The exercise was repeated with benzyl substituents (70, R = H) which reduced the overall log *P* of the compounds and improved solubility but resulted in a small drop in potency, typically 0.5 log unit compared to the corresponding benzhydryl analogue. Finally replacements for the piperazine were investigated focusing mainly on piperazines (70 R = Ph, D = CH). The replacement was tolerated in terms of potency but increased the lipophilicity of the compounds resulting in poor drug like properties. All compounds described were active with pIC_{50} values in the range of 5.5–6.0. Finally selected compounds were profiled in in vitro DMPK assays and in in vivo DMPK and efficacy assays with (16) having the optimal profile. The full profile of both (16) and (70, A-686085) was described in a subsequent publication[138] which is summarized in **Tables 4** and **5**.

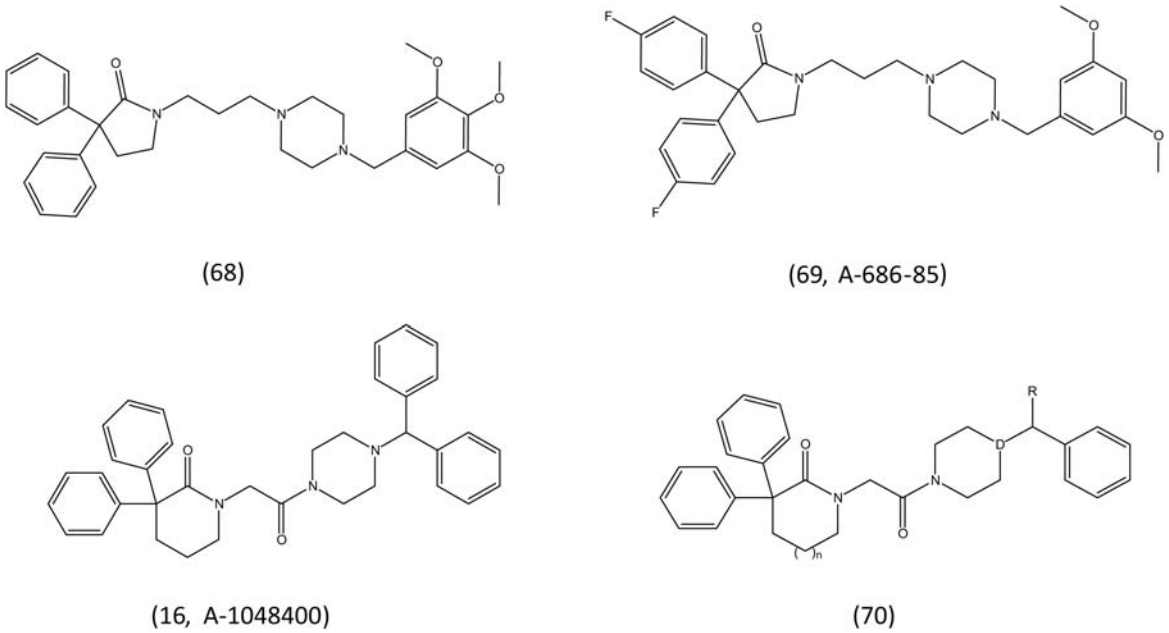

Fig. 18 Compounds prepared by Abbott during the identification of A-686085 and A-1048400.

Table 4 Comparison of A-686085 and A-1048400

Assay	*A-686085*	*A-1048400*
FLIPR IC_{50} μM		
N	0.8	1.4
T	4.6	1.2
Relaxation of rat aortic ring (EC_{50}, μM)	0.6	28
Effect on MAP (iv)	58% (0.7 μg mL^{-1})	NSE (4.9 μg mL^{-1})

Table 5 Biological profile of A-1048400 (16)

Assay	*Result*	
Electrophysiology	Closed state IC_{50} (μM)	Inactivated state IC_{50} (μM)
Cav2.1	16.1	1.3
Cav2.2	4.1	0.8
Cav3.2	2.6	0.9
Selectivity		
CEREP (80) panel	$IC_{50} > 80$ ion channels GPCRs except NPY2 ($K_i = 0.97$ μM)	
Pharmacokinetics (rat)		
$T_{1/2}$ (h)	2.7	
Vd (L kg^{-1})	5.8	
Clp (l $h^{-1} kg^{-1}$)	1.5	
F (%)	16.6	
Brain/plasma	1:10	
Pain models	ED_{50} (mg kg^{-1}, po)	
MIA	8.9	
CFA	38	
SNL	15	
CCI	53	
Safety		
Rotorod	No significant effects up to and including 300 mg kg^{-1}	

The two compounds were profiled together initially in selectivity assays and in an in vivo study which examined the effects of the compounds on cardiovascular parameters. Neither compound showed appreciable selectivity over the Cav3 channels but differed in their effects on Cav1.2 channels as determined in a rat aortic ring assay. The original lead A-686085 (70) potently relaxed the tissue with an $IC_{50} = 0.6\ \mu M$, whereas A-1048400 (16) produced only weak inhibition. When profiled in vivo A-686085 caused a marked decrease in mean arterial pressure (MAP) at a concentration of $0.7\ \mu g\ mL^{-1}$ in contrast to A-1048400 which showed no effects on MAP up to and including a concentration of $4.9 \mu g\ mL^{-1}$. Based on the data in **Table 4** A-1048400 was selected for detailed profiling along, and the data is shown in **Table 5**.

When tested in electrophysiology assays A-1048400 was shown to be a potent and state-dependent inhibitor of Cav2.2 channels. Interestingly it showed little or no selectivity for Ca2.1 and Cav3.2 channels. In terms of general selectivity the compound had an excellent profile, only having appreciable binding affinity at the neuropeptide Y2 receptor.

The molecule had a pharmacokinetic profile suitable for testing via oral administration with acceptable bioavailability and reasonable half-life in the rat. The brain to blood ratio was rather low and perhaps surprising given the quite high volume of distribution, suggesting the compound maybe a transporter substrate, although this is not mentioned in the publications. Encouragingly when tested in a battery of pain models A-1048400 showed activity in all modalities being active in models of inflammatory pain—the mono-iodoacetic acid (MIA) model of osteoarthritis pain[139] and the complete Freunds adjuvant (CFA) inflammatory pain model [140] together with models of neuropathic pain, the sciatic nerve ligation model and the chronic constriction injury model. Finally and also encouragingly there appeared to be low potential for CNS side effects as no adverse effects on motor coordination were detected in the rotorod test.[141]

A-1048400 is covered by a single patent[142] and does not appear to have entered development based on currently available information.

A second and possibly related series was later described by the Abbott group[143] which contains a dicyclohexylmethyl group rather than the more common diphenylmethyl (**Fig. 19**). These compounds were also identified through a high-throughput screen. A series of bicyclic compounds were identified as micromolar Cav2.2 blockers in a FLIPR assay (e.g., (71), **Fig. 19**, $IC_{50} = 4.67\ \mu M$) which importantly were devoid of Cav1.2 activity ($IC_{50} > 30\ \mu M$). Initial work focused on studies using racemic material and examined two areas of the molecule (a) introduction of substitution on the benzyl group where it was found that addition of lipophilic groups gave rise to a modest increase in potency but did not affect selectivity over Cav1.2, for example, (72) was shown to have a Cav2.2 $IC_{50} = 1.3\ \mu M$ and Cav1.2 $IC_{50} > 30\ \mu M$. (b) Variation of the amide moiety and a variety of amide substituents were tolerated in dialkylmethyl groups and monoalkylmethyl groups, analysis of the data showed that the dicyclohexyl was optimal both for potency and selectivity of Cav1.2.

Resolution of (72) into separate enantiomers showed (73) to have the superior profile (Cav2.2 $IC_{50} = 0.46\ \mu M$; Cav1.2 $IC_{50} = > 30\ \mu M$) with (74) being slightly less potent (Cav2.2 $IC_{50} = 1.4\ \mu M$; Cav1.2 $IC_{50} = > 30\ \mu M$). Based on this data (73) was selected for further study (**Table 6**).

Compound (73) was shown to be a highly potent state-dependent Cav2.2 blocker which was selective over Cav1.2 channels as demonstrated in the rat aortic ring assay and consequently had no effect on cardiovascular parameters up to a concentration of

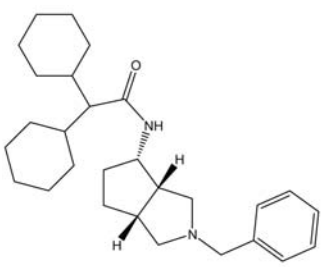

(71)

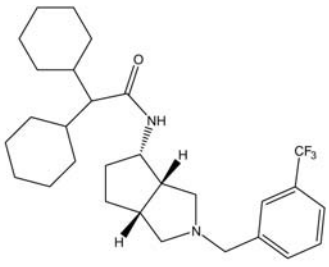

(72)

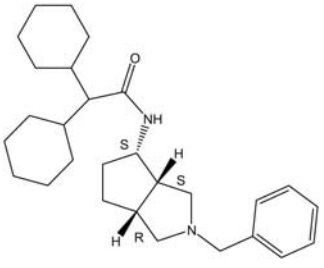

(73)

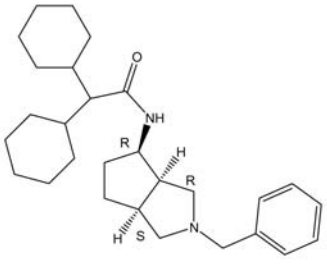

(74)

Fig. 19 Dicyclohexymethyl compounds published by Abbott.

Table 6 Detailed profile of (73)

Assay	*Result*	
Electrophysiology	Closed state	Inactivated state IC_{50} (μM)
Cav2.1	49% inhibition, 0.3 μM	0.041
Relaxation of rat aortic ring (EC_{50}, μM)	46	
Solubility	<3 μM	
Plasma protein binding	$>99\%$	
Bioavailability (ip)	41%	
Pain models (ip)	Effect	
MIA	87% reversal (30 mg kg^{-1})	
Carageenan	67% reversal (30 mg kg^{-1})	
Formalin	51% reversal (10 and 30 mg kg^{-1})	
Safety		
Effect on MAP (iv)	No effect up to 17 μg mL^{-1}	
Rotorod	No significant effects up to and including 30 mg kg	

17 μg mL^{-1} in vivo. Abbott stated that the compound is highly lipophilic (data not given) and that as a consequence the compound was poorly soluble and unstable in both rat and human microsomes ($<5\%$ parent remaining after 30 min incubation). Due to the poor solubility and metabolic instability, its pharmacokinetic profile was evaluated via ip administration and shown to be suitable for efficacy and safety profiling. In a variety of pain models (73) demonstrated efficacy and showed no sign of CNS side effects in the rotorod model. The compounds are covered by two patents[144,145]; however, to date there is no evidence that any of these compounds entered development.

7.03.5.3.5.4 Diphenylmethylpiperazines and related structures published only in the patent literature

A number of companies have patented novel Cav2.2 blockers containing diphenylmethyl groups linked to a saturated nitrogen containing heterocyclic ring. These are summarized in Fig. 20. The majority of compounds have been identified by Shionogi or

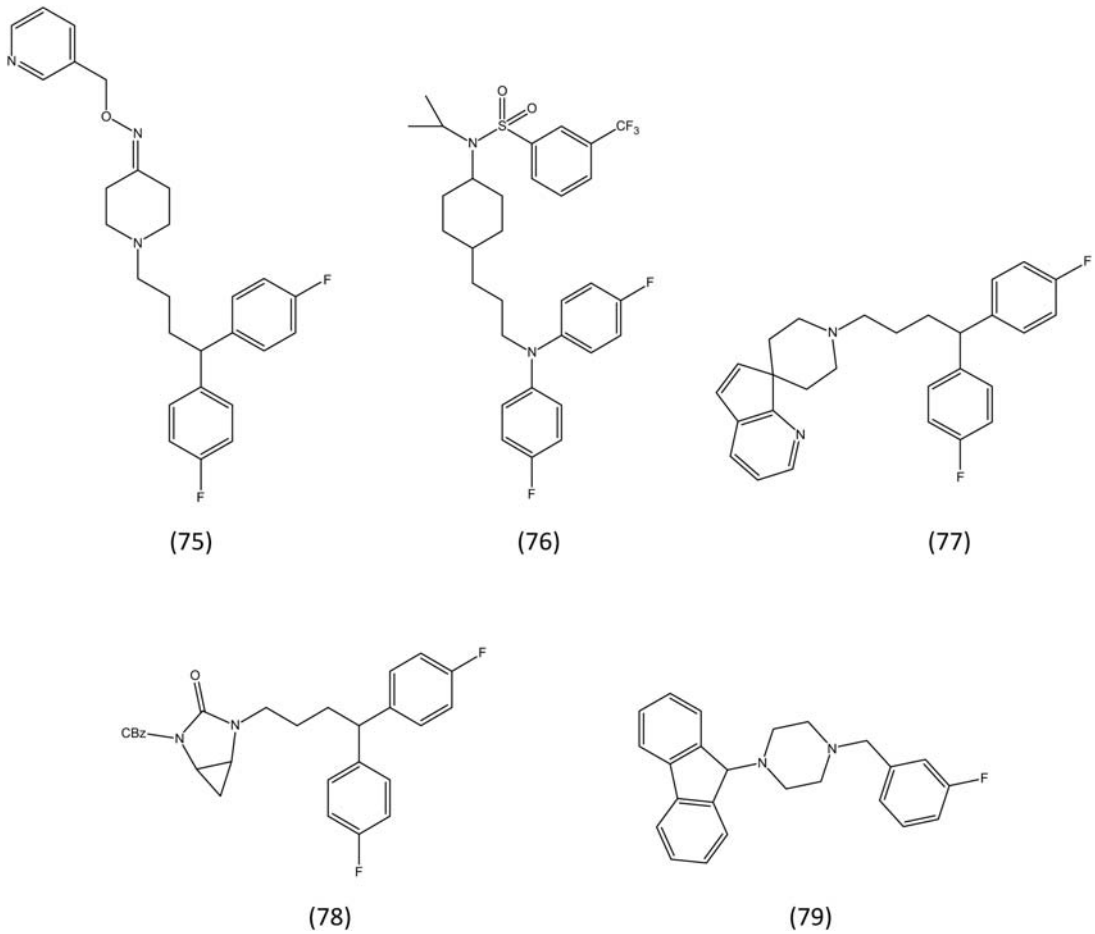

Fig. 20 Diphenylmethylpiperazines published in the patent literature.

Shionogi/Euro-Celtique who have published four patent filings covering compounds containing this template or related structures. The only patent which contains screening data describes a series of oximes with (75) reported to have an IC_{50} of 6.6 μM in a Cav2.2 FLIPR assays.[146] Other filings cover a range of different group including aminocyclohexylsulfonamides (76),[147] spiro indanes (77),[148] and cyclic ureas (78).[149] A recent filing from Institute of Pharmacology and Toxicology, Academy of Military Medical Sciences, PLA, Peoples Republic of China covers a series in which the diphenylmethyl group is fused producing a tricyclic system (79).[150] No data is provided.

7.03.5.3.6 Sulfones and sulfonamides

7.03.5.3.6.1 Merck compounds

Another template which has been reported by a number of groups is that based on a core structure of a saturated cyclic amine capped with a sulfonamide or the corresponding sulfone. Many examples of this template have appeared in the patent literature during recent years but as yet relatively few scientific articles have been published. Merck has published the details of one series of compounds.[151,152] Sulfonamide (80, Fig. 21) was identified by high-throughput screening and showed promising activity in a FLIPR assay (Cav2.2 $IC_{50} = 0.12$ μM), the compound however displayed poor selectivity over Cav1.2 ($IC_{50} = 0.12$ μM) and hERG (91% inhibition (1 μM). Additionally (80) had a poor pharmacokinetic profile when tested in the rat having a clearance in excess of liver blood flow ($Clp = 169$ mL $min^{-1} kg^{-1}$). Initial modification of the propyl group on the sulfonamide gave (81) which showed increased Cav2.2 potency ($IC_{50} = 0.06$ μM) but retained similar activity at hERG (70% inhibition (1 μM)), and this template was selected for further SAR investigation. Modification of the left-hand phenyl ring (phenyl ring of the benzyl group) substituents revealed that (a) a wide range of lipophilic groups were tolerated but retained the profile of the original hit; (b) polar, hydrogen bond donor groups reduced potency at Cav2.2; and (c) introduction of a sulfonyl group at the 2-position improved both potency and selectivity (82). Several compounds were selected for further profiling of which (82) is described in the most detail (Table 7).

Compound (82) has slightly reduced activity at Cav2.2 in the FLIPR assay but an improved selectivity profile both against Cav2.1 and hERG. The compound had an excellent pharmacokinetic profile in the rat and showed efficacy in models of both inflammatory and neuropathic pain. Unfortunately the in vivo efficacy results were rendered equivocal with the finding that a metabolite which circulated in appreciable concentrations (83) showed efficacy in both pain models but was devoid of Cav2.2 activity, hence the compound was not progressed further. It also inhibited cytochrome P450 3A4 ($IC_{50} = 5.1$ μM) and showed the potential to induce

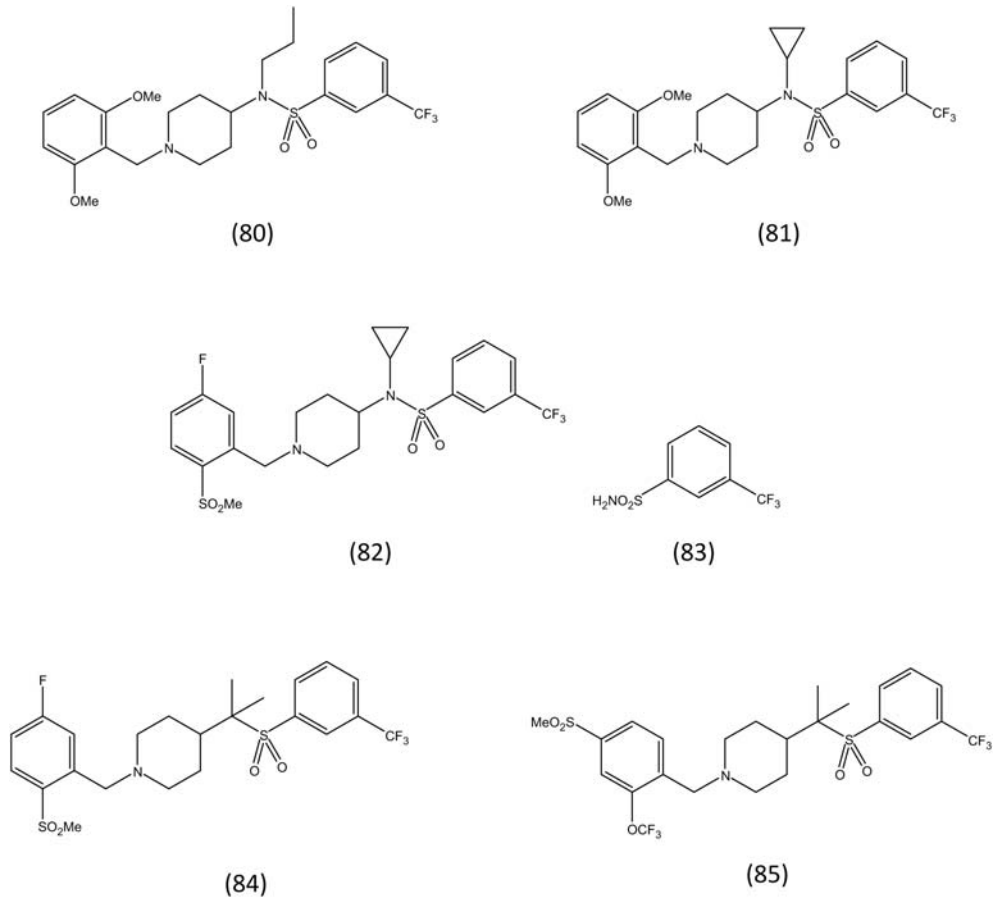

Fig. 21 Sulfonamides and sulfones published by Merck.

Table 7 Detailed profile of compounds 82, 84, and 85

Compound	*82*	*84*	*85*
Assay	Result		
FLIPR			
Cav2.2 (IC_{50}, μM)	0.56	0.51	0.092
Cav2.1	34% inhibition (3 μM)	$IC_{50} > 10$ μM	$IC_{50} > 10$ μM
Electrophysiology			
Cav2.2	84% block @ 3 μM (−40 mV) 34% block @ 10 μM (−90 mV)	–	–
Binding[a]			
hERG	32% inhibition of binding @ 10 μM	$IC_{50} > 10$ μM	$IC_{50} > 10$ μM
CYP induction			
PXR EC_{50} (μM)	0.43	2.5	>30
Pharmacokinetics			
F (%)	99	24	95
Clp (mL min^{-1} kg^{-1})	35	29	27
$T_{1/2}$ (h)	1.3	–	2.3
Pain models (po)			
FCA (% reversal, 30 mg kg^{-1})	66 (1 h), 57 (3 h)—mechanical allodynia	57 (1 h), 54 (3 h)—mechanical allodynia	–
FCA (% reversal, 10 mg kg^{-1})	–	36 (1 h), 49 (3 h)—mechanical allodynia	21(1 h), 30 (3 h)—mechanical allodynia
SNL (% reversal, 30 mg kg^{-1})	59—mechanical allodynia	–	–

[a]Displacement of [^{35}S]MK-499, a well-characterized hERG K^+ channel blocker.

the same enzyme through its activity at the PXR receptor ($EC_{50} = 0.43$ μM). These results did however initiate further chemistry studies[152] to identify related compounds with similar Cav2.2 activity but which did not produce the same metabolite.

Efforts initially focused on two areas (a) further modification of the left-hand phenyl ring substituents and (b) replacement of the central piperidine with alternative saturated heterocycles. While many of the modifications resulted in potent Cav2.2 blockers, where tested compounds retained cytochrome P450 inhibitory and induction together with producing (83) when incubated with liver microsomes. The successful strategy which ultimately prevented formation of the undesired metabolite was to replace the nitrogen of the sulfonamide with a tertiary carbon atom thus creating a sulfone and avoiding a potential metabolic pathway involving initial hydroxylation of the carbon atom to which the nitrogen atom of the sulfonamide is attached. The profiles of two compounds (84) and (85) resulting from the work are described. Both compounds retained potent Cav2.2 activity in the FLIPR assay and good selectivity over Ca1.2 and hERG. Compound (84) showed a slight improvement in PXR activity and (85) had a much better profile. Both compounds had moderate clearance in the rat with (85) having higher bioavailability compared to (84); no reason is suggested for this difference. Both compounds demonstrate modest efficacy in the FCA inflammatory pain model. Compound (85) is reported to be a substrate for the transporter P glycoprotein (P-gp, efflux ratio 4.2) compared to (84) which is reported to have an efflux ration of 1.8. Neither compound was considered to be suitable for further progression. The compounds are covered by two patent filings.[153,154]

7.03.5.3.6.2 Janssen compounds

Janssen has also described a structurally distinct series of sulfonamides[155] derived from hits identified by high-throughput screening (**Fig. 22**). A series of diphenyl pyrazoles were identified from the screen which showed excellent potency in a functional calcium indicator dye assay (FDSS), ((86) $IC_{50} = 97$ nM) but demonstrated poor in vitro metabolic stability (14% remaining after 10 min incubation with rat liver microsomes). Additionally the hits were not chemically novel. In an attempt to achieve novelty and improved metabolic stability a series of substituted piperidines (87) were synthesized. A number of alkyl sulfonamides all demonstrated promising activity in the FDSS assay ($IC_{50} < 100$ nM). The compound (87, $R = MeSO_2$) was selected for full profiling (**Table 8**). The compound is a potent Cav2.2 blocker in both the FDSS and automated patch clamp assays; in the latter the compound showed evidence of frequency-dependent inhibition unlike ω conotoxin. Additionally selectivity of Cav1.2 is reported. What is interesting about Janssen's approach is they report data in a biochemical functional assay where (87) potently inhibits CGRP release from rat spinal cord slices evoked by potassium chloride treatment. Compound (87) is much more stable in liver microsomes compared to the original hit and when tested in the rat demonstrated had an encouraging pharmacokinetic profile. Surprisingly given the encouraging bioavailability (87) was subsequently profiled in two pain studies via ip administration where it showed efficacy in models of both inflammatory and neuropathic pain. SAR investigation around both of the benzene rings is reported and additionally the replacement of the chlorophenyl group with either saturated or heterocyclic systems. Limited studies around the methoxyphenyl group suggest that hydrophobic groups are preferred, and that the relative position of the chlorine on the other ring is important. However insufficient compounds are reported to draw strong conclusions. A similar trend regarding

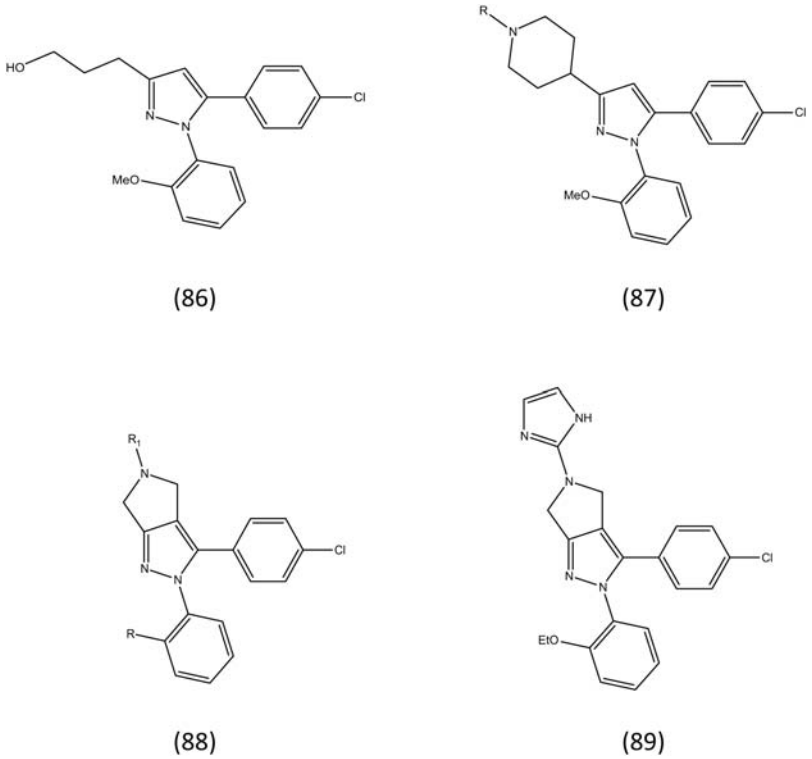

Fig. 22 Sulfonamides and related compounds published by Janssen.

a preference for hydrophobic groups is observed with the chlorophenyl ring. Attempts to replace the chlorophenyl group with fully saturated rings resulted in a small loss of potency which could be restored through introduction of a double bond. Heterocycles also appear to be tolerated although only a few examples are reported.

In two subsequent publications[88,156] Janssen described further studies based around optimization of (86). An alternative strategy to that previously described was to fuse a saturated nitrogen containing heterocycle onto the core pyrazole (88). Initial studies investigated a variety of phenyl substituents (R) in combination with nitrogen substituents (R1). Sulfonamides and sulfamides in combination with R as methoxy were optimal for both potency but did not afford stability in microsomes, for example, the methylsulfonamide derivative (R = OMe, R1 = SO_2Me) is reported to have Cav2.2 $IC_{50} = 21$ nM (FDSS assay) but following 10 min incubation with human liver microsomes only 3% compound remained. An extensive investigation of different sulfonamides in combination with different phenyl substituents produced a number of active compounds but failed to solve the metabolic stability issue in microsomes. The only way to achieve both potency and in vitro stability was to replace the sulfonamide

Table 8 Detailed profile of (87)

Assay	*Result*
FDSS	
Cav2.2 (IC_{50} μM)	0.027
Electrophysiology (Q Patch)	
Cav2.2 (IC_{50} nM)	0.2 (high frequency, 0.57 (low frequency)
Selectivity	
Cav1.2	52% inhibition @5 μM
Functional activity	
Inhibition of KCl-stimulated CGRP release in rat spinal cord slices	91% and 100% @ 1 μM (2 separate batches)
Liver microsomes	
% remaining after 10 min incubation	86 (h), 45 (r)
Pharmacokinetics	
F (%)	42.5
Clp (mL $min^{-1} kg^{-1}$)	26
$T_{1/2}$ (h)	1.5
Pain models (ip)	
Carageenan	82% reversal @ 30 mg kg^{-1}
CCI	41–51% reversal @ 30 mg kg^{-1} (cold allodynia)

group within this series, the optimal compound being the imidazole derivative (89). It should be highlighted that in their article Janssen does not specify which imidazole isomer was prepared however from the perspectives of both chemical stability and bioisosterism the isomer depicted by (89) is the most likely. Compound (89) is reported to have Cav2.2 activity ($IC_{50}=38$ nM, FDFSS assay), was active in the QPatch assay (13% inhibition at low frequency and 29% at high frequency when tested at 0.1 μM), inhibited CGRP release from rat spinal cord slices (21%@ 1 μM), and was stable in rat liver microsomes (81% remaining after 10 min incubation). No further scientific articles have been published by the Janssen group; however a number of patents have published covering structures related to those described. Compound (87) does not appear to have been covered by any patent filing; however bicyclic sulfonyl derivatives (88) are covered by a 2014 patent.[157] A number of related nonsulfonyl compounds are covered by patent filings but not covered by scientific publications and are briefly described in the following section.

7.03.5.3.6.2.1 Related compounds described in the patent literature

In addition to the sulfonamides and related structures that have been described in the scientific literature a number of closely related nonsulfonamide structures have been the subject of patent filings (**Fig. 23**). Three patents cover pyrazoles[158–160] with a cyclic oxygen containing substituent which is directly linked (90), fused as part of a cyclic ketal (91), or attached through a linker (92). In a more recent filing imidazole analogues (93) are also described.[161]

7.03.5.3.6.3 Sulfones and sulfonamides only published in the patent literature

The sulfonyl class of channel blocker is by far the most common in terms of publications, and while some templates have been described in detail in the scientific literature, many more are covered by patent filings. A summary of patents published in the last 10 years is shown in **Table 9**. A wide variety of sulfonamides have been patented which typically, but not exclusively, have an aryl sulfonyl group attached to a saturated ring which can bear a wide variety of functionality, suggesting that the phenyl sulfonyl moiety is in some way a privileged fragment. In many cases little or no data is given so drawing conclusions regarding SAR or the preferred compound in the patent is difficult.

Zalicus has filed one patent covering diaryl sufonyl derivatives, and compound (94) is reported to have an $IC_{50}=320$ nM in a FLIPR assay.[162] Shionogi has filed a total of eight patents all covering arylsufonamides some of which are filed by Shionogi and Euro-Celtique. Euro-Celtique SA acts as a patent holding agent for various companies. Four patents cover phenyl sulfonyl piperidines and vary in the nature of the group appended to the 4-position of the piperidine, which may be a vinyl amide, for example, (95) with the compound reported to have $IC_{50}=550$ nM (FLIPR assay).[163] *N*-acyl hydroxyamines (96),[164] oxycarbamates (97, $IC_{50}=240$ nM),[165] as well as glycine amides (98, $IC_{50}=440$ nM)[166] are claimed. The remaining four filings cover 4-piperidine sulfonamides (99, 100, and 101)[147,167–169] or 3-piperidine sulfonamides (102)[149] with the ring nitrogen capped by either acyl, sulfonyl, or alkyl groups. Compound (102) is reported to have $IC_{50}=130$ nM (FLIPR).

Convergence has filed a number of patents covering different sulfonamides. Five related patents cover piperazine sulfonamides (103–107). The first three patents[170–172] cover simple piperazine sulfonamides (103–105) capped with an amide and differ that in one case the piperazine is substituted with an alkyl group.[171] A further case covers similar structures, but the piperazine is capped

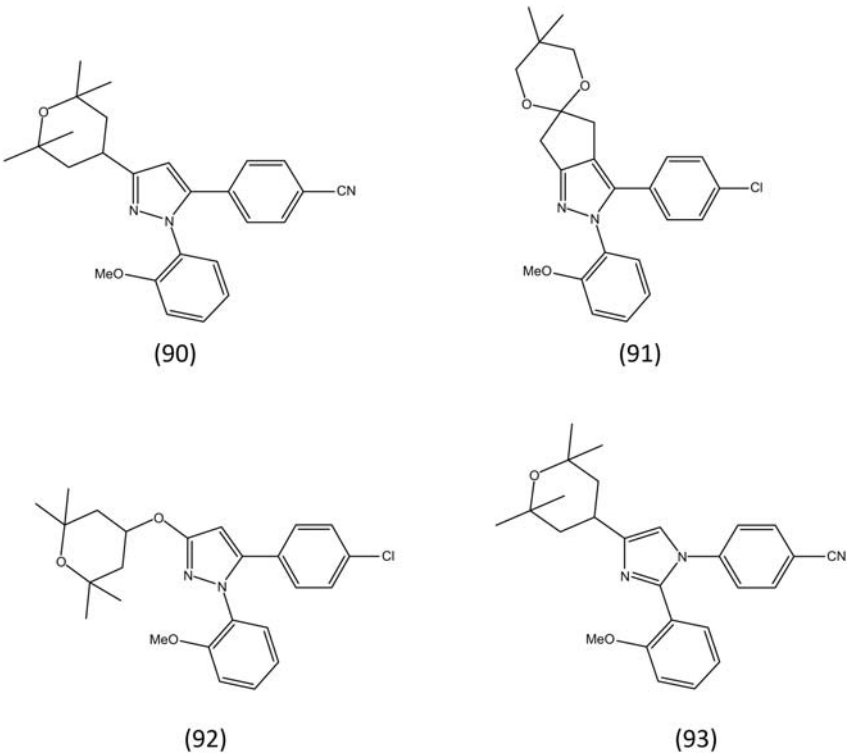

Fig. 23 Nonsulfonyl pyrazoles and imidazoles covered by Janssen patent filings.

Table 9 Sulfones and sulfonamides published in the patent literature

Organization	*Structures*
Zailcus	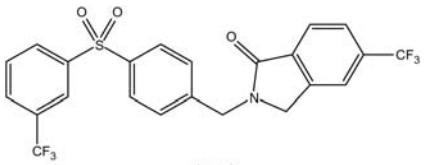 (94)
Shionogi/Shionogi Euroceltique	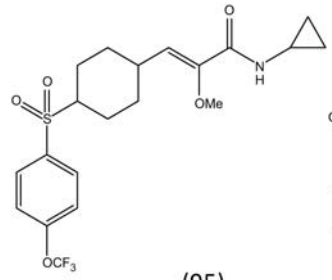 (95) 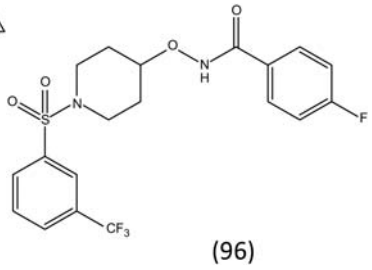 (96) 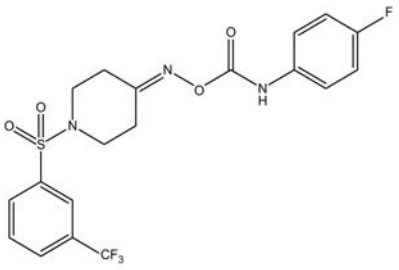 (97) 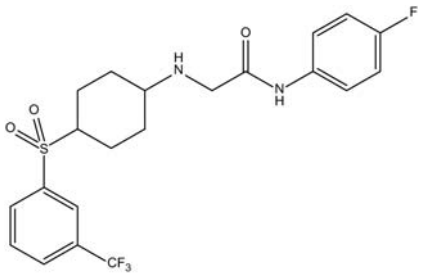 (98) 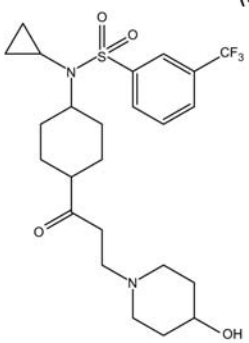 (99) 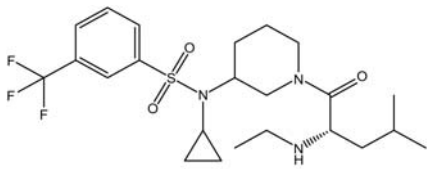 (100) 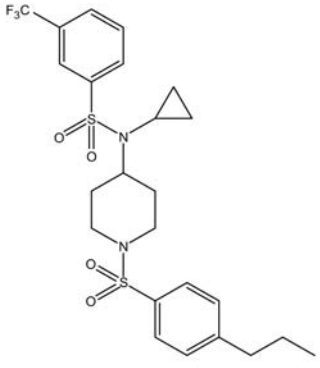 (101) 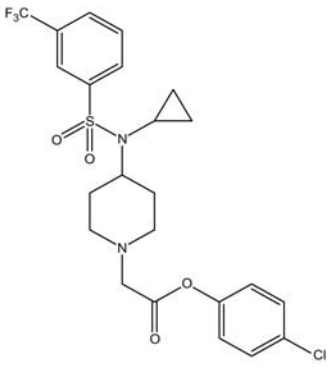 (102)

(Continued)

Table 9 Sulfones and sulfonamides published in the patent literature—cont'd

Organization	*Structures*
Convergence	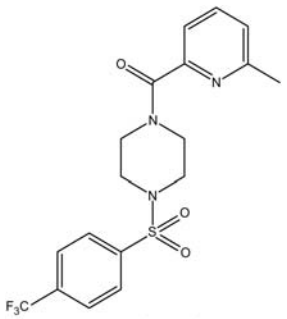 (103)
	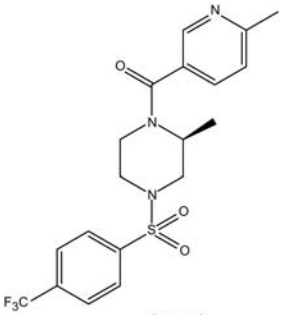 (104)
	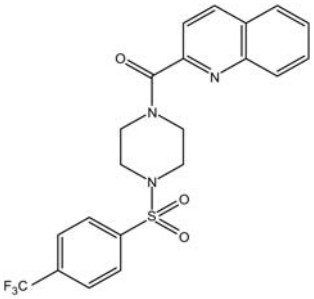 (105)
	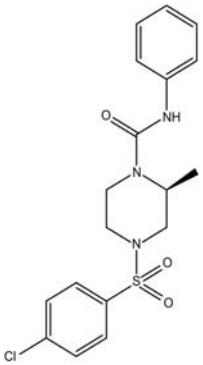 (106)
	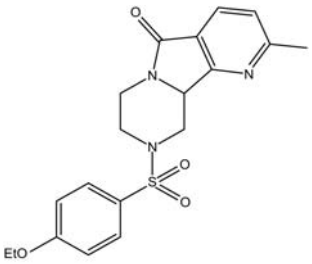 (107)
	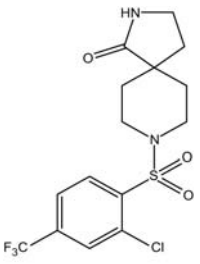 (108)

Table 9 Sulfones and sulfonamides published in the patent literature—cont'd

Organization	*Structures*
Pfizer	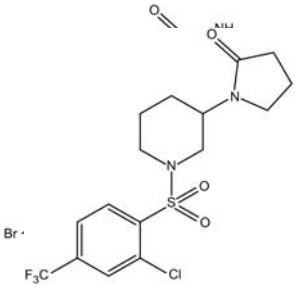 (110) 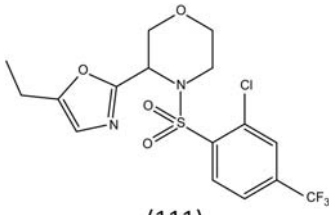 (111)
Grunenthal	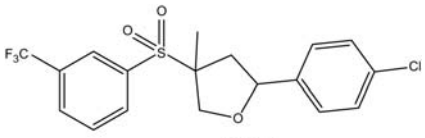 (112) 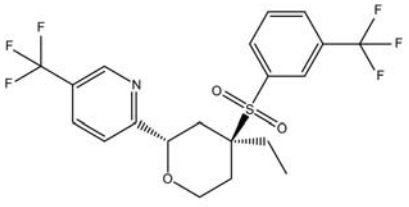 (113)
Ono	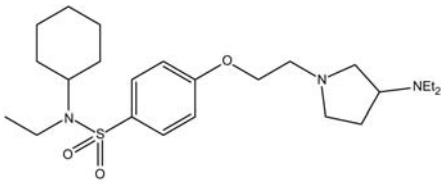 (114)
Vernalis	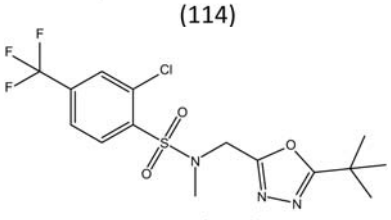 (115)
Ionix	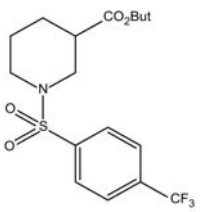 (116)

with a urea (106),[173] and in a fifth case the capping group is fused to the piperazine ring to form a tricyclic structure (107).[174] Three further cases cover piperidine sulfonamides (108–110) with an additional ring either attached as a spiro system at the 3-position[175] or 4-position[176] or appended directly to the 3-position of the piperidine.[177] In each case limited data is given, but the compounds shown are all described as being use-dependent blockers ($pUID_{30} > 5$) with at least 10-fold selectivity over the resting state of the channel tonic inhibition ($pIC_{50} < 4.5$ in an ionworks assay). No scientific publications have yet emerged from GSK or Convergence describing the discovery of these compounds, and the structure and biological profile of the clinical development candidate CNV2197944 still remains unknown.

Pfizer has filed a single patent[178] covering various saturated heterocyclic sulfonamides, and the morpholine (111) is reported to have $IC_{50} = 70$ nM (NTCC assay). Recently Grunenthal has filed two applications covering phenylsulfones with a tetrahydrofuran (112)[179] or tetrahydropyran (113) core[180]; both (112) and (113) are reported to inhibit Cav2.2 by >95% when tested at 3 μM (FLIPR). Ono has filed one patent covering benzenesulfonamides[181] with (114) reported to inhibit Cav2.2 by 82% (1 μM (FLIPR). Vernalis has filed a single patent[182] covering acyclic sulfonamides (115), no data is given. And Ionix has filed a patent[183] covering piperidine sulfonamides (116) with most compounds inhibiting Cav2.2 in the single-digit micromolar range (FLIPR).

7.03.5.3.7 Indole-derived structures

7.03.5.3.7.1 Merck compounds

Merck has published the profiles of several structurally diverse compounds with an indole ring as the core structure. The oxindole (18, TROX-1) is described in two biology publications[184,185] which detail the compounds pharmacological profile in detail. No medicinal chemistry around this template has been described to date, but the compound and analogues are covered by two patent filings.[186,187] It is also unclear exactly how TROX-1 was identified, but an assay development paper[188] published at a similar time to the biology papers suggest it might have been identified by screening. TROX-1 is a state-dependent Cav2.2 blocker (**Table 10**) and shows encouraging activity in several assay formats. It is selective over a wide range of targets, but poorly selective among the subtypes of the Cav2 family, particularly when tested in the depolarized state where it is an equipotent blocker of Cav2.1, Cav2.2, and Cav2.3 channels. The compound has an encouraging pharmacokinetic profile in the rat with high bioavailability a good plasma half-life and a brain to plasma ratio of unity. When tested in a range of pain models at 30 mg kg^{-1} the compound shows similar analgesic effects to standard marketed compounds such as pregabalin. In the rotorod assay while the compound did show the potential for CNS side effects at 100 mg kg^{-1}, no adverse effects were seen at lower doses suggesting the potential for an acceptable therapeutic index. When tested in a dog cardiovascular model, dose-related effects on heart rate and MAP were seen at doses of 3 and 10 mg kg^{-1}. The authors suggest that the effects are Cav2 mechanism related and that potentially the state

Table 10 Biological profile of TROX-1 (18)

Assay	*Result*	
FLIPR	Depolarised state IC_{50} (μM)	Hyperpolarised state IC_{50} (μM)
Cav2.2	0.27	>10
Electrophysiology		
Cav2.2 (DRG)	0.4	2.6
Cav2.1 (bMHN-4 cell line)	0.29	37
Cav2.2 (bMHN-4 cell line)	0.19	1.1
Cav2.3 (bMHN-4 cell line)	0.28	1.3
Selectivity	IC_{50} (μM)	
Cav1.2 (FLIPR)	18	
Cav3.1 (FLIPR)	15	
Cav3.2 (FLIPR)	>20	
166 target panel	All binding < 50% inhibition of binding @ 10 μM except adrenergic a2A (IC_{50} 8.2 μM),[a] 5-HT6 (IC_{50} 8.8 μM)[a] and phosphodiesterase(IC_{50} 7.6 μM)[b]	
Pharmacokinetics (rat)		
$T_{1/2}$ (h)	2.2	
F (%)	89	
Brain/plasma	~1:1	
Pain models	% reversal (30 mg kg^{-1}, *po*)	
MIA	49	
CFA	81	
SNL	72	
Capsaicin	Equivalent activity to pregabalin	
Safety		
Rotorod	Significant observed at 100 mg kg^{-1}	
Dog cardiovascular	Dose dependent reduction in heart rate and MAP at 3 and 10 mg kg^{-1}. No significant effects observed at 1 mg kg^{-1}	

[a]No significant functional activity.
[b]Functional IC_{50}.

dependency is not optimal. It was felt that the profile was not suitable for progression largely due to the lack of selectivity among Cav2 family members.

TROX-1 and related analogues are covered by two patent filings.[186,187] Ref.[186] covers TROX-1 and a close set of analogues[187] covers structurally related compounds but with either no nitrogen substituent or those containing a methylene linker between the oxindole core and the nitrogen substituent, for example, (117). Little data is given in the patents hence it is difficult to have an idea of detailed SAR, but general trends can be observed.

In a related publication[189] Merck described the discovery of a series of indoles (118–121, **Fig. 24**). The series was identified through a screening campaign with the original hit being (118) having Cav2.2 $IC_{50} = 0.88$ μM (FLIPR) and encouraging selectivity over Cav1.2 and sodium channels (Nav1.5 channels). Preliminary SAR studies led to the identification of (119) which retained the potency and selectivity of the original hit. The initial focus was to simplify the structure, and Merck hypothesized that the C3 substituent might not be required for activity which was indeed the case. Focus then turned to SAR at the 5-position with compounds unsubstituted at C3. It was found that the gem dimethyl group was required for activity and that the bicyclic amide could be simplified to a *t*-butyl group which gave lead structure (120), having a very similar profile to (118) (Cav2.2 $IC_{50} = 0.88$ μM, similar selectivity). Further optimization showed that *t*-butyl acetamides at both N1 and C5 were optimal for potency, and isosteric replacements resulted in loss of activity. When tested, compounds with the 3,5 diphenyl group at C2 were unstable in both rat and human liver microsomes. Modifying the substituents on the phenyl ring afforded improved stability (for (121), 20% compound

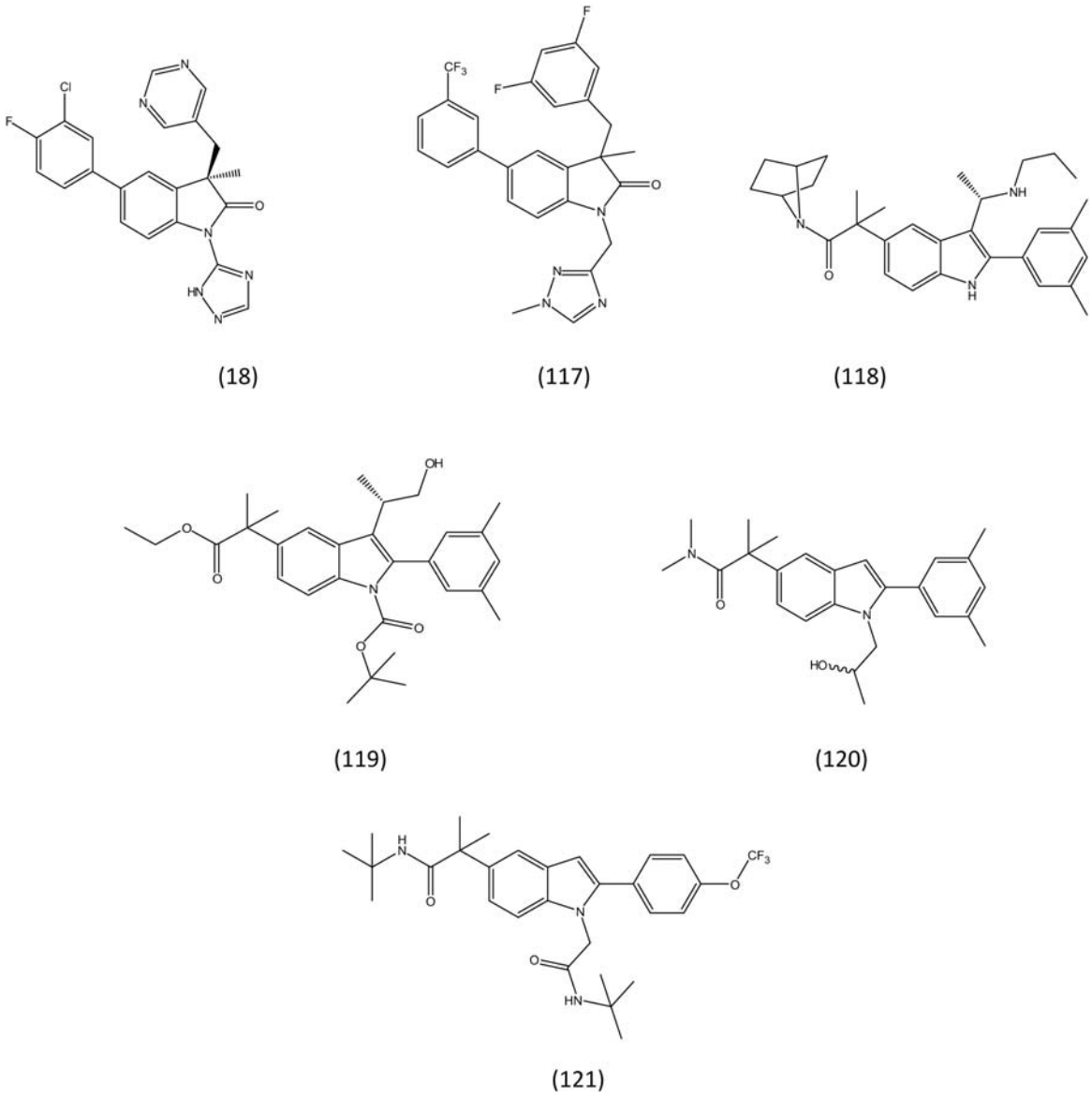

Fig. 24 Indole based compounds published by Merck.

remaining after 60 min incubation with both rat and human liver microsomes). The 2-trifluoromethoxy analogue of B was more stable in microsomal assays, but in vivo (121) had the better bioavailability and was chosen for further study. The indole derivative (121) was a potent Cav2.2 inhibitor in the FLIPR assay ($IC_{50}=0.15$ μM) with modest selectivity over Cav1.2 ($IC_{50}=0.91$ μM). It has a pharmacokinetic profile in the rat suitable for profiling in pain models (high clearance (64 mL $min^{-1}kg^{-1}$), $T_{1/2}=1.4$ h and 68% bioavailable). When profiled in models of both inflammatory and neuropathic pain it demonstrated robust efficacy at a dose of 30 mg kg^{-1} (*po*). However when dosed to dogs it showed effects on both heart rate and MAP at doses between 1 and 10 mg kg^{-1}. Plasma levels from the experiments suggest that the effects are consistent with the poor selectivity over Cav1.2. No further studies have been reported with this class of compounds. The indole compounds are covered by a single patent filing.[190]

7.03.5.3.7.2 Structures only disclosed in patents

Merck filed a patent[191] covering the tetrahydroisoquinoline derivatives (**Fig. 25**, (122) and (123)). The compounds are not indoles specifically, but given their structural similarity to TROX-1 (16) it is appropriate that they are included in this section. Compounds containing the mono and dioxo core are covered. They differ from TROX-1 in that no compounds are claimed with a pendant heterocycle corresponding to the triazole in (18). The compounds are potent Cav2.2 blockers with (122) and (123) have IC_{50} values of 023 and 0.02 μM, respectively. Preferred compounds are also described as having activity at Cav3 channels although no data is given. Lectus has filed two patents[192,193] covering indoles with a glyoxamide at the 3-position. The compounds are claimed to act by blocking interaction between the channels α1 and β subunits. The patent[192] covers simple oxamide derivatives, and compound (124) is reported to inhibit Cav2.2 activity by 44% at 1 μM in a rat DRG electrophysiology assay. The second patent[193] covers aminoacetic acid derivatives (125). Little data is given although (125) is described at inhibiting Cav2.2 currents in a rat DRG assay when applied at 50 μM.

7.03.5.3.8 Miscellaneous templates

7.03.5.3.8.1 Miscellaneous structures disclosed in the scientific literature

The 2-bromofuran ZC88 (126, **Fig. 26**) is reported to be a potent Cav2.2 blocker ($IC_{50}=0.45$ μM in oocytes) with high selectivity over Cav1.2 and Cav2.1 channels[194]; however it is also reported to be a hERG blocker.[195] The compound has been profiled in pain models where it demonstrates encouraging efficacy.[196] However, the presence of a 2-bromofuran moiety raises the question to the stability of the compound and its utility as a tool. The triazine T4 (127) has recently been reported by Abbvie scientists as a highly state-dependent blocker.[197] No patents have been published covering either of these compounds.

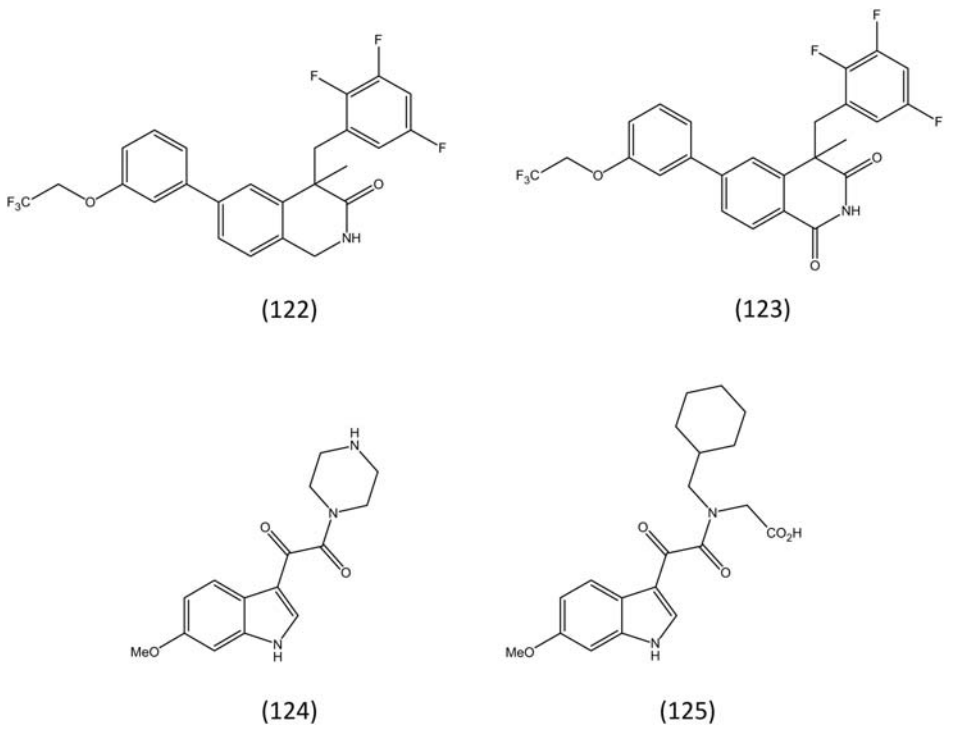

Fig. 25 Indole based scaffolds only disclosed in the patent literature.

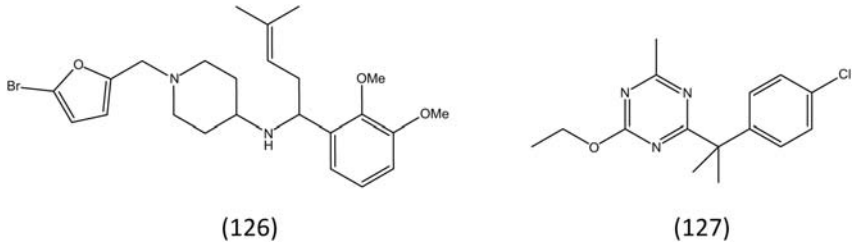

Fig. 26 Miscellaneous structures disclosed in the scientific literature.

7.03.5.3.8.2 Miscellaneous structures disclosed in the patent literature

A number of patent filings cover compounds not disclosed in the scientific literature and which do not belong to classes reported by other organizations (Fig. 27). Astellas has a single filing[198] which covers tetrahydroisoquinolines (128), and the compound is reported to actively block calcium influx into IMR 2 cells when tested at 1 μM, and when tested in the formalin pain model at 100 mg kg^{-1} produced a 52% reversal of response. Vertex has filed a patent covering quinazolines (129), but no data is given.[199] Neuromed has filed a patent[200] covering amino acid derivatives (130) distinct from other templates they have disclosed. GSK/Convergence has filed one patent[201] which covers structurally distinct compounds from the sulfonamides around which their other patents are based. This case covers phenyltetrazoles (131), similar to the other cases compounds are reported to be use-dependent blockers and not display any tonic inhibition ($IC_{50} < 4.5$) in an ionworks assay. Grunenthal has filed four patents[202–204,306] covering pyrrole derivative (132).

7.03.5.4 Cav2.3 Blockers

There have been recent reports which suggest that Cav2.3 plays a role in pain signaling and that this channel might also be a pain target.[14] Validation data comes from studies with the tarantula toxin SNX-482 demonstrating efficacy in preclinical pain models.[205] It important to highlight that while SNX-482 selectively blocks Cav2.3 channels it does have some activity at Cav1 channels. Mice lacking the Cav2.3 gene demonstrate reduced sensitivity to pain,[206] and clinically it has been suggested that polymorphisms of the gene may be responsible for different responses to fentanyl in patients undergoing surgery.[14] Currently no selective small-molecule

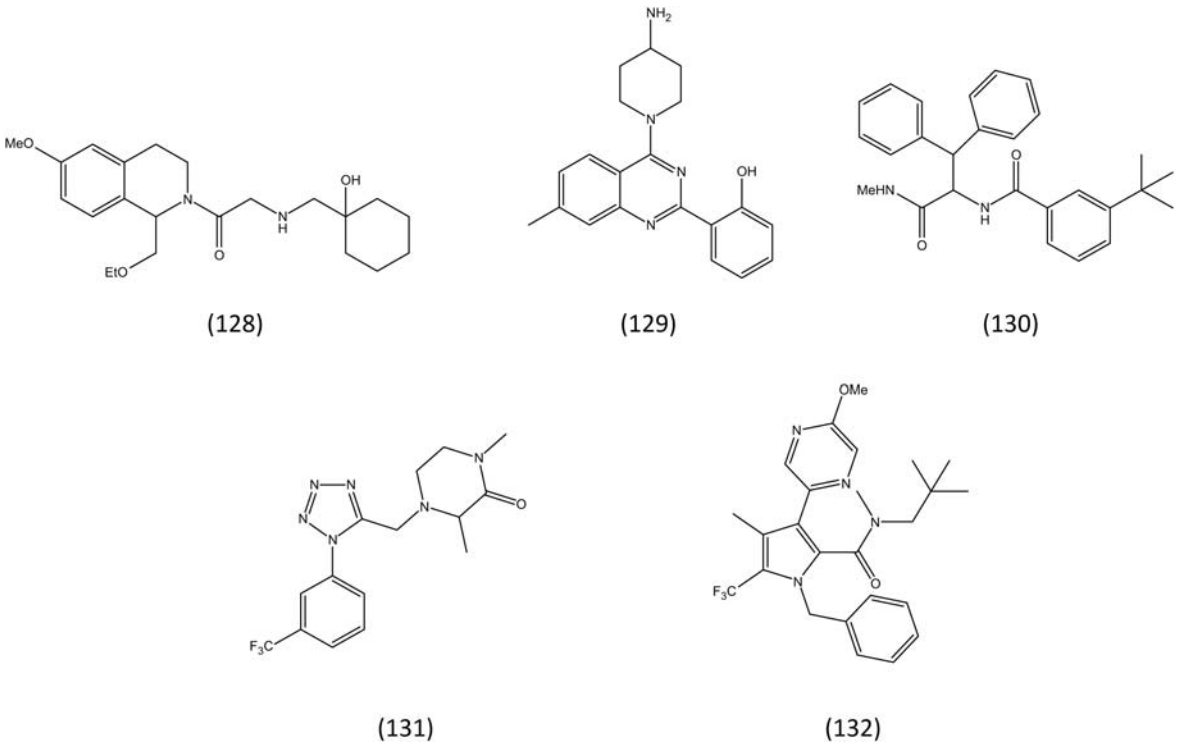

Fig. 27 Miscellaneous structures disclosed in the patent literature.

Cav2.3 inhibitors have been reported. There are publications showing that drugs such as lamotrigine and topiramate block Cav2.3 in addition to other channels.[14]

7.03.5.5 Cav3 Blockers

The Cav3 or T-type family has received much attention and is alongside Cav2.2 with respect to the level of interest based on volume of publications. Unlike Cav2.2 the T-type family has three well-characterized subtypes, Cav3.1, Ca3.2, and Ca3.3 all of which are validated pain targets. Most workers have focused on the identification of nonselective Cav3 blockers rather than subtype selective agents, and all three will be covered together in this section and molecules which have demonstrated selectivity will be highlighted. Unlike the Cav2.2 there are relatively few toxins reported to be potent and selective inhibitors of Cav3 channels. A number of agents have been reported that block Cav3 channel but are also potent blockers of other channels. The only toxin reported to date with any genuine selectivity is PsPTx3, a peptide isolated from Theraphosidae tarantula that has apparent selectivity for Cav3.2 calcium channels.[207] The preferred tools for Cav3 block in electrophysioloigical characterization studies are metal ions such as nickel. Thus there has been no small-molecule inhibitors designed using peptides as starting points. It should be pointed out that there is strong target validation for the role of Cav3 channel in neurological disorders other than pain, including epilepsy, Parkinson's disease, hypertension, and regulation of arousal state.[11,208–210] As a result many of the compounds reported have been profiled in models of several indications. While the therapeutic potential of Cav3 blockers in other indications is well validated a detailed discussion is beyond the scope of this article and discussion will be limited to pain studies where available.

7.03.5.5.1 Early molecules

A number of early compounds which are currently in clinical use for non-pain indications have been reported to have activity at the Cav3 family (Fig. 28). One of the first small-molecule Cav3 blockers reported was amiloride (133) which has multiple other activities has been shown to block Cav3.2 channels with about 10-fold selectivity over Cav3.1 and 3.3. Ethosuximide (4) has been shown to be a weak, nonselective, state-dependent Cav3 blocker[72] and is currently used clinically as a treatment for epilepsy. Recently a study commenced to investigate the clinical potential of ethosuximide to treat neuropathic pain.[71] It has previously demonstrated efficacy in a number of preclinical pain models. The first compound which emerged which was claimed to be a potent and selective blocker of Cav3 channels was Mibefradil (134). The compound was marketed for the treatment of hypertension in 1997, however withdrawn a year later due to an issue with drug–drug interactions mediated by cytochrome P450 inhibition.[211] Mibefradil has subsequently been shown to be a nonselective Cav channel inhibitor with activity at most family members. NMP7 (135) has been reported to be a Cav3 blocker and demonstrates activity in a number of animal pain models however also possesses activity at cannabinoid receptors thus making data difficult to interpret.[212]

The most advanced compounds have been identified by Abbott and Epirus who both currently have compounds undergoing clinical studies ABT-639 (2) and Z944 (3), respectively. The Epirus compound is derived from a previously reported series of Cav2.2 blockers. The Abbott molecule represents a new structural class of calcium channel blocker.

7.03.5.5.2 Sulfonamides

7.03.5.5.2.1 ABT-639 and related compounds

The discovery and ADME optimization which led to ABT639 has been published[69] together with the detailed biological profile.[213] ABT-639 (2) is derived from screening hits (136) and (137) (Fig. 29). The hits were identified from a high-throughput screen using

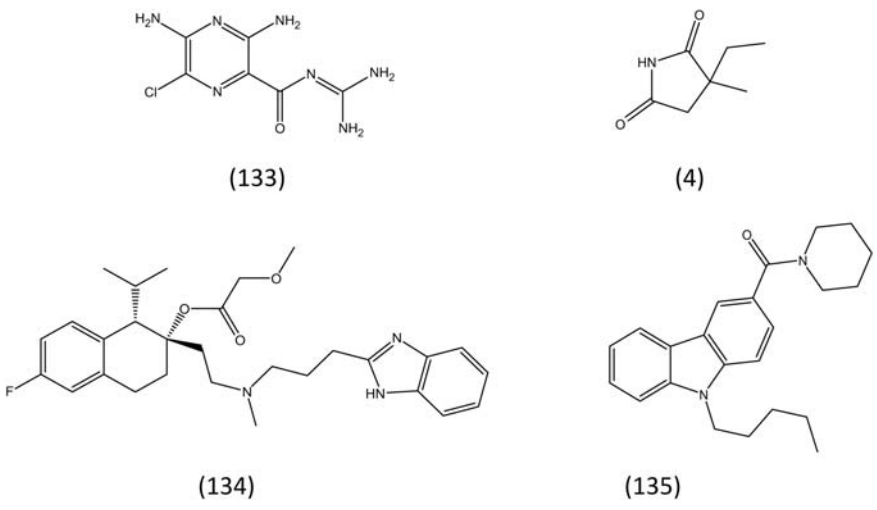

Fig. 28 Early small-molecule Cav3 blockers.

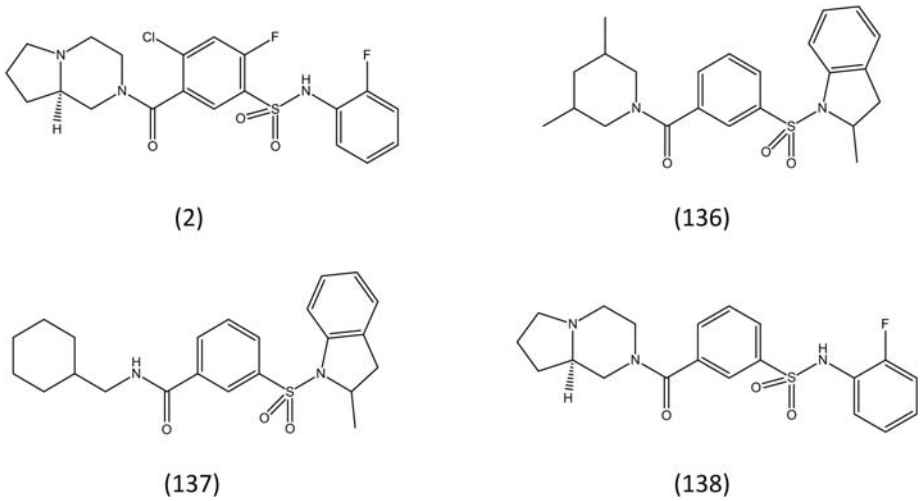

Fig. 29 ABT-639 and key molecules which led to its identification.

a FLIPR assay and a cell line expressing Cav3.2 and had IC_{50} values in the micromolar range (136, $IC_{50}=3$ μM ; 137, $IC_{50}=5$ μM); the compounds were however very unstable in rat liver microsomes (0.5% and 0.1% remaining, respectively, after 30 min incubation). Both compounds were also highly lipophilic (136, cLogP = 4.4; 137 cLogP = 5.3), and it was suggested that this was responsible for the metabolic instability. Following an exercise to reduce lipophilicity through changes to both the left- and right-hand sides of the molecule (138) was identified which had reduced lipophilicity (cLogP = 2.8) and an improved DMPK profile (68% compound remaining after 30 min incubation in rat liver microsomes) and when tested in vivo (rat) had acceptable bioavailability (35%) but was still highly cleared ($1.79\ L\ h^{-1}\ kg^{-1}$). The paper focuses on optimization of the ADME profile, and no Cav3.2 SAR is reported. Investigation of the relative clearance (138) and its enantiomer together with several other enantiomeric pairs showed the R enantiomers to be more stable than the corresponding S isomers, thus (138) was the preferred isomer from an ADME perspective. Further improvement in stability was achieved by substitution of the central aromatic core to give the final compound ABT-639.

The detailed biological profile of ABT-639 was published in a separate article[213] and is shown in **Table 11**. The compound is a selective state-dependent blocker of Cav3.2 channels with a pharmacokinetic profile in the rat suitable of supporting efficacy

Table 11 Biological profile of ABT-639

Assay	*Result*	
Electrophysiology	Inactivated state IC_{50} (μM)	Resting state IC_{50} (μM)
Cav3.2	$IC_{50}=2.3$ μM	NSE @ 30 μM
Cav3.1	50% inhibition (10 μM)	17% inhibition (10 μM)
Cav3.3	39% inhibition (10 μM)	17% inhibition (10 μM)
Cav2.2	11.8% inhibition (30 μM)	<10% inhibition (30 μM)
Cav2.1	NSE @ 30 μM	
Cav1.2	NSE @ 30 μM	
Selectivity	IC_{50} (μM)	
hERG	>200 μM	
CEREP panel	No off target activity detected (exact panel not given)	
Pharmacokinetics (rat)		
$T_{1/2}$ (h)	3.9	
F (%)	73	
Brain/plasma	0.05	
Pain models (*po*)		
MIA	ED_{50} 2 mg kg^{-1}	
CFA	25% reversal (100 mg kg^{-1})	
Carageenan	30% reversal (30 mg kg^{-1})	
SNL	Dose dependent efficacy (10–100 mg kg^{-1})	
CCI	Dose dependent efficacy (3–100 mg kg^{-1})	
Safety		
Edge test (*po*)	No effect observed up to and including 300 mg kg^{-1}	
Rat cardiovascular (iv)	No effect observed up to and including a dose of 30 mg kg^{-1}	

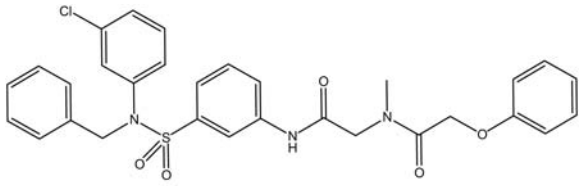

(139)

Fig. 30 Sulfonamide published by Bristol Myers Squibb.

studies, and it is peripherally restricted. When tested in rat pain models it was highly efficacious in models on neuropathic pain but poorly effective in models of inflammatory pain. In vivo electrophysiology studies supported these results as an iv infusion of ABT-639 (3 mg kg^{-1}) had no effect on spinal cord neuron firing in FCA-treated rats when stimulated with Von Frey hairs yet attenuated neuron firing in rats with spinal nerve ligation (SNL model). The compound had an encouraging safety profile when investigated for the potential to cause CNS-mediated effects and cardiovascular adverse effects. As discussed in Section "**Compounds Under Clinical Evaluation**" ABT-639 has recently failed to show efficacy in a clinical study for reason which are not clear, maybe central penetration could have been an advantage or possible selective inhibition of a single Cav3 subtype is not optimal. The compound is covered by two patent filings.[214,215]

7.03.5.5.2.2 Sulfonamides reported by Bristol Myers Squibb

Bristol Myers Squibb has reported a structurally distinct series of Cav3.2 blocker (139, **Fig. 30**) designed by computational methods using the structure of known antihypertensives which have been demonstrated to act via Cav3 blockade.[216] The compound has $IC_{50} = 110$ nM (patch clamp). Both the pharmacological profile and the compounds physicochemical properties do not lend it to being an analgesic agent however and the full profile will not be discussed.

7.03.5.5.2.3 Sulfonamides, sulfones, and related structures only reported in the patent literature

In addition to the detailed description of the discovery of ABT-639 in the scientific literature there are also a number of related templates that have been disclosed in the patent literature in recent years (**Fig. 31**). In a 2015 patent[217] Korea Institute of Science and Technology described a series of pyrazole containing sulfonamides with (140) being an example disclosed with relatively weak activity (61.42% of inhibition at 10 μM). A second patent[218] from the same group describes amide derivatives (141) with a similar right hand side, suggesting that the sulfonamide is not essential for activity (141) and are reported to have similar activity to (140). In a 2010 patent[219] Zalicus claims a series of sulfones a specific example being (143) which has micromolar activity at Cav3.1 ($IC_{50} = 2.79$ μM) and Cav3.2 ($IC_{50} = 4.66$ μM). Only limited in vitro data is given for key compounds.

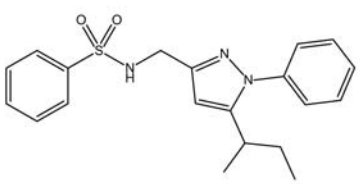

(140)

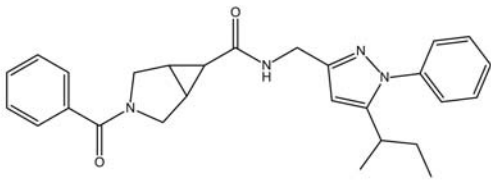

(141)

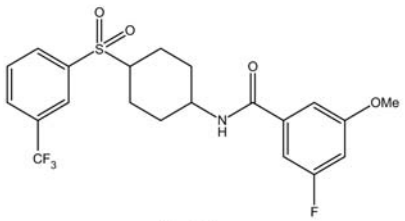

(142)

Fig. 31 Sulfonamides, sulfones and related structures reported in the patent literature.

7.03.5.5.3 Piperidine- and piperazine-based structures

A number of groups have reported a diverse range of structures containing a piperidine or piperazine ring as a core structure. In each case the core ring is flanked on either side by a hydrophobic group commonly linked by an amide function. The most advanced example of a compound from this series is Z944 (3) currently being developed by Epirus.

7.03.5.5.3.1 Z944 and related compounds

The discovery of Z944 (3) and a related compound Z941 (143) has recently been described[220] (**Fig. 32**). Both compounds were originally identified as treatments for epilepsy for which there is much precedent[208]; however it appears that currently the major clinical focus on Z944 is for its potential as an analgesic agent. Epirus described the chemistry strategy which initiated from Z160 (1) thus maintaining the beneficial properties of the compound, namely, lack of off target activity, potential for a good pharmacokinetic profile, particularly high central penetration, and ease of synthesis while optimizing Cav3.2 activity and enhancing solubility. The steps taken during the optimization are described in the publication, but no data is provided for the intermediates. The detailed profile of Z944 (3) is shown in **Table 12**. A less complete data package has been published on Z941 (1) and is therefore not included in the table although the reported Cav3.2 IC_{50} (inactivated state) is 150 nM. Both compounds are potent inhibitors of Cav3 channels with selectivity for the inactivated state. Z944 (3) shows selectivity for Cav2.2 and Cav1.2 channels. No pharmacokinetic information is given for either compound. Z944 (3) was profiled in a number of pain models[221] where it showed significant reversal of effects in the CFA model, the formalin test and in a butyric acid model of visceral pain. In a recent study Z944 (3) reversed

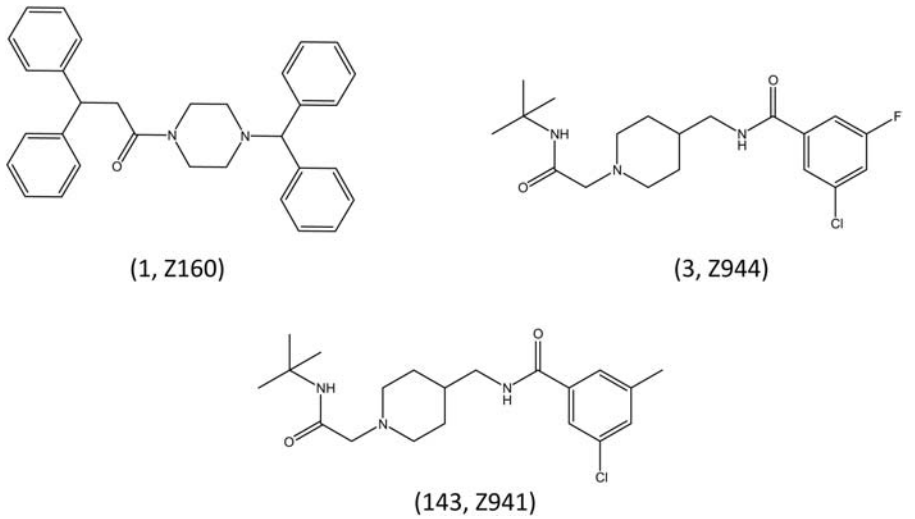

Fig. 32 Epirus compounds Z941 and Z944.

Table 12 Biological profile of Z944

	Z944	
Assay	*Result*	
Electrophysiology	Inactivated state IC_{50} (μM)	Closed state IC_{50} (μM)
Cav3.2	0.16	0.54
Cav3.1	0.05	0.13
Cav3.3	0.11	0.26
Cav2.2	11.0	150.0
Cav1.2	32	–
hERG	7.8	–
Nav1.5	>100	–
Pain models		
CFA (*po*)	Efficacious at 3 and 10 mg kg^{-1}	
CCI	Reversal of thermal hyperalgesia	
Formalin (*ip*)	Complete reversal of acute and late stage responses at 60 mg kg^{-1} (*ip*)	
Butyric acid (*po*)	Efficacious at 10 and 30 mg kg^{-1}	
Safety		
Monkey cardiovascular (*po*)	No effects on heart rate, MAP, RR and QTc intervals up to and including a dose of 45 mg kg^{-1}	

thermal hyperalgesia in the rat CCI model and encouragingly reduced neuronal firing when examined in an in vivo electrophysiology study.[222] Z944 (3) has also been profiled extensively in epilepsy models where it demonstrates an encouraging profile.[223] Both compounds were originally covered by a 2009 Neuromed patent.[224]

7.03.5.5.3.2 Merck TTA derivatives

Merck has reported the discovery of a number of structurally distinct series of Cav3 blockers all prefixed TTA which were all developed from hits identified by high-throughput screening using a FLIPR assay.[225] The first series of compounds (Fig. 33) is structurally related to Z941 and Z944, the most advanced compounds being TTA-P2 (147) and TTA-P1 (148). Details of two hit compounds arising from screening hits (144) and (145) have been published.[226,227] Compounds were tested in a membrane potential assay at two different holding potentials −20 mV (representative of the depolarized state and −60 mV (representative of the hyperpolarized state) in a cell line expressing Cav3.3 channels. Both hits had encouraging potency (144, $IC_{50}=185$ nM (−60 mV), $IC_{50}=215$ nM (−20 mV); 145, $IC_{50}=342$ nM (−60 mV), $IC_{50}=373$ nM (−20 mV)) but were not selective over hERG or Cav1.2. Initial SAR studies revealed that the optimal combination of substituents for potency at Cav3.3 and selectivity were those in (146) (Cav3.3 $IC_{50}=98$ nM (−60 mV), $IC_{50}=61$ nM, hERG $IC_{50}=1930$ nM, Cav1.2 $IC_{50}=1190$ nM); however when (146) was tested against a panel of GPCRs and other ion channels, it demonstrated a poor overall profile inhibiting eight other targets by more than 50% at 10 μM. Merck hypothesized that the strongly basic center might be responsible for the selectivity

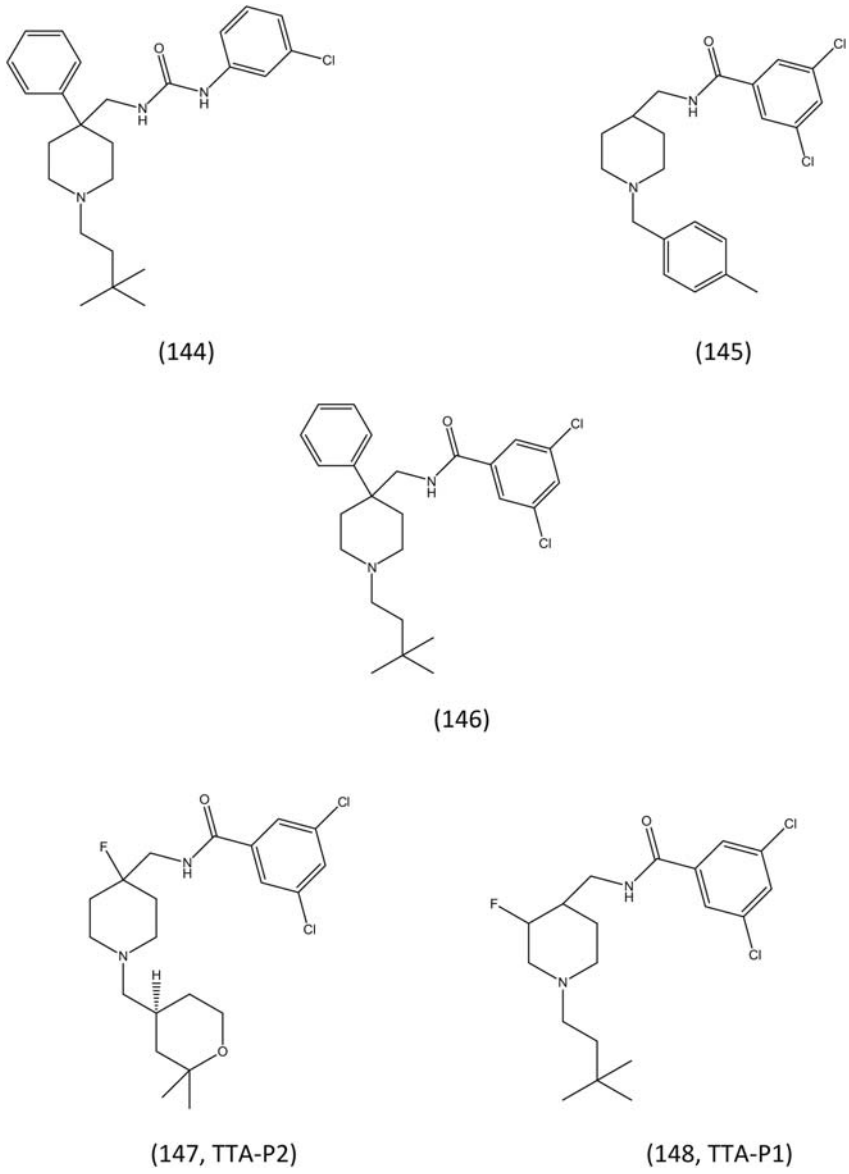

Fig. 33 Piperidine based compounds reported by Merck.

Table 13 Biological profile of (147, TTA-P2) and (148, TTA-P1)

Compound	*(A)*		*(B)*	
Assay	*Result*			
Membrane potential	Hyperpolarised state (−60 mV) IC_{50} (μM)	Depolarised state (−20 mV) IC_{50} (μM)	Hyperpolarised state (−60 mV) IC_{50} (μM)	Depolarised state (−20 mV) IC_{50} (μM)
Cav3.3	181	84	–	32
Electrophysiology	Hyperpolarised state (−100 mV) IC_{50} (μM)	Depolarised state (−80 mV) IC_{50} (μM)	Hyperpolarised state (−100 mV) IC_{50} (μM)	Depolarised state (−80 mV) IC_{50} (μM)
Cav3.1	93	–	62	44
Cav3.2	196	–	–	–
Cav3.3	84	115	43	25
Cav1.2	6330[a]	–	14,900	–
Selectivity	IC_{50} (μM)			
hERG	3790		2400	
Pharmacokinetics (rat)				
$T_{1/2}$ (h)	1.8		4.9	
F (%)	36		30	
Safety				
Dog cardiovascular (iv)	No effect observed on heart rate, MAP or ECG parameters up to and including a dose of 4.3 mg kg^{-1}		No effect on, with modest bradycardia Seen at 1–3 mg kg^{-1}	

[a]Binding assay.

issue and investigated potential substituents which had the potential to modulate basicity. Introduction of a fluorine at the 4-position of the piperidine proved successful and following further SAR studies led to (147) and (148) whose profiles are shown in Table 13. Both compounds are potent CaV3 blockers with little selectivity for Cav3 subtypes. The compounds show some activity at hERG and Cav1.2 although a true comparison is not possible as different assay formats are used in the two papers describing the profile of each compound. Compound (147), also known as TTA-P2, was well tolerated and without issue when tested in a dog cardiovascular study having no effect on ECG, heart rate, or MAP, where (148, also known as TTA-P1) produced no changes in ECG but did cause mild bradycardia, suggesting that it does not have the desired level of functional selectivity over Cav1.2. Both compounds had good pharmacokinetics in all species tested. Compounds were evaluated in models of epilepsy where they demonstrated encouraging effects. TTA-P2 (A) has been profiled in models of neuropathic pain. *i.p.* injections of 5 or 7.5 mg kg^{-1} TTA-P2 reduced pain responses in mice in phases 1 and 2 of the formalin test. Furthermore, TTA-P2, at 10 mg kg^{-1} *i.p.*, selectively and completely reversed thermal hyperalgesia in diabetic rats treated with streptozocin but had no effect on the nociceptive response of healthy animals. The antihyperalgesic effects of TTA-P2 in diabetic rats were completely abolished by administration of oligonucleotide antisense for Cav3.2 isoform of T channels. The compounds are covered by patents.[228,229] No development has been reported for the compounds reported from this series.

7.03.5.5.3.3 Piperidines reported by Astra Zeneca

Astra Zeneca has reported a series of piperidines[307] closely related to TTA-P2 (147) in terms of structure (Fig. 34); however these compounds are tonic Cav3.2 blockers rather than state-dependent and thus produce strong reductions in heart rate and blood pressure and were prepared with a cardiovascular indication in mind. Given their different therapeutic indication a detailed discussion is beyond the scope of this article. The lead compound (150) was derived from a screening hit (149). It is not clear from the publications which structural features are responsible for driving the different mechanisms of action, but the structural

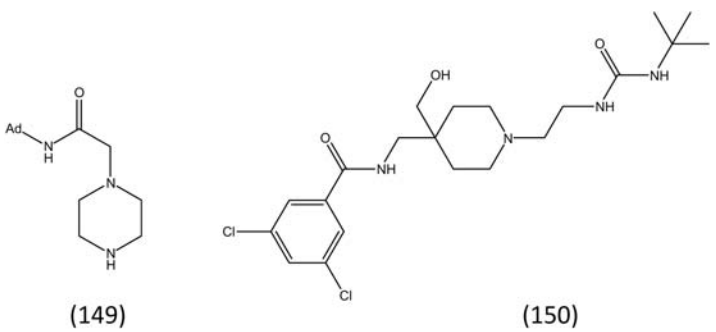

Fig. 34 Cav3.2 blockers reported by Astra Zeneca with strong cardiovascular effects.

similarities between TTA-P2 (147) and (150) indicate that subtle modifications can result dramatic changes in electrophysiological profile.

7.03.5.5.3.4 Piperidine amide templates reported in the patent literature

Toa Eiyo Ltd., Japan, has filed one patent[230] covering tropane derivatives (151) related to the compounds described by Zalicus, and Merck is reported to have $IC_{50} = 68$ nM (FLIPR), although it is not clear which Cav3 subtype was used in the screen (Fig. 35).

7.03.5.5.3.5 Hybrid compounds

The University of Calgary has identified a series of carbazole derivative (152, 153) which were derived from hybrids of NMP7 (135) and TTA-P2 (Fig. 36).[231] The rationale was that the hybrid structures would potentially enhance the Cav3 blocking activity of NMP7 and remove or reduce the activity at cannabinoid receptors. Preliminary work demonstrated that attaching a cyclic amine via an aliphatic chain to the amide group of NMP7 increased activity at Cav3.2 channels. Further optimization produced two compounds which were potent Cav3.2 blockers (152) and (153) but while being structurally similar had very different selectivity profiles when tested at cannabinoid receptors. Compounds (152) and (153) inhibited Cav3.2 channels with IC_{50} values of 1.48 and 3.68 μM, respectively. In addition (153), when tested in a radioligand binding assay (152) showed no affinity for either the CB1 or CB2 receptor ($K_i > 5$ μM), where (153) showed high affinity for CB1 ($pK_i = 15$ nM) and weaker, but measurable affinity for CB2 receptors ($pK_i = 1.9$ μM). The authors present SAR data to show that the chain length between the amide and the basic center is the key driver for selectivity over cannabinoid receptors. Compound (152) was tested for selectivity at other Cav3 channels using a single concentration of 3 μM where it blocked Cav3.1 by 44% and Cav3.3 by 42.5% and Cav3.2 by 69%. Finally (152) was profiled

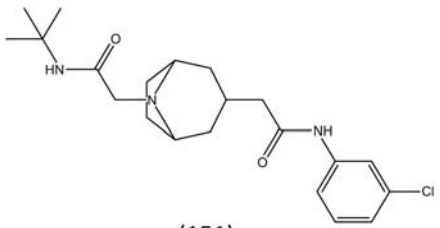

(151)

Fig. 35 Cav blocker patented by Toa Eiyo.

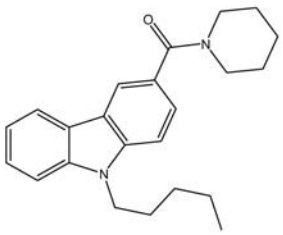

(135)

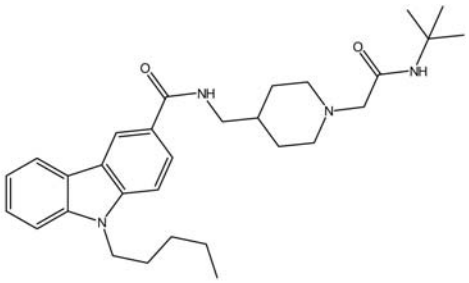

(152)

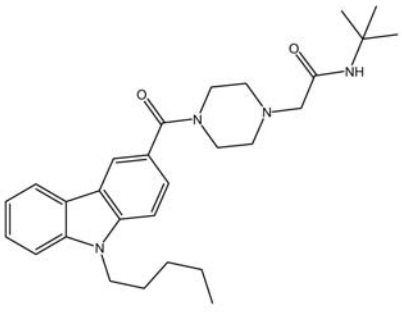

(153)

Fig. 36 Hybrids of TTA-P2 and NMP7 reported by the University of Calgary.

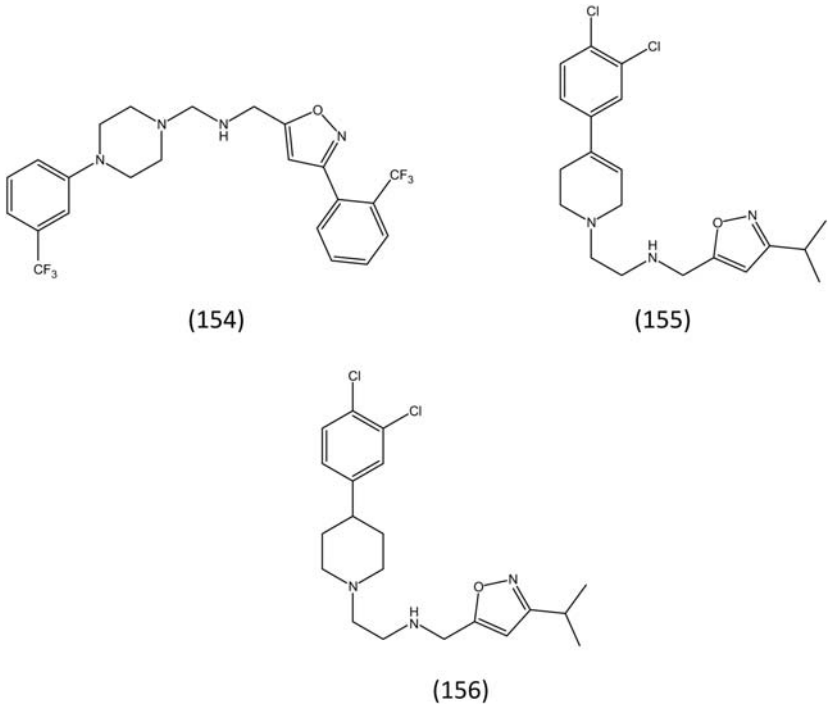

Fig. 37 Piperidines published by the Korea Institute of Science and Technology.

in vivo where it showed positive effects in a mouse formalin test inhibiting both early and late stage responses when dosed at 1–10 μg (*it*) and 10–100 mg kg^{-1} (*ip*) the response being slightly greater following *it* administration. Encouragingly none of the animals dosed *ip* showed any disturbance in locomotor activity. Compound (152) was also efficacious in a mouse peripheral nerve injury model of neuropathic pain when dosed at 30 mg kg^{-1} (*ip*) producing significant reversal of mechanical hyperalgesia for greater than 3 h.

7.03.5.5.3.6 Piperidines reported by The Korea Institute of Science and Technology

The Korea Institute of Science and Technology has also reported the discovery of a series of piperidines and tetrahydropydinedines.[232] The compounds (**Fig. 37**) originate from early work which identified micromolar Cav3.2 inhibitors, for example, (154, Cav3.2 $IC_{50} = 1$ μM). These compounds were based on Cav3 blockers reported in the early 2000s with a strategy of introducing an amide isostere to produce more stable compounds. Recently following the reports of other piperidine based blockers such as TTA-P1 and TTA-P2examination of the model showed that proposed targets (155) and (156) mapped well with a five point pharmacophore having three hydrophobic regions, one positively ionized center and a H bond acceptor. TTA-P1 also mapped well with the model. Synthesis of a set of analogues containing either a piperidine or a tetrahydropiperidine core with diverse substituents on the phenyl ring and the isoxazole showed (155) and (156) to have optimal activity. The full profiles are shown in **Table 14**.

Both (155) and (156) inhibit Cav3.1 and Cav3.2 channel in a whole cell patch clamp assay with micromolar potency although no information regarding state dependency is given. Both compounds are also potent inhibitors of hERG. Interestingly the

Table 14 Profiles of piperidines published by the Korea Institute of Science and Technology

Compound	*(155)*	*(156)*
Assay		
Electrophysiology		
Cav3.1 (IC_{50} (μM))	0.8	1.47
Cav3.2 (IC_{50} (μM))	1.3	1.36
hERG (IC_{50} (uM))	0.2	1.18
Pharmacokientics (rat, in vivo)		
F (%)	47.8	11.9
Clp (mL min^{-1} kg^{-1})	49	168
$T_{1/2}$ (h)	1.3	1.3

tetrahydropyrine has a better pharmacokinetic profile in the rat. Both compounds were profiled in the sciatic nerve ligation model of neuropathic pain (Chung model) at 100 mg kg^{-1} orally. Both showed similar efficacy in reversing both cold and mechanical allodynia which was comparable with gabapentin (100 mg kg^{-1}) for cold allodynia but slightly weaker for mechanical allodynia. The compounds are covered by two Korean patents.[233,234] No further development of these compounds is reported.

7.03.5.5.3.7 Spiro piperidine derivatives

Icagen has reported a series of spiro piperidine derivatives by (157) identified initially by phamacophore modeling using a similar strategy to that described the scientists at The Korea Institute of Science and Technology[235] (Fig. 38). The modeling led to the spiro scaffold present in (157). Investigations around the scaffold showed that all of the pharmacophoric elements present were needed for optimal potency (157; 58% inhibition Cav3.2 (30 nM) and 31% inhibition Cav1.2 (100 nM)). In particular removal of the diphenylmethyl group or the carbonyl function results in loss of activity.

7.03.5.5.3.8 Fused piperidines

A group from the Vanderbilt Centre for Neuroscience Drug Discovery has reported the identification of a series of fused piperidine derivatives (Fig. 39)[236] represented by ML218 (160). The compound is derived from a screening hit (158, Cav3.2 $IC_{50} = 810$ nM, FLIPR assay). The Vanderbilt scientists used scaffold hopping techniques in the process to remove the undesirable oxadiazole ring and increase potency. Initial efforts focused on piperdines (159) and resulted in similar potency. Further optimization through the use of a phamacophore led to ML218 which had slightly improved potency (Cav3.2 $IC_{50} = 120$ nM (FLIPR)). Activity was confirmed in electrophysiology studies where the compounds had Cav3.2 $IC_{50} = 310$ nM and Cav3.3 $IC_{50} = 274$ nM. When tested in a rat pharmacokinetic study the compound had moderate clearance (56 mL min^{-1} kg^{-1}) and a long-terminal half-life (7 h). When tested in a panel of 68 different molecular targets ML218 was highly selective including against other calcium channels thus rendering it a highly attractive chemical probe for studying the pharmacology and role of Cav3 channels in different disease indications. ML218 was made available to the research community for such purposes.

7.03.5.5.3.9 Related compounds disclosed in the patent literature

In addition to the filings from the Korea Institute of Science and Technology around this template other groups have also filed patents on similar chemotypes. Pfizer has published a patent[237] covering molecules related to (161) which is described as having $IC_{50} = 19$ nM at Cav3, however it is not clear from the patent how selective the compounds are over Cav2 and Cav1 channels (Fig. 40).

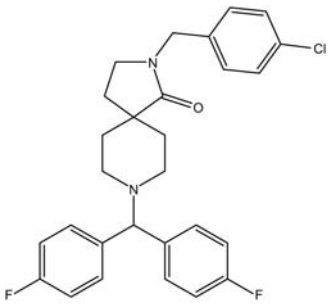

(157)

Fig. 38 Compound reported by Icagen.

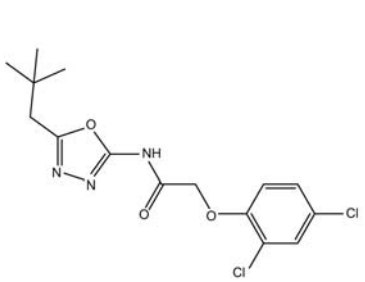

(158)

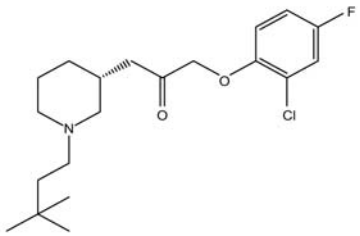

(159)

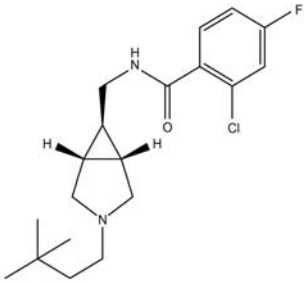

(160, ML218)

Fig. 39 ML218 (160) a fused piperidine identified by Vanderbilt Centre for Neuroscience Drug Discovery.

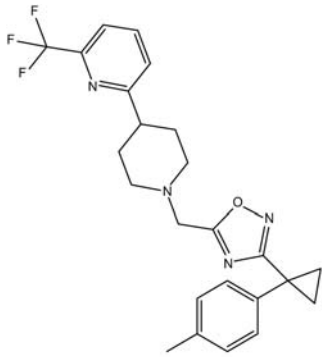

(161)

Fig. 40 Pfizer Cav3 blocker covered by a recent patent filing.

7.03.5.5.4 Piperazines and homopiperazines

7.03.5.5.4.1 Homopiperazines

A series of studies from the Korea Institute of Science and Technology describe the discovery of a series of homopiperazines (Fig. 41) represented by lead compound (164). Initial work generated a pharmacophore from available data and structures of Cav3 blockers published at the time.[238] This led to the preparation of a library of phthalimides (163). Screening of the library identified two lead compounds (R = Me, Cav3.2 IC_{50} = 0.96 μM, R = H, Cav3.2 IC_{50} = 0.96 μM). Further refinement of the pharmacophore led to the generation of a series of homopiperazines[239] with a pendant benzimidazole of which (163) had the optimal profile from the set of compounds prepared (Cav3.2 IC_{50} = 1.23 μM, Cav2.2 IC_{50} = 28.7 μM, hERG IC_{50} = 3.9 μM). Compound (163) was also profiled in DMPK studies (F = 43%, $T_{1/2}$ = 5.7 h, brain/plasma ratio = 0.43). The group next focused on increasing Cav3.2 potency and reexamination of the pharmacophore suggested that increasing the hydrophobicity of the left-hand side was the preferred option. A library of different bicyclic and monocyclic heterocycles was prepared[240] from which (164) emerged with the highest potency (IC_{50} = 0.2 μM). No further reports describing more detailed profiles of these compounds have been published. The compounds are covered by patent filings.[241]

7.03.5.5.4.2 Homopiperazine and piperazine disclosed in the patent literature

In addition to the compounds described in the scientific literature Korea Institute of Science and Technology has filed a large number of patents covering this area. Representative structures (168–167, Fig. 42) and corresponding patents are shown below.[242–244]

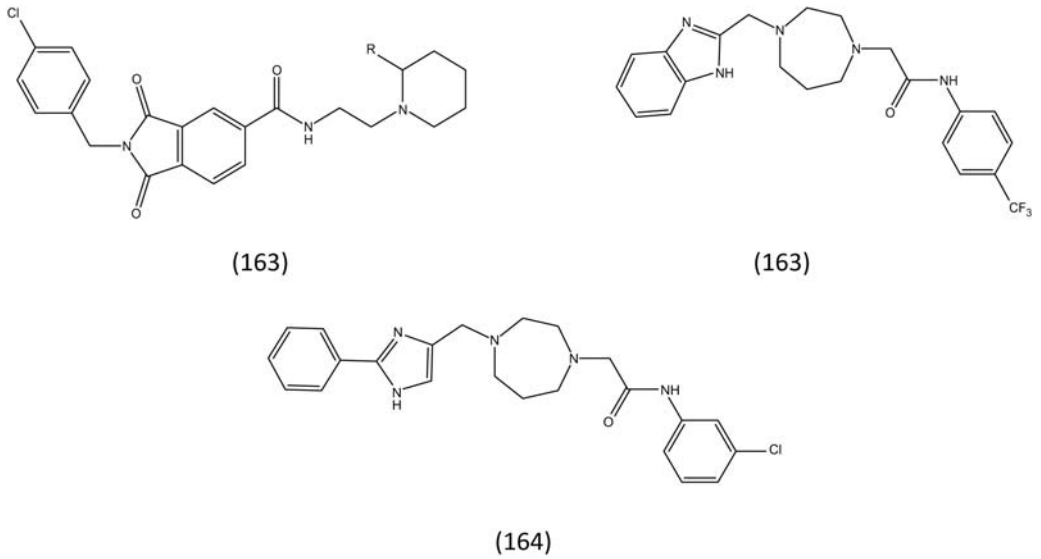

(163) (163)

(164)

Fig. 41 Homopiperazines published by the Korea Institute of Science and Technology.

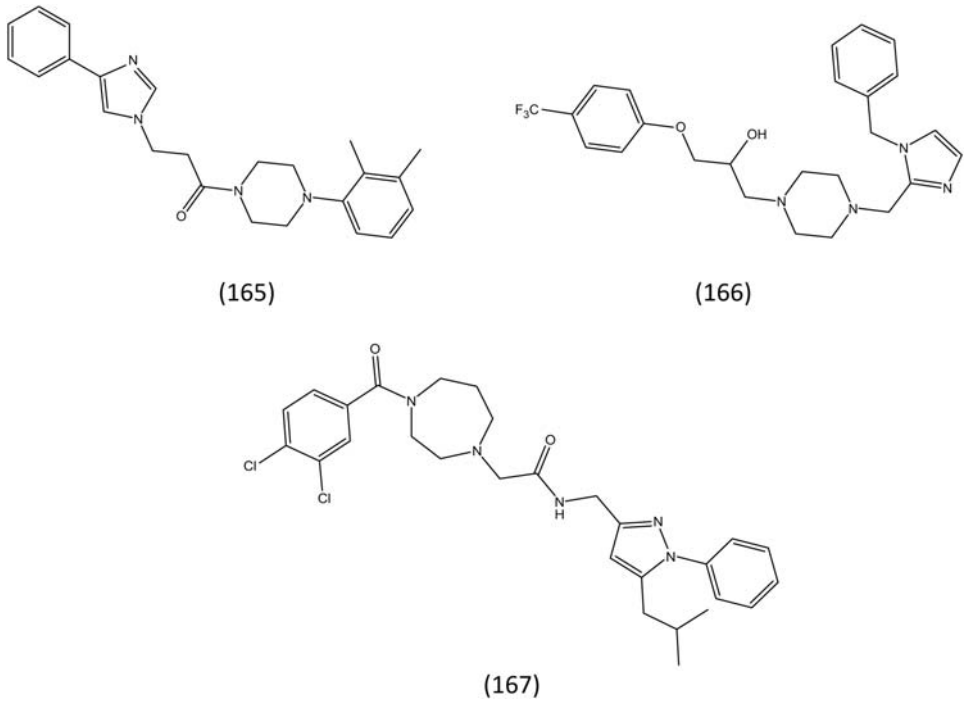

Fig. 42 Homopiperazines and piperazine covered by patents filed by the Korea Institute of Science and Technology.

7.03.5.5.5 Pyridyl amides

Merck has also reported[245] the identification of a series of pyridyl amides (Fig. 43), the most advanced of which is (171, TTA-A2), which was derived from screening hit (168) having encouraging activity at Cav3.3 in a FLIPR assay (IP* = 235 nM, When describing the TTA-A series Merck change the format in which the primary assay data is reported and quote IP (inflection point) values rather than IC_{50} values for the FLIPR assay. The infection point[245] is defined as the point of the concentration response curve where the curvature changes direction, for compounds producing a traditional sigmoidal concentration response this value is close to the

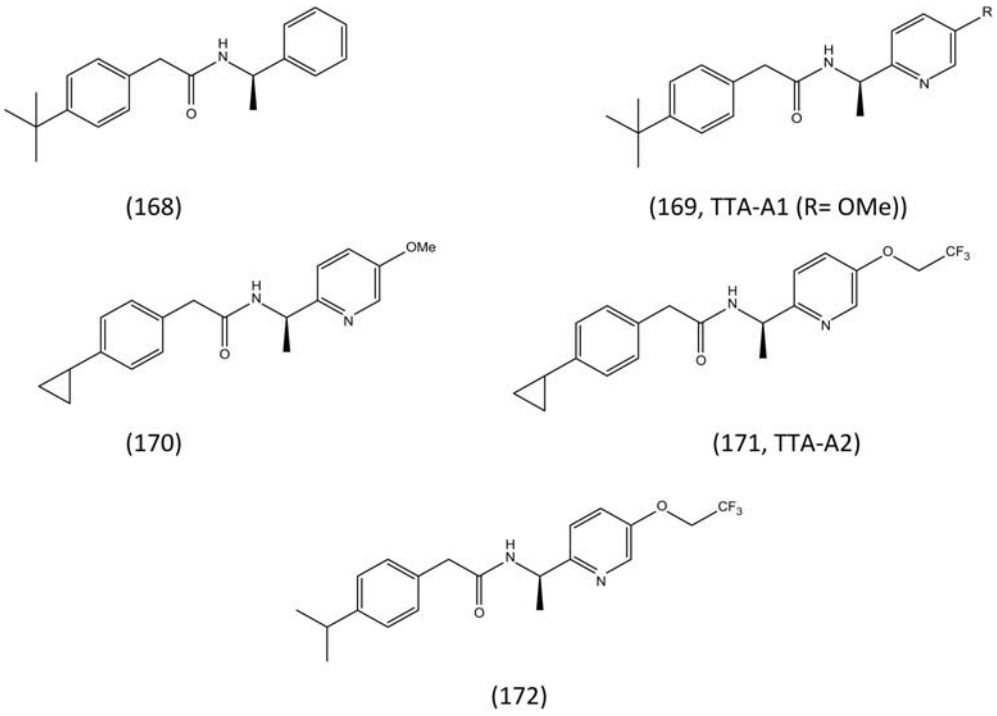

Fig. 43 Pyridyl amide compounds reported by Merck.

Table 15 Biological profile of TTA-A2 (171)

FLIPR	IP (nM)	
Cav3.3	6	
Electrophysiology	Closed state (−100 mV) IC_{50} (μM)	Inactivated state (−80 mV) IC_{50} (μM)
Cav3.1	4.1	0.089
Cav3.2	5.6	0.092
Cav3,3	3.7	0.098
Binding	IC_{50} (μM)	
Cav3.3	0.0012	
Cav1.2	>10	
hERG	>10	
In vitro ADME		
PXR (10uM)	14% rifamapacin response	
Pgp (A-B/B-A)	0.7	
Pharmacokinetics (rat)		
$T_{1/2}$ (h)	1.5	
F (%)	68	
Clp (mL $min^{-1}kg^{-1}$)	6	

IC_{50}.). Early investigations showed that the S-enantiomer as depicted was the preferred isomer with the R-isomer and the gem dimethyl analogues showing little activity. Exploration of the SAR around the right-hand aromatic ring showed that potency could be increased by replacing the phenyl group with a 2-pyridyl having a lipophilic 5-substituent ((169); R = Cl, Cav3.3 IP = 30 nM, R = OMe, Cav3.3 IP = 22 nM). The methoxy derivative (169, TTA-A1) was profiled further but revealed to be a potent PXR activator (87% rifampicin response at 10 μM). Molecular modeling studies suggested that changing the tert-butyl group to a less lipophilic substituent would reduce the PXR liability. Extensive studies revealed that introduction of polar groups reduced the PXR liability but also reduced calcium channel activity of the compounds. Ultimately it was shown that a slight reduction in the size of the lipophilic group was able to remove the CYP induction potential (170, Cav3.3 IP = 70 nM, 22% PXR activation relative to rifampacin (10 μM)). A further gain in potency was achieved by modification of the ether on the pyridyl ring to give (171, TTA-A2).

The full biological profile of TTA-A2[246,247] is summarized in Table 15. The compound is a highly potent, and nonselective state-dependent blocker of Cav3 channels. Binding data suggests it is selective over Cav1.2 and hERG channels. Compared with close analogues TTA-A2 is a weak activator of the PXR receptor and when tested in a permeability assay it showed no potential to be a P-gp substrate. The compound has an excellent pharmacokinetic profile in rats being highly bioavailable with low clearance and a long half-life. When tested in an in vivo model of epilepsy at 10 mg kg (*po*) TTA-A2 showed a robust response with a 87% reduction in seizures over 4 h. Like other TTA compounds, Merck investigated the effect of TTA-A2 on sleep patterns in mice, where significant changes were observed. A reduction in active wake was observed soon after dosing with a concurrent increase in delta sleep and decrease in REM sleep, the effects lasted for 4 hours. Similar effects have also been reported for other TTA compounds suggesting that Cav3 channels are involved. TTA-A2 has also been profiled in a number of different in vivo pain models where it shows efficacy.[154] Merck has recently reported progressing a Cav3 blocker MK-8998 into clinical studies for schizophrenia.[248] The exact structure of the compound has not been published by the company, but a compound of that name is available from a number of chemical suppliers; however the precise nature of the structure is still confusing, particularly the chirality which varies from supplier to supplier. Based on published SAR the structure of MK-8998 is believed to be (172). Little data is available but the compound is a potent Cav3 blocker (Cav3.3 IP = 5 nM) and a modest PXR activator (30% rifampicin response at 10 μM). When tested in acutely psychotic patients with schizophrenia at doses of 6–8 mg twice a day MK-8998 showed no difference to placebo on all primary outcome measures and had a similar side effect profile to olanzapine (5–15 mg twice daily).[248] These compounds are covered by a single patent.[249]

7.03.5.5.6 Quinazoline derivatives

The quinazoline series is another structurally distinct series of Cav3 blocker reported by Merck arising from high-throughput screening.[250] The original hit was (173) which demonstrated encouraging activity in a FLIPR assay (IC_{50} = 2174 nM, hyperpolarized state, and 847 nM, depolarized state). Resolution of enantiomers quickly showed that the activity lay mainly in the isomer depicted in Fig. 44. Initial profiling of compounds with an unsubstituted pendant phenyl ring revealed an encouraging profile but a tendency for time dependent cytochrome P450 inhibition which was resolved by the introduction of an electron withdrawing group in the 4-position. A trifluoroethyl group at the 3-position was reported to be optimal both for potency and metabolic stability. The initial chemistry led to a number of highly potent compounds of which (174, TTA-Q3) and (175, TTA-Q6) are examples which were extensively profiled (Table 15). Further SAR investigation produced further compounds of which (176) was the most extensively profiled. Their second publication focused on this template.[251] Merck has reported that replacement of the pendant phenyl resulted in a drop in potency, as did substitution of the N1 atom of the quinazoline ring with few exceptions and that enhancement of metabolic stability can be achieved through fluorination of the aliphatic C4 substituent. Profiles of the most advanced compounds are shown in Table 16.

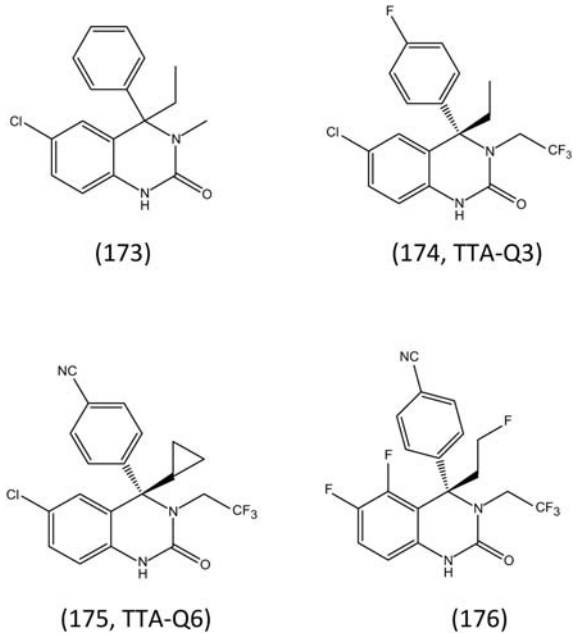

Fig. 44 Quinazolines reported by Merck.

Both TTA-Q3 (174) and TTA-Q6 (175) are potent blockers of Cav3.3 with evidence of state dependence as shown by the FLIPR data and are selective over Cav1.2 and Cav2.2. Compound (176) is a potent Cav3.3 blocker when tested in a FLIPR assay with channels in the depolarized state; it is also state dependent as evidenced by the reported whole cell patch clamp data. When tested at holding potentials of −100 mV and −80 mV (176) blocked Cav3.3 current with IC_{50} values of 190 and 31 nM, respectively. No selectivity data is given for this compound. None of the compounds were Pgp substrate but did have a cytochrome P450 induction liability. TTA-Q3 (174) and TTA-Q6 (175) had the better rat pharmacokinetic profiles both being low clearance compounds with good bioavailability and encouraging half-lives. All three compounds were tested in the WAG/Rij epilepsy model where they showed robust efficacy in reversing seizures (174) and (175) at 3 mg kg^{-1} and (176) at 10 mg kg^{-1}. When tested in sleep models they displayed similar profiles to other compounds reported by Merck. The quinazoline compounds are covered by two patent applications.[251,252]

In a follow-up article[225] Merck has compared the properties of all of their identified Cav3 blockers. Of interest is a series of binding experiments performed with labeled TTA-A1 (169) where they show that all of the compounds binding competitively with this ligand as do literature standards including mibefradil and flunarizine. The only exception being the quinazoline series which are not competitive and suggesting they bind at an allosteric site.

Table 16 Profiles of quinazolines reported by Merck

Compound *Assay*	*174*	*175*	*176*
FLIPR			
Cav3.3 depolarised (IC_{50} nM)	61	14	14
Cav3.3 hyperpolarised (IC_{50} nM)	1155	590	–
Cav1.2 (IC_{50} μM)	>10	4.5	–
Cav2.2 (IC_{50} μM)	>10	>10	
In vitro ADME			
PXR	63	66	35
Pgp (B:A/A:B)	1.5	1.1	
In vivo ADME (rat)			
F (%)	100	49	15
$T_{1/2}$ (h)	4.3	5.9	1.6
Clp (mL $min^{-1}kg^{-1}$)	22	12	55

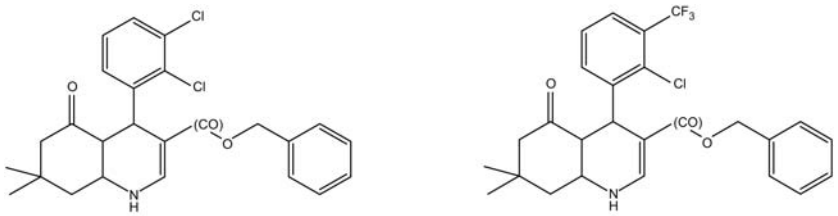

Fig. 45 Dihydropyridines reported by the University of Calgary.

7.03.5.5.7 Dihydropyridine derivatives

A group from the University of Calgary, some of whom had been previously associated with Neuromed and subsequent companies has recently described a series of dihyropyridine ester (Fig. 45) which show some selectivity over Ca1 channels and are active in neuropathic pain models.[253,254] In the initial publication a series of compounds are described with a saturated ring fused onto the dihydropyridine ring. Compounds (178) and (179) were shown to have optimal in vitro profiles, potently inhibiting Cav3.2 (178, $IC_{50}=257$ nM, 179, $IC_{50}=177$ nM) when tested in an electrophysiology assay and showing selectivity over Cav1.2 (179, 40% inhibition @ 10 μM). The key groups which enhance potency at Cav3.2 are described as being the gem dimethyl group on the saturated ring, and their position is critical for potency as moving them to the alpha position results in an approximate 10-fold loss in Cav3.2 potency. Compound (179) was profiled in a pain model (formalin test) using Cav3.2 null mice where it showed no activity, but when profiled in wild-type animals at 10 mg kg^{-1} (*ip*) it produced almost complete reversal of both initial and late phase responses and importantly showed no effects on locomotor function in wild-type mice at the same dose. When tested in a sciatic nerve ligation model of neuropathic pain in mice, (179) produced near maximal reversal of mechanical hyperalgesia at 10 mg kg^{-1} (*ip*) when tested 1 h post dose with 50% reversal when tested at 3 h. The more recent article[254] has investigated potential structural explanations for the SAR reported by the Calgary group and proposed further studies which might add confidence to the hypothesis.

7.03.5.5.8 Indoles

In addition to the three structurally diverse series of Cav3 blockers which have been extensively profiled, Merck has also reported a further compound (Fig. 46), the indole derivative TTA-I1 (180). Little data is given for this compound except that it was identified through high-throughput screening.[255]

7.03.5.5.9 Dihydroquinazolines

A group from the Korean institute of science and Technology was the first to pioneer work in the area of Cav3 blockers and have published work on a number of different templates. The first template explored was the dihydroquinazolines from which they identified a number of interesting compounds (Fig. 47). Early examples are KYS05044 (181, R=H) and KYS05050 (182, R=H)

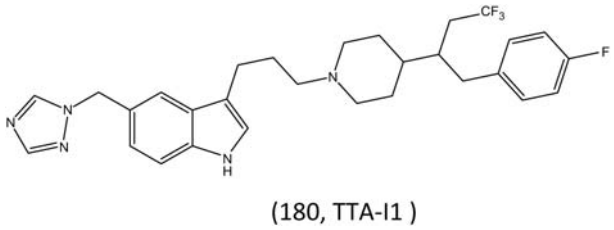

Fig. 46 TTA-I1 Recently described by Merck.

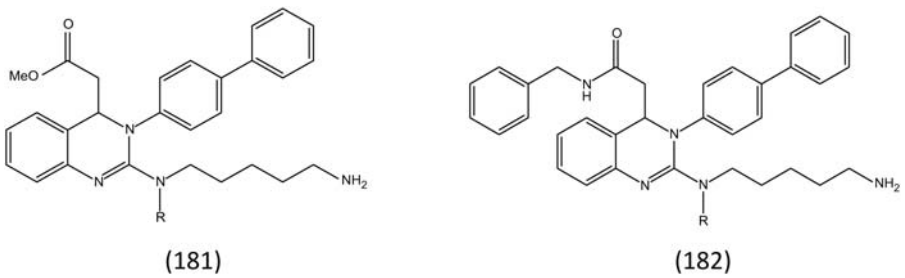

Fig. 47 KYS05044 and KYS05050.

reported to be equipotent with mibefradil but more selective. Published data shows KYS05044 to have Cav3.2 $IC_{50} = 0.56$ μM when tested in a whole cell manual patch clamp assay with >100-fold selectivity over Cav2.2 and KYS05050 Cav3.2 $IC_{50} = 0.13$ μM and 10-fold selectivity over Cav2.2. Extensive SAR investigations have been published, and ultimately KYS05090 (182, R = Me) was identified with Cav3.2 $IC_{50} = 0.04$ μM and 119-fold selectivity over Cav2.2. Interestingly N-methylation of (181) has little effect on potency and selectivity of the parent compound. The authors state that the series did not progress further due to not being able to achieve the desired pharmaceutical properties.[256] This area will not be reviewed in detail given that the chemistry was performed more than 10 years ago but for completeness it is included given a recent report describing the in vivo profile of KYS05090. In a recent study KYS05090 has been profiled in mouse models of acute and neuropathic pain. KYS-05090S (10 μg/10 μL delivered intrathecally) significantly reduced acute pain induced by formalin in both the tonic and inflammatory phases. Its antinociceptive effect was not observed when delivered to Cav3.2 null mice revealing a Cav3.2-dependent mechanism. KYS-05090S also reduced neuropathic pain in a model of partial sciatic nerve injury.[257] However caution should be applied when interpreting results with these compounds as KYS-05090S has also recently be shown to be a highly potent TRPV1 antagonist.[258]

7.03.5.5.10 Miscellaneous chemotypes disclosed only in the patent literature

In addition to the diverse array of chemotypes reported in the scientific literature a similar number of equally diverse templates have been disclosed in the recent patent literature (Table 17).

Astellas has filed two patents covering benzyltriazole (183) and benzylpyrazole amides (184).[259,260] The compounds shown are potent Cav3.2 blockers (FLIPR assay) having IC_{50} values of 21 nM (183) and 14 nM (184). Nissan Chemical Industries have filed three patents covering triazinone structures.[261–263] Cav3.2 data is reported (FLIPR assay) with the compounds becoming increasingly potent (185, $IC_{50} = 220$ nM; 186 $IC_{50} = 67$ nM; and 187, $IC_{50} = 4.7$ nM). A number of bicyclic heterocyclic structures have been published. Kyowa Hakko Kirin has published two patents[264,265] covering imidazopyridines (188) and (189); however little data is given on the compounds. Compound (189) is described as having a Cav3.2 $IC_{50} < 100$ nM (FLIPR). Merck has described a series of simple indole structures represented by (190), no data is given in the patent.[266] Two similar structural types have been patented by the University of Naples (191)[267] and the Japanese company Toa Eiyo Ltd.[268]; neither organization has published activity data on the molecules disclosed. Zalicus has published a patent[269] covering more complex structures with a bicyclic pyrimidione core (193) again little data is given. VM Therapeutics has published a patent[270] claiming the bicyclic compound pirenperone (194) as a Cav3 blocker and present in vivo data in the FCA model of inflammatory pain where the compound shows efficacy superior to Naproxen when dosed orally at 30 mg kg^{-1}. The value of this claim is questionable as pirenperone also has activity at 5HT and dopaminergic receptors which could be responsible for the effects in the pain model. Kinki University in Japan has filed a patent claiming T type calcium channel blockers containing flavanones[271] and highlight the natural product 6-prenylnaringenin (195) as an example. Little data is provided. Finally the University of Virginia has filed a patent[272] covering a series of pyrrolidines (196) for the treatment of conditions mediated by splice variants of Cav3.1.

7.03.5.6 Alpha 2 Delta Ligands

Two drugs which bind to the α2δ subunit of voltage-gated calcium channel are currently licensed for the treatment of neuropathic pain and are widely used, namely, gabapentin and pregabalin[273] (Fig. 48). The compounds were not originally designed to target calcium channels nor as analgesic agents. Gabapentin was initially prepared as a more lipophilic analogue of γ aminobutyric acid (GABA) to treat epilepsy and was launched onto the market in 1994 as an adjunct therapy to existing treatments.[274] While it was in clinical use as an anticonvulsant its potential as an analgesic agent was realized. Pregabalin was identified later through a similar chemical approach and has a very similar profile to gabapentin both clinically and preclinically. For many years the mechanism of action of these compounds was not understood and there are many reports of investigations into exactly how they illicit their analgesic effects. It was only recently that the now accepted mechanistic explanation was published. Arising from investigations in rats a group at University College London showed that in rats that had undergone SNL, on the side of the ligation, α2δ expression was increased in various structures. Chronic pregabalin treatment of SNL animals, at a dose that alleviated allodynia, markedly reduced the elevation of α2δ in the spinal cord and ascending axon tracts in vitro, pregabalin reduced plasma membrane expression of α2δ proteinwithout affecting endocytosis. They concluded that the antiallodynic effect of pregabalin in vivo was associated with impaired trafficking of α2δ, resulting in its decrease in presynaptic terminals, which would reduce neurotransmitter release and spinal sensitization, an important factor in the maintenance of neuropathic pain.[275] The discovery of gabapentin and pregabalin and early analogues has been well and extensively reviewed.[273] This section will focus on developments in the last decade. A number of close analogues of gabapentin and pregabalin have been identified and also progressed to clinical development including imagabalin (199, PD-0332334) which advanced as far as phase 3 studies for generalized anxiety disorder,[276] and atagabalin (200, PD-0200390) which entered clinical evaluation for insomnia (Section "Alpha 2 Delta Ligands") but was not progressed into later studies due to unsatisfactory data from initial studies.[277]

7.03.5.6.1 Amino acid-derived structures

The majority of the work has been based around modifications of the GABA skeleton producing compounds related to gabapentin and pregabalin but with different pharmacological properties. Daiichi Sankyo and Pfizer have led the way in this area. The focus of all of the studies has been to identify molecules which are both more potent and more efficacious than the two marketed

Table 17 Cav3 blocker chemotypes covered by recent patent filings

Organization	*Structures*
Astellas	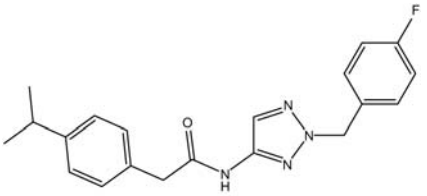 (183)
	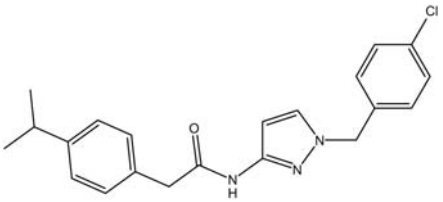 (184)
Nissan Chemical Industries, Ltd.	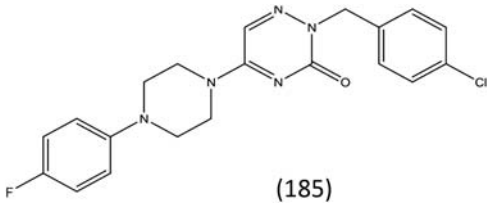 (185)
	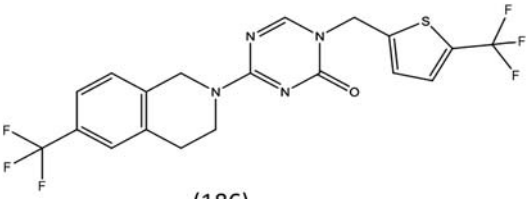 (186)
	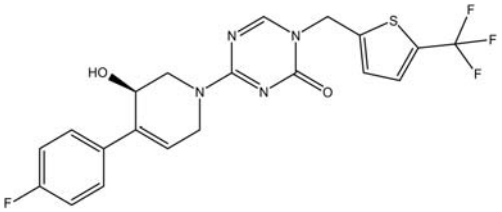 (187)
Kyowa Hakko Kirin Co., Ltd.,	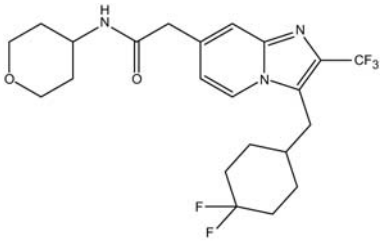 (188)

(Continued)

Table 17 Cav3 blocker chemotypes covered by recent patent filings—cont'd

Organization	*Structures*
	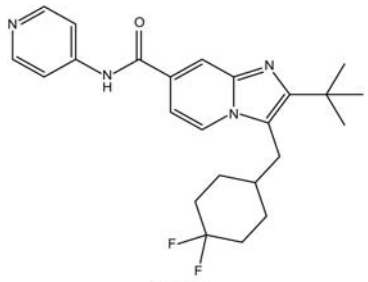 (189)
Merck	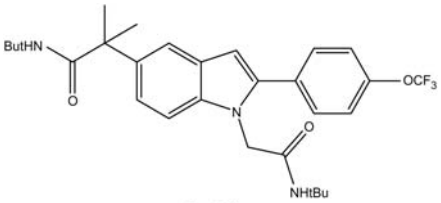 (190)
University of Naples	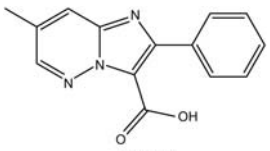 (191)
Toa Eiyo Ltd	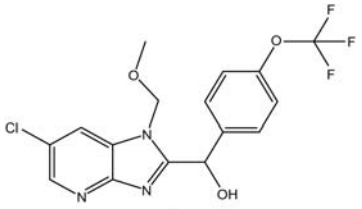 (192)
Zalicus	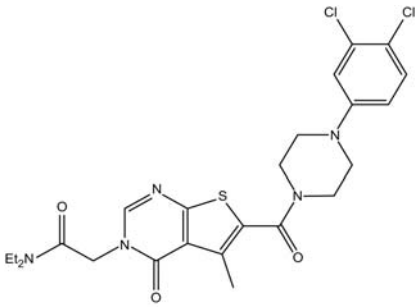 (193)
VM Therapeutics LLC	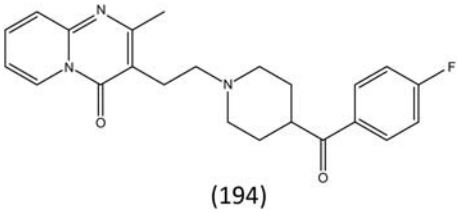 (194)

Table 17 Cav3 blocker chemotypes covered by recent patent filings—cont'd

Organization	*Structures*
Kinki University, Japan; Fuso Pharmaceutical Industries, Ltd	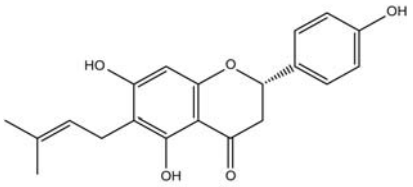 (195)
University of Virginia	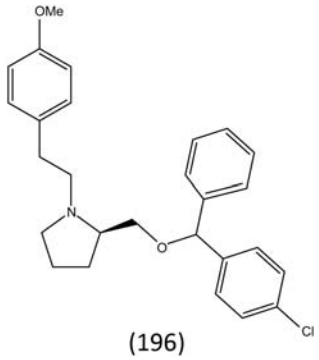 (196)

compounds. Gabapentin and pregabalin are reported by Pfizer to have binding affinities for the α2δ protein of 140 and 80 nM, respectively. Both Daiichi Sankyo and Pfizer have identified molecules with increased potency that have progressed to the clinic. Daiichi Sankyo currently has a compound microgabalin (5, DS-5565) which has shown positive analgesic effects in phase 2 studies and is reported to be entering phase 3 (Section "**Compounds Under Clinical Evaluation**"). Pfizer has progressed two compounds to clinical testing but not for pain indications. Imagabalin (199, PD-0332334) was studied for its potential to treat anxiety and atagabalin (200, PD-0200390) for insomonia. The structures of the two Pfizer molecules are shown in **Fig. 48**, and the Daiichi Sankyo compound is a bicyclic compound (**Fig. 51**) related to a class of compound termed by Pfizer (who also worked in this area) as gababutins (Section "**Alpha 2 Delta Ligands**").

7.03.5.6.1.1 Proline derivatives

A series of proline derivatives has been reported by Pfizer (**Fig. 49**) the most advanced of which is (204) which was evaluated in early clinical studies.[278–280,308] The starting point for the chemistry program was (202, R = H) which is reported to have a binding affinity of 5.4 μM.[278] Preliminary SAR studies showed that potency could be improved through introduction of lipophilic groups on the

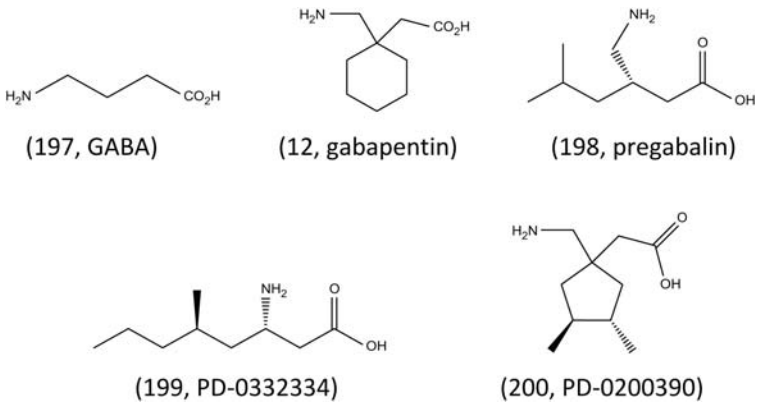

Fig. 48 GABA, gabapentin, and early compounds that have entered clinical development.

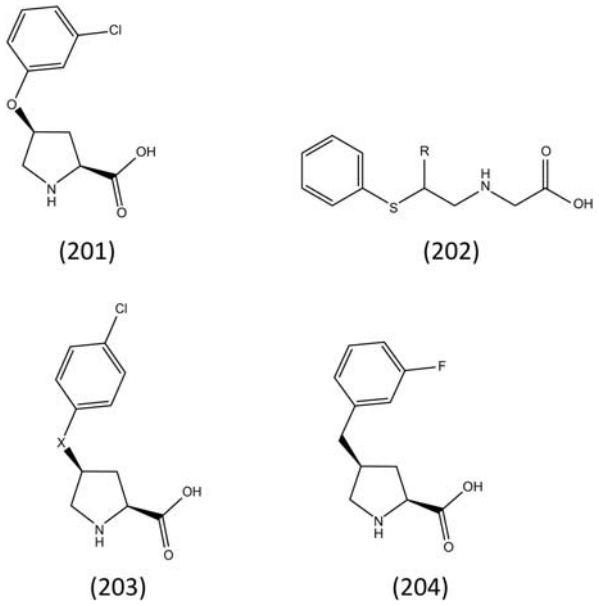

Fig. 49 Proline derivatives reported by Pfizer.

aromatic ring and by adding small lipophilic groups adjacent to the sulfur atom (e.g., (202) R = Me). A sulfur linker was preferred but could be replaced with oxygen with potency being increased through modulation of the chain substituent (R). The naphthyl analogue of (202, R = H) has a binding affinity of 22 nM. The compounds from the initial exploration were highly potent but generally had poor physicochemical properties due to the requirement for lipophilic groups for optimal potency. Conformational restraint of the open chain glycine derivatives was then tried[279] as an approach to enhance potency. The proline derivatives (203, X = O, S) were prepared, and both showed increased potency (203, X = O IC_{50} = 32 nM, X = S IC_{50} = 72 nM) compared to the open chain analogues (ether analogues of (202)—IC_{50} = 523 nM, X = S IC_{50} = 195 nM—both analogues having a methyl alpha to the heteroatom). The activity resided with the isomer of (203) as shown (2*S*, 4*S*). The corresponding (2*R*, 4*R*) isomer was devoid of activity (X = O). Moving the chlorine atom around the phenyl ring gave three isomers all with binding affinities $<$100 nM, the most potent being (201, IC_{50} = 4 nM). When profiled in preclinical species (201) had a relatively short half-life [0.4 h (rat), 1.5 h (dog)] and an unbound clearance higher than glomerular filtration rate. In human studies the compound also had a short half-life (2.3 h), suggesting that it was being renally cleared. Due to the short half-life (201) was not progressed further. Further exploration focussed on the linker atom and a series of benzylprolines were prepared.[280] SAR was similar to that seen with the heteroatom linked series; however these compound were not substrates for the neutral amino acid transporter (believed to be responsible for the active renal excretion) unlike their heteroatom linked analogues. The difference is proposed to be due to the difference in pK_a of the proline nitrogen between the series. The clearance of (204) in the dog is reported to be 0.4 mL $min^{-1} kg^{-1}$, significantly lower than glomerular filtration rate. Compound (204) was reported to have been evaluated in a human pharmacokinetic study[280] but to date the full results have not been published.

7.03.5.6.2 Gabapentins

A second series reported by Pfizer are the gabapentins (Fig. 50), compounds initially derived from studies focused on the gabapentin and pregabalin templates with added conformational constraint. The original compound (205) was weakly active (IC_{50} = 450 nM). The objective was to identify compounds with both increased binding affinity and efficacy. Initial studies[281] focused on the cyclopentane derivatives, and early studies showed that the two isomers (206) and (207) had increased binding affinity (206, IC_{50} = 30 nM, 207, IC_{50} = 71 nM). Both compounds showed similar efficacy to the standard molecules when tested in models of pain and anxiety. Addition of a second methyl group led to the identification of atabagalin (200)[282] which has a similar potency to the monomethyl compounds (IC_{50} = 22 nM); the opposite stereoisomer was also prepared and was weakly active (IC_{50} = 882 nM). The diethyl analogues interestingly showed a dramatic fall in potency (IC_{50} = 1.1 μM). Compound (200) was profiled in the carrageenan model of inflammatory pain where it showed encouraging efficacy and an effect similar to pregabalin producing full reversal of hyperalgesia at a dose of 30 mg kg^{-1}. The pharmacokinetic profile of (200) was investigated in the rat, and it had high bioavailability (Table 18) and a short half-life. The compound was found to be rapidly renally cleared but considered worthy of progression. In humans it had an acceptable half-life and was rapidly absorbed. To date atagabalin has been investigated in three human studies focusing on its potential to treat insomnia.[283–285] No results from these studies have yet been published.

Further investigations identified a series of bicyclic compounds of which (208, IC_{50} = 38 nM) and (209, IC_{50} = 46 nM) had the optimal profiles.[286] Similar to other compounds of this class both compounds had high bioavailabilities and short half-lives. When

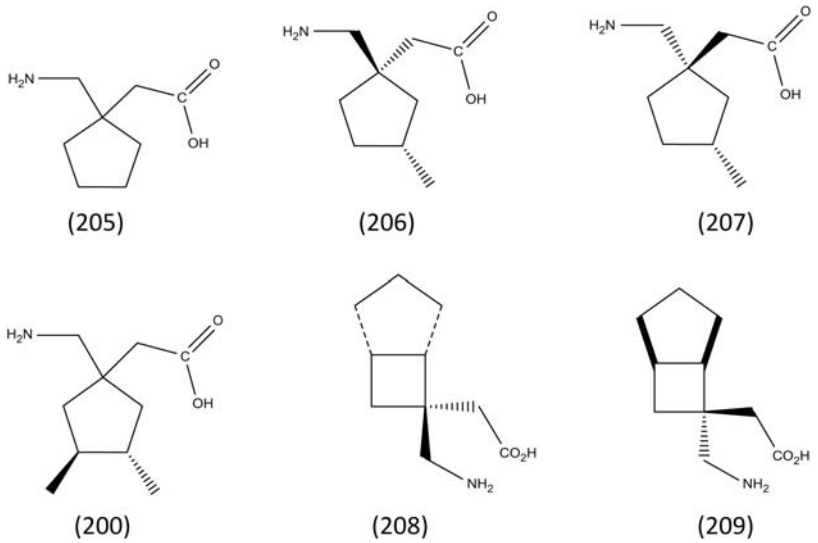

Fig. 50 Gababutins reported by Pfizer.

Table 18 Profile of Atabagalin (200)

Binding	
α2δ (IC_{50} nM)	22
Efficacy (rat)	
Carageenan	Full reversal of mechanical hyperalgesia (30 mg kg^{-1} *po*)
Pharmacokinetics (rat)	
$T_{1/2}$ (h)	2.4
F (%)	87
Clp (mL $min^{-1} kg^{-1}$)	4
Pharmacokinetics (human)	
$T_{1/2}$ (h)	5–6
T_{max} (h)	1.3

tested in the CCI model of neuropathic pain both were more efficacious than gabapentin. No further studies on these compounds have been reported. The compounds described above are covered by a number of patent filings.[309,310]

Daiichi Sankyo is developing a related molecule mirogabalin (DS-5565) (5, Fig. 51) which is reported in the patent literature[287] to be a potent α2δ ligand (binding IC50 = 14 nM) the medicinal chemistry relating to the identification of this compound has not been disclosed, but Daiichi Sankyo has reported clinical data from two phase 2 studies in patients with diabetic neuropathy where it demonstrated positive effects at doses of 15, 20, and 30 mg per day.[288,289] Studies in patients with fibromyalgia are currently ongoing.[73,75] The company is currently recruiting patients to begin phase 3 studies.

7.03.5.6.2.1 Acid bioisosteres

Pfizer has also reported a study into bioisosteres of gabapentin.[290] Oxadiazazolone (210, Fig. 52) and tetrazole derivatives were synthesized and found to have similar affinity to the parent acids to α2δ (IC_{50} = 210 nM). The consequence of modifying the acid was that (210) was no longer a substrate for the transporter which actively uptakes gabapentin into the brain and as a result

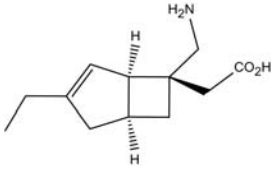

Fig. 51 Mirogabalin (DS-5565).

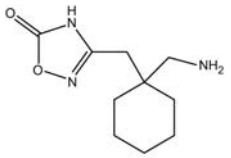

(210)

Fig. 52 Acid bioisotere gabapentin analogue reported by Pfizer.

achieved much lower brain levels when dosed to rats (brain/plasma ration = 0.05). The compound was tested in a number of neuropathic pain models where it showed no efficacy due to poor CNS penetration. It did show efficacy however in a model of osteoarthritis. The compounds are covered by a patent filing.[291]

7.03.5.6.2.2 Silicon containing derivatives

A recent report[292] from a group at Research Foundation ITSUU in Japan has described some silicon containing analogues of pregabalin (Fig. 53). Compounds have excellent pharmacokinetic profiles and show efficacy in models of neuropathic pain at low oral doses yet appear to have only weak affinity for the α2δ protein. When tested in a binding assay (211) and (212) displaced radiolabelled gabapentin with IC_{50} of 1.35 and 2.4 μM, respectively. Given the surprising levels of efficacy compared with the weak binding affinity it is not clear if the analgesia observed is mediated by the α2δ mechanism.

7.03.5.6.2.3 Amino acid derivatives in the patent literature

In addition to the templates described in the previous sections a number of related compounds have been disclosed in patent filings but not in the scientific literature. Few data are disclosed except for binding activity on selected compounds. Key structures are shown in Fig. 54. Daiichi Sankyo has patented[293] a series of β-alanine derivatives (213, $IC_{50} = 25$ nM). Novassay SA has recently filed a patent[294] covering compounds related to microgabalin which contain acid bioisosteres, for example, (214, $IC_{50} = 19$ nM). The Canadian company Bellus Health Inc. has patented[295] a series of low molecular weight amino acid derivatives, for example, (215) but no data is given.

7.03.5.6.3 Nonamino acid structures

7.03.5.6.3.1 Merck compounds

Merck has published a series of structures (Fig. 55) which are reported to bind potency to membranes expressing α2δ which arose from a high-throughput screen. Compound (216) was identified from the screen and bound potently to rat α2δ membranes displacing ^3H with $IC_{50} = 180$ nM. Initial optimization efforts[296] focused on addressing potential issues regarding the functional groups present and attempting to replace the ethoxy group and the methyl groups on the bicycle. Efforts to move or replace the ethoxy group failed as changing its position on the ring or even slight modifications (methoxy or isopropxy) resulted in a large drop in binding affinity. Changing the phenyl ring to pyridine or diazaheterocycles was also unsuccessful. Introduction of an additional alkoxy or alkyl group (218, R1) did produce an increase in activity with (218, R1 = OMe) being the most potent ($IC_{50} = 4$ nM). Modification of one of the methyl groups on the 6-membered ring of the bicycle (217) was also more successful. Introduction of larger alkyl, cycloalkyl, or aryl groups retained activity but produced molecules with inferior physical properties.

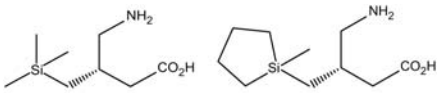

(211) (212)

Fig. 53 Silicon containing pregabalin derivatives.

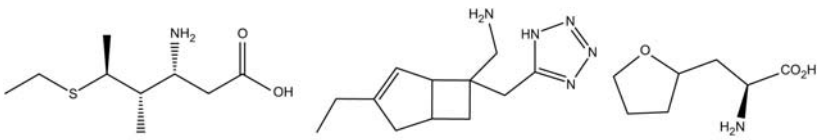

(213) (214) (215)

Fig. 54 Amino acid-derived α2δ ligands reported in the patent literature.

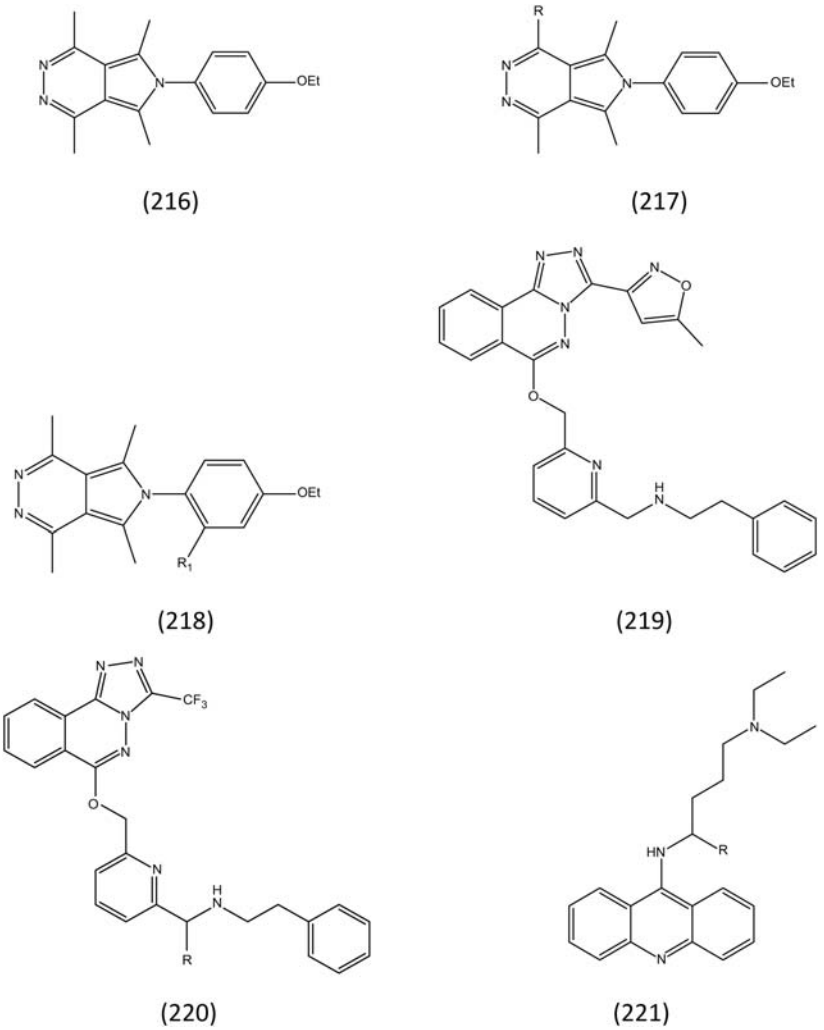

Fig. 55 Nonamino acid α2δ ligands reported by Merck.

Introducing alkoxy groups resulted in a loss of activity. Amino groups were tolerated with (217, R = MeNH) (IC_{50} = 40 nM) and (217, R = PhNH) (IC_{50} = 70 nM) being the most potent.[297]

Compound (216) was progressed to a rat pharmacokinetic study where it showed an encouraging profile (81% bioavailable, half-life 4.5 h) but was slowly absorbed (T_{max} = 2.8 h), and when tested in the Chung model (*ip*) it had a similar response (ID_{50} = 9.4 mg kg^{-1}, ip) to gabapentin (ID_{50} = 39 mg kg^{-1}, *ip*). The compounds are covered by a patent application.[298]

A second hit identified by the Merck screen was the tricyclic compound (219 IC_{50} = 220 nM).[299] Unsurprisingly the compound is described as having poor physical properties, and chemistry focused on attempts to prepare compounds with improved solubility. Replacement of the isoxazole failed to give active compounds with improved profiles, and the trifluoromethyl derivative which had a similar profile to the lead (220 R = H, IC_{50} = 75 nM) was the most potent compound prepared and chosen as the template for further studies. Introduction of an α alkyl group (R) on the benzylic position of the pyridylmethylamine was well tolerated with an α methyl group being optimal, the racemic compound showing increased potency (IC_{50} = 36 nM). Separation of the isomers revealed that the activity largely lay in the (S) enantiomer (IC_{50} = 30 nM) with the (R) enantiomer having only weak affinity (IC_{50} = 10,000 nM). The compounds are covered by a patent filing.[300] There are no reports of further studies with this series of compounds.

A third series identified by screening was represented by amino acridine (221).[301] The original hit was a racemic compound (221, R = Me, IC_{50} = 220 nM). Separation of the enantiomers revealed that much of the activity came from the (S) enantiomer (IC_{50} = 110 nM) with the (R) isomer having very weak affinity (IC_{50} = 11,000 nM). Working with the (S) enantiomers SAR studies revealed that a small increase in size produced a dramatic increase in binding affinity (221, R = (*S*) *n*-propyl, IC_{50} = 9 nM), larger groups such as phenyl were poorly tolerated. The diethylamine appeared to be optimal as all modifications reported produced a large drop in affinity. Saturation on one or both of the carbocyclic rings on the acridine was tolerated but did not improve affinity.

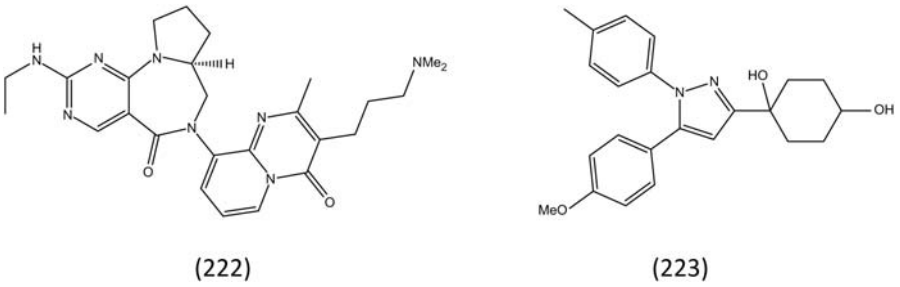

(222) (223)

Fig. 56 Nonamino acid-derived α2δ ligands reported in the patent literature.

No further studies with this series of compounds are reported. The compounds are covered by a patent filing.[302] None of the hits described by Merck appears to have been developed further.

7.03.5.6.3.2 Nonamino acid derivatives in the patent literature

The structures reported by Merck suggest that the α2δ protein is able to accommodate a structurally diverse range of ligands. This is further supported by patent filing covering further structurally distinct templates (**Fig. 56**). Two Japanese companies have filed patents covering new α2δ templates. Kyowa Hakko Kirin Co has filed two patents[303,304] covering pyrimido-diazepinones (e.g., 222, $IC_{50} = 700$ nM), and Toray Industries has filed a single patent describing the diphenyl pyrazole (223),[305] no data is given.

7.03.6 Conclusion

There has been a large volume of work in the area of voltage-gated calcium channels during the last decade as evidenced by the large number of scientific publications and patent filings as well as new chemical entities entering development. This ion channel family represents a highly validated target class with three compounds on the market which are approved for the treatment of pain. These compounds have been on the market for a number of years, and their clinical efficacy and safety profiles are well established. Focus has centered on two areas; the identification of small-molecule state-dependent calcium channel blockers which retain the efficacy of ziconotide yet have an improved safety profile that permits oral administration and α2δ ligands with improved efficacy compared with gabapentin and pregabalin. Unfortunately to date compounds with the desired clinical profiles have not been identified. The results of recent clinical studies with small-molecule inhibitors of Cav2.2 and Cav3 channels are disappointing, and the results of compounds currently undergoing proof of concept studies are eagerly awaited. If the results from studies with CNV2197944 and Z944 are also negative then it will be important to understand fully why the compounds have failed in order to inform any future programs. It would be unadvisable to progress any similar compounds into development unless they are clearly differentiated from the early compounds. Many of these compounds were identified through traditional strategies which relied heavily on the validity of animal pain models to predict clinical efficacy. This is a strategy which is clearly flawed as so many compounds which work in these models have in recent years failed to show efficacy in the clinic. It is therefore encouraging to see the climate changing slightly and groups using in vivo electrophysiology techniques to measure target engagement in preclinical models as Zalicus did in the profiling of Z944. Similarly the studies reported by Janssen which examined their Cav2.2 blockers ability to inhibit neurotransmitter release from spinal cord slices are also a very positive step. Particularly as the effects of ziconotide in similar assays as well as in vivo have also been reported and can be linked to efficacious drug concentrations. Compounds that bind to the α2δ channel subunit with higher affinity than gabapentin or pregabalin have been identified but the increased binding affinity has not translated into increased clinical efficacy.

Another important point to consider is that targeting state-dependent calcium channel blockers clearly produces an excellent safety profile compared with tonic blockers such as ziconotide; however a state-dependent calcium channel blocker has yet to demonstrate clinical efficacy. This poses an important question: is it possible to achieve clinical efficacy with a state-dependent calcium channel blocker? And if so what is the optimal profile?

In future programs, workers should be encouraged to fully determine selectivity across all members of the voltage-gated calcium channel family. This is highlighted by recent reports of compounds such as TROX1 from Merck which was believed to be a selective Ca2.2 blocker, but later shown to inhibit Cav2.1 and Cav2.3 channels with similar potency to Cav2.2. From what has been reported groups only screen against a limited number of family members, and it would be interesting to see how selective many agents really are, if they were to be fully profiled across a full panel of channels.

When reading articles describing the profiles of calcium channel blockers caution should be exercised if trying to compare results from one group with those of another unless identical screening protocols have been used. Potencies and selectivities can vary widely from one assay format to another, thus rendering comparisons very difficult.

From a chemistry perspective the voltage-gated calcium channel family is clearly highly tractable as demonstrated by the diversity of structures that have been published. There also appears to be certain motifs which confer calcium channel activity on a molecule such as the diphenylmethyl group and phenylsulfonyl moiety.

The voltage-gated calcium channel family has a huge potential to deliver future effective and safe pain medicines. To date the potential has not been fully realized with a small molecule that has been designed for the purpose. For future projects there is a huge volume of data now available which has been published during the last decade; data which should be carefully analyzed and the results used to inform the design of the next-generation compounds which will have a higher chance of success.

See also: 7.04. Sodium Channel Blockers for the Treatment of Pain.

References

1. Yu, H.; Li, M.; Wang, W.; Wang, Xiao L. High Throughput Screening Technologies for Ion Channels. *Acta Pharmacol. Sin.* **2016,** *37* (1), 34–43.
2. McManus, O. B. HTS Assays for Developing the Molecular Pharmacology of Ion Channels. *Curr. Opin. Pharmacol.* **2014,** *15,* 91–96.
3. Terstappen, G. C.; Roncarati, R.; Dunlop, J.; Peri, R. Screening Technologies for Ion Channel Drug Discovery. *Future Med. Chem.* **2010,** *2* (5), 715–730.
4. Le, S.; Hwang, S. W. Peptide Neurotoxins Targeting Voltage-Gated Ion Channels and Their Therapeutic Implications. *Front. Clin. Drug Res.: Cent. Nerv. Syst.* **2013,** *1,* 100–165.
5. Sousa, S. R.; Vetter, I.; Lewis, R. J. Venom Peptides as a Rich Source of Cav2.2 Channel Blockers. *Toxins* **2013,** *5* (2), 286–314.
6. Kullman, D. M. Neurological Channelopathies. *Annu. Rev. Neurosci.* **2010,** *33,* 151–172.
7. Pope, J. E.; Deer, T. R. Ziconotide: A Clinical Update and Pharmacologic Review. *Expert Opin. Pharmacother.* **2013,** *14* (7), 957–966.
8. Lee, M. S. Recent Progress in the Discovery and Development of N-Type Calcium Channel Modulators for the Treatment of Pain. *Prog. Med. Chem.* **2014,** *53,* 147–186.
9. Lacinova, L. T-Type Calcium Channel Blockers—New and Notable. *Gen. Physiol. Biophys.* **2011,** *30* (4), 403–409.
10. Lory, P.; Chemin, J. Towards the Discovery of Novel T-Type Calcium Channel Blockers. *Expert Opin. Ther. Targets* **2007,** *11* (5), 717–722.
11. McGivern, J. G. Pharmacology and Drug Discovery for T-Type Calcium Channels. *CNS Neurol. Disord. Drug Targets* **2006,** *5* (6), 587–603.
12. Vink, S.; Alewood, P. F. Targeting Voltage-Gated Calcium Channels: Developments in Peptide and Small-Molecule Inhibitors for the Treatment of Neuropathic Pain. *Br. J. Pharmacol.* **2012,** *167* (5), 970–989.
13. Mohan, C. G.; Gandhi, T. Therapeutic Potential of Voltage Gated Calcium Channels. *Mini Rev. Med. Chem.* **2008,** *8* (12), 1285–1290.
14. Zamponi, G. W. Targeting Voltage-Gated Calcium Channels in Neurological and Psychiatric Diseases. *Nat. Rev. Drug Discov.* **2016,** *15* (1), 19–34.
15. Lee, S. Pharmacological Inhibition of Voltage-Gated Ca^{2+} Channels for Chronic Pain Relief. *Curr. Neuropharmacol.* **2013,** *11* (6), 606–620.
16. Zamponi, G. W.; Striessnig, J.; Koschak, A.; Dolphin, A. C. The Physiology, Pathology, and Pharmacology of Voltage-Gated Calcium Channels and Their Future Therapeutic Potential. *Pharmacol. Rev.* **2015,** *67* (4), 821–870.
17. Tringham, E.; Snutch, T. P. Voltage-Gated N-Type and T-Type Calcium Channels and Excitability Disorders. In *Structure, Function, and Modulation of Neuronal Voltage-Gated Ion Channels;* Gribkoff, Valentin K., Kaczmarek, Leonard K., Eds.; 2009; pp 35–66.
18. Simms, B. A.; Zamponi, G. W. Neuronal Voltage-Gated Calcium Channels: Structure, Function, and Dysfunction. *Neuron* **2014,** *82* (1), 24–45.
19. Zamponi, G. W.; Snutch, T. P. Advances in Voltage-Gated Calcium Channel Structure, Function and Physiology. *Biochim. Biophys. Acta, Biomembr.* **2013,** *1828* (7), 1521.
20. Tyson, J. R.; Snutch, T. P. Molecular Nature of Voltage-Gated Calcium Channels: Structure and Species Comparison. *Wiley Interdiscip. Rev.: Membr. Transp. Signaling* **2013,** *2* (5), 181–206.
21. Catterall, W. A. Voltage-Gated Calcium Channels. In *Functioning of Transmembrane Receptors in Cell Signaling;* Bradshaw, R. A., Dennis, E. A., Eds.; 2011; pp 359–371.
22. Arranz-Tagarro, J.-A.; de los Rios, C.; Garcia, A. G.; Padin, J.-F. Recent Patents on Calcium Channel Blockers: Emphasis on CNS Diseases. *Expert Opin. Ther. Pat.* **2014,** *24* (9), 959–977.
23. Sanford, M. Intrathecal Ziconotide: A Review of Its Use in Patients With Chronic Pain Refractory to Other Systemic or Intrathecal Analgesics CNS. *Drugs* **2013,** *27* (11), 989–1002.
24. Williams, J. A.; Day, M.; Heavner, J. E. Ziconotide: An Update and Review. *Expert Opin. Pharmacother.* **2008,** *9* (9), 1575–1583.
25. Bruel, B. M.; Burton, A. W. Intrathecal Therapy for Cancer-Related Pain. *Pain Med.* **2016,** *1–18.*
26. Salat, K.; Kowalczyk, P.; Gryzlo, B.; Jakubowska, A.; Kulig, K. New Investigational Drugs for the Treatment of Neuropathic Pain. *Expert Opin. Investig. Drugs* **2014,** *23* (8), 1093–1104.
27. Kisilevsky, A. E.; Zamponi, G. W. Pharmacology of Neurotransmitter Release. In *Presynaptic Calcium Channels: Structure, Regulators, and Blockers*; *Handbook of Experimental Pharmacology.* 2008, 184*Handbook of Experimental Pharmacology*; pp 45–75. Springer GmbH.
28. Weiss, N. The First Disease Connection for Cav2.2 Channels. *Gen. Physiol. Biophys.* **2015,** *34* (3), 217–219.
29. Venetucci, L.; Denegri, M.; Napolitano, C.; Priori, S. G. Inherited Calcium Channelopathies in the Pathophysiology of Arrhythmias. *Nat. Rev. Cardiol.* **2012,** *9* (10), 561–575.
30. Jakobsson, J.I.; Palsson, E.; Sellgren, C.; Rydberg, F.; Ekman, A.; Zetterberg, H.; Blennow, K.; Landen, M. CACNA1C Polymorphism and Altered Phosphorylation of Tau in Bipolar Disorder. *Br. J. Psychiatry* **2016,** *208* (2), 195–196. the journal of mental science.
31. Pietrobon, D. Calcium Channels and Migraine. *Biochim. Biophys. Acta, Biomembr.* **2013,** *1828* (7), 1655–1665.
32. Bean, B. P. Classes of Calcium Channels in Vertebrate Cells. *Annu. Rev. Physiol.* **1989,** *51,* 367–384.
33. Nowycky, M. C.; Fox, A. P.; Tsien, R. W. Three Types of Neuronal Calcium Channel With Different Calcium Agonist Sensitivity. *Nature* **1985,** *316,* 440–443.
34. Bourinet, E.; Altier, C.; Hildebrand, M. E.; Trang, T.; Salter, M. W.; Zamponi, G. W. Calcium-Permeable Ion Channels in Pain Signaling. *Physiol. Rev.* **2014,** *94* (1), 81–140.
35. Ellinor, P. T.; Zhang, J. F.; Horne, W. A.; Tsien, R. W. Structural Determinants of the Blockade of N-Type Calcium Channels by a Peptide Neurotoxin. *Nature* **1994,** *372,* 272–275.
36. Zamponi, G. W.; Soong, T. W.; Bourinet, E.; Snutch, T. P. Beta Subunit Coexpression and the Alpha1 Subunit Domain I-II Linker Affect Piperidine Block of Neuronal Calcium Channels. *J. Neurosci.* **1996,** *16,* 2430–2443.
37. Marais, E.; Klugbauer, N.; Hofmann, F. Calcium Channel a2d Subunits—Structure and Gabapentin Binding. *Mol. Pharmacol.* **2001,** *59,* 1243–1248.
38. Catterall, W. A. Structure and Function of Neuronal Ca^{2+} Channels and Their Role in Neurotransmitter Release. *Cell Calcium* **1998,** *24,* 307–323.
39. Meir, A.; Ginsburg, S.; Butkevich, A.; Kachalsky, S. G.; Kaiserman, I.; Ahdut, R.; Demirgoren, S.; Rahamimoff, R. Ion Channels in Presynaptic Nerve Terminals and Control of Transmitter Release. *Physiol. Rev.* **1999,** *79,* 1019–1088.
40. Al-Hasani, R.; Bruchas, M. R. Molecular Mechanisms of Opioid Receptor-Dependent Signaling and Behaviour. *Anesthesiology* **2011,** *115* (6), 1363–1381.
41. Ricoy, U. M.; Frerking, M. E. Distinct Roles for Cav2.1–2.3 in Activity-Dependent Synaptic Dynamics. *J. Neurophysiol.* **2014,** *111,* 2404–2413.
42. Cain, S. M.; Snutch, T. P. T-Type Calcium Channels in Burst-Firing, Network Synchrony, and Epilepsy. *Biochim. Biophys. Acta* **2013,** *1828,* 1572–1578.
43. Dolphin, A. C. The $\alpha 2\delta$ Subunits of Voltage-Gated Calcium Channels. *Biochim. Biophys. Acta, Biomembr.* **2013,** *1828* (7), 1541–1549.

44. Ophoff, R.; Terwindt, G.; Vergouwe, M.; van Eijk, R.; Oefner, P.; Hoffman, S.; Lamerdin, J.; et al. Familial Hemiplegic Migraine and Episodic Ataxia Type-2 are Caused by Mutations in the Ca^{2+} Channel Gene CACNL1A4. *Cell* **1996,** *87* (3), 543–552.
45. Peer, M.; Goadsby, P. J.; Prabhakar, P. Safety and Efficacy of Flunarizine in Childhood Migraine: 11 Years' Experience, With Emphasis on its Effect in Hemiplegic Migraine. *Dev. Med. Child Neurol.* **2012,** *54* (3), 274–277.
46. Souza, I. A.; Gandini, M. A.; Wan, M. M.; Zamponi, G. W. Two Heterozygous Cav3.2 Channel Mutations in a Pediatric Chronic Pain Patient- Recording Condition-Dependent Biophysical Effects. *Pflugers Arch.* **2016,** *468* (4), 635–642.
47. Black, D. F. Sporadic and Familial Hemiplegic Migraine: Diagnosis and Treatment. *Semin. Neurol.* **2006,** *26* (2), 208–216.
48. Wider, B.; Pittler, M. H.; Ernst, E. Feverfew for Preventing Migraine. *Cochrane Database Syst. Rev.* **2015,** *4.* CD002286.
49. Lee, W. Y.; Orestes, P.; Latham, J.; Naik, A. K.; Nelson, M. T.; Vitko, I.; Perez-Reyes, E.; et al. Molecular Mechanisms of Lipoic Acid Modulation of T-Type Calcium Channels in Pain Pathway. *J. Neurosci.* **2009,** *29* (30), 9500–9509.
50. Ziegler, D.; Duan, W. R.; An, G.; Thomas, J. W.; Nothaft, W. A Randomized Double-Blind, Placebo-, and Active-Controlled Study of T-Type Calcium Channel Blocker ABT-639 in Patients With Diabetic Peripheral Neuropathic Pain. *Pain* **2015,** *156* (10), 2013–2020.
51. Serra, J.; Duan, W. R.; Locke, C.; Sola, R.; Liu, W.; Nothaft, W. Effects of a T-Type Calcium Channel Blocker, ABT-639, on Spontaneous Activity in C-Nociceptors in Patients With Painful Diabetic Neuropathy: A Randomized Controlled Trial. *Pain* **2015,** *156* (11), 2175–2183.
52. Parsons, B.; Tive, L.; Huang, S. Gabapentin: A Pooled Analysis of Adverse Events from Three Clinical Trials in Patients With Postherpetic Neuralgia. *Am. J. Geriatr. Pharmacother.* **2004,** *2* (3), 157–162.
53. Chiechio, S.; Zammataro, M.; Caraci, F.; Rampello, L.; Copani, A.; Sabato, A. F.; Nicoletti, F. Pregabalin in the Treatment of Chronic Pain: An Overview. *Clin. Drug Investig.* **2009,** *29* (3), 203–213.
54. Hansson, P.; Bouhassira, D. Failures of Translational Pain Research: Can They Be Due to Misinterpretation of Pain-Related Nomenclature? *Eur. J. Pain* **2015,** *19* (2), 147–149.
55. Barrett, J. E. The Pain of Pain: Challenges of Animal Behavior Models. *Eur. J. Pharmacol.* **2015,** *753,* 183–190.
56. Whiteside, G. T.; Pomonis, J. D.; Kennedy, J. D. An Industry Perspective on the Role and Utility of Animal Models of Pain in Drug Discovery. *Neurosci. Lett.* **2013,** *557(Pt A),* 65–72.
57. Wright, C. E.; Robertson, A. D.; Whorlow, S. L.; Angus, J. A. Cardiovascular and Autonomic Effects of Omega-Conotoxins MVIIA and CVID in Conscious Rabbits and Isolated Tissue Assays. *Br. J. Pharmacol.* **2000,** *131* (7), 1325–1336.
58. Winquist, R. J.; Qian, Pan J.; Gribkoff, V. K. Use-Dependent Blockade of Cav2.2 Voltage-Gated Calcium Channels for Neuropathic Pain. *Biochem. Pharmacol.* **2005,** *70,* 489–499.
59. Adams, D. J.; Berecki, G. Mechanisms of Conotoxin Inhibition of N-Type (Cav2.2) Calcium Channels. *Biochim. Biophys. Acta Biomembr.* **2013,** *1828* (7), 1619–1628.
60. ClinicalTrials.gov Identifier: NCT01655849.
61. ClinicalTrials.gov Identifier: NCT01757873.
62. Snutch T.P.; Fisher D. M.; Method for Increasing the Bioavailability of Benzhydryl Piperazine Containing Compounds By Oral Administration With Food.PCT Int. Appl., WO 2007133481 A2 20071122, 2007.
63. Padval M. V.; Harianawala A.; Grieco E.; Saxena V.; Self-Emulsifying Formulations and Methods of Use Thereof PCT Int. Appl., WO 2012122274 A1 20120913, 2012.
64. Padval M. V.; Gautschi J.T.; SmitheyD.T.; Crew M.D.; Harianawala A.; Solid Dispersion Formulations of 1-(4-Benzhydrylpiperazin-1-yl)-3,3-Diphenylpropan-1-One for Increasing Drug Bioavailability PCT Int. Appl., WO 2012122279 A1 20120913, 2012.
65. ClinicalTrials.gov Identifier: NCT01848730.
66. ClinicalTrials.gov Identifier: NCT01893125.
67. Wallace, M.; Duan, W. R.; Liu, W.; Locke, C.; Nothaft, W. A. Randomized, Double-Blind, Placebo-Controlled, Crossover Study of the T-Type Calcium Channel Blocker ABT-639 in an Intradermal Capsaicin Experimental Pain Model in Healthy Adults. *Pain Med.* **2015**. Dec 16. pii: pnv068. [Epub ahead of print].
68. An, G.; Liu, W.; Duan, W. R.; Nothaft, W.; Awni, W.; Dutta, S. Population Pharmacokinetics and Exposure-Uric Acid Analyses After Single and Multiple Doses of ABT-639, a Calcium Channel Blocker, in Healthy Volunteers. *AAPS J.* **2015,** *17* (2), 416–426.
69. Zhang, Q.; Xia, Z.; Joshi, S.; Scott, V. E.; Jarvis, M. F. Optimization of ADME Properties for Sulfonamides Leading to the Discovery of a T-Type Calcium Channel Blocker, ABT-639. *ACS Med. Chem. Lett.* **2015,** *6* (6), 641–644.
70. Lee, M. Z944: A First in Class T-Type Calcium Channel Modulator for the Treatment of Pain. *J. Peripher. Nerv. Syst.* **2014,** *19 Suppl 2,* S11–S12.
71. ClinicalTrials.gov Identifier: NCT02100046.
72. Matthews, E. A.; Dickenson, A. H. Effects of Ethosuximide, a T-Type Ca(2+) Channel Blocker, on Dorsal Horn Neuronal Responses in Rats. *Eur. J. Pharmacol.* **2001,** *415* (2–3), 141–149.
73. ClinicalTrials.gov Identifier: NCT02187159.
74. ClinicalTrials.gov Identifier: NCT02146430.
75. ClinicalTrials.gov Identifier: NCT02234583.
76. Nimmrich, V.; Gross, G. P/Q-Type Calcium Channel Modulators. *Br. J. Pharmacol.* **2012,** *167,* 741–759.
77. Rajakulendran, S.; Kaski, D.; Hanna, M. G. Neuronal P/Q-Type Calcium Channel Dysfunction in Inherited Disorders of the CNS Nature Reviews. *Neurology* **2012,** *8* (2), 86–96.
78. Wada, T.; Imanishi, T.; Kawaguchi, A.; Mori, M. X.; Mori, Y.; Imoto, K.; Ichida, S. Effects of Calmodulin and Ca^{2+} Channel Blockers on Omega-Conotoxin GVIA Binding to Crude Membranes from alpha1B Subunit (Cav2.2) Expressed BHK Cells and Mice Brain Lacking the alpha1B Subunits. *Neurochem. Res.* **2005,** *30* (8), 1045–1054.
79. Knight, Y. E.; Bartsch, T.; Kaube, H.; Goadsby, P. J. P/Q-Type Calcium-Channel Blockade in the Periaqueductal Gray Facilitates Trigeminal Nociception: A Functional Genetic Link for Migraine? *J. Neurosci.* **2002,** *22* (5). RC213/1-RC213/6.
80. Belardetti, F.; Zamponi, G. W. Calcium Channels as Therapeutic Targets. *Wiley Interdiscip. Rev.: Membr. Transp. Signaling* **2012,** *1* (4), 433–451.
81. Waszkielewicz, A. M.; Gunia, A.; Szkaradek, N.; Sloczynska, K.; Krupinska, S.; Marona, H. Ion Channels as Drug Targets in Central Nervous System Disorders. *Curr. Med. Chem.* **2013,** *20* (10), 1241–1285.
82. Tatalovic, M.; Glazebrook, P. A.; Kunze, D. L. Expression of the P/Q (Cav2.1) Calcium Channel in Nodose Sensory Neurons and Arterial Baroreceptors. *Neurosci. Lett.* **2012,** *520* (1), 38–42.
83. Nachbauer, W.; Nocker, M.; Karner, E.; Stankovic, I.; Unterberger, I.; Eigentler, A.; Schneider, R.; et al. Episodic Ataxia Type 2: Phenotype Characteristics of a Novel CACNA1A Mutation and Review of the Literature. *J. Neurol.* **2014,** *261* (5), 983–991.
84. Gnanasekaran, A.; Bele, T.; Hullugundi, S.; Simonetti, M.; Ferrari, M. D.; van den Maagdenberg, A. M.; Nistri, A.; et al. Mutated Cav2.1 Channels Dysregulate CASK/P2X3 Signaling in Mouse Trigeminal Sensory Neurons of R192Q Cacna1a Knock-in Mice. *Mol. Pain* **2013,** *9,* 62/1–62/6.
85. Dandapani, B. K.; Hanson, M. R. Amlodipine for Migraine Prophylaxis. *Headache* **1998,** *38* (8), 624–626.
86. Leonard, L.; Phillips, W. J. Near-Complete Migraine Prophylaxis With Amlodipine: A Case Report. *J. Pain Symptom Manage.* **2007,** *34* (6), 571–573.
87. Horak, S.; Koschak, A.; Stuppner, H.; Striessnig, J. Use-Dependent Block of Voltage-Gated Cav2.1 Ca^{2+} Channels by Petasins and Eudesmol Isomers. *J. Pharmacol. Exp. Ther.* **2009,** *330* (1), 220–226.
88. Winters, M. P.; Subasingh, N.; Wall, M.; Beck, E.; Brandt, M. R.; Finley, M. F. A.; Liu, Y. I.; et al. Discovery and SAR of Novel Tetrahydropyrrolo[3,4-c]Pyrazoles as Inhibitors of the N-Type Calcium Channel. *Bioorg. Med. Chem. Lett.* **2014,** *24* (9), 2053–2056.
89. Miljanich, G. P.; Ramachandran, J. Antagonists of Neuronal Calcium Channels: Structure, Function, and Therapeutic Implications. *Annu. Rev. Pharmacol. Toxicol.* **1995,** *35,* 707–734.

90. Cox, B. Calcium Channel Blockers and Pain Therapy. *Curr. Rev. Pain* **2000,** *4* (6), 488–498.
91. Cox, B.; Denyer, J. C. N-Type Calcium Channel Blockers in Pain and Stroke. *Expert Opin. Ther. Pat.* **1998,** *8* (10), 1237–1250.
92. Elmslie, K. S. Calcium Channel Blockers in the Treatment of Disease. *J. Neurosci. Res.* **2004,** *75* (6), 733–741.
93. Wood, N. I.; Barone, F. C.; Benham, C. D.; Brown, T. H.; Campbell, C. A.; Cooper, D. G.; et al. The Effects of SB 206284A, a Novel Neuronal Calcium-Channel Antagonist, in Models of Cerebral Ischemia. *J. Cereb. Blood Flow Metab.* **1997,** *17* (4), 421–442.
94. Hu, L.-Y.; Ryder, T. R.; Rafferty, M. F.; Cody, W. L.; Lotarski, S. M.; Miljanich, G. P.; Millerman, E.; et al. N,N-Dialkyl-Dipeptidylamines as Novel N-Type Calcium Channel Blockers. *Bioorg. Med. Chem. Lett.* **1999,** *9* (6), 907–912.
95. Ryder, T. R.; Hu, L.-Y.; Rafferty, M. F.; Lotarski, S. M.; Rock, D. M.; Stoehr, S. J.; Taylor, C. P.; et al. Structure-Activity Relationship at the Proximal Phenyl Group in a Series of Non-Peptidyl N-Type Calcium Channel Antagonists. *Bioorg. Med. Chem. Lett.* **1999,** *9* (16), 2453–2458.
96. Hu, L.-Y.; Ryder, T. R.; Rafferty, M. F.; Feng, M. R.; Lotarski, S. M.; Rock, D. M.; Sinz, M.; et al. Synthesis of a Series of 4-Benzyloxyaniline Analogs as Neuronal N-Type Calcium Channel Blockers With Improved Anticonvulsant and Analgesic Properties. *J. Med. Chem.* **1999,** *42* (20), 4239–4249.
97. Hu, L.-Y.; Ryder, T. R.; Rafferty, M. F.; Taylor, C. P.; Feng, M. R.; Kuo, B.-S.; Lotarski, S. M.; et al. The Discovery of [1-(4-Dimethylamino-Benzyl)-Piperidin-4-yl]-[4-(3,3-Dimethylbutyl)-Phenyl]-(3-Methyl-but-2-Enyl)-Amine, an N-Type Ca+2 Channel Blocker With Oral Activity for Analgesia. *Bioorg. Med. Chem.* **2000,** *8* (6), 1203–1212.
98. Ryder, T. R.; Hu, L.-Y.; Rafferty, M. F.; Feng, M. R.; Lotarski, S. M.; Rock, D. M.; Stoehr, S. J.; et al. Synthesis and Biological Activity of 4-Aminopiperidine Derivatives as N-Type Calcium Channel Antagonists. *Med. Chem. Res.* **2000,** *10* (1), 11–18.
99. Hu, L.-Y.; Ryder, T. R.; Rafferty, M. F.; Siebers, K. M.; Malone, T.; Chatterjee, A.; Feng, M. R.; et al. Neuronal N-Type Calcium Channel Blockers: A Series of 4-Piperidinylaniline Analogs With Analgesic Activity. *Drug Des. Discov.* **2000,** *17* (1), 85–93.
100. Chapdelaine M.; Kemp L.; McCauley J., Preparation of 4-Quinolinamines as N-Type Calcium Channel Antagonists for the Treatment of Pain PCT Int. Appl., WO 2002036569 A1 20020510, 2002.
101. Seko, T.; Kato, M.; Kohno, H.; Ono, S.; Hashimura, K.; Takimizu, H.; Nakai, K.; et al. Structure-Activity Study and Analgesic Efficacy of Amino Acid Derivatives as N-Type Calcium Channel Blockers. *Bioorg. Med. Chem. Lett.* **2001,** *11* (16), 2067–2070.
102. Wheeler-Aceto, H.; Porreca, F.; Cowan, A. The Rat Paw Formalin Test: Comparison of Noxious Agents. *Pain* **1990,** *40* (2), 229–238.
103. Seko, T.; Kato, M.; Kohno, H.; Ono, S.; Hashimura, K.; Takimizu, H.; Nakai, K.; et al. Structure-Activity Study of L-Amino Acid-Based N-Type Calcium Channel Blockers. *Bioorg. Med. Chem.* **2003,** *11* (8), 1901–1913.
104. Austin, P. J.; Wu, A.; Moalem-Taylor, G. Chronic Constriction of the Sciatic Nerve and Pain Hypersensitivity Testing in Rats. *J. Vis. Exp.* **2012,** *13* (61). pii: 3393.
105. Varming, T.; Christophersen, P.; Moeller, A.; Peters, D.; Axelsson, O.; Nielsen, E. O. Synthesis and Biological Activity of the Neuronal Calcium Channel Blocker 2-Amino-1-(2,5-Dimethoxyphenyl)-5-Trifluoromethyl Benzimidazole (NS-649). *Bioorg. Med. Chem. Lett.* **1996,** *6* (3), 245–248.
106. Menzler, S.; Bikker, J. A.; Horwell, D. C. Synthesis of a Non-Peptide Analogue of Omega-Conotoxin MVIIA. *Tetrahedron Lett.* **1998,** *39,* 7619–7622.
107. Menzler, S.; Bikker, J. A.; Suman-Chauhan, N.; Horwell, D. C. Design and Biological Evaluation of Non-Peptide Analogues of Omega-Conotoxin MVIIA. *Bioorg. Med. Chem. Lett.* **2000,** *10,* 345–347.
108. Guo, Z.-X.; Cammidge, A. N.; Horwell, D. C. Dendroid Peptide Structural Mimetics of ω-Conotoxin MVIIA Based on a 2(1H)-Quinolinone Core. *Tetrahedron* **2000,** *56,* 5169–5175.
109. Lew, M. J.; Flinn, J. P.; Pallaghy, P. K.; Murphy, R.; Whorlow, S. L.; Wright, C. E.; Norton, R. S.; Angus, J. A. Structure-Function Relationships of ω-Conotoxin GVIA: Synthesis, Structure, Calcium Channel Binding, and Functional Assay of Alanine Substituted Analogues. *J. Biol. Chem.* **1997,** *272,* 12014–12023.
110. Baell, J. B.; Duggan, P. J.; Forsyth, S. A.; Lewis, R. J.; Lok, Y. P.; Schroeder, C. I. Synthesis and Biological Evaluation of Nonpeptide Mimetics of ω-Conotoxin GVIA. *Bioorg. Med. Chem.* **2004,** *12,* 4025–4037.
111. Baell, J. B.; Duggan, P. J.; Forsyth, S. A.; Lewis, R. J.; Lok, Y. P.; Schroeder, C. I.; Shepherd, N. E. Synthesis and Biological Evaluation of Anthranilamide-Based Non-Peptide Mimetics of ω-Conotoxin GVIA. *Tetrahedron* **2006,** *62,* 7284–7292.
112. Duggan, P. J.; Turk, K. L. Bioactive Mimetics of Conotoxins and Other Venom Peptides. *Toxins* **2015,** *7,* 4175–4198.
113. Gleeson, E.; Graham, J.; Spiller, S.; Vetter, I.; Lewis, R.; Duggan, P.; Tuck, K. Inhibition of N-Type Calcium Channels by Fluorophenoxyanilide Derivatives. *Mar. Drugs* **2015,** *2030–2045,* 13.
114. Tranberg, C. E.; Yang, A.; Vetter, I.; McArthur, J. R.; Baell, J. B.; Lewis, R. J.; Tuck, K. L.; Duggan, P. J. ω-Conotoxin GVIA Mimetics That Bind and Inhibit Neuronal Cav2.2 Ion Channels. *Mar. Drugs* **2012,** *10,* 2349–2368.
115. Knutsen, L. J. S.; Hobbs, C. J.; Fiumana, A.; Radford, F.; et al. Synthesis and SAR of Novel 2-Arylthiazolidinones as Selective Analgesic N-Type Calcium Channel Blockers. *Bioorg. Med. Chem. Lett.* **2007,** *17* (3), 662–667.
116. Knutsen L.J. S.; Hobbs C. J.; Fiumana A.; Radford F.; Preparation of Thiazolidinones as N-Type Calcium Channel Antagonists for Treatment of Chronic and Acute Pain PCT Int. Appl., WO 2004017965 A1 20040304, 2004.
117. Knutsen L. J. S.; Hobbs C.r J.; Radford F.; Fiumana A.; Earnshaw C. G.; Mellor S.L.; Smith N. J.; Preparation of Five-Membered Heterocyclic Ketones as N-Type Calcium Channel Antagonists for Treatment of Chronic and Acute Pain PCT Int. Appl., WO 2004017966 A1 20040304, 2004.
118. Yun L.; Li J.; Zheng J.; Jiang X.; Zhang C.; Wu N.; Zhang S.; 1,3,8-Triazaspiro[4.5]Decan-4-Ones as N-Type Calcium Channel Blockers and Their Preparation, Pharmaceutical Compositions and Use in the Treatment of Pain and Diseases Induced by Opioid Analgesics-Associated Addiction and Tolerance Faming Zhuanli Shenqing, CN 101838269 A 20100922, 2010.
119. Yun L.; Dong G.; Zhang S.; Zhang C.; Wu N.; Wang H.; Pang C.; et al, 3-(1-Arylpiperidin-4-yl)-2-Arylthiazolin-4-One Compounds as N-Type Calcium Channel Blockers and Their Preparation, Pharmaceutical Compositions and Use in the Treatment Of Diseases Faming Zhuanli Shenqing, CN 103130793 A 20130605, 2013.
120. Yamamoto, T.; Niwa, S.; Ohno, S.; Onishi, T.; Matsueda, H.; Koganei, H.; Uneyama, H.; et al. Structure-Activity Relationship Study of 1,4-Dihydropyridine Derivatives Blocking N-Type Calcium Channels. *Bioorg. Med. Chem. Lett.* **2006,** *16* (4), 798–802.
121. Yamamoto, T.; Niwa, S.; Ohno, S.; Tokumasu, M.; Masuzawa, Y.; Nakanishi, C.; Nakajo, A.; et al. The Structure-Activity Relationship Study on 2-, 5-, and 6-Position of the Water Soluble 1,4-Dihydropyridine Derivatives Blocking N-Type Calcium Channels. *Bioorg. Med. Chem. Lett.* **2008,** *18* (17), 4813–4816.
122. Yamamoto, T.; Niwa, S.; Tokumasu, M.; Onishi, T.; Ohno, S.; Hagihara, M.; Koganei, H.; et al. Discovery and Evaluation of Selective N-Type Calcium Channel Blockers: 6-Unsubstituted-1,4-Dihydropyridine-5-Carboxylic Acid Derivatives. *Bioorg. Med. Chem. Lett.* **2012,** *22* (11), 3639–3642.
123. Song, Y.; Bowersox, S. S.; Connor, D. T.; Dooley, D. J.; Lotarski, S. M.; Malone, T.; Miljanich, G.; et al. (S)-4-Methyl-2-(Methylamino)Pentanoic Acid [4,4-bis(4-Fluorophenyl) Butyl]Amide Hydrochloride, a Novel Calcium Channel Antagonist, is Efficacious in Several Animal Models of Pain. *J. Med. Chem.* **2000,** *43* (19), 3474–3477.
124. Yuen, P.-W.; Schelkun, R. M.; Szoke, B.; Tarczy-Hornoch, K. Synthesis and Structure-Activity Relationship of Substituted 1,2,3,4-Tetrahydroisoquinolines as N-Type Calcium Channel Blockers. *Bioorg. Med. Chem. Lett.* **1998,** *8* (18), 2415–2418.
125. Ambler, S. J.; Dell, C. P.; Gilmore, J.; Hotten, T. M.; Sanchiz Suarez, A.; Simmonds, R. G.; Timms, G. H.; et al. Novel N-Substituted Alpha Amino Acid Amides as Calcium Channel Modulators. *Eur. Pat. Appl.* **1997**. EP 805147 A1 19971105.
126. Teodori, E.; Baldi, E.; Dei, S.; Gualtieri, F.; Romanelli, M. N.; Scapecchi, S.; Bellucci, C.; et al. Design, Synthesis, and Preliminary Pharmacological Evaluation of 4-Aminopiperidine Derivatives as N-Type Calcium Channel Blockers Active on Pain and Neuropathic Pain. *J. Med. Chem.* **2004,** *47* (24), 6070–6081.
127. Zamponi, G. W.; Feng, Z.-P.; Zhang, L.; Pajouhesh, H.; Ding, Y.; Belardetti, F.; Pajouhesh, H.; et al. Scaffold-Based Design and Synthesis of Potent N-Type Calcium Channel Blockers. *Bioorg. Med. Chem. Lett.* **2009,** *19* (22), 6467–6472.
128. Snutch T. P.; Zamponi G. W.; Pajouhesh H.; Pajouhesh H.; Belardetti F.; Preparation of 1-Benzhydryl-4-Diphenylpropionylpiperazines as Calcium Channel Blockers U.S. Pat. Appl. Publ., US 20040034035 A1 20040219, 2004.

129. Snutch T. P.; Zamponi G. W.; Pajouhesh H.; Pajouhesh H.; Belardetti F.; Benzhydryl Moiety-Containing Piperazine Compound Calcium Channel Blockers, and Their Therapeutic Use U.S. Pat. Appl. Publ., US 20060084660 A1 20060420, 2006.
130. Pajouhesh, H.; Feng, Z.-P.; Ding, Y.; Zhang, L.; Pajouhesh, H.; Morrison, J.-L.; Belardetti, F. Structure-Activity Relationships of Diphenylpiperazine N-Type Calcium Channel Inhibitors. *Bioorg. Med. Chem. Lett.* **2010,** *20* (4), 1378–1383.
131. Pajouhesh, H.; Feng, Z.-P.; Zhang, L.; Pajouhesh, H.; Jiang, X.; Hendricson, A.; Dong, H.; et al. Structure-Activity Relationships of Trimethoxybenzyl Piperazine N-Type Calcium Channel Inhibitors. *Bioorg. Med. Chem. Lett.* **2012,** *22* (12), 4153–4158.
132. Chung, J. M.; Kim, H. K.; Chung, K. Segmental Spinal Nerve Ligation Model of Neuropathic Pain. *Methods Mol. Med.* **2004,** *99*, 35–45.
133. Borzenko, A.; Pajouhesh, H.; Morrison, J.-L.; Tringham, E.; Snutch, T. P.; Schafer, L. L. Modular, Efficient Synthesis of Asymmetrically Substituted Piperazine Scaffolds as Potent Calcium Channel Blockers. *Bioorg. Med. Chem. Lett.* **2013,** *23* (11), 3257–3261.
134. Snutch T. P.; Zamponi G. W.; Pajouhesh H.; Belardetti F.; Pajouhesh H.; Preparation of Calcium Channel Inhibitors Comprising Benzhydryl Spaced From Piperazine U.S. Pat. Appl. Publ., US 20040266784 A1 20041230, 2004.
135. Snutch T. P.; Zamponi G. W.; Pajouhesh H.; Pajouhesh H.; Belardetti F.; Preparation of Calcium Channel Inhibitors Comprising Benzhydryl Spaced From Piperazine U.S. Pat. Appl. Publ., US 20040044004 A1 20040304, 2004.
136. Snutch T. P.; Pajouhesh H.; Pajouhesh H.; Ding Y.; Preparation of 3-Aminomethylpyrrolidines as N-Type Calcium Channel Blockers PCT Int. Appl., WO 2004105750 A1 20041209, 2004.
137. Doherty, G. A.; Bhatia, P.; Vortherms, T. A.; Marsh, K. C.; Wetter, J. M.; Mack, H.; Scott, V. E. Discovery of Diphenyl Lactam Derivatives as N-Type Calcium Channel Blockers. *Bioorg. Med. Chem. Lett.* **2012,** *22* (4), 1716–1718.
138. Scott, V. E.; Vortherms, T. A.; Niforatos, W.; Swensen, A. M.; Neelands, T.; Milicic, I.; Banfor, P. N.; et al. A-1048400 is a Novel, Orally Active, State-Dependent Neuronal Calcium Channel Blocker That Produces Dose-Dependent Antinociception Without Altering Hemodynamic Function in Rats. *Biochem. Pharmacol.* **2012,** *83* (3), 406–418.
139. Ivanavicius, S. P.; Ball, A. D.; Heapy, C. G.; Westwood, F. R.; Murray, F.; Read, S. J. Structural Pathology in a Rodent Model of Osteoarthritis is Associated With Neuropathic Pain: Increased Expression of ATF-3 and Pharmacological Characterization. *Pain* **2007,** *128* (3), 272–282.
140. Gould, H. J. Complete Freund's Adjuvant-Induced Hyperalgesia: A Human Perception. *Pain* **2000,** *85* (1–2), 301–303.
141. Deacon, R. M. J. Measuring Motor Coordination in Mice. *J. Vis. Exp.* **2013**, (75), e2609. PMC3724562.
142. Bhatia P. A.; Doherty G. A.; Drizin I.; Mack H.; Perner R. J.; Stewart.O.; Zhang Q. W.; Preparation of Pyrrolidinone and Piperidinone Based Compounds as Therapeutic Calcium Channel Blockers PCT Int. Appl., WO 2010039947 A1 20100408, 2010.
143. Beebe, X.; Darczak, D.; Henry, R. F.; Vortherms, T.; Janis, R.; Namovic, M.; Donnelly-Roberts, D.; et al. Synthesis and SAR of 4-Aminocyclopentapyrrolidines as N-Type Ca^{2+} Channel Blockers With Analgesic Activity. *Bioorg. Med. Chem.* **2012,** *20* (13), 4128–4139.
144. Searle X. B.; Yeung M. C.; Didomenico S.; Stewart A.O.; Darczak D.; Schrimpf M.; Rozema M.; Preparation of Novel Substituted Octahydrocyclopenta[c]Pyrrol-4-Amines as Calcium Channel Blockers J U.S. Pat. Appl. Publ., US 20110281870 A1 20111117, 2011.
145. Stewart A.O.; Searle X. B.; Darczak D.; Yeung M. C.; Didomenico S.; Preparation of Novel Substituted Octahydrocyclopenta[c]pyrrol-4-Amines as Calcium Channel Blockers U.S. Pat. Appl. Publ., US 20100130558 A1 20100527, 2010.
146. Matsumura A.; Mikamiyama H.; Tsuno N.; Kyle D. J.; Shao B.; Yao J.; Preparation of Oxime Compounds as Blockers of Calcium Channels Useful in the Treatment of Pain PCT Int. Appl., WO 2008008398 A2 20080117, 2008.
147. Yao J.; Shao B.; Kyle D. J.; Sha D.; Chen Z.; Islam K.; Zhou X.; Benzenesulfonamide Compounds and Their Use as Blockers of Calcium Channels and Their Preparation and Use in the Treatment of Pain PCT Int. Appl., WO 2007118853 A1 20071025, 2007.
148. Chen Z.; Tafesse L.; Yao J.; Islam K.; Preparation of Spiropiperidine-Cyclopenta[b]Pyridine and -Benzocyclopentane Derivatives and Analogs Thereof as Calcium Channel Blockers PCT Int. Appl., WO 2007028638 A1 20070315, 2007.
149. Zhou X.; Preparation of Imidazolidinones, Dihydrobenzimidazolones, and 2,4-Diazabicyclo[3.1.0]Hexanones as Selective N-Type Calcium Channel Blockers for the Treatment of Pain PCT Int. Appl., WO 2007085357 A1 20070802, 2007.
150. Yun L.; Dong G.; Zhang S.; Zhang C.; Wu N.; Wang H.; Pang C.; et al., Faming Zhuanli Shenqing Preparation of Diaryl Pyrazine Compounds as N-Type Calcium Channel Blocker, CN 103130745 A 20130605, 2013.
151. Shao, P. P.; Ye, F.; Chakravarty, P. K.; Varughese, D. J.; Herrington, J. B.; Dai, G.; Bugianesi, R. K.; et al. Aminopiperidine Sulfonamide Cav2.2 Channel Inhibitors for the Treatment of Chronic Pain. *J. Med. Chem.* **2012,** *55* (22), 9847–9855.
152. Shao, P. P.; Ye, F.; Chakravarty, P. K.; Herrington, J. B.; Dai, G.; Bugianesi, R. M.; Haedo, R. J.; et al. Improved Cav2.2 Channel Inhibitors Through a Gem-Dimethylsulfone Bioisostere Replacement of a Labile Sulfonamide. *ACS Med. Chem. Lett.* **2013,** *4* (11), 1064–1068.
153. Chakravarty P.K.; Duffy J. L.; Shao P. P.; Preparation of Substituted Aryl Sulfone Derivatives as Calcium Channel Blockers PCT Int. Appl., WO 2010036589 A1 20100401, 2010.
154. Chakravarty P. K.; Shao P. P.; Substituted Aryl Sulfone Derivatives as Calcium Channel Blockers PCT Int. Appl., WO 2010036596 A1 20100401, 2010.
155. Subasinghe, N. L.; Wall, M. J.; Winters, M. P.; Qin, N.; Lubin, M. L.; Finley, M. F. A.; Brandt, M. R.; et al. A Novel Series of Pyrazolylpiperidine N-Type Calcium Channel Blockers. *Bioorg. Med. Chem. Lett.* **2012,** *22* (12), 4080–4083.
156. Winters, M. P.; Subasinghe, N.; Wall, M.; Beck, E.; Brandt, M. R.; Finley, M. F. A.; Liu, Y.; et al. Discovery and SAR of a Novel Series of 2,4,5,6-Tetrahydrocyclopenta[c] Pyrazoles as N-Type Calcium Channel Inhibitors. *Bioorg. Med. Chem. Lett.* **2014,** *24* (9), 2057–2061.
157. Winters M. P.; Sui Z.; Preparation of Pyrrolopyrazoles as N-Type Calcium Channel Blockers for Treating Pain PCT Int. Appl., WO 2014028805 A1 20140220, 2014.
158. Wall M.; Subasinghe N.; Sui Z.; Flores C.; Preparation of Substituted Pyrazoles as N-Type Calcium Channel Blockers for Treating Inflammatory and Neuropathic Pain PCT Int. Appl., WO 2014028803 A1 20140220, 2014.
159. Wall M.; Subasinghe N.; Sui Z.; Flores C.; Preparation of Substituted Pyrazoles as N-Type Calcium Channel Blockers for Treating Inflammatory and Neuropathic Pain PCT Int. Appl., WO 2014028800 A1 20140220, 2014.
160. Winters M. P.; Sui Z.; Flores C.; Preparation of Cyclopentapyrazoles as N-Type Calcium Channel Blockers for Treating Inflammatory and Neuropathic Pain PCT Int. Appl., WO 2014028801 A1 20140220, 2014.
161. Bakthavatchalam R.; Ahmad I.; Battula S.; Gijsen H.J. M.; Vadivelu S.; Wall M.; Preparation of Substituted Imidazoles as N-Type Calcium Channel Blockers PCT Int. Appl., WO 2015023289 A1 20150219, 2015.
162. Pajouhesh H.; Holland R.; Zhou Y.; Zhu Y.; Grimwood M.E.; Chahal N.; Preparation of Arylsulfone Derivatives for Use as Calcium Channel Blockers PCT Int. Appl., WO 2012061926 A1 20120518, 2012.
163. Mikamiyama H.; Matsumura A.; Masui M.; Anan K.; Hata K.; Preparation of Acrylamide Compounds as Blockers of Calcium Channels for Treating Pain PCT Int. Appl., WO 2010114181 A1 20101007, 2010.
164. Mikamiyama H.; Preparation of oxycarbamoyl compounds as calcium channel blockers PCT Int. Appl., WO 2009151152 A1 20091217, 2009.
165. Tsuno N.; Mikamiyama H.; Masui M.; Oxyimino Compounds for Treatment of Pain PCT Int. Appl., WO 2008150470 A1 20081211, 2008.
166. Kyle D. J.; Yao J.; Preparation of Heterocyclic Benzenesulfonamides as Calcium Channel Blockers for Treating Pain and Other Disorders PCT Int. Appl., WO 2008124118 A1 20081016, 2008.
167. Shao B.; Yao J.; Preparation of Benzenesulfonamide Derivatives as N-Type Calcium Channel Blockers PCT Int. Appl., WO 2009040659 A2 20090402, 2009.
168. Matsumura A.; Mikamiyama H.; Tsuno N.; Yao J.; Shao B.; Benzenesulfonamide Compounds and Their Use as Blockers of Calcium Channels and Their Preparation and Use in the Treatment of Pain PCT Int. Appl., WO 2007118854 A1 2007102, 2007.

169. Chen Z.; Islam K.; Shao B.; Yao J.; Zhou X.; Kyle D. J.; Preparation of Azetidinyl, Pyrrolidinyl, Piperidinyl, and Hexahydroazepinyl Benzenesulfonamides as N-Type Calcium Channel Blockers. PCT Int. Appl., WO 2007110449 A1 20071004, 2007.
170. Beswick P.J.; Campbell A.; Cridland A. P.; Gleave R.J.; Heer J. P.; Nicholson N.H.; Page L.W.; et al Preparation of Piperazine Derivatives as Cav2.2 Calcium Channel Modulators PCT Int. Appl., WO 2010007072 A1 20100121, 2010.
171. Beswick P.J.; Campbell A.; Cridland A. P.; Gleave R.J.; Heer J. P.; Nicholson N.H.; Page L.W.; et al., Preparation of Piperazine Derivatives as Cav2.2 Calcium Channel Modulators PCT Int. Appl., WO 2010007073 A1 20100121, 2010.
172. Heer J. P.; Cridland A. P.; Norton D.; Piperazine Derivatives for Blocking Cav2.2 Calcium Channels PCT Int. Appl., WO 2011086377 A1 20110721, 2011.
173. Beswick P.J.; Campbell A.; Cridland A.; Gleave R. J.; Page L.W.; Preparation of Piperazine Derivatives With Affinity for N-Type Voltage-Gated Calcium Channels for the Treatment of Pain PCT Int. Appl., WO 2010102663 A1 20100916, 2010.
174. Norton D.; Andreotti D.; Ward S. E.; Profeta R.; Spada S.; Price H. S.; Preparation of Tricyclic Piperazine Containing Compounds as Cav2.2 Calcium Channel Blockers for Use in Pain Treatment PCT Int. Appl., WO 2012098400 A1 20120726, 2012.
175. Gleave R. J.; Hachisu S.; Page L. W.; Beswick P.; Preparation of Phenylsulfonyldiazaspirodecanone Derivatives and Analogs for Use as Cav2.2 Calcium Channels Modulators John PCT Int. Appl., WO 2011141728 A1 20111117, 2011.
176. Gleave R. J.; Hachisu S.; Page L. W.; Preparation of Phenylsulfonyldiazaspirodecanone Derivatives and Analogs for Use as Cav2.2 Calcium Channels Modulators PCT Int. Appl., WO 2011141729 A1 20111117, 2011.
177. Beswick P. J.; Gleave R. J.; Preparation of Arylsulfonylpiperidinylpyrrolidinone Derivatives and Analogs for Use in Treatment of Pain PCT Int. Appl., WO 2010091721 A1 20100819, 2010.
178. Inoue T.; Noguchi H.; Sakurada I.; Tatsuta M.; Preparation of Heterocyclic Sulfonamide Compounds Useful in Treatment of Diseases Caused by Overactivation of N-Type Calcium Channels PCT Int. Appl., WO 2007125398 A2 20071108, 2007.
179. Schunk S.; Reich M.; Jakob F.; Koenigs R. M.; Damann N.; Haurand M.; Rogers M.; et al., Preparation of Aryl Substituted Heterocyclyl Sulfones as Voltage Gated Calcium Channel Blockers Useful for the Treatment of Pain U.S. Pat. Appl. Publ., US 20150291573 A1 20151015, 2015.
180. Schunk S.; Reich M.; Jakob F.; Damann N.; Haurand M.; Kless A.; Rogers M.; et al., Preparation of Heteroaryl Substituted Heterocyclyl Sulfones as Voltage Gated Calcium Channel Blockers U.S. Pat. Appl. Publ., US 20150291572 A1 20151015, 2015.
181. Ohtani T.; Kambe T.; Kobayashi K.; Takimizu H.; Ito Y.; Preparation of Benzenesulfonamide Compounds as N-Type Calcium Channel Inhibitors PCT Int. Appl., WO 2006038594 A1 20060413, 2006.
182. Hobbs C. J.; Lynch R.; Mellor S. L.; Radford F.; Gilbert J. C.; Stokes S.; Glen A.; et al., Preparation of Acyclic Sulfonamides as N-Type Calcium Channel Antagonists PCT Int. Appl., WO 2006030211 A2 20060323, 2006.
183. Radford F.; Lynch R.; Mellor S. L.; Hobbs C. J.; Gilbert J. C.; Stokes S.; Glen A.; et al., Sulfonamides, Particularly *N*-(Phenylsulfonyl)Piperidines, as N-Type Calcium Channels Antagonists Useful for Treatment of Pain and Their Preparation PCT Int. Appl., WO 2005068448 A1 20050728, 2005.
184. Swensen, A. M.; Herrington, J.; Bugianesi, R. M.; Dai, G.; Haedo, R. J.; Ratliff, K. S.; Smith, M. M.; et al. Characterization of the Substituted N-Triazole Oxindole TROX-1, a Small-Molecule, State-Dependent Inhibitor of Cav2 Calcium Channels. *Mol. Pharmacol.* **2012,** *81* (3), 488–497.
185. Abbadie, C.; McManus, O. B.; Sun, S.-Y.; Bugianesi, R. M.; Dai, G.; Haedo, R. J.; Herrington, J. B. Analgesic Effects of a Substituted N-Triazole Oxindole (TROX-1), a State-Dependent, Voltage-Gated Calcium Channel 2 Blocker. *J. Pharmacol. Exp. Ther.* **2010,** *334* (2), 545–555.
186. Stevenson C.; N-Substituted Oxindoline Derivatives as Calcium Channel Blockers P. PCT Int. Appl., WO 2009045381 A1 20090409, 2009.
187. Duffy J. L.; Hoyt S. B.; London C.; N-Substituted Oxindoline Derivatives as Calcium Channel Blockers PCT Int. Appl., WO 2009045386 A1 20090409, 2009.
188. Swensen, A. M.; Niforatos, W.; Vortherms, T. A.; Perner, R. J.; Li, T.; Schrimpf, M. R.; Scott, V. E.; et al. An Automated Electrophysiological Assay for Differentiating CaV2.2 Inhibitors Based on State Dependence and Kinetics. *Assay Drug Dev. Technol.* **2012,** *10* (6), 542–550.
189. Tyagarajan, S.; Chakravarty, P. K.; Park, M.; Zhou, B.; Herrington, J. B.; Ratliff, K.; Bugianesi, R. M.; et al. A Potent and Selective Indole N-Type Calcium Channel (Cav2.2) Blocker for the Treatment of Pain. *Bioorg. Med. Chem. Lett.* **2011,** *21* (2), 869–873.
190. Chakravarty P. K.; Duffy J. L.; Park M. K.; Tyagarajan S.; Zhou B.; Preparation of 2-Substituted Indole Derivatives as Calcium Channel Blockers PCT Int. Appl., WO 2008133867 A1 2008110, 2008.
191. Duffy J. L.; Hoyt S. B.; London C.; Stevenson C. P.; Ullman A. M.; Substituted Dihydroisoquinolinone and Isoquinolinedione Derivatives as Calcium Channel Blockers PCT Int. Appl., WO 2010017048 A1 20100211, 2010.
192. Khan N. M.; Burckhardt S.; Cansfield J.E.; Vo N.-T.; Armer R. E.; Boffey R.J.; Preparation of Glyoxyl Indole Compounds as Calcium Ion Channel Modulators & Therapeutic Uses Thereof PCT Int. Appl., WO 2010001179 A2 20100107, 2010.
193. Khan N. M.; Burckhardt S.; Cansfield J. E.; Boffey R. J.; Armer R. E.; Vo N.-T.; Preparation of Indole-3-Glyoxylamide Derivatives for Use as Therapeutic Calcium Ion Channel Modulators PCT Int. Appl., WO 2009133387 A1 20091105, 2009.
194. Zhang, S.; Yang, L.; Zhang, K.; Liu, X.; Dai, W.; Zhang, C.; Yong, Z.; et al. ZC88, a Novel N-Type Calcium Channel Blocker From 4-Amino-Piperidine Derivatives State-Dependent Inhibits Cav2.2 Calcium Channels. *Brain Res.* **2015,** *1605,* 12–21.
195. Wei, X.; Sun, H.; Yan, H.; Zhang, C.; Zhang, S.; Liu, X.; Hua, N.; et al. ZC88, a Novel 4-Amino Piperidine Analog, Inhibits the Growth of Neuroblastoma Cells Through Blocking hERG Potassium Channel. *Cancer Biol. Ther.* **2013,** *14* (5), 450–457.
196. Meng, G.; Wu, N.; Zhang, C.; Su, R.-B.; Lu, X.-Q.; Liu, Y.; Yun, L.-H.; et al. Analgesic Activity of ZC88, a Novel N-Type Voltage-Dependent Calcium Channel Blocker, and its Modulation of Morphine Analgesia, Tolerance and Dependence. *Eur. J. Pharmacol.* **2008,** *586* (1–3), 130–138.
197. Swensen, A. M.; Niforatos, W.; Lee, C.-H.; Jarvis, M. F.; McGaraughty, S. Characterization of the Triazine, T4, a Representative from a Novel Series of CaV2 Inhibitors With Strong State-Dependence, Poor use-Dependence, and Distinctively Fast Kinetics. *Eur. J. Pharmacol.* **2014,** *745,* 234–242.
198. Shishikura J.-I.; Inoue M.; Ogiyama T.; Yonezawa K.; Yamaki S.; Yokoyama K.; Kakimoto S.; et al Preparation of 1-Substituted 2-(Aminoacyl)Tetrahydroisoquinoline Compounds as N-Type Calcium Channel Blockers PCT Int. Appl., WO 2008143263 A1 20081127, 2008.
199. Gonzalez J. E.; Wilson D. M.; Termin A. P.; Grootenhuis P. D. J.; Zhang Y.; Petzoldt B. J.; Fanning L. T. D.; et al., U.S. Pat. Appl. Publ., US 20060217377 A1 20060928, 2006.
200. Galemmo R.; Holland R.; Ding Y.; Zhang L.; Hum G.; Chahal N.; Duffy J.; et al., Amino acid derivatives as calcium channel blockers PCT Int. Appl., WO 2008141446 A1 20081127, 2008.
201. Beswick P. J.; Gleave R. J.; Hachisu S.; Vile S.; Bertheleme N.; Ward S. E.; Preparation of Tetrazole Derivatives as Calcium Channel Blockers for Treating Pain. PCT Int. Appl., WO 2012004604 A1 20120112, 2012.
202. Reich M.; Schunk S.; Jakob F.; Damann N.; Haurand M.; Hamlyn R.; Rogers M.; et al., Fluoromethyl-substituted pyrrole carboxamides as voltage gated calcium channel blockers and their preparation PCT Int. Appl., WO 2015090603 A1 20150625, 2015.
203. Reich M.; Schunk S.; Jakob F.; Steinhagen H.; Damann N.; Haurand M.; Rogers M.; et al., Fluoromethyl-Substituted Pyrrole Carboxamides as Voltage Gated Calcium Channel Blockers and Their Preparation PCT Int. Appl., WO 2015090600 A1 20150625, 2015.
204. Reich M.; Schunk S.; Jakob F.; Steinhagen H.; Damann N. Haurand M.; Hamlyn R.; et al., Fluoromethyl-Pyrrole Carboxamides as CaV2.2 Blockers and Their Preparation, Pharmaceutical Compositions and Use in the Treatment of Pain and Further Diseases PCT Int. Appl., WO 2015090599 A1 20150625, 2015.
205. Matthews, E. A.; Bee, L. A.; Stephens, G. J.; Dickenson, A. H. The Cav2.3 Calcium Channel Antagonist SNX-482 Reduces Dorsal Horn Neuronal Responses in a rat Model of Chronic Neuropathic Pain. *Eur. J. Neurosci.* **2007,** *25* (12), 3561–3569.
206. Yang, L.; Stephens, G. Effects of Neuropathy on High-Voltage-Activated Ca^{2+} Current in Sensory Neurones. *Cell Calcium* **2009,** *46* (4), 248–256.
207. Bourinet E.; Escoubas P.; Merger F.; Nargeot J.; Lazdunski M.; Identification of Novel Antagonist Toxins of T Type Calcium Channels for Analgesia, US8,664,179B2, 2014.

208. Powell, K. L.; Cain, S. M.; Snutch, T. P.; O'Brien, T. J. Low Threshold T-Type Calcium Channels as Targets for Novel Epilepsy Treatments. *Br. J. Clin. Pharmacol.* **2014,** *77* (5), 729–739.
209. Kopecky, B. J.; Liang, R.; Bao, J. T-Type Calcium Channel Blockers as Neuroprotective Agents. *Pflugers Arch.* **2014,** *466* (4), 757–765.
210. Choi, K.-H. The Design and Discovery of T-Type Calcium Channel Inhibitors for the Treatment of Central Nervous System Disorders. *Expert Opin. Drug Discovery* **2013,** *8* (8), 919–931.
211. Connolly, T. M.; Barrow, J. C. Drugs Active at T-Type Ca^{2+} Channels. In *Methods and Principles in Medicinal Chemistry*; *Voltage-Gated Ion Channels as Drug Targets*. 2006, 29*Voltage-Gated Ion Channels as Drug Targets*; pp 84–99.
212. Berger, N. D.; Gadotti, V. M.; Petrov, R. R.; Chapman, K.; Diaz, P.; Zamponi, G. W. NMP-7 Inhibits Chronic Inflammatory and Neuropathic Pain via Block of Cav3.2 T-Type Calcium Channels and Activation of CB2 Receptors. *Mol. Pain* **2014,** *10*, 77/1-77/19.
213. Jarvis, M. F.; Scott, V. E.; McGaraughty, S.; Chu, K. L.; Xu, J.; Niforatos, W.; Milicic, I.; et al. A Peripherally Acting, Selective T-Type Calcium Channel Blocker, ABT-639, Effectively Reduces Nociceptive and Neuropathic Pain in Rats. *Biochem. Pharmacol.* **2014,** *89* (4), 536–544 (Amsterdam, Netherlands).
214. Zhang Q.; Stewart A. O.; Xia Z.; Preparation of Heterocyclic Benzenesulfonamides and Similar Compounds as Therapeutic Calcium Channel Blockers PCT Int. Appl., WO 2010083264 A1 20100722, 2010.
215. Zhang Q.; Stewart A. O.; Zhiren X.; Nothaft W. V.; Benzenesulfonamide Derivative for Use in the Treatment of Diabetic Neuropathy PCT Int. Appl., WO 2013103867 A1 20130711, 2013.
216. Hangeland, J. J.; Cheney, D. L.; Friends, T. J.; Swartz, S.; Levesque, P. C.; Rich, A. J.; Sun, L.; et al. Design and SAR of Selective T-Type Calcium Channel Antagonists Containing a Biaryl Sulfonamide Core. *Bioorg. Med. Chem. Lett.* **2008,** *18* (2), 474–478.
217. Nam G.S.; Choi K. I.; Kim J. H.; Pae A. N.; Hong J. R.; Lee J. K.; Pyrazole Derivatives as Voltage-Gated Calcium Ion Channel Inhibitors and Their Preparation and Use for the Treatment of Diseases U.S. Pat. Appl. Publ., US 20150329533 A1 20151119, 2015.
218. Nam G. S.; Choi K. I.; Pae A. N.; Seo S. H.; Choo H. A.; Keum G. C.; Kim J. H.; Preparation of Novel 6-Pyrazolylamido-3-Substituted Azabicyclo[3.1.0]Hexane Compounds as Calcium Channel Inhibitors U.S. Pat. Appl. Publ., US 20140343295 A1 20141120, 2014.
219. Pajouhesh H.; Galemmo R.; Holland R.; Zhou Y.; Zhu Y.; Simonson E.; Chahal N. et al., Preparation of Phenylsulfone Derivatives for Use as Calcium Channel Blockers PCT Int. Appl., WO 2011035159 A1 20110324, 2011.
220. Tringham, E.; Powell, K. L.; Cain, S. M.; Kuplast, K.; Mezeyova, J.; Weerapura, M.; Eduljee, C.; et al. T-Type Calcium Channel Blockers That Attenuate Thalamic Burst Firing and Suppress Absence Seizures. *Sci. Transl. Med.* **2012,** *4* (121), 14, 121ra19.
221. Lee, M. Z944: A First in Class T-Type Calcium Channel Modulator for the Treatment of Pain. *J. Peripher. Nerv. Syst.* **2014**, (Issue S2), S11–S12. Supplement: Designing Innovative Therapies for Neuropathic Pain: 2014 FPN International Research Symposium(19).
222. LeBlanc, B. W.; Lii, T. R.; Huang, J. J.; Chao, Y.-C.; Bowary, P. M.; Cross, B. S.; Lee, M. S.; et al. T-Type Calcium Channel Blocker Z944 Restores Cortical Synchrony and Thalamocortical Connectivity in a Rat Model of Neuropathic Pain. *Pain* **2016,** *157* (1), 255–263.
223. Casillas-Espinosa, P. M.; Hicks, A.; Jeffreys, A.; Snutch, T. P.; O'Brien, T. J.; Powell, K. L. Z944, a Novel Selective T-Type Calcium Channel Antagonist Delays the Progression of Seizures in the Amygdala Kindling Model. *PLoS One* **2015,** *10* (8). e0130012/1–e0130012/12.
224. Pajouhesh H.; Kaul R.; Ding Y.; Zhu Y.; Zhang L.; Chakka N.; Grimwood M.; et al Yuanxi N-Piperidinyl Acetamide Derivatives as Calcium Channel Blockers and their Preparation, Pharmaceutical Compositions and Use in the Treatment of Obesity PCT Int. Appl., WO 2009146540 A1 20091210, 2009.
225. Uebele, V. N.; Nuss, E.; Fox, S. V.; Garson, S. L.; Cristescu, R.; Doran, S. M.; Kraus, R. L.; et al. Positive Allosteric Interaction of Structurally Diverse T-Type Calcium Channel Antagonists. *Cell Biochem. Biophys.* **2009,** *55,* 81–93.
226. Shipe, W. D.; Barrow, J. C.; Yang, Z.-Q.; Lindsley, C. W.; Yang, F. V.; Schlegel, K.-A. S.; Shu, Y.; et al. Design, Synthesis, and Evaluation of a Novel 4-Aminomethyl-4-Fluoropiperidine as a T-Type Ca^{2+}Channel Antagonist. *J. Med. Chem.* **2008,** *51* (13), 3692–3695.
227. Yang, Z.-Q.; Barrow, J. C.; Shipe, W. D.; Schlegel, K.-A. S.; Shu, Y.; Yang, F. V.; Lindsley, C. W.; et al. Discovery of 1,4-Substituted Piperidines as Potent and Selective Inhibitors of T-Type Calcium Channels. *J. Med. Chem.* **2008,** *51* (20), 6471–6477.
228. Barrow J. C.; Lindsley C. W.; Shipe W. D.; Yang Z.; Wisnoski D.; Preparation of 4-fluoropiperidine derivatives as T-type calcium antagonists PCT Int. Appl., WO 2007002884 A2 20070104, 2007.
229. Barrow J C.; Lindsley C. W.; Shipe W. D.; Yang Z.; Preparation of 3-fluoropiperidine compounds as T-type calcium channel antagonists PCT Int. Appl., WO 2007002361 A2 20070104, 2007.
230. Masaki H.; Iwasaki Y.; Kageyama M.; Uchino Y.; Preparation of Substituted Tropane Derivatives Without Genotoxicity, and Therapeutic Agents and Compositions for T-Type Calcium Channel-Related Diseases PCT Int. Appl., WO 2015182724 A1 20151203, 2015.
231. Bladen, C.; McDaniel, S. W.; Gadotti, V. M.; Petrov, R. R.; Berger, N. D.; Diaz, P.; Zamponi, G. W. Characterization of Novel Cannabinoid Based T-Type Calcium Channel Blockers With Analgesic Effects. *ACS Chem. Neurosci.* **2015,** *6* (2), 277–287.
232. Lee, J.-H.; Seo, S. H.; Lim, E. J.; Cho, N.-C.; Nam, G.; Kang, S. B.; Pae, A. N.; et al. Synthesis and Biological Evaluation of 1-(Isoxazol-5-YImethylaminoethyl)-4-Phenyl Tetrahydropyridine and Piperidine Derivatives as Potent T-Type Calcium Channel Blockers With Antinociceptive Effect in a Neuropathic Pain Model. *Eur. J. Med. Chem.* **2014,** *74,* 246–257.
233. Chu H.A.; Bae A. N.; Cho Y. S.; Lee H. S.; Lee J E.; Cho G. H.; Lim H. W.; et al., Preparation of 5-(Substituted Alkyl-Aminomethyl)Isoxazole Compounds as T-Type Calcium Channel Antagonists Repub. Korean Kongkae Taeho Kongbo, KR 2012096842 A 20120831, 2012.
234. Choo H. A.; Pae A. N.; Cho Y. S.; Lee H. S.; Lee J. E.; Cho G.H.; Rhim H. W.; et al., Preparation of 5-(Substituted Alkyl-Aminomethyl)Isoxazole Compounds as T-Type Calcium Channel Antagonists PCT Int. Appl., WO 2012115446 A2 20120830, 2012.
235. Fritch, P. C.; Krajewski, J. Design, Syntheses, and SAR of 2,8-Diazaspiro[4.5]Decanones as T-Type Calcium Channel Antagonists. *Bioorg. Med. Chem. Lett.* **2010,** *20* (22), 6375–6378.
236. Xiang, Z.; Thompson, A. D.; Brogan, J. T.; Schulte, M. L.; Melancon, B. J.; Mi, D.; Lewis, L. M.; et al. The Discovery and Characterization of ML218: A Novel, Centrally Active T-Type Calcium Channel Inhibitor With Robust Effects in STN Neurons and in a Rodent Model of Parkinson's Disease. *ACS Chem. Neurosci.* **2011,** *2* (12), 730–742.
237. Bornemeier D. A.; Cai C.; Fors K. S.; Hagen T. J.; Holsworth D. D.; Jalaie M.; Leonard D. M.; et al., Preparation of Piperazinylmethyloxadiazoles as Calcium Channel Antagonists PCT Int. Appl., WO 2008050200 A1 20080502, 2008.
238. Kim, H. S.; Kim, Y.; Doddareddy, M. R.; Seo, S. H.; Rhim, H.; Tae, J.; Pae, A. N.; et al. Design, Synthesis, and Biological Evaluation of 1,3-Dioxoisoindoline-5-Carboxamide Derivatives as T-Type Calcium Channel Blockers. *Bioorg. Med. Chem. Lett.* **2007,** *17* (2), 476–481.
239. Gu, S. J.; Lee, J. K.; Pae, A. N.; Chung, H. J.; Rhim, H.; Han, S. Y.; Min, S.-J.; et al. Synthesis and Biological Evaluation of 1,4-Diazepane Derivatives as T-Type Calcium Channel Blockers. *Bioorg. Med. Chem. Lett.* **2010,** *20* (9), 2705–2708.
240. Ullapu, P. R.; Ku, S. J.; Choi, Y. H.; Park, J.; Han, S.-Y.; Baek, D. J.; Lee, J.; et al. Synthesis and Biological Evaluation of 1-Heteroarylmethyl 1,4-Diazepane Derivatives as Potential T-Type Calcium Channel Blockers. *Bull. Korean Chem. Soc.* **2011,** *32* (8), 3063–3073.
241. Cho Y. S.; Min S.J.; Lee J.G.; Ku S. J.; Choi Y. H.; Ullapu P. R.; Ahmed A. W.; et al., Preparation of 2-(4-Substituted-1,4-Diazepan-1-yl)Acetamide Compounds as T-Type Calcium Channel Antagonists Repub. Korean Kongkae Taeho Kongbo, KR 2011115374 A 20111021, 2011.
242. Choi K. I.; Nam G.; Kim H.R.; Rhim H.; Seo S. H.; Kim Y. J.; Shin H. S. et al. Preparation of Imidazolylalkylcarbonyl Derivatives as Calcium Channel Modulators Korea Institute of Science and Technology, S. Korea U.S. Pat. Appl. Publ., US 20090325979 A1 20091231, 2009.
243. Noh E. J.; Park J. E.; Ji W.G.; Shin G. J.; Bae A.N.; Choi G. I.; Kim D. J.; et al., 1-(4-Halophenyl-Oxy/Thio)-3-(4-Substituted Piperazin-1-yl)Propan-2-ol for Inhibiting T-Type Calcium Channel, and Method for the Preparation Thereof Repub. Korean Kongkae Taeho Kongbo, KR 2012066699 A 20120625, 2012.

244. Cho Y. S.; Min S. J.; Bae A. N.; Lee J. G.; Lim H.W.; Choi G. H.; Seo S. H.; et al., Preparation of 1,4-Diazepane Compounds Containing Pyrazole Moiety as T-Type Calcium Channel Antagonists Repub. Korean Kongkae Taeho Kongbo, KR 2012097288 A 20120903, 2012.
245. Reger, T. S.; Yang, Z.-Q.; Schlegel, K.-A. S.; Shu, Y.; Mattern, C.; Cube, R.; Rittle, K. E.; et al. Pyridyl Amides as Potent Inhibitors of T-Type Calcium Channels. *Bioorg. Med. Chem. Lett.* **2011,** *21* (6), 1692–1696.
246. Kraus, R. L.; Li, Y.; Gregan, Y.; Gotter, A. L.; Uebele, V. N.; Fox, S. V.; Doran, S. M.; et al. In Vitro Characterization of T-Type Calcium Channel Antagonist TTA-A2 and in vivo Effects on Arousal in Mice. *J. Pharmacol. Exp. Ther.* **2010,** *335* (2), 409–417.
247. Francois, A.; Kerckhove, N.; Meleine, M.; Alloui, A.; Barrere, C.; Gelot, A.; Uebele, V. N.; et al. State-Dependent Properties of a New T-Type Calcium Channel Blocker Enhance CaV3.2 Selectivity and Support Analgesic Effects. *Pain* **2013,** *154* (2), 283–293.
248. Egan, M. F.; Zhao, X.; Smith, A.; Troyer, M. D.; Uebele, V. N.; Pidkorytov, V.; Cox, K.; et al. Randomized Controlled Study of the T-Type Calcium Channel Antagonist MK-8998 for the Treatment of Acute Psychosis in Patients With Schizophrenia. *Hum. Psychopharmacol.* **2013,** *28* (2), 124–133.
249. Barrow J.C.; Bieber K.-A. S.; Cube R. V.; Mattern M.C.; Reger T.S.; Shu Y.; Yang Z.Q.; Pyridyl Amide Derivatives, Processes for Preparing Them, Pharmaceutical Compositions Containing Them, and Their Use as T-Type Calcium Channel Antagonists PCT Int. Appl., WO 2007120729 A2 20071025, 2007.
250. Barrow, J. C.; Rittle, K. E.; Reger, T. S.; Yang, Z.-Q.; Bondiskey, P.; McGaughey, G. B.; Bock, M. G.; et al. Discovery of 4,4-Disubstituted Quinazolin-2-Ones as T-Type Calcium Channel Antagonists. *ACS Med. Chem. Lett.* **2010,** *1* (2), 75–79.
251. Schlegel, K. A.; Yang, Z.-Q.; Reger, T. S.; Shu, Y.; Cube, R.; Rittle, K. E.; Bondiskey, P.; Bock, M. G.; Hartman, G. D.; Tang, C.; et al. Discovery and Expanded SAR of 4,4-Disubstituted Quinazolin-2-Ones as Potent T-Type Calcium Channel Antagonists. *Bioorg. Med. Chem. Lett.* **2010,** *20* (17), 5147–5152.
252. Barrow J.C.; Cube R. V.; Ngo P.L.; Rittle K. E.; Yang Z.; Young S.D.; Preparation of Quinazolinones as T-Type Calcium Channel Antagonists PCT Int. Appl., WO 2006098969 A2 20060921, 2006.
253. Bladen, C.; Gunduz, M. G.; Simsek, R.; Safak, C.; Zamponi, G. W. Synthesis and Evaluation of 1,4-Dihydropyridine Derivatives With Calcium Channel Blocking Activity. *Pflugers Arch. - Eur. J. Physiol.* **2013,** *466* (7), 1355–1363.
254. Bladen, C.; Gadotti, V. M.; Gunduz, M. G.; Berger, N. D.; Simsek, R.; Safak, C.; Zamponi, G. W. 1,4-Dihydropyridine Derivatives With T-Type Calcium Channel Blocking Activity Attenuate Inflammatory and Neuropathic Pain. *Pflugers Arch.* **2015,** *467* (6), 1237–1247.
255. Uebele, V. N.; Nuss, C. E.; Santarelli, V. P.; Garson, S. L.; Barrow, J. C.; Stauffer, S. R.; Koblan, K. S.; et al. T-Type Calcium Channels Regulate Cortical Plasticity In-Vivo. *NeuroReport* **2009,** *20* (3), 257–262.
256. Rhim, H.; Lee, Y. S.; Park, S. J.; Chung, B. Y.; Lee, J. Y. Synthesis and Biological Activity of 3,4-Dihydroquinazolines for Selective T-Type Ca^{2+} Channel Blockers. *Bioorg. Med. Chem. Lett.* **2005,** *15* (2), 283–286.
257. M'Dahoma, S.; Gadotti, V. M.; Zhang, F. X.; Park, B.; Nam, J. H.; Onnis, V.; Balboni, G.; et al. Effect of the T-Type Channel Blocker KYS-05090S in Mouse Models of Acute and Neuropathic Pain. *Pflugers Arch.* **2016,** *468* (2), 193–199.
258. De Petrocellis, L.; Schiano, Moriello A.; Byun, J. S.; Sohn, J. M.; Lee, J. Y.; Vazquez-Romero, A.; Garrido, M.; et al. Inhibitory Effect of Positively Charged Triazine Antagonists of Prokineticin Receptors on the Transient Receptor Vanilloid Type-1 (TRPV1) Channel. *Pharmacol. Res.* **2015,** *99,* 362–369.
259. Bezencon O.; Gatfield J.; Heidmann B.; Siegrist R.; Stamm S.; Preparation of Triazole Compounds as T-Type Calcium Channel Blockers PCT Int. Appl., WO 2016041892 A1 20160324, 2016.
260. Siegrist R.; Heidmann B.; Stamm S.; Gatfield J.; Bezencon O.; Preparation of Pyrazole Compounds and Their Use as T-Type Calcium Channel Blockers PCT Int. Appl., WO 2015186056 A1 20151210, 2015.
261. Adachi M.; Minami M.; Egi J.; Hirai Y.; Iwamoto T.; Shintani Y.; Okada T.; et al., Preparation of Substituted Triazinones, T-Type Calcium Channel Blockers Containing Them, and Pharmaceuticals for Treatment of Neuropathic Pain PCT Int. Appl., WO 2015093534 A1 20150625, 2015.
262. Niwa M.T.; Inaba Y.; Iwamoto T.; Shintani Y.; Nagai H.; Egi J.; Adachi M.; Hirai Y. Preparation of Triazinone Derivatives as T-Type Calcium Channel Blockers for Therapeutic Agents for Neuropathic Pains PCT Int. Appl., WO 2015050212 A1 20150409, 2015.
263. Niwa M.; Inaba Y.; Iwamoto T.; Shintani Y.; Nagai H.; Egi J.; Adachi M. et al., Preparation of Triazinone Compounds as T-Type Calcium Channel Inhibitors PCT Int. Appl., WO 2013147183 A1, 2013.
264. Furuta T.; Sawada T.; Danjo T.; Nakajima T.; Uesaka N., Preparation of Condensed Ring Heterocyclic Compounds, and Pharmaceuticals and T-Type Calcium Channel Blockers Containing Them for Treatment of Pruritus PCT Int. Appl., WO 2014021383 A1 20140206, 2014.
265. Sawada T.; Danjo T.; Motosawa K.; Furuta T.; Ichioka, M.; Sugawara M.; Uesaka N., Preparation of Ring-Fused Imidazole Heterocyclic Derivatives as Regulators of T-Type Calcium Channel PCT Int. Appl., WO 2012105594 A1 20120809, 2012.
266. Chakravarty P.K.; Duffy J. L.; Park M. K.; Tyagarajan S.; Zhou B., Preparation of 2-Substituted Indole Derivatives as Calcium Channel Blockers PCT Int. Appl., WO 2008133867 A1 20081106, 2008.
267. Abignente E.; Cataldi M.; Citraro R.; Curcio A.; De Lucia S.; De Novellis V.; De Sarro, G., et al., Preparation of 2-Phenyl-Imidazo[1,2-b]Pyridazine Compounds With Analgesic and Antiepileptic Activities Ital. Appl., IT 2007MI2166 A1 20080214, 2008.
268. Masaki H.; Takasugi H.; Nagayama T.; Shimono, R.; Uchino Y.; Takayanagi K., Preparation of Fused Imidazole Derivatives as Antagonists of T-Type Calcium Channel PCT Int. Appl., WO 2011148956 A1 20111201, 2011.
269. Pajouhesh H.; Pajouhesh H.; Ding Y.; Tan J.; Grimwood M.; Belardetti F.; Kaul R., Preparation of Bicyclic Pyrimidine Derivatives as Calcium Channel Blockers U.S. Pat. Appl. Publ., US 20080280900 A1 20081113, 2008.
270. Wu, J. J.-Q., Novel Crystalline Forms of Pirenperone for the Treatment of Diseases, Disorders, or Conditions Associated With T-Type Calcium Ion Channels PCT Int. Appl., WO 2014143915 A1 20140918, 2014.
271. Kawabata A. I; Matsuda H.; Sekiguchi F.; Murata K.; Nishikawa H., T-Type Calcium Channel Blockers Containing Flavanones, and Pharmaceuticals and Neuropathic Pain Treatment Agents Containing the Blockers PCT Int. Appl., WO 2014188980 A1 20141127, 2014.
272. Gray L. S.; Haverstick D. M. T type Calcium Channel Blockers and the Treatment of Diseases U.S. Pat. Appl. Publ., US 20120264804 A1 20121018, 2012.
273. Thorpe, A. J.; Taylor, C. P.; Taylor, J. B.; Triggle, D. J. Calcium Channel α2-δ Ligands: Gabapentin and Pregabalin. *Compr. Med. Chem. II* **2006,** *8,* 227–246.
274. Bryans, J. S.; Wustrow, D. J. 3-Substituted GABA Analogs With Central Nervous System Activity: A Review. *Med. Res. Rev.* **1999,** *19* (2), 149–177.
275. Dolphin, A. C. Calcium Channel Auxiliary α2δ and β Subunits: Trafficking and One Step Beyond. *Nat. Rev. Neurosci.* **2012,** *13* (8), 542–555.
276. Birch, M.; Challenger, S.; Crochard, J.-P.; Fradet, D.; Jackman, H.; Luan, A.; Madigan, E.; Mathew, J. S.; McDowall, N.; Meldrum, K.; et al. A Simplified Process for the Manufacture of Imagabalin Hydrochloride (PD-0332334), an α2δ-Ligand for the Treatment of Generalized Anxiety Disorder. *Org. Process. Res. Dev.* **2011,** *15* (6), 1358–1364.
277. Corriqan, B.; Feltner, D. E.; Ouellet, D.; Werth, J. L.; Moton, A. E.; Gibson, G. Effect of Renal Impairment on the Pharmacokinetics of PD 0200390, a Novel Ligand for the Voltage-Gated Calcium Channel Alpha-2-Delta Subunit. *Br. J. Clin. Pharmacol.* **2009,** *68* (2), 174–180.
278. Thompson, L. R.; Blakemore, D. C.; Brugier, D.; Bryans, J. S.; Chu, W.-L. A.; Maw, G. N.; et al. Part 1: N-Alkylated Glycines as Potent α2δ Ligands. *Bioorg. Med. Chem. Lett.* **2011,** *21* (12), 3764–3766.
279. Rawson, D. J.; Brugier, D.; Harrison, A.; Hough, J.; Newman, J.; Otterburn, J.; Maw, G. N.; et al. Part 2: Design, Synthesis and Evaluation of Hydroxyproline-Derived α2δ Ligands. *Bioorg. Med. Chem. Lett.* **2011,** *21* (12), 3767–3770.
280. Rawson, D. J.; Brugier, D.; Harrison, A.; Hough, J.; Newman, J.; Otterburn, J.; Maw, G. N.; et al. Part 3: Design and Synthesis of Proline-Derived α2δ Ligands. *Bioorg. Med. Chem. Lett.* **2011,** *21* (12), 3771–3773.
281. Blakemore, D. C.; Bryans, J. S.; Carnell, P.; Field, M. J.; Kinsella, N. A.; Kinsora, J. K.; Meltzer, L. T.; et al. Synthesis and in vivo Evaluation of 3,4-Disubstituted Gababutins. *Bioorg. Med. Chem. Lett.* **2010,** *20* (1), 248–251.

282. Blakemore, D. C.; Bryans, J. S.; Carnell, P.; Chessum, N. E. A.; Field, M. J.; Kinsella, N.; Kinsora, J. K. Synthesis and in vivo Evaluation of 3-Substituted Gababutins. *Bioorg. Med. Chem. Lett.* **2010,** *20* (1), 362–365.
283. ClinicalTrials.gov Identifier: NCT00569972.
284. ClinicalTrials.gov Identifier: NCT00551148.
285. ClinicalTrials.gov Identifier: NCT00655369.
286. Blakemore, D. C.; Bryans, J. S.; Carnell, P.; Carr, C. L.; Chessum, N. E. A.; Field, M. J.; Kinsella, N. Synthesis and in vivo Evaluation of Bicyclic Gababutins. *Bioorg. Med. Chem. Lett.* **2010,** *20* (2), 461–464.
287. Shimada, K.; Kawamura, A.; Arakawa, N.; Domon, Y., Preparation of Bicyclic γ-Amino Acid Derivatives as Potential-Dependent Calcium Channel α2δ Subunit Ligands PCT Int. Appl., WO 2009041453 A1 20090402, 2009.
288. Vinik, A.; Rosenstock, J.; Sharma, U.; Feins, K.; Hsu, C.; Merante, D.; et al. Efficacy and Safety of Mirogabalin (DS-5565) for the Treatment of Diabetic Peripheral Neuropathic Pain: A Randomized, Double-Blind, Placebo- and Active Comparator-Controlled, Adaptive Proof-of-Concept Phase 2 Study. *Diabetes Care* **2014,** *37* (12), 3253–3261.
289. Vinik, A.; Sharma, U.; Feins, K.; Hsu, C.; Merante, D. DS-5565 for the Treatment of Diabetic Peripheral Neuropathic Pain: Randomized, Double-Blind, Placebo- and Active Comparator-Controlled Phase II Study (S20.004). *Neurology* **2014,** *82* (10). S20.004.
290. Wustrow, D. J.; Belliotti, T. R.; Capiris, T.; Kneen, C. O.; Bryans, J. S.; Field, M. J.; Williams, D.; et al. Oxadiazolone Bioisosteres of Pregabalin and Gabapentin. *Bioorg. Med. Chem. Lett.* **2009,** *19* (1), 247–250.
291. Bryans, J. S.; Capiris, T.; Horwell, D. C.; Kneen, C. O.; Wustrow, D. J., Preparation of 1-(Azolylmethyl)-1-(Aminomethyl)Cycloalkanes and Related Compounds as Gabapentin Analogues for Treatment of Neurological Disorders PCT Int. Appl., WO 9931075 A1 19990624, 1999.
292. Fukasawa, H. I.; Muratake, H.; Ito, A.; Suzuki, H.; Amano, Y.; Nagae, M.; Sugiyama, K.; Shudo, K. Silicon-Containing GABA Derivatives, Silagaba Compounds, as Orally Effective Agents for Treating Neuropathic Pain Without Central-Nervous-System-Related Side Effects. *ACS Chem. Neurosci.* **2014,** *5* (7), 525–553.
293. Shimada, K.; Kawamura, A.; Onishi, Y.; Watanabe, T., β-Alanine Derivatives as Ligand for Calcium Channel α2δ Subunit 1, Pharmaceutical Compositions Containing Them, and Method for Treating Pain Using Them, Jpn. Kokai Tokkyo Koho, JP 2013245217 A 20131209, 2013.
294. Meghani, P.; Kricek, F., Preparation of Gamma-Aminobutyric Acid (GABA) Analogs for the Treatment of Pain and Other Disorders PCT Int. Appl., WO 2015091463 A1 20150625, 2015.
295. Kong, X.; Levens, N.Lamothe, S.; Atfani, M.; Ciblat, S.; Jette, L., Amino Acid Derivatives for the Treatment of Neuropathic Pain U.S. Pat. Appl. Publ., US 20120208876 A1 20120816, 2012.
296. Stearns, B. A.; Anker, N.; Arruda, J. M.; Campbell, B. T.; Chen, C.; Cramer, M.; Hu, T.; Jiang, X.; Park, K.; Ren, K. K.; et al. Synthesis and Biological Evaluation of 6-Aryl-6H-Pyrrolo[3,4-d]Pyridazine Derivatives: High-Affinity Ligands to the Alpha 2 Delta Subunit of Voltage Gated Calcium Channels. *Bioorg. Med. Chem. Lett.* **2004,** *14* (5), 1295–1298.
297. Hu, T.; Stearns, B. A.; Campbell, B. T.; Arruda, J. M.; Chen, C.; Aiyar, J.; Bezverkov, R.t E.; Santini, A.; Schaffhauser, H.; Liu, W.; et al. Synthesis and Biological Evaluation of 6-Aryl-6H-Pyrrolo[3,4-d]Pyridazine Derivatives as High-Affinity Ligands of the α2δ Subunit of Voltage-Gated Calcium Channels. *Bioorg. Med. Chem. Lett.* **2004,** *14* (9), 2031–2034.
298. Anker, N. B.; Arruda, J. M.; Campbell, B. T.; Munoz, B.; Prasit, P.; Stearns, B. A., Treatment of Neuropathic Pain With 6H-Pyrrolo[3,4-d]Pyridazine Compounds. PCT Int. Appl., WO 2004006836 A2 20040122, 2004.
299. Lebsack, A. D.; Gunzner, J.; Wang, B.; Pracitto, R.; Schaffhauser, H.; Santini, A.; Aiyar, J.; Bezverkov, R.; Munoz, B.; Liu, W.; et al. Identification and Synthesis of [1,2,4] Triazolo[3,4-a]Phthalazine Derivatives as High-Affinity Ligands to the α2δ-1 Subunit of Voltage Gated Calcium Channel. *Bioorg. Med. Chem. Lett.* **2004,** *14* (10), 2463–2467.
300. Lebsack, A. D.; Munoz, B.; Pracitto, R.; Venkatraman, S.; Wang, B.; Gunzner, J., Preparation of Triazolo/Pyridazines Useful in the Treatment of Neuropathic Pain PCT Int. Appl., WO 2005041971 A1 20050512, 2005.
301. Lim, J.; Stock, N.; Pracitto, R.; Boueres, J. K.; Munoz, B.; Chaudhary, A.; Santini, A. M.; Orr, K.; Schaffhauser, H.; Bezverkov, R. E.; et al. N-Acridin-9-yl-Butane-1,4-Diamine Derivatives: High-Affinity Ligands of the α2δ Subunit of Voltage Gated Calcium Channels. *Bioorg. Med. Chem. Lett.* **2004,** *14* (8), 1913–1916.
302. Lim, J.; Boueres, J.K.; Munoz, B.; Pracitto, R.; Stock, N.; Venkatraman, S., Preparation of Pyridin-4-Ylamines Useful in the Treatment of Neuropathic Pain PCT Int. Appl., WO 2005051915 A1 20050609, 2005.
303. Nitta, M.; Sakai, D.; Matsumura, T.; Atago, T.; Matsumiya, S.; Hagihara, K., Method for Producing Pyrimidodiazepinone Compounds From Pyrimidinecarboxylic Acids and (Aminomethyl)Pyrrolidines PCT Int. Appl., WO 2014069626 A1, 2014.
304. Otsubo, N.; Okazaki, S.; Tsukumo, Y.; Iida, K.; Nakoji, M., Preparation of Pyrimido-Diazepinone Compounds as Ligands of α2δ Protein PCT Int. Appl., WO 2012153796 A1 20121115, 2012.
305. Izumimoto, N.; Mochizuki, H., Therapeutic Agent or Prophylactic Agent for Neuropathic Pain PCT Int. Appl., WO 2012015027 A1 20120202, 2012.
306. Schunk S.; Reich M.; Steinhagen H.; Damann N.; Skone P.; Hamlyn R.; Kirby R.; et al., Preparation of Fluoromethyl-Substituted Pyrrole Carboxamides as Voltage Gated Calcium Channel Blockers PCT Int. Appl., WO 2014032801 A1 20140306, 2014.
307. Giordanetto, F.; Waallberg, A.; Knerr, L.; Selmi, N.; Ullah, V.; Thorstensson, F.; Lindeloef, A.; et al. Discovery of N-[[1-[2-(Tert-Butylcarbamoylamino)Ethyl]-4-(Hydroxymethyl)-4-Piperidyl]Methyl]-3,5-Dichloro-Benzamide as a Selective T-Type Calcium Channel (Cav3.2) Inhibitor. *Bioorg. Med. Chem. Lett.* **2013,** *23* (1), 119–124.
308. Rawson, D.J., Proline Derivatives Having Affinity for the Calcium Channel α-2-δ Subunit PCT Int. Appl., WO 2004039367 A1 20040513, 2004.
309. Bryans J. S.; Horwell, D. C.; Thorpe, A. J.; Wustrow, D. J.; Y., P.-W., Synthesis of Cyclic Amino Acids and Derivatives Thereof Useful as Pharmaceutical Agents, PCT Int. Appl., WO 9921824 A1 19990506, 1999.
310. Blakemore, D. C.; Bryans, J.S.; Williams, S. C., Preparation of Fused Bicyclic or Tricyclic Amino Acid PCT Int. Appl., WO 2002085839 A1 20021031, 2002.

7.04 Sodium Channel Blockers for the Treatment of Pain

DR Witty, DT MacPherson, and GMP Giblin, Convergence Pharmaceuticals Limited, a Biogen Company, Cambridge, United Kingdom

© 2017 Elsevier Ltd. All rights reserved.

7.04.1	**Introduction**	131
7.04.2	**Sodium Channel Structure and Function**	132
7.04.2.1	Voltage-Gated Sodium Channels	132
7.04.2.2	Ligand-Gated Sodium Channels	133
7.04.2.3	Mechanisms of Ion Channel Modulation	133
7.04.3	**Voltage-Gated Sodium Channel Blocking Agents**	133
7.04.3.1	Toxins and Peptides	133
7.04.3.2	Antibodies	135
7.04.3.3	Small Molecules	136
7.04.3.3.1	Clinical compounds with a sodium channel mode of action	136
7.04.3.3.2	Multi-channel, partially selective and $Na_V1.7$ selective sodium channel blockers	136
7.04.3.3.3	$Na_V1.8$ blockers	161
7.04.3.3.4	$Na_V1.9$ blockers	165
7.04.4	**Clinical Studies**	165
7.04.5	**Conclusions**	167
References		167

7.04.1 Introduction

Voltage-gated sodium channels[1] (Na_Vs) are ubiquitous proteins found in all known classes of organisms indicating their essential role in the basic functions of life. In multicellular organisms, they are critical mediators of intracellular information transfer along neurons and play a pivotal role in neuronal networks. There is a long history of sodium channel blockers showing utility in the treatment of human diseases, for example, carbamazepine was introduced for the treatment of epilepsy and trigeminal neuralgia in the 1960s,[2] and lamotrigine for epilepsy and bipolar disorder in the 1990s.[3] More recently, driven by discoveries in human sodium channel genetics, there has been a resurgence of effort aimed at discovering novel, subtype selective sodium channel blockers for the treatment of pain.[4]

Sodium channels are transmembrane proteins consisting of a large tetrameric pore-forming α-subunit and smaller auxiliary β-subunits. There are ten known subtypes designated by their respective α-subunits, $Na_V1.1$–1.9 and Na_x, which arise from genes SCN1A to SCN11A (**Table 1**).[6] Sodium channels at resting membrane potential are closed to sodium ion transport but respond to external stimuli by detecting small changes in membrane potential. This triggers activation of the channel via a conformational change, resulting in transient channel opening permitting selective cellular influx of sodium. This leads to further depolarization resulting in neuronal activation and excitation. Channels remain in the open state for a short period before entering an inactivated state that is nonconducting and resistant to activation. An increase in membrane potential known as hyperpolarization causes the channel to return to the resting state. In order to intervene pharmacologically it is preferable to stabilize the inactivated state rather than blocking the open state, which has important roles in homeostasis[7] (*vide infra*).

Table 1 Identification of Na_V channels and inhibition profile with Tetrodotoxin[5]

Channel	*Gene*	*TTX IC_{50} (nM)*	*Occurrence*
Na_V 1.1	SCN1A	6	CNS
Na_V 1.2	SCN2A	13	CNS
Na_V 1.3	SCN3A	4	Embryonic CNS
Na_V 1.4	SCN4A	5	Skeletal muscle
Na_V 1.5	SCN5A	2000	Cardiac
Na_V 1.6	SCN8A	3	CNS, glia, DRG
Na_V 1.7	SCN9A	4	DRG, CNS
Na_V 1.8	SCN10A	31,000	DRG
Na_V 1.9	SCN11A	1500	DRG
Na_X	SCN6(7)A	–	Heart, uterus, lung, DRG, glia, circumventricular organs

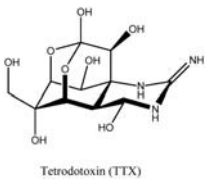

Tetrodotoxin (TTX)

The distribution and function of sodium channels are well characterized.[8] In summary, sodium channels are expressed principally in the central nervous system (CNS) and peripheral nervous system (PNS) on neurons and glial cells. However subtypes $Na_V1.4$ and $Na_V1.5$ are expressed mainly in skeletal and cardiac myocytes. More specifically $Na_V1.1$, 1.2, and 1.3, known as brain sodium channels, are highly expressed in the CNS and are highly sequence homologous. $Na_V1.1$ is also expressed in the dorsal root ganglia (DRG) and is responsible for propagating nociceptive signals from the periphery to the CNS via the dorsal horn of the spinal cord. $Na_V1.2$ is abundant in adult brain whereas $Na_V1.3$ appears to be the dominant brain isoform in the embryonic CNS but is downregulated after birth. $Na_V1.6$ is expressed in the CNS, PNS, and glial cells. $Na_V1.7$ is notable for its high levels of expression in the PNS, particularly in DRG nociceptive neurons, indicating a potential role in pain pathways. $Na_V1.8$ is not expressed in the CNS and occurs mainly in nociceptive neurones in the DRG. $Na_V1.9$ is particularly localized in small DRG neurons and not in the CNS. Hence multiple Na_V channels are associated with cellular locations and cell types that are important for the processing of pain signals and therefore sodium channels are attractive targets for therapeutic intervention in conditions that cause pain.

Human genetic studies[9] have identified a number of mutations that result in interesting pain phenotypes. Certain mutations in the SCN9A gene, which codes for the $Na_V1.7$ channel, result in a rare inherited condition known as erythromelalgia (EM).[10] Patients with EM suffer swelling and painful burning sensations in the extremities, often in the toes but also the ears and face. Electrophysiology studies have demonstrated that mutated $Na_V1.7$ channels from EM patients are constitutively hyperexcited. In addition these mutations cause the voltage sensitivity of inactivation to change resulting in channels that are open for a longer period of time, producing a more prolonged change in membrane potential. Inherited EM became the first neuropathic pain condition with a causal link to genetic mutations. Subsequently other conditions have been genetically linked to SCN9A: paroxysmal extreme pain disorder in which mutant $Na_V1.7$ channels have a disrupted inactivation pathway that prevents channel closure and results in persistent pain; and Congenital Insensitivity to Pain (CIP), a rare condition in which patients experience no pain due to a mutated nonfunctional $Na_V1.7$ channel.

Further genetic linkages to sodium channels[11] have been discovered, including mutations to the SCN10A ($Na_V1.8$ encoding) gene that results in hyperexcitability and decreased pain thresholds in small fiber neuropathy patients, and SCN11A ($Na_V1.9$) mutations, which produce gain-of-function effects in painful peripheral neuropathy and familial episodic pain. Although further genetic studies are warranted in other well-defined human pain populations, it is already evident that mutations in sodium channels can result in either gain-of-function effects or complete loss of pain sensitivity. Evidently multiple channel subtypes are involved in processing pathogenic pain signaling. The specific role of certain subtypes has been defined (e.g., evidence suggests that $Na_V1.7$ acts as a threshold channel which, when activated above a certain membrane voltage, undergoes a slow transition into the inactivated state). However, specific roles of other channels in different cellular population types require further elucidation. Notwithstanding this complexity of subtypes, targeting sodium channels continues to be a focus for pharmacologic and therapeutic intervention in the treatment of human pain conditions.[4]

A considerable number of studies have characterized the effect of sodium channel blockers in animal models of pain. Both nonselective[12] and subtype selective $Na_V1.7$[13,14]and $Na_V1.8$[14,15] molecules have shown efficacy in a range of preclinical pain models, providing further support for these sodium channels as targets for therapeutic intervention.

The last decade has seen major progress in the design of selective sodium channel blockers targeting channel subtypes with a genetic linkage to pain.[11] This progress has been driven by the emergence of an understanding of the structure and function of voltage-gated ion channels, through both detailed electrophysiology studies of particular channels[16] and the solving of the first X-ray crystal structures of sodium channels.[17]

Clinically there have been a number of human studies investigating the efficacy of sodium channel blockers in neuropathic pain. Local anesthetics such as lidocaine are non-selective sodium channel blockers. The analgesic activity of local anesthetics is clinically well characterized although the therapeutic index is low limiting use to local administration. Lamotrigine was developed as a sodium channel blocker with a much improved therapeutic index due to its use- or state-dependency, subsequently shown to be associated with its selective targeting of the inactivated state of the channel. Lamotrigine is effective in reducing pain in patients with diabetic neuropathy at oral doses of 200 mg and above.[18] However it causes a rare life-threatening rash (Stevens–Johnson syndrome), which has limited its use to more severe clinical indications. Recently a new state-dependent small molecule, CNV1014802, has been reported to show efficacy in two Phase II clinical studies in lumbosacral radiculopathy (lower back pain/sciatica) patients and patients suffering from trigeminal neuralgia, a debilitating and excruciatingly painful condition associated with entrapment of the trigeminal nerve in the face.[19] CNV1014802 is reported to be entering Phase III studies in 2016 (*vide infra*).

It is the purpose of this chapter to identify and profile novel classes of sodium channel blockers directed at pain indications. The work comprehensively reviews patent filings and publications from 2012 to 2015 and references all compound classes reported since 2010. Papers describing compounds in which sodium channel blockade is one of a number of polypharmacologic modes of action are not exhaustively covered. The reader is directed to several recent reviews, which also discuss aspects of sodium channel drug discovery.[20]

In addition to small molecule research, modified toxin and antibody approaches are examined. This review will also discuss recently reported clinical findings.

7.04.2 Sodium Channel Structure and Function

7.04.2.1 Voltage-Gated Sodium Channels

Mammalian voltage-gated sodium channels have been characterized by their sensitivity to interaction with tetrodotoxin (**Table 1**) as well as subtype and location. A review of diseases and clinical indications for voltage-gated sodium channels as well as the use of

toxins to characterize channel responses has recently been published.[21] The channels most frequently associated with pain sensation pathways are $Na_V1.2$, 1.3, 1.6, 1.7, 1.8, and 1.9. Much work has been undertaken to discover small molecules with selectivity over the $Na_V1.5$ channel, which is important for cardiac function. Many of the papers and patents discussed report $Na_V1.7/Na_V1.5$ selectivity as a key parameter in drug design. As certain channel subtypes are predominantly found in either peripheral or central locations, designing compounds for a particular compartment has often been a factor in designing blockers for a particular function. For example researchers have reported the design of compounds with low central penetrance as a mechanism by which selective blockade of peripheral sodium channels can be obtained. It is a matter of debate as to whether effective systemic. Sodium channel analgesic agents can be designed without the need to modulate central activity to achieve clinical efficacy.[22]

7.04.2.2 Ligand-Gated Sodium Channels

In contrast to their voltage-gated counterparts, ligand-gated sodium channels are activated by the binding of a ligand rather than a change in membrane potential and have rarely been a target for pain research. However the epithelial sodium channel (ENAC/degenerin family) is known to be ligand gated and has been reported to be associated with pain sensation, but it is also involved with mechanosensation, blood pressure control, and the expression of fear. This channel is predominantly located in the lung, kidney, and colon where it effects transepithelial Na^+ ion transport. It is modulated by the mineral corticosteroid aldosterone and has been shown to be blocked by triamterene or amiloride. The main therapeutic use of these agents is as diuretics and, despite the association, there has been no report of ENAC channel blockers being targeted specifically for pain indications.[23]

7.04.2.3 Mechanisms of Ion Channel Modulation

Both site-directed mutagenesis studies and ligand competition experiments indicate that channel blocking compounds can bind at many differing sites within the ion channel assembly.[24] Certain compounds, such as Tetrodotoxin, block the outer pore which is wide enough to accommodate hydrated sodium ions. Several drugs, such as lidocaine, bind at the "local anesthetic" site on the inside of the pore; this is a broad cavity accessible to small molecules capable of penetrating the cell membrane. Generally there is high sequence homology between channel subtypes in this region but recent structural biology studies using the bacterial sodium channel have indicated that there are fenestrations in the side of the protein assembly that offer a path through which lipophilic molecules can enter and interact with the pore domain.[25] It may be that the shape characteristics of these different openings in the pseudosymmetric assembly of differing channels, and the states of these channels, offer the opportunity of selective binding. In addition it has been established that selective binding to remote voltage sensor and extracellular loop regions, which differ significantly in amino acid sequence between channel subtypes, can be effective at stabilizing particular states of the channel, and hence are accessible drug targets. The differentiated extracellular ion channel surface also provides a potential target for the design of ion channel-specific antibodies, and is the binding site of several toxins and designed peptidic agents (*vide infra*) (**Fig. 1**).

An alternative approach to achieving both specificity and safety with ion channel blockers is to target particular states of the ion channel. Selective stabilization of the inactivated state may reduce the propensity for channel opening in response to high frequency firing. This is important to pain function as pain is typically associated with a high frequency of nerve pulses—often in the hundred hertz region—whereas many other physiological functions, such as heartbeat, also modulated by sodium channel action, are associated with much lower frequency activity. Measurement in the change in conduction after a rapid sequence of action potentials indicates the "use-dependence" of an agent, which blocks the inactivated state of the channel (**Fig. 2**).

An alternative app). The state selectivity of channel blockers and their effect on inhibition of firing frequency is a complex function of compound affinity, binding site location, and binding kinetics; so use-dependency and state selectivity do not always correspond.

By controlling the voltage across a channel within a cell using electrophysiology techniques, it is possible to change the proportion of channels in open, closed, and inactivated states. Therefore testing channel inhibition at differing biasing voltages can also give a measure of the state selectivity of blockers. However, as differing conformations will be present at intermediate voltages and, as channels are necessarily in equilibrium, absolute inhibition constants for specific states are very difficult to establish. Inhibition constants for specific voltages are therefore more typically quoted, but the experimental details may not be disclosed. Furthermore, changes in instrumentation, buffer, cell line, and protocols can have a marked effect on measured values. IC_{50} values are generated by a wide range of techniques from electrophysiological measures in automated or manual patch studies to ion flux assays based on dye concentrations. Consequently, channel inhibition measurements from different experimental groups are not easily compared and this should be borne in mind when assessing inhibition data presented in the rest of this chapter.

7.04.3 Voltage-Gated Sodium Channel Blocking Agents

7.04.3.1 Toxins and Peptides

Several toxins are known to block voltage sodium channels and typically do so in a non-state-selective manner. The best characterized of these agents is tetrodotoxin, a polyhydroxylated bridged alicyclic compound present in the liver of the puffer fish (*Tetraodontidae*), which acts by occupying part of the extracellular end of the channel in an area normally occupied by sodium ions and water. Despite the evident toxicity (deaths are caused each year by ingestion of the tetrodotoxin in specific seafood), research is underway to formulate this agent for treating certain pain conditions.[26,27] The channel selectivity of different toxins has been widely reviewed.[28]

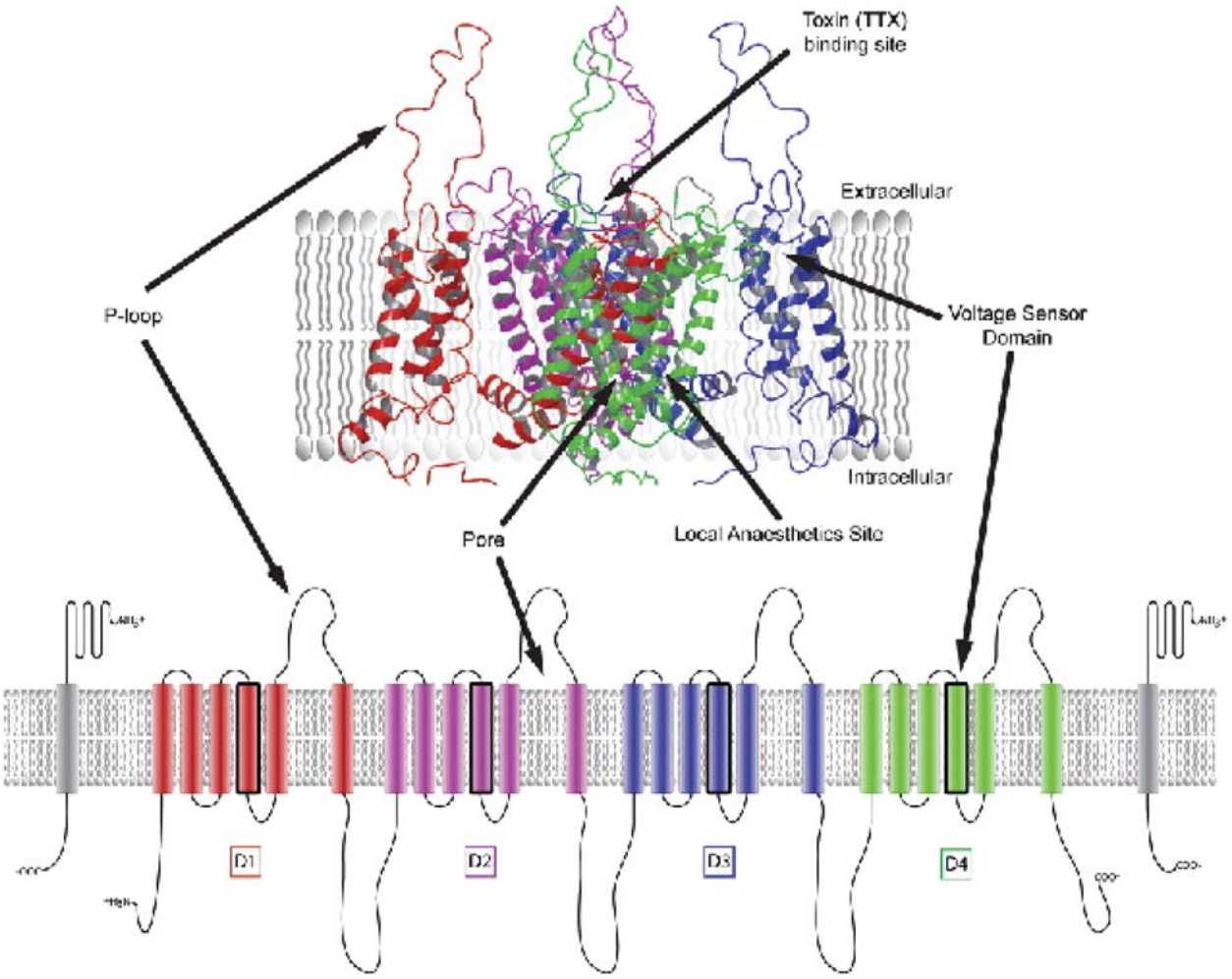

Fig. 1 Na_V channel structural topology, highlighting common ligand binding sites and significant structural features. Domains D1-D4 are represented in different colors while β-subunits are shown in gray.[4] [Reproduced with permission from Taylor and Francis © 2015].

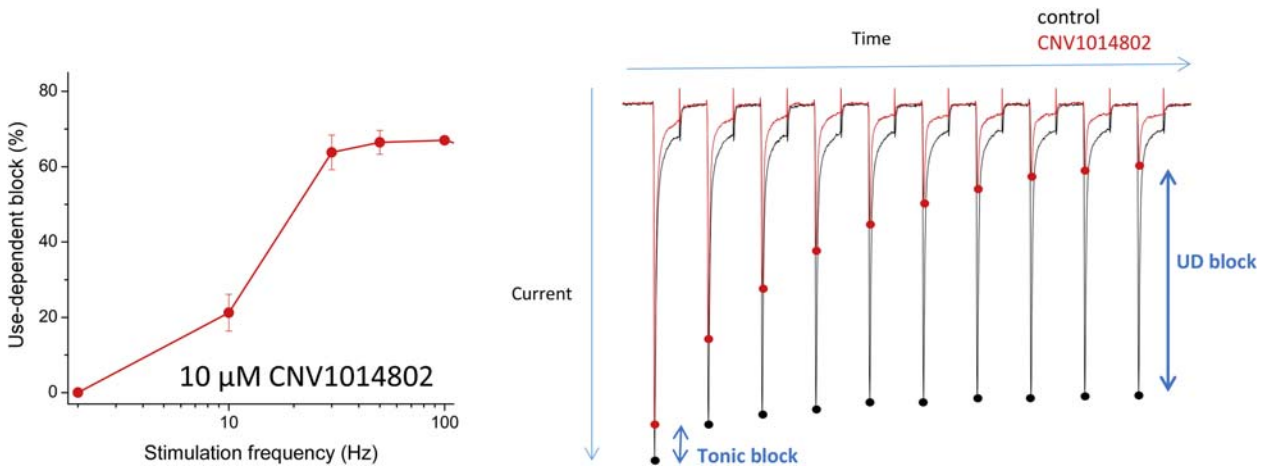

Fig. 2 Illustration of frequency dependent and use-dependent (UD) block of the sodium channel blocker CNV1014802 in a cellular pulse sequence electrophysiology study. Reproduced with permission from Rugiero F, Derjean D, Morisset V, Owen DE, Giblin GMP, Davis JB, Gunn K, Palmer J, and Tate S (2012) CNV1014802, A Novel, Potent Nav 1.7 Selective State-Dependent Sodium Channel Blocker With Broad Preclinical Antihyperalgesic Efficacy. *14th World Congress on Pain (IASP)*, (Milan, Italy).

Other well-characterized isolated small molecule toxins include saxitoxin and neosaxitoxin, members of a related group of compounds isolated from paralytic shellfish toxin which, like tetrodotoxin, bind to an extracellular site on the channel.[29] These agents have been proposed as local anesthetic agents, but not systemic analgesics. Peptidic sodium channel blockers are present in venom produced by a number of invertebrates including cone snails, tarantula spiders, and certain scorpion species.[30] These are typically characterized by their tertiary structure which contains a number of specific disulfide bonds, however these agents also inhibit a range of other ion channels and because of their polypharmacology have not been developed themselves for drug use as sodium channel blocking agents. Other toxins known to bind to specific sites on the sodium channel include α-scorpion toxin, sea-anemone toxin (reported to slow sodium channel inactivation), β-scorpion toxin, brevetoxin, and ciguatoxin.[31] Despite their value as laboratory agents and standards for channel characterization,[32] none of these latter toxins are reported to be developed directly for therapeutic use.

However, peptides from modified toxins have been extensively researched as potential drugs. Amgen in particular has invested significant effort in designing inhibitors utilizing features of the domain II binding peptide present in the tarantula toxin GpTx-1.[33] In a major undertaking, the Amgen team chemically synthesized the toxin and undertook modifications with a range of alterative (including some unnatural) amino acids at all non-cysteine positions on the peptide chain, characterizing the binding site and, through modification, achieving highly selective and potent agents. For example, while the parent toxin has a 10 nM IC_{50} for $Na_V1.7$ and a 20-fold selectivity for $Na_V1.4$, a peptide analogue [Ala5,Phe6,Leu26,Arg28]-GpTx-1 is a 1.6-nM inhibitor with over 10,000-fold selectivity for $Na_V1.7$ over $Na_V1.4$. Aspects of this work are the subject of a patent application.[34]

Janssen has adopted a similar approach in developing selective toxin analogues. Their researchers have designed compounds based on the Peruvian green velvet tarantula venom protoxin-II. Peptides with IC_{50}s for $Na_V1.7$ in the range 2 nM–400 nM have been developed with no measurable activity against $Na_V1.5$.[35] Another set of patent applications describes an approach to variants of huwentoxin-IV from the Chinese bird spider.[36] These disclose effects in a pain model of paw pressure in the rat at low nM concentrations. The spider toxin has also been shown to specifically bind to the voltage sensor β-subunit of the sodium channel, in conjunction with extensive *in silico* docking studies.[37]

Purdue has also engaged in extensive studies on protoxin-II using an approach of making chimeric molecules between protoxin-I and II to modulate channel specificity.[38] This work led to the identification of more potent $Na_V1.7$ blockers, including a methylamino derivative with a 42 pM IC_{50}. The research is associated with a number of patent applications[39] targeting $Na_V1.7$ for pain.

Continuing the theme, researchers at the University of Utah prepared conopeptides from the cone snails *Conus geographus* to act as $Na_V1.7$ blockers.[40] As a class these are known to interact with both sodium and calcium channels and their patent application suggests that novel analogues may have preferred selectivity properties.

The University of Arizona has patented peptides, which have the effect of modulating sodium channels but using an entirely different mechanism, namely inhibiting the trafficking of $Na_V1.7$ ion channels[41] by interacting with the collapsing response mediator protein 2, and affecting the SUMOylation cycle. A patent describes dye studies indicating that a specific peptide can effectively inhibit $Na_V1.7$ currents and claims that spinal delivery of 10 μg of this peptide at a 5 μl dose resulted in a significant long-lasting reversal of both thermal and mechanical hypersensitivity in a rat model.

Saxitoxin has also been a subject of medicinal chemistry optimization for potential therapeutic use, this time by Stanford Junior University in conjunction with SiteOne Therapeutics. The researchers found ester derivatives such as **1** (Fig. 3), which were potent at both $Na_V1.4$ and $Na_V1.7$ while being selective over $Na_V1.5$; however no detailed inhibition data was provided.[42] This work builds on a long-standing interest in modified saxitoxins for treating pain.[43] Another study with this toxin this time at Stanford University involved the preparation of modified forms bearing a cysteine-reactive maleimide group.[44] These were demonstrated to be irreversible inhibitors of sodium conductance.

7.04.3.2 Antibodies

A $Na_V1.7$ blocking antibody has long been mooted as a potential pain therapeutic agent and has attracted both academic and commercial research interest. There has been an expectation that the peripheral distribution of the $Na_V1.7$ channel would be particularly suited to the parenteral route of administration required for antibody delivery, but whether an antibody would be effective against myelinated nerve fibres was unknown. The first academic report of a selective $Na_V1.7$ blocking antibody came from the group of Lee et al. at Duke University in 2014.[45] The Duke team created an antibody that binds to the voltage sensor paddle region of $Na_V1.7$. Their molecule showed between 2 and 3 orders of magnitude selectivity for $Na_V1.7$ over seven other voltage-gated

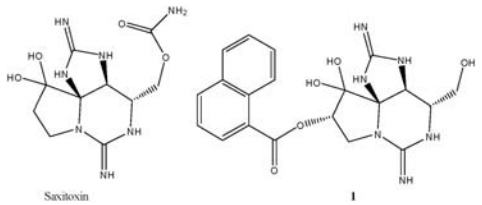

Fig. 3 Small molecule toxin-derived Na_V inhibition.

sodium channels, an IC_{50} of 30 nM, and maximal inhibition of 87%. Efficacy was reported against itch-related synaptic transmission in mouse lamina IIo neurons and this anti-itch activity was borne out in a mouse model. In a model of acute inflammatory pain—formalin induced writhing in mice—only intrathecal activity was recorded, demonstrating a previously unreported central mechanism of $Na_V1.7$ in pain inhibition, and efficacy against myelinated nerve fibres. The activity of the agent was relatively weak compared with other analgesic antibody agents such as the anti-NGF antibody Tanezumab. Interest in an antibody approach has been demonstrated in patent applications filed by UCB,[46] Argen-X,[47] Harvard University,[48] Duke University,[49] and Regeneron.[50] UCB published the earliest claim in 2011 on $Na_V1.7$ monoclonal antibodies. This indicated that the antibodies inhibited evoked action potentials in isolated DRG cells. Argen-X reported that they used a DNA immunization technique to create antibodies that were selective for affinity to the $Na_V1.7$ extracellular loop and these were shown to inhibit inward current in whole-cell voltage-clamp experiments. Regeneron created antibodies that bind to at least one extracellular loop or to the paddle region by immunizing a humanized "VELOCIMMUNE" mouse and generating hybridoma cell lines or isolating anti-$Na_V1.7$ antibodies directly from antigen-positive B cells from immunized animals. The Harvard team described a single-domain antibody that specifically binds both to $Na_V1.7$ and an ion channel toxin in order to have maximal efficacy and selectivity for $Na_V1.7$.

$Na_V1.9$ antibodies have also been the subject of a number of claims from of the CNRS group in France, but the current status of any agents is not clear.[51]

7.04.3.3 Small Molecules

7.04.3.3.1 Clinical compounds with a sodium channel mode of action

Various small molecule agents originating from phenotypic discovery programs aimed at other indications have been discovered that show analgesic effects. Though several act as Na_V blockers, very few have been designed to act specifically by a sodium channel mechanism. It is therefore worth briefly reviewing some therapeutic agents (in addition to lamotrigine and local anesthetics) presently marketed or used in the treatment of pain conditions that are known to act, at least partially, through sodium channel blockade or modulation. An understanding of the properties and deficiencies of these agents has helped inform the design of newer classes of drugs.

Carbamazepine (Tegretol™) and oxcarbazepine (Trieptal™) (Fig. 4) are tricyclic agents developed some 50 years ago as antiepileptics but also with efficacy against neuropathic pain. Their mode of action is likely to be due to a combination of activities, but including sodium channel blockade. Carbamazepine stabilizes the inactivated state of Na_Vs but is also a GABA receptor antagonist and has effects on serotonin release and uptake. Carbamazepine's polypharmacology is compounded by the fact that it interacts strongly with cytochrome P450 enzymes which makes this a difficult agent to use in combination therapies. It also suffers from the potential to induce certain severe skin conditions and anemias, and commonly shows central effects including motor coordination impairment. The structurally related oxcarbazepine has a similar activity but a better metabolic profile and lower propensity to induce anemias, but still with significant central side effects. It is a prodrug of the active component in which the keto carbonyl is reduced to a hydroxyl group *in vivo* ($t_{1/2}=2$ h) but this material, eslicarbazepine, also has a lower half life than carbamazepine.[52]

Lacosamide (Vimpat™) is an anticonvulsant sodium channel blocker marketed by UCB that is approved for the adjunctive treatment of partial onset seizures and neuropathic pain (though it does not presently have FDA approval for the latter indication). It works by enhancing the slow inactivation of Na_Vs without affecting the fast inactivation mechanism. This inactivation prevents the channel from opening, helping to reduce the action potential. However lacosamide has a second mechanism of action as it modulates collapsing response mediator protein 2, preventing the formation of abnormal connections in the brain. For pain, it has been shown to have efficacy in an 18-week Phase III clinical study in diabetic neuropathy compared with placebo. However, it shows significant central and other side effects in at least 10% of patients and has to be titrated to maximal dose over a period of weeks.[53]

7.04.3.3.2 Multi-channel, partially selective and $Na_V1.7$ selective sodium channel blockers

In consideration of the issues presented by the polypharmacology of marketed compounds, the focus of sodium channel drug discovery efforts in pain during the past 5 years has therefore been on discovering sodium channel-specific and subtype selective

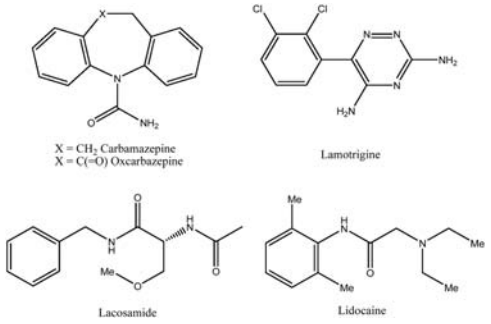

Fig. 4 Some marketed Na_V blockers.

blockers. The majority of research has focused on $Na_V1.7$, and to a lesser extent Na_Vs 1.8 and 1.9. Once thought to be challenging,[54] given the homology in the pore region of sodium channel isoforms, recent studies have shown that it is possible to design small molecules with high levels of channel selectivity as well as specificity for binding to different states of the ion channel.[55] The diversity of Na_V blockers reported, especially in the patent literature, points to multiple targetable binding sites; at least eight have been suggested.[56] However, many Na_V blocking compounds disclosed in the literature cannot readily be allocated to a specific known pharmacophore and there is some evidence that even compounds from well-defined inhibitor classes can have more than one mode of action. Thus the analysis of medicinal chemistry approaches to Na_V inhibition is complex. Furthermore, to date there have been few papers published describing the Structure Activity Relationships (SARs) found in lead optimizing Na_V inhibitor campaigns. In this review we have therefore sought to categorize compounds, predominantly from the patent literature, into agents targeted at particular channels and compare them, where appropriate, in pharmacophoric groups.

The case for $Na_V1.7$ subtype selective inhibitors as therapeutics is very strong, founded on the observation that inherited human familial mutations are known, which render this ion channel inactive and individuals with the phenotype experience no pain,[57] although $Na_V1.7$-independent pain mechanisms are known.[58] Consequently, much research has focused on the design of $Na_V1.7$ blockers, but selectivity is often not reported, especially in the patent literature. Additionally early screens in lead optimization campaigns have often been performed with surrogate ion channels, even though $Na_V1.7$ is the eventual target. This section of the review therefore covers together both $Na_V1.7$ and Na_V blockers of unspecified selectivity, though noting when activity at specific or multiple channels is disclosed or developed as the target profile. The discussion also includes pan-sodium channel blocking agents with selectivity over channels known to be associated with central or peripheral side effects, by virtue of their state- or use-dependency.

7.04.3.3.2.1 Aryl-linked aminoamides

The pharmacophore for a local anesthetic agent such as lidocaine can be described by an aromatic group linked to an amide with a pendant amine, and this has been a starting point for the design of some classes of systemic analgesic agents (Fig. 5), for example by Astellas and EWHA (*vide infra*). However, Convergence has demonstrated that it is possible to obtain state-selective and isoform-selective compounds from a variant of the pharmacophore in which the amino and amide groups are reversed. This aryl-linked aminoamide pharmacophore has been utilized by a number of companies (Fig. 5) and elaborated in different ways. Analogues have been designed to be either brain penetrant or peripherally restricted.

There is significant subtlety in functional group disposition and substitution patterns, which determines the level of state-dependence, inhibition potency, or subtype selective blockade within this pharmacophore. Certain compounds of this class have been reported as showing strong state-dependent selectivity for the $Na_V1.7$ or particular selectivity for the $Na_V1.8$ channel. This first section will therefore discuss both $Na_V1.7$ blockers and unspecified Na_V blockers that related to a particular

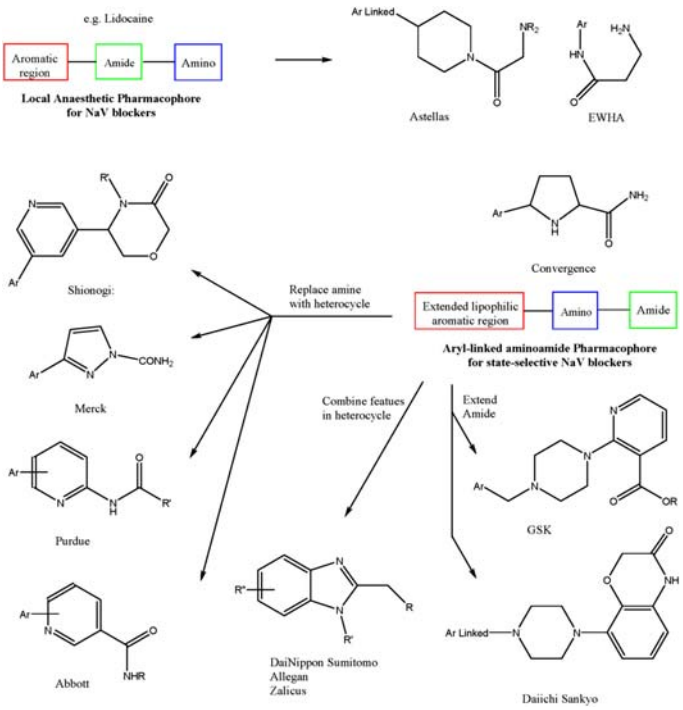

Fig. 5 Compound classes linked to aryl-linked aminoamide and local anesthetic pharmacophores.

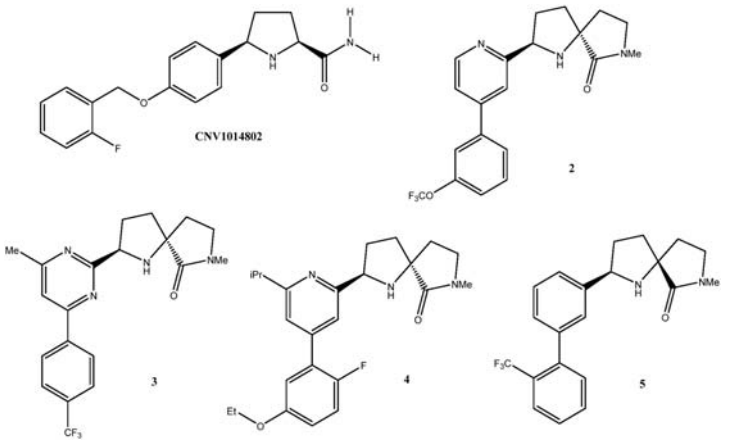

Fig. 6 Convergence Na_V blockers.

pharmacophore. In some cases the scaffold has morphed into other classes of Na_V blocker. In particular, compounds from Purdue Pharma, which have features of two classes, are discussed with triazines (*vide infra*).

CNV1014802 (Fig. 6) is being developed by Convergence Pharmaceuticals for pain and is also discussed under clinical studies as it has recently demonstrated a successful Proof of Concept in Phase II clinical studies for pain (*vide infra*). It shows significant state-dependent selectivity for Na_V 1.7.[59] The compound shows good aqueous solubility, an excellent pharmacokinetic profile, and a low potential for drug–drug interactions.[60]

More recent work has indicated a focus on conformationally restricted spirocyclic aryl-linked aminoamides and this time bearing a biaryl or heterobiaryl feature. A 2014 review[4] noted compounds **2** and **3** as examples from recent Convergence patent applications. Compounds **4** and **5**, which possess differing relative ring stereochemistries, are exemplified as potent $Na_V1.7$ state-dependent blockers with sub-micromolar IC_{50}s against $Na_V1.7$ at V_{half} potential.[61]

One class of Na_V blocker investigated extensively at Merck Sharp and Dohme (MSD) is related to the aryl-linked aminoamide series, but with the basic amino group replaced with a heterocyclic moiety. Three successive publications in 2010 summarized this work, highlighted in Fig. 7.[62] These papers describe the discovery of the three ring class as a development from the semicarbazone sodium channel blocker V102862.[63] A tricyclic aromatic class of Na_V blocker was formed by the replacement of the semicarbazone with a heterocycle-generic structure **9**. Analogues based on the heterocycles **6**, **7**, or **8** were then shown to be able to provide low micromolar or better IC_{50s} for blockade of $Na_V1.7$ in a fluorescence resonance energy transfer (FRET) assay, with compound **8** showing a $Na_V1.7$ IC_{50} of 228 nM. It is interesting to note that the meta-disposition of the three rings was important for activity. The most potent analogue emerging from this work was **10**, a sub-micromolar blocker of $Na_V1.7$ with a good in vitro PK profile and efficacy comparable to gabapentin in the Chung spinal nerve ligation (SNL) model at 30 mg/kg. However, this series suffered from a potential hydrolytic liability, and the final paper in the trio indicated how this was resolved through changing the substitution

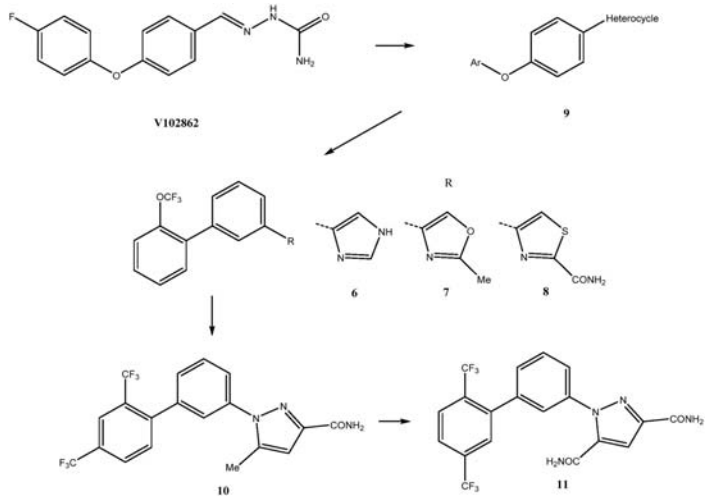

Fig. 7 Evolution of MSD aryl-linked aminoamide Na_V blockers.

pattern on the terminal aromatic ring and introducing a second amide substituent on the heterocycle. This led to the discovery of **11**, a stable molecule which possessed a good *in vitro* PK profile, activity in the SNL model, and which showed 50% reversal of mechanical hyperalgesia in an FCA model of neuropathic pain on oral dosing at 30 mg/kg. The compound also showed little effect on motor function in the mouse at doses of 100 mg/kg.

GlaxoSmithKline (GSK) has pursued inhibition of $Na_V1.7$ and potentially $Na_V1.9$ as a mechanism for suppressing the painful irritation evoking a cough reflex, and have noted that $Na_V1.7$–1.9 are expressed in the vagal sensory neurons that innervate the airways.[64,65] This work has been associated with two patent applications describing series of sodium channel blockers containing 2-piperazinopyridine-3-carboxylates, which fall within an extended amide variant of the aryl-linked aminoamide pharmacophore (**Fig. 5**). In the first,[66] GSK describes over five hundred compounds based on this pharmacophore, with data on compounds which block both $Na_V1.3$ and $Na_V1.7$ to micromolar levels. A representative example **12** is shown in **Fig. 8**.

Compounds in the second application[67] exhibit an extended aromatic region in the pharmacophore and demonstrate higher levels of Na_V blockade, for example, compound **13** which is a sub-micromolar inhibitor of $Na_V1.7$. Detailed ion channel activity data are not recorded in either patent.

Daiichi Sankyo has focused most Na_V patenting activity on the sulfonamide chemotype (*vide infra*); however, in 2015 the company published a summary of work arising from an HTS hit **14** (**Fig. 8**), which was modestly selective for $Na_V1.7$ ($IC_{50} = 3.9$ μM) over $Na_V1.1$ ($IC_{50} > 33$ μM) and $Na_V1.5$ ($IC_{50} = 20$ μM).[68] The initial focus was on replacing the benzoxazinone with a more metabolically stable heterocycle and on reducing the bulk at the right-hand side (as drawn). This work led to the identification of a class of three alternative right-hand side groups, isoindolones, benzamides, and anilides. This latter group was optimized to compound **15**, which is somewhat related to the aryl-linked aminoamide pharmacophore explored by GSK.

Compound **15** continued to show potent human and mouse $Na_V1.7$ inhibitory activities (IC_{50}s of 1.7 and 1.3 μM respectively) with ~10-fold subtype selectivity over $Na_V1.5$, and it successfully demonstrated analgesic efficacy in mice (AcOH-induced writhing $ED_{50} = 19$ mg/kg), comparable to mexiletine, but with an expanded CNS safety margin (5.8-fold) as demonstrated by locomotor activity studies.

Shionogi has filed several related patents targeting blockade of sodium channels with a focus on $Na_V1.7$, which arguably fit the same broad pharmacophore. The first[69] describes a class of over 300 3-oxo-morpholines, linked to a biaryl group—an amide-linked biaryl moiety is a feature seen in various Na_V blockers. Compound **16** (**Fig. 9**) shows blockade of $Na_V1.7$ *in vitro* with an IC_{50} of 1.2 μM. A second patent application[70] provides a similar number of examples based on an imidazoimidazolone core, also typically with IC_{50}s in the micromolar range, for example compound **17** with an IC_{50} of 0.53 μM against $Na_V1.7$.

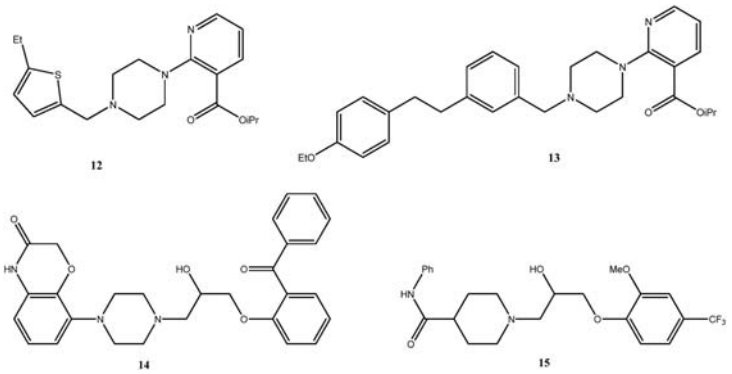

Fig. 8 Extending the aryl-linked amino-amide pharmacophore.

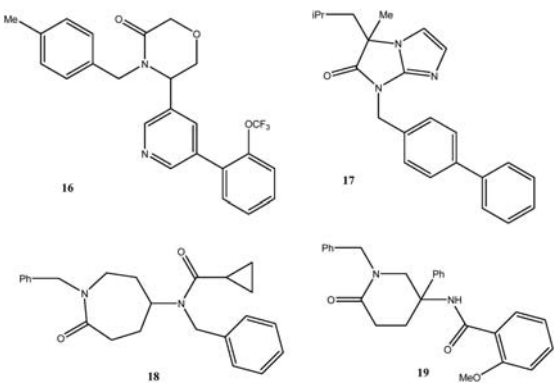

Fig. 9 Extended aryl-linked amino-amide Na_V blockers from Shionogi.

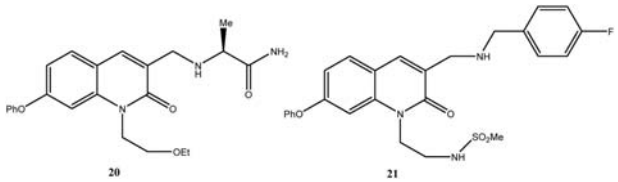

Fig. 10 Quinolone-core Na_V blockers.

A third patent application from this team describes some three hundred more distantly related compounds[71] with a lactam core in either a six- or seven-membered ring, and overall representing a more branched pharmacophore. Compounds **18** and **19** are highlighted as demonstrating potent inhibition of veratridine binding to $Na_V1.7$ with IC_{50}s of 0.58 and 6.3 μM, respectively.

In early studies, DaiNippon Sumitomo had patented a series of quinolone analogues of the aryl-linked aminoamide class bearing a pendant polar side chain (Fig. 10).[72] Such compounds were described as targeting Na_V TTX-resistant channels, rather than identifying the channel by specific subtype. For example, compounds **20** and **21** showed 100% inhibition in the TTX-resistant sodium channel assay at a concentration of 12–13 μM.

More recent work has seen the core shift to a benzimidazole template, replacing the quinolone functionality.[73] The substitution patterns for the 237 exemplified compounds mirror those in the earlier patent with biaryl or aryloxyaryl aromatic portions and a glycine-like amidic region, but the claim is more focused. Table 2 describes examples, which demonstrated 100% inhibition of TTX-sensitive sodium channels expressed in CHO cells at a concentration of 12.5 μM.

Unlike the earlier patent where a wide range of amide and side chain groups are examined, the claims in this patent show an emphasis on fluorinated aromatic substitution patterns which may reflect modulation of developability properties. Notably the benzimidazole compounds contain only one basic group. This, combined with the relatively low molecular weight and low polar surface area of the compounds suggest greater potential for brain penetrance than the quinolone series. Several other companies have also described benzimidazoles as sodium channel blockers (Fig. 11).

Allergan has described benzimidazole sodium channel blockers lacking an aryl substituent. The company has focused patent claims on the target of blocking persistent sodium current. The first case[74] indicates that the compounds may act at a number of ion channels and an emphasis is placed on the *in vivo* studies. These show, for example, that compound **25** (Fig. 12) is effective in a capsaicin model of thermal hyperalgesia in the rat at an oral dose of 10 mg/kg though it was clear that the same compound was much less effective in a spinal nerve ligation model study. This compound, while demonstrating a sub-micromolar IC_{50} in a sodium channel FLIPR assay, was apparently ineffective in an Ionworks electrophysiology study on the same ion channel (either

Table 2 Benzimidazole analogues of aryl-linked aminoamide

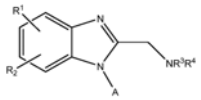

Number		*A*	*NR^3R^4*
22	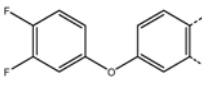		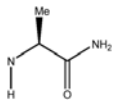
23	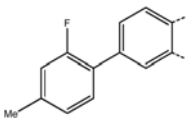		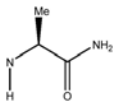
24	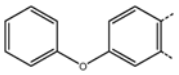	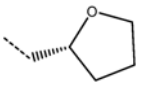	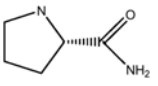

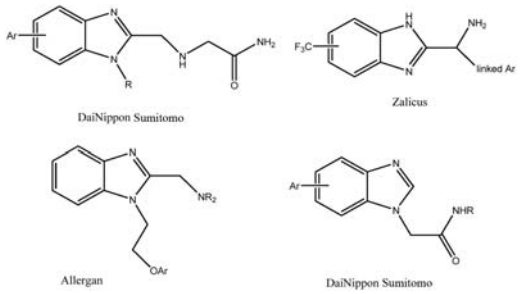

Fig. 11 Classes of benzimidazole-core Na_V blockers.

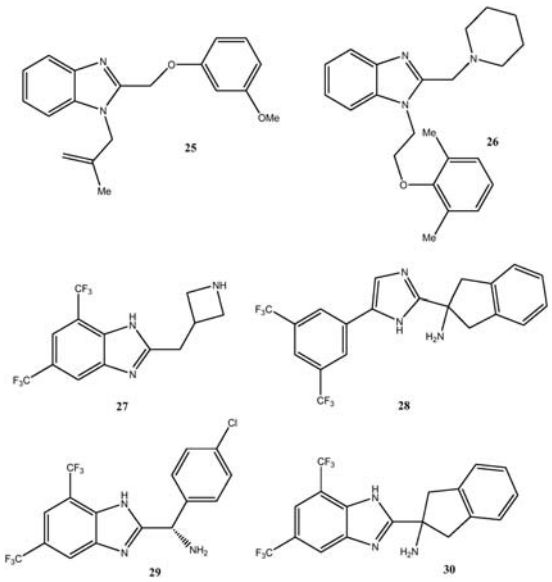

Fig. 12 Substitution patterns of benzimidazole Na_V blockers.

$Na_V1.3$ or $Na_V1.6$). An extension of this series is provided in a second application[75] in which a basic group is included as a benzimidazole substituent. Several compounds are noted as demonstrating significant block of sodium current in either $Na_V1.3$ or $Na_V1.6$ including compound **26,** which inhibited with an IC_{50} of 66 nM in a FLIPR assay. An unspecified close analogue also shows modest efficacy in the capsaicin study.

Zalicus has also worked on the benzimidazole class focused on blocking the slow inactivation process that gives rise to persistent sodium currents as a target for blocking pain. Zalicus filed on a class of ion channel modulators[76] in which inhibitors based on a benzimidazole template are first described. Both amine and amide derivatives are included among 200 examples; however, the only cases which are described as showing activity in pain models were basic. Compound **27** reverses mechanical hyperalgesia in a rat model at 30 mg/kg on oral dosing. Specific ion channel modulatory data is not described for sodium channels on all compounds but some activity at calcium channels is noted, so the compounds may have a mixed mode of action.

The development of this series can be seen in a second patent application[77] where this time the bis-trifluoromethylbenzyl group was not fused with the nitrogen heterocycle. The group investigated hybrid molecules with those of the aryl-linked aminoamide class and other known classes of Na_V blocker. However, in contrast to other patents filed by the group, in this case no data was given describing pain studies and the most potent $Na_V1.7$ modulator of fast inactivation was compound **28** which showed a -19 mV shift in V_{half} for inactivation on exposure at 10 μM. A third application in the series was published in 2014 and while focusing on $Na_V1.7$, emphasized that the compounds may exert their effects by modulation of a broader range of sodium and calcium channels.[78] The same group filed a patent[79] in 2015 covering many of the same compounds with some 90 examples described and data given for the voltage dependence of activation and fast deactivation on human $Na_V1.7$ channels. Zalicus further characterized the compounds by detailed electrophysiology studies indicating which examples were blockers of slow inactivation. Thus compound **29** had an IC_{50} for slow inactivation block of $Na_V1.7$ of 2.9 μM and showed a -27 mV shift in V_{half} for inactivation at 10 μM. In contrast compound **30**, which has much weaker slow activation block and showed a -15 mV shift in V_{half} for inactivation at 10 μM, was reported to show dose-dependent activity in a rat FCA model of pain, with significant activity at 10 mg/kg. The most recent Zalicus Na_V patent application WO 2015130957 starts by exemplifying further compounds from the benzimidazole class but morphs into a disclosure of sulfonamide ion channel modulators and is therefore discussed in that section (Table 4).

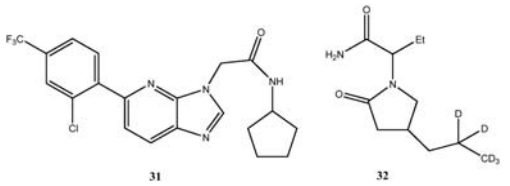

Fig. 13 Recent variations on the aryl-linked amino-amide pharmacophore.

A recent patent filing from DaiNippon Sumitomo[80] also continues to describe work around a benzimidazole template, this time with an N-linked amidic side chain and an emphasis on activity at both $Na_V1.7$ and 1.8. Typical examples include **31** (Fig. 13) with reported Na_V inhibitory activity of 99% at a concentration of 15 μmol/L.

A patent application from Concert Pharmaceuticals suggests that sodium channel blocking activity can be retained in aminoamide derivatives lacking the aryl component.[81] Their examples are also claimed as synaptic vesicle protein 2A (SV2A) ligands and detailed sodium channel activity or selectivity values were not reported. It is interesting to note that their examples included deuterated derivatives such as **32**.

Astellas has published few recent papers on sodium channel blockers; however, the company has disclosed one structure type, arguably most closely related to the local anesthetic pharmacophore.[82] Vinyl piperidines **ASP1120** and **ASP9596** (Fig. 14) are reported to be sodium channel blockers with potent oral analgesic activity in the spinal nerve ligation model in rat ($ED_{50} = 2.1$ and 0.18 mg/kg, for **ASP1120** and **ASP9596**, respectively). Notably the extended aromatic portion extends from the amide rather than from the basic side of the molecule.

Potential inks between the local anesthetic pharmacophore and the aryl-linked amino amide pharmacophore are also indicated in papers published by academic collaborators at several Korean research institutions, including the School of Pharmacy at EWHA Womans University.[83] They indicate that compound **33**, which has been shown to inhibit sodium channels in DRG cells, is also effective in relieving pain in model studies. The compound was effective at reducing both inflammatory and neuropathic pain in the rat on i.p. treatment at 6 mg/kg, while showing no behavioral effects at 60 mg/kg; however, a detailed pharmacological profile of the compound was not given. While demonstrated as inactive at N- and T-type calcium channels, no sodium channel selectivity data was reported. More recently this publication was followed up with a patent filed[84] on sodium channel blockers in which nine further compounds were highlighted and compound **34** was demonstrated to be a 10 μM IC_{50} inhibitor of $Na_V1.7$.

7.04.3.3.2.2 Spirocyclic Na_V blockers

A spirocyclic moiety is a feature of various distinct Na_V blocker series (Fig. 15) and it is interesting to consider why this construct has featured in different compound classes. It is clear that the chiral disposition of different functional groups, fixed by the spirocycles, is critical for aspects of selectivity in at least some of the cases.

A distinct class of spirocyclic indoles is described by Xenon in a series of publications and patent applications, some in collaboration with Genentech and more recently with Teva Pharmaceuticals. Several of these are described as mixed $Na_V1.7$ and $Na_V1.8$ blockers, but for the majority of claims only $Na_V1.7$ data is published. The lead compound XEN402, now TV-45070, is described further in the clinical section. Xenon reported[85] that the series originated from the discovery of oxindole **35** (Fig. 16), which had been identified by high-throughput screening. A series of $Na_V1.7$ blockers was developed by optimization of the oxindole C-3 and N-1 substituents as well as by elimination of metabolically susceptible features. This process led to the simplified analogue **36**, ten times more potent than the original HTS hit.[86] Subsequently a scaffold rigidification strategy gave a number of potential candidate compounds containing the spiro ring including **XEN907 37**, a further 10-fold more potent. A patent application describes the investigation of a several hundred substitution patterns around the phenyl group linked to the spiro center of the oxindole, and it is evident that reducing inhibition of cytochrome 3A4 has been an area of optimization.[87]

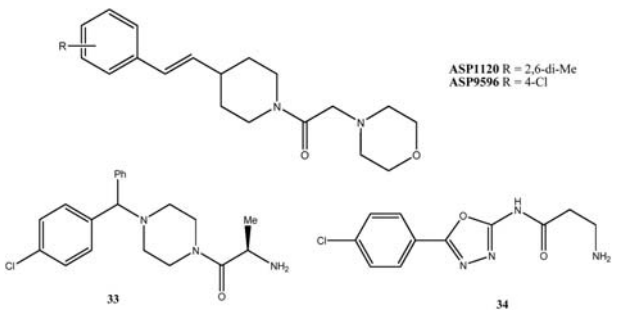

Fig. 14 Systemic Na_V blockers related to the local anesthetic pharmacophore.

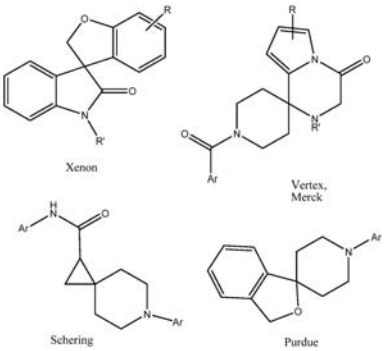

Fig. 15 Spirocycles as sodium channel blockers.

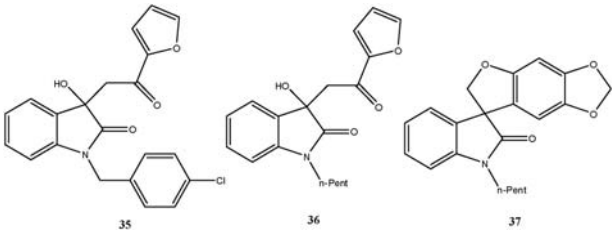

Fig. 16 Discovery of Xenon spirocyclic Na_V blockers.

A selection of spirocyclic indole derivatives from patents filed during the past 5 years by Xenon is described in Table 3. A challenge for this whole class appears to have been the low solubility of the series and formulation has been a significant focus. It is notable that a topical formulation has been developed for their lead compound **XEN402**, identified by Xenon as compound **38**. Significant effort has been applied to developing a bespoke oral formulation.[88] The topical activity of compound **38** in a rat FCA pain model is described as giving a 40% change from baseline in an application with a 4% formulation. Higher dosing levels led to little further change.

The table shows **38** as a single S-enantiomer though the racemate is also claimed in Xenon filings. The preference for the S-enantiomer is described in US 20100331386.[89] Compound **38** is also described in a single compound patent application.[90] *In vitro*, using a guanidinium influx assay, **38** is around 1000 times more potent at blocking the $Na_V1.7$ ion channel than the R-antipode **39**. However a state dependence electrophysiology study suggested that **38** was only fivefold more selective than **39** ($K_i = 0.161$ vs. 0.869 μM) against the inactivated state of $Na_V1.7$, and both compounds had poor affinity for the closed state ($K_i > 10$ μM). A discussion of the atropisomerism of this interesting class has been published.[91]

Further examples illustrate efforts to introduce solubilizing groups into this compound class such as the pyridine containing analogue **40**.[92] In vitro activity was reported based on the block of uptake of C-labeled guanidine in influx assays in cell lines expressing a range of ion channels, and by this means channel selectivity was established, although typically not reported in the patent filings.

The oxindole ring itself could be effectively modified by a further ring fusion, as in **41,** which retained the activity of the parent structure; however, larger ring sizes (**42**) were poorer and incorporation of additional heteroatoms was not tolerated.[93] A range of S-linked imidate variations (such as **43**) is described in WO 2010053998 and while these clearly retain some activity, detailed potency information was not described.[94] Another patent application[95] indicates that attempts were made to introduce solubilizing groups such as pyridines; however, the most potent compounds, including **44**, have only activity range information. It appears that attempts to combine polar features of **40** and **44** in compound **45** led to a lowering of activity. An explicit basic amino group introduced at the end of a chain in **46** lowered the potency in the guanidinium flux assay but actually gave significant potency ($K_i < 300$ nM) in an electrophysiology determination of binding to the inactivated state (of the unspecified channel under test), a contrast to most other examples from the filing.[96]

The Xenon team discussed further aspects of the discovery of the spirocyclic compound class in a paper published in 2013.[97] The group noted that their lead compound at that point, **XEN907** (compound **37** above) while demonstrating high in vitro potency in blocking $Na_V1.7$, showed only moderate bioavailability in the rat, poor solubility in buffer, and only moderate hepatocyte stability across species, with significant inhibition of CYP3A4. This led to efforts to evaluate analogues lacking the methylenedioxy moiety, which was identified as a key liability. A range of analogues was prepared in which this group was replaced with functionality likely to add to stability and solubility, leading to the discovery of **47** (Fig. 17), which was an 8 nM IC_{50} blocker of $Na_V1.7$, but which demonstrated only 29% inhibition of CYP3A4 at 10 μM (c.97% for **37**). This compound also showed around fourfold higher solubility at 25 μg/ml. Increasing the heteroatom incorporation in the aromatic substituent was examined as a next step. Optimization

Table 3 Spirocyclic indoles

Number	*Compound*	*$Na_V1.7$ IC_{50}*[a]	*Patent application*
38	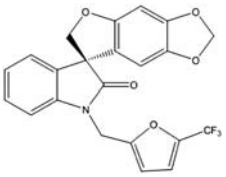	0.003 μM	WO 2011106729
39	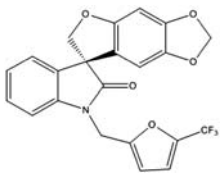	4.2 μM	WO 2011106729
40	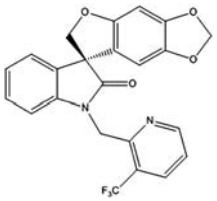	0.005 μM	US 20110087027
41	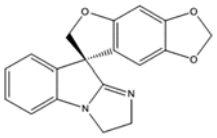	0.0037 μM	WO 2010132352
42	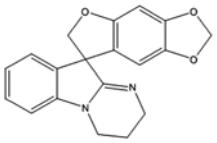	0.31 μM	WO 2010132352
43	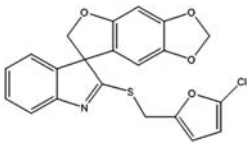	< 100 nM	WO 2010053998
44	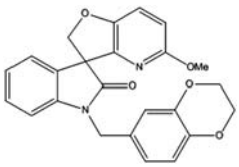	< 100 nM	WO 2010078307
45	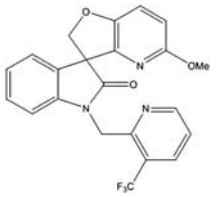	100 nM–1 μM	WO 2010078307
46	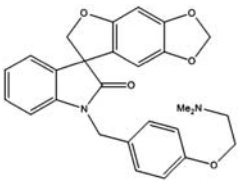	100 nM–1 μM	WO 2010045197

[a]Established by electrophysiology.

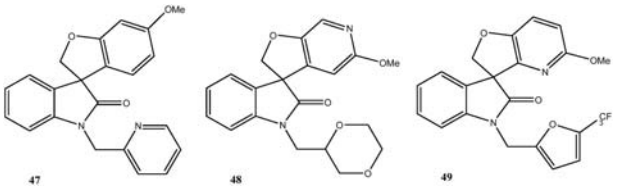

Fig. 17 Xenon spirocycle lead optimization.

of any two of the parameters, $Na_V1.7$ block, solubility, and 3A4 inhibition, was possible, but always at the expense of the other parameter. For example, compound **48** was noted as possessing the best combination of solubility at 67 μg/ml and low CYP3A4 inhibition of 22% at 10 μM, but was a less potent $Na_V1.7$ blocker with an IC_{50} of 0.1 μM. The team went on to demonstrate that, despite poor solubility of less than 5 μM, compound **49**, which was a moderate $Na_V1.7$ blocker with an IC_{50} of 0.13 μM but low CYP3A4 inhibition of 26% at 10 μM, was effective in a Von Frey paw withdrawal rat pain model at 10 mg/kg. However **49** had a relatively short terminal half-life and poor oral bioavailability, and the surprising activity was ascribed to better tissue distribution.

The clinical status and profile of **XEN402 (38)** is described later. The more recent focus of work at Xenon, like many across the industry, has been on compounds of a sulfonamide class and Xenon compounds are described in that section of the review.

Vertex has long had an interest in sodium channel blockers and has patented on a range of chemotypes. In 2011 the company published on a series of spirocycles distinct from those described by Xenon.[98] Variations on the basic template included incorporation of additional nitrogens to form alternative heterocycles in the fused tricyclic ring system, a range of aromatic substituents, and variations in the benzamide portion. The first patent application described several hundred analogues of which about a half fell in the highest activity band disclosed with an IC_{50} of less than or equal to 2.0 μM against $Na_V1.7$, including compound **50** (**Fig. 18**). There is no indication as to which of several screening methodologies was used to generate this figure, only that the ion channels were expressed in HEK cells. A second series[99] retains much of the core structure of the previous case but with a simpler fused heterocycle. Compounds **51** and **52** inhibited the $Na_V1.7$ channel with IC_{50}s of more than 5.0 and less than or equal to 2.0 μM, respectively, using the same assay protocols as earlier. The culmination of this work may be seen in a single compound patent filed in 2014 for solid form formulation of compound **53**, a compound selected from US 20120196869.[100]

Another variant on the same spirocyclic system is described in a case once again representing a simplification on the first described spirocyclic system, and this time with around two hundred examples.[101] Compound **54** (**Fig. 19**) demonstrated an IC_{50} value of less than or equal to 2.0 μM which is typical for most of compounds exemplified. No indication is given as to which

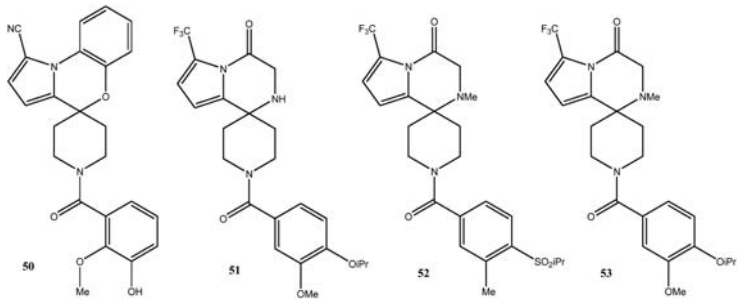

Fig. 18 Vertex spirocyclic Na_V blockers.

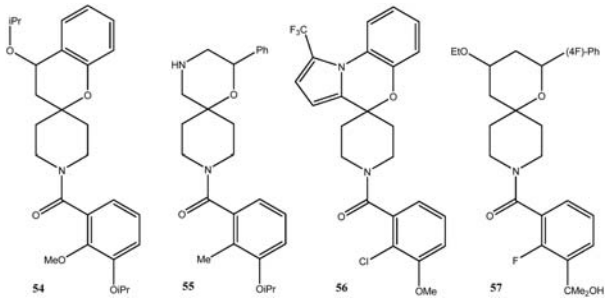

Fig. 19 Evolution of Vertex spirocycle series.

stereochemistry is generally preferred around the spirocyclic system or in aliphatic ring substitution. The same is true of the next patent application in the series[102] in which the morpholine ring at the heart of the spirocycle is not fused with any aromatic. Instead it bears a pendant aromatic substituent, such as phenyl in example **55**. Again, of the approximately three hundred examples, the majority, including **55**, fall into the most active category with an IC_{50} value of less than or equal to 2.0 μM. It is noteworthy that Vertex electrophysiology assays describe a protocol designed to highlight inactivated state block. A further case[103] represents a selection of some eighteen further analogues all in the top potency range and falling under the general description of WO 2011140425 but incorporating a narrow range of substitution patterns, for example, **56**. A later variation replaces the morpholine ring of **55** with a substituted pyran system[104] in which, again, some two hundred examples are claimed, typically with the same preferred substitution patterns represented in analogous series, but perhaps with a greater focus on blocking metabolically vulnerable positions. Compound **57** is typical and like most examples, exhibits the highest reported level of potency with an IC_{50} value of less than or equal to 2.0 μM. The filing discloses that a *cis* arrangement of pyran substituents is significantly favored over the *trans*-form in several examples.

The MSD-Schering merger of 2009 brought together companies actively optimizing different classes of sodium channel blocker. Initial interests in both legacy companies were on constrained amides incorporating conformational restriction through a spiro fusion. These examples are most closely related to the Vertex series. More recent work from MSD has focused on sulfonamide classes.

The first spirocyclic examples are present in a class of compounds described by Schering in patent applications from 2010.[105] These may be considered to be related to the Xenon type of spirocyclic Na_V blocker as they have a similar disposition of features to the parent molecules with no strongly basic center.[106] Compound **58** (**Fig. 20**) is representative, incorporating a conserved fused pyrrole as part of a tricyclic system. Other variations include heterocyclic analogues and changes in substitution pattern around the aromatic amide. Compound **58** is reported as showing an IC_{50} of 13 nM against $Na_V1.7$ in a FLIPR assay. This class was also described in some detail in an MSD publication[107] in which, as well as disclosing the search for selectivity for $Na_V1.7$ over $Na_V1.5$, the authors indicate that compound **59** has oral activity in a rat FCA inflammatory pain model at 100 mg/kg and in a rat spinal nerve ligation neuropathic pain model with an EC_{50} of 75 μM.

Schering also explored blockers based on a linear amidic template, but still incorporating a rigidifying spirocyclic feature, illustrated by compound **60**. In one filing[108] some thirty analogues are claimed with variations in substitution pattern around terminal ring positions, as well as with alternatives to the amide, such as sulfonamides and ureas, e.g., **61**. No detailed activity data is provided, and no indication given of enantiomeric preference, but a focus on $Na_V1.7$ is present in the patent claims.

7.04.3.3.2.3 β-Subunit binding compounds

Between 2005 and 2010 companies started to report compounds containing an aryl sulfonamide feature, typically with a pendant basic side chain, that were reported to be sodium channel blockers. These compounds were later shown to have significant selectivity for the $Na_V1.7$ channel based on the fact that they bound to an entirely different part of the ion channel assembly to the anesthetic binding site that had been the presumed principle binding site for most Na_V blockers hitherto. Recent publications[4] have indicated that the binding site for many molecules of this class is the β-4 subunit, which is known to be quite distinct in sequence between the different voltage-gated sodium channels, thereby providing an explanation for the observed selectivity.[109] A wider range of variants has now been published, though all share a common pharmacophore of an acidic sulfonamide linked through an aryl group to a basic group or pendant heterocycle. Very high levels of $Na_V1.7$ inhibition have been achieved, and it is clear that high levels of channel selectivity are also achievable. Two challenges that medicinal chemistry approaches have sought to overcome have been the relatively poor solubility of this class of, often zwitterionic, compounds, and the tendency for these frequently highly aromatic species to interact with metabolic enzymes and pathways that limit exposure or give rise to significant metabolites.[110] **Table 4** highlights notable or representative compounds described in patent applications from companies active in the area during the past 5 years.

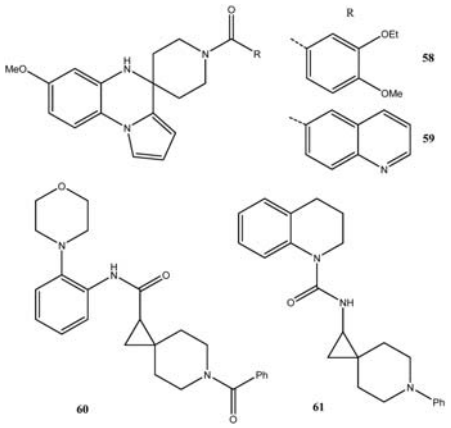

Fig. 20 Schering spirocyclic Na_V blockers.

Table 4 Examples of sulfonamide $Na_V1.7$ blockers from patent applications

#	Structure	$Na_V1.7$ IC_{50}[a] (μM)	Origin	Examples	Comments
62	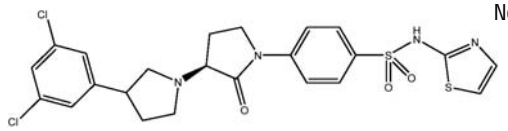	Not recorded	Vertex WO 2010002956	11	Na_V $IC_{50} < 2$ μM (channel unspecified, $Na_V1.1$ and 1.3 noted)
63	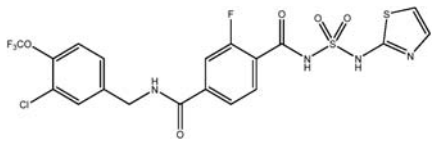	Not recorded	Pfizer, Icagen WO 2010035166	~40	$Na_V1.3$,1.5 IC_{50}s = 0.015, 15.2 μM
64	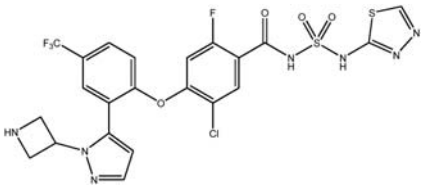	0.0011	Pfizer, Icagen WO 2012004706	21	
65	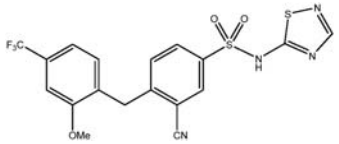	0.0058	Pfizer, Icagen WO 2012004714	24	
66	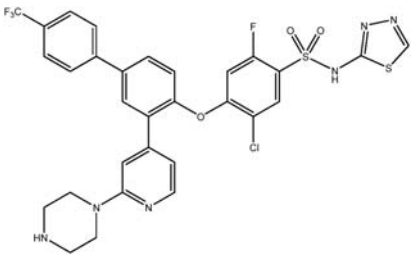	0.0005	Pfizer, Icagen WO 2012004743	40	
67	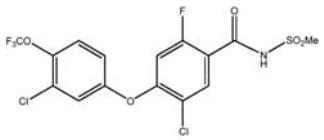	0.025	Pfizer WO 2012007883	327	
68	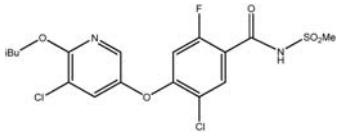	0.0075	Pfizer WO 2012007861	201	
69	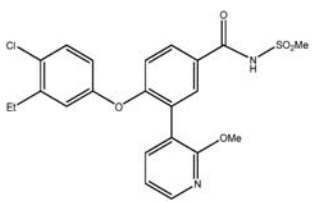	0.018	Pfizer WO 2012007877	95	

(Continued)

Table 4 Examples of sulfonamide $Na_V1.7$ blockers from patent applications—cont'd

#	Structure	$Na_V1.7$ IC_{50}[a] (μM)	Origin	Examples	Comments
70	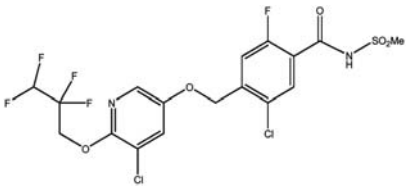	0.0091	Pfizer WO 2012007869	64	
71	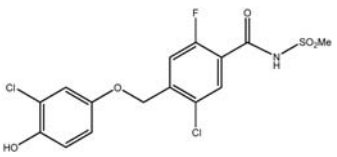	0.0095	Pfizer WO 2012007868	233	
72	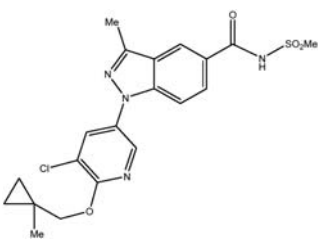	0.008	Pfizer WO 2012095781	163	
73	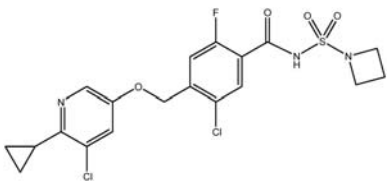	0.15	Pfizer WO 2013088315	~60	
74	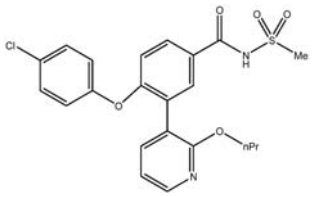	0.014	Pfizer WO 2013093688	9	
75	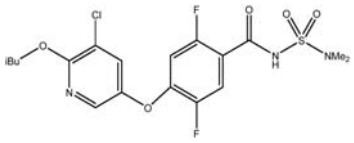	0.13	Pfizer WO 2013102826	~40	
76	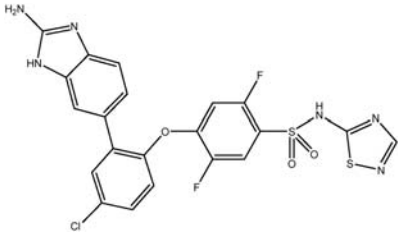	0.0003	Xenon WO 2013064984	~100	$Na_V1.5$ $IC_{50} > 10$ μM

Table 4 Examples of sulfonamide $Na_V1.7$ blockers from patent applications—cont'd

#	Structure	$Na_V1.7$ IC_{50}[a] (μM)	Origin	Examples	Comments
77	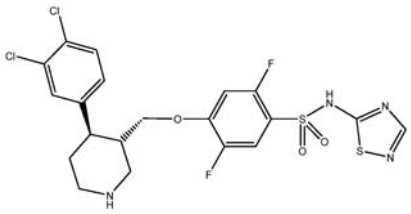	0.0008	Xenon WO 2013064983	~112	$Na_V1.5$ $IC_{50} > 10$ μM
78	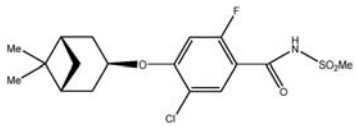	0.0038	Xenon WO 2013177224	~450	$Na_V1.5$ $IC_{50} > 1$ μM
79	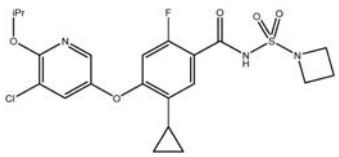	0.0021	Xenon/Genentech WO 2014008458	~100	$Na_V1.5$ $IC_{50} > 1$ μM
80	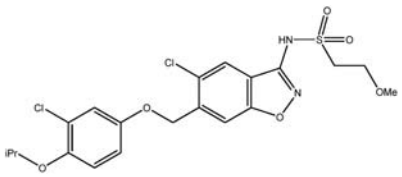	0.002	Xenon/Genentech WO 2014144545	~40	
81	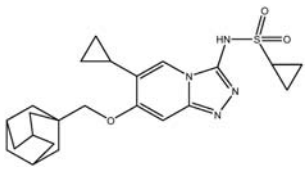	0.002	Xenon/Genentech WO 2014153037	~130	
82	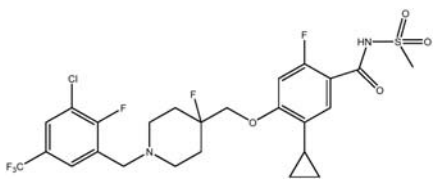	0.0022	Xenon/Genentech WO 2015078374	~600	$Na_V1.5$ $IC_{50} > 0.6$ μM
83	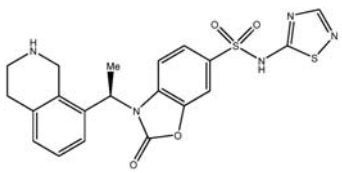	0.026	MSD WO 2013063459	230	$Na_V1.5$ $IC_{50} > 10$ μM
84	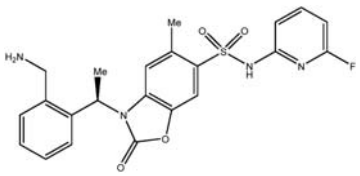	0.006	MSD WO 2014066490	~110	$Na_V1.5$ $IC_{50} > 10$ μM

(Continued)

Table 4 Examples of sulfonamide $Na_V1.7$ blockers from patent applications—cont'd

#	Structure	$Na_V1.7$ IC_{50}[a] (μM)	Origin	Examples	Comments
85	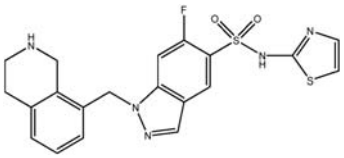	0.02	MSD WO 2014066491	~150	$Na_V1.5$ IC_{50} > 40 μM
86	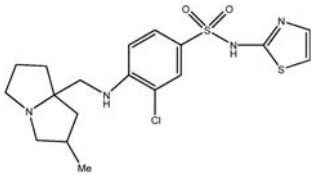	0.005	MSD WO 2015080988	~100	$Na_V1.5$ IC_{50} > 30 μM
87	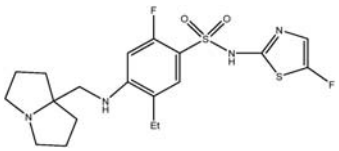	0.005	MSD WO 2015077905	~150	$Na_V1.5$ IC_{50} > 10 μM
88	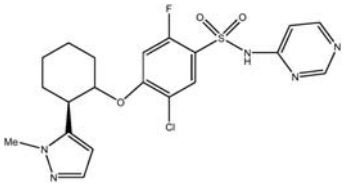	0.02	Daiichi Sankyo WO 2013118854; WO 2014142221	~200; ~70	Tablet formulation described; Selection case
89	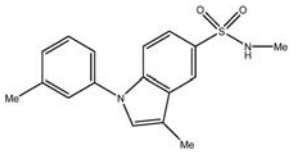	< 0.0098	Daiichi Sankyo JP 2014101287	~200	
90	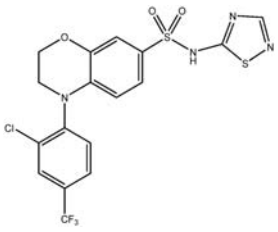	0.008	Amgen WO 2013122897	266	$Na_V1.5$ IC_{50} > 10 μM
91	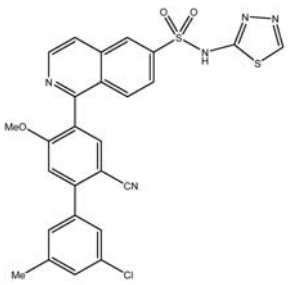	0.011	Amgen WO 2014201173	~570	$Na_V1.5$ IC_{50} > 10 μM

Table 4 Examples of sulfonamide $Na_V1.7$ blockers from patent applications—cont'd

#	Structure	$Na_V1.7$ IC_{50}[a] (μM)	Origin	Examples	Comments
92	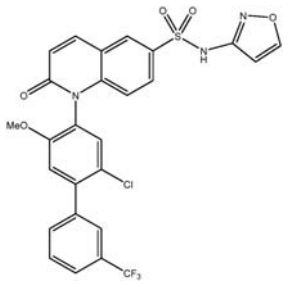	0.004	Amgen WO 2014201206	~1250	$Na_V1.5$ IC_{50} > 30 μM
93	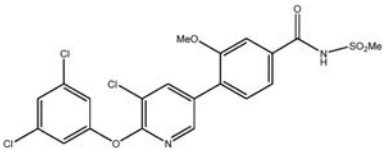	0.035	Amgen WO 2015051043	841	$Na_V1.5$ IC_{50} > 5 μM
94	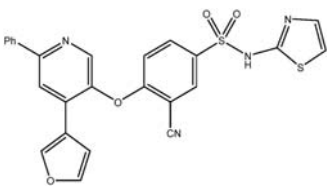	< 0.05	Daewoong WO 214061970	157	
95	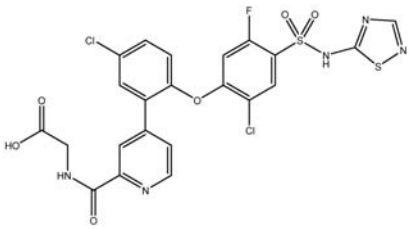	< 0.13	Chromocell WO 201415472, WO 2015038533	33, 70	Examples active in acetic acid, formalin and weight bearing rat in vivo assays at 3–30 mg/kg
96	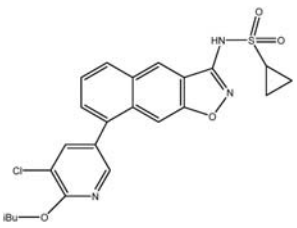	0.01	Novartis US 20150183802	~60	
97	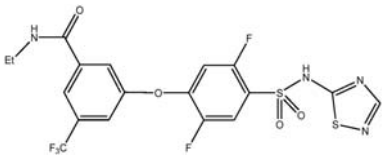	0.26	Zalicus WO 2015130957	65	$Na_V1.2$, 1.5 IC_{50}s > 10, ~5 μM

[a]IC_{50}s by electrophysiology.

The majority of reports of the sulfonamide class of Na_V blockers come from the patent literature. A review including the discovery of early examples has been published by Bagal et al.[4] Initial filings do not disclose specific channel inhibition data but several patent applications from 2010 highlight developments. Vertex, long active in the Na_V blocker area, had filed on a series not specifically claimed as targeted at $Na_V1.7$,[111] but included here (e.g., **62**) as indicative of early work in the area. The potencies of their initially disclosed compounds were not in the nM range recorded by other groups, and Vertex's later filings (*vide infra*) suggest a mainly $Na_V1.8$ focused effort. Vertex aside, Pfizer and Icagen together were the main early drivers in the area and in

a sequence of patent applications published between 2010 and 2012, they explored many aspects of the *N*-heterocyclylaminosulfonyl benzamide class. Their earliest patents also do not disclose $Na_V1.7$ activity (e.g., for **63**) but selective compounds are highlighted in the later cases[112] (e.g., for **64**, **73**) and include *N*-heterocyclylamino benzenesulfonamides (e.g., **65**, **66**)[113] and several series of *N*-methanesulfonyl benzamides (**67–72**, **74**).[114] A key pharmacophoric feature, a 4-*O*-linked-5-chloro-2-fluorophenyl group next to the sulfonamide, is adopted in many examples in different Pfizer patent series (e.g., **64**, **66**, **67**, **68**, **70**, **71**, **73**) and has been adopted by other companies working in the field (e.g., **78**, **88**, **95**). Another related patent application describes a heterocycle utilized to introduce rigidity into the core of the molecules while incorporating a flexible side chain (e.g., **72**).[115] Later filings from the Pfizer group revisit the sulfonylurea functionality, but with aliphatic substituents instead of aromatic heterocycles (**73**, **75**). Some of the examples have a reduced affinity for $Na_V1.7$ which may be compensated for by improved developability properties.[116] Several clinical candidates emerged from this work and some indications of the challenges and properties of the class have been presented at conferences.[117] The location of the sulfonamide binding site has been established as the voltage sensor region in the fourth β-subunit of the ion channel; particular characteristics of the compounds include their acidic character, zwitterionic if, like **64**, they contain a basic center. As a whole, the class is peripherally restricted and evidence from formulation studies suggests that solubility may often be low. Pfizer has also reported that the *in vivo* metabolic stability of compounds of this class has presented development challenges and has been a focus behind the choice of heterocyclic component.[117] A key feature of the class is the exquisite potency for $Na_V1.7$ achieved with examples such as **66,** which demonstrate a sub nM IC_{50}. Channel selectivity data is not included in the Pfizer/Icagen patent filings.

Xenon also sought to exploit this class, combining experience of structurally constraining Na_V blockers with utilization of the reported sulfonamide right-hand portions to create $Na_V1.7$ blockers of similar potency to those described by Pfizer, but also disclosing some selectivity data. For example **76** and **77** are five orders of magnitude selective for $Na_V1.7$ over $Na_V1.5$.[118] Pfizer disclosed[119] that several classes of N-heterocyclyl benzene sulfonamides tend to show metabolic susceptibilities and this finding may have influenced Xenon's pursuit of alternative methane sulfonyl benzamides, such as compound **78**.[119] In collaboration with Genentech, Xenon scientists have explored a wider range of heterocycle-containing sulfonamide classes while retaining a preferred ether-linked lipophilic terminal portion (**79–81**).[120] Incorporation of solubilizing groups such as pyridines and piperidines, illustrated for example by **82**, is a feature of other series.[110]

Merck has pursued a tightly focused strategy aimed at optimizing a core pharmacophore incorporating (see examples **83–87**) differently constrained basic features in combination with a relatively conserved heterocyclyl aminosulfonamide group and has developed a number of aromatic spacers and different lipophilic amines to optimize this class. Its researchers have also achieved $Na_V1.7$ block in the nM range and high $Na_V1.5$ selectivity across their series.[121]

Daiichi Sankyo has focused recent patent applications on the *N*-heterocyclyl benzenesulfonamide class with a heterocycle linked to the aryl core via a constrained ether, a pattern first described in the Pfizer-Icagen series. Compound **88** has been selected as a potential development compound based on a selection case. A recent patent filing suggests that later work has also been directed toward series which do not contain a right-hand heterocycle, such as **89**.[122]

Amgen has had a long established interest in Na_V blockers and has recently also investigated the sulfonamide class,[123] homing in on a preferred thiadiazole component in the early cases (e.g., **90**, **91**) before patenting on the simpler methanesulfonyl benzamide class.[124] Early compounds disclosed are also notable for their high lipophilicity and high level of aromaticity (e.g., **91**, **92**), though later compounds such as **93** have fewer ring systems and are more similar to later Xenon and Pfizer examples in containing a methanesulfonamide.

Daewoong has claimed a stake in the sulfonamide class with a single patent filing exhibiting the ortho ether pattern and an N-heterocyclic sulfonamide group, illustrated by example **94**.[125] In contrast Chromocell has focused on designing compounds which bear a range of peptidic linkers potentially providing solubility handles or acting as prodrugs (see example **95**). It is interesting to note that, in these patent application, the company's therapeutic intent appears directed more toward diabetes than pain as an indication.[126]

Novartis has published a single patent application in the sulfonamide area and its series is unique in having fewest conformational degrees of freedom, sporting a tricyclic heterocyclic core as in **96**.[127] In contrast a recent patent filing from Zalicus describes compounds which are clearly related to early Pfizer–Icagen examples such as **65** but, for example in the case of **97**, incorporating a terminal amidic feature rather than a heterocycle or basic group.[128]

Several papers discuss the properties of the sulfonamide Na_V blocker compound class, but few to date have discussed SAR. The detailed electrophysiological profiles of certain lead compounds, which emerged from the early Pfizer–Icagen collaboration, **ICA-121431** (Fig. 21) and **PF-04856264**, have been described in a paper[29] published in 2013, which also describes the factors influencing the binding profile on the voltage sensor region of the ion channel. These two molecules each exhibit exquisite affinity for binding to specific human ion channel subtypes $Na_V1.3/Na_V1.1$ (**ICA-121431**, $IC_{50} = 19$ nM) and $Na_V1.7$ (**PF-04856264** $IC_{50} = 28$ nM).

Although this sulfonamide class of compounds has been unambiguously shown to exert their effect by binding to the voltage sensor region of the ion channel, their mechanism of action may be more subtle in some cases, hinting at a dual mode of action. For example, the behavior of ion channels can be very sensitive to small structure changes to the inhibitor. In a paper published in 2015, **PF-05661014** is shown to selectively inhibit $Na_V1.3$ over $Na_V1.7$ currents by stabilizing the inactivated state of the channel through an interaction with the D4 voltage sensor.[129] **PF-06526290**, which differs from **PF-05661014** by a single methyl group, exhibits a dual effect, greatly slowing inactivation of Na_V channels in a subtype-independent manner. However, upon prolonged depolarization PF-06526290 becomes a Na_V subtype-selective inhibitor similar to PF-05661014. A key finding was that mutation of the D4

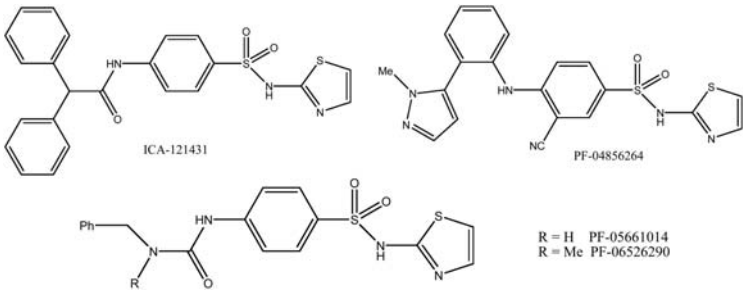

Fig. 21 Evolution of Pfizer sulfonamide Na_V blockers.

region of the ion channel modulates inhibition of $Na_V1.3$ or $Na_V1.7$ by both compounds, but has no effect on the inactivation slowing produced by PF-06526290, suggesting a second mechanism.

The potential for small molecules to bind in different positions in the pseudo-symmetric human ion channel may underlie this behavior and cause the structure sensitivity that has bedevilled attempts to develop clear SAR for small molecule ion channel interactions. Both the site and kinetics of binding will have distinct effects on ion channel behavior, and therefore it is hard to predict physiological effects resulting from channel blockade in vivo.

The Xenon team describe[130] how they explored a class of substituted piperidine methyleneoxy benzenesulfonamides related to the Pfizer compound PF-04856264, typified by compound **98** (Fig. 22). Their starting point was a hybrid compound **99** with the Pfizer right-hand side; however, it was quickly established that substitution on the phenyl ring could give a marked increase in $Na_V1.7$ potency with analogue **100** demonstrating sub nM blockade of $Na_V1.7$ but still high selectivity over $Na_V1.5$. However, the examples proved potent inhibitors of several cytochrome P450 enzymes. The choice of a different right-hand heterocycle could reduce this liability and by selecting the single isomer shown in compound **98,** CYP450 inhibition values of less than 10% across various isoforms at 10 μM were achieved while retaining strong $Na_V1.7$ blockade ($IC_{50} = 11$ nM) and 1000-fold selectivity over $Na_V1.5$.

7.04.3.3.2.4 Aryl triazines and derivatives

The small size of lamotrigine and its activity as a pan-sodium channel blocker has led to the molecule being used a starting point for the development of more selective agents. Some companies have elaborated the core nitrogen containing heterocycle while, in other cases, a triazine structure has been arrived at through lead optimization; analogues are shown in Fig. 23. Optimized compounds may appear unrelated to lamotrigine; however, there are often intermediate structures showing a link to this chemotype. The heterocyclic core has been used to design selective inhibitors of both $Na_V1.7$ and $Na_V1.8$; however, the target profile is not always apparent from the patent literature. Purdue Pharma and Amgen have been most active in exploring this template but it has also been the subject of research by Novartis and various university groups. Abbott and Pfizer have used the template in $Na_V1.8$ blocker design.

Amgen has published a number of patent applications in recent years describing different classes of small molecule sodium channel blockers for the treatment of pain, focused principally on $Na_V1.7$ and in particular on the acyl sulfonamide class also described by Pfizer and others. The earlier patents describe modified toxins, but some publications also include triazines. A patent filing from 2010 describes several hundred compounds including examples with sub-micromolar IC_{50}s in electrophysiology assays.[131] A number of pain model studies are noted including spinal nerve ligation; however, activity data is provided for a small number of compounds including **101,** which showed activity at 10 mg/kg in a rat formalin model of persistent pain when dosed orally. The same molecule gave an IC_{50} against $Na_V1.7$ of 5.0 μM. In contrast, the analgesic activity of the most potent $Na_V1.7$ blocker reported **102** ($IC_{50} = 0.04$ μM) is not recorded. A more detailed description of the discovery and lead optimization of this class is provided in another paper.[132] The origin of this series is revealed to be a high-throughput electrophysiology assay of a compound collection. The authors comment on the need to design compounds based both on $Na_V1.7$ selectivity and state dependence and describe a voltage-dependent protocol for their electrophysiology (E-Phys) assays to enable them to identify compounds, which preferentially bind to the inactivated state of the channel. They reveal that a major hurdle was the need to avoid the hERG blockade and CYP450 liabilities that were identified in their initial lead **103**, which showed an IC_{50} in the partially inactivated state

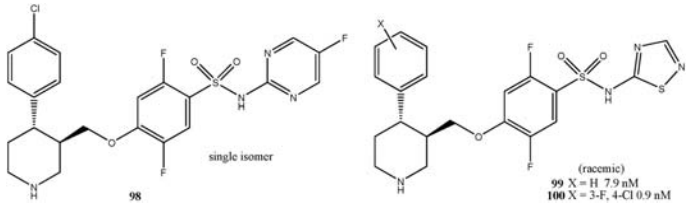

Fig. 22 Optimization of Xenon sulfonamide Na_V blockers.

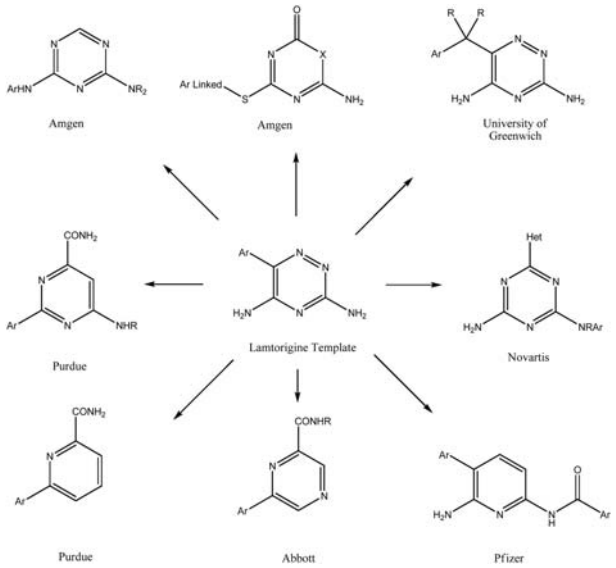

Fig. 23 Relationship of classes of Na_V blockers to Lamotrigine.

E-Phys $Na_V1.7$ assay of 1.9 μM. This issue was overcome by replacement of the tetrahydroisoquinoline with a more flexible and less metabolically susceptible aryl piperidine leading to **104**. This tool compound was between 2- and 12-fold selective for $Na_V1.7$ over other Na_Vs with an IC_{50} of 0.17 μM in a partially inactivated state assay but was much more selective against a wider target class panel. In a rat formalin-induced flinch model, compound **104** showed a dose response with significant efficacy at a minimal oral dose of 10 mg/kg. Interestingly, the group undertook a competition study with tetracaine and batrachotoxin, which suggested that this class of compound does not bind in the Na_V anesthetic binding site (Fig. 24).

In a second related patent application a class of reversed amides was similarly profiled.[133] Among some 300 compounds, example **105** blocked the human $Na_V1.7$ channel with an IC_{50} of 0.52 μM, but no data was given for activity in the pain models described.

Similar compounds have been described in more detail in a series of communications[134] The authors indicated that this series was not specifically modeled on any existing class of sodium channel blocker but was found through an HTS campaign using high-throughput electrophysiology, with a focus on finding state-dependent blockers. The first lead **106** was at least 10-fold selective for the inactivated state over the closed state and showed good developability properties in vitro, but high clearance in vivo. They sought to modify the triazine core to modulate these properties and a pyrazine was found to be suitable as it also gave on average better $Na_V1.5$ selectivity; however, many compounds showed a hERG liability. Further side chain modification led to the discovery of compound **107** with an IC_{50} in a partially inactivated state of 0.24 μM, at least fivefold selectivity over $Na_V1.5$, and IC_{50} against hERG of >30 μM, coupled with low clearance (Fig. 25).

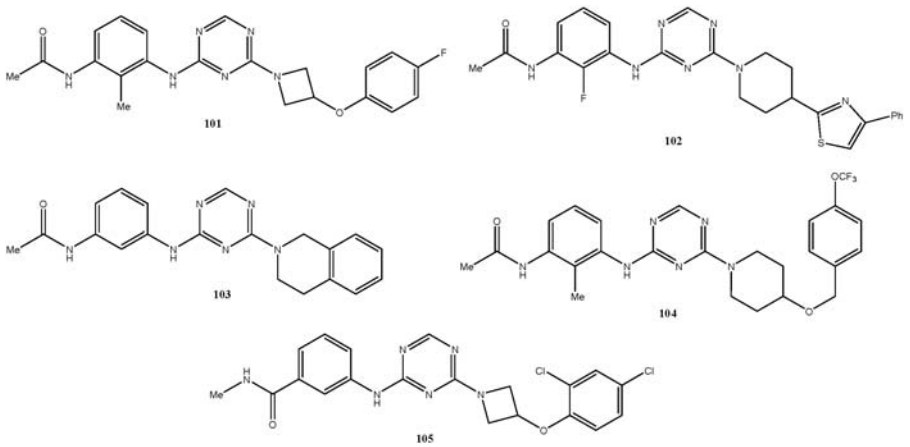

Fig. 24 Amgen Triazine Na_V blockers.

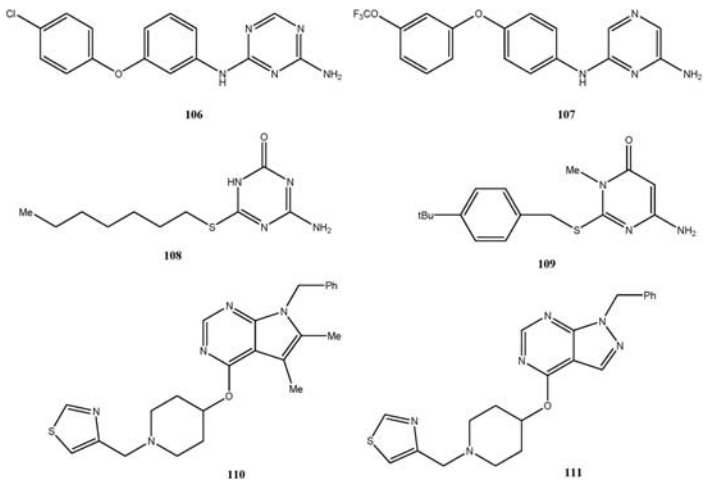

Fig. 25 Evolution of Amgen Na_V blockers.

An even simpler core template has been described in a second paper[135] in which an initial hit **108**, a sub micromolar inhibitor of $Na_V1.7$, was discovered in a screening campaign. It possessed significant activity at $Na_V1.5$ as well, but otherwise possessed a good developability profile. Optimization was effected by varying the thioether side chain and by alkylation on the heterocycle to give an analogue **109**. This showed 10-fold higher potency at $Na_V1.7$ and a low *in vivo* clearance in the rat, though still modest selectivity over $Na_V1.5$. The authors noted that the compound appeared five times more potent under conditions of manual patch testing than when using a Patch Express automated protocol. The clearance had also been reduced fivefold.

Another hit series incorporated a different core heterocycle, replacing the diazine with a pyrrolopyrimidine.[136] A paper describes the lead optimization of a highly potent hit **110** ($Na_V1.7$ $IC_{50} = 0.06$ μM in a partially inactivated state assay) from this class which already showed approximately 100-fold selectivity for this channel over other Na_Vs. This compound had poor stability in human liver microsomes and only modest selectivity over hERG; so these aspects were the focus of the campaign. The methylene thiazole core heterocycle and piperidine linker appeared crucial for activity, and modifications aimed at reducing LogP as a route to lower clearance generally reduced either the potency or selectivity of the series. Aromatic ring substituents offered no advantage. A compromise molecule incorporating a pyrazolopyrimidine (**111**) was therefore selected for further lead optimization based on its better lipophilic efficiency and good microsomal stability despite being a weaker overall inhibitor of $Na_V1.7$ ($IC_{50} = 0.83$ μM).

The patent filings by Purdue illustrate, perhaps better than any other sequence, the links between the aryl-linked aminoamides and triazine Na_V pharmacophores following the evolution of chemotypes through lead optimization in related series. The company has had a long history in sodium channel research and in 2011 published a class of aryl-substituted indoles and azaindoles, which had structural links to the aryl-linked aminoamide class,[137] but included conformational constraint through the indole and biaryl moieties. Compound **112** ($IC_{50} = 0.40$ μM in a $Na_V1.7$ FLIPR assay, Fig. 26) is illustrative. Activity modulation was reported to be

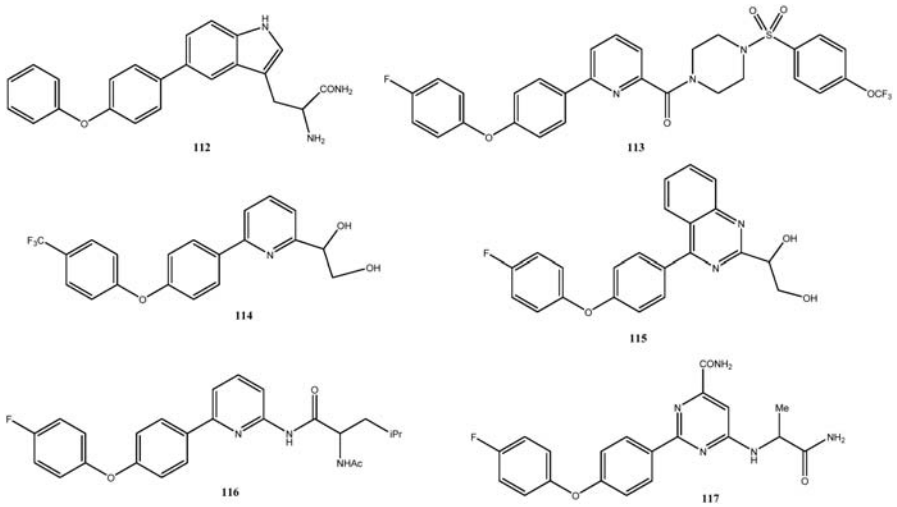

Fig. 26 Early Purdue Na_V blockers.

achieved by either varying the aryl ring substitution pattern or incorporating alkyl or hydroxyl substitutions around the amidic portion. Further patents followed in which the aryl portion was retained while changes were made to the polar amidic region, both by extending (**113** $IC_{50}=0.19$ μM)[138] and contracting (**114** also a micromolar inhibitor) it.[139] The class of compound **114** also included pyrimidines in place of the central pyridine ring and this change is exemplified further with a series of quinazolines highlighted by compound **115**.[140]

Moving from a quinazoline to an amino-pyridine allowed the reincorporation of amidic features, as illustrated by compound **116**, now a potent inhibitor ($IC_{50}=0.042$ μM in FLIPR assay).[141] With the inclusion of a second heteroatom in the pyridine ring **117** ($IC_{50}=0.042$ μM), a link to the lamotrigine chemotype is arguably established, but the similarity to the aryl-linked aminoamide series is also apparent.[142]

Purdue has gone on to explore extensively around these scaffolds, including demonstrating activity with quaternized analogues (Fig. 27) such as **118** ($IC_{50}=0.872$ μM), a feature which would be expected to affect absorption properties.[143] They have also looked to incorporate heteroatoms into the lipophilic aromatic region. For example, compound **119** provides a less amphiphilic molecule ($IC_{50}=0.152$ μM).[144] The significance of incorporating a halogen or CF_3 substituent on the terminal aromatic ring, to both modulate activity and block metabolism, has been demonstrated in other series, which have been subject to patent filings[63] and is a feature in several examples from Purdue including **120** ($IC_{50}=0.098$ μM) another potent $Na_V1.7$ blocker in the FLIPR assay,[145] and **121** ($IC_{50}=0.722$ μM).[146] Triazine carboxamides such as **122** ($IC_{50}=1.8$ μM)[147] are much closer to lamotrigine structurally but still contain the principle aromatic side chain features of the earlier leads; however, they generally appear less potent by the FLIPR assay used throughout this series. Certain compounds incorporate features found in the sulfonamide class of $Na_V1.7$ blockers (such as **123**),[148] but this could be coincidence as sulfonamides are known to bind to a site remote from the pore region believed to be the location where lamotrigine and aryl-linked aminoamide classes are effective.

In a move away from the aromatic dominance of the class and introducing three dimensionality, a more recent series from Purdue incorporated a spiro-linked group through a piperidine substituent **124** with retention of modest $Na_V1.7$ inhibition ($IC_{50}=1.3$ μM).[149] Later filings, however, mostly continue to contain variants on the aryl pyrimidine theme with polar side chains, for example, **125** ($IC_{50}=0.042$ μM) with a glycinamide side chain.[150]

Subsequent patent applications from Purdue have continued the trend of aromatic variation with incorporation of features known to be acceptable in alternative sodium channel pharmacophores (Fig. 28), for example, a benzodiazepine moiety as in **126** ($IC_{50}=0.04$ μM),[151] and indazoles such as **127** ($IC_{50}=0.157$ μM).[152] Compound **128** ($IC_{50}=0.357$ μM) also illustrates attempts within this series to conformationally constrain the aromatic side chain.[153] A further different angled constraint is introduced with a tetrahydroisoquinoline linker in **129** ($IC_{50}=0.428$ μM).[154] It is curious to note that the polar side chain of the original aryl-linked aminoamide series is entirely missing in some of the examples illustrated (such as **126** and **128**) though it is still present

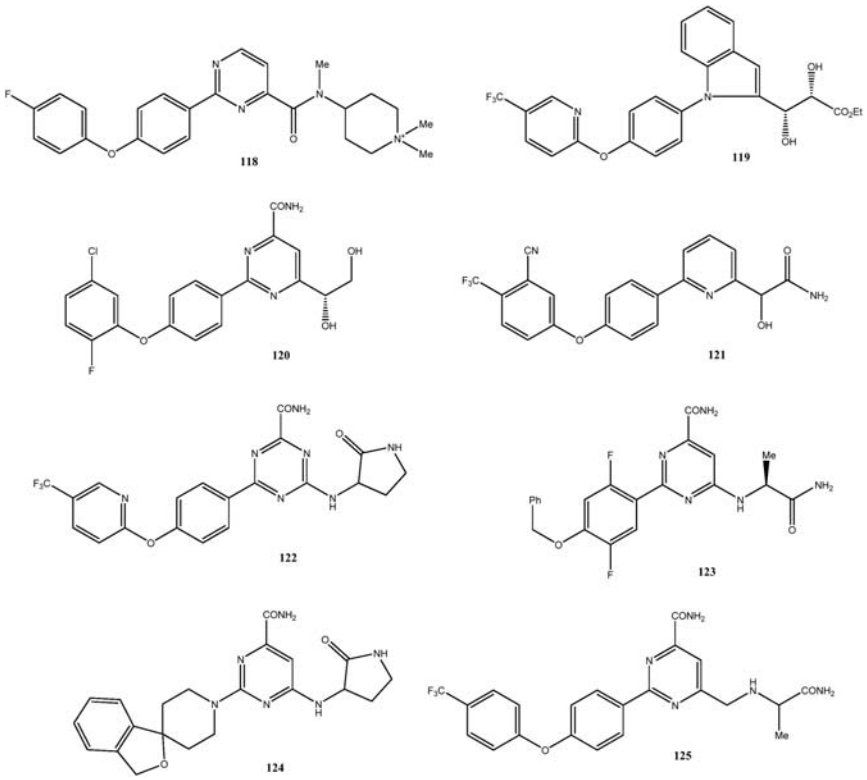

Fig. 27 Diversity of Purdue series.

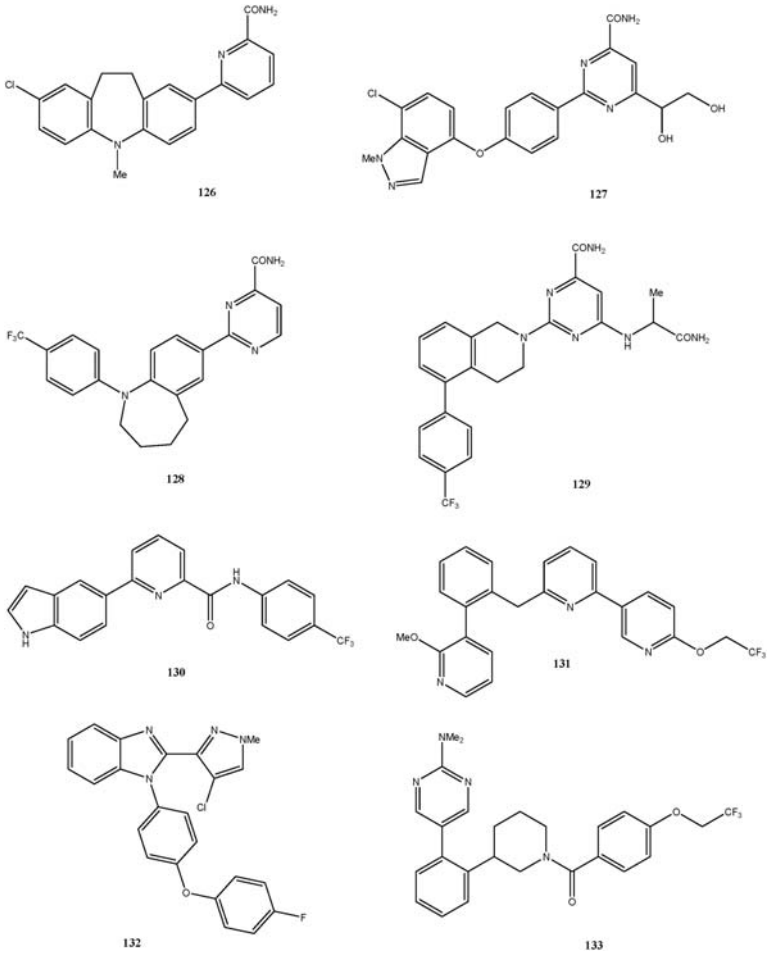

Fig. 28 Combination of Na_V pharmacophores.

within the patent claims, indicating the feature is not by any means essential for Na_V blocking activity. This is perhaps clearest in the most recent patent applications from the group, in which the evolutionary link to the original lead series is scarcely apparent, for example in compound **130** ($IC_{50} = 0.233$ μM)[155] has the glycinamide apparently replaced by anilide, which leads to the question of whether these compounds do bind in the same site as the molecules from which they were derived. Similarly **131**, one of around twenty examples reported as active both in electrophysiological $Na_V1.7$ studies and *in vivo* pain model studies,[156] now just contains four linked aromatic groups and is chemically remote from the original lead series.

Other recent classes of Na_V blockers investigated by Purdue are represented by **132**, a benzimidazole derivative[157] and the piperidine **133**.[158] Compound **132** was reported to have an IC_{50} at $Na_V1.7$ of 0.10 μM and compound **133** 0.096 μM in FLIPR assays. Both represent the most potent of several dozen examples described in their respective patent applications; however, selectivity information was not disclosed.

Purdue has published two papers describing the discovery of certain compound series (Fig. 29). In the first[159] a scaffold hopping strategy takes a previously reported active Na_V blocker **134,** which is close to the aryl-linked aminoamide class, and elaborates it into a series of constrained azepines, illustrated by the generic structure **135**. Some dozen analogues showed potent activity in $Na_V1.7$ electrophysiology assays with IC_{50}s of around 1 μM or less; however, both poor stability in human and rat liver microsomes and low aqueous solubility (~1 μM) made declaration of a lead moot. Compound **136** with a $Na_V1.7$ FLIPR IC_{50} of 1.8 μM was among those highlighted as having the best compromise profile.

The second paper[160] describes a different approach: taking an already identified brain-penetrant sodium channel blocker and rendering it peripherally restricted by modifying the physicochemical profile. The earlier described molecule **134** had previously been elaborated into an azabicyclic derivative **137** (as described above) and the diazepine variant of this moiety was used as a template as the group sought to introduce more polar side chains to limit central penetration. In practice it proved to be a challenge to obtain good gut permeability while limiting brain penetration, but a number of derivatives proved to be substrates for transporters with high MDCK efflux ratios, which potentially offered that prospect. Compound **138**, a sulfonamide with a K_i of 0.23 μM and an efflux ratio of 160, showed high exposure in a rat dosing study and was highlighted as promising, although pharmacodynamic data was not presented nor was evidence of central limitation provided.

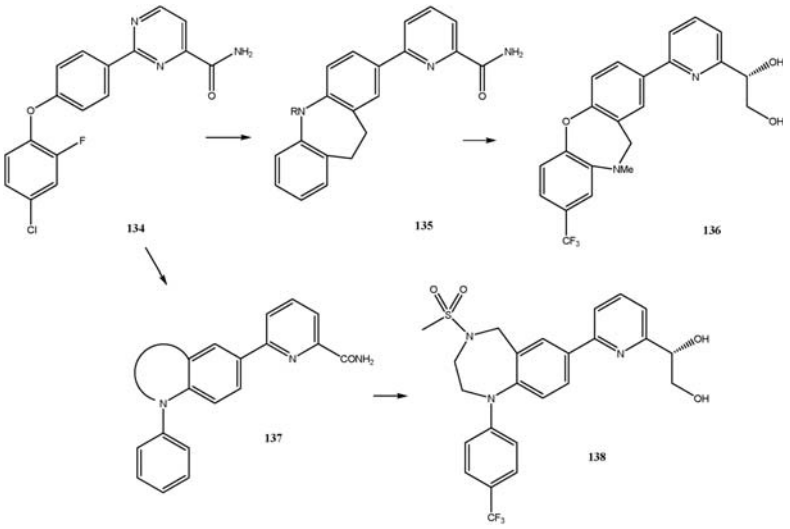

Fig. 29 Optimization of Purdue series.

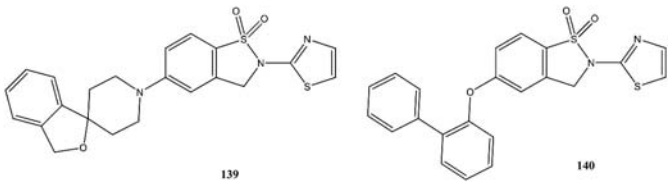

Fig. 30 Cyclic sulfonamides.

Finally, a set of eight cyclic secondary sulfonamides has been described by Purdue.[161] These are, arguably, pharmacophorically more similar to the amidic class of blockers than those sulfonamides that bind to the ion channel allosteric site, as they have neither an acidic proton nor a basic side chain. Several of the compounds claimed do incorporate a spirocyclic feature, including **139** (Fig. 30). Compound **139** is noted as having an IC_{50} of 0.77 μM in a FLIPR assay but no further types of activity data are provided. This spirocycle may provide a link between this class of inhibitor and those discovered by Vertex (e.g., **54**). However, not all compounds have the spirocyclic feature, for example **140** carries a moiety which resembles the β-subunit Na_V binding series; so perhaps this set represents an attempt to marry different pharmacophores.

Novartis has investigated compounds targeted at $Na_V1.7$ based on a triazine template. In a single patent application from 2012 researchers describe some 500 analogues of which compound **141** (Fig. 31) showed the most potent blockade of $Na_V1.7$ at 4 nM, as measured by a patch clamp methodology.[162] Those compounds with the most potency tended to have an extended substituent off the pyridine heterocycle. Data were presented showing that key compounds have a selectivity of at least one order of magnitude over $Na_V1.5$, as measured by high-throughput electrophysiology. The patent disclosed three compounds **142–144,** which were active in a rat FCA model of neuropathic pain and reported unspecified activity between 1 and 3 mg/kg. Notably, this activity does not directly correspond to their measured, blockade, which gave K_is of 110, 560, and 44 nM, respectively.

An interesting twist to the triazine story is seen in compounds which have been the subject of a patent application by the University of Greenwich, UK, who sought to make conformationally restricted lamotrigine derivatives.[163] No characterizing channel

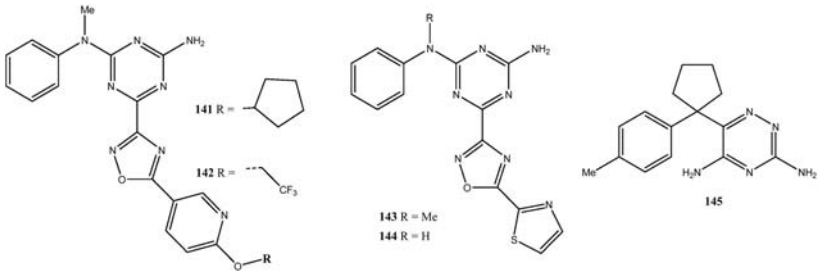

Fig. 31 Novartis triazines and conformationally restricted lamotrigine analogues.

selectivity data was presented and although pain is claimed as an indication, among others, it appears that an objective of this work was a pan-sodium blocker with a better profile than lamotrigine itself. Notable lead compounds included **145,** which exhibited an IC_{50} of less than 0.5 μM in inhibiting the binding of [3H]brevetoxin-B in a sodium channel-blocking assay. An additional claim indicates an interest in the molecule type as antimalarial agents, acting as antifolates, so it is possible that this was their primary interest.

7.04.3.3.2.5 Additional binding classes

RaQualia has identified a class of alkyl-substituted heterocyclic derivatives incorporating an amide side chain, initially described as blockers of both sodium and calcium channels.[164] Their first patent application indicated that around 200 examples out of more than 400 analogues showed IC_{50}s of less than 1 μM in either $Na_V1.7$ or $Na_V1.3$ FRET assays. Most of these compounds, for example **146** (**Fig. 32**), also show T-type calcium channel blocking activity at the same level, and no group of selective compounds is described. Though a wide range of analogues was claimed, a 5-trifluoroethoxy substituent on a 2-substituted pyridine heterocycle is a feature common to most of the claims (e.g., **146**, **149–153**), suggesting a privileged template for their binding site. A wide range of aromatic amides have been incorporated on the right hand side as drawn. Subsequent claims indicated that conformational restriction of the side chain and repositioning of the substitution pattern could focus activity on TTX-sensitive sodium channels and a class of picolinic amides was highlighted, for example, **147**, reported to show TTX blocking with an IC_{50} of less than 0.5 μM.[165] Aromatic groups were also incorporated, linked to the other end of the molecules and described in a patent claiming almost a hundred examples. This application indicates that selectivity over $Na_V1.5$ was being sought but does not provide delineation between $Na_V1.3$ and $Na_V1.7$ inhibitory activity.

A further variation on the constrained aromatic amide theme was highlighted in a third patent application published around the same time.[166] In this case, a substituted piperidine provided the template, usually substituted in the 4-position by an ether-linked aromatic group. The patent indicated that several examples have shown potent but unspecified activity in a FCA-induced thermal hyperalgesia rat model for pain. Compound **148** was highlighted from over 500 examples in showing an IC_{50} of 0.36 μM in a $Na_V1.7$ FRET assay and some 20-fold selectivity over hERG, as measured by dofetilide binding. Another template claimed by RaQualia used piperazine as the amide linker; thus compound **149** is among 40 compounds highlighted from a patent application of some 250 analogues as demonstrating IC_{50}s lower than 3 μM against $Na_V1.7$ and, in this case, some element of selectivity over both $Na_V1.3$ and $Na_V1.5$.[167]

The aryl amide class has proved fertile ground for developing further $Na_V1.7/Na_V1.5$ selective series and two subsequent patent applications indicated a refocus by RaQualia on analogues of **146**.[168] Compounds such as **150** contain a reversed amide, relative to

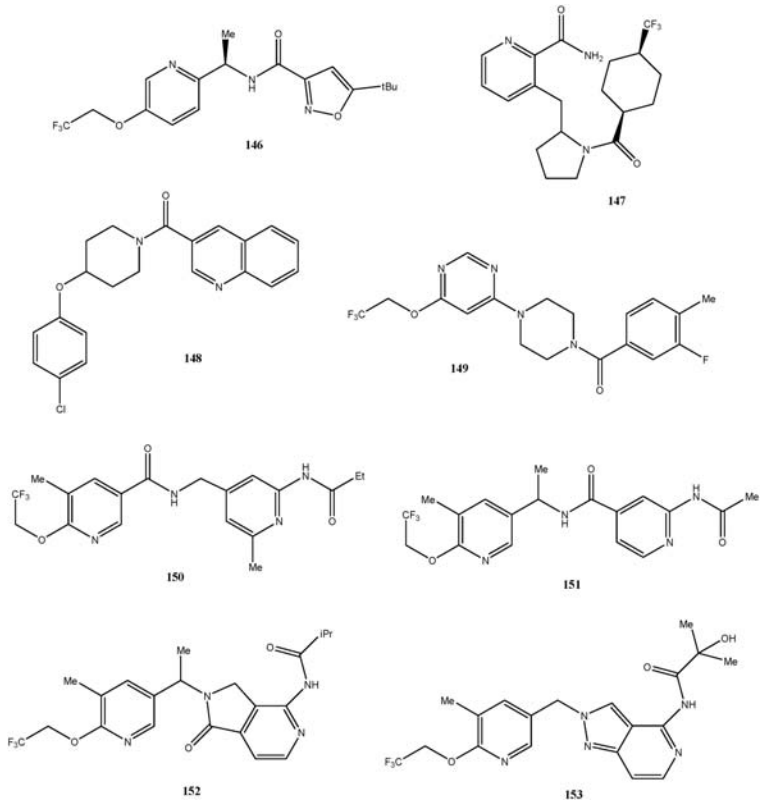

Fig. 32 RaQualia Na_V blockers.

the first series, and a benzylic methyl group is present in most of the example (e.g. **151**, **152**). A wide range of substituents are claimed on the rightmost aromatic right, particularly adjacent to the carbonyl group. Some 350 compounds are exemplified with greater characterization details on just three examples. Compound **150** is highlighted as showing 30-fold selectivity for $Na_V1.7$ ($IC_{50} = 1$ μM) over $Na_V1.5$ in an electrophysiology study while also being an inhibitor of $Na_V1.5$ with an IC_{50} of 0.51 μM in a FRET assay. Likewise in another patent claim[169] over 1000 analogues are described with another amide position varied, typified by **151** which showed K_is of 1.5 μM and 1.3 μM against $Na_V1.3$ and 1.7, respectively in a patch clamp assay based on CHO cells expressing the ion channels. Compound **151** is highlighted in all assay formats and demonstrates activity at 10 mg/kg in a FCA model of static allodynia in the rat.

The two most recent RaQualia patent applications continue the trend but this time with elements of conformational constraint on the right side of the molecule. In the first of these[170] an isoazaindolone forms the basis of the right-hand aromatic portion, exemplified by **152**, one of nearly 700 examples claimed. Again detailed electrophysiology assays are recorded and compound **152** is noted as active in all assay formats including a number of pain models. It is noteworthy that this compound is effective at blocking both $Na_V1.3$ ($K_i = 0.091$ μM) and $Na_V1.7$ ($K_i = 0.014$ μM) in electrophysiology assays on the inactivated state, so a mixed mode of action but state-dependent profile may be the target of RaQualia's research. The most recent filing from this group[171] focuses on a structurally similar chemotype but with a pyrazolopyridine template. Compound **153** was highlighted as showing block of the $Na_V1.3$ and 1.7 inactivated states, but at a lower level than **152** and fewer examples were claimed. *In vivo* activity is claimed in a suite of rat pain models including the formalin-induced nociceptive behavior paradigm, paw incision-induced static allodynia, paclitaxel-induced and FCA-induced weight bearing as well as in established pain models such as chronic constriction injury-induced static allodynia.

An analysis of a series of benzazepinones that had been the subject of earlier Merck patenting activity was published in a paper in 2013.[172] It reports that compound **154** (Fig. 33) achieved good selectivity for $Na_V1.7$ ($IC_{50} = 117$ nM) over other channels ($IC_{50} > 10{,}000$ nM for $Na_V1.5$) and some 10-fold selectivity for blockade of the inactivated state of $Na_V1.7$ compared with $Na_V1.5$, 1.6, and 1.8. In addition oral efficacy in a spinal nerve ligation assay was reported with an ED_{50} of 15 mg/kg. Compound **154** was also reported to have a good selectivity profile across a wide range of assays and to show no significant impairment of motor function at 10-fold higher doses than those shown to be efficacious in the pain model.

UCL filed a patent on a Pan-Na_V blocker for pain including for example compound **155**.[173] However, as the quoted examples showed blockade of $Na_V1.5$ at a level comparable to the other channels, it is not clear on what basis the compounds were expected to be selective for pain indications. The compounds were demonstrated to have some efficacy in an EAE model of relapsing remitting multiple sclerosis (MS); so this may have been the principal target of their investigation.

7.04.3.3.2.6 Dual $Na_V1.7$–1.8 inhibitors

In addition to patenting compounds containing the sulfonamide moiety, which target the voltage sensor region of sodium channels, AbbVie has claimed a class of amidic compounds, with activity at both $Na_V1.7$ and 1.8.[174] The patent application describes over 600 examples based on a quinoline core substituted with an amide-linked ring and an aryl moiety. Most examples were more effective at blocking $Na_V1.7$ than 1.8 in a FRET assay but there were some, such as compound **156** (Fig. 34), with the alternate profile ($Na_V1.7$ $IC_{50} = 0.98$ μM, $Na_V1.8$ $IC_{50} = 0.21$ μM). However, compound **157** ($Na_V1.7$ $IC_{50} = 0.34$ μM, $Na_V1.8$

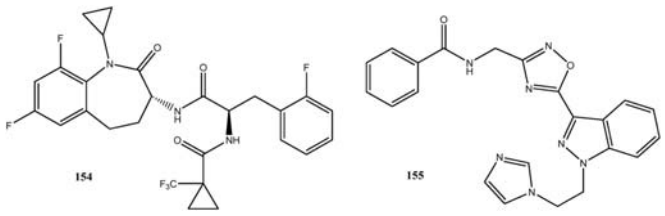

Fig. 33 Alternative Na_V blocker classes.

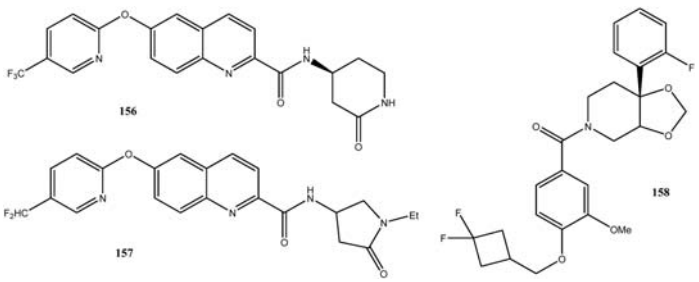

Fig. 34 Dual $Na_V1.7$–1.8 blockers.

$IC_{50} = 0.50\ \mu M$) was effective in rat pain models dosed orally at 30–100 mg/kg. It was clear however that there was no simple correlation between channel blocking efficiency *in vitro* and efficacy in monosodium iodoacetate model of osteoarthritis or spinal nerve ligation studies in the rat.

Vertex has also described classes of compounds with activity at both $Na_V1.7$ and $Na_V1.8$. Compounds from WO 2010002956 are discussed in relation to $Na_V1.7$ sulfonamides (*vide supra*) because of their similarity to compounds of that class. Compounds described in a more recent patent application[175] were suggested to be blockers of both $Na_V1.7$ and Na_V 1.8, and it was indicated that this dual action may make them more efficacious, supporting the hypothesis by noting that double knockouts of $Na_V1.7$ and $Na_V1.8$ in sensory DRG neurons diminish nociceptive behaviors to a greater degree than knockout of either channel alone. Detailed ion channel inhibition values were not disclosed; however, compound **158** is illustrative of the 314 compounds disclosed in this patent filing and was described as active.

7.04.3.3.3 $Na_V1.8$ blockers

$Na_V1.8$ was the first tetrodotoxin-resistant (TTX-r) voltage-gated sodium channel to be identified[176] and its predominant expression in DRG neurons and sensory fibers has led to its attracting interest as a potential target for pain.[177] $Na_V1.8$ knockout mice showed deficits in nociception following inflammation, supporting the involvement of $Na_V1.8$ in inflammatory pain. While some data from knockout mice suggested $Na_V1.8$ is not essential for development of neuropathic pain[178] this is contradicted by findings with selective small molecule blockers of $Na_V1.8$ (*vide infra*), and antisense[179] or siRNA knockdown of $Na_V1.8$ expression,[180] all of which show analgesic effects in neuropathic pain models. Furthermore, gain-of-function mutations of the $Na_V1.8$ channel that produce DRG neuronal excitability have been found in 3% of patients with painful neuropathy.[181] The functional and pharmacological properties of human and rat $Na_V1.8$ channels were explored with a variety of mostly nonselective sodium channel blockers.[182] Over the last decade, the search for potent and selective blockers of $Na_V1.8$ has resulted in the development of several compounds that have helped to define the effects of selective pharmacological block of $Na_V1.8$ and although some compounds emerged as potential treatments for pain, a successful controlled clinical trial of a $Na_V1.8$ blocker has yet to be reported. A recent review linking $Na_V1.8$ with several other disease states such as (MS) and cardiac disorders suggests a more complex role of $Na_V1.8$ in human physiology.[183]

An early report of small molecule blockade of $Na_V1.8$ activity involved the use of ambroxol (**Fig. 35**), a compound which has been used for the treatment of respiratory diseases for several years.[184] Ambroxol has modest selectivity for the $Na_V1.8$ channel over other sodium channels and showed efficacy in several preclinical models of neuropathic and inflammatory pain at doses of 1000 mg/kg.[185] More recently, ambroxol has been shown in uncontrolled studies to have some potential benefit for alleviation of neuropathic pain when applied topically to patients, the effects being attributed to its sodium channel-blocking properties.[186]

It has also recently been reported that the blockade of $Na_V1.8$ currents in nociceptive trigeminal neurons contributes to the anti-trigeminovascular nociceptive effect of several established drugs including the tricyclic antidepressant amitriptyline.[187] Furthermore, interaction with the slow inactivation state of $Na_V1.8$ has also been shown to be a property of carbamazepine,[188] and dexmedetomidine inhibits $Na_V1.8$ sodium channel activity in rat DRG neurons.[189]

The first efforts aimed at optimization of selective small molecule blockers of $Na_V1.8$ were described by Abbott/Icagen and led to the identification of A-803467,[190,191a] a molecule that has been widely studied both *in vitro* and *in vivo*. Proof of concept that a selective small molecule $Na_V1.8$ blocker could be analgesic was provided when A-803467 was shown to be active in preclinical models of inflammatory and neuropathic pain.[173]Further studies showed additive activity with a TRPV1 antagonist in rat neuropathic and inflammatory pain models[192], and more recent studies have shown A-803467 to be active in an animal model of osteoarthritis[193] but it may also have some activity at the cardiac $Na_V1.5$ channel.[194]

The poor solubility and resulting poor oral absorption and pharmacokinetic properties of A-803467 precluded its further development and Abbott/Icagen explored several closely related series in attempts to overcome these issues. Initial studies focused on replacement of the anilide with solubilizing groups leading to the piperazine analogues **159–161** (**Table 5**).[195]

The inclusion of basic nitrogen appeared to give enhanced $Na_V1.8$ blockage but the precise position of the N had only a moderate effect on activity. Introduction of lipophilicity enhanced potency and this was postulated to be important for interaction with hydrophobic regions of the binding site in the $Na_V1.8$ channel; however, these compounds showed only moderate selectivity for the $Na_V1.8$ channel over $Na_V1.2$ and $Na_V1.5$ channels. All three compounds gave sufficient plasma levels after oral administration to enable evaluation in a Chung SNL model of neuropathic pain with **161** having the lowest ED_{50} of 4.7 μmol/kg. Despite significant brain penetration (brain: plasma concentration ratio > 8) for all three analogues, no significant impairment of locomotor

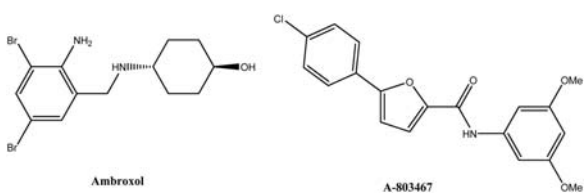

Fig. 35 Discovery of $Na_V1.8$ blockers.

Table 5 Activity of A-803467 analogues at human and rat sodium channels

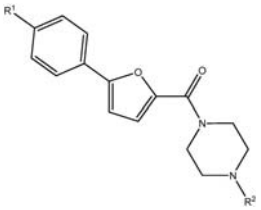

#	R^1	R^2	$hNa_V1.8$[a]	rTTX-R[a]	$hNa_V1.2$[a]	$hNa_V1.5$[a]
159	Cl	H	0.28	0.43	1.1	4.6
160	Cl	Cyclohexyl	0.30	0.39	0.35	2.3
161	t-Bu	Cyclohexyl	0.03	0.09	0.1	0.1

[a]IC_{50}s (μM) by electrophysiology.

activity was observed but compound **161** did show some effects on mean arterial pressure and heart rate at doses that were low concentration multiples of the therapeutic concentration, possibly due to its $Na_V1.5$ activity.

Further studies by Abbot and Icagen focused on replacement of the furyl ring in A-803467 with alternative heterocycles, and several 5- and 6-membered replacements were found to retain activity at $Na_V1.8$.[196] The 3,5-pyridine was chosen for further profiling due to favorable $Na_V1.8$ blocking potency and solubility. Optimization of the anilide portion, aimed at further improvement of solubility by disrupting the planarity of the biaryl anilide system, led to benzyl and picolinyl amides with the picolinyl compounds being favored due to the presence of the basic nitrogen. From these studies, representative compound **162** (Table 6) and the related compound **163** were profiled in a range of *in vitro* pharmacokinetic and *in vivo* studies. Increased solubility and reduced metabolism led to higher plasma levels after oral dosing than the furanamide series and both showed dose-dependant attenuation of mechanical allodynia in the Chung SNL model of neuropathic pain, without discernible side effects.

The closely related analogue **164** (A-887826) has been profiled in a range of electrophysiology assays and was shown to be a state but not frequency-dependent blocker of $Na_V1.8$, a property common to this series of $Na_V1.8$ blockers.[197] It appears that **164** was chosen for further in-depth study due to the higher solubility imparted by the morpholino substituent; however, this substituent also reduces the selectivity against other channels such as $Na_V1.2$. Compound **164** was shown to be approximately 10-fold more potent than A-803467 and dose dependently reduced tactile allodynia in a rat model of neuropathic pain. The analgesic-free plasma concentrations were in the range of 3–10 nM, consistent with the IC_{50} for block of rat DRG TTX-r sodium current.

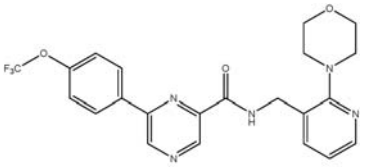

165

Table 6 Second-generation A-803467 analogues

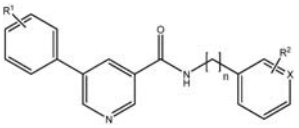

#	R^1	R^2	n	X	$mNa_V1.8$[a] (– 40 mV)	$hNa_V1.8$[a] (– 40 mV)	TTX-r[a] (– 40 mV)	$hNa_V1.2$[a] (– 60 mV)
162	4-CN	3,5-diMe	0	CH	0.19	0.023	0.091	0.091
163	4-Cl	2-OCH_2CF_3	1	N	0.087	0.003	0.028	2.8
164	3-Cl-4-O(n-Bu)	2-*N*-morpholino	1	N	–	0.011	0.0079	66%@0.03

[a]IC_{50}s (μM) by electrophysiology.

A pyrazine central core was also chosen for further SAR investigation[198] leading to compound **165** emerging with favorable solubility and *in vitro* clearance. Further pharmacokinetic profiling indicated modest exposure (oral bioavailability = 18%) and the compound showed dose-dependent inhibition of tactile allodynia in the Chung SNL model of neuropathic pain with an ED_{50} of 78 mg/kg. To date, none of these compounds have been reported to have progressed into human clinical studies.

Pfizer has developed a selective series of $Na_V1.8$ blockers with structural similarities to lamotrigine which is a weak but non-selective a weak but non-selective $Na_V1.8$ blocker.[199] The initial screening lead **166** (**Fig. 36**) was modified to provide **167** with improved $Na_V1.8$ potency and selectivity. Reversal of the amide moiety in **167** gave compound **168** (PF-01247324), a material that has been profiled in some detail[200] and that has been prepared on a kilogram scale.[201] Manual patch electrophysiology indicated that **168** had an IC_{50} at human $Na_V1.8$ of 0.19 μM and >50-fold selectivity over other channels. Furthermore **168** blocked native TTX resistent currents in both human and rat DRG neurons in both frequency-dependent and state-dependent manner. Mutation of key residues in the local anesthetic binding site of the $Na_V1.8$ channel reduced the blocking potency of **168** suggesting some overlap in binding sites. Compound **168** (PF-0127324), has high oral bioavailability ($F = 91\%$ in rat) and showed attenuation of allodynia after oral dosing in rodent models of inflammatory and neuropathic pain, providing pharmacological evidence with this novel chemotype that $Na_V1.8$ channels have a role in these pain states. $Na_V1.8$ channels are upregulated in the cerebellum in multiple sclerosis and $Na_V1.8$ expression is linked to ataxia and MS-like symptoms in mice. Oral dosing of **168** in a mouse MS model led to a significant improvement in motor skills and cerebellar-like symptoms compared to vehicle-treated animals suggesting that $Na_V1.8$ blockers may merit further study for the treatment of MS.[202] Similar but less pronounced reversal of the rapid, asynchronous electrical activity in cerebellar Purkinje neurons had been seen previously with the Abbott compound A-803467 but this required delivery to the CSF by intracerebroventricular injection, due to poor oral bioavailability. Further optimization by Pfizer focused on the instability of the acetamide and on reducing lipophilicity.[201] Small heterocyclic replacements for the acetamide, including pyrazole and isoxazole, retained $Na_V1.8$ potency and selectivity. Further efforts to reduce lipophilicity by replacing the pyridine core with a pyrazine led to a more than 10-fold drop in $Na_V1.8$ inhibition. An analysis of SAR in the pyridine series with the emphasis on lipophilicity, potency, and solubility resulted in the identification of pyrazole **169** and isoxazole **170**. These two derivatives were active in a tibial nerve transection model of neuropathic pain in rat. In addition, **169** (**PF-04531083**) appeared to have little effect on other peripheral or CNS activities. Clinical studies on compound **169** are discussed later.

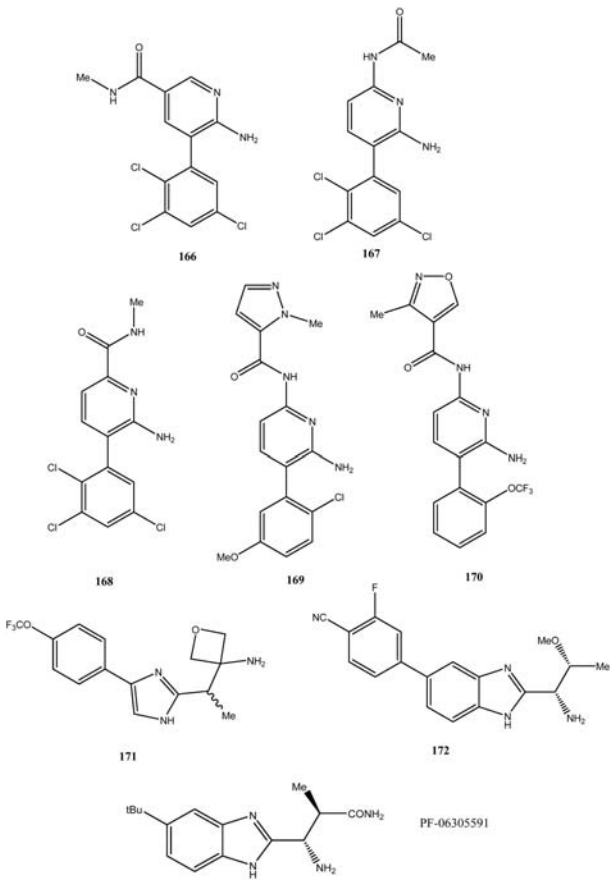

Fig. 36 Pfizer $Na_V1.8$ blockers.

Pfizer has also published patent applications on novel series of aryl imidazoles exemplified by **171**[203] and on related aryl benzimidazoles such as **172**.[204] These show potent block at the inactivated state of $Na_V1.8$ but no Na_V selectivity data was reported. Most recently, the analogue PF-06305591 was disclosed as a clinical candidate at two scientific meetings.[205] It was noted to have a 31 nM IC_{50} against $Na_V1.8$ and a pK_a of 5.9 and a log *D* of 2.1 and is discussed in the clinical section.

Another company with a major interest in $Na_V1.8$ blockers is Vertex; it has published a series of patent applications on structurally related compounds that show potent $Na_V1.8$ blocking activity.[206] Selected examples from these filings are shown in **Table 7**; however, no selectivity data was reported. One application (WO 201508961) describes a series of prodrugs suggesting that there may have been issues with bioavailability in at least some of the series.

Table 7 Vertex $Na_V1.8$ patent examples

Patent application	*No of examples*	*Typical example*	*$Na_V1.8$[a] IC_{50} (μM)*
WO 2014120808	160	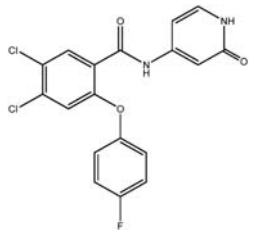	0.006
WO 2014120815	80	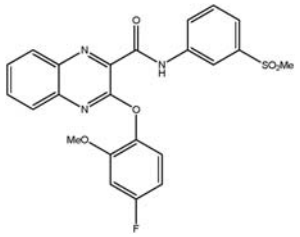	0.001
WO 2014120820	76	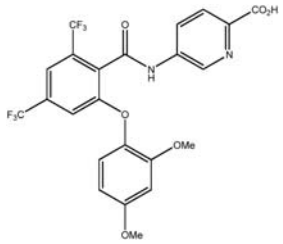	0.006
WO 2015010065	100	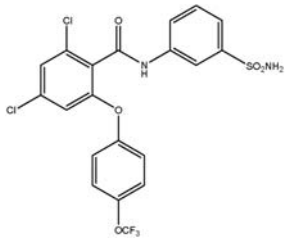	0.004
WO 2015089361	24	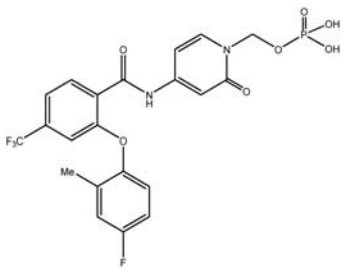	0.33

[a]IC_{50}s assessed by electrophysiology.

Some unrelated compounds have also been shown to be $Na_V1.8$ blockers but with a range of activities at other targets, for example, menthol has been shown to block both $Na_V1.8$ and 1.9 at a high concentration in a use-dependent manner.[207]

7.04.3.3.4 $Na_V1.9$ blockers

$Na_V1.9$ is preferentially expressed in small diameter DRG neurons and in intrinsic myenteric neurons. The status of $Na_V1.9$ as a target for pain has been debated for several years. An early study using $Na_V1.9$ antisense oligodeoxynucleotide treatment did not report amelioration of neuropathic pain but recently clear links to pain conditions have been described.[208] Experimental evidence supports a role for $Na_V1.9$ in inflammatory and diabetic neuropathy pain, although a general role in neuropathic pain is less clear.[209] Expression of $Na_V1.9$ has been shown to increase in DRG neurons following inflammation in rat hind paw.[210] Although expression levels of $Na_V1.9$ do not appear to be altered in small DRG neurons from diabetic rats, increased $Na_V1.9$ levels in large-diameter neurons suggest a contribution to painful diabetic neuropathy.[211] However, $Na_V1.9$ mRNA and protein levels and current density are downregulated in several animal models of neuropathic pain.[212]

A number of painful peripheral neuropathies and familial episodic pain conditions have now been associated with $Na_V1.9$ mutations and shown to be related to increased DRG excitability.[11] Equally, $Na_V1.9$ mutations associated with familial conditions resulting in an inability to experience pain have been related to a decrease in DRG excitability. It has also been shown that the $Na_V1.9$ channel is a key determinant of cold pain sensation.[213] To date, no $Na_V1.9$-specific molecules have been reported; however, it is likely that a portion of the activity of pan-active state-dependent sodium channel blockers will be associated with $Na_V1.9$ inhibition.[214] More specifically, amitriptyline, a tricyclic antidepressant (**Fig. 37**) which is widely used to manage various chronic pain conditions, an activity attributed to its Na_V block, has been shown to have an effect on $Na_V1.9$ currents in nociceptive trigeminal neurons.[215]

A patent application on $Na_V1.9$ was published by the University of Aix-Marseilles claiming the use of cholesterol as a $Na_V1.9$ blocker and describing means of delivering this compound as a transdermal patch. The filing describes the efficacy of cholesterol in a number of pain models including carrageenan-induced pain in the rat treated using a 5.6-mM solution via transdermal delivery.[216] The treatment was shown to be at least as effective as ibuprofen under the test conditions; however, channel selectivity data was not reported. This group also described antibody approaches to channel blockade (*vide infra*).

7.04.4 Clinical Studies

A summary of the reported status of clinical Na_V blockers in early 2016 is shown in **Table 8**. A number of companies have disclosed that they are entering Phase I clinical studies with novel selective sodium channel blockers. DaiNippon Sumitomo[217] has reported

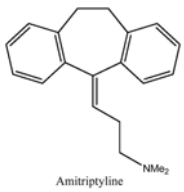

Fig. 37 Amitriptyline—a $Na_V1.9$ blocker.

Table 8 Status of clinical phase sodium channel blockers

Compound	*Mechanism*	*Company*	*Study*	*Comments*
DSP-2230	$Na_V1.7,8$	DaiNippon Sumitomo	Ph I	Target Neuropathic Pain
NKTR-171	Na_V	Necktar Therapeutics	Ph I	Peripheral
DS-1971a	$Na_V1.7$	Daiichi Sankyo	6 Ph I studies completed	PhII planned in Diabetic Neuropathy
PF-05089771	$Na_V1.7$	Pfizer	Ph II studies in dental pain, diabetic peripheral neuropathy, and erythromelalgia	No outcomes reported to date
PF-06305591	$Na_V1.8$	Pfizer	Ph I	Good exposure
CNV1014802	$Na_V1.7$	Convergence	PhII: trigeminal neuralgia; lumbosacral radiculopathy; erythromelalgia.	Phase III plans announced
XEN-402/TV-45070	$Na_V1.7$	Xenon/Teva	Ph II erythromelalgia and post-herpetic neuralgia	
GDC-0276/RG7893	$Na_V1.7$	Xenon/Genentech	Ph I	
GDC-0310	$Na_V1.7$	Xenon/Genentech	Ph I	
Tetrodotoxin	Na_V	WEX	Ph III cancer pain Ph II peripheral neuropathy	
CC8464	$Na_V1.7$	Astellas/Chromocell	Ph I	

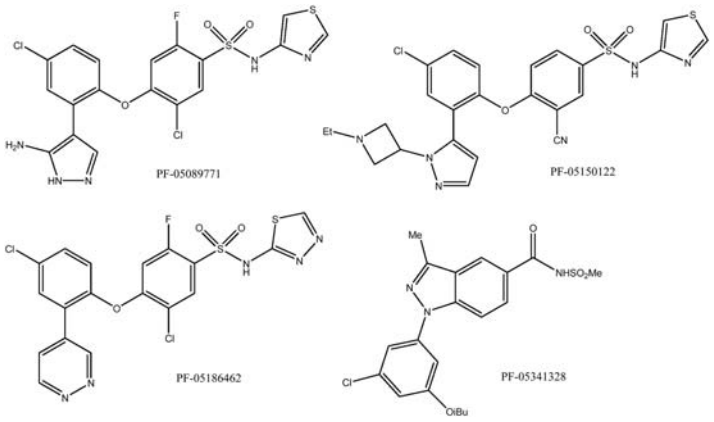

Fig. 38 Pfizer microdosing candidates.

that DSP-2230, an inhibitor of both $Na_V1.7$ and $Na_V1.8$, but of undisclosed structure, is being developed for the treatment of pain and is presently in Phase I; however, to date no outcomes have been reported. Necktar Therapeutics has similarly advanced its undisclosed lead NKTR-171 into Phase I, as a peripherally restricted Na_V blocker but with undisclosed selectivity.[218] Daiichi Sankyo's compound DS-1971a, another sodium channel blocker of undisclosed structure, has completed six Phase I studies and a Phase II study is planned.[219] Pfizer undertook a microdosing study which was used to select a lead $Na_V1.7$ blocker PF-05089771 for full clinical development from four potential candidates (**Fig. 38**), ahead of heterocyclic analogues PF-05186462, PF-05241328, and PF-05150122, which all showed poorer PK properties.[220] This material has now being evaluated in a number of Phase II studies. Likewise the newest Pfizer $Na_V1.8$ blocker PF-06305591 has been selected for clinical evaluation and in Phase I studies showed an exposure of 10 x the IC_{50} at a 40-mg bid dose, and an eight hour-half-life.[207]

Over the past 5 years there have been more than a dozen later phase clinical studies of sodium channel blocking agents against pain conditions. Many of these have looked into the efficacy of currently marketed drugs or compounds with an unselective sodium channel pharmacology[221] or have examined their activity in combination therapies.[222] Several studies are also being conducted into the use of toxins, including tetrodotoxin.[223] The state-dependent pan-Na_V blocking agent ralfinamide[224] was assessed by Newron as a treatment for pain. Ralfinamide is a brain-penetrant molecule, but the compound has a range of additional activities including N-type calcium channel inhibition and NDMA receptor antagonism. In 2010 it failed a Phase IIb/III trial in lower back pain[225] despite earlier success in a Phase II clinical study of neuropathic pain.[226]

A number of studies have now been undertaken with new, more selective agents. In 2014 a study into the efficacy of CNV1014802, a selective and state-dependent $Na_V1.7$ channel blocker, for treatment of the painful facial neuropathy trigeminal neuralgia, reported success.[227] Details of the trial protocol have also been disclosed.[19] Following an initial 21-day open-label treatment period with CNV1014802 at a dose of 150 mg three times a day (tid), patients who showed a successful response in the final week of the period, defined as a 30% or more reduction in numbers of paroxysms, or severity of paroxysms, relative to the run-in period, were then randomized to a 28-day double-blind treatment period with either CNV1014802 150 mg tid or placebo. All patients entering the study had to have a prespecified number of paroxysmal attacks of at least moderate severity. A total of 67 patients were recruited into the study and 69% of those patients completing the open label period were randomized as clear responders into the double-blind phase of the study. CNV1014802 was well tolerated and the study showed a consistent reduction of pain severity and number of paroxysms in all primary and secondary outcomes. In the primary endpoint of the study there was a treatment failure rate of just 33% for CNV1014802 vs. 65% for placebo and a favorable separation from placebo on the Kaplan Meier time to relapse. CNV1014802 showed a 2.3 unit decrease in the numerical rating scale for pain intensity, 60% reduction in paroxysms vs. 12% in placebo, and pain severity dropped by 55% vs. 18% placebo by the end of the study. There were no serious adverse events related to the drug and the adverse event profile of the drug was similar to placebo in the double-blind phase of the study.

CNV1014802 also proved effective in a Phase II study of lumbosacral radiculopathy (sciatic pain) (LSR).[228] The trial was a randomized, double-blind, placebo-controlled cross-over study designed to evaluate the efficacy and safety of orally administered CNV1014802 at a dose of 350 mg twice per day, in 81 patients with pain associated with LSR. There was a statistically significant difference in the primary endpoint between CNV1014802 and placebo (Pain Intensity-Numerical Rating Scale (PI-NRS) mean change at week 3, -0.43; $p=0.0265$). Additional exploratory analyses showed that for the subset treated by CNV1014802 alone, comprising 60% of patients randomized, there was an enhanced statistically significant reduction in pain (PI-NRS mean change at week 3, -0.72; $p=0.0039$). There were no serious adverse events related to the drug in this trial and as seen in all previous clinical studies, CNV1014802 was very well tolerated. The report notes that CNV1014802 was delivered at an effective therapeutic dose without any requirement for dose titration.

A recent report gave notice of plans for the start of a CNV1014802 Phase-III study. This indicated that it is in development for several pain indications. It is anticipated that a Phase III study will be initiated to confirm the efficacy of CNV1014802 in patients

with trigeminal neuralgia. Plans to initiate a Phase II trial in patients with LSR in 2016 were also disclosed and a study into the effect of this compound on erythromelelgia has recently been announced.[229]

Xenon has reported that their clinical candidate XEN402, Funapide, is presently being developed for conditions including osteoarthritis, neuropathic pain, post-herpetic neuralgia, and erythromelalgia. The spirocyclic class typically has low solubility and the compounds are being developed for human use in both topical and oral formulations. A study in 2014 reported success in treatment of inherited erythromelalgia (IEM).[230] An exploratory, randomized, double-blind, 2-period crossover study was conducted in four SCN9A mutation-proven IEM patients. In each treatment period of 2 days, separated by a 2-day washout period, patients were orally administered XEN402 (400 mg twice daily) or matching placebo. In three patients, pain was induced by heat or exercise during each treatment arm. A fourth patient, in constant severe pain, required no induction. Patient-reported outcomes of pain intensity and/or relief were recorded, and the time taken to induce pain was measured. The ability to induce pain in IEM patients was significantly attenuated by XEN402 compared with placebo. XEN402 increased the time to maximal pain induction and significantly reduced the amount of pain (42% less) after induction ($p = 0.014$). This indicated that XEN402 blocks $Na_V1.7$-mediated pain associated with IEM, thereby demonstrating target engagement in humans and underscoring the use of rare genetic disorders with mutant target channels as a novel approach to rapid proof of concept.

Challenges evidently still remain in bringing new classes of sodium channel blocker to market. A Phase IIb study on the XEN402 (now renamed TV-45070 following a transaction between Xenon and with Teva Pharmaceuticals) was conducted into osteoarthritis pain in the knee.[231] Unlike the IEM study, TV-45070 dosed topically at 4% and 8% concentrations did not demonstrate a statistically significant difference from placebo in efficacy endpoints. The companies noted that TV-45070 demonstrated a favorable safety and tolerability profile, with no drug-related serious adverse events. They rationalized that low drug plasma levels coupled with the favorable tolerability profile do support topical application and continued development in neuropathic pain. Results are awaited from the ongoing post-herpetic neuralgia Phase IIb study, expected in the second half of 2016.

Pfizer progressed the first $Na_V1.8$ lead **PF-04531083** (compound **169**) into human clinical studies,[232] the first reported selective $Na_V1.8$ blocker to reach the clinic. However a clinical trial for dental pain was terminated after interim analysis of results, presumably due to a lack of efficacy. No results have been reported for a clinical trial with the same compound aimed at heat pain for UV damaged skin.

7.04.5 Conclusions

This is an exciting time for sodium channel blocker research with success reported in several Phase II studies into pain using agents designed to have specific sodium channel blocking activity, and late-stage trials are expected to report in the next few years. The wealth of research suggests that there are now the tools to answer key questions about the link between specific channel blockers and human disease pharmacology. With the first clinical proof of concept studies reporting positive efficacy data or multiple new chemical entities, there must be a real prospect of novel effective therapies becoming commercially available for the benefit of patients suffering from conditions such as trigeminal neuralgia and other types of chronic neuropathic pain.

See also: 7.03. Progress in the Discovery of Ca Channel Blockers for the Treatment of Pain.

References

1. For a recent review of the field see: de Lera Ruiz, M.; Kraus, R. L. Voltage-Gated Sodium Channels: Structure, Function, Pharmacology, and Clinical Indications *J. Med. Chem.* **2015,** *58* (18), 7093–7118.
2. Scott, D. F. Carbamazepine. In *Chapter 8 in The History of Epileptic Therapy: An Account of How Medication Was Developed*; *History of Medicine SeriesHistory of Medicine Series;* CRC Press, 1993.
3. Lees, G.; Leach, M. J. Studies on the Mechanism of Action of the Novel Anticonvulsant Lamotrigine (Lamictal) Using Primary Neurological Cultures From Rat Cortex. *Brain Res.* **1993,** *612* (1–2), 190–199; Goldberg, J. F.; Calabrese, J. R.; Saville, B. R.; Frye, M. A.; Ketter, T. A.; Suppes, T.; Post, R. M.; Goodwin, F. K. Mood Stabilization and Destabilization During Acute and Continuation Phase Treatment for Bipolar I Disorder With Lamotrigine or Placebo. *J. Clin. Psychiatry* **2009,** *70* (9), 1273–1280.
4. Bagal, S. K.; Chapman, M. L.; Marron, B. E.; Prime, R.; Storer, R. I.; Swain, N. Recent Progress in Sodium Channel Modulators for Pain. *Bioorg. Med. Chem. Lett.* **2014,** *24* (16), 3690–3699.
5. Clare, J. J.; Tate, S. N.; Nobbs, M.; Romanos, M. A. Voltage-Gated Sodium Channels as Therapeutic Targets. *Drug Discov. Today* **2000,** *5*, 506–520.
6. Catterall, W. A.; Goldin, A. L.; Waxman, S. G. International Union of Pharmacology. XLVII. Nomenclature and Structure-Function Relationships of Voltage-Gated Sodium Channels. *Pharmacol. Rev.* **2005,** *57* (4), 397–409.
7. Yu, F. H.; Catterall, W. A. Overview of the Voltage-Gated Sodium Channel Family. *Genome Biol.* **2003,** *4* (3), 207.
8. Ye, C.-I.; Shaw, R. M.; Pitt, G. S.; Yarov-Yarovoy, V.; Sack, J. T.; Abriel, H.; Aldrich, R. W.; Belardinelli, L.; Cannell, M. B.; Catterall, W. A.; et al. Na + Channel Function, Regulation, Structure, Trafficking and Sequestration. *J. Physiol. (Oxford, UK)* **2015,** *593* (6), 1347–1360.
9. Catterall, W. A.; Dib-Hajj, S.; Meisler, M. H.; Pietrobon, D. Inherited Neuronal Ion Channelopathies: New Windows on Complex Neurological Diseases. *J. Neurosci.* **2008,** *28* (46), 11768–11777.
10. Dib-Hajj, S. D.; Yang, Y.; Waxman, S. G. Genetics and Molecular Pathophysiology of $Na_V1.7$-Related Pain Syndromes. *Adv. Genet.* **2008,** *63* (Ion Channel Diseases), 85–110.
11. Bennett, D. L. H.; Woods, C. G. Painful and Painless Channelopathies. *Lancet Neurol.* **2014,** *13* (6), 587–599.
12. Munro, G.; Erichsen, H. K.; Mirza, N. R. Pharmacological Comparison of Anticonvulsant Drugs in Animal Models of Persistent Pain and Anxiety. *Neuropharmacology* **2007,** *53* (5), 609–618.

13. Hoyt, S. B.; London, C.; Abbadie, C.; Felix, J. P.; Garcia, M. L.; Jochnowitz, N.; Karanam, B. V.; Li, X.; Lyons, K. A.; McGowan, E.; et al. A Novel Benzazepinone Sodium Channel Blocker With Oral Efficacy in a Rat Model of Neuropathic Pain. *Bioorg. Med. Chem. Lett.* **2013,** *23* (12), 3640–3645.
14. Rahman, W.; Dickenson, A. H. Osteoarthritis-Dependent Changes in Antinociceptive Action of $Na_V1.7$ and $Na_V1.8$ Sodium Channel Blockers: An In Vivo Electrophysiological Study in the Rat. *Neuroscience (Amsterdam, Netherlands)* **2015,** *295,* 103–116.
15. Payne, C. E.; Brown, A. R.; Theile, J. W.; Loucif, A. J. C.; Alexandrou, A. J.; Fuller, M. D.; Mahoney, J. H.; Antonio, B. M.; Gerlach, A. C.; Printzenhoff, D. M.; et al. A Novel Selective and Orally Bioavailable $Na_V1.8$ Channel Blocker, PF-01247324, Attenuates Nociception and Sensory Neuron Excitability. *Br. J. Pharmacol.* **2015,** *172* (10), 2654–2670.
16. McManus, O. B. HTS Assays for Developing the Molecular Pharmacology of Ion Channels. *Curr. Opin. Pharmacol.* **2014,** *15,* 91–96.
17. Catterall, W. A. Structure and Function of Voltage-Gated Sodium Channels at Atomic Resolution. *Exp. Physiol.* **2014,** *99* (1), 35–51; Ahuja, S.; Mukund, S.; Deng, L.; Khakh, K.; Chang, E.; Ho, H.; Shriver, S.; Young, C.; Lin, S.; Johnson, J. P., Jr.; Wu, P.; Li, J.; Coons, M.; Tam, C.; Brillantes, B.; Sampang, H.; Mortara, K.; Bowman, K. K.; Clark, K. R.; Estevez, A.; Xie, Z.; Verschoof, H.; Grimwood, M.; Dehnhardt, C.; Andrez, J.-C.; Focken, T.; Sutherlin, D. P.; Safina, B. S.; Starovasnik, M. A.; Ortwine, D. F.; Franke, Y.; Cohen, C. J.; Hackos, D. H.; Koth, C. M.; Payandeh, J. Structural Basis of NaV1.7 Inhibition by an Isoform-Selective Small-Molecule Antagonist. *Science* **2015,** *350.*
18. Eisenberg, E.; Lurie, Y.; Braker, C.; Daoud, D.; Ishay, A. Lamotrigine Reduces Painful Diabetic Neuropathy: A Randomized, Controlled Study. *Neurology* **2001,** *57* (3), 505–509.
19. Zakrzewska, J. M.; Palmer, J.; Ettlin, D. A.; Obermann, M.; Giblin, G. M. P.; Morisset, V.; Tate, S.; Gunn, K. Novel Design for a Phase IIa Placebo-Controlled, Double-Blind Randomized Withdrawal Study to Evaluate the Safety and Efficacy of CNV1014802 in Patients With Trigeminal Neuralgia. *Trials* **2013**, *14*, 402/1–402/11. MarketWatch. Convergence Pharmaceuticals' Novel Sodium Channel Blocker CNV1014802 Shows Excellent Efficacy and Safety in Ground-Breaking Phase II Trigeminal Neuralgia Study, 2014.
20. Zuliani, V.; Rapalli, A.; Patel, M. K.; Rivara, M. Sodium Channel Blockers: A Patent Review (2010–2014). *Expert Opin. Ther. Pat.* **2014,** *25* (3), 279–290; Zuliani, V.; Rivara, M.; Fantini, M.; Costantino, G. Sodium Channel Blockers for Neuropathic Pain. *Expert Opin. Ther. Pat.* **2010,** *20* (6), 755–779.
21. Kwong, K.; Carr, M. J. Voltage-Gated Sodium Channels. *Curr. Opin. Pharmacol.* **2015,** *22,* 131–139. http://dx.doi.org/10.1016/j.coph.2015.04.007.
22. Minett, M. S.; Pereira, V.; Sikandar, S.; Matsuyama, A.; Lolignier, S.; Kanellopoulos, A. H.; Mancini, F.; Iannetti, G. D.; Bogdanov, Y. D.; Santana-Varela, S.; Millet, Q.; Baskozos, G.; MacAllister, R.; Cox, J. J.; Zhao, J.; Wood, J. N. Endogenous Opioids Contribute to Insensitivity to Pain in Humans and Mice Lacking Sodium Channel $Na_V1.7$. *Nat. Commun.* **2015,** *6,* 8967. http://dx.doi.org/10.1038/ncomms9967.
23. Hanukoglu, I.; Hanukoglu, A. Epithelial Sodium Channel (ENaC) Family: Phylogeny, Structure-Function, Tissue Distribution, and Associated Inherited Diseases. *Gene* **2016,** *579* (2), 95–132.
24. Mike, A.; Lukacs, P. The Enigmatic Drug Binding Site for Sodium Channel Blockers. *Curr. Mol. Pharmacol.* **2010**, (3), 129–144.
25. Payandeh, J.; Gamal El-Din, T. M.; Scheuer, T.; Zheng, N.; Catterall, W. A. Crystal Structure of a Voltage-Gated Sodium Channel in Two Potentially Inactivated States. *Nature* **2012,** *486* (7401), 135–139. http://dx.doi.org/10.1038/nature11077; Bagneris, C.; DeCaen, P. G.; Naylor, C. E.; Pryde, D. C.; Nobeli, I.; Clapham, D. E.; Wallace, B. A. Prokaryotic NaVMs Channel as a Structural and Functional Model for Eukaryotic Sodium Channel Antagonism. *Proc. Natl. Acad. Sci.* **2014,** *111* (23), 8428–8433. http://dx.doi.org/10.1073/pnas.1406855111; Bagnéris, C.; Naylor, C. E.; McCusker, E. C.; Wallace, B. A. Structural Model of the Open-Closed-Inactivated Cycle of Prokaryotic Voltage-Gated Sodium Channels. *J. Gen. Physiol.* **2015,** *145* (1), 5–16. http://dx.doi.org/10.1085/jgp.201411242.
26. Bane, V.; Lehane, M.; Dikshit, M.; O'Riordan, A.; Furey, A. Tetrodotoxin: Chemistry, Toxicity, Source, Distribution and Detection. *Toxins* **2014,** *6* (2), 693–755. http://dx.doi.org/10.3390/toxins6020693. PMC 3942760. PMID 24566728.
27. Nieto, F. R.; Cobos, E. J.; Tejada, M.Á.; Sánchez-Fernández, C.; González-Cano, R.; Cendán, C. M. Tetrodotoxin (TTX) as a Therapeutic Agent for Pain. *Marine Drugs* **2012,** *10* (2), 281–305. http://dx.doi.org/10.3390/md10020281.
28. Chen, R.; Chung, S.-H. Mechanism of Tetrodotoxin Block and Resistance in Sodium Channels. *Biochem. Biophys. Res. Commun.* **2014,** 2–6. http://dx.doi.org/10.1016/j.bbrc.2014.02.115.
29. Huang, C.-J.; Schild, L.; Moczydlowski, E. G. Use-Dependent Block of the Voltage-Gated Na + Channel by Tetrodotoxin and Saxitoxin: Effect of Pore Mutations That Change Ionic Selectivity. *J. Gen. Physiol.* **2012,** *140* (4), 435–454. http://dx.doi.org/10.1085/jgp.201210853.
30. Chen, R.; Robinson, A.; Chung, S. H. Mechanism of μ-Conotoxin PIIIA Binding to the Voltage-Gated Na + Channel NaV1.4. *PLoS One* **2014,** *9* (3), 1–8. http://dx.doi.org/10.1371/journal.pone.0093267; Cherki, R. S.; Kolb, E.; Langut, Y.; Tsveyer, L.; Bajayo, N.; Meir, A. Two Tarantula Venom Peptides as Potent and Differential NaV Channels Blockers. *Toxicon* **2013,** *77,* 58–67. http://dx.doi.org/10.1016/j.toxicon.2013.10.029; Xu, L.; Li, T.; Liu, H.; Yang, F.; Liang, S.; Cao, Z.; Li, W.; Wu, Y. Functional Characterization of Two Novel Scorpion Sodium Channel Toxins From Lychas mucronatus. *Toxicon* **2014,** *90,* 318–325. http://dx.doi.org/10.1016/j.toxicon.2014.08.075.
31. McCormack, K.; Santos, S.; Chapman, M. L.; Krafte, D. S.; Marron, B. E.; West, C. W.; Krambis, M. J.; Antonio, B. M.; Zellmer, S. G.; Printzenhoff, D.; Padilla, K. M.; Lin, Z.; Wagoner, P. K.; Swain, N. A.; Stupple, P. A.; de Groot, M. Voltage Sensor Interaction Site for Selective Small Molecule Inhibitors of Voltage-Gated Sodium Channels. *Proc. Natl. Acad. Sci. U. S. A.* **2013;** http://dx.doi.org/10.1073/pnas.1220844110.
32. Gilchrist, J.; Olivera, B. M.; Bosmans, F. *Animal Toxins Influence Voltage-Gated Sodium Channel Function. Handbook of Experimental Pharmacology,* 2014; pp 203–229.
33. Murray, J. K.; Ligutti, J.; Liu, D.; Zou, A.; Poppe, L.; Li, H.; Andrews, K. L.; Moyer, B. D.; McDonough, S. I.; Favreau, P.; Stöcklin, R.; Miranda, L. P. Engineering Potent and Selective Analogues of GpTx-1, a Tarantula Venom Peptide Antagonist of the NaV1.7 Sodium Channel. *J. Med. Chem.* **2015,** *58* (5), 2299–2314; Murray, J. K.; Biswas, K.; Ryan Holder, J.; Zou, A.; Ligutti, J.; Liu, D.; Poppe, L.; Andrews, K. L.; Lin, F.-F.; Meng, S.-Y.; Moyer, B. D.; McDonough, S. I.; Miranda, L. P. Sustained Inhibition of the NaV1.7 Sodium Channel by Engineered Dimers of the Domain II Binding Peptide GpTx-1. *Bioorg. Med. Chem. Lett.* **2015,** *25,* 4866–4871.
34. Murray, J. K.; Miranda, L. P.; McDonough, S. I. Potent and Selective Polypeptide Inhibitors of NaV1.3 and NaV1.7 Sodium Channels. PCT Int. Appl., WO 2012125973. Assignee: Amgen Inc., USA, 2012.
35. Flinspach, M.; Wickenden, A.; Fellows, R.; Neff, R.; Liu, Y.; Hagan, R.; Xue, Q. Variants of Thrixopelma Pruriens Protoxin-II as Sodium Channel Antagonists for Use as Analgesics. PCT Int. Appl., WO 2015051216. Assignee: Janssen Biotech, Inc., USA, 2015.
36. Eckert, W.; Flinspach, M.; Hunter, M.; Liu, Y.; Neff, R.; Wickenden, A.; Gibbs, A. Huwentoxin-IV Variants as Human $Na_V1.7$ Peptide Inhibitor for Treatment of Pain. U.S. Pat. Appl. Publ., US 20150087596. Assignee: Janssen Biotech, Inc., USA, 2015; Eckert, W.; Flinspach, M.; Hunter, M.; Liu, Y.; Neff, R.; Wickenden, A.; Gibbs, A. Huwentoxin-IV Polypeptide Variants and Methods of Use Thereof for Treatment of Pain. PCT Int. Appl., WO 2013173706. Assignee: Janssen Biotech, Inc., USA, 2013.
37. Minassian, N. A.; Gibbs, A.; Shih, A. Y.; Liu, Y.; Neff, R. A.; Sutton, S. W.; Wickenden, A. D. Analysis of the Structural and Molecular Basis of Voltage-Sensitive Sodium Channel Inhibition by the Spider Toxin, Huwentoxin-IV (μ-TRTX-Hh2a). *J. Biol. Chem.* **2013,** *288,* 22707–22720. http://dx.doi.org/10.1074/jbc.M113.461392.
38. Park, J. H.; Carlin, K. P.; Wu, G.; Ilyin, V. I.; Musza, L. L.; Blake, P. R.; Kyle, D. J. Studies Examining the Relationship Between the Chemical Structure of Protoxin II and Its Activity on Voltage-Galed Sodium Channels. *J. Med. Chem.* **2014,** *57* (15), 6623–6631. http://dx.doi.org/10.1021/jm500687u.
39. Kyle, D. J.; Park, J. H. Sodium Channel Blocking Peptides and the Use Thereof. PCT Int. Appl., WO 2014016673. Assignee: Purdue Pharma L.P., USA, 2014; Park, J. H.; Kyle, D. J. Preparation and Therapeutic Uses of Peptides and Analogs Thereof for Treatment and Prevention of Diseases Associated With Sodium Channels. PCT Int. Appl., WO 2012004664. Assignee: Purdue Pharma L.P., USA, 2012.
40. Imperial, J.; Green, B. R.; Gajewiak, J.; Zhang, M.; Yoshikami, D.; Bulaj, G.; Olivera, B.; Wickenden, A.; Liu, Y. Sodium Channel Sensitive Conopeptides and Analogs, Including Compositions and Methods Thereof. PCT Int. Appl., WO 2013158800. Assignee: University of Utah Research Foundation, USA, 2013; Janssen Pharmaceutica NV.
41. Khanna, R.; Khanna, M.; Vanderah, T. W.; Dustrude, E. T. Non-narcotic CRMP2-Derived Peptides Targeting Sodium Channels for Pain. PCT Int. Appl., WO 2015134920. Assignee: University of Arizona, USA, 2015.
42. Pajouhesh, H.; Miljanich, G.; Mulcahy, J.; Du Bois, J.; Axtman, M.; Walker, J.; Merit, J. 10',11'-Modified Saxitoxins for the Treatment of Pain. PCT Int. Appl., WO 2015157559. Assignee: Siteone Therapeutics, Inc., USA, 2015, The Board of Trustees of the Leland Stanford Junior University.

43. Dubois, J.; Mulcahy, J.; Andresen, B.; Yeomans, David C.; Biswal, S. Methods and Compositions for Studying, Imaging, and Treating Pain. PCT Int. Appl., WO 2010129864. Assignee: Leland Stanford Junior University, USA, 2010.
44. Parsons, W. H.; Du Bois, J. Maleimide Conjugates of Saxitoxin as Covalent Inhibitors of Voltage-Gated Sodium Channels. *J. Am. Chem. Soc.* **2013,** *135* (29), 10582–10585. http://dx.doi.org/10.1021/ja4019644.
45. Lee, J.-H.; Park, C.-K.; Chen, G.; Han, Q.; Xie, R.-G.; Liu, T.; Ji, R.-R.; Lee, S.-Y. *Cell* **2014,** *157* (6), 1393–1404.
46. Miller, K. M.; De Ryck, M. R.; Wolff, C. G. J.; Lawson, A. D. G.; Finney, H. M.; Baker, T. S. Function Modifying Na_V 1.7 Antibodies. PCT Int. Appl., WO 2011051350. Assignee: UCB Pharma S.A., Belgium, 2011.
47. Ulrichts, P.; Van der Woning, S.; De Boeck, G.; Hofman, E.; Blanchetot, C.; Saunders, M.; De Haard, J. J. W. Antibodies to Complex Targets. PCT Int. Appl., WO 2015032916. Assignee: arGEN-X B.V, Netherlands, 2015.
48. Zhao, H.; Corey, D. P. Bi-Specific Agents, Particularly Pain Inhibitors Comprising a Na_V1.7-Blocking Toxin and an Anti-Na_V1.7 Single Domain Antibody (sdAb). PCT Int. Appl., WO 2015160940. Assignee: President and Fellows of Harvard College, USA, 2015.
49. Lee, S.-Y.; Ji, R.-R. Anti-Human Na_V1.7 Antibodies and Fragments for Treating Pain, Neurogenic Inflammation, Itch or Cough. PCT Int. Appl., WO 2015035173. Assignee: Duke University, USA, 2015.
50. Macdonald, L.; Murphy, A. J.; Papadopoulos, N. J.; Stahl, N.; Alessandri-Haber, N. Human Antibodies to Na_V1.7 and Therapeutic Uses Thereof. PCT Int. Appl., WO 2014159595. Assignee: Regeneron Pharmaceuticals, Inc., USA, 2014.
51. Crest, M.; Delmas, P.; Lonigro-Rame, A.; Osorio, N. Antibodies Against Human Sodium Channel NaV1.9 and Uses Thereof for the Diagnosis of Inflammatory Skin Diseases. PCT Int. Appl., WO 2014207400. Assignee: Galderma Research & Development, France; Centre National de la Recherche Scientifique; Universite d'Aix-Marseille, 2014; Crest, M.; Delmas, P.; Lonigro-Rame, A.; Osorio, N. Antibodies Against the Human Sodium Channel NaV 1.9 and Uses Thereof for Diagnosis. PCT Int. Appl., WO 2014207402. Assignee: Galderma Research & Development, France; Centre National de la Recherche Scientifique; Universite d'Aix-Marseille, 2014.
52. Carbamazepine: The American Society of Health-System Pharmacists. http://www.drugs.com/monograph/carbamazepine.html. Retrieved March 2015.
53. SCHWARZ PHARMA Highlights the Results of 13 Lacosamide Data Presentations at North American Regional Epilepsy Congress in San Diego. Schwarz Pharma. http://www.prnewswire.com/news-releases/schwarz-pharma-highlights-the-results-of-13-lacosamide-data-presentations-at-north-american-regional-epilepsy-congress-in-san-diego-55922847.html (Retrieved 02.04.14).
54. England, S.; Rawson, D. Isoform-Selective Voltage-Gated Na + Channel Modulators as Next-Generation Analgesics. *Future Med. Chem.* **2010,** *2* (5), 775–790.
55. Jukič, M.; Kikelj, D.; Anderluh, M. Isoform Selective Voltage-Gated Sodium Channel Modulators and the Therapy of Pain. *Curr. Med. Chem.* **2013,** *21* (2), 164–186.
56. de Lera Ruiz, M.; Kraus, R. L. Voltage-Gated Sodium Channels: Structure, Function, Pharmacology, and Clinical Indications. *J. Med. Chem.* **2015,** *58* (18), 7093–7118. http://dx.doi.org/10.1021/jm501981g.
57. Cox, J. J.; Reimann, F.; Nicholas, A. K.; Thornton, G.; Roberts, E.; Springell, K.; Karbani, G.; Jafri, H.; Mannan, J.; Raashid, Y.; Al-Gazali, L.; Hamamy, H.; Valente, E. M.; Gorman, S.; Williams, R.; McHale, D. P.; Wood, J. N.; Gribble, F. M.; Woods, C. G. SCN9A Channelopathy Causes Congenital Inability to Experience Pain. *Nature* **2006,** *444* (7121), 894–898.
58. Minett, M. S.; Falk, S.; Santana-Varela, S.; Bogdanov, Y. D.; Nassar, M. A.; Heegaard, A.-M.; Wood, J. N. Pain Without Nociceptors? Na_V1.7-Independent Pain Mechanisms. *Cell Rep.* **2014,** *6* (2), 301–312. http://dx.doi.org/10.1016/j.celrep.2013.12.033.
59. Giblin, G. M. P. CNV1014802, a Novel NaV1.7 Selective State-Dependent Sodium Channel Blocker for the Treatment of Chronic Pain: From Discovery to Phase 2 Clinical Study. Talk presented at European Federation of Medicinal Chemist's International Symposium on Medicinal Chemistry September 7–11, 2014, Lisbon, Portugal.
60. Unpublished data, Convergence Pharmaceuticals, 2016.
61. Giblin, G. M. P.; Witty, D. R.; Macpherson, D. T.; Stanway, S. J.; Wilson, A.; Gleave, L. Preparation of Spiro Derivatives as Voltage-Gated Sodium Channel Modulators. WO 2013179049. Assignee: Convergence Pharmaceuticals Limited, UK.; Preparation of 7-methyl-2-[4-methyl-6-[4-(trifluoromethyl)phenyl]pyrimidin-2-yl]-1,7-diazaspiro[4.4]nonan-6-one Compounds as Modulators of Voltage-Gated Sodium Channels. WO 2013175205; Giblin, G. M. P.; MacPherson, D. T.; Witty, D. R.; Stanway, S. J. Preparation of Pyrimidin-2-yl-1,7-diazaspiro[4.4]nonan-6-one and 1,8-diazaspiro[4.5]decan-7-One Derivatives as Modulators of Voltage-Gated Sodium Channels. WO 20131752068. Assignee: Convergence Pharmaceuticals Limited, UK; Giblin, G. M. P.; MacPherson, D. T.; Witty, D. R.; Stanway, S. J. Assignee: Convergence Pharmaceuticals Limited, UK; Witty, D. R.; Macpherson, D. T.; Giblin, G. M. P.; Stanway, S. J. Preparation of a 2-(pyridin-2-yl)-1,7-diaza-spiro[4.4]nonane-6-one Compound and Its Isomers as Voltage-Gated Sodium Channels Modulators for Therapy. WO 2013093496. Assignee: Convergence Pharmaceuticals Limited, UK; Witty, D. R.; Macpherson, D. T.; Giblin, G. M. P.; Stanway, S. J.; Vong, A. K. K. Preparation of 2-(pyridin-2-yl)-1,7-diaza-spiro[4.4]nonane-6-one Compounds as Voltage-Gated Sodium Channels Modulators for Therapy. WO 2013093497. Assignee: Convergence Pharmaceuticals Limited, UK.
62. Tyagarajan, S.; Chakravarty, P. K.; Zhou, B.; Taylor, B.; Fisher, M. H.; Wyvratt, M. J.; Parsons, W. H. Substituted Biaryl Pyrazoles as Sodium Channel Blockers. *Bioorg. Med. Chem. Lett.* **2010,** *20* (18), 5480–5483. http://dx.doi.org/10.1016/j.bmcl.2010.07.080; Tyagarajan, S.; Chakravarty, P. K.; Zhou, B.; Fisher, M. H.; Wyvratt, M. J.; Lyons, K.; Klatt, T.; Li, X.; Kumar, S.; Williams, B.; Felix, J.; Priest, B. T.; Brochu, R. M.; Warren, V.; Smith, M.; Garcia, M.; Kaczorowski, G. J.; Martin, W. J.; Abbadie, C.; McGowan, E.; Jochnowitz, N.; Parsons, W. H. Substituted Biaryl Oxazoles, Imidazoles, and Thiazoles as Sodium Channel Blockers. *Bioorg. Med. Chem. Lett.* **2010,** *20* (18), 5536–5540. http://dx.doi.org/10.1016/j.bmcl.2010.07.064; Tyagarajan, S.; Chakravarty, P. K.; Zhou, B.; Taylor, B.; Eid, R.; Fisher, M. H.; Parsons, W. H.; Wyvratt, M. J.; Lyons, K. A.; Klatt, T. Discovery of a Novel Class of Biphenyl Pyrazole Sodium Channel Blockers for Treatment of Neuropathic Pain. *Bioorg. Med. Chem. Lett.* **2010,** *20,* 7479–7482. Retrieved from. http://linkinghub.elsevier.com/retrieve/pii/S0960894X1001468X
63. Dimmock, J. R.; Putucode, R. N.; Smith, J. M.; Hetherington, M.; Quail, J. W.; Pugazhentni, U.; Lechler, T.; Stables, J. P. *J. Med. Chem.* **1996,** *39,* 3984; Ilyin, V. I.; Hodges, D. D.; Whitemore, E. R.; Carter, R. B.; Cai, S. X.; Woodward, R. M. *Br. J. Pharmacol.* **2005,** *144,* 801; Ramu, K.; Lam, G. N.; Hughes, H. *Drug Metab. Dispos.* **2000,** *28,* 1153.
64. Carr, M. J. Regulation of Cough and Action Potentials by Voltage-Gated Na Channels. *Pulm. Pharmacol. Ther.* **2013,** *26* (5), 508–509. http://dx.doi.org/10.1016/j.pupt.2013.07.001; Kwong, K.; Carr, M. J.; Gibbard, A.; Savage, T. J.; Singh, K.; Jing, J.; et al. Voltage-Gated Sodium Channels in Nociceptive Versus Non-Nociceptive Nodose Vagal Sensory Neurons Innervating Guinea Pig Lungs. *J. Physiol.* **2008,** *586,* 1321e36.
65. Muroi, Y.; Undem, B. J. Targeting Voltage-Galed Sodium Channels Na_V1.7, Na V1.8, and Na V1.9 for Treatment of Pathological Cough. *Lung* **2014,** *192* (1), 15–20. http://dx.doi.org/10.1007/s00408-013-9533-x.
66. Boehm, J. C.; Davis, R. S.; Kerns, J. K.; Lin, G.; Nie, H. Preparation of Substituted Pyridinecarboxylates as Voltage-Gated Sodium Channel Blockers. PCT Int. Appl., WO 2011088201, 2011.
67. Boehm, J. C.; Davis, R. S.; Kerns, J.; Lin, G.; Murdoch, R. D.; Nie, H. Preparation of 2-Piperazinopyridine-3-Carboxylates as Voltage-Gated Sodium Channel Blockers. PCT Int. Appl., WO 2013006596, 2013.
68. Suzuki, S.; Kuroda, T.; Kimoto, H.; Domon, Y.; Kubota, K.; Kitano, Y.; Yokoyama, T.; Shimizugawa, A.; Sugita, R.; Koishi, R.; Asano, D.; Tamaki, K.; Shinozuka, T.; Kobayashi, H. Discovery of (Phenoxy-2-hydroxypropyl)piperidines as a Novel Class of Voltage-Gated Sodium Channel 1.7 Inhibitors. *Bioorg. Med. Chem. Lett.* **2015,** *25* (22), 7–11. http://dx.doi.org/10.1016/j.bmcl.2015.09.005.
69. Hattori, K.; Takaya, K.; Kawase, K.; Aoki, N. Pyridinylmorpholinone Derivatives as Na_V1.7 Inhibitors, Pharmaceutical Compositions Containing them, and Prevention and/or Treatment of Disease Related to Na_V1.7. PCT Int. Appl., WO 2013161929. Ishida, Yoshihito Assignee: Shionogi & Co., Ltd., Japan, 2013.
70. Nakai, Y. Preparation of Imidazoimidazolone Derivatives as Na_V1.7 Inhibitors and Pharmaceutical Compositions Containing Them. Jpn. Kokai Tokkyo Koho, JP 2014080394. Assignee: Shionogi and Co., Ltd., Japan, 2014.
71. Nakai, Y.; Kawase, K. Preparation of Six- or Seven-Membered Amino Lactam Derivatives as Inhibitors of Voltage-Dependent Sodium Channel Na_V1.7. Jpn. Kokai Tokkyo Koho, JP 2014080395. Assignee: Shionogi and Co., Ltd., Japan, 2014.
72. Tsuboi, K.; Yamai, Y.; Kinoshita, H. Preparation of Quinolinone Derivatives as SNS Inhibitors for Treatment of Pain, Urinary Tract Disorder, or Multiple Sclerosis. PCT Int. Appl., WO 2008069242. Assignee: Dainippon Sumitomo Pharma Co., Ltd., Japan, 2008.

73. Tsuboi, K.; Yamai, Y.; Watanabe, H.; Kinoshita, H. Preparation of N2-[(benzimidazol-2-yl or imidazo[4,5-b]pyridin-2-yl)methyl]amino Acid Amide Derivatives as Inhibitors of Sensory Neuron Specific Sodium Channel (SNS). PCT Int. Appl., WO 2010074193. Assignee: Dainippon Sumitomo Pharma Co., Ltd., Japan, 2010.
74. Ehring, G. R.; Chao, E.; Ng, H.; Ton, H.; Li, J. C.; Adorante, J. S.; Garst, M. E.; Rind, H. B.; Hansen, M. R.; Avey, A. A., Jr.; Dolby, L. J.; Esfandiari, S.; Mackenzie, V. R.; Marsden, J. A.; Muchmore, D. C. Preparation of Benzimidazole Derivatives as Selective Blockers of Persistent Sodium Current. PCT Int. Appl., WO 2013101911. Assignee: Allergan, Inc., USA, 2013.
75. Ehring, G. R.; Garst, M. E.; Avey, A. A., Jr.; Dolby, L. J.; Esfandiari, S.; Mackenzie, V. R.; Marsden, J. A.; Muchmore, D. C. Preparation of Benzimidazole Derivatives as Selective Blockers of Persistent Sodium Current. PCT Int. Appl., WO 2013101926 Assignee: Allergan, Inc., USA, 2013.
76. Pajouhesh, H.; Holland, R.; Zhang, L.; Pajouhesh, H.; Lamontagne, J.; Whelan, B. Preparation of Benzimidazole Inhibitors of the Sodium Channel. PCT Int. Appl., WO 2012116440. Assignee: Zalicus Pharmaceuticals Ltd., Canada, 2012.
77. Pajouhesh, H. A.; Holland, R.; Zhang, L.; Pajouhesh, H. O.; Lamontagne, J.; Whelan, B.; Short, G. F., III; Romero, D. L. Biaryl Compounds as Inhibitors of the Sodium Channel and Their Preparation. PCT Int. Appl., WO 2013131018. Assignee: Zalicus Pharmaceuticals Ltd., USA, 2013.
78. Pajouhesh, H.; Holland, R.; Zhang, L.; Pajouhesh, H.; Lamontagne, J.; Whelan, B. Heterocyclic Inhibitors of the Sodium Channel. PCT Int. Appl., WO 2014134306. Assignee: Zalicus Pharmaceuticals, Ltd., USA, 2014.
79. Pajouhesh, H.; Holland, R.; Zhang, L.; Pajouhesh, H.; Lamontagne, J.; Whelan, B. Preparation of 4,6-bis(trifluoromethyl)-1H-benzo[d]imidazole Derivatives as Sodium Channel Inhibitors. PCT Int. Appl., WO 2015127549. Assignee: Canada, 2015.
80. Komiya, M.; Fujii, Y.; Kataoka, M.; Sawayama, Y. Imidazopyridine Compounds, Medical Compositions, and Method, Usage, Drugs, and Therapeutic Agents for Diseases Caused by Sodium Channels. PCT Int. Appl., WO 2015008861. Assignee: Sumitomo Dainippon Pharma Co., Ltd., Japan, 2015.
81. Liu, J.; Persichetti, R. 2-Oxo-1-pyrrolidine Derivatives for Treatment of Conditions Beneficially Treated With a Synaptic Vesicle Protein 2A Ligand and/or a Sodium Channel Blocker. PCT Int. Appl., WO 2010002869. Assignee: Concert Pharmaceuticals, Inc., USA, 2010.
82. Kikuchi, K.; Honda, S.; Oku, M.; Kuramochi, T.; Kamikawa, A.; Asai, N.; Koga, Y.; Fujiyasu, J.; Kato, K.; Koganemaru, Y.; Hamaguchi, W.; Kinoyama, I.; Akamatsu, S.; Iwai, Y.; Tokuzaki, K.; Yokota, M.; Nagakura, Y.; Suzaka, H.; Ohkura, Y.; Sakamoto, S.; Okada, M.; Watanabe, T.; Tomiyama, H.; Ohta, M.; Tsukamoto, S. Novel Vinylpiperidine Derivatives as Sodium Channel Blockers. *Abstracts of Papers, 241st ACS National Meeting & Exposition, Anaheim, CA, United States, March 27–31, 2011.*
83. Kam, Y. L.; Back, S. K.; Kang, B.; Kim, Y.-Y.; Kim, H.-J.; Rhim, H.; Nah, S.-Y.; Chung, J.-M.; Kim, D. H.; Choi, J.-S.; Na, H. S.; Choo, H.-Y. P. *Pharmacol. Biochem. Behav.* **2012,** *103* (1), 33–42.
84. Park, H. Y.; Yune, T. Y.; Kam, Y. L.; Choi, J.-S. Amide Derivative for Treating Pain and Preparation Method Thereof. PCT Int. Appl., WO 2015102390. Assignee: Ewha University–Industry Collaboration Foundation, South Korea, 2015.
85. Chowdhury, S.; Chafeev, M.; Liu, S.; Sun, J.; Raina, V.; Chui, R.; Young, W.; Kwan, R.; Fu, J.; Cadieux, J. A. Discovery of XEN907, a Spirooxindole Blocker of Na(V)1.7 for the Treatment of Pain. *Bioorg. Med. Chem. Lett.* **2011,** *21* (12), 3676–3681. http://dx.doi.org/10.1016/j.bmcl.2011.04.088.
86. Chafeev, M.; Chowdhury, S.; Fraser, R.; Fu, J.; Kamboj, R.; Liu, S.; Seid Bagherzadeh, M.; Sun, J.; Sviridov, S. Spiroheterocyclic Compounds as Sodium Channel Blockers and Their Preparation, Pharmaceutical Compositions and Use in the Treatment of Diseases. US 7799798. Assignee: Xenon Pharmaceuticals Inc., Canada, 2010.
87. Chafeev, M.; Chowdhury, S.; Fraser, L.; Fu, J.; Langille, J.; Liu, S.; Sun, J.; Sun, S.; Sviridov, S.; Wood, M.; Zenova, A.; Jia, Q.; Cadieux, J.-J.; Gauthier, S. J.; Douglas, A. F.; Hsieh, T.; Chakka, N.; Cikojevic, Z. Spiro-Oxindole Compounds and Their Use as Therapeutic Agents in the Treatment of Sodium Channel-Mediated Diseases and Their Preparation. PCT Int. Appl., WO 2010045251. Assignee: Xenon Pharmaceuticals, Inc., Canada, 2010.
88. Winters, C. S.; Gammill, S. L. Pharmaceutical Compositions for Oral Administration. U.S. Pat. Appl. Publ., US 20110086899. Assignee: Xenon Pharmaceuticals Inc., Canada, 2011.
89. Chafeev, M.; Fu, J.; Cadieux, J.-J. Enantiomers of Spiro-Oxindole Compounds and Their Uses as Therapeutic Agents. U.S. Pat. Appl. Publ., US 20100331386. Assignee: Xenon Pharmaceuticals Inc., Canada, 2010.
90. Winters, C. S.; Yang, M.; Chen, H. Topical Pharmaceuticals of a Spiro-Oxindole Compound for Treatment of Sodium Channel Mediated Disease. WO 2011002708. Assignee: Xenon Pharmaceuticals Inc., Canada, 2011.
91. Palmer, R.a.; Potter, B. S.; Leach, M. J.; Jenkins, T. C.; Chowdhry, B. Z. An Absolute Structure Template for a Unique Voltage-Gated Sodium Channel Binding Site. *Med. Chem. Commun.* **2010,** *1* (1), 45. http://dx.doi.org/10.1039/c0md00043d.
92. Cadieux, J.-J.; Chafeev, M.; Chowdhury, S.; Fu, J.; Jia, Q.; Abel, S.; El-Sayed, E.; Huthmann, E.; Isarno, T. Process for Preparation of Spiro-Oxindole Compounds for Treating Sodium Channel-Mediated Diseases or Conditions. U.S. Pat. Appl. Publ., US 20110087027. Assignee: Xenon Pharmaceuticals Inc., Canada, 2011.
93. Fu, J.; Liu, S.; Sun, S.; Wood, M. Preparation of Spiro Compounds and Their Use as Therapeutic Agents. PCT Int. Appl., WO 2010132352. Assignee: Xenon Pharmaceuticals Inc., Canada, 2010.
94. Chowdhury, S.; Fu, J.; Liu, S.; Qi, J. Preparation of Spiro-Condensed Indole Derivatives as Sodium Channel Inhibitors. PCT Int. Appl., WO 2010053998. Assignee: Xenon Pharmaceuticals, Inc., Canada, 2010.
95. Cadieux, J.-J.; Chafeev, M.; Chowdhury, S.; Douglas, A. F.; Fu, J.; Langille, J.; Sun, S.; Wood, M. Preparation of Spiro-Oxindole Compounds as Therapeutic Sodium Channel Blockers. PCT Int. Appl., WO 2010078307. Assignee: Xenon Pharmaceuticals Inc., Canada, 2010.
96. Chafeev, M.; Chowdhury, S.; Fraser, L.; Fu, J.; Langille, J.; Liu, S.; Sun, J.; Sun, S.; Sviridov, S.; Wood, M.; Zenova, A. Spiro-Oxindole Compounds and Their Use as Therapeutic Agents for the Treatment of Sodium Channel-Mediated Diseases and Their Preparation. PCT Int. Appl., WO 2010045197. Assignee: Xenon Pharmaceuticals, Inc., Canada, 2010.
97. Chowdhury, S.; Liu, S.; Cadieux, J. A.; Hsieh, T.; Chafeev, M.; Sun, S.; Jia, Q.; Sun, J.; Wood, M.; Langille, J.; Sviridov, S.; Fu, J.; Zhang, Z.; Chui, R.; Wang, A.; Cheng, X.; Zhong, J.; Hossain, S.; Khakh, K.; Rajlic, I.; Verschoof, H.; Kwan, R.; Young, W. Tetracyclic Spirooxindole Blockers of hNaV1.7: Activity In Vitro and in CFA-Induced Inflammatory Pain Model. *Med. Chem. Res.* **2013,** *22,* 1825–1836. http://dx.doi.org/10.1007/s00044-012-0180-1.
98. Hadida-Ruah, S. S.; Kallel, E. A.; Miller, M. T.; Pontillo, J.; Anderson, C.; Numa, M.; Frieman, B. A.; Bear, B. R.; Arumugam, V.; Hilgraf, N.; McCartney, J.; Grootenhuis, P. D. J.; Johnson, J. P. Heterocyclic-Fused Spiro[Chromene-Piperidine] Derivatives and Related Compounds as Modulators of Ion Channels and Their Preparation and Use for the Treatment of Diseases. PCT Int. Appl., WO 2011140425. Assignee: Vertex Pharmaceuticals Incorporated, USA, 2011.
99. Hadida Ruah, S. S.; Kallel, E. A.; Miller, M. T.; Arumugam, V.; McCartney, J.; Anderson, C.; Grootenhuis, P. D. J.; Jiang, L. Preparation of Pyrrolopyrazine-Spirocyclic Piperidine Amides as Modulators of Ion Channels. U.S. Pat. Appl. Publ., US 20120196869. Assignee: Vertex Pharmaceuticals Incorporated, USA, 2012.
100. Littler, B. J.; Keshavarz-Shokri, A.; Zhang, B.; Hughes, R. M. Preparation of Solid Form of [3'-4'-dihydro-2'-methyl-6'-(trifluoromethyl)spiro[piperidine-4,1'(2'H) -pyrrolo[1,2-a] pyrazin]-1-yl][3-methoxy-4-(1- methylethoxy)phenyl]methanone as Sodium Channel Inhibitor for the Treatment of Pain. PCT Int. Appl., WO 2014022639. Assignee: Vertex Pharmaceuticals Incorporated, USA, 2014.
101. Hadida-Ruah, S. S.; Miller, M. T.; Kallel, E. A.; Bear, B. R.; Arumugam, V.; Deninno, M. P.; Zhou, J.; Uy, J.; Frieman, B. A. Preparation of Chromanspirocyclic Piperidinylamide Derivatives for Use as Ion Channel Modulators. PCT Int. Appl., WO 2012112743. Assignee: Vertex Pharmaceuticals Incorporated, USA, 2012.
102. Hadida-Ruah, S. S.; Binch, H. M.; Deninno, M. P.; Fanning, L. T. D.; Frieman, B. A.; Grootenhuis, P. D. J.; Hilgraf, N.; Joshi, P.; Kallel, E. A.; Pontillo, J.; Silina, A.; Sheth, U. J.; Hurley, D. J.; Arumugam, V.; Miller, M. T. Preparation of Morpholine-Spirocyclic Piperidine Amides as Modulators of Ion Channels. PCT Int. Appl., WO 2012125613. Assignee: Vertex Pharmaceuticals Incorporated, USA, 2012.
103. Hadida-Ruah, S. S.; Grootenhuis, P. D. J.; Miller, M. T.; Anderson, C.; Pontillo, J.; Kallel, E. A.; Numa, M. M. D.; Frieman, B. A.; McCartney, J.; Worley, J. F.; Arumugam, V.; Uy, J.; Hilgraf, N.; Bear, B. R. Preparation of Spiro Benzoxazine Derivatives as Modulators of Ion Channels. PCT Int. Appl., WO 2013067248. Assignee: Vertex Pharmaceuticals Incorporated, USA, 2013.
104. Hadida-Ruah, S. S.; Arumugam, V.; Deninno, M. P.; Frieman, B. A.; Kallel, E. A.; Miller, M. T.; Uy, J.; Zhou, J. Preparation of Pyranspirocyclic Piperidinylamide Derivatives for Use as Ion Channel Modulators. PCT Int. Appl., WO 2013109521. Assignee: Vertex Pharmaceuticals Incorporated, USA, 2013.

105. Ho, G. D.; Tulshian, D.; Heap, C. R.; Earley, W. G.; Courneya, B. Pyrrolobenzo-1,4-diazines as Sodium Channel Blockers and Their Preparation and Use in the Treatment of Chronic and Neuropathic Pain. WO 2010151597. Assignee: Schering Corporation, USA; Ho, G. D.; Tulshian, D.; Heap, C. R.; Earley, W. G.; Courneya, B. Pyrrolobenzo-1,4-diazines as Sodium Channel Blockers and Their Preparation and Use in the Treatment of Chronic and Neuropathic Pain, PCT Int. Appl., WO 2010151595. Assignee: Schering Corporation, USA, 2010.
106. Ho, G. D.; Tulshian, D.; Bercovici, A.; Tan, Z.; Hanisak, J.; Cooke, S.; Matasi, J.; Heap, C. R.; Earley, W. G.; Courneya, B.; et al. Discovery of Pyrrolo-benzo-1, 4-diazines as Potent NaV1.7 Sodium Channel Blockers. *Abstracts of Papers, 248th ACS National Meeting & Exposition, San Francisco, CA, United States, August 10–14, 2014, MEDI-105.*
107. Yang, S.-W.; Ho, G. D.; Tulshian, D.; Bercovici, A.; Tan, Z.; Hanisak, J.; Brumfield, S.; Matasi, J.; Sun, X.; Sakwa, S. A.; Herr, R. J.; Zhou, X.; Bridal, T.; Urban, M.; Vivian, J.; Rindgen, D.; Sorota, S. Bioavailable Pyrrolo-benzo-1,4-diazines as $Na_V1.7$ Sodium Channel Blockers for the Treatment of Pain. *Bioorg. Med. Chem. Lett.* **2014,** 5–9. http://dx.doi.org/10.1016/j.bmcl.2014.09.038.
108. Ho, G. D.; Tulshian, D.; Heap, C. R. Cyclopropyl-Spiro-Piperidines Useful as Sodium Channel Blockers. PCT Int. Appl., WO 2012047703. Assignee: Schering Corporation, USA, 2012.
109. McCormacka, K.; Santosa, S.; Chapmana, M. L.; Kraftea, D. S.; Marrona, B. E.; Westa, C. W.; Krambisa, M. J.; Antonioa, B. M.; Zellmera, S. G.; Printzenhoffa, D.; Padillaa, K. M.; Lina, Z.; Kay Wagoner, P.; Swainb, N. A.; Stupplec, P. A.; de Grootc, M.; Buttb, R. P.; Castlea, N. A. Voltage Sensor Interaction Site for Selective Small Molecule Inhibitors of Voltage-Gated Sodium Channels. *Proc. Natl. Acad. Sci. U. S. A.* **2013,** *110,* E2724–E2732. http://dx.doi.org/10.1073/pnas.1220844110.
110. Dehnhardt, C. M.; Chowdhury, S.; Focken, T.; Grimwood, M. E.; Hemeon, I. W.; Safina, B.; Sutherlin, D. P. Preparation of Benzamide Derivatives for Use as Sodium Channel Inhibitors. PCT Int. Appl., WO 2014008458. Assignee: Genentech, Inc., USA, 2014; Xenon Pharmaceuticals Inc.; Andrez, J. -C.; Bichler, P. R.; Chen, C. -A.; Chowdhury, S.; Decker, S. M.; Dehnhardt, C. M.; Focken, T.; Grimwood, M. E.; Hemeon, I. W.; Jia, Q.; Li, J.; Liu, Z.; Ortwine, D. F.; Safina, B.; Sutherlin, D.; Sheng, T.; Sun, S.; White, A. D.; Wilson, M. Scott; Zenova, A. Y.; Zhu, J. Substituted benzamides as sodium channel inhibitors and their preparation. PCT Int. Appl., WO 2015078374. Assignee: Genentech, Inc., USA, 2015; Xenon Pharmaceuticals Inc.
111. Zimmermann, N.; Grootenhuis, P. D. J.; Numa, M. M. D.; Stamos, D.; Anderson, C. D.; Whitney, T. Preparation of Thiazolyl Benzenesulfonamides as Modulators of Ion Channels for Treating Pain, Nervous System Disorders, And Other Diseases. PCT Int. Appl., WO 2010002956. Assignee: Vertex Pharmaceuticals Inc., USA, 2010.
112. Markworth, C. J.; Marron, B. E.; Swain, N. A. Benzamide Derivatives as Modulators of SCN3A and SCN5A Sodium Channel Subunits and Their Preparation, Pharmaceutical Compositions and Use in the Treatment of Pain. PCT Int. Appl., WO 2010035166. Assignee: Pfizer Limited, UK, 2010; Icagen, Inc.; Markworth, C. J.; Marron, B. E.; Rawson, D. J.; Storer, R. I.; Swain, N. A.; West, C. W.; Zhou, S. Preparation of sulfonamide Derivatives as NaV1.7 Inhibitors. PCT Int. Appl., WO 2012004706. Assignee: Pfizer Limited, UK, 2012; Icagen, Inc.
113. Greener, B. S.; Marron, B. E.; Millan, D. S.; Rawson, D. J.; Storer, R. I.; Swain, N. A. Preparation of Sulfonamide Derivatives as NaV1.7 Inhibitors. PCT Int. Appl., WO 2012004714. Assignee: Pfizer Limited, UK, 2012; Icagen, Inc.; Brown, A. D.; De Groot, M. J.; Marron, B. E.; Rawson, D. J.; Ryckmans, T.; Storer, R. I.; Stupple, P. A.; Swain, N. A.; West, C. W. Preparation of Benzenesulfonamide Derivatives for Use as Sodium Channel Inhibitors. PCT Int. Appl., WO 2012004743. Assignee: Pfizer Limited, UK, 2012; Icagen, Inc.
114. Bell, A. S.; Brown, A. D.; Lewthwaite, R. A.; Marsh, I. R.; Millan, D. S.; Pacheco, M. P.; Rawson, D. J.; Sciammetta, N.; Storer, R. I.; Stupple, P. A.; Swain, N. A.; De Groot, M. J. Preparation of Sulfonamide Derivatives as NaV1.7 Inhibitors. WO 2012007883. Assignee: Pfizer Limited, UK, 2012; Bell, A. S.; Brown, A. D.; De Groot, M. J.; Lewthwaite, R. A.; Marsh, I. R.; Millan, D. S.; Pacheco, M. P.; Rawson, D. J.; Sciammetta, N.; Storer, R. I.; Swain, N. A.; Gaulier, S. M. Preparation of Heteroaryl Sulfonamide Derivatives as NaV1.7 Inhibitors. WO 2012007861. Assignee: Pfizer Limited, UK, 2012; Bell, A. S.; Brown, A. D.; Lewthwaite, R. A.; Perez Pacheco, M.; Rawson, D. J.; Storer, R. I.; Swain, N. A. Preparation of Sulfonamide Derivatives as NaV1.7 Inhibitors. PCT Int. Appl., WO 2012007877. Assignee: Pfizer Limited, UK, 2012; Brown, A. D.; Rawson, D. J.; Storer, R. I.; Swain, N. A. Preparation of Sulfonamide Derivatives as NaV1.7 Inhibitors. PCT Int. Appl., WO 2012007869. Assignee: Pfizer Limited, UK, 2012; Brown, A. D.; Rawson, D. J.; Storer, R. I.; Swain, N. A. Preparation of Sulfonamide Derivatives as NaV1.7 Inhibitors. PCT Int. Appl., WO 2012007868. Assignee: Pfizer Limited, UK, 2012.
115. Bell, A. S.; De Groot, M. J.; Lewthwaite, R. A.; Marsh, I. R.; Sciammetta, N.; Storer, R. I.; Swain, N. A. Indazole Derivatives as Sodium Channel Inhibitors and Their Preparation and Use in the Treatment of Pain. PCT Int. Appl., WO 2012095781. Assignee: Pfizer Limited, UK, 2012.
116. Preparation of Benzene Sulfonamide Derivatives as NaV 1.7 Inhibitors for Therapy. PCT Int. Appl., WO 2013088315; Storer, R. I.; Swain, N. A. Preparation of Sulfonamide Derivatives and Use Thereof as VGSC Inhibitors. WO 2013093688. Assignee: Pfizer Ltd., UK, 2013; Brown, A. D.; Galan, S. R. G.; Millan, D. S.; Rawson, D. J.; Storer, R. I.; Stupple, P. A.; Swain, N. A. Preparation of Aminosulfonylbenzamide Derivatives for Use as NaV 1.7 Inhibitors. PCT Int. Appl., WO 2013102826. Assignee: Pfizer Limited, UK, 2013.
117. Swain, N. Discovery of Potent, Subtype Selective, Aryl Sulphonamide NaV1.7 Inhibitors for the Treatment of Pain. 18th RSC-SCI Medicinal Chemistry Symposium, PCT Int. Appl. (2013), WO 2013064984; PCT Int. Appl. (2013), WO 2013064983; Cambridge.
118. Liu, S.; Focken, T.; Chahal, N.; Zhang, Z.; Oballa, R. M.; Fonarev, J. Biaryl Ether Sulfonamides, Their Preparation and Use in Treating Sodium Channel-Mediated Diseases. PCT Int. Appl., WO 2013064984. Assignee: Xenon Pharmaceuticals Inc., Canada, 2013; Sun, S.; Zenova, A. Y.; Chafeev, M.; Jia, Q.; Zhang, Z.; Oballa, R. M. Benzenesulfonamide Compounds, Their Preparation, and Use as Voltage-Gated Sodium Channel Blockers for Therapy. PCT Int. Appl., WO 2013064983. Assignee: Xenon Pharmaceuticals Inc., Canada, 2013.
119. Andrez, J. -C.; Chowdhury, S.; Decker, S.; Dehnhardt, C. M.; Focken, T.; Grimwood, M. E.; Hemeon, I. W.; Jia, Q.; Li, J.; Ortwine, D. F.; Safina, B.; Sheng, T.; Sun, S.; Sutherlin, D. P.; Wilson, M. S.; Zenova, A. Y. Preparation of N-Substituted Benzamides and Their Use in the Treatment of Pain. PCT Int. Appl., WO 2013177224. Assignee: Genentech, Inc., USA, 2013; Xenon Pharmaceuticals Inc.
120. Chen, C. -A.; Chowdhury, S.; Dehnhardt, C. M.; Sun, S. Preparation of Benzisoxazole Compounds as Sodium Channel Inhibitors for Treatment of Pain. PCT Int. Appl., WO 2014144545. Assignee: Genentech, Inc., USA, 2014; Xenon Pharmaceuticals Inc.; Bichler, P. R.; Chowdhury, S.; Decker, S. M.; Dehnhardt, C. M.; Focken, T.; Grimwood, M. E.; Hemeon, I. W.; Safina, B.; Sheng, T.; Sun, S.; Wilson, M. S.; Zenova, A. Y. Preparation of Substituted Triazolopyridines as Sodium Channel Inhibitors. PCT Int. Appl., WO 2014153037. Assignee: Genentech, Inc., USA, 2014; Xenon Pharmaceuticals Inc.
121. Layton, M. E.; Pero, J. E.; Fiji, H.; Kelly, M. J., III; De Leon, P.; Rossi, M. A.; Gilbert, K. F.; Roecker, A. J.; Zhao, Z.; Mercer, S. P.; Wolkenberg, S.; Mulhearn, J.; Zhao, L.; Li, D. Preparation of Benzoxazolinone Compounds With Selective Activity in Voltage-Gated Sodium Channels. PCT Int. Appl., WO 2013063459. Assignee: Merck Sharp & Dohme Corp., USA, 2013; Pero, J. E.; Lehman, H. D. G. F.; Kelly, M. J., III; Zhao, L.; Rossi, M. A.; Li, D.; Gilbert, K. F.; Wolkenberg, S.; Mulhearn, J.; Layton, M. E.; De Leon, P. Preparation of Benzoxazolinone Compounds With Selective Activity in Voltage-Gated Sodium Channels. PCT Int. Appl., WO 2014066490. Assignee: Merck Sharp & Dohme Corp., USA, 2014; Pero, J. E.; Lehman, H. D. G. F.; Layton, M. E.; Rossi, M. A.; Kelly, M. J., III. N-Substituted Indazole Sulfonamide Compounds With Selective Activity in Voltage-Gated Sodium Channels. PCT Int. Appl., WO 2014066491. Assignee: Merck Sharp & Dohme Corp., USA, 2014; Li, D.; Layton, M. E.; Roecker, A. J.; Egbertson, M.; Jones, K. L. G.; Wang, X.; Peng, X. Preparation of Bicycloaminebenzenesulfonamide Derivatives for Use as Selective Voltage-Gated Sodium Channel Activity Modulators. PCT Int. Appl., WO 2015080988. Assignee: Merck Sharp & Dohme Corp., USA, 2015; Layton, M. E.; Roecker, A.; Egbertson, M.; Jones, K. L. G.; Wang, X.; Peng, X. Preparation of Bicycloaminebenzenesulfonamide Derivatives for Use as Selective Voltage-Gated Sodium Channel Activity Modulators. PCT Int. Appl., WO 2015077905. Assignee: Merck Sharp & Dohme Corp., USA, 2015.
122. Narayan, K.; Hayashi, N.; Tsuda, S.; Shinozuka, T. Preparation of Indole Derivatives as Sodium Channel Blockers. Jpn. Kokai Tokkyo Koho., JP 2014101287. Assignee: Daiichi Sankyo Co., Ltd., Japan, 2014.
123. Boezio, C.; Boezio, A.; Bregman, H.; Chakka, N.; Coats, J. R.; Copeland, K. W.; Dimauro, E. F.; Dineen, T.; Gao, H.; La, D.; Marx, I. E.; Nguyen, H. N.; Peterson, E. A.; Weiss, M. Preparation of Dihydrobenzoxazine and Tetrahydroquinoxaline Sodium Channel Inhibitors. PCT Int. Appl., WO 2013122897. Assignee: Amgen Inc., USA, 2013; Weiss, M.; Dimauro, E. F.; Dineen, T.; Graceffa, R.; Guzman-Perez, A.; Huang, H.; Kreiman, C.; Marx, I. E.; Nguyen, H. N.; Peterson, E.; Deak, H. L. Bicyclic Sulfonamide Compounds as Sodium Channel Inhibitors and Their Preparation. PCT Int. Appl., WO 2014201173. Assignee: Amgen Inc., USA, 2014; Weiss, M.; Boezio, A.; Boezio, C.; Butler, J. R.; Chu-Moyer, M. Y.; Dimauro, E. F.; Dineen, T.; Graceffa, R.; Guzman-Perez, A.; Huang, H.; Kreiman, C.; La, D.; Marx, I. E.; Milgrim, B. C.; Nguyen, H. N.; Peterson, E.; Romero, K.; Sparling, B. Bicyclic Sulfonamide Compounds as Sodium Channel Inhibitors and Their Preparation. PCT Int. Appl., WO 2014201206. Assignee: Amgen Inc., USA, 2014.
124. Bregman, H.; Chakka, N.; Dimauro, E. F.; Gao, H.; Gunaydin, H.; Huang, H.; Olivieri, P.; Schenkel, L.; Weiss, M. Biarylacyl-sulfonamide compounds as sodium channel inhibitors and their preparation. PCT Int. Appl., WO 2015051043. Assignee: Amgen Inc., USA, 2015.

125. Kim, H. Y.; Kim, I. W.; Jun, S. A.; Na, Y. S.; Lee, H. G.; Cho, M. J.; Lee, J. H.; Kim, H. S.; Yoon, Y. S.; Chung, K. H.; Kim, J. Preparation of Substituted Benzenesulfonamides as Sodium Channel Blockers. PCT Int. Appl., WO 2014061970. Assignee: Daewoong Pharmaceutical Co., Ltd., South Korea, 2014.
126. Babich, O.; Luo, R. Z.; Wang-Fischer, Y.; Palling, D. J.; Venkatachalan, S. P. Preparation of Sodium Channel Modulators for the Treatment of Pain. PCT Int. Appl., WO 201415472. Assignee: Chromocell Corporation, USA, 2014; Babich, O.; Garyantes, T.; Luo, R. Z.; Palling, D. J.; Venkatachalan, S. P.; Wang-Fischer, Y. Preparation of Thiadiazolyl Sulfonamide Derivatives as Sodium Channel Modulators for the Treatment of Pain and Diabetes. PCT Int. Appl., WO 2015038533. Assignee: Chromocell Corporation, USA, 2015.
127. Chen, S.; He, H.; Lagu, B.; Qin, H.; Wu, C.; Xiao, Y. Preparation of tricyclic sulfonamide derivatives as sodium channel inhibitors for treatment of pain. U.S. Pat. Appl. Publ., US 20150183802. Assignee: Novartis AG, Switz, 2015.
128. Short, G. F., III; Romero, D. L.; Lee, M. S. Preparation of heterocyclic compounds as inhibitors of the sodium channel. PCT Int. Appl., WO 2015130957. Assignee: Zalicus Pharmaceuticals, Ltd., USA, 2015.
129. Wang, L.; Zellmer, S. G.; Printzenhoff, D. M.; Castle, N. A. Addition of a Single Methyl Group to a Small Molecule Sodium Channel Inhibitor Introduces a New Mode of Gating Modulation. *Br. J. Pharmacol.* **2015,** *172* (20), 4905–4918.
130. Sun, S.; Jia, Q.; Zenova, A. Y.; Chafeev, M.; Zhang, Z.; Lin, S.; Kwan, R.; Grimwood, M. E.; Chowdhury, S.; Young, C.; Cohen, C. J.; Oballa, R. M. The Discovery of Benzenesulfonamide-Based Potent and Selective Inhibitors of Voltage-Gated Sodium Channel $Na_V1.7$. *Bioorg. Med. Chem. Lett.* **2014,** *24* (18), 4397–4401.
131. Buchanan, J. L.; Bregman, H.; Chakka, N.; Dimauro, E. F.; Du, B.; Nguyen, H. N.; Zheng, X. M. Preparation of Triazine Compounds as Inhibitors of Voltage-Gated Sodium Channels for Treating Chronic Pain Disorders. PCT Int. Appl., WO 2010022055. Assignee: Amgen Inc., USA, 2010.
132. Bregman, H.; Berry, L.; Buchanan, J. L.; Chen, A.; Du, B.; Feric, E.; Hierl, M.; Huang, L.; Immke, D.; Janosky, B.; Johnson, D.; Li, X.; Ligutti, J.; Liu, D.; Malmberg, A.; Matson, D.; McDermott, J.; Miu, P.; Nguyen, H. N.; Patel, V. F.; Waldon, D.; Wilenkin, B.; Zheng, X. M.; Zou, A.; McDonough, S. I.; DiMauro, E. F. Identification of a Potent, State-Dependent Inhibitor of $Na_V1.7$ With Oral Efficacy in the Formalin Model of Persistent Pain. *J. Med. Chem.* **2011,** *54,* 4427–4445. http://dx.doi.org/10.1021/jm200018k.
133. Bregman, H.; Buchanan, J. L.; Chakka, N.; Dimauro, E. F.; Du, B.; Nguyen, H. N.; Zheng, X. M. Preparation of Aryl Carboxamide Derivatives as Sodium Channel Inhibitors for Treatment of Pain. PCT Int. Appl., WO 2011103196. Assignee: Amgen Inc., USA, 2011.
134. Bregman, H.; Nguyen, H. N.; Feric, E.; Ligutti, J.; Liu, D.; McDermott, J. S.; Wilenkin, B.; Zou, A.; Huang, L.; Li, X.; McDonough, S. I.; Dimauro, E. F. The Discovery of Aminopyrazines as Novel, Potent Na(v)1.7 Antagonists: Hit-to-Lead Identification and SAR. *Bioorg. Med. Chem. Lett.* **2012,** *22* (5), 2033–2042. http://dx.doi.org/10.1016/j.bmcl.2012.01.023.
135. Nguyen, H. N.; Bregman, H.; Buchanan, J. L.; Du, B.; Feric, E.; Huang, L.; Li, X.; Ligutti, J.; Liu, D.; Malmberg, A. B.; Matson, D. J.; McDermott, J. S.; Patel, V. F.; Wilenkin, B.; Zou, A.; McDonough, S. I.; Dimauro, E. F. Discovery and Optimization of Aminopyrimidinones as Potent and State-Dependent $Na_V1.7$ Antagonists. *Bioorg. Med. Chem. Lett.* **2011,** *22,* 1055–1060. http://dx.doi.org/10.1016/j.bmcl.2011.11.111.
136. Chakka, N.; Bregman, H.; Du, B.; Nguyen, H. N.; Buchanan, J. L.; Feric, E.; Ligutti, J.; Liu, D.; McDermott, J. S.; Zou, A.; McDonough, S. I.; Dimauro, E. F. Discovery and Hit-to-Lead Optimization of Pyrrolopyrimidines as Potent, State-Dependent Na(v)1.7 Antagonists. *Bioorg. Med. Chem. Lett.* **2012,** *22* (5), 2052–2062. http://dx.doi.org/10.1016/j.bmcl.2012.01.015.
137. Kyle, D. J.; Ni, C.; Tafesse, L.; Yao, J. Preparation of Aryl Substituted Indoles as Sodium Channel Blockers. PCT Int. Appl., WO 2011158108. Assignee: Purdue Pharma L.P., USA, 2011.
138. Kyle, D. J.; Ni, C.; Park, M.; Tafesse, L. Pyridine Compounds as Sodium Channel Blockers and Their Preparation and Use in the Treatment of Pain. PCT Int. Appl., WO 2012007836. Assignee: Purdue Pharma L.P., USA, 2012.
139. Ni, C.; Shao, B.; Tafesse, L.; Yao, J.; Yu, J.; Zhou, X. Preparation of Pyridine Compounds as Voltage-Gated Sodium Channel Blockers Useful in Treatment of Pain. PCT Int. Appl., WO 2012035421. Assignee: Purdue Pharma L.P., USA, 2012.
140. Goehring, R. R.; Tafesse, L.; Yao, J. Preparation of Aryl and Heteroaryl Substituted Quinazoline Compounds as Sodium Channel Blockers. PCT Int. Appl., WO 2012046132. Assignee: Purdue Pharma L.P., USA, 2012.
141. Ni, C.; Park, M.; Shao, B.; Tafesse, L.; Yao, J.; Youngman, M.; Zhou, X. Preparation of Substituted Pyridines as Sodium Channel Blockers. PCT Int. Appl., WO 2012085650. Assignee: Purdue Pharma L. P., USA, 2012.
142. Ni, C.; Park, M.; Shao, B.; Tafesse, L.; Yao, J.; Youngman, M. Preparation of Pyrimidine Derivatives for Use as Sodium Channel Blockers. PCT Int. Appl., WO 2013030665. Assignee: Purdue Pharma L.P., USA, 2013.
143. Engel, J. J. Preparation of Quaternised Amines as Sodium Channel Blockers for Treating Pain. PCT Int. Appl., WO 2013064884. Assignee: Purdue Pharma L.P., USA, 2013.
144. Yao, J. Preparation of Heteroaryl Compounds as Sodium Channel Blockers for Treating Pain. PCT Int. Appl., WO 2013064883. Assignee: Purdue Pharma L.P., USA, 2013.
145. Shao, B. Dihydroxyalkylpyrimidinecarboxamides as Sodium Channel Blockers and Their Preparation. PCT Int. Appl., WO 2013072758. Assignee: Purdue Pharma L. P., USA, 2013.
146. Tafesse, L.; Yao, J. Preparation of Substituted Pyridines and Pyrimidines as Sodium Channel Blockers for Treatment of Diseases Including Pain. PCT Int. Appl., WO 2013136170. Assignee: Purdue Pharma L.P., USA, 2013.
147. Tadesse, D.; Yu, J. Preparation of Triazine Carboxamides as Sodium Channel Blockers Useful in the Treatment of Pain. U.S. Pat. Appl. Publ., US 20140249128. Assignee: Purdue Pharma L.P., USA, 2014.
148. Lockman, J.; Ni, C.; Park, J. H.; Park, M.; Shao, B.; Tafesse, L.; Yao, J.; Youngman, M. A. Preparation of Pyrimidine Carboxamides as Sodium Channel Blockers. PCT Int. Appl., WO 2014135955. Assignee: Purdue Pharma L.P., USA, 2014.
149. Youngman, M. A.; Tafesse, L.; Park, J. H. Preparation of Azaspiro[4.5]decane Derivatives and Use Thereof. PCT Int. Appl., WO 2015031036. Assignee: Purdue Pharma L.P., USA, 2015.
150. Ni, C.; Park, J. H.; Shao, B.; Zhou, X. Preparation of Pyrimidine Derivatives as Sodium Channel Blockers. PCT Int. Appl., WO 2015094443. Assignee: Purdue Pharma L.P., USA, 2015.
151. Lynch, S. M.; Tafesse, L. Preparation of Dibenzazepine Derivatives as Sodium Channel Blockers for Treatment of Pain and Other Disorders. U.S. Pat. Appl. Publ., US 20150175569. Assignee: Purdue Pharma L. P., USA, 2015.
152. Yu, J. Preparation of Indazoles and Use Thereof as Sodium Channel Blockers. PCT Int. Appl., WO 2015099841. Assignee: Purdue Pharma L.P., USA, 2015.
153. Lynch, S. M. Preparation of Pyridines and Pyrimidines as Blockers of Sodium Channels for Treating Pain. PCT Int. Appl., WO 2015112801. Assignee: Purdue Pharma L. P., USA, 2015.
154. Tafesse, L.; Park, J. H. Preparation of Isoquinoline Derivatives for Treating a Disorder Responsive to Blockade of Sodium Channels. PCT Int. Appl., WO 2015123398. Assignee: Purdue Pharma L.P., USA, 2015.
155. Lynch, S. M.; Yao, J.; Park, J. H.; Tafesse, L. Indole Derivatives as Sodium Channel Blockers and Their Preparation and Use for the Treatment of Diseases. U.S. Pat. Appl. Publ., US 20150284383. Assignee: Purdue Pharma L.P., USA, 2015.
156. Park, J. H. Preparation of Pyridine and Piperidine Derivatives as Sodium Channel Blockers. U.S. Pat. Appl. Publ., US 20150141434. Assignee: Purdue Pharma L.P., USA, 2015.
157. Tafesse, L.; Yao, J.; Zhou, X. Benzimidazole Derivatives as Sodium Channel Blockers and Their Preparation and Use for the Treatment of Diseases. U.S. Pat. Appl. Publ., US 20150133500. Assignee: Purdue Pharma L.P., USA, 2015.
158. Tafesse, L.; Park, J. H. Preparation of Substituted Piperidines as Sodium Channel Blockers and Therapeutic Uses Thereof. U.S. Pat. Appl. Publ., US 20150057300. Assignee: Purdue Pharma L.P., USA, 2015.

159. Lynch, S. M.; Tafesse, L.; Carlin, K.; Ghatak, P.; Kyle, D. J. Dibenzazepines and Dibenzoxazepines as Sodium Channel Blockers. *Bioorg. Med. Chem. Lett.* **2014,** *25* (1), 8–12. http://dx.doi.org/10.1016/j.bmcl.2014.11.025.
160. Lynch, S. M.; Tafesse, L.; Carlin, K.; Ghatak, P.; Shao, B.; Abdelhamid, H.; Kyle, D. J. N-Aryl Azacycles as Novel Sodium Channel Blockers. *Bioorg. Med. Chem. Lett.* **2015,** *25,* 48–52. http://dx.doi.org/10.1016/j.bmcl.2014.11.023.
161. Youngman, M. A. Preparation of Cyclic Sulfonamides as Sodium Channel Blockers. PCT Int. Appl., WO 2014096941. Assignee: Purdue Pharma L.P., USA, 2014.
162. Barker, O.; Bentley, J.; Bock, M. G.; Cain, T.; Chovatia, P.; Dod, J. R.; Eustache, F.; Gleave, L.; Hargrave, J.; Heifetz, A.; Law, R.; Raoof, A.; Willows, D. Preparation of Triazine-Oxadiazoles for the Treatment of Chronic Pain. WO 2012035023. Assignee: Novartis AG, Switzerland, 2012.
163. Leach, M.; Franzmann, K.; Riddall, D.; Harbige, L. Preparation of Triazine Compounds as Sodium Channel Blockers. PCT Int. Appl., WO 2011004196, 2011. Assignee: University of Greenwich, UK; Leach, M.; Franzman, K., Preparation of 1,2,4-Triazine Compounds as Sodium Channel Blockers and as Antimalarials. Brit. UK Pat. Appl., GB 2471729, 2011. Assignee: University of Greenwich, UK.
164. Inoue, T.; Watanabe, S.; Yamagishi, T.; Arano, Y.; Morita, M.; Shimada, K. Preparation of Pyridinylcarboxamide Derivatives and Analogues for Use as Calcium or Sodium Channel Blockers. PCT Int. Appl., WO 2010137351. Assignee: RaQualia Pharma Inc., Japan, 2010.
165. Noguchi, H.; Inoue, T.; Morita, M.; Arano, Y. Picolinamide Derivatives as TTX-S Channel Blockers and Their Preparation and Use for the Treatment of Voltage-Galed Sodium Channels-Mediated Diseases. PCT Int. Appl., WO 2011016234. Assignee: RaQualia Pharma Inc., Japan, 2011.
166. Yamagishi, T.; Arano, Y.; Morita, M.; Inoue, T. Aryl Carboxamide Derivatives as TTX-S Channel Blockers, and Use Thereof. PCT Int. Appl., WO 2011058766. Assignee: RaQualia Pharma Inc., Japan, 2011.
167. Morita, M.; Watanabe, S. Preparation of Acylpiperazinylpyrimidine Derivatives for Use as TTX-S Channels Blockers. PCT Int. Appl., WO 2012020567. Assignee: RaQualia Pharma Inc., Japan, 2012.
168. Yamagishi, T.; Kawamura, K.; Morita, M. Amide Derivatives as TTX-S Blockers and Their Preparation. WO 2013161308. Assignee: RaQualia Pharma Inc., Japan, 2013.
169. Yamagishi, T.; Kawamura, K.; Arano, Y.; Morita, M. Preparation of Arylamide Derivatives as Tetrodotoxin-Sensitive (TTX-S) Blockers. PCT Int. Appl., WO 2012053186. Assignee: RaQualia Pharma Inc., Japan, 2012.
170. Kawamura, K.; Morita, M.; Yamagishi, T. Pyrrolopyridinone Derivatives as TTX-S Blockers and Their Preparation. PCT Int. Appl., WO 2013161312. Assignee: RaQualia Pharma Inc., Japan, 2013.
171. Kawamura, K.; Yamagishi, T.; Arano, Y.; Morita, M. Pyrazolopyridine Derivatives as TTX-S Blockers and Their Preparation. PCT Int. Appl., WO 2014068988. Assignee: RaQualia Pharma Inc., Japan, 2014.
172. Hoyt, S. B.; London, C.; Abbadie, C.; Felix, J. P.; Garcia, M. L.; Jochnowitz, N.; Karanam, B. V.; Li, X.; Lyons, K. A.; McGowan, E.; Priest, B. T.; Smith, M. M.; Warren, V. A.; Thomas-Fowlkes, B. S.; Kaczorowski, G. J.; Duffy, J. L. A Novel Benzazepinone Sodium Channel Blocker With Oral Efficacy in a Rat Model of Neuropathic Pain. *Bioorg. Med. Chem. Lett.* **2013,** *23,* 3640–3645. http://dx.doi.org/10.1016/j.bmcl.2013.03.121.
173. Posada, C. G.; Selwood, D.; Garthwaite, J.; Baker, D.; Clutterbuck, L. Preparation of Indazole Derivatives and Their Use for Blockading Voltage Dependent Sodium Channels. PCT Int. Appl., WO 2011061469. Assignee: University College London, UK, 2011.
174. Bogdan, A.; Cowart, M. D.; Degoey, D. A.; Jinkerson, T. K.; Koenig, J. R.; Kort, M. E.; Liu, B.; Matulenko, M. A.; Nelson, D. W.; Patel, M. V.; Peltier, H.; Scanio, M. J.; Wakefield, B. D. Preparation of 6-Heteroaryloxy- or 6-Aryloxyquinoline-2-Carboxamides as Sodium Channel Blockers. WO 2015119998. Assignee: AbbVie, U.S. Pat. Appl. Publ., US 20150218102, 2015.
175. Deninno, M. P.; Anderson, C.; Conroy, E. L.; Frieman, B. A.; Groothenhuis, P. D. J.; Hadida-Ruah, S. S.; Hurley, D. J.; Pierre, F. J. D.; Silina, A.; Uy, J.; Zhou, J. Preparation of Fused Piperidine Amides as Modulators of Ion Channels. PCT Int. Appl., WO 2015006280. Assignee: Vertex Pharmaceuticals Incorporated, USA, 2015.
176. Akopian, A. N.; Sivilotti, L.; Wood, J. N. A Tetrodotoxin-Resistant Voltage-Gated Sodium Channel Expressed by Sensory Neurons. *Nature* **1996,** *379,* 257–262.
177. Akopian, A. N.; Souslova, V.; England, S.; et al. The Tetrodotoxin-Resistant Sodium Channel SNS Has a Specialized Function in Pain Pathways. *Nat. Neurosci.* **1999,** *2,* 541–548.
178. Kerr, B. J.; Souslova, V.; McMahon, S. B.; Wood, J. N. A Role for the TTX-Resistant Sodium Channel NaV1.8 in NGF-Induced Hyperalgesia, But Not Neuropathic Pain. *Neuroreport* **2001,** *12,* 3077–8300; Leoa, S.; D'Hooge, R.; Meert, T. Exploring the Role of Nociceptor-Specific Sodium Channels in Pain Transmission Using $Na_V1.8$ and $Na_V1.9$ Knockout Mice. *Behav. Brain Res.* **2010,** *208,* 149–157.
179. Lai, J.; Gold, M. S.; Kim, C. S.; Bian, D.; Ossipov, M. H.; Hunter, J. C.; Porreca, F. Inhibition of Neuropathic Pain by Decreased Expression of the Tetrodotoxin-Resistant Sodium Channel, $Na_V1.8$. *Pain* **2002,** *95,* 143–152.
180. Dong, X. W.; Goregoaker, S.; Engler, H.; Zhou, X.; Mark, L.; Crona, J.; Terry, R.; Hunter, J.; Priestley, T. Small Interfering RNA-Mediated Selective Knockdown of Na(V)1.8 Tetrodotoxin-Resistant Sodium Channel Reverses Mechanical Allodynia in Neuropathic Rats. *Neuroscience* **2007,** *146,* 812–821.
181. Faber, C. G.; Lauria, G.; Merkies, I. S.; et al. Gain-of-Function of $Na_V1.8$ Mutations in Painful Neuropathy. *Proc. Natl. Acad. Sci. U. S. A.* **2012,** *109,* 19444–19449.
182. Browne, L. E.; Clare, J. J.; Wray, D. Functional and Pharmacological Properties of Human and Rat $Na_V1.8$ Channels. *Neuropharmacology* **2009,** *56,* 905–914.
183. Han, C.; Huang, J.; Waxman, S. G. Sodium Channel $Na_V1.8$, Emerging Links to Human Disease. *Neurology* **2016,** *86,* 473–483.
184. Weiser, T.; Wilson, N. *Mol. Pharmacol.* **2002,** *62* (3), 433.
185. Gaida, W.; Klinder, K.; Arndt, K.; Weiser, T. *Neuropharmacology* **2005,** *49,* 1220.
186. Kern, K.-U.; Weiser, T.; Schmerz, D. Doi:10.1007/s00482-015-0060-y.
187. Jingyao, L.; Xiaoyan, L.; Meiyan, P.; Wei, D.; Zhao, D.; Xiaolin, W.; Ruozhuo, L.; Jianquan, Z.; Shengyuan, Y. Blockade of NaV1.8 Currents in Nociceptive Trigeminal Neurons Contributes to Anti-trigeminovascular Nociceptive Effect of Amitriptyline. *Neuromol Med* **2014,** *16,* 308–321. http://dx.doi.org/10.1007/s12017-013-8282-6.
188. Cardenas, C. A.; Cardenas, C. G.; de Armendi, A. J.; Scroggs, R. S. Carbamazepine Interacts With a Slow Inactivation State of $Na_V1.8$-Like Sodium Channels. *Neurosci. Lett.* **2006,** *408* (2), 129–134.
189. Gu, X.-Y.; Liu, B.-L.; Zang, K.-K.; Yang, L.; Xu, H.; Pan, H.-L.; Zhao, Z.-Q.; Zhang, Y.-Q. Dexmedetomidine Inhibits Tetrodotoxin-Resistant $Na_V1.8$ Sodium Channel Activity Through Gi/o-Dependent Pathway in Rat Dorsal Root Ganglion Neurons. *Mol. Brain* **2015,** *8,* 15. http://dx.doi.org/10.1186/s13041-015-0105-2.
190. Jarvis, M. F.; Honore, P.; Shieh, C. C.; Chapman, M.; Joshi, S. K.; Zhang, X. F.; Kort, M. E.; Carroll, W. A.; Marron, B. E.; Atkinson, R. N.; Thomas, J. B.; Liu, D.; Krambis, M. J.; Liu, Y.; McGaraughty, S.; Chu, K.; Roeloffs, C. R.; Zhong, C.; Mikusa, J. P.; Hernandez, G.; Gauvin, D.; Wade, C.; Zhu, C.; Pai, M.; Scanio, M. J. C.; Shi, L.; Drizin, I.; Gregg, R. J.; Matulenko, M. A.; Ahmed Hakeem, A. H.; Gross, M. F.; Johnson, M. S.; Marsh, K. C.; Wagoner, K.; Sullivan, J. P.; Faltynek, C. R.; Krafte, D. S. *Proc. Natl. Acad. Sci. U. S. A.* **2007,** *104,* 8520.
191. Kort, M. E.; Drizin, I.; Gregg, R. J.; Scanio, M. J. C.; Shi, L.; Gross, M. F.; Atkinson, R. N.; Johnson, M. S.; Pacofsky, G. J.; Thomas, J. B.; Carroll, W. A.; Krambis, M. J.; Liu, D.; Shieh, C.-C.; Zhang, X.; Hernandez, G.; Mikusa, J. P.; Zhong, C.; Joshi, S.; Honore, P.; Roeloffs, R.; Marsh, K. C.; Murray, B. P.; Liu, J.; Werness, S.; Faltynek, C. R.; Krafte, D. S.; Jarvis, M. F.; Chapman, M. L.; Marron, B. E. *J. Med. Chem.* **2008,** *51,* 407.
192. Joshi, S. K.; Honore, P.; Hernandez, G.; Schmidt, R.; Gomtsyan, A.; Scanio, M.; Kort, M.; Jarvis, M. F. *J. Pain* **2009,** *10,* 306.
193. Rahman, W.; Dickenson, A. H. *Neuroscience* **2015,** *295,* 103–116.
194. Han, Z.; Jiang, Y.; Xiao, F.; Cao, K.; Wang, D. W. *Eur. J. Pharmacol.* **2015,** *754,* 52.
195. Drizin, I.; Gregg, R. J.; Scanio, M. J. C.; Shi, L.; Gross, M. F.; Atkinson, R. N.; Thomas, J. B.; Johnson, M. S.; Carroll, W. A.; Marron, B. E.; Chapman, M. L.; Liu, D.; Krambis, M. J.; Shieh, C.-C.; Zhang, X. F.; Hernandez, G.; Gauvin, D. M.; Mikusa, J. P.; Zhu, C. Z.; Joshi, S.; Honore, P.; Marsh, K. C.; Roeloffs, R.; Werness, S.; Krafte, D. S.; Jarvis, M. F.; Faltynek, C. R.; Kort, M. E. *Bioorg. Med. Chem.* **2008,** *16,* 6379.
196. Zhang, X.-F.; Shieh, C.-C.; Chapman, M. L.; Matulenko, M. A.; Hakeem, A. H.; Atkinson, R. N.; Kort, M. E.; Marron, B. E.; Joshi, S.; Honore, P.; Faltynek, C. R.; Krafte, D. S.; Jarvis, M. F. *Neuropharmacology* **2010,** *59,* 201.

197. Kort, M. E.; Atkinson, R. N.; Thomas, J. B.; Drizin, I.; Johnson, M. S.; Secrest, M. A.; Gregg, R. J.; Scanio, M. J. C.; Shi, L.; Hakeem, A. H.; Matulenko, M. A.; Chapman, M. L.; Krambis, M. J.; Liu, D.; Shieh, C.-C.; Zhang, X.; Hernandez, G.; Mikusa, J. P.; Zhong, C.; Joshi, S.; Honore, P.; Roeloffs, R.; Werness, S.; Antonio, B.; Marsh, K. C.; Faltynek, C. R.; Krafte, D. S.; Jarvis, M. F.; Marron, B. E. *Bioorg. Med. Chem. Lett.* **2010,** *20,* 6812.
198. Scanio, M. J. C.; Shi, L.; Drizin, I.; Gregg, R. J.; Atkinson, R. N.; Thomas, J. B.; Johnson, M. S.; Chapman, M. L.; Liu, D.; Krambis, M. J.; Liu, Y.; Shieh, C.-C.; Zhang, X. F.; Simler, G. H.; Joshi, S.; Honore, P.; Marsh, K. C.; Knox, A.; Werness, S.; Antonio, B.; Krafte, D. S.; Jarvis, M. F.; Faltynek, C. R.; Marron, B. E.; Kort, M. E. *Bioorg. Med. Chem.* **2010,** *18,* 7816.
199. Bagal, S. K.; Bungay, P. J.; Denton, S. M.; Gibson, K. R.; Glossop, M. S.; Hay, T. L.; Kemp, M. I.; Lane, C. A. L.; Lewis, M. L.; Maw, G. N.; Million, W. A.; Elizabeth Payne, C.; Poinsard, C.; Rawson, D. J.; Stammen, B. L.; Thompson, L. R. Discovery and Optimization of Selective Na v 1.8 Modulator Series That Demonstrate Efficacy in Preclinical Models of Pain. *ACS Med. Chem. Lett.* **2015,** *6,* 150511124346005. http://dx.doi.org/10.1021/acsmedchemlett.5b00059.
200. Payne, C. E.; Brown, A. R.; Theile, J. W.; Loucif, A. J. C.; Alexandrou, A. J.; Fuller, M. D.; Stevens, E. B. A Novel Selective and Orally Bioavailable Na V 1.8 Blocker PF-01247324 Attenuates Nociception and Sensory Neuron Excitability. *Br. J. Pharmacol.* **2015,** *172,* 2654–2670. http://dx.doi.org/10.1111/bph.13092.
201. Fray, M. J.; Gillmore, A. T.; Glossop, M. S.; McManus, D. J.; Moses, I. B.; Praquin, C. F. B.; Reeves, K. A.; Thompson, L. R. *Org. Process Res. Dev.* **2010,** *14,* 263–271.
202. Waxman, S., et al. Plos One. Doi:10.1371/journal.pone.0119067.
203. Bagal, S.; Kemp, M. I.; Miller, D. C.; Murata, Y. Imidazoles as $Na_V1.8$ Inhibitors and Their Preparation and Use in the Treatment of Pain. PCT Int. Appl., WO 2013061205. Assignee: Pfizer Limited, UK, 2013.
204. Bagal, S. K.; Brown, A. D.; Kemp, M. I.; Klute, W.; Marron, B. E.; Miller, D. C.; Skerratt, S. E.; Suto, M. J.; West, C. W.; Malet Sanz, L. Benzimidazole and Imidazopyridine Derivatives as $Na_V1.8$ Inhibitors and Their Preparation and Use in the Treatment of Pain. PCT Int. Appl., WO 2013114250. Assignee: Pfizer Inc., USA, 2013.
205. Brown, A. Discovery of Potent and Highly Selective $Na_V1.8$ Inhibitors as Potential Pain Therapeutics. *5th SCI-RSC Symposium on Ion Channels as Therapeutic Targets, Cambridge*; Storer, I. Design and Evaluation of Subtype Selective $Na_V1.8$ Inhibitors for the Treatment of Pain. *27th Symposium on Medicinal Chemistry in Eastern England.*
206. Hadida-Ruah, S. S.; Anderson, C.; Arumugam, V.; Asgian, I. L.; Bear, B. R.; Termin, A. P.; Johnson, J. P. Preparation of Pyridone Amides as Modulators of Sodium Channels. U.S. Pat. Appl. Publ., US 20140213616. Assignee: Vertex Pharmaceuticals Incorporated, USA, 2014; Hadida-Ruah, S. S.; Anderson, C.; Arumugam, V.; Asgian, I. L.; Bear, B. R.; Termin, A. P.; Johnson, J. P. Preparation of Quinoline and Quinazoline Amides as Modulators of Sodium Channels. PCT Int. Appl., WO 2014120815. Assignee: Vertex Pharmaceuticals Incorporated, USA, 2014; Hadida-Ruah, S. S.; Anderson, C.; Arumugam, V.; Asgian, L. L.; Bear, B. R.; Termin, A. P.; Johnson, J. P. Preparation of Amides as Modulators of Sodium Channels. PCT Int. Appl., WO 2014120820. Assignee: Vertex Pharmaceuticals Incorporated, USA, 2014; Hadida-Ruah, S. S.; Anderson, C.; Termin, A. P.; Bear, B. R.; Arumugam, V.; Krenitsky, P.; Johnson, J. P. Preparation of Sulfonamides as Modulators of Sodium Channels for Treating of Pain. PCT Int. Appl., WO 2015010065. Assignee: Vertex Pharmaceuticals Inc., USA, 2015; Anderson, C.; Hadida-Ruah, S. S.; Golec, J. M. C.; Zhang, B.; Littler, B. J.; Keshavarz-Shokri, A.; Alcacio, T. E.; Belmont, D. T. Prodrugs of Pyridone Amides Useful as Modulators of Sodium Channels. PCT Int. Appl., WO 2015089361. Assignee: Vertex Pharmaceuticals Incorporated, USA, 2015.
207. Gaudioso, C.; Hao, J.; Martin-Eauclaire, M. F.; Gabriac, M.; Delmas, P. Menthol Pain Relief Through Cumulative Inactivation of Voltage-Gated Sodium Channels. *Pain* **2012,** *153* (2), 473–484.
208. Hockley, J. R. F.; Boundouki, G.; Cibert-Goton, V.; McGuire, C.; Yip, P. K.; Chan, C.; Tranter, M.; Wood, J. N.; Nassar, M.; Blackshaw, L. A.; Aziz, Q.; Michael, G. J.; Baker, M. D.; Winchester, W. J.; Knowles, C. H.; Bulmer, D. C. Multiple Roles for $Na_V1.9$ in the Activation of Visceral Afferents by Noxious Inflammatory, Mechanical, and Human Disease-Derived Stimuli. *Pain* **2014,** *155* (10), 1962–1975. http://dx.doi.org/10.1016/j.pain.2014.06.015.
209. Dib-Hajj, S. D.; Cummins, T. R.; Black, J. A.; et al. Sodium Channels in Normal and Pathological Pain. *Annu. Rev. Neurosci.* **2010,** *33,* 325–347.
210. Tate, S.; Benn, S.; Hick, C.; et al. Two Sodium Channels Contribute to the TTX-R Sodium Current in Primary Sensory Neurons. *Nat. Neurosci.* **1998,** *1,* 653–655.
211. Craner, M. J.; Klein, J. P.; Renganathan, M.; et al. Changes of Sodium Channel Expression in Experimental Painful Diabetic Neuropathy. *Ann. Neurol.* **2002,** *52,* 786–792.
212. Cummins, T. R.; Waxman, S. G. Downregulation of Tetrodotoxin-Resistant Sodium Currents and Upregulation of a Rapidly Repriming Tetrodotoxinsensitive Sodium Current in Small Spinal Sensory Neurons After Nerve Injury. *J. Neurosci.* **1997,** *17,* 3503–3514; Genetic aspects of sodium channelopathy in SFN Dib-Hajj, S. D.; Tyrrell, L.; Black, J. A.; et al. NaN, a Novel Voltage-Gated Na Channel, Is Expressed Preferentially in Peripheral Sensory Neurons and Down-Regulated After Axotomy. *Proc. Natl. Acad. Sci. U. S. A.* **1998,** *95,* 8963–8968; Cummins, T. R.; Black, J. A.; Dib-Hajj, S. D.; et al. Glial-Derived Neurotrophic Factor Upregulates Expression of Functional SNS and NaN Sodium Channels and Their Currents in Axotomized DRG Neurons. *J. Neurosci.* **2000,** *20,* 8754–8761; Decosterd, I.; Ji, R. R.; Abdi, S.; et al. The Pattern of Expression of the Voltage-Gated Sodium Channels Na(v)1.8 and Na(v)1.9 Does Not Change in Uninjured Primary Sensory Neurons in Experimental Neuropathic Pain Models. *Pain* **2002,** *96,* 269–277; Sleeper, A. A.; Cummins, T. R.; Dib-Hajj, S. D.; et al. Changes in Expression of Two Tetrodotoxin-Resistant Sodium Channels and Their Currents in Dorsal Root Ganglion Neurons After Sciatic Nerve Injury but Not Rhizotomy. *J. Neurosci.* **2000,** *20,* 7279–7289.
213. Lolignier, S.; Bonnet, C.; Gaudioso, C.; Ruel, J.; Amsalem, M.; Ferrier, J.; Rodat-Despoix, L.; Bouvier, V.; Aissouni, Y.; Prival, L.; Chapuy, E.; Padilla, F.; Eschalier, A.; Delmas, P.; Busserolles, J. The $Na_V1.9$ Channel Is a Key Determinant of Cold Pain Sensation and Cold Allodynia. *Cell Rep.* **2015,** *11,* 1067–1078. http://dx.doi.org/10.1016/j.celrep.2015.04.027.
214. Dib-Hajj, S. D.; Black, J. A.; Waxman, S. G. $Na_V1.9$: A Sodium Channel Linked to Human Pain. *Nat. Rev. Neurosci.* **2015,** *16* (9), 511–519. http://dx.doi.org/10.1038/nrn3977.
215. Liang, J.; Liu, X.; Zheng, J.; Yu, S. Effect of Amitriptyline on Tetrodotoxin-Resistant $Na_V1.9$ Currents in Nociceptive Trigeminal Neurons. *Mol. Pain* **2013,** *9* (1), 31. http://dx.doi.org/10.1186/1744-8069-9-31.
216. Delmas, P.; Amsalem, M. E.; Roubinet, F. M. -D. Voltage-gated sodium channel $Na_V1.9$ inhibitors and uses thereof for treating pain. PCT Int. Appl., WO 2014128240. Assignee: Universite d'Aix-Marseille, Fr.; Centre National de la Recherche Scientifique, 2014.
217. DaiNippon Sumitomo Company Report for Third Quarter of year ending March 31, 2016—http://www.ds-pharma.com/pdf_view.php?id=474.
218. Gursahani, H., Kim, G., Gogas, K., et al., NKTR-171: A Novel Sodium Channel Blocker for Neuropathic Pain with Reduced CNS Side Effects. Abstract # 8106/Poster #JJ11: Presented at the Society for Neuroscience 42nd Annual Meeting: Neuroscience 2012, October 13–17th, 2012, New Orleans, LA.
219. Clinicaltrials.gov—A Randomised, Double-Blind, Placebo-Controlled Multiple Dose Study Designed to Explore the Safety, Tolerability and PK of DS-1971a Following Oral Administration Over 14 days to Healthy Male and Female Subjects. https://clinicaltrials.gov/ct2/show/NCT02564861.
220. Jones, H. M.; Butt, R. P.; Webster, R. W.; Gurrell, I.; Dzygiel, P.; Flanagan, N.; Fraier, D.; Hay, T.; Iavarone, L. E.; Luckwell, J.; Pearce, H.; Phipps, A.; Segelbacher, J.; Speed, B.; Beaumont, K. Clinical micro-dose studies to explore the human pharmacokinetics of four selective inhibitors of human $Na_V1.7$ voltage-dependent sodium channels. *Clin. Pharmacokinet.* **2016,** *55,* 875–887 (Epub ahead of print).
221. Demant, D. T.; Lund, K.; Vollert, J.; Maier, C.; Segerdahl, M.; Sindrup, S. H. The Effect of Oxcarbazepine in Peripheral Neuropathic Pain Depends on Pain Phenotype: A Randomised, Double-Blind, Placebo-Controlled Phenotype-Stratified Study. *Pain* **2014,** *155* (11), 2263–2273; Movassaghian, S.; Afzalifar, R.; Alaeddini, M. Clinical Anesthetic Effectiveness of Intraoral Mucoadhesive Tablets of Amitriptyline in Healthy Volunteers. *J. Oral Maxillofac. Surg.* **2013,** *71* (1), 23–28; Statland, J. M.; Bundy, B. N.; Wang, Y.; Rayan, D. R.; Trivedi, J. R.; Sansone, V. A.; Salajegheh, M. K.; Venance, S. L.; Ciafaloni, E.; Matthews, E.; et al. Mexiletine for Symptoms and Signs of Myotonia in Nondystrophic Myotonia: A Randomized Controlled Trial. *JAMA* **2012,** *308* (13), 1357–1365.
222. Lobo, K.; Donado, C.; Cornelissen, L.; Kim, J.; Ortiz, R.; Peake Roy, W. A.; Kellogg, M.; Alexander, M. E.; Zurakowski, D.; Kurgansky, K. E.; et al. A Phase 1, Dose-Escalation, Double-Blind, Block-Randomized, Controlled Trial of Safety and Efficacy of Neosaxitoxin Alone and in Combination With 0.2% Bupivacaine, With and Without Epinephrine, for Cutaneous Anesthesia. *Anesthesiology* **2015,** *123* (4), 873–885.
223. ClinicalTrials.gov—Safety & Efficacy Study of Subcutaneous Tetrodotoxin for Moderate to Severe Inadequately Controlled Cancer-related Pain (TEC-006)—https://clinicaltrials.gov/ct2/show/NCT00725114.
224. Sinatra, R. S.; Jahr, J. S.; Watkins-Pitchford, J. M.. *The Essence of Analgesia and Analgesics;* Cambridge University, 2010.
225. http://www.bloomberg.com/apps/news?pid=conewsstory&tkr=NP5:GR&sid=af0gKdEDHRDA—Newron reports SERENA trial top-line results for ralfinamide.
226. Newron Announces Positive Results With Ralfinamide From Phase II Trial in Neuropathic Pain. http://www.prnewswire.com/news-releases/newron-announces-positive-results-with-ralfinamide-from-phase-ii-trial-in-neuropathic-pain-74976442.html.

227. Convergence Pharmaceuticals Press Release 2014. http://www.convergencepharma.com/userfiles/file/140616_Convergence_TGN%20vFINALFINAL.pdf; Study report *in press* in Lancet Neurology
228. Convergence Pharmaceuticals Press Reslease 2014. http://www.convergencepharma.com/userfiles/file/140923_LSR_FINAL.pdf.
229. Biogen Press release. http://www.biotechnologyevents.com/node/11063; https://clinicaltrials.gov/ct2/show/NCT02917187.
230. Goldberg, Y. P.; Price, N.; Namdari, R.; Cohen, C. J.; Lamers, M. H.; Winters, C.; Price, J.; Young, C. E.; Verschoof, H.; Sherrington, R.; Pimstone, S. N.; Hayden, M. R. Treatment of Na(v)1.7-Mediated Pain in Inherited Erythromelalgia Using a Novel Sodium Channel Blocker. *Pain* **2014,** *155* (4), 837–838.
231. Teva Pharmaceuticals Press Resease. http://www.tevapharm.com/news/teva_and_xenon_provide_update_on_tv_45070_phase_2b_study_in_osteoarthritis_pain_07_15.aspx.
232. https://clinicaltrials.gov/ct2/results?term=PF-04531083.

7.05 CGRP Receptor Antagonists for the Treatment of Migraine

GM Dubowchik, Bristol-Myers Squibb Co., Wallingford, CT, United States
IM Bell, Merck & Co., Inc., West Point, PA, United States

© 2017 Elsevier Ltd. All rights reserved.

7.05.1	**Introduction**	177
7.05.1.1	Migraine Prevalence and Symptoms	177
7.05.1.2	Migraine Pathophysiology	177
7.05.1.3	Medications for Migraine	178
7.05.1.4	Older Acute Migraine Drug Classes	178
7.05.1.4.1	Ergot alkaloids	178
7.05.1.4.2	5-$HT_{1B/1D}$ agonists (triptans)	179
7.05.2	**Calcitonin Gene-Related Peptide**	181
7.05.2.1	CGRP and Migraine	181
7.05.2.2	CGRP Receptor Structure and Function	181
7.05.2.3	CGRP Receptor Antagonist Binding	183
7.05.3	**Small-Molecule CGRP Receptor Antagonists**	184
7.05.3.1	CGRP Receptor Antagonists From Boehringer Ingelheim	184
7.05.3.1.1	BIBN4096 BS	184
7.05.3.1.2	BI 44370	188
7.05.3.2	CGRP Receptor Antagonists From Merck	189
7.05.3.2.1	Caprolactam-based CGRP receptor antagonists	189
7.05.3.2.2	Spiroindane-based CGRP receptor antagonists	195
7.05.3.3	CGRP Receptor Antagonists From Bristol–Myers Squibb	200
7.05.3.3.1	Intranasal BMS-694153	200
7.05.3.3.2	Intranasal BMS-742413	205
7.05.3.3.3	Orally delivered rimegepant (BMS-927711)	207
7.05.3.4	Other Small-Molecule CGRP Receptor Antagonists	213
7.05.3.4.1	SmithKline Beecham and GlaxoSmithKline	213
7.05.3.4.2	Vertex	215
7.05.3.4.3	Neurogen	215
7.05.3.4.4	Grünenthal	215
7.05.4	**Biologics**	216
7.05.4.1	Monoclonal Antibodies	216
7.05.4.1.1	AMG-334 (Amgen)	216
7.05.4.1.2	LY2951742 (Lilly)	216
7.05.4.1.3	ALD403 (Alder BioPharmaceuticals)	216
7.05.4.1.4	TEV-48125 (formerly known as LBR-101, Teva Pharmaceuticals)	216
7.05.4.2	Spiegelmers	217
7.05.5	**Conclusion**	217
References		218
Relevant Websites		224

Abbreviations

5-HT 5-hydroxytryptamine (serotonin)
ADME absorption, distribution, metabolism, and excretion
AE adverse event
AM adrenomedullin
AMY amylin
Arg L-arginine
AUC area under the curve
BBB blood–brain barrier
BFC 7-benzyloxy-4-trifluoromethylcoumarin
BZR 7-benzyloxyresorufin
cAMP cyclic adenosine monophosphate
CGRP calcitonin gene-related peptide
CIDV capsaicin-induced dermal vasodilation
CLR calcitonin receptor-like receptor
CNS central nervous system
CSD cortical spreading depression
CSF cerebrospinal fluid
CT calcitonin
CTR calcitonin receptor
CV cardiovascular

CYP cytochrome P450
DHE dihydroergotamine
ECD extracellular domain
f_u fraction unbound
GIP gastric inhibitory polypeptide
GPCR G-protein-coupled receptor
hERG human Ether-à-go-go-related gene
HS human serum
HTS high-throughput screen
Ile L-isoleucine
IN intranasal
IV intravenous
kcal kilocalories
LE ligand efficiency
Lys L-lysine
Met L-methionine
MW molecular weight
nM nanomolar
NSAID nonsteroidal anti-inflammatory drug
PAMPA parallel artificial membrane permeability assay
PD pharmacodynamic
PDB protein database
PEG polyethylene glycol
PET positron emission tomography
P-gp P-glycoprotein
Phe L-phenylalanine
PK pharmacokinetic
pM picomolar
PO Latin "per os" (by mouth)
PSA polar surface area
PTH parathyroid hormone
RAMP receptor activity-modifying protein
SAR structure–activity relationship
SC subcutaneous
TGVS trigeminovascular system
Thr L-threonine
Trp L-tryptophan

7.05.1 Introduction

7.05.1.1 Migraine Prevalence and Symptoms

Migraine is a debilitating neurological syndrome, usually presenting with severe headache pain, nausea, and heightened sensitivity to sound (phonophobia), light (photophobia), smell, and tactile sensations.[1,2] Beyond the individual suffering, it is also recognized as a significant source of lost productivity. In 2009, it was estimated that migraine attacks cost the US economy at least 17 billion dollars per year in direct costs, missed workdays, and reduced performance.[3] Severe migraine is considered by the World Health Organization to be comparable to quadriplegia in its impact on the daily life of individual sufferers. Despite many decades of research, the vast majority of migraineurs are underserved by existing therapies, because of both inadequate efficacy and treatment-limiting side effects.[4]

It is estimated that migraine affects 12–20% of the global population, with women sufferers more than twice as compared to men sufferers. Unlike most other neurological conditions, migraine mainly afflicts those in middle age or younger. In women, prevalence increases until about age 40, after which it begins to decrease and approach that of men.[5] Although the frequency of attacks varies widely, about 1% of Americans are considered to have chronic migraine, defined as more than 15 days with headache per month, with prevalence inversely related to income.[6]

Migraine is increasingly recognized to be a highly complex disorder with multiple, patient-specific factors determining the character of a given episode. This may partly explain the heterogeneity of treatment responses seen with various therapies. Duration of attacks vary widely, from a few hours to several days or more.[7] Since everyday tasks usually aggravate the symptoms, migraineurs often require immobility and isolation during attacks. A typical migraine episode usually consists of several phases.[8] In the prodromal phase, experienced by roughly 80% of patients, the individual is aware that an attack is imminent hours or even days before the onset of pain. Many migraineurs (20–30%) experience visual auras—moving rings or spots of light—before and/or during the initial phase of headache pain. The overall headache phase, where the pain is often unilateral, typically lasts from 4 to 72 h and is usually accompanied by one or more associated symptoms such as nausea, photophobia, phonophobia, and tactile sensitivities. Finally, the postdromal phase is marked by physical and mental fatigue, along with residual signs of neuronal hyperexcitability such as allodynia. There is a strong hereditary component in migraine with many reports of positive family histories. This is especially true of familial hemiplegic migraine where approximately 50% of sufferers possess a mutation in a voltage-gated Ca^{2+} channel gene, *CACNA1A*, strong evidence for the involvement of ion channels in the aura that is a hallmark of this condition.[9]

7.05.1.2 Migraine Pathophysiology

In many individuals, migraines are brought on by specific stimuli or triggers. These can vary greatly between migraineurs and include specific foods (chocolate, cheeses, and red wine, in particular), changes in weather, hormone levels, disrupted sleep patterns, and stress. However, many sufferers need no obvious trigger to bring on an attack. Migraineurs may have an increased tendency toward intermittent neuronal excitability, possibly due to inherited mutations in, for example, ion channels[10,11] that

lower their threshold for neuronal firing in reaction to modest physiological changes such as menstrual hormone fluctuations, emotional stress, and even awakening from sleep.

The basic causal mechanisms that lead to migraine pain and associated symptoms are still matters of investigation and debate. Through the last half of the 20th century, a "vascular-only" hypothesis prevailed.[12] According to this model, migraine headache pain could be explained by the physical dilation of dural and extracranial blood vessels. Briefly, a given migraine trigger results in vasoconstriction leading to localized ischemia. This is followed by an excessive compensatory response by the trigeminovascular system (TGVS) in which blood vessels are dilated by neuronal secretion of vasoactive peptides such as calcitonin gene-related peptide (CGRP), neuropeptide Y, and substance P, leading to activation of the perivascular sensory nerve projecting to the brain.[13] In this model, the TGVS, which innervates the face and the meningeal blood vessels surrounding the brain, is responsible for migraine pain. In addition, cortical spreading depression (CSD), a self-propagating wave of neuronal depolarization in the cortex of the brain, is thought to be directly responsible for the visual aura that precedes headache for approximately one-third of migraineurs.

Many researchers believe that a combination of environmental factors and a lowered threshold for cortical hyperexcitability leads to CSD, possibly in all migraineurs since aura may only manifest itself when CSD occurs in visual areas of the brain.[11] CSD, which may be promoted by low magnesium concentrations leading to enhanced *N*-methyl-D-aspartate receptor activation, results in extracellular release of a number of neuronally active substances that may activate or sensitize meningeal nociceptors.[14] It is thought that the activated TGVS secretes neuropeptides that cause vasodilation and increase blood vessel permeability, leading to plasma extravasation and mast cell degranulation, all resulting in dural inflammation.[15] Other vasoactive substances have been identified in afferents supplying intracranial vessels including serotonin (5-HT), nitric oxide, substance P, neurokinin A, and vasoactive intestinal peptide.[16] Most of these can also mediate neurotransmission in the central nervous system (CNS) and thus may have multiple functions in migraine pathophysiology, complicating the interpretation of mechanism-based therapies.[17]

Recent findings, especially from positron emission tomography (PET) imaging studies,[18] have stressed the potential importance of central dysfunction in migraine, in particular, the periaqueductal gray (PAG), a region of the brain well known to be involved in the pain desensitization pathway. A number of researchers now believe that altered brainstem activity may be critically important in both triggering and lowering the threshold for migraine attacks.[1] The lowered threshold for neuronal hyperexcitability that many or most migraineurs possess may be triggered by what would normally be considered minor day-to-day stresses or stimuli. Repeated migraine attacks could result in a chronic state of dysregulation of pain pathways that might explain the resistance to acute therapy that some migraineurs eventually experience.[19] A recent meta-analysis of 40 published clinical studies of acute and chronic migraine patients sought to identify common biomarkers in cerebrospinal fluid (CSF) and blood.[20] As expected, CGRP was commonly found to be increased in both compartments. Other potential biomarkers frequently identified were nerve growth factor (NGF, only increased in CSF), glutamate, and beta-endorphin (significantly decreased in migraineurs), suggesting pathways for further investigation.

7.05.1.3 Medications for Migraine

The majority of migraine sufferers remain undiagnosed or misdiagnosed, commonly with either sinus- or tension-type headache, despite efforts to motivate patients to seek physician care and treatment.[21] Among the undiagnosed population, there is a high degree of self-treatment with over-the-counter medications. Antimigraine drugs can be divided into two classes: abortive and preventative. The former has been dominated by over-the-counter analgesics, such as acetaminophen and nonsteroidal anti-inflammatory drugs (NSAIDs) and, since the early 1990s, by the triptans (5-$HT_{1B/1D}$ agonists) most of which are now available as generics. Overuse of several types of acute migraine medications has been shown to result in progression to increasingly chronic migraine conditions in some patients.[22]

Preventative treatments are primarily used by frequent and chronic migraineurs along with acute treatments and include a wide range of drug classes (**Table 1**). Most of these prophylactic agents are older drugs whose mechanisms of action are often incompletely understood and whose biological activities and/or side effect profile determines who can use them. Notably, there are no approved disease-specific treatments for migraine prevention. NSAIDs are also used for migraine prophylaxis, either intermittently or daily, especially if migraine triggers are predictable.[23] However, their adverse effects on the GI tract, a result of cyclooxygenase-1 (COX-1) inhibition, can make chronic use problematic.

7.05.1.4 Older Acute Migraine Drug Classes

7.05.1.4.1 Ergot alkaloids

Ergotamine (**1**, **Fig. 1**) has been used as an acute antimigraine agent since 1925. Prominent side effects such as severe nausea and chest tightness were common until it was largely replaced by dihydroergotamine (**2**, DHE) in 1945.[25] DHE, especially in its intravenous (IV) and subcutaneous (SC) formulations, remains a highly effective abortive treatment for severe migraine. Ergotamines display complex pharmacology through interactions with a variety of neurotransmitter targets, including not only the serotonin 5-HT_{1B} and 5-HT_{1D} receptors ($IC_{50} \leq 1$ nM), known to be involved in the antimigraine activity of the triptans, but also 5-HT_{2B} and 5-HT_{2C} receptors ($IC_{50} < 10$ nM) that may contribute to efficacy.[26] They also bind with high affinity ($IC_{50} < 10$ nM) to 5-HT_{1A} and 5-HT_{2A} receptors; noradrenaline α_{1A}, α_{2A}, and α_{2B} receptors; and dopamine D_{2L}, D_3, and D_4 receptors. Antimigraine activity was long thought to be solely due to constriction of meningeal arteries, but newer evidence suggests that ergotamines, like

Table 1 Currently used preventative migraine therapies[24]

Drug class	*Examples*
Anticonvulsants	Topiramate
	Valproate
	Gabapentin
Antidepressants	Tricyclics
	Duloxetine
ACE inhibitors	Lisinopril
Calcium channel blockers	Verapamil
	Flunarizine
Beta adrenergic blockers	Atenolol
	Propranolol
Melatonin agonists	Ramelteon
Miscellaneous	Vitamin B12
	Botulinum toxin
	Coenzyme Q10
	Magnesium
	Glucocorticoids

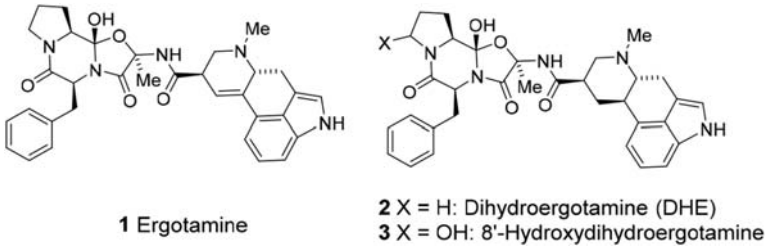

Fig. 1 Ergotamine, dihydroergotamine (DHE), and the metabolite of DHE, 8′-hydroxydihydroergotamine.

the triptans, exert additional effects on neurotransmission and neurogenic inflammation.[27] DHE has been used as both an abortive and an preventative migraine therapy, but recently, the European Union has limited ergot alkaloids to acute indications, in part due to an increased risk of fibrosis with chronic use.[28] DHE has low oral bioavailability due to extensive oxidative metabolism in the liver and poor gut penetration. However, upon repeated oral administration, a prominent active metabolite, 8′-hydroxydihydroergotamine (**3**, 8′-OH-DHE), is formed, which has a long half-life (10–13 h). This has been postulated to account for the low rate of headache recurrence seen with DHE.

7.05.1.4.2 5-HT$_{1B/1D}$ agonists (triptans)

The vascular theory of migraine, supported by the efficacy of the ergotamines, led to an effort in the last quarter of the 20th century to develop more selective abortive medications, focusing on the role of serotonin (**Fig. 2**). This work specifically targeted agonism of the 5-HT$_{1B/1D}$ receptor subtypes known to be involved in vasoconstriction,[29] in order to avoid the multiplicity of pharmacological effects serotonin can elicit.[30]

Sumatriptan (**5**) was introduced by Glaxo in 1991 and was a milestone in migraine treatment, being not only the first rationally designed compound for this indication but also the first that was free of severe side effects in most patient populations.[31,32] By bismethylation of the amino group and replacement of the hydroxyl of the serotonin indole core with a sulfonamide side chain, a great degree of selectivity had been obtained for 5-HT$_{1B/1D}$ over the 14 other known 5-HT$_1$ receptors. Sumatriptan has fairly low oral bioavailability (see **Table 2**[33,34]) and is also available in SC and intranasal (IN) formulations. Interestingly, there has been no simple pharmacodynamic/pharmacokinetic (PK/PD) relationship for migraine efficacy in humans, leading to speculation regarding the importance of rate of absorption on activity.[35] In general, SC injection provides not only the most rapid and profound migraine relief but also the most pronounced on-target side effects. Sumatriptan remains the most prescribed triptan, and numerous reviews on it have been written.[36,37]

The six subsequent "second-generation" triptans developed by Glaxo and other companies, mostly through the 1990s, with the intention of improving pharmacological and pharmaceutical properties, all retain the tryptamine core of serotonin. Rizatriptan, zolmitriptan, and almotriptan utilize the indole C3 dimethylaminoethyl group found in sumatriptan and differ in the indole C5 substituent. Frovatriptan and eletriptan contain conformationally restricted aminoethyl groups—frovatriptan with its *N*-methylaminocyclohexeno group fused at C2 and C3 of the indole scaffold and eletriptan with its indole C3 *N*-methylpyrrolidin-2-ylmethyl side chain. All "second-generation" triptans are potent 5-HT$_{1B/1D}$ receptor agonists, differing somewhat in their

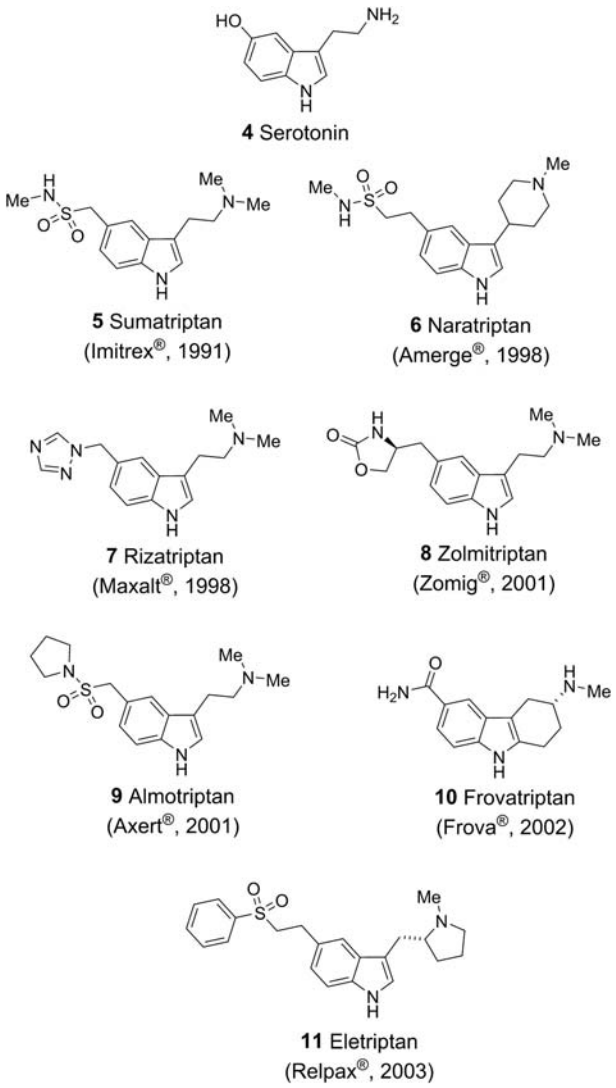

Fig. 2 Serotonin and the triptans, including the year of FDA approval for triptans.

off-target 5-HT_1 profiles.[38] They also differ, sometimes greatly, in their physiochemical and absorption, distribution, metabolism, and excretion (ADME) properties, as well as CNS penetrance (Table 2). At the time of their discovery and development, there was hope that these differences would lead to superiority in clinical efficacy and a reduction in adverse events compared to sumatriptan. However, there are still insufficient data to show clear distinctions between the individual triptans.[39] As shown in Table 2, the triptans provide relief in approximately 60% of migraine attacks with significant headache recurrence after 24 h for all members. Differences experienced in patients are likely due to individual variations in metabolism or genetics. As a result, migraineurs will

Table 2 Comparison of clinical pharmacokinetic and efficacy of marketed triptans

Drug, PO dose	*Company*	F_{PO} *(%)*	T_{max} *(h)*	$T_{1/2}$ *(h)*	*Onset of relief (h)*	*Pain relief at 2 h (%)*	*Pain free at 2 h (%)*	*Headache recurrence at 24 h (%)*
Sumatriptan, 50 mg	Glaxo	15	2.5	2	0.5–1	50–61	30–32	29–34
Naratriptan, 2.5 mg	Glaxo	40–48	2–3	6	0.75	NA	NA	27–45
Rizatriptan, 10 mg	Merck	70	3–4	3	1–3	67–77	40–44	28–47
Zolmitriptan, 2.5 mg	AstraZeneca	45	1–1.5	2	0.5–2	62–65	22–39	13–39
Almotriptan, 12.5 mg	Johnson & Johnson	70	1–3	3–4	1–3	57–65	18	18–27
Frovatriptan, 2.5 mg	Elan	20–30	1–2	26	1–2	38–40	NA	9–14
Eletriptan, 80 mg	Pfizer	50	2	4	1–2	65–80	37	21–33

often switch to a new triptan until they find the most effective one for them or when the efficacy of a given triptan begins to diminish.

Sumatriptan has direct, dose-dependent vasoconstrictive effects on intracranial blood vessels that have been correlated with its antimigraine activity.[40] All triptans share this property, and accordingly, the majority of adverse events associated with triptan use are a result of vasoconstriction of tissues other than cranial arteries, including cardiac vessels and other vasoactive tissues. In rare cases, ischemic cardiac events have been reported with triptan use.[41] Off-target blood vessel and tissue vasoconstriction is the major adverse event with this class, limiting the number of doses allowed per migraine attack and during the course of a month. CGRP receptor antagonists represent a newer mechanism that does not involve active vasoconstriction and may provide safer antimigraine agents.

7.05.2 Calcitonin Gene-Related Peptide

7.05.2.1 CGRP and Migraine

Migraine is a complex and heterogeneous neurological disorder that defies simple explanations.[42,43] Nonetheless, significant progress in understanding the nature of migraine and its underlying causes has been made over the past few decades. Multiple lines of evidence have pointed to a key role for CGRP in migraine pathophysiology and led to interest in the peptide as a therapeutic target.[44] CGRP, a 37-amino acid neuropeptide that was first described in 1982,[45] is widely expressed in the peripheral and central nervous systems and has been implicated in a range of biological functions,[46] including vasodilation,[47,48] nociception,[42,49] inflammation,[50,51] and regulation of insulin release.[52,53]

Based on its apparent role in cerebrovascular regulation, Edvinsson postulated that the peptide could be involved in migraine pathophysiology over 30 years ago.[54] This hypothesis has subsequently been substantiated by a number of key studies, including some that resulted from an important collaboration between Edvinsson and Goadsby. Examining the craniovascular levels of several neuropeptides during migraine attacks, they observed a significant increase in the levels of CGRP in migraineurs during an attack, while the concentrations of other neuropeptides, such as neuropeptide Y or substance P, were unchanged.[55] In a follow-up experiment, it was found that these migraine-associated elevations of CGRP could be returned to baseline by successful treatment of the headache with sumatriptan.[56] Further compelling evidence for the importance of CGRP in migraine was provided by another study in migraineurs demonstrating that IV infusion of the peptide could induce a migraine-like headache.[57] These and other studies have pointed to a crucial role for CGRP in migraine and, by the late 1990s, led to significant interest in the development of novel therapeutics that could block the effects of the neuropeptide.

7.05.2.2 CGRP Receptor Structure and Function

CGRP, calcitonin (CT), amylin (AMY), and adrenomedullin (AM) comprise the calcitonin family of peptides.[58,59] In spite of significant differences at the level of amino acid sequence, these related peptides share key structural features, including an *N*-terminal cyclic structure formed with a Cys–Cys disulfide bond and a C-terminal amide group.[58] The cyclic moiety at the *N*-terminus of CT family peptides is important for receptor activation, and its removal can convert the endogenous agonist into an antagonist. For example, deletion of the first seven amino acids from CGRP affords a functional antagonist of the CGRP receptor ($CGRP_{8-37}$).[59] Like CGRP, the other CT family peptides are widely distributed and involved in a variety of biological processes.[58] Two forms of CGRP are known: α-CGRP, produced by alternate splicing of the CT gene, and β-CGRP, which is encoded by a separate gene.[59] Fig. 3 details the primary structures of human α-CGRP and β-CGRP, which differ by three amino acids. Although α-CGRP and β-CGRP possess very similar activities, they differ in terms of distribution, with α-CGRP being more prevalent in primary neurons while β-CGRP predominates in enteric neurons.[60]

The CGRP receptor (CGRP-R) is a multimeric protein and consists of the calcitonin receptor-like receptor (CLR) and receptor activity-modifying protein (RAMP) 1, with the RAMP1 protein being essential for production and function of the CGRP-R.[61,62] CLR is highly homologous to the calcitonin receptor (CTR), and both proteins are known to associate with RAMPs.[63] CLR and CTR are members of the secretin family (family B) of G-protein-coupled receptors (GPCRs), and they share a number of structural features with other family B GPCRs, including seven-transmembrane domains and large *N*-terminal extracellular domains (ECDs) that are essential for binding of their peptide agonists.[63] Like these GPCRs, the RAMPs are also transmembrane proteins, and each RAMP possesses a single-transmembrane domain attached to a significant *N*-terminal ECD.[61] The association of CLR and CTR with different RAMPs leads to pharmacologically distinct receptors.[63] As already mentioned, the CGRP-R results from coexpression of CLR and RAMP1. However, CLR is also known to form high-affinity AM receptors, known as the AM_1 and AM_2 receptors, by association with RAMP2 or RAMP3, respectively.[62] The coexpression of CTR with RAMP1, RAMP2, or RAMP3 is known to produce

α-CGRP NH_2-ACDTATCVTHRLAGLLSRSGGVVKNNFVPTNVGSKAF-NH_2

β-CGRP NH_2-ACNTATCVTHRLAGLLSRSGGMVKSNFVPTNVGSKAF-NH_2

Fig. 3 Primary structures of human α-CGRP and β-CGRP.

receptors for AMY, designated the AMY_1, AMY_2, and AMY_3 receptors, respectively.[62] Because CTR is similar to CLR in terms of primary structure, the AMY_1 receptor (CTR/RAMP1) is structurally similar to the CGRP-R (CLR/RAMP1) so it is not surprising that some small-molecule CGRP receptor antagonists also bind to the AMY1 receptor (*vide infra*).

In principle, the RAMPs could exert their effect on the binding of endogenous ligands, such as CGRP and AM, via an allosteric mechanism in which they alter the peptide binding site on CLR or by interacting directly with the ligand. The experimental evidence has favored the latter possibility since the earliest reports on CLR/RAMP1 (the CGRP-R). Cross-linking studies using [^{125}I]CGRP showed that the agonist appears to interact with both CLR and RAMP1.[61,64] Experiments with both chimeric receptors and deletion mutants demonstrated that the ECDs of both CLR and RAMP1 are important for agonist binding and selectivity.[65,66] Site-directed mutagenesis of human RAMP1 revealed that Trp84 in the ECD of this protein is particularly important for the potency of CGRP.[67] Antagonists of the CGRP-R also appear to interact with the ECDs of both CLR and RAMP1. A number of residues in both ECDs have been shown to contribute to binding of antagonists, with CLR Met42, RAMP1 Trp74, and RAMP1 Trp84 being especially important for receptor affinity.[62,67–70] It should be noted that some small-molecule CGRP receptor antagonists do not appear to interact with the ECD. For example, the hydroxypyridine class of antagonists block CGRP in a RAMP-independent manner[71] and are believed to interact with transmembrane domain 7 (TM7) in CLR and make no contact with the ECDs of either CLR or RAMP1 (*vide infra*).[69]

Therefore, before any detailed structural information on the CGRP-R was obtained, the available evidence indicated that both CGRP and CGRP receptor antagonists made a number of key interactions with the ECDs of both CLR and RAMP1. Indeed, the known data are consistent with the two-domain model for family B GPCRs described by Hoare more than a decade ago.[72] A schematic representation of this model for the CGRP receptor is illustrated in **Fig. 4**. Consistent with the mutagenesis and cross-linking studies, the two-domain model emphasizes a key role for the ECD in binding of both the peptide agonist and antagonists. According to the model, the C-terminal portion of CGRP initially binds to the ECD of the receptor, formed by the *N*-termini of CLR and RAMP1. Thus, anchored to the receptor by its C-terminal region, the CGRP *N*-terminus is brought into proximity with the juxtamembrane portion of CLR. This "affinity trap" greatly increases the local concentration of the CGRP *N*-terminal region, enabling it to interact with CLR and induce a conformational change that results in activation of the receptor. Based on the known mutagenesis data, most small-molecule antagonists are thought to block the effects of CGRP by preventing the peptide's initial interaction with the ECD of CLR/RAMP1.[62]

For many years, detailed structural data were available for only a few GPCRs, although significant progress has been made in past decade.[73] Even today, obtaining such information is complicated by the membrane-bound nature of GPCRs and the challenges of expressing, isolating, and purifying the proteins.[74] The CGRP receptor has the added complication of being a heterodimer. However, since most small-molecule antagonists of the CGRP-R apparently bind to the ECD, a team at Vertex Pharmaceuticals attempted to obtain structural data for this extracellular portion. They successfully expressed, purified, and refolded a soluble form of the CGRP-R ECD comprising a complex of the truncated *N*-terminal domains of CLR and RAMP1.[75] This soluble CGRP-R ECD bound the peptide CGRP with relatively low affinity ($IC_{50} = 12\ \mu M$) but had much higher affinity for known small-molecule antagonists ($K_D < 0.02\ \mu M$), consistent with the two-domain model (**Fig. 4**) in which the peptide also interacts with other portions of the CGRP-R.[75] Importantly, the CGRP-R ECD complex was crystallized, and the structure of the CLR–RAMP1 ectodomain was solved (**Fig. 5**).[76]

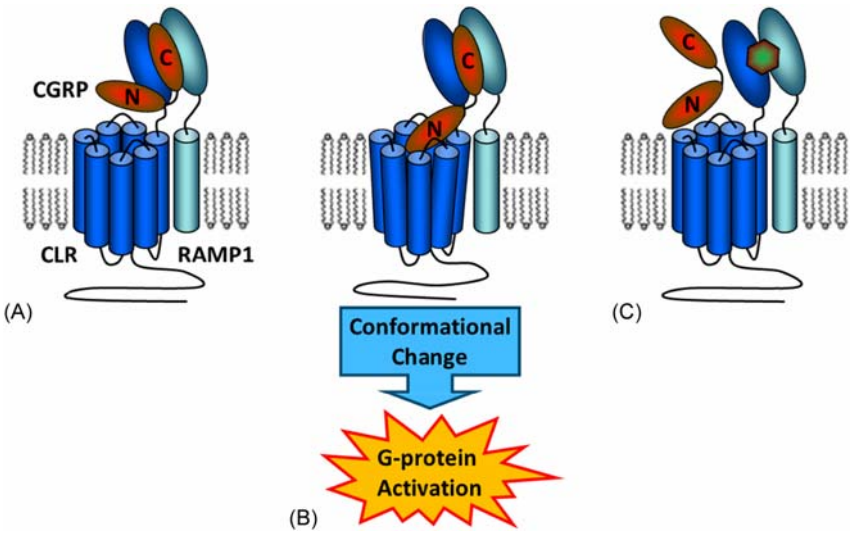

Fig. 4 Schematic two-domain model of CGRP receptor activation. (A) The C-terminal portion of CGRP *(red)* binds to the extracellular domains of CLR *(blue)* and RAMP1 *(teal)*, producing an increase in the local concentration of the CGRP *N*-terminus. (B) The *N*-terminal portion of CGRP interacts with the CLR juxtamembrane region, producing a conformational change in the GPCR that leads to G-protein activation and signaling. (C) A small-molecule antagonist *(green)* blocks binding of CGRP to the extracellular domains of both CLR and RAMP1, preventing receptor activation.

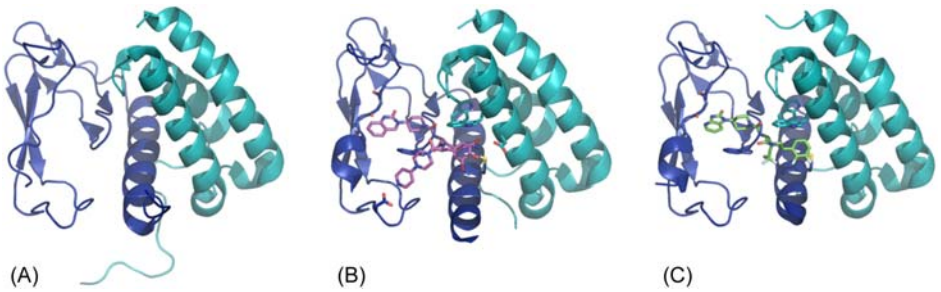

Fig. 5 Crystal structures of CLR–RAMP1 ectodomain complexes depicted as ribbon diagrams.[76] CLR *(blue)* and RAMP1 *(teal)* are shown as (A) unliganded (PDB ID 3N7P), (B) complexed with olcegepant *(magenta)* (PDB ID 3N7S), and (C) complexed with telcagepant *(green)* (PDB ID 3N7R).

The crystal structure of the unliganded CGRP-R ectodomain complex is shown in Fig. 5A. The ECD of CLR (shown in blue) exhibits some features that are similar to known structures of the ECDs of other family B GPCRs, such as those of the parathyroid hormone (PTH) receptor[77] or gastric inhibitory polypeptide (GIP) receptor.[78] Common features in these GPCR structures include a helix (residues 35–53 in CLR) and a finger-like structural motif (residues 65–81 in CLR) that is stabilized by a pair of disulfide bonds.[76] The RAMP1 ectodomain (shown in teal) contains a three-helix bundle, and two of these helices pack against the *N*-terminal helix in CLR in a perpendicular fashion, forming an interface at which multiple interactions that apparently stabilize the CLR–RAMP1 heterodimer occur. The overall structure of the RAMP1 ECD reported by ter Haar et al. is similar to a previously described crystal structure of the RAMP1 ECD alone.[79] The structures of other family B GPCR ectodomains, for example, the PTH1 receptor and the GIP receptor, have been reported as complexes with their respective endogenous ligands (PTH and GIP), in which the peptides bind in a helical conformation.[77,78] Based on the similar overall structure of the CLR ECD, the Vertex group suggested that the CGRP peptide might bind in the pocket formed at the interface between CLR and RAMP1.[76] This binding mode would place the peptide ligand close to residues that have been shown to be important for the interaction of CGRP with its receptor by mutagenesis studies.[59]

7.05.2.3 CGRP Receptor Antagonist Binding

Since the description of the first small-molecule CGRP receptor antagonists, there has been speculation about how they were able to block the binding of a 37-amino acid peptide, and a basic model for their action was developed (Fig. 4). It was recognized that many of the small-molecule antagonists possessed some common features, including a terminal cyclic amide or urea moiety that appeared to be a crucial element in the so-called "privileged structure"[80] found in these molecules (Fig. 6). In both olcegepant[81] (**12**) and telcagepant[82] (**13**), for example, a bicyclic *N*-aryl urea at one end of the structure was known to be critical for potency (Fig. 6).

The Vertex team revealed how these privileged structures and other key moieties contribute to binding to the CGRP-R when they solved the crystal structures of the CGRP ECD complex bound to both olcegepant (**12**) and telcagepant (**13**) (Figs. 5 and 7).[76] These structures demonstrated how a small molecule could bind to and antagonize a family B GPCR (Fig. 7). In the crystal structures of the complexes with **12** and **13**, the privileged structure amide moiety is involved in hydrogen-bonding interactions with the backbone elements of CLR Thr122.[76] Additionally, these structures revealed the important role of several residues that have been shown to function in antagonist binding by mutagenesis studies.[67–70] For example, CLR Met42, RAMP1 Trp74, and RAMP1 Trp84 contribute to the formation of a hydrophobic pocket at the interface of the two proteins. In the crystal structures of the complexes, this pocket

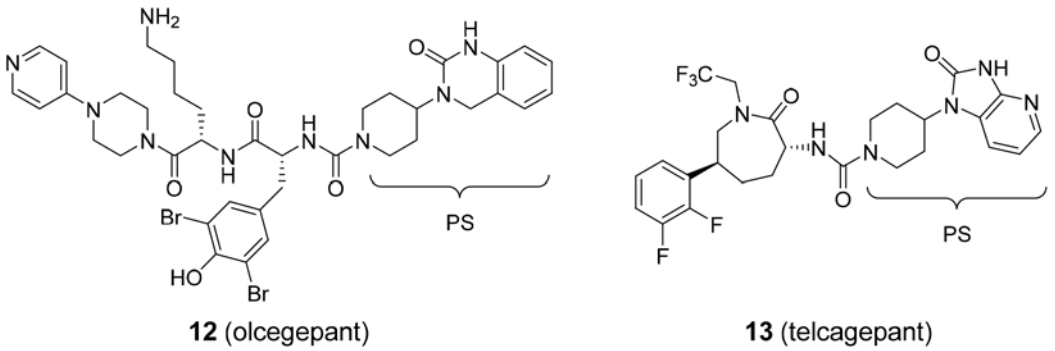

Fig. 6 Structures of olcegepant and telcagepant showing the privileged structure (PS) moiety in each.

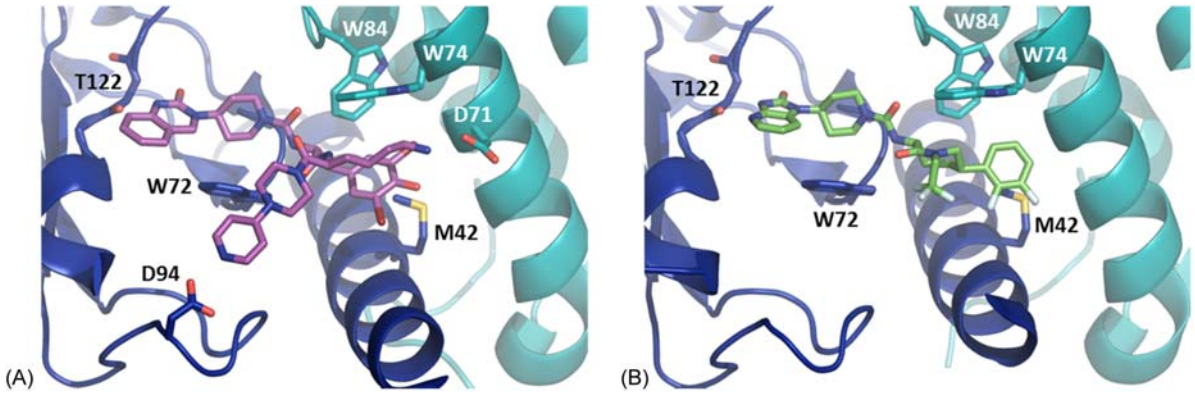

Fig. 7 Crystal structures of the CLR–RAMP1 ectodomain complexes with small-molecule antagonists bound.[76] View of small-molecule antagonist binding site formed by CLR *(blue)* and RAMP1 *(teal)* complexed with (A) olcegepant *(magenta)* (PDB ID 3N7S) and (B) telcagepant *(green)* (PDB ID 3N7R). Side chains of selected residues involved in antagonist binding are shown and labeled in *black* (CLR residues) or *white* (RAMP1 residues).

accommodates aromatic rings in the antagonists that contribute significantly to receptor affinity: the dibromophenol in **12** and the difluorophenyl ring in **13**. Other residues appear to interact with the antagonists in these complexes, notably CLR Trp72, which stacks against the piperidine rings of the privileged structures and also forms a hydrogen bond from the indole NH to carbonyl groups in both **12** and **13**.[76]

The X-ray crystallography work also revealed that both **12** and **13** exhibit a similar binding topology, with an extended conformation that allows them to bridge a distance of about 18 Å from the Thr122 hydrogen bonding interactions with the privileged structure to the hydrophobic pocket at the CLR/RAMP1 interface.[76] Overall, it appears that these small-molecule antagonists need to span this appreciable distance in order to effectively block binding of CGRP.[76] This observation is consistent with reported structure–activity data for analogs of olcegepant and telcagepant, which clearly reveal the importance of the hydrogen bond donor–acceptor pair in the privileged structure and the aromatic ring that binds in the hydrophobic pocket.[81,82] The requirement to bridge across this binding site, coupled with the apparent need for other hydrogen-bonding interactions, such as those with CLR Trp72, may explain why so many potent small-molecule CGRP-R antagonists are relatively large molecules with multiple amide groups. The nature of the antagonist-binding site therefore appears to favor these structures that, by their nature, do not conform to known guidelines for orally bioavailable drugs such as the Lipinski "rule of five."[83] This observation highlights the difficulty of designing orally acting compounds that target this family B GPCR.

Thus, the hydrophobic pocket at the interface of CLR and RAMP1 appears to be crucial for binding of antagonists, and the residues CLR Met42, RAMP1 Trp74, and RAMP1 Trp84 have been shown to affect antagonist-binding affinity and, in the case of RAMP1 Trp84, agonist potency.[67,84] One of these residues can also have a profound impact on the species selectivity observed for most small-molecule antagonists, which typically display much higher affinity for the CGRP receptors of primates compared with nonprimates.[62] This selectivity can make it difficult to achieve meaningful CGRP blockade in rodents, and consequently, nonhuman primate models have been developed to allow in vivo evaluation of CGRP-R antagonism. Examples include models based on facial flushing in marmosets[85] or capsaicin-induced dermal vasodilation in rhesus monkeys.[86] A team at Merck demonstrated that this species selectivity appeared to be controlled by a section of the RAMP1 protein, specifically by RAMP1 residue 74, which is Trp in most primates but Lys in rat and mouse. Interestingly, mutation of this residue in rat RAMP1 to Trp produced a mutant rat CGRP receptor with humanlike pharmacology.[68] The demonstration that a humanlike CGRP-R could be produced in rodents via a single-amino-acid substitution inspired studies that led to the production of transgenic mice with humanized CGRP receptors and such engineered animals could prove to be valuable tools for investigating the in vivo properties of CGRP and its receptor.[87]

7.05.3 Small-Molecule CGRP Receptor Antagonists

7.05.3.1 CGRP Receptor Antagonists From Boehringer Ingelheim

7.05.3.1.1 BIBN4096 BS

The first small-molecule CGRP receptor antagonist discovery effort was carried out by scientists at Boehringer Ingelheim (BI), and it was successful in demonstrating the first clinical proof of concept for CGRP receptor antagonism in the acute treatment of migraine with BIBN4096 BS (olcegepant, compound **12**).[81] A high-throughput screen against the human CGRP receptor expressed in SK-N-MC cells (a human neuroblastoma cell line) led to the identification of a dipeptide analog containing L-Lys and an unusual amino acid, D-3,5-dibromotyrosine (**14**, Fig. 8) as a weakly potent but verifiable hit ($IC_{50} = 17\ \mu M$). The related aniline (**15**) also showed some activity. The other three combinations of amino acid stereoisomers were inactive ($IC_{50} > 300\ \mu M$), fixing the stereochemical preference of the receptor for this chemotype. Related 3,5-dibromoanilines in the BI compound collection were

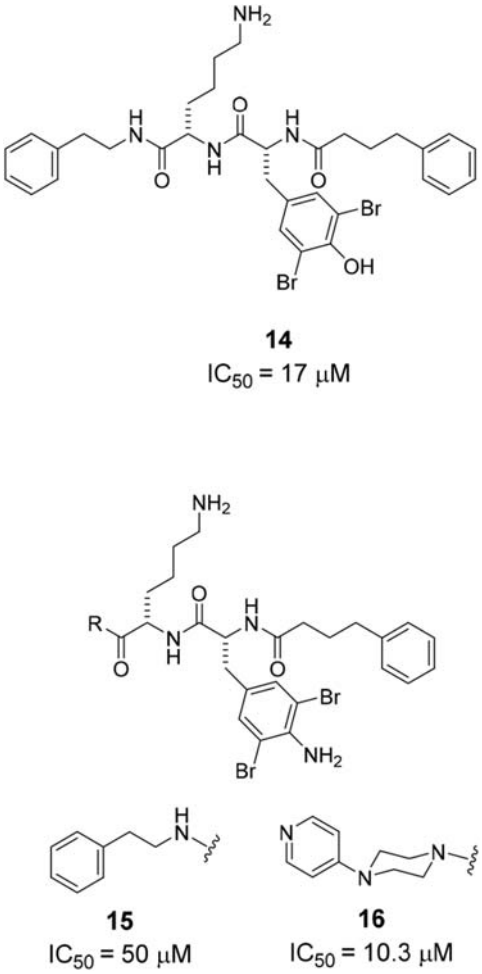

Fig. 8 Early lead structures in the development of olcegepant.

tested, and significantly better activity was seen for the constrained, heterocyclic *N*-4-pyridylpiperazine (**16**, $IC_{50} = 10.3$ μM). This Lys substituent was the mainstay of subsequent structure–activity relationship (SAR) and indeed remained in olcegepant.

Further SAR work was carried out using the somewhat more potent D-dibromotyrosine core. Table 3 shows the evolution of what became the first of a series of GPCR-privileged structures that confer specificity and potent antagonist activity against the CGRP receptor (*vide supra*). Some advantage had already been seen with ureas as *N*-terminal substituents, and methoxy-substituted phenethylamines **17** ($IC_{50} = 1000$ nM) and **18** ($IC_{50} = 200$ nM) brought activity down to the submicromolar level. Exploration of isosteric piperazine- and piperidine-constrained anisoles **19** ($IC_{50} = 226$ nM) and **20** ($IC_{50} = 250$ nM) maintained activity, while a presumably better hydrogen bond accepting cyclic urethane further enhanced CGRP receptor binding by fivefold (**21**, $IC_{50} = 44$ nM). Profound improvements in potency were realized by the further addition of a hydrogen bond-donating urea NH_2 (**22**, $IC_{50} = 4.7$ nM), incorporation of this into an imidazolone (**23**, $IC_{50} = 0.2$ nM), and ring expansion into a tetrahydroisoquinolone (**12**, BIBN4096 BS, olcegepant, $IC_{50} = 0.03$ nM). Olcegepant possesses higher affinity for the human CGRP-R than the endogenous ligand and is 150-fold more potent than the peptide antagonist $CGRP_{8-37}$. Compound **24** is comparably potent. However, the phenylimidazolone in **24** has been shown to be oxidatively unstable.[88] The BI scientists have not yet reported SAR for alternatives to the core amino acids, but it is surely notable that the L-Lys-D-dibromotyrosine portion of the screening lead remained in the compound that entered clinical trials.

BIBN4096 BS (Fig. 9) was shown to be a highly potent, full antagonist ($pA_2 = 11.1$) in a cyclic AMP (cAMP) assay in SK-N-MC cells. The compound is three log units less potent against rat and other nonprimate CGRP receptors ($IC_{50} = 6.4$ nM).[85] This is not seen with the peptide antagonist $CGRP_{8-37}$, but has been found to be a common feature among small-molecule CGRP antagonists. As described earlier, this divergence has been ascribed to the critical difference in hydrophobicity of residue 74 of the RAMP1 component protein of the CGRP-R, which for primates is Trp, while nonprimates have Lys or Arg.[68] Interestingly, BIBN4096 BS is reported to be a competitive antagonist at the human receptor, expressed in SC arteries, at low concentrations (c.0.01 nM), but noncompetitive at higher concentrations (0.1–1 nM).[89]

Table 3 Human CGRP receptor binding affinities of dipeptide CGRP antagonists

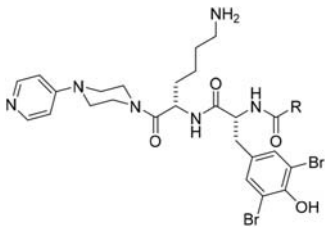

Compound	*R^1*	*hCGRP-R IC_{50} (nM)*
17	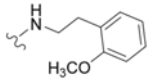	1000
18	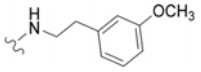	200
19	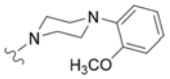	226
20	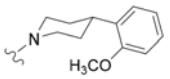	250
21	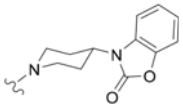	44
22	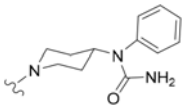	4.7
23	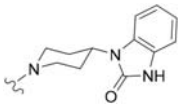	0.2
12	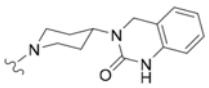	0.03
24	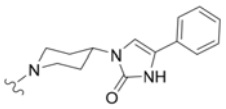	0.05

Aspects of the SAR leading to olcegepant can be better appreciated in the context of the Vertex CGRP receptor ectodomain X-ray structural studies, in which the compound was cocrystallized with the protein complex (Fig. 10).[76] As expected, since the compound spans a portion of the interface between CLR and the RAMP1 protein, it binds in a highly extended state, covering about 18 Å. The GPCR-privileged tetrahydroisoquinolone urea, which has been postulated to mimic the C-terminal Phe-NH_2 of the CGRP peptide,[90,91] forms highly optimized donor–acceptor-pair hydrogen-bonding interactions with the Thr122 carbonyl and NH. This structural picture makes it easier to understand the evolution of the pharmacophore comparing, for example, compound **21** (Table 3; no hydrogen bond donor, $IC_{50}=44$ nM) with compound **23** (Table 3; benzimidazolone NH, $IC_{50}=0.2$ nM). Further significant improvements in potency were then achieved as the aryl ring was further extended into a largely lipophilic pocket with olcegepant ($IC_{50}=0.03$ nM) and compound **25** ($IC_{50}=0.05$ nM).

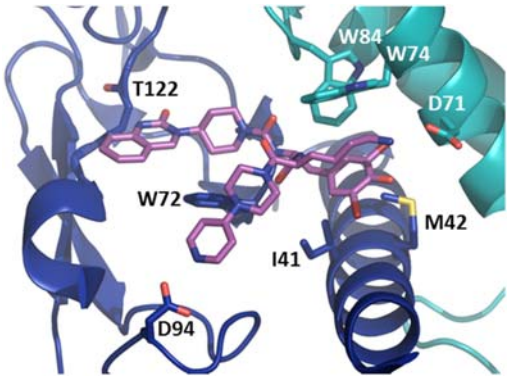

Fig. 9 Crystal structure of the CLR–RAMP1 ectodomain complex with olcegepant (compound **24**) *(magenta)* showing the binding site formed by CLR *(blue)* and RAMP1 *(teal)*.[76] Side chains of selected residues involved in antagonist binding are shown and labeled in *black* (CLR residues) or *white* (RAMP1 residues).

The importance of the Trp74 residue of RAMP1 for binding of compounds like olcegepant to the primate CGRP-R is illustrated in Fig. 10, where, as discussed earlier, it forms a hydrophobic pocket, along with RAMP1 Trp84, CLR Met42, and CLR Ile43, which interacts with the dibromotyrosine side chain and the alkyl portion of the lysine. Replacement of RAMP1 Trp74 with Lys or Arg would remove the lipophilic ceiling to this pocket and significantly alter the electrostatic environment.

Olcegepant has been used as a biochemical tool compound in numerous studies that have elucidated the mechanisms and consequences of CGRP receptor antagonism.[92] In order to differentiate it from the triptans as a "nonvasoconstricting" antimigraine agent, olcegepant was tested in ex vivo preparations of dog and human coronary arteries. In contrast to sumatriptan but in accordance with the expected mechanism of CGRP receptor antagonism, it was found to have no inherent vasoconstrictive properties.[93]

In a marmoset model of neurogenic vasodilation in which TGVS-mediated secretion of CGRP was induced by direct electrical stimulation of the trigeminal ganglion, IV-administered olcegepant was found to inhibit the resulting increases in facial blood flow (a surrogate marker for vasodilation) in a potent, dose-dependent manner with $ED_{50} = 3\ \mu g\ kg^{-1}$.[85] The compound was similarly tested in rats in both a facial blood flow and a intravital model. Electric stimulation resulted in dilation of the middle meningeal artery and cortical pial arterioles. However, olcegepant only caused a significant reduction in dilation of the former, which is not protected by the blood–brain barrier (BBB), suggesting a purely peripheral action of the compound.[94]

As might be expected for a fairly large (MW = 870) and highly polar molecule containing more than 10 hydrogen-bonding groups and several ionizable functionalities, olcegepant showed very low oral bioavailability in animals ($F_{PO} < 1\%$ in rat and dog) and was largely unbound by plasma proteins.[81] As a result, clinical proof of concept and safety studies were carried out using an IV formulation.

A phase I study in healthy volunteers specifically addressed the potential cardiovascular safety issues around CGRP-R antagonism. No significant changes in electrocardiogram, blood pressure, pulse rate, or forearm blood flow were seen with IV doses up to 10 mg.[95] Other phase I studies examined cerebrovascular effects of olcegepant (2.5 or 10 mg, IV) using brain imaging[96] and the ability of the compound (at a 2.5 mg dose) to prevent CGRP-induced headache in healthy volunteers.[97] Again, no undesired effects were observed. The compound effectively inhibited CGRP-induced headache in the 6 of 10 patients in which it manifested itself, and imaging appeared to confirm that pain relief, at least in this model, occurred without significant effects on major CNS blood vessels, including the middle cerebral artery.

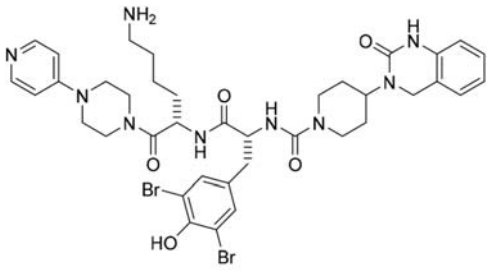

12

Olcegepant (BIBN4096 BS)

Fig. 10 Olcegepant (BIBN4096 BS), the first CGRP antagonist to be tested in the clinic.

A multicenter, double-blind, randomized phase II clinical trial of olcegepant was carried out in 126 patients with migraine receiving placebo or total doses of 0.25, 0.5, 1.0, 2.5, 5.0, or 10.0 mg (IV, total dose) infused over a period of 10 min.[98] No serious adverse events were observed up to the highest dose. Mild paresthesia (8%) was the only significant adverse event reported. Mean maximal C_{max} levels were dose-proportional. Human V_d (20 L) generally reflects a highly polar molecule with limited bilayer membrane permeability. Total plasma clearance (C_L) was 12 L h^{-1} and terminal $T_{1/2} = 2.5$ h.

Two hours following a 2.5 mg dose, 66% of patients reported significant migraine pain relief. The therapeutic response was similar to that observed for oral triptans in previous clinical trials, though less than that reported for sumatriptan, dosed SC.[99] No further improvement in the primary or secondary end points was seen at higher doses, and no significant efficacy was seen at the next lower dose (1 mg). Patients treated with olcegepant also exhibited significant superiority over the placebo group with regard to most secondary end points, including pain-free response rate at 2 h; rate of sustained response over 24 h; rate of headache recurrence; improvement in nausea, photophobia, phonophobia, and functional capacity; and time to meaningful pain relief. It is worth noting that a total plasma $C_{max} > 200$ nM appeared necessary for olcegepant ($K_i = 0.014$ nM) to demonstrate robust clinical efficacy. If indeed peripheral CGRP-Rs are the target for olcegepant, this may represent at least a 1000-fold required coverage over binding K_i. On the other hand, if the target receptors are on the abluminal side of the dilated blood vessels, then this may partly reflect a permeability barrier for the highly polar molecule. A further possibility involves the hypothesis that the blood–brain barrier is somewhat compromised during migraine attack. Olcegepant on its own would not be expected to be significantly brain-penetrant. However, a leaky BBB might allow a fraction of the compound in plasma into the CNS to act on central CGRP receptors. This is a controversial issue, and it has been argued that it is not necessary to invoke a leaky BBB in this regard and that if even a small fraction of the 200 nM total plasma olcegepant entered the CNS, it might be sufficient to act on central CGRP-Rs.[100] In May 2006, BI announced that it had discontinued development of olcegepant.[101]

From a marketing point of view, an injectable CGRP antagonist may be unlikely to be more than a niche product. There is evidence in the patent literature that BI had explored noninjectable formulations of olcegepant, most prominently a powder inhalation form.[102]

7.05.3.1.2 BI 44370

Further work at BI resulted in a small-molecule CGRP receptor antagonist, BI 44370 (compound **41**, **Fig. 16**),[88] which could be dosed orally, and that was tested in clinical trials for acute migraine.[103] However, published reports describing the evolution of this compound from olcegepant have not yet appeared. In their medicinal chemistry paper on the work leading to olcegepant,[81] the authors state that progress had been made on "novel CGRP antagonists of reduced size and structural complexity," perhaps implying that oral or at least non-IV dosing was a further goal of the program. In the published applications cited in that paper, some idea of the approaches tried can be gleaned from looking at the many examples prepared, even though no discrete biological data are provided. Selected exemplified compounds that show some of the structural variety explored are shown in **Figs. 11–14**. They demonstrate a clear focus on reducing polar surface area and suggest that alternative D-amino acids were investigated early on.[104] Not surprisingly, the Lys residue in olcegepant is missing from all but a handful of exemplified compounds, and the central urethane NH is often replaced by a methylene[105] and later an oxygen.[106] Several series were investigated in which the entire C-terminal substituent and the carboxyl itself on the D-amino acid core were eliminated, with or without structural constraint.[107,108]

BI has disclosed two orally bioavailable CGRP receptor antagonists that were in late-stage phases of preclinical development.[88] The first, BIBP 5371 (compound **40**, **Fig. 15**), contains the succinimidyl diamide core seen in WO 2004037810 (**Fig. 14**) in place of the more polar ureidoamide in olcegepant and a chlorotrifluoromethylaniline replacing the dibromophenol. The tetrahydroisoquinolone portion of the olcegepant GPCR-privileged structure, which was found to be prone to benzylic oxidation under fairly mild conditions[88], was subjected to ring expansion to a more lipophilic and presumably more stable benzodiazepinone.

Despite lacking the L-Lys portion of olcegepant, BIBP 5371 suffered only a fourfold reduction in binding potency ($K_i = 0.14$ nM), while oral bioavailability was greatly improved compared with olcegepant (for BIBP 5371, rat $F_{PO} = 43\%$, dog $F_{PO} = 22\%$, and rhesus monkey $F_{PO} = 19\%$). Unfortunately, toxicological studies demonstrated species-dependent phospholipidosis that was significant enough to halt development based on fears of potential organ damage. In response, an in vitro assay was developed to measure intracellular phospholipid content in a U937 cell line challenged with 12.5–400 μM compound concentrations.

Further optimization led to BI 44370 (compound **41**, **Fig. 16**),[88] containing an amidourethane core and a dimethylphenol residue. The *N*-methylpiperazine of BIBP 5371 that presumably contributes to its phospholipidosis activity was replaced by a less basic morpholine ($pK_a = 6.5$). BI 44370 is 10-fold less potent against the human CGRP-R than olcegepant and showed somewhat poorer oral bioavailability than BIBP 5371 (rat $F_{PO} = 31\%$, dog $F_{PO} = 11\%$, and rhesus monkey $F_{PO} = 10\%$), but it did not cause phospholipidosis. In addition, the compound retained a fairly low degree of plasma protein binding ($f_u = 10\%$ and 13% for human and rat, respectively).

On the basis of its overall preclinical profile, BI 44370 was advanced to phase I clinical trials, where it was well tolerated.[103] Subsequent phase II efficacy studies were carried out with BI 44370 at three doses (50, 200, and 400 mg) in comparison with an active comparator, eletriptan (40 mg), and placebo, with the primary end point being pain freedom at 2 h. Only the 400 mg dose showed significant superiority in response rate compared with placebo (27.4% vs. 8.6%). The 200 mg dose showed a trend toward activity (21.5% response rate) that was statistically significant for some secondary end points, while the 50 mg dose was similar to placebo (7.8% response rate). The primary response rate for eletriptan in this study was 34.8%. The occurrence of adverse events at all doses of BI 44370 was similar to placebo, as was that of eletriptan at 40 mg. The current development status of BI 44370 is unknown.

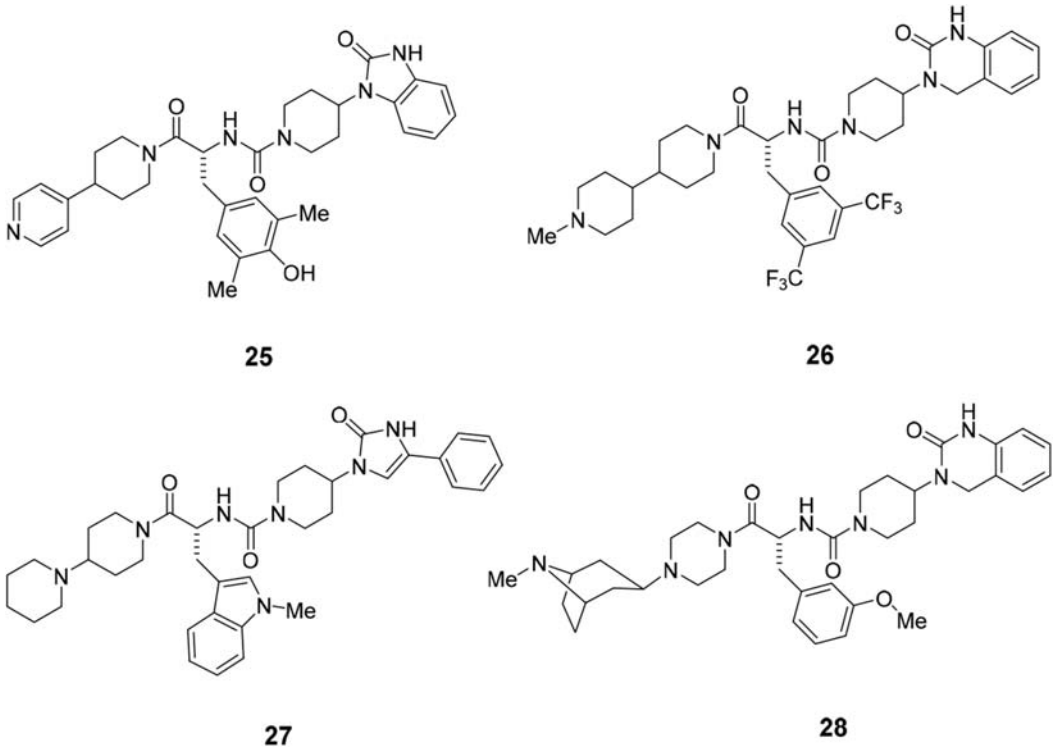

Fig. 11 Selected examples from WO 1998011128, published Mar. 19, 1998.

7.05.3.2 CGRP Receptor Antagonists From Merck

7.05.3.2.1 Caprolactam-based CGRP receptor antagonists

The program to develop orally acting CGRP receptor antagonists at Merck started from the micromolar benzodiazepinone-based lead **42** (Fig. 17), which was identified in a high-throughput screen.[91] Compound **42** had modest binding affinity ($K_i = 4.8$ μM) and similar potency in a functional assay based on CGRP-stimulated production of cAMP in cells (cAMP $IC_{50} = 6$ μM).[91] It is worth noting that **42** was not an optimal lead for discovering an orally bioavailable drug: it had relatively poor ligand efficiency (LE = 0.18 kcal mol^{-1}) and a significant number of hydrogen bond donors and acceptors, which correlated with a calculated polar surface area that predicted poor passive permeability (PSA = 147 $Å^2$).[109] However, the structure was novel with respect to other

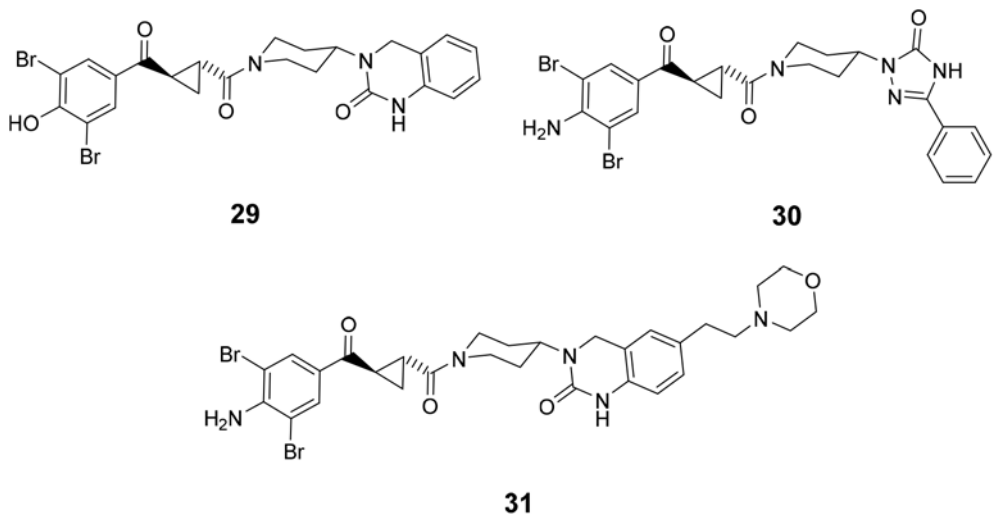

Fig. 12 Selected examples from WO 2001032648, published May 10, 2001.

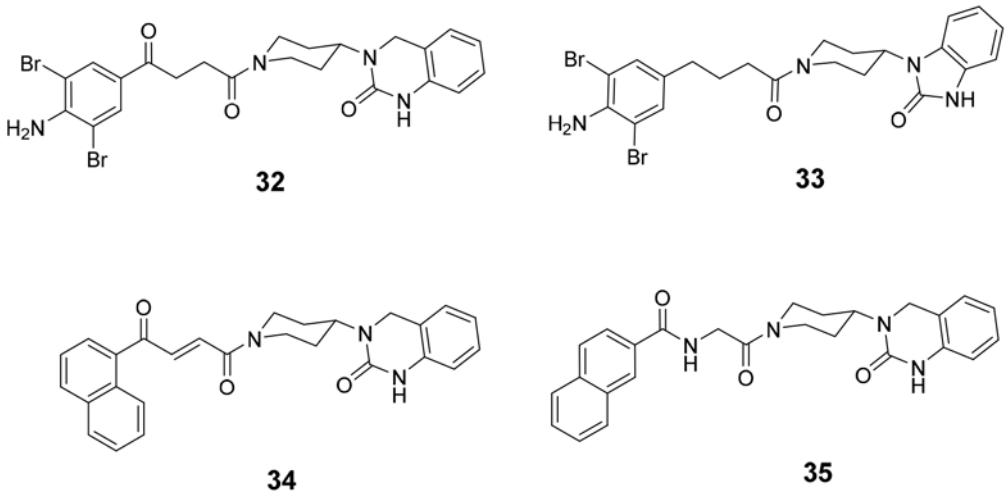

Fig. 13 Selected examples from WO 2001032649, published May 10, 2001.

CGRP receptor antagonists known at the time, many of which were based on a D-tyrosine backbone like the BI antagonist olcegepant (**12**), and the Merck team explored a number of approaches to optimize this benzodiazepinone lead.

One such approach was based on the hypothesis that the spirohydantoin moiety in compound **42** could be a "privileged structure" analogous to the piperidinyldihydroquinazolinone in olcegepant (**12**); both contained a secondary amide hydrogen bond donor–acceptor pair embedded in a heterocycle. To test this hypothesis, the 2-aminotetralin spirohydantoin in **42** was replaced with the piperidinyl-based privileged structure from **12** to provide compounds with similar receptor affinity to the high-throughput screen (HTS) lead.[91] The team built upon this encouraging result by discovering that replacement of the *N*-methyl substituent on the benzodiazepine with a trifluoroethyl group led to a nanomolar CGRP receptor antagonist (**43**, Fig. 17). This

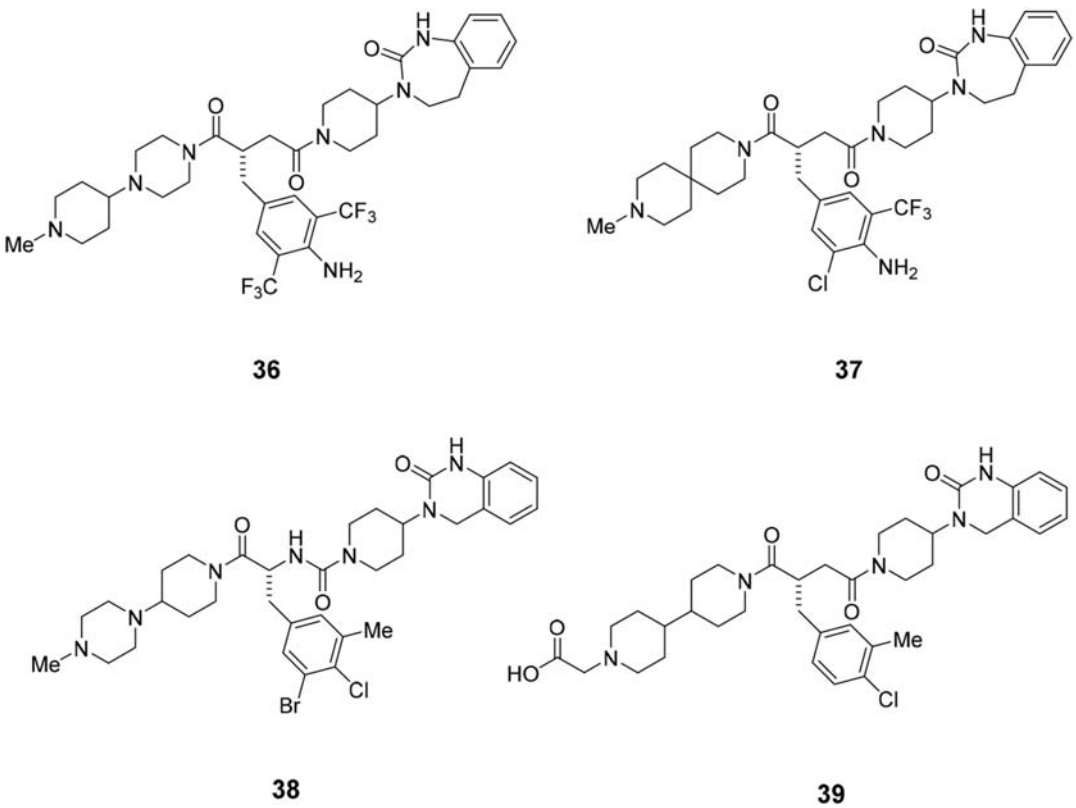

Fig. 14 Selected examples from WO 2004037810, published May 6, 2004.

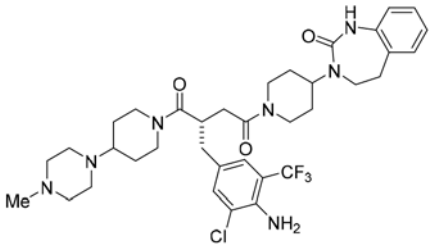

40

BIBP 5371

IC_{50} = 0.14 nM

Fig. 15 The structure of BIBP 5371.

hybrid antagonist **43** ($K_i = 44$ nM; cAMP $IC_{50} = 38$ nM) had modest oral bioavailability in rats ($F_{PO} = 10\%$) but represented a promising start to the quest for an orally acting agent.[91]

One drawback of the piperidinyldihydroquinazolinone privileged structure was that it was found to be chemically unstable. In analogy with the reported instability of **12** (*vide supra*), compound **43** was found to undergo oxidation of the quinazolinone benzylic site under mild conditions.[110] To address this liability, a survey of alternative piperidinyl-based privileged structures was undertaken, with an emphasis on quinazolinone replacements that eliminated the oxidation-prone benzylic position but maintained the hydrogen bond donor–acceptor pair. This study identified a number of alternative privileged structures, most notably the piperidinylazabenzimidazolone found in **44** ($K_i = 23$ nM; cAMP $IC_{50} = 49$ nM), which provided good potency and improved stability.[110] This privileged structure has been used widely in small-molecule CGRP receptor antagonist discovery.

In parallel with the effort to identify alternative privileged structures to the piperidinyldihydroquinazolinone in **43**, work to improve upon the benzodiazepinone portion of such compounds was underway. In general, the benzodiazepinone derivatives possessed poor pharmacokinetic properties with low oral bioavailability, and believing that poor solubility and high lipophilicity were in part to blame, the team sought to identify other scaffolds that could have improved physicochemical properties. One successful strategy was to replace the benzodiazepinone with a simple caprolactam and attempt to optimize the substitution and stereochemistry of this system.[111] This systematic investigation identified a (3*R*,6*S*)-3-amino-6-aryl substitution pattern as being optimal, to give antagonists like **45** (**Fig. 17**; $K_i = 25$ nM; cAMP $IC_{50} = 36$ nM), which had reduced MW compared with the earlier **43**.[111]

Combining the structural changes embodied in **44** and **45** led directly to compound **46** ($K_i = 11$ nM; cAMP $IC_{50} = 38$ nM), which exhibited significant oral bioavailability in rat and dog.[82] When the cell-based cAMP assay was conducted in the presence of 50% human serum, the potency of **46** shifted about ninefold (cAMP + HS $IC_{50} = 340$ nM), suggesting that plasma protein binding would lead to more modest in vivo potency. In order to improve CGRP receptor antagonist potency, an exploration of substitution around the caprolactam system was conducted.[82] Initial investigation of the C-6 position was conducted in the absence of a substituent on the caprolactam nitrogen atom, and this survey is summarized in **Table 4**. Replacement of phenyl with alkyl (e.g., isopropyl) or benzyl groups led to reduced CGRP-R affinity, as did incorporation of a pyridyl nitrogen to give **51** or **52**. A variety of substituents on the phenyl ring were explored, including hydroxy, methoxy, and methyl, but all such groups resulted in decreased in vitro potency with the exception of some halogen substituents.[82] Notably, 2-fluorophenyl (**56**, $K_i = 22$ nM) and 3-fluorophenyl (**57**, $K_i = 51$ nM) appeared to offer modest advantages over phenyl (**47**, $K_i = 83$ nM), and the combination of these two substituents

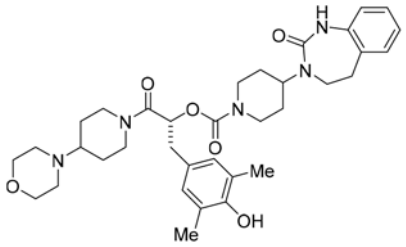

41

BI 44370

IC_{50} = 0.3 nM

Fig. 16 The structure of BI 44370.

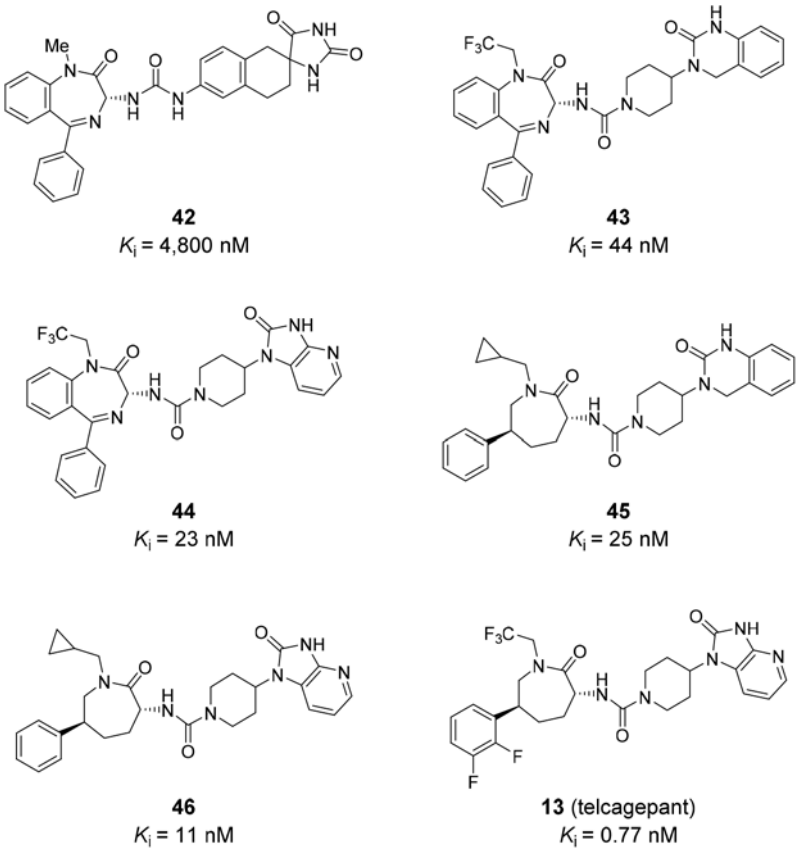

Fig. 17 Benzodiazepinone and caprolactam CGRP receptor antagonists from Merck.

Table 4 Caprolactam CGRP receptor antagonists[a]

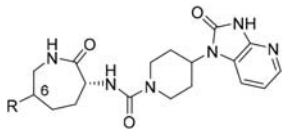

Compound	*Stereo*[b]	*R*	*K_i*[c] *(nM)*	*cAMP IC_{50}*[d] *(nM)*
47	*S*	Phenyl	83	520
48	*RS*	Isopropyl	470	380
49	*RS*	Benzyl	610	920
50	*RS*	4-Hydroxyphenyl	770	1000
51	*RS*	2-Pyridinyl	4400	
52	*RS*	3-Pyridinyl	9900	
53	*RS*	3-Thienyl	470	750
54	*RS*	2-Methoxyphenyl	1700	
55	*RS*	4-Methylphenyl	1100	
56	*S*	2-Fluorophenyl	22	65
57	*S*	3-Fluorophenyl	51	220
58	*S*	2,3-Difluorophenyl	3.6	14

[a]Data reported in Ref. 82.
[b]Stereochemistry at C-6 of caprolactam ring.
[c]K_i value for inhibition of ^{125}I-hCGRP binding determined using membranes from HEK293 cells stably expressing human CLR/RAMP1.
[d]Inhibition of CGRP-induced cAMP production in HEK293 cells stably expressing human CLR/RAMP1.

led to a 20-fold increase in affinity in the 2,3-difluorophenyl analog (**58**, $K_i = 3.4$ nM). This modification along with a trifluoroethyl substituent on the caprolactam nitrogen, which provided a good balance of potency and pharmacokinetics, led to telcagepant (MK-0974, **13**, Fig. 17), which had significantly improved binding affinity for the human CGRP-R ($K_i = 0.77$ nM) compared with compound **46**.[82]

Telcagepant (**13**) was also found to have high binding affinity for the rhesus monkey CGRP-R ($K_i = 1.2$ nM) but significantly lower affinity for nonprimate CGRP-Rs, such as those from dog ($K_i = 1200$ nM) or rat ($K_i = 1190$ nM).[112] Telcagepant was highly selective, demonstrating little to no affinity for human AM receptors AM_1-R and AM_2-R and >10,000-fold selectivity against a panel of over 160 receptors, enzymes, and transporters.[82,112] Studies with the radiotracer [^{3}H]telcagepant demonstrated saturable and reversible binding to native human CGRP-R in SK-N-MC cell membranes ($K_D = 1.9$ nM), and the radioligand could be displaced in competition binding studies by both agonist CGRP and antagonist $CGRP_{8-37}$.[113] In kinetic binding studies, the off rate of [^{3}H]telcagepant was found to be 0.51 min^{-1} with a half-life of 1.3 min.[113]

The published crystal structure of telcagepant bound to the ectodomain CGRP-R complex revealed the details of how this orally bioavailable small molecule is able to block binding of the 37-amino acid agonist CGRP to its receptor (Fig. 18).[76] Although telcagepant is significantly smaller than olcegepant, they exhibit similar binding topology, spanning approximately 18 Å from the CLR Thr122 hydrogen bond donor–acceptor site to the hydrophobic pocket that accommodates the difluorophenyl ring of telcagepant. The key azabenzimidazolone ring in the privileged structure of telcagepant is involved in hydrogen-bonding interactions with the backbone amide nitrogen and carbonyl of CLR Thr122, and the piperidinyl moiety forms an edge-to-face stack with CLR Trp72, while a weak hydrogen bond is apparent between the CLR Trp72 indole nitrogen atom and the carbonyl of the caprolactam ring.[76] The caprolactam trifluoroethyl substituent of telcagepant makes a significant hydrophobic interaction with the side chain of CLR Ile41, and the difluorophenyl ring binds in the previously described hydrophobic pocket, making productive interactions with both RAMP1 Trp74 and RAMP1 Trp84. Interestingly, the difluorophenyl ring of telcagepant binds deeper in this pocket than the dibromophenol ring of olcegepant and appears to be closer to CLR Met42, consistent with published data that revealed telcagepant to be more sensitive than olcegepant to mutation of this methionine residue.[70] It was hypothesized that enhanced binding to this hydrophobic pocket in combination with an additional hydrogen bond from the azabenzimidazolone group led to the increased ligand efficiency of telcagepant compared with olcegepant.[76]

In the functional cAMP assay, telcagepant was a potent antagonist of human CGRP-R (cAMP $IC_{50} = 2.2$ nM), and this functional potency shifted fivefold in the presence of 50% human serum (cAMP + HS $IC_{50} = 11$ nM).[112] This shift suggested a significant degree of plasma protein binding, and experimental results were consistent: human plasma $f_u = 4.1\%$. Because of the pronounced species selectivity of telcagepant and other small-molecule CGRP receptor antagonists, in vivo potency was assessed in nonhuman primates using the rhesus monkey capsaicin-induced dermal vasodilation (CIDV) model.[86] In this model, capsaicin is applied to the forearm of an anesthetized rhesus monkey, causing local CGRP release and vasodilation of dermal blood vessels. The resulting increase in blood flow is quantitated using laser Doppler imaging, and this effect may be blocked by a CGRP receptor antagonist, allowing the in vivo potency of the compound to be measured. Importantly, this noninvasive pharmacodynamic assay could be translated to the clinic, providing a direct link between the preclinical and clinical studies on a compound.[114] In the rhesus monkey CIDV assay, telcagepant blocked the effects of CGRP with EC_{50} and EC_{90} values of 127 and 994 nM, respectively.[112] The fact that the in vivo EC_{50} (127 nM) is about 10-fold higher than the in vitro serum-shifted IC_{50} (11 nM) suggests that a higher level of CGRP receptor occupancy is required to block the CIDV signal in vivo compared with the level of occupancy required to block cAMP production in cells.

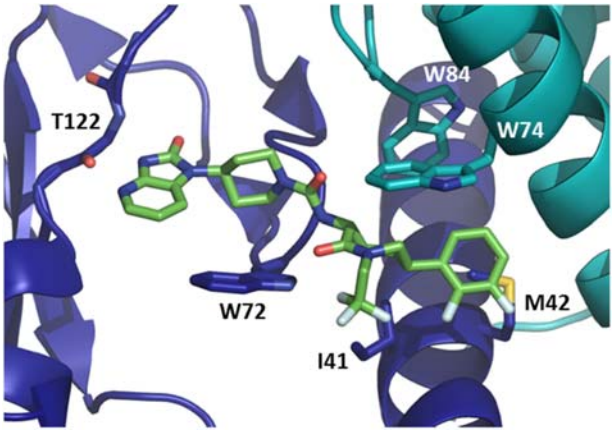

Fig. 18 Crystal structure of the CLR–RAMP1 ectodomain complex with telcagepant bound.[76] View of small-molecule antagonist binding site formed by CLR *(blue)* and RAMP1 *(teal)* complexed with telcagepant *(green)* (PDB ID 3N7R). Side chains of selected residues involved in antagonist binding are shown and labeled in *black* (CLR residues) or *white* (RAMP1 residues).

Table 5 Preclinical pharmacokinetics of telcagepant

Species	*Dose (mg kg^{-1})*	F_{PO} *(%)*	Cl_p[c] *(mL min^{-1} kg^{-1})*	*IV* $T_{1/2}$[c] *(h)*
Rat	15 (PO); 2 (IV)	22[a]	9.4	1.6
Dog	1 (PO); 0.5 (IV)	35[b]	17	0.67
Monkey	5 (PO); 10 (IV)	6[a]	14	3.2

[a]Compound dosed PO in 1:1 Imwitor-742/Tween-80 vehicle.
[b]Compound dosed PO 1% Methocel vehicle.
[c]Compound dosed IV in DMSO vehicle.

The preclinical pharmacokinetic properties of telcagepant are summarized in Table 5. The compound had low to moderate plasma clearance and short plasma half-lives in rat, dog, and monkey.[115,116] Although this profile was indicative of a relatively short plasma half-life in humans, this was not considered a liability for acute treatment of migraine. While telcagepant had good oral bioavailability in rat (F_{PO} = 22%) and dog (F_{PO} = 35%), the oral bioavailability in rhesus monkey was low and not dose-proportional: after oral dosing of monkeys, the area under the curve (AUC) was found to be 0.48 μM · h after a 5 mg kg^{-1} dose but 42 μM · h after a 30 mg kg^{-1} dose.[116] Further studies indicated that saturable, intestinal first-pass metabolism contributed to the low oral bioavailability and nonlinear oral pharmacokinetics in rhesus monkeys.[116] Overall, the preclinical studies on telcagepant revealed it to be a potent and selective orally bioavailable CGRP receptor antagonist and it was selected as the first orally acting compound in this class to be advanced to clinical trials.

Initial studies on the pharmacokinetics and tolerability of telcagepant confirmed that it was orally bioavailable in humans, with a T_{max} of approximately 1–2 h and oral bioavailability of about 45–50% at clinically relevant doses.[117,118] Consistent with preclinical observations, oral administration of telcagepant produced greater than dose proportional increases in exposure.[118] After IV dosing, the terminal half-life of telcagepant was found to be 8–9 h.[118] Telcagepant was found to be generally well tolerated in these studies.[117,118]

One attractive feature of the rhesus monkey capsaicin-induced dermal vasodilation pharmacodynamic model was that, by virtue of its noninvasive nature, it could be readily translated into the clinical setting.[114] Assessment of telcagepant in this human CIDV assay after oral dosing determined that the human CIDV EC_{90} value was 909 nM, in excellent agreement with the preclinical value found in rhesus monkey (CIDV EC_{90} = 994 nM).[119] This PD assay, which translated predictably from the preclinical to the clinical setting, became a key tool for evaluation of subsequent compounds of interest.

In a phase II randomized controlled trial of telcagepant in acute treatment of migraine, seven doses of telcagepant (from 25 to 600 mg) were evaluated along with placebo and an active comparator—rizatriptan (10 mg).[120] For the primary end point of pain relief at 2 h, doses of 300 mg (68.1%) and 600 mg (67.5%) of telcagepant were superior to placebo (46.3%) and similar to rizatriptan (69.5%), indicating that these doses of telcagepant were effective for the acute treatment of migraine.[120] Telcagepant was generally well tolerated, with a similar incidence of adverse events (AEs) to placebo in this study,[120] and it was subsequently evaluated in a number of phase III trials.

A placebo-controlled study of two doses of telcagepant (150 or 300 mg, administered using a liquid-filled capsule formulation) demonstrated that the 300 mg dose was effective as an acute treatment for migraine with efficacy comparable with that of zolmitriptan at 5 mg but with fewer associated AEs.[121] Another placebo-controlled phase III trial evaluated three doses of telcagepant (50, 150, and 300 mg) and showed that the 150 and 300 mg doses were effective in terms of pain relief and reduction of other symptoms, including nausea, photophobia, and phonophobia.[122] The 300 mg dose was slightly more effective than the 150 mg dose, and both were generally well tolerated, consistent with earlier reports.[122] Telcagepant was also shown to be effective for intermittent treatment of up to four migraine attacks.[123] A long-term tolerability study showed that telcagepant 300 mg (dosed using the 300 mg liquid-filled capsule or a bioequivalent 280 mg tablet formulation) was generally well tolerated when used for intermittent treatment of migraine for up to 18 months, with a lower incidence of drug-related AEs than rizatriptan at 10 mg.[124]

As already noted, CGRP receptor antagonists, in contrast to triptans, do not appear to cause direct vasoconstriction. This issue has been studied experimentally using human isolated coronary arteries, in which telcagepant was found to antagonize CGRP-mediated relaxation with a pA_2 value of 8.43,[125] consistent with other measures of its in vitro potency.[112] While zolmitriptan induced concentration-dependent contraction of these arteries, telcagepant produced no changes in their contractile tone at concentrations of up to 30 μM.[126] These preclinical studies suggest that CGRP receptor antagonists could offer improved cardiovascular safety compared with triptans.[125] A number of clinical studies have examined the cardiovascular safety profile of telcagepant, for example, in patients with stable coronary artery disease,[127,128] or stable angina,[129] and they have concluded that telcagepant was generally well tolerated in these patients. Other studies have indicated that telcagepant does not affect nitroglycerin-induced vasodilation in healthy subjects[130] and does not appear to have a hemodynamic interaction with sumatriptan.[131]

More recently, the results of studies examining the use of telcagepant for migraine prevention have been reported. In a placebo-controlled trial, telcagepant was administered twice daily at two doses (140 and 280 mg).[132] Unfortunately, this trial was terminated prematurely because a small number of patients were found to have elevated levels of liver transaminases, indicating a risk of hepatotoxicity. Although this study was not completed, the data obtained showed that in migraine patients, telcagepant reduced the number of headache days by 1.4 days per month compared with placebo, suggesting that a CGRP receptor antagonist could be useful for migraine prophylaxis.[132] In another placebo-controlled study conducted with more than 4000 female migraine

patients, telcagepant 140 mg was dosed once daily perimenstrually for seven days to evaluate the safety and efficacy of this treatment for headache prophylaxis.[133] Although telcagepant did not reduce monthly headache frequency, the incidence of perimenstrual headaches was lower with telcagepant compared with placebo. In this study, telcagepant was found to be generally well tolerated, with a similar incidence of AEs for the drug-treated and placebo-treated patients. However, dosing of telcagepant was associated with a low incidence of liver transaminase elevations.[133] Based on an assessment of data across the clinical program, Merck announced that the development of telcagepant was discontinued.[134]

After telcagepant was selected as a clinical candidate, the Merck team sought to identify a compound that would have a lower projected clinical dose.[135] The team focused on improving both pharmacokinetic properties and potency in order to achieve this goal. One approach to improving pharmacokinetics that was explored was replacement of the caprolactam ring by a simpler and more rigid pyridinone, which was hypothesized to be less subject to oxidative metabolism.[136] A systematic exploration of substitution of the pyridinone core identified the optimal substituents for CGRP-R affinity as trifluoroethyl at the 1-position and 2,3-difluorophenyl at the 5-position, consistent with observations in the caprolactam series and leading to compound **59** (Fig. 19).[136] Although pyridinone **59** ($K_i = 17$ nM and cAMP $IC_{50} = 18$ nM) was not equipotent with telcagepant, it did exhibit improved pharmacokinetics in rat and dog, with low plasma clearances and longer half-lives (rat, $Cl_p = 0.8$ mL min^{-1} kg^{-1} and $T_{1/2} = 6.3$ h and dog, $Cl_p = 0.2$ mL min^{-1} kg^{-1} and $T_{1/2} = 3.3$ h).[136]

Another approach to reducing oxidative metabolism in compounds like telcagepant was modification of the piperidinyl-based privileged structure, which was known to undergo oxidative metabolism and *N*-dealkylation with loss of the azabenzimidazolone.[137] To address this potential liability, a number of novel privileged structures based on spiropiperidines were synthesized and evaluated. This study led to the identification of a number of interesting CGRP receptor antagonists with comparable potency to telcagepant, including **60** (Fig. 19, $K_i = 1.7$ nM and cAMP $IC_{50} = 3.3$ nM) and **61** (Fig. 19, $K_i = 1.1$ nM and cAMP $IC_{50} = 2.7$ nM), and as hypothesized, these compounds had reduced propensity for metabolism on the terminal ring of the spirocyclic system.[137] Combining the spirocyclic privileged structure from **61** with a fused imidazoazepane, designed to improve solubility, followed by optimization of the imidazole C5 substituent, led to preclinical candidate MK-2918 (**62**, Fig. 19).[135]

MK-2918 had high CGRP-R affinity ($K_i = 0.05$ nM) and was more potent than telcagepant in vitro (cAMP + HS $IC_{50} = 0.63$ nM) and in vivo (rhesus monkey, CIDV $EC_{90} = 300$ nM). MK-2918 had an excellent overall selectivity profile but modest oral bioavailability in rat, dog, and monkey ($F_{PO} = 5$–16%), in part because of significant formation of an active metabolite: the alcohol that results from *O*-dealkylation of the methyl ether. Further analysis suggested that this active metabolite should contribute significantly to clinical efficacy and the clinical dose was therefore anticipated to be lower than that of telcagepant.[135] On the basis of this lower projected dose and its overall profile, MK-2918 was selected as a preclinical candidate, but no clinical data for the compound have been reported.

7.05.3.2.2 Spiroindane-based CGRP receptor antagonists

As described, the initial approach to optimization of HTS lead **42** was to replace the aminotetralin part of the structure with a piperidinyl-based privileged structure, and this led to telcagepant and MK-2918. In a complementary approach, the spirohydantoin portion of **42** was retained and formed the basis of a screen for alternatives to the benzodiazepinone using a rapid analog strategy.[138] This approach quickly led to submicromolar lead structures that were modified to provide **63** (Fig. 20, $K_i = 21$ nM; cAMP $IC_{50} = 78$ nM), in which the benzodiazepinone was replaced with a simpler substituted benzimidazolone

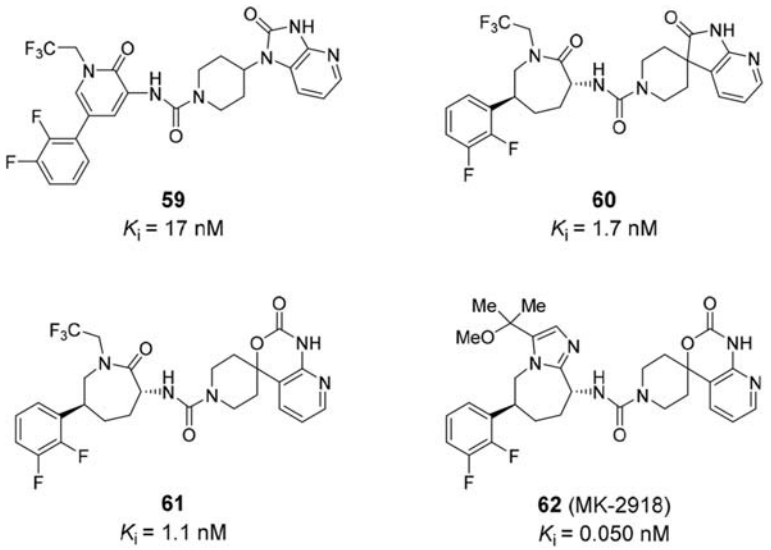

Fig. 19 Pyridinone and azepane CGRP receptor antagonists from Merck.

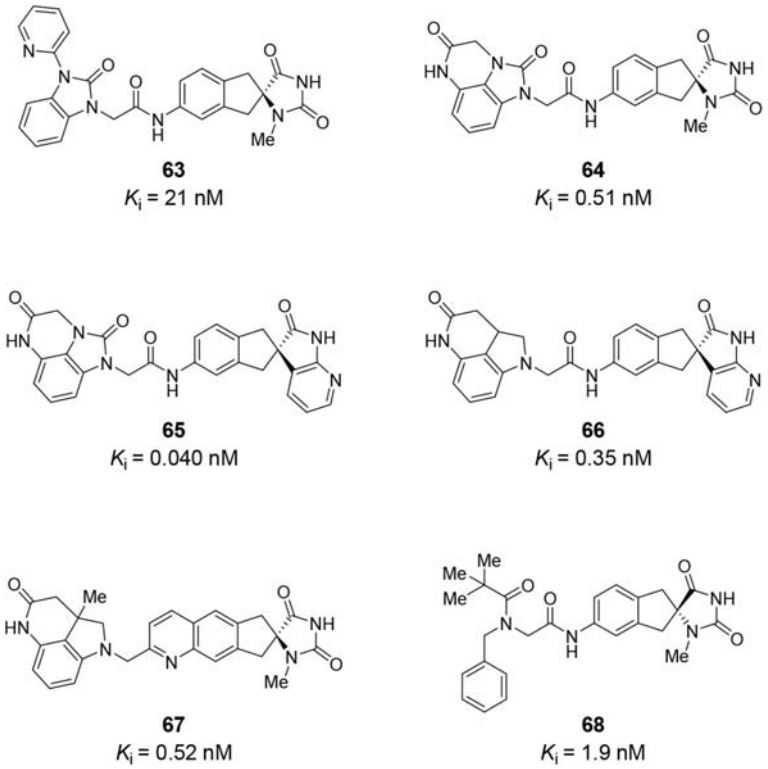

Fig. 20 Spiroindane-based CGRP receptor antagonists from Merck.

and the (*R*)-enantiomer of the spirohydantoin was preferred in terms of CGRP-R affinity.[138] Compound **63** had good oral bioavailability in rat, dog, and monkey (F_{PO} = 29–83%), and further optimization was directed at improving CGRP receptor antagonist potency.

An interesting approach to potency enhancement was realized when a glycine substituent on the benzimidazolone was constrained to give the tricyclic moiety found in **64** (Fig. 20; K_i = 0.51 nM and cAMP IC_{50} = 2.4 nM).[139] Compared to the pyridyl-substituted **63**, the tricyclic benzimidazolone conferred a 40-fold increase in CGRP-R affinity. Potency was enhanced further by rational modification of the spirohydantoin moiety based on analogy with the key role played by the azabenzimidazolone privileged structure in compounds like telcagepant. Specifically, the spirohydantoin was replaced with a spiroazaoxindole to give compounds like **65** (Fig. 20; K_i = 0.04 nM and cAMP IC_{50} = 0.28 nM), which was about 500-fold more potent than **63** in the radioligand binding assay.[140]

While **65** was a highly potent CGRP receptor antagonist, it was not orally bioavailable in rat or dog. In related compounds, it was observed that the probability of good oral exposure was significantly higher when the calculated PSA < 130 Å^2, suggesting that membrane permeability was a key limitation to absorption.[109,138] Compound **65** had a high PSA (149 Å^2) and low aqueous solubility (0.24 μg mL^{-1} at pH 7.4 for amorphous material), and attempts to improve both of these parameters led to indoline **66** (Fig. 20, K_i = 0.35 nM and cAMP IC_{50} = 2.4 nM).[141] Indoline **66** was about 10-fold less potent than benzimidazolone **65** in vitro, but it had reduced PSA (125 Å^2), and it was anticipated that the weakly basic indoline nitrogen would help to enhance solubility at acidic pH. Indeed, **65** was found to be orally bioavailable in rat, dog, and monkey (F_{PO} = 25–49%), consistent with the design hypothesis, and it had in vitro and in vivo potency that was similar to telcagepant.[141]

Another approach to reducing PSA in this series was to replace the central amide bond, and conformational analysis indicated that a quinoline-based central constraint may be a good mimic of the bioactive conformation of amides like **63**.[142] This hypothesis led to compounds like quinoline **67** (Fig. 20, K_i = 0.52 nM and cAMP IC_{50} = 2.2 nM), in which the spirohydantoin was reintroduced, in part to improve solubility.[142] Not only did this central constraint prove to be an effective mimic of the amide's bioactive conformation, but also it helped improve the pharmacokinetic profile, and **67** had good oral bioavailability in rat, dog, and monkey (F_{PO} = 38–59%).[142] Quinolines like **67** also served as inspiration for the design of compound **68** (Fig. 20, K_i = 1.9 nM), which resulted from a strategy of structural simplification to facilitate rapid exploration of SAR.[143] Intriguingly, the preferred stereochemistry of the spirohydantoin **68** had switched to (*S*) from (*R*) in earlier compounds like **63**, and this stereochemical change correlated, not surprisingly, with very different SAR for this new series.

Compound **68** had many positive attributes. It was a structurally simple CGRP receptor antagonist with nanomolar receptor affinity and good ligand efficiency (LE = 0.35 kcal mol^{-1}). For comparison, LE = 0.27 kcal mol^{-1} for olcegepant and 0.31 kcal mol^{-1} for telcagepant. However, it was not potent enough to have a low projected clinical dose, and it lacked optimal

selectivity for the CGRP-R over the AM_2 receptor (CLR/RAMP3): for **68**, AM_2/CGRP selectivity = 370-fold.[143] The early exploration of SAR in this new series established that fluoro substitution of the terminal phenyl ring increased CGRP-R affinity and selectivity against the AM_2 receptor. It was also discovered that the acyclic *N*-benzylpivalamide end group could be cyclized to give a substituted piperidinone ring. Combining these modifications with the potency-enhancing spiroazaoxindole replacement for spirohydantoin afforded the picomolar antagonist piperidinone **69** (Fig. 21, $K_i = 0.039$ nM and cAMP $IC_{50} = 0.16$ nM).[143]

The excellent receptor affinity of **69** was matched by good selectivity versus the AM_2 receptor (AM_2/CGRP selectivity = 4100-fold) and translated into very good cell-based functional potency in the presence of 50% human serum (cAMP + HS $IC_{50} = 0.35$ nM). Unfortunately, while it had moderate oral bioavailability in rat ($F_{PO} = 12\%$) and dog ($F_{PO} = 44\%$), it was not orally bioavailable in monkey ($F_{PO} = 0\%$), which precluded full evaluation of its in vivo pharmacology because such antagonists have significantly reduced potency at nonprimate CGRP receptors (*vide supra*).[144] It was thought that the low oral bioavailability in monkey was due in part to intestinal first-pass metabolism, in analogy with telcagepant. Since the piperidinone ring of **69** was known to be subject to significant metabolism in vitro, the team sought to incorporate polar functionality into this ring with the dual goals of reducing metabolism and increasing aqueous solubility. These design considerations led to morpholinones like **71** and piperazinones like **74** (Fig. 21 and Table 6).[144]

In analogy with the earlier caprolactam-based antagonists, a difluorophenyl substituent on the lactam ring led to increased CGRP receptor affinity (compare compounds **69** and **70** in Table 6), although in this context, a 3,5-difluorophenyl was preferred to 2,3-difluorophenyl.[143] This similarity suggested that the 3,5-difluorophenyl ring in compounds like **69** might be binding to the same hydrophobic pocket as the 2,3-difluorophenyl of telcagepant.

Incorporation of an oxygen atom to give a morpholinone ring produced compounds like **71**, which maintained the high receptor affinity of the corresponding lactam **70**. It was discovered that replacement of the geminal methyl substituents in **71** with the ethyl substituents in **72** led to improvements in the rat PK profile.[144] Addition of the potency-enhancing fluoro substituents afforded morpholinone **73**, which was highly potent ($K_i = 0.018$ nM and cAMP $IC_{50} = 0.32$ nM) and had superior oral bioavailability to lactam **69** in rat ($F_{PO} = 59\%$) and dog ($F_{PO} = 72\%$) but not in monkey ($F_{PO} = 0\%$).[144]

Piperazinone **74** was also potent ($K_i = 0.034$ nM and cAMP $IC_{50} = 0.17$ nM) and more soluble than the morpholinone, especially at acidic pH, and this correlated with at least measurable oral bioavailability in monkey ($F_{PO} = 7\%$).[144] The piperazinone series became a major focus for the team, and it was discovered that incorporation of geminal diethyl substituents on the piperazinone ring (compound **75**; Table 6) led to improved rat pharmacokinetics, in analogy with results for the morpholinone

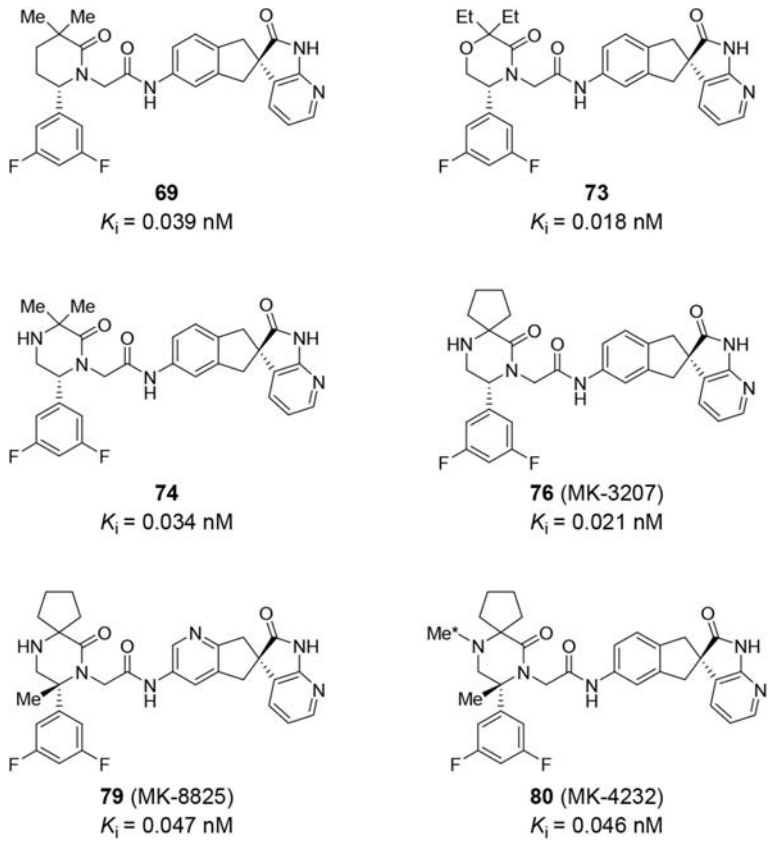

Fig. 21 Spiroindane-based CGRP receptor antagonists from Merck. Position of [^{11}C]-methyl group in [^{11}C]**80** indicated by asterisk.

Table 6 Spiroindane-based CGRP receptor antagonists[a]

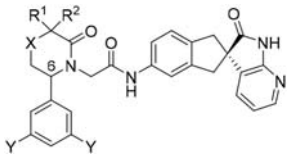

Compound	R^1	R^2	X	Y	Stereo[b]	K_i[c] (pM)	cAMP IC_{50}[d] (nM)	cAMP + HS IC_{50}[e] (nM)
69	Me	Me	CH_2	F	*S*	39	0.16	0.35
70	Me	Me	CH_2	H	*S*	120	0.59	1.4
71	Me	Me	O	H	*R*	82	0.22	0.27
72	Et	Et	O	H	*R*	67	0.23	0.37
73	Et	Et	O	F	*R*	18	0.32	0.44
74	Me	Me	NH	F	*R*	34	0.17	0.25
75	Et	Et	NH	F	*R*	20	0.14	0.18
76	$-(CH_2)_4-$		NH	F	*R*	21	0.12	0.17
77	$-(CH_2)_5-$		NH	F	*S*	570	10	11
78	$-(CH_2)_5-$		NH	F	*R*	17	0.22	0.33

[a]Data reported in Ref. 144.
[b]Stereochemistry at C-6 of heterocycle.
[c]K_i value for inhibition of ^{125}I-hCGRP binding determined using membranes from HEK293 cells stably expressing human CLR/RAMP1.
[d]Inhibition of CGRP-induced cAMP production in HEK293 cells stably expressing human CLR/RAMP1.
[e]Assay conditions as for footnote *d* but in presence of 50% human serum.

antagonists. The importance of the difluorophenyl substituent to CGRP-R affinity of these piperazinones is illustrated by the spirocyclohexyl analogs **77** and **78**, in which inverting the C6 stereocenter from *R* to *S* leads to a potency loss of more than 30-fold (**Table 6**). The optimal balance of potency, selectivity, and pharmacokinetics in this series was obtained by replacing the gem dimethyl substituents on the piperazinone ring in **74** with a spirocyclopentyl ring, leading to MK-3207 (**76**) (**Fig. 21**, $K_i = 0.021$ nM), a picomolar CGRP receptor antagonist with oral bioavailability in rat, dog, and monkey.[144]

The high affinity and binding kinetics of MK-3207 were investigated using the [^{3}H]MK-3207 tracer, revealing that the K_D was 60 pM and that the higher affinity compared with telcagepant (**13**) ($K_D = 1.9$ nM) resulted from a reduced off rate (0.012 min^{-1}) and longer dissociation half-life (59 min).[145] MK-3207 had excellent cell-based potency (cAMP $IC_{50} = 0.12$ nM) that was slightly shifted in the presence of 50% human serum (cAMP + HS $IC_{50} = 0.17$ nM), consistent with a good unbound fraction in plasma. Interestingly, while the plasma unbound fraction of MK-3207 was similar in human ($f_u = 9.4\%$) and monkey ($f_u = 9.6\%$), it was significantly lower in rat ($f_u = 0.8\%$).[144] The high in vitro potency of MK-3207 translated to the in vivo CIDV monkey PD model, in which it was determined to have an EC_{90} value of 7 nM.[145] Based on these data, MK-3207 was about 50-fold more potent than telcagepant in vitro and approximately 100-fold more potent in vivo.

As expected, MK-3207 also had high affinity for rhesus monkey CGRP-R ($K_i = 0.024$ nM) but significantly reduced affinity for nonprimate CGRP receptors, such as those of rat ($K_i = 10$ nM) and dog ($K_i = 10$ nM).[145] The compound was found to have high selectivity for the human CGRP-R versus the related AM_1 (>600,000-fold), AM_2 (>6500-fold), and AMY_3 (>5000-fold) receptors but relatively low selectivity against the AMY_1 receptor (30-fold). When tested in a panel of 169 receptors, enzymes, and transporters, MK-3207 was found to >50,000-fold selective for human CGRP-R versus any of these other targets.[145]

The preclinical pharmacokinetic profile of MK-3207 is summarized in **Table 7**. In rat and dog, it had low plasma clearance and excellent oral bioavailability ($F_{PO} = 67$–74%). However, in rhesus monkey, the clearance was moderate, and the oral bioavailability was modest at low doses ($F_{PO} = 9\%$ at 2 mg kg^{-1}) but increased at higher doses ($F_{PO} = 41\%$ at 20 mg kg^{-1}), suggesting that saturable first-pass metabolism played a role, in analogy with telcagepant. The plasma half-life was short in all three preclinical species but compatible with acute treatment of migraine in the clinic. Overall, MK-3207 had an attractive profile in terms of potency, selectivity, and pharmacokinetics, and it was selected as a development candidate with the potential for a low clinical dose.[146]

Table 7 Preclinical pharmacokinetics of MK-3207

Species	Dose (mg kg^{-1})	F_{PO}[a] (%)	Cl_p[b] (mL min^{-1} kg^{-1})	IV $T_{1/2}$[b] (h)
Rat	10 (PO); 2 (IV)	74	11	0.6
Dog	2 (PO); 0.5 (IV)	67	8.0	1.0
Monkey	2 (PO); 0.5 (IV)	9	15	1.5

[a]Compound dosed PO in 1% Methocel vehicle.
[b]Compound dosed IV in DMSO vehicle.

MK-3207 was found to be orally bioavailable in humans with rapid absorption (T_{max} = 1–2 h) and a terminal plasma half-life after oral dosing of around 9–18 h.[147] The human CIDV PD assay was, once again, found to translate well from the preclinical setting, providing a human CIDV $EC_{90} \approx 14$ nM.[147] A detailed PK/PD analysis suggested that a 20 mg dose of MK-3207 would effectively block the CGRP receptor peripherally and that this dose should provide similar clinical efficacy to telcagepant.[147] In a placebo-controlled phase II study, seven doses of MK-3207 (from 2.5 to 200 mg) were evaluated with a primary end point of pain freedom at 2 h.[148] For this primary end point, doses of 10, 100, and 200 mg were found to be superior to placebo. It was not possible to conclude that the 200 mg dose was more effective than any dose from 10 to 100 mg, and 10 mg may have represented the plateau of efficacy,[148] a suggestion that is consistent with the PK/PD modeling.[147] Although MK-3207 was generally well tolerated in this study, in extended phase I clinical trials, delayed liver test abnormalities were observed, usually after cessation of dosing, and the development of MK-3207 was discontinued.[148] The observation of liver transaminase elevations with both telcagepant and MK-3207 raises the possibility that these effects could be mechanism-related. However, the patterns of clinical findings with telcagepant and MK-3207 were quite different from one another, suggesting that these effects may be specific to these compounds.[132]

The ability to evaluate CGRP receptor antagonists in a variety of rat and mouse models could provide key insights into the in vivo activity of CGRP and the consequences of inhibiting its actions. Unfortunately, the pronounced species selectivity observed with most small-molecule CGRP receptor antagonists presents significant challenges for evaluation of their in vivo pharmacology in rodents; most orally bioavailable antagonists are simply not potent at rodent CGRP receptors. MK-3207 offered some promise because, even though it was >400-fold less potent at the rat CGRP-R, it was still a nanomolar antagonist (K_i = 10 nM). Unfortunately, MK-3207 was significantly less potent as a CGRP receptor antagonist in vivo in the rat CIDV PD model (EC_{50} = 58 μM), and its low unbound fraction in rat plasma (f_u = 0.8%) was thought to contribute to this.[149] Based on these observations, the team tried to identify a potent rat CGRP receptor antagonist with reduced plasma protein binding.

It was known that the C-6 piperazinone stereocenter in MK-3207 could have a profound influence of plasma unbound fraction in rat and addition of a methyl substituent at this position led to a significant increase in rat unbound fraction.[144,149] This modification was combined with a spiroazaindane privileged structure to give MK-8825 (**79**, Fig. 21), which possessed improved unbound fraction (rat f_u = 23%) and nanomolar potency at the rat CGRP-R (K_i = 17 nM). MK-8825 was orally bioavailable in rat (F_{PO} = 28%) and had improved potency compared with MK-3207 in the rat CIDV model (EC_{50} = 7.4 μM).[149] Importantly, MK-8825 has been successfully used to study the effects of CGRP receptor antagonism in a number of rodent studies.[150–153]

Analogs of MK-3207 also proved to be useful starting points for development of a PET tracer to enable an assessment of central CGRP receptor occupancy (RO) with compounds like telcagepant. The high receptor affinity of MK-3207 was excellent, but its P-glycoprotein (P-gp) transport ratio (25) was far from optimal for a potential PET ligand. It was known that the C6 methyl substituent, in addition to increasing rat plasma unbound fraction, also led to reduced P-gp susceptibility, perhaps because of increased steric bulk that shielded the piperazinone amide moiety.[154] Substituting the piperazinone 4-position with another methyl group produced compound **80** (MK-4232, Fig. 21), which had attenuated P-gp efflux (transport ratio = 1.7) and appeared to achieve significantly higher CNS penetrance compared with MK-3207. This *N*-Me substituent also provided a convenient location for introduction of an ^{11}C-label to produce [^{11}C]MK-4232, the first PET tracer for the CGRP receptor.[154]

[^{11}C]MK-4232 has been used to address one of the key controversies in the field, whether CGRP receptor antagonists like telcagepant work in the periphery or the CNS, an issue that has been discussed in detail elsewhere.[42,155] The PET tracer allows a direct way to determine the extent of central CGRP receptor occupancy (RO) achieved by a clinically efficacious dose of a CGRP receptor antagonist. Administration of [^{11}C]MK-4232 to healthy volunteers revealed the highest level of tracer binding in the cerebellum, consistent with autoradiography experiments with [^{3}H]MK-3207.[145,156] The PET tracer was used to evaluate central CGRP RO achieved by two doses of telcagepant: the clinically efficacious dose of 140 mg and a supratherapeutic dose of 1120 mg.[156] Although the high dose produced moderate levels of occupancy (CGRP RO = 43–58%), the efficacious dose produced little or no central occupancy (CGRP RO ≤ 10%).[156] Even the level of occupancy achieved by the 1120 mg dose is unlikely to block the CGRP-R effectively, since orthosteric antagonists usually require high levels of occupancy to exert a therapeutic effect.[157] These results indicate that central CGRP-R occupancy is not necessary for antimigraine efficacy by a CGRP receptor antagonist and that the clinical results achieved are due to peripheral modes of action.[156] It is, of course, possible that greater antimigraine efficacy could be achieved by a compound that effectively antagonized the CGRP-R in both the periphery and the CNS. There have been reports of CGRP receptor antagonists with enhanced CNS penetrance, and the hypothesis could be tested directly if such a compound can be advanced into clinical trials.[158,159]

A number of other novel CGRP receptor antagonists have been reported by the Merck team. Attempts to incorporate a quinoline central constraint to replace the central amide in compounds like **69** (Fig. 21) led to a different substitution pattern compared with earlier quinoline CGRP receptor antagonists like **67** (Fig. 20). This initially unexpected result is exemplified by **81** (Fig. 22, K_i = 0.30 nM), and it was consistent with the change in stereochemical preference observed with this novel series of antagonists.[143,160] Related work in the same structural series described the replacement of the central amide with hydrocarbon linkers such as the (*E*)-alkene found in **82** (Fig. 22, K_i = 0.040 nM).[158] These compounds generally had reduced susceptibility for P-gp efflux, indicating the potential for making truly brain-penetrant CGRP receptor antagonists. For example, **82** was not a P-gp efflux substrate (transport ratio = 1.4) and was orally bioavailable in rat (F_{PO} = 51%).[158]

More recently, a series of oxazolidinone CGRP receptor antagonists, derived from MK-3207 via a scaffold-hopping approach, were described.[161] This work led to the identification of compound **83** (Fig. 22, K_i = 0.15 nM and cAMP IC_{50} = 0.15 nM), which

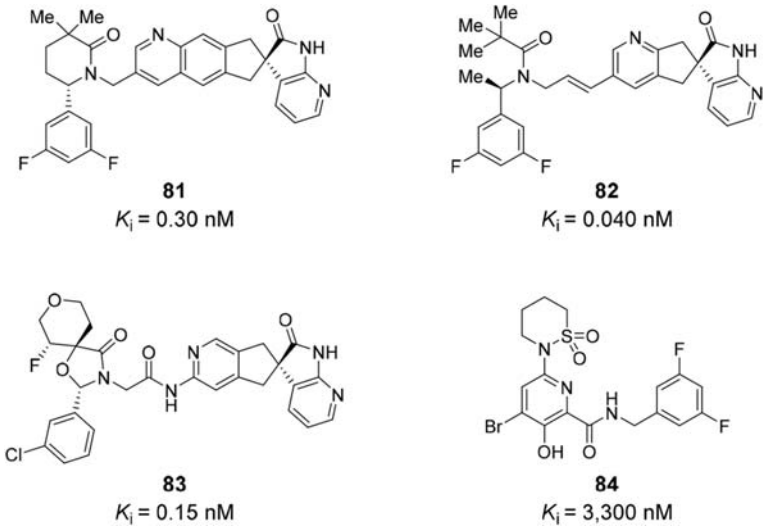

Fig. 22 Other CGRP receptor antagonists from Merck.

had excellent rat pharmacokinetics (F_{PO} = 100% and IV $T_{1/2}$ = 7 h) and in which the 3-fluoro substituent on the tetrahydropyran ring provided a substantial potency boost.[161]

All the Merck small-molecule CGRP receptor antagonists described herein were derived from the same HTS lead (**42**) and are believed to bind to the same site in the CGRP ECD as olcegepant and telcagepant. An interesting exception to this binding mode is compound **84** (Fig. 22; K_i = 3300 nM and cAMP IC_{50} = 2700 nM),[71] which was derived not from **42** but from the HIV integrase inhibitor L-870,810.[162] In contrast to other small-molecule CGRP receptor antagonists, the binding affinity of **84** was dependent upon the presence of a divalent cation such as Mg^{2+}, and **84** apparently interacts with transmembrane domain 7 in CLR and not with the ECDs of either CLR or RAMP1.[69,71]

7.05.3.3 CGRP Receptor Antagonists From Bristol–Myers Squibb

7.05.3.3.1 Intranasal BMS-694153

Researchers at Bristol–Myers Squibb began a small-molecule CGRP antagonist program attempting to improve the oral pharmacokinetics of published leads such as olcegepant and **85**[163] (Fig. 23) by balancing polarity and lipophilicity and reducing the number of rotatable bonds.

To this effect, a series of compounds based on D-benzothiophen-3-ylalanine were prepared to explore various spirocyclic GPCR-privileged components.[164] Selected examples are shown in Fig. 24 along with IC_{50} data from competition binding experiments with [^{125}I]CGRP against the human CGRP receptor expressed in SK-N-MC cells. In comparison with the compound containing the benzimidazolone (**86**) component used by BI and Merck, most of these compounds lose some degree of potency. Notably, there seems to be no preference for the location of the critical hydrogen bond-donating NH on either side of the carbonyl in dihydroquinolinone (**88**, IC_{50} = 23 nM) or dihydroisoquinolinone (**89**, IC_{50} = 29 nM). There is an enhanced effect of having two urea NH's (**91**, IC_{50} = 5 nM) that is not seen with the carbamate (**90**, IC_{50} = 20 nM). It appears that other spatial relationships, that is, between the aryl ring and the carbonyl (**92** and **93** vs. **88** and **89**), are more important for binding.

In general, the benzothiophenes showed good in vitro metabolic stability but poor Caco-2 cell permeability, possibly due to active efflux. Although compounds such as **91**, **86**, and **101** (Tables 8 and 9) demonstrated good CGRP binding affinity (for **101**, K_i = 0.55 nM), the chemotype presented an obvious liability with extremely potent CYP3A4 inhibition with the 7-benzyloxyresorufin (BZR) substrate (IC_{50} = 0.084 μM). SAR studies identified purely hydrophobic aromatic residues such as benzothiophene as being primarily responsible for this strong interaction. A number of benzimidazolone-containing analogs containing various D-amino acid side chains were prepared (Table 8).[165] It was found that CGRP-R binding potency and CYP inhibition did not track (**94** and **95**), and increasing polarity distal to the attachment point of the side chain residue resulted in reduced CYP3A4 inhibition (**96** vs. **94** and **98** vs. **97**, in particular).

With the more optimized quinazolinone GPCR-privileged component, the 5-substituted indazole (**102**, K_i = 0.23 nM) and benzoxazolone (**103**, K_i = 0.27 nM) were identified as attractive leads (Table 9).[166] Further SAR work showed that substitution at the 7-position with small, lipophilic groups such as methyl, ethyl, or chloro boosted CGRP-R binding potency into the picomolar range with compounds like **104** (K_i = 0.010 nM), **105** (K_i = 0.0050 nM), and **106** (K_i = 0.039 nM). It can be seen, however, that CYP3A4 inhibition is significantly increased with compound **105**, possibly due to shielding of the polar NH by the larger ethyl group. Interestingly, the nitrile group, not often considered highly polar, reduces the potency of **107** almost 300-fold in comparison with the 7-chloro compound, **106**.

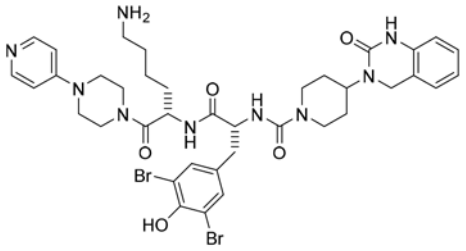

12
Olcegepant (BIBN4096 BS)

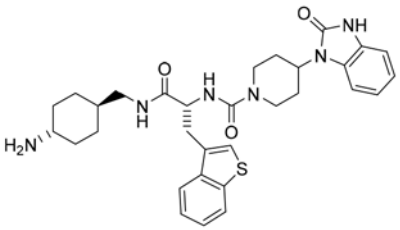

85 Example from WO 2000018764, published April 6, 2000

Fig. 23 Lead structures for the Bristol–Myers Squibb intranasal CGRP antagonist program.

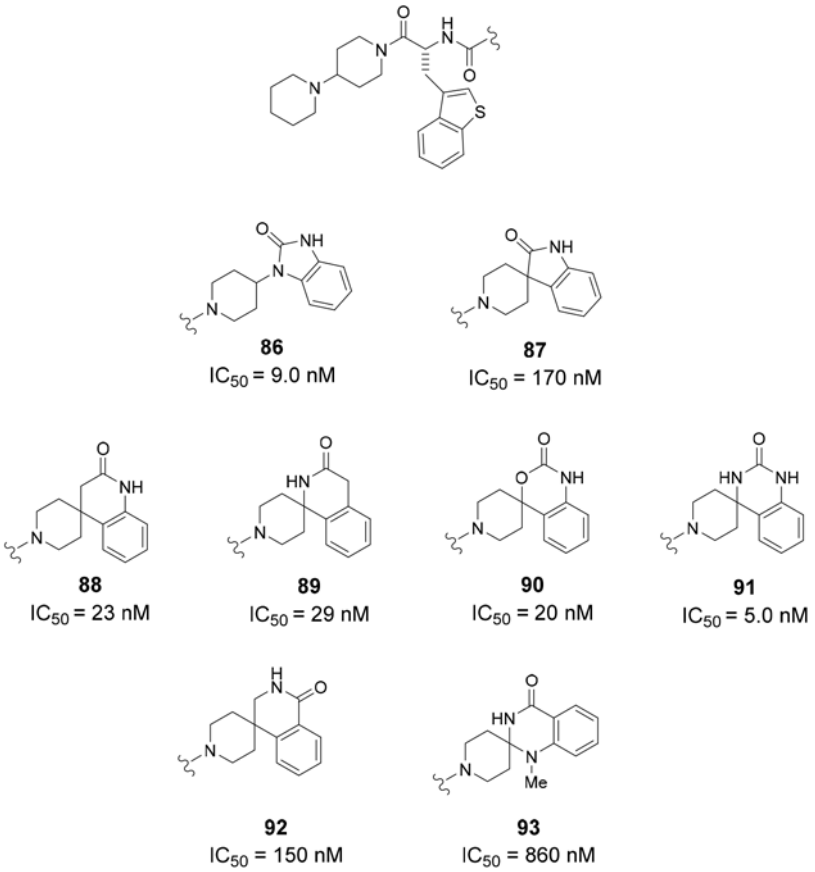

Fig. 24 Benzothiophene-containing CGRP antagonists from BMS.[164]

Table 8 Benzimidazolone-containing CGRP receptor antagonists from BMS containing various D-amino acid side chains[a]

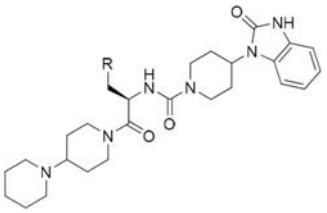

Compound	R	hCGRP-R K_i (nM)[b]	CYP3A4 BZR, IC_{50} (μM)[c]
86		4.3	0.22
94		7.2	0.03
95	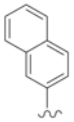	230	0.03
96	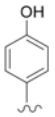	2.5	>40
97	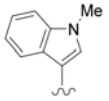	16	0.1
98		84	>40
99	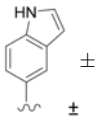	32	2.5
100	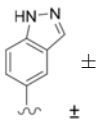	68	17

[a]Data reported in Ref. 165.
[b]K_i value for inhibition of ^{125}I-hCGRP binding determined using membranes from SK-N-MC cells stably expressing human CLR/RAMP1.
[c]Inhibition of recombinant human cytochrome P450 3A4 (CYP3A4) degradation of 7-benzyloxyresorufin (BZR).

Compound **104** represented an attractive lead, but this class of CGRP-R antagonists demonstrated poor oral bioavailability, most likely due to very limited absorption of these large (MW > 600), polar molecules. The BMS group therefore investigated IN delivery as an alternative and potentially more attractive mode of administering these compounds to treat migraine attacks.[167]

Traditionally formulated oral medications can require several hours before they reach effective concentrations in plasma or target tissues due to passage and absorption through the gut. For migraine, it would be greatly advantageous to have a convenient, faster-acting formulation. In principle, this not only would shorten the duration of headache pain but also, by aborting the attack in its early stages, might reduce its severity.[168] In addition, migraine-associated nausea can limit the effectiveness of oral delivery.[169] Injectable agents are generally fast-acting but are not yet convenient for individual patient use. IN delivery would seem well suited

Table 9 Quinazolinone-containing CGRP receptor antagonists containing various D-amino acid side chains[a]

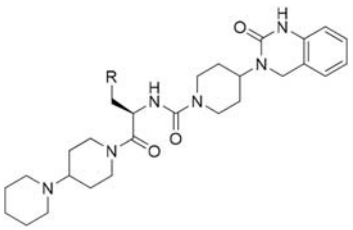

Compound	R	hCGRP-R K_i (nM)[b]	CYP3A4 BZR, IC_{50} (μM)[c]
101		0.55	0.084
102	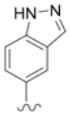	0.23	4.0
103	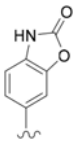	0.27	30
104	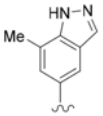	0.010	6.0
105	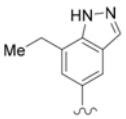	0.0050	0.45
106	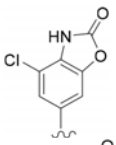	0.039	17
107	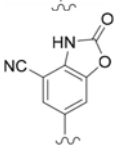	11	-

[a]Data reported in Ref. 166.
[b]IC_{50} value for inhibition of ^{125}I-hCGRP binding determined using membranes from SK-N-MC cells stably expressing human CLR/RAMP1.
[c]Inhibition of recombinant human cytochrome P450 3A4 (CYP3A4) degradation of 7-benzyloxyresorufin (BZR).

for migraine treatment, given a compound with appropriate target potency and physical properties. Two triptans, sumatriptan (Imitrex®) and zolmitriptan (Zomig®), are available as IN formulations. The efficacy of sumatriptan nasal spray has been reported to be inconsistent, with patients showing the lack of tolerance for its unpleasant taste.[170] In contrast, zolmitriptan nasal spray has shown a rapid onset of action in comparison with oral triptans,[171] high response rates, and an improved tolerability profile, though "unusual taste," possibly a human sensory characteristic of the common tryptamine core, remains the most prominent adverse event.[172]

Compound properties necessary for IN delivery are somewhat different than for oral dosing, and the formulation options available for optimization are more limited.[173] The molecule must be very potent at the biological target because of the need to deliver a relatively small dose to the nasal cavity.[174] In addition, the compound must have very good aqueous solubility, as the

Table 10 Human CGRP-R binding affinities, recombinant CYP3A4 inhibitory activities, and aqueous solubility values for BMS intranasal CGRP receptor antagonist leads

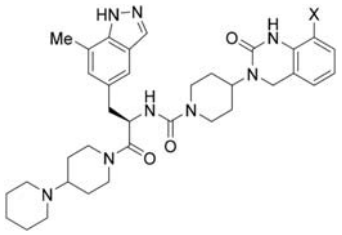

Compound[a]	*X*	*hCGRP-R K_i (nM)*[b]	*CYP3A4 BFC, IC_{50} (μM)*[c]	*CYP3A4 BZR, IC_{50} (μM)*[c]	*Aqueous solubility (mg mL^{-1})*[d]
104	H	0.010	36	6.0	15
108	F	0.013	26	7.8	>500
BMS-694153					

[a]Data reported in Ref. 167.
[b]K_i value for inhibition of ^{125}I-hCGRP binding determined using membranes from SK-N-MC cells stably expressing human CLR/RAMP1.
[c]Inhibition of recombinant human cytochrome P450 3A4 (CYP3A4) degradation of 7-benzyloxyresorufin (BZR) and 7-benzyloxy-4-trifluoromethylcoumarin (BFC).
[d]Aqueous solubilities from solid (for details, see aforementioned text).

maximum volume of liquid that can be delivered in each human nostril is only about 0.1 mL.[175] Despite the high degree of polar surface area that these properties imply, the compound must also show sufficient permeability at the nasal membrane.

The aqueous solubility of compound **104** (15 mg mL^{-1} at pH 5.0 from amorphous solid) was not sufficient to support intranasal dosing (Table 10). Interestingly, simple addition of a fluorine atom at C-8 of the quinazolinone (compound **108**, BMS-694153) had the dramatic effect of increasing aqueous solubility to >500 mg mL^{-1} from crystalline free base (pH 1.0–6.8) while preserving CGRP-R binding potency (K_i = 0.013 nM) and acceptable CYP3A4 inhibition (IC_{50} = 6.7 μM). The compound was shown to be a full antagonist at the human CGRP receptor in SK-N-MC cells (cAMP EC_{50} = 0.034 nM), highly selective (>10,000-fold) against related human AMY, AM, and CT receptors, but essentially inactive against the rat CGRP receptor.

In two ex vivo experiments using preparations of human intracranial arteries, BMS-694153 both reversed (EC_{50} = 0.06 nM) and prevented (K_b = 0.028 nM) CGRP-induced blood vessel dilation with potency comparable to its receptor activity. In contrast, BMS-694153 did not cause active vasoconstriction of ex vivo human coronary artery rings at concentrations up to 10 μM. In these experiments, sumatriptan produced concentration-dependent vessel contraction up to 59% of maximum (induced by addition of 10 μM serotonin) with EC_{50} = 311 nM. As a surrogate for the cardiovascular side effects seen with triptans, these results again suggest that BMS-694153 and other CGRP receptor antagonists may be free of the mechanism-based cardiovascular (CV) liabilities displayed by the triptans.

Along with the reduced risk of "triptan-like" cardiovascular liabilities predicted by the ex vivo blood vessel studies, BMS-694153 also showed a low likelihood for ion channel-mediated CV adverse events. At 30 μM, the compound produced 19% inhibition of human Ether-à-go-go-related gene (hERG) channel activity and showed minimal effect on sodium channel activity. In addition, BMS-694153 demonstrated no significant potential for other off-target liabilities in a broad panel of receptors, ion channels, and enzymes.

As a measure of in vivo efficacy, the BMS group employed a marmoset facial blood flow model similar to that used by BI. However, instead of electrical stimulation-induced CGRP release, α-CGRP was given IV (10 μg kg^{-1}) prior to and at three time points following SC dosing of BMS-694153. This allowed assessment of individual baseline response to CGRP and duration of in vivo inhibition by the antagonist. At a dose of 0.03 mg kg^{-1}, BMS-694153 demonstrated robust inhibition (>60%) of CGRP-induced increases in facial blood flow at 15, 60, and 105 min. At 0.01 mg kg^{-1}, 50% inhibition was observed at 60 and 105 min, while modest activity (c.30%) was seen at 15 min. No inhibition was seen at 0.003 mg kg^{-1}. Comparing exposure with efficacy, total plasma levels of approximately 10 nM were associated with robust activity in this model.

IN pharmacokinetics were assessed in the rabbit. When sprayed as an aqueous solution, BMS-694153 was efficiently absorbed from the nasal cavity. The IN bioavailabilities at 1.0 and 0.3 mg kg^{-1} were 59% (C_{max} = 1200 nM) and 55% (C_{max} = 360 nM), respectively with T_{max} occurring within 10 min for both doses, suggesting the potential for rapid onset of efficacy. When dosed IV (0.5 mg kg^{-1}), mean clearance was 13 mL min^{-1} kg^{-1}, volume of distribution (steady state) was 2.7 L kg^{-1}, and $T_{1/2}$ was 11 h. BMS-694153 also showed good bioavailability when dosed intratracheally (F_{IT} = 73%) and SC (F_{SC} = 43–100%, depending on the vehicle) in rats. Oral bioavailability in cynomolgus monkey and rat was very low (F_{PO} < 0.3%), probably due to active efflux and/or poor bilayer permeability (Caco-2 P_c < 15 nm s^{-1}). The compound at 10 μM demonstrated very low binding to plasma proteins from several species including human (f_u = 35–77%).

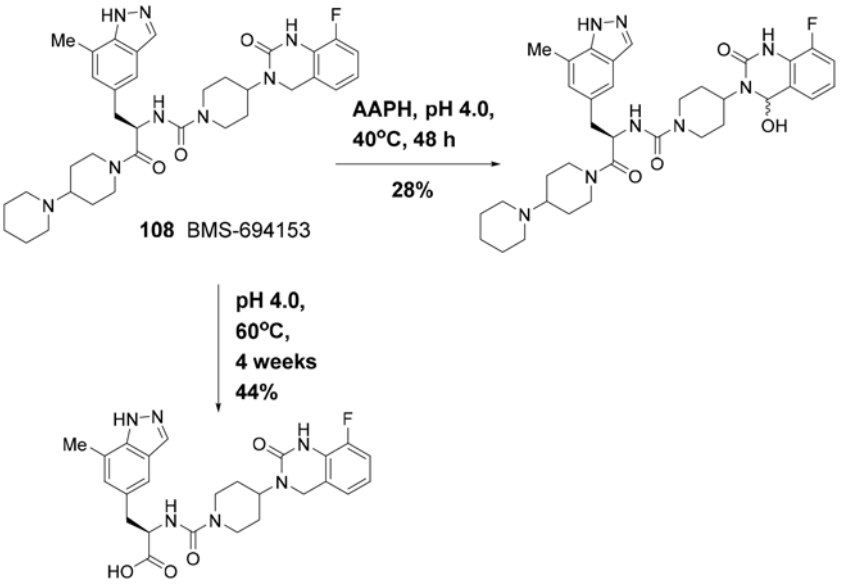

Fig. 25 Degradation pathways of BMS-694153.

7.05.3.3.2 Intranasal BMS-742413

Preclinical development of BMS-694153 was hampered by two issues: chemical stability and IN irritation.[176] Oxidative degradation of the fluorodihydroquinazolinone benzylic methylene group in aqueous solution occurred slowly, and this was accelerated by light. There was also some degree of hydrolytic instability of the carboxamide (illustrated in Fig. 25).[177] Nasal irritation and atrophy of the olfactory epithelium were observed in rat toxicological studies, and these issues were more difficult to design around since their cause was not well understood.

In order to address the chemical stability issue, the fluorodihydroquinazolinone in BMS-694153 was replaced by a 2-quinolone in **109** (BMS-742413, Fig. 26), effectively making a formerly sensitive, electron-rich position electron deficient and oxidatively stable. A second change was the inclusion of an additional protonatable nitrogen in the form of an *N*-methylpiperidinylpiperazine amide.

BMS-742413 ($K_i = 0.023$ nM) demonstrated binding potency that was comparable with BMS-694153 ($K_i = 0.013$ nM) and was a full antagonist at the human CGRP-R (cAMP $EC_{50} = 0.022$ nM). In the human ex vivo intracranial artery model mentioned earlier, the compound reversed and prevented CGRP-induced dilation with subnanomolar potency ($EC_{50} = 0.88$ nM and $K_b = 0.091$ nM, respectively).

BMS-742413 also showed robust activity in the marmoset facial blood flow model. At 0.03 mg kg^{-1} (SC), strong inhibition of CGRP-induced increases in facial blood flow was observed at 15 (48%), 60 (80%), and 105 min (70%). Total plasma levels from 15 to 105 min, associated with significant activity, ranged from 25 to 31 nM.

The inclusion of a second amino group may have mitigated any negative effect on solubility of exchange of the fluorodihydroquinazolinone with the quinolone. With a high-polar surface area (116 $Å^2$), BMS-742413 retained excellent aqueous solubility from crystalline material (105 mg mL^{-1} at pH 8.5 and >300 mg mL^{-1} at lower pH values) and low plasma protein binding (human $f_u = 37\%$). As a consequence, bilayer permeability (Caco-2 and parallel artificial membrane permeability assay (PAMPA))

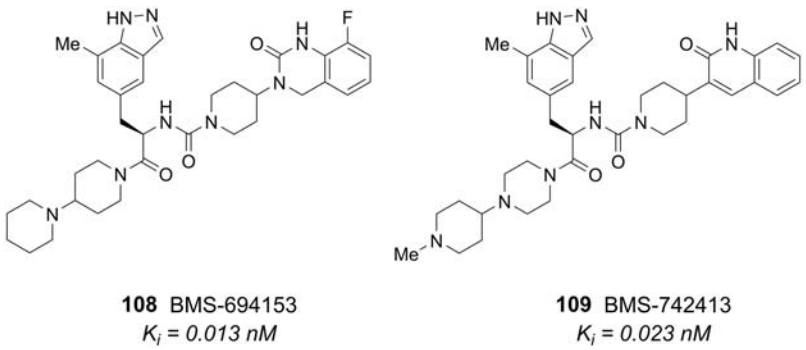

Fig. 26 Structures of BMS-694153 and BMS-742413.

was poor, and oral exposures in mouse and cynomolgus monkey were very low ($F_{PO}=1.4\%$ and 0.3%, respectively). In contrast, absorption of BMS-742413 in rabbit after IN dosing appeared to be rapid and quite efficient. Absolute bioavailabilities were found to be dependent on solution concentrations, with $F_{IN}=13\%$ at 10 mg mL^{-1} ($C_{max}=0.12$ μM) and $F_{IN}=30\%$ at 100 mg mL^{-1} ($C_{max}=2.0$ μM). T_{max} occurred within 20 min for each dose. The compound also showed excellent exposure in rat when dosed SC ($F_{SC}=82\%$). Despite the presence of two tertiary amines and two aromatic rings, but perhaps as a result of its high overall polarity, BMS-742413 caused a low degree of hERG inhibition in a patch clamp assay (9.5% and 22% inhibition at 10 and 30 μM, respectively).

Regarding the two issues that complicated development of BMS-694163, both the solution stability and toxicological profile of BMS-742413 were significantly improved. A 40 mg mL^{-1} solution in succinate buffer (pH 6, 40°C) showed only 0.3% degradation after 3 months. This may suggest that the protonated distal piperidine nitrogen in BMS-694153 intramolecularly activates the amide carbonyl toward hydrolysis and that neither of the two new protonatable nitrogens are properly placed to do this. The potential for off-target systemic toxicity was deemed low based on a 10-day rat study at doses up to 30 mg kg^{-1} day^{-1} (SC). The critical IN toxicity studies showed no significant findings at doses and volumes (75 and 175 mg mL^{-1} in 12.5 μL succinate buffer) matching those where BMS-694153 demonstrated irritation and olfactory epithelial atrophy. Importantly, the dosing volume used in rats was allometrically scaled from the human. At higher concentrations and volumes, dose-dependent irritation, including epithelial inflammation and atrophy, was seen, but these issues were markedly less severe than for BMS-694153. Overall, BMS-742413 represents a promising antimigraine agent that has the potential to provide rapid relief when delivered either IN or SC.

The BMS team also explored carbamates as core urea replacements in this chemotype, with the hope that they might be less susceptible to amide hydrolysis and that loss of the hydrogen bond donor would favorably modulate ADME properties.[177] As shown in Fig. 27, the carbamate backbone was highly tolerant to typical variations used by the BMS group in the GPCR-privileged structure component, with compounds **110**, **111**, and **112** showing CGRP-R potencies that were perhaps somewhat better than corresponding ureidoamides. In addition, even the simplified isoquinoline (**113**) demonstrated subnanomolar affinity ($IC_{50}=0.18$ nM).

A small set of amides that was also prepared showed nothing superior to the piperidyl-piperidine. However, the importance of the distal piperidine was emphasized by the simple piperidine amide, **114** (Fig. 28), which was 100-fold less potent ($IC_{50}=1.8$ nM).

The chemical stability of **112** was clearly superior to BMS-694153 under both the oxidative (97% remaining after 48 h) and hydrolytic (99% remaining after 4 weeks) conditions shown in Fig. 25. The latter result suggests anchimeric assistance of the backbone urea in the degradation of the ureidoamide. Compound **112** also possessed very good aqueous solubility (>50 mg mL^{-1} at pH 7.0 from amorphous solid).

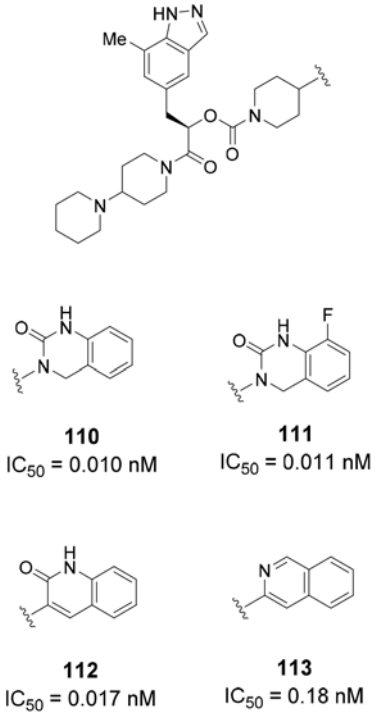

Fig. 27 BMS CGRP receptor antagonists containing carbamate core structures.

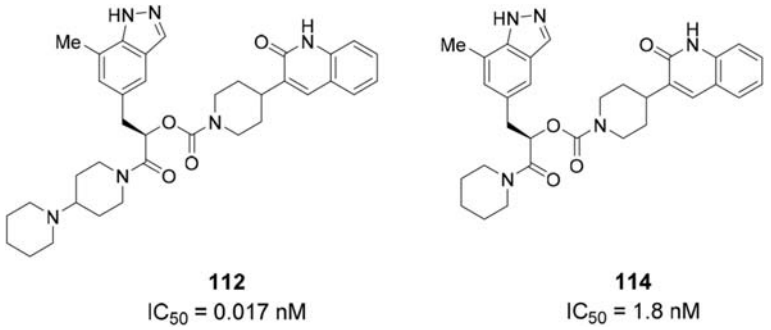

Fig. 28 BMS CGRP receptor antagonists containing carbamate core structures.

7.05.3.3.3 Orally delivered rimegepant (BMS-927711)

The BMS group continued to try to optimize their lead structures for oral delivery. Further backbone modification of the carbamates to corresponding succinyl diamides again yielded compounds that showed potent, though somewhat diminished, hCGRP-R binding and antagonist activities.[178] As shown in Table 11, methylene substitution (compounds **115**, **116**, and **118**) resulted in a fairly consistent reduction in binding potency compared to either ureas or carbamates. Like the carbamates, potent compounds tested were full antagonists with potencies comparable to their binding affinities. However, the succinyl diamides had neither the aqueous solubility needed for intranasal delivery nor the inherent bilayer permeability (assessed in the PAMPA assay) that would justify testing for oral bioavailability.

Radical simplification of the GPCR-privileged component to minimize hydrogen bonding potential was explored using the BMS-694153 core (examples shown in Table 12).[180] In comparison with the simple phenylpiperidine (**119**), moderate binding potency was seen with compounds having a chloro substituent, perhaps a modestly polarizable mimic of the amide carbonyl oxygen, in the 2-position (**120**), or naphthylene (**121**), which is nearly isosteric with the quinolone and quinazolinone privileged structure components. Combining these two elements resulted in subnanomolar potency for chloronaphthylene, **122**, and for the corresponding cyanonaphthylene, **123**. Several of these compounds showed measurable but still modest PAMPA permeability, where the parent, BMS-694153, showed none at all. However, Caco-2 permeabilities remained poor, perhaps due to active efflux.

Another approach taken by the group was to constrain the D-amino acid side chain indazole with the C-terminal amide nitrogen into a cyclic structure that might approximate the CGRP-R binding conformation and reduce the number of rotatable bonds. This work remains unpublished except in the patent literature, and two examples reported to possess both hCGRP-R binding, and functional activities in the most potent category ($IC_{50} = 0.1–10$ nM) are shown in Fig. 29.

Table 11 A comparison of backbone structures for BMS CGRP receptor antagonists[a]

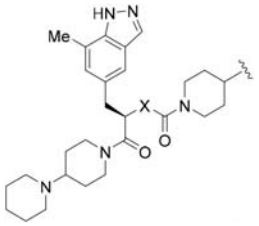

Compound	*Structure*	*X*	*hCGRP-R IC_{50} (nM)*[b]
104	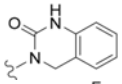	**NH**	0.010
110		**O**	0.010
115		**CH_2**	0.074
Y BMS-694153	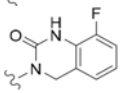	**NH**	0.013
111		**O**	0.011
116		**CH_2**	0.089
117[c]	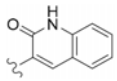	**NH**	0.025
112		**O**	0.017
118		**CH_2**	0.12

[a]Data reported in Ref. 178.
[b]IC_{50} value for inhibition of ^{125}I-hCGRP binding determined using membranes from SK-N-MC cells stably expressing human CLR/RAMP1.
[c]Data from Ref. 179.

Table 12 BMS CGRP receptor antagonists containing simplified GPCR-privileged structure components[a]

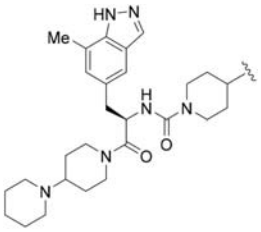

Compound	*Structure*	*hCGRP-R* K_i *(nM)*[b]	*PAMPA (nm* s^{-1}*)*[c]
119	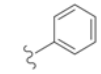	460	-
120	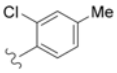	16	120
121	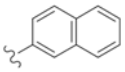	14	61
122	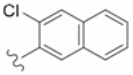	0.23	57
123	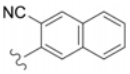	0.11	-

[a]Data reported in Ref. 180.
[b]K_i value for inhibition of ^{125}I-hCGRP binding determined using membranes from SK-N-MC cells stably expressing human CLR/RAMP1.
[c]Parallel artificial membrane permeability assay (PAMPA) at pH 4.

Since bilayer permeability of these compounds that contain multiple amide bonds was generally poor, the BMS group investigated replacement of the D-amino acid carboxy amide group with various heterocycles (**Fig. 30**). This approach typically involves using an sp^2 nitrogen that mimics the amide carbonyl oxygen and tends to rely on the heterocycle to provide additional lipophilicity and substitution vectors to further explore SAR. It is often used in neuroscience drug discovery as a means to improve CNS penetration of a given chemotype.[181]

A series of imidazoles were prepared that kept the 7-methylindazole side chain and the quinazolinone GPCR-privileged component constant and probed substitutions that would yield favorable target potency and significantly improve ADME properties.[182] Selected compounds are shown in **Table 13**. The diversity of substituents reported is limited but suggests that groups on the 2-nitrogen of the imidazole may be taking advantage of the mostly hydrophobic part of the receptor occupied by the pyridylpiperazine in olcegepant[76] and where the imidazole NH is certainly disfavored (**126**, $IC_{50}=97$ nM vs. **127**, $IC_{50}=4.8$ nM). Various fluoro-substituted benzyl analogs showed subnanomolar binding potency with favorable in vitro metabolic stability. However, unlike the IN compounds, these apparently had poor aqueous solubility. When the more polar pyridylmethyl derivatives were made, subnanomolar potency was again achieved, but metabolic stability was greatly diminished. The possibility that this was due to pyridyl *N*-oxidation was addressed by steric blocking with methyl (**134**, $IC_{50}=0.13$ nM) and both chloro and methyl (**135**,

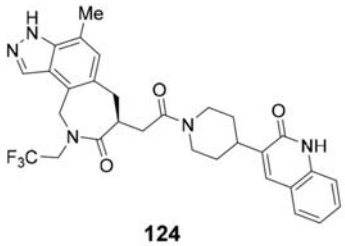

124

From WO 2007131020, published November 15, 2007

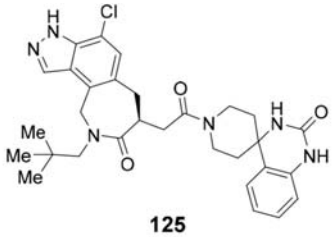

125

From WO 2007130927, published November 15, 2007

Fig. 29 Selected examples of BMS indazoloazepinone CGRP receptor antagonists.

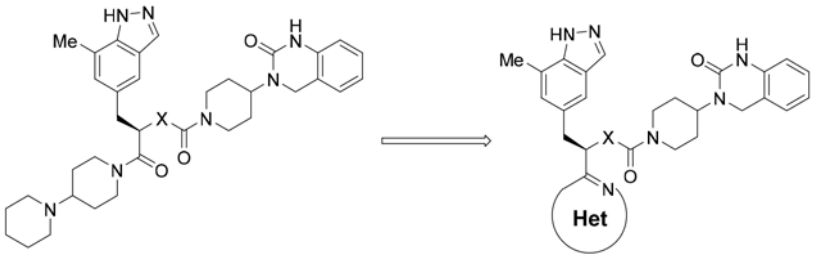

Fig. 30 Heterocyclic bioisostere replacement of the amide functionality in BMS CGRP receptor antagonists.

$IC_{50} = 0.078$ nM). This failed to improve stability. Compound **135** demonstrated only modest PAMPA permeability (33 nm s^{-1} at pH 7.4) but was taken into a rat PK study where it showed high IV clearance and no detectable oral exposure at 1 mg kg^{-1}.

A further small set of imidazole carbamates was made to remove the core urea NH and more closely mimic the structure of the IN compounds (Table 14).[182] Hydrophobic groups such as cyclohexyl (**137**) and benzyl (**138**) again provided subnanomolar binding activity, with somewhat improved PAMPA permeability in the case of the former. However, in vitro metabolic stabilities were still too poor to justify progression.

Table 13 Imidazole-containing CGRP receptor antagonists[a]

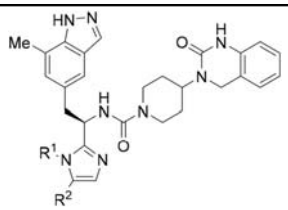

Compound	*R^1*	*R^2*	*hCGRP-R IC_{50} (nM)*[b]	*Metabolic stability, % remaining (H, R, M)*[c]
126	H	H	97	-
127	Me	H	4.8	-
128	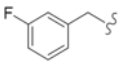	H	0.63	-
129	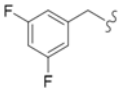	H	0.39	84, 78, 66
130	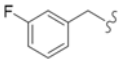	Me	0.37	100, 87, 85
131	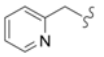	H	1.6	1, 1, 0
132	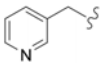	H	0.42	4, 20, 2
133	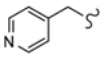	H	0.83	-
134	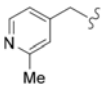	H	0.13	1, 2, 1
135	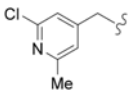	H	0.078	2, 2, 0

[a]Data reported in Ref. 182.
[b]IC_{50} value for inhibition of ^{125}I-hCGRP binding determined using membranes from SK-N-MC cells stably expressing human CLR/RAMP1.
[c]Percent of parent remaining after 10 min incubation in human (H), rat (R), and mouse (M) liver microsomes.

Table 14 Imidazolopiperazine-containing CGRP receptor antagonists from BMS[a]

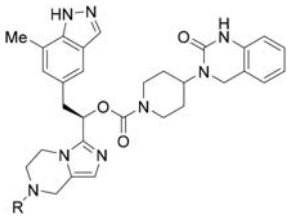

Compound	*R*	*hCGRP-R IC_{50} (nM)*[b]	*Metabolic stability, % remaining (H, R, M)*[c]	*PAMPA (nm s^{-1})*[d]
136	**Et**	1.7	-	-
137		0.22	41, 30, 21	15
138	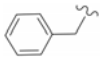	0.26	41, 32, 9	71

[a]Data reported in Ref. 182.
[b]IC_{50} value for inhibition of ^{125}I-hCGRP binding determined using membranes from SK-N-MC cells stably expressing human CLR/RAMP1.
[c]Percent of parent remaining after 10 min incubation in human (H), rat (R), and mouse (M) liver microsomes.
[d]Parallel artificial membrane permeability (PAMPA) at pH 4.

More extensive work was done using pyridine as an amide bioisostere with its potential advantages such as somewhat higher lipophilicity and different substitution vectors (Fig. 31).[183] As with the intranasal compounds, ureas (**139**) and carbamates (**140**) were somewhat more potent than the corresponding amides (**141**). Unusually, for CGRP-R antagonists, reasonable Caco-2 permeability was observed for several modestly potent examples in the succinyl diamide series. However, these compounds did not show good oral exposure in rats, possibly due to poor metabolic stability (Table 15).

Attempting to incorporate protonatable nitrogens that might improve physical properties, the BMS group found that the 4-position on the pyridine was optimal. In Table 16, it is seen that moderate Caco-2 permeability can still be achieved with a highly potent piperidine analog such as **147**. Interestingly, the corresponding morpholine, **148**, suffers an eightfold loss of potency, suggesting that the ring is binding in a hydrophobic pocket. No oral exposure data are disclosed for these compounds, but they are reported to be rapidly metabolized in human and rat microsomes.

Further work led to a small set of 6-chloro, 4-*N*,*N*-dimethylamides in which the effect of the GPCR-privileged structure component was explored (Table 17). Only one of these highly potent compounds, the quinolone (**150**), showed significant Caco-2 permeability, and as with other compounds in this series, rat oral exposure was low (F_{PO} = 4.5%). It was noted that these compounds, in contrast to the intranasal agents discussed earlier, possessed poor aqueous solubility.[183] One compound, the azabenzimidazolone, **152** (IC_{50} = 0.071 nM), was tested in the marmoset facial blood flow model using oral dosing. Somewhat surprisingly, the compound showed moderate activity (31% inhibition of CGRP-induced increases in facial blood flow), albeit at a rather high dose (10 mg kg^{-1}).[184]

The failure to optimize physiochemical properties and achieve good oral exposure with CGRP-R antagonists containing the 7-methylindazole led the BMS group to combine several previous design approaches,[184] namely, cyclic constraint, a carbamate linkage to the GPCR-privileged component, the pyridine-amide bioisostere, and a 2,3-difluorophenyl ring, the hydrophobic residue used by the Merck group in telcagepant.[82] As mentioned earlier, a cocrystal structure of telcagepant with the CGRP-R ectodomain

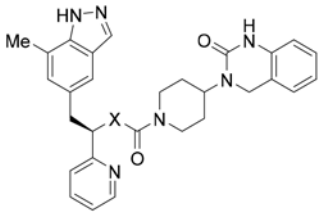

139 X = NH: IC_{50} = 3.1 nM
140 X = O: IC_{50} = 1.5 nM
141 X = CH_2: IC_{50} = 8.6 nM

Fig. 31 Simple pyridyl-containing CGRP receptor antagonists from BMS.

Table 15 Pyridyl-containing CGRP receptor antagonists from BMS[a]

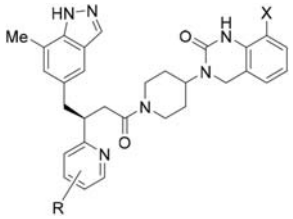

Compound	*R*	*X*	*hCGRP-R IC_{50} (nM)*[b]	*Caco-2 P_c (A-B) (nm s^{-1})*[c]	*Rat F_{PO}*[d]
141	H	H	8.6	120	3%
142	H	F	35	210	3%
143	4-Et	H	10	140	2%
144	5-Me	H	12	64	1%

[a]Data reported in Ref. 183.
[b]IC_{50} value for inhibition of ^{125}I-hCGRP binding determined using membranes from SK-N-MC cells stably expressing human CLR/RAMP1.
[c]Apical to basolateral permeability in Caco-2 cell monolayer.
[d]Rat oral bioavailability (dose and vehicle not reported).

showed the difluorophenyl ring to bind in the same pocket as the dibromophenol of olcegepant but, more deeply, displacing a bridging water molecule that formed a hydrogen bond to the latter.[76] Its lack of an obvious hydrogen bond donor was considered advantageous in the context of a chemotype that is still somewhat large (MW > 500) and rich in hydrogen-bonding groups. The resulting compound, **153** (BMS-846372, Fig. 32), showed very potent binding (K_i = 0.070 nM) and functional antagonist (cAMP IC_{50} = 0.22 nM) activities. As expected, the enantiomer of BMS-846372 was much less active (K_i = 920 nM).

In the marmoset facial blood flow model, the compound was dosed SC at 7 mg kg^{-1} and showed strong (52–60%) inhibition of CGRP-induced effects at 60 and 105 min post dose. Robust in vivo activity was associated with rather high total plasma levels of BMS-846372 (≥1000 nM), especially in comparison with the first intranasal compound, BMS-694153, where much lower levels (>10 nM) were similarly effective.[167] BMS-846372 binds to plasma proteins to a much greater extent (human f_u = 2.3%) than the intranasal compounds (human f_u > 30%), and this may be largely responsible for the difference. BMS-846372 showed good PAMPA permeability (800–1000 nm s^{-1}) and reasonable human microsomal stability ($T_{1/2}$ = 24 min). The compound

Table 16 Pyridyl-containing CGRP receptor antagonists from BMS[a]

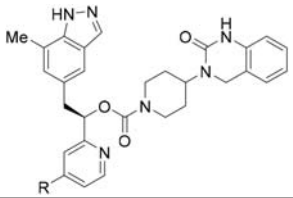

Compound	*R*	*hCGRP-R IC_{50} (nM)*[b]	*Caco-2 P_c (A-B) (nm s^{-1})*[c]
145	$CONMe_2$	0.33	-
146		0.27	-
147	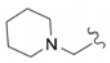	0.16	85
148	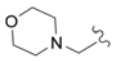	1.2	99
149	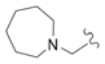	0.095	28

[a]Data reported in Ref. 183.
[b]IC_{50} value for inhibition of ^{125}I-hCGRP binding determined using membranes from SK-N-MC cells stably expressing human CLR/RAMP1.
[c]Apical to basolateral permeability in Caco-2 cell monolayer.

Table 17 Pyridylamide-containing CGRP receptor antagonists from BMS[a]

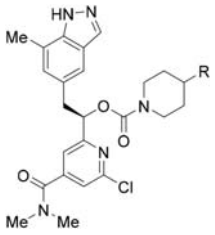

Compound	*R*	*hCGRP-R IC_{50} (nM)*[b]	*Caco-2 P_c (A-B) (nm s^{-1})*[c]	*Rat F_{PO}*[d]
150	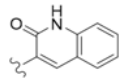	0.077	52	4.5%
151	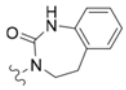	0.093	<15	-
152	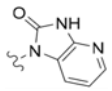	0.071	16	BLLQ

[a]Data reported in Ref. 183.
[b]IC_{50} value for inhibition of ^{125}I-hCGRP binding determined using membranes from SK-N-MC cells stably expressing human CLR/RAMP1.
[c]Apical to basolateral permeability in Caco-2 cell monolayer.
[d]Rat oral bioavailability (dose and vehicle not reported).

demonstrated good oral bioavailability in rat ($F_{PO}=29\%$), dog ($F_{PO}=34\%$), and cynomolgus monkey ($F_{PO}=38\%$), especially in comparison with previous program compounds.

Despite the significant improvement in oral exposure, development of BMS-846372 was hampered by poor physical properties. Crystalline solubility of the free base was very poor (<2 μg mL^{-1}), and salt formation with various acids led to hydrolysis of the carbamate linkage, presumably through activation by the protonated pyridine.[185] A search for positions on the core structure that were tolerant of helpful polarity led to synthesis of the *S*-hydroxyl derivative, **154** (**Fig. 33**), which showed activity comparable to the parent ($K_i=0.081$ nM) and was 50-fold more potent than the *R*-isomer (**155**, $K_i=4.3$ nM). As might be expected, **154** had a somewhat higher free fraction in human plasma ($f_u=4.1\%$), improved aqueous solubility (66 μg mL^{-1}, from amorphous solid), and better human microsomal stability ($T_{1/2}=70$ min).

Further optimization led to the corresponding amine, **156** (rimegepant, BMS-927711).[185] This provided even better binding potency ($K_i=0.027$ nM) and a higher human serum free fraction ($f_u=6.9\%$). As a result, the plasma protein-adjusted affinity of rimegepant was much improved over BMS-846372 (0.39 nM vs. 3.0 nM). Human microsomal stability was also superior ($T_{1/2}=83$ min vs. 24 min), but the most dramatic improvement was in aqueous solubility from crystalline material (50 μg mL^{-1} vs. <2 μg mL^{-1}).

Despite the addition of a primary amine, bilayer permeability of rimegepant was still reasonable, though with some expected pH dependency ($P_C=190$ nm s^{-1} at pH 5.5 and $P_C=320$ nm s^{-1} at 7.4). This suggests that steric crowding may mitigate the absolute polarity of the amino group. With this good balance of physical properties, oral exposures with solution dosing were quite good in

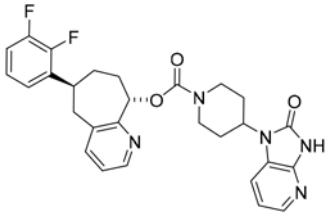

153
BMS-846372
K_i = 0.070 nM

Fig. 32 Structure of BMS-846372.

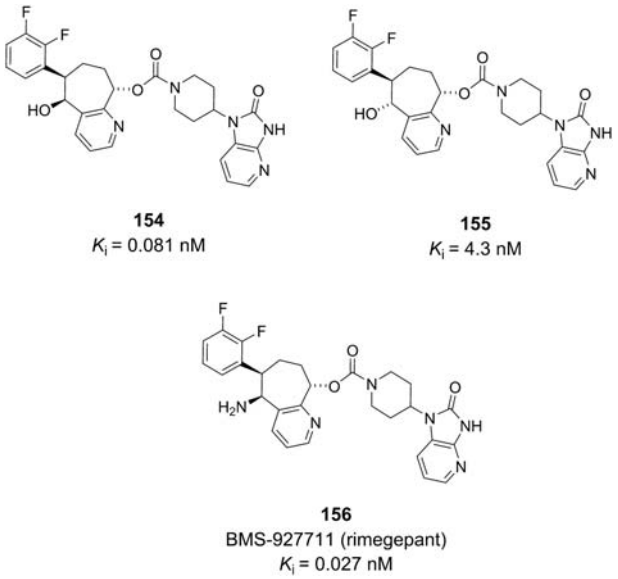

Fig. 33 Substituted analogs of BMS-846372 leading to rimegepant.

rat (F_{PO} = 45%) and cynomolgus monkey (F_{PO} = 67%). Indeed, even when dosed as a crystalline suspension, bioavailability in the monkey remained favorable (F_{PO} = 48%).

When dosed SC at 7 mg kg^{-1} in the marmoset facial blood flow model, rimegepant showed strong (>65%) inhibition of CGRP-induced effects at all time points 15, 60, and 105 min post dose. The magnitude of the effect at 15 min (c.65%), associated with total rimegepant plasma levels of 400 nM, was comparable with that seen with the more lipophilic BMS-846372 at 1900 nM and increased to c.80% at 105 min (total plasma levels c.800 nM). These observations were consistent with the higher intrinsic potency and f_u of rimegepant compared with BMS-846372.

A potential risk in incorporating an amino group into a lipophilic compound is blockade of various ion channels, leading to, among other things, cardiovascular liabilities. However, rimegepant caused <30% inhibition of the hERG potassium channel at 30 μM and had no significant effect on L-type sodium and calcium channels expressed in HEK293 cells. Against a panel of eight recombinant human CYP isoforms, the compound showed low levels of inhibition (IC_{50} > 20 μM, except for CYP3A4, where IC_{50} = 17 μM).

Limited further exploration was carried out on this chemotype (Fig. 34),[186] primarily by replacement of the core pyridine with pyrazine (**157**), thiazole (**159**), and 2-trifluoromethylthiazole (**160**). It is interesting that compound **158**, the urea analog of **157**, suffers a 10-fold loss in binding potency. Although the carbamates in this series demonstrated binding potency that was comparable to rimegepant, their microsomal stability was poor in comparison.

Based on its favorable overall profile and promising pre-IND toxicological study results, BMS decided to proceed with clinical development of rimegepant. Preclinical studies in the marmoset facial blood flow model in conjunction with multispecies pharmacokinetics suggested that a 75 mg oral dose in humans might be efficacious. In a phase I study in healthy subjects, a single 75 mg dose did indeed result in plasma levels ($T_{1/2}$ 10–12 h) commensurate with robust activity in the primate model (≥700 nM).[187] In addition, the compound was well tolerated up to 1500 mg as a single dose and at a daily dose of 600 mg for up to 14 days. Interestingly, food intake delayed T_{max} from 1 to 4 h, and famotidine (antacid) coadministration reduced C_{max} by 26% and AUC by 42%.

In a randomized, double-blind, placebo-controlled, dose-finding study, rimegepant was tested in 885 patients as an abortive migraine therapy at six single doses (10, 25, 75, 150, 300, and 600 mg).[188] High-dose (100 mg) sumatriptan was included as an active comparator. The primary end point was pain freedom at 2 h, with a number of secondary and exploratory outcomes, and safety evaluations. As predicted by the preclinical PK/PD studies, rimegepant was significantly superior to placebo (15.3%) at doses of 75 mg (31.4%), 150 mg (32.9%), and 300 mg (29.7%) and comparable to 100 mg sumatriptan (35%), in the 2-h pain freedom measure of efficacy (though the study was not powered to make direct comparisons with sumatriptan[189]). There were no serious adverse events in the trial, and the side effect profile was "placebo-like," with no marked pattern (unlike the triptans and ergot alkaloids).

7.05.3.4 Other Small-Molecule CGRP Receptor Antagonists

7.05.3.4.1 SmithKline Beecham and GlaxoSmithKline

The earliest reported small-molecule CGRP receptor antagonists were discovered by researchers at SmithKline Beecham.[190] A high-throughput screen identified quinine analog **161** (Fig. 35) as a micromolar antagonist of the CGRP-R: it displaced ^{125}I-CGRP from SK-N-MC cell membranes with an IC_{50} value of 5.9 μM and exhibited a functional IC_{50} value of 26 μM in a cell-based cAMP assay.

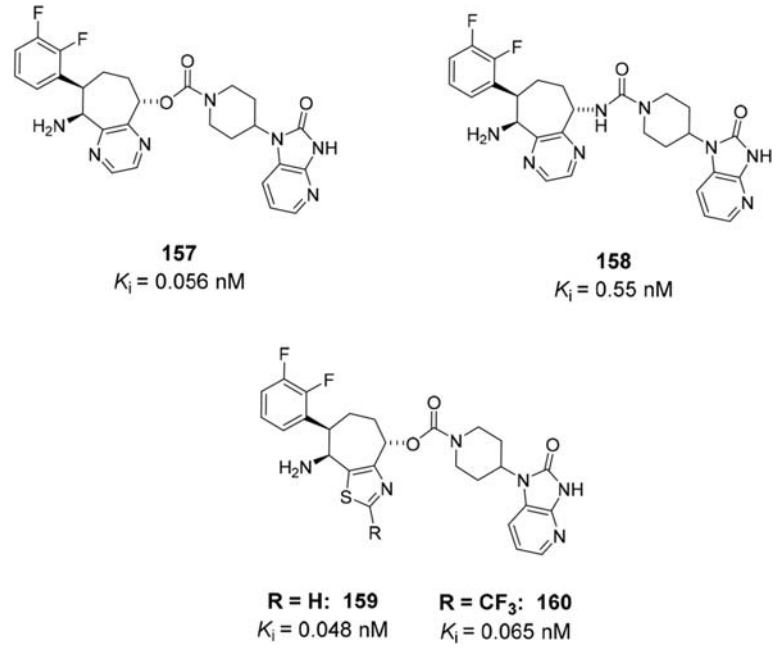

Fig. 34 Alternate heterocyclic analogs of rimegepant.

Limited SAR exploration demonstrated that the 4-chlorophenyl substituent was important for CGRP-R affinity. Compound **161** was also found to be selective for the human CGRP-R with respect to other receptors, including the AM receptor ($IC_{50} > 30$ μM).[190]

Another high-throughput screening lead identified at SmithKline Beecham was SB-211973 (**162**, Fig. 35), which exhibited activity in a binding assay with $IC_{50} = 1.9$ μM.[191] Optimization of this HTS lead led to a series of nitrobenzanilides exemplified by SB-(+)-273779 (**163**, Fig. 35), which had reduced molecular weight and improved in vitro potency: Binding $IC_{50} = 310$ nM; cAMP $IC_{50} = 390$ nM. Compound **163** was also shown to block CGRP-induced hypotension in rats at a dose of 10 mg kg^{-1} IV, although other data indicated that the compound may bind irreversibly to the CGRP-R.[191]

More recently, a group at GlaxoSmithKline focused on the development of novel, orally acting CGRP receptor antagonists.[192] They developed a pharmacophore model based on earlier reported small-molecule antagonists from Merck and BMS and used this to identify a novel series of oxadiazole-based antagonists represented by **164** (Fig. 35, cAMP $K_i \approx 13$ nM). Compound **164** reportedly had the most optimal balance of solubility and permeability in this series, and it exhibited oral bioavailability in rat ($F_{PO} \approx 14\%$) albeit with a delayed absorption profile that was considered suboptimal for acute treatment of migraine.[192]

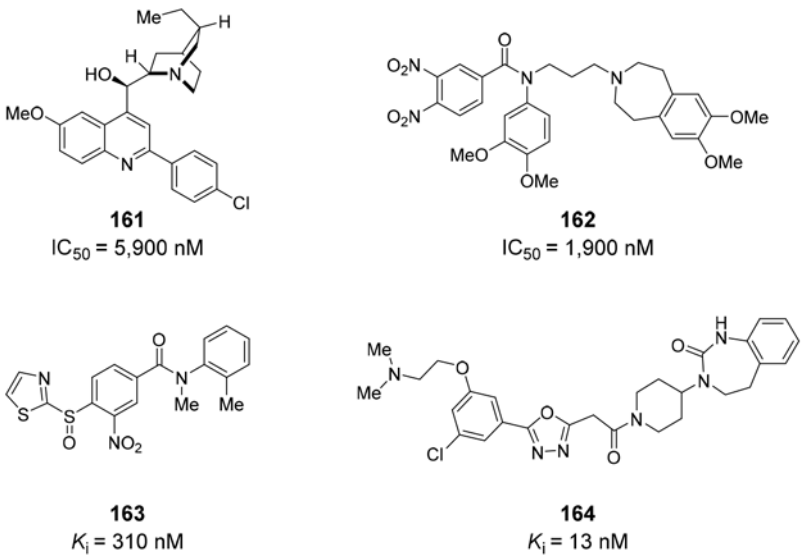

Fig. 35 CGRP receptor antagonists from SmithKline Beecham and GlaxoSmithKline.

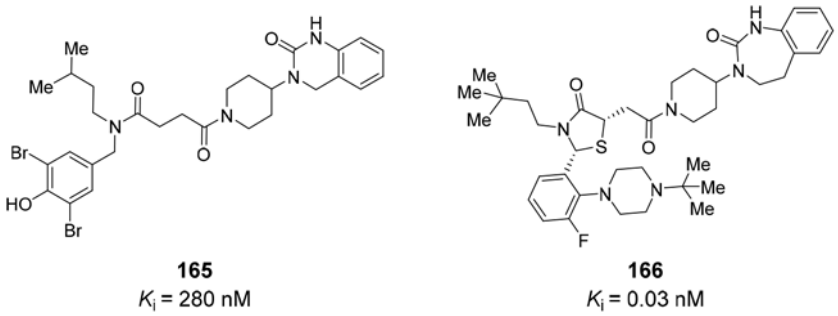

Fig. 36 CGRP receptor antagonists from Vertex.

7.05.3.4.2 Vertex

The Vertex CGRP program was focused on identifying potent, orally bioavailable CGRP receptor antagonists that, in contrast to olcegepant and telcagepant, would be CNS-penetrant.[159] Starting from truncated analogs of olcegepant, they identified **165** (Fig. 36, $K_i = 280$ nM) and optimized this flexible lead structure by incorporating conformational constraints. The most successful of these led to thiazolidinone **166** ($K_i = 0.03$ nM and cAMP $IC_{50} = 1$ nM), which was orally bioavailable in rat ($F_{PO} = 13\%$) and exhibited a moderate brain–plasma ratio (B:P = 0.51), suggesting that such compounds could be optimized to give potent, CNS-penetrant, orally acting receptor antagonists.[159]

7.05.3.4.3 Neurogen

Two patent applications from Neurogen claim small-molecule CGRP receptor antagonists: biaryl ketones such as **167**[193] and aryl amides such as **168**[194] (Fig. 37). A number of the aryl amide compounds were reported to have cell-based IC_{50} values of less than 2 μM. Interestingly, some of the claimed compounds appear to be similar to those claimed in patent applications from BI.[195,196]

7.05.3.4.4 Grünenthal

Grünenthal GmbH disclosed a series of cyclopentenone-based compounds with micromolar activity against the CGRP-R represented by **169** and **170** (Fig. 38).[197] The compounds are closely related to known inhibitors of cyclooxygenase-2[198] but have a dimethylaminomethyl substituent on the cyclopentenone ring. They were reported to functionally antagonize the CGRP receptor with IC_{50} values of 13 μM (compound **169**) and 32 μM (compound **170**).[197]

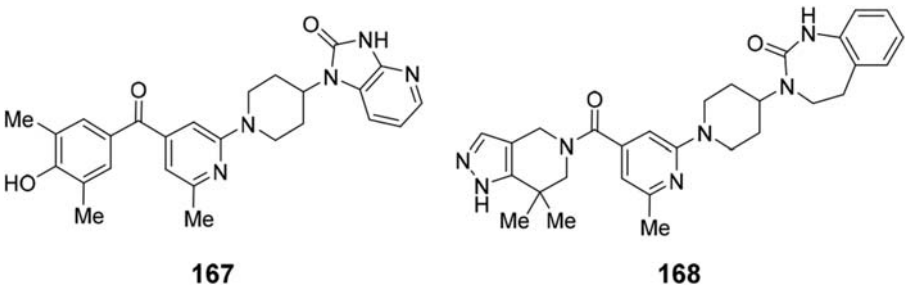

Fig. 37 CGRP receptor antagonists from Neurogen.

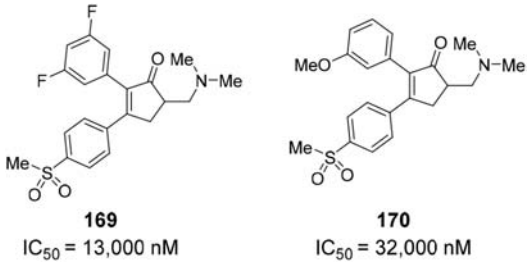

Fig. 38 CGRP receptor antagonists from Grünenthal.

7.05.4 Biologics

7.05.4.1 Monoclonal Antibodies

By virtue of their extended pharmacokinetics, monoclonal antibodies (IgG1 MW approx. 150 kDa) are potentially attractive agents for preventative therapy since they can be dosed with reduced frequency compared with most small molecules, potentially improving compliance and providing long-term coverage against disease-causing targets. It is not clear if the chronic blockade of CGRP or its receptor could lead to adverse events. Since CGRP is the most potent known vasodilator peptide, the possibility of cardiovascular effects has been raised, and long-term safety studies with CGRP-blocking monoclonal antibodies will be needed to address such potential concerns.[199] There are currently four humanized antibodies in development for migraine prevention. Three of these are targeted to CGRP itself, while the fourth binds to the CGRP receptor.

7.05.4.1.1 AMG-334 (Amgen)

AMG-334 is a fully human monoclonal antibody that binds with high affinity ($K_i = 0.020$ nM) to the human CGRP-R and competes with ^{125}I-CGRP.[200] Like the small-molecule agents already discussed, it behaves as a full antagonist at the human (cAMP $IC_{50} = 2.3$ nM) and cynomolgus monkey (cAMP $IC_{50} = 5.7$ nM) receptors. Also like the small-molecule antagonists, it shows >5000-fold reduced activity against nonprimate receptors. Preclinical in vivo assessment was thus carried out in a capsaicin-induced dermal blood flow model in cynomolgus monkeys, where it demonstrated dose-dependent activity measured at days 2 and 4 post dose.

In a 12-week phase II study, patients with frequent episodic migraine (4–14 migraine days/month) were given monthly SC doses of AMG-334 (7, 21, and 70 mg) or placebo, with reduction in monthly migraine days being the primary end point.[199] Only the 70 mg dose showed superiority over placebo (−3.4 days vs. −2.3 days), reducing the average number of monthly migraine days by 1.1 in comparison. Treatment was well tolerated, with adverse events being "placebo-like." Only 3% of patients developed neutralizing antibodies to AMG-334, and this was not associated with adverse events.

7.05.4.1.2 LY2951742 (Lilly)

LY2951742 is a neutralizing humanized monoclonal antibody against human ($K_D = 0.031$ nM) and rat ($K_D = 0.246$ nM) CGRP, respectively.[201] It effectively reduces cAMP production in human SK-N-MC cells with $IC_{50} = 0.35$ nM against human CGRP and $IC_{50} = 1.05$ nM against rat CGRP. In a rat capsaicin-induced dermal blood flow model, LY2951742 (4 mg kg^{-1}, SC) showed an approximately 65% reduction in increased blood flow when dosed 5 days before the capsaicin challenge. The antibody also showed significant activity in two arthritis pain models. [201]

LY2951742 was tested in a 12-week, placebo-controlled migraine prevention study at one dose level (150 mg, SC) given every 2 weeks.[202] Results for the primary end point were similar to those seen for AMG-334 in a similar patient population, with the net difference in monthly migraine days between placebo and antibody being −1.2. LY2951742 had a long elimination half-life (28 days) and was well tolerated.

7.05.4.1.3 ALD403 (Alder BioPharmaceuticals)

ALD403 is another anti-CGRP antibody that is reported to have very high affinity ($K_D < 0.020$ nM) for both the alpha and beta forms of human CGRP.[203] A proof-of-concept phase II study in frequent migraineurs was carried out to assess the safety and efficacy of a single 1000 mg IV dose of ALD403 or placebo. The primary end points were the change from baseline to trial weeks 5–8 in the frequency of migraine days and safety after 12 weeks. There were no obvious safety concerns in this short trial. The difference in migraine days between antibody treatment (−5.6 days) and placebo (−4.6 days) was 1 day.

7.05.4.1.4 TEV-48125 (formerly known as LBR-101, Teva Pharmaceuticals)

The anti-CGRP (IgG2) antibody, TEV-48125, reported to bind with high affinity to the alpha and beta forms of human CGRP, was originally discovered by scientists at Rinat, a small biotechnology company in South San Francisco that was acquired by Pfizer.[204] TEV-48125 (formerly known as PF-04427429) was characterized preclinically in several rat and cynomolgus monkey PD studies. Impressively, a single dose of TEV-48125 was able to inhibit CGRP-induced vasodilation upon weekly capsaicin challenges over 2 months. TEV-48125 was assessed for safety and tolerability in a series of phase I studies in healthy volunteers.[205] By the time the results were reported, the asset had been acquired by Labrys Biologics and renamed LBR-101. When given as a single IV infusion of up to 2000 mg or in two 300 mg doses 1 week apart, the antibody was well tolerated. Mean terminal half-lives for the 30–2000 mg doses ranged from 40 to 48 days, with dose-dependent C_{max} levels. In the meantime, Teva Pharmaceuticals acquired Labrys.

TEV-48125 was reformulated for SC dosing and tested in two large phase II migraine prevention studies in both frequent episodic and chronic (8–14 days of headache per month) migraineurs.[204] In the chronic migraine study, TEV-48125 was given in three SC injections every 28 days over 3 months in two dosing paradigms, (1) 675 mg/225 mg/225 mg and (2) 900 mg/900 mg/900 mg, and compared with placebo.[206] The primary end point was change from baseline in the number of hours with headache in the third month. The differences compared with placebo were −22.74 h for the 675/225 mg group and −30.41 h for the 900 mg group. In the frequent episodic migraine trial, TEV-48125 was given in three SC injections, 28 days apart, in two dosages, 275 and 675 mg, with the primary end point being change from baseline in the number of migraine days during the last 3 weeks. The results for the primary efficacy measure were comparable for the two dosing groups (difference from placebo

for 275 mg is −2.81 days and for 675 mg is −2.64 days). All dosing regimens in these two trials were well tolerated, and there were no serious adverse events.

In summary, the four antibodies so far in clinical trials have shown strikingly similar degrees of efficacy in these initial phase II preventative migraine studies. In theory, monoclonal antibodies should not readily cross the BBB, though there is controversy over its integrity during a migraine attack in some patients.[207] Therefore, considering that all of the small-molecule CGRP-R antagonists that have reached phase II have shown at least "triptan-like" efficacy, this supports the idea that inhibiting the activity of peripheral CGRP can both abort and prevent a significant proportion of migraine attacks. It is reassuring that there were no obvious safety issues, especially concerning cardiovascular function, during these trials. Larger phase III studies, already in progress, will be needed to further define the efficacy and safety of these monoclonal antibodies.

7.05.4.2 Spiegelmers

A German company, NOXXON, has developed a class of artificial oligonucleotides that are mirror-image aptamers,[208] called Spiegelmers, which can bind with high affinity to proteins and other targets.[209] Unlike aptamers, these agents use unnatural ribonucleic acids made from L-ribose. This imparts a great deal of in vivo stability toward degradation (though not renal clearance) since they are not recognized by endogenous nucleases. The unnatural stereochemistry of these oligonucleotides also means that typical selection techniques used against natural targets cannot be used to produce Spiegelmers. Instead, mirror-image protein targets must be generated, conventional aptamers selected against those, and L-ribose versions of the best binders synthesized. These Spiegelmers bind to the natural target with the same affinity as the aptamer leads but are resistant to degradative nucleases. Importantly, evidence so far suggests that Spiegelmers are nonimmunogenic.[210] In order to avoid rapid renal clearance, Spiegelmers are conjugated to a sizable (e.g., 40 kDa) polyethylene glycol (PEG) chain.

NOXXON had progressed an anti-CGRP Spiegelmer, NOX-C89, which was selected against rat D-CGRP and had modest affinity for the human peptide ($IC_{50}=16$ nM) and no selectivity against AMY ($IC_{50}=27$ nM).[211] Subsequently, it was replaced by a more potent and selective Spiegelmer, NOX-L41, which had been selected against human D-CGRP ($IC_{50}=0.5$ nM) and showed no detectable binding to human AMY and other members of the CT family.[212] Affinity had also been improved by direct modification of the ribonucleic acid (RNA) backbone, by replacement of cytidine-41 with deoxycytidine. Conjugation of a branched 40 kDa PEG chain to the 5′ end of the 50-mer, NOX-L41, modulated association/dissociation rates, but did not change the equilibrium binding constant for human CGRP ($K_D=0.4$ nM). NOX-L41 also bound with good affinity to rat CGRP ($IC_{50}=4.0$ nM).

Pharmacokinetics in rat at 10 mg kg^{-1} resulted in nearly identical IV and SC half-lives (8.1 h and 8.2 h, respectively), with a T_{max} approximately 24 h for the SC dose. Clinical pharmacokinetics has been shown with three other Spiegelmers against other targets to be improved on going from rat ($T_{1/2}=6$–8 h) to human ($T_{1/2}=23$–50 h).[209] NOX-L41 at 10 mg kg^{-1} (SC and IV) was tested in a rat neurogenic inflammation model, where it effectively inhibited plasma protein extravasation (PPE) in dura mater upon electrical stimulation of the trigeminal ganglia. Intravital two-photon microscopy was used to show a somewhat delayed accumulation of the Spiegelmer in the dura (equilibrium reached after 2 h), even with IV dosing, potentially explaining the lower activity seen at earlier time points.

7.05.5 Conclusion

The last few decades have seen significant advances in the understanding of migraine attacks and their causes. Importantly, the first migraine-specific class of drugs, the triptans, was introduced, and triptans have had a significant positive impact for many patients, although some concerns remain about their tolerability and vasoconstrictive properties. While there are still many unanswered questions about migraine pathology, the fact that CGRP plays an important role has become widely accepted.

The data implicating CGRP led to interest in agents that could block its effects as potential migraine therapeutics. Gratifyingly, there have been multiple clinical studies on both small molecules and monoclonal antibodies that achieve the goal of CGRP blockade and have shown efficacy for the treatment of migraine. However, none of these have achieved regulatory approval as of the time of this writing.

The dosing frequency and properties of monoclonal antibodies have led to interest in using them for migraine prevention. The available clinical data suggest that antibodies that target either the CGRP peptide or the CGRP receptor may have utility for this purpose. The studies published to date also indicate that these biologics are generally well tolerated. Larger, phase III clinical trials will be needed to assess the safety and efficacy of these agents, but the initial results are certainly encouraging.

In the small-molecule field, the first demonstration of clinical efficacy with a CGRP receptor antagonist was reported more than a decade ago with the IV-administered olcegepant. Since that time, four orally acting CGRP receptor antagonists have been evaluated for the acute treatment of migraine. Overall, the data from these clinical trials are consistent and demonstrate that CGRP receptor antagonists can provide similar efficacy to the triptans but with a much lower incidence of adverse events. Moreover, a variety of preclinical and clinical studies have demonstrated that CGRP receptor antagonists do not cause vasoconstriction, in contrast to triptans, and these studies suggest that CGRP receptor antagonists may have a superior cardiovascular safety profile compared with triptans.

Concerns have been raised about the possible association of CGRP blockade with liver injury, following the observation of elevated levels of liver transaminases after dosing with both MK-3207 and telcagepant. The possibility that these observations could

be due, in part, to CGRP receptor antagonism cannot be ruled out at this time. However, the pattern of findings with these two compounds was reportedly quite different, suggesting that these effects may be specific to these molecules rather than mechanism-based.[132] Additional studies with other CGRP receptor antagonists should lead to a better understanding of these issues.

Perhaps, one of the lessons to be taken from the work reviewed here is that developing an orally bioavailable small-molecule antagonist for a family B GPCR is not trivial. In the present case, such a small molecule must effectively block binding of the 37-amino acid CGRP peptide to an extensive binding site on its receptor. The structural studies reported for the CGRP-R ectodomain complex with olcegepant and telcagepant highlight these challenges and help to explain why potent CGRP receptor antagonists tend to be large, somewhat rigid molecules with multiple hydrogen bond donors and acceptors. Understandably, it has often been challenging to reconcile these properties with good oral pharmacokinetics. A potential solution is intranasal delivery of a molecule such as BMS-742413, although compound design for that route of delivery is, in many ways, just as difficult. While four orally acting CGRP receptor antagonists have demonstrated clinical efficacy, two have been discontinued, and the status of the others (BI 44370 and rimegepant) is unclear. Nonetheless, CGRP blockade is a clinically validated mechanism, and we remain hopeful that one of these compounds or another CGRP receptor antagonist may become an approved treatment for migraine. Such an achievement would represent the first new migraine-specific therapeutic agent in some time and would surely provide great benefit to the many patients who frequently suffer from this complex disorder.

See also: 7.03. Progress in the Discovery of Ca Channel Blockers for the Treatment of Pain. 7.04. Sodium Channel Blockers for the Treatment of Pain.

References

1. Goadsby, P. J.; Lipton, R. B.; Ferrari, M. D. Migraine-Current Understanding and Treatment. *N. Engl. J. Med.* **2002,** *346,* 257–270.
2. Diener, H. C.; Charles, A.; Goadsby, P. J.; Holle, D. New Therapeutic Approaches for the Prevention and Treatment of Migraine. *Lancet* **2015,** *14,* 1010–1022.
3. Hazard, E.; Munakata, J.; Bigal, M. E.; Rupnow, M. F. T.; Lipton, R. B. The Burden of Migraine in the United States: Current and Emerging Perspectives on Disease Management and Economic Analysis. *Value Health* **2009,** *12* (1), 55–64.
4. Harwood, R. H.; Sayer, A. A.; Hirschfeld, M. Current and Future Worldwide Prevalence of Dependency, Its Relationship to Total Population, and Dependency Ratios. *Bull. World Health Organ.* **2004,** *82,* 251–258.
5. Stewart, W. F.; Shechter, A.; Rasmussen, B. K. Migraine Prevalence. A Review of Population-Based Studies. *Neurology* **1994,** *44* (6 Suppl 4), S17–S23.
6. Buse, D. C.; Manack, A. N.; Fanning, K. M.; Serrano, D.; Reed, M. L.; Turkel, C. C.; Lipton, R. B. Chronic Migraine Prevalence, Disability, and Sociodemographic Factors: Results From the American Migraine Prevalence and Prevention Study. *Headache* **2012,** *52* (10), 1456–1470.
7. *The International Classification of Headache Disorders*, 2nd ed, International Headache Society, 52–53 Russell Square London, WC1B 4HP. United Kingdom. Available at http://ihs-classification.org/en/.
8. Linde, M. Migraine: A Review and Future Directions for Treatment. *Acta Neurol. Scand.* **2006,** *114* (2), 71–83.
9. van den Maagdenberg, A. M.; Pietrobon, D.; Pizzorusso, T.; Kaja, S.; Broos, L. A.; Cesetti, T.; van de Ven, R. C.; Tottene, A.; van der Kaa, J.; Plomp, J. J.; Frants, R. R.; Ferrari, M. D. A Cacna1a Knockin Migraine Mouse Model with Increased Susceptibility to Cortical Spreading Depression. *Neuron* **2004,** *41* (5), 701–710.
10. Welch, K. M. Contemporary Concepts of Migraine Pathogenesis. *Neurology* **2003,** *61* (8 Suppl. 4), S2–S8.
11. Pietrobon, D.; Striessnig, J. Neurobiology of Migraine. *Nat. Rev. Neurosci.* **2003,** *4* (5), 386–398.
12. Ashina, M. Vascular Changes Have a Primary Role in Migraine. *Cephalalgia* **2012,** *32* (5), 428–430.
13. Parsons, A. A.; Strijbos, P. J. The Neuronal Versus Vascular Hypothesis of Migraine and Cortical Spreading Depression. *Curr. Opin. Pharmacol.* **2003,** *3* (1), 73–77.
14. Zhang, X.; Levy, D.; Noseda, R.; Kainz, V.; Jakubowski, M.; Burstein, R. Activation of Meningeal Nociceptors by Cortical Spreading Depression: Implications for Migraine with Aura. *J. Neurosci.* **2010,** *30* (26), 8807–8814.
15. Longoni, M.; Ferrarese, C. Inflammation and Excitotoxicity: Role in Migraine Pathogenesis. *Neurol. Sci.* **2006,** *27* (Suppl. 2), S107–S110.
16. Edvinsson, L.; Jansen, I.; Cunha e Sa, M.; Gulbenkian, S. Demonstration of Neuropeptide Containing Nerves and Vasomotor Responses to Perivascular Peptides in Human Cerebral Arteries. *Cephalalgia* **1994,** *14* (2), 88–96.
17. Dodick, D.; Silberstein, S. Central Sensitization Theory of Migraine: Clinical Implications. *Headache* **2006,** *46* (Suppl. 4), S182–S191.
18. Sprenger, T.; Goadsby, P. J. What Has Functional Neuroimaging Done for Primary Headache and for the Clinical Neurologist? *J. Clin. Neurosci.* **2010,** *17,* 547–553.
19. Ramadan, N. M. Current Trends in Migraine Prophylaxis. *Headache* **2007,** *47* (Suppl. 1), S52–S57.
20. Van Dongen, R. M.; Zielman, R.; Noga, M.; Dekkers, O. M.; Hankemeier, T.; van den Maagdenberg, A. M.; Terwindt, G. M.; Ferrari, M. D. Migraine Biomarkers in Cerebrospinal Fluid: A Systematic Review and Meta-Analysis. *Cephalalgia* **2016;** http://dx.doi.org/10.1177/0333102415625614.
21. Lipton, R. B.; Serrano, D.; Holland, S.; Fanning, K. M.; Reed, M. L.; Buse, D. C. Barriers to the Diagnosis and Treatment of Migraine: Effects of Sex, Income, and Headache Features. *Headache* **2013,** *53* (1), 81–92.
22. Bigal, M. E.; Lipton, R. B. Excessive Acute Migraine Medication Use and Migraine Progression. *Neurology* **2008,** *71* (22), 1821–1828.
23. Goadsby, P. J. Migraine: Nonvascular/Neurally Acting Drugs as Novel Treatment Strategies. *Drugs Future* **2006,** *31* (11), 969–977.
24. MacGregor, E. A. Menstruation, Sex Hormones and Migraine. *Neurol. Clin.* **1997,** *15* (1), 125–141.
25. Colman, I.; Brown, M. D.; Innes, G. D.; Grafstein, E.; Roberts, T. E.; Rowe, B. H. Parenteral Dihydroergotamine for Acute Migraine Headache: A Systematic Review of the Literature. *Ann. Emerg. Med.* **2005,** *45* (4), 393–401.
26. Schaerlinger, B.; Hickel, P.; Etienne, N.; Guesnier, L.; Maroteaux, L. Agonist Actions of Dihydroergotamine at 5-HT2B and 5-HT2C Receptors and Their Possible Relevance to Antimigraine Efficacy. *Br. J. Pharmacol.* **2003,** *140* (2), 277–284.
27. Baron, E. P.; Tepper, S. J. Revisiting the Role of Ergots in the Treatment of Migraine and Headache. *Headache* **2010,** *50* (8), 1353–1381.
28. Allen, M. B.; Tosh, G.; Walters, G.; Muers, M. F. Pleural and Pericardial Fibrosis After Ergotamine Therapy. Pleural and Pericardial Fibrosis After Ergotamine Therapy. *Respir. Med.* **1994,** *88* (1), 67–69.
29. Muller-Schweinitzer, E.; Fanchamps, A. Effects on Arterial Receptors of Ergot Derivatives Used in Migraine. *Adv. Neurol.* **1982,** *33,* 343–356.
30. Johnson, K. W.; Phebus, L. A.; Cohen, M. L. Serotonin in Migraine: Theories, Animal Models and Emerging Therapies. *Prog. Drug Res.* **1998,** *51,* 219–244.
31. Doenicke, A.; Brand, J.; Perrin, V. L. Characterization of 5-HT Receptors Mediating Contraction of Canine and Primate Basilar Artery by Use of GR43175, a Selective 5-HT1-Like Receptor Agonist. *Lancet* **1988,** *331* (8598), 1309–1311.

32. Perrin, V. L.; Färkhilä, M.; Goasguen, J.; Doenicke, A.; Brand, J.; Tfelt-Hansen, P. Overview of Initial Clinical Studies with Intravenous and Oral GR43175 in Acute Migraine. *Cephalalgia* **1989,** *9* (Suppl. 9), 63–72.
33. Tepper, S. J.; Rapoport, A. M.; Sheftell, F. D. Mechanisms of Action of the 5-HT1B/1D Receptor Agonists. *JAMA Neurol.* **2002,** *59* (7), 1084–1088.
34. Winner, P.; Linder, S. L.; Lipton, R. B.; Almas, M.; Parsons, B.; Pitman, V. Eletriptan for the Acute Treatment of Migraine in Adolescents: Results of a Double-Blind, Placebo-Controlled Trial. *Headache* **2007,** *47* (4), 511–518.
35. Freidank-Mueschenborn, E.; Fox, A. Resolution of Concentration-Response Differences in Onset of Effect Between Subcutaneous and Oral Sumatriptan. *Headache* **2005,** *45* (6), 632–637.
36. Dahlöf, C. Update on Sumatriptan: New Progress in Migraine Treatment. *Therapy* **2005,** *2* (3), 349–356.
37. Cady, R.; Schreiber, C. Sumatriptan: Update and Review. *Expert. Opin. Pharmacother.* **2006,** *7* (11), 1503–1514.
38. Tfelt-Hansen, P.; De Vries, P.; Saxena, P. R. Triptans in Migraine—A Comparative Review of Pharmacology, Pharmacokinetics and Efficacy. *Drugs* **2000,** *60* (6), 1259–1287.
39. Mett, A.; Tfelt-Hansen, P. Acute Migraine Therapy: Recent Evidence from Randomized Comparative Trials. *Curr. Opin. Neurol.* **2008,** *21* (3), 331–337.
40. Humphrey, P. P. A.; Goadsby, P. J. The Mode of Action of Sumatriptan is Vascular? A Debate. *Cephalalgia* **1994,** *14* (6), 401–410.
41. Mueller, L.; Gallagher, R. M.; Ciervo, C. A. Vasospasm-Induced Myocardial Infarction with Sumatriptan. *Headache* **1996,** *36* (5), 329–331.
42. Ho, T. W.; Edvinsson, L.; Goadsby, P. J. CGRP and Its Receptors Provide New Insights into Migraine Pathophysiology. *Nat. Rev. Neurol.* **2010,** *6* (10), 573–582.
43. Russo, A. F. Calcitonin Gene-Related Peptide (CGRP): A New Target for Migraine. *Annu. Rev. Pharmacol. Toxicol.* **2015,** *55,* 533–552.
44. Karsan, N.; Goadsby, P. J. Calcitonin Gene-Related Peptide and Migraine. *Curr. Opin. Neurol.* **2015,** *28* (3), 250–254.
45. Amara, S. G.; Jonas, V.; Rosenfeld, M. G.; Ong, E. S.; Evans, R. M. Alternative RNA Processing in Calcitonin Gene Expression Generates mRNAs Encoding Different Polypeptide Products. *Nature* **1982,** *298,* 240–244.
46. Edvinsson, L.; Ho, T. W. CGRP Receptor Antagonism and Migraine. *Neurotherapeutics* **2010,** *7* (2), 164–175.
47. Brain, S. D.; Williams, T. J.; Tippins, J. R.; Morris, H. R.; MacIntyre, I. Calcitonin Gene-Related Peptide is a Potent Vasodilator. *Nature* **1985,** *313,* 54–56.
48. Shen, Y.-T.; Pittman, T. M.; Buie, P. S.; Bolduc, D. L.; Kane, S. A.; Koblan, K. S.; Gould, R. J.; Lynch, J. J. Functional Role of α-Calcitonin Gene-Related Peptide in the Regulation of the Cardiovascular System. *J. Pharmacol. Exp. Ther.* **2001,** *298* (2), 551–558.
49. Ambalavanar, R.; Dessem, D.; Moutanni, A.; Yallampalli, C.; Yallampalli, U.; Gangula, P.; Bai, G. Muscle Inflammation Induces a Rapid Increase in Calcitonin Gene-Related Peptide (CGRP) mRNA That Temporally Relates to CGRP Immunoreactivity and Nociceptive Behavior. *Neuroscience* **2006,** *143,* 875–884.
50. Kilo, S.; Harding-Rose, C.; Hargreaves, K. M.; Flores, C. M. Peripheral CGRP Release as a Marker for Neurogenic Inflammation: A Model System for the Study of Neuropeptide Secretion in Rat Paw Skin. *Pain* **1997,** *73* (2), 201–207.
51. Benemei, S.; Nicoletti, P.; Capone, J. G.; Geppetti, P. CGRP Receptors in the Control of Pain and Inflammation. *Curr. Opin. Pharmacol.* **2009,** *9,* 1–6.
52. Gram, D. X.; Ahrén, B.; Nagy, I.; Olsen, U. B.; Brand, C. L.; Sundler, F.; Tabanera, R.; Svendsen, O.; Carr, R. D.; Santha, P.; Wierup, N.; Hansen, A. J. Capsaicin-Sensitive Sensory Fibers in the Islets of Langerhans Contribute to Defective Insulin Secretion in Zucker Diabetic Rat, an Animal Model for Some Aspects of Human Type 2 Diabetes. *Eur. J. Neurosci.* **2007,** *25,* 213–223.
53. Riera, C. E.; Huising, M. O.; Follett, P.; Leblanc, M.; Halloran, J.; Van Andel, R.; de Magalhaes Filho, C. D.; Merkwirth, C.; Dillin, A. TRPV1 Pain Receptors Regulate Longevity and Metabolism by Neuropeptide Signaling. *Cell* **2014,** *157* (5), 1023–1036.
54. Edvinsson, L. Functional Role of Perivascular Peptides in the Control of Cerebral Circulation. *Trends Neurosci.* **1985,** *8,* 126–131.
55. Goadsby, P. J.; Edvinsson, L.; Ekman, R. Vasoactive Peptide Release in the Extracerebral Circulation of Humans During Migraine Headache. *Ann. Neurol.* **1990,** *28* (2), 183–187.
56. Goadsby, P. J.; Edvinsson, L. The Trigeminovascular System and Migraine: Studies Characterizing Cerebrovascular and Neuropeptide Changes Seen in Humans and Cats. *Ann. Neurol.* **1993,** *33* (1), 48–56.
57. Lassen, L. H.; Haderslev, P. A.; Jacobsen, V. B.; Iversen, H. K. CGRP May Play a Causative Role in Migraine. *Cephalalgia* **2002,** *22* (1), 54–61.
58. Poyner, D. R.; Sexton, P. M.; Marshall, I.; Smith, D. M.; Quirion, R.; Born, W.; Muff, R.; Fischer, J. A.; Foord, S. M. International Union of Pharmacology. XXXII. The Mammalian Calcitonin Gene-Related Peptides, Adrenomedullin, Amylin, and Calcitonin Receptors. *Pharmacol. Rev.* **2002,** *54* (2), 233–246.
59. Woolley, M. J.; Conner, A. C. Comparing the Molecular Pharmacology of CGRP and Adrenomedullin. *Curr. Protein Pept. Sci.* **2013,** *14* (5), 358–374.
60. Edvinsson, L. Novel Migraine Therapy with Calcitonin Gene-Related Peptide Receptor Antagonists. *Expert Opin. Ther. Targets* **2007,** *11* (9), 1179–1188.
61. McLatchie, L. M.; Fraser, N. J.; Main, M. J.; Wise, A.; Brown, J.; Thompson, N.; Solari, R.; Lee, M. G.; Foord, S. M. RAMPs Regulate the Transport and Ligand Specificity of the Calcitonin Receptor-Like Receptor. *Nature* **1998,** *393,* 333–339.
62. Moore, E. L.; Salvatore, C. A. Targeting a Family B GPCR/RAMP Receptor Complex: CGRP Receptor Antagonists and Migraine. *Br. J. Pharmacol.* **2012,** *166* (1), 66–78.
63. Barwell, J.; Gingell, J. J.; Watkins, H. A.; Archbold, J. K.; Poyner, D. R.; Hay, D. L. Calcitonin and Calcitonin-Like Receptors: Common Themes with Family B GPCRs? *Br. J. Pharmacol.* **2012,** *166* (1), 51–65.
64. Hilairet, S.; Foord, S. M.; Marshall, F. H.; Bouvier, M. Protein-Protein Interaction and Not Glycosylation Determines the Binding Specificity of Heterodimers Between the Calcitonin Receptor-Like Receptor and the Receptor Activity-Modifying Proteins. *J. Biol. Chem.* **2001,** *276* (31), 29575–29581.
65. Koller, D.; Born, W.; Leuthauser, K.; Fluhmann, B.; McKinney, R. A.; Fischer, J. A.; Muff, R. The Extreme N-Terminus of the Calcitonin-Like Receptor Contributes to the Selective Interaction with Adrenomedullin or Calcitonin Gene-Related Peptide. *FEBS Lett.* **2002,** *531* (3), 464–468.
66. Kuwasako, K.; Kitamura, K.; Nagoshi, Y.; Cao, Y.-N.; Eto, T. Identification of the Human Receptor Activity-Modifying Protein 1 Domains Responsible for Agonist Binding Specificity. *J. Biol. Chem.* **2003,** *278* (25), 22623–22630.
67. Moore, E. L.; Gingell, J. J.; Kane, S. A.; Hay, D. L.; Salvatore, C. A. Mapping the CGRP Receptor Ligand Binding Domain: Tryptophan-84 of RAMP1 is Critical for Agonist and Antagonist Binding. *Biochem. Biophys. Res. Commun.* **2010,** *394* (1), 141–145.
68. Mallee, J. J.; Salvatore, C. A.; LeBourdelles, B.; Oliver, K. R.; Longmore, J.; Koblan, K. S.; Kane, S. A. Receptor Activity-Modifying Protein 1 Determines the Species Selectivity of Non-Peptide CGRP Receptor Antagonists. *J. Biol. Chem.* **2002,** *277* (16), 14294–14298.
69. Salvatore, C. A.; Mallee, J. J.; Bell, I. M.; Zartman, C. B.; Williams, T. M.; Koblan, K. S.; Kane, S. A. Identification and Pharmacological Characterization of Domains Involved in Binding of CGRP Receptor Antagonists to the Calcitonin-Like Receptor. *Biochemistry* **2006,** *45* (6), 1881–1887.
70. Miller, P. S.; Barwell, J.; Poyner, D. R.; Wigglesworth, M. J.; Garland, S. L.; Donnelly, D. Non-Peptidic Antagonists of the CGRP Receptor, BIBN4096BS and MK-0974, Interact with the Calcitonin Receptor-Like Receptor via Methionine-42 and RAMP1 via Tryptophan-74. *Biochem. Biophys. Res. Commun.* **2010,** *391* (1), 437–442.
71. Zartman, C. B.; Bell, I. M.; Gallicchio, S. N.; Graham, S. L.; Kane, S. A.; Mallee, J. J.; Rutledge, R. Z.; Salvatore, C. A.; Vacca, J. P.; Williams, T. M. Identification of a Novel RAMP-Independent CGRP Receptor Antagonist. *Bioorg. Med. Chem. Lett.* **2011,** *21* (22), 6705–6708.
72. Hoare, S. R. J. Mechanisms of Peptide and Nonpeptide Ligand Binding to Class B G-Protein-Coupled Receptors. *Drug Discov. Today* **2005,** *10* (6), 417–427.
73. Cooke, R. M.; Brown, A. J.; Marshall, F. H.; Mason, J. S. Structures of G Protein-Coupled Receptors Reveal New Opportunities for Drug Discovery. *Drug Discov. Today* **2015,** *20* (11), 1355–1364.
74. Rosenbaum, D. M.; Rasmussen, S. G. F.; Kobilka, B. K. The Structure and Function of G-Protein-Coupled Receptors. *Nature* **2009,** *459,* 356–363.
75. Koth, C. M.; Abdul-Manan, N.; Lepre, C. A.; Connolly, P. J.; Yoo, S.; Mohanty, A. K.; Lippke, J. A.; Zwahlen, J.; Coll, J. T.; Doran, J. D.; Garcia-Guzman, M.; Moore, J. M. Refolding and Characterization of a Soluble Ectodomain Complex of the Calcitonin Gene-Related Peptide Receptor. *Biochemistry* **2010,** *49* (9), 1862–1872.
76. ter Haar, E.; Koth, C. M.; Abdul-Manan, N.; Swenson, L.; Coll, J. T.; Lippke, J. A.; Lepre, C. A.; Garcia-Guzman, M.; Moore, J. M. Crystal Structure of the Ectodomain Complex of the CGRP Receptor, a Class-B GPCR, Reveals the Site of Drug Antagonism. *Structure* **2010,** *18* (9), 1083–1093.
77. Pioszak, A.; Xu, H. Molecular Recognition of Parathyroid Hormone by Its G Protein-Coupled Receptor. *Proc. Natl. Acad. Sci. U. S. A.* **2008,** *105* (13), 5034–5039.

78. Parthier, C.; Kleinschmidt, M.; Neumann, P.; Rudolph, R.; Manhart, S.; Schlenzig, D.; Fanghänel, J.; Rahfeld, J.; Demuth, H.; Stubbs, M. Crystal Structure of the Incretin-Bound Extracellular Domain of a G Protein-Coupled Receptor. *Proc. Natl. Acad. Sci. U. S. A.* **2007,** *104* (35), 13942–13947.
79. Kusano, S.; Kukimoto-Niino, M.; Akasaka, R.; Toyama, M.; Terada, T.; Shirouzu, M.; Shindo, T.; Yokoyama, S. Crystal Structure of the Human Receptor Activity-Modifying Protein 1 Extracellular Domain. *Protein Sci.* **2008,** *17* (11), 1907–1914.
80. Evans, B. E.; Rittle, K. E.; Bock, M. G.; DiPardo, R. M.; Freidinger, R. M.; Whitter, W. L.; Lundell, G. F.; Veber, D. F.; Anderson, P. A.; Chang, R. S. L.; Lotti, V. J.; Cerino, D. J.; Chen, T. B.; Kling, P. J.; Kunkel, K. A.; Springer, J. P.; Hirshfield, J. Methods for Drug Discovery: Development of Potent, Selective, Orally Effective Cholecystokinin Antagonists. *J. Med. Chem.* **1988,** *31* (12), 2235–2246.
81. Rudolf, K.; Eberlein, W.; Engel, W.; Pieper, H.; Entzeroth, M.; Hallermayer, G.; Doods, H. Development of Human Calcitonin Gene-Related Peptide (CGRP) Receptor Antagonists. 1. Potent and Selective Small Molecule CGRP Antagonists. 1-[N^2-[3,5-Dibromo-*N*-[[4-(3,4-dihydro-2(1*H*)-oxoquinazolin-3-yl)-1-piperidinyl]carbonyl]-D-tyrosyl]-L-lysyl]-4-(4-pyridinyl)piperazine: The First CGRP Antagonist for Clinical Trials in Acute Migraine. *J. Med. Chem.* **2005,** *48* (19), 5921–5931.
82. Paone, D. V.; Shaw, A. W.; Nguyen, D. N.; Burgey, C. S.; Deng, J. Z.; Kane, S. A.; Koblan, K. S.; Salvatore, C. A.; Mosser, S. D.; Johnston, V. K.; Wong, B. K.; Miller-Stein, C. M.; Hershey, J. C.; Graham, S. L.; Vacca, J. P.; Williams, T. M. Potent, Orally Bioavailable Calcitonin Gene-Related Peptide Receptor Antagonists for the Treatment of Migraine: Discovery of N-[(3R,6S)-6-(2,3-difluorophenyl)-2-oxo-1-(2,2,2-trifluoroethyl)azepan-3-yl]-4-(2-oxo-2,3-dihydro-1H-imidazo[4,5-b]pyridin-1-yl)piperidine-1-carboxamide (MK-0974). *J. Med. Chem.* **2007,** *50* (23), 5564–5567.
83. Lipinksi, C. A.; Lombardo, F.; Dominy, B. W.; Feeney, P. J. Experimental and Computational Approaches to Estimate Solubility and Permeability in Drug Discovery and Development Settings. *Adv. Drug Deliv. Rev.* **1997,** *23* (1–3), 3–25.
84. Hay, D. L.; Christopoulos, G.; Christopoulos, A.; Sexton, P. M. Determinants of BIBN4096BS Affinity for Calcitonin Gene-Related Peptide and Amylin Receptors—The Role of Receptor Activity Modifying Protein 1. *Mol. Pharmacol.* **2006,** *70,* 1984–1991.
85. Doods, H.; Hallermayer, G.; Wu, D.; Entzeroth, M.; Rudolf, K.; Engel, W.; Eberlein, W. Pharmacological Profile of BIBN4096BS, the First Selective Small Molecule CGRP Antagonist. *Br. J. Pharmacol.* **2000,** *129* (3), 420–423.
86. Hershey, J. C.; Corcoran, H. A.; Baskin, E. P.; Salvatore, C. A.; Mosser, S.; Williams, T. M.; Koblan, K. S.; Hargreaves, R.; Kane, S. A. Investigation of the Species Selectivity of a Nonpeptide CGRP Receptor Antagonist Using a Novel Pharmacodynamic Assay. *Regul. Pept.* **2005,** *127,* 71–77.
87. Salvatore, C.; Breese, R.; Chen, R.; Lyle, E.; Corcoran, H.; Hershey, J.; Vogt, T.; Williams, T.; Koblan, K.; Kane, S. Humanization of Mouse RAMP1 via Targeted Recombination Confers Human-Like Pharm acology of CGRP Receptor Antagonists. Presented at the 35th Annual Meeting of the Society for Neuroscience, Washington, DC, November 12–16.
88. Rudolf, K.; Mueller, S.; Stenkamp, D.; Lustenberger, P.; Dreyer, A.; Schaenzle, G.; Bauer, E.; Santagostino, M.; Paleari, F.; Nolte, T.; Beilmann, M.; Schindler, M.; Arndt, K.; Doods, H. Abstracts of Papers. 241st National Meeting and Exposition of the American Chemical Society, Anaheim, CA, March 27–31, 2011**;** American Chemical Society: Washington, DC, 2011. MEDI 11.
89. Sheykhzade, M.; Lind, H.; Edvinsson, L. Noncompetitive Antagonism of BIBN4096BS on CGRP-Induced Responses in Human Subcutaneous Arteries. *Br. J. Pharmacol.* **2004,** *143* (8), 1066–1073.
90. Carpenter, K. A.; Schmidt, R.; von Mentzer, B.; Haglund, U.; Roberts, E.; Walpole, C. Turn Structures in CGRP C-Terminal Analogues Promote Stable Arrangements of Key Residue Side Chains. *Biochemistry* **2001,** *40* (28), 8317–8325.
91. Williams, T. M.; Stump, C. A.; Nguyen, D. N.; Quigley, A. G.; Bell, I. M.; Gallicchio, S. N.; Zartman, C. B.; Wan, B. L.; Penna, K. D.; Kunapuli, P.; Kane, S. A.; Koblan, K. S.; Mosser, S. D.; Rutledge, R. Z.; Salvatore, C.; Fay, J. F.; Vacca, J. P.; Graham, S. L. Non-Peptide Calcitonin Gene-Related Peptide Receptor Antagonists from a Benzodiazepinone Lead. *Bioorg. Med. Chem. Lett.* **2006,** *16* (10), 2595–2598.
92. Doods, H.; Arndt, K.; Rudolf, K.; Just, S. CGRP Antagonists: Unravelling the Role of CGRP in Migraine. *Trends Pharmacol. Sci.* **2007,** *28* (11), 580–587.
93. Doods, H. Development of CGRP Antagonists for the Treatment of Migraine. *Curr. Opin. Investig. Drugs* **2001,** *2* (9), 1261–1268.
94. Petersen, K. A.; Birk, S.; Doods, H.; Edvinsson, L.; Olesen, J. Inhibitory Effect of BIBN4096BS on Cephalic Vasodilatation Induced by CGRP or Transcranial Electrical Stimulation in the Rat. *Br. J. Pharmacol.* **2004,** *143* (6), 697–704.
95. Iovino, M.; Feifel, U.; Yong, C. L.; Wolters, J. M.; Wallenstein, G. Safety, Tolerability and Pharmacokinetics of BIBN 4096 BS, the First Selective Small Molecule Calcitonin Gene-Related Peptide Receptor Antagonist, Following Single Intravenous Administration in Healthy Volunteers. *Cephalalgia* **2004,** *24* (8), 645–656.
96. Petersen, K. A.; Birk, S.; Lassen, L. H.; Kruuse, C.; Jonassen, O.; Lesko, L.; Olesen, J. The CGRP-Antagonist, BIBN4096BS Does Not Affect Cerebral Or Systemic Haemodynamics in Healthy Volunteers. *Cephalalgia* **2005,** *25* (2), 139–147.
97. Petersen, K. A.; Lassen, L. H.; Birk, S.; Lesko, L.; Olesen, J. BIBN4096BS Antagonizes Human Alpha-Calcitonin Gene Related Peptide-Induced Headache and Extracerebral Artery Dilatation. *Clin. Pharmacol. Ther.* **2005,** *77* (3), 202–213.
98. Olesen, J.; Diener, H. C.; Husstedt, I. W.; Goadsby, P. J.; Hall, D.; Meier, U.; Pollentier, S.; Lesko, L. M. Calcitonin Gene-Related Peptide (CGRP) Receptor Antagonist BIBN4096BS for the Acute Treatment of Migraine. *N. Engl. J. Med.* **2004,** *350,* 1104–1110.
99. The Subcutaneous Sumatriptan International Study Group. Treatment of Migraine Attacks with Sumatriptan. *N. Engl. J. Med.* **1991,** *325* (5), 316–321.
100. Edvinsson, L.; Tfelt-Hansen, P. The Blood–Brain Barrier in Migraine Treatment. *Cephalalgia* **2008,** *28* (12), 1245–1258.
101. Boehringer-Ingelheim Announcement (lDdb3), May 15, 2006.
102. US20030191068A1, Published October 9, 2003.
103. Diener, H. C.; Barbanti, P.; Dahlöf, C.; Reuter, U.; Habeck, J.; Podhorna, J. BI 44370 TA, an Oral CGRP Antagonist for the Treatment of Acute Migraine Attacks: Results from a Phase II Study. *Cephalalgia* **2011,** *31* (5), 573–584.
104. WO 9811128, Published March 19, 1998.
105. WO 2004037810, Published May 6, 2004.
106. US 20050234067, Published October 20, 2005 and others.
107. WO 200132648, Published May 10, 2001.
108. WO 200132649, Published May 10, 2001.
109. Clark, D. E. Rapid Calculation of Polar Molecular Surface Area and Its Application to the Prediction of Transport Phenomena. 1. Prediction of Intestinal Absorption. *J. Pharm. Sci.* **1999,** *88* (8), 807–814.
110. Burgey, C. S.; Stump, C. A.; Nguyen, D. N.; Deng, J. Z.; Quigley, A. G.; Norton, B. R.; Bell, I. M.; Mosser, S. D.; Salvatore, C. A.; Rutledge, R. Z.; Kane, S. A.; Koblan, K. S.; Vacca, J. P.; Graham, S. L.; Williams, T. M. Benzodiazepine Calcitonin Gene-Related Peptide (CGRP) Receptor Antagonists: Optimization of the 4-Substituted Piperidine. *Bioorg. Med. Chem. Lett.* **2006,** *16* (19), 5052–5056.
111. Shaw, A. W.; Paone, D. V.; Nguyen, D. N.; Stump, C. A.; Burgey, C. S.; Mosser, S. D.; Salvatore, C. A.; Rutledge, R. Z.; Kane, S. A.; Koblan, K. S.; Graham, S. L.; Vacca, J. P.; Williams, T. M. Caprolactams as Potent CGRP Receptor Antagonists for the Treatment of Migraine. *Bioorg. Med. Chem. Lett.* **2007,** *17* (17), 4795–4798.
112. Salvatore, C. A.; Hershey, J. C.; Corcoran, H. A.; Fay, J. F.; Johnston, V. K.; Moore, E. L.; Mosser, S. D.; Burgey, C. S.; Paone, D. V.; Shaw, A. W.; Graham, S. L.; Vacca, J. P.; Williams, T. M.; Koblan, K. S.; Kane, S. A. Pharmacological Characterization of MK-0974 [N-[(3R,6S)-6-(2,3-difluorophenyl)-2-oxo-1-(2,2,2-trifluoroethyl)azepan-3-yl]-4-(2-oxo-2,3-dihydro-1H-imidazo[4,5-b]pyridin-1-yl)piperidine-1-carboxamide], a Potent and Orally Active Calcitonin Gene-Related Peptide Receptor Antagonist for the Treatment of Migraine. *J. Pharmacol. Exp. Ther.* **2008,** *324* (2), 416–421.
113. Moore, E. L.; Burgey, C. S.; Paone, D. V.; Shaw, A. W.; Tang, Y. S.; Kane, S. A.; Salvatore, C. A. Examining the Binding Properties of MK-0974: A CGRP Receptor Antagonist for the Acute Treatment of Migraine. *Eur. J. Pharmacol.* **2009,** *602* (2–3), 250–254.
114. Van der Schueren, B. J.; de Hoon, J. N.; Vanmolkot, F. H.; Van Hecken, A.; Depre, M.; Kane, S. A.; De Lepeleire, I.; Sinclair, S. R. Reproducibility of the Capsaicin-Induced Dermal Blood Flow Response As Assessed by Laser Doppler Perfusion Imaging. *Br. J. Clin. Pharmacol.* **2007,** *64* (5), 580–590.

115. Paone, D. V.; Shaw, A.; Nguyen, D.; Burgey, C.; Deng, J.; Stump, C.; Quigley, A.; DeSolms, J.; Kane, S.; Koblan, K.; Bednar, R.; Mallee, J.; Mosser, S.; Salvatore, C.; McMasters, D.; Hershey, J.; Corcoran, H.; Lyle, B.; Wong, B.; Roller, S.; Miller-Stein, C.; Rowe, J.; Yu, S.; Graham, S.; Vacca, J.; Williams, T. Abstracts of Papers. 233rd ACS National Meeting & Exposition, Chicago, IL, March 25–29, 2007; American Chemical Society: Washington, DC, 2007. MEDI 20.
116. Roller, S.; Cui, D.; Laspina, C.; Miller-Stein, C.; Rowe, J.; Wong, B.; Prueksaritanont, T. Preclinical Pharmacokinetics of MK-0974, an Orally Active Calcitonin Gene-Related Peptide (CGRP)-Receptor Antagonist, Mechanism of Dose Dependency and Species Differences. *Xenobiotica* **2009,** *39* (1), 33–45.
117. Han, T. H.; Blanchard, R. L.; Palcza, J.; McCrea, J. B.; Laethem, T.; Willson, K.; Xu, Y.; Ermlich, S.; Boyle, J.; Lines, C.; Gutierrez, M.; Van Bortel, L.; Xiao, A. J.; Sinclair, S.; Hickey, L.; Panebianco, D.; Murphy, M. G. Single- and Multiple-Dose Pharmacokinetics and Tolerability of Telcagepant, an Oral Calcitonin Gene-Related Peptide Receptor Antagonist, in Adults. *J. Clin. Pharmacol.* **2010,** *50* (12), 1367–1376.
118. Han, T. H.; Blanchard, R. L.; Palcza, J.; Martucci, A.; Miller-Stein, C. M.; Gutierrez, M.; Panebianco, D.; Rippley, R. K.; Lines, C.; Murphy, M. G. The Dose Proportionality of Telcagepant After Administration of Single Oral and Intravenous Doses in Healthy Adult Subjects. *Arch. Drug Info.* **2010,** *3* (4), 55–62.
119. Sinclair, S. R.; Kane, S. A.; Van der Schueren, B. J.; Xiao, A.; Willson, K. J.; Boyle, J.; de Lepeleire, I.; Xu, Y.; Hickey, L.; Denney, W. S.; Li, C.-C.; Palcza, J.; Vanmolkot, F. H. M.; Depré, M.; Van Hecken, A.; Murphy, M. G.; Ho, T. W.; de Hoon, J. N. Inhibition of Capsaicin-Induced Increase in Dermal Blood Flow by the Oral CGRP Receptor Antagonist, Telcagepant (MK-0974). *Br. J. Clin. Pharmacol.* **2010,** *69* (1), 15–22.
120. Ho, T. W.; Mannix, L. K.; Fan, X.; Assaid, C.; Furtek, C.; Jones, C. J.; Lines, C. R.; Rapoport, A. M. Randomized Controlled Trial of an Oral CGRP Receptor Antagonist, MK-0974, in the Acute Treatment of Migraine. *Neurology* **2008,** *70* (16), 1304–1312.
121. Ho, T. W.; Ferrari, M. D.; Dodick, D. W.; Galet, V.; Kost, J.; Fan, X.; Leibensperger, H.; Froman, S.; Assaid, C.; Lines, C.; Koppen, H.; Winner, P. K. Efficacy and Tolerability of MK-0974 (Telcagepant), an New Oral Antagonist of Calcitonin Gene-Related Peptide Receptor, Compared with Zolmitriptan for Acute Migraine: A Randomised, Placebo-Controlled, Parallel-Treatment Trial. *Lancet* **2008,** *372,* 2115–2123.
122. Connor, K. M.; Shapiro, R. E.; Diener, H.-C.; Lucas, S.; Kost, J.; Fan, X.; Fei, K.; Assaid, C.; Lines, C.; Ho, T. W. Randomized, Controlled Trial of Telcagepant for the Acute Treatment of Migraine. *Neurology* **2009,** *73* (12), 970–977.
123. Ho, A. P.; Dahlöf, C. G. H.; Silberstein, S. D.; Saper, J. R.; Ashina, M.; Kost, J. T.; Froman, S.; Leibensperger, H.; Lines, C. R.; Ho, T. W. Randomized, Controlled Trial of Telcagepant Over Four Migraine Attacks. *Cephalalgia* **2010,** *30* (12), 1443–1457.
124. Connor, K. M.; Aurora, S. K.; Loeys, T.; Ashina, M.; Jones, C.; Giezek, H.; Massaad, R.; Williams-Diaz, A.; Lines, C.; Ho, T. W. Long-Term Tolerability of Telcagepant for Acute Treatment of Migraine in a Randomized Trial. *Headache* **2011,** *51* (1), 73–84.
125. Chan, K. Y.; Edvinsson, L.; Eftekhari, P. O.; Kimblad, S. A.; Kane, S. A.; Lynch, J.; Hargreaves, R. J.; de Vries, R.; Garrelds, I. M.; van den Bogaerdt, A. J.; Danser, A. H. J.; MaassenVanDenBrink, A. Characterization of the Calcitonin Gene-Related Peptide Receptor Antagonist Telcagepant (MK-0974) in Human Isolated Coronary Arteries. *J. Pharmacol. Exp. Ther.* **2010,** *334* (3), 746–752.
126. Lynch, J. J.; Regan, C. P.; Edvinsson, L.; Hargreaves, R. J.; Kane, S. A. Comparison of the Vasoconstrictor Effects of the Calcitonin Gene-Related Peptide Receptor Antagonist Telcagepant (MK-0974) and Zolmitriptan in Human Isolated Coronary Arteries. *J. Cardiovasc. Pharmacol.* **2010,** *55* (5), 518–521.
127. Ho, T. W.; Ho, A. P.; Chaitman, B. R.; Johnson, C.; Mathew, N. T.; Kost, J.; Fan, X.; Aurora, S. K.; Brandes, J. L.; Fei, K.; Beebe, L.; Lines, C.; Krucoff, M. W. Randomized, Controlled Study of Telcagepant in Patients With Migraine and Coronary Artery Disease. *Headache* **2012,** *52* (2), 224–235.
128. Behm, M. O.; Blanchard, R. L.; Murphy, M. G.; Palcza, J.; Harris, D. E.; Butterfield, K. L.; Smith, W. B.; Preston, R. A.; Chodakewitz, J. A.; Krucoff, M. W. Effect of Telcagepant on Spontaneous Ischemia in Cardiovascular Patients in a Randomized Study. *Headache* **2011,** *51* (6), 954–960.
129. Chaitman, B. R.; Ho, A. P.; Behm, M. O.; Rowe, J. F.; Palcza, J.; Laethem, T.; Heirman, I.; Panebianco, D.; Kobalava, Z.; Martsevich, S. Y.; Free, A. L.; Bittar, N.; Chrysant, S. G.; Ho, T. W.; Chodakewitz, J. A.; Murphy, M. G.; Blanchard, R. L. A Randomized, Placebo-Controlled Study of the Effects of Telcagepant on Exercise Time in Patients With Stable Angina. *Clin. Pharmacol. Ther.* **2012,** *91* (3), 459–466.
130. Van der Schueren, B. J.; Blanchard, R.; Murphy, M. G.; Palcza, J.; de Lepeleire, I.; Van Hecken, A.; Depré, M.; de Hoon, J. N. The Potent Calcitonin Gene-Related Peptide Receptor Antagonist, Telcagepant, Does Not Affect Nitroglycerin-Induced Vasodilation in Healthy Men. *Br. J. Clin. Pharmacol.* **2011,** *71* (5), 708–717.
131. Depré, M.; MacLeod, C.; Palcza, J.; Behm, M. O.; de Lepeleire, I.; Han, T.; Panebianco, D.; Smith, W. B.; Blanchard, R.; Chodakewitz, J. A.; Murphy, M. G.; de Hoon, J. N. Lack of Hemodynamic Interaction Between CGRP-Receptor Antagonist Telcagepant (MK-0974) and Sumatriptan: Results From a Randomized Study in Patients With Migraine. *Cephalalgia* **2013,** *33* (16), 1292–1301.
132. Ho, T. W.; Connor, K. M.; Zhang, Y.; Pearlman, E.; Koppenhaver, J.; Fan, X.; Lines, C.; Edvinsson, L.; Goadsby, P. J.; Michelson, D. Randomized Controlled Trial of the CGRP Receptor Antagonist Telcagepant for Migraine Prevention. *Neurology* **2014,** *83* (11), 958–966.
133. Ho, T. W.; Ho, A. P.; Ge, Y.; Assaid, C.; Gottwald, R.; MacGrergor, E. A.; Mannix, L. K.; van Oosterhout, W. P. J.; Koppenhaver, J.; Lines, C.; Ferrari, M. D.; Michelson, D. Randomized Controlled Trial of the CGRP Receptor Antagonist Telcagepant for Prevention of Headache in Women With Perimenstrual Migraine. *Cephalalgia* **2014,** *36* (2), 148–161.
134. Merck News Release. Merck Announces Second Quarter 2011 Financial Results. July 29, 2011.
135. Paone, D. V.; Nguyen, D. N.; Shaw, A. W.; Burgey, C. S.; Potteiger, C. M.; Deng, J. Z.; Mosser, S. D.; Salvatore, C. A.; Yu, S.; Roller, S.; Kane, S. A.; Selnick, H. G.; Vacca, J. P.; Williams, T. M. Orally Bioavailable Imidazoazepanes as Calcitonin Gene-Related Peptide (CGRP) Receptor Antagonists: Discovery of MK-2918. *Bioorg. Med. Chem. Lett.* **2011,** *21* (9), 2683–2686.
136. Nguyen, D. N.; Paone, D. V.; Shaw, A. W.; Burgey, C. S.; Mosser, S. D.; Johnston, V.; Salvatore, C. A.; Leonard, Y. M.; Miller-Stein, C. M.; Kane, S. A.; Koblan, K. S.; Vacca, J. P.; Graham, S. L.; Williams, T. M. Calcitonin Gene-Related Peptide (CGRP) Receptor Antagonists: Investigations of a Pyridinone Template. *Bioorg. Med. Chem. Lett.* **2008,** *18* (2), 755–758.
137. Burgey, C. S.; Potteiger, C. M.; Deng, J. Z.; Mosser, S. D.; Salvatore, C. A.; Yu, S.; Roller, S.; Kane, S. A.; Vacca, J. P.; Williams, T. M. Optimization of Azepanone Calcitonin Gene-Related Peptide (CGRP) Receptor Antagonists: Development of Novel Spiropiperidines. *Bioorg. Med. Chem. Lett.* **2009,** *19* (22), 6368–6372.
138. Bell, I. M.; Bednar, R. A.; Fay, J. F.; Gallicchio, S. N.; Hochman, J. H.; McMasters, D. R.; Miller-Stein, C.; Moore, E. L.; Mosser, S. D.; Pudvah, N. T.; Quigley, A. G.; Salvatore, C. A.; Stump, C. A.; Theberge, C. R.; Wong, B. K.; Zartman, C. B.; Zhang, X.-F.; Kane, S. A.; Graham, S. L.; Vacca, J. P.; Williams, T. M. Identification of Novel, Orally Bioavailable Spirohydantoin CGRP Receptor Antagonists. *Bioorg. Med. Chem. Lett.* **2006,** *16* (24), 6165–6169.
139. Theberge, C. R.; Bednar, R. A.; Bell, I. M.; Corcoran, H. A.; Fay, J. F.; Hershey, J. C.; Johnston, V. K.; Kane, S. A.; Mosser, S.; Salvatore, C. A.; Williams, T. M.; Zartman, C. B.; Zhang, X.-F.; Graham, S. L.; Vacca, J. P. Potent Benzimidazolone-Based CGRP Receptor Antagonists. *Bioorg. Med. Chem. Lett.* **2008,** *18* (23), 6122–6125.
140. Stump, C. A.; Bell, I. M.; Bednar, R. A.; Bruno, J. G.; Fay, J. F.; Gallicchio, S. N.; Johnston, V. K.; Moore, E. L.; Mosser, S. D.; Quigley, A. G.; Salvatore, C. A.; Theberge, C. R.; Zartman, C. B.; Zhang, X.-F.; Kane, S. A.; Graham, S. L.; Vacca, J. P.; Williams, T. M. The Discovery of Highly Potent CGRP Receptor Antagonists. *Bioorg. Med. Chem. Lett.* **2009,** *19* (1), 214–217.
141. Bell, I. M.; Bednar, R. A.; Corcoran, H. A.; Fay, J. F.; Gallicchio, S. N.; Johnston, V. K.; Hershey, J. C.; Miller-Stein, C. M.; Moore, E. L.; Mosser, S. D.; Roller, S. A.; Salvatore, C. A.; Theberge, C. R.; Wong, B. K.; Zartman, C. B.; Kane, S. A.; Williams, T. M.; Graham, S. L.; Vacca, J. P. The Identification of Potent, Orally Bioavailable Tricyclic CGRP Receptor Antagonists. *Bioorg. Med. Chem. Lett.* **2009,** *19* (16), 4740–4742.
142. Stump, C. A.; Bell, I. M.; Bednar, R. A.; Fay, J. F.; Gallicchio, S. N.; Hershey, J. C.; Jelley, R.; Kreatsoulas, C.; Moore, E. L.; Mosser, S. D.; Quigley, A. G.; Roller, S. A.; Salvatore, C. A.; Sharik, S. S.; Theberge, C. R.; Zartman, C. B.; Kane, S. A.; Graham, S. L.; Selnick, H. G.; Vacca, J. P.; Williams, T. M. The Identification of Potent, Orally Bioavailable Tricyclic CGRP Receptor Antagonists. *Bioorg. Med. Chem. Lett.* **2010,** *20* (8), 2572–2576.
143. Wood, M. R.; Schirripa, K. M.; Kim, J. J.; Quigley, A. G.; Stump, C. A.; Bell, I. M.; Bednar, R. A.; Fay, J. F.; Bruno, J. G.; Moore, E. L.; Mosser, S. D.; Roller, S.; Salvatore, C. A.; Vacca, J. P.; Selnick, H. G. Novel CGRP Receptor Antagonists Through a Design Strategy of Target Simplification With Additional Molecular Flexibility. *Bioorg. Med. Chem. Lett.* **2009,** *19* (19), 5787–5790.

144. Bell, I. M.; Gallicchio, S. N.; Wood, M. R.; Quigley, A. G.; Stump, C. A.; Zartman, C. B.; Fay, J. F.; Li, C.-C.; Lynch, J. J.; Moore, E. L.; Mosser, S. D.; Prueksaritanont, T.; Regan, C. R.; Roller, S.; Salvatore, C. A.; Kane, S. A.; Vacca, J. P.; Selnick, H. G. Discovery of MK-3207: A Highly Potent, Orally Bioavailable CGRP Receptor Antagonist. *ACS Med. Chem. Lett.* **2010,** *1* (1), 24–29.
145. Salvatore, C. A.; Moore, E. L.; Calamari, A.; Cook, J. J.; Michener, M. S.; O'Malley, S.; Miller, P. J.; Sur, C.; Williams, D. L.; Zeng, Z.; Danziger, A.; Lynch, J. J.; Regan, C. R.; Fay, J. F.; Tang, Y. S.; Li, C.-C.; Pudvah, N. T.; White, R. B.; Bell, I. M.; Gallicchio, S. N.; Graham, S. L.; Selnick, H. G.; Vacca, J. P.; Kane, S. A. Pharmacological Properties of MK-3207, a Potent and Orally Active Calcitonin Gene-Related Peptide Receptor Antagonist. *J. Pharmacol. Exp. Ther.* **2010,** *333* (1), 152–160.
146. Bell, I. M. Abstracts of Papers. *237th ACS National Meeting & Exposition, Salt Lake City, UT, March 22–26, 2009*; American Chemical Society: Washington, DC, 2009. MEDI 28.
147. Li, C.-C.; Vermeersch, S.; Denney, W. S.; Kennedy, W. P.; Palcza, J.; Gipson, A.; Han, T. H.; Blanchard, R.; De Lepeleire, I.; Depré, M.; Murphy, M. G.; Van Dyck, K.; de Hoon, J. N. Characterizing the PK/PD Relationship for Inhibition of Capsaicin-Induced Dermal Vasodilatation by MK-3207, an Oral Calcitonin Gene Related Peptide Receptor Antagonist. *Br. J. Clin. Pharmacol.* **2015,** *79* (5), 831–837.
148. Hewitt, D. J.; Aurora, S. K.; Dodick, D. W.; Goadsby, P. J.; Ge, Y. J.; Bachman, R.; Taraborelli, D.; Fan, X.; Assaid, C.; Lines, C.; Ho, T. W. Randomized Controlled Trial of the CGRP Receptor Antagonist MK-3207 in the Acute Treatment of Migraine. *Cephalalgia* **2011,** *31* (6), 712–722.
149. Bell, I. M.; Stump, C. A.; Gallicchio, S. N.; Staas, D. D.; Zartman, C. B.; Moore, E. L.; Sain, N.; Urban, M.; Bruno, J. G.; Calamari, A.; Kemmerer, A. L.; Mosser, S. D.; Fandozzi, C.; White, R. B.; Zrada, M. M.; Selnick, H. G.; Graham, S. L.; Vacca, J. P.; Kane, S. A.; Salvatore, C. A. MK-8825: A Potent and Selective CGRP Receptor Antagonist With Good Oral Activity in Rats. *Bioorg. Med. Chem. Lett.* **2012,** *22* (12), 3941–3945.
150. Feistel, S.; Albrecht, S.; Messlinger, K. The Calcitonin Gene-Related Peptide Receptor Antagonist MK-8825 Decreases Spinal Trigeminal Activity During Nitroglycerin Infusion. *J. Headache Pain* **2013,** *14* (1), 93/1–93/9.
151. Greco, R.; Mangione, A. S.; Siani, F.; Blandini, F.; Vairetti, M.; Nappi, G.; Sandrini, G.; Buzzi, M. G.; Tassorelli, C. Effects of CGRP Receptor Antagonism in Nitroglycerin-Induced Hyperalgesia. *Cephalalgia* **2014,** *34* (8), 594–604.
152. Michot, B.; Kayser, V.; Hamon, M.; Bourgoin, S. CGRP Receptor Blockade by MK-8825 Alleviates Allodynia in Infraorbital Nerve-Ligated Rats. *Eur. J. Pain* **2015,** *19* (2), 281–290.
153. Romero-Reyes, M.; Pardi, V.; Akerman, S. A Potent and Selective Calcitonin Gene-Related Peptide (CGRP) Receptor Antagonist, MK-8825, Inhibits Responses to Nociceptive Trigeminal Activation: Role of CGRP in Orofacial Pain. *Exp. Neurol.* **2015,** *271,* 95–103.
154. Bell, I. M.; Gallicchio, S. N.; Stump, C. A.; Bruno, J. G.; Fan, H.; Gantert, L. T.; Hostetler, E. D.; Kemmerer, A. L.; McWherter, M.; Moore, E. L.; Mosser, S. D.; Purcell, M. L.; Riffel, K.; Salvatore, C. A.; Sanabria-Bohórquez, S.; Staas, D. D.; White, R. B.; Williams, M.; Zartman, C. B.; Cook, J. J.; Hargreaves, R. J.; Kane, S. A.; Graham, S. L.; Selnick, H. G. [11C]MK-4232: The First Positron Emission Tomography Tracer for the Calcitonin Gene-Related Peptide Receptor. *ACS Med. Chem. Lett.* **2013,** *4* (9), 863–868.
155. Bell, I. M. Calcitonin Gene-Related Peptide Receptor Antagonists: New Therapeutic Agents for Migraine. *J. Med. Chem.* **2014,** *57* (19), 7838–7858.
156. Hostetler, E. D.; Joshi, A. D.; Sanabria-Bohórquez, S.; Fan, H.; Zeng, Z.; Purcell, M.; Selnick, H. G.; Gallicchio, S. N.; Bell, I. M.; Salvatore, C. A.; Kane, S. A.; Li, C.-C.; Hargreaves, R.; de Groot, T.; Bormans, G.; Van Hecken, A.; Derdelinckx, I.; de Hoon, J.; Reynders, T.; Declercq, R.; De Lepeleire, I.; Kennedy, W. D.; Blanchard, R.; Marcantonio, E. E.; Sur, C.; Cook, J. J.; van Laere, K.; Evelhoch, J. L. In Vivo Quantification of Calcitonin Gene-Related Peptide (CGRP) Receptor Occupancy by Telcagepant in Rhesus Monkey and Human Brain Using the Positron Emission Tomography (PET) Tracer [11C]MK-4232. *J. Pharmacol. Exp. Ther.* **2013,** *347* (2), 478–486.
157. Grimwood, S.; Hartig, P. R. Target Site Occupancy: Emerging Generalizations From Clinical and Preclinical Studies. *Pharmacol. Ther.* **2009,** *122* (3), 281–301.
158. Kim, J. J.; Wood, M. R.; Stachel, S. J.; de Leon, P.; Nomland, A.; Stump, C. A.; McWherter, M. A.; Schirripa, K. M.; Moore, E. L.; Salvatore, C. A.; Selnick, H. G. (*E*)-Alkenes as Replacements of Amide Bonds: Development of Novel and Potent Acyclic CGRP Receptor Antagonists. *Bioorg. Med. Chem. Lett.* **2014,** *24* (1), 258–261.
159. Joshi, P.; Anderson, C.; Binch, H.; Hadida, S.; Yoo, S.; Bergeron, D.; Decker, C.; terHaar, E.; Moore, J.; Garcia-Guzman, M.; Termin, A. Identification of Potent CNS-Penetrant Thiazolidinones as Novel CGRP Receptor Antagonists. *Bioorg. Med. Chem. Lett.* **2014,** *24* (3), 845–849.
160. Wood, M. R.; Schirripa, K. M.; Kim, J. J.; Bednar, R. A.; Fay, J. F.; Bruno, J. G.; Moore, E. L.; Mosser, S. D.; Roller, S.; Salvatore, C. A.; Vacca, J. P.; Selnick, H. G. Novel CGRP Receptor Antagonists From Central Amide Replacements Causing a Reversal of Preferred Chirality. *Bioorg. Med. Chem. Lett.* **2010,** *20* (22), 6827–6830.
161. Crowley, B. M.; Stump, C. A.; Nguyen, D. N.; Potteiger, C. M.; McWherter, M. A.; Paone, D. V.; Quigley, A. G.; Bruno, J. G.; Cui, D.; Culberson, J. C.; Danziger, A.; Fandozzi, C.; Gauvreau, D.; Kemmerer, A. L.; Menzel, K.; Moore, E. L.; Mosser, S. D.; Reddy, V.; White, R. B.; Salvatore, C. A.; Kane, S. A.; Bell, I. M.; Selnick, H. G.; Fraley, M. E.; Burgey, C. S. Novel Oxazolidinone CGRP Receptor Antagonists for the Acute Treatment of Migraine. *Bioorg. Med. Chem. Lett.* **2015,** *25* (21), 4777–4781.
162. Hazuda, D. J.; Anthony, N. J.; Gomez, R. P.; Jolly, S. M.; Wai, J. S.; Zhuang, L.; Fisher, T. E.; Embrey, M.; Guare, J. P., Jr.; Egbertson, M. S.; Vacca, J. P.; Huff, J. R.; Felock, P. J.; Witmer, M. V.; Stillmock, K. A.; Danovich, R.; Grobler, J.; Miller, M. D.; Espeseth, A. S.; Jin, L.; Chen, I.-W.; Lin, J. H.; Kassahun, K.; Ellis, J. D.; Wong, B. K.; Xu, W.; Pearson, P. G.; Schleif, W. A.; Cortese, R.; Emini, E.; Summa, V.; Holloway, M. K.; Young, S. D. A Naphthyridine Carboxamide Provides Evidence for Discordant Resistance Between Mechanistically Identical Inhibitors of HIV-1 Integrase. *Proc. Natl. Acad. Sci. U. S. A.* **2004,** *101* (31), 11233–11238.
163. WO 00018764, Published April 6, 2000.
164. Chaturvedula, P. V.; Pin, S.; Tholady, G.; Conway, C. M.; Macor, J. E.; Dubowchik, G. M. Design and Synthesis of Potent Antagonists Containing Rigid Spirocyclic Privileged Structures for the CGRP Receptor. *Bioorg. Med. Chem. Lett.* **2012,** *22* (14), 4719–4722.
165. Han, X.; Civiello, R. L.; Conway, C. M.; Cook, D. A.; Davis, C. D.; Macci, R.; Pin, S. S.; Ren, S. X.; Schartman, R.; Signor, L. J.; Thalody, G.; Widmann, K. A.; Xu, C.; Chaturvedula, P. V.; Macor, J. E.; Dubowchik, G. M. The Synthesis and SAR of Calcitonin Gene-Related Peptide (CGRP) Receptor Antagonists Derived From Tyrosine Surrogates. Part 1. *Bioorg. Med. Chem. Lett.* **2012,** *22* (14), 4723–4727.
166. Han, X.; Civiello, R. L.; Conway, C. M.; Cook, D. A.; Davis, C. D.; Degnan, A. P.; Jiang, X. J.; Macci, R.; Mathias, N. R.; Moench, P.; Pin, S. S.; Schartman, R.; Signor, L. J.; Thalody, G.; Tora, G.; Whiterock, V.; Xu, C.; Macor, J. E.; Dubowchik, G. M. The Synthesis and SAR of Calcitonin Gene-Related Peptide (CGRP) Receptor Antagonists Derived From Tyrosine Surrogates. Part 2. *Bioorg. Med. Chem. Lett.* **2013,** *23* (6), 1870–1873.
167. Degnan, A. P.; Chaturvedula, P. V.; Conway, C. M.; Cook, D. A.; Davis, C. D.; Denton, R.; Han, X.; Macci, R.; Mathias, N. R.; Moench, P.; Pin, S. S.; Ren, S. X.; Schartman, R.; Signor, L. J.; Thalody, G.; Widmann, K. A.; Xu, C.; Macor, J. E.; Dubowchik, G. M. Discovery of (R)-4-(8-fluoro-2-oxo-1,2-dihydroquinazolin-3(4H)-yl)-N-(3-(7-methyl-1H-indazol-5-yl)-1-oxo-1-(4-(piperidin-1-yl)piperidin-1-yl)propan-2-yl)piperidine-1-carboxamide (BMS-694153): A Potent Antagonist of the Human Calcitonin Gene-Related Peptide Receptor for Migraine With Rapid and Efficient Intranasal Exposure. *J. Med. Chem.* **2008,** *51* (16), 4858–4861.
168. Goadsby, P. J.; Zanchin, G.; Geraud, G.; de Klippel, N.; Diaz-Insa, S.; Gobel, H.; Cunha, L.; Ivanoff, N.; Falques, M.; Fortea, J. Early vs. Non-Early Intervention in Acute Migraine-'Act When Mild (AwM)'. A Double-Blind, Placebo-Controlled Trial of Almotriptan. *Cephalalgia* **2008,** *28* (4), 383–391.
169. Rapoport, A. M.; Bigal, M. E.; Tepper, S. J.; Sheftell, F. D. Intranasal Medications for the Treatment of Migraine and Cluster Headache. *CNS Drugs* **2004,** *18* (10), 671–685.
170. Dahlöf, C. Clinical Applications of New Therapeutic Deliveries in Migraine. *Neurology* **2003,** *61* (8 Suppl. 4), S31–S34.
171. Dodick, D.; Brandes, J.; Elkind, A.; Mathew, N.; Rodichok, L. Speed of Onset, Efficacy and Tolerability of Zolmitriptan Nasal Spray in the Acute Treatment of Migraine: A Randomised, Double-Blind, Placebo-Controlled Study. *CNS Drugs* **2005,** *19* (2), 125–136.
172. Dowson, A. J.; Charlesworth, B. R.; Green, J.; Färkkilä, M.; Diener, H. C.; Hansen, S. B.; Gawel, M.; INDEX Study Group. Zolmitriptan Nasal Spray Exhibits Good Long-Term Safety and Tolerability in Migraine: Results of the INDEX Trial. *Headache* **2005,** *45* (1), 17–24.
173. Bitter, C.; Suter-Zimmermann, K.; Surbera, C. Nasal Drug Delivery in Humans. In *Topical Applications and the Mucosa;* Surber, C., Elsner, P., Farage, M. A., Eds.; *Curr. Probl. Dermatol*; Karger: Basel, 2011; pp 20–35.
174. Wermeling, D. P.; Miller, J. L.; Rudi, A. C. Systemic Intranasal Drug Delivery: Concepts and Applications. *Drug Deliv. Technol.* **2002,** *2* (1), 56–61.
175. Merkus, P.; Guchelaar, H. J.; Bosch, D. A.; Merkus, F. W. Direct Access of Drugs to the Human Brain After Intranasal Drug Administration? *Neurology* **2003,** *60* (10), 1669–1671.

176. Chaturvedula, P. V.; Mercer, S. E.; Pin, S. S.; Thalody, G.; Xu, C.; Conway, C. M.; Keavy, D.; Signor, L.; Cantor, G. H.; Mathias, N.; Moench, P.; Denton, R.; Macci, R.; Schartman, R.; Whiterock, V.; Davis, C.; Macor, J. E.; Dubowchik, G. M. Discovery of (R)-N-(3-(7-methyl-1H-indazol-5-yl)-1-(4-(1-methylpiperidin-4-yl)-1-oxopropan-2-yl)-4-(2-oxo-1,2-dihydroquinolin-3-yl)piperidine-1-carboxamide (BMS-742413): A Potent Human CGRP Antagonist With Superior Safety Profile for the Treatment of Migraine Through Intranasal Delivery. *Bioorg. Med. Chem. Lett.* **2013,** *23* (11), 3157–3161.
177. Degnan, A. P.; Conway, C. M.; Dalterio, R. A.; Macci, R.; Mercer, S. E.; Schartman, R.; Xu, C.; Dubowchik, G. M.; Macor, J. E. Carbamates as Potent Calcitonin Gene-Related Peptide Antagonists With Improved Solution Stability. *Bioorg. Med. Chem. Lett.* **2009,** *19* (13), 3555–3558.
178. Luo, G.; Chen, L.; Pin, S. S.; Xu, C.; Conway, C. M.; Macor, J. E.; Dubowchik, G. M. Calcitonin Gene-Related Peptide (CGRP) Receptor Antagonists: Novel Aspartates and Succinates. *Bioorg. Med. Chem. Lett.* **2012,** *22* (8), 2912–2916.
179. Chaturvedula, P.; Dubowchik, G. M.; Degnan, A. D.; Han, X.; Conway, C. M.; Cook, D.; Davis, C. D.; Denton, R.; Macci, R.; Mathias, N. R.; Pin, S. S.; Signor, L.; Thalody, G.; Schartman, R.; Widmann, K. A.; Xu, C.; Macor, J. E. Design and Synthesis of Potent CGRP Antagonists for Migraine. Abstracts of Papers. 234th National Meeting and Exposition of the American Chemical Society, Boston, MA, August 19–23, 2007**;** American Chemical Society: Washington, DC, 2007. MEDI 220.
180. Civiello, R. L.; Han, X.; Beno, B. R.; Chaturvedula, P. V.; Herbst, J. J.; Xu, C.; Conway, C. M.; Macor, J. E.; Dubowchik, G. M. Synthesis and SAR of Calcitonin Gene-Related Peptide (CGRP) Antagonists Containing Substituted Aryl-Piperazines and Piperidines. *Bioorg. Med. Chem. Lett.* **2016,** *26* (4), 1229–1232.
181. Meanwell, N. A. The Influence of Bioisosteres in Drug Design: Tactical Applications to Address Developability Problems. In *Tactics in Contemporary Drug Design;* Meanwell, N. A., Ed.; *Topics in Medicinal Chemistry*; Springer Berlin: Heidelberg, 2014; pp 283–381.
182. Tora, G.; Degnan, A. P.; Conway, C. M.; Kostich, W. A.; Davis, C. D.; Pin, S. S.; Schartman, R.; Xu, C.; Widmann, K. A.; Macor, J. E.; Dubowchik, G. M. Preparation of Imidazoles as Potent Calcitonin Gene-Related Peptide (CGRP) Antagonists. *Bioorg. Med. Chem. Lett.* **2013,** *23* (20), 5684–5688.
183. Luo, G.; Chen, L.; Civiello, R.; Pin, S. S.; Xu, C.; Kostich, W.; Kelley, M.; Conway, C. M.; Macor, J. E.; Dubowchik, G. M. Calcitonin Gene-Related Peptide (CGRP) Receptor Antagonists: Pyridine as a Replacement for a Core Amide Group. *Bioorg. Med. Chem. Lett.* **2012,** *22* (8), 2917–2921.
184. Luo, G.; Chen, L.; Conway, C. M.; Denton, R.; Keavy, D.; Gulianello, M.; Huang, Y.; Kostich, W.; Lentz, K. A.; Mercer, S. E.; Schartman, R.; Signor, L.; Browning, M.; Macor, J. E.; Dubowchik, G. M. Discovery of BMS-846372, a Potent and Orally Active Human CGRP Receptor Antagonist for the Treatment of Migraine. *ACS Med. Chem. Lett.* **2012,** *3* (4), 337–341.
185. Luo, G.; Chen, L.; Conway, C. M.; Denton, R.; Keavy, D.; Signor, L.; Kostich, W.; Lentz, K. A.; Santone, K. S.; Schartman, R.; Browning, M.; Tong, G.; Houston, J. G.; Dubowchik, G. M.; Macor, J. E. Discovery of (5S,6S,9R)-5-amino-6-(2,3-difluorophenyl)-6,7,8,9-tetrahydro-5H-cyclohepta[b]pyridin-9-yl 4-(2-oxo-2,3-dihydro-1H-imidazo[4,5-b]pyridin-1-yl)piperidine-1-carboxylate (BMS-927711): An Oral Calcitonin Gene-Related Peptide (CGRP) Antagonist in Clinical Trials for Treating Migraine. *J. Med. Chem.* **2012,** *55* (23), 10644–10651.
186. Luo, G.; Chen, L.; Conway, C. M.; Kostich, W.; Macor, J. E.; Dubowchik, G. M. Asymmetric Synthesis of Heterocyclic Analogues of a CGRP Receptor Antagonist for Treating Migraine. *Org. Lett.* **2015,** *17* (24), 5982–5985.
187. Tong, G.; Savant, I.; Jariwala, N.; Burt, D.; Zheng, N.; Buzescu, A.; Bertz, R.; Keswani, S.; Marcus, R. Phase I Single and Multiple Dose Study to Evaluate the Safety, Tolerability, and Pharmacokinetics of BMS-927711 in Healthy Subjects. *J. Headache Pain* **2013,** *14* (Suppl. 1), 118.
188. Marcus, R.; Goadsby, P. J.; Dodick, D.; Stock, D.; Manos, G.; Fischer, T. Z. BMS-927711 for the Acute Treatment of Migraine: A Double-Blind, Randomized, Placebo Controlled, Dose-Ranging Trial. *Cephalalgia* **2014,** *2,* 114–125.
189. Bigal, M. E. BMS-927711 for the Acute Treatment of Migraine. *Cephalalgia* **2014,** *34* (2), 90–92.
190. Daines, R. A.; Sham, K. K.; Taggart, J. J.; Kingsbury, W. D.; Chan, J.; Breen, A.; Disa, J.; Aiyar, N. Quinine Analogs as Non-Peptide Calcitonin Gene-Related Peptide (CGRP) Receptor Antagonists. *Bioorg. Med. Chem. Lett.* **1997,** *7* (20), 2673–2676.
191. Aiyar, N.; Daines, R. A.; Disa, J.; Chambers, P. A.; Sauermelch, C. F.; Quiniou, M.-J.; Khandoudi, N.; Gout, B.; Douglas, S. A.; Willette, R. N. Pharmacology of SB-273779, a Nonpeptide Calcitonin Gene-Related Peptide 1 Receptor Antagonist. *J. Pharmacol. Exp. Ther.* **2001,** *296* (3), 768–775.
192. Nichols, P. L.; Brand, J.; Briggs, M.; D'Angeli, M.; Farge, J.; Garland, S. L.; Goldsmith, P.; Hutchings, R.; Kilford, I.; Li, H. Y.; MacPherson, D.; Nimmo, F.; Sanderson, F. D.; Sehmi, S.; Shuker, N.; Skidmore, J.; Stott, M.; Sweeting, J.; Tajuddin, H.; Takle, A. K.; Trani, G.; Wall, I. D.; Ward, R.; Wilson, D. M.; Witty, D. Potent Oxadiazole CGRP Receptor Antagonists for the Potential Treatment of Migraine. *Bioorg. Med. Chem. Lett.* **2010,** *20* (4), 1368–1372.
193. WO 2008070014, Published June 12, 2008.
194. WO 2008060568, Published May 22, 2008.
195. WO 2009050232, Published April 23, 2009.
196. WO 2009065919, Published May 28, 2009.
197. US Patent 7,109,214, September 19, 2006.
198. Zhao, D.; Xu, F.; Chen, C.; Tillyer, R. D.; Grabowski, E. J. J.; Reider, P. J. Efficient Syntheses of 2-(3′,5′-difluorophenyl)-3-(4′-methylsulfonylphenyl)cyclopent-2-enone, a Potent COX-2 Inhibitor. *Tetrahedron* **1999,** *55* (19), 6001–6018.
199. Sun, H.; Dodick, D. W.; Silberstein, S.; Goadsby, P. J.; Reuter, U.; Ashina, M.; Saper, J.; Cady, R.; Chon, Y.; Dietrich, J.; Lenz, R. Safety and Efficacy of AMG 334 for Prevention of Episodic Migraine: A Randomised, Double-Blind, Placebo-Controlled, Phase 2 Trial. *Lancet Neurol.* **2016,** *15* (4), 382–390.
200. Shi, L.; Lehto, S. G.; Zhu, D. X.; Sun, H.; Zhang, J.; Smith, B. P.; Immke, D. C.; Wild, K. D.; Xu, C. Pharmacologic Characterization of AMG 334, a Potent and Selective Human Monoclonal Antibody Against the Calcitonin Gene-Related Peptide Receptor. *J. Pharmacol. Exp. Ther.* **2016,** *356* (1), 223–231.
201. Benschop, R. J.; Collins, E. C.; Darling, R. J.; Allan, B. W.; Leung, D.; Conner, E. M.; Nelson, J.; Gaynor, B.; Xu, J.; Wang, X. F.; Lynch, R. A.; Li, B.; McCarty, D.; Nisenbaum, E. S.; Oskins, J. L.; Lin, C.; Johnson, K. W.; Chambers, M. G. Development of a Novel Antibody to Calcitonin Gene-Related Peptide for the Treatment of Osteoarthritis-Related Pain. *Osteoarthr. Cartil.* **2014,** *22* (4), 578–585.
202. Dodick, D. W.; Goadsby, P. J.; Spierings, E. L.; Scherer, J. C.; Sweeney, S. P.; Grayzel, D. S. Safety and Efficacy of LY2951742, a Monoclonal Antibody to Calcitonin Gene-Related Peptide, for the Prevention of Migraine: A Phase 2, Randomised, Double-Blind, Placebo-Controlled Study. *Lancet Neurol.* **2014,** *13* (9), 885–892.
203. Dodick, D. W.; Goadsby, P. J.; Silberstein, S. D.; Lipton, R. B.; Olesen, J.; Ashina, M.; Wilks, K.; Kudrow, D.; Kroll, R.; Kohrman, B.; Bargar, R.; Hirman, J.; Smith, J. ALD403 Study Investigators, Safety and Efficacy of ALD403, an Antibody to Calcitonin Gene-Related Peptide, for the Prevention of Frequent Episodic Migraine: A Randomised, Double-Blind, Placebo-Controlled, Exploratory Phase 2 Trial. *Lancet Neurol.* **2014,** *13* (11), 1100–1107.
204. Walter, S.; Bigal, M. E. TEV-48125: A Review of a Monoclonal CGRP Antibody in Development for the Preventive Treatment of Migraine. *Curr. Pain Headache Rep.* **2015,** *19* (3), 6.
205. Bigal, M. E.; Escandon, R.; Bronson, M.; Walter, S.; Sudworth, M.; Huggins, J. P.; Garzone, P. Safety and Tolerability of LBR-101, a Humanized Monoclonal Antibody That Blocks the Binding of CGRP to Its Receptor: Results of the Phase 1 Program. *Cephalalgia* **2013,** *34* (7), 483–492.
206. Bigal, M. E.; Edvinsson, L.; Rapoport, A. M.; Lipton, R. B.; Spierings, E. L.; Diener, H. C.; Burstein, R.; Loupe, P. S.; Ma, Y.; Yang, R.; Silberstein, S. D. Safety, Tolerability, and Efficacy of TEV-48125 for Preventive Treatment of Chronic Migraine: A Multicentre, Randomised, Double-Blind, Placebo-Controlled, Phase 2b Study. *Lancet Neurol.* **2015,** *14* (11), 1091–1100.
207. Edvinsson, L.; Villalón, C. M.; MaassenVanDenBrink, A. Basic Mechanisms of Migraine and Its Acute Treatment. *Pharmacol. Ther.* **2012,** *136* (3), 319–333.
208. Cox, J. C.; Hayhurst, A.; Hesselberth, J.; Bayer, T. S.; Georgiou, G.; Ellington, A. D. Automated Selection of Aptamers Against Protein Targets Translated In Vitro: From Gene to Aptamer. *Nucleic Acids Res.* **2002,** *30* (20), e108.
209. Vater, A.; Klussmann, S. Turning Mirror-Image Oligonucleotides into Drugs: The Evolution of Spiegelmer(**®**) Therapeutics. *Drug Discov. Today* **2015,** *20* (1), 147–155.
210. Wlotzka, B.; Leva, S.; Eschgfäller, B.; Burmeister, J.; Kleinjung, F.; Kaduk, C.; Muhn, P.; Hess-Stumpp, H.; Klussmann, S. In Vivo Properties of an Anti-GnRH Spiegelmer: An Example of an Oligonucleotide-Based Therapeutic Substance Class. *Proc. Natl. Acad. Sci. U. S. A.* **2002,** *99* (13), 8898–8902.

211. Vater, A.; Jarosch, F.; Buchner, K.; Klussmann, S. Short Bioactive Spiegelmers to Migraine-Associated Calcitonin Gene-Related Peptide Rapidly Identified by a Novel Approach: Tailored-SELEX. *Nucleic Acids Res.* **2003,** *31* (21), e130.
212. Hoehlig, K.; Johnson, K. W.; Pryazhnikov, E.; Maasch, C.; Clemens-Smith, A.; Purschke, W. G.; Vauléon, S.; Buchner, K.; Jarosch, F.; Khiroug, L.; Vater, A.; Klussmann, S. A Novel CGRP-Neutralizing Spiegelmer Attenuates Neurogenic Plasma Protein Extravasation. *Br. J. Pharmacol.* **2015,** *172* (12), 3086–3098.

Relevant Websites

http://www.americanheadachesociety.org/—American Headache Society.
http://www.americanmigrainefoundation.org/—American Migraine Foundation.
http://www.ihs-headache.org/—International Headache Society.
http://www.mayoclinic.org/diseases-conditions/migraine-headache/basics/definition/con-20026358—Mayo Clinic Migraine website.
http://www.headaches.org/—National Headache Foundation.
http://www.neurotransmitter.net/migrainecgrp.html—Neurotransmitter.net site dedicated to scientific literature on CGRP and Migraine.
https://www.migrainetrust.org/—The Migraine Trust (UK).

7.06 Orexin Receptor Antagonists

BT Shireman and MA Letavic, Janssen Research & Development, L.L.C., San Diego, CA, United States

© 2017 Elsevier Ltd. All rights reserved.

7.06.1	**Introduction**	226
7.06.2	**Actelion**	227
7.06.2.1	Tetrahydroisoquinolines	227
7.06.2.2	Substituted Lactams	231
7.06.2.3	Proline Sulfonamide ACT-462206	232
7.06.2.4	1-Acyl-2-benzylpyrrolidines	233
7.06.2.5	*N*-Glycine-Sulfonamides	234
7.06.3	**Banyu**	237
7.06.3.1	Tetrahydroisoquinolines	237
7.06.4	**Eisai**	238
7.06.4.1	N-Aryl-2-Phenylcyclopropanecarboxamides	238
7.06.4.1.1	E2006	239
7.06.5	**GlaxoSmithKline**	239
7.06.5.1	SB-649868 and Substituted Piperidines	239
7.06.5.2	GSK Early Selective OX1R Tool Compounds	244
7.06.5.3	Triazolo-Thioamides	246
7.06.6	**Heptares**	246
7.06.6.1	2*H*-pyrido[2,3-*e*][1,2,4]thiadiazin-3(4*H*)-one 1,1-dioxides	246
7.06.7	**International Institute for Integrative Sleep Medicine**	247
7.06.7.1	OX2R Agonists	247
7.06.8	**Johnson & Johnson/Janssen Pharmaceuticals**	250
7.06.8.1	4-Phenyl-[1,3]dioxanes	250
7.06.8.2	Octahydropyrrolo[3,4-*c*]pyrroles	250
7.06.8.2.1	JNJ-42847922	252
7.06.9	**Merck**	253
7.06.9.1	Proline bis-Amides	253
7.06.9.2	Diamines/MK-4305 (Suvorexant)	253
7.06.9.3	MK-4305 (Suvorexant/Belsomra)	255
7.06.9.4	Piperidines/MK-6096 (Filorexant)	255
7.06.9.5	2,5-Diarylnicotinamides	257
7.06.9.6	MK-1064	258
7.06.9.7	MK-3697	258
7.06.9.8	Piperidine Ethers	260
7.06.9.9	Diazepanes	260
7.06.9.10	MK-8133	260
7.06.10	**Novartis**	263
7.06.10.1	Spirocyclic Amino-Amides	263
7.06.10.2	Pyrazolopyridines	265
7.06.11	**Research Triangle Institute**	267
7.06.11.1	Tetrahydroisoquinolines	267
7.06.11.2	Diarylureas related to SB-334867	268
7.06.12	**Rottapharm**	269
7.06.12.1	Bicyclic [5.2.0] and [4.2.0] Diamines	269
7.06.13	**The Scripps Research Institute**	271
7.06.13.1	Piperidin-2-ylmethanamines	271
7.06.14	**Taisho**	271
7.06.14.1	TASP0428980	271
7.06.15	**Takeda**	271
7.06.15.1	Spiropiperidine-Based Selective Orexin-2 Antagonists	271
7.06.15.2	Benzoxazepine-Based Selective Orexin-2 Antagonists	272
7.06.16	**Summary of Compounds That Progressed to Clinical Trials**	274
References		277

Abbreviations

bl Blood
br Brain
CB1 Ligand cannabinoid-1 ligand
CL Clearance
CNS Central nervous system
CYP Cytochrome P450
EEG Electroencephalogram
FLIPR assay Fluorometric Imaging Plate Reader assay
Hcrt-1 Hypocretin-1
Hcrt-2 Hypocretin-2
hERG Human Ether-à-go-go Related Gene
HTS High-throughput screen
i.c.v. Intracerebroventricular
LLE Ligand lipophilic efficiency
LPS Latency to persistent sleep
NMR Nuclear magnetic resonance
NREM sleep Nonrapid eye movement sleep
OX1R Orexin-1 receptor
OX2R Orexin-2 receptor
PET Positron emission tomography
P-pg P-Glycoprotein
REM sleep Rapid eye movement sleep
SAR Structure activity relationship
TDI Time-dependent inhibition
WASO Wake after sleep onset

7.06.1 Introduction

The orexin ligands are a pair of excitatory neuropeptides that are most often termed orexin-A and orexin-B, or hypocretin-1 and hypocretin-2, respectively. Sakurai identified these neuropeptides in 1998 and demonstrated their ability to invoke an increase in intracellular Ca^{2+} concentrations by activation of what was at that time an orphan G-protein coupled receptor (GPCR).[1] The receptors were characterized by Sakurai and given the names orexin-1 (OX1R) and orexin-2 (OX2R). In an independent manuscript, De Lecea showed that mRNA originating in the hypothalamus coded for the prepro-orexin peptide, which is the precursor to orexin-A and orexin-B.[2] This precursor peptide is expressed in the hypothalamus in neurons that project into areas of the central nervous system that have been associated with sleep regulation, addiction and reward, panic, and food intake among other behaviors. De Lecea used the hypocretin nomenclature (Hcrt-1 and Hcrt-2) to describe these new peptides. For the remainder of this article we will use the term orexin. These independent publications by Sakurai and De Lecea describing the orexin system were the motivation behind nearly two decades of research in academic and industrial laboratories that continue to develop and prosper. This research has been the subject of various reviews.[3]

In regard to the roles of the orexin receptors in the CNS, one interesting aspect in terms of drug discovery is the localization of the receptors.[4] While some areas of the CNS contain both receptors, differentiated roles of the receptors are suggested by selective receptor expression in areas of the brain thought to play a role in sleep–wake, reward, addiction, stress, anxiety, and other neuropsychiatric disorders. For example, localization of the OX2R primarily in histaminergic neurons in the tuberomammillary nucleus is consistent with what is now understood for the OX2Rs with respect to their role in wake promotion and as an important modulator of arousal. Piper et al. demonstrated that intracerebroventricular (i.c.v.) administration of orexin caused rats to spend more time awake.[5] A phenotype similar to narcolepsy was observed in rodents whose prepro-orexin gene had been knocked out, or whose orexigenic neurons have been ablated.[6] Further support for the role of orexin in the modulation of sleep–wake cycles came from Stanford University[7] when it was shown by Mignot that a colony of narcoleptic canines had mutated or nonfunctional OX2 receptors. In addition, human narcoleptic patients were shown to have attenuated orexin levels and reduced orexinergic neurons, providing clinical evidence for the modulation of orexin signaling as a potential treatment for sleep disorders.[8] Over the years, there has been a debate in the literature on whether to target both orexin receptors or only the OX2 receptor. This began with a publication from Janssen, which demonstrated that selective antagonism of the OX2R is sufficient to induce and prolong sleep in rodents.[9] Furthermore, a selective OX1R antagonist had no effect on these parameters. These findings have since been replicated by others.[10] In the Janssen study, it was demonstrated that a dual orexin receptor antagonist failed to induce sleep in mice lacking the OX2 receptor but succeeded in the OX1 knockout mice. Subsequent manuscripts suggested that antagonism of the OX1R concurrent with the OX2R reduced REM sleep latency and duration to a greater extent than nonrapid eye movement (NREM), which disrupts the physiological balance of REM and NREM sleep.[11] In contrast to the OX2R, the OX1Rs are selectively located in the bed nucleus of the striata, amygdala, cingulate cortex, and noradrenergic neurons of the locus coeruleus. These areas of the brain are commonly thought to play a role in anxiety, stress, or reward. Studies corroborating the role of the orexins, specifically the OX1R in complex psychiatric disorders, are emerging that is consistent with brain localization in these areas.[12] For example, in an animal model of panic disorders, selective activation of orexinergic neurons via lactate infusion also correlates with anxiety measures in the social interaction test or open field test.[12a,13] These responses are blocked or attenuated with either siRNA or selective OX1R antagonists. Another method to induce panic is CO_2.[14] It has been shown that activation of the OX1R is a critical component of CO_2-mediated anxiety and hypertension attenuated hypercapnic gas-induced pressor and anxiety

responses. Interestingly, the anxiety measures and autonomic responses are attenuated with a selective OX1R antagonist or an OX1R/OX2R antagonist, but not a selective OX2R antagonist. Both dual and selective OX1R antagonists have demonstrated efficacy in other models of conditioned fear or stress such as the fear-conditioned startle paradigm.[15] Colocalization of both receptors in the ventral tegmental area is consistent with a variety of studies that have appeared, suggesting the possibility that OX1R antagonists would be useful for the treatment of addictive disorders and withdrawal. As examples, selective OX1R antagonists have attenuated conditioned place preference and reinstatement induced by morphine, stress-induced cocaine reinstatement, cocaine-induced behavioral and synaptic plasticity, precipitated morphine withdrawal, and nicotine self-administration. A reduction in the self-administration of ethanol was recently reported using a selective OX2R antagonist. However, most studies have demonstrated an attenuation using selective OX1R antagonists in the intake, cue- and stress-induced reinstatement of ethanol. As will be covered in the section regarding clinical candidates, the work that was summarized earlier has led to dual OX1R/OX2R or selective OX2 antagonists entering the clinic for the treatment of insomnia or related disorders.[3a] All of these data prompted numerous pharmaceutical companies and academic researchers to further investigate the pharmacological effects of modulation of the orexin system, and as such, many dual OX1R/OX2R receptor antagonists and selective OX1R or OX2R antagonists have been studied,[3b] primarily with the goal of treating sleep disorders by antagonizing the OX2 receptors.[16] Considering that most OXR antagonists are primarily undergoing clinical trials for the treatment of insomnia and related sleep disorders, many of the medicinal chemistry efforts described in this article have focused on an appropriate duration of action in human and as such, compounds with a relatively short predicted half-life have been advanced into the clinic, given the likelihood that longer acting compounds would be expected to have detrimental effects, including next-day drowsiness. Although a significant amount of literature exist studying OX1R antagonists, to date, no known selective OX1R antagonist has entered human clinical trials. A synopsis of the medicinal chemistry related to various dual and selective orexin receptor ligands is reviewed herein.

7.06.2 Actelion

7.06.2.1 Tetrahydroisoquinolines

Actelion was the first to demonstrate efficacy in human patients for the treatment of sleep disorders with an orexin antagonist.[17] In 2007, Actelion published a Nature Medicine paper describing **ACT-078573**, a compound that is now known as almorexant (**1**), which is shown in **Fig. 1**. This publication represented a turning point in the orexin field as it was the first disclosure of an OXR antagonist in human patients with insomnia. At doses of 200 mg or greater patients receiving almorexant showed signs of decreased wakefulness consistent with preclinical studies in rat and dog without signs of cataplexy. Subsequent to this initial report, phase III clinical trials of almorexant were discontinued due to safety concerns in Jan. 2011.

Actelion has published a variety of medicinal chemistry papers describing the tetrahydroisoquinoline template before and after the disclosure of almorexant.[15b,18] The primary goal of these initial investigations was to replace the 6,7-dimethoxy-tetrahydroisoquinoline with 1-ethyl-3-methyl-tetrahydro-1*H*-pyrazolo[4,3-c]pyridine as shown in **Table 1**. The initial studies focused on the SAR of the pendant phenethyl moiety represented as R_1.[18a] Generally speaking, mono-*para*-substituted phenyls tended to have the most effect on OX1R potency, for example, **2**–**5**. For example, although compound **2** demonstrated that this replacement was tolerated for the OX2R, potency for the OX1R receptor was diminished giving a selective OX2R antagonist. Certain di- and trisubstituted analogs, such as **6**–**8**, were shown to provide dual OX1R/OX2R antagonists with excellent potency. Compounds **7** and **8** were progressed into an EEG study and showed to increase time spent in non-REM sleep to a lesser extent than that observed for almorexant after a 100 mg/kg PO dose. Noteworthy here was that replacement of the $-CH_2CH_2-$ linker in **5** with a $-CH_2O-$ in **9** completely depleted OX1R potency.

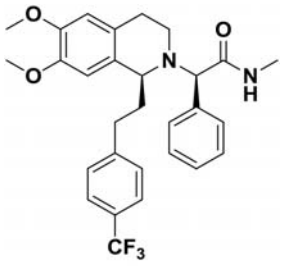

1, Almorexant

(ACT-078573)
OX2R IC_{50}=13 nM
OX1R IC_{50}=8 nM

Fig. 1 Structure- and FLIPR-based data for almorexant.

Table 1 Cell-based FLIPR assay data for the human OX2 and OX1 receptor for compounds **2–9**

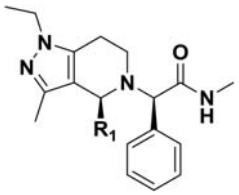

Compound	*R_1*	*OX2R IC_{50} (nM)*	*OX1R IC_{50} (nM)*
2	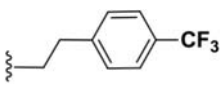	3	128
3	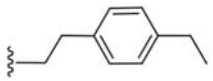	3	63
4	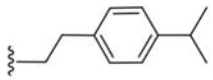	9	161
5, Mix of diastereomers	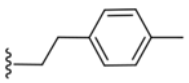	6	108
6	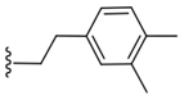	3	7
7	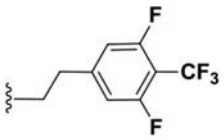	4	5
8	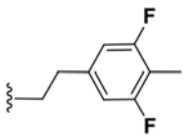	5	16
9	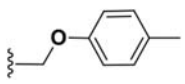	19	>10,000

Further studies focused on 5,6,7,8-tetrahydroimidazo[1,5-*a*]pyrazines as illustrated in Table 2.[18c] Interestingly, replacement of the pyrazole in **2**, with the imidazole in **10**, resulted in slightly diminished OX2R potency, but a complete loss in OX1R potency. Further replacements, such as a cyano (**11**) or CF_3 (**12**), began to restore potency for the OX1R. Eventually, the researchers at Actelion found that a chlorine in this position improved potency at both receptors providing the dual OX1R/OX2R antagonist **13**.

With the chlorine held constant, in order to investigate the effect of substitutions in this area of the molecule, further SAR was generated as shown in Table 3. Going from the ethyl in **13** to the methyl in **14** had minimal impact on potency at both receptors as shown. However, the *n*-propyl substituted analog **15** began to reduce OX1R potency. The *i*-propyl or cyclopropyl analogs **16** and **17** were found to be similar to the ethyl-substituted analog **13**. Compounds **13** and **17** were evaluated in vivo in rats for their ability to penetrate into the brain. After a 100 mg/kg PO dose brain/plasma (B/P) ratios were determined to be 0.06 and 0.07, respectively. This can be compared to the B/P ratios for **1**, which were shown to be 0.32.

Next, the focus was placed on the pendant phenethyl substituent with aims of increasing brain penetration and potency.[18b] Shown in Table 4 is the representative SAR in regard to potency and selectivity for the OX1 and OX2 receptors. Generally

Table 2 Cell-based FLIPR assay data for the human OX2 and OX1 receptor for compounds **10–13**

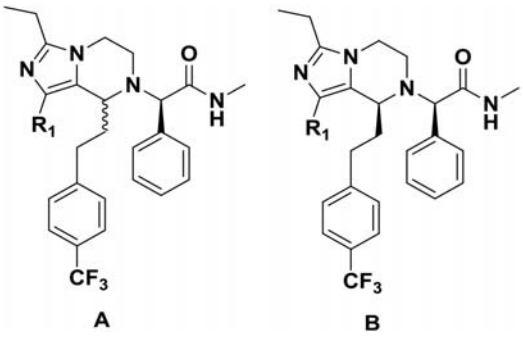

Compound	*A or B*	*R_1*	*OX2R IC_{50} (nM)*	*OX1R IC_{50} (nM)*
10	A	Me	24	>10,000
11	A	CN	10	537
12	B	CF_3	11	1066
13	B	Cl	9	40

Table 3 Cell-based FLIPR assay data for the human OX2 and OX1 receptor for compounds **14–17**

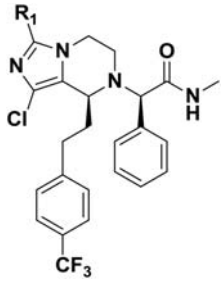

Compound	*R_1*	*OX2R IC_{50} (nM)*	*OX1R IC_{50} (nM)*
14	Me	13	90
15		60	459
16		11	313
17		9	31

speaking most substitutions on the phenethyl portion had minimal impact on OX2R potency. As observed in the pyrazolo-tetrahydropyridines series, replacement of the $-CH_2CH_2-$ linker with $-CH_2O-$ was detrimental to OX1R potency, for example, **13** versus **18**. Although replacement of the $-CF_3$ in **13** with an $-OCF_3$ (**19**) resulted in a loss of potency at both receptors, a $-OCHF_2$ (**20**) resulted in a potent and selective OX2R antagonist. The disubstituted analogs **21–23** further demonstrate that subtle changes in structure seem to affect the OX1R potency more so than the OX2R potency. Cyclopropyl-substituted compounds were studied next. As shown for compounds **24–26**, similar trends were observed as with the ethyl-substituted compounds. In general, only minor improvements in brain penetration were observed for these compounds, and none of these compounds appeared to be superior to almorexant in this regard. However, compound **21** did show similar efficacy in promoting sleep as demonstrated by a significant decrease in the amount of time spent in active wake after a 100 mg/kg PO dose.

Additional studies related to the almorexant core that were conducted by Actelion resulted in the selective OX1R antagonist **ACT-335827**, Table 5.[15b] Beginning with tetrahydroisoquinoline **27**, Actelion began an investigation in library format using an Ugi four-component coupling. The initial campaign yielded **28**, which was shown to be a potent and selective OX1R antagonist

Table 4 Compounds **13** and **18–26**

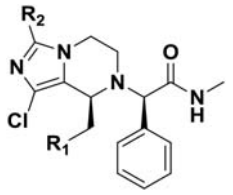

Compound	R_1	R_2	OX2R IC_{50} (nM)	OX1R IC_{50} (nM)
13	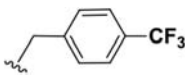		9	40
18	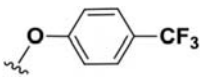		9	431
19	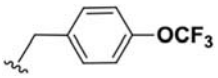		18	203
20	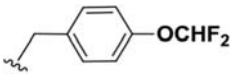		1	74
21	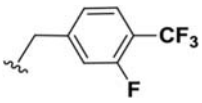		7	18
22	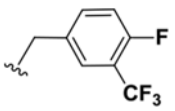		16	378
23	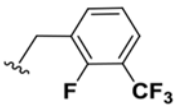		9	16
24	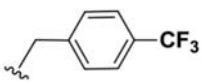		9	30
25	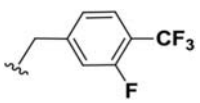		10	53
26	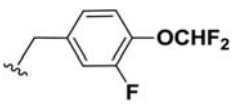		2	170

with limited penetration into the CNS. Subsequent to the identification of **28**, compound **29** was also identified. Although OX1R potency and selectivity for OX1R was reduced for **29**, improved brain penetration and plasma levels after an oral dose provided a rationale for further refinement. Additional modifications to the amide portion of the molecule while keeping the phenyl substituent R_2 constant resulted in the *n*-butyl amide **30**. In this case, both potency and selectivity were improved relative to **29** while maintaining good penetration into the CNS after a 100 mg/kg PO dose. Further modifications led to the identification of **ACT-335827** (**31**). This molecule maintained potency, selectivity, and brain penetration with increased plasma levels after an oral dose relative to **31**. Analogous to almorexant, at a high dose (300 mg/kg PO), the selective OX1R antagonist **ACT-335827**

Table 5 Human OX2R and OX1R FLIPR-based data and B/P for compounds **27–32**

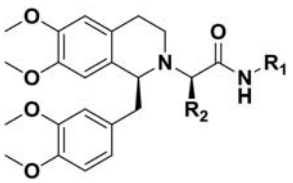

Compound	*R_1*	*R_2*	*OX2R IC_{50} (nM)*	*OX1R IC_{50} (nM)*	*B/P*
27	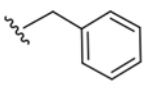	H	8447	63	
28	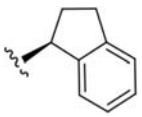	H	244	3	Reported as not significant
29	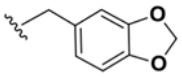	H	170	15	0.7
30	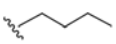	Ph	365	7	0.6
31 ACT-335827		Ph	417	6	0.6
32	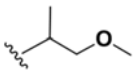	Ph	191	4	0.3

(**31**) was effective decreasing reactions in the fear-potentiated startle paradigm, suggesting that OX1 antagonism is responsible for efficacy. This compound was tested in a variety of stress-related paradigms and shown to be efficacious without decreasing wakefulness, as would be expected from a selective OX1R antagonist.

7.06.2.2 Substituted Lactams

In an effort to identify new templates, Actelion disclosed their work which began with the lead compound **33** shown in Fig. 2.[19] The primary goals were the improvement of potency at both OX1R and OX2R concurrent with improvements in metabolic stability. In vitro studies indicated that the primary site of metabolism in **33** was oxidation of the sulfur to the sulfone or sulfoxide. Based on this, carbon-linked replacements were studied. As such, the corresponding pyrrolidin-2-one (**34**), piperidin-2-one (**35**), and azepin-2-one (**36**) were evaluated. The piperidin-2-one **35** was chosen for further follow-up based on improved potency at the OX2R relative to **34** and **36**. Additional SAR allowed the team to identify compound **37**, which was shown to have improved potency at the OX1R and a good brain to plasma ratio. However, high predicted metabolism of **37** necessitated further studies. Metabolism on the substituted dimethoxy aryl ring was predicted to be the main driver of the observed metabolic instability. While replacements for this moiety did result in potent molecules at both receptors, it was reported that these changes did not result in improved microsomal stability.

Further modifications to the core included morpholine (**38**), piperazines (**39–40**), and the [3.1.0] bicycle (**41**), all of which were detrimental to potency as is shown in Fig. 3. A key finding in regard to improvements in intrinsic clearance for the series was methylation alpha to the amide carbonyl of the pyrrolidinone template. This resulted in the racemic diastereomers **42** and **43**. Although the *trans*-diastereomer **42** was shown to be only moderately potent at both receptors, an improvement in microsomal stability warranted further investigation.

Further studies focused primarily on manipulation of the methyl group to substituents such as ethyl, fluoro, chloro, amino, and hydroxyl led to compound **44**, Fig. 4, which exhibited low predicted clearance in human microsomes. In order to improve OXR potency, changes to the benzyl moiety were performed.[19] This resulted in **45**, a compound that maintained favorable clearance along with good potency at both the OX1R and OX2R. Changes to the 2,5-dimethoxyphenyl group led to the identification of **46**, which in this case is a selective OX2R antagonist with good brain penetration and low predicted clearance. The authors proposed

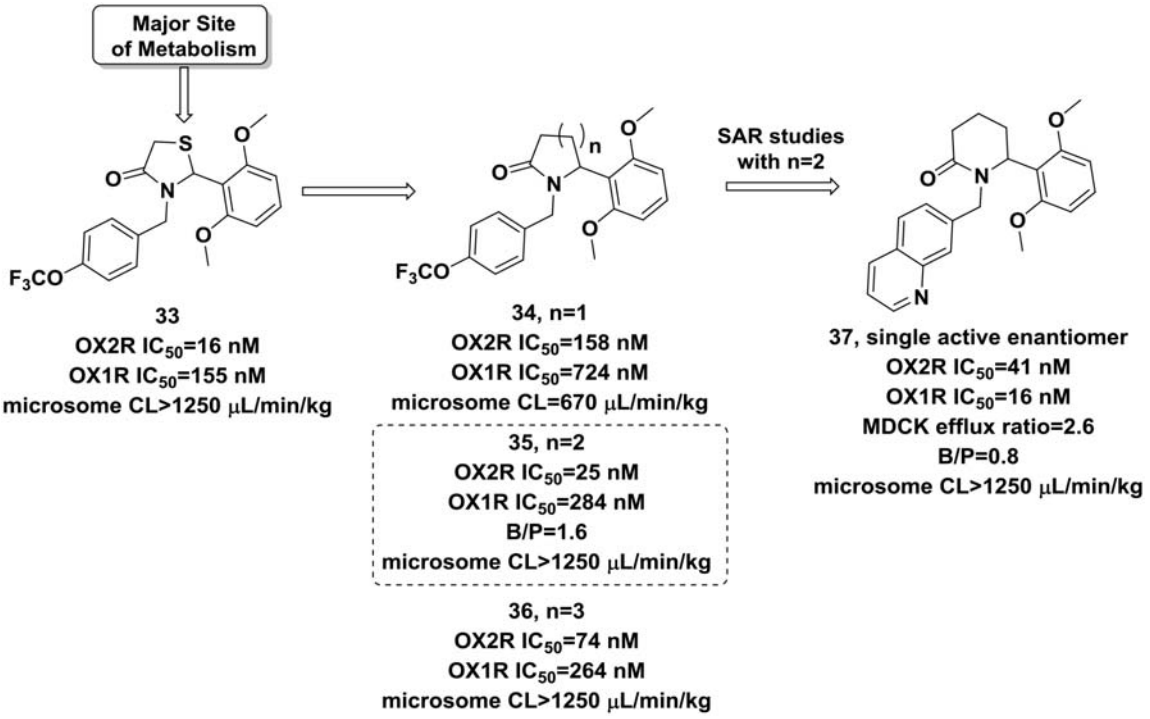

Fig. 2 Evolution of compound **37**.

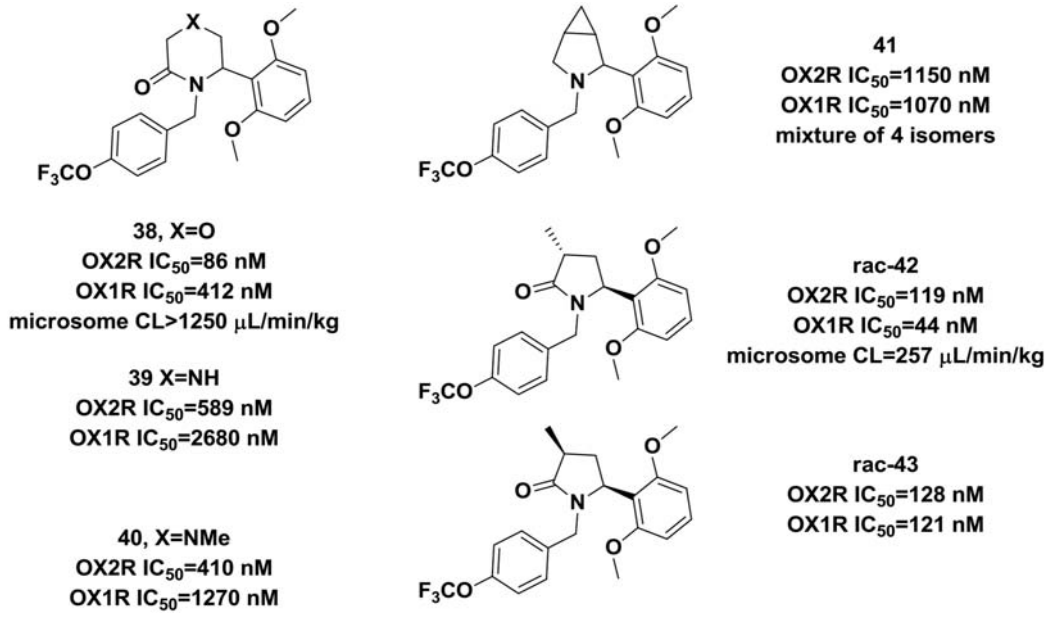

Fig. 3 Modifications to the piperidine core.

an intramolecular hydrogen bond which may mask the influence of the hydroxyl group in regard to brain permeability. Subsequent evaluation of **46** in male rats to determine its effects on sleep–wake cycles demonstrated that compound **46** had activity similar to almorexant after a 100 mg/kg PO dose.

7.06.2.3 Proline Sulfonamide ACT-462206

Actelion has also studied proline-based sulfonamides based on the high-throughput screening (HTS) hit **47**, which is shown in Fig. 5.[15c,20] While this molecule possesses recognized structural alerts, potency, brain penetration, and moderate clearance were

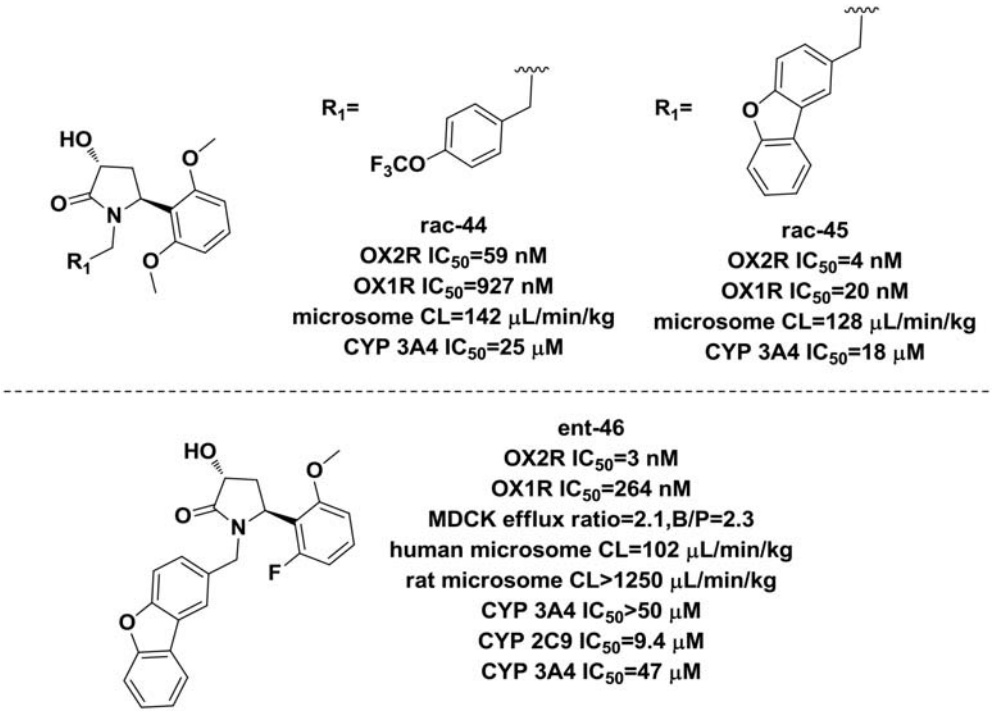

Fig. 4 Compound **46**, a selective OX2R antagonist with good drug-like properties.

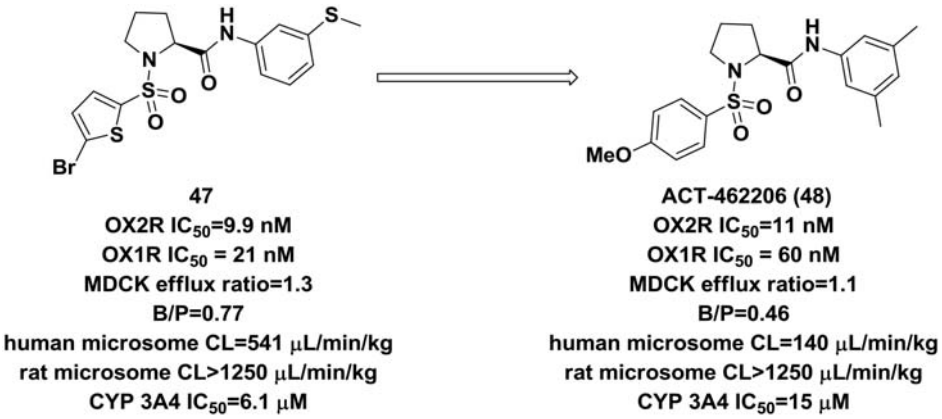

Fig. 5 Characterization of ACT-462206 (**48**).

all in acceptable ranges for an insomnia indication. Specifically, the authors were interested in exploring variations to the bromothiophene, the anilide, and the thioether moiety. Alternatives to the proline core were also investigated, and it was determined that the proline-based core was optimal. These variations led to the identification of compound **48** (ACT-462206), which is a compound that showed a dose-dependent reduction in sleepiness in human volunteers at doses of 200 mg and above. Preclinically compound **48** was also assessed in models of stress and anxiety and shown to be efficacious. A summary of these studies is shown in Table 6.

7.06.2.4 1-Acyl-2-benzylpyrrolidines

A series of 1-acyl-2-benzylpyrrolidines were also disclosed by Actelion.[21] This work began with the acylthienopiperidine **49** as shown in Fig. 6. Recognizing that the thiophene was not relevant for activity, the team quickly transformed the lead structure into piperidine **50** and subsequently pyrrolidine **51**. Both of these compounds had the advantage of improved metabolic stability, and in addition to that the calculated lipophilic ligand efficiency (LLE) of these molecules was increased from 3.5 to 4.8 and 4.7,

Table 6 In vivo data and results for the OX1R/OX2R antagonist **ACT-462206**

Test	*Result*
Fear-potentiated startle	Decreased startle reflexes at doses of 100 and 300 mg/kg
Resident intruder rat model	Decreased the social stress-induced increases of locomotion, body temperature, and heart rate at 100 mg/kg
Conditioned place preference induced	Decreased locomotor without affecting conditioned place preference induced by Morphine conditioning at 100 mg/kg
Morris water maze	No effect
Passive avoidance learning paradigm	No effect up to 300 mg/kg
Rotarod	No effect
Sleep promoting effects in rats and dogs	Dose-dependent decrease in total wake with conserved sleep architecture

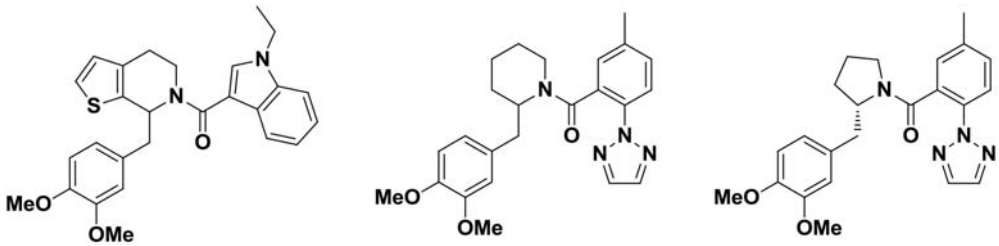

Fig. 6 Discovery of 1-acyl-2-benzylpyrrolidine **51**.

respectively. Based on these attributes, the enantiomerically pure pyrrolidine template **51** was chosen for the development of additional SAR as will be outlined here.

In attempts to further improve upon the human microsomal stability, SAR was carried out on the acylbenzamide portion of the molecule.[21] Representative examples are shown in Table 7. With the presumption that the toluyl methyl was a metabolic hot spot, compound **52** was prepared and characterized. As shown in the table, this compound maintains potency at OX2R, has slightly reduced potency at OX1R, and improved microsomal stability. The compound was brain penetrant with a brain to plasma ratio of 0.4. Further studies were focused on further reducing the Log P. Replacement of the triazole with the pyrimidine **53** gave a molecule with similar properties and a slightly lower brain to plasma ratio. The picolinic amide **54** possessed good stability in microsomes; however a loss in OXR potency was observed. Replacing the central core with a thiazole led to the identification of compound **55**, a potent OXR antagonist with moderate stability in microsomes and a good brain to plasma ratio of 0.97. Although **55** had the lowest LLE, it was chosen as the lead molecule for further follow-up due to improved penetration into the CNS.

Replacement of the pendant aryl ring with alternative substituted aryls eventually led to the identification of **56** shown in Fig. 7. Although the brain to plasma ratio of this compound is 0.3, the authors point out the increased plasma levels that were obtained after an oral dose. This led to free brain concentrations of 60 nM which are well above the measured IC_{50} at either receptor. Compound **56** was demonstrated to be an insurmountable antagonist with similar effects on sleep–wake cycles in male rats as has been reported for other dual orexin receptor antagonists.

7.06.2.5 *N*-Glycine-Sulfonamides

In 2008, Actelion reported a series of *N*-glycine-sulfonamides as dual OX1R/OX2R antagonists.[22] Workers at Actelion began with the HTS hit **57** (Fig. 8). Although this molecule possessed excellent selectivity for the OX2R over the OX1R, the goal of the research was to improve potency at the OX1R. Highlighting a common issue in the orexin field, especially at the time, this molecule had an oral bioavailability of 1%.

Initial efforts of the Actelion team focused on the SAR of the *tert*-butyl phenyl sulfonamide, specifically on the aryl portion. A summary of these data is outlined in Table 8. Replacement of the *tert*-butyl substituent with the dimethoxy (**58**) resulted in a slight loss in affinity while maintaining excellent selectivity. Alternative monosubstituted aryls were not tolerated as shown in the table for compounds **59**–**63**. Interestingly, although the *para*-methylphenyl compound **61** was shown to result in a loss in OX2R potency,

Table 7 Cell-based FLIPR data for the human OX2 and OX1 receptor for compounds **52–55**

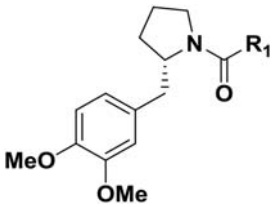

Compound	*R_1*	*OX2R IC_{50} (nM)*	*OX1R IC_{50} (nM)*	*HLM Cl(mL/min/kg)*	*LLE*	*B/P*
52	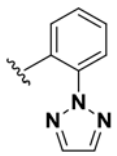	3.5	16	104	4.7	0.4
53	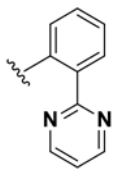	4.7	16	102	4.5	0.18
54	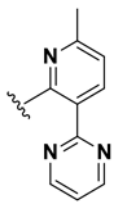	71	60	17	3.8	n.d.
55	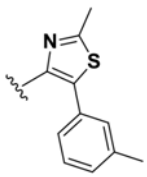	3.1	3.5	338	3.3	0.97

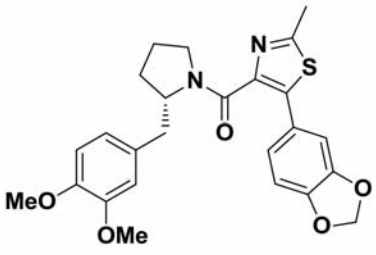

56
OX2R IC_{50}=6.6 nM
OX1R IC_{50} = 11 nM
MDCK efflux ratio=7
B/P=0.3
100 mg/kg po [B]=698 ng/g/[P]=2328 ng/mL
$[B]_{free}$=60 nM
[CSF]=133 nM
human microsome CL=197 μL/min/kg
rat microsome CL>1250 μL/min/kg

Fig. 7 Characterization of compound **56**.

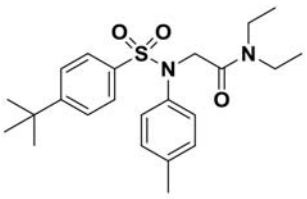

57
OX2R IC_{50}=5 nM
OX1R IC_{50} > 10,000 nM
F=1%

Fig. 8 Compound **57**, a selective OX2R antagonist.

moving the methyls around (**62** and **63**) the ring to the *meta*- and *ortho*- increased OX2R potency relative to **61**. The team at Actelion reported that they were most interested in dual OX2R/OX1R antagonists.

The Actelion team then focused on the anilide portion of the molecule, shown as R_1 in Table 9. SAR studies quickly determined that placing substituents in a 2,5-disubstituted arrangement maintained OX2R potency and increased OX1R potency as shown in compounds **64** and **65**. Expanding the SAR of the diethyl amide resulted in the identification of heterocycles that yielded a further increase in OX1R potency as shown for the pyridine, pyrazine, and pyrazole substituents in **66–69**. These compounds have the added benefit of improved oral bioavailability in rat. Specifically, compound **66** was shown to have an oral bioavailability of 35%. Although brain penetration of this compound was quite low, it was shown to be effective in increasing the time spent in non-REM and REM sleep. Following this publication, Roche reported on the in vitro activity of a tool compound now known as EMPA which is a selective OX2R antagonist from the same structural class. This compound has been found to have tremendous utility in the orexin field as a radioligand tracer for ex vivo autoradiography and in vitro binding assays.[23]

Table 8 Binding data for the human OX2 and OX1 receptor for compounds **58–63**

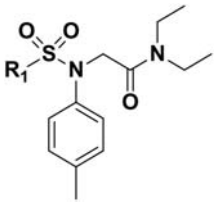

Compound	*R_1*	*OX2R K_i (nM)*	*OX1R K_i (nM)*
58	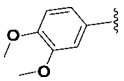	19	>10,000
59	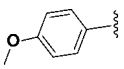	661	>10,000
60	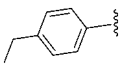	89	>10,000
61	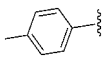	232	>10,000
62	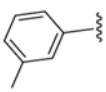	60	>10,000
63	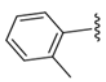	58	>10,000

Table 9 Binding data for the human OX2 and OX1 receptor for compounds **64–69**

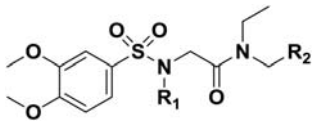

Compound	*R_1*	*R_2*	*OX2R K_i (nM)*	*OX1R K_i (nM)*
64	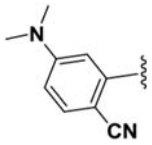	Me	10	166
65	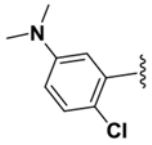	Me	5	119
66	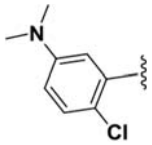	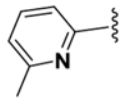	5	17
67	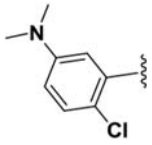	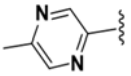	3	5
68	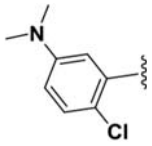	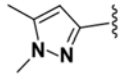	7	12
69	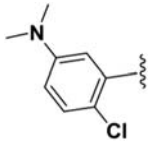	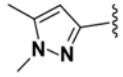	4	6

7.06.3 Banyu

7.06.3.1 Tetrahydroisoquinolines

In 2003 a team at Banyu Tsukuba Research Institute disclosed the first nonpeptide selective OX2R receptor antagonists based on a tetrahydroisoquinoline scaffold. First, an HTS screen uncovered **70** (Table 10), which is a nonselective and weak OXR antagonist. Simply removing the bromine (**71**) gave a 30-fold increase in OX2R potency, without any significant change in OX1R potency. Attempts were made to improve the physicochemical properties of these compounds (mainly poor solubility), and this work lead to compounds such as **72**. Subsequent modifications of the benzyl moiety provided more soluble, selective OX2R antagonists, including **74**.[24]

Table 10 Human OX2 and OX1 receptor IC_{50}'s for compounds **70–74**

Compound	*Structure*	*OX2R IC_{50} (nM)*	*OX1R IC_{50} (nM)*
70	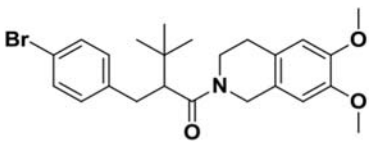	2000	7000
71	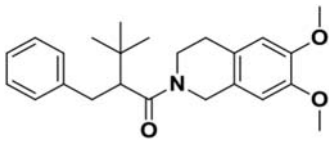	56	5500
72	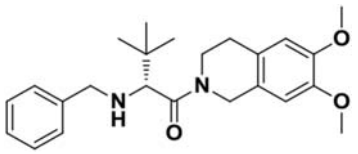	130	>10,000
73	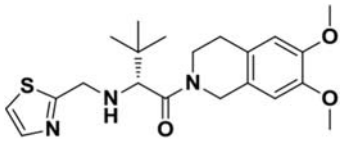	59	>10,000
74	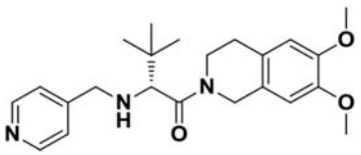	40	>10,000

7.06.4 Eisai

7.06.4.1 N-Aryl-2-Phenylcyclopropanecarboxamides

Eisai has published several reports on cyclopropanecarboxamides as potent orexin receptor antagonists. The Eisai team reported the serendipitous discovery of cyclopropane **75** (Fig. 9) as a weak OX2R antagonist while pursuing this chemotype in another discovery program.[25] Notably, this chemotype contains the dimethoxyphenyl moiety found in many other orexin antagonists and also adopts the "U-shaped" conformation found in other orexin chemotypes. The authors added a hydrogen bond acceptor donor to this lead compound and very quickly were able to generate high-affinity OXR antagonists. The 2-pyridyl analog **77** resulted in a significant loss of OX1R affinity, and removal of the 3,4-dimethoxy moiety results in a very weak OXR antagonist. The authors focused on pyridyl and heteroaromatic substituents in order to remove the potential liabilities associated with the aniline. Thiazoles (**80**

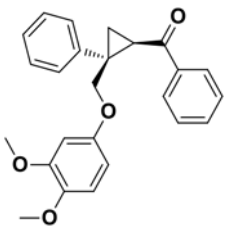

75
OX2R K_i=8.7 μM
OX1R K_i=>10 μM

Fig. 9 Compound **75**.

and **81**) and isoxazoles were tolerated; however compounds with these substituents showed P-gp efflux. In the end the cyanopyridine **82** had the best balance of affinity and physicochemical properties; therefore this compound was profiled in more detail (and as the single enantiomer). It should be noted that compounds **75–81** shown in Table 11 were tested as racemic mixtures. Compound **82** reduced locomotor activity in a mouse and, at high doses (30 and 100 mg/kg PO), decreased wakefulness and increased non-REM sleep.

7.06.4.1.1 E2006

The medicinal chemistry group at Eisai later reported that compound **82** was not suitable for clinical development because of time-dependent CYP3A inhibition, poor solubility, and some reversible CYP inhibition. For these reasons, further optimization of this series was explored in order to find a clinical candidate. Given that the time-dependent CYP inhibition was most likely related to the 3,4-dimethoxy moiety, the researchers made modifications to this portion of the molecule to try to reduce the CYP liability while at the same time improving solubility. As such, numerous heteroaromatic substituents were installed, including those shown in Table 12.[26] The pyridine compounds **83** and **84** were much less potent than **82** and in some cases retained the time-dependent cytochrome P450 inhibition (TDI) liability. However, other heterocycles including a pyrazole (**85**), pyrimidine (**86** and **87**), or a pyrazine (**88**) provided high-affinity compounds with improved TDI and solubility. Compounds **86–88** were tested as single enantiomers. Compound **86** was chosen for further optimization, primarily due to improved solubility and TDI potential.

The optimization of **86** led to the compounds shown in Table 13. In this work, a variety of substituted pyridines were profiled as single enantiomers, with variable results in affinity, solubility, and TDI liability. For the most part TDI was reduced (**94** is the exception). Compounds **91** and **93** were found to have high affinity, and both compounds reduced wake time when dosed at 30 mg/kg. Moving to the phenyl ring attached to the cyclopropane ring, the researchers were able to generate very high-affinity OXR ligands (**95–98**). Based on an analysis of all the in vitro data, compound **96** appeared most promising and was selected for further profiling. Compound **96** has good physicochemical properties, is metabolically stable, and has low efflux and reduced CYP interactions. The compound effectively distributes into the CNS and induces sleep following oral administration. In contrast to earlier compounds from the series, compound **96** increased both non-REM and REM sleep. Finally, **96** (E2006) was chosen as a candidate for clinical development. E2006 advanced into efficacy trials in 2015 (NCT02350309).[27] The doses tested were 5 and 10 mg in subjects with insomnia disorder. No results have been posted.

An analog of **96** was also evaluated as a positron emission tomography (PET) radioligand in rat and monkey. In this study, the researchers evaluated several potential ligands including compounds **99** and **100** shown in Fig. 10. However, they were unable to identify a PET ligand that was suitable for use in rat or nonhuman primate.[28] This is most likely due to a requirement for more potent compounds, given the low B_{max} value for OX2R (the measured B_{max} value for [^{3}H]-EMPA was 6.5 nM). The authors assert that the B_{max}/K_i should be greater than 5 in order to generate a successful OXR PET ligand.

7.06.5 GlaxoSmithKline

7.06.5.1 SB-649868 and Substituted Piperidines

While a review of the patent literature is not the subject of this article, a patent literature search revealed numerous patent applications from GSK related to the piperidine template contained in the compounds shown in Fig. 11. Although GSK has not published extensively on the SAR related to this series, one manuscript appeared in 2011 describing the SAR leading to **SB-649868** (**105**) which was reported to promote sleep in healthy volunteers.[29] The program began with a lead molecule related to compound **101**. Potency could be improved through the installation of the 2-arylbenzamide shown in **102** and **103**. Rapid in vitro clearance values (>50 mL/min/kg in rat) of **103** were attributed to the ether functionality in these compounds. Replacement of the ether linkage with the amide **104** was tolerated and resulted in lower predicted clearance of 19 mL/min/kg in rat and 23 mL/min/kg in human. Subsequent to these findings, additional SAR studies on both amide molecules resulted in the discovery of **SB-649868 (105)**, which has rat and human in vitro clearance values of 8.7 and 15.1 mL/min/kg, respectively, suggestive of a low to moderate clearance. Preclinical in vivo studies in rat revealed a clearance of 24 mL/min/kg, an oral bioavailability of 85% and demonstrated that the compound was brain penetrant. Following this manuscript and the discontinuation of **SB-649868**, a report appeared discussing the metabolic fate in humans.[29d] Although the half-life of **SB-649868** was 4–6 h, the radioactive half-life was measured at approximately 40 h. The circulating metabolites were found to be compounds **106** and **107**. A mechanism for the formation of these metabolites was proposed by the authors and summarized in a recent review from Merck.[3a] The proposed mechanism was supported by trapping of an epoxide intermediate with glutathione.

In addition to the molecules mentioned earlier, two other tool compounds originally discovered by GSK that have found utility as selective OX1R antagonists are **GSK1059865** (**108**) and the cyclopropyl compound **109**, Fig. 12.[13a,30] Although both of these molecules are only disclosed in the patent literature, but appear to offer advantages to existing tool compounds. The neuroanatomy or neuronal substrate responsible for behavior outcomes of **GSK1059865** and the selective OX2R antagonist from Janssen, **JNJ-10307049** (**134**), were mapped using fMRI. Consistent with previous reports, the OX2R antagonist was shown to promote sleep, whereas the OX1R antagonist had no effect in an EEG study. However, **GSK1059865** was able to inhibit a cocaine-induced conditioned place preference in rat and 10 and 30 mg/kg s.c. consistent with previous findings using other selective OX1R antagonists. In this initial report, theoretical brain receptor occupancy was calculated based on plasma pharmacokinetics and brain to blood ratios to estimate the dose required to occupy the OX1R. This has since been confirmed using ex vivo

Table 11 Human OX2 and OX1 receptor K_i's for compounds **76–82**

Compound	*Structure*	*OX2R* K_i *(nM)*	*OX1R* K_i *(nM)*
76	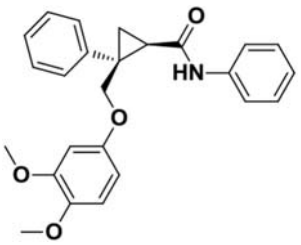	7.2	7.2
77	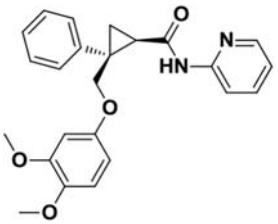	36	1068
78	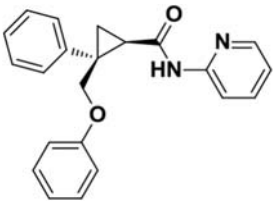	967	6841
79	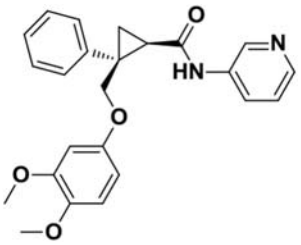	51	206
80	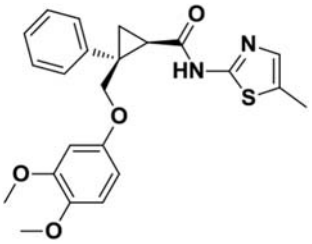	35	291
81	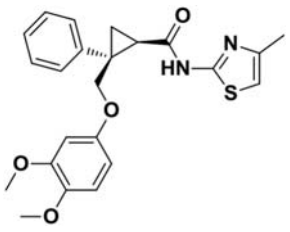	14	831
(−)-82	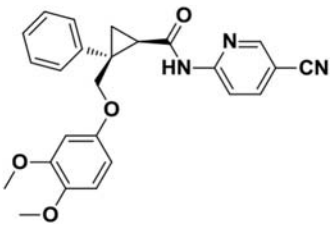	5.0	106

Table 12 Human OX2 and OX1 receptor K_i's for compounds **83–88**

Compound	*Structure*	*OX2R* K_i *(nM)*	*OX1R* K_i *(nM)*
(±)-83	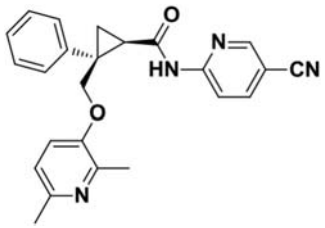	222	938
(±)-84	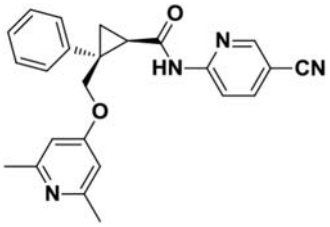	>2000	>2000
(−)-85	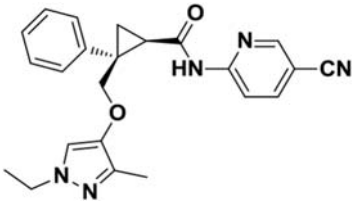	8	171
86	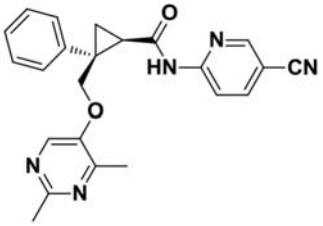	49	2491
87	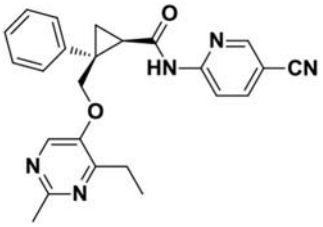	7	121
88	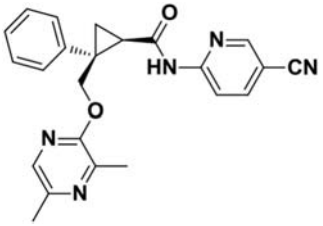	21	73

Table 13 Human OX2 and OX1 receptor K_i's for compounds **89–98**

Compound	*Structure*	*OX2R* K_i *(nM)*	*OX1R* K_i *(nM)*
89	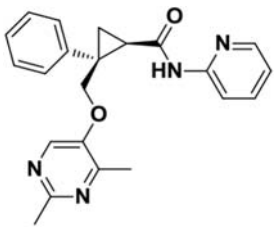	80	1016
90	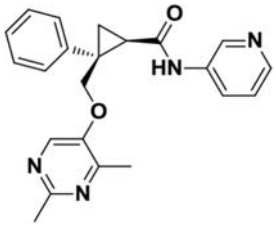	50	391
91	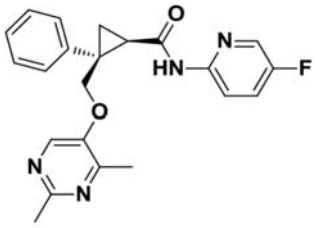	7	137
92	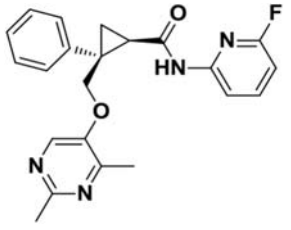	56	138
93	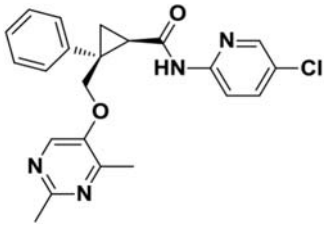	2	39
94	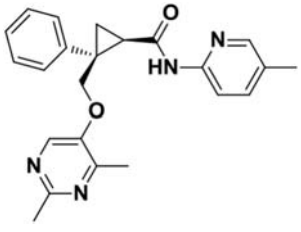	34	124

Table 13 Human OX2 and OX1 receptor K_i's for compounds **89**–**98**—cont'd

Compound	*Structure*	*OX2R* K_i *(nM)*	*OX1R* K_i *(nM)*
95	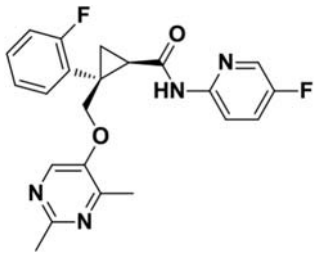	17	81
96	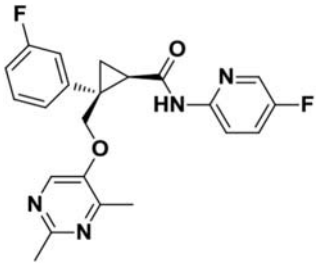	3	6
97	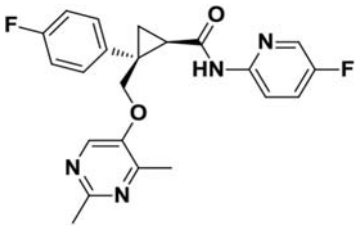	8	39
98	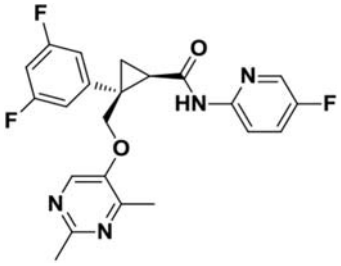	3	7

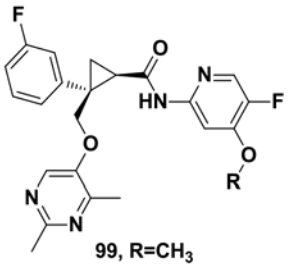

99, R=CH_3
OX2R K_i=2 nM
OX1R K_i=3 nM
[^{11}C]-99, R=$^{11}CH_3$

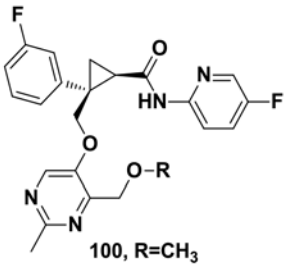

100, R=CH_3
OX2R K_i=1 nM
OX1R K_i=1 nM
[^{11}C]-100, R=$^{11}CH_3$

Fig. 10 Potential PET tracers.

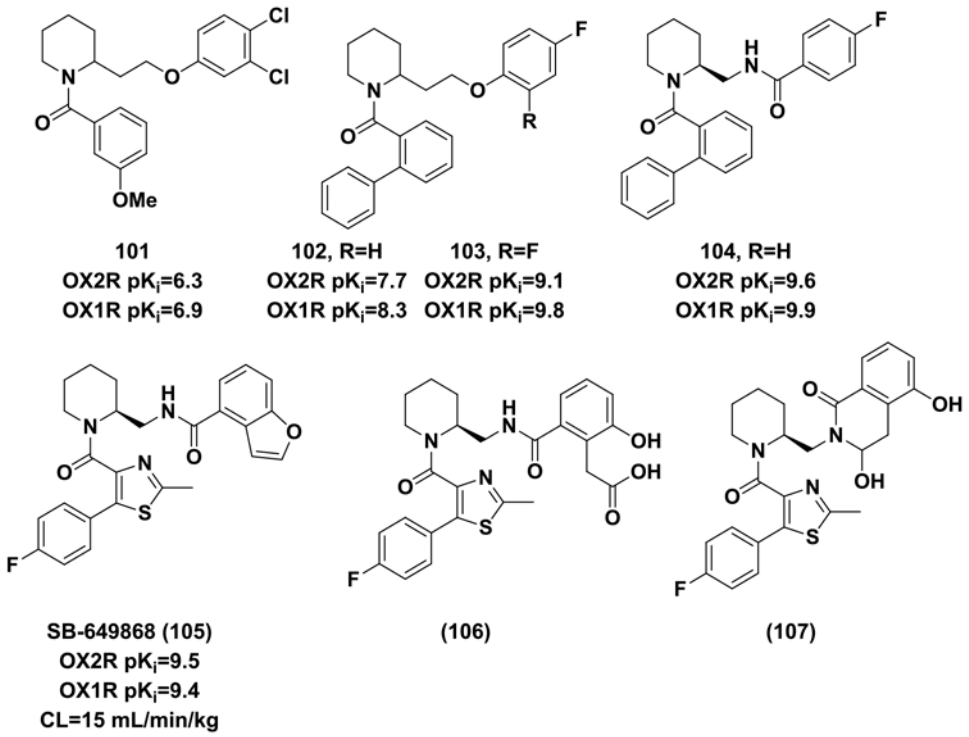

Fig. 11 SAR leading to SB-649868.

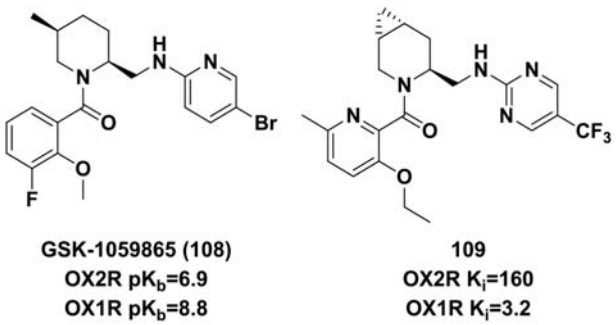

Fig. 12 2-Substituted-piperidine-based selective orexin-1 antagonists.

autoradiography by Janssen.[13a] Additional investigations by Janssen and researchers at Indiana University demonstrated that compound **109** was able to attenuate the anxiety-like behaviors induced by sodium lactate or CO_2.[13b] Interestingly in the CO_2-induced panic model, a dual orexin receptor antagonist and a selective OX1R antagonist were both efficacious. However, the selective OX2R antagonist **JNJ-10397049** did not attenuate the effects of CO_2.

7.06.5.2 GSK Early Selective OX1R Tool Compounds

The first medicinal chemistry paper describing nonpeptidic orexin antagonists was published by GSK in 2001.[31] This paper detailed the progression of the HTS hit **110** to SB-334867 (**111**), Table 14. Although the starting point **110** was selective over the OX2R receptor, selectivity over the serotonin 5-HT_{2B} and 5-HT_{2C} receptors was an issue that needed to be addressed in order for this series of molecules to provide useful tool compounds. In order to improve the selectivity profile of **110**, efforts were focused on changes to both sides of the diaryl urea. This culminated in the discovery of **SB-334867**. Hydrolytic instability of **SB-334867** has also been reported by researchers at Research Triangle Institute. Although **SB-334867** is not ideal with regard to off-target affinities, solubility and stability at low pH, it has been the most widely utilized tool compound used to elucidate the role of the OX1R in vivo. This compound was essential in the early understanding of the orexin system; however given the issues associated with **SB-334867**, many of the in vivo behavioral data should be analyzed and interpreted carefully.

Table 14 Cell-based FLIPR data for the human OX2 and OX1 receptor and off-target activities for compounds **110** and **SB-334867 (111)**

Compound	*R_1*	*OX1R pK_B*	*OX1R pK_B*	*5HT2B pK_i*	*5HT2C pK_i*
110	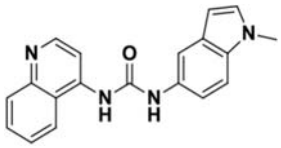	7.5	5.6	8.6	7.6
111 **SB-334867**	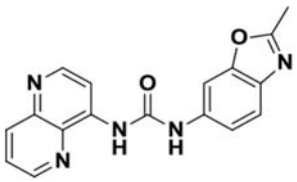	7.4	5.7	5.4	<5.3

Following the initial report of **SB-334867**, additional selective nonpeptidic selective OX1R antagonists were described that have also served as tool compounds. These are shown in **Table 15**. While the relative benefits of **SB-408124 (112)** and **SB-410220 (113)** are unclear, these analogs do not contain the methylbenzoxazole, the reactive moiety in **SB-334867**. Also shown in the table is **SB-67042 (114)**. Although, this compound, when R=H is not an acceptable in vivo tool due to poor solubility, the tritiated compound, that is, when R=^{3}H, has been crucial to the orexin field as a radioligand for both binding assays and ex vivo receptor occupancy studies.

Table 15 Binding data for the human OX2 and OX1 receptor for compounds **111–114**

Compound	*R_1*	*OX1R K_i*	*OX2R K_i*
111 **SB-334867**	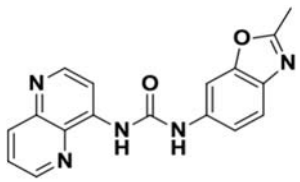	27.8	1704
112 **SB-408124**	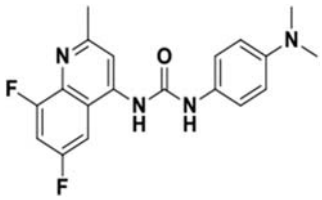	21.7	1405
113 **SB-410220**	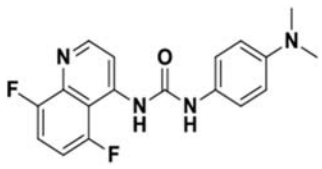	8.7	503
114 **SB-674042**	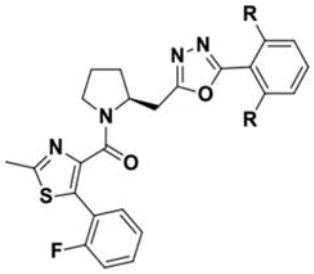	1.1	129

7.06.5.3 Triazolo-Thioamides

Unrelated to the compounds mentioned earlier, GSK has also reported on compound **115**.[32] This compound is a high-affinity selective OX2 receptor antagonist obtained from a HTS (Fig. 13). Attempts to make improvements in potency first focused on screening commercially available libraries which did not result in meaningful improvements in potency. While the in vivo properties of **115** were not described, the reported high intrinsic clearance would be expected to limit its utility. The compound does have excellent selectivity versus the OX1 receptor and a panel of 300 other receptors.

7.06.6 Heptares

7.06.6.1 2*H*-pyrido[2,3-*e*][1,2,4]thiadiazin-3(4*H*)-one 1,1-dioxides

Hetpares recently disclosed a series of 2*H*-pyrido[2,3-*e*][1,2,4]thiadiazin-3(4*H*)-one 1,1-dioxides that are dual OX2R/OX1R receptor antagonists. The team at Heptares had a number of screening strategies which lead to the identification of **116** as a viable lead compound with a structure unlike most of the known chemotypes at the time (Fig. 14).[33]

Initial exploration of this chemotype resulted in significant improvements in OX2R affinity. First, the undesirable methylenedioxy substituent was removed. This change also improved OX2R affinity slightly. Further improvements in OX2R and OX1R affinity were realized with the addition of substituents on the benzyl ring in the 2,4- and 2,6-positions as exemplified by compounds **118** and **119** in Table 16. Substitution in the 4-position was desirable for metabolic stability, and multiple substitutions proved most advantageous for affinity as shown for compounds **120** and **121**.

In order to reduce lipophilicity and optimize physicochemical properties, the authors' next goals were to remove the potentially risky dimethoxyphenyl substituent, modify the masked aniline moiety, and add heteroatoms to the core in order to reduce the lipophilicity of the resulting compounds.

Some key compounds in this exploration are shown in Table 17. A nitrogen is tolerated at several positions of the dimethoxyphenyl moiety, and a nitrogen was tolerated in the 5-position of the core. Balancing the overall compound profile including an analysis of microsomal stability, in vivo pharmacokinetics, and OX2R receptor kinetics, compound **125** was chosen for further profiling. Compound **125** has fast OXR kinetics with a dissociation half-life of 4.2 min at OX2R and 0.8 min at OX1R. The authors compared this to the much slower dissociation $t_{1/2}$'s for suvorexant of 210 and 24 min (OX2R and OX1R, respectively), and they assert that this property (fast dissociation) may provide a better profile for a sleep drug, in particular with respect to next-day somnolence effects. The authors demonstrated that compound **125** is permeable, Ames negative; has no hERG affinity (>10 μM), or measurable CYP inhibition; and has no reactive metabolites in their assays. The compound efficiently binds to the OX2R in rat frontal cortex as measured by ex vivo autoradiography and promoted sleep in rat, primarily through an increase in REM sleep,

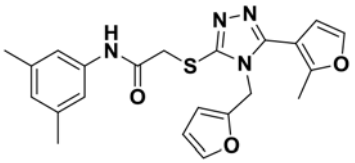

115
OX2R pK_i=8.8
OX1R pK_i=6.1

Fig. 13 Structure of compound **115**.

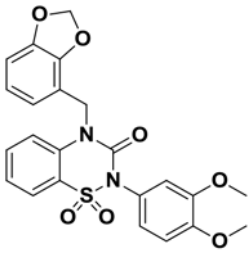

116
OX2R pK_i=6.6

Fig. 14 Compound **116**.

Table 16 Human OX2 and OX1 receptor pK_i's for compounds **117–121**

Compound	*Structure*	*OX2R* pK_i	*OX1R* pK_i
117	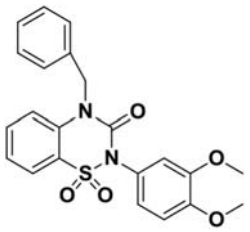	7.1	5.7
118	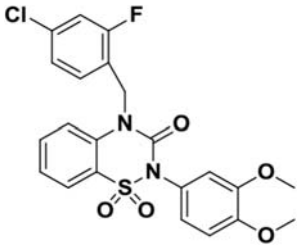	8.0	7.2
119	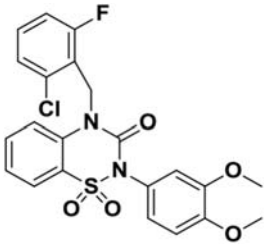	9.1	8.1
120	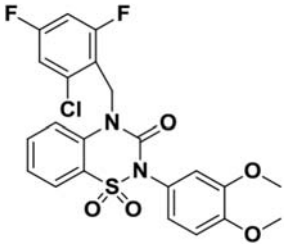	9.0	7.6
121	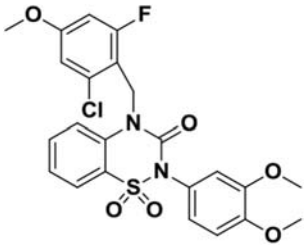	10.0	9.4

as expected. Overall, compound **125 (HTL6641)** was considered the best compound in the series, given the requirements for the treatment of insomnia (rapid onset, relatively short human half-life, and rapid dissociation kinetics).

7.06.7 International Institute for Integrative Sleep Medicine

7.06.7.1 OX2R Agonists

Research groups at the International Institute for Integrative Sleep Medicine in collaboration with Kitasato and Showa Universities and the University of Texas Southwestern Medical Center became interested in OX2R agonists in order to investigate their effects on

Table 17 Human OX2 and OX1 receptor pK_i's for compounds **122–125**

Compound	*Structure*	*OX2R* pK_i	*OX1R* pK_i
122	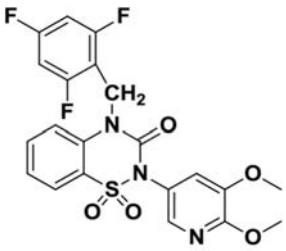	8.3	7.9
123	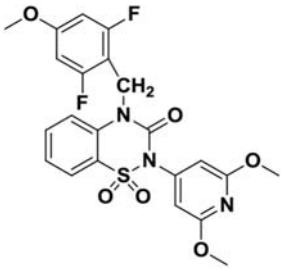	9.6	9.0
124	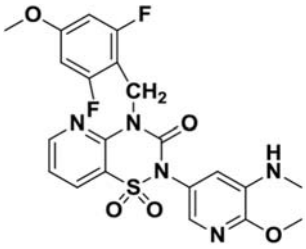	9.2	8.9
125	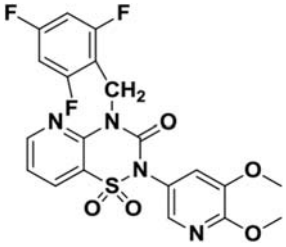	8.6	7.7

excessive sleepiness and narcolepsy. First, a HTS campaign identified a weak hit compound (**126**).[34] The authors then made numerous modifications to the core structure and to the substitution patterns on all the aromatic rings in order to improve stability and affinity. These efforts led to compounds with both improved potency and efficacy as shown in Table 18. Modifications to **126** quickly demonstrated that a diamine linker could provide similar efficacy, and after some additional SAR investigations the authors identified the *m*-phenylenediamine core as shown in **127** as a viable starting point. Small changes quickly lead to the more potent and efficacious compounds **128–131**. The authors note that these compounds show moderate to good selectivity over OX1R agonism (60- to 280-fold, for those reported). Compound **131** was docked into a model of OX2R based on the crystal structure reported for suvorexant,[35] and the authors assert that slight movements in TM5 and TM6 may account for the difference between agonism and antagonism.[34,36] Finally, the dimethylamino compound **132** was prepared in order to improve solubility since compounds **130** and **131** were insoluble in water, precluding in vivo work. Compound **132** also has good selectivity over OX1R ($EC_{50} = 2.75\ \mu M$) and promoted wake in mice after i.c.v. injection (Fig. 15).

Table 18 Human OX2 and OX1 receptor EC_{50}'s for compounds **127–132**

Compound	*Structure*	*OX2R EC_{50} (μM)*	*OX2R E_{max}*
127	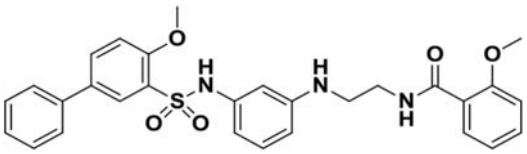	>10	48% @10 μM
128	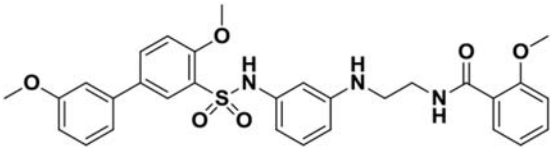	0.800	54% @1 μM
129	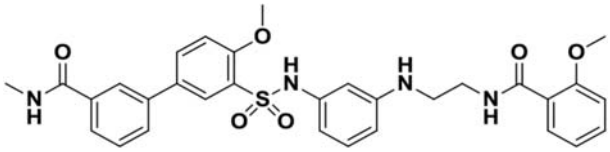	0.182	98% @1 μM
130	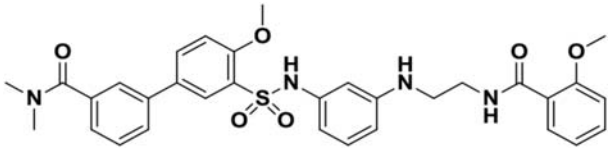	0.050	74% @1 μM
131	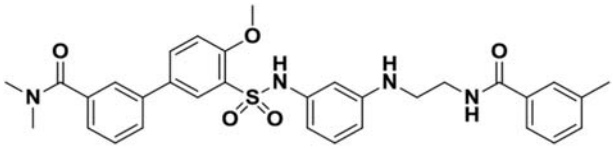	0.023	98%
132	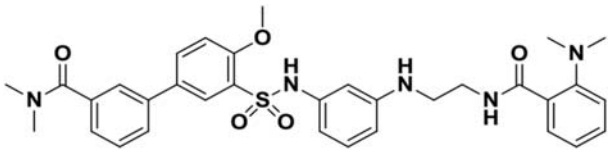	0.028	94%

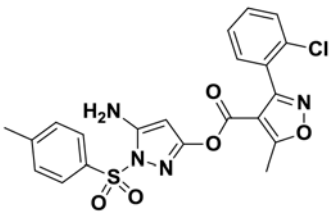

126
36% inc. in OX2R mediated luciferace activity at 5 μM)

Fig. 15 Compound **126**.

7.06.8 Johnson & Johnson/Janssen Pharmaceuticals

7.06.8.1 4-Phenyl-[1,3]dioxanes

Johnson & Johnson/Janssen has had a long-standing interest in the discovery and development of selective OX2R antagonists. In 2004, the team at Johnson & Johnson reported on a series of 4-phenyl-[1,3]dioxanes that are highly selective OX2R antagonists.[37] A HTS campaign yielded the dioxane **133**, and some limited medicinal chemistry led to the identification of **JNJ-10397049** (**134**), which is a potent and selective (600-fold over OX1R) OX2R antagonist. **JNJ-10397049** also has good selectivity over a panel of 50 receptors, ion channels, and transporters. In a subsequent report, the same group reported that **JNJ-10397049** achieved high levels of OX2R receptor occupancy in a rat brain following subcutaneous administration as measured by ex vivo autoradiography.[9] **JNJ-10397049** was also shown to decrease the latency to persistent sleep, demonstrating that OX2R antagonism is sufficient to promote sleep. The authors also showed that coadministration of an OX1R antagonist with an OX2R antagonist attenuated the effects of a selective OX2R antagonist. This leads them to conclude that a selective OX2R antagonist may provide an advantageous sleep profile as compared to dual OX1R/OX2R antagonists.[9,11] Later, **JNJ-10379049** was also shown to attenuate ethanol self-administration in rat (Fig. 16).[38]

7.06.8.2 Octahydropyrrolo[3,4-*c*]pyrroles

The researchers at Janssen have also reported on a series of octahydropyrrolo[3,4-*c*]pyrroles that are selective OX2R antagonists.[39] In this case, they stated that the dioxane moiety in **JNJ-10379049** proved essential for activity and was also the cause of poor oral bioavailability due to its inherent acid instability. For this reason, another HTS was conducted which provided numerous lead compounds, including the diazepane **135**, a compound which was also used as a lead for the team at Merck.[40] After exploring a variety of diamine core structures, the team settled on the octahydropyrrolo[3,4-*c*]pyrrole core, as exemplified by structure **136**, which proved to be a modest OX2R antagonist with >10-fold selectivity over OX1R. This compound was optimized for potency and selectivity by making changes to both the benzamide and the heteroaromatic substituents (examples include compounds **137–140**); however all the compounds in this set suffer from poor metabolic stability, likely due to the physicochemical properties of the compounds. In this series the dimethylpyrimidine generally provided good selectivity over OX1R, and the substituent on the benzamide was then used to optimize the physicochemical properties in order to improve the pharmacokinetic profile (Fig. 17).

A variety of benzamides were evaluated and are shown in Table 19. The 2-triazolophenyl substituent shown in compounds **141–144** provided relatively potent compounds with good physicochemical properties and good selectivity over OX1R. Overall, compound **144** (**JNJ-42847922**) had the best in vitro and in vivo profile, and this compound was chosen as a clinical candidate and is currently in development.

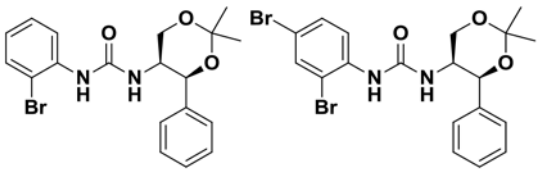

133
OX2R pK_i = 7.0
OX1R pK_i = 5.7

JNJ-10397049, 134
OX2R pK_i = 8.3
OX1R pK_i = 5.5

Fig. 16 Compounds **133–134**.

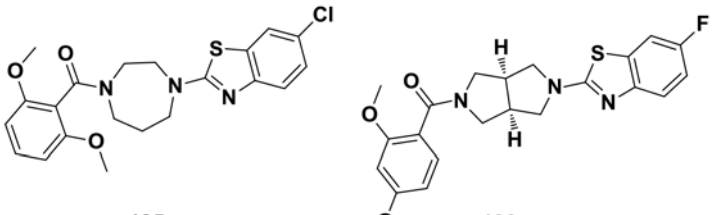

135
OX2R K_i=25 nM
OX1R K_i=216 nM

136
OX2R K_i=746 nM
OX1R K_i=>10000 nM

Fig. 17 Compounds **135–136**.

Table 19 Binding data for the human OX2 and OX1 receptor for compounds **137–144**

Compound	*Structure*	*OX2R* K_i *(nM)*	*OX1R* K_i *(nM)*
137	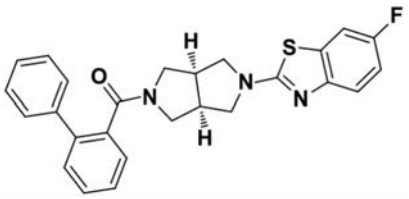	294 ± 53	925 ± 84
138	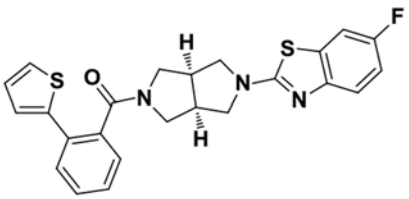	137 ± 15	267 ± 25
139	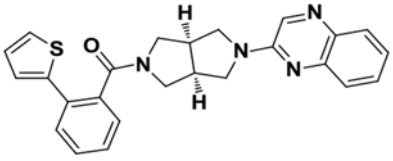	106 ± 95	623 ± 282
140	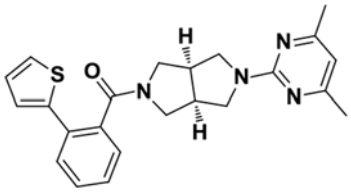	9.8 ± 3.8	471 ± 71
141	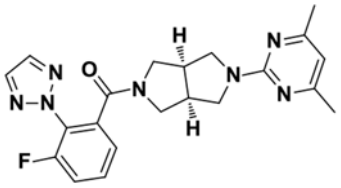	14 ± 5	2280 ± 1500
142	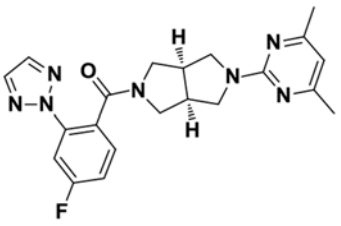	10 ± 3	1960 ± 2180
143	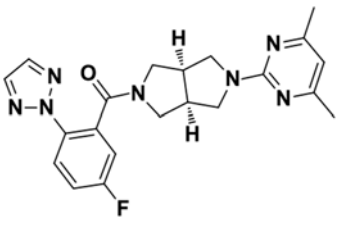	30 ± 15	5780 ± 2860
144	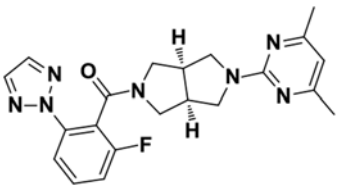	10 ± 1	800 ± 220

7.06.8.2.1 JNJ-42847922

JNJ-42847922 (**144**, Fig. 18) is a high-affinity OX2R antagonist with 80-fold selectivity over OX1R and has no other measurable effects in a panel of ion channels transporters or receptors. The compound has no affinity (>10 μM) for the hERG channel and was found to have modest microsomal stability in rat and human (ER 0.85 and 0.84). In rat, **JNJ-42847922** has relatively high clearance (CL = 40.0 mL/min/kg) and modest bioavailability (%F = 24%). **JNJ-42847922** dose-dependently occupies the OX2R in rat with an EC_{50} of 171 ng/mL and induced sleep in rat following oral administration. The compound has relatively high clearance in all preclinical species and based on these data was predicted to have a short human $t_{1/2}$ of between 1.2 and 1.8 h.[39] The dose estimation in human was calculated to be 250 mg, which was based on a calculated human EC_{50} of 330 ng/mL.

The synthesis of **JNJ-42847922** that was used to support 5-day rat and dog toleration studies is shown in Fig. 19. First, the carboxylic acid **145** is converted to 2-fluoro-6-[1,2,3]triazol-2-yl-benzoic acid and activated as the acid chloride to give **146**, which is then coupled with (3a*R*,6a*S*)-2-(4,6-dimethylpyrimidin-2-yl)octahydropyrrolo[3,4-*c*]pyrrole(**148**) (which was prepared in a two-step procedure from 2-benzyl-5-(4,6-dimethylpyrimidin-2-yl)-octahydropyrrolo[3,4-*c*]pyrrole(**147**)). Finally, recrystallization provided in excess of 100 g of **JNJ-42847922**.

JNJ-42847922 dose-dependently induces and prolongs sleep in rats, these effects persist upon 7-day repeated dosing, and the compound shows no effect in the OX2R knockout mouse, indicating that the sleep effects observed in the wild-type mouse are OX2R dependent. The compound does not induce a place preference in rat and has no effect on motor coordination. **JNJ-42847922** has entered human clinical trials, and pharmacokinetic data for a single dose of 10, 20, 40, and 80 mg were recently reported.[41] In human, **JNJ-42847922** has a half-life of approximately 2 h and a t_{max} of 0.33–0.5 h. Somnolence was reported at all doses, and the incidence of somnolence appeared to be dose dependent. In early 2016 Janssen's development partner Minerva Neurosciences issued a press release indicating that **JNJ-42847922** (MIN-202) had positive efficacy signals on key sleep parameters in patients with insomnia disorder.[42]

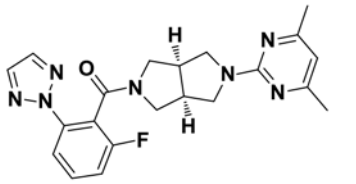

JNJ-42847922, 144
OX2R K_i=10 nM
OX1R K_i=800 nM
moderate %F in mouse, rat, dog and monkey
high receptor occupancy in rat
human predicted $t_{1/2}$ = 1.2 - 1.8 h

Fig. 18 Compound **144**, **JNJ-42847922**.

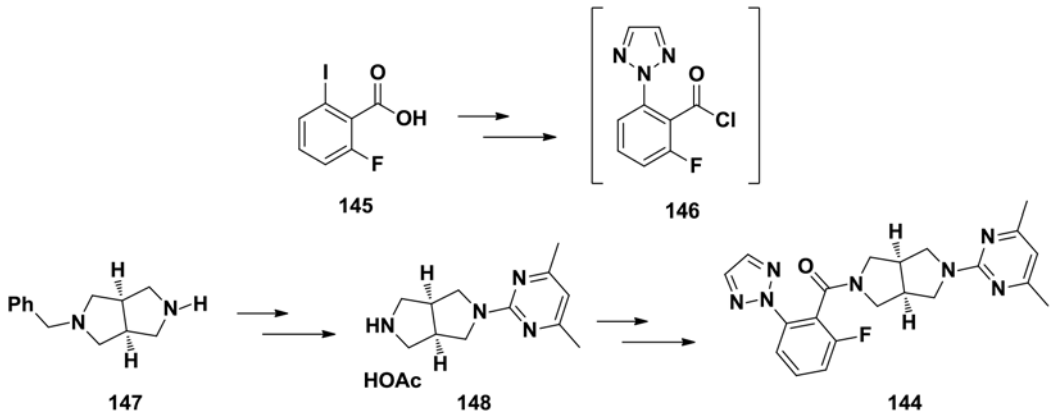

Fig. 19 Optimized synthesis of compound **144**.

7.06.9 Merck

7.06.9.1 Proline bis-Amides

The research group at Merck has published extensively on their efforts to progress orexin antagonists into the clinic. The efforts at Merck have been reviewed several times recently[3a] and are summarized here as well. One of the first reports from Merck noted that HTS efforts identified the proline bis-amide **149** of unknown stereochemistry as a potent OX2R and OX1R antagonist.[43] Medicinal chemistry efforts designed to optimize potency and brain penetration led to compound **150**, a compound that effectively entered the CNS and showed efficacy in a model of induced locomotion inhibition (Fig. 20).

7.06.9.2 Diamines/MK-4305 (Suvorexant)

Merck also discovered a diazepane lead via HTS (**135**), and after significant optimization compound **152** was identified and found to dose-dependently reduce locomotor activity and induce sleep in rat.[40] Unfortunately, **152** has low bioavailability in rat due to high clearance, a characteristic of many potent OXR antagonists. The team also noted that this compound existed in solution as two major rotamers and an NMR analysis revealed that the low energy conformations had a U-shaped structure (nuclear overhauser effects between the amide phenyl ring and the quinazoline).[44] Preference for this U-shaped conformation was confirmed in the solid state by an X-ray crystal structure of **152**. A macrocyclic analog of **152** was subsequently prepared (**153**), and this compound also proved to be a potent OX2R and OX1R antagonist, as shown in Fig. 21. These data also suggest that the bioactive conformation

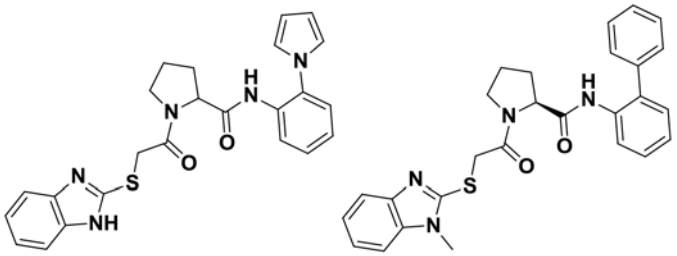

149
OX2R K_i=1 nM
OX1R K_i=28 nM

150
OX2R K_i=0.2 nM
OX1R K_i=3 nM

Fig. 20 Compounds **149**–**150**.

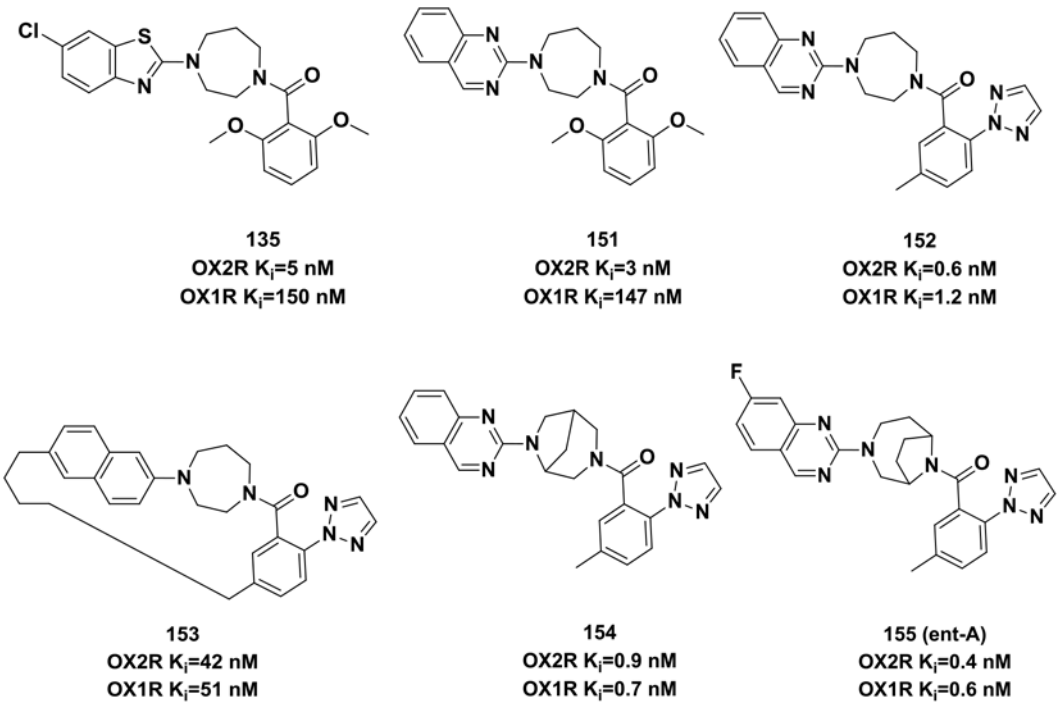

135
OX2R K_i=5 nM
OX1R K_i=150 nM

151
OX2R K_i=3 nM
OX1R K_i=147 nM

152
OX2R K_i=0.6 nM
OX1R K_i=1.2 nM

153
OX2R K_i=42 nM
OX1R K_i=51 nM

154
OX2R K_i=0.9 nM
OX1R K_i=0.7 nM

155 (ent-A)
OX2R K_i=0.4 nM
OX1R K_i=0.6 nM

Fig. 21 Compounds **135** and **151**–**155**.

of all of these OXR antagonists is the U-shaped structure. Many other groups subsequently utilized a variety of core structures to induce such a U-shaped conformation and produce potent OXR antagonists. One example from the Merck team is shown as compound **154**.[45] This compound is a potent OXR antagonist; however the 2,3-diazabicyclo[3.2.1] octane core did not improve the pharmacokinetics of this analog over the diazepane structure (e.g., **152**). Related work produced the 2-carbon bridged version **155** which also offered no improvements in pharmacokinetic parameters.[46] In efforts to overcome the metabolic liabilities associated with **152** and **154**, a series of substituted diazepanes were prepared and profiled.[35] Several of these are shown in **Table 20**. Compound **158** had reasonable bioavailability in dog and decreased active wake in rat; however it was subject to bioactivation and the formation of reactive metabolites. The fluoroquinazoline was thought to be responsible for the bioactivation, and consequently a series of heterocyclic replacements were investigated, including the benzoxazoles **159** and **160**. The benzoxazole **160** had low dog clearance, good bioavailability, and a low propensity to produce reactive metabolites. The compound readily penetrates the CNS, is permeable, not a substrate for efflux, and was shown to be very selective over a large panel of other target enzymes, receptors, and ion channels. Compound **160** significantly increased delta and REM sleep in rats at 30 mg/kg. Based on the overall preclinical profile of **160**, the compound was predicted to have low to moderate clearance in human with a rapid onset of action. Ultimately, this compound (**160**, suvorexant) was chosen for clinical development and is the first OXR antagonist to be approved for use in humans.

Table 20 Human OX2 and OX1 receptor K_i's for compounds **156–160**

Compound	*Structure*	*OX2R* K_i	*OX1R* K_i
156	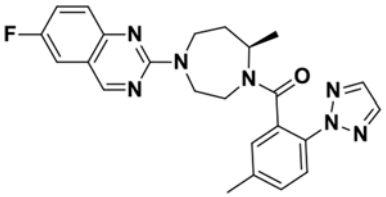	0.17	1.8
157	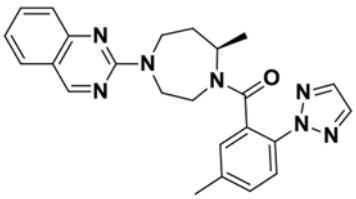	0.36	0.39
158	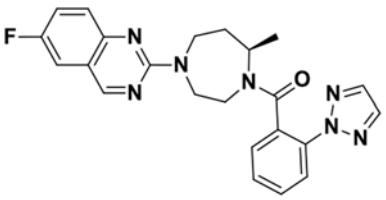	0.17	1.8
159	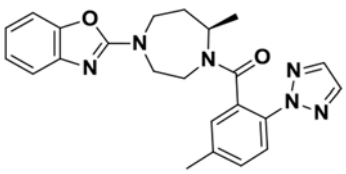	3.2	4.1
160	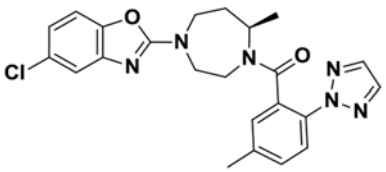	0.35	0.55

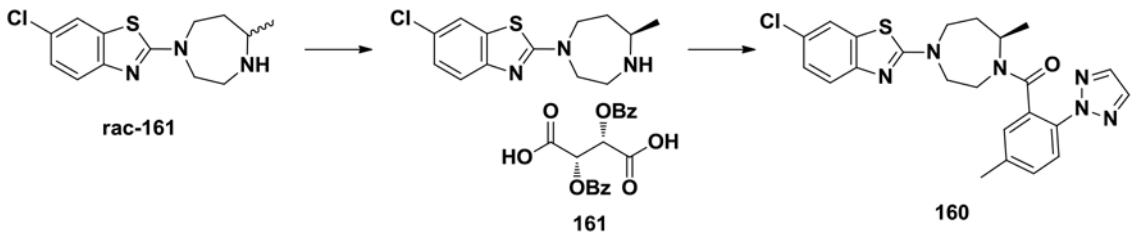

Fig. 22 Process synthesis of **160**.

7.06.9.3 MK-4305 (Suvorexant/Belsomra)

A summary of the work that lead to the discovery of MK-4305 (**160**) was described in the last section and in 2010 Merck reported that **MK-4305** entered Phase III clinical trials for the treatment of primary insomnia.[35] In 2011, Merck reported on the synthesis of over 25 kg of **MK-4305** via preparation of racemic **161**, classical resolution of **161** following crystallization as the dibenzoyltartrate salt, and coupling with 5-methyl-2-(2*H*-1,2,3-triazol-2-yl)benzoic acid to form **MK-4305** in an overall yield of 19% in five steps.[47] The sequence is summarized in Fig. 22.

In 2011, Merck reported that **MK-4305** dose-dependently promoted sleep in rats, dogs, and monkeys[48] and in 2014 the results of a 12-month clinical trial assessing safety, toleration, and efficacy in human.[49] The authors note that they concluded that 30 or 40 mg of suvorexant appeared to be safe and well tolerated in that trial; the authors also noted that the FDA thought the data supported 10–20 mg doses of suvorexant. In 2014, the FDA approved the use of suvorexant (Belsomra) for use in the treatment of insomnia. Belsomra remains the only orexin antagonist approved for use in humans.

7.06.9.4 Piperidines/MK-6096 (Filorexant)

Additional OXR antagonists include the 2,5 disubstituted piperidines **162–168**.[50] The 2,5 trans substitution on the piperidine was designed to enforce a diaxial structure, thereby inducing a U-shaped conformation which should be optimal for OXR binding. Several examples are shown in Table 21. The goal was to improve the pharmacokinetic properties of **(±)-162**. A number of heterocycles were profiled, and some were not tolerated (e.g., **163**); however the 2-pyridyl substituent produced high-affinity OXR antagonists (**164–168**). Modifications of the amide also lead to high-affinity compounds, and the authors note that the 5-methyl substituent on the benzamide was needed for optimal OX1R activity. From this work, compound **167** (**MK-6096**, Filorexant) emerged as the most interesting compound in the series. **MK-6096** is a potent OXR antagonist with good preclinical

Table 21 Human OX2 and OX1 receptor K_i's for compounds **162–168**

Compound	*Structure*	*OX2R* K_i	*OX1R* K_i
(±)-162	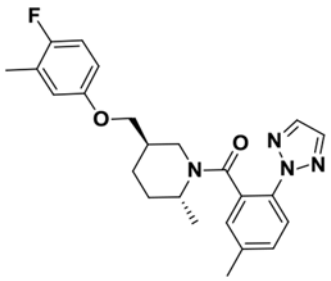	0.1	0.3
163	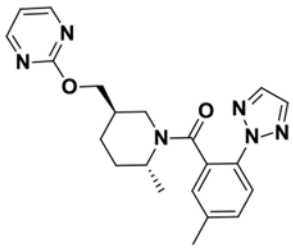	55	340

(Continued)

Table 21 Human OX2 and OX1 receptor K_i's for compounds **162–168**—cont'd

Compound	*Structure*	*OX2R* K_i	*OX1R* K_i
164	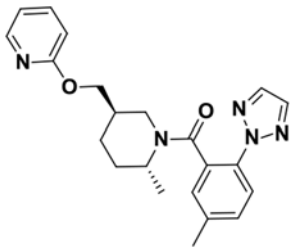	4	11
165	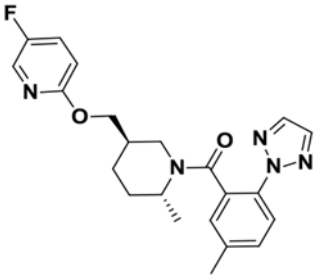	0.2	1.0
166	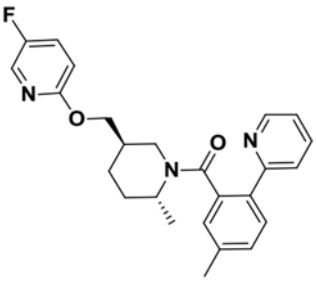	0.4	3.2
167	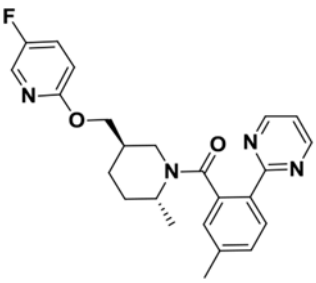	0.3	2.5
168	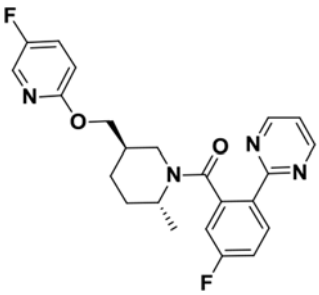	0.6	10

pharmacokinetics in dog and high clearance in rat. Efficacy in sleep was demonstrated for **MK-6096** in dog. Based on microsomal clearance, the human pharmacokinetics was expected to be similar to dog. **MK-6096** is not a CYP inhibitor, showed no TDI, is selective in a broad screening panel, and shows no cardiovascular liabilities. Based on these and other data,[51] **MK-6096** was chosen as a candidate for clinical development. In 2012, the team at Merck reported using a biocatalytic transamination as a key step to prepare the substituted piperidine core of this molecule and subsequently to synthesize **MK-6096** in multikilogram quantities.[52] **MK-6096** has been in several clinical trials. In one trial, **MK-6096** (Filorexant) was dosed at 10 mg for 3 months and efficacy in migraine was assessed. The compound had no statistically significant effect in this study.[53] **MK-6096** was also clinically evaluated in patients with insomnia. In this Phase II study, **MK-6096** showed a significant decrease to sleep onset and improvements in sleep maintenance.[54]

Related piperidines have also been evaluated as OXR antagonists.[55] In this case, the ether linker on the molecule was replaced with a carbon linker and the resulting compound (**169**) had reasonably good OX2R affinity. The authors also prepared the olefin **170** and some acetylenes, as represented by **171** shown in **Fig. 23**. These changes lead to high-affinity OXR antagonists, and **171** had good pharmacokinetics and showed efficacy in increasing sleep however; compound **171** and all other acetylene analogs produced time-dependent CYP 3A4 inhibition and, as such, work on this series was terminated.

7.06.9.5 2,5-Diarylnicotinamides

The team at Merck has also reported on selective OX2R receptor antagonists. Starting with lead structure **172** (**Fig. 24**), the team prepared a series of diarylnicotinimides.[56] Several modifications of the benzyl moiety revealed the dimethoxy compound **173** as a potent and selective OX2R antagonist; however this compound had high clearance in rat, prompting further investigations on this series. Focusing on the dimethylphenyl substituent, several 2,5-disubstituted nicotinamides were profiled. From this group **174** emerged as a viable candidate for further profiling. Compound **174** is an extremely high-affinity OX2R antagonist; however the exposure of this compound in the brain is limited, likely due to the fact that the compound is a P-gp substrate. Despite this, **174** did show efficacy in a rat sleep EEG model.

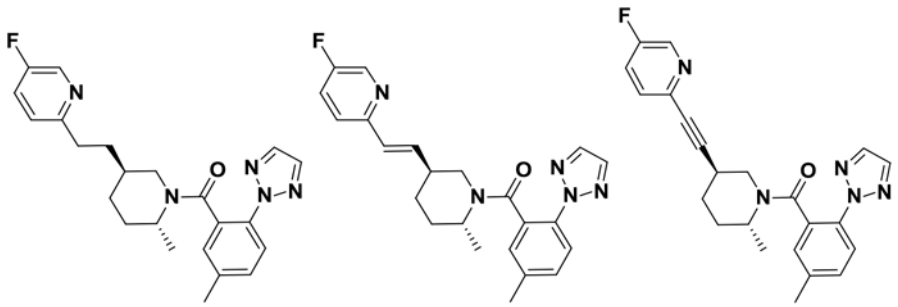

Fig. 23 Compounds **169–171**.

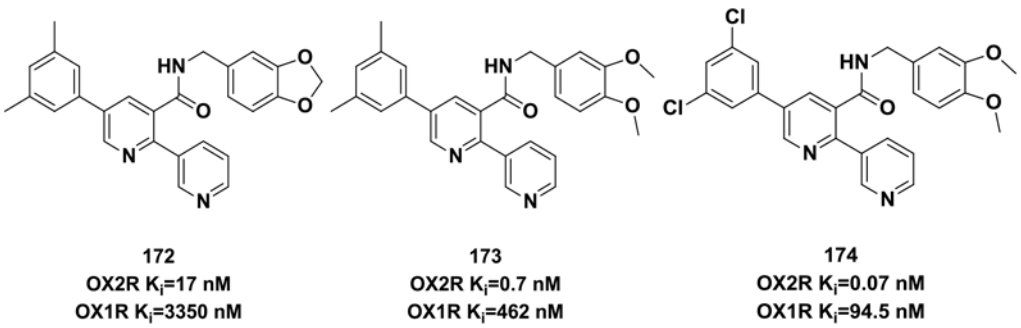

Fig. 24 Compounds **172–174**.

7.06.9.6 MK-1064

Compound **174** was subsequently reported to be a CYP 3A4 inhibitor, and follow-up efforts to optimize this series included work that resulted in the selection of an OX2R antagonist suitable for clinical development.[57] This work focused primarily on optimization of the benzamide while closely monitoring CYP inhibition, reactive metabolite formation, P-gp activity, and metabolic stability. Compounds **175** and **176** (Fig. 25) are examples of compounds with improved physical properties, unfortunately **175** suffered from a P-gp liability and **176** produced reactive metabolites. Since the reactive metabolites were thought to arise from the reactivity of the dimethoxyphenyl ring, several variations of this substituent were prepared and profiled. Compound **177** (**MK-1064**) was ultimately selected for additional profiling because it had high OX2R affinity, an acceptable P-gp profile, and low bioactivation potential. **MK-1064** has reasonable pharmacokinetics in rat, dog, and rhesus monkey; effectively occupies the OX2R in rat brain; and promoted sleep in mouse, rat, dog, and rhesus monkey. **MK-1064** was predicted to have low clearance in human, and the human half-life was estimated to be 2–16 h. In toleration studies in rat, no drug-related changes were noted, and in CV studies in dog, no signals were observed. **MK-1064** was chosen as a candidate for clinical trials, and it appears that a Phase I trial was conducted at doses of 50, 120, and 250 mg. In the clinic, MK-1064 was found to decrease latency to persistent sleep (LPS) and wake after sleep onset (WASO).[58] No further data has been reported for this compound.

7.06.9.7 MK-3697

After it was determined that the 2-pyridyl moiety on the nicotinamide was responsible for hydrolysis of the amide observed during salt screening exercises (compare **177** and **178**, Fig. 26),[59] efforts also focused on optimizing the nicotinamides for chemical stability. For this portion of the research, the SAR of the nicotinamide was explored with the goals of maintaining OX2R selectivity and optimizing clearance in dog.

The OX2R and OX1R affinities are very sensitive to the position of the nitrogen on the nicotinamide ring (compare **179–180** and **181** in Table 22). Overall, **181** had the best profile, and this compound was also found to have the lower clearance in dog; therefore it was used as a lead for further optimization. Compound **181** was found to be stable at low pH; however it also had CYP 3A4 TDI potential, similar to that seen for **MK-1064**. This work produced a number of substituted 2-aryl analogs, including **183–188**. Substitution is tolerated with variable selectivity, and some 5-membered heterocycles are tolerated. Compounds **183**, **184**, **186**, and **188** also had relatively low clearance in dog. Compound **187** was also stable at pH 2 and showed reduced risk for TDI, and as such, it was chosen for further profiling. This compound had good bioavailability in rat and dog and showed significant reductions in active wake in mouse, rat, and dog. Ultimately **187** (**MK-3697**) was chosen as a preclinical candidate. To our knowledge no clinical data has been reported for **MK-3697** although one report indicated that the compound was in Phase II clinical trials.[60]

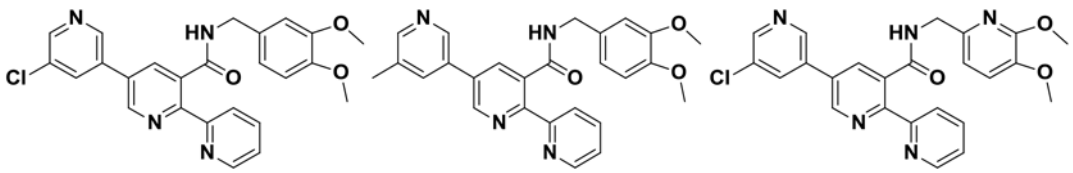

Fig. 25 Compounds **175–177**.

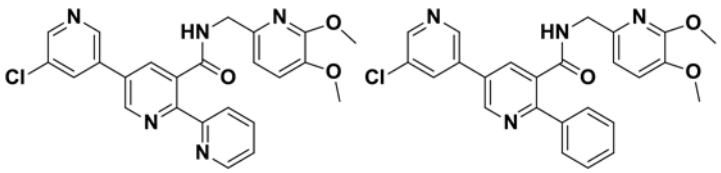

Fig. 26 Compounds **177** and **178**.

Table 22 Human OX2 and OX1 receptor K_i's for compounds **179–188**

Compound	*Structure*	*OX2R* K_i	*OX1R* K_i
179	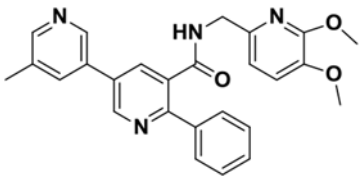	0.3	720
180	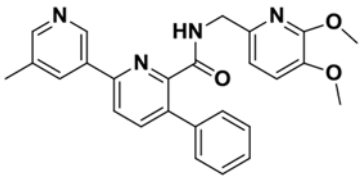	43	2400
181	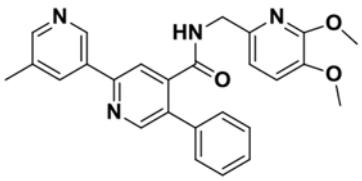	0.5	2700
182	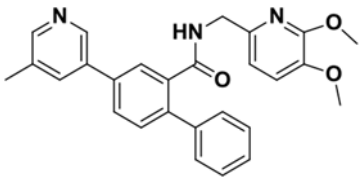	0.3	1000
183	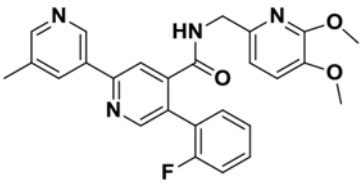	1.4	2700
184	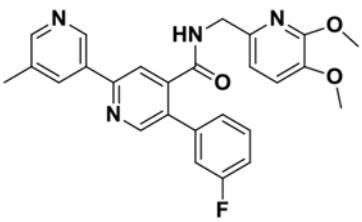	0.9	4000
185	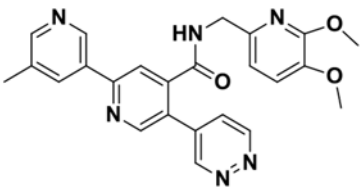	193	39,000
186	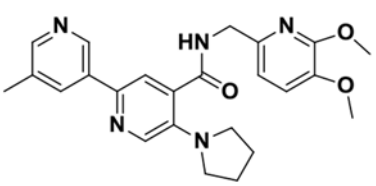	4.5	1400

(Continued)

Table 22 Human OX2 and OX1 receptor K_i's for compounds **179–188**—cont'd

Compound	*Structure*	*OX2R* K_i	*OX1R* K_i
187	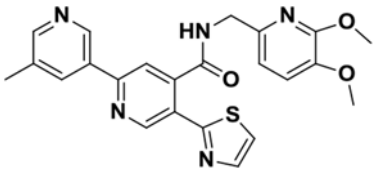	1.1	3600
188	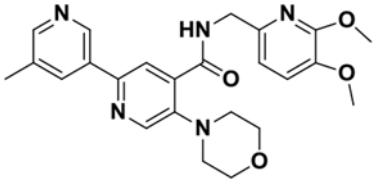	75	1500

7.06.9.8 Piperidine Ethers

Modifications of the MK-6096 core structure also lead to selective OX2R antagonists, as exemplified by **189** and **190** shown in Fig. 27. In this work, **(±)-189**, a compound with a shorter linker to the aryl ether attached to the piperidine, provided a lead compound which was further elaborated with the correct substitution and stereochemistry on the piperidine to give **191**, a potent OX2R antagonist with modest OX1R selectivity.[61] Additional exploration of the aryl ether produced **191**, a potent and selective OX2R antagonist. Compound **191** also promotes sleep in rat although this compound has a shorter duration of action than **MK-6096**.

7.06.9.9 Diazepanes

Recently Merck also disclosed a series of diazepanes that were prepared as a follow-up to the quinazoline-based compounds such as **158**. Select compounds from this set are shown in Table 23. As mentioned earlier, some of the quinazolines suffered from bioactivation and it was thought that monocyclic replacements for the quinazoline, with the proper substitution, may reduce the bioactivation potential for these compounds. Indeed, high-affinity OXR antagonists were prepared (**189–192**).[62] Compound **192** had the best preclinical profile, reduced GSH adducts, and showed efficacy, reducing wake in rats. Further exploration, which included removal of the methyl group on the benzamide (known to reduce OX1R affinity in other analogs) and modification of the pyrimidine, provided the selective OX2R antagonists **193–196**. Compound **196** induced sleep in mouse; however due to its pharmacokinetic profile high doses were required, and this compound would be expected to have a relatively short duration of action.

7.06.9.10 MK-8133

In a separate report, Merck disclosed further optimization of the piperidine core, with the goals of preparing selective OX2R antagonists, and this work lead to the identification of another clinical candidate, **MK-8133**.[63] The team first explored the SAR of methyl substituted pyridines (**197–200**, Table 24) and found that the 4-methylpyridine **199** provided the best OX2R affinity

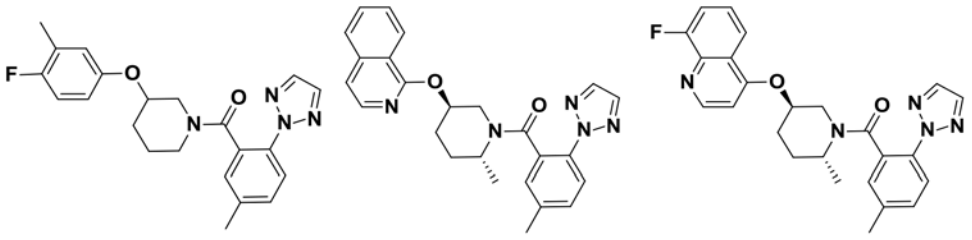

(±)-189
OX2R K_i=55 nM
OX1R K_i=106 nM

190
OX2R K_i=0.3 nM
OX1R K_i=10.5 nM

191
OX2R K_i=0.6 nM
OX1R K_i=965 nM

Fig. 27 Compounds **189–191**.

Table 23 Human OX2 and OX1 receptor K_i's for compounds **189–196**

Compound	*Structure*	*OX2R* K_i	*OX1R* K_i
189	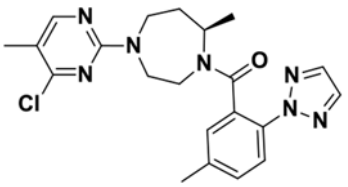	0.4	3.9
190	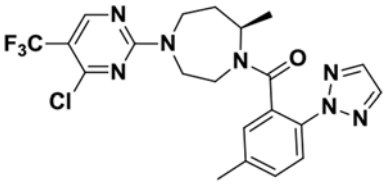	0.6	0.7
191	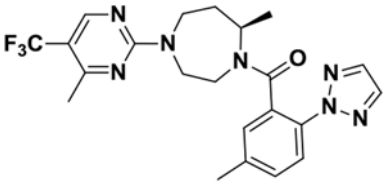	0.5	1.6
192	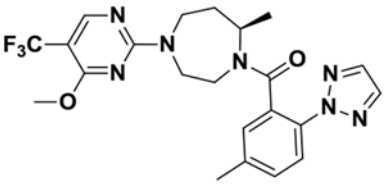	0.4	1.5
193	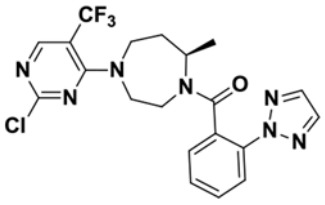	7.7	1100
194	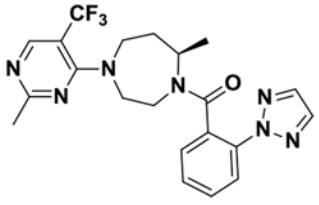	31	4200
195	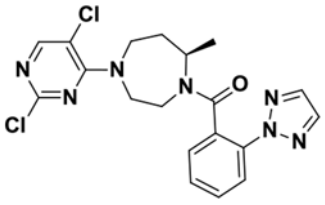	1.1	850
196	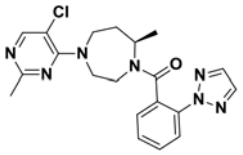	3.6	1800

Table 24 Human OX2 and OX1 receptor K_i's for compounds **197–207**

Compound	*Structure*	*OX2R* K_i	*OX1R* K_i
197	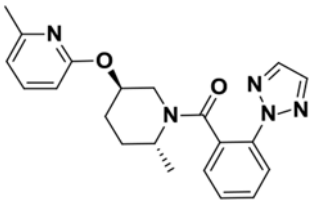	7.6	11
198	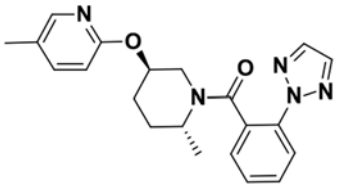	2.6	37
199	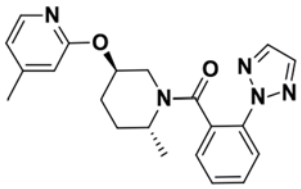	2.6	166
200	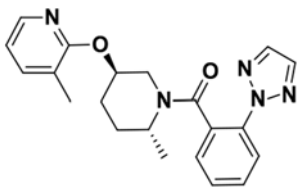	621	4756
201	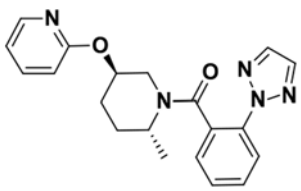	2400	14,000
202	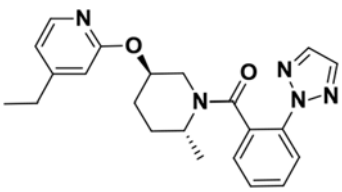	0.6	57
203	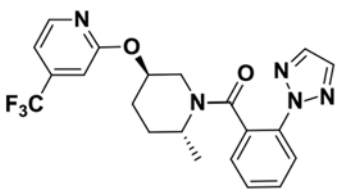	0.2	64
204	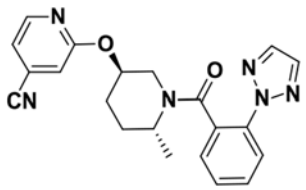	1.6	830

Table 24 Human OX2 and OX1 receptor K_i's for compounds **197–207**—cont'd

Compound	*Structure*	*OX2R* K_i	*OX1R* K_i
205	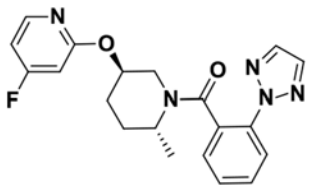	3.9	430
206	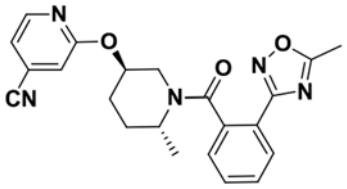	25	8400
207	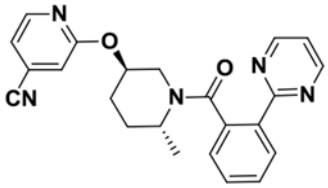	28	4900

and OX1R selectivity. Further optimization of the substituent in the 4-position of the pyridine produced numerous compounds, represented by **201–205** here. These changes produced compounds with variable OX2R affinity and selectivity, as one might expect. Ultimately, larger substituents in the 4-position gave the best profile and cyano (**204**) proved to have the best balance of OX2R affinity, selectivity over OX1R, and functional activity (FLIPR assay). As such, this is the substituent that was installed for subsequent optimization of the benzamide substituent. This work led to the identification of compounds **206** and **207** as interesting leads. Compounds **204**, **206**, and **207** were characterized further in rat and dog, and it was compound **207** that had the best overall profile in rat and dog (high %F and moderate clearance). In addition, this compound was not a significant substrate for P-gp, had no off-target activities, had improved solubility over compound **204**, and distributed into the CNS. After oral administration to mice, rats, or dogs, compound **207** decreased active wake, as expected. Compound **207** (**MK-8133**) was subsequently identified as a potential clinical candidate.

7.06.10 Novartis

7.06.10.1 Spirocyclic Amino-Amides

Novartis's interest in orally active selective OX2R antagonist began with the spirocycle **208**.[64] As summarized in Fig. 28, the initial iterations were aimed at attempting to understand the role of the amide carbonyl or putative hydrogen bond acceptor highlighted in blue. For example, was this carbonyl in fact acting as a hydrogen bond acceptor or was it necessary to force a particular

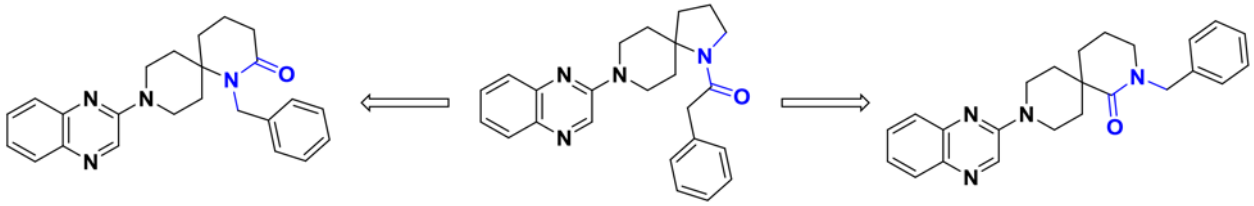

209
OX2R pK_i=6.52
OX1R pK_i=5.83
OX2R LE=0.32

208
OX2R pK_i=6.73
OX1R pK_i=6.02

210
OX2R pK_i=6.75
OX1R pK_i=5.81
OX2R LE=0.22

Fig. 28 Spirocycles **208–210**.

conformation? In order to mimic the *E* and *Z* isomers of the amide bond, reverse amides **209** and **210** were synthesized to probe this question. Interestingly, both were found to have near equal potency for both orexin receptors as the lead **208**. This led to the conclusion that the amide carbonyl was only present to either fix a particular conformation or that these three molecules had alternative binding modes which were forming hydrogen bonds with different residues in the active site.

Based on ligand efficiency (LE), the Novartis team began their SAR studies with compounds related to **209**, Table 25. A good increase in potency for both receptors was realized by substitution on the pendant phenyl ring, as exemplified by compound **211**. Although the LE was maintained in this case due to the increased potency, the overall cLogP had increased. Therefore efforts

Table 25 Human OX2 and OX1 receptor K_i's for compounds **211–218**

Compound	R_1	*OX2R* pK_i	*OX1R* pK_i
211	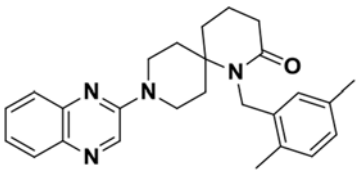	7.89	7.23
212	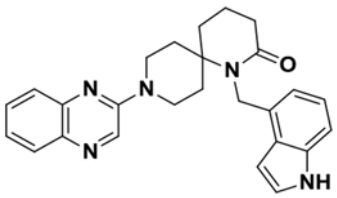	9.34	8.04
213	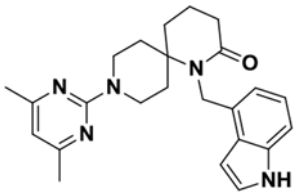	9.07	6.43
214	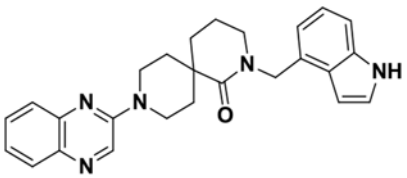	7.2	6.3
215	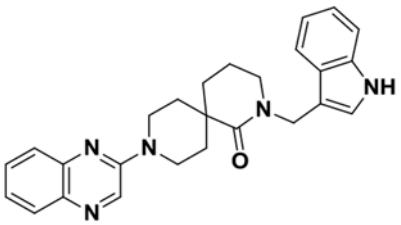	7.2	6.5
216	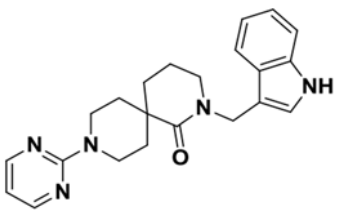	6.4	5

Table 25 Human OX2 and OX1 receptor K_i's for compounds **211–218**—cont'd

Compound	*R_1*	*OX2R pK_i*	*OX1R pK_i*
217	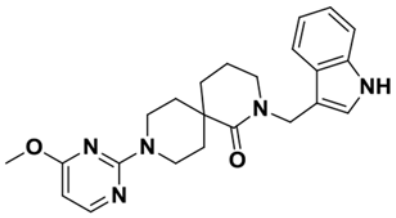	7.85	6.29
218	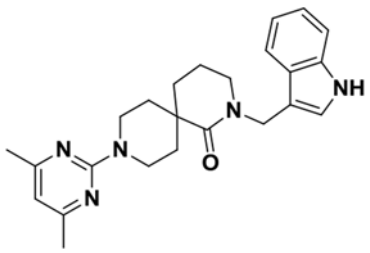	8.16	6.18

were focused on decreasing cLogP while maintaining potency by incorporating heterocyclic replacements, such as substituted indoles, for the benzyl group. The resulting 4-substituted indole **212** provided a further improvement in OX2R potency. Additional selectivity over the OX1R was evident as well. Next, modifications were focused on the quinoxaline portion. The OX2R selectivity inherent in this series was further improved by utilizing the 4,6-dimethylpyrimidine as shown in **213**. In rat PK experiments all of these compounds were found to have high clearance resulting in poor exposure after an oral dose. This was exemplified by compound **212** which has a clearance greater than hepatic blood flow, a C_{max} of 18 nM, an oral bioavailability (F) of 5%, and a low brain to blood ratio of 0.2. Next, the team investigated further analogs related to compound **210**. Using this isomer and applying the same substituents as found in **212** gave compound **214**, which was found to be less potent at both orexin receptors. Moving the attachment point to the 3-position (**215**) gave a molecule with similar potency and a slight improvement in LE (not shown). Additional examples here included compounds **216–218**. Although the unsubstituted pyrimidine **216** has a relatively dramatic loss in OX2R potency, this could be restored by monosubstitution in the 4-position (**217**) or disubstitution in the 4,6-position (**218**). Selectivity over the OX1R was also maintained with these heterocycles. Compound **217**, which is now known as IPSU, was chosen for further characterization. In vivo, this molecule gave improved pharmacokinetics and brain penetration relative to compound **212** as shown in Table 26. Interestingly, OX1/OX2 selectivity was decreased in **217** slightly in mouse and reported to have only a 10-fold selectivity window due to a lower potency for the OX2R. This is an important characteristic that should be considered when evaluating **217** in mouse in vivo experiments.

7.06.10.2 Pyrazolopyridines

From a structural point of view, a distinct series of molecules was published by Novartis in 2015.[65] The initial hit from a HTS campaign designed to identify dual OX1R/OX2R antagonists was the racemic version of **219**. After establishing that potency resided with a single enantiomer (**219**), potency was improved at both receptors by replacing the R_1 benzamide with a 4-methoxyphenyl (**220**) or the substituted pyrazole **221** as shown in Table 27.

After identifying that the 3-position aryl ring could be modified with only a moderate loss in potency, for example a cyclopropyl as in compound **222**, this area of the molecule was targeted to reduce lipophilicity. Select examples are shown in Table 28. In addition, after identifying the major metabolic pathways in vitro, compounds **223–225** were designed to reduce metabolism on the 3-position phenyl ring. Although potency was good for compound **224** and moderate for **225**, metabolism was not improved

Table 26 OX1R/OX2R binding and pharmacokinetic data for compounds **212** and **217**

Compound	*CL (mL/min/kg)*	*C_{max} (nM)*	*%F (po)*	*Brain/blood*	*OX2R mouse pK_i*	*OX1R mouse pK_i*
212	188	18	5	0.2	not tested	not tested
217	28	864	47	1.1	7.23	6.34

Table 27 Binding data for the human OX2 and OX1 receptor for compounds **219–221**

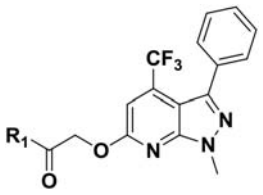

Compound	*R_1*	*OX2R K_i (nM)*	*OX1R K_i (nM)*
219	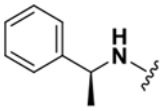	108	175
220	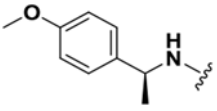	2	14
221	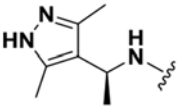	2	5

Table 28 Binding data for the human OX2 and OX1 receptor for compounds **222–225**

Compound	*R_1*	*OX2R K_i (nM)*	*OX1R K_i (nM)*
222	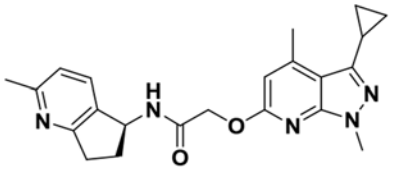	22	109
223	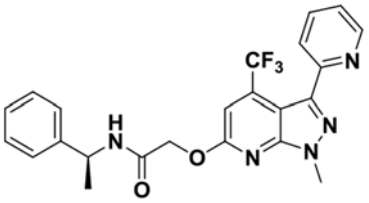	367	660
224	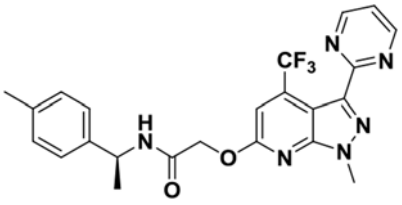	5	4
225	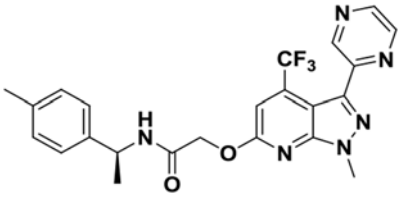	15	52

with this strategy. According to the authors, the cyclopropyl compound **222** (16%F and a [br]/[bl] ratio of 0.13) provided an optimal balance of good plasma exposure after an oral dose along with sufficient brain penetration. Clearly, improvements in oral bioavailability and brain penetration are still desired.

7.06.11 Research Triangle Institute

7.06.11.1 Tetrahydroisoquinolines

Following up on the HTS hit **226** (**27**) reported by Actelion, researchers at Research Triangle Institute (RTI) have published SAR around the tetrahydroisoquinoline template shown in Table 29.[66] These studies initially focused on SAR at the 7-position (R_1) and the benzamide (R_2). All of the compounds shown in this table have a reported K_e of >10,000 nM at the OX2 receptor. Focusing first on R_1, increasing the size of the substituent from Me (**226**) to Et (**227**) to CH_2CF_3 (**228**) resulted in a progressive increase in potency. On the benzamide, a variety of changes were evaluated. Highlighted here are the 2-, 3-, and 4-pyridyl analogs (**229–231**). The 2- and 3-pyridyl were comparable to the benzyl group. As previously noted, the potency could be improved by incorporating the $-CH_2CF_3$ group in the 7-position as shown for compound **232**. While in vivo data related to pharmacokinetics or brain penetration were not provided, after a 20 mg/kg i.p. dose compound **232** did attenuate development of place preference induced by cocaine, consistent with other OX1R antagonists. In a subsequent paper, further exploration of the SAR resulted in the identification of the selective OX1R antagonists **233** and **234** (Fig. 29).[67] Similar to results obtained using **SB-334867**, compound **233** was able to attenuate the development of cocaine-induced behavioral sensitization at 10 mg/kg i.p. after repeated dosing.

Table 29 Binding data for the human OX2 and OX1 receptor for compounds **226–232**

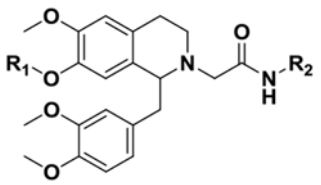

Compound	*R_1*	*R_2*	*OX1R K_e (nM)*
226 (27)	Me	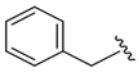	199
227	Et	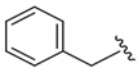	30
228	CF_3CH_2-	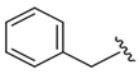	9.4
229	Me	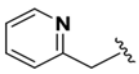	261
230	Me	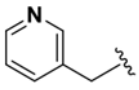	152
231	Me	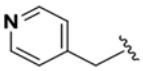	1010
232	CF_3CH_2-	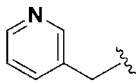	8.5

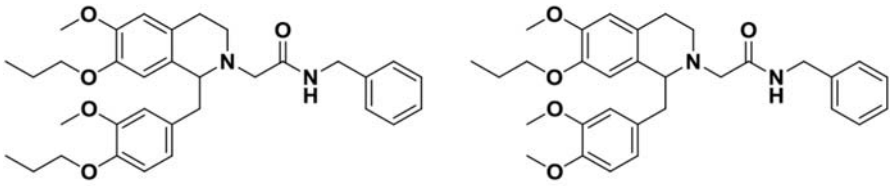

233
OX2R K_e>10,000 nM
OX1R K_e=16.1 nM

234
OX2R K_e=2550 nM
OX1R K_e=23.7 nM

Fig. 29 Compounds **233** and **234**.

7.06.11.2 Diarylureas related to SB-334867

Researchers from Research Triangle Institute have also reported on additional SAR related to **SB-334867 (111)**, Table 30.[68] The goal of these initial studies was to identify parts of the molecule, wherein linkers could be installed. These linkers were then envisioned as an attachment point for CB1 ligands resulting in bivalent ligands for the OX1 and CB1 receptors. After replacement of the naphthyridine in **SB-334867 (111)** with the 8-fluoroquinoline, studies were shifted to replacement of the benzoxazole. These efforts resulted in the identification of anilines **235–237**. The conclusions by the authors that this could be an area of the molecule that would tolerate further substitutions.

An additional paper from RTI has appeared detailing the hydrolytic instability of SB-334867.[69] The general observations from the paper were that when the HCl salt of SB-334867 is utilized, caution needs to be taken because of the fact that hydrolysis occurs to generate the ring-opened compound **238** as shown in Fig. 30 Although the free base of SB-334867 was found to be stable for at least 1 year, when the HCl salt was stored as a solid at 15°C for 15 months under argon in a sealed container, new resonances that appeared in the ^{1}H NMR spectrum were observed due to the formation of **238**. A refrigerated solution of

Table 30 **SB-334867**-based analogs **235–237**

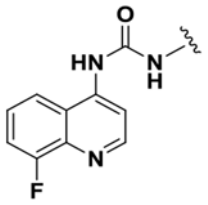

Compound	*R_1*	*OX2R K_e (nM)*	*OX1R K_e (nM)*
235	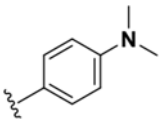	171	2.4
236	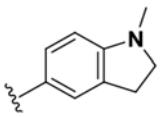	491	4.9
237	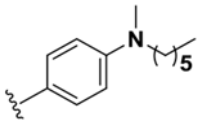	2410	64.2

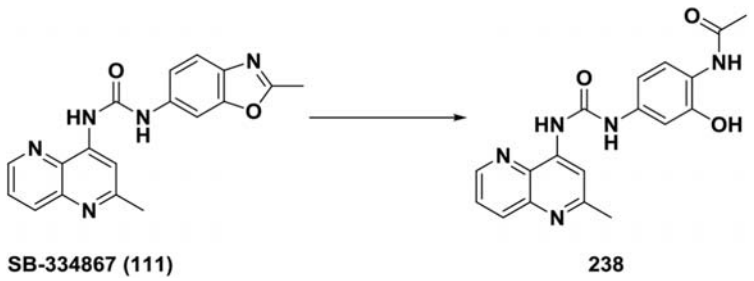

Fig. 30 Decomposition of **SB-334867** to **238.**

SB-334867 as the free base was stable for 3 months in 100% DMSO in a tightly capped vial. This is in contrast to a solution that was not protected from moisture and stored at room temperature. In this case, the hydrolysis product was observed in 33% after 3 months. These studies lead to the concern that many studies that have utilized either the free base of **SB-334867** or the HCl salt should be analyzed closely. The free base is notoriously insoluble in aqueous media, and the HCl salt could decompose if not handled properly.

7.06.12 Rottapharm

7.06.12.1 Bicyclic [5.2.0] and [4.2.0] Diamines

Rottapharm has also investigated bicyclic [5.2.0] and [4.2.0] analogs as shown in Table 31.[70] Initially, the [5.2.0] piperidine analog **239** was first compared with the [4.2.0] pyrrolidine analog **240**. Although **240** did show improved potency for OX1, selectivity over the OX2R was similar in both cases. In addition moderate oral bioavailability (40% F, 1 mg/kg PO) and low brain

Table 31 Spirocyclics **239–247**

Compound	R_1	*OX2R* pK_b	*OX1R* pK_b
239	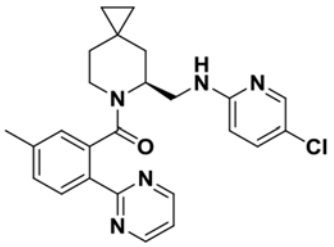	<5.0	7.6
240	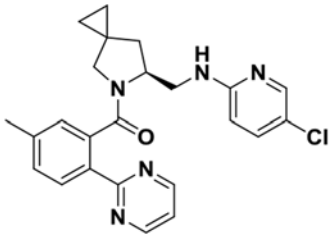	<5.0	8.2
241	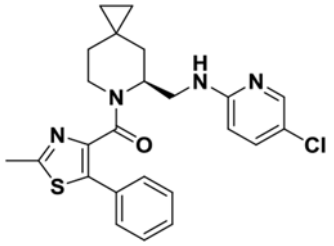	<5.0	7.9

(Continued)

Table 31 Spirocyclics **239–247**—cont'd

Compound	*R_1*	*OX2R pK_b*	*OX1R pK_b*
242	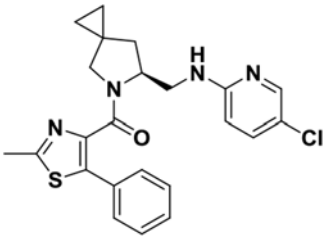	7.1	8.3
243	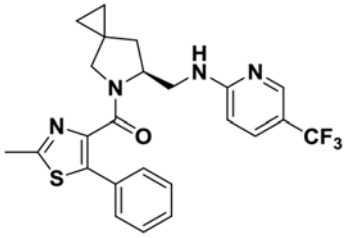	7.7	8.4
244	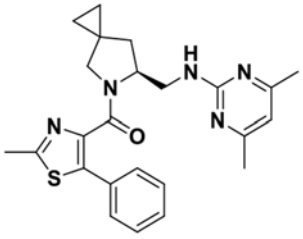	8.6	7.5
245	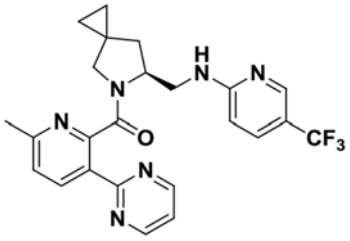	7.5	8.4
246	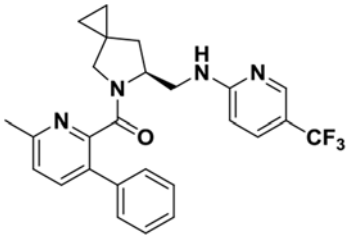	8.0	8.6
247	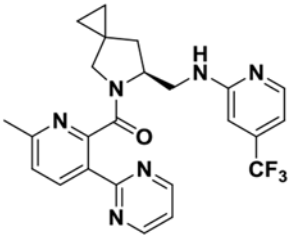	8.1	6.0

penetration (B/P = 0.03) were reported for compound **240**. Further efforts were focused on modifications to the amide portion of these templates. Changing the phenyl pyrimidine to a thiazolo-phenyl benzamide, which is present in **SB-649686**, gave diverging results for these templates. Both molecules, **241** and **242**, retained their potency for the OX1R, while the pyrrolidine **242** gained a significant amount of potency for the OX2R. Since the goals of the Rottapharm team were to discover dual OX1/OX2 receptor antagonists, further efforts were focused on the pyrrolidine template as this template had already been shown to provide dual antagonists. This was apparent in the trifluoromethyl substituted compound **243** as well. Utilization of the 4,6-dimethylpyrimidine reversed this trend to give the moderately selective antagonist **244**. Efforts to reduce cLogP resulted in compounds **245** and **246** which maintained activity for the OX1 receptors. Unfortunately these molecules were CYP 3A4 time-dependent inhibitors. This issue was alleviated by replacing the pyrimidine ring with a phenyl ring. A key compound of note is the trifluoromethyl pyridine **247**. Simply moving the trifluoromethyl group from the 5-position to the 4-position gave a potent and selective OX2R antagonist that was a result of decreased OX1R potency. This theme has been discussed by others and reiterated here. Often times in the orexin field the pharmacology associated with a particular core can be modified with the pendant substituents to give dual or selective OX1R/OX2R antagonists.

7.06.13 The Scripps Research Institute

7.06.13.1 Piperidin-2-ylmethanamines

Based on patent disclosures and the work that has been disclosed in the primary literature surrounding **SB-649868**, workers at Scripps investigated the effect of methyl substitution on the piperidine ring of structures related to **SB-649868**.[71] Similarities between this work and **GSK1059865 (108)** are also apparent. This work began with compound **248** (Table 32) which was used as a benchmark for comparisons. The effect of methylation in the 3-position in a *cis*-orientation gave an OX1R antagonist with good potency and 100-fold selectivity over the OX2R. This is evident by comparing compounds **248** and **249**. Subsequent SAR led to compounds **250** and **251**. Both compounds maintained selectivity over the OX2R. Both of these molecules were also shown to have increased brain levels after 50 mg/kg ip dose when compared to **248**. Alternatively substituted piperidines in the three- and other positions on the piperidine ring did not appear to offer any advantages in regard to potency.

7.06.14 Taisho

7.06.14.1 TASP0428980

The research group at Taisho recently reported on a series of benzamides that were designed using ligand-based drug design. Using the U-shaped conformation disclosed by Merck and others, these researchers pursued the development of novel, short acting OXR antagonists in order to prevent any residual next-day effects in the clinic.[72] This work led to the preparation of **252**, a potent OXR antagonist. In efforts designed to reduce the lipophilicity of this lead other heterocyclic linkers (e.g., **253**, Table 33) were also prepared; however OXR affinity was reduced in most cases. The researchers also modified the alkyl substituent on the amide nitrogen and made changes to the substituents on the benzamide. In the end, the typical substituents that have been utilized in a variety of core series proved to have the best balance of affinity and lipophilicity and as such, compounds **255** and **256** were characterized further. Both were relatively short acting compounds, and **255** was chosen for additional studies due to the better brain distribution measured for this compound in rat. Compound **255 (TASP0428980)** was found to be very selective over >90 other targets, the brain to plasma ratio was measured at 0.17 in rat, and the predicted human half-life was assessed at between 1.2 and 1.4 h based on single species scaling in rat and dog.

7.06.15 Takeda

7.06.15.1 Spiropiperidine-Based Selective Orexin-2 Antagonists

Based on a template disclosed by Merck, workers at Takeda utilized the spirodiamine **257** (Fig. 31) as a lead for further optimization.[73] The template was chosen based on its desirable molecular properties. The initial work focused on modification of the pyrolidine ring to generate a fused aminal, as exemplified by compound **258**. This modification gave a moderately potent OX2R antagonist with poor selectivity over the OX1R and poor human microsomal stability. Replacement of the amino-quinoxaline with the phenyl urea as shown for compound **259** gave decreased potency, similar selectivity but slightly improved microsomal stability. In addition to that observation, the authors commented on the poor solubility and acid instability of the cyclic aminal of **259**. The strategy used to address these two issues was to reduce the electron density at the aminal carbon atom, which was expected to help stabilize the aminal. This was also thought to help with solubility by decreasing the symmetry in the molecule. An example of this is the fluorinated compound **260**, which was shown to decrease predicted

Table 32 Methylated piperidines **248–251**

Compound	R_1	*OX2R IC_{50} (nM)*	*OX1R IC_{50} (nM)*
248	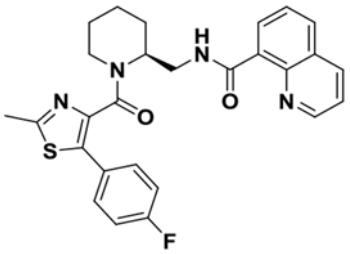	23	5
249	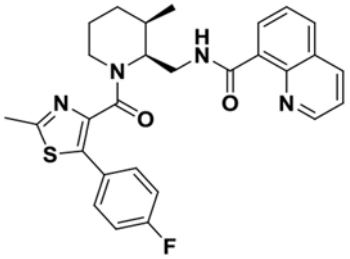	858	8
250	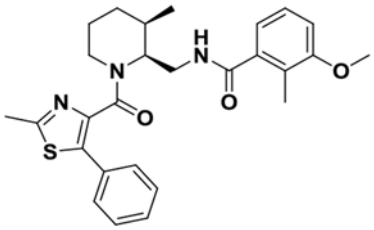	>10,000	145
251	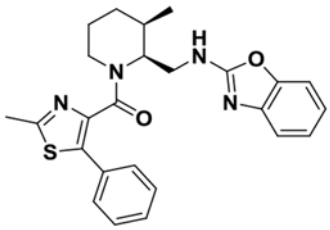	447	6

clearance to 2 mL/min/kg. In order to improve potency, substitution on the phenyl sulfonamide was explored. From this, the 3,4-dimethoxy phenyl compound **261** was identified as a potent OX2R antagonist with excellent selectivity over the OX1R receptor. Predicted human metabolic stability was measured as < 1 mL/min/kg. No information was disclosed on this molecule in relation to in vivo PK studies or brain penetration.

7.06.15.2 Benzoxazepine-Based Selective Orexin-2 Antagonists

Takeda also disclosed work beginning with the benzoxazepine **262**,[74] which was identified from a HTS campaign. The predicted rapid clearance for this compound initiated an investigation focusing on the likely metabolic hot spot, the 7-position methyl as indicated by R_1 in Table 34. The SAR was guided by analysis of Hammet (σ_p) and Hansch (π) parameters in this position. Replacement of the OMe in **262** with a less electron donating and lipophilic methyl group led to both a decrease in OX2R potency and microsomal stability. A small polar electron withdrawing group such as cyano (**265**) or lipophilic electron withdrawing

Table 33 Human OX2 and OX1 receptor K_i's for compounds **252–256**

Compound	*Structure*	*OX2R* K_i	*OX1R* K_i
252	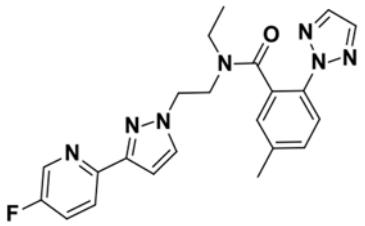	0.43	0.89
253	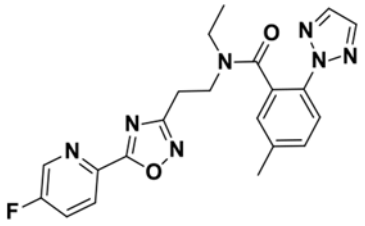	8.09	22.99
254	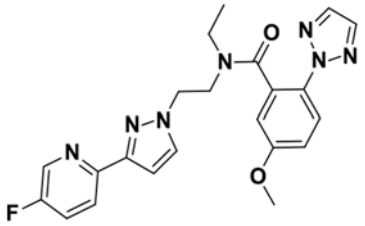	119.30	638.10
255	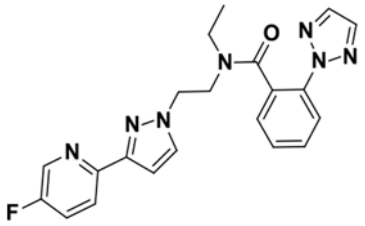	5.00	13.06
256	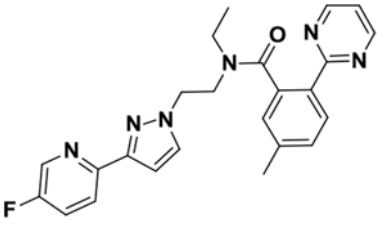	2.52	4.01

fluoro (**266**) resulted in reduced OX2R potency. However, increasing lipophilicity by replacement with a trifluoromethyl (**267**) or trifluromethoxy (**268**) restored OX2R potency and provided an improvement in microsomal stability. Ultimately the difluoromethoxy (**269**) substituted compound gave a potent OX2R receptor antagonist with excellent microsomal stability. Further profiling of **269** demonstrated selectivity over the OX1R receptor (OX1R $IC_{50} = 3000$ nM), good oral bioavailability in rat (52%), and low clearance 90 mL/h/kg. This compound was also able to reverse the orexin-A induced locomotion in rat suggesting central penetration. Brain exposure was predicted by the low efflux ratio of 0.4.

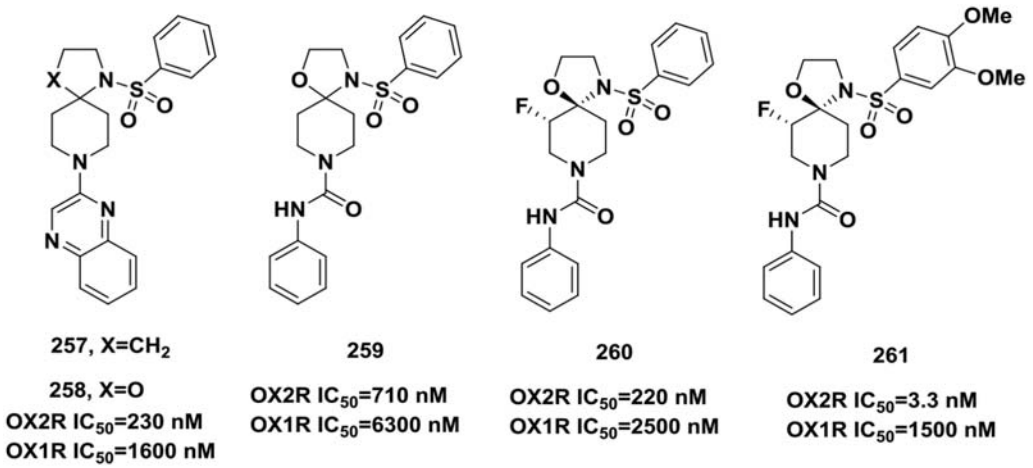

Fig. 31 Discovery of compound **261**.

Table 34 Cell-based FLIPR and human microsome data for compounds **262–269**

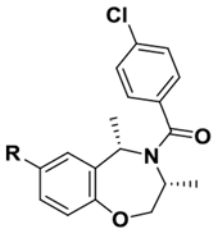

Compound	*R_1*	*OX2R IC_{50} (nM)*	*HLM*
262	OMe	74	98
263	Me	150	115
264	Et	160	146
265	CN	8200	<1
266	F	3000	15
267	CF_3	270	30
268	OCF_3	140	7
269	$OCHF_2$	27	<1

7.06.16 Summary of Compounds That Progressed to Clinical Trials

This section gives a summary of the OXR compounds that have progressed into human clinical trials and details the human doses that were given, the PK parameters of the compounds and select clinical efficacy/toleration data.

As shown in Table 35, many years of work by multiple research groups have resulted in the identification of numerous nonselective OXR and selective OX2R receptor antagonists that were deemed suitable to progress into human clinical trials. Several of these compounds have dropped out of the clinic for safety and/or efficacy reasons; however several compounds are still progressing, with promising efficacy results on sleep parameters. To date, one nonselective OXR antagonist, Belsomra, has been approved for use in humans. Given the sustained activity in the orexin field, it seems likely that other compounds will also eventually be approved for a variety of CNS indications.

Table 35 OXR antagonists that have progressed into clinical trials

Compound	Compound identifier/company name	Structure	OX2R IC_{50} (nM)	OX1R IC_{50} (nM)	Clinical doses tested	Human PK parameters	Comments	Status	Refs.
1	**ACT-078573 almorexant Actelion**	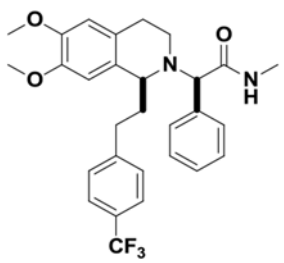	13	8	100, 200, 400, 600 mg	$t_{1/2}=1.6$ h $T_{max}=1.5$ h	Dose-dependent reduction in latency to sleep at doses >200 mg	Phase III, discontinued due to safety concerns	17,75
48	**ACT-462206 Actelion**	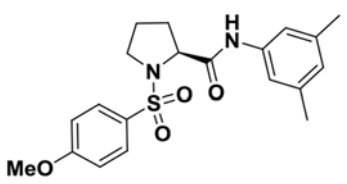	11 (K_i)	60 (K_i)	5, 25, 100, 200, 400, 1000, 1500 mg	$t_{1/2}=\sim$10 h @≥100 mg $T_{max}=1.5$–4.0 h	Well-tolerated without dose-limiting toxicity with a profile consistent with a sleep-inducing agent	Completed Phase I	15c,20
96	**E2006 Eisai**	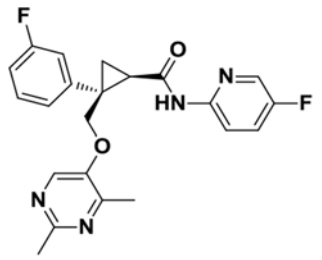	3	6	5, 10 mg	Not reported	Tested in subjects with somnolence, no data reported	Phase I	27
105	**SB-649868 GlaxoSmithKline**	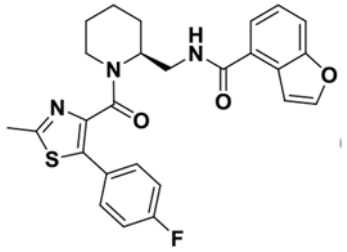	0.3 nM (K_i)	0.4 nM (K_i)	5, 15, 30 mg in RD, 10–80 mg in SD	RD $t_{1/2}=3$–6 h	Well-tolerated after single and repeated dose. Clinically relevant dose-dependent sleep promoting effects were observed	Completed Phase I, discontinued	29b–d
144	**JNJ-42847922 MIN-202 Janssen/Minerva**	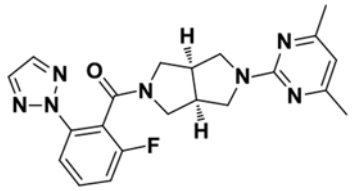	10	800	10, 20, 40, 80 mg	$t_{1/2}=\sim$2 h $T_{max}=0.33$–0.5 h	Somnolence reported at all doses in healthy volunteers Efficacy reported in patients with insomnia disorder	Phase IIa	39,41

(Continued)

Table 35 OXR antagonists that have progressed into clinical trials—cont'd

Compound	Compound identifier/company name	Structure	OX2R IC_{50} (nM)	OX1R IC_{50} (nM)	Clinical doses tested	Human PK parameters	Comments	Status	Refs.
160	**MK-4305 Suvorexant Merck**	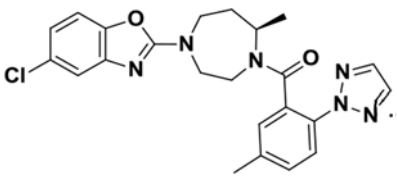	0.35	0.55	10, 15, 20, 30, 40 mg	$t_{1/2}$ = 8–14 T_{max} = 1.5–4 h	Improvements in sleep efficiency at all doses	Marketed as Belsomra	3a,76
167	**MK-6096 Filorexant Merck**	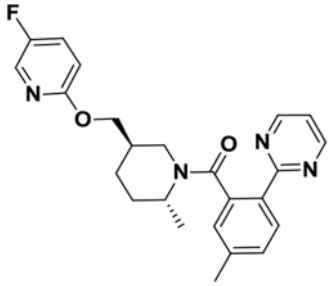	0.3	2.5	5, 10, 20 mg	Not reported	Negative clinical trial for migraine prophylaxis	Phase II	50,53,54,57,58
177	**MK-1064 Merck**	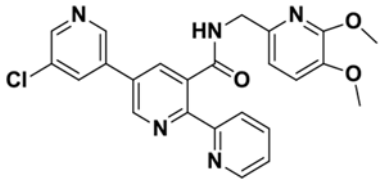	0.5	1584	50, 120, 250 mg	$t_{1/2}$ = 1.6–4.0 T_{max} = 1–2 h	Decreased LPS Decreased WASO	Phase I	3a,58
187	**MK-3697 Merck**	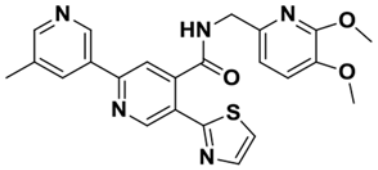	1.1	3600	Not reported	Not reported	No data reported	Phase II?	3a
207	**MK-8133 Merck**	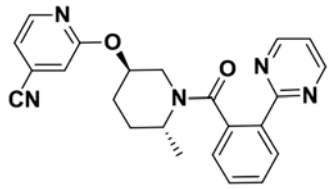	28	4900	Not reported	Not reported	No data reported		63

References

1. Sakurai, T.; Amemiya, A.; Ishii, M.; Matsuzaki, I.; Chemelli, R. M.; Tanaka, H.; Williams, S. C.; Richardson, J. A.; Kozlowski, G. P.; Wilson, S.; Arch, J. R.; Buckingham, R. E.; Haynes, A. C.; Carr, S. A.; Annan, R. S.; McNulty, D. E.; Liu, W. S.; Terrett, J. A.; Elshourbagy, N. A.; Bergsma, D. J.; Yanagisawa, M. Orexins and Orexin Receptors: A Family of Hypothalamic Neuropeptides and G Protein-Coupled Receptors That Regulate Feeding Behavior. *Cell* **1998,** *92* (4), 573–585.
2. de Lecea, L.; Kilduff, T. S.; Peyron, C.; Gao, X.; Foye, P. E.; Danielson, P. E.; Fukuhara, C.; Battenberg, E. L.; Gautvik, V. T.; Bartlett, F. S., 2nd; Frankel, W. N.; van den Pol, A. N.; Bloom, F. E.; Gautvik, K. M.; Sutcliffe, J. G. The Hypocretins: Hypothalamus-Specific Peptides With Neuroexcitatory Activity. *Proc. Natl. Acad. Sci. U. S. A.* **1998,** *95* (1), 322–327.
3. (a) Roecker, A. J.; Cox, C. D.; Coleman, P. J. Orexin Receptor Antagonists: New Therapeutic Agents for the Treatment of Insomnia. *J. Med. Chem.* **2016,** *59* (2), 504–530; (b) Lebold, T. P.; Bonaventure, P.; Shireman, B. T. Selective Orexin Receptor Antagonists. *Bioorg. Med. Chem. Lett.* **2013,** *23* (17), 4761–4769; (c) Boss, C.; Roch, C. Recent Trends in Orexin Research—2010 to 2015. *Bioorg. Med. Chem. Lett.* **2015,** *25* (15), 2875–2887; (d) Gotter, A. L.; Roecker, A. J.; Hargreaves, R.; Coleman, P. J.; Winrow, C. J.; Renger, J. J. Orexin Receptors as Therapeutic Drug Targets. *Prog. Brain Res.* **2012,** *198,* 163–188; (e) Gotter, A. L.; Webber, A. L.; Coleman, P. J.; Renger, J. J.; Winrow, C. J. International Union of Basic and Clinical Pharmacology. LXXXVI. Orexin Receptor Function, Nomenclature and Pharmacology. *Pharmacol. Rev.* **2012,** *64* (3), 389–420; (f) Winrow, C. J.; Renger, J. J. Discovery and Development of Orexin Receptor Antagonists as Therapeutics for Insomnia. *Br. J. Pharmacol.* **2014,** *171* (2), 283–293; (g) Gatfield, J.; Brisbare-Roch, C.; Jenck, F.; Boss, C. Orexin Receptor Antagonists: A New Concept in CNS Disorders? *ChemMedChem* **2010,** *5* (8), 1197–1214; (h) Kukkonen, J. P. Physiology of the Orexinergic/Hypocretinergic System: A Revisit in 2012. *Am. J. Physiol. Cell Physiol.* **2013,** *304* (1), C2–C32.
4. (a) Peyron, C.; Tighe, D. K.; van den Pol, A. N.; de Lecea, L.; Heller, H. C.; Sutcliffe, J. G.; Kilduff, T. S. Neurons Containing Hypocretin (Orexin) Project to Multiple Neuronal Systems. *J. Neurosci. Off. J. Soc. Neurosci.* **1998,** *18* (23), 9996–10015; (b) Nambu, T.; Sakurai, T.; Mizukami, K.; Hosoya, Y.; Yanagisawa, M.; Goto, K. Distribution of Orexin Neurons in the Adult Rat Brain. *Brain Res.* **1999,** *827* (1–2), 243–260; (c) Sakurai, T. The Neural Circuit of Orexin (Hypocretin): Maintaining Sleep and Wakefulness. *Nat. Rev. Neurosci.* **2007,** *8* (3), 171–181; (d) Marcus, J. N.; Aschkenasi, C. J.; Lee, C. E.; Chemelli, R. M.; Saper, C. B.; Yanagisawa, M.; Elmquist, J. K. Differential Expression of Orexin Receptors 1 and 2 in the Rat Brain. *J. Comp. Neurol.* **2001,** *435* (1), 6–25; (e) Trivedi, P.; Yu, H.; MacNeil, D. J.; Van der Ploeg, L. H.; Guan, X. M. Distribution of Orexin Receptor mRNA in the Rat Brain. *FEBS Lett.* **1998,** *438* (1–2), 71–75.
5. Piper, D. C.; Upton, N.; Smith, M. I.; Hunter, A. J. The Novel Brain Neuropeptide, Orexin-A, Modulates the Sleep-Wake Cycle of Rats. *Eur. J. Neurosci.* **2000,** *12* (2), 726–730.
6. (a) Chemelli, R. M.; Willie, J. T.; Sinton, C. M.; Elmquist, J. K.; Scammell, T.; Lee, C.; Richardson, J. A.; Williams, S. C.; Xiong, Y.; Kisanuki, Y.; Fitch, T. E.; Nakazato, M.; Hammer, R. E.; Saper, C. B.; Yanagisawa, M. Narcolepsy in Orexin Knockout Mice: Molecular Genetics of Sleep Regulation. *Cell* **1999,** *98* (4), 437–451; (b) Hara, J.; Beuckmann, C. T.; Nambu, T.; Willie, J. T.; Chemelli, R. M.; Sinton, C. M.; Sugiyama, F.; Yagami, K.; Goto, K.; Yanagisawa, M.; Sakurai, T. Genetic Ablation of Orexin Neurons in Mice Results in Narcolepsy, Hypophagia, and Obesity. *Neuron* **2001,** *30* (2), 345–354.
7. Lin, L.; Faraco, J.; Li, R.; Kadotani, H.; Rogers, W.; Lin, X.; Qiu, X.; de Jong, P. J.; Nishino, S.; Mignot, E. The Sleep Disorder Canine Narcolepsy Is Caused by a Mutation in the Hypocretin (Orexin) Receptor 2 Gene. *Cell* **1999,** *98* (3), 365–376.
8. (a) Peyron, C.; Faraco, J.; Rogers, W.; Ripley, B.; Overeem, S.; Charnay, Y.; Nevsimalova, S.; Aldrich, M.; Reynolds, D.; Albin, R.; Li, R.; Hungs, M.; Pedrazzoli, M.; Padigaru, M.; Kucherlapati, M.; Fan, J.; Maki, R.; Lammers, G. J.; Bouras, C.; Kucherlapati, R.; Nishino, S.; Mignot, E. A Mutation in a Case of Early Onset Narcolepsy and a Generalized Absence of Hypocretin Peptides in Human Narcoleptic Brains. *Nat. Med.* **2000,** *6* (9), 991–997; (b) Mignot, E.; Lin, L.; Rogers, W.; Honda, Y.; Qiu, X.; Lin, X.; Okun, M.; Hohjoh, H.; Miki, T.; Hsu, S.; Leffell, M.; Grumet, F.; Fernandez-Vina, M.; Honda, M.; Risch, N. Complex HLA-DR and -DQ Interactions Confer Risk of Narcolepsy-Cataplexy in Three Ethnic Groups. *Am. J. Hum. Genet.* **2001,** *68* (3), 686–699.
9. Dugovic, C.; Shelton, J. E.; Aluisio, L. E.; Fraser, I. C.; Jiang, X.; Sutton, S. W.; Bonaventure, P.; Yun, S.; Li, X.; Lord, B.; Dvorak, C. A.; Carruthers, N. I.; Lovenberg, T. W. Blockade of Orexin-1 Receptors Attenuates Orexin-2 Receptor Antagonism-Induced Sleep Promotion in the Rat. *J. Pharmacol. Exp. Ther.* **2009,** *330* (1), 142–151.
10. Mang, G. M.; Durst, T.; Burki, H.; Imobersteg, S.; Abramowski, D.; Schuepbach, E.; Hoyer, D.; Fendt, M.; Gee, C. E. The Dual Orexin Receptor Antagonist Almorexant Induces Sleep and Decreases Orexin-Induced Locomotion by Blocking Orexin 2 Receptors. *Sleep* **2012,** *35* (12), 1625–1635.
11. Dugovic, C.; Shelton, J. E.; Yun, S.; Bonaventure, P.; Shireman, B. T.; Lovenberg, T. W. Orexin-1 Receptor Blockade Dysregulates REM Sleep in the Presence of Orexin-2 Receptor Antagonism. *Front. Neurosci.* **2014,** *8,* 28.
12. (a) Johnson, P. L.; Truitt, W.; Fitz, S. D.; Minick, P. E.; Dietrich, A.; Sanghani, S.; Traskman-Bendz, L.; Goddard, A. W.; Brundin, L.; Shekhar, A. A Key Role for Orexin in Panic Anxiety. *Nat. Med.* **2010,** *16* (1), 111–115; (b) Johnson, P. L.; Molosh, A.; Fitz, S. D.; Truitt, W. A.; Shekhar, A. Orexin, Stress, and Anxiety/Panic States. *Prog. Brain Res.* **2012,** *198,* 133–161; (c) Sakurai, T. The Role of Orexin in Motivated Behaviours. *Nat. Rev. Neurosci.* **2014,** *15* (11), 719–731.
13. (a) Bonaventure, P.; Yun, S.; Johnson, P. L.; Shekhar, A.; Fitz, S. D.; Shireman, B. T.; Lebold, T. P.; Nepomuceno, D.; Lord, B.; Wennerholm, M.; Shelton, J.; Carruthers, N.; Lovenberg, T.; Dugovic, C. A Selective Orexin-1 Receptor Antagonist Attenuates Stress-Induced Hyperarousal Without Hypnotic Effects. *J. Pharmacol. Exp. Ther.* **2015,** *352* (3), 590–601; (b) Johnson, P. L.; Federici, L. M.; Fitz, S. D.; Renger, J. J.; Shireman, B.; Winrow, C. J.; Bonaventure, P.; Shekhar, A. Orexin 1 and 2 Receptor Involvement in Co2 -Induced Panic-Associated Behavior and Autonomic Responses. *Depression Anxiety* **2015,** *32* (9), 671–683.
14. Johnson, P. L.; Samuels, B. C.; Fitz, S. D.; Lightman, S. L.; Lowry, C. A.; Shekhar, A. Activation of the Orexin 1 Receptor Is a Critical Component of CO2-Mediated Anxiety and Hypertension But not Bradycardia. *Neuropsychopharmacology* **2012,** *37* (8), 1911–1922.
15. (a) Steiner, M. A.; Lecourt, H.; Jenck, F. The Brain Orexin System and Almorexant in Fear-Conditioned Startle Reactions in the Rat. *Psychopharmacology* **2012,** *223* (4), 465–475; (b) Steiner, M. A.; Gatfield, J.; Brisbare-Roch, C.; Dietrich, H.; Treiber, A.; Jenck, F.; Boss, C. Discovery and Characterization of ACT-335827, an Orally Available, Brain Penetrant Orexin Receptor Type 1 Selective Antagonist. *ChemMedChem* **2013,** *8* (6), 898–903; (c) Boss, C.; Roch-Brisbare, C.; Steiner, M. A.; Treiber, A.; Dietrich, H.; Jenck, F.; von Raumer, M.; Sifferlen, T.; Brotschi, C.; Heidmann, B.; Williams, J. T.; Aissaoui, H.; Siegrist, R.; Gatfield, J. Structure-Activity Relationship, Biological, and Pharmacological Characterization of the Proline Sulfonamide ACT-462206: A Potent, Brain-Penetrant Dual Orexin 1/Orexin 2 Receptor Antagonist. *ChemMedChem* **2014,** *9* (11), 2486–2496.
16. Roecker, A. J.; Cox, C. D.; Coleman, P. J. Orexin Receptor Antagonists: New Therapeutic Agents for the Treatment of Insomnia. *J. Med. Chem.* **2016,** *59,* 504–530.
17. Brisbare-Roch, C.; Dingemanse, J.; Koberstein, R.; Hoever, P.; Aissaoui, H.; Flores, S.; Mueller, C.; Nayler, O.; van Gerven, J.; de Haas, S. L.; Hess, P.; Qiu, C.; Buchmann, S.; Scherz, M.; Weller, T.; Fischli, W.; Clozel, M.; Jenck, F. Promotion of Sleep by Targeting the Orexin System in Rats, Dogs and Humans. *Nat. Med.* **2007,** *13* (2), 150–155.
18. (a) Sifferlen, T.; Boss, C.; Cottreel, E.; Koberstein, R.; Gude, M.; Aissaoui, H.; Weller, T.; Gatfield, J.; Brisbare-Roch, C.; Jenck, F. Novel Pyrazolo-Tetrahydropyridines as Potent Orexin Receptor Antagonists. *Bioorg. Med. Chem. Lett.* **2010,** *20* (5), 1539–1542; (b) Sifferlen, T.; Koberstein, R.; Cottreel, E.; Boller, A.; Weller, T.; Gatfield, J.; Brisbare-Roch, C.; Jenck, F.; Boss, C. Structure-Activity Relationship Studies and Sleep-Promoting Activity of Novel 1-chloro-5,6,7,8-tetrahydroimidazo[1,5-a]pyrazine Derivatives as Dual Orexin Receptor Antagonists. Part 2. *Bioorg. Med. Chem. Lett.* **2013,** *23* (13), 3857–3863; (c) Sifferlen, T.; Koberstein, R.; Cottreel, E.; Boller, A.; Weller, T.; Gatfield, J.; Brisbare-Roch, C.; Jenck, F.; Boss, C. Synthesis, Structure-Activity Relationship Studies, and Identification of Novel 5,6,7,8-tetrahydroimidazo[1,5-a]pyrazine derivatives as Dual Orexin Receptor Antagonists. Part 1. *Bioorg. Med. Chem. Lett.* **2013,** *23* (7), 2212–2216.
19. (a) Sifferlen, T.; Boller, A.; Chardonneau, A.; Cottreel, E.; Hoecker, J.; Aissaoui, H.; Williams, J. T.; Brotschi, C.; Heidmann, B.; Siegrist, R.; Gatfield, J.; Treiber, A.; Brisbare-Roch, C.; Jenck, F.; Boss, C. Discovery of Substituted Lactams as Novel Dual Orexin Receptor Antagonists. Synthesis, Preliminary Structure-Activity Relationship Studies and Efforts Towards Improved Metabolic Stability and Pharmacokinetic Properties. Part 1. *Bioorg. Med. Chem. Lett.* **2014,** *24* (4), 1201–1208; (b) Sifferlen, T.; Boller, A.; Chardonneau, A.; Cottreel, E.; Gatfield, J.; Treiber, A.; Roch, C.; Jenck, F.; Aissaoui, H.; Williams, J. T.; Brotschi, C.; Heidmann, B.; Siegrist, R.; Boss, C. Substituted Pyrrolidin-2-Ones: Centrally Acting Orexin Receptor Antagonists Promoting Sleep. Part 2. *Bioorg. Med. Chem. Lett.* **2015,** *25* (9), 1884–1891.
20. Hoch, M.; van Gorsel, H.; van Gerven, J.; Dingemanse, J. Entry-Into-Humans Study With ACT-462206, a Novel Dual Orexin Receptor Antagonist, Comparing Its Pharmacodynamics With Almorexant. *J. Clin. Pharmacol.* **2014,** *54* (9), 979–986.

21. Williams, J. T.; Gatfield, J.; Roch, C.; Treiber, A.; Jenck, F.; Bolli, M. H.; Brotschi, C.; Sifferlen, T.; Heidmann, B.; Boss, C. Discovery and Optimisation of 1-acyl-2-benzylpyrrolidines as Potent Dual Orexin Receptor Antagonists. *ChemMedChem* **2015,** *6* (6), 1054–1064.
22. Aissaoui, H.; Koberstein, R.; Zumbrunn, C.; Gatfield, J.; Brisbare-Roch, C.; Jenck, F.; Treiber, A.; Boss, C. N-Glycine-Sulfonamides as Potent Dual Orexin 1/Orexin 2 Receptor Antagonists. *Bioorg. Med. Chem. Lett.* **2008,** *18* (21), 5729–5733.
23. Malherbe, P.; Borroni, E.; Gobbi, L.; Knust, H.; Nettekoven, M.; Pinard, E.; Roche, O.; Rogers-Evans, M.; Wettstein, J. G.; Moreau, J. L. Biochemical and Behavioural Characterization of EMPA, a Novel High-Affinity, Selective Antagonist for the OX(2) Receptor. *Br. J. Pharmacol.* **2009,** *156* (8), 1326–1341.
24. Hirose, M.; Egashira, S.; Goto, Y.; Hashihayata, T.; Ohtake, N.; Iwaasa, H.; Hata, M.; Fukami, T.; Kanatani, A.; Yamada, K. N-acyl 6,7-dimethoxy-1,2,3,4-tetrahydroisoquinoline: The First Orexin-2 Receptor Selective Non-peptidic Antagonist. *Bioorg. Med. Chem. Lett.* **2003,** *13* (24), 4497–4499.
25. Yoshida, Y.; Terauchi, T.; Naoe, Y.; Kazuta, Y.; Ozaki, F.; Beuckmann, C. T.; Nakagawa, M.; Suzuki, M.; Kushida, I.; Takenaka, O.; Ueno, T.; Yonaga, M. Design, Synthesis, and Structure-Activity Relationships of a Series of Novel N-aryl-2-Phenylcyclopropanecarboxamide That Are Potent and Orally Active Orexin Receptor Antagonists. *Bioorg. Med. Chem.* **2014,** *22* (21), 6071–6088.
26. Yoshida, Y.; Naoe, Y.; Terauchi, T.; Ozaki, F.; Doko, T.; Takemura, A.; Tanaka, T.; Sorimachi, K.; Beuckmann, C. T.; Suzuki, M.; Ueno, T.; Ozaki, S.; Yonaga, M. Discovery of (1R,2S)-2-{[(2,4-Dimethylpyrimidin-5-yl)oxy]methyl}-2-(3-fluorophenyl)-N-(5-fluor opyridin-2-yl)cyclopropanecarboxamide (E2006): A Potent and Efficacious Oral Orexin Receptor Antagonist. *J. Med. Chem.* **2015,** *58* (11), 4648–4664.
27. NCT02350309.
28. Oi, N.; Suzuki, M.; Terauchi, T.; Tokunaga, M.; Nakatani, Y.; Yamamoto, N.; Fukumura, T.; Zhang, M. R.; Suhara, T.; Higuchi, M. Synthesis and Evaluation of Novel Radioligands for Positron Emission Tomography Imaging of the Orexin-2 Receptor. *J. Med. Chem.* **2013,** *56* (16), 6371–6385.
29. (a) Di Fabio, R.; Pellacani, A.; Faedo, S.; Roth, A.; Piccoli, L.; Gerrard, P.; Porter, R. A.; Johnson, C. N.; Thewlis, K.; Donati, D.; Stasi, L.; Spada, S.; Stemp, G.; Nash, D.; Branch, C.; Kindon, L.; Massagrande, M.; Poffe, A.; Braggio, S.; Chiarparin, E.; Marchioro, C.; Ratti, E.; Corsi, M. Discovery Process and Pharmacological Characterization of a Novel Dual Orexin 1 and Orexin 2 Receptor Antagonist Useful for Treatment of Sleep Disorders. *Bioorg. Med. Chem. Lett.* **2011,** *21* (18), 5562–5567; (b) Bettica, P.; Squassante, L.; Zamuner, S.; Nucci, G.; Danker-Hopfe, H.; Ratti, E. The Orexin Antagonist SB-649868 Promotes and Maintains Sleep in Men With Primary Insomnia. *Sleep* **2012,** *35* (8), 1097–1104; (c) Bettica, P.; Nucci, G.; Pyke, C.; Squassante, L.; Zamuner, S.; Ratti, E.; Gomeni, R.; Alexander, R. Phase I Studies on the Safety, Tolerability, Pharmacokinetics and Pharmacodynamics of SB-649868, a Novel Dual Orexin Receptor Antagonist. *J. Psychopharmacol.* **2012,** *26* (8), 1058–1070; (d) Renzulli, C.; Nash, M.; Wright, M.; Thomas, S.; Zamuner, S.; Pellegatti, M.; Bettica, P.; Boyle, G. Disposition and Metabolism of [14C]SB-649868, an Orexin 1 and 2 Receptor Antagonist, in Humans. *Drug Metab. Dispos.* **2011,** *39* (2), 215–227.
30. Gozzi, A.; Turrini, G.; Piccoli, L.; Massagrande, M.; Amantini, D.; Antolini, M.; Martinelli, P.; Cesari, N.; Montanari, D.; Tessari, M.; Corsi, M.; Bifone, A. Functional Magnetic Resonance Imaging Reveals Different Neural Substrates for the Effects of Orexin-1 and Orexin-2 Receptor Antagonists. *PLoS One* **2011,** *6* (1), e16406.
31. (a) Porter, R. A.; Chan, W. N.; Coulton, S.; Johns, A.; Hadley, M. S.; Widdowson, K.; Jerman, J. C.; Brough, S. J.; Coldwell, M.; Smart, D.; Jewitt, F.; Jeffrey, P.; Austin, N. 1,3-Biarylureas as Selective Non-peptide Antagonists of the Orexin-1 Receptor. *Bioorg. Med. Chem. Lett.* **2001,** *11* (14), 1907–1910; (b) Smart, D.; Sabido-David, C.; Brough, S. J.; Jewitt, F.; Johns, A.; Porter, R. A.; Jerman, J. C. SB-334867-A: The First Selective Orexin-1 Receptor Antagonist. *Br. J. Pharmacol.* **2001,** *132* (6), 1179–1182; (c) Langmead, C. J.; Jerman, J. C.; Brough, S. J.; Scott, C.; Porter, R. A.; Herdon, H. J. Characterisation of the Binding of [3H]-SB-674042, a Novel Nonpeptide Antagonist, to the Human Orexin-1 Receptor. *Br. J. Pharmacol.* **2004,** *141* (2), 340–346.
32. Micheli, F.; Antolini, M.; Di Fabio, R.; Pellacani, A.; Pozzan, A. 2-Methyl-3-furanyl-4H-1,2,4-triazol-3-ylthioamides: A New Class of Selective Orexin 2 Antagonists. *Bioorg. Med. Chem. Lett.* **2010,** *20* (22), 6405–6407.
33. Christopher, J. A.; Aves, S. J.; Brown, J.; Errey, J. C.; Klair, S. S.; Langmead, C. J.; Mace, O. J.; Mould, R.; Patel, J. C.; Tehan, B. G.; Zhukov, F. H.; Marshall, F. H.; Congreve, M. Discovery of HTL6641, a Dual Orexin Receptor Antagonist With Differentiated Pharmacodynamic Properties. *Med. Chem. Commun.* **2015,** *6,* 947–955.
34. Nagahara, T.; Saitoh, T.; Kutsumura, N.; Irukayama-Tomobe, Y.; Ogawa, Y.; Kuroda, D.; Gouda, H.; Kumagai, H.; Fujii, H.; Yanagisawa, M.; Nagase, H. Design and Synthesis of Non-Peptide, Selective Orexin Receptor 2 Agonists. *J. Med. Chem.* **2015,** *58* (20), 7931–7937.
35. Cox, C. D.; Breslin, M. J.; Whitman, D. B.; Schreier, J. D.; McGaughey, G. B.; Bogusky, M. J.; Roecker, A. J.; Mercer, S. P.; Bednar, R. A.; Lemaire, W.; Bruno, J. G.; Reiss, D. R.; Harrell, C. M.; Murphy, K. L.; Garson, S. L.; Doran, S. M.; Prueksaritanont, T.; Anderson, W. B.; Tang, C.; Roller, S.; Cabalu, T. D.; Cui, D.; Hartman, G. D.; Young, S. D.; Koblan, K. S.; Winrow, C. J.; Renger, J. J.; Coleman, P. J. Discovery of the Dual Orexin Receptor Antagonist [(7R)-4-(5-chloro-1,3-benzoxazol-2-yl)-7-methyl-1,4-diazepan-1-yl][5-methyl-2-(2H −1,2,3-triazol-2-yl)phenyl]methanone (MK-4305) for the Treatment of Insomnia. *J. Med. Chem.* **2010,** *53* (14), 5320–5332.
36. Heifetz, A.; Bodkin, M. J.; Biggin, P. C. Discovery of the First Selective, Nonpeptidic Orexin 2 Receptor Agonists. *J. Med. Chem.* **2015,** *58* (20), 7928–7930.
37. McAtee, L. C.; Sutton, S. W.; Rudolph, D. A.; Li, X.; Aluisio, L. E.; Phuong, V. K.; Dvorak, C. A.; Lovenberg, T. W.; Carruthers, N. I.; Jones, T. K. Novel Substituted 4-phenyl-[1,3]dioxanes: Potent and Selective Orexin Receptor 2 (OX(2)R) Antagonists. *Bioorg. Med. Chem. Lett.* **2004,** *14* (16), 4225–4229.
38. Shoblock, J. R.; Welty, N.; Aluisio, L.; Fraser, I.; Motley, S. T.; Morton, K.; Palmer, J.; Bonaventure, P.; Carruthers, N. I.; Lovenberg, T. W.; Boggs, J.; Galici, R. Selective Blockade of the Orexin-2 Receptor Attenuates Ethanol Self-administration, Place Preference, and Reinstatement. *Psychopharmacology* **2011,** *215* (1), 191–203.
39. Letavic, M. A.; Bonaventure, P.; Carruthers, N. I.; Dugovic, C.; Koudriakova, T.; Lord, B.; Lovenberg, T. W.; Ly, K. S.; Mani, N. S.; Nepomuceno, D.; Pippel, D. J.; Rizzolio, M.; Shelton, J. E.; Shah, C. R.; Shireman, B. T.; Young, L. K.; Yun, S. Novel Octahydropyrrolo[3,4-c]pyrroles Are Selective Orexin-2 Antagonists: SAR Leading to a Clinical Candidate. *J. Med. Chem.* **2015,** *58* (14), 5620–5636.
40. Whitman, D. B.; Cox, C. D.; Breslin, M. J.; Brashear, K. M.; Schreier, J. D.; Bogusky, M. J.; Bednar, R. A.; Lemaire, W.; Bruno, J. G.; Hartman, G. D.; Reiss, D. R.; Harrell, C. M.; Kraus, R. L.; Li, Y.; Garson, S. L.; Doran, S. M.; Prueksaritanont, T.; Li, C.; Winrow, C. J.; Koblan, K. S.; Renger, J. J.; Coleman, P. J. Discovery of a Potent, CNS-Penetrant Orexin Receptor Antagonist Based on an n,n-Disubstituted-1,4-diazepane Scaffold That Promotes Sleep in Rats. *ChemMedChem* **2009,** *4* (7), 1069–1074.
41. Bonaventure, P.; Shelton, J.; Yun, S.; Nepomuceno, D.; Sutton, S.; Aluisio, L.; Fraser, I.; Lord, B.; Shoblock, J.; Welty, N.; Chaplan, S. R.; Aguilar, Z.; Halter, R.; Ndifor, A.; Koudriakova, T.; Rizzolio, M.; Letavic, M.; Carruthers, N. I.; Lovenberg, T.; Dugovic, C. Characterization of JNJ-42847922, a Selective Orexin-2 Receptor Antagonist, as a Clinical Candidate for the Treatment of Insomnia. *J. Pharmacol. Exp. Ther.* **2015,** *354* (3), 471–482.
42. MIN202 Phase 2a https://www.morningstar.com/news/globe-news-wire/GNW_6118250/minerva-neurosciences-announces-favorable-top-line-results-from-min202-phase-2a-clinical-trial-in-insomnia-disorder.html.
43. Bergman, J. M.; Roecker, A. J.; Mercer, S. P.; Bednar, R. A.; Reiss, D. R.; Ransom, R. W.; Meacham Harrell, C.; Pettibone, D. J.; Lemaire, W.; Murphy, K. L.; Li, C.; Prueksaritanont, T.; Winrow, C. J.; Renger, J. J.; Koblan, K. S.; Hartman, G. D.; Coleman, P. J. Proline bis-Amides as Potent Dual Orexin Receptor Antagonists. *Bioorg. Med. Chem. Lett.* **2008,** *18* (4), 1425–1430.
44. Cox, C. D.; McGaughey, G. B.; Bogusky, M. J.; Whitman, D. B.; Ball, R. G.; Winrow, C. J.; Renger, J. J.; Coleman, P. J. Conformational Analysis of N, N-disubstituted-1,4-diazepane Orexin Receptor Antagonists and Implications for Receptor Binding. *Bioorg. Med. Chem. Lett.* **2009,** *19* (11), 2997–3001.
45. Coleman, P. J.; Schreier, J. D.; McGaughey, G. B.; Bogusky, M. J.; Cox, C. D.; Hartman, G. D.; Ball, R. G.; Harrell, C. M.; Reiss, D. R.; Prueksaritanont, T.; Winrow, C. J.; Renger, J. J. Design and Synthesis of Conformationally Constrained N, N-disubstituted 1,4-diazepanes as Potent Orexin Receptor Antagonists. *Bioorg. Med. Chem. Lett.* **2010,** *20* (7), 2311–2315.
46. Coleman, P. J.; Schreier, J. D.; Roecker, A. J.; Mercer, S. P.; McGaughey, G. B.; Cox, C. D.; Hartman, G. D.; Harrell, C. M.; Reiss, D. R.; Doran, S. M.; Garson, S. L.; Anderson, W. B.; Tang, C.; Prueksaritanont, T.; Winrow, C. J.; Renger, J. J. Discovery of 3,9-diazabicyclo[4.2.1]nonanes as Potent Dual Orexin Receptor Antagonists With Sleep-Promoting Activity in the Rat. *Bioorg. Med. Chem. Lett.* **2010,** *20* (14), 4201–4205.
47. Baxter, C. A.; Cleator, E.; Brands, K. M. J.; Edwards, J. S.; Reamer, R. A.; Sheen, F. J.; Stewart, G. W.; Strotman, N. A.; Wallace, D. J. The First Large-Scale Synthesis of MK-4305: A Dual Orexin Receptor Antagonist for the Treatment of Sleep Disorder. *Org. Process Res. Dev.* **2011,** *15* (2), 367–375.
48. Winrow, C. J.; Gotter, A. L.; Cox, C. D.; Doran, S. M.; Tannenbaum, P. L.; Breslin, M. J.; Garson, S. L.; Fox, S. V.; Harrell, C. M.; Stevens, J.; Reiss, D. R.; Cui, D.; Coleman, P. J.; Renger, J. J. Promotion of Sleep by Suvorexant-a Novel Dual Orexin Receptor Antagonist. *J. Neurogenet.* **2011,** *25* (1–2), 52–61.

49. Michelson, D.; Ellen, S.; Paradis, E.; Chengan-Liu, M.; Snavely, D. B.; Hutzelmann, J.; Walsh, J. K.; Krystal, A. D.; Benca, R. M.; Cohn, M.; Lines, C.; Roth, T.; Herring, W. J. Safety and Efficacy of Suvorexant During 1-Year Treatment of Insomnia With Subsequent Abrupt Treatment Discontinuation: A Phase 3 Randomised, Double-Blind, Placebo-Controlled Trial. *Lancet Neurol.* **2014,** *13* (5), 461–471.
50. Coleman, P. J.; Schreier, J. D.; Cox, C. D.; Breslin, M. J.; Whitman, D. B.; Bogusky, M. J.; McGaughey, G. B.; Bednar, R. A.; Lemaire, W.; Doran, S. M.; Fox, S. V.; Garson, S. L.; Gotter, A. L.; Harrell, C. M.; Reiss, D. R.; Cabalu, T. D.; Cui, D.; Prueksaritanont, T.; Stevens, J.; Tannenbaum, P. L.; Ball, R. G.; Stellabott, J.; Young, S. D.; Hartman, G. D.; Winrow, C. J.; Renger, J. J. Discovery of [(2R,5R)-5-[[(5-fluoropyridin-2-yl)oxy]methyl}-2-methylpiperidin-1-yl][5-methyl-2-(pyrimidin-2-yl)phenyl]methanone (MK-6096): A Dual Orexin Receptor Antagonist With Potent Sleep-Promoting Properties. *ChemMedChem* **2012,** *7* (3), 415–424, 337.
51. Winrow, C. J.; Gotter, A. L.; Cox, C. D.; Tannenbaum, P. L.; Garson, S. L.; Doran, S. M.; Breslin, M. J.; Schreier, J. D.; Fox, S. V.; Harrell, C. M.; Stevens, J.; Reiss, D. R.; Cui, D.; Coleman, P. J.; Renger, J. J. Pharmacological Characterization of MK-6096—A Dual Orexin Receptor Antagonist for Insomnia. *Neuropharmacology* **2012,** *62* (2), 978–987.
52. Girardin, M. O.; Ouellet, S. G.; Gauvreau, D.; Moore, J. C.; Hughes, G.; Devine, P. N.; O'Shea, P. D.; Campeau, L.-C. Convergent Kilogram-Scale Synthesis of Dual Orexin Receptor Antagonist. *Org. Process Res. Dev.* **2013,** *17* (1), 61–68.
53. Chabi, A.; Zhang, Y.; Jackson, S.; Cady, R.; Lines, C.; Herring, W. J.; Connor, K. M.; Michelson, D. Randomized Controlled Trial of the Orexin Receptor Antagonist Filorexant for Migraine Prophylaxis. *Cephalalgia* **2015,** *35* (5), 379–388.
54. Zisapel, N. Current Phase II Investigational Therapies for Insomnia. *Expert Opin. Investig. Drugs* **2015,** *24* (3), 401–411.
55. Kuduk, S. D.; Skudlarek, J. W.; Di Marco, C. N.; Bruno, J. G.; Pausch, M. A.; O'Brien, J. A.; Cabalu, T. D.; Stevens, J.; Brunner, J.; Tannenbaum, P. L.; Gotter, A. L.; Winrow, C. J.; Renger, J. J.; Coleman, P. J. Synthesis and Evaluation of Carbon-Linked Analogs of Dual Orexin Receptor Antagonist Filorexant. *Bioorg. Med. Chem. Lett.* **2014,** *24* (7), 1784–1789.
56. Mercer, S. P.; Roecker, A. J.; Garson, S.; Reiss, D. R.; Meacham Harrell, C.; Murphy, K. L.; Bruno, J. G.; Bednar, R. A.; Lemaire, W.; Cui, D.; Cabalu, T. D.; Tang, C.; Prueksaritanont, T.; Hartman, G. D.; Young, S. D.; Winrow, C. J.; Renger, J. J.; Coleman, P. J. Discovery of 2,5-diarylnicotinamides as Selective Orexin-2 Receptor Antagonists (2-SORAs). *Bioorg. Med. Chem. Lett.* **2013,** *23* (24), 6620–6624.
57. Roecker, A. J.; Mercer, S. P.; Schreier, J. D.; Cox, C. D.; Fraley, M. E.; Steen, J. T.; Lemaire, W.; Bruno, J. G.; Harrell, C. M.; Garson, S. L.; Gotter, A. L.; Fox, S. V.; Stevens, J.; Tannenbaum, P. L.; Prueksaritanont, T.; Cabalu, T. D.; Cui, D.; Stellabott, J.; Hartman, G. D.; Young, S. D.; Winrow, C. J.; Renger, J. J.; Coleman, P. J. Discovery of 5''-chloro-N-[(5,6-dimethoxypyridin-2-yl)methyl]-2,2':5',3''-terpyridine-3'-carbo xamide (MK-1064): A Selective Orexin 2 Receptor Antagonist (2-SORA) for the Treatment of Insomnia. *ChemMedChem* **2014,** *9* (2), 311–322.
58. NCT02549027. https://clinicaltrials.gov/ct2/show/NCT02549027.
59. Roecker, A. J.; Reger, T. S.; Mattern, M. C.; Mercer, S. P.; Bergman, J. M.; Schreier, J. D.; Cube, R. V.; Cox, C. D.; Li, D.; Lemaire, W.; Bruno, J. G.; Harrell, C. M.; Garson, S. L.; Gotter, A. L.; Fox, S. V.; Stevens, J.; Tannenbaum, P. L.; Prueksaritanont, T.; Cabalu, T. D.; Cui, D.; Stellabott, J.; Hartman, G. D.; Young, S. D.; Winrow, C. J.; Renger, J. J.; Coleman, P. J. Discovery of MK-3697: A Selective Orexin 2 Receptor Antagonist (2-SORA) for the Treatment of Insomnia. *Bioorg. Med. Chem. Lett.* **2014,** *24* (20), 4884–4890.
60. Sleepdex. http://www.sleepdex.org/newdrugs.htm.
61. Raheem, I. T.; Breslin, M. J.; Bruno, J.; Cabalu, T. D.; Cooke, A.; Cox, C. D.; Cui, D.; Garson, S.; Gotter, A. L.; Fox, S. V.; Harrell, C. M.; Kuduk, S. D.; Lemaire, W.; Prueksaritanont, T.; Renger, J. J.; Stump, C.; Tannenbaum, P. L.; Williams, P. D.; Winrow, C. J.; Coleman, P. J. Discovery of Piperidine Ethers as Selective Orexin Receptor Antagonists (SORAs) Inspired by Filorexant. *Bioorg. Med. Chem. Lett.* **2015,** *25* (3), 444–450.
62. Roecker, A. J.; Mercer, S. P.; Bergman, J. M.; Gilbert, K. F.; Kuduk, S. D.; Harrell, C. M.; Garson, S. L.; Fox, S. V.; Gotter, A. L.; Tannenbaum, P. L.; Prueksaritanont, T.; Cabalu, T. D.; Cui, D.; Lemaire, W.; Winrow, C. J.; Renger, J. J.; Coleman, P. J. Discovery of Diazepane Amide DORAs and 2-SORAs Enabled by Exploration of Isosteric Quinazoline Replacements. *Bioorg. Med. Chem. Lett.* **2015,** *25* (21), 4992–4999.
63. Kuduk, S. D.; Skudlarek, J. W.; DiMarco, C. N.; Bruno, J. G.; Pausch, M. H.; O'Brien, J. A.; Cabalu, T. D.; Stevens, J.; Brunner, J.; Tannenbaum, P. L.; Garson, S. L.; Savitz, A. T.; Harrell, C. M.; Gotter, A. L.; Winrow, C. J.; Renger, J. J.; Coleman, P. J. Identification of MK-8133: An Orexin-2 Selective Receptor Antagonist With Favorable Development Properties. *Bioorg. Med. Chem. Lett.* **2015,** *25* (12), 2488–2492.
64. Betschart, C.; Hintermann, S.; Behnke, D.; Cotesta, S.; Fendt, M.; Gee, C. E.; Jacobson, L. H.; Laue, G.; Ofner, S.; Chaudhari, V.; Badiger, S.; Pandit, C.; Wagner, J.; Hoyer, D. Identification of a Novel Series of Orexin Receptor Antagonists With a Distinct Effect on Sleep Architecture for the Treatment of Insomnia. *J. Med. Chem.* **2013,** *56* (19), 7590–7607.
65. Behnke, D.; Cotesta, S.; Hintermann, S.; Fendt, M.; Gee, C. E.; Jacobson, L. H.; Laue, G.; Meyer, A.; Wagner, T.; Badiger, S.; Chaudhari, V.; Chebrolu, M.; Pandit, C.; Hoyer, D.; Betschart, C. Discovery of 1H-pyrazolo[3,4-b]pyridines as Potent Dual Orexin Receptor Antagonists (DORAs). *Bioorg. Med. Chem. Lett.* **2015,** *25* (23), 5555–5560.
66. Perrey, D. A.; German, N. A.; Gilmour, B. P.; Li, J. X.; Harris, D. L.; Thomas, B. F.; Zhang, Y. Substituted Tetrahydroisoquinolines as Selective Antagonists for the Orexin 1 Receptor. *J. Med. Chem.* **2013,** *56* (17), 6901–6916.
67. (a) Perrey, D. A.; German, N. A.; Decker, A. M.; Thorn, D.; Li, J. X.; Gilmour, B. P.; Thomas, B. F.; Harris, D. L.; Runyon, S. P.; Zhang, Y. Effect of 1-Substitution on Tetrahydroisoquinolines as Selective Antagonists for the Orexin-1 Receptor. *ACS Chem. Neurosci.* **2015,** *6* (4), 599–614; (b) Perrey, D. A.; Decker, A. M.; Li, J. X.; Gilmour, B. P.; Thomas, B. F.; Harris, D. L.; Runyon, S. P.; Zhang, Y. The Importance of the 6- and 7-Positions of Tetrahydroisoquinolines as Selective Antagonists for the Orexin 1 Receptor. *Bioorg. Med. Chem.* **2015,** *23* (17), 5709–5724.
68. Perrey, D. A.; Gilmour, B. P.; Runyon, S. P.; Thomas, B. F.; Zhang, Y. Diaryl Urea Analogues of SB-334867 as Orexin-1 Receptor Antagonists. *Bioorg. Med. Chem. Lett.* **2011,** *21* (10), 2980–2985.
69. McElhinny, C. J., Jr.; Lewin, A. H.; Mascarella, S. W.; Runyon, S.; Brieaddy, L.; Carroll, F. I. Hydrolytic Instability of the Important Orexin 1 Receptor Antagonist SB-334867: Possible Confounding Effects on In vivo and In vitro Studies. *Bioorg. Med. Chem. Lett.* **2012,** *22* (21), 6661–6664.
70. Stasi, L. P.; Artusi, R.; Bovino, C.; Buzzi, B.; Canciani, L.; Caselli, G.; Colace, F.; Garofalo, P.; Giambuzzi, S.; Larger, P.; Letari, O.; Mandelli, S.; Perugini, L.; Pucci, S.; Salvi, M.; Toro, P. Discovery, Synthesis, Selectivity Modulation and DMPK Characterization of 5-azaspiro[2.4]heptanes as Potent Orexin Receptor Antagonists. *Bioorg. Med. Chem. Lett.* **2013,** *23* (9), 2653–2658.
71. Jiang, R.; Song, X.; Bali, P.; Smith, A.; Bayona, C. R.; Lin, L.; Cameron, M. D.; McDonald, P. H.; Kenny, P. J.; Kamenecka, T. M. Disubstituted Piperidines as Potent Orexin (Hypocretin) Receptor Antagonists. *Bioorg. Med. Chem. Lett.* **2012,** *22* (12), 3890–3894.
72. Suzuki, R.; Nozawa, D.; Futamura, A.; Nishikawa-Shimono, R.; Abe, M.; Hattori, N.; Ohta, H.; Araki, Y.; Kambe, D.; Ohmichi, M.; Tokura, S.; Aoki, T.; Ohtake, N.; Kawamoto, H. Discovery and In vitro and In vivo Profiles of N-ethyl-N-[2-[3-(5-fluoro-2-pyridinyl)-1H-pyrazol-1-yl]ethyl]-2-(2H-1,2,3-triazol – 2-yl)-benzamide as a Novel Class of Dual Orexin Receptor Antagonist. *Bioorg. Med. Chem.* **2015,** *23* (6), 1260–1275.
73. Fujimoto, T.; Kunitomo, J.; Tomata, Y.; Nishiyama, K.; Nakashima, M.; Hirozane, M.; Yoshikubo, S.; Hirai, K.; Marui, S. Discovery of Potent, Selective, Orally Active Benzoxazepine-Based Orexin-2 Receptor Antagonists. *Bioorg. Med. Chem. Lett.* **2011,** *21* (21), 6414–6416.
74. Fujimoto, T.; Tomata, Y.; Kunitomo, J.; Hirozane, M.; Marui, S. Discovery of Spiropiperidine-Based Potent and SELECTIVE OREXIN-2 RECEPTOR Antagonists. *Bioorg. Med. Chem. Lett.* **2011,** *21* (21), 6409–6413.
75. Hoever, P.; Hay, J.; Rad, M.; Cavallaro, M.; van Gerven, J. M.; Dingemanse, J. Tolerability, Pharmacokinetics, and Pharmacodynamics of Single-Dose Almorexant, an Orexin Receptor Antagonist, in Healthy Elderly Subjects. *J. Clin. Psychopharmacol.* **2013,** *33* (3), 363–370.
76. (a) Sun, H.; Kennedy, W. P.; Wilbraham, D.; Lewis, N.; Calder, N.; Li, X.; Ma, J.; Yee, K. L.; Ermlich, S.; Mangin, E.; Lines, C.; Rosen, L.; Chodakewitz, J.; Murphy, G. M. Effects of Suvorexant, an Orexin Receptor Antagonist, on Sleep Parameters as Measured by Polysomnography in Healthy Men. *Sleep* **2013,** *36* (2), 259–267; (b) Herring, W. J.; Snyder, E.; Budd, K.; Hutzelmann, J.; Snavely, D.; Liu, K.; Lines, C.; Roth, T.; Michelson, D. Orexin Receptor Antagonism for Treatment of Insomnia: A Randomized Clinical Trial of Suvorexant. *Neurology* **2012,** *79* (23), 2265–2274.

7.07 Targeting γ-Secretase for the Treatment of Alzheimer's Disease

A Hall, UCB, Braine l'Alleud, Belgium
Al Velter, Janssen Pharmaceutica NV, Beerse, Belgium

© 2017 Elsevier Ltd. All rights reserved.

7.07.1	**Introduction**	281
7.07.1.1	Structural Determination of Gamma Secretase	281
7.07.1.2	GS as Pharmaceutical Target for AD	282
7.07.2	**Modulators From Acturum Life Science**	284
7.07.3	**Modulators From Amgen**	284
7.07.4	**Modulators From Ares Trading/Merck KGAA**	284
7.07.5	**Modulators From Astellas**	285
7.07.6	**Modulators From AstraZeneca**	286
7.07.7	**Modulators From Biogen**	288
7.07.8	**Modulators From Bristol-Myers Squibb**	289
7.07.9	**Modulators From Boehringer-Ingelheim**	292
7.07.10	**Modulators From Dainippon Sumitomo**	292
7.07.11	**Modulators From Eisai**	293
7.07.12	**Modulators From Forum/EnVivo**	294
7.07.12.1	Carboxylic Acid Derivatives	294
7.07.12.2	Aryl-Imidazole Derivatives	295
7.07.13	**Modulators From GlaxoSmithKline**	296
7.07.13.1	Carboxylic Acid Derivatives	296
7.07.13.2	Arylimidazole Derivatives	296
7.07.14	**Modulators From Janssen**	298
7.07.14.1	Carboxylic Acid Derivativess	298
7.07.14.2	Aryl Imidazole Derivatives	299
7.07.15	**Modulators From Merck**	302
7.07.15.1	Carboxylic Acid Derivatives	302
7.07.15.2	Aryl-Piperazine Derivatrives	303
7.07.15.3	Aryl Imidazole Derivatives	304
7.07.16	**Modulators From Pfizer**	304
7.07.16.1	Carboxylic Acid Derivatives	304
7.07.16.2	Aryl-Imidazole Derivatives	305
7.07.17	**Modulators From Roche**	307
7.07.17.1	Aryl Imidazole Derivatives	307
7.07.17.2	Other Derivatives	308
7.07.18	**Modulators From Satori**	308
7.07.19	**Modulators From Schering-Plough**	311
7.07.20	**Modulators From Shionogi**	312
7.07.21	**Modulators From Takeda**	313
7.07.22	**Modulators From UCSD/Neurogenetics Inc/Torrey Pines Therapeutics**	314
7.07.23	**Photo-Activity Ligands**	315
7.07.24	**Clinical Compounds**	318
7.07.25	**Conclusion**	320
Acknowledgments		321
References		321

Abbreviations

AD Alzheimer's disease
Aph1 Anterior pharynx-defective 1
APP Amyloid precursor protein
BACE β-Site APP cleaving enzyme (β-secretase)
CHO Chinese hamster ovary
CTD C-terminal domain
DAPT *N*-[*N*-(3,5-difluorophenacetyl)-L-alanyl]-*S*-phenylglycine *t*-butyl ester
ECD Ectodomain
FAD Familial Alzheimer's disease
GSI γ-Secretase inhibitor
HBA Hydrogen bond acceptor

 http://dx.doi.org/10.1016/B978-0-12-409547-2.13789-8

HBD Hydrogen bond donor
MAD Multiple ascending dose
NCT Nicastrin
NSAID Nonsteroidal antiinflammatory drug
PAL Photo-affinity labeling
PCN Primary cortical neurons
PD Pharmacodynamics
Pen2 Presenilin enhancer protein-2
PK Pharmacokinetic
PS1 Presenilin 1
SAD Single ascending dose
sAPP Soluble APP
SCAM Surface cysteine availability methods

7.07.1 Introduction

7.07.1.1 Structural Determination of Gamma Secretase

γ-Secretase (GS) is a membrane-bound, multiprotein complex, which belongs to the aspartyl protease family of enzymes. In addition to amyloid precursor protein (APP), it processes several other type I integral membrane proteins, including Notch,[1] Jagged,[2] and CD44.[3] GS contains at least four components: anterior pharynx-defective 1 (Aph-1), presenilin enhancer protein-2 (Pen2), presenilin (PS1), and nicastrin (NCT),[4] comprising a total of 20 transmembrane domains (TMs). In human cells, two presenilin isoforms, PS1 and PS2, have been identified and two Aph1 homologues, Aph1a and Aph1b.[5] Together with NCT and Pen2, this can lead to six distinct GS complexes. All four components of the GS complex are required for protease activity. Presenilin-1, which comprises nine TMs, is endoproteolyzed during the assembly process of the GS complex to produce N- and C-terminal fragments, NTF and CTF, respectively, which remain associated as heterodimeric integral membrane proteins. The NTF protein contains TM domains TM1–6, whereas the CTF fragment contains the remaining three, TM7–9. The active site of GS consists of two aspartic residues (Asp257 and Asp385), which are found at the interface of the PS heterodimer, in TM6 and TM7. Aph1 contains seven TMs and plays an important role in the assembly, stabilization, and trafficking of GS complex. NCT contains a large, highly glycosylated ectodomain (ECD), which might be involved in the recognition of N-terminus of substrate protein, and one TM domain. Pen2 binds PS-1 directly and is important in the endoproteolysis of presenilin, as well as for GS activity.[6,7]

A considerable amount of work has been done to elucidate the structure of GS. Due to the complexity of GS, and therefore the difficulties in its isolation and purification, structural elucidation has been performed by electron microscopy (EM) experiments.[8,9] A first cryo-EM study was done at a resolution of 12 Å. The low resolution allowed the identification of only 19 of the 20 TM domains. Also, the identified TMs could not be assigned to the four components of GS complex and therefore could not provide any functional insight. More recently, Lu et al. reported a cryo-EM study at 4.5 Å, which revealed the three-dimensional structure of an intact human GS complex, in which the 19 TMs and a large, bi-lobed extracellular domain of NCT form a horseshoe-shaped TM domain. The low-resolution structure also allowed for the construction of a partial atomic model for NCT, which was found to be homologous in sequence and structure to glutamate carboxyl peptidase PSMA.[10] However, in this experiment, the 4.5 Å resolution could be applied only to ECDs, whereas the resolution for TM domains was of 5–7 Å. Further improvements in cryo-EM resolution have allowed structural refinement. At a resolution of 4.32 Å, a third TM domain was identified in Pen2, resulting in a total of 20 TMS for the GS complex.[11] This time, the 20 TMs could be assigned to the four components of the protease complex. Most recently, the same research group has reported elucidation of the first atomic structure of GS via single particle cryo-EM at a resolution of 3.4 Å Å, **Fig. 1**.[12] This model contains 598 residues in the TMs and 632 residues in the ECD and it confirms the previous TMs assignment to the GS subunits.

The model also confirms the horseshoe shape of TM domain of GS, which has a thin end, composed of the three TMs of Pen2, and a thick end, comprising the NCT TM domain. PS1 and Aph1 are located in the center of the horseshoe, whilst the TM domain of NCT interacts with TM1/5/7 of Aph1 via hydrophobic interactions. The remaining Aph1 TMs interact with TM8/9 of PS1. All three Pen2 TM domains bind to TM4 of PS1 and as a result the catalytic residues Asp257 and Asp385 are placed on the convex side of the horseshoe, and ~10.6 Å apart. The authors suggest that substrate binding, for instance, an inhibitor or a modulator, might trigger a conformational change that would bring the two aspartate residues in closer proximity, which is needed for proteolysis.

Most of the GS ECD is occupied by NCT ECD, which contains 11 glycans and interacts with the two ends of the TM horseshoe. The NCT ECD contains a small lobe and a large lobe. In the large lobe, a hydrophilic pocket containing residues Glu333 and Tyr337, previously reported as important in substrate recognition, is covered by an extended surface loop known as the lid and which comes from the small lobe, **Fig. 2**. The authors suggest that rotation of the large lobe relative to the small lobe around a central pivot (Phe 287) would cause the lid to open and allow substrate access to the putative binding site. This movement would also align the putative binding pocket in NCT with the cleavage site in PS1, positioning thus the substrate for cleavage.

Furthermore, the high resolution allowed for mapping and analysis of the mutations in presenilin known to be linked to familial Alzheimer's disease (FAD). Thus, more than two-thirds of the mutations present in the patients with FAD are derived from the PS-1 component of presenilin, the rest being attributed to PS-2 and APP.

In order to help elucidate the binding site of compounds to GS, in the absence of high-resolution protein structures, when drug discovery efforts were initiated, many groups have employed photoaffinity labeling (PALs) chemical probes. This work is discussed later, Section "**Photo-Activity Ligands**", once the different structural classes have been reviewed.

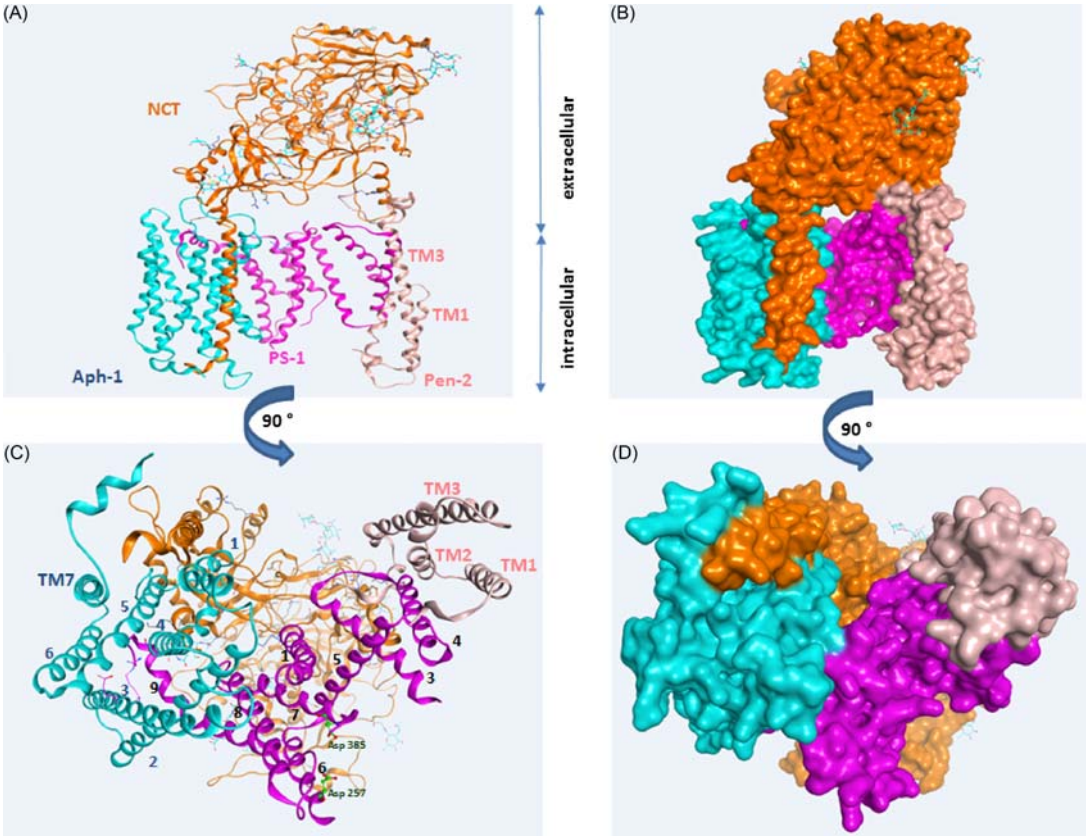

Fig. 1 Atomic model of GS, prepared using MOE software, from the deposited pdb 5A63 file.[12] (A) Ribbon representation; (B) surface view; (C) ribbon view from intracellular side, showing the TM domains. From the pdb deposited structure, TM2 of PS-1 could not be identified; (D) surface view from intracellular side.

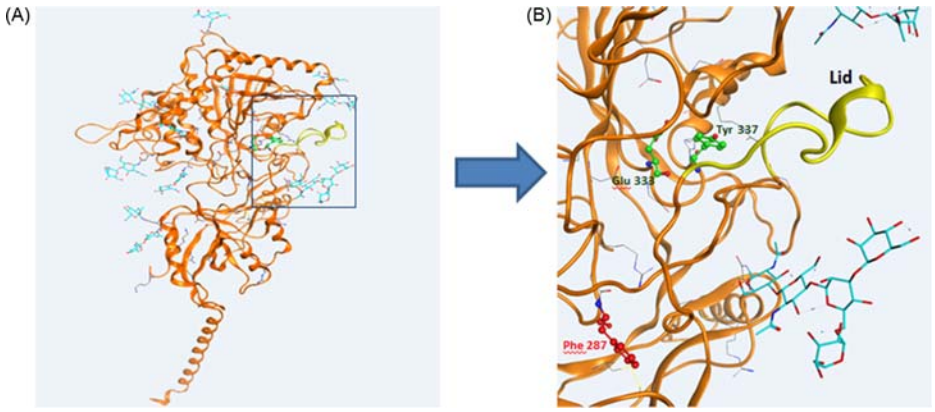

Fig. 2 Atomic structure of nicastrin, prepared using MOE software, from the deposited pdb 5A63 file.[12] (A) Ribbon representation, (B) enlarged view of the lid covering the hydrophilic pocket of Glu333 and Tyr337.

7.07.1.2 GS as Pharmaceutical Target for AD

The initial proteolytic cleavage of the TM APP by β secretase (β-site aPP cleaving enzyme (BACE)) forms two products, soluble APP (containing the extracellular domain of APP) and C99, a membrane-bound carboxy-terminal fragment (CTF). Subsequent cleavage of C99 in the TM domain of GS generates the Aβ peptides, with lengths of 37–43 aminoacids. Initial proteolysis at the membrane cytoplasm boundary, known as the ε site, releases APP intracellular domain into the cytoplasm, while leaving either $A\beta_{48}$ or $A\beta_{49}$ peptides embedded in the membrane. Each of these peptides is then successively cleaved by GS every three aminoacids, generating two product lines: $\varepsilon A\beta_{48}$-ζ $A\beta_4$-γ $A\beta_{42}$ or $\varepsilon A\beta_{49}$-ζ $A\beta_{46}$-γ $A\beta_{43}$-γ$A\beta_{40}$. The generated $A\beta_{40}$ and $A\beta_{42}$ can either be released in the

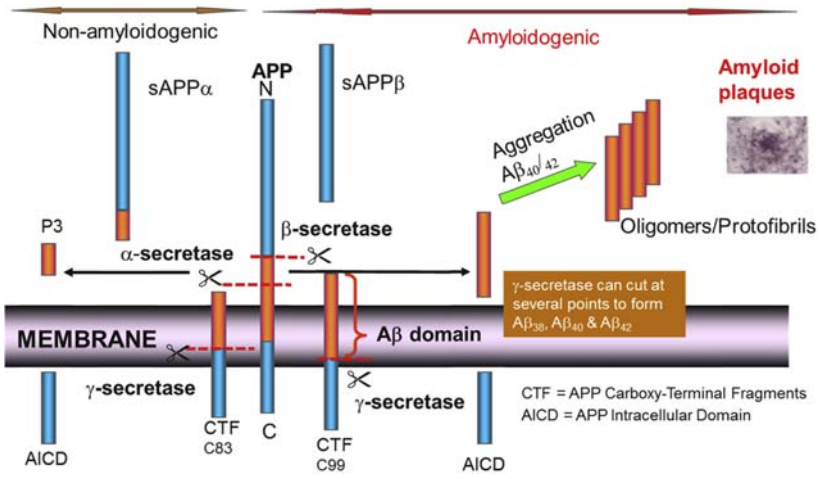

Fig. 3 Schematic of the amyloid pathway depicting the sequential cleavage of APP by β-secretase and γ-secratase. Also depicted, the alternative, nonamyloidogenic, sequential processing of APP by α-secretase and γ-secretase.

extracellular domain, or further cleaved to shorter isoforms, namely $A\beta_{39}$ and $A\beta_{38}$ from $A\beta_{42}$ product line and, respectively, $A\beta_{37}$ from $A\beta_{40}$ product line, Fig. 3.

The predominant forms of Aβ resulting from this process, $A\beta_{40}$ and $A\beta_{42}$, are known to have high propensity to aggregate and therefore comprise the main components of the senile plaques. Moreover, the amount of the longer isomer, $A\beta_{42}$, is selectively increased by mutations in the APP and presenilin genes, which are observed in familial AD. Therefore, many research groups consider $A\beta_{42}$ to be the main culprit in the pathogenesis of AD.[13]

Even in the absence of a molecular mechanism for the second cleavage step of APP, the GS complex has become one of the prime targets in the search for a disease modifying anti-AD drug.[14] A first major strategy to reduce the levels of $A\beta_{42}$ was via inhibition of GS. Various classes of γ-secretase inhibitors (GSIs) have been synthesized, including peptidomimetic compounds such as DAPT, aryl sulfonamides, cycloalkylcarboxamides, pyrazole-derived GSIs, to name just a few.[156] A number of GSIs have advanced into phase II and phase III clinical trials such as Semagacestat/LY-450149, ELND006, Avagacestat/BMS-708163, and Begacestat/GSI-953. However, the progression of all these compounds has been halted however due to the numerous side effects observed: liver toxicity, gastrointestinal effects, dermatological effects, and the absence of an effect on cognition. It became evident that GS has proteolytic activity on other substrates, such as Notch, which is essential for normal biological functions and whose inhibition leads to several undesirable side effects in the thymus, spleen, and intestine. While one approach to circumvent the problem has been the search for selective inhibitors with an acceptable degree of separation between APP and Notch activity, another has been the design of γ-secretase modulators (GSMs),[16] a class of compounds which are able to reduce the level of longer, neurotoxic Aβ peptides while maintaining the total Aβ level constant.

The first modulators of GS were nonsteroidal anti-inflammatory drugs (NSAIDs), discovered when epidemiological studies reported a reduced prevalence of AD among users of NSAIDs. Thus, drugs such as ibuprofen, indomethacin, and sulindac sulfide were able to decrease the production of $A\beta_{42}$ levels and stimulate those of $A\beta_{38}$ both in vitro and in vivo. Tarenflurbil (**1**), Fig. 4, was the first GSM to enter clinical trials. It was discontinued in PhIII, however, due to lack of efficacy resulting from insufficient potency and poor brain penetration, *vide infra*.

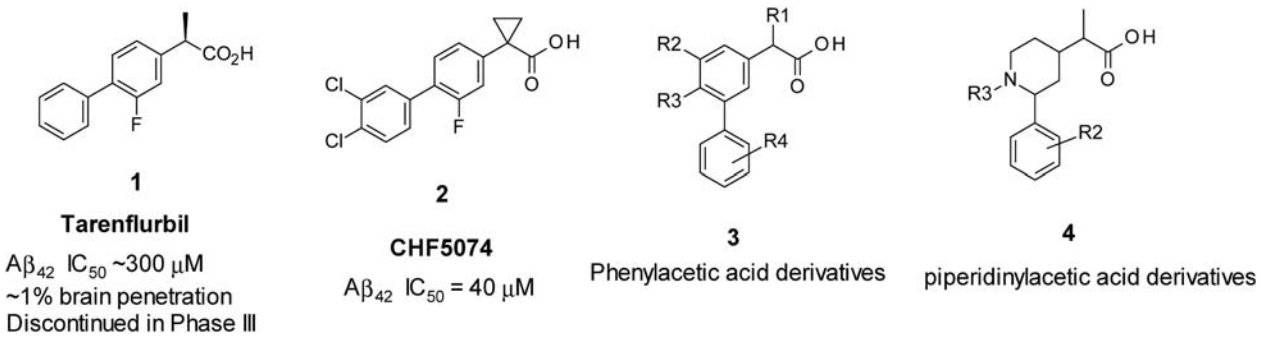

Fig. 4 Examples of NSAID and NSAID-derived GSMs.

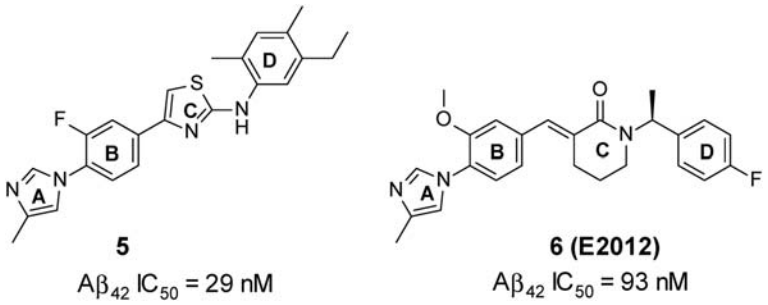

Fig. 5 Non-NSAID aryl-imidazole-derived GSMs.

This initial clinical trial was followed by a considerable amount of work aimed at discovery of more potent and more brain penetrant GSMs.[17] Initial design centered around the tarenflurbil structure, resulting either in direct analogs, such as CHF5074 (**2**), Fig. 4, *vide infra*, or in compounds in which the phenylacetic acid core of tarenflurbil was preserved, while the substituents at 3-, 4-, or/and 5-position were extensively explored, for example, **3**, Fig. 4, *vide infra*. Another class of NSAID-derived GSMs is represented by the piperidinyl-acetic acid derivatives targeting GSMs **4**, Fig. 4, with reduced lipophilicity (*vide infra*). In general, the NSAID-derived GSMs selectively reduce $A\beta_{42}$ levels and do not affect $A\beta_{40}$ levels, whilst compensating by increasing the levels of $A\beta_{37}$ and $A\beta_{38}$.

A second class of GSMs is represented by the non-NSAID, or aryl-imidazoles. The first compounds in this class were anilinothiazole **5**, followed by related cinnamide **E2012 (6)**, Fig. 5, *vide infra*.

As will become evident during this review, these two compounds represented the starting point in the design of novel series of non-NSAID GSMs for many research groups. The aryl-imidazole on left hand side has proven essential in most cases for the in vitro potency of GSMs and therefore difficult to replace. Thus, there are many similarities between the various (sub)-classes of GSMs, sometimes even overlaps. Since most of the exemplified compounds contain the four consecutive (heteroaromatic) rings, these were designated as **A**-**B** for the imidazo-aryl left hand side, **C**- for the central core, and **D**- for the (aromatic) appendage and referred to as such during the text. The pharmacophore consists of what is believed to be a hydrogen bond acceptor (HBA) moiety, fulfilled by the A-ring imidazole, and central HBA moiety, denoted by the C-ring/amide, and a lipophilic/aromatic moiety, as shown by the D-ring. In general, compounds from this series reduce $A\beta_{42}$ selectively over $A\beta_{40}$, but the levels of both proteins are generally reduced. To compensate, the shorter chain amino acids such as $A\beta_{37}$, $A\beta_{38}$, and $A\beta_{39}$ are generally increased.

This review steps through the work of each research group, by alphabetical order, and highlights key compounds from each series from both the primary peer-reviewed literature and the patent literature.

7.07.2 Modulators From Acturum Life Science

Formed in 2013 and based in the Biovation Park on the former AstraZeneca Sodertalje site, and with some of the former AstraZeneca chemists who worked on the GSM project, Acturum Life Science chemists have recently disclosed some of their work in the field. Although the compounds still include the aryl-imidazole moiety, linked via an amide to a triazole or pyrimidine, they do offer some structural diversity. Published examples have data in both HEK cells overexpressing APPSwe and mouse primary cortical neurons (PCN). Examples include the diaminotriazole derivatives with an azetidine on the right hand side, **7** and **8**,[18] the related benzyl analog, **9**,[19] and the diaminopyrimidine derivatives **10** and **11**,[20] Fig. 6.

7.07.3 Modulators From Amgen

Amgen have had a long standing interest in the amyloid field, directed mainly at the identification of BACE inhibitors, however they have also had a brief foray to the GS field. Published patent applications describe compounds from the aryl-imidazole template, where the methylimidazole has been replaced by a methylpyridine and the typical heterocycle has been replaced by an amide such as **12**[21] or a urea such as **13**,[22] Fig. 7. Analysis of the data on each series suggest that achieving sufficient potency appears to have been challenging, and the physicochemical properties also appear suboptimal.

7.07.4 Modulators From Ares Trading/Merck KGAA

Whilst still active in the neuroscience field, Merck KGAA (Merck Serono at the time) had an interest in GSMs and has a published patent application in collaboration with the chemistry group at BioFocus in the UK. The exemplified compounds come from the aryl-imidazole chemotype and resemble compounds disclosed by other companies. A typical example is shown by **14**,[23] Fig. 8.

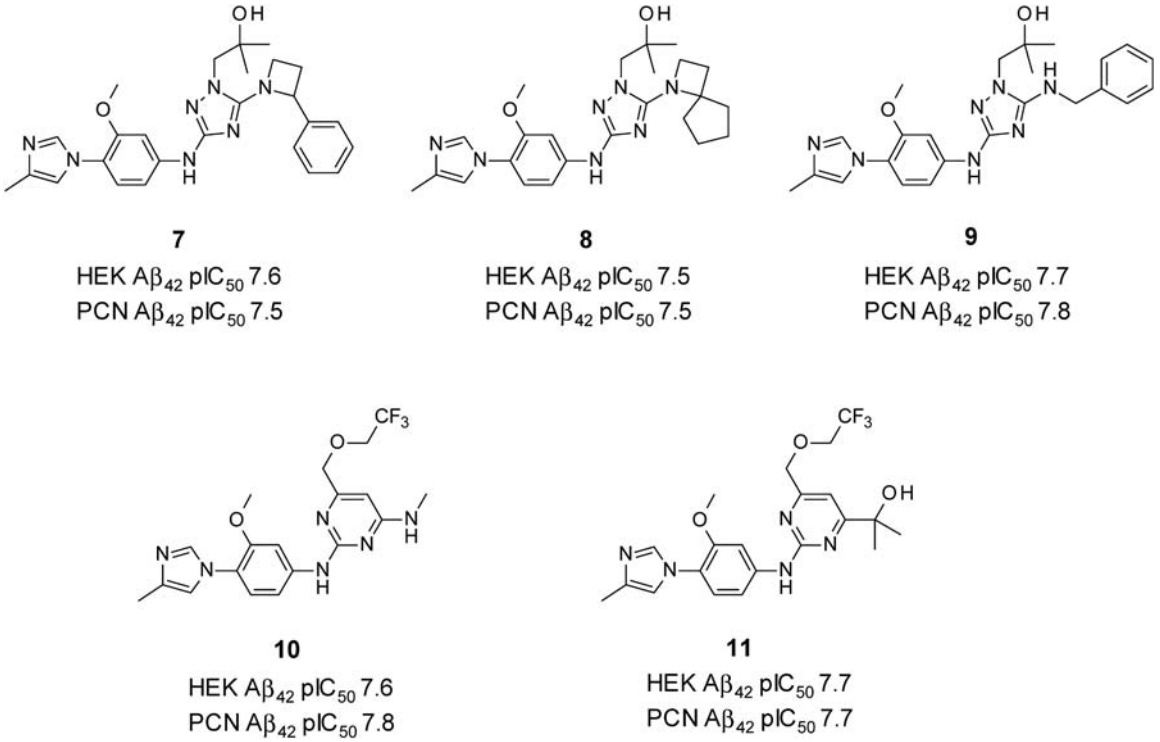

Fig. 6 Diamino-triazole derivatives (**7–9**) and diamino-pyrimidine derivatives (**10** and **11**) from Acturum Life Science.

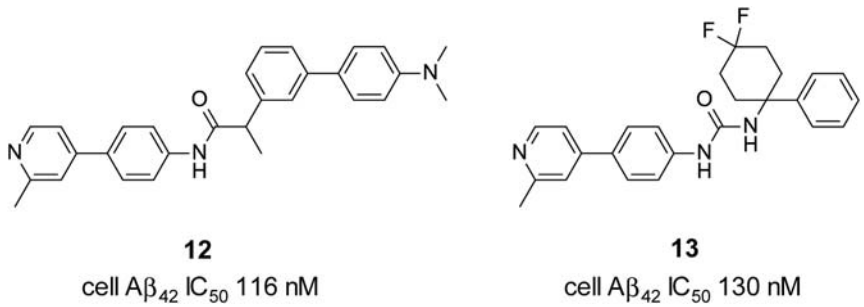

Fig. 7 Selected compounds covering the amide (**12**) and urea (**13**) series from Amgen.

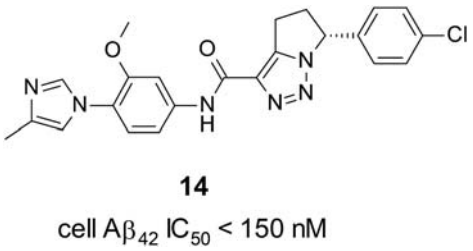

Fig. 8 Example from Ares Trading patent application.

7.07.5 Modulators From Astellas

The Astellas group has worked on carboxylic acid-derived GSM, which contains the familiar acetic acid moiety, which is linked to a central cyclohexane ring. Saturation of the central ring allows incorporation of a basic center, similar to derivatives disclosed by Pfizer (e.g., **118**, Fig. 35). The other key pharmacophoric elements project from the cyclohexane ring either from the 3,4-positions,

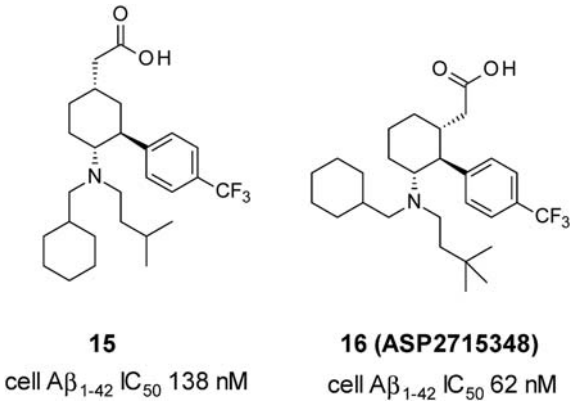

Fig. 9 Selected compounds from Astellas patent application, with ASP2715348 highlighted.

15, or in the 2,3-position, **16**, Fig. 9.[24] **15** was reported to reduce hippocampal $A\beta_{42}$ in vivo in a dose-dependent manner at doses of 3, 10, and 30 mg kg^{-1} with 25%, 45%, and 61% reductions, respectively, whilst **16** was reported to reduce hippocampal $A\beta_{42}$ in vivo by 29% following a 30 mg kg^{-1} dose.

Astellas have recently described the pharmacology of AS2715348 (**16**), Fig. 9,[25] in more detail. AS2715348 was found to inhibit $A\beta_{42}$ production in a cell-free system, IC_{50} 450 nM, and in H4 cells overexpressing APP, IC_{50} 128 nM, whilst exhibiting no inhibition of Notch up to 10 μM in the same cell line. The compound displayed little difference in activity across species; human $A\beta_{42}$ IC_{50} 62 nM (SK-N-BE(2) cells), mouse $A\beta_{42}$ IC_{50} 156 nM (neuro2A cells), rat $A\beta_{42}$ IC_{50} 121 nM (primary cortical neurons). In a time course study in rats, AS2715348 was found to reduce $A\beta_{42}$ in brain, CSF, and plasma following a 5 mg kg^{-1} oral dose, with maximal reductions of 33%, 32%, and 56%, respectively. The Br:Pl AUC was 0.22 showing reasonable penetration into the CNS, whilst the CSF C_{max} was 13 ng mL^{-1} and brain C_{max} was 379 ng g^{-1}. In a rat dose–response study, 1–10 mg kg^{-1} doses of AS2715348 caused a dose-dependent decrease in brain $A\beta_{42}$ (15–49%) 4.5 h after administration. In cynomolgus monkeys, a 10 mg kg^{-1} dose of AS2715348 caused a 34% reduction in plasma and brain $A\beta_{42}$, 34% in plasma, 21% in hippocampus, and 16% reduction in cortex, respectively, 4 h postdose, with a Br:Pl of ~0.4. The ability of the compound to reverse the cognitive deficits in 5.5-month-old Tg2576 mice was also assessed. In this model, the effect on cognition was assessed using the Y-maze 3 h after a single dose and again after a further 7 days, that is, a total of 8 days dosing. On day 1, a dose–response reversal of cognitive impairment was seen in three dose groups, 0.3, 1, and 3 mg kg^{-1}, with the 3 mg kg^{-1} group giving full reversal and a 0.1 mg kg^{-1} having no effect. After 8 days of dosing, the 0.3 and 1 mg kg^{-1} groups both had full efficacy whilst the 3 mg kg^{-1} group was efficacious also, but with lower significance. Interestingly, analysis of brain $A\beta_{42}$ levels at the end of the study showed the 0.3 mg kg^{-1} dose group had no effect on $A\beta_{42}$ levels, whilst the 1 mg kg^{-1} group had a slight effect and the 3 mg kg^{-1} group had $A\beta_{42}$ levels 31% lower than vehicle controls. Thus, although these data show a GSM is able to reverse the cognitive deficit in Tg2576 mice, the relationship between brain $A\beta_{42}$ and cognition is not clear.

Analysis of the Astellas pipeline reveals there are currently no GSMs undergoing clinical development and review of previous pipeline updates shows it is unlikely that they progressed a GSM to clinical trials.

7.07.6 Modulators From AstraZeneca

AstraZeneca disclosed in 2010 two series of potent GSMs having the classical imidazolo-anisole system linked to bicyclic aminopyrimidines (**17**) or pyridines (**18**), Fig. 10.[26,27] A subsequent patent application disclosed a series of potent analogs of **18**,[28] highly

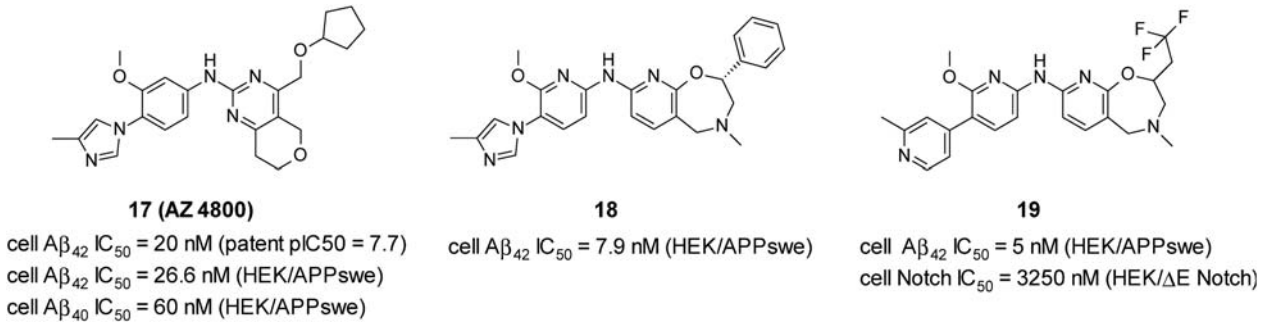

Fig. 10 AstraZeneca's bicyclic amino heterocycles.

selective over Notch, in which the aromatic appendage was replaced by aliphatic side chains (**19**, Fig. 10). This resulted in compounds with reduced aromaticity and lipophilicity.

The modulatory properties of **17**, also known as **AZ-4800**, were described in a report published at a later date. Thus, when tested in HEK cell lines expressing APP with Swedish mutation (APPswe), **AZ-4800** decreased the levels of both $A\beta_{42}$ ($IC_{50} = 26.6$ nM) and $A\beta_{40}$ ($IC_{50} = 60$ nM), while increasing the levels of $A\beta_{37}$ by 750% and $A\beta_{38}$ by 300%. **AZ4800** did not inhibit NICD translocation, showing about ~1000-fold selectivity for Aβ modulation over NICD formation. Furthermore, in vivo efficacy studies indicated that **AZ-4800** was able to penetrate the CNS and could decrease $A\beta_{42}$ levels in the brain of wild-type (C5BL7/6) mice.[29] Thus, acute p.o. dosing of **AZ-4800** at 75, 150, and 300 μmol kg^{-1} decreased $A\beta_{42}$ levels in brain homogenates by 26%, 40%, and 46%, respectively, 1.5 h postadministration. At these doses, the corresponding free concentrations of **AZ-4800** in the mouse brain were ~130, 340, and 880 nM, respectively, with a Br:Pl ratio of 2.4 (average of doses).

An analog belonging to the bicyclic aminopyridine series, **AZ-4126**, was also extensively used for in vivo studies.[30] This analog, presumably **18** based on the reported molecular weight ($MW = 442.52$ g mol^{-1})[31] and reference to the patent describing its preparation, was a potent GSM, causing a reduction in the levels of $A\beta_{42}$ ($IC_{50} = 6$ nM) and $A\beta_{40}$ ($IC_{50} = 22.5$ nM) in HEK/APPswe cells, while leaving the total level of Aβ unaffected. **AZ-4126** was tested at three doses in wild-type mice (C57BL/6), at doses of 10, 25, 50, and 75 μmol kg^{-1}, where it showed a dose-dependent reduction of both $A\beta_{42}$ (9, 17, 33, and 40%) and $A\beta_{40}$ (9, 19, 29, and 36%), 2 h postadministration. A more recent study evaluated the central effects of **AZ-4126** in guinea pig, which is also used as a preclinical model.[6] Thus, when **AZ-4126** was administered to the guinea pig at 30, 75, and 150 μmol kg^{-1}, it was able to significantly reduce the brain $A\beta_{42}$ levels in a dose-dependent manner by 16%, 34%, and 49%, respectively, 2.5 h after administration. In the same time, the brain $A\beta_{40}$ levels were reduced by 36%, 47%, and 68%, respectively. These reductions corresponded to unbound brain concentrations ($C_{u,b}$) of 6, 12, and 53 nM, respectively. In CSF, it significantly reduced $A\beta_{42}$ only at the highest dose (150 μmol kg^{-1}), by 53%. On the other hand, in a time course study, **AZ-4126** was administered at 150 μmol kg^{-1} and the effect on CSF Aβ peptides was assessed at 1, 6, 16, and 24 h after administration. The maximum effect was observed 1 h postdosing, when $A\beta_{37}$ levels increased to 170%, with return to vehicle levels after 24 h, while $A\beta_{40}$ decreased to ~70% and then returned to vehicle levels after 24 h, with no rebound effect. At 1 h postdose, the $C_{u,b}$ had the maximum value of 62 nM. Because $A\beta_{42}$ levels were below the limit of detection for some samples, they were excluded from further analysis.

In a report from 2013,[32] Astra Zeneca disclosed a series of analogs in which the amino-linked C-ring/core was replaced with a bicyclic triazole. The starting point for this series were GSMs possessing a triazolopiperidine core, already described in the literature by research groups at Eisai (**E2212**, compound **6**, Figs. 5 and 18), Roche (**131**, Fig. 38), and Janssen[33] depicted by structure **20** in Fig. 11. AstraZeneca's initial optimization efforts focused on replacing the classical A–B imidazole-anisole system. It was observed that two main factors were important to preserve GSM potency: (a) conservation of the aromatic character of A and B rings and (b) the strength and position of the HBA in the A-ring. The most potent analog resulting from this exploration was **21**, in which the imidazole A-ring was replaced by a pyridazine. Another noteworthy analog was **22**, which still showed modest potency despite having the aromatic ring replaced by an acetonitrile side chain.

AstraZeneca's next efforts were directed at identification of novel core structures, distinct from the ones reported by Janssen and Roche, and with improved overall physicochemical and drug-like properties. In order to decrease lipophilicty of compounds such as **20**, the fused piperidine ring was replaced with a fused tetrahydropyrimidone moiety. This resulted in identification of **23**, Fig. 12, a potent GSM which suffered from poor solubility (6 μM) and showed micromolar inhibition of the hERG channel (hERG $IC_{50} = 3.7$ μM). Pharmacokinetic (PK) profiling in mouse showed that **23** had good brain penetration, with Br:Pl of 0.72, moderate clearance (Cl = 21 mL min^{-1} kg^{-1}), short half-life ($t_{½} = 0.6$ h) and low oral bioavailability ($F = 32\%$). When administered orally to wild-type mice (C57BL/6) at 150 μmol kg^{-1}, it reduced $A\beta_{42}$ peptides by 24%, 1.5 h postadministration, while at lower dose of 50 μmol kg^{-1} it was inactive.

Attempts to increase the solubility of the tetrahydropyrimidone-derived GSMs were successful only when the amide bond on the core was reduced to an amine, yielding tetrahydropyrimidine derivatives. One of the most interesting examples from this new subseries was **24**, Fig. 12, which combined good in vitro potency with an improved overall profile. Not only was the kinetic solubility improved (63 μM), but this compound did not significantly inhibit the hERG channel (hERG $IC_{50} = 33$ μM). The PK profile was

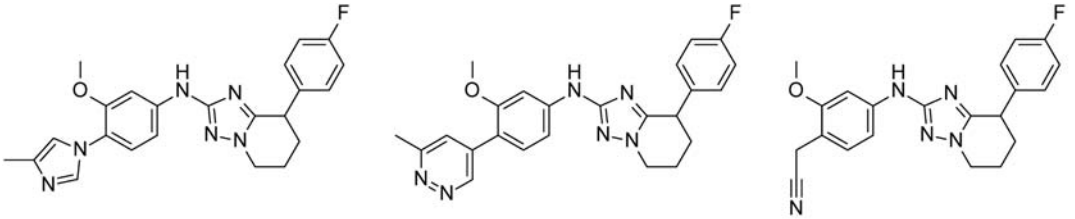

Fig. 11 Exploration around classical GSM arylimidazole ring system by AstraZeneca.

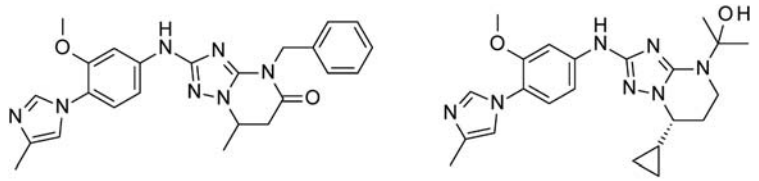

23
cell $A\beta_{42}$ pIC_{50} = 8 (HEK)
cell $A\beta_{42}$ pIC_{50} = 7.7 (PCN)

24
cell $A\beta_{42}$ pIC_{50} = 7.5 (PCN)

Fig. 12 Bicyclic aminotriazole analogs from AstraZeneca.

also improved, **24** having an excellent oral bioavailability of $F = 91\%$. Interestingly, an analysis of the GSM profiles of **23** and **24**, incubated for 5 h in HEK/APPswe cells, showed different behavior for the two compounds. Thus, **23** behaved as a typical GSM, lowering the levels of $A\beta_{42}$ and $A\beta_{40}$ and increasing the level of shorter $A\beta_{38}$ and $A\beta_{37}$. At concentrations of 10 nM, it inhibited the production of $A\beta_{42}$ without affecting the $A\beta_{total}$ levels and Notch cleavage. On the other hand, **24** switched its GSM characteristic to that of inhibitor of APP processing. In this case, 10 nM concentrations of **24** reduced the $A\beta_{total}$ levels, without affecting however the Notch processing.

7.07.7 Modulators From Biogen

GSM research at Biogen focused on the carboxylic acid series, aiming to improve potency and CNS penetration of the NSAID-like GSMs.[34] An early Biogen lead, **25** (**Fig. 13**), which reduced the $A\beta_{42}$ levels in APP-CHO cellular assay by 50% at 1 μM, was poorly brain penetrant, reaching 0.6 μM 4 h after being dosed at 50 mg kg^{-1}. To address this issue, more rigid analogs, which also incorporated basic amines (**26**, **Fig. 13**), were designed, by conformationally restricting the *i*-butyl side chain in **25** into a cyclic amine, while swapping the *N*-(trifluoromethylphenyl) substituent from the benzylic nitrogen to the benzylic position. Optimization of **26** structures led to the identification of preclinical candidate **BIIB042**, (**27** in **Fig. 13**). When tested in Chinese hamster ovary (CHO) cells overexpressing APP V717F mutation, this compound showed good lowering of $A\beta_{42}$ levels ($IC_{50} = 170$ nM) and increase of $A\beta_{38}$ ($EC_{50} = 150$ nM), while the $A\beta_{40}$ levels remained unchanged. The in vitro potency translated into 40% lowering of $A\beta_{42}$ in the brain of wild-type mice at 10 mg kg^{-1}, 4 h after administration. This effect corresponded to a total brain exposure of 4.6 μM and a Br:Pl ratio of 0.46.

More recently, **BIIB042** was assessed in efficacy studies in vivo.[35] First, the in vitro potency was confirmed in human H4 cells expressing human APP, where **BIIB042** reduced the levels of $A\beta_{42}$ ($IC_{50} = 64$ nM), increased $A\beta_{38}$ ($EC_{50} = 146$ nM), and had limited effect on $A\beta_{40}$. **BIIB042** demonstrated similar pharmacodynamic (PD) effects when tested in vivo across species. For instance, acute p.o. dosing of **BIIIB042** to CF1-mice at 3, 10, 30, and 100 mg kg^{-1} produced a significant modulation of Aβ peptides in a dose-dependent manner, both in brain and in plasma, when measured 4 h after dosing. For instance, at 100 mg kg^{-1} dose, $A\beta_{42}$ levels were reduced by ~60% in brain and 45% in plasma, whereas $A\beta_{38}$ levels increased by ~98% in brain and 82% in plasma. On the other hand, $A\beta_{40}$ peptides showed a more modest, non dose-dependent decrease, at 100 mg kg^{-1} being reduced by ~16% in brain

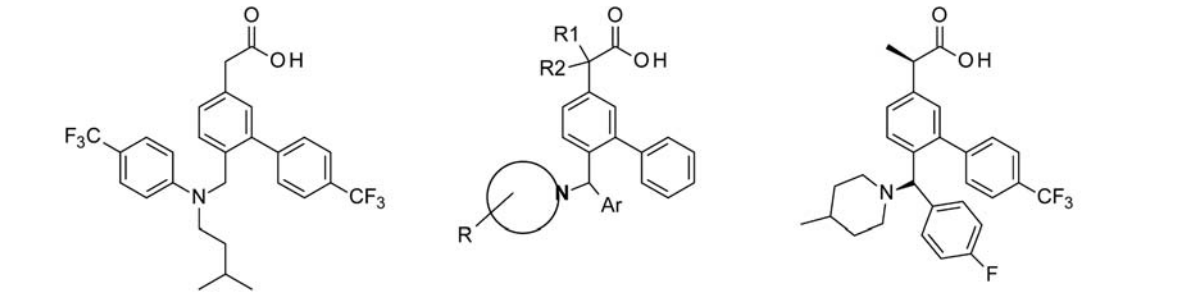

25
cell $A\beta_{42}$ IC_{50} = 1 μM (CHO/APP V717F)

26

27
BIIB042
cell$A\beta_{42}$ IC_{50} = 170 nM (CHO/APP V717F)
cell$A\beta_{42}$ IC_{50} = 64 nM (H4 /APP)

Fig. 13 Carboxylic acid derivatives from Biogen.

and ~25% in plasma. Br:Pl ratio was ~0.8 across all doses. Furthermore, it was determined that a compound brain concentration of 2.8 μM was required to reduce the brain $A\beta_{42}$ by 29%. Similar PK/PD effects were observed in brain, plasma, and CSF of the F344 rat. In a time course study, **BIIB042** was administered at a single dose of 10, 30, or 100 mg kg^{-1} to CF1 mice, and the PD effects were evaluated up to 48 h after dosing. At 10 mg kg^{-1}, a maximum 40% inhibition of brain $A\beta_{42}$ production was observed 4 h postdosing, whereas a maximum ~50% stimulation of $A\beta_{38}$ occurred 16 h postdoing. No effect was observed on $A\beta_{40}$ levels. At 10 mg kg^{-1}, the maximum brain exposure of **BIIB042** was achieved 4 h postdosing and reached a concentration of 7.5 μM. After 48 h, Aβ peptide levels returned to normal. Cynomolgus monkeys were also treated with a single 10 mg kg^{-1} dose of **BIIB042** in a 72 h time course experiment. A PK/PD relationship similar to that in rodents was observed. Subchronic administration of **BIIB042** to 5-month-old Tg2576 mice, at doses of 3, 10, 30, and 60 mg kg^{-1} day^{-1} for a total of 65 days produced a similar modulation of Aβ peptides to those observed in WT mice, for both soluble and insoluble peptides. Soluble brain $A\beta_{42}$ levels were reduced in a dose-dependent fashion, with a maximum ~50% reduction at 60 mg kg^{-1} day^{-1}. Soluble brain $A\beta_{38}$ levels showed a maximum 60% increase at 30 mg k^{-1} day^{-1}, while soluble brain $A\beta_{40}$ were unaffected. Insoluble brain $A\beta_{42}$ were also significantly and dose dependently reduced, at 60 mg kg^{-1} day^{-1} being reduced by 80%. Insoluble $A\beta_{40}$ were also reduced, a significant effect being observed only at a 60 mg kg^{-1} day^{-1} dose. **BIIIB042** was dosed chronically in 10 months old Tg2576 mice, at doses of 0.3, 1, 10, or 30 mg kg^{-1} day^{-1} and the PD effects analyzed 6 months after treatment. Both soluble and insoluble brain $A\beta_{42}$ levels were significantly decreased at 10 and 30 mg kg^{-1} day^{-1}. Soluble and insoluble brain $A\beta_{40}$ levels showed an increase at 0.3 and 1 mg kg^{-1} day^{-1}, no effect at 10 mg kg^{-1} day^{-1} and a significant decrease at 30 mg kg^{-1} day^{-1}. Soluble and insoluble brain $A\beta_{38}$ were increased at 0.3, 1, and 10 mg kg^{-1} day^{-1}, the effect being more pronounced for insoluble fractions at 0.3 and 1 mg kg^{-1}. At 30 mg kg^{-1} day^{-1} soluble $A\beta_{38}$ showed a slight decrease, while insoluble fractions were unaffected. Animals treated with 30 mg kg^{-1} day^{-1} of **BIIB042** had a significantly lower parenchymal plaque staining in the cortex and in the hippocampus.

Based on its PD effects and reduction of plaque pathology, BIIB042 was reported to have entered into advanced safety and tolerability studies, before its planned progression to clinical trials.[35] However, it appears that the compound did not reach the clinic and there has been no recent patent activity from Biogen in the GSM arena, suggesting that they are no longer working in the field.

7.07.8 Modulators From Bristol-Myers Squibb

The group at Bristol-Myers Squibb (BMS) has had a long standing interest in GS, having taken the GSI avagacestat (BMS-708163) to the clinic.[36] Since then they have switched focus to GSMs and publications are now emerging, which delineate their research. An HTS in human H4 cells expressing APP751 Swe mutant identified triazine hit **28**, which was homologated to give the benzyl analog **29**, which displayed a sixfold improvement in potency, Fig. 14.[37]

The introduction of a conformational constraint with simultaneous replacement of the triazine by a thiazole resulted in **30**, Table 1. Replacement of the imidazole HBA moiety was explored on this template as exemplified by **31–34**, all of which resulted in a substantial decrease in potency, Table 1.

Although found to be a potent inhibitor of CYP3A4, IC_{50} 700 nM, and having very high plasma protein binding (ppb, >99.8% in mouse and human), **30** was profiled in vivo in a 3×Tg mouse model at doses of 1, 3, 10, 30, and 100 mg kg^{-1} p.o., which resulted in 30%, 50%, and 50% reductions in brain $A\beta_{1-42}$ at the three highest doses, respectively. The brain concentration was measured at 8900 nM, with corresponding plasma concentration of 800 nM at the 30 mg kg^{-1} dose, 3 h postdose, which resulted in a Br:Pl of 1.1. Thus, the compound elicited moderate reductions in brain amyloid at relatively high doses and exposure, especially when considered in the context of CYP3A4 inhibition.

Another manuscript describes alternative cyclization strategies to optimize **29**, which resulted in compounds such as **35**, Fig. 15.[38] Despite promising in vitro activity, **35** failed to show efficacy in vivo at 30 mg kg^{-1} p.o., which was attributed to low CNS exposure.

Despite this, alternative cyclization strategies appeared more fruitful as shown by the patent literature and recent pharmacological data. Thus, scaffold hopping to give fused amino-triazole derivatives, such as **36**, and **37** (**BMS-869780**),[39] Fig. 15, resulted in potent cellular activity. Interestingly, both compounds incorporate the chloroimidazole, which would be expected to decrease the HBA ability of the imidazole N-atom, as shown by the activity of **32**. This moiety may also provide other favorable properties

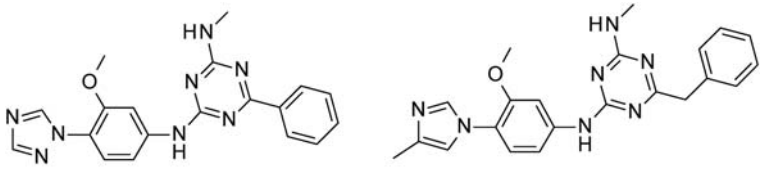

28
cell $A\beta_{42}$ IC_{50} 180 nM

29
cell $A\beta_{42}$ IC_{50} 29 nM

Fig. 14 BMS HTS hit **28** and initial lead **29**.

Table 1 Tricyclic derivatives derived from a scaffold hop from initial lead **29**

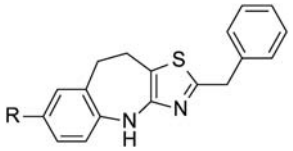

Compound	*R*	*Aβ$_{42}$ cell IC$_{50}$ (nM)*
30	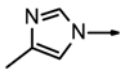	35
31	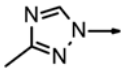	140
32	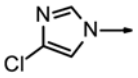	140
33	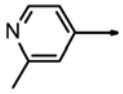	50
34		1200

including intellectual property as its use is not widespread. BMS-869780 (**37**) has been characterized in detail.[40] In mouse embryonic fibroblasts (MEF,M146V), to align data for experiments in 3×Tg mice, BMS-869780 reduced $A\beta_{1-42}$ and $A\beta_{1-40}$ with IC_{50} values of 22 nM and 34 nM, respectively. In the rat, ip administration of doses from 0.3 to 100 mg kg^{-1}, with efficacy assessed 5 h postdose resulted in significant reductions in brain $A\beta_{1-42}$ with the 3 mg kg^{-1} dose achieving nearly 50% reduction and the 30 and 100 mg kg^{-1} doses reaching essentially full reduction, c.75%. Brain $A\beta_{1-40}$ paralleled $A\beta_{1-42}$ but was reduced by ~90% at doses of 30 and 100 mg kg^{-1}. In a separate experiment, doses of 1.9, 22, 100, and 235 mg kg^{-1} BMS-869780 were given to rats, and brain amyloid peptides were measured 24 h later. Doses of 200 and 235 mg kg^{-1} resulted in strong reductions in $A\beta_{1-42}$ and $A\beta_{1-40}$, with the reductions compensated by increases in $A\beta_{1-37}$ (largest increase) and $A\beta_{1-38}$, resulting in no overall change in total Aβ levels. Time course studies on rats (10 mg kg^{-1} p.o.) and 3×Tg mice (30 and 100 mg kg^{-1} p.o.) resulted in calculated plasma concentrations of 1.9 μM and 4.0 μM to reduce brain $A\beta_{1-42}$ by 50%, respectively. Employing ppb data (99.5% in rat and 99.6% in mouse), resulted in calculated free plasma concentrations of 5.1 nM and 22 nM, respectively, which are in line with the in vitro the in vitro cellular data. Utilizing the in vivo activity data in conjunction with allometric scaling resulted in predicted human doses of 700 mg BMS-869780 to achieve 25% reductions in brain $A\beta_{1-42}$. In addition, BMS-869780 was found to activate PXR and to increase CYP3A4 expression in human hepatocytes at concentrations of 300 nM and above, with EC_{50} values in the 1 μM range. Furthermore, in a rat 4 day safety study (10, 30, 100 mg kg^{-1}), BMS-869780 showed signs of lipidosis in the liver at doses of 10 mg kg^{-1} (C_{max} 1.9 μM) and above, thus showing no separation between efficacy and hepatotoxicity. As a consequence, the further investigation of BMS-869780 was halted in search for compounds with increased in vivo potency and better separation over off-target effects.

A subsequent patent application describes examples, where the fused aminotriazole core has been replaced by a fused diaminopyrimidine core, such as **38**, **39**, and **40 (BMS932481)**,[41] Fig. 15, which are closer to the original HTS, **28** and early lead **29**. Ultimately, BMS-932481 (**40**) was progressed to PhI single ascending dose (SAD) and multiple ascending dose (MAD) clinical studies, and the detailed pharmacological profile[42] and clinical data[43] have recently been disclosed. As with other GSMs, BMS-932481 was found not to affect total Aβ levels in cellular assays, as the reduction in $A\beta_{1-42}$ and $A\beta_{1-40}$ were compensated by increase in $A\beta_{1-37}$ and $A\beta_{1-38}$. Profiling in vivo was conducted across several preclinical species, including rat, dog, and monkey. In the rat, doses of 1, 5, and 10 mg kg^{-1} i.v. of BMS-932481 resulted in up to 75% reductions in brain and CSF $A\beta_{1-42}$ with similar decreases in $A\beta_{1-40}$ levels, which was compensated by increases in $A\beta_{1-37}$ and $A\beta_{1-38}$ levels. The Br_{AUC}:Pl_{AUC} was ~0.6. In the dog, oral doses of 2, 5, and 30 mg kg^{-1} reduced CSF $A\beta_{1-42}$ and $A\beta_{1-40}$ levels to a similar extent, with the maximal effect being a 65% reduction in $A\beta_{1-42}$ 24 h postdose. There was a weak increase in $A\beta_{1-38}$, but $A\beta_{1-37}$ increased up to fivefold. In the monkey, i.v. administration of doses of 5 and 15 mg kg^{-1} resulted in pronounced parallel reductions of CSF $A\beta_{1-42}$ and $A\beta_{1-40}$ levels, with a maximal effect of 75% 12–24 h after the higher dose. $A\beta_{1-38}$ and $A\beta_{1-37}$ levels showed maximal increases of threefold and eightfold, respectively. In a human SAD study (10, 30, 100, 300, 600, 900, 1200 mg), CSF Aβ levels were monitored serially for 24 h after a 900 mg dose.

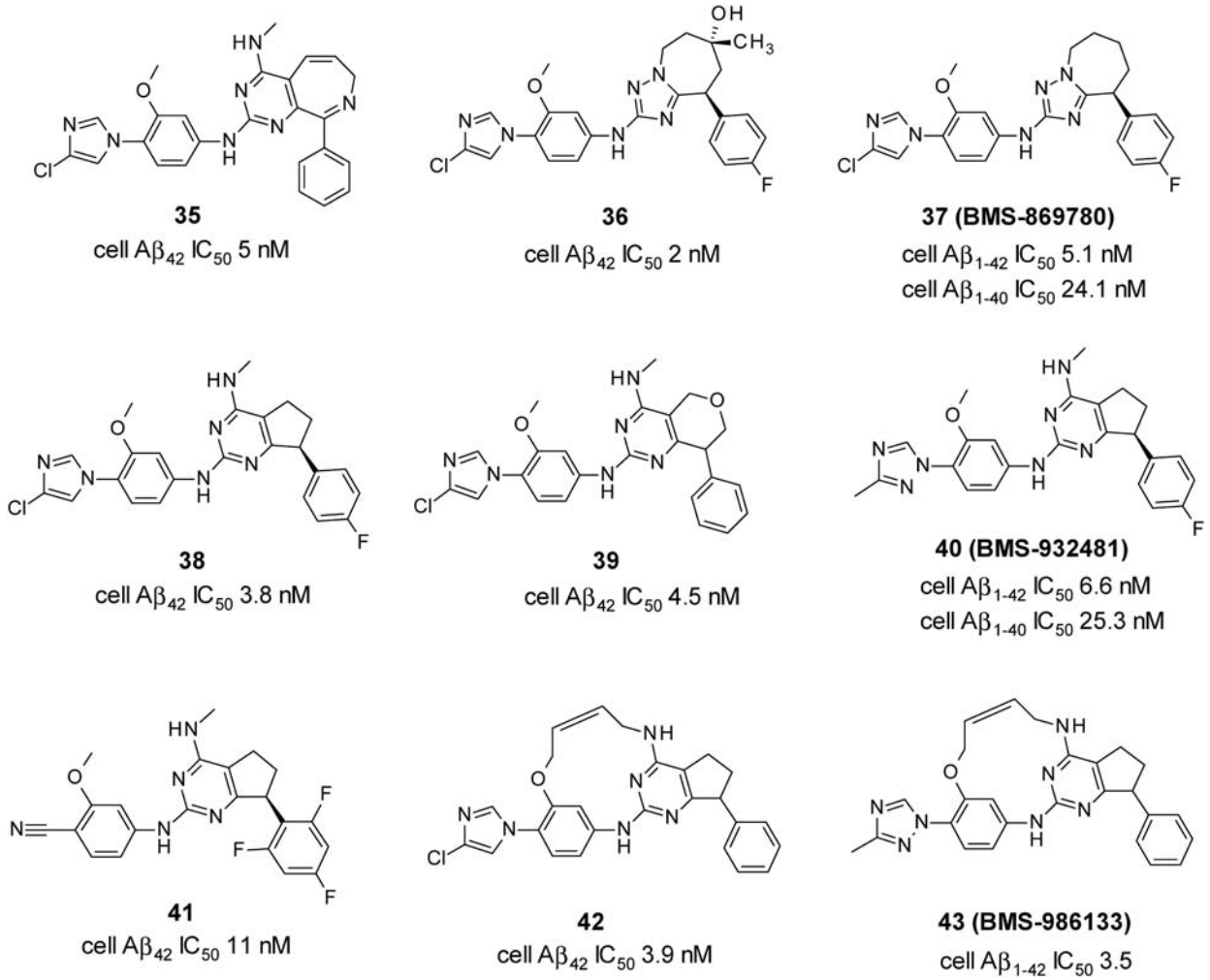

Fig. 15 Further compounds from BMS, including key compounds BMS-869780 (**37**), BMS-932481 (**40**), and BMS-986133 (**43**).

After initial increases (60% vs. predose), CSF $A\beta_{1-42}$ levels decreased slowly with maximal reductions of around 50% of predose levels 24 h postdose. The placebo treated volunteers also showed increased $A\beta_{1-42}$ (and $A\beta_{1-40}$) versus predose followed by a gradual return to near predose levels. The reductions in $A\beta_{1-40}$ levels were similar to those of $A\beta_{1-42}$, whilst $A\beta_{1-38}$ levels increased approximately twofold, there were stronger increases in $A\beta_{1-37}$, which increased by 12-fold. The CSF drug exposure was less than 1% ($\sim$10 nM at the 900 mg dose) that of the plasma exposure, with T_{max} 6 h postdose, in line with the plasma T_{max}. Repeat dose studies (MAD) were conducted with doses of 50, 100, and 200 mg for 28 days (50 and 100 mg) and 14 days (200 mg), with all doses resulting in increased C_{max} and AUC values after repeat dosing. CSF Aβ levels were measured 72 h postdose and showed concentration-dependent reductions; 38%, 46%, and $\sim$70% ($A\beta_{1-42}$), 36%, 44%, and $\sim$70% ($A\beta_{1-40}$), or increases; 292%, 518%, and 545% ($A\beta_{1-37}$) and 20%, 69%, and 68% ($A\beta_{1-38}$). As has been seen in other studies, placebo treated volunteers showed increased amyloid levels, thus drug effects were normalized to predose levels, rather than placebo. CSF amyloid levels were also measured 48 and 96 h after the 200 mg dose, and showed a similar magnitude of effect. The corresponding CSF concentrations were $\sim$3 nM (50 mg), 7 nM (100 mg), and 16 nM (200 mg). In the MAD study, several adverse events were detected, such as elevated bilirubin (all doses) and at the 200 mg dose there was a decrease in creatinine clearance and increases in ALT/AST levels. As a result, a sufficient therapeutic index could not be established and the progression of BMS-932481 was thus terminated.

A further patent application demonstrates that the imidazole can be replaced by a nitrile moiety in the fused diaminopyrimidine series, for example, **41**,[44] Fig. 15. In this instance, the nitrile presumably accepts a hydrogen bond in the same way as the imidazole, but does not result in marked decrease in potency, unlike previous compounds, that is, **30** versus **34**.

The BMS group has also described macrocylic aminopyridine analogs such as **42**[45] and **43** (**BMS-986133**), Fig. 15. Further data on BMS-986133 has recently been disclosed.[42] In the rat doses of 2.5, 5, and 15 mg kg^{-1} i.v. produced similar effects on brain Aβ peptides to that of BMS-932481.

Thus, despite considerable commitment to the amyloid field with particular focus on GS, having progressed both a GSI and a GSM to the clinic, it is disappointing that all of the compounds were terminated. Subsequently BMS have announced their

discontinuation in the neuroscience field. It can be seen from the clinical data with BMS-932481 that achieving sufficient efficacy with a suitable therapeutic index has proved a considerable challenge for GSMs. Although BMS-932481 showed a reduction in CSF amyloid in humans, the efficacy was limited compared to that seen for BACE inhibitors. Despite the fact that the efficacious CSF concentrations were low, total plasma concentrations and doses were relatively high. Thus, perhaps the lipophilic nature of the compounds, coupled with off-target activity and relatively high total exposures results in a narrow TI.

7.07.9 Modulators From Boehringer-Ingelheim

Boehringer Ingelheim entered the GSM field in 2013,[46–48] when they reported a series of aryl-imidazole GSMs in which the conserved left hand side was attached to bicyclic aminopyrimidines, fused to five- or six-membered aliphatic heterocycles. GSMs with a similar pattern were reported by BMS (*vide supra*, Section "Modulators From Bristol-Myers Squibb"). A dihydrothienodiaminopyrimidine series provided moderate modulators of GS, the most potent analog in this series being **44**, Fig. 16, with an $IC_{50} = 90$ nM for lowering $A\beta_{42}$ in H4 neuroglioma cells stably expressing human APP695 isoform. An interesting analog was **45**, in which the ubiquitous imidazole moiety of the aryl-imidazole left hand side was replaced by a 5-methyl-oxazole. This analog was somewhat less potent than **44**, but had higher selectivity for reduction of $A\beta_{42}$ over $A\beta_{total}$. Improved potency was obtained when the central pyrimidine ring was fused to six-membered saturated heterocycles, such as in dihydropteridinones **46**–**48**, Fig. 16. Interestingly, in all these series, an RHS aromatic appendix on the central core did not seem to be required for potency.

7.07.10 Modulators From Dainippon Sumitomo

Researchers at Dainippon Sumitomo appear to have entered the GSM latterly with patent applications appearing in 2011. They have focused their efforts on the aryl-imidazole chemotype, and have recently detailed their lead generation strategy.[49] Starting from what is believed to be E2012 (**6**), Figs. 5 and 18, the group prepared an aryl-imidazole acid (**49**) and combined it with amines (**50**) to generate a library of compounds which were screened at 2.5 μM. Optimization of the amine substituent resulted in the identification of **51**, Fig. 17, which exhibited similar potency to **E2012**, **5**, (IC_{50} 250 nM) in a rat-fetus primary neuronal cellular assay. A 100 mg kg^{-1} oral dose of **51** reduced $A\beta_{42}$ by 55% and 66% in the hippocampus and plasma of the mouse. The group has disclosed several other series, all based on the aryl-imidazole template, such as amino-oxadiazole **52**,[50] amide derivative **53**,[51] Fig. 17, which shows some similarity to derivatives from Pfizer (**120** and **121**, Fig. 36), and trans-olefin **54**,[52] an analog of **59** (proposed to be E2212, Fig. 18), where the methylimidazole has been replaced by a methylpyridine (Fig. 17).

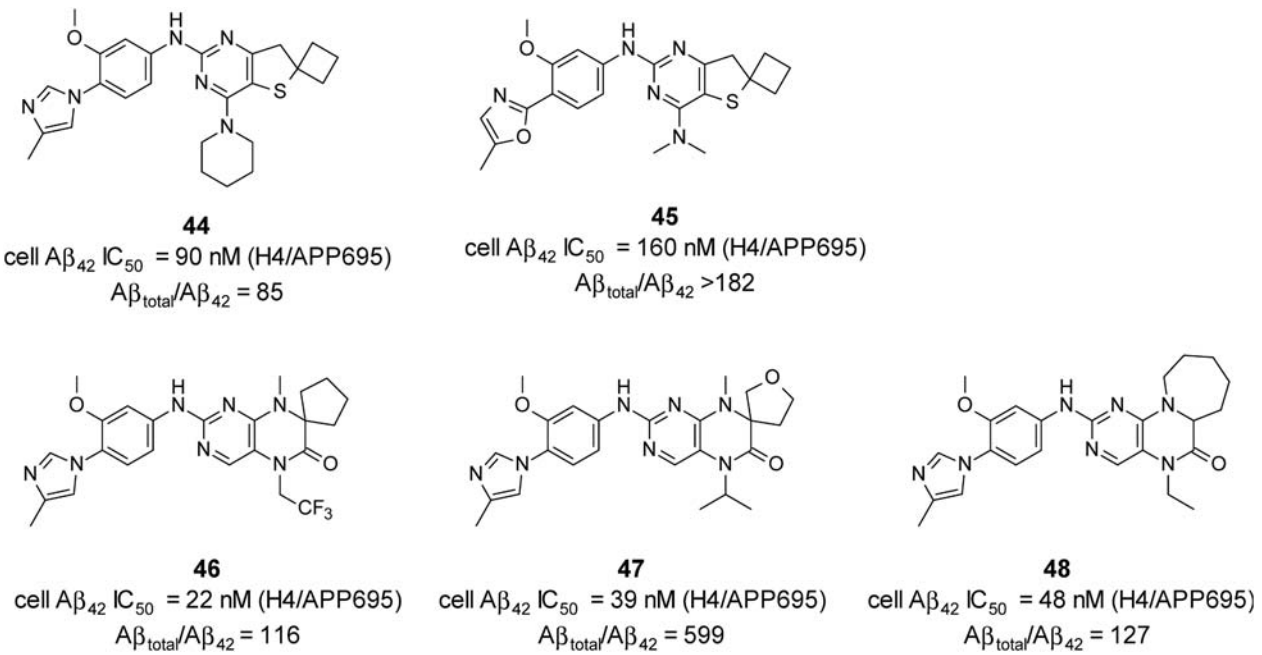

Fig. 16 Selected imidazole-phenyl derivatives from Boehringer Ingelheim.

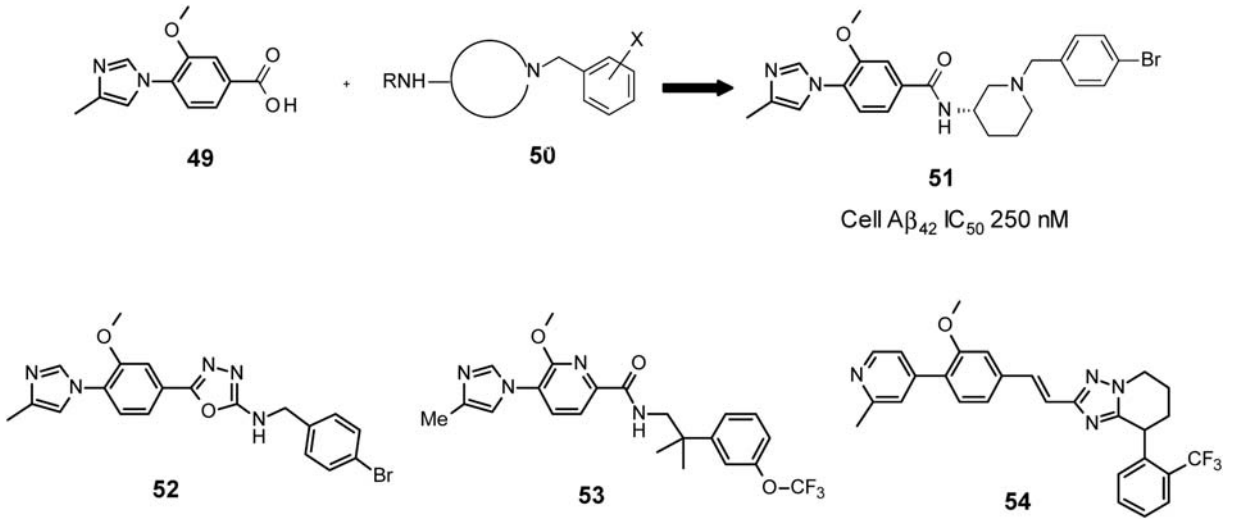

Fig. 17 Lead generation to give **51** with selected other examples from Dainippon Sumitomo.

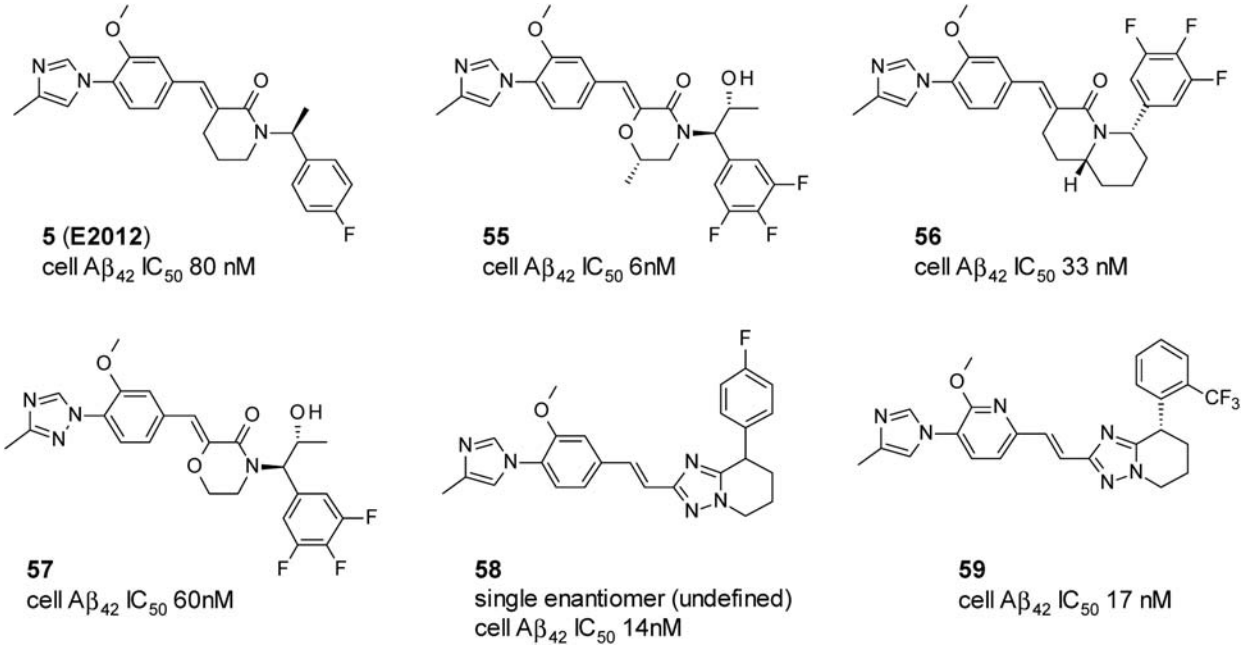

Fig. 18 Key compounds from Eisai patent applications, including the proposed structures of E2102 (**6**) and E2212 (**59**).

7.07.11 Modulators From Eisai

Eisai was one of the pioneers in the GSM arena, where they have focused on the aryl-imidazole structural class. The first patent application appeared in 2005,[53] detailing more than 100 examples, of particular note was **6**, Fig. 18, widely accepted to be E2012, which inhibits $A\beta_{42}$ production in cells with an IC_{50} of 80 nM. Analysis of the structure, in conjunction with the significant body of the literature on its analogs, allows one to propose that the key pharmacophoric elements are an HBA on the left hand side, represented by the imidazole, an HBA in the central region, fulfilled by the amide, and a lipophilic/aromatic moiety on the right hand side.

Following this publication, many groups have prepared and profiled **6** and initiated drug discovery projects delivering related analogs. E2012 entered phase 1 clinical trials in 2006, but was terminated due to effects on cholesterol metabolism, however data are only now beginning to appear. A recently published manuscript demonstrates that E2012 was found to induce cataracts in rats, and that this was not mediated by GS inhibition or modulation.[54] The formation of cataracts was found to be due to 3β-hydroxysterol Δ24-reductase (DHCR24) inhibition, which mediates the last step of cholesterol synthesis, and inhibition results in increased levels of desmosterol, with concomitant reductions in cholesterol levels. It was found that prolonged dosing was required

to see the effect as this was first observed in 13-week-rat toxicology studies, but could be detected after 2 weeks dosing. In the rat, doses of 3 and 10 mg kg^{-1} for 91 days did not affect desmosterol or cholesterol levels, however doses of 30 and 60 mg kg^{-1} had a clear effect. Thus, there was insufficient separation between amyloid lowering doses and those which affected desmosterol conversion to cholesterol.

Subsequent patent applications highlight several derivatives, such as the morpholinone derivative **55**,[55] including follow-up applications,[56] the constrained piperidone derivative **56**.[57] Other patent disclosures include analogs of **55**, where the imidazole has been replaced by a triazole to give compounds such as **57**.[58] The series also evolved to include olefin derivatives with a substituted heterocycle, most notably triazolopiperidine derivatives such as **58**,[59] which were ultimately optimized to **59**, which is widely speculated in the literature to be **E2212**,[60] Fig. 18. Details of the PhI study with E2212 have recently been published.[61] In the SAD study, volunteers received doses of 10, 20, 25, 50, 75, 100, 125, 150, 200, or 150 mg. The compound was well tolerated and it was concluded that the maximum tolerated dose had not been reached. The C_{max} and AUC were found to increase linearly with dose and the half-life ranged from 12.5–19.0 h with renal excretion being the major route of elimination. The effect of E2212 on plasma $A\beta_{x-42}$ was assessed, with ~50% reduction observed following 200 and 250 mg doses, with weaker effects seen at lower doses, that is, ~40% reduction following 100, 125, or 150 mg doses. The authors note that the PKPD relationship and modeling indicate that further increases in dose might not result in further reduction of $A\beta_{x-42}$, although they conclude that E2212 is suitable for further progression.

The group at Pfizer has published data on the characterization of E2012 (**6**) and **59** in preclinical species.[62] **6** was dosed to the guinea pig at doses of 32 and 100 mg kg^{-1} p.o. with effects on brain and CSF amyloid assessed a several time points postdose. Maximal reductions in brain $A\beta_{42}$ of 60% were recorded 9 h after the 100 mg kg^{-1} dose, whilst CSF $A\beta_{42}$ was reduced by 84% and 68% 4 and 9 h after the 100 mg kg^{-1} dose, respectively. PK–PD modeling of the time course study resulted in free brain concentration of 98 nM to reduce brain $A\beta_{42}$ by 50%.

59 was dosed to the rat (15 and 100 mg kg^{-1} p.o.) and the guinea pig (1, 3, 10, 30, and 100 mg kg^{-1} p.o.). In the rat, the lower dose produced 48% and 64% reductions in brain and CSF $A\beta_{42}$ levels, respectively, whilst the higher dose resulted in sustained reductions with the maximal effect at 20 h postdose (70% reduction of brain $A\beta_{42}$ and 97% reduction of CSF $A\beta_{42}$). PK–PD modeling resulted in a calculated free brain concentration of 1.3 nM to reduce brain $A\beta_{42}$ by 50%. In the guinea pig, Eisai-6 showed significantly enhanced potency over E2012, with a 1 mg kg^{-1} dose reducing $A\beta_{42}$ by 55% and 43% in the brain and CSF after 4 h, whilst the 10 mg kg^{-1} dose caused 68% and 82% reductions, respectively. A time course study showed maximal effects at 6 and 9 h postdose with prolonged effects. PK–PD modeling resulted in a calculated free brain concentration of 2.1 nM to reduce brain $A\beta_{42}$ by 50%, thus showing an almost 50-fold improvement over E2012.

The Eisai group has also investigated cinnamide isosteres, including ureas,[63] but it would appear that no compounds of significant interest have emerged from this chemotype.

Thus, after many years of research and pioneering the field with the aryl-imidazole class of GSMs, it seems that the Eisai group is no longer active in the field. Despite having progressed two compounds to the clinic, analysis of the company pipeline would suggest that the development of E2012 and E2212 is not being actively pursued, and at least E2012 has been terminated. Since this period, Eisai has been extremely active in the BACE inhibitor field and is currently progressing the BACE inhibitor E2609 in the clinic in partnership with Biogen.

7.07.12 Modulators From Forum/EnVivo

The group at Forum, originally called EnVivo, has shown long-term commitment to the identification of GSMs, having first prepared carboxylic acid derivatives, then latterly aryl-imidazole and related derivatives.

7.07.12.1 Carboxylic Acid Derivatives

Early work from the Forum (then EnVivo) group identified several carboxylic acid derivatives, which are closely related to the NSAID template.[64–67] The preclinical profile of EVP-0015962 (**60**), Fig. 19, which is believed to be EVP-0962, a GSM that reached PhII clinical trials, has recently been disclosed.[68] In a cellular assay (human neuroglioma H4 cells stably transfected with wild-type human APP751) the EVP-0015962 (**60**) showed high potency for a carboxylic acid derivative, reducing $A\beta_{42}$ with an IC_{50} of 67 nM and increasing $A\beta_{38}$ with an EC_{50} of 33 nM. Further analysis revealed that $A\beta_{42}$ and $A\beta_{39}$ were decreased whilst $A\beta_{38}$ and $A\beta_{33}$ levels were increased, and $A\beta_{40}$ and $A\beta_{37}$ did not change. Surprisingly, the potency was found to be almost 10-fold lower in rat primary neocortical cultures, $A\beta_{42}$ IC_{50} of 427 nM and an $A\beta_{38}$ EC_{50} of 384 nM. In a Tg2576 mouse study, a 30 mg kg^{-1} p.o. dose reduced brain $A\beta_{42}$ levels by 39% with corresponding brain concentrations of 4.3 μM 4 h postdose, but a 10 mg kg^{-1} was inefficacious, despite brain levels of 1.3 μM. A 50 week study in Tg2576 mice, at doses of 20 and 60 mg kg^{-1} p.o. showed 53% and 89% reductions of brain $A\beta_{42}$, respectively. Both doses also reduced plaque area and number relative to vehicle treated animals. In this study, the brain concentrations were measured at 2.5 and 8.3 μM for the 20 and 60 mg kg^{-1} doses, respectively. EVP-0015962 (**60**) also showed a reversal in the contextual fear conditioning model following 11 weeks treatment at 20 and 60 mg kg^{-1} in Tg2576 mice.

EVP-0962 has progressed to clinical studies, where it was assessed in a small PhII trial, *vide infra*. However, the status of the compound is currently unknown, but it seems that it is no longer being progressed. Furthermore, due to recent issues with its nAChR

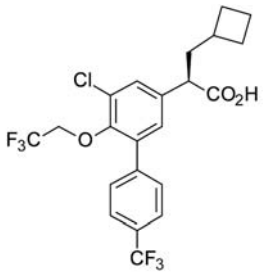

EVP-0015962 (**60**)
cell $A\beta_{42}$ IC_{50} 67 nM (H4-APP_{751})
cell $A\beta_{42}$ IC_{50} 427 nM (rat PCN)
measured logD 3.88

Fig. 19 Structure of EVP-0015962 (**60**), thought to be EVP-0962.

α7 agonist/PAM, encenicline (EVP-6124), it appears that Forum Pharmaceuticals no longer exists, thus the progression of all assets would also cease.

7.07.12.2 Aryl-Imidazole Derivatives

Recently, the focus of the Forum group has shifted to the aryl-imidazole-derived templates, with the publication of several recent patent applications. The compounds all contain a morpholine moiety fused to a heterocycle, such as an aminopyrimidine. Prominent derivatives include **61**, Fig. 20.[69] Related examples, typified by **62**,[70] display a piperidine moiety in place of the typical methoxyphenyl ring, in conjunction with a methoxy-pyridine as the HBA motif, Fig. 20.

Subsequent patent applications demonstrate the aryl motif on the morpholine N-atom can be moved to the adjacent C-atom, that is, **63**, and even be replaced by alkyl groups such as **64**.[71] These chemotypes have then been combined to yield compounds such as **65**, and the related THP derivative, **66**,[72] Fig. 20.

Thus, although there is no published information on why the Forum group has changed focus to the aryl-imidazole template, the fact is suggestive that the carboxylic acid derivatives may have encountered some issues and that the aryl-imidazole template is seen as more attractive.

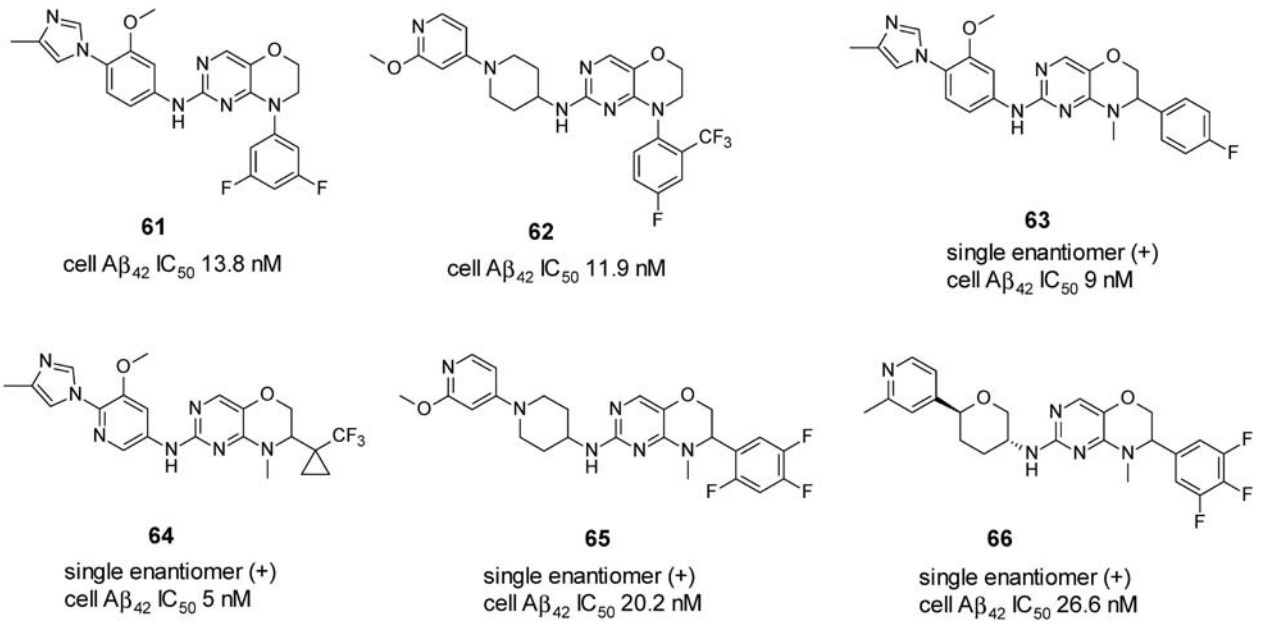

Fig. 20 New derivatives from Forum Pharmaceuticals.

7.07.13 Modulators From GlaxoSmithKline

7.07.13.1 Carboxylic Acid Derivatives

In 2010, scientists at GSK disclosed their research aimed at identifying novel carboxylic acid GSMs.[73] Their interest focused on the piperidine analogs similar to the ones reported by Merck (**103** Fig. 30, *vide infra*) which, although still suffering from suboptimal drug-like properties, had reduced lipophilicity versus earlier carboxyllic acid GSMs reported in the literature (such as **76**, Fig. 24 and **101**, Fig. 30). To further lower the lipophilicity of **103**, various heterocyclic aromatic groups were introduced on the 1-position of the piperidine ring. Optimization efforts resulted in identification of compounds **67** and **68**, Fig. 21. These compounds showed moderate inhibition of $A\beta_{42}$ production in SHSY5Y cells, after 48 h incubation, no significant effect on $A\beta_{40}$ production and showed selectivity over Notch (Notch $IC_{50} > 20$ μM in both cases). Compound **68**, also known as **GSM-10 h**, was further profiled. After 24 h incubation in SHSY5Y cells, **GSM-10 h** showed a typical GSM profile, inhibiting $A\beta_{42}$ production ($IC_{50} = 1$ μM), stimulating $A\beta_{38}$ ($EC_{50} = 500$ nM) showing no significant effect on $A\beta_{40}$ and $A\beta_{total}$. **GSM-10 h** displayed consistent PK across species, with low blood clearance ($Cl_b = 4$ mL $min^{-1} kg^{-1}$ in mouse and rat and 3 mL $min^{-1} kg^{-1}$ in dog), moderate volumes of distribution ($V_{dss} = 1.4$, 2.3 and 1.1 L kg^{-1} in mouse, rat and dog, respectively), a moderate half-life ($t_{1/2} = 4.3$, 6.6, and 5.2 h in mouse, rat, and dog), and high oral bioavailability ($F_{po} > 100\%$ in mouse and rat and 75% in dog). When dosed orally at 5 mg kg^{-1} in a mouse CNS penetration study, **GSM-10 h** demonstrated good CNS exposures with concentrations of 5.6 μM, 2 h postdose, and a Br:Bl ratio of 0.74.

GSM-10 h was further assessed in a rat model of endogenous Aβ production.[74] The in vitro potency was confirmed in primary rat cortical neurons, where, after a 48-h incubation, **GSM-10 h** reduced $A\beta_{42}$ with an IC_{50} of 350 nM and had no significant effect on $A\beta_{40}$ levels. Acute p.o. dosing of **GSM-10 h** to the rat at 3, 10, 30, and 100 mg kg^{-1} significantly reduced $A\beta_{42}$ levels in a dose-dependent manner in plasma and in CSF, 6 h postadministration. At the highest (100 mg kg^{-1}) dose, $A\beta_{42}$ levels were reduced by 75% in plasma and 66% in CSF, corresponding to brain and plasma concentrations of 34 and 28 μM, respectively. In the brain, **GSM 10 h** had weaker efficacy, showing only 21% and 30% reductions in $A\beta_{42}$ at doses of 30 and 100 mg kg^{-1}, respectively. The authors remarked that brain amyloid was extracted with guanidine hydrochloride, which extracts both soluble and deposited amyloid, the latter representing a larger proportion of the extracted amyloid. Since the compound could only reduce soluble amyloid, this would explain the difference in **GSM-10 h** effect on $A\beta_{42}$ in brain versus CSF (which contains only soluble amyloid). Upon subchronic, 5-day oral administration, **GSM-10 h** showed an increased effect on lowering brain $A\beta_{42}$, by 38% and 48% at 30 and 100 mg kg^{-1}, respectively, 6 h postadministration. The profile of decreasing CSF and plasma $A\beta_{42}$ was similar to that of the acute dosing. The corresponding brain and plasma concentrations at 100 mg kg^{-1} dose were 52 μM and 79 μM, respectively, higher than in the acute study, which could account for the marginal increase in efficacy. In a time course study, rats were orally dosed with 30 mg kg^{-1} of **GSM-10 h**, the PD effects in the three compartments being assessed up to 72 h postdose. Maximum compound exposure was observed 3 h postdose (17.8 μM in brain and 18.3 μM in plasma), whereas the maximum $A\beta_{42}$ lowering occurred 6 h postdose in all three compartments. The amyloid levels returned to baseline 24 h after administration, and showed no rebound, unlike the effects observed with GSIs.

7.07.13.2 Arylimidazole Derivatives

An HTS campaign at GSK identified **69**, Fig. 22, a compound which in cellular assays inhibited both the production of $A\beta_{42}$ peptides as well as Notch processing. In **69**, the classical GSM A-B left hand side was linked via a C—C bond to a pyridazine central core containing a benzamide appendage.[75] An optimization program focused on improving the potency of **69**, as well as the selectivity over Notch. Replacing the amide in **69** with a benzyl amine led to significant increase in $A\beta_{42}$ and $A\beta_{40}$ potency, as in **70** and **71**. Interestingly, it was found that minor modifications could switch the profile from GSMs to Notch agonists, at high concentrations.

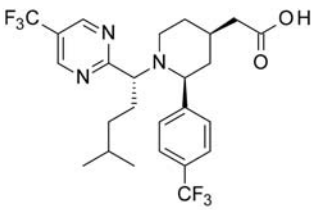

67

cellular $A\beta_{42}$ IC_{50} = 794 nM (SHSY5Y/APPswe)
cellular $A\beta_{40}$ IC_{50} > 20 μM (SHSY5Y/APPswe)
cellular Notch IC_{50} = 25 μM

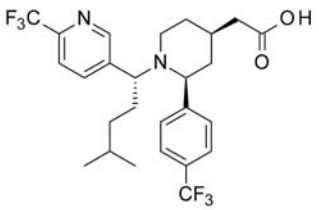

68
GSM-10h

cellular $A\beta_{42}$ IC_{50} = 316 nM (SHSY5Y/APPswe)
cellular $A\beta_{40}$ IC_{50} = 6.3 μM (SHSY5Y/APPswe)
cellular Notch IC_{50} > 20 μM

Fig. 21 GSK carboxylic acid GSMs.

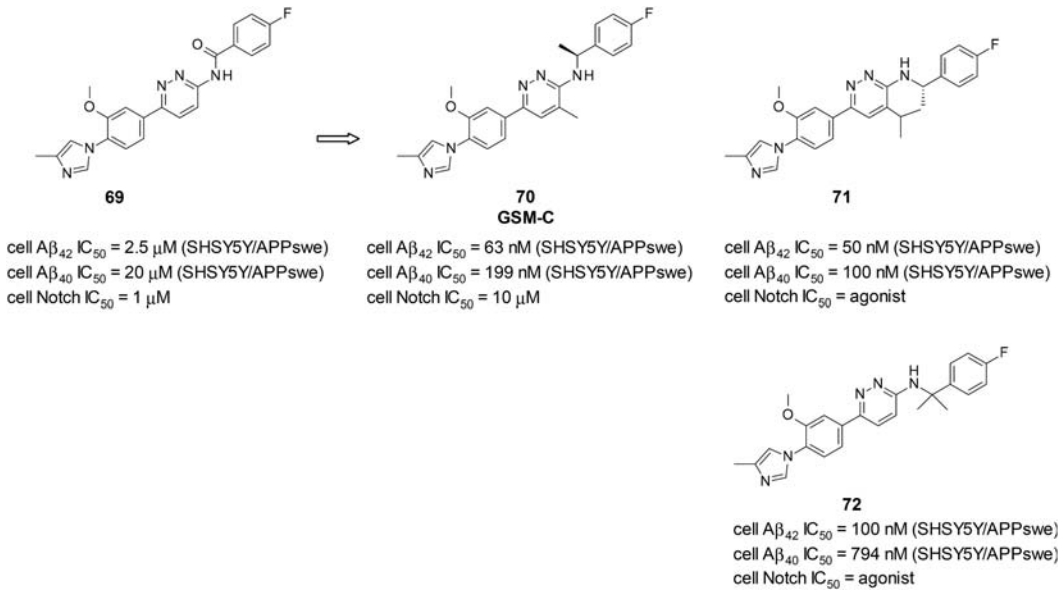

Fig. 22 Aryl imidazole derivatives with substituted aminopyridazine cores from GSK.

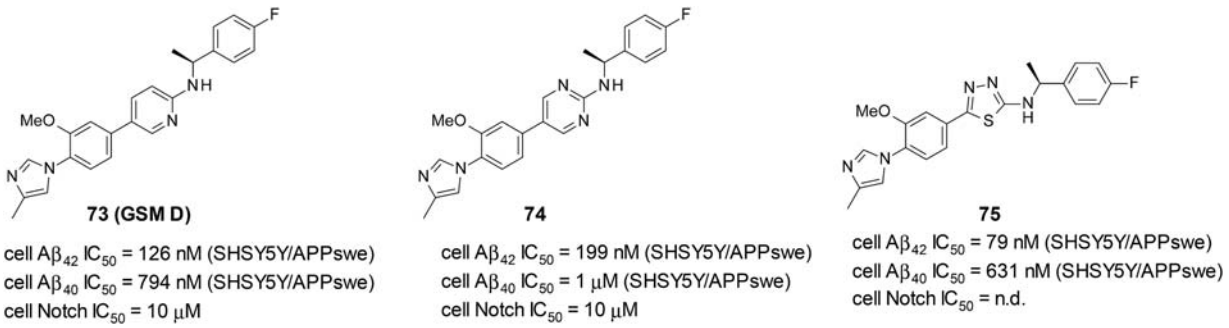

Fig. 23 Aryl imidazole derivatives with different amino heterocycle cores from GSK.

For instance, while **70** showed a 60-fold improvement for $A\beta_{42}$ inhibition, replacement of the Me substituent on the pyridazine ring with an iPr group as in **71** enhanced Notch processing, showing a greater than 30% increase of luciferase activity at 10 μM concentrations. The same was observed for analogs in which the benzylic position was disubstituted (**72**), Fig. 22.

Explorations around the central pyridazine core in **69** showed that it could be replaced by other heterocycles, such as pyridine in **73** and thiadiazole in **75** (Fig. 23).[76] Explorations around the arylimidazole left-hand side in **73** failed to provide an alternative to the ubiquitous imidazole ring.

Based on their favorable ADME profiles, **70** and **73** were further profiled in vivo in the rat, where both compounds displayed a good overall PK profile, with low clearance (5.2 and 12.2 mL $min^{-1} kg^{-1}$), acceptable half-life ($t_{1/2}$ = 3.1 and 3.3 h), and excellent bioavailability (F_{po} = 98% and 100%). Upon oral administration to rat, at 30 mg kg^{-1}, **70** and **73** displayed high (total) brain concentrations of 9.1 μM and 8.7 μM, respectively. Both compounds were then assessed in vivo efficacy studies, in Sprague Dawley rats.[77] Thus, in a dose–response study, oral administration of **70** at 3, 10, 30, and 100 mg kg^{-1} produced a significant reduction of $A\beta_{40}$ and $A\beta_{42}$ levels in plasma, CSF, and brain, in a dose-dependent manner, as determined 6 h postdosing. Under these conditions, **73** showed weaker reduction of $A\beta_{40}$ and $A\beta_{42}$ levels in brain and CSF. For **70**, the necessary doses to reduce the $A\beta_{42}$ by 50% in the three compartments were 77 mg kg^{-1} in brain; 66 mg kg^{-1} in CSF and 2.8 mg kg^{-1} in plasma. In a time course experiment, rats were orally dosed with 30 mg kg^{-1} of **70** and **73**, the PD effects in the three compartments being assessed up to 51 h postdosing. Compound **70** was again more efficacious than **73**. For **70**, the maximum compound exposure was observed 6 h postdosing (13 μM in brain and 26 μM in plasma), whereas the maximum reduction in $A\beta_{42}$ occurred at ~12 h postadministration in brain (~40% reduction) and 16 h in plasma (~91% reduction). After 51 h the amyloid levels returned to baseline and showed no rebound. Upon subchronic, 5-day oral administration of a 30 mg kg^{-1} dose of **70** and **73**, significant reduction of both $A\beta_{40}$ and $A\beta_{42}$ was observed, both in brain (63% and 58% for **70** and 17% and 23% for **73**) and in plasma (82% and 93% for **70** and 36% and 63% for **74**) at the end of the treatment.

7.07.14 Modulators From Janssen

7.07.14.1 Carboxylic Acid Derivativess

Janssen has been long active in the field of GSMs. Starting in 2007, researchers at OrthoMcNeil/Janssen in collaboration with Cellzome published a series of patents around NSAID-derived GSMs. These applications claimed a series of 3,5-disubstituted aryl acetic acid analogs, resulting from the explorations around the methyleneoxy linker in arylacetic acid GSM **76**, Fig. 24, developed by Cellzome.[78] Analogs from these patent applications are shown in Fig. 24, and they include ether (**77**), amine (**78**), amide (**79**), or carbon (**80** and **81**) linkers.[79–82] Compounds **77** and **78** were tested in vivo in mice and it was found that at a 30 mg kg^{-1} oral dose, **77** displayed a more pronounced, 43% reduction, of $A\beta_{42}$ levels versus the 18% $A\beta_{42}$ reduction shown by **78**, 4 h after administration.[79] On the other hand, when tested in rat, **78** showed a slightly improved 30% reduction in the $A\beta_{42}$ levels 4 h after treatment.

Analogs of **76** in which the linker was completely removed, leading to terphenyl derivatives, were also claimed in the 2009 patent application (**82** and **83**, Fig. 25).[83]

Apart from cellular potencies, the patent also discloses results from the in vivo testing of these compounds in mice and rats (species not specified). Compound **85**, the (S) form of **83**, Fig. 25, showed a 40% reduction of $A\beta_{42}$ levels in both species, 4 h after an oral administration of a 30 mg kg^{-1} dose. Compounds with reduced aromaticity and lipophilicity, which incorporated cyclic amines such as the piperidinyl derivative **86**, Fig. 25, were also disclosed in a different patent application.[84] Compound **86**, one of the most potent in this series, still incorporates a highly lipophilic trifluoromethyl group. A Janssen report from 2013 described

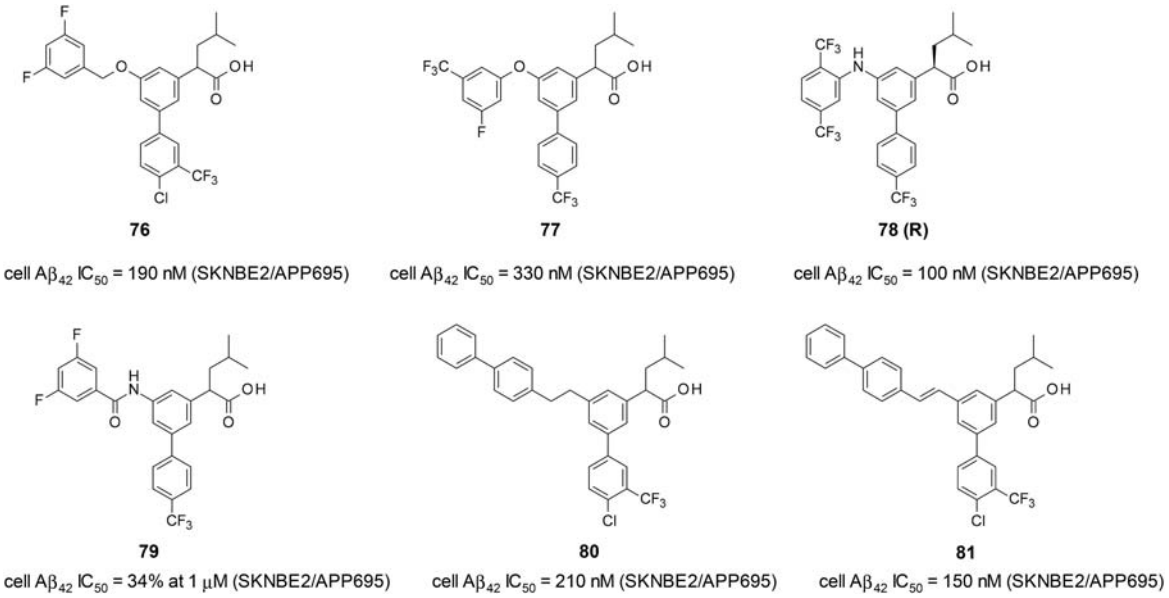

Fig. 24 Cellzome and OrthoMcNeil/Janssen carboxylic acid GSMs.

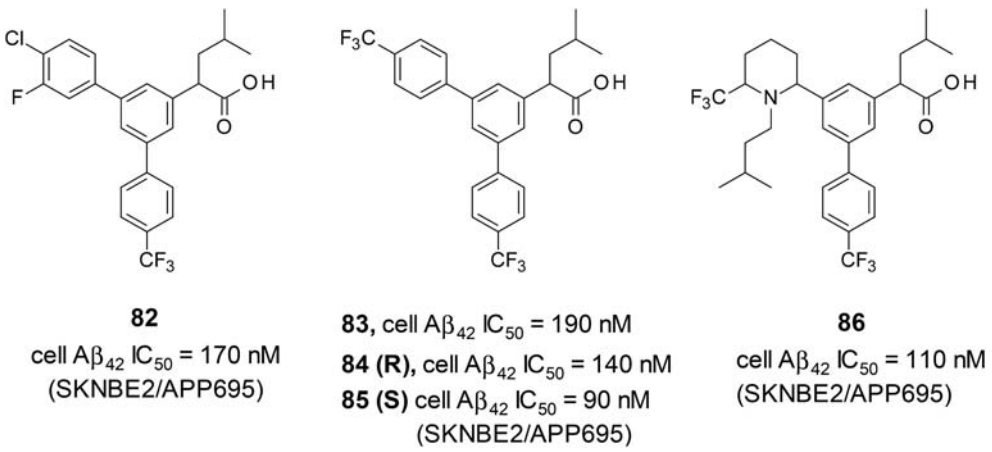

Fig. 25 Cellzome and OrthoMcNeil/Janssen terphenyls and piperidines GSMs.

the behavior of **85**, also known as JNJ-40418677, in efficacy studies in vivo in mice.[85] First, the in vitro potency was confirmed in SKNBE-2/(WT)APP cells, when **85** inhibited $A\beta_{42}$ production with an IC_{50} of 200 nM after a 16 h incubation, and in rat primary cortical neurons, where IC_{50} was 185 nM after a 48 h incubation. The levels of $A\beta_{total}$ remained unchanged in both cellular tests. When dosed at 10, 30, 100, and 300 mg kg^{-1} in nontransgenic mice, **85** showed a dose-dependent reduction in brain $A\beta_{42}$ of 18%, 36%, 61%, and 69%, respectively, 4 h after administration. In a time course experiment, nontransgenic mice were orally dosed with 30 mg kg^{-1} of **85**, the PD effects in the brain being assessed up to 24 h postdosing. The maximum compound exposure in brain was observed 6 h postdosing (~13 μM) whereas the maximum reduction (55%) of $A\beta_{42}$ and the maximum increase (78%) in $A\beta_{38}$ occurred at 6 h postadministration. After 24 h, $A\beta_{42}$ levels remained ~16% below baseline. The levels of $A\beta_{total}$ in brain remained unchanged at all time points after treatment with **85**. Following 7 months of chronic administration of **85** to 6-month-old transgenic Tg2576 mice, the compound produced a significant reduction in brain $A\beta_{42}$ and $A\beta_{40}$ levels, both soluble and deposited, at doses of 60 and 120 mg kg^{-1} day^{-1}. Unlike the effect observed in nontransgenic mice, there was no increase in the $A\beta_{38}$ levels at 20 and 60 mg kg^{-1} day^{-1}, whereas at 120 mg kg^{-1} day^{-1} a decrease in $A\beta_{38}$ deposition was observed. The chronic administration of **85** produced also a significant inhibition in the formation of plaques in the brain of Tg2576 mice, as well as a dose-dependent reduction in the number of plaques formed.

Further development of compound **85** was halted[86] due to liver toxicity and related side effects, such as increases in bilirubin and liver enzymes (ALT/AST), which were observed in an advanced canine model.

7.07.14.2 Aryl Imidazole Derivatives

As with many other research groups, Janssen's research into aryl imidazole GSMs was inspired by **E2012** (**5**, Figs. 6 and 18).[87] Computational studies suggested that replacement of the E-double bond in **E2012** with an NH-linker would provide an amino-pyridone in which the preferred, low energy conformation would be as drawn in **87**, Fig. 26. This compound would preserve a similar geometry to that of **E2012**, due to favorable electrostatic interactions. Schering/Merck also described a series of GSMs with similar amino-pyridone C-ring (**150**, Fig. 41, *vide infra*). Compound **87** was sevenfold less potent than **E2012** and did not show a significant effect on amyloid peptides when tested in vivo in mice. Conformational restriction of **87** via cyclization of the benzylic side-chain into the pyridone central ring provided imidazopyridine **88**, Fig. 26, in which the aromatic appendage needed to be attached to the 2-position of the imidazopyridine ring for potency.

Although **88** was still approximately twofold less potent than **E2012**, it produced a 35% lowering of $A\beta_{42}$ levels in mouse brain, 4 h after an oral administration of a 30 mg kg^{-1} dose. Isosteric replacement of the imidazopyridine core resulted several subseries of potent in vitro and in vivo analogs, which suffered however from suboptimal drug-like properties, such as high lipophilicity, poor solubility, and binding to the hERG channel. Further optimization led to the identification of **89**, Fig. 26, in which the

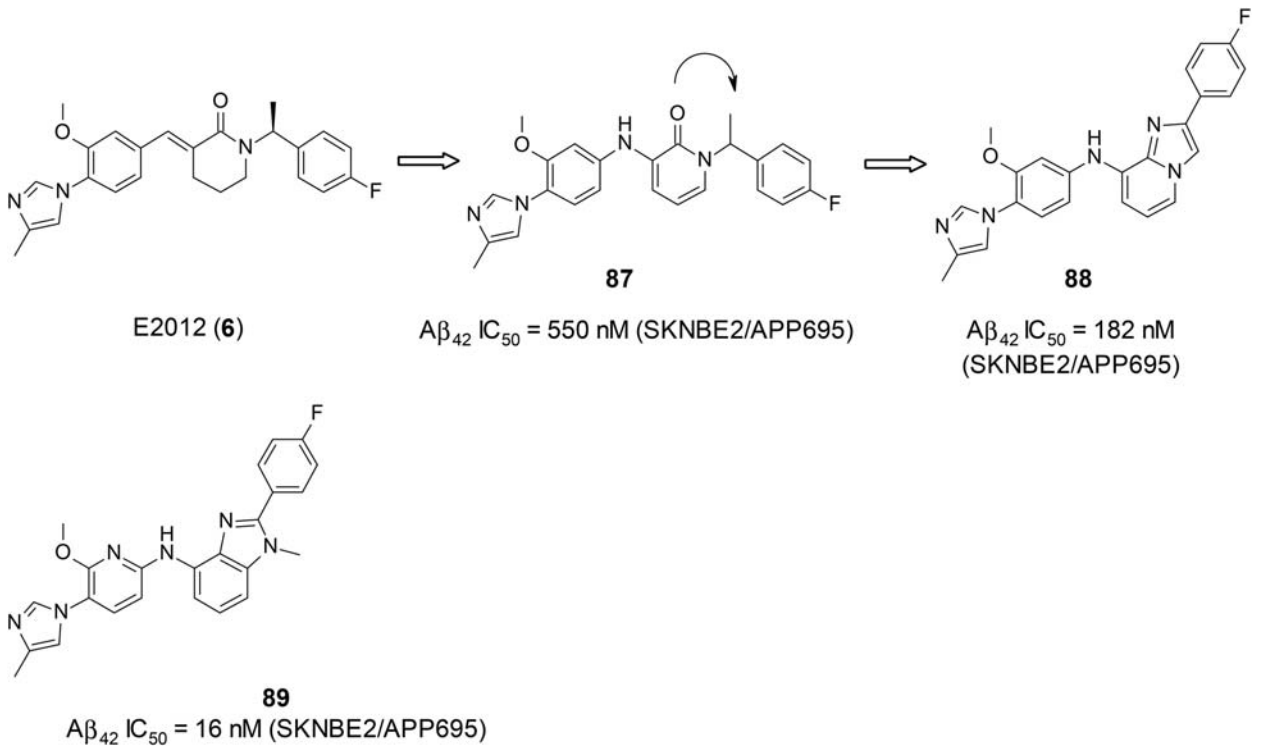

Fig. 26 Bicyclic GSMs from Janssen.

imidazopyridine was replaced by a benzimidazole isostere and, in order to decrease lipophilicity, the left hand side anisole ring was replaced by a methoxypyridine. This compound showed weak affinity for binding to the hERG channel ($IC_{50} = 8.5$ μM), which translated into a weak inhibition of the potassium membrane current recorded with an automatic patch clamp system (30% inhibition at 3 μM vs. 17% for the vehicle). Upon evaluation of the PK profile across species, **89** displayed good, and rapid, absorption in mouse ($C_{max} = 2293$ ng mL^{-1}, $T_{max} = 0.5$ h at 10 mg kg^{-1} p.o.) and dog ($C_{max} = 648$ ng mL^{-1}, $T_{max} = 0.8$ h at 5 mg kg^{-1} p.o.), and a good, but slow, absorption in rat ($C_{max} = 1973$ ng mL^{-1}, $T_{max} = 4$ h at 10 mg kg^{-1} p.o.). High bioavailability was observed in all species, 64% in dog, 95% in rat, and 100% in mouse. In a 24 h time course experiment, **89** was administered orally to mice, at 10 and 30 mg kg^{-1}, where it displayed a dose-dependent reduction of $Aβ_{42}$ and an increase in $Aβ_{38}$ levels in plasma and brain. The maximal effect for modulation of Aβ peptides was observed 4 h postdosing at 10 mg kg^{-1}, when the production $Aβ_{42}$ was inhibited by 51%, while that of $Aβ_{38}$ stimulated by 41%. Maximum brain exposure of **89** was 2.8 μM, also achieved 4 h postdosing. At 30 mg kg^{-1}, a maximum 65% increase in $Aβ_{38}$ levels was observed 4 h postdoing, whereas a maximal decrease in $Aβ_{42}$ levels, of 71%, occurred 8 h postdosing. The maximum brain exposure of 15.6 μM was achieved after 4 h. No significant effect was observed on the total level of Aβ peptides, although there was a trend for reduction at the 8 h time point. After 24 h, Aβ levels returned to normal, with the exception of $Aβ_{42}$, for which, at the 30 mg kg^{-1} dose, the levels were still reduced versus vehicle. An additional analysis performed in this experiment showed that at 48 h, the $Aβ_{42}$ levels had returned to normal. In a 24 h time course experiment performed in the beagle dog, **89** was administered orally at 20 mg kg^{-1}. The maximum PD effect in dog CSF was observed 8 h postdosing, when $Aβ_{38}$ levels were increased by 84%, whereas $Aβ_{42}$ and $Aβ_{40}$ decreased by 48% and 36%, respectively. The maximum compound exposure in dog CSF (4.1 μM) was observed 4 h postdosing. Finally, **89** showed good modulation of Aβ peptides in the brain and CSF of rat, where it was dosed at 10 mg kg^{-1} in a 25 h time course experiment. A decrease in $Aβ_{40}$ and $Aβ_{42}$ was observed in both compartments, as well as an increase in $Aβ_{38}$. A particularly strong increase was observed in $Aβ_{37}$ levels in both compartments, namely fourfold in brain and eightfold in CSF. Compound **89** still suffered from suboptimal physicochemical properties, that is, high logP, high aromaticity, and low solubility, which manifested in signs of liver toxicity after dosing in the dog at 20 mg kg^{-1}.[88] A parallel Hit Hopping search starting with **87** resulted in the identification of amide **90**, Fig. 27, which displayed a approximately fivefold loss in potency.[89] Pfizer also reported their work around a similar series of benzamides (*vide infra*, Fig. 36). Cyclization of the benzylic moiety in **90** onto the amide carbonyl moiety provided the conformationally restricted **91**, Fig. 27, having a triazole core directly linked to the A-B system. Further optimization included removal of the hydrogen bond donor (HBD) by introduction of a methyl substituent on the triazole N-atom, and introduction of a linker between the triazole core and the aromatic appendage. A methylene linker provided **92**, Fig. 27. Further restriction of the free rotation in **92** led to the identification of a series of bicyclic triazolo-amines, which allowed for the discovery of **93**, Fig. 27, a compound with reduced lipophilicity compared to **89**.[90] Compound **93** combined high in vitro potency with favorable ADME parameters. When tested in vivo in mice, it demonstrated a 62% reduction of brain $Aβ_{42}$ levels, together with a 66% increase in $Aβ_{38}$ levels, 4 h postdosing, which corresponded to a brain concentration of 2.8 μM and a Br:Pl ratio of 0.23. The free fraction of **93** in brain was $f_{u,b} = 2.2\%$, relatively high when compared to other reported GSMs. When screened in the dog, at an oral dose of 20 mg kg^{-1}, **93** demonstrated a strong, 50%,

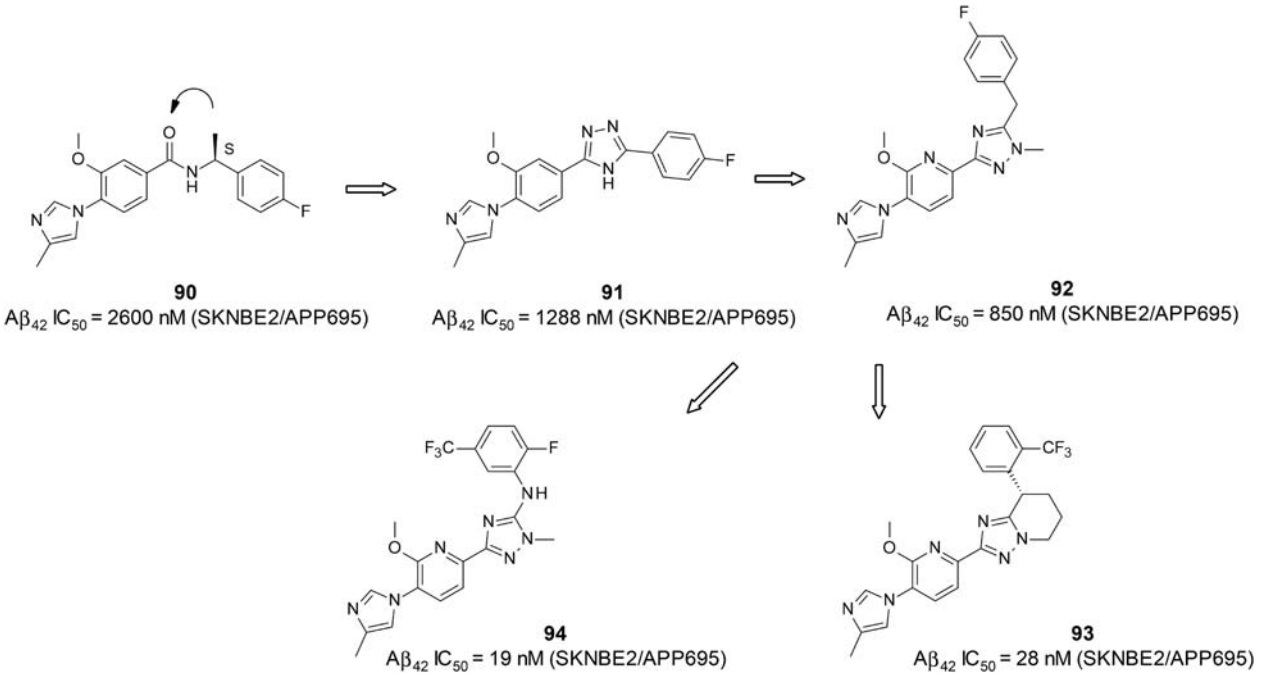

Fig. 27 Assorted triazole-derived GSMs from Janssen.

reduction in $A\beta_{42}$ levels in CSF, and a 28% increase in $A\beta_{38}$ levels, 8 h postadministration. This corresponded to a 19 μM concentration of compound in dog plasma. No increases in liver enzymes were observed despite the high plasma levels, suggesting that the liver toxicity observed with **89** was due to the high lipophilicity of the compound, and not target related.

In a parallel effort, replacement of the methylene linker in **92** with an amino-linker led to an anilinotriazole series of potent GSMs.[91] Upon subsequent optimization of this series, it was observed that for some analogs there was a disconnect between the in vitro potency and in vivo activity. The authors remarked that the presence of an ortho-substituent on the aromatic appendage was of crucial importance to obtain in vivo active compounds. In this series, **94**, Fig. 27, was identified as a GSM which combined good in vitro potency with improved physicochemical and ADME properties. For instance, when it was compared to **89**, **94** demonstrated reduced aromaticity and lipophilicity (c log *P* 4.6 vs. 5.9), better lipophilic efficiency (3.1 vs. 1.8), better kinetic solubility (39 μM vs. 3 μM), and displayed a weaker potential to inhibit CYP450 enzymes (all $IC_{50} > 10$ μM). The potential cardiovascular risk raised by the moderate inhibition of the potassium membrane current (52% at 3 μM, i.e., higher than that of **89**) did not translate in vivo in anesthetized guinea pigs. When it was orally administered to mice at 30 mg kg^{-1}, **94** showed a strong 55% reduction of $A\beta_{42}$ levels, accompanied by a strong 53% stimulation of $A\beta_{38}$, 4 h after dosing. At this time, the brain concentration of **94** was 14 μM and the Br:Pl was 0.8. As a typical GSM, **94** was highly bound to plasma and brain proteins; for instance, the brain-free fraction was $f_{u,b} = 0.5$ %, which was however improved versus that of **89** ($f_{u,b} < 0.05$ %). This resulted in a free brain concentration (69 nM), which was higher than the in vitro IC_{50} by a factor 3.6. The authors also noted that due to the low $f_{u,b}$ observed in this series, high exposure of compounds in mouse brain were required to achieve in vivo activity. In a 24 h time course experiment, **94** was administered orally to mice at 30 mg kg^{-1}, where it displayed a maximum reduction of $A\beta_{42}$ levels (61%) 6 h after treatment, while the maximum stimulation (67%) of $A\beta_{38}$ levels was observed 2 h postdosing, after which time it plateaued until 8 h postdosing. No effect was observed on the total level of Aβ peptides. After 24 h, $A\beta_{42}$ levels returned to normal, while a slight decrease from vehicle (19%) was observed for $A\beta_{38}$. Upon oral administration of 20 mg kg^{-1} of **94** to the dog, a maximal 56% reduction of CSF $A\beta_{42}$ was observed 8 h postdosing, combined with a 54% reduction of $A\beta_{40}$ and 31% increase in $A\beta_{38}$ levels. The corresponding concentration of **94** in dog plasma was 6.7 μM. The authors also mentioned that in a one week repeated dose study in dog, at 10 and 20 mg kg^{-1}, no increase in liver enzymes (ALT and AST) was observed.

A subsequent patent application from Janssen described GSMs with imidazolo-indoles for the left hand A-B system, as well as compounds in which the imidazole was replaced by a nitrile moiety.[92] GSMs having the ubiquitous imidazole replaced by a nitrile moiety were also reported by BMS, *vide supra*, for example, **34**, Table 1 and **41**, Fig. 15. Notably, this modification preserved the modulation of Aβ peptides both in vitro and in vivo, as shown for compounds **95** and **96** in Fig. 28. As can be inferred from the reported in vivo effects of the claimed compounds, compound **96** was a particular example of a potent GSM which, upon oral administration of a 30 mg kg^{-1} oral dose to nontransgenic mice, strongly inhibited the production of $A\beta_{42}$ peptides, but it did not show a significant increase in the $A\beta_{38}$ levels from the baseline, 4 h postadministration.

More recent applications from Janssen disclosed yet another chemical class of GSMs, in which a central piperazino-pyridone core is substituted with the conserved imidazole or triazole on the left hand side, while various substituents are claimed on the piperazinone right hand side (**97–99**, Fig. 29).[93,94] As will be described later in this review, Pfizer has also claimed GSMs containing a piperazino-pyridone core,[95] *vide infra* (Fig. 36), which appeared a few months before a similar publication of Janssen, WO 2013171712. The most interesting compounds from the Janssen applications are illustrated in Fig. 29 and Table 2. To be noted is **99**, which upon oral administration to nontransgenic mice at a 30 mg kg^{-1} dose, produced a strong modulatory effect on the amyloid peptides 4 h after administration. Finally, restriction of the piperazinone substituents into the piperazinone ring led to novel tricyclic GSMs, such as **100**, Fig. 29, in which a fused 6,6,5-tricycle has a flexible aromatic appendage at position 3.[96]

Further progression of compound **89**, also known as JNJ-42601572, was halted, due to the aforementioned liver toxicity. Moreover, in a tissue distribution study in rats, **89** showed a liver:plasma ratio of 8.5.[86] Compound **94** was described as the next generation of GSM and may have been selected for further development, although no active work with this compound has yet been reported.

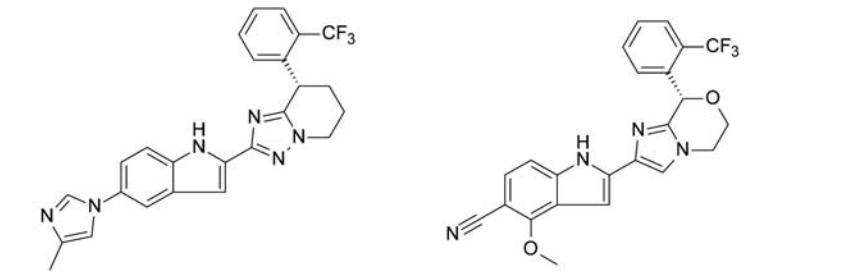

95
cell $A\beta_{42}$ = 46 nM (SKNBE2/APP695)
cell $A\beta_{total}$ > 10 μM (SKNBE2/APP695)

96
cell $A\beta_{42}$ = 21 nM (SKNBE2/APP695)
cell $A\beta_{total}$ > 10 μM (SKNBE2/APP695)

Fig. 28 Triazolo-derivatives with an indole core (**95**) and cyano-indole derivative as the aryl-imidazole (A-B) replacement (**96**) from Janssen.

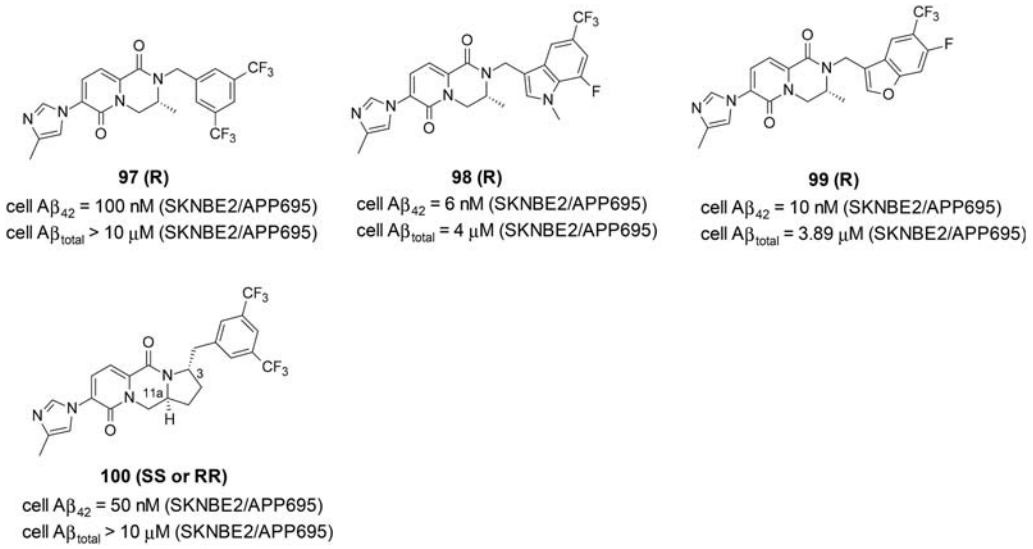

Fig. 29 Janssen piperazino-pyridones.

Table 2 Effect of Janssen GSMs on nontransgenic mice, 4 h after oral administration of a 30 mg kg^{-1} dose

Compound	*%Aβ 42 lowering*	*%Aβ 40 lowering*	*%Aβ 38 increase*
95	59	N.A.	81
96	73	69	10
97	45	N.A.	37
99	75	79	137
100	53	31	36

7.07.15 Modulators From Merck

7.07.15.1 Carboxylic Acid Derivatives

Research in the GSM area started at Merck more than a decade ago, when they reported carprofen-derived modulators.[97] Their initial work on the phenyl-acetic acid class of GSMs focused on the exploration of 3,4-positions of the phenyl ring.[98] This led to analogs such as trifluoromethylaryl **101** (Fig. 30). Subsequent work focused on reducing the lipohilicity in this series by replacing the central aromatic core with a piperidine ring. This exercise led to compounds such as **102** and **103**,[99] Fig. 30, in which however the c log *P* remained suboptimal. Compound **103**, also known as **GSM-1**,[100] is a potent carboxylic acid GSM, which was further evaluated in in vivo studies. Thus, when it was administered to transgenic mice expressing APP_{Swe} at 3, 10, and 30 mg kg^{-1} dose, **103** demonstrated a dose-dependent reduction in $A\beta_{42}$ levels, with a maximum 69% reduction at 30 mg kg^{-1}, 4 h after treatment.[101] Simultaneously, the levels of $A\beta_{38}$ increased in a dose-dependent manner, while $A\beta_{40}$ and $A\beta_{total}$ levels were not significantly changed.

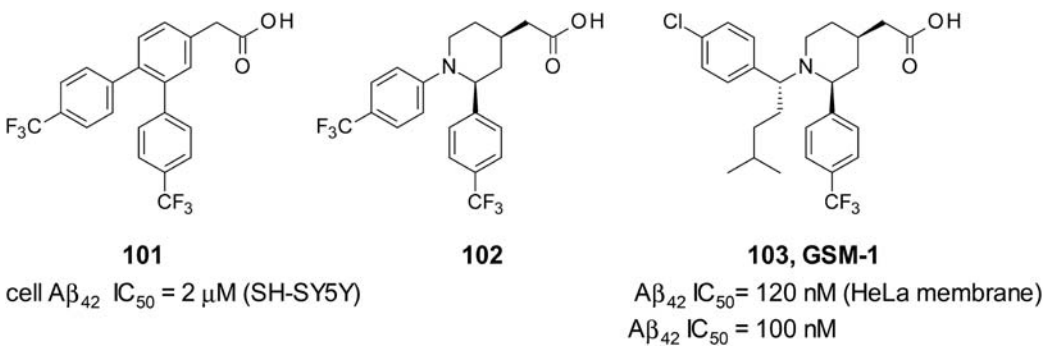

Fig. 30 Merck aryl and piperidine acetic acid GSMs.

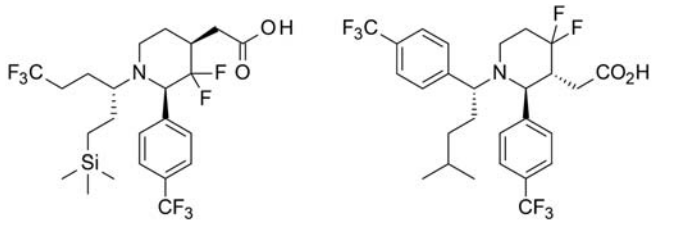

Fig. 31 Merck difluorpiperidine GSMs.

During optimization efforts around the piperidine acetic acid derivatives **103**, Merck researchers incorporated a di-F substitution on the piperidine ring, both at the 3- and at the 4-positions.[102] Two representative examples from this series, **104** and **105**, are shown in Fig. 31. Not only was the di-fluoro substitution tolerated at both 3- and 4-positions of the piperidine, but replacement of the aromatic substituents on the piperidine nitrogen with alkyl moieties was also allowed.

Despite the moderate in vitro potency of **104** and **105**, both compounds showed a robust reduction of $A\beta_{42}$ levels of 64% and 84%, respectively, when dosed at 10 mg kg^{-1} in APP-YAC transgenic mice, after 7 h p.o. administration. For compound **105**, this effect was achieved at a brain concentration of 0.58 μM and a Br:Pl of 0.51. Moreover, **105** demonstrated a dose-dependent lowering of $A\beta_{42}$ in rats, when dosed orally, at 1, 3, 10, and 30 mg kg^{-1}, and with an $ED_{50} = 5$ mg kg^{-1}, brain $EC_{50} = 1$ μM, and plasma $EC_{50} = 3.7$ μM. No adverse Notch effects were observed when **105** was tested in a 7-day oral rat safety study, at 250 mg kg^{-1} day^{-1}.

7.07.15.2 Aryl-Piperazine Derivatrives

A piperazinyl-pyrimidine derivative identified at Merck after an HTS campaign showed weak modulation of Aβ peptides and inhibited the production of $A\beta_{42}$ versus $A\beta_{40}$ by a factor ~2 (**106**, Fig. 32).[103] Initial SAR studies provided **107**, which incorporated a di-methyl substituent on the piperazine ring. When compared to **106**, **107**, Fig. 32, showed improved potency for $A\beta_{42}$ inhibition, which resulted in a 17-fold selectivity over the inhibition of $A\beta_{40}$. A round of optimization focused on improving potency and selectivity for $A\beta_{42}$ over $A\beta_{40}$, and led to the identification of a *tert*-butyl-aniline as an optimal substituent on the pyrimidine ring. Upon optimization of the physicochemical parameters of the series, it was found that polar groups were tolerated on the central pyrimidine ring. This resulted in the identification of **108**, Fig. 32, as a potent inhibitor of $A\beta_{42}$ production, with high selectivity (24-fold) over inhibition of $A\beta_{40}$ and 180-fold selectivity over Notch. Importantly, this is an example of non-NSAID GSMs structurally different from the aryl-imidazole class. The modulation pattern of Aβ peptides is also different, resembling more the NSAID-like GSMs.

Speculating that the high potency in **108** was due to hydrogen-bond interactions of the hydroxymethyl moiety on the pyrimidine ring, subsequent optimization focused on finding isosteres that would enhance this interaction. This led to the identification of purine analog **109**, Fig. 33, a potent GSM with high selectivity over $A\beta_{40}$ and Notch. Exploration around the 4-methoxyphenyl-piperazine left hand side revealed that this region was now more tolerant to substitution than in the pyrimidine series. For instance, it allowed the identification of **110**, Fig. 33, in which the piperazine ring was replaced with a piperidine and the anisole ring with a pyrimidine connected to the piperidine ring via an O-linker. The pyrimidine ring in **110** preserved the HBA properties of the methoxy moiety in **109**.

Compounds **109** and **110** were administered to APP-YAC transgenic mice at an oral dose 100 mg kg^{-1} and the effect on Aβ peptides was evaluated 6 h postdosing. Both compounds demonstrated a strong reduction of $A\beta_{42}$ peptides, corresponding to 73% for **109** and 69% for **110**. Only **110** showed a slight 26% reduction of $A\beta_{40}$ levels. The corresponding brain concentrations were 7.8 μM for both compounds.

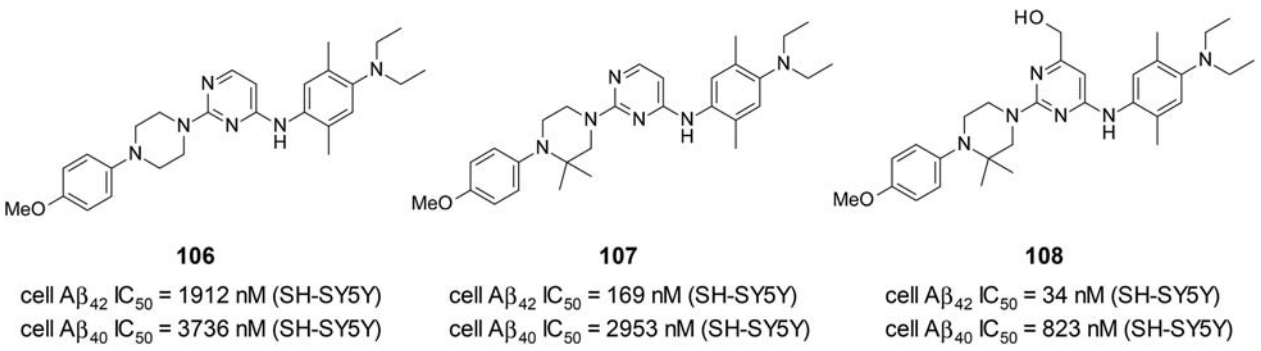

Fig. 32 Merck piperazinyl-pyrimidine GSMs.

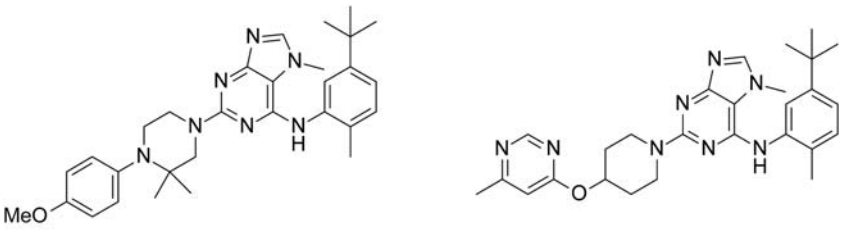

Fig. 33 Merck purine GSMs.

7.07.15.3 Aryl Imidazole Derivatives

In order to identify novel non-carboxyllic acid GSMs, scientists at Merck considered modifications of Eisai cinnamide series.[104] Starting from **E2012** (**6**, Figs. 5 and 18), their initial efforts focused on investigating amide replacements. This exploration allowed identification of **111**, an olefinic quinazolinone with modest in vitro potency. While this compound displayed an acceptable rat PK profile (Cl_p 6.8 mL $min^{-1}kg^{-1}$, $V_{dss}=1.8$ L kg^{-1}, $t_{1/2}=5.8$ h, $F_{po}=59\%$), the quinazolinone series in general suffered from suboptimal properties, that is, poor solubility, which resulted in low oral bioavailability, and hERG liabilities. To address these issues, in a subsequent exploration the double bond linker was replaced by various five-membered ring heterocycles.[105] Compounds in which the double bond was substituted by a 1,2,3-triazole central core (ring C) were selected for further optimization. Analogs with benzyl substituents on the triazole core had low potencies, **112**, being the most potent of the series. Replacement of the hydrophobic benzyl substituent in **112** with amides provided analogs with a slight increase in potency (**113**),[106] Fig. 34. Conformational restriction of the amides to give lactams, as shown by **114**, allowed the identification of triazolo-azepinones with improved in vitro potency. Such an example is **115**, Fig. 34, which combined good in vitro potency ($IC_{50}=9$ nM) with low hERG binding ($IC_{50}=5$ μM). Unfortunately, these compounds had no effect on Aβ peptides when tested p.o. in SD rats or APP YAC mice, at 50 mg kg^{-1}, due to low brain exposures and suboptimal brain:plasma ratios, in general <0.1.

More recently, Merck disclosed their optimization studies towards improving central lowering of $Aβ_{42}$ of triazolo-azepinones. In a first optimization round, a series of triazolo-benzazepinones was identified,[107] with analogs which lowered $Aβ_{42}$ levels in Sprague Dawley rats and transgenic APP-YAC mice brains in a dose-dependent manner after single oral dose. A lead in this series, **116**, Fig. 34, displayed an ED_{50} of 15 mg kg^{-1} when dosed orally in both species. When tested at highest dose (100 mg kg^{-1}) in a dose-dependent study in SD rat, **116** showed a total brain concentration $C_b=35$ μM, 6 h after dosing, and a 92% reduction of $Aβ_{42}$ levels in rat brain. This compound displayed an acceptable rat PK profile with good bioavailability (Cl_p 38 mL $min^{-1}kg^{-1}$, $V_{dss}=4.8$ L kg^{-1}, $t_{1/2}=0.8$ h, $F_{po}=190\%$). In dog, **116** had high clearance ($Cl_p=82$ mL $min^{-1}kg^{-1}$) and no oral bioavailability. Rhesus PK for **116** showed moderate plasma clearance ($Cl_p=17$ mL $min^{-1}kg^{-1}$) but no oral bioavailability. Compound **116** was then evaluated in an acute PK/PD study in a cisterna-magna-ported rhesus model, when it was administered via i.v. infusion at a dose of 50 mg kg^{-1}. Compound **116** significantly lowered the $Aβ_{42}$ levels in rhesus CSF, with sustained $Aβ_{42}$ reduction over 20 h. Further profiling of **116** revealed that it was a potent inhibitor of serotonin re-uptake transporter, with an $IC_{50}=32$ nM.

Optimization of the benzoazepinone series focused on improving the PK parameters, via modification of the conserved methylimidazole-anisole moiety (A-B ring), which was identified as a potential metabolic liability.[108] Fluoroaryl derivative **117**, Fig. 34, one of the leads identified after this exploration, showed good in vitro potency (58 nM), low hERG binding (hERG $IC_{50}=8.3$ μM), and an improved Br:pl ratio of 1. When dosed at 100 mg kg^{-1} in APP YAC Tg-mice, **117** demonstrated significant lowering of $Aβ_{42}$ brain levels (74%) 6 h postdosing. It also showed an ED_{50} of 5.8 mg kg^{-1} in SD rats. Compound **117** had an improved PK profile in both SD rat and dog, with low clearance (Cl = 17 and 22 mL $min^{-1}kg^{-1}$, respectively) and good oral bioavailability ($F_{po}=55$ and 74%, respectively).

From the latest report, which occurred in 2015, it would appear that Merck might have advanced compounds from the benzazepinone series (exemplified by **116**) to preclinical development. As of yet, there is no subsequent publication around **116** and analogs.

7.07.16 Modulators From Pfizer

7.07.16.1 Carboxylic Acid Derivatives

Researchers at Pfizer disclosed in 2011 a series of carboxylic acid GSMs, which contained aminocyclohexanes or aminotetrahydropyrans as central core,[109] similar to those reported by Merck (vide supra). GSMs **118** and **119**, Fig. 35, were among the most potent and most tested analogs. Similar potencies were observed for both compounds, however, **119** is less lipophilic. These derivatives are

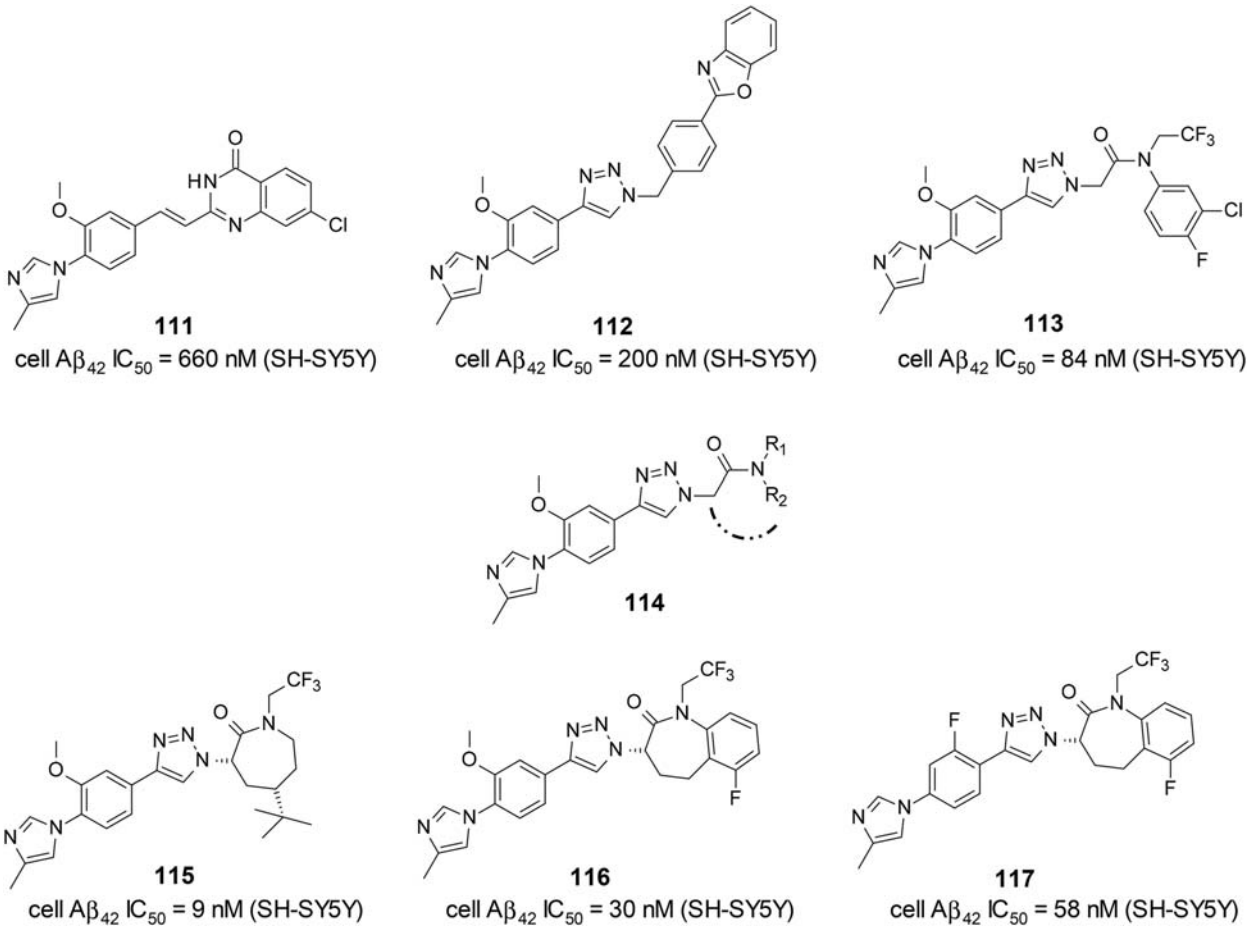

Fig. 34 Merck 1,2,3-triazole GSMs.

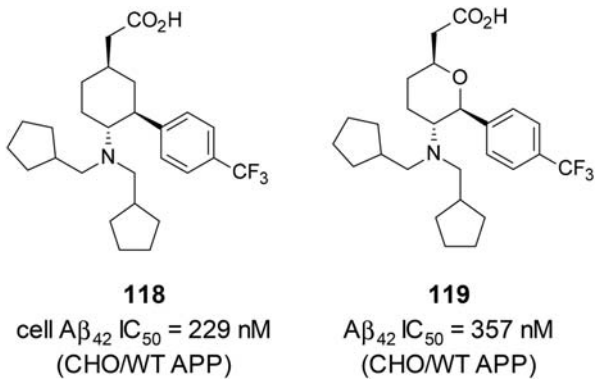

Fig. 35 Carboxylic acid containing modulators from Pfizer.

similar to those reported by Astellas, *vide supra*, for example, compound **15**, Fig. 9. It appears that interest in this series was short-lived as the focus of the Pfizer group's research has changed to the aryl-imidazole template.

7.07.16.2 Aryl-Imidazole Derivatives

Researchers at Pfizer started their search for novel non-NSAID GSMs from **E2012**, (**6**, Figs. 5 and 18) aiming to reduce lipophilicity in order to improve the overall drug-like profile. Replacement of the undesirable cinnamide olefin moiety in **E2012** with an amide bond,[110] as in **90**, Fig. 36, led to a significant decrease in potency. Amide-containing GSMs were also reported by Janssen (*vide supra*, Fig. 27). Optimization, which focused on the right hand side phenyl appendage delivered analogs with restored

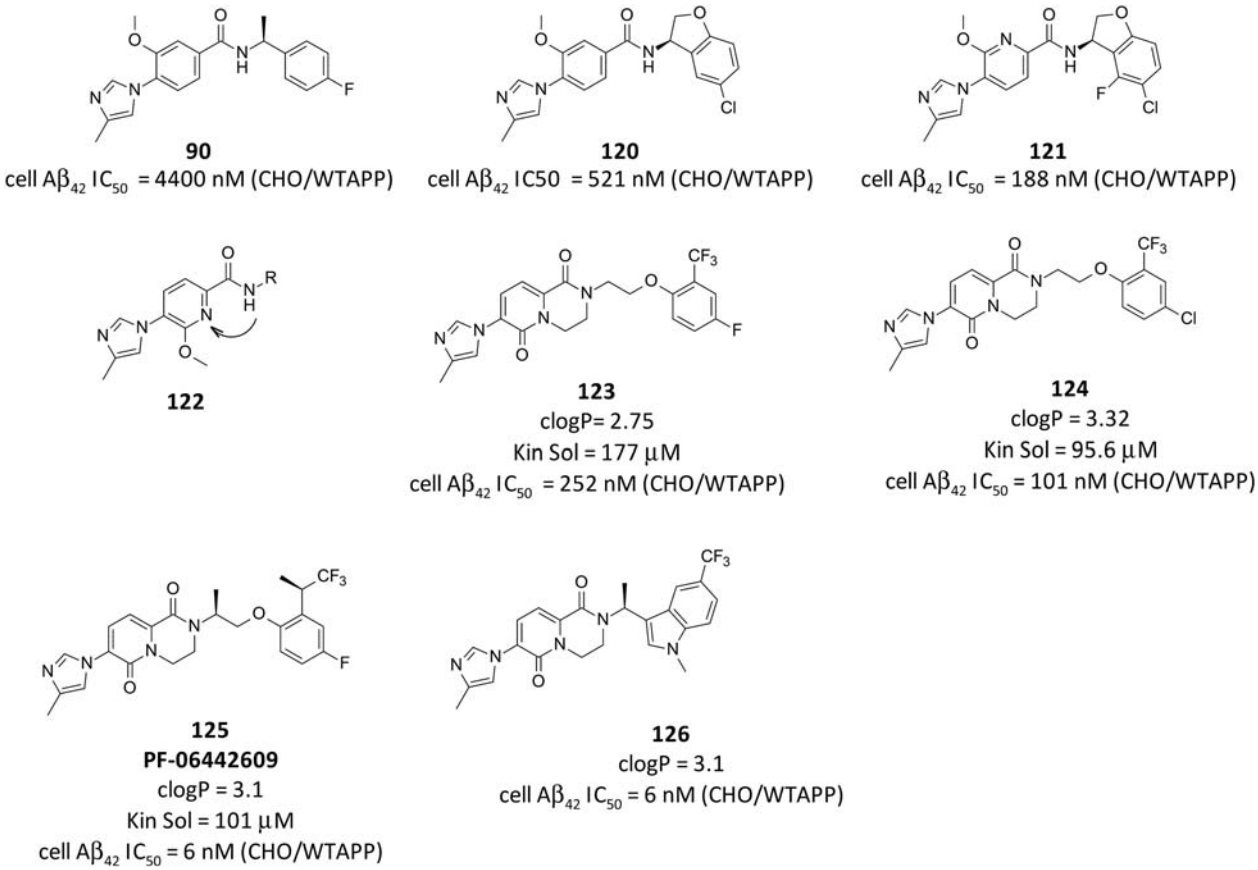

Fig. 36 Pfizer amide derivatives (**90**, **120**, and **121**) and piperazino–pyridone (**123–126**) GSMs.

potency, such as **120**, and **121**, Fig. 36. The PK profile of these compounds was evaluated in rat. **120** had a better overall profile than **121**, with lower clearance (Cl = 9.63 vs. 31.4 mL $min^{-1} kg^{-1}$), longer half-life ($t_{½}$ = 2.43 vs. 0.64 h), and better bioavailability (F = 100% vs. 51%). When tested in vivo in guinea pigs, at 100 mg kg^{-1}, **120** showed a better, 57% reduction of brain $Aβ_{42}$ levels 4 h postdosing versus 36% displayed by **121**. Bioanalysis revealed that the free brain concentration for **120** was 1038 nM, twofold higher than the IC_{50}; while for **121** the free brain concentration was $C_{u,b}$ = 89 nM, lower than the IC_{50} ($C_{u,b}/IC_{50}$ = 0.31). This might explain the difference in the in vivo potency of **120** and **121** and it is consistent with the trend observed for GSMs, that is, their characteristic high lipophilicity leads to compounds that are highly bound to brain tissue. As a result, a high total brain concentration is required for in vivo efficacy.

Cyclization of the amide N-atom in **122** onto the methoxypyridyl ring, Fig. 36, led to a novel type of GSMs, in which the conserved aryl-imidazole ring was replaced with a less lipophilic piperazino-pyridone scaffold.[111] GSMs containing a similar template have been disclosed also by Janssen, for example, compounds **97–99**, Fig. 29. GSM potency was maintained in this new series, as can be seen by examples **123** and **124**, Fig. 36. These compounds have an improved overall profile versus the majority of reported GSMs, being less lipophilic and having excellent kinetic solubilities, for instance. Compound **124** had a good PK profile in rat, with low clearance (Cl = 1.4 mL $min^{-1} kg^{-1}$), rather long half-life ($t_{½}$ = 6.88 h) and high oral bioavailability (F = 88%). The in vivo activity was assessed in a guinea pig efficacy model, at 10, 30, and 90 mg kg^{-1} oral doses. In this case, a dose-dependent reduction of Aβ peptides in brain was observed, which was more pronounced for $Aβ_{42}$ than for $Aβ_{40}$. For instance, when it was dosed at 30 mg kg^{-1} and 4 h postoral dosing, **124** showed a significant decrease of brain $Aβ_{42}$ (44%) levels, combined with a moderate decrease of $Aβ_{40}$ (31%). At this dose, no significant effect was observed on $Aβ_{38}$ peptides (8% increase). Bioanalysis revealed that the free brain concentration of **124** at 30 mg kg^{-1} was 72 nM ($F_{u,Br}$ = 0.8%). Optimization efforts aimed to improve the cellular potency of **124**, and identified highly potent compounds such as **125** and **126**,[112,113] Fig. 36. Indole-substituted piperazinone derivatives have also been disclosed in a patent application from Janssen, which published sooner, for example, compounds **97–99**, Fig. 29, covering compounds with an indole appendage as in **126**.[114] Compound **125**, also known as PF-06442609, has an F-atom strategically introduced on the phenyl ring to block oxidative metabolism. This compound combined excellent single-digit in vitro potency with good physicochemical and ADME properties. Rat PK parameters were acceptable, **125** showing moderate clearance (Cl = 34.1 mL min^{-1}), acceptable half-life, and oral bioavailability ($t_{½}$ = 1.15 h, F = 51%). Compound **125** was evaluated in a guinea pig time-course experiment, when it was dosed orally at 60 mg kg^{-1}. The lowering of Aβ peptides and the corresponding brain exposures were measured at 1, 3, 6, 9, and 24 h postdose. The maximal effect seemed to be obtained 3 h

postdose, when $A\beta_{42}$ and $A\beta_{40}$ were significantly reduced by 41% and 50%, respectively, while $A\beta_{38}$ levels increased by 46%. This corresponded to an unbound brain concentration of 225 nM.

Compound **126** was also examined in an in vivo efficacy study in rat. Despite its high in vitro potency and acceptable intrinsic apparent clearance in human liver microsomes (28.3 mL $min^{-1}kg^{-1}$), when dosed orally at 30 mg kg^{-1}, **126** showed a low reduction of brain $A\beta_{42}$ and $A\beta_{40}$ 4 h after exposure (21% and 20%, respectively). This corresponded to low compound exposures in brain ($C_{u,b}=5$ nM, and Br:Pl of 0.7), which were attributed to PgP-mediated efflux after comparison with brain exposures in Pgp knockout mice.

According to the Pfizer pipeline, it appears that Pfizer has identified a GSM, PF-06648671 with suitable properties to progress to clinical studies, *vide infra*. Thus, it appears that long-term commitment to the field has paid off. Whether this compound will differentiate over the previously terminated GSMs from this structural class, *vide infra*, remains to be seen.

7.07.17 Modulators From Roche

7.07.17.1 Aryl Imidazole Derivatives

The group at Roche has published details of their early work on aryl-imidazole-related temples. An HTS delivered **127**,[115] which selectively lowered $A\beta_{42,}$ in human neuroglioma H4 cells overexpressing human APP. Optimization resulted in the discovery of RO5220778 (**128**),[116] Fig. 37. As **128** displayed adequate PKs in the mouse, Cl_p 18.3 mL $min^{-1}kg^{-1}$, V_{dss} 4.6 L kg^{-1}, $t_{½}$ 2.5 h, F_{po} 25%, Br:Pl 0.4–2.1, it was profiled in an efficacy study in the APPSwe Tg mouse. Doses of 10, 30, and 100 mg kg^{-1} p.o. reduced brain $A\beta_{42}$ by 18%, 35%, and 65%, respectively, 4 h postdose, resulting in a calculated ED_{50} of 40 mg kg^{-1}.

Subsequent iterations of this series have been disclosed in a series of patent applications. Analogs have been divulged with either an aminotriazole, such as **129**, or amino-pyrazole, such as **130**,[117] with a substituted *N*-benzyl group on the right hand side, Fig. 38. It is noteworthy that these compounds also have a nitrile group in place of the methoxy group, however this might be reflected by suboptimal potency. Related fused triazolopyridine derivatives have also been described, such as **131** and **132**,[118] Fig. 38, which offer enhanced potency.

Alternatively, replacement of the aminotriazole in compounds such as **129** by an aminopyrimidine results in compounds such as RO5434400 (**133**),[116,119] Fig. 38. Whilst displaying modest potency in H4 cells, enhanced potency was observed in rat primary neurons, $A\beta_{42}$ IC_{50} 31 nM. Doses of 3–100 mg kg^{-1} p.o. to APP-Swe resulted in dose-dependent reductions in brain $A\beta_{42}$, with around 60% at 100 mg kg^{-1}. Furthermore, a 30 mg kg^{-1} dose of RO54434400 reduced CSF $A\beta_{42}$ in the rat by around 50% 6 h postdose. However, RO54434400 was found to inhibit multiple CYP enzymes, 3A4 IC_{50} 1.4 μM, 2D6 IC_{50} 1.1 μM, 2C9 IC_{50} 1.5 μM, and display time-dependent CYP inhibition and produce reactive metabolites. It was also found to block the hERG channel, IC_{50} 1.5 μM, thus making it unattractive for further progression.

This series was modified further to deliver amino-triazines such as **134**,[120] which displayed weak activity, Fig. 38. The replacement of the methoxyphenyl moiety has been described for a range of derivatives. For example, replacement of the methoxyphenyl moiety in **131** and **133** resulted in piperidine derivatives with a C-linked heterocyclic replacement for the methylimidazole, to give **135** (RO5506284) and **136**, respectively,[121] Fig. 38. Further derivatives have also been disclosed whereby a bicyclic piperidine has been incorporated, such as **137**,[122] Fig. 38. RO5506284 (**135**) has been the subject of a recent publication detailing a longitudinal study in APP-Swe mice whereby amyloid levels were tracked with the use of positron emission tomography (PET).[123] Interestingly, the potency quoted in the literature implies the compound is 10-fold more potent than originally denoted in the patent application. In an acute dose–response study in the APP-Swe mouse, RO5506284 (**135**) reduced brain $A\beta_{42}$ in a dose-dependent manner, with reductions of 20%, 48%, and 73% 4 h after oral doses of 10, 30, and 100 mg kg^{-1}, respectively. Subsequently, a 30 mg kg^{-1} oral dose of RO5506284 (**135**) was administered to APP-Swe mice for 6 months, starting at 12 months of age, and amyloid reductions monitored temporally by PET as well as upon termination by PET, ELISA, and histochemistry. The results showed a 56% reduction in fibrillary Aβ plaques compared to vehicle controls, primarily due to the lower number and density of smaller plaques, showing that RO5506284 prevents new plaque formation. It has been reported that RO5506284 inhibits CYP2D6, IC_{50} 1 μM, and shows GSH adducts when incubated with human liver microsomes, which was attributed the thiadiazole moiety.[116] Thus, it seems that RO5506284 did not progress beyond preclinical investigation.

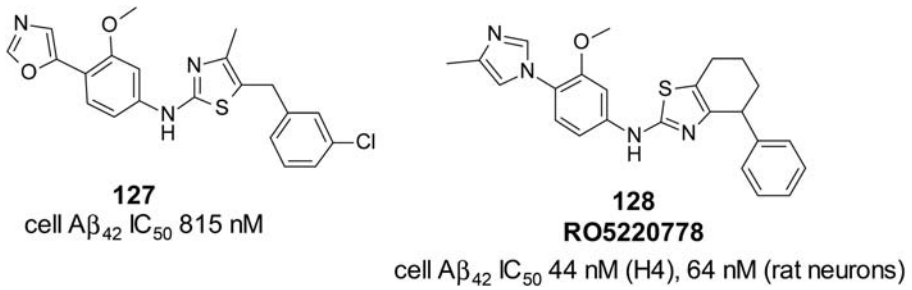

Fig. 37 Early compounds from Roche, including HTS hit **127** and optimized lead, **128**.

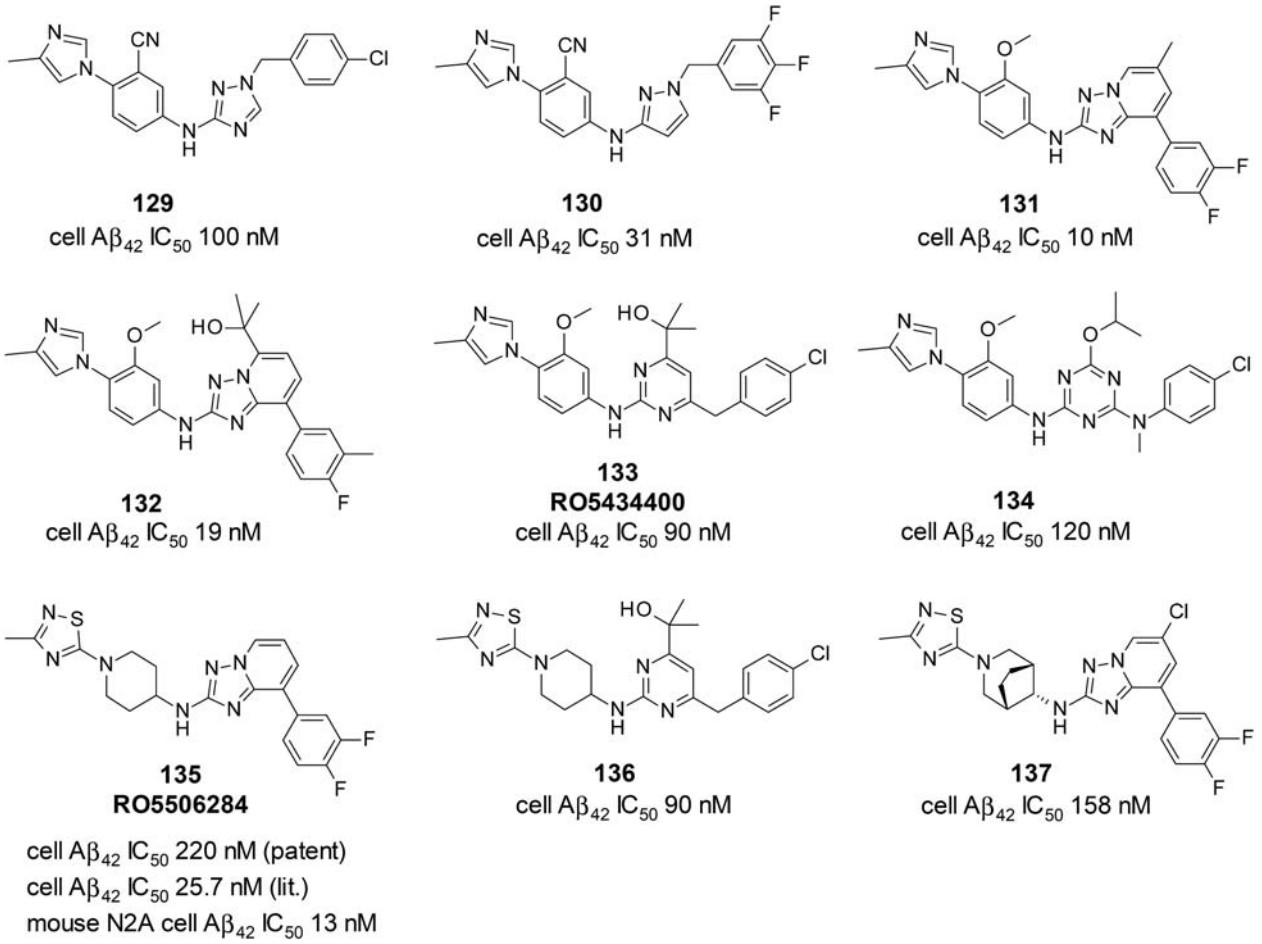

Fig. 38 Selected derivatives from Roche patent applications, including RO5506284 (**135**).

7.07.17.2 Other Derivatives

A more recent patent application details a novel chemotype that had not previously been described. The compounds consist of an indole core with an anilide in the 2-position, usually containing a fluorinated aniline, often 3-fluoro aniline. The 5-position of the indole contains some polar or basic functionality, such as substituted piperidines. Although the potency described is moderate, the discovery of a new template offers the possibility of a completely different profile and therefore different properties and off-target activities. Pertinent examples include **138** and **139**,[124] Fig. 39.

In summary, Roche have invested significant effort to the GSM field, but despite this prolonged research on multiple templates it does not seem that Roche have progressed any GSMs to clinical studies. Overall, it appears that CYP450 issues (inhibition, TDI, and reactive metabolites) in addition to the high efficacious concentrations of compounds and suboptimal physicochemical properties have precluded further advancement.

7.07.18 Modulators From Satori

The Satori group tackled the identification of GSIs by taking a different approach to all other groups and screening natural products, using a cellular assay (H4 cells expressing human wild-type APP).[125] This resulted in the identification of **140**, $A\beta_{42}$ IC_{50} 100 nM, $A\beta_{40}$ IC_{50} 6300 nM, the extract of the black cohosh plant, Fig. 40. Compound **140** displayed an unusual modulatory profile compared to other modulator chemotypes. In CHO cells (either expressing APP_{wt} or mutant APP_{V717F}), 1 μM **140** decreased $A\beta_{42}$ and $A\beta_{38}$, whilst it increased $A\beta_{37}$ and $A\beta_{39}$ and marginally lowered $A\beta_{40}$.

Initial optimization investigated reduction of the enol ether with concomitant replacement of the xylopyranose by esters.[126] However, more fruitful changes resulted when the xylopyranose was replaced by a morpholine, with the rationale of incorporating a basic center to increase CNS penetration. This resulted in the identification of compounds such as **141** and **142**, Table 3.[127] A mouse PK study revealed an encouraging profile for **141**, having a longer half-life than **142** by virtue of its greater volume of

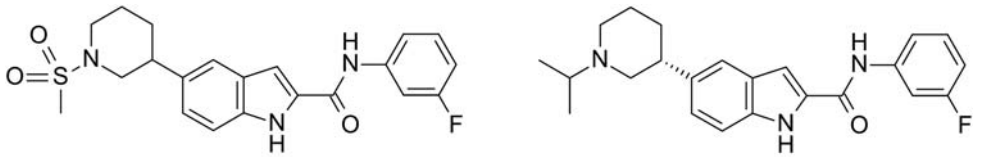

138
cell $A\beta_{42}$ IC_{50} 148 nM

139
cell $A\beta_{42}$ IC_{50} 116 nM

Fig. 39 Novel indole derivatives disclosed by Roche.

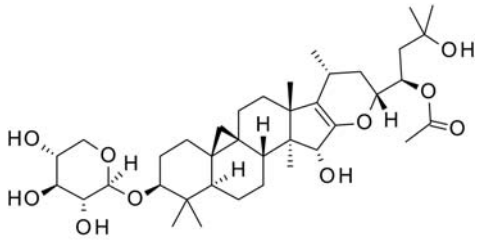

140
Cell $A\beta_{42}$ IC_{50} 100 nM
Cell $A\beta_{40}$ IC_{50} 6300 nM
PSA 155.1

Fig. 40 Structure of **140**, an extract of the black cohosh plant.

distribution, which was thought to be due to the higher pKa of **141**. Neither **141** nor **142** was efficacious in a mouse efficacy study, even though **141** demonstrated good levels of exposure in the brain, 2117 nM and 3586 nM at 4 and 8 h after a 30 mg kg^{-1} dose, respectively. The lack of efficacy for **142** could be due to its low brain exposure, 269 nM and 658 nM, 4 and 6 h after a 100 mg kg^{-1} dose.

Further optimization resulted in replacement of the labile acetate group by an ethyl ether, to give derivatives such as **143** and **144**, Table 3.[128] The ability of **143** and **144** to penetrate the CNS was assessed in the mouse via i.v. administration, with samples collected 6 h postdose. Compound **143** showed moderate CNS penetration, Br:Pl 0.26 when using total levels but low Br_u:Pl_u (0.025). Compound **144** showed better CNS penetration, with Br:Pl 0.49 and Br_u:Pl_u 0.11, however the Br_u:Pl_u implies both are subject to active efflux. Profiling **143** in vivo (mouse) a 100 mg kg^{-1} i.p., resulted in a 46% decrease in brain $A\beta_{42}$ levels 6 h after dosing. Consistent with the in vitro profile, $A\beta_{38}$ levels were also reduced (31%), however the $A\beta_{40}$ levels were also reduced by a similar magnitude (30%), which would not be expected by the in vitro profile. In this study, **143** showed high exposure in the brain (23 μM total, 23 nM free) and plasma (12 μM, 132 nM free), which resulted in a Br:Pl 2, remarkably different from the i.v. study, however the Br_u:Pl_u 0.17 is still low. A similar study with **144** at 100 mg kg^{-1} p.o. elicited a 26% reduction in brain $A\beta_{42}$ levels 6 h postdose. A similar reduction in brain $A\beta_{38}$ (31%) was observed, whilst the reduction in $A\beta_{40}$ was not statistically significant. In this study, the brain concentration was 20 μM (40 nM free), with corresponding plasma concentration 15 μM (120 nM free), Br_u:Pl_u 0.3. Finally, in a 5-day efficacy study, **144** administered at 50 mg kg^{-1} p.o. produced a 42% reduction in brain $A\beta_{42}$ 8 h after final dose. The brain concentration was 31 μM (unbound brain 62 nM) with corresponding plasma concentration 16 μM (free 128 nM). A lower dose (10 mg kg^{-1} p.o.) failed to deliver statistically significant reductions in brain $A\beta_{42}$ or $A\beta_{38}$.

It appears that despite the structural diversity over other series, CYP inhibition was also an issue for this series as it was reported that **143** potently inhibits CYP3A4, IC_{50} 1.1 μM, whilst **144** has weaker activity, IC_{50} 12 μM.[129] It was also reported that time-dependent CYP inhibition was a general problem for the series. Ultimately, overcoming these issues led to the identification of SPI-1865 (**145**), Table 3, cell $A\beta_{42}$ IC_{50} 110 nM, CYP450 3A4 IC_{50} 37 μM. A rat PK study (1 mg kg^{-1} i.v. and 100 mg kg^{-1} p.o.) showed low clearance (0.5 mL min^{-1} kg^{-1}), moderate V_d (5.8 L kg^{-1}), and long $t_{½}$ (129 h), with moderate bioavailability (50%). PKs in the mouse have been described in less detail but appear similar, Table 3.[130] It was also noted that the T_{max} was extremely long, 40 h, which was hypothesized to be due to lymphatic absorption, which may be related to the lipophilicity of SPI-1865, clogP 5.7. This slow T_{max} appears general to the series. In vivo efficacy in the rat was assessed 24 h after a 100 mg kg^{-1} oral dose. SPI-1865 had measured plasma and brain concentrations of 14 and 33 μM, respectively, resulting in a Br:Pl of 2.4. A reduction in brain $A\beta_{42}$ of 50% was observed, representing moderate efficacy, but at a very high dose.[129] In a 14 day exploratory safety study, SPI-1865 was found to be tolerated at 90 mg kg^{-1} day^{-1}, with a corresponding average plasma concentration of 40 μM. Thus, there would appear to be no therapeutic window between efficacious dose and a tolerated dose, although there may be a narrow window in terms of concentrations.[129]

Table 3 Summary of key derivatives (**141**–**145**) from Satori, including development compound SPI-1865 (**145**)

Compound	*141*	*142*	***143*** *(SPI-1802)*	***144*** *(SPI-1810)*	***145*** *(SPI-1865)*
structure	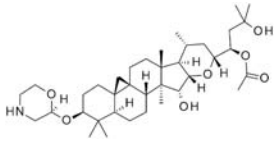	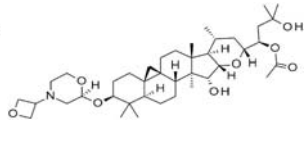	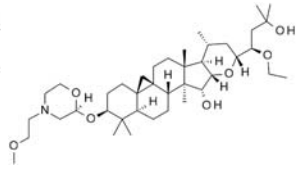	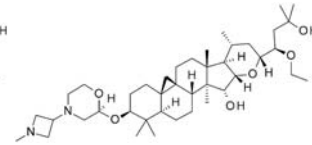	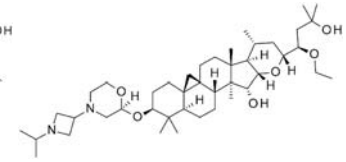
$A\beta_{42}$ IC_{50} (nM)	55	270	270	100	106
$A\beta_{40}$ IC_{50} (nM)	1400	14,100	9900	2100	2800
$A\beta_{38}$ IC_{50} (nM)	80	300	380	160	259
PSA	106.5	106.9	89.9	83.9	83.9
Mouse Cl (mL $min^{-1} kg^{-1}$)	51.7	55	4.8	3.2	
Mouse V_d (L kg^{-1})	12.1	0.6	0.42	5.3	9.2
Mouse $t_{½}$ (h)	6.5	0.3			83
Mouse F_{po}	37%	11%	19%	75%	
Mouse Br:Pl	1.86 ($AUC_{4–24h}$), 1.7 (6 h)	0.39 ($AUC_{2–6h}$), 0.23 (6 h)	0.26		0.4–1.4
Ppb			98.9%	99.2%	97.6%
Btb			99.9%	99.8%	99.9%

In a rat dose–response study, oral doses of 10, 30, and 100 mg kg^{-1}, SPI-1865 reduced brain $A\beta_{42}$ levels by 21%, 37%, and 50%. The corresponding brain concentrations were 2.8, 11, and 33 μM and plasma concentrations were 3.3, 8.5, and 14 μM, respectively, resulting in Br:Pl 0.9–2.4. A follow up repeat dose (6 days) study in the rat was conducted at oral doses of 10, 30, and 60 mg kg^{-1}, which resulted in 24%, 44%, and 66% reductions of brain $A\beta_{42}$ 24 h after the final dose. Brain and plasma concentrations were similar for both studies.

A 6-day dosing study was also conducted in Tg2576 mice, with doses of 10, 30, 60, and 90 mg kg^{-1} being administered once daily and efficacy assessed 24 h after the final dose. None of the doses produced a statistically significant reduction in brain or CSF $A\beta_{42}$ levels, although plasma $A\beta_{42}$ was reduced at the top two doses. Total brain concentrations of 0.5, 1.3, 3.9, and 6.9 μM were achieved (Br:Pl 0.5–1.1), thus based on the rat efficacy and exposure, one would have expected to see reductions in brain $A\beta_{42}$ in the highest dose groups. In a follow up study, the efficacy of SPI-1865 was assessed in CD1 mice at dose of 15, 30, and 50 mg kg^{-1} b.i.d. for 6 days, with efficacy measured 6 h after the final dose. Brain $A\beta_{42}$ levels were reduced at all doses, 22%, 39%, and 47%, respectively. The brain concentrations from this study were measured at 3.6, 8.7, and 22 μM (Br:Pl 1.1–2.9) at doses of 15, 30, and 50 mg kg^{-1}, respectively. Thus similar levels of brain $A\beta_{42}$ reduction were observed in the CD1 mouse and the rat at similar brain concentrations but no effects were seen in the Tg2576 mouse. Calculated Br_u:Pl_u ratios for the three ascending dose groups in the CD1 mouse are 0.05, 0.08, and 0.12, which implies active efflux. Direct PK–PD modeling predicted a brain concentration of 3.8 μM (total, 27 nM unbound) to reduce brain AB42 levels by 50%, with 25.2 μM (176 nM unbound) to reduce the levels by 50%, thus showing good agreement with the cellular data.

Based on these data, SPI-1865 was selected as a development candidate, however, it has recently been disclosed that the development of SPI-1865 has been halted due to the finding that it disrupted adrenal function in monkeys, an observation that is believed to be unrelated to GS modulation.

Whilst the Satori work has established that complex natural product derivatives with multiple HBA/HBD motifs can penetrate the CNS to some extent, the preclinical efficacy appears somewhat limited compared to other series. It is also concerning that SPI-1865 was not efficacious in the Tg2576 model despite achieving similar free and total brain concentrations to those in the wild-type mouse and rat where efficacy was demonstrated.

7.07.19 Modulators From Schering-Plough

Prior to the merger with Merck in 2009, Schering-Plough were also active in the field of aryl-imidazole GSMs. Some of their disclosed structures are shown in the Fig. 41. The design of these compounds originated from E2012 (**6**, Figs. 5 and 18), in which the cinnamide double bond and carbonyl moiety were incorporated into five-membered ring heterocycles.[131] This modification generated a novel class of fused 5,6-bicyclic heterocycles GSMs, such as the tetrahydrotriazolopyrimidine **146** and pyrazolopiperidine **147** (Fig. 41). When tested in vivo in rat, **146** showed no efficacy at 30 mg kg^{-1} 3 h postadministration, which might be attributed to insufficient brain concentration (0.49 μM). Compound **147** on the other hand showed modest reduction of $A\beta_{42}$ levels in the rat CSF (16%) 3 h after a 30 mg kg^{-1} dose. Further optimization, via aromatization of the piperidine ring in **147**, led to a novel pyrazolopyridine series of GSMs.[132] The PgP efflux observed in analogs of this series was mitigated by introduction of a Cl atom on the pyridine ring. The best chloropyridine analog was **148**, Fig. 41, which, in a single dose rat efficacy study, reduced CSF $A\beta_{42}$ by 45% 3 h postdose (30 mg kg^{-1}), with corresponding brain and plasma concentrations of 1.22 and 5.02 μM, respectively.

Other modifications of **E2012** involved replacement of the double bond linker.[133] For instance, compound **149**, Fig. 41, mimicked the *E*-configuration of the double bond in **E2012** via a H-bond between the hydroxyl group and the carbonyl moiety of the pyridazinone ring. This modification led however to a drastic loss in potency. Optimization of **149** led to aminopyridinone **150**, a potent GSM in which the amine linker locks the molecule in an active conformation via intramolecular hydrogen bonding to the carbonyl moiety of the pyridine ring. Pyridone-type GSMs were also described by Janssen, for example, compound **87**, Fig. 26. Compound **150** however demonstrated weak efficacy in rat, when dosed orally at 100 mg kg^{-1}, reducing the $A\beta_{42}$ by 26% in brain and 40% in CSF.

In 2010–2013, Schering-Plough disclosed yet another class of aryl imidazole GSMs derived from **E2012** template. Recognizing that in **151** (Fig. 42), a potent analog of **E2012**, a bulky tetrahydropyranyl moiety allows hydrogen bonding interactions only for the LHS lone pair of electrons of the lactam carbonyl moiety,[134] a formal cyclization from the carbonyl moiety into the benzylic position provided oxadiazolines (**152**, Fig. 42) and oxadiazines (**153**, Fig. 42) as bioisosteres, which maintain the LHS HBA capabilities of **151**.

Further exploration of **152** allowed the identification of more potent GSM **154**, Fig. 42. When dosed orally in rat at 10 mg kg^{-1}, **154** reduced $A\beta_{42}$ by 66% in CSF and 37% in the cortex, 3 h postdosing and with a brain exposure of 0.54 μM. In the same study, oxadiazine **153** reduced $A\beta_{42}$ by 65% in CSF and 63% in the cortex, 3 h after oral administration of a 3 mg kg^{-1} dose to rat. The corresponding brain exposure was found to be 1.47 μM. The PK profile of **SP-7** in rat showed that this compound had a low clearance of 1.4 mL min^{-1} kg^{-1}, a low V_{dss} of 0.4 L kg^{-1} and a moderate half-life of 3.5 h together with 100% oral bioavailability. Furthermore, **153** showed no QTc prolongation in the dog, despite exhibiting 76% inhibition of hERG at 10 μM. Further optimization of **153** aimed to improve its overall profile and focused on modification of the central core. This resulted in the identification of **155** and **156**,[135,136] Fig. 42. A highly potent GSM, morpholino oxadiazine **155** reduced $A\beta_{42}$ levels in rat CSF by 60% of 3 h after a 20 mg kg^{-1} oral dose. Compound **156**, having similar activities in vitro ($A\beta_{42}$ IC_{50} = 39 nM) and in vivo (61% reduction of $A\beta_{42}$ in CSF) with **153**, proved to be a weaker hERG inhibitor (33% inhibition at 10 μM). Compound **155** employs a similar cyclization strategy to that used by Eisai, for example, compound **55**, Fig. 18.

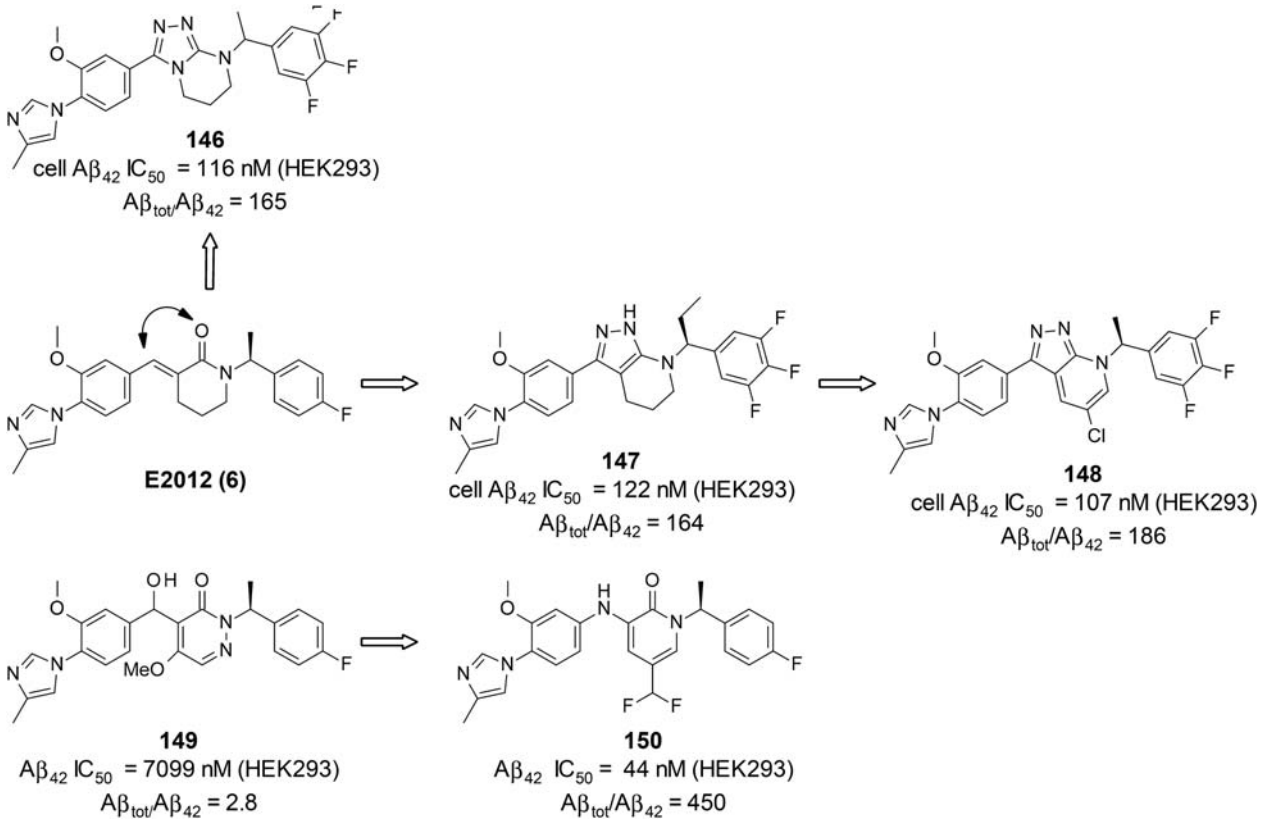

Fig. 41 Schering-Plough aryl imidazole GSMs.

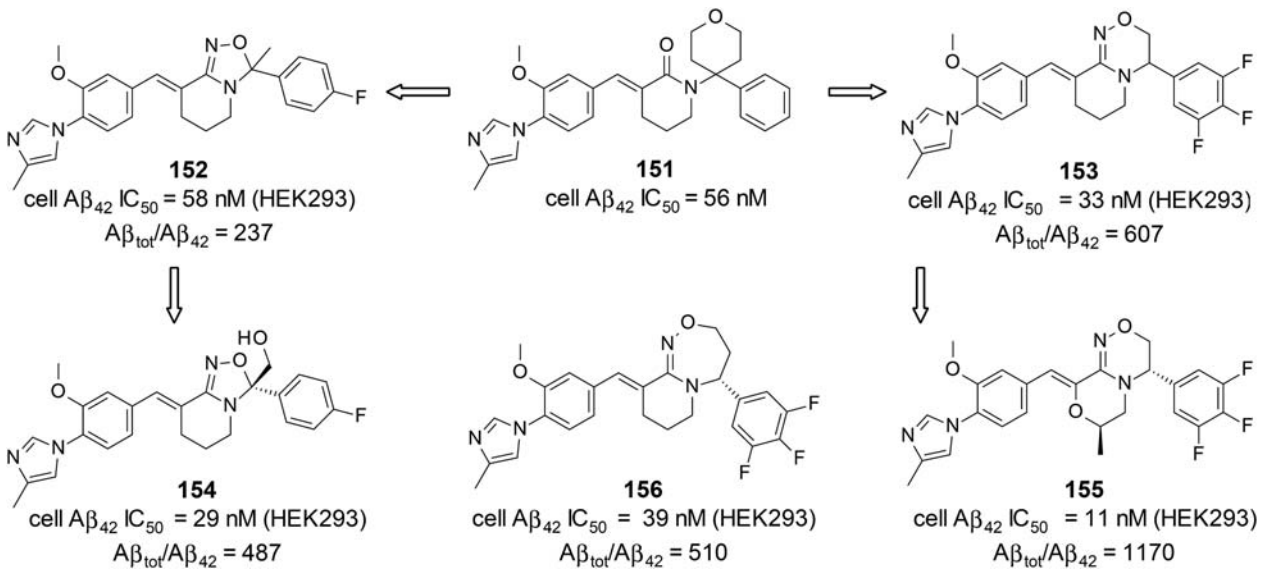

Fig. 42 Schering-Plough. Fused oxadiazolines and oxadiazines as GSMs.

7.07.20 Modulators From Shionogi

In a patent application from 2010,[137] researchers at Shionogi claimed GSMs in which the aryl-imidazolo GSM A-B system was linked to give a central sulfonamide core linked to a substituted thiophene. These compounds were weakly potent in lowering $A\beta_{42}$, with IC_{50}'s being in micromolar range. The best compounds claimed in the patent are **156** and **157**, Fig. 43.

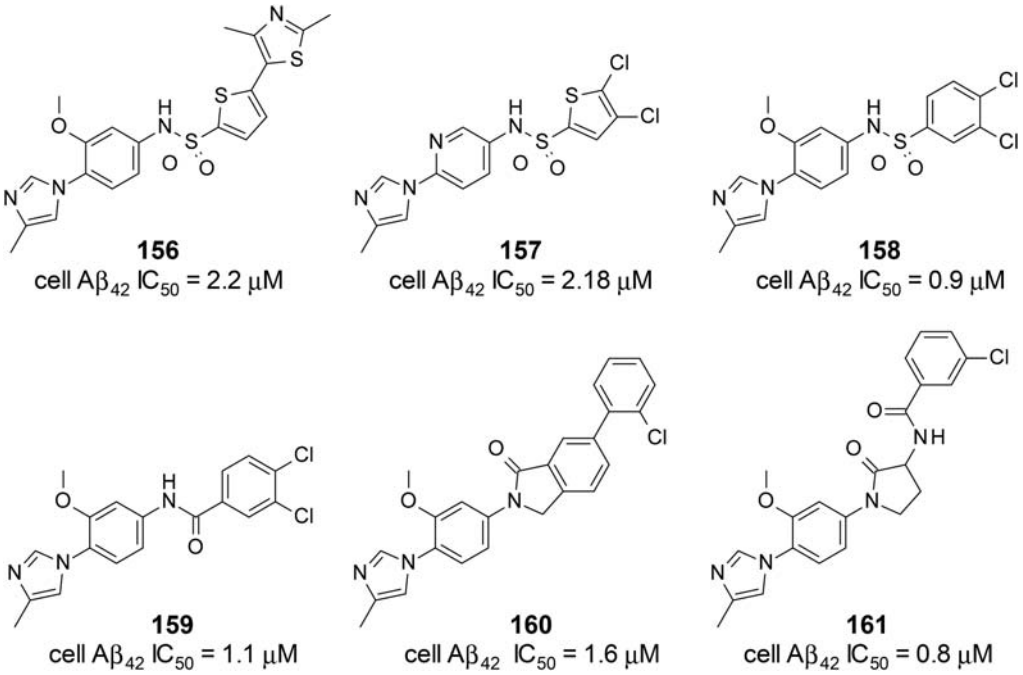

Fig. 43 Sulfonamide derivatives (**156–158**) and amide/lactam (**159–161**) GSMs from Shionogi.

In a subsequent application,[138] the thiophene was replaced with a phenyl ring, as in **158**, which showed a slight, twofold, increase in potency when compared to the thiophene analog. Replacement of the sulfonamide with a reversed amide, as in **159**, kept the potency within the same (1 μM) range. Cyclization of the reversed amide into a lactam ring generated analogs such as fused lactam **160** and more flexible **161**, Fig. 43.

7.07.21 Modulators From Takeda

An HTS screening campaign of Takeda's in-house compound collection identified a piperazine derivative with GSM properties.[139] Initial modifications led to **162**, Fig. 44, which lowered $A\beta_{42}$ in primary neuronal cells and had no effect on $A\beta_{40}$ levels. In vivo in mice, however, **162** did not show significant lowering of $A\beta_{42}$ 3 h after being dosed orally at 100 mg kg^{-1}. This result could be partially explained by a suboptimal bioavailabity of **162**, as suggested by its high clearance in mouse hepatic microsomes (Cl = 150 mL min^{-1} mg^{-1}). Further optimization around **162** focused on replacing the ubiquitous imidazole moiety and identified a methyloxazole analog with improved primary potency over **162**, but which still had high metabolic clearance. Subsequent optimization around the central piperazine core (C-ring) and the naphtylethylurea (D-ring) allowed identification of **163**, Fig. 44. This compound was a potent GSM with high selectivity over Notch and low metabolic clearance (Cl = 67 mL min^{-1} kg^{-1}) in mouse hepatic microsomes, and it was further profiled. When tested in IMR-32 neuroblastoma cells in a concentration-dependent manner (0.001–1 μM), **163** significantly inhibited $A\beta_{42}$ production (up to ~50% at ~0.55 μM), while $A\beta_{40}$ levels showed a slight increase

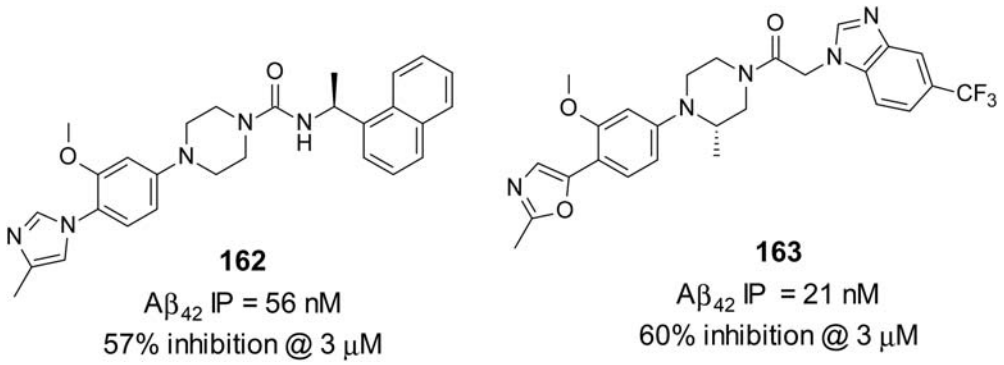

Fig. 44 Takeda aryl-imidazole GSMs. *Note*: *IP*, inflection point.

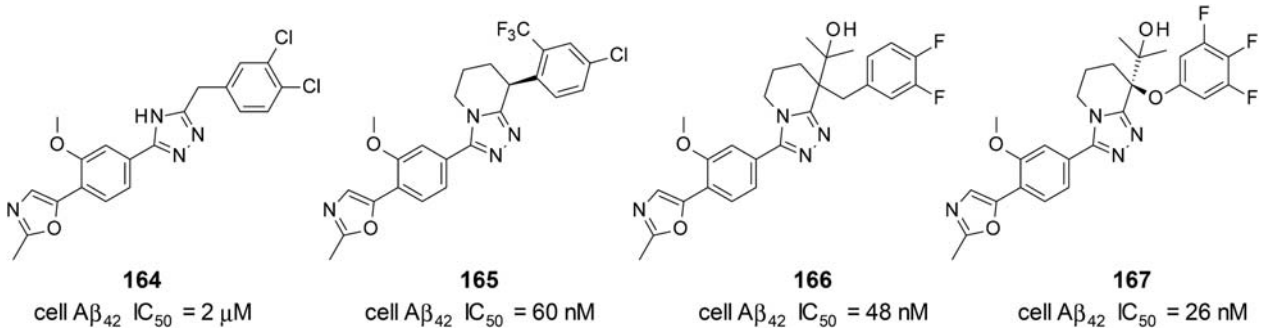

Fig. 45 Takeda bicyclic triazole GSMs.

(up to ~25% at 0.55 μM) and $A\beta_{total}$ remained unchanged. Compound **163** showed an acceptable PK profile in mice, having a low total clearance (Cl_{tot} = 117 mL h^{-1} kg^{-1}) and a good bioavailability (F = 46%).

When tested in vivo in C57BL/6 mice, **163** reduced brain $A\beta_{42}$ by 41% 3 h after being dosed orally at 100 mg kg^{-1} and had no significant effect on $A\beta_{40}$ levels. No corresponding brain exposure was reported.

In a new round of optimization, researchers at Takeda considered attaching the previously identified oxazolylphenyl moiety to various right-hand C–D systems existing in reported GSMs, such as the 3-benzyl-1,2,4 triazole derivatives reported by Janssen (such as **92**, Fig. 27).[140] These modifications led to **164**, Fig. 45, a weakly active GSM. Addition of a conformational constraint to fix the active conformation of **164** and further optimization led to the identification of **165**, Fig. 45, in which the central triazole core was fused into a triazolopiperidine. This was a potent GSM with improved physicochemical properties and drug-like parameters (LLE = 3.6). Compound **165** produced a strong reduction of $A\beta_{42}$ (50%) and $A\beta_{40}$ (75%) in brain of C57BL/6 mice, 3 h after oral administration, which corresponded to a brain exposure of 4.76 μM and Br:Pl ratio of 0.36. Given the high brain and plasma concentrations at the pharmacological dose of **165**, researchers at Takeda applied an LLE-based optimization approach to find safer analogs that could show pharmacological effect at lower drug exposures.[141] This led in a first step to **166**, Fig. 45, in which a polar hydroxypropyl moiety was introduced at the 8-position of the triazolopiperidine core. Equipotent to **165**, with increased LLE (4.3), **166** however suffered from high clearance in mouse liver microsomes (Cl = 93 mL min^{-1} mg^{-1}). The suboptimal metabolic stability of **166** was then addressed, by modification of the metabolically labile benzyl and hydroxypropyl moieties. This led to the identification of **167**, Fig. 45, a potent GSM which preserved the high LLE and had good microsomal stability (Cl = 7 mL min^{-1} kg^{-1}). When it was orally administered to C57BL/6 J mice at 6 mg kg^{-1}, this compound showed a strong, 60%, decrease in brain $A\beta_{42}$ which corresponded to exposures of 1.3 μM in brain and 6.4 μM in plasma, significantly improved with respect to **164**.

In a recently reported in vivo efficacy study,[142] the GSM behavior of **167** was first confirmed in Neuro2A mouse cells expressing human Swedish mutant APP(N2a-APPsw), when dose-dependent decreases in $A\beta_{42}$ and $A\beta_{40}$ and increase in $A\beta_{37}$ levels were observed. The total Aβ levels were not affected and there was no activity against Notch (IC_{50} > 10 μM). A chronic 58-day oral administration study with **167** to Tg2576 mice, at 10 and 30 mg kg^{-1} day^{-1}, led to significant and dose-dependent reductions of both soluble and insoluble brain $A\beta_{42}$ levels. At the highest 30 mg kg^{-1} day^{-1} dose, this corresponded to a ~60% reduction of soluble $A\beta_{42}$ in brain and ~50% reduction of insoluble $A\beta_{42}$. The reported brain concentrations after treatment with **167** at 10 and 30 mg kg^{-1} day^{-1} were 0.301 and 1.325 μg g^{-1} (0.58 and 2.57 μM), respectively. At both doses, **167** was reported to display a tendency to inhibit plaque deposition. In addition, in the novel object recognition test, treatment with **167** significantly recovered preference ratios to 65% and 67% at 10 mg kg^{-1} and 30 mg kg^{-1}, respectively. Moreover, continuous cognitive improvement was observed up to 7 days after cease of **167** administration. Compound **167** was described as a potential candidate therapy for disease modification in AD. As expected for a GSM **167** did not display any of the adverse effects observed with GSIs and Notch-sparing GSIs. The current status of **167** is unclear but perhaps more reports around **167** will follow in the literature.

7.07.22 Modulators From UCSD/Neurogenetics Inc/Torrey Pines Therapeutics

The University of California, San Diego, in collaboration with the Tanzi group and spin out companies of different guises were early entrants to the GSM field. Neurogenetics Inc. changed name to Torrey Pines Therapeutics in Mar. 2005 and under the latter name, the group disclosed the aryl-imidazole template, which was exemplified by compounds such as **168** and **5**,[143] Fig. 46. These compounds were extremely important and essentially seeded the field. A recent publication describes the identification of their series. Compound **168** was discovered from a screen of 80 k compounds and was found to reduce $A\beta_{42}$ production in CHO cells overexpressing wild-type APP695, with an IC_{50} of 1512 nM.[144] Optimization of the series utilized an SH-SY5Y cellular assay, overexpressing APP751, and resulted in the identification of **5**, which displayed significantly improved activity, Fig. 46. Further characterization of **5** in mixed brain cell cultures from Tg2576 mice confirmed the activity; $A\beta_{42}$ IC_{50} 29 nM, $A\beta_{40}$ IC_{50} 90 nM, $A\beta_{38}$ EC_{50} 170 nM. In vivo profiling in the mouse at 50 mg kg^{-1} for 3 days showed that **5** penetrated the CNS with a Br:Pl of 0.93. Efficacy was initially assessed by dosing **5** to Tg2576 mice for 3 days at 12.5, 25, 50, and 100 mg kg^{-1} p.o., with read out 6 h after final dose. Analysis revealed strong affects on

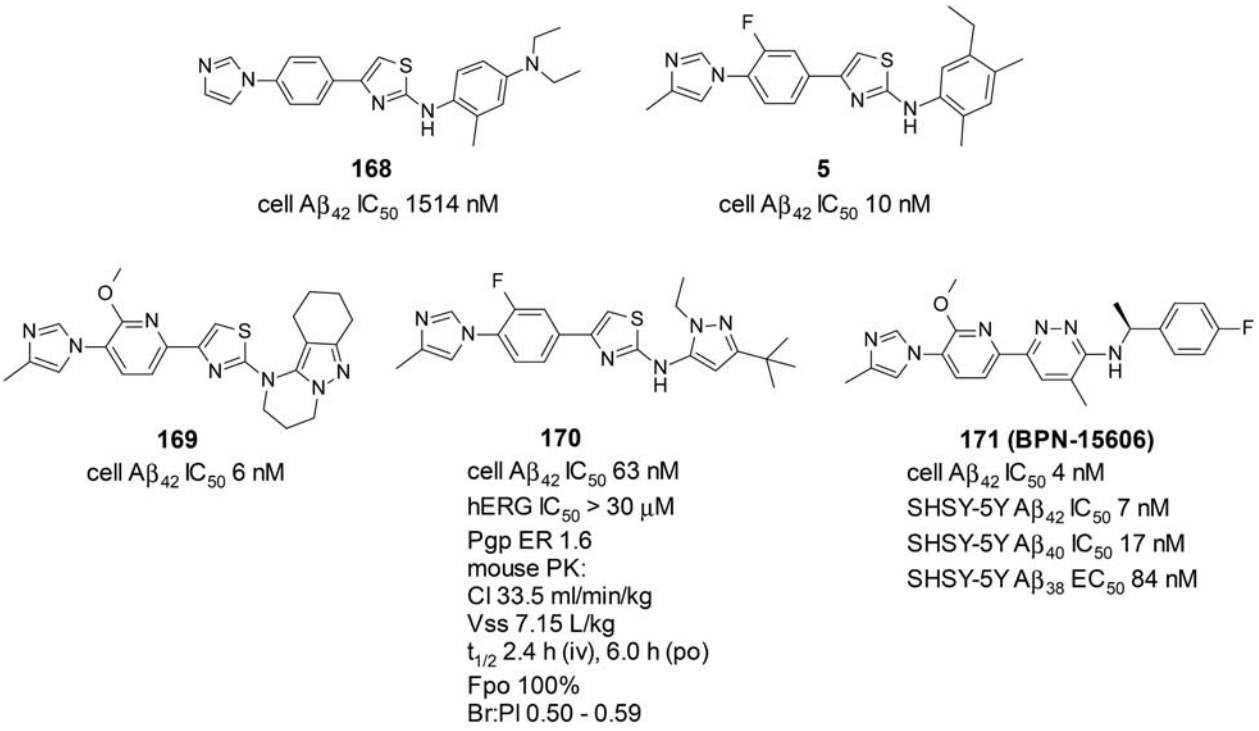

Fig. 46 HTS hit **168** and optimized compound **5**, with more recent examples from the patent literature from UCSD/Neurogenetics/Torrey Pines Therapeutics.

plasma $A\beta_{42}$ levels but weak, ~30% and 40% reductions on brain $A\beta_{42}$ following 30 and 100 mg kg^{-1} doses, respectively, despite high total brain concentrations (29.5 and 66.4 μM, respectively). A follow on study assessed the effect of a 50 mg kg^{-1} p.o. dose of **5** for 7 months to preplaque bearing Tg2576 mice. Quantification of the effect was assessed by two different Aβ extraction methods—DEA and formic acid, the former showing the larger effect. Analysis of DEA-extracted brain Aβ showed a 76% reduction of brain $A\beta_{42}$, and a similar reduction of brain $A\beta_{40}$ (73%). Surprisingly, $A\beta_{38}$ in the brain was also reduced by 76%, in contrast to the in vitro profile where $A\beta_{38}$ levels are increased. The reduction in soluble amyloid levels were accompanied by a reduction in plaque area in the cortex and hippocampus relative to vehicle treated control mice.

The group at UCSD has maintained an active interest in the area as shown by patent activity. Thus, more recent publications from the group have reported aminothiazoles such as **169**,[145] Fig. 46. A related manuscript also describes close analogs of **169**, or which **170**, Fig. 46, represented the most interesting example.[146] The prime drive in the optimization was to improve the solubility over examples such as **170**, as this series generally had very low solubility, <0.1 μM at neutral pH. Compound **169** showed moderate activity in a SH-SY5Y cell assay, but showed no major CYP450 interactions and minimal hERG activity as well as a suitable PK profile in the mouse. Solubility was also marginally improved at 4.7 μM at pH 7.4.

Finally, a very recent patent application hints that the group may have moved away from the aminothiazole series as, working with Albany Molecular Inc., they have disclosed a series of aminopyridazines, such as **171**,[147] Fig. 46. Compound **171** is an extremely close analog of the well-characterized compound **70** from gsk, Fig. 22, Section "Modulators From GlaxoSmithKline", first disclosed some 7 years ago,[148] where the methoxyphenyl ring has been replaced by a methoxypyridyl ring. In addition to the in vitro characterization, in vivo profiling was also conducted with **171**. PKs in the rat showed low clearance (1.5 mL min^{-1} kg^{-1}) and good half-life (5.9 h) and oral bioavailability (60%). Efficacy was assessed in both the mouse and the rat. In the mouse doses of 10, 25, and 50 mg kg^{-1} for 7 days resulted in 36%, 69%, and 85% reductions in brain $A\beta_{42}$ levels, with similar effects on $A\beta_{40}$. Similar efficacy was observed in the rat with doses of 5, 25, and 50 mg kg^{-1} producing reductions of 43%, 73%, and 85% in $A\beta_{42}$ levels. Again, the effect on $A\beta_{40}$ levels was very similar to those on $A\beta_{42}$. In addition to brain amyloid levels, $A\beta_{42}$ was also measured in CSF where reductions of 43%, 73%, and 86% were measured, again showing high concordance with the reductions in the brain. Thus, it would appear that **171** is of significant interest to the group and may be further advanced.

7.07.23 Photo-Activity Ligands

As mentioned in the introduction, the lack of high resolution protein crystallography has presented researchers with challenges to understand the binding mode and binding site of GSMs. In the absence of a crystal structure of a GSM-protein complex, one

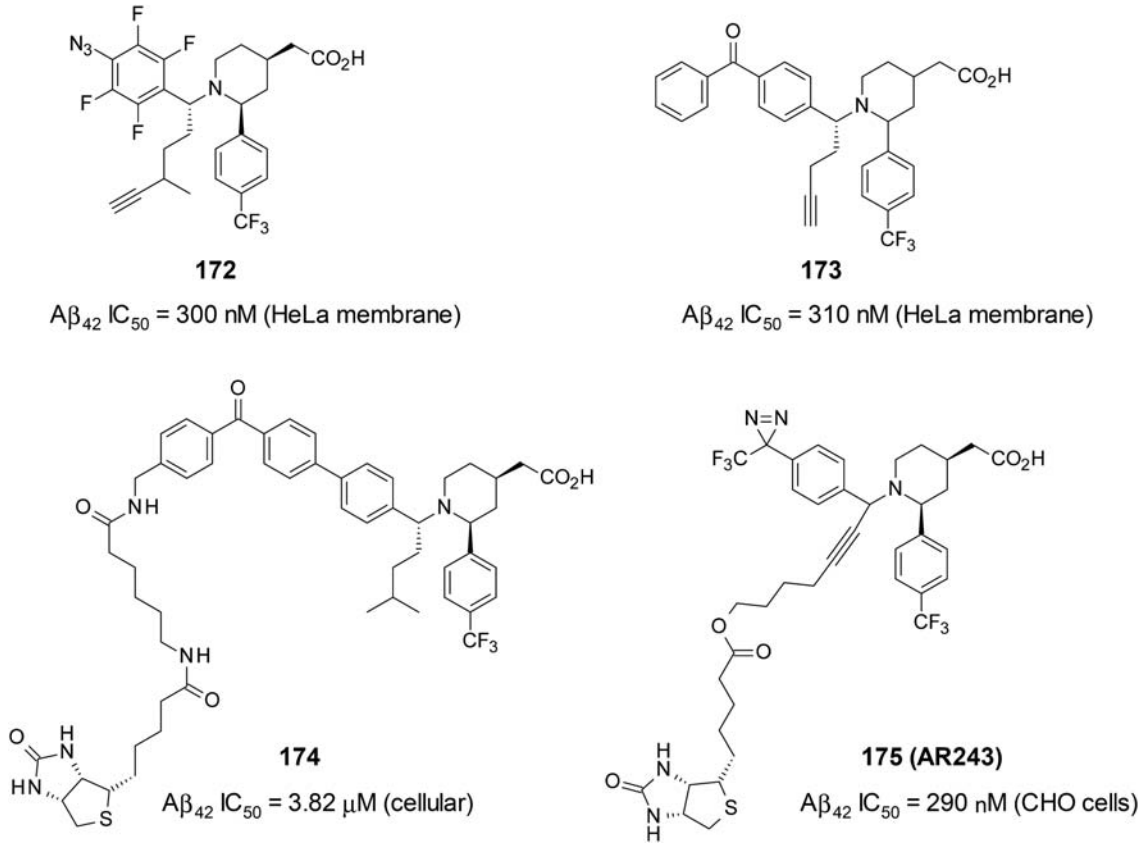

Fig. 47 PALs derived from GSM-1 (**103**).

technique that has been applied to improve the understanding of the mode of action of GSMs is photoaffinity labeling.[149] This method involves introducing a photolabile group into a biologically active molecule, which under UV irradiation can form a covalent bond with the target protein, at its binding site. Most commonly used photolabile moieties include azides, trifluormethyl diazirines, and benzophenone.

In the NSAID class of GSMs, compound GSM-1 (**103**, Fig. 30) has been extensively utilized in photoaffinity labeling studies. For instance, researchers at Pfizer and academic collaborators developed a GSM-derived photoprobe in which the parent molecule incorporated both a photolabile group,[150] such as an azide (**172**) or benzophenone (**173**), Fig. 47, and an alkyne moiety. After crosslinking, the alkyne was subjected to click chemistry conjugation with an azide-linked biotin tag which allowed isolation and purification of the target protein–ligand complex via immobilization on an avidin column, using the strong binding interaction between avidin and biotin.[151] The pure, biotynilated protein–ligand complex can then be obtained by washing it off the column, with the aid of a buffer. Western blot analysis showed that **172** and **173** labeled PS1-NTF and that labeling was diminished in the presence of two GSMs from the same class—meaning it was specific binding. Moreover, the authors report that GSM-1 (**103**) enhanced the photolabeling of GSI-derived photoprobes. This result implies that the binding of GSM-1 (**103**) to an allosteric site of PS-1 causes a conformational change in the active site thus increasing GS binding of an orthosteric ligand (a gain of function).

These findings were confirmed in a study by Ohki et al.,[152] in which they utilized photoprobe **174**, Fig. 47, having the biotin tag already attached to the PAL. In addition, using fluorescence lifetime imaging and surface cysteine availability (SCAM) methods, the study suggested that GSM-1-type of modulators bind to a hydrophobic extracellular/luminal side of the TMD1 in PS1, which provokes the conformational changes in GS active site. Moreover, the authors demonstrated that GSM-1 (**103**) affects the γ-cleavage site of GS, and not the ε or ζ-sites.

In a third independent report, Jumpertz et al. confirmed the PS1-NTF binding site of GSM-1 (**103**) in living cells.[153] Their PAL incorporated a biotin label on the aliphatic side chain of GSM-1, whereas the photosensitive group used was an (trifluoromethyl) diazirine. This resulted in a PAL with nanomolar potency, **175**, much improved over **174**. In addition to previous studies, competition experiments suggested that GSMs from the same class, such as **85** (Fig. 25), bind to the same site as GSM-1 (fully displace **175** PS-NTF binding), whereas some of the aryl-imidazole GSMs tested (an analog of **107**, Fig. 32 and E2012) only partially overlapped, showing reduced displacement of **175**. Intriguingly, the GSK aryl-imidazole derivative, **70** (Fig. 22), fully displaced **175**, suggesting an identical binding site.

The binding site of different types of aryl-imidazole GSMs (Fig. 48) has also been investigated. Early work done by Ebke et al. on a photoprobe derived from compounds such as Ro-57-BpB (**134**, Fig. 38),[154] identified binding to PS2-NTF as well to PS1 NTF.

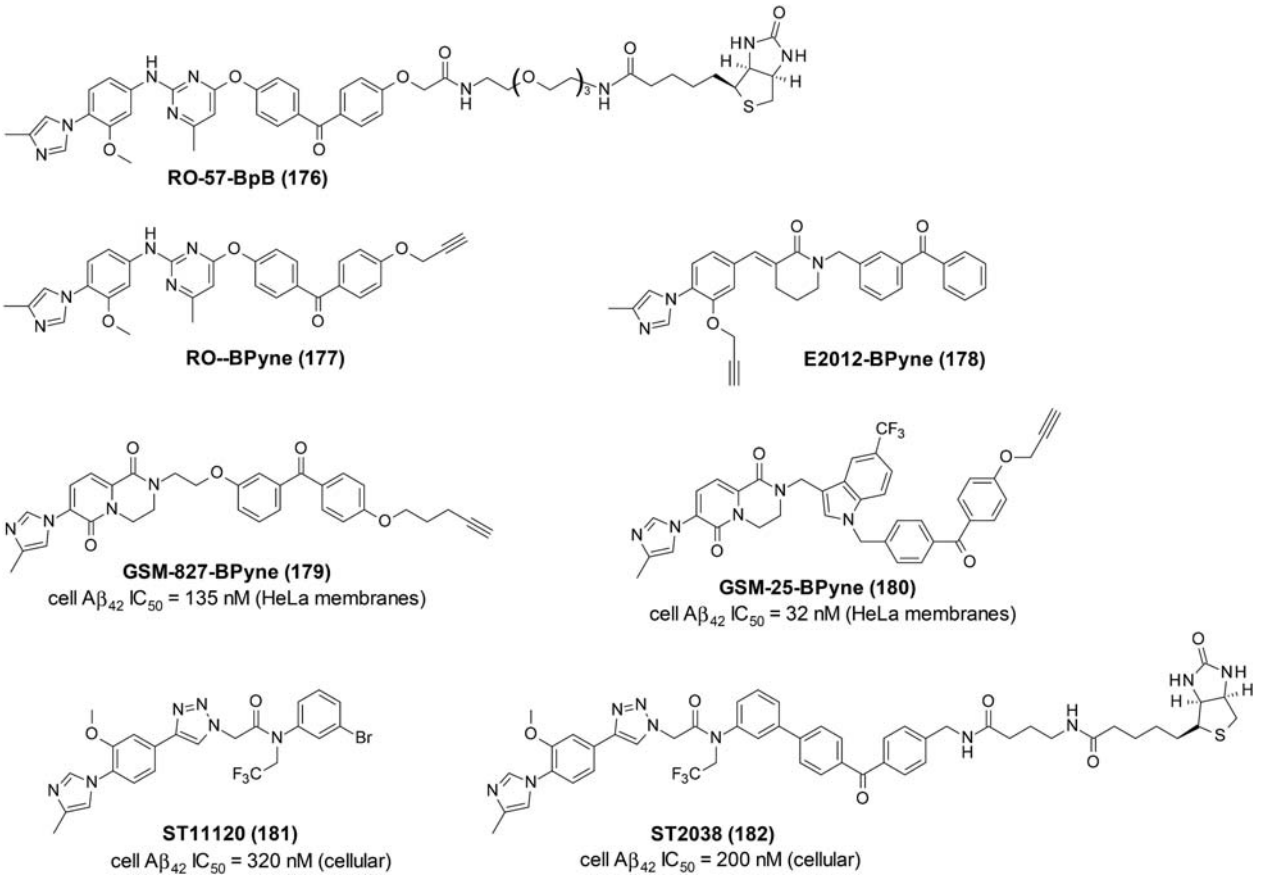

Fig. 48 Aryl-imidazole-derived GSM photoprobes.

Competition experiments revealed that the binding to PS-NTF was completely displaced by E2012 analogs, but only partially by Torrey-Pines analogs. On the other hand, carboxylic acid GSM-1 (**103**) only partially competed for PS1-NTF (confirming previous findings), however, GSM-1 completely displaced Ro-BpB from PS2-NTF binding site. Finally, transition state analog L-685,458 displayed moderate competition, whereas GSIs such as begacestat competed very weakly or not at all. These findings were partially confirmed in a later study by Pozdnyakov et al. by cross-linking experiments of a clickable photoprobe, RO-Bpyne (**177**, Fig. 48)[155] with PS1-NTF, however no mention was made of PS2-NTF crosslinking.

The research group in Pozdnyakov et al. also investigated the binding of an E2012-derived clickable photoprobe, E2012 B-Pyne, **178**, Fig. 48.[155] This probe specifically labeled PS1-NTF in cell membranes, live HeLa cells and primary neuronal cultures. The photolabeling of E2012-B-Pyne (**178**) was enhanced when the crosslinking was performed in the presence of active-site directed GSI, L-685,458 (L458). The authors suggest that the binding of L-685,458 to the active site of PS-1 produces a conformational change that leads to a better fit of E2012 to the binding site. This observation opposes the Ro-57BpB experiment (*vide supra*), suggesting a different binding site for GSMs belonging to the same aryl-imidazole class. Neither GSM-1 (**103**) nor BMS-708,163 inhibited the binding of **178** to PS1-NTF in competition experiments, suggesting different binding sites for E2012 and both GSM-1 and GSIs.

Recently, Pfizer prepared clickable photoprobes of a new type of GSM scaffolds, in order to verify whether their binding site is similar to that reported for other aryl-imidazole-type GSMs.[111,113] (X REF J Med Chem 2014, 57, 1046 and BMCL 2015, 25, 908) Thus, cross-linking experiments performed with 1 μM of a clickable photoprobe derived from **126** (Fig. 36), GSM25-Pyne (**180**, Fig. 48), revealed that GSM25-BPyne (**180**) also labeled PS1-NTF. The labeling was diminished in the presence of GSMs belonging to the same series as **126**, showing specific binding. Similarly, GSM-827 B-Pyne (**179**, Fig. 48), derived from the **124** series (Fig. 36) showed specific binding to PS1-NTF. Moreover, unlike E2012-BPyne, crosslinking of **179** in the presence of GSI L-685,458 did not produce a significant increase in the binding to PS1-NTF.

In a recent report,[156] Takeo et al. investigated GSM mode of action utilizing cross-linking experiments performed with two photoprobes derived from **113** (Fig. 34), namely ST2038 (**181**, Fig. 48) and ST1120 (**182**, Fig. 48), in addition to systematic mutagenesis. A first PAL experiment was aimed at understanding the effect of GSMs on the conformation of GS. To this end, ST-1120 (**181**) was incubated with two GSI PALs prior to crosslinking: 31C-Bpa, a PAL derived from a transition-state-type GSI, which binds to PS1-NTF and CTF, and Pep.11-Bt, a PAL derived from helical-peptide-type GSI pep.11, which binds to the initial substrate binding site within PS1-NTF. The authors observed that **181** enhanced the binding of 31C-Bpa, and decreased the binding of

Pept11-Bt. This result would suggest that **181** might affect the conformation of the GS active site by facilitating the formation of the transition state of GS. This finding is also in agreement with the previous observations of Crump et al. (*vide infra*) from cross-linking experiments done in the presence of GSM-1. Furthermore, the authors also tested ST1120 (**181**) in PS2-containing GS cultured cells, which confirmed the results of Ebke et al. (with RO-57, *vide infra*), indicating a preference of ST1120 to bind to PS2 over PS1 (IC_{50} $A\beta_{40}/A\beta_{42}$ for PS2 = 271/51 nM vs. IC_{50} $A\beta_{40}/A\beta_{42}$ = 5538/320 nM for PS1).

Photoaffinity labeling experiments with ST2038 (**182**) incubated in membrane fractions isolated from mouse brain, indicated that **182** binds to both PS-NTF and Aph-1. Again, competition experiments with GSM-1 (**103**) suggested that **103** and **182** binding sites partially overlap, whereas **182** does not share the same binding site with GSIs 31C and peptide Pep.11. An alanine scanning analysis, in which each of the amino acid residues from PS2 that is conserved in PS1 was replaced by alanine, was performed in order to identify the specific PS2 residues to which **181**-type GSMs bind. The potency and labeling of **182** to the resultant mutants was verified, which showed that labeling efficiencies of **182** to PS2 Y112A, N141A, and Y246 mutants were decreased. This therefore suggests that these aminoacid residues could be directly involved in the binding of **182**. As the authors mention, there is of course the possibility that the alanine substitution affects the architecture of the binding site (i.e., and as a result the GSM does not bind in it anymore). Utilization of a homology model of human PS1 derived from the reported crystal structure of the archaea PSH[157] allowed the identification of the ST-1120 binding pocket. This was found to be an extracellular pocket formed by HL1/TM2/TM5 of PS. Further analysis using the SCAM method provided evidence that the binding of ST1120-type GSMs to the extracellular pocket provokes conformational changes in the catalytic site of PS which, in turn leads to an increase in the cleavage activity of GS.

In conclusion, more light has been shed on the mode of action of GSMs via the use of PALs. Thus, it seems that, regardless of chemical class, GSMs consistently bind to PS1-NTF, some of them showing even better binding to PS2-NTF. For both types of GSMs, the binding site seems to be placed in different extracellular pockets of PS1. Most of the time, GSMs from the same class seem to bind to the same site, but there are also exceptions. The consensus is that the allosteric binding of GSMs induces a conformational change in the catalytic site of GS, which generates a GS gain of function, ultimately resulting in increased production of shorter Aβ peptides at the expense of the longer isoforms. Another recent advance is represented by the determination of the first atomic structure of GS, with the aid of high-resolution cryo-EM. Perhaps further refinement/understanding of GSM binding sites in PS/GS will allow for the design of more drug-like GSMs is after all not so distant.

7.07.24 Clinical Compounds

Several GSMs are now known to have entered clinical trials, and key compounds from the carboxylic acid and aryl-imidazole derivatives are listed in **Tables 4** and **5**. Unfortunately, the picture painted by the clinical development is not one of optimism, but highlights the challenges/difficulties which have been encountered.

In the carboxylic acid series, the most progressed derivative, (*R*)-flurbiprofen (**1**), **Table 4** and **Fig. 4**, failed in PhIII. However, this may not be unexpected as the compound has extremely weak GSM activity, $A\beta_{42}$ IC_{50} 307 μM,[158] and failed to impact CSF $A\beta_{42}$ levels in the clinic and minimally impacted plasma $A\beta_{42}$ levels.[159] As a result, although there was initial encouragement from a 24-month trial in mild to moderate AD patients,[160] this was not confirmed in a large 18 month trial, where there were no improvements in the rate of cognitive decline or loss of activities of daily living in patients with mild AD.[161] Retrospective analysis of published preclinical data in Tg2576 mice may help shine light on possible reasons for failure.[162] Oral administration at doses of 10, 25, and 50 mg kg^{-1} for 3 days, with three mice per dose reduced brain $A\beta_{42}$ were observed at all doses, but there was no dose–response; the reductions were 26%, 60%, and 34% at the 10, 25, and 50 mg kg^{-1} doses, respectively. The plasma concentrations were also not linear with dose; 83, 117, and 78 μM at 10, 25, and 50 mg kg^{-1}, respectively, whilst the corresponding brain concentrations were 1.5, 2.6, and 2.5 μM, respectively. Thus, the total brain exposures are far inferior to the estimated in vitro IC_{50}, and an in vivo concentration response relationship was also lacking. In addition to the low animal numbers in the in vivo study, these may be confounding factors in the failure of this compound.

CHF5074 shares a similar structure to flurbiprofen, **Table 4**, and has also been investigated in the clinic. Preclinical data indicates CHF5074 has weak GSM activity, IC_{50} = 3.6 μM,[163] although it is still some 85-fold more potent than flurbiprofen. Again, CHF5074 has failed to show modulation of $A\beta_{42}$ in the clinic despite having progressed to PhII trials. Despite this, the compound has been licensed by Cerespir and renamed CSP-1103.[164] The mechanism of action has been rebranded and it is claimed to have several modes of action[165] in addition to its primary GSM pharmacology, namely to reduce tau pathology[166] and restore normal microglial function by increasing phagocytosis and decreasing the production of pro-inflammatory cytokines.[167] According to the Cerespir website they are working with regulators to finalize PhIII protocols.

A third compound from the carboxylic acid series, EVP-0962 (**60**), **Table 4** and **Fig. 19**, from Forum/EnVivo Pharmaceuticals has also progressed to PhII,[168] showing considerably improved in vitro potency over the two aforementioned compounds. In the PhII study, EVP-0962 was dosed (10, 50, 100, and 200 mg) for 14 days to patients with MCI or early AD and CSF amyloid levels were assessed,[169] however no data have been published on the outcome.

Recently, it has been shown that ibuprofen does not impact Aβ levels in plasma or CSF in human or monkey. Thus, this support the fact that the low CSF penetration (~1% that of plasma, with a human CSF conc ~12 μM), coupled with weak modulatory activity (IC_{50} ~250 μM) is insufficient to deliver efficacy.[170]

In the aryl-imidazole series, the picture is not much better than the carboxylic acid series. Despite the promise of a different template with increased potency and CNS penetration, this series has also struggled to deliver compounds to the clinic. Despite the huge effort expended by numerous research groups, a limited number of compounds have progressed to clinical studies, **Table 5**.

Table 4 Summary of compounds from the carboxylic acid series that have entered clinical trials

Compound	*Company*	*Stucture*	*IC_{50} (nM)*	*Status*
MPC-7869 (*R*)-flurbiprofen/tarenflurbil (Flurizan)	Myriad/Lundbeck	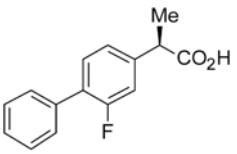	307,000	Terminated
CHF5074	Chiesi/Cerespir	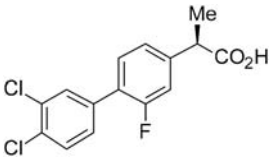	3600	Unknown
EVP-0962	Forum/EnVivo	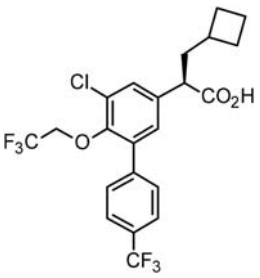	67 (H4-APP_{751}) 427 (rat PCN)	Unknown

Table 5 Summary of key aryl-imidazole derivatives to progress to human clinical trials, including purported structure of E2212

Compound	*Company*	*(Proposed) structure*	*IC_{50} (nM)*	*Status*
E2012 (6)	Eisai	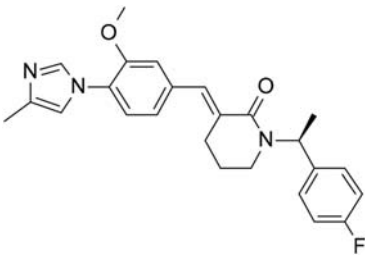	80	Terminated (PhI), lenticular opacity
E2212 (59)	Eisai	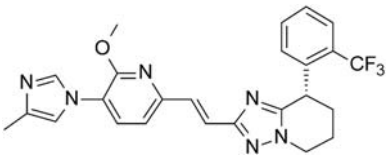	17	Terminated (PhI)
BMS-932481 (40)	BMS	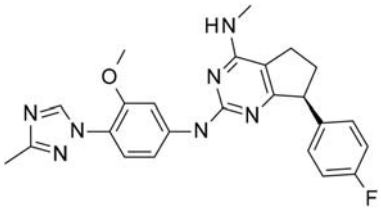	6.6	Terminated (PhI), liver toxicity
PF-06648671	Pfizer	Not disclosed	Not known	PhI

The aryl-imidazole class was led by E2012, which was the first compound from this class to enter clinical. There is still little published information on this compound, but some data has been presented at conferences. In rat primary cortical neurons E2012 reduced both $A\beta_{42}$ and $A\beta_{40}$ with an IC_{50} of 100 nM,[171] and the modulatory mechanism of action was confirmed by demonstrating lack of accumulation of APP-CTF and lack inhibition of notch processing.[172] Preclinical efficacy in the rat was observed at doses of 10 and 30 mg kg^{-1} p.o., which effected reductions in CSF $A\beta_{40}$ and $A\beta_{42}$ levels.[53] The PhI study commenced in 2006, with doses ranging from 1–800 mg.[173] Lowering of plasma $A\beta_{42}$ was reported, with a 53% reduction observed following the 400 mg dose. As discussed under the Eisai section (**Modulators From Eisai**) it has now been publicly disclosed that the progression of E2012 has been terminated, due to lenticular opacity/cataracts in preclinical toxicology studies.

A second compound from Eisai, E2212 has one SAD trial listed, which was scheduled for completion in Nov. 2012.[174] As there are no further trials ongoing and the compound has not been listed on the company pipeline since the FY2012 Financial Results Presentation on May 13, 2013, it is assumed that its progression has been halted.[175] The widely purported structure of E2212 is depicted in **Table 5**, however, there has not been an official link between this structure and compound number from Eisai.

More recent efforts have seen the progression of BMS-932481 to PhI studies. However, the development of this compound was terminated following the MAD arm of the PhI trial due to liver toxicity, which occurred at doses required to effect changes on $A\beta_{42}$ levels. The effects on CSF $A\beta_{42}$ in the clinic appear modest, considering the potency of the compound. This may be a result of suboptimal CNS pentration and high nonspecific binding. These issues appear to have dogged the series in general, in addition to CYP inhibition, hERG inhibition, and high lipophilicity. However, there are also some positives to be taken from this data as it is the first time that a GSM has demonstrated efficacy by modulating CSF $A\beta_{42}$ levels.

Most recently, Pfizer have advanced PF-06648671 to PhI studies. Until lately the mechanism of action had not been confirmed for this compound, however, the PhI trial detailed the biomarkers, which were measured and included $A\beta_{42}$, $A\beta_{40}$, $A\beta_{37}$, $A\beta_{38}$, and $A\beta_{tot}$, thus implying that this compound is indeed a GSM.[176] Currently, the compound has completed SAD study (Dec. 2014–Mar. 2015)[177] and a 14-day MAD (Dec. 2015–Oct. 2016)[178] is ongoing. The doses detailed for the MAD study, which includes a CYP3A4 interaction arm, are 4, 12, 40, 100, 200, and 360 mg.

A recent presentation has confirmed the mechanism of action of this compound and provides further details.[179] In the phase 1, SAD study two cohorts were examined, with each subject receiving up to three doses of PF-06648671 and a placebo. Single doses of 2, 4, 12, and 40 mg were tested in Cohort 1, and 120, 240, and 360 mg were tested in Cohort 2. PF-06648671 was found to be generally safe and well tolerated in healthy subjects after single oral doses up to 360 mg (no clinical abnormalities were identified and no significant changes on safety ECG, telemetry, vital signs, or labs were observed). The maximum tolerated dose was not been established.

Following single doses under fasted condition, PF-06648671 was absorbed rapidly with a median T_{max} of 1–1.5 h. The mean terminal $t_{½}$ ranged from 13.9 to 23.1 h. The C_{max} and AUC_{inf} increased by ~88- and 140-fold over the dose range of 2–360 mg. The food effect was also assessed at 120 mg with a high-fat breakfast. In this case, a delayed median T_{max} of 4 h was observed. The AUC_{inf} slightly increased by 23%, whilst the C_{max} decreased by 24% compared to the fasted state.

Significant, dose-dependent reductions in plasma $A\beta_{42}$, $A\beta_{40}$, and $A\beta_{total}$ were observed. The placebo-adjusted maximal change from baseline was −56.9% and −68.8% for plasma $A\beta_{42}$ and $A\beta_{40}$, respectively, after a single dose of 360 mg. The authors reported that a multiple ascending dose study in healthy adult and elderly is ongoing with the effect on CSF Aβ being evaluated at steady state.

Thus, although the full picture is not yet available for PF-06648671, the effects on plasma $A\beta_{42}$ can be compared to those published for E2012 and BMS-932481, as the data is available from the SAD studies with each compound. Thus, at a dose of 400 mg, E2012 reduced plasma $A\beta_{42}$ by 53%, whilst 300 mg of BMS-932481 reduced plasma $A\beta_{42}$ by ~40%. The effects of BMS-932481 on plasma $A\beta_{42}$ appeared to plateau at 600 mg, as doses of 600 and 900 mg both produced ~60% reductions of plasma $A\beta_{42}$. As noted, recently released data on PF-06648671 reveals that a 360 mg dose produced a 57% reduction in plasma $A\beta_{42}$. Thus, taken together, the effects of PF-06648671 on plasma Aβ do not appear stringer than either of the two forerunner compounds, which have both been terminated. Therefore, unless the CNS penetration and efficacy of PF-06648671 is significantly improved realtive to E2012 and BMS-932481, it would appear unlikely that greater central efficacy will be observed. However, if PF-06648671 shows sufficient efficacy and progresses beyond this stage, it would represent a major breakthrough for the field and perhaps encourage other groups to return to the field. Conversely, Pfizer also have a BACE inhibitor (PF-06751979) which is progressing in parallel in clinical trials. Based on other publicly available data from a range of companies, BACE inhibitors appear to offer improved efficacy over GSMs and are further advanced with Verubecestat/MK-8931 from Merck currently undergoing PhIII trials. Thus, Pfizer will be in the unique position of being able to compare contemporaneous clinical trial data on a GSM and BACE inhibitor and decide on their progression.

Thus, a decade after the first GSM from this class entered PhI studies, no compound has yet progressed beyond this stage. PF-06648671, from Pfizer, is the latest GSM to enter clinical trials but has only progressed to PhI so far, which highlights the challenging nature of this field.

7.07.25 Conclusion

From this review, it is evident that a considerable amount of research has been conducted in the GS field. Early work centered on the carboxylic acid series, following on from the identification of the GSM profile of some NSAIDs. As can be seen, this series has

encountered issues in trying to optimize potency to the single-digit nanomolar range. In addition, the high lipophilicity has also proved challenging to modulate. Furthermore, optimizing CNS penetration and nonspecific (plasma protein and brain tissue) binding (ppb and btb) represents further challenges. Few groups have published detailed PK–PD relationships on compounds from this series, however, the relationship between free drug concentrations and efficacy is not always apparent. Currently, it seems that no research groups are actively working on carboxylic acid derivatives and most have switched to the aryl-imidazole-derived template, typified by the UCSD/Torrey Pines and Eisai compounds. Despite appearing more CNS drug-like and offering the promise of better CNS penetration and better potency, this class of compounds has not been without challenges. Compounds generally show good PK profiles in preclinical species as demonstrated by multiple compounds. However, many groups have struggled to manage CYP inhibition, hERG inhibition, as well as high ppb and btb, which is in part due to the high lipophilicity of these derivatives. The latter appear to manifest in high total concentrations to drive efficacy, which may ultimately be linked to off-target and toxicological issues. Despite several derivatives showing good levels of in vitro potency, in vivo efficacy has generally been weak, and is certainly weaker than that observed with BACE inhibitors. As data emerges on compounds which have entered the clinic, it can be seen that three out of four have been stopped, thus not boding well for further derivatives. Despite this, it appears that some research groups are active in the area, although many also appear to have stopped work, as inferred from patent activity.

Thus, ultimately it appears that weak clinical effects on central amyloid levels, coupled with suboptimal safety profiles, mean that it currently looks unlikely that GSMs will make it to launch. Comparative efficacy data would suggest BACE inhibitors offer the highest likelihood of delivering a drug and they are currently making excellent progress, with a number of compounds in late stage clinical trials. Despite this,there are many lessons that can be learned from the GSM field.

Acknowledgments

The authors would like to thank Dr E. Jacoby for his contribution to the Figs. 1 and 2.

See also: 7.08. Targeting β-Secretase (BACE) for the Treatment of Alzheimer's Disease.

References

1. De Strooper, B.; Annaert, W.; Cupers, P.; Saftig, P.; Craessaerts, K.; Mumm, J. S.; Schroeter, E. H.; Schrijvers, V.; Wolfe, M. S.; Ray, W. J.; Goate, A.; Kopan, R. *Nature* **1999,** *398,* 518–522.
2. La Voie, M. J.; Selkoe, D. J. *J. Biol. Chem.* **2003,** *278,* 34427–34437.
3. Lammich, S.; Okochi, M.; Takeda, M.; Kaether, C.; Capell, A.; Zimmer, A. K.; Edbauer, D.; Walter, J.; Steiner, H.; Haass, C. *J. Biol. Chem.* **2002,** *22,* 44754–44759.
4. Selkoe, D. J.; Wolfe, M. S. *Cell* **2007,** *131,* 215–221.
5. Kaether, C.; Haass, C.; Steiner, H. *Neurodegener. Dis.* **2006,** *3,* 275–283.
6. Oehlrich, D.; Berthelot, D.; Gijsen, H. J. *Med. Chem.* **2011,** *54,* 669–698.
7. Crump, C. J.; Johnson, D. S.; Li, Y.-M. *Biochemistry* **2013,** *52,* 3197–3216.
8. Osenkowski, P.; Ye, W.; Wang, R.; Wolfe, M. S.; Selkoe, D. J. *J. Biol. Chem.* **2008,** *283,* 22529–22540.
9. Osenkowski, P.; Li, H.; Ye, W.; Li, D.; Aeschbach, L.; Fraering, P. C.; et al. *J. Mol. Biol.* **2009,** *385,* 642–652.
10. Lu, P.; Bai, X.-C.; Ma, D.; Xie, T.; Yan, C.; Sun, L.; Yang, G.; Zhao, Y.; Zhou, R.; Scheres, S. H. W.; Shi, Y. *Nature* **2014,** *512,* 166–170.
11. Sun, L.; Zhao, L.; Yang, G.; Yan, C.; Zhou, X.; Xie, T.; Zhao, Y.; Wu, S.; Li, X.; Shi, Y. *PNAS* **2015,** *112,* 6003–6008.
12. Bai, X-c.; Yan, C.; Yang, G.; Lu, P.; Ma, D.; Sun, L.; Zhou, R.; Scheres, S. W.; Shi, Y. *Nature* **2015,** *525,* 212–217.
13. Hardy, J. A.; Higgins, G. A. Alzheimer's Disease: The Amyloid Cascade Hypothesis. *Science* **1992,** *256,* 184–185; Bergmans, B. A.; De Strooper, B. γ-Secretases: From Cell Biology to Therapeutic Strategies. *Neurology* **2010,** *9,* 215–225.
14. Marjaux, E.; De Strooper, B. *Drug Discov. Today Ther. Strateg.* **2004,** *1,* 1–6.
15. Larner, A. J. *Expert Opin. Ther. Pat.* **2004,** *14,* 1403–1420.
16. (a) Garofalo, A. W. Expert Opin. Ther. Pat. 2008, 693.
(b) Griffiths, H. H.; Morten, I. J.; Hooper, N. M. *Expert Opin. Ther. Targets* **2008,** *12* (6), 693–704; Lukiw, W. J. *Expert Opin. Emerg. Drugs* **2008,** *13* (2), 257–271.
17. Recent reviews on GSMs include: (a) Bursavich, M. G.; Harrison, B.A.; Blain, J. *Med. Chem.* **2016**, *59*, 7389–7409
(b) Hall, A.; Patel, T. R. *Prog. Med. Chem.* **2014,** *53,* 101–145; (c) Pettersson, M.; Stepan, A. F.; Kauffman, G. W.; Johnson, D. S. *Expert Opin. Ther. Pat.* **2013,** *23,* 1349–1365. See also Ref. 6.
18. Besidski, Y.; Yngve, U.; Paulsen, K.; Linde, C.; Nordvall, G.; Macsari, I.; Malmborg, J. Triazole Compounds and Their Use as Gamma Secretase Modulators. PCT Patent Application WO 2014195321, Published December 11, 2014.
19. Besidski, Y.; Yngve, U.; Paulsen, K.; Linde, C.; Malmborg, J. Triazole Compounds and Their Use as Gamma Secretase Modulators. PCT Patent Application WO 2014195322, Published December 11, 2014.
20. Besidski, Y.; Yngve, U.; Paulsen, K.; Linde, C.; Macsari, I.; Malmborg, J.; Paptchikhine, A.; Arvidsson, P. Pyrimidine Compounds and Their Use as Gamma Secretase Modulators. PCT Patent Application WO 2014195323, Published December 11, 2014.
21. Hitchcock, S.; Chen, J. J.; Ncube, M.; Nixey, T.; Amegadzie, A.; Kunz, R.; Qian, W.; Chen, N.; Tegley, C. M.; Demorin, F.; Yuan, C. C.; Liu, Q.; Zhu, J.; Peterkin, T.; Adams, J. A.; Hu, E.; Chavez, Jr, F. Gamma Secretase Modulators. PCT Patent Application WO 2009075874, Published June 18, 2009.
22. Biswas, K.; Chen, J. J.; Falsey, J. R.; Gore, V. K.; Liu, Q.; Ma, V. V.; Mercede, S. J.; Rzasa, R. M.; Tegley, C. M.; Zhu, J. Urea Compounds as Gamma Secretase Modulators. PCT Patent Application WO 2009137404, Published November 12, 2009.
23. Whittaker, B.; Steele, C.; Hardick, D.; Mitchell, D.; Pomel, V.; Quattopani, A.; Beher, D. Fused Triazole Derivatives as Gamma Secretase Modulators. PCT Patent Application WO 2014012614, Published January 23, 2014.

24. Yamasaki, S.; Honjo, E.; Samizu, K.; Kuroda, A.; Yonezawa, K.; Hayashibe, S.; Suzuki, T.; Hoshii, H.; Mitani, Y.; Akashiba, H. Cycloalkane Compound. PCT Patent Application WO 2012046771, Published April 12, 2012.
25. Mitani, Y.; Akashiba, H.; Saita, K.; Yarimizu, J.; Uchino, H.; Okabe, M.; Asai, M.; Yamasaki, S.; Nozawa, T.; Ishikawa, N.; Shitaka, Y.; Ni, K.; Matsuoka, N. *Neuropharmacology* **2014,** *79,* 412–419.
26. Forsblom, R.; Paulsen, K.; Rotticci, D.; Santangelo, E.; Waldman, M. Modulators of Amyloid Beta. Patent Application WO 2010053438, Published May 14, 2010.
27. Lo-Alfredsson, Y.; Paulsen, K.; Rakos, L.; Rotticci, D.; Waldman, M. Preparation of Pyridooxazepine Derivatives for Use as Gamma Secretase Modulators and Treatment of Aβ-Related Diseases Pathologies, Such as Alzheimer's Disease. Patent Application WO 2010132015, Published November 18, 2010.
28. Macsari, I.; Paulsen, K.; Rakos, L.; Rotticci, D.; Swahn, B. M.; Von Berg, S.; Waldman, M. Preparation of Pyrido[3,2-f][1,4]oxazepine Compounds and Their Use for Treatment of Aβ-Related Diseases. Patent Application WO 2012064269, Published May 18, 2012.
29. Borgerad, T.; Jureus, A.; Olsson, F.; Rosqvist, S.; Sabirsh, A.; Rottici, D.; Paulsen, K.; et al. *J. Biol. Chem.* **2012,** *287,* 11810–11819.
30. Wanngren, J.; Ottervald, J.; Parpal, S.; Portelius, E.; Stroemberg, K.; Borgergard, T.; et al. *J. Biol. Chem.* **2012,** *287,* 32640–32650.
31. Portelius, E.; Appelkvist, P.; Stromberg, K.; Hoeglund, K. *Curr. Pharm. Des.* **2014,** *20,* 2484–2490.
32. Yngve, U.; Paulsen, K.; Macsari, I.; Sundstrom, M.; Santangelo, E.; Linde, C.; Bogar, K.; Lake, F.; Besidski, Y.; Malmborg, J.; et al. *Med. Chem. Commun.* **2013,** *4,* 422–431.
33. De Cleyn, M. A. J.; Van Brandt, S. F. A.; Gijsen, H. J. M.; Berthelot, D. J.-C.; Oehlrich, D. Triazole Derivatives as γ-Secretase Modulators and Their Preparation and Use for the Treatment of Diseases. PCT Patent Application WO 2011086098 published July 21, 2011.
34. Peng, H.; Talreja, T.; Xin, Z.; Cuervo, J. H.; Gnanasambandam, K.; Humora, M.; Xu, L.; et al. *ACS Med. Chem. Lett.* **2011,** *2,* 786–791.
35. Scannevin, R. H.; Sowmya, C.; Brennan, M. S.; Snodgrass-Belt, P. A.; Peng, H.; Xu, L.; Jung, M.; Bussiere, T.; et al. *Neuropharmacology* **2016,** *103,* 57–68.
36. Gillman, K. W.; Starrett, J. E., Jr.; Parker, M. F.; Xie, K.; Bronson, J. J.; Marcin, L. R.; McElhone, K. E.; Bergstrom, C. P.; Mate, R. A.; Williams, R.; Meredith, J. E., Jr.; Burton, C. R.; Barten, D. M.; Toyn, J. H.; Roberts, S. B.; Lentz, K. A.; Houston, J. G.; Zaczek, R.; Albright, C. F.; Decicco, C. P.; Macor, J. E.; Olson, R. E. *ACS Med. Chem. Lett.* **2010,** *1,* 120–124.
37. Shi, J.; Zuev, D.; Xu, L.; Lentz, K. A.; Grace, J. E.; Toyn, J. H.; Olson, R. E.; Macor, J. E.; Thompson, L. A. *Bioorg. Med. Chem. Lett.* **2016,** *26,* 1498–1502.
38. Wu, Y.-J.; Zhang, Y.; Toyn, J. H.; Macor, J. E.; Thompson, L. A. *Bioorg. Med. Chem. Lett.* **2016,** *26,* 1554–1557.
39. Marcin, L. R.; Thompson III, L. A.; Boy, K. M.; Guernon, J. M.; Higgins, M. A.; Shi, J.; Wu, Y-J.; Zhang, Y.; Macor, J. E. Bicyclic Compounds for the Reduction of Beta-Amyloid Protein Production. PCT Patent Application WO 2010083141A1, Published July 22, 2010.
40. Toyn, J. H.; Thompson, L. A.; Lentz, K. A.; Meredith, J. E., Jr.; Burton, C. R.; Sankaranararyanan, S.; Guss, V.; Hall, T.; Iben, L. G.; Frause, C. M.; Krause, R.; Lin, X.-A.; Pierdomenico, M.; Polson, C.; Robertson, A. S.; Denton, R. R.; Grace, J. E.; Morrison, J.; Raybon, J.; Zhuo, X.; Snow, K.; Padmanabha, R.; Agler, M.; Esposito, K.; Harden, D.; Prack, M.; Verma, S.; Wong, V.; Zhu, Y.; Zvyaga, T.; Gerritz, S.; Marcin, L. R.; Higgins, M. A.; Shi, J.; Wei, C.; Cantone, J. L.; Drexler, D. M.; Macor, J. E.; Olson, R. E.; Ahlijanian, M. K.; Albright, C. F. *Int. J. Alzheimers Dis.* **2014,** *2014*, 431858.
41. Boy, K. M.; Guernon, J. M.; Macor, J. E.; Olson, R. E.; Shi, J.; Thompson III, L. A.; Wu, Y-J.; Xu, L.; Zhang, Y.; Zuev, D. Compounds as Modulators of β-Amyloid Production. PCT Patent Application WO 2011014535, Published February 3, 2011.
42. Toyn, J. H.; Boy, K. M.; Raybon, J.; Meredith, J. E., Jr.; Robertson, A. S.; Guss, V.; Hoque, N.; Sweeney, F.; Zhuo, X.; Clarke, W.; Snow, K.; Denton, R. R.; Zuev, D.; Thompson, L. A.; Morrison, J.; Grace, J.; Berisha, F.; Furlong, M.; Wang, J.-S.; Lentz, K. A.; Padmanabha, R.; Cook, L.; Wei, C.; Drexler, D. M.; Macor, J. E.; Albright, C. F.; Gasior, M.; Olson, R. E.; Hong, Q.; Soares, H. M.; AbuTarif, M.; Ahlijanian, M. K. *J. Pharmacol. Exp. Ther.* **2016,** *358,* 125–137.
43. Soares, H. M.; Gasior, M.; Toyn, J. H.; Wang, J.-S.; Hong, Q.; Berisha, F.; Furlong, M. T.; Raybon, J.; Lentz, K. A.; Sweeney, F.; Zheng, N.; Akinsanya, B.; Berman, R. M.; Thompson, L. A.; Olson, R. E.; Morrison, J.; Drexler, D. M.; Macor, J. E.; Albright, C. F.; Ahlijanian, M. K.; AbuTarif, M. *J. Pharmacol. Exp. Ther.* **2016,** *358,* 138–150.
44. Boy K. M.; Guernon, J. M.; Macor, J. E.; Olson, R. E.; Shi, J.; Thompson III, L. A.; Wu, Y-Y.; Xu, L.; Zhang, Y.; Zuev, D. Compounds for the Reduction of β-Amyloid Production. PCT Patent Application WO 2012103297, Published August 2, 2012.
45. Boy, K.M.; Guernon, J. M.; Macor, J. E.; Thompson III, L. A.; Wu, Y. J.; Zhang, Y. Compounds for the Reduction of Beta-Amyloid Production. PCT Patent Application WO 2012009309, Published January 19, 2012.
46. Gerlach, K.; Heine, N. Hobson, S.; Hoenke, C.; Weber, A. Preparation of Dihydrothienopyrimidines as γ-Secretase Modulators. PCT Patent Application WO 2013020992A1, Published February 14, 2013.
47. Gerlach, K; Eickheimer, C.; Heine, C.; Heine, N.; Weber, A. Preparation of Dihydropteridinones as Modulators of γ-Secretase for Treating Alzheimer's Disease. PCT Patent Application US20130225549A1, Published August 29, 2013.
48. Eickheimer, C.; Gerlach, K; Heine, C.; Heine, N.; Weber, A.; Gross U. Preparation of Spiroheterocyclodihydropteridinones as Modulators of γ-Secretase for Treating Alzheimer's Disease. PCT Patent Application US20130225593A1, Published August 29, 2013.
49. Kobayashi, T.; Iwama, S.; Fusano, A.; Kato, Y.; Ikeda, A.; Teranishi, Y.; Nishihara, A.; Tobe, M. *Bioorg. Med. Chem. Lett.* **2014,** *24,* 378–381.
50. Iwama, S.; Nakagawa, H.; Kato, Y. Novel Oxadiazole Derivative. PCT Patent Application WO 2011001931, Published January 6, 2011.
51. Iwama, S.; Kato, Y.; Kobayashi, T.; Fusano, A. Novel Amide Derivative. PCT Patent Application WO 2011059048, Published May 19, 2011.
52. Iwama, S.; Ikeda, T.; Kobayashi, T. Novel Pyridine Derivative. PCT Patent Application WO 2012057300, Published May 3, 2012.
53. Kimura, T.; Kawano, K.; Doi, E.; Kitazawa, N.; Shin, K.; Miyagawa, T.; Kaneko, T.; Takaishi, M.; Sasaki, T.; Hagiwara, H. Cinnamide Compound. PCT Patent Application WO 2005115990, Published December 8, 2005.
54. Nakano-Ito, K.; Fujikawa, Y.; Hihara, T.; Shinjo, H.; Kotani, S.; Suganuma, A.; Aoki, T.; Tsukidate, K. *Toxicol. Sci.* **2014,** *137,* 249–258.
55. Kimura, T.; Kawano, K.; Doi, E.; Kitazawa, N.; Takaishi, M.; Ito, K.; Kaneko, T.; Sasaki, T.; Sato, N.; Miyagawa, T.; Hagiwara, H. Morpholine Type Cinnamide Compound. PCT Patent Application WO 2007060810, Published May 31, 2007.
56. Kimura, T.; Kawano, K.; Doi, E.; Kitazawa, N.; Takaishi, M.; Koichic, I.; Kaneko, T.; Sasaki, T.; Sato, N.; Miyagawa, T.; Hagiwara, H. Bicyclic Odomorpholine Derivative. PCT Patent Application WO 2008108378, Published September 12, 2008.
57. Kimura, T.; Kawano, K.; Doi, E.; Kitazawa, N.; Takaishi, M.; Ito, K.; Kaneko, T.; Sasaki, T.; Miyagawa, T.; Hagiwara, H.; Yoshida, Y. Bicyclic Cinnamide Compound. PCT Patent Application WO 2007060821, Published May 31, 2007.
58. Kimura, T.; Kawano, K.; Doi, E.; Kitazawa, N.; Miyagawa, T.; Sato, N.; Kaneko, T.; Shin, K.; Ito, K.; Takaishi, M.; Sasaki, T.; Hagiwara, H. Heterocyclic Type Cinnamide Derivative. PCT Patent Application WO 2007135970, Published November 29, 2007.
59. Kimura, T.; Kitazawa, N.; Kaneko, T.; Sato, N.; Kawano, K.; Ito, K.; Doi, E.; Takaishi, M.; Sasaki, T.; Doko, T.; Miyagawa, T.; Hagiwara, H. Polycyclic Cinnamide Derivative. PCT Patent Application WO 2007102580, Published September 13, 2007.
60. Kimura, T.; Kitazawa, N.; Kaneko, T.; Sato, N.; Kawano, K.; Ito, K.; Takaishi, M.; Sasaki, T.; Yohda, Y.; Uemura, T.; Doko, T.; Shinmyo, D.; Hasegawa, D.; Miyagawa, T.; Hagiwara, H. Polycyclic Compound. PCT Patent Application WO 2009028588, Published March 5, 2009.
61. Yu, Y.; Logovinsky, V.; Schuck, E.; Kaplow, J.; Chang, M.; Miyagawa, T.; Wong, N.; Ferry, J. *J. Clin. Pharmacol.* **2014,** *54,* 528–536.
62. Lu, Y.; Riddell, D.; Hajos-Korcsok, E.; Bales, K.; Wood, K. M.; Nolan, C. E.; Robshaw, A. E.; Zhang, L.; Leung, L.; Becker, S. L.; Tseng, E.; Barricklow, J.; Miller, E. H.; Osgood, S.; O'Neill, B. T.; Brodney, M. A.; Johnson, D. S.; Pettersen, M. *J. Pharmacol. Exp. Ther.* **2012,** *342,* 366–375.
63. Kimura, T.; Kawano, K.; Doi, E.; Kitazawa, N.; Miyagawa, T.; Sato, N.; Kaneko, T.; Shin, K.; Ito, K.; Takaishi, M.; Sasaki, T.; Miyagawa, T.; Hagiwara, H. Urea Type Cinnamide Derivative. PCT Patent Application WO 2007135969, Published November 29, 2007.
64. Shapiro, G.; Chesworth, R. 1,3,4-Trisubstituted Benzenes. PCT Patent Application WO 2009036428, Published March 19, 2009.
65. Chesworth, R.; Shapiro, G. 1,3,5-Trisubstituted Benzenes for Treatment of Alzheimer's Disease and Other Disorders. PCT Patent Application WO 2009067943, Published May 28, 2009.
66. Shapiro, G.; Chesworth, R.; Tetrasubstituted Benzens. PCT Patent Application WO 2009086277, Published July 9, 2009.

67. Koenig, G.; Blain, J-F. Tetrasubstituted Benzenes for Treatment of Early Onset Alzheimer's Disease. PCT Patent Application WO 2013106328, Published July 18, 2013.
68. Rogers, K.; Felsenstein, K. M.; Hrdlicka, L.; Tu, Z.; Albayya, F.; Lee, W.; Hopp, S.; Miller, M.-J.; Spaulding, D.; Yang, Z.; Hodgdon, H.; Nolan, S.; Wen, M.; Costa, D.; Blain, J.-F.; Freeman, E.; De Strooper, B.; Vulsteke, V.; Scrocchi, L.; Zetterberg, H.; Portelius, E.; Hutter-Paier, B.; Havas, D.; Ahlijanian, M.; Flood, D.; Leventhal, L.; Shapiro, G.; Patzke, H.; Chesworth, R.; Koenig, G. *Mol. Neurodegener.* **2012,** *7,* 61.
69. Burnett, D. A.; Bursavich, M. G.; Mcriner, A. J. Fused Morpholinopyrimidines and Methods of Use Thereof. PCT Patent Application WO 2015066697, Published May 7, 2015.
70. Burnett, D. A.; Bursavich, M. G.; Mcriner, A. J. Fused Morpholinopyrimidines and Methods of Use Thereof. PCT Patent Application WO 2015066696, Published May 7, 2015.
71. Burnett, D. A.; Bursavich, M. G.; Mcriner, A. J. Fused Morpholinopyrimidines and Methods of Use Thereof. PCT Patent Application WO 2015109109, Published July 23, 2015.
72. Burnett, D. A.; Bursavich, M. G.; Mcriner, A. J. Fused Morpholinopyrimidines and Methods of Use Thereof. PCT Patent Application WO 2015138689, Published September 17, 2015.
73. Hall, A.; Elliot, R. L.; Giblin, G. M. P.; Hussain, I.; Musgrave, J.; Naylor, A.; Sasse, R.; Smith, B. *Bioorg. Med. Chem. Lett.* **2010,** *20,* 1306–1311.
74. Hawkings, J.; Harrison, D. C.; Ahmed, S.; Davis, R. P.; Chapman, T.; Marshall, I.; Smith, B.; Mead, T. L.; Medhurst, A.; Giblin, G. M. P.; et al. *Neurodegener. Dis.* **2011,** *8,* 455–464.
75. Wan, Z.; Hall, A.; Jin, Y.; Xiang, J.-N.; Yang, E.; Eatherton, A.; Smith, B.; Yang, G.; Yu, H.; Wang, J.; et al. *Bioorg. Med. Chem. Lett.* **2011,** *21,* 4016–4019.
76. Wan, Z.; Hall, A.; Sang, Y.; Xiang, J.-N.; Yang, E.; Smith, B.; Harrison, D. C.; Yang, G.; Yu, H.; Price, H. S.; et al. *Bioorg. Med. Chem. Lett.* **2011,** *21,* 4832–4835.
77. Huang, Y.; Li, T.; Eatherton, A.; Mitchell, W.; Rong, N.; Ye, L.; yang, X.-J.; Jin, S.; Ding, Y.; Zhang, J. *Neuropharmacology* **2013,** *70,* 278–286.
78. Ho, C. Y. Preparation of Biphenyl Carboxylic Acids and Derivatives as Modulators of γ-Secretase for Treatment of Alzheimer's Disease. PCT Patent Application WO 2009051948A1, Published April 23, 2009.
79. Wilson, F.; Reid, A.; Reader, V.; Harrison, R.J.; Sunose, M.; Hernandez-Perni, R.; Major, J.; Boussard, C.; Smelt, K.; Taylor, J. et al. Substituted Biphenyl Carboxyllic Acids and Derivatives Thereof. PCT Patent Application WO 2007124394, Published November 1, 2007.
80. Ho, C. Y. Preparation of Biphenyl Derivatives as Modulators of γ-Secretase for Treatment of Alzheimer's Disease. PCT Patent Application WO 2009052350, Published April 23, 2009.
81. Ho, C. Y. Preparation of Biphenyl Derivatives as Modulators of γ-Secretase for Treatment of Alzheimer's Disease. PCT Patent Application WO 2009052079, Published April 23, 2009.
82. Ho, C. Y. Preparation of Carbon-Linked Modulators of γ-Secretase. PCT Patent Application WO 2009052334, Published April 23, 2009.
83. Wilson, F.; Reid, A.; Reader, V.; Harrison, R. J.; Sunose, M.; Hernandez-Perni, R.; Major, J.; Boussard, C.; Smelt, K.; Taylor, J. et al. Terphenyl Derivatives for Treatment of Alzheimer Disease. PCT Patent Application WO 2007124351, Published November 1, 2007.
84. Ho, C. Y. Preparation of Biphenylpiperidines and Piperazines as Modulators of γ-Secretase. PCT Patent Application WO 2009052126, Published April 23, 2009.
85. Van Broeck, B.; Chen, J.-M.; Treton, G.; Desmidt, M.; Hopf, C.; Ramsden, N.; Karran, E.; Mercken, M.; Rowley, A. *Br. J. Pharmacol.* **2011,** *163,* 375–389.
86. Gijsen, H. J. M.; Mercken, M. *Int. J. Alzheimers Dis.* **2012,** *2012,* 295207.
87. Bischoff, F.; Berthelot, D.; De Cleyn, M.; Macdonald, G.; Minne, G.; Oehlrich, D.; Pieters, S.; Surkyn, M.; Trabanco, A. A.; Tresadern, G.; Van Brandt, S.; Velter, I.; Zaja, M.; Borghys, H.; Masungi, C.; Mercken, M.; Gijsen, H. J. M. J. *Med. Chem.* **2012,** *55,* 9089–9106.
88. Borghys, H.; Tuefferd, M.; Van Broeck, B.; Clessens, E.; Dillen, L.; Cools, W.; Vinken, P.; Straetemans, R.; de Ridder, F.; Gijsen, H.; Mercken, M. *J. Alzheimer's Dis.* **2012,** *28,* 809–822.
89. Oehlrich, D.; Rombouts, F. J. R.; Berthelot, D.; Bischoff, F. P.; De Cleyn, M.; Jaroskova, L.; Macdonald, G.; Mercken, M.; Surkyn, M.; Trabanco, A. A.; Tresadern, G.; Van Brandt, S.; Velter, A. I.; Wu, T.; Gijsen, H. J. M. *Bioorg. Med. Chem. Lett.* **2013,** *23,* 4794–4800.
90. Similar triazole-containig GSMs were also reported by Eisai in: (a) Kitazawa, N.; Shinmyo, D.; Ito, K.; Sato, N.; Hasegawa, D.; Uemura, T.; Watanabe, T. Nitrogen-Containing Fused Heterocyclic Compounds and Their Use as Beta Amyloid Production Inhibitors. PCT Patent Application WO 2010098487, Published September 2, 2010. (b) Kimura, T; Doi, E.; Doko, T.; Shinmyo, D.; Ito, K.; Sato, N.; Hashizume, M.; Watanabe, T. Preparation of Aryl Imidazole Compounds and Their Use as Beta Amyloid Production Inhibitors. PCT Patent Application WO 2010098488, Published September 2, 2010.
91. Velter, A. I.; Bischoff, F. P.; Berthelot, D.; De Cleyn, M.; Oehlrich, D.; Jaroskova, L.; Macdonald, G.; Minne, G.; Pieters, S.; Rombouts, F. *Bioorg. Med. Chem. Lett.* **2014,** *24,* 5805–5813.
92. Minne, G.; Bischoff, F. P.; Gijsen, H. J. M.; Velter, A. I.; Pieters, S. M. A.; Berthelot, D. J-C. Preparation of Substituted Indole Derivatives as Gamma Secretase Modulators. PCT Patent Application WO 2013010904, Published January 24, 2013.
93. Rombouts, F. J. R.; Trabanco, A. A.; Gijsen, H. J. M.; Macdonald, G. J.; Bischoff, F. P.; Alonso de Diego, S.; A.; Velter, A. I.; Van Roosbroeck, Y. E. M. Substituted 3,4-Dihydro-2*H*-pyrido[1,2-A]pyrazine-1,6-dione Derivatives Useful for the Treatment of (Inter Alia) Alzheimer's Disease. PCT Patent Application WO 2013171712A1, Published November 21, 2013.
94. Bischoff, F. P.; Velter, A. I.; Rombouts, F. J. R.; De Cleyn, M.; Van Brandt, S.; Gijsen, H. J. M.; Zavattaro, C.; Van Den Keybus, F. A. M. Novel Substituted Pyrido-Piperazinone Derivatives as Gamma Secretase Modulators. PCT Patent Application WO 2014111457, Published July 24, 2014.
95. Am Ende, C. W.; Fish, B. A.; Green, M. E.; Johnson, D. S.; Mullins, P. B.; O'Donnell, C. J.; Pettersson, M. Y.; Stiff, C. M.; Subramanyam, Ch.; Tran, T. P.; Navaratnam, T. Preparation of Pyrido[1,2-a]pyrazine-1,6-dione Derivatives as γ-Secretase Modulators. PCT Patent Application WO 2012131539, Published October 4, 2012.
96. Bischoff, F. P.; Gijsen, H. J. M.; Van Den Keybus, F. A. M.; Rombouts, F. J. R. Novel Tricyclic 3,4-dihydro-2*H*-pyrido[1,2-a]pyrazine-1,6-dione Derivatives as Gamma Secretase Modulators PCT Patent Application WO 2014096212, Published June 26, 2014.
97. Beher, D.; Bettati, M.; Checksfield, G. D.; Churcher, I.; Doughty, V. A.; Oakley, P. J.; Quddus, A.; Teall, M. R.; Wrigley, J. D. Treatment for Alzheimer's Disease and Related Conditions. PCT Patent Application WO 2005013985, Published February 17, 2005.
98. Blurton, P.; Burkamp, F.; Churcher, I.; Harrison, T.; Neduvelil, J. Arylacetic Acids and Related Compounds and Their Preparation, Pharmaceutical Composition and Their Use for the Treatment of Diseases Associated With Depositions of β-Amyloid Peptides in the Brain Such as Alzheimer's Disease. PCT Patent Application WO 2006008558, Published January 26, 2006.
99. Hannam, J. C.; Kulagowski, J. J.; Madin, A.; Ridgill, M. P.; Seward, E. M. Preparation of Piperidines and Related Compounds for Treatment of Alzheimer's Disease. PCT Patent Application WO 2006043064, Published April 27, 2006.
100. Bulic, B.; Ness, J.; Hahn, S.; Rennhack, A.; Jumpertz, T.; Weggen, S. *Curr. Neuropharmacol.* **2011,** *9,* 598–622.
101. Page, R. M.; Baumann, K.; Tomioka, M.; Perez-Revuelta, B. I.; Fukumori, A.; Jacobsen, H.; Flohr, A.; Luebbers, T.; Ozmen, L.; Steiner, H.; Haas, C. J. *Biol. Chem.* **2008,** *283,* 677–683.
102. Stanton, M. G.; Hubbs, J.; Sloman, D.; Hamblett, C.; Andrade, P.; Angagaw, M.; et al. *Bioorg. Med. Chem. Lett.* **2010,** *20,* 755–758.
103. Rivkin, A.; Ahearn, S. P.; Chichetti, S. M.; Kim, Y. R.; Li, C.; Rosneau, A.; Kattar, S. D.; Jung, J.; Shah, S.; Hughes, B. *Bioorg. Med. Chem. Lett.* **2010,** *20,* 1269–1271.
104. Fischer, C.; Shah, S.; Hughes, B. L.; Nikov, G. N.; Crispino, J. L.; Middleton, R. E.; et al. *Bioorg. Med. Chem. Lett.* **2011,** *21,* 773–776.
105. Fischer, C.; Zultanski, S. L.; Zhou, H.; Methot, J. L.; Brown, W. C.; Mampreian, D. M.; et al. *Bioorg. Med. Chem. Lett.* **2011,** *21,* 4083–4087.
106. Fischer, C.; Zultanski, S. L.; Zhou, H.; Methot, J. L.; Shah, S.; Nuthall, H.; et al. *Bioorg. Med. Chem. Lett.* **2012,** *22,* 3140–3146.
107. Fischer, C.; Zultanski, S. L.; Zhou, H.; Methot, J. L.; Shah, S.; Hayashi, I. *Bioorg. Med. Chem. Lett.* **2015,** *25,* 3488–3494.
108. Methot, J. L.; Fischer, C.; Li, C.; Rivkin, A.; Ahearn, S. P.; Brown, W. C.; et al. *Bioorg. Med. Chem. Lett.* **2015,** *25,* 3495–3500.
109. Am Ende, C. W.; Fish, B.A.; Johnson, D. S.; Lira, R.; O'Donnell, C. J.; Pettersson, M. Y.; Stiff, C. M. Aminocyclohexanes and Aminotetrahydropyrans and Related Compounds as γ-Secretase Modulators. WO 2011092611A1, August 4, 2011.

110. Petterson, M.; Johnson, D. S.; Subramanyam, C.; Bales, K. R.; Am Ende, C. W.; Fish, B. A.; Green, M. A.; Kaufmann, G. W.; Lira, R.; Mullins, P. B.; et al. *Bioorg. Med. Chem. Lett.* **2012,** *22,* 2906–2911.
111. Petterson, M.; Johnson, D. S.; Subramanyam, C.; Bales, K. R.; Am Ende, C. W.; Fish, B. A.; Green, M. A.; Kaufmann, G. W.; Mullins, P.; Navaratnam, T.; et al. *J. Med. Chem.* **2014,** *57,* 1046–1062.
112. Petterson, M.; Johnson, D. S.; Humphrey, J. M.; Butler, T. W.; Am Ende, C.; Fish, B. A.; Green, M. E.; Kaufmann, G. W.; Mullins, P. B.; O'Donnel, C. J.; et al. *ACS Med. Chem. Lett.* **2015,** *6,* 596–601.
113. Petterson, M.; Johnson, D. S.; Humphrey, J. M.; am Ende, C.; Evrard, E.; Efremov, I.; Kaufmann, G. W.; Stepan, A. F.; Stiff, C. M.; Xie, L.; et al. *Bioorg. Med. Chem. Lett.* **2015,** *25,* 908–913.
114. The Pfizer patent application describing indole-substituted piperazino pyridones was published in 2015: Pettersson, M. Y.; Johnson, D. S.; Subramanyam, C.; O'Donnell, C. J.; Am Ende, C. W.; Green, M. E.; Patel, N. C.; Stiff, C. M.; Tran, T. P.; Kauffman, G. W.; Stepan, A. F.; Verhoest, P. R. Preparation of Novel Bicyclic Pyridinones as Gamma-Secretase Modulators. PCT Patent Application WO 2015049616, Published April 9, 2015.
115. Lübbers, T.; Flohr, A.; Jolidon, S.; David-Pierson, P.; Jacobsen, H.; Ozmen, L.; Baumann, K. *Bioorg. Med. Chem. Lett.* **2011,** *21,* 6554–6558.
116. Luebbers, T. Optimization of γ-Secretase Modulators Through Variation of Scaffolds. Proteinase 2013—8th RSC/SCI Symposium on Proteinase Inhibitor Design. Basel, 15-16th April *2013.*
117. Baumann, K.; Goetschi, E.; Jolidon, S.; Limberg, A.; Luebbers, T. Heterocyclic Gamma Secretase Modulators. PCT Patent Application WO 2010052199, Published May 14, 2010.
118. Baumann, K.; Goetschi, E.; Green, L.; Jolidon, S.; Knust, H.; Limberg, A.; Luebbers, T.; Thomas, A. Gamma Secretase Modulaters. PCT Patent Application WO 2011092272, Published August 4, 2011.
119. Baumann, K.; Flohr, A.; Goetschi, E.; Jacobsen, H.; Jolidon, S.; Luebbers, T. Modulators for Amyloid Beta. PCT Patent Application WO 2009103652, Published August 27, 2009.
120. Goetschi, E.; Jolidon, S.; Luebbers, T. Modulators for Amyloid Beta. PCT Patent Application WO 2010040661, Published April 14, 2010.
121. Baumann, K.; Flohr, A.; Goetschi, E.; Green, L.; Jolidon, S.; Knust, H.; Limberg, A.; Luebbers, T.; Thomas, A. Piperidine Derivatives. PCT Patent Application WO 2011101304, Published August 25, 2011.
122. Baumann, K.; Green, L.; Limberg, A.; Luebbers, T.; Thomas, A. Bridged Piperidine Derivatives. PCT Patent Application WO 2012116965, Published September 7, 2012.
123. Brendel, M.; Jaworska, A.; Herms, J.; Trambauer, J.; Rotzer, C.; Gildehaus, F.-J.; Carlsen, J.; Cumming, P.; Bylund, J.; Luebbers, T.; Bartenstein, P.; Steiner, H.; Haass, C.; Baumann, K.; Rominger, A. *Mol. Psychiatry* **2015,** *20,* 1179–1187.
124. Baumann, K.; Flohr, A.; Jolidon, S.; Knust, H.; Limberg, A.; Luebbers, T.; Nettekoven, M. Indola-Amide Compounds as Beta-Amyloid Inhibitors. PCT Patent Application WO 2015060386, Published April 24, 2014.
125. Findeis, M. A.; Schroeder, F.; McKee, T. D.; Yager, D.; Fraering, P. C.; Creaser, S. P.; Austin, W. F.; Clardy, J.; Wang, R.; Selkoe, D.; Eckman, C. B. *ACS Chem. Neurosci.* **2012,** *3,* 941–951.
126. Austin, W. F.; Hubbs, J. L.; Fuller, N. O.; Creaser, S. P.; McKee, T. D.; Loureiro, R. M. B.; Findeis, M. A.; Tate, B.; Ives, J. L.; Bronk, B. S. *Med. Chem. Commun.* **2013,** *4,* 569–574.
127. Fuller, N. O.; Hubbs, J. L.; Austin, W. F.; Creaser, S. P.; McKee, T. D.; Loureiro, M. B.; Tate, B.; Xia, W.; Ives, J. L.; Findeis, M. A.; Bronk, B. S. *ACS Med. Chem. Lett.* **2012,** *3,* 908–913.
128. Hubbs, J. L.; Fuller, N. O.; Austin, W. F.; Shen, R.; Creaser, S. P.; McKee, T. D.; Loureiro, M. B.; Tate, B.; Xia, W.; Ives, J.; Bronk, B. S. J. *Med. Chem.* **2012,** *55,* 9270–9282.
129. Hubbs, J. L.; Fuller, N. O.; Austin, W. F.; Shen, R.; Ma, J.; Gong, Z.; Li, J.; McKee, T. D.; Loureiro, R. M. B.; Tate, B.; Dumin, J. A.; Ives, J.; Bronk, B. S. *Bioorg. Med. Chem. Lett.* **2015,** *25,* 1621–1626.
130. Loureiro, R. M.; Dumin, J. A.; McKee, T. D.; Austin, W. F.; Fuller, N. O.; Hubbs, J. L.; Shen, R.; Jonker, J.; Ives, J.; Bronk, B. S.; Tate, B. *Alzheimers Res. Ther.* **2013,** *5,* 19.
131. Qin, J.; Dhondi, P.; Huang, X.; Mandal, M.; Zhao, Z.; Pissarnitski, D.; Zhou, W.; Aslanian, R.; Zhu, Z.; Greenlee, W.; et al. *Bioorg. Med. Chem. Lett.* **2011,** *21,* 664–669.
132. Quin, J.; Zhou, W.; Huang, X.; Dhondi, P.; Palani, A.; Aslanian, R.; Zhu, Z.; Greenle, W.; Cohen-Williams, M.; Jones, N.; Hyde, L.; Zhang, L. *ACS Med. Chem. Lett.* **2011,** *2,* 471–476.
133. Huang, X.; Aslanian, R.; Zhou, W.; Zhu, X.; Qin, J.; Greenlee, W.; Zhu, Z.; Zhang, L.; Hyde, L.; Chu, I.; Cohen-Williams, M.; Palani, A. *ACS Med. Chem. Lett.* **2010,** *1,* 184–187.
134. Sun, Z.-Y.; Asberom, T.; Bara, T.; Bennet, C.; Burnett, D.; Chu, I.; Clader, J.; Cohen-Williams, M.; Cole, D.; Czarniecki, M.; Durkin, J.; et al. *J. Med. Chem.* **2011,** *55,* 489–502.
135. Huang, X.; Zhou, W.; Liu, X.; Li, H.; Sun, G.; Mandal, M.; Vicarel, M.; Zhu, X.; Bennet, C.; McCracken, T.; Pissarnitski, D.; et al. *ACS Med. Chem. Lett.* **2012,** *3,* 931–935.
136. Li, H.; Qin, J.; Dhondi, P.; Zhou, W.; Vicarel, M.; Bara, T.; Cole, D.; Josien, H.; Pissarnitski, D.; Zhu, Z.; et al. *Bioorg. Med. Chem. Lett.* **2013,** *23,* 466–471.
137. Nishitomi, K.; Jano, K.; Kato, I.; Sako, Y. Preparation of Pharmaceutical Products Containing Heterocyclic Sulfonamide Compounds as γ-secretase modulators. PCT Patent Application WO 2010126002A1, Published November 4, 2010.
138. Kato, Y.; Kano, K. Preparation of Lactam or Benzenesulfonamide Compounds as Inhibitors for Production of Amyloid β Protein. PCT Patent Application WO 2011007819A1, Published January 20, 2011.
139. Takai, T.; Koike, T.; Honda, E.; Kajita, Y.; Nakamura, M.; Morimoto, S.; Hoashi, Y.; Kamata, M.; Watanabe, T.; Igari, T.; Terauchi, J. *Bioorg. Med. Chem.* **2015,** *23,* 1923–1934.
140. Takai, T.; Hoashi, Y.; Tomata, Y.; Morimoto, S.; Nakamura, M.; Watanabe, T.; Igari, T.; Koike, T. *Bioorg. Med. Chem. Lett.* **2015,** *25,* 4245–4249.
141. Takai, T.; Koike, T.; Nakamura, M.; Kajita, Y.; Yamashita, T.; Taya, N.; Tsukamoto, T.; Watanabe, T.; Murakami, K.; Igari, T.; Kamata, M. *Bioorg. Med. Chem.* **2016,** *24,* 3192–3206.
142. Murakami, K.; Watanabe, T.; Koike, T.; Kamata, M.; Igari, T.; Kondo, S. *Brain Res.* **2016,** *1633,* 73–86.
143. Cheng, S.; Comer, D. D.; Mao, L.; Balow, G. P.; Pleynet, D.; Reiter, S. E. Compositions and Uses Thereof in Modulating Amyloid Beta. PCT Patent Application WO 2004110350, Published December 23, 2004.
144. Kounnas, M. Z.; Danks, A. M.; Cheng, S.; Tyree, C.; Ackerman, E.; Zhang, X.; Ahn, K.; Nguyen, P.; Comer, D.; Mao, L.; Yu, C.; Pleynet, D.; Digregorio, P. J.; Velicelebi, G.; Stauderman, K. A.; Comer, W. T.; Mobley, W. C.; Li, Y.-M.; Sisodia, S. S.; Tanzi, R. E.; Wagner, S. L. *Neuron* **2010,** *67* (5), 769–780.
145. Tanzi, R. E.; Wagner, S. L.; Cheng, S.; Mobley, W. C. Gamma-Secretase Modulators. PCT Patent Application WO 2014165263, Published October 9, 2014.
146. Rynearson, K. D.; Buckle, R. N.; Barnes, K. D.; Herr, R. J.; Mayhew, N. J.; Paquette, W. D.; Sakwa, S. A.; Nguyen, P. D.; Johnson, G.; Tanzi, R. E.; Wagner, S. L. *Bioorg. Med. Chem. Lett.* **2016,** *26,* 3928–3937.
147. Wagner, S. L.; Mobley, W. C.; Tanzi, R. E.; Johnson, G.; Buckle, R.; Mayhew, N.; Herr, R. J.; Rynearson, K. D. Potent Gamma-Secretase Modulators. PCT Patent Application WO 2016070107, Published May 6, 2016.
148. Eatherton, A. J.; Giblin, G. M. P.; Hall, A.; Johnson, M. R.; Le, J.; Mitchell, W. L.; Myatt, J.; Norton, D.; Price, H. S. Pyridazine Derivatives for Inhibiting Beta Amyloid Peptide Production. PCT Patent Application WO 2009050227, Published April 23, 2009.
149. Bayley, H. Photogenerated Reagents in Biochemistry and Molecular Biology. In *Laboratory techniques in Biochemistry and Molecular Biology;* Work, T. S., Burdon, R. H., Eds.; Elsevier: Amsterdam, 1983; (b) Kotzyba-Hibert, F.; Kapfer, I.; Goeldner, M. *Angew. Chem. Int. Ed.* **1995,** *34,* 1296–1312; (c) Dorman, G.; Prestwich, G. D. *Trends Biotechnol.* **2000,** *18* (2), 64–77.
150. Crump, C. J.; Fish, B. A.; Castro, S. V.; Chau, D.-M.; Gertsik, N.; Ahn, K.; Stiff, C.; Pozdnyakov, N.; Bales, K. R.; Johnson, D. S.; Li, Y.-M. *ACS Chem. Neurosci.* **2011,** *2,* 705–710.

151. (a) Green, N. M. *Adv. Protein Chem.* **1975,** *29,* 85; (b) Romovacek, H.; Finn, F.; Hofmann, K. *Biochemistry* **1983,** *22,* 904–909.
152. Ohki, Y.; Higo, T.; Uemura, K.; Shimada, N.; Osawa, S.; Berezovska, O.; Yokoshima, S.; Fukuyama, T.; Tomita, T.; Iwatsubo, T. *EMBO J.* **2011,** *30,* 4815–4824.
153. Jumpertz, T.; Rennhack, A.; Ness, J.; Baches, S.; Pietrzik, C. U.; Bulic, B.; Weggen, S. *PLoS ONE* **2012;**, e30484.
154. Ebke, A.; Luebbers, T.; Fukumori, A.; Shirotani, K.; Haas, C.; Baumann, K.; Steiner, H. J. *Biol. Chem.* **2011,** *286,* 37181–37186.
155. Pozdnyakov, N.; Murrey, H. E.; Crump, C. J.; Petersson, M.; Ballard, T. E.; Am Ende, C. W.; Ahn, K.; Li, H.-M.; Bales, K. R.; Johnson, D. S. J. *Biol. Chem.* **2013,** *288,* 9710–9720.
156. Takeo, K.; Tanimura, S.; Shinoda, T.; Osawa, S.; Zahariev, I. K.; Takegami, N.; Ishizuka-Katsura, Y.; Shinya, N.; Takagi-Niidome, S.; Tominaga, A.; et al. *PNAS* **2014,** *111,* 10544–10549.
157. Li, X.; Dang, S.; Yan, C.; Gong, X.; Wang, J.; Shi, Y. *Nature* **2013,** *493,* 56–61.
158. Narlawar, R.; Perez Revuelta, B. I.; Haass, C.; Steiner, H.; Schmidt, B.; Baumann, K. *J. Med. Chem.* **2006,** *49,* 7588–7591.
159. Galasko, D. R.; Graff-Radford, N.; May, S.; Hendrix, S.; Cottrell, B. A.; Sagi, S. A. *Alzheimer Dis. Assoc. Disord.* **2007,** *21* (4), 292–299.
160. Wilcock, G. K.; Black, S. E.; Hendrix, S. B.; Zavitz, K. H.; Swabb, E. A.; Laughlin, M. A. *Lancet Neurol.* **2008,** *7* (6), 483–493.
161. Green, R. C.; Schneider, L. S.; Amato, D. A.; Beelen, A. P.; Wilcock, G.; Swabb, E. A.; Zavitz, K. H. *JAMA* **2009,** *302* (23), 2557–2564.
162. Eriksen, J. L.; Sagi, S. A.; Smith, T. E.; Weggen, S.; Das, P.; McLendon, D. C.; Ozols, V. V.; Jessing, K. W.; Zavitz, K. H.; Koo, E. H.; Golde, T. E. *J. Clin. Invest.* **2003,** *112* (3), 440–449.
163. Imbimbo, B. P.; Del, G. E.; Colavito, D.; D'Arrigo, A.; Dalle, C. M.; Villetti, G.; Facchinetti, F.; Volta, R.; Pietrini, V.; Baroc, M. F.; Serneels, L.; De Strooper, B.; Leon, A. *Pharmacol. Exp. Ther.* **2007,** *323* (3), 822–830.
164. CereSpir Announcement. http://www.cerespir.com/072613b.htm (accessed 01.08.13).
165. Sivilia, S.; Lorenzini, L.; Giuliana, A.; Gusciglio, M.; Fernandez, M.; Baldassarro, V. A.; Mangano, C.; Ferraro, L.; Pietrini, V.; Baroc, M. F.; Viscomi, A. R.; Ottonello, S.; Villetti, G.; Imbimbo, B. P.; Calza, L.; Giardino, L. *BMC Neurosci.* **2013,** *14,* 44.
166. Lanzillotta, A.; Sarnico, I.; Benareses, M.; Branca, C.; Baiguera, C.; Hutter-Paier, B.; Windisch, M.; Spano, P.; Imbimbo, B. P.; Pizzi, M. *J. Mol. Neurosci.* **2011,** *45,* 22–31.
167. Ross, J.; Sharma, S.; Winston, J.; Nunez, M.; Bottini, G.; Franceschi, M.; Scarpini, E.; Frigerio, E.; Fiorentini, F.; Fernandez, M.; Sivilia, S.; Giardino, L.; Calza, L.; Norris, D.; Cicirello, H.; Casula, D.; Imbimbo, B. P. *Curr. Alzheimer Res.* **2013,** *10* (7), 742–753.
168. EnVivo EVP-0962 Press Release. http://www.envivopharma.com/news-item.php?id=44, 2013.
169. EVP-0962 PhII Trial. https://clinicaltrials.gov/show/NCT01661673.
170. Ling, I. F.; Golde, T. E.; Galasko, D. R.; Koo, E. H. *Alzheimers Res. Ther.* **2015,** *7,* 55.
171. Hashimoto, T.; Ishibashi, A.; Hagiwara, H.; Murata, Y.; Takenaka, O.; Miyagawa, T. E2012: A novel gamma-secretase modulator-pharmacology part. *Alzheimers Dement.* **2012,** *6* (4), S242.
172. Amino, H.; Hagiwara, H.; Murata, Y.; Watanabe, H.; Sasaki, T.; Miyagawa, T. E2012: A novel gamma-secretase modulator-mechanism of action. *Alzheimers Dement.* **2010,** *6* (4), S541–S542.
173. Nagy, C.; Schuck, E.; Ishibashi, A.; Nakatani, Y.; Rege, B.; Logovinsky, V. E2012, a novel gamma-secretase modulator, decreases plasma amyloid-beta levels in humans. *Alzheimers Dement.* **2010,** *6* (4), S574.
174. E2212 Clinical Trials. http://clinicaltrials.gov/ct2/show/NCT01221259?intr=E2212&rank=1, 2013.
175. Eisai Financial Update 1st May 2013. http://www.eisai.com/pdf/eir/emat/e4523_130513.pdf (accessed 01.05.13).
176. PF-06648671 Biomarkers. https://clinicaltrials.gov/ct2/show/NCT02407353?intr=PF-06648671&rank=2.
177. PF-06648671 SAD. https://clinicaltrials.gov/ct2/show/NCT02316756?intr=PF-06648671&rank=3.
178. PF-06648671 SAD. https://clinicaltrials.gov/ct2/show/NCT02440100?intr=PF-06648671&rank=1.
179. Qiu, R.; Liu, R.; Wills, A. M.; He, P.; Leurent, C.; Hajos-Korcsok, E.; Mendes da Costa, L.; Alexander, R. C. P2009 PF06648671 a Novel Gamma Secretase Modulator: Safety, Tolerability, Pharmacokinetics and Effects on Plasma Amyloid-β Levels Following Single Oral Ascending Doses in Healthy Volunteers. In AAIC, July 22–28, Toronto, Canada 2016.

7.08 Targeting β-Secretase (BACE) for the Treatment of Alzheimer's Disease

A Hall, UCB Pharma, Braine l'Alleud, Belgium
HJM Gijsen, Janssen Research & Development, Janssen Pharmaceutica NV, Beerse, Belgium

© 2017 Elsevier Ltd. All rights reserved.

7.08.1	**Introduction**	327
7.08.1.1	Alzheimer's Disease and the Amyloid Hypothesis	327
7.08.1.2	Challenges With Early BACE Inhibitor Discovery	327
7.08.2	**Inhibitors Reported by Amgen**	330
7.08.3	**Inhibitors Reported by Astellas**	333
7.08.4	**Inhibitors Reported by AstraZeneca**	333
7.08.5	**Inhibitors Reported by Boehringer Ingelheim/Vitae**	335
7.08.6	**Inhibitors Reported by BMS**	337
7.08.7	**Inhibitors Reported by Eisai**	338
7.08.8	**Inhibitors Reported by Elan**	341
7.08.9	**Inhibitors Reported by Genentech/Array BioPharma**	342
7.08.10	**Inhibitors Reported by Janssen**	342
7.08.11	**Inhibitors Reported by Lilly**	344
7.08.12	**Inhibitors Reported by Lundbeck**	349
7.08.13	**Inhibitors Reported by Merck Serono/Merck KGAA**	349
7.08.14	**Inhibitors Reported by Noscira**	350
7.08.15	**Inhibitors Reported by Novartis**	350
7.08.16	**Inhibitors Reported by Pfizer**	353
7.08.16.1	Spiropiperidine Derivatives	353
7.08.16.2	Spiropyrrolidine Derivatives	354
7.08.16.3	Isothioureas and Related Derivatives	354
7.08.17	**Inhibitors Reported by Roche**	358
7.08.18	**Inhibitors Reported by Schering-Plough/Merck**	363
7.08.18.1	Early Peptidomimetic Inhibitors	363
7.08.18.2	Spiropiperidine Derivatives	364
7.08.18.3	Amidine and Guanidine Derivatives	364
7.08.19	**Inhibitors Reported by Shionogi**	367
7.08.20	**Inhibitors Reported by Wyeth**	370
7.08.21	**Inhibitors Reported by vTv/TransTech/HighPoint**	372
7.08.22	**Summary of Clinical Development Compounds and Clinical Outlook**	372
7.08.23	**Conclusion**	375
Acknowledgments		375
References		375

Abbreviations

AD Alzheimer's disease
APP Amyloid precursor protein
AUC Area under the curve
BACE β-site APP cleaving enzyme (β-secretase)
BBB Blood brain barrier
Br:Pl Brain plasma ratio
CSF Cerebrospinal fluid
CYP Cytochrome P450
HBD Hydrogen bond donor
MAD Multiple ascending dose
PD Pharmacodynamics
PK Pharmacokinetic
SAD Single ascending dose
SAR structure activity relationship
SBDD Structure-based drug discovery
THF Tetrahydrofuran
THP Tetrahydropyran
(T)PSA (topological) Polar surface area

7.08.1 Introduction

7.08.1.1 Alzheimer's Disease and the Amyloid Hypothesis

Alzheimer's disease (AD) continues to represent a huge unmet, global need. According to the Alzheimer's Association, more than 5 million Americans are currently living with AD, who require support from 15 million caregivers. The net estimate is that AD and other dementias will cost $236 million in the United States alone in 2016.[1] Worldwide, in 2015, it was estimated that 46.8 million people were suffering from Alzheimer's and related dementia, with an associated cost of $818 billion.[2] AD was first described in 1906 in a lecture by Alois Alzheimer.[3] In this seminal report, the key pathological hallmarks were characterized as amyloid plaques and neurofibrillary tangles, consisting of aggregated tau protein.[4] Despite this, it took considerable time before our understanding of the disease pathology progressed to a level to enable informed drug discovery. Key events were the genetic associations found between amyloid precursor protein (APP) and the disease via the amyloid cascade,[5–8] which uncovered links to the disease at multiple points.[9] APP exists in three different isoforms, which vary in length, having either 695, 751, or 770 amino acids, with the 695 variant being predominantly expressed in the CNS.[10] APP is processed sequentially by β-secretase (BACE1) and γ-secretase, to generate amyloid proteins of varying length, most commonly $A\beta_{1-40}$ and $A\beta_{1-42}$, the latter of which is considered the main pathogen (Fig. 1A). Several mutations in APP have been uncovered and linked to the progression of AD. Of particular note are the Swedish mutations (K670N and M671L) which are proximal to the BACE cleavage site—which cleaves between M671 and D672, and render the protein more susceptible to cleavage by BACE (Fig. 1B). Further mutations in APP, proximal to the BACE cleavage site, namely A673T and A673V, have been found to be protective (causing approximately 50% reduction in BACE cleavage) and pathogenic, respectively.[11] Although these mutations confer strong support, recent literature suggests that the neuropathology associated with the recessive A673V mutation may be somewhat distinct from other forms of AD (sporadic AD or familial AD (FAD) linked with a dominant trait),[12] thus highlighting the potential need for careful patient selection in clinical studies.

Further support of the amyloid cascade hypothesis comes from individuals with Down's syndrome. APP is expressed on chromosome 21, thus individuals with Down's syndrome, who have a triplication of chromosome 21, express higher levels of APP. As a result, these individuals produce higher levels of Aβ and suffer from cognitive impairment, although the correlation is the subject of debate.[13] Furthermore, there is a report of a 78-year-old female with Down's syndrome that did not suffer from dementia. Autopsy revealed incomplete triplication of chromosome 21, with no triplication of the APP gene, thus conferring additional support to the link between APP/Aβ and dementia.[14]

However, the amyloid cascade hypothesis has received scrutiny as some posit that amyloid deposit accumulation may be a consequence of the disease, rather than the cause.[15]

Taken together, the pathology and the genetic evidence make a strong case for the involvement of the amyloid cascade in disease pathology, thus highlighting β- and γ-secretase as attractive points of intervention. Both targets have received intensive effort in terms of drug discovery, while some companies have worked on both simultaneously. At times progress has been made on one more than the other, only for the pendulum to swing back to the other. Neither target has been without challenge; however, currently BACE seems to be the more tractable of the two and inhibitors continue to progress clinically. This article will deal exclusively with BACE inhibitors, while a companion chapter will deal with γ-secretase.

7.08.1.2 Challenges With Early BACE Inhibitor Discovery

Since its discovery in 1999,[16–19] BACE has proven an appealing target to the scientific community. Chemists flocked to start drug discovery projects to identify BACE inhibitors as it was assumed to be a druggable target, based on previous experience in the protease inhibitor field, for example, HIV protease and related targets. However, High Throughput Screening (HTS) campaigns in multiple companies drew blanks, and hence chemists turned to substrate-based drug design. Progress was made quickly with the availability of a crystal structure with a high affinity peptide, transition state inhibitor OM-99-2[20] which aided design and facilitated the identification of potent in vitro inhibitors. The structure, residue labeling, and binding mode to BACE are depicted in Fig. 2, which shows the hydroxyl moiety acting as the transition state mimic for the cleaved amide bond, and interacts with the catalytic aspartic acid diad (Asp32 and Asp228), while the inhibitor makes a further 10 hydrogen bonds with BACE. The availability of BACE crystal structures has provided another advantage over γ-secretase, which is a complex of several proteins and lacks structural information. However, this has not been the deciding factor in the success of BACE inhibition.

Unfortunately, the rapid progress was soon hampered by a series of problems, which ultimately proved insurmountable. Firstly, it was found that CNS penetration was extremely limited, predominantly due to P-gp mediated efflux. Further problems were to come when chemists discovered that many inhibitors had very poor exposure after oral dosing, found to be mainly due to extremely rapid metabolism by CYP3A. Peptidomimetic derivatives have been reviewed extensively and there are many excellent reviews on this subject.[21–25] Some groups tried to pursue the peptidomimetic derivatives and increase potency to subnanomolar levels in order to try to compensate for the extremely low CNS penetration, however to no avail. The challenges outlaid earlier are exemplified by seminal work from GSK, Bristol Myers Squibb (BMS), and Merck. Researchers at GSK devoted significant effort to the discovery of peptidomimetic BACE inhibitors, from which GSK188909 (**2**) (Fig. 3) was identified as an advanced lead. However, administration of this compound at a dose of 250 mg/kg i.p. to TASTPM mice[26] resulted in a brain concentration of only 0.62 μM and no significant effect of brain $A\beta_{40}$ levels. When the P-gp inhibitor GF120918 was administered 5 h prior to GSK188909 (**2**), the brain concentration of GSK188909 (**2**) was measured at 5.43 μM, that is, approximately ninefold higher. The increased brain concentrations resulted in a 68% reduction in brain $A\beta_{40}$ levels compared to vehicle controls.[27] One further complicating factor of this work is

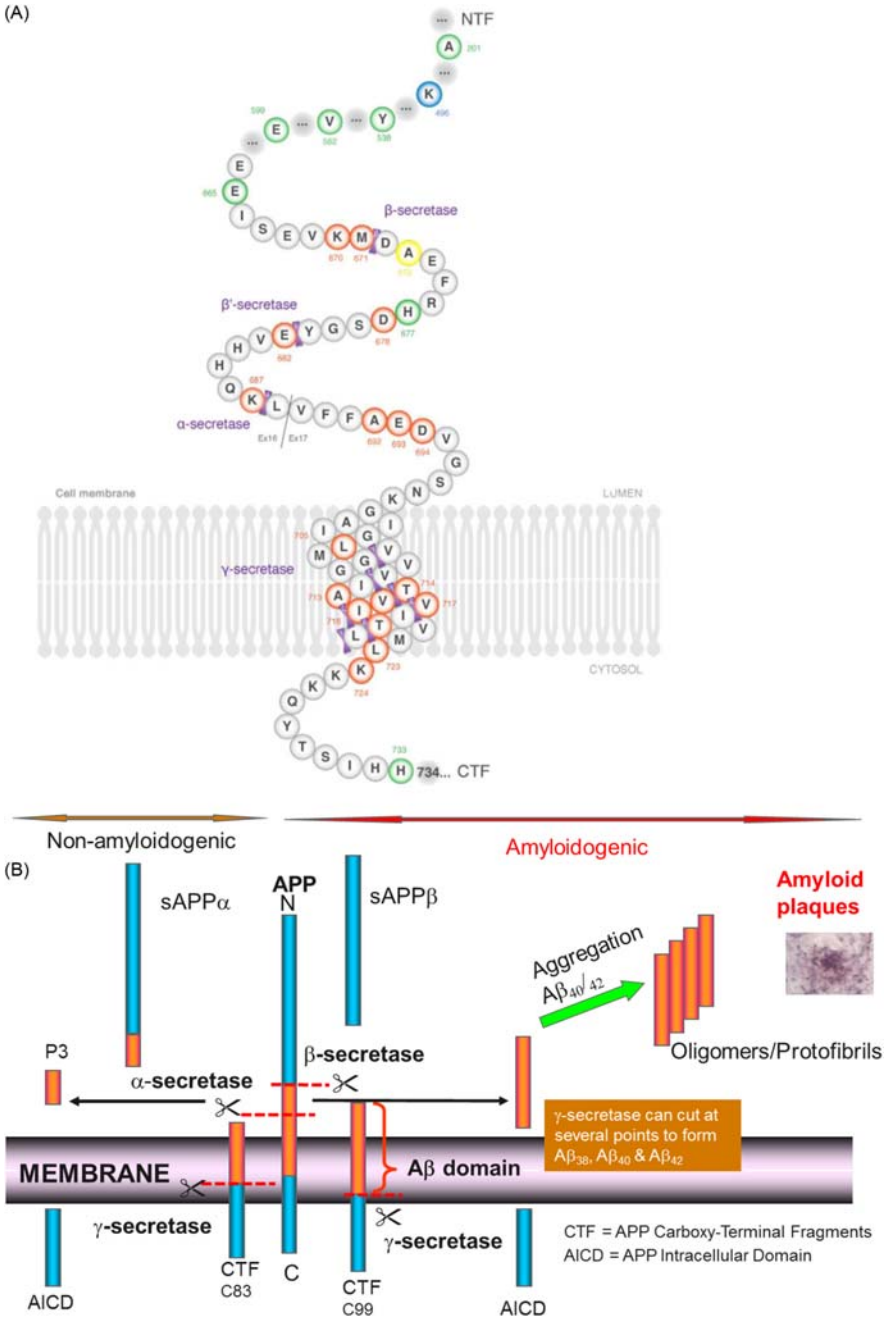

Fig. 1 (A) Sequence of APP with known mutations highlighted, Courtesy of Alzforum. *Red*=pathogenic mutation, *green*=nonpathogenic mutation, *yellow*=protective mutation, *blue*=unclear. (B) Depiction of sequential cleavage of APP by β- and γ-secretase to yield $A\beta_{40}$ and $A\beta_{42}$, and subsequent oligomerization.

that TASTPM mice express APP with the Swedish double mutation, K595N/M596L (in addition to a PS-1 mutation, M146V). This makes APP a better substrate for BACE cleavage, thus resulting in higher IC_{50} values, exemplified by GSK188909 (**1**), which shows sixfold lower activity in APP_{Swe} expressing cells than in cells expressing APP_{wt}. Similarly, BMS found that it was possible to reduce plasma $A\beta_{40}$ levels, but not brain $A\beta_{40}$ levels in the mouse with BACE peptidomimetic derivatives, such as compound **3** (Fig. 3).[28] This compound showed potent activity in biochemical and cellular assays. Subcutaneous dosing resulted in effective reductions in plasma $A\beta_{1-40}$ levels in the wild-type mouse, ED_{50} 0.6 mg/kg s.c., with an identical ED_{50} in P-gp KO mice. However, compound **3** had no effect on brain $A\beta_{1-40}$ levels in the wild-type mouse up to the highest dose of 100 mg/kg, whereas in P-gp KO mice the ED_{50} was estimated at 30 mg/kg s.c. for an effect on brain $A\beta_{1-40}$. This again highlights the challenge of overcoming P-gp mediated efflux with peptidomimetic BACE inhibitors. Researchers from Merck succeeded in overcoming the challenge of identifying peptidomimetic BACE inhibitors which were not P-gp substrates, for example, TC-1 (**4**) (Fig. 3), P-gp ER 2.3 (mouse), 2.5 (monkey), and

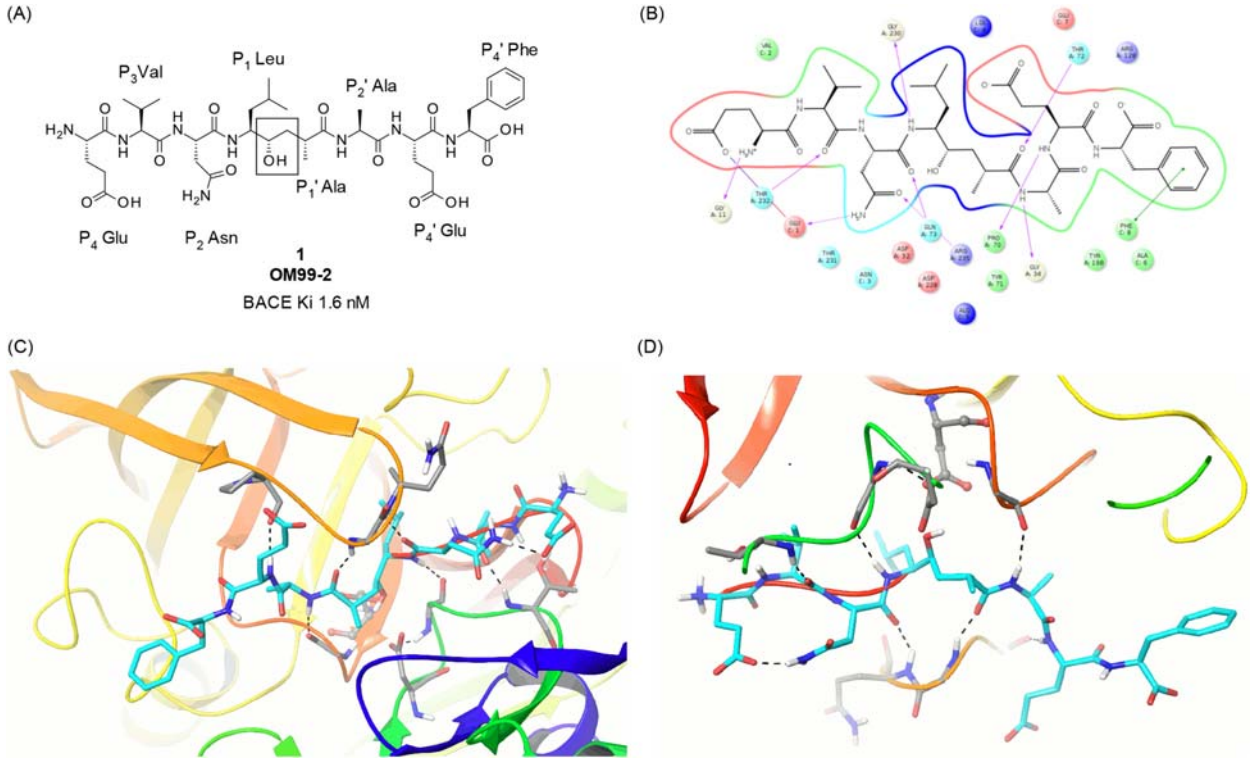

Fig. 2 (A) Structure of OM99–2 (**1**) indicating the substrate pocket numbering. (B) Depiction of the interactions between OM99–2 (**1**) and BACE. (C) and (D) Crystal structure of OM99-2 (**1**) bound to BACE. (C) depicted in the same orientation as shown in (B). PDB code 2ZHR.

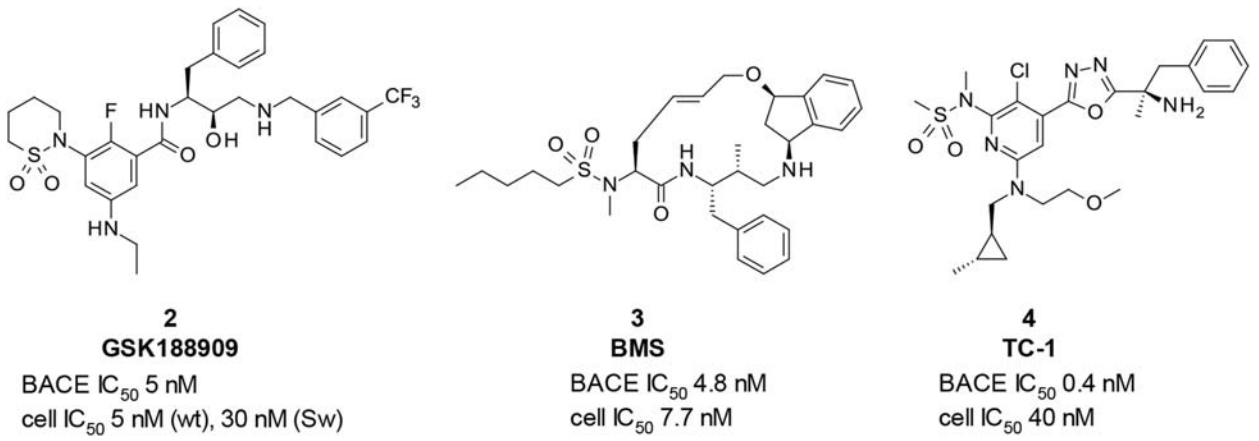

Fig. 3 Structures of hydroxyethylamine (HEA) peptidomimetic inhibitors GSK188909 (**2**) from GSK, (**3**) from BMS, and TC-1 (**4**) from Merck.

human (1.9). Despite this, TC-1 (4) was still found to be heavily metabolized by CYP3A4 and required coadministration with a CYP3A4 inhibitor, ritonavir, in order to demonstrate efficacy.[29] When TC-1 (4) was administered to rhesus monkeys, in the presence of ritonavir, the plasma clearance decreased from 24 to 7 mL/min/kg, while the $t½$ increased from 1 to 3 h and the oral bioavailability increased dramatically from $<1\%$ to 83%. In the rhesus monkey, ritonavir administration 2 h before an oral dose of TC-1 (4) at 15 mg/kg twice daily for 3.5 days resulted in average free plasma and CSF concentrations of 13.5 and 25 nM, respectively, thus showing free permeation of the compound into the CNS. Furthermore, this resulted in an average reduction of $A\beta_{40}$ by 61% in plasma and 42% in CSF, respectively.

Thus, these publications exemplify the challenges to identify peptidomimetic BACE inhibitors devoid of P-gp efflux with low metabolic clearance suitable for clinical progression. Only one peptidomimetic BACE inhibitor appears to have progressed to the clinic, CTS-21166/ASP1702 (structure not disclosed), which entered PhI studies in Jun. 2007.[30] Intravenous (iv) administration at doses from 7.5 to 225 mg led to reductions of up to 60% in plasma amyloid, however no effect was reported on CSF amyloid

levels.[31] Thus, the clinical data appear to recapitulate the challenges observed preclinically. While the initial results offered a breakthrough and resulted in a partnership with Astellas, the development of CTS-21166/ASP1702 was ultimately terminated, presumably due to the issues discussed earlier, and Astellas and CoMentis officially ended their agreement in Oct. 2014.[32] Ultimately these challenges appear to have been insurmountable and all research groups eventually switched to focus their research efforts on guanidine-derived BACE inhibitors, which proved extremely fruitful, despite significant challenges.

The breakthrough came when research groups utilized fragment or high concentration screening. Multiple groups identified compounds containing a guanidine derivative that bound to the active site and made highly complementary interactions with the catalytic aspartic acid diad. Although initial inhibitors were weak in terms of potency, the use of SBDD enabled rapid gains in potency. Despite this, several challenges still existed, namely CYP2D6 metabolism/inhibition, hERG inhibition (both mainly due to the basic center), and CNS penetration.

This article illustrates how multiple research groups have addressed these issues and, that the result of long-term commitment to the field has resulted in a fruitful return, with a range of inhibitors from multiple groups now in late-stage clinical trials. It thus seems that after nearly 17 years of research, the dedication will pay off, and the field is now poised at a stage which could provide the biggest breakthrough in neuroscience, with compounds having the potential to slow or even halt the progression of AD. Research from each group is reviewed in turn, based on the alphabetical order of lead company or research group.

7.08.2 Inhibitors Reported by Amgen

Amgen's interest in BACE dates back to the early 2000s with considerable activity in optimizing hydroxethylamine (HEA) type inhibitors. A focus on reduction of molecular weight, hydrogen bond donors (HBDs) and acceptors, and TPSA resulted in a potent and orally efficacious compound **5** (Fig. 4).[33] However, lowering of brain amyloid levels remained suboptimal, with a 100 mg/kg

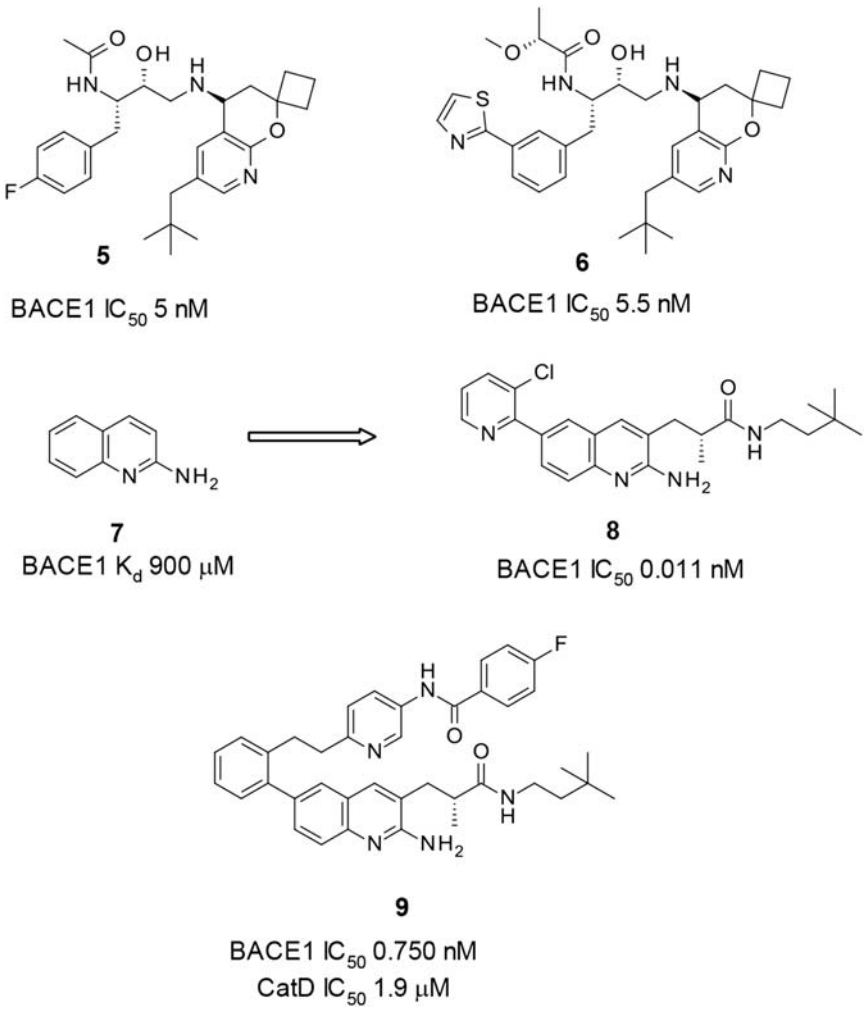

Fig. 4 Structures of peptidomimetic derivatives **5** and **6**, and FBDD ligands **7–9** from Amgen.

p.o. dose only achieving 35% $A\beta_{40}$ reduction in rat brain after 4 h. Analogous compounds with a strongly reduced P-gp efflux, such as **6** (Fig. 4), did demonstrate more robust Aβ lowering in brain and CSF after a PO dose of 30 mg/kg, but their increased size may have attributed to a suboptimal pharmacokinetic (PK) profile.[34]

Amgen has also described a series of 2-aminoquinolones originating from a fragment-based Surface Plasmon Resonance (SPR). Optimization of the initial 2-aminoquinolone hit **7** was guided by ligand efficiency (LE) and SBDD and led to compounds with subnanomolar potency. Physical property optimization led to compound **8** (Fig. 4). When tested in rats, a 60 mg/kg oral dose showed 42% reduction in CSF after 2 h. Lipophilicity of **8** remains high with a clogP of 4.4, and metabolic stability was again suboptimal. In a recent addition to this work, a second-site fragment screen using ^{19}F NMR spectroscopy delivered a fragment targeting the S3 binding site of BACE1.[35] Linking this fragment to a suitable analog of **8** delivered highly potent inhibitors as demonstrated by **9** (Fig. 4). The crystal structure of **9** bound to BACE is depicted in Fig. 5 and shows the multiple pockets being filled by this type of inhibitor. The fluorophenyl group of **9** extends deep into the S3 pocket providing potency. In addition, a significantly enhanced selectivity over Cathepsin D (>2000-fold) is achieved due to the structural differences in the S3 pocket between BACE1 and Cathepsin D. With a molecular weight over 600 and a cLogP above 7, the physicochemical properties remain far from optimal for a CNS drug.

Most of the Amgen efforts focused on the reported 5,5-diaryl substituted aminohydantoin inhibitors, which display an optimal hydrogen-bonding interaction with the catalytic aspartyl diad in the BACE enzyme. Replacement of the hydantoin core in **10** by an oxazoline heterocycle and linking of the two aryl substituent to form a tricyclic xanthane system led to **11** (Fig. 6).[36,37] These compounds suffered from hERG[36] inhibition, which could be mitigated by the introduction of a nitrogen atom in the 3- or 4-position.[36,38] Additionally, the nitrogen at these positions resulted in the formation of direct or water-bridged hydrogen bond with Trp76 near the flap of the enzyme, resulting in an increase in BACE1 potency. Optimization of the P3 and P2′ side chains for both aza-analog series led to **12** and **13**, respectively, which showed robust and sustained Aβ lowering in vivo. Both compounds have been progressed into toxicological studies. **12** displayed numerous toxicities, including retinal toxicity. Although no direct link to Cathepsin D inhibition could be made, **12** did show submicromolar inhibition of this enzyme in vitro ($IC_{50}=0.66$ μM).[36] In a 1-month rat toxicity study, also **13** (AMG-8718) displayed retinal thinning.[39]

The investigations of Amgen have since then focused on 6-ring warheads with vectors allowing deeper interaction into the S3 pocket. The data indicate they are significantly more selective over Cathepsin D, as shown by earlier, similar competitor series. Fig. 7 shows six examples of six patent applications in chronological order. The first application still exemplifies compounds containing the typical tricyclic core explored previously, but with an amide-linked P3 substituent, exemplified by **14**.[40] While highly potent, the molecular weight of these compounds greatly exceeds 400, making them unlikely candidates for a CNS drug. A number of patent applications describe compounds containing monocyclic, spirocyclic, tricyclic, and bridged 5-amino-1,4-thiazine 1, 1-dioxide warheads. These have similarity to earlier compounds from Schering/Merck, and several observations can be derived from them. A typical exemplification in the first patent in this series is **15**[41] which bears some resemblance to compounds from Roche, for example, **167** (Fig. 48), and Schering-Plough/Merck, for example, **189** (Fig. 52). The fluoromethyl substituent will lower the pK_a of the amidine group, and in **15** this may contribute to the loss of cellular potency versus enzymatic inhibition. The replacement of the often used heretoacryl amide P3 substituent with a bioisosteric 2-aminonaphthtyridine system still results in potent molecules. Cyclization between the 1,4-thiazine 1,1-dioxide warhead and the P1-phenyl core led to tricyclic structures as in **16**.[42] Interestingly, both 4aR and 4aS diastereomers are reported to have almost equal potency for BACE1 inhibition. In rat, an

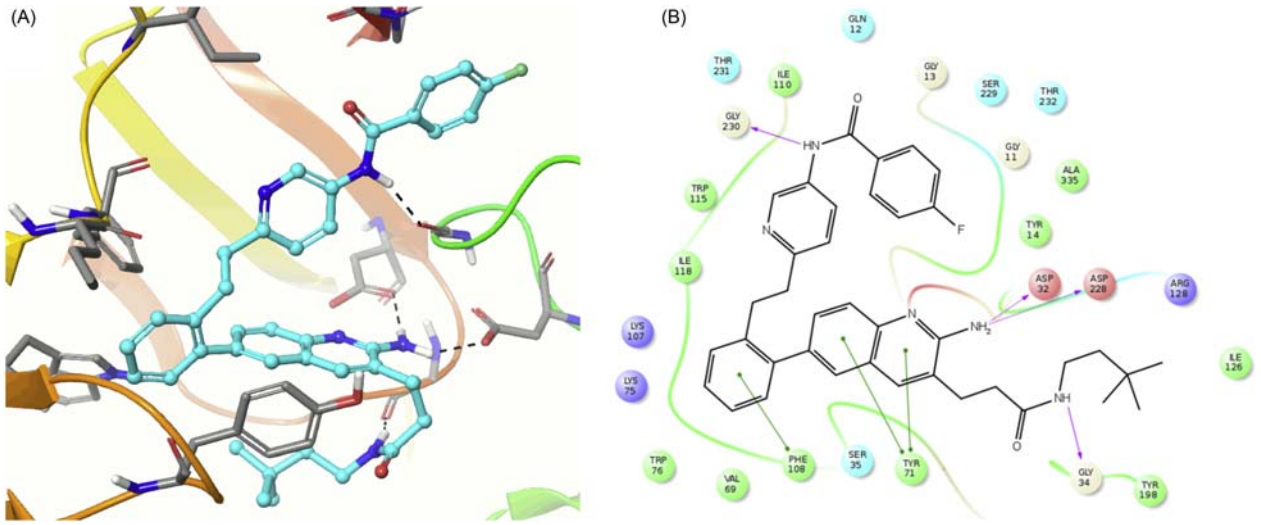

Fig. 5 (A) Crystal structure of compound **9** bound to BACE with key hydrogen bonds highlighted (PDB code 5I3Y). (B) Depiction of residues and interactions between **50** and BACE.

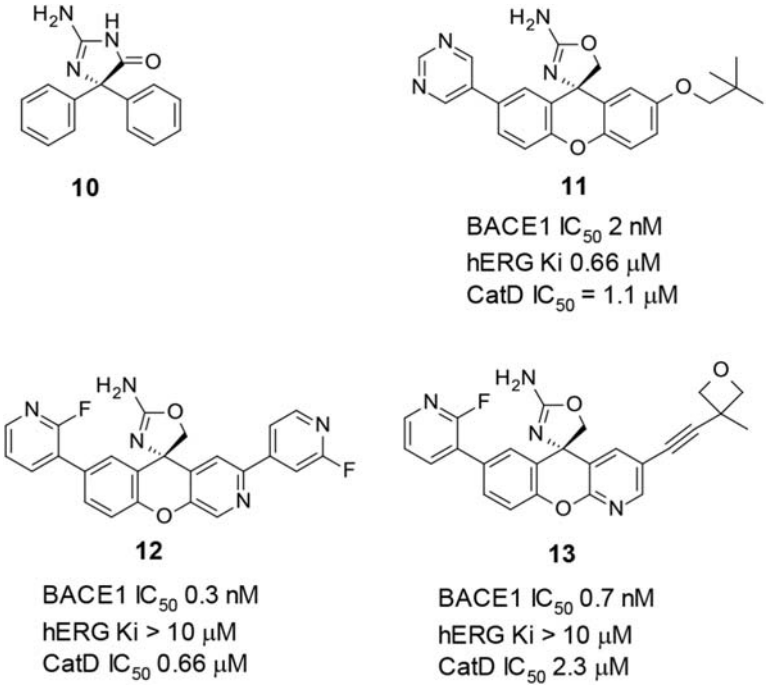

Fig. 6 Acylguanidine **10** and isourea derivatives **11**–**13** from Amgen.

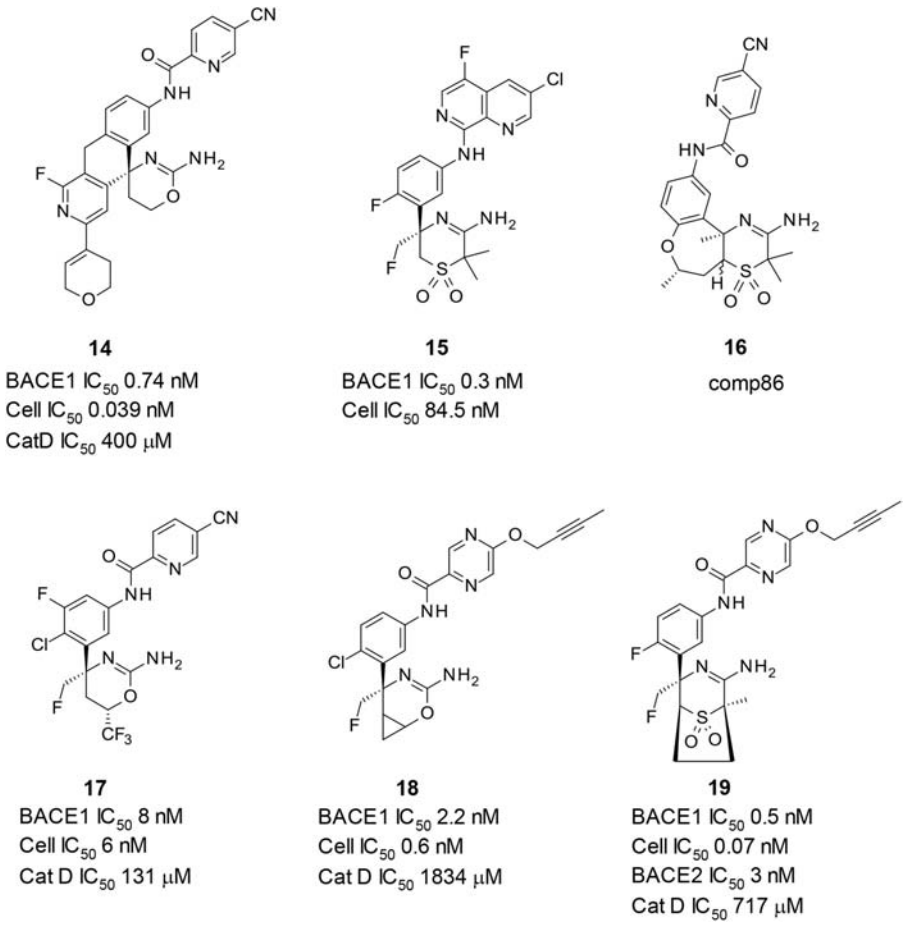

Fig. 7 Isourea and sulfonyl amidine derivatives from Amgen.

oral dose of 10 mg/kg resulted in a 79% Aβ reduction in CSF and brain, 4 h after dosing. Utilizing the isourea/1,3-dihydro-oxazine warhead, researchers from Amgen have described compounds such as 17,[43] which bears similarity to compounds from Roche, for example, **155** (Fig. 43), and **18**,[44] with a cyclopropyl ring fused to the 1,3-dihydro-oxazine ring. The last application around this series describes bridged amino thiazine dioxide compounds as exemplified by **19**.[45] These examples highlight the significantly improved selectivity over Cathepsin D inhibition compared to the earlier tricyclic compounds in Fig. 6. Exemplified compounds in the later patent applications replacing the amide P3 linker with fused and monocyclic heterocycles generally resulted in poorly active compounds.[43–45] Most compounds bear fluoro-containing electron-withdrawing groups on the warhead, expected to modulate the pK_a of the amidine. The most potent compounds have additional acetylene substituents as in **18**, penetrating deep into the S3 pocket, as demonstrated before by other companies (e.g., **162**, Fig. 47 from Roche and **215**, Fig. 54 from Shionogi).

Thus, after sustained commitment to the field from the outset, despite significant effort expended on a range of chemotypes, ultimately ending up with amidine and isourea derivatives with S3 pocket targeting anilides, it appears that Amgen were not successful in achieving the balance of properties required in a single molecule for progression to the clinic. However, they have since entered into a collaboration with Novartis to codevelop and cocommercialize the Novartis BACE inhibitor CNP520 (see what follows), which is currently progressing this compound through clinical trials.

7.08.3 Inhibitors Reported by Astellas

Astellas entered the BACE inhibitor field through a collaboration with Comentis on their peptidomimetic series. Although the lead compound from Comentis, CTS-21166, was one of the first compounds to progress to the clinic it was rapidly terminated, presumably due to low oral exposure and low levels of CNS penetration and efficacy.[32] Data reported at a conference demonstrated that CTS-21166/ASP1702 was a potent BACE inhibitor, enzyme IC_{50} 2.5 nM, cell IC_{50} 3.9 nM. Single or multiple doses of 100 mg/kg p.o. to the rat resulted in modest reductions of soluble $A\beta_{40}$, c. 23% or 30% versus vehicle. In a rat microdialysis time course study, a single iv dose of 15 mg/kg resulted in ~50% reduction of CSF $A\beta_{40}$ levels. In a baboon microdialysis study, an iv dose of 1 mg/kg resulted in a 28% reduction of brain $A\beta_{40}$ levels. Brain penetration (Br:Pl) was assessed in the mouse (0.5), rat (0.18–0.39), dog (1.3), and baboon (0.37), which implied some degree of CNS penetration; however, CSF:Pl levels were much lower in rat (0.02–0.09) and baboon (0.02).[46] Since this early entry, Astellas and Comentis have shifted their focus to spirocyclic isoureas. This series has been disclosed in a relatively large patent application, which highlights three key compounds, including their hERG data and in vivo efficacy. Thus, **20**, **21**, and **22** (Table 1) all show potent cellular activity and weak hERG activity[47]. All three compounds reduced brain amyloid levels in the rat at reasonable doses, even though they are not single enantiomers.

7.08.4 Inhibitors Reported by AstraZeneca

AstraZeneca obtained their initial amidine-type hit **23** from a fragment-based approach using Nuclear Magnetic Resonance (NMR) screening. In collaboration with Astex, structure-based drug design led to **24** with the ethyl linker required for optimal filling of the P1/P3 pocket (Fig. 8).[48] The relatively modest potency of this compound may be related to the flexibility of the ethyl linker, and subsequent efforts by AZ show a focus on series with high conformational constraint, often resulting in more potent BACE inhibition.

Starting from the dihydroisocytosine warhead present in **24** and **25**, scaffold hopping via the ring contracted aminohydantoin **26** led to bicyclic aminoimidazole **27**.[48] Interestingly, the evolution from 6-ring warheads to 5-ring warheads is the opposite from the

Table 1 Summary of data for three key isourea derivatives from Astellas

Compound	**20**	**21**	**22**
Structure	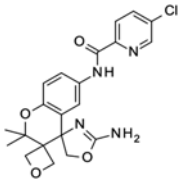	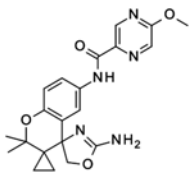	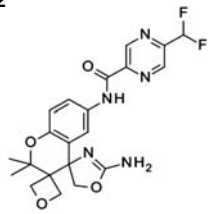
BACE FRET IC_{50} (nM)	44.7	99.1	91.4
BACE FRET Ki (nM)	10.3	61.2	52.7
Cell IC_{50} (nM)	0.78	3.1	0.63
hERG IC_{50} (μM)	20.67	20.77	15.1
Rat brain ↓$A\beta_{40}$ @ 1 mg/kg (time)	Not tested	19% (3 h)	21% (3 h)
Rat brain ↓$A\beta_{40}$ @ 3 mg/kg (time)	24% (2.5 h)	34% (3 h)	35% (3 h)
Rat brain ↓$A\beta_{40}$ @ 10 mg/kg (time)	31% (2.5 h)	Not tested	Not tested

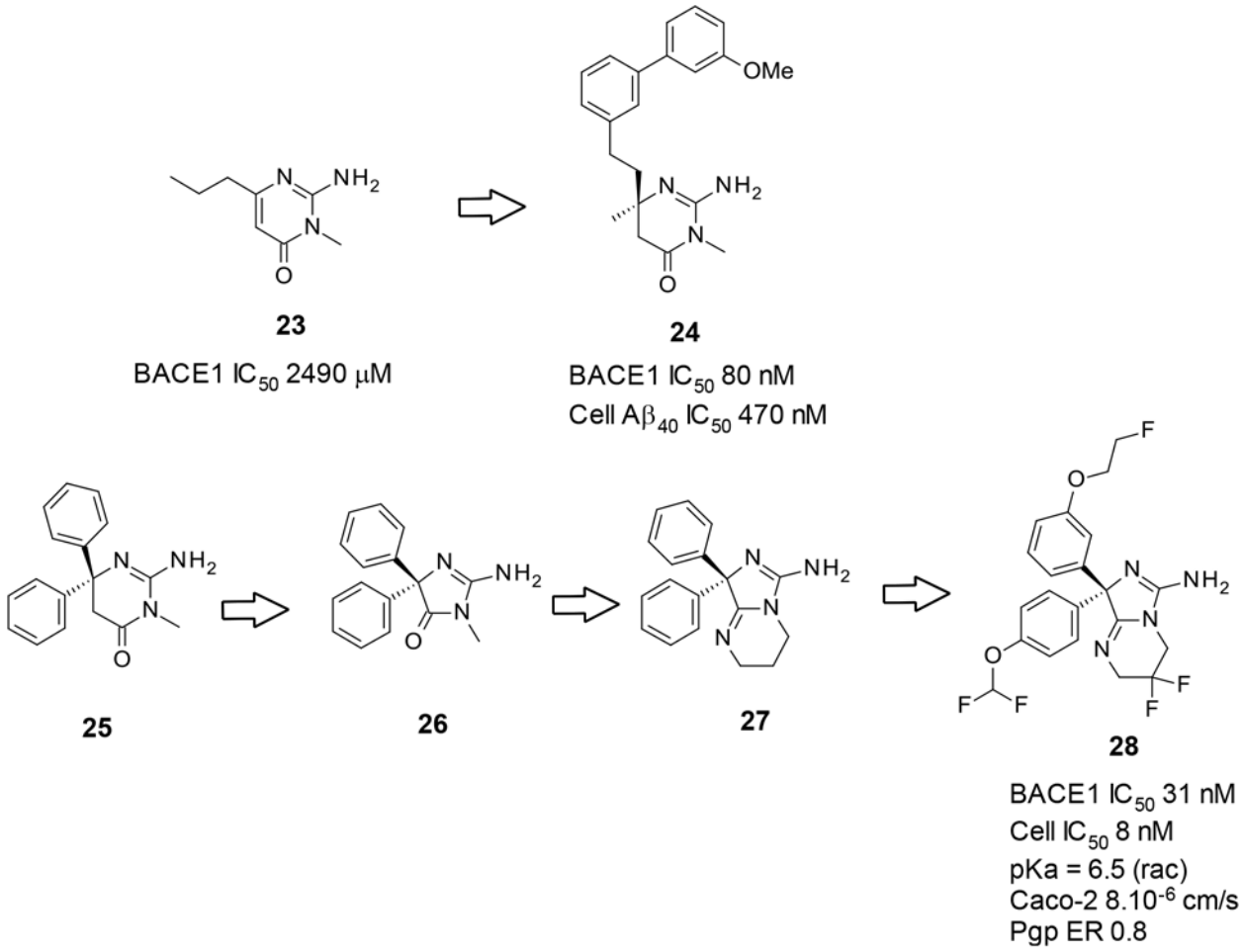

Fig. 8 Early compounds and lead generation summary of work from AstraZeneca.

evolution in the Schering–Merck BACE program (see later). Optimization of the aminoimidazole **27** led to **28** (Fig. 8) with the difluoro substitution lowering the pK_a of by about 1 log unit, leading to improved permeability. The alkoxy substituents in **28** resulted in a further improved permeability and efflux profile compared to the more often used biaryl substitution pattern. Nevertheless, **28** still suffered from significant efflux in vivo, only resulting in significant lowering of amyloid in mouse brain when coadministered with the pan-efflux inhibitor GF120918.[48]

In a further elaboration of the fused 5-ring warheads, a series of amino-isoindoles was optimized.[50] The introduction of a fluorine atom adjacent to the amidine reduced the pK_a, presumably by forming a weak internal hydrogen bond with the exocyclic amidine nitrogen, and was key in achieving central amyloid lowering activity. The series displayed significant affinity for the hERG channel, attributed to the combination of relatively high basicity and lipophilicity. However, reduced lipophilicity was linked to increased efflux. Optimization and balancing of lipophilicity led to compounds **29** and **30** (Fig. 9). The 5-propynyl-3-pyridinyl group in **30** has a deep interaction within the S3 subpocket which leads to subnanomolar cellular potency, translating into a larger in vitro margin to hERG inhibition of **30** versus **29**. However, in vivo, **29** had a superior profile to **30**, attributed to the high unbound brain/plasma ratio for **29**, which could be explained by the reduced lipophilicity of **29** versus **30** and other analogs. Based on the overall best properties, **29** was selected for clinical evaluation (AZD3839).[51] In a Phase 1 clinical study, AZD3839 reduced plasma $A\beta_{40}$ and $A\beta_{42}$ in healthy volunteers, with estimated potencies (EC_{50}) of 46 and 59 nM, respectively.[52] The maximum effect obtained after a dose of 300 mg was ~55%, which is rather moderate considering the high dose. In addition, the compound also caused a dose-dependent prolongation in QTc, which can be linked to hERG inhibition. The combination of moderate efficacy and QTc prolongation has likely contributed to the termination of further development of AZD3839.

Recognizing that the core, amidine containing structures play a crucial role in the druglike profile of the final compounds, AstraZeneca has published on their workflow to identify novel promising amidine containing cores.[53] Profiling of de novo designed ideas was carried out as an iterative creation and prioritization process of core structures using in silico models for permeability, hERG activity, and BACE1 inhibition, followed by a manual evaluation of metabolic liabilities and synthetic feasibility. A number of new cores with promising activity and reduced hERG activity have been identified using this approach.[54] The fact that several of

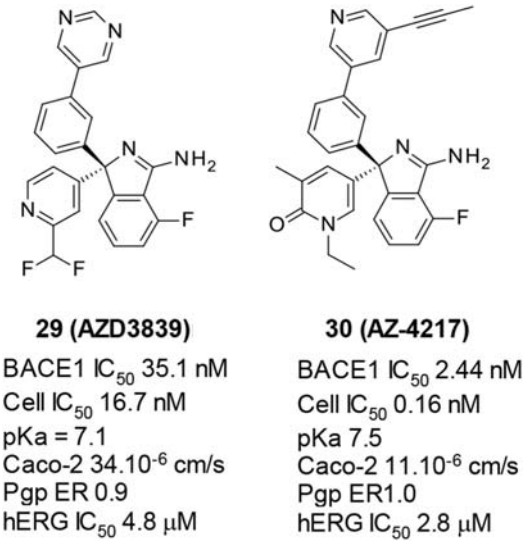

Fig. 9 Structures of AZD3839 (**29**) and AZ-4217 (**30**) from AstraZeneca.

these cores were subsequently and independently reported by other companies illustrates the success of this approach. While not necessarily originating from this work, a monocyclic series of aminoimidazoles were also reported as a promising series of BACE inhibitors and exemplified by **31**, showing good target potency, low hERG inhibition, and decent CNS exposure in vivo (Fig. 10). This particular core has since appeared in multiple AstraZeneca patent applications describing double spiro aminoimidazoles. The replacement of one of the aryl substituents in **31** by a cyclohexyl ring, spiro-cyclized to the warhead and aryl substituent resulted in series of compounds exemplified in Fig. 10. In the first patent in this series, **32** was one of the exemplified compounds, for which a subsequent process patent was published describing the large-scale synthesis of a camsylate salt.[55,56] This compound is also known as AZD3293 or LY3314814, and is currently in Phase2/3 clinical trials in collaboration with Eli Lilly.[57] The in vitro and in vivo pharmacological profile has been reported, indicating subnanomolar enzymatic and cellular potency with a markedly slow target off-rate ($t½ \sim 9$ h).[58] AZD3293 shows high potency in vitro in a range of assays, but is approximately 100-fold less potent in Tg2576 mouse neurons. Despite showing low efflux in a CaCo-2 assay, it appears to be a strong P-gp substrate. It was also found that AZD3293 produces a major active metabolite in vivo which is also a P-gp substrate (ER > 30). Although the structure of the metabolite has not been disclosed, one may hypothesize that it is the O-desmethyl analog, the presence of a hydroxyl group could explain the P-gp efflux and decreased plasma protein binding (ppb). In the mouse and dog, this slow off-rate may have contributed to a prolongation of the amyloid lowering effect beyond its plasma and CSF exposure. Despite the long duration of action, the compound shows a moderate maximal reduction of brain $A\beta_{42}$ in the mouse, ~40%, after a 100 μmol/kg p.o. dose. Maximal reductions in $A\beta_{42}$ were significantly greater in the guinea pig; Ab42 reduced by ~80% (brain after 4 h) and ~90% (CSF after 8 h) following a 30 mmol/kg p.o. dose. While selective for Cathepsin D, the compound did not show selectivity over BACE2.

In a Phase 1 multiple ascending dose (MAD) trial, AZD3293 was dosed for 14 days in mild to moderate AD patients at 15, 50, or 150 mg.[59] At steady state, the mean effective half-life was 16–21 h. Significant amyloid reduction was seen in plasma and CSF at all doses tested. At day 14, $A\beta_{42}$ levels in CSF were reduced by 52%, 76%, and 90% for the 15, 50, and 150 mg doses, respectively. Additional patent applications describe further variations on this class of double spiro BACE inhibitors, exemplified by the most potent analogs in Fig. 10: **33**,[60] **34**,[61] **35**,[62] **36**,[63] and **37**.[64] In **37**, the aminoimidazole is replaced with an aminopyrrole with the additional fluoro-substituent likely having a similar effect on basicity as described for **29** and **30** (Fig. 9).

In conclusion, sustained commitment from the AZ group has resulted in the identification of at least two development compounds which have progressed to clinical studies. Furthermore, both AZD3839 and AZD3293 represent a different structural class from most of the compounds in clinical development. Whether this will offer any benefit remains to be seen, but they do avoid the presence of an aniline structural alert present in many of the competitor BACE inhibitors in clinical development. Since announcing their withdrawal from neuroscience, AZD3293 is being advanced under an alliance with Lilly (see later), whereby Lilly lead the clinical development. The compound is currently undergoing PhII/III clinical trials.

7.08.5 Inhibitors Reported by Boehringer Ingelheim/Vitae

After initial efforts on ethylenediamine peptidometic BACE inhibitors, Boehringer Ingelheim started exploring guanidine containing warheads incorporated in 2-aminobenzimidazoles **38**[65] and 2-aminoquinazolones **39** (Fig. 11).[66]

As appreciated by other companies, both types of BACE inhibitor series apparently did not yield the desired combination of in vitro potency and in vivo efficacy, because in 2009 an alliance was established between Boehringer and Vitae Pharmaceuticals

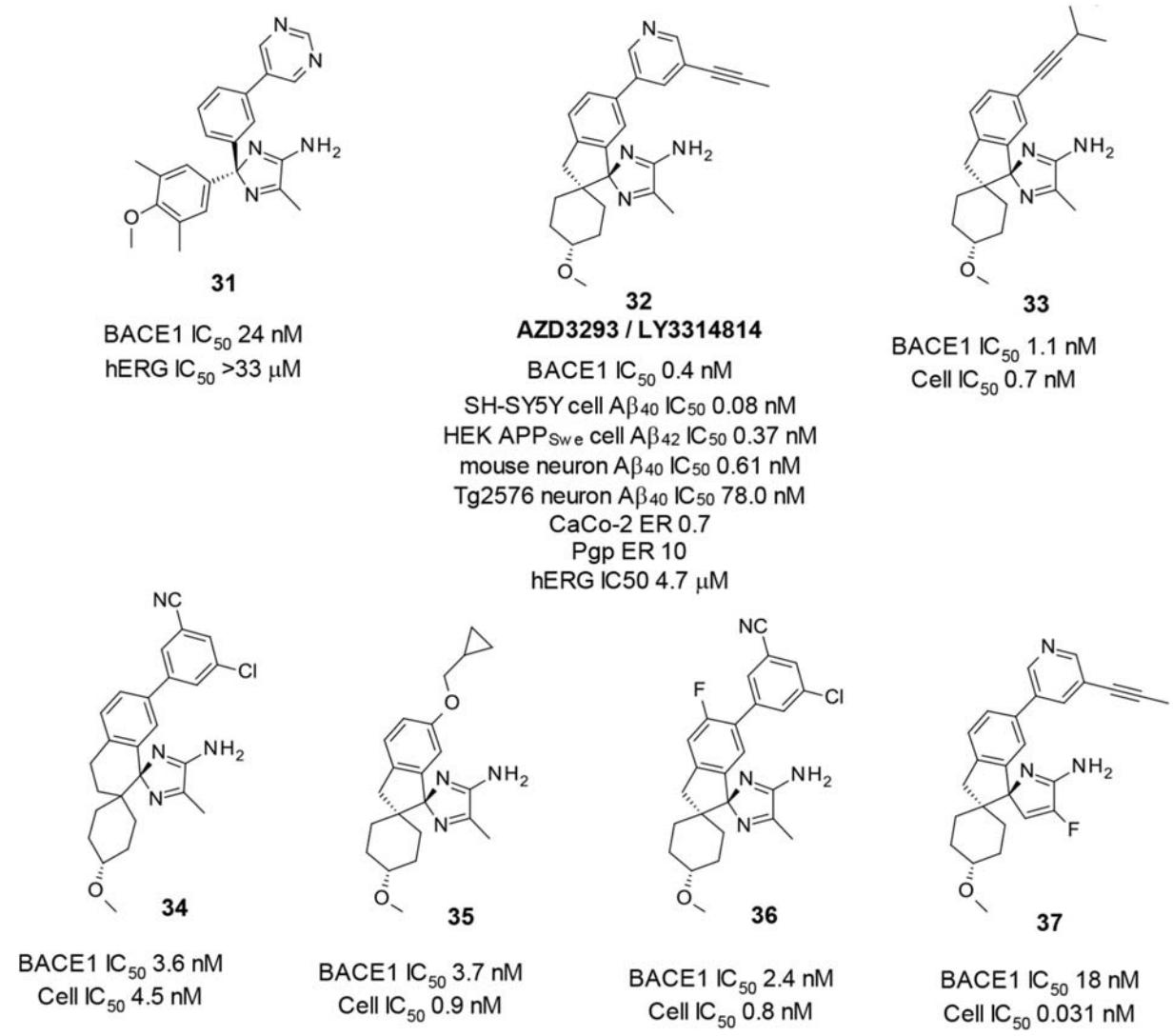

Fig. 10 Spiro-imidazolines from AstraZeneca.

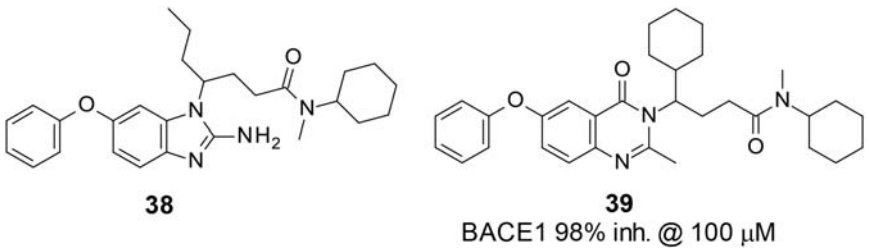

Fig. 11 Early derivatives from Boehringer Ingelheim.

focusing on aminohydantoin inhibitors. The first patent in this series describes conformationally restricted, double spiro aminohydantoins of relatively large molecular weight, for example, **40** (Fig. 12).[67] Another application describes fused bicyclic warhead variations as exemplified by **41** (Fig. 12) having considerable similarity to series described by AstraZeneca.[68] Overlap with AstraZeneca series is also clear for another application, describing variations containing an aminoimidazole warhead, as exemplified by **46**.[69] Additional patent applications claim aminohydantoin subseries with reduced molecular weight and reduced aromatic ring count with variations of hydantoin N-alkyl groups directed toward P1′, and small substituents on both the cyclohexyl moiety directed to P2′ and on the aryl moiety directed into P3, for example, **42** and **43** (Fig. 12).[70] The more recent patent applications

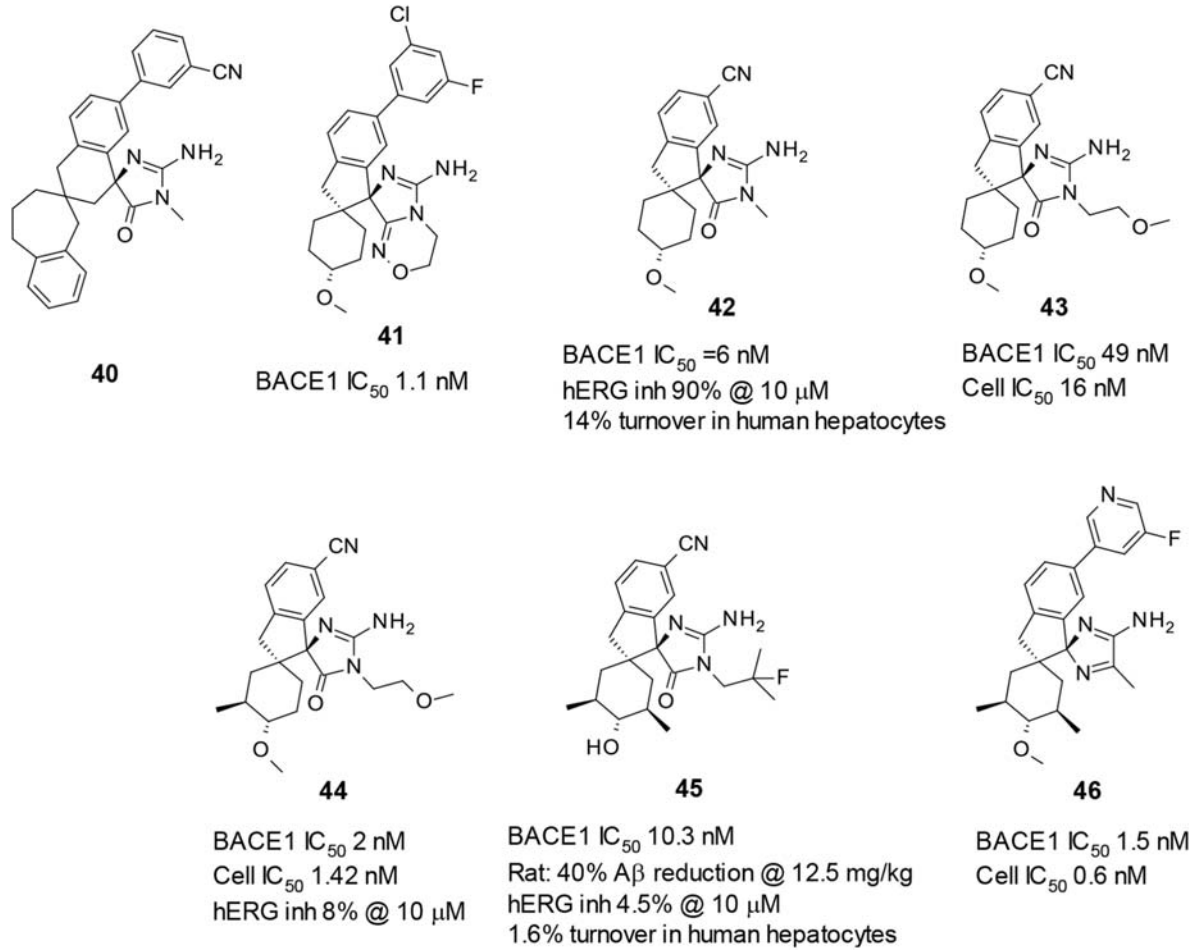

Fig. 12 Recent examples from Boehringer Ingelheim/Vitae.

around this series contain close analogs with additional methyl substituents directed into P2′, for example, **44** and **45** (Fig. 12).[71,72] Comparative data over the earlier applications indicate improvements in potency, reduced hERG inhibition, lower propensity to cause phospholipidosis, and increased metabolic stability in human hepatocytes, as illustrated by the data in Fig. 12.

From this series, BI1181181 has been progressed into Phase I clinical trials, and single doses of this compound induced a sustained reduction in CSF Aβ peptide concentrations in healthy volunteers: a single dose of 50 or 100 mg resulted in a 63.6% or 82.7% reduction 24 h after dosing, respectively.[73] During the MAD trial, skin reactions were observed in some participants. Further progression of BI1181181 has been put on hold, and the alliance between Boehringer and Vitae has been dissolved.[74]

7.08.6 Inhibitors Reported by BMS

Despite being late entrants to the BACE field, BMS have managed to find novel chemical matter. To date, three patent applications have been published, all employing the isothiourea warhead. The first patent application described THF-fused isothioureas, such as **47** (Fig. 13).[75] Compounds from this series are isomeric to the compounds detailed by Eisai who have detailed the other two isomeric series (see later) and would be expected to bind in a similar manner. Compounds such as **47** display moderate cellular activity, IC_{50} 24 nM, however, as they are aminals it is unclear how stable they are to hydrolytic conditions. The second patent application detailed tricylic derivatives such as **48**, cell IC_{50} 8.8 nM (Fig. 13).[76] These derivatives would also be expected to bind in a similar mode, with the amide donating an H-bond to the carbonyl group of Gly 230.

A third patent application detailed compounds which appear to be of more interest, highlighted by **49** and **50** (Fig. 14).[77] Both compounds possess the 2,5-dimethylisoxazol-3yl group. Interestingly, the amide **49**, IC_{50} 5 nM, and biaryl derivative **50**, IC_{50} 8 nM, display similar levels of activity, whereas in other series the amides generally show much higher activity than the corresponding biaryl analogs (Lilly and Eisai, described later). In the biaryl series, the methyl group in the 4-position on the dihydrothiazine ring enhances potency 7.5-fold, as the corresponding desmethyl derivative displays an IC_{50} of 60 nM.

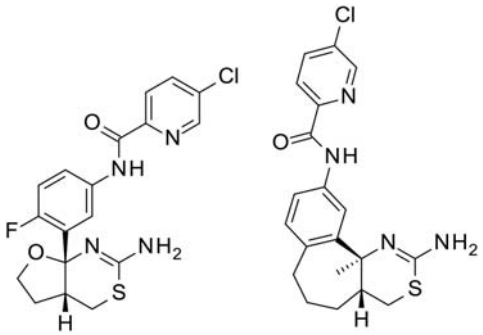

Fig. 13 Initial isothiourea derivatives from BMS.

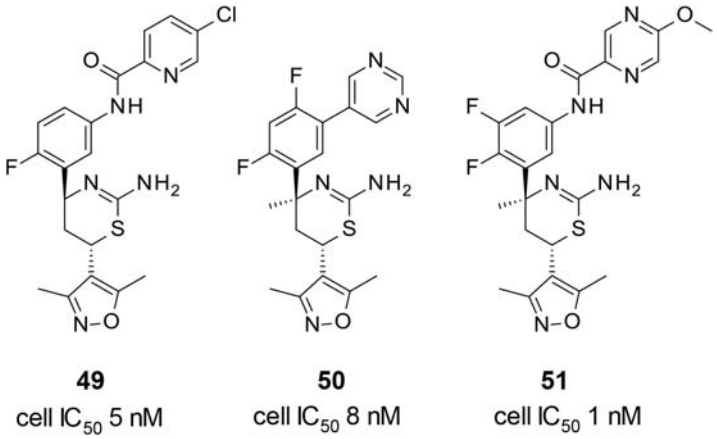

Fig. 14 Later isothiourea derivatives from BMS.

A subsequent publication from BMS has provided further detail in **49** and **50** (Fig. 14)[78] including crystallographic information on the binding modes, as depicted in Fig. 15 for **50**. Whereas in the acylguanidine/dihydroiminopyrimidine series from Merck (see later) the 4-methyl group was essential to place the phenyl ring in a pseudoaxial position, with **50** calculations revealed that the methyl group to have little effect on the orientation of the phenyl ring. Thus, the major role of the 4-methyl group appears to be hydrophobic interaction with isoleucine 118. The pseudoaxial orientation of the phenyl ring may be favored due to the pseudoequitorial orientation of the dimethylisoxazole. Furthermore, the dimethylisoxazole is perpendicular to the dihydroisothiazine and accepts two hydrogen bonds from Gln73 and Thr72. Despite promising in vitro results, **50** displayed weak in vivo activity at 30 mg/kg p.o., due to a combination of poor metabolic stability and low CNS penetration. As the metabolic issues were attributed to oxidation of the pyrimidine, emphasis shifted to the amide series, exemplified by **49**. A crystal structure with **49** revealed similar binding interactions to **50**, with the amide forming the expected H-bond interaction with the C═O of Gly230. Further optimization resulted in the identification of **51** (Fig. 14), which demonstrated potent cellular activity, IC_{50} 1 nM. In vivo efficacy was demonstrated in the mouse where a 10 mg/kg oral dose resulted in an 85% reduction in brain amyloid. In the rat, a dose response study (5 h time point) resulted in an ED_{50} of ~3 mg/kg p.o. Estimated EC_{50} concentrations in plasma and brain were 260 nM (13 nM free) and 160 nM respectively. CNS exposure was moderate with Br:Pl 0.30–0.46. **51** demonstrated minimal CYP interactions, but quite potent hERG inhibition, IC_{50} 0.64 μM, although this was argued to deliver a 49-fold separation over the free plasma EC_{50} (13 nM). The parent compound was found to be nonmutagenic in an Ames assay, and although the aniline was confirmed as an in vivo metabolite its mutagenicity was not assessed. Despite the progress made, it is unlikely that compounds have progressed beyond the preclinical stage as BMS recently announced that they have stopped research in the neuroscience area.

7.08.7 Inhibitors Reported by Eisai

Eisai have been active in the amyloid field for a considerable time, tackling both γ-secretase and β-secretase. The efforts on BACE involved a global collaboration spanning the United Kingdom and Japan and have resulted in at least one development compound,

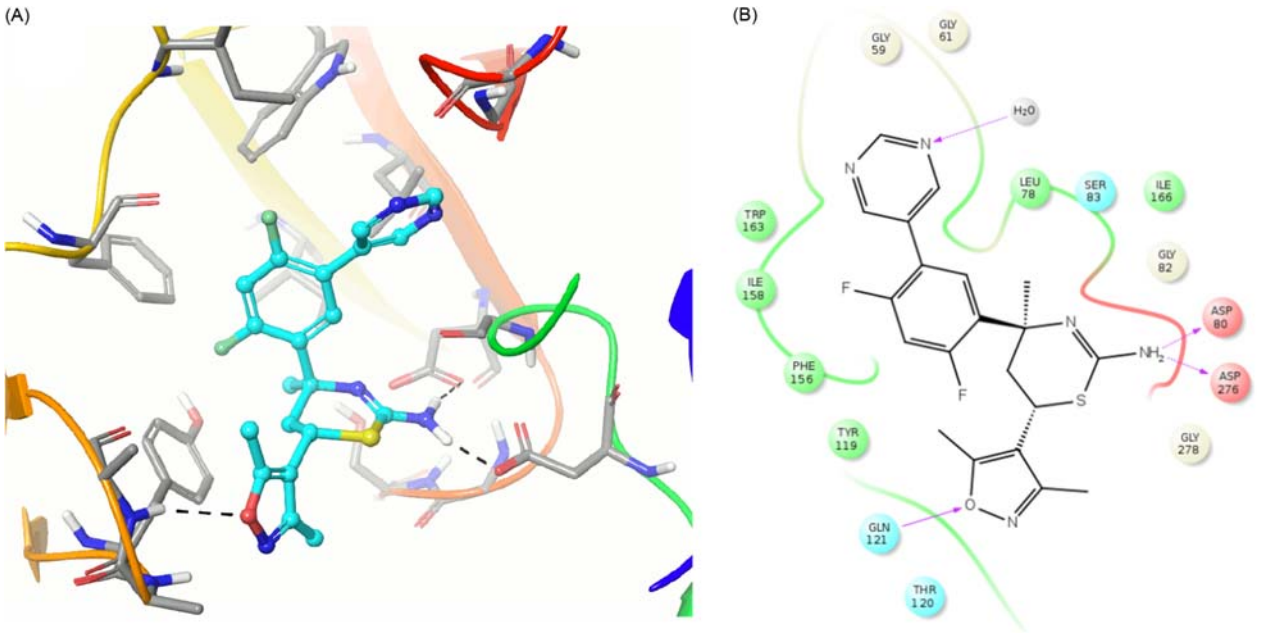

Fig. 15 (A) Crystal structure of **50** bound to BACE (PDB 5ENK). (B) Depiction of the interactions of compound **50** with BACE.

E2609, which is currently undergoing PhII/III trials in collaboration with Biogen. The compounds disclosed by Eisai center primarily on the isothiourea/aminodihydrothiazine template exemplified by spiro cycles, THF-fused and pyrrolidine-fused derivatives. In addition to these derivatives, Eisai have also described THF-fused acylguanidines and were the first to disclose the isourea/aminodihydrooxazine warhead, fused to a THF ring. Examples illustrating each of the series are highlighted.

A patent application published in 2009, detailing aminodihydrothiazine derivatives with a fused ring, including cyclopentyl, cyclohexyl, THP, THF, and pyrrolidine.[79] Pertinent examples from this application are **52** and **53**, both of which inhibit $A\beta_{42}$ production in cellular assays with IC_{50} 7 nM (Fig. 16). A subsequent patent application has recently published detailing pharmaceutical compositions and salts of **52**.[80] THP-fused aminodihydroisothiazine derivatives have also been the subject of a patent application, with selected examples including **54** (Pfizer, described later), **55**, and **56** (Fig. 16).[81] The addition of the methyl group next to the S-atom on the 1,3-thiazine ring, as in **56**, was also detailed.

Further in vivo data on **53** has been disclosed in subsequent patent applications.[82] While **53** displays good Br:Pl of 0.8, when total levels are used, further analysis of free levels, Br_u:Pl_u 0.15 and CSF:Pl_u 0.21, shows potential efflux, P-gp ER 20.7. Despite this, **53** shows potent reduction of CSF and brain $A\beta_{40}$ levels, 76% and 59% reductions in CSF and brain, respectively, 4 h after a 10 mg/kg oral dose.

Further patent applications on the THF-fused aminodihydrothiazine series have described biaryl derivatives[83] and two filings have covered fluoromethyl and difluoromethyl-substituted THF derivatives, with a methoxy pyrazine amide (four examples), exemplified by **57**, and trifluoromethyl-substituted THF derivatives, exemplified by **58** and **59**.[84] In the case of **57**, compounds from this

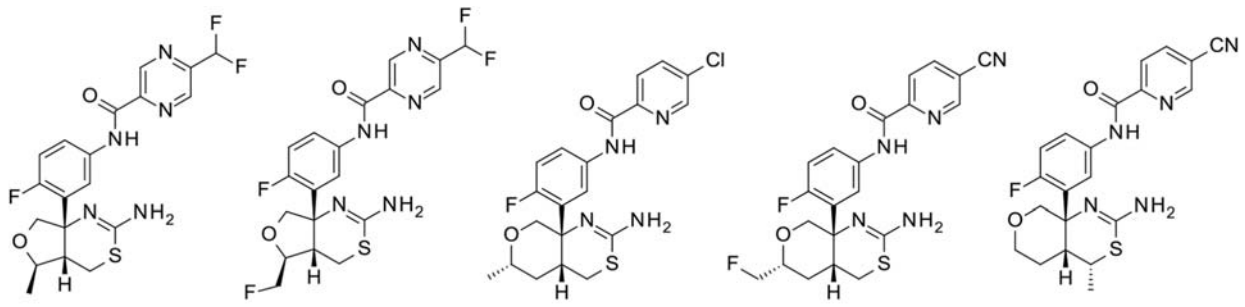

Fig. 16 Early examples from Eisai patent applications.

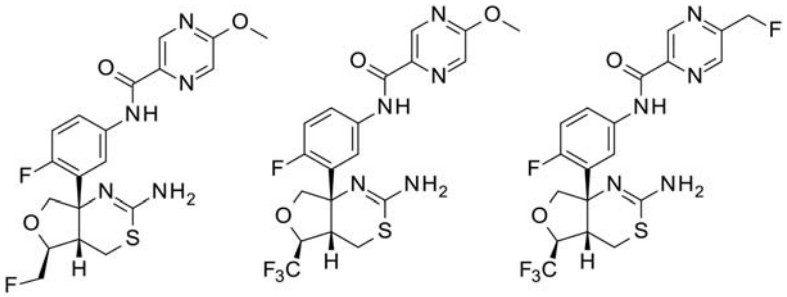

Fig. 17 Further prominent THF-fused isothiourea derivatives from Eisai.

series appear to have improved metabolic stability over close analogs in human liver microsomes.[82] **57** demonstrated potent in vitro, cell IC_{50} 4 nM, and in vivo activity in the rat, where an oral dose of 10 mg/kg resulted in 85% and 63% reductions of $A\beta_{40}$ in CSF and brain, respectively, 4 h postdose. Derivatives in this application also appeared to show improved CNS penetration over **53**, for example, **57** showed Br_u:Pl_u 0.5–0.6 and CSF:Pl_u 0.6–1.2.

Both **58** and **59** were well characterized in rat in vivo efficacy studies (Fig. 17). **58** showed marked reductions in brain (70%) and CSF (85%) $A\beta_{40}$ levels, 6 h after an oral dose of 10 mg/kg. As predicted by low in vitro P-gp efflux, ER 0.7, **58** readily penetrated the CNS in the same study, with Br_u:Pl_u 1.3 and CSF:Pl_u 1.0, 2 h postdose, with resultant free brain concentration of 30 nM.

59 also effectively penetrated the CNS, displaying Br_u:Pl_u 0.8 and CSF:Pl_u 0.5, in line with minimal P-gp efflux, ER 1.7. In the rat, **59** caused a 68% and 82% reduction of brain and CSF $A\beta_{40}$, respectively, 4 h after an oral dose of 10 mg/kg. The highest free brain concentration (87 nM) was measured 2 h postdose.

A UK patent application has published detailing the structures of three metabolites (**60–62**, Fig. 18) of **59** with their cellular activity.[85]

The isomeric THF-fused aminodihydrothiazine derivatives were exemplified in a GB patent application.[86] Overall, these derivatives, as exemplified by **63** with a cell IC_{50} of 8 nM (Fig. 19), appear to have a similar profile to compounds from the isomeric THF series, although there are only three examples. Rat in vivo data for **63** revealed marked lowering of brain and CSF $A\beta_{40}$, 56% and 84%, respectively, 6 h postdose at 30 mg/kg. At this time point, the free brain and CSF concentrations were 108 and 101 nM, respectively, giving good coverage of the cell IC_{50}. While the total Br:Pl was 1.0, the Br_u:Pl_u and CSF:Pl_u were 0.2.

An ensuing patent has also described pyrrolidine-fused aminodihydrothiazines, of which **64** is of particular note (Fig. 19).[87] **64** displays good activity in cellular assays, IC_{50} 14 nM, and a P-gp ER 7.4. Despite this, in vivo assessment in the rat at 60 mg/kg p.o. revealed good CNS penetration with a Br_u:Pl_u 0.9 and CSF:Pl_u 0.8, 3 h postdose. The Br_u and CSF concentrations were 8 and 6 nM, respectively, which resulted in a 47% decrease in CSF $A\beta_{40}$ levels but no effect on brain $A\beta_{40}$. It was noted that the lack of efficacy in brain could be due to low plasma levels in rat, which could be due to low metabolic stability, and that metabolic stability is better in human than rat, implying that the compound may be efficacious in human. In rat, **64** has moderate CLb, 53.3 mL/min/kg, and Vd, 2.62 L/kg, resulting in a $t½$ of 1.4 h.

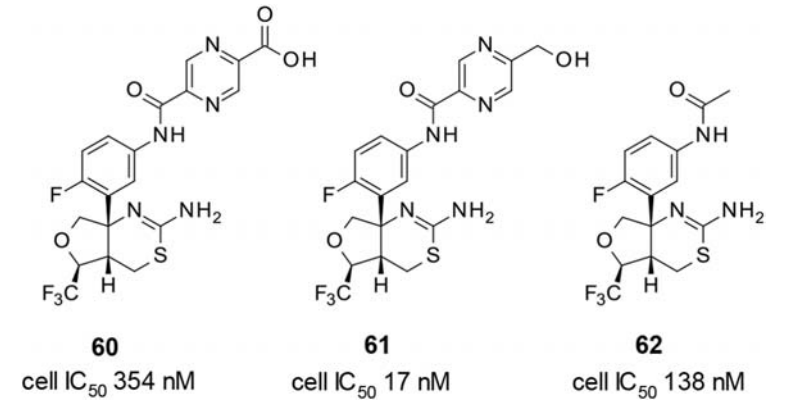

Fig. 18 Metabolites of compound **59**.

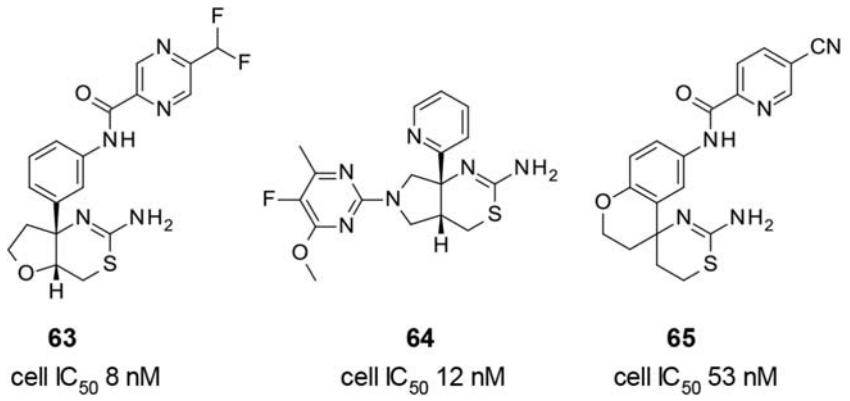

Fig. 19 Further selected chemotypes from Eisai.

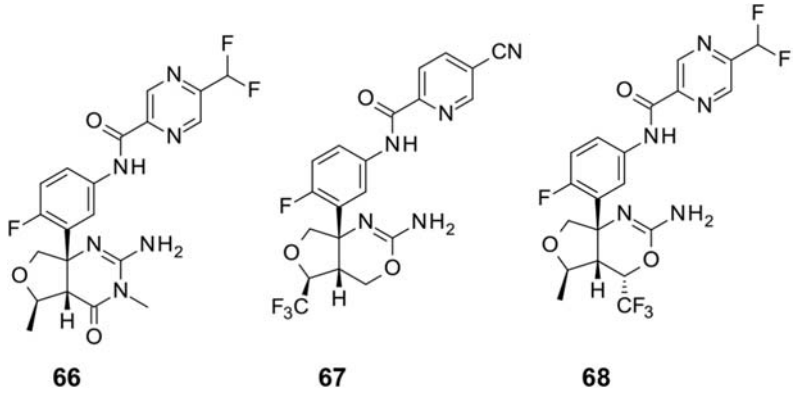

Fig. 20 THF-fused derivatives with alternative warheads from Eisai.

A patent application detailing spirocyclic analogs of the aminodihydrothiazines, such as **65,**[88] shows these derivatives appear to have weaker activity in general (Fig. 19). However, similar structural modifications have been tried on other templates by multiple groups, for example, Merck Serono and Roche on several templates (see later).

In addition to the isothiourea warhead, the Eisai group have also patented other THF-fused warheads, such as the acylguanidines, for example, **66**,[89] and isoureas, for example, **67** and **68** (Fig. 20).[90]

From conference activity, it is clear that Eisai have progressed at least one compound into clinical development, that is, E2609, although the structure of this compound has not been disclosed. In a single ascending dose (SAD) study, E2609 was administered at doses of 5, 10, 25, 50, 100, 200, 400, and 800 mg. The plasma Cmax increased proportionally with dose and the half-life ranged from 7.3 to 16.1 h. Plasma $A\beta_{1-x}$ levels were reduced by ~80% at doses from 25 to 100 mg, while higher doses resulted in prolonged reductions of >90%.[91] Repeat dosing for 14 days demonstrated that E2609 penetrated the CNS, with a CSF:Plasma (total) of ~0.2. Dose-dependent reductions in CSF $A\beta_{1-x}$ levels were demonstrated at a single time point, 12 h postfinal dose, whereby 56% (25 mg), 71% (50 mg), 83% (100 mg), and almost 90% (200 mg) absolute changes were shown.[92] This resulted in placebo-corrected reductions of 46% (25 mg), 62% (50 mg), 74% (100 mg), and 80% (200 mg).[93] Based on these results, E2609 was progressed to a Ph2 study in partnership with Biogen, whereby the compound will be dosed for 18 months to subjects with mild cognitive impairment (MCI) due to AD, and to subjects with mild to moderate AD.[94]

7.08.8 Inhibitors Reported by Elan

Elan have had a long standing interest in the amyloid field, focusing mainly on γ-secretase; however, they have also explored BACE inhibition and have a published patent application describing isothioureas/1,3-thiazines and isoureas/1,3oxazines. These compounds contain the common fluorophenyl anilides but offer diversity by means of a spiro ring on the 6-position of the oxazine/thiazine. Key compounds are depicted by **69**, **70**, and **71** which highlight the improved potency of the isothioureas over the isoureas (Fig. 21). In vivo efficacy proved moderate as at doses of **69** at 10, 30, 60, and 100 mg/kg an reduced brain $A\beta_{x-40}$ levels (guanidine extracted) by 23%, 31%, 31%, and 40%, respectively, 3 h postdose. A rat time course study at 30 mg/kg p.o. with **70** is

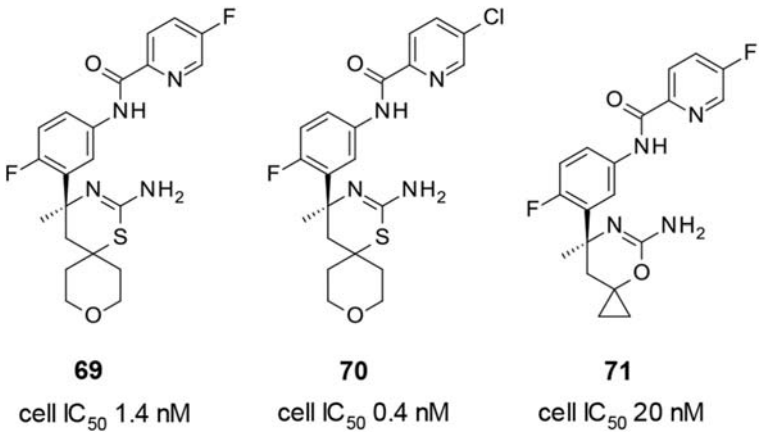

Fig. 21 Key compounds from Elan.

claimed to reduce $A\beta_{x-40}$ in brain and CSF for more than 12 h. As well as showing weaker in vitro activity, the isourea **71** showed weaker in vivo activity, whereby a 100 mg/kg oral dose to the rat resulted in only a 25% reduction of brain $A\beta_{x-40}$ 3 h postdose.

7.08.9 Inhibitors Reported by Genentech/Array BioPharma

Investigators from Genentech and Array BioPharma have collaborated around the optimization of spirocyclic BACE inhibitors. Structure-based design and a focus on conformational restriction led to low molecular weight BACE inhibitor **72** with only one rotatable bond (Fig. 22).[95] Despite being a significant substrate for P-gp-mediated efflux, **72** reduced CSF Aβ in rodents and monkey, with monkey showing a 65% reduction in $A\beta_{40}$ 8 h after a 100 mg/kg dose. Compounds from this series suffered from μ- and κ-opioid agonistic activity[96] as well as Cathepsin D inhibition. Both undesired activities could be diminished during further elaboration of this series into tricyclic tetrahydropyranyl chromanes, leading to **73** (Fig. 22).[97] The profile of this series was further tuned by shifting the position of the oxygen in the tetrahydropyranyl ring, and introduction of a bridgehead β-methyl group giving **74** (Fig. 22).[98] The β-methyl group was postulated to form a favorable hydrophopic interaction with Tyr132 in the BACE1 active site, but to clash with the flexible loop in CatD. As in the other series, compounds with the acyl guanidine Asp-binding moiety provided the most potent analogs, but the aminooxazolines had a more favorable efflux ratio. In rats, **74** reduced CSF $A\beta_{40}$ by 69%, 5 h after a 60 mg/kg dose, despite a relatively low coverage ratio of 2.1. In yet another attempt to improve BACE1 potency in this series, the oxygen of the tetrahydropyranyl was moved to the 6-position, supported by the possibility of forming a hydrogen bond with the NH of Trp76.[99] From this series, **75** (Fig. 22) was tested in rat at 60 mg/kg and although achieving a coverage ratio of free brain concentration over cellular IC_{50} of >10, the maximal Aβ reduction reached was only 40%.

In a parallel approach to target the BACE1 enzyme, Genentech has been developing bispecific antibodies with arms targeting both BACE1 and the transferrin receptor (TfR). A low affinity for TfR has been shown to take advantage of the receptor-mediated transcytosis properties of TfR resulting in a significantly increased trafficking of the antibodies across the BBB. This concept has now been proven to reduce amyloid levels in CSF in both mice and monkeys.[100]

Thus, despite a considerable investment, it does not appear that Genentech have progressed a BACE inhibitor to clinical trials. However, their parent company Roche has also had a significant interest in the BACE field and progressed at least one compound to the clinic.

7.08.10 Inhibitors Reported by Janssen

The initial work of Janssen on BACE inhibitors describes a series of 2-aminoquinazolines exemplified by **76** (Fig. 23).[101] Similarly substituted 2-aminoquinazolones were later on reported by Boehringer (**39**, Fig. 11). Cocrystallization of **76** with the BACE1 enzyme showed the typical amidine hydrogen bond network of two of the nitrogens of the aminoquinazoline with the catalytic aspartate dyad. The large side chain from the third nitrogen formed a hairpin loop with itself to position the N-cyclohexyl group into the S1 pocket. The α-cyclohexyl group was added to occupy the S1′ pocket, resulting in a compound with low nanomolar potency. An oral dose of 30 mg/kg of **76** in rats lowered $A\beta_{40}$ levels by 40–70% in plasma, but significant efflux prevented central activity. Compared to other series, the requirement of a bend conformation to optimally reach the S1 binding pocket prevents an energetically favored binding pose and the required linkers do not allow for achieving high LE. In addition the high basicity with pK_a values around 11 and high lipophilicity of this series was thought to be detrimental for a CNS lead. Subsequent efforts reported by Janssen focused on alternative series with cyclic amidines of moderate basicity and providing more optimal vectors into the

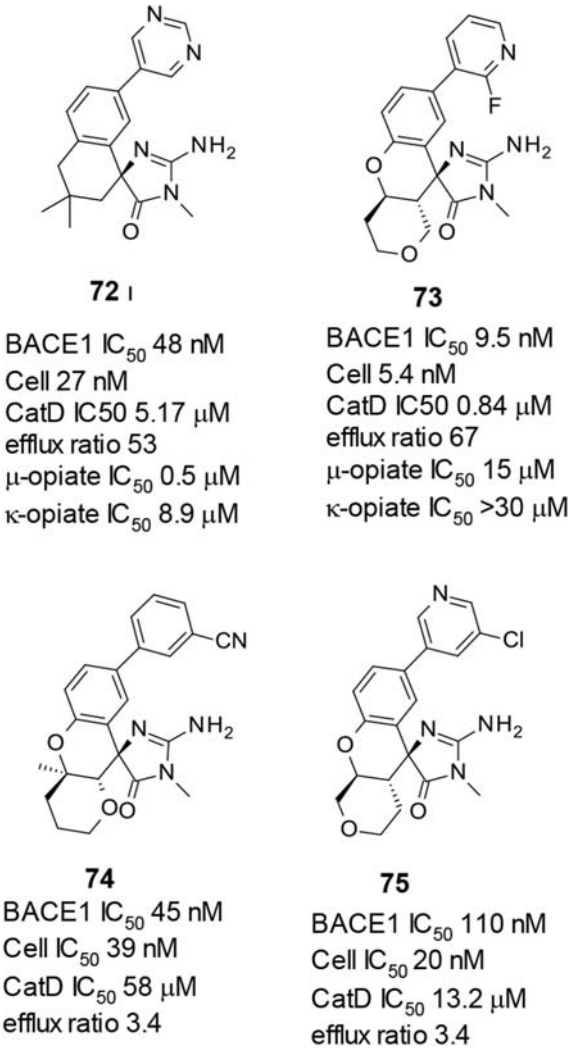

Fig. 22 Selected derivatives from Genentech/Array BioPharma.

various binding pockets. This resulted in two series of isomeric aminopiperazinones, exemplified by **77** and **78** (Fig. 23) of which **78** can be considered as a reverse amide isomer of aminodihydropyrimidones such as **24** (Fig. 8).[102] Both **77** and **78** were evaluated in a mouse in vivo model for brain penetration and **78** was also assessed for central lowering of Aβ levels. Both compounds showed low (**77**) to moderate (**78**) brain penetration, and a rapid decrease in plasma concentration attributed to low metabolic stability. Nevertheless, a relatively high dose of 60 mg/kg of **78** given subcutaneously led to a 73% reduction in brain Aβ levels, 4 h after dosing. Further work has been reported around a similar series of 3-amino-1,4-oxazine compounds, and fine-tuning of the basicity of the amidine group via the introduction of electron-withdrawing substituents.[103] Compounds with an unsubstituted 3-amino-1,4-oxazine had a pK_a of 9–9.6 and showed poor brain penetration due to P-gp-mediated efflux. Introduction of a 6-fluoro-susbtituent reduced the pK_a to values below 8 and led to compounds with a significant and long-lasting central amyloid reduction in mice and dogs. For example, a single oral dose of 2.5 mg/kg **79** (Fig. 23) in dog led to 90% reduction of CSF $A\beta_{42}$ up to 50 h postdosing.

Two subsequent patent applications describe further variations of the substituted 3-amino-1,4-oxazine series. One application describes compounds with a difluoromethyl substituent as the electron-withdrawing group, exemplified by **80** (Fig. 23),[104] and the other one replacing the common amide linker with amino linked heterocycles (**81**) (Fig. 23).[105] The iminomorpholine template is closely related to that described by Roche and Novartis, the latter of whom appear to have secured the patent space with the first published patent application (see later).

In what can be considered a continuation of the aminopiperazinone series, a number of patents have appeared incorporating 5-ring heteroaryl isosteric replacements of the piperazinone amide. This resulted in fused heteroaryl aminopiperazine compounds, exemplified by **82–88** (Fig. 24).[106–108] The synthesis of the tricyclic version **89** (Fig. 24) of the pyrrolopiperazines series has also been described, with the aim to reduce the high pK_a (~10) of the unsubstituted aminopyrrolopiperazines.[109] As with the 1,4-oxazines such as **79**, electron-withdrawing groups have also been incorporated in the bicyclic piperazines as shown in **84** and **88**,[110] with **84** showing 84% reduction in brain $A\beta_{42}$, 4 h after an oral dose of 30 mg/kg in mouse.[111] Central activity is not obvious

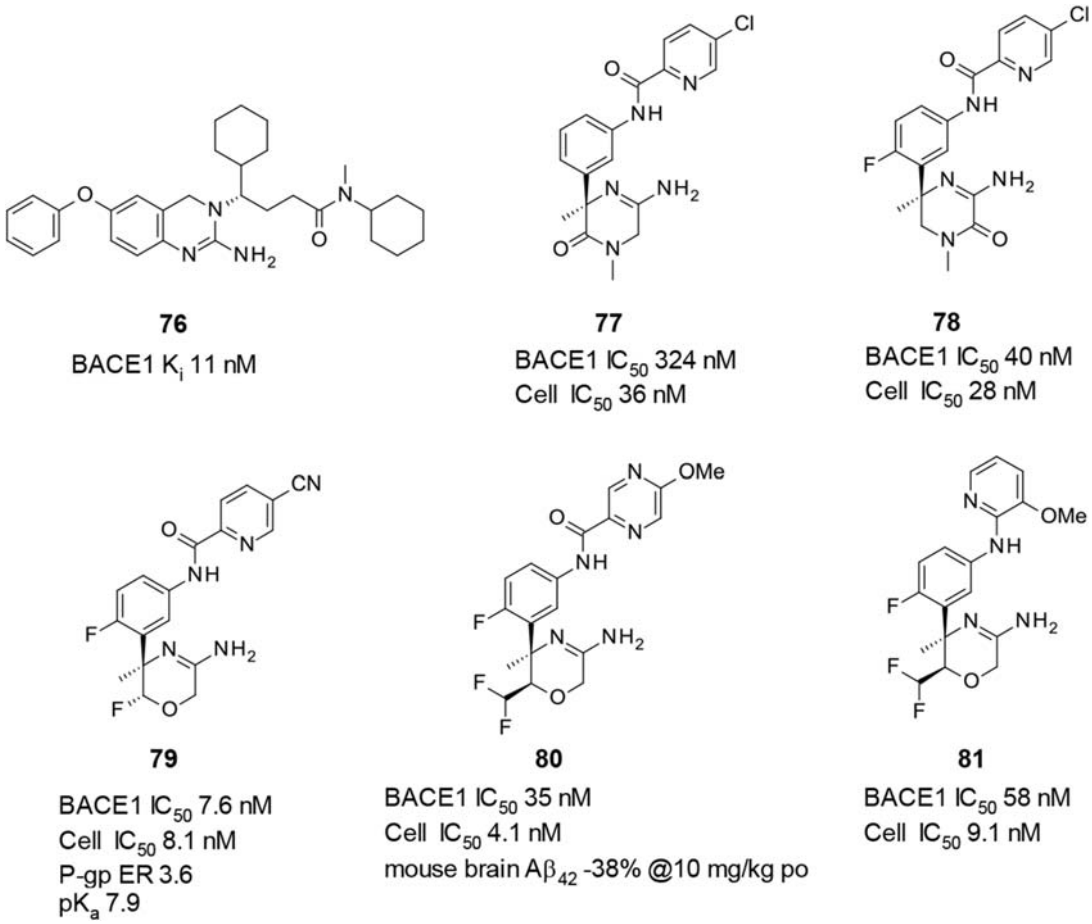

Fig. 23 Initial examples from Janssen.

for all of the fused piperazine subseries, as **86** and **87** and their analogs were not able to significantly lower amyloid levels in mouse at the tested dose of 10 mg/kg s.c.[112,113]

In another example of pK_a modulation of the basic amidine via decoration of the amidine containing heterocycle with electron-withdrawing groups, the synthesis and activity was described for a pair of 2-amino-pyrrolidine containing compounds, **90** and **91**.[114] The basicity of the CF_3-substituted analog **91** was reduced by over 2 log units versus **90**, in addition to a fivefold increase in potency (Fig. 25).

In summary, the Janssen group have been extremely active in the field and have published compounds covering a range of chemotypes, although most contain an amidine-derived warhead with an S3 pocket targeting anilide. Despite this, there has been no public disclosure of a compound progressing to the clinic. Ultimately, however, the group have progressed a compound to clinical trials in partnership with Shionogi (see later).

7.08.11 Inhibitors Reported by Lilly

The research group at Lilly has been a stalwart in the amyloid field, having tackled both γ-secretase and latterly BACE. In addition to having progressed semagacestat (γ-secretase inhibitor) to PhIII, they have progressed several BACE inhibitors to clinical development, pioneering the path and being the first group to publicly demonstrate clinical effects on central amyloid levels with a BACE inhibitor.

The chemical matter from the group at Lilly has been focused almost exclusively on isothioureas/aminodihydrothiazines. The initial compounds were simple derivatives, but these were succeeded by THF-fused and the pyrrolidine-fused derivatives. Two compounds have been terminated in clinical development, for nontarget related reasons, and at the time of writing Lilly are progressing LY3314814/AZD3293 (**32**, Fig. 10) licensed from AstraZeneca, currently PhII/III and LY3202626 (structure undisclosed), currently PhI.

For their first foray into clinical development, researchers at Lilly identified LY2811376 (**92**, Table 2). This compound was shown to lower Aβ species in a FRET assay, IC_{50} 239 nM, and cellular assays, HEK SwAPP IC_{50} 300 nM ($A\beta_{1-40}$) and 299 nM

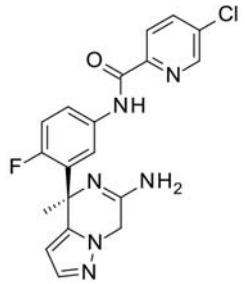

82

BACE1 IC_{50} 43 nM
Cell IC_{50} 4.3 nM
mouse brain $A\beta_{42}$ -29%
@ 30 mg/kg sc

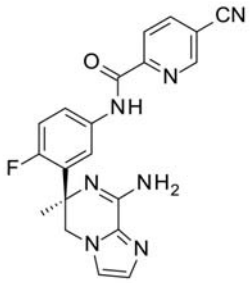

83

BACE1 IC_{50} = 53 nM
Cell IC_{50} = 6.3 nM
mouse brain $A\beta_{42}$ -62%
@30 mg/kg po

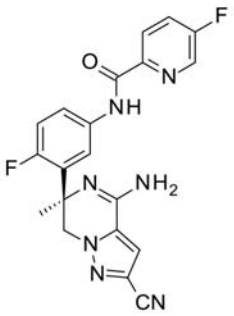

84

BACE1 IC_{50} = 32 nM
Cell IC_{50} = 3.3 nM
mouse brain $A\beta_{42}$ -84%
@ 30 mg/kg po

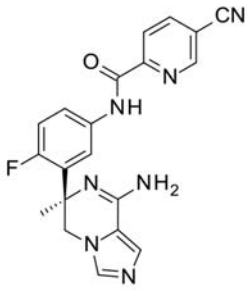

85

BACE1 IC_{50} 3.3 nM
Cell IC_{50} 5.2 nM
BACE2 IC_{50} 19 nM
mouse brain $A\beta_{42}$ no effect
@10 mpk sc

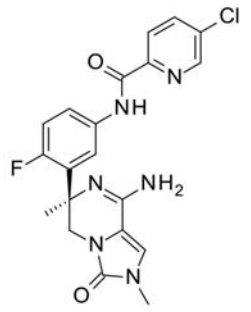

86

BACE1 IC_{50} 3.9 nM
Cell IC_{50} 6.3 nM
BACE2 IC_{50} = 4.3 nM
mouse brain $A\beta_{42}$ no effect
@10 mpk sc

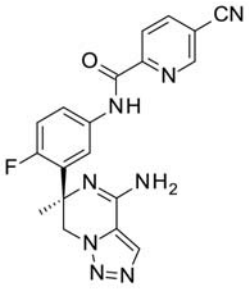

87

BACE1 IC_{50} 1.7 nM
Cell IC_{50} 1 nM
BACE2 IC_{50} 5.3 nM
mouse brain Aβ42 -39%
@10 mpk sc

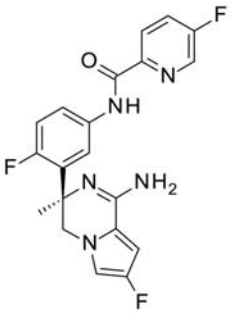

88

BACE1 IC_{50} 41 nM
Cell IC_{50} .6 nM
mouse brain $A\beta_{42}$ -27%
@30 mpk po

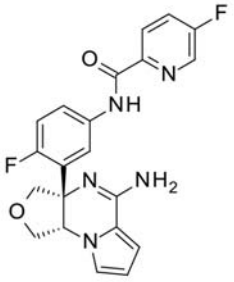

89

BACE1 IC_{50} submicromolar

Fig. 24 Bicyclic and tricyclic derivatives from Janssen.

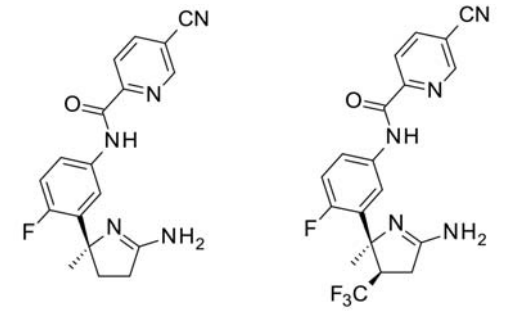

90
BACE1 IC_{50} 1047 nM
pK_a 11.1

91
BACE1 IC_{50} 182 nM
pK_a 9.0

Fig. 25 Further amidine derivatives from Janssen.

Table 2 Summary of Lilly clinical compounds **92** and **93** with further derivatives **94** and **95**

Compound Structure	LY2811376 (**92**)	LY2886721 (**93**)	**94**	**95**
	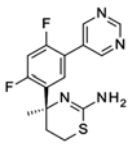	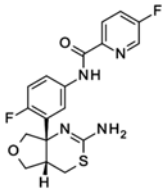	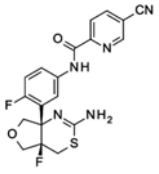	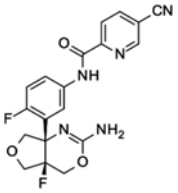
FRET IC_{50} (nM)	239	20.3	6.66	45
HEK SwAPP $A\beta_{1-40}$ IC_{50} (nM)	300	18.5	n.d.	n.d.
HEK SwAPP $A\beta_{1-42}$ IC_{50} (nM)	299	19.7	n.d.	n.d.
PDAPP neuron $A\beta_{1-40}$ IC_{50} (nM)	102	10.7	20.2	49.9
PDAPP neuron $A\beta_{1-42}$ IC_{50} (nM)	94.7	9.23	16.3	36.5

($A\beta_{1-42}$), PDAPP mouse neuron IC_{50} 102 nM ($A\beta_{1-40}$) and 94.7 nM ($A\beta_{1-42}$).[115] Initial data demonstrated that LY2811376 (**92**) reduced amyloid levels in the PDAPP mouse, 3 h postdose CSF $A\beta_{1-x}$ was reduced by 60% following a 10 mg/kg s.c. dose, whereas brain $A\beta_{1-x}$ was reduced by 50% at 30 mg/kg s.c. Further characterization in the PDAPP mouse showed 47%, 64%, and 68% reductions in cortical $A\beta_{1-x}$ 3 h after 10, 30, and 100 mg/kg oral doses, respectively, with a corresponding Br:Pl 1.7–2.2.[116] In vivo efficacy was confirmed in the dog, where a 5 mg/kg oral dose resulted in ~70% reduction in CSF $A\beta_{1-x}$ 9 h postdose.

LY2811376 (**92**) entered PhI clinical trials in Dec. 2008[117] and completed SAD and MAD studies demonstrating 58% reduction of CSF $A\beta_{1-40}$ and $A\beta_{1-42}$ approximately 18 h after an oral dose of 90 mg, in healthy volunteers. The effect in CSF was slightly less pronounced than that in plasma, 80% reduction ~7 h postdose. The T_{max} in CSF was reached ~5 h postdose, somewhat delayed compared to the plasma T_{max} 2 h, and the CSF:Pl_{tot} AUC was ~0.3, showing good distribution into the human CNS. Disappointingly, further development of this compound was halted due to a finding in a preclinical 3-month rat toxicological study, where autofluorescent material was found in the retinal epithelium at doses ≥30 mg/kg. This finding was adjudged to be compound specific and not related to BACE inhibition as the same effects were not seen in BACE KO mice.[116]

Ultimately, these issues resulted in Lilly progressing a second compound, LY2886721 (**93**, Table 2) into clinical studies. Initial data reported in a patent application showed improved in vitro activity over its predecessor, BACE FRET IC_{50} 20.3 nM, and cellular assays, HEK SwAPP IC_{50} 18.5 nM ($A\beta_{1-40}$) and 19.7 nM ($A\beta_{1-42}$), and PDAPP mouse neuron IC_{50} 10.7 nM ($A\beta_{1-40}$) and 9.23 nM ($A\beta_{1-42}$).[118] In vivo, PDAPP mouse, LY2886721 (**93**) reduced $A\beta_{1-x}$ by 54% in brain cortex 3 h postdose following 10 mg/kg oral administration. Further characterization of this compound has recently been detailed.[119] In the dog, a 1.5 mg/kg oral dose of LY2886721 (**93**) resulted in strong reductions of $A\beta_{1-x}$ in CSF, 80% reduction 9 h postdose, with slightly stronger effects seen in plasma. In this study, the CSF_{AUC}:free $plasma_{AUC}$ was ~0.9, demonstrating excellent CNS penetration. In healthy volunteers, doses of 5–70 mg LY2886721 (**93**) were assessed in a SAD, showing ~80% reduction in plasma amyloid levels at the highest dose, which did not significantly differentiate from the 35 mg dose. Following a single 35 mg dose to healthy volunteers, the maximal CSF $A\beta_{1-40}$ reduction, 40%, was observed ~17 h postdose. Following 14 days administration of the 35 mg dose, CSF $A\beta_{1-40}$ levels were reduced by 58%, whereas a 70 mg dose resulted in a maximal 74% reduction of CSF $A\beta_{1-40}$ levels. Unfortunately PhII studies were terminated due to effects on liver enzymes, again not related to BACE inhibition.

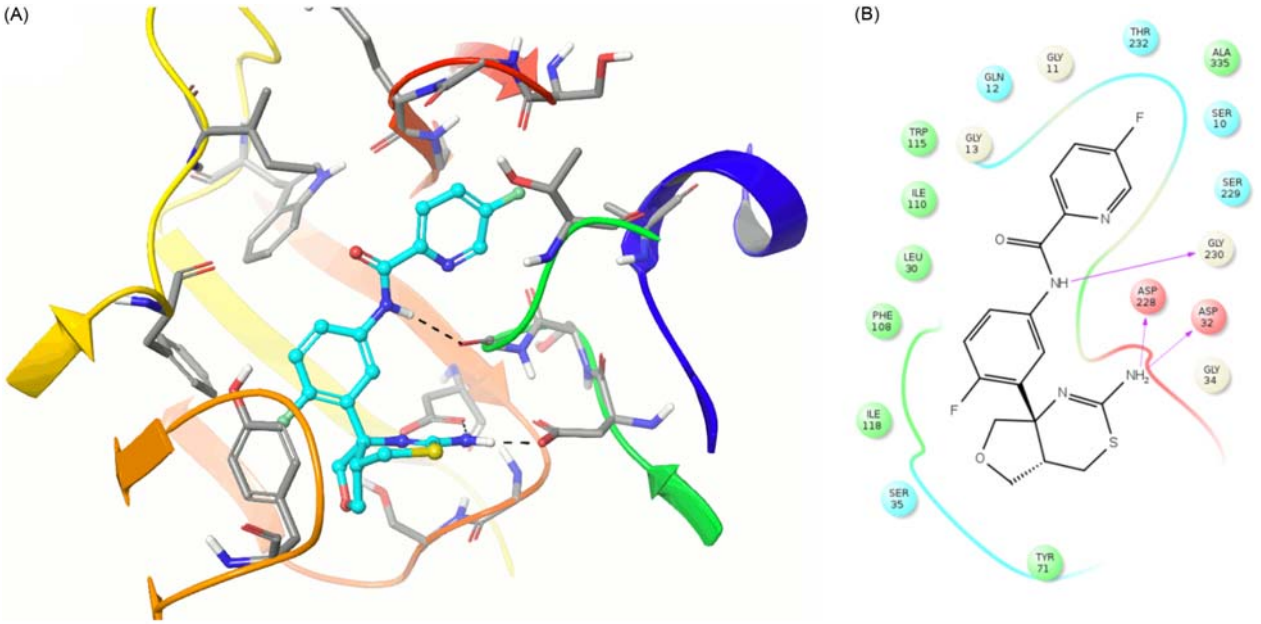

Fig. 26 (A) X-ray crystal structure of LY2886721 (**93**) bound to BACE (PDB code 4X7I). (B) Depiction of LY2886721 (**93**) interactions.

The crystal structure of LY2886721 (**93**) bound to BACE has been published, and is depicted in Fig. 26. The isothiourea interacts with the catalytic aspartic acid diad, while the anilide forms a hydrogen bond with Gly230 and the pyridyl moiety extends into the S3 pocket.

The final patent application from this series has appeared more recently, the key difference being the addition of a fluorine atom at the ring junction,[120] presumably to modulate the basicity of the warhead. The application covers isothioureas, for example, **94**, as well as isoureas, for example, **95**, Table 2, which are generally more basic, and may therefore benefit more from the presence of the fluorine atom (Table 2). Head to head data for a matched pair shows that the isoureas have weaker in vitro activity, **95** BACE FRET IC_{50} 45 nM, PDAPP neuron IC_{50} 49.9 ($A\beta_{1-40}$) and 36.5 nM ($A\beta_{1-42}$) than the isothioureas, **94** BACE FRET IC_{50} 6.66 nM, PDAPP neuron IC_{50} 20.2 ($A\beta_{1-40}$) and 16.3 nM ($A\beta_{1-42}$), respectively (Table 2). The potency difference in vivo was less pronounced, with a 10 mg/kg oral dose of **94** resulting in a 34% and 46% reduction of $A\beta_{1-x}$ in hippocampus and cortex, whereas **95** at the same dose resulted in a 26% and 26% or 24% reduction, respectively. In addition to the two highlighted compounds, the methoxypyrazine amide analog of **94** also appears to be a favored compound, showing 40% and 45% reduction of $A\beta_{1-x}$ in hippocampus and brain amyloid level after a 10 mg/kg oral dose. Both **94** and **95** are specifically claimed, and given the strength of the in vitro and in vivo results for these compounds, versus previous development compounds, either one of these compounds could have been nominated as a development candidate.

Following on from the THF-fused derivatives, the focus of the Lilly group appears to have shifted to pyrrolidine-fused aminodihydrothiazines, which are related to the aminodihydropyrimidone series from Merck and Eisai. Moving to this series meant an initial step back in terms of in vitro potency, to similar or weaker levels than displayed by LY2811376 (**92**, Table 2). A first patent application disclosed **96**, BACE FRET IC_{50} 172 nM, PDAPP neuron IC_{50} 2240 ($A\beta_{1-40}$) and 2870 nM ($A\beta_{1-42}$) respectively (Table 3).[121] Despite the much weaker activity in the PDAPP neuron assay, **96** still demonstrated efficacy in vivo in the PDAPP mouse, at an oral dose of 30 mg/kg it reduced $A\beta_{1-x}$ by 45% and 52% in hippocampus and cortex, respectively. This compound

Table 3 Initial pyrrolidine-fused isothiourea derivatives from Lilly

Compound	**96**	**97**
Structure	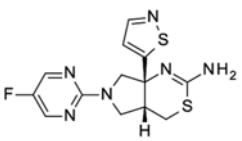	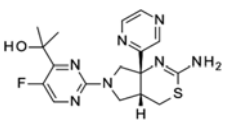
FRET IC_{50} (nM)	172	105
PDAPP neuron $A\beta_{1-40}$ IC_{50} (nM)	2240	455
PDAPP neuron $A\beta_{1-42}$ IC_{50} (nM)	2870	412

in addition to the 5-cyano-thiophene-2-yl analog were both specifically claimed, thus representing key compounds. A subsequent patent application detailed three key compounds, the most prominent being **97** with improved in vitro activity, particularly in cellular assays, FRET IC_{50} 105 nM, PDAPP neuron IC_{50} 455 ($A\beta_{1-40}$) and 412 nM ($A\beta_{1-42}$), respectively (**Table 3**).[122] Thus the in vitro activity levels were in line with the initial clinical candidate, LY2811376 (**92**), providing confidence that human efficacy could be observed. In vivo efficacy was demonstrated in the PDAPP mouse at 10 and 30 mg/kg p.o., with amyloid measured 3 h postdose. The lower dose provided marginal efficacy, reducing $A\beta_{1-x}$ by 19% and 23% in hippocampus and cortex, respectively, whereas the higher dose resulted in $A\beta_{1-x}$ reductions of 46% and 53% in hippocampus and cortex, respectively.

In order to increase potency in the pyrrolidine-fused series, the group at Lilly have added the amide substituent present in the most potent BACE inhibitors to pick up additional interactions, principally the HBD interaction with Gly230. Thus, recent patent applications have described **98** and **99** (**Table 4**).[123] Both compounds demonstrated subnanomolar activity in vitro **98** BACE FRET 0.6 nM, PDAPP neuron IC_{50} 0.5 nM ($A\beta_{1-40}$) and 0.5 nM ($A\beta_{1-42}$), Lilly-6 BACE FRET 0.6 nM, PDAPP neuron IC_{50} 0.13 nM ($A\beta_{1-40}$) and 0.135 nM ($A\beta_{1-42}$). **98** displayed potent in vivo efficacy in the PDAPP mouse, with 43%, 59%, and 66% reductions in cortical $A\beta_{1-x}$ after 1, 3, and 10 mg/kg oral doses, respectively. Similar effects on amyloid were seen in the hippocampus. **99** has been the subject of a subsequent patent application, detailing the synthesis, crystalline forms, and its use in the treatment of AD.[124] Additional in vivo efficacy data was provided in this application, demonstrating potent amyloid lowering activity in the PDAPP mouse; 31%, 39%, and 61% reduction in hippocampal $A\beta_{1-x}$ at oral doses of 0.3, 1, and 3 mg/kg 3 h postdose, respectively.

A recent patent application has published, describing a single compound, **100**, this compound having the central phenyl ring replaced by a pyridine (**Table 4**).[125] Only in vitro activity data were presented. As with analogs, **100** showed potent in vitro activity, BACE FRET 0.9 nM, PDAPP neuron IC_{50} 0.65 nM ($A\beta_{1-40}$) and 0.91 nM ($A\beta_{1-42}$) respectively. An even more recent patent application has published, again containing a single compound, **101**, which differs from **100** by the replacement of the central pyridine ring by a fluorophenyl ring (**Table 4**).[126] The patent application describes a similar level of characterization to other patent applications, whereby **101** shows extremely potent in vitro activity, PDAPP neuron IC_{50} 0.275 nM ($A\beta_{1-40}$), 0.228 nM ($A\beta_{1-42}$), and strong in vivo efficacy in a dose–response study in the PDAPP mouse—doses of 0.3, 1, and 3 mg/kg p.o. resulted in reductions of 28%, 42%, and 64% in brain cortex, respectively, 3 h postdose. A subsequent patent application discloses the combination of a BACE inhibitor, such as **101** and very close analogs, with an Aβ antibody.[127]

The analysis here further commentary on Lilly's patenting strategy relative to their clinical studies. Thus, clinical studies with LY2811376 (**92**) commenced in Dec. 2008, while the patent application only published on 5th Nov. 2008. For LY2886721 (**93**), the fist clinical studies commenced in Jun. 2010, while the patent application covering the compound did not publish until 13th Jan. 2011. Thus, one can see that Lilly are happy to aggressively push compounds forward while carrying significant patent risks due to the extremely competitive nature of the field.

Based on the analysis presented here, one may posit that Lilly have identified several further development candidates, however it would appear that only one further compound discovered by the Lilly group has progressed to the clinic, namely LY3202626. The analysis reveals that LY3202626 is most likely represented by **99**, **100**, or **101**. The publication of a recent patent application describing the tosylate salt of **101**[128] would suggest that this compound is LY3202626.

Lilly's commitment to the AD field, and in particular the BACE inhibitor field should be commended. The company has expended significant research efforts over the years to identify BACE inhibitors. This work has resulted in exciting and challenging times as early compounds demonstrated efficacy on pharmacodynamics (PDs) and disease biomarkers, but disappointment as compounds were discontinued due to toxicological issues. A third proprietary compound is currently undergoing clinical development, in addition to AZD3293/LY3314814 (**32**, **Fig. 10**), licensed from AZ which is undergoing PhII/III studies

Table 4 Follow-on pyrrolidine-fused isothiourea derivatives from Lilly, incorporating the S3-pocket-binding amides

Compound	**98**	**99**	**100**	**101**
Structure	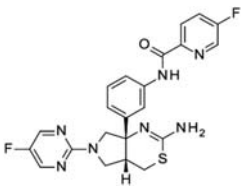	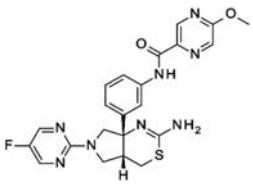	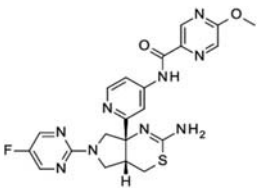	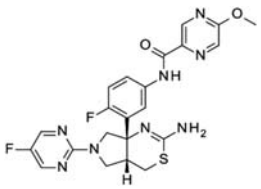
FRET IC_{50} (nM)	0.610	0.482	0.90	0.569/0.615
HEK SwAPP $A\beta_{1-40}$ IC_{50} (nM)	0.619	0.324		
HEK SwAPP $A\beta_{1-42}$ IC_{50} (nM)	0.437	0.289		
PDAPP neuron $A\beta_{1-40}$ IC_{50} (nM)	0.487	0.244	0.65	0.134/0.275
PDAPP neuron $A\beta_{1-42}$ IC_{50} (nM)	0.591	1.22	0.91	0.131/0.228

7.08.12 Inhibitors Reported by Lundbeck

Lundbeck have also been late entrants to the field, with five published patent applications, three of which published in May 2016. The first publication describes thiazole isothiourea derivatives, where a second aromatic group is attached via a methylene linker. Overall these compounds display weak activity, as shown by **102**, with a BACE1 binding Ki of 1.9 μM (Fig. 27).[129] A second application describes fluorinated amidine derivatives, exemplified by **103** (Fig. 27).[130] Several derivatives show potent binding to BACE1, and five analogs are reported to lower $A\beta_{40}$ in rat brain 3 h after oral administration at 30 mg/kg. Three compounds including **103** also have activity reported at 10 mg/kg. Of these, **103** appears to be the most active, displaying good CNS penetration, Br:Pl 0.5, and reducing brain amyloid by 66% and 61% at doses of 10 and 30 mg/kg, respectively. The total brain concentrations achieved were 412 and 1606 ng/g following doses of 10 and 30 mg/kg, respectively.

Recently, three further patent applications have appeared, which described related analogs. One of the patent applications describes analogs of **103**, such as **104** (Fig. 27)[131] which have only one fluorine atom at the 5-postion of the iminopiperidine ring. **104** was found not to be a P-gp substrate in vitro and displayed the strongest in vivo activity to date among the compounds they have described, whereby a 3 mg/kg oral dose to the rat resulted in a 52% decrease in brain $A\beta_{40}$ 3 h postdose. A Br:Pl of 2.2 was also recorded in this study, with a total brain concentration of 610 ng/g. No data on free brain or plasma concentrations was provided. **105** (Fig. 27) with additional fluorination on the central phenyl ring as well as the 6-fluoromethyl group displayed a similar in vitro profile.[132] Rat in vivo data for **105** was provided only at doses of 10 and 30 mg/kg p.o., whereby the compound lowered brain $A\beta_{40}$ by 43% and 50% 3 h postdose, respectively. The Br:Pl ranged from 1.3 to 1.8, with total brain exposure of 1758 and 4210 ng/g at 10 and 30 mg/kg, respectively. The third patent is best exemplified by **106** (Fig. 23).[133] It can be seen that the increased fluorination results in a more potent series, however in vivo activity appears weaker than other series. Doses of 10 and 30 mg/kg of **106** resulted in 24% and 38% decreases in brain $A\beta_{40}$ levels in the rat. The weaker efficacy could be due to the lower Br:Pl (0.3) than other series, for example, **104** and **105**, which resulted in lower total brain concentrations of 511 and 2284 ng/g at doses of 10 and 30 mg/kg, respectively. It could also be that there are differences in brain tissue binding between the subseries which may also impact the in vivo efficacy, as the total brain concentration for **106** were similar to **103** which displays much better in vivo efficacy.

In the three most recent patent applications, it can be seen that the amidines were generally not P-gp substrates, however there were certain amide motifs which clearly resulted in P-gp efflux, reflecting a specific recognition pattern. Overall, the amidines appear to demonstrate acceptable levels of in vitro potency while not being subjected to P-gp efflux. The in vivo activity appears moderate, with some subseries, that is, **104** and **105** appearing more potent than others. However, it is not known whether α-fluoro-amidine, present in **103** and **104**, is stable to hydrolysis and whether this template suffers from hERG and CYP2D6 inhibition.

Currently, there are no BACE inhibitors listed on the Lundbeck pipeline, so it is unclear if any compounds have progressed beyond the preclinical stage.

7.08.13 Inhibitors Reported by Merck Serono/Merck KGAA

Another late entrant to the BACE field, Merck Serono, who under the name Ares Trading SA, have published a single patent application on their work.[134] The compounds are related to the spirocyclic series from Eisai, for example, **65** (Fig. 19), whereby the phenyl ring has been replaced by a thiophene, to give compounds such as **107**, which is claimed to display submicromolar activity in enzymatic and cellular assays (Fig. 28). Other warheads such as acylguanidine **108** are also described, with similar activity (Fig. 28). It would appear that Merck Serono are no longer active in the field.

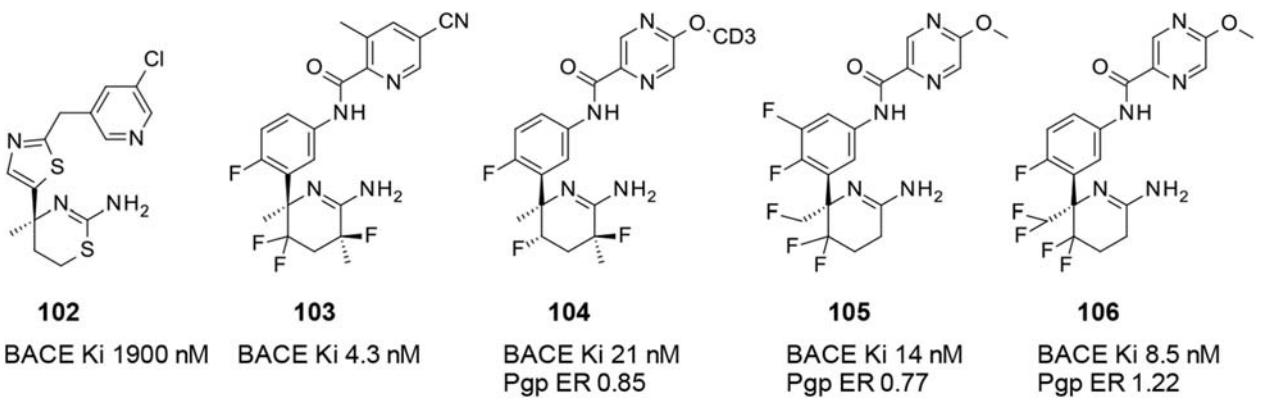

Fig. 27 Isothiourea derivative **102**, and fluorinated amidine derivatives (**103–106**) from Lundbeck.

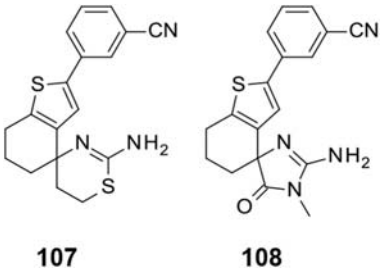

Fig. 28 Examples from Merck-Serono.

7.08.14 Inhibitors Reported by Noscira

Noscira, based in Spain, have published one patent application, describing conjugated acylguanidine derivatives, such as **109**, with weak in vitro activity, IC_{50} 220 nM in a recombinant enzyme assay, cell IC_{50} 1.15 μM (Fig. 29).[135] No further publications have appeared and it does not look like these derivatives have progressed beyond early preclinical characterization.

7.08.15 Inhibitors Reported by Novartis

Novartis have expended a significant effort in the field and analysis of the published patents reveal several key compounds, all based on the iminomorpholine/1,4-oxazine template, with the exception of the latest published patent application. It appears that several companies, including Janssen, had been interested in this template, but Novartis managed to secure the primary published patent application. The first patent application from Novartis, covering **110** and **111** (Fig. 30) published on 27th Jan. 2011, just 4 weeks ahead of that from Roche, covering **144** and **145** (Fig. 41), which published on 24th Feb. 2011. Similarly, patents from Janssen covering **79**, **80**, and **81** (Fig. 23), published on 13th Jun. 2013. Again, this serves to highlight the competitive nature of the field.

Initial compounds, centered on the iminomorpholine template as depicted by **110**,[136] Fig. 30, the difluoromethyl group presumably serves to orient the fluoro-anilide in the axial location while reducing the pK_a of the guanidine moiety, as it may be expected that the β-oxygen atom does not sufficiently modulate the basicity of the guanidine. This series was quickly followed up by more key examples, such as **111** and **112** (Fig. 30), which have been described in several patent applications.[137–139] The close analog of **112**, namely **113** (Fig. 30), appeared in the second patent application,[137] the addition of a methyl group *ortho* to the amide may have been intended to reduce amide cleavage. The addition of fluorine atoms either on the 5-methyl, as shown by **112** and **113**, or at the 2-position are presumably to reduce the pK_a on the guanidine moiety, which is probably still too basic despite the β-oxygen on the morpholine.

Further pharmacological data on **111**, also known as **NBI-360**, have recently been published.[140] In vitro characterization of **NBI-360** revealed BACE1 enzyme inhibition IC_{50} of 5 nM (human and mouse, slightly more potent than the original report). Significantly weaker activity was observed in a HEK cell line overexpressing SwAPP IC_{50} 33 nM, than that against wild-type APP, IC_{50} 3 nM, presumably due to the fact that SwAPP is a better BACE substrate than wild-type APP. **NBI-360** is not a P-gp substrate (ER 1.9) and shows good CNS penetrations, rat Br:Bl 0.86 (AUC), which equates to a Br_u:Bl_u of 0.32, assuming brain tissue and ppb are equal. In the dog, the compound also penetrated the CNS, CSF:Pl 0.023, which when corrected for free plasma concentrations equates to CSF:Pl_u of $\geq$2.3, although this value could be significantly overestimated due to the high ppb in the dog. The PK profile was characterized in the mouse, rat, and dog which were all used to investigate efficacy. Low clearance and volume of distribution was observed in the dog, perhaps due to high ppb, but the $t^1/_2$ was 36.2 h. In the mouse and rat the $t^1/_2$ was 3.6 and 2.7 h,

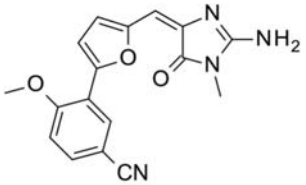

109

BACE IC_{50} 220 nM

cell IC_{50} 1150 nM

Fig. 29 Selected example from Noscira patent application.

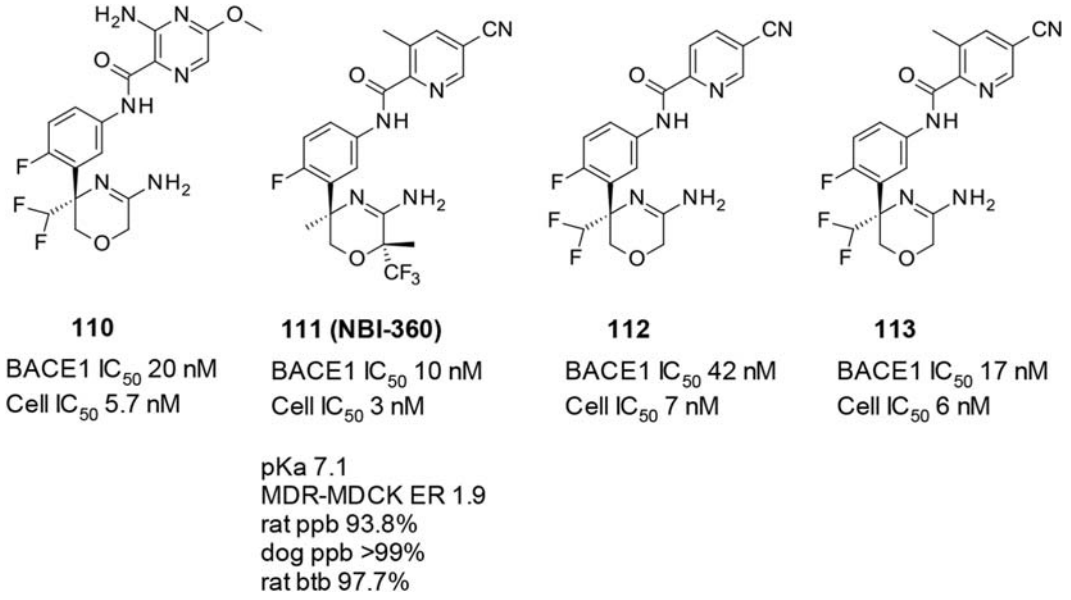

Fig. 30 Initial iminomorpholine derivatives from Novartis, including NBI-360 (**111**).

respectively, and both showed moderate to high oral bioavailability. A dose–response time course study in the rat showed a strong reduction of $A\beta_{40}$ levels in CSF and forebrain with a maximal effect in brain of 91% 4 h postdose (30 μmol/kg). This resulted in a calculated ED_{50} of 1.6 μmol/kg for $A\beta_{40}$ lowering in the forebrain at the 4 h time point (direct modeling). In the dog, an oral dose of 0.5 mg/kg (1.1 μmol/kg) p.o. resulted in ~80% reduction of CSF $A\beta_{40}$ 12–24 h postdose, resulting in a calculated plasma concentration of 59 nM to reduce CSF $A\beta_{40}$ by 50%, which corresponds to a CSF concentration of 1.4 nM, which is similar to the cell IC_{50}. In preplaque APP51/16 transgenic mice (3–5 months of age), a single dose of 30 μmol/kg resulted in ~80% decrease of brain $A\beta_{40}$ 4 h postdose. A follow-up study in older mice (8 months of age) with dosing for 4 days resulted in 15% and 52% reduction of brain $A\beta_{40}$ 24 h postdose at 30 and 100 μmol/kg, respectively. Finally, a chronic (6 weeks) study in older mice (starting at 14.5 months of age) at a dose of 100 μmol/kg p.o. showed >90% reduction of CSF $A\beta_{40}$ at 4 h and approximately 60% at 24 h postfinal dose. Analysis of plaque growth compared to baseline showed that **NBI-360** treatment prevented plaque growth over the 6-week treatment period, thus demonstrating the potential of a BACE inhibitor to halt disease progression.

Although the characterization of **NBI-360** demonstrates an encouraging profile, it would appear that this compound may not have progressed to the clinic. No mention is made of the hERG or cardiovascular safety profile, which have represented significant challenges in the BACE inhibitor field. In addition, during the chronic (6 weeks) mouse study patches of gray hair appeared on **NBI-360**-treated mice. This has been attributed to BACE2 inhibition.[141]

A related patent application disclosed further analogs with a variety of substituents on the pyridyl amide as well as additional fluorination on the central phenyl ring.[142] Of more interest, a subsequent patent application described further examples of **111** and **113**, where the central phenyl group has been replaced by a pyridine ring.[143] Pertinent examples are highlighted by **114**, **115**, and **116** (Fig. 31). This change appears not to affect BACE potency, although the in vivo profile may be improved (see later). It is unclear if they offer any other benefit apart from avoidance of an aniline structural alert.

Additional analogs in this series have been disclosed where the amide has been replaced by isosteres, for example, **117** and **118**,[144] where the amide has been replaced by a fused pyridine or by a fused pyrimidine respectively (Fig. 32). Many research groups have tried this type of strategy on other templates, but other issues would be anticipated, and as such it is unlikely that compounds have progressed from this subseries.

Finally, the group at Novartis applied the pyridine replacement in the isourea/dihydroaminooxazine series. The patent discloses head to head in vivo data with the corresponding phenyl analogs patented by Roche. The pyridine not only maintains potency in vitro but drastically improves the in vivo efficacy, demonstrated by in vivo efficacy studies in the SD rat at a dose of 10 μmol/kg, with sampling 4 h postdose. With the data provided, it is unclear whether this improvement is due to increased metabolic stability, increased CNS penetration, or a combination of both. However, it is clear that there are several key compounds in this patent application, such as **119**, **120**, **121**, and **122** (Fig. 33). In particular **119** and **120** demonstrated potent in vivo efficacy. The Novartis patent application takes advantage of the fact that Roche patents covering the 1,3-oxazine derivatives only claim substituted phenyl ring. The Novartis patent published on 28th Feb. 2013, ahead of near neighbors Roche, who were just over 18 months behind with their pyridyl analogs, for example, **152** and **153** (Fig. 43) (see later), which published on 16th Oct. 2014.

From this analysis it seems there have been several key compounds identified by the group at Novartis. It is not known how many of these compounds have completed toxicology studies, however it appears that only one compound has progressed to clinical trials. Due to a strategic decision to exit neuroscience, it was announced in Sep. 2015 that the Novartis BACE inhibitor

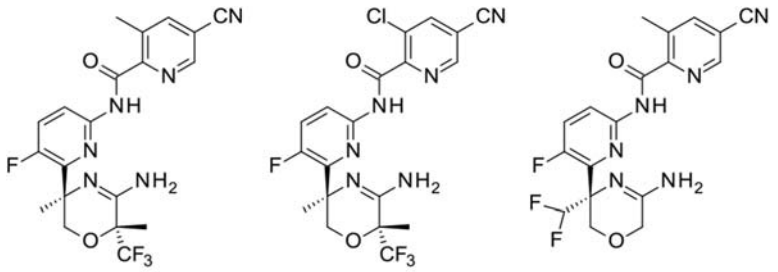

Fig. 31 Follow-on iminomorpholine derivatives with a central pyridine ring from Novartis.

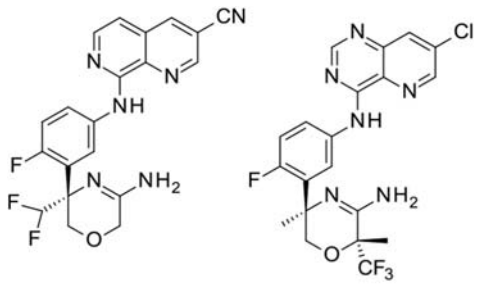

Fig. 32 Amide isosteres from Novartis.

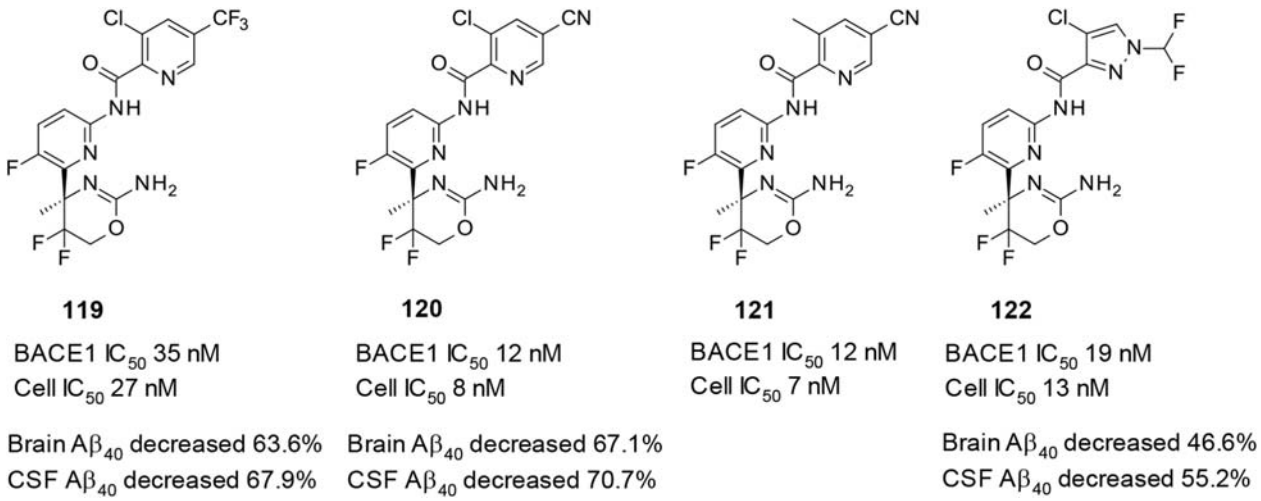

Fig. 33 Key isourea derivatives from Novartis containing a central pyridine ring.

undergoing clinical development (PhI/IIa), **CNP-520** has been partnered with Amgen.[145] This compound is currently in PhII, and in addition to a standard safety and tolerability trial over 13 weeks, **CNP-520** is also being tested in a 5-year prevention trial in APOE4 carriers. This study is being conducted in partnership with the Banner Alzheimer's Institute as part the Alzheimer's Prevention Initiative (API) and will also include an arm with the Aβ vaccine CAD-106.[146] The trial seeks to treat cognitively normal, healthy older (60–75 years of age) individuals who have a higher risk of developing AD due to them possessing two copies of the APOE4 gene. All

participants are required to undergo at least two amyloid Positron Emission Tomography (PET) scans (18F-florbetapir), although CSF collection is voluntary. It is anticipated that 430 individuals will be treated with **CNP-520** and the trial is expected to complete in 2023. It may be hypothesized that **CNP-520** is represented by one of the key compounds highlighted here, for example, **114**, **115**, **116**, **119**, or **120**.

7.08.16 Inhibitors Reported by Pfizer

Pfizer have had a long standing interest in the amyloid field, tackling both β- and γ-secretase. Their work has covered several areas, with the initial focus being on fragment hits and spiropiperidine derivatives, as well as alternative lead generation strategies including fragment screens, before shifting to amidine derivatives. The following section highlights pertinent examples from each area.

7.08.16.1 Spiropiperidine Derivatives

Before Pfizer turned their attention to the amidine derivatives, which ultimately proved successful, they had directed research on several other series. One prominent series, which produced a clinical development candidate, was the spirocyclic piperidine series, which is closely related to that from Schering-Plough/Merck ("Inhibitors Reported by Schering-Plough/Merck" section). The main difference between the Pfizer and Merck compounds is that the Pfizer compounds contain a spiro sulfamide, whereas those from Merck contain a spiro aminohydantoin, which displays additional substitution (cyclohexyl) on the exocyclic N-atom.

The Pfizer compounds are exemplified by **123–125** in Table 5.[147] The starting point, **123**, displayed weak in vitro activity and was found to be a weak P-gp substrate. The P-gp efflux was confirmed in vivo in the mouse. The sulfamide NH was capped with a methyl group to reduce the HBDs, resulting in **124** which displayed reduced P-gp efflux and increased CNS penetration in the mouse. A crystal structure of **124** with BACE revealed that the protonated piperidine N-atom interacts directly with the catalytic water, which site directly between the two carboxylates of the aspartic acid diad. Furthermore, the compound was found to display a folded conformation whereby the two phenyl rings π-stack with one another. One oxygen of the sulfamide was found to accept hydrogen bonds from the backbone NH of Thr272 and Gln73. This information also allowed the group to hypothesize that adding a hydroxyl group ortho to the isopropoxy moiety could make a HBD interaction with the carbonyl of Phe108 (not shown), which was confirmed by crystallography, **125**, depicted in Fig. 34. This change resulted in a dramatic increase in potency, however P-gp efflux also increased somewhat, reflected also by the in vivo CNS penetration.

Mouse in vivo studies with **125**, subcutaneous dosing, revealed reductions of brain $A\beta_{40}$ of 40% and 60% at 100 and 300 mg/kg, respectively. Lower doses, 10 and 30 mg/kg, did not achieve statistically significant effects. CSF $A\beta_{40}$ levels were also reduced by 44% and 54% at 100 and 300 mg/kg, respectively. The authors note that **125** still lacks sufficient potency for progression. Potency was enhanced by changing from the sulfamine to a cyclic urea and then eventually to the dehydrolactam **126** (**PF-05297909**) (Table 5).[148] Although enzymatic activity was not altered, the cellular inhibition was improved threefold compared to **125**.[149] In the rat, doses of 30 and 100 mg/kg resulted in 35% and 50% reductions in brain $A\beta_{40}$, and 69% and 80% reductions in CSF $A\beta_{40}$. Efficacy was confirmed in the monkey, where a 30 mg/kg subcutaneous dose resulted in a 60% reduction of CSF amyloid ~6 h postdose. Efficacy was also confirmed in the dog, where **PF-05297909** showed ~10-fold increased potency compared with other preclinical species (mouse, rat, monkey). Modeling predicted the effective human dose to be 525 mg. As there were concerns about whether clinical efficacy could be achieved at a tolerated dose, **PF-05297909** (**126**) was advanced to the clinic under an exploratory Investigational New Drug (IND) application. This allowed the compound to progress to a clinical setting with a reduced toxicology package, and only 150 g drug substance,[150] to assess whether the desired reductions of $A\beta_{40}$ could be seen in human CSF.

Table 5 Summary of key compounds from the Pfizer spiropiperidine series

Compound	**123**	**124** (**PF-04976081**)	**125**	**126** (**PF-05297909**)
Structure	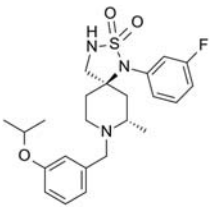	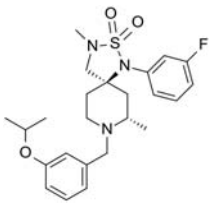	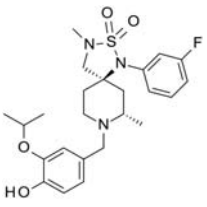	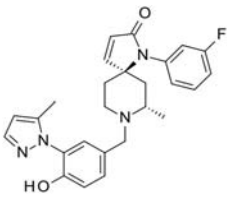
BACE 1 IC_{50} (nM)	1300	2400	100	80
Cell IC_{50} (nM)	2900	1800	100	32
Pgp ER	3.8	1.7	3.4	3.3
Mouse Br:Pl	0.67	0.97	0.35	n.d.
Mouse Br_u:Pl_u	0.22	0.65	0.27	n.d.

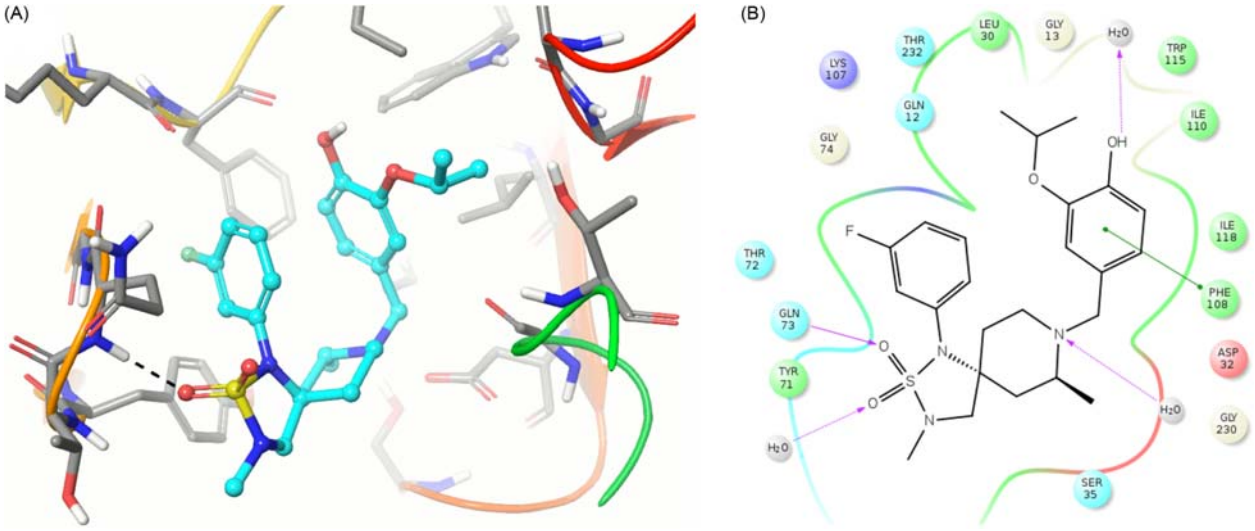

Fig. 34 (A) **125** bound to BACE showing key interactions and the folded conformation with intramolecular π-stacking (PDB code 4FM7). (B) Residues around **125** with interactions.

A two-part PhI study was initiated in Sep. 2011, commencing with a SAD study at doses of 25, 100, 250, and 525 mg[151] which demonstrated lowering of plasma amyloid at 250 and 325 mg[152] (note discrepancy between higher doses quoted in two references). This was followed by a human PK/PD study measuring CSF amyloid levels after the Maximum Tolerated Dose (MTD) of 325 mg.[151] Unfortunately, it was found that the maximum tolerated dose of 325 mg did not result in sufficient reductions in CSF amyloid levels, despite showing robust effects on plasma amyloid.[151] Based on this data, the progression of **PF-05297909** was terminated and the search for a compound with increased potency and CNS penetration was initiated, which resulted in a change of chemotype (see later).

7.08.16.2 Spiropyrrolidine Derivatives

The group from Pfizer also described a somewhat related spiropyrrolidine series, where the amine moiety was found to directly interact with both of the catalytic aspartic acids. This series was discovered through an X-ray fragment screen which produced a single hit, **127** (Fig. 35), with an estimated K_D of 1.4 mM, LE 0.31 kcal/mol/atom.[153] Elaboration via SBDD culminated in the identification of **128** (Fig. 35), with a K_D of 1 μM, determined by NMR, and a cellular IC_{50} of 4 μM.

This work highlights the challenges in the identification of highly potent BACE inhibitors and demonstrates the criticality of optimal binding interactions with the catalytic aspartic acid diad in order to be able to deliver compounds of sufficient potency.

7.08.16.3 Isothioureas and Related Derivatives

Having initially preferred alternative chemotypes, it was only latterly that Pfizer turned to the amidine derivatives in order to improve potency, focusing on the isothiourea/aminodihydroisothiazine class. A recent publication details their initial work, whereby they chose to avoid the S1/S3 subpocket of BACE, occupied by the aryl amide of most compounds, in order to try to increase CNS penetration. To this end, it was found that a THP-fused aminodihydrothiazine allowed the appendage of groups to interact with the flap region (see later), and resulted in the identification of **129** (Fig. 36).[154] **129** shows low P-gp efflux and good CNS penetration in the mouse, Br_u:Pl_u 1.42. In vivo efficacy was demonstrated in the rat (brain and CSF) at doses of 10 and 150 mg/kg s.c., whereby both doses achieved a seemingly maximal reduction of brain amyloid, ~70% but the higher dose

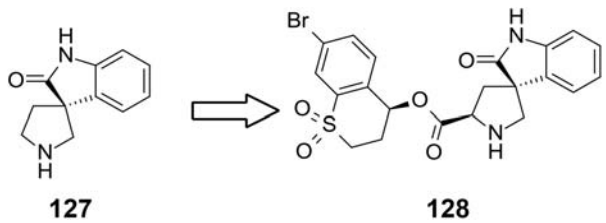

127 **128**

Fig. 35 Summary of fragment hit, **127**, from X-ray fragment screen and optimization to **128**.

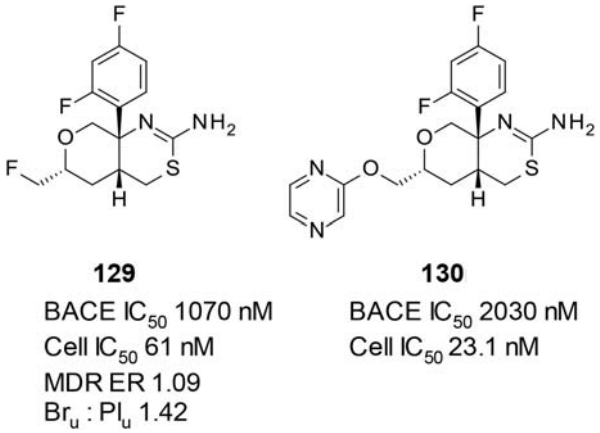

Fig. 36 Initial THP-fused isothiourea derivatives from Pfizer.

resulted in a more sustained reduction. The effect on CSF amyloid levels was somewhat stronger than the brain. This resulted in an efficacious free brain concentration of 371 nM. A single dose of 18 mg/kg p.o. to the dog resulted in up to 74% reduction in CSF amyloid levels compared to vehicle. In transgenic PS1/APP mice (8–9 months of age), a dose of 30 mg/kg s.c. lowered CSF $A\beta_{40}$ by 79%. A further study in transgenic PS1/APP mice at 100 mg/kg p.o. for 2 months (starting from 6.5 months of age) using two photon imaging demonstrated that **129** was able to prevent plaque growth. Finally, a 14-day rat toxicology study with **129**, at doses of 25 and 75 mg/kg, indicated no overt toxicity and no retinal toxicology. These data indicate the potential of this series to yield a safe and efficacious compounds suitable to progress to clinical evaluation, however the group noted that an enhancement in potency was required compared to **129**. Many groups have speculated that this phenomenon is due to compounds displaying higher concentrations in the lysosome, where BACE is located, due to the acidic nature of this compartment.

The structure of **129** bound to BACE has been published and is shown in Fig. 37. The binding mode is similar to other structures with the isothiourea binding to the catalytic aspartates, and **129** has also been the subject of a patent application,[155] along with several related analogs that represented initial attempts to interact with the flap region, including ether-linked heterocycles such as **130** (Fig. 36).[156] Interestingly, both compounds display weak activity in a BACE enzyme assay, but significantly improved activity in a cellular assay, **129** showing 17-fold improved activity and **130** displaying nearly 100-fold more potent activity in a cellular assay.

Subsequent patent applications have detailed addition of aromatic groups in place of the fluoromethyl group in **129** which resulted in a significant increase in potency. Examples include **131** (Fig. 38),[157] which maintains the 2,4-difluorophenyl ring and adds the 4-pfluorphenyl ring on the THP ring. Interestingly, in addition to showing potent cellular activity, these derivatives

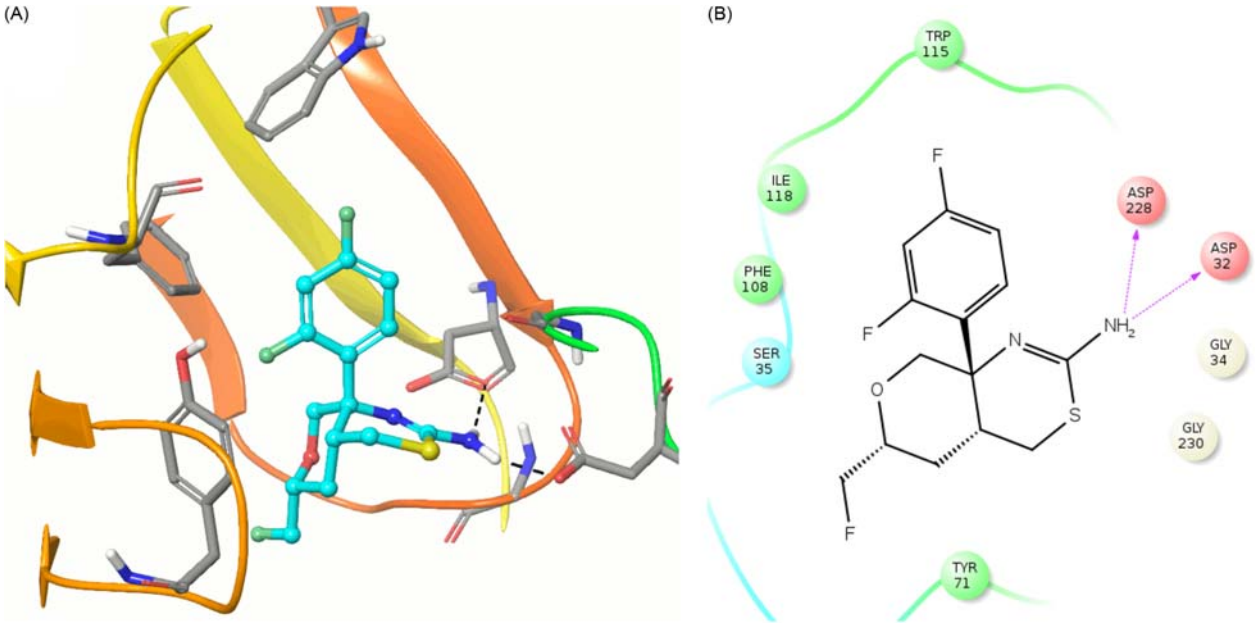

Fig. 37 (A) Crystal structure of **129** bound to BACE (PDB code 4WY6). (B) Depiction of residues interacting with **129**.

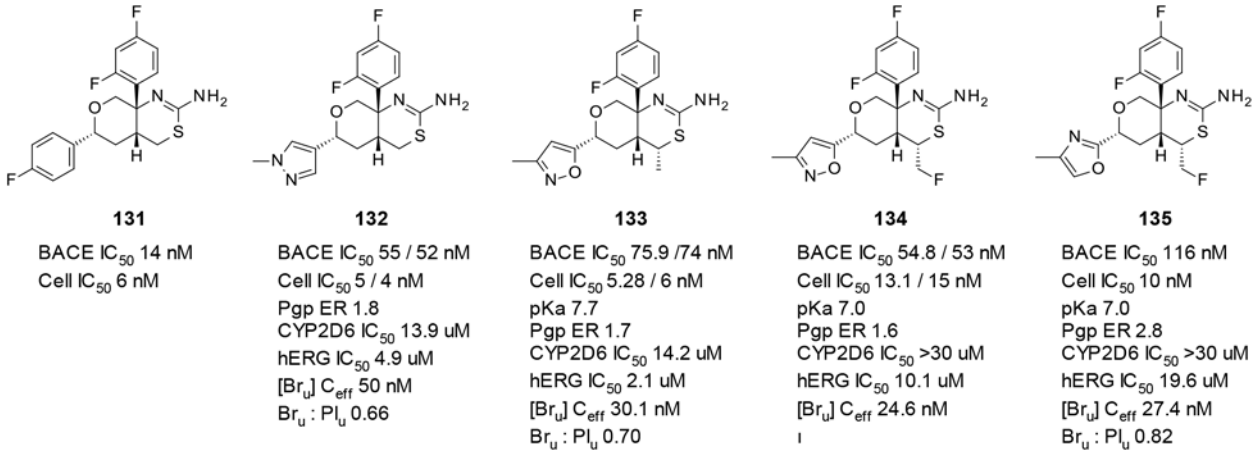

Fig. 38 Follow-on THP-fused isothioureas from Pfizer. Note, there is a slight discrepancy between biological data reported in the patent literature and journal literature for some compounds, for example, **132**, **133**, **134**. Where this is the case the patent literature data is reported first, followed by the peer-reviewed literature data.

also show potent inhibition in a BACE enzyme assay, which is in stark contrast to initial derivatives such as **129** and **130**. It appears that 5-membered heteroaryl groups are particularly preferred. In particular, the methyl pyrazole derivative, **132** (Fig. 38)[158] has been the subject of a recent publication[159] where it has shown a very good overall profile with low P-gp efflux (ER 1.8) and good CNS penetration in the mouse, Br_u:Pl_u 0.66. In vivo efficacy was demonstrated in the mouse (brain and CSF) at doses of 10 and 50 mg/kg s.c. Maximal effects on $A\beta_{x-42}$ were observed 6 h postdose where the 50 mg/kg dose caused a 60% reduction and the 10 mg/kg dose demonstrated ~40% reduction in brain $A\beta_{x-42}$. Using indirect modeling, the free brain concentration to effect a 25% reduction in brain $A\beta_{x-42}$ at steady state ($[Br_u]$ C_{eff}) was calculated to be 50 nM, which would require a free plasma concentration of 76 nM. It should be noted that this is the concentration to reduce brain amyloid levels by 25%, which many believe would be the minimal amount necessary, and it may optimally be able to reduce amyloid levels by at least 50% or 90%. However, it was found that **132** undergoes oxidative demethylation by CYP2D6. The desmethyl metabolite is a weak BACE inhibitor (BACE IC_{50} 599 nM), but a potent CYP 2D6 inhibitor (IC_{50} 370 nM). The deuteromethyl analog is described in a subsequent patent application,[160] presumably in an attempt to slow demethylation. **132** was crystallized with CYP2D6 and this information was used to identify additional analogs, which resulted in the addition of a methyl group on the aminodihydrothiazine ring which reduces CYP2D6 binding by virtue of a steric clash and thus results in decreased metabolism. Switching the N-methyl pyrazole to the 3-methyl isoxazole to give **133** (Fig. 38) is well tolerated and as the methyl group is no longer attached to a heteroatom, demethylation cannot occur. However, it is not known if the methyl on the isoxazole is still oxidized and whether this leads to the formation of an active metabolite. Replacement of the methyl group on the dihydrothiazine ring by a fluoromethyl group resulted in the optimized derivatives **134** and **135** (Fig. 38). Both compounds retain the desired BACE activity and low P-gp efflux, while having lower hERG and CYP2D6 inhibition. Furthermore, both compounds maintain good levels of CNS penetration in the mouse and also satisfactory $[Br_u]$ C_{eff} levels. As a result of these data, both **134** and **135** were progressed to long-term safety studies.

The structure of **132** bound to BACE has been published and is shown in Fig. 39. Overall the binding mode is very similar to **129** (Figs. 36 and 37).

A related patent application has detailed nonaromatic groups, such as the THF-derivative **136** (Fig. 40),[161] although this results in a significant drop in potency, both in enzymatic and cellular assays. It is not known whether these derivatives show improved metabolic stability or whether the newly installed THF ring is subjected to oxidation.

The latest set of derivatives from this series was also disclosed in a 2014 patent application.[162] Key compounds, such as **137** and **138** (Fig. 40), maintain the methyl pyrazole and methyl isoxazole respectively but include the benzonitrile rather than the difluorophenyl of previous examples. One further prominent example, **139** (Fig. 40), has a substituted benzylamine moiety, presumably to try to pick up the HBD interaction with Gly120.

In Oct. 2015, a patent application disclosed a series of thiazole amides with comparative data showing advantages over close analogs,[163] including examples disclosed by Eisai, "Inhibitors Reported by Genentech/Array BioPharma" section. The most prominent examples, **140** and **141**, are detailed in Table 6. Both compounds show potent activity while balancing CYP2D6 and hERG activity with low P-gp efflux. In addition, both show low clearance in human hepatocytes. The ability to balance the profile is attributed to the thiazole which reduces the basicity, as denoted by pK_a, of the isothiourea. Although the regioisomeric thiazole, **142**, has a similar pK_a, it is almost inactive at BACE. Interestingly, while maintaining the same pK_a as **141**, **142** appears to be a stronger P-gp substrate. Comparative examples from Pfizer, (**143**) and Eisai (**54**), Table 6, show that these analogs with a central fluorophenyl ring in place of the thiazole have a worse overall profile, most notably in terms CYP2D6 and hERG inhibition, which may be due to the stronger basicity of the isothiourea in these analogs. Furthermore, **143** shows stronger P-gp-mediated efflux and both

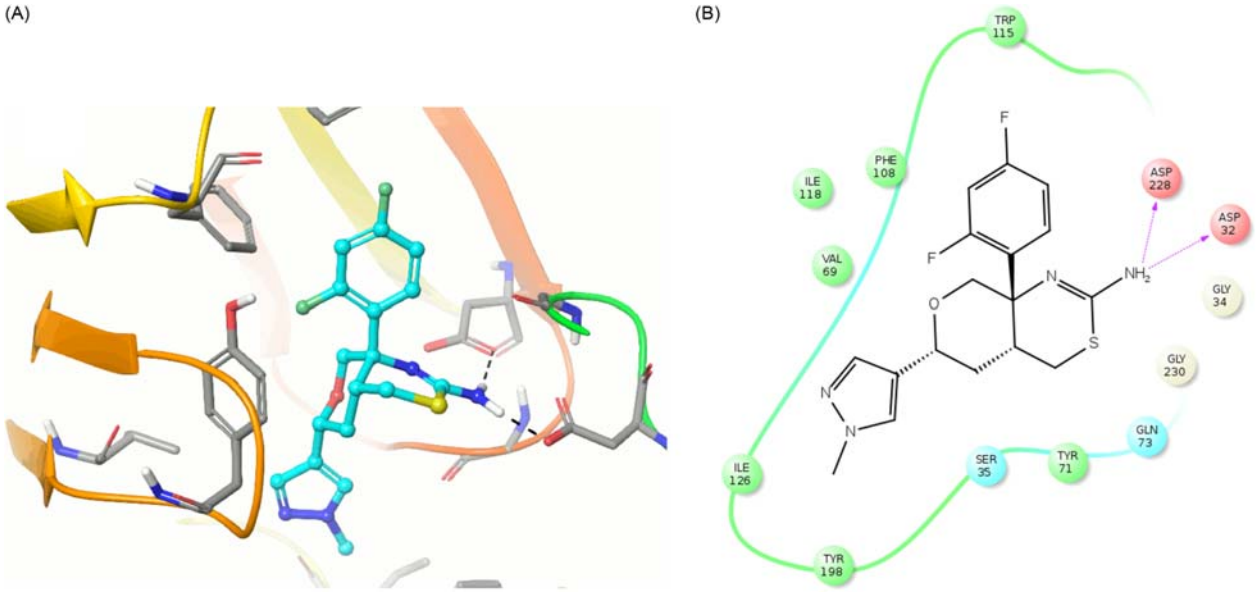

Fig. 39 (A) Structure of **132** bound to BACE (PDB code 4XXS). (B) Depiction of residues interacting with **132**.

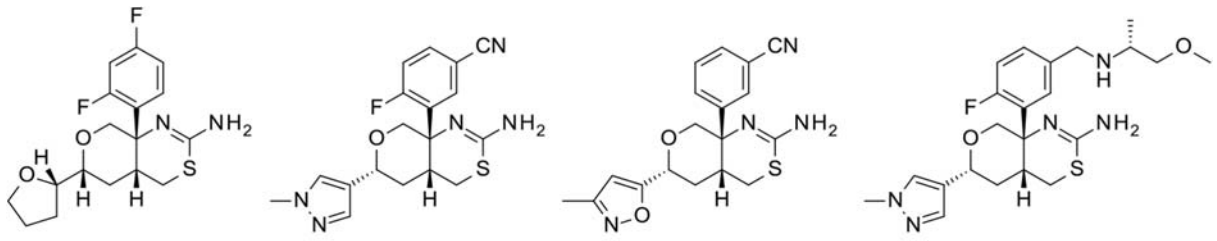

Fig. 40 Further THP-fused isothiourea derivatives from Pfizer.

Table 6 Summary of the latest key compounds from Pfizer

Compound	**140**	**141**	**142**	**143**	**54**
Structure	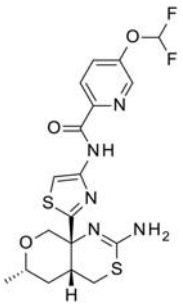	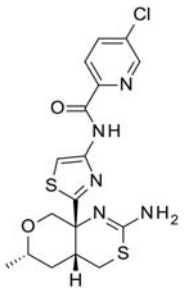	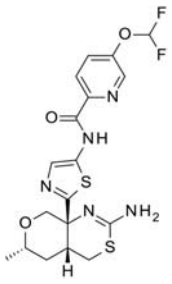	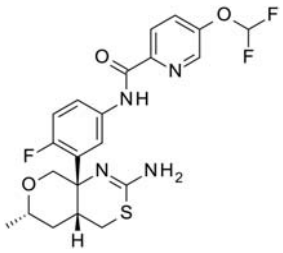	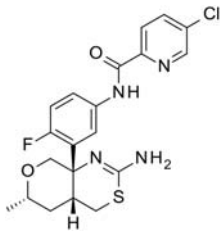
BACE1 IC_{50} (nM)	41	33	>100,000	3	1
Cell IC_{50} (nM)	5	4	13600	<1	<1
CYP 2D6 IC_{50} (μM)	>30	>30	15% I @ 3 μM	<0.030	<0.030
hERG IC_{50} (μM)	9.9	9.0	11.97	0.4	0.2
Pgp ER	2.2	2.4	7.1	5.1	3.0
pK_a	6.8	6.9	7.0	8.3	8.7
GSH trapping	Negative	Negative	Not determined	Not determined	Not determined

143 and **54** display higher clearance in human liver microsomes. Finally, it is also pointed out that compounds such as **143** and **54** contain an aniline structural alert, whereas **140** and **141** do not. Whilst this is correct, both **140** and **141** contain an aminothiazole, which may also present the same (mutagenic) risk as the aniline fragment. Hence, despite a lot of effort spent on nonamide derivatives, it seems the Pfizer group may have come full circle and ended up with an amide derivative as their best compound.

Currently, inspection of the Pfizer development pipeline indicates three compounds undergoing phase 1 trials for AD. Of these, PF-02521729 has completed a single Phase 1 study, but does not appear to affect the amyloid pathway as no measurement of amyloid species was undertaken. PF-06648671 appears to be a γ-secretase modulator as the one trial aims to measure CSF levels of $A\beta_{37}$ and $A\beta_{38}$, in addition to $A\beta_{40}$ and $A\beta_{42}$, following a 300 mg dose. This trial is expected to complete in Mar. 2016. A third compound, PF-06751979, is undergoing a 14-day MAD study, which will assess CSF Aβ fragments including $A\beta_{1-40}$, $A\beta_{1-42}$, Aβ total, $A\beta_{x-40}$, $A\beta_{x-42}$, sAPPα, and sAPPβ, indicating it to be a BACE inhibitor. Thus PF-06751979 could be represented by one of the above structures, quite possibly **140**.

In summary, it is evident that Pfizer have progressed at least two compounds to candidate selection and beyond. The piperidine series highlights some of the challenges and confirms the translatability of preclinical efficacy. Continued research from the group resulted in similar chemotypes to those described by other groups, however it appears that the sustained effort has been rewarded by the identification of a compound which is currently undergoing clinical trials.

7.08.17 Inhibitors Reported by Roche

The group at Roche have devoted considerable effort to BACE for a sustained period of time, which has resulted in the publication of over 30 patents which cover a range of templates, including acylguanidines[164,165] (as BACE2 inhibitors), dihydroisothiazine/isothioureas (also initially as BACE 2 inhibitors),[166] 1,3-thiazepines/isothioureas[167] iminomorpholines, homo-iminomorpholines, as well as others. However, the majority of their effort has been directed toward dihydrooxazines/isoureas. The disclosed research also includes a collaboration with Siena Biotech.

The competition in the field is also evident, as Roche appear to have lost the battle to gain intellectual property on several templates, as will be discussed here.

The iminomorpholine/1,4-oxazines offer an interesting insight to the competiveness of the BACE field. The first patent from Roche on this template published on 24th Feb. 2011, just 4 weeks after a similar patent claiming the same core from Novartis, which published on 27th Jan. 2011, Novartis section. Pertinent examples in the Roche application include **144** and **145** (Fig. 41), which show potent in vitro activity.[168] It might be anticipated, from the key examples disclosed by Novartis and from the homomorpholine derivatives disclosed by Roche, that further control of the basicity of the guanidine moiety is necessary on this template. Follow-up application on the same template covered analogs with amide replacements[169] and biaryl derivatives with an additional aryl ring in place of the methyl group.[170]

A subsequent series of patent applications described examples with a homologated ring template, namely the homomorpholines or 1,4-oxazepines. Pertinent examples from the key patent application are exemplified by **146**, **147**, and **148** (Fig. 41), which contain additional fluorine atoms to reduce the basicity of the guanidine moiety.[171] Related examples with amide surrogates were the subject of subsequent disclosures,[172,173] as well as biaryl derivatives.[174]

The mainstay of work from Roche has been directed to the isourea/1,3-oxazine series, from which at least 16 patent applications have been disclosed. An early patent application described biaryl derivatives with a 5-membered ring isourea, but these derivatives had weak in vitro activity.[175] The next patent application in this series described the simple 6-membered ring isourea/1,3-oxazine derivatives, as denoted by **149** (Fig. 42).[176,177] In addition, one example detailing a fused THF-derivative, **150** (Fig. 42), was also disclosed. Hence, it appears that Roche may have been in the process of investigating the THF-fused analogs when a patent

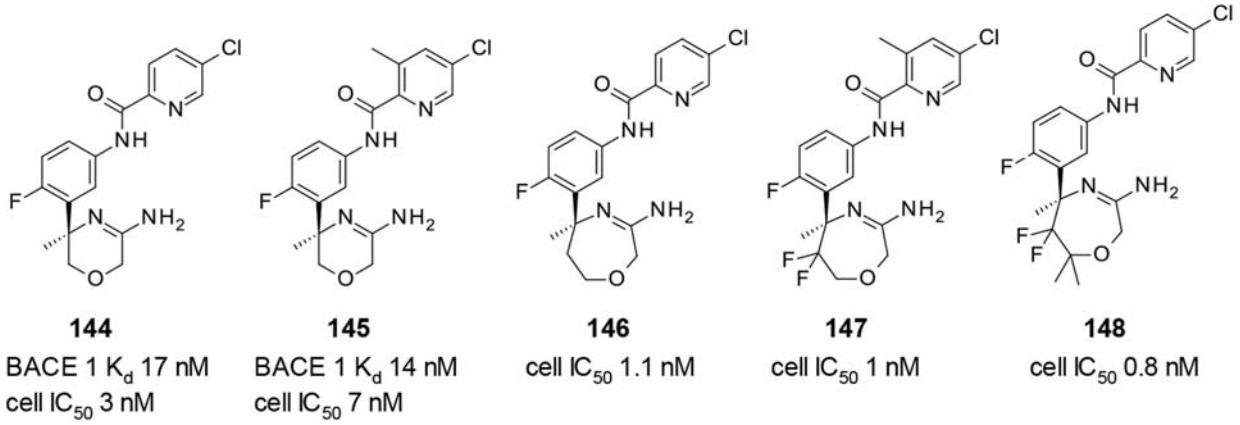

Fig. 41 Early chemotypes from Roche, including iminomorpholines **144** and **145**, and the homologous derivatives **146–148**.

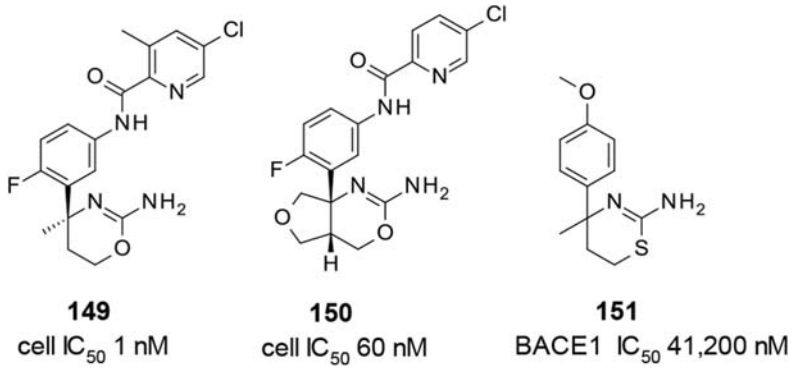

Fig. 42 Early isoureas from Roche, **149** and **150**, with HTS hit, isothiourea derivative **151**.

published from Eisai, claiming the same compounds—Eisai patent application published on 11th Jan. 2011, whereas the Roche case published on 16th Jun. 2011, Eisai section. Again, this highlights the extreme competiveness of the field.

A recent manuscript describes an overview of the Roche BACE research project, including the identification of the hit matter, that is, isothiourea derivative **151** (Fig. 42), which originated from an HTS campaign. It is noted that **151** had been synthesized more than 30 years ago as part of an analgesic project. This is one of the few HTS campaigns to identify any hits. It may have been easy to overlook **151** due to its weak potency, however, in the context of fragment hits, this compound displays good LE, 0.41 kcal/mol/nonhydrogen atom.[178,179] The manuscript details many of the subseries and the effect of degrees of fluorination on the basicity of the isourea as well as in vitro and in vivo potency.[180] The unfluorinated 1,3-oxazine was found to be strongly basic, pK_a 9.8, which resulted in weak in vivo activity. Addition of 2-fluorine atoms was found to reduce the pK_a of the isourea moiety by 2.5 log units. The reduction in pK_a was found not only to improve in vivo activity, via reduction of P-gp-mediated efflux, but also to reduce hERG and CYP2D6 activity. The basicity could be decreased substantially without negatively impacting potency, compounds with pK_a 5.8 still showed potent enzyme and cell inhibition, whereas when the pK_a reached 5.1 this appeared to have a negative impact on cellular activity with an approximate drop of 20-fold. Prominent examples from this article are shown in Fig. 43 and include **152** (**RO5508887**),[181] **153**, **154** (pK_a 7.0, P-gp ER 1.9, hERG: 75% inhibition at 10 μM),[182] **155** (pK_a 6.3, P-gp ER 1.6, hERG: 39% inhibition at 10 μM),[183,184] (two separate patent applications), and **156** (pK_a 5.9, P-gp ER 1.5, hERG: 48% inhibition at 10 μM)[181] which have been described in patent applications. All compounds displayed potent in vivo activity, by reduction of brain Aβ_{40} in the mouse 4 h postoral dose of 10 mg/kg; **152** (**RO5508887**) 78%, **153** 66%, and **155** 88%. Furthermore, two compounds produced efficacy at lower doses: **154** 78%, 88%, and 95%; **156** 41%, 71%, and 93% reductions at 1, 3, and 10 mg/kg, respectively. Despite the strongest efficacy, **154** did not appear to be profiled further, perhaps because of its hERG inhibition. Instead, **152** (**RO5508887**) was studied in further detail. A single time point (4 h) dose–response study in the mouse revealed strong efficacy with approximately 32%, 78%, 95%, 97%, and 99% reductions in brain Aβ_{40} at doses of 0.3, 1, 3, 10, and 30 mg/kg and good CNS penetration, with Br:Pl 1–1.5 (0.3–3 mg/kg) and 2.3–3.4 (10–30 mg/kg). In a rat time course study, an oral dose of 1 mg/kg produced robust reductions in CSF Aβ_{40} and Aβ_{42} levels, with maximal reductions of around 70% 4–8 h postdose. PK/PD modeling resulted in a free plasma/brain EC_{50} of 20 nM which corresponds well with the cellular activity, IC_{50} 12 nM. In addition,

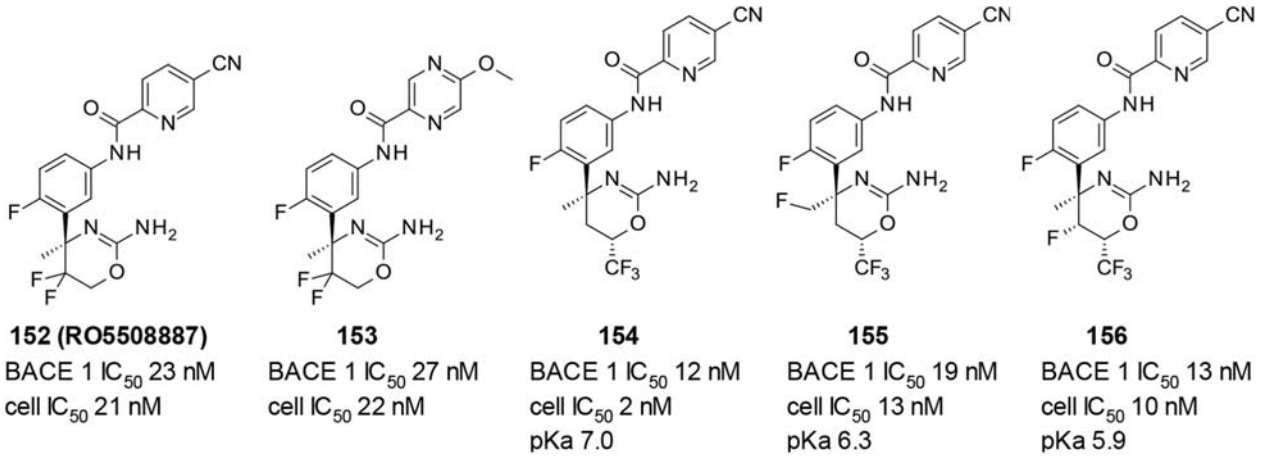

Fig. 43 Further isourea derivatives from Roche with varying degrees of fluorination.

152 (**RO5508887**) was found to have an acceptable PK profile in the rat, CL 16.8 mL/min/kg, Vdss 11.5 L/kg, $t½$ 8.9 h, and Fpo 68%. The compound appeared free of CYP450 liabilities with $IC_{50} > 25$ μM at 2C9, 2D6, and 3A4. Further pharmacological characterization of the compound has been described recently.[185] Cellular activity was confirmed in rat cortical neurons, IC_{50} 55 nM, showing considerably weaker activity than Eisai compounds in a similar same assay ("Inhibitors Reported by Genentech/Array BioPharma" section). Characterization in APP transgenic mouse models revealed similar efficacy in APP_{Lon} mice to wild-type mice, but much weaker efficacy in APP_{Swe} mice, presumably due to the increased propensity for APP_{Swe} cleavage by BACE. When dosed chronically (4 months) to APP_{Lon} mice, 13–14 months of age, **152** (**RO5508887**) reduced brain $Aβ_{42}$ by 28% and 69% and $Aβ_{40}$ by 45% and 69% at doses of 30 and 90 mg/kg, respectively. CSF amyloid was measured at several time points and revealed near complete reduction (almost equivalent to untreated wild-type mice) of $Aβ_{40}$ and $Aβ_{42}$ 5 h postdose. CSF amyloid levels had almost returned to baseline 8 h postdose, whereas the higher dose resulted in sustained (70–80%) reductions 8 h postdose. A dose proportional reduction in plaque area and number was seen in the cortex and hippocampus, however both measurements exceed the baseline values at the start of the study, indicating the BACE inhibitor treatment did not fully prevent new plaque formation. Based on these data, **152** (**RO5508887**) was selected as a development candidate and advanced to clinical trials (see later).

Several of the Roche compounds have been crystallized with BACE, including **152** and **154**. The structure of **154** is shown to illustrate the binding mode, with is similar to other BACE inhibitors which contain an anilide, with the anilide NH donating a hydrogen bond to the Gly230 carbonyl and the picolinamide moiety extending into the S3 pocket (Fig. 44).

In addition to these compounds, further analogs have been described with varying degrees of fluorination, for example monofluorination (rather than difluorination at the 5-position)[186] have been disclosed. A further patent application discloses derivatives where the fluorophenyl ring has been replaced by a fluoropyridine, for example, **157** (Fig. 45).[187] As mentioned under the Novartis

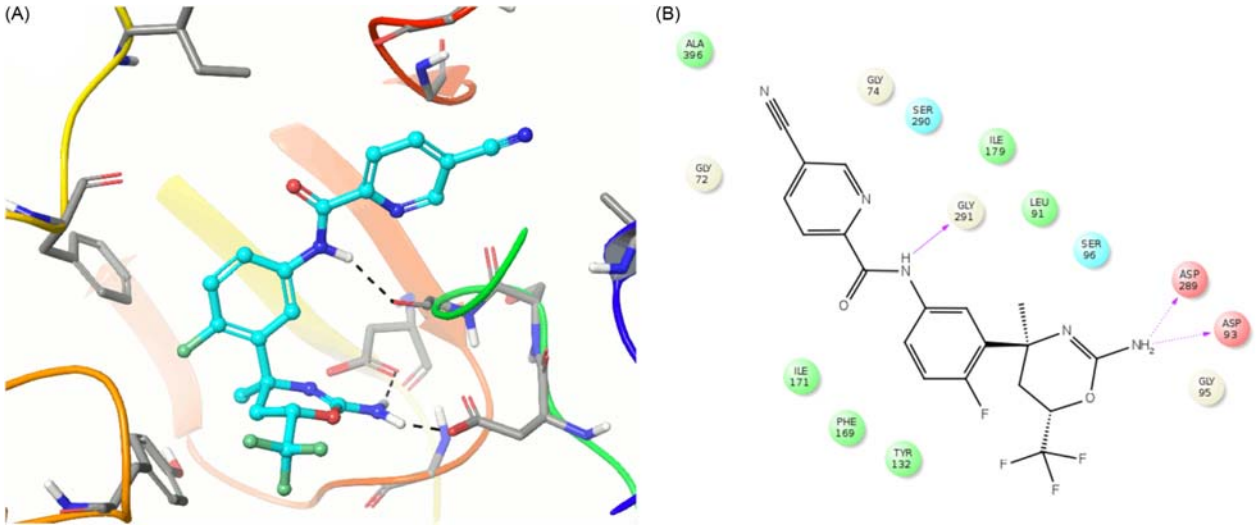

Fig. 44 (A) **154** bound to BACE (PDB code 4J1F). (B) Depiction of key residues interacting with **154**.

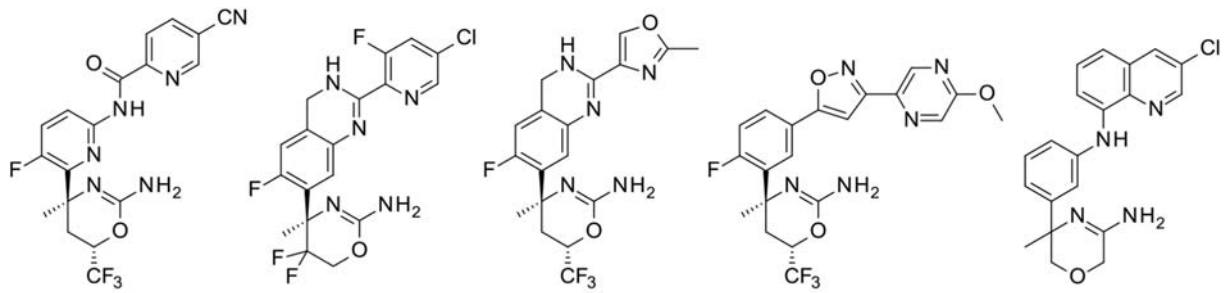

Fig. 45 Isourea derivative, **157**, with a central pyridine ring, isourea derivatives with amide isosteres, **158** and **159**, isourea **160** which lacks the amide and iminomorpholine derivative **161** with amide isothere.

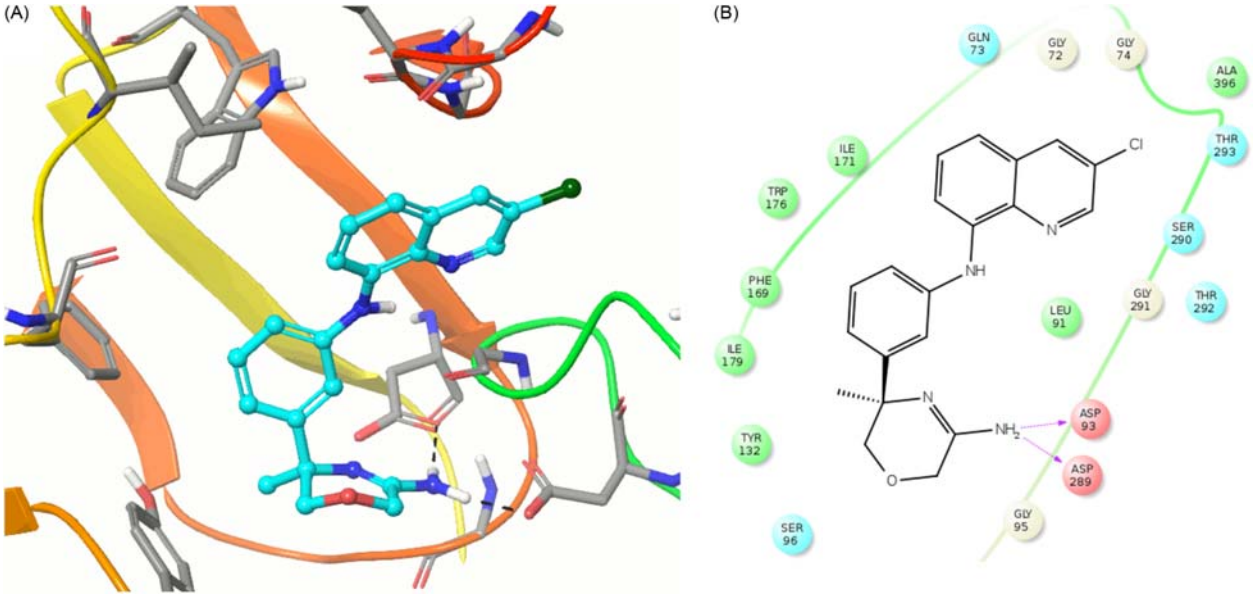

Fig. 46 (A) Binding mode of **161** with BACE (PDB code 5F00). (B) Depiction of vicinal residues to **161**.

section, the Roche patent published just over 18 months (10th Oct. 2014) after a similar patent from Novartis (28th Feb. 2013). Several patent applications also describe examples where the amide has been replaced by various groups,[188] the most pertinent include the dihydroquinazolines **158**[189] and **159**[190] as well as the isoxazole **160**,[191] Fig. 45. It is claimed that derivatives such as **158** are sufficiently basic, pK_B 7.15, that they are protonated when bound to BACE and therefore mimic the amide by being able to act as HBDs. Taken together, these examples highlight the prominence of the 5,5-difluoro[1,3]oxazine and the 6-trifluoromethyl[1,3]oxazine templates.

A recent manuscript shows that compounds with amide isosteres, such as iminomorpholine **161** (Fig. 45) can bind to BACE in the same manner, and make the same interactions, as their amide counterparts.[192] The binding mode of **161** is depicted in Fig. 46. Closely related analogs to 161 have been described by Novartis, "Inhibitors Reported by Novartis" section, compounds **117** and **118** (Fig. 32).

Other compounds of note include the PET ligand **162** (Fig. 47).[193] This compound was tritium labeled for in vitro autoradiography studies in the Sprague–Dawley rat which showed widespread binding in the brain, but highest density in the dentate gyrus and CA3 regions of the hippocampus, cerebellum, pallidum, and substantia nigra. Similar binding was seen in both monkey and human brain slices. Furthermore, the in vitro data was confirmed ex vivo in the rat. The methyl group on the acetylene was labeled

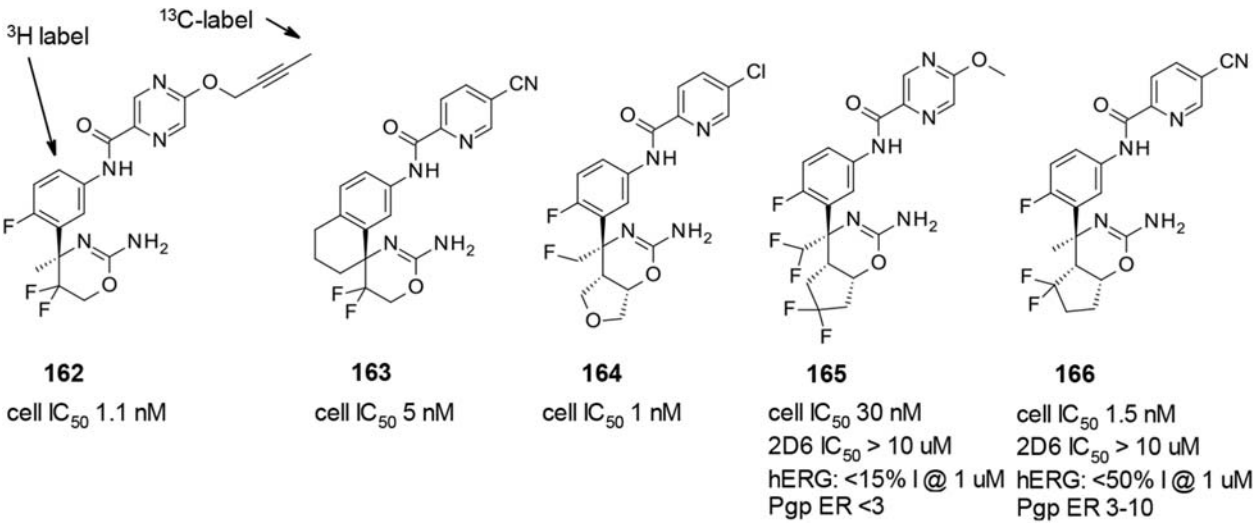

Fig. 47 Radiolabelled isourea derivative **162**, spirocyclic isourea derivative **163**, and fused-isourea derivatives **164–166** from Roche.

with ^{11}C to enable in vivo PET studies in the baboon, which showed very similar results to the rat studies. While this data appears encouraging, it is unclear if this ligand offers sufficient signal to noise and whether any further studies were conducting in humans. In addition, several companies have shown that it is possible to reduce CSF Aβ in humans, thus providing target engagement and disease biomarker modulation, thereby limiting the need for PET enzyme occupancy studies.

Spirocyclic derivatives have also been the subject of a patent application, for example, **163** (Fig. 47). A range of ring sizes were investigated in this series, thus both 5- and 6-membered rings, that is, indane and tetralin substructures, were assessed with the indanes yielding weaker activity. Similarly, 6-membered isoureas proved better than the homologous 7-membered counterparts. Thus, although **163** shows potent in vitro activity, the series appears to be generally weaker that other series.[194]

Although the intellectual property for the initial THF-fused [1,3]oxazines/isoureas may have been secured by Eisai, Roche found additional ways to fuse a 5-membered ring to the [1,3]oxazine template, yielding the bicyclic THF series exemplified by **164**,[195] Fig. 47, and the analogous series where the THF has been replaced by a difluorocyclopentyl ring, such as **165** (Fig. 47).[196] In addition to potent in vitro activity, examples such as **165** were found to have weak CYP2D6 activity and P-gp efflux as well as moderately weak hERG inhibition and >50% lowering of Aβ in vivo after a 30 mg/kg dose (no further details described). Finally, the isomeric-fluorinated cyclopentyl derivatives have also been described, as exemplified by **166** (Fig. 47).[197] This series displayed almost identical in vitro activity to the regioisomeric series, in vivo activity also appears good (>70% reduction of Aβ) however, P-gp ER and hERG may not have been as good.

Latterly the group at Roche have returned to amidine and guanidine moieties as the key warhead motif and control the basicity coming from a moiety in the beta-position, for example, β-sulfonyl amidines such as **167** (Fig. 48),[198] which is closely related to compounds from Schering-Plough/Merck ("**Inhibitors Reported by Schering-Plough/Merck**" section), such as **189** (Fig. 52). The patent application covering these derivatives from Roche published on 18th Nov. 2013, with an initial application date of 24th May 2012, some 5 months before the publication of the Schering-Plough/Merck application, which published on 18th Oct. 2012. Interestingly, several identical compounds are exemplified by both applications. The corresponding 7-membered homologs appear somewhat weaker in terms of in vitro activity.[199] It is not known whether the basicity of the amidine is sufficiently tempered in this series, however no further fluorination to this end has been disclosed. Replacement of the sulfone moiety by a sulfoxime with concomitant cyclization has yielded some potent compounds with in vivo activity, for example, **168** and **169** (Fig. 48).[200] Interestingly, all four stereoisomers of **168** were prepared and tested in vitro and in vivo. While all four compounds (S- and C-atom α- to the

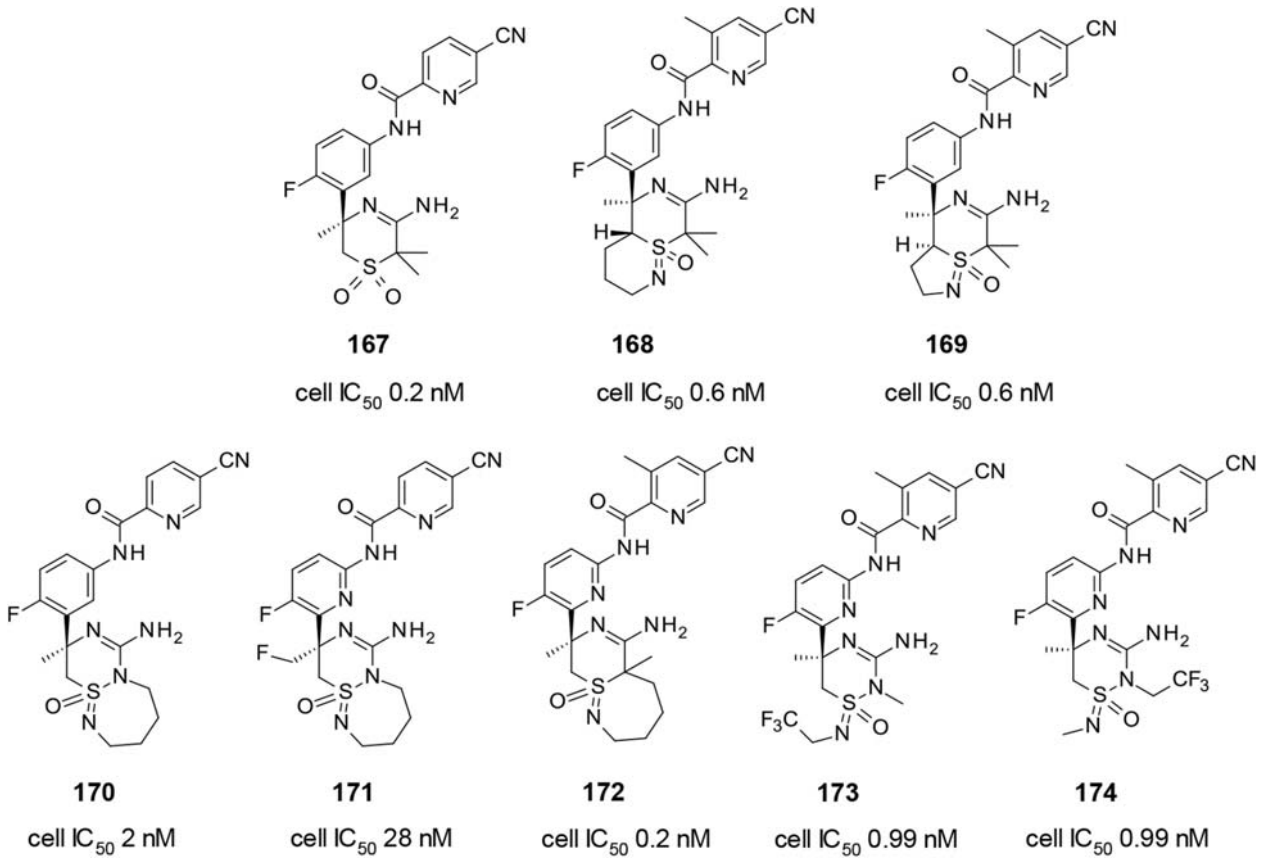

Fig. 48 Amidine derivatives containing sulfone (**167**) and sulfoximine groups (**168** and **169**) and bicyclic analog (**172**). Sulfoximinylguanidine derivatives (**173** and **174**) including bicycles (**170** and **171**).

sulfur) displayed similar in vitro activity, only **168** showed good levels of in vivo activity in the mouse, reducing Aβ in the brain by 62% 4 h after a 30 mg/kg oral dose. Furthermore, when in the fused 5-membered ring analogs, such as **169** (Fig. 48), the stereochemistry at the C-atom α- to the S-atom is inverted. Again, **168** showed potent in vivo activity, causing a 60% reduction in brain Aβ 4 h after a 30 mg/kg dose in the mouse.

The next iteration of analogs has described sulfoximinylguanidines containing a fused alkyl ring linking the guanidinyl N-atom to the sulfonimidamide N-atom. Examples have been described with both a central fluorophenyl ring, for example, **170**,[201] and with a central fluoropyridyl ring, for example, **171** (Fig. 48),[202] although the latter appear to have significantly weaker in vitro activity in general. A follow-on patent application has described analogs of **171** where the bridgehead N-atom has been replaced by a C-atom, resulting again in an amidine warhead, for example, **172** (mixture of diastereomers) (Fig. 48).[203] Despite showing potent cellular activity, these derivatives show comparatively weak in vivo activity; a 30 mg/kg oral dose of **172** resulted in a 52% reduction of brain $A\beta_{40}$ in the mouse. Monocyclic sulfoximinylguanidines, such as **173** and **174** (Fig. 48), have also been described.[204] It is noteworthy that control of basicity can be achieved by substitution on the N-atom of the sulfonimidamide (**173**) or on the guanidine N-atom (**174**), even though the latter may no longer be basic.

Thus, this analysis demonstrates the significant commitment the Roche group have invested in the BACE field. The work has delivered several compounds which appear to have good overall profiles, balancing primary activity with off-target activities, such as hERG, CYP2D6 inhibition while simultaneously minimizing P-gp efflux. Although it is not possible to assess how many compounds have entered preclinical development, or even progressed into toxicological studies, to date it appears only one compound has entered clinical development, namely **RO0550887** (**152**, presumed to be RG7129). This compound entered clinical trials in Oct. 2011, completing SAD studies which measured plasma PK and $A\beta_{1-40}$ and $A\beta_{1-42}$.[205] A PhI MAD study commenced in Jul. 2012, which measured similar parameters following daily administration for up to 30 days.[206] A PK/PD study commenced in May 2012, measuring plasma and CSF amyloid following a single oral dose in healthy volunteers has also been conducted.[207] The development of **RO5508887** was terminated in 2013. The reasons have not been disclosed, although there were rumors it was due to liver toxicity. Roche have remained highly committed to the BACE field but so far, despite several compounds displaying at least similar profiles to **RO5508887** no compounds have entered clinical development. In the meantime, the field has advanced significantly which now leaves Roche perhaps too far behind.

7.08.18 Inhibitors Reported by Schering-Plough/Merck

7.08.18.1 Early Peptidomimetic Inhibitors

Before the merger of Merck and Schering Plough, both companies had independent programs aimed at BACE inhibitors, with early efforts mainly directed toward HEA peptidomimetic BACE inhibitors, as exemplified by TC-1 (4, Fig. 3), as discussed in the "Introduction" section. Merck explored isophthalamide derived subseries, which generally suffered from strong efflux and lacking central activity in vivo models. In addition to compounds such as TC-1 (**4**), Schering has also explored isophthalamide HEA inhibitors, with the amine conformationally restrained into various saturated heterocycles, such as pyrrolidine **175**[208,209] and piperazinone **176** (Fig. 49).[210] Although potent BACE1 inhibitors were obtained, cellular activity was suboptimal, and in vivo central Aβ lowering could not be achieved.

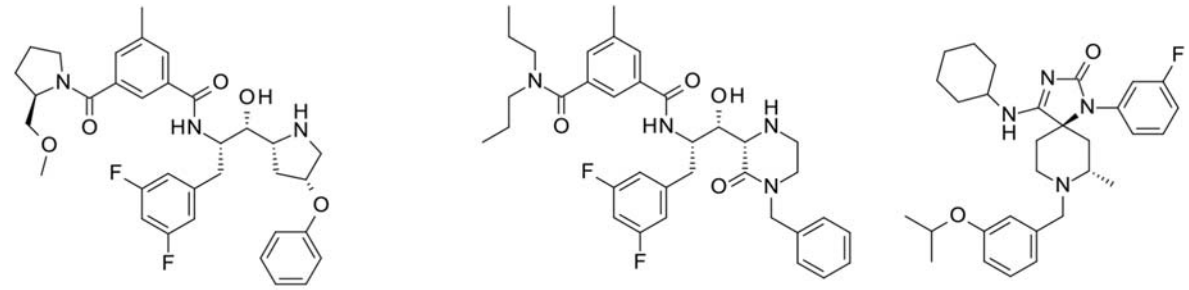

175

BACE1 IC_{50} 0.7 nM
Cell IC_{50} 21 nM
CaCo-2 ER 174
Br:PI <0.1
Tg CRND8 Mouse 100 mg/kg (3h):
Plasma $A\beta_{40}$ 70% (po), 88% (sc) reduction

176

BACE1 IC_{50} 3 nM
Cell IC_{50} 300 nM
CaCo-2 ER 17
Br:PI 0.07
Tg CRND8 Mouse 100 mg/kg sc:
Plasma $A\beta_{40}$ 65% (3h)

177

BACE1 IC_{50} 6 nM
Cell IC_{50} 63 nM

Fig. 49 Early HEA inhibitors (**175** and **176**) and spiropiperidine derivative **177** from Schering Plough/Merck.

7.08.18.2 Spiropiperidine Derivatives

Moving away from the HEA-type inhibitors, Merck has reported on a series of aminohydantoin spiropiperidine inhibitors, originating from a high-throughput screening.[211] In this series, exemplified by **177** (Fig. 49), the key interaction with the catalytic aspartic acid residues takes place via hydrogen bonding of the protonated piperidine nitrogen through intermediary water molecules. Modeling indicated that the actual ligand-bound conformation is a relatively high energy conformation. Substitution of the piperidine with a 2-methyl group induced a favorable conformational restraint stabilizing the bioactive conformation and optimized the occupation of the binding pocket, resulting in a 200-fold potency increase compared to the desmethyl analog.[212] The binding mode of **177** to BACE is similar to that of compounds **124** and **125**, Table 5 and Fig. 34, from Pfizer.

7.08.18.3 Amidine and Guanidine Derivatives

The efforts of the Schering group have subsequently also evolved around nonpeptidic BACE1 inhibitors. Fragment-based NMR screening led to the identification of the isothiourea fragment hit **178** (Fig. 50), which displayed an optimal hydrogen bond donor–acceptor interaction with the catalytic aspartate dyad in BACE1.[213,214] Guided by structure-based design, fragment **178** was evolved into diphenyl iminohydantoin **179** (Fig. 50), a fragment with high LE also identified and used by other companies (Amgen, AstraZeneca, Wyeth).[215] In fact, the amidine containing heterocycle motif has since then become the main focus in BACE inhibitor design offering optimal vectors toward P1, P3, and P2′, and seems to have completely taken over the more classical transition state inhibitor approaches. Expansion of **179** into the S3 pocket led to the high-affinity iminohydantoin **180** (Fig. 50).[216] In rat, this compound was shown to have reasonable brain penetration with a Br:Pl of 0.3 and was able to reduce CSF $A\beta_{40}$ by 54% after a single oral dose of 30 mg/kg. The reduced cellular activity of **180** compared to the enzymatic activity was addressed by increasing the pK_a of the basic amidine via ring-expansion of the aminohydantoin core into a slightly more basic 6-membered amino-dihydropyrimidinone. An increased pK_a should lead to accumulation of the compound into the acidic endosomes where BACE1 is acting. In addition, to the change in pK_a, by adding an additional sp^3 carbon the orientation of the substituents into P1 and P2′ is also affected. Larger groups such as the cyclopropyl in **180** or aryl in **179** now tend to clash with Ile 118 so smaller substituents like methyl are therefore optimal. Optimization of the aminodihydropyrimidone series led to the highly ligand efficient inhibitor **181** (Fig. 50), with in rat a further enhanced Br:Pl ratio and in vivo efficacy, showing 81% reduction in CSF $A\beta_{40}$ after a 10 mg/kg oral dose.[217]

Fusion of the aminodihydropyrimidone heterocycle with N-substituted pyrrolidine allowed targeting of the S2′ pocket.[218] A first round of exploration led to **182** (Fig. 50), which occupies both S1–S3 and S2′ pockets. Although **182** did show central amyloid lowering in rats, efficacy was reduced compared to **181**. Overall the size and PSA of this molecule rendered the properties unsuitable for a CNS drug, having modest brain penetration, significant hERG inhibition, and time-dependent CYP3A4 inhibition attributed to bioactivation of the fluoropyrimidine moiety leading to a reactive metabolite. Further efforts were directed toward reducing molecular weight and lipophilicity via removal of the S3 targeting cyanophenyl group, and to regain activity via optimization of the S2′ group.[219] X-ray cocrystallization of **182** and analogs indicated a key hydrogen-bonding network with Trp76 via a water molecule in a subpocket termed S2″. Substitution of the pyrimidine with a 4-methoxy group led to a shift of the pyrimidine group in the S2′ pocket, allowing displacement of two conserved water molecules, and burying the methoxy substituent deeply in the S2″ pocket (**183**) (Fig. 50). The addition of a methyl substituent directed into S2′ enhanced the potency significantly and resulted in a reduction of the time-dependent CYP3A4 inhibition. The improvement on time-dependent CYP3A4 inhibition was attributed to increased steric demand around the pyrimidine or redirecting metabolism to the methyl substituent. These variations culminated with the identification of **183**, which was extensively profiled. Clearance in rat, dog, and monkey was relatively high, exceeding liver blood flow in rat and, which was attributed to low plasma stability in these species. Despite being a P-gp substrate (ER >30), **183** showed good CNS penetration in the rat, Br:Pl 0.8, and monkey, Br:Pl 3.2. However, when considering CSF exposure, the CNS penetration appears lower; rat CSF:Pl 0.008, monkey CSF:Pl 0.01, although it should be noted that the extent of ppb cannot be taken into account due to plasma stability issues. A rat dose–response study revealed $A\beta_{40}$ ED_{50} of 5.2 mg/kg (for effect in CSF) and 12.7 mg/kg (for effect in cortex), with complete reduction in both compartments seen at doses ≥ 30 mg/kg. In the monkey a 100 mg/kg oral dose resulted in a 77% reduction of CSF $A\beta_{40}$ after 24 h. In the same study, a 10 mg/kg dose resulted in a 22% reduction of CSF $A\beta_{40}$ after 12 h. In a separate, acute dose terminal study, a 10 mg/kg oral dose resulted in a 58% reduction in $A\beta_{40}$ in the cortex and a 35% reduction in CSF.

The binding mode of **183** to BACE is depicted in Fig. 51 and shows the acylguanidine interacting with the aspartic acid diad and the pyrimidine extending into the S2′pocket.

In a further extension of the amino-dihydropyrimide series, the planar carbonyl group in this heterocycle was replaced with a tetrahydral sulfonyl group, which was predicted to lead to an overall similar shape and orientation of substituents.[220] Indeed, this yielded equipotent iminothiadiazine dioxide compounds (**181** vs. **184**) (Fig. 50). The lower basicity of **184** compared to **181** resulted in a reduced cellular potency, but in vivo potency was enhanced, explained by an improved permeability and CNS penetration. **184** was not progressed further due to only modest Cathepsin D selectivity and formation of glutathione adducts, attributed to the propynylpyridine moiety. Replacement of this moiety with a substituted picolinamide group, as also seen in other BACE programs, strongly reduced Cathepsin D affinity, due to the CatD S3 subpocket being smaller than that in BACE1. BACE1 affinity was further increased fivefold via the introduction of a 6-fluoro-substituent, in analogy with the chloro-substituent in **184**. The pyridyl nitrogen is thought to play an important beneficial role by forming an internal hydrogen bond to the amide hydrogen. This allows an optimal coplanar conformation, positioning the picolinamide into S3, and the masking of the amide H-bond donor helped to enhance permeability and reduce efflux. As a consequence compounds such as **185** (Fig. 50) display robust CNS activity

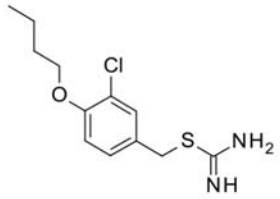

178

BACE1 K_i > 200 μM

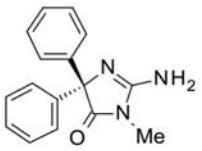

179

BACE1 K_i 3.7 μM
(LE 0.37)
Cell IC_{50} 13 μM

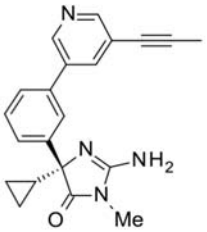

180

BACE1 K_i 5 nM (LE 0.43)
Cell IC_{50} 84 nM
rat Br:PI 0.3
rat CSF $A\beta_{40}$ -54% @ 30 mg/kg po

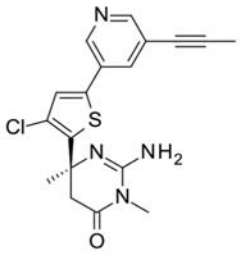

181

BACE1 K_i 2 nM (LE 0.48)
Cell IC_{50} 11 nM
Br:PI 2.9
CatD/BACE1 21
rat CSF/cortex $A\beta_{40}$ -81%/53%
@ 10 mg/kg po

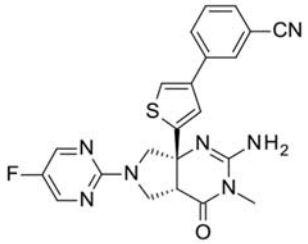

182

BACE1 K_i 4 nM (LE 0.36)
Cell IC_{50} 16 nM
Br:PI 0.1
rat CSF $A\beta_{40}$ -52% @ 10 mg/kg po

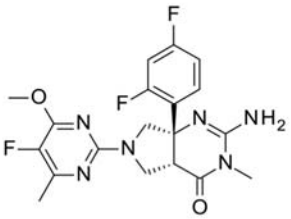

183

BACE1 K_i 5 nM
Cell IC_{50} 14 nM
Br:PI 1.1
monkey CSF $A\beta_{40}$ -77% @ 100 mg/kg po

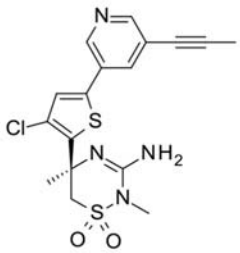

184

BACE1 K_i 2.4 nM
Cell IC_{50} 55 nM
pKa 6.6
Br:PI 2.3
CatD/BACE1 47
rat CSF/cortex $A\beta_{40}$ -82%/61%
@ 10 mg/Kg po

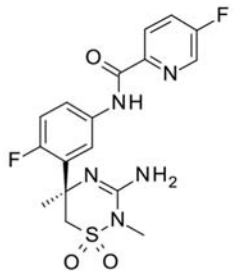

185 (MK8931, verubecestat)

BACE1 K_i 2.2 nM
BACE2 Ki 0.38 nM
Cell IC50 ($A\beta_{40}$) 2.1 nM
pKa 7.5
Br:PI 0.57
CatD Ki > 100 μM
monkey CSF $A\beta_{40}$ -81%
@ 10 mg/Kg po

Fig. 50 Evolution of HTS hit **178–179** and **180–181** and S2′ pocket targeting derivatives **182** and **183** and sulfonyl gaunadines **184** and **185** (MK8931, verubecestat).

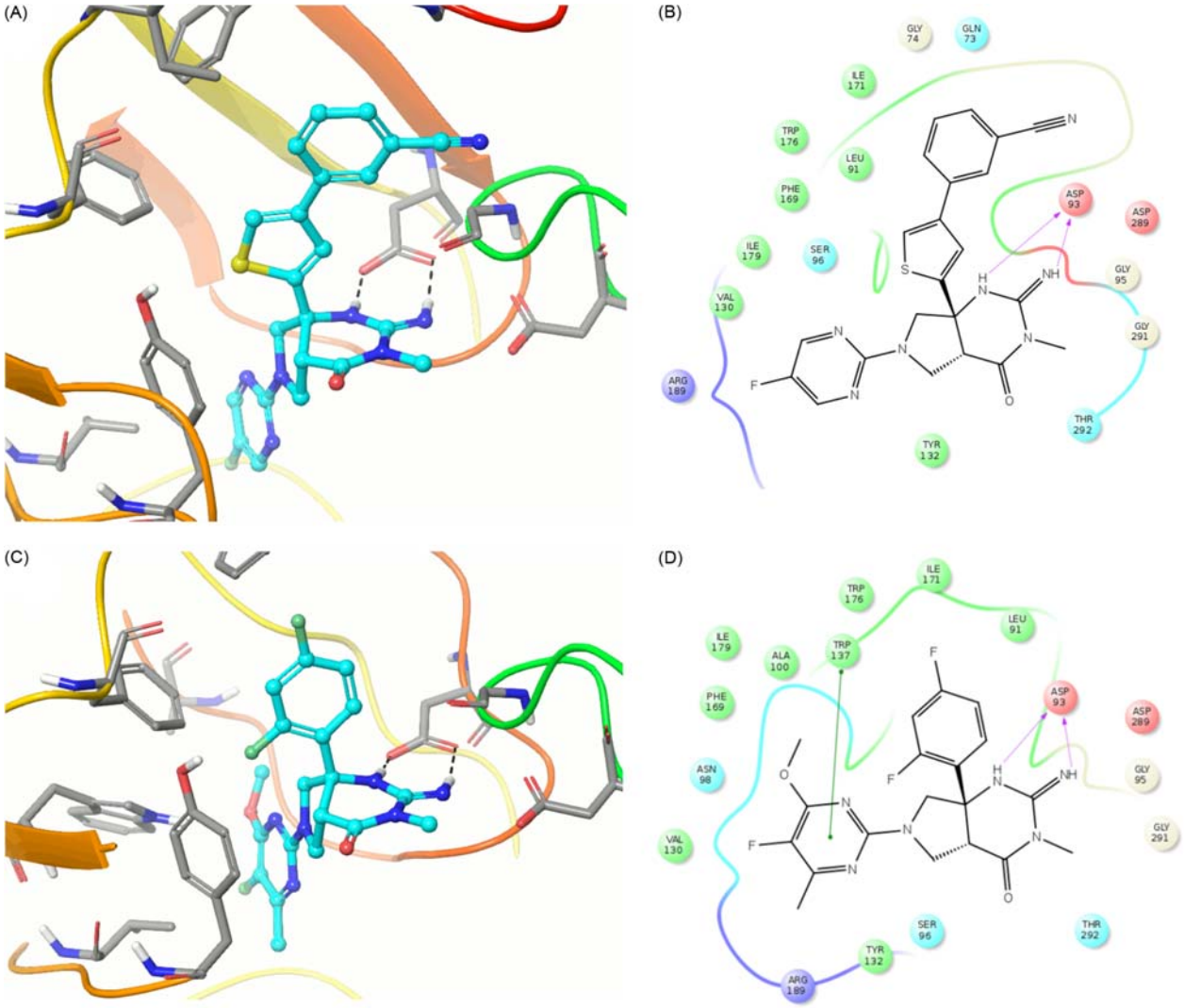

Fig. 51 X-ray structure of (A) **182** bound to BACE (PDB code 5HD0). (B) Depiction of residues around / interacting with **182**. (C) **183** bound to BACE (PDB code 5HE7). (D) Depiction of residues around/interacting with **183**.

in both rat and monkey, despite a rather high PSA (calculated at 115 $Å^2$), for a CNS drug. The Br:Pl ratio in rat for **185** was 0.57, again an improvement over the direct amino-dihydropyrimidine analog. In vitro, **185** inhibited the hERG channel with an IC_{50} of 2.2 μM, which was estimated to be sufficiently higher (~27-fold) than the projected human Cmax exposure levels. Combining all desired properties, **185** was selected for further development and is currently progressing in Phase 3 clinical trials (MK8931 or verubecestat). Initial data indicate a good translation of amyloid reduction in preclinical species in CSF Aβ reductions in healthy volunteers and patients. The terminal half-life of MK8931 was 14–24 h, and dose-dependent reductions in CSF Aβ peptides levels were observed, with over 90% reduction of $Aβ_{40}$ levels at the highest dose tested (550 mg). This was confirmed in a Phase 1b study, where patients with mild-to-moderate AD received a daily dose of 12, 40, and 60 mg doses for 7 days, achieving a sustained reduction in CSF $Aβ_{40}$ levels of 57%, 79%, and 84%, respectively. Phase 3 trials are ongoing targeting prodromal and mild-to-moderate AD. The selected doses of 12 and 40 mg are predicted to achieve >50% and >75% reductions in CSF Aβ peptides, respectively.

Further work of the Merck team seems to have focused around further exploration and securing the chemical space around the iminothiadiazine dioxide type of BACE inhibitors. Analogs without S3 targeting substituent, but having substituents directed toward S2′ are exemplified by **186**[221] and **187** (Fig. 52).[222] Comparative data indicate an enhanced solution stability of the iminothiadiazine dioxide analogs over their corresponding aminidihydropyrimidone analogs, as well as reduced efflux, with **187** having a reported P-gp efflux ratio of 1.6 versus 7.7 for the corresponding pyrimidone **183**. The THF-fused **188** (Fig. 52) can be considered a direct analog of LY2886721 (**93**, Table 2).[223] A one atom modification (sp^2 N to sp^3 C) led to multiple patent applications on iminothiazine dioxide analogs, such as **189**,[224] **190**,[225] and **191** (Fig. 52),[226] having similar or enhanced enzymatic potency compared to their iminothiadiazine dioxide analogs. For example, spiro-cyclized iminothiazine dioxide **195**[227] showed a BACEi Ki of 8 versus 70 nM for the corresponding imino thiadiazine analog **194** (Fig. 52).[228] Reinsertion of a nitrogen in the

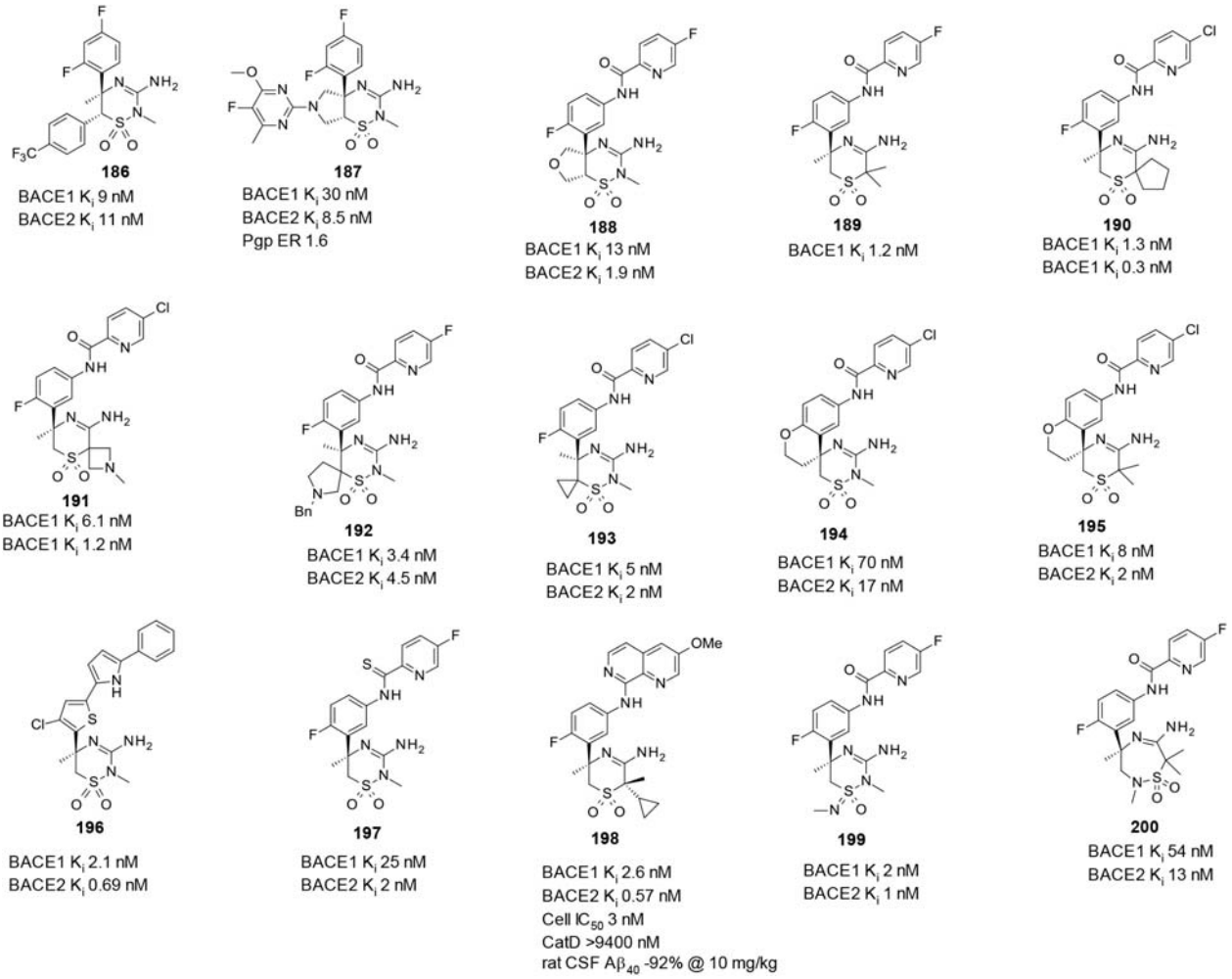

Fig. 52 Selected recent examples from patent applications from Schering-Plough/Merck.

ring led to reversed sulfonamides exemplified by **200** (Fig. 52) in general having reduced potency.[229] Additional variations include C2- and C-6 spiro-substituted analogs such as **190**, **192**,[230] and **193** as well as S-imino-S-oxo iminothiazine derivatives (**199**) (Fig. 52).[231] Most applications contain a multitude of variations on the S1–S3 targeting substituents, for example, **198** which showed excellent in vivo central activity in rat (Fig. 52).[232] A few applications specifically claim bioisosteric amide modifications such a heteroaromatic rings (**196**)[233] or thioamides (**197**) (Fig. 52).[234] In most patent applications, BACE1 and BACE2 enzymatic data have been reported. In general, no to minimal selectivity is observed for the various subseries, in agreement with the lack of selectivity reported for MK-8931 (**185**).

The intensive and persistent efforts toward BACE inhibitors by the Schering/Merck teams have clearly paid off with MK8931 (**185**) now furthest ahead in clinical development. Initiated by FBDD and guided by SBDD, their program has established the optimal vectors toward the various pockets culminating in the highly ligand efficient **185**. Although the high intrinsic TPSA of the iminothiadiazine dioxide warhead would perhaps be counterintuitive for a CNS drug, the acceptable brain penetration and demonstrated efficacy in clinical trials have proven its worth and illustrate the value of exploring beyond the traditional boundaries of CNS druglike properties.

7.08.19 Inhibitors Reported by Shionogi

Initial patent applications of Shionogi describe 2-amino-1,3-thiazine containing BACE inhibitors.[235,236] These are among the first examples of BACE inhibitors with data indicating very efficient lowering of amyloid peptide levels in the brain. For example, **201** (Fig. 53) reduced $A\beta_{40}$ levels in mice by 79%, 3 h after a 10 mg/kg oral dose. Very similar 2-amino-1,3-thiazine examples have been described by Roche as BACE2 inhibitors,[165] and the isothiourea warhead has since been used by multiple companies as evidenced in several of the previous paragraphs. Subsequent applications by Shionogi describe analogs with various substitution patterns on

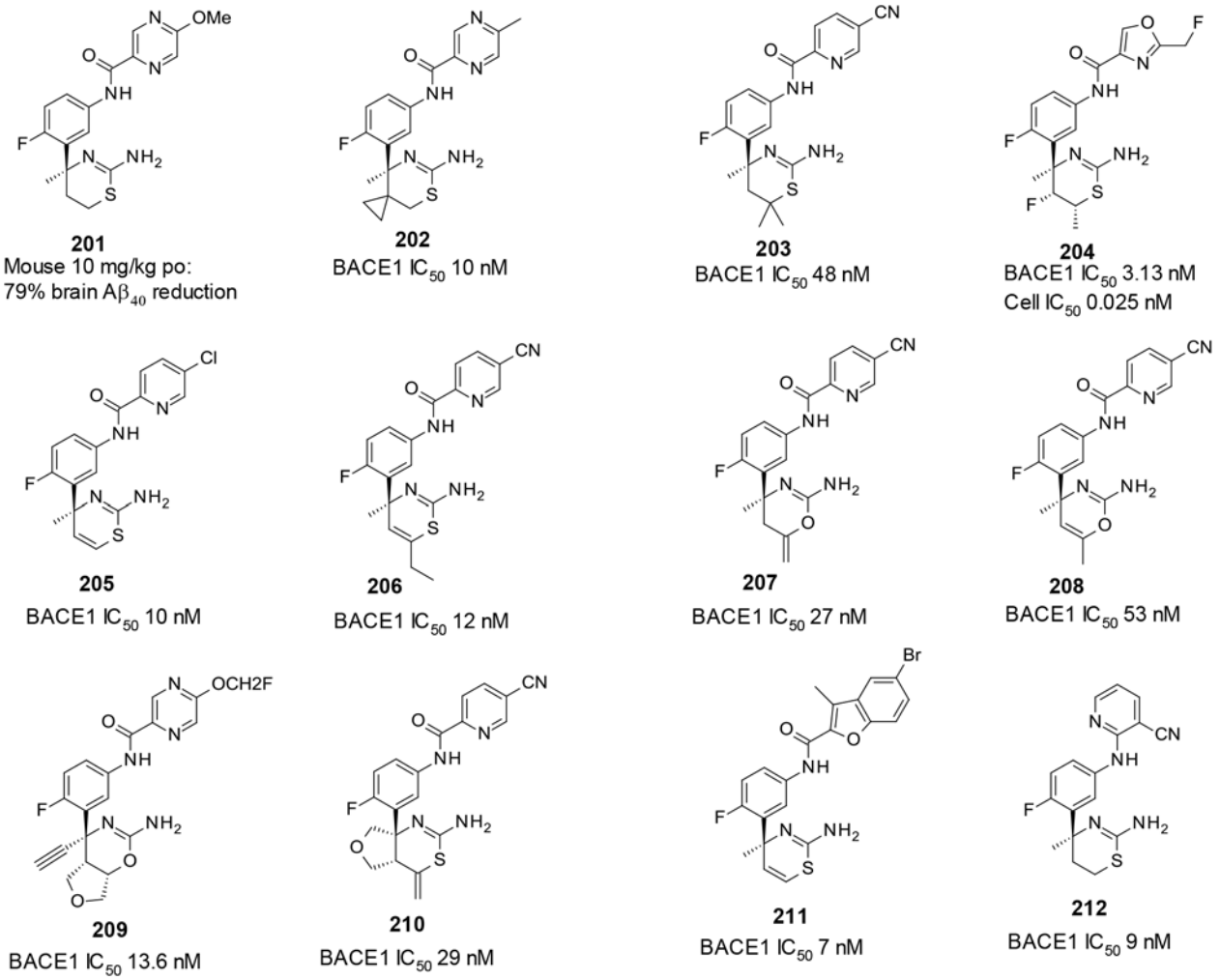

Fig. 53 Selected examples covering multiple patent applications from Shionogi.

the thiazine ring including spirocyclic **202**,[237] dialkyl substituted **203**,[238] and electron-withdrawing groups such as fluoro- and fluoroalkyl substituted thiazines such as **204** (Fig. 53).[239] Also compounds incorporating endo- or exocyclic double bonds have been described in various patent applications (**205**, **206**, Fig. 53).[240,241] Similarly substituted 2-amino-1,3-oxazine congeners also appear in several of these or separate patent applications, as exemplified by **207**[242] and **208** (Fig. 53).[243] Fused bicyclic oxazines, such as **209**,[244] and thiazines are also claimed, with **210** (Fig. 53), having similarity to LY2886721 (**93**, Table 2).[245] While most analogs contain the usual picolinamide moiety targeting the S3 pocket, interesting alternatives are also exemplified showing good potency such as **211**[239] and **212** (Fig. 53).[246] The 2-aminopyridyl substituted **212** shows resemblance to Amgen's **15** (Fig. 7) with the aminopyridyl being a successful bioisosteric replacement of the more common amide linker. Similar S3-binding groups have also been described by Roche.[168]

In addition to 2-amino-1,3-thiazines and oxazines, Shionogi has also explored a diversity of other warhead variations. Staying within the theme of sulfur-containing warheads, isomeric 4-amino-1,3-thiazines such as **213**[247] and noncyclic isothioureas such as **214**[248] have been described (Fig. 54). In another application, a series of aminopyrimidone BACE inhibitors such as **215** are described, but also a series of 2,3-diaminopyridine containing compounds (**216**), although the latter series seems to suffer from reduced potency (Fig. 54).[249] Several types of fused bicyclic warheads have been described, such as napthyridine derivatives (**217**)[250] and fused aminodihydropyrimidines exemplified by **218** (Fig. 54), which can be considered a bioisosteric version of the aminopyrimidone inhibitors described by Shionogi and other companies.[251]

A few papers describe a conformational restriction approach on the ethyl-linked aminopyrimidone series of BACE inhibitors, previously described by AstraZeneca (**23**, Fig. 8).[252,253] Replacement of the flexible ethyl linker in **219** with a rigid cyclopropyl linker having the optimal cis-(1*S*,2*R*) configuration triggered an induced fit of BACE1, leading to a novel binding mode, with the *para*-bisaryl containing **220** showed significantly higher potency than the corresponding ethyl analog (Fig. 55). X-ray analysis revealed a CH–π interaction of the cyclopropane ring with Tyr71 in BACE1. For metasubstituted bisaryl analogs, no potency improvement was observed for the cyclopropyl-linked compounds. However, introduction of an additional ethyl spacer between the two aryl

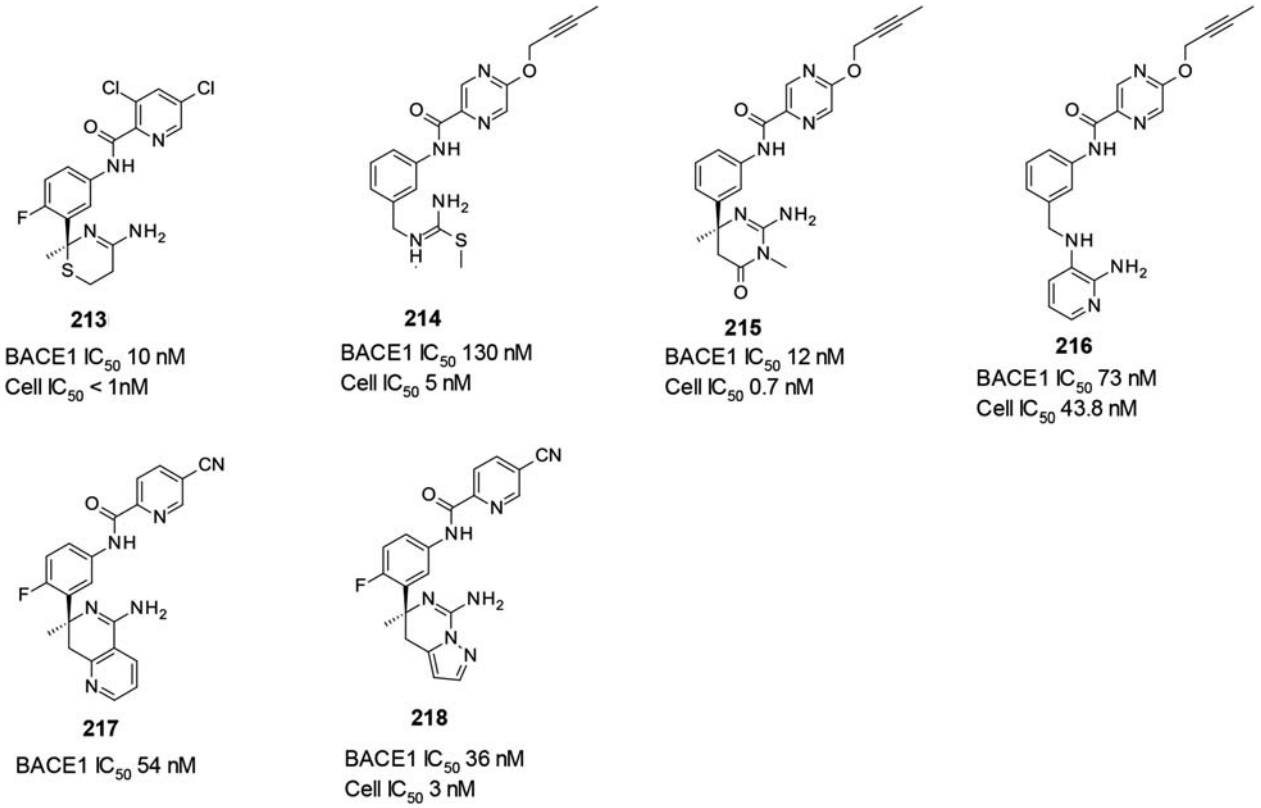

Fig. 54 Selected derivatives with alternative warheads and templates from Shionogi.

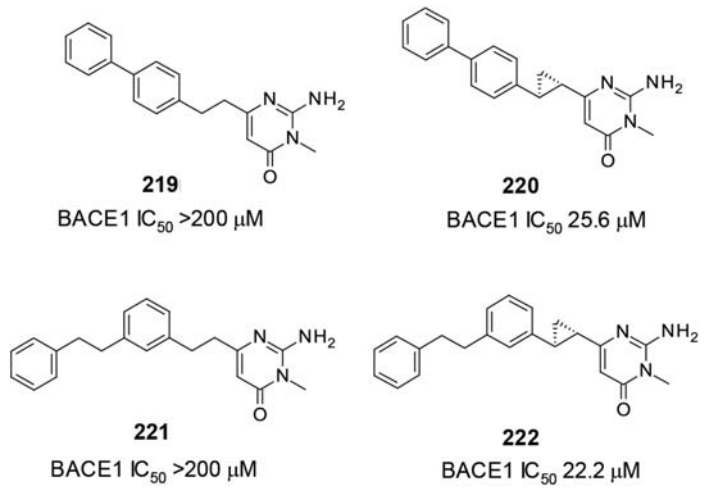

Fig. 55 Conformationally constrained aminopyrimidone derivatives from Shionogi.

rings again resulted in inhibitory activity for the rigidified **222** compared with undetectable activity for the flexible ethyl analog **221** (Fig. 55). Overall, potency of these rigid analogs remained in a very moderate micromolar range, illustrating the importance of having a quaternary center next to the amidine to optimally direct substitution into S1–S3.

Shionogi were one of the earliest entrants to the amidine-derived template, with particular focus on isothioureas. The group have published multiple patent applications and have ultimately identified at least one development candidate, JNJ-54861911, which has progressed to clinical studies in collaboration with Janssen. Results from a Phase 1 MAD study indicated that this compound reduced CSF $A\beta_{40}$ levels by 50% after 2 weeks of treatment, while the 30, 50, and 90 mg doses reduced levels by more than 80%, indicating a comparative efficacy versus competitor clinical candidates.[254]

7.08.20 Inhibitors Reported by Wyeth

Wyeth was among the first companies to identify guanidine containing scaffolds as having an optimal interaction with the catalytic Asp-dyad. Two series of BACE inhibitor have been developed, originating from hits **223** and **224** (Fig. 56) both identified via high-throughput screening using a FRET assay screen. Note that **224** has also been reported by AstraZeneca. Initial publications describe the optimization of the more potent acylguanidine hit **223**, already displaying single-digit micromolar BACE inhibition. A cocrystal structure of BACE1 with **223** indicated four key hydrogen-bonding interactions between the acylguanidine group in **223** and the two catalytic aspartic acid residues Asp32 and Asp228.[255] In addition, the two phenyl groups extended into the S1 and S2′ pockets. It also provided guidance for further optimization of the hit: substitution of the *para* position of the P1 phenyl group should provide a vector into the S3 pocket, and substitution of the non-Asp interacting third nitrogen of the guanidine should allow access to the S1′ pocket. Exploration of the SAR around these regions led to **225** (Fig. 56) having a significantly improved potency for BACE1. Difficulties in the synthesis of these trisubstituted pyrroles prompted the replacement of the pyrrole by a thiophene as in **226** (Fig. 56), allowing a more facile exploration of this series.[256] The *n*-propoxyphenyl group covered the S1–S3 pocket with minimal strain, contributing to the potency of **225**. While *para*-substituents of more significant size did fit into the S1–S3 pocket, the potency increase was suboptimal, attributed to a significant strain in these molecules.[257] Polar substituents targeting the S1′ pocket as in **225** showed relatively high levels of BACE1/Cathepsin D selectivity (85-fold for **225**), while analogs containing aromatic groups had poor selectivity.[258] To overcome the poor brain penetration of these acylguanidine-containing compounds, bioisosteric replacement of this polar group was investigated resulting in a series of 2-aminopyridine containing derivatives.[259] A crystal structure comparison of **223** with prototype **227** (Fig. 56) showed an almost perfect overlap of the acylguanidine and aminopyridine groups, and the reduced TPSA of **227** resulted in a significantly enhanced brain to plasma ratio of 1.7 compared to 0.04 for

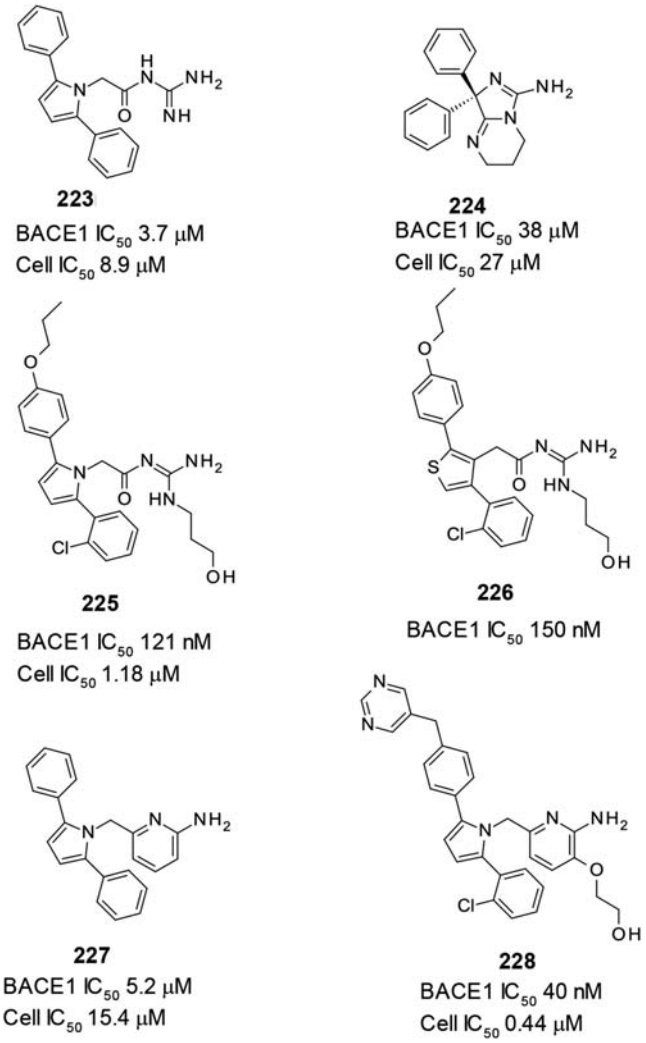

Fig. 56 Acylguanidine and related derivatives from Wyeth.

223. Potency could also be maintained, with optimized compound **228** (Fig. 56), having low nanomolar potency, albeit reduced brain penetration due to the introduction of the additional alkyl alcohol group.

Hit **224** was also explored using a traditional SAR approach supported by molecular modeling studies based on the cocrystal structure of BACE1 with **224**.[260] Similarly to **223**, the two phenyl groups extend into the S1 and S2′ pockets, but in **224** the meta-position of the P1 phenyl group offered the optimal vector into the S3 pocket. SAR exploration led to the identification of the 3-pyridyl substituent with the pyridyl nitrogen having an interaction through a water bridge with Ser229 in the S3 pocket. Interaction within the S2′ pocket was enhanced by the introduction of a *para*-trifluorometoxy group, resulting in a further 15-fold potency boost. Optimized compound **229** (Fig. 57) had a more than 1000-fold improvement in potency over **224**. The introduction of the additional fluoro-substituent in **229** was not driven by potency but based on metabolic properties. **229** was also evaluated in vivo using Tg2576 mice. A dose of 30 mpk led to a 71% reduction in $A\beta_{40}$ plasma levels 6 h after dosing, but no significant reduction in brain $A\beta_{40}$ was observed, presumably due to poor brain exposure of **229**.

The tetrahydropyrimidine ring in **224** and **229** extends toward solvent, therefore further improvements in potency via changes in this region were difficult to attain. Removal of this ring led to compounds containing an aminohydantoin core such as in **230** (Fig. 57) which was also explored by other groups. Compared to **224**, the less lipophilic and lower molecular weight **230** showed a 10-fold improvement of both enzymatic and cellular potency.[261] Saturation of the P2′ phenyl group, and optimization into S3 led to compounds such as **231** (Fig. 57) having low nanomolar potency. In a further exploration of this series, it was recognized that a 4-pyridyl P2′ group created a hydrogen-bonding interaction with Trp76, contributing to an increased potency, as exemplified by **232** (Fig. 57).[262] Taking advantage of the differences in amino acid sequence in the S2′ pocket of BACE1 and BACE2, further substitution of the pyridyl group led to highly selective BACE1 ligands such as **233** (Fig. 57) with over 500-fold selectivity against BACE2.[263] The large steric ethyl-substituents apparently clash with the BACE2 enzyme backbone, but were shown to interact with Tyr71, Val69, and Ser35 in the S2′ pocket of BACE1, with one of the ethyl groups also displacing two conserved waters. Selectivity over Cathepsin D was >5000-fold. Replacement of the pyridyl P2′ group with substituted pyrazole or thiophene heterocycles also provided potent and selective compounds.[264] With all of these compounds still suffering from poor brain penetration, a stepwise exploration of the S3 and S2′ regions was carried out to reduce the efflux liability in this series, attributed to the electron richness of the heterocycle substituents used before (pyridyl as in **229**, **232** pyrimidyl as in **233**).[265] Replacement of the heteroaryl

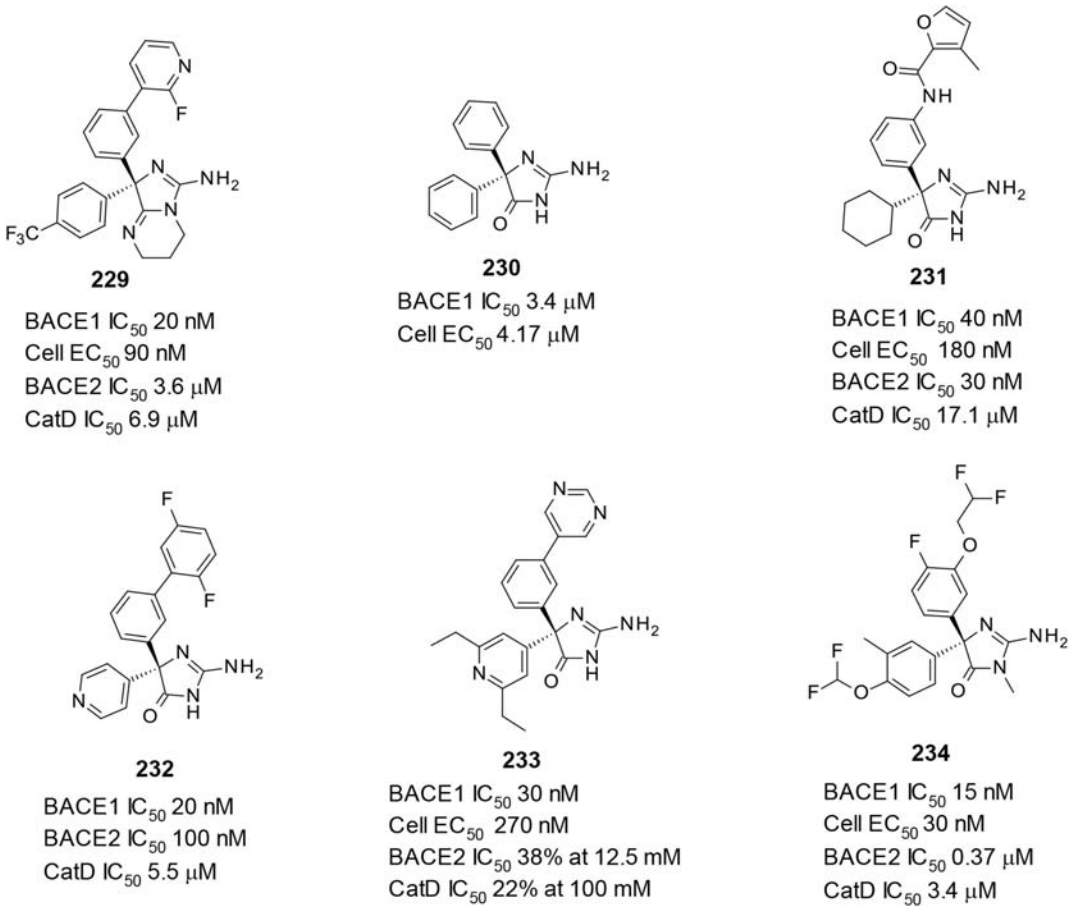

Fig. 57 Further examples from Wyeth.

substituents at the *meta*-P1 phenyl with alkyl and alkoxy groups led to **234** (Fig. 57). The additional *para*-fluoro-substituent decreased CYP450-mediated metabolism, and the overall improved physicochemical properties resulted in an enhanced brain permeability of 40–70% compared to 5–10% for previously described analogs. Despite this increase in brain penetration, **234** was not able to reduce $A\beta_{40}$ levels in the brain of Tg2576 mice after a 30 mg/kg p.o. dose. This was attributed to a significant increase in brain tissue binding, resulting in low central free drug exposure.

After the merger of Wyeth with Pfizer, further development of this series seems to have been halted in favor of the efforts described in the section of Pfizer (see earlier text).

7.08.21 Inhibitors Reported by vTv/TransTech/HighPoint

TransTech, subsequently rebranded to HighPoint Pharmaceuticals, now vTv Therapeutics, has disclosed a series of imidazole-based BACE inhibitors. The series have been covered by a series of patent applications, with the culmination of one compound, HPP854, entering PhI clinical trials. The first application[266] covered compounds with weak affinity, but subsequent applications detailed compounds such as **235**,[267] **236**,[268] and **237** (Fig. 58),[269] all of which apparently display reasonable activity in enzyme and cellular assays.

Inspection of the structures shows no similarity with other published BACE inhibitors and no peer-reviewed publications or crystal structures have appeared to shed light on the mode of action. However, the compounds contain a very high proportion of aromatic rings in addition to probably intramolecular hydrogen bonds, hence it would be anticipated that they would display low solubility. Furthermore, it seems that no other groups have shown interest in these series, hence the profile of these compounds appears not to have proven of interest to the BACE community. Despite this, ultimately one compound, HPP854, progressed to a PhI study and was investigated in subjects with MCI or mild AD. The trial started in Oct. 2011 and assessed doses of 5–800 mg HPP854.[270] The study was terminated and no further development has been reported.

7.08.22 Summary of Clinical Development Compounds and Clinical Outlook

As highlighted, multiple groups have identified and progressed development compounds into clinical development, although several have been terminated. Table 7 summarizes the development compounds, the companies developing them, and their current status.

Merck are the furthest progressed with MK-8931/verubecestat. Two large PhII/III trials, APECS and EPOCH, are currently underway. APECS, a PhIII trial, is assessing MK-8931/verubecestat in patients with prodromal AD in a total of 1500 participants. The primary efficacy outcome of the study is change from baseline in the Clinical Dementia Rating Scale-Sum of Boxes (CDR-SB) score following 104 weeks of treatment. EPOCH, a Phase II/III of MK-8931/verubecestat in patients with mild-to-moderate AD, commenced in Nov. 2012, and is currently estimated to complete in mid-2017. Efficacy will be assessed by change from baseline in the Alzheimer's Disease Assessment Scale Cognitive Subscale (ADAS-Cog) score, as well as the change from baseline in the Alzheimer's Disease Cooperative Study–Activities of Daily Living (ADCS–ADL) score, following 78 weeks of treatment.

Other companies, such as Eisai/Biogen, Lilly/AstraZeneca, and Janssen, appear to be following closely behind, pushing compounds rapidly through PhII and into PhIII trials. Eisai have recently announced the successful completion of the PhII trial of E2609, which will subsequently progress to two PhIII studies at 50 mg/day, each of 24 months duration.[271] Lilly recently announced that AZD3293 has been granted a fast track designation by the FDA. In addition to the ongoing PhII/III trial (AMARANTH), a second PhIII trial (DAYBREAK-ALZ) in people with mild AD has begun enrolling participants in the 3rd quarter of 2016.[272]

Analysis of the compounds in development and the compounds covered by each of the companies reveals that a lot of the compounds have similar features, such as an anilide. In addition, it is likely that a lot of companies are developing compounds which contain the isothiourea warhead, for example, Eisai, Janssen, Lilly, and Pfizer, although MK-8931 (Merck) has the sulfonyl-guanidine warhead and AZD3293 (Lilly/AZ) utilizes an amidine and lacks the typical anilide, RG7129 (Roche) utilized an isourea and CNP-520 (Novartis/Amgen) likely employs an isourea or iminomorpholine/β-alkoxyamidine. LY2811376 and LY2811376,

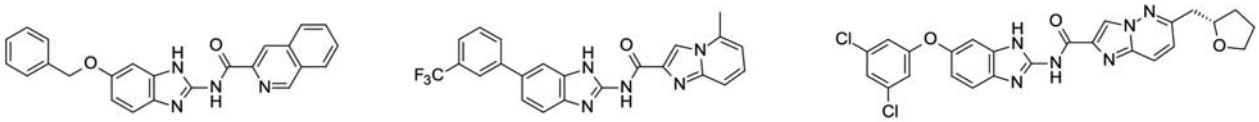

235
BACE IC_{50} 85 nM
cell IC_{50} 120 nM

236
BACE IC_{50} 320 nM
cell IC_{50} 530 nM

237
BACE IC_{50} 207 nM
cell IC_{50} 270 nM

Fig. 58 Selected examples from vTv/TransTech/HihPoint Pharma patent applications.

Table 7 Summary of key compounds which have progressed to clinical studies with their current status

Compound	Lead company/discoverer	Structure	Current status	Doses	Comment	Patient population
CNP520	Amgen/Novartis	Not disclosed	PhII/III	1, 10, 25, and 75 mg	NCT02791191 NCT02565511	Prevention in APOE4 carriers
CTS-21166	Astellas/Comentis	Not disclosed	Terminated (PhI)		NCT00621010 HEA peptidomimetic showed plasma amyloid reduction after iv administration	N/A
AZD3839	AstraZeneca	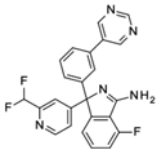	Terminated (PhI) due to QTc prolongation		NCT01348737	
BI 1181181/VTP 37948	Boehinger Ingelheim/Vitae	Not disclosed	Terminated (PhI)		NCT02254161	
E2609	Eisai/Biogen	Not disclosed	PhII started Nov. 2014	5, 15, and 50 mg	NCT02322021 18-Month trial with 700 participants. Primary endpoint slowing of cognitive decline (ADCOMS)	MCI due to AD or prodromal AD plus positive amyloid PET scan
JNJ-54861911	Janssen/Shionogi	Not disclosed	PhII/III started Oct. 2015	5 and 25 mg	NCT02569398 54-Month trial in 1650 participants with read out in 2023. Primary endpoint slowing of cognitive decline (ADAS-PACC)	Patient population: asymptomatic people at risk
LY2811376	Lilly		Terminated (PhI)		NCT00838084 Terminated due to retinal toxicity	
LY2886721	Lilly	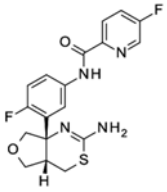	Terminated (PhII)		NCT01561430 Terminated due to liver toxicity	
LY3202626	Lilly	Not disclosed	PhII		NCT02791191	52-week mild AD

(Continued)

Table 7 Summary of key compounds which have progressed to clinical studies with their current status—cont'd

AZD3293/ LY3314814	Lilly/AstraZeneca	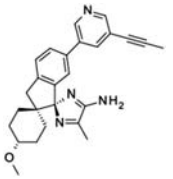	PhII/III (AMARANTH)	20 and 50 mg	NCT02245737	24-Month study in early AD, e.g., MCI
MK-8931 Verubecestat	Merck	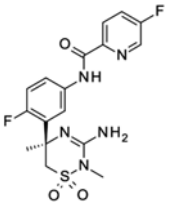	PhII/III	12 and 40 mg	EPOCH: NCT01739348 APECS: NCT01953601	Prodromal and mild-to-moderate
PF-05297909	Pfizer	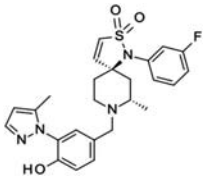	Discontinued PhI	25, 100, 250, and 525 mg	NCT01462851 Compound did not achieve sufficient lowering of CSF Aβ at 325 mg dose despite lowering plasma Aβ	Sep. 2011–Feb. 2012
PF-06751979	Pfizer	Not disclosed	PhI	SAD: 3, 12, 40, and 125 mg MAD: 5, 15, 50, and 70 mg	NCT02509117 SAD plus human CSF PK/PD at 525 mg dose	Combined SAD and MAD (14d)
RO5508887/ RG7129	Roche	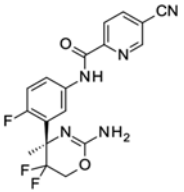	Discontinued PhI	N/A	NCT01461967	N/A
HPP854	TransTech/High Point Pharmaceuticlas	Not disclosed	Discontinued (PhI)		NCT01482013	May not be a BACE inhibitor

containing the isothiourea warhead, were both terminated due to nontarget related toxicity, albeit from a different origin. However, a structurally differentiated warhead does not guarantee success, as shown by the termination of the isourea RG7129 from Roche. Several compounds have now passed the hurdle of initial Phase I and II safety trials and are progressing in late-stage clinical trials. This indicates that intrinsic toxicity can be avoided with BACE inhibitors. However, the safety profile of chronic exposure to BACE inhibitors, as likely required for a successful treatment, still needs to be firmly established.

7.08.23 Conclusion

After many years of arduous research by multiple competing groups around the world, the BACE inhibitor field is currently poised at a very exciting moment in time. Not only has the extremely competitive field become collaborative, turning foes into allies, in order to share the risks and costs of the clinical development projects, but also multiple compounds have now progressed into PhII clinical trials and beyond. It would appear that sustained research in the field has resulted in success in terms of the delivery of compounds which are suitable to assess the mechanism in a clinical setting. There are many things that can be learned from this research, for example, alternative screening approaches such as fragment screening may make undruggable targets druggable and chemists should not be fixated with the identification of highly potent hits from HTS campaigns. As clinical data and preclinical data become available, it is possible to correlate human CNS penetration ($CSF:Pl_u$) with preclinical data and this will help to guide future discovery. Furthermore, the field has shown the persistency and ingenuity of medicinal chemists and their ability to overcome multiple issues, including hERG inhibition, P-gp efflux, CYP inhibition, and metabolism. Modulation of the pK_a of the amidine-containing warheads has been instrumental, especially in dealing with hERG inhibition and P-gp efflux. As illustrated by many examples throughout this article, this has been achieved by incorporation of the amidine function into various heterocyclic ring systems, and by decoration of these heterocycles with electron-withdrawing groups.

Over the many years of BACE research, most companies have had considerably sized teams of chemists dedicated to this target. This is understandable when considering the difficulty of the target, the high competitiveness, as illustrated by the many overlapping patent scopes, and last but not least, the complexity of the synthesis. Most of the compounds shown in this overview contain multiple chiral centers, fused or bridged nonaromatic ring systems, and require 10–20 synthesis steps to prepare. BACE therefore highlights the importance of synthetic organic chemistry, as illustrated nicely by the work of Lilly on conformationally restricted BACE inhibitor prototypes.[273] Most of the compounds that have progressed do not show selectivity over BACE2. The consequences of this are currently unknown, but the more recent patents tend to show inhibition constants for both BACE1 and BACE2, indicating a raised interest in selectivity ratios. Furthermore, new substrates are being identified for BACE1 and the impact of potentially chronic inhibition of the processing of other proteins is currently unknown.[274]

Several important questions remain, such as: How much amyloid reduction should be targeted? How does the amyloid reduction in human CSF relate to the reduction in human brain? Which patient population should be treated, at which stage of the disease and for how long? Which other proteins does BACE cleave and what will the relevance of these be? The ongoing suite of clinical trials with multiple compounds is set to provide answers to these questions. Improved biomarkers to select patients and follow disease progression, targeting of various stages of the disease including prevention, and the multiyear exposure to BACE inhibition in humans should ensure a thorough testing of the amyloid hypothesis and targeting it via BACE inhibition. The combined treatment with a BACE inhibitor and drugs targeting other mechanisms may also prove beneficial. For example, Roche has reported that the combined treatment of APP_{London} transgenic mice with the BACE inhibitor RO5508887 (**152**) and the anti-Aβ antibody gantenerumab significantly enhanced the antiamyloid effect, including an enhanced clearance of preexisting amyloid plaques.[275] A similar effect of targeting both synthesis and clearance in the amyloid cascade has been presented by Lilly via the combination of LY2811376 (**92**) and the plaque targeting antibody N3pG.[276]

The field is now poised to deliver what could be the biggest results ever seen in neuroscience. Should one of these compounds manage to deliver a slowing, or even, a halting, of disease progression, the results would have a huge impact on the lives of millions of AD sufferers and their carers and families. Although several challenges remain to be addressed, if successful, the field of AD will have changed dramatically and it will no longer be viewed as a life sentence.

Acknowledgments

The authors would like to thank Yogesh Sabnis (UCB) for the preparation of the Figures depicting X-ray crystal structures.

See also: 7.07. Targeting γ-Secretase for the Treatment of Alzheimer's Disease. 8.09. Verubecestat.

References

1. Alzheimer's Association. 2016 Alzheimer's Disease Facts and Figures, http://www.alz.org/documents_custom/2016-facts-and-figures.pdf.
2. Alzheimer's Disease International, World Alzheimer Report, https://www.alz.co.uk/research/statistics.
3. Maurer, K.; Volk, S.; Gerbaldo, H. Auguste D and Alzheimer's disease. *Lancet* **1977,** *349,* 1546–1549.

4. Hardy, J. A hundred years of Alzheimer's disease research. *Neuron* **2006,** *52,* 3–13.
5. Selkoe, D. J. *Neuron* **1991,** *6,* 487–498.
6. Hardy, J. A.; Higgins, G. A. Alzheimer's disease: the amyloid cascade hypothesis. *Science* **1992,** *256,* 184–185.
7. Hardy, J.; Selkoe, D. J. The amyloid hypothesis of Alzheimer's disease: progress and problems on the road to therapeutics. *Science* **2002,** *297,* 353–356.
8. Goate, A.; Hardy, J. Twenty years of Alzheimer's disease-causing mutations. *J. Neurochem* **2012,** *120* (Suppl. 1), 3–8.
9. Alzforum APP Mutation List, http://www.alzforum.org/mutations.
10. O'Brien, R. J.; Wong, P. C. Amyloid precursor protein processing and Alzheimer's disease. *Ann. Rev. Neurosci.* **2011,** *34,* 185–204.
11. Jonsson, T.; Atwal, J. K.; Steinberg, S.; Snaedal, J.; Jonsson, P. V.; Bjornsson, S.; Stefansson, H.; Sulem, P.; Gudbjartsson, D.; Maloney, J.; Hoyte, K.; Gustafson, A.; Liu, Y.; Lu, Y.; Bhangale, T.; Graham, R. R.; Huttenlocher, J.; Bjornsdottir, G.; Andreassen, O. A.; Jonsson, E. G.; Palotie, A.; Behrens, T. W.; Magnusson, O. T.; Kong, A.; Thorsteinsdottir, U.; Watts, R. J.; Stefansson, K. A mutation in APP protects against Alzheimer's disease and age-related cognitive decline. *Nature* **2012,** *488,* 96–99.
12. Giaccone, G.; Morbin, M.; Moda, F.; Botta, M.; Mazzoleni, G.; Uggetti, A.; Catania, M.; Moro, M. L.; Redaelli, V.; Spagnoli, A.; Rossi, R. S.; Salmona, M.; Di Fede, G.; Tagliavini, F. Neuropathology of the recessive A673V APP mutation: Alzheimer disease with distinctive features. *Acta Neuropathol.* **2010,** *120,* 803–812.
13. Wiseman, F. K.; Al-Janabi, T.; Hardy, J.; Karmiloff-Smith, A.; Nizetic, D.; Tybulewicz, V. L. J.; Fisher, E. M.; Strydom, A. A genetic cause of Alzheimer disease: mechanistic insights from Down syndrome. *Nat. Rev. Neurosci.* **2015,** *16,* 564–574.
14. Prasher, V. P.; Farrer, M. J.; Kessling, A. M.; Fisher, E. M.; West, R. J.; Barber, P. C.; Butler, A. C. Molecular mapping of Alzheimer-type dementia in Down's syndrome. *Ann. Neurol.* **1998,** *43,* 380–383.
15. Hardy, J. The amyloid hypothesis for Alzheimer's disease: a critical reappraisal. *J. Neurochem.* **2009,** *110,* 1129–1134.
16. Hussain, I.; Powell, D.; Howlett, D. R.; Tew, D. G.; Meek, T. D.; Chapman, C.; Gloger, I. S.; Murphy, K. E.; Southan, C. D.; Ryan, D. M.; Smith, T. S.; Simmons, D. L.; Walsh, F. S.; Dingwall, C.; Christie, G. Identification of a novel aspartic protease (Asp 2) as beta-secretase. *Mol. Cell. Neurosci.* **1999,** *14,* 419–427.
17. Vassar, R.; Bennett, B. D.; Babu-Khan, S.; Kahn, S.; Mendiaz, E. A.; Denis, P.; Teplow, D. B.; Ross, S.; Amarante, P.; Loeloff, R.; Luo, Y.; Fisher, S.; Fuller, J.; Edenson, S.; Lile, J.; Jarosinski, M. A.; Biere, A. L.; Curran, E.; Burgess, T.; Louis, J.-C.; Collins, F.; Treanor, J.; Rogers, G.; Citron, M. Beta-secretase cleavage of Alzheimer's amyloid precursor protein by the transmembrane aspartic protease BACE. *Science* **1999,** *286,* 735–741.
18. Yan, R.; Bienkowski, M. J.; Shuck, M. E.; Miao, H.; Tory, M. C.; Pauley, A. M.; Brashler, J. R.; Stratman, N. C.; Mathews, W. R.; Buhl, A. E.; Carter, D. B.; Tomasselli, A. G.; Parodi, L. A.; Heinrikson, R. L.; Gurney, M. E. Membrane-anchored aspartyl protease with Alzheimer's disease beta-secretase activity. *Nature* **1999,** *402,* 533–537.
19. Sinha, S.; Anderson, J. P.; Barbour, R.; Basi, G. S.; Caccavello, R.; Davis, D.; Doan, M.; Dovey, H. F.; Frigon, N.; Hong, J.; Jacobson-Croak, K.; Jewett, N.; Keim, P.; Knops, J.; Lieberburg, I.; Power, M.; Tan, H.; Tatsuno, G.; Tung, J.; Schenk, D.; Seubert, P.; Suomensaari, S. M.; Wang, S.; Walker, D.; Zhao, J.; McConlogue, L.; John, V. Purification and cloning of amyloid precursor protein beta-secretase from human brain. *Nature* **1999,** *402,* 537–540.
20. Hong, L.; Koelsch, G.; Lin, X.; Wu, S.; Terzyan, S.; Ghosh, A. K.; Zhang, X. C.; Tang, J. Structure of the protease domain of memapsin 2 (beta-secretase) complexed with inhibitor. *Science* **2000,** *290,* 150–153.
21. Iserloh, I.; Cumming, J. N. Peptidomimetic BACE1 Inhibitors for the Treatment of Alzheimer's Disease: Design and Evolution. In *Aspartic Acid Proteases as Therapeutic Targets;* Ghosh, A. K., Ed.; WILEY-VCH Verlag Gmbh & Co KGaA. ISBN: 97-3-527-31811-7 (chapter 16).
22. Baxter, E. W.; Reitz, A. B. Inhibitors for the Treatment of Alzheimer's Disease. *Annu. Rep. Med. Chem.* **2005,** *40,* 35–48.
23. Hills, I. D.; Vacca, J. P. Progress toward a practical BACE-1 inhibitor. *Curr. Opin. Drug Discov. Devel.* **2007,** *10,* 383–391.
24. Probst, G.; Xu, Y.-Z. Small-molecule BACE1 inhibitors: a patent literature review (2006–2011). *Expert Opin. Ther. Pat.* **2012,** *22,* 511–540.
25. Holloway, M. K.; Hunt, P.; McGaughey, G. B. Structure and modeling in the design of β- and γ-secretase inhibitors. *Drug Dev. Res.* **2009,** *70,* 70–93.
26. Howlett, D. R.; Richardson, J. C.; Austin, A.; Parsons, A. A.; Bate, S. T.; Davies, D. C.; Gonzalez, M. I. Cognitive correlates of Abeta deposition in male and female mice bearing amyloid precursor protein and presenilin-1 mutant transgenes. *Brain Res.* **2004,** *1017,* 130–136.
27. Hussain, I.; Hawkins, J.; Harrison, D.; Hille, C.; Wayne, G.; Cutler, L.; Buck, T.; Walter, D.; Demont, E.; Howes, C.; Naylor, A.; Jeffrey, P.; Gonzalez, M. I.; Dingwall, C.; Michel, A.; Redshaw, S.; Davis, J. B. Oral administration of a potent and selective non-peptidic BACE-1 inhibitor decreases β-cleavage of amyloid precursor protein and amyloid-β production in vivo. *J. Neurochem.* **2007,** *100,* 802–809.
28. Meredith, J. E., Jr.; Thompson, L. A.; Toyn, J. H.; Marcin, L.; Barten, D. M.; Marcinkeviciene, J.; Kopcho, L.; Kim, Y.; Lin, A.; Guss, V.; Burton, C.; Iben, L.; Polson, C.; Cantone, J.; Ford, M.; Drexler, D.; Fiedler, T.; Lentz, K. A.; Grace, J. E., Jr.; Kolb, J.; Corsa, J.; Pierdomenico, M.; Jones, K.; Olson, R. E.; Macor, J. E.; Albright, C. F. P-glycoprotein efflux and other factors limit brain amyloid β reduction by β-site amyloid precursor protein-cleaving enzyme 1 inhibitors in mice. *J. Pharmacol. Exp. Ther.* **2008,** *326,* 502–513.
29. Sankaranarayanan, S.; Holahan, M. A.; Colussi, D.; Crouthamel, M.-C.; Devanarayan, V.; Ellis, J.; Espeseth, A.; Gates, A. T.; Graham, S. L.; Gregro, A. R.; Hazuda, D.; Hochman, J. H.; Holloway, K.; Jin, L.; Kahana, J.; Lai, M.-T.; Lineberger, J.; McGaughey, G.; Moore, K. P.; Nantermet, P.; Pietrak, B.; Price, E. A.; Rajapakse, H.; Stauffer, S.; Steinbeiser, M. A.; Seabrook, G.; Selnick, H. G.; Shi, X.-P.; Stanton, M. G.; Swestock, J.; Tugusheva, K.; Tyler, K. X.; Vacca, J. P.; Wong, J.; Wu, G.; Xu, M.; Cook, J. J.; Simon, A. J. First demonstration of cerebrospinal fluid and plasma A beta lowering with oral administration of a beta-site amyloid precursor protein-cleaving enzyme 1 inhibitor in nonhuman primates. *J. Pharmacol. Exp. Ther.* **2009,** *328,* 131–140.
30. CTS21166 Phase I Trial https://clinicaltrials.gov/ct2/show/NCT00621010.
31. Comentis Company Website Accessed 08.08.08.
32. Astellas & COMentis Press Release 6th October 2014, http://comentis.com/wp-content/uploads/2014/10/Astellas-CoMentis-Press-Release-Oct-16-2015.pdf.
33. Kaller, M. R.; Harried, S. S.; Albracht, B.; Amarante, P.; Babu-Khan, S.; Bartberger, M. D.; Brown, J.; Brown, R.; Chen, K.; Cheng, Y.; et al. A potent and orally efficacious, hydroxyethylamine-based inhibitor of β-secretase. *ACS Med. Chem. Lett.* **2012,** *3,* 886–891.
34. Wood, S.; Wen, P. H.; Zhang, J.; Zhu, L.; Luo, Y.; Babu-Kahn, S.; Chen, K.; Pham, R.; Esmay, J.; Dineen, T. A.; Kaller, M. R.; Weiss, M. M.; Hitchcock, S. A.; Citron, M.; Zhong, W.; Hickman, D.; Williamson, T. Establishing the relationship between in vitro potency, pharmacokinetic, and pharmacodynamic parameters in a series of orally available, hydroxyethylamine-derived β-secretase inhibitors. *J. Pharmacol. Exp. Ther.* **2012,** *343,* 460–467.
35. Jordan, J. B.; Whittington, D. A.; Bartberger, M. D.; Sickmier, E. A.; Chen, K.; Cheng, Y.; Judd, T. Fragment-linking approach using ^{19}F NMR spectroscopy to obtain highly potent and selective inhibitors of β-secretase. *J. Med. Chem.* **2016,** *59,* 3732–3749.
36. Chen, J. J.; Liu, Q.; Yuan, C.; Gore, V.; Lopez, P.; Ma, V.; Amegadzie, A.; Qian, W.; Judd, T. C.; Minatti, A. E.; et al. Development of 2-aminooxazoline 3-azaxanthenes as orally efficacious β-secretase inhibitors for the potential treatment of Alzheimer's disease. *Bioorg. Med. Chem. Lett.* **2015,** *25,* 767–774.
37. Huang, H.; La, D. S.; Cheng, A. C.; Whittington, D. A.; Patel, V. F.; Chen, K.; Dineen, T. A.; Epstein, O.; Graceffa, R.; Hickman, D.; Kiang, Y.-H.; Louie, S.; Luo, Y.; Wahl, R. C.; Wen, P. H.; Wood, S.; Fremau, R. T., Jr. Structure- and property-based design of aminooxazoline xanthenes as selective, orally efficacious, and CNS penetrable BACE inhibitors for the treatment of Alzheimer's disease. *J. Med. Chem.* **2012,** *55,* 9156–9169.
38. Dineen, T. A.; Chen, K.; Cheng, A. C.; Derakhchan, K.; Epstein, O.; Esmay, J.; Hickman, D.; Kreiman, C. E.; Marx, I. E.; Wahl, R. C.; Wen, P. H.; Weiss, M. M.; Whittington, D. A.; Wood, S.; Fremau, R. T., Jr.; White, R. D.; Patel, V. F. Inhibitors of β-site amyloid precursor protein cleaving enzyme (BACE1): identification of (*s*)-7-(2-fluoropyridin-3-yl)-3-((3-methyloxetan-3-yl)ethynyl)-5′*h*-spiro[chromeno[2,3-*b*]pyridine-5,4′-oxazol]-2′-amine (AMG-8718). *J. Med. Chem.* **2014,** *57,* 9811–9831.
39. Fielden, M. R.; Werner, J.; Jamison, J. A.; Coppi, A.; Hickman, D.; Dunn, R. T.; Trueblood, E.; Zhou, L.; Afshari, C. A.; Lightfoot-Dunn, R. Retinal toxicity induced by a novel β-secretase inhibitor in the sprague-dawley rat. *Toxicol. Pathol.* **2015,** *43,* 581–592.
40. White, R.; Cheng, Y.; Minatti, A. El.; Yang, B.; Zheng, X. M.; Lopez, P.; Human, J. B.; Epstein, O.; Judd, T.; Sham, K.; et al. Preparation of Amino-Oxazine and Amino-Dihydrothiazine Compounds as β-Secretase Modulators. PCT Int. Appl. WO2013044092 published March 28, 2013.
41. Lewis, R. T.; Choquette, D.; Epstein, O.; Guzman-Perez, A.; Hua, Z.; Human, J. B.; Judd, T.; Liu, Q.; Lopez, P.; Minatti, A. E.; et al. Aminodihydrothiazine and Aminodioxidodihydrothiazine Compounds as Beta-Secretase Antagonists and Their Preparation. PCT Int. Appl. WO2014059185 published April 17, 2014.

42. White, R.; Allen, J. R.; Epstein, O.; Hong, F.-T.; Hua, Z.; Human, J. B.; Lopez, P.; Olivieri, P. R.; Romero, K.; Schenkel, L.; et al. Fused Multi-Cyclic Sulfone Compounds as Inhibitors of Beta-Secretase and Methods of Use and Preparation Thereof. U.S. Pat. Appl. 20140213581 published July 31, 2014.
43. Minatti, A. E.; Low, J. D.; Allen, J. R.; Chen, J.; Chen, N.; Cheng, Y.; Judd, T.; Liu, Q.; Lopez, P.; Qian, W.; et al. Preparation of Perfluorinated 5,6-Dihydro-4H-1,3-Oxazin-2-Amine Compounds as β-Secretase Inhibitors and Methods of Use. PCT Int. Appl. WO2014134341 published September 4, 2014.
44. Minatti, A. E.; Low, J. D.; Allen, J. R.; Amegadzie, A.; Brown, J.; Frohn, M. J.; Guzman-Perez, A.; Harrington, P. E.; Lopez, P.; Ma, V. V.; et al. Preparation of Cyclopropyl Fused 1,3-Oxazin-2-Amine Compounds as Beta-Secretase Inhibitors and Methods of Use. PCT Int. Appl. WO2014138484 published September 12, 2014.
45. Lewis, R. T.; Allen, J. R.; Brown, J.; Guzman-Perez, A.; Hua, Z.; Judd, T.; Liu, Q.; Olivieri, P. R.; Schenkel, L.; Stellwagen, J.; et al. Bridged Bicyclic Aminothiazine Dioxide Compounds as Inhibitors of Beta-Secretase and Their Preparation. PCT Int.WO2015017407 published February 5, 2015.
46. Yu, J.; Koelsch, G.; Li, A.; Turner, R. T.; Bilcer, G. M.; Grove, C.; Hsu, H. H.; Shitaka, Y.; Hamakawa, N.; Terashita, S.; Matsuoka, N.; Tang, J.; Ghosh, A. K.; Hey, J. A. In Vivo Efficacy of BACE-1 Inhibitor CTS21166 (ASP1702) in Rat CNS Compartments. *Alzheimer's Dement.* **2009,** *5* (4), 430–431. supplement P3-298.
47. Munakata, R.; Inoue, M.; Tominaga, H.; Yamasaki, S.; Shiina, Y.; Samizu, K.; Hamaguchi, H.; Hong, L. Chromane Compounds. PCR Patent Application WO2013181202 published December 5, 2013.
48. Edwards, P. D.; Albert, J. S.; Sylvester, M.; Aharony, D.; Andisik, D.; Callaghan, O.; Campbell, J. B.; Carr, R. A.; Chessari, G.; Congreve, M.; Frederickson, M.; Folmer, R. H. A.; Geschwindner, S.; Koether, G.; Kolmodin, K.; Krumrine, J.; Mauger, R. C.; Murray, C. W.; Olsson, L.-L.; Patel, S.; Spear, N.; Tian, G. Application of fragment-based lead generation to the discovery of novel, cyclic amidine β-secretase inhibitors with nanomolar potency, cellular activity, and high ligand efficiency. *J. Med. Chem.* **2007,** *50,* 5912–5925.
49. Swahn, B.-M.; Holenz, J.; Kihlström, J.; Kolmodin, K.; Lindström, J.; Plobeck, N.; Rotticci, D.; Sehgelmeble, F.; Sundström, M.; von Berg, S.; Fälting, J.; Georgievska, B.; Gustavsson, S.; Neelissen, J.; Ek, M.; Olsson, L. L.; Berg, S. Aminoimidazoles as BACE-1 inhibitors: The challenge to achieve in vivo brain efficacy. *Bioorg. Med. Chem. Lett.* **2012,** *22,* 1854–1859.
50. Swahn, B.-M.; Kolmodin, K.; Karlström, S.; von Berg, S.; Söderman, P.; Holenz, J.; Berg, S.; Lindström, J.; Sundström, M.; Turek, D.; Kihlström, J.; Slivo, C.; Andersson, L.; Pyring, D.; Rotticci, D.; Öhberg, L.; Kers, A.; Bogar, K.; Von Kieseritzky, F.; Bergh, M.; Olsson, L.-L.; Janson, J.; Eketjäll, S.; Georgievska, B.; Jeppsson, F.; Fälting, J. Design and synthesis of β-site amyloid precursor protein cleaving enzyme (BACE1) inhibitors with in vivo brain reduction of β-amyloid peptides. *J. Med. Chem.* **2012,** *55,* 9346–9361.
51. Jeppsson, F.; Eketjäll, S.; Janson, J.; Karlström, S.; Gustavsson, S.; Olsson, L.-L.; Radesäter, A.-R.; Ploeger, B.; Cebers, G.; Karin Kolmodi, K.; Swahn, B.-M.; von Berg, S.; Fälting, S. Discovery of AZD3839, a potent and selective BACE1 inhibitor clinical candidate for the treatment of alzheimer disease. *J. Biol. Chem.* **2012,** *287,* 41245–41257.
52. Quartino, A.; Huledal, G.; Sparve, E.; Lüttgen, M.; Bueters, T.; Karlsson, P.; Olsson, T.; Paraskos, J.; Maltby, J.; Claeson-Bohnstedt, K.; Lee, C.-M.; Alexander, R.; Fälting, J.; Paulsson, B. Population pharmacokinetic and pharmacodynamic analysis of plasma $A\beta_{40}$ and $A\beta_{42}$ following single oral doses of the BACE1 inhibitor AZD3839 to healthy volunteers. *Clin. Pharmacol. Drug Dev.* **2015,** *3,* 396–405.
53. Viklund, J.; Kolmodin, K.; Nordvall, G.; Swahn, B.-M.; Svensson, M.; Gravenfors, Y.; Rahm, F. Creation of novel cores for β-secretase (BACE-1) inhibitors: A multiparameter lead generation strategy. *ACS Med. Chem. Lett.* **2014,** *5,* 440–445.
54. Ginman, T.; Viklund, J.; Malmstrom, J.; Blid, J.; Emond, R.; Forsblom, R.; Johansson, A.; Kers, A.; Lake, F.; Sehgelmeble, F.; Streky, K. J.; Bergh, M.; Lindgren, A.; Johansson, P.; Jeppsson, F.; Fälting, J.; Gravenfors, Y.; Rahm, F. Core refinement toward permeable β-secretase (BACE-1) inhibitors with low hERG activity. *J. Med. Chem.* **2013,** *56,* 4181–4205.
55. Csjernyik, G.; Karlström, S.; Kers, A.; Kolmodin, K.; Nylöf, M.; Öhberg, L.; Rakos, L.; Öhberg, L.; Rakos, L.; Sandberg, L.; Sehgelmeble, F.; Söderman, P.; Swahn, B-M.; Von Berg, S. Compounds and Their Use as Bace Inhibitors. PCT Int. Appl. WO2012087237 published June 28, 2012.
56. Bohlin, M.H.; Stewart, C.R. Camsylate Salt. PCT Int. Appl. WO2013190302 published December 27, 2013.
57. https://clinicaltrials.gov/ct2/show/NCT02245737?term=AZD3293&rank=8.
58. Eketjäll, S.; Janson, J.; Kaspersson, K.; Bogstedt, A.; Jeppsson, F.; Fälting, J.; Budd Haeberlein, S.; Kugler, A. R.; Alexander, R. C.; Cebers, G. AZD3293: A novel, orally active BACE1 inhibitor with high potency and permeability and markedly slow off-rate kinetics. *J. Alzheimers Dis.* **2016,** *50,* 1109–1123.
59. Alexander, R.; Budd Haeberlein, S.; Rosen, L.; Russell, M.; Kugler, A.; Cebers, G.; Naidong, Y.; Olsson, T.; Han, D.; Ereshefsky, L. AZD3293 a Novel BACE1 Inhibitor: Pharmacokinetics and Effects on Plasma and CSF A-Beta Peptides Following Multiple-Dose Administration in Alzheimer's Disease Patients. ADPD Conference, Nice, March 18–22, 2015. *Neurodegener. Dis.* **2015,** *352,* 702 (1969).
60. Karlström, S.; Csjernyik, G.; Swahn, B.-M.; Sandberg, L.; Kolmodin, K.; Söderman, P.; Öhberg, L. 2H-Imidazol-4-Amine Compounds and Their Use as Bace Inhibitors. PCT Int. Appl. WO2013190298 published December 27, 2013.
61. Karlström, S.; Sandberg, L.; Söderman, P; Kolmodin, K.; Öhberg, L. Cyclohexane-1,2′-Naphthalene-1′,2″-Imidazole Compounds and Their Use as Bace Inhibitors. PCT Int. Appl. WO2013190300 published December 27, 2013.
62. Karlström, S.; Söderman, P.; Swahn, B.-M.; Laszlo, R.; Öhberg, L. Cycloalkyl Ether Compounds and Their Use as Bace Inhibitors. PCT Int. Appl. WO2013190301 published December 27, 2013.
63. Karlström, S.; Söderman, P.; Rakos, L.; Öhberg, L.; Kolmodin, K.; Sandberg, L. Cyclohexane-1,2′-Indene-1′,2″-Imidazol Compounds and Their Use as Bace Inhibitors. PCT Int. Appl. WO2013190299 published April 18, 2013.
64. Minidis, A.; Rahm, F.; Viklund, J. Mono-Fluoro Beta-Secretase Inhibitors. PCT Int. Appl. WO2013054108 published December 27, 2013.
65. Fuchs, K.; Dorner-Ciossek, C.; Handschuh, S.; Heine, N.; Hoerer, S.; Klinder, K. Substituted Amino-Benzimidazoles, Medicaments Comprising Said Compound, Their Use and Their Method of Manufacture. PCT Int. Appl. WO2009092566 published July 30, 2009.
66. Fuchs, K.; Heine, N.; Eickmeier, C.; Handschuh, S.; Dorner-Ciossek, C.; Hoerer, S. Substituted Amino-Quinazolinones, Medicaments Comprising Said Compound, Their Use and Their Method of Manufacture. PCT Int. Appl. WO2009007300 published June 4, 2009.
67. Dillard, L.W.; Yuan, J.; Jia, L.; Zheng, Y. Inhibitors of Beta-Secretase. PCT Int. Appl. WO2010021680, April 15, 2010.
68. Dillard, L.W. Yuan, J.; Leftheris, K.; Venkatraman, S.; Wu, G.; Jia, L.; Xu, Z.; Cacatian, S.; Morales-Ramos, A.; Singh, S.; Zheng, Y. Inhibitors of Beta-Secretase. PCT Int. Appl. WO2011106414 published September 1, 2011.
69. Venkatraman, S.; Yuan, J.; Zheng, Y. Inhibitors of Beta-Secretase. PCT Int. Appl. WO2014052398 published January 29, 2015.
70. Cacatian, S.; Claremon, D. A.; Dillard, L. W.; Fuchs, K.; Heine, N.; Jia, L.; Leftheris, K.; Mckeever, B.; Morales-Ramos, A.; Singh, S.; et al. Inhibitors of Beta-Secretase. PCT Int. Appl. WO2010105179 published September 16, 2010.
71. Bukhtiyarov, Y.; Cacatian, S.; Dillard, L. W.; Dorner-Ciossek, C.; Fuchs, K.; Jia, L.; Lala, D. S.; Morales-Ramos, A.; Rast, G.; Reeves, J.; Singh, S. B.; Venkatraman, S.; Xu, Z.; Yuan, J.; Zhao, Y.; Zheng, Y. Spirocyclic Acylguanidine Derivatives as β-Secretase Inhibitors Useful in Treatment of Diseases Characterized by Production of β-Amyloid Aggregates and Their Preparation. PCT Int. Appl. WO2013134085 published September 12, 2013.
72. Bukhtiyarov, Y.; Cacatian, S.; Dillard, L. W.; Dorner-Ciossek, C.; Fuchs, K.; Gross, U.; Heine, N.; Jia, L.; Lala, D. S;. Morales-Ramos, A.; et al. Inhibitors of Beta-Secretase. PCT Int. Appl. WO2014035860 published January 15, 2015.
73. Borta, A.; Nicolas, L.; Kleiner, O.; Kammerer, K.-P.; Schaible, J.; Pietzko, K.; Podhorna, J.; Dorner-Ciossek, C.; Scholpp, J. Single Oral Doses of the Novel BACE Inhibitor BI 1181181 Significantly Reduce Concentrations of Cerebrospinal Fluid Amyloid-Beta Peptides in Healthy Subjects. Alzheimer's Association International Conference, Washington, DC, 2015. *Alzheimers Dement.* **2015,** *11* (Suppl.), 740.
74. http://www.alzforum.org/news/research-news/bace-inhibitor-trial-put-hold.
75. Wu, Y.-J. Compounds for the reduction of beta-amyloid production. PCT Application WO2012162334 published November 29, 2012.
76. Thompson III, L. A.; Shi, J.; Wu, Y-J.; Marcin, L. R.; Rajamani, R.; Higgins, M. A. Tricyclic compounds as inhibitors for the production of beta-amyloid. PCT Application WO2012162330 published November 29, 2012.

77. Wu, Y.-J.; Gueron, J. M. 4,6-diarylaminothiazines as bace1 inhibitors and their use for the reduction of beta-amyloid production. PCT Application WO2014098831 published June 26, 2014.
78. Wu, Y.-J.; Guernon, J.; Yang, F.; Snyder, L.; Shi, J.; McClure, A.; Rajamani, R.; Park, H.; Ng, A.; Lewis, H.; Chang, C.; Camac, D.; Toyn, J. H.; Ahlijanian, M. K.; Albright, C. F.; Macor, J. E.; Thompson, L. A. Targeting the BACE1 active site flap leads to a potent inhibitor that elicits robust brain aβ reduction in rodents. *ACS Med. Chem. Lett.* **2016,** *7,* 271–276.
79. Suzuki, Y.; Motoki, T.; Kaneko, T.; Takaishi, M.; Ishida, T.; Takeda, K.; Kita, Y.; Yamamoto, N.; Khan, A.; Dimopoulos, P. Condensed aminodihydrothiazine derivative. PCT Application WO2009091016 published July 23, 2009.
80. Zaima, Y.; Kazama, K.; Arase, S.; Nagane, K.; Horie, K, Ueki, Y. Pharmaceutical composition of fused aminodihydrothiazine derivative. PCT Application WO2016056638 published April 14, 2016.
81. Motoki, T.; Takeda, K.; Kita, Y.; Takaishi, M.; Suzuki, Y.; Ishida, T. Novel fused aminodihydrothiazine derivative. PCT Application WO2010038686 published April 8, 2010.
82. Takaishi, M.; Ishida, T. Fused aminodihydrothiazine derivatives. PCT Application WO2012098461 published August 15, 2013.
83. Dimopoulos, P.; Hall, A.; Kita, Y.; Madin, A.; Shuker, N. L. Fused aminodihydrothiazine derivatives. PCT Application WO2012093148 published July 12, 2012.
84. Hall, A.; Farthing, C. N.; Castro Pineiro, J. L. Fused Aminodihydrothiazine Derivatives Useful as BACE Inhibitors. PCT Patent Application WO2012098213 published July 26, 2012.
85. Hall, A.; O'Connor, D. M. Preparation of furo[3,4-d][1,3]thiazinyl compounds as BACE1 inhibitors for treating neurodegenerative diseases. UK Patent Application GB2504615 published February 5, 2014.
86. Castro Pineiro, J. L.; Guerot, C. Preparation of 4a,6,7,7a-tetrahydro-4H-furo[3,2-d][1,3]thiazin-2-amine derivatives for the treatment of Alzheimer-type dementia. UK Patent Application GB2512975 published October 16, 2014.
87. Hall, A.; Farthing, C. N.; Eatherton, A. J. Hexahydropyrrolothiazine compounds. PCT Application WO2014013076 published January 23, 2014.
88. Motoki, T.; Kaneko, T.; Yamamoto, N.; Khan, A. Spiroaminodihydrothiazine derivatives. PCT Application WO2010013794 published February 4, 2010.
89. Castro Pineiro, J. L.; Hall, A.; Madin, A.; Vo, N.-T. Fused Aminodihydropyrimidone Derivatives. PCT Patent Application WO2011009897 published January 27, 2011.
90. Ellard, J. M.; Farthing, C. N.; Hall, A. Fused Aminodihydro-Oxazine Derivatives. PCT Patent Application WO2011009898 published January 27, 2011.
91. Lai, R.; Albala, B.; Kaplow, J. M.; Aluri, J.; Yen, M.; Satlin, A. First-in-human study of E2609, a novel BACE1 inhibitor, demonstrates prolonged reductions in plasma beta-amyloid levels after single dosing. *Alzheimers Dement.* **2012,** *8* (4 Suppl.), P96. 01-06-05.
92. Albala, B.; Kaplow, J. M.; Lai, R.; Matijevic, M.; Aluri, J.; Satlin, A. CSF amyloid lowering in human volunteers after 14 days' oral administration of the novel BACE1 inhibitor E2609. *Alzheimers Dement.* **2012,** *8* (4 Suppl.), S743. S4-04-01.
93. Lai, R. Y. K. First-in-Human Study of E2609, a Novel BACE1 Inhibitor, Demonstrates Prolonged Reductions in Plasma Ab Levels After Single Dosing. *Alzheimer's Association International Conference, Vancouver, July 14– 19, 2012.*
94. https://clinicaltrials.gov/ct2/show/NCT02322021?intr=E2609&rank=3.
95. Hunt, K. W.; Cook, A. W.; Watts, R. J.; Clark, C. T.; Vigers, G.; Smith, D.; Metcalf, A. T.; Gunawardana, I. W.; Burkard, M.; Cox, A. A.; Geck Do, M. K.; Dutcher, D.; Thomas, A. A.; Rana, S.; Kallan, N. C.; DeLisle, R. K.; Rizzi, J. P.; Regal, K.; Sammond, D.; Groneberg, R.; Siu, M.; Purkey, H.; Lyssikatos, J. P.; Marlow, A. X.; Tang, T. P. Spirocyclic β-site amyloid precursor protein cleaving enzyme 1 (BACE1) inhibitors: from hit to lowering of cerebrospinal fluid (CSF) amyloid β in a higher species. *J. Med. Chem.* **2013,** *56,* 3379–3403.
96. Diaz, D.; Dambach, D.; Siu, M.; Hunt, K.; Thomas, A.; Lyssikatos, J.; Liu, X.; Lewin-Koh, S.; McCray, B.; Ford, K. Mitigation of opioid off-target effects and identification of structural drivers of opioid receptor engagement for BACE-1 small molecule inhibitors. *Toxicol. Mech. Methods* **2015,** *25,* 478–486.
97. Thomas, A. A.; Hunt, K. W.; Volgraf, M.; Watts, R. J.; Liu, X.; Vigers, G.; Smith, D.; Sammond, D.; Tang, T. P.; Rhodes, S. P.; et al. Discovery of 7-tetrahydropyran-2-yl chromans: β-site amyloid precursor protein cleaving enzyme 1 (BACE1) inhibitors that reduce amyloid β-protein (Aβ) in the central nervous system. *J. Med. Chem.* **2014,** *57,* 878–902.
98. Thomas, A. A.; Hunt, K. W.; Newhouse, B.; Watts, R. J.; Liu, X.; Vigers, G.; Smith, D.; Rhodes, S. P.; Brown, K. D.; Otten, J. N.; et al. 8-Tetrahydropyran-2-yl chromans: highly selective beta-site amyloid precursor protein cleaving enzyme 1 (BACE1) inhibitors. *J. Med. Chem.* **2014,** *57,* 10112–10129.
99. Volgraf, M.; Chan, L.; Huestis, M. P.; Purkey, H. E.; Burkard, M. L.; Geck Do, M.; Harris, J.; Hunt, K. W.; Liu, X.; Lyssikatos, J. P.; Rana, S.; Thomas, A. A.; Vigers, G. P. A.; Siu, M. Synthesis, characterization, and PK/PD studies of a series of spirocyclic pyranochromene BACE1 inhibitors. *Bioorg. Med. Chem. Lett.* **2014,** *24,* 2477–2480.
100. Yu, Y. J.; Atwal, J. K.; Zhang, Y.; Tong, R. K.; Wildsmith, K. R.; Tan, C.; Bien-Ly, N.; Hersom, M.; Maloney, J. A.; Meilandt, W. J. Therapeutic bispecific antibodies cross the blood-brain barrier in nonhuman primates. *Sci. Transl. Med.* **2014,** *6. 261ra154/1–261ra154/11, 11 pp.*
101. Baxter, E. W.; Conway, K. A.; Kennis, L.; Bischoff, F.; Mercken, M. H.; De Winter, H. L.; Reynolds, C. H.; Tounge, B. A.; Luo, C.; Scott, M. K.; Huang, Y.; Braeken, M.; Pieters, S. M. A.; Berthelot, D. J. C.; Masure, S.; Bruinzeel, W. D.; Jordan, A. D.; Parker, M. H.; Boyd, R. E.; Qu, J.; Alexander, R. S.; Brenneman, D. E.; Reitz, A. B. 2-Amino-3,4-dihydroquinazolines as inhibitors of BACE-1 (β-site app cleaving enzyme): use of structure based design to convert a micromolar hit into a nanomolar lead. *J. Med. Chem.* **2007,** *50,* 4161–4264.
102. Tresadern, G.; Delgado, F.; Delgado, O.; Gijsen, H.; Macdonald, G. J.; Moechars, D.; Rombouts, F.; Alexander, R.; Spurlino, J.; Van Gool, M.; et al. Rational design and synthesis of aminopiperazinones as β-secretase (BACE) inhibitors. *Bioorg. Med. Chem. Lett.* **2011,** *21,* 7255–7260.
103. Rombouts, F. J.; Tresadern, G.; Delgado, O.; Martínez-Lamenca, C.; Van Gool, M.; García-Molina, A.; Alonso de Diego, S. A.; Oehlrich, D.; Prokopcova, H.; Alonso, J. M.; Austin, N.; Borghys, H.; Van Brandt, S.; Surkyn, M.; De Cleyn, M.; Vos, A.; Alexander, R.; Macdonald, G.; Moechars, D.; Gijsen, H.; Trabanco, A. A. 1,4-Oxazine β-secretase 1 (BACE1) inhibitors: From hit generation to orally bioavailable brain penetrant leads. *J. Med. Chem.* **2015,** *58,* 8216–8235.
104. Trabanco-Suarez, A. A.; Gijsen, H. J. M.; Surkyn, M.; Prokopcova, H. 6-Difluoromethyl-5,6-Dihydro-2H-[1,4]Oxazin-3-Amine Derivatives. Int. Appl. WO2013083557 published June 13, 2013.
105. Gijsen, H. J. M.; Van Brandt, S. F. A. 5-(3-Aminophenyl)-5-Alkyl-5,6-Dihydro-2H-[1,4]Oxazin-3-Amine Derivatives. PCT Int. Appl. WO2013083556 published June 13, 2013.
106. Trabanco-Suarez, A. A.; Tresadern, G. J.; Delgado-Jimenez, F. 4,7-Dihydro-Pyrazolo[1,5-a]Pyrazin-6-Ylamine Derivatives Useful as Inhibitors of Beta-Secretase (BACE). PCT Int. Appl. WO2012038438 published March 29, 2012.
107. Trabanco-Suarez, A. A.; Delgado-Jimenez, F.; Vega Ramiro, J. A.; Tresadern, G. J.; Gijsen, H. J. M.; Oehlrich, D. 5,6-Dihydroimidazo[1,2-a]Pyrazine-8-Ylamine Derivatives Useful as Inhibitors of Beta-Secretase (BACE). PCT Int. Appl. WO2012085038 published June 28, 2012.
108. Oehlrich, D.; Gijsen, H. J. M. 4-Amino-6-Phenyl-6,7-Dihydro[1,2,3]Triazolo[1,5-A]Pyrazine Derivatives as Inhibitors of Beta-Secretase (BACE). PCT Int. Appl. WO2014198854 published December 18, 2014.
109. Bel Abed, H.; Van Brandt, S. F. A.; Vega, J.-A.; Gijsen, H. J. M. Simple approach to the synthesis of novel tricyclic BACE1 inhibitor warhead through β-lactam opening. *Tetrahedron Lett.* **2015,** *56,* 4028–4030.
110. Trabanco-Suarez, A. A.; Delgado-Jimenez, F. 3,4-Dihydro-Pyrrolo[1,2-a]Pyrazin-1-Ylamine Derivatives Useful as Inhibitors of Beta-Secretase (BACE). PCT Int. Appl. WO2012120023 published September 13, 2012.
111. Trabanco-Suarez, A. A.; Gijsen, H. J. M.; Van Gool, M. L. M.; Vega Ramiro, J. A.; Delgado-Jimenez, F. 6,7-Dihydropyrazolo[1,5-a]Pyrazine-4-Ylamine Derivatives Useful as Inhibitors of Beta-Secretase (BACE). Int. Appl. WO2012117027 published September 7, 2012.
112. Oehlrich, D.; Gijsen, H. J. M. 4-Amino-6-Phenyl-5,6-Dihydroimidazo[1,5-a]Pyrazine-3(2H)-One Derivatives as Inhibitors of Beta-Secretase (BACE). PCT Int. Appl. WO2014198851 published December 18, 2014.
113. Oehlrich, D.; Gijsen, H. J. M. 4-Amino-6-Phenyl-5,6-Dihydroimidazo[1,5-a]Pyrazine Derivatives as Inhibitors of Beta-Secretase (BACE). PCT Int. Appl. WO2014198853, December 18, 2014.

114. Mateu, N.; Ciordia, M.; Delgado, O.; Sanchez-Rosello, M.; Trabanco, A. A.; Van Gool, M.; Tresadern, G.; Perez-Benito, L.; Fustero, S. A versatile approach to CF_3-containing 2-pyrrolidones by tandem Michael addition–cyclization: Exemplification in the synthesis of amidine class BACE1 inhibitors. *Chem. A Eur. J.* **2015,** *21,* 11719–11726.
115. Audia, J. E.; Mergott, D. J.; Sheehan, S. M.; Watson, B. M. PCT Application WO2009134617 published November 5, 2009.
116. May, P. C.; Dean, R. A.; Lowe, S. L.; Martenyi, F.; Sheehan, S. M.; Boggs, L. N.; Monk, S. A.; Mathes, B. M.; Mergott, D. J.; Watson, B. M.; Stout, S. L.; Timm, D. E.; LaBell, E. S.; Gonzales, C. R.; Nakano, M.; Jhee, S. S.; Yen, M.; Ereshefsky, L.; Lindstrom, T. D.; Calligaro, D. O.; Cocke, P. J.; Hall, D. G.; Friedrich, S.; Citron, M.; Audia, J. E. Robust central reduction of amyloid-β in humans with an orally available, non-peptidic β-secretase inhibitor. *J. Neurosci.* **2011,** *31,* 16507–16516.
117. https://clinicaltrials.gov/ct2/show/NCT00838084?intr=LY2811376&rank=1.
118. Audia, J. E.; Mergott, D. J.; Shi, C. E.; Vaught, G. M.; Watson, B. M.; Winneroski Jr., L. L. Bace inhibitors. PCT Application WO2011005738 published January 13, 2011.
119. May, P. C.; Willis, B. A.; Lowe, S. L.; Dean, R. A.; Monk, S. A.; Cocke, P. J.; Audia, J. E.; Boggs, L. N.; Borders, A. R.; Brier, R. A.; Calligaro, D. O.; Day, T. A.; Ereshefsky, L.; Erickson, J. A.; Gevorkyan, H.; Gonzales, C. R.; James, D. E.; Jhee, S. S.; Komjathy, S. F.; Li, L.; Lindstrom, T. D.; Mathes, B. M.; Martenyi, F.; Sheehan, S. M.; Stout, S. L.; Timm, D. E.; Vaught, G. M.; Watson, B. M.; Winneroski, L. L.; Yang, Z.; Mergott, D. J. The potent BACE1 inhibitor LY2886721 elicits robust central Aβ pharmacodynamic responses in mice, dogs, and humans. *J. Neurosci.* **2015,** *35,* 1199–1210.
120. Green, S. J.; Hembre, E. J.; Mergott, D. J.; Shi, Y.; Watson, B. M.; Winneroski Jr., L. L. Bace inhibitors. PCT Application WO2014204730 published December 24, 2014.
121. Beck, J. P.; Grenn, S. J.; Lopez, J. E.; Mathes, B. M.; Mergott, D. J.; Porter, W. J.; Rankovic, Z.; Shi, Y.; Watson, B. M.; Winneroski Jr., L. L. Tetrahydropyrrolothiazine compounds. PCT Application WO2013151832 published October 10, 2013.
122. Martin, F. M.; Mergott, D. J.; Owton, W. M. Bace inhibitors. PCT Application WO2014066132 published May 1, 2014.
123. Green, S. J.; Mergott, D. J.; Watson, B. M.; Winneroski Jr., L. L. Tetrahydropyrrolothiazine compounds. PCT Application WO2014143579 published September 18, 2014.
124. Coates, D. A.; Losada, P. G. A Tetrahydropyrrolo[3,4-D][1,3]Thiazine-Derivative as BACE Inhibitor. WO2016043996 published March 24, 2016.
125. Martin, F. M. Aminothiazine compounds. PCT Application WO2015138208 published September 17, 2015.
126. Coates, D. A.; Losada, P. G. A tetrahydropyrrolo[3,4-d][1,3]thiazine-derivative as bace inhibitor. PCT Application WO2016043996 published March 24, 2016.
127. May, P. C.; Mergott, D. J. Combination Alzheimer Therapy Using Anti-N3pGlu Abeta Antibodies + a BACE Inhibitor. PCT Patent application published March 24, 2016.
128. Coates, D. A.; Wolfangel, C. D. Tosylate Salt of N-[3-[(4aR, 7aS)-2amino-6-(5-fluoropyrimidin-2-yl)-4,4a,5,7-tetrahydropyrrolo[3,4-d][1,3]thiazin-7a-yl]-4-fluoro-phenyl]-5-methoxy-pyrazine-2-carboxamide. PCT Patent Application WO2016122968 published August 4, 2016.
129. Juhl, K.; Tagmose, L.; Marigo, M. 2-Aminothiazinylheteroaryls as BACE1 inhibitors for the treatment Alzheimer's disease. PCT Application WO2013182638 published December 12, 2013.
130. Juhl, K.; Marigo, M.; Tagmose, L.; Jensen, T. 2-Amino-3, 5, 5-trifluoro-3, 4, 5, 6-tetrahydropyridines as BACE1 inhibitors for treatment of Alzheimer's disease. PCT Application WO2015124576 published August 27, 2015.
131. Juhl, K.; Tagmose, L.; Marigo, M. 2-Amino-3,5-difluoro-3,6-dimethyl-6-phenyl-3,4,5,6-tetrahydropyridines as BACE1 Inhibitors for Treating Alzheimer's Disease. PCT Patent Application WO2016075062 published May 19, 2016.
132. Juhl, K.; Tagmose, L.; Marigo. M. 2-Amino-5,5-difluoro-6-(fluoromethyl)-6-phenyl-3,4,5,6-tetrahydropyridines as BACE1 Inhibitors. PCT Patent Application WO2016075064 published May 19, 2016.
133. Juhl, K.; Tagmose, L.; Marigo. 2-Amino-6-(difluoromethyl)-5,5-difluoro-6-phenyl-3,4,5,6-tetrahydropyridines as BACE1 Inhibitors. PCT Patent Application WO2016075063 published May 19, 2016.
134. Quattropani, A.; Swinnen, D. 2-Amino-6-(difluoromethyl)- 5,5-difluoro-6-phenyl-3,4,5,6-tetrahydropyridines as BACE1 inhibitors. PCT WO2013178322, published December 5, 2013.
135. Medina Padilla, M.; Herrero Santos, S.; Garcia Palomero, E. Spiro tetrahydro - benzothiophen derivatives useful for the treatment neurodegenerative diseases. PCT Application WO2011015646 published February 10, 2011.
136. Tintelnot-Blomley, M.; Veenstra, S. J. Pyrazine Derivatives and Their Use in the Treatment of Neurological Disorders. WO2011080176 published July 7, 2011.
137. Badiger, S.; Chebrolu, M.; Frederiksen, M.; Holzer, P.; Hurth, K.; Lueoend, R. M.; Machauer, R.; Moebitz, H.; Neumann, U.; Ramos, R.; Rueeger, H.; Tintelnot-Blomley, M.; Veenstra, S. J.; Voegtle, M. Oxazine Derivatives and Their Use as BACE Inhibitors for the Treatment of Neurological Disorders. WO201100943 published January 27, 2011.
138. Badiger, S.; Chebrolu, M.; Frederiksen, M.; Holzer, P.; Hurth, K.; Li, L.; Liu, H.; Lueoend, R. M.; Machauer, R.; Moebitz, H.; Neumann, U.; Ramos, R.; Rueeger, H.; Schaefer, M.; Tintelnot-Blomley, M.; Veenstra, S. J.; Voegtle, M.; Xiong, X. Oxazine Derivatives and Their Use as BACE Inhibitors for the Treatment of Neurological Disorders. WO2012006953 published January 19, 2012.
139. Rueeger, H. BACE2 Inhibitors for the Treatment of Metabolic Disorders. WO2012095521 published July 19, 2012.
140. Neumann, U.; Rueeger, H.; Machauer, R.; Veenstra, S. J.; Lueoend, R. M.; Tintelnot-Blomley, M.; Laue, G.; Beltz, K.; Vogg, B.; Schmid, P.; Frieauff, W.; Shimshek, D. R.; Staufenbiel, M.; Jacobson, L. H. A novel BACE inhibitor NB-360 shows a superior pharmacological profile and robust reduction of amyloid-β and neuroinflammation in APP transgenic mice. *Mol. Neurodegener.* **2015,** *10,* 44.
141. Shimshek, D. R.; Jacobson, L. H.; Kolly, C.; Zamurovic, N.; Balavenkatraman, K. K.; Morawiec, L.; Kreutzer, R.; Schelle, J.; Jucker, M.; Bertschi, B.; Theil, D.; Heier, A.; Bigot, K.; Beltz, K.; Machauer, R.; Brzak, I.; Perrot, L.; Neumann, U. Pharmacological BACE1 and BACE2 inhibition induces hair depigmentation by inhibiting PMEL17 processing in mice. *Sci. Rep.* **2016,** *6,* 21917.
142. Hurth, K.; Lueoend, R. M.; Machauer, R.; Neumann, U.; Rueeger, H.; Schaefer, M.; Tintelnot-Blomley, M.; Veenstra, S. J.; Voegtle, M. Oxazine Derivatives and Their Use in the Treatment of Neurological Disorders. WO2012095463 published July 19, 2012.
143. Badiger, S.; Chebrolu, M.; Hurth, K.; Jacquier, S.; Lueoend, R. M.; Machauer, R.; Rueeger, H.; Tintelnot-Blomley, M.; Veenstra, S. J.; Voegtle, M. Novel Heterocycle Derivatives and Their Use in the Treatment of Neurological Disorders. WO2012095469 published July 19, 2012.
144. Hurth, K.; Jacquier, S.; Machauer, R.; Rueeger, H.; Tintelnot-Blomley, M.; Veenstra, S. J.; Voegtle, M. Novel Oxazine Derivatives and Their Use in the Treatment of Disease. WO2013054291 published April 18, 2013.
145. https://www.novartis.com/news/media-releases/novartis-announces-global-partnership-amgen-develop-and-commercialize-pioneering.
146. A Study of CAD106 and CNP520 Versus Placebo in Participants at Risk for the Onset of Clinical Symptoms of Alzheimer's Disease (Generation), https://clinicaltrials.gov/ct2/show/NCT02565511.
147. Brodney, M. A.; Barreiro, G.; Ogilvie, K.; Hajos-Korcsok, E.; Murray, J.; Vajdos, F.; Ambroise, C.; Christoffersen, C.; Fisher, K.; Lanyon, L.; Liu, J. H.; Nolan, C. E.; Withka, J. M.; Borzilleri, K. A.; Efremov, I.; Oborski, C. E.; Varghese, A.; O'Neill, B. T. Spirocyclic Sulfamides as β-Secretase 1 (BACE-1) Inhibitors for the Treatment of Alzheimer's Disease: Utilization of Structure Based Drug Design, WaterMap, and CNS Penetration Studies To Identify Centrally Efficacious Inhibitors. *J. Med. Chem.* **2012,** *55,* 9224–9239.
148. O'Neill, B. T.; Brodney, M.; Hajos-Korcsok, E.; Karanian, D.; Leung, L.; Lu, Y.; Leil, T.; Nicholas, T.; Borzilleri, K.; Barreiro, G.; Ogilvie, K.; Vandal, G.; Bell, J.; Huang, Y.; Zhou, J.; Washman, L.; Billing, B.; Proud, A.; Fisher, K. β-Secretase Inhibitors for the Treatment of Alzheimer's Disease. *Proteinase 2013—8th RSC/SCI Symposium on Proteinase Inhibitor Design, 15–16th April 2013, Basel, Switzerland.*
149. Brodney, M. A. Lactams as Beta Secretase Inhibitors. PCT Patent Application WO2012172449 published December 20, 2012.
150. Henegar, K. E.; Lira, R.; Kim, H.; Gonzalez-Hernandez, J. Process Development and Scale-up of a β-Secretase Inhibitor via a Stereospecific Jocic Reaction. *Org. Process. Res. Dev.* **2013,** *17,* 985–990.
151. A Study to Observe Safety and Concentrations of PF-05297909 and Proteins in Both Blood and Cerebrospinal Fluid After a Single Dose of PF-05297909 in Healthy Adults, NCT01462851, https://clinicaltrials.gov/ct2/show/NCT01462851?intr=PF-05297909&rank=1.
152. Bell, J.; O'Neill, B. T.; Brodney, M.; Hajos-Korcsok, E.; Lu, Y.; Riddell, D.; Ito, K.; Ueckert, S.; Nichols, T. A Novel BACE Inhibitor (PF-05297909): A Two-Part Adaptive Design to Evaluate Safety, Pharmacokinetics and Pharmacodynamics for Modifying Beta-Amyloid in a First-in-Human Study. *Alzheimers Dement.* **2013,** *9* (4 Suppl.), 287. http://dx.doi.org/10.1016/j.jalz.2013.05.578. Poster abstract P 1–351.

153. Efremov, I. V.; Vajdos, F. F.; Borzilleri, K. A.; Capetta, S.; Chen, H.; Dorff, P. H.; Dutra, J. K.; Goldstein, S. W.; Mansour, M.; McColl, A.; Noell, S.; Oborski, C. E.; OÇonnell, T. N.; O'Sullivan, T. J.; Pandit, J.; Wang, H.; Wei, B. Q.; Withka, J. M. Discovery and Optimization of a Novel Spiropyrrolidine Inhibitor of β-Secretase (BACE1) through Fragment-Based Drug Design. *J. Med. Chem.* **2012,** *55,* 9069–9088.
154. Butler, C. R.; Brodney, M. A.; Beck, E. M.; Barreiro, G.; Nolan, C. E.; Pan, F.; Vajdos, F.; Parris, K.; Varghese, A. H.; Helal, C. J.; Lira, R.; Doran, S. D.; Riddell, D. R.; Buzon, L. M.; Dutra, J. K.; Martinez-Alsina, L. A.; Ogilvie, K.; Murray, J. C.; Young, J. M.; Atchison, K.; Robshaw, A.; Gonzales, C.; Wang, J.; Zhang, Y.; O'Neill, B. T. Discovery of a Series of Efficient, Centrally Efficacious BACE1 Inhibitors through Structure-Based Drug Design. *J. Med. Chem.* **2015,** *58,* 2678–2702.
155. Beck, E. M.; Brodney, M. A.; Butler, C. R.; Davoren, J. E. Alkyl-substituted hexahydropyrano[3,4-d] [1,3]thiazin-2-amine compounds. PCT Application WO2014045162 published March 27, 2014.
156. Brodney, M. A.; Butler, C. R.; Helal, C. J.; O'Neill, B. T. Hexahydropyrano [3,4-d][1,3] thiazin-2-amine compounds. PCT Application WO2013030713 published March 7, 2013.
157. Beck, E. M.; Brodney, M. A.; Butler, C. R.; O'Neill, B. T. Substituted phenyl hexahydropyrano[3,4-d][1,3]thiazin-2-amine compounds. PCT Application WO2014125397 published August 21, 2014.
158. Beck, E. M.; Brodney, M. A.; Butler, C. R.; Davoren, J. E.; O'Neill, B. T. Heterocyclic substituted hexahydropyrano [3,4-D] [1,3] thiazin- 2 -amine compounds as inhibitors of APP, BACE1 and BACE 2. PCT Application WO2013164730 published November 7, 2013.
159. Brodney, M. A.; Beck, E. M.; Butler, C. R.; Barreiro, G.; Johnson, E. F.; Riddell, D.; Parris, K.; Nolan, C. E.; Fan, Y.; Atchison, K.; Gonzales, C.; Robshaw, A. E.; Doran, S. D.; Bundesmann, M. W.; Buzon, L.; Dutra, J.; Henegar, K.; LaChapelle, E.; Hou, X.; Rogers, B. N.; Pandit, J.; Lira, R.; Martinez-Alsina, L.; Mikochik, P.; Murray, J. C.; Ogilvie, K.; Price, L.; Sakya, S. M.; Yu, A.; Zhang, Y.; O'Neill, B. T. Utilizing Structures of CYP2D6 and BACE1 Complexes To Reduce Risk of Drug–Drug Interactions with a Novel Series of Centrally Efficacious BACE1 Inhibitors. *J. Med. Chem.* **2015,** *58,* 3223–3252.
160. Brodney, M. A.; Butler, C. R.; Beck, E. M.; Davoren, J. E.; Lachapelle, E. A.; O'Neill, B. T. PCT Application WO2014125394 published August 21, 2014.
161. Brodney, M. A.; Butler, C. R.; Lachapelle, E. A.; O'Neill, B. T. PCT Application WO2014097038 published June 26, 2014.
162. Brodney, M. A.; Beck, E. M.; Butler, C. R.; Davoren, J. E.; O'Neill, B. T. PCT Application WO2014091352 published June 19, 2014.
163. Brodney, M. A.; Beck, E. M.; Butler, C. R.; Zhang, L.; O'Neill, B. T.; Barreiro, G.; Lachapelle, E. A.; Rogers, B. N. 2-Amino-6-methyl-4,4a,5,6-tetrahydropyrano[3,4-d][1,3] thiazin-8a(8H)-yl-1,3-thiazol-4-yl amides. PCT Patent Application WO2015155626 published October 15, 2015.
164. Banner, D.; Hilpert, H.; Humm, R.; Mauser, H.; Mayweg, A. V.; Ricklin, F.; Rogers-Evans, M. Dihydropyrimidones for Use as BACE 2 Inhibitors. PCT Patent Application WO2010128058 published November 11, 2010.
165. Banner, D.; Gabellieri, E.; Guba, W.; Hilpert, H.; Hornsperger, B.; Humm, R.; Mauser, H.; Mayweg, A. V.; Narquizian, R.; Pinard, E.; Rogers-Evans, M.; Woltering, T.; Wostl, W. 1,4,5,6-Tetrahydro-pyrimidin-2-ylamine Compounds. PCT Patent Application WO2012019966 published February 16, 2012.
166. Beauchamp, J.; Benardeau, A.; Hilpert, H.; Migliorini, C.; Riboulet, W.; Wang, W. 2-Aminodihydro[1,3]thiazines as BACE 2 Inhibitors for the Treatment of Diabetes. PCT Patent Application WO2011029803.
167. Woltering, T. Cyclopropyl-Fused-1,3-Thiazepines As BACE 1 Inhibitors. PCT Patent Application WO2013004676 published January 10, 2013.
168. Andreini, M.; Banner, D.; Guba, W.; Hilpert, H.; Mauer, H.; Mayweg, A. V.; Narquizian, R.; Power, E.; Rogers-Evans, M.; Travagli, M; Valacchi, M.; Woltering, T.; Wostl, W. 3-Amino-5-phenyl-5,6-dihydro-2H-[1,4]oxazine Derivatives. PCT Patent Application WO2011020806 published February 24, 2011.
169. Andreini, M.; Gabellieri, E.; Guba, W.; Hilpert, H.; Mauser, H.; Mayweg, A. V.; Narquizian, R.; Power, E.; Travagli, M.; Woltering, T.; Wostl, W. 1,4-Oxazines as BACE1 and/or BACE2 inhibitors. PCT Patent Application WO2012098064 published July 26, 2012.
170. Andreini, M.; Gaallieir, E.; Narquizian, R.; Travagli, M.; Wostl, W. 1,4-Oxazines as BACE1 and/or BACE2 Inhibitors. PCT Patent Application WO2012104263 published August 9, 2012.
171. Banner, D.; Guba, W.; Hilpert, H.; Humm, R.; Mauser, H.; Mayweg, A. V.; Narquizian, R.; Power, E.; Rogers-Evans, M.; Rombach, D.; Woltering, T.; Wostl, W. 2,5,6,7-Tetrahydro-[1,4]oxazepin-3-ylamine or 2,3,6,7-Tetrahydro-[1,4]oxaepin-5-ylamine Compounds. PCT Patent Application WO2011138293 published November 10, 2011.
172. Gabellieri, E.; Guba, W.; Hilpert, H.; Mauser, H.; Mayweg, A. V.; Rogers-Evans, M.; Rombach, D.; Thomas, A.; Woltering, T.; Wostl, W. 1,4-Oxazines as BACE1 and/or BACE2 Inhibitors. PCT Patent Application WO2012126791 published September 27, 2012.
173. Hilpert, H.; Narquizin, R. 1,4-Oxazines as BACE1 and/or BACE2 Inhibitors. PCT Patent Application WO2012110459 published August 23, 2012.
174. Narquizian, R.; Woltering, T.; Wostl, W. 1,4-Oxazines as BACE1 and/or BACE2 Inhibitors. PCT PATENT Application WO2012136603 published October 11, 2012.
175. Anreini, M.; Gabellieri, E.; Guba, W.; Marconi, G.; Narquizian, R.; Power, E.; Travagli, M.; Woltering, T.; Wostl, W. 4,5-Dihydro-oxazol-2-ylamine Derivatives. PCT Patent Application WO2009103626 published August 27, 2009.
176. Banner, D.; Hilpert, H.; Mauser, H.; Mayweg, A. V.; Rogers-Evans, M. Amino Oxazine Derivatives. PCT Application WO2011070029 published June 16, 2011.
177. Hopkins, A. L.; Groom, C. R.; Alex, A. Ligand efficiency: a useful metric for lead selection. *Drug Discov. Today* **2004,** *9,* 430–431.
178. Kuntz, I. D.; Chen, K.; Sharp, K. A.; Kollman, P. A. The maximal affinity of ligands. *Proc. Natl. Acad. Sci. U. S. A.* **1999,** *96,* 9997–10002.
179. Hopkins, A. L.; Groom, C. R.; Alex, A. Ligand efficiency: a useful metric for lead selection. *Drug Discov. Today* **2004,** *9,* 430–431.
180. Hilpert, H.; Guba, W.; Woltering, T. J.; Wostl, W.; Pinard, E.; Mauser, H.; Mayweg, A. V.; Rogers-Evans, M.; Humm, R.; Krummenacher, D.; Muser, T.; Schnider, C.; Jacobsen, H.; Ozmen, L.; Bergadano, A.; Banner, D. W.; Hochstrasser, R.; Kuglstatter, A.; David-Pierson, P.; Fischer, H.; Polara, A.; Narquizian, R. β-Secretase (BACE1) Inhibitors with High in Vivo Efficacy Suitable for Clinical Evaluation in Alzheimer's Disease. *J. Med. Chem.* **2013,** *56,* 3980–3995.
181. Banner, D.; Guba, W.; Hilpert, H.; Mauser, H. Mayweg, A. V.; Narquizian, R.; Pinard, E.; Power, E.; Rogers-Evans, M.; Woltering, T.; Wostl, W. 2-Amino-5, 5-Difluoro-5, 6-Dihydro-4H-oxazines as BACE 1 and/or BACE 2 Inhibitors. PCT Patent Application WO2011069934 published June 16, 2011.
182. Guba, W.; Hilpert, H. Kuglstatter, H.; Limberg, A.; Obst Sander, U.; Pinard, E.; Wostl, W. Fluoro-[1,3]oxazines as BACE1 Inhibitors. PCT Patent Application WO2014114532 published July 31, 2014.
183. Woltering, T. Halogen-alkyl-1,3 Oxazines as BACE1 and/or BACE2 Inhibitors. PCT Patent Application WO2012168164 published December 13, 2012.
184. Hilpert, H.; Humm, R.; Woltering, T. Fluoromethyl-5,6-dihydro-4H-[1,3]oxazines. PCT Patent Application WO2013110622 published August 1, 2013.
185. Jacobsen, H.; Ozmen, L.; Caruso, A.; Narquizian, R.; Hilpert, H.; Jacobsen, B.; Terwel, D.; Tanghe, A.; Bohrmann, B. Combined Treatment with a BACE Inhibitor and Anti-Aβ Antibody Gantenerumab Enhances Amyloid Reduction in APP_{London} Mice. *J. Neurosci.* **2014,** *34,* 11621–11630.
186. Hilpert, H.; Wostl, W. 1,3-Oxazines as BACE1 and/or BACE2 Inhibitors. PCT Patent Application WO2012139993 published October 18, 2012.
187. Hilpert, H.; Humm, R.; Muser, T.; Schnider, C.; Wermuth, R.; Woltering, T. BACE1 Inhibitors. PCT Patent Application WO2014166906 published October 16, 2014.
188. Hilpert, H.; Narquizian, R.; Pinard, E.; Polara, A.; Rogers-Evans, M.; Woltering, T.; Wostl, W. 1,3-Oxazines as BACE1 and/or BACE2 Inhibitors. PCT Patent Application WO2012156284 published November 22, 2012.
189. Guba, W.; Kuglstatter, A.; Obst Sander, U.; Peters, J.-U.; Woltering, T. 1,3-Oxazine-2-amine Derivatives Acting as BACE Inhibitors for the Treatment of Alzheimer's Disease. PCT Patent Application WO2015132141 published September 11, 2015.
190. Dolente, C.; Bartels, B.; Guba, W.; Haap, W.; Obst Sander, U.; Peters, J.-U.; Rogers-Evans, M.; Woltering, W. Trifluormethyloxazine Amidines as BACE1 Inhibitors. PCT Patent Application WO2016012384 published January 28, 2016.
191. Guba, W.; Haap, W.; Obst Sander, U.; Peters, J.-U.; Woltering, T. Fluoro-[1,3]oxazines as BACE1 Inhibitors. PCT Patent Application WO2016001266 published January 7, 2016.
192. Kuhn, B.; Guba, W.; Hert, W.; Banner, D.; Bissantz, C.; Ceccarelli, S.; Haap, W.; Korner, M.; Kuglstatter, A.; Lerner, C.; Mattei, P.; Neidhart, W.; Pinard, E.; Rudolph, M. G.; Schulz-Gasch, T.; Woltering, T.; Stahl, M. A Real-World Perspective on Molecular Design. *J. Med. Chem.* **2016,** *59,* 4087–4102.
193. Borrinin, E.; Gobbi, L.; Hilpert, H.; Honer, M.; Muri, D.; Narquizian, R.; Polara, A. [1,3]oxazines. PCT Patent Application WO2012168175 published December 13, 2013.

194. Narquizian, R.; Pinard, E.; Wostl, W. Spiro-[1,3]-oxazines and Spiro-[1,4]-oxazepines as BACE1 and/or BACE2 Inhibitors. PCT Patent Application WO2012163790 published December 6, 2012.
195. Hilpert, H.; Humm, R. N-[3-(5-Amino-3,3A,7,7A-tetrahydro-1h-2,4-dioxa-6-aza-inden-7-yl)-phenyl]-amides as BACE1 and/or BACE2 Inhibitors. PCT Patent Application WO2012107371 published August 16, 2012.
196. Hilpert, H.; Pinard, E.; Woltering, T. N-(3-(2-amino-6,6-difluoro-4,4a,5,6,7,7a-hexahydro-cyclopenta[e][1,3]oxazin-4-yl)-phenyl)-amides as BACE1 Inhibitors. PCT Patent Application WO2013041499 published March 28, 2013.
197. Hilpert, H. Difluoro-Hexahydro-Cyclopentaoxazinyls and Difluoro-Hexahydro-Benzooxazinyls as BACE1 Inhibitors. PCT Patent Application WO2014001228 published January 3, 2014.
198. Hilpert, H.; Woltering, T. 5-Amino[1,4]thiazines as BACE 1 Inhibitors. PCT Patent Application WO2013174781 published November 28, 2013.
199. Hilpert, H.; Rogers-Evans, M.; Rombach, D. 1,4-Thiazepines/Sulfones as BACE1 and/or BACE2 Inhibitors. PCT Patent Application WO2012119883 published September 13, 2012.
200. Bartels, B.; Cueni, P.; Dolente, C.; Guba, W.; Haap, W.; Kuglstatter, A.; Obst Sander, U.; Peters, J.-U.; Rogers-Evans, M.; Vifian, W.; Woltering, T. BACE1 Inhibitors. PCT Patent Application WO2016055496 published April 14, 2016.
201. Guba, W.; Haap, W.; Kuglstatter, A.; Peters, J.-U.; Obst Sander, U.; Schnider, C.; Wermuth, R.; Woltering, T. 5-Aryl-1-imino-1-oxo-[1,2,4]thiadiazines. PCT Patent Application WO2015091595 published June 25, 2015.
202. Bartels, B.; Dolente, C.; Guba, W.; Haap. W.; Kuglstatter, A.; Obst Sander, U.; Peters, J.-U.; Rogers-Evans, M.; Woltering, T.; Schnider, C.; Wermuth, R. Pyridyl-Triazabicycles. PCT Patent Application WO2016012422 published January 28, 2016.
203. Bartels, B.; Dolente, C.; Guba, W.; Haap, W.; Obst Sander, U.; Peters, J.-U.; Rogers-Evans, M.; Rombach, D.; Woltering, T. BACE1 Inhibitors. PCT Patent Application WO2016071211 published May 12, 2016.
204. Anselm, L.; Bartels, B.; Dolente, C.; Guba, W.; Haap, W.; Peters, J.-U.; Woltering, T.; Obst Sander, U.; Rogers-Evans, M. 2,2,2-Trifluoroethyl-thiadiazines. PCT Patent Application WO2016023927 published February 18, 2016.
205. RO550887 Single Ascending Dose study NCT01461967, https://clinicaltrials.gov/ct2/show/NCT01461967?intr=RO5508887&rank=3.
206. RO5508887 Multiple Ascending Dose study NCT01664143, https://clinicaltrials.gov/ct2/show/NCT01664143?intr=RO5508887&rank=1.
207. RO5508887 human PK/PD study NCT01592331, https://clinicaltrials.gov/ct2/show/NCT01592331?intr=RO5508887&rank=2.
208. Iserloh, U.; Wu, Y.; Cumming, J. N.; Pan, J.; Wang, L. Y.; Stamford, A. W.; Kennedy, M. E.; Kuvelkar, R.; Chen, X.; Parker, E. M.; Strickland, C.; Voigt, J. Potent pyrrolidine- and piperidine-based BACE-1 inhibitors. *Bioorg. Med. Chem. Lett.* **2008,** *18,* 414–417.
209. Iserloh, U.; Pan, J.; Stamford, A. W.; Kennedy, M. E.; Zhang, Q.; Zhang, L.; Parker, E. M.; McHugh, N. A.; Favreau, L.; Strickland, C.; Voigt, J. Discovery of an orally efficaceous 4-phenoxypyrrolidine-based BACE-1 inhibitor. *Bioorg. Med. Chem. Lett.* **2008,** *18,* 418–422.
210. Cumming, J. N.; Le, T. X.; Babu, S.; Carroll, C.; Chen, X.; Favreau, L.; Gaspari, P.; Guo, T.; Hobbs, D. W.; Huang, Y.; Iserloh, U.; Kennedy, M. E.; Kuvelkar, R.; Li, G.; Lowrie, J.; McHugh, N. A.; Ozgur, L.; Pan, J.; Parker, E. M.; Saionz, K.; Stamford, A. W.; Strickland, C.; Tadesse, D.; Voigt, J.; Wang, L.; Wu, Y.; Zhang, L.; Zhang, Q. Rational design of novel, potent piperazinone and imidazolidinone BACE1 inhibitors. *Bioorg. Med. Chem. Lett.* **2008,** *18,* 3236–3241.
211. Barrow, J. C.; Stauffer, S. R.; Rittle, K. E.; Ngo, P. L.; Yang, Z.-Q.; Selnick, H. G.; Graham, S. L.; Munshi, S.; McGaughey, G. B.; Holloway, M. K.; Simon, A. J.; Price, E. A.; Sankaranarayanan, S.; Colussi, D.; Tugusheva, K.; Lai, M.-T.; Espeseth, A. S.; Xu, M.; Huang, Q.; Wolfe, A.; Pietrak, B.; Zuck, P.; Levorse, D. A.; Hazuda, D.; Vacca, J. P. Discovery and X-ray Crystallographic Analysis of a Spiropiperidine Iminohydantoin Inhibitor of β-Secretase. *J. Med. Chem.* **2008,** *51,* 6259.
212. Egbertson, M.; McGaughey, G. B.; Pitzenberger, S. M.; Stauffer, S. R.; Coburn, C. A.; Stachel, S. J.; Yang, W.; Barrow, J. C.; Neilson, L. A.; McWherter, M.; Perlow, D.; Fahr, B.; Munshi, S.; Allison, T. J.; Holloway, K.; Selnick, H. G.; Yang, Z.; Swestock, J.; Simon, A. J.; Sankaranarayanan, S.; Colussi, D.; Tugusheva, K.; Lai, M.-T.; Pietrak, B.; Haugabook, S.; Lixia Jin, L.; Chen, I.-W.; Holahan, M.; Stranieri-Michener, M.; Cook, J. J.; Vacca, J. L.; Graham, S. L. Methyl-substitution of an iminohydantoin spiropiperidine β-secretase (BACE-1) inhibitor has a profound effect on its potency. *Bioorg. Med. Chem. Lett.* **2015,** *25,* 4812–4819.
213. Wang, Y.-S.; Strickland, C.; Voigt, J. H.; Kennedy, M. E.; Beyer, B. M.; Senior, M. M.; Smith, E. M.; Nechuta, T. L.; Madison, V. S.; Czarniecki, M.; McKittrick, B. A.; Stamford, A. W.; Parker, E. M.; Hunter, J. C.; Greenlee, W. J.; Wyss, D. F. Application of Fragment-Based NMR Screening, X-ray Crystallography, Structure-Based Design, and Focused Chemical Library Design to Identify Novel μM Leads for the Development of nM BACE-1 (β-Site APP Cleaving Enzyme 1) Inhibitors. *J. Med. Chem.* **2010,** *53,* 942–950.
214. (a) Wyss, D. F.; Cumming, J. N.; Strickland, C. O.; Stamford, A. W. BACE Inhibitors. In *Fragment-based Drug Discovery: Lessons and Outlook,* 67, Erlanson, D. A., Jahnke, W., Eds.; Wiley: New Jersey, NJ, 2016; pp 329–353; (b) Stamford, A.; Strickland, C. Inhibitors of BACE for Treating Alzheimer's Disease: A Fragment-based Drug Discovery Story. *Curr. Opin. Chem. Biol.* **2013,** *17,* 320–328.
215. Zhu, Z.; Sun, Z.-Y.; Ye, Y.; Voigt, J.; Strickland, C.; Smith, E. M.; Cumming, J.; Wang, L.; Wong, J.; Wang, Y.-S.; Wyss, D. F.; Chen, X.; Kuvelkar, R.; Kennedy, M. E.; Favreau, L.; Parker, E.; McKittrick, B. A.; Stamford, A.; Czarniecki, M.; Greenlee, W.; Hunter, J. C. Discovery of Cyclic Acylguanidines as Highly Potent and Selective β-Site Amyloid Cleaving Enzyme (BACE) Inhibitors: Part I—Inhibitor Design and Validation. *J. Med. Chem.* **2010,** *53,* 951–965.
216. Cumming, J. N.; Smith, E. M.; Wang, L.; Misiaszek, J.; Durkin, J.; Pan, J.; Iserloh, U.; Wu, Y.; Zhu, Z.; Strickland, C.; Voigt, J.; Chen, X.; Kennedy, M. E.; Kuvelkar, R.; Hyde, L. A.; Cox, K.; Favreau, L.; Czarniecki, M. F.; Greenlee, W. J.; McKittrick, B. A.; Parker, E. M.; Stamford, A. W. Structure based design of iminohydantoin BACE1 inhibitors: Identification of an orally available, centrally active BACE1 inhibitor. *Bioorg. Med. Chem. Lett.* **2012,** *22,* 2444–2449.
217. Stamford, A. W.; Scott, J. D.; Li, S. W.; Babu, S.; Tadesse, D.; Hunter, R.; Wu, Y.; Misiaszek, J.; Cumming, J. N.; Gilbert, E. J.; Huang, C.; McKittrick, B. A.; Hong, L.; Guo, T.; Zhu, Z.; Strickland, C.; Orth, P.; Voigt, J. H.; Kennedy, M. E.; Chen, X.; Kuvelkar, R.; Hodgson, R.; Hyde, L. A.; Cox, K.; Favreau, L.; Parker, E. M.; Greenlee, W. J. Discovery of an Orally Available, Brain Penetrant BACE1 Inhibitor That Affords Robust CNS Aβ Reduction. *ACS Med. Chem. Lett.* **2012,** *3,* 897–902.
218. Mandal, M.; Zhu, Z.; Cumming, J. N.; Liu, X.; Strickland, C.; Mazzola, R. D.; Caldwell, J. P.; Leach, P.; Grzelak, M.; Hyde, L.; Zhang, Q.; Terracina, G.; Zhang, L.; Chen, X.; Kuvelkar, R.; Kennedy, M. E.; Favreau, L.; Cox, K.; Orth, P.; Buevich, A.; Voigt, J.; Wang, H.; Kazakevich, I.; McKittrick, B. A.; Greenlee, W.; Parker, E. M.; Stamford, A. W. Design and Validation of Bicyclic Iminopyrimidinones As Beta Amyloid Cleaving Enzyme-1 (BACE1) Inhibitors: Conformational Constraint to Favor a Bioactive Conformation. *J. Med. Chem.* **2012,** *55,* 9331–9345.
219. Mandal, M.; Wu, Y.; Misiaszek, J.; Li, G.; Buevich, A. V.; Caldwell, J. P.; Voigt, J. H.; Wang, H.; Zhu, Z.; Chen, X.; et al. Structure-Based Design of an Iminoheterocyclic β-Site Amyloid Precursor Protein Cleaving Enzyme (BACE) Inhibitor that Lowers Central Aβ in Nonhuman Primates. *J. Med. Chem.* **2016,** *59,* 3231–3248.
220. Scott, J. D.; Li, S. W.; Brunskill, A. P. J.; Chen, X.; Cox, K.; Cumming, J. N.; Forman, M.; Gilbert, E. J.; Hodgson, R. A.; Hyde, L. A.; Jiang, Q.; Iserloh, U.; Kazakevich, I.; Kuvelkar, R.; Mei, H.; Meredith, J.; Misiaszek, J.; Orth, P.; Rossiter, L. M.; Slater, M.; Stone, J.; Strickland, C.; Voigt, J. H.; Wang, G.; Wang, H.; Wu, Y.; Greenlee, W. J.; Parker, E. M.; Kennedy, M. E.; Stamford, A. W. Discovery of the 3-Imino-1,2,4-thiadiazinane 1,1-Dioxide Derivative Verubecestat (MK-8931)–A β-Site Amyloid Precursor Protein Cleaving Enzyme 1 Inhibitor for the Treatment of Alzheimer's Disease. *J. Med. Chem.* **2016,** *59* (23), 10435–10450. http://dx.doi.org/10.1021/acs.jmedchem.6b00307; (b) Kennedy, M. E.; Stamford, A. W.; Chen, X.; Cox, K.; Cumming, J. N.; Dockendorf, M. F.; Egan, M.; Ereshefsky, L.; Hodgson, R. A.; Hyde, L. A.; Jhee, S.; Kleijn, H. J.; Kuvelkar, R.; Li, W.; Mattson, B. A.; Mei, H.; Palcza, J.; Scott, J. D.; Tanen, M.; Troyer, M. D.; Tseng, J. L.; Stone, J. A.; Parker, E. M.; Forman, M. S. The BACE1 inhibitor verubecestat (MK-8931) reduces CNS β-amyloid in animal models and in Alzheimer's disease patients. *Sci. Transl. Med.* **2016,** *8,* 363ra150.
221. Scott, J. D.; Stamford, A. W.; Gilbert, E. J.; Cumming, J. N.; Iserloh, U.; Wang, L.; Li, W. Iminothiadiazine Dioxide Compounds as BACE Inhibitors and Their Preparation, Compositions and Use in the Treatment of Pathologies Associated With Beta-Amyloid Protein. PCT Int. Appl. WO2011044187 published April 14, 2011.
222. Stamford, A. W.; Gilbert, E. J.; Cumming, J. N. Preparation of Pyrrolidine-fused Thiadiazine Dioxide Compounds as Beta Site APP Cleaving Enzyme (BACE) Inhibitors, Pharmaceutical Compositions, and Their Use. PCT Int. Appl. WO2012138590 published October 11, 2012.
223. Cumming, J. N.; Gilbert, E. J.; Stamford, A. W. Preparation of C5–C6 Oxacyclic-fused Thiadiazine Dioxide Compounds as Beta Site APP Cleaving Enzyme (BACE) Inhibitors, Pharmaceutical Compositions, and Their Use. PCT Int. Appl. WO2012138734 published October 11, 2012.

224. Wu, W.-L.; Burnett, D. A.; Stamford, A. W.; Cumming, J. N.; Bennett, C. E.; Gilbert, E. J.; Peng, X.; Scott, J. D.; Yu, Y. Preparation of 5-Substituted Iminothiazines and Their Mono- and Dioxides as BACE Inhibitors. PCT Int. Appl. WO2012139425 published October 18, 2012.
225. Wu, W.-L.; Burnett, D. A.; Stamford, A.; Cumming, J. N.; Asberom, T.; Bennett, C.; Sasiskumar, T. K.; Scott, J. D. Preparation of Spiroiminothiazine Derivatives for Use as BACE Inhibitors. PCT Int. Appl. WO2013028670 published February 28, 2013.
226. Gilbert, E. J.; Cumming, J. N.; Scott, J. D.; Wu, W.-L.; Burnett, D. A.; Stamford, A. W. Preparation of C2-Azaspiro Iminothiazine Dioxides as BACE Inhibitors. PCT Int. Appl. WO2014150344 published September 25, 2014.
227. Scott, J. D.; Wu, W.-L.; Cumming, J. N. Preparation of C5-spiro Iminothiazine Dioxide Compounds as BACE Inhibitors for Treatment of Amyloid β Pathologies. PCT Int. Appl. WO2015038446 published March 19, 2015.
228. Cumming, J. N.; Scott, J. D.; Stamford, A. W.; Iserloh, U.; Neelamkavil, S. F.; Shao, P. P.; Wilson, J. E. C5-spiro Iminothiadiazine Dioxides and Application for Treating Alzheimer's Disease. PCT Int. Appl. WO2014099788 published June 26, 2014.
229. Dai, X.; Cumming, J. N.; Scott, J. D.; Liu, H.; Palani, A. Preparation of Iminothiadiazepane Dioxide Compounds as BACE Inhibitors Useful in Treatment of Diseases. PCT Int. Appl. WO2015095104 published June 25, 2015.
230. Cumming, J. N.; Kaelin Jr., D. E.; Scott, J. D.; Stamford, A. W.; Iserloh, U. Preparation of C6-azaspiroiminothiadiazine Dioxides as BACE Inhibitors. PCT Int. Appl. WO2014099768 published June 26, 2914.
231. Khan, T. A.; Scott, J. D.; Cumming, J. N. S-Imino-s-oxo Iminothiadiazine Compounds as BACE Inhibitors, Compositions, and Their Use. PCT Int. Appl. WO2014150340 published September 25, 2014.
232. Walsh, S. P.; Cumming, J. N.; He, S.; Taoka, B. M.; Truong, Q. T.; Wu, W.-L. Preparation of C2-carbocyclic Iminothiazine Dioxides as BACE Inhibitors, Compositions, and Their Use. PCT Int. Appl. WO2015187437 published December 10, 2015.
233. Gilbert, E. J.; Cumming, J. N.; Stamford, A. W.; Yu, Y.; Scott, J. D.; Iserloh, U. Preparation of Tricyclic Substituted Thiadiazine Dioxide Compounds as BACE Inhibitors, Compositions, and Their Therapeutic Use. PCT Int. Appl. WO2014062549 published April 24, 2014.
234. Cumming, J. N.; Scott, J. D.; Biftu, T. Preparation of Iminothiadiazine Dioxides as BACE Inhibitors. PCT Int. Appl. WO2014093190 published June 19, 2014.
235. Kobayashi, N.; Ueda, K.; Itoh, N.; Suzuki, S.; Sakaguchi, G.; Kato, A.; Yukimasa, A.; Hori, A.; Kooriyama, Y.; Haraguchi, H. K.; Kanda, Y. Aminodihydrothiazine Derivative. PCT Int. Appl. WO2007049532 published May 3, 2007.
236. Kobayashi, N.; Ueda, K.; Itoh, N.; Suzuki, S.; Sakaguchi, G.; Kato, A.; Yukimasa, A.; Hori, A.; Kooriyama, Y.; Haraguchi, H.; K.; Kanda, Y. Pharmaceutical Composition for Treatment of Alzheimer's Disease. PCT Int. Appl. WO2008133273 published November 6, 2008.
237. Tamura, Y.; Suzuki, S.; Tada, Y.; Yonezawa, S.; Fujikoshi, C.; Matsumoto, S.; Kooriyama, Y.; Ueno, T. Aminodihydrothiazine Derivatives Substituted with Cyclic Groups. PCT Int. Appl. WO2008133274 published November 6, 2008.
238. Tada, Y.; Kusakabe, K.-I.; Tadano, G. Pyridine Derivative and Bace-1 Inhibitor Containing Same. PCT Int. Appl. WO2012147762 published November 2, 2012.
239. Kusakabe, K.-I.; Tadano, G.; Komano, K.; Fuchino, K.; Nakahara, K. Dihydrothiazine and Dihydrooxazine Derivatives Having Bace1 Inhibitory Activity. PCT Int. Appl. WO2015156421 published October 15, 2015.
240. Hori, A.; Yonezawa, S.; Fujikoshi, C.; Matsumoto, S.; Kooriyama, Y.; Ueno, T.; Kato, T. Preparation of Thiazole and Thiazine Derivatives as β-secretase Inhibitors. PCT Int. Appl. WO2009151098 published.December 17, 2009.
241. Anan, K.; Tada, Y.; Hori, A.; Masui, M. Preparation of Substituted 2-Amino-4H-1,3-Thiazine Derivatives as β-secretase (BACE1) Inhibitors. PCT Int. Appl. WO2011070781 published June 16, 2011.
242. Masui, M.; Hori, A. Oxazine Derivative. PCT Int. Appl. WO2011071135 published June 16, 2011.
243. Kurose N.; Kusakabe K.-I.; Masui M.; Mitsuoka Y.; Onodera N.; Yoshida S. Oxazine Derivative and Bace 1 Inhibitor Containing Same. PCT Int. Appl. WO2012147763 published November 2, 2012.
244. Kusakabe, K.-I.; Yoshida, S.; Nakahara, K.; Hasegawa, T.; Tadano, G.; Fuchino, K. Dihydrooxazine or Oxazepine Derivatives Having Bace1 Inhibitory Activity. PCT Int. Appl. WO2014065434 published May 1, 2014.
245. Yoshida, S.; Kato, I.; Fuchino, K.; Kooriyama, Y.; Baba, Y.; Tanimoto, N. Fused Heterocyclic Compound Having Amino Group. PCT Int. Appl. WO2011071109 published June 16, 2011.
246. Masui, M.; Anan, K. Aminothiazine or Aminooxazine Derivative Having Amino Linker. PCT Int. Appl. WO2011058763 published May 19, 2011.
247. Suzuki, S.; Kooriyama, Y. 4-Amino-1,3-thiazine or Oxazine Derivative. PCT Int. Appl. WO2011077726 published June 30, 2011.
248. Tamura, Y.; Suzuki, S.; Matsumoto, S.; Hori, A.; Kooriyama, Y. Isothiourea Derivative or Isourea Derivative Having Bace1 Inhibitory Activity. PCT Int. Appl. WO2010113848 published October 7, 2010.
249. Yonezawa S.; Tamura Y.; Kooriyama Y.; Sakaguchi G. 2-Aminopyridin-4-one and 2-aminopyridine Derivative Both Having Bace1-Inhibiting Activity. PCT Int. Appl. WO2010047372 published April 29, 2010.
250. Mitsuoka, Y.; Kooriyama, Y. Naphthyridine Derivative. PCT Int. Appl. WO2012057248 published May 3, 2012.
251. Masui, M.; Tadano, G. Fused Aminodihydropyrimidine Derivative. PCT Int. Appl. WO2012057247 published May 3, 2012.
252. Yonezawa, S.; Yamamoto, T.; Yamakawa, H.; Muto, C.; Hosono, M.; Hattori, K.; Higashino, K.; Yutsudo, T.; Iwamoto, H.; Kondo, Y.; Sakagami, M.; Togame, H.; Tanaka, Y.; Nakano, T.; Takemoto, H.; Arisawa, M.; Shuto, S. Conformational Restriction Approach to β-Secretase (BACE1) Inhibitors: Effect of a Cyclopropane Ring To Induce an Alternative Binding Mode. *J. Med. Chem.* **2012,** *55,* 8838–8858.
253. Yonezawa, S.; Yamakawa, H.; Muto, C.; Hosono, M.; Yamamoto, T.; Hattori, K.; Sakagami, M.; Togame, H.; Tanaka, Y.; Nakano, T.; Takemoto, H.; Arisawa, M.; Shuto, S. Conformational restriction approach to BACE1 inhibitors II: SAR study of the isocytosine derivatives fixed with a cis-cyclopropane ring. *Bioorg. Med. Chem. Lett.* **2013,** *23,* 2912–2915.
254. Timmer, M.; Van Broeck, B.; Slemmon, J.; De Waepenaert, K.; Russu, A.; Bogert, J.; Moechars, D.; Mercken, M.; Sinha, V.; Tritsmans, L.; Streffer, J. Profiling the Dynamics of CSF and Plasma Abeta Reduction with JNJ-54861911, an Oral Bace Inhibitor. ADPD Conference, Nice, March 18–22, 2015. *Neurodegener. Dis.* **2015,** 289–351; p. 310.
255. Cole, D. C.; Manas, E. S.; Stock, J. R.; Condon, J. S.; Jennings, L. D.; Aulabaugh, A.; Chopra, R.; Cowling, R.; Ellingboe, J. W.; Fan, K. Y.; et al. Acylguanidines as small-molecule beta-secretase inhibitors. *J. Med. Chem.* **2006,** *49,* 6158–6161.
256. Fobare, W. F.; Solvibile, W. R.; Robichaud, A. J.; Malamas, M. S.; Manas, E.; Turner, J.; Hu, Y.; Wagner, E.; Chopra, R.; Cowling, R.; et al. Thiophene substituted acylguanidines as BACE1 inhibitors. *Bioorg. Med. Chem. Lett.* **2007,** *17,* 5353–5356.
257. Cole, D. C.; Stock, J. R.; Chopra, R.; Cowling, R.; Ellingboe, J. W.; Fan, K. Y.; Harrison, B. L.; Hu, Y.; Jacobsen, S.; Jennings, L. D.; et al. Acylguanidine inhibitors of beta-secretase: optimization of the pyrrole ring substituents extending into the S1 and S3 substrate binding pockets. *Bioorg. Med. Chem. Lett.* **2008,** *18,* 1063–1066.
258. Jennings, L. D.; Cole, D. C.; Stock, J. R.; Sukhdeo, M. N.; Ellingboe, J. W.; Cowling, R.; Jin, G.; Manas, E. S.; Fan, K. Y.; Malamas, M. S.; et al. Acylguanidine inhibitors of beta-secretase: optimization of the pyrrole ring substituents extending into the S1' substrate binding pocket. *Bioorg. Med. Chem. Lett.* **2008,** *18,* 767–771.
259. Malamas, M. S.; Barnes, K.; Hui, Y.; Johnson, M.; Lovering, F.; Condon, J.; Fobare, W.; Solvibile, W.; Turner, J.; Hu, Y.; et al. Novel pyrrolyl 2-aminopyridines as potent and selective human beta-secretase (BACE1) inhibitors. *Bioorg. Med. Chem. Lett.* **2010,** *20,* 2068–2073.
260. Malamas, M. S.; Erdei, J.; Gunawan, I.; Barnes, K.; Johnson, M.; Hui, Y.; Turner, J.; Hu, Y.; Wagner, E.; Fan, K.; et al. Aminoimidazoles as potent and selective human beta-secretase (BACE1) inhibitors. *J. Med. Chem.* **2009,** *52,* 6314–6323.
261. Nowak, P.; Cole, D. C.; Aulabaugh, A.; Bard, J.; Chopra, R.; Cowling, R.; Fan, K. Y.; Hu, B.; Jacobsen, St; Jani, M. Discovery and initial optimization of 5,5'-disubstituted aminohydantoins as potent beta-secretase (BACE1) inhibitors. *Bioorg. Med. Chem. Lett.* **2010,** *20,* 632–635.
262. Zhou, P.; Li, Y.; Fan, Y.; Wang, Z.; Chopra, R.; Olland, A.; Hu, Y.; Magolda, R. L.; Pangalos, M.; Reinhart, P. H.; et al. Pyridinyl aminohydantoins as small molecule BACE1 inhibitors. *Bioorg. Med. Chem. Lett.* **2010,** *20,* 2326–2329.

263. Malamas, M. S.; Barnes, K.; Johnson, M.; Hui, Y.; Zhou, P.; Turner, J.; Hu, Y.; Wagner, E.; Fan, K.; Chopra, R.; et al. Di-substituted pyridinyl aminohydantoins as potent and highly selective human beta-secretase (BACE1) inhibitors. *Bioorg. Med. Chem.* **2010,** *18,* 630–639.
264. Malamas, M. S.; Erdei, J.; Gunawan, I.; Barnes, K.; Hui, Y.; Johnson, M.; Robichaud, A.; Zhou, P.; Yan, Y.; Solvibile, W.; et al. New pyrazolyl and thienyl aminohydantoins as potent BACE1 inhibitors: exploring the S2' region. *Bioorg. Med. Chem. Lett.* **2011,** *21,* 5164–5170.
265. Malamas, M. S.; Robichaud, A.; Erdei, J.; Quagliato, D.; Solvibile, W.; Zhou, P.; Morris, K.; Turner, J.; Wagner, E.; Fan, K.; et al. Design and synthesis of aminohydantoins as potent and selective human β-secretase (BACE1) inhibitors with enhanced brain permeability. *Bioorg. Med. Chem. Lett.* **2010,** *20,* 6597–6605.
266. Mjalli, A. M. M.; Jones, D.; Gohimmukkula, D. R.; Huang, G.; Zhu, J.; Rao, M.; Andrews, R. C.; Ren, T. Benzazole Derivatives, Compositions, and Methods of Use as β-secretase Inhibitors. PCT Patent Application WO2006099379 published September 21, 2006.
267. Mjalli, A. M. M.; Gaddam, B.; Gohimukkula, D. R.; Polisetti, D. R.; El Abdellaoui, H.; Rao, M.; Wang, P.; Andrews, R. C.; Xie, R.; Ren, T. Substituted Isoquinoline Derivatives, Pharmaceutical Compositions, and Methods of Use as β-secretase Inhibitors. PCT Patent Application WO2010126743 published November 4, 2010.
268. Mjalli, A. M. M.; Hari, A.; Gaddam, B.; Gohimukkula, D. R.; Polisetti, D. R.; El Abdellaoui, H.; Rao, M.; Andrews, R. C.; Xie, R.; Ren, T. Substituted Imidazo[1,2-a]pyridine Derivatives, Pharmaceutical Compositions, and Methods of Use as β-secretase Inhibitors. PCT Patent Application WO2010126745 published November 4, 2010.
269. Mjalli, A. M. M.; Hari, A.; Gaddam, B.; Gohimukkula, D. R.; Polisetti, D. R.; Rao, M.; Andrews, R. C.; Xie, R.; Sahoo, S. P.; Ren, T.; Banner, W. K. Substituted imidazo[1,2-b] pyridazine Derivatives, Pharmaceutical Compositions, and Methods of Use as Beta-Secretase Inhibitors. PCT Patent Application WO2011119465 published September 29, 2011.
270. HPP854 Phl Clinical Trail, https://clinicaltrials.gov/ct2/show/NCT01482013?intr=HPP854&rank=1.
271. Eisai Press Release August 9th 2016, U.S. FDA Confirms Sufficient Data to Advance Investigational Bace Inhibitor E2609 for Treatment of Early Alzheimer's Disease to Phase III, http://www.eisai.com/news/news201659.html.
272. Lilly Press Release August 22nd 2016, Lilly and AstraZeneca Receive FDA Fast Track Designation for AZD3293, an Investigational Treatment for Early Alzheimer's Disease. https://investor.lilly.com/releasedetail.cfm?ReleaseID=985052.
273. Winneroski, L. L.; Schiffler, M. A.; Erickson, J. A.; May, P. C.; Monk, S. A.; Timm, D. E.; Audia, J. E.; Beck, J. P.; Boggs, L. N.; Borders, A. R.; et al. Preparation and biological evaluation of conformationally constrained BACE1 inhibitors. *Bioorg. Med. Chem.* **2015,** *23,* 3260–3268.
274. Vassar, R.; Kuhn, P. H.; Haass, C.; Kennedy, M. E.; Rajendran, L.; Wong, P. C.; Lichtenthaler, S. F. Function, therapeutic potential and cell biology of BACE proteases: current status and future prospects. *J. Neurochem.* **2014,** *130,* 4–28.
275. Jacobsen, H.; Ozmen, L.; Caruso, A.; Narquizian, R.; Hilpert, H.; Jacobsen, B.; Terwel, D.; Tanghe, A.; Bohrmann, B. Combined Treatment with a BACE Inhibitor and Anti-Aβ Antibody Gantenerumab Enhances Amyloid Reduction in APP_{London} Mice. *J. Neurosci.* **2014,** *34,* 11621–11630.
276. DeMattos, R.; May, P.; Racke, M.; Hole, J.; Tzaferis, J.; Liu, F.; DeLong, C.; Day, T.; Yang, Z.; Boggs, L.; et al. Combination Therapy With a Plaquespecific Abeta Antibody and Bace Inhibitor Results in Dramatic Plaque Lowering in Aged PDAPP Transgenic Mice. Alzheimer's Association International Conference, Kopenhagen, 2014. *Alzheimers Dement.* **2014,** *10* (Suppl. 149).

7.09 Targeting Phosphodiesterases in the CNS

J Kehler, H. Lundbeck A/S, Valby, Denmark

© 2017 Elsevier Ltd. All rights reserved.

7.09.1	Introduction	384
7.09.2	PDE Structure and PDE Binding Site Topology	386
7.09.3	CNS Drug-Like Properties	387
7.09.4	PDE Inhibitors	389
7.09.4.1	PDE1	389
7.09.4.2	PDE2	392
7.09.4.3	PDE4	395
7.09.4.4	PDE9	399
7.09.4.5	PDE10	400
7.09.5	Conclusion	404
References		404

7.09.1 Introduction

When the British physician Henry Hyde Salter in 1860 discovered that his asthmatic breathing eased when he drank two strong cups of coffee on an empty stomach,[1] he was little aware, that the bronchodilator properties was caused by the alkaloid constituents caffeine (**3**), theophylline (**4**), and theobromine (**5**) (Fig. 1). Two morning cups of strong coffee contain a mixture of xanthines (**1**) corresponding to a dose of ~300 mg theophylline. At the same time, the three xanthines had been isolated from beans of coffee and cacao and from tea leaves in 1820, 1842, and 1888, respectively. Their chemical structures were proven via chemical synthesis in 1895.[2] The stimulatory effects on the central nervous system (CNS) were later shown to be caused by these same heterocyclic purines[3] although most of the available data suggest that caffeine, in the doses that are commonly consumed, acts primarily by blocking adenosine A1 and A2A receptors.[4] Subsequently, theophylline was successfully introduced as treatment, first as a diuretic and for cardiovascular disease and later for airway disease. In spite of being unselective phosphodiesterase (PDE) inhibitors, the xanthine-scaffold has played an important role in PDE drug discovery, and many chemical series and drug candidates have been derived from this bicyclic purine.

The mechanism of action (MoA) of xanthines at the time was unknown; however, in 1958 Sutherland and Rall found that caffeine and theophylline were acting as nonselective, albeit weak, inhibitors of the newly discovered PDE enzyme.[5] The PDE was found to be a metallohydrolase present in tissue extracts from the heart, brain, and liver and was activated by magnesium ions. The PDE was found to be responsible for the degradation of the heat-stable cyclic nucleotide (cN) 3′–5′ cyclic adenosine monophosphate (cAMP) first isolated from liver extracts.[6] PDE was later also shown to degrade 3′–5′ cyclic guanosine monophosphate (cGMP) first isolated from rat urine.[7] The cyclic nucleotides were shown to be intracellular second messengers, which mediated many of the cellular effects of neurotransmitters and hormones. It became apparent that steady-state levels of cAMP and cGMP in cells and tissues are determined by the balance of syntheses by adenylyl cyclase (AC) and guanylyl cyclase (GC), degradation by PDEs, and extrusion out of the cell by ABC transporter multidrug resistance-associated protein 4 and 5, MRP4 and MRP5[8] (Fig. 2).

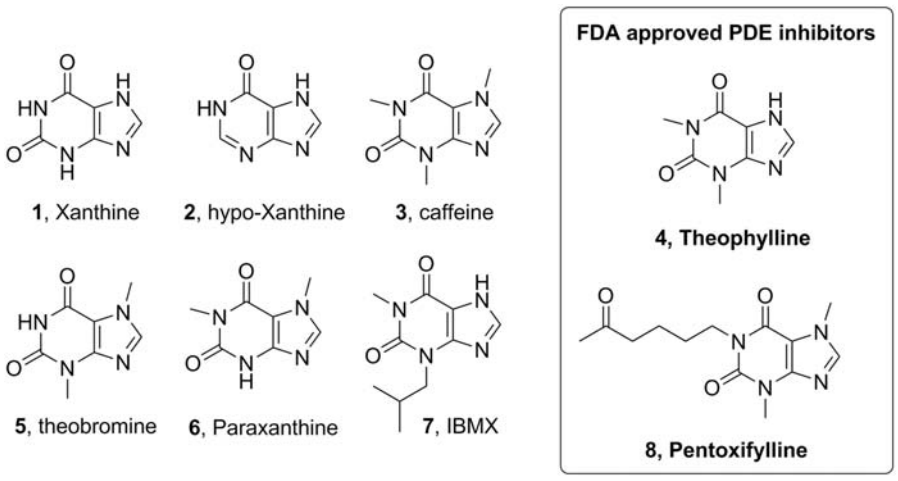

Fig. 1 Xanthine and xanthine analogues pioneered the PDE drug discovery and were among the first PDE inhibitors to be approved drugs.

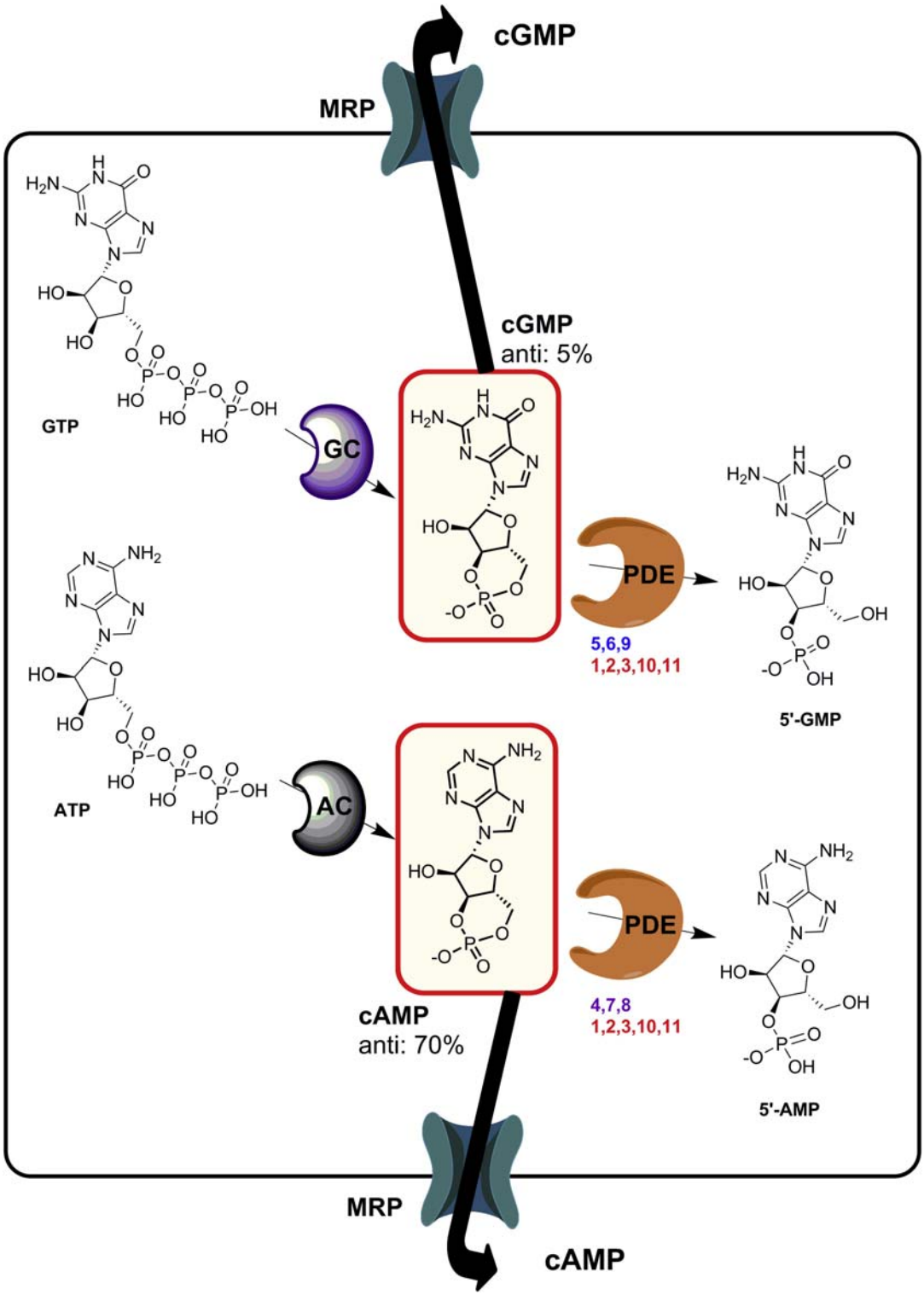

Fig. 2 Overview of the cellular systems responsible for regulating cyclic nucleotide (cN) levels in the cell. An enzyme system responsible for the formation of cAMP in the presence of ATP, named adenylate cyclase, AC (EC 4.6.1.1) and the corresponding system responsible for the formation of cGMP in the presence of GTP, named guanylate cyclase, GC (EC 4.6.1.2) are shown. Another enzyme system, 3′,5′-cyclic-AMP phosphodiesterase (PDE, EC 3.1.4.17) and 3′,5′-cyclic-GMP phosphodiesterase (PDE, EC 3.1.4.35), is responsible for hydrolyzing cNs. Furthermore, cNs are known to be effluxed from cultured cells or isolated tissues by members of the multidrug resistance protein family, MRP4 and MRP5. For Enzyme nomenclature, see http://enzyme.expasy.org/.

Table 1 Cyclic nucleotide phosphodiesterase gene families

PDE	*PDE isozyme families*	*Substrate selectivity*	*Localization in the brain*
PDE1	CaM-dependent PDEs	cGMP and cAMP (dual)	Hippocampus, cortex, olfactory bulb, striatum (highest expression levels), thalamus, amygdala, cerebellum; expression levels are in general highest for 1A and lowest for 1C
PDE2	cGMP- stimulated PDEs	cGMP and cAMP (dual)	Hippocampus, cortex, striatum, hypothalamus, amygdala, midbrain
PDE3	cGMP-inhibited PDEs	cGMP and cAMP (dual)	Throughout the brain low expression levels
PDE4	cAMP-specific PDES	cAMP	Hippocampus, cortex, olfactory bulb, striatum, thalamus, hypothalamus, amygdala, midbrain, cerebellum; expression levels are in general highest for 4A–4D (differs per brain structure) and lowest for 4C
PDE5	cGMP-specific PDEs	cGMP	Hippocampus, cortex, cerebellum
PDE6	Photoreceptor PDEs	cGMP	Pineal gland
PDE7	HCP1–PDE	cAMP	Hippocampus, cortex, olfactory bulb, striatum, thalamus, hypothalamus, midbrain; expression levels are in general highest for 7B
PDE8		cAMP	Hippocampus, cortex, olfactory bulb, striatum, thalamus, hypothalamus, midbrain; expression levels are in general highest for 8B
PDE9		cGMP	Hippocampus, cortex, olfactory bulb, striatum, thalamus, hypothalamus, amygdala, midbrain, cerebellum
PDE10	Striatal-enriched PDE	cGMP and cAMP (dual)	Hippocampus, cortex, striatum (highest expression levels), midbrain, cerebellum
PDE11		cGMP and cAMP (dual)	Throughout the brain low expression levels

The cell membrane-bound anion transporters MRP4 and MRP5 are low-affinity cN transporters that function as overflow pumps, decreasing steep increases in cGMP and cAMP levels under conditions where cN synthesis is strongly induced and PDE activity is limiting. In some cells, this export might be of similar importance for intracellular cGMP and cAMP signals as degradation by PDEs.[9]

Early nomenclature categorized the different PDEs according to their chromatographic eluent properties, their order of discovery, their substrate specificity, and kinetic and regulatory properties. The completion of the Human Genome Project in 2001 established that there are 21 PDE genes in humans, which are subdivided into 11 PDE families (**Table 1**). It has been shown that each PDE isoform exhibits a unique expression pattern across the brain (**Table 1**), and this expression pattern is highly conserved between rats, mice, and humans. Furthermore, it has been shown that PDE1B, PDE1C, PDE2A, PDE4A, PDE4D, PDE5A, PDE7A, PDE8A, PDE8B, PDE10A, and PDE11A showed an age-related increase or decrease in mRNA expression in at least one of the four brain regions examined (hippocampus, cortex, striatum, and cerebellum). In contrast, mRNA expression of PDE1A, PDE3A, PDE3B, PDE4B, PDE7A, PDE7B, and PDE9A did not change with age.[10]

When AC is activated, it continuously catalyzes the conversion of ATP into cAMP, and when GC is activated, it continuously catalyzes the conversion of GTP into cGMP. This results in high concentrations of cAMP or cGMP and a strong amplification of the signal. Once cAMP and cGMP are synthesized, these cNs transduce signal-encoded information by acting through a number of cellular effectors. These include cAMP- or cGMP-activated protein kinases [protein kinase A (PKA) or PKG, respectively], cyclic nucleotide-gated ion channels, a family of two cAMP-activated guanine nucleotide exchange proteins [exchange factors directly activated by cAMP 1 (EPAC1) and EPAC2], and a limited group of enzymes from the PDE family, which contain allosteric cN-binding sites in addition to their catalytic sites.[11] Divergent N- and C-termini allow differential regulation of PDEs by other intracellular signaling pathways. A simplified view of the signaling pathways is summarized in **Fig. 3**.

7.09.2 PDE Structure and PDE Binding Site Topology

Since the first publication in 2000 of a PDE crystal structure of the APO-structure of the PDE catalytic domain of PDE4B,[12] there are now structures of the catalytic domains of 9 of the 11 human PDE families, the structures of PDE6 and PDE11 being the only ones still lacking. The number of PDE crystal structures continues to grow with a rate of about 20 per year, and more than 230 PDE crystal structures were deposited in the Protein Data Bank in the beginning of 2016. PDE structures of 5 of the 13 PDE inhibitors that have been approved for use as pharmaceuticals have been published crystallized in complex with their respective PDE targets. Five comprehensive reviews of PDE crystal structures have been published.[13]

The PDE families have relatively rigid pockets at the active sites. The catalytic domains of PDEs are composed of approximately 350 amino acids and have been shown to share a similar topography, folded into 16 helices (H1–H16). An overlay of all published PDE crystal structures showed that PDEs share a highly conserved fold, with an overall RMSD of C-α atoms of 1.2 Å,[13,14] underscoring the high degree of topological homology and similarity within their catalytic domains. However, slight structural differences in these domains determine whether the PDE has dual substrate specificity (PDE1, PDE2, PDE3, PDE10, and PDE11) or is cGMP-specific (PDE5, PDE6, and PDE9) or cAMP-specific (PDE4, PDE7, and PDE8). Importantly, the subtle structural differences also form the basis for subtype-selectivity among PDE ligands. All PDE inhibitors crystallized to date have been found to bind to the

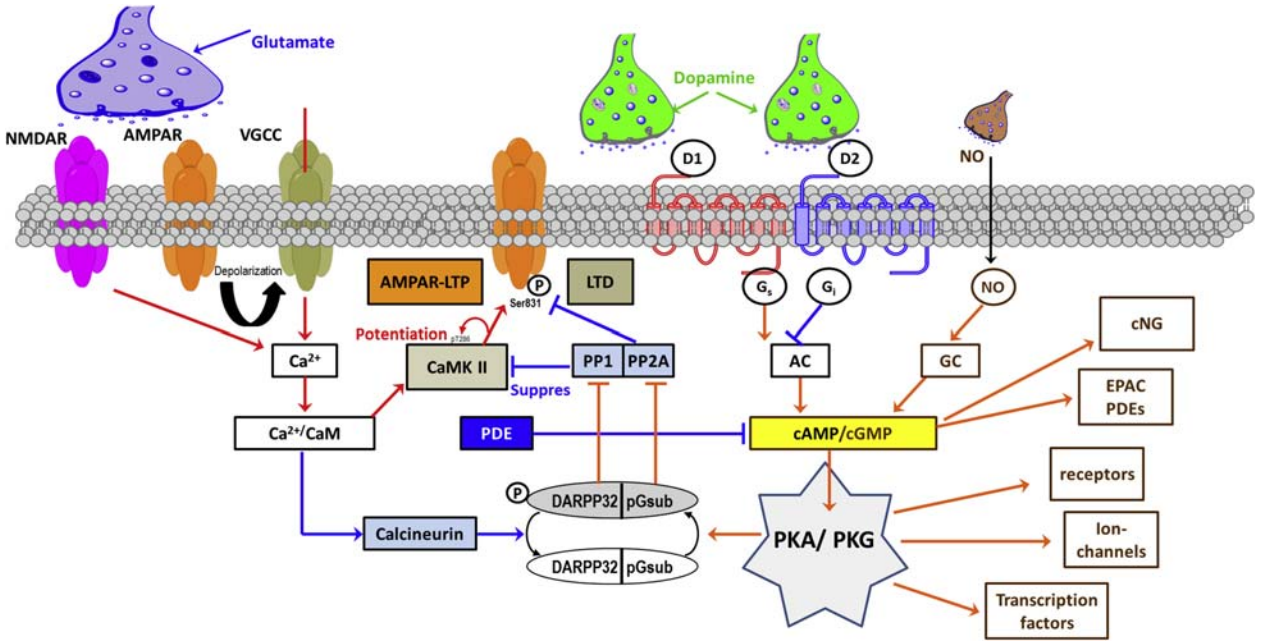

Fig. 3 A simplified view of the signaling pathways, where PDEs are involved.

substrate binding pocket of the PDE catalytic domain. The catalytic active site forms a deep hydrophobic pocket with a total of 57 residues identified as pocket residues[14] and includes a substrate binding region formed between H13 and H16. The pocket has a metal binding (MB) region at the apex of H6–H13, that contains a PDE-specific, histidine-containing signature motif, HD(X2)H(X4)N, that forms the binding sites for the two divalent metal ions that are essential for the catalytic function of PDEs. One of the histidines (His160 in PDE4D2) has been proposed to serve as a general acid for catalysis. Thirteen of the 57 pocket residues are conserved across all PDEs, and 11 of these are in MB regions. The two other conserved amino acids play important roles in substrate and inhibitor binding and are an invariant glutamine residue (Gln-369 in PDE4D2, Gln-453 in PDE9A2, and Gln-726 in PDE10A2), and a phenylalanine residue (Phe372 in PDE4D2 and Trp621 in PDE11A2). To describe the interactions between the ligands and the substrate binding pocket in a consistent manner, a systematic nomenclature for the residues of the binding pocket has been proposed (Fig. 4).[14] The pocket is divided into 10 regions consisting of: The invariant glutamine (Q) and neighboring regions Q1 and Q2; the hydrophobic clamp (HC) regions HC, HC1, and HC2; the MB regions MB, MB1, and MB2; and the solvent filled (S) region S. Based on the alignment of the pocket residues, a nomenclature was introduced numbering the 57 pocket residues according to its position from number 1 to number 57. In addition, a prefix is given indicating in which pocket region the amino acid is placed. In this nomenclature, the invariant glutamine is named QQ.50 since the residue is a glutamine (Q), placed in the Q-pocket (Q) in position 50. Correspondingly, in this nomenclature the conserved phenylalanine in the "roof" of the HC is named FHC.52. This nomenclature allows an easy and consistent way of comparing different structures and interactions cross PDE families.

7.09.3 CNS Drug-Like Properties

The concept of drug-likeness was introduced in the late 1990s as a guide for molecule design in hit- and lead optimization. Drug-like was defined as those compounds that have sufficiently acceptable ADME properties and sufficiently acceptable toxicity properties to survive through the completion of human phase 1 clinical trials. Analysis of the distribution of physicochemical properties of marketed drugs shows that they fall within a relatively narrow range of possible values. Therefore, the term "drug-like" is used to describe physicochemical properties of compounds that fall within this range. It appears that CNS drugs fall within an even more narrow range. Physicochemical properties determine important drug parameters like solubility, permeability, metabolic stability, transporter effects, and plasma- and tissue-free fractions, thereby impacting oral bioavailability and exposure to drug targets in vivo (pharmacokinetics), which is a prerequisite to pharmacodynamics (PDs) and toxicity. Drug-likeness, therefore, can be understood as a way to relate physicochemical properties to ADME-T and other in vivo parameters. The meaning of "drug-like" is dependent on mode of administration. The route of drug administration associated with the greatest patient compliance is the oral route, which is also the most cost effective and most convenient. This is why most of the drugs that are available in the marketplace are administered via the oral route. Oral-drug space is a generic term that describes the area of chemical space in which oral drugs have a high probability of being found. It can in principle be defined using any number of physicochemical or

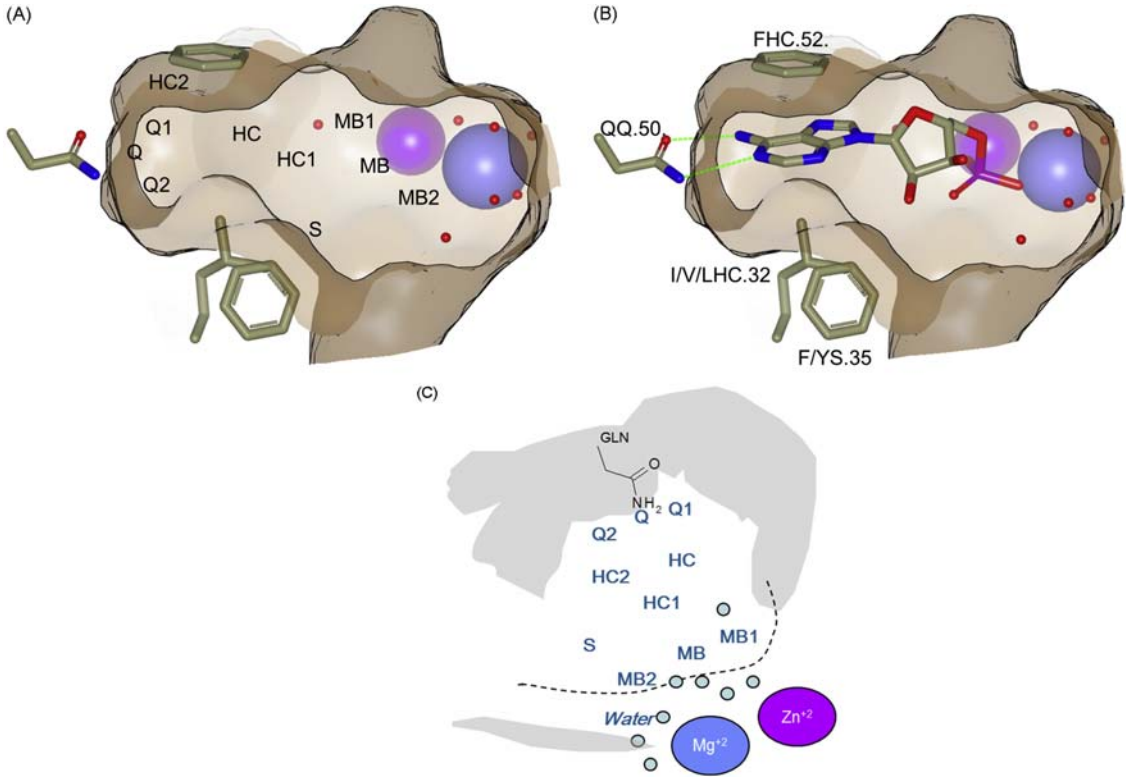

Fig. 4 (A) The PDE pocket is divided into 10 defined regions of the substrate binding site. The substrate binding site includes the Q, Q1, and Q2 regions that surround the important invariant glutamine residue QQ.50, the HC, HC1, and HC2 regions that surround the hydrophobic clamp (I/V/LHC.32 and FHC.52) and the S region solvent filled subpockets. The metal binding (MB) site is divided into the MB, MB1, and MB2 regions. (B) The PDE pocket shown with AMP in the binding site and some key-residues involved in substrate and inhibitor binding are highlighted. (C) The PDE pocket shown schematic, seen from the top.

theoretical descriptors. A descriptor is a structural or physicochemical property of a molecule or part of a molecule. Examples include log *P*, molecular mass (MW), and polar surface area (PSA). Most commonly the assessment of drug-likeness is performed by the use of rules, the original and most well-known of which is Lipinski's rule of five (Ro5, see **Table 2**).[15]

In 1997 Lipinski et al. analyzed the physicochemical properties of drugs in a database of about 2500 orally active drugs that had entered at least phase 2, based on United States Adopted Name (USAN) or International Nonproprietary Name (INN) names. From this analysis, the Ro5 was developed (see **Table 2**, rules of drug-likeness). The Ro5 is so named because all the essential physical properties are parameters of five, and it defines four simple physicochemical parameter ranges (MW $\leq$ 500, log $P \leq 5$, H-bond donors, HBD $\leq$ 5, H-bond acceptors, HBA $\leq$ 10) associated with 90% of orally active drugs that have achieved phase 2 clinical status. These physicochemical parameters are associated with acceptable aqueous solubility and intestinal permeability and comprise the first steps in oral bioavailability. When the Lipinski type analysis was applied to CNS-active compounds, a stricter CNS rule-of-4 (Ro4) was found (see **Table 2**). Of especially high importance for a CNS-active PDE ligand is that it is able to cross the blood–brain barrier (BBB) and have a good permeability across cell membrane in order to reach the intracellularly PDE-target. A small molecule

Table 2 Rules of drug-likeness and pgp substrates

Lipinski's Ro5	*Pgp substrates: Petrauskas*
– Molecular mass $<$500	Pgp substrates:
– Calculated log $P<5$	– N+O >8
– $<$5 Hydrogen-bond donors	– MW $>$400
– $<$10 hydrogen-bond acceptors	– Acid with p$K_a>4$
Lipinski's CNS Ro4	
– Molecular mass $<$400	● Pgp nonsubstrates:
– Calculated log $P<4$	– N+O <4
– $<$4 Hydrogen-bond donors	– MW $<$400
– $<$8 Hydrogen-bond acceptors	– Base with p$K_a>8$

with a low molecular weight (~<400 Da), a relatively high lipophilicity (cLogP in the range of 2–4) and low PSA (<80–90 Å^2), appears to be optimal for diffusion across the lipophilic BBB. It has become increasingly apparent that the endothelial cells in the CNS vasculature express many efflux proteins such as P-glycoprotein (P-gp), which protects the brain by actively pumping out molecules that enters the brain. In order to facilitate the design of compounds with higher likelihood of penetrating the brain, Petrauskas et al. made a classification analysis of P-gp substrate specificity and found that in order to avoid molecular features of P-gp, it is often advisable to keep the Ro4 (see **Table 2**).[16] However, since P-gp is a protein, its recognition of substrates is not governed only by physicochemical properties but by specific molecular recognition elements. Some attempts have been made to define this pharmacophore. Based on a comparison of a hundred compounds previously tested as P-gp substrates, Seelig proposed[17] that a set of well-defined structural elements is required for an interaction with P-gp. The recognition elements are formed by two (type I unit) or three electron donor groups (type II unit) with a fixed spatial separation. Type I units consist of two HBAs with a spatial separation of 2.5 ± 0.3 Å. Type II units contain either two HBAs with a spatial separation of 4.6 ± 0.6 Å or three HBAs with a spatial separation of the outer two groups of 4.6 ± 0.6 Å. In a similar attempt, Pajeva and Wiese proposed[18] a general pharmacophore model of P-gp drugs consisting of two hydrophobic points, three HBA points, and one HBD point. Since Lipinski's seminal report, a large number of additional analyses have been performed on huge datasets and generally have confirmed the central role of physicochemistry. During such an analysis, it was observed that the polarity and molecular weight of in vitro permeable and low clearance compounds are concentrated within an area with a base-line from log $D = -2.0$ to log $D = 5.0$ at MW = 200 and an apex at log $D = 1.0$–2.0 and MW = 450. These trends lead to a triangular-shaped area known as the golden triangle centered at log D 1.5, MW 350, and molecules within this area that are low clearance and permeable are said to obey the golden triangle rule.

7.09.4 PDE Inhibitors

There are 13 FDA approved PDE inhibitors, namely, the unselective PDE-inhibitors theophylline, pentoxifylline, and papaverine; the PDE3-inhibitors cilostazol, milrinone, amrinone, and enoximone; the PDE4-inhibitors roflumilast and apremilast; the PDE5-inhibitors sildenafil, vardenafil, tadalafil, and avanafil. Currently many PDE inhibitors are under development by the pharmaceutical industry across multiple indications. Within therapies to treat CNS diseases the interest for PDEs as targets continues to grow particularly for cognitive decline associated with aging and/or neuropsychiatric diseases such as Alzheimer's disease. The most active areas of research are within the PDE subtypes PDE1, PDE2, PDE4, PDE9, and PDE10, which are reviewed in the following sections.

7.09.4.1 PDE1

PDE1 was one of the first PDE families to be identified in 1970 when it was isolated from bovine and rat brain and was previously called calcium- and calmodulin-dependent PDE, due to its unique Ca^{2+}-dependent activation via calmodulin, thus representing an interesting regulatory link between cyclic nucleotides and intracellular Ca^{2+}.[19] PDE1 isoenzymes are encoded by three genes, PDE1A, PDE1B, and PDE1C. The N-terminal regions contain the regulatory calcium/calmodulin binding sites that activate the enzyme to increase V_{max}. Despite high structural homology within the C-terminal catalytic regions, the three PDE1 isoforms differ in substrate affinity. The affinity for cGMP is similar ($K_m \sim 1$ μM) across the three PDE1-subtypes; however, their affinities for cAMP differ up to 100-fold with the PDE1C having K_m around 1 μM, PDE1B has a K_m of 10–24 μM, and PDE1A has a K_m of 72–124 μM.[20]

The three isoforms have a differential distribution throughout the brain and the body; PDE1B is highly expressed in the striatum, whereas PDE1A is mainly found in the cortical areas, hippocampus, and vascular smooth muscle cells; and PDE1C is particularly highly expressed in the olfactory epithelium, heart, and bladder. In spite of the early discovery of PDE1, a lack of suitable potent and selective, permeable PDE1-inhibitors has hampered extensive understanding of its biological functions. However, during recent years, a growing interest has provided new discoveries and progress in the PDE1 field with a particular focus on the use of PDE1 inhibitors within neurodegenerative and neurologic diseases.[21,22]

Although currently there are no marketed drugs which sole MoA is via PDE1, the indole alkaloid vinpocetine (**9**) and the dihydropyridine nimodipine (**10**) (**Fig. 5**) both have been shown to be PDE1 inhibitors, albeit with relatively low to moderate potency (low micromolar IC_{50}). Both drugs are clinically used vasodilators. Vinpocetine is an alkaloid extracted from the periwinkle plant, and reported to have cerebral blood-flow enhancing and neuroprotective effects, and is used as a drug in Eastern Europe for the treatment of cerebrovascular disorders and age-related memory impairment.[23] Vinpocetine is not approved in the United States for pharmaceutical use, but it can be sold as a dietary supplement. With a dose of 10 mg vinpocetine, the C_{max} plasma concentration of vinpocetine has been measured to lie between 62 and 67 ng mL^{-1} (total conc.),[24] which is significantly lower than its potency on PDE1 (IC_{50}–10 μM), hence the reported effects of vinpocetine are unlikely to be caused by PDE1 inhibition, since this inhibition occurs at a fairly large dose and may not apply to standard supplemental dosages of vinpocetine. It appears that the main MoA of vinpocetine is that it blocks several ion channels (sodium, potassium, and calcium) and is an IKK kinase inhibitor.[25]

Nimodipine is an L-type voltage-gated calcium channel blocker but has additionally been found to act as an antagonist of the mineralocorticoid receptor. Nimodipine was originally developed for the treatment of high blood pressure due to the potent vasodilating effects of calcium antagonists, but the main use is in the prevention of cerebral vasospasm and resultant ischemia, a complication of subarachnoid hemorrhage. The regular dosage is 60 mg tablets every 4 hours, and the average, maximum nimodipine plasma concentrations (C_{max}) at a dose of 30 mg were 16.6 ng mL^{-1} (total concentration),[26] which is significantly lower than its potency on PDE1 (IC_{50}–1 μM), hence the reported effects of Nimodipine is unlikely to be mainly caused by PDE1 inhibition.

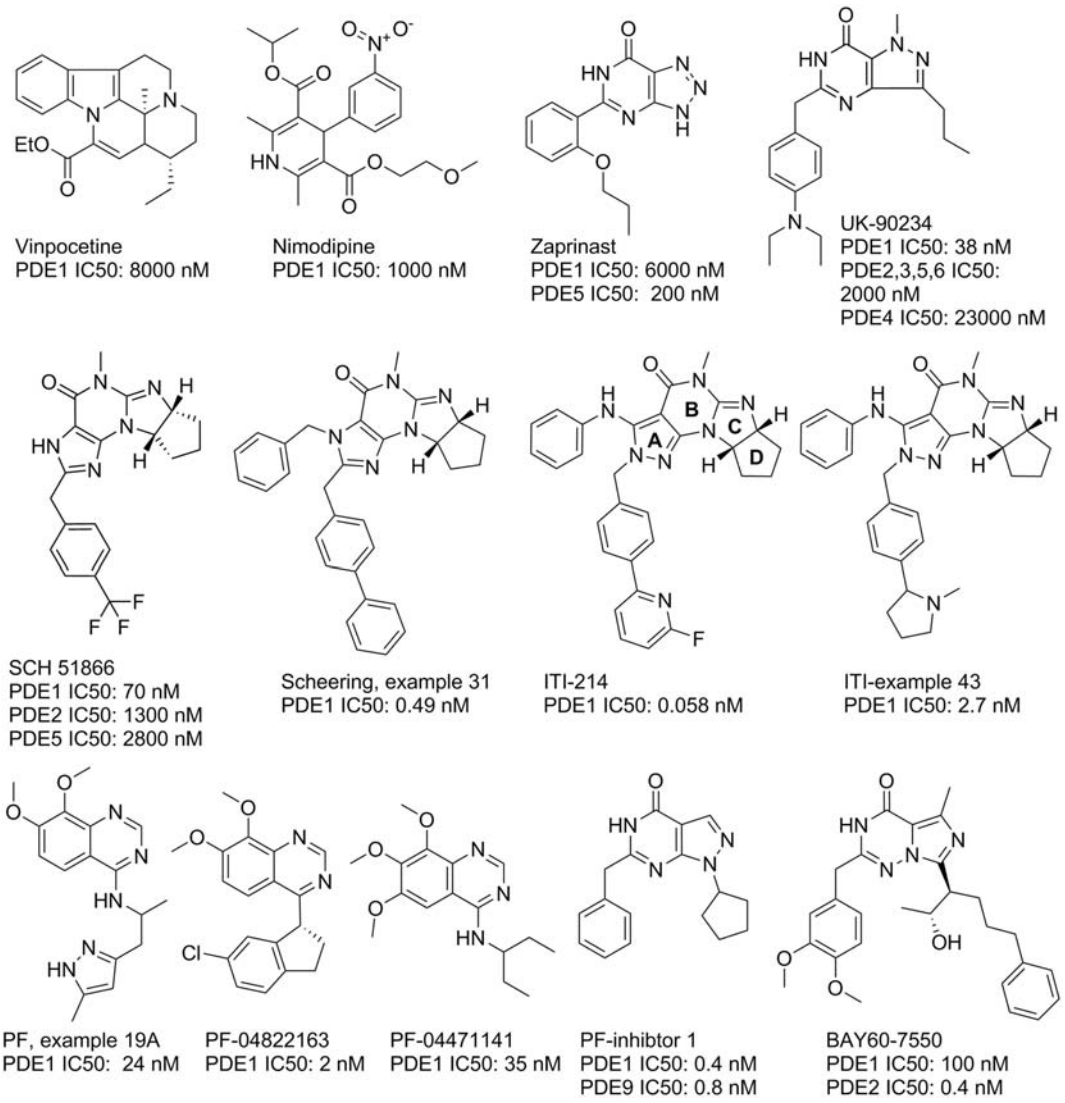

Fig. 5 Structures and IC_{50} values of some inhibitors of PDE1.

Another well-known nonpotent, nonselective inhibitor is zaprinast (**11**), which still lacks selectivity versus other PDE families and is a more potent PDE5 inhibitor. Although Zaprinast was an unsuccessful clinical drug candidate, it has found widespread use as a pharmacological tool.[27]

The recent era of selective PDE1 inhibitors begins with efforts from Schering in the 1990s to "hybridize" the nonselective xanthines like, for example, IBMX (**7**) (Fig. 1) to make them more guanine like resulting in a series of tetracyclic guanines, an example of which is SCH 51866 (**12**) (Fig. 5), which has undergone extensive pharmacological characterization. For unknown reasons, there are conflicting reports on the relative potency and selectivity of SCH 51866 in the literature. The original report from Schering reported SCH 51866 to be a dual inhibitor of PDE1 and PDE5 with equal potency and IC_{50} values of 70 and 60 nM, respectively.[28] However, more recently, SCH 51866 was reported to be PDE1-prefering (for recent IC_{50} values, see Fig. 5).[29] Initial research with SCH 51866 focused on use as a peripheral acting antihypertensive agent, but recent data showed that SCH 51866 also demonstrates CNS effect as it dose-dependently elevated brain striatal levels of cGMP, suggesting the compound to be CNS permeable and CNS-active. Further work in this series led to the highly potent and selective PDE1 inhibitor compound 31 (**13**) (Fig. 5) with subnanomolar potency on PDE1, which however lacked oral activity in contrast to SCH 51866, likely reflecting that compound 31 does not fulfill CNS drug-like properties.[30,31]

In the late 1990s Pfizer described a series of pyrazolopyrimidinones exemplified with UK-90,234 (**14**) (Fig. 5). The UK-90,234 series of compounds are relatively small in size compared with the tetracyclic guanine 31 (**13**) but still might be considered to be distant analogs of guanosine due to the 6,5-fused pyrimidinone ring system, and the PDE1 IC_{50} of 38 nM shows some selectivity versus PDEs 2–6 of 52–640-fold.[32] Although the potency toward PDE9 has not been revealed, subtle structural changes leading to

a structurally isomeric pyrazole pyrimidinone, PF-inhibitor 1 (**15**) and the structurally more distant BAY60-7550 (**16**) (Fig. 5), show that these types of 6,5-fused pyrimidinone lactam-ring systems can fulfill the structural and pharmacophoric requirements for affinity at the PDE9- or PDE2-binding site, since PF-inhibitor 1 has been reported to be an unselective dual PDE1 and PDE9 inhibitor with subnanomolar affinity for both PDE subtypes.[33]

Recently, the Pfizer group published a series of quinazoline derivatives, exemplified with the 3-pentyl amine derivative PF-04471141 (**17**) and the chloroindane derivative PF-04822163 (**18**) (Fig. 5).[34] For the first time within the PDE1 field, now the medicinal chemistry program gets support from X-ray structure showing the binding mode of the ligand PF-04471141 (**17**) (accession code 4NPV). The X-ray structure reveals that the quinazoline 7- and 8-methoxy groups accept a bifurcated H-bond from the side chain nitrogen of the PDE1 Gln-421 residue (Fig. 6A). Furthermore, the quinazoline N1-atom accepts a H-bond from the imidazole side chain of His-373, a signature amino acid specific for PDE1. The requirement for a quinazoline core in this series is further explained by the hydrogen bonding pattern at quinazoline-N3, which is 2.8 Å from a conserved water molecule, which is coordinated by H-bonds to the side chain phenol of Tyr-222, to the carbonyl of Asp-370, and to the catalytic Zn atom via a second well-ordered crystallographic water molecule. This network of water-mediated H-bonds is likely important for quinazoline potency, since both the cinnoline and quinoline templates, which retain N1 but lack the HBA at position 3, show no activity against PDE1.[34]

From the same series, another X-ray was deposited in PDB, namely, 8-dimethoxy-*N*-(1-(5-methyl-1*H*-pyrazol-3-yl)propan-2-yl) quinazolin-4-amine (**19**, PF example 19A, accession code 4NPW). This ligand showed the same binding mode with the same orientation of the quinazoline in the HC (HC, Fig. 6B), thereby demonstrating the ability of the quinazoline to be a purine mimetic.

Recently, Intracellular therapies (ITI) announced completion of a series of phase 1 studies for ITI-214, (6a*R*,9a*S*)-2-(4-(6-fluoropyridin-2-yl)benzyl)-5-methyl-3-(phenylamino)-5,6a,7,8,9,9ahexahydrocyclopenta[4,5]imidazo[1,2-*a*]pyrazolo[4,3-*e*]pyrimidin-4-(2*H*)-one (**20**, Fig. 5), a tetracyclic structure which has some similarity to Schering's earlier tetracyclic guanines.[35] The X-ray crystal structure of the catalytic domain of the human recombinant PDE1B complexed with ITI-214 was reported (accession code 5B25) and gave some insight into the interesting binding mode of this class of compounds. The pyrazolo[3,4-*d*]pyrimidinone

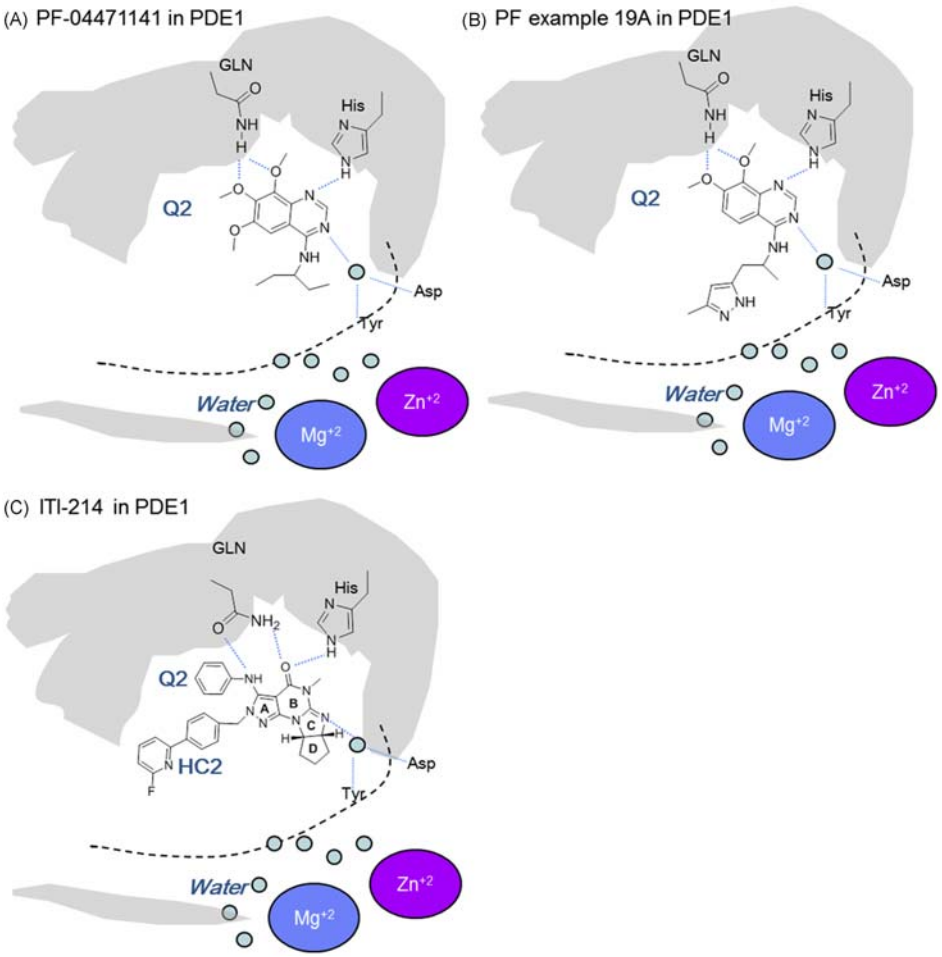

Fig. 6 (A) Cartoon of binding mode of PF-04471141 (**17**) in PDE1 based on X-ray PDB code 4NPV. (B) Cartoon of binding mode of PF example 19A (**19**) in PDE1 based on X-ray PDB code 4NPW. (C) Cartoon of binding mode of ITI-214 (**20**) in PDE1B, based on X-ray pdb code 5B25.

(ring **A**+B in **20**, Fig. 6C) core is held tightly by the HC formed by F424, L388, and F392 located above and below the aromatic core of ITI-214. The π–π stacking and hydrophobic interactions between these contact residues and the planar guanine-mimetic core contribute significantly to the picomolar affinity of ITI-214, which also seems to adopt a binding pose where the conserved Q421 is tilted out of the plane forming bidentate hydrogen bonds with the exocyclic carbonyl group of the pyrimidone and the anilino group. The HBD of the aniline N−H group at position 3 of the A-ring seem to play an important role in contributing to the affinity, supported by an observation, that removal of the hydrogen by N,N-substitution resulted in compounds that were significantly weaker inhibitors than monosubstituted analogues. In addition, replacing this N−H at position 3 with O, S, or CH_2 caused 35–90-fold decrease in PDE1 binding affinity.[35]

The ITI-214 compound is an important contribution to the PDE1 research since it is the first example of a PDE1 inhibitor that reached the clinic. Importantly, it was reported that multiple human clinical phase 1 studies have been completed. In these studies, ITI-214 demonstrated a favorable safety profile and was generally well tolerated across a broad range of doses both in healthy volunteers and in patients with schizophrenia with a pharmacokinetic profile that supports once daily dosing. According to the Company homepage, ITI is currently evaluating ITI-214 for several indications including cognition in patients with Parkinson's disease, dementia, schizophrenia, and other CNS and non-CNS disorders. Based on preclinical studies, ITI-214 may also have the potential to treat cardiac and vascular hypertrophy associated with diseases such as congestive heart failure and may also possess antiinflammatory activity for use in treating neuroinflammation and other major inflammatory diseases. The preclinical characterization of ITI-214 in rats was also reported, and ITI-214 showed procognitive properties in rodents.[36]

The elucidation of the biological function and role of PDE1 was previously hampered by lack of subtype selective compounds; however, recently the field has been moved significantly by the publication of novel PDE1 inhibitors and the pharmacological properties are emerging indicating a potential within cognitive dysfunction. However, PDE1 does also play a significant role in the regulation of the vascular tone, and PDE1 inhibitors might have a potential for treatment of non-CNS disorders in the cardiovascular system and might also be limiting the clinical use within the CNS indication space. In spite of the cardiovascular PDE1-effects reported in preclinical species, the most progressed PDE1 inhibitor from intracellular therapies (ITI-214) has currently completed phase 1 clinical studies and was reported to be safe and well tolerated.

7.09.4.2 PDE2

Native human PDE2A is a protein of 941 amino acids that is organized in four domains: (1) [N-terminus (1–214), (2) GAF-A (215–372), (3) GAF-B (393–541), and (4) catalytic (579–941)] and that functions as a homodimer. The near full length enzyme was crystallized and gave valuable insight to the structure and function of PDEs.[37] PDE2 is a dual substrate PDE, which is activated by cGMP. It is expressed in forebrain regions of the brain, including the cerebral cortex and hippocampus, regions known to be involved in learning and memory, and therefore has been pursued as a target to address CNS disorders, and especially AD.[22,38] It is also expressed in peripheral organs, particularly in the heart, where it plays a role in the regulation of the cardiac cyclic nucleotide cross-talk signaling network.[39]

One of the early reported PDE2 inhibitors was the adenine derivative EHNA, **22** (Fig. 7); however, this compound was subsequently found to lack the requisite selectivity and potency for conclusive pharmacological evaluation.[38] Nevertheless, an X-ray structure of EHNA in complex with the PDE2 catalytic site[40] showed (Fig. 8A) that EHNA binds in the binding pocket of PDE2 via bidentate H-bonds to the invariant Gln-859 which adopts the AMP-mode. The Q2 pocket in PDE2 is relatively small. However, a main finding was the observation of a "binding-induced hydrophobic pocket" (H-pocket, Fig. 8A). The deep H-pocket is generated by induced fit when EHNA binds to the PDE2A enzyme, where the aliphatic side chain of EHNA pushes Leu-770 out to the solvent-exposed surface of the protein and thereby opens up the deep H-pocket. This pocket is closed/blocked by Leu-770 in the absence of ligand (APO-structure—PDB 1Z1) and the pocket is also closed in structures where ligands bind in the binding site, but where a substituent is not protruding into the pocket. An improved tool compound for evaluating PDE2 inhibition was the imidazotriazinone compound BAY-60-7550, **23** (Fig. 7), which is selective with respect to other PDE isoforms (50-fold over PDE1C, >100-fold selectivity vs. other PDE isoforms). While the poor pharmacokinetic properties of BAY-60-7550 probably preclude its use in clinical studies, the compound has been a critical tool to validate the potential therapeutic utility of PDE2 inhibition and has demonstrated enhanced learning and memory and procognitive effects in a range of animal models.[38,41] However, BAY-60-7550 demonstrated poor brain uptake in rats 30 min after administration of a 10 mg kg^{-1} oral dose (B/P = 0.05, [P] = 72.9 ng mL^{-1}, and [B] = 3.6 ng g^{-1}), meaning that in vivo data with this compound should be treated with caution.[42]

The crystal structure of a PDE2a catalytic domain in complex with BAY-60-7550 has been published at a resolution of 1.9 Å.[43] BAY-60-7550 was shown to bind to the active site of PDE2 and interact with the conserved glutamine residue Gln-859 in a GMP-mode (Fig. 8B). The observation that the adenine derivative EHNA interacts with the GLN in AMP-mode and that the "guanine" core of the imidazotriazinone BAY-60-7550 interacts with the GLN in GMP-mode, support that the so-called glutamine-switch is responsible for the dual cAMP/cGMP specificity of PDE2a. Importantly, the authors, who were the first to report the discovery of the hydrophobic subpocket in PDE2 and named it the "H-pocket," describe in detail how the propylphenyl group of BAY-60-7550 was found to bind to the H-pocket between helices H11 and H14, which is formed mainly by hydrophobic residues: Leu770, Leu809, Ile866, Ile870, His773, and Leu774.[43] The authors argued that the origin of the high PDE2a selectivity of BAY-60-7550 is a combination of binding to the glutamine-switch, and to this new induced hydrophobic pocket as a specific selectivity pocket for PDE2, since it is not yet described in any other published PDE-inhibitor complexes.

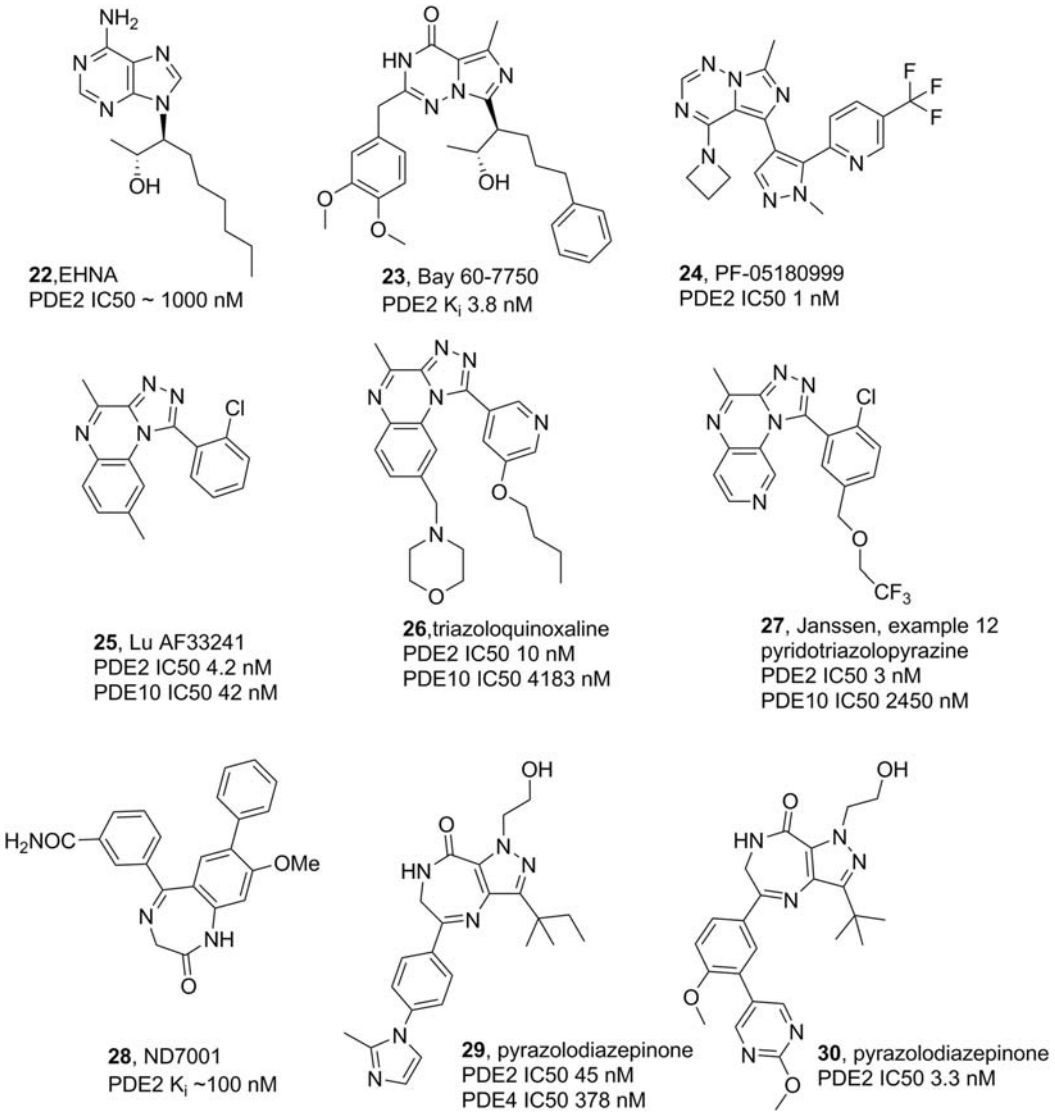

Fig. 7 Structures and IC_{50} values of some inhibitors of PDE2.

Other research groups have also found and used this H-pocket as a mean to develop PDE2 selective compounds. The clinically most progressed efforts have been reported by Pfizer, which presented the clinical candidate, PF-05180999, **24** (Fig. 7).[44] Docking experiments of PF-05180999 suggest that the high PDE2-potency and selectivity is obtained by the 2-(2-methyl-2*H*-pyrazol-3-yl)-5-trifluoromethyl-pyridine group occupying the H-pocket (Fig. 8B).[45] A PDE2 PET-ligand candidate was also reported from this series.[46]

Another compound developed by Takeda, TAK-915, has also been progressed to clinical trials (ClinicalTrials.gov Identifier: NCT02584569). This phase 1 study was conducted to examine the degree and duration of brain PDE2A enzyme occupancy/target engagement as a function of TAK-915 plasma concentration in order to guide dosing and schedule for future clinical studies in schizophrenia with TAK-915.

Several other groups also reported the observation and effective use of the H-pocket to obtain potent and selective PDE2 inhibitors. A series of [1,2,4]triazolo[4,3-*a*]quinoxalines was identified as dual PDE2/PDE10 inhibitors, originally invented by Biotie Therapies GMBH (later Biocrea) and later codeveloped with Wyeth/Pfizer and later again with Boehringer Ingelheim International Gmbh.[38] Simultaneously this series was actively explored by the Janssen group and the Lundbeck group. The Lundbeck group reported on the compound Lu AF33241, **25** (Fig. 7) as a novel, brain-penetrant, dual inhibitor of PDE2A and PDE10A.[47] The Janssen Group has published several reports on the optimization work in this series, for example, **26** (Fig. 7). Following the design hypothesis of utilizing the H-pocket as a selectivity pocket, structure-guided design led to the identification of the novel, potent, and selective PDE2 inhibitor *triazolo-quinoxaline example* **12**, **27** (Fig. 7).[42] An X-ray structure of *triazolo-quinoxaline* **26** in complex with the catalytic domain of PDE2 (PDB 4D08) confirmed that the lipophilic butyloxy-chain was positioned in the induced H-pocket. A

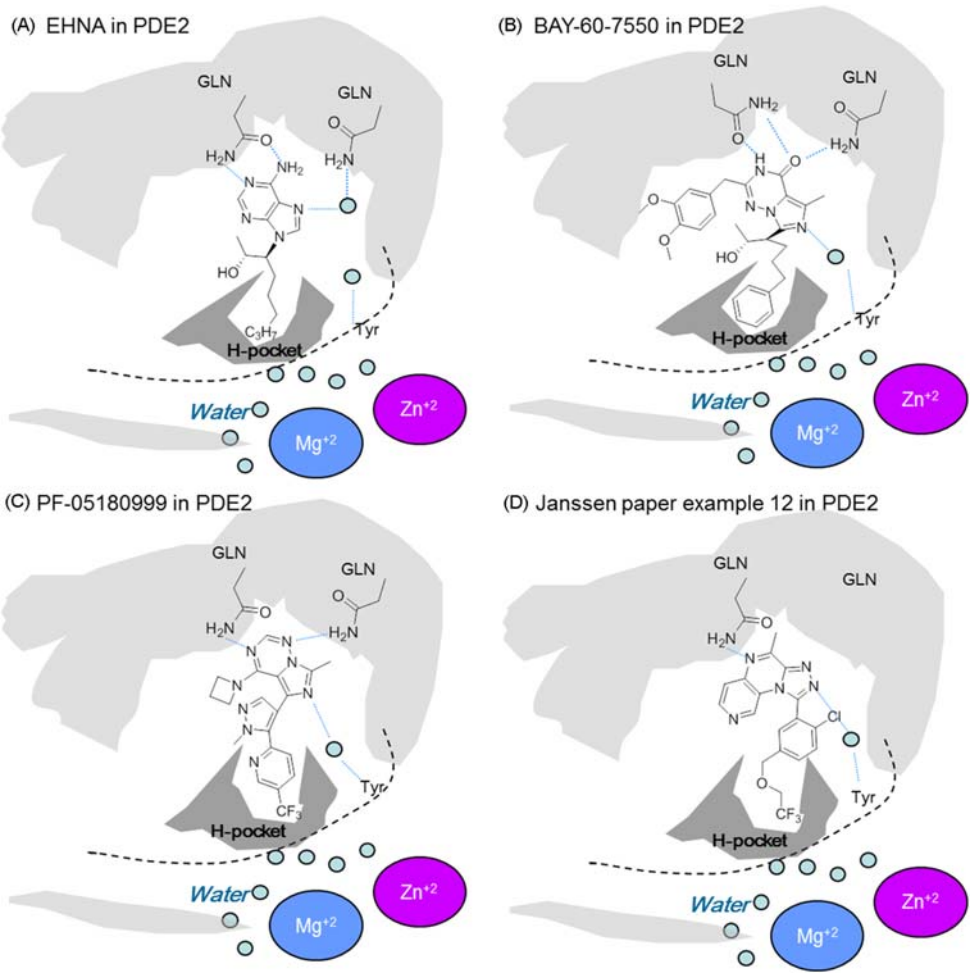

Fig. 8 (A) Cartoon of binding mode of EHNA, **22** in PDE2 based on X-ray. (B) Cartoon of binding mode of BAY-60-7550, **23** in PDE2 based on X-ray. (C) Cartoon of binding mode of PF-05180999, **24** in PDE2, based on docking. (D) Cartoon of binding mode of Janssen, paper example 12 pyridotriazolopyrazine **27**, in PDE2, based on X-ray.

tritiated version of the triazolo[4,3-*a*]quinoxaline was used to demonstrate central occupancy of PDE2 inhibitors in a consistent dose–response manner and in vivo evaluation provided evidence that this series of compounds is able to engage the target and to increase cGMP levels in relevant brain regions. While solubility was increased compared with original HTS-hit, poor metabolic stability led to further lead optimization and introduction of pyridyl-like nitrogen in the benzene ring of the quinoxaline moiety resulting in series and a pyrido[4,3-*e*][1,2,4]triazolo[4,3-*a*]pyrazine series, for example, **27** (Fig. 7) maintaining high ligand efficiency and good overall physicochemical and ADME properties.[48] Also here, the H-pocket was being used to obtain potency and PDE2 selectivity (Fig. 8D). Due to the roof-like position of the H-pocket, very strict geometric requirements must be fulfilled in order to be able to reach this pocket. Since all compounds occupy the clamp-region with a purine isostere, the H-pocket can only be reached by a perpendicular 90-degree orientation of the substituent. In the dual inhibitors triazolo[4,3-*a*]quinoxalines like for example, Lu AF33241, this is achieved by introduction of an ortho-chlorine in the phenyl group, forcing the phenyl out of plane. Alternatively, a pyridyl nitrogen is introduced in the meta-position, which pick up a H-bond in the "floor" and thereby orients the butyloxy group towards the roof pocket. Notably, from this tricyclic series, both the Janssen group and the Biocrea group have identified PDE2 PET-ligand candidates.[49]

Another, older, well-characterized PDE2 inhibitor is the benzodiazepinone compound ND-7001 (IC_{50}–50-100 nM) from Neuro3d (now Evotec). Although structural information is not available with this compound, a molecular modeling study reported by Hamza and Zhan,[50] proposed that the phenyl-amide of ND-7001 serves as the primary anchor point with the amide hooking up in H-bonds with Gln-859 and the phenyl group in the clamp. Although the H-pocket was not known at that time, the ligand pose has the 7-phenyl group pointing toward the H-pocket. Biochemically, ND-7001 increases cGMP levels in primary neuronal cultures of rat cerebral cortical neurons, and in spite of being a pgp-substrate,[40] it was reported to have anxiolytic effects in a number of tests.[40] A clinical phase 1 trial was conducted with ND-7001, and the compound was reported to be safe and well tolerated to high doses and produced no sedation, memory disturbance, or withdrawal effects, but no further development has been reported since 2008.

Pfizer recently published articles discussing the discovery of a series of potent PDE2 inhibitors identified from a PDE4 diazepinone scaffold, for example, **29** in Fig. 7, mainly aimed at for non-CNS indications. In silico modeling studies suggested that this series of inhibitors would adopt a cGMP-like binding mode due to the orientation of the ligand with Gln-859. It was thought that this orthogonal binding mode, compared to cAMP-like binding mode found for PDE4, would allow for greater PDE2/PDE4 selectivity. After extensive SAR studies, the researchers identified the diazepinone compound **30** in Fig. 7 with good PDE2a potency ($IC_{50} = 0.003$ μM) and improved PDE4B selectivity (PDE4B $IC_{50} = 0.562$ μM). Based on the cLogP and TPSA values, the researchers did not expect this PDE2 tool compound to show good brain penetration.

In summary, several groups have invented potent and selective brain-penetrant PDE2 inhibitors and demonstrated procognitive properties of PDE2 inhibitors in rodent models. PET-ligands assisting target engagement studies in the clinic have been published, and several groups have advanced PDE2 clinical candidates into phase 1 studies, reporting them to be safe and well tolerated with Pfizer currently having the compound PF-05180999 (**24**) on clinical hold, whereas Takeda is progressing the compound TAK-915 for cognitive dysfunction associated with schizophrenia.

7.09.4.3 PDE4

PDE4 is a cAMP-specific hydrolase, which is the major enzyme responsible for the degradation of cAMP in the body and is represented by four genes (PDE4A, B, C, and D). PDE4A, B, and D are expressed in the brain. PDE4 isoforms differ in N-terminal sequences that determine cellular sublocalization and regulatory properties. All four proteins contain signature regulatory domains, called upstream conserved region 1 (UCR1; ~55 amino acids) and upstream conserved region 2 (UCR2; ~78 amino acids). UCR2 negatively regulates cAMP hydrolysis and is also needed for high-affinity binding of the PDE4 inhibitor rolipram, **37** (Fig. 9). Based on the variation of UCR1/2 of the N-terminus, the PDE4 isoforms can be divided into three classes: long, short, and super short. The long class of enzymes has both UCR1 and UCR2; the short has UCR2 only; and the supershort has only a truncated UCR2. UCR1 and UCR2 form a regulatory module that is disrupted by protein kinase A (PKA) by phosphorylation of UCR1, which increases enzymatic activity and sensitivity to rolipram. Another characteristic of the PDE4 enzymes is an extreme C-terminal sequence that is unique to each PDE4, and which is important in the design of PDE4 subtype selective inhibitors.

PDE4-selective inhibitors have potential therapeutic use in many disease areas but have had particularly high interest for CNS, inflammatory and respiratory diseases. More than 30 different PDE4 inhibitors have been developed and advanced to human clinical trials, mostly for the treatment of inflammatory diseases. Two PDE4 drugs are now on the market, roflumilast **31** (Fig. 9), showing clinical effectiveness in chronic obstructive pulmonary disease (COPD), and apremilast, **32** (Fig. 9) approved for the treatment of certain types of psoriasis and psoriatic arthritis. The development of PDE4 inhibitors as therapeutic drugs has been hampered by the dose-limiting emetic side effects (nausea and even vomiting) in humans. Currently, PDE4 inhibitors are being developed that show a strong reduction in emetic side effects, particularly the effect of roflumilast on nausea is mostly mild or moderate in intensity and occurs in only 5% of the subjects. The improved tolerability in comparison to other PDE4 inhibitors has been attributed to a pharmacokinetic profile with a lower peak-to-trough ratio, allowing a stable plasma concentration so that the drug remains in a narrow free concentration range.[51] Recently, CNS effects of roflumilast were demonstrated, and it was shown to improve memory in rodents at nonemetic doses.[52] Based on the results in rodents, a clinical trial involving healthy 18- to 35-year-old adults was performed using a single oral administration of a capsulated formulation containing 100, 300, or 1000 μg roflumilast.[53] In this clinical trial the group of healthy adults receiving a single oral dose of 100 mg of roflumilast showed a considerable improvement with respect to the number of correct words recalled (an average 2.5 words improvement after the third trial) in the verbal learning task (VL-T). EEG measurements performed simultaneously with VL-T testing revealed that event-related potential (ERP), P600 demonstrated the strongest increase of amplitude, also in the group of healthy adults receiving a single oral dose of 100 μg of roflumilast. In order (a) to confirm the results seen in the clinical trial with the healthy 18- to 35-year-old adults and (b) to detect whether perhaps even more substantial improvement might be observed in aged adults with a certain degree of cognitive impairment, a small clinical study was conducted with forty 60- to 80-year-old subjects with one group having a more pronounced cognitive decline (assessed with VL-T) as well as with an aged matched control group.[53] The two patients groups were tested for cognitive battery (Verbal Learning Task, Spatial Memory Task, and Stroop Task) and EEG battery (ERP's, sensory gating and novelty oddball task) tests. The data obtained from an interim analysis of that clinical trial based on nine subjects of the impaired group and four subjects of the control group appears to confirm the effects seen in the VL-T in the earlier trial with healthy adults after administration of 100 mg of roflumilast. All these data indicate that roflumilast administered in doses considerably lower than the approved once a day dose for the treatment of severe COPD (500 μg) is effective in improving cognitive impairment. Roflumilast has undergone two clinical studies, one proof of mechanism study in schizophrenia with roflumilast plus antipsychotics (ClinicalTrials.gov Identifier: NCT02079844) evaluating cognitive improvement. Another clinical trial investigated roflumilast and Donepezil ability to reverse scopolamine-induced cognitive deficits in healthy adults (clinicaltrials.gov identifier: NCT02051335). Results of the studies have not yet been published.

The other PDE4 inhibitor on the market, apremilast, has not yet been investigated for its potential CNS effects, but apremilast has been reported to be a pgp-substrate and the concentrations measured in the CNS were consistently low, indicating that penetration of the blood/brain barrier was poor.[54]

The prototypic PDE4 inhibitor, rolipram, **37**, showed efficacy in a small, open-label depression study in the early 1980s,[55] and since then an extensive body of preclinical and clinical efficacy data has been accumulated, however its development was

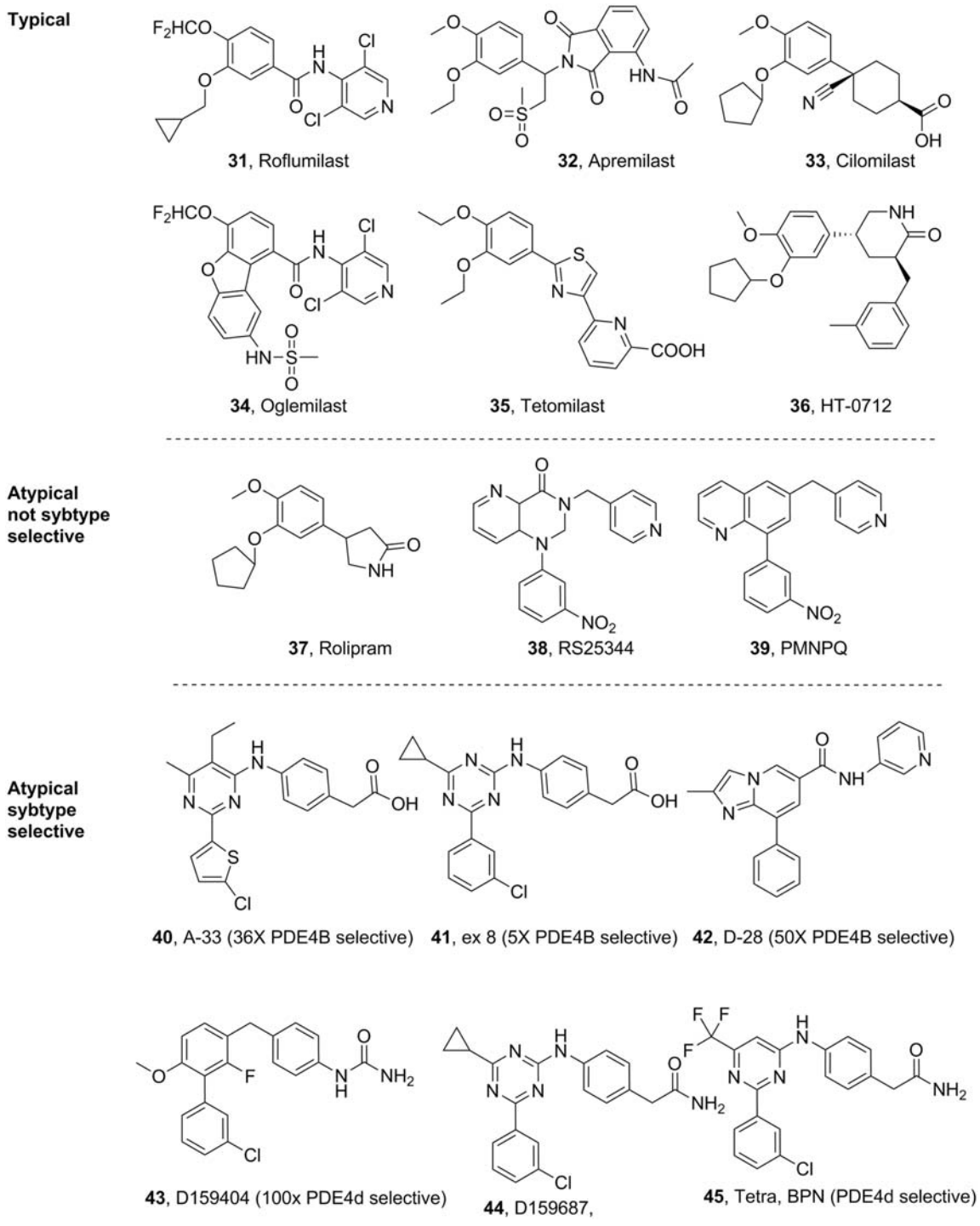

Fig. 9 Structures of some inhibitors of PDE4.

discontinued owing to its side effects. Nevertheless, Rolipram is a widely used PDE4 inhibitor that has been evaluated in multiple models of learning and memory and has been shown to reverse memory deficits in mouse models of AD and provide cognitive benefit in a range of rodent models.[22,56]

Detailed overviews of the binding mode of PDE4 inhibitors have been published, in which PDE4 inhibitors have been divided into three groups, based on their PDE4 subtype-selectivity and binding mode: (1) typical PDE4 inhibitors including roflumilast, **31**, and apremilast, **32**; (2) atypical inhibitors which are not PDE4-subtype selective including rolipram; and (3) atypical inhibitors which are PDE4-subtype selective including the PDE4D-preferring tool compound D159404, **43** (see Fig. 9).[57]

Inhibitors of PDE4 may be classified as "typical" or "atypical" (Fig. 9) based on whether they interact with the catalytic domain alone (like roflumilast) or with the catalytic domain plus one of the regulatory domains, that is either the UCR2 domain (like rolipram) or the C-terminal domain (like A-33, **40** see Fig. 9).[57] Atypical inhibitors are much more potent against long forms of PDE4 that contain both UCR1 and UCR2 compared to those containing only the catalytic domain. For example, PMNPQ, **39** (Fig. 9) is >10,000 more potent against the long-form variant PDE4D7 than against PDE4D catalytic domain.[57] By contrast, typical inhibitors, such as roflumilast, bind with nearly equal affinity to long isoforms and catalytic domain constructs. Both roflumilast and rolipram belong to the class of dialkoxyphenyl PDE4 inhibitors. This class also includes HT-0712, **36** (Fig. 9), which has been reported to have completed a clinical trial versus placebo in subjects with age-associated memory impairment, although no study results have been posted yet (ClinicalTrials.gov Identifier: NCT02013310). Several compounds from the dialkoxyphenyl family of compounds have been crystallized in the PDE4 catalytic domain, and they all share a common binding mode (Fig. 10).[58] The catechol ethers make a H-bond with the conserved GLN, and the phenyl group is sandwiched by the P-clamp. Substituents on the phenyl ring are exploring the ribose binding site and to some extent the phosphate binding site. The dialkoxyphenyl family of compounds almost all contains one carbon ether, for example, methoxy or difluoromethoxy, and a cyclic multicarbon ether, for example, cyclopentyloxy or cyclopropylmethyl. The smaller methoxy or difluoromethoxy group on the phenyl ring is tucked into a small pocket at the deep side of the Q1 pocket formed by Y233(PDE4B), N395(PDE4B), T407(PDE4B), and Y403(PDE4B).[58] The other alkoxy-group tends to be a larger hydrophobic group such as cyclopentyl, which occupy the larger hydrophobic Q2 pocket formed by F414(PDE4B), M411(PDE4B), M431(PDE44B), and F446(PDE4B).

The various substituents on the nonalkoxy positions of the phenyl scaffold explore the deep pocket close to the MB site, and how well they form interactions with residues lining this pocket determines their relative binding affinity. The relatively smaller pyrrolidinone substituent in rolipram has resulted in somewhat lower binding affinity of 570 nM. The pyrrolidinone group is stabilized mainly through hydrophobic interactions with M347(PDE4B), I410(PDE4B), and F414(PDE4B). Roflumilast binds similar to rolipram. The difluromethoxy group binds at the Q1 pocket, while the cyclopropyl methoxy group binds at the Q2 pocket. The difluromethoxy group fits the Q1 pocket better and makes more hydrophobic interactions with residues than the methoxy group. However, due to the relatively lower lipophilic surface area of the cyclopropylmethylether group, it makes fewer hydrophobic interactions than the larger cyclopentylether group. The dichloropyridyl group extends to the dimetal ion site and forms one H-bond to a water molecule that is coordinated to Mg^{2+}. The dichloro-atoms also form additional hydrophobic interactions with residues in the M-pocket. The dichloropyridyl substitution has compensated for the negative effect of the cyclopropylmethyl ether group and as a result has increased the potency significantly ($IC_{50}=0.84$ nM).

When it comes to binding mode of roflumilast and rolipram to long-form PDE4, however, there is a marked difference in observed interactions between ligand and binding site compared to binding to the catalytic domain only. Rolipram has been shown to bind to PDE4 possessing two binding sites, high-affinity (1–50 nM) and low-affinity (500–1000 nM) rolipram binding sites, and recently, it has been shown that these represent two different conformational states of the enzyme.[59] It has been shown that there is a difference between the interactions of rolipram binding in the catalytic site alone (the low-affinity binding site) compared to the interactions of rolipram binding in the long-form PDE4, where UCR2 of one subunit interacts with the catalytic domain of the other subunit and thereby introduces further interactions that identifies the basis of the high-affinity rolipram binding site (Fig. 10).[59] In the high-affinity binding mode, Tyr274 from the regulatory UCR2 helix forms one wall of the hydrophobic pocket occupied by the cyclopentyl group, and its phenolic hydroxyl oxygen from the tyrosine forms a hydrogen bond with the amide carbonyl oxygen in rolipram. Both these interactions are absent in the low-affinity binding mode. So, the difference is that rolipram makes two significant additional interactions with the regulatory helix. The hydrophobic cyclopentyl group is now completely buried in

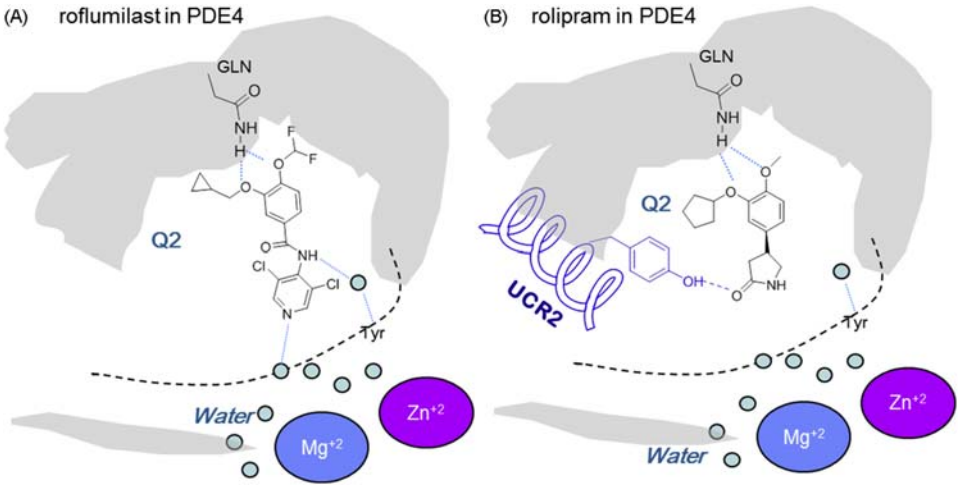

Fig. 10 Cartoon of binding mode of PDE4 inhibitors roflumilast and rolipram in PDE4 based on X-ray.

a hydrophobic pocket, whereas it was partially exposed to solvent in the catalytic domain structure. These additional interactions, which contribute to high-affinity rolipram binding, are only possible in dimeric PDE4 where the autoinhibitory domain of one subunit can interact with the catalytic domain of the other subunit.[59]

Recent progress in understanding the structural basis of PDE4 regulation has made it possible to design selective PDE4D and PDE4B inhibitors, which have been called negative allosteric modulators (NAMs) due to the interaction with either the UCR2 or the C-terminal domains. These act by modulating the closure of N- and C-terminal PDE4 regulatory domains across the active site, thereby inhibiting the enzyme.

PDE4B and PDE4D are therapeutic targets of high interest for CNS; however, it has been difficult to discover selective PDE4B and PDE4D inhibitors as there are no amino acid sequence differences in the active site that distinguish PDE4B from the other PDE4 subtypes.

It is possible to design small-molecule negative allosteric modulators of PDE4D that act through closing UCR2 over the active site. Indeed, rolipram inhibits PDE4 through that mechanism. Examples of such compounds are D159404, **43** (100× PDE4d selective); D159687, **44**; and Tetra, BPN-compounds, for example, **45** (**Figs. 9** and **11**). Notably, the UCR2-directed, partial inhibitor D159687 was 300-fold less emetic than rolipram, despite equal potency in cognition assays, and D159687 was 3000-fold less emetic than rolipram in the beagle dog, and 500-fold less emetic in monkey.[60] Thus, there is a striking difference between full and partial PDE4D selective-inhibitors directed against UCR2 with respect to PD tolerability. This could indicate that allosteric modulators that only partially inhibit PDE4D activity may achieve improved tolerability by maintaining temporal and spatial aspects of cAMP signaling.[60] Compounds able to bind UCR2, when located in the active site, share a common pharmacophore and binding pose. The pharmacophore consists of three elements: (1) a planar scaffold providing a hydrogen bond to Gln-535, (2) a linker, and (3) two aromatic substituents which create a clamp that holds UCR2 in the closed conformation. Key to the design of partial inhibitors was the deliberate weakening of the P-clamp interaction with the hydrophobic walls of the active site.[60]

Besides the role of UCR2 to function as a regulatory part when closing over the active site, a second, downstream C-terminal helix, termed CR3 (conserved region 3) is present in all PDE4 isoforms and was also shown to close over the active site by weakly engaging inhibitors (e.g., PMNPQ, **39** **Fig. 9**; PDB ID: 3G58). Recently, selective PDE4B inhibitors have been reported, which act by engaging the C-terminal CR3 regulatory domain, thereby locking the enzyme in a closed conformation and therefore closing the active site to access by cAMP.[61] Examples of PDE4B selective compounds are A-33,[62] ex-8,[63] and D-28 (**Figs. 9** and **11**). Notably, allosteric modulators that only partially inhibit PDE4D activity may achieve improved tolerability by maintaining temporal and spatial aspects of cAMP signaling.

In summary, whereas the use of PDE4 inhibitors for several peripheral diseases is now well established, the application within the CNS area has been lacking behind due to target-mediated side effects. Strategies to avoid particularly the emetic side effects by either utilizing pharmacokinetic strategies like with roflumilast or pursuing PDE4-subtpe selective compounds have resulted in several companies now having PDE4 compounds in clinical trials for cognitive dysfunction.

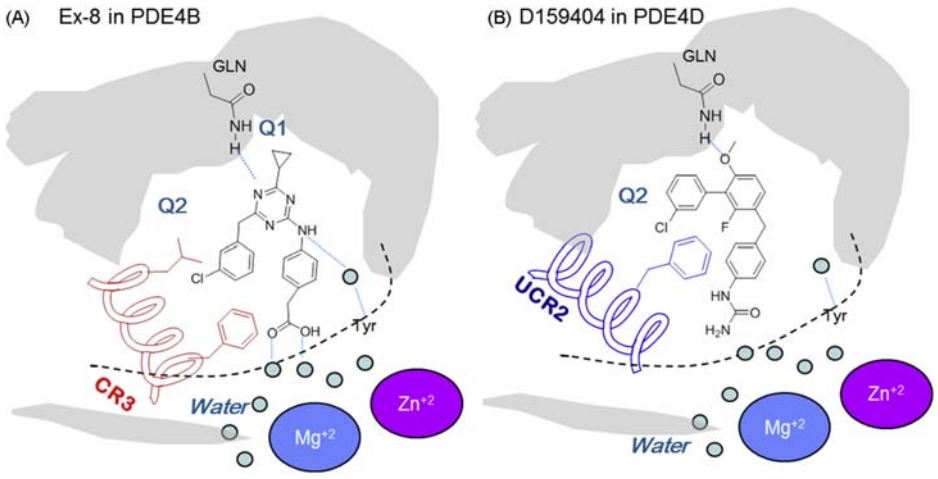

Fig. 11 Binding mode of PDE4 negative allosteric modulators (NAMs). (A) Binding of compound **41** in PDE4B showing key interactions. PDE4B NAMs are directed against CR3. The CR3 regulatory domain (*red*) is closed in cis across the active site of the same monomer. The cyclopropyl group has good shape complimentarily and fills the Q1 hydrophobic pocket in the active site. The amine in the Ar1 linker region is in position to make a H-bond to a conserved water molecule. Both Ar1 and Ar2 groups modulate PDE4B vs. PDE4D selectivity in the triazine series and reach out of the active site and engage the CR3 regulatory helix. The chlorophenyl Ar2 group on the triazine is in position to make hydrophobic interactions with CR3 Phe678 and Leu674, and the carboxylic acid group of Ar1 hydrogen bonds to multiple water molecules which engage CR3 (PDB: 4NW7). (B) Binding of D159404, compound **43** in PDE4D. PDE4D NAMs close the UCR2 regulatory domain (*blue*) in trans over the active site of the opposite catalytic domain in the PDE4 dimer, thereby preventing access by cyclic adenosine monophosphate and inhibiting the enzyme. D159404 forms a H-bond to the invariant GLN (Q610 in PDE4D7), while two arms project outward toward UCR2. Binding of the inhibitor completes a hydrophobic interaction surface for the closure of UCR2 by displacing water from the active site (PDB: 3IAD).

7.09.4.4 PDE9

PDE9 is a family of cGMP-specific enzymes first described in 1998 and has the lowest K_m among cGMP-specific PDE families (cGMP $K_m = 170$ nM, cAMP $K_m = 230$ μM), which might suggest that it could play a role in modulating basal levels of cGMP. Neuronal PDE9 expression has been detected in the cerebellum, cerebral cortex, caudate-putamen, and hippocampus.[64] Selective PDE9 inhibitors have been studied as potential therapeutics for the treatment of diabetes and CNS diseases such as Alzheimer's disease,[65] and several reports have been published demonstrating that PDE9 inhibitors showed memory improving effects in many animal pharmacological deficit models.[65]

PF-4447943, **46** (Fig. 12), a potent, selective, and brain-penetrant PDE9A inhibitor, has been reported to have been dosed in humans where it was well tolerated, and increased CSF cGMP levels, supporting central target engagement and demonstrating the translation of cGMP-measurement between humans and rodents.[66] However, despite strong preclinical efficacy in a range of rodent cognition models,[67] PF-4447943 did not improve cognition or behavior compared with placebo in a 12-week phase 2 clinical trial evaluating the efficacy in mild to moderate Alzheimer's disease.[68] This result is one of many, which highlights the general challenge of translation from preclinical animal models to human clinical efficacy trials, and particularly, finding the right clinical dose is challenging. Nevertheless, Starting in 2011, Boehringer Ingelheim thus far has conducted 10 phase 1 studies, testing both tablets and liquid formulations in a total of about 500 people in Germany, Belgium, South Korea, and the United States on their clinical candidate BI-409306 (chemical structure not disclosed, but examples from patent applications are compounds **48** and **49**, Fig. 12).[69] Eight studies were in healthy volunteers, while three in people with Alzheimer's disease and schizophrenia. The studies assessed safety, tolerability, pharmacokinetics and -dynamics, single or ascending doses given once or twice daily, as well as the effect of food on the drug's metabolism. In Dec. 2014 and Jan. 2015, respectively, two 3-month, multinational phase 2 trials of BI-409306 began in patients with prodromal AD. One study will compare four doses of BI-409306 to placebo in 288 people with mild to moderate AD who have not taken an acetylcholine esterase inhibitor or memantine in the past 3 months; the other will compare the same doses as add-on therapy in 336 patients who also take donepezil. For both studies, the primary outcome measure is the neuropsychological test battery, and secondary outcomes include the clinical scales: ADCS-MCI-ADL, CDR-SB, ADAS-Cog11, and ADCS-ADL. In Mar. 2015, data were presented at the 15th International Congress on Schizophrenia Research, Colorado, USA[70] from a randomized, parallel-group, double-blind, double-dummy, single dose, placebo-controlled trial on healthy male volunteers ($n = 20$), assessing the effect of different doses (25, 50, 100, and 200 mg qd po) of BI-409306 on cGMP CSF levels. Plasma levels of BI-409306 increased rapidly with a delay in reaching maximum CSF concentration. There was

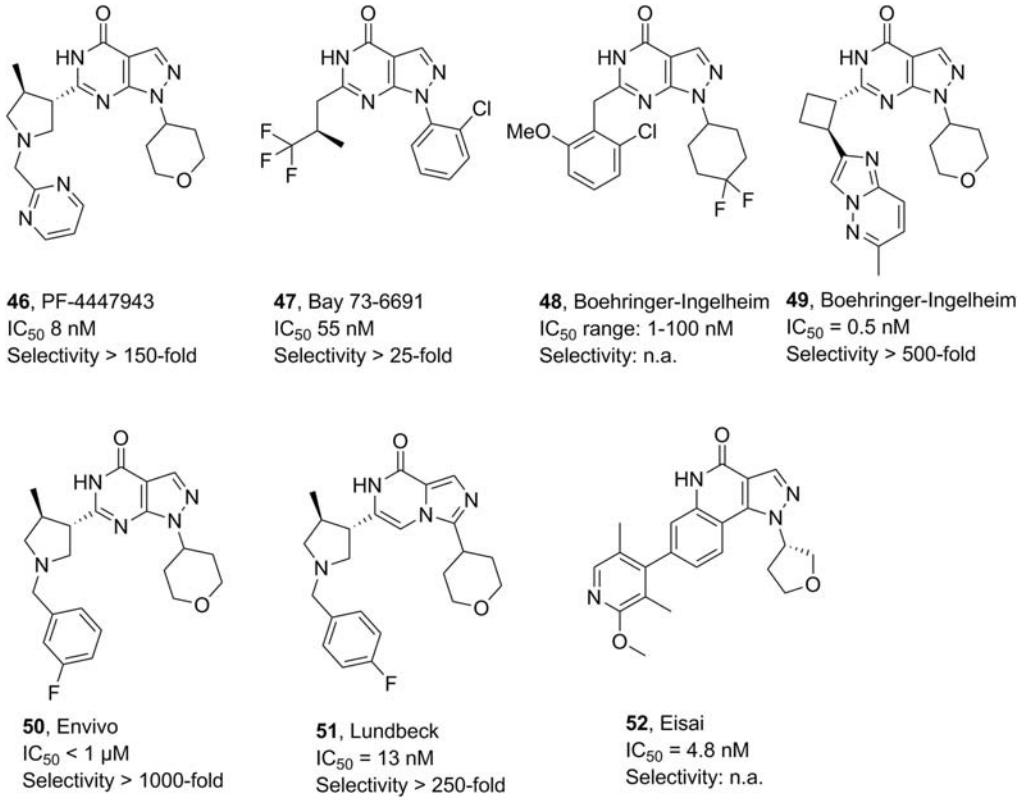

Fig. 12 Structures and IC_{50} values of some inhibitors of PDE9.

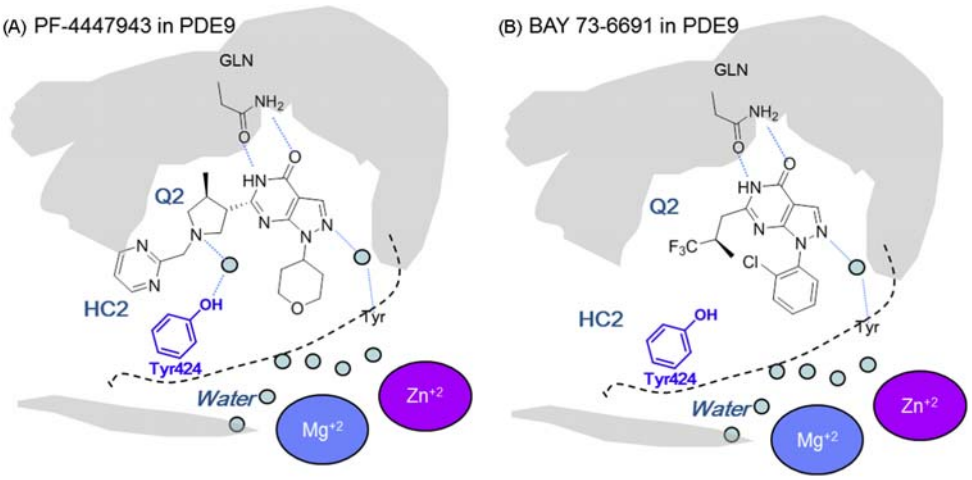

Fig. 13 Cartoon of binding mode of PDE9-inibitors PF-4447943, **46**, and BAY 73-6691, **47**, in PDE9 based on X-ray.

a dose-dependent increase in the cGMP level in CSF, thus validating the use of this biomarker. The drug was found to be safe and well tolerated at all doses.

Another PDE9 inhibitor from Eisai has also been progressed into clinical trials targeting Alzheimer's disease (E-2027, the chemical structure was not yet reported, but a patent application has been published on the Eisai-compound **52** shown in Fig. 12). This first-in-human study (ClinicalTrials.gov Identifier: NCT02415790), designed to assess the safety, tolerability, and pharmacokinetics (PK) of single oral ascending doses of E2027, will be administered to healthy adult participants to determine the maximum tolerated dose. Thereafter, the PD effects of single doses of E2027 on elevation of cGMP in the CSF in healthy adult participants will be evaluated across a broad dose range, to establish the PK/PD relationship.

The crystal structures of the PDE9A catalytic domain in complex with the substrate and with inhibitors reveal that the purine recognizing conserved GLN is locked in a conformation that facilitates a preference for cGMP. The mechanism of the catalytic process of PDE9 and the substrate specificity of PDE9 in the actual hydrolytic reaction was revealed by an unusual series of elegant experiments by X-ray studies by freeze-trapping of isolated structures of reaction intermediates accumulated at the reaction steady state in PDE9-crystal.[71] The X-ray structure of the clinical compound PF-4447943 (PDB code: 4E90)[72] is one of several examples[73] illustrating that a guanine-like motif is needed. The pyrimidinone core interacts with the donor–acceptor pair of the invariant Gln-453 in the GMP-mode (Fig. 13), and the GMP-mode of action promotes selectivity against the AMP preferring PDEs. Further selectivity enhancement is obtained by addressing the small Q2 pocket and particularly selectivity against the structurally similar PDE1 is obtained by forming a H-bond from the amino-group in the pyrrolidine to the PDE9 unique Tyr-424. Another clinical PDE9 compound is BAY 73-6691, **47**, which was the first reported potent and selective PDE9A inhibitor,[74] has also shown significant procognitive effects in animal models[75] and particularly in a transgenic animal model of AD.[76] An X-ray crystallographic study[65] of BAY 73-6691 and its enantiomer (PDB ID 3K3E and 3K3H) bound to PDE9A show a similar binding of the pyrimidinone lactam to Gln-435, the HC being occupied by the 1*H*-pyrazolo[3,4-*d*]pyrimidin-4(5*H*)-one core, the *N*-1 2-chlorophenyl in the ribose region, and 3,3,3-trifluoro-2-methylpropyl in Q2.[77]

Several other research groups have investigated PDE9 inhibitors for the treatment of cognitive impairment, specifically targeting Alzheimer's disease (Fig. 12),[40,65] for example, Boehringer Ingelheim, Envivo Pharmaceuticals, **50**, H. Lundbeck A/S, **51**, and notably there is a very strong similarity of the core structures for many of these and a strong preference among the known PDE9 inhibitors for a guanine like-motif like for example, 1*H*-pyrazolo[3,4-*d*]pyrimidin-4(5*H*)-ones, and it seems as if the PDE9 binding pocket is very strict in recognizing only a small narrow of chemotypes.

In brief, several PDE9 inhibitor compounds have been evaluated to be safe and well tolerated in the clinic, and clinical evaluation of the potential for testing cognitive impairment in patients is underway, with Boehringer Ingelheim being most progressed with their clinical candidate BI-409306.

7.09.4.5 PDE10

PDE10A has a narrow distribution pattern, with expression primarily limited to the brain and testes, and within the brain, PDE10A protein is expressed at high levels in the basal ganglia.[78] Inhibition of PDE10A as a mechanism to address the core symptom domains of schizophrenia has received considerable attention.[79] Inhibitors of PDE10 have been shown to be efficacious in multiple preclinical models thought to be predictive of antipsychotic action, and PDE10A inhibitors increase the functionality of striatal medium spiny neurons and produce antipsychotic-like effects in rodents by blocking PDE10A-mediated hydrolysis of cAMP and cGMP. By using a radiolabeled PDE10A inhibitor and an ex vivo PDE10 binding autoradiographic assay to explore the relationship between the PDE10 binding site occupancy and the observed biochemical and behavioral effects of PDE10 inhibitors in mice, it was

shown that PDE10A occupancy was positively correlated with striatal pCREB expression levels. PDE10A occupancy was also correlated with antipsychotic-like effects measured using the conditioned avoidance response model; a minimum of ~40% occupancy was typically required to achieve efficacy. In contrast, a clear relationship between PDE10A occupancy and catalepsy scores (a potential extrapyramidal symptom readout in rodent) was not evident.[80] Unfortunately, the sparse published clinical studies to date with selected PDE inhibitors have not revealed a procognitive or antipsychotic benefit in humans.[81] A recent trial with the PDE-10 inhibitor MP-10 (**53**, PF-02545920,[82] **Fig. 14**) for the adjunctive treatment of suboptimally controlled symptoms of schizophrenia was stopped based on interim analysis that indicated efficacy would not be achieved (ClinicalTrials.gov). However, phase 2 clinical trials within Huntington's Disease is still ongoing, including a 12-month open-label extension study of PF-02545920 20 mg dosed BID

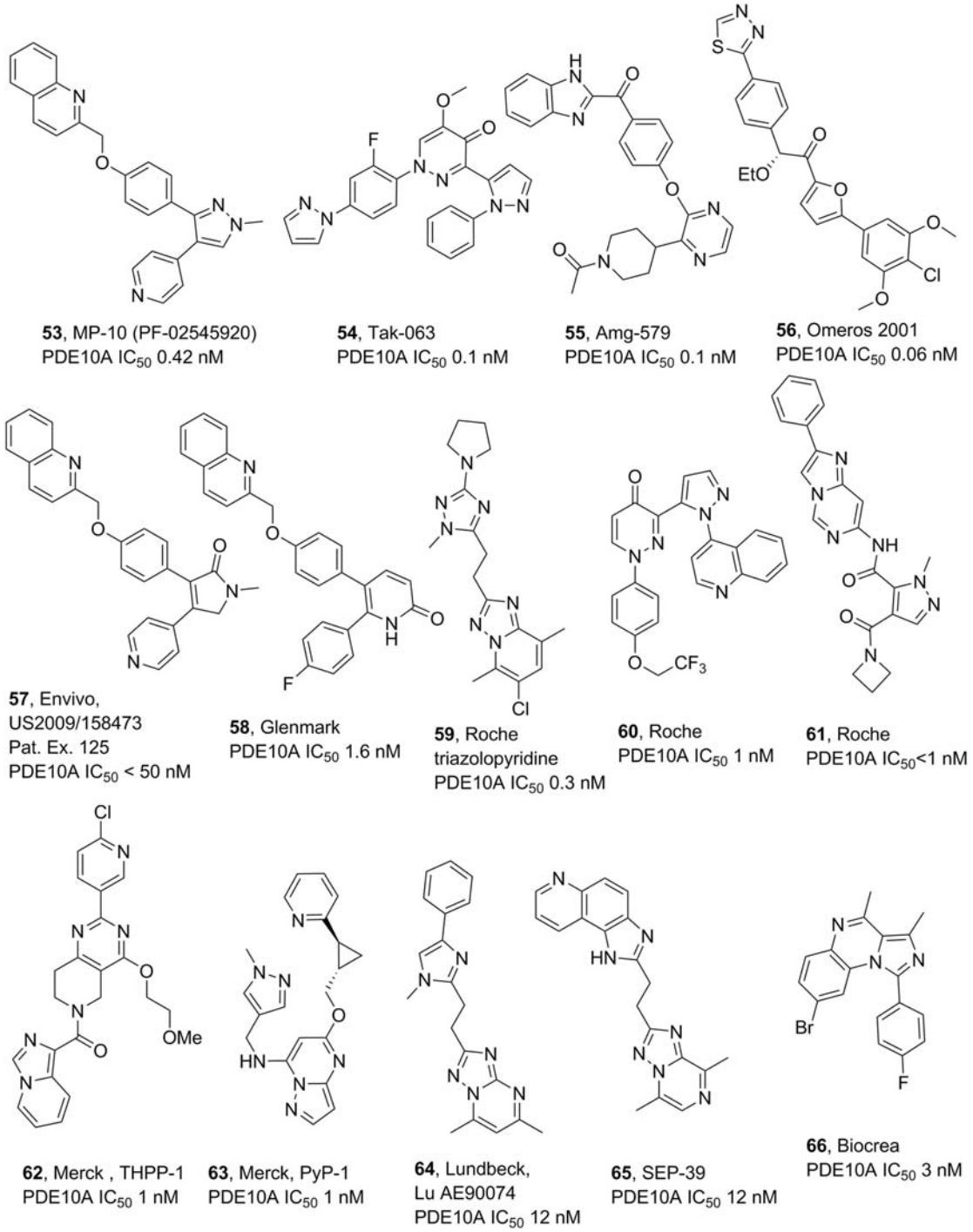

Fig. 14 Structures and IC_{50} values of some inhibitors of PDE10.

following a study in subjects with HD (ClinicalTrials.gov Identifier: NCT02342548). Several companies are currently pursing PDE10 inhibitors in the clinic (see Table 2).

Many X-ray structures of ligands in complex with the catalytic domain of PDE10 have been published, and many drug discovery programs have heavily used structure-based drug design approaches. One hit-finding strategy has been to conduct a fragment screen in the search for chemical matter to serve as starting points for lead optimization. The fragment approach, in which low-molecular-weight, weakly binding fragment hits are evolved toward drug-like compounds, has been more frequently practiced in recent years, with several reported examples applied to PDE10A.[83] Many research groups also report on SBDD used in the lead identification and lead optimization, and structural information on advanced preclinical and clinical compounds is publically available. A few key compounds are illustrated in Fig. 14, chosen in order to illustrate both the structure of some clinical candidates and also to show the high diversity among PDE10 chemotypes and binding modes.

The chemical structure of the clinical candidate TAK-063, **54** (Fig. 14) and the binding mode in PDE10 (Fig. 15) have been reported[84] along with extensive pharmacological profiling and target validation.[85] This compound has been progressed to clinical phase 2 in a PoC study targeting schizophrenia. Radiolabeled versions in the form of tritiated and [^{14}C]-labeled versions of TAK-063 have been developed and used in autoradiography studies to demonstrate that TAK-063 selectively accumulated in PDE10A expressing brain regions.[86] A close structural analogue from the same chemical series has also been developed as a [^{11}C]-PET ligand.[87]

Another clinical compound AMG 579, **55** (Fig. 14) was reported along with its binding mode in the X-ray of the catalytic domain of PDE10, and the pharmacological profile showed antipsychotic properties; however, the phase 1 trial has been terminated (ClinicalTrials.gov Identifier: NCT01568203).[88]

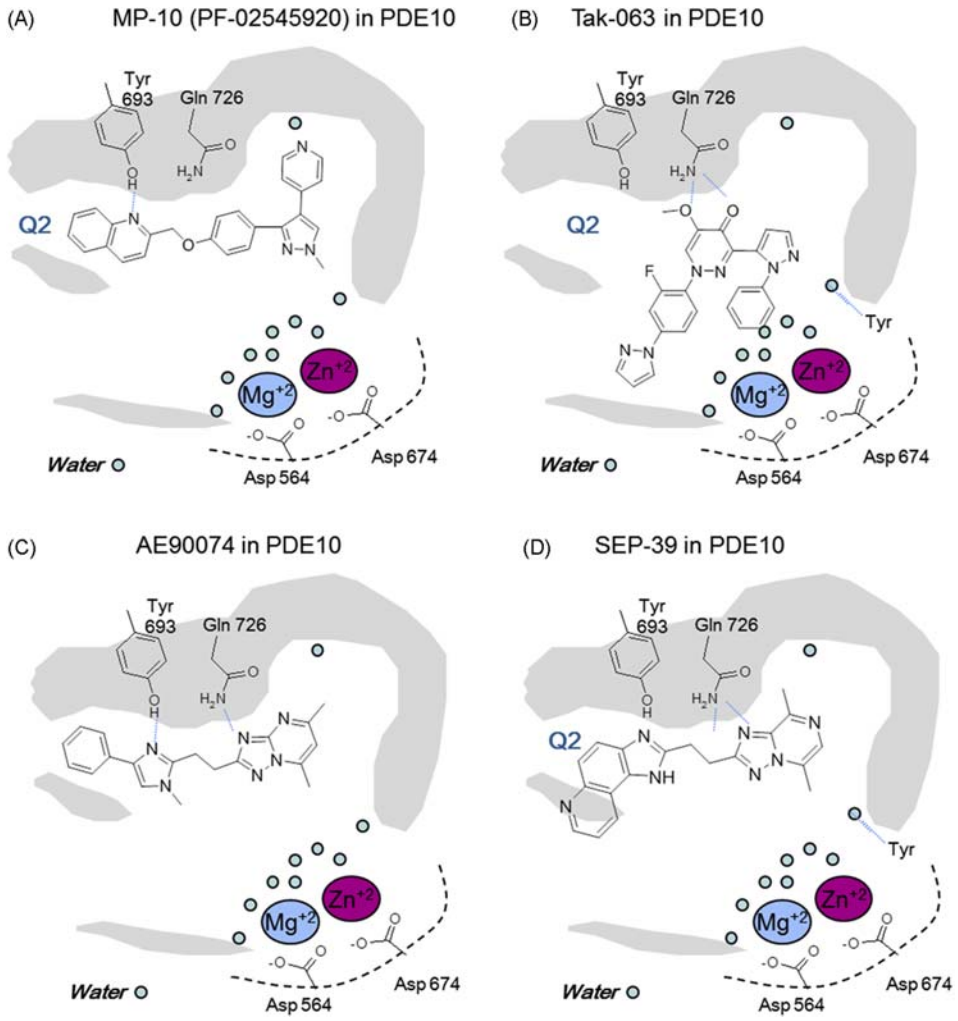

Fig. 15 (A) Cartoon of binding mode of MP-10, **53** in PDE10 based on X-ray. (B) Cartoon of binding mode of TAK-063, **54** in PDE10 based on X-ray. (C) Cartoon of binding mode of LU AE90074, **64** in PDE10, based on X-ray. (D) Cartoon of binding mode of SEP-39, **65** in PDE10, based on X-ray.

The chemical structure of other clinical compounds, OMS-824, RG-7203, FRM-6308, and LU AF11167, have not yet been disclosed, but a few selected PDE10 inhibitors from the companies behind those clinical programs are shown in Fig. 14 in order to illustrate the chemical space covered by these companies.[89] The Omeros group reported on the discovery, SAR studies and optimization studies of some of their PDE10 inhibitors,[90] but did not disclose the structure of their clinical candidate. The Roche group also has not yet disclosed the structure of their clinical candidate, but recently reported on a triazolopyridine, **59** and 3-pyrazolylpyridazin-4-one, **60** (Fig. 14) in a publication describing series of small-molecule drug discovery case studies where computational methods were prospectively employed to impact Roche research projects.[91] The binding mode of the triazolopyridine in the PDE10 binding pocket of the catalytic domain was revealed by an X-ray structure and it showed a similar binding mode to the Lundbeck compound Lu AE90074 **64**,[40] and the recently reported Sunovion compound SEP-39 **65**,[92] which all occupy the central clamp with a purine isostere hooking up with H-bonds to the conserved GLN and furthermore obtain potency and selectivity by occupying the Q2-pocket (Fig. 15). Extensive pharmacological profiling of SEP-39 showed it to be a potent (1.0 nM) inhibitor of PDE10A, with good selectivity (16,000-fold) against other PDEs.[93] In an in vivo occupancy study, the RO50 value was determined to be 0.7 mg kg^{-1} (p.o.), corresponding to plasma and brain exposures of 28 ng mL^{-1} and 43 ng g^{-1}, respectively, and 3 mg kg^{-1} (p.o.) SEP-39 significantly increased rat striatal cGMP concentrations. Furthermore, SEP-39 inhibits PCP-induced hyperlocomotion at doses of 1 and 3 mg kg^{-1} (p.o.) corresponding to 59–86% occupancy. In an EEG study, 3 and 10 mg kg^{-1} (p.o.) SEP-39 suppressed REM intensity and increased the latency to REM sleep, as also shown for other PDE10 inhibitors. SEP-39 had precognitive effects in the rat novel object recognition assay, and the precognitive effects appear to require less PDE10A inhibition than the reversal of PCP-induced hyperlocomotion or EEG effects.

The Merck group has published on two structurally different PDE10 inhibitor chemotypes. The results of an optimization from a novel HTS tetrahydropyridopyrimidine hit led to the compound, THPP-1, **62** (Fig. 14), which exhibits nanomolar potency, excellent pharmacokinetic properties, and a clean off-target profile.[94] It displays in vivo target engagement as measured by increased rat striatal cGMP levels upon oral dosing. It shows dose-dependent efficacy in a key PD assay predictive of antipsychotic activity. It was also reported to improve cognition in the rat and rhesus monkey.[95] More recently, the same group reported the discovery of PyP-1, **63** (Fig. 14), a potent, highly selective, and orally bioavailable pyrazolopyrimidine inhibitor of PDE10A.[96] PyP-1 exhibits subnanomolar potency (PDE10A $K_i = 0.23$ nM), excellent pharmacokinetic and physicochemical properties, and a clean off-target profile. PyP-1 displays dose-dependent efficacy in numerous PD assays that measure potential for antipsychotic activity and cognitive improvement. PyP-1 also has a clean preclinical profile with respect to cataleptic potential in rats, prolactin secretion, and weight gain, common adverse events associated with currently marketed therapeutics. Further, PyP-1 displays in vivo preclinical target engagement as measured by PET enzyme occupancy in concert with [^{11}C]MK-8193, a novel PDE10A PET tracer.[97] Interestingly, the tetrahydropyridopyrimidine has a binding mode in PDE10 (Fig. 16), where THPP-1 has a lack of interaction with Y693 in the PDE10A "selectivity pocket," which likely explains its suboptimal PDE5A, PDE6A, and PDE11A selectivities. In contrast, Pyp-1 was deliberately designed to make the requisite critical interactions in the selectivity pocket. The Envivo group (now Forum)[79] and the Glenmark group have both worked on chemotypes related to the quinoline based MP-10-like structures (Fig. 14), and presumably, they therefore may have the same binding modes (Fig. 15). The Envivo group replaced the central pyrazole of MP-10 with a 1-methyl-1,5-dihydro-2*H*-pyrrol-2-one (**57**), whereas the Glenmark group pursued a pyridin-2(1*H*)-one (**58**) replacement.[98] However, the Glenmark group also reported on a series of polycyclic heteroarene ethers, which exhibited high peripheral and adequate brain levels upon oral dosing in rodents and showed efficacy in multiple preclinical animal models related to psychiatric disorders, particularly schizophrenia.[99]

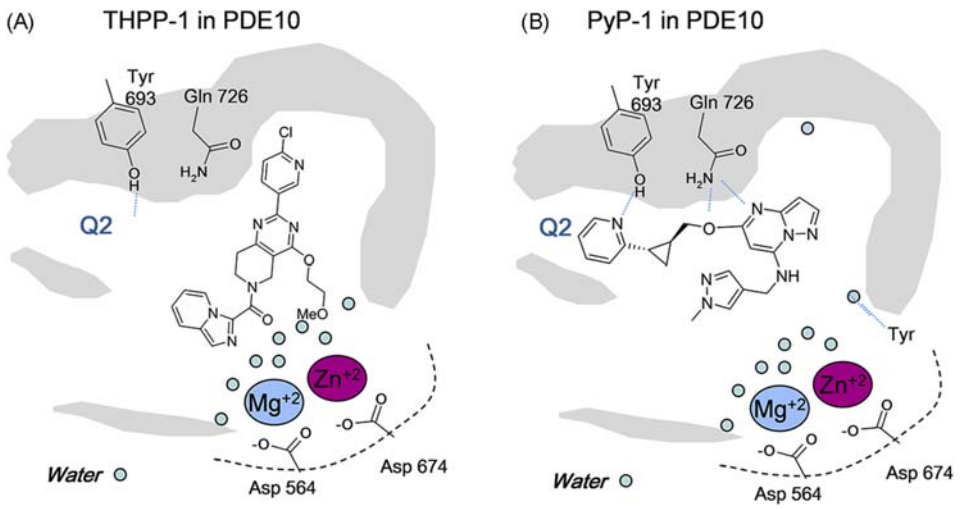

Fig. 16 (A) Cartoon of binding mode of THPP-1, **62** in PDE10 based on X-ray. (B) Cartoon of binding mode of PyP-1, **63** in PDE10 based on X-ray.

To further illustrate the diversity of possible chemotypes within the PDE10 inhibitor field, the tricyclic scaffold from Biocrea (**66** in Fig. 14)[100] is just one out of numerous tricyclic scaffolds which inhibits PDE10 but also other PDEs.[101]

In summary, numerous PDE10 inhibitors have been developed to date, and several compounds have been progressed to the clinic with Takeda and Pfizer currently having the most advanced PDE10 inhibitors which are being pursued for basal ganglia disorders like Huntington's disease and schizophrenia.

7.09.5 Conclusion

PDE inhibitors have been considered as possible therapeutic agents to treat impaired cognitive function linked to several brain disorders, including depression, schizophrenia, Huntington's disease, and Alzheimer's disease. The design of novel, selective inhibitors is being increasingly driven by improved understanding of the biology of PDEs and PDE inhibitors, as well as by structural insights from X-ray crystallography of PDE catalytic cores and PDE inhibitor cocrystal complexes. In addition to providing the basis for structure-based drug design, these studies have yielded information about the unique allosteric interactions between the regulatory and catalytic domains of PDEs. Whereas PDE inhibitors have been successfully marketed for a number of peripheral diseases, we have yet to see the first PDE inhibitor on the market for CNS diseases. With the current intense focus of CNS PDE drug discovery and with the many ongoing clinical trials with PDE inhibitors within CNS areas, the first CNS PDE inhibitor might be approved already in the near future.

References

1. (a) May, C. D. History of the Introduction of Theophylline Into the Treatment of Asthma. *Clin. Allergy* **1974,** *4,* 211–217; (b) Persson, C. G. On the Medical History of Xanthines and Other Remedies for Asthma: A Tribute to HH Salter. *Thorax* **1985,** *40,* 881–886.
2. Fischer, E.; Ach, L. Synthese des Caffeins. *Ber. Dtsch. Ges.* **1895,** *28,* 3135.
3. Nehlig, A.; Daval, J. L.; Debry, G. Caffeine and the Central Nervous System: Mechanisms of Action, Biochemical, Metabolic and Psychostimulant Effects. *Brain Res. Brain Res. Rev.* **1992,** *17* (2), 139–170.
4. Fredholm, B. B.; Bättig, K.; Holmén, J.; Nehlig, A.; Zvartau, E. E. Actions of Caffeine in the Brain With Special Reference to Factors That Contribute to Its Widespread Use. *Pharmacol. Rev.* **1999,** *51* (1), 83–133.
5. Rall, T. W.; Sutherland, E. W. Formation of a Cyclic Adenine Ribonucleotide by Tissue Particles. *J. Biol. Chem.* **1958,** *232,* 1065–1091.
6. A brief history of PDE discoveries is summarized in: Beavo, J. A.; Brunton, L. L. Cyclic Nucleotide Research—Still Expanding After Half a Century *Nat. Rev. Mol. Cell Biol.* **2002,** *9,* 710–718.
7. Ashman, D. F.; Lipton, R.; Melicow, M. M.; Price, T. D. Isolation of Adenosine 3′, 5′-Mono-Phosphate and Guanosine 3′, 5′-Monophosphate From Rat Urine. *Biochem. Biophys. Res. Commun.* **1963,** *11,* 330–334.
8. Wielinga, P. R.; van der Heijden, I.; Reid, G.; Beijnen, J. H.; Wijnholds, J.; Borst, P. Characterization of the MRP4- and MRP5-Mediated Transport of Cyclic Nucleotides From Intact Cells. *J. Biol. Chem.* **2003,** *278,* 17664–17671.
9. Krawutschke, C.; Koesling, D.; Russwurm, M. Export Is of Similar Importance as Degradation. *Arterioscler. Thromb. Vasc. Biol.* **2015,** *35,* 2011–2019.
10. Kelly, M. P.; Adamowicz, W.; Bove, S.; Hartman, A. J.; Mariga, A.; Pathak, G.; Reinhart, V.; Romegialli, A.; Kleiman, J. Select 3′,5′-Cyclic Nucleotide Phosphodiesterases Exhibit Altered Expression in the Aged Rodent Brain. *Cell. Signal.* **2014,** *26,* 383–397.
11. (a) Some comprehensive and timely: reviews of PDEs are: Conti, M.; Beavo, J. Biochemistry and Physiology of Cyclic Nucleotide Phosphodiesterases: Essential Components in Cyclic Nucleotide Signaling *Annu. Rev. Biochem.* **2007,** *76,* 481–511; (b) Francis, S.; Blount, M.; Corbin, J. Mammalian Cyclic Nucleotide Phosphodiesterases: Molecular Mechanisms and Physiological Functions. *Physiol. Rev.* **2011,** *91,* 651–690; (c) Keravis, T.; Lugnier, C. Cyclic Nucleotide Phosphodiesterase (PDE) Isozymes as Targets of the Intracellular Signalling Network: Benefits of PDE Inhibitors in Various Diseases and Perspectives for Future Therapeutic Developments. *Br. J. Pharmacol.* **2012,** *165,* 1288–1305; (d) Maurice, D. H.; Ke, H.; Ahmad, F.; Wang, Y. Advances in Targeting Cyclic Nucleotide Phosphodiesterases. *Nat. Rev. Drug Discov.* **2014,** *13,* 290–314.
12. Xu, R. X.; Hassell, A. M.; Vanderwall, D.; Lambert, M. H.; Holmes, W. D.; Luther, M. A.; Rocque, W. J.; Milburn, M. V.; Zhao, Y.; Ke, H.; Nolte, R. T. Atomic Structure of PDE4: Insights Into Phosphodiesterase Mechanism and Specificity. *Science* **2000,** *288,* 1822–1825.
13. (a) Jeon, Y. H.; Heo, Y. S.; Kim, C. M.; Hyun, Y. L.; Lee, T. G.; Ro, S.; Cho, J. M. Phosphodiesterase: Overview of Protein Structures, Potential Therapeutic Applications and Recent Progress in Drug Development. *Cell. Mol. Life Sci.* **2005,** *62,* 1198–1220; (b) Card, G. L.; England, B. P.; Suzuki, Y.; Fong, D.; Powell, B.; Lee, B.; Luu, C.; Tabrizizad, M.; Gillette, S.; Ibrahim, P. N.; Artis, D. R.; Bollag, G.; Milburn, M. V.; Kim, S.-H.; Schlessinger, J.; Zhang, K. Y. J. Structural Basis for the Activity of Drugs That Inhibit Phosphodiesterases. *Structure* **2004,** *12,* 2233–2247; (c) Manallack, D. T.; Hughes, R. A.; Thompson, P. E. The Next Generation of Phosphodiesterase Inhibitors: Structural Clues to Ligand and Substrate Selectivity of Phosphodiesterases. *J. Med. Chem.* **2005,** *48,* 3449–3462; (d) Ke, H.; Wang, H. Crystal Structures of Phosphodiesterases and Implications on Substrate Specificity and Inhibitor Selectivity. *Curr. Top. Med. Chem.* **2007,** *7,* 391–403; (e) Jansen, C.; Kooistra, A. J.; Kanev, G. K.; Leurs, R.; de Esch, I. J. P.; de Graaf, C. PDEStrIAn: A Phosphodiesterase Structure and Ligand Interaction Annotated Database as a Tool for Structure-Based Drug Design. *J. Med. Chem.* **2016,** *59,* 3449–3462.
14. Jansen, C.; Kooistra, A. J.; Kanev, G. K.; Leurs, R.; de Esch, I. J. P.; de Graaf, C. PDEStrIAn: A Phosphodiesterase Structure and Ligand Interaction Annotated Database As a Tool for Structure-Based Drug Design. *J. Med. Chem.* **2016,** *59,* 3449–3462.
15. Lipinski, C. A.; Lombardo, F.; Dominy, B. W.; Feeney, P. J. Experimental and Computational Approaches to Estimate Solubility and Permeability in Drug Discovery and Development Settings. *Adv. Drug Deliv. Rev.* **1997,** *23,* 3–25.
16. Didziapetris, R.; Japertas, P.; Avdeef, A.; Petrauskas, A. Classification Analysis of P-Glycoprotein Substrate Specificity. *J. Drug Target.* **2003,** *11,* 391–406.
17. Seelig, A. A General Pattern for Substrate Recognition by P-Glycoprotein. *Eur. J. Biochem.* **1998,** *251* (1–2), 252–261.
18. Pajeva, I. K.; Wiese, M. Pharmacophore Model of Drugs Involved in P-Glycoprotein Multidrug Resistance: Explanation of Structural Variety (Hypothesis). *J. Med. Chem.* **2002,** *45* (26), 5671–5686.
19. Bender, A. T.; Beavo, J. A. Cyclic Nucleotide Phosphodiesterases: Molecular Regulation to Clinical Use. *Pharmacol. Rev.* **2006,** *58,* 488–520.
20. Keravis, T.; Lugnier, C. Cyclic Nucleotide Phosphodiesterase (PDE) Isozymes as Targets of the Intracellular Signaling Network: Benefits of PDE Inhibitors in Various Diseases and Perspectives for Future Therapeutic Developments. *Br. J. Pharmacol.* **2012,** *165,* 1288–1305.
21. Medina, A. E. Therapeutic Utility of Phosphodiesterase Type I Inhibitors in Neurological Conditions. *Front. Neurosci.* **2011,** *5,* 21.
22. Umar, T.; Hoda, N. Selective Inhibitors of Phosphodiesterases: Therapeutic Promise for Neurodegenerative Disorders. *Med. Chem. Commun.* **2015,** *6,* 2063–2080.

23. (a) Szilágyi, G. Z.; Nagy, Z. N.; Balkay, L. S.; Boros, I. N.; Emri, M. S.; Lehel, S.; Márián, T. Z.; Molnár, T. S.; Szakáll, S.; Trón, L.; Bereczki, D. N.; Csiba, L. S.; Fekete, I. N.; Kerényi, L.; Galuska, L. S.; Varga, J. Z.; Bönöczk, P. T.; Vas, Á. M.; Gulyás, B. Z. Effects of Vinpocetine on the Redistribution of Cerebral Blood Flow and Glucose Metabolism in Chronic Ischemic Stroke Patients: A PET Study. *J. Neurol. Sci.* **2005,** *229–230,* 275–284; Dézsi, L.; Kis-Varga, I.; Nagy, J.; Komlódi, Z.; Kárpáti, E. Neuroprotective Effects of Vinpocetine in vivo and in Vitro. Apovincaminic Acid Derivatives as Potential Therapeutic Tools in Ischemic Stroke. *Acta Pharm. Hung.* **2002,** *72,* 84–91.
24. Abd Elbary, A.; Foda, N.; El-Gazayerly, O.; El Khatib, M. Reversed Phase Liquid Chromatographic Determination of Vinpocetine in Human Plasma and its Pharmacokinetic Application. *Anal. Lett.* **2002,** *35* (6), 1041–1054.
25. Medina, A. E. Vinpocetine as a Potent Antiinflammatory Agent. *PNAS* **2010,** *107,* 9921–9922.
26. Michelson, G.; Wärntges, S.; Leidig, S.; Lötsch, J.; Geisslinger, G. Nimodipine Plasma Concentration and Retinal Blood Flow in Healthy Subjects. *Invest. Ophthalmol. Vis. Sci.* **2006,** *47,* 3479–3486.
27. Dumaitre, B.; Dodic, N. Synthesis and Cyclic GMP Phosphodiesterase Inhibitory Activity of a Series of 6-Phenylpyrazolo[3,4-*d*]Pyrimidines. *J. Med. Chem.* **1996,** *39,* 1635–1644.
28. Vemulapalli, S.; Watkins, R. W.; Chintala, M.; Davis, H.; Ahn, H.-S.; Fawzi, A.; Tulshian, D.; Chiu, P.; Chatterjee, M.; Lin, C.-C.; Sybertz, E. J. Antiplatelet and Antiproliferative Effects of SCH 51866, a Novel Type 1 and Type 5 Phosphodiesterase Inhibitor. *J. Cardiovasc. Pharmacol.* **1996,** *28,* 862–869.
29. Beaumont, V.; Park, L.; Rassoulpour, A.; Dijkman, U.; Heikkinen, T.; Lehtimaki, K.; Kontkanen, O.; Al Nackkash, R.; Bates, G. P.; Gleyzes, M.; Steidl, E.; Ramboz, S.; Murphy, C.; Beconi, M. G.; Dominguez, C.; Munoz-Sanjuan, I. The PDE1/5 Inhibitor SCH-51866 Does Not Modify Disease Progression in the R6/2 Mouse Model of Huntington's Disease. *PLoS Currents* **2014,** *6.* http://dx.doi.org/10.1371/currents.hd.3304e87e460b4bb0dc519a29f4deccca. Feb. 13. Edition 1.
30. Ahn, H. S.; Bercovici, A.; Boykow, G.; Bronnenkant, A.; Chackalamannil, S.; Chow, J.; Cleven, R.; Cook, J.; Czarniecki, M.; Domalski, C.; Fawzi, A.; Green, M.; Gündes, A.; Ho, G.; Laudicina, M.; Lindo, N.; Ma, K.; Manna, M.; McKittrick, B.; Mirzai, B.; Nechuta, T.; Neustadt, B.; Puchalski, C.; Pula, K.; Silverman, L.; Smith, E.; Stamford, A.; Tedesco, R. P.; Tsai, H.; Tulshian, D.; Vaccaro, H.; Watkins, R. W.; Weng, X.; Witkowski, J. T.; Xia, Y.; Zhang, H. Potent Tetracyclic Guanine Inhibitors of PDE1 and PDE5 Cyclic Guanosine Monophosphate Phosphodiesterases With Oral Antihypertensive Activity. *J. Med. Chem.* **1997,** 2196–2210.
31. Xia, Y.; Chackalamannil, S.; Czarniecki, M.; Tsai, H.; Vaccaro, H.; Cleven, R.; Cook, J.; Fawzi, A.; Watkins, R.; Zhang, H. Synthesis and Evaluation of Polycyclic Pyrazolo[3,4-*d*] Pyrimidines as PDE1 and PDE5 cGMP Phosphodiesterase Inhibitors. *J. Med. Chem.* **1997,** *40* (26), 4372–4377. Dec 19.
32. Humphrey, J. M. Selective New Small-Molecule Inhibitors of Phosphodiesterase 1. In *Phosphodiesterases and Their Inhibitors;* Liras, S., Bell, A. S., Eds.; 1st ed.; Wiley-VCH Verlag GmbH & Co: Weinheim, Germany, 2014. KGaA.
33. Verhoest, P. R.; Fonseca, K. R.; Hou, X.; Proulx-Lafrance, C.; Corman, M.; Helal, C. J.; Claffey, M. M.; Tuttle, J. B.; Coffman, K. J.; Liu, S.; Nelson, F.; Kleiman, R. J.; Menniti, F. S.; Schmidt, C. J.; Vanase-Frawley, M.; Liras, S. Design and Discovery of 6-[(3S,4S)-4-Methyl-1-(Pyrimidin-2-Ylmethyl)Pyrrolidin-3-yl]-1-(Tetrahydro-2*H*-Pyran-4-yl)-1,5-Dihydro-4*H*-Pyrazolo[3,4-*d*]Pyrimidin-4-one (PF-04447943), a Selective Brain Penetrant PDE9A Inhibitor for the Treatment of Cognitive Disorders. *J. Med. Chem.* **2012,** *55,* 9045–9054.
34. Humphrey, J. M.; Yang, E. X.; Am Ende, C. W.; Arnold, E. P.; Head, J. L.; Jenkinson, S.; Lebel, L. A.; Liras, S.; Pandit, J.; Samas, B.; Vajdos, F.; Simons, S. P.; Evdokimova, A.; Mansour, M.; Menniti, F. S. Small-Molecule Phosphodiesterase Probes: Discovery of Potent and Selective CNS-Penetrable Quinazoline Inhibitors of PDE1. *Med. Chem. Commun.* **2014,** *5,* 1290–1296.
35. Li, P.; Zheng, H.; Zhao, J.; Zhang, L.; Yao, W.; Zhu, H.; Beard, J. D.; Ida, K.; Lane, W.; Snell, G.; Sogabe, S.; Heyser, C. J.; Snyder, G. L.; Hendrick, J. P.; Vanover, K. E.; Davis, R. E.; Wennogle, L. P. Discovery of Potent and Selective Inhibitors of Phosphodiesterase 1 for the Treatment of Cognitive Impairment Associated With Neurodegenerative and Neuropsychiatric Diseases. *J. Med. Chem.* **2016,** *59,* 1149–1164.
36. Snyder, G. L.; Prickaerts, J.; Wadenberg, M.-L.; Zhang, L.; Zheng, H.; Yao, W.; Akkerman, S.; Zhu, H.; Hendrick, J. P.; Vanover, K. E.; Davis, R. E.; Li, P.; Mates, S.; Wennogle, L. P. Preclinical Profile of ITI-214, an Inhibitor of Phosphodiesterase 1, for Enhancement of Memory Performance in Rats. *Psychopharmacology (Berl)* **2016,** *233,* 3113. http://dx.doi.org/10.1007/s00213-016-4346-2.
37. Pandit, J.; Forman, M. D.; Fennell, K. F.; Dillman, K. S.; Menniti, F. S. Mechanism for the Allosteric Regulation of Phosphodiesterase 2A Deduced From the X-ray Structure of a Near Full-Length Construct. *Proc. Natl. Acad. Sci. U. S. A.* **2009,** *106,* 18225–18230.
38. Gomez, L.; Breitenbucher, J. G. PDE2 Inhibition: Potential for the Treatment of Cognitive Disorders. *Bioorg. Med. Chem. Lett.* **2013,** *23,* 6522–6527.
39. Zhao, C. Y.; Greenstein, J. L.; Winslow, R. L. Roles of Phosphodiesterases in the Regulation of the Cardiac Cyclic Nucleotide Cross-Talk Signaling Network. *J. Mol. Cell. Cardiol.* **2016,** *91,* 215–227.
40. Jørgensen, M.; Kehler, J.; Langgård, M.; Svenstrup, N.; Tagmose, L. Selective Inhibitors of PDE2, PDE9, and PDE10: Modulators of Activity of the Central Nervous System. In *Annual Reports in Medicinal Chemistry,* vol. 48, Desai, M. C., Ed.; Academic Press: Burlington, 2013; pp 37–55.
41. Lueptow, L. M.; Zhan, C.-G.; O'Donnell, J. M. Cyclic GMP–Mediated Memory Enhancement in the Object Recognition Test by Inhibitors of Phosphodiesterase-2 in Mice. *Psychopharmacology (Berl)* **2016,** *233,* 447–456.
42. Buijnsters, P.; De Angelis, M.; Langlois, X.; Rombouts, F. J.; Sanderson, W.; Tresadern, G.; Ritchie, A.; Trabanco, A. A.; VanHoof, G.; Roosbroeck, Y. V.; Andrés, J. I. Structure-Based Design of a Potent, Selective, and Brain Penetrating PDE2 Inhibitor With Demonstrated Target Engagement. *ACS Med. Chem. Lett.* **2014,** *5,* 1049–1053.
43. Zhu, J.; Yang, Q.; Dai, D.; Huang, Q. X-Ray Crystal Structure of Phosphodiesterase 2 in Complex With a Highly Selective, Nanomolar Inhibitor Reveals a Binding-Induced Pocket Important for Selectivity. *J. Am. Chem. Soc.* **2013,** *135,* 11708–11711.
44. (a) Helal, C. J.; Chappie, T. A.; Humphrey, J. M.; Verhoest, P. R.; Yang, E. US 20,120,214,791.
(b) Helal, C. J. Identification of a Brain Penetrant, Highly Selective Phosphodiesterase 2A Inhibitor for the Treatment of Cognitive Impairment Associated With Schizophrenia (CIAS) Abstracts of Papers. 244th ACS National Meeting & Exposition, Philadelphia, PA, United States, August 19–23.
45. am Ende, C. W.; Kormos, B. L.; Humphrey, J. M. The State of the Art in Selective PDE2A Inhibitor Design. In *Phosphodiesterases and Their Inhibitors;* Liras, S., Bell, A. S., Eds.; 1st ed**;** Wiley-VCH Verlag GmbH & Co, 2014; pp 83–104. KGaA.
46. Zhang, L.; Villalobos, A.; Beck, E. M.; Bocan, T.; Chappie, T. A.; Chen, L.; Grimwood, S.; Heck, S. D.; Helal, C. J.; Hou, X.; et al. Design and Selection Parameters to Accelerate the Discovery of Novel Central Nervous System Positron Emission Tomography (PET) Ligands and Their Application in the Development of a Novel Phosphodiesterase 2A PET Ligand. *J. Med. Chem.* **2013,** *56,* 4568–4579.
47. Redrobe, J. P.; Rasmussen, L. K.; Christoffersen, C. T.; Bundgaard, C.; Jørgensen, M. Characterisation of Lu AF33241: A Novel, Brain-Penetrant, Dual Inhibitor of Phosphodiesterase (PDE) 2A and PDE10A. *Eur. J. Pharmacol.* **2015,** *761,* 7980–7985.
48. Rombouts, F. J.; Tresadern, G.; Buijnsters, P.; Langlois, X.; Tovar, F.; Steinbrecher, T. B.; Vanhoof, G.; Somers, M.; Andrés, J. I.; Trabanco, A. A. Pyrido[4,3-e][1,2,4]Triazolo [4,3-a]Pyrazines as Selective, Brain Penetrant Phosphodiesterase 2 (PDE2) Inhibitors. *ACS Med. Chem. Lett.* **2015,** *6,* 282–286.
49. (a) Andres, J.I.; Rombouts, F.J.R.; Trabanco, A.A.; Vanhoof, G.C.P.; de Angelis, M.; Buijnsters, P.J.J.A.; Guillemont, J.E.G.; Bormans, G.M.R.; Celen, S.J.L. 1-Aryl-4-Methyl-[1,2,4]Triazolo[4,3- *a*]Quinoxaline Derivatives. Patent WO 2013/000924 A1, 03 January 2013.
(b) Schröder, S.; Wenzel, B.; Deuther-Conrad, W.; Teodoro, R.; Egerland, U.; Kranz, M.; Scheunemann, M.; Höfgen, N.; Steinbach, J.; Brust, P. Synthesis, 18 F-Radiolabelling and Biological Characterization of Novel Fluoroalkylated Triazine Derivatives for In Vivo Imaging of Phosphodiesterase 2A in Brain via Positron Emission Tomography. *Molecules* **2015,** *20,* 9591–9615.
50. Hamza, A.; Zhan, C. G. Determination of the Structure of Human Phosphodiesterase-2 in a Bound State and Its Binding With Inhibitors by Molecular Modeling, Docking, and Dynamics Simulation. *J. Phys. Chem. B* **2009,** *113,* 2896.
51. Darout, E.; Menhaji-Klotz, E.; Chappie, T. A. PDE4: Recent Medicinal Chemistry Strategies to Mitigate Adverse Effects. In *Phosphodiesterases and Their Inhibitors;* Liras, S., Bell, A. S., Eds.; 1st ed.; Wiley-VCH Verlag GmbH & Co: Weinheim, Germany, 2014; pp 45–64. KGaA.
52. Vanmierlo, T.; Creemers, P.; Akkerman, S.; van Duinen, M.; Sambeth, A.; De Vry, J.; Uz, T.; Blokland, A.; Prickaerts, J. The PDE4 Inhibitor Roflumilast Improves Memory in Rodents at Non-Emetic Doses. *Behav. Brain Res.* **2016,** *303,* 26–33.

53. Prickaerts, J.; Van Duinen, M.; Sambeth, A.; Blokland, A., Treatment of cognitive impairment with phosphodiesterase 4 inhibitor, PCT Int. Appl., WO 2015022418, 2015.
54. Assessment Report Otezla International Non-Proprietary Name: Apremilast Procedure No. EMEA/H/C/003746, http://www.celgene.nl/content/uploads/sites/11/2-OTZ-EPAR-WC500182629.pdf.
55. Zeller, E.; Stief, H. J.; Pflug, B.; Sastre-y-Hernandez, M. Results of a Phase II Study of the Antidepressant Effect of Rolipram. *Pharmacopsychiatry* **1984,** *17,* 188–190.
56. (a) Garcia-Osta, A.; Cuadrado-Tejedor, M.; Garcia-Barroso, C.; Oyarzabal, J.; Franco, R. Phosphodiesterases as Therapeutic Targets for Alzheimer's Disease. *Chem. Neurosci.* **2012,** *3,* 832–844; (b) Soares, L. M.; De Vry, J.; Steinbusch, H. W. M.; Milani, H.; Prickaerts, J.; WeffortdeOliveira, R. M. Rolipram Improves Cognition, Reduces Anxiety- and Despair-Like Behaviors and Impacts Hippocampal Neuroplasticity After Transient Global Cerebral Ischemia. *Neuroscience* **2016,** *326,* 69–83; (c) Heckman, P. R. A.; Wouters, C.; Prickaerts, J. Phosphodiesterase Inhibitors as a Target for Cognition Enhancement in Aging and Alzheimerμs Disease: A Translational Overview. *Curr. Pharm. Des.* **2015,** *21,* 317–331.
57. (a) Pandit, J. PDE4: New Structural Insights Into the Regulatory Mechanism and Implications for the Design of Selective Inhibitors. In *Phosphodiesterases and Their Inhibitors;* Liras, S., Bell, A. S., Eds., 1st ed.; Wiley-VCH Verlag GmbH & Co: Weinheim, Germany, 2014; pp 29–43. KGaA; (b) Fox, D., 3rd; Burgin, A. B.; Gurney, M. E. Structural Basis for the Design of Selective Phosphodiesterase 4B Inhibitors. *Cell. Signal.* **2014,** *26,* 657–663; (c) Gurney, M. E.; D'Amato, E. C.; Burgin, A. B. Phosphodiesterase-4 (PDE4) Molecular Pharmacology and Alzheimer's Disease. *Neurotherapeutics* **2015,** *12,* 49–56.
58. Card, G. L.; England, B. P.; Suzuki, Y.; Fong, D.; Powell, B.; Lee, B.; Luu, C.; Tabrizizad, M.; Gillette, S.; Ibrahim, P. N.; Artis, D. R.; Bollag, G.; Milburn, M. V.; Kim, S.-H.; Schlessinger, J.; Zhang, K. Y. J. Structural Basis for the Activity of Drugs That Inhibit Phosphodiesterases. *Structure* **2004,** *12,* 2233–2247.
59. Cedervall, P.; Aulabaugh, A.; Geoghegan, K. F.; McLellan, T. J.; Pandit, J. Engineered Stabilization and Structural Analysis of the Autoinhibited Conformation of PDE4. *Proc. Natl. Acad. Sci. U. S. A.* **2015,** *112,* E1414–E1422.
60. Gurney, M. E.; Burgin, A. B.; Magnusson, O. T.; Stewart, L. J. Small Molecule Allosteric Modulators of Phosphodiesterase 4. In *Phosphodiesterases as Drug Targets, Handbook of Experimental Pharmacology 204;* Francis, S. H.; et al., Eds.; Springer-Verlag: Berlin, Heidelberg, 2011.
61. Fox, D., 3rd; Burgin, A. B.; Gurney, M. E. Structural Basis for the Design of Selective Phosphodiesterase 4B Inhibitors. *Cell. Signal.* **2014,** *26,* 657–663.
62. Naganuma, K.; Omura, A.; Maekawara, N.; Saitoh, M.; Ohkawa, N.; Kubota, T.; Nagumo, H.; Kodama, T.; Takemura, M.; Ohtsuka, Y.; Nakamura, J.; Tsujita, R.; Kawasaki, K.; Yokoi, H.; Kawanishi, M. Discovery of Selective PDE4B Inhibitors. *Bioorg. Med. Chem. Lett.* **2009,** *19,* 3174.
63. Hagen, T. J.; Mo, X.; Burgin, A. B.; Fox, D., 3rd; Zhang, Z.; Gurney, M. E. Discovery of Triazines as Selective PDE4B Versus PDE4D Inhibitors. *Bioorg. Med. Chem. Lett.* **2014,** *24,* 4031–4034.
64. Lakics, V.; Karran, E. H.; Boess, F. G. Quantitative Comparison of Phosphodiesterase mRNA Distribution in Human Brain and Peripheral Tissues. *Neuropharmacology* **2010,** *59* (6), 367–374.
65. Claffey, M. M.; Helal, C. J.; Hou, X. PDEs as CNS Targets: PDE9 Inhibitors for Cognitive Deficit Diseases. In *Phosphodiesterases and Their Inhibitors;* Liras, S., Bell, A. S., Eds.; 1st ed.; Wiley-VCH Verlag GmbH & Co: Weinheim, Germany, 2014. KGaA.
66. Nicholas, T. E.; Styren, S.; Qui, R.; Wang, E. Q.; Nelson, F.; Le, V.; Grimwood, S.; Christoffersen, C.; Banerjee, S.; Corrigan, B.; Kocan, G.; Geoghegan, K.; Carrieri, C.; Raha, N.; Verhoest, P.; Soares, H. PF-04447943, a Novel PDE9A Inhibitor, Increases cGMP Levels in Cerebrospinal Fluid: Translation From Nonclinical Species to Healthy Human Volunteers. *Alzheimers Dement.* **2009,** *5,* 330.
67. Kleiman, R. J.; Chapin, D. S.; Christoffersen, C.; Freeman, J.; Fonseca, K. R.; Geoghegan, K. F.; Grimwood, S.; Guanowsky, V.; Hajós, M.; Harms, J. F.; Helal, C. J.; Hoffmann, W. E.; Kocan, G. P.; Majchrzak, M. J.; McGinnis, D.; McLean, S.; Menniti, F. S.; Nelson, F.; Roof, R.; Schmidt, A. W.; Seymour, P. A.; Stephenson, D. T.; Tingley, F. D.; Vanase-Frawley, M.; Verhoest, P. R.; Schmidt, C. J. Phosphodiesterase 9A Regulates Central cGMP and Modulates Responses to Cholinergic and Monoaminergic Perturbation In Vivo. *J. Pharmacol. Exp. Ther.* **2012,** *341,* 396–409.
68. Schwam, E.; Evans, R.; Nicholas, T.; Chew, R.; Davidson, W.; Ambrose, D.; Altstiel, L. PF-04447943: A Phase II Controlled Clinical Trial of a Selective PDE9A Inhibitor in Alzheimer's Disease. *Alzheimers Dement.* **2011,** *7* (4), S695.
69. http://www.alzforum.org/therapeutics/bi-409306.
70. Boland, K.; Moschetti, V.; Dansirikul, C.; Pichereau, S.; Gheyle, L.; Sand, M. Randomized, Double-Blind, Placebo-Controlled, Parallel-Group Proof of Mechanism Study to Assess the Pharmacokinetics and Pharmacodynamic Effect of Different Single Oral Doses of BI-409306 in Healthy Male Volunteers. *International Congress on Schizophrenia Research*, 15th (March 29) Abs SUN-114.
71. Li, J.; Liu, C. N.; Wei, N.; Li, X. D.; Liu, Y. Y.; Yang, R.; Jia, Y. J. Protective Effects of BAY 73–6691, a Selective Inhibitor of Phosphodiesterase 9, on Amyloid-β Peptides-Induced Oxidative Stress in in-Vivo and in-Vitro Models of Alzheimer's Disease. *Brain Res.* **2016**. http://dx.doi.org//10.1016/j.brainres.2016.04.011 pii: S0006–8993(16)30204-9. [Epub ahead of print].
72. Verhoest, P. R.; Fonseca, K. R.; Hou, X.; Proulx-Lafrance, C.; Corman, M.; Helal, C. J.; Claffey, M. M.; Tuttle, J. B.; Coffman, K. J.; Liu, S.; Nelson, F. R.; Kleiman, R. J.; Menniti, F. S.; Schmidt, C. J.; Vanasse-Frawley, M. A.; Liras, S. Design and Discovery of 6-[(3S,4S)-4-Methyl-1-(Pyrimidin-2-Ylmethyl)Pyrrolidin-3-yl]-1-(Tetrahydro-2*H*-pyran-4-yl)-1,5-Dihydro-4*H*-Pyrazolo[3,4-*d*]Pyrimidin-4-one (PF-04447943) a Selective Brain Penetrant PDE9A Inhibitor for the Treatment of Cognitive Disorders. *J. Med. Chem.* **2012,** *55,* 9045–9054.
73. Verhoest, P. R.; Proulx-Lafrance, C.; Corman, M.; Chenard, L.; Helal, C. J.; Hou, X.; Kleiman, R.; Liu, S.; Marr, E.; Menniti, F. S.; Schmidt, C. J.; Vanase-Frawley, M.; Schmidt, A. W.; Williams, R. D.; Nelson, F. R.; Fonseca, K. R.; Liras, S. Identification of a Brain Penetrant PDE9A Inhibitor Utilizing Prospective Design and Chemical Enablement as a Rapid Lead Optimization Strategy. *J. Med. Chem.* **2009,** *52,* 7946–7949.
74. Wunder, F.; Tersteegen, A.; Rebmann, A.; Erb, C.; Fahrig, T.; Hendrix, M. Characterization of the First Potent and Selective PDE9 Inhibitor Using a cGMP Reporter Cell Line. *Mol. Pharmacol.* **2005,** *68* (6), 1775–1781.
75. van der Staay, F. J.; Rutten, K.; Baerfacker, L.; DeVry, J.; Erb, C.; Heckroth, H.; Karthaus, D.; Tersteegen, A.; van Kampen, M.; Blokland, A.; Prickaerts, J.; Reymann, K. G.; Schroeder, U. H.; Hendrix, M. The Novel Selective PDE9 Inhibitor BAY 73-6691 Improves Learning and Memory in Rodents. *Neuropharmacology* **2008,** *55,* 908–918.
76. Kroker, K. S.; Mathis, C.; Marti, A.; Cassel, J.-C.; Rosenbrock, H.; Dorner-Ciossek, C. PDE9A Inhibition Rescues Amyloid Beta-Induced Deficits in Synaptic Plasticity and Cognition. *Neurobiol. Aging* **2014,** *35,* 2072–2078.
77. Hou, J.; Xu, J.; Liu, M.; Zhao, R.; Luo, H.-B.; Ke, H. Structural Asymmetry of Phosphodiesterase-9, Potential Protonation of a Glutamic Acid, and Role of the Invariant Glutamine. *PLoS One* **2011,** *6,* e18092.
78. Coskran, T. M.; Morton, D.; Menniti, F. S.; Adamowicz, W. O.; Kleiman, R. J.; Ryan, A. M.; et al. Immunohistochemical Localization of Phosphodiesterase 10A in Multiple Mammalian Species. *J. Histochem. Cytochem.* **2006,** *54,* 1205–1213.
79. Kehler, J.; Nielsen, J. PDE10A Inhibitors: Novel Therapeutic Drugs for Schizophrenia. *Curr. Pharm. Des.* **2011,** *17,* 137–150; (b) Kehler, J. Phosphodiesterase 10A Inhibitors: A 2009–2012 Patent Update. *Expert Opin. Ther. Pat.* **2013,** *23,* 31–45; (c) Chappie, T. A.; Helal, C. J.; Hou, X. Current Landscape of Phosphodiesterase 10A (PDE10A) Inhibition. *J. Med. Chem.* **2012,** *55,* 7299–7331; (d) Kehler, J.; Kilburn, J. P. Patented PDE10A Inhibitors: Novel Compounds Since 2007. *Expert Opin. Ther. Pat.* **2009,** *19,* 1715–1725; (e) Kehler, J.; Ritzen, A.; Greve, D. R. The Potential Therapeutic Use of Phosphodiesterase 10 Inhibitors. *Expert Opin. Ther. Pat.* **2007,** *17,* 147–158.
80. Li, Y. W.; Seager, M. A.; Wojcik, T.; Heman, K.; Molski, T. F.; Fernandes, A.; Langdon, S.; Pendri, A.; Gerritz, S.; Tian, Y.; Hong, Y.; Gallagher, L.; Merritt, J. R.; Zhang, C.; Westphal, R.; Zaczek, R.; Macor, J. E.; Bronson, J. J.; Lodge, N. J. Biochemical and Behavioral Effects of PDE10A Inhibitors: Relationship to Target Site Occupancy. *Neuropharmacology* **2016,** *102,* 121–135.
81. Wilson, L. S.; Brandon, N. J. Emerging Biology of PDE10A. *Curr. Pharm. Des.* **2015,** *21,* 378–388.
82. Chappie, C. T. A.; Helal, C. J.; Hou, X. Current Landscape of Phosphodiesterase 10A (PDE10A) Inhibition. *J. Med. Chem.* **2012,** *55,* 7299–7331.
83. Shipe, W. D.; Sharik, S. S.; Barrow, J. C.; McGaughey, G. B.; Theberge, C. R.; Uslaner, J. M.; Yan, Y.; Renger, J. J.; Smith, S. M.; Coleman, P. J.; Cox, C. D. Discovery and Optimization of a Series of Pyrimidine-Based Phosphodiesterase 10A (PDE10A) Inhibitors Through Fragment Screening, Structure-Based Design, and Parallel Synthesis. *J. Med. Chem.* **2015,** *58,* 7888–7894. and references therein.

84. Kunitomo, J.; Yoshikawa, M.; Fushimi, M.; Kawada, A.; Quinn, J. F.; Oki, H.; Kokubo, H.; Kondo, M.; Nakashima, K.; Kamiguchi, N.; Suzuki, K.; Kimura, H.; Taniguchi, T. Discovery of 1-[2-Fluoro-4-(1*H*-Pyrazol-1-yl)Phenyl]-5-Methoxy-3-(1-Phenyl-1*H*-Pyrazol-5-yl)Pyridazin-4(1*H*)-one (TAK-063), a Highly Potent, Selective, and Orally Active Phosphodiesterase 10A (PDE10A) Inhibitor. *J. Med. Chem.* **2014,** *57,* 9627–9643.
85. Suzuki, K.; Harada, A.; Shiraishi, E.; Kimura, H. In Vivo Pharmacological Characterization of TAK-063, a Potent and Selective Phosphodiesterase 10A Inhibitor With Antipsychotic-Like Activity in Rodents. *J. Pharmacol. Exp. Ther.* **2015,** *352* (3), 471–479.
86. Harada, A.; Suzuki, K.; Kamiguchi, N.; Miyamoto, M.; Tohyama, K.; Nakashima, K.; Taniguchi, T.; Kimura, H. Characterization of Binding and Inhibitory Properties of TAK-063, a Novel Phosphodiesterase 10A Inhibitor. *PLoS One* **2015,** *10,* e0122197.
87. (a) Takano, A.; Stepanov, V.; Gulyás, B.; Nakao, R.; Amini, N.; Miura, S.; Kimura, H.; Taniguchi, T.; Halldin, C. Evaluation of a Novel PDE10A PET Radioligand, [(11) C]T-773, in Nonhuman Primates: Brain and Whole Body PET and Brain Autoradiography. *Synapse* **2015,** *69,* 345–355; (b) Harada, A.; Suzuki, K.; Miura, S.; Hasui, T.; Kamiguchi, N.; Ishii, T.; Taniguchi, T.; Kuroita, T.; Takano, A.; Stepanov, V.; Halldin, C.; Kimura, H. Characterization of the Binding Properties of T-773 as a PET Radioligand for Phosphodiesterase 10A. *Nucl. Med. Biol.* **2015,** *42,* 146–154.
88. Hu, E.; Chen, N.; Bourbeau, M. P.; Harrington, P. E.; Biswas, K.; Kunz, R. K.; Andrews, K. L.; Chmait, S.; Zhao, X.; Davis, C.; Ma, J.; Shi, J.; Lester-Zeiner, D.; Danao, J.; Able, J.; Cueva, M.; Talreja, S.; Kornecook, T.; Chen, H.; Porter, A.; Hungate, R.; Treanor, J.; Allen, J. R. Discovery of Clinical Candidate 1-(4-(3-(4-(1*H*-Benzo[d]Imidazole-2-Carbonyl)Phenoxy)Pyrazin-2-yl)Piperidin-1-yl)Ethanone (AMG 579), a Potent, Selective, and Efficacious Inhibitor of Phosphodiesterase 10A (PDE10A). *J. Med. Chem.* **2014,** 6632–6641. *57*.
89. Roche, Forum and Lundbeck: see Ref.[78] and Ref.[38]; Omeros: Cutshall, N.S.; Ferguson, K.M.; Zuta, C.P., (S)-1-(5-(4-Chloro-3,5-Dimethoxyphenyl)Furan-2-yl)-2-Ethoxy-2-(4-(5-Methyl-1,3,4-Thiadiazol-2-yl)Phenyl)Ethanone as PDE10 Inhibitor and Its Preparation and Use for the Treatment of Neurological Disorders PCT Int. Appl., WO 2015167968. Roche: http://www.hra.nhs.uk/news/research-summaries/a-pet-study-to-assess-brain-uptake-of-ro5545965-version-1/, 2015.
90. (a) Gage, J. L.; Onrust, R.; Johnston, D.; et al. N-Acylhydrazones as Inhibitors of PDE10A. *Bioorg. Med. Chem. Lett.* **2012,** *21,* 4155–4159; (b) Cutshall, N. S.; Onrust, R.; Rohde, A.; et al. Novel 2-Methoxyacylhydrazones as Potent, Selective PDE10A Inhibitors With Activity in Animal Models of Schizophrenia. *Bioorg. Med. Chem. Lett.* **2012,** *22,* 5595–5599.
91. Kuhn, B.; Guba, W.; Hert, J.; Banner, D.; Bissantz, C.; Ceccarelli, S.; Haap, W.; Körner, M.; Kuglstatter, A.; Lerner, C.; Mattei, P.; Neidhart, W.; Pinard, E.; Rudolph, M. G.; Schulz-Gasch, T.; Woltering, T.; Stahl, M. A Real-World Perspective on Molecular Design. *J. Med. Chem.* **2016,** *59* (9), 4087–4102. http://dx.doi.org/10.1021/acs.jmedchem.5b01875. Article ASAP.
92. Burdi, D. F.; Campbell, J. E.; Wang, J.; Zhao, S.; Zhong, H.; Wei, J.; Campbell, U.; Shao, L.; Herman, L.; Koch, P.; Jones, P. G.; Hewitt, M. C. Evolution and Synthesis of Novel Orally Bioavailable Inhibitors of PDE10A. *Bioorg. Med. Chem. Lett.* **2015,** *25,* 1864–1868.
93. Jones, P. G.; Hewitt, M. C.; Campbell, J. E.; Quinton, M. S.; Engel, S.; Lew, R.; Campbell, U.; Burdi, D. F. Pharmacological Evaluation of a Novel Phosphodiesterase 10A Inhibitor in Models of Antipsychotic Activity and Cognition. *Pharmacol. Biochem. Behav.* **2015,** *135,* 46–52.
94. Raheem, I. T.; Breslin, M. J.; Fandozzi, C.; Fuerst, J.; Hill, N.; Huszar, S.; Kandebo, M.; Kim, S. H.; Mac, B.; McGaughey, G.; Renger, J. J.; Schreier, J. D.; Sharma, S.; Smith, S.; Uslaner, J.; Yan, Y.; Coleman, P. J.; Cox, C. D. *Bioorg. Med. Chem. Lett.* **2012,** *22,* 5903–5908.
95. Smith, S. M.; Uslaner, J. M.; Cox, C. D.; Huszar, S. L.; Cannon, C. E.; Vardigan, J. D.; Eddins, D.; Toolan, D. M.; Kandebo, M.; Yao, L.; Raheem, I. T.; Schreier, J. D.; Breslin, M. J.; Coleman, P. J.; Renger, J. J. *Neuropharmacology* **2013,** *64,* 215–223.
96. Raheem, I. T.; Schreier, J. D.; Fuerst, J.; Gantert, L.; Hostetler, E. D.; Huszar, S.; Joshi, A.; Kandebo, M.; Kim, S. H.; Li, J.; Ma, B.; McGaughey, G.; Sharma, S.; Shipe, W. D.; Uslaner, J.; Vandeveer, G. H.; Yan, Y.; Renger, J. J.; Smith, S. M.; Coleman, P. J.; Cox, C. D. Discovery of Pyrazolopyrimidine Phosphodiesterase 10A Inhibitors for the Treatment of Schizophrenia. *Bioorg. Med. Chem. Lett.* **2016,** *26,* 126–132.
97. Cox, C. D.; Hostetler, E.; Flores, B. A.; Evelhoch, J. L.; Fan, H.; Gantert, L.; Holahan, M.; Eng, W.; Joshi, A.; McGaughey, G.; Meng, X.; Purcell, M.; Raheem, I. T.; Riffel, K.; Yan, Y.; Renger, J. J.; Smith, S. M.; Coleman, P. J. Discovery of [^{11}C]MK-8193 as a PET Tracer to Measure Target Engagement of Phosphodiesterase 10A (PDE10A) Inhibitors. *Bioorg. Med. Chem. Lett.* **2015,** *25,* 4893–4898.
98. Lingam, V. S.; Dahale, D. H.; Rathi, V. E.; Shingote, Y. B.; Thakur, R. R.; Mindhe, A. S.; Kummari, S.; Khairatkar-Joshi, N.; Bajpai, M.; Shah, D. M.; Sapalya, R. S.; Gullapalli, S.; Gupta, P. K.; Gudi, G. S.; Jadhav, S. B.; Pattem, R.; Thomas, A. Design, Synthesis, and Pharmacological Evaluation of 5,6- Disubstituted Pyridin-2(1*H*)-One Derivatives as Phosphodiesterase 10A (PDE10A) Antagonists. *J. Med. Chem.* **2015,** *58,* 8292–8308.
99. (a) Das, S.; Shelke, D. E.; Harde, R. L.; Avhad, V. B.; Khairatkar-Joshi, N.; Gullapalli, S.; Gupta, P. K.; Gandhi, M. N.; Bhateja, D. K.; Bajpai, M.; Joshi, A. A.; Marathe, M. Y.; Gudi, G. S.; Jadhav, S. B.; Mahat, M. Y.; Thomas, A. Design, Synthesis and Pharmacological Evaluation of Novel Polycyclic Heteroarene Ethers as PDE10A Inhibitors: Part I. *Bioorg. Med. Chem. Lett.* **2014,** *24,* 2073–2078; (b) Das, S.; Shelke, D. E.; Harde, R. L.; Avhad, V. B.; Khairatkar-Joshi, N.; Gullapalli, S.; Gupta, P. K.; Gandhi, M. N.; Bhateja, D. K.; Bajpai, M.; Joshi, A. A.; Marathe, M. Y.; Gudi, G. S.; Jadhav, S. B.; Mahat, M. Y.; Thomas, A. Design, Synthesis and Pharmacological Evaluation of Novel Polycyclic Heteroarene Ethers as PDE10A Inhibitors: Part II. *Bioorg. Med. Chem. Lett.* **2014,** *24,* 3238–3242.
100. Wagner, S.; Scheunemann, M.; Dipper, K.; Egerland, U.; Hoefgen, N.; Steinbach, J.; Brust, P. Development of Highly Potent Phosphodiesterase 10A (PDE10A) Inhibitors: Synthesis and In Vitro Evaluation of 1,8-Dipyridinyl- and 1-Pyridinyl-Substituted Imidazo[1,5-*a*]Quinoxalines. *Eur. J. Med. Chem.* **2016,** *107,* 97–108.
101. Asproni, B.; Dore, A.; Murineddu, G.; Pinna, G. A. Chemistry of Tricyclic-Based Heterocycles as Useful Scaffolds for Phosphodiesterase 10A Ligands. *Mini-Rev. Org. Chem.* **2013,** *10* (2), 123–140.

7.10 Inhibiting Kinases in the CNS

H Tsui, Q Zeng, K Chen, and X Zhang, Innovative Medicines and Early Development, Astrazeneca, Shanghai, People's Republic of China

© 2017 Elsevier Ltd. All rights reserved.

7.10.1	**Introduction**	408
7.10.2	**Kinases Implicated in CNS Pathology**	409
7.10.2.1	Neurodegeneration	409
7.10.2.2	Oncology	409
7.10.3	**Challenges in Development of Kinase Inhibitors for CNS**	410
7.10.4	**Designing Kinase Inhibitors for CNS Indications**	410
7.10.4.1	Chemistry Approaches for Physicochemical Property Optimization	410
7.10.5	**Small Molecule Kinase Inhibitors for CNS Disorders**	412
7.10.5.1	Leucine-Rich Repeat Kinase 2	412
7.10.5.2	Cyclin-Dependent Kinase 5	414
7.10.5.3	Mitogen-Activated Protein Kinase Kinase 1/2	414
7.10.5.4	c-Jun N-Terminal Kinase	415
7.10.5.6	Casein Kinase 1	415
7.10.5.7	Mixed-Lineage Kinase	416
7.10.5.8	Death-Associated Protein Kinase 1	417
7.10.5.9	Glycogen Synthase Kinase 3	417
7.10.5.10	Rho-Associated Protein Kinase	419
7.10.5.11	p38 Mitogen-Activated Protein Kinase	420
7.10.5.12	Polo-Like Kinase 2	422
7.10.5.13	p21-Activated Kinase	425
7.10.5.14	Dual Leucine Zipper Kinase	426
7.10.5.15	Tropomyosin Receptor Kinase	428
7.10.5.16	Epidermal Growth Factor Receptor	428
7.10.5.17	Anaplastic Lymphoma Kinase	431
7.10.5.18	Human Epidermal Growth Factor Receptor 2	433
7.10.5.19	Phosphoinositide 3-Kinase	434
7.10.20	Ataxia-Telangiectasia Mutated Kinase	436
7.10.6	**Assessment of CNS Exposure in Drug Discovery**	436
7.10.6.1	Barriers Within CNS System	436
7.10.6.2	In Vitro Methodology to Identify Permeability and Efflux Liability at BBB	437
7.10.6.3	In Vivo Methodology to Measure the Extent of Brain Penetration	438
7.10.7	**Conclusion and Future Perspectives**	439
References		439

7.10.1 Introduction

Protein kinases are essential in many biological processes. Protein phosphorylation by their corresponding kinases maintains signaling transductions, which are essential for cellular functions, such as growth, survival, and proliferation.[1] Of the about 518 known kinases, a small portion have been investigated and their dysfunction has been linked to various human diseases. Targeting the activity of those aberrant kinases as a therapeutic intervention for a variety of disorders has attracted a great amount of effort in pharmaceutical research over the last few decades. Of the 29 kinase inhibitors approved by the FDA since 2001, majority of them are in oncology and only two are for noncancer indications.[2–4] Nintedanib, a multikinases inhibitor inhibiting Vascular Endothelial Growth Factor Receptor (VEGFR), Fibroblast Growth Factor Receptor (FGFR), and Platelet Derived Growth Factor Receptor (PDGFR), was approved for idiopathic pulmonary fibrosis. The JAK1,3 inhibitor, tofacitinib, was approved for rheumatoid arthritis (RA). Although there are no approved kinase inhibitors indicated for central nervous system (CNS) diseases so far, kinase inhibitors have demonstrated activity against tumors that have metastasized to the brain.[5] However, at standard doses, they are not as efficacious in controlling metastasized brain tumors compared to their ability to control peripheral tumors, mainly due to their poor brain penetration, which leads to insufficient drug concentrations for target coverage in CNS. In addition, recent advances in the understandings of some neurodegenerative diseases have been linked to the aberrant signaling pathways that are controlled by different kinases. Inhibiting those malfunctioning kinase-mediated signaling pathways may be useful in providing therapeutic

benefits to patients. To this end, designing kinase inhibitors specifically indicated for CNS diseases requires special attention. A different set of physicochemical properties is needed to design candidates that can efficiently cross the blood–brain barrier (BBB). In this article, recent efforts in developing kinase inhibitors for both noncancer- and cancer-related diseases targeting CNS are reviewed. Two excellent reviews in this area have been published a few years back and this work will try to provide readers with some updates on the progress that researchers have made in the intervening years.[6,7]

7.10.2 Kinases Implicated in CNS Pathology

7.10.2.1 Neurodegeneration[8–11]

As the aging population continues to increase, the incidence of disability caused by neurodegenerative disorders will affect many people. The medical burden on the individual as well as the health care system will be significant. Common neurodegenerative diseases include Parkinson's disease (PD), Alzheimer's disease (AD), Huntington's disease (HD), amyotrophic lateral sclerosis, and atypical parkinsonian disorder among others. Unfortunately, there are no disease-modifying treatment options for these neurodegenerative diseases. Neurodegenerative disorders are mostly believed to be caused by several related processes such as hyperphosphorylation of the tau protein (tauopathies), $A\beta_{42}$ accumulation, neuronal apoptosis, and brain inflammation. Aberrant phosphorylation of tau by several key kinases has been identified in the process of tauopathies. Selective kinase inhibitors targeting their cognate kinases with some brain penetration information, either in vitro or in vivo, are summarized in the section "Small Molecule Kinase Inhibitors for CNS Disorders" (Fig. 1). The most active areas of research to develop kinase inhibitors targeting tau protein or α-synuclein hyperphosphorylation include targeting leucine-rich repeat kinase 2 (LRRK2), p38 mitogen-activated protein kinase (MAPK), and GSK3β. Kinases with newly identified roles, which may contribute to the pathology of neurodegenerative diseases, continue to emerge. For example, a connection was recently identified between 3-phosphoinositide-dependent protein kinase 1 and AD.[11]

7.10.2.2 Oncology[1,12]

Targeting aberrant kinase signaling with small molecule inhibitors has been one of the main frames in cancer therapy. Although most of the targeted malignancies are of peripheral origin, certain cancer types inevitably and preferentially undergo metastasis into the CNS, including the brain tissues and cerebrospinal fluid (CSF). Besides the highly metastasizing nature of the tumors, other reasons attributed to increasing cases of brain metastasis identified may be due to the prolonged systemic control with new drugs and the wider availability of CNS diagnostic tools. Lung[13] and breast[4] cancers are two examples where CNS metastases represent one of the major reasons for treatment failure and disease progression. Glioblastoma multiforme (GBM)[14] is a form of primary brain malignancy for which therapeutic intervention is desperately needed. Oncogenic kinase targets included in this article concerning recent developments in brain-penetrant small molecule kinase inhibitors specifically targeting CNS metastases are anaplastic lymphoma kinase (ALK), epidermal growth factor receptor (EGFR), phosphoinositide 3-kinase (PI3Kα), human epidermal growth factor receptor 2 (HER2), and ataxia-telangiectasia mutated kinase (ATM).

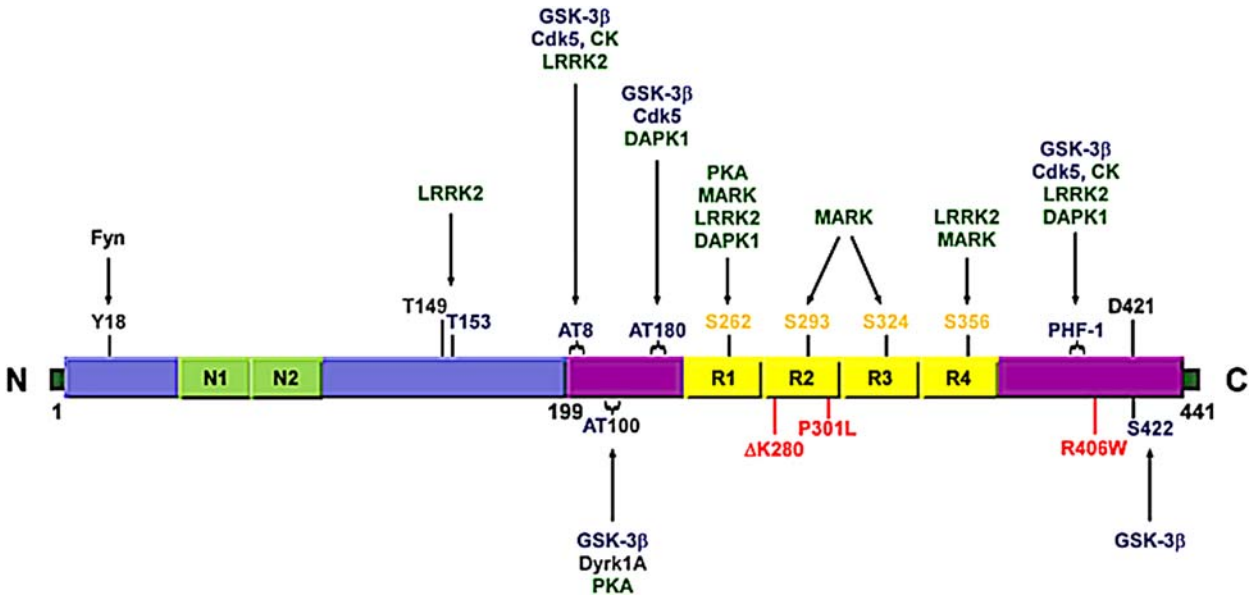

Fig. 1 Kinases involved in tau protein hyperphosphorylation. Adapted from Tenreiro, S.; Eckermann, K.; Outeiro, T. F. Protein Phosphorylation in Neurodegeneration: Friend or Foe? *Front. Mol. Neurosci.* **2014**, *7*, 42.

7.10.3 Challenges in Development of Kinase Inhibitors for CNS

Recently, Wu et al. nicely summarized all of the 28 kinase inhibitors approved by the FDA up to late 2015.[2,3] Their analysis showed that most compounds are in good compliance with the Lipinski's rule of five, except for the molecule weight (MW). About 30% of them have MW > 500. A new kid on the block came in late 2015 with the FDA approval of Tagrisso (AstraZeneca), which is an irreversible EGFR inhibitor for nonsmall cell lung cancer (NSCLC) with L858R, Exon19Del activating mutations, and T790M resistance mutation.[15] Similar to the analysis reported by Wu, we performed a study on the physicochemical properties of all 29 FDA-approved kinase inhibitors. Comparing these parameters against the literature reported median values for CNS drugs;[16] it is apparent that most of these marketed kinase inhibitors may have limited CNS penetration simply through passive diffusion (Table 1 and Fig. 2).

Most noticeable are the lower values for all of these physicochemical properties for CNS drugs compared with the kinase inhibitors. It may be challenging to maintain the activity for the primary pharmacology and selectivity with lower molecular weight compounds, especially designing type II kinase inhibitors to gain selectivity. However, this analysis may give a direction for future modification of currently approved kinase inhibitors or a new compound design to favor CNS penetration.

7.10.4 Designing Kinase Inhibitors for CNS Indications

7.10.4.1 Chemistry Approaches for Physicochemical Property Optimization

Over the years, several analytical tools and models have been developed to help medicinal chemists design compounds with good CNS penetration.[17–22] A number of excellent reviews have been published recently to summarize the chemistry strategies to facilitate efficient design of efficacious CNS drugs. The physicochemical properties that favor a drug's CNS permeability are reasonably clear, but to achieve a balance across all of these properties together with optimal target potency is challenging. The modification of a compound to satisfy one parameter to favor brain penetration will often affect other attributes that render the drug impenetrable to the brain or even to lose its target potency. A successful CNS drug development program depends on the medicinal chemist's ability to perform a highly balanced maneuver of different properties of a molecule at once to deliver a CNS drug candidate. Please find literature references for the successful design of CNS drugs summarized later.

The main mechanisms that allow small molecule drugs to penetrate into CNS are passive diffusion and/or active transport. Key compound properties that help increase the chance of having good brain penetration include: (1) minimized intrinsic clearance. Adequate drug exposure in systemic circulation can allow it to equilibrate into the CNS; (2) non-BBB efflux transporter substrates. There are several key efflux transporters that can be found on the BBB, with P-glycoprotein (P-gp, MDR1) and breast cancer resistance protein (BCRP) being the two most important transporters. In addition to them not being transporter substrates, compounds with a $P_{app} > 150–200$ nm s^{-1} are more favorable to counteract the transporters' efflux process.

In order to meet the above criteria to facilitate brain entry, the physicochemical properties of a compound need to be within certain boundaries.[23] The median values of the reported physicochemical properties of marketed drugs are: molecular weight = 305; hydrogen bond donor (HBD) = 1; TPSA = 45; c log P = 2.8; c log D = 1.7; pK_a = 8.4; rotatable bond = 4.5.[16]

Based on these values and other similar analysis, a good CNS drug designer should focus on optimizing compounds with properties: (1) molecular weight (< 450); (2) lipophilicity (c log P < 5; log $D \sim 2–3$); (3) polar surface area (PSA ~ 60–70 Å^2); (4) pK_a (7.5–10.5); (5) rotational bonds (< 8); (6) hydrogen bonding (H-bond donor < 3; H-bond acceptor < 7).

It has also been shown that the most important molecular properties affecting CNS penetration relate to the H-bonding propensity of the molecule. The higher hydrogen-bonding capability of a molecule will increase the risk of it being a transporter substrate and decrease its intrinsic permeability through the BBB. Another interesting observation is the lack of correlation between lipophilicity and free drug brain exposure. For a molecule with a higher molecular weight, a corresponding higher lipophilicity is required for optimal permeability in the absence of an active transport mechanism.

Besides considering these physicochemical property parameters individually, different models have been developed to consider them as a whole in a composite index. Recently, Raevsky and colleagues reported a comparative study of five different models including "rule of five", multiparameter optimization (MPO), logistic regression, random forest (RF), and support vector machine (SVM), for predicting brain permeability.[24] The authors suggested that focusing on a single parameter is unlikely to correctly predict

Table 1 Comparing the physicochemical properties of FDA approved kinase inhibitors (n = 29) with CNS drugs on the market

Kinase inhibitors (n = 29)	*MW*	*HDA*	*HBD*	*PSA*	*c log* P	*AZ log* D *(pH 7.4)*	*pK$_a$ (base)*	*# Ring*	*# Rotable bonds*
Ave	470.7	6.517	2.103	87.852	4.318	3.157	5.968	4.172	7.690
Median	482.8	7.000	2.000	87.755	4.490	3.320	6.341	4.000	7.000
CNS drugs	*MW*	*HDA*	*HBD*	*PSA*	*c log* P	*c log* D	*pK$_a$ (base)*	*# Ring*	*# Rotable bonds*
Median	305	–	1	45	2.8	1.7	8.4	–	–

Part of the data was adapted from Wager, T. T.; Chandrasekaran, R. Y.; Hou, X.; Troutman, D. M.; Verhoest, P. R.; Villalobos, A.; Will, Y. Defining Desirable Central Nervous System Drug Space Through the Alignment of Molecular Properties, in vitro ADME, and Safety Attributes. *ACS Chem. Neurosci.* **2010**, *1*(6), 420–434.

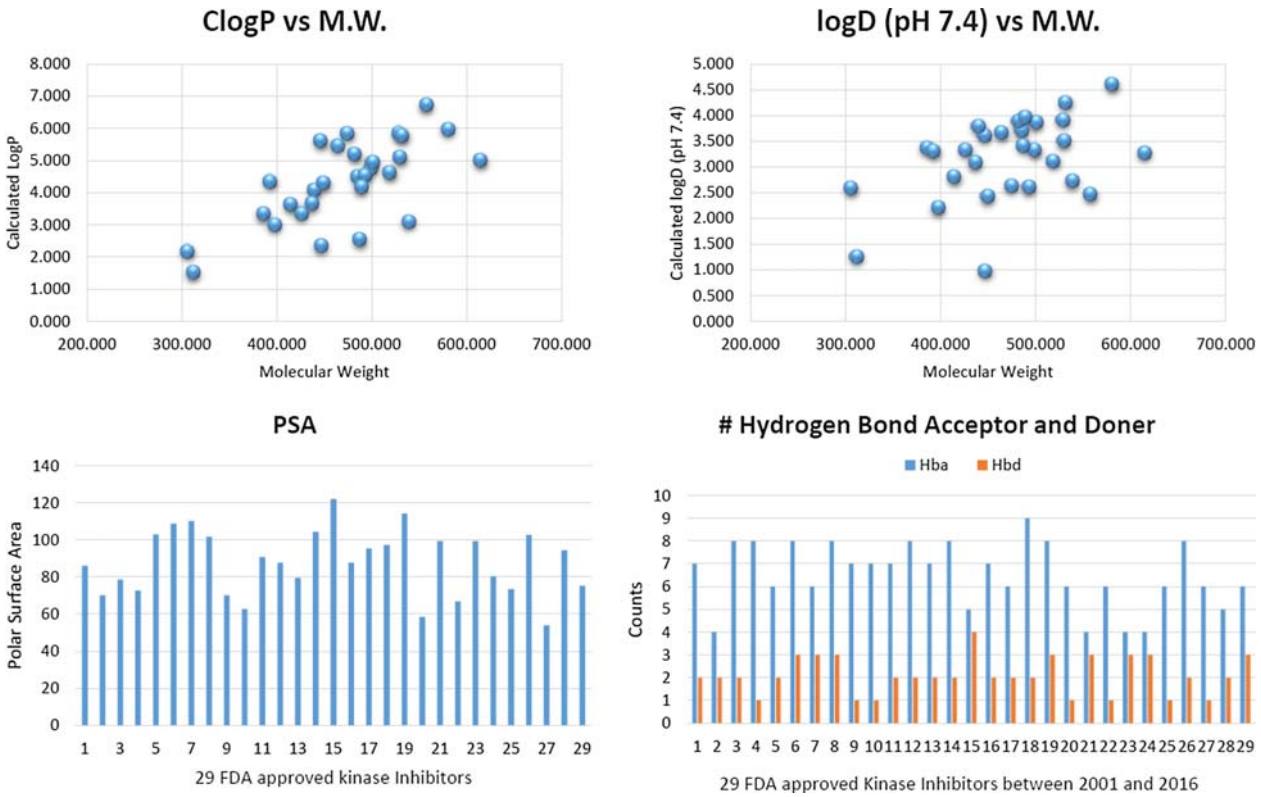

Fig. 2 Correlation of physicochemical properties of all 29 FDA-approved kinase inhibitors.

CNS+ or CNS− for a compound. Out of the five models compared, the RF and SVM models are superior in terms of accuracy compared with the other three models in classifying brain-penetrable compounds in their test set of compounds. Based on the modeling results for a set of selected compounds, the importance of physicochemical parameters affecting brain penetration was ranked in the order as follows: (1) TPSA, (2) H-bond acceptor and donor groups, and (3) electrostatic potential (H-bond ability of the strongest acceptor). The characteristic chemical functional groups in the tested compounds are represented in Fig. 3. A higher percentage of compounds with a tertiary amine moiety are predicted as CNS+ while the presence of a hydroxyl group in a molecule has a higher chance of brain penetration failure.

Recently, a new model using probabilistic MPO (pMPO) scoring function was proposed by Gunaydin from Merck.[25] In this approach, the author tried to combine two scoring functions (MPO & QED) into a more predictive model with one scoring function. The pMPO model minimizes the number of parameters needed to define an MPO score for a molecule by imposing boundaries with a probability distribution in a desired molecular space. This approach claimed to be less prone to the "double-counting error" presented in other scoring approaches. The scoring functions have been used to correlate two different end points in drug discovery. As an example, Gunaydin used the pMPO model to illustrate that the prediction of the "CNS drug-likeness" of a molecule

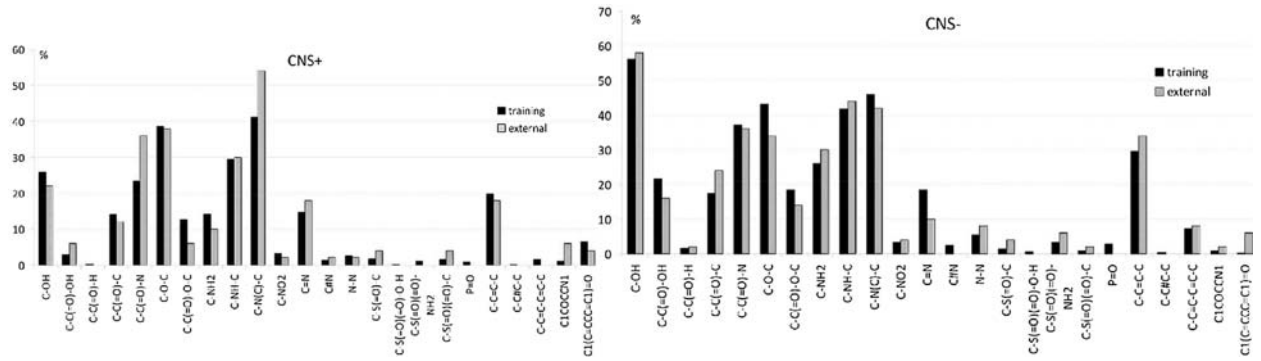

Fig. 3 Chemical functional groups present in studied CNS+ and CNS− data sets. Adapted from Raevsky, O. A.; Grigorev, V. Y.; Polianczyk, D. E.; Sandakov, G. I.; Solodova, S. L.; Yarkov, A. V.; Bachurin, S. O.; Dearden, J. C. Physicochemical Property Profile for Brain Permeability: Comparative Study by Different Approaches. *J. Drug Target.* **2016**, Published online, http://dx.doi.org/10.3109/1061186X.2015.1132224.

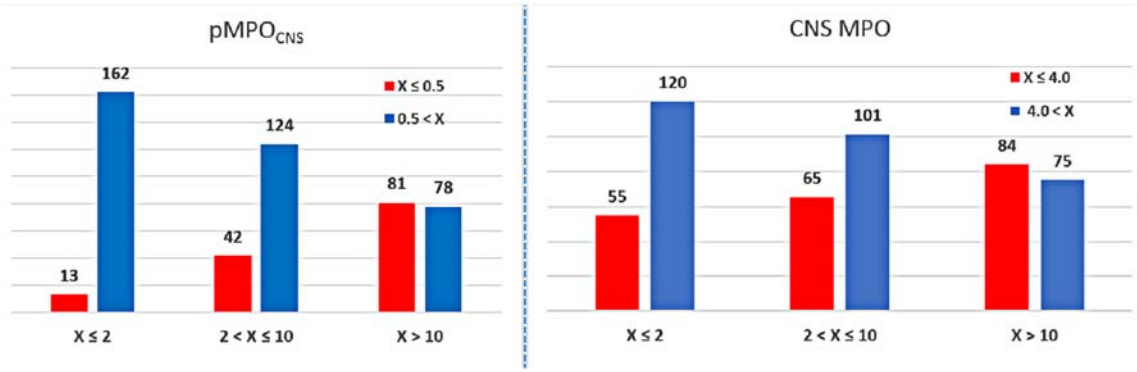

Fig. 4 Enrichment of benefit achieved with $pMPO_{CNS}$ and CNS MPO scores for predicting efflux liability of molecules (*x*-axis = effective efflux ratio; *y*-axis = number of compounds; CNS penetration: *blue* = favorable; *red* = unfavorable). Reproduced from Gunaydin, H. Probabilistic Approach to Generating MPOs and Its Application as a Scoring Function for CNS Drugs. *ACS Med. Chem. Lett.* **2016**, *7*, 89–93.

could correlate with the liability of its being a P-gp substrate. Analysis of a set of ~500 Merck internal compounds suggested that the $pMPO_{CNS}$ scoring function is better than the more commonly used CNS MPO scoring function[26] in predicting efflux liability (Fig. 4).

Other avenues to bring drugs into the CNS have also been explored when CNS penetration of a compound is not sufficient simply by using a passive diffusion mechanism to achieve the required drug concentration. Strategies include the use of transporter-mediated brain uptake (e.g., PEPT1) or liposomes/nanoparticles approach.[27–31] However, such methodologies are still in their infancy. With more experimentation, their practical application in the clinical setting may be realized in the near future.

7.10.5 Small Molecule Kinase Inhibitors for CNS Disorders

7.10.5.1 Leucine-Rich Repeat Kinase 2

The LRRK2 is a large protein (monomer ~240 kDa). It is widely distributed throughout the body and is found in elevated concentrations in brain, kidney, and heart tissues, as well as various immune cells.[32,33] LRRK2 protein sequence contains multiple domains, including ATP-binding kinase domain, GTPase domain, and several protein–protein interaction domains, such as ankyrin-like (ANK) domain, leucine-rich repeat domain, C-terminal of ROC-COR domain, and C-terminal WD40 domain.[34] However, most of the pathogenic LRRK2 variants are located in either the enzymatically active serine–threonine kinase domain or the GTPase domain of the protein. There is no published structure of LRRK2 or any of the individual protein domains due to its complexity. More recent studies suggested that several residue variants may affect LRRK2 kinase activity by modulating LRRK2 dimerization kinetics or by altering interactions between the ROC and COR domains. Activating mutants such as G2019S enhance LRRK2 kinase activity. Modulation of kinase function with small molecules might be achieved by interfering with ATP binding in the kinase domain, GTP binding and hydrolysis in the GTPase domain, or the LRRK2 dimerization equilibrium.

LRRK2 gene mutations are considered as a key driver of PD and several generic variants such as G2019S, R1441C/G, Y1699C, and I2020T have been confirmed as pathogenic contributors to the disease.[35–37] These variants are located in the activation loop of the kinase domain, the ROC domain, and on the dimerization interface of the COR domain. In particular, the most common and extensively characterized variant, LRRK2 G2019S, counts for 6% of all hereditary, and 1–2% of all idiopathic cases of PD.

As an attractive therapeutic target for the treatment of PD, LRRK2 has received increased attention in academic institutions and in the pharmaceutical industry. Multiple programs have been launched in different institutions and several small molecule LRRK2 inhibitors have been identified in recent years. Early reported LRRK2 inhibitors include staurosporine, K252A7, sunitinib, H-11529, and GW5074.[38–40] These compounds, however, are nonspecific inhibitors against LRRK2. More recently, LRRK2-IN-1 was identified and exhibited excellent activity and selectivity.[41] In biochemical assays with 0.1 mM ATP concentration, this compound inhibited both wild-type LRRK2 and G2019S mutant with activities (IC_{50}) of 13 nM and 6 nM, respectively. In addition, it inhibited only 12 kinases in a 442-kinase panel assay with a score of < 10% of the DMSO control at a concentration of 10 μM. As a tool compound, LRRK2-IN-1 has demonstrated that the inhibition of LRRK2 induces the dephosphorylation of Ser910/Ser935 and the accumulation of LRRK2 within aggregate structures in mice kidneys. In contrast, no dephosphorylation of LRRK2 Ser910 or Ser935 was observed in brain tissue, indicating that LRRK2-IN-1 is likely unable to efficiently cross the BBB. CZC-251469 is another potent, highly selective, and metabolically stable LRRK2 inhibitor.[33] It has been demonstrated that CZC-251469 prevents mutant LRRK2-induced injury of cultured rodent and human neurons with midnanomolar potency. This agent, however, displayed poor brain penetration (~4%), which limited its utility in PD models and eventual translation into human clinical trials.

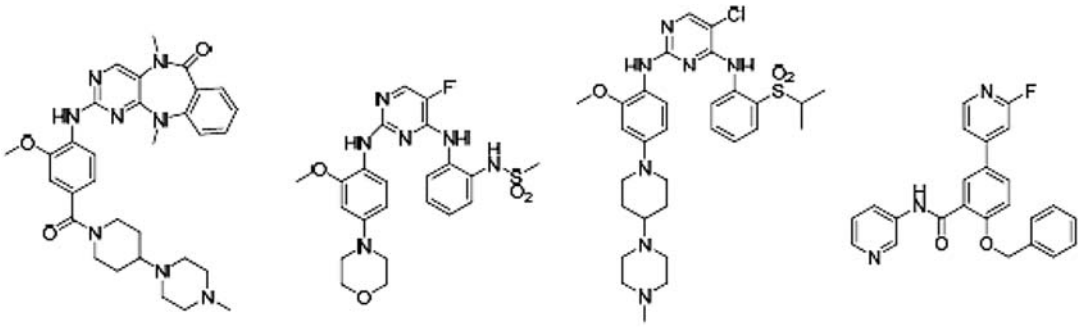

Recently, it was reported that TAE684, a previously reported inhibitor of ALK, is also a potent inhibitor of LRRK2 kinase activity (IC_{50} of 7.8 nM against wild-type LRRK2, 6.1 nM against the G2019S mutant).[42] At a concentration of 0.1–0.3 μM in cells TAE684 substantially inhibits Ser910 or Ser935 phosphorylation of both wild-type LRRK2 and G2019S mutants. The mouse pharmacokinetic (PK) profile of TAE684 demonstrated excellent oral bioavailability (83%), a half-life of 11.3 h and excellent plasma exposure (AUC of 6374 h ng mL^{-1}) at a dose of 10 mg kg^{-1}. Furthermore, TAE684 exhibited a brain-to-plasma AUC ratio of 2, indicating its superior BBB penetration property. In addition, complete Ser910 or Ser935 dephosphorylation of LRRK2 in the kidney and spleen at an oral dose of 50 mg kg^{-1} and slightly lower effects at 10 mg kg^{-1} were observed. Unfortunately, no inhibition of Ser910 or Ser935 phosphorylation of LRRK2 was observed in the mouse brain.

In 2012, a research group from GlaxoSmithKline reported a novel LRRK2 inhibitor GSK2578215A.[43] This agent exhibited biochemical IC_{50}s of around 10 nM against both wild-type LRRK2 and the G2019S mutants. GSK2578215A also substantially inhibited Ser910 or Ser935 phosphorylation of both wild-type LRRK2 and G2019S mutants at a concentration of 0.3–1.0 μM in cells. Evaluation of the PK profile of GSK2578215A in wild-type mice demonstrated that the compound achieved exposure in the brain with a brain-to-plasma ratio of 1.9. However, GSK2578215A exhibits low oral bioavailability (12%), short half-life (1.14 h), and limited plasma exposure (AUC = 635.3 h ng mL^{-1}) at an oral dose of 10 mg kg^{-1}. Complete Ser910 or Ser935 dephosphorylation of LRRK2 was observed in the kidney and spleen after intraperitoneal (i.p.) injections with 100 mg kg^{-1} of GSK2578215A in normal mice. Again, despite the significant exposure of GSK2578215A in the brain, no inhibition of LRRK2 Ser910 or Ser935 phosphorylation was observed in the brain, a finding similar to that observed for TAE684. Recently, Estrada et al. at Genentech Inc. reported the first BBB-penetrant, CNS-active, highly selective LRRK2 inhibitor, GNE-7915.[44] GNE-7915 demonstrated excellent LRRK2 inhibitory activity in biochemical (K_i = 1 nM) and cellular assays (IC_{50} = 9 nM) and high selectivity in a kinase panel screen. In addition, GNE-7915 exhibited excellent in vitro DMPK and in vivo rat PK profiles including good brain penetration in rats (unbound brain/unbound plasma AUC ratio = 0.50 and CSF/unbound plasma AUC ratio = 0.60). Furthermore, GNE-7915 was dosed to BAC transgenic mice expressing human LRRK2 protein with the G2019S PD mutation via either a single oral dose (p.o.) or i.p. injection. A robust, concentration-dependent knockdown of pLRRK2 in the brain was observed after an oral dose of 15 and 50 mg kg^{-1} and an i.p. dose of 10 and 50 mg kg^{-1}. GNE-7915 was also tolerable in the genotoxic study and 7-day repeat-dose toxicity studies in rats (10, 50, and 100 mg kg^{-1}) and cynomolgus monkeys (10, 25, and 65 mg kg^{-1}).

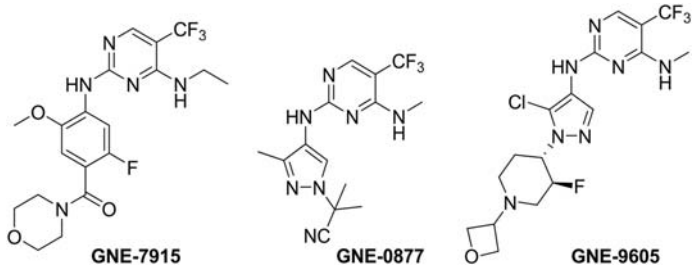

In an effort to improve aqueous solubility and eliminate the potential ortho-quinone-imine reactive metabolite formation of GNE-7915, the Genentech group successfully designed aminopyrazole inhibitors GNE-0877 and GNE-9605.[45] GNE-0877 and GNE-9605 exhibited excellent potency in cellular assays (3 and 19 nM of IC_{50}s, respectively) and good selectivity in kinase panel screening. Furthermore, GNE-0877 showed clearance of 44 mL min^{-1} kg^{-1} and oral bioavailability of 88% at a dose of 50 mg kg^{-1} in rats. Crystalline GNE-0877 also demonstrated good thermodynamic solubility (solubility = 100 μg mL^{-1} under neutral conditions). Importantly, the absence of P-gp efflux (efflux ratio = 0.8) translated to an in vivo rat-free brain/plasma AUC ratio (0.6) and corresponding CSF/free plasma AUC ratio (0.9). However, GNE-0877 was found to be a reversible CYP1A2 inhibitor (IC_{50} = 0.7 μM) although this compound did not exhibit time-dependent inhibition of CYP1A2. Additional profiling suggested that GNE-0877 was a pan inducer of CYP enzymes in human hepatocytes. Another LRRK2 inhibitor GNE-9605, which possessed

the same pyrimidine unit as GNE-0877 but with a different substitution pattern on the pyrazole moiety, was also described. A basic piperidine, which is a favorable fragment for solubility and brain penetration, was incorporated into GNE-9605. It was very potent toward LRRK2 in both biochemical ($K_i = 2.0$ nM) and cellular assays and highly selective in kinase panel screening. This agent is not a CYP inhibitor or inducer of any major CYP isoforms. In addition, in vivo rat PK studies with GNE-9605 demonstrated a total plasma clearance of 26 mL $min^{-1} kg^{-1}$ with excellent oral bioavailability (90%). Unbound brain-to-plasma and CSF-to-unbound plasma AUC ratios of GNE-9605 were between 0.5 and 1.0, respectively.

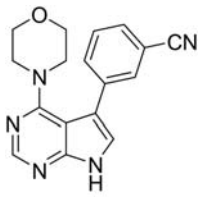

PF-06447475

More recently, Pfizer scientists reported a novel LRRK2 inhibitor PF-06447475.[46] This agent exhibited IC_{50} values against wild-type LRRK2 at 3 nM and the G2019S mutant at 11 nM in biochemical assays and 25 nM of IC_{50} in LRRK2 whole cell assay. PF-06447475 achieved approximately equal distribution of the free drug between rat brain, plasma, and kidney tissues. However, despite high permeability and moderate clearance, oral bioavailability was poor across species. Therefore, this agent was not progressed into clinic.

7.10.5.2 Cyclin-Dependent Kinase 5

Cyclin-dependent kinase 5 (CDK5) is a proline-directed serine/threonine kinase belonging to the family of cyclin-dependent kinases. It requires association with a regulatory partner, p35 and p39, for kinase activation. CDK5 plays a pivotal role in the development of the CNS. In addition to maintaining neuronal architecture, CDK5 plays an important role in the regulation of synaptic plasticity, neurotransmitter release, neuron migration, and neurite outgrowth.[47–50] The hyperactivity of CDK5 has been linked to the development of AD. Although CDK5 is important in the development of CNS and neuronal survival, many questions, such as what is the precise mechanism in disease progression, remain unanswered. Brain-penetrant CKD5 inhibitors have not yet been reported.

7.10.5.3 Mitogen-Activated Protein Kinase Kinase 1/2

MEK is a Ser/Thr protein kinase that phosphorylates extracellular signal-regulated kinase (ERK) in the Ras/Raf/MEK/ERK pathway. Mitogen-activated protein kinase kinase 1/2 (MEK1/2) has been an attractive therapeutic target in drug development for the treatment of a number of cancers. Highly selective and potent MEK1/2 inhibitors have been identified and assessed in recent years. Trametinib received US FDA approval in 2013 for the treatment of melanoma. Several other inhibitors are in clinical trials for cancer therapy.[51,52] Although oncology is the major area of focus, MEK1/2 has been investigated as a potential CNS target. Several MEK1/2 kinase inhibitors such as PD-98059, U0126, and PD198306 have shown efficacy in treating preclinical animal models of cerebral ischemia, traumatic brain injury, and neuropathic pain.[53] However, no MEK1/2 inhibitors for the treatment of CNS disorders are currently under clinical investigation, partly because the precise mechanism by which MEK inhibition relates to CNS disorders still remains unknown. Several inhibitors such as PD325901, cobimetinib (GDC-0973), and trametinib, designed for cancer therapy, have been screened and demonstrated that their brain penetration levels were very low.[6,54,55] The unfavorable physicochemical properties of these agents such as excessive HBDs might limit their brain exposure. Both cobimetinib and trametinib were determined to be substrates of the P-gp efflux transporter.

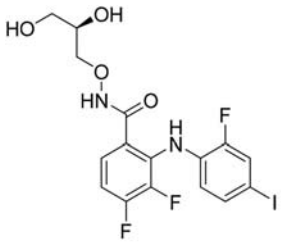

PD325901

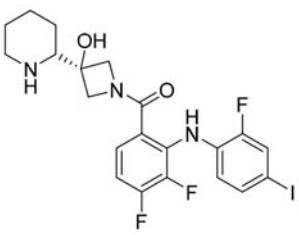

Cobimetinib

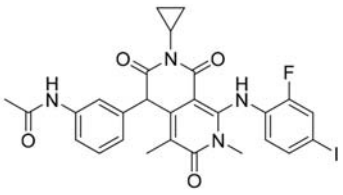

Trametinib

7.10.5.4 c-Jun N-Terminal Kinase

The c-jun N-terminal kinases (JNKs) are members of the MAPK family and they regulate the serine/threonine phosphorylation of several transcription factors when they are activated in response to a variety of stress-based stimuli such as cytokines, ultraviolet irradiation, heat shock, fatty acids, and osmotic shock. Despite the fact that JNK1 and JNK2 are expressed throughout the body, JNK3 is predominantly expressed in the brain and at lower levels in the heart and testis. Recent studies have suggested that JNK1 plays a central role in the development of obesity-induced insulin resistance and JNK2 is linked to autoimmune disorders such as RA and asthma. On the other hand, JNK3 has been shown to play an important role in the brain, by mediating neurodegeneration, such as beta amyloid processing, Tau phosphorylation, and neuronal apoptosis in AD, as well as mediating neurotoxicity in a rodent model of PD. Therefore, interest in developing selective JNK inhibitors as therapeutics for CNS disorders has been increasing over the past few years although no JNK kinase inhibitors are currently under clinical investigation.[56,57] A recent excellent review article described several brain-penetrant JNK3 kinase inhibitors.[58]

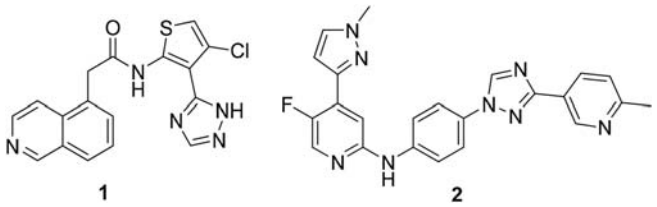

In 2011, Bowers et al. reported the JNK inhibitor 1.[59] This compound exhibited a favorable combination of potency, selectivity for JNK over p38α and ERK2 (JNK3 $IC_{50}=11$ nM, JNK1 $IC_{50}=14$ nM, JNK2 $IC_{50}=43$ nM, p38α $IC_{50}>50$ μM, and ERK2 $IC_{50}>50$ μM in biochemical assays), metabolic stability, permeability, and P-gp efflux. It was dosed to mice in kainic acid animal model study and the effect of JNK inhibition was tested. Pretreatment with a single, oral dose of compound 1 at 300 mg kg^{-1} resulted in a significant 51% reduction of phospho-c-jun in the hippocampus of FVB mice 4 h after an i.p. injection of 25 mg kg^{-1} kainic acid, indicating the in vivo effect on JNK activity of the inhibitor. The brain penetration level of this compound, however, was not reported. In the same year, Noel et al. independently disclosed a novel JNK inhibitor 2.[60] This agent displayed IC_{50} of 0.2 μM against JNK3 and >20 μM against p38α. The concentrations of the compound were determined at 9 and 10 μM in mouse plasma and in mouse brain, respectively, 2 h after IP dosing of 10 mg kg^{-1}. In addition, the compound exhibited good oral bioavailability (69%) and moderate terminal half-life ($T_{1/2}=2.3$ h).

7.10.5.6 Casein Kinase 1

Casein kinase 1 (CK1) is a Ser/Thr kinase that is ubiquitously expressed in eukaryotic organisms.[61] Seven CK1 isoforms (α, β, γ1, γ2, γ3, δ, and ε), highly homologous within their kinase domains and significantly different in the length and primary structure of their N-terminal and C-terminal noncatalytic domains, have been characterized.[62–65] Recent review articles have summarized the pharmacology studies that linked CK1 to several CNS-associated disorders, such as movement- and motivation-related behaviors, acceleration of the mammalian clock in brain regions and peripheral tissues, and AD.[66,67] AD is associated with the accumulation of the neurotoxic peptide amyloid-β (Aβ), which is produced by the sequential cleavage of amyloid precursor protein by the aspartyl protease β-secretase and the presenilin-dependent protease γ-secretase. Elevated CK1 activity has been reported to be associated with the pathological accumulation of the tau protein.[68] Inhibition of CK1 has been shown to reduce fibrillar lesions and to inhibit the production of the neurotoxic peptide (Aβ).

CKI-7 was the first reported CK1 inhibitor, which was characterized as an ATP-competitive inhibitor. However, this agent displayed poor selectivity against CK1 isoforms and was not suitable to proceed as a drug candidate. PF-4800567 and PF-670462 are the first reported brain-penetrable CK1 inhibitors.[69] Activity results of both compounds are summarized in **Table 2**. When tested in an in vitro assay against purified CK1ε and CK1δ, PF-4800567 had an IC_{50} of 32 nM for CK1ε, whereas its CK1δ IC_{50} was 711 nM, 22-fold less potent than toward CK1ε. In contrast, PF-670462, an inhibitor of both CK1ε and CK1δ, showed a small preference in the opposite direction and was approximately sixfold more potent toward CK1δ.

Table 2 Enzyme and whole cell IC_{50} values for PF-4800567 and PF-670462

	Enzymes		*Whole cell*	
	CK1ε IC_{50} *(μM)*	*CK1δ* IC_{50} *(μM)*	*CK1ε* IC_{50} *(μM)*	*CK1δ* IC_{50} *(μM)*
PF-4800567	0.032	0.711	0.13	2.65
PF-670462	0.080	0.013	0.55	0.14

Reproduced from Walton, K. M.; Fisher, K.; Rubitski, D.; Marconi, M.; Meng, Q.-J.; Sládek, M.; Adams, J.; Bass, M.; Chandrasekaran, R.; Butler, T.; Griffor, M.; Rajamohan, F.; Serpa, M.; Chen, Y.; Claffey, M.; Hastings, M.; Loudon, A. Maywood, E.; Ohren, J.; Doran, A.; Wager, T. T. Selective Inhibition of Casein Kinase 1 Epsilon Minimally Alters Circadian Clock Period. *J. Pharmacol. Exp. Ther.* **2009**, *330*(2), 430–439.

Table 3 Pharmacokinetic parameters of PF-4800567 and PF-670462

	PF-4800567		*PF-670462*	
	Plasma	*Brain*	*Plasma*	*Brain*
Dose (mg kg^{-1})	100		32	
AUC (ng h mL^{-1})	6030	11,400	2880	3410
Total C_{max} (ng mL^{-1})	5250	9250	2760	2800
T_{max} (h)	0.5	0.5	0.5	0.5
f_u	0.069	0.016	0.12	0.046
Free C_{max} (nM)	1007	411	982	393

Reproduced from Walton, K. M.; Fisher, K.; Rubitski, D.; Marconi, M.; Meng, Q.-J.; Sládek, M.; Adams, J.; Bass, M.; Chandrasekaran, R.; Butler, T.; Griffor, M.; Rajamohan, F.; Serpa, M.; Chen, Y.; Claffey, M.; Hastings, M.; Loudon, A. Maywood, E.; Ohren, J.; Doran, A.; Wager, T. T. Selective Inhibition of Casein Kinase 1 Epsilon Minimally Alters Circadian Clock Period. *J. Pharmacol. Exp. Ther.* **2009**, *330*(2), 430–439.

The in vivo PKs of PF-4800567 and PF-670462 were determined in C57BL/6J mice at a single 100 mg kg^{-1} subcutaneous dose. The results are shown in **Table 3**. The brain-to-plasma ratios were constant throughout the period of 24 h with an average value of 2.1 and 1.3 for PF-4800567 and PF-670462, respectively.

More recently, the efficacy of PF-670462 against alcoholism in rats was reported.[70] CK1ε/δ inhibition with PF-670462 decreased the alcohol deprivation effect dose-dependently and prevented alcohol intake during the days following treatment.

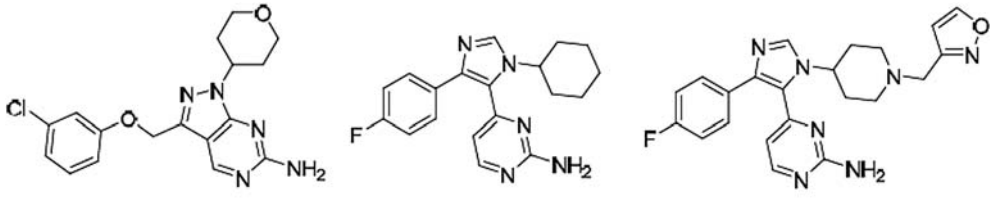

PF-5006739 is another CK1δ/ε inhibitor.[71] The crystal structure of the complex of PF-5006739 and CK1δ has revealed that the aminopyrimidine moiety binds to residue Leu85 in the hinge area by two-point hydrogen bonding. PF-5006739 exhibited potency against CK1δ and ε at a nanomolar range (CK1δ $IC_{50} = 3.9$ nM; CK1ε $IC_{50} = 17$ nM) in enzymatic assays and in whole cell screening ($EC_{50} = 15.2$ and 83 nM, respectively). PF-5006739 exhibited P_{app} value of 22×10^{-6} cm s^{-1} in permeability assay. Its MDR1 efflux ratio is 3.2. The maximum free concentration of PF-5006739 in the mouse brain was estimated to be 117 nM, with sufficient free drug exposure to cover the whole cell EC_{50} at a 10 mg kg^{-1} subcutaneous dose. PF-5006739 also demonstrated in vivo responses downstream of CK1δ/ε inhibition. It dose-dependently modulated circadian rhythm in both nocturnal and diurnal animal models.

7.10.5.7 Mixed-Lineage Kinase

Mixed lineage kinases (MLKs) are members of a large family of MAPK kinase kinases that activate MAPKs, including JNK, ERK 1/2, ERK5/BMK1, and p38.[72] MLK3 is the most widely expressed MLK family member. It is expressed in neurons and activates a neuronal cell death signal transduction pathway.[73,74] Inhibition of MLK3 has been a strategy for the prevention or treatment of neurodegenerative diseases such as AD and PD.[75,76]

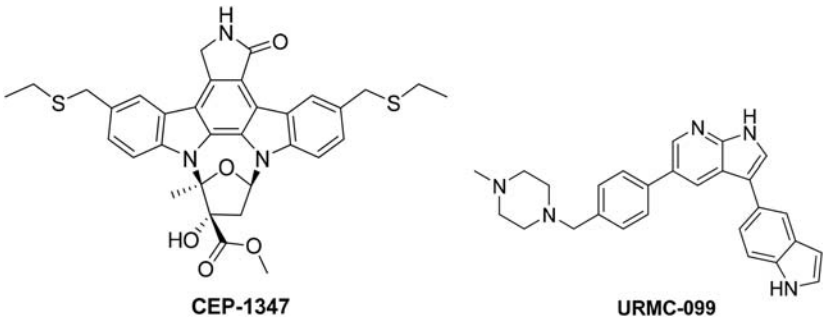

CEP-1347 is a semisynthetic inhibitor in the MLK family. As a tool compound, it demonstrated the promotion of neuronal survival at dosages that inhibit activation of the JNKs in primary embryonic cultures and differentiated PC12 cells after trophic withdrawal in animal models.[77–84] CEP-1347 was advanced into clinical investigation stage and was found to be safe and well tolerable

Table 4 Blood–brain barrier penetration data of URMC-099 (C-57/BL/6 mice, i.v., 10 mg kg^{-1})

	Concentrations (ng mL^{-1} in plasma and ng g^{-1} in brain) (min)			*Brain/plasma ratio*		
Sample	*30*	*60*	*180*	*30*	*60*	*180*
Plasma	4163	2920	1167	0.68	0.77	0.81
Brain	2833	2249	950			

Reproduced from Marker, D. F.; Tremblay, M. È.; Puccini, J. M.; Barbieri, J.; Gantz Marker, M. A.; Loweth, C. J.; Muly, E. C.; Lu, S. M.; Goodfellow, V. S.; Dewhurst, S.; Gelbard, H. A. The New Small-Molecule Mixed-Lineage Kinase 3 Inhibitor URMC-099 Is Neuroprotective and Anti-inflammatory in Models of Human Immunodeficiency Virus-Associated Neurocognitive Disorders. *J. Neurosci.* **2013**, *33*(24), 9998–10010.

during 4 weeks in PD patients. Unfortunately, it failed to show efficacy in phase II clinical trials for early stage PD.[85] The brain exposure of CEP-1347 was not reported. However, the undesired properties such as high molecular weight (MW = 615) could limit its BBB penetration.

URMC-099, a new MLK3 inhibitor, possesses more favorable CNS drug-like properties with molecular weight of 421 Da, c log *P* of 3.8, c log *D* of 2.5, and PSA of 51 $Å^2$.[86] As a result, this agent exhibited excellent brain penetration in mice at an intravenous (i.v.) dose of 10 mg kg^{-1}. The brain and plasma levels were measured at three time points utilizing averages from three mice per time point (Table 4). The brain/plasma ratios across the three time points are fairly consistent. In addition, further PK evaluation in mice indicated that this agent displayed the clearance rate of 1.8 L $h^{-1}kg^{-1}$, volume of distribution of 5.6 L kg^{-1}, terminal half-life of 2.1 h, and bioavailability of 41%. This potent (IC_{50} = 14 nM) compound inhibits LPS-induced TNFα release in microglial cells, human immunodeficiency virus 1 (HIV-1) Tat-induced release of cytokines in human monocytes, and the upregulation of phospho-JNK in Tat-injected brains of mice. The antiinflammatory and neuroprotective effects of URMC-099 in multiple murine and rodent models of HIV-associated neurocognitive disorders were also demonstrated.[87]

7.10.5.8 Death-Associated Protein Kinase 1

Death-associated protein kinase (DAPK1) is a serine/threonine protein kinase that participates in apoptotic cell death, growth factor signaling, and autophagy.[88,89] It consists of a protein kinase domain, a calcium–calmodulin binding region, an ankyrin repeat domain, two putative P loops, a cytoskeletal binding region, and a death domain.[90] Emerging evidence suggests that elevated DAPK1 activity is linked to neuronal injury, such as ischemic injury and seizure-related injury.[91–93] Therefore, DAPK1 has been proposed as a target in CNS drug discovery and several DAPK1 inhibitors have been identified recently (3–6).[94–97] All these compounds, however, are in an early stage of the drug discovery process. No brain penetration data were reported and no DAPK1 inhibitors are in clinical investigation to date.

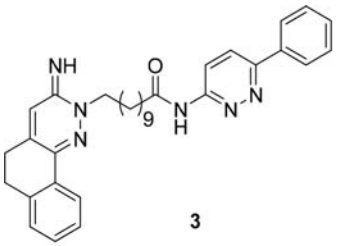

3

DAPK IC_{50} = 13 μM

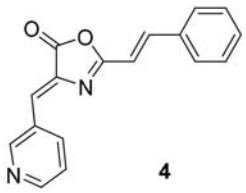

4

DAPK1 IC_{50} = 69 nM

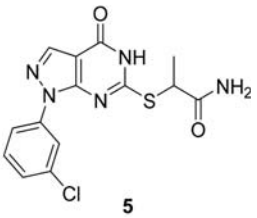

5

DAPK1 IC_{50} = 200 nM

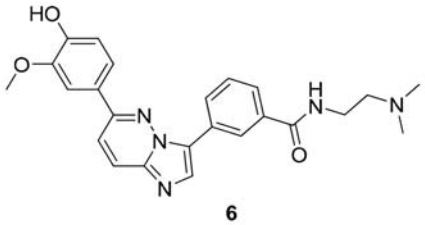

6

DAPK1 IC_{50} = 250 nM

7.10.5.9 Glycogen Synthase Kinase 3

In the late 1970s, two constitutively active isoforms of glycogen synthase kinase 3 (GSK3), with 98% homology in their catalytic domains, were identified in mammals: GSK3α and GSK3β.[98] The expression of GSK3 isoforms was found with greater abundance

in the brain compared to other tissues. GSK3 was originally identified as one of the kinases that modulates the activity of glycogen synthase (GS) for the conversion of glucose to glycogen.[99] Other kinases involved in the deactivation of GS are PKA, AMPK, and CK2. Upstream signaling, including the insulin or Wnt pathways, controls the activity of GSK3. GSK3α is inactivated by phosphorylation at Ser21 while GSK3β is inactivated at Ser9. The initial recognition of GSK3's regulation of GS suggested the possibility of using GSK3 inhibitors for treating diabetes mellitus type 2. Other therapeutically useful indications by the inhibition of GSK3 include bipolar disorder, inflammation, neuropathic pain, cancers, and fragile X syndrome (FXS).[100–104] However, much of the research focus was toward identifying GSK3 inhibitors for neurodegenerative AD.[105,106] The pathological link between GSK3 and AD was suggested when the involvement of GSK3β isoform in Tau protein phosphorylation was discovered. One of the histological hallmarks of AD is the formation of neurofibrillary tangles (NFTs) and intraneuronal aggregates of paired helical filaments. Hyperphosphorylation of Tau protein at the microtubule-binding motif by GSK3 leads to Tau protein aggregation (formation of NFTs) and microtubule destabilization within brain cells. Other important functions of GSK3 within the CNS include the regulation of the neuronal network's synaptic plasticity that may have an effect on depression, memory, and learning. In light of the multiple biological functions of GSK3β in the brain, the effort to identify clinically useful brain-penetrant GSK3β inhibitors has been intensified in the past few years. Although most of the inhibitors reported in the literature were claimed GSK3β selective, the selectivity between GSK3α and GSK3β isoforms is minimal because of the high homology of their kinase domains. Developing an isoform-selective GSK3β kinase inhibitor presents great challenges and pan-GSK inhibitors may not be disadvantageous. The first GSK3 inhibitor identified was lithium, which has been used to safely treat bipolar disorder for over 60 years. Readers who are interested in the history of using lithium for the treatment of bipolar disorder are referred in Refs. [107,108]. Over the years, numerous GSK3 inhibitors have been reported. The following section will focus on the recent development of potent synthetic small molecule GSK3 inhibitors with disclosed data on brain penetration.

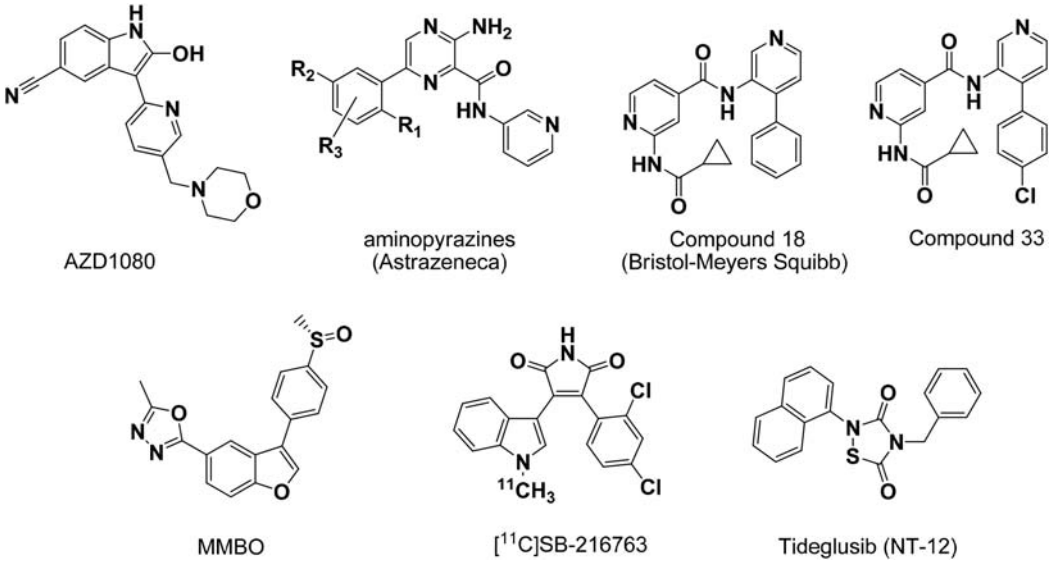

AstraZeneca reported a low-molecular-weight (MW = 334 g mol^{-1}) GSK3 inhibitor, AZD1080, which was in the phase I clinical trial targeting AD.[109] In an animal model, AZD1080 was able to rescue synaptic plasticity deficits in rodent brains after animals were challenged with a low dose of MK-801 (a N-Methyl-D-Aspartate (NMDA) blocker for behavioral testing). The ability of AZD1080 to penetrate the BBB was evaluated using an in vitro bovine endothelial cell assay. The high permeability (8×10^{-3} cm min^{-1}) of AZD1080 determined in the assay predicted that AZD1080 could achieve significant brain exposure in vivo. A PK/PD study in a rat model with AZD1080 with the administration of 3 and 10 μmol kg^{-1} of AZD1080 showed a 38% and 48% maximum inhibitory effect of tau phosphorylation (Thr-231) in hippocampus at 6 h. AZD1080 could achieve a 0.5–0.8 brain-to-plasma ratio at C_{max} in rats. Although AZD1080 possessed two HBDs; its other physicochemical properties were within the range for a good brain penetrant (e.g., MW = 334). The morpholine moiety of AZD1080 could help improve drug solubility and brain penetration. Tertiary amines are one of the common structural elements that can be found in numerous CNS pharmaceuticals. Unfortunately, further development of AZD1080 was halted due to nephrotoxicity observed in a phase I clinical trial.[107]

Another different chemotype targeting GSK3 reported by AstraZeneca was aminopyrazine.[110] The same in vitro bovine endothelial cell assay was used to evaluate the compound's brain penetration ability. Given the presence of an amino group on a pyrazine core and an amide functionality (both can act as HBDs), poor permeability was expected. However, good measured permeability in both Caco-2 and bovine endothelial cell assays was observed. These data suggest that the masking of the HBDs through intramolecular interaction could be beneficial for both oral absorption and brain penetration. Although compounds in this pyrazine series were identified with good in vitro permeability, in vivo confirmation of their brain-to-plasma ratio was not reported.

Recently, researchers at Bristol-Meyers Squibb reported a bis-amide series of GSK3 inhibitors.[111] In their case, a vinblastine-resistance carcinoma (KBV) cell line with overexpression of human tau protein was used in compounds profiling for target activity

and permeability. Using the same cell line in assays with or without a P-gp inhibitor (tariquidar), the compound's permeability was evaluated and used as guidance for predicting brain penetration efficacy. Compounds with efflux ratio >2 were believed to have a low chance for good brain penetration. An amide is reported as one of the structural moieties that favors P-gp efflux because amide compounds tend to have more HBDs and a high polar surface area. It was interesting that most of the compounds reported in the bis-amide series had a high passive permeability and efflux ratios <2, despite the presence of two amide functionalities in the scaffold. Several lead compounds, such as compounds 18 and 33, were tested in vivo in a transgenic mouse AD model with elevated pTau levels. At oral doses of 10 and 30 mg kg^{-1}, both compounds showed dose-response activity and brain-to-plasma ratios of 0.2–0.3 and ≥ 0.5, respectively. The liability associated with those compounds was high PK variability probably due to their high clearance and the metabolic instability in mouse plasma. However, the same instability was not observed in human plasma.

A benzofuran scaffold GSK3 inhibitor, MMBO, was published by researchers at Takeda focusing on AD.[112,113] MMBO was classified as a brain-penetrant potent GSK3 inhibitor superior to lithium. An oral dose of 3 mg kg^{-1} of MMBO in C57BL/6N mice showed a brain-to-plasma ratio (AUC) = 1.6. In addition, MMBO showed a dose-dependent in vivo efficacy and the measured Tau phosphorylation (pT205-tau) in the hippocampus of mice was decreased maximally after 30 min of dose administration, which corresponded to T_{max}. The physicochemical properties of low molecular weight (338), tPSA (60 $Å^2$), and without HBDs were all in favor of MMBO being a good brain penetrant.

For a successful CNS drug development program, it is key to quantify compound's brain exposure for a PK/PD/efficacy correlation. A commonly used technique to quantify tissues drug exposure is the use of radiotracers in positron emission tomography (PET). Some GSK3 inhibitor PET tracers had been reported and they had demonstrated limited BBB penetration. Their unfavorable physicochemical properties for brain penetration such as their high PSA and/or the presence of an excess number of HBDs might be the culprit for the observation. Recently, Aigbirhio et al. reported a successful case study using [^{11}C]SB-216763 as a brain-penetrant GSK-3 inhibitor radiotracer.[114] The arylindole maleimide SB216763 is a potent GSK-3 inhibitor with $K_i = 9$ nM and $IC_{50} = 34$ nM. PET imaging study in a nonhuman primate showed SB216763 to have significant brain uptake and the highest exposure is in thalamus, striatum, cortex, and cerebellum areas in the brain. Uniform distribution of the radiotracer within the brain revealed by PET imaging also suggests the ubiquitous distribution of GSK3 in brain tissue.

Tideglusib (NT-12) is the most advanced GSK3 inhibitor ever reported in a phase II clinical trial.[115,116] Evidence has indicated that tideglusib is an irreversible non-ATP-competitive GSK3 inhibitor. Preclinical models have confirmed that tideglusib could decrease tau phosphorylation and lower brain amyloid plaque. Although no PK data have been released on tideglusib to understand its brain penetrative ability, the small MW and high lipophilicity may predict a favorable brain exposure. Recent data release from the ARGO phase II study showed that tideglusib had an acceptable safety profile but unfortunately, no clinical benefit was observed in this trial for AD.

Over the past years, many GSK3 inhibitors with different scaffolds and inhibition modes have been developed. However, candidates successfully moved into clinical trials were scarce. The negative results in the recent clinical trial observed in tideglusib suggested that there are challenges ahead to validate anti-GSK3 as an intervention point for treating neurodegenerative disorders such as AD.

7.10.5.10 Rho-Associated Protein Kinase

Rho-associated protein kinases (ROCKs) are the downstream effectors of the small GTPase RhoA.[117] A recent review by Feng gave a comprehensive summary for a large number of ROCK inhibitors developed in the past decades.[118] Two isoforms, ROCK I and II, were identified as ~160 kDa serine/threonine kinases. The expressions of both ROCKs are considered ubiquitous, but a higher expression of ROCK II was found in the brain compared to ROCK I. ROCK's kinase activity is auto-inhibited by its carboxy terminal. Interaction with GTPase RhoA activates ROCKs by binding to the Rho-binding domain located in the coiled-coil region of ROCK proteins and conformational changes release the auto-inhibitory carboxy terminal from the kinase domain. A number of downstream effectors of ROCKs have been identified and their biological functions on smooth muscle cell contraction, cell proliferation, adhesion, and migration have been delineated. Because of the important functions of ROCKs in the regulation of the cytoskeleton of cells, ROCK inhibitors have been proposed for the treatment of cardiovascular, respiratory, and renal diseases including hypertension, asthma, chronic obstructive pulmonary disease (COPD), inflammatory bowel disease, glaucoma, age-related macular degeneration, optical nerve and spinal cord injuries, stroke, and AD. In 1995, Japan approved the first ROCK inhibitor Fasudil (Eril®) for the treatment of cerebral vasospasm, followed by China in 2010 for the same indication.[119] Fasudil was notably the first small molecule kinase inhibitor approved for clinical use 40 years later after the discovery of protein kinases in 1954. In 2014, another structurally similar ROCK inhibitor, ripasudil, reached the market place for very different indications. Ripasudil (Glanatec®) was approved, also in Japan, as a twice daily dosing eye drop for glaucoma and ocular hypertension treatment. Research in developing ROCK inhibitors has been intensified in the past decade and numerous ROCK inhibitors have been reported either in preclinical or in different phases of clinical trials.[120] The most advanced AR13324 is in phase III for the same indications as for ripasudil. Some examples of other ROCK inhibitors currently in clinical trials are KD-025, Y39983, AT13148, LX-7101, and a few others. Although ROCK inhibitors have successfully been proven for some clinical use, continuous systemic inhibition of ROCKs may be problematic. Major safety concerns related to systemic ROCK inhibition include the induction of significant hypotension and a reversible reduction in lymphocyte counts. ROCK I, but not ROCK II, is believed to be related to the observed toxicity. Almost all reported inhibitors are pan-ROCK inhibitors, with the exception of KD-025 which shows higher inhibitory activity for ROCK II.

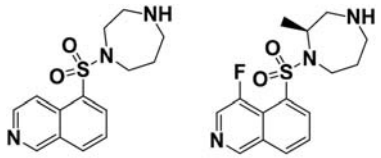

The biological functions of ROCKs related to the CNS have been explored in the last decade.[121,122] The RhoA/ROCK signaling axis regulates myelin-associated axon growth inhibitors, including Nogo, myelin-associated glycoprotein, oligodendrocyte-myelin glycoprotein, and repulsive guidance molecule. Following nerve injuries or developing neurological disorders, ROCKs are activated and neurite growth is inhibited. Inhibiting ROCK's signaling may abolish the effects of the axon growth inhibitors and promote axonal growth for recovery. On this basis, ROCK inhibitors may be therapeutically important for the treatment of some neurodegenerative disorders and brain/spinal cord injuries.

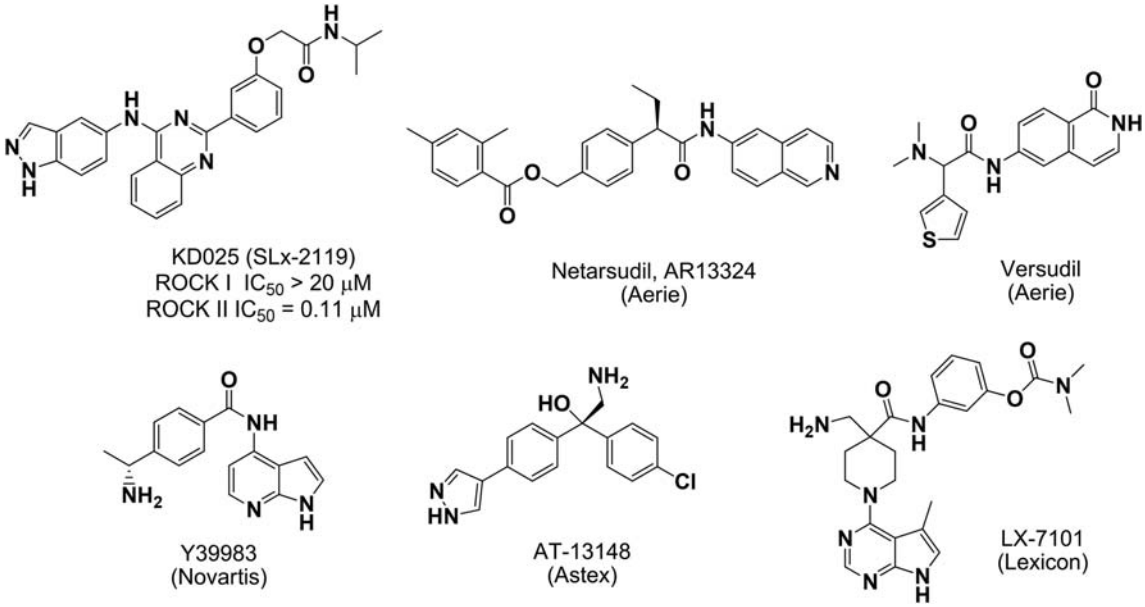

Although therapeutic effects have been demonstrated in animal models for targeting ROCK inhibition in numerous CNS diseases, successful use of ROCK inhibitors in clinical trials for CNS-related neurodegenerative diseases has yet to be reported. One probable reason may be the toxicity related to ROCK I inhibition and the fact that designing a ROCK II isoform-selective inhibitor is extremely challenging. Currently, SLx-2119 (KD-025) is the most advanced ROCK II isoform-selective inhibitor designed by researchers at Surface-Logix Inc. in order to reduce the ROCK I-related toxicity (e.g., hypotension). KD-025 is about 200-fold more potent against ROCK II ($IC_{50} = 105$ nmol L^{-1}) compared to ROCK I ($IC_{50} = 24$ μmol L^{-1}). Since the physicochemical properties and in vivo data of those ROCK inhibitors were not detailed in any publications, their CNS penetration could not be evaluated. The marketed drug Fasudil has been reported to have therapeutic effects against several CNS disorders in clinical and animal models. However, Fasudil was found to have low brain penetration and special strategies, such as liposome preparation, myelin injection, or prodrug, to enhance CNS penetration have been exploited for CNS targeting. The aforementioned ROCK II-selective inhibitor KD-025 was recently studied in focal cerebral ischemia in mice.[123,124] At a dose of 100 mg kg^{-1}, total KD-025 concentration (AUCs) in plasma and brain tissue are 51.93 and 2.37 (h μg mL^{-1}), respectively. Although the peak level of KD-025 in plasma and brain tissue is more than 10-fold of the ROCK II IC_{50}, inhibitors with a significantly higher free plasma-to-brain ratio are more desirable. Until the CNS penetration and selectivity issues can be properly addressed with newer ROCK II-selective inhibitors,[9] intervening in the ROCK signaling pathway in the clinical setting for the treatment of medically unmet CNS-related disorders such as AD and PD will remain challenging.

7.10.5.11 p38 Mitogen-Activated Protein Kinase

Cellular signaling through one of the three major MAPK (ERKs, JNKs, p38s), the cytoplasmic p38 MAPK, is activated in response to stress stimuli and proinflammatory cytokines (e.g., interleukins and TNFα). The importance of p38 MAPK as a therapeutic target in inflammatory diseases and cancer has been recognized since 1994 soon after it was first isolated and characterized as a 38 kDa protein, which regulates proinflammatory cytokine syntheses. The rationale of using p38 MAPK inhibitors as therapeutics has been the focus of

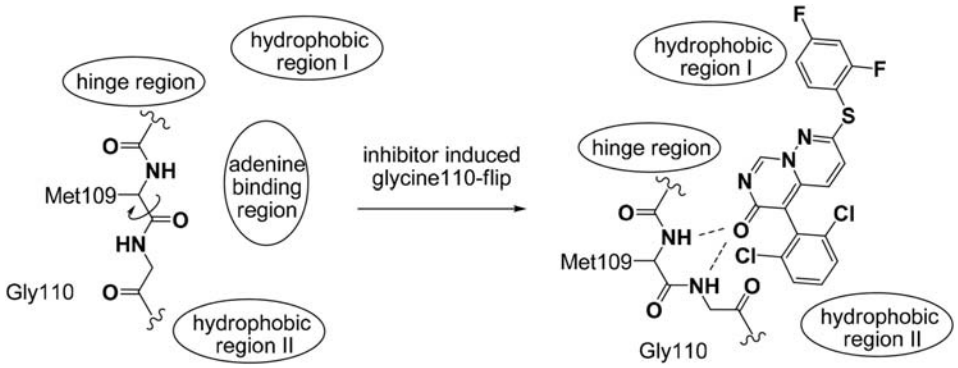

Fig. 5 Gly110 flip induced by inhibitor binding to the ATP-binding pocket. Reproduced from Fischer, S.; Koeberle, S. C.; Laufer, S. A. p38a Mitogen-Activated Protein Kinase Inhibitors, a Patent Review (2005–2011). *Expert Opin. Ther. Pat.* **2011**, *21* (12), 1843–1866.

several excellent reviews.[125–130] The original development of p38 inhibitors was motivated by an interest in targeting peripheral inflammatory diseases such as RA, cancer, and COPD.[131,132] However, the efficacy of p38 MAPK inhibition is compromised by the observation that a feedback loop mechanism, which led to the activation of other proinflammatory pathways, such as JNK. In addition, studies have shown that p38 MAPK may act as a tumor suppressor in some cell types and its inhibition may cause tumorigenesis. Recent understanding of several CNS disease pathologies suggested that the activation of p38 MAPK was responsible for disease progression. Proinflammatory cytokines produced *via* p38α MAPK activation are implicated in CNS ailments such as Alzheimer disease (AD), PD, multiple sclerosis (MS), neuropathic pain, neuronal injury, and depression.[133–139] In Alzheimer's disease, for example, hyperphosphorylation of the Tau protein by p38α MAPK is thought to cause Tau protein aggregation (formation of NFTs), which leads to microtubule destabilization within brain cells. Recently, the p38α MAPK signaling pathway was suggested to be important for effecting CNS axons myelination and remyelination in diseases such as MS and periventricular leukomalacia.[140]

The p38 MAPK has four isoforms (α, δ, γ, δ). Based on sequence homology, the four isoforms can be separated into two groups, group I (α and β) and group II (γ and δ). The most studied isoform p38α is mainly responsible for the biosynthesis of proinflammatory cytokines. Over the past 20 years, extensive efforts by major pharmaceutical companies and smaller outfits have produced numerous p38α MAPK inhibitors for preclinical and clinical testing. For a clinically useful p38α inhibitor, besides selectivity among other off-targets, the main hurdle was to achieve selectivity over other p38 isoforms. Up-to-date, small molecule p38α MAPK inhibitors involved interaction with the ATP-binding pocket and selectivity was achieved with a design using three key strategies. The first and the most selective strategy involved the use of the so-called glycine flip with Gly110 at the hinge (Fig. 5). When a suitable hydrogen bond acceptor (e.g., a carbonyl) of the inhibitor was directed toward Gly110 within the hinge motif, the glycine's amide bond (HBD) rotated to engage a hydrogen bond with the carbonyl of the inhibitor. Such a bond flip along the hinge region is only possible for a small amino acid such as glycine; hence, it imposed a high selectivity of the inhibitor among other kinases. The second approach for a selective inhibitor design made use of a Aspartic acid-Phenylalanine-Glycine (DFG)-pocket in an inactive state of the enzyme. When an enzyme was in its inactive state (DFG-out), the DFG motif rotates outward into the ATP-binding pocket. An inhibitor designed with an extended moiety could occupy the space vacated by the DFG motif. The third strategy involved the use of p38's gatekeeper residue, Thr160. The small amino acid Thr160 in p38 allowed the designs of inhibitors with substituents large enough to reach the hydrophobic region I. Kinases with larger gatekeeper residues would not accommodate such inhibitors. Summarized in the following sections are different chemotypes which use the three aforementioned methods for the design of selective p38α MAPK inhibitors. The availability of p38 X-ray crystallographic structural data also facilitated the design of novel inhibitors. Drug discovery efforts targeting p38α MAPK were mainly focused on targeting peripheral diseases such as RA. Unfortunately, a p38α MAPK inhibitor has not achieved regulatory agency approval for such a disease indication. Toxicity appears to be the main reason for their clinical failure.

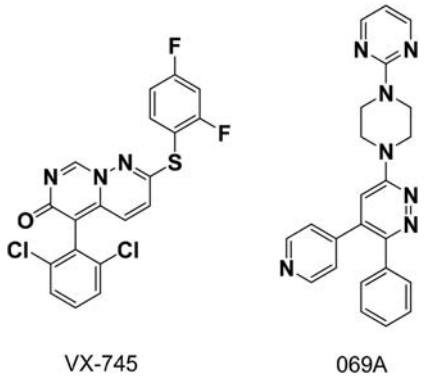

VX-745 069A

Due to earlier p38α MAPK inhibitors, which showed signs of CNS toxicity in a preclinical animal study, nonbrain-penetrant p38α MAPK inhibitors have been the focus in the past decades and less effort was dedicated to CNS. CNS toxicity was reported in a dog study for VX-745, and the development of the compound was discontinued in the early 2000s. Interestingly, VX-745 reemerged recently as an effective tool to target AD. EIP Pharma reported a preclinical study using VX-745 as an antagonist to modulate the effects of microglia-mediated inflammatory responses related to p38α MAPK activation.[141] The total drug concentration of VX-745 brain-to-plasma ratio is about 1.7 in rats after a single oral dose. The same brain-to-plasma ratio was also observed in dogs after 2 weeks of dosing with VX-745. In the same dog study, a $K_{p,uu,csf}=2$ was achieved. The low molecular weight (MW = 436), polar surface area (tPSA = 45), and the absence of HBDs all favor VX-745 as a brain penetrant.

In 2007, Munoz et al. reported a brain-penetrant p38α MAPK inhibitor 069A with a pyridazine scaffold.[133] Experimental values of lipophilicity and aqueous solubility were used to predict brain penetration of newly designed compounds. The experimentally determined c log *P* and solubility for 069A were 3.18 and 9.54 μg mL^{-1}, respectively. The solubility value of 9.54 μg mL^{-1} translated to a log *S* = −2.02 and a c log *P* = 3.18 are both within the preferred range for good brain penetration. In addition, compound 069A has MW = 395, tPSA = 68, and with no HBDs. All of these physicochemical properties of 069A support its being a good brain penetrant. In an in vivo efficacy study using an AD-relevant mouse model, compound 069A was able to suppress excess proinflammatory cytokine upregulation (IL-1, TNFα, and S100B) and improved neurological outcome was observed. Comparable total exposure of 069A to both plasma and the brain tissue was observed after an oral dose of 2.5 mg kg^{-1} to C57Bl/6 mice.

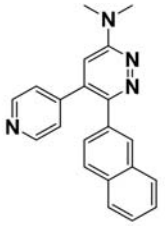

MW-108
p38α MAPK Ki = 114 nM
Kp (brain/blood) = 0.9

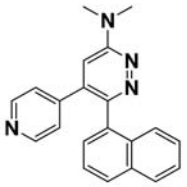

MW-181
p38α MAPK Ki = 114 nM
Kp (brain/blood) = 0.7

A similar brain-penetrant pyridazine-based chemical probe p38α inhibitor MW-108 was reported by Watterson et al. in a study of synaptic dysfunction in neurodegenerative diseases.[142] MW-108 is a selective p38α small molecule inhibitor with favorable CNS drug-like physicochemical properties (MW = 326; cPSA = 41.9; c log *P* = 3.4). In a PK study, a brain-to-blood ratio of 0.9 was achieved at C_{max} after an oral dose. A similar analog MW-181 (MW = 326; cPSA = 41.9; c log *P* = 3.4) with an isomeric naphthalene substitution also showed good penetration (brain-to-blood ratio = 0.7). In an in vivo animal model relevant to AD, attenuation of $A\beta_{42}$-induced synaptic and cognitive dysfunction by MW-108 administration was observed.

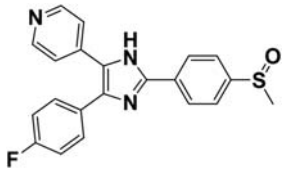

SB203580

A trisubstituted imidazole SB203580 has been the most investigated tool compound in preclinical CNS disease models.[134] However, the imidazole core was believed to be the culprit for severe hepatotoxicity and different scaffolds were used in later inhibitor designs. Drug delivery to the CNS was also limited for the trisubstituted imidazole series and resorted to unconventional dosing routes. I.c.v./intrathecal/osmotic infusions into cisterna magna were reported to have been used in those studies.

Very few p38α MAPK inhibitors have ever been advanced into clinical trials to target CNS diseases.[143] A few compounds related to pain treatment and major depressive disorders were tested in phase II/III clinical trials but subsequent development was discontinued. The development of p38α MAPK inhibitors for the treatment of RA has been slowed by the lack of clinical efficacy and toxicity associated with the drug candidates. Another disease focus for p38α MAPK inhibitors is for COPD. With more specific tissue delivery of the inhibitors, systemic toxicity observed with early generation compounds could be minimized. Targeting CNS diseases with p38α MAPK inhibitors is still in its infancy, and more understanding of the underlying biology associated with those CNS diseases related to the p38α signaling pathway is needed. Developing more brain-penetrant p38α MAPK inhibitors in the future will no doubt be very helpful but challenging.

7.10.5.12 Polo-Like Kinase 2

The Polo-like kinases (PLKs) family consists of five members (PLK1–5).[144] They belong to the serine/threonine protein kinase family primarily expressed in dividing cells and are essential in cell cycle control and in the regulation of mitosis. Unlike

PLK1–4, PLK5 is different in that it lacks a functional kinase domain and is not involved in cell cycle control.[145] All PLKs possess binding motifs called "polo-boxes," which interact specifically with their corresponding substrates.

The most studied member, PLK1, was a key kinase in directing mitotic entry, centrosome maturation and separation, formation of the bipolar spindle, transition from metaphase to anaphase, and the initiation of cytokinesis. Not only being overexpressed in a number of human tumor tissues, PLK1 is also activated in response to DNA damage and replication stress.[146–151] Since the biological function of PLK1 is key to cell division, the inhibition of PLK1 signaling is expected to have an antimitotic effect on rapidly dividing tumor cells. In addition, embryonic lethality was observed in PLK1 knockout mouse.

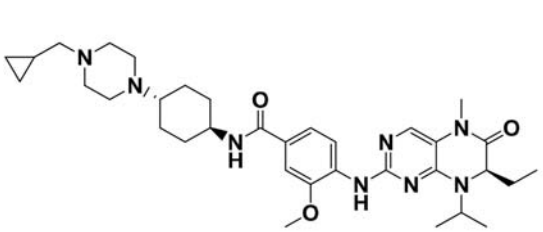

Volasertib (BI-6727)

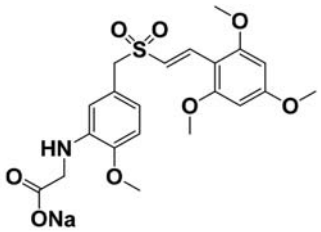

Rigosertib (ON-01910)

Several PLK inhibitors have entered clinical trials and two of them have recently reached phase III clinical trials for hematological malignancies, including Acute Lymphoblastic Leukemia (ALL), acute myeloid leukemia (AML), Chronic Lymphocytic Leukemia (CLL), Chronic Myeloid Leukemia (CML), and myelodysplastic syndrome (MDS).[152–154] Volasertib, in combination with cytarabine, is being evaluated in older patients with AML who are ineligible for intensive induction therapy. Rigosertib, a dual PLK/PI3K inhibitor, is being investigated in patients with MDS. Clinical observations however showed PLK1 inhibitors inevitably causing undesirable myelosuppressive toxicities. In this regard, more isoform-selective PLK inhibitors were needed as useful therapeutic agents. More importantly, different members in the PLK family have been suggested to have opposite functions. For example, the function of PLK1 is inhibited as a consequence of DNA damage-induced ATM signaling while PLK3 is activated by the same signal.

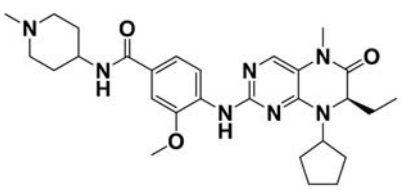

BI-2536

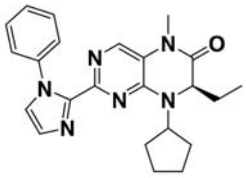

compound 9

Besides oncology, PLKs have been implicated in certain neurodegenerative diseases. One member of the PLKs family, Polo-like kinase 2 (PLK2), is of special interest for targeting CNS diseases.[155] PLK2 is believed to play an important role in the neurological disorder, PD. Phosphorylation of α-synuclein at Ser-129 represents one of the key proteins in the pathology of PD, and PLK2 has been implicated as a major contributor to the formation of phosphor-S129 α-synuclein. α-Synuclein is a major component in Lewy bodies, which was found in intracytoplasmic dopaminergic neurons. Lewy bodies are considered the prime histological marker for PD. The design of isoform-selective PLK2 inhibitors is essential for targeting CNS diseases to avoid the potential toxicity associated with PLK1 inhibition in dividing cells. Because of the high homology of PLK isoforms, developing an isoform-selective PLK2 inhibitor for the treatment of PD is very challenging. Researchers at Boehringer Ingelheim first reported a selective PLK inhibitor, BI-2536, which showed > 10,000 fold selectivity against a panel of other kinases. Unfortunately, PLK1/PLK2 selectivity was not achieved with BI-2536 (PLK2/PLK1 selectivity = 0.10). Scientists at Elan Pharmaceutical later analyzed the crystal structure of BI-2536 bound to PLK2, which revealed that selectivity could be achieved by exploiting the PLK2-specific gatekeeper + 2 Tyr-161 residue in the kinase ATP-binding pocket (**Fig. 6**).[156–157] Different heterocyclic rings at C2 of the pteridinone core achieved optimization of PLK2 selectivity over other PLK isoforms. Crystal structure analysis showed an edge-to-face interaction between the C2-heteroaryls and Tyr-161, which improved both the compound's PLK2 activity and their selectivity against PLK1 and PLK3. Based on the crystal information, two similar chemical series, a pteridinone and a tricyclic pteridinone, were reported as PLK2 isoform-selective inhibitors.

In the first report, design criteria favoring metabolic stability and CNS penetration were included. Design criteria included are: (1) incorporation of fluorine atoms, (2) lowering the compounds' c log *P* to improve metabolic stability, (3) selecting compounds with high permeability and low P-gp efflux for favorable CNS penetration. Ultimately, optimization resulted in compound 10 (PLK2/PLK1 selectivity = 193) as a brain-penetrant PLK2-selective inhibitor, which showed in vivo activity. In a rat model, compound 37 was able to reduce phospho-S129 α-synuclein by 41–45% at 6 h after a single oral dose of 100 and 200 mg kg^{-1}. The brain-to-plasma level at 6 h was determined to be 0.36 and 0.28 at 100 mg kg^{-1} and 200 mg kg^{-1}, respectively. The total drug

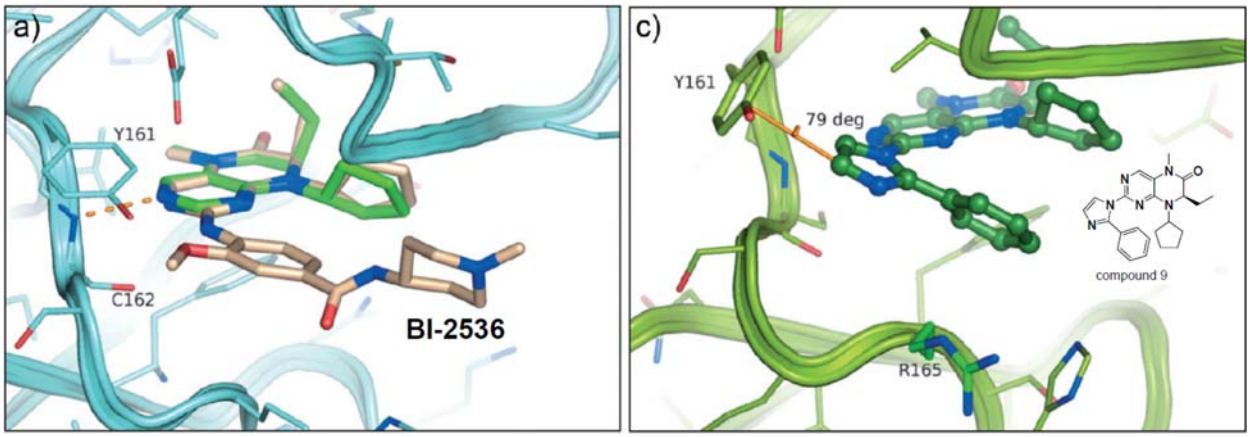

Fig. 6 Binding of BI-2536 and Compound 9 to PLK2. Reproduced from Aubele, D. L.; Hom, R. K.; Adler, M.; Galemmo, R. A., Jr.; Bowers, S.; Truong, A. P.; Pan, H.; Beroza, P.; Neitz, R. J.; Yao, N.; Lin, M.; Tonn, G.; Zhang, H.; Bova, M. P.; Ren, Z.; Tam, D.; Ruslim, L.; Baker, J.; Diep, L; Fitzgerald, K.; Hoffman, J.; Motter, R.; Fauss, D.; Tanaka, P.; Dappen, M.; Jagodzinski, J.; Chan, W.; Konradi, A. W.; Latimer, L.; Zhu, Y. L.; Sham, H. L.; Anderson, J. P.; Bergeron, M.; Artis, D. R. Selective and Brain-Permeable Polo-Like Kinase-2 (Plk-2) Inhibitors That Reduce a-Synuclein Phosphorylation in Rat Brain. *ChemMedChem* **2013**, *8* (8), 1295–1313. (a) Plk-2 protein is shown with cyan carbon atoms, the structure of BI2536 in pink, (c) Compound 9: PDB code 4I6F, 2.9 Å resolution, showing the corresponding edge-to-face angle.

exposure at these two dosing levels was well above the PLK2 cellular IC_{50} value. Unfortunately, the free drug concentration and $K_{p,uu}$ were not available.

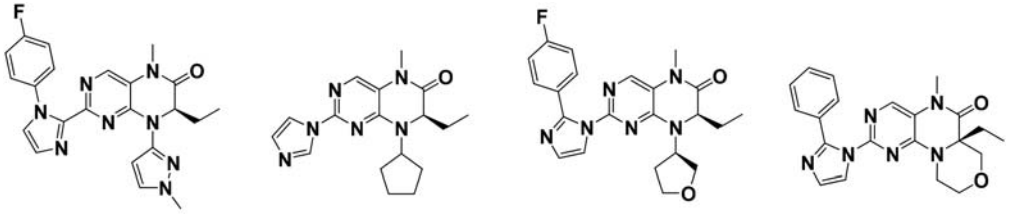

Another PLK2-selective inhibitor based on a tricyclic pteridinone was detailed in a second publication by the same group at Elan.[157] After optimization, three short-listed compounds (11, 12, and 13) were evaluated in vivo for brain exposure in mouse (i.v.) and PK in rat (i.v./p.o.). Compounds 11, 12, and 13 showed total brain/plasma AUC ratios of 1.7, 0.03, and 0.3, respectively. Taking into account of other DMPK parameters, the tricyclic pteridinone, compound 13, was identified with high PLK2 potency ($IC_{50} = 39$ nM) together with a PLK2/PLK1 selectivity ratio = 700. A subsequent target engagement (phospho-S129 α-synuclein) study with a single oral dose of compound 13 in rats at 100 or 200 mg kg^{-1} resulted in 34.5% and 41.4% decrease of phospho-S129 α-synucleins level, respectively, in the cerebral cortex. Although the free drug concentrations of the compound were not reported, the total concentration of compound 13 in the rat brain at 6 h was fivefold (@100 mg kg^{-1}) and sevenfold (@200 mg kg^{-1}) higher than the PLK2 IC_{50} value. With the properties of a non-P-gp substrate with good permeability and oral bioavailability, compounds 10 and 13 have become useful tools to aid the understanding of the role of PLK2/α-synuclein system in the pathology of PD.

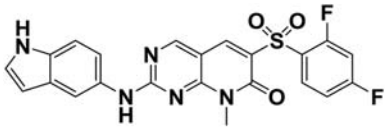

ON1231320
PLK2 selective
(Onconova)

Recently, another PLK2-selective chemotype, pyrido[2,3-d]pyrimidine, was reported by researchers at Onconova Therapeutics.[158] Phenotypic screening of a library of compounds using cell death as a readout identified ON1231320 as a PLK2-specific small molecule inhibitor. The identified isoform-selective PLK2 inhibitor ON1231320 caused apoptotic cell death in cultured tumor cell lines and showed significant tumor growth inhibition in a triple-negative breast tumor xenograft model (MDA-MB-231). Since the inhibitors reported by the authors are primarily targeting peripheral human tumors, CNS exposure information for this class of PLK2-selective inhibitors is not available.

In addition to PLK1 and PLK2, the structurally distinct isoform PLK4 (with only one polo-box instead of two) was also found to be overexpressed in triple-negative breast cancer with basal-like subtype and upregulation of PLK4 causes centriole overduplication.[159,160] Several potent and selective PLK4 inhibitors have been reported and tumor growth inhibition was observed in a preclinical mouse xenograft model with a triple-negative breast cancer cell line (MDA-MB-468). The rest of the PLKs—PLK3 and PLK5—are considered to be tumor suppressors and they regulate cellular responses to DNA damage and cellular stress. No selective PLK3 and PLK5 inhibitors have been reported. In the past few years, most PLK inhibitors were developed for oncology focusing on peripheral diseases and their brain penetration levels were not reported. However, it would be beneficial to patients if some of the developed PLK inhibitors could penetrate the CNS in order to treat metastatic tumors therein.

7.10.5.13 p21-Activated Kinase

p21-activated kinases (PAKs), a family of serine/threonine kinases, were identified as effectors of small GTPase-activating proteins such as Ras-related C3 botulinum toxin substrate 1 (Rac1) and cell division control protein 42 (Cdc42) in 1994.[161] The PAKs are classified into two subgroups (group I: PAK1–3; group II: PAK4–6) based on protein sequence and structural homology.[162] Expression of PAK in different tissues was characterized in rodents and it was found that PAKs are expressed at significant levels in the brain. Activation of PAK occurs *via* the binding of Rac1 or Cdc42 to their N-terminal regulatory domain (the CRIB motif). Research has suggested that PAK plays important roles in both neurodegenerative diseases and cancers. Historically, group I PAK1–3 have been the main focus of the research community and much of the understanding of PAK biology was from PAK1–3. Because of the important roles of group 2 PAK4–6 in many fundamental cellular processes, recent research focus on PAK4–6 is on oncology indications.[163–165]

In neurodegenerative diseases such as Alzheimer disease (AD), dysregulation of PAK1 and PAK3 is associated with the buildup of amyloid (Aβ) extracellular plaques and intraneuronal NFTs. Huntingtin protein aggregation is enhanced by PAK1 activity in HD. Abnormal activation of PAK1 is also related to a family of genetic diseases called neurofibromatosis caused by dysfunctional NF1/NF2 genes.[166] PAK3 gene mutations found in fetal and adult brain tissues are believed to be responsible for X-linked mental retardation. FXS, a form of mental illness, was recently found to be related to the activation of the RAC/PAK signaling.[167] In some human tumor cells, PAKs are overexpressed and amplified, which transduce signal *via* Ras, Raf, NFκB, Akt, Bad, and p53 to effect cell proliferation, survival, anti-apoptosis, and invasion. As the biological roles of PAKs become clearer in relation to the aforementioned diseases, therapeutic intervention with selective PAK inhibitors might be a useful strategy.[168]

Paradoxically, some PAK activities were recently found to have a positive impact in some disease settings where compounds with agonistic rather than inhibitory activity might be desirable. A recent study suggested that the inhibition of the RAC/PAK axis induced autism-like deficits in normal mice,[169] and in another study, PAK1/2 kinase activity was shown to be essential for neurite growth.[170] The cardiac protective function of PAK1 was also recently highlighted in an animal study.[171] PAK1 may function in preventing arrhythmogenesis associated with ischemia/reperfusion injury.

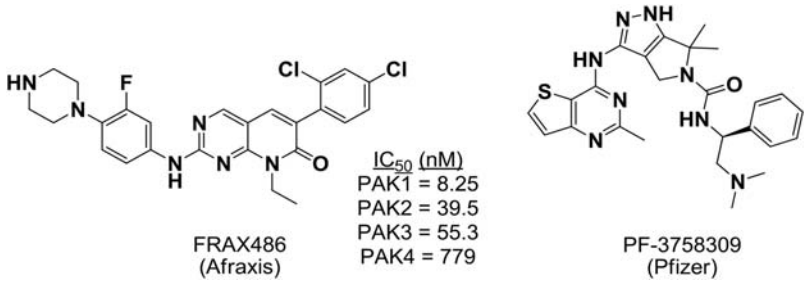

Recently, Rudolph et al. published a perspective review on the current status of PAK inhibitors.[162] Most reported structural types are ATP-competitive binders and only a few allosteric PAK inhibitors have been identified so far. The only PAK inhibitor with reported CNS penetration information is FRAX486, which was developed by Afraxis to study FXS in *Fmr1* KO mice.[167] FRAX486 is a pyrido[2,3-d]pyrimidine-7-one derivative with selectivity against group I PAK1–3. The subcutaneous injection of a dose of 20 mg kg^{-1} FRAX486 to mice achieved PAK1,2,3 coverage in the brain of about 36, 7.6, and 5.4 folds, respectively, based on the total drug concentration. In addition, FRAX486 can achieve total drug concentration in the brain tissue that is higher than in plasma (**Fig. 7**). However, the free fractions of the compound in the brain tissue and in plasma were not reported in this study to reveal the $K_{p,uu}$ value. Nevertheless, an injection of FRAX486 was able to reverse the phenotypes in the *Fmr1* KO mice model for FXS in a dose-dependent manner.

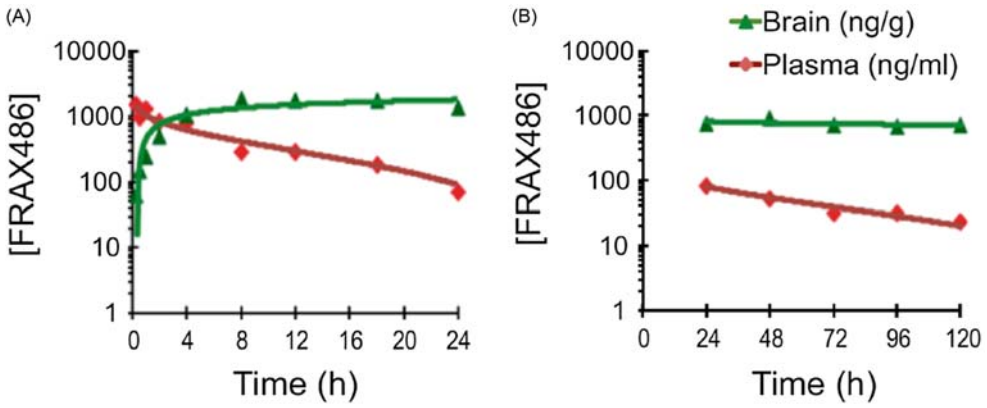

Fig. 7 Pharmacokinetics of FRAX486. (A) A single s.c. injection; (B) daily administration of 20 mg kg^{-1}. Adapted from Dolan, B. M.; Duron, S. G.; Campbell, D. A.; Vollrath, B.; Shankaranarayana Rao, B. S.; Ko, H. Y.; Lin, G. G.; Govindarajan, A.; Choi, S. Y.; Tonegawa, S. Rescue of Fragile X Syndrome Phenotypes in Fmr1 KO Mice by the Small-Molecule PAK Inhibitor FRAX486. *Proc. Natl. Acad. Sci. USA* **2013**, *110*(14), 5671–5676.

Although the importance of PAKs in CNS diseases as mentioned earlier has been proposed, the majority of the PAK inhibitors reported are antitumor agents, including both group 1 and 2 PAKs. For example, researchers at Pfizer focused on designing potent PAK4 inhibitors with a pyrroloaminopyrazole scaffold targeting colon, ovarian, and pancreatic tumors.[172,173] PF-3758309 (PAK4 $K_d = 2.7$ nM) was advanced into phase I clinical trials for solid tumors but was eventually discontinued due to poor human PKs. Optimization to increase permeability and reduce the efflux ratio due to P-gp-mediated efflux were the focus of the design of the next-generation compounds; however, no brain penetration data of the newly designed compounds were reported.

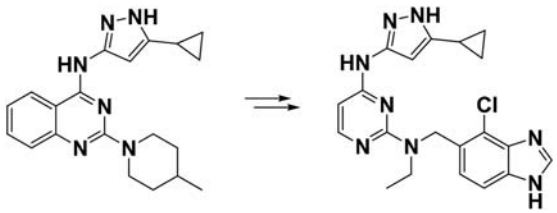

14
PAK1 Ki = 100 nM
PAK4 Ki = 49 nM

15
PAK1 Ki = 5 nM
PAK4 Ki = 547 nM

The Genentech group focused on developing selective PAK1 inhibitors for the luminal B subtype of breast cancer, which is known to have focal amplification of PAK1. Structure Activity Relationship (SAR) development was described in detail for improving PAK1 selectivity over Group 2 PAKs.[174,175] Starting with PAK4-selective lead compound 14, replacing the quinazoline core in 14 with a pyrimidine scaffold and changing the piperidine to a substituted benzimidazole, the researchers were able to identify compounds which are PAK1-selective inhibitors as demonstrated in compound 15. Most compounds reported therein have an efflux liability, which may impede their brain penetration ability. Interestingly, the highlighted compound 15 is not a P-gp substrate (MDCK P_{app} AB:BA = 7.4/11.1). Further optimization of this series is needed to minimize off-target activity against Aurora A. Although many kinase inhibitors are primarily developed against peripheral tumors as shown in this section and other sections, brain metastasis is one of the reasons for treatment resistance in certain types of cancers such as in lung and breast carcinomas. Developing a kinase inhibitor that has sufficient brain penetration will undoubtedly be beneficial for patients who have developed brain metastasis.

7.10.5.14 Dual Leucine Zipper Kinase

Dual leucine zipper kinase (DLK, MAP3K12), one of the upstream regulators of JNK, has recently been proposed as an alternative target for treating neurodegenerative diseases, such as Alzheimer's and Parkinson's.[176] The expression of DLK is neuronal-specific and animal models have demonstrated that DLK plays an important regulatory role in neuronal degeneration. Genentech researchers conducted a high-throughput screening using an enzymatic inhibition assay of DLK kinase domain catalytic activity followed by a measurement of p-JNK levels in a DLK overexpressed cell-based assay for lead identification.[1] Based on the physicochemical properties required for brain penetration, compound 16 was selected for optimization.

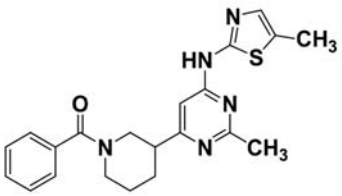

16
DLK IC_{50} = 0.035 μM
p-JNK IC_{50} = 0.641 μM
MDR1 BA/AB = 2.2; AB = 4.3 X10^6 cm s^{-1}

ClogP and ClogD = 3.9
LipE = 3.6
tPSA = 71
cpKa = 6.8
HBD = 1
MW = 398
CNS MPO score = 4.2

Lead optimization was focused around replacing the potential toxicophore aminothiazole and reducing metabolic liability. Including design parameters, such as maintaining PSA < 80 Å^2, avoiding HBD, and adjusting basicity, can lead to favorable brain penetrants. The aminothiazole moiety was successfully replaced by 2-amino-4-cyanopyridine with a slight loss in potency. Modification of the central pyrimidine core to pyridine reduced tPSA by more than 10 units. Further optimization on compound 17 by replacing the benzamide moiety with an oxetane gave a potent DLK inhibitor compound 18 (GNE-3511) with desirable PK properties (Table 5). The oxetane was essential for reducing the basicity of the piperidine nitrogen to reduce efflux liability.

In a PTP (1-methyl-4-phenyl-1,2,3,6-tetrahydropyridine)-induced phosphorylation of c-Jun PD model, a dose-dependent reduction of p-c-Jun positive neurons was observed in brain tissue with compound 18. PK analysis in rodents showed that compound 18 is brain penetrant with a $K_{p,uu} = 0.7$ in rat at 6 h (Table 6). Compound 18 was the first selective DLK inhibitor reported with in vivo brain penetration activity so far. The availability of tools like compound 18 will allow for a better understanding of the DLK biology and its implication in neurodegenerative diseases.

Table 5 DLK inhibitors

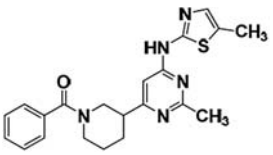

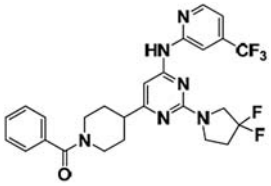

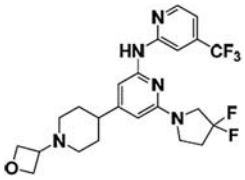

	16	*17*	*18 (GNE-3511)*
K_i (nM)	35	33	< 0.5
p-Jun IC_{50} (nM)	641	300	30
tPSA	71	74	77
LM CI_{hep} (mL $min^{-1} kg^{-1}$) H/R/M	na	16/32/75	13/29/76
MDR1 BA/AB (AB $\times 10^6$ cm s^{-1})	na	na	2 (6)

Reproduced from Patel, S.; Cohen, F.; Dean, B. J.; De La Torre, K.; Deshmukh, G.; Estrada, A. A.; Ghosh, A. S.; Gibbons, P.; Gustafson, A.; Huestis, M. P.; Le Pichon, C. E.; Lin, H.; Liu, W.; Liu, X.; Liu, Y.; Ly, C. Q.; Lyssikatos, J. P.; Ma, C.; Scearce-Levie, K.; Shin, Y. G.; Solanoy, H.; Stark, K. L.; Wang, J.; Wang, B.; Zhao, X.; Lewcock, J. W.; Siu, M. Discovery of Dual Leucine Zipper Kinase (DLK, MAP3K12) Inhibitors With Activity in Neurodegeneration Models. *J. Med. Chem.* **2015**, *58*(1), 401−418.

Table 6 PK properties of DLK inhibitor 18[a]

Species	*CL_p (mL $min^{-1} kg^{-1}$)*	*V_{dss} (L kg^{-1})*	*$T_{1/2}$ (h)*	*F (%)*	*B_u/P_u*[b]	*CSF/P_u*[c]
Mouse	56	2.5	0.6	45	0.24 at 6 h	–
Rat	30	3.7	1.8	63	0.7	0.4
Dog	41	6.5	4	32	–	0.4
Cynomolgous	16	3.1	2.4	19	–	0.6

[a]Compounds were dosed i.v. (1 mg kg^{-1}) as a 60% PEG solution and p.o. (5 mg kg^{-1}) as an aqueous suspension with 1% methylcellulose.
[b]Unbound brain/unbound plasma AUC (unless noted otherwise).
[c]CSF/unbound plasma AUC ratio.
Reproduced from Patel, S.; Cohen, F.; Dean, B. J.; De La Torre, K.; Deshmukh, G.; Estrada, A. A.; Ghosh, A. S.; Gibbons, P.; Gustafson, A.; Huestis, M. P.; Le Pichon, C. E.; Lin, H.; Liu, W.; Liu, X.; Liu, Y.; Ly, C. Q.; Lyssikatos, J. P.; Ma, C.; Scearce-Levie, K.; Shin, Y. G.; Solanoy, H.; Stark, K. L.; Wang, J.; Wang, B.; Zhao, X.; Lewcock, J. W.; Siu, M. Discovery of Dual Leucine Zipper Kinase (DLK, MAP3K12) Inhibitors With Activity in Neurodegeneration Models. *J. Med. Chem.* **2015**, *58*(1), 401−418.

7.10.5.15 Tropomyosin Receptor Kinase

Tropomyosin receptor kinases (Trks) are believed to be possible druggable targets for both neurological diseases and cancers.[177] There exist three Trk isoforms (TrkA, TrkB, and TrkC). Each Trk isoform is activated by its own ligands. Ligands such as nerve growth factor, brain-derived neurotropic factor and neurotrophin-4/5, and neurotrophin-3 activate TrkA, TrkB, and TrkC, respectively. Several Trk isoform-selective inhibitors have been reported but no related CNS penetration data are available. The development of Trk-selective brain-penetrant PET ligands can help understanding of target distribution in brain tissue and target occupancy by inhibitors. Recently, brain-penetrant 3-indolydene 4-aza-2-oxindole-based [^{11}C] and [^{18}F] radiolabeled ligands against Trk have been reported.[178] Several design parameters related to brain penetration were considered: (1) BBB permeation and neuroreceptor imaging binding potential (ideally BP $= B_{max}/K_d > 10$), (2) molecular weight (MW) ≤ 305, (3) calculated distribution coefficient (c log $D_{7.4}$) in the range of 2.0–3.5, (4) topological polar surface area of 30–80 Å^2, and (5) HBD ≤ 1. Eventually, potent pan-Trk inhibitors [^{11}C]-19 and [^{18}F]-20 were chosen as the early generation ligands for development as Trk PET probes.

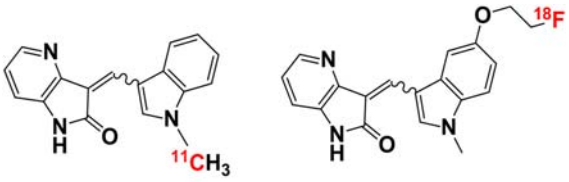

(*E*)/(*Z*)-[^{11}C]-**19**
[^{11}C]-GW441759

(*E*)/(*Z*)-[^{18}F]-**20**

PET imaging studies in rodents with compounds 19 and 20 showed high level of brain uptake but nonspecific distribution within the CNS. Obvious drawbacks with compounds 19 and 20 are the isomeric alkene functionalities in addition to the metabolic instability of the "labeled" alkyl groups. Thus, further structural optimization may be necessary to provide better tools to improve the understanding of Trk biology in the CNS.

7.10.5.16 Epidermal Growth Factor Receptor

NSCLC accounts for more than 85% of all lung cancer cases and is one of the leading causes of cancer death worldwide.[179] It is estimated that in 2014 there were 224,210 new lung cancer cases and 159,260 NSCLC related deaths in the United States alone.[180] Genetic aberrations in the tyrosine kinase domain of EGFR have been identified as one of the key drivers of NSCLC progression.[181] EGFR kinase inhibitors, such as gefitinib, erlotinib, and afatinib, deliver significant patient benefit and have been approved for the treatment of advanced NSCLC with EGFR activating mutations.[182–185]

An increased incidence of CNS metastases has been reported as patients live longer with treatment and with the improvement of imaging technology and routine screening.[186,187] Studies have suggested that around 40–50% of patients with lung cancer will develop CNS metastases, including brain metastases and leptomeningeal metastases, in their life span.[188,189] Currently approved drugs can neither effectively treat lung cancer CNS metastases nor prevent the development of metastases under standard dosing regimens, due to their limited BBB penetration of the currently marketed compounds.[190,191] For patients with symptomatic brain metastases, selective use of radiation therapy and surgery are still the mainstay of treatment, but provide limited benefit.[192,193] Given the effectiveness of EGFR TKIs in treating tumors in the lung, there is a major unmet medical need for an agent which can effectively penetrate the CNS and treat tumors in brain tissue.

In order to design a brain-penetrant EGFR kinase inhibitor, scientists at the AstraZeneca Innovation Center in China re-engineered Gefitinib, a nonbrain-penetrant EGFR kinase inhibitor, by creating an intra-molecular hydrogen bonding interaction between F and adjacent NH, reducing the polar surface area and molecular weight of the molecule, and decreasing the number of rotatable bonds to give lead compound 21 (**Table 7**).[194] As a result, good CNS drug-like properties, such as a low efflux ratio (0.33) and good permeability ($P_{app,A\ to\ B} = 32 \times 10^{-6}$ cm s^{-1}), were achieved. Encouragingly, this compound exhibited inhibitory potency (IC_{50}) at 3.8 and 6.6 nM in PC-9 and H3255 cell line EGFR phosphorylation assays, which were comparable to that of gefitinib (at 6.2 and 6.5 nM, respectively). Furthermore, compound 21 demonstrated an acceptable human CYP450 inhibition profile ($IC_{50} > 10$ μM for CYP2C9, CYP2D6, and CYP3A4) and low hERG inhibition liability (hERG $IC_{50} = 17$ μM, patch clamp assay). More importantly, the preferred CNS drug-like properties of the compound translated into much improved brain and CSF penetration ($K_{puu,brain}$ and $K_{puu,CSF}$ were 0.47 and 0.76, respectively). Furthermore the compound showed reasonable exposure in both brain and blood ($AUC_{0-7\ h}$ at 2 mg kg^{-1} were 1013 and 834 nM h, respectively). The excellent in vitro potency and promising CNS penetration results were achieved while maintaining reasonable PK properties in rats (oral bioavailability 44%, elimination half-life 1.1 h, clearance 59 mL min^{-1} kg^{-1}, and volume of distribution at steady state 2.8 L kg^{-1}).

Table 7 Properties of Gefitinib and compound 21

Compound	*Gefitinib*	*21*
Molecular weight	446.7	402.9
PSA (Å^2)	62.6	53.5
Rotatable bonds[a]	10	7
Exon 19Del pEGFR IC_{50} (nM)	6.2	4.6
L858R pEGFR IC_{50} (nM)	6.5	4.2
MDCKII–MDR1 P_{app}, A to B (10^{-6} cm s^{-1})	8.3	32
Efflux ratio	3.0	0.33
$f_{u,blood}$ (%)	3.3	7.8
$f_{u,brain}$ (%)	0.39	3.0
$K_{puu,brain}$	0.021	0.47
$K_{puu,CSF}$	0.088	0.76

[a]The rotatable bond number is calculated using the equation of $N_{rot} = N_{rot,ac} + \Sigma(size - 4 - N_{ring,ac} - N_{fused})$, where N_{rot} is the rotatable bond number in the molecule, $N_{rot,ac}$ is the number of rotatable acyclic bonds, *Size* is the size of the nonaromatic ring, $N_{rig,cyc}$ is the number of rigid bonds within the ring, and N_{fused} is the number of bonds which belong to more than one ring system.
Reproduced from Zeng, Q.; Wang, J.; Cheng, Z.; Chen, K.; Johnström, P.; Varnäs, K.; Li, D. Y.; Yang, Z. F.; Zhang, X. Discovery and Evaluation of Clinical Candidate AZD3759, a Potent, Oral Active, Central Nervous System-Penetrant, Epidermal Growth Factor Receptor Tyrosine Kinase Inhibitor. *J. Med. Chem.* **2015**, *58*(20), 8200−8215.

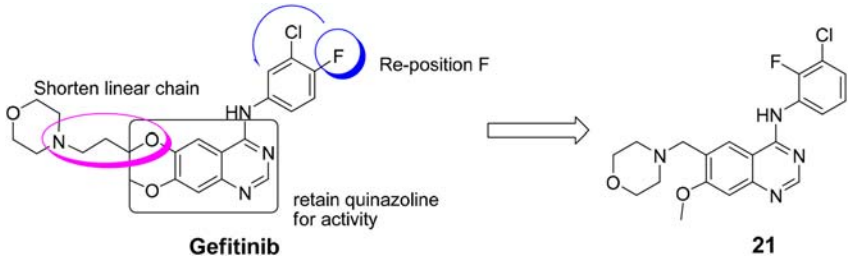

The further optimization of this compound led to the discovery of the clinical candidate AZD3759, a compound with an improved DMPK profile and enhanced brain exposure. AZD3759 achieved excellent levels of CNS penetration as demonstrated by $K_{puu,brain}$ and $K_{puu,CSF}$ around unity (both $K_{puu,brain}$ and $K_{puu,CSF}$ are 1.3). This compound possesses optimal CNS–drug-like properties, while maintaining the same binding mode as Gefitinib. It was found that the terminal basic nitrogen atom in the piperazine moiety promotes solubility and also brain penetration. AZD3759 exhibited excellent potency against EGFR activating mutants (L858R and Exon 19Del) and a good PK profile with moderate blood clearance at 17 mL min^{-1} kg^{-1} and the volume of distribution at 5.2 L kg^{-1}. The intrinsic clearance (Cl_{int}) is 11.4 μL min^{-1} 10^{-6} cells in human hepatocytes and the predicted clearance of the agent in human is 7.7 mL min^{-1} kg^{-1} by in vitro–in vivo extrapolation (IVIVe).[195,196] The liver blood flow (LBF) method with blood protein binding correction was applied to generate individual estimates of unbound human hepatic clearance ($CL_{hepatic}$) using available data from the preclinical studies in each species.[197–199] Using the LBF method, the predicted human clearance from rats is 8.1 mL min^{-1} kg^{-1}, which is very similar to that derived from IVIVe. Following oral dosing in rats at 2 mg kg^{-1}, absorption of AZD3759 was rapid with blood C_{max} of 0.58 μM achieved at 1.0 h. Subsequently, blood concentrations of AZD3759 declined mono-exponentially with a mean elimination half-life of 4.3 h, which was close to the same parameter obtained from i.v. dosing (4.1 h). The bioavailability following an oral dose in rats was 91%.

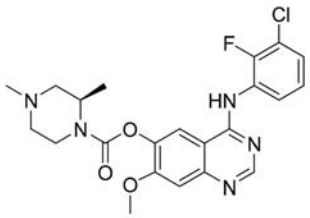

AZD3759

L858R pEGFR IC_{50} = 7.2 nM
Exon 19Del pEGFR IC_{50} = 7.4 nM
$K_{puu,brain}$ = 1.3
$K_{puu,CSF}$ = 1.3

To substantiate the PK and CNS penetration data in rats, the brain distribution of AZD3759 was further investigated in monkeys by microdosing PET.[200] Radio-labeled [^{11}C]-AZD3759 (0.28 μg, 150 MBq and 0.35 μg, 155 MBq, respectively) was injected into

Table 8 Unbound brain/plasma ratio for [^{11}C]-AZD3759 in cynomolgus monkey[a]

	Injected mass and radioactivity	V_T *(mL cm^{-3})*	$f_{u,\ plasma}$ [b]	$f_{u,\ brain}$ [c]	$C_{u,\ brain}/C_{u,\ plasma}$
PETA	0.28 μg, 150 MBq	3.0	0.12	0.02	0.50
PETB	0.35 μg, 155 MBq	3.7	0.14	0.02	0.53

[a]PET microdosing studies were performed after a single dose of [^{11}C]-AZD3759 (phosphate buffered saline, pH 7.4) *via* intravenous bolus route.
[b]The unbound fraction in plasma was determined in the PET experiment using ultrafiltration.
[c]Data obtained from in vitro equilibrium dialysis of rat brain homogenate were used as an estimate of the unbound fraction in monkey brain tissue.
Reproduced from Zeng, Q.; Wang, J.; Cheng, Z.; Chen, K.; Johnström, P.; Varnäs, K.; Li, D. Y.; Yang, Z. F.; Zhang, X. Discovery and Evaluation of Clinical Candidate AZD3759, a Potent, Oral Active, Central Nervous System-Penetrant, Epidermal Growth Factor Receptor Tyrosine Kinase Inhibitor. *J. Med. Chem.* **2015**, *58*(20), 8200−8215.

two male cynomolgus monkeys (PETA and PETB, respectively). The PET distribution volume (V_T) was estimated for the whole brain region using the two-tissue compartment model. The distribution volume and estimated free brain to plasma partition coefficient ($C_{u,brain}/C_{u,plasma}$) are summarized in **Table 8**. The partition coefficient values (0.50 and 0.53 for PETA and PETB, respectively) indicated that AZD3759 penetrated extensively into monkey brain tissue. PET images (**Fig. 8**) for both monkeys also suggested that the radio-labeled compound was well distributed throughout the brain.

In late 2015 the FDA approved Tagrisso (AstraZeneca), which is an irreversible EGFR inhibitor for nonsmall lung cancer with L858R, Exon19Del activating mutants, and the T790M resistance mutation. Its clinical investigations for the treatment of brain metastases are ongoing. Recently, Bao et al. from Hansoh Pharmaceuticals reported a compound code named HS-10269 (structure not disclosed), which is also a T790M mutant active EGFR inhibitor.[201] The brain penetration results in mice of Tagrisso and HS-10269 are shown in **Table 9**.

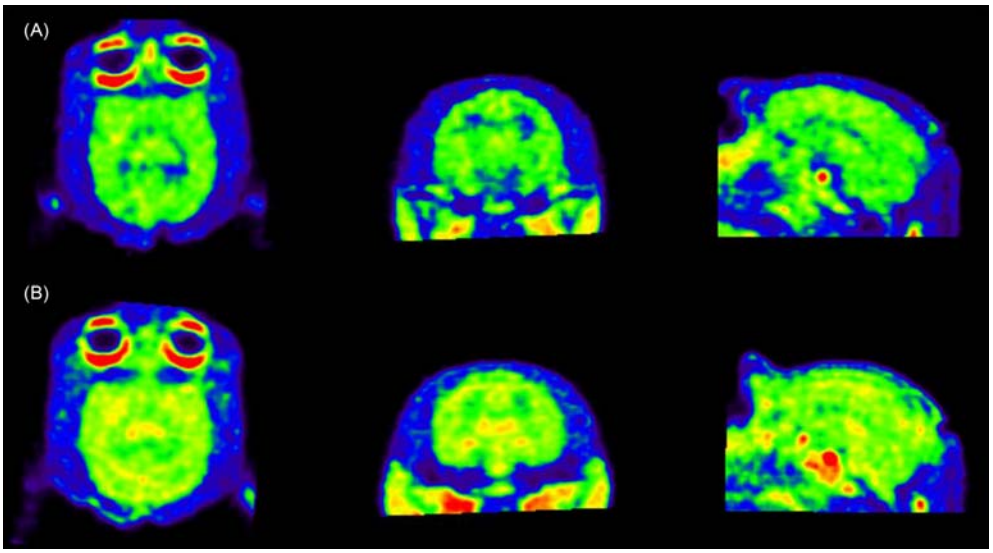

Fig. 8 Color-coded PET images showing the distribution of radioactivity in the monkey brains following administration of [^{11}C]-AZD3759. Horizontal *(left panel)*, coronal *(middle panel)*, and sagittal *(right panel)* projections for monkey PET1 (A) and monkey PET2 (B). Images created from summation images from 5 to 123 min and image intensity is normalized for injected radioactivity. Adapted from Zeng, Q.; Wang, J.; Cheng, Z.; Chen, K.; Johnström, P.; Varnäs, K.; Li, D. Y.; Yang, Z. F.; Zhang, X. Discovery and Evaluation of Clinical Candidate AZD3759, a Potent, Oral Active, Central Nervous System-Penetrant, Epidermal Growth Factor Receptor Tyrosine Kinase Inhibitor. *J. Med. Chem.* **2015**, *58*(20), 8200−8215.

Table 9 Comparison of AZD9291 and HS-10269

	EGFR enzymatic activity, IC_{50} (nM)					*Mouse @ 5 mg kg^{-1} @ 6 h*	
Compound	*Wild-type*	*L858R*	*Del19*	*L858R/T790M*	*Del19/T790M*	*Plasma (ng mL^{-1})*	*Brain (ng mL^{-1})*
AZD9291	5.55	2.26	1.21	0.46	0.29	24.2	165
HS-10269	3.39	1.5	0.88	0.29	0.21	102	139

Reproduced from Bao, R.; Gao, P.; Zhang, F.; Tong, Z.; Yu, H.; Xu, Y. Discovery of a Third-Generation EGFR Inhibitor, Which Is Highly Selective and Potent Against Both Resistant and Activating EGFR Mutations for NSCLC Therapy. In *Annual Meeting of the American Association for Cancer Research,* New Orleans, Louisiana (LA), Apr 16–20, 2016; Abstract nr 3063.

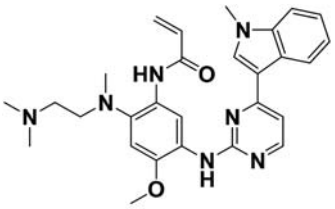

AZD9291 (Tagrisso)

HS-10269 has a similar in vitro activity profile to AZD9291 (Tagrisso). Total HS-10269 drug brain-to-plasma ratio is ~1.4 at 6 h time point, after a single dose of 5 mg kg^{-1} in mice which is lower compared to that with AZD9291 (brain-to-plasma ratio = 6.8).

7.10.5.17 Anaplastic Lymphoma Kinase

ALK, which belongs to the insulin receptor superfamily, was first discovered in 1994 and has subsequently been linked to a subtype of non-Hodgkin lymphoma.[202] Chromosomal translocation results in the expression of a fusion protein of the nucleophosmin to the truncated form of ALK, which is constitutively activated the cytoplasmic ALK kinase activity and led to aberrant downstream signaling. Lung cancer represents the highest cancer death among all cancer types and the oncogenic addiction through the ALK signaling pathway accounted for about 8% as the driver mutation in this cancer type.[203] The main ALK-related driver mutation involves a fusion protein of the N-terminal of echinoderm microtubule-associated protein-like 4 and the intracellular portion of ALK (EML4–ALK), which renders the kinase activity of the protein constitutively activated. The quest for clinically useful ALK inhibitors has intensified over the past decade.[204–208] The first ALK fusion protein kinase inhibitor, crizotinib (Xalkori), was approved by the US FDA in 2011 for the treatment of NSCLC. In addition to anti-ALK, Crizotinib also has activity against the kinases ROS and MET. Ceritinib (Zykadia), the second ALK inhibitor for the same patient group, was approved by the US FDA in 2014. Similar to crizotinib, ceritinib is also a multi-kinase inhibitor with activity against ROS. In 2015, the third ALK inhibitor Alectinib (Alecensa), also targeting crizotinib resistant patients, gained US FDA approval for treating NSCLC with ALK abnormality. Unlike crizotinib and ceritinib, alectinib is a more selective ALK inhibitor and does not act against ROS and/or MET. Although initially effective, resistance to the approved ALK inhibitors nevertheless will emerge due to mutations and/or tumor metastasis to distal organs which the current drugs show limited access. The CNS represents the most common site of metastasis and up to 60% of NSCLC patients either present with CNS disease at first diagnosis, or they eventually develop brain and/or leptomeningeal metastases during the course of therapy. Therefore, developing inhibitors, which can treat both peripheral and CNS malignancies, are urgently needed.[209]

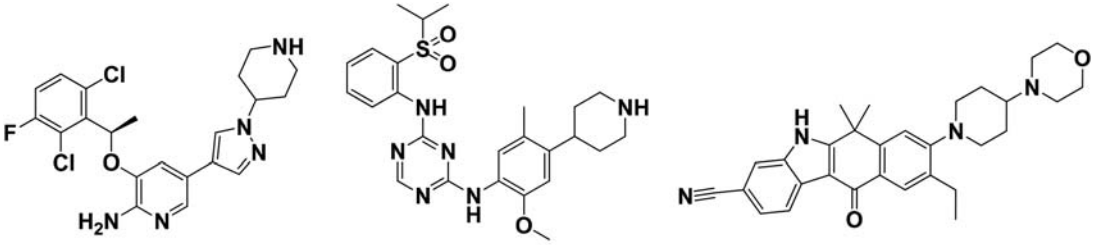

Crizotinib (Pfizer)

Ceritinib (Novartis)

Alectinib, CH5424802 (Roche)

The importance of multidrug transporters (P-gp and BCRP) in the systemic and brain availability of ceritinib was studied by Schinkel et al. Using genetic strains of P-gp and BCRP transporter knockout mice as well as the co-administration of zosuquidar (a P-gp inhibitor) and/or Ko143 (a BCRP inhibitor) with ceritinib in mice, the authors showed that the oral bioavailability of ceritinib was not significantly affected in the absence of P-gp and/or BCRP.[210] Saturation of transporters in the gastrointestinal tract by the oral administration of ceritnib might limit the effect of transporter efflux on the absorption of ceritinib, therefore resulting in oral exposure. However, the concentration of ceritinib in the mouse brain was significantly increased (62-fold) in a P-gp knockout mouse study. A double knockout of both P-gp and BCRP provided another threefold increase in ceritinib brain exposure (193-fold). The results strongly suggested that both P-gp and BCRP restrict ceritinib's access to the CNS. Importantly, the concentration of ceritinib did not show a relevant increase in either the liver or kidneys.

In a recent study by Kodama et al. with alectinib in a preclinical intracranial metastases model, alectinib showed superior antitumor efficacy compared to the first-generation ALK inhibitor crizotinib.[211–213] Both survival benefit and tumor regression were observed in the alectinib group at an oral daily dose of 60 mg kg^{-1}. The higher CNS activity of alectinib could be explained by the fact that it is not a P-gp substrate (Caco-2 B − A/A − B = 1.32) while crizotinib is a substrate for P-gp. A ^{14}C-labeled alectinib study in rats confirmed that a brain-to-plasma ratio of 0.63–0.94 was achieved at T_{max}. Comparing the physicochemical properties of all three approved ALK inhibitors, alectinib has the lowest tPSA value, the lowest number of HBDs, and the highest c log *P*, suggesting that alectinib would have the highest brain penetration of the three. Another phase I ALK inhibitor, ASP3026 (discontinued in 2014),

which is structurally similar to ceritinib, had been studied for its brain penetration by PET ^{11}C-labeling.[214,215] A quantitative measurement of [^{11}C]ASP3026 showed a higher drug concentration in tumors Standard Uptake Value (SUV = 3.0) compared to brain parenchyma (SUV = 0.8). In addition, a PK study on ASP3026 showed a brain-to-plasma ratio = 0.72 ($AUC_{0-24\ h}$) after an oral dose of 10 mg kg^{-1} in mice. In a similar experiment, a much lower brain-to-plasma ratio = 0.18 ($AUC_{0-24\ h}$) was observed for crizotinib. The higher brain penetration and tumor concentration of ASP3026 might be the result of the presence of extra basic nitrogen.

Another ALK inhibitor TAE684 (ALK IC_{50} = 3 nM; LRRK2 IC_{50} = 6.8 nM), which is structurally very similar to ASP3026, was reported to have a K_p = 2 though it did not demonstrate target modulation.[42,216,217] It was speculated that free drug concentration in the brain was not enough to cause any biological response based on the free drug hypothesis.

A recent review by Klempner et al. gave an overview of current ALK inhibitors and their CNS activity.[209] Poor CSF-to-plasma drug concentration has been reported for crizotinib and alectinib. Although intracranial responses were observed in both untreated and patients with brain metastasis who were previously treated with alectinib, the overall response rate was significantly lower than the systemic overall response rate. This might suggest suboptimal target engagement due to insufficient free drug concentration within the CNS, which hence results in disease progression.

PF-06463922, a macrocyclic analog of crizotinib, was specifically designed as an ALK-mutants active and brain-penetrant dual ALK-ROS inhibitor.[218] At the outset of the design of the next-generation brain-penetrant ALK inhibitors, transporter-mediated efflux should be minimized in order to lead to higher drug concentrations within the CNS and tumor cells. Overexpression of efflux transporters is a common resistance mechanism adopted by cancer cells to evade therapeutic agents. The expression of efflux transporters, such as P-gp and BCRP in particular, along the BBB is a way to protect the brain from exogenous contaminants. Several critical parameters, including lipophilic efficiency, log *D*, and molecular weight (MW), were incorporated into the design of new compound to achieve the goal of discovering brain-penetrant ALK inhibitors. Macrocyclic compounds provided several attributes favoring CNS Absorption, Distribution, Metabolism, and Excretion (ADME) properties, including less flexible conformation (reinforced binding), reduced number of rotatable bonds, and more compact structures compared to their acyclic counterparts. With the key structural information provided by inhibitor bound cocrystals, the novel approach of employing macrocycles was proven to be a viable strategy. The U-shaped binding conformation of crizotinib brought the halogen-substituted phenyl ring in close proximity with the pyrazole. Optimization, by forming an amide macrocycle, ultimately provided PF-06463922 as an ALK inhibitor with activity against the L1169M mutant (pALK-L1169M cell IC_{50} = 21 nM). PF-06463922 is stable in an in vitro human liver microsome assay (< 8), is highly permeable, is not a P-gp substrate [MDR ER (B − A/A − B) = 1.5], and has a log *D* value of 2.3. A preclinical rat PK study with PF-06463922 showed a half-life of 2.7 h with 100% bioavailability. At an oral dose of 10 mg kg^{-1}, PF-06463922 demonstrated a free brain-to-plasma AUC ratio = 0.21. Exposure of PF-06463922 in CSF is also significant with free CSF-to-plasma AUC ratio = 0.31 which may have an important therapeutic value for leptomeningeal metastatic cancer in the ALK disease setting. It was found that amide macrocycles in the PF-06463922 series were superior in CNS penetration compared to ether macrocycles. The amide-macrocycles display significantly lower lipophilicity (log *D* = 2–3), exhibit low clearance, and are not P-gp substrates. It was estimated that the solvent-accessible areas (SASAs) for macrocyclic compounds are about 10% less than their acyclic analogs within the same range of molecular weight. SASA has been suggested as a better descriptor for molecular size than molecular weight as a way of predicting CNS penetration. The authors also discussed analysis of > 115,000 compounds from the Pfizer compound collection with MDR BA/AB efflux ratio data. They concluded that one should focus on compounds with a log *D* range from 2 to 3 with a minimal number of HBDs, and a lower molecular weight (or SASA) in order to favor CNS penetration.

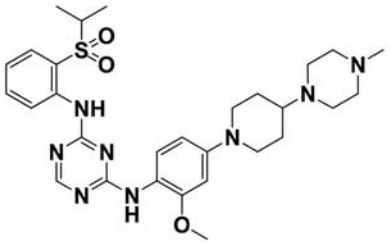

ASP3026
(Astellas)

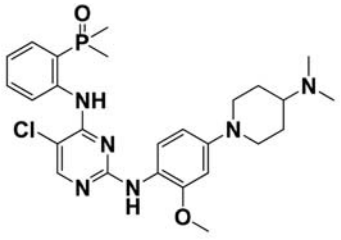

AP26113
(Ariad)

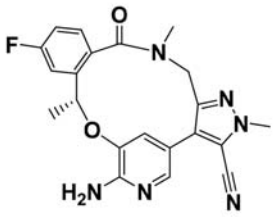

PF-06463922
(Pfizer)

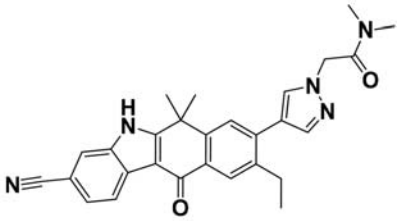

JH-VIII-157-02
EML4-ALK (WT) IC_{50} = 2 nM
EML4-ALK (G120R) IC_{50} = 2 nM
mouse brain-to-plasma ratio = 0.1

A newer generation of ALK inhibitors targeting resistance mutation continues to emerge in the literature. Although most reports provide superior activity against crizotinib resistant mutations, their brain penetration still requires improvement. Gary et al. recently disclosed an alectinib analog, JH-VIII-152-02, which targets the G1202R and other mutations, which were resistant to both alectinib and ceritinib.[219] Although JH-VIII-152-02 has good oral bioavailability and a half-life of 1.69 h, its brain-to-plasma ratio is only 0.1 at 2 h after a 10 mg kg^{-1} oral dose. Another ALK inhibitor, Brigatinib (AP26113), is now in a phase II clinical trial with a secondary objective measuring CNS response in the setting of brain metastases.[207] More understanding of the physicochemical properties of these new comers in the ALK-targeted therapeutic area will be important and helpful for designing CNS-penetrable compounds for other diseases.

7.10.5.18 Human Epidermal Growth Factor Receptor 2

The accurate measurement of free drug concentration in the CNS is important for the development of a valid PK/PD model for CNS diseases. However, developing such an accurate and reliable analytical method is not without difficulties, especially for highly protein-bound lipophilic molecules. TAK-285 (HER2 $IC_{50} = 17$ nM; EGFR $IC_{50} = 23$ nM) was a dual HER2/EGFR kinase inhibitor developed for the treatment of metastatic breast cancer with overexpression of HER2. In a preclinical animal model, microdialysis was used to determine the free drug concentration in rat brain tissue.[220,221] The adsorption of TAK-285 (>99% plasma protein bound) to the microdialysis apparatus tubing unfortunately hindered the accurate measurement of free drug concentration. Optimization of the assay protocol, by adding bovine serum albumin (4% w/v) to the perfusion fluids and using a flow rate (from 1.0 to 0.5 μL min^{-1}), allowed more reliable detection of TAK-285 in the rat brain. Using AUC curve values, the brain-to-blood ratio ($K_{p,uu,brain} = 0.24$) for unbound TAK-285 was determined. Unfortunately, further clinical development of TAK-285 targeting brain metastasis for breast cancer patients has not yet been reported.

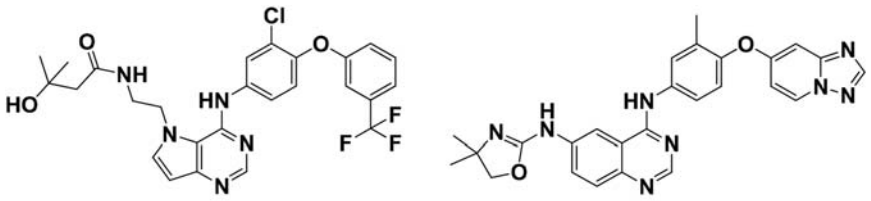

Another HER2 small molecule kinase inhibitor reported to have CNS activity is ONT-380 (original Arry-380).[222–225] ONT-380 is a selective HER2 inhibitor (HER2 $K_i = 1.8$ nM; EGFR $K_i = 72$ nM) with high selectivity against EGFR, another member in the Erbb family. A compound such as ONT-380, which has low activity against wild-type EGFR, is believed to have a better tolerability profile. Inhibition of wild-type EGFR correlated with adverse events including diarrhea and skin rashes when patients are treated with EGFR inhibitors. ONT-380 has been reported to have about a 30% overall response rate in a phase I clinical trial focusing on brain metastasis in HER2 positive breast cancer patients. Analysis of the CNS activity of ONT-380 is complicated by the presence of an active metabolite (AR00440993), which was considered to be a brain penetrant (**Fig. 9**). However, the structure of the elusive brain-penetrant metabolite was not disclosed. Further evaluation of ONT-380 in a phase II clinical trial is currently in the planning stages.

Shionogi recently reported S-222611 (structure not disclosed) as an orally active, reversible, dual EGFR/HER2 inhibitor.[226] In a preclinical study, S-222611 (25–100 mg kg^{-1}) showed better efficacy compared to lapatinib (50–200 mg kg^{-1}) in the intracranial implantation brain metastasis model with BT474 breast cancer cells. Unfortunately, no details of the brain exposure for S-222611 were included in the report; hence it is not possible to relate exposure of the drug to the observed efficacy in the CNS.

One of the greatest hurdles to developing brain-penetrant therapeutics is the lack of CNS drug exposure data in the clinical setting. In a rare instance, the drug disposition of capecitabine (and metabolites) and lapatinib in surgically resected brain metastases from metastatic breast cancer patients was investigated.[227,228] Although the results showed high variability, both capecitabine (and metabolites) and lapatinib showed significant drug concentrations in the resected brain tumor tissues from patients, even though lapatinib was classified as a nonbrain penetrant in a preclinical model, due to the fact that it is a P-gp substrate. In this study, brain tumor tissue-to-serum ratio of lapatinib in a range of 0.19–9.8 was observed.

With only a few brain-penetrant HER2 inhibitors such as TAK-285 and ONT-380 reported, further discovery of brain-penetrant HER2 inhibitors to treat breast cancer patients with HER2 overexpression and brain metastases is urgently needed.

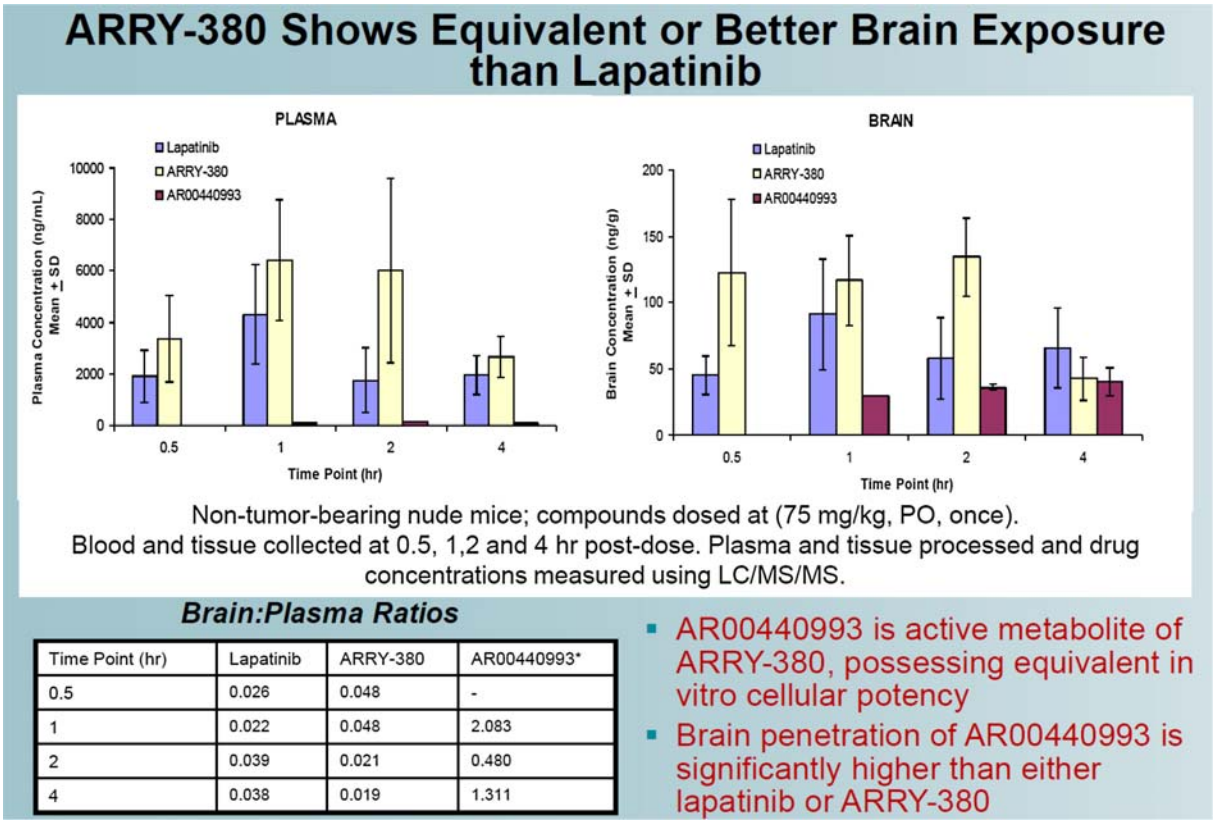

Time Point (hr)	Lapatinib	ARRY-380	AR00440993*
0.5	0.026	0.048	-
1	0.022	0.048	2.083
2	0.039	0.021	0.480
4	0.038	0.019	1.311

Fig. 9 Plasma and brain exposure of ARRY-380 and its metabolite. Adapted from Dinkel, V.; Anderson, D.; Winski, S.; Winkler, J.; Koch, K.; A. Lee, P. A. ARRY-380, a Potent, Small Molecule Inhibitor of ErbB2, Increases Survival in Intracranial ErbB2+ Xenograft Models in Mice. In *Proceedings of the 103rd Annual Meeting of the American Association for Cancer Research*, Chicago, IL, Mar 31 to Apr 4, 2012; Philadelphia (PA): AACR; *Cancer Res.* **2012**, *72*(8 Suppl): Abstract nr 852. doi:1538-7445.AM2012-852.

7.10.5.19 Phosphoinositide 3-Kinase

GBM is a form of primary brain malignancy for which therapeutic intervention is desperately in need. The current standard of care includes surgery, radiotherapy, and cytotoxic chemotherapy drugs. In GBM, aberrant PI3K signaling is implicated in more than 80% of cases. One of the common mechanisms of PI3K pathway signaling dysregulation in GBM is through PI3Kα amplification or mutations. Researchers at Genentech recently disclosed two classes of brain-penetrant pan-PI3K inhibitors originating from their nonbrain-penetrant PI3K inhibitor assets, namely the thienopyrimidine and the purine-based series.[229] Design criteria for new inhibitors were focused on reducing efflux transporter liability (P-gp and BCRP) compared to the original leads. It was demonstrated that minimizing the number of HBDs could reduce the chance of molecules becoming efflux transporter substrates (Table 10).

Throughout the lead optimization process, a CNS MPO scoring system was used to guide compound design. The MPO scoring system assigns a score between 0 (low chance of being brain penetrant) and 6 (high) to a compound based on a weighted formula from the six descriptors (c log *P*, c log *D*, MW, TPSA, HBDm, and pK_a). A correlation between high MPO scores and low efflux liability was observed in the thienopyrimidine series. Based on the design criteria and MPO scores, several compounds with good PI3Kα activity were identified and were confirmed to be brain penetrant, in vivo. It was emphasized that an "out-of-range" parameter can sometimes be compensated by other parameters included in the composite MPO scoring system and thus a compound should not be precluded from CNS penetration assessment. Eventually, compounds 22 (PI3Kα $K_{iapp} = 1$ nM) and 23 (PI3Kα $K_{iapp} = 2$ nM) were selected for in vivo study in the U-87 MG/M GBM subcutaneous xenograft model, which is a surrogate for an intracranial model. A dose-dependent inhibition of tumor growth was observed in this model, together with evidence of downstream target modulation (pAKT and pS6RP).

Table 10 SAR of hydrogen bond donor and transporter efflux for PI3Kα inhibitors

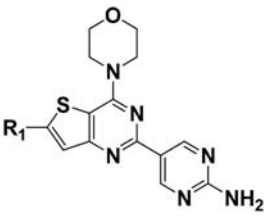

R1	*B-A/A-B (MDR1)*	*B-A/A-B (BCRP)*
	5.0	37
	0.9	3.7
	37	7.1
	1.8	1.3

Data reproduced from Heffron, T. P.; Salphati, L.; Alicke, B.; Cheong, J.; Dotson, J.; Edgar, K.; Goldsmith, R.; Gould, S. E.; Lee, L. B.; Lesnick, J. D.; Lewis, C.; Ndubaku, C.; Nonomiya, J.; Olivero, A. G.; Pang, J.; Plise, E. G.; Sideris, S.; Trapp, S.; Wallin, J.; Wang, L.; Zhang, X. The Design and Identification of Brain Penetrant Inhibitors of Phosphoinositide 3-Kinase α. *J. Med. Chem.* **2012**, *55*(18), 8007−8020.

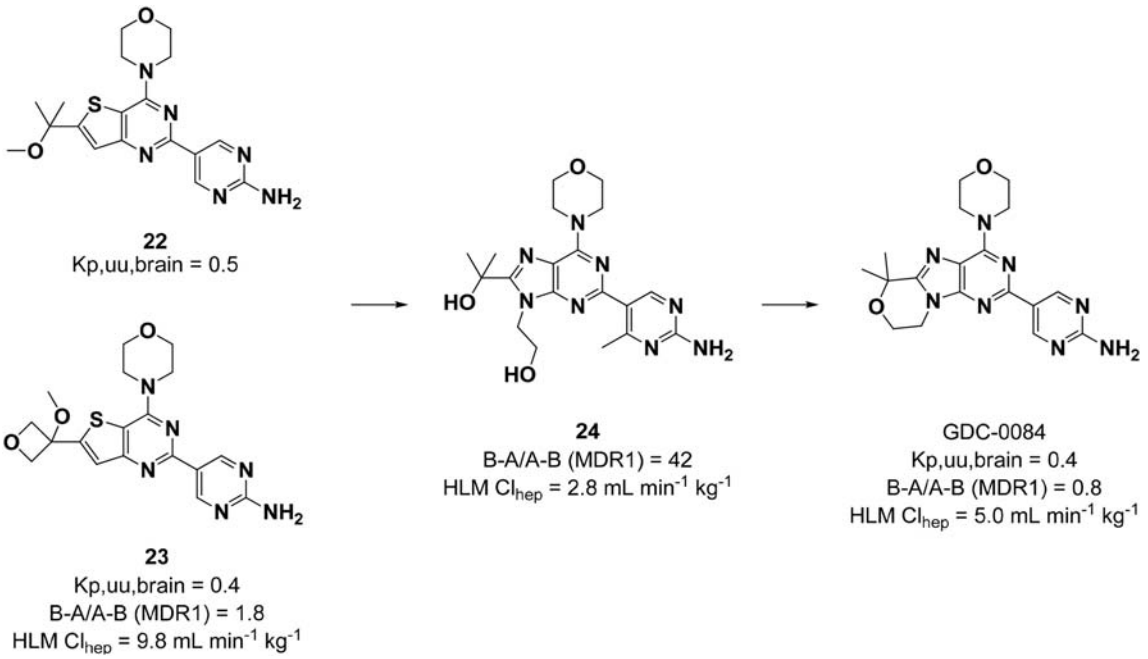

Unfortunately, the thienopyrimidine compound 23 was not further developed because it was predicted to have high clearance in humans. Recently, the same research group disclosed purine-based, brain-penetrant, scaffold of PI3Kα inhibitors which addressed the metabolic issues of the previously disclosed thienopyrimidine series.[230] Utilizing the same SAR from the thienopyrimidine series, a purine-based series with good PI3Kα potency and human microsomal stability was identified. The original concern that high PSA would adversely affect brain penetration for the purine-based scaffold was dispelled as compounds from the purine series were shown not to be P-gp or BCRP substrates, displaying low efflux ratios. Optimization of lead compound 24 (PI3Kα $K_{iapp} = 3$ nM), using the same design criteria described previously for the thienopyrimidine series, led to the development candidate GDC0084 (PI3Kα $K_{iapp} = 2$ nM). Cyclization of the hydroxyethyl substituent to the isopropanol moiety in 24, to form a tricyclic ring

system, significantly reduced the efflux liability observed with compound 24. In addition to having good metabolic stability, GDC0084 is also a good brain penetrant with $K_{p,uu,brain} = 0.4$ in mice. Dose-dependent inhibition of tumor growth was observed, and tumor regression was achieved at a daily subcutaneous dose of 17.5 mg kg^{-1} in an in vivo GBM U87 MG/M xenograft model in mice. Further evidence to support the CNS penetration of GDC0084 was demonstrated by a dose-dependent modulation of pAKT in the brain tissue of normal mice. Based on its PI3Kα activity and good pharmaceutical properties, GDC0084 was selected as a clinical development candidate for the treatment of glioblastoma, targeting the aberrant PI3K signaling pathway. Due to the current lack of effective treatment for a devastating disease like glioblastoma, a highly brain-penetrant inhibitor targeting the relevant oncogenic PI3K signaling pathway will definitely provide another option to benefit patients.

7.10.20 Ataxia-Telangiectasia Mutated Kinase

In addition to PI3Kα (5.18) mentioned earlier, another potentially important targeted therapy for glioblastoma is chemosensitization for radiotherapy. Irradiation of tumors causes both a single- and double-strand DNA break. The inhibition of the cellular repair mechanism of the damaged DNA can be lethal to all cells. ATM is one of the key components for cells to respond to such DNA damage. Thus, inhibiting ATM should sensitize tumors to radiotherapy.

Durant et al. at AstraZeneca recently presented potent inhibitors of the ATM.[231]

The original lead AZ31 is not CNS penetrant ($K_{p,uu} = 0.07$) due to its poor physicochemical properties with a high PSA = 99. AZ31 is also a P-gp transporter substrate with efflux ratio = 10.7 in a MDCK-MDR1 assay (**Table 11**). Structural modification of AZ32 focused on reducing PSA (reduce number of O-atoms) and eliminating the efflux liability (by reducing the number of HBDs) and resulted in the identification of AZ32 ($K_{p,uu} = 0.26$), which has greatly improved brain penetration. In this case, reducing the number of HBDs has a profound effect on the compound's efflux liability. Although AZ32 is less potent against ATM in the cellular assay, its physicochemical properties are another example to support the guidelines discussed previously on what makes for a good brain penetration (e.g., low MW, PSA, and not a transporter substrate). Further potency optimization in this series will provide important validation tools to test the hypothesis that ATM inhibition together with radiotherapy will be beneficial for patients with GBM.

7.10.6 Assessment of CNS Exposure in Drug Discovery

7.10.6.1 Barriers Within CNS System

Sufficient exposure at the site of action is responsible for pharmacological activity and ultimately delivers the desired therapeutic effects during the course of disease. For most organs, there is no restriction on compound diffusion between blood and extracellular space, consequently leading to a steady state of free drug equilibrium. However, the brain is separated from blood by the barriers, which regulate homeostasis and prevent the entry of exogenous and harmful compounds into the brain.[232,233] There are two important barriers to protect the brain, namely the BBB and the blood–cerebrospinal fluid barrier (BCSFB).

The BBB consists of monolayer of polarized endothelial cells, situated in the brain microvasculature, with a large surface area but tight intercellular junctions. Therefore the BBB acts as a major barrier to CNS penetration for compounds which are the subject of

Table 11 Profile of ATM inhibitors from AstraZeneca

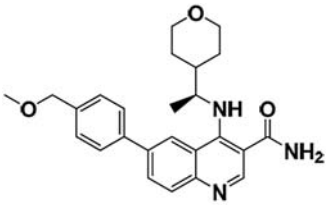

AZ31

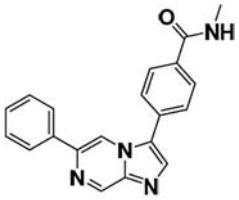

AZ31

	AZ31	*AZ32*
Potency ATM Enz IC_{50} (μM)	<0.0012	<0.006
Potency ATM cell IC_{50} (μM)	0.046	0.31
Molecular weight	421	328
Polar surface area ($Å^2$)	99	54
Efflux: MDCK–MDR1 P_{app} A–B/ER	55/10.7	33.7/0.4
Free brain: plasma ratio: $K_{p,uu}$ (mouse 2 h)	0.07	0.26

Adapted from Durant, S. T.; Karlin, J.; Pike, K.; Colclough, N.; Mukhopadhyay, N.; Ahmad, S. F.; Bekta, J. M.; Tokarz, M.; Bardelle, C.; Hughes, G.; Patel, B.; Thomason, A.; Cadogan, E.; Barrett, I.; Lau, A.; Pass, M.; Valerie, K. Blood-Brain Barrier Penetrating ATM inhibitor (AZ32) Radiosensitises Intracranial Gliomas in Mice. In *Annual Meeting of the American Association for Cancer Research*, New Orleans, Louisiana (LA), Apr 16–20, 2016; Abstract nr 3041.

transcellular diffusion. Efflux transporters in the BBB, such as P-gp and BCRP, present a hurdle to efficient brain delivery. The BCSFB creates a similar barrier at the choroid plexus epithelium, which is situated between fenestrated blood vessels and the CSF, but it is 5000 times smaller in surface area than BBB and less important with regard to drug uptake into the brain.[234,235]

Retrospective analysis of human brain exposure was performed on a set of 32 structurally diversified Pfizer candidate drugs with clinical data by Di et al. The results demonstrated that those compounds with high passive permeability, were not efflux transporter substrates and showed good CNS distribution in preclinical animals at equilibrium, predicted good human brain penetration.[236] Consistent with this, the current strategy for CNS drug discovery relies on optimizing permeability and reducing efflux across BBB in vitro. The ratio of unbound drug in brain to unbound drug in plasma was used to determine the extent of in vivo brain penetration in rodents, which allows optimization cycles to balance physiochemical properties for favorable CNS penetration and achieve high unbound brain concentration. Additionally, brain PKs provides guidance design of subsequent pharmacological studies and thereafter enhances the understanding of target engagement. Integrated approaches are established to build SAR and to design compounds with favorable physiochemical properties and therefore identify compounds with an optimal extent of brain penetration.

This section does not give a full overview of all the techniques and models available today, but focuses on the assays widely used across the pharmaceutical industry and some of the new techniques available due to recent advances in technology.

7.10.6.2 In Vitro Methodology to Identify Permeability and Efflux Liability at BBB

BBB permeability is expressed in the same units (mL $min^{-1}g^{-1}$ brain) as cerebral blood flow (CBF), which will limit the maximal amount of compound delivered to the brain.[237] Obviously, compounds with low passive permeability tend to have low free brain exposure given that most systemically exposed drugs will be carried away by CBF if drug permeability is less than CBF, 0.15–0.6 mL $min^{-1}g^{-1}$ brain.[238] For example, mannitol has low passive permeability, less than 1 μL $min^{-1}g^{-1}$ brain, and consequently shows a low $K_{puu,brain}$ (0.01). In contrast, caffeine (not P-gp substrate) with a passive permeability of 13 μL $min^{-1}g^{-1}$ brain shows a much better $K_{puu,brain}$ (1.0).[239] It has been reported that 46 of 48 CNS drugs have an apparent permeability of greater than 15×10^{-6} cm s^{-1}, and non-CNS drugs show a sevenfold higher incidence of having permeability $< 15 \times 10^{-6}$ cm s^{-1}.[240] Thus, this cut-off value has been recommended by the authors to help predict CNS candidates. However, data accumulated so far suggest that permeability criteria have been considered as one of the important parameters to be optimized during the screening cascade for the CNS drug project. However, high value passive permeability alone cannot deliver good brain penetration when active efflux processes in the BBB are involved in drug transport.[241]

It is desirable to have an in vitro methodology to identify high efflux liability in a screening cascade, for example by capturing asymmetric drug transport in a quantitative manner and identifying the potential of BBB efflux. There is a great potential for human in vitro BBB models to make a large impact on the evaluation of BBB permeability and efflux potential as complements to human in vivo assessment. Unfortunately, primary and immortalized brain endothelial cells are not suitable for routine screening due to the fact that they have loose junctions, down-regulated transporter expression, and are costly.[242] MDCK cells are neither endothelial cells nor do they originate from the brain; however the tight junctions of the MDCK monolayer provide transcellular permeability which correlates well with in vivo BBB permeation.[242] BBB efflux can be predicted by using an MDCK monolayer transfected with P-gp or BCRP transporters. The rate of transcellular transport and the susceptibility of a drug to efflux are expressed as an apparent permeability coefficient (P_{app})

$$P_{app} = \frac{dC}{dt} \times \frac{V_r}{A \times C_0}$$

where dC/dt represents the concentration change with time in the receiver chamber, V_r is the volume of the receiver chamber, A is the surface area of a semi-permeable membrane, and C_0 is the initial concentration in the donor chamber.

An efflux ratio (ER) can also be calculated from the bidirectional permeability assessment.

$$ER = \frac{P_{app\ (basolateral\ to\ apical)}}{P_{app\ (apical\ to\ basolateral)}}$$

It is beneficial to establish the correlation between the efflux ratio observed in the in vitro assay of choice and $K_{puu,brain}$ obtained in vivo. Once a predictive relationship has been established, more confidence can be built on these first tier assays, such as P-gp efflux, to filter out compounds that fail to meet the cut-off value. When running the assay, it is desirable to test compounds at a reasonable concentration, for example 1 μM.

BCRP expression at the human microvascular vessel is slightly higher than P-gp. P-gp is a dominant efflux transporter and can prevent the entry of drugs into brain, but some non-P-gp substrates still have limited brain penetrance in rodents. Cooperative effects between P-gp and BCRP have been reported for dual substrates, which further limits the entry of compounds into the brain.[243,244] Thus, MDCK cells transfected with both P-gp and BCRP transporters enable one to simultaneously detect the efflux liability of both P-gp and BCRP at BBB. Unpublished data from AZ have found that 37 out of 48 non-P-gp substrate compounds ($ER < 2$ in MDCK–MDR1 assay) still demonstrated poor CNS penetration in rodents in vivo ($K_{puu,brain} < 0.5$). However a higher efflux ratio ($ER > 2$), in doubly transfected MDCK cells, was found to predict poor CNS penetration ($K_{puu,brain} < 0.5$). (Internal data not published.) Thus, we believe that the inclusion of efflux from both P-gp and BCRP could significantly increase the throughput and sensitivity to identify BBB efflux liability from an in vitro platform.

7.10.6.3 In Vivo Methodology to Measure the Extent of Brain Penetration

The extent of brain delivery should be considered separately from BBB permeability. The extent of brain delivery can be estimated in vivo by the ratio of $C_{u,brain}$ to $C_{u,plasma}$ at a steady state, alternatively the ratio of free AUC_{brain} to free AUC_{plasma} following a single dose. Meanwhile, CSF serves as a surrogate for free brain concentration that can be represented in the following equation.

$$K_{puu,brain} = \frac{C_{u,brain\ (steady\ state)}}{C_{u,plasma\ (steady\ state)}} = \frac{\text{free AUC}_{brain}}{\text{free AUC}_{plasma}}$$

There are only two in vivo methodologies to directly measure free drug levels in the CNS, namely intracerebral micro-dialysis and CSF sampling. The technique of microdialysis enables sampling and collecting of small molecular weight substance from the interstitial space of brain; however it suffers from several limitations including invasiveness, low throughput, the requirement of surgical skills, and nonspecific binding to the device for highly lipophilic compounds. On the plus side, microdialysis can directly measure free drug concentration in a specific region in the brain CSF; it is sometimes used as a surrogate for unbound drug concentrations in brain interstitial fluid. CSF samples are usually taken via lumbar puncture in humans and from the cisterna magna in nonclinical species, such as rodents and nonhuman primates. The CSF-to-plasma ratio can vary along the path of CSF flow since drug exchange may be different at different sampling sites. Therefore, a CSF readout should be interpreted with caution since there are many factors governing the equilibrium between brain and CSF;[245] however, it is still best if the compounds show high permeability and are not a substrate of BBB transporters. $K_{puu,CSF}$ can be estimated using the following equation.

$$K_{puu,CSF} = \frac{C_{u,CSF\ (steady\ state)}}{C_{u,plasma\ (steady\ state)}} = \frac{\text{free AUC}_{CSF}}{\text{free AUC}_{plasma}}$$

In order to come up with suitable methods of a higher capacity, unbound brain concentrations can be calculated by combining in vivo whole brain measurements with in vitro estimates of the unbound/free fraction in brain tissue. Typically, animals are orally administrated with test compounds, and plasma and brain samples are harvested at predefined time points. Alternatively, test compounds are infused intravenously until steady state is reached, and plasma and brain tissues are taken at only one, that is, the terminal, time point. Homogenization of the brain destroys the tissue and thus this method cannot reveal drug levels in a specific brain region. In vitro equilibrium dialysis of brain homogenate can determine free fractions in brain tissue and plasma in a high-throughput manner. There was a poor correlation between $f_{u,brain}$ and $f_{u,plasma}$ given that there were different levels of lipids and proteins present in plasma and brain tissue. The in vivo brain penetration study determines the total brain to plasma ratio. Thus, the ratio of $f_{u,brain}$ to $f_{u,plasma}$ varies significantly with physiochemical properties. K_p reflects both the extent of the brain penetration and the partition coefficient mainly driven by relative binding ratios between brain and plasma tissue; thus the optimization of K_p for better brain penetration generally ends with a compound with high lipophilicity as already discussed in many papers.[236]

$$K_p = K_{puu,brain} \times \frac{f_{u,brain}}{f_{u,plasma}}$$

A simple animal model, namely short oral absorption, attempts to address multiple DMPK properties in one assay with a minimum number of animals (one animal per time point), such as brain penetration, oral exposure, and the extent of hepatic extraction.[246] Blood samples are taken via portal vein, and cardiac puncture, while brain tissue in addition to CSF from cisterna magna is taken from individual animals at a pre-defined time point. The extent of hepatic extraction can be roughly estimated from the ratio of blood concentrations in the portal vein relative to the cardiac sample (extraction ratio $= 1 - C_{cardiac}/C_{portal\ vein}$). For brain penetration assessment, time course profile of brain concentration provides dynamic brain penetration data and more accurately measures brain penetration as compared to a single time point approach since distribution equilibrium may not be achieved at single time point and data could be misleading. For example, K_p value at 2 h time point may underestimate brain penetrance of AZ-2 (**Fig. 10**).

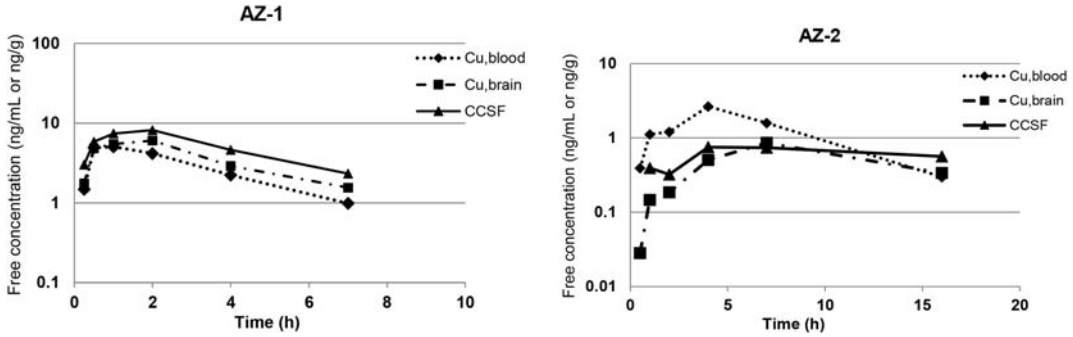

Fig. 10 The graph on the left demonstrates the parallel or overlap of free blood, free brain, and CSF concentrations; the graph on the right shows delayed T_{max} in free brain and CSF concentrations as compared to free blood.

Noninvasive techniques, such as PET, have multiple applications. PET allows the direct measurement of brain uptake and BBB permeability in humans, which is not feasible for other approaches. Following a trace dose of radiolabeled (^{11}C and ^{18}F) test compound, administrated intravenously, PET can monitor bio-distribution of the test compound into the brain and plasma and offer a readout of the brain partition coefficient K_p. After correcting for the unbound fraction in plasma and brain, the extent of brain penetration can be estimated.[247,248] Secondly, targeting specific PET tracers can serve as a biomarker for early disease diagnosis and disease progression monitoring given that the expression levels of neurological targets may alter during the course of the progression of a neurological disease, even before clinical symptoms present. Several PET tracers for Aβ plaque have been approved by the FDA for the diagnosis of AD.[249] In neurological disease, the tight junctions of the BBB may have become compromised and expression levels of efflux transporters may alter as well. To understand the scientific rationale of drug resistance in patients and to stratify patients for appropriate treatments, a metabolically activated, ^{18}F labeled PET tracer was developed to monitor P-gp and BCRP functions.[250] These efforts toward the advancement of noninvasive PET imaging enable us to directly monitor the alterations of drug disposition in the CNS due to the compromisation of the BBB in the course of disease.

However, a drawback of PET is that it is not able to differentiate between the parent molecule and metabolites in brain tissue. This shortcoming can be overcome by mass spectrometry imaging (MSI) since mass spectrometry can differentiate between metabolites and parent, if they have different molecular weights, based upon their m/z values or different mass transitions. The spatial distribution of multiple molecules can thus be obtained simultaneously in a given tissue slice. Signals from heme proteins have been used as robust MSI markers to localize the boundaries between the tissue blood vessels. Multiplex imaging of heme distribution has been related to the distribution of the therapeutics and their metabolites and ultimately utilized to provide a spatial/temporal map of drug transit into the brain parenchyma.[251] If a target site is located in the interstitial space of the brain and is accessible, microdialysis is available to measure the unbound concentration. No method exists to measure the intracellular unbound drug concentration if the target site is inside the cell. Current imaging tools allow one to obtain the total amount of drug in the vicinity of the target. Pharmacodynamic responses or modulation of biomarkers can be used as a readout for active concentrations in the target site. Another approach is PBPK modeling to enhance the understanding of intracellular disposition of drugs and link it to pharmacodynamic changes and thereafter therapeutic efficacy.

7.10.7 Conclusion and Future Perspectives

Research efforts during the past decades have provided scientists with a much deeper understanding of the underpinning biology of both proliferative and neurodegenerative diseases. Protein kinases have been demonstrated as key players in either activating or deactivating various proteins, via phosphorylation, for normal cell function. However, hyperphosphorylated proteins have been linked to protein aggregation and ultimately lead to tissue inflammation in disorders such as AD. Therefore the inhibition of an aberrant protein phosphorylation status may provide an avenue to control disease. Although there have been many successful developments in the use of kinase inhibitors in oncology, efforts to develop kinase inhibitors for noncancer-related diseases have been less successful. There are 29 FDA approved kinase inhibitors available but only two are for noncancer-related diseases. More importantly, no successful kinase inhibitor for neurodegenerative diseases has yet been approved. This data reflects the difficulties in developing kinase inhibitors to target diseases beyond oncology. Even in the oncology area, a need for brain-penetrant kinase inhibitors as a potential therapy is of equal importance. Brain metastasis is one of the pathways for disease progression. Although kinase inhibitors are successful in controlling peripheral diseases, their CNS efficacy is usually not realized. One of the key reasons may be due to the challenges of incorporating target potency and selectivity within the desired CNS DMPK parameters. Over the years, the required physicochemical properties to favor CNS penetration have become better understood. It is clear that the currently used kinase inhibitor chemical scaffolds may not be suitable for CNS penetration.

New chemistry design strategies are necessary to develop brain-penetrable compounds. Several theoretical models have been developed in the past few years to help medicinal chemists to achieve their goals of developing drug candidates that achieve effective CNS penetration. In addition, only a small fraction of all kinases have been studied. More kinases may be involved in the pathology of CNS diseases than is currently recognized. If more than one signaling pathway is involved in the underlying diseases, selective multikinase inhibition may be more efficacious and beneficial. The recent development of many in vitro/in vivo DMPK methodologies has also facilitated more efficient and productive workflows for the identification of compounds with desirable CNS penetration properties. Ultimately, the key lies in designing new chemical scaffolds, which will lead to more candidates entering clinical studies by biologists/physicians for proof-of-concept studies. We should be optimistic that some of the research efforts may result in the creation of medicines for the treatment of patients with CNS diseases in the near future.

References

1. Zhang, J.; Yang, P. L.; Gray, N. S. Targeting Cancer With Small Molecule Kinase Inhibitors. *Nat. Rev. Cancer* **2009,** *9* (1), 28–39.
2. Wu, P.; Nielsen, T. E.; Clausen, M. H. FDA-Approved Small-Molecule Kinase Inhibitors. *Trends Pharmacol. Sci.* **2015,** *36* (7), 422–439.
3. Wu, P.; Nielsen, T. E.; Clausen, M. H. Small-Molecule Kinase Inhibitors: An Analysis of FDA-Approved Drugs. *Drug Discov. Today* **2016,** *21* (1), 5–10.
4. Rostami, R.; Mittal, S.; Rostami, P.; Tavassoli, F.; Jabbari, B. Brain Metastasis in Breast Cancer: A Comprehensive Literature Review. *J. Neurooncol.* **2016,** *127* (3), 407–414.

5. Porkka, K.; Koskenvesa, P.; Lundán, T.; Rimpiläinen, J.; Mustjoki, S.; Smykla, R.; Wild, R.; Luo, R.; Arnan, M.; Brethon, B.; Eccersley, L.; Hjorth-Hansen, H.; Höglund, M.; Klamova, H.; Knutsen, H.; Parikh, S.; Raffoux, E.; Gruber, F.; Brito-Babapulle, F.; Dombret, H.; Duarte, R. F.; Elonen, E.; Paquette, R.; Zwaan, C. M.; Lee, F. Y. Dasatinib Crosses the Blood-Brain Barrier and Is an Efficient Therapy for Central Nervous System Philadelphia Chromosome-Positive Leukemia. *Blood* **2008,** *112* (4), 1005–1012.
6. Chico, L. K.; Van Eldik, L. J.; Watterson, D. M. Targeting Protein Kinases in Central Nervous System Disorders. *Nat. Rev. Drug Discov.* **2009,** *8* (11), 892–909.
7. Amigoni, F.; Legnaghi, E.; Pevarello, P. Kinase Inhibitors for CNS Diseases: An Analysis of the Recent Patent Literature. *Pharm. Pat. Anal.* **2012,** *1* (2), 177–192.
8. Bulic, B.; Pickhardt, M.; Schmidt, B.; Mandelkow, E. M.; Waldmann, H.; Mandelkow, E. Development of Tau Aggregation Inhibitors for Alzheimer's Disease. *Angew. Chem. Int. Ed. Engl.* **2009,** *48* (10), 1740–1752.
9. Mohamed, T.; Shakeri, A.; Rao, P. P. Amyloid Cascade in Alzheimer's Disease: Recent Advances in Medicinal Chemistry. *Eur. J. Med. Chem.* **2016,** *113,* 258–272.
10. Tenreiro, S.; Eckermann, K.; Outeiro, T. F. Protein Phosphorylation in Neurodegeneration: Friend or Foe? *Front. Mol. Neurosci.* **2014,** *7,* 42.
11. Pietri, M.; Dakowski, C.; Hannaoui, S.; Alleaume-Butaux, A.; Hernandez-Rapp, J.; Ragagnin, A.; Mouillet-Richard, S.; Haik, S.; Bailly, Y.; Peyrin, J. M.; Launay, J. M.; Kellermann, O.; Schneider, B. PDK1 Decreases TACE-Mediated α-Secretase Activity and Promotes Disease Progression in Prion and Alzheimer's Diseases. *Nat. Med.* **2013,** *19* (9), 1124–1131.
12. Gross, S.; Rahal, R.; Stransky, N.; Lengauer, C.; Hoeflich, K. P. Targeting Cancer With Kinase Inhibitors. *J. Clin. Invest.* **2015,** *125* (5), 1780–1789.
13. Berger, L. A.; Riesenberg, H.; Bokemeyer, C.; Atanackovic, D. CNS Metastases in Non-Small-Cell Lung Cancer: Current Role of EGFR-TKI Therapy and Future Perspectives. *Lung Cancer* **2013,** *80,* 242–248.
14. van Tellingen, O.; Yetkin-Arik, B.; de Gooijer, M. C.; Wesseling, P.; Wurdinger, T.; de Vries, H. E. Overcoming the Blood-Brain Tumor Barrier for Effective Glioblastoma Treatment. *Drug Resist. Updat.* **2015,** *19,* 1–12.
15. Finlay, M. R.; Anderton, M.; Ashton, S.; Ballard, P.; Bethel, P. A.; Box, M. R.; Bradbury, R. H.; Brown, S. J.; Butterworth, S.; Campbell, A.; Chorley, C.; Colclough, N.; Cross, D. A.; Currie, G. S.; Grist, M.; Hassall, L.; Hill, G. B.; James, D.; James, M.; Kemmitt, P.; Klinowska, T.; Lamont, G.; Lamont, S. G.; Martin, N.; McFarland, H. L.; Mellor, M. J.; Orme, J. P.; Perkins, D.; Perkins, P.; Richmond, G.; Smith, P.; Ward, R. A.; Waring, M. J.; Whittaker, D.; Wells, S.; Wrigley, G. L. Discovery of a Potent and Selective EGFR Inhibitor (AZD9291) of Both Sensitizing and T790M Resistance Mutations That Spares the Wild Type Form of the Receptor. *J. Med. Chem.* **2014,** *57* (20), 8249–8267.
16. Wager, T. T.; Chandrasekaran, R. Y.; Hou, X.; Troutman, D. M.; Verhoest, P. R.; Villalobos, A.; Will, Y. Defining Desirable Central Nervous System Drug Space Through the Alignment of Molecular Properties, In Vitro ADME, and Safety Attributes. *ACS Chem. Neurosci.* **2010,** *1* (6), 420–434.
17. Segall, M. Advances in Multiparameter Optimization Methods for De Novo Drug Design. *Expert. Opin. Drug Discov.* **2014,** *9* (7), 803–817.
18. Segall, M. D. Multi-Parameter Optimization: Identifying High Quality Compounds With a Balance of Properties. *Curr. Pharm. Des.* **2012,** *18,* 1292–1310.
19. Segall, M.; Champness, E.; Leeding, C.; Lilien, R.; Mettu, R.; Stevens, B. Applying Medicinal Chemistry Transformations and Multiparameter Optimization to Guide the Search for High-Quality Leads and Candidates. *J. Chem. Inf. Model.* **2011,** *51,* 2967–2976.
20. Di, L., Kerns, E. H., Eds. *Blood–Brain Barrier in Drug Discovery: Optimizing Brain Exposure of CNS Drugs and Minimizing Brain Side Effects for Peripheral Drugs;* Wiley: Hoboken, NJ, 2015.
21. Rankovic, Z. CNS Drug Design: Balancing Physicochemical Properties for Optimal Brain Exposure. *J. Med. Chem.* **2015,** *58,* 2584–2608.
22. Lanevskij, K.; Japertas, P.; Didziapetris, R. Improving the Prediction of Drug Disposition in the Brain. *Expert Opin. Drug Metab. Toxicol.* **2013,** *9* (4), 473–486.
23. Pajouhesh, H.; Lenz, G. R. Medicinal Chemical Properties of Successful Central Nervous System Drugs. *NeuroRx* **2005,** *2,* 541–553.
24. Raevsky, O. A.; Grigorev, V. Y.; Polianczyk, D. E.; Sandakov, G. I.; Solodova, S. L.; Yarkov, A. V.; Bachurin, S. O.; Dearden, J. C. Physicochemical Property Profile for Brain Permeability: Comparative Study by Different Approaches. *J. Drug Target.* **2016,** http://dx.doi.org/10.3109/1061186X.2015.1132224.
25. Gunaydin, H. Probabilistic Approach to Generating MPOs and Its Application as a Scoring Function for CNS Drugs. *ACS Med. Chem. Lett.* **2016,** *7,* 89–93.
26. Wager, T. T.; Hou, X.; Verhoest, P. R.; Villalobos, A. Moving Beyond Rules: The Development of a Central Nervous System Multiparameter Optimization (CNS MPO) Approach to Enable Alignment of Druglike Properties. *ACS Chem. Neurosci.* **2010,** *1,* 435–449.
27. Malakoutikhah, M.; Teixid, M.; Giralt, E. Shuttle-Mediated Drug Delivery to the Brain. *Angew. Chem. Int. Ed.* **2011,** *50,* 7998–8014.
28. Tashima, T. Intriguing Possibilities and Beneficial Aspects of Transporter-Conscious Drug Design. *Bioorg. Med. Chem.* **2015,** *23,* 4119–4131.
29. Martel, S. Learning From Our Failures in Blood–Brain Permeability: What Can Be Done for New Drug Discovery? *Expert. Opin. Drug Discov.* **2015,** *10* (3), 207–211.
30. Zuchero, Y. J.; Chen, X.; Bien-Ly, N.; Bumbaca, D.; Tong, R. K.; Gao, X.; Zhang, S.; Hoyte, K.; Luk, W.; Huntley, M. A.; Phu, L.; Tan, C.; Kallop, D.; Weimer, R. M.; Lu, Y.; Kirkpatrick, D. S.; Ernst, J. A.; Chih, B.; Dennis, M. S.; Watts, R. J. Discovery of Novel Blood-Brain Barrier Targets to Enhance Brain Uptake of Therapeutic Antibodies. *Neuron* **2016,** *89* (1), 70–82.
31. Bank, W. A. From Blood-Brain Barrier to Blood-Brain Interface: New Opportunities for CNS Drug Delivery. *Nat. Rev. Drug Discov.* **2016,** *15* (4), 275–292.
32. Paisán-Ruíz, C.; Jain, S.; Evans, E. W.; Gilks, W. P.; Simón, J.; van der Brug, M.; López de Munain, A.; Aparicio, S.; Gil, A. M.; Khan, N.; Johnson, J.; Martinez, J. R.; Nicholl, D.; Carrera, I. M.; Pena, A. S.; de Silva, R.; Lees, A.; Martí-Massó, J. F.; Pérez-Tur, J.; Wood, N. W.; Singelton, A. B. Cloning of the Gene Containing Mutations That Cause PARK8-Linked Parkinson's Disease. *Neuron* **2004,** *44,* 595–600.
33. Ramsden, N.; Perrin, J.; Ren, Z.; Lee, B. D.; Zinn, N.; Dawson, V. L.; Tam, D.; Bova, M.; Lang, M.; Drewes, G.; Bantscheff, M.; Bard, F.; Dawson, T. M.; Hopf, C. Chemoproteomics-Based Design of Potent LRRK2-Selective Lead Compounds That Attenuate Parkinson's Disease-Related Toxicity in Human Neurons. *ACS Chem. Biol.* **2011,** *6* (10), 1021–1028.
34. Ray, S.; Liu, M. Current Understanding of LRRK2 in Parkinson's Disease: Biochemical and Structural Features and Inhibitor Design. *Future Med. Chem.* **2012,** *4,* 1701–1713.
35. Bonifati, V. Parkinson's Disease: The *LRRK2*–G2019S Mutation: Opening a Novel Era in Parkinson's Disease Genetics. *Eur. J. Hum. Genet.* **2006,** *14,* 1061–1062.
36. Seol, W. Biochemical and Molecular Features of LRRK2 and Its Pathophysiological Roles in Parkinson's Disease. *BMB Rep.* **2010,** *43,* 233–244.
37. Mata, I. F.; Wedemeyer, W. J.; Farrer, M. J.; Taylor, J. P.; Gallo, K. A. LRRK2 in Parkinson's Disease: Protein Domains and Functional Insights. *Trends Neurosci.* **2006,** *29,* 286–293.
38. Covy, J. P.; Giasson, B. I. Identification of Compounds That Inhibit the Kinase Activity of Leucine-Rich Repeat Kinase 2. *Biochem. Biophys. Res. Commun.* **2009,** *378* (3), 473–477.
39. Anand, V. S.; Reichling, L. J.; Lipinski, K.; Stochaj, W.; Duan, W.; Kelleher, K.; Pungalliya, P.; Brown, E. L.; Reinhart, P. H.; Someberg, R.; Hirst, W. D.; Riddle, S. M.; Braithwaiste, S. P. Investigation of Leucine-Rich Repeat Kinase 2: Enzymological Properties and Novel Assays. *FEBS J.* **2009,** *276* (2), 466–478.
40. Nichols, R. J.; Dzamko, N.; Hutti, J. E.; Cantley, L. C.; Deak, M.; Moran, J.; Bamborough, P.; Reith, A. D.; Alessi, D. R. Substrate Specificity and Inhibitors of LRRK2, a Protein Kinase Mutated in Parkinson's Disease. *Biochem. J.* **2009,** *424* (1), 47–60.
41. Deng, X.; Dzamko, N.; Prescott, A.; Davies, P.; Liu, Q.; Yang, Q.; Lee, J. D.; Patricelli, M. P.; Nomanbhoy, T. K.; Alessi, D. R.; Gray, N. S. Characterization of a Selective Inhibitor of the Parkinson's Disease Kinase LRRK2. *Nat. Chem. Biol.* **2011,** *7* (4), 203–205.
42. Zhang, J.; Deng, X.; Choi, H. G.; Alessi, D. R.; Gray, N. S. Characterization of TAE684 as a Potent LRRK2 Kinase Inhibitor. *Bioorg. Med. Chem. Lett.* **2012,** *22* (5), 1864–1869.
43. Reith, A. D.; Bamborough, P.; Jandu, K.; Andreotti, D.; Mensah, L.; Dossang, P.; Choi, H. G.; Deng, X.; Zhang, J.; Alessi, D. R.; Gray, N. S. GSK2578215A, a Potent and Highly Selective 2-Arylmethyloxy-5-substitutent-N-arylbenzamide LRRK2 Kinase Inhibitor. *Bioorg. Med. Chem. Lett.* **2012,** *22* (17), 5625–5629.
44. Estrada, A. A.; Liu, X.; Baker-Glenn, C.; Beresford, A.; Burdick, D. J.; Chambers, M.; Chan, B. K.; Chen, H.; Ding, X.; DiPasquale, A. G.; Dominguez, S. L.; Dotson, J.; Drummond, J.; Flagella, M.; Flynn, S.; Fuji, R.; Gill, A.; Gunzner-Toste, J.; Harris, S. F.; Heffron, T. P.; Kleinheinz, T.; Lee, D. W.; Le Pichon, C. E.; Lyssikatos, J. P.; Medhurst, A. D.; Moffat, J. G.; Mukund, S.; Nash, K.; Scearce-Levie, K.; Sheng, Z.; Shore, D. G.; Tran, T.; Trivedi, N.; Wang, S.; Zhang, S.; Zhang, X.; Zhao, G.; Zhu, H.; Sweeney, Z. K. Discovery of Highly Potent, Selective, and Brain-Penetrable Leucine-Rich Repeat Kinase 2 (LRRK2) Small Molecule Inhibitors. *J. Med. Chem.* **2012,** *55* (22), 9416–9433.

45. Estrada, A. A.; Chan, B. K.; Baker-Glenn, C.; Beresford, A.; Burdick, D. J.; Chambers, M.; Chen, H.; Dominguez, S. L.; Dotson, J.; Drummond, J.; Flagella, M.; Fuji, R.; Gill, A.; Halladay, J.; Harris, S. F.; Heffron, T. P.; Kleinheinz, T.; Lee, D. W.; Le Pichon, C. E.; Liu, X.; Lyssikatos, J. P.; Medhurst, A. D.; Moffat, J. G.; Nash, K.; Scearce-Levie, K.; Sheng, Z.; Shore, D. G.; Wong, S.; Zhang, S.; Zhang, X.; Zhu, H.; Sweeney, Z. K. Discovery of Highly Potent, Selective, and Brain-Penetrant Aminopyrazole Leucine-Rich Repeat Kinase 2 (LRRK2) Small Molecule Inhibitors. *J. Med. Chem.* **2014,** *57* (3), 921–936.
46. Henderson, J. L.; Kormos, B. L.; Hayward, M. M.; Coffman, K. J.; Jasti, J.; Kurumbail, R. G.; Wager, T. T.; Verhoest, P. R.; Noell, G. S.; Chen, Y.; Needle, E.; Berger, Z.; Steyn, S. J.; Houle, C.; Hirst, W. D.; Galatsis, P. Discovery and Preclinical Profiling of 3-[4-(Morpholin-4-yl)-7*H*-pyrrolo[2,3-*d*]pyrimidin-5-yl]benzonitrile (PF-06447475), a Highly Potent, Selective, Brain Penetrant, and In Vivo Active LRRK2 Kinase Inhibitor. *J. Med. Chem.* **2015,** *58* (1), 419–432.
47. Mushtaq, G.; Greig, N. H.; Anwar, F.; Al-Abbasi, F. A.; Zamzami, M. A.; Al-Talhi, H. A.; Kamal, M. A. Neuroprotective Mechanisms Mediated by CDK5 Inhibition. *Curr. Pharm. Des.* **2016,** *22* (5), 527–534.
48. Liu, S. L.; Wang, C.; Jiang, T.; Tan, L.; Xing, A.; Yu, J. T. The Role of CDK5 in Alzheimer's Disease. *Mol. Neurobiol.* **2016,** *53* (7), 4328–4342.
49. Lai, K. O.; Ip, N. Y. CDK5: A Key Player at Neuronal Synapse With Diverse Functions. *Mini Rev. Med. Chem.* **2015,** *15* (5), 390–395.
50. Rosenblum, J. S. CDK5 Acts as a Surveillance System in the Nervous System. In *New Developments on Signal Transduction Research;* Yamaguchi, M., Ed.; Nova Science Publishers, Inc., 2013; pp 67–112. Chapter 4.
51. Zhao, Y.; Adjei, A. A. The Clinical Development of MEK Inhibitors. *Nat. Rev. Clin. Oncol.* **2014,** *11,* 385–400.
52. Miller, C. R.; Oliver, K. E.; Farley, J. H. MEK1/2 Inhibitors in the Treatment of Gynecologic Malignancies. *Gynecol. Oncol.* **2014,** *133* (1), 128–137.
53. Hartung, I. V.; Hammer, S.; Hitchcock, M.; Neuhaus, R.; Scholz, A.; Siemeister, G.; Bohlmann, R.; Hillig, R. C.; Pühler, F. Optimization of Allosteric MEK Inhibitors. Part 2: Taming the Sulfamide Group Balances Compound Distribution Properties. *Bioorg. Med. Chem. Lett.* **2016,** *26* (1), 186–193.
54. Choo, E. F.; Ly, J.; Chan, J.; Shahidi-Latham, S. K.; Messick, K.; Plise, E.; Quiason, C. M.; Yang, L. Role of P-Glycoprotein on the Brain Penetration and Brain Pharmacodynamic Activity of the MEK Inhibitor Cobimetinib. *Mol. Pharm.* **2014,** *11* (11), 4199–4207.
55. Vaidhyanathan, S.; Mittapalli, R. K.; Sarkaria, J. N.; Elmquist, W. F. Factors Influencing the CNS Distribution of a Novel MEK-1/2 Inhibitor: Implications for Combination Therapy for Melanoma Brain Metastases. *Drug Metab. Dispos.* **2014,** *42* (8), 1292–1300.
56. Yarza, R.; Vela, S.; Solas, M.; Ramirez, M. J. c-Jun N-Terminal Kinase (JNK) Signaling as a Therapeutic Target for Alzheimer's Disease. *Front. Pharmacol.* **2016,** *6,* 321.
57. Mehan, S.; Meena, H.; Sharma, D.; Sankhla, R. JNK: A Stress-Activated Protein Kinase Therapeutic Strategies and Involvement in Alzheimer's and Various Neurodegenerative Abnormalities. *J. Mol. Neurosci.* **2011,** *43* (3), 376–390.
58. Graczyk, P. P. JNK Inhibitors as Anti-inflammatory and Neuroprotective Agents. *Future Med. Chem.* **2013,** *5* (5), 539–551.
59. Bowers, S.; Truong, A. P.; Neitz, R. J.; Neitzel, M.; Probst, G. D.; Hom, R. K.; Peterson, B.; Galemmo, R. A., Jr.; Konradi, A. W.; Sham, H. L.; Tóth, G.; Pan, H.; Yao, N.; Artis, D. R.; Brigham, E. F.; Quinn, K. P.; Sauer, J. M.; Powell, K.; Ruslim, L.; Ren, Z.; Bard, F.; Yednock, T. A.; Prenner, G. I. Design and Synthesis of a Novel, Orally Active, Brain Penetrant, Tri-Substituted Thiophene Based JNK Inhibitor. *Bioorg. Med. Chem. Lett.* **2011,** *21* (6), 1838–1843.
60. Noël, R.; Shin, Y.; Song, X.; He, Y.; Koenig, M.; Chen, W.; Ling, Y. Y.; Lin, L.; Ruiz, C. H.; LoGrasso, P.; Cameron, M. D.; Duckett, D. R.; Kamenecka, T. M. Synthesis and SAR of 4-(Pyrazol-3-yl)-pyridines as Novel c-Jun N-Terminal Kinase Inhibitors. *Bioorg. Med. Chem. Lett.* **2011,** *21* (9), 2732–2735.
61. Peters, J. M.; McKay, R. M.; McKay, J. P.; Graff, J. M. Casein Kinase I Transduces Wnt Signals. *Nature* **1999,** *401* (6751), 345–350.
62. Gross, S. D.; Anderson, R. A. Casein Kinase I: Spatial Organization and Positioning of a Multifunctional Protein Kinase Family. *Cell. Signal.* **1998,** *10* (10), 699–711.
63. Rowles, J.; Slaughter, C.; Moomaw, C.; Hsu, J.; Cobb, M. H. Purification of Casein Kinase I and Isolation of cDNAs Encoding Multiple Casein Kinase I-Like Enzymes. *Proc. Natl. Acad. Sci. U. S. A.* **1991,** *88* (21), 9548–9552.
64. Knippschild, U.; Gocht, A.; Wolff, S.; Huber, N.; Lohler, J.; Stoter, M. The Casein Kinase 1 Family: Participation in Multiple Cellular Processes in Eukaryotes. *Cell. Signal.* **2005,** *17* (6), 675–689.
65. Oumata, N.; Bettayeb, K.; Ferandin, Y.; Demange, L.; Lopez-Giral, A.; Goddard, M. L.; Myrianthopoulos, V.; Mikros, E.; Flajolet, M.; Greengard, P.; Meijer, L.; Galons, H. Roscovitine-Derived, Dual Specificity Inhibitors of Cyclin-Dependent Kinases and Casein Kinases 1. *J. Med. Chem.* **2008,** *51* (17), 5229–5242.
66. Perez, D. I.; Gil, C.; Martinez, A. Protein Kinases CK1 and CK2 as New Targets for Neurodegenerative Diseases. *Med. Res. Rev.* **2011,** *31* (6), 924–954.
67. Cozza, G.; Pinna, L. A. Casein Kinases as Potential Therapeutic Targets. *Expert Opin. Ther. Targets* **2016,** *20* (3), 319–340.
68. Schwab, C.; DeMaggio, A. J.; Ghoshal, N.; Binder, L. I.; Kuret, J.; McGeer, P. L. Casein Kinase 1 Delta Is Associated With Pathological Accumulation of Tau in Several Neurodegenerative Diseases. *Neurobiol. Aging* **2000,** *21* (4), 503–510.
69. Walton, K. M.; Fisher, K.; Rubitski, D.; Marconi, M.; Meng, Q.-J.; Sládek, M.; Adams, J.; Bass, M.; Chandrasekaran, R.; Butler, T.; Griffor, M.; Rajamohan, F.; Serpa, M.; Chen, Y.; Claffey, M.; Hastings, M.; Loudon, A.; Maywood, E.; Ohren, J.; Doran, A.; Wager, T. T. Selective Inhibition of Casein Kinase 1 Epsilon Minimally Alters Circadian Clock Period. *J. Pharmacol. Exp. Ther.* **2009,** *330* (2), 430–439.
70. Perreau-Lenz, S.; Vengeliene, V.; Noori, H. R.; Merlo-Pich, E. V.; Corsi, M. A.; Corti, C.; Spanagel, R. Inhibition of the Casein-Kinase-1-Epsilon/Delta Prevents Relapse-Like Alcohol Drinking. *Neuropsychopharmacology* **2012,** *37* (9), 2121–2131.
71. Wager, T. T.; Chandrasekaran, R. Y.; Jenifer Bradley, J.; Rubitski, D.; Berke, H.; Mente, S.; Butler, T.; Doran, A.; Chang, C.; Fisher, K.; Knafels, J.; Shenping Liu, S.; Ohren, J.; Marconi, M.; DeMarco, G.; Sneed, B.; Walton, K.; Horton, D.; Amy Rosado, A.; Mead, A. Casein Kinase 1δ/ε Inhibitor PF-5006739 Attenuates Opioid Drug-Seeking Behavior. *ACS Chem. Neurosci.* **2014,** *5* (12), 1253–1265.
72. Gallo, K. A.; Johnson, G. L. Mixed-Lineage Kinase Control of JNK and p38 MAPK Pathways. *Nat. Rev. Mol. Cell Biol.* **2002,** *3* (9), 663–672.
73. Maroney, A. C.; Finn, J. P.; Connors, T. J.; Durkin, J. T.; Angeles, T.; Gessner, G.; Xu, Z.; Meyer, S. L.; Savage, M. J.; Greene, L. A.; Scott, R. W.; Vaught, J. L. Cep-1347 (KT7515), a Semisynthetic Inhibitor of the Mixed Lineage Kinase Family. *J. Biol. Chem.* **2001,** *276* (27), 25302–25308.
74. Gotoh, I.; Adachi, M.; Nishida, E. Identification and Characterization of a Novel MAP Kinase Kinase Kinase MLTK. *J. Biol. Chem.* **2001,** *276* (6), 4276–4286.
75. Silva, R. M.; Kuan, C. Y.; Rakic, P.; Burke, R. E. Mixed Lineage Kinase-c-jun N-Terminal Kinase Signaling Pathway: A New Therapeutic Target in Parkinson's Disease. *Mov. Disord.* **2005,** *20* (6), 653–664.
76. Wang, L. H.; Besirli, C. G.; Johnson, E. M., Jr. Mixed-Lineage Kinases: A Target for the Prevention of Neurodegeneration. *Annu. Rev. Pharmacol. Toxicol.* **2004,** *44,* 451–474.
77. Borasio, G. D.; Horstmann, S.; Anneser, J. M. H.; Neff, N. T.; Glicksman, M. A. CEP-1347/KT7515, a JNK Pathway Inhibitor, Supports the In Vitro Survival of Chick Embryonic Neurons. *Neuroreport* **1998,** *9* (7), 1435–1439.
78. Maroney, A. C.; Glicksman, M. A.; Basma, A. N.; Walton, K. M.; Knight, E.; Murphy, C. A.; Bartlett, B. A.; Finn, J. P.; Angeles, T.; Matsudam, Y.; Neff, N. T.; Dionne, C. A. Motoneuron Apoptosis Is Blocked by CEP-1347 (KT 7515), a Novel Inhibitor of the JNK Signaling Pathway. *J. Neurosci.* **1998,** *18* (1), 104–111.
79. Maroney, A. C.; Finn, J. P.; Bozyczko-Coyne, D.; O'Kane, T.; Neff, N. T.; Tolkovsky, A. M.; Park, D. S.; Yan, C. Y. I.; Troy, C. M.; Greene, L. A. CEP-1347 (KT7515), an Inhibitor of JNK Activation, Rescues Sympathetic Neurons and Neuronally Differentiated PC12 Cells From Death Evoked by Three Distinct Insults. *J. Neurochem.* **1999,** *73* (5), 1901–1912.
80. Glicksman, M. A.; Chiu, A. Y.; Dionne, C. A.; Harty, M.; Kaneko, M.; Murakata, C.; Oppenheim, R. W.; Prevette, D.; Sengelaub, D. R.; Vaught, J. L.; Neff, N. T. CEP-1347/KT7515 Prevents Motor Neuronal Programmed Cell Death and Injury-Induced Dedifferentiation *In Vivo*. *J. Neurobiol.* **1998,** *35* (4), 361–370.
81. Saporito, M. S.; Brown, E. R.; Carswell, S.; DiCamillo, A. M.; Miller, M. S.; Murakata, C.; Neff, N. S.; Vaught, J. L.; Haun, F. A. Preservation of Cholinergic Activity and Prevention of Neuron Death by CEP-1347/KT7515 Following Excitotoxic Injury of the Nucleus Basalis Magnocellularis. *Neuroscience* **1998,** *86* (2), 461–472.
82. Saporito, M. S.; Brown, E. M.; Miller, M. S.; Carswell, S. CEP-1347/KT-7515, an Inhibitor of *c-jun* N-Terminal Kinase Activation, Attenuates the 1-Methyl-4-phenyl Tetrahydropyridine-Mediated Loss of Nigrostriatal Dopaminergic Neurons In Vivo. *J. Pharmacol. Exp. Ther.* **1999,** *288* (2), 421–427.
83. Saporito, M. S.; Hudkins, R. L.; Maroney, A. C. Discovery of CEP-1347/KT-7515, an Inhibitor of the JNK/SAPK Pathway for the Treatment of Neurodegenerative Diseases. *Prog. Med. Chem.* **2002,** *40,* 23–62.

84. Bozyczko-Coyne, D.; O'Kane, T. M.; Wu, Z. L.; Dobrzanski, P.; Murthy, S.; Vaught, J. L.; Scott, R. W. CEP-1347/KT-7515, an Inhibitor of SAPK/JNK Pathway Activation, Promotes Survival and Blocks Multiple Events Associated With Abeta-Induced Cortical Neuron Apoptosis. *J. Neurochem.* **2001,** *77* (3), 849–863.
85. Parkinson Study Group PRECEPT Investigators. Mixed Lineage Kinase Inhibitor CEP-1347 Fails to Delay Disability in Early Parkinson Disease. *Neurology* **2007,** *69* (15), 1480–1490.
86. Goodfellow, V. S.; Loweth, C. J.; Ravula, S. B.; Wiemann, T.; Nguyen, T.; Xu, Y.; Todd, D. E.; Sheppard, D.; Pollack, S.; Polesskaya, O.; Marker, D. F.; Dewhurst, S.; Gelbard, H. A. Discovery, Synthesis, and Characterization of an Orally Bioavailable, Brain Penetrant Inhibitor of Mixed Lineage Kinase 3. *J. Med. Chem.* **2013,** *56* (20), 8032–8048.
87. Marker, D. F.; Tremblay, M.È.; Puccini, J. M.; Barbieri, J.; Gantz Marker, M. A.; Loweth, C. J.; Muly, E. C.; Lu, S. M.; Goodfellow, V. S.; Dewhurst, S.; Gelbard, H. A. The New Small-Molecule Mixed-Lineage Kinase 3 Inhibitor URMC-099 Is Neuroprotective and Anti-inflammatory in Models of Human Immunodeficiency Virus-Associated Neurocognitive Disorders. *J. Neurosci.* **2013,** *33* (24), 9998–10010.
88. Bialik, S.; Kimchi, A. The Death-Associated Protein Kinases: Structure, Function, and Beyond. *Annu. Rev. Biochem.* **2006,** *75,* 189–210.
89. Stevens, C.; Hupp, T. R. Novel Insights Into DAPK Autophagic Signalling Using Peptide Aptamer Combinatorial Protein Interaction Screens. *Autophagy* **2008,** *4* (4), 531–533.
90. Nair, S.; Hagberg, H.; Krishnamurthy, R.; Thornton, C.; Mallard, C. Death Associated Protein Kinases: Molecular Structure and Brain Injury. *Int. J. Mol. Sci.* **2013,** *14* (7), 13858–13872.
91. Schumacher, A. M.; Velentza, A. V.; Watterson, D. M.; Wainwright, M. S. DAPK Catalytic Activity in the Hippocampus Increases During the Recovery Phase in an Animal Model of Brain Hypoxic-Ischemic Injury. *Biochim. Biophys. Acta* **2002,** *1600* (1–2), 128–137.
92. Shamloo, M.; Soriano, L.; Wieloch, T.; Nikolich, K.; Urfer, R.; Oksenberg, D. Death-Associated Protein Kinase Is Activated by Dephosphorylation in Response to Cerebral Ischemia. *J. Biol. Chem.* **2005,** *280* (51), 42290–42299.
93. Henshall, D. C.; Araki, T.; Schindler, C. K.; Shinoda, S.; Lan, J. Q.; Simon, R. P. Expression of Death-Associated Protein Kinase and Recruitment to the Tumor Necrosis Factor Signaling Pathway Following Brief Seizures. *J. Neurochem.* **2003,** *86* (5), 1260–1270.
94. Velentza, A. V.; Wainwright, M. S.; Zasadzki, M.; Mirzoeva, S.; Schumacher, A. M.; Haiech, J.; Focia, P. J.; Egli, M.; Watterson, D. M. An Aminopyridazine-Based Inhibitor of a Pro-apoptotic Protein Kinase Attenuates Hypoxia-Ischemia Induced Acute Brain Injury. *Bioorg. Med. Chem. Lett.* **2003,** *13* (20), 3465–3470.
95. Okamoto, M.; Takayama, K.; Shimizu, T.; Ishida, K.; Takahashi, O.; Furuya, T. Identification of Death-Associated Protein Kinases Inhibitors Using Structure-Based Virtual Screening. *J. Med. Chem.* **2009,** *52* (22), 7323–7327.
96. Carlson, D. A.; Franke, A. S.; Weitzel, D. H.; Speer, B. L.; Hughes, P. F.; Hagerty, L.; Fortner, C. N.; Veal, J. M.; Barta, T. E.; Zieba, B. J.; Somlyo, A. V.; Sutherland, C.; Deng, J. T.; Walsh, M. P.; MacDonald, J. A.; Haystead, T. A. J. Fluorescence Linked Enzyme Chemoproteomic Strategy for Discovery of a Potent and Selective DAPK1 and ZIPK Inhibitor. *ACS Chem. Biol.* **2013,** *8* (12), 2715–2723.
97. Wilbek, T. S.; Skovgaard, T.; Sorrell, F. J.; Knapp, S.; Berthelsen, J.; Strømgaard, K. Identification and Characterization of a Small-Molecule Inhibitor of Death-Associated Protein Kinase 1. *Chembiochem* **2015,** *16* (1), 59–63.
98. Kramer, T.; Schmidt, B.; Lo Monte, F. Small-Molecule Inhibitors of GSK-3: Structural Insights and Their Application to Alzheimer's Disease Models. *Int. J. Alzheimers Dis.* **2012,** 381029.
99. Cohen, P.; Frame, S. The Renaissance of GSK3. *Nat. Rev. Mol. Cell Biol.* **2001,** *2* (10), 769–776.
100. King, M. K.; Pardo, M.; Cheng, Y.; Downey, K.; Jope, R. S.; Beurel, E. Glycogen Synthase Kinase-3 Inhibitors: Rescuers of Cognitive Impairments. *Pharmacol. Ther.* **2014,** *141* (1), 1–12.
101. Beurel, E.; Grieco, S. F.; Jope, R. S. Glycogen Synthase Kinase-3 (GSK3): Regulation, Actions and Diseases. *Pharmacol. Ther.* **2015,** *148,* 114–131.
102. O'Leary, O.; Nolan, Y. Glycogen Synthase Kinase-3 as a Therapeutic Target for Cognitive Dysfunction in Neuropsychiatric Disorders. *CNS Drugs* **2015,** *29* (1), 1–15.
103. Martins, D. F.; Rosa, A. O.; Gadotti, V. M.; Mazzardo-Martins, L.; Nascimento, F. P.; Egea, J.; López, M. G.; Santos, A. R. The Antinociceptive Effects of AR-A014418, a Selective Inhibitor of Glycogen Synthase Kinase-3 Beta, in Mice. *J. Pain* **2011,** *12* (3), 315–322.
104. Franklin, A. V.; King, M. K.; Palomo, V.; Martinez, A.; McMahon, L. L.; Jope, R. S. Glycogen Synthase Kinase-3 Inhibitors Reverse Deficits in Long-Term Potentiation and Cognition in Fragile X Mice. *Biol. Psychiatry* **2014,** *75* (3), 198–206.
105. Hernandeza, F.; Lucasa, J. J.; Avila, J. GSK and Tau: Two Convergence Points in Alzheimer's Disease. *J. Alzheimers Dis.* **2013,** *33* (Suppl. 1), S141–S144.
106. Hernández, F.; Barredaa, E. G.; Fuster-Matanzoa, A.; Lucasa, J. J.; Avila, J. GSK3: A Possible Link Between Beta Amyloid Peptide and Tau Protein. *Exp. Neurol.* **2010,** *223* (2), 322–325.
107. Eldar-Finkelman, H.; Martinez, A. GSK-3 Inhibitors: Preclinical and Clinical Focus on CNS. *Front. Mol. Neurosci.* **2011,** *4,* 32.
108. Freland, L.; Beaulieu, J. M. Inhibition of GSK3 by Lithium, From Single Molecules to Signaling Networks. *Front. Mol. Neurosci.* **2012,** *5,* 14.
109. Georgievska, B.; Sandin, J.; Doherty, J.; Mörtberg, A.; Neelissen, J.; Andersson, A.; Gruber, S.; Nilsson, Y.; Schött, P.; Arvidsson, P. I.; Hellberg, S.; Osswald, G.; Berg, S.; Johanna Fälting, J.; Bhat, R. V. AZ1080, a Novel GSK3 Inhibitor, Rescues Synaptic Plasticity Deficits in Rodent Brain and Exhibits Peripheral Target Engagement in Humans. *J. Neurochem.* **2013,** *125,* 446–456.
110. Berg, S.; Bergh, M.; Hellberg, S.; Högdin, K.; Lo-Alfredsson, Y.; Söderman, P.; Berg, S.; Weigelt, T.; Ormö, M.; Xue, Y.; Tucker, J.; Neelissen, J.; Jerning, E.; Nilsson, Y.; Bhat, R. Discovery of Novel Potent and Highly Selective Glycogen Synthase Kinase-3β (GSK3β) Inhibitors for Alzheimer's Disease: Design, Synthesis, and Characterization of Pyrazines. *J. Med. Chem.* **2012,** *55* (21), 9107–9119.
111. Luo, G.; Chen, L.; Burton, C. R.; Xiao, H.; Sivaprakasam, P.; Krause, C. M.; Cao, Y.; Liu, N.; Lippy, J.; Clarke, W. J.; Snow, K.; Raybon, J.; Arora, V.; Pokross, M.; Kish, K.; Lewis, H. A.; Langley, D. R.; Macor, J. E.; Dubowchik, G. E. Discovery of Isonicotinamides as Highly Selective, Brain Penetrable, and Orally Active Glycogen Synthase Kinase-3 Inhibitors. *J. Med. Chem.* **2016,** *59* (3), 1041–1051.
112. Onishi, T.; Iwashita, H.; Uno, Y.; Kunitomo, J.; Saitoh, M.; Kimura, E.; Fujita, H.; Uchiyama, N.; Kori, M.; Takizawa, M. A Novel Glycogen Synthase Kinase-3 Inhibitor 2-Methyl-5-(3-{4-[(S)-methylsulfinyl]phenyl}-1-benzofuran-5-yl)-1,3,4-oxadiazole Decreases Tau Phosphorylation and Ameliorates Cognitive Deficits in a Transgenic Model of Alzheimer's Disease. *J. Neurochem.* **2011,** *119* (6), 1330–1340.
113. Saitoh, M.; Kunitomo, J.; Kimura, E.; Iwashita, H.; Uno, Y.; Onishi, T.; Uchiyama, N.; Kawamoto, T.; Tanaka, T.; Mol, C. D.; Dougan, D. R.; Textor, G. P.; Snell, G. P.; Takizawa, M.; Itoh, F.; Kori, M. 2-{3-[4-(Alkylsulfinyl)phenyl]-1-benzofuran-5-yl}-5-methyl-1,3,4-oxadiazole Derivatives as Novel Inhibitors of Glycogen Synthase Kinase-3β With Good Brain Permeability. *J. Med. Chem.* **2009,** *52* (20), 6270–6286.
114. Li, L.; Shao, X.; Cole, E. L.; Ohnmacht, S. A.; Ferrari, V.; Hong, Y. T.; Williamson, D. J.; Fryer, T. D.; Quesada, C. A.; Sherman, P.; Riss, P. J.; Scott, P. J.; Aigbirhio, F. I. Synthesis and Initial In Vivo Studies With [^{11}C]SB-216763: The First Radiolabeled Brain Penetrative Inhibitor of GSK-3. *ACS Med. Chem. Lett.* **2015,** *6* (5), 548–552.
115. Domínguez, J. M.; Fuertes, A.; Orozco, L.; del Monte-Millán, M.; Delgado, E.; Medina, M. Evidence for Irreversible Inhibition of Glycogen Synthase Kinase-3β by Tideglusib. *J. Biol. Chem.* **2012,** *287* (2), 893–904.
116. Lovestone, S.; Boada, M.; Dubois, B.; Hüll, M.; Rinne, J. O.; Huppertz, H. J.; Calero, M.; Andrés, M. V.; Gómez-Carrillo, B.; León, T.; del Ser, T.; ARGO Investigators. A Phase II Trial of Tideglusib in Alzheimer's Disease. *J. Alzheimers Dis.* **2015,** *45* (1), 75–88.
117. Riento, K.; Ridley, A. J. ROCKS: Multifunctional Kinases in Cell Behavior. *Nat. Rev. Mol. Cell Biol.* **2003,** *4* (6), 446–456.
118. Feng, Y.; LoGrasso, P. V.; Defert, O.; Li, R. Rho Kinase (ROCK) Inhibitors and Their Therapeutic Potential. *J. Med. Chem.* **2016,** *59* (6), 2269–2300.
119. Chen, M.; Liu, A.; Ouyang, Y.; Huang, Y.; Chao, X.; Pi, R. Fasudil and Its Analogs: A New Powerful Weapon in the Long War Against Central Nervous System Disorders? *Expert Opin. Investig. Drugs* **2013,** *22* (4), 537–550.
120. Daneshvar, R.; Amini, N. Rho-Associated Kinase Inhibitors: Potential Future Treatments for Glaucoma. *J. Ophthalmic Vis. Res.* **2014,** *9* (3), 395–398.
121. Kubo, T.; Yamaguchi, A.; Iwata, N.; Yamashita, T. The Therapeutic Effects of Rho-ROCK Inhibitors on CNS Disorders. *Ther. Clin. Risk Manag.* **2008,** *4* (3), 605–615.
122. Tönges, L.; Koch, J. C.; Bähr, M.; Lingor, P. ROCKing Regeneration: Rho Kinase Inhibition as Molecular Target for Neurorestoration. *Front. Mol. Neurosci.* **2011,** *4,* 39.

123. Lee, J. H.; Zheng, Y.; von Bornstadt, D.; Wei, Y.; Balcioglu, A.; Daneshmand, A.; Yalcin, N.; Yu, E.; Herisson, F.; Atalay, Y. B.; Kim, M. H.; Ahn, Y. J.; Balkaya, M.; Sweetnam, P.; Schueller, O.; Poyurovsky, M. V.; Kim, H. H.; Lo, E. H.; Furie, K. L.; Ayata, C. Selective ROCK2 Inhibition in Focal Cerebral Ischemia. *Ann. Clin. Transl. Neurol.* **2014,** *1* (1), 2–14.
124. Boland, S.; Bourin, A.; Alen, J.; Geraets, J.; Schroeders, P.; Castermans, K.; Kindt, N.; Boumans, N.; Panitti, L.; Fransen, S.; Vanormelingen, J.; Stassen, J. M.; Leysen, D.; Defert, O. Design, Synthesis, and Biological Evaluation of Novel, Highly Active Soft ROCK Inhibitors. *J. Med. Chem.* **2015,** *58* (10), 4309–4324.
125. Yong, H. Y.; Koh, M. S.; Moon, A. The p38 MAPK Inhibitors for the Treatment of Inflammatory Diseases and Cancer. *Expert Opin. Investig. Drugs* **2009,** *18* (12), 1893–1905.
126. Cuendaa, A.; Rousseau, S. p38 MAP-Kinases Pathway Regulation, Function and Role in Human Diseases. *Biochim. Biophys. Acta* **2007,** *1773* (8), 1358–1375.
127. Coulthard, L. R.; White, D. E.; Jones, D. L.; McDermott, M. F.; Burchill, S. A. p38 MAPK: Stress Responses From Molecular Mechanisms to Therapeutics. *Trends Mol. Med.* **2009,** *15* (8), 369–379.
128. Kim, E. K.; Choi, E. J. Pathological Roles of MAPK Signaling Pathways in Human Diseases. *Biochim. Biophys. Acta* **2010,** *1802* (4), 396–405.
129. Bühler, S.; Laufer, S. A. p38 MAPK Inhibitors: A Patent Review (2012–2013). *Expert Opin. Ther. Pat.* **2014,** *24* (5), 535–554.
130. Fischer, S.; Koeberle, S. C.; Laufer, S. A. p38α Mitogen-Activated Protein Kinase Inhibitors, a Patent Review (2005–2011). *Expert Opin. Ther. Pat.* **2011,** *21* (12), 1843–1866.
131. Norman, P. Investigational p38 Inhibitors for the Treatment of Chronic Obstructive Pulmonary Disease. *Expert Opin. Investig. Drugs* **2015,** *24* (3), 383–392.
132. Marengo, B.; De Ciucis, C. G.; Ricciarelli, R.; Furfaro, A. L.; Colla, R.; Canepa, E.; Traverso, N.; Marinari, U. M.; Pronzato, M. A.; Domenicotti, C. p38 MAPK Inhibition: A New Combined Approach to Reduce Neuroblastoma Resistance Under Etoposide Treatment. *Cell Death Dis.* **2013,** *4,* e589.
133. Munoz, L.; Ralay, R. H.; Roy, S. M.; Hu, W.; Craft, J. M.; McNamara, L. K.; Chico, L. W.; Van Eldik, L. J.; Watterson, D. M. A Novel p38α MAPK Inhibitor Suppresses Brain Proinflammatory Cytokine Up-regulation and Attenuates Synaptic Dysfunction and Behavioral Deficits in an Alzheimer's Disease Mouse Model. *J. Neuroinflammation* **2007,** *4,* 21.
134. Yasuda, S.; Sugiura, H.; Tanaka, H.; Takigami, S.; Yamagata, K. p38 MAP Kinase Inhibitors as Potential Therapeutic Drugs for Neural Diseases. *Cent. Nerv. Syst. Agents Med. Chem.* **2011,** *11* (1), 45–59.
135. Bachstetter, A. D.; Van Eldik, L. J. The p38 MAP Kinase Family as Regulators of Proinflammatory Cytokine Production in Degenerative Diseases of the CNS. *Aging Dis.* **2010,** *1* (3), 199–211.
136. Xing, B.; Bachstetter, A. D.; Van Eldik, L. J. Microglial p38α MAPK Is Critical for LPS-Induced Neurodegeneration, Through a Mechanism Involving TNFα. *Mol. Neurodegener.* **2011,** *6,* 84.
137. Bachstetter, A. D.; Xing, B.; de Almeida, L.; Dimayuga, E. R.; Watterson, D. M.; Van Eldik, E. J. Microglial p38α MAPK Is a Key Regulator of Proinflammatory Cytokine Up-regulation Induced by Toll-Like Receptor (TLR) Ligands or Beta-Amyloid (Aβ). *J. Neuroinflammation* **2011,** *8,* 79.
138. Munoz, L.; Ammit, A. J. Targeting p38 MAPK Pathway for the Treatment of Alzheimer's Disease. *Neuropharmacology* **2010,** *58* (3), 561–568.
139. Legos, J. J.; Erhardt, J. A.; White, R. F.; Lenhard, S. C.; Chandra, S.; Parsons, A. A.; Tuma, R. F.; Barone, F. C. SB239063, a Novel p38 Inhibitor, Attenuates Early Neuronal Injury Following Ischemia. *Brain Res.* **2001,** *892* (1), 70–77.
140. Chung, S. H.; Biswas, S.; Selvaraj, V.; Liu, X. B.; Sohn, J.; Jiang, P.; Chen, C.; Chmilewsky, F.; Marzban, H.; Horiuchi, M.; Pleasure, D. E.; Deng, W. The p38α Mitogen-Activated Protein Kinase Is a Key Regulator of Myelination and Remyelination in the CNS. *Cell Death Dis.* **2015,** *6,* e1748.
141. Alam, J. J. Selective Brain-Targeted Antagonism of p38 MAPKα Reduces Hippocampal IL-1β Levels and Improves Morris Water Maze Performance in Aged Rats. *J. Alzheimers Dis.* **2015,** *48* (1), 219–227.
142. Watterson, D. M.; Grum-Tokars, V. L.; Roy, S. M.; Schavocky, J. P.; Bradaric, B. D.; Bachstetter, A. D.; Xing, B.; Dimayuga, E.; Saeed, F.; Zhang, H.; Staniszewski, A.; Pelletier, J. C.; Minasov, G.; Anderson, W. F.; Arancio, O.; Van Eldik, L. J. Development of Novel In Vivo Chemical Probes to Address CNS Protein Kinase Involvement in Synaptic Dysfunction. *PLoS One* **2013,** *8* (6), e66226.
143. Goldstein, D. M.; Kuglstatter, A.; Lou, Y.; Soth, M. J. Selective p38α Inhibitors Clinically Evaluated for the Treatment of Chronic Inflammatory Disorders. *J. Med. Chem.* **2010,** *53* (6), 2345–2353.
144. Zitouni, S.; Nabais, C.; Jana, S. C.; Guerrero, A.; Bettencourt-Dias, M. Polo-Like Kinases: Structural Variations Lead to Multiple Functions. *Nat. Rev. Mol. Cell Biol.* **2014,** *15* (7), 433–452.
145. Andrysik, Z.; Bernstein, W. Z.; Deng, L.; Myer, D. L.; Li, Y. Q.; Tischfield, J. A.; Stambrook, P. J.; Bahassi el, M. The Novel Mouse Polo-Like Kinase 5 Responds to DNA Damage and Localizes in the Nucleolus. *Nucleic Acids Res.* **2010,** *38* (9), 2931–2943.
146. Kothe, M.; Kohls, D.; Low, S.; Coli, R.; Cheng, A. C.; Jacques, S. L.; Johnson, T. L.; Lewis, C.; Loh, C.; Nonomiya, J.; Sheils, A. L.; Verdries, K. A.; Wynn, T. A.; Kuhn, C.; Ding, Y. H. Structure of the Catalytic Domain of Human Polo-Like Kinase 1. *Biochemistry* **2007,** *46* (20), 5960–5971.
147. McInnes, C.; Wyatt, M. D. PLK1 as an Oncology Target: Current Status and Future Potential. *Drug Discov. Today* **2011,** *16* (13–14), 619–625.
148. Chopra, P.; Sethi, G.; Dastidar, S. G.; Ray, A. Polo-Like Kinase Inhibitors: An Emerging Opportunity for Cancer Therapeutics. *Expert Opin. Investig. Drugs* **2010,** *19* (1), 27–43.
149. Duffey, M. O.; Vos, T. J.; Adams, R.; Alley, J.; Anthony, J.; Barrett, C.; Bharathan, I.; Bowman, D.; Bump, N. J.; Chau, R.; Cullis, C.; Driscoll, D. L.; Elder, A.; Forsyth, N.; Frazer, J.; Guo, J.; Guo, L.; Hyer, M. L.; Janowick, D.; Kulkarni, B.; Lai, S. J.; Lasky, K.; Li, G.; Li, J.; Liao, D.; Little, J.; Peng, B.; Qian, M. G.; Reynolds, D. J.; Rezaei, M.; Scott, M. P.; Sells, T. B.; Shinde, V.; Shi, Q. J.; Sintchak, M. D.; Soucy, F.; Sprott, K. T.; Stroud, S. G.; Nestor, M.; Visiers, I.; Weatherhead, G.; Ye, Y.; D'Amore, N. Discovery of a Potent and Orally Bioavailable Benzolactam-Derived Inhibitor of Polo-Like Kinase 1 (MLN0905). *J. Med. Chem.* **2012,** *55* (1), 197–208.
150. Beria, I.; Ballinari, D.; Bertrand, J. A.; Borghi, D.; Bossi, R. T.; Brasca, M. G.; Cappella, P.; Caruso, M.; Ceccarelli, W.; Ciavolella, A.; Cristiani, C.; Croci, V.; De Ponti, A.; Fachin, G.; Ferguson, R. D.; Lansen, J.; Moll, J. K.; Pesenti, E.; Posteri, H.; Perego, R.; Rocchetti, M.; Storici, P.; Volpi, D.; Valsasina, B. Identification of 4,5-Dihydro-1H-pyrazolo[4,3-h]quinazoline Derivatives as a New Class of Orally and Selective Polo-Like Kinase 1 Inhibitors. *J. Med. Chem.* **2010,** *53* (9), 3532–3551.
151. Casolaro, A.; Golay, J.; Albanese, C.; Ceruti, R.; Patton, V.; Cribioli, S.; Pezzoni, A.; Losa, M.; Texido, G.; Giussani, U.; Marchesi, F.; Amboldi, N.; Valsasina, B.; Bungaro, S.; Cazzaniga, G.; Rambaldi, A.; Introna, M.; Pesenti, E.; Alzani, R. The Polo Like Kinase 1 (PLK1) Inhibitor NMS-P937 Is Effective in a New Model of Disseminated Primary CD56+ Acute Monoblastic Leukaemia. *PLoS One* **2013,** *8* (3), e58424.
152. Talati, C.; Griffiths, E. A.; Wetzler, M.; Wang, E. S. Polo-Like Kinase Inhibitors in Hematologic Malignancies. *Crit. Rev. Oncol. Hematol.* **2016,** *98,* 200–210.
153. Kobayashi, Y.; Yamauchi, T.; Kiyoi, H.; Sakura, T.; Hata, T.; Ando, K.; Watabe, A.; Harada, A.; Taube, T.; Miyazaki, Y.; Naoe, T. Phase I Trial of Volasertib, a Polo-Like Kinase Inhibitor, in Japanese Patients With Acute Myeloid Leukemia. *Cancer Sci.* **2015,** *106* (11), 1590–1595.
154. Gjertsen, B. T.; Schöffski, P. Discovery and Development of the Polo-Like Kinase Inhibitor Volasertib in Cancer Therapy. *Leukemia* **2015,** *29* (1), 11–19.
155. Inglis, K. J.; Chereau, D.; Brigham, E. F.; Chiou, S. S.; Schöbel, S.; Frigon, N. L.; Yu, M.; Caccavello, R. J.; Nelson, S.; Motter, R.; Wright, S.; Chian, D.; Santiago, P.; Soriano, F.; Ramos, C.; Powell, K.; Goldstein, J. M.; Babcock, M.; Yednock, T.; Bard, F.; Basi, G. S.; Sham, H.; Chilcote, T. J.; McConlogue, L.; Griswold-Prenner, I.; Anderson, J. P. Polo-Like Kinase 2 (PLK2) Phosphorylates α-Synuclein at Serine129 in Central Nervous System. *J. Biol. Chem.* **2009,** *284* (5), 2598–2602.
156. Bowers, S.; Truong, A. P.; Ye, M.; Aubele, D. L.; Sealy, J. M.; Neitz, R. J.; Hom, R. K.; Chan, W.; Dappen, M. S.; Galemmo, R. A., Jr.; Konradi, A. W.; Sham, H. L.; Zhu, Y. L.; Beroza, P.; Tonn, G.; Zhang, H.; Hoffman, J.; Motter, R.; Fauss, D.; Tanaka, P.; Bova, M. P.; Ren, Z.; Tam, D.; Ruslim, L.; Baker, J.; Pandya, D.; Diep, L.; Fitzgerald, K.; Artis, D. R.; Anderson, J. P.; Bergeron, M. Design and Synthesis of Highly Selective, Orally Active Polo-Like Kinase-2 (Plk-2) Inhibitors. *Bioorg. Med. Chem. Lett.* **2013,** *23* (9), 2743–2749.
157. Aubele, D. L.; Hom, R. K.; Adler, M.; Galemmo, R. A., Jr.; Bowers, S.; Truong, A. P.; Pan, H.; Beroza, P.; Neitz, R. J.; Yao, N.; Lin, M.; Tonn, G.; Zhang, H.; Bova, M. P.; Ren, Z.; Tam, D.; Ruslim, L.; Baker, J.; Diep, L.; Fitzgerald, K.; Hoffman, J.; Motter, R.; Fauss, D.; Tanaka, P.; Dappen, M.; Jagodzinski, J.; Chan, W.; Konradi, A. W.; Latimer, L.; Zhu, Y. L.; Sham, H. L.; Anderson, J. P.; Bergeron, M.; Artis, D. R. Selective and Brain-Permeable Polo-Like Kinase-2 (Plk-2) Inhibitors That Reduce α-Synuclein Phosphorylation in Rat Brain. *ChemMedChem* **2013,** *8* (8), 1295–1313.

158. Reddy, M. V.; Akula, B.; Jatiani, S.; Vasquez-Del Carpio, R.; Billa, V. K.; Mallireddigari, M. R.; Cosenza, S. C.; Venkata Subbaiah, D. R.; Bharathi, E. V.; Pallela, V. R.; Ramkumar, P.; Jain, R.; Aggarwal, A. K.; Reddy, E. P. Discovery of 2-(1H-Indol-5-ylamino)-6-(2,4-difluorophenylsulfonyl)8-methylpyrido[2,3-d]pyrimidin-7(8H)-one (7ao) as a Potent Selective Inhibitor of Polo Like Kinase 2 (PLK2). *Bioorg. Med. Chem.* **2016,** *24* (4), 521–544.
159. Laufer, R.; Forrest, B.; Li, S. W.; Liu, Y.; Sampson, P.; Edwards, L.; Lang, Y.; Awrey, D. E.; Mao, G.; Plotnikova, O.; Leung, G.; Hodgson, R.; Beletskaya, I.; Mason, J. M.; Luo, X.; Wei, X.; Yao, Y.; Feher, M.; Ban, F.; Kiarash, R.; Green, E.; Mak, T. W.; Pan, G.; Pauls, H. W. The Discovery of PLK4 Inhibitors: (E)-3-((1H-Indazol-6-yl)methylene) indolin-2-ones as Novel Antiproliferative Agents. *J. Med. Chem.* **2013,** *56* (15), 6069–6087.
160. Sampson, P. B.; Liu, Y.; Patel, N. K.; Feher, M.; Forrest, B.; Li, S. W.; Edwards, L.; Laufer, R.; Lang, Y.; Ban, F.; Awrey, D. E.; Mao, G.; Plotnikova, O.; Leung, G.; Hodgson, R.; Mason, J. M.; Wei, X.; Kiarash, R.; Green, E.; Qiu, W.; Chirgadze, N. Y.; Mak, T. W.; Pan, G.; Pauls, H. W. The Discovery of Polo-Like Kinase 4 Inhibitors: Design and Optimization of Spiro[cyclopropane-1,3′[3H]indol]-2′(1′H)-ones as Orally Bioavailable Antitumor Agents. *J. Med. Chem.* **2015,** *58* (1), 130–146.
161. Segev, N. Special Issue Focuses on PAKs. *Cell Logist.* **2012,** *2* (2), 53–135.
162. Rudolph, J.; Aliagas, I.; Crawford, J. J.; Mathieu, S.; Lee, W.; Chao, Q.; Dong, P.; Rouge, L.; Wang, W.; Heise, C.; Murray, L. J.; La, H.; Liu, Y.; Manning, G.; Diederich, F.; Hoeflich, K. P. Leveraging the Pre-DFG Residue Thr-406 to Obtain High Kinase Selectivity in an Aminopyrazole-Type PAK1 Inhibitor Series. *ACS Med. Chem. Lett.* **2015,** *6* (6), 711–715.
163. Shao, Y. G.; Ning, K.; Li, F. Group II p21-Activated Kinases as Therapeutic Targets in Gastrointestinal Cancer. *World J. Gastroenterol.* **2016,** *22* (3), 1224–1235.
164. Pandolfi, A.; Stanley, R. F.; Yu, Y.; Bartholdy, B.; Pendurti, G.; Gritsman, K.; Boultwood, J.; Chernoff, J.; Verma, A.; Steidl, U. PAK1 Is a Therapeutic Target in Acute Myeloid Leukemia and Myelodysplastic Syndrome. *Blood* **2015,** *126* (9), 1118–1127.
165. Yeo, D.; He, H.; Patel, O.; Lowy, A. M.; Baldwin, G. S.; Nikfarjam, M. FRAX597, a PAK1 Inhibitor, Synergistically Reduces Pancreatic Cancer Growth When Combined With Gemcitabine. *BMC Cancer* **2016,** *16,* 24.
166. Maruta, H. Effective Neurofibromatosis Therapeutics Blocking the Oncogenic Kinase PAK1. *Drug Discov. Ther.* **2011,** *5* (6), 266–278.
167. Dolan, B. M.; Duron, S. G.; Campbell, D. A.; Vollrath, B.; Shankaranarayana Rao, B. S.; Ko, H. Y.; Lin, G. G.; Govindarajan, A.; Choi, S. Y.; Tonegawa, S. Rescue of Fragile X Syndrome Phenotypes in Fmr1 KO Mice by the Small-Molecule PAK Inhibitor FRAX486. *Proc. Natl. Acad. Sci. USA* **2013,** *110* (14), 5671–5676.
168. Crawford, J. J.; Hoeflich, K. P.; Rudolph, J. p21-Activated Kinase Inhibitors: A Patent Review. *Expert Opin. Ther. Pat.* **2012,** *22* (3), 293–310.
169. Duffney, L. J.; Zhong, P.; Wei, J.; Matas, E.; Cheng, J.; Qin, L.; Ma, K.; Dietz, D. M.; Kajiwara, Y.; Buxbaum, J. D.; Yan, Z. Autism-Like Deficit in Shank3-Deficient Mice Are Rescued by Targeting Actin Regulators. *Cell Rep.* **2015,** *11* (9), 1400–1413.
170. Ding, Y.; Li, Y.; Lu, L.; Zhang, R.; Zeng, L.; Wang, L.; Zhang, X. Inhibition of Nischarin Expression Promotes Neurite Outgrowth Through Regulation of PAK Activity. *PLoS One* **2015,** *10* (12), e0144948.
171. Ke, Y.; Lei, M.; Wang, X.; Solaro, R. J. Novel Roles of PAK1 in the Heart. *Cell Logist.* **2012,** *2* (2), 89–94.
172. Murray, B. W.; Guo, C.; Piraino, J.; Westwick, J. K.; Zhang, C.; Lamerdin, J.; Dagostino, E.; Knighton, D.; Loi, C. M.; Zager, M.; Kraynov, E.; Popoff, I.; Christensen, J. G.; Martinez, R.; Kephart, S. E.; Marakovits, J.; Karlicek, S.; Bergqvist, S.; Smeal, T. Small-Molecule p21-Activated Kinase Inhibitor PF-3758309 Is a Potent Inhibitor of Oncogenic Signaling and Tumor Growth. *Proc. Natl. Acad. Sci. U. S. A.* **2010,** *107* (20), 9446–9451.
173. Guo, C.; McAlpine, I.; Zhang, J.; Knighton, D. D.; Kephart, S.; Johnson, M. C.; Li, H.; Bouzida, D.; Yang, A.; Dong, L.; Marakovits, J.; Tikhe, J.; Richardson, P.; Guo, L. C.; Kania, R.; Edwards, M. P.; Kraynov, E.; Christensen, J.; Piraino, J.; Lee, J.; Dagostino, E.; Del-Carmen, C.; Deng, Y. L.; Smeal, T.; Murray, B. W. Discovery of Pyrroloaminopyrazoles as Novel PAK Inhibitors. *J. Med. Chem.* **2012,** *55* (10), 4728–4739.
174. Rudolph, J.; Crawford, J. J.; Hoeflich, K. P.; Wang, W. Inhibitors of p21-Activated Kinases (PAKs). *J. Med. Chem.* **2014,** *58* (1), 111–129.
175. Crawford, J. J.; Lee, W.; Aliagas, I.; Mathieu, S.; Hoeflich, K. P.; Zhou, W.; Wang, W.; Rouge, L.; Murray, L.; La, H.; Liu, N.; Fan, P. W.; Cheong, J.; Heise, C. E.; Ramaswamy, S.; Mintzer, R.; Liu, Y.; Chao, Q.; Rudolph, J. Structure-Guided Design of Group I Selective p21-Activated Kinase Inhibitors. *J. Med. Chem.* **2015,** *58* (12), 5121–5136.
176. Patel, S.; Cohen, F.; Dean, B. J.; De La Torre, K.; Deshmukh, G.; Estrada, A. A.; Ghosh, A. S.; Gibbons, P.; Gustafson, A.; Huestis, M. P.; Le Pichon, C. E.; Lin, H.; Liu, W.; Liu, X.; Liu, Y.; Ly, C. Q.; Lyssikatos, J. P.; Ma, C.; Scearce-Levie, K.; Shin, Y. G.; Solanoy, H.; Stark, K. L.; Wang, J.; Wang, B.; Zhao, X.; Lewcock, J. W.; Siu, M. Discovery of Dual Leucine Zipper Kinase (DLK, MAP3K12) Inhibitors With Activity in Neurodegeneration Models. *J. Med. Chem.* **2015,** *58* (1), 401–418.
177. Bernard-Gauthier, V.; Aliaga, A.; Aliaga, A.; Boudjemeline, M.; Hopewell, R.; Kostikov, A.; Rosa-Neto, P.; Thiel, A.; Schirrmacher, R. Syntheses and Evaluation of Carbon-11- and Fluorine-18-Radiolabeled Pan-Tropomyosin Receptor Kinase (Trk) Inhibitors: Exploration of the 4-Aza-2-oxindole Scaffold as Trk PET Imaging Agents. *ACS Chem. Neurosci.* **2015,** *6* (2), 260–276.
178. Piel, M.; Vernaleken, I.; Rösch, F. Positron Emission Tomography in CNS Drug Discovery and Drug Monitoring. *J. Med. Chem.* **2014,** *57* (22), 9232–9258.
179. Molina, J. R.; Yang, P.; Cassivi, S. D.; Schild, S. E.; Alex, A.; Adjei, A. A. Non-Small Cell Lung Cancer: Epidemiology, Risk Factors, Treatment, and Survivorship. *Mayo Clin. Proc.* **2008,** *83* (5), 584–594.
180. Siegel, R.; Ma, J.; Zou, Z.; Jemal, A. Cancer Statistics, 2014. *CA Cancer J. Clin.* **2014,** *64* (1), 9–22.
181. Sharma, S. V.; Bell, D. W.; Settleman, J.; Haber, D. A. Epidermal Growth Factor Receptor Mutations in Lung Cancer. *Nat. Rev. Cancer* **2007,** *7* (3), 169–181.
182. Mok, T. S.; Wu, Y. L.; Thongprasert, S.; Yang, C. H.; Chu, D. T.; Saijo, N.; Sunpaweravong, P.; Han, B.; Margono, B.; Ichinose, Y.; Nishiwaki, Y.; Ohe, Y.; Yang, J. J.; Chewaskulyong, B.; Jiang, H.; Duffield, E. L.; Watkins, C. L.; Armour, A. A.; Fukuoka, M. Gefitinib or Carboplatin-Paclitaxel in Pulmonary Adenocarcinoma. *N. Engl. J. Med.* **2009,** *361* (10), 947–957.
183. Shepherd, F. A.; Pereira, J. R.; Ciuleanu, T.; Tan, E. H.; Hirsh, V.; Thongprasert, S.; Campos, D.; Maoleekoonpiroj, S.; Smylie, M.; Martins, R.; Kooten, M. V.; Dediu, M.; Findlay, B.; Tu, D.; Johnston, D.; Bezjak, A.; Clark, G.; Santabarbara, P.; Seymour, L. Erlotinib in Previously Treated Non-Small-Cell Lung Cancer. *N. Engl. J. Med.* **2005,** *353* (2), 123–132.
184. Cataldo, V. D.; Gibbons, D. L.; Pérez-Soler, R.; Quintás-Cardama, A. Treatment of Non-Small-Cell Lung Cancer With Erlotinib or Gefitinib. *N. Engl. J. Med.* **2011,** *364* (10), 947–955.
185. Wu, Y. L.; Zhou, C.; Hu, C. P.; Feng, J.; Lu, S.; Huang, Y.; Li, W.; Hou, M.; Shi, J. H.; Lee, K. Y.; Xu, C. R.; Massey, D.; Kim, M.; Shi, Y.; Geater, S. L. Afatinib Versus Cisplatin Plus Gemcitabine for First-Line Treatment of Asian Patients With Advanced Non-Small-Cell Lung Cancer Harbouring EGFR Mutations (LUX-Lung 6): An Open-Label, Randomised Phase 3 Trial. *Lancet Oncol.* **2014,** *15* (2), 213–222.
186. Barajas, R. F., Jr.; Cha, S. Imaging Diagnosis of Brain Metastasis. *Prog. Neurol. Surg.* **2012,** *25,* 55–73.
187. Nguyen, N. P.; Nguyen, M. L.; Vock, J.; Lemanski, C.; Kerr, C.; Vinh-Hung, V.; Chi, A.; Khan, R.; Woods, W.; Altdorfer, G.; D'Andrea, M.; Karlsson, U.; Hamilton, R.; Ampil, F. Potential Applications of Imaging and Image-Guided Radiotherapy for Brain Metastases and Glioblastoma to Improve Patient Quality of Life. *Front. Oncol.* **2013,** *3,* 284.
188. Nayak, L.; Lee, E. Q.; Wen, P. Y. Epidemiology of Brain Metastases. *Curr. Oncol. Rep.* **2012,** *14* (1), 48–54.
189. Gril, B.; Evans, L.; Palmieri, D.; Steeg, P. S. Translational Research in Brain Metastasis Is Identifying Molecular Pathways That May Lead to the Development of New Therapeutic Strategies. *Eur. J. Cancer* **2010,** *46* (7), 1204–1210.
190. Grommes, C.; Oxnard, G. R.; Kris, M. G.; Miller, V. A.; Pao, W.; Holodny, A. I.; Clarke, J. L.; Lassman, A. B. Pulsatile High-Dose Weekly Erlotinib for CNS Metastases From EGFR Mutant Non-Small Cell Lung Cancer. *Neuro Oncol.* **2011,** *13* (12), 1364–1369.
191. Jackman, D. M.; Holmes, A. J.; Lindeman, N.; Wen, P. Y.; Kesari, S.; Borras, A. M.; Bailey, C.; Jong, F. D.; Jänne, P. A.; Johnson, B. E. Response and Resistance in a Non-Small-Cell Lung Cancer Patient With an Epidermal Growth Factor Receptor Mutation and Leptomeningeal Metastases Treated With High-Dose Gefitinib. *J. Clin. Oncol.* **2006,** *24* (27), 4517–4520.
192. Owonikoko, T. K.; Arbiser, J.; Zelnak, A.; Shu, H.-K. G.; Shim, H.; Robin, A. M.; Kalkanis, S. N.; Whitsett, T. G.; Salhia, B.; Tran, N. L.; Ryken, T.; Moore, M. K.; Egan, K. M.; Jeffrey, J.; Olson, J. J. Current Approaches to the Treatment of Metastatic Brain Tumours. *Nat. Rev. Clin. Oncol.* **2014,** *11* (4), 203–222.

193. Gow, C. H.; Chien, C. R.; Chang, Y. L.; Chiu, Y. H.; Kuo, S. H.; Shih, J. Y.; Chang, Y. C.; Yu, C. J.; Yang, C. H.; Yang, P. C. Radiotherapy in Lung Adenocarcinoma With Brain Metastases: Effects of Activating Epidermal Growth Factor Receptor Mutations on Clinical Response. *Clin. Cancer Res.* **2008,** *14* (1), 162–168.
194. Zeng, Q.; Wang, J.; Cheng, Z.; Chen, K.; Johnström, P.; Varnäs, K.; Li, D. Y.; Yang, Z. F.; Zhang, X. Discovery and Evaluation of Clinical Candidate AZD3759, a Potent, Oral Active, Central Nervous System-Penetrant, Epidermal Growth Factor Receptor Tyrosine Kinase Inhibitor. *J. Med. Chem.* **2015,** *58* (20), 8200–8215.
195. Riley, R. J.; McGinnity, D. F.; Austin, R. P. A Unified Model for Predicting Human Hepatic, Metabolic Clearance From In Vitro Intrinsic Clearance Data in Hepatocytes and Microsomes. *Drug Metab. Dispos.* **2005,** *33* (9), 1304–1311.
196. Sohlenius-Sternbeck, A. K.; Jones, C.; Ferguson, D.; Middleton, B. J.; Projean, D.; Floby, E.; Bylund, J.; Afzelius, L. Practical Use of the Regression Offset Approach for the Prediction of in vivo Intrinsic Clearance From Hepatocytes. *Xenobiotica* **2012,** *42* (9), 841–853.
197. Mahmood, I. Prediction of Clearance in Humans From In Vitro Human Liver Microsomes and Allometric Scaling. A Comparative Study of the Two Approaches. *Drug Metab. Drug Interact.* **2002,** *19* (1), 49–64.
198. Mahmood, I. Prediction of Human Drug Clearance From Animal Data: Application of the Rule of Exponent and fu Corrected Intercept Method (FCIM). *J. Pharm. Sci.* **2006,** *95* (8), 1810–1821.
199. Ward, K. W.; Smith, B. R. A Comprehensive Quantitative and Qualitative Evaluation of Extrapolation of Intravenous Pharmacokinetic Parameters From Rat, Dog and Monkey to Humans. I. Clearance. *Drug Metab. Dispos.* **2004,** *32* (6), 603–611.
200. Varnäs, K.; Varrone, A.; Farde, L. Modeling of PET Data in CNS Drug Discovery and Development. *J. Pharmacokinet. Pharmacodyn.* **2013,** *40* (3), 267–279.
201. Bao, R.; Gao, P.; Zhang, F.; Tong, Z.; Yu, H.; Xu, Y. Discovery of a Third-Generation EGFR Inhibitor, Which Is Highly Selective and Potent Against Both Resistant and Activating EGFR Mutations for NSCLC Therapy. In *Annual Meeting of the American Association for Cancer Research*, New Orleans, Louisiana (LA), Apr 16–20, 2016; Abstract nr 3063.
202. Bossi, R. T.; Saccardo, M. B.; Ardini, E.; Menichincheri, M.; Rusconi, L.; Magnaghi, P.; Orsini, P.; Avanzi, N.; Borgia, A. L.; Nesi, M.; Bandiera, T.; Fogliatto, G.; Bertrand, J. A. Crystal Structures of Anaplastic Lymphoma Kinase in Complex With ATP Competitive Inhibitors. *Biochemistry* **2010,** *49* (32), 6813–6825.
203. Kris, M. G.; Johnson, B. E.; Berry, L. D.; Kwiatkowski, D. J.; Iafrate, A. J.; Wistuba, I. I.; Varella-Garcia, M.; Franklin, W. A.; Aronson, S. L.; Su, P. F.; Shyr, Y.; Camidge, D. R.; Sequist, L. V.; Glisson, B. S.; Khuri, F. R.; Garon, E. B.; Pao, W.; Rudin, C.; Schiller, J.; Haura, E. B.; Socinski, M.; Shirai, K.; Chen, H.; Giaccone, G.; Ladanyi, M.; Kugler, K.; Minna, J. D.; Bunn, P. A. Using Multiplexed Assays of Oncogenic Drivers in Lung Cancers to Select Targeted Drugs. *JAMA* **2014,** *311* (19), 1998–2006.
204. Ott, G. R.; Wells, G. J.; Thieu, T. V.; Quail, M. R.; Lisko, J. G.; Mesaros, E. F.; Gingrich, D. E.; Ghose, A. K.; Wan, W.; Lu, L.; Cheng, M.; Albom, M. S.; Angeles, T. S.; Huang, Z.; Aimone, L. D.; Ator, M. A.; Ruggeri, B. A.; Dorsey, B. D. 2,7-Disubstituted-pyrrolo[2,1-f][1,2,4]triazines: New Variant of an Old Template and Application to the Discovery of Anaplastic Lymphoma Kinase (ALK) Inhibitors With In Vivo Antitumor Activity. *J. Med. Chem.* **2011,** *54* (18), 6328–6341.
205. Gridelli, C.; Peters, S.; Sgambato, A.; Casaluce, F.; Adjei, A. A.; Ciardiello, F. ALK Inhibitors in the Treatment of Advanced NSCLC. *Cancer Treat. Rev.* **2014,** *40,* 300–306.
206. Muller, I. B.; De Langen, A. J.; Honeywell, R. J.; Giovannetti, E.; Peters, G. J. Overcoming Crizotinib Resistance in ALK-Rearranged NSCLC With the Second-Generation ALK-Inhibitor Ceritinib. *Expert Rev. Anticancer Ther.* **2016,** *16* (2), 147–157.
207. Zhang, I.; Zaorsky, N. G.; Palmer, J. D.; Mehra, R.; Lu, B. Targeting Brain Metastases in ALK-Rearranged Non-Small-Cell Lung Cancer. *Lancet Oncol.* **2015,** *16* (13), e510–e521.
208. Huang, Q.; Johnson, T. W.; Bailey, S.; Brooun, A.; Bunker, K. D.; Burke, B. J.; Collins, M. R.; Cook, A. S.; Cui, J. J.; Dack, K. N.; Deal, J. G.; Deng, Y. L.; Dinh, D.; Engstrom, L. D.; He, M.; Hoffman, J.; Hoffman, R. L.; Johnson, P. S.; Kania, R. S.; Lam, H.; Lam, J. L.; Le, P. T.; Li, Q.; Lingardo, L.; Liu, W.; Lu, M. W.; McTigue, M.; Palmer, C. L.; Richardson, P. F.; Sach, N. W.; Shen, H.; Smeal, T.; Smith, G. L.; Stewart, A. E.; Timofeevski, S.; Tsaparikos, K.; Wang, H.; Zhu, H.; Zhu, J.; Zou, H. Y.; Edwards, M. P. Design of Potent and Selective Inhibitors to Overcome Clinical Anaplastic Lymphoma Kinase Mutations Resistant to Crizotinib. *J. Med. Chem.* **2014,** *57* (4), 1170–1187.
209. Klempner, S. J.; Ou, S. H. Anaplastic Lymphoma Kinase Inhibitors in Brain Metastases From ALK+ Non-Small Cell Lung Cancer: Hitting the Target Even in the CNS. *Chin. Clin. Oncol.* **2015,** *4* (2), 20.
210. Kort, A.; Sparidans, R. W.; Wagenaar, E.; Beijnen, J. H.; Schinkel, A. H. Brain Accumulation of the EML4-ALK Inhibitor Ceritinib Is Restricted by P-Glycoprotein (P-GP/ABCB1) and Breast Cancer Resistance Protein (BCRP/ABCG2). *Pharmacol. Res.* **2015,** *102,* 200–207.
211. Kodama, T.; Hasegawa, M.; Takanashi, K.; Sakurai, Y.; Kondoh, O.; Sakamoto, H. Antitumor Activity of the Selective ALK Inhibitor Alectinib in Models of Intracranial Metastases. *Cancer Chemother. Pharmacol.* **2014,** *74* (5), 1023–1028.
212. Song, Z.; Wang, M.; Zhang, A. Alectinib: (ALK) Inhibitor for Over Coming Clinically-Acquired Resistance. *Acta Pharm. Sin. B* **2015,** *5* (1), 34–37.
213. Seto, T.; Kiura, K.; Nishio, M.; Nakagawa, K.; Maemondo, M.; Inoue, A.; Hida, T.; Yamamoto, N.; Yoshioka, H.; Harada, M.; Ohe, Y.; Nogami, N.; Takeuchi, K.; Shimada, T.; Tanaka, T.; Tamura, T. CH5424802 (RO5424802) for Patients With ALK-Rearranged Advanced Non-Small-Cell Lung Cancer (AF-001JP Study): A Single-Arm, Open-Label, Phase 1–2 Study. *Lancet Oncol.* **2013,** *14* (7), 590–598.
214. Mori, M.; Ueno, Y.; Konagai, S.; Fushiki, H.; Shimada, I.; Kondoh, Y.; Saito, R.; Mori, K.; Shindou, N.; Soga, T.; Sakagami, H.; Furutani, T.; Doihara, H.; Kudoh, M.; Kuromitsu, S. The Selective Anaplastic Lymphoma Receptor Tyrosine Kinase Inhibitor ASP3026 Induces Tumor Regression and Prolongs Survival in Non-Small Cell Lung Cancer Model Mice. *Mol. Cancer Ther.* **2014,** *13* (2), 329–340.
215. Fushiki, H.; Saito, R.; Jitsuoka, M.; Shimada, I.; Kondoh, Y.; Sakagami, H.; Funatsu, Y.; Noda, A.; Murakami, Y.; Miyoshi, S.; Ueno, Y.; Konagai, S.; Soga, T.; Nishimura, S.; Mori, M.; Kuromitsu, S. First Demonstration of in vivo PET Imaging for ALK Inhibitor Using [11C]ASP3026, a Novel Brain-Permeable Type of ALK Inhibitor. In *Proceedings of the 104th Annual Meeting of the American Association for Cancer Research*; Washington, DC, Apr 6–10, 2013. Philadelphia (PA): AACR; *Cancer Res.* **2013**; *73*(8 Suppl): Abstract nr 2678.
216. Galkin, A. V.; Melnick, J. S.; Kim, S.; Hood, T. L.; Li, N.; Li, L.; Xia, G.; Steensma, R.; Chopiuk, G.; Jiang, J.; Wan, Y.; Ding, P.; Liu, Y.; Sun, F.; Schultz, P. G.; Gray, N. S.; Warmuth, M. Identification of NVP-TAE684, a Potent, Selective, and Efficacious Inhibitor of NPM-ALK. *Proc. Natl. Acad. Sci. U. S. A.* **2007,** *104* (1), 270–275.
217. Rodrigues, F. S.; Yang, X.; Nikaido, M.; Liu, Q.; Kelsh, R. N. A Simple, Highly Visual in vivo Screen for Anaplastic Lymphoma Kinase Inhibitors. *ACS Chem. Biol.* **2012,** *7* (12), 1968–1974.
218. Johnson, T. W.; Richardson, P. F.; Bailey, S.; Brooun, A.; Burke, B. J.; Collins, M. R.; Cui, J. J.; Deal, J. G.; Deng, Y. L.; Dinh, D.; Engstrom, L. D.; He, M.; Hoffman, J.; Hoffman, R. L.; Huang, Q.; Kania, R. S.; Kath, J. C.; Lam, H.; Lam, J. L.; Le, P. T.; Lingardo, L.; Liu, W.; McTigue, M.; Palmer, C. L.; Sach, N. W.; Smeal, T.; Smith, G. L.; Stewart, A. E.; Timofeevski, S.; Zhu, H.; Zhu, J.; Zou, H. Y.; Edwards, M. P. Discovery of (10R)-7-Amino-12-fluoro-2,10,16-trimethyl-15-oxo-10,15,16,17-tetrahydro-2H-8,4-(metheno)pyrazolo[4,3-h][2,5,11]-benzoxadiazacyclotetradecine-3-carbonitrile (PF-06463922), a Macrocyclic Inhibitor of Anaplastic Lymphoma Kinase (ALK) and c-ros Oncogene1 (ROS1) With Preclinical Brain Exposure and Broad-Spectrum Potency Against ALK-Resistant Mutations. *J. Med. Chem.* **2014,** *57* (11), 4720–4744.
219. Hatcher, J. M.; Bahcall, M.; Choi, H. G.; Gao, Y.; Sim, T.; George, R.; Jänne, P. A.; Gray, N. S. Discovery of Inhibitors That Overcome the G1202R Anaplastic Lymphoma Kinase Resistance Mutation. *J. Med. Chem.* **2015,** *58* (23), 9296–9308.
220. Ishikawa, T.; Seto, M.; Banno, H.; Kawakita, Y.; Oorui, M.; Taniguchi, T.; Ohta, Y.; Tamura, T.; Nakayama, A.; Miki, H.; Kamiguchi, H.; Tanaka, T.; Habuka, N.; Sogabe, S.; Yano, J.; Aertgeerts, K.; Kamiyama, K. Design and Synthesis of Novel Human Epidermal Growth Factor Receptor 2 (HER2)/Epidermal Growth Factor Receptor (EGFR) Dual Inhibitors Bearing a Pyrrolo[3,2-d]pyrimidine Scaffold. *J. Med. Chem.* **2011,** *54* (23), 8030–8050.
221. Erdo, F.; Gordon, J.; Wu, J. T.; Sziráki, I. Verification of Brain Penetration of the Unbound Fraction of a Novel HER2/EGFR Dual Kinase Inhibitor (TAK-285) by Microdialysis in Rats. *Brain Res. Bull.* **2012,** *87* (4–5), 413–419.
222. Dinkel, V.; Anderson, D.; Winski, S.; Winkler, J.; Koch, K.; Lee, P. A. ARRY-380, a Potent, Small Molecule Inhibitor of ErbB2, Increases Survival in Intracranial ErbB2+ Xenograft Models in Mice. In *Proceedings of the 103rd Annual Meeting of the American Association for Cancer Research*, Chicago, IL, Mar 31 to Apr 4, 2012; Philadelphia (PA): AACR; *Cancer Res.* **2012**, *72* (8 Suppl): Abstract nr 852. doi:1538-7445.AM2012-852.

223. Murthy, R. K.; Hamiltonb, E.; Borges, V.; Moulder, S.; Aucoin, N.; Welch, S.; Chaves, J.; Falkson, C. I.; Walker, L.; Ferrario, C. ONT-380 in the Treatment of HER2+ Breast Cancer Central Nervous System (CNS) Metastases. In *Proceedings of the Thirty-Eighth Annual CTRC-AACR San Antonio Breast Cancer Symposium*, San Antonio, TX, Dec 8–12, 2015; Philadelphia (PA): AACR; *Cancer Res.* **2016,** *76* (4 Suppl): Abstract nr P4-14-19.
224. Ferrario, C.; Welch, S.; Chaves, J. M.; Walker, L. N.; Krop, I. E.; Hamilton, E. P.; Borges, V. F.; Moulder, S. L. ONT-380 in the Treatment of HER2+ Breast Cancer Central Nervous System (CNS) Metastases. *J. Clin. Oncol.* **2015,** *33* (Suppl). Abstr 612.
225. Dinkel, V.; Anderson, D.; Winski, S.; Winkler, J.; Koch, K.; A. Lee, P. A. ARRY-380, a Potent, Small Molecule Inhibitor of ErbB2, Increases Survival in Intracranial ErbB2+ Xenograft Models in Mice. In *Proceedings of the 103rd Annual Meeting of the American Association for Cancer Research*, Chicago, IL, Mar 31 to Apr 4, 2012; Philadelphia (PA): AACR; *Cancer Res.* **2012**, *72*(8 Suppl): Abstract nr 852. doi:1538-7445.AM2012-852.
226. Tanaka, H.; Hirata, M.; Shinonome, S.; Wada, T.; Iguchi, M.; Dohi, K.; Inoue, M.; Ishioka, Y.; Hojo, K.; Yamada, T.; Sugimoto, T.; Masuno, K.; Nezasa, K.; Sato, N.; Matsuo, K.; Yonezawa, S.; Frenkel, E. P.; Shichijo, M. Preclinical Antitumor Activity of S-222611, an Oral Reversible Tyrosine Kinase Inhibitor of Epidermal Growth Factor Receptor and Human Epidermal Growth Factor Receptor 2. *Cancer Sci.* **2014,** *105* (8), 1040–1048.
227. Morikawa, A.; Peereboom, D. M.; Thorsheim, H. R.; Samala, R.; Balyan, R.; Murphy, C. G.; Lockman, P. R.; Simmons, A.; Weil, R. J.; Tabar, V.; Steeg, P. S.; Smith, Q. R.; Seidman, A. D. Capecitabine and Lapatinib Uptake Insurgically Resected Brain Metastases From Metastatic Breast Cancer Patients: A Prospective Study. *Neuro Oncol.* **2015,** *17* (2), 289–295.
228. Polli, J. W.; Humphreys, J. E.; Harmon, K. A.; Castellino, S.; O'Mara, M. J.; Olson, K. L.; John-Williams, L. S.; Koch, K. M.; Serabjit-Singh, C. J. The Role of Efflux and Uptake Transporters in N-{3-Chloro-4-[(3-fluorobenzyl)oxy]phenyl}-6-[5-({[2-(methylsulfonyl)ethyl]amino}methyl)-2-furyl]-4-quinazolinamine (GW572016, Lapatinib) Disposition and Drug Interactions. *Drug Metab. Dispos.* **2008,** *36* (4), 695–701.
229. Heffron, T. P.; Ndubaku, C. O.; Salphati, L.; Alicke, B.; Cheong, J.; Drobnick, J.; Edgar, K.; Gould, S. E.; Lee, L. B.; Lesnick, J. D.; Lewis, C.; Nonomiya, J.; Pang, J.; Plise, E. G.; Sideris, S.; Wallin, J.; Wang, L.; Zhang, X.; Olivero, A. G. Discovery of Clinical Development Candidate GDC-0084, a Brain Penetrant Inhibitor of PI3K and mTOR. *ACS Med. Chem. Lett.* **2016,** *7* (4), 351–356.
230. Heffron, T. P.; Salphati, L.; Alicke, B.; Cheong, J.; Dotson, J.; Edgar, K.; Goldsmith, R.; Gould, S. E.; Lee, L. B.; Lesnick, J. D.; Lewis, C.; Ndubaku, C.; Nonomiya, J.; Olivero, A. G.; Pang, J.; Plise, E. G.; Sideris, S.; Trapp, S.; Wallin, J.; Wang, L.; Zhang, X. The Design and Identification of Brain Penetrant Inhibitors of Phosphoinositide 3-Kinase α. *J. Med. Chem.* **2012,** *55* (18), 8007–8020.
231. Durant, S. T.; Karlin, J.; Pike, K.; Colclough, N.; Mukhopadhyay, N.; Ahmad, S. F.; Bekta, J. M.; Tokarz, M.; Bardelle, C.; Hughes, G.; Patel, B.; Thomason, A.; Cadogan, E.; Barrett, I.; Lau, A.; Pass, M.; Valerie, K. Blood-Brain Barrier Penetrating ATM Inhibitor (AZ32) Radiosensitises Intracranial Gliomas in Mice. In *Annual Meeting of the American Association for Cancer Research*, New Orleans, Louisiana (LA), Apr 16–20, 2016; Abstract nr 3041.
232. Abbott, N. J.; Rönnbäck, L.; Hansson, E. Astrocyte-Endothelial Interactions at the Blood-Brain Barrier. *Nat. Rev. Neurosci.* **2006,** *7* (1), 41–53.
233. Dejana, E. Endothelial Cell-Cell Junctions: Happy Together. *Nat. Rev. Mol. Cell Biol.* **2004,** *5* (4), 261–270.
234. Begley, D. J.; Brightman, M. W. Structural and Functional Aspects of the Blood-Brain Barrier. *Prog. Drug Res.* **2003,** *61,* 39–78.
235. Wong, A. D.; Ye, M.; Levy, A. F.; Rothstein, J. D.; Bergles, D. E.; Searson, P. C. The Blood-Brain Barrier: An Engineering Perspective. *Front. Neuroeng.* **2013,** *6,* 7.
236. Di, L.; Rong, H.; Feng, B. Demystifying Brain Penetration in Central Nervous System Drug Discovery. *J. Med. Chem.* **2013,** *56* (1), 2–12.
237. Rowland, M.; Tozer, T. N. *Clinical Pharmacokinetics and Pharmacodynamics: Concepts and Applications,* 4th ed.; Wolters Kluwer Health/Lippincott William & Wilkins: Philadelphia, 2011.
238. Fung, E. K.; Carson, R. E. Cerebral Blood Flow With [^{15}O]Water PET Studies Using an Image-Derived Input Function and MR-Defined Carotid Centerlines. *Phys. Med. Biol.* **2013,** *58* (6), 1903–1923.
239. Hansen, D. K.; Scott, D. O.; Otis, K. W.; Lunte, S. M. Comparison of In Vitro BBMEC Permeability and In Vivo CNS Uptake by Microdialysis Sampling. *J. Pharm. Biomed. Anal.* **2002,** *27* (6), 945–958.
240. Doan, K. M.; Humphreys, J. E.; Webster, L. O.; Wring, S. A.; Shampine, L. J.; Serabjit-Singh, C. J.; Adkison, K. K.; Polli, J. W. Passive Permeability and P-Glycoprotein-Mediated Efflux Differentiate Central Nervous System (CNS) and Non-CNS Marketed Drugs. *J. Pharmacol. Exp. Ther.* **2002,** *303* (3), 1029–1037.
241. Deo, A. K.; Theil, F. P.; Nicolas, J. M. Confounding Parameters in Preclinical Assessment of Blood-Brain Barrier Permeation: An Overview With Emphasis on Species Differences and Effect of Disease States. *Mol. Pharm.* **2013,** *10* (5), 1581–1595.
242. Palmer, A. M.; Alavijeh, M. S. Overview of Experimental Models of the Blood-Brain Barrier in CNS Drug Discovery. *Curr. Protoc. Pharmacol.* **2013,** *62*. Unit 7.15.
243. Lagas, J. S.; van Waterschoot, R. A.; Sparidans, R. W.; Wagenaar, E.; Beijnen, J. H.; Schinkel, A. H. Breast Cancer Resistance Protein and P-Glycoprotein Limit Sorafenib Brain Accumulation. *Mol. Cancer Ther.* **2010,** *9* (2), 319–326.
244. Römermann, K.; Helmer, R.; Löscher, W. The Antiepileptic Drug Lamotrigine Is a Substrate of Mouse and Human Breast Cancer Resistance Protein (ABCG2). *Neuropharmacology* **2015,** *93,* 7–14.
245. de Lange, E. C.; Danhof, M. Considerations in the Use of Cerebrospinal Fluid Pharmacokinetics to Predict Brain Target Concentrations in the Clinical Setting: Implications of the Barriers Between Blood and Brain. *Clin. Pharmacokinet.* **2002,** *41* (10), 691–703.
246. Zhang, J.; Fu, T.; Chen, Y.; Pu, D.; Lu, S.; Liu, H.; Cheng, Z. Short Oral Absorption Model: One Stone to Shoot Multiple Birds. CPSA 2012 poster.
247. Bergström, M.; Grahnén, A.; Långström, B. Positron Emission Tomography Microdosing: A New Concept With Application in Tracer and Early Clinical Drug Development. *Eur. J. Clin. Pharmacol.* **2003,** *59* (5–6), 357–366.
248. Lee, C. M.; Farde, L. Using Positron Emission Tomography to Facilitate CNS Drug Development. *Trends Pharmacol. Sci.* **2006,** *27* (6), 310–316.
249. Dubois, B.; Feldman, H. H.; Jacova, C.; Dekosky, S. T.; Barberger-Gateau, P.; Cummings, J.; Delacourte, A.; Galasko, D.; Gauthier, S.; Jicha, G.; Meguro, K.; O'brien, J.; Pasquier, F.; Robert, P.; Rossor, M.; Salloway, S.; Stern, Y.; Visser, P. J.; Scheltens, P. Research Criteria for the Diagnosis of Alzheimer's Disease: Revising the NINCDS–ADRDA Criteria. *Lancet Neurol.* **2007,** *6* (8), 734–746.
250. Sander, K.; Galante, E.; Gendron, T.; Yiannaki, E.; Patel, N.; Kalber, T. L.; Badar, A.; Robson, M.; Johnson, S. P.; Bauer, F.; Mairinger, S.; Stanek, J.; Wanek, T.; Kuntner, C.; Kottke, T.; Weizel, L.; Dickens, D.; Erlandsson, K.; Hutton, B. F.; Lythgoe, M. F.; Stark, H.; Langer, O.; Koepp, M.; Årstad, E. Development of Fluorine-18 Labeled Metabolically Activated Tracers for Imaging of Drug Efflux Transporters With Positron Emission Tomography. *J. Med. Chem.* **2015,** *58* (15), 6058–6080.
251. Nilsson, A.; Goodwin, R. J.; Shariatgorji, M.; Vallianatou, T.; Webborn, P. J.; Andrén, P. E. Mass Spectrometry Imaging in Drug Development. *Anal. Chem.* **2015,** *87* (3), 1437–1455.

7.11 Modulating AMPA Receptors for the Treatment of CNS Disorders

Tristan Reuillon, Simon E Ward, and Paul Beswick, University of Sussex, Brighton, United Kingdom

© 2017 Elsevier Ltd. All rights reserved.

7.11.1	**Introduction**	447
7.11.2	**AMPA Receptor Function and Structure**	447
7.11.2.1	Glutamate and Its Implication in Neuropsychiatric and Neurological Disorders	447
7.11.2.2	Structure and Modulation of AMPA Receptors	448
7.11.3	**AMPA Receptor Positive Allosteric Modulators**	450
7.11.3.1	Clinical Studies With AMPAR Potentiators	450
7.11.3.2	Chemotypes of AMPAR Positive Allosteric Modulators	451
7.11.3.3	Recent Medicinal Chemistry of AMPAR Potentiators	452
7.11.3.3.1	Two novel templates from GSK	452
7.11.3.3.2	HTS and hybridization strategies by Pfizer	459
7.11.3.3.3	Evolution and optimization of the Cortex CX614 series	467
7.11.3.3.4	Optimization of an HTS-derived hit by Organon using SBDD	469
7.11.3.3.5	Work from other pharmaceutical and academic groups	473
7.11.4	**AMPA Receptor Antagonists**	473
7.11.5	**Conclusion and Future Perspective**	476
7.11.6	**Conflict of Interest**	476
Acknowledgment		476
References		476

7.11.1 Introduction

This article will focus on the medicinal chemistry of ligands selective for the α-amino-3-hydroxy-5-methyl-4-isoxazolepropionic acid (AMPA) receptor which have been reported in the last decade. The AMPA receptor (AMPAR) is a ligand gated ion channel of the glutamate family, which plays a pivotal role in the biological processes that underpin learning and memory. This renders the AMPA ion channel a highly attractive target for the treatment of cognitive impairment, in particular for conditions linked to reduced levels of glutamate neurotransmission. Excess levels of glutamate are also detrimental and can lead to potentially serious adverse conditions, most notably seizures, which are in part attributed to overstimulation of the AMPAR. Hence, inhibitors of the AMPA ion channel have also been researched and represent an attractive option for the treatment of epilepsy. In addition, high levels of glutamate have strongly been linked with neurodegenerative processes underlying a number of diseases. The majority of work during the last decade has focused on the identification of positive allosteric modulators (PAMs), which will be the main focus of this article. The medicinal chemistry of negative modulators was thoroughly reviewed in the second edition of *Comprehensive Medicinal Chemistry*,[1] and little or no new work has been reported during recent years. However, it is worth mentioning that a number of the compounds previously reported have been progressed into clinical studies, where they have shown encouraging results in epilepsy studies.[2] A brief summary is contained in the section "**AMPA Receptor Antagonists**" together with a description of a recent, novel approach to the identification of AMPA antagonists involving targeting transmembrane AMPA receptor regulatory proteins (TARPs).

7.11.2 AMPA Receptor Function and Structure

7.11.2.1 Glutamate and Its Implication in Neuropsychiatric and Neurological Disorders

In the mammalian central nervous system (CNS), fast excitatory signaling is mediated through binding of the neurotransmitter glutamate, released from presynaptic terminals, to glutamatergic receptors widely distributed on postsynaptic neurons and glia.[3] Fast synaptic neurotransmission plays a major role in controlling diverse sensory, behavioral and cognitive processes, including learning and memory. Glutamate binds to two distinct classes of receptors: ionotropic (ion channels) and metabotropic (G-protein coupled receptors).[4] Three types of ionotropic glutamate receptors (iGluRs) have been identified and are named according to the chemical entity originally discovered to selectively activate each channel: AMPA, NMDA (*N*-methyl-D-aspartate), and kainate ((3*S*,4*S*)-3-(carboxymethyl)-4-isopropenyl-L-proline).[5] Although they share common structural features and act by depolarizing the postsynaptic membrane in response to glutamate, each type of iGluRs has distinct kinetic and pharmacological properties, and plays a disparate role in cognition. iGluRs are involved in several aspects of nervous system development and function, and glutamate neurotransmission dysfunction has been linked to the pathophysiology of several psychiatric and neurological disorders, such as schizophrenia, mood disorders, epilepsy, Alzheimer's disease, and Parkinson's disease.[6–8] As a result,

alteration of glutamatergic neurotransmission with small-molecule drugs attracted the interest of the pharmaceutical research community, since it could possibly lead to the discovery of innovative treatments for a range of diseases. However, the complex pharmacology of the glutamatergic signaling pathway and the absence of highly selective chemical probes have restricted major advancement in this area of neuroscience for many years. Recent developments in the understanding of this multireceptor physiological pathway,[9] the expanding knowledge on the structure and composition of the AMPAR complexes,[10] and the identification of novel, rationally designed, AMPAR ligands with targeted pharmacokinetic profiles represent great promise and could lead to new therapies for a number of neurological and psychiatric conditions in the near future.

Hypofunction of fast excitatory synaptic transmission has been linked to cognition deficit, a major symptom in Alzheimer's disease and schizophrenic patients.[6] In the case of schizophrenia, it has been proposed that the disease predominantly originates from NMDA receptors' (NMDARs) glutamatergic synaptic underactivity, with nonselective NMDAR antagonists, such as ketamine, causing schizophrenia-like symptoms in healthy volunteers.[11,12] In addition, postmortem analysis of schizophrenic hippocampus has revealed a subnormal density of AMPARs and an increased concentration of the glutamate receptor antagonist *N*-acetylaspartyl glutamate, emphasizing the link with hypoglutamatergic neurotransmission.[13] Dynamic regulation of AMPARs in postsynaptic membranes and activation of the receptor are intimately associated with synaptic plasticity, a mechanism believed to underlie learning and memory.[14,15] Under normal physiological conditions, repetitive AMPAR stimulation induces postsynaptic neuronal membrane depolarization, provoking colocalized NMDARs activation through release of the Mg^{2+} block. This enhances NMDAR Ca^{2+}-gating,[16] which concomitantly with AMPAR-mediated cation influx (Na^{+} and K^{+}) eventually results in synapse strengthening, an effect named synaptic plasticity.[15,17] In turn, the increased NMDAR synaptic signaling influences receptor trafficking and additional AMPARs are inserted into the synapses.[18] The rapid response of the AMPAR enables accurate transmission of high-frequency presynaptic impulse.

7.11.2.2 Structure and Modulation of AMPA Receptors

Similarly, to the other iGluRs, AMPARs have a modular tetrameric architecture, organized as dimers of dimers.[19,20] Four different subunits (GluA1 to GluA4), composed of about 900 amino acids and sharing 65%–75% sequence homology, can combine to form homo- or heterodimers, which subsequently combine to form a heterotetramer, composed of at least two types of subunits.[21] Distribution of AMPAR subunits in the CNS has been demonstrated to be uneven between the various brain regions, with different cellular expression within each region.[22] Although they are not expressed by nerve cells, recombinant AMPAR homotetramers are fully functional and have been used to study the structure and pharmacology of the channel. Over the last decade, single electron microscopy and X-ray crystallography have enabled researchers to develop a better understanding of the structure and assembly of the AMPAR subunits.[23] Until recently, only the structure of extracellular subregions of the AMPAR complex and the structure of functional homotetramers in complex with ligands had been resolved by X-ray crystallography.[23,24] These studies provided insights into the mechanism and conformational changes, that occur during AMPAR-gating, and resulted in the elaboration of possible gating models.[24,25] The combined use of X-ray crystallography and cryogenic electron microscopy has now enabled scientists to obtain structural information for GluA2-containing AMPAR heteromers and has revealed new insights into the dynamic arrangement of the extracellular region of the receptor.[26] Each subunit is composed of an extracellular domain, a transmembrane domain and an intracellular domain.[27] The extracellular domain comprises a large *N*-terminal region with binding sites for regulatory proteins, and a ligand binding domain (LBD) consisting of two discontinuous polypeptides, S1 and S2 arranged in a clamshell motif allowing glutamate binding. The LBD is responsible for agonist and antagonist recognition. The transmembrane section is composed of three α-helices (TM1, TM3, and TM4) and a re-entrant hairpin loop (TM2), which constitute part of the cation conducting pore and contribute to the receptor tetrameric assembly.[28] The intracellular section of each subunit displays the C-terminal domain, which possesses interaction sites for a range of accessory proteins, contributing to AMPARs trafficking and regulation of the receptor kinetics.[29–32] Experiment data suggest that the amino-terminal domain (NTD) is critical in regulating the subunit assembly, and, as a result, it has attracted a lot of attention to determine the molecular basis guiding the receptor oligomerization.[20] The NTD has also been shown to control other processes, such as receptor trafficking, channel gating, agonist potency, and allosteric modulation. The traditional gating view is based on the assumption that the LBD is highly mobile and adopts a close clamshell conformation upon binding of an agonist. This conformational change induces disruption of transmembrane segment interactions and formation of a cation pore.

A diverse range of subunit assemblies can lead to functional AMPARs. The composition of the channel in vivo is extremely complicated and influences receptor kinetics and glutamate binding. Despite this diversity in composition, the signaling properties of AMPARs are dominated by the GluA2 subunit, which has been detected in the majority of the receptor complexes.[26] An extra layer of structural diversity arises from the presence of sites of posttranslational modifications and the existence of splice isoforms, known as flip (i) (Ser775; UniProt ascension number P42262-2) and flop (o) (Asn775; UniProt ascension number P42262-1).[33,34] The flip/flop variation, found in the S2 subdomain of the LBD, controls the kinetics of channel closure and desensitization, the reduction of AMPAR-mediated currents in the continuous presence of glutamate.[35,36] Incorporation of flip or flop isoforms in a tetrameric complex is influenced by transmembrane proteins.[29]

In view of the connection of glutamatergic neurotransmission dysfunction with diverse neurological and psychiatric disorders, generation of glutamate receptor ligands has been of interest and a range of different approaches have been

investigated. In particular, according to the mechanism of synaptic plasticity and the causes of cognitive deficit in diseases, such as schizophrenia, enhancement of AMPAR-mediated synaptic transmission has been extensively explored.[37,38] Originally, direct or partial AMPAR agonists were sought, but it quickly became clear that such compounds were associated with a high risk of toxicity following overexcitation of the receptor signaling.[39,40] This approach precluded the precise and refined spatial and temporal control, required for optimal cognitive functioning, and was overcome by the discovery of AMPAR PAMs, termed potentiators, which lack intrinsic activity in the absence of glutamate. Nonetheless, when AMPARs are functionally activated *via* binding of the endogenous substrate, they enhance the agonistic effect by modulating the channel's biophysical properties.[41] Potentiators enhance AMPAR response through two distinct effects on synaptic currents: inhibiting desensitization and/or slowing deactivation.[42] Unlike orthosteric agonists, PAMs maintain the magnitude and/or duration of channel opening during synaptic activity. However, AMPAR potentiators can still cause excitotoxicity, resulting in motor coordination disruption and/or convulsion,[43,44] and therefore carefully determining preclinical therapeutic indexes (TIs) of these molecules is critical for onward development. The majority of modulators described to date have limited subunit selectivity but excellent selectivity against the other ionotropic and metabotropic glutamate receptors. It has been hypothesized that some AMPAR subtypes might govern the "positive" pharmacology of AMPAR PAMs whereas other subtypes might cause the undesired adverse events. Hence, selectively targeting the "positive" subtypes would prevent side-effects and offer an optimal TI. Unfortunately, it is currently impossible to biologically test this assumption. Recent structural studies have revealed a marked vertical compression in AMPAR heteromers, giving rise to novel NTD/LBD interfaces, which may enable subunit-specific allosteric modulation. Alteration of receptor signaling with NTD ligands has been successfully explored with NMDARs. On the other hand, inhibition or negative modulation of AMPARs is an attractive strategy to mediate CNS disorders characterized by excessive neuronal activity. Hence, AMPAR antagonists which dampen aberrant neurotransmission have been developed to treat stroke and epilepsy. However, a number of clinical trials with this class of drug have indicated a narrow therapeutic window and shown associated side-effects, such as ataxia, sedation, and dizziness.[45]

After years of intense research, recent studies have established that AMPARs are part of macromolecular complexes with a large molecular diversity.[46] The complexes result from the assembly of the GluA heterotetramer with auxiliary proteins, including the transmembrane AMPAR regulatory proteins (TARPs), the cornichon homologs, and the CKAMP44 protein.[47] The finding that AMPARs are heteromultimeric in nature indicates that the receptor functions beyond glutamate binding may be largely influenced by non-GluA subunit constituents, which increase the ability of neurons to tune the response to presynaptic excitation. In particular, it has been established that members of the TARP family of proteins dramatically regulate AMPAR trafficking, gating, and pharmacology, but also control sensitivity to AMPAR ligands.[47–49] TARPs comprise γ2 (stargazing), γ3, γ4, γ5, γ7, and γ8 subunits, which are differentially localized in specific neuronal and glial populations throughout the CNS.[50,51] Recently, the molecular architecture of the AMPAR–TARP-γ2 complex has been reported in two separate studies and defines the molecular basis for TARP modulation of AMPAR gating and pharmacology.[52,53] The stoichiometry of the TARP–AMPAR complex is still unclear, but distinct interactions between the two component TMDs have been elucidated. Electrostatic interactions between the "palm" section of TARPs and the lower part of the AMPAR LBD also contribute to the complex formation. It is assumed that the contraction of AMPARs upon activation enhances this electrostatic attraction, accounting for the TARP-mediated stabilization of the opened state AMPARs.[53] Interaction mapping studies have also revealed that the distal AMPAR NTD also possesses TARP interaction regions, which impact on AMPAR gating.[54] An increasing number of studies into neuropsychiatric and neurodegenerative illnesses are demonstrating an emerging pathological role for TARPs. Members of the TARP protein family have distinct regional expression across the CNS, resulting in physiologic differentiation of the AMPAR activity.[55] This discrete distribution provides the innovative and attractive opportunity to modulate AMPARs in specific brain regions to access modulators with potential therapeutic advantage, which would not globally affect synaptic transmission.[56] This would be achieved by identifying TARP-dependent AMPAR ligands and a similar strategy has recently been successfully implemented by Lilly and Janssen in their search for safer AMPAR antagonists for the treatment of epilepsy,[57,58] demonstrating that accessory proteins are novel pharmacological targets. Positive emission tomography studies with a range of AMPAR modulators have indicated that different concentrations of potentiators are required to selectively activate the CNS regions associated with procognitive and undesired effects, suggesting a potential role of localized auxiliary proteins, resulting in AMPAR complexes with different biophysical properties.[59]

The LBD of the channel has an opened bilobate structure which closes upon binding of glutamate, initiating the gating cascade.[60,61] According to X-ray cocrystal structures of positive modulators bound to the LBD of AMPAR, all potentiators bind at the S1S2 interface of the LBD, resulting in increased stability of the closed glutamate-bound dimer.[62] Several studies have demonstrated that the isolated LBD possesses similar pharmacological properties to the native membrane-bound AMPAR.[63] This has enabled significant advance in the understanding of the biophysical and structural properties of the channel, allowing structure-based drug design (SBDD) of agonists and antagonists, but also the identification of binding sites for PAMs.[64] Irrespective of their mechanistic properties and mode of action, AMPAR potentiators have been shown to enhance glutamatergic synaptic activity in several in vitro experiments both on recombinant and on native tissue preparation,[17,65] and improve cognition in preclinical animal models and in small but not all clinical trials.[66–70] In addition, AMPAR PAMs have been therapeutically beneficial to treat a range of neuropsychiatric and neurological conditions in animal models, such as anxiety, attention-deficit hyperactivity disorder (ADHD), Parkinson's disease, and depression.[71–75]

7.11.3 AMPA Receptor Positive Allosteric Modulators

7.11.3.1 Clinical Studies With AMPAR Potentiators

A number of candidates have been identified that have entered clinical development. Encouragingly no major mechanism-related safety issues have been reported and some compounds have shown promising efficacy in early patient-based studies, however, no compounds have yet demonstrated sufficient efficacy to merit large scale efficacy studies. Table 1 summarizes compounds that have entered clinical evaluation many of which have been terminated.

Cortex pioneered early work in the area and reported encouraging results with early compounds such as CX516, which demonstrated positive effects in studies with healthy volunteers[70] and as an adjunct therapy in patients with schizophrenia.[76,77] Unfortunately, CX516 failed to demonstrate efficacy in a number of later studies when tested in patients with mild cognitive impairment,[78] autism[79], or Alzheimer's disease.[80] A later compound, CX717 (structure currently unknown) was also progressed to clinical studies, where it failed to demonstrate beneficial effects in healthy subjects,[88] but showed some efficacy in ADHD patients.[89] Cortex were unable to obtain funding to follow up on the positive results seen in patients with ADHD, but they are currently developing CX717 for respiratory depression (Table 2). Cortex have also taken a third compound CX691 into the clinic either alone or following licensing deals with other companies, but the compound failed to demonstrate beneficial effects.[81–83] Organon, Lilly, and GlaxoSmithKline (GSK) have also progressed molecules into the clinic but all have reported negative data.[78,84–87] Understanding why some compounds have shown hints of efficacy, yet others have failed, is an important challenge and the answer will be key in the design of the next generation of AMPA modulators.

A number of AMPAR modulators remain under clinical investigation (Table 2). Cortex is again leading the way, but has changed therapeutic focus to respiratory conditions, and recently the company name changed to RespireRx. They are currently progressing three compounds for sleep apnea and drug-induced respiratory depression.[91] The only company currently known to be active in the psychiatry area is Pfizer with a compound PF-4958242 **11** in phase I studies. A total of 11 phase I studies have been conducted over an extended period,[90] many of these studies focus on pharmacokinetic evaluation and investigation of drug–drug interaction potential, suggesting that there are potentially a number of safety concerns with the compound. The results of one study with PF-04958242 have been published, where it failed to show beneficial effects in treating age-related hearing loss.[92]

Table 1 AMPAR positive modulators clinically evaluated but whose progression has been terminated

Molecule	*Trial*	*Status*
CX516 (**2**) Ampalex	Cognitive performance in healthy young and aged volunteers[70,76]	Improved cognitive performance
	CX516 added to Clozapine, Olanzapine, or Risperidone in patients with schizophrenia[77]	Inconsistent cognitive benefits
	Efficacy and safety of CX516 in elderly participants with mild cognitive impairment[78]	Completed
	Effects of CX516 on functioning in fragile X syndrome and autism[79]	Completed
	Treatment of Alzheimer's disease with CX516[80]	Completed
CX691 (**3**)	Cardiac safety study of phase I and phase II ORG24448 patients[81]	95 patients Completed
ORG24448	Depression: 8 week treatment, includes PET analysis	180 patients
SCH900460	Excluded patients with propensity for seizure following EEG assessment[82]	Completed
Faramaptor	TUNRS NIMH-funded cognitive impairments in schizophrenia: 8 weeks adjunctive therapy to existing atypical antipsychotic medication[83]	Terminated
ORG26576 (**4**)	Phase II major depressive disorder: 54 patients[84] Part 1: 100–600 mg bid up to 16 days Part 2: 30 subjects; high dose group and low dose group; 28 days dosing	Completed
	ADHD: 60 patients[85]; 100–300 mg BID; 8 weeks	Completed
LY451395 (**7**) (Mibampator)	Aggression and agitation in Alzheimer's disease: 132 patients; 3 mg bid 12 weeks[78]	Comparable to placebo on all endpoint except Frontal Systems Behavior Inventory where a significant improvement was demonstrated ($p=0.007$) (38)
	Alzheimer's disease: 200 patients[86]	Negative
GSK729327 (**9**)	Phase I: safety and tolerability in healthy volunteers: 79 volunteers, 1–6 mg[87]	Completed

Table 2 AMPAR potentiators still under clinical investigation in 2016

Molecule	*Trial*	*Status*
CX717	DARPA-funded small scale trial in healthy volunteers subjected to simulated night shift work[88]	No improvement in cognitive performance
	ADHD small (n=23–28) study of 200 mg bid and 800 mg bid for 3 weeks in adults with moderate-severe symptoms	Significant improvements at highest dose on hyperactivity and inattention indices
	Drug-induced respiratory depression	Pending
CX1739	Sleep apnea	No effect on mean apnea/hypopnea index, however significantly reduced apnea time
	Drug-induced respiratory depression	
CX1942	Respiratory depression (intravenous)	Pending
PF-04958242 (**11**)	Phase I[90]	On-going

7.11.3.2 Chemotypes of AMPAR Positive Allosteric Modulators

A number of excellent comprehensive reviews, describing the historical chemotypes originally explored as selective AMPAR positive modulators (Fig. 1), have been published in recent years.[93–95] Briefly, three major classes have been explored: the benzamides, the thiadiazines, and the phenethyl sulfonamides. Chronologically, the benzamide series, derived from the nootropic agent aniracetam **1**, was first investigated and developed by Cortex into derivatives such as CX516 **2**, CX691 **3**, and ORG26576 **4**, which were all tested in the clinic. Then the thiadiazine series, originating from the diuretic agent cyclothiazide **5**, was also extensively investigated, leading to Servier's clinical candidate S-18986 **6**. Finally, a class of phenethyl sulfonamides, discovered by Lilly, generated significant interest with a number of subsequent patent applications from several pharmaceutical companies also covering sulfonamide

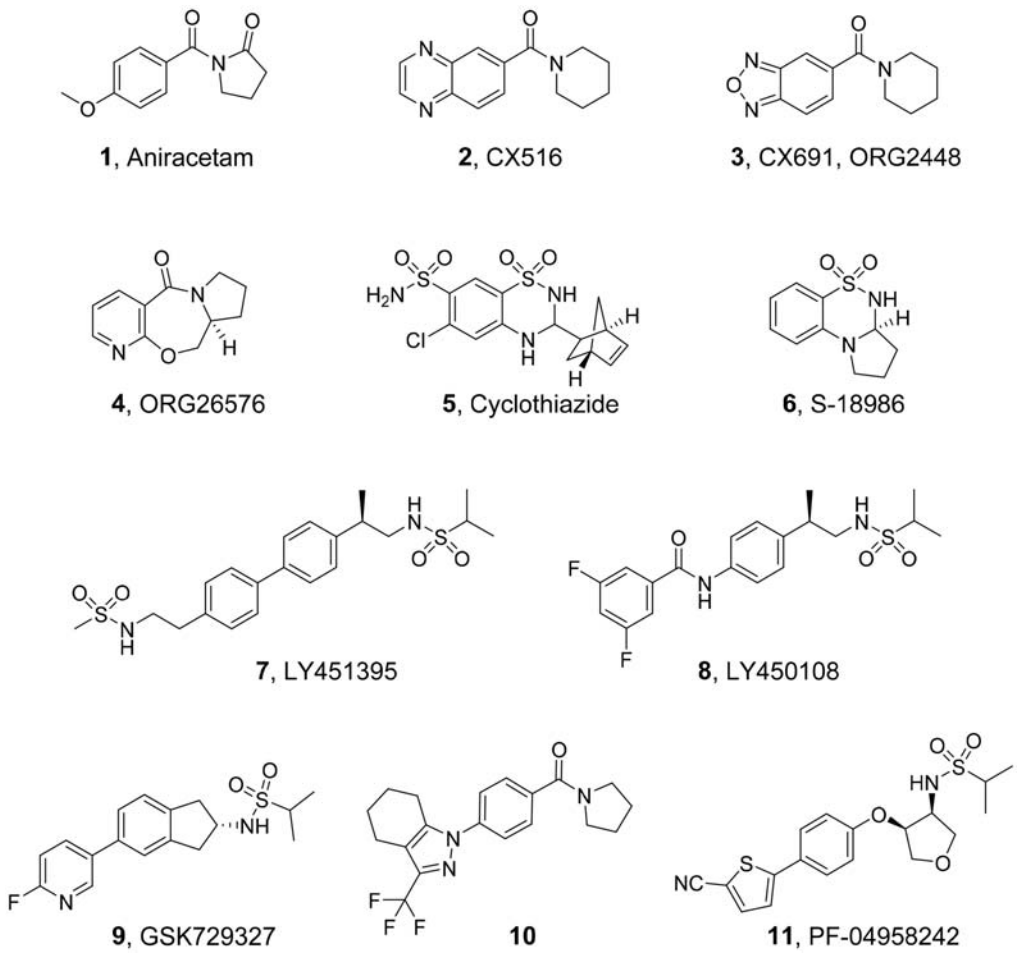

Fig. 1 Representative chemotypes of AMPAR positive allosteric modulators.

derived structures. This class has yielded candidate compounds including LY451395 **7** and LY450108 **8** from Lilly, GSK729327 **9** from GSK and PF-04958242 **11** from Pfizer. In recent years, GSK also filed a number of patents describing novel AMPAR potentiators, all displaying a trifluoromethylpyrazole group, and later reported the discovery of clinical candidate **10**, a benzamide derivative with a fused trifluoromethylpyrazole scaffold at the *para* position.[96] It is worth noting that since, trifluoromethylpyrazole derivatives have become common functionality in AMPAR potentiator structures that have been claimed by a number of pharmaceutical groups and can be considered as the latest class of AMPA PAMs. Over time the modulators developed have become increasingly more potent for the AMPAR, with the original benzamides being weaker than the phenethylsulfonamides.[93]

As highlighted in our 2015 review of the AMPAR potentiator patent literature,[97] a number of novel chemotypes have recently been discovered, some of which are suggested to have a different mode of action and potentially a different clinical profile. This article will concentrate on new developments reported in the scientific literature over the last ten years and not fully covered by previous reviews. We will mainly focus on the new core templates, some derived from high-throughput screens (HTS), with an emphasis on structure–activity relationships (SARs), drug metabolism and pharmacokinetics (DMPK) properties, and pharmacological profiles of these series. While only GSK and Pfizer have described in detail the discovery and profiles of development candidates (**9**, **10**, and **11**),[59,96,98] other organizations have published descriptions of a range of different chemotypes for which no development has been reported. It is also interesting to note that many recent scientific articles and patents in this area have been published by academic groups with a reduced number coming from industrial laboratories, this perhaps has been influenced by the decision of many companies to withdraw from the neuroscience area, and also in some cases the move of experts in this area from industry to the academic sector.

7.11.3.3 Recent Medicinal Chemistry of AMPAR Potentiators

7.11.3.3.1 Two novel templates from GSK

Between 2005 and 2010, GSK have filed a large number of patent applications for novel AMPAR modulators, indicating strong interest from the company in this area of neuroscience.[99–110] In the period covered by this article, they published three scientific articles, each focusing on a different chemotype.[96,98,111]

In a short communication,[111] they reported the discovery of a series of *N*-substituted pyrrolidines and tetrahydrofurans (THF), related to the phenethyl sulfonamide modulators described by Lilly. One may assume that this exploratory work, based on existing literature, was conducted when the company first started to develop an interest in this area and can be considered as GSK's initial attempt to identify AMPAR positive modulators. The original Lilly phenethyl sulfonamide series generally suffered from poor physicochemical properties, such as low solubility, high polar surface area (PSA), and high lipophilicity, which might have contributed to the failure of the compounds which progressed to the clinic (LY451395 **7** and LY450108 **8**). By introducing heteroatoms on the phenethyl moiety, using a 3,4-disubstituted pyrrolidine (**Fig. 2**) or a 3,4-disubstituted THF (**Fig. 3**) linker, and exploring replacement for the *N*-phenyl methanesulfonamide motif, the GSK team attempted to modulate these undesired properties. Interestingly the reported pyrrolidine linker derivatives have *trans* relative stereochemistry whereas the THF linker derivatives have *cis* relative stereochemistry. This renders direct comparisons between the two subseries challenging and it is assumed that direct matched-pairs have not been prepared, since according to the authors these stereochemistry were only selected because of their synthetic tractability. The compounds were screened for their ability to potentiate glutamate-induced calcium influx against recombinant hGluA2i receptors in a fluorometric imaging plate reader (FLIPR)-based assay, with the maximal response of cyclothiazide defined as 100%.

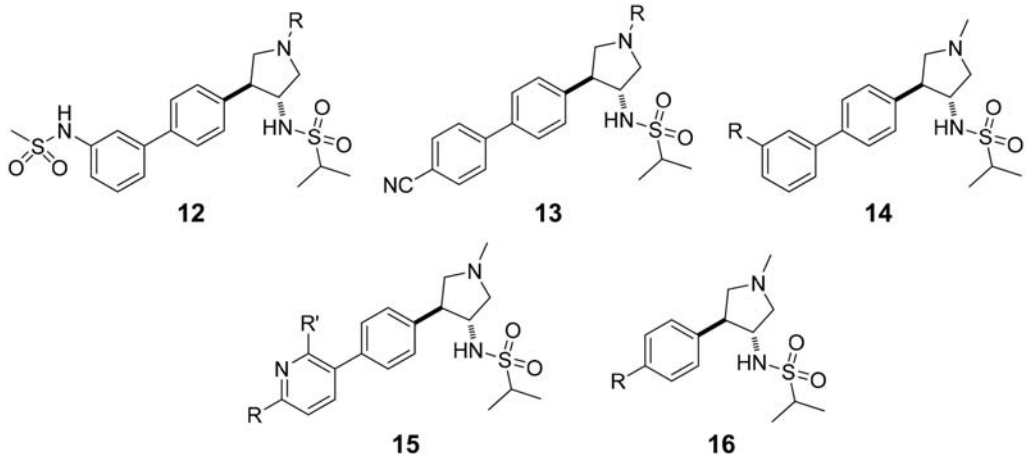

Fig. 2 Representative structures of the pyrrolidine-linked *iso*propylsulfonamide derivatives.

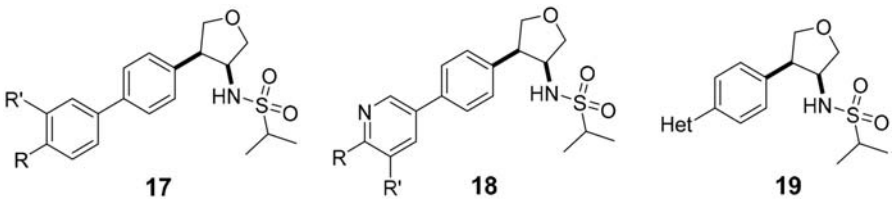

Fig. 3 Representative structures of the tetrahydrofuran-linked *iso*propylsulfonamide derivatives.

Rigidification of the linker and introduction of a heteroatom in this part of the template was well tolerated since the first derivative prepared **12** (R = Me) induced strong potentiation of the hGluA2i recombinant receptor (EC_{50} = 0.3 μM, Asym Max = 124%). Different substituents on the pyrrolidine nitrogen atom were investigated (**12** and **13**, R = Me, Et, ^{i}Pr, Ph) and showed that *N*-methylated pyrrolidines afforded the best activities, with bulkier groups leading to decreased potentiation. Reduction of the PSA was examined by replacing the *meta* methylsulfonamide moiety by a *para* nitrile, as in **13** or various *meta* substituents, as in **14**, such as a methylsulfone, an acetamide, a methylketone, or a trifluoromethyl group. All of these modifications resulted in at least a 10-fold loss in potency. Changing the phenyl ring for a pyridyl, **15** (R = R′ = H) or a substituted pyridyl **15** (R = H, R′ = F or R = F, R′ = H) produced compounds with higher EC_{50}s than **12** (R = Me), in the micromolar range (2.5–5 μM). Thiophenes were also explored as potential phenyl replacements but afforded weaker compounds (**16**, R = 2-thiophene, EC_{50} = 20 μM; **16**, R = 3-thiophene, EC_{50} = 3.2 μM, Fig. 2).

A major downside of the majority of these pyrrolidine-linked *iso*propylsulfonamides was an undesired off-target inhibition of the hERG cardiac channel. Despite a reduction in lipophilicity, these molecules contain a basic center, a common feature in compounds with affinity for hERG, and some derivatives were very potent hERG inhibitors, such as **12** (R = Ph, hERG IC_{50} = 1.3 μM) or **15** (R = F, R′ = H, hERG IC_{50} = 1.0 μM), Fig. 2. An increase in solubility was successfully achieved, with compound **12** (R = Me) and **13** (R = Me), Fig. 2, which achieved levels of >9 mg/mL and >2.7 mg/mL, respectively. Intrinsic clearance was high in both rat and human liver microsomes (RLM and HLM) for *N*-methylated derivatives, with *N*-dealkylation being identified as a major route of metabolism. Compounds with larger *N*-substituents generally achieved good microsomal stability but had similar or higher affinity for hERG relative to AMPAR. It was hypothesized that substituting the pyrrolidine ring by a THF could mitigate the hERG and metabolic liabilities of this series and afford selective compounds with a better pharmacokinetic profile.

All the THF analogs reported (seven in total) showed excellent potentiation of the AMPAR (EC_{50} 112%) and were significantly more active than the *N*-methyl pyrrolidine derivatives. This could be explained by the reduced steric bulk of the THF and also possibly by the different relative stereochemistry. The calculated lipophilicity and PSA of the THF derivatives was lower than that of the pyrrolidine analogs. With the exception of **17** (R = CN, R′ = H) and **18** (R = F, R′ = H), Fig. 3, all the molecules in this subseries had more than 100-fold selectivity for hGluA2i over hERG. Unfortunately, only a limited set of in vitro DMPK data was reported for these THF modulators and it is impossible to know if these molecules successfully achieved the targeted properties discussed earlier. Indeed, the intrinsic clearance of only two analogs, **18** (R = H, R′ = F) and **19** (Het = 2-(5-F)-pyridyl), Fig. 3, was disclosed and both compounds had high turnover in RLM. In addition, no solubility or CNS permeability data are given for the THF derivatives.

The limited success in identifying AMPAR modulators with desirable physicochemical and pharmacokinetic properties starting from a literature chemotype probably prompted GSK to identify their own chemical hits through screening of in-house compound libraries. Hence in a second publication from 2010, scientists at GSK reported the discovery and optimization of indane clinical candidate **9**.[98] From this publication, it appears that the indane series was the first novel chemical core extensively explored by GSK in their search for AMPAR positive modulators. Interestingly in addition to high potency, scientists at GSK were also targeting a specific pharmacokinetic profile, which would deliver high unbound compound concentrations. In this respect, the article not only presents the SAR around the indane core but also detailed in vitro and in vivo DMPK data, which led to the selection of the clinical candidate.

The exploratory work in this series started with the identification of lead amino indane **20**, Table 3, a rigid analog of the phenethyl series, which comprises the two sulfonamide moieties of Lilly's clinical candidate LY451395 **7**. Compound **20** induced significant potentiation of the AMPAR-mediated response against recombinant hGluA2i receptors in a FLIPR-based fluorescent-indicator dye assay (pEC_{50} = 6.1, Asym Max = 123%). Owing to its encouraging calculated physicochemical properties (see Table 3), lead **20** was profiled in an array of in vitro assays, and found to have acceptable rat protein plasma binding (95.9%) and good selectivity for AMPAR over closely related ion channels. Additionally, it did not cause CYP450 inhibition at low concentrations but was identified as a moderate P-gp substrate with a moderate efflux ratio (ER = 5.8) in a MDCK–MDR1 permeability assay. This was assumed to be caused by the high PSA (92 Å^2) and resulted in low CNS penetration in a rat oral pharmacokinetic study (Table 1, brain:blood ratio = 0.1) despite good systemic exposure.

With the preliminary SAR indicating that modulation of the *iso*propylsulfonamide moiety was not tolerated, attention turned to modification of the phenyl ring. Deletion of the *meta* substituent and introduction of *ortho* or *para* groups led to a significant reduction in potency. A broad range of alternative *meta* substituents were investigated but none retained the activity of compound

Table 3 Physicochemical and DMPK properties of lead compound **20**

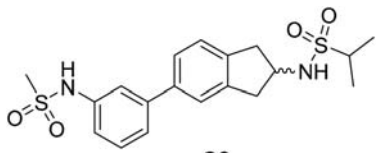

20

PSA (Å^2)	*MWt g/mol)*	*clogP*[a]	*PPB*[b]	*AUC_{0-t} (ng h/mL)*	*Brain:blood (AUC_{0-t} ratio*	P_{app} *(+ inh) (nm/s)*[c]	*ER*[d]
92	409	2.7	95.9%	1130	0.1	608	5.8

[a]clogP Daylight Chemical Information Systems Inc., Alisa Viejo, CA, http://www.daylight.com.
[b]Rat plasma protein binding determined *via* a dialysis method at 1 μg/mL.
[c]Apical (A) to basolateral (B) transport rates of molecules (0.5 μM) across MDCK–MDR1 cells in the presence of a potent P-gp inhibitor.
[d]Efflux ratio: the ratio of transport from B–A/A–B in the absence of a P-gp inhibitor.

20, with the exception of sulfonamide derivatives (secondary and tertiary), but which also maintained undesirable high PSA. In vivo exposure of some of these potent analogs was determined in rat pharmacokinetic studies but similarly to **20** all suffered from poor CNS penetration. As a result, a number of aromatic rings with significantly lower PSA was explored, with the objective to reduce affinity for P-gp while maintaining high free drug concentration and good potency. This led to the identification of 3-pyridyl and 2-pyridyl indane analogs (Fig. 4: **21**, R = H and **22**, R = H), Fig. 4. Although, unsubstituted 3-pyridyl analog **21** (R = H) had lower potency in the FLIPR assay (pEC_{50} = 4.8, Asym Max = 101%), inhibited CYP1A2 (IC_{50} = 0.6 μM) and was moderately stable in rat microsomes (Cli = 2.1 mL/min/g), it possessed significantly improved physicochemical properties, such as lower PSA (59 Å^2), molecular weight (316 g/mol), and clogP (2.3). These pyridyl derivatives were deemed interesting starting points for the identification of compounds with improved CNS penetration and a series of close analogs was prepared. To avoid an increase of the PSA (PSA < 60 Å^2), pyridyl substituents were limited to alkyl and halo groups.

In the 3-pyridyl indane series, represented by **21**, Fig. 4, introduction of a single substituent at any position of the pyridyl ring reduced CYP450 inhibition, but only *para*-substitution provided stronger potentiators (**21**, R = 6-F, pEC_{50} = 5.3, Asym Max = 106%; **21**, R = 6-Me, pEC_{50} = 5.5, Asym Max = 107%). Intrinsic clearance across this set of substituted 3-pyridyl analogs was variable, all compounds had noticeably higher human microsomal turnover than the unsubstituted pyridyl **21** (R = H) and the fluoro analogs were generally more stable than the methyl substituted pyridines. The same pattern in terms of potency (**22**, R = 5-F, pEC_{50} = 5.2, Asym Max = 114%; **22**, R = 5-Me, pEC_{50} = 5.5, Asym Max = 90%), CYP450 inhibition and microsomal stability was observed in the 2-pyridyl indane series, represented by **22**. To validate the initial hypothesis that a reduction in PSA would increase CNS exposure, a selection of compounds from these series (**21** and **22**) with lower PSA than **20** were assessed in rat in vivo pharmacokinetic studies and found to have significantly improved brain to blood ratios (**21**, R = 2-F, brain:blood ratio = 1.5; **22**, R = 6-Me, brain:blood ratio = 1.4).

The exploratory work described above was conducted using racemic mixtures of indanes, comprising *R* and *S* enantiomers. Testing of single enantiomers indicated that the *S* enantiomers were significantly more potent, hence further exploration and characterization then focused on derivatives with the *S* stereochemistry. Three enantiomerically pure modulators (Fig. 5: **9**, **23**, and **24**) were profiled in detail. Indanes **9**, **23**, and **24** all produced good potentiation of AMPAR in the FLIPR assay, did not inhibit the CYP450 isoforms tested and retained the good microsomal clearance of the racemic mixtures, with methyl derivative **23** having higher intrinsic turnover than fluoro derivatives **9** and **24**. In a whole-cell patch clamp electrophysiology assay, these compounds also showed clear potentiation of AMPAR-mediated currents over a range of concentrations in HEK293 cells expressing hGluA2i homomeric receptors. Furthermore, all three derivatives (**9**, **23**, and **24**) had excellent selectivity against a wide range of ion channels, enzymes, and GPCRs. When tested in two in vivo behavioral cognition models, compounds **9** and **24** had a significant effect. Administration of both compounds at 0.3 mg/kg (PO) improved recognition memory in male rats, in the 24 h delay-induced deficit in a novel object recognition (NOR) experiment.[112] In the passive avoidance task assay,[113] modulator **9** attenuated the scopolamine-induced amnesic effect when administered at 3 and 10 mg/kg (PO), while compound **24** was active at 1 and

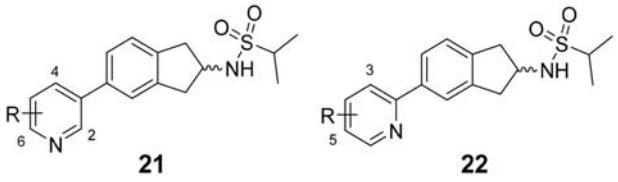

21 **22**

Fig. 4 Chemical structure of the racemate pyridyl indane derivatives.

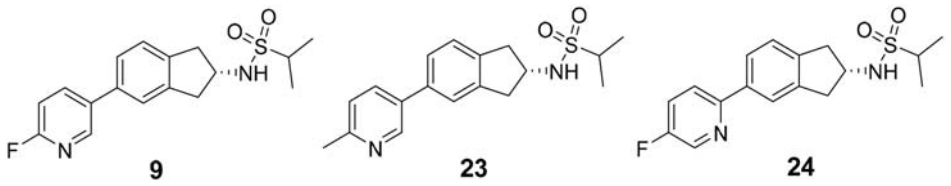

Fig. 5 Structure of the three enantiopure indanes extensively profiled.

3 mg/kg (PO). Based on the efficacy and DMPK data, only derivatives **9** and **24** were progressed to safety and tolerability studies. From these studies (no direct comparison is given), **9** was selected as the development compound.

The binding mode of the indane series was determined from a 1.8 Å resolution crystal structure of the functional hGluA2i S1S2 LBD in complex with modulator **9** (PDB code 2xhd; Fig. 6). The compound was found to bind in an analogous manner to the phenethyl sulfonamides described by Lilly: the *iso*propylsulfonamide moiety points into one of the two deep hydrophobic pockets present at the dimer interface, having displaced a network of four water molecules, and the sulfonamide NH makes a hydrogen bond with the backbone carbonyl of Pro515. The aromatic ring of the indane core sits in a narrow tunnel between the two lobs of the binding pocket, while the fluoropyridyl ring points toward the top of the symmetrical end of the inverted U-shaped binding pocket and is only making hydrophobic contacts with the protein.

Clinical candidate **9** had low equilibrium solubility ($\leq$0.1 mg/mL) across the range of pH (2–10) and physiological fluids (water, simulated gastric fluid, and simulated intestinal fluid) tested, but high permeability (P_{app} (+inh) = 688 nm/s; ER = 1.1), which delivered an attractive pharmacokinetic profile across different species. Indeed, **9** had good oral bioavailability (51%–61%) and low blood clearance (3%–11% liver blood flow) in the three preclinical species tested (rat, dog, and monkey). In addition to these suitable developability properties, compound **9** had excellent solid and solution stability under a range of conditions and did not induce time-dependent inhibition of CYP450. Furthermore, no formation of glutathione conjugates was detected, eliminating the potential liability associated with the presence of the α-fluoropyridine. AMPAR modulator **9** induced weak PXR activation in both rat and human, and as such only had a low propensity for drug–drug interactions through induction of CYP3A4. The in vitro plasma protein binding of the compound was measured in five species (mouse, rat, dog, monkey, and human), found to be moderate (from 79.5% to 90.8%) with low interspecies variability, and was fitting with the targeted pharmacokinetic profile sought by the GSK group.

A metabolite identification study was conducted using in vitro rat, dog, monkey, and human microsomes. Five metabolites were observed at low abundance relative to the parent drug, and all metabolites detected in HLM were also present in the other microsomal species. Three metabolites resulted from hydroxylation of the aliphatic part of the indane ring and one of these was a major metabolite across all species. Oxidation of the *iso*propyl moiety was also detected but represented a minor route. Aryl hydroxylation was the final metabolic route identified and was only significant in rat microsomes. Furthermore, development compound **9** was not genotoxic in the selected in vitro genetic toxicity screens and did not exhibit any cardiovascular risk in an in vitro hERG assay or following single oral dosing up to 2.5 mg/kg in cynomolgus monkeys. Finally, clinical candidate **9** had no observed adverse effect levels and acceptable safety margins in preclinical safety screening up to 6 weeks. All of these results prompted evaluation of **9** in the clinic.

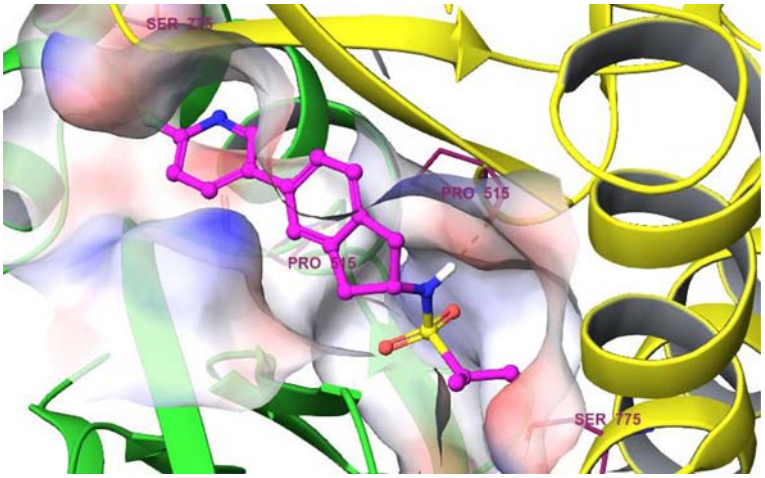

Fig. 6 X-ray crystal structure of clinical candidate 9 in complex with hGluA2i S1S2 LBD (PDB code 2xhd, 1.8 Å resolution). All the X-ray images presented in this review were generated using Maestro, version 10.5, Schrödinger, LLC, New York, NY, 2016.

An initial phase I study was conducted in healthy volunteers to explore the safety and tolerability of the candidate, as well as its pharmacokinetics in human. Two dosing regimens were investigated: single doses (0.25–6 mg) and multiple doses of 0.1 mg administered daily for 28 days. In both cases, indane **9** was rapidly absorbed (C_{max} reached between 0.5 and 3 h postadministration) and had a very long half-life (107–168 h). This resulted from a very low apparent oral clearance and a large apparent volume of distribution, in excess of total body water. This pharmacokinetic profile was not predicted from preclinical species and prevented further clinical evaluation of the compound. Importantly, both dosing regimens were well tolerated with no safety issues raised or withdrawal caused by adverse events.

In a third publication from 2011, GSK reported the identification of a novel chemical series originating from a HTS and optimized using ligand-bound X-ray crystal structures.[96] The optimization work in that series led to the identification of a second clinical candidate, compound **10**. The HTS was run using a FLIPR-based fluorescent-indicator dye protocol in HEK cells expressing recombinant hGluA2i receptors, indicating the ability of the screened molecules to potentiate glutamate-induced calcium influx. Despite a moderate AMPAR potentiation ($pEC_{50}=4.6$, Asym Max = 94%) in the FLIPR assay relative to other hits, compound **25** (Fig. 8) was selected as an attractive starting point from the screen output because of its superior preliminary developability profile. Indeed, hit **25** had good physicochemical properties (MWt = 337 g/mol and logD = 3.0) and performed well in a battery of in vitro assays. The molecule had moderate protein binding (plasma and brain), was devoid of significant CYP450 inhibitory activity, and had good selectivity against a range of ion channels, receptors, and enzymes. Low kinetic solubility and high metabolic turnover in microsomes (rat Cli = 12.7 mL/min/g; human Cli = 3.5 mL/min/g) were identified as the major shortcomings of **25** and resulted in low systemic exposure ($AUC_{0-t}=78$ ng h/mL) when the compound was tested in a rat pharmacokinetic assay. However in that assay hit **25** had good CNS exposure (brain:blood AUC_{0-t} ratio = 1.3), suggesting high permeability.

In order to rapidly identify a development candidate, the screening cascade used in the optimization work not only relied on in vitro functional efficacy screens (FLIPR assay and electrophysiology), but also extensively on calculated physicochemical properties. Unusually for a membrane-bound ion channel target, X-ray crystallography was also routinely employed enabling SBDD and a focused exploration of chemical space to quickly access highly potent modulators and ultimately, the identification of a clinical candidate. The crystal structure of tetrahydroindazole **25** in complex with the rat GluA2i S1S2 LBD and glutamate was determined at 1.55 Å (PDB code 2xx8; Fig. 7), and indicated that the phenyl ring sits at the S1–S2 interface on the twofold axis, similarly to other AMPAR PAMs. The trifluoromethyl group occupies one end of the inverted U-shaped binding pocket, making hydrophobic contacts with the protein, and has displaced the same cluster of four water molecules as the isopropyl group in compound **9**, while the carbonyl of the amide points down into the symmetrical end of the inverted U, making a hydrogen bond with one of the four water molecules. The aliphatic part of the tetrahydroindazole heterocycle makes contact with solvent, suggesting that modification of this ring might be tolerated, but such changes may not impact potency. Several serine residues (Ser518, Ser750, and Ser775), which can interact with a small-molecule modulator *via* hydrogen bonding, are detected in the binding pocket from the crystal structure, but were not exploited by hit **25**. The dimethylamide group was identified as amenable for modification and as a handle to potentially reach Ser750, Ser775 or the water molecules as hydrogen bonding partners.

The hit optimization campaign focused on improving potency, solubility, and metabolic stability. The high metabolic clearance of compound **25** was assumed to be caused by the dimethylamide moiety and other acyclic amides (Fig. 8: **26**, R = CH_2CH_2Ph or R = Bu) where one of the methyl groups was replaced by a larger substituent were prepared. These derivatives retained similar potency to **25** but had reduced solubility and similar or higher microsomal instability. Attention then turned to cyclic amides (Fig. 8: **10** and **27** (X = CH_2 or O)), which were predicted to fit optimally in the binding pocket according to the crystal structure of **25** (Fig. 7) and were expected to have reduced metabolic instability. Interestingly in the FLIPR assay pyrrolidine derivative **10** was

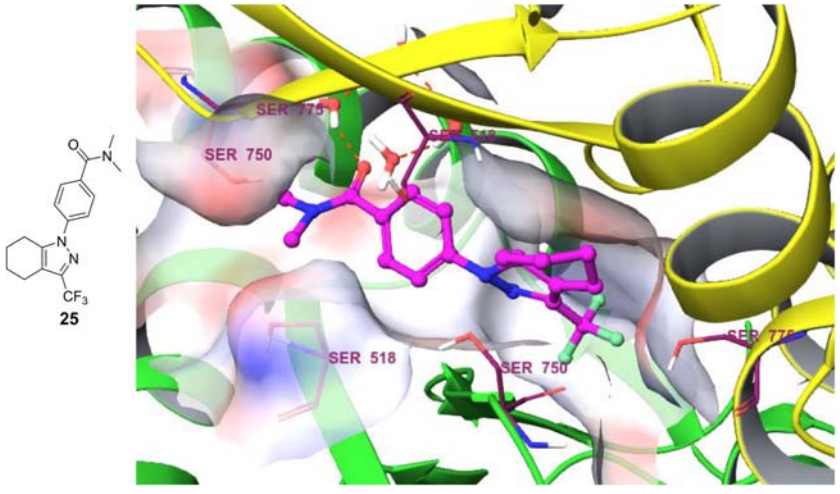

Fig. 7 Chemical structure of hit 25 and its X-ray crystal structure with the hGLuA2i S1S2 LBD (PDB code 2xx8, 1.55 Å resolution).

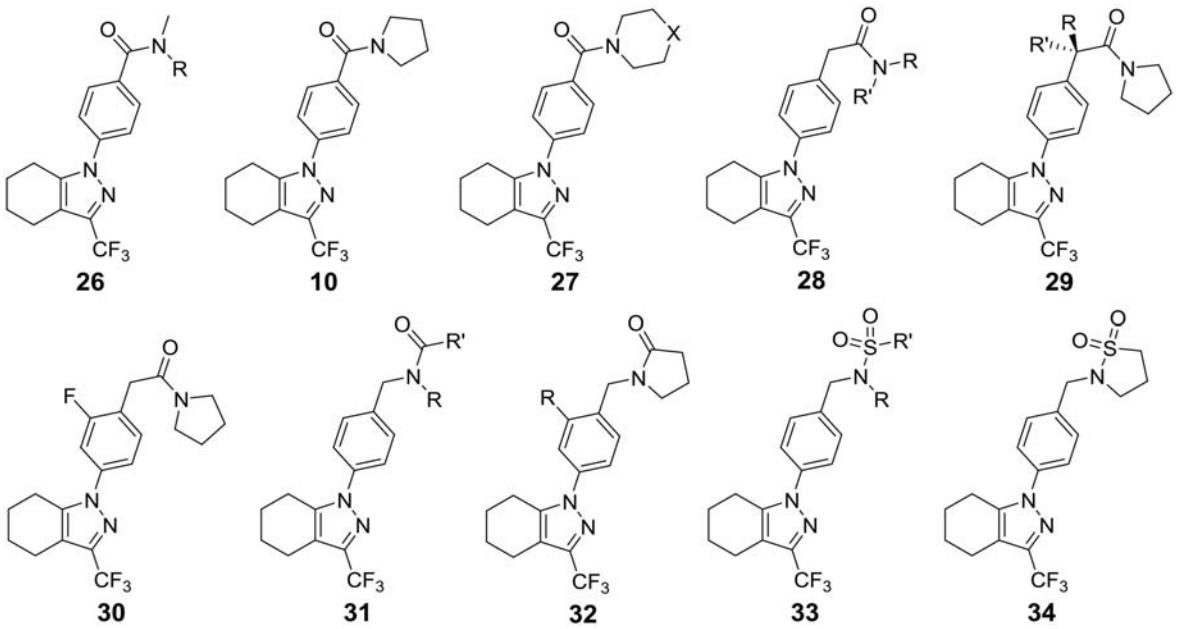

Fig. 8 Chemical structures of the tetrahydroindazole derivatives investigated during the lead optimization program.

more potent than **25** ($pEC_{50}=5.0$, Asym Max = 123%), while 6-membered ring analogs **27** were less active (X = CH_2, $pEC_{50}<4$, Asym Max = 100%; X = O, $pEC_{50}<4.7$, Asym Max = 81%). Despite its moderate potency, morpholine derivative **27** (X = O) had an attractive profile since it retained similar solubility to **25**, did not cause CYP450 inhibition and had significantly improved metabolic stability in both RLM and HLM (rat Cli < 0.5 mL/min/g; human Cli = 1.3 mL/min/g). Encouragingly, compound **10** was also more stable than **25** when tested in microsomes (rat Cli = 2.4 mL/min/g; human Cli < 0.5 mL/min/g). Derivatives **10** and **27** (X = O) had good physicochemical properties (MWt < 380 g/mol and logD < 3.1), high permeability in an artificial membrane permeability assay (**10**, 415 nm/s; **27** (X = O), 455 nm/s) and moderate to high rat plasma and brain protein binding. Owing to their favorable in vitro profile, compounds **10** and **27** (X = O) were progressed to rat in vivo pharmacokinetic studies and found to have good systemic exposure (**10**, $AUC_{0-t}=472$ ng h/mL; **27** (X = O), $AUC_{0-t}=1984$ ng h/mL) with reduced blood clearance relative to the HTS hit. Both compounds also retained high CNS penetration (brain:blood AUC_{0-t} ratio > 1) comparable to **25**. Interestingly, a cocrystal structure of amide **10** (PDB code 2xx7; Fig. 9) showed a similar binding mode to compound **25**, with an unpredicted reorientation of the amide carbonyl and differences in the network of water molecules. The carbonyl group of **10** makes a hydrogen bond with a water molecule, sitting at the top of the benzene ring, which is itself makes a second hydrogen bond

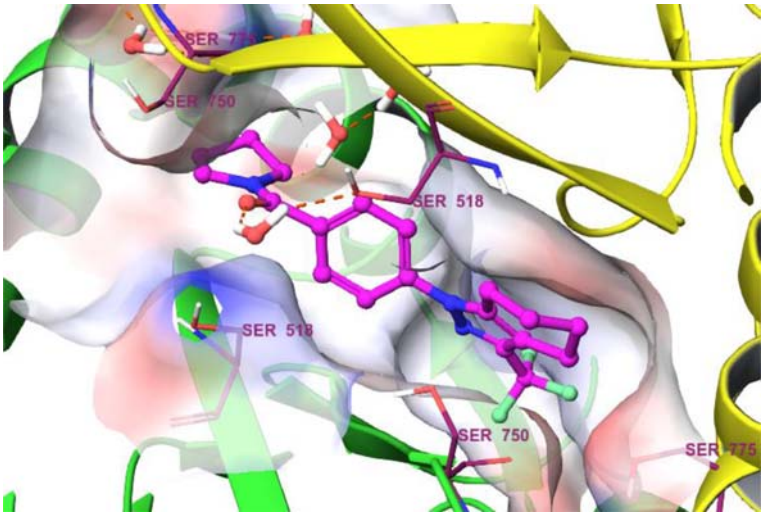

Fig. 9 X-ray crystal structure of pyrrolidine amide 10 in complex with the hGLuA2i S1S2 LBD (PDB code 2xx7, 2.2 Å resolution).

with Ser518. In the meantime, the pyrrolidine ring has displaced one of the four water molecules found at the end of the inverted U-shaped binding pocket.

Replacement of the amide moiety with a sulfonamide, a ketone or a sulfone was also investigated but afforded compounds with lower or at best similar potency to hit **25**. Kinetic solubility of these derivatives was also low. Owing to the difficulties in balancing high potency and DMPK properties, introduction of a linker atom between the phenyl and the amide group was explored as this modification was suggested to be tolerated by docking studies. Such molecules were expected to have an increased flexibility that would lead to superior solubility. The homologated analog of **25**, compound **28** (Fig. 8: R = R′ = Me), induced a substantial increase in calcium influx in the FLIPR assay ($pEC_{50} = 5.7$, Asym Max = 107%) but retained high microsomal turnover. The SAR in this series appeared to be quite narrow since a close acyclic homologated amide **28** (Fig. 8: R = ^{c}Pen, R′ = H) had reduced efficacy and very high microsomal clearance (rat and human Cli > 45 mL/min/g). The successful improvement in metabolic stability with cyclic amides **10** and **27** (X = O), prompted the GSK team to look at similar structural transformation in the homologated series (**29** and **30**). Derivative **29** (Fig. 8: R = R′ = H) maintained the improved potency of **28** (Fig. 8: R = R′ = Me) ($pEC_{50} = 5.5$, Asym Max = 82%) but also the undesired high microsomal instability (rat Cli = 14.6 mL/min/g; human Cli = 24.9 mL/min/g). When both compounds were tested in a rat in vivo pharmacokinetic experiment, moderate systemic exposure and high blood clearance were observed, emphasizing the need to identify compounds with much improved metabolic stability. The initial attempt to enhance metabolic stability focused on blocking the benzylic position of **29** (R = R′ = H), a likely site of metabolism, by the introduction of small alkyl and fluorine groups. Monomethyl, cyclopropyl, mono and bis-fluorinated analogs **29** were prepared, but all gave reduced potency relative to methylene benzylic modulator **29** (R = R′ = H) and retained high metabolic turnover. The methylene spacer not only created a potential site of metabolism but also increased the electron density of the phenyl ring, making it more prone to oxidation. Lowering the aromatic electron density by introducing substituents was considered, but was limited to fluorine atoms since the crystal structure of **29** (R = R′ = H) (PDB code 2xxh; Fig. 10) indicated that the benzene ring was in a narrow channel and that large substituents would not be tolerated. Fluorophenyl analog **30**, Fig. 8, was synthesized and had superior potency to **29** (R = R′ = H) ($pEC_{50} = 5.9$, Asym Max = 79%), slightly better human microsomal stability but significantly reduced solubility.

The lack of success in identifying homologated amides with a favorable in vitro DMPK profile prompted scientists at GSK to consider reversed amides with an embedded benzylamine core motif (Fig. 8: **31** and **32**). Tertiary, **31** (R = R′ = Me) and secondary, **32** (Fig. 8, R = H, R′ = Et and R = H, R′ = Me), acyclic amides were prepared and found to be highly potent ($pEC_{50} > 5.6$), but retained high to moderate intrinsic clearance in both RLM and HLM (3.3 < Cli < 22.4 mL/min/g). With the previous success of cyclic amides **10** and **27** (X = O) to yield compounds with reduced turnover, pyrrolidinone **32** (R = H) was synthesized and induced excellent potentiation of the AMPA ion channel ($pEC_{50} = 6.0$, Asym Max = 132%). Despite similar moderate rat microsomal clearance to **10** (Cli = 2.4 mL/min/g), modulator **32** (Fig. 8, R = H) had lower systemic exposure ($AUC_{0-t} = 231$ ng h/mL) and notably higher estimated blood clearance when tested in rats in vivo. Blocking a potential site of metabolism by introduction of a fluorine on the phenyl ring in **32** (R = F) successfully afforded a potent compound ($pEC_{50} = 6.0$, Asym Max = 112%) with slightly higher intrinsic stability in microsomes (rat Cli = 2.0 mL/min/g; human Cli = 2.9 mL/min/g). However this did not translate to a remarkably superior in vivo pharmacokinetic profile and compound **32** (Fig. 8, R = F) did not achieve the blood and brain levels observed with **10**. The majority of the reversed amides retained some undesired CYP450 inhibition, and solubility in this series was variable with the cyclic derivatives being the most soluble. Replacement of the amide moiety by sulfonamides, such as in **33** (Fig. 8: R = H or Me, R′ = Me or ^{c}Pr or ^{i}Pr) or in **34** (Fig. 8), produced active compounds, although moderately less potent than the amide analogs, but lacking any CYP450 inhibitory activity. These compounds also successfully achieved moderate to high microsomal stability in both rat and human microsomes (Cli < 2.5 mL/min/g) but were unfortunately, for the vast majority, too poorly soluble to be tested in vivo.

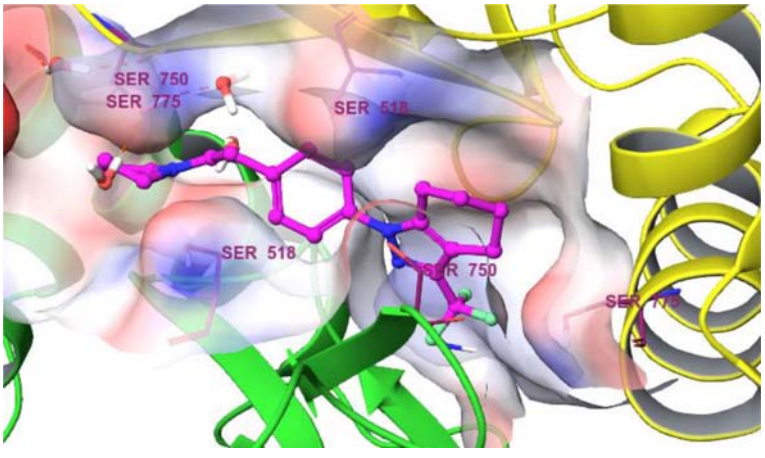

Fig. 10 X-ray crystal structure of homologated amide 29 with the hGLuA2i S1S2 LBD (PDB code 2xxh, 1.5 Å resolution).

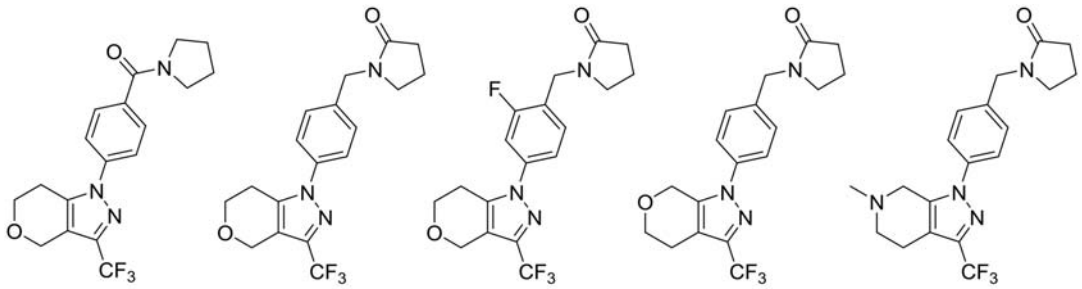

Fig. 11 Indazole derivatives containing a heteroatom in the saturated ring.

Having failed to identify compounds with low in vitro and in vivo turnover using a range of strategies, a selection of compounds was progressed to an in vitro metabolite identification study to develop a better understanding of the metabolic liabilities of the series. Interestingly the saturated part of the tetrahydroindazole was detected as a major site of metabolism and stabilization of this heterocycle was subsequently investigated. Introduction of heteroatoms (oxygen or nitrogen) in the aliphatic part of the tetrahydroindazole moiety was explored (**Fig. 11**) and successfully delivered active compounds with much improved in vitro properties. Overall, modulators **35**–**39**, **Fig. 11**, had lower intrinsic clearance in rat and human microsomes, higher solubility, lower logD, higher free fraction in both plasma and brain, and did not inhibit CYP450 enzymes. This resulted in high oral exposure, with low blood clearance and good CNS penetration, when the compounds were tested in rat pharmacokinetic experiments. These molecules, alongside the ones which previously gave the best exposures when profiled in vivo ($AUC_{0-t} > 400$ ng h/mL), were tested in electrophysiology, selectivity, developability, and early toxicology screens. From the results of these assays (data not disclosed), a set of five molecules (**10**, **27** (X = O), **33** (R = H, R′ = Me), **35**, and **37**), with excellent wider selectivity and clear potentiation of AMPAR-mediated currents in patch clamp assays, were identified as potential development candidates.

As mentioned earlier, AMPAR positive modulators have a tendency to induce convulsion, a recognized side-effect of this class of drugs.[43] The maximum electroshock seizure threshold (MEST) assay enables the identification of compounds which reduce seizure threshold and possess an undesirable proconvulsant activity.[114] The five selected compounds were profiled in MEST experiments and found to be devoid of any proconvulsant adverse effects. With the exception of compound **33** (R = H, R′ = Me), all the modulators were clean in preliminary genotoxic screens and were subsequently tested in in vivo cognition models. In the passive avoidance task model,[113] only modulators **10**, **35**, and **37** attenuated the scopolamine-induced amnesic deficit while modulator **27** (X = O) showed no effect. The three active molecules were then assessed in the NOR experiment,[112] a second in vivo behavioral model to evaluate cognition. In this model, only compound **10** showed a significant procognitive effect when administered at doses ranging from 0.1 to 1 mg/kg (PO). Hence tetrahydroindazole derivative **10**, which was identified early in the program, was selected as the preclinical candidate and evaluated further in a battery of in vitro and in vivo assays.

Similarly to hit **25**, development candidate **10** exhibited low solubility in water, simulated gastric fluid and fasted simulated intestinal fluid. Nonetheless the compound had excellent solution stability in all media tested and also high solid stability over time. In addition, compound **10** did not induce time-dependent inhibition of CYP450 isoforms 2D6 and 3A4, and did not inhibit hERG currents at 10 μM. Intrinsic turnover of the molecule was studied in both microsomes and hepatocytes across five different species: rat, dog, minipig, monkey, and human. Microsomal and hepatocyte clearances were correlated well and highlighted interspecies differences, with low to moderate instability in rat, dog, and human, and high turnover in minipig and monkey. In vivo pharmacokinetic profiling of modulator **10** in four species (rat, dog minipig, and monkey) indicated good tissue distribution, with a volume of distribution at steady state in excess of total body water, a rapid oral absorption (0.5–1 h) and variable blood clearance across species (moderate in rat and high in the others). This resulted in short half-lives (0.5–1.6 h) and moderate to low oral bioavailability (2%–54%). The general good agreement between in vitro and in vivo clearances suggested a likely high systemic exposure in humans. In single and repeat dose oral toxicity studies of up to 4 weeks in rats and dogs, the clinical candidate exhibited a safe profile, giving a large therapeutic window. Surprisingly, AMPAR PAM **10** never entered clinical evaluation and GSK did not report or patent further exploratory work in the trifluoromethylpyrazole series.

7.11.3.3.2 HTS and hybridization strategies by Pfizer

Pfizer is another pharmaceutical group which has shown a strong interest in AMPAR modulation and has filed four patent applications between 2008 and 2010.[115–118] The company has published the most recent scientific literature in the area, with three journal articles since 2013,[59,119,120] and is probably the last pharmaceutical group to have joined the race to discover and commercialize an AMPAR PAM. In these recent publications, Pfizer describes the discovery and optimization of two chemical series, one of which has led to the discovery of clinical candidate PF-04958242,[59] believed to be the only AMPAR potentiator still actively evaluated in clinical trials for neurological disorders.

The majority of AMPAR modulators described in the literature were identified and characterized in vitro using recombinant systems, which do not reproduce the structural complexity of AMPARs found in vivo (see section **Introduction**) and possess

Table 4 Physicochemical and DMPK properties of DHI 40

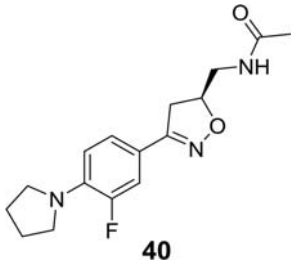

40

TPSA ($Å^2$)	*MWt(g/mol)*	*clogP*	$Cl_{int,\ app}$ (*μL/min/mg*)	P_{app} (*cm/s*)[a]	*ER*[b]
54	305	2.0	26	35×10^{-6}	0.98

[a]Absorptive apparent permeability of a potentiator (2 μM) across a population of MDCK cells with reduced transporter expression.
[b]Efflux ratio: the ratio of secretory (B to A) to absorptive (A to B) apparent permeabilities of a potentiator (2 μM) in MDR1 transfected MDCK cells.

a risk that data generated using homotetrameric receptors will not translate reliably to native tissues. To mitigate this risk early, Pfizer developed an assay employing mouse embryonic stem (mES) cell-derived neurons, which are expected to represent more accurately the considerable heterogeneity of composition of AMPARs found in biological organisms and afford composite pharmacological values.[121] This assay, which was optimized for a HTS campaign and ran on a FLIPR platform, provided two quantifiable parameters: an EC_{50} obtained from a 9-point concentration-response curve and a maximal efficacy percentage (E_{max}), normalized to the average response to 100 μM of AMPA in the presence of 32 μM of cyclothiazide, which was defined as 100%. Screening the Pfizer compound library using this newly developed assay led to the identification of dihydroisoxazole (DHI) hit **40**, **Table 4**.[119] Despite showing moderate potency in the FLIPR mES assay ($EC_{50} = 4.4$ μM), modulator **40** had favorable calculated physicochemical properties and was, as a result, profiled in an array of in vitro DMPK assays (see **Table 4**). Interestingly, compound **40** had good permeability with no P-gp liability and moderate clearance in HLM, confirming that it was an attractive starting point for an optimization program that would primarily focus on improving the potency while maintaining optimal CNS physicochemical and ADME (absorption, distribution, metabolism, and excretion) properties.

A cocrystal structure of DHI **40** with the LBD of hGluA2o was determined (PDB code 4lz7; **Fig. 12**) and revealed that the phenyl ring sits on the twofold axis and that the acetamide projects into one of the deep hydrophobic pockets, similar to the *iso*propyl sulfonamide group in LY451395 **7**. The pyrrolidine ring approaches Asn775 but does not participate in any distinct interaction. Intriguingly, unlike GSK researchers, scientists at Pfizer did not comment on the network of water molecules present at the dimer interface of the two LBD subunits and their potential displacement or interaction with modulator **40**.

From this crystal structure, it was initially suggested that replacement of the acetamide by a sulfonamide could afford molecules with superior binding affinity since docking of a sulfonamide group provided a better fit for the hydrophobic pocket. The *iso*propylsulfonamide of the phenethyl series was introduced on the DHI core, giving **41** (**Fig. 13**), which was 35-fold more active than **40**

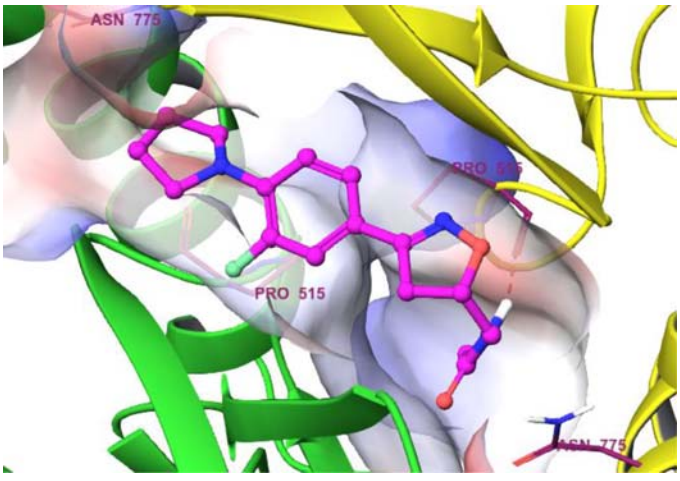

Fig. 12 X-ray crystal structure of DHI hit 40 with the hGLuA2o S1S2 LBD (PDB code 4lz7, 2.1 Å resolution).

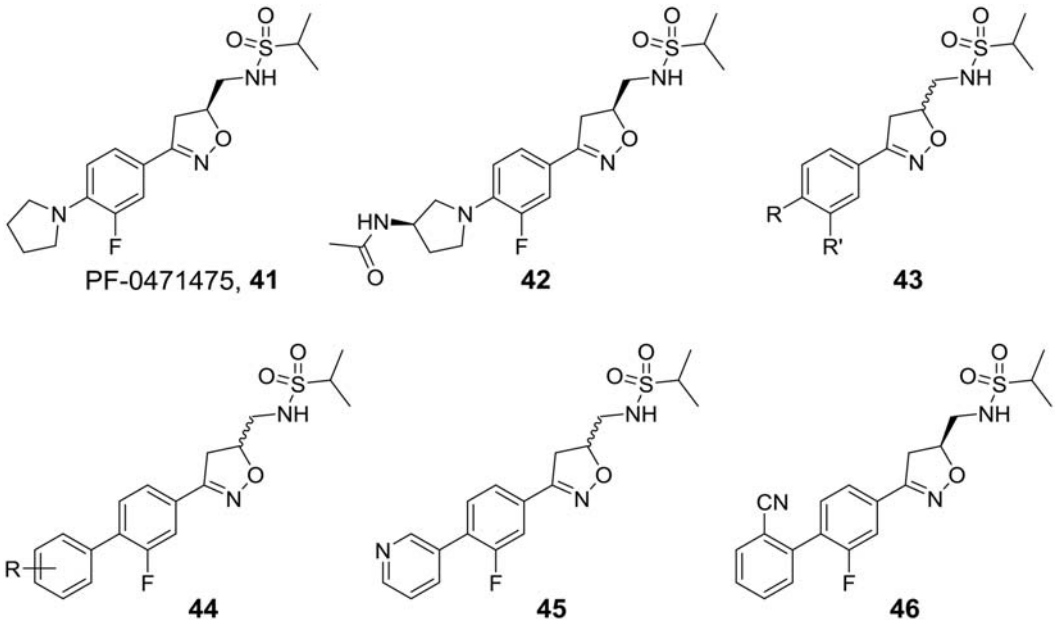

Fig. 13 Representative structures of DHI derivatives prepared during the lead optimization campaign.

($EC_{50}=123$ nM, $E_{max}=147\%$), confirming the design hypothesis. Compound **41** retained desirable CNS drug-like properties (MWt = 369 g/mol, clogP = 3.0, TPSA = 79 Å^2), had moderate predicted human blood clearance (Cl = 13.5 mL/min/kg), showed good permeability with no P-gp efflux in the MDR1-MDCK assay ($P_{app}=18.6\times10^{-6}$ cm/s, ER = 1.45). The enantiomer of **41** was significantly less active, confirming that molecules with the *S* stereochemistry provided the best fit in the binding pocket. A variety of small amides and sulfonamides were prepared to probe the SAR of this part of the scaffold, but all induced a loss of potency. Replacing the amide with carbamates or ureas was also unsuccessfully investigated. Removal of the pyrrolidine produced an inactive compound (Fig. 13: **43**; R = H, R′ = F; $EC_{50}>32$ μM), while des-fluoro racemate **43** (R = pyrrolidine, R′ = H) was only slightly less active ($EC_{50}=253$ nM, $E_{max}=169\%$) but was attractively slightly less lipophilic (clogP = 2.75).

Docking of **41** into the crystal structure of **40** was performed to help identify additional means to increase the functional potency of this series, and indicated that the second symmetrical hydrophobic pocket could be accessed through substitution of the pyrrolidine. Hence an acetamide was introduced at the 3-position of the pyrrolidine affording **42**, Fig. 13, an exceptionally active potentiator ($EC_{50}<10$ nM, $E_{max}=143\%$), whose postulated binding interactions were confirmed by X-ray cocrystal structure (Fig. 14, PDB code 4lz8). A tritiated form of this potent modulator was prepared to develop an in-house AMPAR competition binding assay.

The development of a low nanomolar potentiator which occupies both hydrophobic pockets of the LBD was done at the expense of the physicochemical properties of **42** (MWt = 427 g/mol, TPSA = 109 Å^2) and resulted in poor permeability and P-gp mediated efflux ($P_{app}=3.9\times10^{-6}$ cm/s, ER = 12.1). Consequently, compound **42** had low CNS exposure in a mouse pharmacokinetic study,

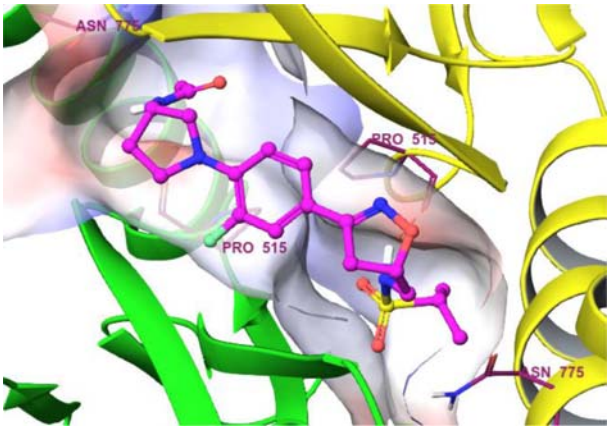

Fig. 14 X-ray crystal structure of compound 42 with the hGLuA2o S1S2 LBD (PDB code 4lz8, 1.85 Å resolution).

precluding its use in vivo. Therefore the SAR around the pyrrolidine ring was revisited with the objective to obtain compounds with lower TPSA and also to remove the aniline moiety which represented well-documented concerns.[122,123] From the crystal structure of **40** and **42**, it appeared that replacing the pyrrolidine with a second aromatic ring would be tolerated, and a series of biaryl derivatives was prepared. While phenyl analog **44** (Fig. 13, R = H) had low affinity for AMPARs ($EC_{50} = 3.2$ μM, $E_{max} = 138\%$), pyridyl derivative **45**, Fig. 13, retained acceptable potency ($EC_{50} = 294$ nM, $E_{max} = 157\%$). Molecular modeling of the biaryl template suggested that a nitrile group at the *ortho* position of the distal aromatic could access the hydrophobic pocket, providing superior binding affinity. This design hypothesis was confirmed since racemate **44** (Fig. 13, R = 2-CN) had similar potency to **41** ($EC_{50} = 87$ nM, $E_{max} = 152\%$) and the *S*-enantiomer **46** was again the most potent ($EC_{50} < 10$ nM). Modulator **46** retained good calculated physicochemical properties (MWt = 401 g/mol, clogP = 3.8, TPSA = 100 $Å^2$), had moderate predicted human hepatic clearance (Cl = 9.67 mL/min/kg) and was highly permeable ($P_{app} = 29.1 \times 10^{-6}$ cm/s; ER = 1.18). Disappointingly, no additional ADME, selectivity or in vivo pharmacokinetic data were given for this very promising compound. In addition, it should be noted that no solubility or CYP450 inhibitory data are communicated on any of the compounds described earlier.[119]

In this publication, detailed pharmacokinetics and pharmacodynamics were only reported for compound **41**, despite modulator **46** being in appearance the most attractive compound. In their in vivo assessment, the Pfizer group demonstrated a marked interest to the unbound brain compound concentration ($C_{b,u}$), which determines AMPAR LBD interactions, and developed a $C_{b,u}$-normalized AMPAR-mediated exposure-response continuum to define an acute dose rodent-based TI. Such studies were carried out since AMPAR overstimulation has been associated with excitotoxicity[39,43,44] and for this reason defining the toxicity threshold in rodents was viewed as crucial by Pfizer scientists before advancing any drug of this pharmacological class to large animal safety and efficacy models.

Potentiator **41** had high rat protein plasma binding (97.3%) and rat brain tissue binding in brain homogenates (98.6%). In a rat pharmacokinetic study, following single subcutaneous (SC) dosing (0.2 mg/kg), compound **41** had a short terminal half-life ($t_{1/2} = 0.4$ h), a total brain to total plasma concentration ratio of 1.04 and an unbound brain to unbound plasma concentration ratio of 0.54, confirming that DHI **41** was CNS-penetrant. The convulsion liability, a recognized side-effect of AMPAR PAMs,[44] was first studied in CD-1 mice and detected 5–11 min postdose in one third of the animals following SC administration of 0.32 mg/kg of **41** and in all animals at a higher dose (0.56 mg/kg, SC). Bioanalysis of brain samples from these mice indicated that a 2.1 nM mean $C_{b,u}$ of potentiator induced convulsion. The same study was repeated in Sprague-Dawley rats where the exposure convulsion threshold was similar with a toxic $C_{b,u}$ of 2.3 nM.

The efficacy of potentiator **41** was first assessed in a modified version of the cerebellum cyclic guanosine monophosphate (cGMP) assay, published by Lilly[124] to evaluate the effect of their AMPAR modulators on the accumulation of cGMP, a downstream messenger involved in a signaling cascade regulating excitatory neurotransmission and neuroplasticity. It was determined that cGMP levels increased with statistical significance in CD-1 mouse cerebellum 30 min after SC dosing of 0.32 mg/kg of **41**, corresponding to a mean $C_{b,u}$ of 0.4 nM. Surprisingly, it is not mentioned if the effect of **41** on cGMP elevation occurred in a dose-dependent manner and as mentioned earlier, this same dosing regimen (0.32 mg/kg, SC) also induced convulsion in one third of the mice, supporting the idea that lower doses must have been investigated but for which no result is reported. Urethane-anesthetized rats, treated with the NMDAR antagonist MK-801, which induces a schizophrenic state, were used as an in vivo model to measure the nootropic electrophysiological effects of **41** administered intravenously. A minimal effective dose of 0.003 mg/kg (IV) of **41** was required to significantly reverse the MK-801-induced schizophrenic effect. From a pilot rat IV pharmacokinetic study (0.01 mg/kg), it was extrapolated that the reversal effect, which occurred after 5 min, corresponded to a $C_{b,u}$ of 0.004 nM, giving a 500-fold TI for convulsion relative to procognitive electrophysiological enhancement in rats. In the majority of the pharmacokinetic and pharmacodynamic experiments described earlier, DHI **41** was administered subcutaneously and no justification was given in this first publication for choosing this preferred mode of administration, which is not desired for clinical evaluation. However in a subsequent article,[120] it was mentioned that SC administration was predominantly used to control the variability in C_{max} and prevent the generation of any potential first-pass active metabolites. Pfizer did not mention if further biological studies were being undertaken with this compound, such as in vivo cognition behavioral experiments, or assessment of memory related effects in nonrodent species or if focus had shifted to potentiator **46**. No additional data have been reported on either compound since 2013. From this study, it should be noted that the use of SBDD positively informed GluA2-based SAR and allowed the group to quickly prepare potent modulators.

In a second publication from 2013,[120] Pfizer presented extensive efficacy and safety profiling on a single compound, PF-04778574 **47** (Fig. 15), which was originally disclosed in a patent[115] and for which no medicinal chemistry rational design

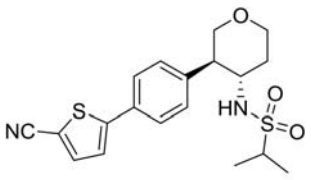

PF-04778574, **47**

Fig. 15 Chemical structure of PF-04778574.

has yet been revealed. As previously mentioned, AMPAR overstimulation can be excitotoxic and AMPAR potentiators have been associated with marked adverse events in preclinical studies.[43] Conscious of this risk, Pfizer designed a sequence of in vitro and in vivo assays to aid the selection of preclinical species to assist in the identification of safe compounds early in lead optimization campaigns and understand potentiator exposures causing desired versus harmful effects. In this article, the Pfizer scientists reported how they applied their safety and efficacy assessment cascade to carefully define a PF-04778574 mechanism-based TI in mice and study its translatability from rodents to higher-order species, by developing an interspecies exposure-response model.

In the in vitro mES FLIPR assay, which was used for the screening campaign in the work described earlier, PF-04778574 concentration-dependently enhanced *S*-AMPA calcium influx through the heterogeneous mixture of AMPARs expressed ($pEC_{50} = 6.05 \pm 0.19$ and $E_{max} = 162\% \pm 24\%$). In the in-house competitive binding assay, modulator PF-04778574 had a Ki of 85 nM and was also found to be devoid of any agonistic effect in three different assays, corroborating the assumed mode of action. Results from these two experiments confirmed that PF-04778574 was a subtype-independent AMPAR PAM. As expected, the compound also potentiated the effect of *S*-AMPA on HEK293 cells expressing either recombinant hGluA2i or hGluA2o in a FLIPR assay, with similar efficacy on both isoforms (flip: $pEC_{50} = 7.35 \pm 0.11$ and $E_{max} = 111\% \pm 6\%$; flop: $pEC_{50} = 7.05 \pm 0.07$ and $E_{max} = 112\% \pm 5\%$), demonstrating an absence of selectivity between these two receptor subtypes. Whole-cell patch clamp electrophysiology on primary cultures of rat cortical neurons, expressing native populations of AMPARs, was used to study the functional potency of PF-04778574 on *S*-AMPA-evoked currents. In that assay, PF-04778574 clearly increased the electric current induced by 30 μM of *S*-AMPA from a concentration of 30 nM and had an EC_{50} of 282 nM.

The protein plasma binding of PF-04778574 was measured across a range of species (CD-1 mice, Sprague-Dawley rats, beagle dogs, cynomolgus monkeys) and found to be moderate (91.2% –95.2%). Interestingly the brain tissue binding was markedly higher (98.0%) and considered species-independent.[125] These two parameters were used to calculate the unbound drug concentration in the plasma ($C_{p,u}$) and the brain ($C_{b,u}$) from measured total plasma and total brain concentrations. To reduce the number of animals sacrificed in the efficacy and safety pharmacodynamic studies, $C_{b,u}$:$C_{p,u}$ ratios in four animal models (mouse, rat, dog, and monkey) were experimentally determined to subsequently allow calculation of a $C_{b,u}$ from a measured $C_{p,u}$, when brain tissues were not collected. This conversion of a $C_{p,u}$ into a $C_{b,u}$ relies on the assumption that $C_{b,u}$:$C_{p,u}$ ratios are constant over time, which is not always the case. The free drug ratios determined in neuropharmacokinetic experiments ranged from 0.42 (mouse) to 0.73 (monkey), indicating good CNS permeability and low interspecies variability from rodents to large animals (< 1.7-fold differences). A number of acute pharmacokinetic experiments in different animal models, using alternative mode of administration and various doses of PF-04778574, were then conducted to obtain a selection of dose–$C_{b,u}$–time relationships.

From these experiments, it should be noted that following intravenous administration of PF-04778574 (0.2 mg/kg) in rat, the blood clearance was more than twice in excess of total liver blood flow (Cl = 250 mL/min/kg), the volume of distribution was high ($V_d = 4.59$ L/kg) and the half-life very short ($t_{1/2} = 0.24$ h), indicating poor systemic stability of PF-04778574 in rats. The compound was noticeably more stable in dogs following oral dosage (0.1 mg/kg) with a moderate blood clearance (Cl = 8.01 mL/min/kg), a high volume of distribution ($V_d = 2.1$ L/kg), and a moderate half-life ($t_{1/2} = 3.1$ h). PF-04778574 was rapidly absorbed in dogs ($T_{max} = 0.75$ h) and had acceptable systemic exposure ($C_{max} = 56.0$ ng/mL and $AUC_{0-\infty} = 210$ ng h/mL). In monkeys, PF-04778574 was administered subcutaneously at two doses (0.1 and 0.32 mg/kg) affording a moderate mean half-life ($t_{1/2} = 3.4$ h) and a T_{max} around 2 h. Positively, maximal plasma drug concentration (C_{max}) and $AUC_{0-\infty}$ values suggested linear pharmacokinetics across this dosing range. Unfortunately, no in vitro clearance assessments in microsomes or hepatocytes were given and it is impossible to say if the overall high in vivo metabolic turnover of PF-04778574 could have been predicted from the in vitro data.

Once all the pharmacokinetic studies had been carried out, modulator PF-04778574 was characterized in a selection of in vivo pharmacodynamic models to correlate the unbound brain drug concentration ($C_{b,u}$) with the observed pharmacological effects. To rule out any non-AMPAR-mediated in vivo pharmacological effect, PF-04778574 was screened at 10 μM against a panel of 118 enzymes and receptors, and found to express a high degree of selectivity for the AMPAR with only minimal inhibitory activity on the dopamine transporter ($IC_{50} = 0.95$ μM).

The in vivo efficacy of PF-04778574 was first assessed in the cGMP assay similarly to compound **41**. cGMP elevation in the cerebellum of CD-1 mice occurred dose-dependently and was statistically significant from a SC dose of 0.32 mg/kg of drug, the other doses evaluated being 0.1 and 1 mg/kg SC. Using the pharmacokinetic models developed in CD-1 mice and assuming linear pharmacokinetics across the doses tested, it was determined that $C_{b,u}$ superior to 1.7 nM would induce a significant increase in cerebellar cGMP levels. In this article, Pfizer also suggested that changes in cerebellar cGMP levels correlate with the potential of compounds to display adverse events. However it should be noted that this assay was originally developed to study the efficacy of the AMPAR modulators but not their safety.[124] In urethane-anesthetized rats, a dose of 0.1 mg/kg (IV) of PF-04778574 significantly overcame the electrophysiological hypoglutamatergic conditions induced by the NMDAR antagonist MK-801. The restorative effect occurred between 5 and 25 min postdose and was projected to correspond to $C_{b,u}$ ranging between 0.98 and 0.35 nM, respectively. Additionally, a 0.03 mg/kg dose (IV) of the compound, translating to a maximal projected $C_{b,u}$ of 0.30 nM, was ineffective in this assay, indicative of a minimal effective $C_{b,u}$ close to 0.30 nM. Since modulator **47** improved impaired synaptic transmission over a large concentration range, it was then tested in a behavioral cognition model, the monkey ketamine-disrupted spatial delayed response task.[68] In this behavioral model, PF-04778574 was tested over a 100-fold dose range (0.001, 0.01, and 0.1 mg/kg, SC), but only significantly reversed the ketamine-induced impaired performance at 0.01 mg/kg (SC), suggesting that the compound had a hormetic exposure-response,[126] typical of nootropic drugs. From the pharmacokinetic model

experiments in primate, this dose projected to a mean $C_{b,u}$ of 0.38 nM. Interestingly the readouts of the two in vivo efficacy models were consistent and suggested that **47** induced procognitive effects from an unbound brain drug concentration of around 0.35 nM.

The amplitude of adverse events caused by AMPAR potentiators is generally progressive, first manifesting as disruption of motor coordination and ultimately leading to convulsion. The tremorgenic potential of AMPAR modulator **47** was evaluated in mice undergoing an accelerating rotarod assay 30 min postdose. In this assay, low doses (0.178 and 0.32 mg/kg, SC) were not associated with a decrease animal fall latency and only a dose of 0.56 mg/kg (SC) of PF-04778574, projecting to a $C_{b,u}$ of 4.8 nM, induced statistically meaningful motor deficits. In addition to the motor coordination disruption observed in the rotarod test, a number of tremorgenic events were unexpectedly recorded during the initial pharmacokinetic studies. Hence general tremor was observed in dogs at $C_{b,u}$ ranging from 6.0 to 15.6 nM and movement-related tremor/ataxia was detected in monkeys at $C_{b,u}$ ranging from 8.0 to 24.1 nM. In these two species, the $C_{b,u}$ inducing tremorgenic side-effects were similar but were two to three times higher than in mice. Convulsion, a more severe side-effect, which has been associated with a significant number of AMPAR PAMs, was assessed in dose-response studies across three species (mice, rats, and dogs) to evaluate a potential interspecies consistency in $C_{b,u}$ causing convulsions. In CD-1 mice, among the three doses tested (1, 1.78, and 3 mg/kg, SC), only the highest two induced general convulsions and this extrapolated to a minimal convulsion-causing $C_{b,u}$ of 9.6 nM. The delay to observe convulsions following dosing was greater for the 1.78 mg/kg (SC) group (23 min) relative to the 3.2 mg/kg (SC) group (7 min), which was consistent with the "threshold" nature of this adverse event. In rats, the two highest doses evaluated (3.2 and 5.6 mg/kg, SC) induced convulsions and the same dose-dependent adverse event delay as in mice was observed. The convulsive-exposure threshold in this species translated to a projected $C_{b,u}$ of 10.7 nM. In dogs, tremorgenic events were observed at the low doses investigated (0.2 and 0.25 mg/kg, PO), but generalized convulsions only occurred following a dose of 0.5 mg/kg (PO) of **47**, corresponding to a $C_{b,u}$ of 17.4 nM. The PF-04778574 $C_{b,u}$ causing convulsion was consistent in rodents (9.6 and 10.7 nM), slightly higher in dogs (17.4 nM) and could be expected to be even higher in primates, since tremorgenic events happened at doses of up to 24.1 nM.

The data generated showed that motor coordination disruption was the dose-capping adverse effect and that PF-04778574 showed adequate separation between $C_{b,u}$ linked to efficacy and harmful effects with TI of 7–13, 16–29, and 22–42 in mice, dogs, and monkeys, respectively. Overall, the exposure-response physiological effects were mainly consistent across species, suggesting a translatable relationship from rodent to higher-order species. Escalating unbound brain concentrations progressively led from efficacy to cerebellar cGMP elevation to motor coordination disruptions to convulsion. From these studies and a number of subsequent assumptions, the scientists at Pfizer concluded that PF-04778574, with a projected 8–16-fold TI in humans for self-limiting tremor, might be safely evaluated clinically as a nootropic drug in schizophrenic patients. Despite this conclusion, the compound never entered clinical evaluation and no further results with this AMPAR potentiator have been reported since 2013.

In a final publication from 2015, scientists at Pfizer reported the discovery, SAR and optimization of clinical candidate PF-04958242 **11**.[59] In addition to the identification of new templates from HTS such as the DHI series described previously, Pfizer also explored modification of Lilly's biaryl *iso*propylsulfonamide LY451646 **48** (Fig. 16), with the objective to discover a series with improved efficacy, selectivity, and metabolic stability relative to **48**. Synthetic tractability strongly influenced chemistry route design to enable library synthesis and quick expansion of the SAR around the biaryl scaffold. From their initial studies with AMPAR modulators, the scientists at Pfizer understood the importance of identifying compounds with low human pharmacokinetic

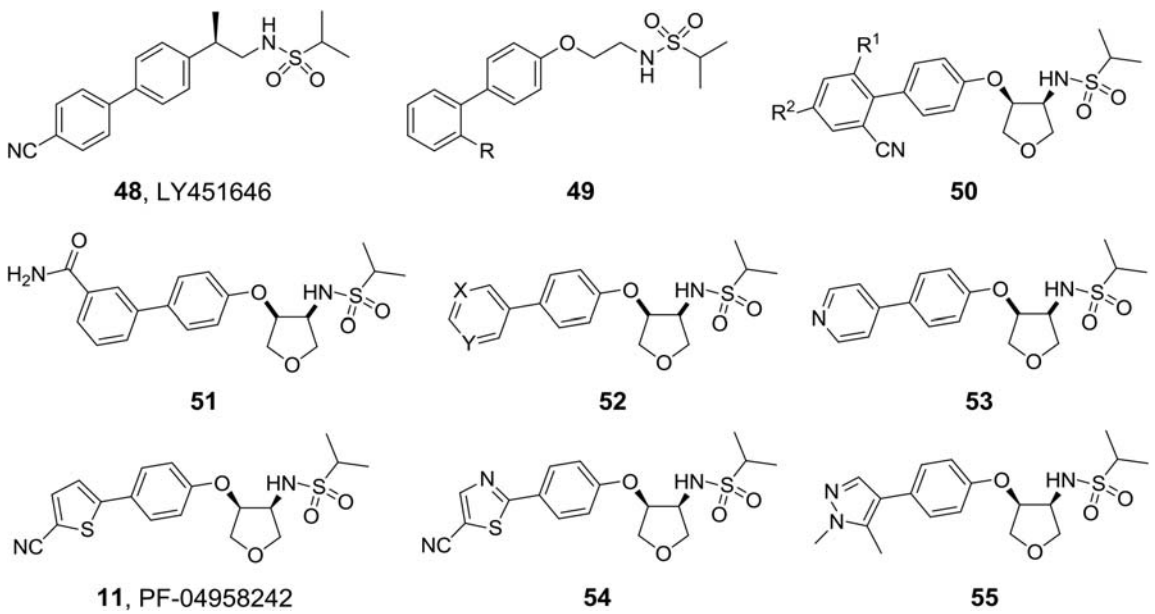

Fig. 16 Representative structures of the derivatives investigated during the lead optimization which led to the identification of PF-04958242.

variability to accurately predict the C_{max} and prevent occurrence of threshold-mediated adverse events.[127] With this in mind, physicochemical properties of virtual targets imparting ADME properties were carefully examined to only prepare compounds likely to develop into good oral CNS drugs with the targeted pharmacokinetic profile.

LY451646 **48** was tested in the FLIPR mES assay developed by Pfizer to set a benchmark and only produced moderate activity ($EC_{50}=3.4$ μM, $E_{max}=132\%$). A number of initial design hypotheses, including investigation of different vectors around the central aryl ring, replacement of the middle benzene with a heteroaliphatic ring and sulfonamide variation/replacement were unsuccessfully explored and afforded inactive compounds. Modulation of the linker was more successful, in particular introduction of an oxygen between the phenyl and the two-carbon linker resulted in active modulators, such as **49** (Fig. 16). In this ether subset, *para*-substitution was preferred, mimicking the SAR of the all-carbon linker series. Interestingly while the unsubstituted distal aromatic analog **49** (R = H) had similar potency to **48** but was significantly less efficacious ($EC_{50}=2.44$ μM, $E_{max}=32\%$), introduction of an *ortho*-cyano **49** (R = CN) had an opposite effect, giving a less potent compound with greater efficacy ($EC_{50}=7.35$ μM, $E_{max}=218\%$), suggesting a potential functionally favorable contact of the cyano with the AMPAR LBD interface.

The X-ray crystal structure of LY451646 **48** in complex with the LBD of hGluA2o (PDB code 4lz5) indicated that the *iso*propylsulfonamide NH forms a hydrogen bond with the carbonyl oxygen of Pro515 and occupies one of the deep lipophilic pockets, similarly to modulators of the sulfonamide class. The biaryl core was sitting along the twofold axis, projecting to the symmetrical binding pocket. Docking of **49** (R = CN) into this crystal structure indicated that the *ortho*-cyano was ideally positioned to access the symmetrical hydrophobic space occupied by the *iso*propylsulfonamide at the other end of the inverted U-shaped binding pocket. This binding model prompted the team at Pfizer to conformationally restrict the amido-alkoxyethane linker to preorganize the ligand for binding and obtain potentiators with superior pharmacological activity. Hence a number of *cis* and *trans* 1,2-dihalo 5- and 6-membered rings were designed and prepared. Examination of the physicochemical properties of these molecules and consideration of prior findings from GSK on an almost identical series, incited Pfizer to focus on *cis*-THF ether analogs.

A significant improvement in functional efficacy was observed following the introduction of the THF-ether linker and chiral separation indicated that the (3*S*,4*S*)-isomers were notably more potent than their (3*R*,4*R*)-counterparts. Despite high functional efficacy ($EC_{50}=217$ nM, $E_{max}=143\%$) and good permeability with no P-gp efflux in the in vitro MDR1–MDCK assay ($P_{app}=32.3\times10^{-6}$ cm/s; ER = 1.39), compound **50** (Fig. 16: $R^1=H$, $R^2=H$) suffered from undesirable high turnover in HLM (Cli = 158 mL/min/kg). To improve the metabolic stability, fluorine atoms were introduced on the distal phenyl, which was a likely source of CYP450-mediated hydroxylation, and afforded functionally active compounds with improved but still suboptimal human microsomal turnover, such as **50** ($R^1=F$, $R^2=H$, $EC_{50}=14.1$ nM, $E_{max}=126\%$, Cli = 89 mL/min/kg) and **50** ($R^1=H$, $R^2=F$, $EC_{50}<10$ nM, $E_{max}=190\%$, Cli = 39 mL/min/kg). Addition of polar groups to the phenyl ring successfully lowered the clearance but concomitantly induced a reduction of potency (Fig. 16: **51**, $EC_{50}=1.11$ μM, $E_{max}=102\%$) and negatively impacted properties governing CNS permeability (**51**, $P_{app}=17.4\times10^{-6}$ cm/s; ER = 7.84). Replacement of the *ortho*-cyanophenyl with 6-membered heteroaromatics such as **52** (Fig. 16: X = N, Y = C, or X = Y = N) and **53** caused a reduction of clogP and delivered compounds with low HLM clearance, high permeability, no P-gp liability and acceptable functional potency ($0.62<EC_{50}<1.16$ μM, $110<E_{max}<161\%$). A selection of substituted 5-membered heteroaromatic derivatives (Fig. 16: **11**, **54**, **55**) was also synthesized and afforded compounds with superior functional activity compared to the 6-membered heteroaromatics. Of these compounds, potentiator **11** which had good activity in the FLIPR mES assay ($EC_{50}=310$ nM, $E_{max}=110\%$), low HLM clearance (Cli < 8 mL/min/kg) and high predicted CNS exposure from the MDR1–MDCK assay ($P_{app}=19.3\times10^{-6}$ cm/s; ER = 1.05) was selected for further profiling.

An X-ray cocrystal structure of **11** bound to the LBD interface of hGluA2o (PDB code 4x48, Fig. 17) indicated that the *iso*propylsulfonamide was making similar contacts with the protein as **48**, and that the cyano group was in the vicinity of Asn775 possibly impacting on the flip/flop selectivity of modulator **11**.

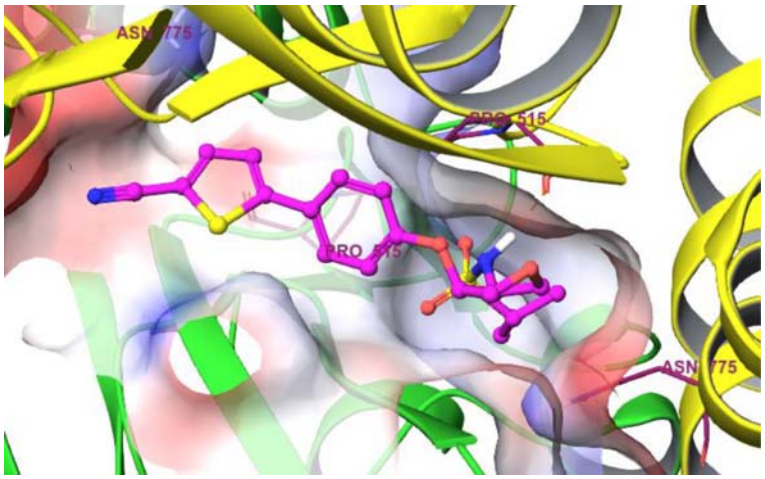

Fig. 17 X-ray crystal structure of 11 bound to hGluA2o S1S2 LBD (PDB code 4x48, 1.89 Å resolution).

The in vitro potency and efficacy of PF-04958242 **11** was assessed in a selection of assays to evaluate its species, subunit and splice variant selectivity profile. Although no data are given, the authors mentioned that **11** was equipotent in mouse and human ES cell-derived neurons, indicating interspecies uniformity. In cells expressing recombinant hGluA2 receptors, compound **11** increased *S*-AMPA-mediated Ca^{2+} influx with some selectivity for the flip (hGluA2i (Ser775), $EC_{50} = 24$ nM, $E_{max} = 124\%$) over the flop isoform (hGluA2o (Asn775), $EC_{50} = 880$ nM, $E_{max} = 124\%$). In a whole-cell patch clamp electrophysiology experiment on primary cultures of rat cortical neurons, modulator **11** significantly enhanced *S*-AMPA-evoked current ($EC_{50} = 43 \pm 10$ nM). To ascertain that the pharmacological effects observed when testing PF-04958242 in vivo were solely AMPAR-mediated, the selectivity of **11** was determined against a panel of 118 human-based ion channels, receptors, and enzymes. At the concentration tested (10 μM), compound **11** had good selectivity for AMPAR with detectable affinity for only three other receptors and enzymes, the most potent interaction being with the serotonin transporter (Ki = 530 nM). The plasma protein binding of **11** was moderate in the three species tested (rat: 95.2%; dog: 93.0%; monkey: 89%) while its rat brain protein binding was relatively high (98.1%), consistent with the moderate calculated lipophilicity of **11** (clogP = 3.54). Inhibition of seven major CYP450 isoforms by modulator **11** was low, with only detectable inhibition of CYP2D6 ($IC_{50} = 18$ μM). Unfortunately only this limited set of in vitro ADME properties was given, and important parameters, such as compound solubility, hERG inhibition, CYP induction, reactivity with glutathione, and genotoxicity, were not discussed.

A similar approach to the one used to study the effects of PF-04778574 in vivo was employed and $C_{b,u}$ (unbound brain concentrations) were calculated for each animal/dose/time/administration mode to establish a $C_{b,u}$-normalized AMPAR-mediated exposure-response continuum for clinical candidate **11**, enabling the assessment of AMPAR-dependent activities related to nootropic effects and safety. Single-dose neuropharmacokinetic experiments were conducted in CD-1 mice and Sprague-Dawley rats to determine $C_{b,u}$:$C_{p,u}$ ratios, treated as constant over time, and subsequently allow calculation of a $C_{b,u}$ from a measured $C_{p,u}$ at multiple time-points. The experimentally measured C_b:C_p and $C_{b,u}$:$C_{p,u}$ ratios ranged from 0.59 to 1.5, confirming the good CNS permeability of **11**, as predicted by the MDR1-MDCK assay. The neuropharmacokinetic experiments in rat (1 mg/kg, SC; 0.01 mg/kg, IV) indicated that **11** had similar terminal half-life, ranging from 0.53 h to 0.76 h, and T_{max} (0.75 h) in plasma, cerebrospinal fluid, and brain. Following intravenous administration in rat (0.2 mg/kg), PF-04958242 had very high blood clearance (Cl = 169 mL/min/kg), very short half-life ($t_{1/2} = 0.31$ h), high volume of distribution ($V_d = 3.6$ L/kg), and low systemic exposure ($AUC_{0-\infty} = 20.1$ ng h/mL), indicating poor plasma stability in rats. When administered orally to rats (3 mg/kg), **11** was rapidly absorbed ($T_{max} = 0.25$ h), had a longer half-life ($t_{1/2} = 0.84$ h) and acceptable systemic exposure ($C_{max} = 134.0$ ng/mL and $AUC_{0-\infty} = 175$ ng h/mL), gave rat oral bioavailability of 58%. In higher-order species, the half-life was greater ($t_{1/2} = 6.21$ h in dogs (0.1 mg/kg, PO), $t_{1/2} = 12.3$ h in monkey (0.032 mg/kg, SC)), the C_{max} was lower and the systemic exposure consistent (in dogs, $C_{max} = 23.9$ ng/mL and $AUC_{0-\infty} = 158$ ng h/mL; in monkeys, $C_{max} = 6.87$ ng/mL and $AUC_{0-\infty} = 149$ ng h/mL).

Elevation of cerebellar cGMP in CD-1 mice occurred dose-dependently 30 min after administration of compound **11** and was statistically significant from a dose of 1 mg/kg (SC). From the neuropharmacokinetic models previously established in CD-1 mice following SC dosing of **11**, it was determined that a projected $C_{b,u}$ of 6.7 nM induced cGMP elevation in CD-1 mice cerebellum. In urethane-anesthetized rats, a dose of 0.01 mg/kg (IV) of **11** significantly overcame the electrophysiological hypoglutamatergic conditions induced by the NMDAR antagonist MK-801, projecting to $C_{b,u}$ ranging between 0.23 and 0.18 nM. The compound was then tested in a second behavioral cognition model, the ketamine-disrupted spatial working memory in the radial arm maze, in which it attenuated the ketamine-evoked memory loss at doses ranging from 0.0032 to 0.032 mg/kg (SC), protecting to $C_{b,u}$ between 0.029 and 0.29 nM according to the SC rat pharmacokinetic study. Higher doses (0.1 and 0.32 mg/kg, SC) were ineffective, indicating a hormetic exposure-response for this nootropic agent.

The tremorgenic potential of potentiator **11** was assessed in C57BL/6J mice undergoing an accelerating rotarod assay 30 min postdose. In this test, low doses (0.1 and 0.178 mg/kg) were safe and only 0.32 mg/kg (SC) of PF-04958242, projecting to a $C_{b,u}$ of 10.8 nM, induced statistically meaningful motor deficits. The convulsion liability of potentiator **11** was not described, although it can be assumed from the previous studies that $C_{b,u}$ superior to 10.8 nM will be required to cause convulsion. From these studies, PF-04958242 had a 37-fold TI in rodents.

The intrinsic turnover of **11** was studied in rat and dog hepatocytes (rat Cli ≤ 63.6 mL/min/kg and dog Cli ≤ 7.4 mL/min/kg) and found to be consistent with the respective in vivo clearance. The good agreement between in vitro and in vivo clearances, and the moderate human hepatocyte clearance of the molecule (Cli ≤ 7.1 mL/min/kg) suggested a likely moderate to high systemic exposure in humans. Metabolite identification studies, indicated that compound **11** underwent similar turnover in dog and human systems, with THF hydroxylation and *O*-dealkylation identified as the major routes of metabolism. Studies using major recombinant human cytochrome P450 isoforms indicated that hepatic turnover *via* CYP2C19 and CYP3A4 would be the predominant human clearance pathways.

These positive results prompted Pfizer to evaluate PF-04958242 in 90 day regulatory toxicology studies in rats and dogs, in which clinical candidate **11** achieved adequate TIs, suggesting that the compound could be safely evaluated in the clinic. Simcyp software was used to project clinical pharmacokinetic parameters from experimentally determined preclinical data and predicted an efficacious dose of 0.3 mg with a 12 h dosing interval. At the time of publication, AMPAR potentiator **11** had been tested in 11 phase I clinical trials and found to be safe and well tolerated in healthy volunteers, in patients with age-related sensorineural hearing loss and schizophrenic subjects on stable doses of antipsychotics and other psychotropic medications. The authors claimed that further clinical studies would focus on evaluating the nootropic effects of **11** in select neurodisease populations.

7.11.3.3.3 Evolution and optimization of the Cortex CX614 series

Cortex has worked in the area of AMPAR positive modulators for many years and has progressed several compounds into clinical trials, as described in the introduction of this article (see Tables 1 and 2). Nonetheless, the company has only published a limited number of medicinal chemistry papers and the majority of the chemical information was until recently contained within patents.[128–132] In particular, the structures of the early development compounds (CX516, CX546, CX614, and CX691, Fig. 18) are in the public domain, but little information, describing the SAR and DMPK properties of these molecules, has been disclosed. Four recent publications from the Cortex group describe the discovery of some later compounds, based on CX614 as a starting point.[133–136]

In the first scientific article,[135] the authors described the design of CX614 **57**, using an understanding of the mode of binding of aniracetam **1** to the AMPA protein and the application of conformational restriction to the benzamide scaffold to increase potency to low micromolar levels and obtain compounds with superior chemical stability. The pharmacological effect of the modulators developed by Cortex was evaluated using patch clamp electrophysiology on cultured rat hippocampal neurons. The activities were reported as EC_{2x}, defined as the concentration of potentiator required to double the current flow through the perfused neuron.

Initial work centered on exploration of the importance of the fused dioxane ring present in CX614. Close analogs indicated that the oxygen at position 1 was essential for activity; analogs, in which this oxygen had been replaced, were significantly less active, with the exception of a compound with a carbonyl group at position 1 which retained activity. On the contrary, the SAR exploration demonstrated that the oxygen at position 4 was not required for AMPAR potentiation. Hence, the introduction of a carbonyl group at position 4, together with a fused pyrrolidine, to increase the rigidity of the modulator, encouragingly produced a more potent derivative (**58**, $EC_{2x}=0.06$ μM) than CX614. The positive results with this symmetrical molecule prompted further work, which initially focused on simple *N*-alkyl analogs **59**. Biological evaluation of an array of compounds (**59**, R=alkyl) showed that a small alkyl group was optimal for potency, with the methyl derivative being the most active ($EC_{2x}=0.1$ μM). Analogs bearing larger groups, including cycloalkyls and branched alkyls, had reduced activity, while the unsubstituted analog (**59**, R=H, $EC_{2x}=5$ μM) had similar potency to CX614. AMPAR modulators from this series were also tested in a ligand binding assay, where a good correlation with the electrophysiology data was observed. Some of the molecules with good activity in the hippocampal neuron electrophysiology assay were tested in a rat hippocampal slice preparation, where weak activity was observed.

In a second paper,[136] Cortex published further SAR studies around the *N*-substituent of **59**. Initial work focused on short alkyl chains bearing substituents. Starting from the *N*-ethyl derivative (**59**, R=Et, Fig. 18) work investigated the effect of introducing a range of functionality on the terminal carbon atom. A wide array of groups was tolerated, the majority of substituents afforded compounds with similar potency to the *N*-ethyl derivative (**59**, R=Et, $EC_{2x}=0.2$ μM). Two modifications, which showed small increase in potency, were the introduction of the chemically reactive groups azide (**59**, R=$N_3(CH_2)_2$–, $EC_{2x}=0.08$ μM) and isothiocyanate (**59**, R=$NCS(CH_2)_2$–, $EC_{2x}=0.06$ μM). Extending the chain length by one carbon atom and appending a nitrile group resulted in a potent butanenitrile derivative (**59**, R=$NC(CH_2)_3$–, $EC_{2x}=0.05$ μM). This work indicated that a wide range of *N*-substituents is tolerated with retention of potency, possibly suggesting that these groups do not interact with the target protein.

Further studies investigated the effect of aromatic groups on the terminus of the alkyl chain (**60**, R=$Ar(CH_2)_n$). Modulation of the chain length was initially studied (Ar=phenyl, **60a–60d**) and the activity found to be optimal with two carbon atoms

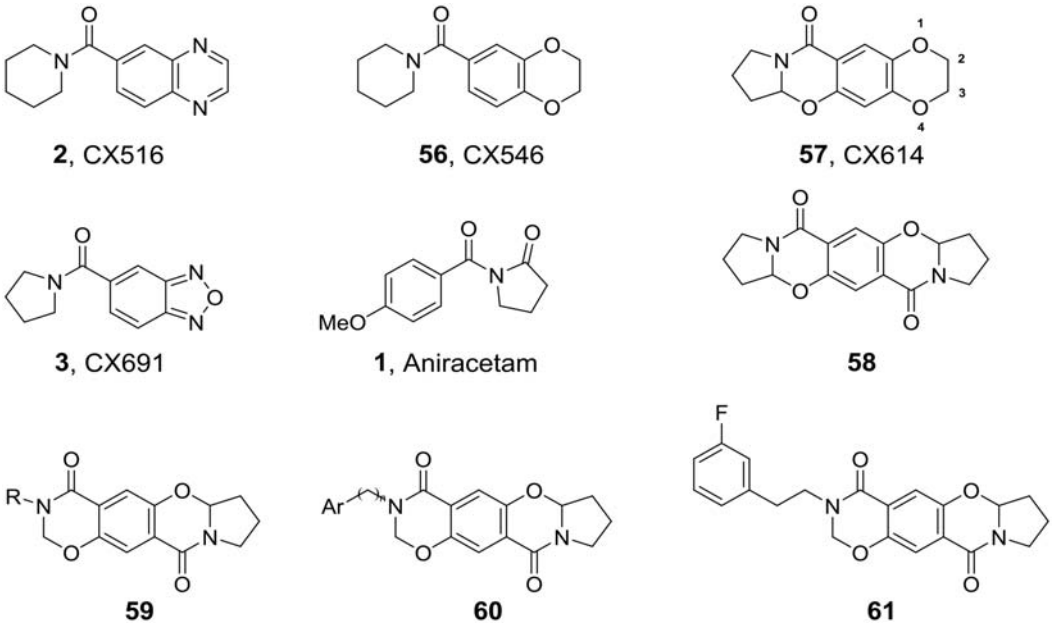

Fig. 18 Evolution of the AMPAR modulators, described by Cortex, containing the benzamide motif.

(**60c**, $EC_{2x}=0.25$ μM), longer (**60d**) and shorter (**60b**) chains gave compounds with activity similar to CX614 (Table 5). In this optimized two carbon linker series, introduction of small halogen substituents (**60e** and **60f**) at the *meta* position of the phenyl ring resulted in a 10-fold increase in potency, larger or more polar groups (**60 g** and **60 h**) led to reduced activity or at best retention. Appending substituents at the *ortho* or *para* position of the phenyl ring reduced potency in all cases (**60i** and **60j**). Interestingly, bis-meta substitution was tolerated and the 3,5-difluorophenyl derivative **60k** had high potency in both the electrophysiology ($EC_{2x}=0.005$ μM) and the binding assay (Ki = 0.3 μM). Following exploration of the SAR of substitution around the phenyl ring, the final area of investigation looked at phenyl replacement with heterocycles, all linked to the core through a two carbon chain. Six-membered heteroaromatic did not provide any advantages with the three regioisomeric pyridines (**60l–60n**) being equipotent to the unsubstituted phenyl analog (Table 5). The general trend among unsubstituted 5-membered heterocycles was a raise in potency, typically 10-fold compared to the pyridyl groups. The limited range of substituents, described for each heterocycle, make it difficult to draw conclusions regarding the SAR. However, there is a suggestion that in the case of the pyrazoles described, introduction of a small lipophilic group, such as chlorine, provided a further increase in potency.

In a subsequent publication,[133] Cortex scientists mentioned phenethyl compound **61**, Fig. 18, stating that despite its very good potency in a rat in vitro electrophysiology assay ($EC_{2x}=0.011$ μM), it was only weakly active when tested in an in vivo electrophysiology experiment, similar to related compounds. High clearance was suggested to explain the discrepancy between in vitro potency and in vivo efficacy. Metabolite identification studies in RLM showed the major sites of metabolism to be the ethyl chain and the saturated carbon atoms of the oxazinone and pyrrolidine rings. The initial strategy adopted to improve the metabolic stability was to substitute the alkyl chain linking the phenyl group to tetracyclic core, such as in **62** and **63** (Fig. 19). Substitution adjacent to the phenyl group represented by **62**, Fig. 19, resulted in a large reduction of the in vitro potency of all analogs. Substitution of the methylene adjacent to the tetracyclic core, represented by **63**, Fig. 19 (X = H, $R^1=CO_2Me$, $R^2=H$; X = F, R^1 = ethynyl, $R^2=H$), did result in compounds with similar potency to the parent compound (**61**, Fig. 18), but, unfortunately, these derivatives failed to demonstrate superior metabolic stability.

The second strategy investigated was to replace the oxazinone ring with pyrimidinone (Fig. 19: **64**, X = CH) or triazinone rings (Fig. 19: **64**, X = N). This approach proved successful with both the pyrimidinone and the triazinone showing similar effects in an in vivo electrophysiology assay at 5 mg/kg (IP), when compared to **61**, which showed very little response. The SAR of the pyrimidinones and triazinones regarding chain substitution matched that described for **62** and **63**, with small lipophilic groups on the carbon atom adjacent to the heterocycle producing increased potency, but substituents adjacent to the phenyl ring not being tolerated. Replacement of the pendant 3-fluorophenyl group with a 2-tetrazolyl group resulted in improved potency in the in vivo electrophysiology assay. This was particularly evident in the triazinone series and was also reported to correlate with increased exposure. Having identified compounds with superior metabolic stability, Cortex focused on removing the chiral center present in the pyrrolidinooxazinone motif, this was achieved by substituting the nitrogen of the oxazinone with a cyclopropyl group. Combining the achiral ring system with the modifications, which resulted in optimal metabolic stability and potency, afforded

Table 5 Influence of chain length and appended aromatic groups on AMPAR modulation

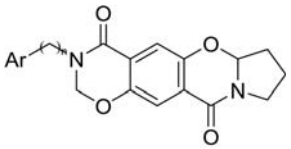

60

	Ar	*n*	*EC2x (μM)*
60a	Ph	0	Inactive
60b	Ph	1	6.0
60c	Ph	2	0.25
60d	Ph	3	3.6
60e	3-F-Ph	2	0.011
60f	3-Cl-Ph	2	0.02
60g	3-Br-Ph	2	1.6
60h	3-MeO-Ph	2	14
60i	2-F-Ph	2	5.4
60j	4-F-Ph	2	1.2
60k	3,5-F_2-Ph	2	0.005
60l	2-Pyridyl	2	0.6
60m	3-Pyridyl	2	0.2
60n	4-Pyridyl	2	0.24

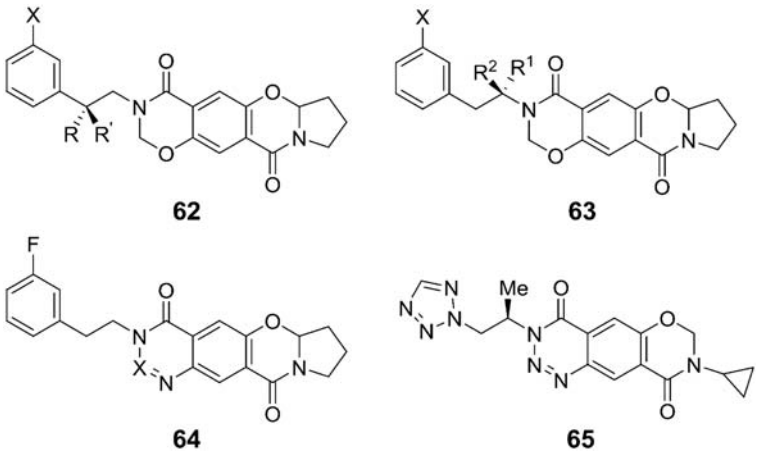

Fig. 19 *N*-substituted derivatives with improved potency.

65 (Fig. 19), which was active in a rat native tissue electrophysiology assay ($EC_{2x}=0.46$ μM), produced an increase in the amplitude of fEPSP in vivo (39% at 5 mg/kg, IP) and induced LTP in the rat (1 mg/kg, IP).

The main issue with compound **65**, Fig. 19, was its short plasma half-life (0.27 h) and in a fourth publication[134] Cortex described how the pharmacokinetic profile of this series was optimized. In addition to the short half-life, it was also suggested that **65** had low brain penetration, although no data were presented to support this. Initially investigation of the core ring system was performed, and replacement of the oxazinone with either pyrimidinone or triazinone was investigated, leading to the discovery of compound **66** (Fig. 20), which had an encouraging profile. Potentiator **66** was 100% bioavailable in the rat with a good half-life in all species (rat: $t_{1/2}=1.7$ h; dog: $t_{1/2}=3$ h; monkey $t_{1/2}=9.5$ h), and retained the electrophysiological profile of **65** ($EC_{2x}=0.28$ μM; 37% increase in fEPSP amplitude at 5 mg/kg, IP). All four possible combinations of pyrimidinone and triazinone were prepared with **66** having the best profile. Extensive SAR investigations were subsequently performed looking at modifications of the tetrazole, pendant methyl, and cyclopropyl groups. Few transformations gave a profile superior to **66**. Wider SAR investigation showed that dimeric tetrazole **67** (Fig. 20) was more potent than **66** ($EC_{2x}=0.016$ μM; 59% increase in fEPSP amplitude at 1 mg/kg, IP), but no pharmacokinetic data were provided on the later compound. Since the publication of these data, Cortex has not published any further medicinal chemistry papers.

7.11.3.3.4 Optimization of an HTS-derived hit by Organon using SBDD

Organon (now Merck) have published four patent applications between 2008 and 2010,[137–140] and shortly after published a series of papers[141–143] which describe the discovery of advanced lead compounds derived from a screening hit, compound **68**, Fig. 22.

In the first publication,[143] they describe the profile of **68** (Fig. 22) and strategies used to improve the in vitro developability profile with retention of potency. AMPAR modulator **68** had very encouraging in vitro functional potency ($pEC_{50}=6.7$; calcium assay in HEK cells overexpressing hGluA1) but was poorly soluble (<1 mg/L) and highly unstable in both rat and human liver microsomes (Cli >270 μL/min/mg). To direct the medicinal chemistry, the group utilized X-ray structures of compounds in complex with the LBD of the hGluA2i subunit. Analysis of the binding mode of **68** (PDB code 3O28, Fig. 21) indicated that the key interactions potentially responsible for the activity were predominantly hydrophobic and were those made by (a) the trifluoromethyl on the tetrahydroindazole and also (b) the cyclohexyl ring of the tetrahydrobenzothiophene.

Initial efforts concentrated on opening of the saturated ring of the tetrahydrobenzothiophene which resulted in dimethyl or methyl and ethyl thiophene analogs (Fig. 22: **69**) or introduction of heteroatoms into the saturated ring (Fig. 22:**70**). These analogs all exhibited reduced potency (≈ 30-fold) but encouragingly a modest increase in kinetic solubility (10 mg/L) in some cases. Introduction of an oxygen atom into the saturated ring produced compound **70** which retained potency, but still showed poor solubility and microsomal stability. Attempts to modify the saturated ring of the tetrahydroindazole gave similar results and truncation

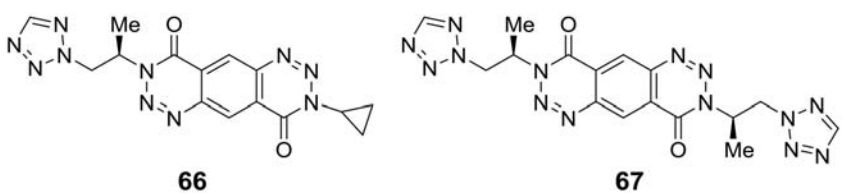

Fig. 20 Tetrazole derivatives with improved DMPK profiles.

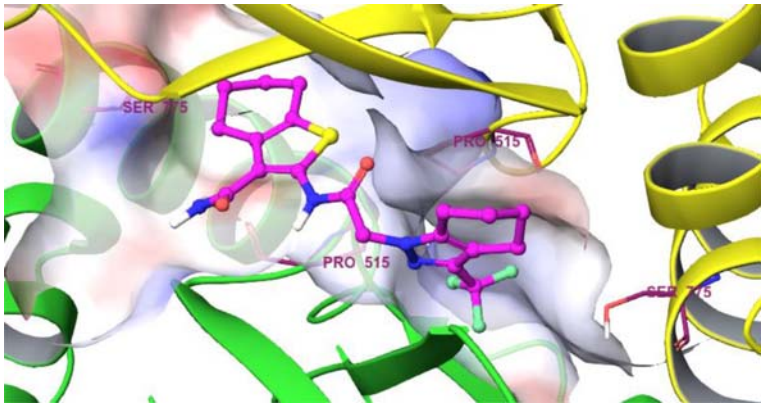

Fig. 21 X-ray structure of hit compound 68 in complex with the S1S2 LBD of hGluA2i (PDB code 3O28, 2.0 Å resolution).

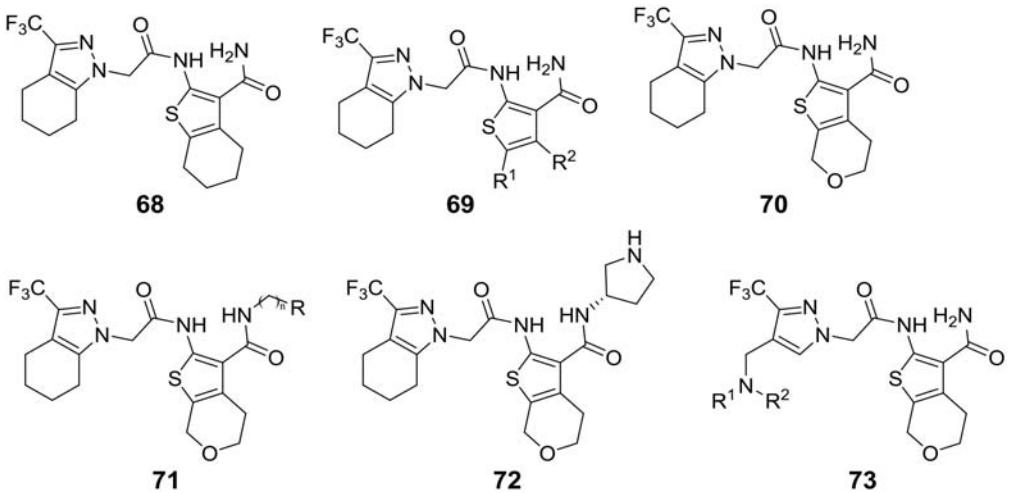

Fig. 22 Key compounds in the optimization of screening hit 68 published by Organon.

was generally poorly tolerated. Active compounds were obtained when the system was fully aromatized preferably with nitrogen atoms in the 6-membered ring, but this failed to improve the developability characteristics.

Further examination of the structural information revealed a hydrophilic pocket close to the space occupied by the primary amide function. Thus, a series of analogs were prepared in which various groups were appended to the amide of **71** (Fig. 22). One of the early analogs (**71**, R = NMe_2, $n = 2$) showed modest potency ($pEC_{50} = 5.2$) but was successfully crystallized with the hGluA2 LBD (PDB code 3O29, Fig. 23). Analysis of the structure revealed a weak interaction with an aspartic acid residue (Asp781), which had the potential for further optimization. Interestingly both the tetrahydroindazole and the tetrahydrobenzothiophene moieties occupied similar regions to the hit **68**.

Further modification led to a more potent analog (**71**, R = NH_2, $n = 3$; $pEC_{50} = 6.4$) which also showed an improved developability profile (solubility: 38 mg/L; Cli = 17 μL/min/mg (HLM), Cli = 77 μL/min/mg (RLM)). The ADME properties still required work as the permeability (Caco-2 assay) was low, but encouragingly the compound was not a P-gp substrate (A–B = 34 nm/s, B–A = 55 nm/s). Unfortunately, when **71** (R = NH_2, $n = 3$) was tested in an in vivo rat pharmacokinetic study, the poor permeability contributed to low oral bioavailability (7.7%) and poor CNS penetration (brain to plasma ratio = 0.05), despite having moderate blood clearance (21 mL/min/kg). Further analysis of X-ray data suggested that conformationally constrained analogs, would bind well to the protein. Compound **72** (Fig. 22) was prepared and showed good potency ($pEC_{50} = 6.6$), which was slightly superior to the corresponding enantiomer ($pEC_{50} = 5.8$). **72** possessed promising solubility (20 mg/L) and microsomal stability (Cli = 41 μL/min/mg (HLM), Cli = 50 μL/min/mg (RLM)). However, the permeability was still low, as was bioavailability (3.8%) despite low in vivo clearance (2.3 mL/min/kg, rat). Surprisingly the brain to plasma ratio was found to be 1:1.

Following extensive exploration of the tetrahydrobenzothiophene motif, which failed to deliver molecules with the desired in vivo profile, attention focused on the tetrahydroindazole group.[142] Structural data suggested that introduction of polar groups in this region was possible and could potentially interact with two key residues, namely Pro515 and Ser750. Compounds with an

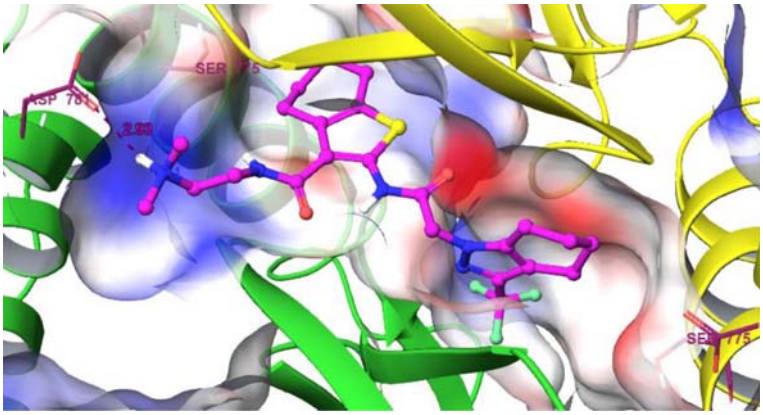

Fig. 23 Biostructure of lead 71 (R = NMe_2, n = 2) bound to the S1S2 LBD of hGluA2i (PDB code 3O29, 2.02 Å resolution).

opened saturated ring and basic functionality appended to the pyrazole ring were modeled and appeared to have the greatest potential. A series of analogs **73** (Fig. 22) was prepared; a wide variety of small alkyl groups were tolerated and good activity ($pEC_{50} \geq 6$) was observed with both secondary and tertiary amines. Two secondary amines were chosen for further study: **73**, R^1 = Me, R^2 = H; pEC_{50} = 6.5, Cli < 12 μL/min/mg (RLM), Cli = 33 μL/min/mg (HLM) and kinetic solubility = 65 mg/L and **73**, R^1 = Et, R_2 = H; pEC_{50} = 6.1, Cli < 19 μL/min/mg (RLM), Cli < 12 μL/min/mg (HLM) and kinetic solubility = 107 mg/L, Fig. 22. The pharmacokinetics of both compounds were studied in vivo and showed improved oral bioavailability in the rat compared to previous analogs (R^1 = Me, F = 15%; R^1 = Et, F = 43%). The ethyl compound was progressed further but found to have low CNS penetration (brain to plasma ratio = 0.05). However, despite the poor CNS penetration, it showed positive effects in a rat in vivo electrophysiology assay, increasing the amplitude of evoked activity at a dose of 0.3 mg/kg (IV). The crystal structure of **73** (R^1 = Et, R_2 = H) bound to the S1S2 LBD of hGluA2i was obtained and confirmed the initial designed hypothesis (PDB code 3O6H, Fig. 24). The authors conclude by saying that at the time of publication the advanced compound was under detailed investigation and further results will be published at a later date.

In the final publication,[141] further evolution of the template to structurally diverse scaffolds was explored using a hybridization strategy (Fig. 25). Structural components of other reported AMPA modulators were combined with key elements of the newly discovered scaffold, in order to identify a back-up series. The work resulted in the identification of compound **77**, Fig. 25. Examination of available X-ray structures suggested that **74** (hGluA1 pEC_{50} = 6.4, solubility = 20 mg/L) had the potential to be hybridized with the previously reported Lilly compound (LY451646, **48**) by replacing the cyanophenyl group with the pyrazole moiety of **74** to give **75**, Fig. 25. The results were initially encouraging with **75** having the desired in vitro profile (pEC_{50} = 6.3, solubility = 73 mg/L and Cli < 12 μL/min/mg (rat and human)), combined with reasonable permeability (Caco-2) and no evidence of transporter interaction. However, the in vivo rat profile was less than desired with moderate-high plasma clearance (49.7 mL/min/kg). It was hypothesized that introducing a conformational constraint might reduce CYP-mediated metabolism leading to decreased clearance.

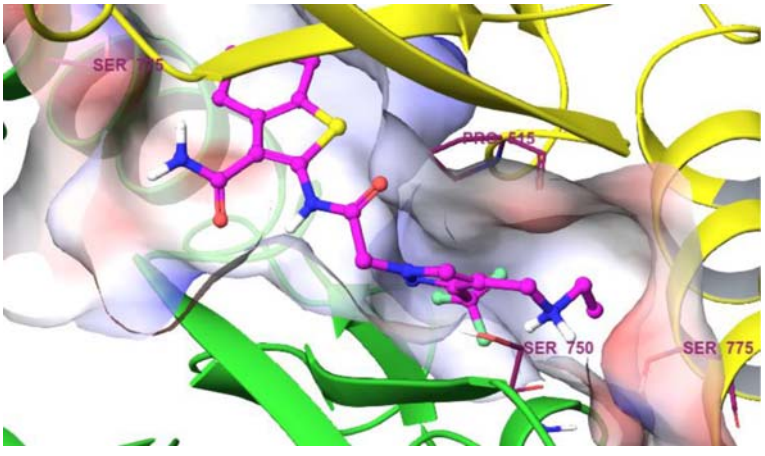

Fig. 24 X-ray structure of 73 (R^1 = Et, R^2 = H) in complex with the S1S2 LBD of hGluA2i (PDB code 3O6H, 2.1 Å resolution).

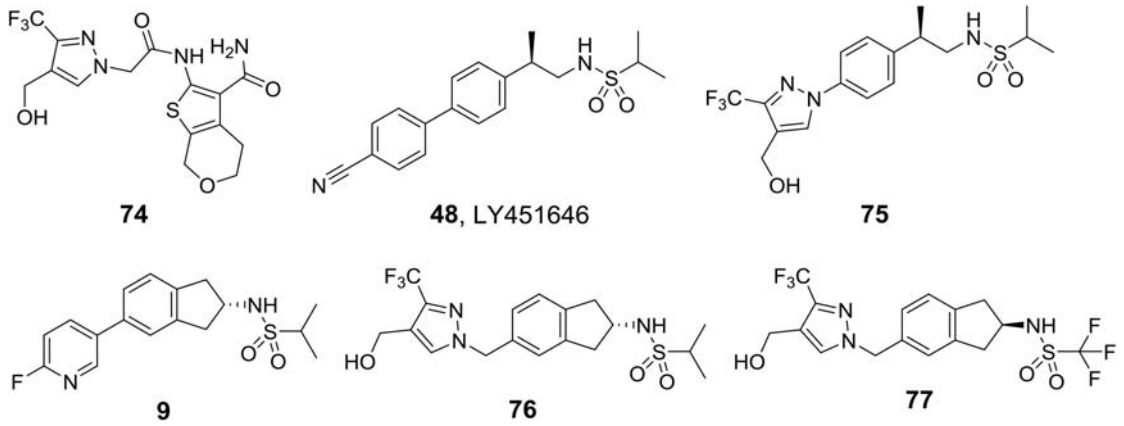

Fig. 25 Advanced compounds from Organon and comparison with similar templates from other groups.

A second hybridization strategy was employed to achieve the conformational restraint, incorporating features of a template described by GlaxoSmithKline 9[98] producing **76** (PDB code 3PMW, Fig. 26). A linker was introduced between the indane and the pyrazole as molecular modeling suggested the directly linked pyrazole would not fit the binding site optimally. Derivative **76** had a very encouraging profile ($pEC_{50}=6.3$, Cli = 31 μL/min/mg (RLM), 23 μL/min/mg (HLM)), improved in vivo clearance (21.6 mL/min/kg, rat) and excellent oral bioavailability ($F\%=95$). Having identified **76** as a promising new scaffold, the Organon group explored further the SAR around the template. Changing the stereochemistry of these compounds had little effect on the overall profile. The pyrazole ring could be replaced by other 5-membered heterocycles including furan and pyrrole. A range of substituents in place of the alcohol were tolerated including hydrophobic groups, such as an additional trifluoromethyl, and polar groups, such as secondary amines. Exploration of the sulfonamide demonstrated that a wide range of hydrophobic groups were tolerated in this position including aromatic groups, such as methoxyphenyl and trifluoromethyl pyrazole. Compound **77**, Fig. 25, resulted from this exploration and it was noted that replacement of the isopropyl sulfonamide by the corresponding trifluoromethyl analog gave a compound which retained much of the potency of **76** but with further improved metabolic stability. The profile of **77** is as follows: $pEC_{50}=5.6$, solubility = 83 mg/L, Cli < 12 μL/min/mg (RLM and HLM), in vivo (rat) Cl = 1.9 mL/min/kg, $t_{1/2}=7.4$ h, $F\%=100$, and evidence of good CNS penetration. No report describing the in vivo pharmacological effects of the AMPAR potentiators is described in these three papers and it is unclear if these series are still being developed.

A recent publication from one of the Organon authors currently working at the University of Strathclyde described another hybridization strategy,[144] in which the hydroxymethyl pyrazole used in the design of **77** is combined with a template related to those previously described by Cortex to produce hybrid **79** (Fig. 27). Only in vitro activity data are described in an electrophysiology assay with compounds being tested on both flip and flop isoforms of GluA2. Modulator **79** is significantly more potent than **74** and shows activity at both receptor subtypes. Also described in the paper are the sulfonamide analog **80** (Fig. 27) and the compound in which the pyrazole is directly attached to the tricyclic core, **81** (Fig. 27), both compounds are less potent than **79**.

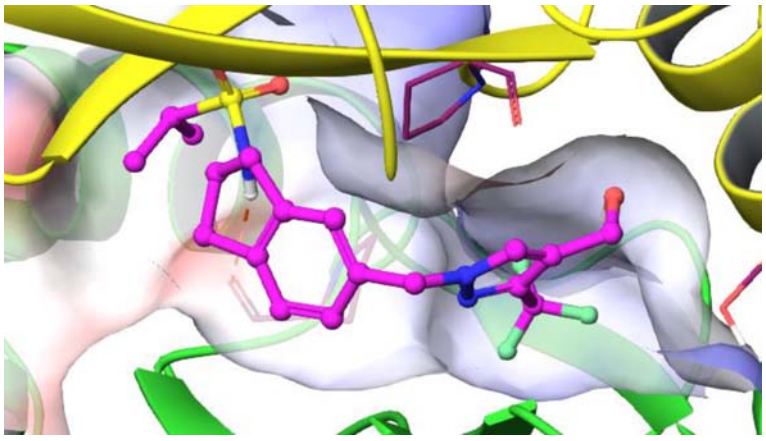

Fig. 26 X-ray structure of 76 bound to the S1S2 LBD of hGluA2i (PDB code 3PMW, 2.2 Å resolution).

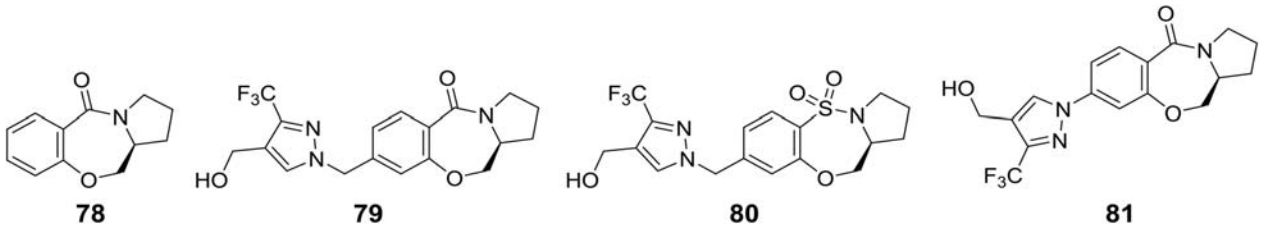

Fig. 27 Conformationally restrained molecules published by the University of Strathclyde.

7.11.3.3.5 Work from other pharmaceutical and academic groups

A number of groups at the universities of Liege, Copenhagen, and Modena have published work centered around the cyclothiazide core **5**, Fig. 1.[145–152] Servier also worked for many years on this template but have not described any new chemotypes related to this scaffold in the period covered by this article. This work has been comprehensively reviewed elsewhere.[153]

Takeda have demonstrated an interest in this area of neuroscience through a significant number of patent applications between 2009 and 2012 (Fig. 28).[154–159] However, until now, no scientific publication reporting on their strategy and discovery of advanced AMPAR PAMS has been published. Lilly which had a strong interest in the area before 2010[160–163] seems to have stopped working on AMPAR PAMS, since no patent or scientific articles originating from them has been reported in the last 10 years.

7.11.4 AMPA Receptor Antagonists

The medicinal chemistry of AMPAR negative modulators was thoroughly reviewed in the second edition of *Comprehensive Medicinal Chemistry*[1] and little or no new work has been reported during recent years. AMPAR antagonists have been shown to be potent anticonvulsants and, as a result, have been developed as antiseizure agents. A number of the compounds previously reported have been progressed into clinical studies where they have shown encouraging results in epilepsy studies. One molecule perampanel **87**[164] has reached the market with a number of others currently in late stage clinical trials: selurampanel **88**, talampanel **89**, and GYKI 53784 **90** (Fig. 29).[165]

A recent, novel approach, to the identification of AMPA negative modulators has recently been published, by both Lilly and Janssen.[57,58] It involves targeting of AMPAR accessory proteins, more precisely TARPs, and represent an innovative approach to

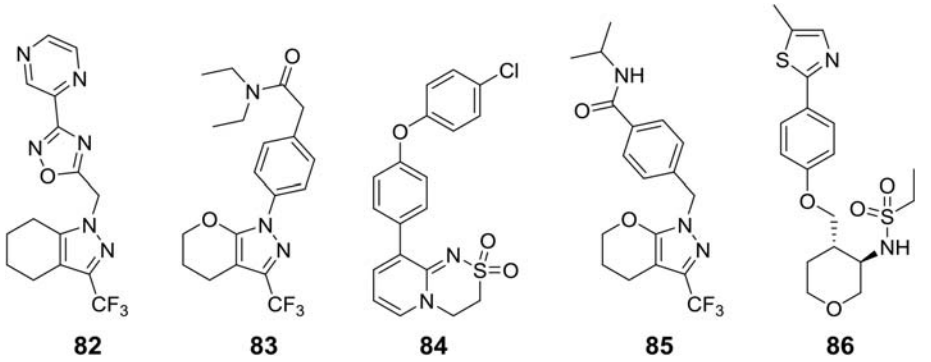

Fig. 28 Representative structures of the AMPAR modulators claimed by Takeda.

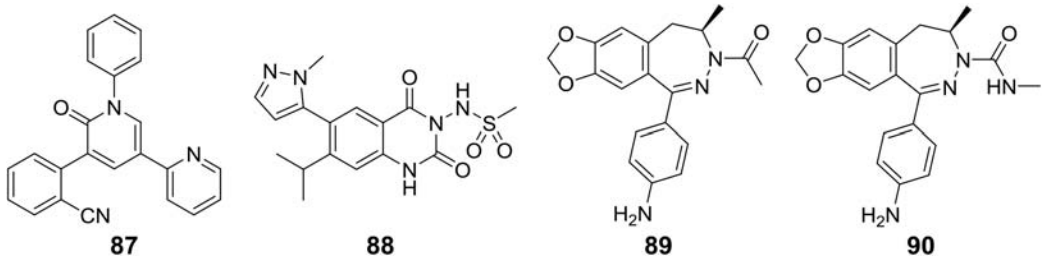

Fig. 29 Advanced AMPA negative allosteric modulators.

modulate AMPAR in specific brain regions. Indeed, while relative concentrations of GluA subunits vary between brain regions, they are generally present throughout the brain and inhibition in specific brain compartments is challenging to achieve. To date, no AMPAR inhibitors have been found to exhibit regional specificity or AMPAR subunit selectivity.

Since AMPAR are ubiquitously expressed within the CNS, general AMPAR antagonists have very narrow therapeutic windows and are associated with side effects, such as motor impairment, dizziness, ataxia, and falling.[166] The variable regional expression of members of the TARP protein family across the CNS provide the opportunity to identify AMPAR modulators dependent on the co-expression of AMPAR with a specific TARP protein.[167] For instance, TARP-γ8 has significantly higher expression within the hippocampus relative to other major brain areas, while TARP-γ2 is mainly found in the cerebellum. Since the hippocampus is the region of the brain associated with the etiology of epilepsy and the cerebellum the region controlling motor function, the identification of a selective AMPAR–TARP-γ8 antagonist selective over TARP-γ2 could provide a therapeutic advantage over previously reported AMPA negative modulators that bind to the LBD. In addition, hippocampal excitotoxicity caused by kainate, an AMPAR partial agonist, is overturned in TARP-γ8 knockout mice.[168] Hence, ligands targeting the AMPAR–TARP-γ8 complex are of interest and two pharmaceutical companies have recently reported the identification of selective TARP-γ8 modulators. The novel class of AMPAR antagonists is assumed to work by disrupting the interaction between TARP-γ8 and the pore-forming region of the GluA subunits. These molecules, which represent the first AMPAR modulators to exhibit regional specificity, have an encouraging preclinical profile and the potential for progression to clinical evaluation.

A screening campaign was initiated at Lilly to identify compounds which inhibited calcium entry (FLIPR assay) into CHO cells, exclusively expressing AMPAR complexes formed a recombinant of GluA1 tetramer (flip isoform) and TARP-γ8. Cell lines, expressing alternative AMPAR complexes, composed of the GluA1 homotetramer and other single TARPs, were generated and used to assess selectivity for the GluA1–TARP-γ8 complex. The screen identified phenol **91** (Fig. 30) which was modestly potent (TARP-γ8 $IC_{50} = 2.97$ μM), selective over TARP-γ2 ($IC_{50} \geq 83$ μM), but was unstable in rat and human liver microsomes (81% and 84% metabolism, respectively, following 5 min incubation). Hepatocyte studies also indicated the presence of phase II metabolism. Unsurprisingly, when tested in vivo (rat), **91** had a clearance well in excess of liver blood flow (234 mL/min/kg). The first stage of hit optimization focused on reducing the phase II metabolic liability, and a series of phenol isosteres were prepared (Fig. 30: **92**, **93**, and **94**). Encouragingly, all three compounds were more potent than the original hit (TARP-γ8 $IC_{50} = 0.147$ μM (**92**), 0.35 μM (**93**), 0.07 μM (**94**)). While compound **92** was poorly stable in both rat and human liver microsomes, the other two compounds had improved stability: **93** 52% and 65% metabolism in rat and human liver microsomes respectively following 5 min incubation and **94** 36% and 32% metabolism in rat and human liver microsomes respectively. Analog **94** was progressed to an in vivo pharmacokinetic study in rats where it showed encouraging blood clearance (61 mL/min/kg). However, when **92**, **93**, and **94** were profiled against a panel of cytochrome P450 enzymes, it was discovered that all three compounds were potent inhibitors of CYP1A2, with IC_{50} values of 0.22, 0.23, and 0.36 μM, respectively. CY1A2 was also shown to be the predominant metabolic enzyme for all three compounds.

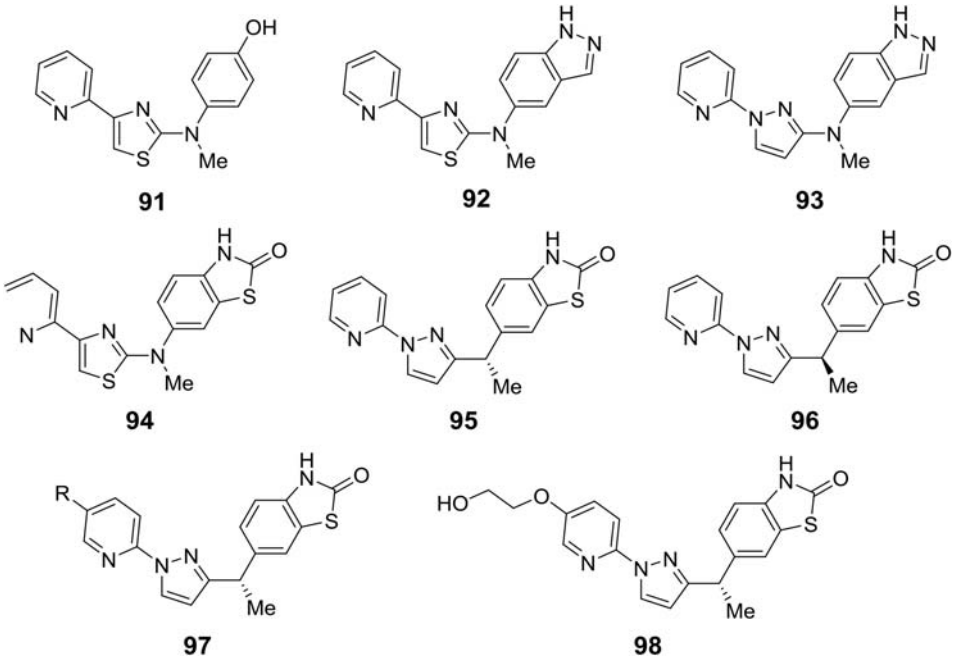

Fig. 30 Selective AMPA modulators which act through binding to TARPγ-8.

The Lilly group used structure-based design to solve this issue by predicting binding modes of the three compounds at the CYP enzyme. They hypothesized that replacing the nitrogen atom of the tertiary amine linker in **92**, **93**, and **94** by a sp^3-hybridized carbon should not affect the binding to the AMPA protein since it would maintain the overall shape and size of the molecules, but would distort the planarity of the molecule sufficiently to reduce the potential to bind to CYP1A2. The enantiomeric carbon linked compounds **95** and **96** were prepared (Fig. 30). Encouragingly both compounds showed little or no inhibition of CYP1A2, having IC_{50} values of >10 and 4.67 μM respectively, but retained activity in the TARP-γ8 assay and were highly selective over TARP-γ2. Unfortunately, both compounds displayed poor metabolic stability both in vitro and in vivo having clearances greater than liver blood flow in rats. Using in silico methods to predict sites of metabolism indicated that the main site of oxidative metabolism was the pyridine ring. A series of analogs, exemplified by **97**, were prepared from which **98**, LY3130481, Fig. 30, emerged as the preferred molecule. Compound **98** showed encouraging potency in the TARP-γ8 assay ($IC_{50}=0.065$ μM) with no detectable activity at TARP-γ2 or affinity for GluA1 protein. Modulator **98** has an encouraging pharmacokinetic profile in the rat with low clearance (11 mL/min/kg), high bioavailability (97%) and was highly efficacious in the PTZ epilepsy model ($ED_{50}=1.7$ mg/kg). Importantly, **98** was clearly differentiated in its side effect profile from agents which act elsewhere at the AMPAR, such as perampanel. When tested in the inverted screen model, **98** showed little potential to alter climbing behavior at low doses and had an inverted index (ratio of TD_{50} in inverted screen model to ED_{50} in PTZ test) superior to 58, much greater than perampanel which showed and index of 0.4.

Similarly to Lilly, Janssen initiated a HTS campaign targeting the AMPAR–TARP-γ8 complex. Hits were identified and following extensive medicinal chemistry optimization led to the discovery of JNJ-55511118 **99** and JNJ-56022486 **100** (Fig. 31). No publication describing the optimization campaign behind these molecules has yet been disclosed. In a calcium flux assay, **99** and **100** inhibited glutamate-evoked calcium influx in HEK293 cells, expressing GluAx subunit and TARP-γ8. In the absence of TARP-γ8 or in the presence of other TARP subunits, little or no inhibition was observed, demonstrating the selectivity of these molecules. The broad selectivity of JNJ-55511118 **99** and JNJ-56022486 **100** was evaluated at 1 μM against a panel of 52 receptors, ion channels and transporters. Both compounds were highly selective, with at least 100-fold selectivity against all tested targets. The effect and selectivity of other TARP family members was confirmed using patch clamp electrophysiology in CHO cells expressing heterologous GluA1o–TARP-γ8. A similar effect on glutamate-evoked currents was recorded on neuronal cells, with no effect on cerebellar granule cells expressing native AMPAR–TARP-γ2, and a significant inhibition on hippocampal neurons expressing native AMPAR–TARP-γ8. These positive results indicate that the presence of other interaction partners in the native system does not affect the binding of the compounds or their functional impact. Extensive additional electrophysiological studies were conducted and concluded that JNJ-55511118 does not cause dissociation of TARP-γ8 from the AMPAR, but modifies the protein-protein interaction between these two components of the receptor complex.

From a radioligand binding assay, the binding affinity (K_i) of JNJ-55511118 **99** and JNJ-56022486 **100** was found to be 26 and 19 nM respectively. In brain slices, the tritiated version of 100 was shown to bind at high concentrations to regions of high TARP-γ8 expression. The in vivo pharmacokinetic profile of both molecules was evaluated in rat and mouse, and JNJ-55511118 **99** showed the best profile in these studies, prompting further in vivo experiments to focus on that compound. Compound **99** had good oral bioavailability, with acceptable clearance (4.8 mL/min/kg) and volume of distribution (1.8 L/kg) in rats. It also demonstrated high CNS penetration and high target occupancy following oral dosing in both rat and mouse. Free fraction of JNJ-55511118 in rat and mouse plasma was generally low (1.48% and 0.88%, respectively), as was the free fraction in rat brain tissue (0.24%).

JNJ-55511118 **99** showed strong anticonvulsant properties in the corneal kindling and PTZ models in mice, and in the amygdala kindling model in rats. The compound also demonstrated partial protection in the 6 Hz and MES tests in mice. Potential side effects of **99** on learning and memory, resulting from AMPAR negative modulation in the hippocampus, were tested in rats using two cognition models (V-maze and Morris water maze). Although JNJ-55511118 induced memory impairment in both tests, the effect was significantly milder to that caused by the NMDAR antagonists dizocilpine and phencyclidine. Positively, other severe side effects, such as loss of motor coordination or sedation, were not observed in animals dosed with AMPAR modulator **99**, even when saturating doses were used.

Inhibition of excitatory neurotransmission with AMPAR–TARP-γ8 modulators, such as LY3130481 and JNJ-55511118, has a strong potential clinical utility top prevent convulsion, in particular in patients whose epilepsy has a strong hippocampal component. The absence of effect in the midbrain and hindbrain with such inhibitors is expected to attenuate seizures without the side effects seen with classical anticonvulsants, such as sedation or ataxia.

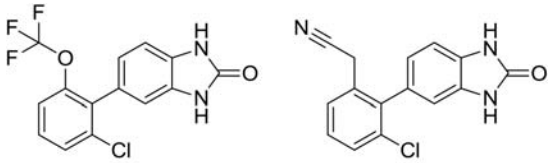

JNJ-55511118, **99** JNJ-56022486, **100**

Fig. 31 TARP-γ8 selective AMPAR modulators identified by Janssen.

7.11.5 Conclusion and Future Perspective

The large number of publications on AMPAR potentiators within the period covered by this article proves that it remains a fertile area of drug discovery and that interest will remain for the foreseeable future. It appears that the field has learnt from the failure of the early AMPAR PAMs which entered clinical evaluation and that more precise and defined properties are now sought. The use of SBDD has clearly assisted a number of projects and allowed the identification of very potent potentiators, active at very low doses in cognition behavioral models in vivo. Some pharmaceutical groups such as Pfizer and GSK have also aimed for a specific pharmacokinetic profile with the objective to achieve large TI, low intersubject pharmacokinetics variability and prevent the occurrence of the recognized adverse events associated with AMPAR modulators. We can expect a number of compounds derived from series described in this review to enter clinical evaluation in the next few years, thus expectation of positive readouts of clinical trial data continues. The recent report from Lilly scientists of ligands which modulate AMPA function through binding to TARPs offers a novel strategy to modulate the channel function and potentially a pathway to the identification of modulators with greater safety profiles.

7.11.6 Conflict of Interest

S. Ward holds a grant from the Wellcome Trust entitled "Transforming the treatment of schizophrenia: Design and development of AMPA receptor modulators with a much improved safety profile as novel drugs for treating the cognitive dysfunction associated with schizophrenia and other CNS disorders."

The authors have no other relevant affiliations or financial involvement with any organization or entity with a financial interest in or financial conflict with the subject matter or materials discussed in the manuscript apart from those disclosed.

Acknowledgment

The authors thank Dr Ben Wahab for crystal structure processing and computational support.

References

1. Taylor, J. B., Triggle, D. J., Eds. *Comprehensive Medicinal Chemistry II;* Elsevier Science: Amsterdam, 2006.
2. Russo, E.; Gitto, R.; Citraro, R.; Chimirri, A.; De Sarro, G. New AMPA Antagonists in Epilepsy. *Expert Opin. Investig. Drugs* **2012,** *21,* 1371–1389.
3. Dingledine, R.; Borges, K.; Bowie, D.; Traynelis, S. F. The Glutamate Receptor Ion Channels. *Pharmacol. Rev.* **1999,** *51,* 7–61.
4. Kew, J. N. C.; Kemp, J. A. Ionotropic and Metabotropic Glutamate Receptor Structure and Pharmacology. *Psychopharmacology (Berl)* **2005,** *179,* 4–29.
5. Ozawa, S.; Kamiya, H.; Tsuzuki, K. Glutamate Receptors in the Mammalian Central Nervous System. *Prog. Neurobiol.* **1998,** *54,* 581–618.
6. Zarate, C. A.; Manji, H. K. The Role of AMPA Receptor Modulation in the Treatment of Neuropsychiatric Diseases. *Exp. Neurol.* **2008,** *211,* 7–10.
7. Sanacora, G.; Zarate, C. A.; Krystal, J. H.; Manji, H. K. Targeting the Glutamatergic System to Develop Novel, Improved Therapeutics for Mood Disorders. *Nat. Rev. Drug Discov.* **2008,** *7,* 426–437.
8. Goff, D. C.; Coyle, J. T. The Emerging Role of Glutamate in the Pathophysiology and Treatment of Schizophrenia. *Am. J. Psychiatry* **2001,** *158,* 1367–1377.
9. Partin, K. M. AMPA Receptor Potentiators: From Drug Design to Cognitive Enhancement. *Curr. Opin. Pharmacol.* **2015,** *20,* 46–53.
10. Gan, Q.; Salussolia, C. L.; Wollmuth, L. P. Assembly of AMPA Receptors: Mechanisms and Regulation. *J. Physiol.* **2015,** *593,* 39–48.
11. Coyle, J. T. NMDA Receptor and Schizophrenia: A Brief History. *Schizophr. Bull.* **2012,** *38,* 920–926.
12. Javitt, D. C. Glutamate and Schizophrenia: Phencyclidine, *N*-Methyl-D-Aspartate Receptors, and Dopamine–Glutamate Interactions. *Int. Rev. Neurobiol.* **2007,** *78,* 69–108.
13. Meador-Woodruff, J.; Healy, D. J. Glutamate Receptor Expression in Schizophrenic Brain. *Brain Res. Rev.* **2000,** *31,* 288–294.
14. Lynch, M. A. Long-Term Potentiation and Memory. *Physiol. Rev.* **2004,** *84,* 87–136.
15. Morris, R. G. M. Long-Term Potentiation and Memory. *Philos. Trans. R. Soc. B Biol. Sci.* **2003,** *358,* 643–647.
16. Lynch, G. Memory Enhancement: The Search for Mechanism-Based Drugs. *Nat. Neurosci.* **2002,** *5,* 1035–1038.
17. Lynch, G.; Gall, C. M. Ampakines and the Threefold Path to Cognitive Enhancement. *Trends Neurosci.* **2006,** *29,* 554–562.
18. Sun, X.; Zhao, Y.; Wolf, M. E. Dopamine Receptor Stimulation Modulates AMPA Receptor Synaptic Insertion in Prefrontal Cortex Neurons. *J. Neurosci.* **2005,** *25,* 7342–7351.
19. Tichelaar, W.; Safferling, M.; Keinänen, K.; Stark, H.; Madden, D. R. The Three-Dimensional Structure of an Ionotropic Glutamate Receptor Reveals a Dimer-of-Dimers Assembly. *J. Mol. Biol.* **2004,** *344,* 435–442.
20. Jin, R.; Singh, S. K.; Gu, S.; Furukawa, H.; Sobolevsky, A. I.; Zhou, J.; Jin, Y.; Gouaux, E. Crystal Structure and Association Behaviour of the GluR2 Amino-Terminal Domain. *EMBO J.* **2009,** *28,* 1812–1823.
21. Mansour, M.; Nagarajan, N.; Nehring, R. B.; Clements, J. D.; Rosenmund, C. Heteromeric AMPA Receptors Assemble With a Preferred Subunit Stoichiometry and Spatial Arrangement. *Neuron* **2001,** *32,* 841–853.
22. Beneyto, M.; Meador-Woodruff, J. H. Expression of Transcripts Encoding AMPA Receptor Subunits and Associated Postsynaptic Proteins in the Macaque Brain. *J. Comp. Neurol.* **2004,** *468,* 530–554.
23. Sobolevsky, A. I.; Rosconi, M. P.; Gouaux, E. X-Ray Structure, Symmetry and Mechanism of an AMPA-Subtype Glutamate Receptor. *Nature* **2009,** *462,* 745–756.
24. Yelshanskaya, M. V.; Li, M.; Sobolevsky, A. I. Structure of an Agonist-Bound Ionotropic Glutamate Receptor. *Science* **2014,** *345,* 1070–1074.
25. Dürr, K. L.; Chen, L.; Stein, R. A.; De Zorzi, R.; Folea, I. M.; Walz, T.; Mchaourab, H. S.; Gouaux, E. Structure and Dynamics of AMPA Receptor GluA2 in Resting, Pre-Open, and Desensitized States. *Cell* **2014,** *158,* 778–792.
26. Herguedas, B.; Garcia-Nafria, J.; Cais, O.; Fernandez-Leiro, R.; Krieger, J.; Ho, H.; Greger, I. H. Structure and Organization of Heteromeric AMPA-Type Glutamate Receptors. *Science* **2016,** *352,* aad3873.
27. Mayer, M. L.; Armstrong, N. Structure and Function of Glutamate Receptor Ion Channels. *Annu. Rev. Physiol.* **2004,** *66,* 161–181.
28. Gouaux, E. Structure and Function of AMPA Receptors. *J. Physiol.* **2004,** *554,* 249–253.

29. Traynelis, S. F.; Wollmuth, L. P.; McBain, C. J.; Menniti, F. S.; Vance, K. M.; Ogden, K. K.; Hansen, K. B.; Yuan, H.; Myers, S. J.; Dingledine, R. Glutamate Receptor Ion Channels: Structure, Regulation, and Function. *Pharmacol. Rev.* **2010,** *62,* 405–496.
30. Milstein, A. D.; Nicoll, R. A. Regulation of AMPA Receptor Gating and Pharmacology by TARP Auxiliary Subunits. *Trends Pharmacol. Sci.* **2008,** *29,* 333–339.
31. Tigaret, C.; Choquet, D. More AMPAR Garnish. *Science* **2009,** *323,* 1295–1296.
32. Schwenk, J.; Harmel, N.; Zolles, G.; Bildl, W.; Kulik, A.; Heimrich, B.; Chisaka, O.; Jonas, P.; Schulte, U.; Fakler, B.; Klöcker, N. Functional Proteomics Identify Cornichon Proteins as Auxiliary Subunits of AMPA Receptors. *Science* **2009,** *323,* 1313–1319.
33. Sommer, B.; Keinanen, K.; Verdoorn, T.; Wisden, W.; Burnashev, N.; Herb, A.; Kohler, M.; Takagi, T.; Sakmann, B.; Seeburg, P. H. Flip and Flop: A Cell-Specific Functional Switch in Glutamate-Operated Channels of the CNS. *Science* **1990,** *249,* 1580–1585.
34. Seeburg, P. H.; Single, F.; Kuner, T.; Higuchi, M.; Sprengel, R. Genetic Manipulation of Key Determinants of Ion Flow in Glutamate Receptor Channels in the Mouse. *Brain Res.* **2001,** *907,* 233–243.
35. Partin, K. M.; Fleck, M. W.; Mayer, M. L. AMPA Receptor Flip/Flop Mutants Affecting Deactivation, Desensitization, and Modulation by Cyclothiazide, Aniracetam, and Thiocyanate. *J. Neurosci.* **1996,** *16,* 6634–6647.
36. Pei, W.; Huang, Z.; Wang, C.; Han, Y.; Park, J. S.; Niu, L. Flip and Flop: A Molecular Determinant for AMPA Receptor Channel Opening. *Biochemistry* **2009,** *48,* 3767–3777.
37. Menniti, F. S.; Lindsley, C. W.; Conn, P. J.; Pandit, J.; Zagouras, P.; Volkmann, R. A. Allosteric Modulators for the Treatment of Schizophrenia: Targeting Glutamatergic Networks. *Curr. Top. Med. Chem.* **2013,** *13,* 26–54.
38. Chang, P. K.-Y.; Verbich, D.; McKinney, R. A. AMPA Receptors as Drug Targets in Neurological Disease – Advantages, Caveats, and Future Outlook. *Eur. J. Neurosci.* **2012,** *35,* 1908–1916.
39. Garthwaite, G.; Garthwaite, J. Mechanisms of AMPA Neurotoxicity in Rat Brain Slices. *Eur. J. Neurosci.* **1991,** *3,* 729–736.
40. Brorson, J. R.; Manzolillo, P. A.; Gibbons, S. J.; Miller, R. J. AMPA Receptor Desensitization Predicts the Selective Vulnerability of Cerebellar Purkinje Cells to Excitotoxicity. *J. Neurosci.* **1995,** *15,* 4515–4524.
41. Jin, R.; Clark, S.; Weeks, A. M.; Dudman, J. T.; Gouaux, E.; Partin, K. M. Mechanism of Positive Allosteric Modulators Acting on AMPA Receptors. *J. Neurosci.* **2005,** *25,* 9027–9036.
42. Hansen, K. B.; Yuan, H.; Traynelis, S. F. Structural Aspects of AMPA Receptor Activation Desensitization and Deactivation. *Curr. Opin. Neurobiol.* **2007,** *17,* 281–288.
43. Yamada, K. A. Modulating Excitatory Synaptic Neurotransmission: Potential Treatment for Neurological Disease? *Neurobiol. Dis.* **1998,** *5,* 67–80.
44. Qi, J.; Wang, Y.; Jiang, M.; Warren, P.; Chen, G. Cyclothiazide Induces Robust Epileptiform Activity in Rat Hippocampal Neurons Both In Vitro and In Vivo. *J. Physiol.* **2006,** *571,* 605–618.
45. Ko, D.; Yang, H.; Williams, B.; Xing, D.; Laurenza, A. Perampanel in the Treatment of Partial Seizures: Time to Onset and Duration of Most Common Adverse Events From Pooled Phase III and Extension Studies. *Epilepsy Behav.* **2015,** *48,* 45–52.
46. Schwenk, J.; Harmel, N.; Brechet, A.; Zolles, G.; Berkefeld, H.; Müller, C. S.; Bildl, W.; Baehrens, D.; Hüber, B.; Kulik, A.; Klöcker, N.; Schulte, U.; Fakler, B. High-Resolution Proteomics Unravel Architecture and Molecular Diversity of Native AMPA Receptor Complexes. *Neuron* **2012,** *74,* 621–633.
47. Jackson, A. C.; Nicoll, R. A. The Expanding Social Network of Ionotropic Glutamate Receptors: TARPs and Other Transmembrane Auxiliary Subunits. *Neuron* **2011,** *70,* 178–199.
48. Schober, D. A.; Gill, M. B.; Yu, H.; Gernert, D. L.; Jeffries, M. W.; Ornstein, P. L.; Kato, A. S.; Felder, C. C.; Bredt, D. S. Transmembrane AMPA Receptor Regulatory Proteins and Cornichon-2 Allosterically Regulate AMPA Receptor Antagonists and Potentiators. *J. Biol. Chem.* **2011,** *286,* 13134–13142.
49. Kato, A. S.; Gill, M. B.; Yu, H.; Nisenbaum, E. S.; Bredt, D. S. TARPs Differentially Decorate AMPA Receptors to Specify Neuropharmacology. *Trends Neurosci.* **2010,** *33,* 241–248.
50. Tomita, S.; Chen, L.; Kawasaki, Y.; Petralia, R. S.; Wenthold, R. J.; Nicoll, R. A.; Bredt, D. S. Functional Studies and Distribution Define a Family of Transmembrane AMPA Receptor Regulatory Proteins. *J. Cell Biol.* **2003,** *161,* 805–816.
51. Klugbauer, N.; Dai, S.; Specht, V.; Lacinová, L.; Marais, E.; Bohn, G.; Hofmann, F. A Family of γ-Like Calcium Channel Subunits. *FEBS Lett.* **2000,** *470,* 189–197.
52. Twomey, E. C.; Yelshanskaya, M. V.; Grassucci, R. A.; Frank, J.; Sobolevsky, A. I. Elucidation of AMPA Receptor-Stargazin Complexes by Cryo-Electron Microscopy. *Science* **2016,** *353,* 83–86.
53. Zhao, Y.; Chen, S.; Yoshioka, C.; Baconguis, I.; Gouaux, E. Architecture of Fully Occupied GluA2 AMPA Receptor–TARP Complex Elucidated by Cryo-EM. *Nature* **2016,** *536,* 108–111.
54. Cais, O.; Herguedas, B.; Krol, K.; Cull-Candy, S. G.; Farrant, M.; Greger, I. H. Mapping the Interaction Sites Between AMPA Receptors and TARPs Reveals a Role for the Receptor N-Terminal Domain in Channel Gating. *Cell Rep.* **2014,** *9,* 728–740.
55. Straub, C.; Tomita, S. The Regulation of Glutamate Receptor Trafficking and Function by TARPs and Other Transmembrane Auxiliary Subunits. *Curr. Opin. Neurobiol.* **2012,** *22,* 488–495.
56. Gill, M. B.; Bredt, D. S. An Emerging Role for TARPs in Neuropsychiatric Disorders. *Neuropsychopharmacology* **2011,** *36,* 362–363.
57. Gardinier, K. M.; Gernert, D. L.; Porter, W. J.; Reel, J. K.; Ornstein, P. L.; Spinazze, P.; Stevens, F. C.; Hahn, P.; Hollinshead, S. P.; Mayhugh, D.; Schkeryantz, J.; Khilevich, A.; De Frutos, O.; Gleason, S. D.; Kato, A. S.; Luffer-Atlas, D.; Desai, P. V.; Swanson, S.; Burris, K. D.; Ding, C.; Heinz, B. A.; Need, A. B.; Barth, V. N.; Stephenson, G. A.; Diseroad, B. A.; Woods, T. A.; Yu, H.; Bredt, D.; Witkin, J. M. Discovery of the First α-Amino-3-Hydroxy-5-Methyl-4-Isoxazolepropionic Acid (AMPA) Receptor Antagonist Dependent Upon Transmembrane AMPA Receptor Regulatory Protein (TARP) γ-8. *J. Med. Chem.* **2016,** *59,* 4753–4768.
58. Maher, M. P.; Wu, N.; Ravula, S.; Ameriks, M. K.; Savall, B. M.; Liu, C.; Lord, B.; Wyatt, R. M.; Matta, J. A.; Dugovic, C.; Yun, S.; Ver Donck, L.; Steckler, T.; Wickenden, A. D.; Carruthers, N. I.; Lovenberg, T. W. Discovery and Characterization of AMPA Receptor Modulators Selective for TARP-8. *J. Pharmacol. Exp. Ther.* **2016,** *357,* 394–414.
59. Shaffer, C. L.; Patel, N. C.; Schwarz, J.; Scialis, R. J.; Wei, Y.; Hou, X. J.; Xie, L.; Karki, K.; Bryce, D. K.; Osgood, S. M.; Hoffmann, W. E.; Lazzaro, J. T.; Chang, C.; McGinnis, D. F.; Lotarski, S. M.; Liu, J.; Obach, R. S.; Weber, M. L.; Chen, L.; Zasadny, K. R.; Seymour, P. A.; Schmidt, C. J.; Hajós, M.; Hurst, R. S.; Pandit, J.; O'Donnell, C. J. The Discovery and Characterization of the α-Amino-3-Hydroxy-5-Methyl-4-Isoxazolepropionic Acid (AMPA) Receptor Potentiator N -{(3S,4S)-4-[4-(5-Cyano-2-Thienyl)phenoxy]tetrahydrofuran-3-Yl}propane-2-Sulfonamide (PF-04958242). *J. Med. Chem.* **2015,** *58,* 4291–4308.
60. Jin, R.; Banke, T. G.; Mayer, M. L.; Traynelis, S. F.; Gouaux, E. Structural Basis for Partial Agonist Action at Ionotropic Glutamate Receptors. *Nat. Neurosci.* **2003,** *6,* 803–810.
61. Mayer, M. L. Glutamate Receptors at Atomic Resolution. *Nature* **2006,** *440,* 456–462.
62. Ptak, C. P.; Ahmed, A. H.; Oswald, R. E. Probing the Allosteric Modulator Binding Site of GluR2 With Thiazide Derivatives. *Biochemistry* **2009,** *48,* 8594–8602.
63. Kuusinen, A.; Arvola, M.; Keinänen, K. Molecular Dissection of the Agonist Binding Site of an AMPA Receptor. *EMBO J.* **1995,** *14,* 6327–6332.
64. Meyerson, J. R.; Kumar, J.; Chittori, S.; Rao, P.; Pierson, J.; Bartesaghi, A.; Mayer, M. L.; Subramaniam, S. Structural Mechanism of Glutamate Receptor Activation and Desensitization. *Nature* **2014,** *514,* 328–334.
65. Arai, A.; Kessler, M.; Ambros-Ingerson, J.; Quan, A.; Yigiter, E.; Rogers, G.; Lynch, G. Effects of a Centrally Active Benzoylpiperidine Drug on α-Amino-3-Hydroxy-5-Methyl-4-Isoxalepropionic Acid Receptor Kinetics. *Neuroscience* **1996,** *75,* 573–585.
66. Black, M. D. Therapeutic Potential of Positive AMPA Modulators and Their Relationship to AMPA Receptor Subunits. A Review of Preclinical Data. *Psychopharmacology (Berl)* **2005,** *179,* 154–163.
67. Hampson, R. E.; España, R. A.; Rogers, G. A.; Porrino, L. J.; Deadwyler, S. A. Mechanisms Underlying Cognitive Enhancement and Reversal of Cognitive Deficits in Nonhuman Primates by the Ampakine CX717. *Psychopharmacology (Berl)* **2009,** *202,* 355–369.
68. Roberts, B. M.; Holden, D. E.; Shaffer, C. L.; Seymour, P. A.; Menniti, F. S.; Schmidt, C. J.; Williams, G. V.; Castner, S. A. Prevention of Ketamine-Induced Working Memory Impairments by AMPA Potentiators in a Nonhuman Primate Model of Cognitive Dysfunction. *Behav. Brain Res.* **2010,** *212,* 41–48.

69. Woolley, M. L.; Waters, K. A.; Gartlon, J. E.; Lacroix, L. P.; Jennings, C.; Shaughnessy, F.; Ong, A.; Pemberton, D. J.; Harries, M. H.; Southam, E.; Jones, D. N. C.; Dawson, L. A. Evaluation of the Pro-cognitive Effects of the AMPA Receptor Positive Modulator, 5-(1-Piperidinylcarbonyl)-2,1,3-Benzoxadiazole (CX691), in the Rat. *Psychopharmacology (Berl)* **2009,** *202,* 343–354.
70. Ingvar, M.; Ambros-Ingerson, J.; Davis, M.; Granger, R.; Kessler, M.; Rogers, G. A.; Schehr, R. S.; Lynch, G. Enhancement by an Ampakine of Memory Encoding in Humans. *Exp. Neurol.* **1997,** *146,* 553–559.
71. Gainetdinov, R. R.; Mohn, A. R.; Bohn, L. M.; Caron, M. G. Glutamatergic Modulation of Hyperactivity in Mice Lacking the Dopamine Transporter. *Proc. Natl. Acad. Sci. U. S. A.* **2001,** *98,* 11047–11054.
72. Fan, W.; Wu, X.; Pan, Y.; Li, C.; Niu, Y.; Zhai, Y.; Mei, Q. 1-(1,3-Benzodioxol-5-Yl-Carbo-Nyl) Piperidine, a Modulator of α-Amino-3-Hydroxy-5-Methyl-4-Isoxazole Propionic Acid Receptor, Ameliorates Exercise-Induced Fatigue in Mice. *Biol. Pharm. Bull.* **2014,** *37,* 13–17.
73. Silverman, J. L.; Oliver, C. F.; Karras, M. N.; Gastrell, P. T.; Crawley, J. N. AMPAKINE Enhancement of Social Interaction in the BTBR Mouse Model of Autism. *Neuropharmacology* **2013,** *64,* 268–282.
74. Knapp, R. J.; Goldenberg, R.; Shuck, C.; Cecil, A.; Watkins, J.; Miller, C.; Crites, G.; Malatynska, E. Antidepressant Activity of Memory-Enhancing Drugs in the Reduction of Submissive Behavior Model. *Eur. J. Pharmacol.* **2002,** *440,* 27–35.
75. Li, X.; Tizzano, J. P.; Griffey, K.; Clay, M.; Lindstrom, T.; Skolnick, P. Antidepressant-like Actions of an AMPA Receptor Potentiator (LY392098). *Neuropharmacology* **2001,** *40,* 1028–1033.
76. Lynch, G.; Granger, R.; Ambros-Ingerson, J.; Davis, C. M.; Kessler, M.; Schehr, R. Evidence That a Positive Modulator of AMPA-Type Glutamate Receptors Improves Delayed Recall in Aged Humans. *Exp. Neurol.* **1997,** *145,* 89–92.
77. Goff, D. C.; Leahy, L.; Berman, I.; Posever, T.; Herz, L.; Leon, A. C.; Johnson, S. A.; Lynch, G. A Placebo-Controlled Pilot Study of the Ampakine CX516 Added to Clozapine in Schizophrenia. *J. Clin. Psychopharmacol.* **2001,** *21,* 484–487.
78. Chappell, A. S.; Gonzales, C.; Williams, J.; Witte, M. M.; Mohs, R. C.; Sperling, R. AMPA Potentiator Treatment of Cognitive Deficits in Alzheimer Disease. *Neurology* **2007,** *68,* 1008–1012.
79. Berry-Kravis, E.; Krause, S. E.; Block, S. S.; Guter, S.; Wuu, J.; Leurgans, S.; Decle, P.; Potanos, K.; Cook, E.; Salt, J.; Maino, D.; Weinberg, D.; Lara, R.; Jardini, T.; Cogswell, J.; Johnson, S. A.; Hagerman, R. Effect of CX516, an AMPA-Modulating Compound, on Cognition and Behavior in Fragile X Syndrome: A Controlled Trial. *J. Child Adolesc. Psychopharmacol.* **2006,** *16,* 525–540.
80. Tolerability and Primary Efficacy of CX516 in Alzheimer's Disease. https://clinicaltrials.gov/ct2/show/NCT00001662 (accessed on March 23, 2016).
81. A Follow Up Safety Study of Patients Who Participated in Previous Studies of the Drug Org 24448. https://clinicaltrials.gov/ct2/show/NCT0078058 (accessed on March 23, 2016).
82. Org 24448 to Treat Major Depression. https://clinicaltrials.gov/ct2/show/NCT00113022 (accessed on March 23, 2016).
83. Org 24448 (Ampakine) for Cognitive Deficits in Schizophrenia. https://clinicaltrials.gov/ct2/show/NCT00425815 (accessed on March 23, 2016).
84. Nations, K. R.; Dogterom, P.; Bursi, R.; Schipper, J.; Greenwald, S.; Zraket, D.; Gertsik, L.; Johnstone, J.; Lee, A.; Pande, Y.; Ruigt, G.; Ereshefsky, L. Examination of Org 26576, an AMPA Receptor Positive Allosteric Modulator, in Patients Diagnosed With Major Depressive Disorder: An Exploratory, Randomized, Double-Blind Placebo-Controlled Trial. *J. Psychopharmacol.* **2012,** *26,* 1525–1539.
85. Adler, L. A.; Kroon, R. A.; Stein, M.; Shahid, M.; Tarazi, F. I.; Szegedi, A.; Schipper, J.; Cazorla, P. A Translational Approach to Evaluate the Efficacy and Safety of the Novel AMPA Receptor Positive Allosteric Modulator Org 26576 in Adult Attention-Deficit/Hyperactivity Disorder. *Biol. Psychiatry* **2012,** *72,* 971–977.
86. Trzepacz, P. T.; Cummings, J.; Konechnik, T.; Forrester, T. D.; Chang, C.; Dennehy, E. B.; Willis, B. A.; Shuler, C.; Tabas, L. B.; Lyketsos, C. Mibampator (LY451395) Randomized Clinical Trial for Agitation/Aggression in Alzheimer's Disease. *Int. Psychogeriatrics* **2013,** *25,* 707–719.
87. Evaluation of Single and Repeat Doses of GSK729327 in Healthy Volunteers. https://clinicaltrials.gov/ct2/show/NCT00448890 (accessed on March 23, 2016).
88. Wesensten, N. J.; Reichardt, R. M.; Balkin, T. J. Ampakine (CX717) Effects on Performance and Alertness During Simulated Night Shift Work. *Aviat. Space Environ. Med.* **2007,** *78,* 937–943.
89. Swanson, G. T. Targeting AMPA and Kainate Receptors in Neurological Disease: Therapies on the Horizon? *Neuropsychopharmacology* **2009,** *34,* 249–250.
90. Registered Clinical Studies for PF-04958242. https://clinicaltrials.gov/ct2/results?term=pf-04958242&Search=Search (accessed on March 23, 2016).
91. RespireRx Product Pipeline. http://www.respirerx.com/product/index.html (accessed on March 23, 2016).
92. Bednar, M. M.; DeMartinis, N.; Banerjee, A.; Bowditch, S.; Gaudreault, F.; Zumpano, L.; Lin, F. R. The Safety and Efficacy of PF-04958242 in Age-Related Sensorineural Hearing Loss. *JAMA Otolaryngol. Neck Surg.* **2015,** *141,* 607.
93. Ward, S. E.; Bax, B. D.; Harries, M. Challenges for and Current Status of Research Into Positive Modulators of AMPA Receptors. *Br. J. Pharmacol.* **2010,** *160,* 181–190.
94. Ward, E. S.; Harries, M. Recent Advances in the Discovery of Selective AMPA Receptor Positive Allosteric Modulators. *Curr. Med. Chem.* **2010,** *17,* 3503–3513.
95. Grove, S. J. A.; Jamieson, C.; Maclean, J. K. F.; Morrow, J. A.; Rankovic, Z. Positive Allosteric Modulators of the α-Amino-3-Hydroxy-5-Methyl-4-Isoxazolepropionic Acid (AMPA) Receptor. *J. Med. Chem.* **2010,** *53,* 7271–7279.
96. Ward, S. E.; Harries, M.; Aldegheri, L.; Austin, N. E.; Ballantine, S.; Ballini, E.; Bradley, D. M.; Bax, B. D.; Clarke, B. P.; Harris, A. J.; Harrison, S. A.; Melarange, R. A.; Mookherjee, C.; Mosley, J.; Dal Negro, G.; Oliosi, B.; Smith, K. J.; Thewlis, K. M.; Woollard, P. M.; Yusaf, S. P. Integration of Lead Optimization With Crystallography for a Membrane-Bound Ion Channel Target: Discovery of a New Class of AMPA Receptor Positive Allosteric Modulators. *J. Med. Chem.* **2011,** *54,* 78–94.
97. Ward, S. E.; Pennicott, L. E.; Beswick, P. AMPA Receptor-Positive Allosteric Modulators for the Treatment of Schizophrenia: An Overview of Recent Patent Applications. *Future Med. Chem.* **2015,** *7,* 473–491.
98. Ward, S. E.; Harries, M.; Aldegheri, L.; Andreotti, D.; Ballantine, S.; Bax, B. D.; Harris, A. J.; Harker, A. J.; Lund, J.; Melarange, R.; Mingardi, A.; Mookherjee, C.; Mosley, J.; Neve, M.; Oliosi, B.; Profeta, R.; Smith, K. J.; Smith, P. W.; Spada, S.; Thewlis, K. M.; Yusaf, S. P. Discovery of N-[(2S)-5-(6-Fluoro-3-Pyridinyl)-2,3-Dihydro-1H-Inden-2-Yl]-2-Propanesulfonamide, a Novel Clinical AMPA Receptor Positive Modulator. *J. Med. Chem.* **2010,** *53,* 5801–5812.
99. Bertheleme, N.; Bradley, D. M.; Cardullo, F.; Merlo, G.; Pozzan, A.; Scott, J. S.; Thewlis, K. M.; Ward, S. E. Compounds Which Potentiate AMPA Receptor and Uses Thereof In Medicine. WO 2008/113795 A1, 2008.
100. Bertheleme, N.; Chan, W. N.; Scott, J. S.; Ward, S. E. Compounds Which Potentiate the AMPA Receptor and Uses Thereof in Medicine. WO 2009/080637 A1, 2009.
101. Bradley, D. M.; Cardullo, F.; Marshall, H.; Marzorati, P.; Pozzan, A.; Ward, S. E. Compounds Which Potentiate The AMPA Receptor And Uses Thereof In Medicine. WO 2010/066658 A1, 2010.
102. Bradley, D. M.; Chan, W. N.; Harrison, S. A.; Thewlis, K. M.; Ward, S. E. Compounds Which Potentiate AMPA Receptor and Uses Thereof in Medicine. WO 2008/110566 A1, 2008.
103. Bradley, D. M.; Chan, W. N.; Thewlis, K. M.; Ward, S. E. Compounds Which Potentiate AMPA Receptor and Uses Thereof in Medicine. WO 2008/053031 A1, 2008.
104. Bradley, D. M.; Chan, W. N.; Ward, S. E. Compounds Which Potentiate AMPA Receptor and Uses Thereof in Medicine. WO 2008/148836 A1, 2008.
105. Bradley, D. M.; Thewlis, K. M.; Ward, S. E. Compounds Which Potentiate AMPA Receptor and Uses Thereof in Medicine. WO 2008/148832 A1, 2008.
106. Chan, W. N.; Harrison, S.; Hughes, O. R.; Neesom, J. K.; Thewlis, K. M.; Ward, S. E. Compounds Which Potentiate AMPA Receptor and Uses Thereof in Medicine. WO 2009/053448 A1, 2009.
107. Chan, W. N.; Thewlis, K. M.; Ward, S. E. Thiazoles Which Potentiate AMPA Receptor and Medicinal Uses Thereof. WO 2009/053449 A1, 2009.
108. Thewlis, K. M.; Ward, S. E. Compounds Which Potentiate the AMPA Receptor and Uses Thereof in Medicine. WO 2009/092713 A1, 2009.
109. Thewlis, K. M.; Ward, S. E. Compounds Which Potentiate the AMPA Receptor and Uses Thereof in Medicine. WO 2009/092712 A1, 2009.
110. Ward, S. E.; Bertheleme, N. Compounds Which Potentiate AMPA Receptor and Uses Thereof in Medicine. WO 2010/037760 A1, 2010.

111. Thewlis, K. M.; Aldegheri, L.; Harries, M. H.; Mookherjee, C.; Oliosi, B.; Ward, S. E. N-Substituted Pyrrolidines and Tetrahydrofurans as Novel AMPAR Positive Modulators. *Bioorg. Med. Chem. Lett.* **2010,** *20,* 7116–7119.
112. Ennaceur, A.; Delacour, J. A New One-Trial Test for Neurobiological Studies of Memory in Rats. 1: Behavioral Data. *Behav. Brain Res.* **1988,** *31,* 47–59.
113. Foley, A. G.; Murphy, K. J.; Hirst, W. D.; Gallagher, H. C.; Hagan, J. J.; Upton, N.; Walsh, F. S.; Regan, C. M. The 5-HT(6) Receptor Antagonist SB-271046 Reverses Scopolamine-Disrupted Consolidation of a Passive Avoidance Task and Ameliorates Spatial Task Deficits in Aged Rats. *Neuropsychopharmacology* **2004,** *29,* 93–100.
114. Löscher, W.; Fassbender, C. P.; Nolting, B. The Role of Technical, Biological and Pharmacological Factors in the Laboratory Evaluation of Anticonvulsant Drugs II. Maximal Electroshock Seizure Models. *Epilepsy Res.* **1991,** *8,* 79–94.
115. Estep, K. G.; Fliri, A. F. J. J. G.; O'Donnell, C.; Patel, N. C.; Schwarz, J. B.; Xie, L. Oxopiperidinyl and Pyranyl Sulfonamides as AMPA Potentiators. WO 2010/038167 A1, 2010.
116. Estep, K. G.; Fliri, A. F. J.; O'Donnell, C. J. Sulfonamides and Pharmaceutical Compositions Thereof. WO 2008/120093 A1, 2008.
117. Estep, K. G.; O'Donnell, C. J.; Xie, L. Tetrahydrofuranyl Sulfonamides for Use as AMPA Modulators in the Treatment of CNS Disorders. WO 2010/041162 A1, 2010.
118. Fliri, A. F. J. J.; Gallaschun, R. J.; O'Donnell, C. J.; Schwarz, J. B.; Segelstein, B. E. Heterocyclic Sulfonamides, Uses and Pharmaceutical Compositions Thereof. WO 2010/150192 A1, 2010.
119. Patel, N. C.; Schwarz, J.; Hou, X. J.; Hoover, D. J.; Xie, L.; Fliri, A. J.; Gallaschun, R. J.; Lazzaro, J. T.; Bryce, D. K.; Hoffmann, W. E.; Hanks, A. N.; McGinnis, D.; Marr, E. S.; Gazard, J. L.; Hajós, M.; Scialis, R. J.; Hurst, R. S.; Shaffer, C. L.; Pandit, J.; O'Donnell, C. J. Discovery and Characterization of a Novel Dihydroisoxazole Class of α-Amino-3-Hydroxy-5-Methyl-4-Isoxazolepropionic Acid (AMPA) Receptor Potentiators. *J. Med. Chem.* **2013,** *56,* 9180–9191.
120. Shaffer, C. L.; Hurst, R. S.; Scialis, R. J.; Osgood, S. M.; Bryce, D. K.; Hoffmann, W. E.; Lazzaro, J. T.; Hanks, A. N.; Lotarski, S.; Weber, M. L.; Liu, J.; Menniti, F. S.; Schmidt, C. J.; Hajos, M. Positive Allosteric Modulation of AMPA Receptors From Efficacy to Toxicity: The Interspecies Exposure-Response Continuum of the Novel Potentiator PF-4778574. *J. Pharmacol. Exp. Ther.* **2013,** *347,* 212–224.
121. McNeish, J.; Roach, M.; Hambor, J.; Mather, R. J.; Weibley, L.; Lazzaro, J.; Gazard, J.; Schwarz, J.; Volkmann, R.; Machacek, D.; Stice, S.; Zawadzke, L.; O'Donnell, C.; Hurst, R. High-Throughput Screening in Embryonic Stem Cell-Derived Neurons Identifies Potentiators of Amino-3-Hydroxyl-5-Methyl-4-Isoxazolepropionate-Type Glutamate Receptors. *J. Biol. Chem.* **2010,** *285,* 17209–17217.
122. Stepan, A. F.; Walker, D. P.; Bauman, J.; Price, D. A.; Baillie, T. A.; Kalgutkar, A. S.; Aleo, M. D. Structural Alert/Reactive Metabolite Concept as Applied in Medicinal Chemistry to Mitigate the Risk of Idiosyncratic Drug Toxicity: A Perspective Based on the Critical Examination of Trends in the Top 200 Drugs Marketed in the United States. *Chem. Res. Toxicol.* **2011,** *24,* 1345–1410.
123. Kalgutkar, A.; Gardner, I.; Obach, R.; Shaffer, C.; Callegari, E.; Henne, K.; Mutlib, A.; Dalvie, D.; Lee, J.; Nakai, Y.; O'Donnell, J.; Boer, J.; Harriman, S. A Comprehensive Listing of Bioactivation Pathways of Organic Functional Groups. *Curr. Drug Metab.* **2005,** *6,* 161–225.
124. Ryder, J. W.; Falcone, J. F.; Manro, J. R.; Svensson, K. A.; Merchant, K. M. Pharmacological Characterization of cGMP Regulation by the Biarylpropylsulfonamide Class of Positive, Allosteric Modulators of -Amino-3-Hydroxy-5-Methyl-4-Isoxazolepropionic Acid Receptors. *J. Pharmacol. Exp. Ther.* **2006,** *319,* 293–298.
125. Di, L.; Umland, J. P.; Chang, G.; Huang, Y.; Lin, Z.; Scott, D. O.; Troutman, M. D.; Liston, T. E. Species Independence in Brain Tissue Binding Using Brain Homogenates. *Drug Metab. Dispos.* **2011,** *39,* 1270–1277.
126. Calabrese, E. J. Hormesis and Medicine. *Br. J. Clin. Pharmacol.* **2008,** *66,* 594–617.
127. Shaffer, C. L.; Scialis, R. J.; Rong, H.; Obach, R. S. Using Simcyp to Project Human Oral Pharmacokinetic Variability in Early Drug Research to Mitigate Mechanism-Based Adverse Events. *Biopharm. Drug Dispos.* **2012,** *33,* 72–84.
128. Mueller, R.; Lee, S.; O'Hare, S.; Rogers, G.; Rachwal, S.; Street, L. Benzotriazinone Derivatives as AMPA Receptor Enhancers and Their Preparation, Pharmaceutical Compositions and Use in the Treatment of Diseases. WO 2008/085505 A1, 2008.
129. Mueller, R.; Street, L.; Rachwal, S.; Alisala, K. Preparation of Substituted Triazinone Derivatives and Analogs as Glutamatergic Synaptic Response Enhancers. WO 2009/038752 A2, 2009.
130. Cordi, A.; Desos, P.; Lestage, P.; Danober, L. Benzothiadiazepine Derivatives Used as AMPA and NMDA Receptor Modulators. WO 2010/106249 A1, 2010.
131. Cordi, A.; Desos, P.; Lestage, P. Dihydrobenzoxathiazepine Derivatives, Preparation Thereof, Pharmaceutical Compositions and Use as AMPA Receptor Modulators. WO 2012/035216 A1, 2012.
132. Cordi, A.; Rogers, G. 3-Substituted-[1,2,3]-Benzotriazinone Compound for Enhancing Glutamatergic Synaptic Responses. WO 2008/085506 A1, 2008.
133. Mueller, R.; Rachwal, S.; Varney, M. A.; Johnson, S. A.; Alisala, K.; Zhong, S.; Li, Y.-X.; Haroldsen, P.; Herbst, T.; Street, L. J. Benzobistriazinones and Related Heterocyclic Ring Systems as Potent, Orally Bioavailable Positive Allosteric AMPA Receptor Modulators. *Bioorg. Med. Chem. Lett.* **2011,** *21,* 7455–7459.
134. Mueller, R.; Rachwal, S.; Lee, S.; Zhong, S.; Li, Y.-X.; Haroldsen, P.; Herbst, T.; Tanimura, S.; Varney, M.; Johnson, S.; Rogers, G.; Street, L. J. Benzotriazinone and Benzopyrimidinone Derivatives as Potent Positive Allosteric AMPA Receptor Modulators. *Bioorg. Med. Chem. Lett.* **2011,** *21,* 6170–6175.
135. Mueller, R.; Li, Y.-X.; Hampson, A.; Zhong, S.; Harris, C.; Marrs, C.; Rachwal, S.; Ulas, J.; Nielsson, L.; Rogers, G. Benzoxazinones as Potent Positive Allosteric AMPA Receptor Modulators: Part I. *Bioorg. Med. Chem. Lett.* **2011,** *21,* 3923–3926.
136. Mueller, R.; Rachwal, S.; Tedder, M. E.; Li, Y.-X.; Zhong, S.; Hampson, A.; Ulas, J.; Varney, M.; Nielsson, L.; Rogers, G. Substituted Benzoxazinones as Potent Positive Allosteric AMPA Receptor Modulators: Part II. *Bioorg. Med. Chem. Lett.* **2011,** *21,* 3927–3930.
137. Gillen, K. J.; Jamieson, C.; Maclean, J. K. F.; Moir, E. M.; Rankovic, Z.; Gillen Craig; Maclean, John Kinnaird Ferguson; Moir, Elizabeth Margaret; Rankovic, Zoran., K. J. J. Preparation of Pyrazolealkanamide Substituted Thiophenes as AMPA Potentiators. WO 2008/003452 A1, 2008.
138. Gillespie, J.; Jamieson, C.; Maclean, J. K. F.; Moir, E. M.; Rankovic, Z. Indane Derivatives as AMPA Receptor Modulators. WO 2009/147167 A1, 2009.
139. Gallagher, M. G.; Jamieson, C. C.; Lyons, A. J.; Maclean, J. K. F.; Moir, E. M.; Gallagher Craig, M. G. J. Heterocyclic Derivatives. WO 2009/131455 A1, May 2009.
140. Gillen, K. J.; Gillespie, J.; Jamieson, C.; Maclean, J. K. F.; Moir, E. M.; Rankovic, Z. Indane Derivatives. WO 2010/115952 A1, 2010.
141. Jamieson, C.; Maclean, J. K. F.; Brown, C. I.; Campbell, R. A.; Gillen, K. J.; Gillespie, J.; Kazemier, B.; Kiczun, M.; Lamont, Y.; Lyons, A. J.; Moir, E. M.; Morrow, J. A.; Pantling, J.; Rankovic, Z.; Smith, L. Structure Based Evolution of a Novel Series of Positive Modulators of the AMPA Receptor. *Bioorg. Med. Chem. Lett.* **2011,** *21,* 805–811.
142. Jamieson, C.; Campbell, R. A.; Cumming, I. A.; Gillen, K. J.; Gillespie, J.; Kazemier, B.; Kiczun, M.; Lamont, Y.; Lyons, A. J.; Maclean, J. K. F.; Martin, F.; Moir, E. M.; Morrow, J. A.; Pantling, J.; Rankovic, Z.; Smith, L. A Novel Series of Positive Modulators of the AMPA Receptor: Structure-Based Lead Optimization. *Bioorg. Med. Chem. Lett.* **2010,** *20,* 6072–6075.
143. Jamieson, C.; Basten, S.; Campbell, R. A.; Cumming, I. A.; Gillen, K. J.; Gillespie, J.; Kazemier, B.; Kiczun, M.; Lamont, Y.; Lyons, A. J.; Maclean, J. K. F.; Moir, E. M.; Morrow, J. A.; Papakosta, M.; Rankovic, Z.; Smith, L. A Novel Series of Positive Modulators of the AMPA Receptor: Discovery and Structure Based Hit-to-Lead Studies. *Bioorg. Med. Chem. Lett.* **2010,** *20,* 5753–5756.
144. Caldwell, N.; Harms, J. E.; Partin, K. M.; Jamieson, C. Rational Design of a Novel AMPA Receptor Modulator Through a Hybridization Approach. *ACS Med. Chem. Lett.* **2015,** *6,* 392–396.
145. Dintilhac, G.; Arslan, D.; Dilly, S.; Danober, L.; Botez, I.; Lestage, P.; Pirotte, B.; de Tullio, P. New Substituted Aryl Esters and Aryl Amides of 3,4-Dihydro-2H-1,2,4-Benzothiadiazine 1,1-Dioxides as Positive Allosteric Modulators of AMPA Receptors. *Med. Chem. Commun.* **2011,** *2,* 509.
146. Carrozzo, M. M.; Battisti, U. M.; Cannazza, G.; Puia, G.; Ravazzini, F.; Falchicchio, A.; Perrone, S.; Citti, C.; Jozwiak, K.; Braghiroli, D.; Parenti, C.; Troisi, L. Design, Stereoselective Synthesis, Configurational Stability and Biological Activity of 7-Chloro-9-(Furan-3-Yl)-2,3,3a,4-Tetrahydro-1H-benzo[e]pyrrolo[2,1-c][1,2,4]thiadiazine 5,5-Dioxide. *Bioorg. Med. Chem.* **2014,** *22,* 4667–4676.
147. Francotte, P.; Goffin, E.; Fraikin, P.; Graindorge, E.; Lestage, P.; Danober, L.; Challal, S.; Rogez, N.; Nosjean, O.; Caignard, D.; Pirotte, B.; de Tullio, P. Development of Thiophenic Analogues of Benzothiadiazine Dioxides as New Powerful Potentiators of 2-Amino-3-(3-Hydroxy-5-Methylisoxazol-4-Yl)propionic Acid (AMPA) Receptors. *J. Med. Chem.* **2013,** *56,* 7838–7850.

148. Francotte, P.; Goffin, E.; Fraikin, P.; Lestage, P.; Van Heugen, J.-C.; Gillotin, F.; Danober, L.; Thomas, J.-Y.; Chiap, P.; Caignard, D.-H.; Pirotte, B.; de Tullio, P. New Fluorinated 1,2,4-Benzothiadiazine 1,1-Dioxides: Discovery of an Orally Active Cognitive Enhancer Acting through Potentiation of the 2-Amino-3-(3-Hydroxy-5-Methylisoxazol-4-Yl)propionic Acid Receptors. *J. Med. Chem.* **2010,** *53,* 1700–1711.
149. Francotte, P.; Nørholm, A.-B.; Deva, T.; Olsen, L.; Frydenvang, K.; Goffin, E.; Fraikin, P.; de Tullio, P.; Challal, S.; Thomas, J.; Iop, F.; Louis, C.; Botez-Pop, I.; Lestage, P.; Danober, L.; Kastrup, J. S.; Pirotte, B. Positive Allosteric Modulators of 2-Amino-3-(3-Hydroxy-5-Methylisoxazol-4-Yl)propionic Acid Receptors Belonging to 4-Cyclopropyl-3,4-Dihydro-2H -1,2,4-Pyridothiadiazine Dioxides and Diversely Chloro-Substituted 4-Cyclopropyl-3,4-Dihydro-2H-1,2,4-Benzot. *J. Med. Chem.* **2014,** *57,* 9539–9553.
150. Nørholm, A.; Francotte, P.; Goffin, E.; Botez, I.; Danober, L.; Lestage, P.; Pirotte, B.; Kastrup, J. S.; Olsen, L.; Oostenbrink, C. Thermodynamic Characterization of New Positive Allosteric Modulators Binding to the Glutamate Receptor A2 Ligand-Binding Domain: Combining Experimental and Computational Methods Unravels Differences in Driving Forces. *J. Chem. Inf. Model.* **2014,** *54,* 3404–3416.
151. Nørholm, A.-B.; Francotte, P.; Olsen, L.; Krintel, C.; Frydenvang, K.; Goffin, E.; Challal, S.; Danober, L.; Botez-Pop, I.; Lestage, P.; Pirotte, B.; Kastrup, J. S. Synthesis, Pharmacological and Structural Characterization, and Thermodynamic Aspects of GluA2-Positive Allosteric Modulators With a 3,4-Dihydro-2H -1,2,4-Benzothiadiazine 1,1-Dioxide Scaffold. *J. Med. Chem.* **2013,** *56,* 8736–8745.
152. Larsen, A. P.; Francotte, P.; Frydenvang, K.; Tapken, D.; Goffin, E.; Fraikin, P.; Caignard, D.-H.; Lestage, P.; Danober, L.; Pirotte, B.; Kastrup, J. S. Synthesis and Pharmacology of Mono-, Di-, and Trialkyl-Substituted 7-Chloro-3,4-Dihydro-2H -1,2,4-Benzothiadiazine 1,1-Dioxides Combined with X-Ray Structure Analysis to Understand the Unexpected Structure–Activity Relationship at AMPA Receptors. *ACS Chem. Neurosci.* **2016,** *7,* 378–390.
153. Pirotte, B.; Francotte, P.; Goffin, E.; de Tullio, P. AMPA Receptor Positive Allosteric Modulators: A Patent Review. *Expert Opin. Ther. Pat.* **2013,** *23,* 615–628.
154. Mochizuki, M.; Imaeda, T. Heterocyclic Compound. WO 2010/140339 A1, 2010.
155. Mochizuki, M.; Imaeda, T.; Aso, K. Heterocyclic Compound. WO 2011/036885 A1, 2011.
156. Mochizuki, M.; Miura, S. Heterocyclic Compound. WO 2009/119088 A1, 2009.
157. Aso, K.; Mochizuki, M.; Miura, S.; Imaeda, T.; Toyofuku, M. Heterocyclic Compound. WO 2011/036889 A1, 2011.
158. Kori, M.; Imaeda, T.; Nakamura, S.; Toyofuku, M.; Honda, E.; Asano, Y.; Ujikawa, O.; Mochizuki, M. Heterocyclic Compound and Use Thereof. WO 2012/020848 A1, 2012.
159. Fukumoto, S.; Ujikawa, O.; Morimoto, S.; Asano, Y.; Mikami, S.; Tokunaga, N.; Kori, M.; Imaeda, T.; Fukuda, K.; Nakamura, S.; Iwanaga, K. Sulfonamide Derivative and Use Thereof. WO 2012/137982 A2, 2012.
160. Shepherd, T. A.; Aikins, J. A.; Bleakman, D.; Cantrell, B. E.; Rearick, J. P.; Simon, R. L.; Smith, E. C. R.; Stephenson, G. A.; Zimmerman, D. M.; Mandelzys, A.; Jarvie, K. R.; Ho, K.; Deverill, M.; Kamboj, R. K. Design and Synthesis of a Novel Series of 1,2-Disubstituted Cyclopentanes as Small, Potent Potentiators of 2-Amino-3-(3-Hydroxy-5-Methyl-Isoxazol-4-Yl)propanoic Acid (AMPA) Receptors. *J. Med. Chem.* **2002,** *45,* 2101–2111.
161. Quirk, J. C.; Nisenbaum, E. S. LY404187: A Novel Positive Allosteric Modulator of AMPA Receptors. *CNS Drug Rev.* **2006,** *8,* 255–282.
162. Zarrinmayeh, H.; Tromiczak, E.; Zimmerman, D. M.; Rankl, N.; Ho, K. H.; Dominguez, E.; Castaño, A.; Escribano, A.; Fernandez, C.; Jimenez, A.; Hornback, W. J.; Nisenbaum, E. S. A Novel Class of Positive Allosteric Modulators of AMPA Receptors: Design, Synthesis, and Structure–Activity Relationships of 3-Biphenyl-4-Yl-4-Cyano-5-Ethyl-1-Methyl-1H-Pyrrole-2-Carboxylic Acid, LY2059346. *Bioorg. Med. Chem. Lett.* **2006,** *16,* 5203–5206.
163. Fernandez, M.-C.; Castaño, A.; Dominguez, E.; Escribano, A.; Jiang, D.; Jimenez, A.; Hong, E.; Hornback, W. J.; Nisenbaum, E. S.; Rankl, N.; Tromiczak, E.; Vaught, G.; Zarrinmayeh, H.; Zimmerman, D. M. A Novel Class of AMPA Receptor Allosteric Modulators. Part 1: Design, Synthesis, and SAR of 3-Aryl-4-Cyano-5-Substituted-Heteroaryl-2-Carboxylic Acid Derivatives. *Bioorg. Med. Chem. Lett.* **2006,** *16,* 5057–5061.
164. Hibi, S.; Ueno, K.; Nagato, S.; Kawano, K.; Ito, K.; Norimine, Y.; Takenaka, O.; Hanada, T.; Yonaga, M. Discovery of 2-(2-Oxo-1-Phenyl-5-Pyridin-2-Yl-1,2-Dihydropyridin-3-Yl) benzonitrile (Perampanel): A Novel, Noncompetitive α-Amino-3-Hydroxy-5-Methyl-4-Isoxazolepropanoic Acid (AMPA) Receptor Antagonist. *J. Med. Chem.* **2012,** *55,* 10584–10600.
165. Mattes, H.; Carcache, D.; Kalkman, H. O.; Koller, M. Alpha-Amino-3-Hydroxy-5-Methyl-4-Isoxazolepropionic Acid (AMPA) Antagonists: From Bench to Bedside. *J. Med. Chem.* **2010,** *53,* 5367–5382.
166. Rogawski, M. A. Revisiting AMPA Receptors as an Antiepileptic Drug Target. *Epilepsy Curr.* **2011,** *11,* 56–63.
167. Tomita, S. Regulation of Ionotropic Glutamate Receptors by Their Auxiliary Subunits. *Physiology* **2010,** *25,* 41–49.
168. Tomita, S.; Byrd, R. K.; Rouach, N.; Bellone, C.; Venegas, A.; O'Brien, J. L.; Kim, K. S.; Olsen, O.; Nicoll, R. A.; Bredt, D. S. AMPA Receptors and Stargazin-Like Transmembrane AMPA Receptor-Regulatory Proteins Mediate Hippocampal Kainate Neurotoxicity. *Proc. Natl. Acad. Sci. U. S. A.* **2007,** *104,* 18784–18788.

7.12 GLP-1 Receptor Agonists for the Treatment of Diabetes and Obesity

A Palani, Y-Y Zhou, M Halleck, and P Carrington, Merck Research Laboratories, Kenilworth, NJ, United States

© 2017 Elsevier Ltd. All rights reserved.

7.12.1	**Introduction**	482
7.12.1.1	T2D Background	482
7.12.1.2	GLP-1 History and Background	482
7.12.2	**Mechanism of Action**	482
7.12.2.1	GLP-1 Synthesis and Expression	482
7.12.2.2	GLP-1 Synthesis and Expression	482
7.12.3	**Effects on Food Intake**	483
7.12.3.1	Inhibition of Feeding in Rodents and Humans	483
7.12.4	**Interactions With the GLP-1R**	483
7.12.4.1	Brief Overview of GLP-1 Structure	483
7.12.5	**GLP-1R Agonists**	483
7.12.6	**Structure Activity Relationships of GLP-1**	484
7.12.6.1	Exenatide	485
7.12.6.2	Lixienatide	485
7.12.6.3	Taspoglutide	485
7.12.6.4	Liraglutide	485
7.12.6.5	Semaglutide	486
7.12.6.6	Albiglutide	486
7.12.6.7	Dulaglutide	486
7.12.7	**Summary of GLP-1R Agonist Toxicity**	487
7.12.7.1	Gastrointestinal Effects	487
7.12.7.2	Heart Rate Effects	487
7.12.7.3	Thyroid C-Cell Tumor	487
7.12.7.4	Pancreatitis	487
7.12.7.5	Gall Bladder Events	488
7.12.7.6	ADA Generations	488
7.12.8	**Future Directions**	488
References		489

Abbreviations

ADA Antidrug antidody
Aib Aminoisobutyric acid
API Active pharmaceutical ingredient
ATP Adenosine triphosphate
BID Twice daily
BP Blood pressure
cAMP Cyclic adenosine monophosphate
DPP4 Dipeptidyl protease 4
F Oral bioavailability
FDA Federal drug administration
FFAs Free fatty acids
GI Gastrointestinal
GLP-1 Glucagon-like peptide 1
GLP-1R Glucagon-like peptide 1 receptor
GLP2 Glucagon-like peptide 2
GPCRs G-protein-coupled receptors
HbA1c Hemoglobin A1c
HR Heart rate
i.v. Intravenous
ICV Intracerebroventricular
IP Intellectual property
IVP Intravesicular pressure
PD Pharmacodynamic
PEG Polyethylene glycol
PI-3 Phosphoinositide 3-kinase
PK Pharmacokinetic
PKA Protein kinase activator
QD Once daily
QW Once weekly
$T_{1/2}$ Half-life
T2DM Type 2 diabetes
TGs Triglycerides
ZDF Zucker diabetic fatty

7.12.1 Introduction

7.12.1.1 T2D Background

The incidence of Type 2 Diabetes (T2DM) is increasing rapidly in both the developed and developing world. The disease is characterized by hyperglycemia as a consequence of increased insulin resistance and a deterioration of the ability of the pancreas to compensate through increased insulin secretion.[1] For the majority of T2DM patients, the etiology is exacerbated by underlying excess body weight and obesity.[2] While, several therapeutics have been developed for control of elevated blood glucose levels, including sulfonyl ureas and metformin, these are not generally associated with weight-loss that would contribute to improvement in the underlying disease state.[3] One class of therapeutics that has shown promise in this respect is the glucagon-like peptide 1 receptor (GLP-1R) agonists.[4] In addition to effective glucose control through increased insulin secretion and decreased glucagon secretion, the most prominent of these, liraglutide (Novo Nordisk), has been shown to provide dose-dependent weight loss. Liraglutide is approved for T2DM at a subcutaneously approved dose of up to 1.8 mg/day. At a relatively higher 3.0 mg/day subcutaneous dose, liraglutide has recently been shown to provide meaningful body weight reduction in both diabetic and non-diabetic obese subjects.[5]

7.12.1.2 GLP-1 History and Background

GLP-1 was initially identified in the early 1980s and was subsequently shown to increase insulin secretion from the pancreatic β-cells in a glucose-dependent manner.[6] GLP-1 is secreted from intestinal endocrine cells in response to a meal, stimulating a postprandial release of insulin.[7] Human studies comparing matched levels of glucose following intravenous versus oral administration indicated that an oral glucose challenge provides a much greater increase in secreted insulin, a phenomenon known as the incretin effect, leading to early efforts to develop GLP-1 as a drug.[8,9] However, due to rapid cleavage and inactivation by the peptidase, DPP-4, the native peptide does not lend itself to development as a therapeutic agent[10]. Therefore, DPP-4 inhibitors were identified that target GLP-1 action through stabilization of the endogenous hormone. These compounds have proven effective at controlling hyperglycemia, particularly in combination with metformin, which has been shown to potentiate the release of endogenous GLP-1.[11,12]

In parallel to the development of DPP-4 inhibitors, more stable analogs of the native GLP-1 hormone were sought. Exenatide, a synthetic version of the hormone exendin-4 identified from the saliva of the Gila monster, was the first peptide GLP-1 agonist to be commercialized.[13] Exenatide is a longer peptide than GLP-1, but shares approximately 55% homology.[14] Most notably, the position 2 alanine of GLP-1, which is the site of cleavage by DPP-4, is a glycine in exenatide. This mutation, together with other sequence changes, provides significant resistance to peptidase-mediated degradation, thus significantly enhancing the plasma half-life.

A number of modified GLP-1 and exenatide-based analogs have since been identified, taking different approaches to provide enhanced duration of action.[15] Together with amino acid alternations, these include conjugation to PEG, albumin, Fc fragments, and acyl modifications. In addition, alternative delivery systems to subcutaneous injection have also been trialed, including transdermal patches and, more notably, subcutaneous osmotic minipumps.[16,17]

7.12.2 Mechanism of Action

7.12.2.1 GLP-1 Synthesis and Expression

GLP-1 is synthesized and subsequently processed from the preproglucagon gene in the intestinal endocrine cells.[18] In the α-cell, preproglucagon is processed into active glucagon and the major proglucagon fragment, while in intestinal L-cells in the gut, the pro-hormone is processed by the enzyme PC1/3 into GLP-1, GLP-2, and glicentin and oxyntmodulin.[19] The GLP-1 peptide was discovered in the early 1980s, sharing approximately 50% sequence homology with glucagon, and was later shown to induce glucose-stimulated insulin secretion from pancreatic β-cells.[6] Active, circulating GLP-1 is found in two forms, predominantly GLP-1(7–36 amide) and to a lesser extent, GLP-1(7–37).[20] The peptide is rapidly inactivated by the enzyme DPP-4, via truncation the N-terminal His-Ala dipeptide, a discovery which led to the DPP-4 inhibitor class of drugs, which thus prolong the lifetime of the active form of the peptide.[10,21] Removal of the two N-terminal amino acids completely abrogates agonist activity of both forms of GLP-1. A similar truncation of exendin-4, from Gila monster venom, results in the GLP-1 receptor (GLP-1R) antagonist exendin9-39.[14,22]

7.12.2.2 GLP-1 Synthesis and Expression

The GLP-1R is expressed in multiple tissues, including pancreatic islets, the brain, and GI tract.[23,24] GLP-1R is a $G_{\alpha s}$-coupled family B GPCR, characterized by a large extracellular domain.[25,26] Activation of the receptor on the pancreatic β-cell results in an increase in cAMP, activation of PKA, and an increase in insulin biosynthesis.[7,27] Under hyperglycemic conditions, the downstream effect of cAMP accumulation results in an increase in insulin secretion from the β-cell. Under normal conditions, stimulation of insulin secretion via activation of the GLP-1R occurs in a glucose-dependent fashion.[28] However, under euglycemic or even hypoglycemic conditions, concomitant exposure of rat pancreas to GLP-1 and a sulfonylurea results in increased insulin secretion. This indicates that the glucose sensitive response of GLP-1 is controlled by the K_{ATP} channel.[29–31]

In addition to stimulating cAMP through $G_{\alpha s}$, the GLP-1R has also been shown to stimulate other cellular pathways.[7] For example, stimulation of mouse β-cells with GLP-1 increases intracellular Ca^{2+}, likely mediated by PI-3 kinase, resulting in transcriptional changes that include increased insulin biosynthesis.[32] It has been demonstrated that prolonged exposure to GLP-1 may result in cumulative effects that include enhanced β-cell survival.[33,34]

GLP-1 may also play a role in control of fasting glycemia through inhibition of glucagon secretion.[35,36] While the mechanism of suppression is not well understood, in addition to stimulating insulin secretion, the use of GLP-1 analogs in diabetic patients may serve to diminish the rise in postprandial glucagon often observed in these patients.[37]

7.12.3 Effects on Food Intake

7.12.3.1 Inhibition of Feeding in Rodents and Humans

GLP-1R is expressed in the hypothalamus, the center of regulation of feeding.[38] Elegant studies involving intracerebroventricular (ICV) administration of GLP-1 to fasted rats resulted in inhibition of food intake.[39] Interestingly, inhibition of feeding in diabetic rodents can also be achieved following peripheral administration of long-acting GLP-1R agonists, such as liraglutide. While, liraglutide may cross the blood-brain barrier, evidence suggests that GLP-1 receptors in the arcuate nucleus may play a role in mediating food intake effects.[40]

In humans, a number of studies have demonstrated that GLP-1 dose dependently reduces food intake and slows gastric emptying.[41] This has been shown in type 2 diabetics as well as obese and healthy subjects.[42,43] Furthermore, prolonged activation of the receptor results in reduced bodyweight, most likely as a result of suppressed gastric emptying and decreased food intake. [44]

Together, the biological effects on insulin secretion, hepatic glucose production, food intake, and body weight make activation of the GLP-1R an ideal target for treatment of obesity and T2DM. However, the short half-life and physical properties of the endogenous ligand present multiple challenges to developing a suitable therapeutic agent.[45]

7.12.4 Interactions With the GLP-1R

7.12.4.1 Brief Overview of GLP-1 Structure

The GLP-1R was first cloned in the early 1990s.[46] It has been characterized as a family B GPCR with a predicted seven alpha helix transmembrane domain and an extracellular N-terminal domain. While a structure of the intact receptor is yet to be published, in 2007 Runge et al. expressed the isolated N-terminal domain and determined the X-ray crystal structure bound to the GLP-1 analog, exendin(9–39).[47] The structure indicated that the central alpha helix of exendin(9–39) forms both hydrophobic and hydrophilic interactions within a ligand-binding groove in the extracellular domain of the receptor. Binding of GLP-1 to its receptor is believed to be a two-step process. The first part is recruitment of the peptide to the N-terminal domain and the second is the interaction of the N-terminal region of the peptide with seven transmembrane cores of the receptor.[48]

7.12.5 GLP-1R Agonists

GLP-1R agonists, exenatide, lixisenatide, liraglutide, dulaglutide, and albiglutide have been approved for the treatment of T2DM.[49,50] Structures of these GLP-1 analogs and natural GLP-1 are shown in Fig. 1. Natural GLP-1 is an incretin hormone produced by intestinal L-cells and released in response to food intake to induce insulin secretion from pancreatic β-cells.

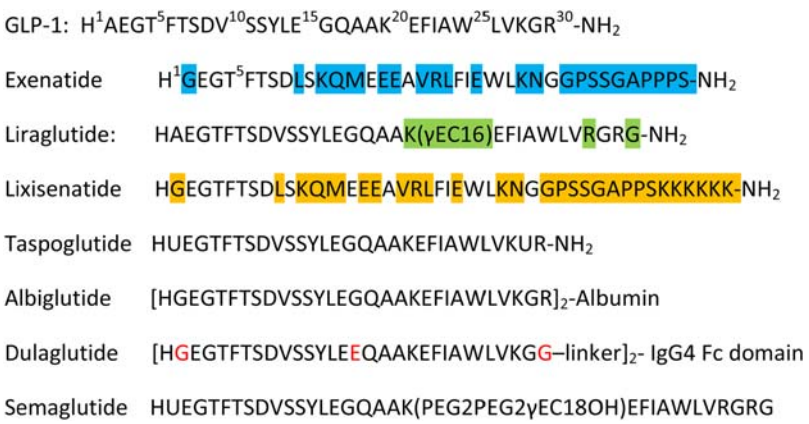

Fig. 1 Sequence of natural GLP-1 and its analogs.

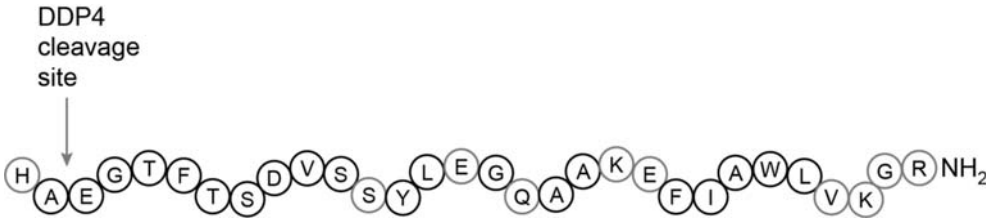

Fig. 2 DDP4 cleavage site of GLP-1.

GLP-1(7–36) amide is a biologically active form of GLP-1 and it binds to GLP-1R to trigger conformational change of the receptor, which in turn produces an increase in secondary messengers such as cAMP and Ca^{2+} levels. Natural GLP-1 has a very short half-life in plasma and it is degraded by serum protease DDP4 (Fig. 2) and other enzymes such as NEP, kallikurin, and plasmin. Therefore, to increase the plasma stability of the peptide and in turn to increase the $T_{1/2}$, scientists have used strategies such as DDP4 inhibitors, alteration of the *N*-terminal AA sequence to prevent degradation by DPP-4, and also design of sequences by attaching fatty acids that bind tightly to human serum albumin. [51–53]

7.12.6 Structure Activity Relationships of GLP-1

Adelhorst and co-workers as well as others investigated the importance of each residue on the GLP-1 backbone using alanine scanning, and these studies have shown that the *N*-terminal end of the GLP-1 is critical for receptor activation.[54] Furthermore, these studies also demonstrated that the C-terminal end residues of GLP-1 are responsible for binding to extracellular domain.

Pos 1. Histidine was found to be a key and important residue for GLP-1R binding and activation. This amino acid is present in all the GLP-1 agonists. The presence of this intact *N*-terminal α-amino group is required for DPP-4 cleavage, and modifications of *N*-terminal His can confer resistance to proteolysis. Also, *N*-methylation, α-methylation, des-amination, and imidazole lactic acid confer stabilization against DPP-4 proteolysis. Complete removal of histidine resulted in loss of activity. Replacement of histidine with other positive-charged amino acids Arginine and Lysine resulted in significantly reduced activity. However, histidine can be substituted for Phenylalanine with minimum loss of activity indicating importance of interaction of aromatic group with the receptor.

Pos 2. At the N-terminal end, modification to the second AA (Ala) has been extensively investigated to address metabolic instability due to processing by DPP-4. Substitution of Ala for Gly as in liraglutide is only slightly detrimental to GLP-1 activity and it improved the stability to DPP-IV. Replacement of Ala with polar AAs such as Ser provided modest resistance to proteolysis with approximately 10-fold loss of activity toward GLP-1R. Sterically hindered amino acids such as Leu and isoLeu resulted in a significant loss of potency. Substitution of Aib (2-aminobutyric acid) gave comparable binding and activity to native GLP-1 with complete resistance to DPP-4. In addition, both D- and L-Ala exhibited similar potency and activity and thus stereochemical configuration has minimal effect on activity.[55]

Pos 3. Negatively charged amino acids Glu and Asp are important for receptor interaction and they confer good receptor binding affinity and potency. Replacement of Glu with a basic amino acid such as Lys resulted in significant loss of potency. Substitution with Ala, Ser, and Val resulted in reduced potency. The stereochemical configuration is very critical for this position and thus replacement with D-Glu led several fold reduction in potency. Replacement of Glu with Pro, Phe, and Tyr showed comparable insulinotropic effect relative to GLP-1; however with slight loss of potency and binding affinity.

Pos 4. Gly at pos4 is very important for interaction with GLP-1R and all the GLP-1 agonists prepared to-date all have Gly at this position.

Pos 5, 6, 7, and 8 are represented by Thr, Phe, Thr, and Ser, respectively, and this combination of sequence is key for activity.

Pos 9. Negatively charged amino acid Asp is critical for activity and the only alternate AA that is tolerated here is Glu with slight loss in affinity. D-Asp substitution gave significant loss of binding affinity indicating importance of stereochemical configuration.

Pos 10–15. Val at pos10 can be replaced with Tyr, Ala, and other hydrophobic amino acids with some loss in affinity and activity. Substitution of position 12 Ser with Ala did not affect receptor binding and activity while replacement with Lys gave fourfold reduction in binding affinity. Replacement of Glu at pos 15 with smaller amino acids such as Gly and Ala resulted in significantly reduced affinity. Ser at pos11, Tyr at pos13, and Leu at pos14 are important for GLP-1R binding and activity.

Pos 16–20. Gly at pos16 can be replaced by a variety of other amino acids including branched amino acids without loss of activity. Aib is well tolerated at this position and exhibited binding affinity and potency comparable to GLP-1. Lys at pos20 has been used as a conjugation site for attaching fatty acids directly or via γ-glutamyl spacer to prolong the half-life by means of increased albumin binding. Similarly, conjugation with PEG2 linker also provided long $T_{1/2}$ with minimal loss of activity. Gln at pos17, Ala at pos18, and Ala at pos19 are critical for GLP-1 activity.

Pos 21–25. Glu at pos21 can be replaced with other amino acids with very minimal loss of GLP-1R binding. Pos21 can also be replaced with Lys, a basic amino acid without loss of activity. Phe at pos22 is an important AA for both receptor binding and activity

and can be replaced with hexafluoroleucine with modest loss in GLP-1 activity. lle at pos23 is also important for receptor binding and can be replaced with hexafluoroleucine. Ala at pos24 and Trp at pos25 are both critical for GLP-1 activity.

Pos 26–31. Leu at pos26 is also an important residue for activity and can be replaced with hexafluoro analog with slight loss of potency and affinity. Similarly, Val at pos27 is an important AA and is present in both natural and synthetic GLP-1 agonists. Lys at pos28 is found to be another good conjugation site for PEGylation and lipidation with only a twofold loss in potency relative to Lys at pos20. Gly at pos29 can be substituted for Aib to provide more potent GLP-1 agonist with excellent resistance to DPP-IV. This alteration was important in the discovery of taspoglutide. Arg at pos30 and Gly at pos31 are critical for GLP-1R binding and activation.

The endogenous GLP-1 is rapidly cleaved by serum proteases, particularly dipeptidyl peptidase 4 (DPP-4) at the His-Ala position as mentioned before. Therefore, therapeutic utility of natural GLP-1 is very limited. This difficulty can be overcome by using metabolically stable GLP-1 analogs or DPP-IV inhibitors. Also, a number of other strategies have been introduced including pegylation, D-amino acids, α,α-dialkylated aminoacids, β-amino acids, *N*-alkylated amino acids, stapling, and other conformational restriction to protect the peptides from proteolysis.[16,56] Exenatide showed a terminal half-life of ~2.4 h after subcutaneous administration and was consequently dosed 10 μg twice daily.[57]

7.12.6.1 Exenatide

The first GLP-1 agonist (exenatide) brought to the market for the treatment of diabetes (Fig. 3). It has Gly at pos2 and it provides stability to DPP-4-mediated degradation. In addition leucine at pos21 and serine at pos39 form a compact conformation that shields the side chain of Trp25 from solvent exposure that results in increased peptide stability and α-helicity.

7.12.6.2 Lixienatide

Lixisenatide contains amino acid residues similar to Exenatide at positions 1 to 39 with one less proline and additional six Lys residues at the C-terminal end (Fig. 4). Lixisenatide exhibiting a terminal half-life of 3 h is dosed 20 μg once daily. Lixisenatide showed improved HbA1c reduction in combination with metformin compared to exenatide with less hypoglycemia.

7.12.6.3 Taspoglutide

Taspoglutide is closely similar to natural GLP-1 analog with presence of Aib at positions 2 and 29 (Fig. 5). These modifications provided stability to DPP-4 and other plasma enzymes such as kallikerin and plasmin. In phase 3 studies the sustained release formulation of taspoglutide showed very good profile with consistent HbA1c reductions, however further progress on this molecule was terminated due to immunogenicity issues as well as allergic reactions at the injection site.

7.12.6.4 Liraglutide

Liraglutide is structurally similar to natural GLP-1(7–37) with 97% identical amino acid residues to natural hormone (Fig. 6). It differs at position 28 with Arg instead of Lys and in addition palmitic acid is conjugated via glutamate spacer at Lys in position 20. This fatty acid conjugation provides the prolonged duration of action facilitated by binding to serum albumin as well self-association at the subcutaneous space. Furthermore, the tight albumin binding action protects liraglutide sequence from DPP-4 and NEP enzymatic degradation. The mean plasma half-life in humans is 11–13 h. Once daily human dose of 1.2 mg provides good glycemic control and with increasing doses up to 1.8 mg show significant improvements in HbA1c reduction compared to exenatide (1.1% vs. 0.79%). Further increase in dose of up to 3 mg of liraglutide gave ~6% weight reduction in overweight Type 2 diabetics compared to placebo.

Fig. 3 Sequence of exenatide.

Fig. 4 Sequence of lixisenatide.

Fig. 5 Sequence of taspoglutide.

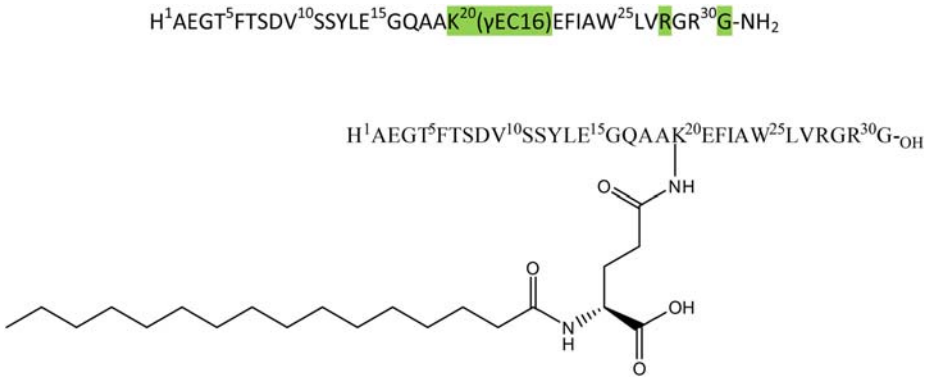

Fig. 6 Sequence and structure of liraglutide.

7.12.6.5 Semaglutide

Semaglutide is a long-acting GLP-1 agonist from Novo Nordisk, currently in phase 3 clinical trials as a once weekly treatment for T2DM (Fig. 7).[58] Semaglutide's structure differs from liraglutide at two places. Pos2 Gly is substituted with Aib (U) and this modification provides significant protection to enzymatic degradation by DPP-4. In addition, a modified fatty acid chain and the two PEG2 spacers turned out to be optimal for both in vitro and in vivo prolonged duration of action. As a result of these two modifications, the half-life for semaglutide in human is 160 h and a dose of 0.2 mg and above dose dependently reduced HbA1c by 1.7%. More importantly, semaglutide is currently being investigated in clinical trial for once daily oral treatment.

7.12.6.6 Albiglutide

In albiglutide, two copies of GLP-1 analog fused as repeat units to *N*-terminus of human serum albumin in a recombinant manner (Fig. 8). The GLP-1 analog has Gly instead of Ala at position 2 to provide resistance to DPP-4. These tandem repeat units of GLP-1 analog are critical and provide improved potency upon conjugation to albumin. Albiglutide has a half-life of 6–8 days in humans and it demonstrated good efficacy in humans with HbA1c reduction of 0.78% from baseline.

7.12.6.7 Dulaglutide

Dulaglutide is developed by Eli Lilly and is a recombinant fusion protein consists of two GLP-1 peptides covalently linked by a small peptide to human IgG4 Fc domain (Fig. 9). Ala at pos2 and Arg at pos30 are replaced with Gly to provide protection from DPP-4

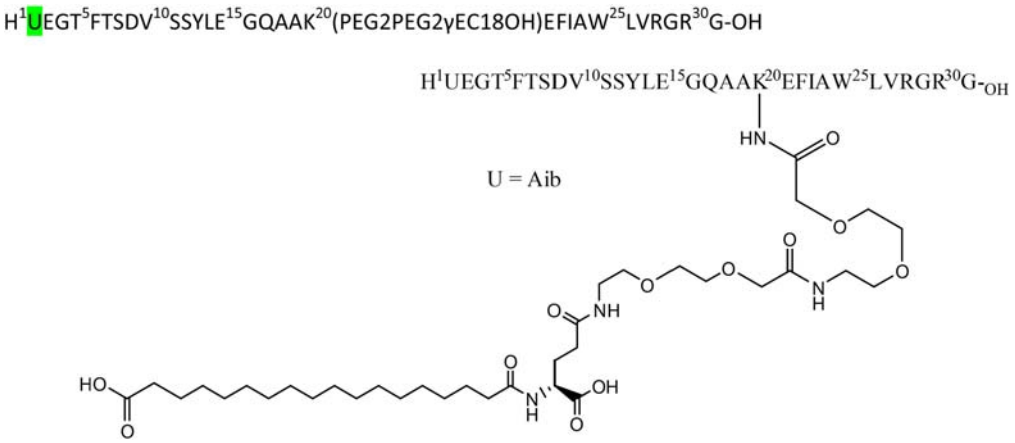

Fig. 7 Sequence and structure of semaglutide.

Fig. 8 Sequence of albiglutide.

Fig. 9 Sequence of dulaglutide.

cleavage as well as to maintain potency. Glu at pos16 provides improved potency. Dulaglutide has a half-life of ~4 days and showed significant dose-dependent reduction in HbA1c of 1.5% at 1.5 mg dose after 12 weeks.

7.12.7 Summary of GLP-1R Agonist Toxicity

All approved GLP-1R agonist drugs are modified GLP-1-like peptides, which are expected to have high specificity and low risk of off-target effects. Common findings observed in nonclinical toxicity studies of GLP-1R agonists are pharmacologically mediated reductions in food consumption accompanied by decreased body weight gain and/or body weight loss.[59–62] Food restriction in rats, significantly affecting body weight in the absence of any pharmacologic treatment, is associated with changes in hematology and serum chemistry parameters as well as histopathologic changes.[63] This association makes it particularly challenging to determine which changes observed after treatment with GLP-1R agonists are primary effects and which are secondary to effects on food consumption and body weight. Despite these challenges, several class effects, common to GLP-1R agonists, have emerged in nonclinical and/or clinical studies.

7.12.7.1 Gastrointestinal Effects

Administration of GLP-1R agonists is associated with gastrointestinal (GI) symptoms such as nausea and vomiting. These GI effects are believed to be mediated by local stimulation of GI tract, activation of GLP-1Rs in the central nervous system, and/or peripheral stimulation of the vagal afferent leading to a polysynaptic activation of neurons in the hypothalamus and brain stem.[64,65] In animal studies, including animal models of nausea, nausea and/or vomiting were observed in monkeys after albiglutide or dulaglutide treatment,[60,62,66] in pigs after liraglutide treatment,[67] and in cats and mice after exenatide treatment.[68,69] Clinically, patients have discontinued treatment due to adverse GI effects; however, gradual dose escalation doses of new patients has been shown to lessen these GI effects.

7.12.7.2 Heart Rate Effects

Increased heart rate is another common finding in animal studies for GLP-1 or GLP-1R agonists.[61,62,70] Even though GLP-1Rs are expressed in the cardiac sinoatrial node, the exact mechanisms mediating these hemodynamic changes are still under investigation.[71–73] A small increase in heart rate (a few beats per minute) is also the most common finding in the patients and is usually associated with nausea and a small blood pressure decrease.[74,75] Even though changes in heart rate are associated with increased cardiac mortality, recent preliminary data from large cardiovascular outcome trial of Victoza® (LEADER),[76] which spanned a period of up to 5 years and included more than 9000 adult T2DM patients, showed superior reduction in major adverse cardiovascular events including cardiovascular death, non-fatal myocardial infarction, or non-fatal stroke. A previous cardiovascular outcome study of lixisenatide (ELIXA)[77] did not demonstrate an increase or decrease in the rate of cardiovascular events compared to placebo.

7.12.7.3 Thyroid C-Cell Tumor

Class labeling GLP-1R agonists marketed in the United States include a black box warning for risk of thyroid C-cell tumors.[62,78–81] This warning is based on the increased incidence of thyroid C-cell adenomas and/or carcinomas observed in rodents treated for 2 years with GLP-1R agonists. These tumors were sometimes observed at clinically relevant exposures. It has been hypothesized that thyroid C-cell hyperplasia, adenomas and/or carcinomas observed in repeat dose toxicity studies, or carcinogenicity studies in rats and/or mice are likely due to the activation of GLP-1Rs on rodent thyroid C-cells.[78,80] The relevance of these findings to other species is not known. Activation of GLP-1Rs receptor in rodent thyroid C-cells was associated with transient elevations in calcitonin levels.[78,82] Neither elevated calcitonin levels nor thyroid C-cell tumors were observed in monkeys given liraglutide for up to 87 weeks.[78] Little or no significant rise in calcitonin levels was identified in long-term clinical studies of liraglutide.[82,83] The density of GLP-1Rs on C-cells of rodents has been reported to be higher than that observed in monkey or human thyroid.[73,78,84,85] Taken together, these data suggest but do not prove that the thyroid C-cell tumors observed in rats and mice treated with GLP-1R agonists may be a rodent-specific phenomena; however, the relevance of these findings to human remains uncertain.[66]

7.12.7.4 Pancreatitis

Xu and colleagues have reported that GLP-1Rs are expressed on pancreatic ductal cells of rats and humans and have demonstrated that treatment of diabetic rodents and isolated human pancreatic islets with exendin-4, a long-acting GLP-1R agonist, increases β-cell differentiation/proliferation.[86,87] Although these data suggest that GLP-1R agonists could have a beneficial effect on

pancreatic function, pancreas has been identified as a potential target organ of toxicity. Pancreatitis has not been observed in mice, rats, or monkeys in repeated toxicity studies with liraglutide[88], exenatide,[59] and dulaglutide[80]. However, low-grade chronic pancreatitis was noted in rats treated with exenatide and elevated GLP-1 levels were suspected to cause pancreatitis in a transgenic rat model of T2DM.[89,90] In contrast, prolonged exposure of Zucker diabetic fatty rats to liraglutide did not reveal any evidence of drug-induced pancreatitis.[91] Clinically, isolated cases of acute pancreatitis have been reported in T2DM patients treated with GLP-1R agonists including exenatide and liraglutide;[82,92] however, an exposure-response relationship for the increased incidence of pancreatitis was not evident in clinical trials of GLP-1R agonsits. [93] It is well known that T2DM patients have up to three times higher risk for pancreatitis than patients without diabetes,[94] suggesting a better understanding of the relationship between treatment with GLP-1R agonists and pancreatitis is needed.[95,96]

7.12.7.5 Gall Bladder Events

For high-dose liraglutide, gall bladder has been identified as another potential target organ of toxicity based on clinical observations of cholelithiasis and cholecystitis in Saxenda®-treated subjects.[81] In most nonclinical toxicity studies, no adverse effects were observed in the gall bladders of animals administered GLP-1R agonists. However, an increased incidence of cholecystitis was observed in mouse gall bladder after repeated dosing of dulaglutide[62] and liraglutide[61]. Although treatment with liraglutide[61] was associated with other gall bladder findings such as abnormal contents and/or dilation/distention enlargement of the gall bladder in mouse, usually there were no histomorphologic correlates to these macroscopic observations. It should be noted that T2DM patients have almost twofold greater risk of biliary disease than patients without diabetes,[94] and substantial or rapid weight loss itself can increase the risk of cholelithiasis.[81] Increased incidences of cholelithiasis and cholecystitis were observed in patients treated with high-dose liraglutide (>1.8 mg) for weight management but not in patients treated with lower dose liraglutide (≤ 1.8 mg) for management of T2DM.[61,81] Furthermore, exposure-response analysis of several liraglutide clinical trials with more than 4000 patients did not reveal any relationship between liraglutide exposure and the incidence of documented gall bladder events.[93]

7.12.7.6 ADA Generations

Formation of anti-drug antibodies (ADA) has been reported for several GLP-1R agonists. The carcinogenic potential of albiglutide could not be assessed due the formation of ADA.[60] Monkeys treated with exenatide developed ADA within one month of treatment.[59]. At high titers, these anti-exenatide antibodies altered pharmacokinetics but did not affect the pharmacologic activity (reduced body weight effect) or toxicity in the monkey studies. Clinically ADA formation was more frequently identified in exenatide once weekly (~45% low titer, 12% high titer at 24–30 weeks) than exenatide BID (~32% low titer, 5% high titer at 30 weeks).[97,98] The incidence of injection site reactions appears higher in subjects with ADAs as compared to those without ADAs (24% vs. 15%). No significant correlation has been observed between low titer antiexenatide antibodies and efficacy, but higher titer antibodies were associated with a statistically significant attenuation in HbA1c reduction.[97] Potential ADA-related hypersensitivity, skin reactions, and GI symptoms have been described in a few patients ($<1\%$) in clinical phase 3 clinical studies of taspoglutide.[98,99] Low incidences of ADA formation (4–10%, low titers) have been reported for liraglutide but did not have a significant impact on efficacy and safety.[61]

7.12.8 Future Directions

There has been tremendous progress made in the discovery of novel GLP-1 agonists. Almost all of approved products are injectable as either once daily or once weekly subcutaneous treatment. In addition, Novo-Nordisk and vIV therapeutics are developing newer oral GLP-1 agents that can provide clear advantage in the GLP-1 space. The ongoing clinical studies will determine whether these new oral drugs will be advantageous in terms of safety and efficacy compared to current treatment options. The clinical use of GLP-1 agonists is moving greatly toward the direction of combination with other agents such as insulin and incretins. Coformulation is one of the attractive approaches to provide better glycemic efficacy and additional weight loss and CV benefits. IDegLira as developed by Novo Nordisk is one of the examples of co-formulation approach. In addition to Novo, a number of other companies have the potential to develop co-administration regimens of insulin with incretins. Sanofi has access to insulin glargine (Lantus) and the GLP-1R agonist lixisenatide. In addition, Roche is in early development with GLP-1R/GIPR dual agonist, which could also be combined with human insulin. Similarly, Lilly is seeking approval of basal PEGylated insulin analog (peglyspro), which could be combined with recently approved dulaglutide. The ongoing studies will determine the clinical efficacy, tolerability, and superiority compared to already available GLP-1 agents.

See also: 7.14. DPP-4 Inhibitors.

References

1. Kahn, S. E.; Cooper, M. E.; Del Prato, S. *Lancet* **2014,** *383,* 1068.
2. Kahn, S. E.; Hull, R. L.; Utzschneider, K. M. *Nature* **2006,** *444,* 840.
3. DeFronzo, R. A.; Triplitt, C. L.; Abdul-Ghani, M.; Cersosimo, E. *Diabetes Spectr.* **2014,** *27,* 100.
4. Van Gaal, L.; Scheen, A. *Diabetes Care* **2015,** *38,* 1161.
5. Pi-Sunyer, X.; Astrup, A.; Fujioka, K.; Greenway, F.; Halpern, A.; Krempf, M.; Lau, D. C. W.; le Roux, C. W.; Violante Ortiz, R.; Jensen, C. B.; Wilding, J. P. H. *N. Engl. J. Med.* **2015,** *373,* 11.
6. Mojsov, S.; Weir, G. C.; Habener, J. F. *J. Clin. Investig.* **1987,** *79,* 616.
7. Doyle, M. E.; Egan, J. M. *Pharmacol. Ther.* **2007,** *113,* 546.
8. Nauck, M. A. *Diabetologia* **1999,** *42,* 373.
9. Nauck, M. A.; Homberger, E.; Siegel, E. G.; Allen, R. C.; Eaton, R. P.; Ebert, R.; Creutzfeldt, W. *J. Clin. Endocrinol. Metab.* **1986,** *63,* 492.
10. Mentlein, R.; Gallwitz, B.; Schmidt, W. E. *Eur. J. Biochem.* **1993,** *214,* 829.
11. Yasuda, N.; Inoue, T.; Nagakura, T.; Yamazaki, K.; Kira, K.; Saeki, T.; Tanaka, I. *Biochem. Biophys. Res. Commun.* **2002,** *298,* 779.
12. Cho, Y. M.; Kieffer, T. *J. Diabetologia* **2011,** *54,* 219.
13. Malhotra, R.; Singh, L.; Eng, J.; Raufman, J. P. *Regul. Pept.* **1992,** *41,* 149.
14. Furman, B. L. *Toxicon* **2012,** *59,* 464.
15. Meier, J. J. *Nat. Rev. Endocrinol.* **2012,** *8,* 728.
16. Lorenz, M.; Evers, A.; Wagner, M. *Bioorg. Med. Chem. Lett.* **2013,** *23,* 4011.
17. Trujillo, J. M.; Nuffer, W.; Ellis, S. L. *Ther. Adv. Endocrinol. Metab.* **2015,** *6,* 19.
18. Lim, G. E.; Brubaker, P. L. *Diabetes* **2006,** *55,* S70.
19. Dhanvantari, S.; Seidah, N. G.; Brubaker, P. L. *Mol. Endocrinol.* **1996,** *10,* 342.
20. Orskov, C.; Rabenhoj, L.; Wettergren, A.; Kofod, H.; Holst, J. *J. Diabetes* **1994,** *43,* 535.
21. Deacon, C. F.; Wamberg, S.; Bie, P.; Hughes, T. E.; Holst, J. *Endocrinology* **2002,** *172,* 355.
22. Raufman, J. P.; Singh, L.; Eng, J. *J. Biol. Chem.* **1991,** *266,* 2897.
23. Campos, R. V.; Lee, Y. C.; Drucker, D. *Endocrinology* **1994,** *134,* 2156.
24. Bullock, B. P.; Heller, R. S.; Habener, J. F. *Endocrinology* **1996,** *137,* 2968.
25. Hobai, S. V. *Revista Romana De Medicina De Laborator* **2008,** *12,* 7.
26. Runge, S.; Thogersen, H.; Madsen, K.; Lau, J.; Rudolph, R. *J. Biol. Chem.* **2008,** *283,* 11340.
27. Dyachok, O.; Isakov, Y.; Sagetorp, J.; Tengholm, A. *Nature* **2006,** *439,* 349.
28. Kjems, L. L.; Holst, J. J.; Volund, A.; Madsbad, S. *Diabetes* **2003,** *52,* 380.
29. de Heer, J.; Holst, J. *J. Diabetes* **2007,** *56,* 438.
30. Light, P. E.; Fox, J. E. M.; Riedel, M. J.; Wheeler, M. B. *Mol. Endocrinol.* **2002,** *16,* 2135.
31. Light, P. E.; Riedel, M. J.; Manning, J. E. *Biophys. J.* **2002,** *82,* 593A.
32. MacDonald, P. E.; El-kholy, W.; Riedel, M. J.; Salapatek, A. M. F.; Light, P. E.; Wheeler, M. B. *Diabetes* **2002,** *51,* S434.
33. Soleimanpour, S. A.; Crutchlow, M. F.; Ferrari, A. M.; Raum, J. C.; Groff, D. N.; Rankin, M. M.; Liu, C.; De Leon, D. D.; Naji, A.; Kushner, J. A.; Stoffers, D. A. *J. Biol. Chem.* **2010,** *285,* 40050.
34. Toso, C.; McCall, M.; Emamaullee, J.; Merani, S.; Davis, J.; Edgar, R.; Pawlick, R.; Kin, T.; Knudsen, L. B.; Shapiro, A. M. *J. Transplant Int.l* **2010,** *23,* 259.
35. Rodriguez-Gallardo, J.; Silvestre, R. A.; Marco, J. *Int. J. Obes.* **1999,** *23,* 787.
36. Holst, J. *J. Physiol. Rev.* **2007,** *87,* 1409.
37. Meier, J. J.; Ritter, P. R.; Jacob, A.; Menge, B. A.; Deacon, C. F.; Schmidt, W. E.; Nauck, M. A.; Holst, J. *J. Clin. Endocrinol. Metab.* **2010,** *95,* 4061.
38. Merchenthaler, I.; Lane, M.; Shughrue, P. *J. Comp. Neurol.* **1999,** *403,* 261.
39. Meeran, K.; O'Shea, D.; Edwards, C. M. B.; Turton, M. D.; Heath, M. M.; Gunn, I.; Abusnana, S.; Rossi, M.; Small, C. J.; Goldstone, A. P.; Taylor, G. M.; Sunter, D.; Steere, J.; Choi, S. J.; Ghatei, M. A.; Bloom, S. R. *Endocrinology* **1999,** *140,* 244.
40. Secher, A.; Jelsing, J.; Baquero, A. F.; Hecksher-Sorensen, J.; Cowley, M. A.; Dalboge, L. S.; Hansen, G.; Grove, K. L.; Pyke, C.; Raun, K.; Schaffer, L.; Tang-Christensen, M.; Verma, S.; Witgen, B. M.; Vrang, N.; Knudsen, L. B. *J. Clin. Investig.* **2014,** *124,* 4473.
41. Willms, B.; Werner, J.; Holst, J. J.; Orskov, C.; Creutzfeldt, W.; Nauck, M. A. *J. Clin. Endocrinol. Metab.* **1996,** *81,* 327.
42. Acosta, A.; Camilleri, M.; Burton, D.; O'Neill, J.; Eckert, D.; Carlson, P.; Zinsmeister, A. R. Physiological Reports 2015, 12610.
43. Wishart, J. M.; Horowitz, M.; Morris, H. A.; Jones, K. L.; Nauck, M. A. *Peptides* **1998,** *19,* 1049.
44. Ladenheim, E. E. *Drug Design Develop.Therapy* **2015,** *9,* 1867.
45. Holst, J. *J. Diabetes-Metabol. Res. Rev.* **2002,** *18,* 430.
46. Thorens, B. *Proc. Natl. Acad. Sci. U. S. A.* **1992,** *89,* 8641.
47. Runge, S.; Schimmer, S.; Oschmann, J.; Schiodt, C. B.; Knudsen, S. M.; Jeppesen, C. B.; Madsen, K.; Lau, J.; Thogersen, H.; Rudolph, R. *Biochemistry* **2007,** *46,* 5830.
48. Al-Sabah, S.; Donnelly, D. *Br. J. Pharmacol.* **2003,** *140,* 339.
49. Tomlinson, B.; Hu, M.; Zhang, Y.; Chan, P.; Liu, Z.-M. *Expert Opin. Drug Metab. Toxicol.* **2016,** *25,* 145.
50. Kaspar, A. A.; Reichert, J. M. *Drug Discov. Today* **2013,** *18,* 807.
51. Knudsen, L. B.; Nielsen, P. F.; Huusfeldt, P. O.; Johansen, N. L.; Madsen, K.; Pedersen, F. Z.; Thogersen, H.; Wilken, M.; Agerso, H. *J. Med. Chem.* **2000,** *43,* 1664.
52. Manandhar, B.; Ahn, J.-M. *J. Med. Chem.* **2015,** *58,* 1020.
53. Johnson, L. M.; Barrick, S.; Hager, M. V.; McFedries, A.; Homan, E. A.; Rabaglia, M. E.; Keller, M. P.; Attie, A. D.; Saghatelian, A.; Bisello, A.; Gellman, S. H. *J. Am. Chem. Soc.* **2014,** *136,* 12848.
54. Adelhorst, K.; Hedegaard, B. B.; Knudsen, L. B.; Kirk, O. *J. Biol. Chem.* **1994,** *269,* 6275.
55. Santoprete, A.; Capito, E.; Carrington, P. E.; Pocai, A.; Finotto, M.; Langella, A.; Ingallinella, P.; Zytko, K.; Bufali, S.; Cianetti, S.; Veneziano, M.; Bonelli, F.; Zhu, L.; Monteagudo, E.; Marsh, D. J.; SinhaRoy, R.; Bianchi, E.; Pessi, A. *J. Pept. Sci.* **2011,** *17,* 270.
56. Finan, B.; Clemmensen, C.; Mueller, T. D. *Mol. Cell. Endocrinol.* **2015,** *418,* 42.
57. Tibble, C. A.; Henry, R. R. *Expert. Rev. Endocrinol. Metab.* **2013,** *8,* 247.
58. Lau, J.; Bloch, P.; Schaffer, L.; Pettersson, I.; Spetzler, J.; Kofoed, J.; Madsen, K.; Knudsen, L. B.; McGuire, J.; Steensgaard, D. B.; Strauss, H. M.; Gram, D. X.; Knudsen, S. M.; Nielsen, F. S.; Thygesen, P.; Reedtz-Runge, S.; Kruse, T. *J. Med. Chem.* **2015,** *58,* 7370.
59. Byetta, Summary Basis of Approval, FDA Review, 2004.
60. Tanzeum, Summary Basis of Approval, FDA review, 2013.
61. Victoza, Summary Basis of Approval, FDA Review, *2010.*
62. Trulicity, Summary Basis of Approval, FDA Review, 2009.
63. Levin, S.; Semler, D. Ruben Z. *Toxicol. Pathol.* **1993,** *21,* 1.

64. Kanoski, S. E.; Rupprecht, L. E.; Fortin, S. M.; De Jonghe, B. C.; Hayes, M. R. *Neuropharmacology* **2012,** *62,* 1916.
65. Consoli, A.; Formoso, G. Expert opin. *Drug Saf.* **2015,** *14,* 207.
66. Jespersen, M. J.; Knop, F. K.; Christensen, M. *Expert Opin. Drug Metab. Toxicol.* **2013,** *9,* 17.
67. Emamaullee, J. A.; Merani, S.; Toso, C.; Kin, T.; Al-Saif, F.; Truong, W.; Pawlick, R.; Davis, J.; Edgar, R.; Lock, J.; Bonner-Weir, S.; Knudsen, L. B.; Shapiro, A. M. *Endocrinology* **2009,** *150,* 2145.
68. Padrutt, I.; Lutz, T. A.; Reusch, C. E.; Zini, E. *Res. Vet. Sci.* **2015,** *99,* 23.
69. Patel, K. N.; Joharapurkar, A. A.; Patel, V.; Kshirsagar, S. G.; Bahekar, R.; Srivastava, B. K.; Jain, M. R. *Can. J. Physiol. Pharmacol.* **2014,** *92,* 975.
70. Goodwill, A. G.; Mather, K. J.; Conteh, A. M.; Sassoon, D. J.; Noblet, J. N.; Tune, J. D. *Rev. Endocr. Metab. Disord.* **2014,** *15,* 209.
71. Gardiner, S. M.; March, J. E.; Kemp, P. A.; Bennett, T.; Baker, D. J. *Br. J. Pharmacol.* **2010,** *161,* 92.
72. Yamamoto, H.; Lee, C. E.; Marcus, J. N.; Williams, T. D.; Overton, J. M.; Lopez, M. E.; Hollenberg, A. N.; Baggio, L.; Saper, C. B.; Drucker, D. J.; Elmquist, J. K. *J. Clin. Investig.* **2002,** *110,* 43.
73. Pyke, C.; Heller, R. S.; Kirk, R. K.; Orskov, C.; Reedtz-Runge, S.; Kaastrup, P.; Hvelplund, A.; Bardram, L.; Calatayud, D.; Knudsen, L. B. *Endocrinology* **2014,** *155,* 1280.
74. Katout, M.; Zhu, H.; Rutsky, J.; Shah, P.; Brook, R. D.; Zhong, J.; Rajagopalan, S. *Am. J. Hypertens.* **2014,** *27,* 130.
75. Robinson, L. E.; Holt, T. A.; Rees, K.; Randeva, H. S.; O'Hare, J. P. *BMJ Open* **2013,** *3.*
76. Top-line data from LEADER Trial, www.diabetesincontrol.com; www.medscape.com/viewarticle/803916_8.
77. Top-line data from ELIXA Trial, www.ndei.org/expert-commentary-ELIXA-cardiovascular-safety-study-GLP-1-recept; www.medscape.com/viewarticle/846074.
78. Knudsen, L. B.; Madsen, L. W.; Andersen, S.; Almholt, K.; de Boer, A. S.; Drucker, D. J.; Gotfredsen, C.; Egerod, F. L.; Hegelund, A. C.; Jacobsen, H.; Jacobsen, S. D.; Moses, A. C.; Molck, A.-M.; Nielsen, H. S.; Nowak, J.; Solberg, H.; Thi, T. D. L.; Zdravkovic, M. *Endocrinology* **2010,** *151,* 1473.
79. Bydureon, Summary Basis of Approval, FDA Review, 2011.
80. Byrd, R. A.; Sorden, S. D.; Ryan, T.; Pienkowski, T.; LaRock, R.; Quander, R.; Wijsman, J. A.; Smith, H. W.; Blackbourne, J. L.; Rosol, T. J.; Long, G. G.; Martin, J. A.; Vahle, J. L. *Endocrinology* **2015,** *156,* 2417.
81. FDA product label for Saxenda, 2014.
82. Parks, M.; Rosebraugh, C. *NEJM* **2010,** *362* (9), 774.
83. Hegedus, L.; Moses, A. C.; Zdravkovic, M.; Tu Le, T.; Daniels, G. H. *J. Clin. Endocrinol. Metab.* **2011,** *96,* 853.
84. Vahle, J. L.; Byrd, R. A.; Blackbourne, J. L.; Martin, J. A.; Sorden, S. D.; Ryan, T.; Pienkowski, T.; Wijsman, J. A.; Smith, H. W.; Rosol, T. *Endocrinology* **2015,** *156,* 2409.
85. Waser, B.; Beetschen, K.; et al. *Neuroendocrinology* **2011,** *94,* 291.
86. Xu, G.; Stoffers, D. A.; Habener, J. F.; Bonner-Weir, S. *Diabetes* **1999,** *48,* 2270.
87. Xu, G.; Kaneto, H.; Lopez-Avalos, M. D.; Weir, G. C.; Bonner-Weir, S. *Diabetes Res. Clin. Pract.* **2006,** *73,* 107.
88. Nyborg, N. C. B.; Molck, A.-M.; Madsen, L. W.; Knudsen, L. B. *Diabetes* **2012,** *61,* 1243.
89. Nachnani, J. S.; Bulchandani, D. G.; Nookala, A.; Herndon, B.; Molteni, A.; Pandya, P.; Taylor, R.; Quinn, T.; Weide, L.; Alba, L. M. *Diabetologia* **2010,** *53,* 153.
90. Matveyenko, A. V.; Dry, S.; Cox, H. I.; Moshtaghian, A.; Gurlo, T.; Galasso, R.; Butler, A. E.; Butler, P. C. *Diabetes* **2009,** *58,* 1604.
91. Vrang, N. J.; Simonsen, L.; et al. *Am. J. Physiol. Endocrinol. Metab.* **2012,** *303,* E253.
92. Elashoff, M.; Matveyenko, A. V.; Gier, B.; Elashoff, R.; Butler, P. C. *Gastroenterology* **2011,** *141,* 150.
93. Wilding, J. P. H.; Overgaard, R. V.; et al. Diabetes. *Obes. Metab.* **2016,** *18,* 491.
94. Noel, R. A.; Braun, D. K.; Patterson, R. E.; Bloomgren, G. L. *Diabetes Care* **2009,** *32,* 834.
95. Jensen, T. M.; Saha, K.; Steinberg, W. M. *Diabetes Care* **2015,** *38,* 1057.
96. Li, L.; Shen, J.; et al. *BMJ* **2014,** *348,* g2366.
97. Fineman, M. S.; Mace, K. F.; Diamant, M.; Darsow, T.; Cirincione, B. B.; Porter, T. K. B.; Kinninger, L. A.; Trautmann, M. E. *Diabetes Obes. Metab.* **2012,** *14,* 546.
98. Rosensatock, J.; Boldrin, M.; et al. *Diabetes Care* **2013,** *36,* 498.
99. Madsbad, S.; Kielgast, U.; Asmar, M.; Deacon, C. F.; Torekov, S. S.; Holst, J. *Diabetes Obes. Metab.* **2011,** *13,* 394.

7.13 Sodium–Glucose Cotransporters

G Bebernitz, Novartis Institutes for Biomedical Research, Cambridge, MA, United States

© 2017 Elsevier Ltd. All rights reserved.

7.13.1	**Introduction**	492
7.13.2	**Sodium–Glucose Cotransporters**	492
7.13.2.1	Human SGLT Loss-of-Function Patients	492
7.13.2.2	SGLT Knockout Animals	493
7.13.2.3	Other SGLTs	494
7.13.2.4	SGLT Structure and Glucose-Binding Motif	494
7.13.2.5	Inhibitor Binding Characteristics	496
7.13.2.6	Expression Levels of Glucose Transporters With Disease	497
7.13.2.6.1	Kidney	497
7.13.2.6.2	Intestine	497
7.13.3	**SGLT Inhibitors**	497
7.13.3.1	O-Glycosides	497
7.13.3.2	T-1095 (hSGLT2 $IC_{50}=4.4$ nM: hSGLT1 $IC_{50}=260$ nM)	498
7.13.3.3	Sergliflozin (hSGLT2 $IC_{50}=7.5$ nM: hSGLT1 $IC_{50}=2100$ nM)	498
7.13.3.4	Remogliflozin (hSGLT2 $IC_{50}=12.4$ nM: hSGLT1 $IC_{50}=6500$ nM)	499
7.13.3.5	SGLT1-Selective Analogs of Remogliflozin (hSGLT2 $IC_{50}=1730$ nM: hSGLT1 $IC_{50}=50$ nM)	499
7.13.4	**Origin of C-Glucoside**	499
7.13.4.1	Dapagliflozin (hSGLT2 $IC_{50}=1.1$ nM: hSGLT1 $IC_{50}=1400$ nM)	500
7.13.4.2	Canagliflozin (hSGLT2 $IC_{50}=4.4$ nM: hSGLT1 $IC_{50}=684$ nM)	501
7.13.4.3	Ipragliflozin (hSGLT2 $IC_{50}=7.4$ nM: hSGLT1 $IC_{50}=1880$ nM)	502
7.13.4.4	Empagliflozin (hSGLT2 $IC_{50}=3.1$ nM: hSGLT1 $IC_{50}=8300$ nM)	502
7.13.4.5	Tofogliflozin (hSGLT2 $IC_{50}=2.9$ nM: hSGLT1 $IC_{50}=8444$ nM)	503
7.13.4.6	Ertugliflozin (hSGLT2 $IC_{50}=0.88$ nM: hSGLT1 $IC_{50}=1960$ nM)	503
7.13.4.7	Sotagliflozin (Lexicon LX4211) (hSGLT2 $IC_{50}=1.8$ nM: hSGLT1 $IC_{50}=36$ nM)	504
7.13.4.8	Luseogliflozin TS071 (hSGLT2 $IC_{50}=2.3$ nM: hSGLT1 $IC_{50}=3990$ nM)	505
7.13.4.9	A-Ring Replacements	505
7.13.4.10	Nonnucleoside Inhibitors	505
7.13.5	**Limitations on Effects of SGLT Inhibitors**	506
7.13.5.1	Target Engagement	506
7.13.5.2	Competition With Glucose	506
7.13.5.3	Other Transporters	506
7.13.5.4	Patients With Kidney Damage	506
7.13.5.5	Drug Metabolism and Clearance	506
7.13.5.6	Increased Glucagon Response	507
7.13.6	**Potential Safety Concerns**	507
7.13.6.1	Hypoglycemia	507
7.13.6.2	Urinary Tract Infections	507
7.13.6.3	Diabetic Ketoacidosis (DKA)	507
7.13.6.4	SGLT in Heart	508
7.13.7	**Added Beneficial Effects**	508
7.13.7.1	Effects on Blood Pressure	508
7.13.7.2	Added GLP-1 Effects	508
7.13.7.3	Weight Loss	508
7.13.8	**Summary**	508
References		509

Abbreviations

AEs adverse events
AMG α-methylglucose
AUC area under the curve
BBM brush border membrane
BID pill taken twice daily
BW body weight
CKD chronic kidney disease
DBP diastolic blood pressure
DDI drug–drug interaction
DKA diabetic ketoacidosis

DOG deoxyglucose
EGP endogenous glucose production
eGFR estimated glomerular filtration rate
FPG fasting plasma glucose
FRG familial renal glucosuria
GGM glucose–galactose malabsorption
GLUT facilitative glucose transporters
HbA1c glycosylated hemoglobin—measure of diabetes
OGTT oral glucose tolerance test
QD pill taken once daily
SBP systolic blood pressure
TG triglycerides
UGE urinary glucose excretion

7.13.1 Introduction

Diabetes is a chronic disease that affects nearly 400 million individuals worldwide, the majority of these being Type 2 diabetics, whose disease is driven by insulin insufficiency and peripheral insulin resistance. A wealth of therapies are employed to treat this disease, but all come with the potential for serious events such as hypoglycemia, and most cause increases in body weight (BW) that further exacerbates the disease. New mechanisms are sorely needed that maintain their efficacy as the disease progresses, possess a low risk of serious adverse events, are weight neutral at a minimum,[1] and decrease the metabolic and cardiovascular risk factors associated with the disease.

Each day, all of the glucose in the blood, roughly 180 g, enters the kidney, is filtered by the glomerulus, and is then reabsorbed in the proximal tubule of the kidney by sodium–glucose cotransporters (SGLTs) that effectively recover >99% of the filtered amount. However, in diabetics, the high levels of glucose being filtered can exceed the capacity of the SGLTs to recover the glucose leading to glucosuria, the spillage of glucose into the urine. As glucosuria is not harmful to the patient and is an excellent way of eliminating excess energy, the inhibition of SGLTs has become a recent focus of the pharmaceutical industry as a way of reducing glucose levels. This should provide a novel way of reducing the hyperglycemia associated with diabetes and potentially provide benefit to a multitude of metabolic diseases.

The theoretical benefits of inhibiting SGLTs for diabetes and metabolic diseases are

- low risk for hypoglycemia as glucosuria decreases as blood glucose levels normalize;
- an effective treatment independent of insulin levels or sensitivity (will work in all patients!);
- the ability to pass 180 g (720 kcal) of glucose/day, the body's daily glucose requirement;
- reduction in glucose levels and glucose toxicity, therefore sparing the pancreatic beta cell;
- beneficial effects on hypertension and cardiovascular disease via reductions in blood pressure;
- weight loss, reducing stress on the body and improving cardiovascular risk factors.

7.13.2 Sodium–Glucose Cotransporters

The sodium–glucose transporters are a family of transporters from the SLC5 gene family that couple sodium to the transport of sugars most often glucose, galactose, and mannose and, in addition, myoinositol and short-chain fatty acids. Unlike the GLUTs that are facilitative glucose transporters and simply assist in moving glucose down a concentration gradient, the SGLTs are capable of collecting and transporting glucose against a concentration gradient, using the electrochemical force of the sodium gradient to accomplish this. The Na^+/K^+ pump continually maintains the gradient by pumping sodium out of the cell at the basolateral membrane. SGLTs work similarly in either proximal tubule cells or intestinal cells transporting glucose into the requisite cell at the luminal surface followed by GLUT-mediated transport of glucose into the bloodstream at the basolateral membrane. The main SGLTs of interest are SGLT1, a high-affinity/low-capacity transporter, and SGLT2, a low-affinity/high-capacity transporter. Substrates bind in an ordered fashion with Na^+ binding first, followed by a conformational change that opens up the site for glucose to bind.

The location of the high-capacity SGLT2 in the upper S1–S2 segment of the kidney proximal tubule functions to rapidly reabsorb the majority of the glucose (~90%). The high-affinity SGLT1 in the lower S3 segment acts to collect any remaining glucose (~10%) escaping SGLT2. The process is very efficient with >99% of the glucose recovered and a loss into urine of <0.5 g day^{-1} up to a filtered serum concentration near 11 mM (200 mg dL^{-1}). When this transport maximum (T_m) is reached, glucose begins passing the transporters and reaches the bladder to be excreted in the urine, one of the more common ways of identifying early-stage diabetics.[2] This threshold for glucose is altered in diabetics due to increased expression of SGLT2 ($T_{m\text{-}Glucose}=420$ vs. 317 mg min^{-1} in normal patients), and this increased preservation of glucose by the kidney only serves to exacerbate the diabetic condition. SGLT1 is also found in all three segments of the small intestine and is solely responsible for glucose and galactose absorption from the intestinal brush border of the gut. Some of the properties of SGLTs are shown in Fig. 1.[3]

7.13.2.1 Human SGLT Loss-of-Function Patients

Familial renal glucosuria (FRG) is a consequence of genetic defects in renal SGLT2 that results in varying amounts of glucose excreted in the urine.[4] In general, FRG is a mild disorder with patients living normal lives, experiencing no resulting kidney disease

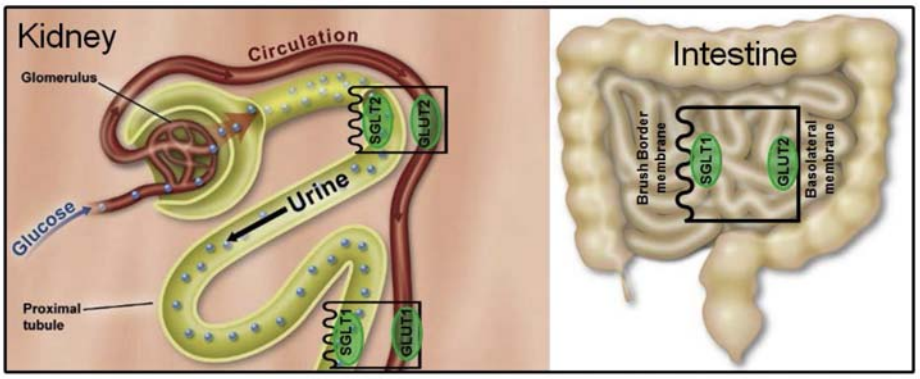

	SGLT1 K_i (mM)	SGLT2 K_i (mM)
$K_{0.5}$ (D-glucose)	0.4	5
$K_{0.5}$ (Na+)	3	100
Na:glucose transport ratio	2	1
Sugar specificity	Glucose, galactose	Glucose
Localization	Intestine, trachea, kidney, heart, brain, testes, prostate	Kidney, brain, liver, thyroid, muscle, heart
Size	664 AA	672 AA

Fig. 1 Schematic and properties of SGLT1 and SGLT2.

or early kidney failure and hypoglycemia or hypovolemia only rarely. Homozygous and multidefect heterozygous individuals can pass anywhere from 10 to 162 g of glucose per day depending on the extent of the defect or truncation of the protein, whereas heterozygous individuals appear normal and show only a very mild glucosuria ($<10\ g\ day^{-1}$). The rather benign nature of this defect along with the lack of any long-term pathophysiology associated with FRG, in addition to the ability to pass calories with a low chance of hypoglycemia, is the main reason that SGLT2 inhibition is a recent target for pharmaceutical intervention. Interestingly, FRG patients do not experience urinary tract infections, a concern reported with SGLT2 inhibitors investigated in clinic, suggesting that glucose levels in themselves are not responsible for these infections.[2]

Glucose–galactose malabsorption (GGM) is a genetic defect in SGLT1 protein, and to varying degrees, these patients are glucose-intolerant. The most severe cases are commonly diagnosed at birth due to severe osmotic diarrhea that is life-threatening unless glucose, galactose, and lactose are excluded from the diet. A study of GGM patients indicates that the defect is normally a missense mutation, most commonly D28N, which prevents viable SGLT1 from reaching the cell membrane. The outcome is that sugar and Na^+ along with the ~250 molecules of water/glucose molecule that would be normally absorbed in the upper intestinal tract are passed further down into the intestine. The nonabsorbed sugar and Na^+ extract water from the intestinal cells due to osmotic forces resulting in osmotic diarrhea. Bacteria further down in the gut exacerbate the situation as they metabolize the excess sugar releasing hydrogen and methane as by-products. GGM patients may also experience a minor renal glucosuria reflective of the role SGLT1 plays in the kidney.[5] In a study of GGM patients from an Amish population, it is observed that as these patients age, their glucose intolerance eases and they are able to tolerate carbohydrate in their diets by their teenage years.[6] It is uncertain whether this is an adaptive change in glucose transporter subtype or simply improved management of sugar disposal as probiotics accelerate the tolerance.[7] Finally, the amount of water absorbed along with sodium and glucose through SGLT1 in the intestine is significant and has been employed as an oral rehydration therapy in severely dehydrated cholera patients employing a salt/glucose solution.

7.13.2.2 SGLT Knockout Animals

SGLT1 knockout mice ($SGLT1^{-/-}$) are found to experience similar symptoms to GGM patients with an inability to absorb glucose and galactose, resulting in diarrhea when these carbohydrates are present in the diet.[8] In $SGLT1^{-/-}$ mice, little if any compensation through overexpression of GLUT transporters is reported as suggested elsewhere in response to hyperglycemia. $SGLT1^{-/-}$ mice do not exhibit glucose-induced activation of insulin release through GLP-1 and GIP indicating that glucose transport into L and K cells through SGLT1 may be necessary in order to trigger these responses. A minor reduction in renal glucosuria is observed in $SGLT1^{-/-}$ mice (~3%) as would be expected based on SGLT1's role in the kidney.

$SGLT2^{-/-}$ mice are healthy and show a similar growth rate compared with wild-type (wt) littermates except for being modestly hyperphagic and consuming twice the normal daily amounts of water.[9] Renal SGLT2 mRNA expression is absent although GLUT1 and GLUT2 expression is normal. SGLT1 expression and protein are reduced unexpectedly by 40% in $SGLT2^{-/-}$ mice compared with wt mice suggesting that under these conditions, a reduction in glucose reabsorption in early segments of the proximal tubule does not result in a compensatory increase in SGLT1 protein and glucose uptake in later segments of the proximal tubule. Reabsorption of glucose early in the proximal tubule is roughly 78% of the filtered load in wt mice and 0% in $SGLT2^{-/-}$ mice indicating

total loss of SGLT2 activity. Cumulative reabsorption assessed later in the proximal tubule totaled 93% of the filtered load in wt mice vs. 21% in SGLT2$^{-/-}$ mice indicating SGLT1 activity is still present and perhaps contributing more than expected to glucose recovery. Reabsorption is reduced overall suggested as a mechanism to protect the later proximal tubule from glucose toxicity. Systolic blood pressure (SBP), estimated glomerular filtration rate (eGFR), hematocrit, and plasma osmolality are normal as are plasma and urine levels of Na^+ and K^+, although modest changes in renin and aldosterone may reflect adjustments that prevent volume depletion. Knockout of SGLT2 on top of a diabetic *db*/*db* mouse background is hyperphagic (+20%) with a threefold increase in urine output and a 500-fold increase in glucosuria. However, even on a high-fat diet, these animals are protected from hyperglycemia and have preserved β-cell function and normal insulin sensitivity.[10] In another group, SGLT2$^{-/-}$ mice subsequently subjected to streptozotocin-induced diabetes showed protection from hyperglycemia, increased glucosuria, and renal hyperfiltration, an early marker of renal injury.[11] This suggests that pharmacological inhibition of SGLT2 should also prevent the renal injury common in diabetic patients by reducing glucose flux through the proximal tubule, thereby preventing proximal tubule hypertrophy and maintaining normal eGFR.[12]

7.13.2.3 Other SGLTs

SGLT3 is also found in the proximal tubule, shares 70% identity to SGLT1, and is located distal to SGLT1.[13] Examination of the function of SGLT3 indicates it is not a glucose/carbohydrate transporter but instead serves as a glucose-stimulated Na^+ transporter (see **Table 1**). SGLT3 expression is elevated in diabetes, which may lead to enhanced Na^+ transport postulated to promote hyperfiltration and ultimately renal damage. This suggests that inhibiting the SGLTs including SGLT3 in the proximal tubule could be beneficial in diabetics as it could also prevent the renal injury characteristic of advanced diabetes. However, none of the inhibitors described thus far inhibit SGLT3 in any significant way. Examination of the amino acid sequence of SGLT3 compared with SGLT1/2 indicates that a single-point change of glutamine-457 to glutamate (Q457E) relegates SGLT3 to the role of a glucose sensor/Na^+ transporter rather than glucose transporter. Interestingly, restoring glutamine-457 (E457Q) in SGLT3 protein reinstates its glucose transport function.[14] SGLT3 is also found in cholinergic neurons of the small intestine and the neuromuscular junction of skeletal muscle suggesting a role in the regulation of muscle contraction.[15]

SGLT4 is mainly expressed in the intestine and kidney with mannose as the preferred substrate. Mannose undergoes glomerular filtration by the kidney and is necessary for the normal glycosylation of proteins, making a specific mannose transporter necessary in the kidney.[16]

SGLT5 is expressed primarily in the S3 segment of the kidney proximal tubule and is responsible for fructose reabsorption after glomerular filtration. SGLT5$^{-/-}$ mice show complete elimination of Na^+-dependent fructose (and mannose) reuptake from the proximal tubule.[17] As metabolism of fructose in the liver leads to the synthesis and accumulation of liver triglycerides (TG) resulting in nonalcoholic fatty liver disease (NAFLD) and nonalcoholic steatohepatitis (NASH), it is thought that selective inhibition of renal SGLT5 would be an appropriate treatment for these diseases. Surprisingly, the SGLT5$^{-/-}$ mice demonstrate an exacerbated fatty liver phenotype coexisting with increased hepatic insulin resistance. Marketed SGLT2-selective inhibitors are in general biased against SGLT5, although remogliflozin appears only 16-fold selective signifying an added benefit for treating metabolic syndrome is possible.[18]

SGLT6, also referred to as SMIT2, is expressed primarily in the brain and CNS and is responsible for myoinositol transport and has been associated with infantile convulsion diseases.[19]

7.13.2.4 SGLT Structure and Glucose-Binding Motif

Prior to the advent of crystallographic information, the binding of various sugar analogs provided a basic understanding of the requirements of sugar binding to the different SGLTs (see **Table 2**). AMG (α-methylglucose), a nonmetabolized glucose analog

Table 1 Characteristics of other SGLT homologues

	SGLT3 (mM)	*SGLT4 (mM)*	*SGLT5 (mM)*	*SGLT6 (mM)*
K0.5 (D-glucose)	20	2	ND	ND
K0.5 (Na+)	Noninteracting	0.15	ND	ND
Na–glucose transport ratio	2	?		
Sugar specificity	Glucose	Mannose, glucose	Glucose, mannose, galactose, fructose	Myoinositol
Localization	Intestine, muscle, lung, brain, thyroid, uterus, testis, kidney	Intestine, trachea, kidney, liver, brain, lung, uterus, pancreas	Kidney	*Brain*, spinal cord, intestine, kidney, skeletal muscle
Size	659 AA	699 AA	596 AA	661 AA
Purpose	Sensor—not transporter	Protein glycosylation	Fructose/mannose recovery	Psychiatric conditions

Table 2 Substrate affinity to hSGLT1

Sugar	*hSGLT1 affinity*	*Sugar*	*hSGLT1 affinity nM*
D-Glucose	0.5	L-Glucose	≫ 100
D-Galactose	0.5	4F4DOGa	1.3
α- or β-Methyl glucose	0.5	D-xylose	50
1DOG	10		
2DOG	>100	2F2DOG	≫ 100
3DOG	>100	3F3DOG	9
4DOG	0.4	4F4DOG	0.07
6DOG	3	6F6DOG	5
D-Fructose	No interaction	D-Mannose	No interaction

used in cell assays to assess glucose transport, and D-glucose and D-galactose all bind to hSGLT1 in the 0.5–1 mM range. Removing the anomeric hydroxyl in 1-deoxyglucose (1DOG) results in a 10-fold shift in affinity to 10 mM. 2DOG and 3DOG lose another order of magnitude in binding affinity indicating the importance of these two hydroxyls to the binding of the sugar. Replacement of the 2- or 3-hydroxyls with fluorine shows opposing results with 2F2DOG remaining > 100 mM, while 3F3DOG recovers some of its binding (9 mM). 3-*O*-Methyl glucose (3OMG) retains affinity (3.5 mM) compared with 3DOG. Interestingly, 4DOG is no different than glucose, while the corresponding F-analog, 4F4DOG, actually gains some affinity (0.070 mM) compared to glucose itself. 6DOG and 6F6DOG are nearly equivalent binders indicating that in comparison with the 2- and 3-hydroxyls that are vital, the 4- and 6-positions are much less critical to tight binding to the transporter. However, the C6 methylene does appear important for affinity as the corresponding xylose derivatives are transported poorly. Fructose and mannose do not bind and are not transported. An understanding of these attributes can potentially provide an advantage in modifying the binding affinity and physiochemical properties of inhibitors. The low-affinity transporter, SGLT2, exhibits weaker binding constants with AMG and D-glucose at ~5 mM and does not interact with D-galactose.[5]

SGLTs' secondary structure is composed of 14 transmembrane (TM) helices with both the C- and N-terminal ends in the extracellular matrix. Although no crystal structures exist for human SGLT1/SGLT2 proteins, a homology model built using an X-ray of the bacterial galactose transporter from *Vibrio parahaemolyticus*[20] is available and employed to better understand the sugar binding site and the possible aglycone binding site.[21] The bacterial sugar binding site consists of residues from TM helices 1, 2, 6, 7, and 10. The Na^+ binding site is located ~10 Å away and is composed mainly of serine interactions S354/S355 and backbone carbonyls of A62, I65, and A361 in TM helices 1 and 8. The homology model for hSGLT1 indicates key interactions between each of the hydroxyls and protein as shown in Fig. 2.

As with ion channels, the SGLT transporters are dependent on the membrane potential, which accelerates initial sodium binding and leads to transport of more glucose at higher potentials. Na^+ is suggested to bind first, which then allows for a conformational change that exposes the sugar binding site. Subsequent to sugar binding, a conformational shift of the 12- and 6-helices opens the transporter pocket to the inside of the cell where the sodium ions and glucose diffuse out of the pocket. Na^+ is the best ion trigger for SGLT1 with a $k_{0.5}$ of 4 mM. Li^+ ($k_{0.5} = 12$ mM) is somewhat weaker and H^+, which is almost 1000-fold more potent ($k_{0.5} = 0.007$ mM), is also possible, but neither are important physiologically due to a 10–100-fold decrease in sugar binding

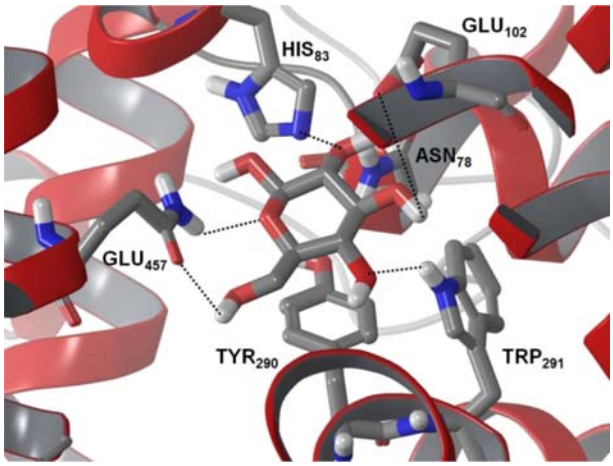

Fig. 2 Glucose binding interactions from homology model of hSGLT1 (from bacterial X-ray).

affinity. Expression of the high-affinity/low-capacity SGLT1 transporter in the gut, where large concentrations of glucose are present, is unexpected, although, as SGLT1 is located throughout the entire length of the small intestine, transporter efficiency is most relevant.

7.13.2.5 Inhibitor Binding Characteristics

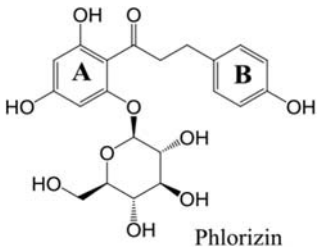

Phlorizin

Initial small-molecule X-ray and computational analyses of the binding conformations of various inhibitors, of which phlorizin is the prototype (see O-glycosides), suggest that the distal B-ring either can adopt a position coplanar with the proximal A-ring and sugar or can fold up over the A-ring. Adoption of a model where B-ring is folded up over A-ring would increase the overall space occupied by the molecule, allowing a better filling of the intended cavity. This supports the observation that simple single ring phenylglycosides are transported, while other inhibitors with a sufficiently large aglycone are not transported. Examination of the SGLT homology model suggests the aglycone may bind in the loop between helices 13 and 14 corresponding to residues 604–610 in rabbit SGLT1. This sequence contains an FCG motif that is conserved across all SGLT isoforms.[22] A key residue in inhibitor binding in rabbit SGLTs, rbCys608, also shows equivalent human homologues, hSGLT1 (Cys610) and hSGLT2 (Cys615). Mutation of this residue in hSGLT1 (C610K) results in a significant loss of AMG transport and a corresponding 10-fold decrease in phlorizin binding.[23] In contrast, mutation of the equivalent residue in hSGLT2 (C615K) maintains AMG transport along with a twofold improvement in phlorizin binding. Along with other mutations that have been studied, this argues that these residues are key in forming a hydrophobic binding pocket but do not possess direct H-bonding interactions with the aglycone portion of SGLT inhibitors.

Comparisons of the activity of known SGLT inhibitors have shown clear discrimination over hSGLT3, hSGLT4, hSGLT6, and hSMIT1 with varying selectivity against hSGLT1 and hSGLT5 (see **Table 3**).[24] Homology is relatively high among family members with 67–84% similarity (50–70% identity) although species differences in homologues have been observed to vary activity 10-fold.

In general, all SGLT selectivity ratios as reported are determined in cell-based assays with the transporter overexpressed and with IC_{50}s based on steady-state conditions. However, when looking deeper into the initial rate constants, the selectivity can be quite different. Whereas steady-state IC_{50}s do provide a relative selectivity ratio, that is, >1200-fold for dapagliflozin, they do not explain the initial rate constants where dapagliflozin is shown to have only ~100-fold selectivity over SGLT1.[25] The overall effect an inhibitor has on SGLTs requires an understanding of the various on and off rate constants where in this case, the very slow off rate of dapagliflozin against SGLT2 and relatively short off rate against SGLT1 helps explain the actual selectivity (see **Table 4**). This could explain a continued effect on glucosuria after plasma concentrations have fallen below their IC_{50}s for compounds such as dapagliflozin, in addition to the vastly different doses of different SGLT2 inhibitors required for efficacy given that all known inhibitors have similar low nM binding affinities.

Table 3 hSGLT IC_{50}s and selectivity against other known homologues

Compound	*hSGLT2 IC_{50}*	*Selectivity relative to SGLT2*					
		hSGLT1	*hSGLT3*	*hSGLT4*	*hSGLT5*	*hSGLT5*	*hSMIT1*
Phlorizin	16.4 nM	11	1300	490	36	1000	25,000
T-1095A	4.4 nM	60		500	250	750	
Sergliflozin	7.5 nM	280		800	147	1900	
Remogliflozin	12 nM	542		125	16	517	
Dapagliflozin	1.3 nM	610	190,000	3000	210	1300	22,000
Canagliflozin	6.7 nM	290	52,000	2800	180	200	5600
Empagliflozin	3.6 nM	1100	62,000	2200	110	1100	8300
Ipragliflozin	2.8 nM	860	7700	4500	87	3500	21,000
Tofogliflozin	2.9 nM	2900	19,000	1500	540	6200	28,000
Ertugliflozin	1.4 nM	1300	>71,000	2300	3400	980	26,000
Sotagliflozin	1.8 nM	20					
Luseogliflozin	3.1 nM	1600	8100	9800	280	220	7800

Table 4 Assessment of rate constants for phlorizin and dapagliflozin

	SGLT2			*SGLT1*		
	Initial rate, K_i (nM)	*$t^{1/2}$ off s^{-1}*	*Steady-state IC_{50} (nM)*	*Initial rate K_i (nM)*	*$t^{1/2}$ off s^{-1}*	*Steady-state IC_{50} (nM)*
Phlorizin	65	24	36	400	4	330
Dapagliflozin	6	$\gg$ 300	1	400–800	1.8	1390

7.13.2.6 Expression Levels of Glucose Transporters With Disease

7.13.2.6.1 Kidney

Hyperglycemia, whether in animal models or humans, leads to concomitant increases in mechanisms that increase or preserve carbohydrate energy reserves. In diabetic ZDF rats, the expression levels of renal SGLT1 and SGLT2 are increased 1.6- and 4.8-fold, respectively.[26] In other models of diabetes, increased renal SGLT2 mRNA levels and activity are driven by hyperglycemia, are under the control of HNF-1, and are reversed by normalizing glucose levels.[27] Renal proximal tubule cells collected from diabetic patients show a concomitant fourfold increase in SGLT2 mRNA and a threefold increase in GLUT2 mRNA compared with nondiabetic patients indicating an adaptive change to maximize glucose recovery. These cells demonstrate a threefold increase in AMG uptake.[28]

7.13.2.6.2 Intestine

A similar increase in glucose uptake is observed in the intestine of diabetic individuals. This is due to both hypertrophy of the small intestine's absorptive surface and an increase in the quantity of transporters SGLT1 and/or GLUT2 at the brush border and basolateral membrane, respectively. Using antibody recognition, a 4.3-fold increase in SGLT1 protein in brush border membrane (BBM) vesicles is found in diabetic vs. normal patients corresponding to a 3.3-fold increase in glucose transport capacity. The question of whether GLUT transporter expression at the BBM surface also plays a role has been investigated comparing phloretin-/phlorizin-[29] and cytochalasin B[30]-dependent transport with the body of evidence currently suggesting SGLT1 and not GLUT as the major effector of transport. As an added observation, GGM would not be as serious a condition in infants if the GLUTs were able to mediate transport. Indications of additional regulation involving phosphorylation through PKA/PKC are also suggested.[31]

7.13.3 SGLT Inhibitors

The potential effect of SGLT2 inhibitors in reducing glucose levels in diabetic patients has resulted in a wealth of agents entering the clinic and on the market. The purpose of this section is to highlight the genesis of various chemotypes both in terms of chemical diversity and summarize their clinical outcomes.[32]

7.13.3.1 O-Glycosides

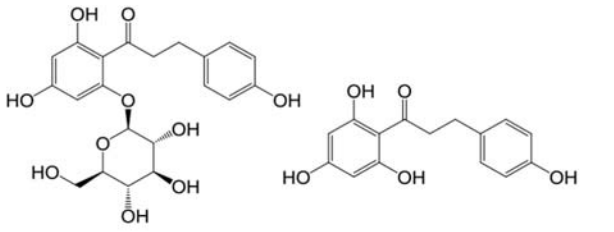

Phlorizin
SGLT2 IC_{50} 21 nM
SGLT1 IC_{50} 290 nM

Phloretin
SGLT2 IC_{50} 25000 nM
SGLT1 IC_{50} 50000 nM
GLUT IC_{50}~400 nM

Phlorizin, isolated originally from the bark of apple trees, is a potent inhibitor of human SGLT1 (290 nM) although this is species-dependent with the IC_{50} being an order of magnitude more potent (12 nM) in rat and considerably less potent against rabbit SGLT1 (760 nM). Phlorizin is an even better inhibitor of human SGLT2 (21 nM), the low-affinity/high-capacity transporter.[33] Phlorizin suffers from poor bioavailability requiring rather large oral doses in order to assess its effect on SGLT2 in the kidney, which results

in significant inhibition of SGLT1 in the gut along with the accompanying diarrhea observed in GGM patients. IV administration to patients at doses above 12 mg kg^{-1} results in complete inhibition of glucose reuptake by the kidney.[34] In addition to poor exposure when delivered orally, phlorizin is also unstable due to hydrolysis of the O-glycosidic bond by intestinal glucosidases, generating the aglycone, phloretin. Phloretin is well absorbed and has a variety of functions including inhibition of the GLUT transporters and uncoupling of oxidative phosphorylation. As the GLUTs are the major cellular glucose transporters, their inhibition could severely compromise a tissue's ability to maintain essential energy supplies, thereby making phlorizin unsuitable as a potential agent for the treatment of diabetes. Phlorizin has been shown to block glucose uptake into the brain and specifically glucose uptake into glucose-sensitive neurons in the hypothalamus. Injection of phlorizin into the brain of normal rats causes a marked increase in food intake although injection into the brains of ZDF rats has no effect.[35] For these reasons, it would be prudent to keep SGLT inhibitors out of the brain.[36] The recent evaluation of apple cider in healthy volunteers, which contains a plethora of polyphenolic compounds including phlorizin, confirms sufficient exposures to affect increases in glucosuria along with reductions in blood glucose and plasma insulin.[37] Phlorizin is the starting point for design of all sugar-containing SGLT inhibitors.

7.13.3.2 T-1095 (hSGLT2 $IC_{50} = 4.4$ nM: hSGLT1 $IC_{50} = 260$ nM)

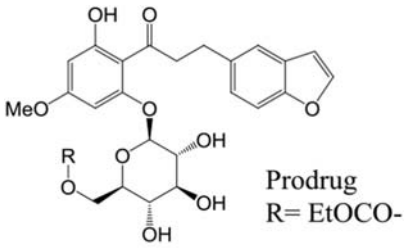

T1095 R=H

T-1095 provides a modest improvement over phlorizin in terms of activity/selectivity by derivatization of one of the hydroxyls as a methyl ether and incorporation of the phenol oxygen into a benzofuran ring. It appears to be hydrolytically more stable and overcomes the poor bioavailability of phlorizin by using a carbonate prodrug situated on the 6-position of the sugar. As it is expected that the prodrug will be absorbed intact to be cleaved in the liver, this would serve to both limit the effect on SGLT1 in the gut and increase the plasma exposure of active drug.

7.13.3.3 Sergliflozin (hSGLT2 $IC_{50} = 7.5$ nM: hSGLT1 $IC_{50} = 2100$ nM)

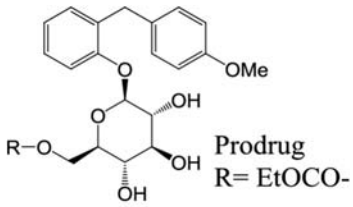

Sergliflozin R=H

Sergliflozin is the next key compound, maintaining a β-O-glycoside similar to phlorizin and T-1095 but reconstituting the aglycone to remove the phenols and make the compound more drug-like. Selectivity is improved with a ratio of 200-fold over SGLT1. Sergliflozin is still an O-glucoside and requires a prodrug to escape glucosidases in the gut and achieve sufficient exposures. Early clinical outcomes show glucosuria of approximately 20 g day^{-1} in healthy volunteers and 36 g day^{-1} in T2DM patients, along with a reduction in glucose area under the curve (AUC) during an oral glucose tolerance test (OGTT) when administered at 500 mg day^{-1}. The activity is limited due to poor exposure with a short half-life and would require frequent dosing in order to be a successful drug.[38] A study of carbocyclic versions of sergliflozin indicates that removal of the ring oxygen substantially improves stability to glucosidases. Even though half-life and efficacy improve, selectivity and other physiochemical liabilities limit clinical advancement.[39]

7.13.3.4 Remogliflozin (hSGLT2 IC_{50} = 12.4 nM: hSGLT1 IC_{50} = 6500 nM)

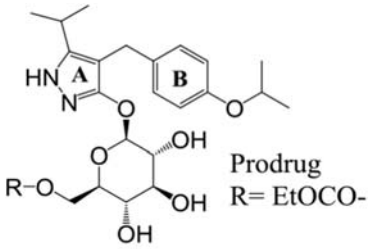

Remogliflozin R=H

Remogliflozin substitutes the A-ring phenyl with a pyrazole and is optimized for improved properties although it still requires dosing as a prodrug to avoid cleavage by the glucosidases.[40] A report of the early clinical studies looks promising with 1000 mg QD dosing in diabetic patients resulting in a urinary glucose excretion (UGE) of 165 g day^{-1}, nearly that of the maximum filtered load of 180 g day^{-1}. Unfortunately, this dose only results in a minor reduction in fasting plasma glucose (FPG) of 5.4 mg dL^{-1}, which is puzzling. Doses of 100 mg BID and 1000 mg BID produce roughly equivalent daily UGE values of 91.6 and 103 g/24 h and FPG reductions of 23.4 and 41.4 mg dL^{-1}, respectively.[41] Subsequent 12-week studies confirm reductions in HbA1c of 0.73–1.07% with doses ranging from 50 to 1000 mg QD.[42]

7.13.3.5 SGLT1-Selective Analogs of Remogliflozin (hSGLT2 IC_{50} = 1730 nM: hSGLT1 IC_{50} = 50 nM)

This template was further investigated with the goal of generating selective SGLT1 agents. With suitable modifications, 24-fold selective SGLT1 agents with improved intestinal stability are identified, showing no effect on renal glucosuria and complete inhibition of carbohydrate absorption during an OGTT.[43] Continued efforts to improve activity and stability are needed as glucosidases are still an issue in vivo leading to the expected aglycone cleavage and producing undesirable pharmacology. Along with further improvements in stability, the aglycone portion is modified with functional groups that prevent absorption should cleavage occur. These compounds proved superior to acarbose, an alpha-glucosidase inhibitor, in preventing glucose absorption in animal models and with reduced side effects (diarrhea).[44]

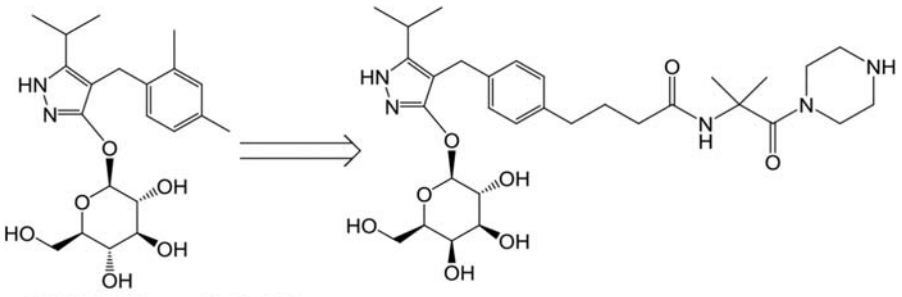

SGLT2 IC_{50}= 6010nM
SGLT1 IC_{50}= 246nM

SGLT2 IC_{50}= 1730nM
SGLT1 IC_{50}= 50nM

7.13.4 Origin of C-Glucoside

In an attempt to reduce the instability of the O-glycosides, a conservative O- to C-replacement on the sergliflozin template loses nearly 60-fold potency against SGLT2. Removing the oxygen altogether generates the first C-arylglycoside where the activity tumbles even further to 4000 nM. However, examination of a pharmacophore model suggests that shifting the B-ring connectivity from an orthobenzyl to a metabenzyl should better approximate the O-glycoside conformation. Indeed, this allows recovery of most of the activity of the original structure while more importantly removing the instability inherent in the O-glycosides.[30]

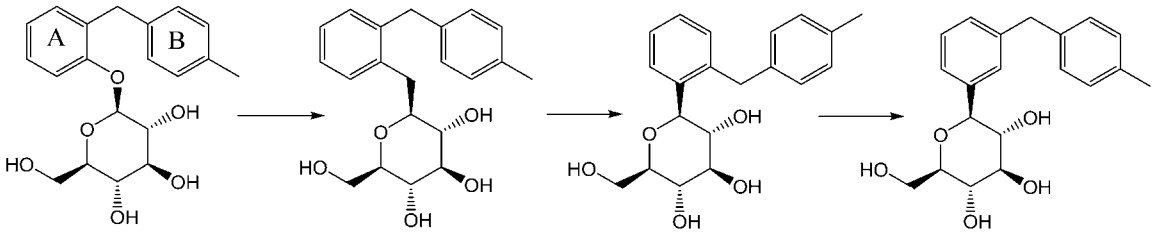

Initial optimization of the newly identified aglycone reveals that alteration of the aromatic linker along with suitable substitution of the B-ring produces effects on both potency and selectivity over SGLT1.[45]

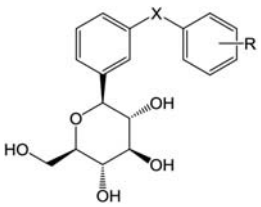

Cmpd	*hSGLT IC_{50} (nM) (hSGLT2 selectivity ratio over hSGLT1)*				
	X = CH_2	X = Bond	X = CH_2CH_2	X = S	X = O
R = H	190	623	710		
R = 4-Me	22 (600-fold)	290 (30-fold)	430 (20-fold)	69 (100-fold)	540 (15-fold)
R = 3-Me	510	1200	970		

7.13.4.1 Dapagliflozin (hSGLT2 IC_{50} = 1.1 nM: hSGLT1 IC_{50} = 1400 nM)

Additional rounds of optimization of the A-ring and the B-ring give the best combination of potency and selectivity in dapagliflozin with selectivity over hSGLT1 of 1200:1.

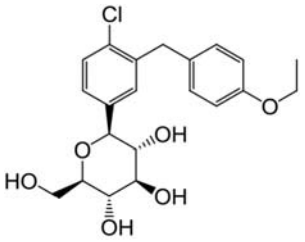

Dapagliflozin

Early clinical evaluation reveals that at doses of 5–100 mg day^{-1}, glucosuria reaches a maximum of 82 g day^{-1} on day one and then moderates to 64 g day^{-1} as the hyperglycemia normalizes, resulting in less glucose to filter and excrete. This is the first reported example where drug-induced glucosuria is limited providing only 44% of the total possible 180 g of glucose recovered each day. On day 13, fasting serum glucose is reduced by 15.4 mg dL^{-1}, and an OGTT allows a 17.4% reduction in glucose AUC compared with placebo control.[46] Hypoglycemia is observed in 10% of the patients, although metformin cotherapy could contribute to this. As dapagliflozin is highly selective and unlikely to inhibit SGLT1 activity in the gut, the reduction in OGTT is likely in response to glucosuria and improved insulin-mediated glucose disposal due to reduced glucotoxicity. Longer-term studies demonstrate consistent reductions in HbA1c of 0.72–0.66% as monotherapy with corresponding decreases in BW of up to 2.2 kg and SBP of up to 4 mmHg.[47] In more recent examinations in diabetic patients, dapagliflozin increases glucosuria by 78–91 g glucose/day, enhances whole-body glucose disposal, primarily in the muscle, decreases insulin levels as a result of decreased hyperglycemia, and counters glucose toxicity increasing insulin sensitivity. Unexpectedly, an increase in endogenous glucose production (EGP) in response to increases in glucagon occurs.[48] Increases in both glucagon levels (23%) and EGP result in an increase of ~47 g glucose/day offsetting the effect of glucosuria and reducing the expected effect on plasma glucose by 50%. As other SGLT inhibitors also show this increase in EGP

following drug treatment, this effect along with the limitations on glucosuria noted earlier significantly undercuts the overall benefit to patient.

Dapagliflozin was evaluated in both naive early-stage diabetics and late-stage diabetics on insulin therapy with similar renal function. Although dapagliflozin is effective in both groups, higher starting FPG, HbA1c, and weight translate into better outcomes on glucosuria, HbA1c reductions, and weight loss in the late-stage patients.[49]

Carba-analogs of the C-linked glycosides are also interesting. In this case, retention of the hydroxyl at the previous anomeric center (R3) gives varying effects on potency but always improves the SGLT2 selectivity. Addition of a group at the C6 center of the A-ring (R2) improves selectivity dramatically but unexpectedly only when the C4-position (R1) is vacant in contrast to previous findings by others.[50]

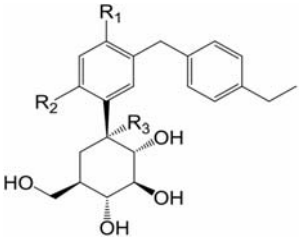

R_1	R_2	R_3	hSGLT2 IC_{50}	Selectivity
H	H	H	49	670
OMe	H	H	8.3	61
OMe	H	OH	100	310
H	OMe	H	12	6100
H	OMe	OH	14	>7100
OMe	OMe	H	8.5	530
OMe	OMe	OH	10	860

7.13.4.2 Canagliflozin (hSGLT2 IC_{50} = 4.4 nM: hSGLT1 IC_{50} = 684 nM)

Soon after the discovery of C-aryl glycosides as preferential to O-glycosides, an explosion of SAR commenced. Replacement of the B-ring phenyl as in phlorizin and dapagliflozin with heteroaromatics proves equally attractive. Although the initial furan was disappointing, the thiophene shows much better activity, while pyrazole and pyridine are ~10-fold weaker.[51] Optimization of the A-ring substituents shows that chloro and methyl substitutions provide a significant advantage. Aromatic substitution of the thiophene proves even better both in terms of in vivo activity and chemical stability and provides the clinical candidate canagliflozin.[52]

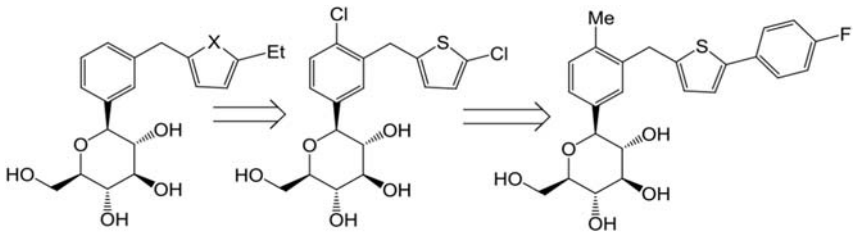

As canagliflozin has only a modest selectivity of ~155-fold over SGLT1, one could expect that at higher dose regimens, it would begin to show some of the positive and negative effects of SGLT1 inhibition in the gut. Patients administered 300 mg of canagliflozin show a 20% inhibition of glucose uptake in the gut over the first 2 h. However, this is followed by a substantial increase in glucose uptake of 34% over the next 4 h producing a 6% net reduction in intestinal glucose uptake as compared with the first 6 h.[53] Delayed gastric emptying, as assessed by acetaminophen absorption is observed in this study although it is insufficient to explain the entirety of the effect. Increases in gut peptides GLP-1 and PYY with corresponding reductions in GIP suggest that inhibition of SGLT1 is delaying glucose absorption sufficient to trigger these responses by L cells. As the delay of early glucose absorption is then countered by a faster rate at later times, this transient effect would not result in a real inhibition of total glucose uptake, but would reduce the postprandial glucose spike and trigger an incretin response; and perhaps, independent of the kidney effects has a beneficial effect on glucose homeostasis. However, as a hydrogen breath test is negative, this suggests little if any glucose persists into the lower gut where bacteria would metabolize it releasing hydrogen in the process.

Continuation of this heterocyclic SAR expansion provides additional subnanomolar compounds when the B-ring is a suitably decorated thiazole. Further substitution of the thiazole with a simple alkyl chain or aromatic does not increase potency, although furans and thiophenes show considerable improvement.[54] Additional heteroatoms in either of the heterocyclic rings do not provide any further benefit. The need for the aglycone to consist of a nonpolar somewhat planar assembly is clear. Attempts to instill solubilizing polar groups such as carboxylic acid are entirely unacceptable even as a B-ring substituent. The furan and thiophene compounds with maximal potency still possess poor physiochemical properties that preclude clinical examination.

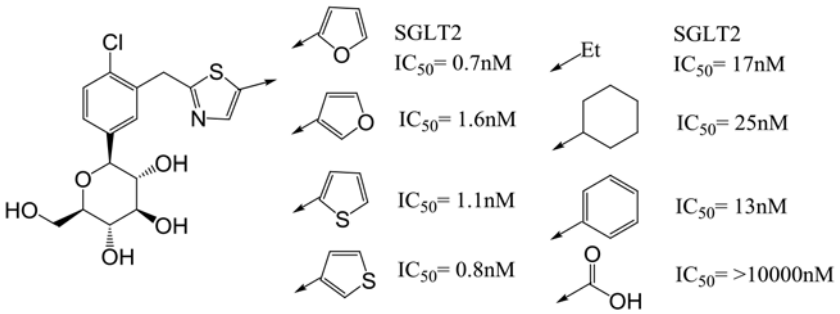

7.13.4.3 Ipragliflozin (hSGLT2 IC_{50} = 7.4 nM: hSGLT1 IC_{50} = 1880 nM)

Expanding the scope of the B-ring to fused aromatics results in limited success, with benzothiophene proving the best option, although 10–100-fold losses of activity are observed with modest changes in heterocycle. Optimization of the A-ring substituents leads to the discovery of clinical candidate ipragliflozin. Additional evaluation of R_1 substitution, generally ignored since phlorizin, suggests that this position can also tolerate substitution to generate improved SGLT2-selective agents.[55]

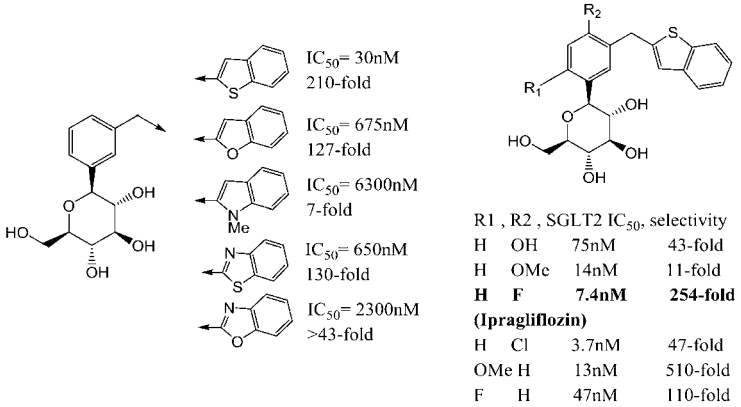

R1	R2	SGLT2 IC_{50}	selectivity
H	OH	75nM	43-fold
H	OMe	14nM	11-fold
H	**F**	**7.4nM**	**254-fold**
(Ipragliflozin)			
H	Cl	3.7nM	47-fold
OMe	H	13nM	510-fold
F	H	47nM	110-fold

Initial dose-range finding trials in diabetic patients provide a maximum placebo-adjusted reduction in FPG of 60 mg dL^{-1} along with reductions in BW and SBP. Gastrointestinal disorders are common and reported in 50% of the study population. A 12-week study of ipragliflozin dosed from 12.5 to 150 mg provides a placebo-adjusted HbA1c reduction of 0.61–1.31% (placebo HbA1c increases by 0.5%). FPG is reduced by 27.6–58.9 mg dL^{-1}, and a reduction in BW of 1.61 kg is observed at the highest dose. Adverse events (AEs) are typical of this class including GI, UTI, and polyuria.[56]

7.13.4.4 Empagliflozin (hSGLT2 IC_{50} = 3.1 nM: hSGLT1 IC_{50} = 8300 nM)

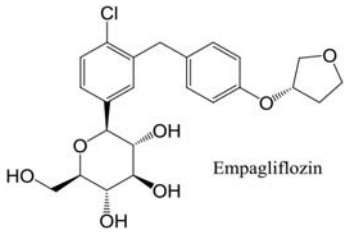

No publications examining the SAR of empagliflozin exist, but it would appear the efforts are aimed at optimizing the 4-position of the B-ring. When examined in diabetic patients, the highest dose of 25 mg produces placebo-corrected reduction in HbA1c of 0.70%, with FPG reduction of 24 mg dL^{-1}, and modest effects on weight loss (2.1 kg) and SBP (3.4 mm) over 12 weeks of treatment. Modest reductions in eGFR are noted as have been observed with other SGLT2 inhibitors and are reversible once treatment is discontinued. Examination of individual patients suggests that those with normal eGFR have no change during treatment, while patients with hyperfiltration, a hallmark of early diabetes, do see a reduction. Significant loss of efficacy is observed in patients with progressively worsening eGFR with a 50% reduction in glucosuria in stage-3 chronic kidney disease (CKD) and total loss in stage-4 CKD typical of SGLT2/kidney centric agents.[57]

7.13.4.5 Tofogliflozin (hSGLT2 IC_{50} = 2.9 nM: hSGLT1 IC_{50} = 8444 nM)

Efforts toward tofogliflozin focus on the orientation between the sugar and the aglycone using a pharmacophore approach based on known SGLT inhibitors. This exercise suggests that insertion of a spiro-sugar connection maintains the proper shape and provides novelty of structure. Optimization of the remaining aglycone follows the traditional bibenzyl path with slightly different outcomes.

			SGLT2 IC_{50} (nM)	*Selectivity SGLT1/2*
Dapagliflozin			1.3	800
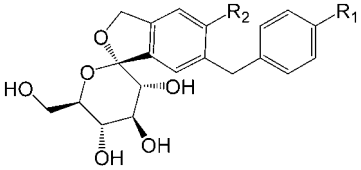	R1	R2		
Tofogliflozin	Et	H	2.9	2912
1	iPr	H	3.2	3855
2	F	H	123	152
3	CN	H	118	691
4	Et	Cl	1.3	122
5	Et	Me	1.4	90

Interestingly, 4-substitutions on the A-ring degrade selectivity and so are intentionally absent. Electron-withdrawing groups on the B-ring (compounds 2 and 3) are also found detrimental to both selectivity and activity.[58] Comparative in vivo studies select tofogliflozin over other analogs due to superior PK parameters, with improved exposure and reduced clearance. A 52-week trial in diabetics demonstrates a reduction in HbA1c of approximately 0.67% at both 20 and 40 mg QD doses against patients own baseline values (no placebo controls). Modest effects on TG, HDL-C, LDL-C, and SBP are observed along with increases in eGFR. Ketone bodies, a new safety concern for this class of compounds, nearly double (108–211 μmol L^{-1}) in the tofogliflozin-treated groups.[59]

Close derivatives of spiro glucoside are also prepared where the spiro-ring oxygen is replaced with carbon. This effort produces clearly the most selective compounds to date due to near total loss of SGLT1 activity. These compounds, however, are rapidly cleared in vivo, which limits their effects on glucosuria in rats.[60]

Cmpd	*X*	*SGLT IC_{50} (nM)*	*Selectivity SGLT1/2*
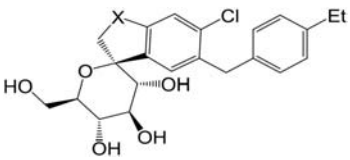	Dapagliflozin	6.7	132[a]
	$-CH_2-$	0.3	18,667
	$-CHOH-$	40	3450
	$-CHF-$	0.9	56,667
	$-CHOMe-$	1.8	55,000
	$-CH_2CH_2-$	33	>6060

[a]Selectivity values for dapagliflozin are usually ~1000 as reported elsewhere.

7.13.4.6 Ertugliflozin (hSGLT2 IC_{50} = 0.88 nM: hSGLT1 IC_{50} = 1960 nM)

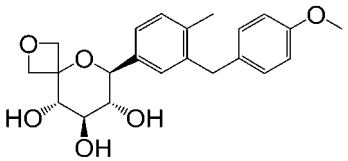

SGLT2 IC_{50} 6.98 nM
SGLT1 IC_{50} 1540nM
HLM Cl= 12 uL/min/mg
HHep Cl= 44 uL/min
Rat plasma Cl = 22 mL/min/kg

This approach investigates modification of the sugar rather than the aglycone. Starting with sequential modification and removal of hydroxyls around the ring, the critical requirement of the C2 and C3 hydroxyls for binding coupled with flexibility at the C4 and C5 positions is soon rediscovered.[61] The first spirocyclic sugar has relatively good potency, sufficient selectivity, low microsomal clearance, and good physiochemical properties and oral exposures. However, clearance in human hepatocytes is much higher than observed in microsomes, possibly due to the lack of an H-bond donor in the 5 position, and, in addition, effects on UGE in a rat model are unimpressive.

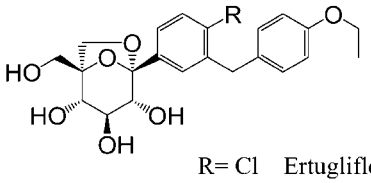

R= Me	R= Cl Ertugliflozin
SGLT2 IC_{50} 1.07 nM	SGLT2 IC_{50} 0.93 nM
SGLT1 IC_{50} 506nM	SGLT1 IC_{50} 2050nM
HLM Cl= <8 uL/min/mg	HLM Cl= 12 uL/min/mg
HHep Cl= <2.1 uL/min	HHep Cl= 4.5 uL/min
Rat plasma Cl=37 mL/min/kg	Rat plasma Cl=4 mL/min/kg

An alternate bicyclic series proves much more amenable with regard to acceptable activity and in vitro clearance. The first compound (R=Me) has the appropriate activity with good microsomal and human hepatocyte stability but inordinately high in vivo rat clearance. Employing the dapagliflozin aglycone then provides ertugliflozin with near 2000-fold selectivity and good in vitro and in vivo PK characteristics.[62] The authors claim that this substitution pattern at the C5 position of the sugar solves supposed issues with genotoxicity that are common in previous compounds tested across the industry using the standard in vitro micronucleus assay.[63] Clinical evaluation of ertugliflozin in diabetic patients over 12 weeks demonstrates placebo-adjusted reductions of HbA1c (0.72%), FPG (32 mg dL^{-1}), and BW (1.9 kg) at the highest dose (25 mg). Reductions in SBP (3.4 mm) and DBP (2.6 mm) are observed along with reductions in fasting insulins indicating relief of glucotoxicity. Serum lipids (cholesterol, LDL, and HDL) are increased similar to other SGLT2i. AEs are moderate across dosing groups, and UTIs, common with SGLT2i compounds, are only seen in the 10 mg group, notably the only group with near equal distribution of women.[64]

7.13.4.7 Sotagliflozin (Lexicon LX4211) (hSGLT2 IC_{50} = 1.8 nM: hSGLT1 IC_{50} = 36 nM)

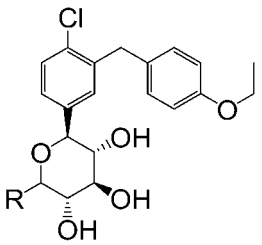

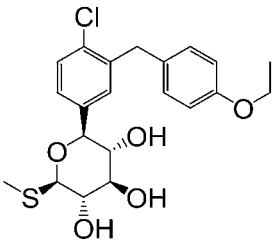

R,	hSGLT2 IC_{50}
βOMe	14nM
αOMe	4800nM
β OiPr	33nM
β OBn	620nM

LX4211
hSGLT2 IC_{50}= 1.8nM
hSGLT1 IC_{50}= 36nM

LX4211 is the first compound reported that intentionally adds SGLT1 inhibition to its profile. Addition of SGLT1 could potentially improve glucosuria further over the nine SGLT2-selective agents as explained earlier. However, SGLT1 in the kidney is only reported to account for 10% of the glucose recovery, questioning whether this effect would be measurable. Inhibition of SGLT1's effect on reducing or eliminating glucose uptake in the intestine has the potential to be truly meaningful if it does not produce the diarrhea observed in the SGLT1-deficient GGM patients. This approach utilizes a different sugar, xylose, which ultimately reduces the C5 methanol unit of glucose to an alcohol. Stereochemistry at the C5 position requires the β-configuration as the α-configuration lost more than 100-fold in activity. Activity also degrades with increasing size of the alkoxy unit.[65] The clinical candidate, LX4211, has a thioether substituent at C5, an interesting choice as one would expect that increased metabolism would limit exposures.

The effects of LX4211 in a 4-week trial show promising results with reductions in FPG of 39 and 55 mg dL^{-1} at the 150 and 300 mg dose levels, respectively, along with corresponding reductions in HbA1c of 0.66 and 0.76 (placebo-corrected).[66] Additional reductions in LDL and HDL are also observed in contrast to most SGLT2-selective agents. Activation of the GLP-1 pathway is evident, which also

improves glucose homeostasis by improving insulin action and delaying gastric emptying. An assessment of timing of dose with effect on postprandial glucose levels indicates that LX4211's effect is dependent on the presence of compound in the gut irrespective of systemic concentrations.[67] A 12-week study supports HbA1c reductions of 0.83%, similar to values seen with the SGLT2-selective agents, although with only a 29 mg dL^{-1} drop in FPG.[68] BID dosing provides the best weight loss of 2.6% (200 mg BID @ 12 weeks). As BID dosing should inhibit gut SLGT1 at least enough to cover an additional meal, the effect is somewhat disappointing as it did not differentiate from SGLT2-selective agents. AEs are generally mild with reports of urinary tract infections (UTIs) and diarrhea, but these did not differentiate from placebo. The lack of significant intestinal effects expected with gut SGLT1 inhibition suggests either that the concern is overblown or that LX4211 has only transient effects in the gut similar to that observed with canagliflozin.

7.13.4.8 Luseogliflozin TS071 (hSGLT2 IC_{50} = 2.3 nM: hSGLT1 IC_{50} = 3990 nM)

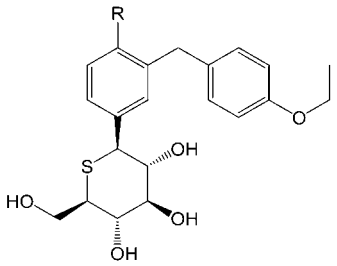

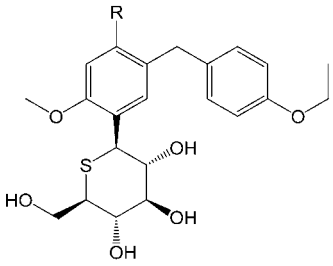

R,	hSGLT2 IC_{50}	SGLT1/2
H	74nM	355-fold
OMe	13nM	42-fold
Me	2.3nM	293-fold
Cl	1.8nM	684-fold

R,	hSGLT2 IC_{50}	SGLT1/2	
H	38nM	2640-fold	
OMe	11nM	395-fold	
Me	2.3nM	1770-fold	(luscogliflozin)

Conversion of the pyranose ring O to S results in similar SAR as seen previously including A-ring 4-substitution preferences. The addition of a methoxy group in the 6-position of the A-ring leads to improvement in potency and selectivity ultimately resulting in luseogliflozin as the clinical candidate.[69] Early clinical trials with luseogliflozin show reductions in HbA1c of 0.82% (placebo-adjusted) at the highest dose of 5 mg along with reductions in FPG of 27 mg dL^{-1}.[70] BW losses and SBP reductions of 1.7 kg and ~6.6 mmHg are in line with other SGLT2 inhibitors. AEs are minimal, and UTIs are not observed, although the patient population is skewed toward men in all groups. As with other SGLT2 inhibitors, decreases in insulin are matched by increases in glucagon, although not triggered by hypoglycemia as glucose levels remain above 100 mg dL^{-1} assessed by continuous glucose monitoring.[71]

7.13.4.9 A-Ring Replacements

Very few replacements of the A-ring are described. In these manuscripts, two different indole replacements, one as an N-glycoside and the other as a C-glycoside, produce moderate activity although selectivity remains elusive.[72] A similar attempt utilizing a thiophene, ordinarily considered a direct phenyl replacement, produces compounds of only modest activity.[73]

7.13.4.10 Nonnucleoside Inhibitors

Little if any effort has been directed toward finding nonglucoside SGLT inhibitors, although one effort uncovered a rather potent starting point using high throughput screening (HTS).[74] This series was then optimized to eliminate metabolic liabilities and improve potency.

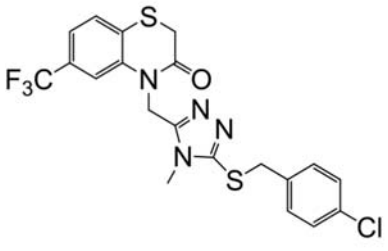

hSGLT2 IC_{50} = 1400nM
hSGLT1 IC_{50} = 7000nM

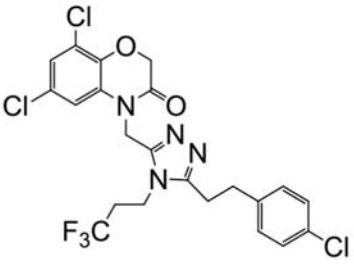

hSGLT2 IC_{50} = 10nM
hSGLT1 IC_{50} = 6300nM

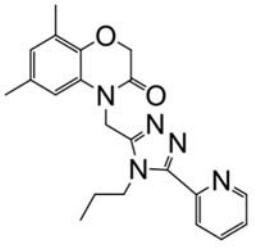

hSGLT2 IC_{50} = 12nM
hSGLT1 IC_{50} NA

Through the course of these efforts, very little change in SGLT1 inhibition is observed with the best compounds showing approximately 1000-fold selectivity of SGLT2/1 similar to that of dapagliflozin. Although metabolic liabilities are partially addressed, the compound still does not meet development criteria, and further, SAR minimizes many of these liabilities while retaining SGLT2 potency and increasing solubility.[75]

7.13.5 Limitations on Effects of SGLT Inhibitors

Ever since SGLT2 inhibitors have been evaluated in clinic, a significant limitation becomes apparent with inhibitors providing only 30–50% of the 180 g maximum possible glucosuria per day. Potential reasons for this have been postulated resulting in various scenarios that could account for this deficiency, although currently no single explanation accounts for this reduced effect on glucosuria.[76]

7.13.5.1 Target Engagement

Examination of different agents suggests that varying dosing regimens generate sufficient systemic exposure to fully inhibit SGLT2 although activity does persist longer with some inhibitors potentially due to slower off rates. Another limitation is the ability of the inhibitor to physically reach the target, the luminal side of the transporter in the proximal tubule, and disposition of the inhibitor once dissociated from the transporter. As very few inhibitors are recovered as unchanged drug in the urine, most are likely reabsorbed and only eliminated after metabolism indicating repeated access to target is not an issue. Although overexpression of SGLT2 transporters in response to hyperglycemia is expected, a deficiency of drug is unlikely as dose adjustment would be expected to compensate. Other less likely scenarios posit whether newly expressed SGLT2 transporters, as a result of hyperglycemia, could be in a different location anatomically or are inserted into the membrane in such a way as to be blind to SGLT2 inhibitors but not to glucose.

7.13.5.2 Competition With Glucose

Increasing concentrations of glucose in the proximal tubule as a result of hyperglycemia could compete with the inhibitor, although as the activity of most known inhibitors is low nM, while the binding constant for glucose is $\sim$5 mM, a million-fold less, it is unlikely that glucose itself could effectively compete with most of the known inhibitors.

7.13.5.3 Other Transporters

Expression of other glucose transporters such as GLUTs on the BBM has been considered and tested extensively, although current evidence suggests that this potential bypass mechanism to enhance glucose absorption is not functional. Otherwise, one would expect GGM patients to be able to express transporters to absorb glucose making their side effects less severe. Alternatively, the remaining SGLT1 could simply take the place of SGLT2 and reabsorb the majority of the glucose; however, this is not shown to be the case in terms of expression or transport rate and as well with the dual SGLT1/2 inhibitor, LX4211.

7.13.5.4 Patients With Kidney Damage

One of the accompanying comaladies associated with diabetes is kidney disease that presents initially with hyperfiltration but then proceeds with continual reductions in eGFR that eventually leads to kidney failure.[77] This is driven by increased glucose flux through the proximal tubule cells, which triggers a hypertrophic phase aided by paracrine factors, EGF, and angiotensin II. This causes an increase in reactive oxygen species leading to tubule cell damage and ultimately apoptosis. Hyperglycemia is shown to increase the levels and transport capacity of the SGLT transporters and results in even larger flux through the tubule cell.[78] In the development of SGLT inhibitors, a question remains as to whether they will prevent or protect the kidney from this pathophysiology.[79] As SGLT2 inhibitors work in the kidney, a question of loss of efficacy with decreasing renal function is an important consideration in this patient population. As proximal tubule cells collected from diabetic patients elicit a reduction in oxidative stress and apoptosis when exposed to various SGLT inhibitors, there is hope that this effect will be observed in patients as well. However, to date, it would appear that most SGLT2 inhibitors cause a modest reduction in eGFR. The effect of dapagliflozin and other SGLT2 inhibitors on glucosuria, however, is severely encumbered ($>$5-fold) under conditions of moderate to severe renal impairment.[80]

7.13.5.5 Drug Metabolism and Clearance

The extent of exposure of a particular agent can also be altered based on both renal function and individual drug metabolism and clearance pathways. Although the exposure profiles of most of the SGLT2 inhibitors do not vary extensively with changes in renal function, exposure maximums increase as clearance is generally reduced. Multiple elimination pathways are preferred so as not to stress one pathway or result in changes in exposure or clearance of other drugs (DDI). The metabolism and route of elimination of dapagliflozin were extensively studied in normal patients and patients with varying stages of kidney disease. In the case of dapagliflozin, the primary route of metabolism is phase-2 glucuronidation at the 3 position of the sugar with 61% of this metabolite being

recovered in the urine of patients. Decreasing eGFR nearly doubles the drug AUC as renal clearance decreases. As less than 1% of unchanged drug is cleared renally and as drug effect requires the drug be on the luminal side of the transporter where the drug could be easily excreted, a reabsorption pathway in the lower proximal tubule is necessary. Many of the known SGLT2 inhibitors, such as canagliflozin, empagliflozin, ertugliflozin, and ipragliflozin, are extensively glucuronidated prior to excretion, although empagliflozin is excreted to some extent as unchanged drug in the urine (28.6%) and tofogliflozin is predominantly excreted in the urine as unchanged drug and oxidative metabolites.[81,82]

7.13.5.6 Increased Glucagon Response

Additional studies with dapagliflozin and empagliflozin[83] demonstrate that increases in glucagon and EGP occur upon drug treatment and produce significant limitations in the agent's effect on hyperglycemia in diabetic patients. Using tracer studies in diabetic patients, reductions in postprandial glucose levels would be fourfold greater if enhanced EGP did not compensate. Although the actual cause of this is unknown, it could be a direct consequence of lower glucose levels attenuating insulin release, which subsequently reduces glucose uptake in insulin-sensitive tissues along with a maintained or higher glucagon–insulin ratio that induces glucose production. It is possible that immediate corrections of the diabetic phenotype by SGLT2 inhibitors through improvements in glucose toxicity, insulin sensitivity, hyperinsulinemia, and glucose uptake are not immediately sensed in the pancreas where islet hyperplasia results in increased islet cell mass. The reduction in insulin release from the β-cell may remove the local paracrine restraint on the α-cell allowing for either maintained or even larger glucagon release from the α-cell. An alternative explanation suggests SGLTs as the major glucose transporters on the α-cell,[84] and as a result, inhibition of transport into the α-cell signals an intracellular hypoglycemia resulting in increased glucagon release. As the addition of phlorizin, a dual SGLT1/2 inhibitor, has no additional effect on glucagon release, the effects are likely SGLT2-selective.

7.13.6 Potential Safety Concerns

7.13.6.1 Hypoglycemia

One of the biggest concerns of patients and physicians is the potential for hypoglycemia with any therapy for diabetes, and many of the current standards of care do have this potential especially when combined with other therapies. The potential for hypoglycemia with the known SGLT2 inhibitors has proved very low, an expected finding as the drug effect is dependent on blood glucose levels and hepatic glucose production will maintain euglycemia.

7.13.6.2 Urinary Tract Infections

Urinary tract and genitourinary infections, predominantly fungal *candidiasis* and bacterial infections, respectively, could be expected to limit the use of SGLT inhibitors in the diabetic population. These infections are considered a direct result of the increased glucose passing through the bladder due to inhibition of glucose reuptake by SGLTs. Indeed, an increased incidence of infections is observed with SGLT inhibitors, which are much more often reported in women ($>85\%$ of reported cases) than men likely due to anatomical considerations and are usually mild and self-treated. More recent clinical trials have sought to limit the number of patients entering the evaluation with a history of UTI in order to assess the actual drug-related increase in these events. Diabetics are more prone to these types of infections due to increased adherence of bacteria to the uroepithelial cells and account for why the FRG population with extensive glucosuria does not experience infections. Secondly, a glucose-rich environment has been shown to affect leukocyte function altering immune function and promoting a higher risk of infections in diabetics.[85]

7.13.6.3 Diabetic Ketoacidosis (DKA)

Moderate ketosis is common when glucose is scarce and the alternative is burning fat to satisfy the body's energy needs. Ketone bodies such as β-hydroxybutyrate occur normally in circulation and are an energy source for the brain when glucose levels are low. DKA occurs when enough ketone bodies are present that acidification of the blood results. Many diabetics will experience an occasional bout of DKA with 10% of Type 1 diabetics experiencing DKA at least once a year. The present concern focuses on significant DKA in the absence of hyperglycemia due to the effects of the SGLT2 inhibitors on glucose levels, which make it difficult for health care professionals to recognize the symptoms and treat the patient accordingly. Clinical studies with SGLT2i including dapagliflozin, empagliflozin, and others have shown that the frequency of DKA is very low, $<0.1\%$, and further profiling of the affected patients indicates many present as either Type 2 diabetics who are on insulin therapy or Type 1 diabetics who either have been misdiagnosed or are trying to reduce their insulin use by reducing their glucose levels with SGLT2i (off label). In Type 2 diabetics who are normally hyperinsulinemic due to whole-body insulin resistance, SGLT2i reduces glucose levels resulting in a rapid drop of insulin levels. This results in glucagon excess that drives lipolysis and fatty acid oxidation increasing the likelihood of ketoacidosis. This effect is further exacerbated due to increased levels of unabsorbed sodium in the proximal tubule that activate the sodium-monocarboxylate carrier increasing recovery of ketone bodies that would normally be excreted in the urine.[86] It is important that a better means for identifying euglycemic DKA be available for both patients and physicians in order to correctly diagnose this potentially life-threatening condition.[87]

7.13.6.4 SGLT in Heart

Cardiac myocytes can burn either fatty acid or glucose in order to meet energy needs. Although fatty acids are the preferential fuel under conditions where oxygen supply is plentiful, under situations such as ischemia where oxygen supply is low, glucose becomes the preferred substrate. SGLT1 mRNA has been identified in the sarcolemma of cardiac myocytes in rodents and humans although its function is unclear as both GLUT1 and GLUT4 are also highly expressed.[88] Addition of insulin to mice results in no change in SGLT1 mRNA levels although it produces a near sevenfold increase in cardiac 2DOG uptake indicative of the action of insulin-sensitive GLUT4 transporters. This transport capacity is reduced by ~50% when phlorizin is added suggesting SGLT1 could be playing a role in glucose uptake. Insulin is shown to have a dramatic effect on the force of contraction in both ischemic and dilated cardiomyopathic human heart strips and is related to increases in GLUT4 translocation to the cell surface. GLUT4 mRNA is increased as an adaptive change in cardiomyopathy without changes in GLUT1 or SGLT1 expression, although SGLT inhibitors do have an effect to reduce contractive force in failing hearts perhaps as an adaptive change due to the lack of sufficient insulin action through GLUTs.[89] As these studies use phlorizin as the SGLT1 inhibitor, which breaks down to generate phloretin, a GLUT inhibitor, these effects are difficult to ascribe to SGLT1 alone. However, as the effects of GLUT4 are reduced under conditions of insulin resistance present in Type 2 diabetes, an increase in SGLT1 could occur as an adaptive change to maintain the necessary glucose uptake when conditions necessitate.

7.13.7 Added Beneficial Effects

7.13.7.1 Effects on Blood Pressure

Hypertension comes with an increased risk of stroke, coronary artery disease, nephropathy, retinopathy, and neuropathy, and the risk increases substantially in patients with diabetes. Any additional effect a drug may have that reduces blood pressure (BP) would have a beneficial outcome to the patient. The UK Prospective Diabetes study shows a 32% risk reduction for diabetes-related death and a 44% reduction for stroke when patients are under tight BP control.[90] A comprehensive compilation of BP effects for different SGLT2 inhibitors during the course of clinical trials suggests reductions in both systolic and diastolic BP of 3–5 mmHg and 1–3 mmHg, respectively.[91,92] This reduction in BP is likely due to inhibition of SGLT that increases Na^+ on the luminal side of the proximal tubule and promotes osmotic diuresis leading to a reduction in plasma volume and an increase in urine output. Interestingly, add-on cotherapies such as sitagliptin, metformin, and sulfonylureas tend to reduce or actually reverse the beneficial effect of SGLT2 inhibition on BP. This seemingly positive effect on BP must be managed carefully in poorly controlled elderly patients concurrently on hypertension medications where extensive BP reduction has the potential to lead to dizziness and syncope resulting in falls and potential bone fractures.

7.13.7.2 Added GLP-1 Effects

In a cell model of intestinal L cells, the presence of SGLT1 allows for glucose uptake, metabolism, and activation of GLP-1 release.[93] Processes that drive glucose further down in the small intestine toward the ileum such as α-glucosidase inhibitors or SGLT1 inhibitors are shown to activate this pathway in the distal L cell. In contrast, direct effects of phlorizin, which inhibits SGLT1, prevent GLP-1 release in this cell line suggestive of SGLT1-mediated glucose uptake in these cells in order to activate the incretin response. As LX4211 elicits a GLP-1 response in vivo, it would appear that the SGLT1 inhibitors do not likely remain in the lumen of the intestine as far down as the ileum and are absorbed earlier, although they likely delay the absorption of glucose that reaches the L cell and activates GLP-1 and the other incretins, GIP, and PPY.

7.13.7.3 Weight Loss

All of the SGLT2 inhibitors elicit effects on weight loss, usually 1–3 kg, which represents about 2–3% of BW and goes along with the intended mechanism of reducing metabolic excess by excreting glucose. Whereas this is insufficient BW reduction as a registrable endpoint for an obesity indication, it certainly plays a part in risk reduction from a cardiovascular and diabetic standpoint. The hope is that adding SGLT1 inhibition would not only increase glucosuria from the kidney but also prevent glucose absorption from the diet triggering incretin responses, and this could substantially increase the potential weight loss. Unfortunately, the only dual SGLT1/2 inhibitor, LX4211, does not appear to differentiate from the SGLT2-selective agents and produces a similar 2–3% reduction in BW.

7.13.8 Summary

As the effects of the SGLT2 inhibitors are directed specifically to enhancing glucosuria, it appears that the reduction of metabolic load reduces glucose toxicity and is disease-modifying, which drives other positive effects such as reduced insulin levels, increased beta cell insulin content, improved insulin sensitivity, and enhanced postprandial glucose disposal.[94] Additional therapeutic interventions such as insulin or insulin secretagogues increase the possibility of hypoglycemia, and increased vigilance for possible euglycemic

diabetic ketoacidosis needs to be managed moving forward. Adverse events such as UTIs, thought to be limiting early on, seem to be manageable, and the incidence seems to wane over time. Additional benefits on BW and BP could further prevent disease progression and improve cardiovascular risk factors. This has recently been borne out in studies in Type 2 diabetic patients at high risk of cardiovascular events when administered empagliflozin and produces a 38% relative risk reduction of death from cardiovascular causes over the 4-year study duration.[95] Although the limitations of efficacy based on incomplete glucosuria and the compensating glucagon effects are significant and need to be better understood and addressed, this therapy is showing considerable benefit and is an important tool in the arsenal used to manage diabetes. Glucagon-driven ketogenesis resulting in DKA in a small number of patients is serious but suggests agents that also activate GLP-1 and maintain sufficient insulin effect could potentially counter these effects. Other side effects of SGLT inhibition not discussed earlier include increased LDL levels, predicted for a long time to be a negative risk factor for cardiovascular diseases, and effects on electrolytes that can lead to loss of bone density, and these will need to be factored into the risk–benefit analysis of this new drug class. Although most agents maximize their selectivity against SGLT1, a few explore whether additional benefit can be gleaned from inhibiting SGLT1, including activation of GLP-1 pathway along with reductions in glucose uptake from the gut further reducing metabolic load. Whether this can be accomplished without increasing gastrointestinal complications is yet to be seen.

See also: 8.14. Canagliflozin.

References

1. Hermansen, K.; Mortensen, L. S. Bodyweight Changes Associated With Antihyperglycemic Agents in Type 2 Diabetes Mellitus. *Drug Saf.* **2007,** *30,* 1127–1142.
2. Bays, H. From Victim to Ally: The Kidney as an Emerging Target for the Treatment of Diabetes Mellitus. *Curr. Med. Res. Opin.* **2009,** *25,* 671–681.
3. Wright, E. M. Renal Na^+-Glucose Cotransporters. *Am. J. Physiol. Renal Physiol.* **2001,** *280,* F10–F18.
4. Wright, E. M.; Hirayama, B. A.; Loo, D. F. Active Sugar Transport in Health and Disease. *J. Intern. Med.* **2007,** *261,* 32–43.
5. Wright, E. M.; Loo, D. F.; Hirayama, B. A. Biology of Human Sodium Glucose Transporters. *Physiol. Rev.* **2011,** *91,* 733–794.
6. Xin, B.; Wang, H. Multiple Sequence Variations in *SLC5A1* Gene are Associated With Glucose–Galactose Malabsorption in a Large Cohort of Old Order Amish. *Clin. Genet.* **2011,** *79,* 86–91.
7. Probiotics such as *Lactobacillus acidophilus* have been known to adhere to the mucosa of intestinal cells and used in treatment of lactose intolerance providing preferential metabolism of complex sugars and avoid some of the negative outcomes of sugars passing further down in the intestinal tract.
8. Gorboulev, V.; Schurrmann, A.; Vallon, V.; Kipp, H.; Jaschke, A.; Klessen, D.; et al. Na^+ D-Glucose Cotransporter SGLT1 is Pivotal for Intestinal Glucose Absorption and Glucose-Dependent Incretin Secretions. *Diabetes* **2012,** *61,* 187–196.
9. Vallon, V.; Platt, K. A.; Cunard, R.; Schroth, J.; Whaley, J.; Thomson, S. C.; Koepsell, H.; Rieg, T. SGLT2 Mediates Glucose Reabsorption in the Early Proximal Tubule. *J. Am. Soc. Nephrol.* **2011,** *22,* 104–112.
10. Jurczak, M.; Lee, H.; Birkenfeld, A. L.; Jornayvaz, F. R.; Frederick, D. W.; Pongratz, R. L.; Zhao, X.; et al. SGLT2 Deletion Improves Glucose Homeostasis and Preserves Pancreatic β Cell Function. *Diabetes* **2011,** *60,* 890–898.
11. Vallon, V.; Rose, M.; Gerasimova, M.; Satriano, J.; Platt, K.; et al. Knockout of Na-Glucose Transporter SGLT2 Attenuates Hyperglycemia and Glomerular Hyperfiltration but not Kidney Growth or Injury in Diabetes Mellitus. *Am. J. Physiol. Renal Physiol.* **2013,** *304,* F156–F167.
12. Thomas, M. C. Renal Effects of Dapagliflozin in Patients With Type 2 Diabetes. *Ther. Adv. Endocrinol. Metab.* **2014,** *5,* 53–61.
13. Kothinti, R. K.; Blodgett, A. B..; North, P. E.; Roman, R. J.; Tabatabai, N. M. A Novel SGLT is Expressed in the Human Kidney. *Eur. J. Pharmacol.* **2012,** *690,* 77–83.
14. Bianchi, L.; Diez-Sampedro, A. A Single Amino Acid Change Converts the Sugar Sensor SGLT3 into a Sugar Transporter. *PLoS ONE* **2010,** *5,* 1–11.
15. Diez-Sampedro, A.; Hirayama, B. A.; Osswald, C.; Gorboulev, V.; Baumgarten, K.; Volk, C.; Wright, E. M.; Koepsell, H. A Glucose Sensor Hiding in a Family of Transporters. *PNAS* **2003,** *100,* 11753–11758.
16. Tazawa, S.; Yamato, T.; Fujikura, H.; Hiratochi, M. SLC5A9/SGLT4, a New Na^+-Dependent Glucose Transporter is an Essential Transporter for Mannose, 1,5-Anhydro-D-Glucitol and Fructose. *Life Sci.* **2005,** *76,* 1039–1050.
17. Fukuzawa, T.; Fukazawa, M.; Ueda, O.; Shimada, H.; Kito, A.; et al. SGLT5 Reabsorbs Fructose in the Kidney but Its Deficiency Paradoxically Exacerbates Hepatic Steatosis Induced by Fructose. *PLoS ONE* **2013,** *8* (2), 1–11.
18. Grempler, R.; Augustin, R.; Froehner, S.; Hildebrandt, T.; Simon, E.; Mark, M.; Eickelmann, P. Functional Characterization of Human SGLT-5 as a Novel Kidney-Specific Sodium-Dependent Sugar Transporter. *FEBS Lett.* **2012,** *586* (3), 248–253.
19. Chen, J.; Williams, S.; Ho, S.; Loraine, H.; Hagan, D.; Whaley, J. M.; Feder, J. N. Quantitative PCR Tissue Expression Profiling of the Human SGLT2 Gene and Related Family Members. *Diabetes Ther.* **2010,** *1* (2), 57–92.
20. Faham, S.; Watanabe, A.; Besserer, G. M.; Cascio, D.; Specht, A.; Hirayama, B. A.; Wright, E. M.; Abramson, J. The Crystal Structure of a Sodium Galactose Transporter Reveals Mechanistic Insights into Na+/Sugar Symport. *Science* **2008,** *321,* 810–814.
21. Raja, M. M.; Tyagi, N. K.; Kinne, R. K. H. Phlorizin Recognition in a C-Terminal Fragment of SGLT1 Studies by Tryptophan Scanning and Affinity Labeling. *J. Biol. Chem.* **2003,** *278,* 49154–49163.
22. Novakova, R.; Homerova, D.; Kinne, R.; Kinne-Saffran, E.; Lin, J. Identification of a Region Critically Involved in the Interaction of Phlorizin With the Rabbit Sodium D-Glucose Cotransporter SGLT1. *J. Membr. Biol.* **2001,** *184,* 55–60.
23. Pajor, A. M.; Randolph, K. M.; Kerner, S. A.; Smith, C. D. Inhibitor Binding in the Human Renal Low- and High-Affinity Na+/Glucose Cotransporter. *J. Pharmacol. Exp. Ther.* **2008,** *324,* 985–991.
24. Sukuki, M.; Honda, K.; Fukazawa, M.; Ozawa, K.; Hagita, H.; et al. Tofogliflozin A Potent and Highly Specific Sodium/Glucose Cotransporter 2 Inhibitor, Improves Glycemic Control in Diabetic Rats and Mice. *J. Pharmacol. Exp. Ther.* **2012,** *341,* 692–701; Grempler, R.; Thomas, L.; Eckhardt, M.; Himmelsbach, F.; Sauer, A.; Sharp, D. E.; Bakker, R. A.; Mark, M.; Klein, T.; Eickelmann, P. Empagliflozin, a Novel Selective Sodium Glucose Cotransporter-2 (SGLT2) Inhibitor: Characterization and Comparison With Other SGLT2 Inhibitors. *Diabetes Obes. Metab.* **2012,** *14,* 83–90.
25. Hummel, C. S.; Lu, C.; Liu, J.; Ghezzi, C.; Hirayama, B. A.; Loo, D. D. F.; Kepe, V.; Barrio, J.; Wright, E. M. Structural Selectivity of Human SGLT Inhibitors. *Am. J. Physiol. Cell Physiol.* **2012,** *302,* C373–C382.
26. Tabatabai, N. M.; Sharma, M.; Blumenthal, S. S.; Petering, D. H. Enhanced Expression of Sodium Glucose Cotransporters in the Kidneys of Diabetic Zucker Rats. *Diabetes Res. Clin. Pract.* **2009,** *83,* e27–e30.
27. Freitas, H. S.; Anhe, G. F.; Melo, K. F. S.; Okamato, M. M.; Oliveira-Souza, M.; Bordin, S.; Machado, U. F. Na^+ Glucose Transporter-2 Messenger Ribonucleic Acid Expression in Kidney of Diabetic Rats Correlates With Glycemic Levels Involvement of Hepatocyte Nuclear Factor-1a Expression and Activity. *Endocrinology* **2008,** *149,* 717–724.

28. Rahmoune, H.; Thompson, P. W.; Ward, J. M.; Smith, C. D.; Hong, G.; Brown, J. Glucose Transporters in Human Renal Proximal Tubular Cells Isolated From the Urine of Patients With Non-Insulin-Dependent Diabetes. *Diabetes* **2005,** *54,* 3427–3434.
29. Kellett, G. L.; Helliwell, P. A. The Diffusive Component of Intestinal Glucose Absorption is Mediated by the Glucose-Induced Recruitment of GLUT2 to the Brush Border Membrane. *Biochem. J.* **2000,** *350,* 155–162.
30. Dyer, J.; Wood, I. S.; Palejwala, A.; Ellis, A.; Shirazi-Beechey, S. P. Expression of Monosaccharide Transporters in Intestine of Diabetic Humans. *Am. J. Physiol. Gastrointest. Liver Physiol.* **2002,** *282,* g241–g248.
31. Poulsen, S. A.; Fenton, R. A.; Rieg, T. Sodium-Glucose Cotransport. *Curr. Opin. Nephrol. Hypertens.* **2015,** *24,* 463–469.
32. Other references available: Washburn, W. N. SGLT2 Inhibitors in Development. In *New Therapeutic Strategies for Type 2 Diabetes: Small Molecule Approaches;* Jones, R. M., Ed.; Royal Society of Chemistry: Cambridge, 2012. Chapter 3; Washburn, W. N.; Poucher, S. M. Differentiating Sodium-Glucose Co-Transporter-2 Inhibitors in Development for the Treatment of Type 2 Diabetes Mellitus. *Expert Opin. Investig. Drugs* **2013,** *22* (4), 463–486.
33. Hirayama, B. A.; Lostao, M. P.; Panayotova-Heiermann, M.; Loo, D. D. F.; Turk, E.; Wright, E. M. Kinetic and Specificity Differences Between rat, Human, and Rabbit Na^+-Glucose Cotransporters (SGLT1). *Am. J. Physiol.* **1996,** *270,* G919–G926.
34. Chasis, H.; Jolliffe, N.; Smith, H. W. The Action of Phlorizin on the Excretion of Glucose, Xylose, Sucrose, Creatinine and Urea by Man. *J. Clin. Invest.* **1933,** *12,* 1083–1090.
35. Tsujii, S.; Bray, G. A. Effects of Glucose, 2-Deoxyglucose, Phlorizin and Insulin on Food Intake of Lean and Fatty Rats. *Am. J. Physiol.* **1990,** *258,* E476–E481.
36. Ehrenkranz, J. R. L.; Lewis, N. G.; Kahn, C. R.; Roth, J. Phlorizin: A Review. *Diabetes Metab. Res. Rev.* **2005,** *21,* 31–38.
37. Schulze, C.; Bangert, A.; Kottr, G.; Geillinger, K. E.; Schwank, B.; Vollert, H.; Blaschek, W.; Daniel, H. Inhibition of the Intestinal Sodium-Coupled Glucose Transporter 1 (SGLT1) by Extracts and Polyphenols From Apple Reduces Postprandial Blood Glucose Levels in Mice and Humans. *Mol. Nutr. Food Res.* **2014,** *58,* 1795–1808.
38. Hussey, E. K.; Clark, R. V.; Amin, D. M.; Kipnes, M. S.; et al. Single-Dose Pharmacokinetics and Pharmacodynamics of Sergliflozin Etabonate, a Novel Inhibitor of Glucose Reabsorption, in Healthy Volunteers and Patients With Type 2 Diabetes Mellitus. *J. Clin. Pharmacol.* **2010,** *50,* 623–635.
39. Ohtake, Y.; Sato, T.; Matsuoka, H.; Nishimoto, M.; Taka, N.; et al. 5a-Carba-β-D-Glucopyranose Derivatives as Novel Sodium-Dependent Glucose Cotransporter 2 (SGLT2) Inhibitors for the Treatment of Type 2 Diabetes. *Bioorg. Med. Chem.* **2011,** *19,* 5334–5341.
40. Fujimori, Y.; Katsuno, K.; Nakashima, I.; Ishikawa-Takemura, Y.; Fujikura, H.; Isaji, M. Remogliflozin Etabonate in a Novel Category of Selective low-Affinity Sodium Glucose Cotransporter SGLT2 Inhibitors Exhibits Antidiabetic Efficacy in Rodent Models. *J. Pharmacol. Exp. Ther.* **2008,** *327,* 268–276.
41. Dobbins, R. L.; O'Connor-Semmes, R.; Kapur, A.; Kapitza, C.; Golor, G.; Mikoshiba, I.; Tao, W.; Hussey, E. K. Remogliflozin Etabonate, a Selective Inhibitor of the Sodium-Dependent Transporter 2 Reduces Serum Glucose in Type 2 Diabetes Mellitus Patients. *Diabetes Obes. Metab.* **2012,** *14,* 15–22.
42. Sykes, A. P.; O'Connor-Semmes, R.; Dobbins, R.; Dorey, D. J.; Lorimer, J. D.; Walker, S.; Wilkison, W. O.; Kler, L. Randomized Trial Showing Efficacy and Safety of Twice-Daily Remogliflozin Etabonate for the Treatment of Type 2 Diabetes. *Diabetes Obes. Metab.* **2015,** *17,* 94–97.
43. Fushimi, N.; Fujikura, H.; Shiohara, H.; Teranishi, H.; Shimizu, K.; et al. Structure–Activity Relationship Studies of 4-Benzyl-1H-Pyrazol-3-yl-β-D-Glucopyranoside Derivatives as Potent and Selective Sodium Glucose Co-Transporter 1 (SGLT1) Inhibitors With Therapeutic Activity on Postprandial Hyperglycemia. *Bioorg. Med. Chem.* **2012,** *20,* 6598–6612.
44. Fushimi, N.; Teranishi, H.; Shimizu, K.; Yonekubo, S.; Ohno, K.; et al. Design, Synthesis, and Structure–Activity Relationships of a Series of 4-Benzyl-5-Isopropyl-1H-Pyrazol-3-yl β-D-Glycopyranosides Substituted With Novel Hydrophilic Groups as Highly Potent Inhibitors of Sodium Glucose co-Transporter 1 (SGLT1). *Bioorg. Med. Chem.* **2013,** *21,* 748–765.
45. Ellsworth, B. A.; Meng, W.; Patel, M.; Girotra, R. N.; Wu, G.; Sher, P. M.; Hagan, D. L.; et al. Aglycone Exploration of C-Arylglucoside Inhibitors of Renal Sodium-Dependent Glucose Transporter SGLT2. *Bioorg. Med. Chem. Lett.* **2008,** *18,* 4770–4773.
46. Komoroski, B.; Vachharajani, N.; Feng, Y.; Li, L.; Kornhauser, D.; Pfister, M. Dapagliflozin, a Novel, Selective SGLT2 Inhibitor, Improved Glycemic Control Over 2 Weeks in Patients With Type 2 Diabetes Mellitus. *Clin. Pharmacol. Ther.* **2009,** *85,* 513–519.
47. Bailey, C. J.; Day, C. SGLT2 Inhibitors: Glucuretic Treatment for Type 2 Diabetes. *Br. J. Diabetes Vasc. Dis.* **2010,** *10,* 193–199.
48. Merovci, A.; Solis-Herrera, C.; Daniele, G.; Eldor, R.; Fiorentino, T. V.; Tripathy, D.; Xiong, J.; Perez, Z.; Norton, I.; Muhammad, A.; Abdul-Ghani, A.; DeFronzo, R. A. Dapagliflozin Improves Muscle Insulin Sensitivity but Enhances Endogenous Glucose Production. *J. Clin. Invest.* **2014,** *124,* 509–514.
49. Zhang, L.; Feng, Y.; List, J.; Kasichayanula, S.; Pfister, M. Dapagliflozin Treatment in Patients With Different Stages of Type 2 Diabetes Mellitus: Effect on Glycemic Control and Body Weight. *Diabetes Obes. Metab.* **2010,** *12,* 510–516.
50. Ohtake, Y.; Sato, T.; Matsuoka, H.; Kobayashi, T.; Nishimoto, M.; Taka, N.; et al. C-Aryl 5a-Carba-β-D-Glucopyranosides as Novel Sodium Glucose Cotransporter 2 (SGLT2) Inhibitors for the Treatment of Type 2 Diabetes. *Bioorg. Med. Chem.* **2012,** *20,* 4117–4127.
51. Liang, Y.; Arakawa, K.; Ueta, K.; Matsushita, Y.; Kuriyama, C.; Martin, T.; et al. Effect of Canagliflozin on Renal Threshold for Glucose, Glycemia, and Body Weight in Normal and Diabetic Animal Models. *PLoS ONE* **2012,** *7* (2), 1–7.
52. Nomura, S.; Sakamaki, S.; Hongu, M.; Kawanishi, E.; Koga, Y.; Sakamoto, T.; et al. Discovery of Canagliflozin, a Novel C-Glucoside With Thiophene, as Sodium Dependent Glucose Transporter 2 Inhibitor for the Treatment of Type 2 Diabetes Mellitus. *J. Med. Chem.* **2010,** *53,* 6355–6360.
53. Polodori, D.; Sha, S.; Mudaliar, S.; Ciraldi, T.; Ghosh, A.; Vaccaro, N.; Farrell, K.; Rothenberg, P.; Henry, R. R. Canagliflozin Lowers Postprandial Glucose and Insulin by Delaying Intestinal Glucose Absorption in Addition to Increasing Urinary Glucose Excretion. *Diabetes Care* **2013,** *36,* 2154–2161.
54. Song, K. S.; Lee, S. H.; Kim, M. J.; Seo, H. J.; Lee, J.; et al. Synthesis and SAR of Thiazolylmethylphenyl Glucoside as Novel C-Aryl Glucoside SGLT2 Inhibitors. *ACS Med. Chem. Lett.* **2011,** *2,* 182–187. See also; Lee, J.; Lee, S. H.; Seo, H. J.; Son, E. J.; Lee, S. H.; et al. Novel C-Aryl Glucoside SGLT2 Inhibitors as Potential Antidiabetic Agents: 1,3,4-Thiadiazolylmethylphenyl Glucoside Congeners. *Bioorg. Med. Chem.* **2010,** *18,* 2178–2194.
55. Imamura, M.; Nakanishi, K.; Suzuki, T.; Ikegai, K.; Shiraki, R.; Ogiyama, T.; Murakami, T. Discovery of Ipragliflozin (ASP1941): A Novel C-Glucoside With Benzothiophene Structure as a Potent and Selective Sodium Glucose co-Transporter 2 (SGLT2) Inhibitor for the Treatment of Type 2 Diabetes Mellitus. *Bioorg. Med. Chem.* **2012,** *20,* 3263–3279.
56. Kashiwagi, A.; Kazuta, K.; Yoshida, S.; Nagase, I. Randomized, Placebo-Controlled, Double-Blind Glycemic Control Trial of Novel Sodium-Dependent Glucose Cotransporter 2 Inhibitor Ipragliflozin in Japanese Patients With Type 2 Diabetes Mellitus. *J. Diabetes Investig.* **2014,** *5,* 382–391.
57. White, J. R. Empagliflozin, an SGLT2 Inhibitor for the Treatment of Type 2 Diabetes Mellitus: A Review of the Evidence. *Ann. Pharmacother.* **2015,** *49,* 582–598.
58. Ohtake, Y.; Sato, T.; Kobayashi, T.; Nishimoto, M.; Taka, N.; et al. Discovery of Tofogliflozin, a Novel C-Arylglucoside With an O-Spiroketal Ring System, as a Highly Selective Sodium Glucose Cotransporter 2 (SGLT2) Inhibitor for the Treatment of Type 2 Diabetes. *J. Med. Chem.* **2012,** *55,* 7828–7840.
59. Tanizawa, Y.; Kaku, K.; Araki, E.; Tobe, K.; Terauchi, Y.; et al. Long Term Safety and Efficacy of Tofogliflozin, a Selective Inhibitor of Sodium Glucose Cotransporter 2, as Monotherapy or in Combination With Other Oral Antidiabetic Agents in Japanese Patients With Type 2 Diabetes Mellitus: Multicenter, Open Label, Randomized Controlled Trials. *Expert. Opin. Pharmacother.* **2014,** *15,* 749–766.
60. Lv, B.; Feng, Y.; Dong, J.; Xu, M.; Zhang, W.; Sheng, Z.; Welihinda, A.; Seed, B.; Chen, Y. Conformationally Constrained Spiro C-Arylglucosides as Potent and Selective Renal Sodium-Dependent Glucose Co-transporter 2 (SGLT2) Inhibitors. *ChemMedChem* **2010,** *5,* 827–831.
61. Robinson, R. P.; Mascitti, V.; Boustany-Kari, C. M.; Carr, C. L.; Foley, P. M.; Kimoto, E.; Leininger, M. T.; et al. C-Aryl Glycoside Inhibitors of SGLT2: Exploration of Sugar Modifications Including C-5 Spirocyclization. *Bioorg. Med. Chem. Lett.* **2010,** *20,* 1569–1572.
62. Mascitti, V.; Maurer, T. S.; Robinson, R. P.; Bian, J.; Boustany-Kari, C. M.; Brandt, T.; Collman, B. M.; et al. Discovery of a Clinical Candidate From the Structurally Unique Dioxa-Bicyclo[3.2.1]Octane Class of Sodium-Dependent Glucose Cotransporter 2 Inhibitors. *J. Med. Chem.* **2011,** *54,* 2952–2960.
63. Mascitti, V.; Preville, C. Steroselective Synthesis of a Dioxa-Bicyclo[3.2.1]Octane SGLT2 Inhibitor. *Org. Lett.* **2010,** *12,* 2940–2943.
64. Amin, N. B.; Wang, X.; Jain, S. M.; Lee, D. S.; Nucci, G.; Rusnak1, J. M. Dose-Ranging Efficacy and Safety Study of Ertugliflozin, a Sodium-Glucose co-Transporter 2 Inhibitor, in Patients With Type 2 Diabetes on a Background of Metformin. *Diabetes Obes. Metab.* **2015,** *17,* 591–598.

65. Goodwin, N. C.; Mabon, R.; Harrison, B. A.; Shadoan, M. K.; Almstead, Z. Y.; et al. Novel L-Xylose Derivatives as Selective Sodium Dependent Glucose Cotransporter 2 (SGLT2) Inhibitors for the Treatment of Type 2 Diabetes. *J. Med. Chem.* **2009,** *52,* 6201–6204. Dapagliflozin comparison values in this publication are quite different from what is reported in literature.
66. Zambrowicz, B.; Freiman, J.; Brown, P. M.; Frazier, K. S.; Turnage, A.; et al. LX4211, a Dual SGLT1/SGLT2 Inhibitor, Improved Glycemic Control in Patients with Type 2 Diabetes in a Randomized, Placebo-Controlled Trial. *Clin. Pharmacol. Ther.* **2012,** *92,* 158–169.
67. Zambrowicz, B.; Ogbaa, I.; Frazier, K.; Banks, P.; Turnage, A.; Freiman, J.; Boehm, K. A.; Ruff, D.; Powell, D.; Sands, A. Effects of LX4211, a Dual Sodium-Dependent Glucose Cotransporters 1 and 2 Inhibitor, on Postprandial Glucose, Insulin, Glucagon-like Peptide 1, and Peptide Tyrosine Tyrosine in a Dose-Timing Study in Healthy Subjects. *Clin. Ther.* **2013,** *35* (8), 1162–1173.
68. Rosenstock, J.; Cefalu, W. T.; Lapeurta, P.; Zambrowicz, B.; Ogbaa, I.; Banks, P.; Sands, A. Greater Dose-Ranging Effects on A1C Levels Than on Glucosuria With LX4211, a Dual Inhibitor of Sodium Glucose Transporters SGLT1 and SGLT2, in Type 2 Diabetes on Metformin Monotherapy. *Diabetes Care* **2015,** *38,* 431–438.
69. Kakinuma, H.; Oi, T.; Hashimoto-Tsuchiya, Y.; Arai, M.; Kawakita, Y.; Fukasawa, Y.; et al. (1S)-1,5-Anhydro-1-[5-(4-Ethoxybenzyl)-2-Methoxy-4-Methylphenyl]-1-Thio-D-Glucitol (TS-071) is a Potent, Selective Sodium-Dependent Glucose Cotransporter 2 (SGLT2) Inhibitor for Type 2 Diabetes Treatment. *J. Med. Chem.* **2010,** *53,* 3247–3261.
70. Seino, Y.; Sasaki, T.; Fukatsu, A.; Sakai, S.; Samukawa, Y. Efficacy and Safety of Luseogliflozin Monotherapy in Japanese Patients With Type 2 Diabetes Mellitus: A 12-Week, Randomized, Placebo-Controlled, Phase II Study. *Curr. Med. Res. Opin.* **2014,** *30* (7), 1219–1230.
71. Nishimura, R.; Osonoi, T.; Kanada, S.; Jinnouchi, H.; Sugio, K.; Omiya, H.; Ubukata, M.; Sakai, S.; Samukawa, Y. Effects of Luseogliflozin, a Sodium–Glucose co-Transporter 2 Inhibitor, on 24-h Glucose Variability Assessed by Continuous Glucose Monitoring in Japanese Patients With Type 2 Diabetes Mellitus: A Randomized, Double-Blind, Placebo-Controlled, Crossover Study. *Diabetes Obes. Metab.* **2015,** *17,* 800–804.
72. Yao, C. H.; Song, J. S.; Chen, C. T.; Yeh, T. K.; Hung, M. S.; Chang, C. C.; et al. Discovery of Novel N-β-D-Xylosylindole Derivatives as Sodium-Dependent Glucose Cotransporter 2 (SGLT2) Inhibitors for the Management of Hyperglycemia in Diabetes. *J. Med. Chem.* **2011,** *54,* 166–178; Yao, C. H.; Song, J. S.; Chen, C. T.; Yeh, T. K.; Hsieh, T. C.; Wu, S. H. Synthesis and Biological Evaluation of Novel C-Indolylxylosides as Sodium-Dependent Glucose co-Transporter 2 Inhibitors. *Eur. J. Med. Chem.* **2012,** *55,* 32–38.
73. Lee, S. H.; Song, K. S.; Kim, J. Y.; Kang, M.; Lee, S.; Cho, S. H.; Park, H. J.; Kim, J.; Lee, J. Novel Thiophenyl C-Aryl Glucoside SGLT2 Inhibitors as Potential Antidiabetic Agents. *Bioorg. Med. Chem.* **2011,** *19,* 5813–5832.
74. Li, A. R.; Zhang, J.; Greenberg, J.; Lee, T. W.; Liu, J. Discovery of Non-Glucoside SGLT2 Inhibitors. *Bioorg. Med. Chem. Lett.* **2011,** *21,* 2472–2475.
75. Du, X.; Lizarzaburu, M.; Turcotte, S.; Lee, T.; Greenberg, J.; Shan, B.; Fan, P.; Ling, Y.; Medina, J. C.; Houze, J. Optimization of Triazoles as Novel and Potent Nonphlorizin SGLT2 Inhibitors. *Bioorg. Med. Chem. Lett.* **2011,** *21,* 3774–3779.
76. Liu, J.; Lee, T.; DeFronzo, R. Why do SGLT2 Inhibitors Inhibit Only 30–50% of Renal Glucose Reabsorption in Humans. *Diabetes* **2012,** *61,* 2199–2204.
77. Stages of kidney disease—CKD1 normal $>=$ 90 mL/min/1.73 m^2, CKD2 60–90, CKD3 30–59, CKD4 15–29, CKD5 $<$ 15 (kidney failure).
78. Ishibashi, Y.; Matsui, T.; Yamagishi, S. Tofogliflozin, a Highly Selective Inhibitor of SGLT2 Blocks Proinflammatory and Proapoptotic Effects on Glucose Overload in Proximal Tubular Cells Partly by Suppressing Oxidative Stress Generation. *Horm. Metab. Res.* **2016,** *48* (3), 191–195.
79. Lee, Y. J.; Lee, Y. J.; Han, H. J. Regulatory Mechanism of N+/Glucose Cotransporters in Renal Proximal Tubule Cells. *Kidney Int.* **2007,** *72,* s27–s35.
80. Kasichayanula, S.; Liu, X.; Pe Benito, M.; Yao, M.; Pfister, M.; LaCreta, F. P.; Humphreys, W. G.; Boulton, D. W. The Influence of Kidney Function on Dapagliflozin Exposure, Metabolism and Pharmacodynamics in Healthy Subjects and in Patients With Type 2 Diabetes. *Br. J. Clin. Pharmacol.* **2012,** *76,* 432–444.
81. Scheen, A. J. Pharmacokinetics, Pharmacodynamics and Clinical Use of SGLT2 Inhibitors in Patients With Type 2 Diabetes Mellitus and Chronic Kidney Disease. *Clin. Pharmacokinet.* **2015,** *54,* 691–708. This manuscript also provides a good summary of the PK/Pd of marketed SGLT2 inhibitors.
82. Miao, Z.; Nucci, G.; Amin, N.; Sharma, R.; Mascitti, V.; Tugnait, M.; Vaz, A. D.; Callegari, E.; Kalgutkar, A. S. Pharmacokinetics, Metabolism, and Excretion of the Antidiabetic Agent Ertugliflozin (PF-04971729) in Healthy Male Subjects. *Drug Metab. Dispos.* **2013,** *41,* 445–456.
83. Ferrannini, E.; Muscelli, E.; Frascerra, S.; Baldi, S.; Mari, A.; Heisse, T.; Broedl, U. C.; Woerle, H. J. Metabolic Response to Sodium-Glucose Cotransporter 2 Inhibition in Type 2 Diabetic Patients. *J. Clin. Invest.* **2014,** *124,* 499–508.
84. Bonner, C.; Kerr-Conte, J.; Gmyr, v.; Queniat, G.; et al. Inhibition of Glucose Transporter SGLT2 With Dapagliflozin in Pancreatic Alpha Cells Triggers Glucagon Secretion. *Nat. Med.* **2015,** *21,* 512–517.
85. Geerlings, S.; Fonseca, V.; Castro-Diaz, D.; List, J.; Parikh, S. Genital and Urinary Tract Infections in Diabetes: Impact of Pharmacologically-Induced Glucosuria. *Diabetes Res. Clin. Pract.* **2014,** *103,* 373–381.
86. Taylor, S. I.; Blau, J. E.; Rother, K. I. SGLT2 Inhibitors may Predispose to Ketoacidosis. *J. Clin. Endocrinol. Metab.* **2015,** *100* (8), 2849–2852.
87. Rosenstock, J.; Ferrannini, E. Euglycemic Diabetic Ketoacidosis: A Predictable, Detectable, and Preventable Safety Concern with SGLT2 Inhibitors. *Diabetes Care* **2015,** *38,* 1638–1642.
88. Banerjee, S. K.; McGaffin, K. R.; Pastor-Soler, N. M.; Ahmad, F. SGLT1 is a Novel Cardiac Glucose Transporter That is Perturbed in Disease States. *Cardiovasc. Res.* **2009,** *84,* 111–118.
89. Lewinski, D.; Gasser, R.; Rainer, P. P.; Huber, M.; Wilhalm, B.; Roessl, U.; Haas, T.; Wasler, A.; Grimm, M.; Bisping, E.; Pieske, B. Functional Effects of Glucose Transporters in Human Ventricular Myocardium. *Eur. J. Heart Fail.* **2010,** *12,* 106–113.
90. UKPDS. Effect of Intensive Blood-Glucose Control With Metformin on Complications in Overweight Patients. With Type 2 Diabetes (UKPDS 34). UK Prospective Diabetes Study (UKPDS) Group. *Lancet* **1998,** *352,* 854–865.
91. Oliva, R. V.; Bakris, G. L. Blood Pressure Effects of Sodium-Glucose Cotransport 2 (SGLT2) Inhibitors. *J. Am. Soc. Hypertens.* **2014,** *8,* 330–339.
92. Imprialos, K. P.; Sarafidis, P. A.; Karagiannisa, A. I. Sodium-Glucose Cotransporter-2 Inhibitors and Blood Pressure Decrease: A Valuable Effect of a Novel Antidiabetic Class. *J. Hypertens.* **2015,** *33,* 2185–2197.
93. Gribble, F. M.; Williams, L.; Simpson, A. K.; Reimann, F. A Novel Glucose-Sensing Mechanism Contributing to the Glucagon-Like Peptide-1 Secretion From the GLUTag Cell Line. *Diabetes* **2003,** *52,* 1147–1154.
94. Sheen, A. J.; Paquot, N. Metabolic Effects of SGLT2 Inhibitors Beyond Increased Glucosuria: A Review of the Clinical Evidence. *Diabetes Metab.* **2014,** *40,* S4–S11.
95. Zinman, B.; Wanner, C.; Lachin, J. M.; Fitchett, D.; Bluhmki, E.; Hantel, S.; Mattheus, M.; et al. Empagliflozin, Cardiovascular Outcomes, and Mortality in Type 2 Diabetes. *N. Engl. J. Med.* **2015,** *373,* 2117–2128.

7.14 DPP-4 Inhibitors

T Biftu, Merck Research Laboratories, Kenilworth, NJ, United States
R SinhaRoy, Janssen Pharmaceuticals, Inc., Raritan, NJ, United States

© 2017 Elsevier Ltd. All rights reserved.

7.14.1	**Introduction**	513
7.14.2	**Scientific Rationale for DPP-4 Inhibitors in the Treatment of Type 2 Diabetes**	514
7.14.3	**Biology of DPP-4**	514
7.14.3.1	Gene Structure, Expression, and Related Enzymes	514
7.14.3.2	Substrate Specificity	515
7.14.3.3	Processing of Glucagon Superfamily Peptides	515
7.14.3.4	Cleavage of Neuropeptide Y and Peptide YY	516
7.14.3.5	Chemokine and Cytokine Substrates	516
7.14.3.6	Processing of Vasoactive Peptides	517
7.14.4	**Crystal Structure of DPP-4**	517
7.14.5	**DPP-4 Inhibitors**	518
7.14.5.1	Approved and Marketed DPP-4 Inhibitors	518
7.14.5.1.1	β-Amino butanoic acid derivatives	518
7.14.5.1.2	Pyrrolidine analogs	524
7.14.5.1.3	Pyrimidinedione/xanthine analogs	531
7.14.5.2	DPP-4 Inhibitors in Phase III	534
7.14.5.2.1	Dutogliptin (PHX1149, Phenomix Corp)	534
7.14.5.2.2	Gosogliptin (PF-00734200, Pfizer)	534
7.14.5.2.3	Denagliptin (GSK-823093, GlaxoSmithKline)	536
7.14.5.2.4	Melogliptin (GRC 8200, Glenmark)	536
7.14.5.2.5	Retagliptin (SP-2086, Jiangsu Hengrui Medicine)	538
7.14.5.3	DPP-4 Inhibitors in Phase II	538
7.14.5.4	DPP-4 Inhibitors in Phase I	540
7.14.5.5	DPP-4 Inhibitors in Preclinical Development	542
7.14.6	**Natural DPP-4 Inhibitors**	544
7.14.6.1	Natural Products as DPP-4 Inhibitors	544
7.14.6.2	DPP-4 Inhibitors From Natural Extracts	545
7.14.7	**Summary**	545
Acknowledgment		547
References		547

Abbreviations

ACE Angiotensin-converting enzyme
AEs Adverse events
Ala Alanine
ANC Anthocyanin
Arg Arginine
AUC Area under the curve
b.i.d Twice-daily dosing
$BnONH_2 \cdot HCl$ Benzyloxyhydroxyl amine hydrochloride
BNP Brain natriuretic peptide
Boc *tert*-Butyloxycarbonyl
Cbz Carboxybenzyl or benzyloxy carbamate
CD26 T-cell activation antigen CD26 (EC 3.4.14.5.)
CLp Plasma clearance
C_{max} Maximum plasma concentration
CVD Cardiovascular disease
CXCR4 Chemokine receptor type 4
CYP Cytochrome P450 isozymes
DASH DPP-4 activity and/or structural homologue
DCC *N,N′*-Dicyclohexylcarbodiimide
DCM Dichloromethane
DHIM 16,17-Dihydro-17b-hydroxy isomitraphylline
DIAD Diisopropyl azodicarboxylate
DIO Diet-induced obese
DIPEA Diisopropyl ethylamine
DKR Diketoreductase
DMAP Dimethylaminopyridine
DMF-DMA *N,N*-Dimethylformamide dimethyl acetal
DPP-4 Dipeptidyl peptidase 4
DPP-8 Dipeptidyl peptidase 8
DPP-9 Dipeptidyl peptidase 9
DPP-II Dipeptidyl peptidase II
EDC *N*-(3-Dimethylaminopropyl)-*N*-ethylcarbodiimide hydrochloride
Epo Erythropoietin

F Oral bioavailability
FAP Fibroblast-activating protein-α
FMO Flavin-containing monooxygenase
FPG Fasting plasma glucose
GHRH Growth hormone–releasing hormone
GI Gastrointestinal
GIP Glucose-dependent insulinotropic polypeptide
GLP-1 Glucagon-like peptide-1
GLP-2 Glucagon-like peptide-2
Gly Glycine
GM-CSF Granulocyte-macrophage colony-stimulating factor
GSIS Glucose-stimulated insulin secretion
HbA1c Hemoglobin A1c
hERG Human ether-a-go-go-related gene channel
HFD High-fat diet
HOBt Hydroxybenzotriazole
HOMA-β Homeostasis model assessment of β-cell
IBCF Isobutyl chloroformate
IL-10 Interleukin 10
KFDA Korean Food and Drug Administration
LHMDS Lithium bis(trimethylsilyl)amide
Lys Lysine
MeCN Acetonitirile
NEP Neutral endopeptidase
NPY Neuropeptide Y
OGTT Oral glucose tolerance test
Oxm Oxyntomodulin
PACAP38 Pituitary adenylate cyclase-activating polypeptide-(1–38)
PD Pharmacodynamics
Pd/C Palladium on carbon
PK Pharmacokinetic
PO Per os (by mouth)
PPA Polyphosphoric acid
PPG Postprandial glucose
PPh_3 Triphenylphosphine
Pro Proline
PYY Peptide YY
q.d. Once-daily dosing
QPP Quiescent cell proline dipeptidase
RT Room temperature
SAD Single ascending dose
SDF-1α/CXC12 Stromal cell-derived factor 1α
Ser Serine
SP Substance P, tachykinin
STZ Streptozotocin
$T_{1/2}$ Half-life
T2DM Type 2 diabetes mellitus
TEA Triethylamine
TECOS Trial Evaluating Cardiovascular Outcomes with Sitagliptin
TFA Trifluoroacetic acid
TFAA Trifluoroacetic anhydride
TGF-β Transforming growth factor β
T_{max} Time to maximum concentration
Trp Tryptophan
TZDs Thiazolidinediones
USFDA US Food and Drug Administration
Y1R NPY receptor type 1
Y5R NPY receptor type 5
ZDF Zucker diabetic fatty rats

7.14.1 Introduction

Type 2 diabetes mellitus (T2DM) is a complex metabolic disease that is characterized by hyperglycemia and reduced insulin biosynthesis/secretion in the context of whole-body insulin resistance. A hallmark of the disease is the inability of insulin-producing β-cells in the pancreas to cope with the increased secretory demand of insulin-resistant organs and tissue, which over time leads to a vicious cycle of progressive loss of glycemic control and β-cell dysfunction. This relentless decline in pancreatic β-cell function due to increased metabolic stress underlies the progressive nature of T2DM. Both lifestyle factors such as overeating and physical inactivity that cause obesity and a genetic predisposition to β-cell dysfunction play significant roles in the etiology of T2DM. The ensuing chronic hyperglycemia, if left untreated, can lead to serious microvascular complications including retinopathy, nephropathy, and peripheral vascular disease. In addition, metabolic derangements such as dyslipidemia and hypertension that often accompany T2DM increase the risk of cardiovascular complications including atherosclerosis, myocardial infarction, heart failure, and stroke.

The global epidemic of diabetes afflicts more than 415 million people, and its worldwide prevalence is anticipated to exceed 642 million by 2040.[1] T2DM is the leading cause of kidney disease, nontraumatic amputations, and new cases of blindness. Approximately 5 million people aged between 20 and 79 years died from diabetes in 2015, equivalent to one death every 6 s.[1] A large majority of people with diabetes live in developing nations, and their numbers are projected to exceed 274 million by 2040 in India and China alone.[1] In the United States, 29.1 million people (9.3% of the population) have diabetes, 27.8% of whom are undiagnosed.[2] It is estimated that one out of every three adults in the United States could have diabetes by 2050.[3] In addition to the human toll, diabetes confers a significant financial burden to society. The estimated annual global cost of treating diabetes was $673 billion in 2015, and it is expected to exceed $750 billion in 2040.[1] In the United States alone, the direct medical cost to treat diabetes was $176 billion in 2012, with an additional $69 billion in indirect costs due to lost productivity and early death.[3]

Based on their mechanisms of action, 12 classes of oral and injectable medications are currently approved for the treatment of T2DM.[4] Unfortunately, none of these agents halt disease progression, and the initial correction of hyperglycemia with current oral agents is typically not sustained beyond a few years. Hence, initial oral monotherapy is typically followed by oral combination therapies and subsequently by the addition of insulin or other injectable agents to control blood glucose. Several established oral T2DM therapies are associated with significant side effects such as hypoglycemia (sulfonylureas), weight gain (sulfonylureas and TZDs), GI intolerance (metformin), and increased risk of fractures, bladder cancer, and cardiovascular morbidity (TZDs). Over the last decade, however, dipeptidyl peptidase 4 (DPP-4) inhibitors (gliptins) have emerged as a new class of oral agents with good efficacy and few side effects, including a low risk of hypoglycemia and no weight gain. Sitagliptin, the first marketed DPP-4 inhibitor,[5,6] and the gliptin class in general have consequently enjoyed significant clinical and commercial success. Together with the injectable glucagon-like peptide-1 (GLP-1) analogs, these medicines work to increase the activation of incretin receptors, which are key molecular targets involved in glucose-stimulated insulin secretion (GSIS) and energy homeostasis. Specifically, DPP-4 inhibitors inhibit cleavage and inactivation of the peptide incretin hormones GLP-1 and glucose-dependent insulinotropic polypeptide (GIP) by the serine protease, DPP-4. The stabilized endogenous circulating GLP-1 and GIP incretins increase signaling via their cognate G protein-coupled receptors, resulting in enhanced GSIS from islets and improved glucose control with a low risk of hypoglycemia.

The biology of incretins, the pharmacology of DPP-4 inhibitors, and their clinical use in the treatment of T2DM have all been well reviewed elsewhere.[7–10] Beyond its catalytic activity, the complex biology of DPP-4 as a multidomain cell surface protein identical to the T-cell activation antigen CD26, which interacts with multiple proteins, has also been recently summarized.[11] This review in contrast focuses primarily on a comparison of the medicinal chemistry and clinical pharmacology of the DPP-4 inhibitors. It summarizes marketed gliptins, compounds in development, and natural DPP-4 inhibitors. The first section introduces incretins and reviews relevant aspects of the human biology and structure of DPP-4 to provide the necessary context for the second section that reviews the synthesis and pharmaceutical properties of the various gliptins.

7.14.2 Scientific Rationale for DPP-4 Inhibitors in the Treatment of Type 2 Diabetes

The observation that oral nutrients (glucose) stimulate higher levels of insulin secretion in humans than an intravenous isoglycemic infusion led to development of the incretin concept[12,13] and identification of an entero-insular axis,[14] wherein gut-derived factors (intestine secretion insulin, incretins) enhance GSIS from pancreatic β-cells. Subsequent reports in human subjects of potent insulinotropic activity for the gut-derived peptides GIP[15] (secreted by enteroendocrine K cells of the proximal intestine[16]) and GLP-1[17] (secreted from L cells primarily in the ileum[18]) and elucidation of their primary sequences[19,20] led to intense interest in peptide incretins and associated pathways as potential therapeutic targets for the treatment of T2DM. The insulinotropic activities of GLP-1 and GIP are additive and fully account for the incretin effect in healthy human subjects.[21,22] Early research efforts focused primarily on GLP-1, however, after demonstration of its preserved incretin activity in T2DM subjects[23] unlike that of GIP, which is significantly diminished in the diabetic state.[23,24]

GLP-1 and GIP signal through activation of corresponding Gs protein-coupled receptors that rapidly increase intracellular cAMP and calcium levels in β-cells and stimulate glucose-dependent insulin secretion.[25–28] Of note, the bioactive forms of circulating GLP-1 (GLP-1[7–36]-amide and GLP-1[7–37]) and GIP (GIP[1–42]) are rapidly degraded in human plasma and in vivo[29–32] with clearance half-lives of only a few minutes.[33] Proteolytic removal of two residues from the N-terminal of each peptide results in the formation of inactive des-dipeptidyl metabolites.[34–36] With identification of the inactivating protease in both instances as the cell surface-associated dipeptidyl peptidase 4 (DPP-4),[36] two strategies emerged for the development of incretin-based therapeutics for T2DM: the pursuit of injectable DPP-4-resistant GLP-1 peptide mimetics as incretin replacement therapy and the development of oral small-molecule DPP-4 inhibitors to increase pools of endogenous active GLP-1 and GIP. Although there is considerable overlap in the pharmacologies of these two classes of incretin-based therapeutics, important differences regarding the modest weight loss and gastrointestinal side effects observed for the GLP-1 class derive from pharmacological activation of the GLP-1 receptor by supraphysiological levels of exogenously administered peptides, in contrast to DPP-4 inhibitors, which effect physiological activation of GLP-1 and GIP receptors by their endogenous ligands, are weight-neutral and well tolerated in comparison.

7.14.3 Biology of DPP-4

7.14.3.1 Gene Structure, Expression, and Related Enzymes

Dipeptidyl peptidase 4 [EC3.4.14.5] was first identified in 1966 as an aminopeptidase with the relatively unique ability to cleave a prolyl amide bond.[37] As a serine protease with an α,β hydrolase fold, DPP-4 is representative of the peptidase family S9b and together with prolyl endopeptidase (PEP, S9a) and acylaminoacyl peptidase (S9c) comprises the prolyl oligopeptidase family.[38] DPP-4 is also identical to the T-cell activation antigen cluster of differentiation (CD) 26.[39] DPP-4 is a type II transmembrane protein consisting of short cytoplasmic and transmembrane domains, a flexible stalk region, and a predominant extracellular domain (residues 40–766) containing the C-terminal active site, a cysteine-rich area, and a glycosylated region. The enzyme exists predominantly as a homodimer,[40] formation of which is required for enzyme activity. DPP-4 can also form heterodimers with related peptidases such as fibroblast-activating protein-α (FAP/seprase), each enzyme retaining its activity within such complexes.[41,42] The human DPP-4 gene is located on chromosome 2 and consists of 26 exons spanning 70 kb.[43–45] DPP-4 is a ubiquitous enzyme, present

on epithelial and endothelial cells, and expressed in numerous tissues including the liver, gut, placenta, lung, and kidney.[45,46] The enzyme is shed from the plasma membrane as soluble circulating DPP-4, the activity of which can be readily detected in human plasma and serum.[47] DPP-4 is the founding member of the DPP-4 activity and/or structural homologue (DASH) family of peptidases (dipeptidyl peptidase 4 activity and/or structure homologues),[48] which includes FAP/seprase,[41] dipeptidyl peptidase II/quiescent cell proline dipeptidase (DPP-II/QPP),[49] dipeptidyl peptidase 8 (DPP-8),[50] and dipeptidyl peptidase 9,[51] all of which cleave prolyl amide bonds within peptide substrates.[52–54] While DPP-4 is widely expressed and is a cell surface-associated or soluble peptidase, the remaining DASH family members are either restricted in expression or activity (FAP/seprase) or intracellular in localization (DPP-II/QPP, DPP-8, and DPP-9). Hence, DPP-4 has relatively better access to diverse circulating and secreted bioactive peptides as potential substrates, several of which, in addition to GLP-1 and GIP, are physiological substrates that are regulated by the enzyme.

7.14.3.2 Substrate Specificity

In vitro, DPP-4 is a prolyl-aminodipeptidase that cleaves NH_2-X-Pro dipeptides from the amino terminus of peptide substrates. Although Pro is the preferred P1 residue (using the protease active site nomenclature of Schechter and Berger[55]), DPP-4 can also cleave peptides that contain a penultimate Ala at the N-terminal (e.g., GLP-1 and GIP). Incubation of soluble DPP-4 with positional-scanning libraries[56] of dipeptides conjugated to 7-amino-4-carbamoylmethylcoumarin (AMC) as a fluorogenic reporter of cleavage has confirmed the P1 Pro/Ala specificity of DPP-4 while revealing a relatively relaxed specificity for the P2 position (i.e., for the amino terminal residue of the substrate).[53] The peptidase is unable to cleave Pro–Pro bonds but otherwise accommodates diverse residues at the P1′ position adjacent to the scissile amide. Not surprisingly, the in vitro cleavage by DPP-4 of numerous bioactive peptides, hormones, neuropeptides, and chemokines that contain the canonical X-Pro/Ala amino terminal sequence has been reported,[57–59] and corresponding hypotheses have been generated for diverse roles of this peptidase in human physiology and disease. A key limitation of these studies, however, is that they typically use conditions of limited physiological relevance for in vivo substrate cleavage (e.g., supraphysiological concentrations of DPP-4 and substrate and/or prolonged incubation times). In addition, efficient cleavage of a specific peptide by DPP-4 in vitro or upon pharmacological infusion of the exogenous peptide in animals or human subjects has limited bearing on whether the peptidase and its putative endogenous substrate are otherwise exposed to each other in vivo for similar cleavage to occur physiologically. Indeed, redundant or other specific proteolytic pathways may be more relevant to the in vivo clearance of a particular putative DPP-4 substrate. Of note, very few of the bioactive substrates tested in vitro have been shown to satisfy all of the following prerequisites necessary to qualify as physiologically relevant substrates that are regulated by DPP-4 cleavage, namely, (1) demonstration of in vivo cleavage of the *endogenous* peptide by DPP-4, (2) blockade of this cleavage by administration of a DPP-4 inhibitor or in animals genetically deficient in DPP-4, (3) concomitant increase in endogenous levels of intact peptide, and (4) modulation of endogenous peptide bioactivity as a consequence of DPP-4 cleavage or its blockade. A key challenge in this regard has been the lack of suitable assays to measure levels of intact versus cleaved peptides with the requisite selectivity and sensitivity necessitated by the low abundance of these putative endogenous substrates. Our discussion therefore focuses only on those bioactive peptides that have been established as physiologically relevant substrates regulated by DPP-4 cleavage in humans. We also discuss select peptides, however, that may be processed by DPP-4 in humans but for which additional clinical data are needed to unequivocally establish their contributory role to the established pharmacology of DPP-4 inhibitors.

7.14.3.3 Processing of Glucagon Superfamily Peptides

With demonstration of GLP-1 and GIP as short-lived physiological incretins and identification of DPP-4 as the key inactivating enzyme, intense efforts led to the development of small-molecule DPP-4 inhibitors and demonstration of antihyperglycemic efficacy of these agents in rodents.[60,61] Proof of concept in humans was subsequently obtained upon demonstration of glucose-lowering efficacy in a 4-week study in diabetic subjects using the DPP-4 inhibitor NVP-DPP728.[62] Since then, the cumulative preclinical and clinical data for DPP-4 inhibitors indicate that the acute antihyperglycemic efficacy of these agents can be fully accounted for by stabilization of the incretin substrates GLP-1 and GIP.[7,63] Infusion of the GLP-1 receptor antagonist exendin (9–39) in diabetic subjects reverses the acute glucose-lowering efficacy of sitagliptin by only 50%,[64] highlighting the importance of both GLP-1 and GIP as physiological incretins. This finding is also consistent with the complete lack of acute glucose-lowering efficacy of a DPP-4 inhibitor in double incretin receptor knockout (DIRKO) mice lacking both GLP-1 and GIP receptors.[65]

It is possible that DPP-4 substrates besides GLP-1 and GIP contribute to the long-term efficacy of DPP-4 inhibitors since the peptidase can cleave and inactivate additional glucagon superfamily peptides in vitro with catalytic efficiencies comparable to that of GLP-1 and GIP cleavage.[66] For most of these peptides, however, including growth hormone-releasing hormone (GHRH), glucagon-like peptide-2 (GLP-2), and gastrin releasing peptide, increased in vivo bioactivity as a physiological substrate that is stabilized by DPP-4 inhibition appears unlikely.[67–69] Intriguingly, oxyntomodulin (Oxm) and pituitary adenylate cyclase-activating polypeptide (1–38) (PACAP38) are also efficiently cleaved by DPP-4 in vitro despite both peptides containing a P1 serine residue.[66] Endogenous Oxm has insufficient bioactivity to act as a physiological hormone,[70] although long-acting DPP-4-resistant Oxm analogs are being actively pursued as dual GLP-1/glucagon receptor agonists for the treatment of obesity and diabetes.[71,72] Exogenously infused PACAP38 is rapidly cleaved by DPP-4 in mice but not in DPP-4-deficient animals.[66] The acute insulinotropic activity of PACAP38 is also augmented by a DPP-4 inhibitor in mice.[69] Since the peptide also stimulates glucagon secretion, which

counteracts insulin action, its role in islet function remains unclear. Additional clinical data are therefore needed to determine whether PACAP38 contributes to the long-term metabolic effects of DPP-4 inhibitors.

7.14.3.4 Cleavage of Neuropeptide Y and Peptide YY

Neuropeptide Y (NPY) is a 36-residue peptide produced in the hypothalamus and secreted into cerebrospinal fluid. The peptide plays several roles in the central and peripheral nervous system, including the regulation of energy intake, stress, and vascular remodeling.[73,74] NPY and the related peptide YY (PYY), which is secreted by GLP-1-producing L cells in the gut following a meal, mediate their actions through a family of related receptors (Y1R–Y5R). Both peptides are cleaved by DPP-4 in vitro,[75] and the corresponding metabolites (NPY(3–36) and PYY(3–36)) show increased selectivity for Y2R versus Y1R activation; PYY(3–36) is a potent anorectic peptide in humans due to its Y2R agonist activity.[76]

While there is no clinical evidence for a role of NPY in the action of DPP-4 inhibitors, increased levels of intact NPY(1–36) and increased Y1R activation/peripheral sympathetic tone have been recently invoked to explain skin lesions and necrosis observed in cynomolgus monkeys treated with the DPP-4 inhibitor vildagliptin.[77] In the absence of measurements of endogenous NPY in this study, however, and given the lack of cutaneous toxicity in primates treated with sitagliptin, it is unlikely that these findings reflect NPY stabilization as a mechanism-based class effect for all DPP-4 inhibitors. In addition, NPY is cleaved by multiple DASH peptidases in vitro,[78] suggesting the potential for redundant proteolytic clearance pathways of the intact peptide in vivo. As an alternate hypothesis, off-target inhibition of the related DASH family dipeptidyl peptidases DPP-8 and DPP-9 had previously been shown to associate with the preclinical toxicity of nonselective DPP-4 inhibitors in rats and dogs.[79] Sitagliptin, a highly selective DPP-4 inhibitor, does not exhibit any of these liabilities. The importance of DPP-4 inhibitor selectivity for safety has been questioned,[80,81] but the predominantly intracellular localization of DPP-8 and DPP-9[82] and the challenge of isolating their activities from that of other DASH family members have precluded a valid assessment of the endogenous inhibition of these enzymes by the various gliptins and any corresponding active metabolites. Notwithstanding, activity-based dipeptidyl peptidase profiling studies in rats and cynomolgus monkeys have identified DPP-8 and DPP-9 expression and activity in lymphoid cells, in epithelial and capillary endothelia of multiple tissues, and in the skin of both species.[83] These data are more consistent with the view that the observed experimental differences in preclinical toxicity of various gliptins reflect different off-target activities and selectivities of the inhibitors and/or their active metabolites (as determined by species-dependent biodistribution, intracellular permeability, and access to various intracellular compartments and DASH peptidases), although local stabilization of putative DPP-4 substrates such as NPY by select gliptins such as vildagliptin that distribute widely into tissue and extravascular spaces cannot be discounted.

Endogenous levels of PYY(1–36) and PYY(3–36) have been measured using specific immunoassays after a standard mixed meal in T2DM subjects administered sitagliptin or placebo for 12 weeks.[68] While the ratio of intact to cleaved PYY increased ~50% to 0.78 with DPP-4 inhibition, levels of total PYY and PYY(3–36) both decreased after treatment by 25% and more than 60%, respectively, likely due to negative feedback on PYY-secreting cells. The same study reported no differences in the levels of endogenous intact GLP-2 with sitagliptin treatment. Hence, PYY but not GLP-2 appears be an endogenous DPP-4 substrate in humans. The absence of increased PYY(3–36) levels, however, is consistent with the weight-neutral profile of DPP-4 inhibitors in the clinic, and the peptide remains unlikely to contribute to the long-term efficacy of DPP-4 inhibitors.

7.14.3.5 Chemokine and Cytokine Substrates

Chemokines are cytokines that modulate the chemotaxis of responsive cells. Several chemokines and cytokines contain an N-terminal X-Pro dipeptide sequence that is efficiently cleaved in vitro by DPP-4,[58] often with changes in bioactivity of the signaling molecule.[84,85] Since these molecules play a key role in cell recruitment and immunity and given that DPP-4 is identical to the T-cell coactivation antigen CD26, numerous hypotheses have been made regarding both the potential therapeutic utility and liability of DPP-4 inhibitors in modulating T cell and immune function.[86] Pharmacological infusions of exogenous cytokines that are in vitro substrates of DPP-4, such as granulocyte-macrophage colony-stimulating factor (GM-CSF) and erythropoietin (Epo), result in increased bioactivity in DPP-4-deficient mice compared with wild-type animals. Consistent with these observations, increased CSF activity and hematopoiesis after chemotherapy or radiation have been reported in DPP-4-deficient mice or in mice treated with sitagliptin, although endogenous cytokine levels were not measured in these studies.[85] Despite numerous studies in cell-based systems and in preclinical models of immune disease, however, a definitive role for the catalytic activity of DPP-4 in human immune function has yet to be established.[87] The only chemokine for which there is good evidence of in vivo processing by DPP-4 in preclinical species is stromal cell-derived factor 1α (SDF-1α, CXCL12). Increased levels of endogenous intact SDF-1α and decreased levels of the des-dipeptidyl fragment have been measured in rhesus monkeys treated with the DPP-4 inhibitor MK-0626 using immunoenrichment and mass spectrometry assays with the requisite sensitivity and selectivity.[88] Similar results have also been reported in DPP-4-deficient mice.[89] SDF-1α is a pro-inflammatory chemokine that signals through its receptor chemokine receptor type 4 (CXCR4) and regulates homing of hematopoietic stem/progenitor cells during various physiological processes including organogenesis and tumor metastasis.[90] T-cell (T)-tropic HIV-1 strains use CXCR4 as the entry coreceptor, and the intact SDF-1α ligand blocks HIV entry.[91] A study in a limited number of T2DM subjects has reported that treatment with sitagliptin increases the number of $CD34^{+}CXCR4^{+}$ cells that are responsive to SDF-1α.[92] Plasma levels of SDF-1α were decreased by 50% after 12 weeks of treatment, however, similar to the negative feedback observed for PYY secretion in humans. Additional clinical studies

are needed to determine whether SDF-1α or other cytokines contribute to the pharmacology of DPP-4 inhibitors, although the excellent clinical safety profile of these agents is reassuring,[93] as is a preliminary report that sitagliptin does not appear to compromise immune or virological status in HIV-infected individuals.[94]

7.14.3.6 Processing of Vasoactive Peptides

Brain natriuretic peptide (BNP) is a 32-residue cardioactive peptide secreted by the ventricles of the heart in response to mechanical stretch. The peptide promotes natriuresis and reduces vascular resistance and venous pressure.[95] Cleavage of the amino-terminal Ser-Pro dipeptide of intact BNP by DPP-4 in vitro produces BNP (3–32),[96] which exhibits reduced vasodilatory and natriuretic activity when infused in dogs.[97] Vasodilation induced by BNP infused in healthy subjects, however, is not potentiated by the administration of sitagliptin.[98]

Substance P (SP, tachykinin) is an 11-residue sensory neuropeptide that is ubiquitously distributed and is associated with numerous physiological and pathological processes including vasodilation, nociception, emesis, depression, angioedema, and adverse cardiac remodeling.[99,100] DPP-4 processing results in sequential removal of Arg-Pro and Lys-Pro dipeptide sequences from the amino terminus of SP to produce SP[3–11] and SP[5–11], respectively, the latter being further cleaved by aminopeptidase M.[101] SP is also a substrate for angiotensin-converting enzyme (ACE) and neutral endopeptidase (NEP).[102] Plasma levels of SP were doubled in DPP-4-deficient mice,[103] however, suggesting modulation of endogenous SP bioactivity. In T2DM subjects, increased levels of SP have been suggested to contribute to the rare cases of angioedema that have been reported for gliptin therapy,[103] especially in the background of ACE inhibitors being used to treat hypertension, which is common in diabetes. Infused SP increases heart rate and sympathetic activity in healthy volunteers only after coadministration of both sitagliptin and an ACE inhibitor (enalapril) and not when each agent is administered individually.[104] In addition, sitagliptin does not potentiate SP-induced cutaneous wheal and flare responses[105] in human subjects, consistent with clearance of SP by the other proteolytic pathways.

The potential modulation of cardioactive peptides such as SP, NPY, and/or SDF-1α has been invoked[106] to explain an increased risk of heart failure hospitalization related to treatment with the DPP-4 inhibitor saxagliptin in high cardiovascular disease (CVD)-risk T2DM patients.[107] No such signal for increased heart failure risk has been observed in the cardiovascular outcomes trial for sitagliptin,[108] however, suggesting that this is not a class effect. While the neutral cardiovascular safety profile of sitagliptin is reassuring, ongoing trials with linagliptin in high CVD-risk T2DM patients[109,110] should provide further experience into the use of gliptins in high-risk populations.

7.14.4 Crystal Structure of DPP-4

The X-ray crystal structure of recombinant soluble human DPP-4 bound to the dipeptide mimetic inhibitor valine pyrrolidide reveals a homodimeric enzyme with each subunit comprising an N-terminal eight-bladed β-propeller domain and a classical C-terminal α/β hydrolase domain.[111] A large cavity of ~30–45 Å in the α/β hydrolase domain incorporates a small pocket containing the peptidase active site, with the catalytic triad (Ser630, Asp708, and His740) located at the interface of the two domains. The active site can be accessed by two passages – one funnel-shaped tunnel defined by the propeller domain that extends from the lower face of the propeller to the active site is itself connected to a second larger opening on the side, at the interface of the propeller and hydrolase domains. The side entrance is calculated to have negative electrostatic potential, which interacts favorably with the positively charged amino-termini of peptide substrates to facilitate their entry into the active site. The crystal structure of DPP-4 bound to a fragment of NPY[112] confirms that two acidic residues (Glu205 and Glu206) within a short α-helix insertion protruding from the propeller domain toward the active site anchor the amino-terminus of the substrate via salt bridges to align the peptide for cleavage. This α-helix together with residues Tyr 662 and Tyr666 restricts the size of the P1 residue that can be accommodated in the S1 pocket, explaining the restricted P1 selectivity of DPP-4. The P2 residue of the substrate points into the large cavity, interacting with water molecules partially occupying the S2 pocket and making no specific contacts with the enzyme, consistent with the broad specificity of the hydrophobic S2 subsite. The catalytic Ser630 residue is located within a "nucleophilic elbow" (Gly-Trp-Ser630-Tyr-Gly) and oriented by a network of hydrogen bonds with proximal residues. The oxyanion hole that stabilizes the tetrahedral intermediate is formed by Tyr547 and the backbone NH of Tyr631. The carbonyl oxygen of the P1′ residue hydrogen bonds to Arg125, which together with residues Phe357, Tyr547, Pro550, Tyr631, and Tyr666, forms the hydrophobic S2 pocket.

The common binding pockets and key interactions of the various gliptins with residues at the DPP-4 active site (discussed in the next section) predict similar pharmacologies of these inhibitors, which is confirmed by the similar glucose-lowering efficacies of these compounds in the clinic[113] that correlate with the extent of plasma DPP-4 inhibition. The latter is a useful pharmacodynamic (PD) marker for efficacy.[114] It should be emphasized that in the absence of standardized plasma DPP-4 activity assays and methods of analyzing DPP-4 inhibition data, varying extents of plasma DPP-4 inhibition (typically uncorrected for assay dilution and for the competitive effects of added substrate) have been reported for the various gliptins. Upon correction for these effects,[115] however, all marketed gliptins likely achieve similar and effective (>95%) inhibition of plasma DPP-4 activity at their prescribed doses.

7.14.5 DPP-4 Inhibitors

7.14.5.1 Approved and Marketed DPP-4 Inhibitors

Currently, 10 orally active DPP-4 inhibitors have been approved for the treatment of T2DM (Table 1, Fig. 1). These are sitagliptin **1**, gemigliptin **2**, evogliptin **2a**, omarigliptin **3**, vildagliptin **4**, saxagliptin **5**, teneligliptin **6**, anagliptin **7**, linagliptin **8**, alogliptin **9**, and trelagliptin **10**. These approved drugs[116,117] can be grouped into three structural classes, namely, β-amino butanoic acid derivatives **1**,**2**, pyrrolidine analogs **3**–**7**, and pyrimidone/xanthine analogs **8**–**10**. The preclinical pharmacokinetic (PK) profiles of the approved DPP-4 inhibitors are summarized in Table 2. These drugs have different half-lives in the clinic, corresponding to oral dosing regimens ranging from twice-daily (vildagliptin), to once-weekly (trelagliptin and omarigliptin), to once-daily for the remaining seven DPP-4 inhibitors. A metaanalysis[129] of six of the above DPP-4 inhibitors (alogliptin, dutogliptin, linagliptin, saxagliptin, sitagliptin, and vildagliptin) as monotherapy or in combination therapy with metformin in patients with T2DM has shown that the combination therapy displays better efficacy than metformin monotherapy alone, which in turn achieves slightly greater reductions in hemoglobin A1c (HbA1c), fasting plasma glucose (FPG), and body weight than DPP-4 inhibitor monotherapy. Gliptin monotherapy was associated with a lower risk of adverse cardiovascular events, hypoglycemia, and gastrointestinal adverse effects compared with metformin monotherapy, while combination therapy did not increase the number of such adverse events. Hence, DPP-4 inhibitors are well suited in combination with metformin as second-line agents.

7.14.5.1.1 β-Amino butanoic acid derivatives

7.14.5.1.1.1 Sitagliptin (MK-0431, Merck)

Sitagliptin **1**, a triazolopiperazine derivative containing a β-amino amide moiety, was the first DPP-4 inhibitor approved by the US FDA in 2006. It is a potent DPP-4 inhibitor ($IC_{50} = 18$ nM) and has good selectivity over DPP-8 ($IC_{50} \sim 48{,}000$ nM), DPP-9 ($IC_{50} > 100{,}000$ nM), and other DASH peptidases.[118] Sitagliptin exhibits excellent oral bioavailability in preclinical species (100% in dogs and 61% in rats at a dose of 2 mg kg^{-1}). Administration of single oral doses of sitagliptin in lean mice reduced the blood glucose excursion in an oral glucose tolerance test (OGTT) in a dose-dependent manner from 0.1 mg kg^{-1} (23% reduction) to 3.0 mg kg^{-1} (55% reduction) when administered 60 min before an oral dextrose challenge (5 g kg^{-1}). In a parallel experiment in lean mice, its PD profile was determined; plasma DPP-4 inhibition, compound concentration, and active GLP-1 levels were measured 20 min after a dextrose challenge. Reduction of blood glucose excursion at 1 mg kg^{-1} corresponded to a plasma sitagliptin concentration of 190 nM and 69% inhibition of plasma DPP-4 activity. A 3 mg kg^{-1} dose, corresponding to a plasma concentration of 600 nM, provided 84% inhibition of plasma DPP-4. Maximal glucose-lowering efficacy at 3 mg kg^{-1} was accompanied by a two- to threefold increase in plasma active GLP-1 levels, analogous to what is observed upon glucose

Table 1 Approval dates and potencies of marketed DPP-4 inhibitors

Common name	*Originator*	*Status*	*Dose (dosing frequency)*	*DPP-4 IC_{50} and K_i (nM)*
1 Sitagliptin	Merck & Co.	Approved by US FDA 2006	25/50/100 mg (QD)	$IC_{50} = 18$ $K_i = 9$ Reversible, slow binding
2 Gemigliptin	LG Life Sciences Ltd.	Approved by Korea FDA 2012	50 mg (QD)	$IC_{50} = 16$ $K_i = 15.2$ Reversible
2a Evogliptin	Dong-A	Approved in Korea 2015	5 mg (QD)	$IC_{50} = 0.9$
3 Omarigliptin	Merck	Approved in Japan 2015	12.5/25 mg (QW)	$IC_{50} = 1.6$ Reversible, long acting
4 Vildagliptin	Novartis	Approved by EMEA 2008	50 mg (BID or QD)	$IC_{50} = 3.5$ $K_i = 17$ Reversible, covalently bound inhibitor
5 Saxagliptin	Bristol–Myers Squibb	Approved by US FDA 2009	2.5/5 mg (QD)	$IC_{50} = 3.37$ $K_i = 0.6$ Reversible, covalent bound
6 Teneligliptin	Mitsubishi Tanabe Pharma	Approved in Japan 2012	20/40 (QD)	$IC_{50} = 0.37$
7 Anagliptin	Sanwa Kagaku Kenkyushu/Kowa	Approved in Japan 2013	200/400 mg (QD)	$IC_{50} = 3.3$ Reversible, covalently bound
8 Linagliptin	Boehringer Ingelheim/Lilly	Approved by US FDA 2011	5 mg (QD)	$IC_{50} = 1.0$ Reversible, long acting
9 Alogliptin	Takeda/Furiex	Approved by US FDA 2013	6.25/12/5/25 mg (QD)	$IC_{50} = 7$ Reversible, long acting
10 Trelagliptin	Takeda/Furiex	Approved in Japan 2015	100 mg (QW)	$IC_{50} = 4$ Reversible, long acting

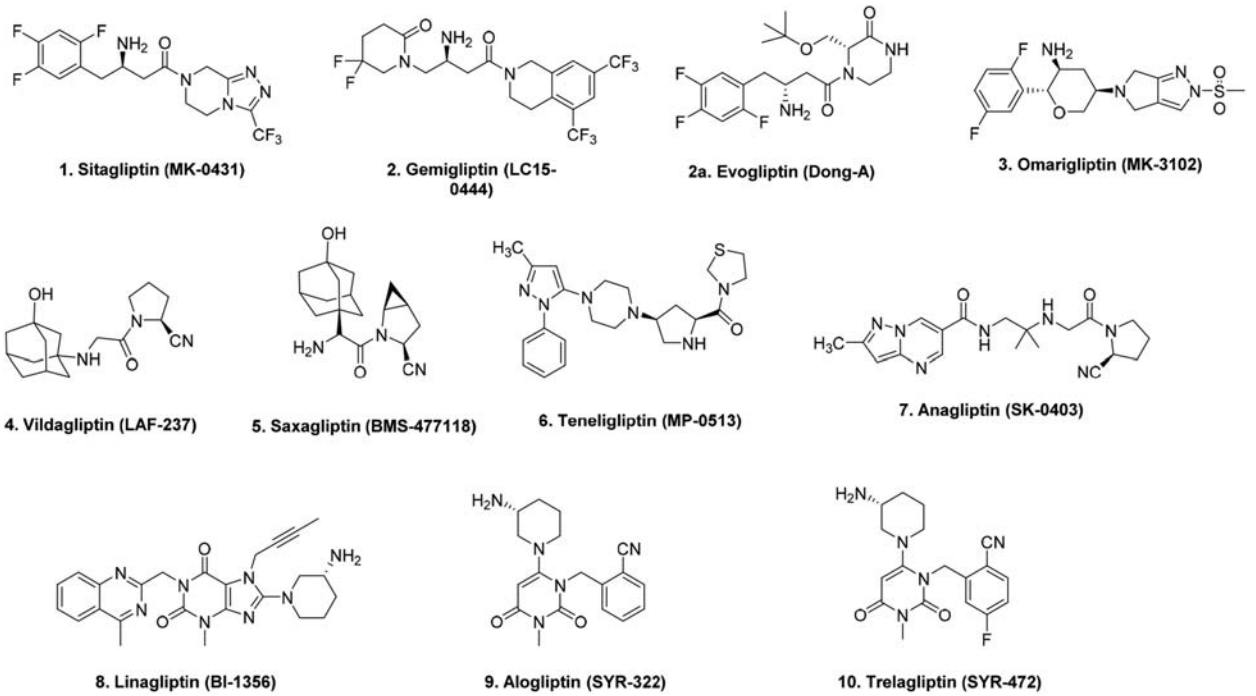

Fig. 1 Chemical structures of approved and marketed DPP-4 inhibitors.

Table 2 Summary of preclinical pharmacokinetic properties of approved DPP-4 inhibitors

DPP-4 inhibitors	T_{max} *(h)*	C_{max} *(μM)*	*CLp (L kg^{-1} h^{-1})*	$T_{1/2}$ *(h)*	F *(%)*	*Species*	*Active metabolite*	*Elimination route*
Sitagliptin[118,119]	1–4	0.3	3.6	1.7	61	Rat	No	Renal
		2.2	0.36	4.9	100	Dog		
		0.3	1.7	3.7	67	Monkey		
Vildagliptin[120]	1.75	0.3	1.5	1.5	85	Monkey	No	Renal
Saxagliptin[121]	2	24	–	2.1	75	Rat	BMS-510849	Renal
Alogliptin[122]	2.5	0.4	–	2.77	45	Rat	No	Renal
		0.7	–	3.04	86	Dog		
		0.5–9.6	–	5.7	72–88	Monkey		
		2.7	–	3.8	90	Dog		
		1.1	–	6.3	90	Monkey		
Linagliptin[123]	0.7–3.0	–	–	113–131	51	–	No	Biliary
Trelagliptin[124]	–	–	–	4.8	–	Dog	–	–
				6.2	–	Monkey		
Omarigliptin[125]	1.0	9.0	1.1	11	~100	Rat	Pyrrolo-pyrimidine metabolite	Renal
	1.3	5.9	0.9	22	~100	Dog		
Teneligliptin[126]	0.8–0.9	5.5–152.4		8–16	63–86	Rat	–	Biliary
	0.50–1.38	28.3–273.5	–	15–19	44–83	Monkey		
Gemigliptin[127]	1.8	511–2230	–	16–20	96	Rat	No	Renal
					73	Dog		
					26	Monkey		
Anagliptin[128]	0.8	309	2.0	1.9	23	Rat	–	Renal and biliary
	1.56	261	0.65	1.0	100	Dog		

T_{max} = time to maximum concentration observed in plasma, C_{max} = maximum plasma concentration, CLp = plasma clearance, $T_{1/2}$ = half-life, and F = oral bioavailability.

challenge in DPP-4-deficient mice. Acute lowering of blood glucose was also demonstrated in diet-induced obese (DIO) mice, which are hyperglycemic and hyperinsulinemic, and shows impaired glucose tolerance similar to that observed in T2DM.[118,119]

Based on X-ray studies, the trifluorophenyl moiety of sitagliptin fits into the S1 pocket of the DPP-4 active site, and the binding orientation of the amide carbonyl is reversed relative to that of α-amino acid scaffold-containing peptidomimetic inhibitors. The β-amino amide moiety binds in the S2 pocket. The primary amino group forms a salt bridge and hydrogen bonding interactions with Glu205 and Glu206 and with Tyr662, respectively. The carbonyl group exhibits a water bridge hydrogen-bonding interaction

with Tyr547. The triazolopiperazine moiety occupies the S2 extended pocket and stacks against Phe357. The trifluoromethyl group exhibits interactions with Arg358 and Ser209.[118]

Sitagliptin has good oral bioavailability of 87% in the clinic[130] and a terminal half-life ($T_{1/2}$) of 10–12 h at doses of 25–100 mg.[131] The drug is 80% renally cleared as the parent compound,[131] and exposure is 2.3- to 4.5-fold higher in patients with moderate to severe renal insufficiency, including end-stage renal disease.[132] Hence, a dose adjustment is recommended in such patients, with the nominal 100 mg dose being reduced to 50 mg or even 25 mg depending on the degree of renal dysfunction.[133] Sitagliptin inhibits plasma DPP-4 activity by over 80% for 24 h (corresponding to estimated in vivo plasma DPP-4 inhibition of $>90\%$) at doses ≥ 100 mg in healthy subjects.[131] Postprandial active GLP-1 levels are increased two- to threefold, but total GLP-1 levels are decreased, suggestive of negative feedback as has been reported for PYY. In patients with T2DM, a single 200 mg dose of sitagliptin inhibited plasma DPP-4 activity by 90% over 24 h and doubled active GLP-1 and GIP levels in response to oral glucose challenges at 2 and 24 h post dose, resulting in significant reductions in glucose excursions.[134] A once-daily treatment regimen was further supported by phase II studies in T2DM patients, where similar HbA1c and FPG reductions from baseline were obtained after 12 weeks of dosing with 100 mg qd and 50 mg bid.[283] Sitagliptin was well tolerated with single doses up to 800 mg and multiple doses up to 400 mg day^{-1} over 28 days.[133] In a 24-week phase III study in T2DM patients (HbA1c mean baseline 8.0%) treated with sitagliptin 100 or 200 mg, similar placebo-subtracted reductions in HbA1c (-0.8% and -0.9%), fasting plasma glucose (FPG, -17 and -21 mg dL^{-1}), and 2 h postprandial glucose (PPG, -47 and -54 mg dL^{-1}) were obtained with hypoglycemia incidence similar to placebo,[135] supporting the rationale for a recommended dose of 100 mg in patients with normal renal function. Rates of overall adverse events (AEs) with sitagliptin treatment in clinical trials have been similar to placebo, typically including nasopharyngitis, upper respiratory tract infection, and headache.[133] Add-on therapy studies have demonstrated the benefits of adding sitagliptin therapy to metformin or pioglitazone (-0.7% incremental HbA1c reductions from a baseline of $\sim 8.0\%$), although addition to a sulfonylurea (glimepiride) resulted in a higher incidence of hypoglycemia compared with placebo.[285] Sitagliptin and glipizide both reduced HbA1c by 0.7% when added to metformin (mean baseline HbA1c 7.5%), demonstrating noninferiority of sitagliptin to a sulfonylurea.[136] In addition, the incidence of hypoglycemia was significantly reduced with sitagliptin (5%) compared with glipizide (32%), and sitagliptin-treated patients lost 1.5 kg after 52 weeks compared with patients on glipizide who gained 1.1 kg. These data underscore the superior safety and tolerability profile of sitagliptin, which induces glucose-dependent insulin secretion in contrast to a conventional sulfonylurea secretagogue.

Sitagliptin increased the number of insulin-positive pancreatic β-cells, islet insulin content, and GSIS and reduced glucagon-positive α-cells in a high-fat-fed streptozotocin (STZ)-induced mouse model of diabetes.[137] In the clinic, sitagliptin improved HOMA-β, the proinsulin-to-insulin ratio, the insulinogenic index, and the overall responsiveness of the β-cell to glucose.[133] Islet-protective effects leading to disease modification similar to that observed in animal models, however, have not been observed in the clinic to date for sitagliptin or for the gliptin class in general.

The cardiovascular safety of sitagliptin was evaluated over a median follow-up of 3 years in Trial Evaluating Cardiovascular Outcomes with Sitagliptin (TECOS) in patients with T2DM and established CVD.[108] Sitagliptin was noninferior to placebo for the primary composite cardiovascular endpoint of cardiovascular death, nonfatal myocardial infarction, nonfatal stroke, or hospitalization for unstable angina. In addition, rates of hospitalization for heart failure, which had raised concern after prior cardiovascular outcomes trials with two other gliptins, were the same for the two groups. There were also no significant differences in rates of pancreatitis or pancreatic cancer, which had been suggested as potential mechanism-based adverse effects of GLP-1 receptor activation.[138] TECOS was therefore a key trial in establishing the long-term safety profile of sitagliptin in high-risk populations.

Three approaches for the synthesis of sitagliptin are outlined in Schemes 1–3. Each method involves coupling the trifluorophenyl-containing "left-hand" moiety with the triazolopiperazine moiety **15**. Triazolopiperazine **15** was prepared from chloropyrazine **11** by treatment with hydrazine to generate hydrazinopyrazine **12** followed by conversion to compound **13** by acylation with trifluoroacetic anhydride (TFAA). Intramolecular cyclization of compound **13** with polyphosphoric acid gave compound **14**, which on catalytic hydrogenation over Pd/C provided the desired triazolopiperazine **15**.

In the first synthetic approach to sitagliptin, treatment of the Schollkopf reagent **16** with 2,4,5-trifluorobenzyl bromide gave compound **17**, which upon treatment with acid and Boc protection gave the ester **18**, which was subsequently converted to the Boc-protected amino acid **19**. Using a mixed anhydride procedure, intermediate **19** was converted to the diazoketone **20** using diazomethane. **20** was converted subsequently to the desired β-amino acid **21** by sonication in the presence of silver benzoate.[139] Coupling of **21** with triazolopiperazine intermediate **15** followed by Boc deprotection provided sitagliptin **1**, which was converted to the corresponding hemifumarate salt (Scheme 1).[118]

The first step of another method for synthesis of sitagliptin is asymmetrical reduction of β-ketoester **23** with the (*S*)-BinapRuCl2 complex and a catalytic amount of HBr in methanol followed by hydrolysis to provide the β-hydroxy acid **24**. Subsequently, lactam **25** was synthesized by coupling of **24** with $BnONH_2 \cdot HCl$ using N-(3-dimethylaminopropyl)-N-ethylcarbodiimide hydrochloride (EDC), followed by cyclization with diisopropyl azodicarboxylate (DIAD) and PPh_3.[140] Treatment of **25**, a catalytic amount of 0.1% sodium hydroxide, directly provided the β-amino acid **26**, which was coupled with triazolopiperazine **15** using EDC·HCl and N-methylmorpholine to give compound **27**. Hydrogenation of **27** using Pd/C and treatment with phosphoric acid provided the phosphate salt of sitagliptin 1 (Scheme 2).

A third approach for the synthesis of sitagliptin is outlined in Scheme 3. Trifluorophenylacetic acid **28** was converted to a mixed anhydride with pivaloyl chloride. Subsequent treatment with Meldrum's acid **29**, dipropyamine ethyl amine (DIPEA), and a catalytic amount of dimethylamino pyridine (DMAP) in acetonitrile provided the Meldrum adduct **30**. Treatment of **30** with

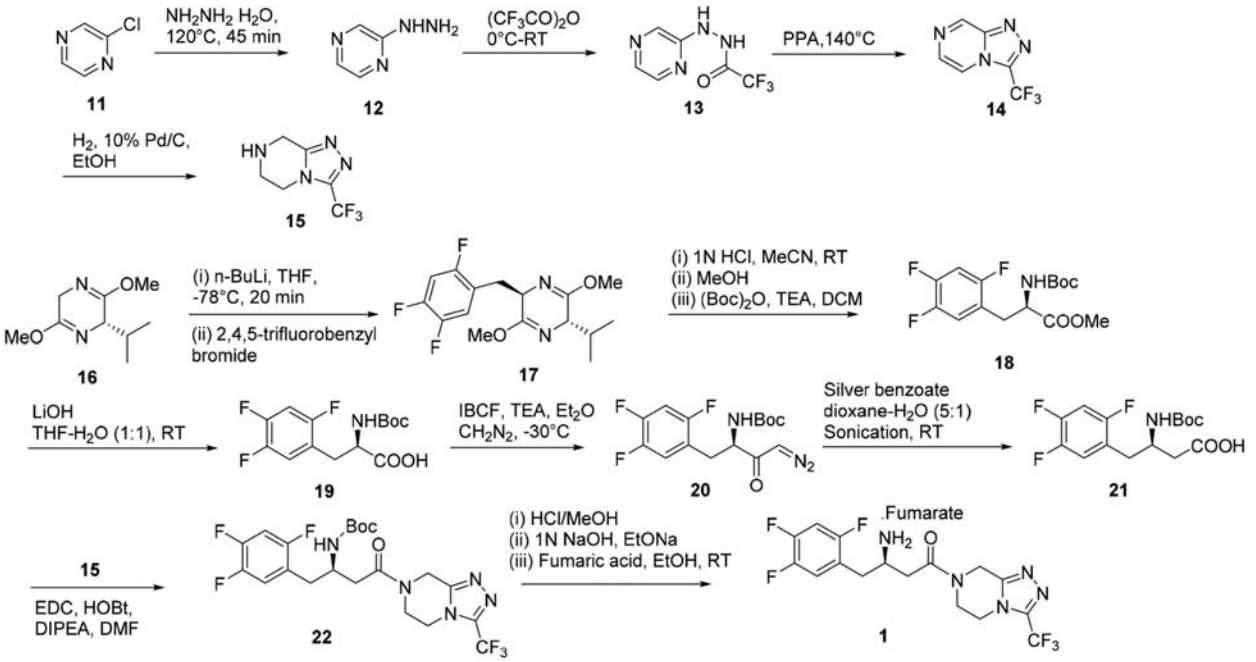

Scheme 1 First-generation approach for sitagliptin synthesis.

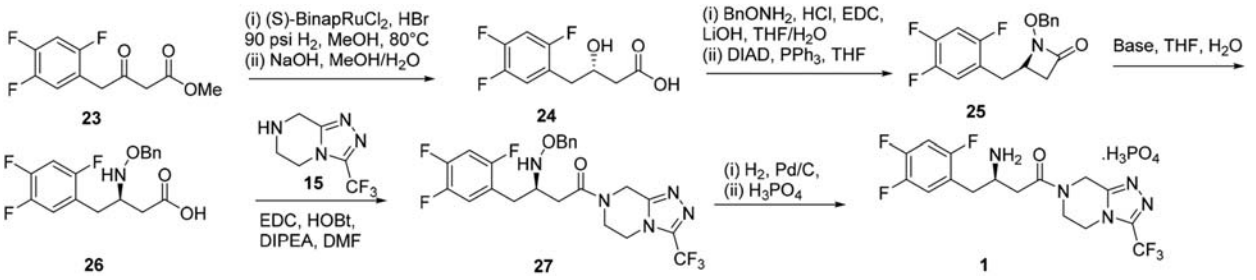

Scheme 2 Second approach to sitagliptin synthesis.

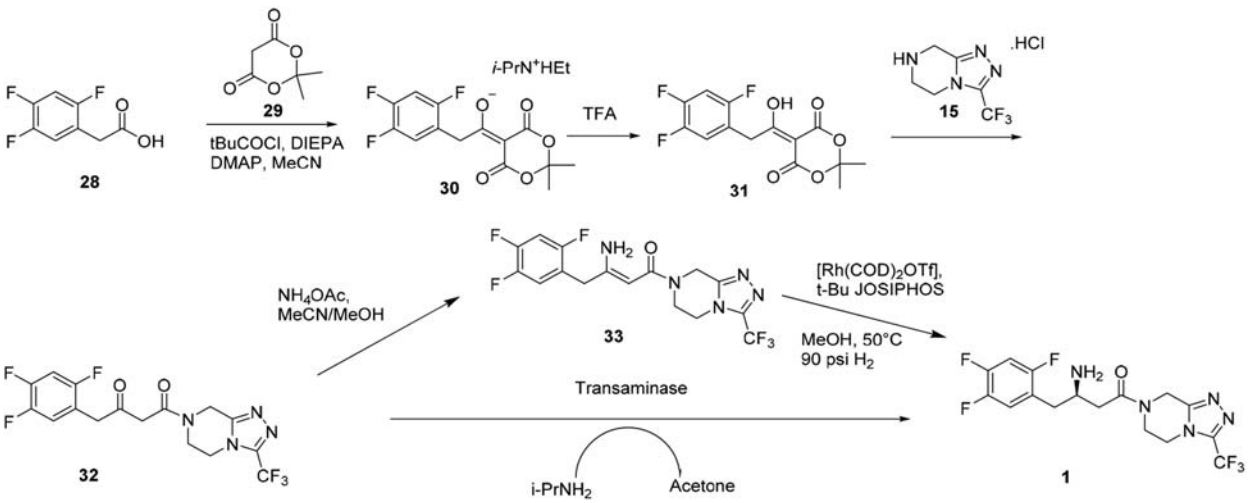

Scheme 3 Third approach to sitagliptin synthesis.

trifluoroacetic acid (TFA) gave compound **31**. Reaction of **31** with the HCl salt triazolopiperazine **15** gave β-keto amide **32**, which upon further treatment with ammonium acetate in methanol gave the enamine amide, dehydrositagliptin **33**. Finally, sitagliptin **1** with 95% ee was synthesized by enantioselective hydrogenation of **33** in the presence of [Rh(COD)2OTf] 12,13 and tBu JOSIPHOS in excellent yield.[141,142] An efficient biocatalytic process[141] to replace the rhodium-catalyzed asymmetrical enamine reduction for the large-scale manufacture of sitagliptin has been reported. The authors applied a substrate walking, modeling, and mutation approach to create a transaminase with marginal activity for the synthesis of the chiral amine and then further engineered via directed evolution for efficient, economical, and environmentally benign processes for the manufacture of pure sitagliptin (**Scheme 3**).

7.14.5.1.1.2 Gemigliptin (LC15-0444, LG Life Sciences)

Gemigliptin (LC15-0444) tartrate sesquihydrate is a potent, selective, competitive, and long-acting DPP-4 inhibitor discovered by modifying compounds from published patents. It was approved by the Korean Food and Drug Administration (KFDA) in June 2012. Gemigliptin is 3000-fold selective for DPP-4 ($IC_{50} = 16$ nM) over other proteases such as DPP-8 and DPP-9. The absorption, distribution, metabolism, and excretion of gemigliptin were examined following single oral administration of (14)C-labeled gemigliptin to rats. The (14)C-labeled gemigliptin was rapidly absorbed after oral administration, and its bioavailability was 95.2% (by total radioactivity). Distribution to specific tissues other than the digestive organs was not observed. Within 7 days after oral administration, 43.6% of the administered dose was excreted via urine, and 41.2% was excreted via feces. Biliary excretion of the radioactivity was about 17.7% for the first 24 h. After oral administration of gemigliptin to rats, the in vivo metabolism of gemigliptin was investigated in bile, urine, feces, plasma, and liver samples. The major metabolic pathway was hydroxylation, and the major circulating metabolites were dehydrated and hydroxylated metabolites.[127,143] Gemigliptin was rapidly absorbed after single oral dosing, and the compound was eliminated with a half-life of 3.6, 5.2, and 5.4 h in the rat, dog, and monkey, respectively. Gemigliptin produced a dose-dependent inhibition of plasma DPP-4 activity, with 80% inhibition of plasma DPP-4 activity observed at plasma gemigliptin levels of 9, 7, and 2 ng mL^{-1} in rats, dogs, and monkeys, respectively. Gemigliptin improved glycemic control after a single dose during an OGTT and reduced HbA1c levels following chronic treatment in high-fat diet (HFD)-fed mice.[127,144]

In clinical studies, gemigliptin was well tolerated in both a single ascending dose (SAD) study[145] from 25 to 600 mg and a multiple ascending dose (MAD) study[146] from 200 to 600 mg in healthy Korean male subjects. It was readily absorbed after single oral dosing with median T_{max} at 2.0 h (0.5–5.1 h) post dose and mean terminal elimination half-life of 16.7–21.3 h at all dose levels. Gemigliptin exhibited linear PK properties over the range of 50–400 mg in the SAD study and dose-dependently inhibited of plasma DPP-4 in both studies.

The efficacy and safety of gemigliptin (50, 100, or 200 mg once daily) in patients with T2DM were evaluated in a placebo-controlled, double-blind phase II study in Korea.[147] At week 12, gemigliptin significantly reduced HbA1c (placebo-subtracted reduction of 0.68–0.92% from a baseline of ~8.2%) and FPG at all doses compared with placebo, without significant differences among doses. Glucose tolerance was also significantly improved at all doses compared with placebo based on the results from an OGTT performed at week 12. Gemigliptin was well tolerated, and the incidences of AEs were not different from placebo. The efficacy of 50 mg gemigliptin as monotherapy was assessed in a 24-week phase III study in patients with T2DM.[148] Placebo-subtracted HbA1c reduction of 0.71% (baseline HbA1c ~8.2%) and corresponding FPG reduction of 19.80 mg dL^{-1} were observed. The HbA1c-lowering effects of gemigliptin were proportional to the baseline HbA1c as reported with other DPP-4 inhibitors. The overall incidence rates for AEs were similar in both gemigliptin and placebo groups.

The efficacy of gemigliptin (25 mg twice daily or 50 mg once daily) as a combination therapy was assessed in a 24-week phase III study in patients with T2DM inadequately controlled with metformin alone.[149] Sitagliptin 100 mg was used as an active comparator. At week 24, both dose regimens of gemigliptin were noninferior to sitagliptin. The proportion of patients achieving HbA1c <7% with gemigliptin 25 mg twice daily (50%) or 50 mg once daily (54%) was comparable to that of sitagliptin (49%). There were significant decreases in FPG and postprandial glucose, improvements in glucose tolerance during OGTT, and increases in GLP-1 and β-cell sensitivity to glucose. There was no increased risk of AEs with gemigliptin compared with sitagliptin. Unlike sitagliptin, however, which does not interfere with the P450 cytochrome enzymes and has no reported significant drug–drug interactions, gemigliptin is a substrate of both CYP3A4 and P-glycoprotein. Coadministration of a single dose of gemigliptin (50 mg) and multiple once-daily doses of ketoconazole (400 mg), a strong inhibitor of CYP3A4 and P-glycoprotein, increased total active drug exposure by 1.94-fold based on both the systemic exposure and the relative activities of gemigliptin and active metabolite. Rifampin (600 mg once daily), a strong inducer of CYP3A4 and P-glycoprotein, significantly decreased the total drug exposure by 70%. These data suggest that gemigliptin may need a dose adjustment when coadministered with drugs that alter CYP3A4 activity.[150] In addition, coadministration of multiple once-daily doses of gemigliptin (200 mg) and pioglitazone (30 mg) decreased the plasma C_{max} and area under the curve (AUC) of pioglitazone by 16% and 15%, respectively, while it caused no alteration in the PKs of gemigliptin.[151]

Analogous to the synthesis of sitagliptin, the synthesis of gemigliptin **2** (**Scheme 4**) involved coupling[152,153] of two key intermediates, dihydropyrido[3,4-d] pyrimidine **37** and β-amino acid **41**, using EDC/hydroxybenzotriazole (HOBt) to yield **42** followed by Boc deprotection. Treatment of the enolate made from compound **34** using LHMDS and adding trifluoroacetate gave **35**, which upon reflux condition gave **36**. Boc deprotection of **36** afforded the key intermediate **37**. Cyclization of **38** with **39** yielded the β-amino derivative **40**. Benzyl deprotection of **40** using Pd/C gave the desired intermediate **41**.

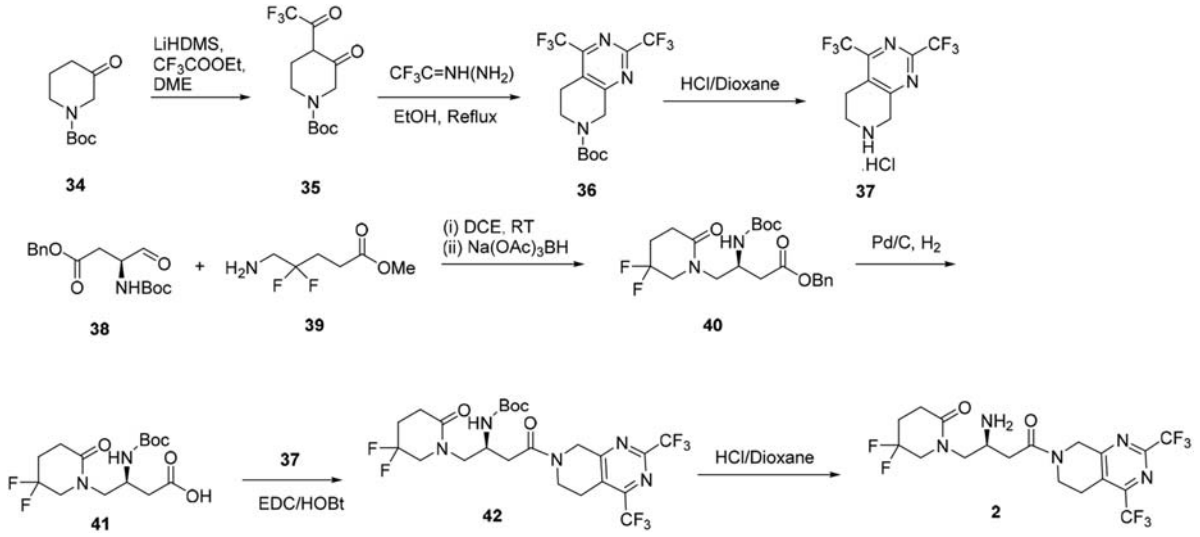

Scheme 4 Synthetic approach for gemigliptin.

7.14.5.1.1.3 Evogliptin (DA-1229, Dong-A)

Evogliptin (DA-1229) is a long-acting DPP-4 inhibitor and a β-amino amide-containing piperazine-2-one derivative[154] discovered by pharmaceutical in Korea. Evogliptin (5 mg oral dose) has been approved by the South Korean Ministry of Food and Drug Safety in October 2015. Evogliptin is a potent ($IC_{50} = 0.98$ nM), reversible, competitive, long-acting DPP-4 inhibitor and is selective (6000-fold) against other proteases such as DPP-8 and DPP-9. X-ray structure analysis reveals that the trifluorophenyl ring of evogliptin occupies the hydrophobic S1 pocket at the active site of DPP-4 and interacts with Tyr547, Tyr662, and Tyr666. The β-amino amide group binds at the S2 pocket where the amine group forms a salt bridge and hydrogen bonds with the side chains of Glu205 and Tyr662. The piperazine-2-one moiety occupies the S2 extended pocket. Evogliptin (0.1–3 mg kg^{-1}) dose-dependently inhibited plasma DPP-4, increased levels of insulin and GLP-1, and lowered blood glucose levels in mice. Evogliptin effected >80% of DPP-4 inhibition at 24 h following a single dose of 100 mg kg^{-1} in mice maintained on a HFD.[154]

In a phase I trial,[286] evogliptin achieved >80% plasma DPP-4 inhibition after a single dose of 5.0 mg. In a phase II trial, evogliptin was efficacious, safe, and well tolerated at all doses.[288] Evogliptin treatment produced a significant reduction in HbA1c levels of 0.56%, 0.66%, and 0.61% at doses of 2.5, 5.0, and 10.0 mg, respectively.

Synthesis of evogliptin started with the preparation of piperazine-2-one moiety **190** from the boron trifluoride-catalyzed ring opening of N-protected aziridine carboxyl ester **184** with tertiary butanol. The resulting compound **185**, after hydrogenation, gave compound **186**, which after reductive amination with sodium triacetoxyborohydride followed by Boc deprotection, and cbz protection provided compound **188** via **187**. Compound **188** was conducted using trimethylaluminum followed by cbz deprotection that gave the key intermediate **188**. The coupling of this key intermediate with β-amino acid **21** offered **191**, which after Boc deprotection using hydrochloride in ether provided evogliptin **176** (Scheme 5).[154] Long-term treatment with evogliptin for 8 weeks in mice maintained on a HFD showed significant improvement in impaired glucose tolerance and insulin resistance.[287]

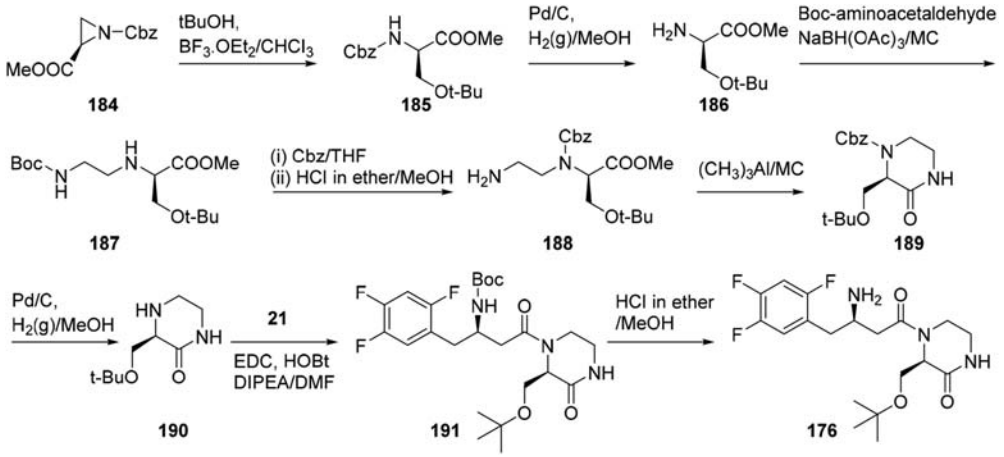

Scheme 5 Synthesis of evogliptin.

7.14.5.1.1.4 Omarigliptin (MK-3102, Merck)

Omarigliptin (MK-3102) 3 is a novel long-acting aminotetrahydropyran-based DPP-4 inhibitor targeted at achieving better medication compliance in T2DM patients. It was designed by replacing the middle "linker" in sitagliptin with a rigid cyclohexylamine/aminotetrahydropyran moiety. It exhibits an order of magnitude-enhanced potency (DPP-4 $IC_{50} = 1.6$ nM) compared with sitagliptin and has excellent selectivity ($IC_{50} > 67$ μM) against the other DASH peptidases.[125] It is a once-weekly oral antidiabetic agent as opposed to most other existing gliptin therapies, which are administered once or twice daily. Omarigliptin has a clinical half-life of 11–22 h and oral bioavailability of 100% in rat and dog.[155]

In X-ray studies conducted with a trifluorophenyl analog of omarigliptin, the inhibitor binds in the DPP-4 active site analogous to sitagliptin and shares the same interactions. The 2-F atom in the trifluorophenyl group occupies the S1 pocket and hydrogen bonds with the side chain of Arg125. The aminotetrahydropyran group binds at the S2 pocket where the primary amine group makes salt bridges with the carboxylates of Glu205 and Glu206. The fused ring π–π stacks with the side chain of Phe347.[125,155]

In an OGTT in lean mice, omarigliptin significantly reduced blood glucose excursion in a dose-dependent manner from 0.01 mg kg^{-1} (7% reduction in glucose AUC) to 0.3 mg kg^{-1} (51% reduction). The efficacy of glucose lowering in this model was similar to that achieved with sitagliptin. In the corresponding PD assay, plasma DPP-4 activity was inhibited by 85% at the 0.3 mg kg^{-1} dose. In addition, the administration of omarigliptin dose-dependently increased plasma concentrations of active GLP-1 in this study, with maximal increase observed at the 0.3–1 mg kg^{-1} doses.[155]

Omarigliptin dose-dependently inhibited plasma DPP-4 activity in healthy subjects and in patients with T2DM, with 80.7% plasma DPP-4 inhibition at the prescribed clinical dose of 25 mg and a doubling of postprandial 4 h-weighted mean active GLP-1 levels compared with placebo.[156] Omarigliptin is rapidly absorbed in healthy volunteers with a bioavailability of ≥74%. At steady state following three weekly doses of omarigliptin 25 mg, AUC was 22.3 μmol L^{-1} h^{-1}, C_{max} was 701 nM, T_{max} was 1.5 h, and the half-life was 82.5 h.[156] In a 12-week dose range-finding study in T2DM patients, omarigliptin (25 mg once weekly) significantly reduced HbA1c (placebo-subtracted reduction of 0.72% from a baseline of 8.1%).[12] Plasma DPP-4 activity was inhibited by 80.7% at trough. Omarigliptin is generally well tolerated with safety and efficacy comparable to that of sitagliptin.[156] Omarigliptin was approved in Japan in 2015, but its filing in the United States was recently abandoned due to business reasons.[157]

The synthesis of omarigliptin illustrated in Scheme 6 involved the coupling of methylsulfonylpyrrolopyrazole **48** and tetrahydropyranone **56b**. The pyrrolopyrazole intermediate **43** was made by heating a solution of the Boc-protected ketone **45** with *N*,*N*-dimethylformamide dimethyl acetal (DMF-DMA) to form the enamine **44**, which was subsequently dissolved in ethanol and heated under pressure with hydrazine then heated with hydrogen chloride in dry ethyl acetate. Neutralization with aqueous sodium hydroxide gave **43**. The methyl sulfonyl pyrrolopyrazole **48** was made from the Boc-protected intermediate **46** by sequential treatment with sodium hydride, methane sulfonyl chloride, and deprotection with benzene sulphonic acid and neutralization with ammonium hydroxide.

The tetrahydropyranone intermediates **56a** and **56b** were made in the following manner. The nitroketone **51** was made by reacting aldehyde **49** with nitromethane in the presence of a catalytic amount of sodium hydroxide as a base and oxidizing the resulting nitroalcohol **50** with Jones or Dess–Martin reagent. Heating the nitroketone **51** with 3-iodo-2-(iodomethyl)prop-1-ene gave the pyran **52**, which, when reduced with sodium borohydride, gave a mixture of racemic trans-**53** and racemic *cis*-**54** isomers, which were separated by flash column chromatography. The *cis* isomer **54** was readily converted to the transisomer **53** by treatment with 1,8-diazabicyclo[5.4.0]undec-7-ene (DBU). The nitro-substituted pyrans **53** were then reduced using zinc and hydrochloric acid. The resulting amines were protected as Boc derivatives by treatment with di-*tert*-butyl dicarbonate and separated by chiral column chromatography to give **55a** and **55b**. Treatment of **55b** with osmium tetroxide and *N*-methylmorpholine *N*-oxide followed by treatment with sodium periodate gave ketone **56b**.[125]

A second convergent manufacturing route of omarigliptin (MK-3102) synthesis[158] through a diastereoselective reductive amination of pyranone **56b** with a mesylated pyrazole **48** followed by deprotection of a Boc group is displayed in Scheme 7.

The synthesis of the pyranone **56b** relies on three Ru-catalyzed reactions: (1) a DKR reduction of a rac-α-aminoketone to set the two contiguous stereogenic centers, (2) a cycloisomerization of a bis-homopropargylic alcohol to a dihydropyran, and, finally, (3) a Ru-catalyzed oxidation of a pyranol to the desired pyranone. The regioselective synthesis of an *N*-Boc-1-mesyl pyrazole fragment was achieved via base-promoted mesyl group isomerization to afford 30:1 selectivity. A highlight of the endgame process development is telescoping a Boc deprotection and reductive amination followed by direct crystallization of the penultimate intermediate from the reaction mixture.

7.14.5.1.2 Pyrrolidine analogs

7.14.5.1.2.1 Vildagliptin (LAF-237, Novartis)

Vildagliptin (LAF-237) **3**, the first gliptin of the cyanopyrrolidine class approved for the treatment of T2DM, is a substrate mimic. Vildagliptin is potent (DPP-4 $IC_{50} = 3.5$ nM) and has modest selectivity over DPP-8 (>250-fold) and DPP-9 (23-fold) but is highly selective against other peptidases such as DPP-II and FAP. Vildagliptin was discovered in an attempt to enhance the half-life and potency of a prior-generation inhibitor NVP-DPP-728,[159] which has a short half-life due to formation of an imidate through internal cyclization between the P2-binding amino functionality and the P1-binding nitrile group. Incorporation of a bulky adamantyl group at the glycine nitrogen resolved this drawback and improved PKs. The absolute oral bioavailability of vildagliptin was >90% in cynomolgus monkeys following a 1 μmol kg^{-1} oral dose. Clearance from plasma was ~1.5 L h^{-1} kg^{-1} with

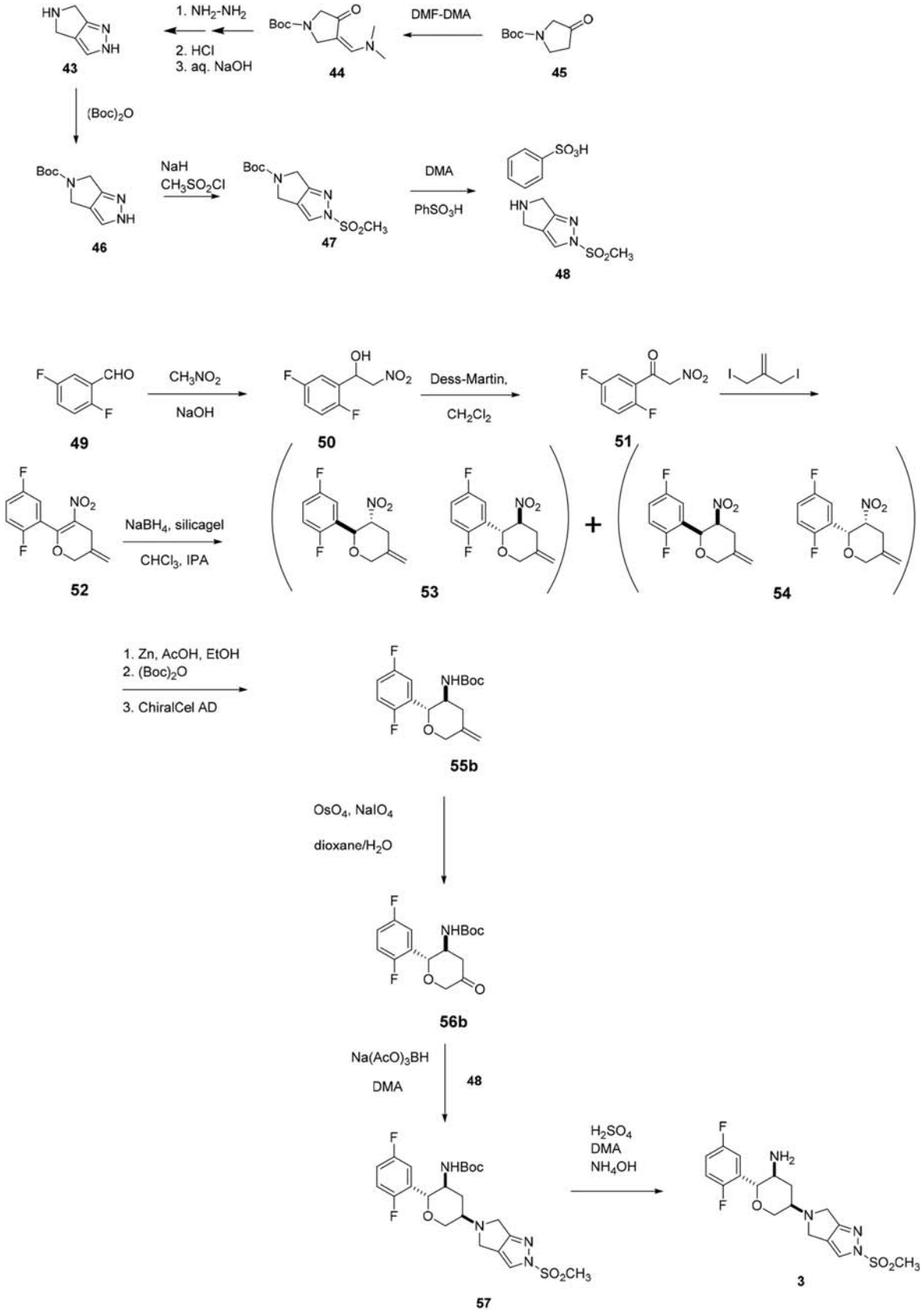

Scheme 6 Synthesis of omarigliptin.

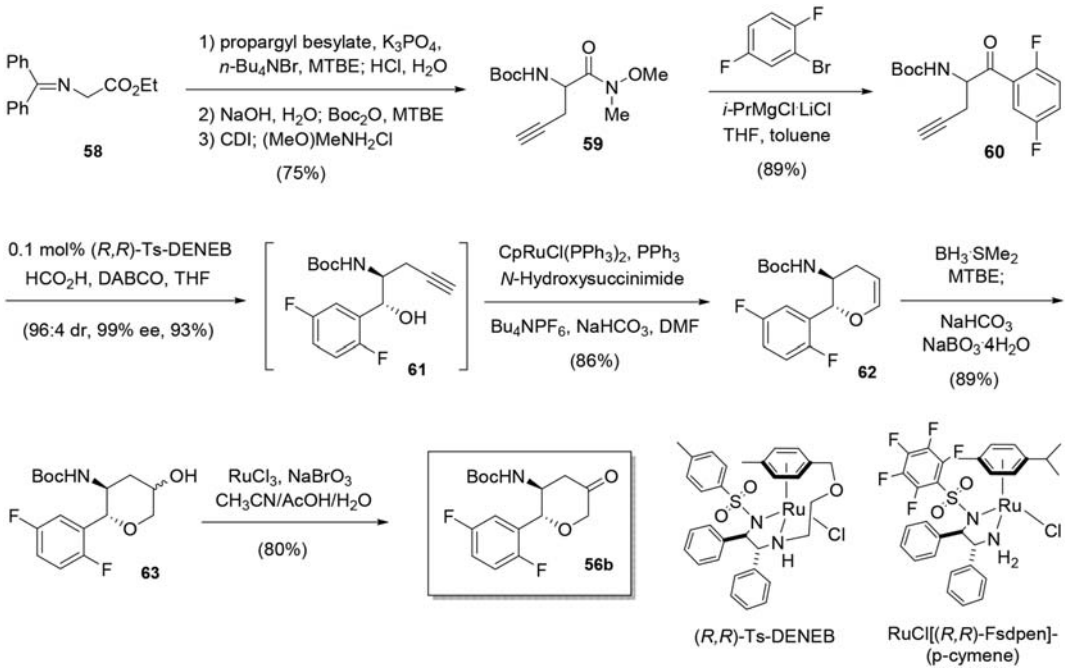

Scheme 7 Process manufacturing route to omarigliptin intermediate pyranone 56b.

a moderate volume of distribution at steady state (0.7 L kg^{-1}). The C_{max} was 293 nM at 72 min, and the terminal elimination half-life was 90 min, longer than that of NVP-DPP-728.[120]

Vildagliptin in an OGTT dosed at 10 μmol kg^{-1} PO 15 min prior to a glucose challenge in obese Zucker (*fa/fa*) rats inhibited plasma DPP-4 activity by >90%, increased active GLP-1 levels fivefold and peak insulin levels approximately twofold, and decreased glucose excursion compared with control-treated rats.[120]

The cyanopyrrolidine moiety of vildagliptin occupies the S1 pocket at the DPP-4 active site. Like saxagliptin, the nitrile group is stabilized through covalent imidate adduct formation with the hydroxyl of catalytic Ser630. The imidate nitrogen–hydrogen bonds with the side chain of Tyr547. The hydrophobic adamantyl moiety occupies the S2 pocket. The hydroxyl-substituent hydrogen bonds with His126 and Ser209 via bridging water molecules. The carbonyl group interacts via hydrogen bonds with the side chain of Asn710, and the secondary amine group is stabilized through salt bridge interactions with Glu205 and Glu206.[160]

Vildagliptin is rapidly absorbed in healthy subjects and T2DM patients with a T_{max} of 1.5 h and a bioavailability of 85% after oral administration.[161] Modeling suggests two absorption sites with lag times of 0.2 and 2.5 h,[162] indicating that vildagliptin may be absorbed via a paracellular pathway. Vildagliptin has a high volume of distribution in healthy subjects (71 L) indicating that it distributes extensively into extravascular spaces. The nitrile moiety in vildagliptin is rapidly hydrolyzed in vivo, likely by DPP-4, to the inactive carboxylic acid metabolite LAY151, which is the major clearance mechanism for the drug. The remaining 33% of vildagliptin total body clearance is via the kidneys as parent (23%) or metabolites. The mean half-life of vildagliptin after multiple doses in T2DM patients is 1.3–2.4 h. Hence, unlike most other gliptins, vildagliptin has to be administered twice daily. There have been no reports of any significant drug–drug interactions with vildagliptin.

In a 24-week dose range-finding phase II study in T2DM patients, vildagliptin (50 mg qd, 50 mg bid, and 100 mg qd) produced placebo-subtracted reductions in HbA1c of 0.5%, 0.7%, and 0.9%, respectively (from a mean baseline HbA1c of 8.4%).[163] Adverse events were similar to that in the placebo group, and no changes in body weight or hypoglycemia were observed. Pooled phase III monotherapy data for vildagliptin 50 mg bid and 100 mg qd from placebo- and active-controlled trials reveal good glucose-lowering efficacy (adjusted mean HbA1c reductions of 1% and 1.1%, respectively) that is consistent with the relatively high corresponding HbA1c baselines of 8.7% and 8.5%.[164] Vildagliptin 50 mg bid was approved by the European Medicines Agency in 2008 as monotherapy and combination therapy with other antihyperglycemic agents, but the drug remains commercially undeveloped in the United States.

Two methods of vildagliptin synthesis are outlined in Scheme 8. In the first method, the amino group of L-prolinamide **64** was acylated using chloroacetyl chloride to give compound **65**, which was converted to compound **66** by dehydration with TFAA. Finally, reaction of 3-hydroxy-1-amino adamantine **67** with **66** gave vildagliptin **4**.[120] An alternative route for the synthesis of intermediate **65** involved the direct *N*-acylation of L-proline **70** with chloroacetyl chloride to afford the chloroacetamide **69**, which was converted to amide **65** by using *N*,*N*′-dicyclohexylcarbodiimide (DCC) and ammonium bicarbonate.[284]

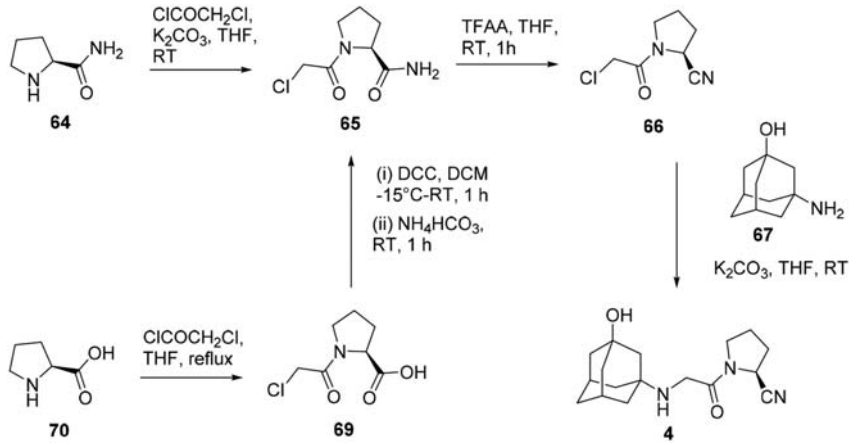

Scheme 8 Combined synthesis of vildagliptin.

7.14.5.1.2.2 Saxagliptin (BMS-477118, Bristol–Myers Squibb*)*

Saxagliptin (**5**) is a substrate-mimicking pyrrolidine-based DPP-4 inhibitor. It contains a cyanomethanoproline moiety at the P1 site and a large hydrophobic adamantyl moiety at the P2 site to fit the S2 pocket. Saxagliptin is highly potent (DPP-4 $K_i = 0.6$ nM) and moderately selective against other DASH peptidases (i.e., DPP-8, DPP-9, FAP, etc.). Like vildagliptin, saxagliptin forms a reversible covalent bond with the catalytic serine residue of DPP-4. This has been used to explain the high potency of saxagliptin versus other gliptins that do not make covalent interactions with DPP-4.[165,166] In addition, the high degree of branching and the presence of a fused cyclopropane scaffold prevent internal cyclization and enhance chemical stability.[121,165,166] Saxagliptin is administered once daily and was approved by US FDA in 2009 either as monotherapy or in combination with other antidiabetic agents.[121]

The PKs of saxagliptin was evaluated in rats, dogs, and monkeys.[167] Saxagliptin was rapidly absorbed and had good bioavailability (50–75%) in the species tested. The plasma clearance (CLp) of saxagliptin was higher in rats (115 mL min^{-1} kg^{-1}) than in dogs (9.3 mL min^{-1} kg^{-1}) and monkeys (14.5 mL min^{-1} kg^{-1}) and was predicted to be low to moderate in humans. The plasma elimination half-life was between 2.1 and 4.4 h in rats, dogs, and monkeys, and both metabolism and renal excretion contributed to overall elimination. The primary metabolic clearance pathway of saxagliptin involved the formation of a pharmacologically active 5-hydroxyl metabolite, which is a reversible DPP-4 inhibitor with twofold lower potency than saxagliptin.[121]

The volumes of distribution for saxagliptin observed in rats, dogs, and monkeys range from 1.3 to 5.2 L kg^{-1}. The in vitro serum protein binding was low ($\leq$30%) in rats, dogs, monkeys, and humans. After intra-arterial administration of saxagliptin to Sprague-Dawley and Zucker diabetic fatty rats, higher levels of saxagliptin and metabolite were observed in the intestine relative to plasma. Saxagliptin displays prolonged PD effects relative to its plasma PK profile, presumably due to a combination of contributions from the active hydroxyl metabolite, distribution of saxagliptin and its metabolite to the intestinal tissue, and slow dissociation of both molecules from DPP-4.[167]

The acute preclinical efficacy of saxagliptin was evaluated in Zucker *fa*/*fa* rats in an OGTT.[121] Saxagliptin (0.3–3 μmol kg^{-1} and 0.13–1.3 mg kg^{-1} PO) dose-dependently increased glucose clearance in this model, and maximal responses in reducing glucose excursion were associated with plasma DPP-4 inhibition of approximately 60%. Saxagliptin was also evaluated in the *ob*/*ob* mouse.[121] An OGTT was performed at 1 h after oral administration of drug at 1, 3, or 10 μmol kg^{-1}. Saxagliptin dose-dependently elevated plasma insulin at 15 min postglucose challenge, with concomitant improvement in the glucose clearance curves at 60 min post challenge.

The cyanopyrrolidine moiety of saxagliptin occupies the S1 pocket of DPP-4 and establishes a covalent bond interaction between the cyano group and side chain of Ser630.[168] The cyclopropyl moiety contributes to binding through hydrophobic interactions with Tyr666. The hydrophobic hydroxyl adamantly group binds at the S2 pocket. The hydroxyl group enhances potency by forming a direct hydrogen bond with the side chain of Tyr547. As with peptide substrates, the primary amine group of saxagliptin in the S2 pocket establishes salt bridges with the carboxylic groups of Glu205 and Glu206.

Saxagliptin exhibited similar PKs in healthy subjects (dosed 40, 100, 150, 200, 300, or 400 mg once daily) and in patients with T2DM (dosed 40, 100, 150, 200, 300, or 400 mg once daily).[169] Drug exposure was dose-proportional, as was exposure to the active 5-hydroxy metabolite BMS-510849, which was 1.7- to 6.9-fold higher than that of the parent molecule. Both saxagliptin and BMS-510849 are cleared from the plasma by the kidney with half-lives of 2.2–3.8 h and 3–7.4 h, respectively.[169] Both, parent drug (12–29% of the administered dose) and active metabolite (21–52% of the dose) were recovered in the urine. Saxagliptin elevated postprandial intact GLP-1 levels up to threefold and dose-dependently inhibited plasma DPP-4 activity (by ~80% to >95%), with maximal DPP-4 inhibition at saxagliptin doses $\geq$150 mg.

In a 12-week study in drug-naive T2DM patients with BMI $\leq$ 37 kg m^{-2}, saxagliptin (2.5, 5, 10, 20, or 40 mg once daily) dose-dependently reduced HbA1c (−0.72% to −0.90%) compared with placebo (−0.27%) from a mean baseline HbA1c of 7.9%.[170] In a 24-week study in drug-naive T2DM subjects, saxagliptin 2.5, 5, or 10 mg once-daily dose-dependently reduced HbA1c compared

with placebo (placebo-subtracted HbA1c reductions of 0.62, 0.65, and 0.73 from a mean baseline of approximately 8.0%).[171] The rates of AEs were similar for treatment and placebo groups, with the most common adverse events (>5% for all saxagliptin groups) being upper respiratory tract infection, headache, urinary tract infection, nasopharyngitis, and sinusitis. Skin AEs were reported more frequently in the treatment groups than in the placebo group, with rash (3.6% in the treatment groups vs. 1.1% in placebo) and pruritus (1.3% in the treatment groups vs none in the placebo) being most common.

The cardiovascular safety of saxagliptin was evaluated in the saxagliptin assessment of vascular outcomes recorded in patients with diabetes mellitus-thrombolysis in myocardial infarction 53 trial (SAVOR-TIMI 53) cardiovascular outcomes study in T2DM subjects, 70% of whom were also on metformin.[172] Saxagliptin met the primary safety objective of noninferiority but did not meet the primary efficacy objective of superiority for a composite endpoint of cardiovascular death, nonfatal myocardial infarction, or nonfatal ischemic stroke. Although there was no increase in all-cause mortality in the trial, the rate of hospitalization for heart failure was 27% higher in the saxagliptin group (3.5%) than placebo (2.8%, $P=0.007$), resulting in an FDA label warning regarding heart failure risk in susceptible populations.[173]

Saxagliptin is made from two key intermediates—the methanoprolinamide **76** and hydroxyadamantylglycine **81**. The methanoprolinamide intermediate **76** was prepared from L-pyroglutamic acid **70**. Compound **70** was esterified to **71**, Boc-protected to yield **71**, and converted to intermediate **73**. Compound **73** was converted into **74** through an amidation reaction. Using a Simmons–Smith cyclization, compound **74** was converted into Boc-protected methanoprolinamide **75**, which after Boc deprotection provided the desired intermediate **76**.

The synthesis of intermediate **81** began from adamantine carboxylic acid methyl ester **77**. Reduction to the aldehyde and its condensation with (R)-2-phenylglycinol and KCN provided compound **78**. Compound **80** was obtained from **78** following acid hydrolysis, hydrogenation-mediated removal of the chiral auxiliary, and Boc protection. Hydroxylation of compound **80** gave the desired intermediate **81**. Thus, saxagliptin **5** was synthesized by coupling of key intermediates, **76** and **81**, using an EDC protocol followed by subsequent TFAA-mediated conversion of amide to nitrile and Boc deprotection (**Scheme 9**).[121]

An asymmetrical synthetic method to make saxagliptin is outlined in **Scheme 10**. Synthesis started with adamantine-1-carboxaldehyde **84** followed by condensation with (*S*)-(+)-*p*-toluenesulfonamide and NaCN to give compound **85**. After acid hydrolysis, compound **86** was subjected to phthalic anhydride protection to give **87**. Hydroxylation of **87** afforded the key intermediate **88**, which was coupled with methanopyrrolidine intermediate **89** to give **90**. Methyl amine-mediated deprotection of phthalic deprotection gave saxagliptin **5**.[174,175]

A third enzymatic approach to saxagliptin synthesis is shown in **Scheme 11**. The key intermediate (*S*)-*N*-Boc-3-hydroxyadamantylglycine **92** was obtained from 2-(3-hydroxy-1-adamantyl)-2-oxoacetic acid **91** by reductive amination with

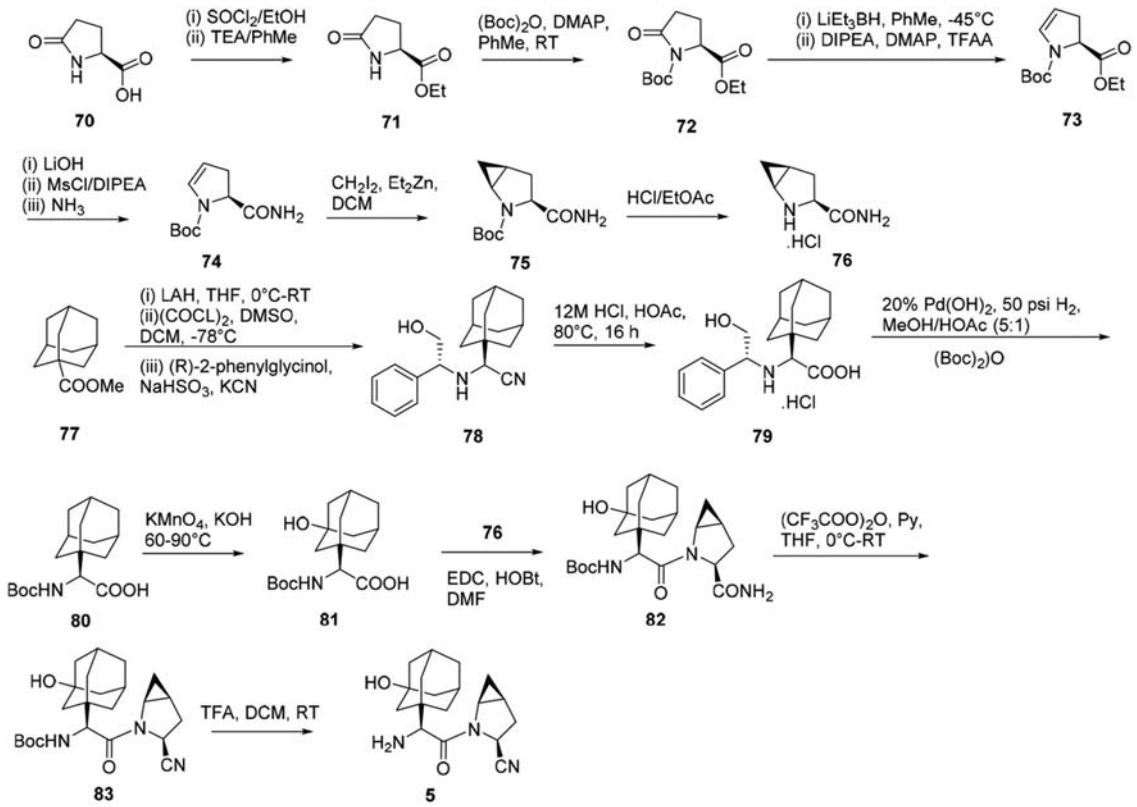

Scheme 9 First method to saxagliptin synthesis.

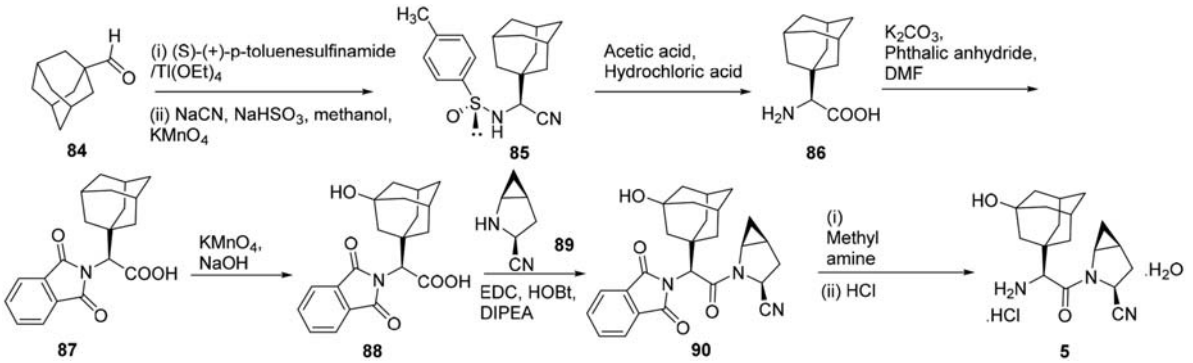

Scheme 10 Second method to saxagliptin synthesis.

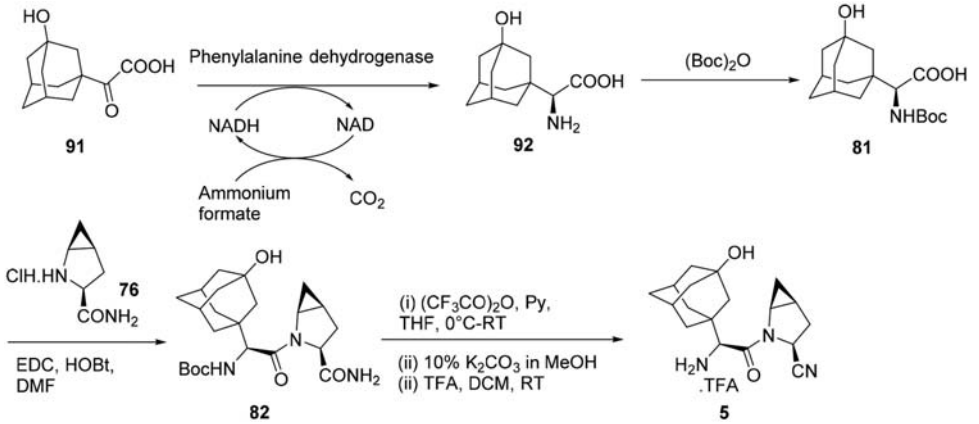

Scheme 11 Third method to saxagliptin synthesis.

a phenylalanine dehydrogenase enzyme. Boc protection followed by coupling with **76** and conversion to the nitrile and deprotection afforded saxagliptin **5**.[176,177]

7.14.5.1.2.3 Teneligliptin (MP-0513, Mitsubishi Tanabe)

Teneligliptin **6** is a proline-based constrained bicyclic heteroarylpiperazine-derived DPP-4 inhibitor. It is extremely potent (DPP-4 $IC_{50} = 0.37$ nM) and selective against DPP-8 (703-fold) and DPP-9 (1460-fold). It has recently been approved in Japan for the treatment of T2DM. Oral administration of teneligliptin (HBr salt) to rats and monkeys at each dose of 0.1, 0.3, and 1.0 mg kg^{-1} reached maximal plasma concentrations (C_{max}) at 0.75–0.88 h in rats and 0.50–1.38 h in monkeys, with corresponding half-lives of 8–16 and 15–19 h. Its bioavailability was 63–86% in rats and 44–83% in monkeys. Drug exposure was dose-proportional, and teneligliptin was mainly excreted into feces via bile in both species.[126]

Teneligliptin (HBr salt) when administered orally to Wistar rats at a dose of 0.03, 0.1, 0.3, or 1 mg kg^{-1} effected dose-dependent, fast-onset, and long-lasting DPP-4 inhibitory activity. Greater than 50% inhibition of plasma DPP-4 level was sustained at a single oral dose of 1 mg kg^{-1} for up to 24 h. In Zucker fatty rats pretreated with compound at doses from 0.03 to 1 mg kg^{-1} in an OGTT, teneligliptin dose-dependently lowered glucose excursions to levels similar to that in lean controls. A 0.03 mg kg^{-1} oral dose of teneligliptin produced >35% DPP-4 inhibition compared with predosing values.[126]

X-ray studies reveal that the thiazolidine moiety of teneligliptin binds to the hydrophobic S1 pocket of DPP-4, while the substituted proline occupies the S2 pocket. The amine functionality of the proline establishes salt bridge interactions with Glu205 and Glu206. The carbonyl group makes a hydrogen-bonding interaction with the side chain of Asn710. The (1-phenylpyrazol-5-yl)piperazine fragment of teneligliptin has been termed an "anchor lock domain" and binds more deeply into the S2 pocket. The pyrazolyl ring is stacked with Phe357. The piperazinyl ring fragment interacts with the Phe357 residue through a CH–n interaction. The phenyl group attached to the pyrazolyl ring forms hydrophobic interactions with Ser209 and Arg358.[126]

Teneligliptin is rapidly absorbed in healthy subjects, with a T_{max} of 1.33 h and an elimination half-life of 26.9 h following a radiolabeled 20 mg dose.[178] The drug is ~78–80% protein-bound in plasma. Teneligliptin is metabolized by CYP3A4 and flavin monooxygenases 1 and 3 to metabolites of uncharacterized biological activity, including a major thiazolidine-1-oxide derivative (14.7% of total AUC). At least 90% of the total radiolabeled dose was excreted by 216 h (45.4% in the urine and the rest in feces). Approximately 21% of teneligliptin is excreted in urine as parent drug. Teneligliptin is a weak CYP2D6, CYP3A4, and FMO inhibitor

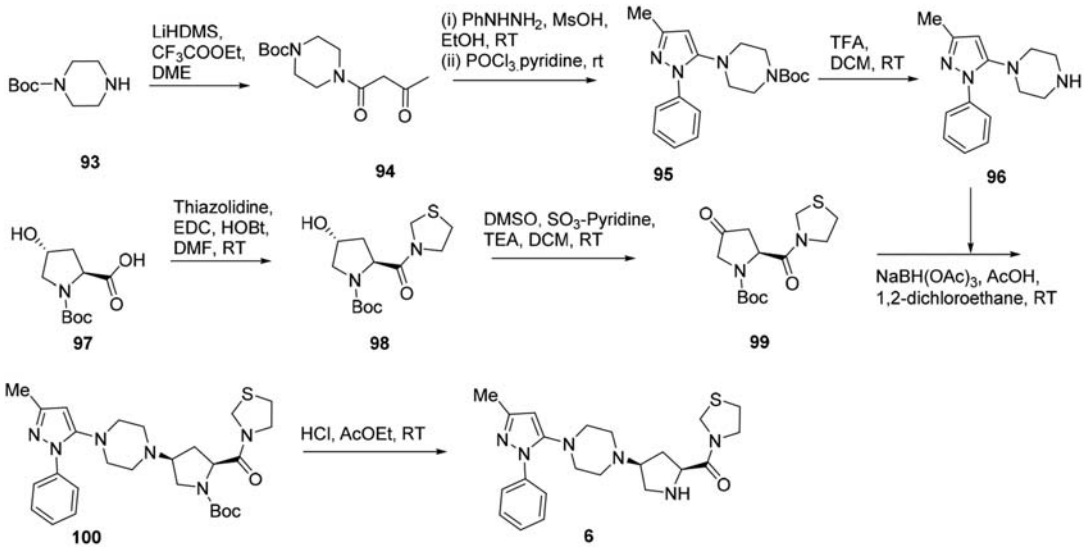

Scheme 12 Synthesis of teneligliptin.

in vitro but did not show any significant drug–drug interactions when coadministered with ketoconazole, metformin, or canagliflozin in healthy subjects.[179] The efficacy of teneligliptin as monotherapy and combination therapy was assessed in T2DM patients in phase II and III trials conducted in Japan and Korea. After 12 weeks of treatment, teneligliptin 20 or 40 mg once daily produced placebo-subtracted HbA1c reductions of 0.9% and 1%, respectively, from corresponding HbA1c mean baselines of 7.8% and 7.7%,[180] similar to efficacy observed in this population for the gliptin class in general. Pooled phase III data from two open-label nonplacebo-controlled monotherapy trials indicate that teneligliptin (20 mg once daily, titrated to 40 mg if inadequate efficacy was observed) reduced HbA1c by 0.63% from a baseline of approximately 7.7%.

Synthesis of teneligliptin **6** (**Scheme 12**) involved the reductive amination of ketone **99** with amine **96** (to afford only the *cis* isomer of compound **100**) and subsequent Boc removal.[126] Intermediate **96** was prepared by treating Boc piperazine **93** with ketene. Subsequent dehydration and cyclodehydration of the resulting β-ketoamide with phenyl hydrazine and phosphorus oxychloride in pyridine, respectively, were followed by Boc deprotection. Intermediate **99** was prepared by coupling of *N*-Boc-*trans*-4-hydroxy-L-proline **97** with thiazolidine followed by oxidation with dimethyl sulfoxide and sulfur trioxide.

7.14.5.1.2.4 Anagliptin (SK-0403, Sanwa Kagaku Kenkyusho)

Anagliptin **7** is a 2-methyl pyrazolopyrimidine-derived cyanopyrrolidine-based DPP-4 inhibitor. It is potent (DPP-4 $IC_{50} = 3.8$ nM) and more than 10,000-fold selective for DPP-4 against DPP-8 and DPP-9.[128] In PK studies,[128] anagliptin had a clearance of 0.65 L h^{-1} kg^{-1} and oral bioavailability of 100% in beagle dogs while showing a relatively higher clearance of 2.00 L h^{-1} kg^{-1} and moderate oral bioavailability of 23% in rats. In bile duct-cannulated rats, 30% and 40% of drug was excreted unchanged from the urine in the 24 h period after IV administration at doses of 1 and 5 mg kg^{-1}, respectively, with recovery of ~13–14% of the doses in bile. Similarly, in dogs dosed at 1 mg kg^{-1} IV, 32% and 24% of anagliptin was excreted unchanged from urine and feces, respectively, in the 24 h period after drug administration. Parent compound was primarily eliminated into urine, and biliary excretion was more significant in dogs than in rats.

In male Wistar/ST rats at oral doses of 0.1, 0.3, 1, or 3 mg kg^{-1}, anagliptin dose-dependently inhibited plasma DPP-4 activity, with sustained inhibition of >90% at 3 mg kg^{-1} over the course of a 2 h OGTT. A significant reduction in glucose AUC was observed at the 1 and 3 mg kg^{-1} doses, with increased insulin levels at 10 min postglucose challenge suggesting augmentation of active GLP-1 levels.[128]

Anagliptin is rapidly absorbed following a 100 mg radiolabeled oral dose in healthy male subjects, with a T_{max} of approximately 1.8 h and a biexponential elimination profile with a terminal half-life of 4.37 h.[181] Hence, like vildagliptin, anagliptin has to be administered twice daily. The drug is moderately protein bound (~37%). Hydrolysis of the cyanopyrrolidine to the corresponding inactive acid, likely in part by DPP-4, forms a major metabolite in vivo (22.3% of the radiolabeled AUC), which has a longer terminal half-life of 9.88 h.[181] Excretion of the radiolabeled dose was primarily by active renal secretion of anagliptin and its acid metabolite in the urine (73.2%), with 25% of the administered dose recovered in feces. In a 24-week phase III study in T2DM patients conducted in Korea, anagliptin 100 or 200 mg bid produced similar placebo-subtracted HbA1c reductions of 0.73% and 0.74%, respectively, from a mean baseline HbA1c of 7.1%.[182] The safety profile was typical for the class, with nonsignificantly higher incidences of pharyngitis, rhinitis, and upper respiratory tract infections compared with placebo. Anagliptin has been approved for use in Japan for the treatment of type 2 diabetes.[183]

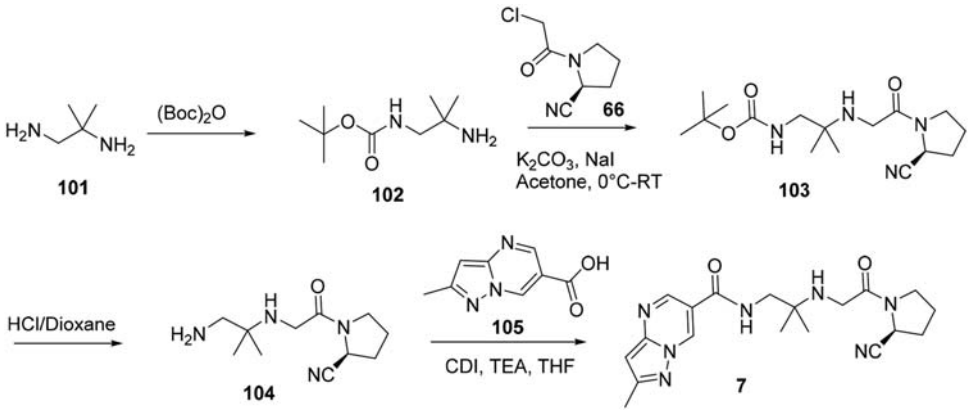

Scheme 13 Synthesis of anagliptin.

The synthesis of anagliptin is summarized in Scheme 13. The selective Boc protection of 2-amino-2-methylpropylamine **101** with Boc anhydride followed by coupling with (*S*)-1-(2-chloroacetyl)pyrrolidine-2-carbonitrile **66** gave compound **103**. After deprotection of the Boc group, compound **103** was coupled with pyrazolo[1,5-a]pyrimidinecarboxylic acid **105** to afford anagliptin **7** in excellent yield.[128]

7.14.5.1.3 Pyrimidinedione/xanthine analogs

7.14.5.1.3.1 Linagliptin (BI-1356, Boehringer Ingelheim)

Linagliptin **8** is a xanthine-based DPP-4 inhibitor. It is highly potent with an IC_{50} of 1.0 nM and is highly selective for DPP-4 over DPP-8 (10,000-fold), DPP-9 (>10,000-fold), and other related peptidases.[123,184,185] Oral bioavailability of linagliptin is reported to be 15–51% in rats, with the drug having a volume of distribution of 5.4–40 L kg^{-1}, a clearance of 37–56 mL min^{-1} kg^{-1}, and a relatively long half-life of 36 h.[123,186] Corresponding values in monkeys are 51%, 16 mL kg^{-1} min^{-1}, and 41 h.[123] The drug is not appreciably metabolized in vivo, with about 80% of radiolabeled linagliptin in the plasma appearing as the parent compound in mice, rats, and humans.[187] After 14 days of repeated oral dosing with radiolabeled linagliptin in rats, approximately 90% of the radioactivity was recovered in the feces, and only ~1% was found in the urine.[188] Multiple oral doses of linagliptin (1, 2.5, 5, or 10 mg qd for 12 days) were administered to patients with type 2 diabetes. The T_{max} was 1–3 h post dose after both single and multiple dosing, and drug exposure (linagliptin AUC) and maximal concentration (C_{max}) values increased dose-dependently but in a less than dose-proportional manner. Steady state was attained within 2–5 days, with only modest drug accumulation (accumulation ratio, 1.18–2.03). At steady state, linagliptin was cleared at a rate of 14–70 mL min^{-1}, and the elimination half-life ranged from 113 to 130 h. Renal excretion of linagliptin was low across all doses, being <1% on day 1 and remaining below 6% on day 12.[189]

Single doses of linagliptin dose-dependently inhibited plasma DPP-4 activity in normal Han–Wistar rats by >70% at 1 mg kg^{-1} and by ~90% at 3 and 10 mg kg^{-1}, measured 7 h post dose.[185] Similar results were obtained in diabetic *db*/*db* mice.[123] In obese insulin-resistant Zucker rats, linagliptin reduced glucose excursion during an OGTT, both when dosed 30 min before the glucose challenge and when dosed 24 h before testing. Acute glucose lowering was associated with increases in intact GLP-1 and insulin levels.[185] In the high-fat diet/STZ-induced mouse model of type 2 diabetes, chronic administration of linagliptin (1, 3, or 10 mg kg^{-1} once daily for 4 weeks) dose-dependently inhibited plasma DPP-4 activity by 59–87% at trough. Oral glucose tolerance was improved to a similar extent after 17 days of treatment at all doses and was associated with improvements in HbA1c after 4 weeks. Basal intact GLP-1 levels 16 h after drug administration were dose-dependently increased up to threefold on day 28.[190] In male Zucker diabetic fatty (ZDF) rats, once-daily administration of linagliptin (3 mg kg^{-1}) for 5 weeks increased intact GLP-1 levels and reduced glucose excursion by ~50% in an OGTT performed at the end of the treatment. In female ZDF rats, which are less severely diabetic, treatment with linagliptin for 7.5 weeks dose-dependently improved glucose tolerance, with the highest dose (3 mg kg^{-1}), leading to a significant reduction in HbA1c.[190]

X-ray crystal structure analysis of the DPP-4-linagliptin complex has revealed that the S1 pocket of DPP-4 is occupied by the butynyl group of linagliptin and the S2 pocket is occupied by the amino piperidine moiety. The amino group of the latter establishes a salt bridge with Glu205 and Glu206 and hydrogen bonds with Tyr662. The aromatic uracil moiety forms a π–π interaction with Tyr547. The carbonyl group at C-6 elicits a hydrogen bond with Tyr631. These interactions enhance binding avidity. The π–π interaction between the quinazoline phenyl and Trp629 is responsible for the enhanced selectivity profile of linagliptin.[123]

Linagliptin is well tolerated with no hypoglycemia in healthy subjects at doses up to 600 mg. The drug exhibits biliary excretion with a terminal half-life of 180 h.[191] In a 12-day study in male T2DM subjects, linagliptin (1, 2.5, 5, or 10 mg once daily) dose-dependently inhibited plasma DPP-4 activity, with >80% inhibition achieved in seven of the eight patients in the 5 mg dose group and in all nine patients in the 10 mg dose group.[189] Moderate accumulation was observed, with the accumulation half-life decreasing with dose from ~24 h at 1 mg dose to ~9 h for the 10 mg dose group. Linagliptin dose-dependently reduced glucose

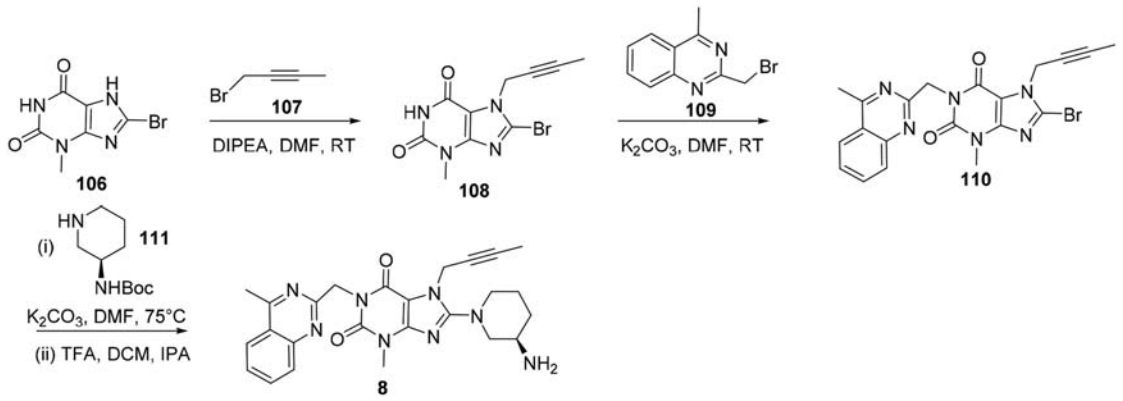

Scheme 14 Synthesis of linagliptin.

excursions and increased active GLP-1 levels during an OGTT both on day 1, and, more markedly, on day 13, reflecting the time to steady state, which ranged between 4 and 6 days for doses up to 5 mg. In a 24-week phase III study in T2DM subjects, linagliptin (5 mg once daily) improved glycemic control with a placebo-subtracted HbA1c reduction of 0.69% from a mean baseline of 8.00%.[192] The drug was well tolerated, with an adverse event profile similar to that of the placebo group. Linagliptin 5 mg was approved by the US FDA in 2011.

Linagliptin reduced kidney fibrosis in STZ-induced diabetic mice independent of glycemic control[193] and inhibited the high glucose-induced increase of the profibrotic cytokine TGFβ1 in human kidney proximal tubular cells.[194] These effects on the TGF-β axis have been attributed to a molecule-specific effect of linagliptin, since they are reportedly not recapitulated by sitagliptin.[195] Linagliptin is currently being assessed for cardiovascular and renal outcomes in T2DM patient in the cardiovascular and renal microvascular outcome study With linagliptin in patients with type 2 diabetes mellitus trial (CARMELINA)[196] and against glimepiride for cardiovascular outcomes in the cardiovascular outcome trial of linagliptin versus glimepiride in type 2 diabetes trial (CAROLINA).[109]

The synthesis of linagliptin presented in **Scheme 14** begins with N-7 alkylation of xanthine analog **106** with 1-bromo-2-butyne **107** to afford compound **108**. N-1 alkylation of **108** with **109** resulted in compound **110**, which on nucleophilic substitution at C-8 by 3-aminopiperidine **111** and subsequent Boc deprotection afforded linagliptin **8**.[123]

An alternative[197–200] route for the synthesis of linagliptin shown in **Scheme 15** involved the preparation of a key intermediate **115** via either the cyclization of 2-aminoacetophenone **112** with chloroacetonitrile **113** or the reaction of quinazoline oxide **114** with PCl_3. N-1 alkylation of **108** with **115** gave the compound **116**. Linagliptin **8** was prepared by nucleophilic substitution at the C-8 position of **116** by piperidine derivative **117** followed by deprotection with 2-aminoethanol.

7.14.5.1.3.2 Alogliptin (SYR-322, Takeda)

Alogliptin 9 is a quinazolinone-based potent inhibitor of DPP-4 exhibiting an IC_{50} of ~6.9 nM and >10,000-fold selectivity for DPP-4 over the other DASH peptidases.[122,201] Alogliptin exhibited favorable PK and PD profiles in rats, dogs, and monkeys.[201]

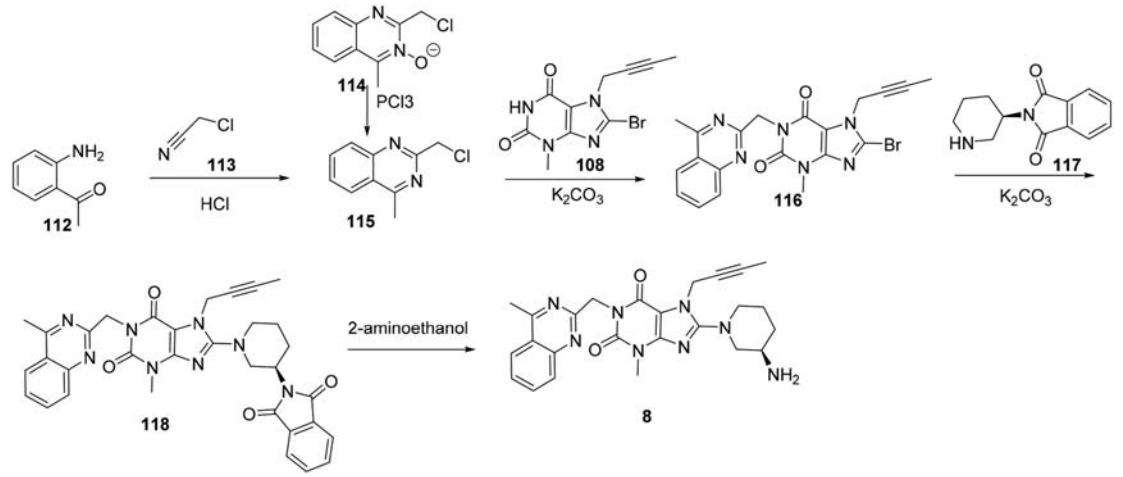

Scheme 15 Second route to the synthesis of linagliptin.

Alogliptin was absorbed rapidly (T_{max} values of 0.4–2.3 h across preclinical species) and exhibited oral bioavailability of 45–88%.[201] Plasma DPP-4 inhibition occurred dose-dependently and rapidly (within 15 min post dose) in all species. Plasma DPP-4 inhibition was sustained in rats (43% DPP-4 inhibition at 12 h following a 10 mg kg^{-1} dose), dogs (65% DPP-4 inhibition at 12 h following a 3 mg kg^{-1} dose), and monkeys (>80% DPP-4 inhibition at 24 h following doses of 2, 10, or 30 mg kg^{-1}), supportive of a once-daily dosing regimen.

Administration of alogliptin to Zucker *fa/fa* rats (0.3–10 mg kg^{-1}) maximally inhibited plasma DPP-4 activity by >90% at all doses, with >65% DPP-4 inhibition measured 24 h after the 10 mg kg^{-1} dose. Alogliptin plasma concentrations of ~5.5 ng mL^{-1} (16.2 nM) were sufficient to inhibit plasma DPP-4 activity by at least 80%. Alogliptin dose-dependently inhibited plasma DPP-4 activity, increased GLP-1 levels, augmented early-phase insulin secretion, and reduced blood glucose excursion in response to an oral glucose challenge. Maximal PD effects were observed at the 10 mg kg^{-1} dose in these animals.[122,201,202]

X-ray studies revealed that the cyanobenzyl group of alogliptin occupies the S1 pocket of DPP-4 and interacts with Arg125. The aminopiperidine scaffold of alogliptin binds into the S2 pocket by making a salt bridge interaction with the carboxylate groups of Glu205 and Glu206. The carbonyl group hydrogen bond with the backbone amide of Tyr631 and the central uracil core forms a π–π interaction with the side chain of Tyr547.[122,124]

In healthy subjects and T2DM patients, alogliptin had a T_{max} of 1–2 h, absolute bioavailability of 100%, and a large volume of distribution (greater than total body water), suggesting wide distribution in tissues.[203,204] The drug was well tolerated at all doses tested from 25 to 800 mg. The drug is minimally metabolized to N-demethylated and N-acetylated derivatives (<1% and <6% of the dose, respectively) and is actively secreted in the urine (60–71%) as parent drug.[205] CYP2D6 and CYP3A4 are the major metabolizing enzymes for alogliptin, but given the minimal metabolism, there have been no reports of any significant drug–drug interactions. The drug has an elimination half-life of 12.5–21 h.[204] In healthy subjects, alogliptin maximally inhibited plasma DPP-4 activity by 93.3–98.8% at all doses tested, with 24 h mean DPP-4 inhibition ranging from 74.3% to 97.0%. Multiple doses of alogliptin (25, 100, and 400 mg once daily) over 14 days inhibited DPP-4 activity by >81% at trough,[205] further supporting the rationale for once-daily dosing. The efficacy of alogliptin monotherapy (12.5 or 25 mg once daily) in T2DM patients was assessed in a 26-week phase III study.[206] The two doses produced placebo-subtracted HbA1c reductions of 0.54% and 0.57%, respectively, from a mean HbA1c baseline of 7.9%. The drug was well tolerated with AEs typical of the class (headache, infection, and gastrointestinal) and comparable to placebo. The incidence of headache (6.8–7.5%) and skin-related events (12.8–15.2%, mainly pruritus) was higher than the placebo group (4.7% and 6.3%, respectively). Alogliptin was approved in Japan in 2010 and by the US FDA in 2013. The recommended drug dosage is 25 mg once daily in patients with normal renal function and 12.5 or 6.25 mg once daily in patients with moderate or severe renal impairment.[207]

The cardiovascular safety of alogliptin was assessed in patients with established ACS in the examination of cardiovascular outcomes with alogliptin versus standard of care in patients with type 2 diabetes mellitus and acute coronary syndrome trial (EXAMINE).[208] The noninferiority primary composite endpoint for death from cardiovascular causes, nonfatal myocardial infarction, or nonfatal stroke was achieved. There was a statistically nonsignificant increased risk of hospitalization for heart failure resulting in a label warning,[173] although all-cause mortality was not increased in the trial.

The synthesis of alogliptin is shown in **Scheme 16**. 4-Chlorouracil **119** was reacted with 2-(bromomethyl) benzonitrile and afforded compound **120**.[209] Methylation of **120** followed by nucleophilic substitution with 3-(R)-aminopiperidine **122** gave alogliptin **8** as the TFA salt.[122,210]

7.14.5.1.3.3 Trelagliptin (SYR-472, Takeda/Furiex)

Trelagliptin **10** is a fluorinated analog of alogliptin. It is a long-acting DPP-4 inhibitor amenable for once-weekly oral administration.[124] It is potent (IC_{50} = 4 nM) with high selectivity (>100,000) against DPP-8 and other related enzymes. Trelagliptin effects a sustained PD effect in dogs and inhibited >80% plasma DPP-4 activity at 24 h after a single oral dose of 7 mg kg^{-1}. It also exhibited favorable PK profiles in dogs and monkeys with half-lives of 4.8 and 8 h, respectively, and oral bioavailability of 90–105%. Trelagliptin 1 mg kg^{-1} exhibited acute antihyperglycemic efficacy in an OGTT conducted in Zucker *fa/fa* rats, with a reduction in glucose excursion and augmented plasma insulin levels.[124]

Due to its structural similarity to alogliptin, trelagliptin exhibits similar interactions with the active site of DPP-4.[124] The aminopiperidine moiety forms salt bridges with Glu205 and Glu206, while the fluorocyanobenzyl group occupies the hydrophobic S1 pocket and interacts with Arg125. The carbonyl at the 2-position forms an important hydrogen bond with the backbone NH of Tyr631 and the uracil core π-stacks with Tyr547.

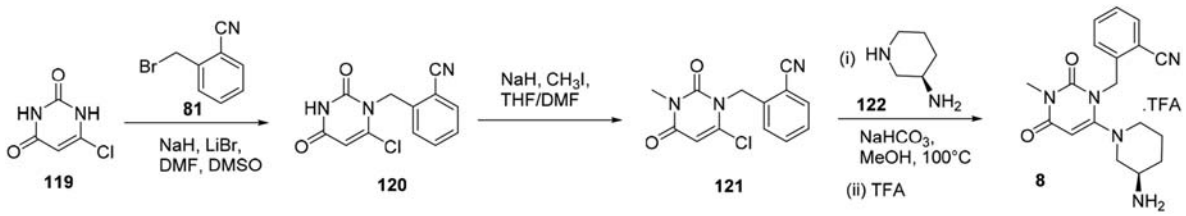

Scheme 16 Synthesis of alogliptin.

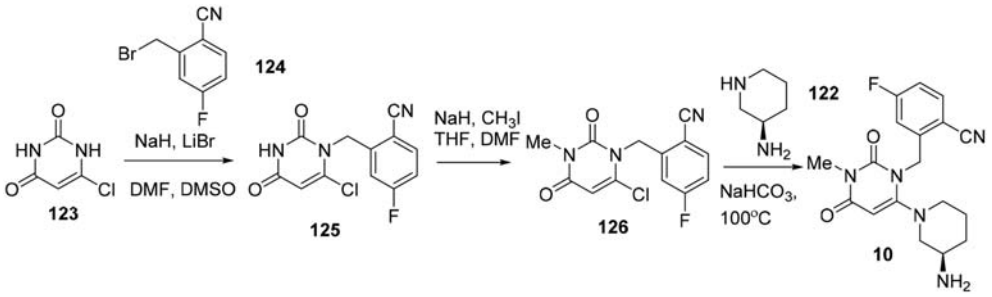

Scheme 17 Synthetic approach toward trelagliptin.

Trelagliptin is rapidly absorbed in healthy subjects following a 100 mg dose, with a T_{max} of 1.3 h.[211] The mean elimination half-life was 18.5–54.3 h. Trelagliptin is metabolized by CYP2D6, and the drug is mainly renally cleared. The marketed dose of 100 mg once weekly is recommended to be reduced to 50 mg in patients with moderate renal impairment.[211] In a phase II dose range-finding study, trelagliptin reduced HbA1c in a dose-dependent manner when administered once weekly for 12 weeks at doses of 12.5–200 mg in Japanese T2DM patients.[212] A maximum placebo-subtracted HbA1c reduction of ~0.9% was obtained at the 100 and 200 mg doses from a baseline of ~8.2%. In a 24-week phase III trial in Japanese T2DM patients, trelagliptin 100 mg once weekly was noninferior to alogliptin 25 mg once daily.[213] Trelagliptin was well tolerated with no serious AEs considered to be related to treatment. It was approved in Japan for the treatment of T2DM in 2014.

Synthesis of trelagliptin is outlined in Scheme 17. Selective alkylation of chlorouracil **123**, followed by methylation, provided compound **126**. The displacement of chloride with 3-(R)-aminopiperidine **122** afforded trelagliptin **10**.[124]

7.14.5.2 DPP-4 Inhibitors in Phase III

Five potent, safe, and well-tolerated peptidomimetic DPP-4 inhibitors are reported to have entered phase III clinical trials as summarized in Table 3. These molecules are dutogliptin (**13**), gosogliptin (**9**), denagliptin (**11**), melogliptin (**10**), and retagliptin (**12**).

7.14.5.2.1 Dutogliptin (PHX1149, Phenomix Corp)

Dutogliptin (PHX1149) **127** is a boronic acid-based DPP-4 inhibitor. Dutogliptin is a highly water-soluble (>2 g mL^{-1}) DPP-4 inhibitor with 15- to 319-fold selectivity over other members of the DPP family and a DPP-4 IC_{50} of 25 nM.[214,215] PK and PD studies indicate that PHX1149 inhibits DPP-4 enzymatic activity across preclinical species in a time- and dose-dependent manner.[214] In a single-dose study of PHX1149 at 50, 100, 200, 300, or 500 mg in healthy male subjects after an overnight fast, mean drug AUC increased in a dose-proportional manner with a median T_{max} of 2–4 h.[215] The half-life for PHX1149 was ~10–13 h. Dose-dependent maximal inhibition of DPP-4 ranging from 64% to 92% was observed 2–4 h post dose. Near-maximal DPP-4 inhibition for 24 h was observed at the 300 and 500 mg doses, and the EC_{50} and EC_{90} values for DPP-4 inhibition by PHX1149 in vivo were ~10 and ~100 ng mL^{-1}, respectively.[215]

Dutogliptin was evaluated in a 12-week phase II study in T2DM patients not optimally controlled with metformin and/or thiazolidinediones.[216] Patients were randomized to receive oral doses of dutogliptin 200 mg and 400 mg once daily. Placebo-subtracted reductions from baseline in HbA1c were 0.34% and 0.52%, from a baseline HbA1c of ~8.4%, and dutogliptin also significantly reduced FPG. The incidence of AEs was similar in treatment and placebo groups, with slightly more headache, arthralgia, sinusitis, and dizziness occurring in the 400 mg group compared with placebo.

Synthesis of dutogliptin begins with pyrrolidine **132**, which, after Boc protection, gave **133**. Treatment of **133** with *sec*-butyllithium and trimethoxyborane resulted in **134**, which, on reaction with (+)-pinanediol, followed by Boc deprotection provided key intermediate **135**. Another core intermediate **138** was prepared from N-protected 3-aminopyrrolidine **136** via alkylation, cbz protection, and hydrolysis of the methyl ester. The coupling of pyrrolidine intermediate **135** with **138** provided **139**, which after cbz and (+)-pinanediol deprotection with hydrogenation and phenyl boronic acid, respectively, afforded dutogliptin **127**.[217] Alternative routes for the synthesis of dutogliptin[218,219] have also been reported (Scheme 18).

7.14.5.2.2 Gosogliptin (PF-00734200, Pfizer)

Gosogliptin **128** is a diprolyl-derived piperazine-containing DPP-4 inhibitor with an IC_{50} of 13 nM and 100-fold selectivity over DPP-II and DPP-8.[220] In rats and dogs, gosogliptin had a half-life of 2.5 and 2.9 h, respectively, with corresponding bioavailability of 109% and 95%.[220,221] In cynomolgus monkey, the half-life of gosogliptin was 7.6 h, with 71% bioavailability.

The X-ray crystal structure of gosogliptin bound to DPP-4 confirms that the hydrophobic difluoropyrrolidide moiety binds to the S1 pocket where it forms hydrophobic interactions with Trp659, Val 656, Tyr631, Ser630, Tyr666, and Tyr662. One of the fluorines forms a hydrogen bond with either Ser630 or the backbone amide of Tyr631. The remaining part of the inhibitor occupies the S2 pocket where the secondary amine of the pyrrolidine makes a salt bridge with the carboxylates of Glu206 and Glu205. The

Table 3 DPP-4 inhibitors in phase III

DPP-4 inhibitors	*Generic/common name*	*Structure*	*Originator*
127 PHX1149	Dutogliptin	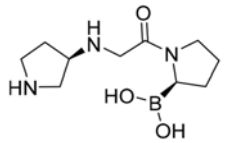	Phenomix Corp.
128 PF-734200	Gosogliptin	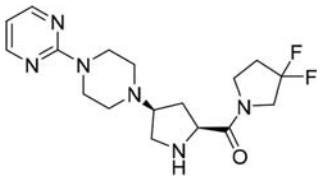	Pfizer
129 GSK-823093 (GW823093)	Denagliptin	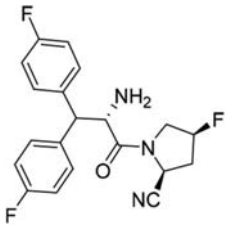	GlaxoSmithKline
130 GRC-8200 (EMD 675992)	Melogliptin	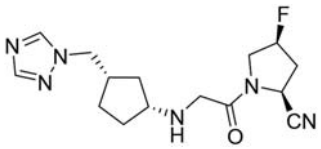	Glenmark
131 SP-2086	Retagliptin	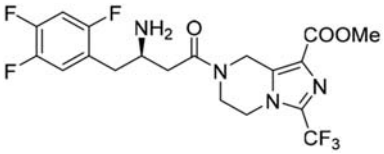	Jiangsu Hengrui Medicine

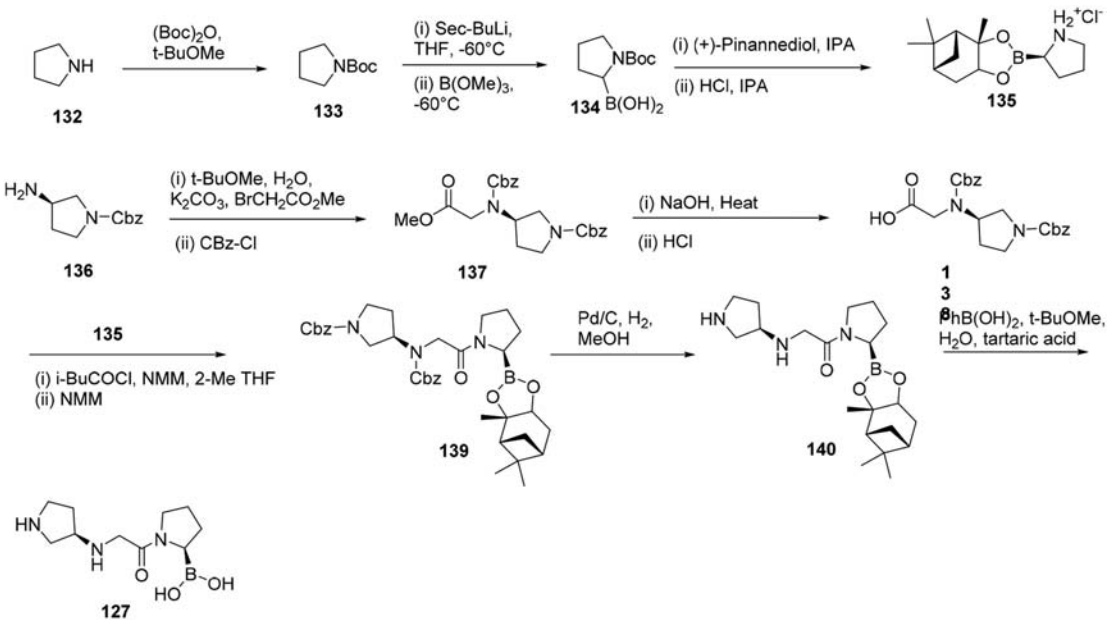

Scheme 18 Synthesis of dutogliptin.

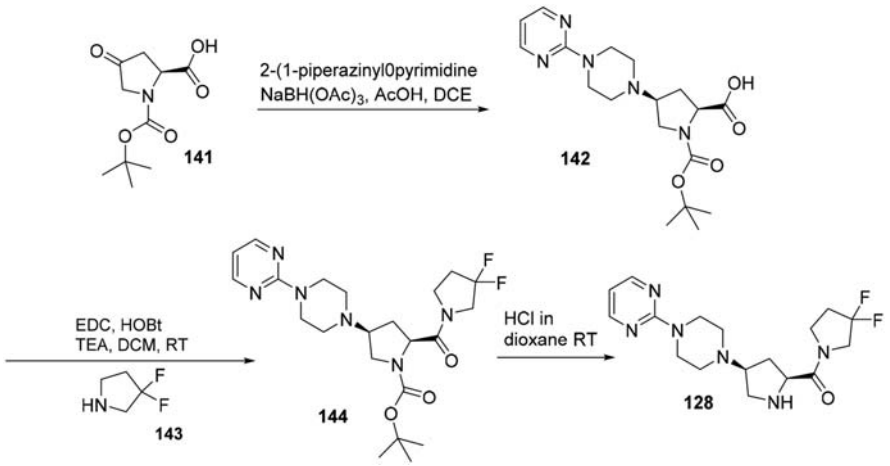

Scheme 19 Synthesis of gosogliptin.

pyrimidine moiety binds in the S2 extended pocket and forms a π–π stacking interaction with the side chain of Phe357, which is responsible for enhancing selectivity.[220]

Gosogliptin was rapidly absorbed in healthy subjects with a mean T_{max} of 1 h and a mean half-life of 63.5 h.[221] Gosogliptin was renally cleared with a cumulative excretion in urine of 76.8% after a single dose. Radiolabeled gosogliptin undergoes moderate metabolism in humans, with parent drug representing 48.9% of total excreted radioactivity and hydroxylation at the 5′ position of the pyrimidine ring by CYP3A4 and CYP2D6 representing a major metabolite (20.6% of the dose).[221] In healthy Japanese subjects, administration of gosogliptin 20 mg once daily for 6 days inhibited DPP-4 activity at steady state by ~75% and enhanced GLP-1 levels twofold after a standardized meal.[222]

In a 12-week add-on study in T2DM patients inadequately controlled with metformin, gosogliptin 20 or 30 mg once daily resulted in placebo-subtracted HbA1c reductions of 0.79% and 0.92% reductions, respectively. The difference in HbA1c reduction between the two doses was not statistically significant.[223]

Gosogliptin was synthesized as shown in Scheme 19. The stereoselective reductive amination reaction of ketone **141** with 2-pyrimidylpiperazine in the presence of triacetoxyborohydride afforded only the *cis* isomer **142**. Coupling **142** with 3,3-difluropyrrolidine **143** using an EDC/HOBt protocol followed by Boc deprotection with HCl in dioxane afforded gosogliptin **128**.[220]

7.14.5.2.3 Denagliptin (GSK-823093, GlaxoSmithKline)

Denagliptin **129** belongs to the cyanofluoropyrrolidine class of DPP-4 inhibitors. It inhibits human DPP-4 with an IC_{50} of 22 nM.[224] Modeling studies show that denagliptin binds in the active site of DPP-4 as a substrate-based inhibitor and forms five strong hydrogen bonds with the side chains of Glu205, Glu206, Asn710, Tyr662, and Arg125.[225]

In phase I studies, denagliptin (25 mg) was rapidly absorbed, with maximal DPP-4 inhibition after 30 min and >80% DPP-4 inhibition after 24 h. In a 7-day, multiple-dose, phase IIA study, denagliptin produced sustained DPP-4 inhibition and elevated levels of GLP-1 and insulin and exhibited no body weight gain.[224]

Denagliptin was synthesized from bisfluorobiphenyl **145**, which was first converted to hydroxy acid **146** and then into acid **148** by successive treatment with H_2SO_4 and catalytic hydrogenation. Compound **148** was converted into oxazolidine amide **149**. Compound **149** on the introduction of an azide moiety provided compound **150**, which after hydrolysis followed by subsequent reduction to amine, and Boc protection gave the desired intermediate **152**. Finally, the coupling of **152** with 4-fluoro-2-pyrrolidinecarbonitrile **153** followed by Boc deprotection afforded denagliptin **129** (Scheme 20).[226,227]

7.14.5.2.4 Melogliptin (GRC 8200, Glenmark)

Melogliptin **130** is a potent DPP-4 inhibitor (IC_{50} = 1.6 nM) containing a triazole moiety. It is 10,000-fold selective against DPP-8 and DPP-9.[228,229] The binding mode of melogliptin with DPP-4 has not been reported, but it likely binds similarly to other substrate mimetics. At a dose of 5 mg kg^{-1}, melogliptin exhibited half-lives of 1.28, 4.31, and 2.15 h with 50–95% bioavailability across preclinical species.[230]

A single oral dose of melogliptin (3 mg kg^{-1}) resulted in a 30% reduction of glucose and twofold enhanced insulin levels in *db*/*db* mice.[228] In overnight fasted beagle dogs, a single oral dose of melogliptin 5 mg kg^{-1} maximally inhibited DPP-4 activity within 1 h and achieved >90% inhibition within 1 h.[228]

In phase II clinical studies, melogliptin 50 mg twice daily or 100 mg once daily inhibited plasma DPP-4 activity by more than 90% within an hour of dosing and reduced HbA1c by 0.75% and 0.60%, respectively.[231]

The synthesis of melogliptin is illustrated in Scheme 21. It starts with Boc protection of ketone **154** to give compound **155**. After palladium-catalyzed reduction of **155**, the resulting compound **156** was reduced with sodium borohydride to give amino alcohol

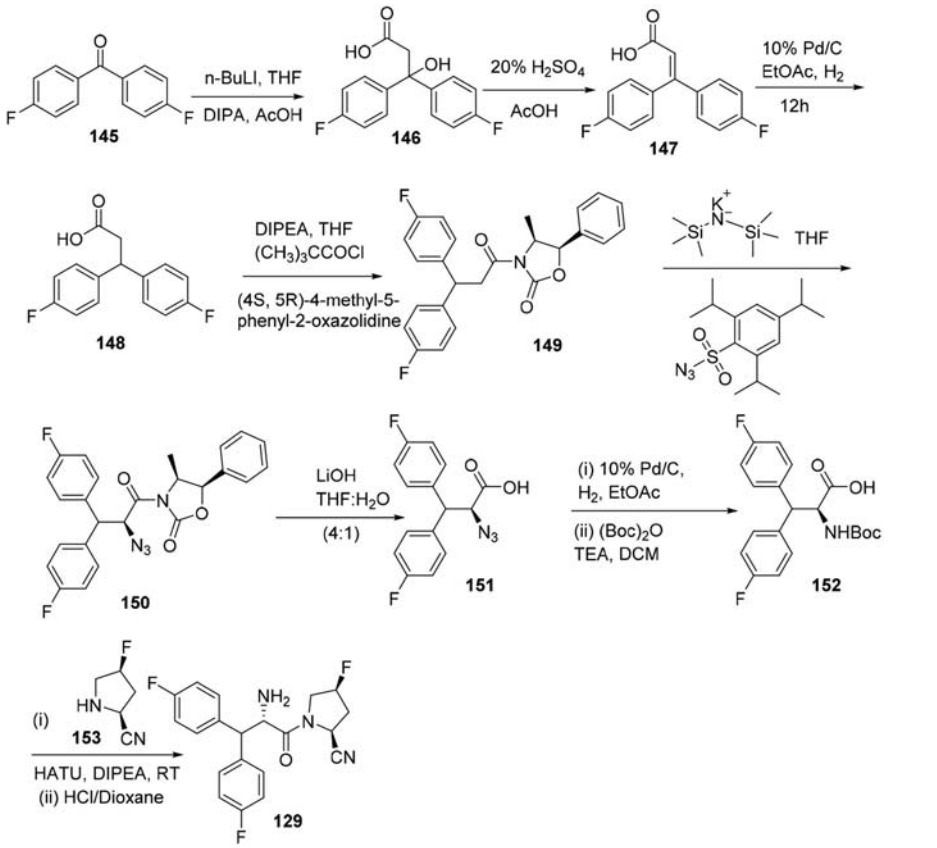

Scheme 20 Synthesis approach of denagliptin.

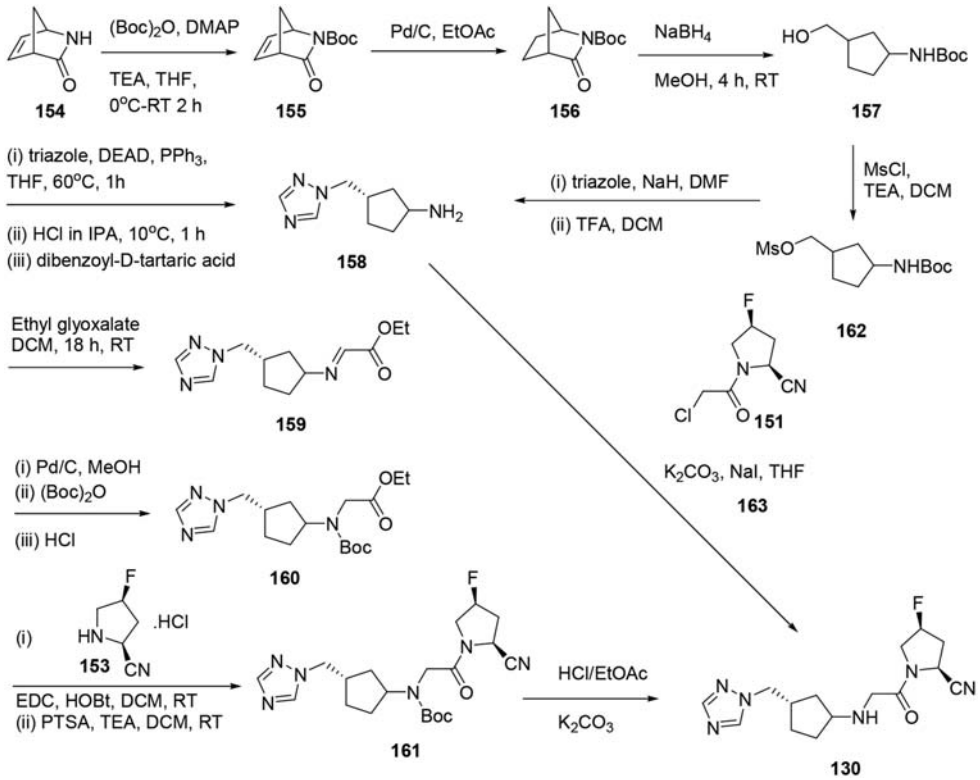

Scheme 21 Synthesis of melogliptin.

157. Compound **158** was prepared via Mitsunobu reaction followed by Boc deprotection and resolution with dibenzoyl D-tartaric acid. Compound **158** after reductive amination and successive Boc protection provided **160** via **159**. Coupling with **153** followed by Boc deprotection then afforded melogliptin **130**.[229]

A second route toward melogliptin synthesis began with the mesylation of compound **157** shown on the right hand side of Scheme 21, to yield **162**, which on reaction with triazole using sodium hydride followed by Boc deprotection afforded compound **158**. Finally, coupling of **158** with chloroacetamide **163** gave melogliptin **130**.[232]

7.14.5.2.5 Retagliptin (SP-2086, Jiangsu Hengrui Medicine)

Retagliptin **131**, a tetrahydro-imidazo[1,5-a] pyrazine analog of sitagliptin. It is twice as potent as sitagliptin ($IC_{50} = 8$ nM) and has good selectivity against DPP-8 (>3000-fold) and DPP-9 (>9000-fold).[233,234]

In clinical studies, retagliptin exhibited a half-life of 1.5 h, and treatment of T2DM patients resulted in meaningful reductions in plasma glucose and HbA1c. It is currently undergoing phase III clinical trials.[234]

The synthesis of retagliptin, which is similar to the method described earlier for sitagliptin, is illustrated in Scheme 22. The sequence involved the preparation of two important intermediates **21** and **173**. The β-amino acid intermediate **21** was synthesized from compound **164**. Treatment with 2,2-dimethyl-[1,3]dioxane-4,6-dione **29** in the presence of DMAP and EDC followed by subsequent heating in ethanol, treatment with ammonium acetate in methanol, Boc protection, stereocontrolled hydrogenation, and hydrolysis afforded intermediate **21** via intermediates **165**, **166**, **167**, and **168**. The tetrahydro-imidazo[1,5-a]pyrazine moiety **173** was prepared from pyrazine-2-carbonitrile **169**, which, following Ni-catalyzed hydrogenation followed by acylation with TFAA, gave compound **171** via **170**. The intramolecular cyclization of compound **171** with phosphorous oxytrichloride gave compound **172**, which on catalytic hydrogenation over Pd/C provided the tetrahydro-imidazo[1,5-a]pyrazine intermediate **173**. The coupling of **21** with **173** provided compound **174**. Treatment with *N*-bromosuccinimide subsequently yielded **175**, which was Boc-protected and successively treated with ethyl chloroacetate in the presence of octacarbonyldicobalt and potassium carbonate. Final Boc deprotection afforded retagliptin **131**.[235,236]

7.14.5.3 DPP-4 Inhibitors in Phase II

Seven DPP-4 inhibitors reported in phase II clinical trials are shown in Table 4. These are R-1579 (carmegliptin, **177**), P32/98 **178**, TS-021 **179**, AMG-222 **180**, NVP-DPP728 **181**, R-1438 **182**, and Ro-0730699 **183**.

Carmegliptin (R-1579) jointly developed by Roche and Chugai comprises a tricyclic moiety. It is a potent DPP-4 inhibitor ($IC_{50} = 6.8$ nM) with >100-fold selectivity over DPP-8 and DPP-9 and >2000-fold selectivity over DPP-II and FAP. Carmegliptin exhibits balanced hepatic and renal excretion with an IV half-life of 6.8 h and 33% oral bioavailability in cynomolgus monkeys. In

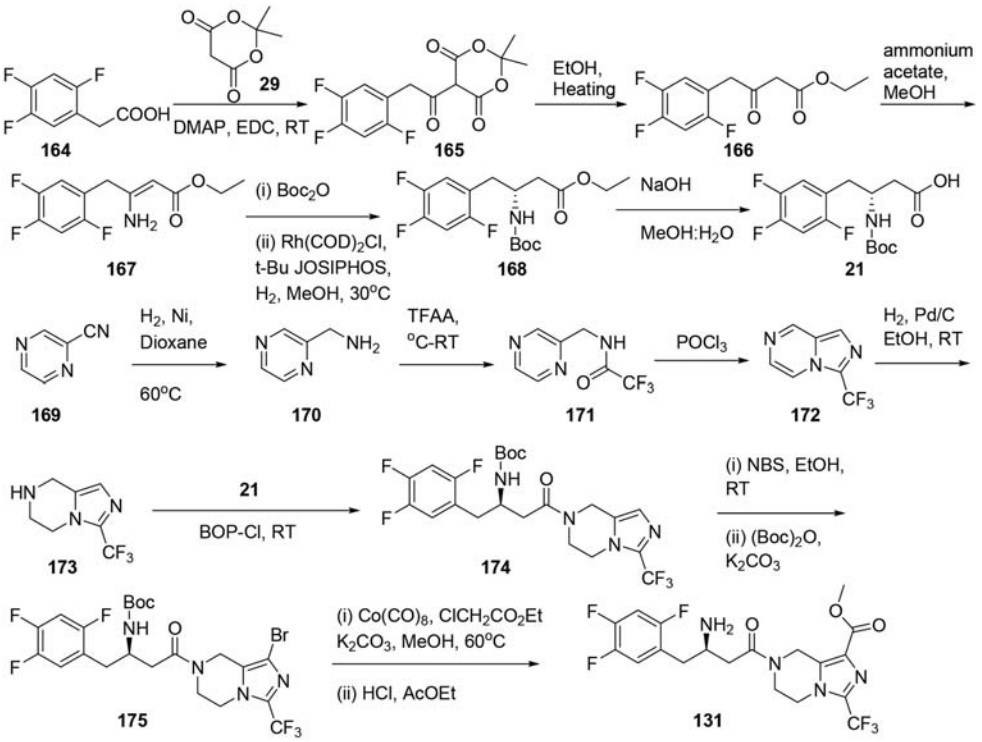

Scheme 22 Synthesis of retagliptin.

Table 4 DPP-4 inhibitors in phase II

DPP-4 inhibitors	*Structure*	*Generic/common name*	*Originator*	*IC_{50} and K_i (nM)*
177 R-1579 (Ro-4876904)	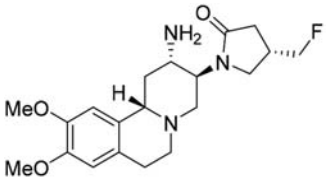	Carmegliptin	F Hoffman-La Roche	$IC_{50}=6.8$
178 P32/98	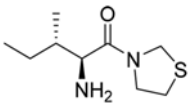	Isoleucine thiazolidide	Probiodrug AG	$IC_{50}=420$ $K_i=80$
179 TS-021	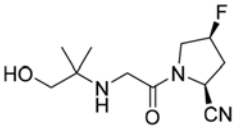	Cyanopyrrolidine analog	Taisho Pharmaceutical Co Ltd./Eli Lilly	$IC_{50}=5.34$ $K_i=4.96$
180 AMG-222 (ALS-2-0426)	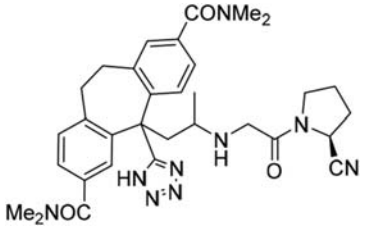	Cyanopyrrolidine analog	Alantos Pharmaceuticals and Amgen Inc.	–
181 NVP-DPP-728	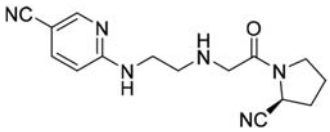	Cyanopyrrolidine analog	Novartis	$IC_{50}=22$ $K_i=11$
182 R-1438	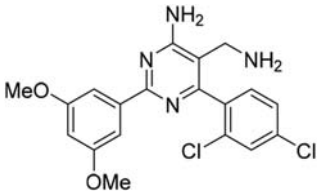	Aminomethylpyridine derivative	Roche	$K_i=0.1$
183 Ro-0730699	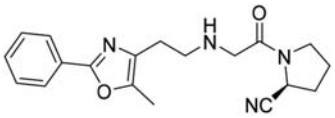	Cyanopyrrolidine derivative	F Hoffman-La Roche	$IC_{50}=75$ $K_i=80$

an OGTT performed in Zucker fatty (*fa/fa*) rats, treatment with carmegliptin (0.3 mg kg^{-1}) resulted in reduced glucose excursion. At a single oral dose of 3 mg kg^{-1}, DPP-4 inhibition reached 40% and 60% 24 and 48 h post dose, respectively. Phase I and II clinical studies have assessed the safety and efficacy of carmegliptin with once-daily dosing.[237] Inhibition of various CYP isozymes and hERG channel inhibition are the major challenges in advancing this compound.

X-ray crystal structure analysis reveals that the 4-fluoromethyl pyrrolidinone moiety of carmegliptin binds in the hydrophobic S1 pocket at the active site of DPP-4. The lactam carbonyl hydrogen bonds with Tyr662 and with the amino side chain of Asn710 and forms a cation–dipole interaction with the guanidine side chain of Arg125. These interactions highlight the similarity between this amide carbonyl group and the carbonyl moiety of substrate-based inhibitors. The tricyclic moiety of carmegliptin appears to fit well into the S2 pocket. The amine group forms a salt bridge with Glu205 and Glu206 and a hydrogen bond with Arg125.

The synthesis of carmegliptin is described in **Scheme 23**. The pyridoisoquinoline amine **199** was prepared from the anhydride **192** via several transformations that included a chiral resolution of **196** to furnish **197**. Compound **197** was converted to **198**, which on treatment with diacetoxyiodosobenzene afforded the desired intermediate **199**. Another key intermediate, acid chloride **203**, was prepared from (*S*)-paraconic acid **200**.[289] The reduction of **200** with borane-dimethyl sulfide complex gave the hydroxymethyl lactone **201**. Since compound **201** is known to racemize rather readily,[238] it was immediately treated with bis(2-methoxyethyl) aminosulfur trifluoride,[239] which gave fluoromethyl lactone **202**. Reaction of **202** with thionyl chloride in the presence of zinc chloride

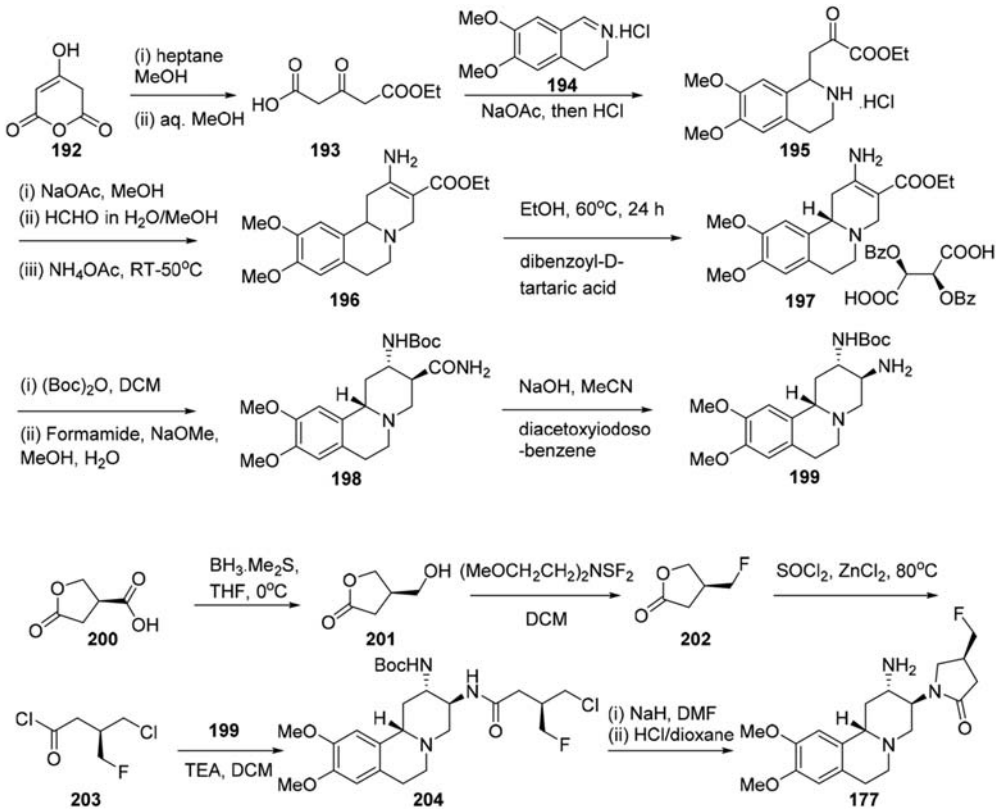

Scheme 23 Synthesis of carmegliptin.

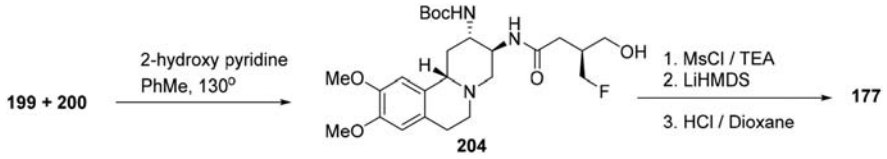

Scheme 24 Second approach for Synthesis of carmegliptin.

provided acid chloride **203** intermediate. The reaction of pyridoisoquinoline amine **199** with acid chloride **203** afforded the compound **204**, which after treatment of sodium hydride followed by Boc deprotection gave carmegliptin **177**.[237]

An alternative route for the synthesis of carmegliptin is outlined in Scheme 24[240,241]

Among the other compounds in early development, P32/98 **178** was discontinued due to adverse findings in animal toxicity studies.[79] NVP-DPP-728 **181** does not appear to provide any advantages over vildagliptin in terms of potency or safety.[159] Compound **183** is an investigational cyanopyrrolidine containing DPP-4 inhibitor with a half-life of 2.3 h and 90% oral bioavailability.[242] Compound **180** is another N-substituted cyanopyrrolidine derivative with a large bulky group at the P1 site. TS-021 **179** is an N-substituted substrate-mimicking glycine containing cyanopyrrolidine-based inhibitor. X-ray crystallographic studies revealed the binding mode of **179** in which the cyanopyrrolidine moiety fits neatly into the S1 pocket and the 2-hydroxy-1,1-dimethylethyl moiety occupies the pocket containing His126, Ser201, Phe357, and Arg358 residues.[290] All of these inhibitors have undergone evaluation for dose-ranging efficacy and tolerability.

7.14.5.4 DPP-4 Inhibitors in Phase I

DPP-4 inhibitors currently undergoing phase I clinical trials based on their potency, selectivity, tolerability, efficacy, and preclinical safety are ABT-279 **205**, ABT-341 **206**, E-3024 **208**, SSR-162369 **211**, TAK-100 **207**, ER-319711 **209**, GSK-23A, and imigliptin **212** **210** (Table 5).

ABT-279 **205** was demonstrated to be a safe and effective DPP-4 inhibitor in ongoing phase I trials. 5-Ethynyl substitution on the cyanopyrrolidine ring of ABT-279 was responsible for the improvement in selectivity over related peptidases such as DPP-8 and

Table 5 DPP-4 inhibitors in phase I[a]

DPP-4 inhibitors	*Structure*	*Generic/common name*	*Originator*	*IC_{50} and K_i (nM)*
205 ABT-279 (A-804693)	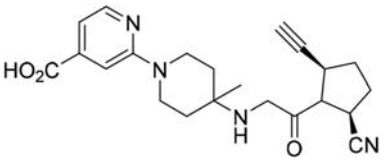	Alkynyl cyanopyrrolidine	Abbott Laboratories	$K_i = 1$
206 ABT-341 (A-916165)	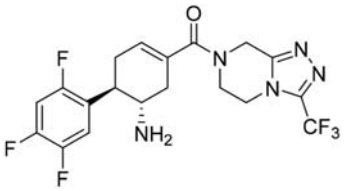	Cyclohexene-constrained phenethyl amine	Abbott	$K_i = 1.3$
ARI-2243			Arisaph Pharma	$K_i = 0027$
207 TAK-100	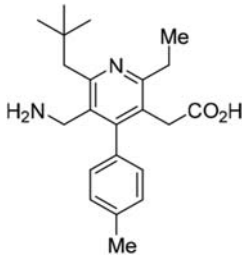	Pyridine derivative	Takeda	$IC_{50} = 5.3$
BMS-477119			Bristol–Myers Squibb	
BMS-686117			Bristol–Myers Squibb	
DSP-7238		Noncyano pyrrolidine analog	Dainippon Sumitomo Pharma	$IC_{50} = 0.58$
208 E-3024	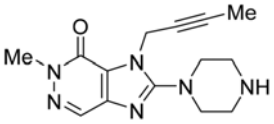	Imidazopyridazinone analog	Eisai Co Ltd.	$IC_{50} = 100$
209 ER-319711-15 (ER-319711)	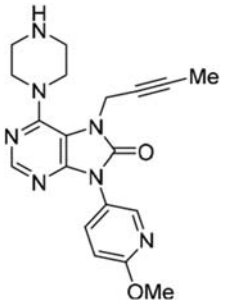	8-Oxo-purine analog	Eisai Co Ltd.	$IC_{50} = 89$
210 GSK-23A	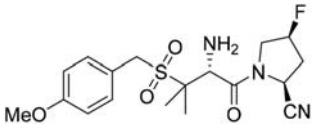	Fluorocyanopyrrolidine analog	GlaxoSmithKline	$K_i = 53$
GSK-825964			GlaxoSmithKline	
NN-7201			Novo-Nordisk	
PBL-1427		Beta-amino acid derivative	Panacea Biotech Ltd.	$IC_{50} = 12$
PSN-357			Prosidion	
R-1499			Roche	
PT-100		Val-BoroPro	Point Therapeutics	$K_i = 0.18$

(Continued)

Table 5 DPP-4 inhibitors in phase I[a]—cont'd

DPP-4 inhibitors	*Structure*	*Generic/common name*	*Originator*	*IC_{50} and K_i (nM)*
211 SSR-162369	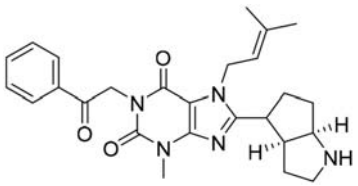	Bicyclic 8-pyrrolidinoxanthine	Sanofi-Aventis	$IC_{50}=18$
TRC-8156		Cyanopyrrolidine deriv.	Torrent Pharmaceuticals	$IC_g=88$
212	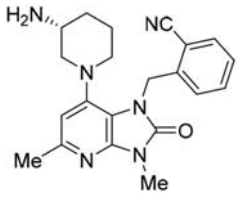	Imigliptin	Sihuan Pharmaceutical	$IC_{50}=9$

[a]Blank cell, data not reported.

DPP-9.[243] ABT-341 **206** is a cyclohexene-based constrained phenethylamine inhibitor of DPP-4. It is potent and selective, and its structure is very similar to sitagliptin. Clinical candidate **206** is orally efficacious and has thus far been deemed safe for the treatment of T2DM patients.[244a] Compound E-3024 **208** exhibits modest potency ($IC_{50}=100$ nM) and high selectivity (>1000-fold).[244b] Its development was discontinued due to observation of rash in healthy volunteers.[244b] SSR-162369 **211** is a bicyclic 8-pyrrolidinoxanthine derivative resembling sitagliptin. It is potent with a DPP-4 IC_{50} of 18 nM.[116,245] TAK-100 **207** is a 3-pyridylacetic acid derivative. It is also potent with a DPP-4 IC_{50} of 5.3 nM and high selectivity (>100,000-fold) against other DASH peptidases. In dogs at a dose of 0.5 mg kg^{-1}, PO, the compound completely inhibited the activity of plasma DPP-4 within 1 h and exhibited 30% inhibition of DPP-4 after 24 h. X-ray studies of TAK-100 bound to the DPP-4 enzyme revealed interactions between the primary amino group and Glu205 and Glu206 residues. The *p*-tolyl group fits into the S1 pocket. The neopentyl group is bound to Phe357 through hydrophobic interactions. The carboxyl group interacts with the side chains of Ser630 and His740. This moiety also forms a salt bridge with the side chain of Arg125.[246]

ER-319711 **209** is an 8-oxo-purine-derived DPP-4 inhibitor. It is potent and selective. In studies comparing the compound with **208**, **209** appears to have a longer glucose-lowering profile suggesting more sustained competitive inhibition of DPP-4.[247]

GSK-23A **210** is a fluorocyanopyrrolidine derivative with a bulky side chain. The steric and electronic effects within a molecule are responsible for the extraordinarily long half-life in buffer (1733 h).[116]

Imigliptin **212** is a pyridinylimidazolone scaffold-based potent ($IC_{50}=9$ nM) and selective (>10,000-fold against DPP-8 and DPP-9) inhibitor of DPP-4. It was discovered via scaffold hopping from alogliptin. It has oral bioavailabilities of 97%, 89%, and 86% in rat, dog, and monkey, respectively. Long-term administration of imigliptin to *db*/*db* mice demonstrated significant lowering of plasma triglycerides and HbA1c and elevated GLP-1 levels. It has good physicochemical properties and a good safety profile. It is currently undergoing phase I clinical trials in China.[248]

7.14.5.5 DPP-4 Inhibitors in Preclinical Development

More than 25 DPP-4 inhibitors have been reported to be in preclinical development (Table 6).

Compounds **213–215**, **217**, and **219**[249] are all cyanopyrrolidine derivatives. In general, these DPP-4 inhibitors in preclinical development are potent and selective. During an OGTT in Zucker fatty rats, RBx-0597 **215** increased the insulin response and ameliorated blood glucose levels.[249] RBx-0597 inhibited human, mouse, and rat plasma DPP-4 activity with IC_{50} values of 32, 31, and 39 nM, respectively. RBx-0597 exhibited significant selectivity (150- to 300-fold) over DPP-8, DPP-9, and other proline-specific proteases (>200- to 2000-fold). Kinetic analysis revealed that RBx-0597 is a competitive and slow-binding DPP-4 inhibitor. In *ob*/*ob* mice, RBx-0597 (10 mg kg^{-1}) inhibited plasma DPP-4 activity up to 50% at 8 h post dose and showed a significant glucose-lowering effect that was sustained through 12 h. The compound also significantly increased active GLP-1 and insulin levels. It showed a favorable PK profile (CLp, 174 mL min^{-1} kg^{-1}, $T_{1/2}$ 0.28 h, T_{max} 0.75 h, and V_{ss} 4.13 L kg^{-1}) in Wistar rats, with oral bioavailability of 65%.[250]

ASP-8497 **214** is potent with DPP-4 IC_{50} of 5.3 nM and excellent selectivity against DPP-8 and DPP-9. Compound **214** inhibits DPP-4 activity in a competitive fashion and significantly reduced glucose excursion during an OGTT in STZ-treated mice.[251] Des-fluoro-sitagliptin **216** is also a potent DPP-4 inhibitor (DPP-4 $IC_{50}=27$ nM) and is highly selective against DPP-8 ($IC_{50}=69{,}000$ nM), DPP-9 ($IC_{50}>100{,}000$ nM), and other DASH peptidases ($IC_{50}>100{,}000$ nM).[79] The inhibitor preserved pancreatic β-cell mass and function in a HFD (STZ)-induced mouse model of type 2 diabetes.[252]

Table 6 DPP-4 inhibitors in preclinical development[a]

DPP-4 inhibitors	*Structure*	*Originator*	*IC_{50} and K_i (nM)*
213 ASP4000	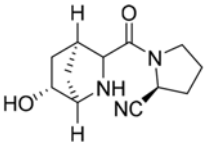	Astellas Pharma Inc.	$IC_{50}=8.7$ $Ki=1.05$
214 ASP-8497	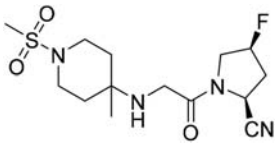	Astellas Pharma Inc.	$IC_{50}=2.6$
215 RBx-0597	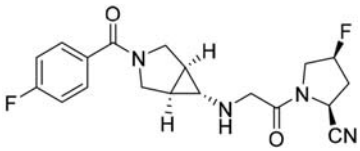	Daiichi Sankyo	
CR-14025		Nuada Pharmaceuticals Inc.	
216 Des-fluoro-sitagliptin	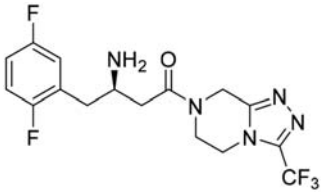	Merck & Co.	$IC_{50}=27$
217 DP-893	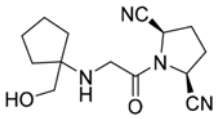	Pfizer Inc.	
218 DSR-12727	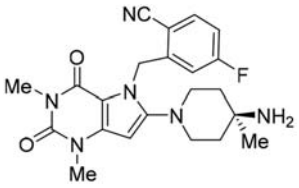	Dainippon Sumitomo Pharma	$IC_{50}=1.1$
GRC-8116 GW-1853		Glenmark Pharmaceuticals Ltd. GlaxoSmithKline	$IC_{50}=6.27$
219 K-579	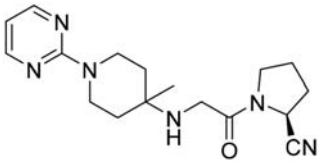	Kyowa Hakko Kogyo Co., Ltd.	$IC_{50}=8$
220 LC-150133	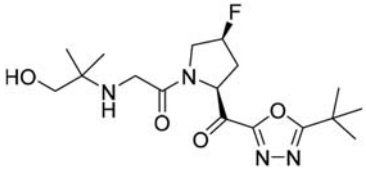	LG Life Sciences Ltd.	$IC_{50}=22$ $K_i=0.247$
221 LY-2463665	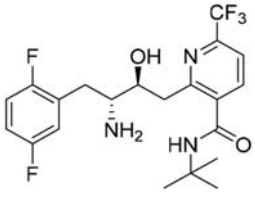	Eli Lilly	$K_i=7$

(Continued)

Table 6 DPP-4 inhibitors in preclinical development[a]—cont'd

DPP-4 inhibitors	*Structure*	*Originator*	*IC_{50} and K_i (nM)*
PHX-1004		Phenomix	
PSN-IV/119-1		Prosidion	$IC_{50}=0.2$
222	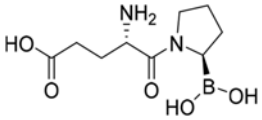	Point Therapeutics	$K_i=1.8$
PT-630			
RBx-0597		Daiichi Sankyo	$IC_{50}=32$
S-40010		Servier	$IC_{50}=2$
S-40755		Servier	
SNT-189379		Santhera Pharmaceuticals	
223	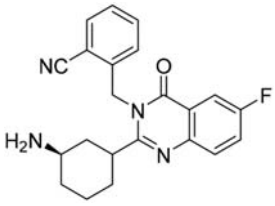	Syrrx	$IC_{50}=4$
Syrrx-106124			

[a]Blank cell, data not reported.

DSR12727 **218** is a potent and selective inhibitor (DPP-4 $IC_{50}=1.1$ nM) with moderate inhibition of CYP3A. It has good PD and PK profiles.[253]

Compound **220** is a potent inhibitor and selective over DPP-II, DPP-8, and DPP-9. It has good PK properties. The crystal structure of its complex with DPP-4 confirms that the pyrrolidine ring occupies the S1 pocket and the fluoride atom interacts with the side chain of Tyr631. The carbonyl oxygen interacts with the hydroxyl group of Tyr631. Both nitrogens of the oxadiazole ring form hydrogen bonds with Arg125 and His740. The secondary amine forms salt bridges with Glu205 and Glu206.[254]

LY 2463665 **221** is a novel ethanolamine inhibitor of DPP-4. It is a potent DPP-4 inhibitor ($IC_{50}=7$ nM) and is selective versus other DASH peptidases (>10,000-fold selectivity against DPP-II, DPP-8, and DPP-9). It shows good PD and PK profiles. It exhibits bioavailabilities of 63% and 76% in rats and dogs with half-lives of 2.5 and 5.7 h, respectively. Like sitagliptin, it exhibits reversible binding to the DPP-4 active site. The aromatic group occupies the S1 pocket.[255]

Compound **223** is a quinazolinone-based potent and selective DPP-4 inhibitor with an IC_{50} of 4.0 nM. The cyanobenzyl moiety occupies the S1 pocket of DPP-4 and interacts with Arg125. The carbonyl group hydrogen bonds with the side chain of Tyr631. The bicyclic heterocycle stacks with Tyr547. The inhibitor achieves 50% plasma DPP-4 inhibition at 12 h following a 10 mg kg^{-1} dose. It lowered glucose excursion and OGTT in mice.[256]

7.14.6 Natural DPP-4 Inhibitors

7.14.6.1 Natural Products as DPP-4 Inhibitors

Several natural dipeptides and tripeptides have been reported to be weak DPP-4 inhibitors. These include several peptides previously identified in dry-cured ham extracts or known to be products of DPP-4 action, which were synthesized and assayed for DPP-4 inhibition. Peptides with amino acid sequences KA and AAATP showed extremely weak DPP-4 inhibitory activity (IC_{50} values of 6.27 and 6.47 mM, respectively). Dipeptides AA, GP, and PL and peptides AAAAG, ALGGA, and LVSGM were also DPP-4 inhibitors, although to an even lesser degree. These findings suggest the potential of Spanish dry-cured ham to be a natural precursor of DPP-4 inhibitory peptides, albeit of very low inhibitory potencies.[257]

Hemorphins are endogenous peptides belonging to the family of "atypical" opioid peptides released sequentially from hydrolyzed hemoglobin, which interact with DPP-4. Hemorphin-7 (H7) is slowly cleaved by the enzyme (k_{cat}/K_M of 137 $mM^{-1}s^{-1}$), but the peptide also acts as a competitive DPP-4 inhibitor. These blood-derived peptides may represent endogenous regulators of enzyme activity.[258]

The diprotins A (Ile-Pro-Ile) and B (Val-Pro-Leu), isolated from culture filtrates of *Bacillus cereus* BMF673-RF1, with IC_{50} values of 1.1 and 5.5 μg mL^{-1}, respectively, also represent natural peptidyl inhibitors of DPP-4.[259] Other examples of reported peptidyl inhibitors include the five sequences HPIK, LPLP, LPVP, MPLW, and GPFP, which inhibited DPP-4 activity with IC_{50} values between 76 and 120 μM.[260] Peptides isolated from tuna cooking juice inhibited DPP-4 with IC_{50} values of 78–116 μM.[261] The peptide Ile-Pro-Ala (also called β-lactosin A) was identified in β-lactoglobulin hydrolysate and inhibited DPP-4 with an IC_{50} value of 49 μM.[262] Another peptide Val-Ala-Gly-Thr-Trp-Tyr, also derived from β-lactoglobulin, was active against DPP-4 with an IC_{50} value of 174 μM.[263] Dipeptide LA and tripeptide IPA isolated from bovine whey are reported to be weak DPP-4 inhibitors ($IC_{50}=454$

and 49 μM, respectively). Two peptides, Gly-Pro-Ala-Glu and Gly-Pro-Gly-Ala, isolated from Atlantic salmon skin gelatin showed inhibition of DPP-4 with IC_{50} values of 49.6 and 41.9 μM, respectively.[264] Peptides derived from amaranth seed proteins after enzymatic digestion also exhibited DPP-4 inhibitory activity ($IC_{50} = 1.1$ mg mL^{-1}).[265]

In addition to peptidyl DPP-4 inhibitors, there are reports of nonpeptide natural products as potential DPP-4 inhibitors. In silico modeling of the xanthone class compound glucosylxanthone, used in traditional Indian medicine, suggests that glucosylxanthone and its analogs may bind to the DPP-4 active site, although no inhibitory data were reported.[266] Triuret, a product of uric acid and peroxynitrite, has been reported to inhibit cell-associated and human recombinant DPP-4. Increasing or decreasing intracellular peroxynitrite levels enhances or decreases the ability of uric acid to inhibit cell-associated DPP-4, respectively.[267]

Organometallic ruthenium(II) complexes of curcumin were evaluated for their DPP-4 inhibitory activity, with the most potent (arene)ruthenium(II) complex having a K_i of ~20 μM.[268]

The DPP-4 inhibitory activities of several flavonoids and phenols (**224–239**,[269] **240**,[270] **241–245**,[271] and **246**[272]) are shown in Fig. 2. Most of these compounds are more potent DPP-4 inhibitors than the positive control diprotin A (Ile-Pro-Ile, $IC_{50} = 4.21 \pm 2.01$ μM).

As shown in Fig. 3, various alkaloids have been reported to be DPP-4 inhibitors (**247–254**[273]).

7.14.6.2 DPP-4 Inhibitors From Natural Extracts

Several natural extracts are reported as inhibitors of DPP-4 activity. However, their inhibitory activities are much lower than those of any of the synthetic compounds in clinical development.

Various alcohol, organic, and water extracts of *Capsicum annuum*, *Capsicum* in Solanaceae, *Rosa gallica*, and *Uncaria tomentosa* are reported to inhibit DPP-4.[273] A hot water extract of *S. chinensis* fruits also inhibited human DPP-4 ($IC_{50} = 10.8 \pm 1.5$ mg mL^{-1}).[274]

The *Castanospermum australe* Cunn. seed (CAS) extract gave a DPP-4 IC_{50} value of 13.96 μg mL^{-1}, while the standard used in the assay, diprotin A, had an IC_{50} value of 1.543 μg mL^{-1}. It was also reported that a 150 mg kg^{-1} dose of the extract normalizes hyperglycemia in T2DM rats.[275] In addition, 16,17-dihydro-17b-hydroxy isomitraphylline (DHIM), an indole alkaloid isolated from *Mitragyna parvifolia*, dose-dependently inhibits DPP-4 in vitro (5, 10, and 20 μg of DHIM inhibits 18%, 56%, and 68% of DPP-4 activity, respectively). Diabetic rats treated with DHIM (100 mg kg^{-1}) for 8 weeks exhibited markedly reduced plasma glucose concentrations and increased glucose tolerance in response to glucose loading. GLP-1 and IL-10 levels were also significantly increased in treated animals.[275]

Grape seed procyanidin extract (GSPE, Vitaceae) inhibits DPP-4 activity in vitro by ~70% upon incubation of the enzyme with 200 mg L^{-1} GSPE. GSPE also weakly inhibits rat intestinal DPP-4 and plasma DPP-4 activities at the same concentration.[276]

Three plants, *Pterocarpus marsupium* (Leguminosae) (PM), *Eugenia jambolana* (Myrtaceae) (EJ), and *Gymnema sylvestre* (Asclepiadaceae) (GS), used in traditional medicine in India, are commonly used for the treatment of hyperglycemia. Their extracts display concentration-dependent inhibition of DPP-4. At an extract concentration of 1000 μg mL^{-1}, both PM and EJ exhibited potent inhibitory activity of DPP-4 with IC_{50} values of 274 and 279 μg mL^{-1}, respectively.[277]

Anthocyanins (ANC) isolated from blueberry–blackberry wine blends (Ericaceae) were investigated for their DPP-4 inhibitory effects in vitro.[269] ANC fractions strongly inhibited DPP-4 activity (IC_{50} values ranging from 0.07 to >300 μM).

Crude extracts of sponge *Xestospongia muta* and the sea anemones *Bunodosoma granulifera* and *Bartholomea annulata* exhibited potent DPP-4 inhibitory activities, with IC_{50} values of 0.80, 1.20, and 0.138 mg mL^{-1}, respectively.[278]

Three kinds of traditional Chinese medicine from Xinjiang, *Trigonella foenum-graecum* L. (Leguminosae) (TF), *Cicer arietinum* L. (Leguminosae) (CA), and *Punica granatum* L. (Leguminosae) (PG), inhibited DPP-4 activity with IC_{50} values of 0.03, 0.09, and 0.19 mg mL^{-1}, respectively.[279]

The extracts of three traditional Chinese herbs, *Hirudo* (Annelida), *Poria cum Radix Pini* (Polyporaceae), and *Buddleja officinalis* Maxim. (Buddlejaceae), were identified as having DPP-4 inhibitory activity. At a concentration of 300 mg L^{-1}, the extent of DPP-4 inhibition by the extracts was 27%, 27%, and 44%, respectively.[280]

7.14.7 Summary

The gliptin class of therapeutics represents a valuable tool in the armamentarium of oral antihyperglycemic agents available to the primary care physician for the treatment of T2DM. While postmarketing surveillance has revealed rare instances of serious side effects such as Stevens–Johnson syndrome (an exfoliative skin condition) associated with sitagliptin or alogliptin use[205,281] and severe joint pain,[282] which appears to be a class effect and is typically relieved after discontinuation of drug, amenability to combination with metformin or other antihyperglycemic agents, an overall excellent safety profile, and glucose dependency of the incretin mechanism have rendered the gliptins popular as monotherapy and add-on therapy. Despite their structural diversity, these agents leverage common interactions in binding to the DPP-4 active site and exhibit similar antihyperglycemic efficacies in the clinic. Long-term cardiovascular outcome data have reinforced the attractive safety profile of sitagliptin while raising some questions regarding saxagliptin and alogliptin use in high-risk patient populations. The recently launched once-weekly DPP-4 inhibitors offer added convenience to T2DM patients facing a large pill burden and may help sustain the clinical and commercial success of the gliptins in the face of newer oral agents such as the SGLT-2 inhibitors.

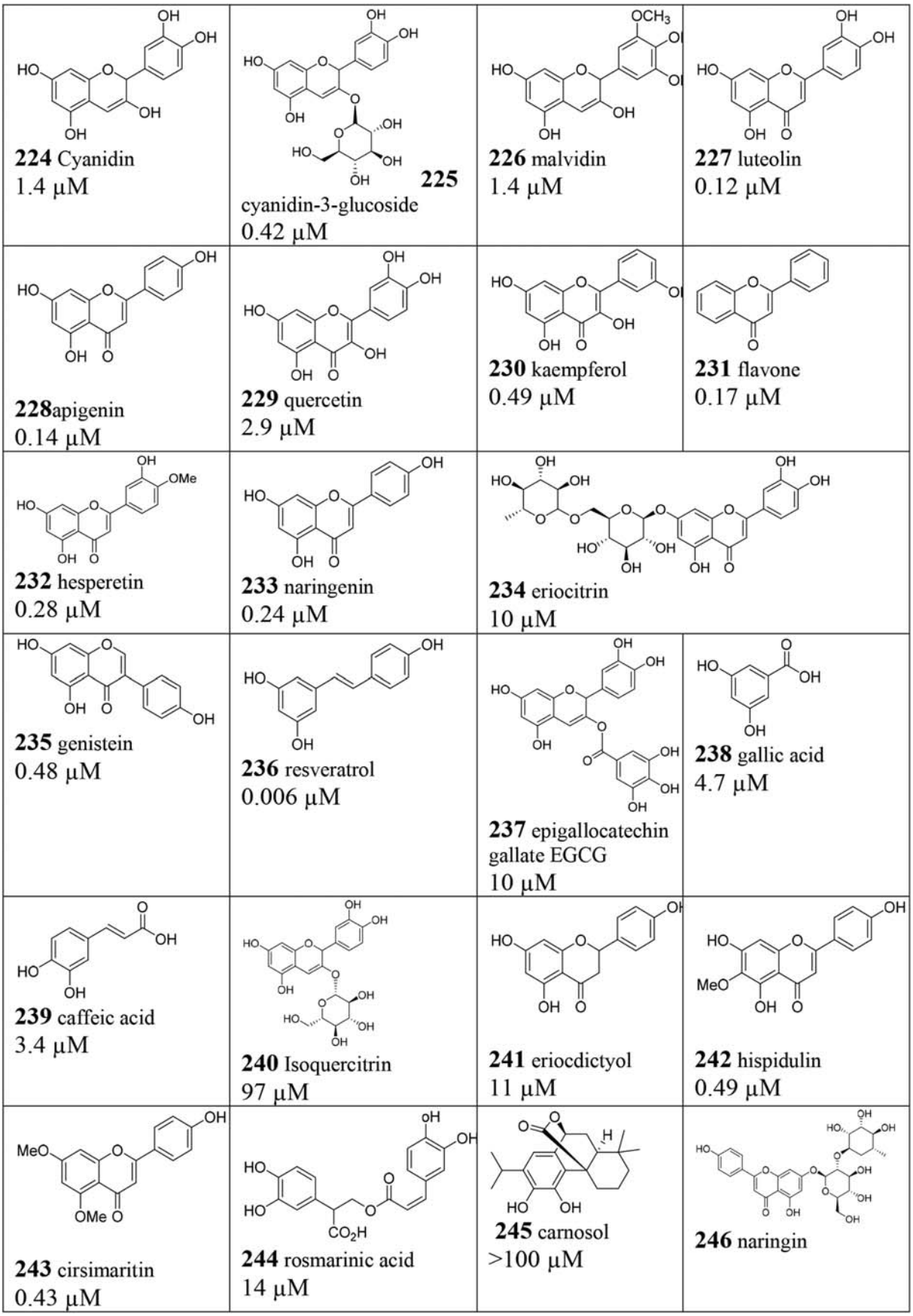

Fig. 2 Structures and inhibitory potencies (IC_{50}) of various flavonoids and phenols reported to be natural DPP-4 inhibitors.

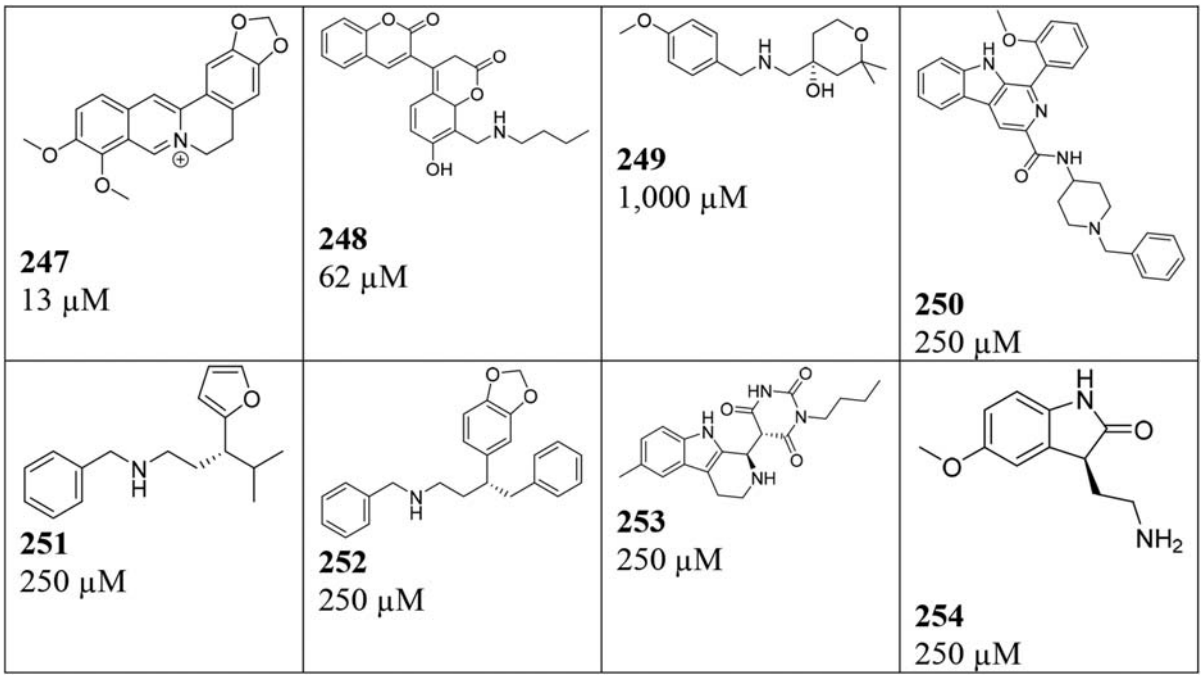

Fig. 3 Structures and inhibitory potencies (IC_{50}) of various alkaloids reported to be natural DPP-4 inhibitors.

Acknowledgment

The authors thank Dr. Xianhai Huang, Dr. Chunhui Huang, Dr. Anil Nair, Dr. Patrick Pengcheng Shao, Sriram Tyagarajan, and Dr. Cheng Zhu for their assistance in the preparation of this manuscript and Dr. Jeff Hale, Dr. Iyassu Sebhat, Dr. Richard Carr, and George Eiermann for their critical reviews.

See also: 7.12. GLP-1 Receptor Agonists for the Treatment of Diabetes and Obesity.

References

1. International Diabetes Federation. *IDF Diabetes Atlas,* 7th ed.; International Diabetes Federation: Brussels, Belgium, 2015.
2. Centers for Disease Control and Prevention. *National Diabetes Statistics Report: Estimates of Diabetes and Its Burden in the United States, 2014;* U.S. Department of Health and Human Services: Atlanta, GA, 2014.
3. Centers for Disease Control and Prevention. *Diabetes Report Card 2014;* Centers for Disease Control and Prevention, US Dept of Health and Human Services: Atlanta, GA, 2015.
4. American Diabetes Association. Approaches to Glycemic Treatment. Sec. 7. In Standards of Medical Care in Diabetes-2016. Diabetes Care 2016;39(Suppl. 1):S52–S59.
5. Thornberry, N. A.; Weber, A. E. Discovery of JANUVIA (Sitagliptin), a Selective Dipeptidyl Peptidase IV Inhibitor for the Treatment of Type 2 Diabetes. *Bioorg. Med. Chem. Lett.* **2007,** *17,* 3384–3387.
6. Parmee, E. R.; SinhaRoy, R.; Xu, F.; Givand, J. C.; Rosen, L. A. Discovery and Development of the DPP-4 Inhibitor JANUVIA™ (Sitagliptin). In *Case Studies in Modern Drug Discovery and Development;* Huang, X., Aslanian, R. G., Eds.; John Wiley & Sons, Inc: Hoboken, NJ, ISBN 978-0-470-60181-5; 2012; pp 10–44.
7. Drucker, D. J. The Biology of Incretin Hormones. *Cell Metab.* **2006,** *3,* 153–165.
8. Nauck, M. A. Unraveling the Science of Incretin Biology. *Am. J. Med.* **2009,** *122,* S3–S10.
9. Mulvihill, E. E.; Drucker, D. J. Pharmacology, Physiology, and Mechanisms of Action of Dipeptidyl Peptidase-4 Inhibitors. *Endocr. Rev.* **2014,** *35,* 992–1019.
10. Davidson, J. A. The Placement of DPP-4 Inhibitors in Clinical Practice Recommendations for the Treatment of Type 2 Diabetes. *Endocr. Pract.* **2013,** *19,* 1050–1061.
11. Röhrborn, D.; Wronkowitz, N.; Eckel, J. DPP4 in Diabetes. *Front. Immunol.* **2015,** *6,* 386.
12. Elrick, H.; Stimmler, L.; Hlad, C. J.; Arai, Y. Plasma Insulin Response to Oral and Intravenous Glucose Administration. *J. Clin. Endocrinol. Metab.* **1964,** *24,* 1076–1082.
13. McIntyre, N.; Holdsworth, C. D.; Turner, D. S. New Interpretation of Oral Glucose Tolerance. *Lancet* **1964,** *2,* 20–21.
14. Unger, R. H.; Eisentraut, A. M. The Entero-Insular Axis. *Arch. Intern. Med.* **1969,** *123,* 261–266.
15. Dupré, J.; Ross, S. A.; Watson, D.; Brown, J. C. Stimulation of Insulin Secretion by Gastric Inhibitory Polypeptide in Man. *J. Clin. Endocrinol. Metab.* **1973,** *37,* 826–828.
16. Buchan, A. M.; Polak, J. M.; Capella, C.; Solcia, E.; Pearse, A. G. Electron-Immunocytochemical Evidence for the K Cell Localization of Gastric Inhibitory Polypeptide (GIP) in Man. *Histochemistry* **1978,** *56,* 37–44.
17. Kreymann, B.; Williams, G.; Ghatei, M. A.; Bloom, S. R. Glucagon-Like Peptide-1 7–36: A Physiological Incretin in Man. *Lancet* **1987,** *2,* 1300–1304.
18. Eissele, R.; Göke, R.; Willemer, S.; Harthus, H. P.; Vermeer, H.; Arnold, R.; Göke, B. Glucagon-Like Peptide-1 Cells in the Gastrointestinal Tract and Pancreas of Rat, Pig and Man. *Eur. J. Clin. Invest.* **1992,** *22,* 283–291.
19. Moody, A. J.; Thim, L.; Valverde, I. The Isolation and Sequencing of Human Gastric Inhibitory Polypeptide (GIP). *FEBS Lett.* **1984,** *172,* 142–148.
20. Lund, P. K.; Goodman, R. H.; Dee, P. C.; Habener, J. F. Pancreatic Preproglucagon cDNA Contains Two Glucagon-Related Coding Sequences Arranged in Tandem. *Proc. Natl. Acad. Sci. U. S. A.* **1982,** *79,* 345–349.

21. Nauck, M. A.; Bartels, E.; Orskov, C.; Ebert, R.; Creutzfeldt, W. Additive Insulinotropic Effects of Exogenous Synthetic Human Gastric Inhibitory Polypeptide and Glucagon-Like Peptide-1-(7–36) Amide Infused at Near-Physiological Insulinotropic Hormone and Glucose Concentrations. *J. Clin. Endocrinol. Metab.* **1993,** *76,* 912–917.
22. Vilsbøll, T.; Krarup, T.; Madsbad, S.; Holst, J. J. Both GLP-1 and GIP Are Insulinotropic at Basal and Postprandial Glucose Levels and Contribute Nearly Equally to the Incretin Effect of a Meal in Healthy Subjects. *Regul. Pept.* **2003,** *114,* 115–121.
23. Nauck, M. A.; Heimesaat, M. M.; Orskov, C.; Holst, J. J.; Ebert, R.; Creutzfeldt, W. Preserved Incretin Activity of Glucagon-Like Peptide 1 [7–36 Amide] But not of Synthetic Human Gastric Inhibitory Polypeptide in Patients With Type-2 Diabetes Mellitus. *J. Clin. Invest.* **1993,** *91,* 301–307.
24. Vilsbøll, T.; Krarup, T.; Madsbad, S.; Larsen, S.; Hansen, T.; Pedersen, O.; Holst, J. J. Defective Amplification of the Late Phase Insulin Response to Glucose by GIP in Obese Type II Diabetic Patients. *Diabetologia* **2002,** *45,* 1111–1119.
25. Dillon, J. S.; Tanizawa, Y.; Wheeler, M. B.; LEng, X.-H.; Ligon, B. B.; Rabin, D. U.; Yoo-Warren, H.; Permutt, M. A.; Boyd, A. E., III. Cloning and Functional Expression of the Human Glucagon-Like Peptide 1-(7–36)-Amide Receptor of Insulin-Secreting β-Cells. *Endocrinology* **1993,** *133,* 1907–1910.
26. Thorens, B.; Porret, A.; Bühler, L.; Deng, S.-P.; Morel, P.; Wildmann, C. Cloning and Functional Expression of the Human Islet GLP-1 Receptor: Demonstration That Exendin-4 Is an Agonist and Exendin-(9–39) an Antagonist of the Receptor. *Diabetes* **1993,** *42,* 1678–1682.
27. Grenlich, S.; Porret, A.; Hani, E. H.; Cherif, D.; Vionnet, N.; Froguel, P.; Thorens, B. Cloning, Functional Expression, and Chromosomal Localization of the Human Pancreatic Islet Glucose-Dependent Insulinotropic Polypeptide Receptor. *Diabetes* **1995,** *44,* 1202–1208.
28. Yamada, Y.; Hayami, T.; Nakamura, K.; Kaisaki, P. J.; Someya, Y.; Wang, C. Z.; Seino, S.; Seino, Y. Human Gastric Inhibitory Polypeptide Receptor: Cloning of the Gene (GIPR) and cDNA. *Genomics* **1995,** *29,* 773–776.
29. Buckley, D. I.; Lundquist, P. Analysis of the Degradation of Insulinotropin [GLP-1(7–37)] in Human Plasma and Production of Degradation Resistant Analogs. *Regul. Pept.* **1992,** *40,* 117.
30. Kieffer, T. J.; McIntosh, C. H. S.; Pederson, R. A. Degradation of Glucose-Dependent Insulinotropic Polypeptide and Truncated Glucagon-Like Peptide 1 In Vitro And in vivo by Dipeptidyl Peptidase IV. *Endocrinology* **1995,** *136,* 3585–3596.
31. Deacon, C. F.; Nauck, M. A.; Toft-Nielsen, M.; Pridal, L.; Willms, B.; Holst, J. J. Both Subcutaneously and Intravenously Administered Glucagon-Like Peptide 1 Are Rapidly Degraded From the NH2-Terminus in Type II Diabetic Patients and in Healthy Subjects. *Diabetes* **1995,** *44,* 1126–1131.
32. Deacon, C. F.; Nauck, M. A.; Meier, J.; Hücking, K.; Holst, J. J. Degradation of Endogenous and Exogenous Gastric Inhibitory Polypeptide in Healthy and in Type 2 Diabetic Subjects as Revealed Using a New Assay for the Intact Peptide. *J. Clin. Endocrinol. Metab.* **2000,** *85,* 3575–3581.
33. Meier, J. J.; Nauck, M. A.; Kranz, D.; Holst, J. J.; Deacon, C. F.; Gaeckler, D.; Schmidt, W. E.; Gallwitz, B. Secretion, Degradation, and Elimination of Glucagon-Like Peptide 1 and Gastric Inhibitory Polypeptide in Patients With Chronic Renal Insufficiency and Healthy Control Subjects. *Diabetes* **2004,** *53,* 654–662.
34. Schmidt, W. E.; Siegel, E. G.; Ebert, R.; Creutzfeldt, W. N-Terminal Tyrosine-Alanine Is Required for the Insulin-Releasing Activity of Glucose-Dependent Insulinotropic Polypeptide (GIP). *Eur. J. Clin. Invest.* **1986,** *16,* A9.
35. Gallwitz, B.; Schmidt, W. E.; Conlon, J. M.; Creutzfeldt, W. Glucagon-Like Peptide-1 (7–36)Amide: Characterization of the Domain Responsible for Binding to Its Receptor on Rat Insulinoma RINm5F Cells. *J. Mol. Endocrinol.* **1990,** *5,* 33–39.
36. Mentlein, R.; Gallwitz, B.; Schmidt, W. E. Dipeptidyl-Peptidase IV Hydrolyses Gastric Inhibitory Polypeptide, Glucagon-Like Peptide-1(7–36)Amide, Peptide Histidine Methionine and Is Responsible for Their Degradation in Human Serum. *Eur. J. Biochem.* **1993,** *214,* 829–835.
37. Hopsu-Havu, V. K.; Glenner, G. G. A New Dipeptide Naphthylamidase Hydrolyzing Glycyl-Prolyl-Beta-Naphthylamide. *Histochemie* **1966,** *7,* 197–201.
38. Barrett, A. J.; Rawlings, N. D. Oligopeptidases and the Emergence of the Prolyl Oligopeptidase Family. *Biol. Chem. Hoppe Seyler* **1992,** *373,* 353–360.
39. Ulmer, A. J.; Mattern, T.; Feller, A. C.; Heymann, E.; Flad, H. D. CD26 Antigen Is a Surface Dipeptidyl Peptidase IV (DPPIV) as Characterized by Monoclonal Antibodies Clone TII-19-4-7 and 4EL1C7. *Scand. J. Immunol.* **1990,** *31,* 429–435.
40. Chien, C. H.; Huang, L. H.; Chou, C. Y.; Chen, Y. S.; Han, Y. S.; Chang, G. G.; Liang, P. H.; Chen, X. One Site Mutation Disrupts Dimer Formation in Human DPP-4 Proteins. *J. Biol. Chem.* **2004,** *279,* 52338–52345.
41. Scanlan, M. J.; Raj, B. K.; Calvo, B.; Garin-Chesa, P.; Sanz-Mncasi, M. P.; Healey, J. H.; Old, L. J.; Rettig, W. J. Molecular Cloning of Fibroblast Activation Protein α, a Member of the Serine Protease Family Selectively Expressed in Stromal Fibroblasts of Epithelial Cancers. *Proc. Natl. Acad. Sci. U. S. A.* **1994,** *91,* 5657–5661.
42. Ghersi, G.; Dong, H.; Goldstein, L. A.; Yeh, Y.; Hakkinen, L.; Larjava, H. S.; Chen, W. T. Seprase-dPPIV Association and Prolyl Peptidase and Gelatinase Activities of the Protease Complex. *Adv. Exp. Med. Biol.* **2003,** *524,* 87–94.
43. Misumi, Y.; Hayashi, Y.; Arakawa, F.; Ikehara, Y. Molecular Cloning and Sequence Analysis of Human Dipeptidyl Peptidase IV, a Serine Proteinase on the Cell Surface. *Biochim. Biophys. Acta* **1992,** *1131,* 333–336.
44. Tanaka, T.; Camerini, D.; Seed, B.; Torimoto, Y.; Dang, N. H.; Kameoka, J.; Dahlberg, H. N.; Schlossman, S. F.; Morimoto, C. Cloning and Functional Expression of the T Cell Activation Antigen CD26. *J. Immunol.* **1992,** *149,* 481–486.
45. Abbot, C. A.; Baker, E.; Sutherland, G. R.; McCaughan, G. W. Genomic Organization, Exact Localization, and Tissue Expression of the Human CD26 (Dipeptidyl Peptidase IV) Gene. *Immunogenetics* **1994,** *40,* 331–338.
46. Fukasawa, K. M.; Fukasawa, K.; Sahara, N.; Harada, M.; Kondo, Y.; Nagatsu, I. Immunohistochemical Localization of Dipeptidyl Aminopeptidase IV in Rat Kidney, Liver, and Salivary Glands. *J. Histochem. Cytochem.* **1981,** *29,* 337–343.
47. Durinx, C.; Lambeir, A. M.; Bosmans, E.; Falmagne, J. B.; Berghmans, R.; Haemers, A.; Scharpe, S.; de Meester, I. Molecular Characterization of Dipeptidyl Peptidase Activity in Serum: Soluble CD26/Dipeptidyl Peptidase IV Is Responsible for the Release of X-Pro Dipeptides. *Eur. J. Biochem.* **2000,** *267,* 5608–5613.
48. Sedo, A.; Malik, R. Dipeptidyl Peptidase IV-Like Molecules: Homologous Proteins or Homologous Activities? *Biochim. Biophys. Acta* **2001,** *1550,* 107–116.
49. Underwood, R.; Chiravuri, M.; Lee, H.; Schmitz, T.; Kabcenell, A. K.; Yardley, K.; Huber, B. T. Sequence, Purification, and Cloning of an Intracellular Serine Protease, Quiescent Cell Proline Dipeptidase. *J. Biol. Chem.* **1999,** *274,* 34053–34058.
50. Abbott, C. A.; Yu, C. M.; Woollatt, E.; Sutherland, G. R.; McCaughan, G. W.; Gorrell, M. D. Cloning, Expression and Chromosomal Localization of a Novel Human Dipeptidyl Peptidase (DPP) IV Homolog, DPP8. *Eur. J. Biochem.* **2000,** *267,* 6140–6150.
51. Ajami, K.; Abbott, C. A.; McCaughan, W.; Gorrell, M. D. Dipeptidyl Peptidase 9 Has Two Forms, a Broad Tissue Distribution, Cytoplasmic Localization, and DPIV-Like Peptidase Activity. *Biochim. Biophys. Acta* **1679,** *2004,* 18–28.
52. Edosada, C. Y.; Quan, C.; Tran, T.; Pham, V.; Wiesmann, C.; Fairbrother, W.; Wolf, B. B. Peptide Substrate Profiling Defines Fibroblast Activation Protein as an Endopeptidase of Strict Gly(2)-Pro(1)-Cleaving Specificity. *FEBS Lett.* **2006,** *580,* 1581–1586.
53. Leiting, B.; Pryor, K. D.; Wu, J.; Marsilio, F.; Patel, R.; Craik, C. S.; Ellman, J. A.; Cummings, R. T.; Thornberry, N. A. Catalytic Properties and Inhibition of Proline-Specific Dipeptidyl Peptidases II, IV and VII. *Biochem. J.* **2003,** *371,* 525–532.
54. Bjelke, J. R.; Christensen, J.; Nielsen, P. F.; Branner, S.; Kanstrup, A. B.; Wagtmann, N.; Rasmussen, H. B. Dipeptidyl Peptidases 8 and 9: Specificity and Molecular Characterization Compared With Dipeptidyl Peptidase IV. *Biochem. J.* **2006,** *396,* 391–399.
55. Schechter, I.; Berger, A. On the Size of the Active Site in Proteases. I. Papain. *Biochem. Biophys. Res. Commun.* **1967,** *27,* 157–162.
56. Backes, B. J.; Harris, J. L.; Leonetti, F.; Craik, C. S.; Ellman, J. A. Synthesis of Positional-Scanning Libraries of Fluorogenic Peptide Substrate Libraries to Define the Extended Substrate Specificity of Plasmin and Thrombin. *Nat. Biotechnol.* **2000,** *18,* 187–193.
57. Mentlein, R. Dipeptidyl-Peptidase IV (CD26)—Role in the Inactivation of Regulatory Peptides. *Regul. Pept.* **1999,** *85,* 9–24.
58. Van Damme, J.; Struyf, S.; Wuyts, A.; Van Coillie, E.; Menten, P.; Schols, D.; Sozzani, S.; de Meester, I.; Proost, P. The Role of CD26/DPP IV in Chemokine Processing. *Chem. Immunol.* **1999,** *72,* 42–56.
59. de Meester, I.; Lambeir, A.-M.; Proost, P.; Scharpé, S. Dipeptidyl Peptidase IV Substrates. An Update on In Vitro Peptide Hydrolysis by Human DPPIV. *Adv. Exp. Med. Biol.* **2003,** *524,* 3–17.

60. Pauly, R. P.; Demuth, H.-U.; Rosche, F.; Schmidt, J.; White, H. A.; Lynn, F.; McIntosh, C. H.; Pederson, R. A. Inhibition of Dipeptidyl Peptidase IV (DP IV) in Rats Results in Improved Glucose Tolerance. *Regul. Pept.* **1996,** *64,* 148.
61. Demuth, H.-U.; Hinke, S. A.; Pederson, R. A.; McIntosh, C. H. Rebuttal to Deacon and Holst: "Metformin Effects on Dipeptidyl Peptidase IV Degradation of Glucagon-Like Peptide-1" Versus "Dipeptidyl Peptidase Inhibition as an Approach to the Treatment and Prevention of Type 2 Diabetes: A Historical Perspective". *Biochem. Biophys. Res. Commun.* **2002,** *296,* 229–232.
62. Ahren, B.; Simonsson, E.; Larsson, H.; Landin-Olsson, M.; Torgeirsson, H.; Jansson, P. A.; Sandqvist, M.; Bavenholm, P.; Efendic, S.; Eriksson, J. W.; Dickinson, S.; Holmes, D. Inhibition of Dipeptidyl Peptidase IV Improves Metabolic Control Over a 4-Week Study Period in Type 2 Diabetes. *Diabetes Care* **2002,** *25,* 869–875.
63. Thornberry, N. A.; Gallwitz, B. Mechanism of Action of Inhibitors of Dipeptidyl-Peptidase-4 (DPP-4). *Best Pract. Res. Clin. Endocrinol. Metab.* **2009,** *23,* 479–486.
64. Aulinger, B. A.; Bedorf, A.; Kutscherauer, G.; de Heer, J.; Holst, J. J.; Goke, B.; Schirra, J. Defining the Role of GLP-1 in the Enteroinsulinar Axis in Type 2 Diabetes Using DPP-4 Inhibition and GLP-1 Receptor Blockade. *Diabetes* **2014,** *63,* 1079–1092.
65. Hansotia, T.; Baggio, L. L.; Delmeire, D.; Hinke, S. A.; Yamada, Y.; Tsukiyama, K.; Seino, Y.; Holst, J. J.; Schuit, F.; Drucker, D. J. Double Incretin Receptor Knockout (DIRKO) Mice Reveal an Essential Role for the Enteroinsular Axis in Transducing the Glucoregulatory Actions of DPP-4 Inhibitors. *Diabetes* **2004,** *53,* 1326–1335.
66. Zhu, L.; Tamvakopoulos, C.; Xie, D.; Dragovic, J.; Shen, X.; Fenyk-Melody, J. E.; Schmidt, K.; Bagchi, A.; Griffin, P. R.; Thornberry, N. A.; Sinha Roy, R. The Role of Dipeptidyl Peptidase IV in the Cleavage of Glucagon Family Peptides: in vivo Metabolism of Pituitary Adenylate Cyclase Activating Polypeptide-(1–38). *J. Biol. Chem.* **2003,** *278,* 22418–22423.
67. Faidley, T. D.; Leiting, B.; Pryor, K. D.; Lyons, K.; Hickey, G. J.; Thompson, D. R. Inhibition of Dipeptidyl-Peptidase IV Does Not Increase Circulating IGF-1 Concentrations in Growing Pigs. *Exp. Biol. Med.* **2006,** *231,* 1373–1378.
68. Aaboe, K.; Knop, F. K.; Vilsboll, T.; Deacon, C. F.; Holst, J. J.; Madsbad, S.; Krarup, T. Twelve Weeks Treatment With the DPP-4 Inhibitor, Sitagliptin, Prevents Degradation of Peptide YY and Improves Glucose and Non-Glucose Induced Insulin Secretion in Patients With Type 2 Diabetes Mellitus. *Diabetes Obes. Metab.* **2010,** *12,* 323–333.
69. Ahren, B.; Hughes, T. E. Inhibition of Dipeptidyl Peptidase-4 Augments Insulin Secretion in Response to Exogenously Administered Glucagon-Like Peptide-1, Glucose-Dependent Insulinotropic Polypeptide, Pituitary Adenylate Cyclase-Activating Polypeptide, and Gastrin-Releasing Peptide in Mice. *Endocrinology* **2005,** *146,* 2055–2059.
70. Pocai, A. Action and Therapeutic Potential of Oxyntomodulin. *Mol. Metab.* **2014,** *3,* 241–251.
71. Pocai, A.; Carrington, P. E.; Adams, J. R.; Wright, M.; Eiermann, G.; Zhu, L.; Du, X.; Petrov, A.; Lassman, M. E.; Jiang, G.; Liu, F.; Miller, C.; Tota, L. M.; Zhou, G.; Zhang, X.; Sountis, M. M.; Santoprete, A.; Capito, E.; Chicchi, G. G.; Thornberry, N.; Bianchi, E.; Pessi, A.; Marsh, D. J.; SinhaRoy, R. Glucagon-Like Peptide 1/Glucagon Receptor Dual Agonism Reverses Obesity in Mice. *Diabetes* **2009,** *58,* 2258–2266.
72. Santoprete, A.; Capito, E.; Carrington, P. E.; Pocai, A.; Finotto, M.; Langella, A.; Ingallinella, P.; Zytko, K.; Bufali, S.; Cianetti, S.; Veneziano, M.; Bonelli, F.; Zhu, L.; Monteagudo, E.; Marsh, D. J.; SinhaRoy, R.; Bianchi, E.; Pessi, A. DPP-4-Resistant, Long-Acting Oxyntomodulin Derivatives. *J. Pept. Sci.* **2011,** *17,* 270–280.
73. Loh, K.; Herzog, H.; Shi, Y. C. Regulation of Energy Homeostasis by the NPY System. *Trends Endocrinol. Metab.* **2015,** *26,* 125–135.
74. Kuo, L. E.; Abe, K.; Zukowska, Z. Stress, NPY and Vascular Remodeling: Implications for Stress-Related Diseases. *Peptides* **2007,** *28,* 435–440.
75. Mentlein, R.; Dahms, P.; Grandt, D.; Krüger, R. Proteolytic Processing of Neuropeptide Y and Peptide YY by Dipeptidyl Peptidase IV. *Regul. Pept.* **1993,** *49,* 133–144.
76. Batterham, R. L.; Cowley, M. A.; Small, C. J.; Herzog, H.; Cohen, M. A.; Dakin, C. L.; Wren, A. M.; Brynes, A. E.; Low, M. J.; Ghatei, M. A.; Cone, R. D.; Bloom, S. R. Gut Hormone PYY(3–36) Physiologically Inhibits Food Intake. *Nature* **2002,** *418,* 650–654.
77. Hofmann, P.; Bentley, P.; Sahota, P.; Schoenfeld, H.; Martin, L.; Longo, L.; Spaet, R.; Moulin, P.; Pantano, S.; Dubost, V.; Lapadula, D.; Burkey, B.; Kaushik, V.; Zhou, W.; Hayes, M.; Flavahan, N.; Chibout, S.-D.; Busch, S. Vascular Origin of Vildagliptin-Induced Skin Effects in Cynomolgus Monkeys: Pathomechanistic Role of Peripheral Sympathetic System and Neuropeptide Y. *Toxicol. Pathol.* **2014,** *42,* 684–695.
78. Frerker, N.; Wagner, L.; Wolf, R.; Heiser, U.; Hoffmann, T.; Rahfeld, J. U.; Schade, J.; Karl, T.; Naim, H. Y.; Alfalah, M.; Demuth, H. U.; von Horsten, S. Neuropeptide Y (NPY) Cleaving Enzymes: Structural and Functional Homologues of Dipeptidyl Peptidase 4. *Peptides* **2007,** *28,* 257–268.
79. Lankas, G. R.; Leiting, B.; Sinha Roy, R.; Eiermann, G. J.; Beconi, M. G.; Biftu, T.; Chan, C.-C.; Edmondson, S.; Feeney, W. P.; He, H.; Ippolito, D. E.; Kim, D.; Lyons, K. A.; Ok, H. O.; Patel, R. A.; Petrov, A. N.; Pryor, K. A.; Qian, X.; Reigle, L.; Woods, A.; Wu, J. K.; Zaller, D.; Zhang, X.; Zhu, L.; Weber, A. E.; Thornberry, N. A. Dipeptidyl Peptidase IV Inhibition for the Treatment of Type 2 Diabetes: Potential Importance of Selectivity Over Dipeptidyl Peptidases 8 and 9. *Diabetes* **2005,** *54,* 2988–2994.
80. Burkey, B. F.; Hoffmann, P. K.; Hassiepen, U.; Trappe, J.; Juedes, M.; Foley, J. E. Adverse Effects of Dipeptidyl Peptidases 8 and 9 Inhibition in Rodents Revisited. *Diabetes Obes. Metab.* **2008,** *10,* 1057–1061.
81. Wu, J.-J.; Tang, H.-K.; Yeh, T.-K.; Chen, C.-M.; Shy, H.-S.; Chu, Y.-R.; Chien, C.-H.; Tsai, T.-Y.; Huang, Y.-C.; Huang, Y.-L.; Huang, C.-H.; Tseng, H.-Y.; Jiaang, W.-T.; Chao, Y.-S.; Chen, X. Biochemistry, Pharmacokinetics, and Toxicology of a Potent and Selective DPP8/9 Inhibitor. *Biochem. Pharmacol.* **2009,** *78,* 203–210.
82. Bank, U.; Heimburg, A.; Wohlfarth, A.; Koch, G.; Nordhoff, K.; Julius, H.; Helmuth, M.; Breyer, D.; Reinhold, D.; Tager, M.; Ansorge, S. Outside or Inside: Role of the Subcellular Localization of DP4-Like Enzymes for Substrate Conversion and Inhibitor Effects. *Biol. Chem.* **2011,** *392,* 169–187.
83. Harstad, E. B.; Rosenblum, J. S.; Gorrell, M. D.; Achanzar, W. E.; Minimo, L.; Wu, J.; Rosini-Marthaler, L.; Gullo, R.; Ordway, N. D.; Kirby, M. S.; Chadwick, K. D.; Cosma, G. N.; Moyer, C. F. DPP8 and DPP9 Expression in Cynomolgus Monkey and Sprague Dawley Rat Tissues. *Regul. Pept.* **2013,** *186,* 26–35.
84. Mentlein, R.; Schiemann, F.; Ludwig, A.; Brandt, E. Modification of the Biological Activity of Chemokines by Dipeptidyl Peptidase IV—A Side Effect in the Use of Inhibitors? *Adv. Exp. Med. Biol.* **2003,** *524,* 37–47.
85. Broxmeyer, H. E.; Hoggatt, J.; O'Leary, H. A.; Mantel, C.; Chitteti, B. R.; Cooper, S.; Messina-Graham, S.; Hangoc, G.; Farag, S.; Rohrabaugh, S. L.; Ou, X.; Speth, J.; Pelus, L. M.; Srour, E. F.; Campbell, T. B. Dipeptidylpeptidase 4 Negatively Regulates Colony-Stimulating Factor Activity and Stress Hematopoiesis. *Nat. Med.* **2012,** *18,* 1786–1796.
86. De Meester, I.; Korom, S.; Van Damme, J.; Scharpe, S. CD26, Let It Cut or Cut It Down. *Immunol. Today* **1999,** *20,* 367–375.
87. Ohnuma, K.; Dang, N. H.; Morimoto, C. Revisiting an Old Acquaintance: CD26 and Its Molecular Mechanisms in T Cell Function. *Trends Immunol.* **2008,** *29,* 295–301.
88. Wang, W.; Choi, B. K.; Li, W.; Lao, Z.; Lee, A. Y.; Souza, S. C.; Yates, N. A.; Kowalski, T.; Pocai, A.; Cohen, L. H. Quantification of Intact and Truncated Stromal Cell-Derived Factor-1 α in Circulation by Immunoaffinity Enrichment and Tandem Mass Spectrometry. *J. Am. Soc. Mass Spectrom.* **2014,** *25,* 614–625.
89. Busso, N.; Wagtmann, N.; Herling, C.; Chobaz-Peclat, V.; Bischof-Delaloye, A.; So, A.; Grouzmann, E. Circulating CD26 Is Negatively Associated With Inflammation in Human and Experimental Arthritis. *Am. J. Pathol.* **2005,** *166,* 433–442.
90. Juarez, J.; Bendall, L.; Bradstock, K. Chemokines and Their Receptors as Therapeutic Targets: The Role of the SDF-1/CXCR4 Axis. *Curr. Pharm. Des.* **2004,** *10,* 1245–1259.
91. Bleul, C. C.; Farzan, M.; Choe, H.; Parolin, C.; Clark-Lewis, I.; Sodroski, J.; Springer, T. A. The Lymphocyte Chemoattractant SDF-1 Is a Ligand for LESTR/Fusin and Blocks HIV-1 Entry. *Nature* **1996,** *382,* 829–833.
92. Aso, Y.; Jojima, T.; Iijima, T.; Suzuki, K.; Terasawa, T.; Fukushima, M.; Momobayashi, A.; Hara, K.; Takebayashi, K.; Kasai, K.; Inukai, T. Sitagliptin, a Dipeptidyl Peptidase-4 Inhibitor, Increases the Number of Circulating CD34(+)CXCR4(+) Cells in Patients With Type 2 Diabetes. *Endocrine* **2015,** *50,* 659–664.
93. Scheen, A. J. Safety of Dipeptidyl Peptidase-4 Inhibitors for Treating Type 2 Diabetes. *Expert Opin. Drug Saf.* **2015,** *14,* 505–524.
94. Goodwin, S. R.; Reeds, D. N.; Royal, M.; Struthers, H.; Laciny, E.; Yarasheski, K. E. Dipeptidyl Peptidase IV Inhibition Does Not Adversely Affect Immune or Virological Status in HIV Infected Men and Women: A Pilot Safety Study. *J. Clin. Endocrinol. Metab.* **2013,** *98,* 743–751.
95. Davidson, N. C.; Struthers, A. D. Brain Natriuretic Peptide. *J. Hypertens.* **1994,** *12,* 329–336.
96. Brandt, I.; Lambeir, A. M.; Ketelslegers, J. M.; Vanderheyden, M.; Scharpe, S.; De Meester, I. Dipeptidyl-Peptidase IV Converts Intact B-Type Natriuretic Peptide Into Its Des-SerPro Form. *Clin. Chem.* **2006,** *52,* 82–87.
97. Boerrigter, G.; Costello-Boerrigter, L. C.; Harty, G. J.; Lapp, H.; Burnett, J. C., Jr. Des-serine-Proline Brain Natriuretic Peptide 3–32 in Cardiorenal Regulation. *Am. J. Physiol. Regul. Integr. Comp. Physiol.* **2007,** *292,* R897–R901.

98. Devin, J. K.; Pretorius, M.; Nian, H.; Yu, C.; Billings, F. T., 4th; Brown, N. J. Dipeptidyl-Peptidase 4 Inhibition and the Vascular Effects of Glucagon-Like Peptide-1 and Brain Natriuretic Peptide in the Human Forearm. *J. Am. Heart Assoc.* **2014,** *3.* http://dx.doi.org/10.1161/JAHA.114.001075.
99. Datar, P.; Srivastava, S.; Coutinho, E.; Govil, G. Substance P: Structure, Function, and Therapeutics. *Curr. Top. Med. Chem.* **2004,** *4,* 75–103.
100. Muñoz, M.; Coveñas, R. Involvement of Substance P and the NK-1 Receptor in Human Pathology. *Amino Acids* **2014,** *46,* 1727–1750.
101. Ahmad, S.; Wang, L.; Ward, P. E. Dipeptidyl(amino)peptidase IV and Aminopeptidase M Metabolize Circulating Substance P In Vivo. *J. Pharmacol. Exp. Ther.* **1992,** *260,* 1257–1261.
102. Skidgel, R. A.; Engelbrecht, S.; Johnson, A. R.; Erdos, E. G. Hydrolysis of Substance P and Neurotensin by Converting Enzyme and Neutral Endopeptidase. *Peptides* **1984,** *5,* 769–776.
103. Byrd, J. S.; Minor, D. S.; Elsayed, R.; Marshall, G. D. DPP-4 Inhibitors and Angioedema: A Cause for Concern? *Ann. Allergy Asthma Immunol.* **2011,** *106,* 436–438.
104. Devin, J. K.; Pretorius, M.; Nian, H.; Yu, C.; Billings, F. T., 4th; Brown, N. J. Substance P Increases Sympathetic Activity During Combined Angiotensin-Converting Enzyme and Dipeptidyl Peptidase-4 Inhibition. *Hypertension* **2014,** *63,* 951–957.
105. Grouzmann, E.; Bigliardi, P.; Appenzeller, M.; Pannatier, A.; Buclin, T. Substance P-Induced Skin Inflammation Is Not Modulated by a Single Dose of Sitagliptin in Human Volunteers. *Biol. Chem.* **2011,** *392,* 217–221.
106. Standl, E.; Erbach, M.; Schnell, O. Dipeptidyl-Peptidase-4 Inhibitors and Heart Failure: Class Effect, Substance-Specific Effect, or Chance Effect? *Curr. Treat. Options Cardiovasc. Med.* **2014,** *16,* 353 http://dx.doi.org/10.1007/s11936-014-0353-y.
107. Scirica, B. M.; Bhatt, D. L.; Braunwald, E.; Steg, P. G.; Davidson, J.; Hirshberg, B.; Ohman, P.; Frederich, R.; Wiviott, S. D.; Hoffman, E. B.; Cavender, M. A.; Udell, J. A.; Desai, N. R.; Mosenzon, O.; McGuire, D. K.; Ray, K. K.; Leiter, L. A.; Raz, I. SAVOR-TIMI 53 Steering Committee and Investigators. Saxagliptin and Cardiovascular Outcomes in Patients With Type 2 Diabetes Mellitus. *N. Engl. J. Med.* **2013,** *369,* 1317–1326.
108. Green, J. B.; Bethel, M. A.; Armstrong, P. W.; Buse, J. B.; Engel, S. S.; Garg, J.; Josse, R.; Kaufman, K. D.; Koglin, J.; Korn, S.; Lachin, J. M.; McGuire, D. K.; Pencina, M. J.; Standl, E.; Stein, P. P.; Suryawanshi, S.; Van de Werf, F.; Peterson, E. D.; Holman, R. R.; TECOS Study Group. Effect of Sitagliptin on Cardiovascular Outcomes in Type 2 Diabetes. *N. Engl. J. Med.* **2015,** *373,* 232–242.
109. Marx, N.; Rosenstock, J.; Kahn, S. E.; Zinman, B.; Kastelein, J. J.; Lachin, J. M.; Espeland, M. A.; Bluhmki, E.; Mattheus, M.; Ryckaert, B.; Patel, S.; Johansen, O. E.; Woerle, H. J. Design and Baseline Characteristics of the CARdiovascular Outcome Trial of LINAgliptin Versus Glimepiride in Type 2 Diabetes (CAROLINA). *Diab. Vasc. Dis. Res.* **2015,** *12,* 164–174.
110. Cardiovascular and Renal Microvascular Outcome Study With Linagliptin in Patients with Type 2 Diabetes Mellitus (CARMELINA). https://clinicaltrials.gov/ct2/show/NCT01897532, 2015.
111. Rasmussen, H. B.; Branner, S.; Wiberg, F. C.; Wagtmann, N. Crystal Structure of Human Dipeptidyl Peptidase IV/CD26 in Complex With a Substrate Analog. *Nat. Struct. Biol.* **2003,** *10,* 19–25.
112. Aertgeerts, K.; Ye, S.; Tennant, M. G.; Kraus, M. L.; Rogers, J.; Sang, B. C.; Skene, R. J.; Webb, D. R.; Prasad, G. S. Crystal Structure of Human Dipeptidyl Peptidase IV in Complex With a Decapeptide Reveals Details on Substrate Specificity and Tetrahedral Intermediate Formation. *Protein Sci.* **2004,** *13,* 412–421.
113. Deacon, C. F.; Holst, J. J. Dipeptidyl Peptidase-4 Inhibitors for the Treatment of Type 2 Diabetes: Comparison, Efficacy and Safety. *Expert. Opin. Pharmacother.* **2013,** *14,* 2047–2058.
114. Krishna, R.; Herman, G.; Wagner, J. A. Accelerating Drug Development Using Biomarkers: A Case Study With Sitagliptin, a Novel DPP4 Inhibitor for Type 2 Diabetes. *AAPS J.* **2008,** *10,* 401–409.
115. Alba, M.; Sheng, D.; Guan, Y.; Williams-Herman, D.; Larson, P.; Sachs, J. R.; Thornberry, N.; Herman, G.; Kaufman, K. D.; Goldstein, B. J. Sitagliptin 100 mg Daily Effect on DPP-4 Inhibition and Compound-Specific Glycemic Improvement. *Curr. Med. Res. Opin.* **2009,** *25,* 2507–2514.
116. Chyan, Y. J.; Chuang, L. M. Dipeptidyl Peptidase-IV Inhibitors: An Evolving Treatment for Type 2 Diabetes From the Incretin Concept. *Recent Pat. Endocr. Metab. Immune Drug Discov.* **2007,** *1,* 15–24.
117. (a) Gupta, R.; Walunj, S. S.; Tokala, R. K.; Parsa, K. V.; Singh, S. K.; Pal, M. Emerging Drug Candidates of Dipeptidyl Peptidase IV (DPP IV) Inhibitor Class for the Treatment of Type 2 Diabetes. *Curr. Drug Targets* **2009,** *10,* 71–87; (b) Verspohl, E. J. Novel Pharmacological Approaches to the Treatment of Type 2 Diabetes. *Pharmacol. Rev.* **2012,** *64,* 188–237; (c) Demuth, H. U.; McIntosh, C. H.; Pederson, R. A. Type 2 Diabetes-Therapy With Dipeptidyl Peptidase IV Inhibitors. *Biochim. Biophys. Acta* **2005,** *1751,* 33–44.
118. Kim, D.; Wang, L.; Beconi, M.; Eiermann, G. J.; Fisher, M. H.; He, H.; Hickey, G. J.; Kowalchick, J. E.; Leiting, B.; Lyons, K.; Mar-silio, F.; McCann, M. E.; Patel, R. A.; Petrov, A.; Scapin, G.; Patel, S. B.; Roy, R. S.; Wu, J. K.; Wyvratt, M. J.; Zhang, B. B.; Zhu, L.; Thornberry, N. A.; Weber, A. E. (2R)-4-Oxo-4-[3-(Trifluoromethyl)-5,6-dihydro [1,2,4]triazolo[4,3-a]pyrazin-7(8H)-yl]-1-(2,4,5-trifluorophenyl) butan-2-amine: A Potent, Orally Active Dipeptidyl Peptidase IV Inhibitor for the Treatment of Type 2 Diabetes. *J. Med. Chem.* **2005,** *48,* 141–151.
119. Thornberry, N. A.; Weber, A. E. Discovery of JANUVIA (Sitagliptin), a Selective Dipeptidyl Peptidase IV Inhibitor for the Treatment of Type 2 Diabetes. *Curr. Top. Med. Chem.* **2007,** *7,* 557–568.
120. Villhauer, E. B.; Brinkman, J. A.; Naderi, G. B.; Burkey, B. F.; Dunning, B. E.; Prasad, K.; Mangold, B. L.; Russell, M. E.; Hughes, T. E. 1-[[(3 Hydroxy-1-adamantyl)amino] acetyl]-2-cyano-(S)-pyrrolidine: A Potent, Selective, and Orally Bioavailable Dipeptidyl Peptidase IV Inhibitor With Antihyperglycemic Properties. *J. Med. Chem.* **2003,** *46,* 2774–2789.
121. Augeri, D. J.; Robl, J. A.; Betebenner, D. A.; Magnin, D. R.; Khanna, A.; Robertson, J. G.; Wang, A.; Simpkins, L. M.; Taunk, P.; Huang, Q.; Han, S. P.; Abboa-Offei, B.; Cap, M.; Xin, L.; Tao, L.; Tozzo, E.; Welzel, G. E.; Egan, D. M.; Marcinkeviciene, J.; Chang, S. Y.; Biller, S. A.; Kirby, M. S.; Parker, R. A.; Hamann, L. G. Discovery and Preclinical Profile of Saxagliptin (BMS-477118): A Highly Potent, Long-Acting, Orally Active Dipeptidyl Peptidase IV Inhibitor for the Treatment of Type 2 Diabetes. *J. Med. Chem.* **2005,** *48,* 5025–5037.
122. Feng, J.; Zhang, Z.; Wallace, M. B.; Stafford, J. A.; Kaldor, S. W.; Kassel, D. B.; Navre, M.; Shi, L.; Skene, R. J.; Asakawa, T.; Takeuchi, K.; Xu, R.; Webb, D. R.; Gwaltney, S. L., II Discovery of Alogliptin: A Potent, Selective, Bioavailable, and Efficacious Inhibitor of Dipeptidyl Peptidase IV. *J. Med. Chem.* **2007,** *50,* 2297–2300.
123. Eckhardt, M.; Langkopf, E.; Mark, M.; Tadayyon, M.; Thomas, L.; Nar, H.; Pfrengle, W.; Guth, B.; Lotz, R.; Sieger, P.; Fuchs, H.; Himmelsbach, F. 8-(3-(R)-Aminopiperidin-1-yl)-7-but-2-ynyl-3- methyl-1-(4-methyl-quinazolin-2-ylmethyl)-3,7-dihydropurine-2,6-dione (BI 1356), a Highly Potent, Selective, Long-Acting, and Orally Bioavailable DPP-4 Inhibitor for the Treatment of Type 2 Diabetes. *J. Med. Chem.* **2007,** *50,* 6450–6453.
124. Zhang, Z.; Wallace, M. B.; Feng, J.; Stafford, J. A.; Skene, R. J.; Shi, L.; Lee, B.; Aertgeerts, K.; Jennings, A.; Xu, R.; Kassel, D. B.; Kaldor, S. W.; Navre, M.; Webb, D. R.; Gwaltney, S. L., II Design and Synthesis of Pyrimidinone and Pyrimidinedione Inhibitors of Dipeptidyl Peptidase IV. *J. Med. Chem.* **2011,** *54,* 510–524.
125. Biftu, T.; Sinha-Roy, R.; Chen, P.; Qian, X.; Feng, D.; Kuethe, J. T.; Scapin, G.; Gao, Y. D.; Yan, Y.; Krueger, D.; Bak, A.; Eiermann, G.; He, J.; Cox, J.; Hicks, J.; Lyons, K.; He, H.; Salituro, G.; Tong, S.; Patel, S.; Doss, G.; Petrov, A.; Wu, J.; Xu, S. S.; Sewall, C.; Zhang, X.; Zhang, B.; Thornberry, N. A.; Weber, A. E. Omarigliptin (MK-3102): A Novel Long-Acting DPP-4 Inhibitor for Once-Weekly Treatment of Type 2 Diabetes. *J. Med. Chem.* **2014,** *57,* 3205–3212.
126. Yoshida, T.; Akahoshi, F.; Sakashita, H.; Kitajima, H.; Nakamura, M.; Sonda, S.; Takeuchi, M.; Tanaka, Y.; Ueda, N.; Sekiguchi, S.; Ishige, T.; Shima, K.; Nabeno, M.; Abe, Y.; Anabuki, J.; Soejima, A.; Yoshida, K.; Takashina, Y.; Ishii, S.; Kiuchi, S.; Fukuda, S.; Tsutsumiuchi, R.; Kosaka, K.; Murozono, T.; Nakamaru, Y.; Utsumi, H.; Masutomi, N.; Kishida, H.; Miyaguchi, I.; Hayashi, Y. Discovery and Preclinical Profile of Teneligliptin (3-[(2S,4S)-4-[4-(3-methyl-1-phenyl-1H-pyrazol-5-yl)piperazin-1-yl]pyrrolidin-2-ylcarbonyl]thiazolidine): A Highly Potent, Selective, Long-Lasting and Orally Active Dipeptidyl Peptidase IV Inhibitor for the Treatment of Type 2 Diabetes. *Bioorg. Med. Chem.* **2012,** *20,* 5705–5719.
127. Hwang, D. M.; Kim, S. H.; Yoon, M. K.; Kwon, O. H.; Koo, K. D.; Min, C. H.; Lee, S. H.; Lee, J. I.; Lee, C. S.; Yim, H. J. LC15-0444 Is a Novel, Potent, Selective, and Orally Active Dipeptidyl Peptidase IV Inhibitor. Poster presented at the annual meeting of American Diabetes Association, San Francisco, CA.

128. Kato, N.; Oka, M.; Murase, T.; Yoshida, M.; Sakairi, M.; Yama-shita, S.; Yasuda, Y.; Yoshikawa, A.; Hayashi, Y.; Makino, M.; Takeda, M.; Mirensha, Y.; Kakigami, T. Discovery and Pharmacological Characterization of N-[2-({2-[(2S)-2-cyanopyrrolidin-1- yl]-2-oxoethyl}amino)-2-methylpropyl]-2-methylpyrazolo[1,5-a]pyrimidine-6-carboxamide Hydrochloride (Anagliptin Hydrochloride Salt) as a Potent and Selective DPP-4 Inhibitor. *Bioorg. Med. Chem.* **2011,** *19,* 7221–7227.
129. Wu, D.; Li, L.; Liu, C. Efficacy and Safety of Dipeptidyl Peptidase-4 Inhibitors and Metformin as Initial Combination Therapy and as Monotherapy in Patients With Type 2 Diabetes Mellitus: A Meta-analysis. *Diabetes Obes. Metab.* **2014,** *16,* 30–37.
130. Bergman, A.; Ebel, D.; Liu, F.; Stone, J.; Wang, A.; Zeng, W.; Chen, L.; Dilzer, S.; Lasseter, K.; Herman, G.; Wagner, J.; Krishna, R. Absolute Bioavailability of Sitagliptin, an Oral Dipeptidyl Peptidase'4 Inhibitor, in Healthy Volunteers. *Biopharm. Drug Dispos.* **2007,** *28,* 315–322.
131. Herman, G. A.; Stevens, C.; Van Dyck, K.; Bergman, A.; Yi, B.; De Smet, M.; Snyder, K.; Hilliard, D.; Tanen, M.; Tanaka, W.; Wang, A. Q.; Zeng, W.; Musson, D.; Winchell, G.; Davies, M. J.; Ramael, S.; Gottesdiener, K. M.; Wagner, J. A. Pharmacokinetics and Pharmacodynamics of Single Doses of Sitagliptin, an Inhibitor of Dipeptidyl Peptidase-IV, in Healthy Subjects: Results From Two Randomized, Double-Blind, Placebo-Controlled Studies With Single Oral Doses. *Clin. Pharmacol. Ther.* **2005,** *78,* 675–688.
132. Bergman, A. J.; Cote, J.; Yi, B.; Marbury, T.; Swan, S. K.; Smith, W.; Gottesdiener, K.; Wagner, J.; Herman, G. A. Effect of Renal Insufficiency on the Pharmacokinetics of Sitagliptin, a Dipeptidyl Peptidase-4 Inhibitor. *Diabetes Care* **2007,** *30,* 1862–1864.
133. Karasik, A.; Aschner, P.; Katzeff, H.; Davies, M. J.; Stein, P. P. Sitagliptin, a DPP-4 Inhibitor for the Treatment of Patients With Type 2 Diabetes: A Review of Recent Clinical Trials. *Curr. Med. Res. Opin.* **2008,** *24,* 489–496.
134. Herman, G. A.; Bergman, A.; Stevens, C.; Kotey, P.; Yi, B.; Zhao, P.; Dietrich, B.; Golor, G.; Schrodter, A.; Keymeulen, B.; Lasseter, K. C.; Kipnes, M. S.; Snyder, K.; Hilliard, D.; Tanen, M.; Cilissen, C.; De Smet, M.; de Lepeleire, I.; Van Dyck, K.; Wang, A. Q.; Zeng, W.; Davies, M. J.; Tanaka, W.; Holst, J. J.; Deacon, C. F.; Gottesdiener, K. M.; Wagner, J. A. Effect of Single Oral Doses of Sitagliptin, a Dipeptidyl Peptidase-4 Inhibitor, on Incretin and Plasma Glucose Levels Following an Oral Glucose Tolerance Test in Patients With Type 2 Diabetes. *J. Clin. Endocrinol. Metab.* **2006,** *91,* 4612–4619.
135. Aschner, P.; Kipnes, M. S.; Lunceford, J. K.; Sanchez, M.; Mickel, C.; Williams-Herman, D. E.; Sitagliptin Study 021 Group. Effect of the Dipeptidyl Peptidase-4 Inhibitor Sitagliptin as Monotherapy on Glycemic Control in Patients With Type 2 Diabetes. *Diabetes Care* **2006,** *29,* 2632–2637.
136. Nauck, M. A.; Meininger, G.; Sheng, D.; Terranella, L.; Stein, P. P.; Sitagliptin Study 024 Group. Efficacy and Safety of the Dipeptidyl Peptidase-4 Inhibitor, Sitagliptin, Compared With the Sulfonylurea, Glipizide, in Patients With Type 2 Diabetes Inadequately Controlled on Metformin Alone: A Randomized, Double-Blind, Noninferiority Trial. *Diabetes Obes. Metab.* **2007,** *9,* 194–205.
137. Mu, J.; Petrov, A.; Eiermann, G. J.; Woods, J.; Zhou, Y. P.; Li, Z.; Zycband, E.; Feng, Y.; Zhu, L.; Sinha Roy, R.; Howard, A. D.; Li, C.; Thornberry, N. A.; Zhang, B. B. Inhibition of DPP-4 With Sitagliptin Improves Glycemic Control and Restores Islet Cell Mass and Function in a Rodent Model of Type 2 Diabetes. *Eur. J. Pharmacol.* **2009,** *623,* 148–154.
138. Butler, P. C.; Elashoff, M.; Elashoff, R.; Gale, E. A. A Critical Analysis of the Clinical Use of Incretin-Based Therapies: Are the GLP-1 Therapies Safe? *Diabetes Care* **2013,** *36,* 2118–2125.
139. Muller, A.; Vogt, C.; Sewald, N. Synthesis of Fmoc-b-Homoamino Acids by Ultrasound-Promoted Wolff Rearrangement. *Synthesis* **1988,** *11,* 837–841.
140. Miller, M. J.; Mattingly, P. G.; Morrison, M. A.; Kerwin, J. F. Synthesis of β-Lactams From Substituted Hydroxamic Acids. *J. Am. Chem. Soc.* **1980,** *102,* 7026–7032.
141. (a) Hansen, K. B.; Yi, H.; Xu, F.; Rivera, N.; Clausen, A.; Kubryk, M.; Krska, S.; Rosner, T.; Simmons, B.; Balsells, J.; Ikemoto, N.; Sun, Y.; Spindler, F.; Malan, C.; Grabowski, E. J. J.; Armstrong, J. D. Highly Efficient Asymmetric Synthesis of Sitagliptin. *J. Am. Chem. Soc.* **2009,** *131,* 8798–8804; (b) Savile, C. K.; Janey, J. M.; Mundorff, E. C.; Moore, J. C.; Jarvis, W. R.; Colbeck, J. C.; Krebber, A.; Fleitz, F. J.; Brands, J.; Devine, P. N.; Huisman, G. W.; Hughes, G. J. Biocatalytic Asymmetric Synthesis of Chiral Amines From Ketones Applied to Sitagliptin Manufacture. *Science* **2010,** *329,* 305.
142. Xiao, Y.; Armstrong, J. D.; Krska, S. W.; Njolito, E.; Rivera, N. R.; Sun, Y., Rosner, T. Process for the Preparation of Chiral Beta Amino Acid Derivatives by Asymmetric Hydrogenation. WO Patent 2004/085378, 2004.
143. Kim, Y.; Kim, U.; Kim, I. S.; Lee, S. H.; Lee, J.; Kim, D. H.; Yoo, H. H. Absorption, Distribution, Metabolism and Excretion of Gemigliptin, a Novel Dipeptidyl Peptidase IV Inhibitor, in Rats. *Xenobiotica* **2014,** *44,* 627–634.
144. Kim, S. H.; Lee, S. H.; Yim, H. J. Gemigliptin, a Novel Dipeptidyl Peptidase 4 Inhibitor: First New Anti-diabetic Drug in the History of Korean Pharmaceutical Industry. *Arch. Pharm. Res.* **2013,** *36,* 1185–1188.
145. Lim, K. S.; Kim, J. R.; Choi, Y. J.; Shin, K. H.; Kim, K. P.; Hong, J. H.; Cho, J. Y.; Shin, H. S.; Yu, K. S.; Shin, S. G.; Kwon, O. H.; Hwang, D. M.; Kim, J. A.; Jang, I. J. Pharmacokinetics, Pharmacodynamics, and Tolerability of the Dipeptidyl Peptidase IV Inhibitor LC15-0444 in Healthy Korean Men: A Dose-Block-Randomized, Double-Blind, Placebo-Controlled, Ascending Single-Dose, Phase I Study. *Clin. Ther.* **2008,** *30,* 1817–1830.
146. Lim, K. S.; Cho, J. Y.; Kim, B. H.; Kim, J. R.; Kim, H. S.; Kim, D. K.; Kim, S. H.; Yim, H. J.; Lee, S. H.; Shin, S. G.; Jang, I. J.; Yu, K. S. Pharmacokinetics and Pharmacodynamics of LC15-0444, a Novel Dipeptidyl Peptidase IV Inhibitor, After Multiple Dosing in Healthy Volunteers. *Br. J. Clin. Pharmacol.* **2009,** *68,* 883–890.
147. Rhee, E. J.; Lee, W. Y.; Yoon, K. H.; Yoo, S. J.; Lee, I. K.; Baik, S. H.; Kim, Y. K.; Lee, M. K.; Park, K. S.; Park, J. Y.; Cha, B. S.; Lee, H. W.; Min, K. W.; Bae, H. Y.; Kim, M. J.; Kim, J. A.; Kim, D. K.; Kim, S. W. A Multicenter, Randomized, Placebo-Controlled, Double Blind Phase II Trial Evaluating the Optimal Dose, Efficacy and Safety of LC 15–0444 in Patients With Type 2 Diabetes. *Diabetes Obes. Metab.* **2010,** *12,* 1113–1119.
148. Yang, S. J.; Min, K. W.; Gupta, S. K.; Park, J. Y.; Shivane, V. K.; Pitale, S. U.; Agarwal, P. K.; Sosale, A.; Gandhi, P.; Dharma-lingam, M.; Mohan, V.; Mahesh, U.; Kim, D. M.; Kim, Y. S.; Kim, J. A.; Kim, P. K.; Baik, S. H. A Multicentre, Multinational, Randomized, Placebo-Controlled, Double-Blind, Phase 3 Trial to Evaluate the Efficacy and Safety of Gemigliptin (LC15-0444) in Patients With Type 2 Diabetes. *Diabetes Obes. Metab.* **2013,** *15,* 410–416.
149. Rhee, E. J.; Lee, W. Y.; Min, K. W.; Shivane, V. K.; Sosale, A. R.; Jang, H. C.; Chung, C. H.; Nam-Goong, I. S.; Kim, J. A.; Kim, S. W.; Gemigliptin Study Group. Efficacy and Safety of the Dipeptidyl Peptidase-4 Inhibitor Gemigliptin Compared With Sitagliptin Added to Ongoing Metformin Therapy in Patients With Type 2 Diabetes Inadequately Controlled With Metformin Alone. *Diabetes Obes. Metab.* **2013,** *15,* 523–530.
150. Noh, Y. H.; Lim, H. S.; Jin, S. J.; Kim, M. J.; Kim, Y. H.; Sung, H. R.; Choi, H. Y.; Bae, K. S. Effects of Ketoconazole and Rifampicin on the Pharmacokinetics of Gemigliptin, a Dipeptidyl Peptidase-IV Inhibitor: A Crossover Drug-Drug Interaction Study in Healthy Male Korean Volunteers. *Clin. Ther.* **2012,** *34,* 1182–1190.
151. Kim, S. E.; Yi, S.; Shin, K. H.; Kim, T. E.; Kim, M. J.; Kim, Y. H.; Yoon, S. H.; Cho, J. Y.; Shin, S. G.; Jang, I. J.; Yu, K. S. Evaluation of the Pharmacokinetic Interaction Between the Dipeptidyl Peptidase IV Inhibitor LC15-0444 and Pioglitazone in Healthy Volunteers. *Int. J. Clin. Pharmacol. Ther.* **2012,** *50,* 17–23.
152. Lee C. S.; Koh J. S.; Koo K. D.; Kim G. T.; Kim K. H.; Hong S. Y.; Kim S.; Kim M. J.; Yim H. J.; Lim D.; Kim H. J.; Han H. O.; Bu S. C.; Kwon O. H.; Kim S. H.; Hur G. C.; Kim J. Y.; Yeom Z. H.; Yeo D. J. Dipeptidyl Peptidase-IV Inhibiting Compounds, Methods of Preparing the Same, and Pharmaceutical Compositions Containing the Same as an Active Agent. WO Patent 2006/104356 A1, 2006.
153. Park, K. S.; Yun, J. M.; Kim, B. C.; Kim, Y. U.; Lee, J. H. Hydrate of 1-{(2S)-2-Amino-4-[2,4-Bis(Trifluoromethyl)-5,8-Di-hydropyrido[3,4-d]Pyrimidin-7(6h)-yl]-4-Oxobutyl}-5,5-Difluoro-Piperidin-2-One Tartrate. WO Patent 2012/060590, 2012.
154. (a) Kim, H. J.; Kwak, W. Y.; Min, J. P.; Lee, J. Y.; Yoon, T. H.; Kim, H. D.; Shin, C. Y.; Kim, M. K.; Choi, S. H.; Kim, H. S.; Yang, E. K.; Cheong, Y. H.; Chae, Y. N.; Park, K. J.; Jang, J. M.; Choi, S. J.; Son, M. H.; Kim, S. H.; Yoo, M.; Lee, B. J. Discovery of DA- 1229: A Potent, Long Acting Dipeptidyl Peptidase-4 Inhibitor for the Treatment of Type 2 Diabetes. *Bioorg. Med. Chem. Lett.* **2011,** *21,* 3809–3812; (b) Tan, X.; Hu, J. Evogliptin: A New Dipeptidyl Peptidase Inhibitor for the Treatment of Type 2 Diabetes. *Expert. Opin. Pharmacother.* **2016,** *17,* 1285–1293.
155. Brunavs, M.; Cowley, P.; Ward, S. E.; Weber, P. Recent Disclosures of Clinical Candidates (SMR Award Lecture) - Highlights from the Society for Medicines Research Symposium, held on December 5th 2012 at the National Heart & Lung Institute (NHLI), London, UK. *Drugs Future* **2013,** *38,* 127–133.
156. (a) Burness, C. B. Omarigliptin: First Global Approval. *Drugs* **2015,** *75,* 1947–1952; (b) Sheu, W. H.; Gantz, I.; Chen, M.; Suryawanshi, S.; Mirza, A.; Goldstein, B. J.; Kaufman, K. D.; Engel, S. S. Safety and Efficacy of Omarigliptin (MK-3102), A Novel Once-Weekly DPP-4 Inhibitor for the Treatment of Patients With Type 2 Diabetes. *Diabetes Care* **2015,** *38,* 2106–2114.
157. Merck Provides Update on Filing Plans for Omarigliptin, an Investigational DPP-4 Inhibitor for Type 2 Diabetes, Merck Press Release, April 8, 2016.

158. Chung, J. Y. L.; Scott, J. P.; Anderson, C.; Bishop, B.; Bremeyer, N.; Cao, Y.; Chen, Q.; Dunn, R.; Kassim, A.; Lieberman, D.; Moment, A. J.; Sheen, F.; Zacuto, M. Evolution of a Manufacturing Route to Omarigliptin, A Long-Acting DPP-4 Inhibitor for the Treatment of Type 2 Diabetes. *Org. Process Res. Dev.* **2015,** *19,* 1760–1768.
159. Villhauer, E. B.; Brinkman, J. A.; Naderi, G. B.; Dunning, B. E.; Mangold, B. L.; Mone, M. D.; Russell, M. E.; Weldon, S. C.; Hughes, T. E. 1-[2[(5-Cyanopyridin-2-yl)amino] Ethylamino]Acetyl-2-(S)-Pyrrolidinecarbonitrile: A Potent, Selective, and Orally Bioavailable Dipeptidyl Peptidase IV Inhibitor With Antihyperglycemic Properties. *J. Med. Chem.* **2002,** *45,* 2362–2365.
160. Nabeno, M.; Akahoshi, F.; Kishida, H.; Miyaguchi, I.; Tanaka, Y.; Ishii, S.; Kadowaki, T. A Comparative Study of the Binding Modes of Recently Launched Dipeptidyl Peptidase IV Inhibitors in the Active Site. *Biochem. Biophys. Res. Commun.* **2013,** *434,* 191–196.
161. He, Y.-L. Clinical Pharmacokinetics and Pharmacodynamics of Vildagliptin. *Clin. Pharmacokinet.* **2012,** *51,* 147–162.
162. He, Y.-L.; Sadler, B. M.; Sabo, R.; Balez, S.; Wang, Y.; Campestrini, J.; Laurent, A.; Ligueros-Saylan, M.; Howard, D. The Absolute Oral Bioavailability and Population-Based Pharmacokinetic Modelling of a Novel Dipeptidylpeptidase-IV Inhibitor, Vildagliptin, in Healthy Volunteers. *Clin. Pharmacokinet.* **2007,** *46,* 787–802.
163. Pi-Sunyer, F. X.; Schweizer, A.; Mills, D.; Dejager, S. Efficacy and Tolerability of Vildagliptin Monotherapy in Drug-Naive Patients With Type 2 Diabetes. *Diabetes Res. Clin. Pract.* **2007,** *76,* 132–138.
164. Rosenstock, J.; Fitchet, M. Vildagliptin: Clinical Trials Programme in Monotherapy and Combination Therapy for Type 2 Diabetes. *Int. J. Clin. Pract.* **2008,** *62* (Suppl 159), 15–23.
165. (a) Duez, H.; Cariou, B.; Staels, B. DPP-4 Inhibitors in the Treatment of Type 2 Diabetes. *Biochem. Pharmacol.* **2012,** *83,* 823–832; (b) Deacon, C. F. Dipeptidyl Peptidase-4 Inhibitors in the Treatment of Type 2 Diabetes: A Comparative Review. *Diabetes Obes. Metab.* **2011,** *13,* 7–18.
166. Magnin, D. R.; Robl, J. A.; Sulsky, R. B.; Augeri, D. J.; Huang, Y.; Simpkins, L. M.; Taunk, P. C.; Betebenner, D. A.; Robertson, J. G.; Abboa-Offei, B. E.; Wang, A.; Cap, M.; Xin, L.; Tao, L.; Sitkoff, D. F.; Malley, M. F.; Gougoutas, J. Z.; Khanna, A.; Huang, Q.; Han, S. P.; Parker, R. A.; Hamann, L. G. Synthesis of Novel Potent Dipeptidyl Peptidase IV Inhibitors With Enhanced Chemical Stability: Interplay Between the N-Terminal Amino Acid Alkyl Side Chain and the Cyclopropyl Group of Alpha-Aminoacyl-l-Cis-4,5-Methanoprolinenitrile-Based Inhibitors. *J. Med. Chem.* **2004,** *47,* 2587–2598.
167. Fura, A.; Khanna, A.; Vyas, V.; Koplowitz, B.; Chang, S. Y.; Caporuscio, C.; Boulton, D. W.; Christopher, L. J.; Chadwick, K. D.; Hamann, L. G.; Humphreys, W. G.; Kirby, M. Pharmacokinetics of the Dipeptidyl Peptidase 4 Inhibitor Saxagliptin in Rats, Dogs, and Monkeys and Clinical Projections. *Drug Metab. Dispos.* **2009,** *37,* 1164–1171.
168. Metzler, W. J.; Yanchunas, J.; Weigelt, C.; Kish, K.; Klei, H. E.; Xie, D.; Zhang, Y.; Corbett, M.; Tamura, J. K.; He, B.; Hamann, L. G.; Kirby, M. S.; Marcinkeviciene, J. Involvement of DPP-4 Catalytic Residues in Enzyme-Saxagliptin Complex Formation. *Protein Sci.* **2008,** *17,* 240–250.
169. Boulton, D. W.; Geraldes, M. Safety, Tolerability, Pharmacokinetics and Pharmacodynamics of Once Daily Oral Doses of Saxagliptin for 2 Weeks in Type 2 Diabetic and Healthy Subjects [Abstract]. *Diabetes* **2007,** *56* (Suppl. 1), A161.
170. Rosenstock, J.; Sankoh, S.; List, J. F. Glucose-Lowering Activity of the Dipeptidyl Peptidase-4 Inhibitor Saxagliptin in Drug-Naive Patients With Type 2 Diabetes. *Diabetes Obes. Metab.* **2008 May,** *10,* 376–386.
171. Rosenstock, J.; Aguilar-Salinas, C.; Klein, E.; Nepal, S.; List, J.; Chen, R.; CV181-011 Study Investigators. Effect of Saxagliptin Monotherapy in Treatment-Naive Patients with Type 2 Diabetes. *Curr. Med. Res. Opin.* **2009,** *25,* 2401–2411.
172. Scirica, B. M.; Bhatt, D. L.; Braunwald, E.; Steg, P. G.; Davidson, J.; Hirshberg, B.; Ohman, P.; Frederich, R.; Wiviott, S. D.; Hoffman, E. B.; Cavender, M. A.; Udell, J. A.; Desai, N. R.; Mosenzon, O.; McGuire, D. K.; Ray, K. K.; Leiter, L. A.; Raz, I.; SAVOR-TIMI 53 Steering Committee and Investigators. Saxagliptin and Cardiovascular Outcomes in Patients With Type 2 Diabetes Mellitus. *N. Engl. J. Med.* **2013,** *369,* 1317–1326.
173. FDA Drug Safety Communication: FDA Adds Warnings About Heart Failure Risk to Labels of Type 2 Diabetes Medicines Containing Saxagliptin and Alogliptin. April 5, 2016. http://www.fda.gov/Drugs/DrugSafety/ucm486096.htm.
174. Kovi, R.; Rapole, K. R.; Naik, A.; Kannapan, J.; Madala, U. K.; Thakor, S. F. Process for Preparing Saxagliptin and its Novel Intermediates Useful in the Synthesis Thereof. U.S. Patent 2013/0023671 A1.
175. Kovi, R.; Rapole, K. R.; Naik, A.; Kannapan, J.; Madala, U. K.; Thakor, S. F. Methods and Compounds Producing Dipeptidyl Peptidase Inhibitors and Intermediates Thereof. WO Patent 2012/162507.
176. Vu, T. C.; Brzozowski, D. B.; Fox, R.; Godfrey, J. D. Jr.; Hanson, R. L.; Kolotuchin, S. V.; Mazzullo, J. A. Jr.; Patel, R. N.; Wang, J.; Wong, K.; Yu, J.; Jason Zhu, J.; Magnin, D. R.; David, J. Augeri, D. A.; Hamann, L. G. Methods and Compounds Producing Dipeptidyl Peptidase iv Inhibitors and Intermediates Thereof. WO Patent 2004/052850 A2.
177. Hanson, L. R.; Goldberg, L. S.; Brzozowski, B. D. Preparation of an Amino Acid Intermediate for the Dipeptidyl Peptidase IV Inhibitor, Saxagliptin, Using a Modified Phenylalanine Dehydrogenase. *Adv. Synth. Catal.* **2007,** *349,* 1369–1378.
178. Nakamaru, Y.; Hayashi, Y.; Ikegawa, R.; Kinoshita, S.; Perez Madera, B.; Gunput, D.; Kawaguchi, A.; Davies, M.; Mair, S.; Yamazaki, H.; Kume, T.; Suzuki, M. Effect of Ketoconazole on the Pharmacokinetics of the Dipeptidyl Peptidase-4 Inhibitor Teneligliptin: An Open-Label Study in Healthy White Subjects in Germany. *Clin. Ther.* **2014,** *36,* 760–769.
179. Scott, L. J. Teneligliptin: A Review in Type 2 Diabetes. *Clin. Drug Invest.* **2015,** *35,* 765–772.
180. (a) Kadowaki, T.; Kondo, K. Efficacy, Safety and Dose–Response Relationship of Teneligliptin, a Dipeptidyl Peptidase-4 Inhibitor, in Japanese Patients With Type 2 Diabetes Mellitus. *Diabetes Obes. Metab.* **2013,** *15,* 810–818; (b) Kadowaki, T.; Marubayashi, F.; Yokota, S.; Katoh, M.; Iijima, H. Safety and Efficacy of Teneligliptin in Japanese Patients With Type 2 Diabetes Mellitus: A Pooled Analysis of Two Phase III Clinical Studies. *Expert. Opin. Pharmacother.* **2015,** *16,* 971–981.
181. Furuta, S.; Smart, C.; Hackett, A.; Benning, R.; Warrington, S. Pharmacokinetics and Metabolism of [14C]Anagliptin, a Novel Dipeptidyl Peptidase-4 Inhibitor, in Humans. *Xenobiotica* **2013,** *43,* 432–442.
182. Yang, H. K.; Min, K. W.; Park, S. W.; Chung, C. H.; Park, K. S.; Choi, S. H.; Song, K. H.; Kim, D. M.; Lee, M. K.; Sung, Y. A.; Baik, S. H.; Kim, I. J.; Cha, B. S.; Park, J. H.; Ahn, Y. B.; Lee, I. K.; Yoo, S. J.; Kim, J.; Park, I. B.; Park, T. S.; Yoon, K. H. A Randomized, Placebo-Controlled, Double-Blind, Phase 3 Trial to Evaluate the Efficacy and Safety of Anagliptin in Drug-Naive Patients With Type 2 Diabetes. *Endocr. J.* **2015,** *62,* 449–462.
183. Graul, A. I.; Lupone, B.; Cruces, E.; Stringer, M. 2012 in Review—Part I. The Year's New Drugs & Biologics. *Drugs Today* **2013,** *49,* 33–68.
184. Deacon, C. F.; Holst, J. J. Linagliptin, a Xanthine-Based Dipeptidyl Peptidase-4 Inhibitor With an Unusual Profile for the Treatment of Type 2 Diabetes. *Expert Opin. Investig. Drugs* **2010,** *19,* 133–140.
185. Thomas, L.; Eckhardt, M.; Langkopf, E.; Tadayyon, M.; Him-melsbach, F.; Mark, M. (R) 8-(3-Amino-Piperidin-1-yl)-7-But-2-ynyl-3-Methyl-1-(4-Methyl-Quinazolin-2-yl-Methyl)-3,7-Dihydro-Purine-2,6-Dione (Bl 1356), a Novel Xanthine-Based Dipeptidyl Peptidase 4 Inhibitor, has a Superior Potency and Longer Duration of Action Compared With Other Dipeptidyl Peptidase-4 Inhibitors. *J. Pharmacol. Exp. Ther.* **2008,** *325,* 175–182.
186. Eckhardt, M.; Hauel, N.; Himmelsbach, F.; Langkopf, E.; Nar, H.; Michael, M. M.; Tadayyon, M.; Thomas, L.; Guth, B.; Lotz, R. 3,5-Dihydro-Imidazo[4,5-d]Pyridazin-4-Ones: A Class of Potent DPP-4 Inhibitors. *Bioorg. Med. Chem. Lett.* **2008,** *18,* 3158–3162.
187. Fuchs, H.; Tillement, J. P.; Urien, S.; Greischel, A.; Roth, W. Concentration-Dependent Plasma Protein Binding of the Novel Dipeptidyl Peptidase 4 Inhibitor Bl 1356 Due to Saturable Binding to Its Target in Plasma of Mice, Rats and Humans. *J. Pharm. Pharmacol.* **2009,** *61,* 55–62.
188. Fuchs, H.; Binder, R.; Greischel, A. Tissue Distribution of the Novel DPP-4 Inhibitor Bl 1356 is Dominated by Saturable Binding to its Target in Rats. *Biopharm. Drug Dispos.* **2009,** *30,* 229–240.
189. Heise, T.; Graefe-Mody, E. U.; Huttner, S.; Ring, A.; Tromme-shauser, D.; Dugi, K. A. Pharmacokinetics, Pharmacodynamics and Tolerability of Multiple Oral Doses of Linagliptin, a Dipeptidyl Peptidase-4 Inhibitor in Male Type 2 Diabetes Patients. *Diabetes Obes. Metab.* **2009,** *11,* 786–794.
190. Thomas, L.; Tadayyon, M.; Mark, M. Chronic Treatment With the Dipeptidyl Peptidase-4 Inhibitor Bl 1356 [(R)-8-(3-Amino-Piperidin-1-yl)-7-But-2-ynyl-3-Methyl-1-(4-Methylquinazolin-2-ylmethyl)-3,7-Dihydro-Purine-2,6-Dione] Increases Basal Glucagon-Like Peptide-1 and Improves Glycemic Control in Diabetic Rodent Models. *J. Pharmacol. Exp. Ther.* **2009,** *328,* 556–563.

191. Huttner, S.; Graefe-Mody, E. U.; Withopf, B.; Ring, A.; Dugi, K. A. Safety, Tolerability, Pharmacokinetics, and Pharmacodynamics of Single Oral Doses of BI 1356, an Inhibitor of Dipeptidyl Peptidase 4, in Healthy Male Volunteers. *J. Clin. Pharmacol.* **2008,** *48,* 1171–1178.
192. Del Prato, S.; Barnett, A. H.; Huisman, H.; Neubacher, D.; Woerle, H. J.; Dugi, K. A. Effect of Linagliptin Monotherapy on Glycaemic Control and Markers of Beta-Cell Function in Patients With Inadequately Controlled Type 2 Diabetes: A Randomized Controlled Trial. *Diabetes Obes. Metab.* **2011,** *13,* 258–267.
193. Kanasaki, K.; Shi, S.; Kanasaki, M.; He, J.; Nagai, T.; Nakamura, Y.; Ishigaki, Y.; Kitada, M.; Srivastava, S. P.; Koya, D. Linagliptin-Mediated DPP-4 Inhibition Ameliorates Kidney Fibrosis in Streptozotocin-Induced Diabetic Mice by Inhibiting Endothelial-to-Mesenchymal Transition in a Therapeutic Regimen. *Diabetes* **2014,** *63,* 2120–2131.
194. Panchapakesan, U.; Gross, S.; Gangadharan Komala, M.; Pegg, K.; Pollock, C. A. DPP4 Inhibition in Human Kidney Proximal Tubular Cells—Renoprotection in Diabetic Nephropathy? *J. Diabetes Metab.* **2013;** http://dx.doi.org/10.4172/2155-6156.S9-007.
195. Shi, S.; Kanasaki, K.; Koya, D. Linagliptin but not Sitagliptin Inhibited Transforming Growth Factor-Beta2-Induced Endothelial DPP-4 Activity and the Endothelial-Mesenchymal Transition. *Biochem. Biophys. Res. Commun.* **2016,** *471,* 184–190.
196. Cardiovascular and Renal Microvascular Outcome Study with Linagliptin in Patients with Type 2 Diabetes Mellitus (CARMELINA), 2015, https://clinicaltrials.gov/ct2/show/NCT01897532.
197. Serradell, N.; Rosa, E.; Castaner, R.; Wang, Y.; Frederick, R. Dipeptidyl-Peptidase IV Inhibitor, Antidiabetic. *Drugs Future* **2008,** *33,* 473–477.
198. Waldemar, P.; Thorsten, P.; Thomas, N; Duran, R. Process for the Preparation of Chiral 8-(−3-Aminopiperidin-1-yl) Xanthines. U.S. Patent 2006/0142310, 2006.
199. Himmelsbach, F.; Langkopf, E.; Eckhardt, M.; Mark, M.; Maier, R.; Lotz, R. H.; Tadayyon, M. 8-[3-Amino-Piperidin-1-yl]-Xanthines, the Preparation Thereof and Their Use as Pharmaceutical Compositions. U.S. Patent 2004/0097510, 2004.
200. Kira, K.; Clark, R.; Yoshikawa, S.; Uehara, T. 1,3-Dihydroimidazole ring compound. U.S. Patent 2006/0111362, 2006.
201. Lee, B.; Shi, L.; Kassel, D. B.; Asakawa, T.; Takeuchi, K.; Christopher, R. Pharmacokinetic, Pharmacodynamic, and Efficacy Profiles of Alogliptin, a Novel Inhibitor of Dipeptidyl Peptidase-4, in Rats, Dogs, and Monkeys. *Eur. J. Pharmacol.* **2008,** *589,* 306–314.
202. Christopher, R. J.; Davenport, J. M.; Gwaltney, S.; Kaldor, S.; Kassel, D.; Lee, B.; Navre, M.; Shi, L.; Stafford, J.; Xu, R.; Zhang, Z. Pharmacokinetic and Pharmacodynamic Profiles of SYR-322, A Novel Inhibitor of Dipeptidyl Peptidase-IV, in Rats, Dogs, and Monkeys. *Diabetes* **2006,** *55.* Abstract 452-P.
203. Christopher, R.; Covington, P.; Davenport, M.; Fleck, P.; Mekki, Q. A.; Wann, E. R.; Karim, A. Pharmacokinetics, Pharmacodynamics and Tolerability of Single Increasing Doses of the Dipeptidyl Peptidase-4 Inhibitor Alogliptin in Healthy Male Subjects. *Clin. Ther.* **2008,** *30,* 513–527.
204. Pratley, R. E. Alogliptin: A New, Highly Selective Dipeptidyl Peptidase-4 Inhibitor for the Treatment of Type 2 Diabetes. *Expert. Opin. Pharmacother.* **2009,** *10,* 503–512.
205. Chen, X. W.; He, Z. X.; Zhou, Z. W.; Yang, T.; Zhang, X.; Yang, Y. X.; Duan, W.; Zhou, S. F. An Update on the Clinical Pharmacology of the Dipeptidyl Peptidase 4 Inhibitor Alogliptin Used for the Treatment of Type 2 Diabetes Mellitus. *Clin. Exp. Pharmacol. Physiol.* **2015,** *42,* 1225–1238.
206. DeFronzo, R. A.; Fleck, P. R.; Wilson, C. A.; Mekki, Q.; Alogliptin Study 010 Group. Efficacy and Safety of the Dipeptidyl Peptidase-4 Inhibitor Alogliptin in Patients With Type 2 Diabetes and Inadequate Glycemic Control: A Randomized, Double-Blind, Placebo-Controlled Study. *Diabetes Care* **2008,** *31,* 2315–2317.
207. FDA Prescribing Information for Alogliptin. http://www.accessdata.fda.gov/drugsatfda_docs/label/2013/022271s000lbl.pdf.
208. White, W. B.; Bakris, G. L.; Bergenstal, R. M.; Cannon, C. P.; Cushman, W. C.; Fleck, P.; Heller, S.; Mehta, C.; Nissen, S. E.; Perez, A.; Wilson, C.; Zannad, F. Examination of CArdiovascular OutcoMes With AlogliptIN Versus Standard of CarE in Patients With Type 2 Diabetes Mellitus and Acute Coronary Syndrome (EXAMINE): A Cardiovascular Safety Study of the Dipeptidyl Peptidase 4 Inhibitor Alogliptin in Patients With Type 2 Diabetes With Acute Coronary Syndrome. *Am. Heart J.* **2011,** *162,* 620–626.e1.
209. Liu, H.; Ko, S. B.; Josien, H.; Curran, D. P. Selective N-Functionalization of 6-Substituted-2-Pyridones. *Tetrahedron Lett.* **1995,** *36,* 8917–8920.
210. Feng, J.; Gwaltney, S. L.; Stafford, J. A.; Kaldor, S. W.; Kassel, D. B.; Zhang, Z.; Bruce, E. J.; Paul, I. K; Grant, P.; Jonathon, S. S.; Luckner, U. Process for the Preparation of Pyrimidinedione Derivatives. WO Patent 2007035629, 2007.
211. McKeage, K. Trelagliptin: First global Approval. *Drugs* **2015,** *75,* 1161–1164.
212. Inagaki, N.; Onouchi, H.; Sano, H.; Funao, N.; Kuroda, S.; Kaku, K. SYR-472, a Novel Once Weekly Dipeptidyl Peptidase-4 (DPP-4) Inhibitor, in Type 2 Diabetes Mellitus: A Phase 2, Randomised, Double Blind, Placebo-Controlled Trial. *Lancet Diabetes Endocrinol.* **2014,** *2,* 125–132.
213. Inagaki, N.; Onouchi, H.; Maezawa, H.; Kuroda, S.; Kaku, K. Once-Weekly Trelagliptin Versus Daily Alogliptin in Japanese Patients With Type 2 Diabetes: A Randomised, Double-Blind, Phase 3, Non-Inferiority Study. *Lancet Diabetes Endocrinol.* **2015,** *3,* 191–197.
214. Li, X.; Winn, D. T.; O'Farrell, A.-M. Preclinical Development of PHX1149, an Orally Available, Potent and Selective DPP4 (Dipeptidyl Peptidase) Inhibitor. *Diabetes* **2006,** *55,* A128. Abstract 538-P.
215. O'Farrell, A. M.; van Vliet, A.; Abou Farha, K.; Cherrington, J. M.; Campbell, D. A.; Li, X.; Hanway, D.; Li, J.; Guler, H. P. Pharmacokinetic and Pharmacodynamic Assessments of the Dipeptidyl Peptidase-4 Inhibitor PHX1149: Double-Blind, Placebo-Controlled, Single- and Multiple-Dose Studies in Healthy Subjects. *Clin. Ther.* **2007,** *29,* 1692–1705.
216. Pattzi, H. M.; Pitale, S.; Alpizar, M.; Bennett, C.; O'Farrell, A. M.; Li, J.; Cherrington, J. M.; Guler, H. P.; PHX1149-PROT202 Study Group. Dutogliptin, a Selective DPP4 Inhibitor, Improves Glycaemic Control in Patients With Type 2 Diabetes: A 12-Week, Double-Blind, Randomized, Placebo-Controlled, Multicentre Trial. *Diabetes Obes. Metab.* **2010,** *12,* 348–355.
217. Wu, Z. P.; Campbell, D. A.; Cherrington, J. M. Synthesis Of Dipeptidyl Peptidase-4 Inhibitors: A Brief Overview. WO Patent 200827273, 2008.
218. Campbell, D. A.; Winn, D. T.; Betancort, J. M. Pyrrolidine Compounds and Methods for Selective Inhibition of Dipeptidyl Peptidase-iv. U.S. Patent 2006/0264400, 2006.
219. Wu, Z. P.; Campbell, D. A.; Leitao, E. P.; Wang, P. Methods and Intermediates for Synthesis of Selective dpp-iv Inhibitors. WO Patent 2008109681, 2008.
220. Ammirati, M. J.; Andrews, K. M.; Boyer, D. D.; Brodeur, A. M.; Danley, D. E.; Doran, S. D.; Hulin, B.; Liu, S.; McPherson, R. K.; Orena, S. J.; Parker, J. C.; Polivkova, J.; Qiu, X.; Soglia, C. B.; Treadway, J. L.; VanVolkenburg, M. A.; Wilder, D. C.; Piotrowski, D. W. (3,3-Difluoro-pyrrolidin-1-yl)-[(2S,4S)-(4-(4-Pyrimidin-2-yl-Piperazin-1-yl)-Pyrrolidin-2-yl]-Methanone: A Potent, Selective, Orally Active Dipeptidyl Peptidase IV Inhibitor. *Bioorg. Med. Chem. Lett.* **2009,** *19,* 1991–1995.
221. Sharma, R.; Sun, H.; Piotrowski, D. W.; Ryder, T. F.; Doran, S. D.; Dai, H.; Prakash, C. Metabolism, Excretion, and Pharmacokinetics of ((3,3-Difluoropyrrolidin-1-yl)((2S,4S)-4-(4-(Pyrimidin-2-yl)Piperazin-1-yl)Pyrrolidin-2-yl)Methanone, a Dipeptidyl Peptidase Inhibitor, in Rat, Dog and Human. *Drug Metab. Dispos.* **2012,** *40,* 2143–2161.
222. Muto, C.; Dai, H. Q.; Teeter, J. G.; Johnson, S.; Cropp, A. B.; Chiba, K.; Suwa, T. The Pharmacokinetics and Pharmacodynamics of PF-00734200, a DPP-IV Inhibitor, in Healthy Japanese Subjects. *Int. J. Clin. Pharmacol. Ther.* **2012,** *50,* 505–509.
223. Rosenstock, J.; Lewin, A. J.; Norwood, P.; Somayaji, V.; Nguyen, T. T.; Teeter, J. G.; Johnson, S. L.; Dai, H.; Terra, S. G. Efficacy and Safety of the Dipeptidyl Peptidase-4 Inhibitor PF-734200 Added to Metformin in Type 2 Diabetes. *Diabet. Med.* **2011,** *28,* 464–469.
224. Geldern, T. W. V.; Trevillyan, J. M. "The Next Big Thing" in Diabetes: Clinical Progress on DPP-4 Inhibitors. *Drug Dev. Res.* **2006,** *67,* 627–642.
225. Anitha, K.; Gopi, G.; Senthil Kumar, P. Molecular Docking Study on Dipeptidyl Peptidase-4 Inhibitors. *Int. J. Res. Dev. Pharm. L. Sci.* **2013,** *2,* 602–610.
226. Haffner, C.; Dougald, D.; L. Randhawa, A. S.; Reister, S.; M. Lenhard J. M. (2S,4S)-4-Fluro-1-[4-Fluoro-Beta-(4-Fluorophenyl)-L-Phenylalanyl]-2-Pyrrolidinecarbonitirle p-Toluenesulfonic Acid Salt and Anhydrous Crystalline Forms Thereof. WO Patent 03/002531, 2003.
227. Igo, D.; H. Johnson, P. R.; Patterson, D. E.; Randhawa A. S. 2s,4s)-4-Fluoro-1-[4-Fluoro-Beta-(4-Fluorophenyl)-l-Phenylalanyl]-2-Pyrrolidinecarbonitrile p-Toluenesulfonic Acid Salt and Anhydrous Crystalline Forms Thereof. WO Patent 2005/009956, 2005.
228. Narayanan, S.; Anupindi, R.; Shah, D. M.; Vakkalanka, S. V. S. Chronic Treatment With GRC 8200, a Novel DPP-IV Inhibitor, Improves Glycemic Control in *db*/*db* Mice. *Diabetes* **2006,** *55,* A324.
229. Thomas, A.; Prasada Rao, L. V. S.; Ashok, K. B.; Suresh, K. M.; Shantaram, P. K.; Deepak, U. V. Novel Processes for the Preparation of DPP IV Inhibitors. WO Patent 2008/001195, 2008.
230. Glenmark Pharmaceuticals Files Phase I Application for It's Anti-Diabetic, DPP-IV Inhibitor GRC 8200 in the UK. Glenmark Pharmaceuticals Ltd Press Release, September 22, 2005.
231. Glenmark's Anti-Diabetic, DPP-IV Inhibitor, GRC 8200 Successfully Completes Phase I. Glenmark Pharmaceuticals Ltd Press Release, February 24, 2006.

232. Thomas, A.; Gopalan, B.; Lingam, P. R. V. S.; Shah, D. M. Novel Dipeptidyl Peptidase IV Inhibitors, Pharmaceutical Compositions Containing Them, and Process for Their Preparation. WO Patent 2006/040625, 2006.
233. Yuan, K.; Ma, S.; Zhu, L.; Liu, H. Salts of Methyl (R)-7-[3-Amino-4-(2,4,5-Trifluoro-Phenyl)-Butyryl]-3-Trifluoromethyl-5,6,7,8-Tetrahydro-Imidazo[1,5-a]Pyrazine-1-Carboxylate. U.S. Patent 2012/0122875 A1, 2012.
234. Sun, P. Y. From Generic Drug to New Drugs: Hengrui's Experience. 5th International Conference and Exhibition, China 2010 Pharmaceutical R&D Summit, Shanghai, April 5–6.
235. Deng, B.; Yang, F.; Fan, J.; Feng, H.; Wang, Y.; Yang, T. Piperazine Derivative, Preparation Thereof and Use Thereof in Medicine. CN Patent 101468988 A, 2009.
236. Tang, P. C.; Yang, F.; Fan, J.; Feng, H.; Wang, Y.; Yang, T. Tetrahydro-Imidazo[1,5-a]Pyrazine Derivatives, Preparation Process and Medicinal Use Thereof. U.S. Patent 2010/0273786, 2010.
237. Mattei, P.; Boehringer, M.; Di Giorgio, P.; Fischer, H.; Hennig, M.; Huwyler, J.; Kocer, B.; Kuhn, B.; Loeffler, B. M.; Macdonald, A.; Narquizian, R.; Rauber, E.; Sebokova, E.; Sprecher, U. Discovery of Carmegliptin: A Potent and Long-Acting Dipeptidyl Peptidase IV Inhibitor for the Treatment of Type 2 Diabetes. *Bioorg. Med. Chem. Lett.* **2010,** *20,* 1109–1113.
238. Mori, K.; Yamane, K. Synthesis of Optically Active Forms of A-Factor, the Inducer of Streptomycin Biosynthesis in Inactive Mutants of Streptomyces Griseus. *Tetrahedron* **1982,** *38,* 2919–2921.
239. Lal, G. S.; Pez, G. P.; Pesaresi, R. J.; Prozonic, F. M.; Cheng, H. Bis(2-methoxyethyl)aminosulfur Trifluoride: A New Broad-Spectrum Deoxofluorinating Agent with Enhanced Thermal Stability. *J. Org. Chem.* **1999,** *64,* 7048–7054.
240. Stefan, A.; Adam, J. M.; Fettes, A.; Joseph, F.; Lohri, B.; Mattei, P.; Moine, G.; Schimd, R.; Zutter U. Preparation of (*S*)-4-Fluoromethyl-Dihydro furan-2-One. WO Patent 2006/125728, 2006.
241. Stefan, A.; Adam, J. M.; Fettes, A.; Hilbrand, S. Process for the Preparation of Pyrido-[2,1-A]Isoquinoline Derivatives Comprising Optical Resolution of an Enamine. WO Patent 2008/031749, 2008.
242. Harrison, A.; Heinig, K.; Fowler, S.; Haas, R.; Pahler, A.; Schmid, P.; Weick, I.; Carlile, D. Non-Cyp Clearance of RO0730699 in Rat, Dog and Man via Cyano Group Hydrolysis—Evidence for Extrahepatic Metabolism. 2012 AAPS Annual Meeting and Exposition, Chicago, October 14–18.
243. Madar, D. J.; Kopecka, H.; Pireh, D.; Yong, H.; Pei, Z.; Li, X.; Wiedeman, P. E.; Djuric, S. W.; Geldern, T. W. V.; Fickes, M. G.; Bhagavatula, L.; McDermott, T.; Wittenberger, S.; Richards, S. J.; Longenecker, K. L.; Stewart, K. D.; Lubben, T. H.; Ballaron, S. J.; Stashko, M. A.; Long, M. A.; Wells, H.; Zinker, B. A.; Mika, A. K.; Beno, D. W. A.; Kempf-Grote, A. J.; Polakowski, J.; Segreti, J.; Reinhart, G. A.; Fryer, R. M.; Sham, H. L.; Trevillyan, J. M. Discovery of 2-[4-{[2-(2S,5R)-2-Cyano-5-Ethynyl-1-Pyrrolidinyl]-2-Oxoethyl]Amino]-4-Methyl-1-Piperidinyl]-4-Pyridinecarboxylic Acid (ABT-279): A Very Potent, Selective, Effective, and Well-Tolerated Inhibitor of Dipeptidyl Peptidase-IV, Useful for the Treatment of Diabetes. *J. Med. Chem.* **2006,** *49,* 6416–6420.
244. (a) Pei, Z.; Li, X.; von Geldern, T. W.; Madar, D. J.; Longenecker, K.; Yong, H.; Lubben, T. H.; Stewart, K. D.; Zinker, B. A.; Backes, B. J.; Judd, A. S.; Mulhern, M.; Ballaron, S. J.; Stashko, M. A.; Mika, A. K.; Beno, D. W.; Reinhart, G. A.; Fryer, R. M.; Preusser, L. C.; Kempf-Grote, A. J.; Sham, H. L.; Trevillyan, J. M. Discovery of ((4R,5S)-5-Amino-4-(2,4,5-Trifluorophenyl)Cyclohex-1-Enyl)-(3-(Trifluoromethyl)-5,6-Dihydro-[1,2,4]Triazolo[4,3-a]Pyrazin-7(8H)-yl)Methanone (ABT-341), a Highly Potent, Selective, Orally Efficacious, and Safe Dipeptidyl Peptidase IV Inhibitor for the Treatment of Type 2 Diabetes. *J. Med. Chem.* **2006,** *49,* 6439–6442; (b) Takeuchi, Y.; Namiki, M.; Kitahara, Y.; Hasegawa, S.; Ohnishi, A.; Yasuda, N.; Inoue, T.; Clark, R.; Safety, K. Y. Tolerability, Pharmacokinetics and Pharmacodynamics of E3024, a Novel and Selective Dipeptidyl Peptidase-IV Inhibitor, in Healthy Japanese Male Subjects: Rash Development in Men and Its Possible Mechanism. *Pharmacol. Pharm.* **2013,** *4,* 663–678. http://dx.doi.org/10.4236/pp. 2013.49093. http://www.scirp.org/journal/pp. Published Online December 2013, Open Access PP 663.
245. Schoenafinger, K.; Jaehne, G.; Defossa, E.; Schwink, L.; Wagner, H.; Buning, C.; Tschank, G.; Werner, U. Substituted Bicyclic 8-Pyrrolidinoxanthines, Method for the Production Thereof and Their Use as Medicaments. WO Patent 2006015701, 2006.
246. Miyamoto, Y.; Banno, Y.; Yamashita, T.; Fujimoto, T.; Oi, S.; Moritoh, Y.; Asakawa, T.; Kataoka, O.; Yashiro, H.; Takeuchi, K.; Suzuki, N.; Ikedo, K.; Kosaka, T.; Tsubotani, S.; Tani, A.; Sasaki, M.; Funami, M.; Amano, M.; Yamamoto, Y.; Aertgeerts, K.; Yano, J.; Maezaki, H. Discovery of a 3-Pyridylacetic Acid Derivative (TAK-100) as a Potent, Selective and Orally Active Dipeptidyl Pepti-Dase IV (DPP-4) Inhibitor. *J. Med. Chem.* **2011,** *54,* 831–850.
247. Yamazaki, K.; Yasuda, N.; Inoue, T.; Nagakura, T.; Kira, K.; Shi-noda, M.; Saeki, T.; Tanaka, I. 7-But-2-ynyl-9-(6-Methoxy-Pyridin-3-yl)-6-Piperazin-1-yl-7,9-Dihydro-Purin-8-One is a Novel competitive and Selective Inhibitor of Dipeptidyl Peptidase IV With an Anti-Hyperglycemic Activity. *J. Pharmacol. Exp. Ther.* **2006,** *319,* 1253–1257.
248. Shu, C.; Ge, H.; Song, M.; Chen, J. H.; Zhou, H.; Qi, Q.; Wang, F.; Ma, X.; Yang, X.; Zhang, G.; Ding, Y.; Zhou, D.; Peng, P.; Shih, C. K.; Xu, J.; Frank Wu, F. Discovery of Imigliptin, a Novel Selective DPP-4 Inhibitor for the Treatment of Type 2 Diabetes. *ACS Med. Chem. Lett.* **2014,** *5,* 921–926.
249. (a) Takasaki, K.; Iwase, M.; Nakajima, T.; Ueno, K.; Nomoto, Y.; Nakanishi, S.; Higo, K. K579, a Slow-Binding Inhibitor of Dipeptidyl Peptidase IV, is a Long-Acting Hypoglycemic Agent. *Eur. J. Pharmacol.* **2004,** *486,* 335–342; (b) Tanaka-Amino, K.; Matsumoto, K.; Hatakeyama, Y.; Takakura, S.; Mutoh, S. ASP4000, a Slow-Binding Dipeptidyl Peptidase 4 Inhibitor, has Antihyperglycemic Activity of Long Duration in Zucker Fatty Rats. *Acta Diabetol.* **2010,** *47,* 43–44.
250. Singh, S.; Roy, S.; Sethi, S.; Benjamin, B.; Sundaram, S.; Khanna, V.; Kandalkar, S. R.; Pal, C.; Kant, R.; Patra, A. K.; Rayasam, G.; Mittra, S.; Saini, K. S.; Paliwal, J.; Chugh, A.; Ahmed, S.; Satti-geri, J.; Cliff, I.; Ray, A. I.; Bansal, V. S.; Bhatnagar, P. K.; Davis, J. A. RBx-0597, a Potent, Selective and Slow-Binding Inhibitor of Dipeptidyl Peptidase-IV for the Treatment of Type 2 Diabetes. *Eur. J. Pharmacol.* **2011,** *652,* 157–163.
251. Matsuyama-Yokono, A.; Tahara, A.; Nakano, R.; Someya, Y.; Nagase, I.; Hayakawa, M.; Shibasaki, M. ASP8497 is a Novel Selective and Competitive Dipeptidyl Peptidase-IV Inhibitor With Anti-Hyperglycemic Activity. *Biochem. Pharmacol.* **2008,** *76,* 98–107.
252. Mu, J.; Woods, J.; Zhou, Y.-P.; Sinha Roy, R.; Li, Z.; Zycband, E.; Feng, Y.; Zhu, L.; Li, C.; Howard, A. D.; Moller, D. E.; Thornberry, N. A.; Zhang, B. B. Chronic Inhibition of Dipeptidyl Peptidase-4 With a Sitagliptin Analog Preserves Pancreatic Beta-Cell Mass and Function in a Rodent Model of Type 2 Diabetes. *Diabetes* **2006,** *55,* 1695–1704.
253. Nishio, Y.; Kimura, H.; Sawada, N.; Sugaru, E.; Horiguchi, M.; Ono, M.; Furuta, Y.; Akai, M.; Masui, Y.; Otani, M.; Hashizuka, T.; Honda, Y.; Deguchi, J.; Nakagawa, T.; Nakahira, H. 2-({6-[(3R)-3-Amino-3-Methylpiperidine-1-yl]-1,3-Dimethyl-2,4-Dioxo-1,2,3,4-Tetrahydro-5H-Pyrrolo[3,2-d]Pyrimidine-5-yl}Methyl)-4-Fluorobenzonitrile (DSR-12727): A Potent, Orally Active Dipeptidyl Peptidase IV Inhibitor Without Mechanism-Based Inactivation of CYP3A. *Bioorg. Med. Chem.* **2011,** *19,* 5490–5499.
254. Koo, K. D.; Kim, M. J.; Kim, S.; Kim, K. H.; Hong, S. Y.; Hur, G. C.; Yim, H. J.; Kim, G. T.; Han, H. O.; Kwon, O. H.; Kwon, T. S.; Koh, J. S.; Lee, C. S. Synthesis, SAR, and X-Ray Structure of Novel Potent DPPIV Inhibitors: Oxadiazolyl Ketones. *Bioorg. Med. Chem. Lett.* **2007,** *17,* 4167–4172, 270.
255. Coghlan, M. J. *Preclinical Profile of LY2463665, a Potent, Highly Selective, Reversible DPP IV Inhibitor for the Treatment of Type 2 Diabetes.* 67th Scientific Sessions; American Diabetes Association: Chicago, IL, 2007. http://professional.diabetes.org/abstract/preclinical-profile-ly2463665-potent-highly-selective-reversible-dpp-iv-inhibitor-treatment.
256. Kushwaha, R. N.; Haq, W.; Katti, S. B. Sixteen-Years of Clinically Relevant Dipeptidyl Peptidase-IV (DPP-IV) Inhibitors for Treatment of Type-2 Diabetes: A Perspective. *Curr. Med. Chem.* **2014,** *21,* 4013–4045.
257. Gallego, M.; Aristoy, M. C.; Toldra, F. Dipeptidyl Peptidase IV Inhibitory Peptides Generated in Spanish Dry-Cured Ham. *Meat Sci.* **2014,** *96,* 757–761.
258. Cohen, M.; Fruitier-Arnaudin, I.; Piot, J. M. Hemorphins: Substrates and/or Inhibitors of Dipeptidyl Peptidase IV. Hemorphins N-Terminus Sequence Influence on the Interaction Between Hemorphins and DPPIV. *Biochimie* **2004,** *86,* 31–37.
259. Umezawa, H.; Aoyagi, T.; Ogawa, K.; et al. Diprotins A and B, Inhibitors of Dipeptidyl Aminopeptidase IV, Produced by Bacteria. *J. Antibiot.* **1984,** *37,* 422–425.
260. Pieter, B. J. W. Protein Hydrolysate Enriched in Peptides Inhibiting DPP-4 and Their Use. WO Patent 2006068480A2, 2006.
261. Huang, S. L.; Jao, C. L.; Ho, K. P.; et al. Dipeptidyl-Peptidase IV Inhibitory Activity of Peptides Derived from Tuna Cooking Juice Hydrolysates. *Peptides* **2012,** *35,* 114–121.
262. Tulipano, G.; Sibilia, V.; Caroli, M. A.; et al. Whey Proteins as Source of Dipeptidyl Dipeptidase IV (Dipeptidyl Peptidase-4) Inhibitors. *Peptides* **2011,** *32,* 835–838.
263. Tulipano, G.; Cocchi, D.; Caroli, A. M. Comparison of Goat and Sheep 442 β-Lactoglobulin to Bovine β-Lactoglobulin as Potential Source of Dipeptidyl Peptidase IV (DPP-4) Inhibitors. *Int. Dairy J.* **2012,** *24,* 97–101.

264. Li-Chan, E. C. Y.; Hunag, S. L.; Jao, C. L.; et al. Peptides Derived from Atlantic Salmon Skin Gelatin as Dipeptidyl-peptidase IV Inhibitors. *J. Agric. Food Chem.* **2012,** *60,* 973–978.
265. Velarde-Salcedo, A. J.; Barrera-Pacheco, A.; Lara-González, S.; et al. *In vitro* Inhibition of Dipeptidyl Peptidase IV by Peptides Derived from the Hydrolysis of Amaranth (*Amaranthus Hypochondriacus L.*) Proteins. *Food Chem.* **2013,** *136,* 758–764.
266. Kumar, K. V.; Pavan, T. S.; Rama, K. C.; Shriram, R.; Murali, P. M. Study of Plant Glucosylxanthone & its Analogs, as DPPIV Inhibitor for Anti-Diabetic Activity. *Int. J. Pharm. Sci. Rev. Res.* **2012,** *15,* 83–87.
267. Mohandas, R.; Sautina, L.; Beem, E.; Schuler, A.; Chan, W.-Y.; Domsic, J.; McKenna, R.; Johnson, R. J.; Segal, M. S. Uric Acid Inhibition of Dipeptidyl Peptidase IV In Vitro is Dependent on the Intracellular Formation of Triuret. *Exp. Cell Res.* **2014,** *326,* 136–142.
268. Antonyan, A.; De, A.; Vitali, L. A.; Pettinari, R.; Marchetti, F.; Gigliobianco, M. R.; Pettinari, C.; Camaioni, E.; Lupidi, G. Evaluation of (Arene)Ru(II) Complexes of Curcumin as Inhibitors of Dipeptidyl Peptidase IV. *Biochimie* **2014,** *99,* 146–152.
269. Fan, J.; Johnson, M. H.; Lila, M. A.; Yousef, G.; de Mejia, E. G. Berry and Citrus Phenolic Compounds Inhibit Dipeptidyl Peptidase IV: Implications in Diabetes Management. *Evid. Based Complement. Alternat. Med.* **2013,** *2013,* 1–13.
270. Zhang, L. *Identification of Isoquercitrin as a Inhibitor of DPP-IV: Implications for Insulin Secretion and Hyperglycemic in Type 2 Diabetes Mice;* Jilin University: Jilin, 2013; pp 1–99.
271. Bower, A. M.; Real Hernandez, L. M.; Berhow, M. A.; et al. Bioactive Compounds from Culinary Herbs Inhibit a Molecular Target for Type-2 Diabetes Management, Dipeptidyl Peptidase-IV. *J. Agric. Food Chem.* **2014,** *62,* 6147–6158.
272. Parmar, H. S.; Jain, P.; Chauhan, D. S.; Gonzalez de Mejia, E. DPP-4 Inhibitory 412 Potential of Naringin: An *In Silico*, *In Vitro* and *In Vivo* Study. *Diabetes Res. Clin. Pract.* **2012,** *97,* 105–111.
273. (a) Guasch, L.; Ojeda, M. J.; Gonza'lez-Abuõ'n, N. G.; Sala, E.; Cereto-Massague, A.; Mulero, M.; Valls, C.; Pinent, M.; Arde'vol, A.; Santiago Garcia-Vallve, S.; Pujadas, G. Identification of Novel Human Dipeptidyl Peptidase-IV Inhibitors of Natural Origin (Part I): Virtual Screening and Activity Assays. *PLoS One* **2012,** *7,* 1–13; ; (b) Hamamoto, A.; Aoki, Y.; Matsukawa, T.; Matsui, Y.; Yamada, Y.; Yamada, I. Dipeptidyl Peptidase IV (DPPIV) Inhibitor Containing Extracts of Capsicum Annuum cv., Rosa Gallica and UNCARINA Tomentosa as Effective Constituent. *Jpn. Kokai Tokkyo Koho*, JP Patent 2007277163 A 20071025, 2007.
274. Sato, Y.; Kawazoe, K.; Mizuguchi, K.; Ota, K. DPP-4 Inhibitors Containing Aqueous Schizandra chinensis Extract, and Pharmaceutical Compositions and Food Compositions Containing the Inhibitors. Jpn. Kokai Tokkyo Koho, JP Patent 2012082172 A 20120426, 2012.
275. (a) Bharti, S. K.; Krishnan, S.; Kumar, A.; Rajak, K. K.; Murari, K.; Bharti, B. K.; Gupta, A. K. Antihyperglycemic Activity With DPP-4 Inhibition of Alkaloids Seed Extract of Castanospermum Australe: Investigation Experimental Validation and Molecular Docking. *Phytomedicine* **2012,** *20* (1), 24–31; (b) Shukla, A.; Srinivasan, B. P. 16,17-Dihydro-17b-Hydroxy Isomitraphylline (DHIM) Alkaloid as an Inhibitor of DPP-4, and its Effect on Incretin Hormone and β-Cell Proliferation in Diabetic Rat. *Eur. J. Pharm. Sci.* **2012,** *47* (2), 512–519.
276. González-Abuín, N.; Martínez-Micaelo, N.; Blay, M.; Pujadas, G.; Garcia-Vallvé, S.; Pinent, M.; Ardévol, A. Grape Seed-Derived Procyanidins Decrease Dipeptidyl-peptidase 4 Activity and Expression. *J. Agric. Food Chem.* **2012,** *60,* 9055–9061.
277. Kosaraju, J.; Dubala, A.; Chinni, S.; Khatwal, R. B.; Satish Kumar, M. N.; Basavan, D. A Molecular Connection of *Pterocarpus Marsupium*, *Eugenia Jambolana* and *Gymnema Sylvestre* with Dipeptidyl Peptidase-4 in the Treatment of Diabetes. *Pharm. Biol.* **2014,** *52,* 268–271.
278. Pascual, I.; Lopéz, A.; Gómez, H.; et al. Screening of Inhibitors of Porcine Dipeptidyl Peptidase IV Activity in Aqueous Extracts from Marine Organisms. *Enzyme Microb. Technol.* **2007,** *40,* 414–419.
279. Yang, Z. Z. *Three Kinds of Plants in Xinjiang on Dipeptidyl Peptidase IV Inhibition Activity*. Masters Thesis; Xinjiang Medical University: Xinjiang, 2012; pp 1–45.
280. Miao, L. *Screening the Dipeptidyl Peptidase IV Inhibitors from the Chinese Herb and It's Pharmacodynamics;* Jiangnan University: Jiangsu, 2008; pp. 1–44.
281. Williams-Herman, D.; Round, E.; Swern, A. S.; Musser, B.; Davies, M. J.; Stein, P. P.; Kaufman, K. D.; Amatruda, J. M. Safety and Tolerability of Sitagliptin in Patients With Type 2 Diabetes: A Pooled Analysis. *BMC Endocr. Disord.* **2008,** *8,* 14. http://dx.doi.org/10.1186/1472-6823-8-14.
282. FDA Drug Safety Communication: FDA Warns that DPP-4 Inhibitors for Type 2 Diabetes may Cause Severe Joint Pain. August 28, 2015, http://www.fda.gov/Drugs/DrugSafety/ucm459579.
283. Hanefeld, M.; Herman, G. A.; Wu, M.; Mickel, C.; Sanchez, M.; Stein, P. P.; Sitagliptin Study 014 Investigators. Once-Daily Sitagliptin, a Dipeptidyl Peptidase 4 Inhibitor, for the Treatment of Patients With Type 2 Diabetes. *Curr. Med. Res. Opin.* **2007,** *23,* 1329–1339.
284. Singh, S. K.; Manne, N.; Pal, M. Synthesis Of (S)-1-(2-Chloroacetyl)Pyrrolidine-2-Carbonitrile: A Key Intermediate For Dipeptidyl Peptidase IV Inhibitors. *Beilstein J. Org. Chem.* **2008,** 4(20). http://dx.doi.org/10.3762/bjoc.4.20.
285. Hermansen, K.; Kipnes, M.; Luo, E.; Fanurik, D.; Khatami, H.; Stein, P. Sitagliptin Study 035 Group. Efficacy and Safety of the Dipeptidyl Peptidase-4 Inhibitor, Sitagliptin, in Patients with Type 2 Diabetes Mellitus Inadequately Controlled on Glimepiride Alone or on Glimepiride and Metformin. *Diabetes Obes. Metab* **2007,** *9,* 733–745.
286. Kim, T. E.; Lim, K. S.; Park, M. K.; Yoon, S. H.; Cho, J. Y.; Shin, S. G.; Jang, I. J.; Yu, K. S. Evaluation of the pharmacokinetics, food effect, pharmacodynamics, and tolerability of DA-1229, a dipeptidyl peptidase IV inhibitor, in healthy volunteers: first-in-human study. *Clin Ther.* **2012,** *34,* 1986–1998.
287. Kim, M. K.; Chae, Y. N.; Kim, H. D.; Yang, E. K.; Cho, E. J.; Choi, S. H.; Cheong, Y. H.; Kim, H. S.; Kim, H. J.; Jo, Y. W.; Son, M. H.; Kim, S. H.; Shin, C. Y. DA-1229, a novel and potent DPP4 inhibitor, improves insulin resistance and delays the onset of diabetes. *Life Sci.* **2012,** *90,* 21–29.
288. Jung, C. H.; Park, C. Y.; Ahn, K. J.; Kim, N. H.; Jang, H. C.; Lee, M. K.; Park, J. Y.; Chung, C. H.; Min, K. W.; Sung, Y. A.; Park, J. H.; Kim, S. J.; Lee, H. J.; Park, S. W. A randomized, double-blind, placebo-controlled, phase II clinical trial to investigate the efficacy and safety of oral DA-1229 in patients with type 2 diabetes mellitus who have inadequate glycaemic control with diet and exercise. *Diabetes Metab. Res. Rev.* **2015,** *31,* 295–306.
289. Crawforth, J. M.; Fawcett, J.; Rawlings, B. J. Asymmetric synthesis of A-factor. *J. Chem. Soc., Perkin Trans.* **1998,** *1,* 1721–1726.
290. Fukushima, H.; Hiratate, A.; Takahashi, M.; Mikami, A.; Saito-Hori, M.; Munetomo, E.; Kitano, K.; Chonan, S.; Saito, H.; Suzuki, A.; Takaoka, Y.; Yamamoto, K. Synthesis and Structure-Activity Relationships of Potent 4-Fluoro-2-cyanopyrrolidine Dipeptidyl Peptidase IV Inhibitors. *Bioorg. Med. Chem.* **2008,** *16,* 4093–4106.

7.15 Advances in Antiplatelet Agents

EA Meyer, E Caroff, and MA Riederer, Actelion Pharmaceuticals Ltd, Allschwil, Switzerland

© 2017 Elsevier Ltd. All rights reserved.

7.15.1	**General Overview**	557
7.15.1.1	Hemostasis and Thrombosis	557
7.15.1.2	Pathology of Thrombotic Diseases	558
7.15.1.3	Epidemiology and Antithrombotic Market	558
7.15.2	**Introduction Into Platelet Function**	559
7.15.2.1	Formation of Platelets	559
7.15.2.2	Endothelial Cell Layer and Extracellular Matrix	559
7.15.2.3	Platelet Adhesion, Activation, Aggregation, and Thrombus Stabilization	559
7.15.2.4	Inhibition of Platelet Aggregation	560
7.15.2.5	Assay Systems to Monitor Platelet Inhibition	560
7.15.2.6	Experimental Thrombosis Models In Vivo	561
7.15.3	**Overview of Current Treatment and Unmet Medical Need**	561
7.15.3.1	Clinical Use of Antiplatelet Drugs	561
7.15.3.2	Need for Novel Antiplatelet Approaches	562
7.15.4	**Overview of Targets for Antiplatelet Therapy**	562
7.15.4.1	Platelet Adhesion and Aggregation Receptors	562
7.15.4.2	GPCRs as Receptors of Released Signaling Molecules	563
7.15.4.3	Mechanism of Intracellular Signaling and Key Intracellular Enzymes	563
7.15.5	**Antagonists of GPCRs**	565
7.15.5.1	Purinergic Receptor Antagonists	565
7.15.5.1.1	$P2Y_{12}$ antagonists	566
7.15.5.1.2	$P2Y_1$ antagonists	572
7.15.5.1.3	$P2X_1$ antagonists	574
7.15.5.2	Protease-Activated Receptor (PAR) Antagonists	574
7.15.5.2.1	PAR-1 antagonists	574
7.15.5.2.3	PAR-4 antagonists	578
7.15.5.3	EP_3 Antagonists	578
7.15.5.4	$5\text{-}HT_{2A}$ Antagonists	579
7.15.5.5	TP Antagonists	580
7.15.5.6	IP Antagonists	580
7.15.6	**Inhibition of Platelet Adhesion and Aggregation**	580
7.15.6.1	Integrin $\alpha_{IIb}\beta_3$ Antagonists	580
7.15.6.1.1	First-generation antagonists	580
7.15.6.1.2	Mechanism of action of integrins and ligand binding mode	581
7.15.6.1.3	Novel approaches in $\alpha_{IIb}\beta_3$ antagonism	581
7.15.6.2	Antagonists of the Adhesion Receptors	582
7.15.6.2.1	$\alpha_2\beta_1$ antagonists	582
7.15.6.2.2	GPVI antagonists	583
7.15.6.2.3	vWF and GPIb receptor antagonists	584
7.15.7	**Inhibitors of Intracellular Enzymes**	584
7.15.7.1	COX Inhibitors	584
7.15.7.1.1	Aspirin	584
7.15.7.1.2	Triflusal	585
7.15.7.1.3	Recent developments	585
7.15.7.2	TXS Inhibitors	586
7.15.7.3	PDE Inhibitors	586
7.15.7.4	Kinase Inhibitors	587
7.15.7.4.1	PI3Kβ inhibitors	587
7.15.7.4.2	Other kinases	588
7.15.8	**New Frontiers in Antiplatelet Therapy**	588
7.15.8.1	Role of Platelets Outside Hemostasis	588
7.15.8.1.1	Platelets in inflammation and immunity	588
7.15.8.1.2	Platelets in cancer	589
7.15.8.2	Emerging Antiplatelet Targets	589

 http://dx.doi.org/10.1016/B978-0-12-409547-2.12431-X

7.15.9 Conclusion 590
Acknowledgments 590
References 590

Abbreviation

AA Arachidonic acid
AC Adenylyl cyclase
ACS Acute coronary syndrome
ADP Adenosine diphosphate
ATC Antiplatelet Trialists' Collaboration
CABG Coronary artery bypass graft
CAD Coronary artery disease
cAMP Cyclic AMP
CD39 Endothelial ADPase
COX-1 Cyclooxygenase-1
DAG Diacylglycerol
DAPT Dual antiplatelet therapy
DP1 PGD_2 receptor
DVT Deep vein thrombosis
ECG Electrocardiogram
ECM Extracellular matrix
EMA European Medicines Agency
ENT1 Equilibrative nucleoside transporter 1
EP PGE_2 receptor
FDA Food and Drug Administration
FVII Coagulation factor VII
Gas6 Growth arrest-specific-6
Gi Gαi subunit
Gla γ-Carboxyglutamic acid
GPCR G protein-coupled receptor
IP PGI_2 receptor
IP3 Inositol phosphate-3
LTA Light transmission aggregometry
MAPKs Mitogen-activated protein kinases
MIDAS Metal ion-dependent adhesion site
NSAIDs Nonsteroidal antiinflammatory drugs
NSTEMI Non-ST-elevated myocardial infarct
PAD Peripheral arterial disease
PAH Pulmonary arterial hypertension
PAOD Peripheral arterial occlusive disease
PAR Protease-activated receptors
PCI Percutaneous intervention
PDE Phosphodiesterase
PE Pulmonary embolism
PGI_2 Prostacyclin
PI3K Phosphoinositol-3-kinase
PKC Protein kinase C
PLA2 Phospholipase A2
PLCβ Phospholipase Cβ
PRP Platelet-rich plasma
PS Phosphatidylserine
RIAM Rap1-GTP-interacting adapter molecule
r-tPA Recombinant tissue-type plasminogen activator
SSc Systemic sclerosis
STEMI ST-elevated myocardial infarct
TF Tissue factor
TI Therapeutic index
TIA Transient ischemic attack
TP Thromboxane receptor
TRAP Thrombin receptor-activating peptide (Ser-Phe-Leu-Leu-Arg-Asn). Peptide fragment (residues 42–47) of PAR1 that acts as a PAR1 agonist
TXA_2 Thromboxane A_2
TXS Thromboxane synthase
UA Unstable angina pectoris
VTE Venous thromboembolism
vWF Von Willebrand factor

7.15.1 General Overview

7.15.1.1 Hemostasis and Thrombosis

The circulation of blood guarantees the supply of oxygen and nutrients, as well as the disposal of catabolic products. Therefore, the integrity of blood vessels is essential at all times. When the vascular integrity is compromised, a highly efficient repair mechanism is activated at the site of injury resulting in the formation of a repair seal to prevent further blood loss. This fundamental biological process is defined as hemostasis.[1] It is mediated by three main components: the endothelial cells, the platelets, and the coagulation system. The endothelial cell layer defines the surface of the blood vessels and thus the interface to the flowing blood. Platelets circulate in a resting state but are able to adhere to the damaged or activated endothelial surface and then stick to each other to form platelet aggregates that seal the damaged surface. Finally, the coagulation system is responsible for the generation of fibrin fibers that stabilize the platelet aggregates. The coagulation cascade and the platelet activation and aggregation are interdependent biological processes: activation of the coagulation cascade leading to efficient formation of fibrin fibers is dependent on the negatively charged membrane surface of activated platelets. On the other hand, platelet activation and stabilization of platelet aggregates depend upon the final product of the coagulation cascade, thrombin.[2] In fact, the key coagulation protease thrombin is responsible for the generation of fibrin fibers, and it is also the most potent activator of platelets.[3] The importance of each

component in the hemostatic system changes with the rheological condition: under high shear rate, that is, in fast-flowing or arterial blood, platelets play a central role, whereas under low shear rate, that is, in slow blood flow characteristic for veins, formation of fibrin clots by the coagulation system is assuming a more dominant role.[4] Although these systems are usually discussed in isolation, it is important to realize that they are mutually dependent and thus cannot optimally perform in the absence of the counterpart.

If the size of a repair seal is exaggerated, such (partially) occlusive platelet/fibrin aggregates, known as platelet- or fibrin-rich thrombi, can block the blood supply to downstream organs, causing ischemic disorders.

Thrombosis is the result of a pathological deviation of one or several components involved in hemostasis. Such deviation can be caused by a plethora of environmental or genetic factors. A differentiation between venous and arterial blood flow is important. In arterial blood vessels, age, gender, race, diabetes mellitus, and a family history of thrombotic events represent risk factors that cannot be influenced and may shift the hemostatic system toward a prothrombotic state. In addition, lifestyle factors such as obesity, hyperlipidemia, smoking, and physical immobilization also contribute to the deviation of the hemostatic system toward higher risk of thrombosis.[5] The effect of these risk factors is thought to be twofold. First, excessive platelet reactivity to activators shifts the balance toward an increased risk of occlusive thrombosis.[6] Second, in a very slow but steady process, these environmental factors trigger changes in the endothelial cell lining of the vascular system and thus support the process of atherosclerosis. Formation of atherosclerotic plaques is triggered by an accumulation of lipid vesicles within the wall of the blood vessels. Macrophages invade the vessel wall and phagocytose the lipids forming the so-called foam cells that accumulate and contribute to the growth of atherosclerotic plaques. With increasing age and size of these plaques, the risk of direct obstruction of blood flow can become symptomatic.[7] Furthermore, if atherosclerotic plaques fissure or rupture, usually triggered by mechanical stress by fast-flowing blood in a partially occluded artery, a prothrombotic surface is exposed, which can initiate the formation of an occlusive platelet thrombus.

7.15.1.2 Pathology of Thrombotic Diseases

Depending on the anatomical location, a limitation of blood flow can have diverse clinical outcomes: occlusion of blood flow to the heart muscle reduces heart performance, which manifests in dyspnea (shortness of breath), vertigo (dizziness), numbness, nausea, or pain. The symptoms of occlusion of blood vessels in the heart are generally described as acute coronary syndrome (ACS). Depending on the stability and induced damage of the vessel occlusion, ACS is further qualified as ST-elevated myocardial infarct (STEMI), non-ST-elevated myocardial infarct (NSTEMI), and unstable angina pectoris (UA). In STEMI, complete and stable vessel occlusion with resultant infarction (death) of distal tissues induces a change in the electrocardiogram (ECG) visible as a change in the ST part of the ECG. In NSTEMI, no functional consequence on the ECG is evident indicating that the vessel occlusion is partial or recent. However, NSTEMI is also associated with an elevation of troponin I or troponin T concentration in blood. The troponins are cytosolic proteins of cardiac muscles and are released into the circulation upon cardiac damage.[8] In contrast, UA is defined by transient signs of the aforementioned symptoms without elevation of troponin levels.[9]

In analogy to coronary blood vessels, if an occlusion arises in the brain, the events are classified as transient ischemic attacks (TIA) or as ischemic stroke if a permanent occlusion of brain arteries occurs. In addition, the occlusion of a peripheral artery in the lower extremities manifests as transient limitation of blood flow and hence leg pain (intermittent claudication) or with stable occlusion as peripheral arterial occlusive disease (PAOD), respectively.

In venous blood vessels, risk factors for the formation of venous thrombi are similar to arterial thrombi. Risk factors that cannot be influenced include genetic predisposition for enhanced coagulation activity, age, gender, race, diabetes mellitus, cancer, orthopedic surgery, and long-term immobilization of patients. Lifestyle factors, which could theoretically be controlled, include obesity, physical inactivity, smoking, and the use of contraceptives.[10] The clinical manifestation of venous thrombosis is different to arterial thrombosis. Occlusion of a vein, usually in the leg, defined as deep vein thrombosis (DVT), results in symptoms such as swollen legs, numbness, redness, and pain in the area of the occlusion. Since veins represent blood vessels with a relatively large diameter, clots can break off from deep vein wall and can be flushed over large distances into the right side of the heart. The right heart chamber pumps the blood into the lung for reoxygenation and thus into the more narrow blood vessels of the lung. There, clots can occlude a pulmonary arterial bed and cause pulmonary embolism (PE). Alternatively, such a clot can be flushed into the brain and cause an embolic stroke. Together, DVT and PE are summarized as venous thromboembolism (VTE). The anti-VTE approaches are described in detail in Book Chapter 7.07. Advances in Anticoagulants.

7.15.1.3 Epidemiology and Antithrombotic Market

Ischemic thrombotic vascular disease is the leading cause of death in developed countries.[11] Despite advances in treatment and prevention, ACS represents an enormous medical, social, and economic burden worldwide. Globally, ACS resulting from myocardial infarction is responsible for almost half of all deaths related to cardiovascular diseases. ACS also claims a high toll in terms of treatment-related and indirect economic costs.[12]

Venous thromboembolism (VTE) represents a significant source of morbidity and mortality. VTE is a common disorder, with an estimated annual incidence of approximately 5–12 cases per 10,000. The prognosis for patients who develop VTE is exacerbated by the risk of recurrent VTE, post-thrombotic syndrome, and chronic pulmonary hypertension as a long-term complication of PE.[13]

The global market of antithrombotics was estimated to exceed 23 billion US dollars in 2013 and is expected to grow in the future.[14] The antiplatelet market is still dominated by clopidogrel, which in 2010 grossed peak sales of over 9 billion US dollars.[15] In light of such significant rewards, efforts within the pharmaceutical industry are benevolently supported. However, the future

success of novel antiplatelet drugs depends on a clear demonstration of excellent efficacy in combination with an improved bleeding risk profile.

In the next sections, after an introduction into platelet biology and a broad overview of the major antiplatelet targets, efforts in medicinal chemistry to generate novel antiplatelet drugs are reviewed. A vast amount of literature that summarizes the different approaches of the past decades is already available.[16] Therefore, in this article, established antiplatelet drugs are described briefly, while the focus is placed on more recent developments.

7.15.2 Introduction Into Platelet Function

7.15.2.1 Formation of Platelets

Platelets, also called thrombocytes, are generated by large progenitor cells known as megakaryocytes. Megakaryocytes release platelets as a result of a complex maturation process. First, megakaryocytes become multinucleated or polyploid and accumulate proteins and membranes. Then, in a cytoskeleton-driven process, they form long branched protrusions termed proplatelets. As these nascent platelets mature, granules and selected organelles are delivered from the megakaryocyte core into the proplatelet tip that then undergoes fission to release platelets. Platelets are devoid of a cell nucleus[17]; nevertheless, they can synthesize proteins *de novo* since they contain messenger RNA.[18] One megakaryocyte may protrude as many as 10–20 proplatelets. Nonactivated, resting platelets circulate as biconvex discoid (lens-shaped), a form defined by internal microtubule and actin cytoskeleton, with an average diameter of 2–4 μm. In healthy individuals, the normal platelet number, usually referred as "platelet count," is 150,000–400,000 per cubic millimeter or $150–400 \times 10^9$ platelets per liter.[19] An average of 10^{11} platelets is produced daily in a healthy adult with an average lifetime of about 10 days.

7.15.2.2 Endothelial Cell Layer and Extracellular Matrix

In the vasculature, the interface between circulating blood and the vessel wall consists of a single layer of endothelial cells. The release of inhibitory mediators, such as nitric oxide (NO), endothelial ADPase (CD39), and prostacyclin (PGI_2), from these endothelial cells contributes to keep circulating platelets in a resting state. Nitric oxide and PGI_2 inhibit platelet activation through intraplatelet signaling, whereas endothelial ADPase degrades ADP, one of the key activators of platelets.

The extracellular matrix (ECM) below the endothelium forms a scaffold that keeps the histological structure of the vessel wall in shape and consists of a complex network of elastic fibers to support vessel stability. ECM is mainly constituted by collagen, laminin, fibronectin, and elastin. The collagens are the most abundant proteins in the ECM where fibril-forming collagens (types I, II, III, V, and XI) represent the most abundant forms.[20]

When the endothelial layer is disrupted and the underlying subendothelial matrix is exposed to the blood flow (e.g., after rupture of an atherosclerotic plaque) or when inflammation perturbs the endothelium, platelets adhere to the ECM and become activated. In addition, the exposed ECM also contains tissue factor (TF). TF exerts its biological activity by forming a catalytic enzyme complex with the coagulation factor VII (FVII). If exposed to blood, it binds to the inactive FVII leading to the active complex TF/FVIIa and subsequent formation of thrombin. As outlined in the preceding text, the relative importance of platelets and the coagulation system for the repair of vascular injuries depends on the rheological conditions.

7.15.2.3 Platelet Adhesion, Activation, Aggregation, and Thrombus Stabilization

Upon adhesion to the ruptured endothelium, platelets become activated via an intraplatelet signaling cascade induced by the adhesion receptors (outside-in signaling). For example, the collagen adhesion receptors trigger synthesis of thromboxane A_2 (TXA_2) via the enzyme cyclooxygenase-1 (COX-1). TXA_2 is then secreted and activates nearby platelets via binding to their thromboxane receptor (TP) and thus contributes to the amplification of platelet aggregation leading to thrombus formation. Furthermore, most adhesion receptors trigger transactivation of other integrin receptors (inside-out signaling). In the active conformation, these integrins can interact with their ECM ligands and thus contribute to the stabilization of the platelet thrombus. Moreover, activated platelets change the composition of the outer membrane resulting in the upregulation of negatively charged phospholipids (mainly phosphatidylserine (PS)) exposed toward the extracellular space. The γ-carboxyglutamic acid (Gla)-containing domain of coagulation factors can interact with the negatively charged membrane that accelerates the coagulation cascade activity.[21] In addition, activated platelets release the content of their dense and alpha-granules.[22] Dense granules contain small molecules such as ADP, ATP, GDP, serotonin, pyrophosphates, and magnesium and calcium ions.[23] Alpha-granules release soluble proteins such as von Willebrand factor (vWF), fibrinogen, thrombospondin, coagulation factors V, XI, and XIII, and prothrombin and, by fusing with the platelet membrane, increase the number of surface receptors, that is, the fibrinogen receptor $\alpha_{IIb}\beta_3$, the collagen receptor GPVI, and the adhesion receptor P-selectin.[24] The released molecules and exposed receptors are major contributors to further activation and recruitment of additional platelets into the initiated platelet thrombus. Specifically, these molecules either activate platelets that are in close proximity of the growing thrombus and thus recruit more platelets or bind to the surface of activated platelets as linker molecules to support thrombus growth or stabilization. For example, ADP binds and activates the purinergic receptors $P2Y_1$ and $P2Y_{12}$ that induce an intraplatelet signaling cascade leading to the activation of resting platelets.

The most important cross-linker is fibrinogen, which binds to the integrin $\alpha_{IIb}\beta_3$ on the surface of platelets and is thus essential for thrombus formation and stabilization.

The platelet response is intertwined at several levels with the coagulation cascade that results in an amplification of the prothrombotic activity. For example, leukocytes, such as monocytes and neutrophils, adhere to the activated platelets and expose the surface molecule TF upon complex formation with FVIIa, one of the strongest activators of the coagulation cascade.[25] In addition, coagulation factors, which are also released from alpha-granules, cooperate with TF to form thrombin. Thrombin activates the receptors PAR-1 and PAR-4 and thereby triggers intraplatelet signaling and further activation of platelets. Finally, thrombin proteolytically cleaves fibrinogen to form fibrin, which then can assemble into a fibrin mesh.

A pleiotropy of additional proteins, enzymes, and receptors has been described to participate in platelet adhesion, activation, aggregation, and stabilization. The precise function of many of these molecules is either not yet fully understood or they have varying importance depending on the specific condition of platelet activation. Rheological conditions, the composition of the prothrombotic surface, the inflammatory status of the endothelial cell layer, and the extent of involvement of the coagulation system might modulate the importance of these factors. While these biological processes are sometimes contradictorily or even confusingly described in the literature, their complexity could be an incentive for the generation of new therapeutic opportunities. Whereas in past decades the focus had been mainly on platelets in thrombotic diseases, recent research suggests additional function of platelets in immunology and tumor biology (see Section **Role of Platelets Outside Hemostasis**). In these processes, different signaling pathways might be more relevant, potentially resulting in novel opportunities for antiplatelet drugs in nonatherothrombotic diseases.

7.15.2.4 Inhibition of Platelet Aggregation

Platelets have been described to contribute to hemostasis and thrombosis since their discovery by Bizzozero in the 1880s.[26] More recently, atherosclerotic lesions in combination with occlusive platelet thrombi have been found in patients with ischemic cardiac death.[27] Inhibition of platelet aggregation is recognized as an effective strategy for the prevention of thrombosis in patients with atherosclerotic disease in the coronary, peripheral, and cerebrovascular circulation.[28] The aforementioned signaling molecules and receptors are among the most important and best studied drivers of thrombus formation in arterial blood flow and thus have been the focus of successful antithrombotic strategies. Briefly, COX-1 is irreversibly inhibited by aspirin, the most widely used agent for prevention of atherothrombotic diseases. The ADP receptor $P2Y_{12}$ is inhibited by the irreversible antagonists, clopidogrel and prasugrel, and the reversible antagonists ticagrelor and cangrelor, which are used for the treatment and prevention of ACS.[28b] The fibrinogen receptor $\alpha_{IIb}\beta_3$ is inhibited by the monoclonal antibody abciximab and by two small molecules tirofiban and eptifibatide, which are used for inhibition of platelet activity in an acute clinical setting. Most recently, the PAR-1 inhibitor vorapaxar gained approval for the prevention of atherothrombotic disease in patients with previous MI.[16d] The properties of these agents and novel development for these targets will be discussed in detail in the following sections.

Furthermore, inhibitors of the coagulation system known as anticoagulants have arisen as powerful antithrombotics. Anticoagulants have been shown to be effective in the treatment and prevention of VTE. However, long-term treatment with anticoagulant therapies in ACS patients was so far only successful with low-dose rivaroxaban, an inhibitor of the coagulation factor Xa. Rivaroxaban has recently been approved by the European Medicines Agency (EMA) but not by the Food and Drug Administration (FDA) for the secondary prevention after ACS.[29] Long-term anticoagulation in addition to dual antiplatelet therapy (DAPT) is required in 5–10% of patients for other conditions, such as atrial fibrillation, mechanical valves, and thromboembolic diseases, but is associated with an increase in major bleeding complications. Bleeding complications separate into minor bleedings like gum or nosebleeds and major bleedings leading to a drop of hemoglobin and the need for medical intervention such as red cell transfusion to guarantee survival.[30] Major bleedings are associated with reduced long-term survival and consequently limitation of bleeding risk is paramount. Therefore, for combination treatments, the safest possible agents and minimal duration of anticoagulant therapy are essential.[31]

7.15.2.5 Assay Systems to Monitor Platelet Inhibition

Inhibition of platelet function can be quantified by multiple assay systems. The classical platelet function assay is termed light transmission aggregometry (LTA). By differential centrifugation, blood cells are separated from platelets to generate platelet-rich plasma (PRP). Resting platelets are in a discoid shape and light transmission through a PRP-containing cuvette is low. However, upon the addition of a soluble platelet activator (ADP, thrombin, collagen, and TXA_2) in combination with stirring, platelets start to aggregate and the transmission of light through the cuvette is increased, hence allowing indirect quantification of platelet aggregation.[32] The quality of PRP preparation and reproducible execution of the protocol is essential to generate reliable results in this very sensitive assay. Although a low-throughput method, LTA still represents the gold standard for investigation of platelet function since inhibition of LTA has been shown to correlate with the antithrombotic effect in vivo. To allow medium throughput in a clinical setting, this principle has been adapted to a whole-blood aggregation assay (VerifyNow®).[33]

Two alternative functional tests using whole blood were developed based on the principle of impedance (time variation in an electric circuit). Two silver electrodes continuously measure the change in impedance in whole blood. Upon stimulation, platelets aggregate and adhere to the electrodes leading to a proportional increase in impedance. The change of impedance over time is graphically displayed and compared relative to control or samples containing various inhibitor concentrations. The identical principle has now been adapted to allow multiple measurements in parallel (Multiplate).[34]

Another functional test system aspirates blood through a capillary that is coated with ADP, collagen, or epinephrine. The platelet activators induce the formation of a platelet plug that closes the capillary (platelet function analyzer).[35] Time to occlusion has been shown to correlate with the extent of platelet inhibition.[36]

Alternatively, platelet activation can be monitored by quantification of intracellular signaling activity. One assay quantifies the phosphorylation of the vasodilator-stimulated phosphoprotein (VASP) that correlates with the extent of platelet activation and inhibition.[37] If the drug target is a G protein-coupled receptor (GPCR), inhibition of G protein signaling can be quantified using labeled GTPγS. Upon activation of the GPCR, labeled GTPγS binds to the G protein. Since GTPγS is not hydrolyzable, the labeled G proteins accumulate and can be quantified. Prevention of accumulation of labeled G protein correlates with inhibition of the GPCR.

Furthermore, the direct binding affinity of antagonists to target proteins can be measured using radiolabeled ligands of the target protein. However, to prevent misinterpretation, the binding affinity of the antagonist has to be put in relation with the binding affinity of the radioligand. Moreover, GTPγS accumulation or binding with radiolabeled ligand is performed in most cases with recombinant cell lines.

7.15.2.6 Experimental Thrombosis Models In Vivo

To confirm antithrombotic activity in animals, various models have been established.[38] The rat ferric chloride ($FeCl_3$) model is one of the most frequently used thrombosis models. In the anesthetized rat, the carotid artery is gently dissected free of connective tissue and a small piece of filter paper, soaked in $FeCl_3$ solution, is topically applied. $FeCl_3$ destroys the endothelial cell layer of the carotid artery and thus induces the formation of an occlusive platelet-rich thrombus. The decrease in blood flow is quantified using a Doppler flow probe.[39] All marketed antiplatelet agents have shown antithrombotic efficacy in this model.[40] In the same animals, quantification of bleeding time, after transection of the rat tail, is often used to evaluate potential side effects on hemostasis. However, in rat, tail bleeding time is reported to vary according to the antithrombotic agent and specific method applied.[41] Therefore, methods to quantify the volume of blood loss after a standardized surgical wound have also been established.[42]

Alternatively, thrombus formation can be induced by mechanical damage of the artery. In the method described by Folts et al. (Folts model), mechanical squeezing of the artery with forceps replaces $FeCl_3$ and induces thrombus formation. In the Folts model, occlusive thrombi are mechanically dislodged to reopen the blood flow. The number of occlusion/reopening cycles (cyclic flow variation) is then compared under various concentrations of antiplatelet agents.[43]

7.15.3 Overview of Current Treatment and Unmet Medical Need

7.15.3.1 Clinical Use of Antiplatelet Drugs

Treatment guidelines for ACS patients are based on a vast amount of clinical evidence. For historical and cultural reasons, not all treatment recommendations are identical. In this paragraph, we summarize the general treatment principles of the North American and European guidelines.

Patients with a STEMI are treated based on the capabilities of the hospital.[44] If the hospital is equipped to perform surgical intervention to reopen the occluded artery, defined as percutaneous intervention (PCI), STEMI patients receive PCI as fast as possible. Briefly, a catheter is inserted into the artery of the leg or the arm and advanced into the heart and finally into the occluded artery. With the help of a small balloon, the occluded artery is dilated to reestablish blood flow. To stabilize the reopened part of the artery, a metal mesh may be inserted into this specific section of the coronary artery (stent placement).

In a non-PCI-capable hospital, patients can be treated with a fibrinolytic agent. Fibrinolytic enzymes, such as tPA and streptokinase, are able to proteolytically cleave fibrin fibers and thus contribute to the dissolution of the occluding thrombus. This therapy, however, is only possible within a narrow time window of up to 6 hours after onset of symptoms. If a fibrinolytic therapy is no longer possible, the patient has to be transported to a hospital with PCI capabilities. Alternatively, if coronary anatomy is not amenable to PCI, coronary artery bypass graft (CABG) surgery is recommended. In this surgical intervention, a healthy artery or vein from the patient (usually from the leg) is grafted upstream and downstream of the blocked coronary artery to form a bypass around the blocked portion of the coronary artery. This creates a new path for oxygen-rich blood to feed the heart muscle and reestablish proper performance.

To support surgical therapy, adjunctive antithrombotic therapy is the standard of care. In all cases, the administration of aspirin (75–325 mg) is recommended to start before procedure and to continue thereafter indefinitely. During surgical intervention until revascularization, anticoagulation with unfractionated heparin, fractionated heparin (enoxaparin), or a synthetic pentasaccharide (fondaparinux) is recommended. In addition, DAPT with $P2Y_{12}$ receptor inhibitors (clopidogrel, prasugrel, and ticagrelor) should start as early as possible or at the time of PCI and continue for at least 12 months. Alternatively, intravenous application of $\alpha_{IIb}\beta_3$ receptor antagonists (abciximab, tirofiban, and eptifibatide) may be used for short-term platelet inhibition (up to 3 days) in combination with anticoagulation therapy. Secondary prevention is then continued with DAPT as described in the preceding text.[44] For UA/NSTEMI patients, treatment guidelines advocate aspirin as soon as possible after hospital presentation, with unlimited duration if tolerated.[45] UA/NSTEMI patients are subsequently treated either invasively with PCI or following a conservative, noninvasive strategy with antiplatelet medication. During invasive PCI, antiplatelet medication follows the same guidelines as described in the preceding text for STEMI patients. For conservative strategies, antiplatelet treatment is limited to DAPT.[45,46]

Treatment guidelines for stroke are well defined.[47] Intravenous application of recombinant tissue-type plasminogen activator (r-tPA) defines the cornerstone of early thrombolysis treatment of acute ischemic stroke. For optimal efficacy, thrombolytic therapy is limited to the first 6 h after onset of symptoms. Three antiplatelet regimens have demonstrated substantial reductions in secondary event risk and are currently recommended by consensus panels: aspirin monotherapy, the combination of aspirin plus extended-release dipyridamole, and clopidogrel monotherapy.[48]

The management of PAOD is multidisciplinary, involving primary care physicians and vascular specialists with varying expertise in diagnostic and treatment modalities. PAOD describes a broad spectrum of diseases from asymptomatic to severe limb ischemia. If the anatomical situation allows, surgical removal of occlusive thrombus or bypass surgery is recommended. In addition, antiplatelet therapy with aspirin, clopidogrel or dipyridamole, and cilostazol is deemed useful to reduce the risk of MI, stroke, or death.[49]

7.15.3.2 Need for Novel Antiplatelet Approaches

The current strategy for treatment and prevention of ACS has significantly reduced morbidity and mortality in this patient population. Unhealthy food choices and sedentary lifestyles in the industrialized world elevate the risk of atherothrombotic disease and thus partially offset the progress achieved by the joint efforts of pharmaceutical and medical research.

The first antiplatelet drug aspirin reduced major cardiovascular events (death, MI, and urgent revascularization) by 22%.[50] The combination of clopidogrel on top of aspirin further decreased major cardiovascular events by an additional 20%.[51] As a next step, prasugrel on top of aspirin achieved a higher platelet inhibition and thus an additional 19% risk reduction of cardiovascular events.[52] Moreover, each improvement in efficacy was accompanied with a statistically significant increase in major bleedings. Nevertheless, despite a higher risk in major bleedings, each of these studies demonstrated a clear medical benefit with a sufficient therapeutic window, which supported market approval and broad use in ACS patients. However, the long-term consequences of increased rates of major bleedings were illustrated by recent post hoc analyses of antiplatelet clinical trials.[53] These analyses revealed that a strong association between major bleeding and increased long-term mortality exists in ACS patients. Therefore, improved antiplatelet agents that are fully effective but show a reduced propensity of major bleeding will be essential to ameliorate current therapeutic strategies.

At present, clopidogrel in combination with aspirin remains the cornerstone of treatment in ACS. However, despite the significant benefits of DAPT, a considerable number of patients experience adverse events such as bleeding and thrombosis. Since the active principle of clopidogrel is a metabolite, and metabolic activation of clopidogrel can be a limiting factor in humans, large interindividual variability of antiplatelet effects is reported. On average, clopidogrel inhibits platelet function only by 40% with a variability of 0 to 80% inhibition.[16b] Those patients with high on-treatment platelet reactivity, that is, $<20\%$ inhibition, are at a higher risk of a thrombotic event.[54] Various approaches have been chosen in the past decades to generate novel antiplatelet therapies with reduced risk of bleeding and improved pharmacokinetic and pharmacodynamic profiles; however, success has been scarce. Encouraging examples are the orally active, reversible $P2Y_{12}$ antagonists ticagrelor and cangrelor and the PAR-1 antagonist vorapaxar.[53a,55] In addition, many more creative approaches for the optimization of known principles or the evaluation of novel targets are still ongoing.

7.15.4 Overview of Targets for Antiplatelet Therapy

7.15.4.1 Platelet Adhesion and Aggregation Receptors

Platelets circulate in a resting state; nevertheless, they can immediately adhere to exposed ECM. The major constituents of the subendothelial matrix, which bind and activate platelets, are collagen, vWF, vitronectin, fibronectin, and laminin.

On the surface of platelets, the most important adhesion receptors are the two main collagen receptors GPVI and integrin $\alpha_2\beta_1$, the vWF receptor GPIb, and the vitronectin receptor integrin $\alpha_V\beta_3$. The two integrins $\alpha_5\beta_1$ and $\alpha_6\beta_1$ are the receptors for fibronectin and laminin, respectively. The key integrin $\alpha_{IIb}\beta_3$ interacts with vWF immobilized on collagen, when acting as an adhesion receptor, and with fibrinogen to trigger aggregation.

Integrin $\alpha_2\beta_1$ is important for the adhesion to collagen, whereas GPVI is required for collagen-induced platelet activation.[56] Upon damage of the endothelial surface, vWF circulating in the blood binds to the exposed collagen fibers and serves as an adhesion partner for the GPIb-V-IX receptor complex. The importance of the GPIb-V-IX receptor complex is increasing with the velocity of the blood. At high blood flow in narrow blood vessels, the role of the GPIb-V-IX receptor is critical for platelet adhesion and thus in the initiation of thrombus formation.[57]

Adhesion receptors are the key initiators of intraplatelet signaling inducing new interactions responsible for the stabilization of platelet adhesion, platelet–platelet contact, platelet spreading, and granule release or clot retraction.[26,58] Ultimately, integrin $\alpha_{IIb}\beta_3$, the most important receptor for fibrinogen, is activated leading to platelet aggregation.

Due to their central role in platelet adhesion and in the early phase of the platelet activation or aggregation process, adhesion receptors have been targeted in antiplatelet approaches (**Table 1** and Section **Antagonists of the Adhesion Receptors**). From a drug discovery perspective, the most successful approach is integrin $\alpha_{IIb}\beta_3$, the major cross-linker between platelets responsible for aggregation (see Section **Integrin $\alpha_{IIb}\beta_3$ Antagonists**).

Table 1 Adhesion and aggregation receptors and selection of corresponding antagonists

Protein	*Receptor*	*Antagonists*	*Marketed*
Collagen	GPVI	Kistomin	No
	$\alpha_2\beta_1$	Revacept	Clin. Dev.
		Various	No
vWF	GPIb-V-IX	Aptamers, proteins, monoclonal antibodies, and nanobodies	Clin. Dev.
Fibrinogen/vWF	$\alpha_{IIb}\beta_3$	Abciximab	Yes
		Eptifibatide	Yes
		Tirofiban	Yes
		RUC-4	Preclin. Dev.

Table 2 The role of GPCRs on platelet activation and inactivation

Agonist	*GPCR*	*G protein*	*Effect on platelets*
ADP	$P2Y_1$	Gq	Activation
	$P2Y_{12}$	Gi	Activation
Thrombin	PAR-1	Gq	Activation
	PAR-4	Gq	Activation
PGE_2	EP3	Gi	Activation
Serotonin	$5\text{-}HT_{2A}$	Gq	Activation
TXA_2	TP	Gq	Activation
PGI_2	IP	Gs	Inactivation
PGD_2	DP1	Gs	Inactivation

Overview of GPCRs described for the activation or inactivation of platelets. Their most relevant associated G protein and their effect on signaling are listed. The GPCRs currently targeted by marketed antiplatelet drugs are highlighted in gray.

7.15.4.2 GPCRs as Receptors of Released Signaling Molecules

Upon adhesion, platelet activation is followed by the release of signaling molecules such as ADP, TXA_2, and thrombin. This triggers an amplification of the hemostatic process through a mechanism initiated by GPCRs.

GPCRs on the platelet surface display differential responses resulting in either further platelet activation or inactivation. As presented in Table 2, these GPCRs fall into two categories. Platelet-activating GPCRs are $P2Y_1$, $P2Y_{12}$, PAR-1, PAR-4, EP3, $5\text{-}HT_{2A}$, and TP. GPCRs that trigger the inactivation of platelets are the prostaglandin receptors IP (PGI_2 receptor) and DP1 (PGD_2 receptor). Most of these important GPCRs have been targeted by the pharmaceutical industry and will be discussed in Section Antagonists of GPCRs.

7.15.4.3 Mechanism of Intracellular Signaling and Key Intracellular Enzymes

Upon interaction with agonists, GPCRs undergo conformational changes and consequently trigger the activation of the bound heterotrimeric G protein complex ($G\alpha\beta\gamma$).[59] Upon GPCR activation, the $G\alpha$ subunit exchanges bound GDP by GTP. As a consequence, the $G\alpha$ subunit detaches from both the GPCR and the $\beta\gamma$ subunits and binds to its downstream signaling partner. Since the $G\alpha$ subunits exist in multiple variations, the ensuing downstream signal is different (Fig. 1). Specifically, the $G\alpha i$ subunit (Gi) inhibits adenylyl cyclase (AC) and thus causes a lowering of cyclic AMP (cAMP). In contrast, the $G\alpha s$ subunit (Gs) activates AC, which leads to elevated cAMP. The third major $G\alpha$ protein $G\alpha q$ (Gq) induces the activation of phospholipase $C\beta$ ($PLC\beta$), which generates inositol phosphate-3 (IP3) leading to an elevation of intraplatelet calcium (Ca^{2+}) levels.[60] Both mediators Ca^{2+} and cAMP play a critical role in platelet stimulation: high calcium and low cAMP levels in the platelet cytosolic space allow full activation of platelets. In contrast, low calcium and high cAMP levels keep the platelet in a resting state.

As shown in Table 2, antiplatelet strategies seek to either stimulate Gi-bound GPCRs, which elevate cAMP, or inhibit Gs-bound GPCRs, which would diminish cAMP concentrations. Alternatively, prevention of cAMP degradation can also interfere with platelet activation. The hydrolysis of cyclic nucleotides such as cAMP and cGMP yields the inactive 5′-AMP and 5′-GMP, respectively, and is mediated by phosphodiesterases (PDEs; Fig. 2). Inhibition of platelet-specific PDEs has already been validated as an antiplatelet approach with two PDE inhibitors approved as antithrombotic drugs.

Cyclooxygenase (COX), also named prostaglandin-endoperoxide synthase, is a pivotal enzyme in the biosynthesis of prostanoids, such as prostacyclin (PGI_2) and TXA_2. In general, after stimulation of a cell, phospholipases are activated and cleave cell membrane phospholipids to liberate arachidonic acid (AA). AA is then converted by COX into PGH_2, a precursor for the prostanoids PGF_2, PGE_2, PGI_2, and PGD_2 and TXA_2. The synthesis of specific prostanoids from PGH_2 depends on the context of activation

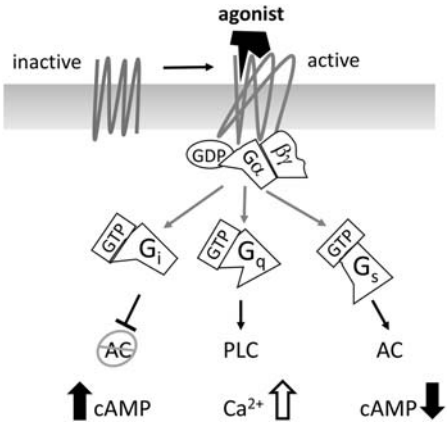

Fig. 1 Schematic representation of G protein-mediated signaling. Binding of an agonist to the GPCR induces a transformation of the GPCR from the inactive to the active conformation, hence triggering an activation of the bound G protein. The G protein is a heterotrimeric protein with three subunits α, β, γ. Only Gα exists in three major forms, termed Gi, Gs, and Gq. Upon activation, the Gα subunit exchanges bound GDP by GTP, detaches from the GPCR, and releases the βγ subunit. Activation and release of Gi result in the suppression of AC activity, while active Gs positively regulates AC, leading to a reduction or increase in cAMP, respectively. Active Gq triggers an increase in the intraplatelet calcium concentration (via activation of PLC and formation of IP3; see also **Fig. 3**). GPCR is symbolically drawn as 7-transmembrane spiral. The membrane surface of platelets is graphically displayed as a *thick gray bar*.

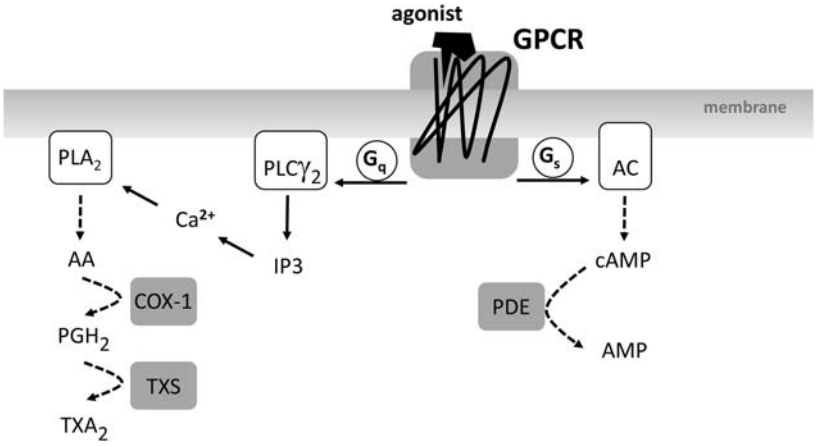

Fig. 2 Schematic representation of GPCR-induced intraplatelet signaling. Agonist binding induces conformational changes allowing an interaction with intracellular G proteins (see also **Fig. 1**). Gs proteins activate AC leading to increased concentrations of cytosolic cAMP. cAMP is hydrolyzed by PDEs into the (inactive) AMP. Gq proteins activate $PLC\gamma_2$, which cleaves phospholipids to liberate IP3 and DAG. IP3 triggers elevation of intraplatelet calcium concentration, which activates phospholipase A_2 (PLA_2). PLA_2 hydrolyses phospholipids to liberate arachidonic acid (*AA*). AA is converted by COX-1 into PGH_2, which, in platelets, is converted by TXS into TXA_2. *Black arrows* indicate an activation step. The dashed arrows point to the formation of an enzymatic product. Current pharmacological targets for the inhibition of platelet activation are highlighted in *gray*.

and the cell type. In thrombosis, two pathways are dominant: (a) in endothelial cells, PGI_2 is mainly produced, and released PGI_2 contributes to the inactivation of circulating platelets, and (b) in platelets, after the activation via the collagen receptor GPVI or thromboxane receptor TP, PGH_2 is converted into TXA_2 by thromboxane synthase (TXS). Secreted TXA_2 is one of the most important activators of circulating platelets and thus of the recruitment of platelets into growing thrombi. Consequently, the prostanoids and TXA_2 biosynthesis pathway contain two targets for antiplatelet approaches: COX-1 and TXS (**Fig. 2**).

Following binding to the exposed ECM ligands, adhesion receptors interact with intracellular effector proteins triggering a signaling cascade.[56,61] Examples of effector proteins are members of the Src kinase family, such as Lyn, Fyn, and Syk.[62] These tyrosine kinases activate phosphoinositol-3-kinase (PI3Kβ) and phospholipase $C\gamma_2$ ($PLC\gamma_2$), which convert membrane lipids into inositol phosphate-3 (IP3) and diacylglycerol (DAG). While IP3 triggers the release of intracellular calcium from internal stores into the platelet cytosol, DAG activates protein kinase C (PKC). Calcium and PKC signaling converge in the induction of granule secretion. In addition, calcium and DAG bind to the nucleotide exchange factor CalDAG-GEF1, which triggers the GTP binding protein Rap1 to exchange GDP by GTP resulting in an active conformation.[63] Active Rap1 associates with the linker protein RIAM (Rap1-GTP-interacting adapter molecule) and talin-1. This ternary complex binds to the

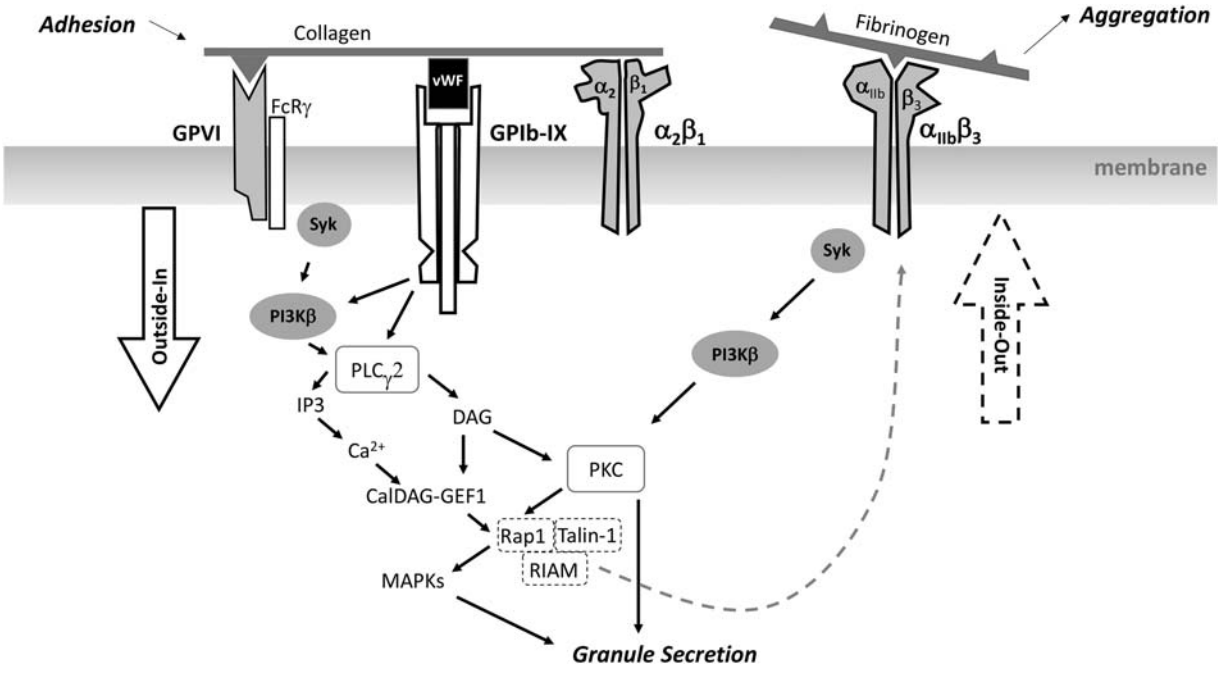

Fig. 3 Intraplatelet signaling induced by adhesion receptors. Adhesion receptors bind to collagen either directly ($\alpha_2\beta_1$, GPVI) or via a linker protein (*vWf*). GPVI using the subunit FcRγ activates Syk, which in turn activates PI3Kβ. PI3Kβ activates PLCγ_2, which cleaves phospholipids releasing IP3 and DAG. IP3 binds and stimulates calcium channels on the surface of intraplatelet organelles to release calcium (Ca^{2+}). Calcium is a key element for platelet activation; thus, this signaling event is termed outside-in signaling. Calcium and DAG bind to CalDAG-GEF1, a nucleotide exchange factor for the GTP binding protein Rap1. CalDAG-GEF1 in turn triggers the formation of the Rap1/RIAM/talin-1 complex, which binds to the intracellular part of integrins, inducing the high-affinity conformation and thus binding of extracellular ligands (inside-out signaling). In parallel, DAG activates PKC and active Rap1 leads to the activation of mitogen-activated protein kinases (*MAPK*s). Both pathways contribute to the phosphorylation of other signaling molecules essential for granule secretion. Upon binding of fibrinogen, additionally induced conformational changes within integrin $\alpha_{IIb}\beta_3$ trigger an interaction with intracellular linker molecules among which Syk activation leads to activation of PI3Kβ. PI3Kβ activates PKC and thus also contributes to the amplification of platelet activation. *Arrows* indicate an activation step within the cascade. Intracellular protein or receptor shapes filled in *gray* indicate current targets of antiplatelet approaches. Integrin $\alpha_{IIb}\beta_3$ is shown as an aggregation receptor only.

intracellular part of integrin $\alpha_{IIb}\beta_3$ triggering the high-affinity conformation with subsequent fibrinogen binding and platelet aggregation (Fig. 3).[64]

Interference with intraplatelet signaling is intended to prevent inside-out signaling and thus initiation of platelet aggregation. Since primary adhesion to exposed ECM is still possible, it is postulated that such an approach is antithrombotic with minimal effect on hemostasis. Antiplatelet approaches targeting enzymes of intraplatelet signaling will be discussed in Section Inhibitors of Intracellular Enzymes.

7.15.5 Antagonists of GPCRs

7.15.5.1 Purinergic Receptor Antagonists

Extracellular nucleotides are ubiquitous signaling molecules, acting via the P2 purinergic receptors. Platelets express three P2 receptor subtypes, the ATP-gated $P2X_1$ cation channel and the ADP-dependent $P2Y_1$ and $P2Y_{12}$ G protein-coupled receptors.[65] Large amounts of ATP released from cells following vascular injury trigger the opening of the $P2X_1$ channel. This results in calcium ion influx leading to shape change, movement of secretory granules, and low levels of $\alpha_{IIb}\beta_3$ integrin activation.[66] $P2X_1$ can also synergize with several other receptors to amplify signaling and functional events in platelets. In addition, when platelets adhere to a prothrombotic surface, they get activated and release the content of their granules including adenosine diphosphate (ADP). ADP stimulates platelet activation through $P2Y_1$ and $P2Y_{12}$.[67]

Coactivation of these two receptors is necessary for normal ADP-induced platelet aggregation; however, they have different functions. In response to ADP, $P2Y_1$ mediates a rise in cytoplasmic calcium that results in platelet shape change and weak, reversible aggregation. Upon ADP binding, $P2Y_{12}$ inhibits AC causing a lowering of cAMP, hence promoting platelet aggregation.[68] Studies with $P2Y_{12}$ knockout mice have demonstrated that the main role of $P2Y_{12}$ is the amplification of aggregation and stabilization of platelet thrombi.[69] $P2Y_{12}$ is also involved in the potentiation of platelet secretion induced by other agents through various intracellular pathways.

The $P2X_1$ receptor is widely distributed, for instance, on smooth muscle cells in different hollow organs (e.g., urinary bladder, artery, intestine, and vas deferens).[70] The $P2Y_1$ receptor is expressed on platelets and in the heart, blood vessels, and various smooth muscles as well as the prostate, ovary, and brain. In contrast, $P2Y_{12}$ is mainly found on platelets and subregions of the brain.[71]

7.15.5.1.1 $P2Y_{12}$ antagonists

In preclinical animal models, inhibition of $P2Y_{12}$ prevented experimental thrombosis with only limited effect on bleeding parameters.[72] Importantly, inhibition of $P2Y_{12}$ as an antiplatelet approach was validated in multiple clinical studies. Several $P2Y_{12}$ antagonists have been demonstrated to effectively reduce the risk of adverse cardiovascular events in patients with ACS and patients undergoing PCI.[68,73] In current treatment guidelines, $P2Y_{12}$ antagonists define the cornerstone therapy for patients with ACS. However, the search for even better $P2Y_{12}$ antagonists is still ongoing. Current efforts are focused on a new generation of molecules with reduced bleeding risk, reduced variability of antiplatelet effects, and preferentially once-a-day treatment. Excellent reviews and book chapters have comprehensively covered the discovery, pharmacology, and clinical use of $P2Y_{12}$ antagonists.[73b,74] In this section, we will provide a short summary of the current available drugs and give an overview of the recent medicinal chemistry efforts with a broad selection of diverse chemical scaffolds.

7.15.5.1.1.1 Indirect $P2Y_{12}$ antagonists: the thienopyridine family

Earlier $P2Y_{12}$ antagonists were developed without knowledge of their pharmacological target. Later studies showed their indirect way of action, that is, they require metabolic activation for biological activity. Three indirect antagonists of the thienopyridine family, which block the ADP-induced platelet activation and aggregation, have reached the market: the orally active ticlopidine, clopidogrel, and prasugrel (Fig. 4).

The first representative of this class was discovered in 1972 at Porcor (later Sanofi) in an effort to find new antiinflammatory drugs based on tinoridine (**1**), a compound previously described by the Yoshitomi company.[75] They chose a phenotypic screening approach: the analogs, synthesized in gram amounts, were directly tested in a wide range of in vivo and ex vivo rodent models, including the ADP-induced platelet aggregation ex vivo assay. In this assay, surprisingly high antiplatelet activity was measured, and one of the most potent analogs, ticlopidine (**2**), was selected for clinical development. It successfully completed several advanced clinical trials and consequently gained global approval in 1991 for the primary and secondary prevention of stroke. Unfortunately, in patients, ticlopidine led to rare but serious hematologic side effects (e.g., thrombocytopenia purpura and neutropenia), and the need for a safer derivative became an urgent priority.

The Sanofi researchers synthesized thousands of analogs and advanced unsuccessfully eight of them into phase I clinical trials before identifying the desired molecule bearing an (*S*)-carboxylic methyl ester at the benzylic position of ticlopidine. Clopidogrel (**3**) was demonstrated to be superior to aspirin in the secondary prevention of vascular events in a huge clinical trial (CAPRIE).[76] Clopidogrel was launched in 1998 worldwide and quickly eclipsed its predecessor ticlopidine due to its higher safety and efficacy profile. In combination with aspirin, it became the therapeutic cornerstone for ACS patients and is widely used during PCI interventions. Clopidogrel rose to the second best-selling drug after atorvastatin before becoming generic in 2012.

Interestingly, clopidogrel and its predecessor ticlopidine were brought to the market without knowledge of their precise biochemical mechanism of action. This mystery could be solved in 2001 with the cloning of the $P2Y_{12}$ receptor and its unequivocal identification as the biological target of the thienopyridines.[77] All thienopyridines are prodrugs that undergo metabolic conversion in the liver to generate the active species. For clopidogrel, the major part of the oral dose (c. 85%) is converted through enzymatic ester hydrolysis in the intestine to the inactive carboxylate derivative. After absorption of the remaining dose, different cytochrome P450 isoforms (mainly CYP2C19) oxidize the thiophene ring to form the intermediate thiolactone (2-oxo-clopidogrel, **6**), which is converted in a second step by CYP-mediated ring opening to an unstable and biologically active metabolite (Fig. 5).[78] $P2Y_{12}$ is covalently modified by the thiol group of the metabolite **7** forming a disulfide bridge with $Cys97^{3.25}$ as a primary attachment site. This metabolite is generated only in small amounts (< 10% of the dose), which leads to a slow onset of the pharmacological effect (up to

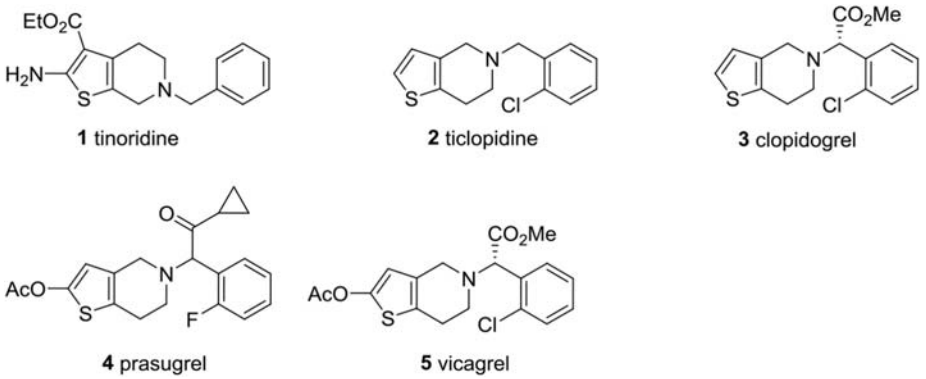

Fig. 4 From tinoridine to ticlopidine and further development to clopidogrel, prasugrel, and hybrid molecule vicagrel.

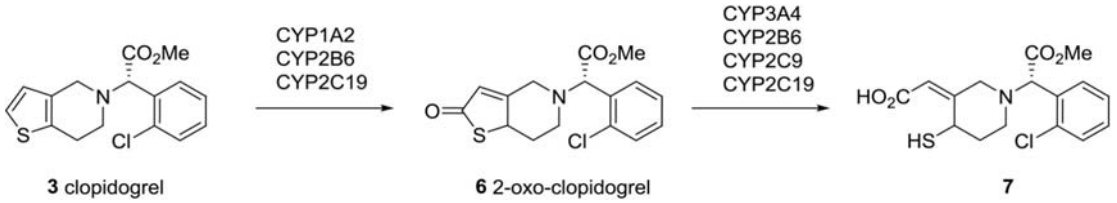

Fig. 5 Metabolism of clopidogrel: CYP-mediated thiophene ring oxidation to 2-oxo-clopidogrel (**6**) followed by a second CYP-mediated oxidation to the active thiol metabolite **7**. Analogous transformations are suggested for ticlopidine. For clopidogrel and 2-oxo-clopidogrel, the inactivation occurs through ester cleavage by carboxyesterases to the corresponding inactive acid. Prasugrel follows after hydrolysis of its acetate, the same second oxidation step as 2-oxo-clopidogrel.

4 days required to achieve steady-state concentration). When high levels of receptor inhibition are rapidly required, a loading dose of 300–600 mg followed by the regular 75 mg clopidogrel dose is prescribed. As for aspirin, irreversible inhibition of the receptor lasts for the lifetime of the platelets, and full restoration of platelet activity may require 7–10 days after the last dosage.

The clinical success of clopidogrel has been overshadowed by the observation that up to 30% of the patients do not achieve the expected level of platelet inhibition ("clopidogrel resistance").[79] The factors contributing to the variable response to this drug are manifold, that is, genetic polymorphism of drug transporter proteins and metabolic enzymes or drug–drug interactions. However, the major determinant for clopidogrel resistance is CYP2C19 polymorphism, which occurs in 30–55% of patients. Loss-of-function variants of CYP2C19 lead to poor conversion of clopidogrel to the active metabolite, and as a consequence, patients showing "high on-treatment platelet reactivity" (i.e., platelets that respond to ADP, despite ongoing anti-$P2Y_{12}$ treatment) are at a higher risk of recurrence of cardiovascular events. Large clinical trials to identify poor responders through platelet function tests with the goal to adjust the dose of clopidogrel were so far unsuccessful.[80]

Consequently, efforts shifted toward the development of compounds relying less on CYP-mediated metabolism. Prasugrel (CS-747, **4**) is a third-generation thienopyridine brought to the market in 2009 by Daiichi Sankyo/Eli Lilly[72b] (**Fig. 4**). The methyl ester moiety of clopidogrel is replaced by a cyclopropyl ketone, which renders the chiral center configurationally labile. Thus, prasugrel has been developed as a racemate. However, similar to its predecessors, it still requires metabolism for biological activity. In contrast to clopidogrel, the crucial thiolactone is provided with less variability by a rapid carboxyesterase-mediated acetate cleavage that takes place already in the intestine. This intermediate undergoes CYP-mediated ring opening to the active metabolite. The higher potency of prasugrel compared with clopidogrel is reflected by the clinical dose of 10 mg/day with a loading dose of 60 mg. In a large clinical phase III trial with ACS patients, prasugrel showed increased efficacy compared with clopidogrel albeit at the cost of higher incidence of major bleeding events in high-risk patients.[81] This safety drawback limits its clinical use.

Two recent studies have described attempts at increasing the systemic exposure of the active metabolite of clopidogrel (**7**). In the first study, a hybrid molecule (vicagrel, **5**) bearing the acetate functionality of prasugrel grafted onto the thiophene ring of clopidogrel was investigated by Shan et al. (**Fig. 4**).[82] Due to faster esterase metabolism, the bioavailability in rats of 2-oxo-clopidogrel (**6**) starting from vicagrel was four- to sixfold higher than with clopidogrel. Vicagrel could therefore overcome the high variability in the pharmacological response due to CYP2C19 polymorphism and thus may attenuate clopidogrel resistance. However, the advantage of vicagrel over prasugrel has yet to be demonstrated since vicagrel showed a lower potency in an ADP-induced platelet aggregation assay in rats. In the second study, the observation of oxidative metabolism at the piperidine ring of clopidogrel, mediated by CYP3A4/5, revealed a novel side pathway decreasing the production of the oxo-clopidogrel intermediate.[83] Based on these findings, Zhu et al. subsequently deuterated the piperidine ring of clopidogrel that moved the metabolism to the thiophene ring, ultimately leading to higher concentration of the deuterated version of metabolite **7**.[84]

7.15.5.1.1.2 The direct $P2Y_{12}$ antagonists

Direct antagonists do not require metabolic activation and therefore display faster onset and offset of action. This is a beneficial profile whenever the recovery of platelet function is required, such as in emergency surgeries or during unforeseen bleeding events. In addition, direct antagonists might cause less bleeding than the irreversible inhibitors since the $P2Y_{12}$ receptor remains responsive to high local concentrations of ADP.[42b,85]

7.15.5.1.1.2.1 Nucleotides analogs: cangrelor, ticagrelor, and regrelor

The audacious decision to launch at Fisons Pharmaceuticals (became the Charnwood site within AstraZeneca) a medicinal chemistry program based on ATP (**8**) paid off with the approval of two drugs, cangrelor (**9**) and ticagrelor (**10**).[86] ATP was known as a competitive albeit weak antagonist of ADP-induced platelet aggregation (later defined as partial agonist of $P2Y_{12}$). It was thus hypothesized that the agonistic and antagonistic behaviors of ADP and ATP, respectively, were derived from the additional negative charges arising from the terminal phosphate in ATP (**Fig. 6**).[87] To avoid the hydrolysis of ATP, which would lead to the agonistic nucleotide ADP, a dichloromethylene bridge was grafted between the β/γ phosphate units. Thioether substitution on the 2-position of the purine ring proved beneficial for affinity and selectivity over other P2 subtypes. The introduction of a lipophilic substituent onto the N6 atom increased the affinity. However, larger side chains (approximately four carbon atoms and longer) led to an

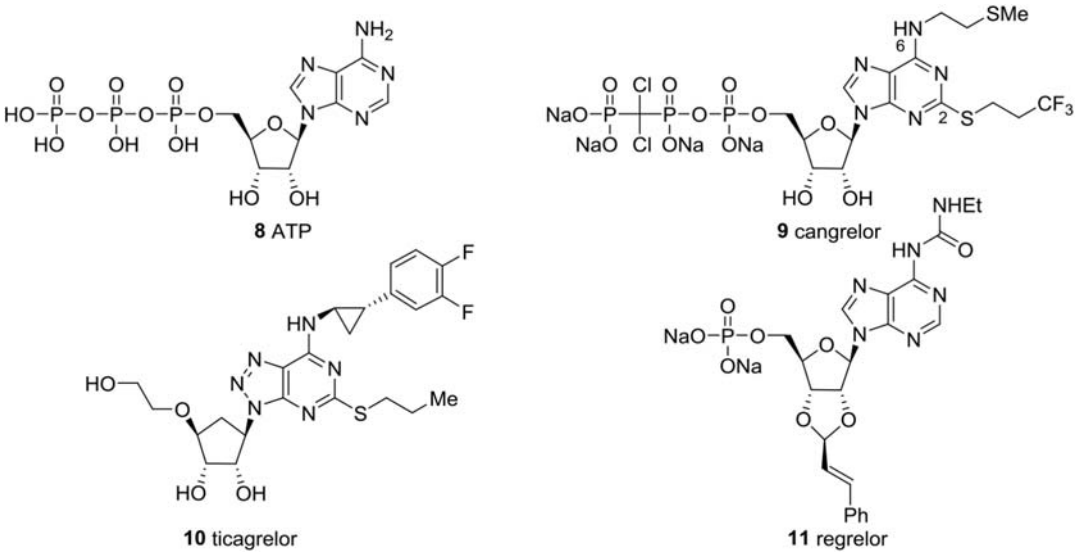

Fig. 6 From ATP to cangrelor (tetrasodium salt) and ticagrelor; the AMP derivative regrelor (disodium salt).

undesired prolonged half-life in dogs. Finally, the optimized combination of substituents resulted in cangrelor (AR-C69931MX), which showed high antiplatelet activity on human platelets (Fig. 6).[88] An infusion during PCI intervention was chosen as primary treatment modality based on the favorable i.v. profile of cangrelor with both its rapid onset (3–6 min) and offset (30–60 min) of action. In large phase III clinical studies (the CHAMPION trials), cangrelor significantly decreased the number of ischemic events during PCI.[89] Despite the minor prolongation of bleeding time at maximally effective antithrombotic doses in a dog model, the occurrence of major bleeding in humans was similar to clopidogrel, along with increased rates of minor bleedings. Cangrelor (out-licensed by AstraZeneca to The Medicines Company) became after the FDA and EMA approval in 2015 the latest addition in the armamentarium of antithrombotic agents.

To develop an orally bioavailable ATP analog, efforts were directed to the replacement of the labile and charged triphosphate side chain of ATP by nonacidic groups.[90] Careful optimization of the hydrophobic substituents of the heterocyclic scaffold, that is, propylthioether and *trans*-2-difluorophenyl cyclopropylamine, enhanced the affinity to the $P2Y_{12}$ receptor. The potentially labile ribose sugar unit was replaced by a cyclopentyl carbocycle, and an additional affinity-enhancing nitrogen was introduced in the purine moiety. The clinical candidate, a neutral cyclopentyl-triazolo-pyrimidine analog, is referred to as ticagrelor (AZD-6140; Fig. 6). Originally described as noncompetitive with respect to ADP, the most recent studies showed that ticagrelor displayed surmountable and competitive antagonism against $P2Y_{12}$.[91] Ticagrelor was evaluated clinically in large patient populations (the PLATO trial)[53a] by AstraZeneca and received marketing authorization in 2010 by the EMA and 1 year later by the FDA for the prevention of atherothrombotic events in patients with ACS.[92] In the PLATO trial, ticagrelor showed an increased effectiveness to lower the rate of death from vascular causes, MI, or stroke compared with clopidogrel, albeit with higher incidence of major bleeding unrelated to CABG. Interestingly, ticagrelor was linked to a significant decrease in overall mortality (see Section Importance of selectivity of receptor and ligand). This finding was however not replicated in other studies.[93] Ongoing clinical trials will help to refine the use of ticagrelor in ACS patients.[16d]

An interesting add-on from the AstraZeneca team is the development of an antibody fragment (Fab) as antidote for ticagrelor.[94] The Fab displays a significantly higher affinity (20 pM) for ticagrelor than ticagrelor shows for its target $P2Y_{12}$. The antidote normalizes bleeding in mice treated with ticagrelor. If this finding translates to humans, it will be an important asset for patients undergoing emergency surgeries.

Several groups have described ticagrelor analogs; however, to the best of our knowledge, no clinical development has been reported.[95]

In 2008, Inspire Pharmaceuticals described AMP/ADP nucleotide and dinucleoside polyphosphate analogs as $P2Y_{12}$ antagonists.[96] Some dinucleoside polyphosphates are endogeneously produced and released into extracellular space where they are able to stimulate several P2 receptors. Recently, their binding mode in the $P2Y_{12}$ receptor was proposed based on its X-ray crystal structure (see Section $P2Y_{12}$ X-ray structure and structure-based modeling).[97] In the course of their work, lipophilic substitution of the ribose ring of AMP by a cinnamaldehyde acetal and apolar N6-urea modification provided the potent antagonist regrelor (INS50589, **11**; $IC_{50} = 16$ nM in the ADP-induced platelet aggregation assay with washed platelets),[96] which was further developed as i.v. drug for CABG surgery (Fig. 6). Its clinical phase II was terminated due to bleeding complications.

7.15.5.1.1.2.2 Sulfonylurea/amide derivatives: AZD1283 and elinogrel

A medicinal chemistry program at Portola Pharmaceuticals aiming at novel $P2Y_{12}$ antagonists started with an HTS hit bearing a crucial sulfonylurea moiety. After SAR optimization, elinogrel (PRT-060128, **12**; acquired in 2009 by Novartis) emerged as an

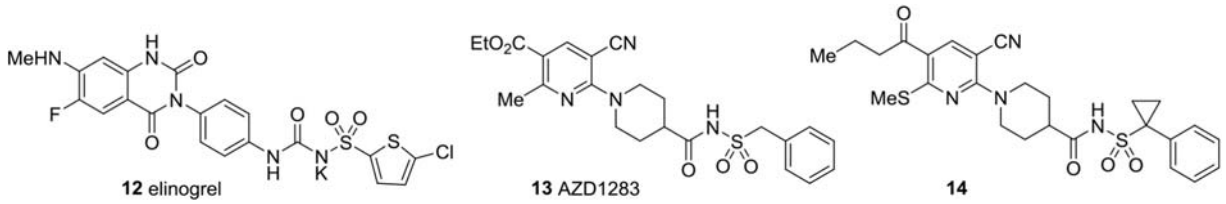

Fig. 7 Elinogrel (potassium salt) with *N*-phenyl quinazoline-2,4-dione and a chlorothiophene subunit connected by the mildly acidic sulfonylurea motif. The acylsulfonamide **13** (AZD1283) and the close derivative **14** with propyl ketone functionality.

in vitro potent ($K_i = 20$ nM) and selective antagonist, showing good activity in the ADP-induced platelet aggregation assay ($IC_{50} = 3–5$ μM) (Fig. 7). It was subsequently developed for both i.v. and oral administration for ACS patients and prevention of secondary thrombotic events,[98] where it has been tested in phase II clinical trials. No public information is available regarding the reasons behind the discontinuation of elinogrel by Portola Pharmaceuticals in 2012.

In 2013, AstraZeneca disclosed the optimization of ethyl 6-aminonicotinate acyl sulfonamides and the selection of their clinical candidate **13** (AZD1283; Fig. 7).[99] The antithrombotic efficacy was assessed in a modified Folts dog model (cyclic flow reduction model), wherein the femoral artery blood flow is measured after mechanical damage of the endothelium followed by c. 80% stenosis. The therapeutic index (TI) of AZD1283 was calculated from the antithrombotic efficacy (ED_{50}) and from the dose leading to 3.5-fold increased bleeding time ($ED_{BT>3.5}$). AZD1283 ($TI > 10$) compared favorably with clopidogrel ($TI = 2.3$) and ticagrelor ($TI > 5.2$). A cocrystal structure of AZD1283 in $P2Y_{12}$ was recently solved (see Section **$P2Y_{12}$ X-ray structure and structure-based modeling**).[97] The clinical development of AZD1283 was stopped for undisclosed reasons in 2012.

In the course of a follow-up program, AstraZeneca explored bioisosteres for the ester functionality of AZD1283.[100] In particular, enhanced stability was desired as its ethyl ester is converted by esterases into inactive metabolites. The closely related propyl ketone derivative **14** showed multiple advantages over AZD1283 in terms of antiplatelet activity and metabolic stability.[101] However, in the modified Folts model in dogs, full inhibition of platelet aggregation was linked with a significant increase in bleeding time, in sharp contrast to the clean profile of AZD1283. It is speculated that the different binding kinetics might account for the unexpected bleeding side effects seen with compound **14** (Fig. 7).

7.15.5.1.1.2.3 Evolution of the Berlex lead compound

In 2007, scientists from Berlex disclosed the antiplatelet effect of the reversible antagonist **15** (BX-667) and its biologically active metabolite **16** (BX-048; Fig. 8).[102] BX-667 inhibits ADP-induced platelet aggregation in human whole blood ($IC_{50} = 97$ nM)

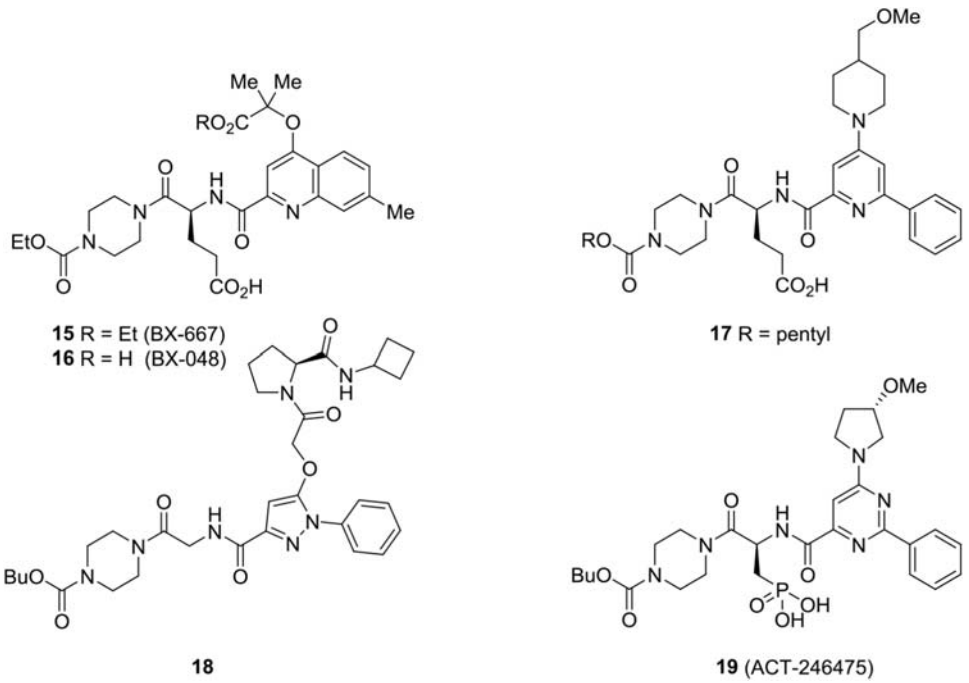

Fig. 8 Medicinal chemistry efforts around the Berlex lead structures (**15** and **16**): representative compounds from Pfizer (**17**), Sanofi (**18**), and Actelion (**19**).

with negligible effect on collagen-induced platelet activation. Both compounds were also able to inhibit AA-induced platelet aggregation albeit at much higher concentrations than those needed after ADP stimulation. Compounds **15** and **16** were studied in three experimental models of thrombosis (A-V shunt model, rat carotid artery injury ($FeCl_3$) model, and dog cyclic flow model), and a wider therapeutic index (less bleeding at maximal efficacy) was achieved with BX-667 compared with clopidogrel. Nevertheless, no further development has been reported for either compound.

The quinoline glutamic acid scaffold of BX-667 and BX-048 was the starting point for an intense medicinal chemistry quest by several companies for improved $P2Y_{12}$ antagonists.

Pfizer published a series of papers whereby the quinoline ring of BX-667 was exchanged with either a pyridine or a pyrimidine heterocycle.[103] Relying on a parallel chemistry approach (polymer-assisted solution-phase synthesis), hundreds of derivatives could be efficiently synthesized. Inhibition of platelet aggregation was assessed in a human PRP assay with ticagrelor as benchmark. The pharmacokinetic profile and the potency of the compounds could be modulated by varying the 4-position of the pyridine. In contrast to most tested substituents, the methoxymethylene-substituted piperidine moiety in compound **17** led to a low clearance in the rat via excretion as unchanged drug in the bile. Compound **17** was found to be orally efficacious in the rat $FeCl_3$ model, where it dose-dependently prevented thrombus formation (Fig. 8).

In 2014, Sanofi reported a detailed SAR study where the glutamic acid piperazine lead structure from Berlex BX-667 was kept constant and the quinoline was replaced by a phenylpyrazole (Fig. 8).[104] To strengthen their investigation, a homology model of $P2Y_{12}$ based on the related $CXCR_4$ receptor was built for structure-based alignment with the Berlex compound. The 5-position of the pyrazole was extensively optimized, and an *N*-acetyl (*S*)-proline cyclobutyl amide moiety was found to deliver highly active antagonists in the glutamic acid series. Surprisingly, with this specific pyrazole substituent, the amino acid could be reduced to a simple glycine spacer while keeping the activity both in the binding assay (**18**, $K_i = 7.7$ nM) and in the ADP-induced platelet aggregation assay in human PRP (**18**, $IC_{50} = 30$ nM).

Actelion recently reported a knowledge-based approach building on the combination of the Berlex compound and a substructure of ticagrelor.[105] Optimization of the substituent at the 4-position of the pyrimidine ring as a replacement of the Berlex quinoline provided compounds with promising biological activity. The glutamic side chain was optimized leading to phosphonate-based antagonists with excellent ex vivo potency in the platelet aggregation assay in human plasma. Specifically, compound **19** (ACT-246475) was profiled to be a reversible and potent $P2Y_{12}$ antagonist with an exceptional selectivity profile (Fig. 8).[42c] ACT-246475 inhibits ADP-induced platelet aggregation in vitro with an apparent IC_{50} of 14 nM. To the best of our knowledge, ACT-246475 currently represents the most potent and selective $P2Y_{12}$ antagonist available. In addition, in a rat thrombosis model, direct comparison of ACT-246475 with clopidogrel, at comparable antithrombotic efficacy, confirmed a clearly improved blood loss profile. Furthermore, preclinical profiling of ACT-246475 confirmed an in vitro and in vivo safety profile that supported further evaluation in humans.[106]

7.15.5.1.1.2.4 Miscellaneous scaffolds

An HTS campaign at Sanofi, resulting in a low micromolar range hit, was the starting point to identify a new series for a clopidogrel follow-up program[107] (Fig. 9). Thorough optimization of the hit **20** yielded the following notable structural improvements: (i) introduction of a ketone motif as metabolically stable ester replacement on the pyrazole, (ii) rigidification and scaffold hopping by switching from an ortho-aminoanisole moiety to an indole ring, (iii) substitution of the indole ring with an optimized carboxamide instead of carboxylic acids to lower the interspecies differences in biological activity and to improve oral bioavailability, and finally (iv) removal of a mutagenic anilinic structural element. The resulting preclinical candidate **21** (SAR216471) is highly potent

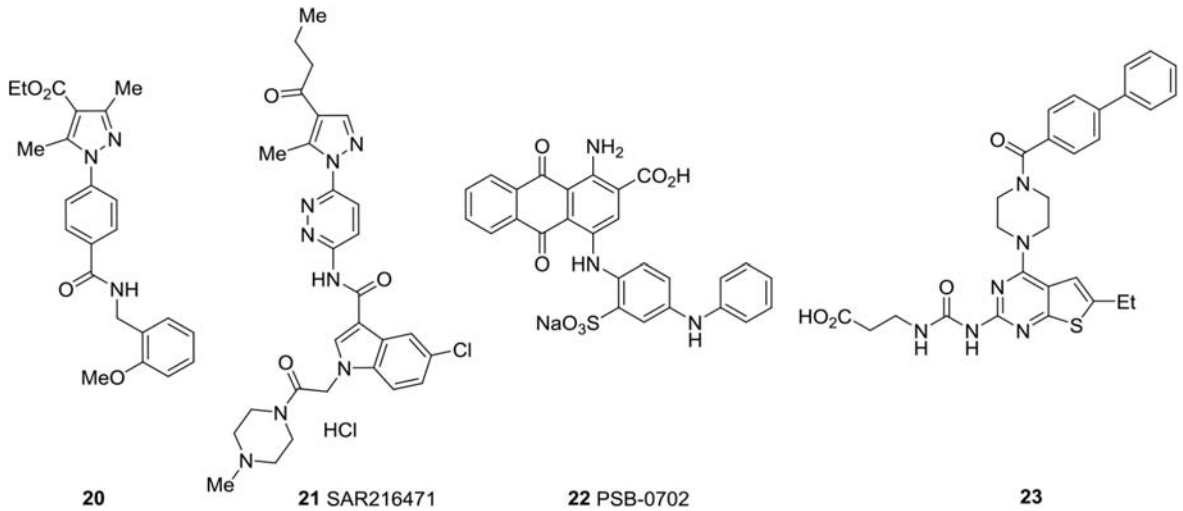

Fig. 9 From the HTS hit **20** to SAR216471 (**21**, Sanofi), PSB-0702 (**22**, University of Bonn), and thienopyrimidine **23** (Pfizer).

in the binding ($IC_{50} = 17$ nM) and in the aggregation assays ($IC_{50} = 108$ nM in human PRP) and has moderate bioavailability in rat but sustained inhibition of platelet aggregation in vivo. The rat tail bleeding experiment revealed a favorable safety profile with the highest therapeutic index in comparison with clopidogrel, prasugrel, and ticagrelor.[108] No recent clinical development has been reported for SAR216471.

The University of Bonn described anthraquinone-derived $P2Y_{12}$ antagonists, thus further demonstrating the capacity of the receptor to accommodate diverse and large ligands.[109] This compound class originates from the dye "reactive blue 2," which interacts with various nucleotide binding proteins, including the P2 family. The most active analog of this series, compound **22** (PSB-0702), exhibits a K_i value of 21 nM and is at least 100-fold selective versus other P2 receptor subtypes (**Fig. 9**).

Potent thienopyrimidines were described by Pfizer and in a patent by Millennium.[110] As it has been observed previously with many compound series, protein binding of the antagonist can lead to a decrease in its activity when measured in human PRP. In the Pfizer thienopyrimidines, as exemplified by compound **23,** highly polar and acidic groups were required to balance out the strong protein binding effect of the biphenyl group (**Fig. 9**).

7.15.5.1.1.3 $P2Y_{12}$ X-ray structures and structure-based modeling

In 2014, X-ray crystal structures of the $P2Y_{12}$ receptor were solved in complex with three different ligands: (i) the non-nucleotide antagonist **13** (AZD1283; **Fig. 7**); (ii) the full agonist 2MeSADP (**24b**; **Fig. 10**; $EC_{50} = 0.3$ nM), which is a more potent close analog of ADP (**24a**, $EC_{50} = 69$ nM); and (iii) the corresponding ATP derivative and partial agonist 2MeSATP.[97,111] The receptor structures in complex with antagonist **13** (AZD1283) or agonists (2MeSADP and 2MeSATP) show markedly different conformations, with an inward shift of two transmembrane helices (TM6 and TM7) toward the agonists making their binding pocket more contracted. In addition, the agonist-bound pocket is closed by an extracellular loop forming a lid through polar interactions. In contrast, binding of the non-nucleotide antagonist AZD1283 prevents lid closure. Two distinct binding pockets could be visualized: pocket 1 (bordered by TM3–7) accommodates the earlier described ligands in different orientations. Thus, AZD1283 and 2MeSADP overlap partially, with superimposition of their nicotinate and adenine moieties, and their aromatic ring undergoes π–π stacking interactions with Tyr105. Pocket 2 (bordered by TM1-3/7) is empty in the AZD1283 structure and may bind diadenosine tetraphosphate and the metabolites of the thienopyridines.

We can anticipate that the availability of structural data of receptor–ligand complexes will reinvigorate the structure-based drug design effort on the $P2Y_{12}$ receptor. Modeling based on these structures has already proposed different binding modes of several ligands described in the preceding text.[112] Moreover, the possibility to target both the orthosteric and allosteric binding sites opens up rich avenues for future drug development programs.

7.15.5.1.1.4 Importance of selectivity of receptor and ligand

Recent studies have challenged the previously restricted expression pattern of $P2Y_{12}$, which is now no longer believed to be confined to platelets and subregions of the brain.[71] This finding may be reflected by numerous extraplatelet effects of $P2Y_{12}$ receptor antagonists described in recent clinical trials.[113] In this context, inhibition of $P2Y_{12}$ on neurons is one of the proposed hypotheses for the observed dyspnea side effect during ticagrelor treatment.[114] Besides the expression pattern of the receptor, the target selectivity of the antagonists plays an important role in the therapeutic efficacy and safety. Comparison of clopidogrel and prasugrel with $P2Y_{12}$ knockout mice suggests that some of the excess bleeding associated with thienopyridines may be due to off-target effects.[69] For ticagrelor, the beneficial effect on mortality observed in the PLATO trial could be due in part to its effect on the adenosine concentration. More specifically, ticagrelor has been found to inhibit the cellular uptake of adenosine, likely by inhibition of equilibrative nucleoside transporter 1 (ENT1). Thus, an additional antiplatelet effect by ticagrelor is mediated by the increase in adenosine levels.[115]

In summary, the fine-tuning of both target selectivity and beneficial polypharmacology represents a great challenge that may lead to new $P2Y_{12}$ antagonists with improved therapeutic window.

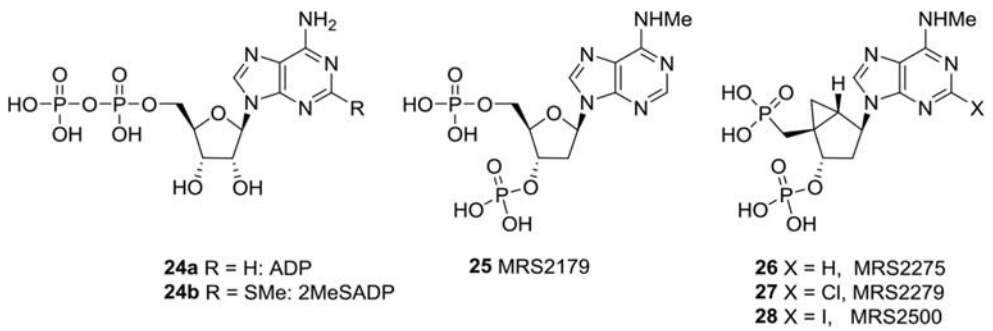

Fig. 10 Endogenous ligand ADP (**24a**) with the closed ADP analog 2MeSADP (**24b**) and adenine nucleotide-based $P2Y_1$ antagonists (**25**–**28**).

7.15.5.1.1.5 Future prospects of $P2Y_{12}$ antagonists

One major unmet goal in $P2Y_{12}$-based therapies is to determine for all patients the optimal therapeutic window in order to maximize therapeutic efficacy while minimizing safety issues (e.g., bleeding).[73a] An important aspect is the level and mode (reversible vs. irreversible) of $P2Y_{12}$ inhibition and its link to excessive bleeding.[85] Will it be therefore possible with newer agents to keep the high level of antiplatelet activity of ticagrelor and decrease its bleeding risk? In combination with a once-daily oral profile and optimized target selectivity, this challenging goal would potentially represent a significant step forward. The duration of therapy, use of dual or triple therapy (e.g., with aspirin and/or an additional antiplatelet agent), and stratification of patients (e.g., diabetes patients) can still be optimized with the current treatment modalities. Finally, although prior trials to improve efficacy, for instance, by testing the platelet reactivity to identify patients with clopidogrel resistance, were so far inconclusive, new concepts in individualized therapy are still being proposed.[116]

7.15.5.1.2 $P2Y_1$ antagonists

In 2001, Léon et al. demonstrated that the deletion of $P2Y_1$ using a $P2Y_1$ knockout mouse led to an antithrombotic effect in a model of thrombin-dependent acute thromboembolism. Similarly, the selective antagonist **25** (MRS2179; **Fig. 10**) showed antithrombotic efficacy in the same model using wild-type mice.[117] Moreover, MRS2179 potentiated the antithrombotic effect of clopidogrel in several in vivo models.[118] Therefore, the $P2Y_1$ receptor represents an attractive target for antiplatelet compounds, alone or in combination with a $P2Y_{12}$ antagonist.

7.15.5.1.2.1 Adenine nucleotide-based antagonists

Several research groups described the discovery of a series of adenine nucleotide-based $P2Y_1$ receptor antagonists that inhibit ADP-induced platelet aggregation, such as **25** (MRS2179), **26** (MRS2275), and **27** (MRS2279; **Fig. 10**).[119] The chemical and enzymatic stability of these tool compounds is suboptimal, which limits their usefulness as potential oral drugs.

7.15.5.1.2.2 Non-nucleotide-based antagonists

7.15.5.1.2.2.1 Bristol-Myers Squibb (BMS)

In search for novel $P2Y_1$ antagonists, scientists at BMS performed an HTS with >1 million compounds using a binding assay with [^{33}P]-2MeSADP as ligand.[120] This campaign uncovered the diarylurea **29** showing high affinity for $P2Y_1$ ($K_i = 75$ nM) and a selectivity >1000-fold against $P2Y_{12}$ (**Fig. 11**). Initial SAR led to the discovery of **30** (BPTU; $K_i = 6$ nM), which showed potency in the ADP-induced platelet aggregation assay in human PRP ($IC_{50} = 2.1$ μM). BPTU provided a significant reduction in thrombus weight in a rat arterial thrombosis model with a limited effect on bleeding. The antithrombotic and bleeding profiles of BPTU were

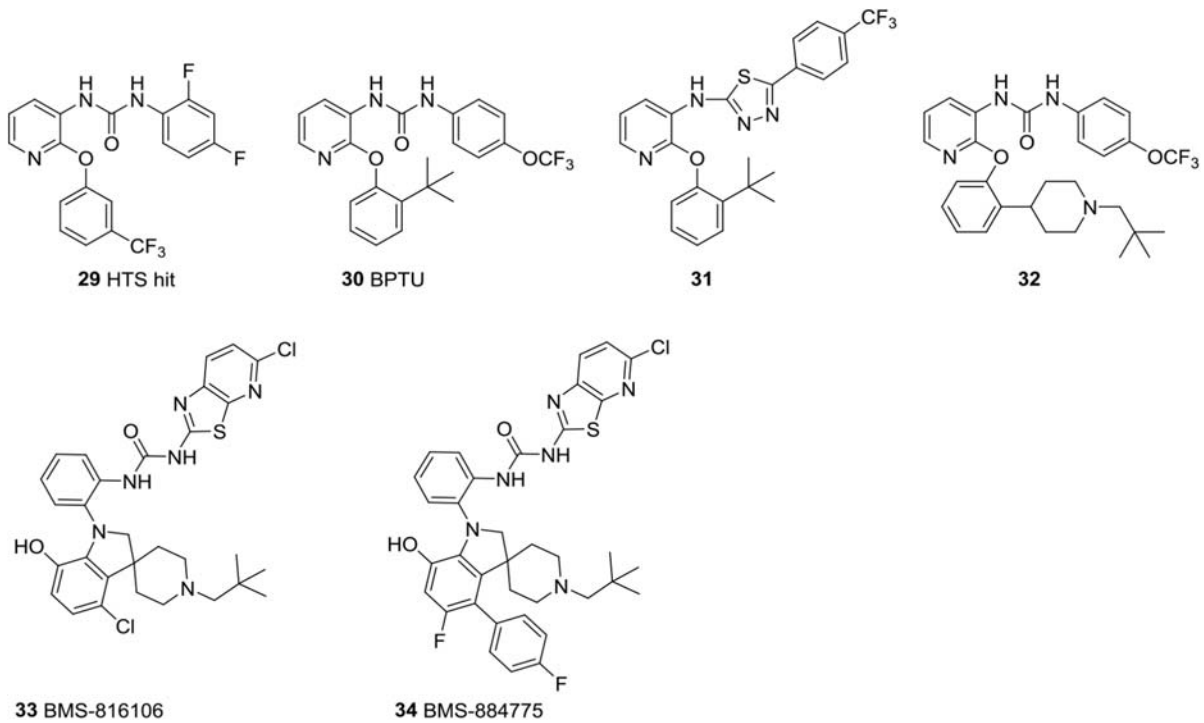

Fig. 11 BMS $P2Y_1$ antagonist program: HTS hit **29** leading to **30** (BPTU), compound **31** containing a urea surrogate, compounds with a basic amino group **32**, **33** (BMS-816106), and **34** (BMS-884775).

favorable in comparison with clopidogrel. However, the compound suffered from low aqueous solubility and high protein binding in human plasma, the latter likely due to a high lipophilicity.

Additional SAR studies targeted the low aqueous solubility of BPTU. Since the urea motif may be detrimental, surrogates were identified, such as aminothiazole or aminothiadiazole moieties[121] (**31**, $K_i = 7$ nM). Alternatively, the introduction of polar groups, such as basic amines, gave compounds such as **32,** which showed a much higher aqueous solubility while retaining affinity and potency ($K_i = 16$ nM and $IC_{50} = 2.4$ μM in human PRP).[122]

In parallel, structural modifications to constrain the tert-butylphenoxy-pyridine region of BPTU were explored, culminating with the introduction of an indoline ring combined with a spiropiperidine moiety.[123] Additional SAR optimization finally led to **33** (BMS-816106), which showed high activity in the FLIPR and platelet aggregation assays (IC_{50} values of 0.12 and 130 nM, respectively), good solubility, and promising PK parameters.[124] The chlorine atom in para position to the solubilizing hydroxyl group decreased the electron density of the 7-hydroxyl indoline ring and led to a high liver microsomal stability and a low level of glutathione addition to the hydroxyindoline moiety. BMS-816106 demonstrated a robust antithrombotic effect with an improved bleeding profile compared with clopidogrel in rat.

Further derivatization of the indoline ring culminated in the discovery of BMS-884775 (**34**, IC_{50} values of 0.12 and 180 nM in FLIPR and platelet aggregation assays, respectively).[125] Its volume of distribution was low, which might reduce potential off-target effects since $P2Y_1$ is expressed widely in the body. BMS-884775 demonstrated antithrombotic efficacy with less bleeding compared with prasugrel in the rabbit models of electrically induced carotid artery thrombosis and cuticle bleeding. To the best of our knowledge, no clinical development of these two advanced molecules has been reported.

7.15.5.1.2.2.2 Pfizer and GlaxoSmithKline (GSK)

An HTS campaign at Pfizer afforded a series of moderately potent diarylurea hits very similar to the BMS hit **29**. Extensive optimization led to the identification of compound **35** ($K_i = 90$ nM), which showed efficacy in a rat ferric chloride arterial thrombosis model (**Fig. 12**).[126] In a similar approach, scientists at GSK reported compounds **36** and **37** as lead $P2Y_1$ antagonists (K_i values of 70 and 140 nM, respectively).[127]

7.15.5.1.2.3 Biologics

Scientists at Western University, Pomona, postulated that an antibody targeting the binding site of ADP within the second extracellular loop of $P2Y_1$ could be used as a function-blocking agent for platelet activation.[128] To test this hypothesis, a rabbit polyclonal antibody was generated against the second extracellular loop of human $P2Y_1$, abbreviated as EL2Ab. It competitively displaced [^{3}H]-MRS2500 ([^{3}H]-**28**; **Fig. 10**) from $P2Y_1$ and dose-dependently inhibited ADP-induced human platelet aggregation in vitro. In a ferric chloride carotid injury thrombosis model in mice, EL2Ab prolonged the time to thrombus occlusion, similarly to MRS2500 (**28**). However, EL2Ab prolonged the tail bleeding in mice, indicating that it impairs hemostasis. Further characterization of the therapeutic window of this approach is required.

7.15.5.1.2.4 Dual $P2Y_1$/$P2Y_{12}$ antagonists

A team at the Boston Children's Hospital reported the discovery of dual $P2Y_1$/$P2Y_{12}$ antagonists based on diadenosine 5′, 5‴-P^1,P^4-tetraphosphate (Ap_4A), an endogenous signaling molecule found in platelet dense granules.[129] Interestingly, compound **38** (**Fig. 12**) inhibited ADP-induced platelet aggregation at a concentration much lower than that required to inhibit either $P2Y_1$ or $P2Y_{12}$ activity, suggesting a synergistic effect. In contrast to Ap_4A, which has a half-life of a few minutes in human blood,[130] compound **38** retained molecular and functional integrity for at least 3 h.[131] The authors conclude that such compounds would cause a rapid onset of platelet inhibition with a rapid clearance from the bloodstream and consequently may be of use when emergency surgery is needed.

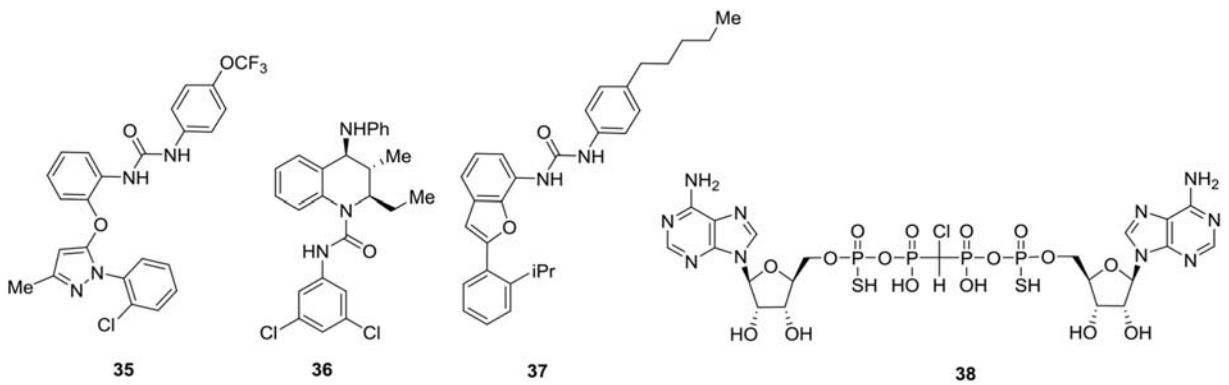

Fig. 12 $P2Y_1$ antagonists reported by Pfizer (**35**), GSK (**36**, **37**), and Boston Children's Hospital (**38**).

7.15.5.1.2.5 X-ray structures

X-ray crystal structures of the human $P2Y_1$ receptor in complex with the nucleotide analog MRS2500 (**28**) or with the nonnucleotide antagonist BPTU (**30**) have been recently solved.[132] MRS2500 is located in a pocket close to the extracellular surface, which is lined up by amino acids from the N-terminus, helices VI and VII, and the extracellular loop 2. In contrast, the $P2Y_1$-BPTU crystal structure surprisingly reveals that BPTU binds at the lipid interface of the transmembrane domain instead of interacting within the helical bundle. The superficial binding pocket, formed by helices I–III and the extracellular loop 1, accommodates BPTU through hydrophobic interactions with a single H bond to the urea carbonyl functionality. Although MRS2500 and BPTU bind to distinct sites in $P2Y_1$, these two ligands stabilize the receptor in similar inactive conformations. The existence of an external hydrophobic binding site suggests that the entry of the allosteric BPTU antagonist occurs through the lipid membrane. This observation opens up new opportunities to target novel allosteric sites outside of the canonical ligand binding pocket.

7.15.5.1.2.6 Summary

Based on in vivo data generated in thrombosis and bleeding models, targeting the $P2Y_1$ receptor represents a relevant strategy for an alternative or a complementary treatment to current antiplatelet drugs. Unfortunately, as of today, the few ongoing drug discovery programs failed to deliver small-molecule $P2Y_1$ antagonists for clinical development. The broad tissue distribution of the receptor and the lack of clinical data represent significant hurdles for the validation of $P2Y_1$ as an antiplatelet target.

7.15.5.1.3 $P2X_1$ antagonists

Only few $P2X_1$ antagonists have been reported.[133] Most are derived from suramin (**39**), a polysulfonated drug used in the treatment of African river blindness (onchocerciasis) and African trypanosomiasis (sleeping sickness). In this context, polysulfonate **40** (NF449) so far represents the most potent and selective antagonist of $P2X_1$ (Fig. 13).[134] In a mouse model of thromboembolism, the chemical probe NF449 decreased intravascular platelet aggregation without prolongation of the bleeding time.[135]

7.15.5.2 Protease-Activated Receptor (PAR) Antagonists

7.15.5.2.1 PAR-1 antagonists

7.15.5.2.1.1 Mechanism of action

In addition to its pivotal role in the coagulation cascade, thrombin directly stimulates platelets via proteolytic activation of specific GPCRs called protease-activated receptors (PARs).[136] Of the four PAR subtypes, only PAR-1 and PAR-4 are expressed on human platelets and only PAR-1 is activated at low thrombin concentrations. Thrombin docks through its positively charged anion binding exosite I to two regions located in the N-terminus of PAR-1, the hirudin-like domain ($K^{51}YEPF^{55}$) and the anionic cluster ($E^{57}DEE^{60}$).[137] Subsequently, thrombin activates PAR-1 by specifically cleaving the N-terminus of the receptor, thus exposing a new N-terminal peptide that begins with the sequence $S^{42}FLLRN^{47}$. This new N-terminus acts as a tethered peptide agonist that binds intramolecularly to the transmembrane core of the receptor, thereby initiating conformational changes and an intracellular signaling cascade. This irreversible "self-activation" of PAR-1 translates into a high local concentration of the tethered agonist peptide (estimated to be 0.4 mM), which is a challenge for the development of high potency antagonists.

Since a PAR-1 antagonist would selectively block the thrombin-mediated platelet activation without inhibiting the fibrin formation or platelet activation by other activators, such as ADP, TXA_2, and collagen, a PAR-1 antagonist might achieve potent antiplatelet activity compared with aspirin and ADP antagonists. Alternatively, a PAR-1 antagonist administered in combination with another antiplatelet agent might lead to higher efficacy in reducing recurrent thrombotic cardiovascular events in ACS patients.

An extensive review enumerating PAR-1 antagonist programs was published in 2006.[138] Therefore, in this article, we will concentrate on recent data and activities, with emphasis on the discovery of vorapaxar, currently, the only approved PAR-1 antagonist.

7.15.5.2.1.2 Vorapaxar (SCH-530348)

Vorapaxar is a first-in-class orally active PAR-1 antagonist discovered by scientists at Schering-Plough and later on developed by Merck. It originated from an HTS performed at Schering-Plough that identified a racemic synthetic analog (±)-**42** of the natural

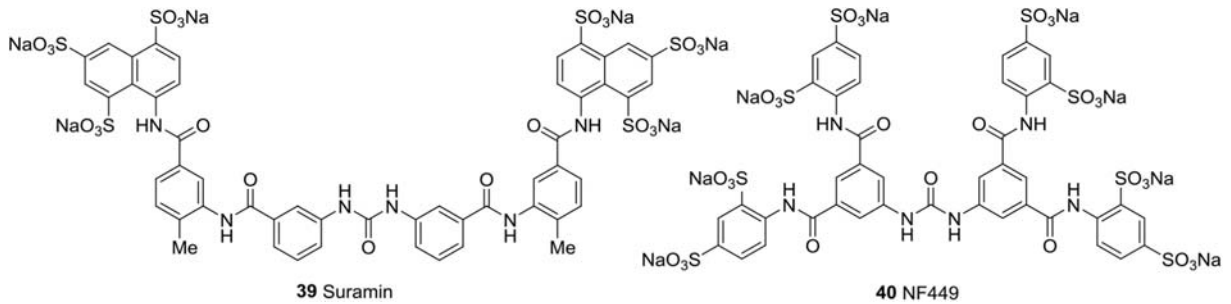

Fig. 13 The $P2X_1$ antagonists suramin and NF449.

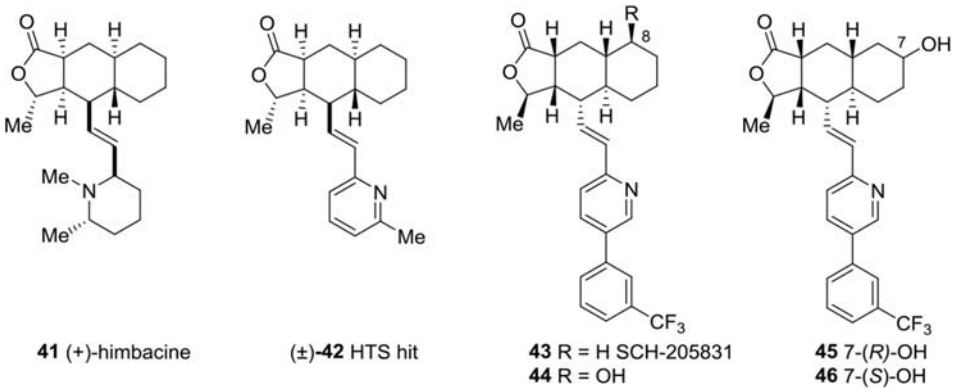

Fig. 14 Racemic HTS hit (±)-**42** derived from (+)-himbacine (**41**) and the ent-himbacine series **43**–**46**.

product (+)-himbacine (**41**) as a hit for the PAR-1 antagonist program (Fig. 14).[139] Optimization of the *ent*-himbacine series started with the pyridine ring and unraveled SCH-205831 (**43**) with a K_i of 2.7 nM against PAR-1.

SCH-205831 showed high oral bioavailability in rat and monkey as well as complete and sustained inhibition of platelet aggregation after a 3 mg/kg oral administration in an ex vivo cynomolgus monkey model. Metabolic profiling revealed three monohydroxylated metabolites **44**–**46** with high circulating levels in several animal species.[140] Further in vivo studies suggested an autoinduction pattern for the hepatic enzymes that might not allow the adequate drug exposure needed for the toxicology studies. Consequently, the development of SCH-205831 was stopped.

The scientists at Schering-Plough adopted two concepts to improve upon **43**. The first approach was to further optimize the structure of the metabolites themselves. The observed low clearance of metabolite **44** in the rat was possibly due to the steric hindrance around the hydroxyl group, which would prevent efficient conjugation and excretion. Therefore, varying the position of the hydroxyl moiety could lead to an analog with higher clearance. In the second approach, the metabolically labile positions 7 and 8 of SCH-205831 were blocked to force the metabolism at alternative sites. The outcome of these efforts was the selection of **45**, devoid of the drawbacks linked to liver enzyme induction. Compound **45** showed a K_i of 11 nM against PAR-1 in the binding assay. It was threefold more potent in the cynomolgus monkey ex vivo platelet aggregation inhibition model than its prototype **43** with an efficacious oral dose of 1 mg/kg. However, an unacceptable off-target activity at the CB2 receptor was observed later in a GPCR counter-screen ($K_i = 38$ nM). The Schering team further optimized the heteroaryl region, that is, the pyridyl ring and its substitution pattern, and in parallel, heteroatoms were incorporated into the C-ring with the goal to modify its metabolic pattern and to increase the overall polarity of the compounds (Fig. 15).[141]

Compound **47** ($IC_{50} = 25$ nM in the binding assay) showed complete inhibition of platelet aggregation at a 1 mg/kg oral dose up to 6 h in the cynomolgus monkey model, comparable with **45**. Nevertheless, considerable amounts of hydroxylated lactol metabolites **48** were quantified in monkey plasma, which led to the termination of this series. Decahydroisoquinoline analogs, in particular ethyl carbamate **49**, showed promising in vitro binding affinities against PAR-1 ($K_i = 4.5$ nM). In the ex vivo platelet aggregation inhibition model in cynomolgus monkeys, **49** exhibited excellent efficacy at a 3 mg/kg oral dose, still inhibiting platelet aggregation by 70% at 24 h. More importantly, contrary to SCH-205831 and **47**, no major hydroxylated metabolite was found in monkey plasma and the metabolic profile of **49** proved to be clean.

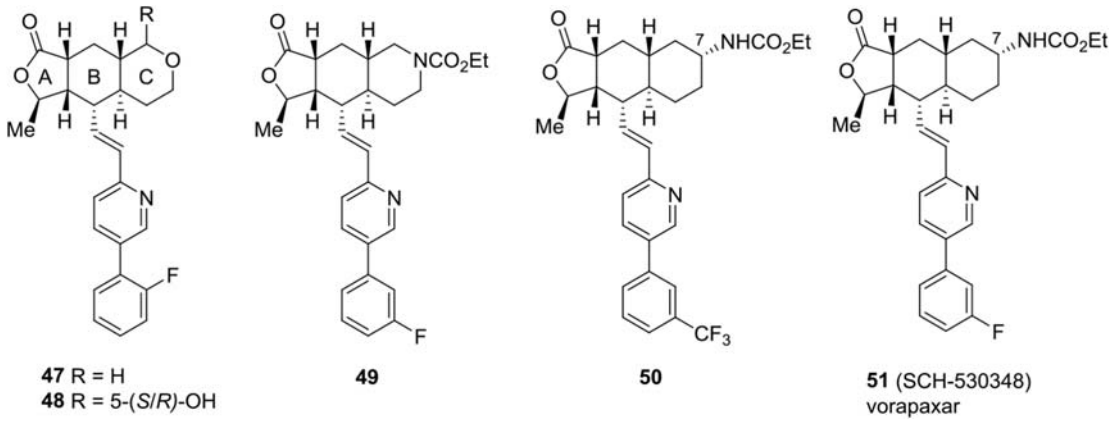

Fig. 15 Further modifications of the C-ring leading to vorapaxar.

A further modification of the C-ring was the replacement of the 7-OH group present in compound **45** by a carbamate group.[142] The optimization of the carbamate chain and of the pyridyl aryl substituent culminated in compounds **50** and **51** displaying similar binding affinity and impressive efficacy in the ex vivo platelet aggregation inhibition model in cynomolgus monkeys, that is, 100% inhibition at 0.1 mg/kg oral dose with 24 h duration. Based on a lower lipophilicity compared with **50** (F-phenyl vs. CF_3-phenyl), compound **51** (SCH-530348, vorapaxar) was further developed in preclinical and clinical studies.

Vorapaxar is a reversible, competitive antagonist with a dissociation half-life of about 20 h allowing effective competition against the tethered ligand. The K_i was 8.1 nM against PAR-1 in the binding assay. The compound showed potent inhibition of thrombin-induced platelet aggregation ($IC_{50} = 47$ nM), whereas no inhibition of platelet aggregation induced by other agonists such as ADP, collagen, and a standard TXA_2 mimetic (U46619) was observed. Vorapaxar was inactive in the PAR-2, PAR-3 binding, and PAR-4 functional assays.

A high-resolution crystal structure of vorapaxar bound to human PAR-1 was reported in 2012.[143] The binding pocket is superficial with a small surface exposed to the aqueous solvent. Vorapaxar may access the binding pocket through the lipid bilayer, possibly between TM6 and TM7, similarly to retinal and S1P with rhodopsin and $S1P_1$, respectively. Despite molecular dynamics simulations and the knowledge of the key amino acids influencing agonist peptide affinity, the mechanism of activation of PAR-1 remains poorly understood.

Vorapaxar was approved in the United States in 2014 for the reduction of thrombotic cardiovascular events in patients with a history of MI or peripheral arterial disease (PAD).[144] In 2015, the drug was approved in the EU for the reduction of atherothrombotic events in adult patients with a history of MI. Vorapaxar is formulated in a 2.5 mg once-daily tablet and is given in combination with aspirin and/or clopidogrel. A black box warning was issued by the FDA regarding an increased bleeding risk in patients with a history of stroke, TIA, intracranial hemorrhage, or active pathological bleeding. Approval of vorapaxar was based on two phase III trials, the TRA2°P-TIMI50 study in patients with MI, PAD, or ischemic stroke and the TRACER study in NSTEMI ACS population.[145] Overall, vorapaxar on top of standard antiplatelet therapy (i.e., aspirin and $P2Y_{12}$ antagonist) significantly reduced the risk of cardiovascular death or ischemic events in patients with a history of MI or ischemic stroke or PAD. Nevertheless, it is associated with an increased risk of bleeding, including serious and potentially fatal bleeding events. Vorapaxar is rapidly and fully absorbed after oral administration in humans, and 80% inhibition of PAR-1 is achieved after one week of treatment at the recommended dose.[146]

The team at Merck is actively searching for follow-up molecules.[147] Notably, efforts addressing vorapaxar's low aqueous solubility led to the discovery of SCH-602539 (**52**; **Fig. 16**).[148] Other vorapaxar analogs were reported by a research group in Korea in collaboration with LG Life Sciences whereby the tricyclic ring was replaced by a bicyclic octahydroindene core.[149] For instance, compounds **53** and **54** showed high potency in the radioligand binding assay and in the platelet aggregation assay (**Fig. 16**).

7.15.5.2.1.3 Atopaxar (E-5555, Eisai)

Atopaxar (**55**, E-5555) is a reversible, orally active PAR-1 antagonist discovered by scientists at Eisai (**Fig. 16**). Atopaxar showed an IC_{50} of 19 nM in the binding assay and in vitro inhibited human platelet aggregation induced by thrombin with an IC_{50} value of 64 nM.[150] The antithrombotic property of atopaxar given orally was studied in a model of photochemically induced thrombosis in guinea pigs. Atopaxar at doses of 30 and 100 mg/kg significantly prolonged the time to occlusion of the femoral artery, demonstrating an antithrombotic effect. Atopaxar administered orally at doses of 30, 300, and 1000 mg/kg did not prolong bleeding time in guinea pigs.

Four phase II clinical trials were performed for the oral treatment of ACS and coronary artery disease (CAD). The LANCELOT ACS study demonstrated that treatment with atopaxar was associated with a significant reduction in the early ischemia without a significant increase in major or minor bleeding.[151] Nevertheless, the development of the compound was discontinued in 2012, possibly due to transient dose-dependent transaminase elevation and cardiotoxicity that were observed with the highest doses of atopaxar.

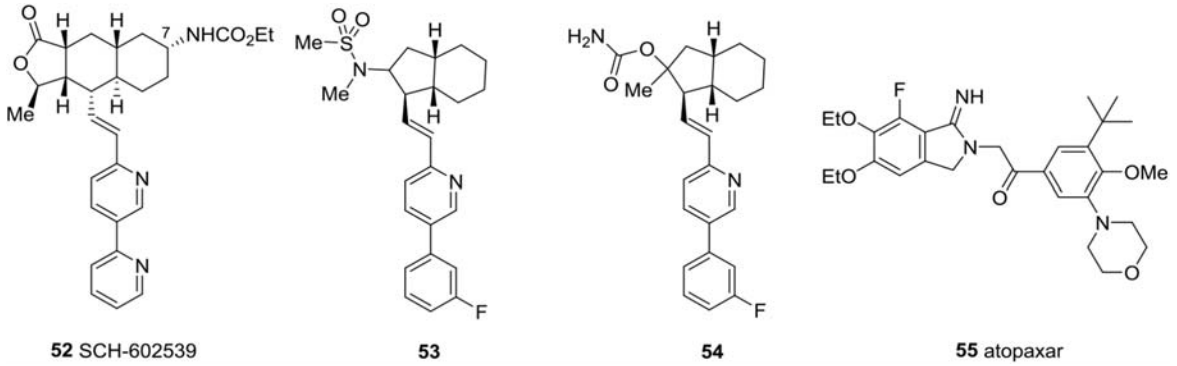

Fig. 16 Modifications of vorapaxar leading to SCH-602539 (**52**) and compounds **53–54;** structure of atopaxar (**55**).

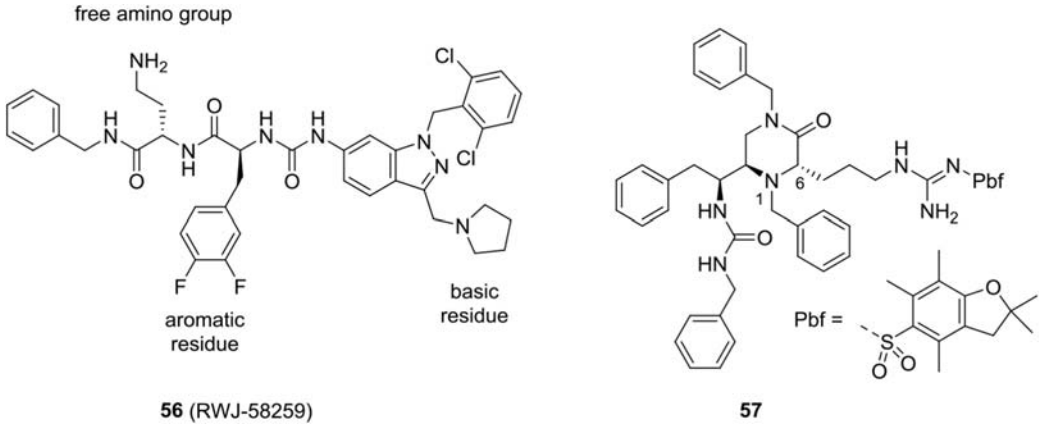

Fig. 17 Peptidomimetic PAR-1 antagonists developed based on the "three-point model," by Johnson & Johnson (RWJ-58259, **56**) and CSIC (**57**).

7.15.5.2.1.4 PZ-128

PZ-128, developed by the Tufts Medical Center (the United States), is a palmitoylated pepducin that targets the cytoplasmic side of PAR-1 and inhibits binding of the G proteins.[152] The structure of PZ-128 mimics the predicted inactive conformation of the third intracellular loop of PAR-1. PZ-128 suppressed platelet aggregation and arterial thrombosis in guinea pigs and baboons and had a synergistic effect in combination with clopidogrel. Full recovery of platelet function occurred after 24 h. Moreover, PZ-128 had no effect on bleeding or coagulation parameters in primates or in blood from patients undergoing PCI. A phase I study is currently evaluating the safety, tolerability, and pharmacodynamics of PZ-128 in patients with vascular disease or with two or more CAD risk factors.

7.15.5.2.1.5 Compounds in early phases

The first generation of peptidomimetic PAR-1 antagonists from Johnson & Johnson was designed based on the SFLLRN motif of the tethered ligand of PAR-1. Three substructures in the tethered peptide were shown to be essential for binding to PAR-1, that is, a free amino group, an aromatic residue, and a basic residue. This "three-point model" eventually led to the discovery of **56** (RWJ-58259) with an IC_{50} value of 150 nM in the binding assay (**Fig. 17**).[153] This compound was not further developed most likely due to low oral bioavailability.

The Spanish research group CSIC used a diversity-oriented synthesis strategy to prepare small libraries with different scaffolds able to orient one to two aromatic and basic groups at variable distances. A first series of peptide-based ureas and thioureas were prepared, including analogs of RWJ-58259.[154] Some protected peptide-based ureas displayed weak antagonistic activity in the TRAP-induced human platelet aggregation assay. In a second step, the pseudodipeptide-based piperazinone scaffold was introduced as to conformationally restrict the urea derivatives.[155] No clear SAR emerged and none of the analogs showed significant antiaggregation activity. The most active compound **57**, wherein the guanidine moiety is protected with a Pbf group, showed 57% inhibition at 150 μM in the TRAP-induced human platelet aggregation assay (**Fig. 17**).

Scientists at Pierre Fabre identified cinnamoyl piperazine and low-molecular-weight imidazole hits as novel PAR-1 antagonists following HTS.[156] Optimization of these two hits delivered compounds **58–60** that were potent in vitro in the FLIPR assay and ex vivo in the agonist peptide SFLLR-induced platelet aggregation assay and displayed high antithrombotic activity in an arteriovenous extracorporal shunt model in rats after i.v. administration (**Fig. 18**).

Among them, **58** (F-16618) was selected based on its reasonable water solubility and DMPK properties and characterized in more depth. F-16618 was found to have strong antithrombotic activity in vivo in several models with no major effects on physiological hemostasis.[157]

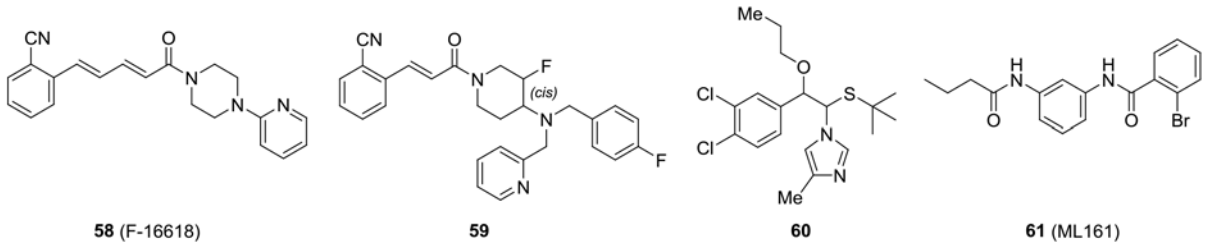

Fig. 18 PAR-1 antagonists developed at Pierre Fabre (**58–60**) and at the Broad Institute of MIT and Harvard (**61**).

Following an HTS screen performed at the Broad Institute of MIT and Harvard, ML161 (**61**) was postulated to inhibit PAR-1 in an allosteric manner (Fig. 18). This feature might provide selective modulation of downstream pathways, thereby potentially decreasing the bleeding risk in the setting of an anti-PAR-1 therapy.[158]

7.15.5.2.1.6 Summary

Despite preclinical and early clinical work indicating that the inhibition of PAR-1 does not interfere with the formation of the first layer of platelets (primary hemostasis) at the damaged vessel wall nor prolong bleeding time, clinical trials of vorapaxar combined with standard antiplatelet therapy showed an increased number of bleeding events. Therefore, current market approval is limited to a clearly defined subpopulation of ACS patients. Additional studies are needed to understand the reasons behind the increase in bleeding and to identify treatment regimens or combinations and patient populations who might optimally profit together with an acceptable increase of bleeding risk. In this regard, two phase IV clinical trials of vorapaxar are reported to be in preparation, on top of prasugrel or ticagrelor, and in patients with diabetes mellitus.

7.15.5.2.3 PAR-4 antagonists

7.15.5.2.3.1 Mechanism of action

PAR-4 lacks the hirudin-like domain found in PAR-1 and has therefore a lower affinity to thrombin. Both receptors differ in their intracellular signaling, which affects their role in thrombus formation. While PAR-1 induces a sharp and short-lived rise in cytosolic calcium and $\alpha_{IIb}\beta_3$ activation, PAR-4 causes a steady and sustained rise in calcium and $\alpha_{IIb}\beta_3$ activation that largely depends on $P2Y_{12}$. PAR-4 and $P2Y_{12}$ heterodimerization may be one mechanism by which the two receptors synergize to stabilize platelet-rich thrombi.[159] An interesting clinical observation was that among patients undergoing CABG surgery, which is associated with excess thrombin generation, bleeding was not increased. To explore the roles of PAR-1 and PAR-4 in thrombin-induced platelet activation, as part of the TRACER study, further studies were conducted in patients receiving vorapaxar or placebo and in healthy volunteers.[160] This study showed that vorapaxar inhibited the PAR-1-mediated component of thrombin-induced calcium mobilization but did not inhibit the PAR-4-mediated delayed increase in intracellular calcium. The authors suggested that under conditions of particularly high thrombin levels, PAR-1-selective antagonists may result in clinical benefits and that the remaining PAR-4 response would help maintain hemostasis. However, the role of PAR-4 in thrombosis and hemostasis is still unclear, and the need for potent and selective PAR-4 antagonists remains.

7.15.5.2.3.2 Clinical and preclinical programs

A phase I clinical study of BMS-986120 assessing safety, tolerability, and pharmacokinetics in healthy subjects has been completed. A second phase I single-dose study is planned to evaluate the effect of BMS-986120 on thrombus formation in an ex vivo thrombosis chamber model, in comparison with aspirin and clopidogrel.

The structure of BMS-986120 has not been publicly revealed. Three patents were published in 2013 disclosing PAR-4 antagonists for the inhibition of platelet aggregation.[161] In particular, a dose–response experiment with compound **62** was performed in the cynomolgus monkey electrically induced arterial thrombosis model, demonstrating in vivo antithrombotic efficacy (Fig. 19).[162]

Compound **63** (YD-3), reported by a research group in Taiwan in 2000, was the first nonpeptidic and selective PAR-4 antagonist.[163] A structural similarity search around the indazole moiety was conducted on the Vanderbilt compound repository unraveling **64** (ML354), with a similar binding affinity as YD-3 in the hundred nanomolar range and a selectivity > 100 versus PAR-1 (Fig. 19). This lead is currently under optimization.[164]

7.15.5.3 EP_3 Antagonists

The prostaglandin PGE_2 (**65**) is involved in various physiological processes, such as inflammation, pain, fever, gastroprotection, and labor.[165] The pharmacological effect of PGE_2 is determined by four receptor subtypes EP_{1-4} and by their tissue distribution. In platelets, the proaggregatory effect of PGE_2 on EP_3 is balanced by the antiplatelet activity of EP_2 and EP_4. As PGE_2 is induced under inflammatory conditions, targeting EP_3 should reduce thrombosis at atherosclerotic sites, which constitutes a state of chronic

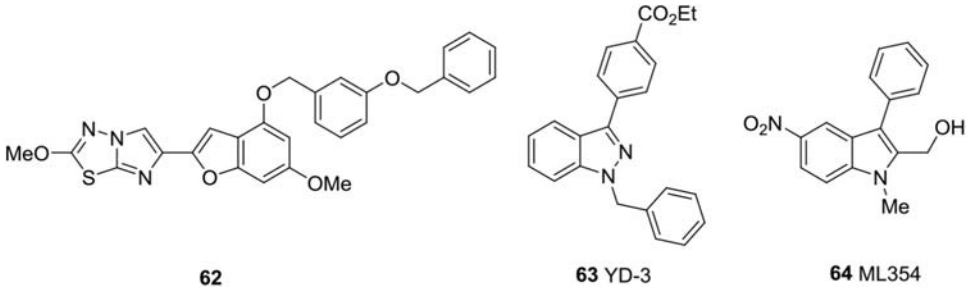

62 **63** YD-3 **64** ML354

Fig. 19 Patent example (**62**) from BMS, the first nonpeptidic selective PAR-4 antagonist **63** (YD-3) and follow-up compound **64** (ML354).

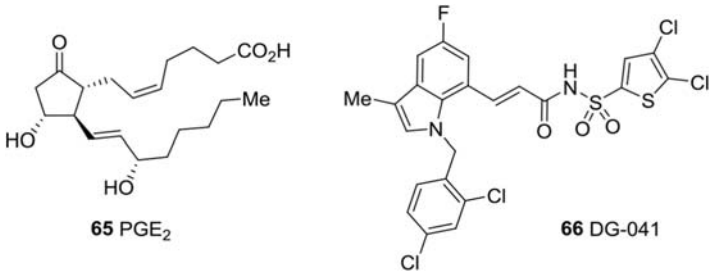

Fig. 20 The natural ligand of EP_3 PGE_2 and the EP_3 antagonist DG-041 (deCODE genetics).

inflammation.[166] In contrast, antagonizing EP_3 should not affect the platelet response to a vessel injury, since collagen and thrombin are the main drivers of platelet activation, while PGE_2 is not induced. As a result, a better safety profile would be expected compared with conventional antiplatelet agents.[167]

deCODE genetics initially identified EP_3 as a target by isolating variants in the gene encoding the EP_3 receptor that significantly increased the risk of PAD.[168] Based on the common pharmacophore of PGE_2 and other early known EP_3 ligands, new EP_3 antagonists were designed bearing a central indole ring as a replacement for the cyclopentanone core of PGE_2 and projecting two arms with apolar anionic and hydrophobic moieties in a 1,7-disubstituted pattern (Fig. 20).[169] Substitution of the indole core with a methyl group and a fluorine atom increased the metabolic stability. Among all tested substituents, the 4,5-dichlorothiophene moiety in combination with the 2,4-dichlorophenyl ring provided adequate in vitro potency along with low plasma protein binding. Compound **66** (DG-041) displayed noncompetitive antagonism of EP_3 due to a slow off-rate and therefore quasi-irreversible binding to the receptor. Importantly, dithiothreitol treatment showed that DG-041 did not behave as a Michael acceptor. Therefore, the formation of a covalent adduct is unlikely. The selectivity against other prostanoid receptors was measured, and no relevant inhibition of the IP receptor was found. As PGE_2 alone does not induce platelet aggregation, the biological activity was measured with collagen as coagonist in an LTA assay. This experimental setting should mimic the specific environment of a ruptured plaque. In different murine models, DG-041 reduced thrombosis without affecting hemostasis.[170] DG-041 was evaluated up to phase IIa clinical trials, but no further development has been reported so far.

7.15.5.4 5-HT_{2A} Antagonists

Following platelet activation, serotonin (5-hydroxytryptamine (5-HT)) is released by dense granules and binds to specific cell surface receptors on neighboring platelets. At least 14 members of serotonin receptors have been described, all belonging to the GPCR family with the exception of the ligand-gated ion channel 5-HT_3.[171] Many receptors are found in the brain, where they mediate the excitatory and inhibitory action of the neurotransmitter serotonin. This has attracted the pharmaceutical community, and as a result, many drugs modulating these receptors have been brought to the market for a variety of indications, such as depression, psychosis, and anorexia.

On platelets, the prominent serotonin receptor is 5-HT_{2A}, which in the brain is the target of psychedelic drugs (e.g., LSD). Serotonin is only a weak activator of platelets and per se is not sufficient to induce platelet aggregation.[172] However, in combination with other agonists, it contributes to the amplification of the platelet response. Preventing the amplification without interfering with the initiation of platelet aggregation should result in a greater separation of bleeding and thrombosis.

Early 5-HT_{2A} receptor antagonists including ketanserin (**67**) and sarpogrelate (**68**) have been shown to reduce restenosis after coronary stenting (Fig. 21). In addition, sarpogrelate (Mitsubishi Tanabe) has been used in some Asian countries for the treatment of PAD. The beneficial effect of 5-HT_{2A} receptor antagonists on the narrowing of arteries could be based on a synergy of an antiplatelet effect, vasodilation, and the inhibition of vascular smooth muscle cell proliferation. So far, serotonin receptor

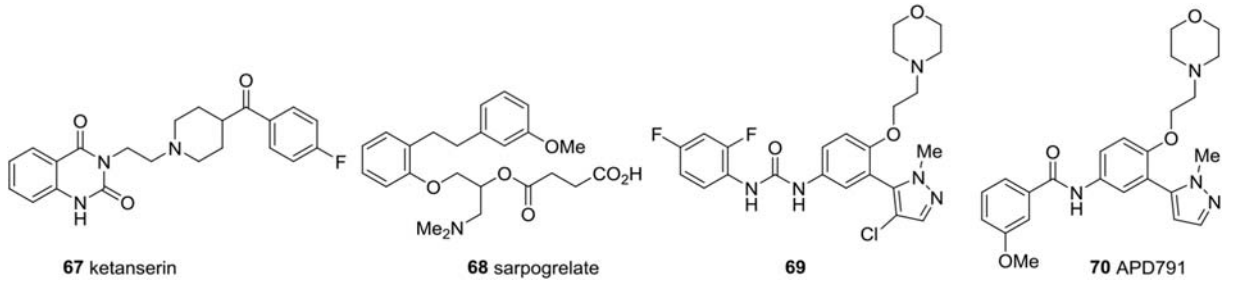

Fig. 21 Ketanserin, sarpogrelate, chloropyrazol **69**, and APD791 (Arena Pharmaceuticals).

antagonists did not achieve FDA approval as antiplatelet agents. The reasons for the challenging development of early-generation antagonists could be the lack of specificity for the 5-HT_{2A} receptor subtype and the complex role of serotonin in many diseases and general homeostasis. Despite positive animal studies, the validity of 5-HT_{2A} as an antithrombotic target for humans has not yet been ascertained and awaits confirmation through clinical trials.[173]

Recently, Arena Pharmaceuticals modified compounds from their own 5-HT_{2A} insomnia program with the goal to improve the selectivity and pharmacokinetic profile of previous 5-HT_{2A} blockers. The discovered functional inverse agonist **69** showed high 5-HT_{2A} selectivity (2700-fold) versus 5-HT_{2C} and low hERG channel inhibition (**Fig. 21**).[174] In a second optimization round, the urea motif was removed to increase the solubility at neutral pH, which led to compound **70** (APD791, temanogrel). In addition to binding assays, compounds were assessed for their antagonistic potential in the serotonin-mediated amplification of ADP-stimulated human platelet aggregation.[175] The low basicity of the morpholine ring of APD791 was key for a reduced hERG interaction. However, the morpholine ring undergoes microsomal ring opening leading to two biologically active metabolites.[176] In the Folts dog model of coronary stenosis, APD791 effectively blocked thrombosis without increasing bleeding time.[177] Despite the short half-life of the clinical candidate APD791 (0.9 h in dogs), the two metabolites may have contributed to the enhanced duration of action (58% inhibition of serotonin-mediated aggregation after 24 h). Finally, limited CNS partitioning in rat was measured, which is beneficial to minimize side effects in the brain. The highly selective and orally active 5-HT_{2A} antagonist APD791 is currently undergoing clinical phase I studies to assess pharmacokinetics, pharmacodynamics, and safety when coadministered with aspirin and clopidogrel.

7.15.5.5 TP Antagonists

The hallmark of platelet activation after adhesion onto collagen is the activation of thromboxane synthesis. PGH_2 is preferentially converted by the thromboxane synthase (TXS) into thromboxane A_2 (TXA_2), which is secreted into the surrounding space of activated platelets (**Fig. 2**).[178] TXA_2 can bind to the thromboxane receptor (TP) on the surface of resting platelets in close proximity. Binding of TXA_2 to TP then triggers signaling through Gq resulting in an elevation of intraplatelet calcium concentrations and hence unleashing further intraplatelet signaling and activation of the platelets.[179]

Blunting of TXA_2 production via inhibition of COX-1 by aspirin is the most successful approach to interfere with atherothrombotic diseases. Alternatively, inhibition of the binding of TXA_2 to its receptor TP was also explored. However, the majority of TP antagonists have been stopped at an early clinical stage due to lack of efficacy and toxicity issues.[180] Terutroban (S-18886, Servier) was the most advanced TP antagonist for antithrombotic therapy. A large phase III clinical trial revealed no benefit for terutroban when compared with aspirin, and its development was terminated. Recently, terutroban analogs have been reported displaying a novel carboxylic group bioisostere.[181] Other TP antagonists currently under clinical investigation have indications outside the antiplatelet field, such as ifetroban (Cumberland Pharmaceuticals), which is in phase II for patients with hepatorenal syndrome. In addition, the inhibitor EV-077/SER150 with TP and TXS dual mode of action (Evolva; outlicensed to Serodus) is evaluated in a clinical phase II study for efficacy in patients with diabetic nephropathy.

7.15.5.6 IP Antagonists

PGI_2 binds to and activates the IP receptor that stimulates AC resulting in elevation of intracellular cAMP.[182] In platelets, activation of IP is essential to keep platelets in a resting state. Elevated cAMP concentrations also lead to the relaxation of smooth muscle cells and thus vasodilation. Therefore, the effect of PGI_2 is twofold: antithrombotic by inhibition of platelet activation and vasodilatory on blood vessels.

PGI_2 is an IP agonist with a very short half-life. Hence, efforts of pharmaceutical research have produced analogs with improved chemical and metabolic stability for use in patients.

7.15.6 Inhibition of Platelet Adhesion and Aggregation

7.15.6.1 Integrin $\alpha_{IIb}\beta_3$ Antagonists

7.15.6.1.1 First-generation antagonists

Stimulation of platelets, independent of the mechanism of activation, always results in the transformation of inactive integrin $\alpha_{IIb}\beta_3$ (glycoprotein GPIIb/IIIa) into its active fibrinogen binding conformation and thus in the initiation of platelet aggregation. This function made $\alpha_{IIb}\beta_3$ a prime target for effective antiplatelet therapy within the pharmaceutical industry for a decade beginning in the late 1980s.[183] Three drugs were successfully developed, all of which are administered intravenously (**Fig. 22**): the human/murine chimeric antibody fragment abciximab (Johnson & Johnson–Eli Lilly) specific for an epitope on the β_3 subunit was the first to be approved in 1994; in 1998, the cyclic heptapeptide eptifibatide (**71**, Merck) was approved, which is derived from the snake venom barbourin; and finally, in the same year, the small molecule tirofiban (**72**, Merck) received as well market approval. These drugs have been widely applied in the treatment of ACS patients. However, compared with the newer $P2Y_{12}$ antagonists, their high antithrombotic efficacy goes along with an increased risk of thrombocytopenia and major bleedings. Therefore, these $\alpha_{IIb}\beta_3$ drugs are preferentially used in high-risk patients undergoing PCI.

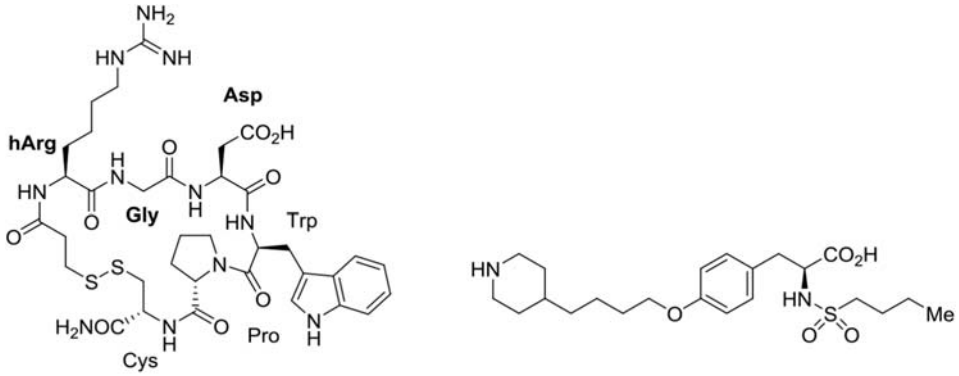

Fig. 22 Eptifibatide contains six amino acids and one mercaptopropionyl (des-amino cysteinyl) residue that forms a disulfide bridge with the cysteine amide. The modified RGD sequence is labeled in bold (*hArg*=homoarginine). Tirofiban mimics with its piperidine and its carboxylic acid moiety the Arg and Asp amino acids of the RGD sequence. The carboxylate group of tirofiban coordinates the Mg^{2+} ion, and the protonated piperidine ring undergoes charge-assisted H-bond interactions with the Asp224.

In contrast to the i.v. drugs, oral $\alpha_{IIb}\beta_3$ antagonists showed little to no benefit in several clinical phase III trials with an unexpected increase in thrombotic events. This resulted in increased mortality in the treatment arms and thus in a discontinuation of the oral antagonist programs across the pharmaceutical industry.[26]

7.15.6.1.2 Mechanism of action of integrins and ligand binding mode

The integrin $\alpha_{IIb}\beta_3$ belongs to a large family of α/β heterodimeric transmembrane proteins that fulfill important roles in cell–cell or cell–extracellular matrix interactions. Integrins are able to transmit signals bidirectionally across the cell membrane. Signaling pathways from numerous agonists of platelet activation (e.g., thrombin, TXA_2, and ADP) converge to activate $\alpha_{IIb}\beta_3$ resulting in fibrinogen cross-linking and platelet aggregation. The "inside-out" signaling is initiated by the binding of the intracellular protein talin to the cytoplasmic tail of the β_3 subunit. Upon this activation event, the integrin undergoes major conformational changes that are described in a simplified fashion thereafter.[184] From the inactive bent conformation in which the extracellular ligand binding domain is masked, $\alpha_{IIb}\beta_3$ converts into an intermediate partially activated ("primed") extended state. In the primed state, the "headpiece" of $\alpha_{IIb}\beta_3$ exposes and opens progressively its binding sites for the docking of the ligand. Finally, upon binding to fibrinogen or other ligands, the integrin switches to a fully extended ligand-bound state, where the rearrangement of the intracellular tails (e.g., tail separation) enables the binding of adaptor proteins (e.g., Syk and $G\alpha_{13}$) and the generation of "outside-in" signaling. Outside-in signaling stabilizes the thrombus and is involved in platelet spreading, granule secretion, and clot retraction (**Fig. 3**).[61,185]

Tirofiban and eptifibatide have been designed based on the RGD (Arg-Gly-Asp) or KGD (Lys-Gly-Asp) sequence found in natural ligands of $\alpha_{IIb}\beta_3$ (e.g., fibrinogen), which enables recognition by the receptor (**Fig. 22**). The binding mode of these antagonists has been elucidated by X-ray crystal structures of receptor–ligand complexes.[186] The basic amine group of the ligands mimics the arginine in the RGD sequence and binds Asp224 in the α_{IIb} subunit, while the carboxyl group replaces the aspartate, which is coordinated to a Mg^{2+} ion in the metal ion-dependent adhesion site (MIDAS) at the β_3 subunit. During complexation of these antagonists, a conformational change of the integrin exposes new epitopes, termed ligand-induced binding sites, which can be detected experimentally by antibodies. In some patients, similar neoepitopes can also be recognized by preformed antibodies. This interaction may lead to antibody-mediated removal of platelets from the circulation resulting in a thrombocytopenia side effect.

7.15.6.1.3 Novel approaches in $\alpha_{IIb}\beta_3$ antagonism

Various hypotheses have been put forward to explain the mortality increase with oral antagonists, but so far, the negative outcome of all different tested drugs could not be attributed to one single factor.[183b,187] RGD sequence-derived inhibitors induce after binding to the integrin a switch to an activated receptor conformation. Some compounds indeed show partial agonistic behavior. For oral antagonists with short half-lives, it was also postulated that the natural ligand agonist (fibrinogen) would directly activate the "primed" receptor after dissociation of the drug. Either effects, partial agonism, or insufficient target engagement with priming of the receptor could lead to outside-in signaling and platelet aggregation. In addition, the low bioavailability of some of the oral antagonists may have resulted in incomplete receptor blockade putting the patients at risk for recurrent thrombosis.

Two novel approaches are currently being pursued in the development of $\alpha_{IIb}\beta_3$ antagonists, which should hopefully lead to compounds with an improved safety profile[61]: (a) antagonist binding to the extracellular domain without eliciting the conformational change leading to receptor activation (in this case, platelet aggregation would still be circumvented due to blockade of the fibrinogen–receptor interaction and outside-in signaling inhibition) and (b) antagonist binding to the intracellular domain.

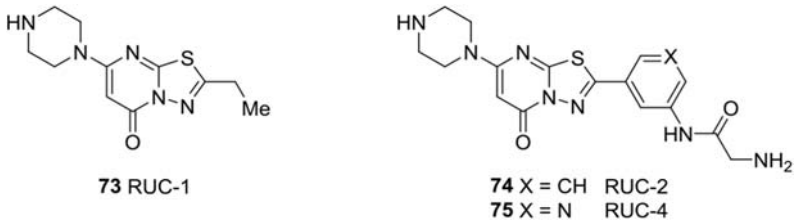

Fig. 23 Novel antagonists of the closed $\alpha_{IIb}\beta_3$ form: RUC-1, RUC-2, and RUC-4 (**73**–**75**).

In the first approach, an HTS screen of >30,000 compounds was performed by Blue et al. to identify novel inhibitors of platelet aggregation.[188] The thiadiazolo-pyrimidinone hit **73** (RUC-1; Fig. 23) was shown to possess promising affinity ($IC_{50} = 13$ μM) for the $\alpha_{IIb}\beta_3$ receptor and high selectivity over other related integrins. In contrast to previous peptidomimetic $\alpha_{IIb}\beta_3$ antagonists that bind to the open form of the integrin, X-ray data confirmed that the inhibitor RUC-1 binds only to the α_{IIb} subunit with no interaction with the Mg^{2+} ion in the β_3 MIDAS region, thus preventing the opening of the headpiece and the adoption of a high-affinity ligand binding conformation.[189] Along the same lines, the ~100-fold more active analog **74** (RUC-2, 90 nM) showed no major conformational changes in the β_3 subunit.[190] It shared the same binding mode as RUC-1, but in addition displaced with its primary amine the Mg^{2+} ion by binding to Glu220, which normally is coordinated to Mg^{2+} in the MIDAS domain.[191] Finally, the exchange of the phenyl ring of RUC-2 by a pyridine ring led to the derivative **75** (RUC-4),[192] showing similar activity but with a more favorable solubility and PK profile. RUC-4 has been further investigated in different animal models of thrombosis, where it protects the mice against thrombus development. For patients experiencing myocardial infarction, a timely exposure to antiplatelet agents is critical for positive outcome. An intramuscular injection of RUC-4 has therefore been proposed by Coller and coworkers as prehospital emergency treatment.[192] Further optimization using pharmacophore modeling identified related $\alpha_{IIb}\beta_3$ antagonists with high affinity for the closed conformation.[193]

The second approach encompasses the intracellular inhibition of the inside-out signaling by targeting the interaction between talin and the cytoplasmic tail of $\alpha_{IIb}\beta_3$. Different cell-permeable peptides containing talin binding sequences have been designed (e.g., palmitoylated peptides)[194] that showed promising antithrombotic activity. However, it is still unclear if this approach would lead to a separation of the antithrombotic activity from the bleeding side effect.

Alternatively, the outside-in signaling, which is believed to be responsible for the formation of an occlusive thrombus from a primary layer of platelets, could be targeted exclusively. In this approach, adhesion to the endothelial lesion and the subsequent primary thrombus formation, both depending on the inside-out mechanism, would not be impeded. This should prevent the undesired bleeding side effects. The ligand-induced outside-in signaling requires $G\alpha_{13}$ docking to the integrin in the same region as talin.[195] A myristoylated (m) ExE motif peptide has been described to disrupt the binding of $G\alpha_{13}$ to $\alpha_{IIb}\beta_3$.[195b] Thus, the hexapeptide m-FEEERA inhibits the early phase of outside-in signaling without interfering with the talin-dependent inside-out mechanism. In two mice models of thrombosis, this novel peptidic agent inhibited occlusive thrombosis without causing bleeding. However, to the best of our knowledge, no small-molecule inhibitors of intracellular $\alpha_{IIb}\beta_3$ tails have been reported so far. Nevertheless, this approach might represent a further step toward the development of $\alpha_{IIb}\beta_3$ antagonists with improved safety profile.

7.15.6.2 Antagonists of the Adhesion Receptors

The initial steps of thrombus formation involve platelet rolling, tethering, and adhesion to the site of vessel injury. Adhesion to the subendothelial exposed collagen is mainly dependent on two platelet receptors: the GPVI immunoglobulin receptor and its coadhesion receptor, the integrin $\alpha_2\beta_1$ (GPIa–IIa). In contrast to the restricted expression pattern of GPVI on platelets and megakaryocytes, $\alpha_2\beta_1$ is also found on epithelial cells, selected immune cells, and a large variety of mesenchymal cells. Several platelet adhesion receptors introduced in Section Platelet Adhesion and Aggregation Receptors have been the target of pharmacological interventions.[196] However, to the best of our knowledge, small-molecule inhibitors have only been described for $\alpha_2\beta_1$.

7.15.6.2.1 $\alpha_2\beta_1$ antagonists

Mouse models revealed diverse potential implications of $\alpha_2\beta_1$ in human diseases, such as infection, immunity, and cancer, with a role in metastasis and angiogenesis. The rationale for targeting $\alpha_2\beta_1$ in thrombosis is supported by the observation that its low expression level in humans is associated with only mild bleeding diathesis, in contrast to the strong bleeding disorder observed in the $\alpha_{IIb}\beta_3$ deficiency subjects (Glanzmann's thrombasthenia). Furthermore, $\alpha_2\beta_1$ gene polymorphism resulting in higher surface-level expression of the $\alpha_2\beta_1$ receptor has been linked to increased risk of myocardial infarction.[196]

The recognition of collagen, and more specifically of the binding sequence GFOGER (where O is hydroxyproline) in type I collagen, is mediated by a MIDAS motif in the αI (insertion) domain. This insertion domain is also common to eight other integrins but is not present in $\alpha_{IIb}\beta_3$ integrin. Binding of collagen triggers a signaling cascade that promotes further platelet adhesion and their subsequent activation and aggregation.

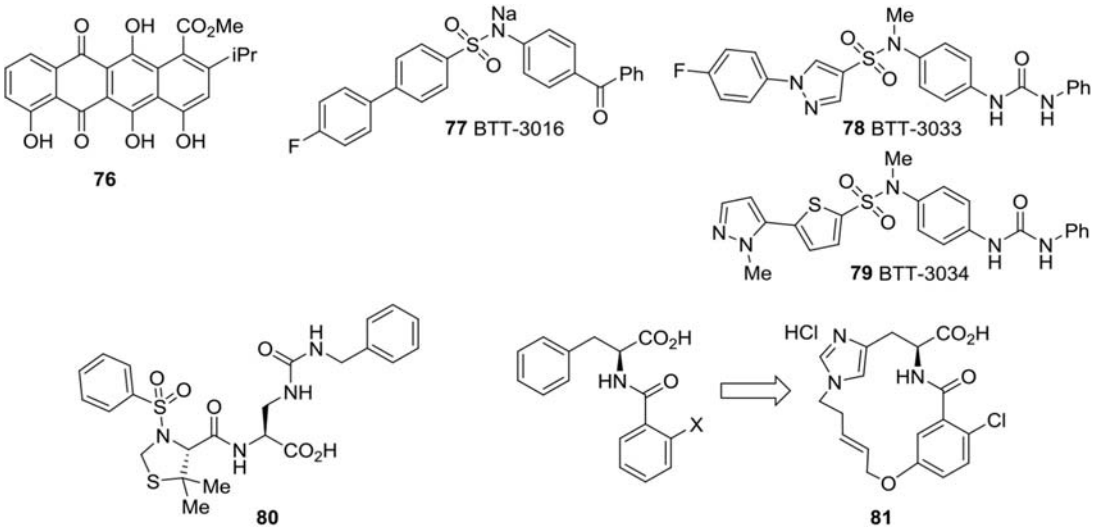

Fig. 24 Collaboration Turku/Jyväskylä Universities with Biotie Therapies: polyketide representative **76** and compounds **77–79**; compound **80** (DeGrado); from the common L-Phe-N-aroyl motif to the 15-membered macrocycle **81** (Sanofi).

From docking experiments of academic and commercial compound libraries, tetracyclic aromatic polyketides were found to be suitable candidates for binding into the closed conformation of the α_2I domain of $\alpha_2\beta_1$. These compounds exemplified by compound **76** (Fig. 24) were able to coordinate to the Mg^{2+} ion (directly or indirectly via water molecules) complexed in the MIDAS domain and showed competitive inhibition against type I collagen with IC_{50} values of 7.5–12 μM.[197] Further structure-based design at the same binding site and lead optimization resulted in a novel potent tool compound **77** (BTT-3016) of the diphenylsulfonamide series. BTT-3016 showed selectivity across the β1 integrin subtypes,[198] and it inhibited thrombus formation in the carotid artery injury model in mice. The bleeding time prolongation in the mouse tail bleeding model was comparable with aspirin. In a next optimization round, a phenylurea moiety replaced the benzophenone substituent, and (hetero)arylpyrazoles were chosen as a substitute for the biphenyl unit. Both compounds **78** (BTT-3033) and **79** (BTT-3034) inhibited cell adhesion to rat tail type I collagen in the submicromolar range. However, only BTT-3033 blocked platelet adhesion under blood flow conditions suggesting two different binding modes, an assumption supported by site-directed mutagenesis.[199] Interestingly, the two inhibitors recognize different $\alpha_2\beta_1$ conformations, and under blood flow conditions, only the targeting of the nonactivated conformation of $\alpha_2\beta_1$ was effective in blocking platelet adhesion.

DeGrado and coworkers combined molecular fragments of previously known $\alpha_4\beta_1$ and $\alpha_{IIb}\beta_3$ integrin inhibitors that led to a series of novel prolyl-2,3-4-diaminopropionic acid (DAP) derivatives with selectivity over other β_1 integrins.[200] Further optimization of the proline ring led to the discovery of thiazolidine-based inhibitors with high affinity (e.g., **80**, $IC_{50} = 12$ nM) toward $\alpha_2\beta_1$ and selectivity toward other platelet integrins (Fig. 24).[201] Based on biochemical studies, it was deduced that the DAP antagonists bind to a second MIDAS site in the β_1I-like domain. Blocking of this allosteric site prevented the opening of the αI-domain in the α_1 subunit to an active collagen binding conformation. In the ferric chloride-induced carotid artery injury model, total time to occlusion for compound **80** (60 mg/kg) was similar to aspirin (10 mg/kg).

In 2014, Sanofi described novel macrocyclic rings that incorporate as a key binding element the L-phenylalanine-N-aroyl motif inspired from $\alpha_4\beta_1$ and $\alpha_2\beta_7$ antagonists.[202] The carboxylic group of these early antagonists binds to the Mg^{2+} ion in the integrin MIDAS domain. The compounds were tested in a collagen interaction solid phase assay using the extracellular part of $\alpha_2\beta_1$. After some optimization, wherein one phenyl was replaced by an imidazole ring, highly active antagonists of $\alpha_2\beta_1$ were obtained (e.g., **81**; $IC_{50} = 4$ nM) with potent activity as well on other β_1 integrins (Fig. 24). The binding mode was rationalized by docking compound **81** to the β_1 MIDAS domain of crystallized $\alpha_5\beta_1$. Disappointingly, the series showed poor cellular permeability and high plasma clearance.

These preliminary studies support $\alpha_2\beta_1$ as an interesting antithrombotic target. Interference with protein–protein interaction was successfully achieved by targeting the α_2I domain. Alternatively, the allosteric pocket in the β_1 subunit could be efficiently targeted with notable selectivity over other integrins. Major efforts are still required to advance new $\alpha_2\beta_1$ integrin antagonists toward clinical evaluation.

7.15.6.2.2 GPVI antagonists

The collagen receptor GPVI is the major platelet receptor that binds to collagen with high affinity and initiates intraplatelet signaling leading to platelet aggregation.[203] The most advanced antagonist is revacept (advanceCor), which is a dimeric GPVI-Fc fusion protein in phase II for the treatment of ischemic stroke and TIA. Preclinical experiments with monoclonal antibodies or genetically modified mice confirmed the essential role of GPVI in collagen-induced platelet activation.[58] Therefore, inhibition of GPVI represents a novel opportunity to interfere with the initiation of thrombus formation.[204]

7.15.6.2.3 vWF and GPIb receptor antagonists

So far, no small-molecular-weight inhibitors of vWF nor of the GPIb-V-IX receptor complex have been reported. Aptamers, monoclonal antibodies, and nanobodies (e.g., ALX-0081) have been generated and have confirmed that targeting the vWF-GPIb-V-IX receptor complex could be a reasonable antithrombotic strategy.[16g,205] Anfibatide (Lee's Pharmaceutical), a snake venom-derived GPIb antagonist, is currently in clinical phase II in ACS patients.[206] Novel approaches or technologies might be needed to enable the identification of small-molecular-weight compounds as GPIb-V-IX receptor inhibitors.[207]

7.15.7 Inhibitors of Intracellular Enzymes

7.15.7.1 COX Inhibitors

COX inhibitors, commonly referred to as nonsteroidal antiinflammatory drugs (NSAIDs), can been classified either based on their chemical structure or by their selectivity profile toward the two cyclooxygenase enzyme isoforms COX-1 and COX-2.[208] For decades, their broad pharmacological effects as analgesic, antipyretic, antiinflammatory, or antiplatelet agents have made them indispensable for human health. The expression pattern of the COX isoforms influences the pharmacological effects of the inhibitors. While COX-2 is inducible under inflammatory conditions, COX-1 is constitutively expressed with high concentrations found in gastric epithelial cells and in platelets.

7.15.7.1.1 Aspirin

High doses of aspirin (**82**, acetylsalicylic acid (ASA)) blunt the synthesis of prostanoids in many tissues, and thus, aspirin is effective to limit prostanoid-mediated inflammation, pain, and thrombosis (Fig. 25).[209] However, long-term treatment with high-dose aspirin is restricted by side effects such as gastric bleeding and impairment of kidney function.[210] Therefore, low-dose regimens of aspirin have been evaluated. Several trials have consistently demonstrated a relevant reduction in cardiovascular events in ACS patients.[50] Due to its good safety profile, aspirin (75–325 mg) is unanimously recommended by health agencies for the prevention of cardiovascular events in ACS patients. Nevertheless, aspirin is a specific (and irreversible) inhibitor of COX-1 and thus ineffective in reducing platelet activation stimulated by other factors such as ADP or thrombin. Therefore, it is usually combined with a $P2Y_{12}$ antagonist.

In contrast, the net benefit of aspirin for the primary prevention of thrombotic events is not clearly established.[211] Particularly, the risk of gastrointestinal and other major bleedings needs to be taken into account when prescribed to healthy individuals. Therefore, primary prevention of ACS with aspirin has not been advocated by health authorities.

The mechanism of action of aspirin involves the transfer of its acetyl group to the hydroxyl group of Ser529 in human COX-1. Aspirin inhibits as well the other isoform COX-2, albeit with lower potency than COX-1 (c. 170-fold selectivity).[212] By such irreversible blockade, the catalytic site of COX enzymes becomes inaccessible to the substrate AA, and hence, the enzymatic conversion to PGG_2 and PGH_2 is hindered. Consequently, the level of PGH_2 that can be converted to TXA_2 in platelets by TXS decreases. It is postulated that the biosynthesis of the prothrombotic TXA_2 should be reduced by $>95\%$ to achieve complete inhibition of platelet aggregation. Being devoid of a nucleus, platelets lack the machinery for protein resynthesis. Thus, the inactivation of COX-1, the major isoform in platelets, lasts for the life span of the platelets (7–10 days). In other cells, irreversible inactivation of COX by aspirin is only of transient nature since they can regenerate COX enzymes through de novo synthesis.

Similar to clopidogrel, aspirin has been linked to high response variability.[213] Indeed, many patients experience recurrent adverse cardiovascular events despite ongoing aspirin therapy ("clinical resistance/treatment failure"). In secondary prevention, aspirin reduces by c. 25% the risk of ACS versus placebo as reported in a large meta-analysis by the Antiplatelet Trialists' Collaboration (ATC).[211] The underlying reasons for its limited efficacy are multifactorial and reflect to a certain extent the heterogeneous nature of the thrombotic diseases, that is, many signaling pathways are responsible for platelet aggregation. Other postulated causes encompass COX-1 polymorphism or higher platelet turnover, drug–drug interactions (e.g., active site competition with ibuprofen leading to decreased aspirin activity), aspirin metabolism or efflux mechanisms, and alternative TXA_2 production. Nevertheless, the "laboratory" resistance of aspirin, as defined by its inability to inactivate COX-1 with an adequate dose, remains a relatively rare phenomenon ($<5\%$). While the contributions of all these individual factors are still a matter of debate, patient compliance and

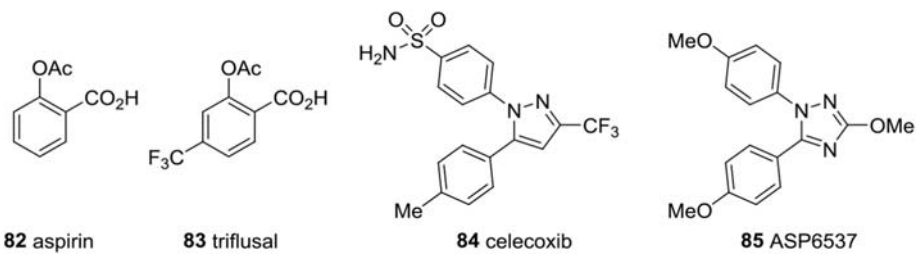

82 aspirin **83** triflusal **84** celecoxib **85** ASP6537

Fig. 25 The COX inhibitors aspirin and triflusal; representative selective COX-2 (celecoxib) and COX-1 inhibitors (ASP6537, Astellas).

pharmacokinetic variability arising, for example, from different aspirin formulations are believed to be major drivers of clinical treatment resistance.

7.15.7.1.2 Triflusal

Triflusal (**83**) is a structural variant of aspirin bearing an additional trifluoromethyl group (**Fig. 25**).[214] Its mechanism of action is similar to aspirin with preferential inactivation of COX-1. It is marketed by Uriach Pharma in some countries for the secondary prevention of ACS as well as to reduce graft occlusion after a coronary bypass. In 2008, based on a favorable efficacy and safety profile, the European Stroke Organization recommended the use of triflusal after strokes and TIA as an alternative to the combination of aspirin and dipyridamole or clopidogrel alone.[215] Triflusal is currently being compared in a clinical trial with clopidogrel for the secondary prevention of ischemic stroke patients based on the CYP2C19 polymorphism.[16i]

7.15.7.1.3 Recent developments

Inhibition of prostaglandin synthesis in the gastrointestinal mucosa is one of the main mechanisms of mucosal damage by NSAIDs and aspirin in particular.[216] The low but clearly increased risk of GI ulceration and bleeds contributes to the reduced patient compliance. Several possibilities have been explored to lower the gastric side effects of aspirin, namely, the development of (i) selective COX-1 inhibitors, (ii) aspirin prodrugs, and (iii) NO hybrids.

7.15.7.1.3.1 Selective COX-1 inhibitors

During the development of improved antiinflammatory drugs, it was initially believed that COX-1 was solely responsible for the gastric side effects of older generation NSAIDs, and therefore, selective COX-2 inhibitors (coxibs, e.g., celecoxib, **84**) were introduced. However, selective COX-2 inhibitors were found to increase adverse cardiovascular side effects that resulted in the withdrawal of rofecoxib (Merck).[217] It was suggested that COX-2 inhibition by the coxibs reduces the production of PGI_2, which possesses antiplatelet activity. This phenomenon may explain why high doses of aspirin have no additional antithrombotic effects compared with low-dose aspirin since simultaneous full inhibition of both COX isoforms may abolish the production of protective PGI_2.

In contrast to the well-defined pharmacology of selective COX-2 inhibitors, the therapeutic advantage of selective COX-1 inhibitors has been only rarely demonstrated. A review from 2010 covers the earlier published examples.[218] The findings that COX-1 knockout mice do not spontaneously develop gastric ulcers[219] and that highly selective COX-2 inhibitors have low gastrointestinal side effects suggest that gastric irritation is linked with the dual inhibition of both enzyme isoforms. Building on these findings, Astellas published the pharmacological profile of ASP6537 (**85**), a diaryltriazole derivative structurally derived from COX-2 inhibitors (**Fig. 25**).[220] The high selectivity profile of ASP6537 (>140,000-fold selective for COX-1 over COX-2) using recombinant human COX enzymes translates into a TXA_2/PGI_2 balance favorably shifted toward TXA_2 production, compared with aspirin. In addition, a significantly higher antithrombotic effect in an induced carotid arterial thrombosis model was measured, and no ulcerogenic effect at an efficacious antithrombotic dose could be observed. ASP6537 (licensed to Cardeus Pharmaceuticals) may be of benefit in both primary and secondary prevention of ACS events. Other recent selective COX-1 inhibitors have been disclosed by Vitale et al. with the investigation of diarylisoxazoles.[221] They could show that the right choice of lipophilic substituents on the central isoxazole determines the high COX-1 selectivity (>1000-fold over COX-2). The binding mode was rationalized by docking simulations using the COX-1 crystal structure.

7.15.7.1.3.2 Aspirin prodrugs

Masking the carboxylic group of aspirin through a prodrug approach would ideally abolish COX inhibition in the GI tract and yield a nonacidic molecule that would spare the gastrointestinal tract. The realization of this concept is challenged by a metabolic issue: in contrast to aspirin, neutral aspirin esters are substrates for butyrylcholinesterase (BuChE) in human plasma. Instead of the desired ester cleavage, a shift to the acetate hydrolysis is observed leading to the undesired formation of salicylic esters. One solution to this problem was proposed by Gilmer and coworkers by using isosorbide as a prodrug moiety (**Fig. 26**).[222] The sugar linker hinders the

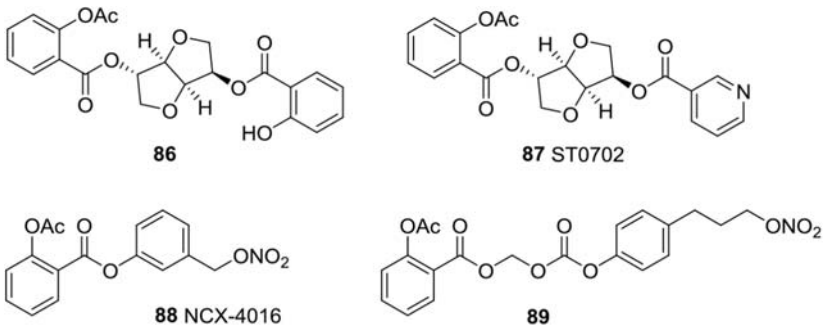

Fig. 26 Isosorbide-derived aspirin prodrugs with salicylate **86** and niacin moieties (**87**, ST0702); NO–aspirin hybrid drugs: compound **88** (NCX-4016) and acyloxymethyl carbonate-based prodrug **89**.

substrate recognition of BuChE, which would cleave the acetate group to the inactive salicylic ester. The aspirin production in **86** is very efficient, with 80–85% conversion. The close analog **87** (ST0702, Solvotrin Therapeutics) possesses a nicotinic acid (niacin) moiety replacing the salicylic acid of **86**.[223] It effectively inhibits human platelet aggregation and is in preclinical development with colorectal cancer as primary indication. In this setting, it is hoped that the released aspirin will have an impact on the platelet-mediated cancer cell metastasis and will concomitantly reduce the prothrombotic state of the disease.[224]

7.15.7.1.3.3 NO–aspirin hybrids

The gaseous messenger nitric oxide (NO) plays an essential role in human physiology, in particular in the cardiovascular system.[225] In blood vessels, the endothelium releases NO, which stimulates the increase in intracellular cGMP in platelets. This mechanism leads to decreased ability of platelet aggregation and to the maintenance of hemostasis[226] In the gastric tract, NO shows a protective effect on the mucosal membrane through multiple mechanisms that could counteract the GI side effects of COX inhibitors. Based on these beneficial effects, combinations of aspirin or other NSAIDs with an NO donor were proposed. This concept has been intensively investigated[227] with a particularly appealing strategy based on the hybrid drug concept (**Fig. 26**), in which aspirin is linked via its carboxylic group to an NO-releasing moiety. Double cleavage of these mutual prodrugs should ideally yield the two desired pharmacological agents in an equimolar ratio. An early compound **88** (NCX-4016, Nicox) has been evaluated up to phase II clinical trials.[228] However, the faster esterase-mediated acetate cleavage compared with the carboxylic ester results in an inhibitory effect on platelet aggregation arising only from the release of NO. Thus, NCX-4016 does not qualify as a "true" aspirin prodrug. Another type of prodrug from the NO–aspirin class of compounds besides the isosorbide moiety[229] has been described by the University of Turin, Italy, with the introduction of (nitrooxyacyloxy)methyl esters and related carbonates of aspirin.[230] The representative prodrug **89** is able to release aspirin quickly in human serum and inhibits collagen-induced platelet aggregation of human PRP.

Despite tremendous efforts, the development of new COX inhibitors with improved antiplatelet and safety profiles compared with aspirin remains a major challenge. However, it is remarkable that being on the market for so long, clinical trials with aspirin are still ongoing to further delimit its potential benefits (i.e., specific patient populations) either as monotherapy or as combination therapy.

7.15.7.2 TXS Inhibitors

Long-term treatment with high-dose aspirin can cause adverse effects such as gastric bleeding. Therefore, the quest for alternative approaches targeting TXA_2 formation has been initiated. In the past decades, the pharmaceutical industry focused on thromboxane synthase (TXS), the enzyme responsible for the conversion of PGH_2 into TXA_2. However, following inhibition of TXS, the PGH_2 produced during prostanoid biosynthesis accumulates and activates the TP receptor. This effect offsets the benefit of TXS inhibition and may explain the negative clinical trial results with TXS inhibitors.[231]

7.15.7.3 PDE Inhibitors

The cytosolic enzymes phosphodiesterases (PDEs) cleave the phosphodiester bond in the second messenger molecules cAMP and cGMP. So far, 11 different families of PDE have been described. In human platelets, the phosphodiesterases PDE2, PDE3, and PDE5 are the key enzymes responsible for cAMP (PDE2/3) and cGMP (PDE2/5) degradation, thereby limiting the intracellular concentration of cAMP and cGMP, respectively.[232]

The PDE3 inhibitor cilostazol (**90**) interferes with cAMP degradation and subsequent platelet activation and is in clinical use for the treatment of intermittent claudication (**Fig. 27**).[233] Cilastazol also antagonizes adenosine uptake and is a weak inhibitor of PDE5. The old drug dipyridamole (**91**) is characterized as a weakly selective PDE5 inhibitor and elevates thus intraplatelet cGMP.[234] It is approved by the FDA in combination with aspirin for the secondary prevention of stroke.[235]

The PDE3 inhibitor **92** (K-134, Kiowa) has been tested for PAD (intermittent claudication) and improved the walking distance in patients.[236] The dual PDE (of unspecified subtype) and $P2Y_{12}$ antagonist **93** (BF061) is an adenosine derivative recently described as a novel antiplatelet agent with similar activity compared with clopidogrel with less bleeding in animal models.[237]

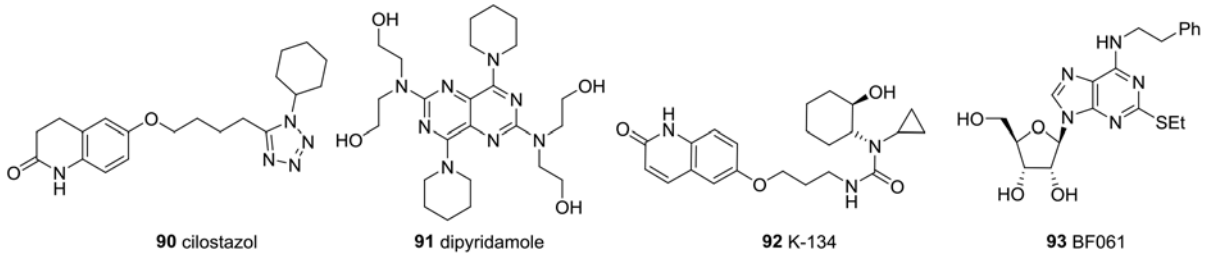

Fig. 27 The marketed PDE inhibitors cilostazol and dipyridamole; early development compounds K-134 (Kiowa) and BF061.

As PDEs display broad distribution in the body, future challenges for novel PDE drugs targeting platelets lie in the design of isoform-specific inhibitors.

7.15.7.4 Kinase Inhibitors

7.15.7.4.1 PI3Kβ inhibitors

PI3Kβ, a member of the PI3K lipid kinase family, has recently been described as a new target for antithrombotic therapy.[238] It is ubiquitously expressed and has been implicated in tumor cell proliferation. In platelets, PI3Kβ is a downstream effector of various cell surface receptors, including GPIb, GPVI, and $P2Y_{12}$.[239] Together with other PI3K isoforms, it regulates signaling of integrins such as $\alpha_{IIb}\beta_3$ (inside-out and outside-in signaling; **Fig. 3**). High shear stress as occurring in narrowed arteries during atherothrombosis activates PI3Kβ, which triggers enhanced $\alpha_{IIb}\beta_3$ adhesive contacts resulting in platelet aggregation. Inhibition of the catalytic subunit 110β of PI3Kβ could selectively decrease pathological thrombus formation while keeping the homeostatic machinery of platelets intact. In 2005, Jackson et al. reported the development of a 110β isoform-selective inhibitor based on compound **94** (LY294002), an early nonselective kinase blocker (**Fig. 28**).[238] After systematic SAR studies, the pyrido[1,2-a]pyrimidin-4-one **95** (TGX-221) was identified as a potent ($IC_{50} = 5$ nM) and selective inhibitor for 110β over a large kinase panel. Importantly, the morpholine ring was kept constant as it is crucial for binding to the hinge region. In a variety of animal models, TGX-221 inhibited thrombus formation with no significant increase in bleeding. Minor structural modifications culminated in the clinical candidate **96** (AZD6482), which was investigated by AstraZeneca up to phase I clinical trials, but no further development has been reported (**Fig. 28**). Similarly to TGX-221, AZD6482 is potent ($IC_{50} = 10$ nM) and selective for PI3Kβ with a short half-life in various species (5–43 min in humans). Owing to its short-acting profile, AZD6482 was administered in a 3 h infusion in human volunteers and showed good tolerability.[240] At maximal antiplatelet effect, it elicited no increase in bleeding time or blood loss. AZD6482 was also evaluated clinically in combination with aspirin or clopidogrel.[241] As a single agent, its antiplatelet effect ranked it between $P2Y_{12}$ and COX_1 antagonists. However, the most effective combination was observed with aspirin, providing enhanced antiplatelet effect with less bleeding complications compared with the clopidogrel–aspirin dual therapy. Short-acting intravenous antiplatelet inhibitors could be of value in the emergency treatment of ischemic stroke or for patients undergoing PCI.

Recently, AstraZeneca published a series of papers describing the follow-up program of AZD6482. The goal was to achieve once-daily oral dosing by improving the bioavailability and the metabolic stability of AZD6482.[242] Another key criterion during the optimization was the selectivity toward 110β over the other isoform 110α, the latter being critical for insulin signaling. Indeed, AZD6482 slightly increased plasma insulin levels in man, which could be linked to its PI3Kα inhibition ($IC_{50} = 0.87$ μM). While this was no issue during short infusions, it was believed that a cleaner profile would be needed for chronic antithrombotic therapies. It was known from TGX-221 that the carboxylic group could be removed without loss of potency but at the expense of an increased lipophilicity and metabolic instability. Therefore, removal of the carboxylic function to avoid the issue of acyl glucuronidation, reintroduction of a polar moiety (hydroxyethylcarboxamide), and exchange of the undesired anilinic nitrogen by an oxygen atom yielded **97** with an improved pharmacokinetic profile. In PRP, the selectivity between the α/β isoforms was sharply increased compared with AZD6482 (25-fold vs. 3.1-fold). Finally, the preclinical candidate **97** was tested in the modified Folts model in dogs to evaluate the safety margin, and no significant bleeding was observed.

Another approach relied on a virtual screening campaign of the AstraZeneca fragment library based on a 110β homology model of the crystallized 110γ structure.[242] The fragment **98** ($IC_{50} = 34$ μM) was chosen as a valid starting point. Introduction of a naphthyl

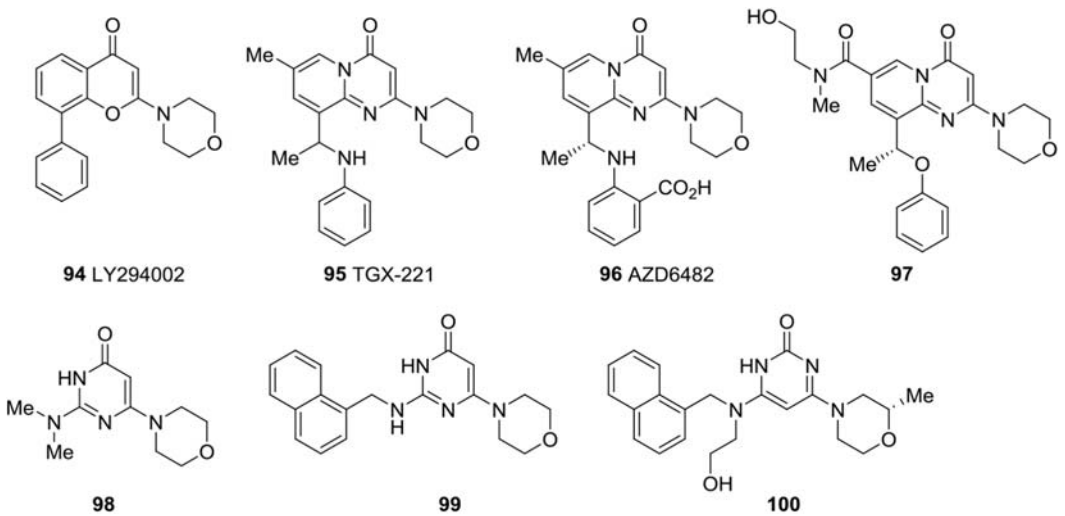

Fig. 28 PI3Kβ inhibitors. From the morpholinochromenone **94** (LY294002) to TGX-221 (**95**) and AZD6482 (**96**). Clinical candidate **97** from AstraZeneca. Follow-up compounds **99** and **100** based on the virtual screening hit **98**.

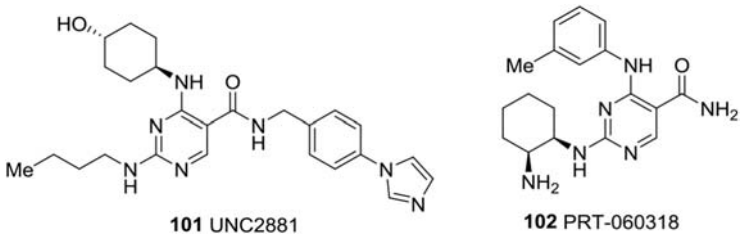

Fig. 29 The Mer inhibitor **101** (UNC2881) and the Syk inhibitor **102** (PRT-060318).

moiety for binding into the selectivity pocket gave the potent lead compound **99** ($IC_{50}=93$ nM), which however displayed low metabolic stability (Fig. 28). Three additional optimization rounds including a shift of the nitrogen within the pyrimidinone core, the introduction of a hydroxyethyl substituent to target the ribose binding subpocket, and a variation of the substituent engaging the hinge region gave **100**. Compound **100** was potent against 110β ($IC_{50}=38$ nM) and inhibited ADP-induced platelet aggregation in whole-blood effectively ($IC_{50}=2.1$ μM). It showed increased 110α/β selectivity translating in minimized risk for insulin resistance. As for AZD6482, a more favorable thrombosis–bleeding separation window was apparent in PK/PD experiments in dogs compared with other antiplatelet agents, such as ticagrelor and clopidogrel.

The enthusiasm for PI3Kβ as an antithrombotic target has been dampened recently by the observation that PI3Kβ activity is required for the stabilization of the thrombus at a high shear rate.[243] In animal models, the inhibition or absence of PI3Kβ in platelets resulted in thrombus instability that led to their enhanced detachment from the vasculature. A defective outside-in signaling from $\alpha_{IIb}\beta_3$ may account for the weakened interplatelet interactions that is required for thrombus consolidation. It is unclear whether these findings may translate into increased emboli and undesired secondary ischemic events during therapeutic intervention.

7.15.7.4.2 Other kinases

Besides PI3Kβ or its isoforms α/γ, other kinase classes have been proposed as antiplatelet targets. Three TAM receptor tyrosine kinases (Tyro3, Axl, and Mer) bind the extracellular protein Gas6 (growth arrest-specific-6), a member of a coagulation factor family. On the platelet surface, Gas6–TAM interaction may activate the integrin $\alpha_{IIb}\beta_3$ in synergy with ADP through a PI3K-dependent mechanism resulting in platelet aggregation. On endothelial cells, Gas6 is an important contributor to the surface expression of TF and therefore to the initiation of the clotting cascade.[244] A recent study from the University of North Carolina on the development of Mer inhibitors has been published.[245] The lead compound **101** (UNC2881; Fig. 29) showed high inhibitory potency on Mer ($IC_{50}=4.3$ nM) with >50-fold selectivity over Axl and Tyro3 ($IC_{50}=360$ and 250 nM, respectively) and activity in the collagen-induced platelet aggregation assay, suggesting a potential use of Mer inhibitors as antiplatelet agents.

Syk is an intracellular kinase with scaffolding properties, which is activated after engagement of several adhesion or aggregation receptors (Fig. 3). Syk plays as well a role in leukocyte recruitment to inflammatory sites. In 2011, Portola Pharmaceuticals reported the selective Syk inhibitor **102** (PRT-060318), which inhibited arterial thrombosis in various animal species and did not affect the bleeding time.[246]

7.15.8 New Frontiers in Antiplatelet Therapy

7.15.8.1 Role of Platelets Outside Hemostasis

7.15.8.1.1 Platelets in inflammation and immunity

Platelets interact with almost all known immune cells and are postulated to play a key role in inflammation and immunity.[247] Dense and alpha-granules contain proinflammatory mediators, such as P-selectin, CD40L, TGF-β, and several growth factors. These signals stimulate other cells to produce proinflammatory cytokines and chemokines, such as IL-1β, IL-8, TNFα, and CCL2.[248]

The role of platelets in various pathological conditions has been described. For example, observational studies suggest that antiplatelet therapy is associated with a reduction in mortality from sepsis.[249] Furthermore, elevated levels of circulating platelet–leukocyte aggregates have been reported in patients with atherothrombosis suggesting a possible role of platelets in inflammation. Not surprisingly, aspirin and $P2Y_{12}$ antagonists possess antiinflammatory action in various experimental systems and clinical conditions.[248]

Pulmonary arterial hypertension (PAH) is a progressive disease that involves pathological remodeling, vasoconstriction, and thrombosis. Although the presence of thrombotic lesions in the pulmonary vasculature is a common pathological finding in PAH, the role of platelets is controversial. Activated platelets may interact with the pulmonary arterial wall and contribute to the functional and structural alterations of pulmonary vessels by releasing vasoactive and mitogenic factors. Further studies are needed to fully understand the role of platelets in the establishment and progression of PAH.[250]

Systemic sclerosis (SSc) is an inflammatory disease of unknown etiology characterized by widespread organ dysfunction due to fibrosis and ischemia. Enhanced activation of platelets and increased tendency to aggregation have long been observed in SSc

patients. Further research has to clarify if aberrant platelet functionality represents the cause or the consequence of initiation and perpetuation of SSc.[251]

Increasing evidence points to an important role for platelets and their secreted products in the pathogenesis of allergic diseases. A variety of changes in platelet function have been observed in patients with asthma, such as alterations in platelet secretion, expression of surface molecules, aggregation, and adhesion. Moreover, platelets have been found to actively contribute to most of the characteristic features of asthma, including bronchial hyperresponsiveness, bronchoconstriction, airway inflammation, and airway remodeling.[252]

Interaction of platelets with viruses is a described pathophysiological phenomenon. Multiple mechanisms are involved including virus-induced platelet destruction, inappropriate platelet activation, and impaired megakaryopoiesis. Viruses can bind platelets through specific receptors that lead to functional alterations of both the platelet and the involved virus.[253]

Furthermore, platelets express a wide range of potential bacterial receptors, including complement receptors, FcγRII (antibody receptor), and Toll-like receptors (danger signal receptor). Platelets are essential for the formation of neutrophil extracellular traps (expelled DNA net), resulting in bacterial clearance by trapping bacteria and concentrating antibacterial factors.[254] Current literature suggests that the interplay of platelets and bacteria is much more complex than currently understood and awaits exciting discoveries.

In conclusion, the identification of platelets in various inflammatory mechanisms suggests an important role in the regulation of innate and adaptive immunity and in the recognition of pathogens.

7.15.8.1.2 Platelets in cancer

Platelet-released factors or platelet-mediated processes play a role in tumor growth and tumor metastasis.[255] An increase in platelet number and activity is seen in patients with tumors. In this context, high platelet number is correlated with low overall survival and poor prognosis. Preclinical data suggest a cross talk between circulating tumor cells and platelets in the blood, thus facilitating tumor metastases through direct interactions and secreted bioactive proteins.[256] In addition, platelets form aggregates with tumor cells in the blood, thereby protecting them from host immune surveillance through physical shielding or release of immunosuppressive signals.[257] Furthermore, inhibitors of the COX enzymes effectively inhibit cancer formation and progression and thus suggest an involvement of platelets or platelet-derived signals.[258]

In summary, a better understanding of the role of platelets in the pathogenesis of these diseases might offer novel opportunities for innovative disease-specific antiplatelet approaches.

7.15.8.2 Emerging Antiplatelet Targets

The newly uncovered role of platelets in inflammation, immunity, and tumor biology offers new insights and thus potentially novel targets. Moreover, recently optimized technologies allow revisiting basic aspects of platelet function and thus have the potential to revive efforts on already well-known targets. In addition, improvements in the methodology of proteomics lead to higher sensitivity and throughput and are expected to unravel novel targets.[259]

In the next paragraph, recently described novel approaches and targets are briefly outlined, and a selection of targets with reported low-molecular-weight molecules is presented in Fig. 30. Available information suggests an important role of these targets

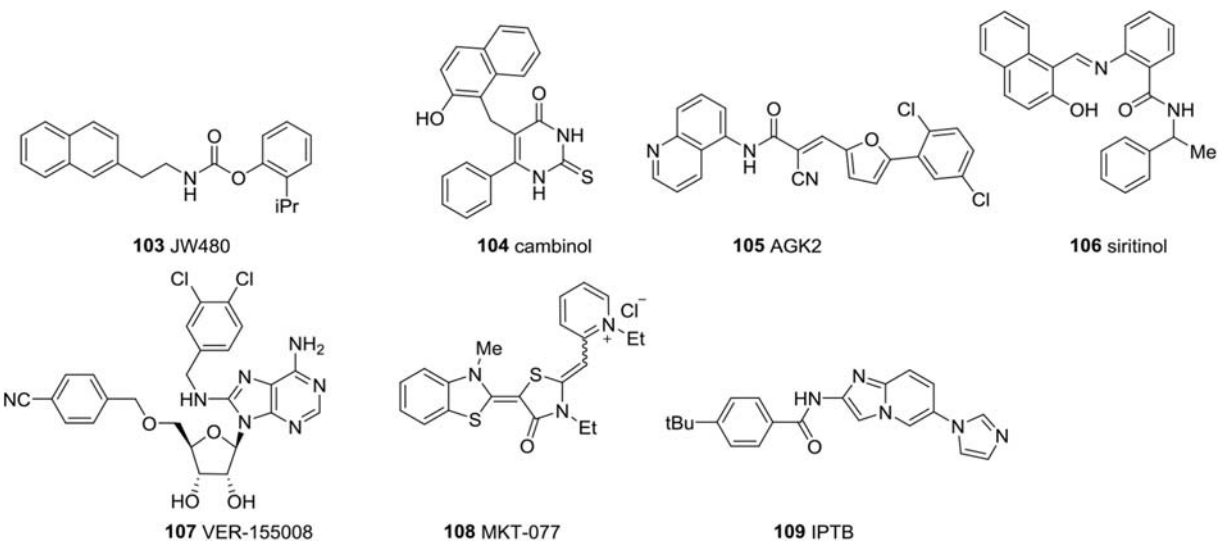

Fig. 30 A selection of inhibitors for various novel antiplatelet targets: JW480 (inhibitor of serine hydrolase); the sirtuin inhibitors cambinol, AGK2, and sirtinol; the HSP70 inhibitors VER-155008 and MKT-077 and IPTB (ASK1 inhibitor).

in platelet function. However, the precise mechanism and the impact of inhibition on the general safety profile and on overall bleeding risk await further investigation.

In a chemoproteomic approach,[260] the new serine hydrolase (AADACL1) was identified as being involved in the regulation of platelet activity. The specific inhibitor JW480 (**103**)[261] was confirmed to inhibit platelet aggregation in vitro and prevents arterial occlusion in an animal thrombosis model.[262]

Clozapine, the antipsychotic of choice for treatment-resistant schizophrenia, has been demonstrated to interfere with platelet function and thus might be the starting point to uncover a novel antiplatelet target.[263]

Protein acetylation is regulated by the activity of acetyltransferases and deacetylases, including sirtuins. Inhibitors of sirtuins, such as cambinol (**104**), AGK2 (**105**), and sirtinol (**106**), were shown to interfere with platelet function.[264] Characterization of the proteins and pathways responsible for this antiplatelet effect awaits further clarification.

Tetrahydrobiopterin (BH4), a cofactor for catecholamines, serotonin, and nitric oxide biosynthesis, was shown to inhibit platelet aggregation by enhancing local NO production within platelets.[265]

Inhibition of the heat shock protein HSP70 with the tool compounds VER-155008 (**107**) and MKT-077 (**108**) suppressed platelet spreading on fibrinogen- but not on collagen-coated surfaces. It was proposed that HSP70 is involved in the regulation of the inside-out signaling of $\alpha_{IIb}\beta_3$ integrin and thus defines a potentially novel antiplatelet approach.[266]

Further profiling of intraplatelet signaling revealed that IPTB (**109**), an inhibitor of the signaling protein ASK1, interfered with platelet aggregation and prevented arterial occlusion in an experimental model of thrombosis.[267]

Many more enzymes, signaling molecules, and surface receptors are expressed in human platelets.[268] In many cases, a potential role in the regulation of platelet function has been proposed based on the reported role of these proteins in other cell types and tissues. So far, mechanistic confirmation has been limited by the availability of research tools or by the inability to find low-molecular-weight inhibitors. We await reinforced efforts toward antiplatelet drugs and are excited to follow future progress in the identification of novel targets.

7.15.9 Conclusion

The last decades have witnessed a major decrease in mortality from cardiovascular diseases, and new antiplatelet drugs have contributed significantly to the medical progress. To interfere with pathological thrombus formation, different stages of the platelet response can be pharmacologically targeted: the adhesion of platelets to the subendothelial layer, the amplification of their biological response through GPCRs, and the concomitant intracellular enzymatic activity that culminates in platelet aggregation. In recent years, new drugs, such as ticagrelor, cangrelor, prasugrel, and vorapaxar, have entered the market and extended the standard treatment of ACS patients with clopidogrel and aspirin. In the field of antithrombotics, the key parameter to control is unwanted bleeding, which defines an upper limit in the optimal therapeutic dose. Therefore, efficacious drugs with a further improved therapeutic window are still needed. Recent studies have provided new antithrombotic targets, and the role of platelets beyond hemostasis has opened up new fields of research.

Acknowledgments

The authors thank Kurt Hilpert, Nathalie Meyer-Schaller, Dorte Renneberg, and Jodi Williams for the critical review of the book chapter.

See also: 7.16. Advances in Anticoagulants.

References

1. (a) Mackie, I. J.; Bull, H. A. Normal Haemostasis and Its Regulation. *Blood Rev.* **1989,** *3* (4), 237–250; (b) Chackalamannil, S. Antiplatelet Agents. In *Burger's Medicinal Chemistry, Drug Discovery, and Development,* vol. 4, Abraham, D. J., Rotella, D. P., Eds.; 7th ed.; John Wiley and Sons, 2010; pp 409–476; (c) Antiplatelet Agents. In *Handbook of Experimental Pharmacology,* vol. 210, Gresele, P., Born, G. V. R., Patrono, C., Page, C. P., Eds.; Springer-Verlag: Berlin, 2012.
2. Jackson, C. M.; Nemerson, Y. Blood Coagulation. *Annu. Rev. Biochem.* **1980,** *49,* 765–811.
3. Coughlin, S. R. How the Protease Thrombin Talks to Cells. *Proc. Natl. Acad. Sci. U. S. A.* **1999,** *96* (20), 11023–11027.
4. Baumgartner, H. R.; Turitto, V.; Weiss, H. J. Effect of Shear Rate on Platelet Interaction With Subendothelium in Citrated and Native Blood. II. Relationships Among Platelet Adhesion, Thrombus Dimensions, and Fibrin Formation. *J. Lab. Clin. Med.* **1980,** *95* (2), 208–221.
5. (a) Kannel, W. B.; Wolf, P. A. Peripheral and Cerebral Atherothrombosis and Cardiovascular Events in Different Vascular Territories: Insights From the Framingham Study. *Curr. Atheroscler. Rep.* **2006,** *8* (4), 317–323; (b) Munger, M. A.; Carter, O. Epidemiology and Practice Patterns of Acute Decompensated Heart Failure. *Am. J. Health Syst. Pharm.* **2003,** *60* (Suppl. 4), S3–S6.
6. (a) Watala, C. Blood Platelet Reactivity and Its Pharmacological Modulation in (People With) Diabetes Mellitus. *Curr. Pharm. Des.* **2005,** *11* (18), 2331–2365; (b) Preston, R. A.; Jy, W.; Jimenez, J. J.; Mauro, L. M.; Horstman, L. L.; Valle, M.; Aime, G.; Ahn, Y. S. Effects of Severe Hypertension on Endothelial and Platelet Microparticles. *Hypertension* **2003,** *41* (2), 211–217; (c) Sener, A.; Ozsavci, D.; Oba, R.; Demirel, G. Y.; Uras, F.; Yardimci, K. T. Do Platelet Apoptosis, Activation, Aggregation, Lipid Peroxidation and Platelet-Leukocyte Aggregate Formation Occur Simultaneously in Hyperlipidemia? *Clin. Biochem.* **2005,** *38* (12), 1081–1087; (d) Valenti, R.; Marcucci, R.; Capodanno, D.; De Luca, G.; Migliorini, A.; Gori, A. M.; Parodi, G.; Giusti, B.; Carrabba, N.; Paniccia, R.; Cantini, G.; Marrani, M.; Gensini, G. F.; Abbate, R.; Antoniucci, D. Residual Platelet Reactivity to Predict Long-Term Clinical Outcomes after Clopidogrel Loading in Patients with Acute Coronary Syndromes: Comparison of Different Cutoff Values by Light Transmission Aggregometry from the Responsiveness to Clopidogrel and Stent Thrombosis 2-Acute Coronary Syndrome (RECLOSE 2-ACS) Study. *J. Thromb. Thrombolysis* **2015,** *40* (1), 76–82.

7. Palomo, I.; Toro, C.; Alarcon, M. The Role of Platelets in the Pathophysiology of Atherosclerosis (Review). *Mol. Med. Rep.* **2008,** *1* (2), 179–184.
8. Antman, E. M.; Tanasijevic, M. J.; Thompson, B.; Schactman, M.; McCabe, C. H.; Cannon, C. P.; Fischer, G. A.; Fung, A. Y.; Thompson, C.; Wybenga, D.; Braunwald, E. Cardiac-Specific Troponin I Levels to Predict the Risk of Mortality in Patients With Acute Coronary Syndromes. *N. Engl. J. Med.* **1996,** *335* (18), 1342–1349.
9. (a) D'Souza, M.; Sarkisian, L.; Saaby, L.; Poulsen, T. S.; Gerke, O.; Larsen, T. B.; Diederichsen, A. C.; Jangaard, N.; Diederichsen, S. Z.; Hosbond, S.; Hove, J.; Thygesen, K.; Mickley, H. Diagnosis of Unstable Angina Pectoris has Declined Markedly With the Advent of More Sensitive Troponin Assays. *Am. J. Med.* **2015,** *128* (8), 852–860; (b) Zhelev, Z.; Hyde, C.; Youngman, E.; Rogers, M.; Fleming, S.; Slade, T.; Coelho, H.; Jones-Hughes, T.; Nikolaou, V. Diagnostic Accuracy of Single Baseline Measurement of Elecsys Troponin T High-Sensitive Assay for Diagnosis of Acute Myocardial Infarction in Emergency Department: Systematic Review and Meta-Analysis. *BMJ* **2015,** *350,* h15.
10. (a) Bleker, S. M.; Coppens, M.; Middeldorp, S. Sex, Thrombosis and Inherited Thrombophilia. *Blood Rev.* **2014,** *28* (3), 123–133; (b) Heit, J. A. Epidemiology of Venous Thromboembolism. *Nat. Rev. Cardiol.* **2015,** *12* (8), 464–474.
11. Lopez, A. D.; Mathers, C. D.; Ezzati, M.; Jamison, D. T.; Murray, C. J. Global and Regional Burden of Disease and Risk Factors, 2001: Systematic Analysis of Population Health Data. *Lancet* **2006,** *367* (9524), 1747–1757.
12. Turpie, A. G. Burden of Disease: Medical and Economic Impact of Acute Coronary Syndromes. *Am. J. Manag. Care* **2006,** *12* (16 Suppl), S430–S434.
13. Ruppert, A.; Lees, M.; Steinle, T. Clinical Burden of Venous Thromboembolism. *Curr. Med. Res. Opin.* **2010,** *26* (10), 2465–2473.
14. Chaudhari, K.; Hamad, B.; Syed, B. A. Antithrombotic Drugs Market. *Nat. Rev. Drug Discov.* **2014,** *13* (8), 571–572.
15. Topol, E. J.; Schork, N. J. Catapulting Clopidogrel Pharmacogenomics Forward. *Nat. Med.* **2011,** *17* (1), 40–41.
16. (a) Michelson, A. D. Advances in Antiplatelet Therapy. *Hematol. Am. Soc. Hematol. Educ. Prog.* **2011,** *2011,* 62–69; (b) Wiviott, S. D.; Tantry, U. S.; Gurbel, P. A. Clinical Applications of Antiplatelet Therapy. *Rev. Cardiovasc. Med.* **2006,** *7* (3), 130–146. quiz 148–9; (c) Choi, J.; Kermode, J. C. New Therapeutic Approaches to Combat Arterial Thrombosis: Better Drugs for Old Targets, Novel Targets, and Future Prospects. *Mol. Interv.* **2011,** *11* (2), 111–123; (d) Franchi, F.; Angiolillo, D. J. Novel Antiplatelet Agents in Acute Coronary Syndrome. *Nat. Rev. Cardiol.* **2015,** *12* (1), 30–47; (e) Jackson, S. P. Arterial Thrombosis—Insidious, Unpredictable and Deadly. *Nat. Med.* **2011,** *17* (11), 1423–1436; (f) Tello-Montoliu, A.; Jover, E.; Rivera, J.; Valdes, M.; Angiolillo, D. J.; Marin, F. New Perspectives in Antiplatelet Therapy. *Curr. Med. Chem.* **2012,** *19* (3), 406–427; (g) Ungerer, M.; Munch, G. Novel Antiplatelet Drugs in Clinical Development. *Thromb. Haemost.* **2013,** *110* (5), 868–875; (h) Grove, E. L.; Wurtz, M.; Thomas, M. R.; Kristensen, S. D. Antiplatelet Therapy in Acute Coronary Syndromes. *Expert Opin. Pharmacother.* **2015,** *16* (14), 2133–2147; (i) Kalantzi, K. I.; Tsoumani, M. E.; Goudevenos, I. A.; Tselepis, A. D. Pharmacodynamic Properties of Antiplatelet Agents: Current Knowledge and Future Perspectives. *Expert Rev. Clin. Pharmacol.* **2012,** *5* (3), 319–336.
17. Machlus, K. R.; Italiano, J. E., Jr. The Incredible Journey: From Megakaryocyte Development to Platelet Formation. *J. Cell Biol.* **2013,** *201* (6), 785–796.
18. Italiano, J. E., Jr.; Shivdasani, R. A. Megakaryocytes and Beyond: The Birth of Platelets. *J. Thromb. Haemost.* **2003,** *1* (6), 1174–1182.
19. Hartwig, J.; Italiano, J., Jr. The Birth of the Platelet. *J. Thromb. Haemost.* **2003,** *1* (7), 1580–1586.
20. Rhodes, J. M.; Simons, M. The Extracellular Matrix and Blood Vessel Formation: Not Just a Scaffold. *J. Cell Mol. Med.* **2007,** *11* (2), 176–205.
21. (a) Forman, S. D.; Nemerson, Y. Membrane-Dependent Coagulation Reaction is Independent of the Concentration of Phospholipid-Bound Substrate: Fluid Phase Factor X Regulates the Extrinsic System. *Proc. Natl. Acad. Sci. U. S. A.* **1986,** *83* (13), 4675–4679; (b) Lentz, B. R. Exposure of Platelet Membrane Phosphatidylserine Regulates Blood Coagulation. *Prog. Lipid Res.* **2003,** *42* (5), 423–438.
22. Golebiewska, E. M.; Poole, A. W. Platelet Secretion: From Haemostasis to Wound Healing and Beyond. *Blood Rev.* **2015,** *29* (3), 153–162.
23. Meyers, K. M.; Holmsen, H.; Seachord, C. L. Comparative Study of Platelet Dense Granule Constituents. *Am. J. Physiol.* **1982,** *243* (3), R454–R461.
24. Blair, P.; Flaumenhaft, R. Platelet Alpha-Granules: Basic Biology and clinical Correlates. *Blood Rev.* **2009,** *23* (4), 177–189.
25. (a) Darbousset, R.; Thomas, G. M.; Mezouar, S.; Frere, C.; Bonier, R.; Mackman, N.; Renne, T.; Dignat-George, F.; Dubois, C.; Panicot-Dubois, L. Tissue Factor-Positive Neutrophils Bind to Injured Endothelial Wall and Initiate Thrombus Formation. *Blood* **2012,** *120* (10), 2133–2143; (b) von Bruhl, M. L.; Stark, K.; Steinhart, A.; Chandraratne, S.; Konrad, I.; Lorenz, M.; Khandoga, A.; Tirniceriu, A.; Coletti, R.; Kollnberger, M.; Byrne, R. A.; Laitinen, I.; Walch, A.; Brill, A.; Pfeiler, S.; Manukyan, D.; Braun, S.; Lange, P.; Riegger, J.; Ware, J.; Eckart, A.; Haidari, S.; Rudelius, M.; Schulz, C.; Echtler, K.; Brinkmann, V.; Schwaiger, M.; Preissner, K. T.; Wagner, D. D.; Mackman, N.; Engelmann, B.; Massberg, S. Monocytes Neutrophils and Platelets Cooperate to Initiate and Propagate Venous Thrombosis in Mice In Vivo. *J. Exp. Med.* **2012,** *209* (4), 819–835.
26. Coller, B. S. Historical Perspective and Future Directions in Platelet Research. *J. Thromb. Haemost.* **2011,** *9* (Suppl. 1), 374–395.
27. Davies, M. J.; Thomas, A. C.; Knapman, P. A.; Hangartner, J. R. Intramyocardial Platelet Aggregation in Patients With Unstable Angina Suffering Sudden Ischemic Cardiac Death. *Circulation* **1986,** *73* (3), 418–427.
28. (a) Davi, G.; Patrono, C. Platelet Activation and Atherothrombosis. *N. Engl. J. Med.* **2007,** *357* (24), 2482–2494; (b) Michelson, A. D. P2Y12 Antagonism: Promises and Challenges. *Arterioscler., Thromb., Vasc. Biol.* **2008,** *28* (3), s33–s38.
29. Huber, K.; Bates, E. R.; Valgimigli, M.; Wallentin, L.; Kristensen, S. D.; Anderson, J. L.; Lopez Sendon, J. L.; Tubaro, M.; Granger, C. B.; Bode, C.; Ohman, E. M.; Steg, P. G. Antiplatelet and Anticoagulation Agents in Acute Coronary Syndromes: What Is the Current Status and What Does the Future Hold? *Am. Heart J.* **2014,** *168* (5), 611–621.
30. (a) Eikelboom, J. W.; Mehta, S. R.; Anand, S. S.; Xie, C.; Fox, K. A.; Yusuf, S. Adverse Impact of Bleeding on Prognosis in Patients With Acute Coronary Syndromes. *Circulation* **2006,** *114* (8), 774–782; (b) Amlani, S.; Nadarajah, T.; Afzal, R.; Pal-Sayal, R.; Eikelboom, J. W.; Natarajan, M. K. Mortality and Morbidity Following a Major Bleed in a Registry Population With Acute ST Elevation Myocardial Infarction. *J. Thromb. Thrombolysis* **2010,** *30* (4), 434–440.
31. (a) Jneid, H. The 2012 ACCF/AHA Focused Update of the Unstable Angina/Non-ST-Elevation Myocardial Infarction (UA/NSTEMI) Guideline: A Critical Appraisal. *Methodist Debakey Cardiovasc. J.* **2012,** *8* (3), 26–30; (b) Steg, P. G.; James, S. K.; Atar, D.; Badano, L. P.; Blomstrom-Lundqvist, C.; Borger, M. A.; Di Mario, C.; Dickstein, K.; Ducrocq, G.; Fernandez-Aviles, F.; Gershlick, A. H.; Giannuzzi, P.; Halvorsen, S.; Huber, K.; Juni, P.; Kastrati, A.; Knuuti, J.; Lenzen, M. J.; Mahaffey, K. W.; Valgimigli, M.; van't Hof, A.; Widimsky, P.; Zahger, D. ESC Guidelines for the Management of Acute Myocardial Infarction in Patients Presenting With ST-Segment Elevation. *Eur. Heart J.* **2012,** *33* (20), 2569–2619.
32. Born, G. V.; Haslam, R. J.; Goldman, M. Comparative Effectiveness of Adenosine Analogues as Inhibitors of Blood-Platelet Aggregation and as Vasodilators in Man. *Nature* **1965,** *205,* 678–680.
33. Patti, G.; Nusca, A.; Mangiacapra, F.; Gatto, L.; D'Ambrosio, A.; Di Sciascio, G. Point-of-Care Measurement of Clopidogrel Responsiveness Predicts Clinical Outcome in Patients Undergoing Percutaneous Coronary Intervention Results of the ARMYDA-PRO (Antiplatelet therapy for Reduction of MYocardial Damage during Angioplasty-Platelet Reactivity Predicts Outcome) Study. *J. Am. Coll. Cardiol.* **2008,** *52* (14), 1128–1133.
34. (a) Karon, B. S.; Tolan, N. V.; Koch, C. D.; Wockenfus, A. M.; Miller, R. S.; Lingineni, R. K.; Pruthi, R. K.; Chen, D.; Jaffe, A. S. Precision and Reliability of 5 Platelet Function Tests in Healthy Volunteers and Donors on Daily Antiplatelet Agent Therapy. *Clin. Chem.* **2014,** *60* (12), 1524–1531; (b) Velik-Salchner, C.; Maier, S.; Innerhofer, P.; Streif, W.; Klingler, A.; Kolbitsch, C.; Fries, D. Point-of-Care Whole Blood Impedance Aggregometry Versus Classical Light Transmission Aggregometry for Detecting Aspirin and Clopidogrel: The Results of a Pilot Study. *Anesth. Analg.* **2008,** *107* (6), 1798–1806.
35. Kundu, S. K.; Heilmann, E. J.; Sio, R.; Garcia, C.; Davidson, R. M.; Ostgaard, R. A. Description of an in vitro Platelet Function Analyzer—PFA-100. *Semin. Thromb. Hemost.* **1995,** *21* (Suppl. 2), 106–112.
36. Madan, M.; Berkowitz, S. D.; Christie, D. J.; Jennings, L. K.; Smit, A. C.; Sigmon, K. N.; Glazer, S.; Tcheng, J. E. Rapid Assessment of Glycoprotein IIb/IIIa Blockade With the Platelet Function Analyzer (PFA-100) During Percutaneous Coronary Intervention. *Am. Heart J.* **2001,** *141* (2), 226–233.
37. Horstrup, K.; Jablonka, B.; Honig-Liedl, P.; Just, M.; Kochsiek, K.; Walter, U. Phosphorylation of Focal Adhesion Vasodilator-Stimulated Phosphoprotein at Ser157 in Intact Human Platelets Correlates With Fibrinogen Receptor Inhibition. *Eur. J. Biochem.* **1994,** *225* (1), 21–27.
38. Day, S. M.; Reeve, J. L.; Myers, D. D.; Fay, W. P. Murine Thrombosis Models. *Thromb. Haemost.* **2004,** *92* (3), 486–494.
39. Kurz, K. D.; Main, B. W.; Sandusky, G. E. Rat Model of Arterial Thrombosis Induced by Ferric Chloride. *Thromb. Res.* **1990,** *60* (4), 269–280.

40. Surin, W. R.; Prakash, P.; Barthwal, M. K.; Dikshit, M. Optimization of Ferric Chloride Induced Thrombosis Model in Rats: Effect of Anti-platelet and Anti-coagulant Drugs. *J. Pharmacol. Toxicol. Methods* **2010,** *61* (3), 287–291.
41. Dejana, E.; Villa, S.; de Gaetano, G. Bleeding Time in Rats: A Comparison of Different Experimental Conditions. *Thromb. Haemost.* **1982,** *48* (1), 108–111.
42. (a) Himber, J.; Refino, C. J.; Burcklen, L.; Roux, S.; Kirchhofer, D. Inhibition of Arterial Thrombosis by a Soluble Tissue Factor Mutant and Active Site-Blocked Factors IXa and Xa in the Guinea Pig. *Thromb. Haemost.* **2001,** *85* (3), 475–481; (b) van Giezen, J. J.; Berntsson, P.; Zachrisson, H.; Bjorkman, J. A. Comparison of Ticagrelor and Thienopyridine P2Y(12) Binding Characteristics and Antithrombotic and Bleeding Effects in Rat and Dog Models of Thrombosis/Hemostasis. *Thromb. Res.* **2009,** *124* (5), 565–571; (c) Caroff, E.; Hubler, F.; Meyer, E.; Renneberg, D.; Gnerre, C.; Treiber, A.; Rey, M.; Hess, P.; Steiner, B.; Hilpert, K.; Riederer, M. A. 4-((*R*)-2-{[6-((*S*)-3-Methoxypyrrolidin-1-yl)-2-phenylpyrimidine-4-carbonyl]amino}-3-phosphonopropionyl)piperazine-1-carboxylic Acid Butyl Ester (ACT-246475) and Its Prodrug (ACT-281959), A Novel P2Y12 Receptor Antagonist With a Wider Therapeutic Window in the Rat Than Clopidogrel. *J. Med. Chem.* **2015,** *58* (23), 9133–9153.
43. (a) Folts, J. An in vivo Model of Experimental Arterial Stenosis, Intimal Damage, and Periodic Thrombosis. *Circulation* **1991,** *83* (6 Suppl), IV3–IV14; (b) Fattorutto, M. A modified Folts Model or the Original Folts Model to Evaluate New Antithrombotics? *Blood* **2003,** *101* (2), 782. author reply 782–3.
44. O'Gara, P. T.; Kushner, F. G.; Ascheim, D. D.; Casey, D. E., Jr.; Chung, M. K.; de Lemos, J. A.; Ettinger, S. M.; Fang, J. C.; Fesmire, F. M.; Franklin, B. A.; Granger, C. B.; Krumholz, H. M.; Linderbaum, J. A.; Morrow, D. A.; Newby, L. K.; Ornato, J. P.; Ou, N.; Radford, M. J.; Tamis-Holland, J. E.; Tommaso, J. E.; Tracy, C. M.; Woo, Y. J.; Zhao, D. X. 2013 ACCF/AHA Guideline for the Management of ST-Elevation Myocardial Infarction: Executive Summary: A Report of the American College of Cardiology Foundation/American Heart Association Task Force on Practice Guidelines. *Circulation* **2013,** *127* (4), 529–555.
45. Jneid, H.; Anderson, J. L.; Wright, R. S.; Adams, C. D.; Bridges, C. R.; Casey, D. E., Jr.; Ettinger, S. M.; Fesmire, F. M.; Ganiats, T. G.; Lincoff, A. M.; Peterson, E. D.; Philippides, G. J.; Theroux, P.; Wenger, N. K.; Zidar, J. P. 2012 ACCF/AHA Focused Update of the Guideline for the Management of Patients With Unstable Angina/non-ST-Elevation Myocardial Infarction (Updating the 2007 Guideline and Replacing the 2011 Focused Update): A Report of the American College of Cardiology Foundation/American Heart Association Task Force on Practice Guidelines. *J. Am. Coll. Cardiol.* **2012,** *60* (7), 645–681.
46. Eisen, A.; Giugliano, R. P. Antiplatelet and Anticoagulation Treatment in Patients With Non ST- Segment Elevation Acute Coronary Syndrome: Comparison of the Updated North American and European Guidelines. *Cardiol. Rev.* **2016,** *24,* 170–176.
47. Powers, W. J.; Derdeyn, C. P.; Biller, J.; Coffey, C. S.; Hoh, B. L.; Jauch, E. C.; Johnston, K. C.; Johnston, S. C.; Khalessi, A. A.; Kidwell, C. S.; Meschia, J. F.; Ovbiagele, B.; Yavagal, D. R. 2015 AHA/ASA Focused Update of the 2013 Guidelines for the Early Management of Patients With Acute Ischemic Stroke Regarding Endovascular Treatment: A Guideline for Healthcare Professionals From the American Heart Association/American Stroke Association. *Stroke* **2015,** *46,* 3020–3035.
48. Guthrie, R. Review and Management of Side Effects Associated With Antiplatelet Therapy for Prevention of Recurrent Cerebrovascular Events. *Adv. Ther.* **2011,** *28* (6), 473–482.
49. Pineda, J. R.; Kim, E. S.; Osinbowale, O. O. Impact of Pharmacologic Interventions on Peripheral Artery Disease. *Prog. Cardiovasc. Dis.* **2015,** *57* (5), 510–520.
50. AntithromboticTrialists' Collaboration. Collaborative Meta-Analysis of Randomised Trials of Antiplatelet Therapy for Prevention of Death, Myocardial Infarction, and Stroke in High Risk Patients. *BMJ* **2002,** *324* (7329), 71–86.
51. Mehta, S. R.; Yusuf, S.; Peters, R. J.; Bertrand, M. E.; Lewis, B. S.; Natarajan, M. K.; Malmberg, K.; Rupprecht, H.; Zhao, F.; Chrolavicius, S.; Copland, I.; Fox, K. A. Effects of Pretreatment With Clopidogrel and Aspirin Followed by Long-Term Therapy in Patients Undergoing Percutaneous Coronary Intervention: The PCI-CURE Study. *Lancet* **2001,** *358* (9281), 527–533.
52. Wiviott, S. D.; Braunwald, E.; McCabe, C. H.; Montalescot, G.; Ruzyllo, W.; Gottlieb, S.; Neumann, F. J.; Ardissino, D.; De Servi, S.; Murphy, S. A.; Riesmeyer, J.; Weerakkody, G.; Gibson, C. M.; Antman, E. M. Prasugrel Versus Clopidogrel in Patients With Acute Coronary Syndromes. *N. Engl. J. Med.* **2007,** *357* (20), 2001–2015.
53. (a) Wallentin, L.; Becker, R. C.; Budaj, A.; Cannon, C. P.; Emanuelsson, H.; Held, C.; Horrow, J.; Husted, S.; James, S.; Katus, H.; Mahaffey, K. W.; Scirica, B. M.; Skene, A.; Steg, P. G.; Storey, R. F.; Harrington, R. A.; Freij, A.; Thorsen, M. Ticagrelor Versus Clopidogrel in Patients With Acute Coronary Syndromes. *N. Engl. J. Med.* **2009,** *361* (11), 1045–1057; (b) Crouch, M. A.; Colucci, V. J.; Howard, P. A.; Spinler, S. A. P2Y(1)(2) Receptor Inhibitors: Integrating Ticagrelor Into the Management of Acute Coronary Syndrome. *Ann. Pharmacother.* **2011,** *45* (9), 1151–1156.
54. (a) Stone, G. W.; Witzenbichler, B.; Weisz, G.; Rinaldi, M. J.; Neumann, F. J.; Metzger, D. C.; Henry, T. D.; Cox, D. A.; Duffy, P. L.; Mazzaferri, E.; Gurbel, P. A.; Xu, K.; Parise, H.; Kirtane, A. J.; Brodie, B. R.; Mehran, R.; Stuckey, T. D. Platelet Reactivity and Clinical Outcomes After Coronary Artery Implantation of Drug-Eluting Stents (ADAPT-DES): A Prospective Multicentre Registry Study. *Lancet* **2013,** *382* (9892), 614–623; (b) Angiolillo, D. J.; Bernardo, E.; Sabate, M.; Jimenez-Quevedo, P.; Costa, M. A.; Palazuelos, J.; Hernandez-Antolin, R.; Moreno, R.; Escaned, J.; Alfonso, F.; Banuelos, C.; Guzman, L. A.; Bass, T. A.; Macaya, C.; Fernandez-Ortiz, A. Impact of Platelet Reactivity on Cardiovascular Outcomes in Patients With Type 2 Diabetes Mellitus and Coronary Artery Disease. *J. Am. Coll. Cardiol.* **2007,** *50* (16), 1541–1547; (c) Tantry, U. S.; Bonello, L.; Aradi, D.; Price, M. J.; Jeong, Y. H.; Angiolillo, D. J.; Stone, G. W.; Curzen, N.; Geisler, T.; Ten Berg, J.; Kirtane, A.; Siller-Matula, J.; Mahla, E.; Becker, R. C.; Bhatt, D. L.; Waksman, R.; Rao, S. V.; Alexopoulos, D.; Marcucci, R.; Reny, J. L.; Trenk, D.; Sibbing, D.; Gurbel, P. A. Consensus and Update on the Definition of On-Treatment Platelet Reactivity to Adenosine Diphosphate Associated With Ischemia and Bleeding. *J. Am. Coll. Cardiol.* **2013,** *62* (24), 2261–2273.
55. (a) Tricoci, P.; Huang, Z.; Held, C.; Moliterno, D. J.; Armstrong, P. W.; Van de Werf, F.; White, H. D.; Aylward, P. E.; Wallentin, L.; Chen, E.; Lokhnygina, Y.; Pei, J.; Leonardi, S.; Rorick, T. L.; Kilian, A. M.; Jennings, L. H.; Ambrosio, G.; Bode, C.; Cequier, A.; Cornel, J. H.; Diaz, R.; Erkan, A.; Huber, K.; Hudson, M. P.; Jiang, L.; Jukema, J. W.; Lewis, B. S.; Lincoff, A. M.; Montalescot, G.; Nicolau, J. C.; Ogawa, H.; Pfisterer, M.; Prieto, J. C.; Ruzyllo, W.; Sinnaeve, P. R.; Storey, R. F.; Valgimigli, M.; Whellan, D. J.; Widimsky, P.; Strony, J.; Harrington, R. A.; Mahaffey, K. W. Thrombin-Receptor Antagonist Vorapaxar in Acute Coronary Syndromes. *N. Engl. J. Med.* **2012,** *366* (1), 20–33; (b) Steg, P. G.; Bhatt, D. L.; Hamm, C. W.; Stone, G. W.; Gibson, C. M.; Mahaffey, K. W.; Leonardi, S.; Liu, T.; Skerjanec, S.; Day, J. R.; Iwaoka, R. S.; Stuckey, T. D.; Gogia, H. S.; Gruberg, L.; French, W. J.; White, H. D.; Harrington, R. A. Effect of Cangrelor on Periprocedural Outcomes in Percutaneous Coronary Interventions: A Pooled Analysis of Patient-Level Data. *Lancet* **2013,** *382* (9909), 1981–1992.
56. Li, Z.; Delaney, M. K.; O'Brien, K. A.; Du, X. Signaling During Platelet Adhesion and Activation. *Arterioscler., Thromb., Vasc. Biol.* **2010,** *30* (12), 2341–2349.
57. Savage, B.; Almus-Jacobs, F.; Ruggeri, Z. M. Specific Synergy of Multiple Substrate–Receptor Interactions in Platelet Thrombus Formation Under Flow. *Cell* **1998,** *94* (5), 657–666.
58. Varga-Szabo, D.; Pleines, I.; Nieswandt, B. Cell Adhesion Mechanisms in Platelets. *Arterioscler., Thromb., Vasc. Biol.* **2008,** *28* (3), 403–412.
59. Bockaert, J.; Pin, J. P. Molecular Tinkering of G Protein-Coupled Receptors: An Evolutionary Success. *EMBO J.* **1999,** *18* (7), 1723–1729.
60. Marinissen, M. J.; Gutkind, J. S. G-Protein-Coupled Receptors and Signaling Networks: Emerging Paradigms. *Trends Pharmacol. Sci.* **2001,** *22* (7), 368–376.
61. Estevez, B.; Shen, B.; Du, X. Targeting Integrin and Integrin Signaling in Treating Thrombosis. *Arterioscler., Thromb., Vasc. Biol.* **2015,** *35* (1), 24–29.
62. Senis, Y. A.; Mazharian, A.; Mori, J. Src Family Kinases: At the Forefront of Platelet Activation. *Blood* **2014,** *124* (13), 2013–2024.
63. Stefanini, L.; Bergmeier, W. RAP1-GTPase Signaling and Platelet Function. *J. Mol. Med. (Ber)* **2016,** *94,* 13–19.
64. Nieswandt, B.; Varga-Szabo, D.; Elvers, M. Integrins in Platelet Activation. *J. Thromb. Haemost.* **2009,** *7* (Suppl. 1), 206–209.
65. Hechler, B.; Gachet, C. Purinergic Receptors in Thrombosis and Inflammation. *Arterioscler., Thromb., Vasc. Biol.* **2015,** *35* (11), 2307–2315.
66. Mahaut-Smith, M. P.; Jones, S.; Evans, R. J. The P2X1 Receptor and Platelet Function. *Purinergic Signal* **2011,** *7* (3), 341–356.
67. Takasaki, J.; Kamohara, M.; Saito, T.; Matsumoto, M.; Matsumoto, S.; Ohishi, T.; Soga, T.; Matsushime, H.; Furuichi, K. Molecular Cloning of the Platelet P2T(AC) ADP Receptor: Pharmacological Comparison With Another ADP Receptor, the P2Y(1) Receptor. *Mol. Pharmacol.* **2001,** *60* (3), 432–439.
68. Cattaneo, M. The Platelet P2Y(1)(2) Receptor for Adenosine Diphosphate: Congenital and Drug-Induced Defects. *Blood* **2011,** *117* (7), 2102–2112.
69. Andre, P.; DeGuzman, F.; Haberstock-Debic, H.; Mills, S.; Pak, Y.; Inagaki, M.; Pandey, A.; Hollenbach, S.; Phillips, D. R.; Conley, P. B. Thienopyridines, but not Elinogrel, Result in Off-Target Effects at the Vessel Wall that Contribute to Bleeding. *J. Pharmacol. Exp. Ther.* **2011,** *338* (1), 22–30.
70. Oury, C.; Lecut, C.; Hego, A.; Wera, O.; Delierneux, C. Purinergic Control of Inflammation and Thrombosis: Role of P2X1 Receptors. *Comput. Struct. Biotechnol. J.* **2015,** *13,* 106–110.
71. Gachet, C. P2Y(12) Receptors in Platelets and Other Hematopoietic and Non-Hematopoietic Cells. *Purinergic Signal* **2012,** *8* (3), 609–619.

72. (a) Umemura, K.; Kawai, H.; Ishihara, H.; Nakashima, M. Inhibitory Effect of Clopidogrel, Vapiprost and Argatroban on the Middle Cerebral Artery Thrombosis in the Rat. *Jpn. J. Pharmacol.* **1995,** *67* (3), 253–258; (b) Sugidachi, A.; Asai, F.; Ogawa, T.; Inoue, T.; Koike, H. The in vivo Pharmacological Profile of CS-747, A Novel Antiplatelet Agent With Platelet ADP Receptor Antagonist Properties. *Br. J. Pharmacol.* **2000,** *129* (7), 1439–1446.
73. (a) Thomas, M. R.; Storey, R. F. The Future of P2Y12 Receptor Antagonists. *Platelets* **2015,** *26* (5), 392–398; (b) Wiviott, S. D.; Steg, P. G. Clinical Evidence for Oral Antiplatelet Therapy in Acute Coronary Syndromes. *Lancet* **2015,** *386* (9990), 292–302; (c) Wallentin, L. P2Y(12) Inhibitors: Differences in Properties and Mechanisms of Action and Potential Consequences for Clinical Use. *Eur. Heart J.* **2009,** *30* (16), 1964–1977.
74. (a) Jacobson, K. A.; Deflorian, F.; Mishra, S.; Costanzi, S. Pharmacochemistry of the Platelet Purinergic Receptors. *Purinergic Signal* **2011,** *7* (3), 305–324; (b) Jakubowski, J. A.; Sugidachi, A. Thienopyridyl and Direct-Acting P2Y12 Receptor Antagonist Antiplatelet Drugs. In *Analogue-Based Drug Discovery III;* Fischer, J., Ganellin, R., Rotella, D. P., Eds.; Wiley-VCH: New York, 2013; pp 141–164.
75. Maffrand, J. P. The Story of Clopidogrel and Its Predecessor, Ticlopidine: Could These Major Antiplatelet and Antithrombotic Drugs be Discovered and Developed Today? *C. R. Chimie* **2012,** *15,* 737–743.
76. CAPRIE Steering Committee. A Randomised, Blinded Trial of Clopidogrel Versus Aspirin in Patients at Risk of Ischaemic Events (CAPRIE). *Lancet* **1996,** *348,* 1329–1339.
77. Hollopeter, G.; Jantzen, H. M.; Vincent, D.; Li, G.; England, L.; Ramakrishnan, V.; Yang, R. B.; Nurden, P.; Nurden, A.; Julius, D.; Conley, P. B. Identification of the Platelet ADP Receptor Targeted by Antithrombotic Drugs. *Nature* **2001,** *409* (6817), 202–207.
78. Savi, P.; Pereillo, J. M.; Uzabiaga, M. F.; Combalbert, J.; Picard, C.; Maffrand, J. P.; Pascal, M.; Herbert, J. M. Identification and Biological Activity of the Active Metabolite of Clopidogrel. *Thromb. Haemost.* **2000,** *84* (5), 891–896.
79. Qureshi, Z.; Hobson, A. R. Clopidogrel "Resistance": Where Are We Now? *Cardiovasc. Ther.* **2013,** *31* (1), 3–11.
80. (a) Paniccia, R.; Priora, R.; Liotta, A. A.; Abbate, R. Platelet Function Tests: A Comparative Review. *Vasc. Health Risk Manag.* **2015,** *11,* 133–148; (b) Lordkipanidze, M.; Pharand, C.; Nguyen, T. A.; Schampaert, E.; Palisaitis, D. A.; Diodati, J. G. Comparison of Four Tests to Assess Inhibition of Platelet Function by Clopidogrel in Stable Coronary Artery Disease Patients. *Eur. Heart J.* **2008,** *29* (23), 2877–2885.
81. Jeong, Y. H.; Tantry, U. S.; Gurbel, P. A. Importance of Potent P2Y(12) Receptor Blockade in Acute Myocardial Infarction: Focus on Prasugrel. *Expert Opin. Pharmacother.* **2012,** *13* (12), 1771–1796.
82. Shan, J.; Zhang, B.; Zhu, Y.; Jiao, B.; Zheng, W.; Qi, X.; Gong, Y.; Yuan, F.; Lv, F.; Sun, H. Overcoming Clopidogrel Resistance: Discovery of Vicagrel as a Highly Potent and Orally Bioavailable Antiplatelet Agent. *J. Med. Chem.* **2012,** *55* (7), 3342–3352.
83. Zhu, Y.; Zhou, J. Identification of the Significant Involvement and Mechanistic Role of CYP3A4/5 in Clopidogrel Bioactivation. *ACS Med. Chem. Lett.* **2012,** *3* (10), 844–849.
84. Zhu, Y.; Zhou, J.; Jiao, B. Deuterated Clopidogrel Analogues as a New Generation of Antiplatelet Agents. *ACS Med. Chem. Lett.* **2013,** *4* (3), 349–352.
85. Becker, R. C.; Gurbel, P. A. Platelet P2Y12 Receptor Antagonist Pharmacokinetics and Pharmacodynamics: A Foundation for Distinguishing Mechanisms of Bleeding and Anticipated Risk for Platelet-Directed Therapies. *Thromb. Haemost.* **2010,** *103* (3), 535–544.
86. Humphries, B.; Dixon, J. "Daring to be Different": The Discovery of Ticagrelor. In *The Handbook of Medicinal Chemistry: Principles and Practice;* Davis, A., Ward, E. W., Eds.; The Royal Society of Chemistry: Cambridge, 2015; pp 699–714.
87. Ingall, A. H.; Dixon, J.; Bailey, A.; Coombs, M. E.; Cox, D.; Mclnally, J. I.; Hunt, S. F.; Kindon, N. D.; Teobald, B. J.; Willis, P. A.; Humphries, R. G.; Leff, P.; Clegg, J. A.; Smith, J. A.; Tomlinson, W. Antagonists of the Platelet P2T Receptor: A Novel Approach to Antithrombotic Therapy. *J. Med. Chem.* **1999,** *42* (2), 213–220.
88. Srinivasan, S.; Mir, F.; Huang, J. S.; Khasawneh, F. T.; Lam, S. C.; Le Breton, G. C. The P2Y12 Antagonists, 2-Methylthioadenosine 5'-Monophosphate Triethylammonium Salt and Cangrelor (ARC69931MX), Can Inhibit Human Platelet Aggregation Through a Gi-Independent Increase in cAMP Levels. *J. Biol. Chem.* **2009,** *284* (24), 16108–16117.
89. (a) Walsh, J. A., Ill; Price, M. J. Cangrelor for Treatment of Arterial Thrombosis. *Expert Opin. Pharmacother.* **2014,** *15* (4), 565–572; (b) Bhatt, D. L.; Stone, G. W.; Mahaffey, K. W.; Gibson, C. M.; Steg, P. G.; Hamm, C. W.; Price, M. J.; Leonardi, S.; Gallup, D.; Bramucci, E.; Radke, P. W.; Widimsky, P.; Tousek, F.; Tauth, J.; Spriggs, D.; McLaurin, B. T.; Angiolillo, D. J.; Genereux, P.; Liu, T.; Prats, J.; Todd, M.; Skerjanec, S.; White, H. D.; Harrington, R. A. Effect of Platelet Inhibition With Cangrelor during PCI on Ischemic Events. *N. Engl. J. Med.* **2013,** *368* (14), 1303–1313.
90. Springthorpe, B.; Bailey, A.; Barton, P.; Birkinshaw, T. N.; Bonnert, R. V.; Brown, R. C.; Chapman, D.; Dixon, J.; Guile, S. D.; Humphries, R. G.; Hunt, S. F.; Ince, F.; Ingall, A. H.; Kirk, I. P.; Leeson, P. D.; Leff, P.; Lewis, R. J.; Martin, B. P.; McGinnity, D. F.; Mortimore, M. P.; Paine, S. W.; Pairaudeau, G.; Patel, A.; Rigby, A. J.; Riley, R. J.; Teobald, B. J.; Tomlinson, W.; Webborn, P. J.; Willis, P. A. From ATP to AZD6140: The Discovery of an Orally Active Reversible P2Y12 Receptor Antagonist for the Prevention of Thrombosis. *Bioorg. Med. Chem. Lett.* **2007,** *17* (21), 6013–6018.
91. Hoffmann, K.; Lutz, D. A.; Strassburger, J.; Baqi, Y.; Muller, C. E.; von Kugelgen, I. Competitive Mode and Site of Interaction of Ticagrelor at the Human Platelet P2Y12 -Receptor. *J. Thromb. Haemost.* **2014,** *12* (11), 1898–1905.
92. Siller-Matula, J. M.; Jilma, B. Ticagrelor: From Discovery to Phase III Clinical Trial. *Future Cardiol.* **2010,** *6* (6), 753–764.
93. Serebruany, V. L. Ticagrelor Shift from PLATO to PEGASUS: Vanished Mortality Benefit, Excess Cancer Deaths, Massive Discontinuations, and Overshooting Target Events. *Int. J. Cardiol.* **2015,** *201,* 508–512.
94. Buchanan, A.; Newton, P.; Pehrsson, S.; Inghardt, T.; Antonsson, T.; Svensson, P.; Sjogren, T.; Oster, L.; Janefeldt, A.; Sandinge, A. S.; Keyes, F.; Austin, M.; Spooner, J.; Gennemark, P.; Penney, M.; Howells, G.; Vaughan, T.; Nylander, S. Structural and Functional Characterization of a Specific Antidote for Ticagrelor. *Blood* **2015,** *125* (22), 3484–3490.
95. (a) Tu, W.; Fan, J.; Zhang, H.; Xu, G.; Liu, Z.; Qu, J.; Yang, F.; Zhang, L.; Luan, T.; Yuan, J.; Gong, A.; Feng, J.; Sun, P.; Dong, Q. Synthesis and Biological Evaluation of Cyclopentyl-Triazolol-Pyrimidine (CPTP) Based P2Y12 Antagonists. *Bioorg. Med. Chem. Lett.* **2014,** *24* (1), 141–146; (b) Zhang, H.; Liu, J.; Zhang, L.; Kong, L.; Yao, H.; Sun, H. Synthesis and Biological Evaluation of Ticagrelor Derivatives as Novel Antiplatelet Agents. *Bioorg. Med. Chem. Lett.* **2012,** *22* (11), 3598–3602; (c) Ye, H.; Chen, C.; Zhang, H. C.; Haertlein, B.; Parry, T. J.; Damiano, B. P.; Maryanoff, B. E. Carba-Nucleosides as Potent Antagonists of the Adenosine 5'-Diphosphate (ADP) Purinergic Receptor (P2Y12) on Human Platelets. *ChemMedChem* **2008,** *3* (5), 732–736.
96. Douglass, J. G.; Patel, R. I.; Yerxa, B. R.; Shaver, S. R.; Watson, P. S.; Bednarski, K.; Plourde, R.; Redick, C. C.; Brubaker, K.; Jones, A. C.; Boyer, J. L. Lipophilic Modifications to Dinucleoside Polyphosphates and Nucleotides that Confer Antagonist Properties at the Platelet P2Y12 Receptor. *J. Med. Chem.* **2008,** *51* (4), 1007–1025.
97. Zhang, K.; Zhang, J.; Gao, Z. G.; Zhang, D.; Zhu, L.; Han, G. W.; Moss, S. M.; Paoletta, S.; Kiselev, E.; Lu, W.; Fenalti, G.; Zhang, W.; Muller, C. E.; Yang, H.; Jiang, H.; Cherezov, V.; Katritch, V.; Jacobson, K. A.; Stevens, R. C.; Wu, B.; Zhao, Q. Structure of the Human P2Y12 Receptor in Complex With an Antithrombotic Drug. *Nature* **2014,** *509* (7498), 115–118.
98. Oestreich, J. H. Elinogrel, a Reversible P2Y12 Receptor Antagonist for the Treatment of Acute Coronary Syndrome and Prevention of Secondary Thrombotic Events. *Curr. Opin. Investig. Drugs* **2010,** *11* (3), 340–348.
99. Bach, P.; Antonsson, T.; Bylund, R.; Bjorkman, J. A.; Osterlund, K.; Giordanetto, F.; van Giezen, J. J.; Andersen, S. M.; Zachrisson, H.; Zetterberg, F. Lead Optimization of Ethyl 6-Aminonicotinate Acyl Sulfonamides as Antagonists of the P2Y12 Receptor. Separation of the Antithrombotic Effect and Bleeding for Candidate Drug AZD1283. *J. Med. Chem.* **2013,** *56* (17), 7015–7024.
100. Bach, P.; Bostrom, J.; Brickmann, K.; Burgess, L. E.; Clarke, D.; Groneberg, R. D.; Harvey, D. M.; Laird, E. R.; O'Sullivan, M.; Zetterberg, F. 5-Alkyl-1,3-oxazole Derivatives of 6-Amino-Nicotinic Acids as Alkyl Ester Bioisosteres Are Antagonists of the P2Y12 Receptor. *Future Med. Chem.* **2013,** *5* (17), 2037–2056.
101. Giordanetto, F.; Bach, P.; Zetterberg, F.; Antonsson, T.; Bylund, R.; Johansson, J.; Sellen, M.; Brown, D.; Hidestahl, L.; Berntsson, P.; Hovdal, D.; Zachrisson, H.; Bjorkman, J. A.; van Giezen, J. J. Optimization of Ketone-Based P2Y(12) Receptor Antagonists as Antithrombotic Agents: Pharmacodynamics and Receptor Kinetics Considerations. *Bioorg. Med. Chem. Lett.* **2014,** *24* (13), 2963–2968.

102. (a) Bryant, J.; Post, J. M.; Alexander, S.; Wang, Y. X.; Kent, L.; Schirm, S.; Tseng, J. L.; Subramanyam, B.; Buckman, B.; Islam, I.; Yuan, S.; Sullivan, M. E.; Snider, M.; Morser, J. Novel P2Y12 Adenosine Diphosphate Receptor Antagonists for Inhibition of Platelet Aggregation (I): in vitro Effects on Platelets. *Thromb. Res.* **2008,** *122* (4), 523–532; (b) Post, J. M.; Alexander, S.; Wang, Y. X.; Vincelette, J.; Vergona, R.; Kent, L.; Bryant, J.; Sullivan, M. E.; Dole, W. P.; Morser, J.; Subramanyam, B. Novel P2Y12 Adenosine Diphosphate Receptor Antagonists for Inhibition of Platelet Aggregation (II): Pharmacodynamic and Pharmacokinetic Characterization. *Thromb. Res.* **2008,** *122* (4), 533–540; (c) Wang, Y. X.; Vincelette, J.; da Cunha, V.; Martin-McNulty, B.; Mallari, C.; Fitch, R. M.; Alexander, S.; Islam, I.; Buckman, B. O.; Yuan, S.; Post, J. M.; Subramanyam, B.; Vergona, R.; Sullivan, M. E.; Dole, W. P.; Morser, J.; Bryant, J. A novel P2Y(12) Adenosine Diphosphate Receptor Antagonist that Inhibits Platelet Aggregation and Thrombus Formation in Rat and Dog Models. *Thromb. Haemost.* **2007,** *97* (5), 847–855.
103. (a) Parlow, J. J.; Burney, M. W.; Case, B. L.; Girard, T. J.; Hall, K. A.; Harris, P. K.; Hiebsch, R. R.; Huff, R. M.; Lachance, R. M.; Mischke, D. A.; Rapp, S. R.; Woerndle, R. S.; Ennis, M. D. Piperazinyl Glutamate Pyridines as Potent Orally Bioavailable P2Y12 Antagonists for Inhibition of Platelet Aggregation. *J. Med. Chem.* **2010,** *53* (5), 2010–2037; (b) Parlow, J. J.; Burney, M. W.; Case, B. L.; Girard, T. J.; Hall, K. A.; Harris, P. K.; Hiebsch, R. R.; Huff, R. M.; Lachance, R. M.; Mischke, D. A.; Rapp, S. R.; Woerndle, R. S.; Ennis, M. D. Part II: Piperazinyl-Glutamate-Pyridines as Potent Orally Bioavailable P2Y12 Antagonists for Inhibition of Platelet Aggregation. *Bioorg. Med. Chem. Lett.* **2010,** *20* (4), 1388–1394.
104. Zech, G.; Hessler, G.; Evers, A.; Weiss, T.; Florian, P.; Just, M.; Czech, J.; Czechtizky, W.; Gorlitzer, J.; Ruf, S.; Kohlmann, M.; Nazare, M. Identification of High-Affinity P2Y(1)(2) Antagonists Based on a Phenylpyrazole Glutamic Acid Piperazine Backbone. *J. Med. Chem.* **2012,** *55* (20), 8615–8629.
105. Caroff, E.; Meyer, E.; Treiber, A.; Hilpert, K.; Riederer, M. A. Optimization of 2-Phenyl-pyrimidine-4-carboxamides Towards Potent, Orally Bioavailable and Selective P2Y(12) Antagonists for Inhibition of Platelet Aggregation. *Bioorg. Med. Chem. Lett.* **2014,** *24* (17), 4323–4331.
106. Baldoni, D.; Bruderer, S.; Krause, A.; Gutierrez, M.; Gueret, P.; Astruc, B.; Dingemanse, J. A New Reversible and Potent P2Y12 Receptor Antagonist (ACT-246475): Tolerability, Pharmacokinetics, and Pharmacodynamics in a First-in-Man Trial. *Clin. Drug Investig.* **2014,** *34* (11), 807–818.
107. Boldron, C.; Besse, A.; Bordes, M. F.; Tissandie, S.; Yvon, X.; Gau, B.; Badorc, A.; Rousseaux, T.; Barre, G.; Meneyrol, J.; Zech, G.; Nazare, M.; Fossey, V.; Pflieger, A. M.; Bonnet-Lignon, S.; Millet, L.; Briot, C.; Dol, F.; Herault, J. P.; Savi, P.; Lassalle, G.; Delesque, N.; Herbert, J. M.; Bono, F. *N*-[6-(4-Butanoyl-5-methyl-1H-pyrazol-1-yl) pyridazin-3-yl]-5-chloro-1-[2-(4-methyl piperazin-1-yl)-2-oxoethyl]-1H-indole-3-carboxamide (SAR216471), a Novel Intravenous and Oral, Reversible, and Directly Acting P2Y12 Antagonist. *J. Med. Chem.* **2014,** *57* (17), 7293–7316.
108. Delesque-Touchard, N.; Pflieger, A. M.; Bonnet-Lignon, S.; Millet, L.; Salel, V.; Boldron, C.; Lassalle, G.; Herbert, J. M.; Savi, P.; Bono, F. SAR216471, an Alternative to the Use of Currently Available P2Y(1)(2) Receptor Inhibitors? *Thromb. Res.* **2014,** *134* (3), 693–703.
109. Baqi, Y.; Atzler, K.; Kose, M.; Glanzel, M.; Muller, C. E. High-Affinity, Non-Nucleotide-Derived Competitive Antagonists of Platelet P2Y12 Receptors. *J. Med. Chem.* **2009,** *52* (12), 3784–3793.
110. (a) Kortum, S. W.; Lachance, R. M.; Schweitzer, B. A.; Yalamanchili, G.; Rahman, H.; Ennis, M. D.; Huff, R. M.; TenBrink, R. E. Thienopyrimidine-Based P2Y12 Platelet Aggregation Inhibitors. *Bioorg. Med. Chem. Lett.* **2009,** *19* (20), 5919–5923; (b) Levy, D. E.; Smyth, M. S.; Scarborough, R. M. *Piperazine and Homopiperazine Compounds,* 2003. WO2003/022214.
111. Zhang, J.; Zhang, K.; Gao, Z. G.; Paoletta, S.; Zhang, D.; Han, G. W.; Li, T.; Ma, L.; Zhang, W.; Muller, C. E.; Yang, H.; Jiang, H.; Cherezov, V.; Katritch, V.; Jacobson, K. A.; Stevens, R. C.; Wu, B.; Zhao, Q. Agonist-Bound Structure of the Human P2Y12 Receptor. *Nature* **2014,** *509* (7498), 119–122.
112. Paoletta, S.; Sabbadin, D.; von Kugelgen, I.; Hinz, S.; Katritch, V.; Hoffmann, K.; Abdelrahman, A.; Strassburger, J.; Baqi, Y.; Zhao, Q.; Stevens, R. C.; Moro, S.; Muller, C. E.; Jacobson, K. A. Modeling Ligand Recognition at the P2Y Receptor in Light of X-ray Structural Information. *J. Comput. Aided Mol. Des.* **2015,** *29,* 737–756.
113. Adamski, P.; Kozinski, M.; Ostrowska, M.; Fabiszak, T.; Navarese, E. P.; Paciorek, P.; Grzesk, G.; Kubica, J. Overview of Pleiotropic Effects of Platelet P2Y12 Receptor Inhibitors. *Thromb. Haemost.* **2014,** *112* (2), 224–242.
114. Cattaneo, M.; Faioni, E. M. Why Does Ticagrelor Induce Dyspnea? *Thromb. Haemost.* **2012,** *108* (6), 1031–1036.
115. Nylander, S.; Femia, E. A.; Scavone, M.; Berntsson, P.; Asztely, A. K.; Nelander, K.; Lofgren, L.; Nilsson, R. G.; Cattaneo, M. Ticagrelor Inhibits Human Platelet Aggregation via Adenosine in Addition to P2Y12 Antagonism. *J. Thromb. Haemost.* **2013,** *11* (10), 1867–1876.
116. Siller-Matula, J. M.; Trenk, D.; Schror, K.; Gawaz, M.; Kristensen, S. D.; Storey, R. F.; Huber, K. How to Improve the Concept of Individualised Antiplatelet Therapy With P2Y12 Receptor Inhibitors–Is an Algorithm the Answer? *Thromb. Haemost.* **2015,** *113* (1), 37–52.
117. Leon, C.; Freund, M.; Ravanat, C.; Baurand, A.; Cazenave, J. P.; Gachet, C. Key Role of the P2Y(1) Receptor in Tissue Factor-Induced Thrombin-Dependent Acute Thromboembolism: Studies in P2Y(1)-Knockout Mice and Mice Treated With a P2Y(1) Antagonist. *Circulation* **2001,** *103* (5), 718–723.
118. (a) Lenain, N.; Freund, M.; Leon, C.; Cazenave, J. P.; Gachet, C. Inhibition of Localized Thrombosis in P2Y1-Deficient Mice and Rodents Treated With MRS2179, a P2Y1 Receptor Antagonist. *J. Thromb. Haemost.* **2003,** *1* (6), 1144–1149; (b) Hechler, B.; Nonne, C.; Roh, E. J.; Cattaneo, M.; Cazenave, J. P.; Lanza, F.; Jacobson, K. A.; Gachet, C. MRS2500 [2-Iodo-N6-methyl-(N)-methanocarba-2'-deoxyadenosine-3',5'-bisphosphate], a Potent, Selective, and Stable Antagonist of the Platelet P2Y1 Receptor With Strong Antithrombotic Activity in Mice. *J. Pharmacol. Exp. Ther.* **2006,** *316* (2), 556–563.
119. (a) Houston, D.; Costanzi, S.; Jacobson, K. A.; Harden, T. K. Development of Selective High Affinity Antagonists, Agonists, and Radioligands for the P2Y1 Receptor. *Comb. Chem. High Throughput Screen* **2008,** *11* (6), 410–419; (b) Costanzi, S.; Tikhonova, I. G.; Ohno, M.; Roh, E. J.; Joshi, B. V.; Colson, A. O.; Houston, D.; Maddileti, S.; Harden, T. K.; Jacobson, K. A. P2Y1 Antagonists: Combining Receptor-Based Modeling and QSAR for a Quantitative Prediction of the Biological Activity Based on Consensus Scoring. *J. Med. Chem.* **2007,** *50* (14), 3229–3241.
120. Chao, H.; Turdi, H.; Herpin, T. F.; Roberge, J. Y.; Liu, Y.; Schnur, D. M.; Poss, M. A.; Rehfuss, R.; Hua, J.; Wu, Q.; Price, L. A.; Abell, L. M.; Schumacher, W. A.; Bostwick, J. S.; Steinbacher, T. E.; Stewart, A. B..; Ogletree, M. L.; Huang, C. S.; Chang, M.; Cacace, A. M.; Arcuri, M. J.; Celani, D.; Wexler, R. R.; Lawrence, R. M. Discovery of 2-(Phenoxypyridine)-3-phenylureas as Small Molecule P2Y1 Antagonists. *J. Med. Chem.* **2013,** *56* (4), 1704–1714.
121. (a) Ruel, R.; L'Heureux, A.; Thibeault, C.; Daris, J. P.; Martel, A.; Price, L. A.; Wu, Q.; Hua, J.; Wexler, R. R.; Rehfuss, R.; Lam, P. Y. New Azole Antagonists With High Affinity for the P2Y(1) Receptor. *Bioorg. Med. Chem. Lett.* **2013,** *23* (12), 3519–3522; (b) Pi, Z.; Sutton, J.; Lloyd, J.; Hua, J.; Price, L.; Wu, Q.; Chang, M.; Zheng, J.; Rehfuss, R.; Huang, C. S.; Wexler, R. R.; Lam, P. Y. 2-Aminothiazole Based P2Y(1) Antagonists as Novel Antiplatelet Agents. *Bioorg. Med. Chem. Lett.* **2013,** *23* (14), 4206–4209.
122. (a) Ruel, R.; L'Heureux, A.; Thibeault, C.; Lapointe, P.; Martel, A.; Qiao, J. X.; Hua, J.; Price, L. A.; Wu, Q.; Chang, M.; Zheng, J.; Huang, C. S.; Wexler, R. R.; Rehfuss, R.; Lam, P. Y. Potent P2Y1 Urea Antagonists Bearing Various Cyclic Amine Scaffolds. *Bioorg. Med. Chem. Lett.* **2013,** *23* (24), 6825–6828; (b) Wang, T. C.; Qiao, J. X.; Clark, C. G.; Jua, J.; Price, L. A.; Wu, Q.; Chang, M.; Zheng, J.; Huang, C. S.; Everlof, G.; Schumacher, W. A.; Wong, P. C.; Seiffert, D. A.; Stewart, A. B..; Bostwick, J. S.; Crain, E. J.; Watson, C. A.; Rehfuss, R.; Wexler, R. R.; Lam, P. Y. Discovery of Diarylurea P2Y(1) Antagonists With Improved Aqueous Solubility. *Bioorg. Med. Chem. Lett.* **2013,** *23* (11), 3239–3243.
123. Qiao, J. X.; Wang, T. C.; Ruel, R.; Thibeault, C.; L'Heureux, A.; Schumacher, W. A.; Spronk, S. A.; Hiebert, S.; Bouthillier, G.; Lloyd, J.; Pi, Z.; Schnur, D. M.; Abell, L. M.; Hua, J.; Price, L. A.; Liu, E.; Wu, Q.; Steinbacher, T. E.; Bostwick, J. S.; Chang, M.; Zheng, J.; Gao, Q.; Ma, B.; McDonnell, P. A.; Huang, C. S.; Rehfuss, R.; Wexler, R. R.; Lam, P. Y. Conformationally Constrained Ortho-Anilino Diaryl Ureas: Discovery of 1-(2-(1'-Neopentylspiro[indoline-3,4'-piperidine]-1-yl)phenyl)-3-(4-(trifluoromet hoxy)phenyl) urea, a Potent, Selective, and Bioavailable P2Y1 Antagonist. *J. Med. Chem.* **2013,** *56* (22), 9275–9295.
124. Jeon, Y. T.; Yang, W.; Qiao, J. X.; Li, L.; Ruel, R.; Thibeault, C.; Hiebert, S.; Wang, T. C.; Wang, Y.; Liu, Y.; Clark, C. G.; Wong, H. S.; Zhu, J.; Wu, D. R.; Sun, D.; Chen, B. C.; Mathur, A.; Chacko, S. A.; Malley, M.; Chen, X. Q.; Shen, H.; Huang, C. S.; Schumacher, W. A.; Bostwick, J. S.; Stewart, A. B..; Price, L. A.; Hua, J.; Li, D.; Levesque, P. C.; Seiffert, D. A.; Rehfuss, R.; Wexler, R. R.; Lam, P. Y. Identification of 1-{2-[4-Chloro-1'-(2,2-dimethylpropyl)-7-hydroxy-1,2-dihydrospiro[indole-3,4'-pip eridine]-1-yl]phenyl}-3-{5-chloro-[1,3]thiazolo[5,4-b]pyridin-2-yl}urea, a Potent, Efficacious and Orally Bioavailable P2Y(1) Antagonist as an Antiplatelet Agent. *Bioorg. Med. Chem. Lett.* **2014,** *24* (5), 1294–1298.
125. Yang, W.; Wang, Y.; Lai, A.; Qiao, J. X.; Wang, T. C.; Hua, J.; Price, L. A.; Shen, H.; Chen, X. Q.; Wong, P.; Crain, E.; Watson, C.; Huang, C. S.; Seiffert, D. A.; Rehfuss, R.; Wexler, R. R.; Lam, P. Y. Discovery of 4-Aryl-7-hydroxyindoline-Based P2Y1 Antagonists as Novel Antiplatelet Agents. *J. Med. Chem.* **2014,** *57* (14), 6150–6164.

126. Pfefferkorn, J. A.; Choi, C.; Winters, T.; Kennedy, R.; Chi, L.; Perrin, L. A.; Lu, G.; Ping, Y. W.; McClanahan, T.; Schroeder, R.; Leininger, M. T.; Geyer, A.; Schefzick, S.; Atherton, J. P2Y1 Receptor Antagonists as Novel Antithrombotic Agents. *Bioorg. Med. Chem. Lett.* **2008,** *18* (11), 3338–3343.
127. (a) Morales-Ramos, A. I.; Mecom, J. S.; Kiesow, T. J.; Graybill, T. L.; Brown, G. D.; Aiyar, N. V.; Davenport, E. A.; Kallal, L. A.; Knapp-Reed, B. A.; Li, P.; Londregan, A. T.; Morrow, D. M.; Senadhi, S.; Thalji, R. K.; Zhao, S.; Burns-Kurtis, C. L.; Marino, J. P., Jr. Tetrahydro-4-Quinolinamines Identified as Novel P2Y(1) Receptor Antagonists. *Bioorg. Med. Chem. Lett.* **2008,** *18* (23), 6222–6226; (b) Thalji, R. K.; Aiyar, N.; Davenport, E. A.; Erhardt, J. A.; Kallal, L. A.; Morrow, D. M.; Senadhi, S.; Burns-Kurtis, C. L.; Marino, J. P., Jr. Benzofuran-Substituted Urea Derivatives as Novel P2Y(1) Receptor Antagonists. *Bioorg. Med. Chem. Lett.* **2010,** *20* (14), 4104–4107.
128. Karim, Z. A.; Vemana, H. P.; Alshbool, F. Z.; Lin, O. A.; Alshehri, A. M.; Javaherizadeh, P.; Paez Espinosa, E. V.; Khasawneh, F. T. Characterization of a Novel Function-Blocking Antibody Targeted Against the Platelet P2Y1 Receptor. *Arterioscler., Thromb., Vasc. Biol.* **2015,** *35* (3), 637–644.
129. Chang, H.; Yanachkov, I. B.; Dix, E. J.; Li, Y. F.; Barnard, M. R.; Wright, G. E.; Michelson, A. D.; Frelinger, A. L., 3rd Modified Diadenosine Tetraphosphates With Dual Specificity for P2Y1 and P2Y12 are Potent Antagonists of ADP-Induced Platelet Activation. *J. Thromb. Haemost.* **2012,** *10* (12), 2573–2580.
130. Zamecnik, P. C.; Kim, B.; Gao, M. J.; Taylor, G.; Blackburn, G. M. Analogues of Diadenosine 5',5'''-P1, P4-Tetraphosphate (Ap4A) as Potential Anti-Platelet-Aggregation Agents. *Proc. Natl. Acad. Sci. U. S. A.* **1992,** *89* (6), 2370–2373.
131. Chan, S. W.; Gallo, S. J.; Kim, B. K.; Guo, M. J.; Blackburn, G. M.; Zamecnik, P. C. P1, P4-Dithio-P2, P3-Monochloromethylene Diadenosine 5',5'''-P1, P4-Tetraphosphate: A Novel Antiplatelet Agent. *Proc. Natl. Acad. Sci. U. S. A.* **1997,** *94* (8), 4034–4039.
132. Zhang, D.; Gao, Z. G.; Zhang, K.; Kiselev, E.; Crane, S.; Wang, J.; Paoletta, S.; Yi, C.; Ma, L.; Zhang, W.; Han, G. W.; Liu, H.; Cherezov, V.; Katritch, V.; Jiang, H.; Stevens, R. C.; Jacobson, K. A.; Zhao, Q.; Wu, B. Two Disparate Ligand-Binding Sites in the Human P2Y1 Receptor. *Nature* **2015,** *520* (7547), 317–321.
133. Lambertucci, C.; Dal Ben, D.; Buccioni, M.; Marucci, G.; Thomas, A.; Volpini, R. Medicinal Chemistry of P2X Receptors: Agonists and Orthosteric Antagonists. *Curr. Med. Chem.* **2015,** *22* (7), 915–928.
134. Kassack, M. U.; Braun, K.; Ganso, M.; Ullmann, H.; Nickel, P.; Boing, B.; Muller, G.; Lambrecht, G. Structure-Activity Relationships of Analogues of NF449 Confirm NF449 as the Most Potent and Selective Known P2X1 Receptor Antagonist. *Eur. J. Med. Chem.* **2004,** *39* (4), 345–357.
135. Hechler, B.; Magnenat, S.; Zighetti, M. L.; Kassack, M. U.; Ullmann, H.; Cazenave, J. P.; Evans, R.; Cattaneo, M.; Gachet, C. Inhibition of Platelet Functions and Thrombosis Through Selective or Nonselective Inhibition of the Platelet P2 Receptors With Increasing Doses of NF449 [4,4',4'',4'''-(Carbonylbis(imino-5,1,3-benzenetriylbis-(carbonylimino)))tetrakis -benzene-1,3-disulfonic acid octasodium salt]. *J. Pharmacol. Exp. Ther.* **2005,** *314* (1), 232–243.
136. Ramachandran, R.; Noorbakhsh, F.; Defea, K.; Hollenberg, M. D. Targeting Proteinase-Activated Receptors: Therapeutic Potential and Challenges. *Nat. Rev. Drug Discov.* **2012,** *11* (1), 69–86.
137. Moschonas, I. C.; Goudevenos, J. A.; Tselepis, A. D. Protease-Activated Receptor-1 Antagonists in Long-Term Antiplatelet Therapy. Current State of Evidence and Future Perspectives. *Int. J. Cardiol.* **2015,** *185,* 9–18.
138. Chackalamannil, S. Thrombin Receptor (Protease Activated Receptor-1) Antagonists as Potent Antithrombotic Agents With Strong Antiplatelet Effects. *J. Med. Chem.* **2006,** *49* (18), 5389–5403.
139. Chackalamannil, S.; Xia, Y.; Greenlee, W. J.; Clasby, M.; Doller, D.; Tsai, H.; Asberom, T.; Czarniecki, M.; Ahn, H. S.; Boykow, G.; Foster, C.; Agans-Fantuzzi, J.; Bryant, M.; Lau, J.; Chintala, M. Discovery of Potent Orally Active Thrombin Receptor (Protease Activated Receptor 1) Antagonists as Novel Antithrombotic Agents. *J. Med. Chem.* **2005,** *48* (19), 5884–5887.
140. Clasby, M. C.; Chackalamannil, S.; Czarniecki, M.; Doller, D.; Eagen, K.; Greenlee, W.; Kao, G.; Lin, Y.; Tsai, H.; Xia, Y.; Ahn, H. S.; Agans-Fantuzzi, J.; Boykow, G.; Chintala, M.; Foster, C.; Smith-Torhan, A.; Alton, K.; Bryant, M.; Hsieh, Y.; Lau, J.; Palamanda, J. Metabolism-Based Identification of a Potent Thrombin Receptor Antagonist. *J. Med. Chem.* **2007,** *50* (1), 129–138.
141. (a) Xia, Y.; Chackalamannil, S.; Clasby, M.; Doller, D.; Eagen, K.; Greenlee, W. J.; Tsai, H.; Agans-Fantuzzi, J.; Ahn, H. S.; Boykow, G. C.; Hsieh, Y.; Lunn, C. A.; Chintala, M. Himbacine Derived Thrombin Receptor (PAR-1) Antagonists: SAR of the Pyridine Ring. *Bioorg. Med. Chem. Lett.* **2007,** *17* (16), 4509–4513; (b) Chelliah, M. V.; Chackalamannil, S.; Xia, Y.; Eagen, K.; Clasby, M. C.; Gao, X.; Greenlee, W.; Ahn, H. S.; Agans-Fantuzzi, J.; Boykow, G.; Hsieh, Y.; Bryant, M.; Palamanda, J.; Chan, T. M.; Hesk, D.; Chintala, M. Heterotricyclic Himbacine Analogs as Potent, Orally Active Thrombin Receptor (Protease Activated Receptor-1) Antagonists. *J. Med. Chem.* **2007,** *50* (21), 5147–5160.
142. Chackalamannil, S.; Wang, Y.; Greenlee, W. J.; Hu, Z.; Xia, Y.; Ahn, H. S.; Boykow, G.; Hsieh, Y.; Palamanda, J.; Agans-Fantuzzi, J.; Kurowski, S.; Graziano, M.; Chintala, M. Discovery of a Novel, Orally Active Himbacine-Based Thrombin Receptor Antagonist (SCH 530348) With Potent Antiplatelet Activity. *J. Med. Chem.* **2008,** *51* (11), 3061–3064.
143. Zhang, C.; Srinivasan, Y.; Arlow, D. H.; Fung, J. J.; Palmer, D.; Zheng, Y.; Green, H. F.; Pandey, A.; Dror, R. O.; Shaw, D. E.; Weis, W. I.; Coughlin, S. R.; Kobilka, B. K. High-Resolution Crystal Structure of Human Protease-Activated Receptor 1. *Nature* **2012,** *492* (7429), 387–392.
144. Poole, R. M.; Elkinson, S. Vorapaxar: First Global Approval. *Drugs* **2014,** *74* (10), 1153–1163.
145. Baker, N. C.; Lipinski, M. J.; Lhermusier, T.; Waksman, R. Overview of the 2014 Food and Drug Administration Cardiovascular and Renal Drugs Advisory Committee Meeting About Vorapaxar. *Circulation* **2014,** *130* (15), 1287–1294.
146. Kosoglou, T.; Reyderman, L.; Tiessen, R. G.; van Vliet, A. A.; Fales, R. R.; Keller, R.; Yang, B.; Cutler, D. L. Pharmacodynamics and Pharmacokinetics of the Novel PAR-1 Antagonist Vorapaxar (formerly SCH 530348) in Healthy Subjects. *Eur. J. Clin. Pharmacol.* **2012,** *68* (3), 249–258.
147. (a) Chelliah, M. V.; Eagen, K.; Guo, Z.; Chackalamannil, S.; Xia, Y.; Tsai, H.; Greenlee, W. J.; Ahn, H. S.; Kurowski, S.; Boykow, G.; Hsieh, Y.; Chintala, M. Himbacine-Derived Thrombin Receptor Antagonists: C_7-Spirocyclic Analogues of Vorapaxar. *ACS Med. Chem. Lett.* **2014,** *5* (5), 561–565; (b) Chelliah, M. V.; Chackalamannil, S.; Xia, Y.; Eagen, K.; Greenlee, W. J.; Ahn, H. S.; Agans-Fantuzzi, J.; Boykow, G.; Hsieh, Y.; Bryant, M.; Chan, T. M.; Chintala, M. Discovery of Nor-Seco Himbacine Analogs as Thrombin Receptor Antagonists. *Bioorg. Med. Chem. Lett.* **2012,** *22* (7), 2544–2549.
148. (a) Xia, Y.; Chackalamannil, S.; Greenlee, W. J.; Wang, Y.; Hu, Z.; Root, Y.; Wong, J.; Kong, J.; Ahn, H. S.; Boykow, G.; Hsieh, Y.; Kurowski, S.; Chintala, M. Discovery of a Vorapaxar Analog With Increased Aqueous Solubility. *Bioorg. Med. Chem. Lett.* **2010,** *20* (22), 6676–6679; (b) Chintala, M.; Strony, J.; Yang, B.; Kurowski, S.; Li, Q. SCH 602539, a Protease-Activated Receptor-1 Antagonist, Inhibits Thrombosis Alone and in Combination With Cangrelor in a Folts Model of Arterial Thrombosis in Cynomolgus Monkeys. *Arterioscler., Thromb., Vasc. Biol.* **2010,** *30* (11), 2143–2149.
149. Lee, S.; Song, J. H.; Park, C. M.; Kim, J. S.; Jeong, J. H.; Cho, W. Y.; Lim, D. C. Discovery of Octahydroindenes as PAR1 Antagonists. *ACS Med. Chem. Lett.* **2013,** *4* (11), 1054–1058.
150. Kogushi, M.; Matsuoka, T.; Kawata, T.; Kuramochi, H.; Kawaguchi, S.; Murakami, K.; Hiyoshi, H.; Suzuki, S.; Kawahara, T.; Kajiwara, A.; Hishinuma, I. The Novel and Orally Active Thrombin Receptor Antagonist E5555 (Atopaxar) Inhibits Arterial Thrombosis Without Affecting Bleeding Time in Guinea Pigs. *Eur. J. Pharmacol.* **2011,** *657* (1-3), 131–137.
151. (a) O'Donoghue, M. L.; Bhatt, D. L.; Wiviott, S. D.; Goodman, S. G.; Fitzgerald, D. J.; Angiolillo, D. J.; Goto, S.; Montalescot, G.; Zeymer, U.; Aylward, P. E.; Guetta, V.; Dudek, D.; Ziecina, R.; Contant, C. F.; Flather, M. D. Safety and Tolerability of Atopaxar in the Treatment of Patients With Acute Coronary Syndromes: The Lessons From Antagonizing the Cellular Effects of Thrombin-Acute Coronary Syndromes Trial. *Circulation* **2011,** *123* (17), 1843–1853; (b) Wiviott, S. D.; Flather, M. D.; O'Donoghue, M. L.; Goto, S.; Fitzgerald, D. J.; Cura, F.; Aylward, P.; Guetta, V.; Dudek, D.; Contant, C. F.; Angiolillo, D. J.; Bhatt, D. L. Randomized Trial of Atopaxar in the Treatment of Patients With Coronary Artery Disease: The Lessons From Antagonizing the Cellular Effect of Thrombin-Coronary Artery Disease Trial. *Circulation* **2011,** *123* (17), 1854–1863; (c) Goto, S.; Ogawa, H.; Takeuchi, M.; Flather, M. D.; Bhatt, D. L. Double-Blind, Placebo-Controlled Phase II Studies of the Protease-Activated Receptor 1 Antagonist E5555 (atopaxar) in Japanese Patients With Acute Coronary Syndrome or High-Risk Coronary Artery Disease. *Eur. Heart J.* **2010,** *31* (21), 2601–2613.
152. Zhang, P.; Gruber, A.; Kasuda, S.; Kimmelstiel, C.; O'Callaghan, K.; Cox, D. H.; Bohm, A.; Baleja, J. D.; Covic, L.; Kuliopulos, A. Suppression of Arterial Thrombosis Without Affecting Hemostatic Parameters With a Cell-Penetrating PAR1 Pepducin. *Circulation* **2012,** *126* (1), 83–91.

153. Zhang, H. C.; Derian, C. K.; Andrade-Gordon, P.; Hoekstra, W. J.; McComsey, D. F.; White, K. B.; Poulter, B. L.; Addo, M. F.; Cheung, W. M.; Damiano, B. P.; Oksenberg, D.; Reynolds, E. E.; Pandey, A.; Scarborough, R. M.; Maryanoff, B. E. Discovery and Optimization of a Novel Series of Thrombin Receptor (par-1) Antagonists: Potent, Selective Peptide Mimetics Based on Indole and Indazole Templates. *J. Med. Chem.* **2001,** *44* (7), 1021–1024.
154. Ventosa-Andres, P.; Valdivielso, A. M.; Pappos, I.; Garcia-Lopez, M. T.; Tsopanoglou, N. E.; Herranz, R. Design, Synthesis and Biological Evaluation of New Peptide-Based Ureas and Thioureas as Potential Antagonists of the Thrombin Receptor PAR1. *Eur. J. Med. Chem.* **2012,** *58,* 98–111.
155. (a) Valdivielso, A. M.; Ventosa-Andres, P.; Tato, F.; Fernandez-Ibanez, M. A.; Pappos, I.; Tsopanoglou, N. E.; Garcia-Lopez, M. T.; Gutierrez-Rodriguez, M.; Herranz, R. Highly Functionalized 2-Oxopiperazine-Based Peptidomimetics: An Approach to PAR1 Antagonists. *Eur. J. Med. Chem.* **2013,** *70,* 199–224; (b) Valdivielso, A. M.; Garcia-Lopez, M. T.; Gutierrez-Rodriguez, M.; Herranz, R. Exploring the Phe-Gly Dipeptide-Derived Piperazinone Scaffold in the Search for Antagonists of the Thrombin Receptor PAR1. *Molecules* **2014,** *19* (4), 4814–4846.
156. (a) Perez, M.; Lamothe, M.; Maraval, C.; Mirabel, E.; Loubat, C.; Planty, B.; Horn, C.; Michaux, J.; Marrot, S.; Letienne, R.; Pignier, C.; Bocquet, A.; Nadal-Wollbold, F.; Cussac, D.; de Vries, L.; Le Grand, B. Discovery of Novel Protease Activated Receptors 1 Antagonists With Potent Antithrombotic Activity In Vivo. *J. Med. Chem.* **2009,** *52* (19), 5826–5836; (b) Rilatt, I.; Mirabel, E.; Le Grand, B.; Perez, M. Discovery and SAR of Small Molecule PAR1 Antagonists. *Bioorg. Med. Chem. Lett.* **2010,** *20* (3), 903–906; (c) Planty, B.; Pujol, C.; Lamothe, M.; Maraval, C.; Horn, C.; Le Grand, B.; Perez, M. Exploration of a New Series of PAR1 Antagonists. *Bioorg. Med. Chem. Lett.* **2010,** *20* (5), 1735–1739.
157. Dumas, M.; Nadal-Wollbold, F.; Gaussem, P.; Perez, M.; Mirault, T.; Letienne, R.; Bourbon, T.; Grelac, F.; Le Grand, B.; Bachelot-Loza, C. Antiplatelet and Antithrombotic Effect of F 16618, a New Thrombin Proteinase-Activated Receptor-1 (PAR1) Antagonist. *Br. J. Pharmacol.* **2012,** *165* (6), 1827–1835.
158. Dockendorff, C.; Aisiku, O.; Verplank, L.; Dilks, J. R.; Smith, D. A.; Gunnink, S. F.; Dowal, L.; Negri, J.; Palmer, M.; Macpherson, L.; Schreiber, S. L.; Flaumenhaft, R. Discovery of 1,3-Diaminobenzenes as Selective Inhibitors of Platelet Activation at the PAR1 Receptor. *ACS Med. Chem. Lett.* **2012,** *3* (3), 232–237.
159. Khan, A.; Li, D.; Ibrahim, S.; Smyth, E.; Woulfe, D. S. The Physical Association of the P2Y12 Receptor With PAR4 Regulates Arrestin-Mediated Akt Activation. *Mol. Pharmacol.* **2014,** *86* (1), 1–11.
160. Judge, H. M.; Jennings, L. K.; Moliterno, D. J.; Hord, E.; Ecob, R.; Tricoci, P.; Rorick, T.; Kotha, J.; Storey, R. F. PAR1 Antagonists Inhibit Thrombin-Induced Platelet Activation Whilst Leaving the PAR4-Mediated Response Intact. *Platelets* **2015,** *26* (3), 236–242.
161. (a) Priestley, E. S.; Posy, S. L.; Tremblay, F.; Martel, A.; Marinier, A.; Lawrence, R. M.; Miller, M. M. Imidazothiadiazole and Imidazopyridazine Derivatives as Protease Activated Receptor 4 (PAR4) Inhibitors for Treating Platelet Aggregation. WO2013/163241, 2013; (b) Banville, J.; Rémillard, R.; Ruediger, E. H.; Deon, D. H.; Gagnon, M.; Dubé, L.; Guy, J.; Priestley, E. S.; Posy, S. L.; Maxwell, B. D.; Wong, P. C.; Lawrence, M. R.; Miller, M. M. Imidazothiadiazole and Imidazopyrazine Derivatives as Protease Activated Receptor 4 (PAR4) Inhibitors for Treating Platelet Aggregation. WO2013/163279, 2013.
162. Lawrence, R. M.; Miller, M. M.; Seiffert, D. A.; Posy, S. L.; Wong, P. C.; Banville, J.; Ruediger, E. H.; Deon, D. H.; Martel, A.; Tremblay, F.; Guy, J.; Lavallee, J.-F.; Gagnon, M. Imidazothiadiazole Derivatives as Protease Activated Receptor 4 (PAR4) Inhibitors for Treating Platelet Aggregation. WO2013/163244, 2013.
163. Wu, C. C.; Huang, S. W.; Hwang, T. L.; Kuo, S. C.; Lee, F. Y.; Teng, C. M. YD-3, a Novel Inhibitor of Protease-Induced Platelet Activation. *Br. J. Pharmacol.* **2000,** *130* (6), 1289–1296.
164. Wen, W.; Young, S. E.; Duvernay, M. T.; Schulte, M. L.; Nance, K. D.; Melancon, B. J.; Engers, J.; Locuson, C. W., II; Wood, M. R.; Daniels, J. S.; Wu, W.; Lindsley, C. W.; Hamm, H. E.; Stauffer, S. R. Substituted Indoles as Selective Protease Activated Receptor 4 (PAR-4) Antagonists: Discovery and SAR of ML354. *Bioorg. Med. Chem. Lett.* **2014,** *24* (19), 4708–4713.
165. Friedman, E. A.; Ogletree, M. L.; Haddad, E. V.; Boutaud, O. Understanding the Role of Prostaglandin E2 in Regulating Human Platelet Activity in Health and Disease. *Thromb. Res.* **2015,** *136* (3), 493–503.
166. Fabre, J. E.; Gurney, M. E. Limitations of Current Therapies to Prevent Thrombosis: A Need for Novel Strategies. *Mol. Biosyst.* **2010,** *6* (2), 305–315.
167. Mawhin, M. A.; Tilly, P.; Fabre, J. E. The Receptor EP3 to PGE2: A Rational Target to Prevent Atherothrombosis Without Inducing Bleeding. *Prostaglandins Other Lipid Mediat.* **2015,** *121,* 4–16.
168. Singh, J.; Kiselyov, A. S. EP3 Receptor Antagonists: Potential for Improving Safety in the Antiplatelet Therapy Field. *Drugs Fut.* **2010,** *35* (1), 21–31.
169. (b) Singh, J.; Zeller, W.; Zhou, N.; Hategan, G.; Mishra, R. K.; Polozov, A.; Yu, P.; Onua, E.; Zhang, J.; Ramirez, J. L.; Sigthorsson, G.; Thorsteinnsdottir, M.; Kiselyov, A. S.; Zembower, D. E.; Andresson, T.; Gurney, M. E. Structure-Activity Relationship Studies Leading to the Identification of (2*E*)-3-[l-[(2,4-dichlorophenyl)methyl]-5-fluoro-3-methyl-lH-indol-7-yl]-*N*-[(4,5-d ichloro-2-thienyl)sulfonyl]-2-propenamide (DG-041), A Potent and Selective Prostanoid EP3 Receptor Antagonist, as a Novel Antiplatelet Agent that does not Prolong Bleeding. *J. Med. Chem.* **2010,** *53* (1), 18–36; (b) Singh, J.; Zeller, W.; Zhou, N.; Hategen, G.; Mishra, R.; Polozov, A.; Yu, P.; Onua, E.; Zhang, J.; Zembower, D.; Kiselyov, A.; Ramirez, J. L.; Sigthorsson, G.; Bjornsson, J. M.; Thorsteinsdottir, M.; Andresson, T.; Bjarnadottir, M.; Magnusson, O.; Fabre, J. E.; Stefansson, K.; Gurney, M. E. Antagonists of the EP3 Receptor for Prostaglandin E2 are Novel Antiplatelet Agents that do not Prolong Bleeding. *ACS Chem. Biol.* **2009,** *4* (2), 115–126.
170. Tilly, P.; Charles, A. L.; Ludwig, S.; Slimani, F.; Gross, S.; Meilhac, O.; Geny, B.; Stefansson, K.; Gurney, M. E.; Fabre, J. E. Blocking the EP3 Receptor for PGE2 With DG-041 Decreases Thrombosis Without Impairing Haemostatic Competence. *Cardiovasc. Res.* **2014,** *101* (3), 482–491.
171. Hoyer, D.; Clarke, D. E.; Fozard, J. R.; Hartig, P. R.; Martin, G. R.; Mylecharane, E. J.; Saxena, P. R.; Humphrey, P. P. International Union of Pharmacology classification of receptors for 5-Hydroxytryptamine (Serotonin). *Pharmacol. Rev.* **1994,** *46* (2), 157–203.
172. Fraer, M.; Kilic, F. Serotonin: A Different Player in Hypertension-Associated Thrombosis. *Hypertension* **2015,** *65* (5), 942–948.
173. Bampalis, V. G.; Dwivedi, S.; Shai, E.; Brandl, R.; Varon, D.; Siess, W. Effect of 5-HT2A Receptor Antagonists on Human Platelet Activation in Blood Exposed to Physiologic Stimuli and Atherosclerotic Plaque. *J. Thromb. Haemost.* **2011,** *9* (10), 2112–2115.
174. Dosa, P. I.; Strah-Pleynet, S.; Jayakumar, H.; Casper, M.; Decaire, M.; Xiong, Y.; Lehmann, J.; Choi, K.; Elwell, K.; Wong, A.; Webb, R. R.; Adams, J. W.; Ramirez, J.; Richman, J. G.; Thomsen, W.; Semple, G.; Teegarden, B. R. Solubilized Phenyl-Pyrazole Ureas as Potent, Selective 5-HT(2A) Inverse-Agonists and Their Application as Antiplatelet Agents. *Bioorg. Med. Chem. Lett.* **2009,** *19* (18), 5486–5489.
175. Xiong, Y.; Teegarden, B. R.; Choi, J. S.; Strah-Pleynet, S.; Decaire, M.; Jayakumar, H.; Dosa, P. I.; Casper, M. D.; Pham, L.; Feichtinger, K.; Ullman, B.; Adams, J.; Yuskin, D.; Frazer, J.; Morgan, M.; Sadeque, A.; Chen, W.; Webb, R. R.; Connolly, D. T.; Semple, G.; Al-Shamma, H. Discovery and Structure-Activity Relationship of 3-methoxy-*N*-(3-(1-methyl-1H-pyrazol-5-yl)-4-(2-morpholinoethoxy)phenyl)benzamide (APD791): A Highly Selective 5-Hydroxytryptamine2A Receptor Inverse Agonist for the Treatment of Arterial Thrombosis. *J. Med. Chem.* **2010,** *53* (11), 4412–4421.
176. Adams, J. W.; Ramirez, J.; Shi, Y.; Thomsen, W.; Frazer, J.; Morgan, M.; Edwards, J. E.; Chen, W.; Teegarden, B. R.; Xiong, Y.; Al-Shamma, H.; Behan, D. P.; Connolly, D. T. APD791, 3-Methoxy-*N*-(3-(1-methyl-1H-pyrazol-5-yl)-4-(2-morpholinoethoxy)phenyl)benzamide, a Novel 5-Hydroxytryptamine 2A Receptor Antagonist: Pharmacological Profile, Pharmacokinetics, Platelet Activity and Vascular Biology. *J. Pharmacol. Exp. Ther.* **2009,** *331* (1), 96–103.
177. Przyklenk, K.; Frelinger, A. L., III; Linden, M. D.; Whittaker, P.; Li, Y.; Barnard, M. R.; Adams, J.; Morgan, M.; Al-Shamma, H.; Michelson, A. D. Targeted inhibition of the Serotonin 5HT2A Receptor Improves Coronary Patency in an in vivo Model of Recurrent Thrombosis. *J. Thromb. Haemost.* **2010,** *8* (2), 331–340.
178. Moncada, S.; Vane, J. R. Pharmacology and Endogenous Roles of Prostaglandin Endoperoxides, Thromboxane A2, and Prostacyclin. *Pharmacol. Rev.* **1978,** *30* (3), 293–331.
179. Jones, R. L.; Giembycz, M. A.; Woodward, D. F. Prostanoid Receptor Antagonists: Development Strategies and Therapeutic Applications. *Br. J. Pharmacol.* **2009,** *158* (1), 104–145.
180. Ting, H. J.; Murad, J. P.; Espinosa, E. V.; Khasawneh, F. T. Thromboxane A2 Receptor: Biology and Function of a Peculiar Receptor that Remains Resistant for Therapeutic Targeting. *J. Cardiovasc. Pharmacol. Ther.* **2012,** *17* (3), 248–259.
181. Wang, X.; Liu, L.; Huang, L.; Herbst-Robinson, K.; Cornec, A. S.; James, M. J.; Sugiyama, S.; Bassetto, M.; Brancale, A.; Trojanowski, J. Q.; Lee, V. M.; Smith, A. B.., III; Brunden, K. R.; Ballatore, C. Potent, Long-Acting Cyclopentane-1,3-Dione Thromboxane (A2)-Receptor Antagonists. *ACS Med. Chem. Lett.* **2014,** *5* (9), 1015–1020.

182. Tanaka, Y.; Yamaki, F.; Koike, K.; Toro, L. New Insights into the Intracellular Mechanisms by which PGI2 Analogues Elicit Vascular Relaxation: Cyclic AMP-Independent, Gs-Protein Mediated-Activation of MaxiK Channel. *Curr. Med. Chem.: Cardiovasc. Hematol. Agents* **2004,** *2* (3), 257–265.
183. (a) Bledzka, K.; Smyth, S. S.; Plow, E. F. Integrin αIIbβ3: From Discovery to Efficacious Therapeutic Target. *Circ. Res.* **2013,** *112* (8), 1189–1200; (b) Armstrong, P. C.; Peter, K. GPIIb/IIIa Inhibitors: From Bench to Bedside and Back to Bench Again. *Thromb. Haemost.* **2012,** *107* (5), 808–814.
184. (a) Cox, D.; Brennan, M.; Moran, N. Integrins as Therapeutic Targets: Lessons and Opportunities. *Nat. Rev. Drug Discov.* **2010,** *9* (10), 804–820; (b) Askari, J. A.; Buckley, P. A.; Mould, A. P.; Humphries, M. J. Linking Integrin Conformation to Function. *J. Cell Sci.* **2009,** *122* (Pt 2), 165–170.
185. Shen, B.; Delaney, M. K.; Du, X. Inside-Out, Outside-In, and Inside-Outside-In: G Protein Signaling in Integrin-Mediated Cell Adhesion, Spreading, and Retraction. *Curr. Opin. Cell Biol.* **2012,** *24* (5), 600–606.
186. Xiao, T.; Takagi, J.; Coller, B. S.; Wang, J. H.; Springer, T. A. Structural Basis for Allostery in Integrins and Binding to Fibrinogen-Mimetic Therapeutics. *Nature* **2004,** *432* (7013), 59–67.
187. Cox, D. Oral GPIIb/IIIa Antagonists: What Went Wrong? *Curr. Pharm. Des.* **2004,** *10* (14), 1587–1596.
188. Blue, R.; Murcia, M.; Karan, C.; Jirouskova, M.; Coller, B. S. Application of High-Throughput Screening to Identify a Novel αIIb-Specific Small-Molecule Inhibitor of αIIbβ3-Mediated Platelet Interaction With Fibrinogen. *Blood* **2008,** *111* (3), 1248–1256.
189. Zhu, J.; Negri, A.; Provasi, D.; Filizola, M.; Coller, B. S.; Springer, T. A. Closed Headpiece of Integrin αIIbβ3 and Its Complex With an αIIbβ3-Specific Antagonist that does not Induce Opening. *Blood* **2010,** *116* (23), 5050–5059.
190. Jiang, J. K.; McCoy, J. G.; Shen, M.; LeClair, C. A.; Huang, W.; Negri, A.; Li, J.; Blue, R.; Harrington, A. W.; Naini, S.; David, G., III; Choi, W. S.; Volpi, E.; Fernandez, J.; Babayeva, M.; Nedelman, M. A.; Filizola, M.; Coller, B. S.; Thomas, C. J. A Novel Class of Ion Displacement Ligands as Antagonists of the αIIbβ3 Receptor that Limit Conformational Reorganization of the Receptor. *Bioorg. Med. Chem. Lett.* **2014,** *24* (4), 1148–1153.
191. Zhu, J.; Choi, W. S.; McCoy, J. G.; Negri, A.; Naini, S.; Li, J.; Shen, M.; Huang, W.; Bougie, D.; Rasmussen, M.; Aster, R.; Thomas, C. J.; Filizola, M.; Springer, T. A.; Coller, B. S. Structure-Guided Design of a High-Affinity Platelet Integrin αIIbβ3 Receptor Antagonist that Disrupts Mg^{2+} Binding to the MIDAS. *Sci. Transl. Med.* **2012,** *4* (125), 125ra32.
192. Li, J.; Vootukuri, S.; Shang, Y.; Negri, A.; Jiang, J. K.; Nedelman, M.; Diacovo, T. G.; Filizola, M.; Thomas, C. J.; Coller, B. S. RUC-4: A Novel αIIbβ3 Antagonist for Prehospital Therapy of Myocardial Infarction. *Arterioscler., Thromb., Vasc. Biol.* **2014,** *34* (10), 2321–2329.
193. Polishchuk, P. G.; Samoylenko, G. V.; Khristova, T. M.; Krysko, O. L.; Kabanova, T. A.; Kabanov, V. M.; Kornylov, A. Y.; Klimchuk, O.; Langer, T.; Andronati, S. A.; Kuz'min, V. E.; Krysko, A. A.; Varnek, A. Design, Virtual Screening, and Synthesis of Antagonists of αIIbβ3 as Antiplatelet Agents. *J. Med. Chem.* **2015,** *58* (19), 7681–7694.
194. Koloka, V.; Christofidou, E. D.; Vaxevanelis, S.; Dimitriou, A. A.; Tsikaris, V.; Tselepis, A. D.; Panou-Pomonis, E.; Sakarellos-Daitsiotis, M.; Tsoukatos, D. C. A Palmitoylated Peptide, Derived from the Acidic Carboxyl-Terminal Segment of the Integrin αIIb Cytoplasmic Domain, Inhibits Platelet Activation. *Platelets* **2008,** *19* (7), 502–511.
195. (a) Gong, H.; Shen, B.; Flevaris, P.; Chow, C.; Lam, S. C.; Voyno-Yasenetskaya, T. A.; Kozasa, T.; Du, X. G Protein Subunit $G\alpha_{13}$ Binds to Integrin $\alpha_{IIb}\beta_3$ and Mediates Integrin "Outside-In" Signaling. *Science* **2010,** *327* (5963), 340–343; (b) Shen, B.; Zhao, X.; O'Brien, K. A.; Stojanovic-Terpo, A.; Delaney, M. K.; Kim, K.; Cho, J.; Lam, S. C.; Du, X. A Directional Switch of Integrin Signalling and a New Anti-Thrombotic Strategy. *Nature* **2013,** *503* (7474), 131–135.
196. Kiefer, T. L.; Becker, R. C. Inhibitors of Platelet Adhesion. *Circulation* **2009,** *120* (24), 2488–2495.
197. Kapyla, J.; Pentikainen, O. T.; Nyronen, T.; Nissinen, L.; Lassander, S.; Jokinen, J.; Lahti, M.; Marjamaki, A.; Johnson, M. S.; Heino, J. Small Molecule Designed to Target Metal Binding Site in the α2I Domain Inhibits Integrin Function. *J. Med. Chem.* **2007,** *50* (11), 2742–2746.
198. Nissinen, L.; Pentikainen, O. T.; Jouppila, A.; Kapyla, J.; Ojala, M.; Nieminen, J.; Lipsanen, A.; Lappalainen, H.; Eckes, B.; Johnson, M. S.; Lassila, R.; Marjamaki, A.; Heino, J. A Small-Molecule Inhibitor of Integrin α2β1 Introduces a New Strategy for Antithrombotic Therapy. *Thromb. Haemost.* **2010,** *103* (2), 387–397.
199. Nissinen, L.; Koivunen, J.; Kapyla, J.; Salmela, M.; Nieminen, J.; Jokinen, J.; Sipila, K.; Pihlavisto, M.; Pentikainen, O. T.; Marjamaki, A.; Heino, J. Novel α2β1 Integrin Inhibitors Reveal that Integrin Binding to Collagen under Shear Stress Conditions Does not Require Receptor Preactivation. *J. Biol. Chem.* **2012,** *287* (53), 44694–44702.
200. Choi, S.; Vilaire, G.; Marcinkiewicz, C.; Winkler, J. D.; Bennett, J. S.; DeGrado, W. F. Small Molecule Inhibitors of Integrin α2β1. *J. Med. Chem.* **2007,** *50* (22), 5457–5462.
201. Miller, M. W.; Basra, S.; Kulp, D. W.; Billings, P. C.; Choi, S.; Beavers, M. P.; McCarty, O. J.; Zou, Z.; Kahn, M. L.; Bennett, J. S.; DeGrado, W. F. Small-Molecule Inhibitors of Integrin α2β1 that Prevent Pathological Thrombus Formation via an Allosteric Mechanism. *Proc. Natl. Acad. Sci. U. S. A.* **2009,** *106* (3), 719–724.
202. Halland, N.; Blum, H.; Buning, C.; Kohlmann, M.; Lindenschmidt, A. Small Macrocycles As Highly Active Integrin α2β1 Antagonists. *ACS Med. Chem. Lett.* **2014,** *5* (2), 193–198.
203. Nieswandt, B.; Brakebusch, C.; Bergmeier, W.; Schulte, V.; Bouvard, D.; Mokhtari-Nejad, R.; Lindhout, T.; Heemskerk, J. W.; Zirngibl, H.; Fassler, R. Glycoprotein VI but not α2β1 Integrin is Essential for Platelet Interaction With Collagen. *EMBO J.* **2001,** *20* (9), 2120–2130.
204. (a) Jiang, P.; Jandrot-Perrus, M. New Advances in Treating Thrombotic Diseases: GPVI as a Platelet Drug Target. *Drug Discov. Today* **2014,** *19* (9), 1471–1475; (b) Dutting, S.; Bender, M.; Nieswandt, B. Platelet GPVI: a Target for Antithrombotic Therapy?!. *Trends Pharmacol. Sci.* **2012,** *33* (11), 583–590.
205. (a) Penz, S. M.; Reininger, A. J.; Toth, O.; Deckmyn, H.; Brandl, R.; Siess, W. Glycoprotein Ibα inhibition and ADP receptor antagonists, but not aspirin, reduce platelet thrombus formation in flowing blood exposed to atherosclerotic plaques. *Thromb. Haemost.* **2007,** *97* (3), 435–443; (b) Ulrichts, H.; Silence, K.; Schoolmeester, A.; de Jaegere, P.; Rossenu, S.; Roodt, J.; Priem, S.; Lauwereys, M.; Casteels, P.; Van Bockstaele, F.; Verschueren, K.; Stanssens, P.; Baumeister, J.; Holz, J. B. Antithrombotic drug candidate ALX-0081 shows superior preclinical efficacy and safety compared With currently marketed antiplatelet drugs. *Blood* **2011,** *118* (3), 757–765.
206. Lei, X.; Reheman, A.; Hou, Y.; Zhou, H.; Wang, Y.; Marshall, A. H.; Liang, C.; Dai, X.; Li, B. X.; Vanhoorelbeke, K.; Ni, H. Anfibatide, a Novel GPIb Complex Antagonist, Inhibits Platelet Adhesion and Thrombus Formation in vitro and in vivo in Murine Models Of Thrombosis. *Thromb. Haemost.* **2014,** *111* (2), 279–289.
207. Firbas, C.; Siller-Matula, J. M.; Jilma, B. Targeting von Willebrand Factor and Platelet Glycoprotein Ib Receptor. *Expert Rev. Cardiovasc. Ther.* **2010,** *8* (12), 1689–1701.
208. Mitchell, J. A.; Warner, T. D. COX Isoforms in the Cardiovascular System: Understanding the Activities of Non-Steroidal Anti-Inflammatory Drugs. *Nat. Rev. Drug Discov.* **2006,** *5* (1), 75–86.
209. Schror, K.; Rauch, B. H. Aspirin and Lipid Mediators in the Cardiovascular System. *Prostaglandins Other Lipid Mediat.* **2015,** *121,* 17–23.
210. (a) Breyer, M. D.; Hao, C.; Qi, Z. Cyclooxygenase-2 Selective Inhibitors and the Kidney. *Curr. Opin. Crit. Care* **2001,** *7* (6), 393–400; (b) Campbell, C. L.; Smyth, S.; Montalescot, G.; Steinhubl, S. R. Aspirin Dose for the Prevention of Cardiovascular Disease: A Systematic Review. *JAMA* **2007,** *297* (18), 2018–2024.
211. Baigent, C.; Blackwell, L.; Collins, R.; Emberson, J.; Godwin, J.; Peto, R.; Buring, J.; Hennekens, C.; Kearney, P.; Meade, T.; Patrono, C.; Roncaglioni, M. C.; Zanchetti, A. Aspirin in the Primary and Secondary Prevention of Vascular Disease: Collaborative Meta-Analysis of Individual Participant Data From Randomised Trials. *Lancet* **2009,** *373* (9678), 1849–1860.
212. Awtry, E. H.; Loscalzo, J. Aspirin. *Circulation* **2000,** *101* (10), 1206–1218.
213. (a) Floyd, C. N.; Ferro, A. Mechanisms of Aspirin Resistance. *Pharmacol. Ther.* **2014,** *141* (1), 69–78; (b) Tantry, U. S.; Gesheff, M.; Liu, F.; Bliden, K. P.; Gurbel, P. A. Resistance to Antiplatelet Drugs: What Progress Has Been Made? *Expert Opin. Pharmacother.* **2014,** *15* (17), 2553–2564.
214. Anninos, H.; Andrikopoulos, G.; Pastromas, S.; Sakellariou, D.; Theodorakis, G.; Vardas, P. Triflusal: An Old Drug in Modern Antiplatelet Therapy. Review of Its Action, Use, Safety and Effectiveness. *Hellenic J. Cardiol.* **2009,** *50* (3), 199–207.
215. Alvarez-Sabin, J.; Quintana, M.; Santamarina, E.; Maisterra, O. Triflusal and Aspirin in the Secondary Prevention of Atherothrombotic Ischemic Stroke: A Very Long-Term Follow-Up. *Cerebrovasc. Dis.* **2014,** *37* (3), 181–187.
216. Wallace, J. L. Prostaglandins, NSAIDs, and Gastric Mucosal Protection: Why Doesn't the Stomach Digest Itself? *Physiol. Rev.* **2008,** *88* (4), 1547–1565.
217. (a) Solomon, D. H.; Schneeweiss, S.; Glynn, R. J.; Kiyota, Y.; Levin, R.; Mogun, H.; Avorn, J. Relationship Between Selective Cyclooxygenase-2 Inhibitors and Acute Myocardial Infarction in Older Adults. *Circulation* **2004,** *109* (17), 2068–2073; (b) Singh, D. Merck Withdraws Arthritis Drug Worldwide. *BMJ* **2004,** *329* (7470), 816.
218. Perrone, M. G.; Scilimati, A.; Simone, L.; Vitale, P. Selective COX-1 Inhibition: A Therapeutic Target to be Reconsidered. *Curr. Med. Chem.* **2010,** *17* (32), 3769–3805.

219. Langenbach, R.; Morham, S. G.; Tiano, H. F.; Loftin, C. D.; Ghanayem, B. I.; Chulada, P. C.; Mahler, J. F.; Lee, C. A.; Goulding, E. H.; Kluckman, K. D.; Kim, H. S.; Smithies, O. Prostaglandin Synthase 1 Gene Disruption in Mice Reduces Arachidonic Acid-Induced Inflammation and Indomethacin-Induced Gastric Ulceration. *Cell* **1995,** *83* (3), 483–492.
220. Sakata, C.; Kawasaki, T.; Kato, Y.; Abe, M.; Suzuki, K.; Ohmiya, M.; Funatsu, T.; Morita, Y.; Okada, M. ASP6537, a Novel Highly Selective Cyclooxygenase-1 Inhibitor, Exerts Potent Antithrombotic Effect Without "Aspirin Dilemma". *Thromb. Res.* **2013,** *132* (1), 56–62.
221. Vitale, P.; Tacconelli, S.; Perrone, M. G.; Malerba, P.; Simone, L.; Scilimati, A.; Lavecchia, A.; Dovizio, M.; Marcantoni, E.; Bruno, A.; Patrignani, P. Synthesis, Pharmacological Characterization, and Docking Analysis of a Novel Family of Diarylisoxazoles as Highly Selective Cyclooxygenase-1 (COX-1) Inhibitors. *J. Med. Chem.* **2013,** *56* (11), 4277–4299.
222. Moriarty, L. M.; Lally, M. N.; Carolan, C. G.; Jones, M.; Clancy, J. M.; Gilmer, J. F. Discovery of a "True" Aspirin Prodrug. *J. Med. Chem.* **2008,** *51* (24), 7991–7999.
223. Harmon, S.; Inkielewicz-Stepniak, I.; Jones, M.; Ledwidge, M.; Santos-Martinez, M. J.; Medina, C.; Radomski, M. W.; Gilmer, J. F. Mechanisms of Aggregation Inhibition by Aspirin and Nitrate-Aspirin Prodrugs in Human Platelets. *J. Pharm. Pharmacol.* **2012,** *64* (1), 77–89.
224. Bambace, N. M.; Holmes, C. E. The Platelet Contribution to Cancer Progression. *J. Thromb. Haemost.* **2011,** *9* (2), 237–249.
225. Lundberg, J. O.; Gladwin, M. T.; Weitzberg, E. Strategies to Increase Nitric Oxide Signalling in Cardiovascular Disease. *Nat. Rev. Drug Discov.* **2015,** *14,* 623–641.
226. Freedman, J. E.; Loscalzo, J. Nitric oxide and Its Relationship to Thrombotic Disorders. *J. Thromb. Haemost.* **2003,** *1* (6), 1183–1188.
227. Serafim, R. A.; Primi, M. C.; Trossini, G. H.; Ferreira, E. I. Nitric Oxide: State of the Art in Drug Design. *Curr. Med. Chem.* **2012,** *19* (3), 386–405.
228. Gresele, P.; Momi, S. Pharmacologic Profile and Therapeutic Potential of NCX 4016, a Nitric Oxide-Releasing Aspirin, for Cardiovascular Disorders. *Cardiovasc. Drug Rev.* **2006,** *24* (2), 148–168.
229. Jones, M.; Inkielewicz, I.; Medina, C.; Santos-Martinez, M. J.; Radomski, A.; Radomski, M. W.; Lally, M. N.; Moriarty, L. M.; Gaynor, J.; Carolan, C. G.; Khan, D.; O'Byrne, P.; Harmon, S.; Holland, V.; Clancy, J. M.; Gilmer, J. F. Isosorbide-Based Aspirin Prodrugs: Integration of Nitric Oxide Releasing Groups. *J. Med. Chem.* **2009,** *52* (21), 6588–6598.
230. (a) Lazzarato, L.; Chegaev, K.; Marini, E.; Rolando, B.; Borretto, E.; Guglielmo, S.; Joseph, S.; Di Stilo, A.; Fruttero, R.; Gasco, A. New Nitric Oxide or Hydrogen Sulfide Releasing Aspirins. *J. Med. Chem.* **2011,** *54* (15), 5478–5484; (b) Rolando, B.; Lazzarato, L.; Donnola, M.; Marini, E.; Joseph, S.; Morini, G.; Pozzoli, C.; Fruttero, R.; Gasco, A. Water-Soluble Nitric-oxide-Releasing Acetylsalicylic Acid (ASA) Prodrugs. *ChemMedChem* **2013,** *8* (7), 1199–1209.
231. Gresele, P.; Arnout, J.; Deckmyn, H.; Huybrechts, E.; Pieters, G.; Vermylen, J. Role of Proaggregatory and Antiaggregatory Prostaglandins in Hemostasis. Studies With Combined Thromboxane Synthase Inhibition and Thromboxane Receptor Antagonism. *J. Clin. Invest.* **1987,** *80* (5), 1435–1445.
232. Rondina, M. T.; Weyrich, A. S. Targeting Phosphodiesterases in Anti-Platelet Therapy. *Handb. Exp. Pharmacol.* **2012,** *210,* 225–238.
233. Gresele, P.; Momi, S.; Falcinelli, E. Anti-Platelet Therapy: Phosphodiesterase Inhibitors. *Br. J. Clin. Pharmacol.* **2011,** *72* (4), 634–646.
234. Aktas, B.; Utz, A.; Hoenig-Liedl, P.; Walter, U.; Geiger, J. Dipyridamole Enhances NO/cGMP-Mediated Vasodilator-Stimulated Phosphoprotein Phosphorylation and Signaling in Human Platelets: in vitro and In Vivo/Ex Vivo Studies. *Stroke* **2003,** *34* (3), 764–769.
235. Ishida, K.; Messe, S. R. Antiplatelet Strategies for Secondary Prevention of Stroke and TIA. *Curr. Atheroscler. Rep.* **2014,** *16* (11), 449.
236. Brass, E. P.; Cooper, L. T.; Morgan, R. E.; Hiatt, W. R. A Phase II Dose-Ranging Study of the Phosphodiesterase Inhibitor K-134 in Patients With Peripheral Artery Disease and Claudication. *J. Vasc. Surg.* **2012,** *55* (2), 381–389. e1.
237. Hu, L.; Fan, Z.; Du, H.; Ni, R.; Zhang, S.; Yin, K.; Ye, J.; Zhang, Y.; Wei, X.; Zhang, X.; Gross, P. L.; Kunapuli, S. P.; Ding, Z. BF061, a Novel Antiplatelet and Antithrombotic Agent Targeting P2Y(1)(2) Receptor and Phosphodiesterase. *Thromb. Haemost.* **2011,** *106* (6), 1203–1214.
238. Jackson, S. P.; Schoenwaelder, S. M.; Goncalves, I.; Nesbitt, W. S.; Yap, C. L.; Wright, C. E.; Kenche, V.; Anderson, K. E.; Dopheide, S. M.; Yuan, Y.; Sturgeon, S. A.; Prabaharan, H.; Thompson, P. E.; Smith, G. D.; Shepherd, P. R.; Daniele, N.; Kulkarni, S.; Abbott, B.; Saylik, D.; Jones, C.; Lu, L.; Giuliano, S.; Hughan, S. C.; Angus, J. A.; Robertson, A. D.; Salem, H. H. PI 3-kinase p110β: A New Target for Antithrombotic Therapy. *Nat. Med.* **2005,** *11* (5), 507–514.
239. Guidetti, G. F.; Canobbio, I.; Torti, M. PI3K/Akt in Platelet Integrin Signaling and Implications in Thrombosis. *Adv. Biol. Regul.* **2015,** *59,* 36–52.
240. Nylander, S.; Kull, B.; Bjorkman, J. A.; Ulvinge, J. C.; Oakes, N.; Emanuelsson, B. M.; Andersson, M.; Skarby, T.; Inghardt, T.; Fjellstrom, O.; Gustafsson, D. Human Target Validation of Phosphoinositide 3-kinase (PI3K)β: Effects on Platelets and Insulin Sensitivity, using AZD6482 a Novel PI3Kβ Inhibitor. *J. Thromb. Haemost.* **2012,** *10* (10), 2127–2136.
241. Nylander, S.; Wagberg, F.; Andersson, M.; Skarby, T.; Gustafsson, D. Exploration of Efficacy and Bleeding With Combined Phosphoinositide 3-Kinase β Inhibition and Aspirin in Man. *J. Thromb. Haemost.* **2015,** *13* (8), 1494–1502.
242. (a) Giordanetto, F.; Barlaam, B.; Berglund, S.; Edman, K.; Karlsson, O.; Lindberg, J.; Nylander, S.; Inghardt, T. Discovery of 9-(1-Phenoxyethyl)-2-morpholino-4-oxo-pyrido [1,2-a]pyrimidine-7-carboxamides as Oral PI3Kβ Inhibitors, Useful as Antiplatelet Agents. *Bioorg. Med. Chem. Lett.* **2014,** *24* (16), 3936–3943; (b) Giordanetto, F.; Wallberg, A.; Ghosal, S.; Iliefski, T.; Cassel, J.; Yuan, Z. Q.; von Wachenfeldt, H.; Andersen, S. M.; Inghardt, T.; Tunek, A.; Nylander, S. Discovery of Phosphoinositide 3-Kinases (PI3K) p110β Isoform Inhibitor 4-[2-Hydroxyethyl(1-naphthylmethyl)amino]-6-[(2S)-2-methylmorpholin-4-yl]-1H-pyrimidin-2-one, an Effective Antithrombotic Agent Without Associated Bleeding and Insulin Resistance. *Bioorg. Med. Chem. Lett.* **2012,** *22* (21), 6671–6676.
243. Laurent, P. A.; Severin, S.; Hechler, B.; Vanhaesebroeck, B.; Payrastre, B.; Gratacap, M. P. Platelet PI3Kβ and GSK3 Regulate Thrombus Stability at a High Shear Rate. *Blood* **2015,** *125* (5), 881–888.
244. Robins, R. S.; Lemarie, C. A.; Laurance, S.; Aghourian, M. N.; Wu, J.; Blostein, M. D. Vascular Gas6 Contributes to Thrombogenesis and Promotes Tissue Factor Up-regulation after Vessel Injury in Mice. *Blood* **2013,** *121* (4), 692–699.
245. Zhang, W.; McIver, A. L.; Stashko, M. A.; DeRyckere, D.; Branchford, B. R.; Hunter, D.; Kireev, D.; Miley, M. J.; Norris-Drouin, J.; Stewart, W. M.; Lee, M.; Sather, S.; Zhou, Y.; Di Paola, J. A.; Machius, M.; Janzen, W. P.; Earp, H. S.; Graham, D. K.; Frye, S. V.; Wang, X. Discovery of Mer Specific Tyrosine Kinase Inhibitors for the Treatment and Prevention of Thrombosis. *J. Med. Chem.* **2013,** *56* (23), 9693–9700.
246. Andre, P.; Morooka, T.; Sim, D.; Abe, K.; Lowell, C.; Nanda, N.; Delaney, S.; Siu, G.; Yan, Y.; Hollenbach, S.; Pandey, A.; Gao, H.; Wang, Y.; Nakajima, K.; Parikh, S. A.; Shi, C.; Phillips, D.; Owen, W.; Sinha, U.; Simon, D. I. Critical Role for Syk in Responses to Vascular Injury. *Blood* **2011,** *118* (18), 5000–5010.
247. Herter, J. M.; Rossaint, J.; Zarbock, A. Platelets in Inflammation and Immunity. *J. Thromb. Haemost.* **2014,** *12* (11), 1764–1775.
248. Schror, K.; Huber, K. Platelets, Inflammation and Anti-Inflammatory Drugs in ACS and CAD. *Thromb. Haemost.* **2015,** *114* (3), 446–448.
249. Akinosoglou, K.; Alexopoulos, D. Use of Antiplatelet Agents in Sepsis: A Glimpse Into the Future. *Thromb. Res.* **2014,** *133* (2), 131–138.
250. (a) Lannan, K. L.; Phipps, R. P.; White, R. J. Thrombosis, Platelets, Microparticles and PAH: More Than a Clot. *Drug Discov Today* **2014,** *19* (8), 1230–1235; (b) Herve, P.; Humbert, M.; Sitbon, O.; Parent, F.; Nunes, H.; Legal, C.; Garcia, G.; Simonneau, G. Pathobiology of Pulmonary Hypertension. The Role of Platelets and Thrombosis. *Clin Chest Med* **2001,** *22* (3), 451–458.
251. Ramirez, G. A.; Franchini, S.; Rovere-Querini, P.; Sabbadini, M. G.; Manfredi, A. A.; Maugeri, N. The Role of Platelets in the Pathogenesis of Systemic Sclerosis. *Front Immunol.* **2012,** *3,* 160.
252. Idzko, M.; Pitchford, S.; Page, C. Role of Platelets in Allergic Airway Inflammation. *J. Allergy Clin. Immunol.* **2015,** *135* (6), 1416–1423.
253. (a) Flaujac, C.; Boukour, S.; Cramer-Borde, E. Platelets and Viruses: An Ambivalent Relationship. *Cell. Mol. Life Sci.* **2010,** *67* (4), 545–556; (b) Chabert, A.; Hamzeh-Cognasse, H.; Pozzetto, B.; Cognasse, F.; Schattner, M.; Gomez, R. M.; Garraud, O. Human Platelets and Their Capacity of Binding Viruses: Meaning and Challenges? *BMC Immunol* **2015,** *16,* 26; (c) Assinger, A. Platelets and Infection – An Emerging Role of Platelets in Viral Infection. *Front Immunol* **2014,** *5,* 649.
254. Hamzeh-Cognasse, H.; Damien, P.; Chabert, A.; Pozzetto, B.; Cognasse, F.; Garraud, O. Platelets and Infections – Complex Interactions With Bacteria. *Front Immunol.* **2015,** *6,* 82.
255. Menter, D. G.; Tucker, S. C.; Kopetz, S.; Sood, A. K.; Crissman, J. D.; Honn, K. V. Platelets and Cancer: A Casual or Causal Relationship: Revisited. *Cancer Metastasis Rev.* **2014,** *33* (1), 231–269.

256. Li, N. Platelets in Cancer Metastasis: To Help the "Villain" to do Evil. *Int. J. Cancer* **2015,** *138,* 2078–2087.
257. Sharma, D.; Brummel-Ziedins, K. E.; Bouchard, B. A.; Holmes, C. E. Platelets in Tumor Progression: A Host Factor that Offers Multiple Potential Targets in the Treatment of Cancer. *J. Cell. Physiol.* **2014,** *229* (8), 1005–1015.
258. Menter, D. G.; Schilsky, R. L.; DuBois, R. N. Cyclooxygenase-2 and Cancer Treatment: Understanding the Risk should be Worth the Reward. *Clin. Cancer Res.* **2010,** *16* (5), 1384–1390.
259. Di Michele, M.; Van Geet, C.; Freson, K. Proteomics to Unravel Platelet-Related Diseases and Identify Novel Anti-platelet Drugs. *Curr. Med. Chem.* **2012,** *19* (27), 4662–4670.
260. Cognetta, A. B.., 3rd; Niphakis, M. J.; Lee, H. C.; Martini, M. L.; Hulce, J. J.; Cravatt, B. F. Selective N-Hydroxyhydantoin Carbamate Inhibitors of Mammalian Serine Hydrolases. *Chem. Biol.* **2015,** *22* (7), 928–937.
261. Chang, J. W.; Nomura, D. K.; Cravatt, B. F. A Potent and Selective Inhibitor of KIAA1363/AADACL1 that Impairs Prostate Cancer Pathogenesis. *Chem. Biol.* **2011,** *18* (4), 476–484.
262. Holly, S. P.; Chang, J. W.; Li, W.; Niessen, S.; Phillips, R. M.; Piatt, R.; Black, J. L.; Smith, M. C.; Boulaftali, Y.; Weyrich, A. S.; Bergmeier, W.; Cravatt, B. F.; Parise, L. V. Chemoproteomic Discovery of AADACL1 as a Regulator of Human Platelet Activation. *Chem. Biol.* **2013,** *20* (9), 1125–1134.
263. (a) Dietrich-Muszalska, A.; Olas, B. The Changes of Aggregability of Blood Platelets in Schizophrenia. *World J. Biol. Psychiatry* **2009,** *10* (2), 171–176; (b) Egan, K. T. J.; Lopes, A.; Dunne, E.; Cooke, N.; Ramperti, N.; Kenny, D. The Antipsychotic Drug Clozapine Is a Potent Antiplatelet Agent. 25th Congr Int Soc Thromb Haemost (ISTH). Abstract PO075-Wed.
264. Latorre, A. M.; Santos, M. T.; Valles, J.; Dasi, M. A.; Moscardo, A. Platelet Function is Regulated by Acetylation and Deacetylation Mechanisms Controlled by Sirtuins. 25th Congr Int Soc Thromb Haemost (ISTH). Abstract PO414-Mon.
265. Suganuma, Y.; Kano, T.; Ikemoto, K.; Ichinose, C.; Nomura, T.; Kondo, K. Orally Administered Tetrahydrobiopterin (BH4) Suppresses Platelet Aggregation via Intraplatelet Production of Nitric Oxide. 25th Congr Int Soc Thromb Haemost (ISTH). Abstract PO432-Wed.
266. Rigg, R. A.; Aslan, J. E.; Pang, J.; Nowak, M. S.; McCarty, O. J. T. Platelet HSP70 Regulates Integrin alphallbbeta3 Activation and Platelet Aggregation. 25th Congr Int Soc Thromb Haemost (ISTH). Abstract PO453-Wed.
267. Naik, M.; Backmann, B.; Maloney, D.; Naik, U. P. A Small Molecule Inhibitor of ASK1 Protects Mice From Thrombosis With Minimal Effect on Hemostasis. 25th Congr Int Soc Thromb Haemost (ISTH). Abstract AS183.
268. (a) Violi, F.; Pignatelli, P. Platelet NOX, a Novel Target for Anti-thrombotic Treatment. *Thromb. Haemost.* **2014,** *111* (5), 817–823; (b) Tautz, L.; Senis, Y. A.; Oury, C.; Rahmouni, S. Perspective: Tyrosine Phosphatases as Novel Targets for Antiplatelet Therapy. *Bioorg. Med. Chem.* **2015,** *23* (12), 2786–2797.

7.16 Advances in Anticoagulants

ML Quan, PW Glunz, and JM Smallheer, Bristol-Myers Squibb Company, Princeton, NJ, United States

© 2017 Elsevier Ltd. All rights reserved.

7.16.1	**Introduction**	600
7.16.2	**Thrombin Inhibitors**	601
7.16.2.1	Target Validation and Proof of Concept	601
7.16.2.2	Small-Molecule Direct Thrombin Inhibitors	601
7.16.3	**Factor Xa Inhibitors**	604
7.16.3.1	Target Validation and Proof of Concept	604
7.16.3.2	Marketed Factor Xa Inhibitors	605
7.16.3.3	Additional FXa Inhibitors Assessed in Clinical Trials	606
7.16.3.4	Preclinical FXa Inhibitors	607
7.16.3.5	Reversal Agents	610
7.16.3.6	Dual Thrombin/FXa Inhibitors	611
7.16.4	**Factor VIIa Inhibitors**	612
7.16.4.1	Target Validation and Proof of Concept	612
7.16.4.2	Agents Advanced to Clinical Development	612
7.16.4.3	Preclinical Compounds	613
7.16.4.3.1	Amidine-based inhibitors and prodrugs	613
7.16.4.3.2	Nonamidine inhibitors	615
7.16.5	**Factor IXa Inhibitors**	617
7.16.6	**Factor XIa Inhibitors**	618
7.16.6.1	Target Validation and Proof of Concept	618
7.16.6.2	Preclinical Small-Molecule FXIa Inhibitors	619
7.16.6.2.1	Irreversible FXIa inhibitors	619
7.16.6.2.2	Reversible FXIa inhibitors	619
7.16.6.2.3	Allosteric FXIa inhibitors	620
7.16.7	**Conclusion**	621
References		621

7.16.1 Introduction

Hemostasis is a process that stops bleeding via clot formation in the event of vascular injury. Conversely, thrombosis is the abnormal propagation of clotting resulting in occlusion of a blood vessel. Clotting is highly regulated to maintain the balance between thrombosis and hemorrhage. In certain pathological states, inappropriate coagulation predominates with serious implications. Arterial thrombosis can lead to myocardial infarction and ischemic stroke, and is the leading cause of mortality and morbidity worldwide, accounting for a combined 25% of all deaths.[1] In a venous setting, deep vein thrombosis (DVT) may result in leg swelling and life-threatening pulmonary embolism (PE), if a clot is dislodged. Overall, effective treatment for thrombosis-related cardiovascular disease remains a major unmet medical need.

Anticoagulant drugs are the primary strategy for the prevention and treatment of thrombosis and its accompanying complications. For about 60 years, the only available anticoagulants were heparin and warfarin. Although both have potent antithrombotic activity, each has limitations.[2] Heparin, a highly sulfated glycosaminoglycan originally isolated from canine liver extracts, is not orally bioavailable and thus requires parenteral administration. With the advent of low molecular weight heparin (LMWH), which is administered subcutaneously, challenges of variable bioavailability and duration of action experienced with unfractionated heparin were overcome. Until recently, warfarin, a vitamin K antagonist (VKA) that acts by preventing maturation of several coagulation proteases through inhibition of vitamin K epoxide reductase, was the only orally bioavailable anticoagulant. Although an efficacious anticoagulant, warfarin is less than an ideal drug due to delayed onset of activity, drug–drug interactions, dietary restrictions, and a narrow therapeutic index, which can result in suboptimal time in therapeutic range, necessitating strict patient monitoring. These limitations spurred research to discover improved anticoagulant drugs that are orally bioavailable with predictable activity, but at the same time do not increase bleeding or require monitoring.

The sequence of enzymatic events leading to clot formation is depicted in the coagulation cascade, a model originally proposed 50 years ago.[3,4] The coagulation cascade model has evolved to consist of three phases: initiation, amplification, and propagation,[5] and is split into the extrinsic and intrinsic pathways (**Fig. 1**). The two pathways converge at the common pathway, in which Factor X (FX) is converted to Factor Xa (FXa). FXa along with its cofactor Va (FVa) then converts prothrombin to thrombin. Thrombin converts fibrinogen to fibrin, which in turn forms the basis for the fibrin clot. Initiation of coagulation occurs in the extrinsic

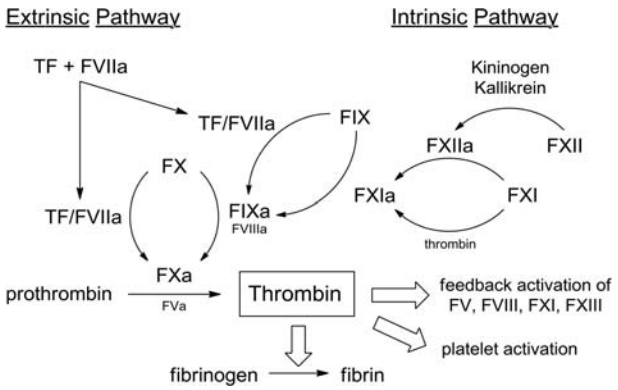

Fig. 1 A representation of the coagulation cascade.

pathway when tissue factor (TF) is exposed upon blood vessel wall injury or atherosclerotic plaque rupture and forms a complex with factor VIIa (FVIIa). The TF/FVIIa complex activates factor IX (FIX) and FX to factor IXa (FIXa) and FXa, respectively. The intrinsic pathway is primarily responsible for the amplification phase of coagulation. This pathway is initiated by the activation of factor XII (FXII) to factor XIIa (FXIIa), facilitated by kininogen and plasma kallikrein. FXIIa activates factor XI (FXI) to factor XIa (FXIa), which in turn activates FIX to FIXa. FIXa forms a complex with factor VIIIa (FVIIIa), which then activates FX to FXa. Additional conversion of FXI to FXIa also occurs via feedback activation by thrombin. Thrombin has multiple functions, including conversion of fibrinogen to fibrin, platelet activation and feedback activation of factor V (FV), factor VIII (FVIII), FXI, and factor XIII (FXIII), which together lead to the propagation of clot formation.

Medicinal chemistry efforts have targeted multiple steps of the coagulation cascade for the discovery of anticoagulant drugs. The main challenge in the anticoagulant drug development effort is balancing antithrombotic efficacy with bleeding safety. The various coagulation targets offer unique profiles with regard to this efficacy/bleeding dichotomy. Significant drug discovery advances have been made, but there continues to be the need for drugs that allow for increased efficacy without dose limitations due to bleeding risk. This review will cover new antithrombotic agents, including inhibitors of thrombin and FXa, several of which have reached the market, as well as inhibitors of TF/FVIIa, FIXa, and FXIa, some of which are currently in development, and highlight the major findings in the quest for better and safer antithrombotic agents since 2006.

7.16.2 Thrombin Inhibitors

7.16.2.1 Target Validation and Proof of Concept

Efforts to identify novel anticoagulants targeting specific serine proteases in the coagulation cascade were initially focused on direct inhibition of thrombin by virtue of its key role both in the formation of fibrin clots and in activation of platelets. Early thrombin inhibitors were i.v. administered polypeptides based on hirudin, a 65-amino acid polypeptide isolated from the salivary gland of the medicinal leech.[6] Two recombinant forms of hirudin, lepirudin and desirudin, were approved for clinical use in the treatment of heparin-induced thrombocytopenia (HIT) and prevention of venous thromboembolism (VTE) in patients undergoing hip-replacement surgery, respectively.[7] A third agent related to hirudin, bivalirudin, a synthetic 20-amino acid polypeptide analog that binds to both the active site and the GPIbα-binding site of thrombin, is approved as an alternate to heparin in patients undergoing percutaneous coronary intervention (PCI).[8]

7.16.2.2 Small-Molecule Direct Thrombin Inhibitors

Structurally, the active site of thrombin, in common with other serine proteases, includes an S1 specificity pocket with Asp189 at the bottom creating a preference for substrates with a basic P1 group.[9,10] Due to an insertion loop that includes Tyr61A, Pro60B, Pro60C, and Trp60D that is unique to thrombin, the S2 pocket in thrombin is relatively small, and the natural substrates typically have small, hydrophobic residues such as proline at P2. The S3/4 pocket is formed by the residues Leu99, Ile174, and Typ215 and accommodates aromatic residues such as Tyr and Phe. In common with other serine proteases is the catalytic triad of Asp102, His57, and Ser195. Hence, medicinal chemistry efforts to identify small-molecule direct thrombin inhibitors (DTIs) focused on Arg–Pro–Phe peptidomimetics and incorporated acid groups to interact with the residues of the catalytic triad. This resulted in the identification of small-molecule inhibitors, such as argatroban (**1**, Fig. 2), a parenteral agent currently approved for the treatment of patients with HIT.[11]

The search for orally bioavailable DTIs was hampered for many years by the presence of the highly basic P1 Arg mimic in combination with the carboxylic acid substituent, which resulted in zwitterionic molecules with poor oral exposure.[12] Ultimately, this lack of oral absorption was addressed using prodrugs. The first such compound to reach the market was ximelagatran (**3**, Fig. 2), a double

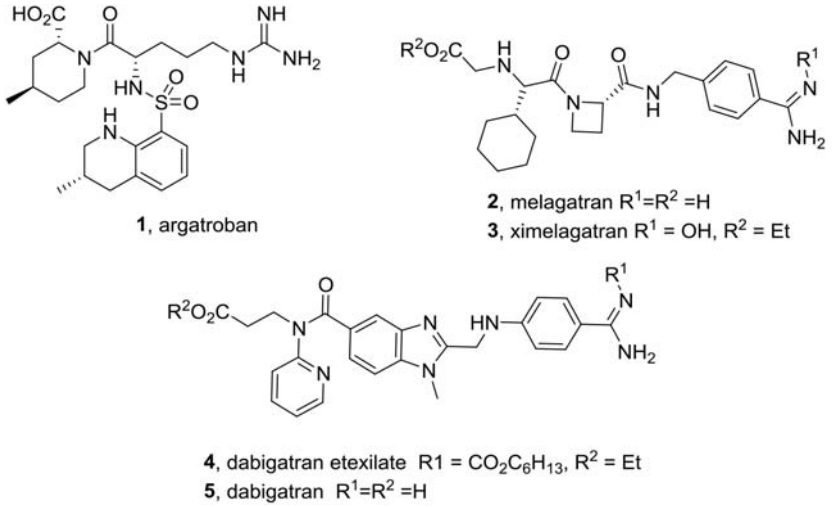

Fig. 2 Small-molecule DTIs: argatroban, ximelagatran, and dabigatran etexilate.

prodrug of melagatran (**2**),[13] which was launched in Europe in 2004, but was subsequently withdrawn from the market due to drug-induced liver toxcity.[14]

A second oral DTI, dabigatran etexilate (**4**, Fig. 2), also a double prodrug of a benzamidine-based inhibitor, dabigatran (**5**), was launched in Europe in 2008 for prevention of VTE[15] and in the United States in 2010 for prevention of stroke and systemic embolism in atrial fibrillation patients (SPAF).[16] Dabigatran etexilate is currently the only orally bioavailable DTI on the market. Dabigatran is a potent inhibitor of thrombin with Ki = 4.5 nM. On oral administration of the double prodrug in humans, the oral bioavailability of **5** is ~6.5%. Concerns over bleeding risk in patients taking DTIs[17,18] led to the introduction of idarucizumab (BI 655075), an antibody fragment that binds to the thrombin-binding site of dabigatran and is a specific antidote for dabigatran recently approved in the United States.[19]

Examples of other DTIs that were advanced into clinical trials are shown in Fig. 3. Efficacy in rat models of venous and arterial thrombosis was demonstrated with AR-H067637 (**7**), the active metabolite of AZD0837 (**6**), with minimal to no increase in bleeding observed.[20] In a Phase II clinical trial, **6** had a good safety profile with low incidence of bleeding and demonstrated effective anticoagulation using standard clotting time measurements.[21] Pyrrolidine LB30870 (**8**) was more potent than melagatran and

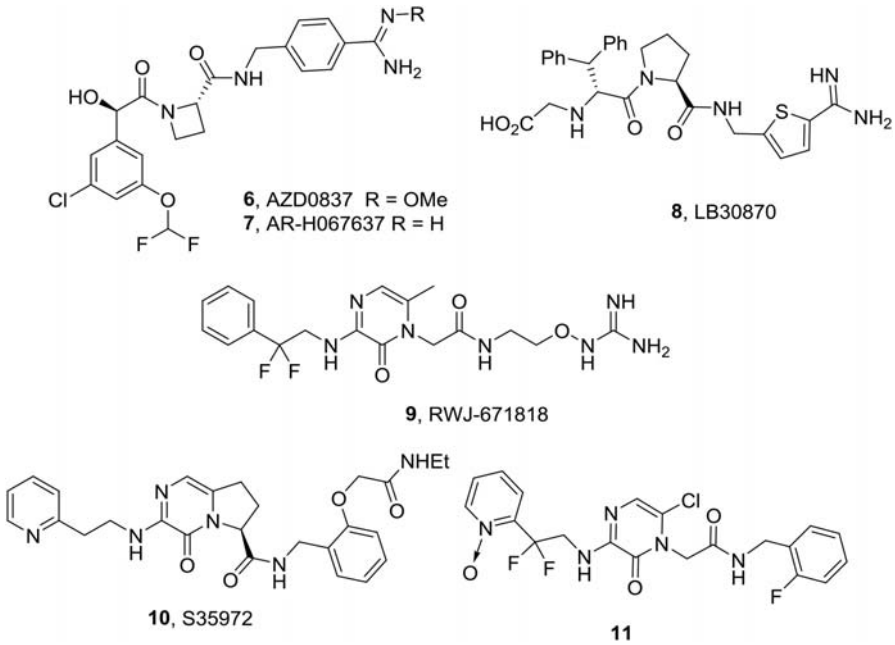

Fig. 3 Examples of additional DTI clinical candidates.

argatroban in inhibiting thrombin in vitro, with a comparable on-rate and slower off-rate compared with melagatran, and showed dose-dependent antithrombotic efficacy in animal models of venous thrombosis.[22] In a Phase I clinical trial to assess pharmacokinetic (PK), pharmacodynamic (PD), and food effects in healthy male subjects, **8** was well tolerated, but showed nonlinear oral PK with a significant, negative food effect.[23]

Ultimately with the aid of structure-based drug design (SBDD), novel DTIs with nonpeptidic scaffolds, less-basic P1 groups, and no acid functionality were identified that obviated the need for prodrugs in order to achieve oral bioavailability. A variety of strategies were explored to replace the basic benzamidine group. RWJ-671818 (**9**, Fig. 3), a pyrazinone core molecule with a weakly basic oxyguanidine P1 group, is a potent inhibitor of thrombin with Ki = 1.3 nM.[24] It is 100% bioavailable in dogs with good stability in human liver microsomes. Compound **9** was highly efficacious in vivo in the electrolytic-mediated carotid arterial thrombosis (ECAT) and DVT models in rats and in the arterial venous (A-V) shunt model in dogs. A Phase I human clinical trial to assess safety, tolerability, PK, and PD of a single oral dose of **9** in healthy male volunteers was completed, and results were described as promising, but no further development has been reported. S35972 (**10**, Fig. 3) is another weakly basic DTI, which is highly selective for thrombin over other serine proteases and shows comparable in vitro potency to dabigatran.[25] Good oral bioavailability was demonstrated with **10** in dogs (F% > 70%), as well as efficacy in both venous and arterial models of thrombosis in the rat, with no food effect. Better efficacy and less bleeding in a rat arterial thrombosis model was reported for **10** when compared with dabigatran etexilate. Based on its positive preclinical profile, **10** was advanced into Phase I clinical trials and was found to be well tolerated at effective anticoagulant doses.[25] In pyrazinone compound **11** (Fig. 3), a pyridine N-oxide was used to impart improved aqueous solubility over a previous lead compound to afford a compound suitable for further clinical development.[26]

While the majority of the effort in anticoagulant research eventually shifted to other targets in the coagulation cascade, additional orally bioavailable DTIs using diverse P1 groups have been reported in the literature. Compounds with pyridone and pyrazinone cores and aminopyridine and imidazole P1 moieties, **12** and **13**, respectively, (Fig. 4) demonstrated modest oral exposure in dogs.[27] Replacement of the P3 imidazole with substituted phenyl groups provided **14** with thrombin Ki = 1.5 nM and excellent trypsin selectivity.[28] The corresponding pyridine N-oxide provided a twofold improvement in functional activity as measured by the activated partial thromboplastin time (aPTT) assay.

In another series of compounds, replacement of the oxyguanidine P1 with 3-(6-methyl-2-aminopyridine) in a series of chlorofluorophenylacetamide P2 thrombin inhibitors provided **15**[29] (Fig. 5) with thrombin Ki = 0.7 nM. In a related series, cyanofluorophenylacetamide **16** was a potent inhibitor with thrombin Ki = 1.2 nM and good oral exposure in dogs (F% = 49%), but lacked oral bioavailability in rats.[30] A thiomorpholine inhibitor **17** with thrombin Ki = 1.1 nM was identified from a screen of six-membered ring heterocycle cores, but while slightly more selective had poor PK compared with the analogous pyrrolidine-based compound **18** (Fig. 5).[31] Benzamidine compound **19**, bearing a benzoxazinone core, was also a potent and selective inhibitor of thrombin in vitro with Ki = 2.6 nM.[32]

Fluorinated dabigatran derivatives **20** and **21** (Fig. 6) where the pyridine ring of **5** was replaced by a substituted *ortho*-fluorobenzene ring, or the terminal benzamidine ring was substituted with fluorine, provided compounds with similar in vitro potency to **5** and in vivo activity of the corresponding double prodrugs **22** and **23** comparable to **4**.[33] N-ethyl analogs **24–26** (Fig. 6) with fluoro-, difluoro-, and trifluoro-substituted methylbenzene rings in place of the pyridyl ring of **5** were also found to be potent DTIs when compared with **1** in vitro.[34] HY023016 (**27**, Fig. 6), a novel tetramethylpyrazine dabigatran prodrug, was efficacious in two animal models of venous thrombosis in rats and demonstrated a lesser effect on bleeding in a mouse tail bleeding model compared with dabigatran etexilate.[35]

Outside the realm of small-molecule inhibitors, both cyclic peptides[36] and DNA aptamers[37,38] have been proposed as thrombin inhibitors which would offer both high specificity and affinity.

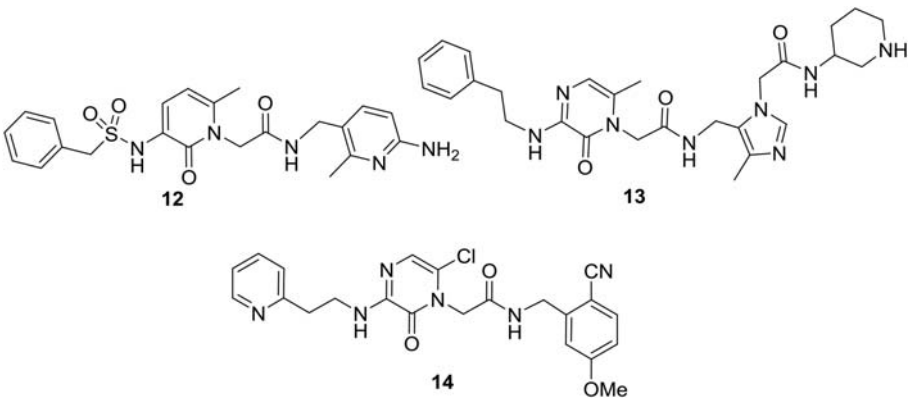

Fig. 4 Pyridone- and pyrimidinone-based DTI examples.

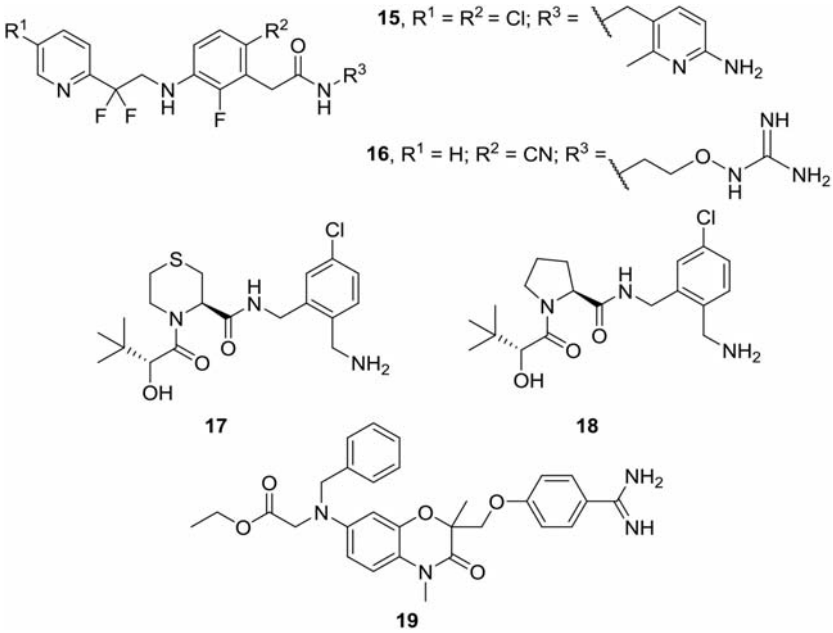

Fig. 5 Phenylacetamide-, thiomorpholine-, pyrrolidine-, and benzoxazinone-based DTI examples.

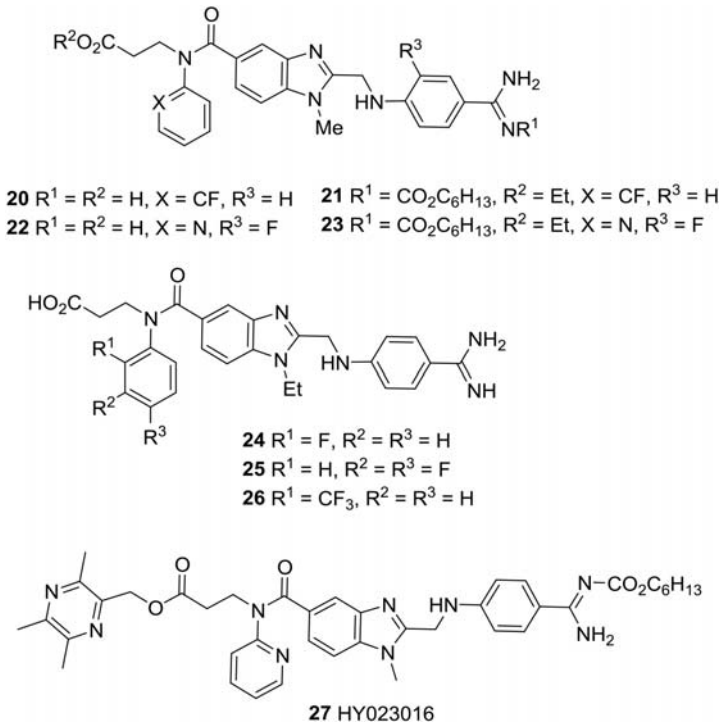

Fig. 6 Analogs of dabigatran.

7.16.3 Factor Xa Inhibitors

7.16.3.1 Target Validation and Proof of Concept

Proof of concept for FXa as an anticoagulant target was provided by polypeptide inhibitors, antistasin, isolated from the salivary glands of the Mexican leech,[39] and the tick anticoagulant peptide (TAP),[40] both of which were shown to be slow, tight-binding inhibitors of FXa. The gradual shift of research focus from thrombin to FXa began in earnest as early preclinical data comparing

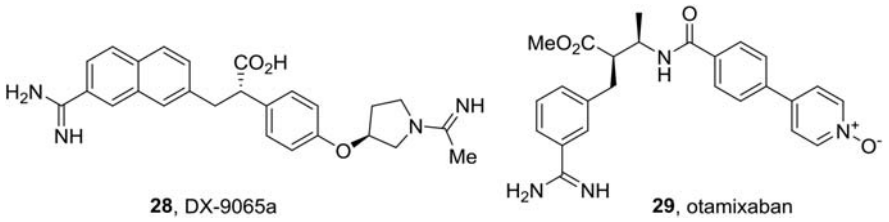

Fig. 7 Benzamidine FXa inhibitors: DX-90651 and otamixaban.

DTIs to selective FXa inhibitors in animal models of thrombosis demonstrated similar or improved efficacy with less bleeding compared with thrombin inhibitors.[41–43] Ensuing clinical success with indirect FXa inhibitors, such as the pentasaccharide fondaparinux, lent further support to the FXa mechanism.[39,44] Early clinical experience with small-molecule FXa inhibitors was obtained with parenteral agents, such as DX-9065a (**28**)[45] and otamixaban (**29**),[46,47] which contain strongly basic amidine moieties and have insufficient oral bioavailability (see **Fig. 7**).

Efforts to identify orally bioavailable direct FXa inhibitors, which have continued over more than two decades, resulted in the identification of numerous novel small-molecule FXa inhibitors. Similar to thrombin inhibitors, this research transitioned from small peptidic inhibitors of FXa to peptidomimetics anchored by a highly basic benzamidine P1 and ultimately to less-basic or neutral small-molecule inhibitors.[48] Extensive systematic structure-activity relationship (SAR) studies beginning from weak inhibitors identified from high-throughput screening, and SBDD using X-ray structures of early inhibitors bound in the active site of FXa, resulted in the identification of potent inhibitors. Key structural features of the FXa-binding site exploited by small-molecule inhibitors are a generally hydrophobic S1 recognition pocket with Asp189 and Tyr228 at the bottom, a hydrophobic S4 pocket formed by residues Phe174, Tyr99, and Trp215 and backed by a "cation hole" formed by the carbonyls of Lys96 and Glu97 that will accommodate positively charged P4 moieties; and backbone interactions with the intervening residues 214–217.[49] While the early benzamidine and other basic P1 groups formed key H-bonding interactions with Asp189, many of the neutral P1 inhibitors instead form hydrophobic interactions with Tyr228 through Cl, Me, or OMe substituents. In addition, the Cys191–Cys220 disulfide bridge above the S1 pocket provides an additional hydrophobic area that is accessed by some small-molecule inhibitors. Further optimization provided compounds with good oral bioavailability and optimal PK profiles suitable for once or twice a day dosing. Large clinical trials comparing FXa inhibitors to the standard of care have now established the safety and efficacy of the FXa mechanism in patients.[50] Currently three FXa inhibitors have been approved and marketed, while several others have entered or completed Phase I and II clinical trials, and the clinical pharmacology of the various compounds has been reviewed.[51]

7.16.3.2 Marketed Factor Xa Inhibitors

Rivaroxaban (**30**, **Fig. 8**),[52] the first FXa inhibitor to be approved for clinical use, utilizes an oxazolidinone core linking a chlorothiophene P1 group and a phenylmorpholinone P4 moiety while forming H-bonds to Gly219, an intervening residue in the active site of FXa. Rivaroxaban is an orally bioavailable, potent, and highly selective inhibitor of FXa with Ki = 0.4 nM. Selectivity over other serine protease is > 10,000 fold. In preclinical animal models of thrombosis, rivaroxaban was efficacious in both venous and arterial models without significant prolongation of bleeding times. Human oral bioavailability is very high (80–100% after a 10 mg dose) with a terminal half-life of 7–11 h.[52] In a large clinical trial comparing rivaroxaban to warfarin in patients with nonvalvular atrial

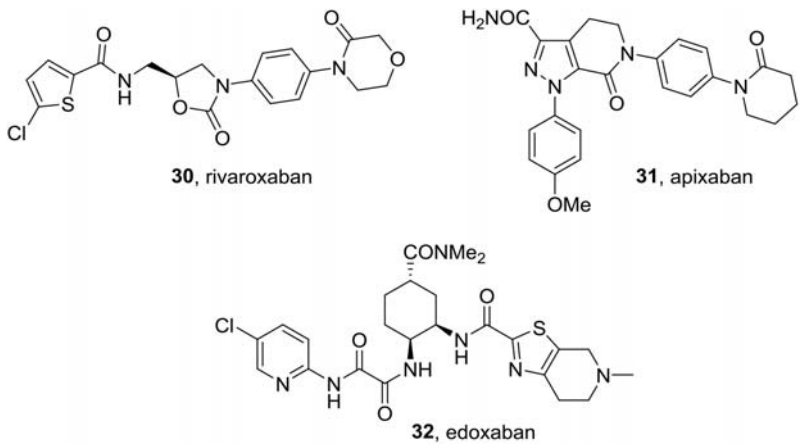

Fig. 8 Marketed FXa inhibitors: rivaroxaban, apixaban, and edoxaban.

fibrillation, rivaroxaban administered once daily was noninferior to warfarin in the prevention of stroke and systemic embolism (SPAF) with similar bleeding occurence.[53]

Apixaban (**31**, Fig. 8),[54] the second FXa inhibitor approved, incorporates a rigid bicyclic tetrahydropyrazolopyridinone core to optimally position its 4-methoxyphenyl P1 and phenylpiperidone P4 groups, while forming key H-bonding interactions to the intervening residues. It is a potent, highly selective FXa inhibitor with FXa Ki = 0.08 nM and >30,000-fold selectivity over other coagulation proteases. In dogs, apixaban demonstrated favorable PK with a small volume of distribution, low clearance, moderate half-life, and good oral bioavailability.[55] Dose-dependent antithrombotic effects in animal models of arterial and venous thrombosis were observed without excessive increase in bleeding times.[56] Apixaban has a terminal half-life in humans of 8–15 h and >50% oral bioavailability and is given twice a day to minimize peak-to-trough fluctuations, which appears to provide a more optimal benefit-to-risk profile.[57] In a clinical trial in 18,201 patients comparing apixaban to warfarin for SPAF, apixaban was superior to warfarin for prevention of stroke and systemic embolism with less bleeding and reduced mortality.[58] In a separate study, apixaban was also shown to be superior to aspirin for SPAF without significant increase in major bleeding.[59]

Edoxaban (**32**, Fig. 8),[60] the third FXa inhibitor to be approved, utilizes a substituted 1,2-diaminocyclohexane core with a chloropyridine P1 and an *N*-methyl-tetrahydrothiazolopyridine P4 group. Its FXa Ki is 0.56 nM with >10,000-fold selectivity for FXa. Oral absorption in rats and monkeys was superior to **28**, and dose-dependent inhibition of thrombus formation was observed in animal models without significant prolongation of bleeding time at an antithrombotic dose. In humans, the terminal half-life is 9–11 h with 50% oral bioavailability. Edoxaban dosed once daily demonstrated noninferiority versus warfarin for SPAF with less bleeding and lower risk of death from a cardiovascular cause.[61,62] The major route of clearance is renal, with 50% of drug excreted unchanged in the urine.[63]

In addition to the above key SPAF trials, these three FXa inhibitors have been assessed in multiple Phase III trials for treatment and prevention of VTE, DVT, or PE and have demonstrated either noninferior or superior efficacy and safety as compared to the standard of care.[64] Indirect analyses of the accumulated trial data suggest, however, that apixaban has a better margin of safety with respect to bleeding.[65] A recent meta-analysis of the combined data from four major SPAF trials with the new oral anticoagulants (dabigatran etexilate, rivaroxaban, apixaban, and edoxaban) found an overall favorable benefit/risk profile, with significant decrease in the incidence of stroke, intracranial bleeding, and mortality.[66] In this pooled analysis, the risk of major bleeding was similar to warfarin.

7.16.3.3 Additional FXa Inhibitors Assessed in Clinical Trials

Razaxaban (**33**, Fig. 9),[67] a forerunner to apixaban, was the first small-molecule oral FXa compound to establish clinical proof of concept (PoC) for the FXa mechanism[68] and advanced through Phase II trials before being superseded by apixaban. Razaxaban has an FXa Ki = 0.19 nM with excellent selectivity over other serine proteases. A unique feature of **33** was the aminobenzisoxazole P1, which was designed using SBDD to provide trypsin selectivity by taking advantage of the larger S1 pocket of FXa. Betrixaban (**34**, Fig. 9),[69] which has completed successful Phase II trials for VTE and SPAF,[70] is an anthranilamide-based compound with a chloropyridine P1 and dimethylbenzamidine P4 group. It is a potent inhibitor of FXa (Ki = 0.12 nM) with a high volume of distribution, long half-life, minimal renal clearance, and low hepatic metabolism.[71] A Phase III study for extended VTE thromboprophylaxis in medical patients is still ongoing.

Optimization of the pyrrolidine N-substituent, which projects into the S1β-pocket of FXa in a series of (3*R*,4*R*)-pyrrolidine-3,4-dicarboxamide core molecules, provided R1663 (**35**, Fig. 9).[72] This inhibitor had good PK and oral bioavailability across multiple species with >33-fold selectivity over other serine proteases. Data from Phase I trials has been reported,[73] and Phase II trials with this compound have since been initiated in Russia.

Letaxaban (**36**, Fig. 9)[74] incorporates a 2-hydroxyethylsulfone moiety to link a chloronaphthyl P1 with a 4-piperidinyltetrahydropyrimidinone P4 group. The tetrahydropyrimidinone P4 group of **36** was discovered from extensive SAR to identify a replacement heterocycle to address a metabolic vulnerability observed in an earlier imidazoimidazolone lead compound. Compound **36** has an FXa IC_{50} = 3.5 nM with favorable PK in monkeys and potent antithrombotic efficacy in a rabbit model of venous thrombosis without affecting bleeding time.[75] Letaxaban was progressed through Phase II clinical trials, but has since been discontinued. Darexaban (**37**, Fig. 9),[76] a phenylene diamine with 4-methoxyphenyl P1 and phenyldiazine P4, is a modestly potent FXa inhibitor with a Ki = 31 nM, which progressed through Phase III clinical trials before being discontinued.[77] Glucuronidation of the phenol in **37** after oral administration leads to the formation of a highly metabolically stable, active metabolite (FXa IC_{50} = 28.6 nM) that plays a major role in the potent anticoagulant activity in plasma.[76]

Eribaxaban[78] (**38**, Fig. 9) is a D-proline-based FXa inhibitor which incorporates a chlorophenyl P1 in combination with a fluorophenylpyridinone P4 group and has a FXa IC_{50} = 0.32 nM. The compound showed good preclinical properties and was advanced through Phase II clinical trials before development was halted.[79] The results of a Phase II proof of concept study with LY517717 (**39**, Fig. 9)[80] were also reported, but no further development is evident. GW813893 (**40**),[81] a pyrrolidinone-based molecule with a 5-chlorothiophene-2-ethenyl P1 and morpholine amide P4 group, was also reportedly advanced into clinical trials based on encouraging preclinical data in animal models,[82] but no results or further development has been reported. Positive results from a first in human (FIH) trial with FXa inhibitor, DY-807f, were recently reported, but the structure of this compound was not disclosed.[83]

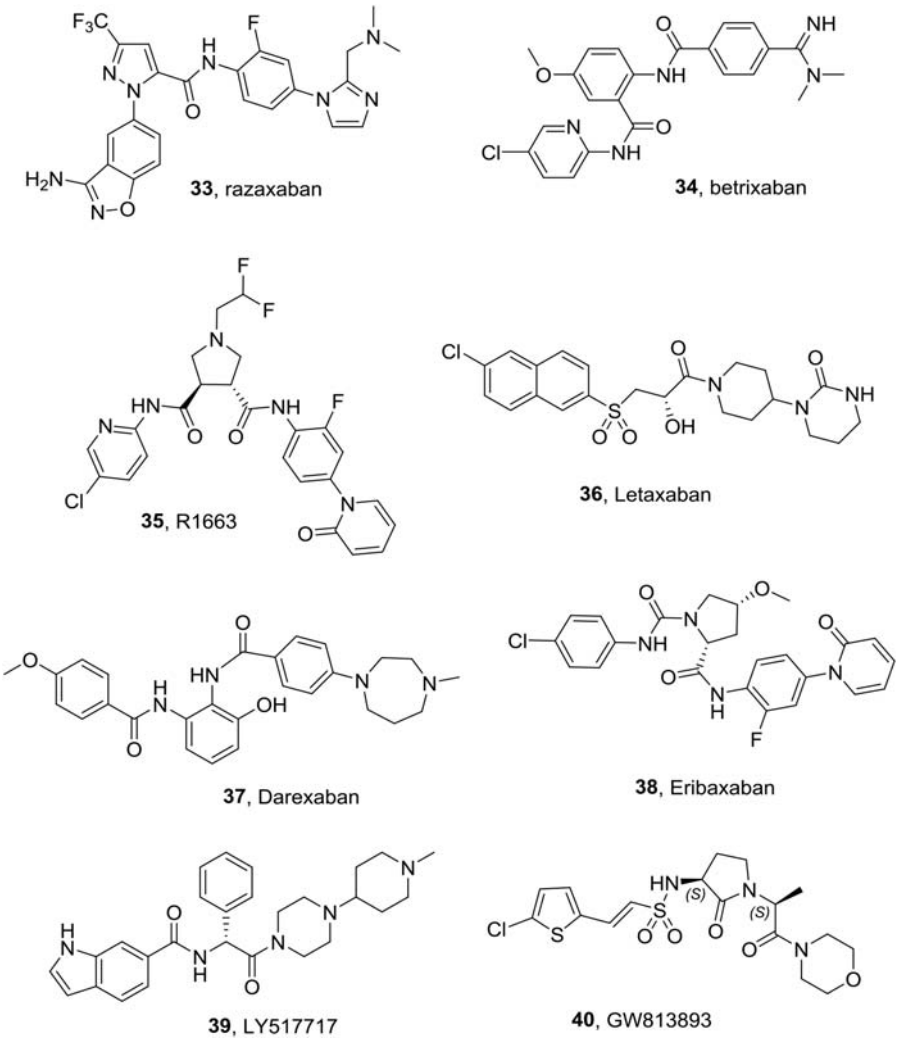

Fig. 9 Structures of additional FXa inhibitors that progressed to clinical trials.

7.16.3.4 Preclinical FXa Inhibitors

Many additional small-molecule inhibitors of FXa that have not advanced to clinical trials have also been described. Potent in vitro inhibition of FXa can be achieved with a wide variety of scaffolds in combination with structurally diverse P1 and P4 moieties, and detailed reviews of the field are available.[48,84,85] Finding drug candidates with the ideal combination of potency, PK and PD, with a good margin of safety is much more challenging and was the cornerstone of the successful efforts that resulted in the FXa inhibitors described earlier. The range of structural diversity explored in the search for viable FXa inhibitors is a testament to the ingenuity of the medicinal chemist. The following additional examples provide a brief survey of recently disclosed novel, potent, and selective inhibitors of FXa, many of which are also efficacious in animal models of thrombosis after oral administration.

A conformationally constrained analog of rivaroxaban (**41**, Fig. 10),[86] which incorporates a novel [6,6,5] tricyclic ring system designed to maintain the preferred coplanar relationship between the oxazolidinone ring and the pendant phenyl, was reported to have improved in vitro and in vivo potency in animal models of thrombosis with similar increase in bleeding times compared with rivaroxaban. The compound had high oral bioavailability in dogs (F% = 92%) and was well tolerated in a 2-week toxicity study in rats.

Various analogs of apixaban have been explored, including triazolinone **42** (Fig. 10), which exhibits a unique binding mode extending the triazolinone ring deeper into the S1 pocket as a result of movement of Asp189 to create a larger pocket.[87] Potential backups to apixaban with gem-dimethyl P4 moieties replacing the terminal lactam were also explored. Compounds **43** and **44** (Fig. 10) had the best combination of FXa affinity, PK, and oral bioavailability, but did not differentiate from apixaban.[88]

In the edoxaban series, compounds with alternate P1 groups were explored including 5-chloroindole compound **45**, which was evaluated as a potential clinical candidate, and chloroisoquinoline **46**,[89] which also incorporates a novel dihydropyrrolo[3,4-*d*]thiazolyl P4 group (See Fig. 11). Compared to **45**, compound **46** showed a reduced food effect in both monkeys and dogs, which was attributed to its greatly improved solubility at both pH 1.2 and 6.8.

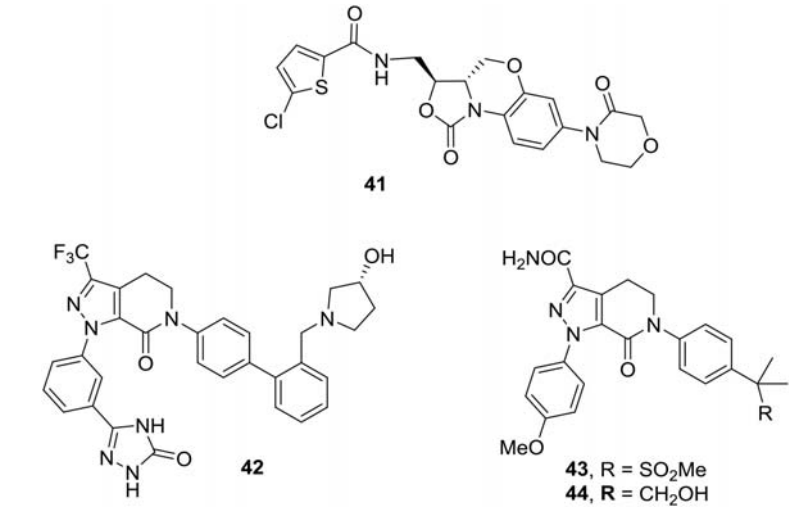

Fig. 10 Analogs of rivaroxaban and apixaban.

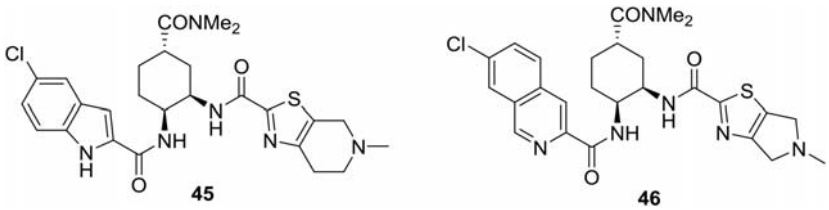

Fig. 11 Analogs of edoxaban.

The biphenylsulfonamide P4, previously pioneered in early examples in the pyrazole series, which led to apixaban, was also used successfully in the SBDD of early examples in the eribaxaban series, such as compound **47** (Fig. 12).[90] Additional analogs of eribaxaban with disubstitution at the 4-position of the central pyrrolidine ring were explored in an attempt to increase the projected human half-life.[91] This was achieved with compound **48** by incorporating a 2,4-difluorophenyl group at this position to achieve a projected human t½ of 23 h compared to 6 h for eribaxaban. An FXa X-ray crystal structure of **48** compared with eribaxaban shows good overlap of the two structures with the aryl group extended above the S1 pocket such that the *ortho*-fluoro substituent occupies the disulfide region. Compound **49**, which uses the P4 of eribaxaban and the P1 of rivaroxaban in combination with a pyrrolidine scaffold, was evolved from a weakly active aminothiazole lead.[92] Further optimization of this series resulted in the identification of clinical candidate, **35** shown earlier.[72]

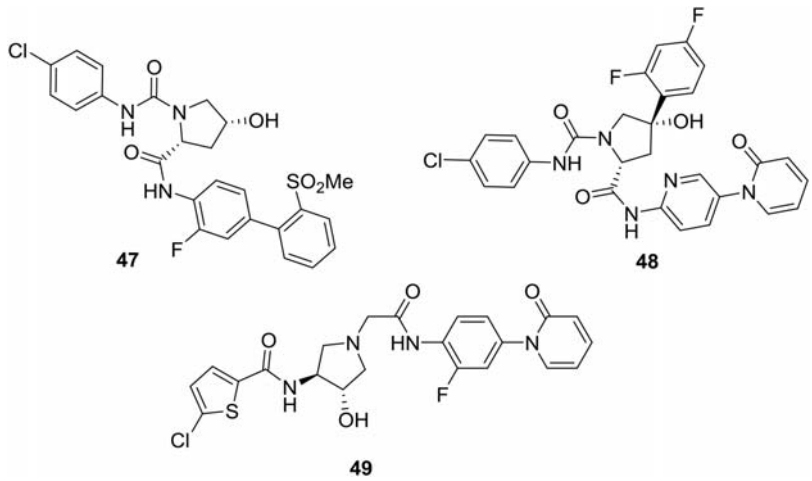

Fig. 12 Analogs of eribaxaban.

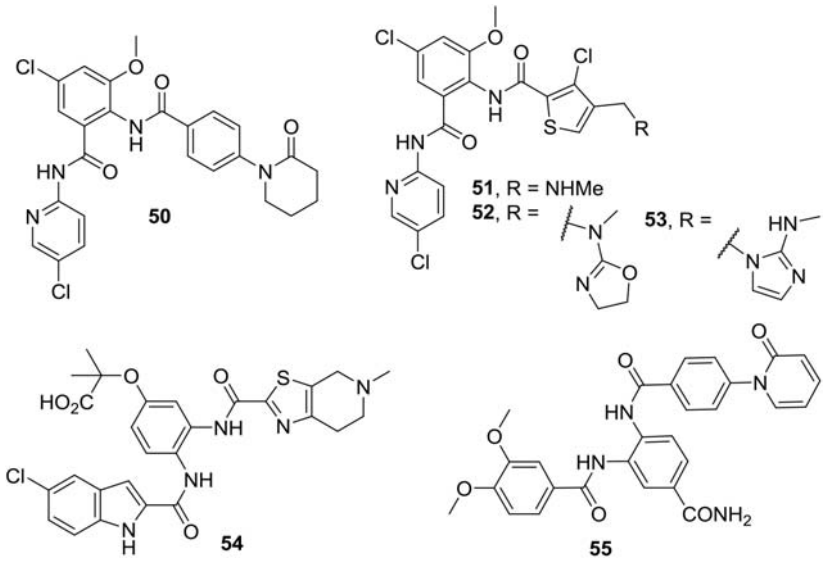

Fig. 13 Analogs of betrixaban.

Numerous examples of anthranilamide-based compounds, of which betrixaban is the most advanced, have been disclosed. The examples depicted in Fig. 13 serve to show the diversity of P1 and P4 groups and substitution patterns on the central phenyl ring that can be combined using this scaffold (ie, **50**[93] and **51–53**[94]), as well as the related phenylene diamine scaffold (ie, **54**[95] and **55**[96]), to provide potent inhibitors of FXa.

To further improve the properties of GW813913, biaryl substituted pyrrolidinones, such as compound **56** (Fig. 14),[97] a subnanomolar inhibitor of FXa that incorporates the P4 group of razaxaban, was prepared. The P1 group of GW813913 was also successfully used in combination with an aminomethyl pyrrolidine core and 4-pyridylpiperidine P4 group in compound **57**.[98]

Various analogs of letaxaban that lack the β-hydroxy group on the ethylsulfone linker and incorporate novel P4 groups were explored. Potent, selective, orally bioavailable inhibitors, such as **58**,[99] **59**,[100] and **60**,[101] (Fig. 15) with reduced CYP3A4 inhibition over earlier analogs were identified as interesting lead molecules.

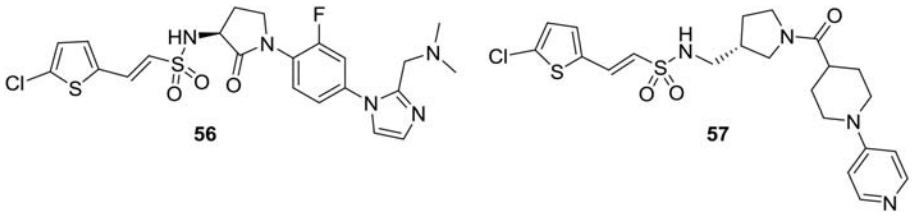

Fig. 14 Analogs of GW813913.

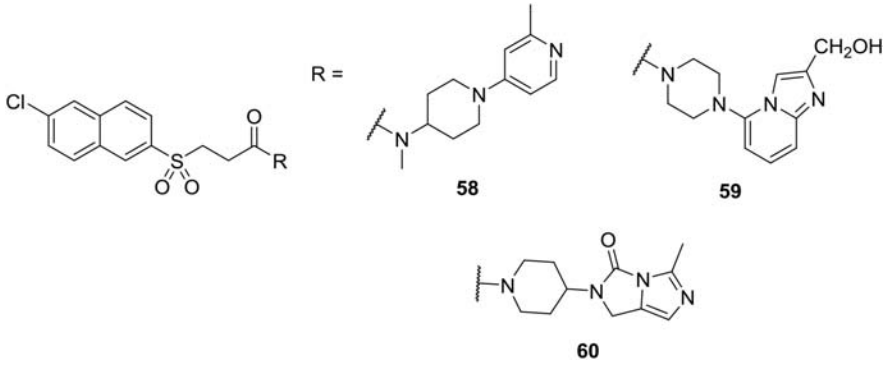

Fig. 15 Analogs of letaxaban.

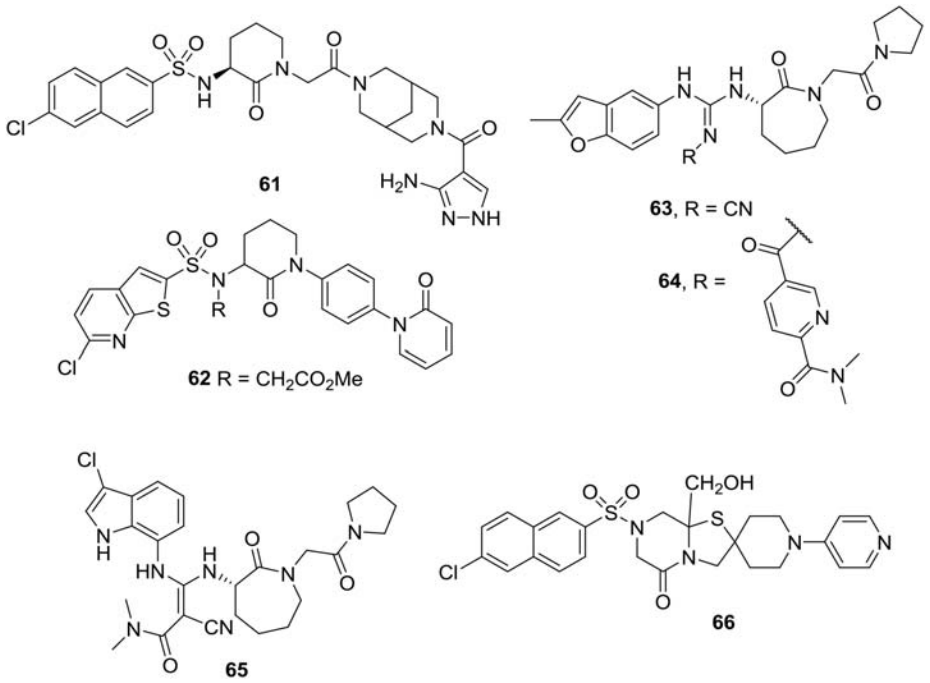

Fig. 16 FXa analogs with alternate cores.

Potent FXa inhibitors have also been reported with lactam cores, such as aminopiperidones **61**[102] and **62**[103] and aminoazepinones **63**,[104] **64**,[105] and **65**[106] (Fig. 16). A final example of a potent FXa inhibitor with a unique tricyclic scaffold, compound **66** utilizes a novel substituted *N,S*-spiroacetal scaffold to position a chloronaphthyl P1 and 4-pyridyl to provide a potent inhibitor of FXa with $IC_{50} = 1.2$ nM.[107]

7.16.3.5 Reversal Agents

The anticoagulant effects of the VKAs can be effectively reversed in 12–24 h by oral or intravenous administration of vitamin K, or more rapidly by intravenous administration of vitamin K-dependent clotting factors in the form of prothrombin complex concentrate to prevent bleeding in the event of trauma, a need for immediate surgery or overdose.[108] With the introduction of new highly potent anticoagulants came concerns over the lack of effective reversal agents for this class of drugs. Consequently, a focused effort was quickly undertaken to identify both general and specific reversal agents for these new anticoagulants.[109] Currently, two potential solutions for reversal of FXa inhibitors have been evaluated in clinical trials.[110,111] Andexanet alfa is a recombinant protein with similar structure to FXa but lacking the γ-carboxyglutamic acid terminal amino acid and incorporating a serine to alanine mutation at the active site, thus rendering it enzymatically inactive, and therefore unable to convert prothrombin to thrombin.[112] This protein effectively binds to FXa inhibitors with a greater affinity than natural FXa, leading to rapid inactivation of the inhibitors. In animal models, the protein effectively reversed the effect of both direct and indirect FXa inhibitors. Phase III clinical trials have demonstrated reversal of the anticoagulant effects of both rivaroxaban and apixaban by adexanet alfa.[113]

Aripazine (PER977, **67**, Fig. 17), a small water-soluble, cationic molecule, was originally developed as a reversal agent for heparin and fondaparinux and works by binding to these anionic drugs through noncovalent H-bonds and charge–charge interactions to inactivate them.[114] Recent studies suggest that this compound may also be effective as a reversal agent for the currently

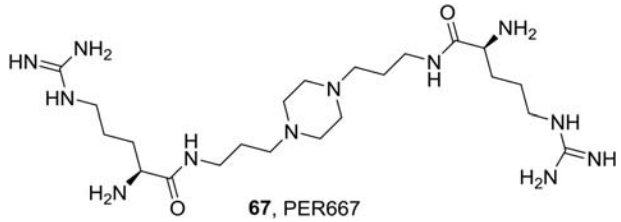

Fig. 17 Structure of PER667.

marketed FXa and thrombin inhibitors. In healthy volunteers pretreated with 60 mg of edoxaban, an i.v. bolus dose of 300 mg of PER977 was shown to return clotting times to normal within 10–30 min.[115]

7.16.3.6 Dual Thrombin/FXa Inhibitors

A number of research groups have proposed dual inhibitors of thrombin and FXa as potentially more effective anticoagulants compared with DTIs or FXa inhibitors alone. A recent publication comparing a thrombin and FXa inhibitor alone or in combination, along with a dual thrombin/FXa inhibitor, RWJ-445167 (**68**, FXa Ki = 230 nM, thrombin Ki = 4 nM, Fig. 18), reported a cooperative antithrombotic effect in vivo in a rat ECAT model when both enzymes were inhibited simultaneously.[116] Based on favorable data in animal models, **68** was studied in Phase I clinical trials; however, oral bioavailability in humans was insufficient for further advancement.[117] A variety of prodrugs were evaluated in rats, but no suitable candidates were identified.

The results of a Phase I clinical trial of another dual thrombin/FXa inhibitor, tanogitran (**69**; thrombin Ki = 2.7 nM, FXa Ki = 26 nM, Fig. 18), in an i.v. model of endotoxin-induced coagulation were published.[118] Plasma aPTT values were prolonged and in vivo thrombin generation (TG) was reduced in a dose-dependent manner. The compound was reported to be safe and well tolerated. No further clinical development has been reported.

The addition of a methyl group to the double bond in vinyl sulfone compound **70** (Fig. 18) converted a 100-fold selective Xa inhibitor into a dual FXa/thrombin inhibitor with 2 nM affinity for both enzymes.[119] This compound had two- to fourfold improved functional potency in plasma-based assays and was orally bioavailable in both dogs and rats. Similarly, using rivaroxaban as a starting point, replacement of the morpholinone P4 group with 2-ethoxycarbonylpiperidine resulted in conversion from a highly potent, selective inhibitor of FXa to a dual FXa/thrombin inhibitor **71**[120] with modest potency for both enzymes, that is, FXa Ki = 62 nM and thrombin Ki = 353 nM. Using docking experiments, the authors proposed that extension of the ethoxycarbonyl group into the S2 pocket of thrombin is responsible for the restoration of thrombin activity. By optimization of a proline analog of another selective FXa inhibitor, the dual thrombin/FXa inhibitor **72**[121] was obtained with FXa Ki = 1.5 nM and thrombin Ki = 3.5 nM. Both this compound and its ethyl ester prodrug had low oral bioavailability and short half-lives in rats that precluded further development.

SAR107375 (**73**, Fig. 18)[122] is a dual inhibitor with FXa Ki = 1 nM and thrombin Ki = 8 nM that was identified from optimization of a thrombin inhibitor with weak FXa affinity. Compound **73** was potent in models of venous and arterial thrombosis in rats and showed reduced bleeding liability compared to either rivaroxaban or dabigatran etexilate. It is orally bioavailable in both dogs and rats (47% and 21%, respectively), and is reportedly in preclinical development.

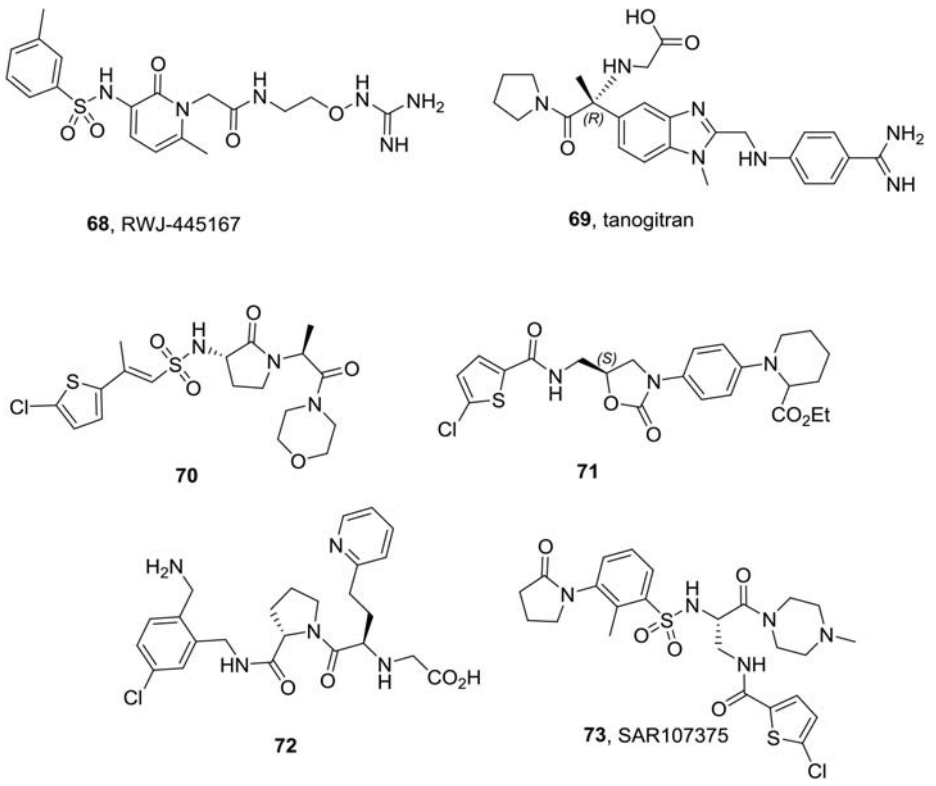

Fig. 18 Dual inhibitors of FXa and thrombin.

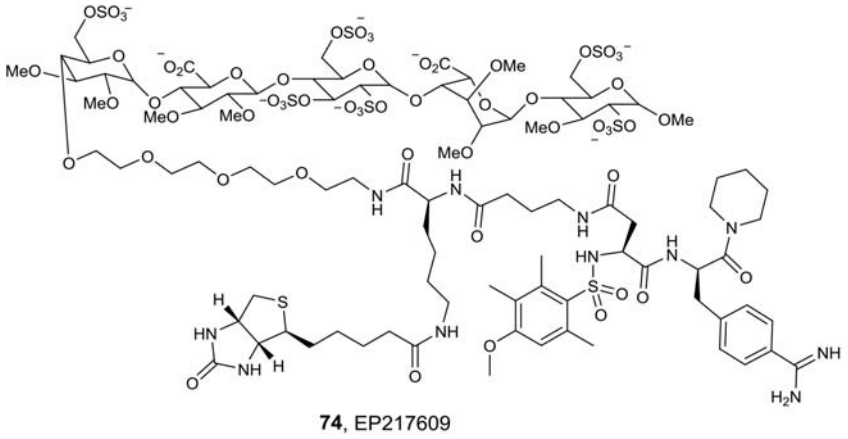

Fig. 19 Structure of parenteral dual inhibitor of FXa and thrombin, EP217609.

EP217609 (**74**, **Fig. 19**),[123] a dual-action parenteral anticoagulant currently in Phase II clinical trials, combines a fondaparinux analog with a peptidomimetic DTI in a single molecule and also incorporates a biotin tag to allow neutralization with avidin. The compound displayed a long half-life with predictable PK, along with the ability to reverse the effects, that cannot be replicated by coadministration of the individual components. It may offer an attractive alternative for use in cardiopulmonary bypass surgery compared to the standard of care.

7.16.4 Factor VIIa Inhibitors

Comparisons of antithrombotic mechanisms have identified the TF–FVIIa complex as a biological target that offers strong antithrombotic efficacy and low bleeding liability in preclinical models.[124–126] Similar to the other serine proteases of the coagulation cascade, a major challenge in the development of drugs inhibiting TF/FVIIa is attaining oral bioavailability. Many TF/FVIIa inhibitors bear a highly basic benzamidine P1 moiety (pKa ~12), a mimetic of the guanidine side-chain of Arg in the natural substrates. Benzamidine-based inhibitors are potent, but due to low permeability of the basic group require administration as a prodrug or replacement with a nonbasic or less-basic moiety to attain orally bioavailability. Replacement of the amidine moiety, which contributes greatly to ligand-binding affinity, requires introduction of compensatory interactions. Neither strategy has yet successfully yielded an orally bioavailable TF/FVIIa clinical compound. TF/FVIIa compounds that have advanced to the clinic thus far have been biological agents[127,128] and a parenterally administered, small-molecule inhibitor.[129]

7.16.4.1 Target Validation and Proof of Concept

Initial evidence for antithrombotic activity for the TF/FVIIa pathway comes from biological agents targeting the complex or its individual components. The anti-TF antibody, AP-1, blocked thrombus formation in a rabbit thrombosis model[130] with reduced bleeding at elevated levels when compared to the DTI napsagatran and heparin.[131] Similarly, inactive mutants of TF showed efficacy in in vivo thrombosis models with decreased bleeding relative to other agents.[132,133] These TF mutants bind FVIIa, but form an enzymatically inactive complex. Active site inactivated FVIIa (FVIIai) showed antithrombotic efficacy in a baboon angioplasty model[134] and a rabbit model of carotid artery thrombosis.[135] These biological agents established a promising efficacy/safety profile for targeting the TF/FVIIa complex.

Following up on initial success of biological agents, many small-molecule inhibitors of TF/FVIIa were advanced into in vivo animal models of thrombosis. In some of the earliest studies of small-molecule TF/FVIIa inhibitors, antithrombotic efficacy in monkeys was reported.[124,125] Addition of a TF/FVIIa inhibitor on top of aspirin increased efficacy in venous thrombosis model without increasing bleeding relative to aspirin alone.[124] In comparisons to other antithrombotic mechanisms, the FVIIa inhibitors showed a superior bleeding profile at equi-efficacious doses or higher multiples.[124–126] Additional in vivo studies of small-molecule inhibitors provide further evidence for TF/FVIIa inhibitors of potent antithrombotic efficacy and minimal bleeding liability, especially when compared to other antithrombotic mechanisms.[136–141]

7.16.4.2 Agents Advanced to Clinical Development

Recombinant nematode anticoagulant protein c2 (rNAPc2) is an 85-amino acid peptide originally isolated from the hookworm, which binds FX and inhibits TF/FVIIa via the formation of a ternary complex.[142] In a Phase II study of patients undergoing total knee replacement surgery, an optimal dose was identified, which balanced antithrombotic efficacy and major bleeding.[127] In a Phase

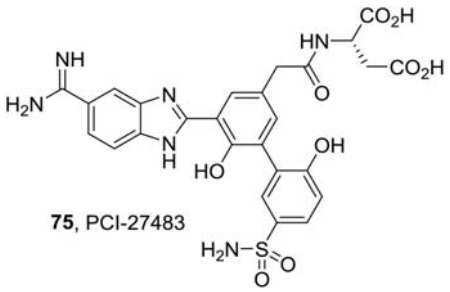

Fig. 20 Structure of parenterally administered TF/FVIIa inhibitor PCI-27483.

II study, rNAPc2 on top of standard therapy in patients undergoing coronary angioplasty suppressed biomarkers of TG and increased minor bleeding only at the highest dose to 27% (vs. 6.7% for placebo).[143] In a Phase II study in patients with non-ST-segment elevation acute coronary syndrome, rNAPc2-suppressed TG, and reduced rates of ischemia by >50%, although the study was not powered to evaluate clinical outcomes.[144] Elevated major bleeding was observed at the highest dose of rNAPc2. No further development as an anticoagulant has been reported.

ALT-836 (also referred to as TNX-832 and Sunol CH36) is an antibody to TF that binds specifically to TF at the FX-binding site, preventing formation of the TF/FVIIa–FX complex, and thus blocks the activation of FX and FIX.[145] In a Phase I study in subjects with stable coronary artery disease, ALT-836 showed dose-dependent anticoagulant effects.[128] Dose-related bleeding was observed, but was limited to minor bleeding events. Preclinically, ALT-836 reduced sepsis-induced respiratory and renal injury in a baboon model.[146] Based upon these results, ALT-836 was subsequently advanced into clinical trials for acute lung injury and acute respiratory distress syndrome (ARDS).[147] A Phase II study to evaluate safety and efficacy in this population is complete and data are pending.[148] A Phase I study of ALT-836 in combination with gemcitabine in patients with locally advanced or metastatic solid tumors is underway.[149]

PCI-27483 (**75**, Fig. 20) is a parenterally administered, small-molecule inhibitor of TF/FVIIa advanced into clinical trials for the treatment of pancreatic cancer. TF is upregulated in cancers and levels correlate with disease progression, making the protein a potential anticancer target.[150] Inhibitors of TF/FVIIa have the potential to prevent cancer-related thromboembolic events and treat cancer by blocking nonhemostatic signaling pathways.[129] In a Phase II study, **75** was dosed parenterally in combination with gemcitabine in patients with advanced pancreatic cancer.[151] Targeted inhibition of coagulation was achieved, but was accompanied by a higher incidence of low-grade bleeding relative to placebo. Clinical endpoints in pancreatic cancer of overall survival versus gemcitabine alone were not achieved.

7.16.4.3 Preclinical Compounds

7.16.4.3.1 Amidine-based inhibitors and prodrugs

Early small-molecule TF/FVIIa inhibitors, like early thrombin and FXa inhibitors, contained an amidine-based P1 moiety (see Fig. 21). A phenylglycine-based TF/FVIIa inhibitor chemotype[137] shows potent inhibitory activity and promising bioavailability upon oral dosing of a prodrug. Compound **76** (TF/FVIIa Ki = 81 nM) showed dose-dependent antithrombotic efficacy upon i.v. infusion in a guinea pig model with little prolongation of bleeding. Oral dosing of the double prodrug **77** showed a similar profile albeit at high doses. In rats, **77** resulted in oral bioavailability of 20%.

A series of amidinobenzimidazole[152,153] and amidinoindole-based[154] inhibitors were disclosed (Fig. 21). Compound **78**[138] potently inhibits TF/FVIIa (Ki = 2 nM) with 3600-fold and >100,000-fold selectivity against FXa and thrombin, respectively. Under i.v. dosing in a baboon thrombosis model, **78** showed potent efficacy, with $EC_{50} = 0.17$ μM. At elevated concentrations, nearly complete inhibition of platelet deposition was reached, accompanied by less than a doubling of bleeding time. Alkoxy and carbamate prodrugs of a related amidinobenzimidazole (**79**)[154] provided low bioavailability (≤2%) of the parent species due to limited cleavage of the highly bioavailable prodrug species. Similarly, oral dosing of amidoxime prodrug **81** in rats gave 11% oral bioavailability of the prodrug, but negligible bioavailability of the parent amidine **80**.[155]

Biaryl acid inhibitor BCX-3607 (**82**, Fig. 21) inhibits TF/FVIIa with an IC_{50} of 4 nM and showed in vivo efficacy in a rat venous thrombosis model.[139] BCX-3607 decreased IL-6 response to LPS (Lipopolysaccharide) in a mouse model of endotoxemia and decreased FVIIa-mediated generation of IL-6 and IL-8 in cells. The combined antithrombotic and antiinflammatory activities of a TF/FVIIa inhibitor may be an attractive profile in treatment of coronary artery disease.[156]

Amidinotetrahydroquinoline-based FVIIa inhibitor BMS-593214 (**83**, Fig. 21) was reported to have a TF/FVIIa Ki = 1.3 nM and >150-fold selectivity versus a panel of 12 serine proteases.[157] In animal studies, **83** showed potent in vivo activities in models of both arterial and venous thrombus formation.[140] Notably, at fully efficacious concentrations, **83** increased bleeding time by only 15%, a favorable efficacy versus bleeding profile.

Prodrug studies of the benzamidine-based TF/FVIIa inhibitor AS1924269 (**84**, Fig. 21) have been reported.[158,159] The carbamate/ester double prodrug **85** resulted in 36% oral bioavailability of the parent species, versus 0.3% for direct dosing of **84**.

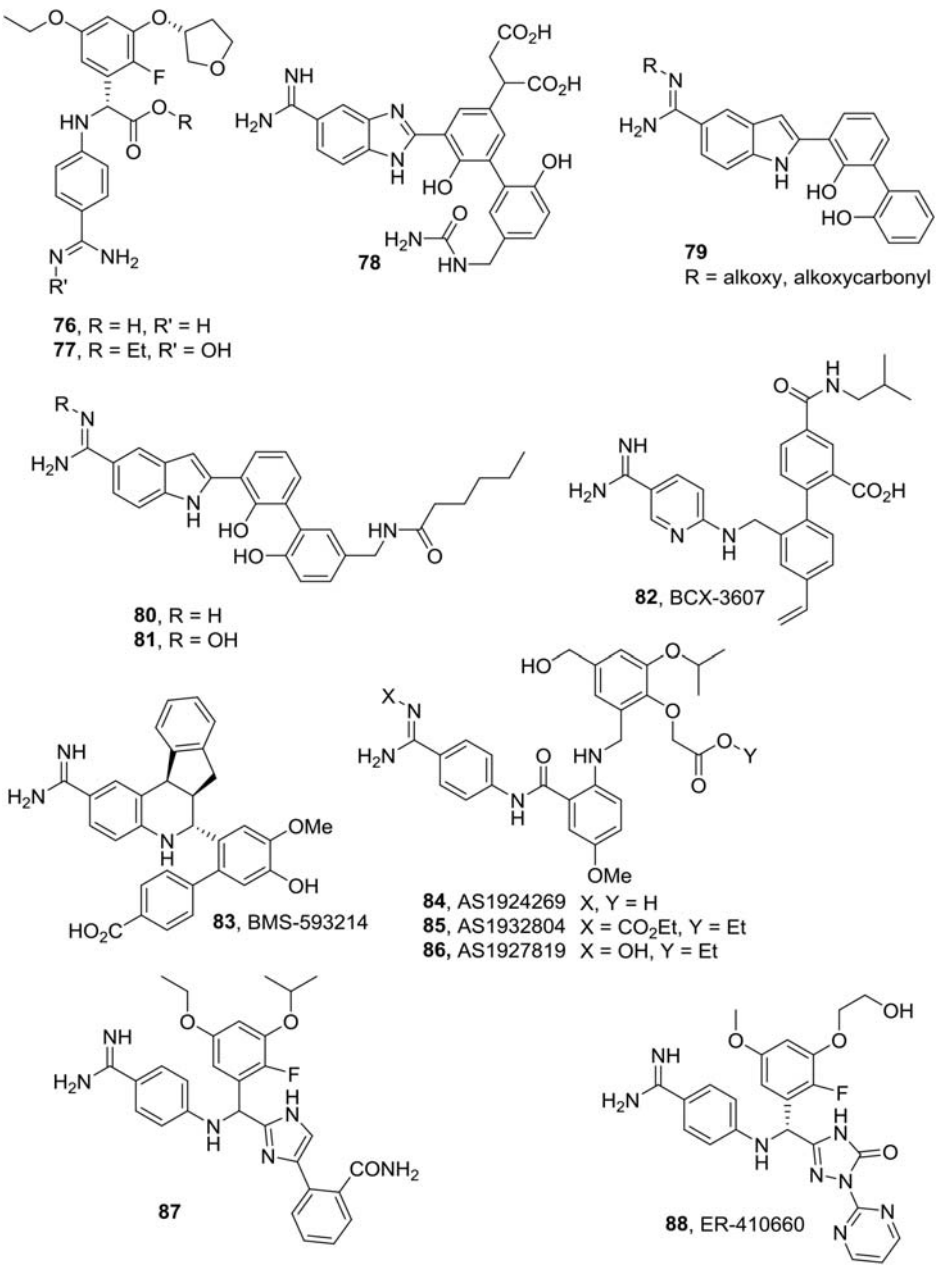

Fig. 21 Structures of amidine-based TF/FVIIa inhibitors.

Alternatively, amidoxime prodrug **86** increased permeability of the intermediate ester-cleaved species, but only 11% of the amidoxime moiety converted to the amidine parent **84**. The high parent oral bioavailability attained with **85** stands out relative to the limited success reported for prodrugs of amidine-based TF/FVIIa inhibitors.

Heterocyclic subunits were incorporated into a phenylglycine chemotype to afford potent FVIIa inhibitors.[160] Compounds were designed to mimic interactions of the carboxylic moiety of compounds such as **76** to the catalytic triad of FVIIa while making additional interactions with the S'_1 pocket. A survey of heterocycles led to the discovery of the optimized phenylimidazole inhibitor **87** (Fig. 21), which was shown by X-ray crystallography to form a key lipophilic interaction with the Cys42–Cys58 disulfide bond of FVIIa.

ER-410660 (**88**, Fig. 21), a structurally similar pyrimidinyltriazolone, along with its prodrug E5539 (structure undisclosed), were studied in vivo.[141] Compound **88** is a potent, selective TF/FVIIa inhibitor with a Ki of 4.9 nM. ER-410660 showed in vivo efficacy in rhesus monkey and rat thrombosis models upon i.v. dosing with reduced bleeding versus both dabigatran and rivaroxaban. The prodrug showed efficacy in a rhesus monkey TF-induced thrombin model after oral dosing, but exposure levels for the parent species **88** were not reported.

7.16.4.3.2 Nonamidine inhibitors

Replacement of the amidinoindole of compound **89** (Fig. 22) with 5-aminopyrrolo[3,2-*b*]pyridine resulted in a 75-fold loss in potency in compound **90** (Ki = 300 nM), but reduced the pKa of the P1 group significantly from ~12 to 8.8.[161] Introduction of additional substitution in **91** (Ki = 20 nM, Fig. 22) recovered much of the lost potency. A related 5-azaindole inhibitor afforded similar potency (**92**, Ki = 62 nM).[162] Incorporation of a 4-amino-5-azaindole P1 group led after further optimization to a potent inhibitor, **93** (Ki = 2.6 nM, Fig. 22).[163] Although the impact of these changes on oral exposure was not reported, these benzamidine replacements may find utility in future serine protease inhibitor design.

Neutral and less-basic benzamidine replacements were also explored in a biaryl chemotype, which led to the discovery of a benzamide P1 group (**95**, Fig. 23), albeit with a 200-fold loss in potency versus benzamidine **94**.[164] Incorporation of an aminomethyl

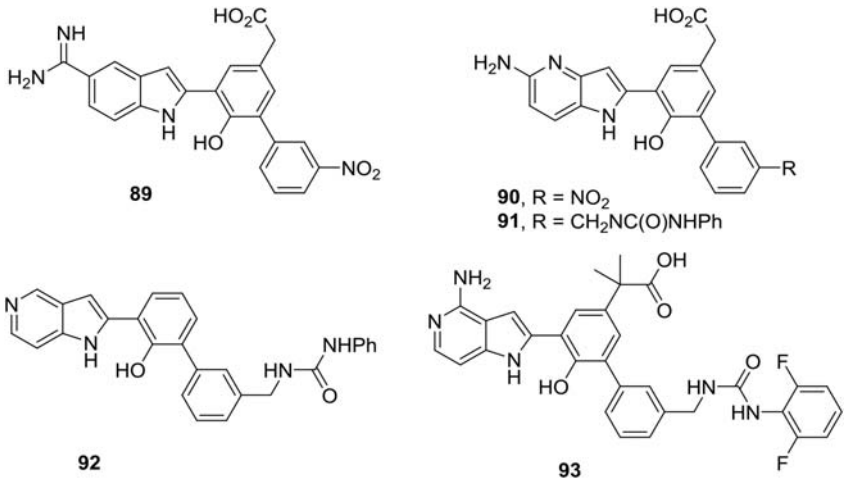

Fig. 22 Nonamidine replacements for amidinoindole and amidinobenzimidazole P1 groups.

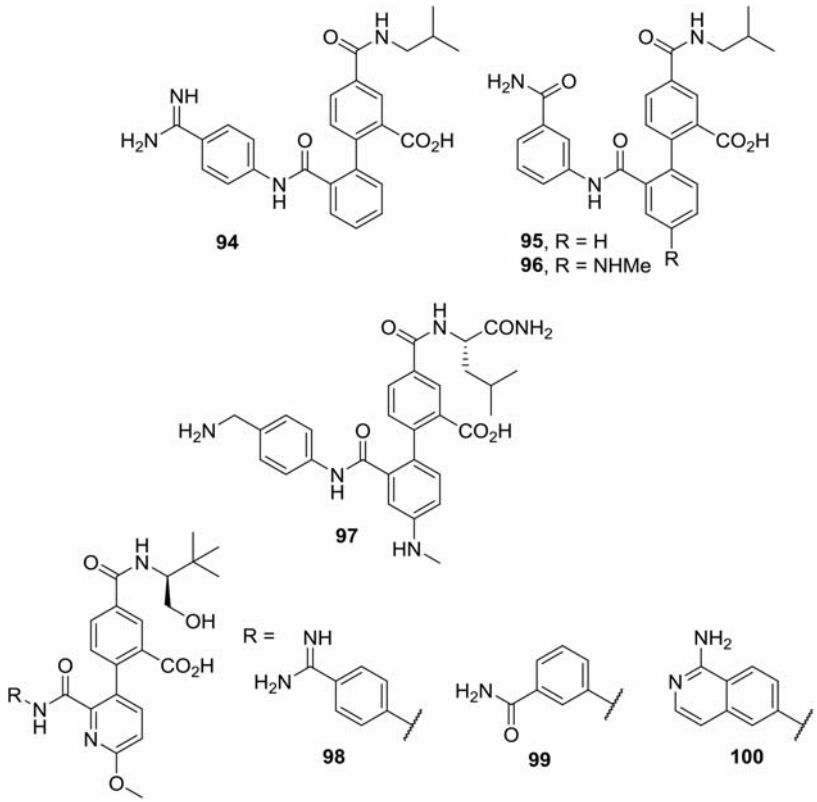

Fig. 23 Nonbenzamidine P1 groups in a biaryl acid chemotype.

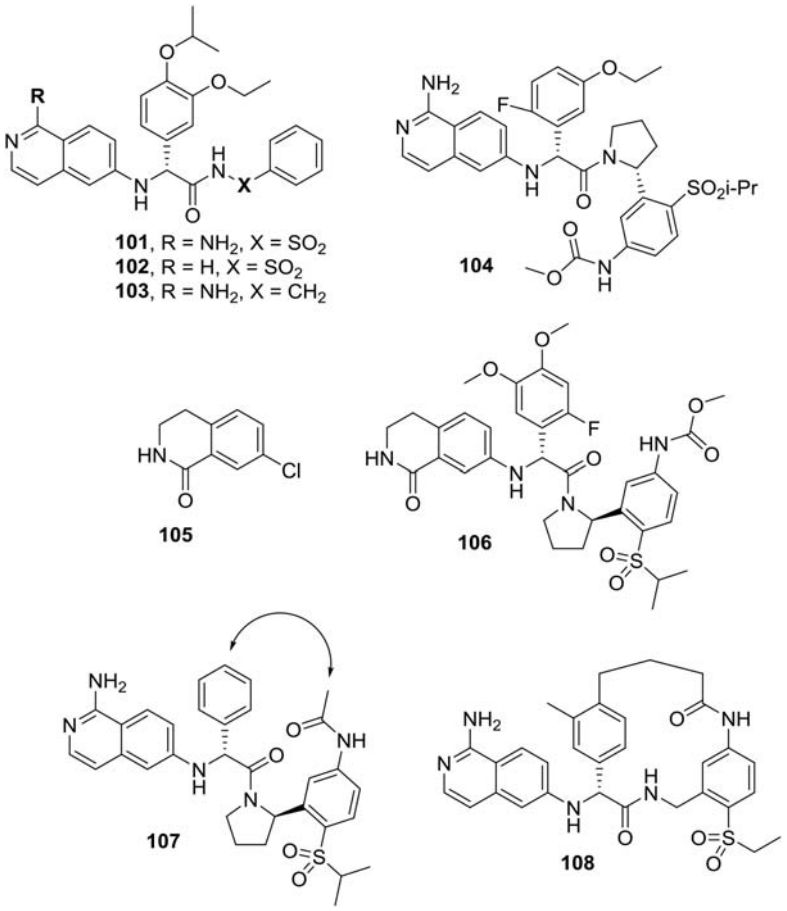

Fig. 24 Nonbenzamidine P1 groups in a phenylglycine chemotype.

group in compound **96** improved potency 30-fold to an IC_{50} of 690 nM. Benzylamine **97** (Fig. 23) showed similar potency (IC_{50} = 590 nM) and reached 2.9 μg mL^{-1} exposure at 1 h after 100 mpk oral dosing, ~10-fold higher than **94**.[165] The same neutral *m*-benzamide P1 group was also identified as a viable benzamidine replacement in a related biaryl acid core example **99** with a 35-fold loss in potency relative to benzamidine **98**.[166] Incorporation of a weakly basic aminoisoquinoline P1 group resulted in a potent inhibitor of TF/FVIIa (**100**, IC_{50} = 7 nM), equipotent with **98**.

Incorporation of the aminoisoquinoline P1 group into a zwitterionic phenylglycine acylsulfonamide core gave another potent inhibitor (**101**, Ki = 10 nM, Fig. 24) with a weakly basic P1 (pKa = 8.9).[167] The compound had low oral bioavailability in dog (F % = 4). The isoquinoline analog (**102**, Ki = 44 nM, Fig. 24) is less basic (pKa = 7.8) and shows improved oral bioavailability in dog of 36%. In a subsequent disclosure, the acidic acylsulfonamide moiety of **102** was replaced with a neutral benzylamide (**103**, Fig. 24).[168] Improved oral bioavailability in dog (45%) and rat (31%) was observed for **103** relative to **102**, but at the expense of potency. Potency was improved while maintaining oral bioavailability by the introduction of a pyrrolidine conformational constraint (**104**, Ki = 1.9 nM, Fig. 24) that maintains good oral bioavailability in dog (45%), but modest bioavailability in rat (8%).

A fragment screen to identify novel, neutral P1 groups was recently described.[169] Fragments were selected computationally using protein ensemble docking in FVIIa. Top-ranked fragments were evaluated in biological and NMR-binding assays yielding a diverse collection of neutral P1 groups. X-ray crystallography of the fragments provided confirmation of binding in the S1 pocket and guided incorporation into inhibitor molecules. Fragment **105** (TF/FVIIa Ki = 8.9 mM, Fig. 24) was grafted onto a phenylglycine amide core to give **106** (Fig. 24) with good potency (TF/FVIIa Ki = 130 nM) and greatly improved parallel artificial membrane permeability assay (PAMPA) permeability when compared to an aminoisoquinoline analog (160 vs. 2 nm s^{-1}).

Novel macrocyclic FVIIa inhibitors have also been reported.[170] A crystal structure of phenylpyrrolidine amide FVIIa inhibitor **107** (Fig. 24) showed close proximity between the P2 phenyl and the P1′ acetanilide and suggested the possibility of macrocyclization. Upon cyclization, the 16-membered macrocycle was 60-fold more potent than the linear counterpart. Further optimization afforded macrocycle **101** (Fig. 24), which is a potent inhibitor of FVIIa (Ki = 1.6 nM) with good selectivity. Macrocyclization provided a potent, structurally well-defined scaffold for FVIIa inhibitor design.

In vivo studies of agents targeting the TF/FVIIa complex show a promising antithrombotic efficacy/bleeding liability profile. Small-molecule inhibitors have made significant advances with regards to oral bioavailability and potency. Promising exposure

levels have been attained with prodrugs of amidine-based inhibitors, and nonamidine compounds have been discovered that combine potency and oral bioavailability. Despite these successes and the advancement of both biological agents and a small-molecule TF/FVIIa inhibitor into clinical trials, a compound targeting this mechanism has yet to reach the market.

7.16.5 Factor IXa Inhibitors

Due to its location in the intrinsic pathway of the coagulation cascade, where it plays a pivotal role in TF-mediated TG, FIXa is also another attractive target for anticoagulant drug development.[171] In a study comparing a humanized anti-FIXa monoclonal antibody, SB249417, to the LMWH, enoxaparin, a superior antithrombotic profile was obtained with SB249217 in a rat model of arterial thrombosis.[172] RB006, an RNA aptamer, a reversible inhibitor with high affinity and specificity for FIXa was evaluated in a Phase II clinical trial in patients undergoing PCI.[173] Dose-dependent aPTT prolongation was achieved with no major bleeding. The effects of RB006 can be reversed by administration of a complementary oligonucleotide antidote, RB007. A Phase III trial comparing the combination of RB006 and RB007 (REG-1) to bivalirudin in patients undergoing PCI has been terminated.[174] Another FIXa inhibitor, TTP889 of undisclosed structure, was evaluated in clinical trials. Phase II clinical trial results for extended prevention of VTE in patients undergoing hip surgery were disappointing. TTP889 was ineffective in reducing biomarkers for TG or the incidence of VTE compared with placebo.[171,175] No further evaluation has been reported.

Early efforts to identify selective, small-molecule FIXa inhibitors by modification of leads obtained from screening of FXa compound collections had limited success, although some potent dual inhibitors were reported.[176–178] Similarly, hydroxy pyrazole based FIXa inhibitor **109** (Fig. 25) was reported to have a FIXa Ki of 50 nM with moderate selectivity over thrombin, FVIIa, FXa, and trypsin.[179] SBDD was employed utilizing a 2-amidinobenzothiphene template to design a series of inhibitors with groups to interact in the S1β and S2–S4 pockets of FIXa.[180,181] Compound **110** was reported to have a FIXa Ki of 8 nM with >200-fold selectivity over FXa and was also shown to be bioavailable in rats.

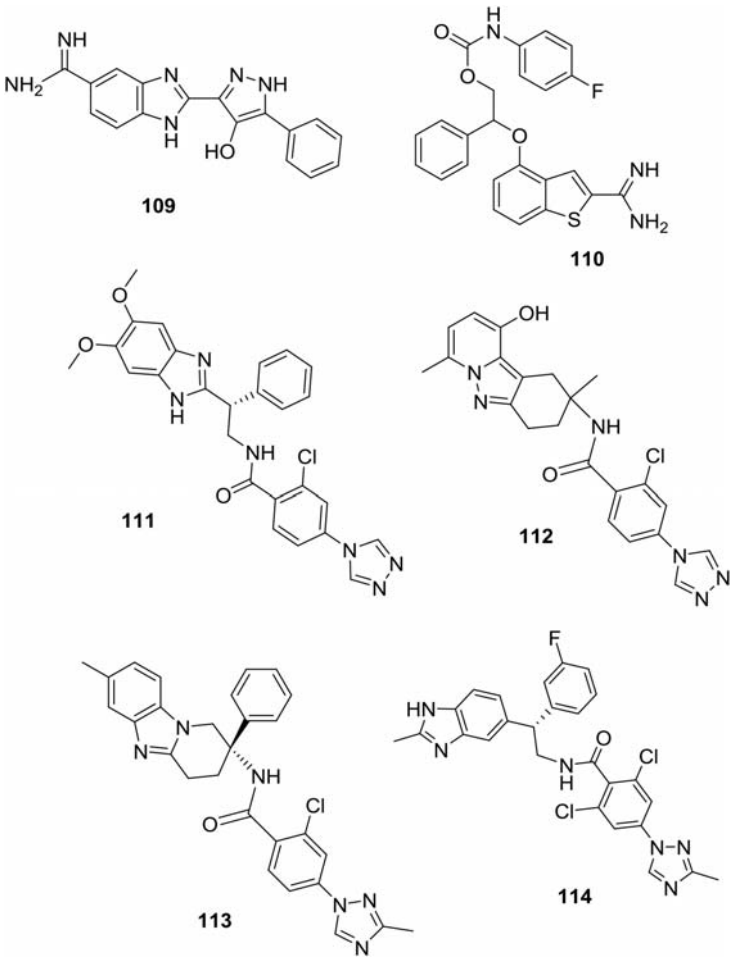

Fig. 25 Factor IXa inhibitors.

Using two screening leads with micromolar potency for FIXa and some selectivity over FXa as a starting point, nanomolar inhibitors of FIXa were identified.[182] Benzimidazole **111** (FIXa Ki = 16 nM, Fig. 25) was 20-fold selective over FXa, and tricyclic compound **112** (FIXa Ki = 90 nM) was > 120-fold selective. Further optimization of both series has been reported. Numerous novel tricyclic scaffolds were explored and compound **113**[183] was identified with improved FIXa affinity (Ki of 5.9 nM), 350-selectivity over FXa, and good oral bioavailability in rat and dog. In a rat A-V shunt model, **113** was as efficacious as apixaban, with little effect on bleeding in a rat cuticle bleeding model. An SAR study beginning with benzamide **111** led to a regioisomeric benzamide analog **114**, with similar potency and selectivity to **113** but lower oral bioavailability in rat.[184] High levels of selectivity versus other coagulation serine proteases were also reported. Both compounds showed aPTT results and a TG profile consistent with inhibition of the intrinsic pathway.

7.16.6 Factor XIa Inhibitors

7.16.6.1 Target Validation and Proof of Concept

FXIa is located upstream in the intrinsic pathway of the coagulation cascade. It plays a major role in the amplification and the propagation of thrombin production. Inhibiting FXIa could disrupt the intrinsic coagulation pathway without affecting either the extrinsic or the common pathways. This approach could provide a reduction in thrombin sufficient to impede occlusive thrombosis, yet allow enough TG to support hemostasis. Therefore, FXIa inhibitors may have the potential to be a promising antithrombotic therapy with a wider therapeutic index.[185,186] Genetic evidence supports this hypothesis. Humans lacking FXI (hemophilia C) have relatively mild bleeding tendencies compared with a deficiency in either FVIII (hemophilia A) or FIX (hemophilia B). Bleeding in individuals with hemophilia C is rarely spontaneous. In addition, clinical studies have shown individuals with a severe FXI deficiency have a lower risk for ischemic stroke and DVT.[187] Similarly, individuals with elevated levels of FXI experience a higher incidence of acute myocardial infarction and DVT.[188,189]

The phenotype observed in FXI-deficient individuals was recapitulated in FXI-deficient mice. Deficiency of mouse FXI provides protection in multiple thrombosis models, and did not show prolonged tail bleeding time when compared with aspirin-treated FXI null and wild-type mice.[190,191] Therefore, studies with FXI null mice are consistent with the tolerable hemostatic defect of human hemophilia C.

Pharmacological studies with FXI-neutralizing antibodies and antisense oligonucleotides (ASOs) in animal models also support the efficacy and safety of the FXI target.[192,193] Antibody 14E11 binds FXI and interferes with the activation of FXI by FXIIa in vitro.[194] Comparable efficacy to total FXI deficiency was obtained with 14E11 in a $FeCl_3$ arterial thrombosis model in mice and reduced thrombus growth was observed in a baboon A-V shunt model. An ASO (ISIS 416858), which blocks the expression of FXI, is the most advanced agent in clinical trials.[195] In a phase II study in arthroplasty, ISIS 416858 reduced the incidence of DVT and showed fewer bleeding events as compared to subcutaneously administered enoxaparin, providing the first PoC in humans.

Pharmacological PoC studies in animal models with small molecules were conducted with irreversible FXIa inhibitors using ketothiazole **115** (FXIa $IC_{50} = 12$ nM)[196,197] and a 4-carboxy-2-azetidinone mechanism-based inhibitor, BMS-262084 (**116**, FXIa $IC_{50} = 2.8$ nM, Fig. 26).[198,199] Ketothiazole **115** was efficacious against $FeCl_2$-induced thrombosis in both the vena cava and carotid artery, and did not alter bleeding time in a rat mesenteric bleeding model.[196] Compound **116** produced dose-dependent antithrombotic effects in rats[198] and rabbits[199] in multiple thrombosis models and did not affect cuticle bleeding time.

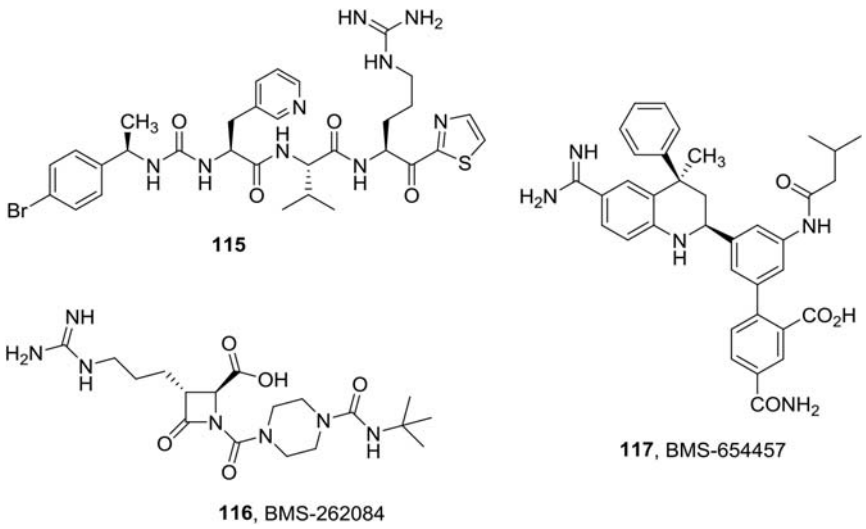

Fig. 26 Small-molecule FXIa Inhibitors used for PoC.

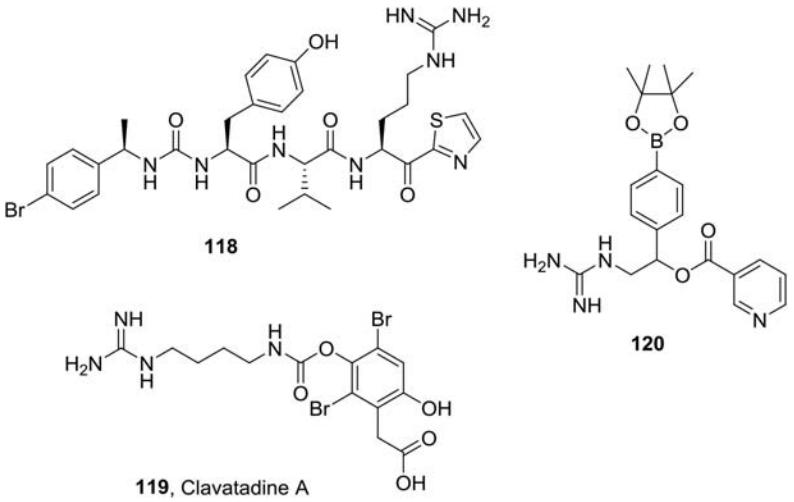

Fig. 27 Irreversible small-molecule FXIa inhibitors.

Proof of concept studies with reversible small-molecule FXIa inhibitors were first reported with BMS-654457 (**117**, Fig. 26),[200,201] a potent FXIa inhibitor (FXIa Ki = 0.20 nM) with >1000-fold selectivity over most of the relevant serine proteases. A dose-dependent antithrombotic effect with an EC_{50} about 300 nM was obtained with **117** in the rabbit ECAT model. A minimal increase in bleeding time was observed for **117** at the dose that gives 80% of thrombosis inhibition. This compares favorably with thrombin inhibitor melagatran, where a significant increase in the bleeding time was observed at the same level of thrombosis inhibition.[201]

7.16.6.2 Preclinical Small-Molecule FXIa Inhibitors

7.16.6.2.1 Irreversible FXIa inhibitors

Keto-arginine-based peptidomimetic FXIa inhibitor 118 (Fig. 27) was reported to have an FXIa IC_{50} of 6 nM with good selectivity over FVIIa, FXa, and thrombin.[196] This series of FXIa inhibitors forms a covalent bond via the keto moiety to the catalytic serine of FXIa. Intravenous infusion of **118** was efficacious in a rat model of venous thrombosis with antithrombotic activity comparable to that of heparin. Modifications to reduce the peptidic character and molecular weight of these inhibitors led to compounds with reduced FXIa affinity.[197] Clavatadine A (**119**), a natural product isolated from a marine sponge, was also reported to be an irreversible inhibitor of FXIa with an IC_{50} of 1300 nM.[202] This compound had no effect on FIXa at a 170-fold greater concentration. A racemic boronate (**120**) was reported to have an FXIa IC_{50} of 1400 nM with 30-fold and eightfold selectivity over FXa and thrombin, respectively.[203]

7.16.6.2.2 Reversible FXIa inhibitors

Several series of reversible small-molecule FXIa inhibitors have been reported (Fig. 28). With the X-ray structure of **117**, SBDD was employed to design and optimize a series of imidazole-based inhibitors. Compound **121** (BMS-724296) was identified as a potent and selective FXIa inhibitor (FXIa Ki = 0.3 nM) that was efficacious in the rabbit AV shunt[204] and ECAT[205] models. The EC_{50} of **121** in the rabbit ECAT model of thrombosis was similar to melagatran. The bleeding time determined at 80% efficacy was fivefold less than melagatran.[205] These results confirm the wider therapeutic index observed with earlier tool compound **117**. Efforts to reduce the basicity of the P1 moiety and polar surface area led to compound **122**. Although the FXIa potency was reduced (FXIa Ki = 6.7 nM), moderate oral exposure was observed in dogs.[206] Further modifications of the P2 and P2′ moieties led to compound **123**, a potent parenteral agent with FXIa Ki of 0.04 nM and dose-dependent efficacy in the rabbit ECAT model with minimal bleeding time prolongation.[207] The imidazole core was replaced with various six-membered ring heterocycles, including pyridine, which showed promising affinity (ie, compound **124**).[208]

A series of diamide FXIa inhibitors was reported (Fig. 29). Compound **125**,[209] derived from fragment screening and SBDD, showed an FXIa Ki of 1.0 nM. Compound **126**,[210] with a different diamide scaffold, was a potent inhibitor with FXIa Ki of 2.0 nM, and efficacy in the rabbit ECAT model.

In addition to the above FXIa inhibitors, data for several additional compounds have been reported, but no structures were disclosed. ONO-8610539[211] is a selective, injectable small-molecule FXIa inhibitor with an FXIa Ki of 1.9 nM. It significantly inhibited thrombus formation in rabbits and monkeys, and did not affect blood loss volume at 33-fold higher than the dose showing the maximum antithrombotic effect compared with enoxaparin. ONO-7750512[211,212] was reported as an orally bioavailable (F = 22% in rats) FXIa inhibitor with an FXIa Ki of 3.8 nM. It has potent antithrombotic efficacy in the $FeCl_3$-induced rabbit venous and the AV-shunt monkey thrombosis models. In the rabbit ear bleeding model, ONO-7750512 had a significantly lower bleeding

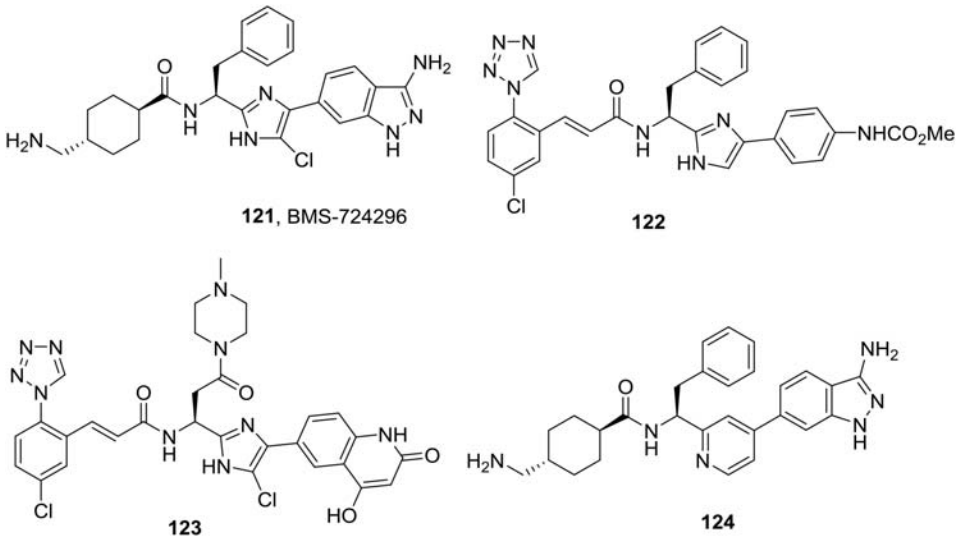

Fig. 28 Reversible small-molecule FXIa inhibitors.

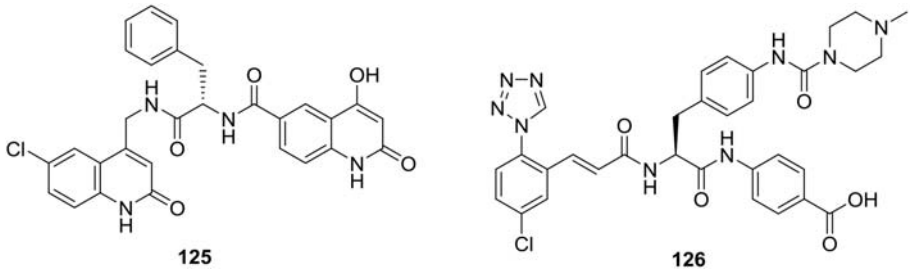

Fig. 29 Diamide FXIa inhibitors.

risk compared with rivaroxaban.[212] DSR-130787 was reported as an orally active prodrug FXIa inhibitor with $IC_{50} < 10$ nM.[213] Intravenous administration of DSR-130787 active form to rabbits produced an antithrombotic effect comparable to that of dabigatran or rivaroxaban with much lower risk of bleeding.

7.16.6.2.3 Allosteric FXIa inhibitors

The FXIa inhibitors described so far all bind to the FXIa active site. A series of allosteric FXIa inhibitors has been published (Fig. 30). Sulfated pentagalloylglucopyranoside **127** was reported to have an IC_{50} of 550 nM with 200-fold selectivity over other relevant

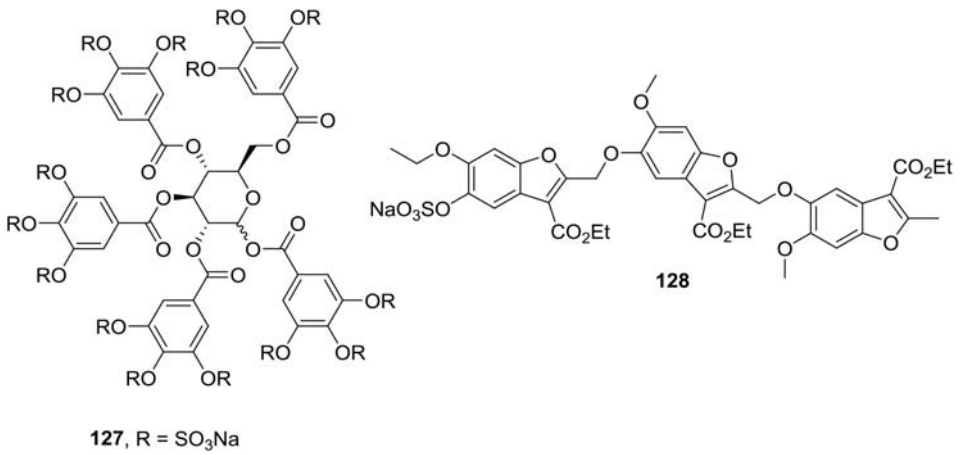

Fig. 30 Allosteric FXIa inhibitors.

enzymes.[214] Competitive binding studies showed that **127** binds in the heparin-binding site of FXIa. A series of allosteric monosulfated benzofuran dimer and trimer FXIa inhibitors that are not competitive with heparin were reported. Compound **128** was the most potent inhibitor with an IC_{50} of 820 nM.[215] Molecular modeling was used to propose a binding site for **128** on the A3 domain of FXIa. As yet these allosteric inhibitors do not have the potent affinity for FXIa demonstrated with active site inhibitors, but they offer an interesting avenue for continued research.

With an FXIa ASO in clinical trials, and reversible, small-molecule inhibitors and an FXI antibody entering clinical trials, the FXIa mechanism may be poised to deliver the next major advance in new anticoagulants since the development of the current class of potent and selective FXa inhibitors.

7.16.7 Conclusion

Through the perseverance of researchers over many years at institutions around the world, patients can now benefit from new oral anticoagulants approved to prevent and treat thromboembolic disorders more effectively, with better overall safety and in particular a lower rate of intracranial hemorrhage, and without the inconvenience of the routine monitoring or dietary restrictions that are associated with VKAs. Direct thrombin and FXa inhibitors have a rapid onset and fixed dosing, thus alleviating the need for initial treatment with a parenteral anticoagulant. Despite these advances in treatment options, however, an increased risk of bleeding still persists to varying degrees with the new thrombin and FXa inhibitors,[216] and an unmet medical need remains for new anticoagulants with even less tendency for bleeding. Preclinical data with FXIa inhibitors and Phase II clinical data with an FXIa ASO suggest that FXIa inhibitors have the potential to provide this added advantage. As the first FXIa inhibitors progress into human clinical trials, further interest in developing novel inhibitors of FXIa and other targets in the intrinsic cascade continues, and the quest for the perfect anticoagulant goes on. Antithrombotic roles for FXIIa[217,218] and plasma kallikrein[219] have been proposed, and may provide new targets for future investigations. For the present, direct thrombin and FXa inhibitors represent major achievements in the identification of safer, more efficacious agents for the treatment of thromboembolic diseases. Their long-term use in patients, along with continued clinical evaluation of inhibitors of other coagulation proteases, will ultimately determine which mechanism offers the optimal benefit/risk profile for specific patient populations.

See also: 7.15. Advances in Antiplatelet Agents.

References

1. Jackson, S. P. Arterial Thrombosis—Insidious, Unpredictable and Deadly. *Nat. Med.* **2011,** *17,* 1423–1436.
2. Hawkins, D. Limitations of Traditional Anticoagulants. *Pharmacotherapy* **2004,** *24,* 62S–65S.
3. Macfarlane, R. G. An Enzyme Cascade in the Blood Clotting Mechanism, and Its Function as a Biochemical Amplifier. *Nature* **1964,** *202,* 498–499.
4. Davie, E. W.; Ratnoff, O. D. Waterfall Sequence for Intrinsic Blood Clotting. *Science* **1964,** *145,* 1310–1312.
5. Adams, R. L.; Bird, R. J. Review Article: Coagulation Cascade and Therapeutics Update: Relevance to Nephrology. Part 1: Overview of Coagulation, Thrombophilias and History of Anticoagulants. *Nephrology* **2009,** *14,* 462–470.
6. Greinacher, A.; Warkentin, T. E. The Direct Thrombin Inhibitor Hirudin. *Thromb. Haemost.* **2008,** *99,* 819–829.
7. Arsenault, K. A.; Hirsh, J.; Whitlock, R. P.; Eikelboom, J. W. Direct Thrombin Inhibitors in Cardiovascular Disease. *Nat. Rev. Cardiol.* **2012,** *9,* 402–414.
8. Baetz, B. E.; Gerstenfeld, E. P.; Kolansky, D. M.; Spinler, S. A. Bivalirudin Use During Radiofrequency Catheter Ablation Procedures in Two Patients With a History of Heparin-Induced Thrombocytopenia. *Pharmacotherapy* **2010,** *30,* 952.
9. Schechter, I.; Berger, A. On the Size of the Active Site in Proteases. I. Papain. *Biochem. Biophys. Res. Commun.* **1967,** *27,* 157–162.
10. Rose, T.; Di Cera, E. Three-Dimensional Modeling of Thrombin-Fibrinogen Interaction. *J. Biol. Chem.* **2002,** *277,* 18875–18880.
11. Grouzi, E. Update on Argatroban for the Prophylaxis and Treatment of Heparin-Induced Thrombocytopenia Type II. *J. Blood Med.* **2014,** *5,* 131–141.
12. Schwienhorst, A. Direct Thrombin Inhibitors - A Survey of Recent Developments. *Cell. Mol. Life Sci.* **2006,** *63,* 2773–2791.
13. Mehta, H. R.; Patel, P. B.; Galani, V. J.; Patel, K. B. Ximelagatran: A New Direct Thrombin Inhibitor. *Int. Res. J. Pharm.* **2011,** *2,* 9–15.
14. Keisu, M.; Andersson, T. B. Drug-Induced Liver Injury in Humans: The Case of Ximelagatran. *Handb. Exp. Pharmacol.* **2010,** *196,* 407–418.
15. Eriksson, B. I.; Smith, H.; Yasothan, U.; Kirkpatrick, P. Dabigatran Etexilate. *Nat. Rev. Drug Discov.* **2008,** *7,* 557–558.
16. Cheng, J. W.; Vu, H. Dabigatran Etexilate: An Oral Direct Thrombin Inhibitor for the Management of Thromboembolic Disorders. *Clin. Ther.* **2012,** *34,* 766–787.
17. Chen, B. C.; Viny, A. D.; Garlich, F. M.; Basciano, P.; Howland, M. A.; Smith, S. W.; Hoffman, R. S.; Nelson, L. S. Hemorrhagic Complications Associated With Dabigatran Use. *Clin. Toxicol.* **2012,** *50,* 854–857.
18. Bloom, B. J.; Filion, K. B.; Atallah, R.; Eisenberg, M. J. Meta-Analysis of Randomized Controlled Trials on the Risk of Bleeding With Dabigatran. *Am. J. Cardiol.* **2014,** *113,* 1066–1074.
19. Pollack, C. V., Jr.; Reilly, P. A.; Eikelboom, J.; Glund, S.; Verhamme, P.; Bernstein, R. A.; Dubiel, R.; Huisman, M. V.; Hylek, E. M.; Kamphuisen, P. W.; Kreuzer, J.; Levy, J. H.; Sellke, F. W.; Stangier, J.; Steiner, T.; Wang, B.; Kam, C. W.; Weitz, J. I. Idarucizumab for Dabigatran Reversal. *N. Engl. J. Med.* **2015,** *373,* 511–520.
20. Pehrsson, S.; Johansson, K.; Kjaer, M.; Elg, M. Evaluation of AR-H067637, the Active Metabolite of the New Direct Thrombin Inhibitor AZD0837, in Models of Venous and Arterial Thrombosis and Bleeding in Anaesthetised Rats. *Thromb. Haemost.* **2010,** *104,* 1242–1249.
21. Lip, G. Y. H.; Rasmussen, L. H.; Olsson, S. B.; Zetterstrand, S.; Stahre, C.; Bylock, A.; Aunes-Jansson, M.; Eriksson, U.; Wahlander, K. Oral Direct Thrombin Inhibitor AZD0837 for the Prevention of Stroke and Systemic Embolism in Patients With Non-Valvular Atrial Fibrillation: A Phase II Study of AZD0837 in Patients Who are Appropriate for but Unable or Unwilling to Take Vitamin K Antagonist Therapy. *Thromb. Res.* **2011,** *127,* 91–99.
22. Park, H. D.; Lee, S.-H.; Kim, T. H.; Lee, S. H.; Cho, K. H.; Kim, A. Antithrombotic Effects of LB30870, a Potent, Orally Active, Selective and Direct Thrombin Inhibitor, and Pharmacokinetics of Its Prodrug. *Bioorg. Med. Chem. Lett.* **2013,** *23,* 4779–4784.
23. Kim, J.; Lee, S.-H.; Boyce, M.; Warrington, S.; Cho, K. H.; Yoon, S. K.; Park, H. D.; Kim, A. Pharmacokinetics, Pharmacodynamics and Food Effect of LB30870, a Novel Direct Thrombin Inhibitor, After Single Oral Doses in Healthy men. *Xenobiotica* **2015,** *45,* 663–671.

24. Lu, T.; Markotan, T.; Ballentine, S. K.; Giardino, E. C.; Spurlino, J.; Brown, K.; Maryanoff, B. E.; Tomczuk, B. E.; Damiano, B. P.; Shukla, U.; End, D.; Andrade-Gordon, P.; Bone, R. F.; Player, M. R. Discovery and Clinical Evaluation of 1-{*N*-[2-(Amidinoaminooxy)Ethyl]Amino}Carbonylmethyl-6-Methyl-3-[2,2-Difluoro-2-Phenylethylamino]Pyrazinone (RWJ-671818), a Thrombin Inhibitor With an Oxyguanidine P1 Motif. *J. Med. Chem.* **2010,** *53,* 1843–1856.
25. Rupin, A.; Marx, I.; Vallez, M. O.; Mennecier, P.; Gloanec, P.; De Nanteuil, G.; Verbeuren, T. J. S35972, a Direct-Acting Thrombin Inhibitor With High Oral Bioavailability and Antithrombotic Efficacy. *J. Thromb. Haemost.* **2011,** *9,* 1375–1382.
26. Burgey, C. S.; Robinson, K. A.; Lyle, T. A.; Nantermet, P. G.; Selnick, H. G.; Isaacs, R. C. A.; Lewis, S. D.; Lucas, B. J.; Krueger, J. A.; Singh, R.; Miller-Stein, C.; White, R. B.; Wong, B.; Lyle, E. A.; Stranieri, M. T.; Cook, J. J.; McMasters, D. R.; Pellicore, J. M.; Pal, S.; Wallace, A. A.; Clayton, F. C.; Bohn, D.; Welsh, D. C.; Lynch, J. J.; Yan, Y.; Chen, Z.; Kuo, L.; Gardell, S. J.; Shafer, J. A.; Vacca, J. P. Pharmacokinetic Optimization of 3-Amino-6-Chloropyrazinone Acetamide Thrombin Inhibitors. Implementation of P3 Pyridine N-Oxides to Deliver an Orally Bioavailable Series Containing P1 N-Benzylamides. *Bioorg. Med. Chem. Lett.* **2003,** *13,* 1353–1357.
27. Isaacs, R. C. A.; Solinsky, M. G.; Cutrona, K. J.; Newton, C. L.; Naylor-Olsen, A. M.; McMasters, D. R.; Krueger, J. A.; Lewis, S. D.; Lucas, B. J.; Kuo, L. C.; Yan, Y.; Lynch, J. J.; Lyle, E. A. Structure-Based Design of Novel Groups for Use in the P1 Position of Thrombin Inhibitor Scaffolds. Part 2: N-Acetamidoimidazoles. *Bioorg. Med. Chem. Lett.* **2008,** *18,* 2062–2066.
28. Isaacs, R. C. A.; Newton, C. L.; Cutrona, K. J.; Mercer, S. P.; Dorsey, B. D.; McDonough, C. M.; Cook, J. J.; Krueger, J. A.; Lewis, S. D.; Lucas, B. J.; Lyle, E. A.; Lynch, J. J.; Miller-Stein, C.; Michener, M. T.; Wallace, A. A.; White, R. B.; Wong, B. K. P3 Optimization of Functional Potency, In Vivo Efficacy and Oral Bioavailability in 3-Aminopyrazinone Thrombin Inhibitors Bearing non-Charged Groups at the P1 Position. *Bioorg. Med. Chem. Lett.* **2011,** *21,* 1532–1535.
29. Lee, L.; Kreutter, K. D.; Pan, W.; Crysler, C.; Spurlino, J.; Player, M. R.; Tomczuk, B.; Lu, T. 2-(2-Chloro-6-Fluorophenyl)Acetamides as Potent Thrombin Inhibitors. *Bioorg. Med. Chem. Lett.* **2007,** *17,* 6266–6269.
30. Kreutter, K. D.; Lu, T.; Lee, L.; Giardino, E. C.; Patel, S.; Huang, H.; Xu, G.; Fitzgerald, M.; Haertlein, B. J.; Mohan, V.; Crysler, C.; Eisennagel, S.; Dasgupta, M.; McMillan, M.; Spurlino, J. C.; Huebert, N. D.; Maryanoff, B. E.; Tomczuk, B. E.; Damiano, B. P.; Player, M. R. Orally Efficacious Thrombin Inhibitors With Cyanofluorophenylacetamide as the P2 Motif. *Bioorg. Med. Chem. Lett.* **2008,** *18,* 2865–2870.
31. Blizzard, T. A.; Singh, S.; Patil, B.; Chidurala, N.; Komanduri, V.; Debnath, S.; Belyakov, S.; Crespo, A.; Struck, A.; Kurtz, M.; Wiltsie, J.; Shen, X.; Sonatore, L.; Arocho, M.; Lewis, D.; Ogletree, M.; Biftu, T. Heterocyclic Core Analogs of a Direct Thrombin Inhibitor. *Bioorg. Med. Chem. Lett.* **2014,** *24,* 1111–1115.
32. Ilaš, J.; Tomašić, T.; Kikelj, D. Novel Potent and Selective Thrombin Inhibitors Based on a Central 1,4-Benzoxazin-3(4H)-One Scaffold. *J. Med. Chem.* **2008,** *51,* 2863–2867.
33. Li, M.-L.; Ren, Y.-J.; Dong, M.-H.; Ren, W.-X. Design, Synthesis and Structural Exploration of Novel Fluorinated Dabigatran Derivatives as Direct Thrombin Inhibitors. *Eur. J. Med. Chem.* **2015,** *96,* 122–138.
34. Chen, H.; Ren, Y. Design, Synthesis, and Anti-Thrombotic Evaluation of Some Novel Fluorinated Thrombin Inhibitor Derivatives. *Arch. Pharm. (Weinheim, Ger.)* **2015,** *348,* 408–420.
35. Li, Y.-Z.; Gong, G.-Q.; Yang, W.-H.; Wang, X.-H.; Jiang, M.-L.; Zhou, Y.; Yang, X.-Z.; Xu, Y.-G.; He, G.-W. Antithrombotic Activity of HY023016, a Novel Dabigatran Prodrug Evaluated in Animal Thrombosis Models. *Thromb. Res.* **2013,** *131,* 425–435.
36. Guillen Schlippe, Y. V.; Hartman, M. C. T.; Josephson, K.; Szostak, J. W. In Vitro Selection of Highly Modified Cyclic Peptides That Act as Tight Binding Inhibitors. *J. Am. Chem. Soc.* **2012,** *134,* 10469–10477.
37. Zavyalova, E.; Golovin, A.; Reshetnikov, R.; Mudrik, N.; Panteleyev, D.; Pavlova, G.; Kopylov, A. Novel Modular DNA Aptamer for Human Thrombin With High Anticoagulant Activity. *Curr. Med. Chem.* **2011,** *18,* 3343–3350.
38. Virno, A.; Randazzo, A.; Giancola, C.; Bucci, M.; Cirino, G.; Mayol, L. A Novel Thrombin Binding Aptamer Containing a G-LNA Residue. *Bioorg. Med. Chem.* **2007,** *15,* 5710–5718.
39. Dunwiddie, C.; Thornberry, N. A.; Bull, H. G.; Sardana, M.; Friedman, P. A.; Jacobs, J. W.; Simpson, E. Antistasin, a Leech-Derived Inhibitor of Factor Xa. Kinetic Analysis of Enzyme Inhibition and Identification of the Reactive Site. *J. Biol. Chem.* **1989,** *264,* 16694–16699.
40. Waxman, L.; Smith, D. E.; Arcuri, K. E.; Vlasuk, G. P. Tick Anticoagulant Peptide (TAP) is a Novel Inhibitor of Blood Coagulation Factor Xa. *Science* **1990,** *248,* 593–596.
41. Sitko, G. R.; Ramjit, D. R.; Stabilito, I. I.; Lehman, D.; Lynch, J. J.; Vlasuk, G. P. Conjunctive Enhancement of Enzymatic Thrombolysis and Prevention of Thrombotic Reocclusion With the Selective Factor Xa Inhibitor, Tick Anticoagulant Peptide. Comparison to Hirudin and Heparin in a Canine Model of Acute Coronary Artery Thrombosis. *Circulation* **1992,** *85,* 805–815.
42. Lynch, J. J.; Sitko, G. R.; Mellott, M. J.; Nutt, E. M.; Lehman, E. D.; Friedman, P. A.; Dunwiddie, C. T.; Vlasuk, G. P. Maintenance of Canine Coronary Artery Patency Following Thrombolysis With Front Loaded Plus low Dose Maintenance Conjunctive Therapy. A Comparison of Factor Xa Versus Thrombin Inhibition. *Cardiovasc. Res.* **1994,** *28,* 78–85.
43. Wong, P. C.; Crain, E. J.; Watson, C. A.; Xin, B. Favorable Therapeutic Index of the Direct Factor Xa Inhibitors, Apixaban and Rivaroxaban, Compared With the Thrombin Inhibitor Dabigatran in Rabbits. *J. Thromb. Haemost.* **2009,** *7,* 1313–1320.
44. Reverter, J. C. Fondaparinux Sodium. *Drugs Today* **2002,** *38,* 185–194.
45. Alexander, J. H.; Yang, H.; Becker, R. C.; Kodama, K.; Goodman, S.; Dyke, C. K.; Kleiman, N. S.; Hochan, J. S.; Berger, P. B.; Cohen, E. A.; Lincoff, A. M.; Burton, J. R.; Bovill, E. G.; Kawai, C.; Armstrong, P. W.; Harrington, R. A. First Experience With Direct, Selective Factor Xa Inhibition in Patients With Non-ST-Elevation Acute Coronary Syndromes: Results of the XaNADU-ACS Trial. *J. Thromb. Haemost.* **2005,** *3,* 439–447.
46. Sabatine, M. S.; Antman, E. M.; Widimsky, P.; Ebrahim, I. O.; Kiss, R. G.; Saaiman, A.; Polasek, R.; Contant, C. F.; McCabe, C. H.; Braunwald, E. Otamixaban for the Treatment of Patients With non-ST-Elevation Acute Coronary Syndromes (SEPIA-ACS1 TIMI 42): A Randomised, Double-Blind, Active-Controlled, Phase 2 Trial. *Lancet* **2009,** *374,* 787–795.
47. Guertin, K. R.; Choi, Y. M. The Discovery of the Factor Xa Inhibitor Otamixaban: From Lead Identification to Clinical Development. *Curr. Med. Chem.* **2007,** *14,* 2471–2481.
48. Pinto, D. J.; Smallheer, J. M.; Cheney, D. L.; Knabb, R. M.; Wexler, R. R. Factor Xa Inhibitors: Next-Generation Antithrombotic Agents. *J. Med. Chem.* **2010,** *53,* 6243–6274.
49. Brandstetter, H.; Kuehne, A.; Bode, W.; Huber, R.; von der Saal, W.; Wirthensohn, K.; Engh, R. A. X-Ray Structure of Active Site-Inhibited Clotting Factor Xa. Implications for Drug Design and Substrate Recognition. *J. Biol. Chem.* **1996,** *271,* 29988–29992.
50. Yeh, C. H.; Hogg, K.; Weitz, J. I. Overview of the New Oral Anticoagulants: Opportunities and Challenges. *Arterioscler. Thromb. Vasc. Biol.* **2015,** *35,* 1056–1065.
51. Rupprecht, H.-J.; Blank, R. Clinical Pharmacology of Direct and Indirect Factor Xa Inhibitors. *Drugs* **2010,** *70,* 2153–2170.
52. Perzborn, E.; Roehrig, S.; Straub, A.; Kubitza, D.; Misselwitz, F. The Discovery and Development of Rivaroxaban, an Oral, Direct Factor Xa Inhibitor. *Nat. Rev. Drug Discov.* **2011,** *10,* 61–75.
53. Patel, M. R.; Mahaffey, K. W.; Garg, J.; Pan, G.; Singer, D. E.; Hacke, W.; Breithardt, G.; Halperin, J. L.; Hankey, G. J.; Piccini, J. P.; Becker, R. C.; Nessel, C. C.; Paolini, J. F.; Berkowitz, S. D.; Fox, K. A. A.; Califf, R. M. Rivaroxaban Versus Warfarin in Nonvalvular Atrial Fibrillation. *New Engl. J. Med.* **2011,** *365,* 883–891.
54. Pinto, D. J. P.; Wong, P. C.; Knabb, R. M.; Wexler, R. R. Case History: Eliquis™ (Apixaban), a Potent and Selective Inhibitor of Coagulation Factor Xa for the Prevention and Treatment of Thrombotic Diseases. *Annu. Rep. Med. Chem.* **2012,** *47,* 123–141.
55. He, K.; Luettgen, J. M.; Zhang, D.; He, B.; Grace, J. E., Jr.; Xin, B.; Pinto, D. J. P.; Wong, P. C.; Knabb, R. M.; Lam, P. Y. S.; Wexler, R. R.; Grossman, S. J. Preclinical Pharmacokinetics and Pharmacodynamics of Apixaban, a Potent and Selective Factor Xa Inhibitor. *Eur. J. Drug Metab. Pharmacokinet.* **2011,** *36,* 129–139.
56. Wong, P. C.; Pinto, D. J. P.; Zhang, D. Preclinical Discovery of Apixaban, a Direct and Orally Bioavailable Factor Xa Inhibitor. *J. Thromb. Thrombolysis* **2011,** *31,* 478–492.
57. Hanna, M. S.; Mohan, P.; Knabb, R.; Gupta, E.; Frost, C.; Lawrence, J. H. Development of Apixaban: A Novel Anticoagulant for Prevention of Stroke in Patients With Atrial Fibrillation. *Ann. N. Y. Acad. Sci.* **2014,** *1329,* 93–106.
58. Granger, C. B.; Alexander, J. H.; McMurray, J. J. V.; Lopes, R. D.; Hylek, E. M.; Hanna, M.; Al-Khalidi, H. R.; Ansell, J.; Atar, D.; Avezum, A.; Bahit, M. C.; Diaz, R.; Easton, J. D.; Ezekowitz, J. A.; Flaker, G.; Garcia, D.; Geraldes, M.; Gersh, B. J.; Golitsyn, S.; Goto, S.; Hermosillo, A. G.; Hohnloser, S. H.; Horowitz, J.; Mohan, P.; Jansky, P.; Lewis, B. S.; Lopez-Sendon, J. L.; Pais, P.; Parkhomenko, A.; Verheugt, F. W. A.; Zhu, J.; Wallentin, L. Apixaban Versus Warfarin in Patients With Atrial Fibrillation. *New Engl. J. Med.* **2011,** *365,* 981–992.

59. Connolly, S. J.; Eikelboom, J.; Joyner, C.; Diener, H.-C.; Hart, R.; Golitsyn, S.; Flaker, G.; Avezum, A.; Hohnloser, S. H.; Diaz, R.; Talajic, M.; Zhu, J.; Pais, P.; Budaj, A.; Parkhomenko, A.; Jansky, P.; Commerford, P.; Tan, R. S.; Sim, K.-H.; Lewis, B. S.; Van Mieghem, W.; Lip, G. Y. H.; Kim, J. H.; Lanas-Zanetti, F.; Gonzalez-Hermosillo, A.; Dans, A. L.; Munawar, M.; O'Donnell, M.; Lawrence, J.; Lewis, G.; Afzal, R.; Yusuf, S. Apixaban in Patients With Atrial Fibrillation. *New Engl. J. Med.* **2011,** *364,* 806–817.
60. Furugohri, T.; Isobe, K.; Honda, Y.; Kamisato-Matsumoto, C.; Sugiyama, N.; Nagahara, T.; Morishima, Y.; Shibano, T. DU-176b, a Potent and Orally Active Factor Xa Inhibitor: In Vitro and In Vivo Pharmacological Profiles. *J. Thromb. Haemost.* **2008,** *6,* 1542–1549.
61. Plitt, A.; Giugliano, R. P. Edoxaban: Review of Pharmacology and key Phase I to III Clinical Trials. *J. Cardiovasc. Pharmacol. Ther.* **2014,** *19,* 409–416.
62. Bounameaux, H.; Camm, A. J. Edoxaban: An Update on the New Oral Direct Factor Xa Inhibitor. *Drugs* **2014,** *74,* 1209–1231.
63. Abramowicz, M.; Zuccotti, G.; Pflomm, J.-M. Edoxaban (Savaysa)—The Fourth New Oral Anticoagulant. *JAMA* **2015,** *314,* 76–77.
64. Mantha, S.; Ansell, J. Indirect Comparison of Dabigatran, Rivaroxaban, Apixaban and Edoxaban for the Treatment of Acute Venous Thromboembolism. *J. Thromb. Thrombolysis* **2015,** *39,* 155–165.
65. Kang, N.; Sobieraj, D. M. Indirect Treatment Comparison of New Oral Anticoagulants for the Treatment of Acute Venous Thromboembolism. *Thromb. Res.* **2014,** *133,* 1145–1151.
66. Ruff, C. T.; Giugliano, R. P.; Braunwald, E.; Hoffman, E. B.; Deenadayalu, N.; Ezekowitz, M. D.; Camm, A. J.; Weitz, J. I.; Lewis, B. S.; Parkhomenko, A.; Yamashita, T.; Antman, E. M. Comparison of the Efficacy and Safety of New Oral Anticoagulants With Warfarin in Patients With Atrial Fibrillation: A Meta-Analysis of Randomised Trials. *Lancet* **2014,** *383,* 955–962.
67. Quan, M. L.; Lam, P. Y. S.; Han, Q.; Pinto, D. J. P.; He, M. Y.; Li, R.; Ellis, C. D.; Clark, C. G.; Teleha, C. A.; Sun, J. H.; Alexander, R. S.; Bai, S.; Luettgen, J. M.; Knabb, R. M.; Wong, P. C.; Wexler, R. R. Discovery of 1-(3'-Aminobenzisoxazol-5'-yl)-3-Trifluoromethyl- *N*-[2-Fluoro-4-[(2'-Dimethylaminomethyl)Imidazol-1-yl]Phenyl] -1*H*-Pyrazole-5-Carboxyamide Hydrochloride (Razaxaban), a Highly Potent, Selective, and Orally Bioavailable Factor Xa Inhibitor. *J. Med. Chem.* **2005,** *48,* 1729–1744.
68. Lassen, M. R.; Davidson, B. L.; Gallus, A. S.; Pineo, G.; Ansell, J.; Deitchman, D. A Phase II Randomized, Double-Blind, Five-arm, Parallel-Group, Dose–Response Study of a New Oral Directly-Acting Factor Xa Inhibitor, Razaxaban, for the Prevention of Deep Vein Thrombosis in Knee Replacement Surgery. *Blood* **2003,** *102,* 111. Abstract 141.
69. Zhang, P.; Wenrong, H.; Wang, L.; Bao, L.; Jia, Z. J.; Bauer, S. M.; Goldman, E. A.; Probst, G. D.; Song, Y.; Su, T.; Fan, J.; Wu, Y.; Li, W.; Woolfrey, J.; Sinha, U.; Wong, P. W.; Edwards, S. T.; Arfsten, A. E.; Clizbe, L. A.; Kanter, J.; Pandey, A.; Park, G.; Hutchaleelaha, A.; Lambing, J. L.; Hollenbach, S. J.; Scarborough, R. M.; Zhu, B. Y. Discovery of Betrixaban (PRT054021), *N*-(5-Chloropyridin-2-yl)-2-(4-(*N, N*-Dimethylcarbamimidoyl)Benzamido)-5-Methoxybenzamide, a Highly Potent, Selective, and Orally Efficacious Factor Xa Inhibitor. *Bioorg. Med. Chem. Lett.* **2009,** *19,* 2179–2185.
70. Chan, N. C.; Bhagirath, V.; Eikelboom, J. W. Profile of Betrixaban and its Potential in the Prevention and Treatment of Venous Thromboembolism. *Vasc. Health Risk Manag.* **2015,** *11,* 343–351.
71. Chan, N. C.; Hirsh, J.; Ginsberg, J. S.; Eikelboom, J. W. Betrixaban (PRT054021): Pharmacology, Dose Selection and Clinical Studies. *Future Cardiol.* **2014,** *10,* 43–52.
72. Anselm, L.; Banner, D. W.; Benz, J.; Zbinden, K. G.; Himber, J.; Hilpert, H.; Huber, W.; Kuhn, B.; Mary, J. L.; Otteneder, M. B.; Panday, N.; Ricklin, F.; Stahl, M.; Thomi, S.; Haap, W. Discovery of a Factor Xa Inhibitor (3*R*,4*R*)-1-(2,2-Difluoro-Ethyl)-Pyrrolidine-3,4-Dicarboxylic Acid 3-[(5-Chloro-Pyridin-2-yl)-Amide] 4-[[2-Fluoro-4-(2-oxo-2*H*-Pyridin-1-yl)-Phenyl]-Amide] as a Clinical Candidate. *Bioorg. Med. Chem. Lett.* **2010,** *20,* 5313–5319.
73. Schmitt, C.; Charoin-Pannier, A.; McIntyre, C.; Zandt, H.; Ciorciaro, C.; Winters, K.; Pepper, T. Safety, Pharmacokinetics and Pharmacodynamics of Multiple Ascending Doses of R1663, an Oral Factor Xa Inhibitor, in Healthy Young Subjects Coupled With Exploration of Influence of Gender and Age. *Thromb. Haemost.* **2012,** *108,* 54–64.
74. Fujimoto, T.; Imaeda, Y.; Konishi, N.; Hiroe, K.; Kawamura, M.; Textor, G. P.; Aertgeerts, K.; Kubo, K. Discovery of a Tetrahydropyrimidin-2(1H)-One Derivative (TAK-442) as a Potent, Selective, and Orally Active Factor Xa Inhibitor. *J. Med. Chem.* **2010,** *53,* 3517–3531.
75. Konishi, N.; Hiroe, K.; Shinozawa, E.; Shofuda, K.-i.; Matsuda, K.; Imaeda, Y.; Fujimoto, T.; Kubo, K.; Kawaramura, M. Antithrombotic Profiles of TAK-442, a Novel Oral Factor Xa Inhibitor, in Venous and Arterial Thrombosis Models. *J. Thromb. Haemost.* **2009,** *7 (Suppl. 2),* 759. Abstract PP-WE-400.
76. Hirayama, F.; Koshio, H.; Ishihara, T.; Hachiya, S.; Sugasawa, K.; Koga, Y.; Seki, N.; Shiraki, R.; Shigenaga, T.; Iwatsuki, Y.; Moritani, Y.; Mori, K.; Kadokura, T.; Kawasaki, T.; Matsumoto, Y.; Sakamoto, S.; Tsukamoto, S.-i. Discovery of *N*-[2-Hydroxy-6-(4-Methoxybenzamido)Phenyl]-4-(4-Methyl-1,4-Diazepan-1-yl)Benzamide (Darexaban, YM150) as a Potent and Orally Available Factor Xa Inhibitor. *J. Med. Chem.* **2011,** *54,* 8051–8065.
77. Vaysman, A. M.; Nutescu, E. A. YM-150, a Factor Xa Inhibitor for the Prevention of Venous Thromboembolism and Coronary Artery Disease. *Curr. Opin. Investig. Drugs* **2010,** *11,* 333–339.
78. Kohrt, J. T.; Bigge, C. F.; Bryant, J. W.; Casimiro-Garcia, A.; Chi, L.; Cody, W. L.; Dahring, T.; Dudley, D. A.; Filipski, K. J.; Haarer, S.; Heemstra, R.; Janiczek, N.; Narasimhan, L.; McClanahan, T.; Peterson, J. T.; Sahasrabudhe, V.; Schaum, R.; Van Huis, C. A.; Welch, K. M.; Zhang, E.; Leadley, R. J.; Edmunds, J. J. The Discovery of (2R,4R)-N-(4-Chlorophenyl)-N- (2-Fluoro-4-(2-Oxopyridin- 1(2H)-yl)Phenyl)-4-Methoxypyrrolidine-1,2-Dicarboxamide (PD 0348292), an Orally Efficacious Factor Xa Inhibitor. *Chem. Biol. Drug Des.* **2007,** *70,* 100–112.
79. Cohen, A. T.; Armstrong, D.; Gazdzik, T.; Ryge, C.; Pak, R.; Mandema, J.; Boyd, R.; McBride, S.; DiCarlo, L. A. An Adaptive-Design Dose-Ranging Study of PD 0348292, a New Oral Factor Xa Inhibitor, for Thromboprophylaxis After Total Knee Replacement Surgery. *Blood (ASH Annual Meeting Abstracts)* **2008,** *112*. Abstract 980.
80. Agnelli, G.; Haas, S.; Ginsberg, J. S.; Krueger, K. A.; Dmitrienko, A.; Brandt, J. T. A Phase II Study of the Oral Factor Xa Inhibitor LY517717 for the Prevention of Venous Thromboembolism After Hip or Knee Replacement. *J. Thromb. Haemost.* **2007,** *5,* 746–753.
81. Chan, C.; Borthwick, A. D.; Brown, D.; Burns-Kurtis, C. L.; Campbell, M.; Chaudry, L.; Chung, C.-W.; Convery, M. A.; Hamblin, J. N.; Johnstone, L.; Kelly, H. A.; et al. Factor Xa Inhibitors: S1 Binding Interactions of a Series of *N*-{(3*S*)-1-[(1*S*)-1-Methyl-2-Morpholin-4-yl-2-Oxoethyl]-2-Oxopyrrolidin-3-yl}Sulfonamides. *J. Med. Chem.* **2007,** *50,* 1546–1557.
82. Abboud, M. A.; Needle, S. J.; Burns-Kurtis, C. L.; Valocik, R. E.; Koster, P. F.; Amour, A. J.; Chan, C.; Brown, D.; Chaudry, L.; Zhou, P.; Patikis, A.; Patel, C.; Pateman, A. J.; Young, R. J.; Watson, N. S.; Toomey, J. R. Antithrombotic Potential of GW813893: A Novel, Orally Active, Active-Site Directed Factor Xa Inhibitor. *J. Cardiovasc. Pharmacol.* **2008,** *52,* 66–71.
83. Ogata, K.; Shimizu, T.; Masumoto, H.; Oguma, T.; Sugiyama, N.; Kunitada, S. Clinical Safety, Tolerability, Pharmacokinetics and Pharmacodynamics of the Novel Factor Xa Inhibitor DY-807f in Healthy Volunteers. *Thromb. Res.* **2015,** *135,* 594–601.
84. Smallheer, J. M.; Quan, M. L. Chapter 9 Recent Advances in Coagulation Serine Protease InhibitorsMacor, J. E., Ed. *Annu. Rep. Med. Chem.* **2009,** *44,* 189–208. Academic Press: New York, NY.
85. Lee, Y.-K.; Player, M. R. Developments in Factor Xa Inhibitors for the Treatment of Thromboembolic Disorders. *Med. Res. Rev.* **2011,** *31,* 202–283.
86. Xue, T.; Ding, S.; Guo, B.; Zhou, Y.; Sun, P.; Wang, H.; Chu, W.; Gong, G.; Wang, Y.; Chen, X.; Yang, Y. Design, Synthesis, and Structure-Activity and Structure-Pharmacokinetic Relationship Studies of Novel [6,6,5] Tricyclic Fused Oxazolidinones Leading to the Discovery of a Potent, Selective, and Orally Bioavailable FXa Inhibitor. *J. Med. Chem.* **2014,** *57,* 7770–7791.
87. Quan, M. L.; Pinto, D. J. P.; Rossi, K. A.; Sheriff, S.; Alexander, R. S.; Amparo, E.; Kish, K.; Knabb, R. M.; Luettgen, J. M.; Morin, P.; Smallwood, A.; Woerner, F. J.; Wexler, R. R. Phenyltriazolinones as Potent Factor Xa Inhibitors. *Bioorg. Med. Chem. Lett.* **2010,** *20,* 1373–1377.
88. Orwat, M. J.; Qiao, J. X.; He, K.; Rendina, A. R.; Luettgen, J. M.; Rossi, K. A.; Xin, B.; Knabb, R. M.; Wexler, R. R.; Lam, P. Y. S.; Pinto, D. J. P. Orally Bioavailable Factor Xa Inhibitors Containing Alpha-Substituted Gem-Dimethyl P4 Moieties. *Bioorg. Med. Chem. Lett.* **2014,** *24,* 3341–3345.
89. Yoshikawa, K.; Kobayashi, S.; Nakamoto, Y.; Haginoya, N.; Komoriya, S.; Yoshino, T.; Nagata, T.; Mochizuki, A.; Watanabe, K.; Suzuki, M.; Kanno, H.; Ohta, T. Design, Synthesis, and SAR of *cis*-1,2-Diaminocyclohexane Derivatives as Potent Factor Xa Inhibitors. Part II: Exploration of 6–6 Fused Rings as Alternative S1 Moieties. *Bioorg. Med. Chem.* **2009,** *17,* 8221–8233.
90. Van Huis, C. A.; Bigge, C. F.; Casimiro-Garcia, A.; Cody, W. L.; Dudley, D. A.; Filipski, K. J.; Heemstra, R. J.; Kohrt, J. T.; Narasimhan, L. S.; Schaum, R. P.; Zhang, E.; Bryant, J. W.; Haarer, S.; Janiczek, N.; Leadley, R. J., Jr.; McClanahan, T.; Thomas Peterson, J.; Welch, K. M.; Edmunds, J. J. Structure-Based Drug Design of Pyrrolidine-1, 2-Dicarboxamides as a Novel Series of Orally Bioavailable Factor Xa Inhibitors. *Chem. Biol. Drug Des.* **2007,** *69,* 444–450.

91. Van Huis, C. A.; Casimiro-Garcia, A.; Bigge, C. F.; Cody, W. L.; Dudley, D. A.; Filipski, K. J.; Heemstra, R. J.; Kohrt, J. T.; Leadley, R. J., Jr.; Narasimhan, L. S.; McClanahan, T.; Mochalkin, I.; Pamment, M.; Thomas Peterson, J.; Sahasrabudhe, V.; Schaum, R. P.; Edmunds, J. J. Exploration of 4,4-Disubstituted Pyrrolidine-1,2-Dicarboxamides as Potent, Orally Active Factor Xa Inhibitors With Extended Duration of Action. *Bioorg. Med. Chem.* **2009,** *17,* 2501–2511.
92. Zbinden, K. G.; Anselm, L.; Banner, D. W.; Benz, J.; Blasco, F.; Decoret, G.; Himber, J.; Kuhn, B.; Panday, N.; Ricklin, F.; Risch, P.; Schlatter, D.; Stahl, M.; Thomi, S.; Unger, R.; Haap, W. Design of Novel Aminopyrrolidine Factor Xa Inhibitors From a Screening Hit. *Eur. J. Med. Chem.* **2009,** *44,* 2787–2795.
93. Corte, J. R.; Fang, T.; Pinto, D. J. P.; Han, W.; Hu, Z.; Jiang, X.-J.; Li, Y.-L.; Gauuan, J. F.; Hadden, M.; Orton, D.; Rendina, A. R.; Luettgen, J. M.; Wong, P. C.; He, K.; Morin, P. E.; Chang, C.-H.; Cheney, D. L.; Knabb, R. M.; Wexler, R. R.; Lam, P. Y. S. Structure-Activity Relationships of Anthranilamide-Based Factor Xa Inhibitors Containing Piperidinone and Pyridinone P4 Moieties. *Bioorg. Med. Chem. Lett.* **2008,** *18,* 2845–2849.
94. Ye, B.; Arnaiz, D. O.; Chou, Y.-L.; Griedel, B. D.; Karanjawala, R.; Lee, W.; Morrissey, M. M.; Sacchi, K. L.; Sakata, S. T.; Shaw, K. J.; Wu, S. C.; Zhao, Z.; Adler, M.; Cheeseman, S.; Dole, W. P.; Ewing, J.; Fitch, R.; Lentz, D.; Liang, A.; Light, D.; Morser, J.; Post, J.; Rumennik, G.; Subramanyam, B.; Sullivan, M. E.; Vergona, R.; Walters, J.; Wang, Y.-X.; White, K. A.; Whitlow, M.; Kochanny, M. Thiophene-Anthranilamides as Highly Potent and Orally Available Factor Xa Inhibitors. *J. Med. Chem.* **2007,** *50,* 2967–2980.
95. Yoshikawa, K.; Yoshino, T.; Yokomizo, Y.; Uoto, K.; Naito, H.; Kawakami, K.; Mochizuki, A.; Nagata, T.; Suzuki, M.; Kanno, H.; Takemura, M.; Ohta, T. Design, Synthesis and SAR of Novel Ethylenediamine and Phenylenediamine Derivatives as Factor Xa Inhibitors. *Bioorg. Med. Chem. Lett.* **2011,** *21,* 2133–2140.
96. Yang, J.; Su, G.; Ren, Y.; Chen, Y. Synthesis of 3,4-Diaminobenzoyl Derivatives as Factor Xa Inhibitors. *Eur. J. Med. Chem.* **2015,** *101,* 41–51.
97. Young, R. J.; Borthwick, A. D.; Brown, D.; Burns-Kurtis, C. L.; Campbell, M.; Chan, C.; Charbaut, M.; Convery, M. A.; Diallo, H.; Hortense, E.; Irving, W. R.; Kelly, H. A.; King, N. P.; Kleanthous, S.; Mason, A. M.; Pateman, A. J.; Patikis, A. N.; Pinto, I. L.; Pollard, D. R.; Senger, S.; Shah, G. P.; Toomey, J. R.; Watson, N. S.; Weston, H. E.; Zhou, P. Structure and Property Based Design of Factor Xa Inhibitors: Biaryl Pyrrolidin-2-Ones Incorporating Basic Heterocyclic Motifs. *Bioorg. Med. Chem. Lett.* **2008,** *18,* 28–33.
98. Shi, Y.; Sitkoff, D.; Zhang, J.; Han, W.; Hu, Z.; Stein, P. D.; Wang, Y.; Kennedy, L. J.; O'Connor, S. P.; Ahmad, S.; Liu, E. C. K.; Seiler, S. M.; Lam, P. Y. S.; Robl, J. A.; Macor, J. E.; Atwal, K. S.; Zahler, R. Amino(Methyl) Pyrrolidines as Novel Scaffolds for Factor Xa Inhibitors. *Bioorg. Med. Chem. Lett.* **2007,** *17,* 5952–5958.
99. Imaeda, Y.; Miyawaki, T.; Sakamoto, H.; Itoh, F.; Konishi, N.; Hiroe, K.; Kawamura, M.; Tanaka, T.; Kubo, K. Discovery of Sulfonylalkylamides: A New Class of Orally Active Factor Xa Inhibitors. *Bioorg. Med. Chem.* **2008,** *16,* 2243–2260.
100. Imaeda, Y.; Kawamoto, T.; Tobisu, M.; Konishi, N.; Hiroe, K.; Kawamura, M.; Tanaka, T.; Kubo, K. Discovery of Piperazinylimidazo[1,2-*a*]Pyridines as Novel S4 Binding Elements for Orally Active Factor Xa Inhibitors. *Bioorg. Med. Chem.* **2008,** *16,* 3125–3140.
101. Imaeda, Y.; Kuroita, T.; Sakamoto, H.; Kawamoto, T.; Tobisu, M.; Konishi, N.; Hiroe, K.; Kawamura, M.; Tanaka, T.; Kubo, K. Discovery of Imidazo[1,5-*c*]Imidazol-3-Ones: Weakly Basic, Orally Active Factor Xa Inhibitors. *J. Med. Chem.* **2008,** *51,* 3422–3436.
102. Shi, Y.; O'Connor, S. P.; Sitkoff, D.; Zhang, J.; Shi, M.; Bisaha, S. N.; Wang, Y.; Li, C.; Ruan, Z.; Michael Lawrence, R.; Klei, H. E.; Kish, K.; Liu, E. C. K.; Seiler, S. M.; Schweizer, L.; Steinbacher, T. E.; Schumacher, W. A.; Robl, J. A.; Macor, J. E.; Atwal, K. S.; Stein, P. D. Arylsulfonamidopiperidone Derivatives as a Novel Class of Factor Xa Inhibitors. *Bioorg. Med. Chem. Lett.* **2011,** *21,* 7516–7521.
103. Smallheer, J. M.; Wang, S.; Laws, M. L.; Nakajima, S.; Hu, Z.; Han, W.; Jacobson, I.; Luettgen, J. M.; Rossi, K. A.; Rendina, A. R.; Knabb, R. M.; Wexler, R. R.; Lam, P. Y.; Quan, M. L. Sulfonamidolactam Inhibitors of Coagulation Factor Xa. *Bioorg. Med. Chem. Lett.* **2008,** *18,* 2428–2433.
104. Shi, Y.; Zhang, J.; Shi, M.; O'Connor, S. P.; Bisaha, S. N.; Li, C.; Sitkoff, D.; Pudzianowski, A. T.; Chong, S.; Klei, H. E.; Kish, K.; Yanchunas, J., Jr.; Liu, E. C. K.; Hartl, K. S.; Seiler, S. M.; Steinbacher, T. E.; Schumacher, W. A.; Atwal, K. S.; Stein, P. D. Cyanoguanidine-Based Lactam Derivatives as a Novel Class of Orally Bioavailable Factor Xa Inhibitors. *Bioorg. Med. Chem. Lett.* **2009,** *19,* 4034–4041.
105. Shi, Y.; Li, C.; O'Connor, S. P.; Zhang, J.; Shi, M.; Bisaha, S. N.; Wang, Y.; Sitkoff, D.; Pudzianowski, A. T.; Huang, C.; Klei, H. E.; Kish, K.; Yanchunas, J., Jr.; Liu, E. C.; Hartl, K. S.; Seiler, S. M.; Steinbacher, T. E.; Schumacher, W. A.; Atwal, K. S.; Stein, P. D. Aroylguanidine-Based Factor Xa Inhibitors: The Discovery of BMS-344577. *Bioorg. Med. Chem. Lett.* **2009,** *19,* 6882–6889.
106. Shi, Y.; Sitkoff, D.; Zhang, J.; Klei, H. E.; Kish, K.; Liu, E. C. K.; Hartl, K. S.; Seiler, S. M.; Chang, M.; Huang, C.; Youssef, S.; Steinbacher, T. E.; Schumacher, W. A.; Grazier, N.; Pudzianowski, A.; Apedo, A.; Discenza, L.; Yanchunas, J., Jr.; Stein, P. D.; Atwal, K. S. Design, Structure-Activity Relationships, X-ray Crystal Structure, and Energetic Contributions of a Critical P1 Pharmacophore: 3-Chloroindole-7-yl-Based Factor Xa Inhibitors. *J. Med. Chem.* **2008,** *51,* 7541–7551.
107. Saitoh, F.; Nishida, H.; Mukaihira, T.; Kosuga, N.; Ohkouchi, M.; Matsusue, T.; Shiromizu, I.; Hosaka, Y.; Matsumoto, M.; Yamamoto, I. Synthesis and Evaluation of 1-Arylsulfonyl-3-Piperazinone Derivatives as Factor Xa Inhibitors VI. A Series of New Derivatives Containing N,S- and N,SO_2-Spiro Acetal Scaffolds. *Chem. Pharm. Bull.(Tokyo)* **2007,** *55,* 317–323.
108. Ansell, J.; Hirsh, J.; Hylek, E.; Jacobson, A.; Crowther, M.; Palareti, G.; American College of Chest Physicians. Pharmacology and Management of the Vitamin K Antagonists: American College of Chest Physicians Evidence-Based Clinical Practice Guidelines (8th Edition). *Chest* **2008,** *133,* 160S–198S.
109. Das, A.; Liu, D. Novel Antidotes for Target Specific Oral Anticoagulants. *Exp. Hematol. Oncol.* **2015,** *4,* 25.
110. Crowther, M.; Crowther, M. A. Antidotes for Novel Oral Anticoagulants: Current Status and Future Potential. *Arterioscler. Thromb. Vasc. Biol.* **2015,** *35,* 1736–1745.
111. Ansell, J. E. Universal, Class-Specific and Drug-Specific Reversal Agents for the New Oral Anticoagulants. *J. Thromb. Thrombolysis* **2016,** *41,* 248–252.
112. Lu, G.; DeGuzman, F. R.; Hollenbach, S. J.; Karbarz, M. J.; Abe, K.; Lee, G.; Luan, P.; Hutchaleelaha, A.; Inagaki, M.; Conley, P. B.; Phillips, D. R.; Sinha, U. A Specific Antidote for Reversal of Anticoagulation by Direct and Indirect Inhibitors of Coagulation Factor Xa. *Nat. Med.* **2013,** *19,* 446–451.
113. Siegal, D. M.; Curnutte, J. T.; Connolly, S. J.; Lu, G.; Conley, P. B.; Wiens, B. L.; Mathur, V. S.; Castillo, J.; Bronson, M. D.; Leeds, J. M.; Mar, F. A.; Gold, A.; Crowther, M. A. Andexanet Alfa for the Reversal of Factor Xa Inhibitor Activity. *New Engl. J. Med.* **2015,** *373,* 2413–2424.
114. Gomez-Outes, A.; Suarez-Gea, M. L.; Lecumberri, R.; Terleira-Fernandez, A. I.; Vargas-Castrillon, E. Specific Antidotes in Development for Reversal of Novel Anticoagulants: A Review. *Recent Pat. Cardiovasc. Drug Discov.* **2015,** *9,* 2–10.
115. Ansell, J. E.; Bakhru, S. H.; Laulicht, B. E.; Steiner, S. S.; Grosso, M.; Brown, K.; Dishy, V.; Noveck, R. J.; Costin, J. C. Use of PER977 to Reverse the Anticoagulant Effect of Edoxaban. *N. Engl. J. Med.* **2014,** *371,* 2141–2142.
116. Giardino, E. C.; Haertlein, B. J.; de Garavilla, L.; Costanzo, M. J.; Damiano, B. P.; Andrade-Gordon, P.; Maryanoff, B. E. Cooperative Antithrombotic Effect From the Simultaneous Inhibition of Thrombin and Factor Xa. *Blood Coagul. Fibrinolysis* **2010,** *21,* 128–134.
117. Maryanoff, B. E.; McComsey, D. F.; Costanzo, M. J.; Yabut, S. C.; Lu, T.; Player, M. R.; Giardino, E. C.; Damiano, B. P. Exploration of Potential Prodrugs of RWJ-445167, an Oxyguanidine-Based Dual Inhibitor of Thrombin and Factor Xa. *Chem. Biol. Drug Des.* **2006,** *68,* 29–36.
118. Leitner, J. M.; Jilma, B.; Mayr, F. B.; Cardona, F.; Spiel, A. O.; Firbas, C.; Rathgen, K.; Stähle, H.; Schühly, U.; Graefe-Mody, E. U. Pharmacokinetics and Pharmacodynamics of the Dual FII/FX Inhibitor BIBT 986 in Endotoxin-Induced Coagulation. *Clin. Pharmacol. Ther.* **2007,** *81,* 858–866.
119. Young, R. J.; Brown, D.; Burns-Kurtis, C. L.; Chan, C.; Convery, M. A.; Hubbard, J. A.; Kelly, H. A.; Pateman, A. J.; Patikis, A.; Senger, S.; Shah, G. P.; Toomey, J. R.; Watson, N. S.; Zhou, P. Selective and Dual Action Orally Active Inhibitors of Thrombin and Factor Xa. *Bioorg. Med. Chem. Lett.* **2007,** *17,* 2927–2930.
120. Trstenjak, U.; Ilaš, J.; Kikelj, D. Transformation of a Selective Factor Xa Inhibitor Rivaroxaban into a Dual Factor Xa/Thrombin Inhibitor by Modification of the Morpholin-3-One Moiety. *Med. Chem. Commun.* **2014,** *5,* 197.
121. Dönnecke, D.; Schweinitz, A.; Stürzebecher, A.; Steinmetzer, P.; Schuster, M.; Stürzebecher, U.; Nicklisch, S.; Stürzebecher, J.; Steinmetzer, T. From Selective Substrate Analogue Factor Xa Inhibitors to Dual Inhibitors of Thrombin and Factor Xa. Part 3. *Bioorg. Med. Chem. Lett.* **2007,** *17,* 3322–3329.
122. Meneyrol, J.; Follmann, M.; Lassalle, G.; Wehner, V.; Barre, G.; Rousseaux, T.; Altenburger, J.-M.; Petit, F.; Bocskei, Z.; Schreuder, H.; Alet, N.; Herault, J.-P.; Millet, L.; Dol, F.; Florian, P.; Schaeffer, P.; Sadoun, F.; Klieber, S.; Briot, C.; Bono, F.; Herbert, J.-M. 5-Chlorothiophene-2-Carboxylic Acid [(S)-2-[2-Methyl-3-(2-Oxopyrrolidin-1-yl) Benzenesulfonylamino]-3-(4-Methylpiperazin-1-yl)-3-Oxopropyl]Amide (SAR107375), a Selective and Potent Orally Active Dual Thrombin and Factor Xa Inhibitor. *J. Med. Chem.* **2013,** *56,* 9441–9456.

123. Olson, S. T.; Swanson, R.; Petitou, M. Specificity and Selectivity Profile of EP217609: A new Neutralizable Dual-Action Anticoagulant That Targets Thrombin and Factor Xa. *Blood* **2012,** *119,* 2187–2195.
124. Szalony, J. A.; Suleymanov, O. D.; Salyers, A. K.; Panzer-Knodle, S. G.; Blom, J. D.; LaChance, R. M.; Case, B. L.; Parlow, J. J.; South, M. S.; Wood, R. S.; Nicholson, N. S. Administration of a Small Molecule Tissue Factor/Factor VIIa Inhibitor in a Non-Human Primate Thrombosis Model of Venous Thrombosis: Effects on Thrombus Formation and Bleeding Time. *Thromb. Res.* **2003,** *112,* 167–174.
125. Suleymanov, O. D.; Szalony, J. A.; Salyers, A. K.; LaChance, R. M.; Parlow, J. J.; South, M. S.; Wood, R. S.; Nicholson, N. S. Pharmacological Interruption of Acute Thrombus Formation With Minimal Hemorrhagic Complications by a Small Molecule Tissue Factor/Factor VIIa Inhibitor: Comparison to Factor Xa and Thrombin Inhibition in a Nonhuman Primate Thrombosis Model. *J. Pharmacol. Exp. Ther.* **2003,** *306,* 1115–1121.
126. Salyers, A. K.; Szalony, J. A.; Suleymanov, O. D.; Parlow, J. J.; Wood, R. S.; South, M. S.; Nicholson, N. S. Assessment of Bleeding Propensity in Non-Human Primates by Combination of Selective Tissue Factor/VIIa Inhibition and Aspirin Compared to Warfarin and Aspirin Treatment. *Pharmacology* **2004,** *70,* 100–106.
127. Lee, A.; Agnelli, G.; Büller, H.; Ginsberg, J.; Heit, J.; Rote, W.; Vlasuk, G.; Costantini, L.; Julian, J.; Comp, P.; van der Meer, J.; Piovella, F.; Raskob, G.; Gent, M. Dose–Response Study of Recombinant Factor VIIa/Tissue Factor Inhibitor Recombinant Nematode Anticoagulant Protein c2 in Prevention of Postoperative Venous Thromboembolism in Patients Undergoing Total Knee Replacement. *Circulation* **2001,** *104,* 74–78.
128. Morrow, D. A.; Murphy, S. A.; McCabe, C. H.; Mackman, N.; Wong, H. C.; Antman, E. M. Potent Inhibition of Thrombin With a Monoclonal Antibody Against Tissue Factor (Sunol-cH36): Results of the PROXIMATE-TIMI 27 Trial. *Eur. Heart J.* **2005,** *26,* 682–688.
129. Versteeg, H. H.; Ruf, W. Emerging Insights in Tissue Factor-Dependent Signaling Events. *Semin. Thromb. Hemost.* **2006,** *32,* 024–032.
130. Pawashe, A. B.; Golino, P.; Ambrosio, G.; Migliaccio, F.; Ragni, M.; Pascucci, I.; Chiariello, M.; Bach, R.; Garen, A.; Konigsberg, W. K. A Monoclonal Antibody Against Rabbit Tissue Factor Inhibits Thrombus Formation in Stenotic Injured Rabbit Carotid Arteries. *Circ. Res.* **1994,** *74,* 56–63.
131. Himber, J.; Kirchhofer, D.; Riederer, M.; Tschopp, T.; Steiner, B.; Roux, S. Dissociation of Antithrombotic Effect and Bleeding Time Prolongation in Rabbits by Inhibiting Tissue Factor Function. *Thromb. Haemost.* **1997,** *78,* 1142–1149.
132. Kelley, R. F.; Refino, C. J.; O'Connell, M. P.; Modi, N.; Sehl, P.; Lowe, D.; Pater, C.; Bunting, S. A Soluble Tissue Factor Mutant is a Selective Anticoagulant and Antithrombotic Agent. *Blood* **1997,** *89,* 3219–3227.
133. Himber, J.; Refino, C. J.; Burcklen, L.; Roux, S.; Kirchhofer, D. Inhibition of Arterial Thrombosis by a Soluble Tissue Factor Mutant and Active Site-Blocked Factors IXa and Xa in the Guinea Pig. *Thromb. Haemost.* **2001,** *85,* 475–481.
134. Harker, L. A.; Hanson, S.; Wilcox, J.; Kelly, A. Antithrombotic and Antilesion Benefits Without Hemorrhagic Risks by Inhibiting Tissue Factor Pathway. *Pathophysiol. Haemost. Thromb.* **1996,** *26,* 76–82.
135. Golino, P.; Ragni, M.; Cirillo, P.; D'Andrea, D.; Scognamiglio, A.; Ravera, A.; Buono, C.; Ezban, M.; Corcione, N.; Vigorito, F. Antithrombotic Effects of Recombinant Human, Active Site–Blocked Factor VIIa in a Rabbit Model of Recurrent Arterial Thrombosis. *Circ. Res.* **1998,** *82,* 39–46.
136. Olivero, A. G.; Eigenbrot, C.; Goldsmith, R.; Robarge, K.; Artis, D. R.; Flygare, J.; Rawson, T.; Sutherlin, D. P.; Kadkhodayan, S.; Beresini, M.; Elliott, L. O.; DeGuzman, G. G.; Banner, D. W.; Ultsch, M.; Marzec, U.; Hanson, S. R.; Refino, C.; Bunting, S.; Kirchhofer, D. A Selective, Slow Binding Inhibitor of Factor VIIa Binds to a Nonstandard Active Site Conformation and Attenuates Thrombus Formation In Vivo. *J. Biol. Chem.* **2005,** *280,* 9160–9169.
137. Zbinden, K. G.; Banner, D. W.; Hilpert, K.; Himber, J.; Lavé, T.; Riederer, M. A.; Stahl, M.; Tschopp, T. B.; Obst-Sander, U. Dose-Dependent Antithrombotic Activity of an Orally Active Tissue Factor/Factor VIIa Inhibitor Without Concomitant Enhancement of Bleeding Propensity. *Bioorg. Med. Chem.* **2006,** *14,* 5357–5369.
138. Young, W. B.; Mordenti, J.; Torkelson, S.; Shrader, W. D.; Kolesnikov, A.; Rai, R.; Liu, L.; Hu, H.; Leahy, E. M.; Green, M. J.; Sprengeler, P. A.; Katz, B. A.; Yu, C.; Janc, J. W.; Elrod, K. C.; Marzec, U. M.; Hanson, S. R. Factor VIIa Inhibitors: Chemical Optimization, Preclinical Pharmacokinetics, Pharmacodynamics, and Efficacy in an Arterial Baboon Thrombosis Model. *Bioorg. Med. Chem. Lett.* **2006,** *16,* 2037–2041.
139. Arnold, C. S.; Parker, C.; Upshaw, R.; Prydz, H.; Chand, P.; Kotian, P.; Bantia, S.; Babu, Y. S. The Antithrombotic and Anti-Inflammatory Effects of BCX-3607, a Small Molecule Tissue Factor/Factor VIIa Inhibitor. *Thromb. Res.* **2006,** *117,* 343–349.
140. Wong, P. C.; Luettgen, J. M.; Rendina, A. R.; Kettner, C. A.; Xin, B.; Knabb, R. M.; Wexler, R.; Priestley, E. S. BMS-593214, an Active Site-Directed Factor VIIa Inhibitor: Enzyme Kinetics, Antithrombotic and Antihaemostatic Studies. *Thromb. Haemost.* **2010,** *104,* 261–269.
141. Nagakura, T.; Tabata, K.; Kira, K.; Hirota, S.; Clark, R.; Matsuura, F.; Hiyoshi, H. Selective Tissue Factor/Factor VIIa Inhibitor, ER-410660, and Its Prodrug, E5539, Have Anti-Venous and Anti-Arterial Thrombotic Effects With a Low Risk of Bleeding. *Thromb. Res.* **2013,** *132,* 271–279.
142. Bergum, P. W.; Cruikshank, A.; Maki, S. L.; Kelly, C. R.; Ruf, W.; Vlasuk, G. P. Role of Zymogen and Activated Factor X as Scaffolds for the Inhibition of the Blood Coagulation Factor VIIa-Tissue Factor Complex by Recombinant Nematode Anticoagulant Protein c2. *J. Biol. Chem.* **2001,** *276,* 10063–10071.
143. Moons, A. H. M.; Peters, R. J. G.; Bijsterveld, N. R.; Piek, J. J.; Prins, M. H.; Vlasuk, G. P.; Rote, W. E.; Büller, H. R. Recombinant Nematode Anticoagulant Protein c2, an Inhibitor of the Tissue Factor/Factor VIIa Complex, in Patients Undergoing Elective Coronary Angioplasty. *J. Am. Coll. Cardiol.* **2003,** *41,* 2147–2153.
144. Giugliano, R. P.; Wiviott, S. D.; Stone, P. H.; Simon, D. I.; Schweiger, M. J.; Bouchard, A.; Leesar, M. A.; Goulder, M. A.; Deitcher, S. R.; McCabe, C. H.; Braunwald, E. Recombinant Nematode Anticoagulant Protein c2 in Patients With Non–ST-Segment Elevation Acute Coronary Syndrome: The ANTHEM–TIMI-32 Trial. *J. Am. Coll. Cardiol.* **2007,** *49,* 2398–2407.
145. Jiao, J.-a.; Kelly, A. B.; Marzec, U. M.; Nieves, E.; Acevedo, J.; Burkhardt, M.; Edwards, A.; Zhu, X.-y.; Chavaillaz, P.-A.; Wong, A.; Wong, J. L.; Egan, J. O.; Taylor, D.; Rhode, P. R.; Wong, H. C. Inhibition of Acute Vascular Thrombosis in Chimpanzees by an Anti-Human Tissue Factor Antibody Targeting the Factor X Binding Site. *Thromb. Haemost.* **2010,** *103,* 224–233.
146. Welty-Wolf, K. E.; Carraway, M. S.; Ortel, T. L.; Ghio, A. J.; Idell, S.; Egan, J.; Zhu, X.; Jiao, J. A.; Wong, H. C.; Piantadosi, C. A. Blockade of Tissue Factor-Factor X Binding Attenuates Sepsis-Induced Respiratory and Renal Failure. *Am. J. Physiol. Lung Cell. Mol. Physiol.* **2006,** *290,* L21–31.
147. Morris, P. E.; Steingrub, J. S.; Huang, B. Y.; Tang, S.; Liu, P. M.; Rhode, P. R.; Wong, H. C. A Phase I Study Evaluating the Pharmacokinetics, Safety and Tolerability of an Antibody-Based Tissue Factor Antagonist in Subjects With Acute Lung Injury or Acute Respiratory Distress Syndrome. *BMC Pulm. Med.* **2012,** *12,* 5.
148. ClinicalTrials.gov. *Anti-TF Antibody (ALT-836) to Treat Septic Patients With Acute Lung Injury or Acute Respiratory Distress Syndrome.* https://clinicaltrials.gov/ct2/show/NCT00879606 (accessed Dec 2, 2015).
149. ClinicalTrials.gov. *A Study of ALT-836 in Combination With Gemcitabine for Locally Advanced or Metastatic Solid Tumors.* https://clinicaltrials.gov/ct2/show/NCT01325558 (accessed Dec 2, 2015).
150. Ruf, W.; Yokota, N.; Schaffner, F. Tissue Factor in Cancer Progression and Angiogenesis. *Thromb. Res.* **2010,** *125 Suppl 2,* S36–38.
151. Mahesh, S. A.; Gabrail, N. Y.; Gandhi, J. G.; Khorana, A. A.; Manges, R.; Shah, S.; Thomas, G. W.; Hamdy, A. M.; Stevens-Brogan, M.; Zhou, C. Phase I/II Study of PCI-27483, a Coagulation Factor VIIa (FVIIa) Inhibitor, in Combination With Gemcitabine in Patients With Advanced Pancreatic Cancer. *J. Clin. Oncol.* **2013,** *31* (suppl; abstr e105014).
152. Kolesnikov, A.; Rai, R.; Young, W. B.; Mordenti, J.; Liu, L.; Torkelson, S.; Shrader, W. D.; Leahy, E. M.; Hu, H.; Gjerstad, E.; Janc, J.; Katz, B. A.; Sprengeler, P. A. Factor VIIa Inhibitors: Improved Pharmacokinetic Parameters. *Bioorg. Med. Chem. Lett.* **2006,** *16,* 2243–2246.
153. Shrader, W. D.; Kolesnikov, A.; Burgess-Henry, J.; Rai, R.; Hendrix, J.; Hu, H.; Torkelson, S.; Ton, T.; Young, W. B.; Katz, B. A.; Yu, C.; Tang, J.; Cabuslay, R.; Sanford, E.; Janc, J. W.; Sprengeler, P. A. Factor VIIa Inhibitors: Gaining Selectivity Within the Trypsin Family. *Bioorg. Med. Chem. Lett.* **2006,** *16,* 1596–1600.
154. Riggs, J. R.; Kolesnikov, A.; Hendrix, J.; Young, W. B.; Shrader, W. D.; Vijaykumar, D.; Stephens, R.; Liu, L.; Pan, L.; Mordenti, J.; Green, M. J.; Sukbuntherng, J. Factor VIIa Inhibitors: A Prodrug Strategy to Improve Oral Bioavailability. *Bioorg. Med. Chem. Lett.* **2006,** *16,* 2224–2228.
155. Vijaykumar, D.; Rai, R.; Shaghafi, M.; Ton, T.; Torkelson, S.; Leahy, E. M.; Riggs, J. R.; Hu, H.; Sprengeler, P. A.; Shrader, W. D.; O'Bryan, C.; Cabuslay, R.; Sanford, E.; Gjerstadt, E.; Liu, L.; Sukbuntherng, J.; Young, W. B. Efforts Toward Oral Bioavailability in Factor VIIa Inhibitors. *Bioorg. Med. Chem. Lett.* **2006,** *16,* 3829–3832.
156. Tousoulis, D.; Charakida, M.; Stefanadis, C. Endothelial Function and Inflammation in Coronary Artery Disease. *Heart* **2006,** *92,* 441–444.

157. Priestley, E. S.; De Lucca, I.; Zhou, J.; Zhou, J.; Saiah, E.; Stanton, R.; Robinson, L.; Luettgen, J. M.; Wei, A.; Wen, X.; Knabb, R. M.; Wong, P. C.; Wexler, R. R. Discovery and Gram-Scale Synthesis of BMS-593214, a Potent, Selective FVIIa Inhibitor. *Bioorg. Med. Chem. Lett.* **2013,** *23,* 2432–2435.
158. Nakabayashi, T.; Gotoh, Y.; Kamada, N.; Fujioka, M.; Ishihara, T.; Hirabayashi, A.; Sato, H. Pharmacokinetics of the Amidine Prodrug of a Novel Oral Anticoagulant Factor VIIa Inhibitor (AS1924269-00) in Rats. *Pharmazie* **2013,** *68,* 349–354.
159. Nakabayashi, T.; Gotoh, Y.; Kamada, N.; Fujioka, M.; Ishihara, T.; Hirabayashi, A.; Sato, H. Characterization of In Vitro Biotransformation of the New Oral Anticoagulants, the Factor VIIa Inhibitors AS1927819-00 and AS1932804-00. *Pharmazie* **2013,** *68,* 406–418.
160. Glunz, P. W.; Cheng, X.; Cheney, D. L.; Weigelt, C. A.; Wei, A.; Luettgen, J. M.; Wong, P. C.; Wexler, R. R.; Priestley, E. S. Design and Synthesis of Potent, Selective Phenylimidazole-Based FVIIa Inhibitors. *Bioorg. Med. Chem. Lett.* **2015,** *25,* 2169–2173.
161. Rai, R.; Kolesnikov, A.; Sprengeler, P. A.; Torkelson, S.; Ton, T.; Katz, B. A.; Yu, C.; Hendrix, J.; Shrader, W. D.; Stephens, R.; Cabuslay, R.; Sanford, E.; Young, W. B. Discovery of Novel Heterocyclic Factor VIIa Inhibitors. *Bioorg. Med. Chem. Lett.* **2006,** *16,* 2270–2273.
162. Riggs, J. R.; Hu, H.; Kolesnikov, A.; Leahy, E. M.; Wesson, K. E.; Shrader, W. D.; Vijaykumar, D.; Wahl, T. A.; Tong, Z.; Sprengeler, P. A.; Green, M. J.; Yu, C.; Katz, B. A.; Sanford, E.; Nguyen, M.; Cabuslay, R.; Young, W. B. Novel 5-Azaindole Factor VIIa Inhibitors. *Bioorg. Med. Chem. Lett.* **2006,** *16,* 3197–3200.
163. Hu, H.; Kolesnikov, A.; Riggs, J. R.; Wesson, K. E.; Stephens, R.; Leahy, E. M.; Shrader, W. D.; Sprengeler, P. A.; Green, M. J.; Sanford, E.; Nguyen, M.; Gjerstad, E.; Cabuslay, R.; Young, W. B. Potent 4-Amino-5-Azaindole Factor VIIa Inhibitors. *Bioorg. Med. Chem. Lett.* **2006,** *16,* 4567–4570.
164. Miura, M.; Seki, N.; Koike, T.; Ishihara, T.; Niimi, T.; Hirayama, F.; Shigenaga, T.; Sakai-Moritani, Y.; Kawasaki, T.; Sakamoto, S.; Okada, M.; Ohta, M.; Tsukamoto, S. Potent and Selective TF/FVIIa Inhibitors Containing a Neutral P1 Ligand. *Bioorg. Med. Chem.* **2006,** *14,* 7688–7705.
165. Miura, M.; Seki, N.; Koike, T.; Ishihara, T.; Niimi, T.; Hirayama, F.; Shigenaga, T.; Sakai-Moritani, Y.; Tagawa, A.; Kawasaki, T.; Sakamoto, S.; Okada, M.; Ohta, M.; Tsukamoto, S. Design, Synthesis and Biological Activity of Selective and Orally Available TF/FVIIa Complex Inhibitors Containing Non-Amidine P1 Ligands. *Bioorg. Med. Chem.* **2007,** *15,* 160–173.
166. Bolton, S. A.; Sutton, J. C.; Anumula, R.; Bisacchi, G. S.; Jacobson, B.; Slusarchyk, W. A.; Treuner, U. D.; Wu, S. C.; Zhao, G.; Pi, Z.; Sheriff, S.; Smirk, R. A.; Bisaha, S.; Cheney, D. L.; Wei, A.; Schumacher, W. A.; Hartl, K. S.; Liu, E.; Zahler, R.; Seiler, S. M. Discovery of Nonbenzamidine Factor VIIa Inhibitors Using a Biaryl Acid Scaffold. *Bioorg. Med. Chem. Lett.* **2013,** *23,* 5239–5243.
167. Glunz, P. W.; Zhang, X.; Zou, Y.; Delucca, I.; Nirschl, A. H.; Cheng, X.; Weigelt, C. A.; Cheney, D. L.; Wei, A.; Anumula, R.; Luettgen, J. M.; Rendina, A. R.; Harpel, M.; Luo, G.; Knabb, R.; Wong, P. C.; Wexler, R. R.; Priestley, E. S. Nonbenzamidine Acylsulfonamide Tissue Factor-Factor VIIa Inhibitors. *Bioorg. Med. Chem. Lett.* **2013,** *23,* 5244–5248.
168. Zhang, X.; Jiang, W.; Jacutin-Porte, S.; Glunz, P. W.; Zou, Y.; Cheng, X.; Nirschl, A. H.; Wurtz, N. R.; Luettgen, J. M.; Rendina, A. R.; Luo, G.; Harper, T. M.; Wei, A.; Anumula, R.; Cheney, D. L.; Knabb, R. M.; Wong, P. C.; Wexler, R. R.; Priestley, E. S. Design and Synthesis of Phenylpyrrolidine Phenylglycinamides as Highly Potent and Selective TF-FVIIA Inhibitors. *ACS Med. Chem. Lett.* **2014,** *5,* 188–192.
169. Cheney, D. L.; Bozarth, J. M.; Metzler, W. J.; Morin, P. E.; Mueller, L.; Newitt, J. A.; Nirschl, A. H.; Rendina, A. R.; Tamura, J. K.; Wei, A.; Wen, X.; Wurtz, N. R.; Seiffert, D. A.; Wexler, R. R.; Priestley, E. S. Discovery of Novel P1 Groups for Coagulation Factor VIIa Inhibition Using Fragment-Based Screening. *J. Med. Chem.* **2015,** *58,* 2799–2808.
170. Priestley, E. S.; Cheney, D. L.; DeLucca, I.; Wei, A.; Luettgen, J. M.; Rendina, A. R.; Wong, P. C.; Wexler, R. R. Structure-Based Design of Macrocyclic Coagulation Factor VIIa Inhibitors. *J. Med. Chem.* **2015,** *58,* 6225–6236.
171. Eikelboom, J. W.; Zelenkofske, S. L.; Rusconi, C. P. Coagulation Factor IXa as a Target for Treatment and Prophylaxis of Venous Thromboembolism. *Arterioscler. Thromb. Vasc. Biol.* **2010,** *30,* 382–387.
172. Toomey, J. R.; Blackburn, M. N.; Storer, B. L.; Valocik, R. E.; Koster, P. F.; Feuerstein, G. Z. Comparing the Antithrombotic Efficacy of a Humanized Anti-Factor IX(a) Monoclonal Antibody (SB 249417) to the Low Molecular Weight Heparin Enoxaparin In a Rat Model of Arterial Thrombosis. *Thromb. Res.* **2000,** *100,* 73–79.
173. Cohen, M. G.; Purdy, D. A.; Rossi, J. S.; Grinfeld, L. R.; Myles, S. K.; Aberle, L. H.; Greenbaum, A. B.; Fry, E.; Chan, M. Y.; Tonkens, R. M.; Zelenkofske, S.; Alexander, J. H.; Harrington, R. A.; Rusconi, C. P.; Becker, R. C. First Clinical Application of an Actively Reversible Direct Factor IXa Inhibitor as an Anticoagulation Strategy in Patients Undergoing Percutaneous Coronary Intervention. *Circulation* **2010,** *122,* 614–622.
174. ClinicalTrials.gov. *A Study to Determine the Efficacy and Safety of REG1 Compared to Bivalirudin in Patients Undergoing PCI (Regulate).* https://www.clinicaltrials.gov/ct2/show/NCT01848106 (accessed Dec 26, 2015).
175. Eriksson, B. I.; Dahl, O.; Lassen, M.; Ward, D.; Rothlein, R.; Davis, G.; Turpie, A. Partial Factor IXa Inhibition With TTP889 for Prevention of Venous Thromboembolism: An Exploratory Study. *J. Thromb. Haemost.* **2008,** *6,* 457–463.
176. Batt, D. G.; Qiao, J. X.; Modi, D. P.; Houghton, G. C.; Pierson, D. A.; Rossi, K. A.; Luettgen, J. M.; Knabb, R. M.; Jadhav, P. K.; Wexler, R. R. 5-Amidinoindoles as Dual Inhibitors of Coagulation Factors IXa and Xa. *Bioorg. Med. Chem. Lett.* **2004,** *14,* 5269–5274.
177. Qiao, J. X.; Cheng, X.; Modi, D. P.; Rossi, K. A.; Luettgen, J. M.; Knabb, R. M.; Jadhav, P. K.; Wexler, R. R. 5-Amidinobenzo[*b*]Thiophenes as Dual Inhibitors of Factors IXa and Xa. *Bioorg. Med. Chem. Lett.* **2005,** *15,* 29–36.
178. Smallheer, J. M.; Alexander, R. S.; Wang, J.; Wang, S.; Nakajima, S.; Rossi, K. A.; Smallwood, A.; Barbera, F.; Burdick, D.; Luettgen, J. M.; Knabb, R. M.; et al. SAR and Factor IXa Crystal Structure of a Dual Inhibitor of Factors IXa and Xa. *Bioorg. Med. Chem. Lett.* **2004,** *14,* 5263–5268.
179. Vijaykumar, D.; Sprengeler, P. A.; Shaghafi, M.; Spencer, J. R.; Katz, B. A.; Yu, C.; Rai, R.; Young, W. B.; Schultz, B.; Janc, J. Discovery of Novel Hydroxy Pyrazole Based Factor IXa Inhibitor. *Bioorg. Med. Chem. Lett.* **2006,** *16,* 2796–2799.
180. Wang, S.; Beck, R.; Blench, T.; Burd, A.; Buxton, S.; Malic, M.; Ayele, T.; Shaikh, S.; Chahwala, S.; Chander, C. Studies of Benzothiophene Template as Potent Factor IXa (FIXa) Inhibitors in Thrombosis. *J. Med. Chem.* **2010,** *53,* 1465–1472.
181. Wang, S.; Beck, R.; Burd, A.; Blench, T.; Marlin, F.; Ayele, T.; Buxton, S.; Dagostin, C.; Malic, M.; Joshi, R. Structure Based Drug Design: Development of Potent and Selective Factor IXa (FIXa) Inhibitors. *J. Med. Chem.* **2010,** *53,* 1473–1482.
182. Parker, D. L., Jr.; Walsh, S.; Li, B.; Kim, E.; Sharipour, A.; Smith, C.; Chen, Y. H.; Berger, R.; Harper, B.; Zhang, T.; Park, M.; Shu, M.; Wu, J.; Xu, J.; Dewnani, S.; Sherer, E. C.; Hruza, A.; Reichert, P.; Geissler, W.; Sonatore, L.; Ellsworth, K.; Balkovec, J.; Greenlee, W.; Wood, H. B. Rapid Development of Two Factor IXa Inhibitors From Hit to Lead. *Bioorg. Med. Chem. Lett.* **2015,** *25,* 2321–2325.
183. Meng, D.; Andre, P.; Bateman, T. J.; Berger, R.; Chen, Y.-H.; Desai, K.; Dewnani, S.; Ellsworth, K.; Feng, D.; Geissler, W. M. Development of a Novel Tricyclic Class of Potent and Selective FIXa Inhibitors. *Bioorg. Med. Chem. Lett.* **2015,** *25,* 5437–5443.
184. Zhang, T.; Andre, P.; Bateman, T. J.; Chen, Y. H.; Desai, K.; Ellsworth, K.; Geissler, W. M.; Guo, L.; Hruza, A.; Jian, T.; Meng, D.; Parker, D. L., Jr.; Qian, X.; Reichert, P.; Sherer, E. C.; Shu, M.; Smith, C. J.; Sonatore, L. M.; Tschirret-Guth, R.; Nolting, A. F.; Orr, R.; Campeau, L. C.; Araki, K.; Nishimura, T.; Sakurada, I.; Wood, H. B. Development of a Novel Class of Potent and Selective FIXa Inhibitors. *Bioorg. Med. Chem. Lett.* **2015,** *25,* 4945–4949.
185. Schumacher, W. A.; Luettgen, J. M.; Quan, M. L.; Seiffert, D. A. Inhibition of Factor XIa as a New Approach to Anticoagulation. *Arterioscler. Thromb. Vasc. Biol.* **2010,** *30,* 388–392.
186. Gailani, D.; Bane, C. E.; Gruber, A. Factor XI and Contact Activation as Targets for Antithrombotic Therapy. *J. Thromb. Haemost.* **2015,** *13,* 1383–1395.
187. Salomon, O.; Steinberg, D. M.; Koren-Morag, N.; Tanne, D.; Seligsohn, U. Reduced Incidence of Ischemic Stroke in Patients With Severe Factor XI Deficiency. *Blood* **2008,** *111,* 4113–4117.
188. Doggen, C. J.; Rosendaal, F. R.; Meijers, J. C. Levels of Intrinsic Coagulation Factors and the Risk of Myocardial Infarction Among Men: Opposite and Synergistic Effects of Factors XI and XII. *Blood* **2006,** *108,* 4045–4051.
189. Meijers, J. C. M.; Tekelenburg, W. L. H.; Bouma, B. N.; Bertina, R. M.; Rosendaal, F. R. High Levels of Coagulation Factor XI as a Risk Factor for Venous Thrombosis. *N. Engl. J. Med.* **2000,** *342,* 696–701.

190. Renne, T.; Pozgajova, M.; Gruner, S.; Schuh, K.; Pauer, H. U.; Burfeind, P.; Gailani, D.; Nieswandt, B. Defective Thrombus Formation in Mice Lacking Coagulation Factor XII. *J. Exp. Med.* **2005,** *202,* 271–281.
191. Wang, X.; Cheng, Q.; Xu, L.; Feuerstein, G. Z.; Hsu, M. Y.; Smith, P. L.; Seiffert, D. A.; Schumacher, W. A.; Ogletree, M. L.; Gailani, D. Effects of Factor IX or Factor XI Deficiency on Ferric Chloride-Induced Carotid Artery Occlusion in Mice. *J. Thromb. Haemost.* **2005,** *3,* 695–702.
192. Crosby, J. R.; Marzec, U.; Revenko, A. S.; Zhao, C.; Gao, D.; Matafonov, A.; Gailani, D.; MacLeod, A. R.; Tucker, E. I.; Gruber, A.; Hanson, S. R.; Monia, B. P. Antithrombotic Effect of Antisense Factor XI Oligonucleotide Treatment in Primates. *Arterioscler. Thromb. Vasc. Biol.* **2013,** *33,* 1670–1678.
193. Zhang, H.; Löwenberg, E. C.; Crosby, J. R.; MacLeod, A. R.; Zhao, C.; Gao, D.; Black, C.; Revenko, A. S.; Meijers, J. C. M.; Stroes, E. S.; Levi, M.; Monia, B. P. Inhibition of the Intrinsic Coagulation Pathway Factor XI by Antisense Oligonucleotides: A Novel Antithrombotic Strategy With Lowered Bleeding Risk. *Blood* **2010,** *116,* 4684–4692.
194. Cheng, Q.; Tucker, E. I.; Pine, M. S.; Sisler, I.; Matafonov, A.; Sun, M. F.; White-Adams, T. C.; Smith, S. A.; Hanson, S. R.; McCarty, O. J.; Renne, T.; Gruber, A.; Gailani, D. A Role for Factor XIIa-Mediated Factor XI Activation in Thrombus Formation In Vivo. *Blood* **2010,** *116,* 3981–3989.
195. Büller, H. R.; Bethune, C.; Bhanot, S.; Gailani, D.; Monia, B. P.; Raskob, G. E.; Segers, A.; Verhamme, P.; Weitz, J. I. Factor XI Antisense Oligonucleotide for Prevention of Venous Thrombosis. *New Engl. J. Med.* **2015,** *372,* 232–240.
196. Lin, J.; Deng, H.; Jin, L.; Pandey, P.; Quinn, J.; Cantin, S.; Rynkiewicz, M. J.; Gorga, J. C.; Bibbins, F.; Celatka, C. A.; Nagafuji, P.; Bannister, T. D.; Meyers, H. V.; Babine, R. E.; Hayward, N. J.; Weaver, D.; Benjamin, H.; Stassen, F.; Abdel-Meguid, S. S.; Strickler, J. E. Design, Synthesis, and Biological Evaluation of Peptidomimetic Inhibitors of Factor XIa as Novel Anticoagulants. *J. Med. Chem.* **2006,** *49,* 7781–7791.
197. Deng, H.; Bannister, T. D.; Jin, L.; Babine, R. E.; Quinn, J.; Nagafuji, P.; Celatka, C. A.; Lin, J.; Lazarova, T. I.; Rynkiewicz, M. J.; Bibbins, F.; Pandey, P.; Gorga, J.; Meyers, H. V.; Abdel-Meguid, S. S.; Strickler, J. E. Synthesis, SAR Exploration, and X-ray Crystal Structures of Factor XIa Inhibitors Containing an Alpha-Ketothiazole Arginine. *Bioorg. Med. Chem. Lett.* **2006,** *16,* 3049–3054.
198. Schumacher, W. A.; Seiler, S. E.; Steinbacher, T. E.; Stewart, A. B.; Bostwick, J. S.; Hartl, K. S.; Liu, E. C.; Ogletree, M. L. Antithrombotic and Hemostatic Effects of a Small Molecule Factor XIa Inhibitor in Rats. *Eur. J. Pharmacol.* **2007,** *570,* 167–174.
199. Wong, P.; Crain, E.; Watson, C.; Schumacher, W. A Small-Molecule Factor XIa Inhibitor Produces Antithrombotic Efficacy With Minimal Bleeding Time Prolongation in Rabbits. *J. Thromb. Thrombolysis* **2011,** *32,* 129–137.
200. Quan, M. L.; Wong, P. C.; Wang, C.; Woerner, F.; Smallheer, J. M.; Barbera, F. A.; Bozarth, J. M.; Brown, R. L.; Harpel, M. R.; Luettgen, J. M.; Morin, P. E.; Peterson, T.; Ramamurthy, V.; Rendina, A. R.; Rossi, K. A.; Watson, C. A.; Wei, A.; Zhang, G.; Seiffert, D.; Wexler, R. R. Tetrahydroquinoline Derivatives as Potent and Selective Factor XIa Inhibitors. *J. Med. Chem.* **2014,** *57,* 955–969.
201. Wong, P. C.; Quan, M. L.; Watson, C. A.; Crain, E. J.; Harpel, M. R.; Rendina, A. R.; Luettgen, J. M.; Wexler, R. R.; Schumacher, W. A.; Seiffert, D. A. In Vitro, Antithrombotic and Bleeding Time Studies of BMS-654457, a Small-Molecule, Reversible and Direct Inhibitor of Factor XIa. *J. Thromb. Thrombolysis* **2015,** *40,* 416–423.
202. Buchanan, M. S.; Carroll, A. R.; Wessling, D.; Jobling, M.; Avery, V. M.; Davis, R. A.; Feng, Y.; Xue, Y.; Oster, L.; Fex, T.; Deinum, J.; Hooper, J. N.; Quinn, R. J. Clavatadine A, a Natural Product With Selective Recognition and Irreversible Inhibition of Factor XIa. *J. Med. Chem.* **2008,** *51,* 3583–3587.
203. Lazarova, T. I.; Jin, L.; Rynkiewicz, M.; Gorga, J. C.; Bibbins, F.; Meyers, H. V.; Babine, R.; Strickler, J. Synthesis and In Vitro Biological Evaluation of Aryl Boronic Acids as Potential Inhibitors of Factor XIa. *Bioorg. Med. Chem. Lett.* **2006,** *16,* 5022–5027.
204. Hangeland, J. J.; Friends, T. J.; Rossi, K. A.; Smallheer, J. M.; Wang, C.; Sun, Z.; Corte, J. R.; Fang, T.; Wong, P. C.; Rendina, A. R.; Barbera, F. A.; Bozarth, J. M.; Luettgen, J. M.; Watson, C. A.; Zhang, G.; Wei, A.; Ramamurthy, V.; Morin, P. E.; Bisacchi, G. S.; Subramaniam, S.; Arunachalam, P.; Mathur, A.; Seiffert, D. A.; Wexler, R. R.; Quan, M. L. Phenylimidazoles as Potent and Selective Inhibitors of Coagulation Factor XIa With In Vivo Antithrombotic Activity. *J. Med. Chem.* **2014,** *57,* 9915–9932.
205. Wong, P.; Quan, M.; Watson, C.; Crain, E.; Luettgen, J.; Wexler, R.; Rendina, A.; Seiffert, D. A. Potent Antithrombotic Effect of a Novel, Small Molecule and Direct Inhibitor of Factor XIa in Prevention and Treatment of Thrombosis in Rabbit Model of Arterial Thrombosis at Doses That Preserve Haemostasis. *J. Thromb. Haemost.* **2015,** *13,* 388–389.
206. Pinto, D. J.; Smallheer, J. M.; Corte, J. R.; Austin, E. J.; Wang, C.; Fang, T.; Smith, L. M., 2nd; Rossi, K. A.; Rendina, A. R.; Bozarth, J. M.; Zhang, G.; Wei, A.; Ramamurthy, V.; Sheriff, S.; Myers, J. E., Jr.; Morin, P. E.; Luettgen, J. M.; Seiffert, D. A.; Quan, M. L.; Wexler, R. R. Structure-Based Design of Inhibitors of Coagulation Factor XIa With Novel P1 Moieties. *Bioorg. Med. Chem. Lett.* **2015,** *25,* 1635–1642.
207. Hu, Z.; Wong, P. C.; Gilligan, P. J.; Han, W.; Pabbisetty, K. B.; Bozarth, J. M.; Crain, E. J.; Harper, T.; Luettgen, J. M.; Myers, J. E., Jr.; Ramamurthy, V.; Rossi, K. A.; Sheriff, S.; Watson, C. A.; Wei, A.; Zheng, J. J.; Seiffert, D. A.; Wexler, R. R.; Quan, M. L. Discovery of a Potent Parenterally Administered Factor XIa Inhibitor With Hydroxyquinolin-2(1*H*)-One as the P2' Moiety. *ACS Med. Chem. Lett.* **2015,** *6,* 590–595.
208. Corte, J. R.; Fang, T.; Hangeland, J. J.; Friends, T. J.; Rendina, A. R.; Luettgen, J. M.; Bozarth, J. M.; Barbera, F. A.; Rossi, K. A.; Wei, A.; Ramamurthy, V.; Morin, P. E.; Seiffert, D. A.; Wexler, R. R.; Quan, M. L. Pyridine and Pyridinone-Based Factor XIa Inhibitors. *Bioorg. Med. Chem. Lett.* **2015,** *25,* 925–930.
209. Fjellstrom, O.; Akkaya, S.; Beisel, H. G.; Eriksson, P. O.; Erixon, K.; Gustafsson, D.; Jurva, U.; Kang, D.; Karis, D.; Knecht, W.; Nerme, V.; Nilsson, I.; Olsson, T.; Redzic, A.; Roth, R.; Sandmark, J.; Tigerstrom, A.; Oster, L. Creating Novel Activated Factor XI Inhibitors Through Fragment Based Lead Generation and Structure Aided Drug Design. *PLoS One* **2015,** *10,* e0113705.
210. Smith, L. M., II; Orwat, M. J.; Hu, Z.; Han, W.; Wang, C.; Rossi, K. A.; Gilligan, P. J.; Pabbisetty, K. B.; Osuna, H.; Corte, J. R.; Rendina, A. R.; Luettgen, J. M.; Wong, P. C.; Narayanan, R.; Harper, T. W.; Bozarth, J. M.; Crain, E. J.; Wei, A.; Ramamurthy, V.; Morin, P. E.; Xin, B.; Zheng, J.; Seiffert, D. A.; Quan, M. L.; Lam, P. Y. S.; Wexler, R. R.; Pinto, D. J. P. Novel Phenylalanine Derived Diamides as Factor XIa Inhibitors. *Bioorg. Med. Chem. Lett.* **2016,** *26,* 472–478.
211. Sakai, M.; Hagio, T.; Koyama, S.; Gohda, M.; Suzuki, K.; Ono, T.; Kondo, T.; Nishiyama, T.; Tanaka, K.; Matsuya, H.; Imagawa, A.; Hirota, Y.; Kawabata, K. Antithrombotic Effect of ONO-8610539, a New, Potent and Selective Small Molecule Factor XIa Inhibitor, in a Monkey Model of Arteriovenous Shunt. *J. Thromb. Haemost.* **2015,** *13 Suppl 2,* 230–231.
212. Koyama, S.; Ono, T.; Harada, K.; Fujioka, A.; Tsukamoto, K.; Sakimoto, S.; Gohda, M.; Hagio, T.; Koda, T.; Matsumura, N.; Yamaura, Y.; Hashimoto, A.; Tanaka, M.; Kondo, T.; Sakai, M.; Tanaka, K.; Matsuya, H.; Imagawa, A.; Hirota, Y.; Kawabata, K. Discovery of ONO-7750512, an Orally Bioavailable Small Molecule Factor XIa Inhibitor: The Pharmacokinetic and Pharmacological Profiles. *J. Thromb. Haemost.* **2015,** *13 Suppl 2,* 389.
213. Mori, M.; Goto, T.; Shintome, M.; Toda, M.; Taga, S.; Matsushita, K.; Fujita, K.; Ikuma, Y.; Iwata, M.; Suzuki, K.; Fukuda, N.; Kato, H.; Shimizu, I. DSR-130787, a Novel Orally-Active Factor XIa Inhibitor With Low Risk of Bleeding. *J. Thromb. Haemost.* **2015,** *13 Suppl 2,* 570–571.
214. Al-Horani, R. A.; Ponnusamy, P.; Mehta, A. Y.; Gailani, D.; Desai, U. R. Sulfated Pentagalloylglucoside is a Potent, Allosteric, and Selective Inhibitor of Factor XIa. *J. Med. Chem.* **2013,** *56,* 867–878.
215. Argade, M. D.; Mehta, A. Y.; Sarkar, A.; Desai, U. R. Allosteric Inhibition of Human Factor XIa: Discovery of Monosulfated Benzofurans as a Class of Promising Inhibitors. *J. Med. Chem.* **2014,** *57,* 3559–3569.
216. Vanassche, T.; Hirsh, J.; Eikelboom, J. W.; Ginsberg, J. S. Organ-Specific Bleeding Patterns of Anticoagulant Therapy: Lessons From Clinical Trials. *Thromb. Haemost.* **2014,** *112,* 918–923.
217. Renne, T.; Gailani, D. Role of Factor XII in Hemostasis and Thrombosis: Clinical Implications. *Expert Rev. Cardiovasc. Ther.* **2007,** *5,* 733–741.
218. Revenko, A. S.; Gao, D.; Crosby, J. R.; Bhattacharjee, G.; Zhao, C.; May, C.; Gailani, D.; Monia, B. P.; MacLeod, A. R. Selective Depletion of Plasma Prekallikrein or Coagulation Factor XII Inhibits Thrombosis in Mice Without Increased Risk of Bleeding. *Blood* **2011,** *118,* 5302–5311.
219. Bird, J. E.; Smith, P. L.; Wang, X.; Schumacher, W. A.; Barbera, F.; Revelli, J. P.; Seiffert, D. Effects of Plasma Kallikrein Deficiency on Haemostasis and Thrombosis in Mice: Murine Ortholog of the Fletcher Trait. *Thromb. Haemost.* **2012,** *107,* 1141–1150.

7.17 Treatments for Heart Failure

W Michael Seganish, Merck Research Laboratories, Kenilworth, NJ, United States
JJ Lynch, Jr., Merck Research Laboratories, West Point, PA, United States
S Sorota, Merck Research Laboratories, Kenilworth, NJ, United States

© 2017 Elsevier Ltd. All rights reserved.

7.17.1 Preface 631
7.17.2 Introduction 631
7.17.2.1 Clinical Description 631
7.17.2.2 Classifications of Chronic Heart Failure 631
7.17.2.2.1 Classification based on disease severity 631
7.17.2.2.2 Classification based on cardiac ejection fraction 631
7.17.2.3 Acute Heart Failure 632
7.17.2.4 Epidemiology 632
7.17.2.5 Prognosis 632
7.17.2.6 Pathophysiology 633
7.17.2.6.1 Neurohomonal 633
7.17.2.6.2 Calcium homeostasis 634
7.17.2.6.3 Extracellular matrix 635
7.17.2.6.4 Mitochondria and metabolism 635
7.17.3 Approved and Future Pharmacological Therapies for Heart Failure 635
7.17.3.1 Antiadrenergics and Anti-RAAS 635
7.17.3.2 Natriuretic Peptide System-Related Approaches 638
7.17.3.2.1 LCZ696 638
7.17.3.2.2 Natriuretic peptide analogs 639
7.17.3.2.3 Corin modulation of natriuretic peptide formation 639
7.17.3.3 Phosphodiesterase Inhibition, Activation of Soluble Guanylate Cyclase, HNO Donors 640
7.17.3.4 Isosorbide Dinitrate–Hydralazine Combination 641
7.17.3.5 Vasopressin Antagonists 642
7.17.3.6 Urocortins 643
7.17.3.7 Positive Inotropic Agents and Sarcomere Targets 643
7.17.3.7.1 Digoxin 643
7.17.3.7.2 cAMP elevating agents 644
7.17.3.7.3 Modulators of sarcomeric proteins 644
7.17.3.8 Correction of Calcium Homeostasis 646
7.17.3.8.1 Mydicar (AAV-1/SERCA2a) 646
7.17.3.8.2 Aladorian 646
7.17.3.8.3 Istaroxime 647
7.17.3.9 Relaxin 648
7.17.3.10 Neuregulin-1 648
7.17.3.11 Ion Channel and Ion Transport Modulators 649
7.17.3.11.1 Diuretics for decongestion in heart failure 649
7.17.3.11.2 Inhibition of the cardiac sino-atrial (SA) node pacemaker current (I_f) 650
7.17.3.11.3 Inhibition of the cardiac late sodium current ($I_{Na,late}$) 651
7.17.3.11.4 Inhibition of the renal outer medullary potassium (ROMK) channel 651
7.17.3.12 Compounds affecting metabolism 652
7.17.3.12.1 Elamipretide 652
7.17.3.12.2 Perhexiline 653
7.17.3.13 MGN-9103 (Antagomir Versus miR-208a/miR499) 654
7.17.4 Summary 654
References 654

Glossary

AI, AII Angiotensin I and angiotensin II.

ACE Angiotensin converting enzyme. The enzyme that converts angiotensin I into the pressor and profibrotic ligand, angiotensin II.

ADHF Acute decompensated heart failure (ADHF). A sudden worsening of the signs and symptoms of heart failure, which typically includes difficulty breathing, swelling of the legs or feet, and fatigue.

AHF Acute heart failure. Heart failure requiring immediate medical attention, which can be either of new onset or from worsening of previously recognized heart failure.

ANP Atrial natriuretic peptide. A peptide agonist that is normally secreted by the atrium in response to volume overload (stretch). This peptide is also secreted by the failing ventricle.

BNP Brain natriuretic peptide. A peptide agonist that is normally secreted from the ventricle in response to stretch.

CNP C-type natriuretic peptide. A peptide agonist synthesized in vascular endothelium in response to shear stress and in response to circulating ANP or BNP. CNP is produced in renal glomerular and tubular cells as well.

Cardiac index Cardiac output divided by the body surface area of the individual, thus relating the pump function of the heart to the size of the individual; a measure of pump function.

Cardiac output The volume of blood ejected or pumped by the heart every minute; cardiac output is the product of two measures, stroke volume, and heart rate; a measure of whole body blood flow that depends on many factors including cardiac function, filling pressures, and vascular resistance.

Chronotropic Pertaining to heart rate.

CCD Cortical collecting duct. A specific segment of nephrons in the kidney.

Diastolic dysfunction Abnormal relaxation of the ventricle after each heartbeat. This can be caused by either increase in passive stiffness of the heart or delay in the relaxation of the contractile apparatus within cardiac myocytes.

Diuresis Renal excretion of water.

Duty ratio The proportion of myosin heads forming strong force-generating interactions or crossbridges with actin during the cardiac actin–myosin ATPase cycle.

Dysguesia An unpleasant taste sensation in the absence of any substance to evoke that taste sensation.

Dyspnea Difficulty in breathing.

É An echocardiography metric from the tissue Doppler approach that evaluates the speed of ventricular relaxation.

E-wave/E-wave deceleration An echocardiography metric determined using Doppler imaging to measure the movement of blood across the mitral valve. The E-wave is the early passive flow of blood from the left atrium to the left ventricle as the left ventricle relaxes. Impaired relaxation is associated with shorter values for E-wave deceleration.

Ejection fraction The fraction of blood volume that is pumped out of the left ventricle during contraction of the heart (systole).

End-diastolic elastance A measure of the relationship between a change in pressure and the change in volume at the end of diastole. A higher value reflects a stiffer ventricle and manifests as a greater change in pressure per unit change of volume.

End-systolic elastance A measure of the relationship between a change in pressure and the change in volume at the end of systole. This metric is used as a load-independent measurement of contractile function.

ECM Extracellular matrix. An extracellular protein scaffold that both signals to and provides a supporting anchor for the parenchymal cells of an organ.

HFpEF Heart failure with preserved ejection fraction in which the major deficit is abnormal relaxation of the heart.

HFrEF Heart failure with reduced ejection fraction in which there is contractile dysfunction and abnormal relaxation.

Inotropic Pertaining to the force of cardiac contractions.

L-type calcium channels An integral membrane protein that selectively allows calcium entry into cells in response to depolarization of the cell membrane. These channels are the primary source for calcium entry in cardiac and vascular smooth muscle.

Left ventricular end-diastolic pressure (LVEDP) Pressure measured in the left ventricle at the end of the cardiac relaxation (diastole), which is prior to the contraction (systole). LVEDP is a primary determinant of preload, the load applied by the volume of blood in the left ventricle that results in the stretching of the left ventricle before the initiation of the next contraction.

Lusitropic Pertaining to relaxation of the heart.

Kaliuresis Renal excretion of potassium.

MI Myocardial infarction.

Orthopnea Positional difficulty in breathing, particularly when lying down.

MRA Mineralocorticoid receptor antagonists. Examples include spironolactone and eplerenone.

Natriuresis Renal excretion of sodium.

NEP Neutral endopeptidase (also known as neprilysin, EC3.4.24.11): enzyme that catabolizes ANP and BNP along with other peptide ligands including bradykinin and angiotensin II.

NP Natriuretic peptide (see NPS).

NPS Natriuretic peptide system (includes ANP, BNP, and CNP). A hormonal system that induces vasodilation and excretion of salt and water through the activation of NPRA and NPRB receptors.

NTproBNP The inactive N-terminal fragment that is released when proBNP is cleaved to release BNP.

PCI Percutaneous coronary intervention. A procedure using a catheter and an intravascular approach to unblock coronary arteries.

Phospholamban A protein in the sarcoplasmic reticulum that modulates the activity of the SR calcium pump, SERCA. Nonphosphorylated phospholamban associates with SERCA and inhibits the ability of SERCA to pump calcium back into the SR. Phosphorylation of phospholamban by protein kinase A causes disinhibition and increases SERCA activity.

Pi/Pi release Pi (inorganic phosphate) release is the rate-limiting step in the cardiac actin–myosin ATPase cycle. Selective enhancement of this step is proposed to increase the percentage of high affinity actin–myosin interactions, thereby increasing the proportion of myosin heads forming strong force-generating interactions or crossbridges with actin and thereby increasing force generation and contractility.

Preload Ventricular filling, resulting in the initial stretching of the left ventricle prior to contraction (systole); the load applied by the volume of blood in the left ventricle that results in the stretching of the left ventricle before the initiation of the next contraction. Preload/ventricular filling is elevated in HFrEF due to ventricular dilation and/or increased blood volume.

Pulmonary capillary wedge pressure (PCWP) PCWP is measured by inserting a balloon-tipped catheter into a peripheral vein and advancing the catheter through the right atrium, right ventricle, pulmonary artery, and into a branch of the pulmonary artery. When the catheter balloon is inflated, a branch of the pulmonary artery is occluded. When this occurs, the pressure measured by the catheter distal to the balloon falls and reaches a value that reflects left atrial pressure. As such PCWP provides an indirect estimate of left atrial pressure and therefore by inference an indirect measure of left ventricular end-diastolic pressure (LVEDP). A reduction in PCWP reflects a reduction in pathologically elevated left atrial pressure, which occurs in heart failure patients as a consequence of elevated left ventricular end-diastolic pressure.

RAAS Renin–angiotensin–aldosterone system. A neurohormonal system with important roles in the regulation of blood pressure, blood volume, and maintenance of appropriate levels of sodium and potassium in serum.

Rales An abnormal crackling sound heard when listening to the lungs with a stethoscope.

Respiratory exchange ratio The ratio between oxygen taken up versus carbon dioxide produced that can be used as an indirect measure of whether glucose or fatty acids are being used as the primary energy source for ATP production. Values close to 1 are consistent with the use of glucose while values close to 0.7 are attributed to fatty acid utilization.

Ryanodine receptors A calcium release channel found in the sarcoplasmic reticulum or endoplasmic reticulum. In striated muscle it is the major cite for release in calcium from the sarcoplasmic reticulum. The channel was named based on the modulation of calcium release by the compound ryanodine.

Sarcolemma The surface or plasma membrane of striated muscle cells.

Sarcoplasmic reticulum An intracellular organelle that is the major site for the intracellular calcium stores used to induce muscle contractions. It is the endoplasmic reticulum of striated muscle cells and also functions in protein translation, processing, and transport.

Schwann cells Cells associated with peripheral nerves that myelinate certain large diameter neurons.

SERCA A calcium pump found in the sarcoplasmic reticulum and endoplasmic reticulum membrane that utilizes the energy from ATP hydrolysis to pump calcium into the SR/ER.

Sodium–calcium exchanger A plasma membrane transport protein that exchanges three sodium ions on one side of the membrane for one calcium ion on the other side of the membrane. This protein generally functions as a mechanism for calcium efflux but can function in the reverse mode if the electrochemical driving force favors calcium influx.

Splanchnic Visceral.

STEMI A relatively severe myocardial infarction with elevation of the ST segment of the electrocardiogram.

Systolic dysfunction Abnormal contraction of the heart resulting in less forceful contractions and less efficient ejection of blood with each beat.

Stroke volume The volume of blood that is ejected or pumped out of the heart with every beat; a measure of pump function.

T-Tubules Tube-like membrane invaginations that are found in striated muscle cells and allow for close approximation of surface membrane calcium channels (L-type calcium channels) and the calcium release channels in the sarcoplasmic reticulum (ryanodine receptors).

TAC Transaortic constriction model of heart failure. A pressure overload model in which the aortic arch is constricted with a clip or a ligature to increase the afterload on the left ventricle.

TALH Thick ascending loop of Henle, a specific segment of nephrons in the kidney.

UCNs Urocortins. The urocortins 1, 2, and 3 (UCN1,2,3) are small (38–40 amino acids) endogenous peptide hormones that belong to the corticotropin-releasing hormone family of hormones that are secreted in response to stress.

7.17.1 Preface

The purpose of this article is to review current and evolving pharmacological therapies used in the treatment of patients with acute and chronic heart failure. To this end, the introduction provides a brief overview of heart failure pathology and epidemiology with the goal of enabling an understanding of currently established and emerging pharmacological therapies for heart failure as well as the unmet medical needs. For more in-depth background information, the interested reader is directed to the most recent Heart Failure Guideline Documents from the American College of Cardiology Foundation/American Heart Association,[1] and the European Society of Cardiology[2] as well as recent review articles and texts.[3–7]

7.17.2 Introduction

7.17.2.1 Clinical Description

Heart failure is not a discrete disease and there is no universally accepted definition. It is a complex syndrome in which the intrinsic function of the heart is compromised such that it is unable to pump blood at a sufficient rate to meet the needs of end organs throughout the body. This deficit in blood pumping can result from impaired ventricular filling, impaired ejection of blood, or a combination of both.[1,2] There are many pathophysiological conditions that can lead to the development of heart failure, including myocardial infarction, cardiac ischemia, hypertension, valvular insufficiency, cardiac toxicity of certain cancer chemotherapies, diabetes, metabolic disorders, and viral myocarditis. Although there may be common symptoms in heart failure of different etiologies, the underlying pathology can vary substantially from patient to patient.

There is agreement with regard to many of the signs and symptoms of heart failure. However, there is no universally utilized set of criteria for diagnosing heart failure and no stand-alone tests that can be used for an unambiguous diagnosis.[1,2,4] Signs and symptoms include fatigue, dyspnea, orthopnea, rales, wheezing, pulmonary edema, splanchnic congestion, peripheral edema, the presence of a third heart sound, and cardiac hypertrophy.[1–4] Many of these signs and symptoms can be attributed to sodium and volume overload and are partially relieved by treatment with diuretics. Common comorbid conditions include hypertension, coronary artery disease, obesity, type 2 diabetes, chronic renal disease, chronic obstructive pulmonary disease, and atrial fibrillation.[1–4]

7.17.2.2 Classifications of Chronic Heart Failure

Chronic heart failure has been classified based on symptom severity (New York Heart Association, NYHA), disease stage (American College of Cardiology Foundation/American Heart Association, ACCF/AHA), and whether or not ejection fraction is compromised. These different approaches to segmenting heart failure patients are discussed in the subsequent sections.

7.17.2.2.1 Classification based on disease severity

NYHA functional classification is based on a patient's symptoms and how well exercise is tolerated. Physical activity is not limited in Class I patients. Class II patients tend to be asymptomatic at rest but heart failure symptoms emerge during physical activity. Class III indicates that patients are comfortable at rest but experience symptoms with even modest physical activity. Class IV patients are either symptomatic at rest or symptomatic with any physical activity.[1]

The following stages are defined by the ACCF/AHA classification system. Unlike the NYHA functional classification system where an individual can improve in class over time, patients do not regress from one ACCF/AHA stage to a less severe stage. Stage A indicates an individual at high risk but without evidence of disease. Stage B patients have structural heart disease but do not exhibit signs or symptoms of heart failure. Once symptoms develop, patients are categorized as Stage C. Refractory disease requiring advanced interventions is classified as Stage D.[1]

7.17.2.2.2 Classification based on cardiac ejection fraction

In many patients, cardiac imaging can document a large reduction in cardiac ejection fraction compared to individuals with healthy hearts. These patients are considered to have heart failure with reduced ejection fraction (HFrEF). Patients with HFrEF typically have dilated ventricles with an increase in left ventricular volumes. A common trigger for the development of HFrEF is myocardial infarction.[8] Typically, HFrEF patients exhibit systolic and diastolic dysfunction.

In approximately half of patients with heart failure, the ejection fraction is either normal or only slightly reduced.[4] These patients are classified as having heart failure with preserved ejection fraction (HFpEF). Women and elderly patients constitute the majority of individuals with HFpEF. In general, HFpEF results from conditions that increase afterload such as hypertension or aortic stenosis.[8] Diastolic dysfunction and left ventricular wall thickening are key features of HFpEF.

Several classes of drugs have shown outcome benefits and/or are approved for the treatment of HFrEF patients. An angiotensin converting enzyme inhibitor (ACEi) is recommended for most HFrEF patients.[1,2] ACE inhibitors, exemplified by enalapril (the ethyl ester prodrug of enalaprilat), have been shown to reduce the risk of death and reduce hospitalization in HFrEF patients with mild, moderate, or severe symptoms of heart failure.[9–11] Clinical data suggest that there are no differences among available ACE inhibitors in their effects on survival or symptoms.[12] In patients who cannot tolerate an ACEi, an angiotensin II (AII) receptor blocker (ARB) is indicated.[1,2] The ARBs valsartan and candesartan have demonstrated benefit by reducing mortality (candesartan) and hospitalization (valsartan and candesartan) in HFrEF patients.[13,14]

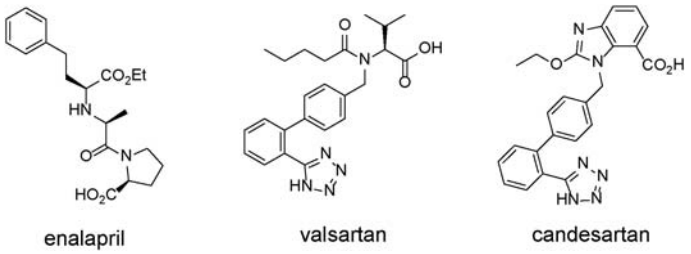

β-Adrenoceptor blockers are also indicated for most HFrEF patients in combination with ACEi or ARBs.[1,2] Three β-adrenoceptor blockers have been shown to reduce death and hospitalization in HFrEF patients: bisoprolol[15] and sustained-release metoprolol[16] which selectively block the β_1-adrenergic receptor, and carvedilol[17,18] which blocks β_1-, β_2-, and α_1-adrenergic receptors. Positive findings with these three agents should not be considered a β-blocker class effect, as other β-adrenoceptor blocking compounds have demonstrated lesser to no significant effects on heart failure outcomes.[1,2] Mineralocorticoid receptor antagonists (MRAs) (vide infra Section **Antiadrenergics and anti-RAAS**) are also recommended for HFrEF patients in whom there are no contraindications.[1,2] The main concerns with MRA include hyperkalemia and renal insufficiency. In a subset of HFrEF patients, particularly those of African American decent, a combination of isosorbide dinitrate and hydralazine can also reduce mortality when added on top of other guideline-directed therapies.[1,2] There are currently no therapies approved for patients with HFpEF.

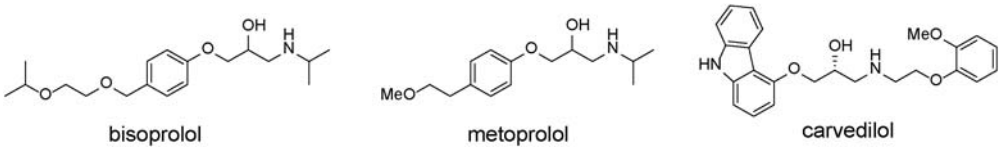

7.17.2.3 Acute Heart Failure

The term acute heart failure (AHF) is used to describe an acute onset or deterioration of the signs and symptoms of heart failure. That is to say that AHF can occur due to worsening of previously existing chronic heart failure (either HFrEF or HFpEF) or it can arise de novo.[2,6,19] AHF is a life-threatening condition requiring immediate medical attention. Most AHF patients present with acute dyspnea, a symptom that is not unique to heart failure.[2,6,19] Measurement of plasma natriuretic peptide levels can be used to support clinical judgment and, if not elevated, to rule out heart failure as the cause of dyspnea.[1,2,6,19] There are multiple triggers and phenotypes encompassed by the term AHF and identification of the trigger can guide the course of care (eg, arrhythmias, acute coronary syndrome, sepsis, noncompliance with recommended drug treatments, volume overload, acute elevation of blood pressure, cardiogenic shock, and acute pulmonary embolism).

Current guideline-directed therapy for the treatment of AHF includes loop diuretics, possibly in combination with other diuretic classes, as the cornerstone of pharmacologic therapy.[1,2] Vasodilators (nitroglycerin, nitrates, and the natriuretic peptides BNP (nesiritide; United States and EU) and ANP (carperitide; Japan)) may be added in hypertensive patients but are generally avoided in patients with low blood pressure.[1,2] In patients with low cardiac output at risk for under-perfusion of vital organs, positive inotropes such as dobutamine or milrinone may be indicated.[1,2] US guidelines state that V2 vasopressin antagonists may be indicated in patients with hyponatremia and cognitive symptoms.[1]

7.17.2.4 Epidemiology

Estimates of the prevalence of heart failure vary widely from 1% to 12% due to differences in methodologies and criteria used to identify patients with this syndrome.[4] Recent statistics from the American Heart Association indicate that there are 5.7 million people in the United States with heart failure, and this number is projected to grow to more than 8 million people by 2030.[5] Worldwide prevalence of heart failure has been estimated at 23 million.[4] The prevalence of heart failure increases with age and is $>10\%$ for individuals ≥ 80 years old.[5,20] The lifetime risk for developing heart failure is estimated as one in five from age 40 and beyond.[5] There are 870,000 new heart failure cases annually in the United States.[5] Estimated annual cost for treating heart failure in the United States in 2014 range from $37 billion to as much as $115 billion.[21] There are reasons to believe that the low end of this range significantly underestimates the true cost of treating heart failure.[21]

7.17.2.5 Prognosis

Survival estimates for patients with heart failure are lower than for patients with most types of cancer.[3] Despite treatment with current standards of care, the 5-year survival for patients with heart failure is $\sim 50\%$ and 10-year survival is $\sim 10\%$.[4] Although there

is a significant noncardiovascular contribution to all-cause mortality, the main causes of death for heart failure patients are pump failure and cardiac arrhythmias.[22–24]

7.17.2.6 Pathophysiology

Patients with heart failure exhibit many changes in cardiac structure and function as well as neurohormonal changes that either correspond with and/or contribute to disease progression. These include neurohormonal changes, hypertrophy at both the cellular and organ levels, fibrosis, altered calcium handling, changes in metabolism, altered mitochondrial structure/function, and increased myocyte apoptosis.[3,8,25–30]

7.17.2.6.1 Neurohomonal

Neurohormonal changes that occur in heart failure include an increase in the activity of the renin/angiotensin/aldosterone system (RAAS), an increase in the activity of the sympathetic nervous system, increase in vasopressin and urocortin (UCN) release, and an elevation of plasma levels of natriuretic peptides.[1–3,31] Each of these neurohormonal systems has served as the basis for pharmacological treatments for heart failure patients and the majority of approved drugs that have been shown to improve outcomes target neurohormonal aspects of heart failure.

The first of the neurohormonal changes to be recognized was activation of the sympathetic nervous system.[28] In response to the development of heart failure, there is an increase in sympathetic tone and cardiac sympathetic nerve activity. The level of sympathetic activation correlates with mortality.[32,33] Excessive neuronally released norepinephrine acts on β_1-adrenoceptors in the heart and renal juxtaglomerular cells and α-adrenoceptors in vascular smooth muscle and renal tubules. Activation of adrenoceptors promotes changes in heart rate, cardiac force of contraction, renin secretion, sodium reabsorption, and vascular resistance.[34] These changes initially serve a compensatory role to help preserve organ perfusion but ultimately contribute to disease progression. Although β-adrenoceptor antagonists (β-blockers) were at one time considered to be contraindicated in heart failure due to the potential to induce an acute decrease of contractility, they have become an established standard of care for the treatment of heart failure.[1,2]

Recognition of the role of the RAAS in heart failure evolved after the development of ACEi.[35] RAAS plays an important role in the control of peripheral vascular resistance as well as sodium and water balance; all of which are dysregulated in heart failure patients. In addition to modulating fluid balance and vascular resistance, AII and aldosterone can also promote cardiac hypertrophy, fibrosis, and activation of the sympathetic nervous system.[35–38] Although the beneficial effects of ACEi in heart failure patients were initially believed to be attributable to vasodilation, there is a more complex role for RAAS activation in heart failure pathophysiology and the benefits of RAAS inhibition are greater than can be observed through vasodilation alone.[31,35,36] Renin activity is elevated in the plasma and hearts of dilated cardiomyopathy patients, particularly those with decompensation.[36,39] However, plasma renin activity may be normal in patients who are not decompensated.[31] A role for nonsystemic, local cardiac RAAS activation has also been proposed. In support of this idea, AII formation in human heart tissue has been shown to increase with heart failure progression.[35,36,40]

The natriuretic peptide system (NPS) is a cardiovascular endocrine system comprised mainly of the following peptides possessing vasodilator, natriuretic, diuretic, antiproliferative, antihypertrophic, and antifibrotic actions: atrial natriuretic peptide (ANP), B-type natriuretic peptide (BNP), and C-type natriuretic peptide (CNP).[41–43] ANP is synthesized in atrial cardiac myocytes and released in response to atrial distension. BNP is synthesized primarily in ventricular cardiac myocytes in response to ventricular pressure and volume stress. CNP is synthesized in vascular endothelium in response to shear stress and in response to circulating ANP or BNP. Additionally, CNP is produced in renal glomerular and tubular cells.

The natriuretic peptides elicit cellular responses through activation of at least two cell surface natriuretic peptide receptors (NPRs). NPRA (also known as NPR1, GC-A) binds ANP and BNP, whereas NPRB (also known as NPR2, GC-B) binds CNP. NPRA and NPRB contain cytoplasmic guanylate cyclase domains, which catalyze the formation of cyclic guanosine monophosphate (cGMP) upon ligand binding. Subsequently, cGMP activation of cGMP-dependent protein kinase I (PKG) is responsible for the cellular response to the natriuretic peptides. A third natriuretic peptide receptor NPRC (also known as NPR3) binds all three natriuretic peptides (see **Fig. 4**). NPRC internalizes and is responsible for clearance of about half of the circulating natriuretic peptides, with the remainder degraded enzymatically by neutral endopeptidase (NEP; neprilysin). NEP is the rate-limiting enzyme in the inactivation of the natriuretic peptides, and accordingly has been pursued as an approach to modulate NPS peptide levels to enhance their salutary effects.

The NPS and RAAS act as counter-regulators in cardiovascular and renal homeostasis. At a physiologic level, the vasodilator, natriuretic, diuretic, antiproliferative/antihypertrophic, and antisympathetic effects of the NPS functionally oppose the vasoconstrictor, cell proliferative and hypertrophic effects, and enhancement of sympathetic tone produced by AII. At a mechanistic level, the NPS and RAAS have complex points of interaction including cross-regulation of synthesis and release.

Vasopressin is a posterior pituitary hormone that is released in response to decreases in plasma osmolarity or blood pressure. Cardiovascular and renal effects of vasopressin are mediated by V_2 receptors in the kidney and V_{1a} receptors in vascular smooth muscle. V_2 activation in the renal collecting ducts increases the reabsorption of free water through elevation of cAMP and increased apical membrane insertion of aquaporin. V_{1a} activation in vascular smooth muscle induces vasoconstriction.[44] Although the mechanism is not understood, plasma vasopressin levels are increased in patients with heart failure.[31,44]

The UCNs are peptide hormones belonging to the corticotrophin-releasing hormone family, and are secreted centrally and peripherally in response to stress. UCN plasma and tissue levels are elevated in experimental and clinical heart failure, and the exogenous administrations of UCNs have been shown to affect cardiac and vascular function.[45]

7.17.2.6.2 Calcium homeostasis

Precise spacial and temporal regulation of cardiac intracellular calcium concentrations is critical for controlling the contraction and relaxation that occurs with each heartbeat.[25] Calcium binds to troponin C on thin myofilaments to permit the progressive "walking" of myosin heads along actin filaments, which leads to muscle contraction and ejection of blood. As calcium levels fall, the myofilaments slide back into their resting position to permit refilling of the cardiac chambers. In heart failure, calcium transients are abnormal with elevated resting calcium levels, a reduced peak, and a slower return to baseline.[46] The suppressed peak calcium contributes to systolic dysfunction in heart failure. The slow return to baseline is one of many pathological changes that contributes to diastolic dysfunction in heart failure patients.

An important subcellular structural component for calcium homeostasis is regions where there is close proximity between L-type calcium channels in the T-tubules and ryanodine receptors in the sarcoplasmic reticulum (SR) to form a "calcium release unit" (Fig. 1).[25,47] The transient elevation of intracellular calcium that drives contractions is attributable to three factors. There is a trigger, a release of calcium from intracellular stores (contained in the SR), and removal of calcium from the cytosol. The trigger comes from action potentials which induce the opening of L-type calcium channels on the sarcolemma, particularly in the T-tubules. Influx of

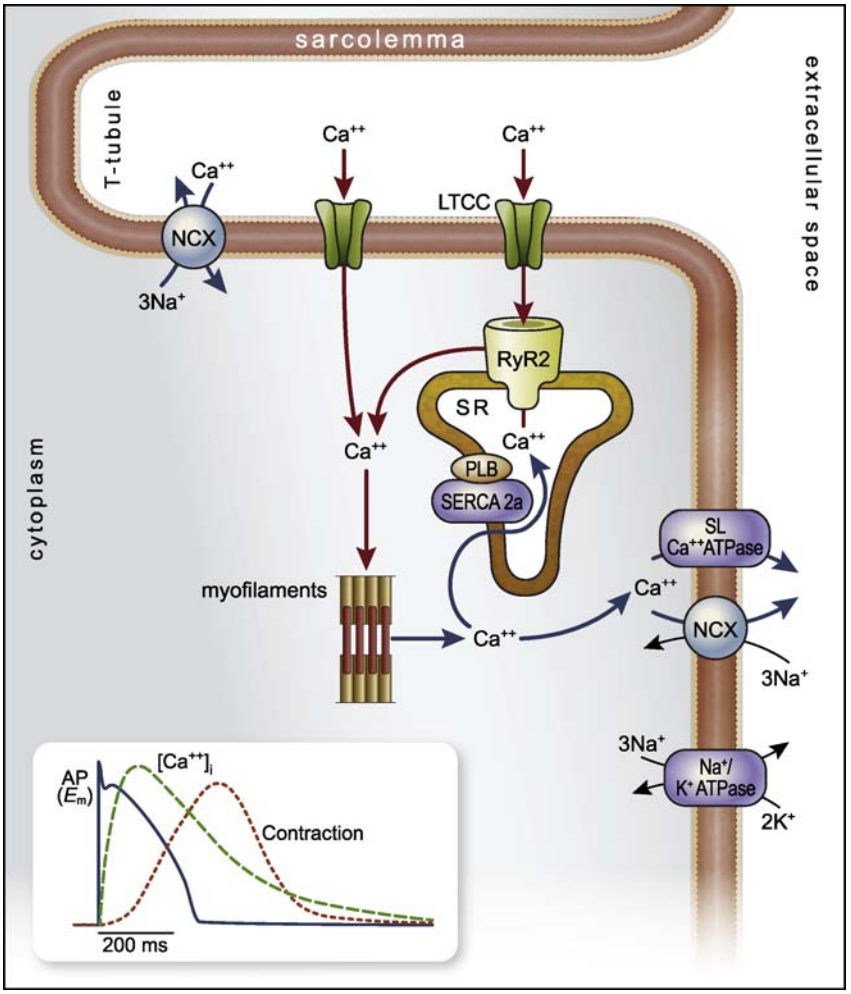

Fig. 1 Schematic representation of key entities involved in intracellular calcium homeostasis in the mammalian ventricle. Action potential propagation into T-tubules induces the opening of voltage gated L-type calcium channels. Close proximity between L-type calcium channels (*LTCC*) and the cardiac ryanodine receptor (*RyR2*) is important for calcium-induced calcium release from the sarcoplasmic reticulum (*SR*), which provides the majority of calcium needed for activation of the cardiac contractile apparatus (myofilaments). Cytoplasmic calcium is then either resequestered into the SR by the sarco/endoplasmic reticulum calcium ATPase (SERCA2a in the heart) or extruded from the cell by either the sarcolemmal sodium-calcium exchanger (*NCX*) or the sarcolemmal calcium ATPase (SL Ca^{++} ATPase). Sodium that enters the cell via the NCX can be extruded by the sodium–potassium ATPase.

calcium across the cell membrane results in a restricted zone of elevated calcium near cardiac ryanodine receptors. Cardiac ryanodine receptors then open by a process referred to as calcium-induced calcium release and allow the efflux of calcium from the SR. Removal of calcium from the cytosol is mediated primarily through the action of an ATP consuming calcium pump on the SR, SERCA2a, but there is also a contribution from the sarcolemmal sodium–calcium exchanger with approximately 70% of cytosolic calcium being resequestered by SERCA2a in large mammals including humans.[25] Two other transporters make minor contributions ($\leq$1% of total each) to the decay of intracellular calcium transients under physiological conditions, the sarcolemmal calcium ATPase, and the mitochondrial calcium uniporter.[25] The function of SERCA2a and the cardiac ryanodine receptor can be modulated by posttranslational modification, notably phosphorylation by protein kinase A (PKA) (to remove phospholamban dependent inhibition of SERCA2a) and calmodulin-activated protein kinase IIδ (CaMKIIδ).

Pathological alterations of calcium handling in the setting of heart failure are caused by changes in cardiac structure, protein expression levels, and posttranslational modifications. First there is a decrease in the expression of SERCA2a, in both animal models and in patients with heart failure.[48] Loss of SERCA2a results in reduced stores of intracellular calcium (weaker contractions) and a slower rate of calcium removal from the cytosol during the relaxation phase (slower relaxation).[48] In addition, there is an increase in the expression of sarcolemmal sodium–calcium exchanger resulting in a larger contribution of this transporter to the decay of calcium transients.[25] Second, phosphorylation of ryanodine receptors by CaMKIIδ or oxidation increases the leakage of calcium from the SR during diastole.[49,50] Somewhat more controversial is a proposed role for PKA-dependent hyperphosphorylation of the ryanodine receptor as an underlying cause of leaky ryanodine receptors.[51–53] The consequences of this increased leak include a further reduction in SR calcium stores and the potential to cause calcium-dependent cardiac arrhythmias. Finally, the close proximity between L-type calcium channels in the T-tubules and ryanodine receptors in the SR can be disrupted in heart failure. One potential reason is a decrease in the density of T-tubules in heart failure.[54] The increased distance between L-type calcium channels and the SR ryanodine receptor can lead to less efficient coupling between trigger calcium from the L-type calcium channel and the calcium-induced opening of the ryanodine receptor resulting in smaller calcium transients and the contractions they induce.[47]

7.17.2.6.3 Extracellular matrix

All forms of heart failure are associated with cardiac remodeling that includes changes in the cardiac extracellular matrix (ECM).[8] In heart failure, there is an increase in the deposition of ECM protein, increased expression of matrix metalloproteinases, altered expression of tissue inhibitors of metalloproteinases, and altered cross-linking of ECM proteins.[8] The increase in ECM contributes to an increase in passive stiffness of the heart. The ECM-dependent increase in passive stiffness, along with the slowing of active relaxation at the level of the myofilaments (primarily via altered kinetics of the intracellular calcium transient), contributes to diastolic dysfunction.[8,29] TGFβ-induced differentiation of fibroblasts into myofibroblasts is an important precursor to ECM remodeling in heart failure.[8] The details of ECM remodeling differ for HFrEF and HFpEF with a more unstable ECM in HFrEF.[8]

7.17.2.6.4 Mitochondria and metabolism

Healthy myocardium utilizes free fatty acids as the preferred source for generating ATP. The heart generally does not produce excess ATP, instead ATP production is finely tuned to match energy demands.[30] In nondiabetic heart failure, there is a decrease in the ability to utilize fatty acids and an increase in glucose metabolism.[26,30] In addition, there is a decrease in the density of mitochondria and alterations of the structure of mitochondria.[30,55] The sum of these phenotypic changes leads to the failing heart persisting in an energy compromised state.[26,30] Although there are no currently approved drugs that target the mitochondria, data from animal models suggests that mitochondrial protection has the potential to be beneficial for heart failure patients.[30]

7.17.3 Approved and Future Pharmacological Therapies for Heart Failure

7.17.3.1 Antiadrenergics and Anti-RAAS

Antisympathetic β-adrenergic receptor antagonists, the anti-RAAS ACE inhibitors, and steroidal MR antagonists have demonstrated significant mortality benefits in large clinical trials and comprise the cornerstones of chronic heart failure therapy in HFrEF patients. While ACE inhibitors are considered first-line therapy, ARBs are also used in HFrEF patients as alternatives when ACE inhibitors are not tolerated.[35,56,57] Consistent with their central roles in heart failure therapy, multiple efforts are investigating alternate means or strategies to elicit and improve upon antiadrenergic and anti-RAAS efficacy.

While the beneficial effects of approved β-adrenergic receptor antagonists in chronic heart failure are attributed primarily to blockade of the β_1-adrenergic receptor, the β_2-adrenergic receptor also plays a significant role in modulating cardiovascular function. In contrast, the β_3-adrenergic receptor is considered to have limited distribution in cardiac tissue at least in normal conditions.[58] Experimental studies have reported that selective β_2-adrenoceptor agonists, exemplified by clenbuterol and fenoterol and administered either alone or in combination with selective β_1-adrenoceptor antagonists, produce beneficial effects potentially relevant to heart failure. In the case of fenoterol, these improvements include increases in cardiac contractile function and remodeling in a rat model of myocardial infarction.[59,60] It also has been reported that β_3-adrenoceptor expression is increased in human heart failure and that the administration of selective β_3-adrenoceptor agonists, exemplified by CGP12177A (β_1, β_2 antagonist, β_3 partial agonist), structurally similar compounds BRL37344, SR58611A, and CL316243, as well as the β_1-adrenoceptor antagonist nebivolol that displays β_3-agonist activity, produce beneficial vasodilator and cardioprotective effects in multiple animal species models of cardiac injury and heart failure.[59,61,62] The observation that the nonselective β_1- and β_2-adrenoceptor antagonist

carvedilol, which has shown mortality benefit in clinical HFrEF trials, induces a change in GPCR conformation leading to β-arrestin-mediated ERK activation has led to the exploration of additional β-adrenergic receptor antagonists with β-arrestin-biased signaling profiles.[59,63–66] β-adrenergic receptor kinase 2 (βARK2) is upregulated in several forms of heart disease and stimulated by excessive catecholamines. This kinase is responsible in part for the desensitization and functional uncoupling of β-adrenoceptors in heart failure and is a potential target for modulating β-adrenoceptor signaling.[67] βARK2ct is a small peptide fragment of the C-terminus of βARK2 that can inhibit βARK2.[68] Delivery of βARK2ct via a recombinant adeno-associated viral vector reversed cardiac contractile dysfunction and normalized β-adrenergic signaling in a rat model of post-MI chronic HF.[69]

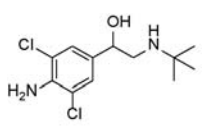
clenbuterol

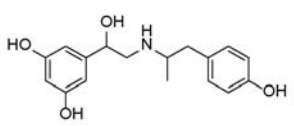
fenoterol

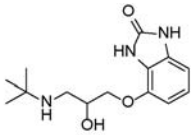
CGP12177

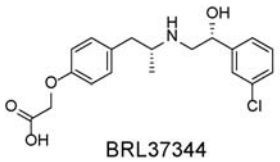
BRL37344

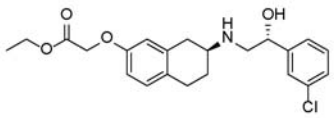
SR58611A

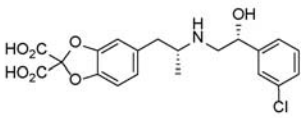
CL316243

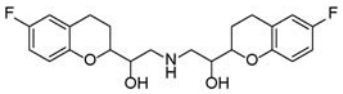
nebivolol

Also of note, an ongoing Phase II study is comparing the efficacies of metoprolol (vida supra Section **Classification based on cardiac ejection fraction**), a selective β_1-adrenoceptor antagonist, and bucindolol, a nonselective β_1- and β_2-adrenoceptor antagonist with weak vasodilator activity, in a genotype-defined population with heart failure and/or reduced ejection fraction at high risk for atrial fibrillation (NCT01970501). For perspective, the previous Phase III BEST trial of bucindolol in HFrEF patients failed to demonstrate significant survival benefit.[70] However, a 1040-patient substudy of the BEST trial identified specific genetic variants of the β_1- and α_{2c}-adrenoceptors that were associated with significant bucindolol benefits on mortality and hospitalization.[71] The ongoing Phase II trial with bucindolol is being conducted in heart failure patients with the specific β_1-adrenoceptor genetic variant to prospectively assess therapeutic efficacy in this patient group.

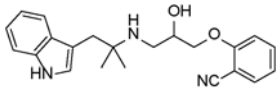
bucindolol

While the beneficial effects of ACE and ARB inhibition are attributed primarily to reduced activation of the ATR1 receptor, experimental studies have assessed other RAAS pathway members that may contribute to or enhance the efficacies of existing anti-RAAS treatments or constitute novel targets (see **Fig. 2**). Stimulation of the ATR2 receptor either as a consequence of AII tone in the setting of ATR1 blockade or by virtue of a selective ATR2 agonist such as compound 21[72] is postulated to mediate cardioprotective and antihypertrophic effects.[59,67] Overall, the "protective arm of RAAS" including ATR2 but also ACE2, angiotensin 1–7, and the Mas receptor are proposed to counteract the actions of AII on ATR1 and elicit antihypertrophic effects. Similarly, the kallikrein–kinin system, which is stimulated by AT2R activation, is thought to counteract the actions of ATR1 stimulation through the actions of bradykinin.[59,73] TRV027 is an 8-amino acid peptide (Sar-Arg-Val-Tyr-Ile-His-Pro-D-Ala-OH) β-arrestin-biased ligand of the ATR1, which blocks AII-stimulated G-protein signaling but stimulates β-arrestin-coupled signaling.[74] In a canine rapid cardiac pacing-induced heart failure model, TRV027 elicited beneficial hemodynamic and renal effects.[57,75] TRV027 currently is in Phase II clinical trial in patients with acute decompensated heart failure (ADHF) (NCT01966601). Upstream of ACE, the direct inhibition of renin to prevent generation of AI and AII is a long-recognized and explored target.[57,76] The Phase III ASTRONAUT trial of aliskiren, one of the first nonpeptide orally bioavailable direct renin inhibitors,[77] in recently hospitalized AHF patients, reported no benefit on cardiovascular death or hospitalization at 6 or 12 months after discharge (NCT00894387).[78] The ongoing ATMOSPHERE Phase III trial is comparing the effects of aliskiren, enalapril, or dual aliskiren plus enalapril treatment in HFrEF patients (NCT00853658). One additional novel RAAS pathway-related approach to heart failure therapy is the development of the combination NEP inhibition plus ARB treatment LCZ696, reviewed in Section **Natriuretic Peptide System-Related Approaches**.

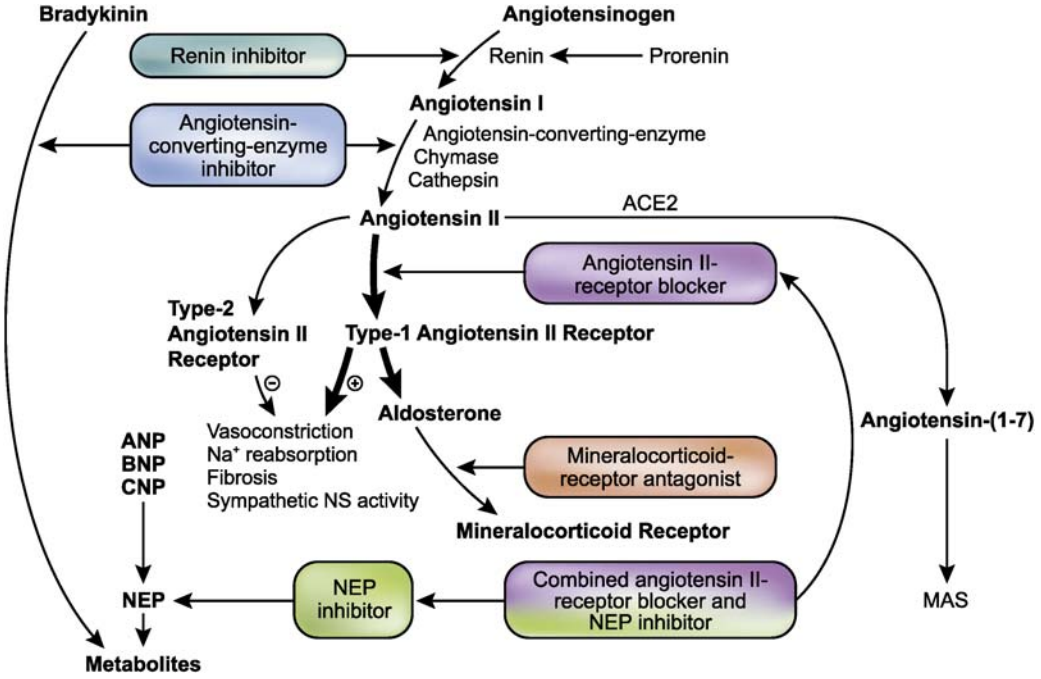

Fig. 2 Schematic of the renin–angiotensin–aldosterone system (*RAAS*) and the natriuretic peptide system. Angiotensinogen is converted to angiotensin II by the sequential action of renin and angiotensin converting enzyme (major). Chymase and cathepsin can also convert angiotensin I to angiotensin II (minor). The main effects of angiotensin II are mediated by the type-1 angiotensin II receptor. In addition, angiotensin II can induce the release of aldosterone, which evokes sodium reabsorption, increased plasma volume and potassium excretion via renal mineralocorticoid receptors. Excessive aldosterone can also promote fibrosis and contribute to the progression of heart failure through tissue remodeling effects. Effects of angiotensin II on type-2 receptors and effects of angiotensin (1–7) on the MAS receptor partially antagonize the pressor and profibrotic effects of angiotensin II. Natriuretic peptides induce vasodilation and sodium excretion through effects on NPRA and NPRB receptors (see **Fig. 4**).

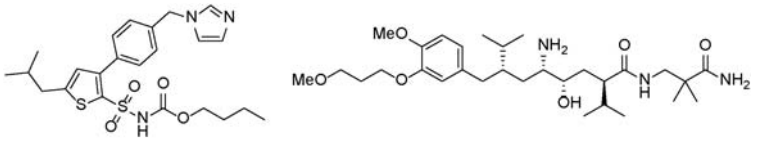

Although short-term treatments with ACE inhibitors and ARBs lower circulating levels of aldosterone, the suppression of aldosterone levels may not be sustained during long-term treatment.[79] Accordingly, MRAs are indicated for use in heart failure patients in order to block aldosterone receptor activation and thereby inhibit the unwanted effects of aldosterone, which include sodium retention, potassium and magnesium loss, sympathetic activation, parasympathetic inhibition, fibrosis, and vascular injury.[80] The Phase III RALES trial demonstrated that the administration of the steroidal MR antagonist spironolactone in HFrEF patients treated with ACE inhibitors reduced the risk of death, reduced the frequency of hospitalization for worsening heart failure, and improved symptoms of heart failure.[80] The Phase III EPHESUS trial assessed the administration of the steroidal MR antagonist eplerenone in patients with myocardial infarction and HFrEF treated with β-blockers, ACE inhibitors, or ARBs. In EPHESUS, eplerenone reduced all-cause mortality as well as cardiovascular death and hospitalization for cardiovascular events.[81] Eplerenone also reduced the risk of death and hospitalization in the Phase III EMPHASIS-HF trial in HFrEF patients with mild symptoms (NYHA Class II) treated with β-blockers, ACE inhibitors, or ARBs (NCT00232180).[82]

A limitation in the use of spironolactone and eplerenone is hyperkalemia due to inhibition of potassium excretion and worsening renal function.[1,2] Accordingly, a number of strategies have been explored to improve upon these steroidal MR antagonists. Novel nonsteroidal MRAs, exemplified by PF-3882845,[83] BR-4628,[84] and BAY94-8862,[85] have been assessed for tissue-selective and renal-sparing actions.[86] PF-3882845 has completed a Phase I safety and tolerability study (NCT00971802). BAY94-8862 (finerenone) has completed a Phase II dose-finding trial in patients with chronic heart failure and mild or moderate kidney disease, with decreases in BNP, NTproBNP, and albuminuria (reflecting reduced ventricular stress and improved renal function) but with significantly smaller elevations in serum potassium compared to spironolactone reported (NCT01345656).[87] BAY94-8862 currently is being studied in a Phase II trial in patients with worsening chronic heart failure and left ventricular systolic dysfunction and either type 2 diabetes mellitus with or without chronic kidney disease or chronic kidney disease alone (NCT01807221).[88] Three Phase III

trials with BAY94-8862 have been announced as soon-to-initiate: the FINESSE-HF study comparing BAY94-8862 to eplerenone in HFrEF patients with type 2 diabetes and/or chronic kidney disease, and FIGARO-DKD (NCT02545049) and FIDELIO-DKD (NCT02540993) assessing BAY94-8862 in diabetic kidney disease patients with moderate and marked albuminuria, respectively.

Aldosterone synthase inhibition constitutes an alternate and/or complementary approach to mineralocorticoid receptor antagonism for attenuating aldosterone activity in disease states, potentially including heart failure.[76] In a rat model of myocardial infarction, the aldosterone synthase inhibitor FAD286 has been reported to elicit beneficial effects on left ventricular function and remodeling.[89] FAD286 is the *R*-(+)-enantiomer of the racemic CYP19 (aromatase) inhibitor CGS016949A (fadrozole).[90] Although its antipode is an aromatase inhibitor, FAD286 potently inhibits human aldosterone synthase in vitro.[91] In a Phase II study in patients with essential hypertension, (NCT00758524) LCI699, a purportedly selective aldosterone synthase inhibitor, was effective in lowering diastolic blood pressure.[92]

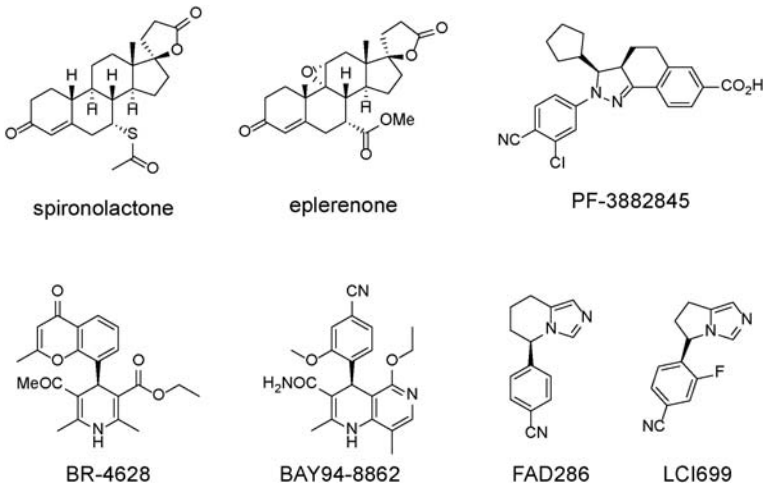

7.17.3.2 Natriuretic Peptide System-Related Approaches

7.17.3.2.1 LCZ696

As noted in the Introduction, the NPS and RAAS act as counter-regulators in cardiovascular and renal homeostasis.[43] Presently, the only approved treatments exploiting the potential benefits of activating the NPS are the short-term intravenous infusions of recombinant BNP (nesiritide; United States and EU) and ANP (carperitide, Japan) for the treatment of ADHF. There has been long-standing interest and effort directed toward longer duration enhancement of NPS tone for the treatment of chronic heart failure. One approach has been that of inhibiting the catabolizing enzyme NEP.[93] Breakdown by NEP constitutes one of two main elimination mechanisms for endogenous NPs, the other being binding to and clearance by the NP receptor NPRC. Clinical studies primarily in patients with hypertension with selective NEP inhibitors demonstrated a lack of sustained efficacy, which was attributed to the promiscuous role of NEP in breaking down multiple vasoactive peptides including bradykinin and AII. Accordingly, patients administered selective NEP inhibitors, exemplified by candoxatril, displayed increases in plasma AII levels, which presumably offset the beneficial actions of increased NP levels.[94–96] Given the latter observation and the known counter-regulatory relationships of the RAAS and NPS, combination NEP plus ACE inhibition in single molecules termed vasopeptidase inhibitors, exemplified by omapatrilat, were pursued in chronic heart failure and hypertension patients. While encouraging clinical efficacy was observed with combined vasopeptidase inhibition,[97,98] the development of vasopeptidase inhibitors was terminated due to the observation of increased rates of angioedema attributed to an excessive accumulation of bradykinin resulting from concomitant inhibition of two catabolizing enzymes for this kinin, ACE, and NEP, as well as inhibition of the catabolizing enzyme aminopeptidase-P in the case of omapatrilat.[93]

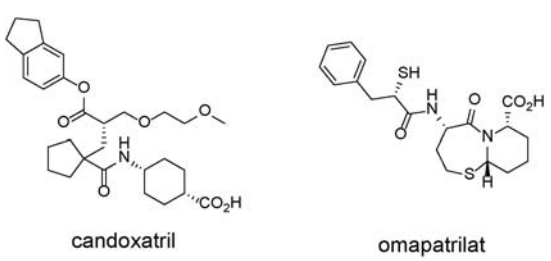

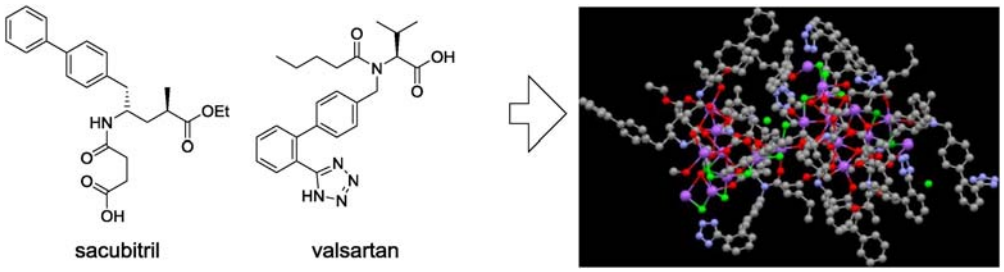

Fig. 3 LCZ696 is a crystalline structure comprising 6 NEP inhibitor prodrug (sacubitril) and 6 ARB (valsartan) molecules in addition to 18 sodium ions and 15 water molecules. Reproduced from Feng, L.; Karpinski, P. H.; Sutton, P.; Liu, Y.; Hook, D. F.; Hu, B.; Blacklock, T. J.; Fanwick, P. E.; Prashad, M.; Godtfredsen, S.; Ziltener, C. LCZ696: A Dual-Acting Sodium Supramolecular Complex. *Tetrahedron Lett.* **2012**, *53*, 275–276.

To circumvent the risk of angioedema, a combination of NEP inhibition plus ARB treatment (LCZ696, cocrystal formulation of the NEP inhibitor prodrug sacubitril (AHU377) plus the ARB valsartan) has been developed in chronic heart failure and hypertension patients. LCZ696 is a unique supramolecular complex consisting of six NEP inhibitor prodrug (AHU377) and six ARB (valsartan) molecules (Fig. 3).[99] Upon oral administration of LCZ696 to healthy volunteers, rapid NEP inhibition and angiotensin receptor blockade is observed with significant elevation of plasma cGMP levels and RAAS biomarkers (renin, PRA, and AII).[100] Importantly, the maximum pharmacodynamic effect (elevated cGMP and RAAS biomarkers) occurred at the same time; 4 h after administration of LCZ696. This is in contrast to omapatrilat where maximum ACE inhibition was observed at 2 h and cGMP elevation was observed at 4 h.[101] The simultaneous effects of the NEP inhibitor and ARB may be responsible for the clinical efficacy of LCZ696.

LCZ696 recently was reported superior to enalapril in reducing the risks of death and of hospitalization in patients with HFrEF in the PARADIGM-HF trial (NCT01035255).[102] LCZ696 was approved for the treatment of patients with HFrEF in the United States, Canada, and the EU in 2015 with approvals in other markets pending. The Phase II clinical trial PARAMOUNT in HFpEF patients has reported encouraging effects of LCZ696 compared to valsartan on the plasma HF biomarker NTproBNP, left atrial dimensions, and NYHA class (NCT00887588),[103] leading to the engagement of the ongoing Phase III PARAGON-HF trial of LCZ696 for the treatment of HFpEF (NCT01920711). ESC guidelines released in May of 2016 recommend that LCZ696 replace ACEi's in ambulatory patients who are symptomatic despite optimal therapy and meet the inclusion/exclusion criteria of the PARADIGM-HF trial.[2]

7.17.3.2.2 Natriuretic peptide analogs

Multiple efforts have been directed toward improving the therapeutic profiles of the natriuretic peptides BNP (nesiritide) and ANP (carperitide) through the synthesis of either modified or chimeric peptides as well as peptide derivatives. These approaches are exemplified by ularitide, cenderitide, PL-3994, and ANX-042.[57,104–107] Ularitide is a synthetically produced form of urodilantin, an endogenous modified version of proANP, which is secreted from the distal tubules of the kidney and regulates renal sodium absorption and water homeostasis through binding to the NPRA receptor. It has been postulated that ularitide/urodilantin possesses greater renal effects with less pronounced peripheral vasodilation compared to BNP and ANP. Two Phase II trials in patients with decompensated heart failure reported that 24 h ularitide IV infusions resulted in reductions in pulmonary capillary wedge pressure (reflecting a reduction in pathologically elevated left atrial pressure that occurs in heart failure patients as a consequence of elevated left ventricular end-diastolic pressure), systemic vascular resistance, and dyspnea.[108,109] The TRUE-AHF Phase III trial assessing the efficacy of ularitide in patients with AHF is ongoing (NCT01661634). Cenderitide (CD-NP) is a chimeric natriuretic peptide that combines CNP and Dendroaspis NP (DNP) and which binds to both the NPRA and NPRB receptors. CNP is a potent venodilator. DNP is a natriuretic peptide family member, which is detected in human circulation and atria by immunoreactivity, activates NPRA, and is a potent natriuretic with additional diuretic and aldosterone-inhibiting activities. It is postulated that this chimeric molecule will display the beneficial effects of predominantly venous vasodilation and natriuresis with reduced risk of hypotension compared to BNP and ANP. A Phase II trial with IV cenderitide in patients with stabilized AHF reported significant reductions in pulmonary capillary wedge pressure and trends toward decreasing right atrial pressure and increasing cardiac output (reflecting more blood being circulated per unit time) (NCT00699712).[110] A Phase II trial with SC cenderitide in chronic HFrEF patients is ongoing (NCT02359227). PL-3994 is a synthetic NPRA receptor agonist with reduced affinity for the NPRC clearance receptor and resistance to degradation by NEP, resulting in an extended in vivo half-life.[104] ANX-042 is a shortened peptide based on an alternative spliced transcript for BNP and is reported to be a renal-selective, nonhypotensive NP.[57] Phase I safety and tolerability studies with PL-3994 (NCT00686803) and ANX-042 (NCT01638104) have been conducted.

7.17.3.2.3 Corin modulation of natriuretic peptide formation

The mature natriuretic peptides ANP, BNP, and CNP are synthesized as preprohormones, with cleavage of the N-terminal signal sequences resulting in the formation of the precursor prohormones proANP, proBNP, and proCNP.[43] The transmembrane serine protease corin is thought to play an important role in the posttranslational cleavage of proANP and proBNP into fully active

ANP and BNP.[111–113] Corin has been shown to be present in human heart, kidney, and circulating in blood, the latter believed to result from the release or shedding of corin from cells.[114,115] In human heart failure, levels of the less active prohormone forms of ANP and BNP have been reported to increase and predominate over the mature forms,[116] whereas circulating levels of corin have been reported to decrease in proportion to increasing heart failure severity.[114] These clinical observations suggest that corin deficiency may contribute to the pathogenesis of heart failure through dysregulation of mature ANP and BNP formation.[114] Preclinically, the potential for corin to impact heart failure development has been assessed in a genetic mouse model of dilated cardiomyopathy (transgenic mice expressing a dominant-negative phosphorylation-resistant cAMP response element-binding protein in the heart). Cardiac-targeted overexpression of corin in this heart failure model reduced the development of fibrosis, increased fractional shortening and ejection fraction (reflecting increased volume of blood ejected per heart beat), and reduced lung water and alveolar congestion.[117] Very recently, in vitro studies have identified proprotein convertase subtilisin/kexin-6 (PCSK6) as the protease responsible for the cleavage of the inactive corin zymogen to active corin.[118] Taken together, these clinical and preclinical findings suggest that PCSK6/corin regulation of ANP and BNP prohormone processing may represent an additional natriuretic peptide-based approach to attenuate heart failure severity.

7.17.3.3 Phosphodiesterase Inhibition, Activation of Soluble Guanylate Cyclase, HNO Donors

Alternate mechanisms to increase myocardial cGMP levels and afford cardioprotective benefit are being explored either as an alternative to, or potentially in combination with, activation of the NPS. One approach being explored is that of inhibiting myocardial phosphodiesterase (PDE) activity to inhibit cGMP degradation (see **Fig. 4**). Inhibition of PDE5A by sildenafil was shown to be effective in preventing cardiac dysfunction and hypertrophy in a mouse pressure overload model of LV hypertrophy and heart failure.[119] However, the administration of sildenafil to HFpEF patients in the Phase III RELAX Trial did not result in significant improvement in exercise capacity or clinical status (NCT00763867).[120] A Phase III study assessing the tolerance, safety, and efficacy of sildenafil in patients with HFrEF and secondary pulmonary hypertension is ongoing (NCT01616381). It has been proposed that cardiac PDE5A primarily regulates nitric oxide (NO)-stimulated, soluble guanylate cyclase-generated cGMP and that NO signaling is often depressed in heart failure.[121,122]

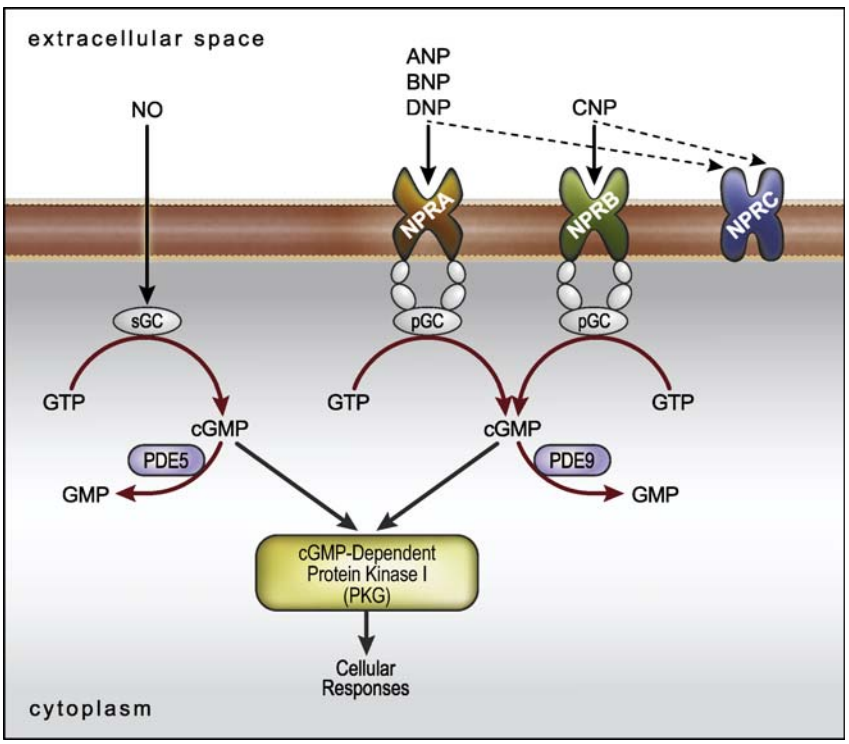

Fig. 4 Overview of the role of cGMP in cardiovascular signaling. Atrial natriuretic peptide (*ANP*), B-type natriuretic peptide (*BNP*), and Dendroaspis natriuretic peptide (*DNP*) activate the NPRA receptor (also termed NPR1, GC-A), which is coupled to particulate guanylate cyclase (*pGC*), thereby stimulating the formation of cGMP. C-type natriuretic peptide (*CNP*) stimulates the generation of cGMP through pGC by activating the NPRB receptor (also termed NPR2, GC-B). Binding of the natriuretic peptides to the NPRC receptor (also termed NPR3) results in receptor internalization and clearance of the natriuretic peptides. Nitric oxide stimulates the formation of cGMP through the activity of soluble guanylate cyclase (*sGC*). The physiologic effects of intracellular cGMP are mediated in great part by activation of cGMP-dependent protein kinase I (*PKG*). It is proposed that PDE9 preferentially regulates the breakdown of natriuretic peptide-generated cGMP, whereas PDE5 regulates the breakdown of NO-generated cGMP.[122]

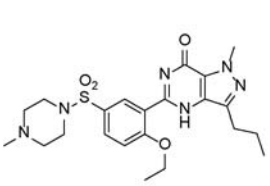
sildenafil

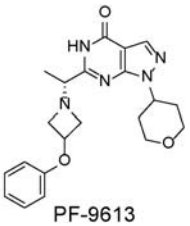
PF-9613

A recent study has suggested that PDE9A, which regulates natriuretic peptide-stimulated and NPRA-associated particulate guanylate cyclase-generated cGMP could be an important target for the treatment of heart failure.[122] PDE9A is expressed in mammalian heart (including human) and is upregulated in human myocardium from patients with HFpEF and patients with left ventricular hypertrophy due to aortic stenosis (pressure overload).[122] A comparison of PDE5A inhibition with sildenafil versus PDE9A inhibition with PF-9613,[123] in the mouse pressure overload heart failure model demonstrated that efficacy in preventing cardiac dysfunction and hypertrophy required active NO synthase activity for sildenafil, whereas comparable efficacy was elicited with PF-9613 independent of NO synthase status.[122] The NO-independence and the upregulation of PDE9A in the setting of heart failure suggest that PDE9A is the preferred PDE isoform (over PDE5A) to target for the treatment of heart failure.

A second approach being explored to enhance myocardial cGMP levels in the setting of heart failure is direct activation of soluble guanylate cyclase.[124] This approach will activate soluble guanylate cyclase in many tissues throughout the body, including vascular smooth muscle. The pulmonary vascular effects of soluble guanylate cyclase activation are responsible for the efficacy of riociguat in the treatment of pulmonary hypertension.[125–127] A Phase II dose-finding study of the soluble guanylate cyclase activator BAY-1021189 (vericiguat) in HFrEF patients with worsening heart failure has been completed (SOCRATES-REDUCED, NCT01951625) and a comparable study in HFpEF patients is ongoing (SOCRATES-PRESERVED, NCT10951638). The primary endpoint of change from the baseline NTproBNP level was not significantly affected when placebo was compared to pooled dosing groups in SOCRATES-REDUCED. However, exploratory analysis indicated that there was a dose-responsiveness with greater reductions in NTproBNP as the dose was increased.[128]

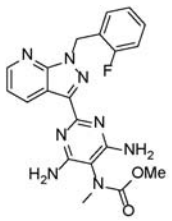
riociguat

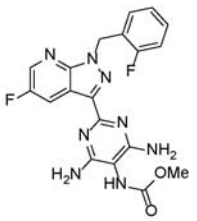
vericiguat

Nitroxyl (HNO) donors exemplified by CXL-1020 and CXL-1427 are being developed to produce beneficial cardiac and vascular effects purportedly via multiple mechanisms. HNO elicits combined venous and arterial dilation attributed at least in part to soluble guanylate cyclase activation, but also has been reported to elicit cAMP- and cGMP-independent positive inotropic and lusitropic effects in cardiac muscle. In a canine model of heart failure induced by coronary microembolization, CXL-1020 reduced left ventricular end-diastolic pressure (reflecting a reduction in elevated ventricular filling/preload) and myocardial oxygen consumption while increasing ejection fraction (reflecting more blood being circulated per beat). In a canine model of heart failure induced by rapid cardiac pacing, CXL-1020 increased contractility as assessed by end-systolic elastance (a load-independent metric reflecting contractile function) and evoked venoarterial dilation.[129] In a Phase II trial in HFrEF patients (NCT01096043), the IV administration of CXL-1020 reduced left and right heart filling pressures and systemic vascular resistance while increasing cardiac index and stroke volume index (reflecting increased circulation of blood). However, the development of this compound was suspended due to the occurrence of inflammatory irritation at the intravenous insertion site.[129] A Phase II study in HFrEF patients is ongoing with CXL-1427, a second generation HNO donor (NCT02157506).

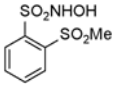
CXL-1020

7.17.3.4 Isosorbide Dinitrate–Hydralazine Combination

The combination of two vasodilator compounds, isosorbide dinitrate and hydralazine, is recommended for African-Americans with symptomatic HFrEF who are being treated optimally with ACE inhibitors and β-adrenergic receptor blockers.[1] Guidelines

also suggest that this combination can be considered in all patients, regardless of race, who cannot tolerate an ACE inhibitor or an ARB.[1,2] Isosorbide dinitrate is an NO donor that can be used on its own to prevent angina. A common issue with isosorbide dinitrate and other nitrates is the development of tolerance. In contrast, the mechanism of action of hydralazine is not completely understood. It has direct relaxing effects on vascular smooth muscles with a preferential action on arterioles. The addition of hydralazine to isosorbide dinitrate can prevent or reverse nitrate intolerance and support sustained NO-mediated vasodilation.[130,131]

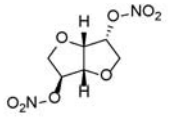

isosorbide dinitrate

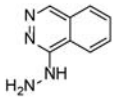

hydralazine

Clinical data supporting the use of isosorbide dinitrate and hydralazine in heart failure comes from three clinical trials; V-HeFT I,[132] V-HeFT II,[10] and A-HeFT.[133–135] V-HeFT I demonstrated that isosorbide dinitrate and hydralazine increased left ventricular ejection fraction in 642 men with impaired cardiac function and reduced exercise tolerance.[132] There was a trend for improvement in survival that was described as being of borderline statistical significance. V-HeFT II compared isosorbide dinitrate–hydralazine to enalapril.[10] Although the mortality benefit was superior with enalapril, isosorbide dinitrate–hydralazine induced greater improvements in ejection fraction and exercise tolerance.[10] The lack of a placebo arm in this study did not permit evaluation of whether there was a mortality benefit with isosorbide dinitrate–hydralazine. However, mortality rates for the isosorbide dinitrate–hydralazine arms were similar in V-HeFT I and V-HeFT II. Retrospective analysis of data from V-HeFT I and II revealed a racial disparity in the response to isosorbide dinitrate–hydralazine. In V-HeFT I African-Americans treated with isosorbide dinitrate had improved survival in comparison to placebo treatment.[136] In contrast, there was no survival benefit in white patients. In V-HeFT II, mortality was not different for African-Americans treated with enalapril versus isosorbide dinitrate.[136] A-HeFT enrolled self-identified black patients with evidence of left ventricular dysfunction that were on optimal therapy. Isosorbide dinitrate–hydralazine improved a composite endpoint of death, heart failure hospitalization, and quality of life as well as each component of the score.[133]

7.17.3.5 Vasopressin Antagonists

Vasopressin, a 9-amino acid neuropeptide hormone, is synthesized in the hypothalamus and secreted by the anterior pituitary. Vasopressin concentrations are elevated in heart failure and contribute to myocardial fibrosis, hypertrophy, vasoconstriction (mediated by vasopressin V_{1a} receptor activation) and water retention and hyponatremia (mediated by vasopressin V_2 receptor activation).[137] Initial work toward vasopressin receptor antagonists focused on small peptides.[138] However, the low bioavailability of the peptides led to the development of small molecule vasopressin receptor antagonists; the first V_{1a} selective antagonist OPC-21268,[139] and the structurally distinct V_{1a} antagonist relcovaptan.[140] Additionally, a class of structurally related V_2 and V_{1a}/V_2 receptor antagonists have been disclosed: mozavaptan (V_2 antagonist),[141] tolvaptan (V_2 antagonist),[142] and conivaptan (V_{1a}/V_2 antagonist).[143] Tolvaptan and conivaptan have been approved for the condition of hyponatremia including hyponatremia-associated heart failure.[144] However, conivapatan is a potent CYP3A4 inhibitor and this has limited its use.[145]

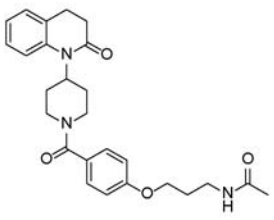

OPC-21268

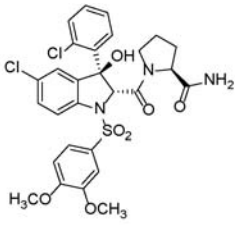

relcovaptan

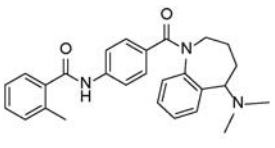

mozavaptan

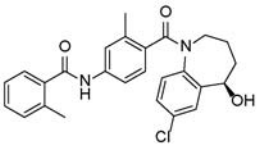

tolvaptan

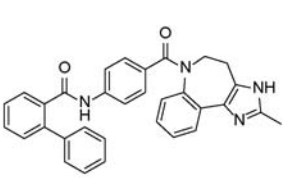

conivaptan

In a Phase III EVEREST trial in HFrEF patients hospitalized for heart failure, tolvaptan displayed improvement in body weight reduction, dyspnea, and edema within the initial 7 days of treatment but had no effect on short-term global clinical status,[146] and no effect observed on long-term mortality or heart failure-related morbidity (NCT00071331).[147] In a Phase II trial in HFrEF patients, the single dose oral administration of tolvaptan reduced pulmonary capillary wedge pressure, right atrial pressure, pulmonary artery pressure, and increased urine output (NCT00132886).[148] A Phase III trial assessing tolvaptan administered intravenously plus the loop diuretic furosemide in patients with ADHF is ongoing (NCT01644331). In a Phase II trial in patients hospitalized for worsening heart failure, the 12 h IV treatment with conivaptan reduced pulmonary capillary wedge pressure and right atrial pressure, and increased urine output (NCT00057356).[149] In a more recent dose-ranging pilot study conducted in patients hospitalized for worsening heart failure, IV conivaptan administered for 48 h increased urine output and decreased body weight, but had no effect on patient or clinical assessments of global and respiratory status at 48 h of treatment.[150]

Efforts to develop novel vasopressin antagonists include the highly selective V_2 antagonists VPA-985 (lixivaptan)[151] and satavaptan.[151–153] Additionally, Bayer has reported the balanced V_{1a}/V_2 antagonist Bay 86-8050 (ribuvaptan). The 8-week oral administration of lixivaptan was assessed in a Phase II trial in patients with heart failure and volume overload, with reductions in body weight and improvements in dyspnea and orthopnea reported (NCT01055912).[154] The Phase III BALANCE trial of lixivaptan in heart failure patients with hyponatremia and volume overload reported significant increases in serum sodium, no significant effect on mortality, but with a numerical increase in mortality in the lixivaptan group (NCT00578695).[155]

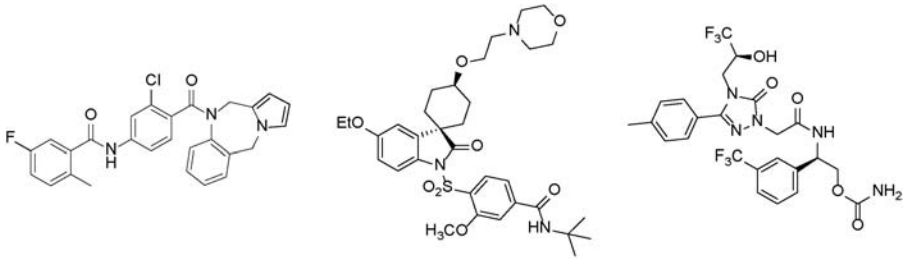

7.17.3.6 Urocortins

The urocortins 1, 2, and 3 (UCN1,2,3) and corticotropin-releasing hormone (CRH) are small (38–40 amino acids) endogenous peptide hormones that belong to the corticotropin-releasing family of hormones that are secreted in response to stress.[45,156] The UCNs signal through the G-protein coupled receptors CRH-R1 and CRH-R2, which are mainly located in the central nervous system and peripheral tissues, respectively. UCN1 binds to both receptors with similar affinities, whereas UCN2 and UCN3 are selective to CRH-R2. An extensive preclinical literature has explored the cardiovascular effects of the UCNs, and has reported these peptides to elicit peripheral vasodilation, positive inotropic effects, and cardioprotection in multiple animal species and models of cardiac injury and heart failure. Plasma and cardiac tissue UCN concentrations also have been reported to be elevated in heart failure.[45,156] Given the preceding observations, several clinical studies have explored the potential therapeutic benefit of exogenous UCN administration in human heart failure. In a small study of subjects with stable HFrEF, the 1 h IV infusion of UCN1 demonstrated increased adrenocorticotropic hormone (ACTH) and cortisol levels, but no effects on cardiovascular or renal parameters.[157] In a similar study of subjects with stable HFrEF, the 1 h IV infusion of UCN2 increased cardiac output and ejection fraction and heart rate while reducing mean arterial pressure and systemic vascular resistance. In this study, UCN2 increased ACTH and NTproBNP plasma concentrations, while other neurohumoral markers including cortisol, AII, aldosterone, and vasopressin were unchanged, and no renal effects were observed.[158] In the Phase II UNICORN trial, the 4 h IV infusion of UCN2 to patients with ADHF significantly reduced diastolic and systolic blood pressure with no effect on heart rate, decreased total peripheral resistance, and increased cardiac output (ACTRN12609000508279).[159] In a Phase II study in patients with stable HFrEF, three sequential rising dose IV infusions of JNJ-39588146 (stresscopin, homologous with UCN3) increased cardiac index and reduced diastolic blood pressure and systemic vascular resistance, with no significant effects on systolic blood pressure, heart rate, or pulmonary capillary wedge pressure observed (NCT01120210).[160]

7.17.3.7 Positive Inotropic Agents and Sarcomere Targets

7.17.3.7.1 Digoxin

Digoxin, the prototypical cardiac glycoside, is a longstanding positive inotropic agent approved for the treatment of HFrEF.[1,2] Cardiac glycosides inhibit sarcolemmal Na^+/K^+ ATPase resulting in a net accumulation of intracellular sodium which, in turn, inhibits the activity of the sarcolemmal Na^+/Ca^{++} exchanger (NCX) resulting in an increase in intracellular calcium concentration which increases contractility (see **Fig. 1**). Several clinical studies have reported that treatment with digoxin improves symptoms, quality of life, and exercise tolerance in patients with mild-to-moderate heart failure.[1,2] In the Phase III DIG trial, the administration

of digoxin to HFrEF patients treated with ACE inhibitors had no effect on all-cause or cardiovascular mortality, but tended to reduce mortality attributable to worsening heart failure. In the DIG trial, digoxin modestly reduced the rate of hospitalization both overall and for worsening heart failure, and modestly reduced the combination endpoint of death and hospitalization.[161] Post-hoc analysis of the DIG trial demonstrated that the subgroup of patients with serum digoxin concentrations of 0.5–0.9 ng mL^{-1} had less mortality and hospitalizations compared to placebo treated patients regardless of baseline ejection fraction or gender.[162]

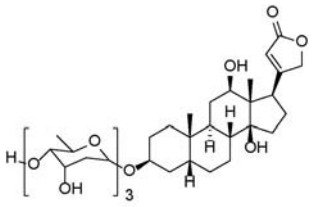

digoxin

7.17.3.7.2 cAMP elevating agents

7.17.3.7.2.1 β-adrenergic receptor agonists and PDE3 inhibitors

β-Adrenergic receptor agonists exemplified by the β_1 selective agonist, dobutamine, and PDE3 inhibitors such as milrinone are positive inotropic agents approved to increase cardiac contractility only in short-term parenteral use in select ADHF patients who are refractory to other therapies and are suffering consequences from end-organ hypoperfusion. β-Adrenergic receptor agonists and PDE3 inhibitors increase cardiac contractility by increasing myocardial cAMP levels, resulting in cAMP-mediated activation of PKA. PKA-dependent enhancement of L-type calcium currents and SERCA2a activity (via phosphorylation of phospholamban and consequent removal of inhibition of SERCA2a) contribute to increases in SR stores of calcium, peak intracellular calcium during contractions, and the rate of calcium resequestration into the SR. In addition, elevation of cAMP in the SA node results in heart rate increases. Although effective in improving cardiac output, β-adrenergic receptor agonists and PDE3 inhibitors are associated with significant adverse effects attributed to increases in intracellular cAMP and calcium concentration, including decreased myocardial efficiency, increased oxygen expenditure, myocardial ischemia, and tachyarrhythmias.[76,163] Consequently, while the acute short-term use of inotropic therapy with β-adrenergic receptor agonists and PDE3 inhibitors can be beneficial in select ADHF patients, their chronic use is generally associated with increased morbidity and mortality.[76]

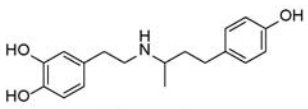

dobutamine

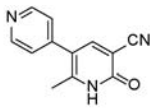

milrinone

7.17.3.7.2.2 Adenylate cyclase gene therapy

In preclinical models and heart failure patients, the expression of adenylate cyclase 6 is reduced.[164] Adenylate cyclase 6 catalyzes the formation of cAMP from ATP in response to G-protein coupled receptors that signal via Gsα. In animal models of heart failure or cardiac dysfunction, enhancing the expression of adenylate cyclase 6 improved cardiac function without affecting basal cAMP levels or heart rate.[164] It has been proposed that this lack of effect on basal cAMP levels could provide a therapeutic advantage over small molecules that induce persistent elevation of cAMP levels (vida supra, Section β-adrenergic receptor agonists and PDE3 inhibitors). RT-100 is a gene therapy vector comprised of a replication-defective adenovirus (serotype 5) that encodes for human adenylate cyclase type 6. Although peer-reviewed data are presently not available, the sponsor has reported that RT-100 safely reduced heart failure hospitalization compared to placebo treated patients in a small Phase 2 clinical trial.[165]

7.17.3.7.3 Modulators of sarcomeric proteins

A different approach to enhance myocardial contractility is the targeting of myocardial sarcomeric proteins. There has been significant effort devoted to the development of "calcium sensitizers," which most generally are characterized as binding to and increasing the sensitivity of troponin C to calcium such that greater contractility is elicited at a given concentration of intracellular calcium. In practice, reported calcium sensitizers have complex and likely multiple mechanisms of action, including many such agents inhibiting PDE3 and/or activating ATP-sensitive potassium channels.[163] Levosimendan presently is the only approved calcium sensitizer (EU, some South American countries) and is used parenterally in ADHF patients.[166] The Phase III SURVIVE trial compared intravenous infusions (minimum of 24 h) of levosimendan versus dobutamine in ADHF patients requiring inotropic support. The levosimendan group displayed greater decreases in plasma BNP levels compared to dobutamine within the first 5 days of treatment, but there were no significant differences between treatment groups in all-cause mortality at 31 days, number of days alive and out of hospital, patient global assessment, patient assessment of dyspnea at 24 h, and cardiovascular mortality at 180 days. Levosimendan

administration in SURVIVE was associated with a higher incidence of atrial fibrillation and ventricular arrhythmia (NCT00348504).[167] In the Phase III REVIVE I and II trials that compared intravenous infusion of levosimendan to placebo in ADHF patients, levosimendan displayed decreases in plasma BNP levels and improvements in composite clinical symptoms related to heart failure within the first 5 days of treatment, but was associated with more frequent hypotension and cardiac arrhythmias during infusion, and a numerically higher risk of mortality (NCT00048425).[168] Several Phase III and IV trials are ongoing assessing the intermittent administration of levosimendan in advanced chronic HFrEF (NCT01290146, NCT0098806, NCT01536132).[163]

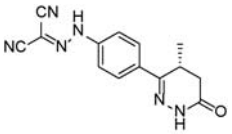

levosimendan

More recently, the targeting of the actin–myosin ATPase cycle has been explored as a means to more directly modulate cardiac contractility through altering the duty ratio, the proportion of myosin heads forming strong force-generating interactions or cross-bridges with actin.[163] Omecamtiv mecarbil (OM) has been described as a cardiac myosin activator that binds to myosin and selectively accelerates the rate-limiting step in the actin–myosin ATPase cycle, Pi release (**Fig. 5**). This results in an increase in the fraction of high affinity myosin–actin interactions (duty ratio), and an increase in contractility in the absence of effects on intracellular calcium levels.[169–171] A potential liability for this mechanism is that the contractions are prolonged resulting in shorter periods of relaxation within each cardiac cycle. As blood flow in the heart is reduced during systole, excessive increases in the duration of contraction could result in ischemia. In an early clinical trial, evidence of ischemia was observed in patients with OM plasma levels ≥ 1350 ng mL^{-1}.[172] Recently, an additional class of flavonoid compounds exemplified by chrysosplenol C have been reported to possess similar activity to OM.[173]

A study with OM in conscious dogs with post myocardial infarction systolic heart failure had indicated that, unlike available inotropes, the effects of OM appeared to be oxygen sparing in the heart.[174] However, a subsequent report studying the effects of OM in pigs with left ventricular dysfunction, ex vivo mouse hearts, and isolated mitochondria indicated that OM significantly increased oxygen wastage in both the contractile and noncontractile (resting) states due to continuous myosin ATPase activation.[175] A clinical study (NCT00748579) to examine this issue was terminated early due to challenges in study design and enrollment. Regardless, in the Phase II ATOMIC-AHF trial (NCT01300013), the 48 h IV administration of OM to patients with ADHF improved symptoms of dyspnea at the highest dose tested, and there was a trend for decreased worsening of HF across all dose groups at 7 days

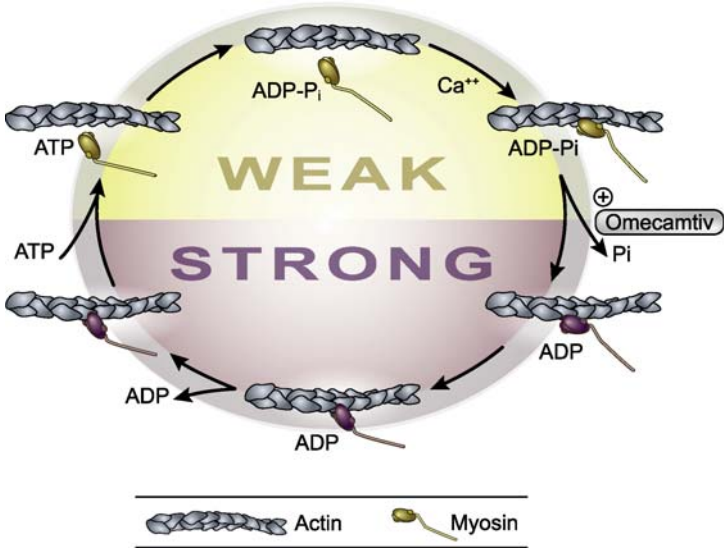

Fig. 5 The actomyosin ATPase cycle. For cardiac myosin the majority of the myosin heads interact weakly with actin, especially in the absence of calcium. Elevation of intracellular calcium removes inhibition of myosin–ADP–Pi interaction with actin by the troponin–tropomyosin complex and promotes the generation of strong crossbridges between myosin heads and actin. The release of inorganic phosphate (Pi) is the rate-limiting step of the cycle and enables the formation of a strong interaction between myosin heads and actin. Subsequently there is a force producing step (power stroke) in which myosin filaments are pulled along the thin filaments. The dissociation of ADP from the myosin heads then enables the binding of an ATP molecule, a weakening of the interaction between actin and myosin and dissociation. The development candidate omecamtiv mecarbil, enhances the release of Pi from actin–myosin–ADP–Pi and in doing so increases the fraction of myosin heads engaged in strong interactions with actin filaments.

after treatment initiation. The Phase II COSMIC-HF trial (NCT01786512) has assessed oral therapy with OM in chronic HFrEF patients.[163] Results of the COSMIC-HF trial were presented at the 2015 American Heart Association Scientific Sessions. Beneficial effects on left ventricular ejection fraction, ventricular size, and NTproBNP were reported at doses that did not raise any major safety concens.[176]

In an analogous approach to targeting the actin–myosin ATPase cycle, albeit to negatively modulate duty ratio and force generation, a preliminary report describes MYK0000461 as stabilizing the detached state of myosin prior to Pi release, thereby inhibiting Pi release and slowing the rate-limiting step in the actin–myosin ATPase cycle.[177] This mechanism potentially would decrease the duration of high affinity myosin–actin interaction, and thereby decrease the duty ratio and decrease contractility. Such a mechanism might be useful in treating hypercontractile disorders such as hypertrophic cardiomyopathy. Multiple Phase I safety and tolerability studies are ongoing with MKY0000461 (NCT02329184, NCT02356289, NCT02480296). These novel approaches targeting of the actin–myosin ATPase cycle to positively or negatively modulate contractility await clinical validation.

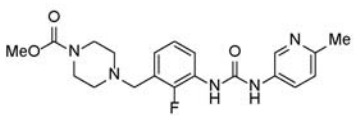

omecamtiv mecarbil

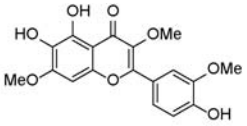

chrysosplenol C

7.17.3.8 Correction of Calcium Homeostasis

7.17.3.8.1 Mydicar (AAV-1/SERCA2a)

Correction of altered intracellular calcium handling in heart failure has been a goal for treatments since the abnormal calcium homeostasis in heart failure was first described.[46] One of the more consistent findings during profiling of either human myocardium or ventricular muscle from animal models of heart failure is a reduction in the expression levels of the SR calcium pump, SERCA2a, which is responsible for calcium reuptake after muscle contraction.[25,48,178] The impact of reduced SERCA2a activity includes a reduction in intracellular stores of calcium and a slower removal of calcium from the cytoplasm after it is released. These changes contribute to systolic and diastolic dysfunction, respectively, and make restoration of normal SERCA2a function an attractive goal for treating heart failure patients.

Mydicar is an adenovirus-associated virus 1 construct in which the cytomegalovirus immediate early promotor drives the expression of human SERCA2a.[179] The aim for this viral construct is to restore normal levels of SERCA2a and correct abnormal calcium homeostasis. SERCA2a encoding viral vectors have been delivered by coronary perfusion in animal models of heart failure and in human clinical trials.[180–185] Due to the nature of the intervention, effects develop over weeks to months. Beneficial effects reported after SERCA2a gene therapy in animal models of heart failure include enhanced survival,[181] increased left ventricular pressure development, increased fractional shortening, a reduction in left ventricular end-systolic volume, enhanced relaxation, improvements in the phosphocreatine/ATP ratio, and a reduction in plasma BNP levels.[180,181,184,185]

Initial clinical results with Mydicar in the CUPID trial appeared promising (NCT00454818).[186] Six months after virus administration to patients in NYHA Class III or IV heart failure with an ejection fraction of 0.35 or less, there was stabilization or improvement of 6 min walk distance, end-systolic volume, and end-diastolic volume in the group receiving the highest dose of virus.[186] In addition, a 3-year follow up of patients in the CUPID trial showed that there was a reduction in cardiovascular events in the high dose group.[187] No safety concerns were identified in the CUPID trial. A limitation of the CUPID trial was the small number of patients (39 in total).[186] A subsequent 250 patient Phase II trial (CUPID 2, NCT01643330) did not meet the prespecified primary endpoint (time-to-recurrent HF-related hospitalizations in the presence of terminal events; all-cause death, heart transplant, LVAD implantation).[182,188] As a consequence of the negative results in CUPID 2, the sponsor has placed all further development for Mydicar on hold.[189]

An issue for gene therapy using adeno-associated virus 1 constructs is the prevalence of neutralizing antibodies in the patient population. For the CUPID 2 trial, 60% of potential subjects were excluded based on the existence of detectable titers of neutralizing antibodies.[179]

There are a number of potential causes of the negative results of the CUPID 2 trial. Although it is clear that viral delivery of a SERCA2a construct can increase myocardial expression of SERCA2a, it is not known if the protein was expressed at a sufficient level or in all the correct locations to correct the calcium mishandling that occurs in heart failure. Because of the caveats of lack of verification of sufficient SERCA2a expression, and/or tissue/cellular/subcellular localization of Mydicar, one cannot exclude the potential benefit of SERCA2a activity augmentation in heart failure, and more exploration of this mechanism is required.

7.17.3.8.2 Aladorian

A second source of calcium mishandling in heart failure is the increased release of calcium from the SR during diastole.[27,190] Potential consequences of diastolic calcium leak include systolic and diastolic dysfunction due to effects on the content of SR calcium stores and the ability of the SR to resequester calcium in the face of an abnormal leak.[190] An additional concern is the potential to initiate calcium-dependent ventricular arrhythmias.[27,190]

The cardiac ryanodine receptor complex contains many proteins including the ryanodine receptor 2 (RyR2), FK binding protein 12/12.6 (FKBP 12/12.6), calmodulin, PKA, calmodulin-dependent protein kinase II δ (CaMKIIδ), and phosphatases.[190] Hyperphosphorylated RyR2 is found in heart failure and is thought to contribute to the enhanced diastolic calcium release.[190] There is controversy in the literature as to whether PKA, CaMKIIδ, or both are responsible for the hyperphosphorylation of ryanodine receptors.[51,190] However, the weight of available evidence appears to favor the notion that CaMKIIδ activity is primarily responsible for calcium leak from the SR in heart failure.[52,53,190] Unfortunately, the development of CaMKIIδ inhibitors appears to be limited by the difficulty in achieving kinase selectivity for the δ isoform, which is the predominant form of CaMKII in the heart, because no highly selective inhibitors have been reported.

A benzothiazepine class of compounds, JTV519 and S107, can function as stabilizers of RyR1–FKBP complexes in vitro. These compounds were developed based on the hypothesis that phosphorylation of RyR2 in heart failure was dependent on PKA, which prevented a stabilizing effect of FKBP 12/12.6 on RyR2 gating. In vitro, S107 was also shown to inhibit *S*-nitrosylation-mediated FKBP12 dissociation from RyR1.[191] A next generation benzothiazepine aladorian (ARM036) has been identified. Preclinically, aladorian has shown favorable effects in a mouse cardiac ischemia reperfusion model.[192] The compound is listed as being in Phase II clinical trials for ventricular arrhythmias in heart failure patients (ISRCTN14227980) and catecholaminergic polymorphic ventricular tachycardia (2011-000579-15).

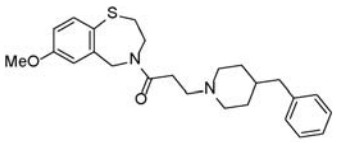

JTV519

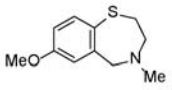

S107

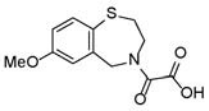

aladorian

7.17.3.8.3 Istaroxime

Istaroxime was identified from efforts to find a less toxic version of the cardiac glycoside, digoxin,[193] which causes cardiac arrhythmias at only two to three times the therapeutically useful doses. Two biochemical mechanisms have been reported for istaroxime and both appear to contribute to the inotropic effects: inhibition of sarcolemmal sodium–potassium ATPase activity and activation of SERCA2a.[194–197] The activation of SERCA2a activity has been attributed to relief of the inhibitory effect of phospholamban (by preventing the interaction between phospholamban and SERCA2a).[198] The addition of SERCA2a activation seems to be beneficial in comparison to the selective inhibition of sodium–potassium ATPase by digoxin. In vitro studies on isolated myocytes and in vivo studies show that istaroxime induces a positive inotropic effect that is comparable to that of digoxin but with a greater therapeutic index.[193,194,199] An important aspect of the effects of istaroxime on contractions is the induction of a positive lusitropic effect. Acute hemodynamic and imaging studies in a canine microembolus model of heart failure demonstrated beneficial effects of istaroxime on left ventricular end-diastolic pressure, chamber volumes (end-diastolic and end-systolic), and ejection fraction without increasing myocardial oxygen consumption or altering heart rate.[200,201] In this model, istaroxime also increased deceleration time of early mitral inflow velocity and diastolic wall stress, effects consistent with improved relaxation of the left ventricle.[201] Additional potential benefits for istaroxime in comparison to digoxin come from its pharmacokinetic properties, which result in a more rapid onset and offset of action.[194]

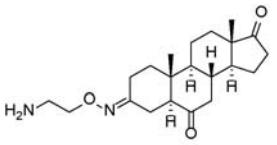

istaroxime

The Horizon HF trial (NCT00616161) evaluated the effects of a 6 h intravenous infusion of istaroxime in hospitalized heart failure patients with AHF, an ejection fraction $<35\%$, and a pulmonary capillary wedge pressure >20 mmHg.[202,203] One hundred twenty patients were normalized to either placebo, 0.5, 1.0, or 1.5 $\mu g\ kg^{-1}\ min^{-1}$ of istaroxime for 6 h. All patients were subjected to pulmonary artery catheterization and echocardiography (two-dimensional Doppler and tissue Doppler) to gather hemodynamic and imaging data at baseline and during treatment. A reduction in pulmonary capillary wedge pressure was observed in all dose groups. Although ejection fraction was not changed, there was a reduction in left ventricular volumes (end-systolic in the 1.0 $\mu g\ kg^{-1}\ min^{-1}$ group and end-diastolic in the 1.5 $\mu g\ kg^{-1}\ min^{-1}$ group).[202] Evidence for reduced diastolic stiffness included an increase in É (reflecting an increase in ventricular relaxation), an increase in E-wave deceleration time, and a decrease in end-diastolic elastance.[203] Side effects of istaroxime included a dose-dependent decrease in the rate-corrected QT interval, vomiting, pain at the infusion site, dysgeusia, and gastrointestinal symptoms.[202]

The Horizon HF study involved a cohort of AHF patients with milder symptoms than would normally be treated with inotropes based on current guidelines. In fact, patients requiring inotropic support were excluded so effects in the target patient population are

unclear. Istaroxime is presently listed as undergoing additional clinical testing in Italy (Phase II) and China (Phase I) CTR20150354; SN-YQ-2015006. The sponsor for istaroxime has also reported data for novel analogs and claim that some have an even greater therapeutic index.[204]

7.17.3.9 Relaxin

Relaxin is a 53-amino acid peptide that is a heterodimer of two peptide chains (24 and 29 amino acids) that are linked together via two disulfide bonds. The secondary structure of relaxin is very similar to insulin, despite the fact that the amino acid sequences between the two have very little similarity. Relaxin was discovered based its ability to relax the pubic ligament of gophers and guinea pigs.[205,206] This peptide has been shown to contribute to renal and cardiovascular adaptations to pregnancy including increased cardiac output, vasodilation resulting in a decreased vascular resistance, and an increase in glomerular filtration rate.[75,207] Molecular biological techniques have revealed that relaxins are a family of seven different insulin-like peptides that bind to and activate a family of four different G-protein coupled receptors.[205] The ligand/receptor pair that has been shown to induce beneficial effects in AHF patients, namely human relaxin-2 and relaxin family peptide receptor 1 (RXFP1), are discussed here.

RXFP1 is expressed in a wide range of reproductive tissues, including ovary, uterus, mammary gland, testis, and prostate. The receptor is also found in kidney, heart, lung, liver, bone, the vasculature, and brain.[205] Signal transduction via RXFP1 activation is complex and involves at least three distinct G-proteins ($G\alpha_s$, $G\alpha_{oB}$, and $G\alpha_{i3}$) to induce changes in cAMP production, activation of ERK 1/2, and production of NO.[205,207]

In animal models, relaxin has pronounced effects on the vasculature including decreases in vascular resistance and increases in arterial compliance.[206,207] There appears to be a species dependence for cardiac inotropic and chronotropic effects with positive effects in rodents and rabbits, whereas there was no effect in sheep and human heart.[207,208] In addition, renal blood flow and sodium excretion are increased in animal models.[209] Preclinical data show that relaxin protects the heart in multiple disease models through vasodilation, angiogenesis, antifibrotic, and antiinflammatory actions.[206,207,210] The renal and vascular effects of relaxin suggested the potential for benefit in the treatment of AHF.

Serelaxin is a recombinant form of human relaxin-2 that is administered by infusion. In the Phase III RELAX-AHF trial (NCT00520806), 1161 patients with a systolic blood pressure >125 mmHg were randomized to 48 h of infusion with 30 $\mu g\ kg^{-1}$ per day of serelaxin or a comparable volume of vehicle within 16 h of presentation. In this study, serelaxin improved one primary endpoint related to dyspnea, the area under the curve of a visual analog score.[211] However, there was not a statistically significant effect on the other primary endpoint related to dyspnea, the Likert score.[211] Surprisingly, a trend toward decreased mortality was observed at 180 days post serelaxin infusion,[211] but not at 60 days. No mechanism has been identified to account for the 6-month survival benefit after 2 days of infusion. Serelaxin is presently approved for use in Russia; however, the US and European regulatory authorities have asked for additional clinical data to support approvals. An ongoing large ($n=6375$ patients) outcomes trial (RELAX-AHF-2, NCT01870778, estimated completion Aug. 2016) is attempting to reproduce the mortality benefit that was found in RELAX-AHF.[75,212]

7.17.3.10 Neuregulin-1

Neuregulin-1 (Nrg-1) is the name used for a group of alternatively spliced protein ligands that belong to the epidermal growth factor (EGF) family. A single Nrg-1 gene encodes for multiple splice variants (≥ 15) of Nrg-1 that contain a common EGF domain. The EGF domain is responsible for ligand binding to its cognate receptors.[213] Nrg-1s are critical for cardiac development and maintenance of a mature working myocardium. They also play important roles in neural development, nerve myelination, and the maintenance of neuromuscular junctions.[214] Receptors for Nrg-1s are expressed in a tissue dependent manner and include the receptor tyrosine kinases, ErbB3 and ErbB4. Adult cardiac muscle expresses and signals primarily through ErbB4 receptors.[214] Most target tissues have a combination of ErbB3 and ErbB4 receptors. However, in contrast to heart, some cell types, such as Schwann cells, signal primarily through ErbB3 receptors.[215] The active form of ErbB receptors is either a homodimer or heterodimer. When heterodimers are induced, the complex frequently includes ErbB2, which has kinase activity but no ligand recognition domain and is structurally poised to dimerize with other ErbB receptors with bound agonist. ErbB3 receptors lack kinase activity and signal exclusively via heterodimers with ErbB2.[216]

The role of Nrg-1s in the heart became apparent from knockout mice and from clinical experience with the anti-ErbB2 antibody, trastuzumab.[214,216] ErbB4 knockout mice, ErbB2 knockout mice, and disruption of the Nrg-1 gene result in a common cardiac phenotype (defects in ventricular trabeculation) and embryonic lethality.[217] Although cardiac myocyte specific deletion of ErbB2 or ErbB4 permits survival of mice beyond birth, in each case a dilated cardiomyopathy develops.[218–220] Treatment of breast cancer patients with anthracyclines plus anti-ErbB2 antibody results in an increased incidence of cardiomyopathy.[221]

Nrg-1s are protective in both in vitro and in vivo animal models of cardiac damage or heart failure including doxorubicin treatment in vitro and in mice, post MI rats, dog tachypacing, and swine post MI models.[214,222,223] Although the mechanistic details remain to be determined, Nrg-1s induce multiple beneficial actions, including improvements in mitochondrial structure and function, improvement of glucose uptake, enhanced expression of sarcomeric proteins, and enhanced contractile function.[214] Biochemical events that are coupled to activation of Erb4 receptors in cardiac myocytes include activation of Akt and MAPK,[214] but it is not clear whether or how these pathways contribute to the beneficial effects of Nrg-1s in damaged myocardium.

Two different Nrg-1 proteins are currently undergoing clinical evaluation in chronic stable heart failure patients. Neucardin is the EGF domain of human Nrg-1 β2a. This 61-amino acid peptide has a short half-life and has been administered via 10 h of infusion on 11 consecutive days. Neucardin treatment of patients with chronic stable heart failure has been reported to induce an increase in ejection fraction, which persists up to 3 months after treatment[224] as well as favorable acute effects on hemodynamics and neurohormones including an increase in cardiac output, a decrease in PCWP, a decrease in systemic vascular resistance, and decreases in plasma norepinephrine and aldosterone.[225] However, there was a steep biphasic dose response observed with Neucardin; at high doses very little improvement in cardiac function was observed. In vitro studies have demonstrated that Nrg-1 can antagonize the enhancement of rabbit papillary muscle contractions by isoproterenol.[226] Whether this effect contributes to the biphasic dose response relationship in clinical trials with Neucardin is not known.

Improvements in ejection fraction in chronic stable heart failure patients have also been reported with a second Nrg-1 isoform, GGF2 (cimaglermin alfa), which can be administered as a single 15 min infusion.[227] This protein is a recombinant version of a longer and naturally occurring Nrg-1 isoform containing domains that could enhance the tissue half-life through binding to the ECM.[228] GGF2 did not exhibit a biphasic dose response in clinical trials but dose limiting liver toxicity was observed.[229] It is not clear if this toxicity was mechanism based. GGF2 is currently undergoing a Phase I pharmacokinetic study to evaluate potential drug–drug interactions with the CNS depressant benzodiazepine, midazolam (NCT01944683), as the observed liver toxicity could impact the elimination kinetics of midazolam. Neucardin is currently undergoing larger clinical trials in China and Australia.[214] A US Phase II trial with Neucardin is listed as being completed in clinicaltrials.gov but no results have been reported (NCT01251406).[230] Despite promising preclinical data and encouraging efficacy readouts in small clinical trials, it remains to be determined whether an acceptable benefit/risk profile can be demonstrated in clinical trials with Nrg-1s.

7.17.3.11 Ion Channel and Ion Transport Modulators

7.17.3.11.1 Diuretics for decongestion in heart failure

Guideline-directed therapy for AHF patients includes the intravenous administration of loop diuretics, such as furosemide (Lasix), bumetanide, and torsemide, in fluid overloaded patients.[1,2] Although the benefit of treating such patients with loop diuretics is well accepted, the level of evidence from controlled clinical trials to support these recommendations is from limited populations and the impact of loop diuretics on outcomes for AHF patients has not been well studied.[1,2,231] In addition, there is some uncertainty regarding optimal dosing regimens.[231]

Loop diuretics work through inhibition of the sodium/potassium/chloride cotransporter, NKCC2, in the thick ascending loop of Henle.[231,232] Preventing the reabsorbtion of sodium and chloride from the renal tubular lumen into the blood results in increased urine volume and increased sodium excretion (Fig. 6). Because loop diuretics have limited permeability across the epithelium of the thick ascending loop of Henle, they must be filtered across the glomerulus in order to reach their site of action on the luminal side of the tubular epithelial cells.[231] Therefore conditions that decrease glomerular filtration can limit the effectiveness of loop diuretics. There is also the potential to evoke undesirable effects with loop diuretics such as reducing glomerular

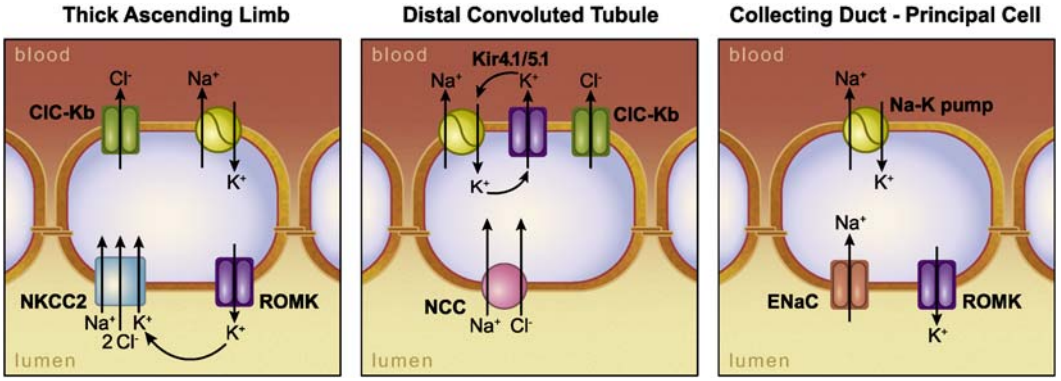

Fig. 6 Ion channels and ion transporters that contribute to transepithelial fluid and electrolyte fluxes within segments of the renal tubule that are targeted by existing diuretics.

filtration rate, activation of counter-regulatory neurohormonal responses, electrolyte disturbances (particularly hypokalemia), and arrhythmias.[231]

Diuretic resistance is a problem in a subset of AHF patients.[232] One approach for overcoming resistance to loop diuretics is to utilize combination therapy with a thiazide, such as chlorothiazide, hydrochlorothiazide, or metolazone.[231,232] Thiazides inhibit the sodium chloride cotransporter, NCC, in the distal convoluted tubule and prevent reabsorbtion of sodium and chloride which results in diuresis and enhanced urinary excretion of sodium (Fig. 6). The addition of a thiazide in a loop diuretic resistant patient can dramatically increase diuresis. However, potential risks of combining a thiazide with a loop diuretic include hypokalemia, hyponatremia, hypotension, and worsening renal function.[232]

Loop diuretics are also recommended for chronic heart failure patients for relief of dyspnea and edema when there is evidence of fluid retention.[1,2] In patients who are hypertensive, oral thiazides may also be considered because they induce a more sustained blood pressure response. Although there are no trials evaluating the effect of diuretics on outcomes in patients with chronic heart failure, controlled trials have demonstrated increases in sodium excretion, relief of fluid retention, and improvements in exercise tolerance.[233–235] Doses of oral diuretics are typically titrated up until the desired effect on body weight is obtained and need to be carefully adjusted to avoid adverse effects such as hypokalemia, hypomagnesemia, hypotension, and renal dysfunction. Hypokalemia risk can be mitigated in some cases through the use of potassium sparing diuretics such as spironolactone (vide supra MR Antagonists) or amiloride which reduces sodium reabsorption by the epithelial sodium channel, ENaC (Fig. 6). Amiloride is a direct inhibitor of this channel. In contrast spironolactone prevents aldosterone-induced stabilization of ENaC channels in the collecting duct.[236]

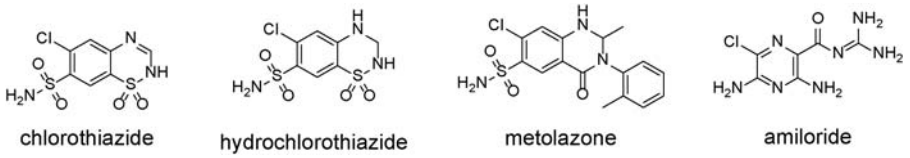

7.17.3.11.2 Inhibition of the cardiac sino-atrial (SA) node pacemaker current (I_f)

The SA node functions as the natural pacemaker of the heart due to the intrinsic ability of its cells to depolarize during diastole, resulting in spontaneous generation of action potentials in this structure, which then propagate throughout the heart. The diastolic depolarization of SA node cells is mediated in large part by the activity of the so-called "funny" current (I_f), which is activated by hyperpolarization and is nonselective for monovalent cations.[237] Ivabradine is a selective inhibitor of I_f, and as such functions as a selective bradycardic, that is heart rate reducing agent.[238] Other compounds have been reported to selectively inhibit I_f including zatebradine, cilobradine (both structurally similar to ivabradine), and ZD 7288; however, these agents have not been advanced beyond preclinical studies.[239,240] Ivabradine has no direct effect on inotropy, blood pressure, or vascular resistance.[241] The ability of ivabradine to selectively lower heart rate without affecting other aspects of cardiac function is in contrast to other heart rate reducing agents, such as β-blockers and cardiac glycosides (digoxin).

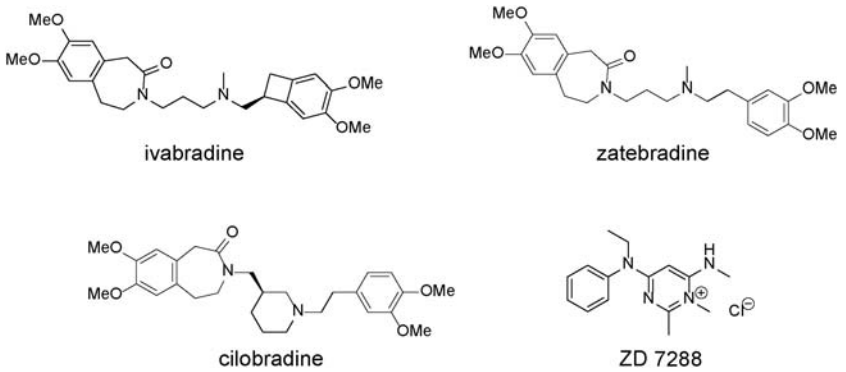

As heart rate is a determinant of myocardial contractile function, coronary blood flow, and myocardial oxygen demand, the therapeutic utility of heart rate reduction with ivabradine has been explored in cardiovascular disease states, such as myocardial ischemia/angina and heart failure.[238,241] The Phase III BEAUTIFUL trial assessed the effect of ivabradine in HFrEF patients with stable coronary artery disease and baseline heart rate $\geq$60 bpm. This trial reported no effect on the primary composite endpoint of cardiovascular death, admission to hospital for acute myocardial infarction, and admission to hospital for new onset or worsening heart failure, whereas a subgroup analysis of patients with baseline heart rate $\geq$70 bpm found that ivabradine reduced admission to hospital for fatal and nonfatal myocardial infarction and coronary revascularization (NCT00143507).[242] A substudy of the BEAUTIFUL trial reported that ivabradine treatment was effective in increasing LV

ejection fraction and decreasing LV end-systolic volume index, reflecting a beneficial effect on remodeling.[243] The subsequent Phase III SHIFT trial assessed the effect of ivabradine in HFrEF patients with baseline heart rate ≥ 70 bpm and reported a reduction in the primary composite endpoint of cardiovascular death or hospital admission for worsening heart failure (NCT02441218).[244] A subanalysis of SHIFT reported that the risk of the primary composite endpoint increased with increasing heart rate, and that the reduction in the primary composite endpoint with ivabradine was accounted for by heart rate reduction.[245] Ivabradine received EU approval in 2012 for the treatment of HFrEF patients in sinus rhythm with a heart rate ≥ 75 bpm and either treated with β-adrenoceptor blockade or for whom β-blockade is not tolerated or contraindicated. Ivabradine received US approval in 2015 for the treatment of HFrEF patients in sinus rhythm with a heart rate ≥ 70 bpm and treated with maximally tolerated β-adrenoceptor blockade or for whom β-blockade is contraindicated. Of note, a small Phase III/IV study in HFpEF patients with baseline sinus heart rate ≥ 60 bpm reported that 7 days administration of ivabradine resulted in improved exercise capacity and peak oxygen uptake associated with an improved left ventricular filling pressure response to exercise.[246] An additional small study in HFpEF patients with baseline sinus heart rate ≥ 75 bpm also has reported that 12 months administration of ivabradine resulted in improved exercise duration, peak oxygen uptake, and NYHA class along with improvements in LV diastolic function.[247] An ongoing Phase II trial is assessing the effect of ivabradine in patients with decompensated heart failure (NCT02236247).

7.17.3.11.3 Inhibition of the cardiac late sodium current ($I_{Na,late}$)

When cardiac myocytes are activated, sarcolemmal sodium channels mainly open transiently and quickly inactivate thereby carrying the peak sodium current (I_{Na} or $I_{Na,peak}$), which underlies cardiac cell depolarization and the upstroke of the cardiac action potential. A small component of sodium current termed late sodium current ($I_{Na,late}$) results from a proportion of sodium channels that remain open, inactivate slowly, or reopen.[248] $I_{Na,late}$ has been reported to be elevated under several cardiac pathological conditions including multiple inherited or acquired arrhythmia syndromes and structural heart disease, including myocardial ischemic injury and heart failure.[249,250] Elevated $I_{Na,late}$ is thought to result in prolongations of and/or dispersions in action potential or QT interval duration that promote arrhythmia.[248,249] Elevated $I_{Na,late}$ also is thought to facilitate intracellular calcium overload through increased NCX activity, which results in diastolic and systolic dysfunction.[248,250] Ranolazine, which is approved worldwide for the treatment of angina, is an inhibitor of $I_{Na,late}$ and has been used to explore the utility of targeting this current in preclinical cardiovascular disease models as well as clinically. In a canine model of coronary microembolization-induced HFrEF, ranolazine was reported to improve left ventricular function when administered acutely, and with chronic treatment prevent progressive LV dysfunction and remodeling when administered alone or in combination with metoprolol or enalapril.[251,252] In the Phase II RALI-DHF proof-of-concept study in HFpEF patients, IV infusion of ranolazine acutely decreased LV end-diastolic pressure and pulmonary capillary wedge pressure, slightly decreased cardiac output but had no effect on LV relaxation parameters.[253] In the same HFpEF study, after 14 days of oral ranolazine treatment, there were no significant changes in echocardiographic or cardiopulmonary exercise test parameters (NCT01163734).[253] Two ongoing Phase II studies are further assessing ranolazine treatment on exercise capacity in HFpEF patients (NCT01505179) as well as in patients with dilated cardiomyopathy (NCT02133911).

Beyond ranolazine, more selective inhibitors of $I_{Na,late}$ have been investigated. In addition to its effects on $I_{Na,late}$, ranolazine inhibits a potassium current that is important for termination of the cardiac action potential, I_{Kr}.[254] Ranolazine also blocks both α- and β-adrenergic receptors,[255] and in one study,[256] but not in another,[257] it was reported to regulate SR calcium release. This lack of selectivity could hinder the interpretation of the mechanism(s) responsible for the beneficial effects of ranolazine. More selective $I_{Na,late}$ inhibitors include GS-967, which has been shown to suppress arrhythmia in preclinical models,[258] and eleclazine (GS-6615), which is being assessed in a Phase II/III study in patients with symptomatic hypertrophic cardiomyopathy (NCT02291237).

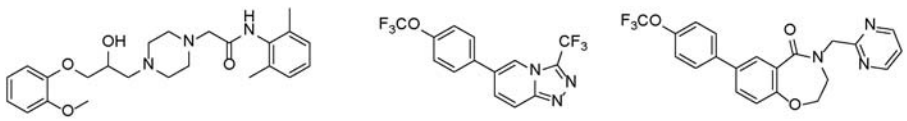

ranolazine GS-967 GS-6615

7.17.3.11.4 Inhibition of the renal outer medullary potassium (ROMK) channel

Currently approved diuretics, which work by reducing sodium and osmotically driven water reabsorption in the nephron, are used extensively in the treatment of heart failure and hypertension. Loop diuretics, exemplified by furosemide (vide supra Diuretics), potentially in combination with other diuretic classes such as the thiazides, exemplified by hydrochlorothiazide (vide supra Diuretics), are first-line treatment of AHF. Hypokalemia is a recognized limitation in the use of loop and thiazide diuretics. Based on human and rodent genetic data, it has been postulated that the selective inhibition of the renal outer medullary potassium (ROMK) channel represents a novel diuretic approach with potential efficacy and safety advantages over existing diuretics. ROMK (designated $K_{ir}1.1$) is a member of the K_{ir} inwardly rectifying family of potassium channels, and is expressed at the apical surface of epithelial cells in two parts of the nephron: the thick ascending loop of Henle (TALH) and the cortical collecting duct

(CCD) (Fig. 6).[259,260] In the TALH, ROMK-dependent efflux of potassium into the lumen is required to maintain luminal potassium at a level that supports $Na^+/K^+/2\ Cl^-$ dependent sodium and chloride reabsorption into the plasma via NKCC2. In the CCD, ROMK is the channel utilized for aldosterone-dependent potassium excretion into the urine and maintaining a cellular resting potential that supports reabsorption of sodium through the epithelial sodium channel, ENaC.[259] It is proposed that by inhibiting sodium reabsorption in the TALH and CCD and blocking potassium secretion in the collecting distal tubules, ROMK inhibitors may induce natriuresis and diuresis but limit the urinary loss of potassium observed with available loop and thiazide diuretics. Furthermore, since ROMK modulates sodium reabsorption in multiple nephron segments, it is possible that ROMK inhibitors may induce natriuresis and diuresis more effectively than available loop and thiazide diuretics which target transport pathways present in single nephron segments (TALH and distal convoluted tubule, respectively). Early screening efforts to identify ROMK inhibitors led to the identification of cryptan VU590 as the first small molecule ROMK inhibitor ($IC_{50}=290$ nM), although selectivity against $K_{ir}7.1$ (also present in the collecting duct) limits this class of compounds.[261] The search for more selective tool compounds (versus $K_{ir}7.1$) led to the discovery of BNBI and VU591.[262] All three compounds share a key nitrophenyl moiety. BNBI possessed modest selectivity versus $K_{ir}7.1$ (at least 10×). Interestingly, the addition of a single oxygen in the tether, generated ROMK inhibitor VU591 and resulted in a 30-fold increase in potency over BNBI due to proposed polar interactions with the ROMK channel.[262] VU591 was also selective (at least 100×) against a large panel of ion channels. VU590 and VU591 were shown to inhibit potassium excretion in vitro in rat isolated collecting duct preparations consistent with ROMK inhibition. More potent and selective inhibitors of ROMK, like Compound 5, were subsequently identified through a high throughput screen.[263] It is interesting to note that compound 5 possesses the same di-nitrophenyl moiety as the previously disclosed inhibitors, although it was actually more potent for hERG (5 nM) than ROMK (52 nM). The metabolic liabilities of the nitro groups could be removed resulting in compound 30 which had good oral bioavailability (64%). Compound 30 was a potent ROMK inhibitor (49 nM) but was still more potent on hERG (17 nM). This series of compounds was evolved to a selective ROMK inhibitor (531-fold versus hERG) resulting in compound 28.[264] Compound 28 was reported to produce dose-dependent natriuretic and diuretic responses with no effect on kaliuresis in vivo in rats and dogs.[264] Further advancement of ROMK inhibition as a novel diuretic target awaits human proof-of-concept studies.

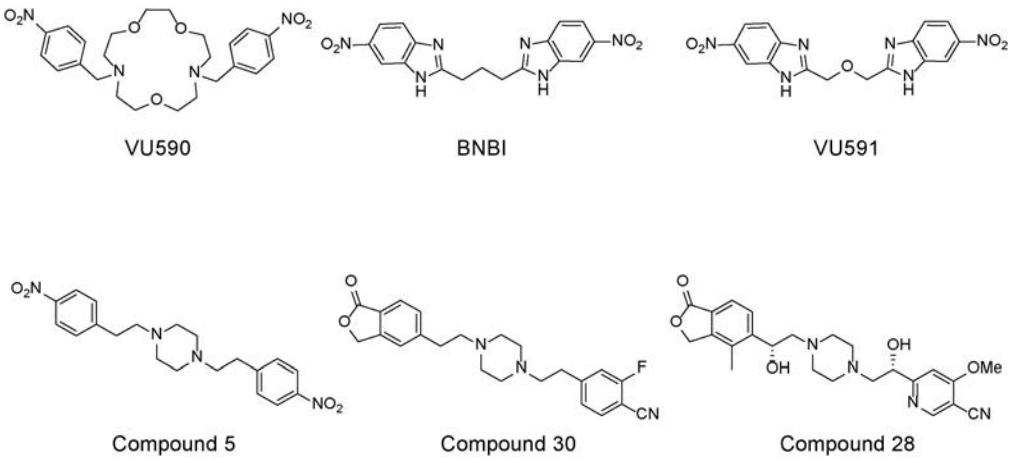

7.17.3.12 Compounds affecting metabolism

7.17.3.12.1 Elamipretide

Elamipretide (aka Bendavia, MPT-131, and SS31) is a tetrapeptide with a cationic 3+ charge at physiological pH that is currently in clinical development for numerous conditions associated with mitochondrial dysfunction, including heart failure.[265–267] This development candidate has unexpected properties for a small highly charged peptide in that it readily permeates cell membranes and crosses the blood brain barrier. A possible mechanism for the observed permeability is the active transport of the peptide through the basolateral peptide transporter.[268] The peptide is also able to be rapidly effluxed from cells despite not being a substrate for P-glycoprotein.[268] The mechanism responsible for cellular efflux is unclear. Elamipretide is concentrated in the inner mitochondrial membrane by >1000-fold relative to plasma and distributes preferentially into the kidney, liver, lung, and heart.[267,268] The proposed mechanism of action is binding to cardiolipin,[269] a phospholipid found exclusively in the inner mitochondrial membrane. The binding to cardiolipin is thought to result in a disruption of interactions between cardiolipin and cytochrome C and consequently reduces oxidative inactivation of cardiolipin by cytochrome C.[265] Cardiolipin plays a role in the formation of mitochondrial cristae, helping to colocalize electron transport complexes in order to promote efficient oxidative phosphorylation, enhance ATP production, and reduce leak of reactive oxygen species.[266]

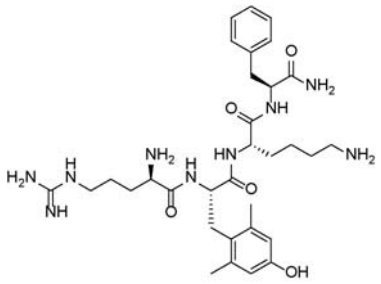

elamipretide

Preclinically, elamipretide protects against hypertrophy and fibrosis in an AII infusion model and a transaortic constriction (TAC) model. Elamipretide also reduces diastolic dysfunction in the AII infusion model.[270,271] In the mouse TAC model, the expression of a large number of mitochondrial proteins was altered and treatment with elamipretide corrected the expression level of many of these proteins.[270] Beneficial effects were also observed in ischemia–reperfusion models with approximately 50% reduction in infarct size but only if the peptide was administered prior to reperfusion.[272] In the dog microembolus model of heart failure, 3 months of subcutaneous treatment with elamipretide (0.5 mg kg^{-1} per day) decreased left ventricular volumes (end-systolic and end-diastolic), decreased end-diastolic pressure while increasing ejection fraction, peak left ventricular rate of pressure development and ATP synthesis.[272]

Phase I clinical data reported at the 2015 Europe Society of Cardiology were encouraging and showed that intravenous elamipretide (for up to 2 h) improved secondary endpoints of end-systolic and end-diastolic volume (NCT02388464, PREVIEW, 36 patients).[273–275] An improvement in left ventricular ejection fraction and cardiac output was also reported.[274] Other clinical trials of interest for elamipretide include the EMBRACE trial (NCT01572909)[275] with intravenous injection of elamipretide in patients with anterior wall STEMI scheduled to undergo primary PCI and stenting and a 7-day Phase I study of an oral formulation (NCT01786915).[276] Besides cardiovascular indications, elamipretide is also being developed for diabetic retinopathy, acute kidney injury, and neuroprotection.[266]

7.17.3.12.2 Perhexiline

Under fasted conditions, the heart normally derives the majority of its ATP production from fatty acids.[277] Carnitine palmitoyl transferase 1 (CPT1), an enzyme located within the mitochondrial outer membrane, is a rate-limiting enzyme for providing substrate for mitochondrial β-oxidation of fatty acids. The use of glucose as a substrate results in greater ATP production per unit of oxygen consumed and is therefore a more energy efficient process.

In nondiabetic heart failure and hypertrophic cardiomyopathy, the heart switches from using primarily fatty acids toward a greater dependence on glucose for generation of ATP. CPT1 inhibitors would be expected to cause a further shift toward glucose utilization and in doing so improve energy efficiency. A potential downside is a reduction in metabolic flexibility and the ability to switch between β-oxidation of fatty acids and glucose as the fuel for ATP production.

Perhexiline is a CPT1 inhibitor that is currently undergoing clinical trials for heart failure and hypertrophic cardiomyopathy. This drug has been used to relieve angina since its initial development in the 1970s.[278] Limitations include metabolism by CYP2D6, which leads to poor metabolism in individuals with polymorphisms of this enzyme, which can predispose these individuals to neurotoxicity and hepatotoxicity upon accumulation of perhexiline.[278] Additionally, in some clinical trials, adverse events (headache, nausea, and dizziness) have been observed in almost 60% of patients.[279] Despite these limitations, initial studies in heart failure patients were encouraging. Eight weeks of treatment with perhexiline increased peak oxygen consumption in chronic stable heart failure patients without any significant side effects.[280] This increase in peak oxygen consumption was superior to that achieved by an ACEi (enalapril), which had been previously shown to induce beneficial effects on this read out.[281,282] Peak oxygen consumption was also increased in patients with nonobstructive hypertrophic cardiomyopathy after 3–6 months of treatment with perhexiline.[283] An additional clinical trial using 1 month of treatment in dilated cardiomyopathy patients has shown improvements in the phosphocreatine/ATP ratio, and improvement in NYHA functional class (NCT00841139).[284,285] Surprisingly, there was no change in respiratory exchange ratio, which reflects the relative use of glucose versus free fatty acids as the fuel used to produce ATP.[285] Pending trials for perhexiline include a Phase II trial in patients with diastolic heart failure (NCT00839228) and a Phase III trial in 350 subjects with hypertrophic cardiomyopathy (NCT02431221).

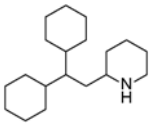

perhexiline

7.17.3.13 MGN-9103 (Antagomir Versus miR-208a/miR499)

Remodeling during heart failure is associated with reactivation of a subset of fetal genes. Downregulation of myosin 6 (Myh6; α-myosin heavy chain) and upregulation of myosin 7 (Myh7; β-myosin heavy chain) occur in heart failure and can affect contractile performance.[286] Micro RNAs (miRs) are small noncoding RNAs that can bind to multiple coding RNA strands and affect their translation. miR-208a is a cardiac specific miR that is encoded by an intron within the Myh6 gene.[287] Related intronic miRs in Myh7 and Myh7b (miR208b and miR-499, respectively) constitute additional members of a family of MyomiRs that control muscle myosin content and muscle performance.[287] Overexpression of miR-208a can induce cardiac hypertrophy in mice and miR208a is upregulated in rodent models of hypertrophy and heart disease.[288] Conversely parenteral treatment of Dahl salt sensitive rats with a locked nucleic acid antisense oligonucleotide (LNA) inhibitor (antagomir) of miR-208a delays mortality in animals placed on high salt, inhibits myosin switching, and improves diastolic function.[289] Co-dosing with an antagomir versus miR-499 accelerates the reduction of Myh7 expression in this model.[289] Additional effects of knocking down the expression of miR-208 in mice have been reported and include resistance to high fat diet and improved insulin sensitivity.[290] The metabolic effects are reportedly dependent on the upregulation of cardiac MED13.[290] Based on these data from animal models MGN-9103, an antagomir versus miR-208a and miR-499 is currently in preclinical development for the treatment of cardiac failure.

7.17.4 Summary

There have been great advances over the past 50 years that have been incorporated into guideline-directed therapies for the treatment of heart failure. However, heart failure remains a therapeutic indication with a high unmet medical need even after the recent approvals for ivabradine and LCZ696. Although current standards of care and newer medications improve long-term outcomes and/or reduce hospitalization, morbidity, and mortality for this syndrome is still disappointingly high, particularly for patients with end-stage disease and those with a recent history of hospitalization for AHF.

Significant research effort remains committed to increasing the efficacy and/or safety of established therapeutic pathways including target subtype-selective or directed biased signaling antiadrenergic and anti-RAAS approaches, as well as alternate or complementary combination approaches to enhance NPS activity and myocardial cGMP generation. While these approaches have the benefit of leveraging validated therapeutic pathways, they face the hurdle of demonstrating significant, greater-than-incremental clinical efficacy over established standard-of-care treatments within the same mechanistic pathway. Alternately, more novel mechanism of action approaches being explored includes the targeting of derangements in intracellular calcium homeostasis, sarcomere targets including modulation of the cardiac actin–myosin ATPase cycle, and interventions aimed at modulating myocardial metabolism and the remodeling process. Recent research also is exploring different modalities for treatment, including gene therapy and microRNA antagomirs. These latter novel approaches await clinical validation.

Although one can never exclude the possibility for identification of new drugs that will benefit all patients with heart failure, recognition of the divergent etiologies that can lead to the development of this syndrome and consequent patient segmentation may be one key for future therapeutic success. HFpEF continues to be problematic, as there are no drugs that have been approved for this indication. Even within this subdivision of heart failure patients further segmentation of the patient population and understanding that there are multiple causes of this condition could be important for delivering the right future drugs to the most responsive patients (eg, pressure overload versus diabetic cardiomyopathy). It is intriguing to speculate whether some of the novel research efforts exploring the modulation of intracellular handling, sarcomere function, and/or remodeling may be relevant to and efficacious in treating diastolic dysfunction in appropriate HFpEF segments.

Our understanding of cardiac biology and integrated cardiovascular biology has also progressed at an incredible pace over the last half century. Despite this, there are still large gaps in our understanding of the physiology and pathophysiology of heart failure. Not discounting the role of serendipity in drug discovery, truly transformational changes in the treatment of heart failure are likely to result from continued attempts to refine our understanding of the molecular triggers for heart failure and the molecular basis for the phenotypic changes that lead down the path to heart failure. The current levels of basic science research, engagement from the pharmaceutical industry, and interest from clinicians suggest that the medical community as a whole will continue to make progress in the treatment of heart failure in the near term and subsequent decades.

See also: 8.12. Discovery of ROMK Inhibitor MK-7145: A Novel Mechanism Diuretic.

References

1. Yancy, C. W.; Jessup, M.; Bozkurt, B.; Butler, J.; Casey, D. E., Jr.; Drazner, M. H.; Fonarow, G. C.; Geraci, S. A.; Horwich, T.; Januzzi, J. L.; Johnson, M. R.; Kasper, E. K.; Levy, W. C.; Masoudi, F. A.; McBride, P. E.; McMurray, J. J.; Mitchell, J. E.; Peterson, P. N.; Riegel, B.; Sam, F.; Stevenson, L. W.; Tang, W. H.; Tsai, E. J.; Wilkoff, B. L. ACCF/AHA Guideline for the Management of Heart Failure: A Report of the American College of Cardiology Foundation/American Heart Association Task Force on Practice Guidelines. *Circulation* **2013,** *2013* (128), e240–e327.
2. Ponikowski, P.; Voors, A. A.; Anker, S. D.; Bueno, H.; Cleland, J. G. F.; Coats, A. J. S.; Falk, V.; GonzÃlez-Juanatey, J. R.; Harjola, V.-P.; Jankowska, E. A.; Jessup, M.; Linde, C.; Nihoyannopoulos, P.; Parissis, J. T.; Pieske, B.; Riley, J. P.; Rosano, G. M. C.; Ruilope, L. M.; Ruschitzka, F.; Rutten, F. H.; van der Meer, P. On behalf of Authors/Task Force Members. 2016 ESC Guidelines for the diagnosis and treatment of acute and chronic heart failure. *Eur. Heart J* **2016**. http://dx.doi.org/10.1093/eurheartj/ehw128.
3. Braunwald, E. Heart Failure. *JACC Heart Fail* **2013,** *1*, 1–20.

4. Roger, V. L. Epidemiology of Heart Failure. *Circ. Res.* **2013,** *113,* 646–659.
5. Mozaffarian, D.; Benjamin, E. J.; Go, A. S.; Arnett, D. K.; Blaha, M. J.; Cushman, M.; de Ferranti, S.; Despres, J. P.; Fullerton, H. J.; Howard, V. J.; Huffman, M. D.; Judd, S. E.; Kissela, B. M.; Mozaffarian, D.; Benjamin, E. J.; Go, A. S.; Arnett, D. K.; Blaha, M. J.; Cushman, M.; de Ferranti, S.; Despres, J. P.; Fullerton, H. J.; Howard, V. J.; Huffman, M. D.; Judd, S. E.; Kissela, B. M.; Lackland, D. T.; Lichtman, J. H.; Lisabeth, L. D.; Liu, S.; Mackey, R. H.; Matchar, D. B.; McGuire, D. K.; Mohler, E. R.; Moy, C. S., 3rd; Muntner, P.; Mussolino, M. E.; Nasir, K.; Neumar, R. W.; Nichol, G.; Palaniappan, L.; Pandey, D. K.; Reeves, M. J.; Rodriguez, C. J.; Sorlie, P. D.; Stein, J.; Towfighi, A.; Turan, T. N.; Virani, S. S.; Willey, J. Z.; Woo, D.; Yeh, R. W.; Turner, M. B.; Muntner, P.; Mussolino, M. E.; Nasir, K.; Neumar, R. W.; Nichol, G.; Palaniappan, L.; Pandey, D. K.; Reeves, M. J.; Rodriguez, C. J.; Sorlie, P. D.; Stein, J.; Towfighi, A.; Turan, T. N.; Virani, S. S.; Willey, J. Z.; Woo, D.; Yeh, R. W.; Turner, M. B. Heart Disease and Stroke Statistics—2015 Update: A Report From the American Heart Association. *Circulation* **2015,** *131,* e29–e322.
6. Poss, J.; Link, A.; Bohm, M. Pharmacological Treatment of Acute Heart Failure: Current Treatment and New Targets. *Clin. Pharmacol. Ther.* **2013,** *94,* 499–508.
7. Marin-Garcia, J. *Heart Failure: Bench to Bedside;* Humana Press: Totowa, NJ, 2010.
8. Spinale, F. G.; Zile, M. R. Integrating the Myocardial Matrix Into Heart Failure Recognition and Management. *Circ. Res.* **2013,** *113,* 725–738.
9. Swedberg, K. Effects of the Early Administration of Enalapril on Mortality in Patients with Acute Myocardial Infarction. Results of the Cooperative New Scandinavian Enalapril Survival Study II (CONSENSUS II). *N. Engl. J. Med.* **1987,** *316,* 1429–1435.
10. Cohn, J. N.; Johnson, G.; Ziesche, S.; Cobb, F.; Francis, G.; Tristani, F.; Smith, R.; Dunkman, W. B.; Loeb, H.; Wong, M.; et al. A Comparison of Enalapril With Hydralazine-isosorbide Dinitrate in the Treatment of Chronic Congestive Heart Failure. *N. Engl. J. Med.* **1991,** *325,* 303–310.
11. Yusuf, S. Effect of Enalapril on Survival in Patients With Reduced Left-ventricular Ejection Fractions and Congestive Heart Failure. *N. Engl. J. Med.* **1991,** *325,* 293–302.
12. Garg, R.; Yusuf, S. Overview of Randomized Trials of Angiotensin-converting Enzyme-inhibitors on Mortality and Morbidity in Patients With Heart-failure. *JAMA* **1995,** *273,* 1450–1456.
13. Cohn, J. N.; Tognoni, G. A Randomized Trial of the Angiotensin-receptor Blocker Valsartan in Chronic Heart Failure. *N. Engl. J. Med.* **2001,** *345,* 1667–1675.
14. Granger, C. B.; McMurray, J. J.; Yusuf, S.; Held, P.; Michelson, E. L.; Olofsson, B.; Ostergren, J.; Pfeffer, M. A.; Swedberg, K. Effects of Candesartan in Patients With Chronic Heart Failure and Reduced Left-ventricular Systolic Function Intolerant to Angiotensin-converting-enzyme Inhibitors: The CHARM-Alternative Trial. *Lancet* **2003,** *362,* 772–776.
15. Lechat, P.; Brunhuber, K. W.; Hofmann, R.; Kuhn, P.; Nesser, H. J.; Slany, J. The Cardiac Insufficiency Bisoprolol Study II (CIBIS-II): A Randomised Trial. *Lancet* **1999,** *353,* 9–13.
16. Hjalmarson, A.; Goldstein, S.; Fagerberg, B.; Wedel, H.; Waagstein, F.; Kjekshus, J.; Wikstrand, J.; El Allaf, D.; Vitovec, J.; Aldershvile, J.; Halinen, M.; Dietz, R.; Neuhaus, K. L.; Janosi, A.; Thorgeirsson, G.; Dunselman, P.; Gullestad, L.; Kuch, J.; Herlitz, J.; Rickenbacher, P.; Ball, S.; Gottlieb, S.; Deedwania, P. Effects of Controlled-release Metoprolol on Total Mortality, Hospitalizations, and Well-being in Patients With Heart Failure—The Metoprolol CR/XL Randomized Intervention Trial in Congestive Heart Failure (MERIT-HF). *JAMA* **2000,** *283,* 1295–1302.
17. Packer, M.; Coats, A. J.; Fowler, M. B.; Katus, H. A.; Krum, H.; Mohacsi, P.; Rouleau, J. L.; Tendera, M.; Castaigne, A.; Roecker, E. B.; Schultz, M. K.; DeMets, D. L. Effect of Carvedilol on Survival in Severe Chronic Heart Failure. *N. Engl. J. Med.* **2001,** *344,* 1651–1658.
18. Dargie, H. J. Effect of Carvedilol on Outcome After Myocardial Infarction in Patients With Left-ventricular Dysfunction: The CAPRICORN Randomised Trial. *Lancet* **2001,** *357,* 1385–1390.
19. Mueller, C.; Christ, M.; Cowie, M.; Cullen, L.; Maisel, A. S.; Masip, J.; Miro, O.; McMurray, J.; Peacock, F. W.; Price, S.; DiSomma, S.; Bueno, H.; Zeymer, U.; Mebazaa, A. European Society of Cardiology-Acute Cardiovascular Care Association Position Paper on Acute Heart Failure: A Call for Interdisciplinary Care. *Eur. Heart J. Acute Cardiovasc. Care* **2015**. http://dx.doi.org/10.1177/2048872615593279.
20. Roger, V. L.; Go, A. S.; Lloyd-Jones, D. M.; Benjamin, E. J.; Berry, J. D.; Borden, W. B.; Bravata, D. M.; Dai, S.; Ford, E. S.; Fox, C. S.; Fullerton, H. J.; Gillespie, C.; Hailpern, S. M.; Heit, J. A.; Howard, V. J.; Kissela, B. M.; Kittner, S. J.; Lackland, D. T.; Lichtman, J. H.; Lisabeth, L. D.; Makuc, D. M.; Marcus, G. M.; Marelli, A.; Matchar, D. B.; Moy, C. S.; Mozaffarian, D.; Mussolino, M. E.; Nichol, G.; Paynter, N. P.; Soliman, E. Z.; Sorlie, P. D.; Sotoodehnia, N.; Turan, T. N.; Virani, S. S.; Wong, N. D.; Woo, D.; Turner, M. B. Heart Disease and Stroke Statistics—2012 Update: A Report From the American Heart Association. *Circulation* **2012,** *125,* e2–e220.
21. Voigt, J.; Sasha John, M.; Taylor, A.; Krucoff, M.; Reynolds, M. R.; Michael Gibson, C. A Reevaluation of the Costs of Heart Failure and its Implications for Allocation of Health Resources in the United States. *Clin. Cardiol.* **2014,** *37,* 312–321.
22. Chugh, S. S.; Reinier, K.; Teodorescu, C.; Evanado, A.; Kehr, E.; Al Samara, M.; Mariani, R.; Gunson, K.; Jui, J. Epidemiology of Sudden Cardiac Death: Clinical and Research Implications. *Prog. Cardiovasc. Dis.* **2008,** *51,* 213–228.
23. Chan, M. M.; Lam, C. S. How Do Patients With Heart Failure With Preserved Ejection Fraction Die? *Eur. J. Heart Fail.* **2013,** *15,* 604–613.
24. Carson, P.; Anand, I.; O'Connor, C.; Jaski, B.; Steinberg, J.; Lwin, A.; Lindenfeld, J.; Ghali, J.; Barnet, J. H.; Feldman, A. M.; Bristow, M. R. Mode of Death in Advanced Heart Failure: The Comparison of Medical, Pacing, and Defibrillation Therapies in Heart Failure (COMPANION) Trial. *J. Am. Coll. Cardiol.* **2005,** *46,* 2329–2334.
25. Bers, D. M. Cardiac Excitation–Contraction Coupling. *Nature* **2002,** *415,* 198–205.
26. Doenst, T.; Nguyen, T. D.; Abel, E. D. Cardiac Metabolism in Heart Failure: Implications Beyond ATP Production. *Circ. Res.* **2013,** *113,* 709–724.
27. Luo, M.; Anderson, M. E. Mechanisms of Altered Ca^{2+} Handling in Heart Failure. *Circ. Res.* **2013,** *113,* 690–708.
28. Parati, G.; Esler, M. The Human Sympathetic Nervous System: Its Relevance in Hypertension and Heart Failure. *Eur. Heart J.* **2012,** *33,* 1058–1066.
29. Wagner, S.; Maier, L. S.; Bers, D. M. Role of Sodium and Calcium Dysregulation in Tachyarrhythmias in Sudden Cardiac Death. *Circ. Res.* **2015,** *116,* 1956–1970.
30. Rosca, M. G.; Tandler, B.; Hoppel, C. L. Mitochondria in Cardiac Hypertrophy and Heart Failure. *J. Mol. Cell. Cardiol.* **2013,** *55,* 31–41.
31. Cohn, J. N. Mechanisms in Heart Failure and the Role of Angiotensin-converting Enzyme Inhibition. *Am. J. Cardiol.* **1990,** *66,* 2D–6D.
32. Cohn, J. N.; Levine, T. B.; Olivari, M. T.; Garberg, V.; Lura, D.; Francis, G. S.; Simon, A. B.; Rector, T. Plasma Norepinephrine as a Guide to Prognosis in Patients With Chronic Congestive Heart Failure. *N. Engl. J. Med.* **1984,** *311,* 819–823.
33. Cohn, J. N. Abnormalities of Peripheral Sympathetic Nervous System Control in Congestive Heart Failure. *Circulation* **1990,** *82,* I-59–I-67.
34. Sorota, S. The Sympathetic Nervous System as a Target for the Treatment of Hypertension and Cardiometabolic Diseases. *J. Cardiovasc. Pharmacol.* **2014,** *63,* 466–476.
35. Lang, C. C.; Struthers, A. D. Targeting the Renin–angiotensin–aldosterone System in Heart Failure. *Nat. Rev. Cardiol.* **2013,** *10,* 125–134.
36. Unger, T.; Li, J. The Role of the Renin–angiotensin–aldosterone System in Heart Failure. *J. Renin. Angiotensin Aldosterone Syst.* **2004,** *5* (Suppl. 1), S7–S10.
37. Zucker, I. H.; Xiao, L.; Haack, K. K. The Central Renin–Angiotensin System and Sympathetic Nerve Activity in Chronic Heart Failure. *Clin. Sci. (Lond.)* **2014,** *126,* 695–706.
38. Sousa-Pinto, B.; Ferreira-Pinto, M. J.; Santos, M.; Leite-Moreira, A. F. Central Nervous System Circuits Modified in Heart Failure: Pathophysiology and Therapeutic Implications. *Heart Fail. Rev.* **2014,** *19,* 759–779.
39. Danser, A. H.; van Kesteren, C. A.; Bax, W. A.; Tavenier, M.; Derkx, F. H.; Saxena, P. R.; Schalekamp, M. A. Prorenin, Renin, Angiotensinogen, and Angiotensin-converting Enzyme in Normal and Failing Human Hearts. Evidence for Renin Binding. *Circulation* **1997,** *96,* 220–226.
40. Zisman, L. S.; Abraham, W. T.; Meixell, G. E.; Vamvakias, B. N.; Quaife, R. A.; Lowes, B. D.; Roden, R. L.; Peacock, S. J.; Groves, B. M.; Raynolds, M. V.; et al. Angiotensin II Formation in the Intact Human Heart. Predominance of the Angiotensin-converting Enzyme Pathway. *J. Clin. Invest.* **1995,** *96,* 1490–1498.
41. Mangiafico, S.; Costello-Boerrigter, L. C.; Andersen, I. A.; Cataliotti, A.; Burnett, J. C., Jr. Neutral Endopeptidase Inhibition and the Natriuretic Peptide System: An Evolving Strategy in Cardiovascular Therapeutics. *Eur. Heart J.* **2013,** *34,* 886–893.
42. McFarlane, S. I.; Winer, N.; Sowers, J. R. Role of the Natriuretic Peptide System in Cardiorenal Protection. *Arch. Intern. Med.* **2003,** *163,* 2696–2704.
43. Potter, L. R.; Abbey-Hosch, S.; Dickey, D. M. Natriuretic Peptides, Their Receptors, and Cyclic Guanosine Monophosphate-dependent Signaling Functions. *Endocr. Rev.* **2006,** *27,* 47–72.
44. Izumi, Y.; Miura, K.; Iwao, H. Therapeutic Potential of Vasopressin-Receptor Antagonists in Heart Failure. *J. Pharmacol. Sci.* **2014,** *124,* 1–6.
45. Garg, V.; Frishman, W. H. A New Potential Approach to Inotropic Therapy in the Treatment of Heart Failure: Urocortin. *Cardiol. Rev.* **2013,** *21,* 160–165.

46. Gwathmey, J. K.; Copelas, L.; MacKinnon, R.; Schoen, F. J.; Feldman, M. D.; Grossman, W.; Morgan, J. P. Abnormal Intracellular Calcium Handling in Myocardium From Patients With End-stage Heart Failure. *Circ. Res.* **1987,** *61,* 70–76.
47. Guo, A.; Zhang, C.; Wei, S.; Chen, B.; Song, L. S. Emerging Mechanisms of T-tubule Remodelling in Heart Failure. *Cardiovasc. Res.* **2013,** *98,* 204–215.
48. Periasamy, M.; Bhupathy, P.; Babu, G. J. Regulation of Sarcoplasmic Reticulum Ca^{2+} ATPase Pump Expression and Its Relevance to Cardiac Muscle Physiology and Pathology. *Cardiovasc. Res.* **2008,** *77,* 265–273.
49. Grimm, M.; Ling, H.; Willeford, A.; Pereira, L.; Gray, C. B.; Erickson, J. R.; Sarma, S.; Respress, J. L.; Wehrens, X. H.; Bers, D. M.; Brown, J. H. CaMKIIδ Mediates Beta-adrenergic Effects on RyR2 Phosphorylation and SR Ca Leak and the Pathophysiological Response to Chronic β-adrenergic Stimulation. *J. Mol. Cell. Cardiol.* **2015,** *85,* 282–291.
50. Oda, T.; Yang, Y.; Uchinoumi, H.; Thomas, D. D.; Chen-Izu, Y.; Kato, T.; Yamamoto, T.; Yano, M.; Cornea, R. L.; Bers, D. M. Oxidation of Ryanodine Receptor (RyR) and Calmodulin Enhance Ca Release and Pathologically Alter, RyR Structure and Calmodulin Affinity. *J. Mol. Cell. Cardiol.* **2015,** *85,* 240–248.
51. Marx, S. O.; Marks, A. R. Dysfunctional Ryanodine Receptors in the Heart: New Insights Into Complex Cardiovascular Diseases. *J. Mol. Cell. Cardiol.* **2013,** *58,* 225–231.
52. Fischer, T. H.; Herting, J.; Tirilomis, T.; Renner, A.; Neef, S.; Toischer, K.; Ellenberger, D.; Forster, A.; Schmitto, J. D.; Gummert, J.; Schondube, F. A.; Hasenfuss, G.; Maier, L. S.; Sossalla, S. Ca^{2+}/Calmodulin-Dependent Protein Kinase II and Protein Kinase A Differentially Regulate Sarcoplasmic Reticulum Ca^{2+} Leak in Human Cardiac Pathology. *Circulation* **2013,** *128,* 970–981.
53. Venetucci, L.; Sankaranarayanan, R.; Eisner, D. A. A Tale of Two Leaks. *Circulation* **2013,** *128,* 941–943.
54. Orchard, C.; Brette, F. t-Tubules and Sarcoplasmic Reticulum Function in Cardiac Ventricular Myocytes. *Cardiovasc. Res.* **2008,** *77,* 237–244.
55. Knowlton, A. A.; Chen, L.; Malik, Z. A. Heart Failure and Mitochondrial Dysfunction: The Role of Mitochondrial Fission/Fusion Abnormalities and New Therapeutic Strategies. *J. Cardiovasc. Pharmacol.* **2014,** *63,* 196–206.
56. Sacks, C. A.; Jarcho, J. A.; Curfman, G. D. Paradigm Shifts in Heart-Failure Therapy-A Timeline. *N. Engl. J. Med.* **2014,** *371,* 989–991.
57. von Lueder, T. G.; Sangaralingham, S. J.; Wang, B. H.; Kompa, A. R.; Atar, D.; Burnett, J. C., Jr.; Krum, H. Renin–Angiotensin Blockade Combined With Natriuretic Peptide System Augmentation: Novel Therapeutic Concepts to Combat Heart Failure. *Circ. Heart Fail.* **2013,** *6,* 594–605.
58. Port, J. D. β-adrenergic Signaling: Complexities and Therapeutic Relevance to Heart Failure. *Curr. Signal Transduction Ther.* **2012,** *7,* 120–131.
59. Chemaly, E. R.; Hajjar, R. J.; Lipskaia, L. Molecular Targets of Current and Prospective Heart Failure Therapies. *Heart* **2013,** *99,* 992–1003.
60. Talan, M. I.; Ahmet, I.; Xiao, R. P.; Lakatta, E. G. β_2-AR Agonists in Treatment of Chronic Heart Failure: Long Path to Translation. *J. Mol. Cell. Cardiol.* **2011,** *51,* 529–533.
61. Gauthier, C.; Rozec, B.; Manoury, B.; Balligand, J. L. β_3-Adrenoceptors as New Therapeutic Targets for Cardiovascular Pathologies. *Curr. Heart Fail. Rep.* **2011,** *8,* 184–192.
62. Rozec, B.; Erfanian, M.; Laurent, K.; Trochu, J.-N.; Gauthier, C. Nebivolol, A Vasodilating Selective β_1-Blocker, Is a β_3-Adrenoceptor Agonist in the Nonfailing Transplanted Human Heart. *J. Am. Coll. Cardiol.* **2009,** *53,* 1532–1538.
63. Baker, A. J. Adrenergic Signaling in Heart Failure: A Balance of Toxic and Protective Effects. *Pflugers Arch. Eur. J. Physiol.* **2014,** *466,* 1139–1150.
64. Kamal, F. A.; Travers, J. G.; Blaxall, B. C. Embracing Bias: β_1-Adrenergic Receptor-biased Ligands and Nuclear miRNA Processing. *Circ. Res.* **2014,** *114,* 742–745.
65. Kim, I.-M.; Wang, Y.; Park, K.-M.; Tang, Y.; Teoh, J.-P.; Vinson, J.; Traynham, C. J.; Pironti, G.; Mao, L.; Su, H.; Johnson, J. A.; Koch, W. J.; Rockman, H. A. Arrestin1-biased β_1-Adrenergic Receptor Signaling Regulates microRNA Processing. *Circ. Res.* **2014,** *114,* 833–844.
66. Patel, C. B.; Noor, N.; Rockman, H. A. Functional Selectivity in Adrenergic and Angiotensin Signaling Systems. *Mol. Pharmacol.* **2010,** *78,* 983–992.
67. Koitabashi, N.; Kass, D. A. Reverse Remodeling in Heart Failure-Mechanisms and Therapeutic Opportunities. *Nat. Rev. Cardiol.* **2012,** *9,* 147–157.
68. Koch, W. J.; Rockman, H. A.; Samama, P.; Hamilton, R. A.; Bond, R. A.; Milano, C. A.; Lefkowitz, R. J. Cardiac Function in Mice Overexpresing the β-adrenergic Receptor Kinase or a βARK Ihnibitor. *Science* **1995,** *268,* 1350–1353.
69. Rengo, G.; Lymperopoulos, A.; Zincarelli, C.; Donniacuo, M.; Soltys, S.; Rabinowitz, J. E.; Koch, W. J. Myocardial Adeno-Associated Virus Serotype 6-βARKct Gene Therapy Improves Cardiac Function and Normalizes the Neurohormonal Axis in Chronic Heart Failure. *Circulation* **2009,** *119,* 89–98.
70. BESTInvestigators. A Trial of the β-blocker Bucindolol in Patients With Advanced Chronic Heart Failure. *N. Engl. J. Med.* **2001,** *344,* 1659–1667.
71. O'Connor, C. M.; Fiuzat, M.; Carson, P. E.; Anand, I. S.; Plehn, J. F.; Gottlieb, S. S.; Silver, M. A.; Lindenfeld, J.; Miller, A. B.; White, M.; Walsh, R.; Nelson, P.; Medway, A.; Davis, G.; Robertson, A. D.; Port, J. D.; Carr, J.; Murphy, G. A.; Lazzeroni, L. C.; Abraham, W. T.; Liggett, S. B.; Bristow, M. R. Combinatorial Pharmacogenetic Interactions of Bucindolol and β_1, α_{2C} Adrenergic Receptor Polymorphisms. *PLoS One* **2012,** *7,* e44324.
72. Wan, Y. Q.; Wallinder, C.; Plouffe, B.; Beaudry, H.; Mahalingam, A. K.; Wu, X. Y.; Johansson, B.; Holm, M.; Botoros, M.; Karlen, A.; Pettersson, A.; Nyberg, F.; Fandriks, L.; Gallo-Payet, N.; Hallberg, A.; Alterman, M. Design, Synthesis, and Biological Evaluation of the First Selective Nonpeptide AT_2 Receptor Agonist. *J. Med. Chem.* **2004,** *47,* 5995–6008.
73. Regoli, D.; Plante, G. E.; Gobeil, F., Jr. Impact of Kinins in the Treatment of Cardiovascular Diseases. *Pharmacol. Ther.* **2012,** *135,* 94–111.
74. Violin, J. D.; DeWire, S. M.; Yamashita, D.; Rominger, D. H.; Nguyen, L.; Schiller, K.; Whalen, E. J.; Gowen, M.; Lark, M. W. Selectively Engaging β-Arrestins at the Angiotensin II Type 1 Receptor Reduces Blood Pressure and Increases Cardiac Performance. *J. Pharmacol. Exp. Ther.* **2010,** *335,* 572–579.
75. Khodjaev, S. D.; Teerlink, J. R.; Malik, F. I. Novel Drug Mechanisms in Development for Heart Failure. *Pflugers Arch. Eur. J. Physiol.* **2014,** *466,* 1219–1225.
76. Aronson, D.; Krum, H. Novel Therapies in Acute and Chronic Heart Failure. *Pharmacol. Ther.* **2012,** *135,* 1–17.
77. Rahuel, J.; Rasetti, V.; Maibaum, J.; Rueger, H.; Goschke, R.; Cohen, N. C.; Stutz, S.; Cumin, F.; Fuhrer, W.; Wood, J. M.; Grutter, M. G. Structure-based Drug Design: The Discovery of Novel Nonpeptide Orally Active Inhibitors of Human Renin. *Chem. Biol.* **2000,** *7,* 493–504.
78. Gheorghiade, M.; Bohm, M.; Greene, S. J.; Fonarow, G. C.; Lewis, E. F.; Zannad, F.; Solomon, S. D.; Baschiera, F.; Botha, J.; Hua, T. A.; Gimpelewicz, C. R.; Jaumont, X.; Lesogor, A.; Maggioni, A. P. Effect of Aliskiren on Postdischarge Mortality and Heart Failure Readmissions among Patients Hospitalized for Heart Failure: The ASTRONAUT Randomized Trial. *JAMA* **2013,** *309,* 1125–1135.
79. Struthers, A. D. Aldosterone Escape During Angiotensin-converting Enzyme Inhibitor Therapy in Chronic Heart Failure. *J. Card. Fail.* **1996,** *2,* 47–54.
80. Pitt, B.; Zannad, F.; Remme, W. J.; Cody, R.; Castaigne, A.; Perez, A.; Palensky, J.; Wittes, J. The Effect of Spironolactone on Morbidity and Mortality in Patients With Severe Heart Failure Randomized Aldactone Evaluation Study Investigators. *N. Engl. J. Med.* **1999,** *341,* 709–717.
81. Pitt, B.; Remme, W.; Zannad, F.; Neaton, J.; Martinez, F.; Roniker, B.; Bittman, R.; Hurley, S.; Kleiman, J.; Gatlin, M. Eplerenone, a Selective Aldosterone Blocker, in Patients With Left Ventricular Dysfunction After Myocardial Infarction. *N. Engl. J. Med.* **2003,** *348,* 1309–1321.
82. Zannad, F.; McMurray, J. J.; Krum, H.; van Veldhuisen, D. J.; Swedberg, K.; Shi, H.; Vincent, J.; Pocock, S. J.; Pitt, B. Eplerenone in Patients With Systolic Heart Failure and Mild Symptoms. *N. Engl. J. Med.* **2011,** *364,* 11–21.
83. Meyers, M. J.; Arhancet, G. B.; Hockerman, S. L.; Chen, X.; Long, S. A.; Mahoney, M. W.; Rico, J. R.; Garland, D. J.; Blinn, J. R.; Collins, J. T.; Yang, S.; Huang, H.-C.; McGee, K. F.; Wendling, J. M.; Dietz, J. D.; Payne, M. A.; Homer, B. L.; Heron, M. I.; Reitz, D. B.; Hu, X. Discovery of (3S,3aR)-2-(3-Chloro-4-cyanophenyl)-3-cyclopentyl-3,3a,4,5-tetrahydro-2H-benzo[g]indazole-7-carboxylic Acid (PF-3882845), an Orally Efficacious Mineralocorticoid Receptor (MR) Antagonist for Hypertension and Nephropathy. *J. Med. Chem.* **2010,** *53,* 5979–6002.
84. Fagart, J.; Hillisch, A.; Huyet, J.; Baerfacker, L.; Fay, M.; Pleiss, U.; Pook, E.; Schaefer, S.; Rafestin-Oblin, M.-E.; Kolkhof, P. A New Mode of Mineralocorticoid Receptor Antagonism by a Potent and Selective Nonsteroidal Molecule. *J. Biol. Chem.* **2010,** *285,* 29932–29940.
85. Baerfacker, L.; Kuhl, A.; Hillisch, A.; Grosser, R.; Figueroa-Perez, S.; Heckroth, H.; Nitsche, A.; Ergueden, J.-K.; Gielen-Haertwig, H.; Schlemmer, K.-H.; Mittendorf, J.; Paulsen, H.; Platzek, J.; Kolkhof, P. Discovery of BAY 94-8862: A Nonsteroidal Antagonist of the Mineralocorticoid Receptor for the Treatment of Cardiorenal Diseases. *ChemMedChem* **2012,** *7,* 1385–1403.
86. Kolkhof, P.; Borden, S. A. Molecular Pharmacology of the Mineralocorticoid Receptor: Prospects for Novel Therapeutics. *Mol. Cell. Endocrinol.* **2012,** *350,* 310–317.

87. Pitt, B.; Kober, L.; Ponikowski, P.; Gheorghiade, M.; Filippatos, G.; Krum, H.; Nowack, C.; Kolkhof, P.; Kim, S. Y.; Zannad, F. Safety and Tolerability of the Novel Non-Steroidal Mineralocorticoid Receptor Antagonist BAY 94-8862 in Patients With Chronic Heart Failure and Mild or Moderate Chronic Kidney Disease: A Randomized, Double-Blind Trial. *Eur. Heart J.* **2013,** *34,* 2453–2463.
88. Pitt, B.; Anker, S. D.; Bohm, M.; Gheorghiade, M.; Kober, L.; Krum, H.; Maggioni, A. P.; Ponikowski, P.; Voors, A. A.; Zannad, F.; Nowack, C.; Kim, S. Y.; Pieper, A.; Kimmeskamp-Kirschbaum, N.; Filippatos, G. Rationale and Design of MinerAlocorticoid Receptor Antagonist Tolerability Study-Heart Failure (ARTS-HF): A Randomized Study of Finerenone vs. Eplerenone in Patients Who Have Worsening Chronic Heart Failure With Diabetes and/or Chronic Kidney Disease. *Eur. J. Heart Fail* **2015,** *17,* 224–232.
89. Mulder, P.; Mellin, V.; Favre, J.; Vercauteren, M.; Remy-Jouet, I.; Monteil, C.; Richard, V.; Renet, S.; Henry, J. P.; Jeng, A. Y.; Webb, R. L.; Thuillez, C. Aldosterone Synthase Inhibition Improves Cardiovascular Function and Structure in Rats With Heart Failure: A Comparison With Spironolactone. *Eur. Heart J.* **2008,** *29,* 2171–2179.
90. Lamberts, S. W. J.; Bruining, H. A.; Marzouk, H.; Zuiderwijk, J.; Uitterlinden, P.; Blijd, J. J.; Hackeng, W. H. L.; Dejong, F. H. The New Aromatase Inhibitor CGS-16949A Supresses Aldosterone and Corticol Production by Human Adrenal-cells In Vitro. *J. Clinical. Endocr. Metab.* **1989,** *69,* 896–901.
91. Trunet, P. F.; Mueller, P.; Girard, F.; Aupetit, B.; Bhatnagar, A. S.; Zognbi, F.; Ezzet, F.; Menard, J. The Effects of Fadrazole Hydrochloride on Aldosterone Secretion in Healthy Male Subjects. *J. Clin. Endocr. Metab.* **1992,** *74,* 571–576.
92. Calhoun, D. A.; White, W. B.; Krum, H.; Guo, W.; Bermann, G.; Trapani, A.; Lefkowitz, M. P.; Menard, J. Effects of a Novel Aldosterone Synthase Inhibitor for Treatment of Primary Hypertension: Results of a Randomized, Double-Blind, Placebo- and Active-controlled Phase 2 Trial. *Circulation* **2011,** *124,* 1945–1955.
93. McMurray, J. J. Neprilysin Inhibition to Treat Heart Failure: A Tale of Science, Serendipity, and Second Chances. *Eur. J. Heart Fail.* **2015,** *17,* 242–247.
94. Bevan, E. G.; Connell, J. M.; Doyle, J.; Carmichael, H. A.; Davies, D. L.; Lorimer, A. R.; McInnes, G. T. Candoxatril, a Neutral Endopeptidase Inhibitor: Efficacy and Tolerability in Essential Hypertension. *J. Hypertens.* **1992,** *10,* 607–613.
95. Richards, A. M.; Wittert, G. A.; Crozier, I. G.; Espiner, E. A.; Yandle, T. G.; Ikram, H.; Frampton, C. Chronic Inhibition of Endopeptidase 24.11 in Essential Hypertension: Evidence for Enhanced Atrial Natriuretic Peptide and Angiotensin II. *J. Hypertens.* **1993,** *11,* 407–416.
96. Richards, A. M.; Wittert, G. A.; Espiner, E. A.; Yandle, T. G.; Ikram, H.; Frampton, C. Effect of Inhibition of Endopeptidase 24.11 on Responses to Angiotensin II in Human Volunteers. *Circ. Res.* **1992,** *71,* 1501–1507.
97. Kostis, J. B.; Packer, M.; Black, H. R.; Schmieder, R.; Henry, D.; Levy, E. Omapatrilat and Enalapril in Patients With Hypertension: The Omapatrilat Cardiovascular Treatment vs. Enalapril (OCTAVE) Trial. *Am. J. Hypertens.* **2004,** *17,* 103–111.
98. Packer, M.; Califf, R. M.; Konstam, M. A.; Krum, H.; McMurray, J. J.; Rouleau, J. L.; Swedberg, K. Comparison of Omapatrilat and Enalapril in Patients With Chronic Heart Failure: The Omapatrilat Versus Enalapril Randomized Trial of Utility in Reducing Events (OVERTURE). *Circulation* **2002,** *106,* 920–926.
99. Feng, L.; Karpinski, P. H.; Sutton, P.; Liu, Y.; Hook, D. F.; Hu, B.; Blacklock, T. J.; Fanwick, P. E.; Prashad, M.; Godtfredsen, S.; Ziltener, C. LCZ696: A Dual-Acting Sodium Supramolecular Complex. *Tetrahedron Lett.* **2012,** *53,* 275–276.
100. Gu, J.; Noe, A.; Chandra, P.; Al-Fayoumi, S.; Ligueros-Saylan, M.; Sarangapani, R.; Maahs, S.; Ksander, G.; Rigel, D. F.; Jeng, A. Y.; Lin, T.-H.; Zheng, W.; Dole, W. P. Pharmacokinetics and Pharmacodynamics of LCZ696, a Novel Dual-acting Angiotensin Receptor-Neprilysin Inhibitor (ARNi). *J. Clin. Pharmacol.* **2010,** *50,* 401–414.
101. Liao, W. C.; Vesterqvist, O.; Delaney, C.; Jemal, M.; Ferreira, I.; Ford, N.; Swanson, B.; Uderman, H. Pharmacokinetics and Pharmacodynamics of the Vasopeptidase Inhibitor, Omapatrilat in Healthy Subjects. *Br. J. Clin. Pharmacol.* **2003,** *56,* 395–406.
102. McMurray, J. J.; Packer, M.; Desai, A. S.; Gong, J.; Lefkowitz, M. P.; Rizkala, A. R.; Rouleau, J. L.; Shi, V. C.; Solomon, S. D.; Swedberg, K.; Zile, M. R. Angiotensin-Neprilysin Inhibition Versus Enalapril in Heart Failure. *N. Engl. J. Med.* **2014,** *371,* 993–1004.
103. Solomon, S. D.; Zile, M.; Pieske, B.; Voors, A.; Shah, A.; Kraigher-Krainer, E.; Shi, V.; Bransford, T.; Takeuchi, M.; Gong, J.; Lefkowitz, M.; Packer, M.; McMurray, J. J. The Angiotensin Receptor Neprilysin Inhibitor LCZ696 in Heart Failure With Preserved Ejection Fraction: A Phase 2 Double-blind Randomised Controlled Trial. *Lancet* **2012,** *380,* 1387–1395.
104. Edelson, J. D.; Makhlina, M.; Silvester, K. R.; Vengurlekar, S. S.; Chen, X.; Zhang, J.; Koziol-White, C. J.; Cooper, P. R.; Hallam, T. J.; Hay, D. W.; Panettieri, R. A., Jr. In Vitro and in vivo Pharmacological Profile of PL-3994, a Novel Cyclic Peptide (Hept-cyclo(Cys-His-Phe-d-Ala-Gly-Arg-d-Nle-Asp-Arg-Ile-Ser-Cys)-Tyr-[Arg mimetic]-NH(2)) Natriuretic Peptide Receptor-A Agonist That Is Resistant to Neutral Endopeptidase and Acts as a Bronchodilator. *Pulm. Pharmacol. Ther.* **2013,** *26,* 229–238.
105. Ezekowitz, J. A. Novel Pharmacologic Therapies in Development for Acute Decompensated Heart Failure. *Curr. Cardiol. Rep.* **2013,** *15,* 329.
106. Selby, V. N.; Teerlink, J. R. What's New in the Treatment of Acute Heart Failure? *Curr. Cardiol. Rep.* **2013,** *15,* 393.
107. Zakeri, R.; Burnett, J. C. Designer Natriuretic Peptides: A Vision for the Future of Heart Failure Therapeutics. *Can. J. Physiol. Pharmacol.* **2011,** *89,* 593–601.
108. Mitrovic, V.; Luss, H.; Nitsche, K.; Forssmann, K.; Maronde, E.; Fricke, K.; Forssmann, W. G.; Meyer, M. Effects of the Renal Natriuretic Peptide Urodilatin (Ularitide) in Patients With Decompensated Chronic Heart Failure: A Double-blind, Placebo-Controlled, Ascending-Dose Trial. *Am. Heart J.* **2005,** *150,* 1239.
109. Mitrovic, V.; Seferovic, P. M.; Simeunovic, D.; Ristic, A. D.; Miric, M.; Moiseyev, V. S.; Kobalava, Z.; Nitsche, K.; Forssmann, W. G.; Luss, H.; Meyer, M. Haemodynamic and Clinical Effects of Ularitide in Decompensated Heart Failure. *Eur. Heart J.* **2006,** *27,* 2823–2832.
110. Rose, R. A. CD-NP, a Chimeric Natriuretic Peptide for the Treatment of Heart Failure. *Curr. Opin. Investig. Drugs* **2010,** *11,* 349–356.
111. Del Ry, S.; Cabiati, M.; Clerico, A. Natriuretic Peptide System and the Heart. *Front. Horm. Res.* **2010,** *43,* 134–143.
112. Ngo, D. T.; Horowitz, J. D.; Sverdlov, A. L. Heart Failure: A Corin-Deficient State? *Hypertension* **2013,** *61,* 284–285.
113. Song, W.; Wang, H.; Wu, Q. Atrial Natriuretic Peptide in Cardiovascular Biology and Disease (NPPA). *Gene* **2015,** *569,* 1–6.
114. Dong, N.; Chen, S.; Yang, J.; He, L.; Liu, P.; Zheng, D.; Li, L.; Zhou, Y.; Ruan, C.; Plow, E.; Wu, Q. Plasma Soluble Corin in Patients With Heart Failure. *Circ. Heart Fail.* **2010,** *3,* 207–211.
115. Ichiki, T.; Huntley, B. K.; Heublein, D. M.; Sandberg, S. M.; McKie, P. M.; Martin, F. L.; Jougasaki, M.; Burnett, J. C., Jr. Corin is Present in the Normal Human Heart, Kidney, and Blood, With Pro-B-type Natriuretic Peptide Processing in the Circulation. *Clin. Chem.* **2011,** *57,* 40–47.
116. Xu-Cai, Y. O.; Wu, Q. Molecular Forms of Natriuretic Peptides in Heart Failure and Their Implications. *Heart* **2010,** *96,* 419–424.
117. Gladysheva, I. P.; Wang, D.; McNamee, R. A.; Houng, A. K.; Mohamad, A. A.; Fan, T. M.; Reed, G. L. Corin Overexpression Improves Cardiac Function, Heart Failure, and Survival in Mice With Dilated Cardiomyopathy. *Hypertension* **2013,** *61,* 327–332.
118. Chen, S.; Cao, P.; Dong, N.; Peng, J.; Zhang, C.; Wang, H.; Zhou, T.; Yang, J.; Zhang, Y.; Martelli, E. E.; Naga Prasad, S. V.; Miller, R. E.; Malfait, A. M.; Zhou, Y.; Wu, Q. PCSK6-Mediated Corin Activation Is Essential for Normal Blood Pressure. *Nat. Med.* **2015,** *21,* 1048–1053.
119. Takimoto, E.; Champion, H. C.; Li, M.; Belardi, D.; Ren, S.; Rodriguez, E. R.; Bedja, D.; Gabrielson, K. L.; Wang, Y.; Kass, D. A. Chronic Inhibition of Cyclic GMP Phosphodiesterase 5A Prevents and Reverses Cardiac Hypertrophy. *Nat. Med.* **2005,** *11,* 214–222.
120. Redfield, M. M.; Chen, H. H.; Borlaug, B. A.; Semigran, M. J.; Lee, K. L.; Lewis, G.; LeWinter, M. M.; Rouleau, J. L.; Bull, D. A.; Mann, D. L.; Deswal, A.; Stevenson, L. W.; Givertz, M. M.; Ofili, E. O.; O'Connor, C. M.; Felker, G. M.; Goldsmith, S. R.; Bart, B. A.; McNulty, S. E.; Ibarra, J. C.; Lin, G.; Oh, J. K.; Patel, M. R.; Kim, R. J.; Tracy, R. P.; Velazquez, E. J.; Anstrom, K. J.; Hernandez, A. F.; Mascette, A. M.; Braunwald, E. Effect of Phosphodiesterase-5 Inhibition on Exercise Capacity and Clinical Status in Heart Failure With Preserved Ejection Fraction: A Randomized Clinical Trial. *JAMA* **2013,** *309,* 1268–1277.
121. Carnicer, R.; Crabtree, M. J.; Sivakumaran, V.; Casadei, B.; Kass, D. A. Nitric Oxide Synthases in Heart Failure. *Antioxid. Redox. Signal.* **2013,** *18,* 1078–1099.
122. Lee, D. I.; Zhu, G.; Sasaki, T.; Cho, G. S.; Hamdani, N.; Holewinski, R.; Jo, S. H.; Danner, T.; Zhang, M.; Rainer, P. P.; Bedja, D.; Kirk, J. A.; Ranek, M. J.; Dostmann, W. R.; Kwon, C.; Margulies, K. B.; Van Eyk, J. E.; Paulus, W. J.; Takimoto, E.; Kass, D. A. Phosphodiesterase 9A Controls Nitric-Oxide-Independent cGMP and Hypertrophic Heart Disease. *Nature* **2015,** *519,* 472–476.
123. Kleiman, R. J.; Chapin, D. S.; Christoffersen, C.; Freeman, J.; Fonseca, K. R.; Geoghegan, K. F.; Grimwood, S.; Guanowsky, V.; Hajos, M.; Harms, J. F.; Helal, C. J.; Hoffmann, W. E.; Kocan, G. P.; Majchrzak, M. J.; McGinnis, D.; McLean, S.; Menniti, F. S.; Nelson, F.; Roof, R.; Schmidt, A. W.; Seymour, P. A.; Stephenson, D. T.; Tingley, F. D.; Vanase-Frawley, M.; Verhoest, P. R.; Schmidt, C. J. Phosphodiesterase 9A Regulates Central cGMP and Modulates Responses to Cholinergic and Monoaminergic Perturbation In Vivo. *J. Pharmacol. Exp. Ther.* **2012,** *341,* 396–409.

124. Gheorghiade, M.; Marti, C. N.; Sabbah, H. N.; Roessig, L.; Greene, S. J.; Bohm, M.; Burnett, J. C.; Campia, U.; Cleland, J. G.; Collins, S. P.; Fonarow, G. C.; Levy, P. D.; Metra, M.; Pitt, B.; Ponikowski, P.; Sato, N.; Voors, A. A.; Stasch, J. P.; Butler, J. Soluble Guanylate Cyclase: A Potential Therapeutic Target for Heart Failure. *Heart Fail. Rev.* **2013,** *18,* 123–134.
125. Ghofrani, H. A.; D'Armini, A. M.; Grimminger, F.; Hoeper, M. M.; Jansa, P.; Kim, N. H.; Mayer, E.; Simonneau, G.; Wilkins, M. R.; Fritsch, A.; Neuser, D.; Weimann, G.; Wang, C. Riociguat for the Treatment of Chronic Thromboembolic Pulmonary Hypertension. *N. Engl. J. Med.* **2013,** *369,* 319–329.
126. Ghofrani, H. A.; Galie, N.; Grimminger, F.; Grunig, E.; Humbert, M.; Jing, Z. C.; Keogh, A. M.; Langleben, D.; Kilama, M. O.; Fritsch, A.; Neuser, D.; Rubin, L. J. Riociguat for the Treatment of Pulmonary Arterial Hypertension. *N. Engl. J. Med.* **2013,** *369,* 330–340.
127. Ghofrani, H. A.; Simonneau, G.; Rubin, L. J. Riociguat for Pulmonary Hypertension. *N. Engl. J. Med.* **2013,** *369,* 2268.
128. Gheorghiade, M.; Greene, S. J.; Butler, J.; Filippatos, G.; Lam, C. S.; Maggioni, A. P.; Ponikowski, P.; Shah, S. J.; Solomon, S. D.; Kraigher-Krainer, E.; Samano, E. T.; Muller, K.; Roessig, L.; Pieske, B. Effect of Vericiguat, a Soluble Guanylate Cyclase Stimulator, on Natriuretic Peptide Levels in Patients With Worsening Chronic Heart Failure and Reduced Ejection Fraction: The SOCRATES-REDUCED Randomized Trial. *JAMA* **2015,** *314,* 2251–2262.
129. Sabbah, H. N.; Tocchetti, C. G.; Wang, M.; Daya, S.; Gupta, R. C.; Tunin, R. S.; Mazhari, R.; Takimoto, E.; Paolocci, N.; Cowart, D.; Colucci, W. S.; Kass, D. A. Nitroxyl (HNO): A Novel Approach for the Acute Treatment of Heart Failure. *Circ. Heart Fail.* **2013,** *6,* 1250–1258.
130. Bauer, J. A.; Fung, H. L. Concurrent Hydralazine Administration Prevents Nitroglycerin-induced Hemodynamic Tolerance in Experimental Heart Failure. *Circulation* **1991,** *84,* 35–39.
131. Gogia, H.; Mehra, A.; Parikh, S.; Raman, M.; Ajit-Uppal, J.; Johnson, J. V.; Elkayam, U. Prevention of Tolerance to Hemodynamic Effects of Nitrates With Concomitant Use of Hydralazine in Patients With Chronic Heart Failure. *J. Am. Coll. Cardiol.* **1995,** *26,* 1575–1580.
132. Cohn, J. N.; Archibald, D. G.; Ziesche, S.; Franciosa, J. A.; Harston, W. E.; Tristani, F. E.; Dunkman, W. B.; Jacobs, W.; Francis, G. S.; Flohr, K. H.; et al. Effect of Vasodilator Therapy on Mortality in Chronic Congestive Heart Failure. Results of a Veterans Administration Cooperative Study. *N. Engl. J. Med.* **1986,** *314,* 1547–1552.
133. Taylor, A. L.; Ziesche, S.; Yancy, C.; Carson, P.; D'Agostino, R., Jr.; Ferdinand, K.; Taylor, M.; Adams, K.; Sabolinski, M.; Worcel, M.; Cohn, J. N. Combination of Isosorbide Dinitrate and Hydralazine in Blacks With Heart Failure. *N. Engl. J. Med.* **2004,** *351,* 2049–2057.
134. Cole, R. T.; Kalogeropoulos, A. P.; Georgiopoulou, V. V.; Gheorghiade, M.; Quyyumi, A.; Yancy, C.; Butler, J. Hydralazine and Isosorbide Dinitrate in Heart Failure: Historical Perspective, Mechanisms, and Future Directions. *Circulation* **2011,** *123,* 2414–2422.
135. Ferdinand, K. C.; Elkayam, U.; Mancini, D.; Ofili, E.; Pina, I.; Anand, I.; Feldman, A. M.; McNamara, D.; Leggett, C. Use of Isosorbide Dinitrate and Hydralazine in African-Americans With Heart Failure 9 Years After the African-American Heart Failure Trial. *Am. J. Cardiol.* **2014,** *114,* 151–159.
136. Carson, P.; Ziesche, S.; Johnson, G.; Cohn, J. N. Racial Differences in Response to Therapy for Heart Failure: Analysis of the Vasodilator-Heart Failure Trials. Vasodilator-Heart Failure Trial Study Group. *J. Card. Fail* **1999,** *5,* 178–187.
137. Teerlink, J. R.; Alburikan, K.; Metra, M.; Rodgers, J. E. Acute Decompensated Heart Failure Update. *Curr. Cardiol. Rev.* **2015,** *11,* 53–62.
138. Manning, M.; Sawyer, W. H. Discovery, Development and Some Uses of Vasopressin and Oxytocin Antagonists. *J. Lab. Clin. Med.* **1989,** *114,* 617–632.
139. Yamamura, Y.; Ogawa, H.; Chihara, T.; Kondo, K.; Onogawa, T.; Nakamura, S.; Mori, T.; Tominaga, M.; Yabuuchi, Y. OPC-21268, an Orally Effective, Nonpeptide Vasopressin-V_1 Receptor Antagonist. *Science* **1991,** *252,* 572–574.
140. Serradeillegal, C.; Wagnon, J.; Garcia, C.; Lacour, C.; Guiraudou, P.; Christophe, B.; Villanova, G.; Nisato, D.; Maffrand, J. P.; Lefur, G.; Guillon, G.; Cantau, B.; Barberis, C.; Trueba, M.; Ala, Y.; Jard, S. Biochemical and Pharmacological Properties of SR-49059, a New, Potent, Nonpeptide Antagonist of Rat and Human Vasopressin V_{1a} Receptors. *J. Clin. Invest.* **1993,** *92,* 224–231.
141. Yamamura, Y.; Ogawa, H.; Yamashita, H.; Chihara, T.; Miyamoto, H.; Nakamura, S.; Onogawa, T.; Yamashita, T.; Hosokawa, T.; Mori, T.; Tominaga, M.; Yabuuchi, Y. Characterization of a Novel Aquaretic Agent, OPC-31260, as an Orally Effective, Nonpeptide Vasopressin V_2 Receptor Antagonist. *Br. J. Pharmacol.* **1992,** *105,* 787–791.
142. Ohnishi, A.; Orita, Y.; Okahara, R.; Fujihara, H.; Inoue, T.; Yamamura, Y.; Yabuuchi, Y.; Tanaka, T. Potent Aquaretic Agent—A Novel Nonpepitde Selective Vasopressin-2 Antagonist (OPC-31260) in Men. *J. Clin. Invest.* **1993,** *92,* 2653–2659.
143. Yatsu, T.; Tomura, Y.; Tahara, A.; Wada, K.; Tsukada, J.; Uchida, W.; Tanaka, A.; Takenaka, T. Pharmacological Profile of YMO87, a Novel Nonpeptide Dual Vasopressin V_{1A} and V_2 Receptor Antagonist, in Dogs. *Eur. J. Pharmacol.* **1997,** *321,* 225–230.
144. Berl, T. Vasopressin Antagonists. *N. Engl. J. Med.* **2015,** *372,* 2207–2216.
145. Ali, F.; Raufi, M. A.; Washington, B.; Ghali, J. K. Conivaptan: A Dual Receptor Vasopressin V-1a/V-2 Antagonist. *Cardiovasc. Drug Rev.* **2007,** *25,* 261–279.
146. Gheorghiade, M.; Konstam, M. A.; Burnett, J. C., Jr.; Grinfeld, L.; Maggioni, A. P.; Swedberg, K.; Udelson, J. E.; Zannad, F.; Cook, T.; Ouyang, J.; Zimmer, C.; Orlandi, C. Short-Term Clinical Effects of Tolvaptan, an Oral Vasopressin Antagonist, in Patients Hospitalized for Heart Failure: The EVEREST Clinical Status Trials. *JAMA* **2007,** *297,* 1332–1343.
147. Konstam, M. A.; Gheorghiade, M.; Burnett, J. C., Jr.; Grinfeld, L.; Maggioni, A. P.; Swedberg, K.; Udelson, J. E.; Zannad, F.; Cook, T.; Ouyang, J.; Zimmer, C.; Orlandi, C. Effects of Oral Tolvaptan in Patients Hospitalized for Worsening Heart Failure: The EVEREST Outcome Trial. *JAMA* **2007,** *297,* 1319–1331.
148. Udelson, J. E.; Orlandi, C.; Ouyang, J.; Krasa, H.; Zimmer, C. A.; Frivold, G.; Haught, W. H.; Meymandi, S.; Macarie, C.; Raef, D.; Wedge, P.; Konstam, M. A.; Gheorghiade, M. Acute Hemodynamic Effects of Tolvaptan, a Vasopressin V_2 Receptor Blocker, in Patients With Symptomatic Heart Failure and Systolic Dysfunction: An International, Multicenter, Randomized, Placebo-controlled Trial. *J. Am. Coll. Cardiol.* **2008,** *52,* 1540–1545.
149. Udelson, J. E.; Smith, W. B.; Hendrix, G. H.; Painchaud, C. A.; Ghazzi, M.; Thomas, I.; Ghali, J. K.; Selaru, P.; Chanoine, F.; Pressler, M. L.; Konstam, M. A. Acute Hemodynamic Effects of Conivaptan, a Dual V_{1A} and V_2 Vasopressin Receptor Antagonist, in Patients With Advanced Heart Failure. *Circulation* **2001,** *104,* 2417–2423.
150. Goldsmith, S. R.; Elkayam, U.; Haught, W. H.; Barve, A.; He, W. Efficacy and Safety of the Vasopressin V_{1a}/V_2-Receptor Antagonist Conivaptan in Acute Decompensated Heart Failure: A Dose-ranging Pilot Study. *J. Card. Fail.* **2008,** *14,* 641–647.
151. Albright, J. D.; Reich, M. F.; Delos Santos, E. G.; Dusza, J. P.; Sum, F. W.; Venkatesan, A. M.; Coupet, J.; Chan, P. S.; Ru, X.; Mazandarani, H.; Bailey, T. 5-Fluoro-2-methyl-N-[4-(5H-pyrrolo[2,1-c][1,4]benzodiazepin-10(11H)-ylca rbonyl)-3-chlorophenyl]benzamide (VPA-985): An Orally Active Arginine Vasopressin Antagonist With Selectivity for V_2 Receptors. *J. Med. Chem.* **1998,** *41,* 2442–2444.
152. Gal, C. S. L. An Overview of SR121463, a Selective Non-peptide Vasopressin V_2 Receptor Antagonist. *Cardiovasc. Drug Rev.* **2001,** *19,* 201–214.
153. Soupart, A.; Gross, P.; Legros, J.-J.; Alfoldi, S.; Annane, D.; Heshmati, H. M.; Decaux, G. Successful Long-term Treatment of Hyponatremia in Syndrome of Inappropriate Antidiuretic Hormone Secretion With Satavaptan (SR121463B), an Orally Active Nonpeptide Vasopressin V_2 Receptor Antagonist. *Clin. J. Am. Soc. Nephrol.* **2006,** *1,* 1154–1160.
154. Ghali, J. K.; Orlandi, C.; Abraham, W. T. The Efficacy and Safety of Lixivaptan in Outpatients With Heart Failure and Volume Overload: Results of a Multicentre, Randomized, Double-Blind, Placebo-Controlled, Parallel-Group Study. *Eur. J. Heart Fail.* **2012,** *14,* 642–651.
155. Zmily, H. D.; Alani, A.; Ghali, J. K. Evaluation of Lixivaptan in Euvolemic and Hypervolemic Hyponatremia and Heart Failure Treatment. *Expert Opin. Drug Metab. Toxicol.* **2013,** *9,* 645–655.
156. Walczewska, J.; Dzieza-Grudnik, A.; Siga, O.; Grodzicki, T. The Role of Urocortins in the Cardiovascular System. *J. Physiol. Pharmacol.* **2014,** *65,* 753–766.
157. Davis, M. E.; Pemberton, C. J.; Yandle, T. G.; Lainchbury, J. G.; Rademaker, M. T.; Nicholls, M. G.; Frampton, C. M.; Richards, A. M. Effect of Urocortin 1 Infusion in Humans With Stable Congestive Cardiac Failure. *Clin. Sci. (Lond.)* **2005,** *109,* 381–388.
158. Davis, M. E.; Pemberton, C. J.; Yandle, T. G.; Fisher, S. F.; Lainchbury, J. G.; Frampton, C. M.; Rademaker, M. T.; Richards, M. Urocortin 2 Infusion in Human Heart Failure. *Eur. Heart J.* **2007,** *28,* 2589–2597.
159. Chan, W. Y.; Frampton, C. M.; Crozier, I. G.; Troughton, R. W.; Richards, A. M. Urocortin-2 Infusion in Acute Decompensated Heart Failure: Findings From the UNICORN Study (Urocortin-2 in the Treatment of Acute Heart Failure as an Adjunct Over Conventional Therapy). *JACC Heart Fail.* **2013,** *1,* 433–441.

160. Gheorghiade, M.; Greene, S. J.; Ponikowski, P.; Maggioni, A. P.; Korewicki, J.; Macarie, C.; Metra, M.; Grzybowski, J.; Bubenek-Turconi, S. I.; Radziszewski, W.; Olson, A.; Bueno, O. F.; Ghosh, A.; Deckelbaum, L. I.; Li, L. Y.; Patel, A. R.; Koester, A.; Konstam, M. A. Haemodynamic Effects, Safety, and Pharmacokinetics of Human Stresscopin in Heart Failure With Reduced Ejection Fraction. *Eur. J. Heart Fail.* **2013,** *15,* 679–689.
161. Perry, G.; Brown, E.; Thornton, R.; Shiva, T.; Hubbard, J.; Reddy, K. R.; et al. The Effect of Digoxin on Mortality and Morbidity in Patients With Heart Failure. *N. Engl. J. Med.* **1997,** *336,* 525–533.
162. Ahmed, A.; Rich, M. W.; Love, T. E.; Lloyd-Jones, D. M.; Aban, I. B.; Colucci, W. S.; Adams, K. F.; Gheorghiade, M. Digoxin and Reduction in Mortality and Hospitalization in Heart Failure: A Comprehensive Post hoc Analysis of the DIG Trial. *Eur. Heart J.* **2006,** *27,* 178–186.
163. Hwang, P. M.; Sykes, B. D. Targeting the Sarcomere to Correct Muscle Function. *Nat. Rev. Drug Discov.* **2015,** *14,* 313–328.
164. Phan, H. M.; Gao, M. H.; Lai, N. C.; Tang, T.; Hammond, H. K. New Signaling Pathways Associated With Increased Cardiac Adenylyl Cyclase 6 Expression: Implications for Possible Congestive Heart Failure Therapy. *Trends Cardiovasc. Med.* **2007,** *17,* 215–221.
165. RT-100. http://renovatherapeutics.com/therapies/rt-100-congestive-heart-failure/ (September 13, 2015).
166. Kasikcioglu, H. A.; Cam, N. A Review of Levosimendan in the Treatment of Heart Failure. *Vasc. Health Risk Manag.* **2006,** *2,* 389–400.
167. Mebazaa, A.; Nieminen, M. S.; Packer, M.; Cohen-Solal, A.; Kleber, F. X.; Pocock, S. J.; Thakkar, R.; Padley, R. J.; Poder, P.; Kivikko, M. Levosimendan vs Dobutamine for Patients With Acute Decompensated Heart Failure: The SURVIVE Randomized Trial. *JAMA* **2007,** *297,* 1883–1891.
168. Packer, M.; Colucci, W.; Fisher, L.; Massie, B. M.; Teerlink, J. R.; Young, J.; Padley, R. J.; Thakkar, R.; Delgado-Herrera, L.; Salon, J.; Garratt, C.; Huang, B.; Sarapohja, T. Effect of Levosimendan on the Short-term Clinical Course of Patients With Acutely Decompensated Heart Failure. *JACC Heart Fail.* **2013,** *1,* 103–111.
169. Liu, Y.; White, H. D.; Belknap, B.; Winkelmann, D. A.; Forgacs, E. Omecamtiv Mecarbil Modulates the Kinetic and Motile Properties of Porcine β-Cardiac Myosin. *Biochem.* **2015,** *54,* 1963–1975.
170. Malik, F. I.; Hartman, J. J.; Elias, K. A.; Morgan, B. P.; Rodriguez, H.; Brejc, K.; Anderson, R. L.; Sueoka, S. H.; Lee, K. H.; Finer, J. T.; Sakowicz, R.; Baliga, R.; Cox, D. R.; Garard, M.; Godinez, G.; Kawas, R.; Kraynack, E.; Lenzi, D.; Lu, P. P.; Muci, A.; Niu, C.; Qian, X.; Pierce, D. W.; Pokrovskii, M.; Suehiro, I.; Sylvester, S.; Tochimoto, T.; Valdez, C.; Wang, W.; Katori, T.; Kass, D. A.; Shen, Y. T.; Vatner, S. F.; Morgans, D. J. Cardiac Myosin Activation: A Potential Therapeutic Approach for Systolic Heart Failure. *Science* **2011,** *331,* 1439–1443.
171. Morgan, B. P.; Muci, A.; Lu, P.-P.; Qian, X.; Tochimoto, T.; Smith, W. W.; Garard, M.; Kraynack, E.; Collibee, S.; Suehiro, I.; Tomasi, A.; Valdez, S. C.; Wang, W.; Jiang, H.; Hartman, J.; Rodriguez, H. M.; Kawas, R.; Sylvester, S.; Elias, K. A.; Godinez, G.; Lee, K.; Anderson, R.; Sueoka, S.; Xu, D.; Wang, Z.; Djordjevic, N.; Malik, F. I.; Morgans, D. J., Jr. Discovery of Omecamtiv Mecarbil the First, Selective, Small Molecule Activator of Cardiac Myosin. *ACS Med. Chem. Lett.* **2010,** *1,* 472–477.
172. Cleland, J. G.; Teerlink, J. R.; Senior, R.; Nifontov, E. M.; Mc Murray, J. J.; Lang, C. C.; Tsyrlin, V. A.; Greenberg, B. H.; Mayet, J.; Francis, D. P.; Shaburishvili, T.; Monaghan, M.; Saltzberg, M.; Neyses, L.; Wasserman, S. M.; Lee, J. H.; Saikali, K. G.; Clarke, C. P.; Goldman, J. H.; Wolff, A. A.; Malik, F. I. The Effects of the Cardiac Myosin Activator, Omecamtiv Mecarbil, on Cardiac Function in Systolic Heart Failure: A Double-blind, Placebo-controlled, Crossover, Dose-Ranging Phase 2 Trial. *Lancet* **2011,** *378,* 676–683.
173. Venkateswararao, E.; Son, M.-J.; Sharma, N.; Manickam, M.; Boggu, P.; Kim, Y. H.; Woo, S.-H.; Jung, S.-H. Exploration of Pharmacophore in Chrysosplenol C as Activator in Ventricular Myocyte Contraction. *ACS Med. Chem. Lett.* **2015,** *6,* 758–763.
174. Shen, Y.-T.; Malik, F. I.; Zhao, X.; Depre, C.; Dhar, S. K.; Abarzua, P.; Morgans, D. J.; Vatner, S. F. Improvement of Cardiac Function by a Cardiac Myosin Activator in Conscious Dogs With Systolic Heart Failure. *Circ. Heart Fail.* **2010,** *3,* 522–527.
175. Bakkehaug, J. P.; Kildal, A. B.; Engstad, E. T.; Boardman, N.; Naesheim, T.; Ronning, L.; Aasum, E.; Larsen, T. S.; Myrmel, T.; How, O. J. Myosin Activator Omecamtiv Mecarbil Increases Myocardial Oxygen Consumption and Impairs Cardiac Efficiency Mediated by Resting Myosin ATPase Activity. *Circ. Heart. Fail* **2015,** *8,* 766–775.
176. Teerlink, J. R.; Felker, G. M.; Mc Murray, J. J.; Solomon, S. D.; Monsalvo, M. L.; Legg, J.; Malik, F. I.; Honarpour, N. *Chronic Oral Study of Myosin Activation to Increase Contractility in Heart Failure: Results From a Double-blind, Randomized, Placebo-controlled, Multicenter Trial;* American Heart Association Scientific Sessions: Orlando, FL, 2015.
177. Rodriguez, H. M.; Whitman-Cox, S.; Kawas, R.; Song, Y.; Sran, A.; Oslob, J. Modulation of the Cardiac Sarcomere by a Small Molecule Agent MYK0000461: A Potential Therapeutic for the Treatment of Genetic Hypertrophic Cardiomyopathies. *Biophys. J.* **2014,** *106,* 562a.
178. Hasenfuss, G.; Reinecke, H.; Studer, R.; Meyer, M.; Pieske, B.; Holtz, J.; Holubarsch, C.; Posival, H.; Just, H.; Drexler, H. Relation Between Myocardial Function and Expression of Sarcoplasmic Reticulum Ca^{2+}-ATPase in Failing and Nonfailing Human Myocardium. *Circ. Res.* **1994,** *75,* 434–442.
179. Greenberg, B. Gene Therapy for Heart Failure. *J. Cardiol.* **2015,** *66,* 195–200.
180. Byrne, M. J.; Power, J. M.; Preovolos, A.; Mariani, J. A.; Hajjar, R. J.; Kaye, D. M. Recirculating Cardiac Delivery of AAV2/1SERCA2a Improves Myocardial Function in an Experimental Model of Heart Failure in Large Animals. *Gene Ther.* **2008,** *15,* 1550–1557.
181. del Monte, F.; Williams, E.; Lebeche, D.; Schmidt, U.; Rosenzweig, A.; Gwathmey, J. K.; Lewandowski, E. D.; Hajjar, R. J. Improvement in Survival and Cardiac Metabolism After Gene Transfer of Sarcoplasmic Reticulum Ca^{2+}-ATPase in a Rat Model of Heart Failure. *Circulation* **2001,** *104,* 1424–1429.
182. Greenberg, B.; Yaroshinsky, A.; Zsebo, K. M.; Butler, J.; Felker, G. M.; Voors, A. A.; Rudy, J. J.; Wagner, K.; Hajjar, R. J. Design of a Phase 2b Trial of Intracoronary Administration of AAV1/SERCA2a in Patients With Advanced Heart Failure: The CUPID 2 Trial (Calcium up-regulation by Percutaneous Administration of Gene Therapy in Cardiac Disease Phase 2b). *JACC Heart Fail.* **2014,** *2,* 84–92.
183. Jaski, B. E.; Jessup, M. L.; Mancini, D. M.; Cappola, T. P.; Pauly, D. F.; Greenberg, B.; Borow, K.; Dittrich, H.; Zsebo, K. M.; Hajjar, R. J. Calcium Upregulation by Percutaneous Administration of Gene Therapy in Cardiac Disease (CUPID Trial), a First-In-Human Phase 1/2 Clinical Trial. *J. Card. Fail.* **2009,** *15,* 171–181.
184. Kawase, Y.; Ly, H. Q.; Prunier, F.; Lebeche, D.; Shi, Y.; Jin, H.; Hadri, L.; Yoneyama, R.; Hoshino, K.; Takewa, Y.; Sakata, S.; Peluso, R.; Zsebo, K.; Gwathmey, J. K.; Tardif, J. C.; Tanguay, J. F.; Hajjar, R. J. Reversal of Cardiac Dysfunction After Long-term Expression of SERCA2a by Gene Transfer in a Pre-Clinical Model of Heart Failure. *J. Am. Coll. Cardiol.* **2008,** *51,* 1112–1119.
185. Miyamoto, M. I.; del Monte, F.; Schmidt, U.; DiSalvo, T. S.; Kang, Z. B.; Matsui, T.; Guerrero, J. L.; Gwathmey, J. K.; Rosenzweig, A.; Hajjar, R. J. Adenoviral Gene Transfer of SERCA2a Improves Left-ventricular Function in Aortic-banded Rats in Transition to Heart Failure. *Proc. Natl. Acad. Sci. USA* **2000,** *97,* 793–798.
186. Jessup, M.; Greenberg, B.; Mancini, D.; Cappola, T.; Pauly, D. F.; Jaski, B.; Yaroshinsky, A.; Zsebo, K. M.; Dittrich, H.; Hajjar, R. J. Calcium Upregulation by Percutaneous Administration of Gene Therapy in Cardiac Disease (CUPID): A Phase 2 Trial of Intracoronary Gene Therapy of Sarcoplasmic Reticulum Ca2+-ATPase in Patients With Advanced Heart Failure. *Circulation* **2011,** *124,* 304–313.
187. Zsebo, K.; Yaroshinsky, A.; Rudy, J. J.; Wagner, K.; Greenberg, B.; Jessup, M.; Hajjar, R. J. Long-Term Effects of AAV1/SERCA2a Gene Transfer in Patients With Severe Heart Failure: Analysis of Recurrent Cardiovascular Events and Mortality. *Circ. Res.* **2014,** *114,* 101–108.
188. CUPID-2/Celladon. http://www.celladon.com/clinical-trials/cupid-2/ (July 28, 2015).
189. Celladon Corporation Provides Business Update. http://ir.celladon.net/releasedetail.cfm?ReleaseID=919606 (July 28, 2015).
190. Bers, D. M. Cardiac Sarcoplasmic Reticulum Calcium Leak: Basis and Roles in Cardiac Dysfunction. *Annu. Rev. Physiol.* **2014,** *76,* 107–127.
191. Mei, Y.; Xu, L.; Kramer, H. F.; Tomberlin, G. H.; Townsend, C.; Meissner, G. Stabilization of the Skeletal Muscle Ryanodine Receptor Ion Channel-FKBP12 Complex by the 1,4-Benzothiazepine Derivative S107. *Plos One* **2013,** *8,* e54208.
192. Wehrens, X. H.; Lehnart, S. E.; Reiken, S.; van der Nagel, R.; Morales, R.; Sun, J.; Cheng, Z.; Deng, S. X.; de Windt, L. J.; Landry, D. W.; Marks, A. R. Enhancing Calstabin Binding to Ryanodine Receptors Improves Cardiac and Skeletal Muscle Function in Heart Failure. *Proc. Natl. Acad. Sci. USA* **2005,** *102,* 9607–9612.
193. De Munari, S.; Cerri, A.; Gobbini, M.; Almirante, N.; Banfi, L.; Carzana, G.; Ferrari, P.; Marazzi, G.; Micheletti, R.; Schiavone, A.; Sputore, S.; Torri, M.; Zappavigna, M. P.; Melloni, P. Structure-based Design and Synthesis of Novel Potent Na+, K+ -ATPase Inhibitors Derived From a 5Alpha,14alpha-androstane Scaffold as Positive Inotropic Compounds. *J. Med. Chem.* **2003,** *46,* 3644–3654.

194. Micheletti, R.; Mattera, G. G.; Rocchetti, M.; Schiavone, A.; Loi, M. F.; Zaza, A.; Gagnol, R. J.; De Munari, S.; Melloni, P.; Carminati, P.; Bianchi, G.; Ferrari, P. Pharmacological Profile of the Novel Inotropic Agent (E, Z)-3-((2-Aminoethoxy)imino)androstane-6,17-dione Hydrochloride (PST2744). *J. Pharmacol. Exp. Ther.* **2002,** *303,* 592–600.
195. Micheletti, R.; Palazzo, F.; Barassi, P.; Giacalone, G.; Ferrandi, M.; Schiavone, A.; Moro, B.; Parodi, O.; Ferrari, P.; Bianchi, G. Istaroxime, a Stimulator of Sarcoplasmic Reticulum Calcium Adenosine Triphosphatase Isoform 2a Activity, as a Novel Therapeutic Approach to Heart Failure. *Am. J. Cardiol.* **2007,** *99,* 24A–32A.
196. Rocchetti, M.; Alemanni, M.; Mostacciuolo, G.; Barassi, P.; Altomare, C.; Chisci, R.; Micheletti, R.; Ferrari, P.; Zaza, A. Modulation of Sarcoplasmic Reticulum Function by PST2744 [Istaroxime; (E, Z)-3-((2-aminoethoxy)imino) androstane-6,17-dione hydrochloride)] in a Pressure-overload Heart Failure Model. *J. Pharmacol. Exp. Ther.* **2008,** *326,* 957–965.
197. Rocchetti, M.; Besana, A.; Mostacciuolo, G.; Micheletti, R.; Ferrari, P.; Sarkozi, S.; Szegedi, C.; Jona, I.; Zaza, A. Modulation of Sarcoplasmic Reticulum Function by Na+/K+ Pump Inhibitors With Different Toxicity: Digoxin and PST2744 [(E, Z)-3-((2-Aminoethoxy)imino)androstane-6,17-dione Hydrochloride]. *J. Pharmacol. Exp. Ther.* **2005,** *313,* 207–215.
198. Ferrandi, M.; Barassi, P.; Tadini-Buoninsegni, F.; Bartolommei, G.; Molinari, I.; Tripodi, M. G.; Reina, C.; Moncelli, M. R.; Bianchi, G.; Ferrari, P. Istaroxime Stimulates SERCA2a and Accelerates Calcium Cycling in Heart Failure by Relieving Phospholamban Inhibition. *Br. J. Pharmacol.* **2013,** *169,* 1849–1861.
199. Alemanni, M.; Rocchetti, M.; Re, D.; Zaza, A. Role and Mechanism of Subcellular Ca^{2+} Distribution in the Action of Two Inotropic Agents With Different Toxicity. *J. Mol. Cell. Cardiol.* **2011,** *50,* 910–918.
200. Mattera, G. G.; Lo Giudice, P.; Loi, F. M.; Vanoli, E.; Gagnol, J. P.; Borsini, F.; Carminati, P. Istaroxime: A New Luso-Inotropic Agent for Heart Failure. *Am. J. Cardiol.* **2007,** *99,* 33A–40A.
201. Sabbah, H. N.; Imai, M.; Cowart, D.; Amato, A.; Carminati, P.; Gheorghiade, M. Hemodynamic Properties of a New-generation Positive Luso-inotropic Agent for the Acute Treatment of Advanced Heart Failure. *Am. J. Cardiol.* **2007,** *99,* 41A–46A.
202. Gheorghiade, M.; Blair, J. E.; Filippatos, G. S.; Macarie, C.; Ruzyllo, W.; Korewicki, J.; Bubenek-Turconi, S. I.; Ceracchi, M.; Bianchetti, M.; Carminati, P.; Kremastinos, D.; Valentini, G.; Sabbah, H. N. Hemodynamic, Echocardiographic, and Neurohormonal Effects of Istaroxime, a Novel Intravenous Inotropic And Lusitropic Agent: A Randomized Controlled Trial in Patients Hospitalized With Heart Failure. *J. Am. Coll. Cardiol.* **2008,** *51,* 2276–2285.
203. Shah, S. J.; Blair, J. E.; Filippatos, G. S.; Macarie, C.; Ruzyllo, W.; Korewicki, J.; Bubenek-Turconi, S. I.; Ceracchi, M.; Bianchetti, M.; Carminati, P.; Kremastinos, D.; Grzybowski, J.; Valentini, G.; Sabbah, H. N.; Gheorghiade, M. Effects of Istaroxime on Diastolic Stiffness in Acute Heart Failure Syndromes: Results From the Hemodynamic, Echocardiographic, and Neurohormonal Effects of Istaroxime, a Novel Intravenous Inotropic and Lusitropic Agent: A Randomized Controlled Trial in Patients Hospitalized With Heart Failure (HORIZON-HF) Trial. *Am. Heart. J.* **2009,** *157,* 1035–1041.
204. Gobbini, M.; Armaroli, S.; Banfi, L.; Benicchio, A.; Carzana, G.; Ferrari, P.; Giacalone, G.; Marazzi, G.; Moro, B.; Micheletti, R.; Sputore, S.; Torri, M.; Zappavigna, M. P.; Cerri, A. Novel Analogues of Istaroxime, a Potent Inhibitor of Na+, K+-ATPase: Synthesis, Structure-Activity Relationship and 3D-Quantitative Structure-Activity Relationship of Derivatives at Position 6 on the Androstane Scaffold. *Bioorg. Med. Chem.* **2010,** *18,* 4275–4299.
205. Bathgate, R. A.; Halls, M. L.; van der Westhuizen, E. T.; Callander, G. E.; Kocan, M.; Summers, R. J. Relaxin Family Peptides and Their Receptors. *Physiol. Rev.* **2013,** *93,* 405–480.
206. Teichman, S. L.; Unemori, E.; Teerlink, J. R.; Cotter, G.; Metra, M. Relaxin: Review of Biology and Potential Role in Treating Heart Failure. *Curr. Heart Fail. Rep.* **2010,** *7,* 75–82.
207. Du, X. J.; Bathgate, R. A.; Samuel, C. S.; Dart, A. M.; Summers, R. J. Cardiovascular Effects of Relaxin: From Basic Science to Clinical Therapy. *Nat. Rev. Cardiol.* **2010,** *7,* 48–58.
208. Han, X.; Habuchi, Y.; Giles, W. R. Relaxin Increases Heart Rate by Modulating Calcium Current in Cardiac Pacemaker Cells. *Circ. Res.* **1994,** *74,* 537–541.
209. Sasser, J. M. The Emerging Role of Relaxin as a Novel Therapeutic Pathway in the Treatment of Chronic Kidney Disease. *Am. J. Physiol. Regul. Integr. Comp. Physiol.* **2013,** *305,* R559–R565.
210. Samuel, C. S.; Bodaragama, H.; Chew, J. Y.; Widdop, R. E.; Royce, S. G.; Hewitson, T. D. Serelaxin Is a More Efficacious Antifibrotic than Enalapril in an Experimental Model of Heart Disease. *Hypertension* **2014,** *64,* 315–322.
211. Teerlink, J. R.; Cotter, G.; Davison, B. A.; Felker, G. M.; Filippatos, G.; Greenberg, B. H.; Ponikowski, P.; Unemori, E.; Voors, A. A.; Adams, K. F., Jr.; Dorobantu, M. I.; Grinfeld, L. R.; Jondeau, G.; Marmor, A.; Masip, J.; Pang, P. S.; Werdan, K.; Teichman, S. L.; Trapani, A.; Bush, C. A.; Saini, R.; Schumacher, C.; Severin, T. M.; Metra, M. Serelaxin, Recombinant Human Relaxin-2, for Treatment of Acute Heart Failure (RELAX-AHF): A Randomised, Placebo-Controlled Trial. *Lancet* **2013,** *381,* 29–39.
212. Efficacy, Safety and Tolerability of Serelaxin When Added to Standard Therapy in AHF (RELAX-AHF-2). https://clinicaltrials.gov/ct2/show/NCT01870778 (13-July-2015).
213. Falls, D. L. Neuregulins: Functions, Forms, and Signaling Strategies. *Exp. Cell. Res.* **2003,** *284,* 14–30.
214. Odiete, O.; Hill, M. F.; Sawyer, D. B. Neuregulin in Cardiovascular Development and Disease. *Circ. Res.* **2012,** *111,* 1376–1385.
215. Vartanian, T.; Goodearl, A.; Viehover, A.; Fischbach, G. Axonal Neuregulin Signals Cells of the Oligodendrocyte Lineage Through Activation of HER4 and Schwann Cells Through HER2 and HER3. *J. Cell Biol.* **1997,** *137,* 211–220.
216. Fuller, S. J.; Sivarajah, K.; Sugden, P. H. ErbB Receptors, Their Ligands, and the Consequences of Their Activation and Inhibition in the Myocardium. *J. Mol. Cell. Cardiol.* **2008,** *44,* 831–854.
217. Meyer, D.; Birchmeier, C. Multiple Essential Functions of Neuregulin in Development. *Nature* **1995,** *378,* 386–390.
218. Crone, S. A.; Zhao, Y. Y.; Fan, L.; Gu, Y.; Minamisawa, S.; Liu, Y.; Peterson, K. L.; Chen, J.; Kahn, R.; Condorelli, G.; Ross, J., Jr.; Chien, K. R.; Lee, K. F. ErbB2 Is Essential in the Prevention of Dilated Cardiomyopathy. *Nat. Med.* **2002,** *8,* 459–465.
219. Garcia-Rivello, H.; Taranda, J.; Said, M.; Cabeza-Meckert, P.; Vila-Petroff, M.; Scaglione, J.; Ghio, S.; Chen, J.; Lai, C.; Laguens, R. P.; Lloyd, K. C.; Hertig, C. M. Dilated Cardiomyopathy in Erb-b4-Deficient Ventricular Muscle. *Am. J. Physiol. Heart Circ. Physiol.* **2005,** *289,* H1153–1160.
220. Ozcelik, C.; Erdmann, B.; Pilz, B.; Wettschureck, N.; Britsch, S.; Hubner, N.; Chien, K. R.; Birchmeier, C.; Garratt, A. N. Conditional Mutation of the ErbB2 (HER2) Receptor in Cardiomyocytes Leads to Dilated Cardiomyopathy. *Proc. Natl. Acad. Sci. USA* **2002,** *99,* 8880–8885.
221. Slamon, D. J.; Leyland-Jones, B.; Shak, S.; Fuchs, H.; Paton, V.; Bajamonde, A.; Fleming, T.; Eiermann, W.; Wolter, J.; Pegram, M.; Baselga, J.; Norton, L. Use of Chemotherapy Plus a Monoclonal Antibody Against HER2 for Metastatic Breast Cancer That Overexpresses HER2. *N. Engl. J. Med.* **2001,** *344,* 783–792.
222. Galindo, C. L.; Kasasbeh, E.; Murphy, A.; Ryzhov, S.; Lenihan, S.; Ahmad, F. A.; Williams, P.; Nunnally, A.; Adcock, J.; Song, Y.; Harrell, F. E.; Tran, T. L.; Parry, T. J.; Iaci, J.; Ganguly, A.; Feoktistov, I.; Stephenson, M. K.; Caggiano, A. O.; Sawyer, D. B.; Cleator, J. H. Anti-Remodeling and Anti-Fibrotic Effects of the Neuregulin-1beta Glial Growth Factor 2 in a Large Animal Model of Heart Failure. *J. Am. Heart Assoc.* **2014,** *3,* e000773.
223. Liu, X.; Gu, X.; Li, Z.; Li, X.; Li, H.; Chang, J.; Chen, P.; Jin, J.; Xi, B.; Chen, D.; Lai, D.; Graham, R. M.; Zhou, M. Neuregulin-1/erbB-Activation Improves Cardiac Function and Survival in Models of Ischemic, Dilated, and Viral Cardiomyopathy. *J. Am. Coll. Cardiol.* **2006,** *48,* 1438–1447.
224. Gao, R.; Zhang, J.; Cheng, L.; Wu, X.; Dong, W.; Yang, X.; Li, T.; Liu, X.; Xu, Y.; Li, X.; Zhou, M. A Phase II, Randomized, Double-blind, Multicenter, Based on Standard Therapy, Placebo-controlled Study of the Efficacy and Safety of Recombinant Human Neuregulin-1 in Patients With Chronic Heart Failure. *J. Am. Coll. Cardiol.* **2010,** *55,* 1907–1914.
225. Jabbour, A.; Hayward, C. S.; Keogh, A. M.; Kotlyar, E.; McCrohon, J. A.; England, J. F.; Amor, R.; Liu, X.; Li, X. Y.; Zhou, M. D.; Graham, R. M.; Macdonald, P. S. Parenteral Administration of Recombinant Human Neuregulin-1 to Patients With Stable Chronic Heart Failure Produces Favourable Acute and Chronic Haemodynamic Responses. *Eur. J. Heart Fail.* **2011,** *13,* 83–92.
226. Lemmens, K.; Fransen, P.; Sys, S. U.; Brutsaert, D. L.; De Keulenaer, G. W. Neuregulin-1 Induces a Negative Inotropic Effect in Cardiac Muscle—Role of Nitric Oxide Synthase. *Circulation* **2004,** *109,* 324–326.

227. Brittain, E.; Muldowney, J.; Geisberg, C.; Caggiano, A.; Eisen, A.; Anderson, S.; Sawyer, D.; Mendes, L.; Lenihan, D. Evaluation of Cardiac Function in Symptomatic Heart Failure Patients in a Single Infusion, Phase 1, Dose Escalation Study of Glial Growth Factor 2. *J. Am. Coll. Cardiol.* **2013,** *61*, E715 (abstract).
228. Hill, M. F.; Patel, A. V.; Murphy, A.; Smith, H. M.; Galindo, C. L.; Pentassuglia, L.; Peng, X.; Lenneman, C. G.; Odiete, O.; Friedman, D. B.; Kronenberg, M. W.; Zheng, S.; Zhao, Z.; Song, Y.; Harrell, F. E., Jr.; Srinivas, M.; Ganguly, A.; Iaci, J.; Parry, T. J.; Caggiano, A. O.; Sawyer, D. B. Intravenous Glial Growth Factor 2 (GGF2) Isoform of Neuregulin-1beta Improves Left Ventricular Function, Gene and Protein Expression in Rats After Myocardial Infarction. *PLoS One* **2013,** *8,* e55741.
229. Single Ascending Doses of GGF2 in Patients With Left Ventricular Dysfunction and Symptomatic Heart Failure (GGF2-1101-1). https://clinicaltrials.gov/ct2/show/results/NCT01258387?term=GGF2&rank=1&sect=X370156#evnt (July 21, 2015).
230. Efficacy and Safety of Human Neuregulin-1 to Treat Stable Chronic Heart Failure (ZS-01-210). https://clinicaltrials.gov/ct2/show/study/NCT01251406?term=Zensun+and+Neucardin&rank=1 (July 21, 2015).
231. Felker, G. M. Loop Diuretics in Heart Failure. *Heart Fail. Rev.* **2012,** *17,* 305–311.
232. Jentzer, J. C.; DeWald, T. A.; Hernandez, A. F. Combination of Loop Diuretics With Thiazide-type Diuretics in Heart Failure. *J. Am. Coll. Cardiol.* **2010,** *56,* 1527–1534.
233. Parker, J. O. The Effects of Oral Ibopamine in Patients With Mild Heart Failure—A Double Blind Placebo Controlled Comparison to Furosemide. The Ibopamine Study Group. *Int. J. Cardiol.* **1993,** *40,* 221–227.
234. Patterson, J. H.; Adams, K. F., Jr.; Applefeld, M. M.; Corder, C. N.; Masse, B. R. Oral Torsemide in Patients With Chronic Congestive Heart Failure: Effects on Body Weight, Edema, and Electrolyte Excretion. *Pharmacotherapy* **1994,** *14,* 514–521.
235. Richardson, A.; Bayliss, J.; Scriven, A. J.; Parameshwar, J.; Poole-Wilson, P. A.; Sutton, G. C. Double-blind Comparison of Captopril Alone Against Frusemide Plus Amiloride in Mild Heart Failure. *Lancet* **1987,** *2,* 709–711.
236. Reilly, R. F.; Jakcson, E. K. Regulation of Renal Function and Vascular Volume. In *Goodman & Gilman's The Pharmacological Basis of Therapeutics;* Brunton, L. L., Chabner, B. A., Knollmann, B. C., Eds., 12th ed.; McGraw Hill: New York, 2011.
237. Accili, E. A.; Proenza, C.; Baruscotti, M.; DiFrancesco, D. From Funny Current to HCN Channels: 20 Years of Excitation. *News Physiol. Sci.* **2002,** *17,* 32–37.
238. Nawarskas, J. J.; Bowman, B. N.; Anderson, J. R. Ivabradine: A Unique and Intriguing Medication for Treating Cardiovascular Disease. *Cardiol. Rev.* **2015,** *23,* 201–211.
239. Bosmith, R. E.; Briggs, I.; Sturgess, N. C. Inhibitory Actions of Zeneca-ZD7288 on Whole-Cell Hyperpolarization-activated Inward Current (I_f) in Guinea-pig Dissociated Sinoatrial Node Cells. *Br. J. Pharmacol.* **1993,** *110,* 343–349.
240. Van Bogaert, P. P.; Pittoors, F. Use-dependent Blockade of Cardiac Pacemaker Current (I_f) by Cilobradine and Zatebradine. *Eur. J. Pharmacol.* **2003,** *478,* 161–171.
241. Reil, J. C.; Bohm, M. Heart Rate and Heart Failure: The Role of Ivabradine Therapy. *Curr. Opin. Cardiol.* **2013,** *28,* 326–331.
242. Fox, K.; Ford, I.; Steg, P. G.; Tendera, M.; Ferrari, R. Ivabradine for Patients With Stable Coronary Artery Disease and Left-Ventricular Systolic Dysfunction (BEAUTIFUL): A Randomised, Double-Blind, Placebo-Controlled Trial. *Lancet* **2008,** *372,* 807–816.
243. Ceconi, C.; Freedman, S. B.; Tardif, J. C.; Hildebrandt, P.; McDonagh, T.; Gueret, P.; Parrinello, G.; Robertson, M.; Steg, P. G.; Tendera, M.; Ford, I.; Fox, K.; Ferrari, R. Effect of Heart Rate Reduction by Ivabradine on Left Ventricular Remodeling in the Echocardiographic Substudy of BEAUTIFUL. *Int. J. Cardiol.* **2011,** *146,* 408–414.
244. Swedberg, K.; Komajda, M.; Bohm, M.; Borer, J. S.; Ford, I.; Dubost-Brama, A.; Lerebours, G.; Tavazzi, L. Ivabradine and Outcomes in Chronic Heart Failure (SHIFT): A Randomised Placebo-Controlled Study. *Lancet* **2010,** *376,* 875–885.
245. Bohm, M.; Swedberg, K.; Komajda, M.; Borer, J. S.; Ford, I.; Dubost-Brama, A.; Lerebours, G.; Tavazzi, L. Heart Rate as a Risk Factor in Chronic Heart Failure (SHIFT): The Association Between Heart Rate and Outcomes in a Randomised Placebo-Controlled Trial. *Lancet* **2010,** *376,* 886–894.
246. Kosmala, W.; Holland, D. J.; Rojek, A.; Wright, L.; Przewlocka-Kosmala, M.; Marwick, T. H. Effect of I_f-Channel Inhibition on Hemodynamic Status and Exercise Tolerance in Heart Failure With Preserved Ejection Fraction: A Randomized Trial. *J. Am. Coll. Cardiol.* **2013,** *62,* 1330–1338.
247. Simantirakis, E. N.; Nakou, E. S.; Kallergis, E. M.; Arkolaki, E. G.; Patrianakos, A. P.; Papakonstantinou, P. E.; Chlouverakis, G. I.; Vardas, P. E. Long-Term Effect of I_f-Channel Inhibition on Diastolic Function and Exercise Capacity in Heart Failure Patients With Preserved Ejection Fraction. *Int. J. Cardiol.* **2015,** *187,* 9–11.
248. Makielski, J. C. Late Sodium Current: A Mechanism for Angina, Heart Failure, and Arrhythmia. *Trends Cardiovasc. Med.* **2015**. http://dx.doi.org/10.1016/j.tcm.2015.05.006.
249. Banyasz, T.; Szentandrassy, N.; Magyar, J.; Szabo, Z.; Nanasi, P. P.; Chen-Izu, Y.; Izu, L. T. An Emerging Antiarrhythmic Target: Late Sodium Current. *Curr. Pharm. Des.* **2015,** *21,* 1073–1090.
250. Maier, L. S.; Sossalla, S. The Late Na Current as a Therapeutic Target: Where Are We? *J. Mol. Cell. Cardiol.* **2013,** *61,* 44–50.
251. Rastogi, S.; Sharov, V. G.; Mishra, S.; Gupta, R. C.; Blackburn, B.; Belardinelli, L.; Stanley, W. C.; Sabbah, H. N. Ranolazine Combined With Enalapril or Metoprolol Prevents Progressive LV Dysfunction and Remodeling in Dogs With Moderate Heart Failure. *Am. J. Physiol. Heart Circ. Physiol.* **2008,** *295,* H2149–H2155.
252. Sabbah, H. N.; Chandler, M. P.; Mishima, T.; Suzuki, G.; Chaudhry, P.; Nass, O.; Biesiadecki, B. J.; Blackburn, B.; Wolff, A.; Stanley, W. C. Ranolazine, a Partial Fatty Acid Oxidation (pFOX) Inhibitor, Improves Left Ventricular Function in Dogs With Chronic Heart Failure. *J. Card. Fail.* **2002,** *8,* 416–422.
253. Maier, L. S.; Layug, B.; Karwatowska-Prokopczuk, E.; Belardinelli, L.; Lee, S.; Sander, J.; Lang, C.; Wachter, R.; Edelmann, F.; Hasenfuss, G.; Jacobshagen, C. RAnoLazIne for the Treatment of Diastolic Heart Failure in Patients With Preserved Ejection Fraction: The RALI-DHF Proof-of-Concept Study. *JACC Heart Fail.* **2013,** *1,* 115–122.
254. Antzelevitch, C.; Belardinelli, L.; Zygmunt, A. C.; Burashnikov, A.; Di Diego, J. M.; Fish, J. M.; Cordeiro, J. M.; Thomas, G. Electrophysiological Effects of Ranolazine, a Novel Antianginal Agent With Antiarrhythmic Properties. *Circulation* **2004,** *110,* 904–910.
255. Zhao, G.; Walsh, E.; Shryock, J. C.; Messina, E.; Wu, Y.; Zeng, D.; Xu, X.; Ochoa, M.; Baker, S. P.; Hintze, T. H.; Belardinelli, L. Antiadrenergic and Hemodynamic Effects of Ranolazine in Conscious Dogs. *J. Cardiovasc. Pharmacol.* **2011,** *57,* 639–647.
256. Parikh, A.; Mantravadi, R.; Kozhevnikov, D.; Roche, M. A.; Ye, Y.; Owen, L. J.; Puglisi, J. L.; Abramson, J. J.; Salama, G. Ranolazine Stabilizes Cardiac Ryanodine Receptors: A Novel Mechanism for the Suppression of Early Afterdepolarization and Torsades De Pointes in Long QT Type 2. *Heart Rhythm* **2012,** *9,* 953–960.
257. Galimberti, E. S.; Knollmann, B. C. Efficacy and Potency of Class I Antiarrhythmic Drugs for Suppression of Ca^{2+} Waves in Permeabilized Myocytes Lacking Calsequestrin. *J. Mol. Cell. Cardiol.* **2011,** *51,* 760–768.
258. Belardinelli, L.; Liu, G.; Smith-Maxwell, C.; Wang, W. Q.; El-Bizri, N.; Hirakawa, R.; Karpinski, S.; Li, C. H.; Hu, L.; Li, X. J.; Crumb, W.; Wu, L.; Koltun, D.; Zablocki, J.; Yao, L.; Dhalla, A. K.; Rajamani, S.; Shryock, J. C. A Novel, Potent, and Selective Inhibitor of Cardiac Late Sodium Current Suppresses Experimental Arrhythmias. *J. Pharmacol. Exp. Ther.* **2013,** *344,* 23–32.
259. Denton, J. S.; Pao, A. C.; Maduke, M. Novel Diuretic Targets. *Am. J. Physiol. Renal Physiol.* **2013,** *305,* F931–F942.
260. Garcia, M. L.; Kaczorowski, G. J. Targeting the Inward-rectifier Potassium Channel ROMK in Cardiovascular Disease. *Curr. Opin. Pharmacol.* **2014,** *15,* 1–6.
261. Lewis, L. M.; Bhave, G.; Chauder, B. A.; Banerjee, S.; Lornsen, K. A.; Redha, R.; Fallen, K.; Lindsley, C. W.; Weaver, C. D.; Denton, J. S. High-Throughput Screening Reveals a Small-Molecule Inhibitor of the Renal Outer Medullary Potassium Channel and Kir7.1. *Mol. Pharmacol.* **2009,** *76,* 1094–1103.
262. Bhave, G.; Chauder, B. A.; Liu, W.; Dawson, E. S.; Kadakia, R.; Nguyen, T. T.; Lewis, L. M.; Meiler, J.; Weaver, C. D.; Satlin, L. M.; Lindsley, C. W.; Denton, J. S. Development of a Selective Small-Molecule Inhibitor of Kir1.1, the Renal Outer Medullary Potassium Channel. *Mol. Pharmacol.* **2011,** *79,* 42–50.
263. Tang, H.; Walsh, S. P.; Yan, Y.; de Jesus, R. K.; Shahripour, A.; Teumelsan, N.; Zhu, Y.; Ha, S.; Owens, K. A.; Thomas-Fowlkes, B. S.; Felix, J. P.; Liu, J.; Kohler, M.; Priest, B. T.; Bailey, T.; Brochu, R.; Alonso-Galicia, M.; Kaczorowski, G. J.; Roy, S.; Yang, L.; Mills, S. G.; Garcia, M. L.; Pasternak, A. Discovery of Selective Small Molecule ROMK Inhibitors as Potential New Mechanism Diuretics. *ACS Med. Chem. Lett.* **2012,** *3,* 367–372.
264. Walsh, S. P.; Shahripour, A.; Tang, H.; Teumelsan, N.; Frie, J.; Zhu, Y.; Priest, B. T.; Swensen, A. M.; Liu, J.; Margulis, M.; Visconti, R.; Weinglass, A.; Felix, J. P.; Brochu, R. M.; Bailey, T.; Thomas-Fowlkes, B.; Alonso-Galicia, M.; Zhou, X.; Pai, L. Y.; Corona, A.; Hampton, C.; Hernandez, M.; Bentley, R.; Chen, J.; Shah, K.; Metzger, J.; Forrest, M.; Owens, K.; Tong, V.; Ha, S.; Roy, S.; Kaczorowski, G. J.; Yang, L.; Parmee, E.; Garcia, M. L.; Sullivan, K.; Pasternak, A. Discovery of a Potent and Selective ROMK Inhibitor With Pharmacokinetic Properties Suitable for Preclinical Evaluation. *ACS Med. Chem. Lett.* **2015,** *6,* 747–752.
265. Szeto, H. H. First-In-Class Cardiolipin-Protective Compound as a Therapeutic Agent to Restore Mitochondrial Bioenergetics. *Br. J. Pharmacol.* **2014,** *171,* 2029–2050.
266. Szeto, H. H.; Birk, A. V. Serendipity and the Discovery of Novel Compounds That Restore Mitochondrial Plasticity. *Clin. Pharmacol. Ther.* **2014,** *96,* 672–683.

267. Szeto, H. H.; Schiller, P. W. Novel Therapies Targeting Inner Mitochondrial Membrane—From Discovery to Clinical Development. *Pharm. Res.* **2011,** *28,* 2669–2679.
268. Zhao, K.; Luo, G.; Zhao, G. M.; Schiller, P. W.; Szeto, H. H. Transcellular Transport of a Highly Polar 3+ Net Charge Opioid Tetrapeptide. *J. Pharmacol. Exp. Ther.* **2003,** *304,* 425–432.
269. Birk, A. V.; Liu, S.; Soong, Y.; Mills, W.; Singh, P.; Warren, J. D.; Seshan, S. V.; Pardee, J. D.; Szeto, H. H. The Mitochondrial-Targeted Compound SS-31 Re-Energizes Ischemic Mitochondria by Interacting With Cardiolipin. *J. Am. Soc. Nephrol.* **2013,** *24,* 1250–1261.
270. Dai, D. F.; Hsieh, E. J.; Chen, T.; Menendez, L. G.; Basisty, N. B.; Tsai, L.; Beyer, R. P.; Crispin, D. A.; Shulman, N. J.; Szeto, H. H.; Tian, R.; MacCoss, M. J.; Rabinovitch, P. S. Global Proteomics and Pathway Analysis of Pressure-Overload-Induced Heart Failure and Its Attenuation by Mitochondrial-Targeted Peptides. *Circ. Heart Fail.* **2013,** *6,* 1067–1076.
271. Dai, W.; Shi, J.; Gupta, R. C.; Sabbah, H. N.; Hale, S. L.; Kloner, R. A. Bendavia, a Mitochondria-Targeting Peptide, Improves Postinfarction Cardiac Function, Prevents Adverse Left Ventricular Remodeling, and Restores Mitochondria-Related Gene Expression in Rats. *J. Cardiovasc. Pharmacol.* **2011,** *64,* 543–553.
272. Sabbah, H. N.; Mengjun, W.; Zhang, K.; Gupta, R. C.; Rastogi, S. Long-Term Therapy With Bendavia (MTP-131), a Novel Mitochondria-Targeting Peptide, Increases Myocardial ATP Synthesis and Improves Left Ventricular Systolic Function in Dogs With Chronic Heart Failure. *J. Am. Coll. Cardiol.* **2013,** *61*, E577.
273. A Study "Investigating the Safety, Tolerability, and Pharmacokinetics of MTP-131 in Subjects With". Congestive Heart Failure. https://clinicaltrials.gov/ct2/show/NCT02388464 (July 24, 2015).
274. Stealth BioTherapeutics Announces Positive Results in Bendavia Heart Failure Study: the PREVIEW Trial http://www.businesswire.com/news/home/20150526005601/en/Stealth-BioTherapeutics-Announces-Positive-Results-Bendavia-Heart (July 24, 2015)
275. Chakrabarti, A. K.; Feeney, K.; Abueg, C.; Brown, D. A.; Czyz, E.; Tendera, M.; Janosi, A.; Giugliano, R. P.; Kloner, R. A.; Weaver, W. D.; Bode, C.; Godlewski, J.; Merkely, B.; Gibson, C. M. Rationale and Design of the EMBRACE STEMI Study: A Phase 2a, Randomized, Double-Blind, Placebo-Controlled Trial to Evaluate the Safety, Tolerability and Efficacy of Intravenous Bendavia on Reperfusion Injury in Patients Treated With Standard Therapy Including Primary Percutaneous Coronary Intervention and Stenting for ST-Segment Elevation Myocardial Infarction. *Am. Heart J* **2013,** *165.*
276. Bendavia Trials in clintrials.gov. https://clinicaltrials.gov/ct2/results?term=bendavia (July 24, 2015).
277. Lopaschuk, G. D.; Ussher, J. R.; Folmes, C. D.; Jaswal, J. S.; Stanley, W. C. Myocardial Fatty Acid Metabolism in Health and Disease. *Physiol. Rev.* **2010,** *90,* 207–258.
278. Ashrafian, H.; Horowitz, J. D.; Frenneaux, M. P. *Perhexiline Cardiovasc. Drug Rev.* **2007,** *25,* 76–97.
279. Killalea, S. M.; Krum, H. Systematic Review of the Efficacy and Safety of Perhexiline in the Treatment of Ischemic Heart Disease. *Am. J. Cardiovasc. Drugs* **2001,** *1,* 193–204.
280. Lee, L.; Campbell, R.; Scheuermann-Freestone, M.; Taylor, R.; Gunaruwan, P.; Williams, L.; Ashrafian, H.; Horowitz, J.; Fraser, A. G.; Clarke, K.; Frenneaux, M. Metabolic Modulation With Perhexiline in Chronic Heart Failure: A Randomized, Controlled Trial of Short-Term Use of a Novel Treatment. *Circulation* **2005,** *112,* 3280–3288.
281. Cooke, G. A.; Williams, S. G.; Marshall, P.; Al-Timman, J. K.; Shelbourne, J.; Wright, D. J.; Tan, L. B. A Mechanistic Investigation of ACE Inhibitor Dose Effects on Aerobic Exercise Capacity in Heart Failure Patients. *Eur. Heart J.* **2002,** *23,* 1360–1368.
282. Vescovo, G.; Dalla Libera, L.; Serafini, F.; Leprotti, C.; Facchin, L.; Volterrani, M.; Ceconi, C.; Ambrosio, G. B. Improved Exercise Tolerance After Losartan and Enalapril in Heart Failure—Correlation With Changes in Skeletal Muscle Myosin Heavy Chain Composition. *Circulation* **1998,** *98,* 1742–1749.
283. Abozguia, K.; Elliott, P.; McKenna, W.; Phan, T. T.; Nallur-Shivu, G.; Ahmed, I.; Maher, A. R.; Kaur, K.; Taylor, J.; Henning, A.; Ashrafian, H.; Watkins, H.; Frenneaux, M. Metabolic Modulator Perhexiline Corrects Energy Deficiency and Improves Exercise Capacity in Symptomatic Hypertrophic Cardiomyopathy. *Circulation* **2010,** *122,* 1562–1569.
284. Beadle, R. M.; Williams, L. K.; Abozguia, K.; Patel, K.; Leon, F. L.; Yousef, Z.; Wagenmakers, A.; Frenneaux, M. P. Metabolic Manipulation in Chronic Heart Failure: Study Protocol for a Randomised Controlled Trial. *Trials* **2011,** *12,* 140.
285. Beadle, R. M.; Williams, L. K.; Kuehl, M.; Bowater, S.; Abozguia, K.; Leyva, F.; Yousef, Z.; Wagenmakers, A. J.; Thies, F.; Horowitz, J.; Frenneaux, M. P. Improvement in Cardiac Energetics by Perhexiline in Heart Failure due to Dilated Cardiomyopathy. *JACC Heart Fail.* **2015,** *3,* 202–211.
286. Gupta, M. P. Factors Controlling Cardiac Myosin-Isoform Shift During Hypertrophy and Heart Failure. *J. Mol. Cell. Cardiol.* **2007,** *43,* 388–403.
287. van Rooij, E.; Quiat, D.; Johnson, B. A.; Sutherland, L. B.; Qi, X.; Richardson, J. A.; Kelm, R. J., Jr.; Olson, E. N. A Family of microRNAs Encoded by Myosin Genes Governs Myosin Expression and Muscle Performance. *Dev. Cell* **2009,** *17,* 662–673.
288. Callis, T. E.; Pandya, K.; Seok, H. Y.; Tang, R. H.; Tatsuguchi, M.; Huang, Z. P.; Chen, J. F.; Deng, Z.; Gunn, B.; Shumate, J.; Willis, M. S.; Selzman, C. H.; Wang, D. Z. MicroRNA-208a Is a Regulator of Cardiac Hypertrophy and Conduction in Mice. *J. Clin. Invest.* **2009,** *119,* 2772–2786.
289. Montgomery, R. L.; Hullinger, T. G.; Semus, H. M.; Dickinson, B. A.; Seto, A. G.; Lynch, J. M.; Stack, C.; Latimer, P. A.; Olson, E. N.; van Rooij, E. Therapeutic Inhibition of miR-208a Improves Cardiac Function and Survival During Heart Failure. *Circulation* **2011,** *124,* 1537–1547.
290. Grueter, C. E.; van Rooij, E.; Johnson, B. A.; DeLeon, S. M.; Sutherland, L. B.; Qi, X.; Gautron, L.; Elmquist, J. K.; Bassel-Duby, R.; Olson, E. N. A Cardiac microRNA Governs Systemic Energy Homeostasis by Regulation of MED13. *Cell* **2012,** *149,* 671–683.

7.18 Advances in Hypercholesterolemia

A Pirillo, E. Bassini Hospital, Cinisello Balsamo, Italy
GD Norata and AL Catapano, University of Milan and IRCCS Multimedica, Milano, Italy

© 2017 Elsevier Ltd. All rights reserved.

7.18.1	**Introduction**	664
7.18.2	**Statins in the Prevention of CV Disease**	665
7.18.3	**Novel Therapeutic Approaches in the Management of Dyslipidemia**	666
7.18.3.1	Targeting Plasma Cholesterol Levels	666
7.18.3.1.1	Ezetimibe	666
7.18.3.1.2	PCSK9 inhibitors	669
7.18.3.1.3	Mipomersen	676
7.18.3.1.4	Lomitapide	679
7.18.3.1.5	CETP inhibitors	681
7.18.3.1.6	ETC-1002	682
7.18.3.2	Targeting Plasma TG Levels	684
7.18.3.2.1	Omega-3 free fatty acids	684
7.18.3.2.2	Alipogene tiparvovec	685
7.18.3.2.3	ISIS-APOCIIIRx	686
7.18.3.2.4	Diacylglycerol *O*-acyltransferase inhibitors	686
7.18.3.3	Conclusions	687
References		687

Abbreviations

ACL Adenosine triphosphate citrate lyase
ALT Alanine aminotransferase
AMPK Adenosine monophosphate-activated protein kinase
apo(a) Apolipoprotein (a)
apoA-I Apolipoprotein A-I
apoB Apolipoprotein B
apoC-III Apolipoprotein C-III
AST Aspartate aminotransferase
CAD Coronary artery disease
CETP Cholesteryl ester transfer protein
CHD Coronary heart disease
CK Creatine kinase
CKD Chronic kidney disease
CV Cardiovascular
CVD Cardiovascular disease
CYP450 Cytochrome P450
DGAT Diacylglycerol *O*-acyltransferase
DHA Docosahexaenoic acid
EPA Eicosapentaenoic acid
ER Endoplasmic reticulum
FCS Familial chylomicronemia syndrome
FH Familial hypercholesterolemia
HDL High-density lipoprotein
HDL-C High-density lipoprotein cholesterol
HeFH Heterozygous familial hypercholesterolemia
HoFH Homozygous familial hypercholesterolemia
HR Hazard ratio
hs-CRP High-sensitivity C-reactive protein
HTG Hypertriglyceridemia
IMT Intima-media thickness
LDL Low-density lipoprotein
LDL-C Low-density lipoprotein cholesterol
LDLR Low-density lipoprotein receptor
Lp(a) Lipoprotein (a)
LPL Lipoprotein lipase
LPLD Lipoprotein lipase deficiency
mAb Monoclonal antibody
MI Myocardial infarction
MTP Microsomal triglyceride transport protein
non-HDL-C Non-high-density lipoprotein cholesterol
NPC1L1 Niemann–Pick C1-like 1
PCSK9 Proprotein convertase subtilisin/kexin type 9
Q2W Every 2 weeks
Q4W Every 4 weeks
RCT Randomized clinical trial
RLP-C Remnant-like particle cholesterol
TC Total cholesterol
TG Triglycerides
ULN Upper limit of normal
VLDL Very-low-density lipoprotein
VLDL-C Very-low-density lipoprotein cholesterol

7.18.1 Introduction

Atherosclerosis is a chronic inflammatory disease of the arterial walls, characterized by a progressive accumulation of lipids. One of the earliest events in the formation of the atherosclerotic lesion is represented by the infiltration of low-density lipoprotein (LDL) within the artery wall. Here, LDL is oxidized by various mechanisms and subsequently greatly internalized by macrophages, which become foam cells.[1] This process, in turn, induces further deposition of lipids and activates a cascade of inflammatory processes that lead to the formation of atherosclerotic plaque. A large number of studies have recognized low-density lipoprotein cholesterol (LDL-C) level as a relevant risk factor for cardiovascular (CV) disease and established the strong and direct relationship between high LDL-C levels and coronary heart disease (CHD), suggesting that decreasing LDL-C levels significantly reduce the CV risk.

From a biological point of view, the "normal" concentrations of LDL-C are much lower than those observed in modern societies. This suggestion derives from the old observation that optimal plasma concentration of LDL-C should be about 25 mg dL^{-1}, since above this value the low-density lipoprotein receptor (LDLR) is constantly saturated.[2] This hypothesis is supported by the observation that individuals with genetically determined low levels of LDL-C are healthy and exhibit very low incidence of CV events.[3,4]

Several clinical trials have shown that reducing LDL-C decreases the incidence of CV events. A meta-analysis of data from trials of statins showed in fact that, during a mean of 5 years, a 12% reduction in all-cause mortality per mmol L^{-1} reduction in LDL-C, a 19% reduction in coronary mortality, and a 17% reduction in any vascular cause of mortality were observed.[5] These effects were independent of the initial lipid profile or other presenting characteristics, and the proportional reductions were similar in all subgroups of patients examined.[5] In addition, the comparison between more intensive and less intensive statin therapy showed that additional reduction in LDL-C levels achieved with more intensive therapy further reduces the incidence of major vascular events (−13% coronary death or nonfatal myocardial infarction (MI), −19% coronary revascularization, and −16% ischemic stroke).[6] These meta-analyses suggest that the higher the degree of reduction of LDL-C levels, the greater the benefit in terms of reduction of CV risk. This means that patients at high CV risk may benefit from achieving the largest LDL-C reduction. Current therapeutic guidelines suggest that in patients at very high CV risk (such as patients with established cardiovascular disease (CVD), diabetes, moderate to severe coronary kidney disease, and familial hypercholesterolemia (FH)), optimal LDL-C is <70 mg dL^{-1} (<1.8 mmol L^{-1}), in those at high CV risk <100 mg dL^{-1} (<2.6 mmol L^{-1}) and in subjects at moderate risk <115 mg dL^{-1} (<3.0 mmol L^{-1}).[7,8] Moreover, the therapeutic goals of LDL-C should be not only achieved but also maintained over time to obtain the clinical benefit; treatments need to be modulated based on the overall CV risk of the individual patient and according to the objectives to be achieved. This means the choice of the drug with the right effectiveness, a dose selection according to the objectives, and eventually the use of additional drugs with complementary mechanisms of action to increase the efficacy of the therapy.

Despite the evidence confirming the beneficial effect of a significant LDL-C level reduction in patients at very high CV risk, many of these patients often do not reach their LDL-C goal with the starting therapy. When a reduction higher than 50% is required, it is necessary to use a high dose of high-potency statins (atorvastatin and rosuvastatin) (**Fig. 1**) or, alternatively, combined lipid-lowering therapies. The choice of the most appropriate therapeutic approach can be done taking into account either the LDL-C target or distance of LDL-C from the target. The achievement of the therapeutic target implies the choice of pharmacological strategies specific to each subject, according to the goal to be achieved; thus, a high distance from the target requires the administration of a high-potency statin or, alternatively, a combination of cholesterol-lowering drugs with different mechanisms of action.

Familial hypercholesterolemia. Among patients with high CV risk, those with FH present a high risk of premature CHD, due to lifelong exposure to high plasma LDL-C levels.[8] FH is caused by mutations in genes encoding proteins involved in the metabolism of LDL, such as LDLR, apolipoprotein B (apoB), proprotein convertase subtilisin/kexin type 9 (PCSK9), and LDLR adaptor protein; mutations in LDLR gene account for the vast majority of FH cases.[8]

Heterozygous familial hypercholesterolemia (HeFH) patients present a residual LDLR activity (up to 50%) and are characterized by two- to threefold elevation in plasma cholesterol levels and development of early coronary atherosclerosis (usually before 50 years); homozygous familial hypercholesterolemia (HoFH) patients may be receptor-defective, with a significantly reduced LDLR pathway (2–10% activity), or receptor-negative, characterized by an LDLR activity $<2\%$. The HoFH presents more severe CV conditions compared with subjects with receptor deficiency.[9] The lack of LDLR in receptor-negative HoFH determines the exposure to very high cholesterol levels (>500 mg dL^{-1} and >12.8 mmol L^{-1}) from childhood, the occurrence of cutaneous xanthomas prior to 4 years of age, childhood CHD, and even death from MI prior to 20 years of age if untreated.[9,10] Lifestyle interventions (low saturated fat, low cholesterol diet, physical activity, and not smoking) are strongly encouraged, but aggressive and adequate lipid-lowering treatments are crucial to lower LDL-C levels drastically. Despite the fact that statins are the first-choice drug for the treatment of hypercholesterolemia,[8,11] their efficacy is strictly related to the presence of a functional LDLR and thus may be effective in HeFH or in receptor-defective HoFH.[8,9] In LDLR-negative HoFH patients, statins, although inducing a modest reduction of LDL-C ($\sim$20%, probably due to alternative mechanism of action independent of LDLR), do not allow the achievement of the recommended LDL-C level target.[12] In addition, some subjects may exhibit intolerance to statins, leading to therapy discontinuation. All these observations suggest the need of new therapeutic options to decrease LDL-C levels in these very high-risk patients, by using combined lipid-lowering therapies (often in addition to apheresis treatment), with drugs having different mechanisms of action as described in the succeeding text, possibly independent of LDLR that may guarantee a higher reduction of LDL-C levels.

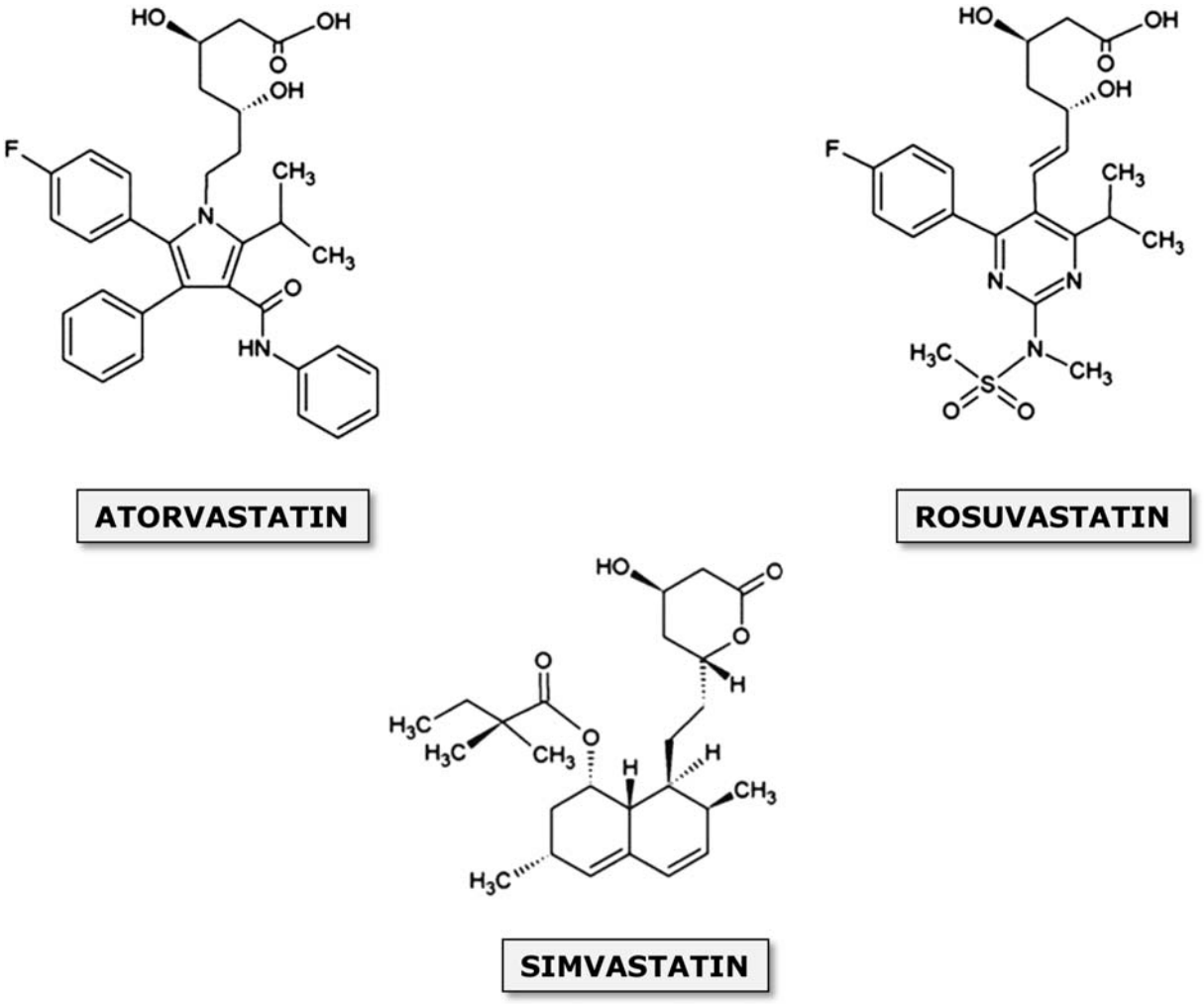

Fig. 1 Structure of atorvastatin, rosuvastatin, and simvastatin.

7.18.2 Statins in the Prevention of CV Disease

Several clinical trials have established the efficacy of statins in reducing CV morbidity and mortality in both primary and secondary prevention.[6,13–18] Statins reduce LDL-C levels by inhibiting 3-hydroxy-3-methylglutaryl coenzyme A (HMG-CoA) reductase, thus inhibiting the endogenous synthesis of cholesterol. This, in turn, results in the upregulation of LDLR and in the subsequent reduction of circulating LDL particles. A meta-analysis of 14 randomized clinical trials with 90,056 participants showed an overall safety and benefit of statin therapy [5]: during a mean of 5 years, there was a 12% proportional reduction in all-cause mortality per mmol L^{-1} reduction in LDL-C, with significant reduction in coronary mortality (-19%, $P<0.0001$), MI or coronary death (-23%, $P<0.0001$), and fatal or nonfatal stroke (-17%, $P<0.0001$).[5] An overall $\sim$20% reduction in the incidence of CV events per mmol L^{-1} LDL reduction was reported.[5] When trials of more intensive versus less intensive statin therapy were analyzed, more intensive regimens produced an additional 15% ($P<0.0001$) reduction in major vascular events,[6] suggesting that further reducing LDL-C levels safely translates into a further clinical benefit.

However, despite the significant reduction of CV events in statin-treated patients, certain patients continue to experience CV events, referred to as "residual risk," even in the presence of well-controlled LDL-C levels.[19] The evidence suggests that atherogenic dyslipidemia, that is, alterations in other lipids (such as high triglycerides (TG) and low high-density lipoprotein cholesterol (HDL-C)), may account for this effect.[20] In addition, an increasing number of subjects are treated with statins, often in combination with other drugs, thus increasing the probability of drug–drug interactions and the occurrence of adverse side effects.[21] Finally, the adherence to statin therapy is not always optimal, as many patients discontinue statin therapy due to adverse events.

The most common adverse events reported with statin are skeletal muscle-related disorders (generally referred to as myopathy). Despite randomized clinical trials reported a 1.5–5% incidence of statin-induced myopathy,[22,23] in clinical practice the frequency appears to be higher.[24] This difference can be partly attributed to the patient inclusion criteria adopted in the clinical trials, which tend to exclude subjects with comorbidities, older subjects, or patients with a history of muscle disorders.[24,25] In addition, increased

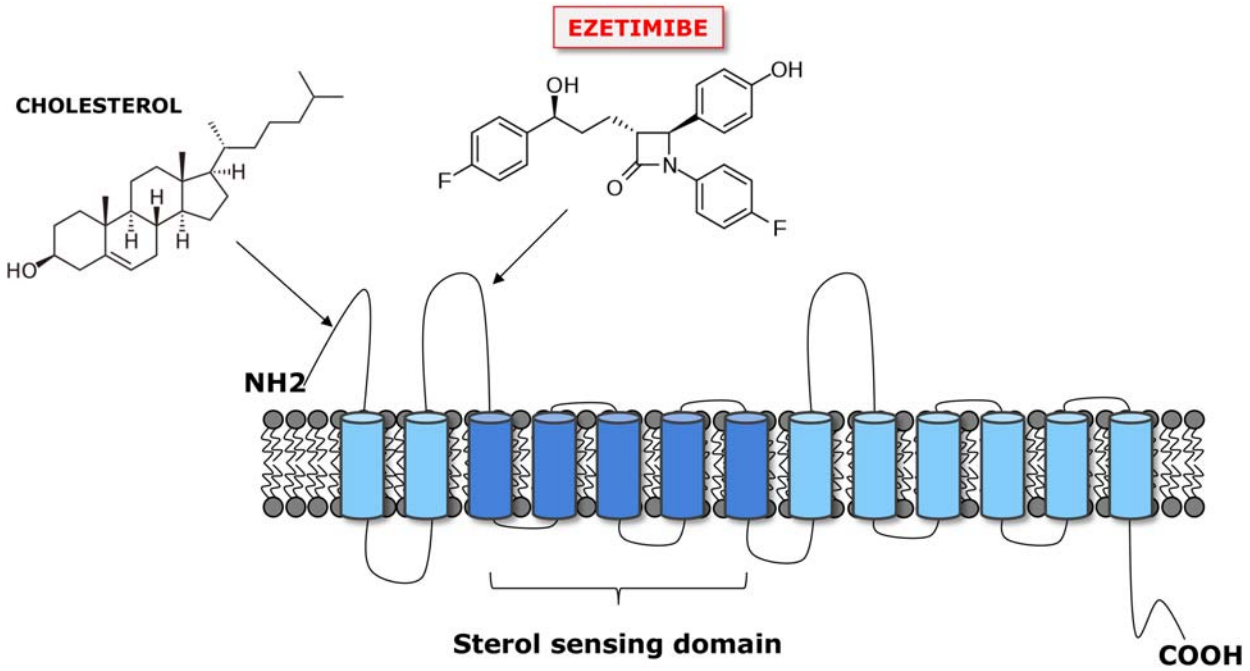

Fig. 2 Structure of human NPC1L1. NPC1L1 contains 13 transmembrane domains, including sterol-sensing domain formed by membrane-spanning helices with short intervening loops. The extracellular N-terminal domain of NPC1L1 directly binds cholesterol; ezetimibe binds to the loop C.

levels of creatine kinase (CK) are used as a marker for statin-induced myopathy, but myopathy occurrence not always associates with these alterations. Finally, less significant signs of myopathy (including fatigability or weakness) are often not considered as relevant.[25] Altogether, these observations may account for the underestimation of muscle-related side effects in statin-treated patients in the clinical trials.

Statin-related myopathy occurs particularly with high-dosage statin regimens, and thus, its incidence is higher in high CV risk patients who need more aggressive lipid-lowering therapies or in patients with comorbidities, due to metabolic interactions with other drugs.[26,27] They include less severe manifestations (asymptomatic moderate serum CK elevation or muscle pain in the absence of CK elevation)[28] up to the most severe and rare rhabdomyolysis.[28,29] Several risk factors may increase the probability of myotoxicity related to statin therapy: chemicophysical properties of statins (lipophilic statins seem to induce myotoxicity more than hydrophilic statins), administration of concomitant drugs that can interact with statins, and patient-related risk factors (age, female gender, and genetic factors).[29] Discontinuation of statin therapy is common among patients experiencing muscle-related adverse effects, but several pharmacological approaches may be adopted to treat patients intolerant to statins. First, a statin rechallenge may be tolerated by patients; the rechallenge may be done by reintroducing the same statin at a lower dose or by introducing a different statin (such as a more potent statin at a low dose) or by using the noneveryday statin administration (this is possible with potent statins with longer half-life, such as rosuvastatin and atorvastatin).[29] Alternatively, the lowest dose of statin tolerated may be combined with nonstatin lipid-lowering drugs.[29] Several nonstatin drugs have been approved for the treatment of dyslipidemia, but, despite an improvement of the lipid profile, results from clinical trials could not support their use as monotherapy or in combination with statins, with the exception of ezetimibe (**Fig. 2**).[30,31] In fact, the addition of niacin to statin therapy did not show any further clinical benefit, compared with statin therapy [32,33]; similarly, clinical trials on fenofibrate showed a benefit only in particular subgroups of patients (i.e., those with high TG and low HDL-C levels).[34,35] In addition, the difficult-to-manage high CV risk patients such as those with FH raised the need of new lipid-lowering drugs that could add significant clinical benefit beyond statin treatment.

7.18.3 Novel Therapeutic Approaches in the Management of Dyslipidemia

In recent years, several therapeutic approaches have been investigated for reducing plasma cholesterol and/or TG levels through different mechanisms of action. Specific therapies were explored not only for the treatment of monogenic homozygous forms of dyslipidemia including familial hypercholesterolemia or chylomicronemia syndrome but also for statin-intolerant patients.

7.18.3.1 Targeting Plasma Cholesterol Levels

7.18.3.1.1 Ezetimibe

Niemann–Pick C1-like 1 (NPC1L1) protein plays a central role in the intestinal absorption of cholesterol and the regulation of cholesterol plasma levels.[36,37] Its expression and localization are strictly regulated by the cellular content of cholesterol: when cells

are enriched in cholesterol, NPC1L1 is localized in the endocytic recycling compartment, but in cells depleted of cholesterol, NPC1L1 translocates to the cell surface to bind extracellular cholesterol[38,39] (Fig. 2). In humans, NPC1L1 is expressed also in the liver, where it prevents excessive loss of biliary cholesterol.[40]

The evidence of the involvement of NPC1L1 in the process of cholesterol absorption derives from observations in animal studies. NPC1L1-deficient mice have a significantly reduced cholesterol absorption (−69%) compared with wild-type mice.[41] In apoE knockout mice, the deficiency of NPC1L1 largely decreased cholesterol absorption, protected them from diet-induced hypercholesterolemia, and prevented atherosclerotic lesion formation.[42,43] On the other hand, NPC1L1 overexpression in cultured cells increased cholesterol uptake in cells,[44] and cholesterol feeding of NPC1L1$^{-/-}$/LDLR$^{-/-}$ knockout mice transgenically expressing human NPC1L1 resulted in significantly increased cholesterol absorption and cholesterol levels compared with the double knockout mice.[45] In humans, carriers of NPC1L1 inactivating mutations exhibit lower LDL-C levels compared with noncarriers and exhibited a relative reduction of 53% in the risk of CHD.[46] These observations suggest that pharmacological inhibition of NPC1L1 can be a therapeutic approach for the treatment of hypercholesterolemia in humans.

Ezetimibe is a selective inhibitor of cholesterol absorption that reduces the cholesterol uptake in enterocytes by inhibiting NPC1L1[47] (Fig. 2). Ezetimibe is rapidly absorbed from the gastrointestinal tract and transformed into its glucuronides. The phenolic glucuronide is the main metabolite detectable in human plasma and accounts for about 90% of the total ezetimibe; it localizes more avidly in the intestine compared with ezetimibe and has similar or even higher cholesterol-lowering activity compared with the parent compound.[48,49]

Statins and ezetimibe have different and complementary mechanisms of action, and thus, the combination statin + ezetimibe may represent a successful approach for the prevention of CV disease and allow the treatment of subjects that manifest intolerance to high-dose statins. In addition, the statin-induced inhibition of cholesterol synthesis results in an increase of absorption markers, and, on the contrary, the reduced cholesterol absorption induced by ezetimibe results in the increase of cholesterol synthesis [50]; this would reduce the efficiency of the single drugs, while the combination decreases both cholesterol synthesis and absorption.[50]

Several clinical trials have shown that adding ezetimibe to statin therapy determines an additional 20% reduction of LDL-C levels[51–54] (Table 1). A pooled analysis of over 21,000 subjects from 27 clinical trials showed that combining ezetimibe with a statin induces a greater lipid-lowering effect than statin monotherapy.[55] Similarly, LDL-C lowering was significantly higher in patients with CHD or CHD equivalent treated with ezetimibe added to current statin therapy compared with patients who titrated the statin doses.[56]

Also, diabetic patients seem to benefit from the combination ezetimibe + statin: the *RESEARCH* (*Recognized Effect of Statin and Ezetimibe Therapy for Achieving LDL-C Goal*) trial reported that the ezetimibe + statin induced a higher LDL-C reduction compared with doubling the statin dose (−24.6% vs. −10.9%, $P<0.0001$)[57]; in addition, more subjects reached their LDL-C goals in the group treated with ezetimibe + statin versus the group treated with a doubled statin dose (89.3% vs. 51%, $P<0.0001$).[57] The combination therapy also improved the atherogenic lipid profile characteristic of diabetes more effectively than statin therapy; this effect can be attributed to a higher reduction of small dense LDL (−20.5% vs. −3.7%) and remnant-like particle cholesterol (RLP-C) (−19.7% vs. +5.5%).[57] Diabetic patients seem to benefit from the combination therapy ezetimibe + statin more than nondiabetic subjects, as they achieve significantly higher reductions in LDL-C and non-high-density lipoprotein cholesterol (non-HDL-C); it has been hypothesized that diabetic patients might have a higher expression of NPC1L1, but a defined explanation is still lacking.[58]

Contrasting results have been reported on the ability of ezetimibe to reduce the carotid intima-media thickness (IMT), a marker of subclinical atherosclerosis. In the *ENHANCE* (*Ezetimibe and Simvastatin in Hypercholesterolemia Enhances Atherosclerosis Regression*, NCT00552097) trial, which compared the effect of ezetimibe + simvastatin (10 + 80 mg) or simvastatin (Fig. 1) alone on the progression of atherosclerosis in HeFH patients, changes in the carotid IMT did not differ in the groups, despite lower LDL-C levels observed in patients treated with the combination therapy (−55.6% vs. −39.1% with statin monotherapy, $P<0.01$)[59] (Table 1). The *ARBITER 6-HALTS* (Arterial Biology for the Investigation of the Treatment Effects of Reducing Cholesterol 6-HDL and LDL Treatment Strategies in Atherosclerosis, NCT00397657) trial, performed in patients with CHD or CHD equivalent to evaluate the effect of ezetimibe or extended-release niacin added to a chronic statin therapy, reported a lack of effect of ezetimibe that instead resulted in carotid IMT progression[60] (Table 1). Lack of effect of ezetimibe added to statin therapy on IMT has been reported also in other studies.[61,62] On the contrary, the *SANDS* (*Stop Atherosclerosis in Native Diabetics Study*, NCT00047424) trial showed that, compared with standard lipid-lowering therapies, aggressive lipid-lowering treatments induced a regression of carotid IMT in type 2 diabetic patients[63] (Table 1). Among subjects treated with aggressive lipid-lowering treatments, those receiving ezetimibe exhibited a greater reduction despite similar LDL-C reductions[64] (Table 1). One possible explanation for these discrepancies is the baseline carotid status: if the patients have IMT values within the normal range, the chance that a cholesterol-lowering therapy may be effective on this parameter is lower than in subjects with significant IMT values.

Two studies have reported a beneficial effect of ezetimibe + statin on coronary atherosclerosis: besides a greater reduction in the plaque volume,[65] a higher increase of the fibrous cap thickness was observed, suggesting a possible role for ezetimibe in the stabilization of atherosclerotic plaque[66] (Table 1).

Ezetimibe in the prevention of cardiovascular disease. Several studies have established the LDL-C-lowering ability of ezetimibe, showing a further reduction of 23% when added to a statin therapy [55,67]; however, few clinical trials have evaluated the clinical benefit of the addition of ezetimibe to statin therapy. The *SHARP* (Study of Heart and Renal Protection, NCT00125593) trial, performed in patients with moderate to severe kidney disease, evaluated the effect of ezetimibe + simvastatin or placebo

Table 1 Effects of ezetimibe combined with a statin versus statin monotherapies on LDL-C levels and clinical outcomes

Clinical trials	*Subjects*	*Duration*	*LDL-C (percent change from baseline)*	*Clinical outcomes*	*P*
RESEARCH[57]	T2DM	12 weeks	Eze + Stat: −24.6% DST: 1–10.9%		
ENHANCE,[59] NCT00552097	FH	24 months	Eze + Simva: −55.6% Simva: −39.1%	Carotid IMT (change from baseline, mm) Eze + Simva: +0.0111 + 0.0038 Simva: +0.0058 + 0.0037	NS
ARBITER 6-HALTS,[60] NCT00397657	CHD or CHD equivalent on stable statin therapy	14 months	Eze: −22.5% Niacin: −12.6%	Carotid IMT (change from baseline, mm) Eze: −0.0007 ± 0.0035 Niacin: −0.0142 ± 0.0041	NS $P=0.001$
SANDS,[63,64] NCT00047424	T2DM	36 months	Aggressive LLT: −31% Standard LLT: +1% Aggressive Eze + Stat: −31.1% Aggressive statin alone: −32.3%	Mean change CIMT (mm) Aggressive LLT: −0.017 ± 0.12 Standard LLT: +0.041 + 0.14 Aggressive Eze + Stat: −0.025 (−0.05 to 0.003) Aggressive statin alone: −0.012 (−0.03 to 0.008)	$P<0.0001$ $P<0.0001$
Masuda et al.[65]	Stable CAD	6 months	Eze + Rosuva: −55.8% Rosuva: −36.8%	% Change in plaque volume Eze + Rosuva: −13.2% Rosuva: −3.1%	$P=0.05$
Habara et al.[66]	Angina pectoris	9 months	Eze + Fluva: −34.0% Fluva: −8.3%	Change in the fibrous cap thickness (mm) Eze + Fluva: +0.08 + 0.08 Fluva: +0.04 ± 0.06	$P<0.001$
SHARP,[68] NCT00125593	CKD	4.9 years	Eze + Simva: −68% Placebo: −14%	Major atherosclerotic events Eze + Simva: 11.3% Placebo: 13.4%	$P=0.0021$
IMPROVE-IT,[31] NCT00202878	ACS	6 years	Eze + Simva: −42.8% Simva: −25.9%	Death from cardiovascular causes, major coronary event, or nonfatal stroke Eze + Simva: 32.7% Simva: 34.7%	$P=0.016$

FH, familial hypercholesterolemia; *CHD*, coronary heart disease; *T2DM*, type 2 diabetes mellitus; *CAD*, coronary artery disease; *CKD*, chronic kidney disease; *ACS*, acute coronary syndrome; *Eze*, ezetimibe; *Stat*, statin; *Simva*, simvastatin; *Fluva*, fluvastatin; *Rosuva*, rosuvastatin; *LLT*, lipid-lowering therapy.

administration for 4.9 years [68]; the combination therapy reduced LDL-C levels by 33 mg dL^{-1} (0.84 mmol L^{-1}) and decreased the incidence of major atherosclerotic events (including nonfatal MI, coronary death, nonhemorrhagic stroke, and arterial revascularization) by 17%[68] (**Table 1**). When considering chronic kidney disease (CKD) patients with LDL-C not at target despite statin therapy (>120 mg dL^{-1} and >3.1 mmol L^{-1}), the combination therapy was more safe than doubling the dose of statins, as the incidence of adverse events was significantly lower.[69] These observations suggest that ezetimibe is a helpful and safe add-on to statin therapy to treat high CV risk patients such as those with CKD.

The *IMPROVE-IT* (*Improved Reduction of Outcomes: Vytorin Efficacy International Trial*, NCT00202878) compared the effect of a 6-year administration of ezetimibe + simvastatin (10/40 mg) or simvastatin (40 mg) alone in patients with a recent acute coronary syndrome and LDL-C levels at target.[31] At the end of the study, the LDL-C level was significantly lower in the group treated with ezetimibe + simvastatin compared with those treated with simvastatin alone (53.7 mg dL^{-1} vs. 69.5 mg dL^{-1}, $P<0.001$) (**Table 1**); furthermore, more patients treated with the combination therapy reached LDL-C levels <70 mg dL^{-1} (<1.8 mmol L^{-1}).[31] This effect on LDL-C level translated into a higher reduction of the primary end point (a composite of CV death, nonfatal MI, unstable angina requiring hospitalization, coronary revascularization, and nonfatal stroke) in the group treated with ezetimibe + simvastatin group (32.7% vs. 34.7% with simvastatin alone, $P=0.016$)[31] (**Table 1**). Secondary analyses of this study have shown the clinical benefit of adding ezetimibe to statin in subgroups of patients; as an example, women receiving the combination therapy exhibited a 12% reduction of the relative risk of the primary end point, compared with a 5% reduction in men [70]; older patients (≥75 years) showed a greater benefit from the combination therapy compared with younger patients (<65 years HR 0.98, ≥65 years HR 0.89, and ≥75 years HR 0.80). Moreover, type 2 diabetic patients seem to benefit more than nondiabetics from the combination therapy (14% reduction of the relative CV risk vs. 2% in nondiabetics).[71] Combined therapy was also superior to simvastatin alone in reducing the incidence of nonhemorrhagic stroke (HR 0.78, $P=0.008$).[72] All these analyses showed that adverse events did not differ among the various subgroups.[72]

Ezetimibe in the treatment of FH. In FH patients treated with the combination ezetimibe + statin, the levels of total cholesterol (TC) and LDL-C were lower than in those treated with statin alone.[59,73,74] However, no difference was observed in the reduction of carotid IMT [59]; this is likely due to the fact that the vast majority of FH patients enrolled in that study were on statin therapy long before entering the trial, resulting in the attenuation of IMT progression, and thus, a further LDL-C reduction was not able to further reduce the carotid IMT. Other studies with statin-naive patients have shown a regression.[75] Despite these considerations, contrasting results have been reported on the effect of the combination ezetimibe + simvastatin, which, in other studies, was reported to decrease significantly the carotid IMT in two groups of HeFH patients, one with a history of acute MI and the other with carotid lesions but no history of CV events.[76]

7.18.3.1.2 PCSK9 inhibitors

PCSK9 is a proteinase that inhibits the recycling of LDLRs by causing their lysosomal degradation, mainly synthesized and secreted by the liver. PCSK9 activity results in reduced expression of hepatic LDLR and increased circulating LDL-C levels (**Fig. 3**). In addition, statins increase PCSK9 expression,[77] which would translate in a reduced efficacy of statin therapy. Thus, inhibiting PCSK9 expression/activity represents a therapeutic approach that can result in the reduction of LDL-C levels. PCSK9 inhibition is obtained by the means of specific monoclonal antibodies (mAbs). Several clinical studies have shown that anti-PCSK9 monoclonal antibody monotherapies significantly decreased TC and LDL-C, with an overall incidence of adverse effects similar between the treatment and placebo groups.[78] Moreover, since statins induce PCSK9 expression, the addition of a PCSK9 mAb to a statin may result in an increased therapeutic effect.[79,80]

Evolocumab, alirocumab and bococizumab are human mAbs against PCSK9 leading to increased hepatic LDLR expression and LDL clearance. Two recent meta-analyses have evaluated the efficacy and safety of PCSK9 antibodies in randomized controlled clinical trials.[81,82] Li et al.[82] analyzed 20 RCTs including 6464 hypercholesterolemic patients and 3416 controls; participants of 16 studies were hypercholesterolemic and included also HeFH patients; three studies were performed only in HeFH and one in HoFH.[82] Most of these trials had a duration of 8–24 weeks. In some studies (10), the PCSK9 mAb was administered as a monotherapy; in the others, the antibodies were administered in addition to other lipid-lowering therapies. The analysis of these trials showed that treatment with PCSK9 mAbs significantly reduces LDL-C levels, with a weighted mean change

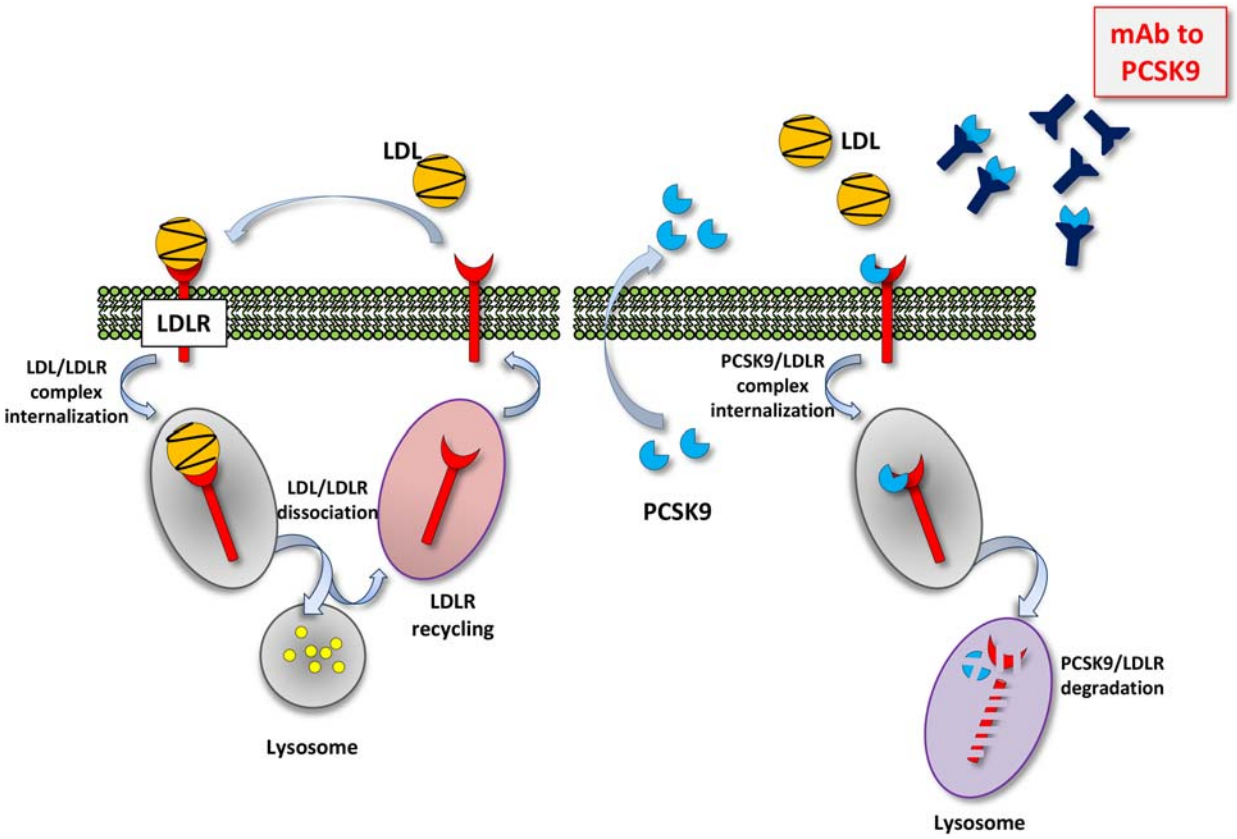

Fig. 3 Mode of action of PCSK9 inhibitors. In the absence of PCSK9, LDL binds to LDLR. After internalization, the LDL-LDLR complex dissociates, LDL undergoes lysosomal degradation, and LDLR is recycled to the cell surface. In the presence of PCSK9, LDLR is degraded within the cells, leading to increased levels of circulating LDL-C. Monoclonal antibodies neutralize secreted PCSK9, rendering it unable to bind to the LDLR. *LDL-C*, LDL cholesterol; *LDLR*, LDL receptor; *PCSK9*, proprotein convertase subtilisin/kexin type 9.

of −65.29 mg dL^{-1}; also, other lipids and apoproteins significantly changed (TC, −60.04 mg dL^{-1}; TG, −12.21 mg dL^{-1}; apoB, −41.01 mg dL^{-1}; HDL-C, +3.40 mg dL^{-1}; and apolipoprotein A-I (apoA-I), +6.75 mg dL^{-1}); lipoprotein (a) (Lp(a)) was significantly reduced following treatment with PCSK9 mAbs (standardized mean difference: −0.94).[82] Despite the reduction of LDL-C levels was greater in patients treated with anti-PCSK9 monotherapy than in those who had received combined therapy (−69.84 mg dL^{-1} vs. −60.16 mg dL^{-1}), the difference was not significant. Patients with HeFH showed a higher LDL-C level reduction compared with patients with non-FH (−79.02 mg dL^{-1} vs. −62.38 mg dL^{-1}). Interestingly, trials with a duration ≤12 weeks obtained greater reductions of LDL-C levels compared with longer trials (−70.89 mg dL^{-1} vs. −55.0 mg dL^{-1}). Mild-to-moderate adverse events as well as serious adverse events did not differ between patients receiving PCSK9 and patients receiving placebo or statin monotherapy. Navarese et al. analyzed 24 RCTs (8 phase 2 and 16 phase 3 trials) including 10,159 patients (6187 receiving anti-PCSK9 and 3972 controls).[81] LDL-C levels were reduced by almost 50% in patients treated with PCSK9 mAb; the reduction was greater when compared with placebo than when compared with ezetimibe (−58.77% vs. −36.17%, $P<0.001$). Also TC and Lp(a) levels were significantly reduced following the treatment with anti-PCSK9 (−31% and −25%, respectively), while HDL-C levels were increased by 6.30% ($P<0.001$). All-cause mortality was significantly reduced in the group of patients receiving anti-PCSK9 (mortality rates: 0.31% vs. 0.53%, $P=0.015$), whereas a nonsignificant reduction of CV mortality was observed (CV mortality rates: 0.19% vs. 0.33%, $P=0.084$) [81]; the rates of unstable angina were similar in the two groups (0.04% vs. 0.08%, $P=0.34$). Treatment with PCSK9 mAb significantly reduced the percentage of patients experiencing an increase in the levels of CK (1.96% vs. 2.31%, $P=0.026$).[81] The overall incidence of serious adverse effects was similar in patients treated with anti-PCSK9 and in patients not receiving the antibodies (9.26% vs. 7.73%, $P=0.879$).[81] Thus, from these two meta-analyses, it appears that anti-PCSK9 antibody treatment effectively corrects lipid abnormalities and reduces the CV mortality in hypercholesterolemic patients.

Evolocumab. A large number of clinical trials have assessed the efficacy and safety of evolocumab in different groups of patients. Most of these studies were 12-week phase 2 and phase 3 trials that reported significant reductions of LDL-C levels compared with either placebo or ezetimibe.[83,84] Tested as monotherapy in *MENDEL* (*Monoclonal Antibody against PCSK9 to Reduce Elevated LDL-C in Subjects Currently Not Receiving Drug Therapy for Easing Lipid Levels*, NCT01375777) and *MENDEL-2* (NCT01763827) trials, the administration of evolocumab for 12 weeks significantly reduced LDL-C levels; similar reductions were observed with 140 mg every 2 weeks (Q2W) or 420 mg every 4 weeks (Q4W) (−50.9% and −48.0% from baseline in MENDEL and −57.0% and −56.1% from baseline in MENDEL-2)[85,86] (**Table 2**). Comparable reductions were reported by other phase 2 trials in different groups of hypercholesterolemic patients.[84]

In *LAPLACE-TIMI 57* (*Low-Density Lipoprotein Cholesterol Assessment with PCSK9 Monoclonal Antibody Inhibition Combined with Statin Therapy*, NCT01380730), hypercholesterolemic patients with LDL-C >85 mg dL^{-1} (>2.2 mmol L^{-1}) despite lipid-lowering therapy (statin with or without ezetimibe), the administration of evolocumab at different doses (70, 105, or 140 mg Q2W or 280, 350, or 420 mg Q4W) for 12 weeks produced a dose-dependent LDL-C reduction[87] (**Table 2**); reductions were comparable in all patient subgroups. Of note, 94% of patients taking evolocumab 140 mg Q2W achieved an LDL-C level <70 mg dL^{-1} (<1.8 mmol L^{-1}), with a mean LDL-C value of 43 mg dL^{-1} (1.1 mmol L^{-1}).[87] In phase 3 *LAPLACE-2* (NCT01763866), patients taking moderate-intensity (atorvastatin 10 mg, simvastatin 40 mg, or rosuvastatin 5 mg) or high-intensity (atorvastatin 80 mg or rosuvastatin 40 mg) therapy were administered with evolocumab (140 mg Q2W or 420 mg Q4W) or placebo or ezetimibe (only in atorvastatin-taking patients).[88] At the mean of weeks 10 and 12, percent reductions were similar across the statin groups and the two evolocumab administration regimens (66–75% with Q2W dosing and 63–75% for Q4W dosing vs. placebo)[88] (**Table 2**). In patients treated with atorvastatin, the addition of evolocumab was significantly more efficacious in reducing LDL-C levels compared with ezetimibe, and greater proportions of patients reached the LDL-C target <70 mg dL^{-1} (<1.8 mmol L^{-1}) with evolocumab than with ezetimibe.[88] When added to a background lipid-lowering therapy for 52 weeks in hypercholesterolemic patients in the *DESCARTES* (*Durable Effect of PCSK9 Antibody Compared with Placebo Study*, NCT01516879) trial, evolocumab significantly reduced LDL-C levels (−57%) either in addition to diet alone or with low-dose (10 mg) or high-dose (80 mg) atorvastatin with or without ezetimibe, and the treatment was well tolerated[89] (**Table 2**). The ongoing *GLAGOV* (*Global Assessment of Plaque Regression with a PCSK9 Antibody as Measured by Intravascular Ultrasound*, NCT01813422) trial will establish whether LDL-C lowering with evolocumab will reduce the percent atheroma volume compared with placebo in subjects with CAD receiving lipid-lowering therapy; the treatment will end after 78 weeks and the trial has an estimated primary completion date in July 2016.

Evolocumab was evaluated in a population of hypercholesterolemic statin-intolerant patients in the phase 2 *GAUSS* (*Goal Achievement after Utilizing an Anti-PCSK9 Antibody in Statin Intolerant Subjects*, NCT01375764) study.[90] Evolocumab was given alone (280, 350, and 420 mg Q4W) or in combination with ezetimibe (420/10 mg) and compared with ezetimibe (10 mg) alone; after 12 weeks, patients who received evolocumab had a dose-dependent reduction of LDL-C levels (−40.8 to −50.7% from baseline), and the association with ezetimibe resulted in a higher decrease compared with ezetimibe alone (−63% vs. −14.8%) (**Table 2**); the maximal reduction was obtained within 2 weeks after starting the treatment.[90] In the group of evolocumab alone, a higher proportion of patients reached the LDL-C targets <100 mg $dL-^{1}$ (<2.6 mmol L^{-1}) or <70 mg dL^{-1} (<1.8 mmol L^{-1}) (54% and 18%) compared with ezetimibe alone (7% and 0%); the combination evolocumab + ezetimibe greatly increased the proportion of patients at target (90% and 62%, respectively).[90] Also TC, non-HDL-C, apoB, and Lp(a) were significantly reduced following evolocumab administration either alone or in combination with ezetimibe; HDL-C and apoA-I increased, although statistically significant differences were observed only with high-dose evolocumab.[90] Overall, the administration of evolocumab was well tolerated, with similar percentages of patients reporting adverse effects in the group of evolocumab and in the group of ezetimibe; myalgia was the most common side effect occurring in 7.4% taking evolocumab alone, in 20% taking evolocumab + ezetimibe, and

Table 2 Results from clinical trials on evolocumab

Clinical trial (ClinicalTrials.gov identification number)	*Subjects*	*Duration*	*Background LLT*	*Intervention*	*LDL-C (percent change from baseline)*	*Primary end point for ongoing trials*
MENDEL, NCT01375777[85]	LDL-C $\geq$100 and <190 mg dL^{-1}; TG <400 mg dL^{-1}	12 weeks	None	70, 105, or 140 mg Q2W 280, 350, or 420 mg Q4W	Q2W: −26.7% to −36.7% versus Eze −37.3% to −47.2% versus placebo Q4W: −25.2% to −34.1% versus Eze −43.6% to −52.5% versus placebo	
MENDEL-2, NCT01763827[86]	LDL-C $\geq$100 and <190 mg dL^{-1}; TG <400 mg dL^{-1}	12 weeks	None	140 mg Q2W 420 mg Q4W	Q2W: −39.3% versus Eze; −57.4% versus placebo Q4W: −37.6% versus Eze; −54.8% versus placebo	
LAPLACE-TIMI 57, NCT01380730[87]	Fasting LDI-C $\geq$85 mg dL^{-1}	12 weeks	Statin ± ezetimibe	70, 105, or 140 mg Q2W 280, 350, or 420 mg Q4W	Q2W: −41.8% to −66.1% versus placebo Q4W: −41.8% to −50.3% versus placebo	
LAPLACE-2, NCT01763866[88]	Fasting LDL-C $\geq$150 mg dL^{-1} if not on statin Fasting LDL-C $\geq$100 mg dL^{-1} if not on intensive statin Fasting LDL-C $\geq$80 mg dL^{-1} if on intensive statin	12 weeks	Atorva 10 ± Eze 10 Atorva 80 ± Eze 10 Rosuva 5 Rosuva 40 Simva 40	140 mg Q2W 420 mg Q4W	Q2W: −66% to −75% versus placebo Q2W: −39.6% to −47.2% versus Eze Q4W: −63% to −75% versus placebo Q4W: −38.9% to −41.1% versus Eze	
DESCARTES, NCT01516879[89]	Fasting LDL-C $\geq$75 mg dL^{-1}	52 weeks	Diet Diet + Atorva 10 mg Diet + Atorva 80 mg Diet + Atorva 80 + Eze 10	420 mg Q4W	−57.0% (48.5-61.6) versus placebo	
GLAGOV, NCT01813422	Fasting LDL-C $\geq$80 mg dL^{-1}	78 weeks	Stable LLT therapy	Evo Q4W (dose not specified)	Ongoing (2016)	Nominal change in percent atheroma volume
GAUSS, NCT01375764[90]	Statin-intolerant	12 weeks	Stable LLT therapy (including statin or low-dose statin)	280, 350, or 420 mg Q4W 420 mg Q4W + Eze 10	−26% to −35.9 versus Eze −47.3% versus Eze	
GAUSS-2, NCT01763905[91]	Statin-intolerant; subjects not at LDL-C goal	12 weeks	Not on statin or on low-dose statin	140 mg Q2W 420 mg Q4W Eze 10	−38.1% versus Eze −37.6% versus Eze	
GAUSS-3, NCT01984424	Statin-intolerant; subjects not at LDL-C goal	Part A: Atorva rechallenge Part B: 24 weeks Part C: 2 years	Stable LLT for at least 4 weeks	Part A: Atorva rechallenge Part B: evo Q4W versus Eze Part C: evo Q2W		Percent change from baseline in LDL-C
FOURIER, NCT01764633	CVD at high risk for a recurrent event LDL-C $\geq$70 mg dL^{-1}	5 years	Effective statin therapy (Atorva 20 mg or equivalent)	140 mg Q2W + effective statin dose 420 mg Q4W + effective statin dose	Ongoing (2017)	Time to CV death, MI, hospitalization for UA, stroke, or coronary revascularization
RUTHERFORD, NCT01375751[92]	HeFH; fasting LDL-C $\geq$100 mg dL^{-1}	12 weeks	Statin ± ezetimibe	350 mg Q4W 420 mg Q4W	−43.8% versus placebo −56.4% versus placebo	

(Continued)

Table 2 Results from clinical trials on evolocumab—cont'd

Clinical trial (ClinicalTrials.gov identification number)	*Subjects*	*Duration*	*Background LLT*	*Intervention*	*LDL-C (percent change from baseline)*	*Primary end point for ongoing trials*
RUTHERFORD-2, NCT01763918[93]	HeFH; fasting LDL-C $\geq$100 mg dL^{-1}	12 weeks	Statin $\pm$ ezetimibe	140 mg Q2W 420 mg 04 W	−59.2% versus placebo −61.3% versus placebo	
TESLA part A, NCT01588496[94]	HOFH; LDL-C $\geq$130 mg dL^{-1}	36 weeks	Stable LLT for at least 4 weeks	420 mg Q4W for 24 weeks + 420 mg Q2W for 12 weeks	Q4W: −16.5% Q2W: −13.9%	
TESLA part B, NCT01588496[95]	HoFH; LDL-C $\geq$130 mg dL^{-1}	12 weeks	Stable LLT for at least 4 weeks	420 mg Q4W	−30.9% versus placebo	
TAUSSIG, NCT01624142	Severe FH	5 years	Stable LLT	Evo Q2W or Q4W	Ongoing (2020)	Subject incidence of treatment-emergent adverse events
OSLER-1, NCT01439880[96]	Subjects from phase 2 evolocumab trials	1 year		420 mg Q4W + standard therapy	−58.4% at week 48 versus standard therapy	Subject incidence of treatment-emergent adverse events
OSLER-2, NCT01854918[97]	Subjects from phase 3 evolocumab trials	1 year			Ongoing (2018)	

FH, familial hypercholesterolemia; *HeFH*, heterozygous familial hypercholesterolemia; *HoFH*, homozygous familial hypercholesterolemia; *LLT*, lipid-lowering therapy; *Q2W*, every 2 weeks; *Q4W*, every 4 weeks; *Eze*, ezetimibe.

in 3.1% taking ezetimibe.[90] In the phase 3 *GAUSS-2* study (NCT01763905), effects of evolocumab 140 mg Q2W or 420 mg Q4W compared with ezetimibe daily were evaluated in hypercholesterolemic patients intolerant to statins and with LDL-C above the recommended target.[91] After a 12-week treatment, evolocumab significantly reduced LDL-C levels compared with ezetimibe (−56.1% with evolocumab 140 mg Q2W and −52.6% with evolocumab 420 mg Q4W, compared with −18.1/−15.1% with ezetimibe), with no difference between the two different evolocumab regimens.[91] Similar results were obtained when considering other biochemical parameters, including non-HDL-C, apoB, and Lp(a).[91] More patients treated with evolocumab reached the LDL-C target goals compared with ezetimibe.[91] Myalgia occurred in 8% of evolocumab patients and 18% of ezetimibe patients.[91] The benefit of evolocumab on CV outcomes is currently under investigation in the GAUSS-3 and the FOURIER (*Further Cardiovascular Outcomes Research with PCSK9 Inhibition in Subjects with Elevated Risk*) studies. The *GAUSS-3* trial (NCT01984424) will include a placebo-controlled reexposure to statin (atorvastatin) before a 24-week double-blind comparison of evolocumab and ezetimibe, followed by 2-year open-label evolocumab extension (**Table 2**). The *FOURIER* study (NCT01764633) will evaluate the effect of evolocumab added to other treatments for dyslipidemia on the risk of CV death, MI, hospitalization for unstable angina, stroke, or coronary revascularization (**Table 2**).

Despite currently used drugs improving the management of HeFH patients, they often do not achieve their LDL-C level target; thus, the *RUTHERFORD* (*Reduction of LDL-C with PCSK9 Inhibition in Heterozygous Familial Hypercholesterolemia Disorder*, NCT01375751) trial evaluated whether evolocumab 350 or 420 mg Q4W was effective in HeFH patients who were unable to achieve LDL-C <100 mg dL^{-1} (<2.6 mmol L^{-1}) despite statin therapy with or without ezetimibe.[92] Percentage reductions of LDL-C were −43.8% and −56.4% versus placebo, respectively[92] (**Table 2**); when compared with patients on ezetimibe or statin alone, similar reductions versus placebo were observed.[92] At week 12, 70% and 89% of patients treated with 350 and 420 mg evolocumab reached LDL-C levels <100 mg dL^{-1} (<2.6 mmol L^{-1}) and 44% and 65% reached LDL-C <70 mg dL^{-1} (<1.8 mmol L^{-1}).[92] Overall, lipid profile was significantly improved, with TC, non-HDL-C, apoB, and Lp(a) significantly reduced.[92] The last finding has a special relevance for FH patients, who commonly exhibit elevated Lp(a) levels. Adverse events were similar in evolocumab-treated patients and in placebo group.[92] The phase 3 *RUTHERFORD-2* (NCT01763918) trial showed that administration of evolocumab 140 mg Q2W or 420 mg Q4W results in similar reductions of LDL-C levels after a 12-week treatment (−59.2% and −61.3% vs. placebo, respectively)[93] (**Table 2**). Reductions were not related to sex, age, body mass index, or type of therapy (intensity of statin therapy or concomitant use of ezetimibe).[93] Among the patients who participated in this study, seven were found to be HoFH or compound heterozygous following the genetic analysis, although they were initially classified as HeFH.[93] They exhibited higher baseline LDL-C levels compared with HeFH, but LDL-C reductions were 68% with 140 mg Q2W and 48% with 420 mg Q4W,[93] which is a much greater response than those reported in trials with selected patients with HoFH. In the pilot study *TESLA* (*Trial Evaluating PCSK9 Antibody in Subjects with LDL Receptor Abnormalities*, NCT01588496) *part A*, eight patients with HoFH (six LDLR-defective and two LDLR-negative) were treated with evolocumab 420 mg Q4W for 24 weeks, followed by 420 mg Q2W for an additional 12 weeks.[94] The treatment resulted in a mean reduction of LDL-C of 17%, with four patients experiencing reductions above 15% and three experiencing reductions above 30%[94] (**Table 2**); the two LDLR-negative patients did not show a reduction of LDL-C levels.[94] In the *TESLA part B*, patients with HoFH not receiving apheresis were administered evolocumab 420 mg or placebo

(33 and 16, respectively) Q4W for 12 weeks in addition to their current lipid-lowering therapy.[95] Evolocumab administration resulted in a reduction versus placebo of 30.9%; one LDLR-negative patient and one patient with autosomal recessive hypercholesterolemia did not respond to the treatment.[95] Among the patients homozygous for the same LDLR mutation, LDL-C reductions were highly heterogeneous and varied from −7.1% to −56%.[95] Overall, the response to evolocumab was related to the genetic defect determining HoFH and ranged from 0% in LDLR-negative patients to 40.8% in more than half of the patients carrying one or two defective LDLR mutations. Patients who completed this study were included in the one-arm open-label extension *TAUSSIG* (*Trial Assessing Long-Term Use of PCSK9 Inhibition in Subjects with Genetic LDL Disorders*, NCT01624142). This study will evaluate the long-term (5 years) efficacy and safety of evolocumab 420 mg Q4W or Q2W in a large cohort (100) of patients with HoFH and has a completion date in March 2020 (**Table 2**). Preliminary data (http://www.athero.org/isa2015/ClinicalBreak/Raal.pdf) show that the reduction of LDL-C persisted up to week 48 and that the administration Q2W results in an incremental 6% reduction compared with evolocumab Q4W in patients not receiving apheresis.

OSLER-1 and *OSLER-2* (*Open-Label Study of Long-Term Evaluation against LDL-C*, NCT01439880 and NCT01854918) are open-label extension trials involving heterogeneous groups of patients that participated in one or more phase 2 or phase 3 studies, respectively, on evolocumab.[96] After 11.1 months, evolocumab reduced LDL-C levels by 61% (**Table 2**).[96] The OSLER-1 study showed that a major part of patients who received evolocumab achieved LDL-C levels below those recommended by current guidelines, with a high percentage of subjects reaching LDL-C levels <50 mg dL^{-1} (1.3 mmol L^{-1}), especially when evolocumab was coadministered with statins.[97] Adverse events, as well as serious adverse events, were similar in placebo- and evolocumab-treated patients.[96,97]

Alirocumab. Alirocumab has a half-life of 6–8 days and is administered subcutaneously every 2 or 4 weeks. In healthy volunteers, alirocumab significantly reduced LDL-C ($>65\%$) and was well tolerated.[98] Three phase 2 trials have evaluated the effects of alirocumab in subjects with hypercholesterolemia. In hypercholesterolemic subjects on stable atorvastatin therapy (*Efficacy and Safety Evaluation of Alirocumab (SAR236553/REGN727) in Patients with Hypercholesterolemia on Stable Atorvastatin Therapy*, NCT01288443), alirocumab when administered for 12 weeks induced a further dose-dependent reduction of LDL-C levels, and the higher efficacy was observed with the Q2W administration compared with higher doses given Q4W[99] (**Table 3**); patients who were not at LDL-C target under atorvastatin therapy achieved this goal after alirocumab treatment.[99] TC, non-HDL-C, and apoB were also significantly reduced.[99] Adverse effects did not differ among groups.[99] Similar results were observed when alirocumab was added to low-dose (10 mg) or high-dose (80 mg) atorvastatin for 8 weeks (*Efficacy and Safety Evaluation of Alirocumab (SAR236553/REGN727) when Coadministered with Atorvastatin in Patients with Primary Hypercholesterolemia*, NCT01288469): a considerable decrease of LDL-C was observed following alirocumab administration compared with atorvastatin alone (−66.2%, −73.2%, and −17.3%, respectively) (**Table 3**), and a greater percentage of patients receiving alirocumab + atorvastatin 80 mg reached the LDL-C target level of <100 mg dL^{-1} (<2.6 mmol L^{-1}) or <70 mg dL^{-1} (<1.8 mmol L^{-1}), without specific safety issues.[100] When tested in a population of HeFH on statin with or without ezetimibe (*Study on the Safety and Efficacy of REGN727/SAR236553 in Patients with HeFH Hypercholesterolemia*, NCT01266876), alirocumab 150 mg Q2W (12-week treatment) reduced LDL-C by 67.9% compared with 10.65% of placebo[101] (**Table 3**).

The *ODYSSEY* program includes 14 phase 3 trials on alirocumab, among a large number of patients ($>23{,}500$) aimed at evaluating the efficacy and safety of alirocumab alone or when combined with other lipid-lowering therapies in several groups of hypercholesterolemic patients. Most of these trials use a dosage of 75 mg Q2W, which is uptitrated to 150 Q2W if the LDL-C target is not reached after 8 weeks. The *ODYSSEY COMBO* studies (I and II) evaluated the efficacy and safety of alirocumab as add-on therapy to stable, maximal tolerated dose of statin, with/without other lipid-lowering drugs in hypercholesterolemic patients of high CV risk. The *COMBO I* trial (*Efficacy and Safety of Alirocumab (SAR236553/REGN727) versus Placebo on Top of Lipid-Modifying Therapy in Patients with High Cardiovascular Risk and Hypercholesterolemia*, NCT01644175) showed that after 24 weeks, LDL-C decreased from baseline by −48.2% with alirocumab and by −2.3% with placebo, and the achieved LDL-C levels were comparable at weeks 24, 36, and 52[102] (**Table 3**); 75% of patients on alirocumab achieved the LDL-C target <70 mg dL^{-1} (<1.8 mmol L^{-1}), compared with 9% of placebo.[102] The incidence of adverse effects was comparable in the two groups.[102] The *COMBO II* trial (*Efficacy and Safety of Alirocumab (SAR236553/REGN727) versus Ezetimibe on Top of Statin in High Cardiovascular Risk Patients with Hypercholesterolemia*, NCT01644188) compared the effect of alirocumab and ezetimibe in a 104-week treatment period in patients with high CV risk and high LDL-C levels despite maximal dose of statin.[103] Mean LDL-C levels decreased rapidly in the first 4 weeks; at week 24, percent change from baseline in LDL-C was −50.6% with alirocumab and −20.7% with ezetimibe (difference between groups: −29.8%) (**Table 3**); these values were maintained up to 52 weeks.[103] Similar incidences of adverse events were observed in the two groups.[103]

In *ODYSSEY FH* studies (FH I, FH II, and HIGH FH), alirocumab was evaluated in the HeFH population.[104] *ODYSSEY FH I* (performed in North America, Europe, and South Africa, NCT01623115) and *FH II* (performed in Europe, NCT01709500) studies, in which patients received alirocumab 75 mg Q2W uptitrated to 150 mg when LDL-C was ≥ 70 mg dL^{-1} (≥ 1.8 mmol L^{-1}) at week 8, showed that HeFH patients with LDL-C levels above the recommended target despite maximal tolerated dose of statin may greatly benefit from alirocumab treatment. In fact, at week 24, LDL-C levels were reduced by 57.9% (FH I) and 51.4% (FH II) versus placebo, respectively (**Table 3**), and these reductions were maintained through week 78.[105] The *ODYSSEY HIGH FH* (NCT01617655) was performed in patients with HeFH with LDL-C ≥ 160 mg dL^{-1} (≥ 4.1 mmol L^{-1}) and treated with alirocumab 150 mg Q2W or placebo for 78 weeks.[104] At week 24, in patients treated with alirocumab, LDL-C levels were reduced by 39% compared with placebo (**Table 3**).

ODYSSEY OPTIONS (I and II) studies were designed to evaluate the efficacy and safety of alirocumab with various therapeutic choices in patients at high CV risk with LDL-C levels not adequately controlled with atorvastatin 20 or 40 mg daily (OPTIONS I) or

Table 3 Results from clinical trials on alirocumab

Clinical trial (ClinicalTrials.gov)	*Subjects*	*Duration*	*Background LLT*	*Treatments*	*LDL-C (percent change from baseline)*	*Primary end point for ongoing trial·*
DFI11565, NCT01288443[99]	LDL-C $\geq$100 mg dL^{-1}	12 weeks	Atorva 10, 20, or 40 mg	Q2W: 50, 100, 150 mg Q4W: 200, 300 mg placebo	Q2W: −39.6% to −72.4% Q4W: −43.2%, −47.7%, −5.1%	
DFI11S66, NCT01288469[100]	LDL-C $\geq$100 mg dL^{-1}	8 weeks	Atorva 10 mg	150 mg Q2W ± Atorva 10 150 mg Q2W + Atorva 80 Atorva 80	−66.2%, −73.2%, −17.3%	
R727-CL-1003, NCT01266876[101]	HeFH; LOL-C $\geq$100 mg dL^{-1}	12 weeks	Diet + statin	150 Q2W 150, 200, 300 Q4W	−57.2% versus placebo −18.2% to −31.9% versus placebo	
ODYSSEY COMBO I, NCT01644175[102]	Established CHD or CUD equivalent, LDL-C $\geq$70 mg dL^{-1}	52 weeks	Max tolerated statin ± other LLT	75 mg Q2W (increased at 150 mg Q2W if LDL-C 270 mg dL^{-1} at week 8)	−45.9% versus placebo at week 24	
ODYSSEY COMBO II, NCT01644188[103]	Established CHD or CHD equivalent, LDL-C $\geq$70 mg dL^{-1} with maximally tolerated dose of statin	52 weeks	High-intensity statins	75 mg Q2W (increased at 150 mg Q2W if LDL-C $\geq$70 mg dL^{-1} at week 8)	−29.8% versus Eze at week 24 −31.2% versus Eze at week 52	
ODYSSEY FH I and FH II, NCT01623115 and NCT01709500[105]	HeFH, LDL-C $\geq$100 mg dL^{-1} (for primary prevention) or LDL-C $\geq$70 mg dL^{-1} (for secondary prevention)	78 weeks	Max tolerated statin ± other LLT	75 mg Q2W (increased at 150 mg Q2W if LDL-C $\geq$70 mg dL^{-1} at week 8)	FH I: −57.9% versus placebo FH II: −51.4% versus placebo	
ODYSSEY HIGH FH, NCT01617655[104]	HeFH LDL-C $\geq$160	78 weeks	Stable LLT	150 mg Q2W	−39% versus placebo at week 24	
ODYSSEY OPTIONS I, NCT01730040[107]	Very high CVD risk and LDL-C $\geq$70 mg dL^{-1} or high CVD risk and LDL-C $\geq$100 mg dL^{-1}	24 weeks	Atorva 20 or 40 mg	75 mg Q2W Eze 10 mg Doubling Atorva dose Atorva 40 → Rosuva 40	Entry statin: Atorva 20 (−44.1%, −20.5%); Atorva 40 (−54%, −22.6%, −21.4%)	
ODYSSEY OPTIONS II, NCT01730053[108]	Very high CVD risk and LDL-C $\geq$70 mg dL^{-1} or high CVD risk and LDL-C $\geq$100 mg dL^{-1}	24 weeks	Rosuva 10 or 20 mg	75 mg Q2W Eze 10 mg Doubling Rosuva dose	Entry statin: Rosuva 10 (−50.6%, −14.4%, −16.3%); Rosuva 20 (−36.3%, −11.0%, −15.9%)	
ODYSSEY ALTERNATIVE, NCT01709513[109]	Moderate or high CV risk with statin intolerance, LDL-C $\geq$100 or $\geq$70 mg dL^{-1}	24 weeks	Nonstatin LLT	75 mg Q2W Eze 10 mg	−34.7% versus Eze	
ODYSSEY MONO, NCT01644474[110]	LDL-C $\geq$100 and $<$190 mg dL^{-1}	24 weeks	None	75 mg Q2W Eze 10 mg	−31.6% versus Eze	
ODYSSEY LONG TERM, NCT01507831[111]	HeFH or established CHD or CHD equivalent LDL-C $\geq$70 mg dL^{-1}	78 weeks	Max tolerated statin ± other LLT	150 mg Q2W	−61.9% versus placebo at week 24	

Table 3 Results from clinical trials on alirocumab—cont'd

Clinical trial (ClinicalTrials.gov)	*Subjects*	*Duration*	*Background LLT*	*Treatments*	*LDL-C (percent change from baseline)*	*Primary end point for ongoing trial·*
ODYSSEY OLE, NCT01954394	HeFH who have completed one of the four parent studies	176 weeks			Ongoing (2017)	Assessment of safety parameters
ODYSSEY OUTCOMES, NCT01663402[112]	Recent ACS (4–52 weeks prior to randomization), LDL-C $\geq$70 mg dL^{-1}	64 months	Atorva 40–80 mg or Rosuva 20–40 or the max tolerated dose	75 mg Q2W 150 mg Q2W	Ongoing (2017)	Time from randomization to first occurrence of CHD death, nonfatal MI, stroke, or UA requiring hospitalization

FH, familial hypercholesterolemia; *HeFH*, heterozygous familial hypercholesterolemia; *HoFH*, homozygous familial hypercholesterolemia; *CHD*, coronary heart disease; *CVD*, cardiovascular disease; *ACS*, acute coronary syndrome; *LLT*, lipid-lowering therapy; *Q2W*, every 2 weeks; *Q4W*, every 4 weeks; *Atorva*, atorvastatin; *Rosuva*, rosuvastatin; *Eze*, ezetimibe.

rosuvastatin 10 or 20 mg daily (OPTIONS II).[106] The *ODYSSEY OPTIONS I* (NCT01730040) trial was performed in patients with very high CVD risk and LDL-C $\geq$70 mg dL^{-1} ($\geq$1.8 mmol L^{-1}) or high CVD risk and LDL-C $\geq$100 mg dL^{-1} ($\geq$2.6 mmol L^{-1}) and compared the efficacy and safety of alirocumab 75 mg Q2W (switched to 150 mg Q2W if LDL-C target was not achieved after 12 weeks) added to atorvastatin 20 or 40 mg with several alternative approaches including adding ezetimibe, doubling atorvastatin dose, or switching from atorvastatin 40 mg to rosuvastatin 40 mg.[107] The addition of alirocumab resulted in the greatest reduction of LDL-C, being reduced by 44.1% and 54.0% with baseline atorvastatin 20 or 40 mg, respectively, by 20.5% and 22.6% after addition of ezetimibe, by 5.0% and 4.8% with doubled atorvastatin dose, and by 21.4% when switching from atorvastatin to rosuvastatin[107] (**Table 3**). A significantly higher proportion of patients receiving alirocumab achieved their LDL-C goals compared with the other treatments[107]; in addition, alirocumab induced a higher reduction of apoB, non-HDL-C, and Lp(a) levels compared with other treatments.[107] Treatment-emergent adverse events were comparable among groups.[107] The *ODYSSEY OPTIONS II* (NCT01730053) evaluated the addition of alirocumab on a background of rosuvastatin 10 or 20 mg in the same type of patients and showed a higher reduction of LDL-C levels with alirocumab ($-$50.6% and $-$36.3%, respectively) compared with the addition of ezetimibe ($-$14.4% and $-$11.0%) or doubling rosuvastatin dose ($-$16.3% and $-$15.9%) after 24 weeks[108] (**Table 3**). Again, similar percentages of treatment-emergent adverse events in the various treatment groups were observed.[108] These trials demonstrated that the addition of PCSK9 antibody achieves LDL-C goals in patients at high/very high CVD risk and not optimally controlled with conventional lipid-lowering treatments.

Statin-intolerant patients with moderate to very high CVD risk with LDL-C $\geq$190 mg dL^{-1} ($\geq$4.9 mmol L^{-1}) were treated with alirocumab 75 mg Q2W (with potential uptitration to 150 mg Q2W) or ezetimibe 10 mg day^{-1} or atorvastatin 20 mg day^{-1} (statin rechallenge; included only as control to define the appropriate patient population) for 24 weeks to evaluate percent change from baseline in LDL-C in the *ODYSSEY ALTERNATIVE* trial (NCT01709513). Alirocumab was superior to ezetimibe in reducing LDL-C levels throughout the study ($-$54.8% and $-$20.1% from baseline, respectively, at week 24, $P<0.0001$) (**Table 3**); a greater proportion of patients receiving alirocumab achieved the LDL-C goals relative to their CV risk compared with those receiving ezetimibe (41.9% vs. 4.4%).[109] TC, non-HDL-C, apoB, and Lp(a) were more significantly reduced with alirocumab than with ezetimibe.[109] Myalgia was the most common adverse event in all groups, but in the alirocumab group, the rate of muscle-related adverse events was significantly lower than in the atorvastatin group (hazard ratio: 0.61, $P=0.042$) with a similar result also compared with the ezetimibe group (HR 0.71, $P=0.096$).[109] Similar results were obtained in the *ODYSSEY MONO* trial (NCT01644474), conducted in hypercholesterolemic patients on no lipid-lowering therapy, with reductions of LDL-C levels of 47.2% with alirocumab and 15.6% with ezetimibe at week 24[110] (**Table 3**).

Two trials have been designed to evaluate the safety of long-term administration of alirocumab. The *ODYSSEY LONG TERM* (NCT01507831) was conducted in high CV risk patients with hypercholesterolemia not adequately controlled by the current lipid-lowering therapy and treated with alirocumab or placebo for up to 86 weeks. The mean percent change in calculated LDL-C was $-$61% with alirocumab and +0.8% with placebo at week 24[111] (**Table 3**) and was similar in HeFH and non-HeFH patients; a consistent reduction of LDL-C levels was obtained after a 4-week treatment and maintained up to 78 weeks.[111] Adverse events occurred similarly in the two groups, but myalgia occurred at a higher frequency in the alirocumab group (5.4% vs. 2.9% in placebo, $P=0.006$).[111] A post hoc analysis suggests a lower rate of major CV events in patients treated with alirocumab than in the placebo group (1.7% vs. 3.3%, HR 0.52, nominal $P=0.02$), with cumulative probability of event curves tending to diverge over time.[111] The ongoing *ODYSSEY OLE* (Open Label Study of Long-Term Safety Evaluation of Alirocumab) (NCT01954394) has as

current primary outcome the assessment of safety parameters (adverse events, laboratory data, and vital signs) following a treatment with alirocumab up to 176 weeks in patients with HeFH. Secondary outcomes are the effects on lipid parameters; the estimated completion date is June 2017.

Finally, the *ODYSSEY OUTCOMES* (NCT01663402) is recruiting patients with a recent acute coronary syndrome to evaluate the effect of adding alirocumab versus placebo to their current therapy on the occurrence of CV events, including CHD death, MI, fatal and nonfatal ischemic stroke, and unstable angina requiring hospitalization.[112]

Bococizumab. Four phase 2 trials on bococizumab have been performed (NCT01342211, NCT01592240, NCT01350141, and NCT02055976); to date, only results from one of these studies have been published. Ballantyne et al. showed that bococizumab (NCT01592240) significantly reduced LDL-C levels across all doses in patients with hypercholesterolemia on stable statin therapy and with fasting LDL-C $\geq$80 mg dL^{-1} ($\geq$2.1 mmol L^{-1})[113] (**Table 4**); however, despite similar reductions with low doses (100 and 150 mg) Q2W or high doses (200 and 300 mg) Q4W, patients who received bococizumab Q2W maintained the LDL-C reductions between dose administration, whereas those who received bococizumab Q4W did not.[113] The frequency of adverse events was similar in all groups.[113] The *SPIRE* (Studies on PCSK9 Inhibition and the Reduction of Vascular Events) program includes eight phase 3 trials (**Table 4**); among these, six are designed to assess the LDL-C-lowering efficiency of bococizumab in several hypercholesterolemic populations (SPIRE-AI, NCT02458287; SPIRE-SI, NCT02135029; SPIRE-FH, NCT01968980; SPIRE-LL, NCT02100514; SPIRE-HR, NCT01968954; and SPIRE-LDL, NCT01968967), whereas the other two will evaluate the effect of long-term bococizumab administration on the occurrence of major CV events in high-risk patients with LDL-C levels 70–100 mg dL^{-1} (1.8-2.6 mmol L^{-1}) (SPIRE-1: NCT01975376) or with LDL-C levels $\geq$100 mg dL^{-1} ($\geq$2.6 mmol L^{-1}) despite high-dose statin (SPIRE-2: NCT01975389).

7.18.3.1.3 Mipomersen

Despite the fact that statins are the most used LDL-C-lowering drug class, certain patients with FH may not benefit from the use of statins or PCSK9 mAbs because their mechanism of action requires the presence of at least partially functional LDLR.[8,9] Thus, HoFH with *ldlr* mutations leading to the absence of LDLR will not benefit from statin- or anti-PCSK9 mAb-based therapies and thus need

Table 4 Results from one clinical trial on bococizumab and list of the ongoing trials

Clinical trial (ClinicalTrials.gov identification number)	*Subjects*	*Duration*	*Background LLT*	*Treatments*	*LDL-C (percent change from baseline)*	*Primary end point for ongoing trials*
NCT01592240[113]	Fasting LDL-C $\geq$80 TG $\leq$400 mg dL^{-1}	24 weeks	Stable statin therapy	Q2W: 50, 100, 150 mg Q4W: 200, 300 mg	Q2W: −35.4%, −52.3%, −54.2% Q4W: −21.3%, −38.3%	
SPIRE-AI, NCT02458287	Hyperlipidemic/dyslipidemic LDL-C $\geq$70 mg dL^{-1} TG $\leq$400 mg dL^{-1}	12 weeks	Statin	75, 150 mg Q2W	Ongoing (2016)	Percent change from baseline in LDL-C
SPIRE-SI, NCT02135029	Hyperlipidemic, statin-intolerant LDL-C $\geq$70 mg dL^{-1} TG $\leq$400 mg dL^{-1}	24 weeks		150 mg Q2W	Ongoing (2015)	Percent change from baseline in fasting LDL-C
SPIRE-FH, NCT01968980	HeFH LDL-C $\geq$70 mg dL^{-1} TG $\leq$400 mg dL^{-1}	52 weeks	Statin	150 mg Q2W	Ongoing (2016)	Percent change from baseline in LDL-C
SPIRE-LL, NCT02100514	High or very high CV risk LDL-C $\geq$100 mg dL^{-1} TG $\leq$400 mg dL^{-1}	52 weeks	Statins	150 mg Q2W	Ongoing (2016)	Percent change from baseline in fasting LDL-C
SPIRE-HR, NCT01968954	High or very high CV risk LDL-C $>$70 mg dL^{-1} TG $\leq$400 mg dL^{-1}	12 months	Statin	150 mg Q2W	Ongoing (2016)	Percent change from baseline in LDL-C
SPIRE-LDL, NCT01968967	High or very high CV risk fasting LDL-C $>$70 mg dL^{-1} TG $\leq$400 mg dL^{-1}	12 months	Statin	150 mg Q2W	Ongoing (2016)	Percent change from baseline in LDL-C
SPIRE-1, NCT01975376	High CV risk LDL-C $\geq$70 and $<$100 mg dL^{-1}	5 years	LLT	150 mg Q2W	Ongoing (2018)	CV death, nonfatal MI or stroke, UA needing urgent revascularization
SPIRE-2, NCT01975389	High CV risk LDL-C $\geq$100 mg dL^{-1}	5 years	LLT	150 mg Q2W	Ongoing (2018)	CV death, nonfatal MI or stroke, UA needing urgent revascularization

HeFH, heterozygous familial hypercholesterolemia; *CV*, cardiovascular; *LLT*, lipid-lowering therapy; *Q2W*, every 2 weeks.

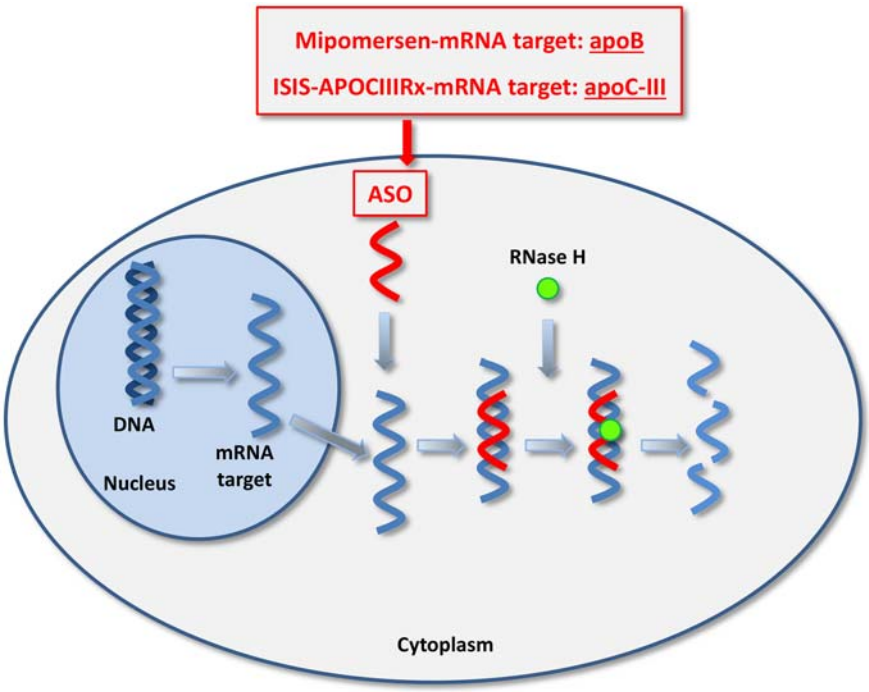

Fig. 4 Mechanism of action of antisense oligonucleotides. Mipomersen and ISIS-APOCIIIRx are second-generation antisense oligonucleotides (ASOs) that inhibit the synthesis of apoB and apolipoprotein C-III, respectively. They bind to the cognate mRNA forming a substrate for ribonuclease H (RNase H), a ubiquitously expressed nuclease, thus resulting in mRNA degradation and reduced production of the encoded protein.

alternative lipid-lowering drugs with mechanisms of action independent of LDLR expression as add-on to the maximal potent statin dose[8] and may include ezetimibe and the most recently approved mipomersen and lomitapide.[9]

High levels of apoB, the main apoprotein of atherogenic lipoproteins [LDL, very-low-density lipoprotein (VLDL), and chylomicrons], represent an established risk factor in atherosclerosis, and the discovery of truncating apoB mutations resulting in low levels of LDL-C indicated it as potential pharmacological target for the treatment of hypercholesterolemia.[114] Mipomersen is a second-generation antisense oligonucleotide (ASO) against the coding region of human apoB mRNA and thus acts as an inhibitor of apoB synthesis[115] (**Fig. 4**). When administered by injection, it is rapidly absorbed, with the liver being one of the organs that accumulate the highest concentrations of this drug,[115] and in humans, it has an elimination half-life of about 30 days.[115] Its administration leads to a dose-dependent reduction of apoB and TC [116]; several studies have shown the lipid-lowering efficacy of mipomersen either as monotherapy or as add-on to current lipid-lowering therapies.[117–124] Mipomersen is not metabolized by the CYP450 system, it does not inhibit major CYP isoenzymes, and it does not show clinically relevant interaction with simvastatin or ezetimibe.[125] The most common adverse reaction associated with mipomersen is the injection site reaction following subcutaneous administration. Due to its characteristics, mipomersen represents an effective approach as lipid-lowering agent in the management of FH but can also be considered in statin-intolerant patients.

Two meta-analyses of randomized clinical trials have reported significant decrease of LDL-C levels induced by mipomersen treatments, as well as beneficial effects on other lipid parameters.[126,127] Both meta-analyses reported as major adverse events associated with mipomersen treatment the risk of injection site reactions, elevated alanine aminotransferase (ALT) $>3\times$ the upper limit of normal (ULN), and hepatic steatosis and flu-like symptoms;[126,127] the most relevant side effect of mipomersen seems to be an increased content of TG in the liver, but though short-term studies revealed an increased steatosis (whose clinical relevance was considered low) in mipomersen-treated subjects, long-term (up to 104 weeks) clinical trials observed a return to normal of hepatic TG level.[128,129] The analysis of liver biopsies of some hypercholesterolemic patients after mipomersen treatment showed a histopathological feature of simple steatosis without signs of inflammation or fibrosis.[130]

In the *ASSIST* (Safety and Efficacy Study of ISIS 301012 (Mipomersen) Administration in High Risk Subjects NCT00707746) trial, mipomersen (200 mg $week^{-1}$) significantly decreased apoB100 and LDL-C levels and reduced small dense proatherogenic LDL, but did not affect high-density lipoprotein (HDL) or apoA-I levels in statin-intolerant hypercholesterolemic patients[124] (**Table 5**); overall, mipomersen was well tolerated.[124] In patients with mild to moderately elevated LDL-C (*Safety and Tolerability of Varying Load and Dose of ISIS 301012 in People with Elevated LDL-C Levels*, NCT00216463) (130 mg dL^{-1} and 3.3 mmol L^{-1}) who did not receive any lipid-lowering therapy in the past month, mipomersen at doses ranging from 50 to 400 mg $week^{-1}$ dose-dependently reduced LDL-C levels (from -8% to -70.6%)[123] (**Table 5**). In hypercholesterolemic patients at high CV risk (*Safety and Efficacy of Mipomersen (ISIS 301012) as Add-on Therapy in High Risk Hypercholesterolemic Patients*, NCT00770146), mipomersen 200 mg significantly reduced LDL-C levels (**Table 5**); after treatment completion, LDL-C levels increased and reached

Table 5 Results from clinical trials on mipomersen and lomitapide

Clinical trial (ClinicalTrials.gov identification number)	*Subjects*	*Duration*	*LDL-C (percent change from baseline)*	*Lp(a) (percent change from baseline)*	*Primary end point for ongoing clinical trials*
Mipomersen					
ASSIST (NCT00707746)[124]	Statin-intolerant, hypercholesterolemic at high CVD risk	26 weeks	−47.3% (200 mg) (vs. −2% placebo)	−27.1% (200 mg) (vs. 0% placebo)	
NCT00216463[123]	LDL-C ≥130 mg dL^{-1}	13 weeks	−8% (50 mg) to 70.6% (400 mg) versus placebo		
NCT00770146[131]	LDL-C ≥100 mg dL^{-1}, at high CHD risk, on stable maximally tolerated dose of statin	28 weeks	−39.6% (200 mg) (−4.5% placebo)	−25.6% (200 mg) (vs. 0.0% placebo)	
NCT00477594[118]	HeFH	6 weeks	−13% (50 mg) to −34% (300 mg) versus placebo	−3% (50 mg) to −24% (300 mg)	
RADICHOL II, NCT00706849[122]	HeFH with CAD on maximally tolerated statin, LDL-C ≥100 mg dL^{-1}	28 weeks	−28% (200 mg) (vs. +5.2% placebo)	−21.1% (200 mg) (vs. +0.0% placebo)	
RADICHOL 1, NCT00607373[121]	HoFH	28 weeks	−21.1% (160 mg) versus placebo	−23.2% (160 mg) versus placebo	
NCT00694109[132]	FH or severe hypercholesterolemia	4.5 years	−28% at week 104	−14% at week 104	
FOCUS FH, NCT01475825	Severe HeFH	60 weeks			Percent change from baseline in LDL-C (completion date: 2016)
Lomitapide					
Cuchel etal.[145]	HoFH	4 weeks for each dose	−24.7% (0.3 mg) −50.9% (1.0 mg)	Unchanged	
NCT00730236[146]	HoFH	26+52 weeks	−50% at week 26 -38% at week 78	−15% at week 26 –0.5% at week 78	
Roeters van Lennep et al.[150]	HoFH		−35% to −73%		

CVD, cardiovascular disease; *CHD*, coronary heart disease; *CAD*, coronary artery disease; *HeFH*, heterozygous familial hypercholesterolemia; *HoFH*, homozygous familial hypercholesterolemia.

baseline levels after 24 weeks.[131] The effect appeared to be greater in women and in patients aged >59 years.[131] Other lipid parameters, including Lp(a), were significantly reduced by mipomersen treatment.[131] All patients treated with mipomersen experienced an injection site reaction, while 23% had an ALT elevation >3× ULN.[123] In a phase 2 study (NCT00477594), 44 patients with HeFH were randomized to mipomersen 50, 100, 200, or 300 mg $week^{-1}$ or placebo for 6 weeks in a background of conventional lipid-lowering therapy, including high-dose statins. Mipomersen reduced apoB and LDL-C by 23% and 21%, respectively, at 200 mg $week^{-1}$ and by 33% and 34%, respectively, at 300 mg $week^{-1}$[118] (**Table 5**). The most common adverse effect with mipomersen was injection site erythema (97%); four patients treated with mipomersen (three of which in the highest dose group) experienced transaminase elevations >3× ULN with signs of hepatic steatosis; no clinically relevant interactions with currently used drugs were observed.[118] LDL-C levels remained lower than baseline levels for 2–3 months after the last injection in the two groups with the highest doses (200 and 300 mg $week^{-1}$), likely due to the long mipomersen half-life.[118] In HeFH patients with CAD (*RADICHOL II*: *Efficacy and Safety Study of ISIS 301012 (Mipomersen) as Add-on in Familial Hypercholesterolemic Patients with Coronary Artery Disease*, NCT00706849), mipomersen treatment induced a −28% reduction from baseline in LDL-C (vs. +5.2% placebo, $P<0.001$) (**Table 5**); the reduction was independent of baseline LDL-C levels and age, but the response was greater in women than in men.[122] ApoB, non-HDL-C, TC, and Lp(a) were significantly reduced in the mipomersen group.[122]

Effective LDL-C reduction with mipomersen (200 mg $week^{-1}$ for 26 weeks) was observed also in 51 patients with HoFH already treated with maximal conventional lipid-lowering therapy (*RADICHOL 1*: *Study to Assess the Safety and Efficacy of ISIS 301012 (Mipomersen) in Homozygous Familial Hypercholesterolemia*, NCT00607373): the mean percent change in LDL-C from baseline was −24.7% (vs. −3.3% with placebo), independently of baseline LDL-C levels.[121] Significant reductions in apoB (−24.2%), non-HDL-C (−21.6%), and Lp(a) (−23.2%) were also reported.[121] Again, the most common adverse event was injection site reactions (76% of mipomersen patients and 24% of placebo patients).[121] ALT elevations ≥3 times ULN occurred in four mipomersen patients, including 1 who had significantly increased hepatic fat.[121] A recent report of 2-year interim results of an ongoing open-label study (conducted in patients with FH or severe hypercholesterolemia on lipid-lowering therapy who had completed one of the described studies, NCT00694109) (**Table 5**) showed that, in HoFH and HeFH patients, mipomersen in

combination with the maximally tolerated dose of lipid-lowering therapy showed that favorable effects on lipid profile were maintained throughout the study and that safety issues were similar to those reported for a 26-week treatment.[132] Data from the 4-year time point will further clarify this finding.

Besides its effect on LDL-C levels, mipomersen has been also evaluated on Lp(a) levels. Lp(a) is a causal, independent genetic risk factor for MI, stroke, and peripheral artery disease.[133–135] Its levels are particularly elevated in patients with FH and are related to severity of hypercholesterolemia,[136] and commonly used lipid-lowering drugs are not effective in reducing Lp(a). Lp(a) has a structure similar to that of LDL, from which it differs in the presence of the glycoprotein apolipoprotein (a) covalently bound to apoB.[137] As mipomersen acts by specifically inhibiting apoB production, it may also affect the formation of Lp(a). In four phase 3 trials, mipomersen significantly reduced Lp(a) levels in various hypercholesterolemic populations[138]; the highest effects were reported in HoFH and in patients with severe hypercholesterolemia at week 26 (−31.8% and −39.1%, respectively).[138] In the pooled analysis of all patients, including HeFH with CAD and hypercholesterolemic patients at high risk for CAD, LDL-C levels were reduced by 26.4%,[138] thus suggesting that mipomersen can efficiently reduce both LDL-C and Lp(a) levels. Whether this can translate into a further clinical benefit remains to be addressed, as the commonly used lipid-lowering drugs do not lower Lp(a).[139]

The ongoing *FOCUS FH* (*A Study of the Safety and Efficacy of Two Different Regimens of Mipomersen in Patients with Familial Hypercholesterolemia and Inadequately Controlled Low-Density Lipoprotein Cholesterol*, NCT01475825) study will determine whether administration of mipomersen for 60 weeks at two different dosing regimens (70 mg thrice weekly or 200 mg once weekly) can significantly reduce LDL-C levels in patients with severe HeFH, thus providing further information on the efficacy and safety of this drug.

7.18.3.1.4 Lomitapide

MTP (microsomal triglyceride transport protein) is a lipid transfer protein crucial for the assembly and secretion of apolipoprotein B-containing lipoproteins, including VLDL and chylomicrons (Fig. 5).[140] MTP localizes in the endoplasmic reticulum (ER) of hepatocytes and enterocytes and acts by transferring TG and cholesteryl esters from the ER membrane to the nascent apoB.[140] Since subjects carrying mutations of the gene encoding for MTP (*MTTP*) exhibit significantly reduced synthesis of VLDL and chylomicrons and increased apoB degradation, thus resulting in reduced circulating VLDL and LDL,[141] it has been hypothesized that inhibition of MTP might be a valuable approach to treat hypercholesterolemia in FH patients. MTP inhibition results in the reduction of both cholesterol and TG plasma levels, due to the inhibition of production of apoB-containing lipoproteins in both the liver (VLDL) and intestine (chylomicrons). Studies in animal models of HoFH have in fact showed that MTP inhibition normalized the levels of atherogenic lipoproteins by greatly reducing the secretion rate of VLDL.[142–144]

Lomitapide is an MTP inhibitor that, by binding MTP, inhibits MTP-mediated synthesis of VLDL and chylomicrons, thus resulting in a significant reduction of LDL-C levels (Fig. 5). Due to the high difficulty to efficiently treat HoFH patients, lomitapide

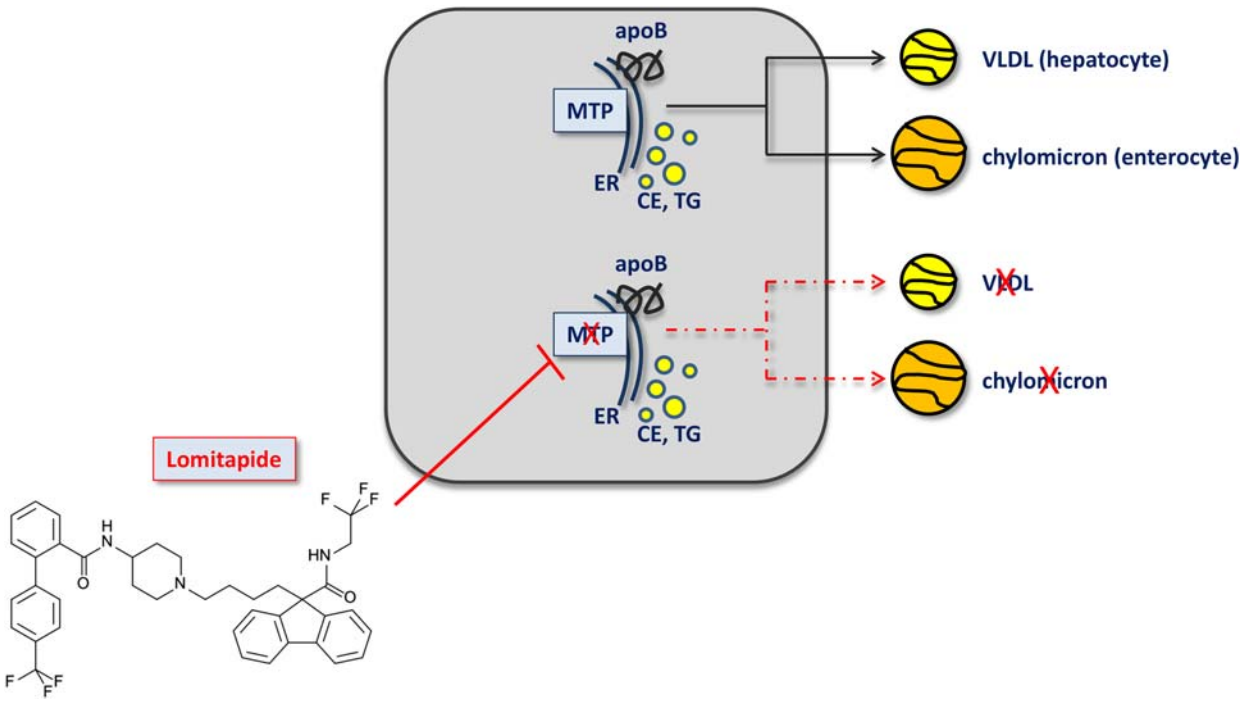

Fig. 5 Mode of action of lomitapide. MTP mediates the transfer of lipid droplet to apoB-100 in the liver and apoB-48 in the intestine, thus resulting in the secretion of VLDL and chylomicrons, respectively. Lomitapide inhibits the activity of MTP in both the liver and intestine.

was considered as a possible approach to reduce LDL-C levels in these patients; to test this possibility, six patients with HoFH (five LDLR-negative and one LDLR-defective) were enrolled in a study in which all lipid-lowering treatments were suspended at least 4 weeks before the baseline visit, and lomitapide was administered at four increasing doses (0.03, 0.1, 0.3, and 1.0 mg kg^{-1} body weight), each for 4 weeks.[145] The mean LDL-C level was reduced by 24.7% after 0.3 mg kg^{-1} for 4 weeks and by 50.9% after 1.0 mg kg^{-1} for 4 weeks[145] (**Table 5**); similarly, TC was reduced by 29.8% and 58.4% from the baseline level, respectively.[145] Both TG and apoB were significantly reduced (TG, −34.1% and −65.2%, and apoB, −14.7% and −55.6%, respectively).[145] The drug was well tolerated and the most serious adverse events were elevations in liver aminotransferase levels and hepatic fat accumulation.[145] Thus, lomitapide was highly effective in reducing LDL-C levels, but the accumulation of fat in the liver requires further investigations to evaluate the long-term safety.

To answer this question, lomitapide was given to 29 HoFH patients in single-arm, open-label, phase 3 study in addition to their lipid-lowering therapy (*A Safety and Efficacy Study of AEGR-733 to Treat Homozygous Familial Hypercholesterolemia*, NCT00730236).[146] This study consisted of a 26-week efficacy study during which lomitapide was initiated at a starting dose of 5 mg day^{-1} for the first 2 weeks and then escalated to 10, 20, 40, and 60 mg day^{-1} at 4-week intervals or until the maximal dose was identified for each subject on the basis of safety and tolerability, and a 52-week safety study that allowed the investigators to modify the concomitant lipid-lowering therapy based on lomitapide effect.[146] Mean LDL-C levels were significantly reduced by 50% at the end of efficacy phase, leading to the discontinuation of LDL apheresis or to the increased interval times between two apheresis processes.[146] At the end of the study (week 78), LDL-C was still significantly reduced, but the reduction was attenuated (−38%) compared with the values at the end of the efficacy study (**Table 5**); this could be due to changes in the concomitant lipid-lowering therapies as well as to the reduction of lomitapide doses in patients experiencing adverse effects.[146] Very-low-density lipoprotein cholesterol (VLDL-C), non-HDL-C, and TG levels were significantly decreased at the end of the efficacy phase (−45%, −50%, and −45%, respectively), and at the end of the study, such reductions resulted attenuated (−31%, −39%, and −31%, respectively), in line with the results obtained for LDL-C levels (**Table 4**).[146] HDL-C and apoA-I levels were significantly reduced at week 26 (−12% and −14%), but returned to levels similar to baseline at the end of the study.[146] During the first period (0–26 weeks), 15 patients reached the LDL-C level target <100 mg dL^{-1} (2.6 mmol L^{-1}), and 8 had LDL-C <70 mg dL^{-1} (<1.8 mmol L^{-1}).[146] The effect of lomitapide on LDL-C level was independent of apheresis treatment, as comparable reductions of LDL-C levels were achieved in patients undergoing apheresis and in those not undergoing apheresis (55.1% vs. 48%).[147] Most patients had mild to moderate gastrointestinal adverse effects during the treatment with lomitapide. Some patients exhibited increased levels of ALT, aspartate aminotransferase (AST), or both, but these changes were transient, were resolved when lomitapide doses were reduced, and were not related to changes of liver function.[146] Mean hepatic fat increased during the efficacy phase but did not further increase (8.6% at week 26 and 8.3% at week 78).[146] The clinical relevance of this rise in liver fat is still unclear and, since lomitapide might be administered lifelong, requires further investigation to assess whether it can progress to hepatic fibrosis or cirrhosis. Comparable results were reported in an Italian subgroup of HoFH patients participating in the described study.[148] These findings, together with the recent data obtained in a HoFH patient treated with lomitapide in addition to other lipid-lowering therapies for 5 years,[149] suggest that lomitapide may be a valuable pharmacological approach for the treatment of these very high-risk patients.

Recently, the use of lomitapide in four HoFH patients (two compound heterozygotes and two homozygotes) in the clinical practice setting has been reported.[150] In all patients, LDL-C levels were significantly reduced (35–73%)[150] (**Table 5**). One compound heterozygous patient having two different severe mutations in the *LDLR* gene, one in each allele, who had LDL-C levels ranging from 290 to 688 mg dL^{-1} (7.4–17.6 mmol L^{-1}) despite atorvastatin + colesevelam therapy, was treated with lomitapide. Lomitapide was started at 5 mg and then escalated to 30 mg day^{-1}; LDL-C levels decreased drastically, reaching very low levels (93 mg dL^{-1} and 2.4 mmol L^{-1}), with a reduction of 83% over 8 months.[150] The second compound heterozygote who had an LDL-C level of about 260 mg dL^{-1} (6.7 mmol L^{-1}) when lomitapide was added to the maximal background LLT (rosuvastatin 40 mg, ezetimibe 10 mg, and colesevelam 2.5 g) had LDL-C reduced by 35%.[150] In one HoFH LDLR-negative patient, who underwent apheresis and was on simvastatin + ezetimibe therapy, lomitapide therapy resulted in LDL-C and TC reductions of 73% and 62%, respectively.[150] The other homozygous patient who had a history of CV disease started lomitapide 5 mg and had a significant decrease of LDL-C within 1 month of treatment.[150] However, when escalated to 10 mg daily, levels of AST and ALT increased by more than 5 × ULN, which resulted in the discontinuation of the drug. Resumption of lomitapide after 4 weeks at 5 mg also increased ALT by three times; thus, the drug was stopped permanently.[150] Altogether, these data indicate that, although lomitapide added to aggressive lipid-lowering therapies may be useful to further reduce LDL-C in HoFH, each patient must be individually monitored to avoid hepatic impairment. Longer follow-ups are required to establish whether lomitapide treatment may effectively prevent CV events.

To date, there are few data on the long-term efficacy and safety of lomitapide. A single case report has been published regarding a patient with a homozygosity for *LPL* gene resulting in the production of noncatalytically active enzyme associated with severe hypertriglyceridemia (HTG) and recurrent pancreatitis.[151] In 1999, lomitapide was given to this patient after stopping all other lipid-lowering treatments; fasting TG levels were significantly reduced, and in the course of 13 years, she had three hospitalizations for pancreatitis during discontinuation of lomitapide or high dietary fat intake.[151] Plasma levels of ALT and AST were within the reference range during the initial 6–7 years and then increased; the fatty liver that was already present before starting lomitapide progressed to hepatitis and fibrosis.[152] It is possible that inhibition of MTP may have reduced the main route by which hepatocytes reduce their fat content. In addition, MTP inhibition increases liver transaminases, and these two different aspects may have interacted and worsened the liver condition.[152]

An ongoing study is evaluating the effect of lomitapide treatment on carotid and aortic atherosclerosis in HoFH patients (NCT02399852) and will measure the percent change from baseline in carotid vessel wall area at the 2-year evaluation as well as the percent change from baseline in carotid aortic vessel wall area and thickness at 1- and 5-year intervals (Table 5).

Lomitapide is a weak inhibitor of CYP3A4 and increases the exposure of statin[153]; thus, caution should be used when administered in combination by monitoring the well-known adverse effects associated with statin therapy.

7.18.3.1.5 CETP inhibitors

Cholesteryl ester transfer protein (CETP) is an enzyme mainly involved in the transfer of cholesteryl esters from HDL to LDL and VLDL; this process results in a reduction and remodeling of HDL particles and in an increase of LDL and VLDL levels (Fig. 6). Under pathological conditions, such as atherosclerosis, CETP activity is increased, while CETP deficiency results in increased HDL-C levels. These observations lead to the hypothesis that CETP inhibition might be a powerful tool to increase HDL cholesterol, decrease LDL and VLDL cholesterol, and reduce the development of atherosclerosis.[154]

The first CETP inhibitor (CETPi) developed, torcetrapib (Fig. 7), although very effective in increasing HDL-C levels (+72%), was withdrawn due to the results of the ILLUMINATE trial that reported an increased risk of CV events and death from any cause.[155] This effect was attributed to an off-target effect of torcetrapib independent of CETP inhibition.[155,156]

The Dalcetrapib HDL Evaluation, Atherosclerosis and Reverse Cholesterol Transport program included three surrogate end point trials, dal-VESSEL, dal-PLAQUE, and dal-PLAQUE 2, and the large phase 3 dal-OUTCOMES trial that evaluated the effects of dalcetrapib (Fig. 7) 600 mg daily added to standard statin therapy on mortality and morbidity in more than 15,000 high-risk CHD patients. In May 2012, however, the development of dalcetrapib was stopped based on the interim analysis of the *dal-OUTCOMES* (NCT00658515) trial that reported lack of efficacy in reducing CV events.[157] One possible explanation for this finding may be the moderate effect of dalcetrapib on HDL-C (+20%) and the lack of effect on LDL-C levels.[157]

Three further CETPi's, anacetrapib, evacetrapib (Fig. 7), and TA-8995, have been developed, and the results of the clinical trials are discussed in the succeeding text.

Anacetrapib. Anacetrapib was initially tested (100 mg daily) in patients with CHD or equivalent conditions (peripheral artery disease, cerebrovascular disease, diabetes, or a 10-year Framingham risk score >20%) resulting in the increase of HDL-C levels and in the decrease of LDL-C and apoB levels either as monotherapy or in combination with a statin.[158–160] The effect of LDL-C reduction is due to an increased rate of apoB fractional clearance.[161] The *DEFINE* (*Determining the Efficacy and Tolerability of CETP Inhibition with Anacetrapib*, NCT00685776) trial showed that in patients at high risk of CHD, anacetrapib increased HDL-C by 138.1% and reduced LDL-C by 39.8% compared with placebo[160] (Table 6), although a subsequent reevaluation of lipid parameters using different methods established an LDL-C level reduction closer to 25–35%.[162] Adverse events were comparable between the two groups.[160] The 2-year extension of the DEFINE study showed that treatment with anacetrapib was well tolerated and determined a 39.9% reduction of LDL-C and 153.3% increase of HDL-C compared with placebo.[163] When analyzed in patient subgroups, defined by age, gender, race, or baseline lipid levels or other conditions such as diabetes status or use of other lipid-modifying therapies, these changes in LDL-C and HDL-C levels were comparable across groups.[164] Only age, gender, and race seem to have a slight effect on anacetrapib-mediated effect, with patients <65 years more responsive than those ≥65 years, men more responsive than women, and whites more responsive than blacks.[164] The *REVEAL* (*Randomized Evaluation of the Effects of Anacetrapib through Lipid-modification*, NCT01252953) trial will determine the occurrence of major coronary events

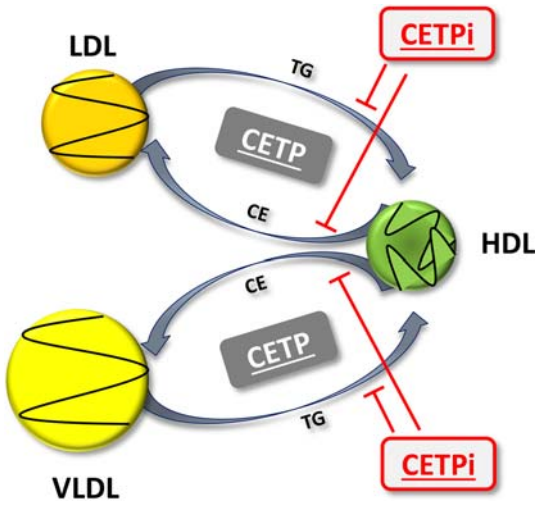

Fig. 6 CETP inhibition. CETP mediates the transfer of cholesteryl ester (CE) from HDL to larger lipoproteins, such as VLDL and LDL, in exchange for triglycerides (TG). This results in the generation of CE-enriched LDL and VLDL and TG-enriched HDL and in the reduction of circulating HDL-C. CETP inhibitors (CETPi's) inhibit the transfer of CE and result in the increase of HDL-C and reduction of LDL-C.

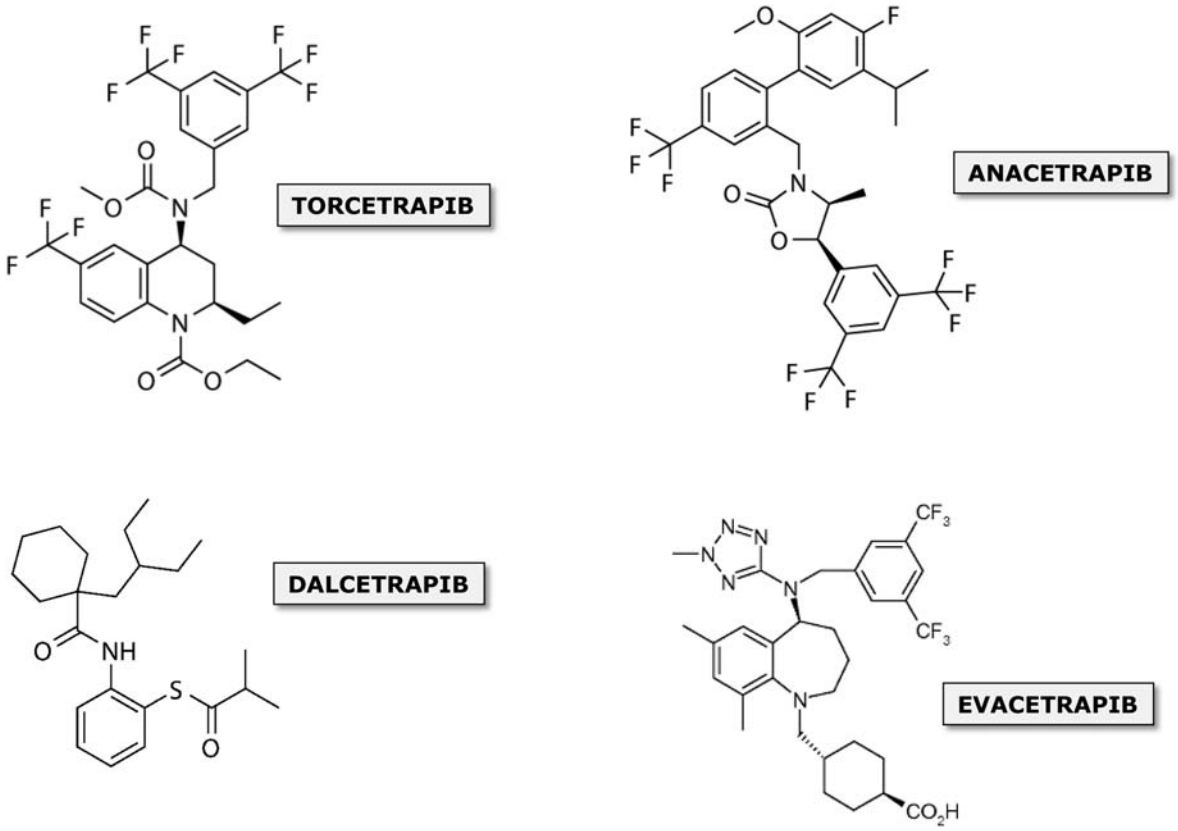

Fig. 7 Structure of CETP inhibitors.

(coronary death, MI, and coronary revascularization procedures) in 30,000 patients with CHD, cerebrovascular atherosclerotic disease, or peripheral artery disease and is estimated to end in 2017.

Anacetrapib has also been tested in patients with HeFH in the phase 3 *REALIZE* study (NCT01524289) that was designed to evaluate the tolerability and efficacy of anacetrapib added to current statin therapy for 52 weeks. This study reported a −39.7% reduction in percent change from baseline in LDL-C versus placebo and a significant increase of HDL-C levels (+105.8% vs. +3.7% with placebo)[165] (Table 6).

Evacetrapib. In a phase 2 study, evacetrapib was effective in reducing LDL-C and increasing HDL-C either as monotherapy (−13.6% to −35.9% and +53.6% to +128.8% from baseline, respectively, vs. +3.9% with placebo) or in combination with statins (Table 6).[166] The *ACCELERATE* (*A Study of Evacetrapib in High-Risk Vascular Disease*, NCT01687998) trial, which enrolled a large population (estimated: 12,000) of patients with diagnosis of high risk of vascular disease to evaluate the time to first occurrence of the composite end point of CV death, MI, stroke, coronary revascularization, or hospitalization for unstable angina in patients administered with evacetrapib or placebo, was stopped early because of futility; in fact, evacetrapib failed to reduce major CV events in these patients when compared with placebo, despite a 130% increase in HDL-C and a 37% decrease in LDL-C.[167]

TA-8995. TA-8995 is a new potent CETPi that demonstrated an almost complete inhibition of CETP, resulting in 96–140% increase of HDL-C and 40–53% reduction of LDL-C in healthy subjects, with no evidence of any off-target effects.[168] The *TULIP* (*TA-8995: Its Use in Patients with Mild Dyslipidemia*, NCT01970215) study evaluated the safety and efficacy of TA-8995 alone or in combination with a statin for 12 weeks.[169] In this trial, TA-8995 reduced LDL-C levels by 45.3% and increased HDL-C by up to 179.1%[169]; when given in combination with a statin, LDL-C levels further decreased (39.8–50.2%)[169] (Table 6). Altogether, we cannot draw a firm conclusion and the results from the REVEAL study will provide a definitive answer.

7.18.3.1.6 ETC-1002

ETC-1002 is a dicarboxylic acid derivative (Fig. 8) that inhibits hepatic adenosine triphosphate citrate lyase (ACL) and activates adenosine monophosphate-activated protein kinase (AMPK), two complementary enzymes involved in the metabolism of lipids and carbohydrates.[170] While ETC-1002-free acid activates liver AMPK, hepatocytes also readily convert the parent compound into ETC-1002-CoA thioester, which has been shown to directly inhibit ACL.[170] The inhibition of ACL results in reduced acetyl coenzyme A (CoA) levels, thus inhibiting both fatty acid and cholesterol synthesis; the activation of AMPK results in the inhibitory phosphorylation of HMG-CoA reductase and acetyl-CoA carboxylase as well as in reduced levels of PEPCK and G6Pase.[170]

Table 6 Effect of new CETP inhibitors

CETP inhibitors	*Subjects*	*Duration*	*LDL-C (percent change from baseline)*	*HDL-C (percent change from baseline)*	*Primary end point for ongoing trials*
Anacetrapib					
DEFINE (NCT00685776)[160]	CHD or CHD risk equivalent Well-controlled LDL-C	76 weeks	−39.8% versus placebo	+138.1% versus placebo	
REVEAL (NCT01252953)	History of MI, cerebrovascular disease, PAD, T2DM with CHD	4 years			Occurrence of major coronary events (coronary death, MI, or coronary revascularization procedure) (completion date: 2017)
REALIZE (NCT01524289)[165]	HeFH treated with optimal dose of statin for at least 6 weeks	52 weeks	−39.7% versus placebo	+102.1% versus placebo	
Evacetrapib					
Nicholls et al.[166]	Low HDL-C or high LDL-C	12 weeks	Monotherapy: −17.6% (30 mg) to −39 8% (500 mg) versus placebo Statin combination: Eva+ Atorva 20, −13.9% versus Atorva 20; Eva+ Simva 40, −11.2% versus Simva 40; Eva+ Rosuva 10, −13.5% versus Rosuva 10	Monotherapy: +56.7% (30 mg) to +131.9% (500 mg) versus placebo Statin combination: Eva+ Atorva 20, +78.5% versus Atorva 20; Eva+ Simva 40, +79.3% versus Simva 40; Eva+ Rosuva 10, +89.5% versus Rosuva 10	
ACCELERATE (NCT01687998)	History of ACS, cerebrovascular disease, PAD, T2DM with stable CAD	4 years			Time to first occurrence of major CV events (CV death, MI, stroke, coronary revascularization, or hospitalization for UA) (completion date: 2016)
TA-8995					
TULIP (NCT01970215)[169]	Mild dyslipidemia	12 weeks	−27.4% to −45.3% (1-10 mg)	+75.8% to +179.0% (1-10 mg)	

CHD, coronary heart disease; *MI*, myocardial infarction; *PAD*, peripheral artery disease; *T2DM*, type 2 diabetes mellitus; *HeFH*, heterozygous familial hypercholesterolemia; *CAD*, coronary artery disease; *ACS*, acute coronary syndrome; *Atorva*, atorvastatin; *Simva*, simvastatin; *Rosuva*, rosuvastatin; Eva, evacetrapib.

ETC-1002 treatment thus results in the reduction of LDL-C and glucose levels. In addition, ETC-1002 possesses anti-inflammatory properties, attenuates leukocyte homing at inflammatory sites, and inhibits adipose tissue inflammation[171] (Fig. 8).

ETC-1002 has been tested in three doses (40, 80, and 120 mg) in 133 subjects with hypercholesterolemia (LDL-C 130–220 mg dL^{-1} and 3.3–5.6 mmol L^{-1}) stratified by baseline normal or elevated TG levels (A Study to Assess the Efficacy and Safety of ETC-1002 in Subjects with Elevated Blood Cholesterol and Either Normal or Elevated Triglycerides, NCT01262638).[172] After 12 weeks of treatment, ETC-1002 significantly reduced LDL-C levels compared with placebo (from −17.9% to −26.6%), independently of baseline TG levels; reduced non-HDL-C, apoB, and LDL particle number in a dose-dependent manner; and was generally safe and well tolerated.[172] A trend in the reduction of high-sensitivity C-reactive protein (hs-CRP) was observed particularly in subjects with higher baseline hs-CRP values.[172] Similar effects were also observed in subjects with type 2 diabetes mellitus and hypercholesterolemia (NCT01607294): ETC-1002 lowered LDL-C levels by 43% and reduced hs-CRP.[173] ETC-1002 has also been tested in hypercholesterolemic patients with a history of statin intolerance (NCT01751984), showing that TC, LDL-C, non-HDL-C, and apoB were significantly decreased by 8-week ETC-1002 treatment compared with placebo (difference from placebo: −18.4%, −28.7%, −20.9%, and −15.3%, respectively).[174] Among the patients in the ETC-1002 treatment arm who were not at LDL-C target 62% reached their goal at the end of the study, while no patients in the placebo arm reached the LDL-C target.[174] Patients treated with ETC-1002 experienced muscle-related adverse events in a percentage similar to those treated with placebo,[174] suggesting that ETC-1002 might be a valuable alternative to statins

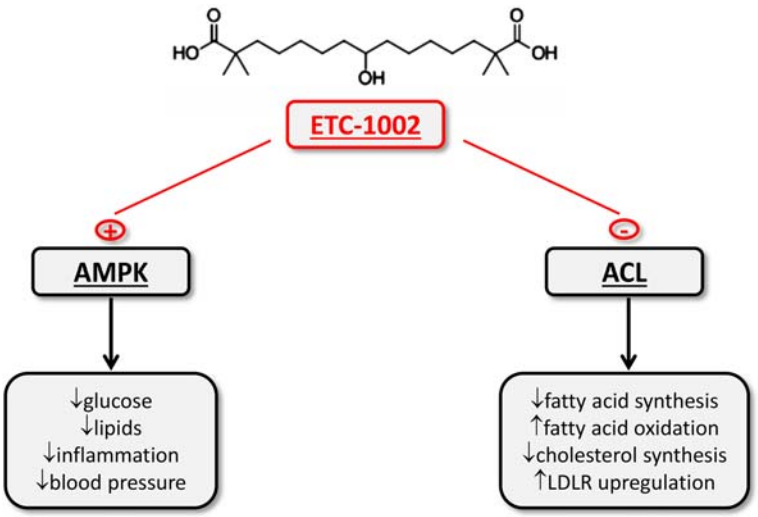

Fig. 8 Dual mechanism of action of ETC-1002. ETC-1002 activates AMP-activated protein kinase (AMPK), thus favorably impacting several metabolic processes, including glucose and lipid metabolism, as well as inflammation. On the other hand, ETC-1002 inhibits ATP citrate lyase (ACL), resulting in the decrease of cholesterol biosynthesis and upregulation of LDLR.

in patients with statin intolerance or as add-on therapy in patients unable to reach LDL-C target despite statin treatment. Future large trials are warranted to confirm these findings.

7.18.3.2 Targeting Plasma TG Levels

High levels of plasma TG are an independent risk factor for atherosclerosis and related CV diseases [175–177]; increased TG levels are usually associated with low HDL-C levels and increased small dense LDL,[178] referred to as atherogenic dyslipidemia.[179] In addition, severe HTG (TG levels $\geq$500 mg dL^{-1} and $\geq$5.65 mmol L^{-1}) significantly increases the risk of acute pancreatitis.[180,181] Thus, several drugs have been developed for the management of HTG, including fibrates, nicotinic acid, and omega-3 polyunsaturated fatty acids. However, new approaches for the management of HTG are now under evaluation.

7.18.3.2.1 Omega-3 free fatty acids

Among the available drugs for the treatment of HTG, there are omega-3 polyunsaturated fatty acids, usually a mixture of eicosapentaenoic acid (EPA) and docosahexaenoic acid (DHA) or EPA alone in their ethyl ester forms. However, to be absorbed in the intestine, the ethyl ester omega-3 polyunsaturated fatty acids need be converted into free acid by pancreatic lipase enzymes.[182] The most recent free fatty acid formulation (Epanova, containing 55% EPA and 20% DHA) is not dependent on pancreatic enzyme activity and is more readily absorbed, even in the condition of a very low fat diet.[182]

The pharmacokinetic parameters of a single dose of omega-3 free fatty acid formulation have been evaluated in comparison with the omega-3 ethyl esters in the *ECLIPSE* (*Epanova® Compared to Lovaza® in a Pharmacokinetic Single-Dose Evaluation*, NCT01208961) study in overweight adults.[183] Under a low fat diet, both EPA and DHA in the free fatty acid form had a higher bioavailability compared with the ethyl ester (ninefold and twofold, respectively).[183] Higher plasma levels of EPA and DHA were found in subjects taking the free fatty acid forms for 14 days compared with subjects taking the ethyl ester form (*ECLIPSE II*), and TG levels were reduced to a greater extent with the free fatty acid form (−21% and −8%, respectively, $P=0.013$),[184] suggesting that omega-3 free fatty acids provide more EPA and DHA under low fat diet conditions, thus resulting in a greater effect on plasma TG levels.

In subjects with severe HTG (TG: $\geq$500 and $\leq$2000 mg dL^{-1}; $\geq$5.65 and $\leq$22.60 mmol L^{-1}) treated with three dosages of 2, 3, and 4 g day^{-1} for 12 weeks in the double-blind, randomized *EVOLVE* (*Epanova for Lowering Very High Triglycerides*, NCT01242527) trial,[185] fasting TG levels were significantly reduced with all doses compared with controls (−25.9%, −25.5%, and −30.9% with 2, 3, and 4 g day^{-1}, respectively, vs. −4.3% of olive oil 4 g day^{-1})[185] (**Table 7**). Despite significant lowering of TC and non-HDL cholesterol, a significant increase of LDL-C was observed (+19.2%, +14.3%, and +19.4% vs. +3.0%) without a concomitant increase of apoB levels,[185] suggesting that the treatment did not increase the number of circulating atherogenic particles. VLDL-C and RLP-C were also significantly reduced in all treatment groups[185] according to the results obtained in studies with the omega-3 ethyl ester formulation[186,187]; also, apolipoprotein C-III (apoC-III) was significantly reduced (−11%, −12%, and −14%, respectively, vs. +1.6%).[185] The analysis of subgroups revealed that high-risk patients with diabetes or baseline TG $\geq$750 mg dL^{-1} ($\geq$8.47 mmol L^{-1}) or the highest tertile of apoC-III or RLP-C may particularly benefit from the treatment with the omega-3 free fatty acid formulation as they reported the most significant reductions in TG and non-HDL-C levels.[188]

The efficacy of free fatty acid formulation of omega-3 as an adjunct to statin therapy and low diet was proved also in high CV risk patients treated with statin and with persistent HTG ($\geq$200 and $<$500 mg dL^{-1}; $\geq$2.26 and $\leq$5.65 mmol L^{-1}) in the *ESPRIT*

Table 7 New TG-lowering drugs

	Subjects	*Duration*	*TG (percent change from baseline)*	*apoC-III (percent change from baseline)*	*Primary end point for ongoing clinical trials*
Omega-3 FFA					
EVOLVE, NCT01242527[185]	HTG	12 weeks	−25.9% (2 g) to −30.9% (4 g)	−10.9% (2 g) to −14.4% (4 g)	
ESPRIT, NCT01408303[189]	Statin-treated patients with residual HTG	6 weeks	−14.6% (2 g) to −20.6% (4 g)		
STRENGTH, NCT02104817[190]	High CVD risk	5 years			Time to the first occurrence of major adverse CV events (completion date: 2019)
ISIS-APOCIIIRx					
Gaudet et al.[200]	FCS	13 weeks	−56% to −86%	−71% to −90%	
NCT01529424[201]	Severe or uncontrolled HTG	13 weeks	Monotherapy: −31.3% (100 mg) to −70.9% (300 mg) Add-on to fibrate: −51% (200 mg) to −64% (300 mg)	Monotherapy: −40.0% (100 mg) to −79.6% (300 mg) Add-on to fibrate: −60.2% (200 mg) to −70.9% (300 mg)	
APPROACH (NCT02211209)	FCS	52 weeks			Percent change in fasting TG from baseline (completion date: 2016)
COMPASS (NCT02300233)	HTG	26 weeks			Percent change in fasting TG from baseline (completion date: 2016)
Pradigastat					
NCT01146522[207]	Hyperlipidemia type I or type V	3 weeks	Fasting TG: −41% (20 mg) to −70% (40 mg) Peak postprandial TG: −38% (20 mg) to −31% (40 mg)		
NCT01514461	FCS	12 weeks	−28.8% (20 mg) −40.9% (40 mg)		

HTG, hypertriglyceridemia; *CVD*, cardiovascular disease; *FCS*, familial chylomicronemia syndrome.

(*Epanova Combined with a Statin in Patients with Hypertriglyceridemia to Reduce Non-HDL Cholesterol*, NCT01408303) trial.[189] TG levels were significantly decreased (−14.6% and −20.6% with 2 and 4 g day^{-1}, respectively) compared with controls (−5.9%, statin + olive oil 4 g day^{-1}) (Table 7); other lipid parameters, including TC, non-HDL-C, and VLDL-C, were significantly improved.[189] Such reductions were higher in patients taking high-potency statins.[189]

The ongoing STRENGTH (*A Long-Term Outcomes Study to Assess Statin Residual Risk Reduction with Epanova in High Cardiovascular Risk Patients with Hypertriglyceridemia*, NCT02104817) trial will evaluate the efficacy of omega-3 free fatty acid formulation in addition to statin therapy in high-risk subjects in the prevention and reduction of major CV events[190] and has as primary outcome the time to the first occurrence of CV death, nonfatal MI, nonfatal stroke, coronary revascularization, or hospitalization for unstable angina (Table 7). The eligible patients that will be in the study for up to 5 years have controlled LDL-C levels ($\leq$100 mg dL^{-1}) but with residual atherogenic dyslipidemia (TG: $\geq$200 and $\leq$500 mg dL^{-1}; HDL-C <40 mg dL^{-1} for men and <45 mg dL^{-1} for women).

Overall, the free fatty acid formulation of EPA and DHA is well tolerated, and the most common adverse effects are mild to moderate gastrointestinal disorders[183–185,189]; in addition, its higher bioavailability may allow treatment with lower doses, thus likely increasing the drug compliance. Whether the lipid-lowering effect of free fatty acid EPA and DHA can translate into a CV benefit remains to be addressed.

7.18.3.2.2 Alipogene tiparvovec

Lipoprotein lipase deficiency (LPLD) is a rare autosomal recessive disease caused by loss-of-function mutations of *LPL* gene and is characterized by hyperchylomicronemia, severe HTG, and high risk of diabetes mellitus and recurrent, acute pancreatitis.[191] Alipogene tiparvovec is the first adeno-associated virus-mediated gene therapy approved for the treatment of LPLD[192]; in fact, the intramuscular administration of alipogene tiparvovec delivers a natural gain-of-function variant of LPL that results in a significant improvement of TG-rich lipoprotein characteristics and relevant reduction in the incidence of pancreatitis.[191] In the initial 12-week study performed in LPLD patients with baseline TG levels >14 mmol L^{-1}, the injection of a single alipogene tiparvovec dose induced local LPL expression and significant but transient reduction of TG levels (27–41%).[193] In an open-label clinical trial,

intramuscular administration of alipogene tiparvovec resulted in a significant improvement of postprandial chylomicron metabolism in LPLD patients, without changes in postprandial nonesterified fatty acids.[194] Overall, there was a reduction in the risk of pancreatitis after up to 6 years follow-up after gene therapy.[191] Alipogene tiparvovec was well tolerated; however, LPLD being a rare disease, it is very difficult to undertake clinical trials to define the safety and efficacy of this therapeutic approach.

7.18.3.2.3 ISIS-APOCIIIRx

apoC-III is a glycoprotein mainly associated with VLDL and chylomicron and, to a lesser extent, with HDL; it plays a critical role in the metabolism of TG-rich lipoproteins as it acts as potent inhibitor of lipoprotein lipase (and, when present at high concentrations, of hepatic lipase) but is also involved in the hepatic VLDL assembly and secretion.[195] apoC-III plasma levels are independently associated with the progression of CV disease[195]; loss-of-function variants of *APOC3* gene are associated with low TG levels and reduced risk of ischemic CV disease.[196,197] Several drugs used for the treatment of HTG also reduce apoC-III levels, including fibrates, peroxisome proliferator-activated receptor agonists, and omega-3 polyunsaturated fatty acids.[195] However, these drugs may decrease apoC-III levels by only 10–30%, while larger apoC-III reductions seem to be required to observe a clinical benefit similar to that reported in subjects carrying genetic mutations in *APOC3*.[196,197]

ISIS-APOCIIIRx is a second-generation 2′-*O*-(2-methoxyethyl)-modified ASO that inhibits the hepatic synthesis of apoC-III (Fig. 4). In healthy human volunteers without HTG, ISIS-APOCIIIRx induced a dose-dependent and prolonged reduction of apoC-III and TG levels.[198] In the multiple-dose phase, healthy subjects were treated for 22 days with six total doses of 50, 100, 200, or 400 mg ISIS-APOCIIIRx, showing median percentage reductions of apoC-III levels from baseline to 19.7%, 17.3%, 70.5%, and >77%, respectively, associated with dose-dependent reductions of TG levels (from −19.5% to 43.8%).[198]

ISIS-APOCIIIRx was also tested in three patients with familial chylomicronemia syndrome (FCS), a rare autosomal recessive disease caused by mutations in the gene encoding LPL or genes encoding proteins involved in LPL function, and characterized by high levels of plasma chylomicrons and severe HTG, with a high risk of recurrent acute pancreatitis.[199] After a 13-week treatment, ISIS-APOCIIIRx significantly reduced apoC-III (71–90%) and TG levels (56–86%)[200] (Table 7). Reductions of TG levels in chylomicrons, apoB-48 levels, and non-HDL-C were also reported; the reduction of non-HDL-C was due to the reduction of chylomicron/VLDL cholesterol, while LDL-C levels that were extremely low at baseline (13–17 mg dL^{-1}) resulted unchanged or increased (up to 35.5 mg dL^{-1}).[200]

In the phase 2 randomized trial, ISIS-APOCIIIRx was given once weekly for 13 weeks to patients with severe or uncontrolled HTG, having fasting TG between 350 and 2000 mg dL^{-1} (4.0–22.6 mmol L^{-1}), and to patients on stable fibrate therapy having fasting TG levels between 225 and 2000 mg dL^{-1} (2.5–22.6 mmol L^{-1}) (NCT01529424). Both groups showed significant reductions of plasma apoC-III and TG levels either when the drug was administered as monotherapy or when it was administered as add-on to stable fibrate therapy[201] (Table 7). The large decrease of TG resulted in a dose-dependent increase of LDL-C levels following the treatment with ISIS-APOCIIIRx, associated with increases in apoB levels and LDL particle size[201]; despite this, non-HDL-C was unchanged.[201] This effect on LDL-C levels may be due to the increased conversion of VLDL to LDL determined by the increased activity of LPL, but other mechanisms may contribute as well. The clinical significance of this increase requires further investigation.

Two ongoing phase 3 trials, the *APPROACH* (*The APPROACH Study: A Study of ISIS-APOCIIIRx in Patients with Familial Chylomicronemia Syndrome*, NCT02211209) and *COMPASS* (*The COMPASS Study: A Study of ISIS-APOCIIIRx in Patients with Hypertriglyceridemia*, NCT02300233) trials, will evaluate the efficacy and safety of ISIS-APOCIIIRx. The APPROACH trial will recruit patients with a history of chylomicronemia and a diagnosis of FCS and fasting TG levels ≥750 mg dL^{-1} (8.4 mmol L^{-1}) who will be treated with 300 mg ISIS-APOCIIIRx administered subcutaneously once weekly for 52 weeks versus placebo. The COMPASS trial will recruit HTG patients with fasting TG ≥500 mg dL^{-1} (≥5.7 mmol L^{-1}) who will be administered 300 mg ISIS-APOCIIIRx versus placebo subcutaneously once weekly for 26 weeks. Both trials have as primary outcome the percent change in fasting TG from baseline.

7.18.3.2.4 Diacylglycerol O-acyltransferase inhibitors

TGs are synthesized in enterocytes and hepatocytes and then assembled into lipoproteins and secreted to transport dietary and endogenous fatty acids. TGs are essential for several functions, among which energy storage and membrane composition represent the most important. However, excess TGs are associated with obesity, insulin resistance, nonalcoholic steatohepatitis, and CV disease.[202]

Diacylglycerol *O*-acyltransferase (DGAT) enzymes catalyze the formation of an ester linkage between a fatty acyl-CoA and diacylglycerol. The two enzymes DGAT1 and DGAT2, encoded by two different genes not sharing significant sequence homology, have a different subcellular localization and are differently regulated, suggesting that they likely participate in different pathways of TG synthesis and thus have distinct physiological functions.[202] DGAT2 seems thus to be involved in the incorporation of endogenously synthesized monounsaturated fatty acids into TG, while DGAT1 appears to be involved in the esterification of exogenous fatty acids taken up by cells.[202]

Mice lacking DGAT1, although capable of synthesizing TG (indicating the existence of alternative mechanisms for TG synthesis), have reduced body TG content and are resistant to diet-induced obesity,[203] while mice lacking DGAT2 have severe lipopenia and die soon after birth [204]; this suggests that DGAT1 and DGAT2 play different roles and that DGAT2 plays an essential role in the synthesis of TG in mammals and is required for survival, while DGAT1 is not. Based on these observations, it has been hypothesized that the pharmacological inhibition of DGAT1 could be an attractive way to control HTG. Several preclinical models have shown that treatment with DGAT1 inhibitors inhibits postprandial plasma TG excursion after a lipid challenge and, when administered chronically, metabolic parameters are improved.[205]

Pradigastat in healthy volunteers suppressed postprandial TG in a dose-dependent manner and reduced postprandial chylomicron numbers (as determined by the apoB-48 reduced levels).[206] The DGAT1 inhibitor pradigastat has been tested in six patients with FCS (NCT01146522), who underwent three consecutive 3-week treatment periods (20, 40, and 10 mg, respectively) separated by 4-week washout periods.[207] Pradigastat 20 and 40 mg reduced plasma TG by 41% and 70%, respectively, in FCS patients, while the lowest dose was ineffective (**Table 7**). More specifically, it mainly reduced the size and TG content of secreted chylomicrons[207] that in FCS transport almost all plasma TG (contrarily to healthy subjects that present their fasting TG almost completely in VLDL, while postprandial TG are equally shared between VLDL and chylomicrons). In a phase 3 study (NCT01514461), a −28.8% with 20 mg and −40.9% with 40 mg pradigastat versus placebo was reported after a 12-week treatment in FCS patients (**Table 7**). When tested in obese patients with type 2 diabetes mellitus in a 2–20 mg dose range (NCT00901979), pradigastat had beneficial effects on several metabolic parameters, including TG, LDL-C, TC, and body weight.[208]

7.18.3.3 Conclusions

Several novel therapeutic approaches have been investigated in the last few years with the aim of reducing plasma cholesterol and TG levels. For cholesterol, with the most potent statins, we have reached a highly effective inhibition of cholesterol biosynthesis in the liver; therefore, from a pharmacological perspective, the development of novel strategies has been focused on different mechanisms of action, including the inhibition of cholesterol absorption in the intestine (ezetimibe), the inhibition of lipoprotein synthesis (lomitapide and mipomersen), and the improvement of lipoprotein catabolism (PCSK9 inhibitors). In FH patients, clinical trials of these new compounds were proved to be successful in decreasing plasma cholesterol levels and reducing the burden of CV diseases.

See also: 8.11. Case Histories: Anacetrapib. 8.13. Fragment-Based Discovery of AZD2716: A Novel, Potent Secreted Phospholipase A_2 ($sPLA_2$) Inhibitor for the Treatment of Coronary Artery Disease.

References

1. Stocker, R.; Keaney, J. F., Jr. Role of Oxidative Modifications in Atherosclerosis. *Physiol. Rev.* **2004,** *84* (4), 1381–1478.
2. Brown, M. S.; Goldstein, J. L. A Receptor-Mediated Pathway for Cholesterol Homeostasis. *Science* **1986,** *232* (4746), 34–47.
3. Glueck, C. J.; Kelley, W.; Gupta, A.; Fontaine, R. N.; Wang, P.; Gartside, P. S. Prospective 10-Year Evaluation of Hypobetalipoproteinemia in a Cohort of 772 Firefighters and Cross-Sectional Evaluation of Hypocholesterolemia in 1,479 Men in the National Health and Nutrition Examination Survey I. *Metabolism* **1997,** *46* (6), 625–633.
4. Cohen, J. C.; Boerwinkle, E.; Mosley, T. H., Jr.; Hobbs, H. H. Sequence Variations in PCSK9, Low LDL, and Protection Against Coronary Heart Disease. *N. Engl. J. Med.* **2006,** *354* (12), 1264–1272.
5. Baigent, C.; Keech, A.; Kearney, P. M.; Blackwell, L.; Buck, G.; Pollicino, C.; Kirby, A.; Sourjina, T.; Peto, R.; Collins, R.; Simes, R. Efficacy and Safety of Cholesterol-Lowering Treatment: Prospective Meta-Analysis of Data From 90,056 Participants in 14 Randomised Trials of Statins. *Lancet* **2005,** *366* (9493), 1267–1278.
6. Baigent, C.; Blackwell, L.; Emberson, J.; Holland, L. E.; Reith, C.; Bhala, N.; Peto, R.; Barnes, E. H.; Keech, A.; Simes, J.; Collins, R. Efficacy and Safety of More Intensive Lowering of LDL Cholesterol: A Meta-Analysis of Data From 170,000 Participants in 26 Randomised Trials. *Lancet* **2010,** *376* (9753), 1670–1681.
7. Catapano, A. L.; Reiner, Z.; De Backer, G.; Graham, I.; Taskinen, M. R.; Wiklund, O.; Agewall, S.; Alegria, E.; Chapman, M. J.; Durrington, P.; Erdine, S.; Halcox, J.; Hobbs, R.; Kjekshus, J.; Filardi, P. P.; Riccardi, G.; Storey, R. F.; Wood, D. ESC/EAS Guidelines for the Management of Dyslipidaemias The Task Force for the Management of Dyslipidaemias of the European Society of Cardiology (ESC) and the European Atherosclerosis Society (EAS). *Atherosclerosis* **2011,** *217* (1), 3–46.
8. Nordestgaard, B. G.; Chapman, M. J.; Humphries, S. E.; Ginsberg, H. N.; Masana, L.; Descamps, O. S.; Wiklund, O.; Hegele, R. A.; Raal, F. J.; Defesche, J. C.; Wiegman, A.; Santos, R. D.; Watts, G. F.; Parhofer, K. G.; Hovingh, G. K.; Kovanen, P. T.; Boileau, C.; Averna, M.; Boren, J.; Bruckert, E.; Catapano, A. L.; Kuivenhoven, J. A.; Pajukanta, P.; Ray, K.; Stalenhoef, A. F.; Stroes, E.; Taskinen, M. R.; Tybjaerg-Hansen, A. Familial Hypercholesterolaemia Is Underdiagnosed and Undertreated in the General Population: Guidance for Clinicians to Prevent Coronary Heart Disease: Consensus Statement of the European Atherosclerosis Society. *Eur. Heart J.* **2013,** *34* (45), 3478-90a.
9. Cuchel, M.; Bruckert, E.; Ginsberg, H. N.; Raal, F. J.; Santos, R. D.; Hegele, R. A.; Kuivenhoven, J. A.; Nordestgaard, B. G.; Descamps, O. S.; Steinhagen-Thiessen, E.; Tybjaerg-Hansen, A.; Watts, G. F.; Averna, M.; Boileau, C.; Boren, J.; Catapano, A. L.; Defesche, J. C.; Hovingh, G. K.; Humphries, S. E.; Kovanen, P. T.; Masana, L.; Pajukanta, P.; Parhofer, K. G.; Ray, K. K.; Stalenhoef, A. F.; Stroes, E.; Taskinen, M. R.; Wiegman, A.; Wiklund, O.; Chapman, M. J. Homozygous Familial Hypercholesterolaemia: New Insights and Guidance for Clinicians to Improve Detection and Clinical Management. A Position Paper From the Consensus Panel on Familial Hypercholesterolaemia of the European Atherosclerosis Society. *Eur. Heart J.* **2014,** *35* (32), 2146–2157.
10. Sniderman, A. D.; Tsimikas, S.; Fazio, S. The Severe Hypercholesterolemia Phenotype: Clinical Diagnosis, Management, and Emerging Therapies. *J. Am. Coll. Cardiol.* **2014,** *63* (19), 1935–1947.
11. Goldberg, A. C.; Hopkins, P. N.; Toth, P. P.; Ballantyne, C. M.; Rader, D. J.; Robinson, J. G.; Daniels, S. R.; Gidding, S. S.; de Ferranti, S. D.; Ito, M. K.; McGowan, M. P.; Moriarty, P. M.; Cromwell, W. C.; Ross, J. L.; Ziajka, P. E. Familial Hypercholesterolemia: Screening, Diagnosis and Management of Pediatric and Adult Patients: Clinical Guidance From the National Lipid Association Expert Panel on Familial Hypercholesterolemia. *J. Clin. Lipidol.* **2011,** *5* (3 Suppl), S1–S8.
12. Hovingh, G. K.; Davidson, M. H.; Kastelein, J. J.; O'Connor, A. M. Diagnosis and Treatment of Familial Hypercholesterolaemia. *Eur. Heart J.* **2013,** *34* (13), 962–971.
13. Naci, H.; Brugts, J. J.; Fleurence, R.; Tsoi, B.; Toor, H.; Ades, A. E. Comparative Benefits of Statins in the Primary and Secondary Prevention of Major Coronary Events and All-Cause Mortality: A Network Meta-Analysis of Placebo-Controlled and Active-Comparator Trials. *Eur. J. Prev. Cardiol.* **2013,** *20* (4), 641–657.
14. Mills, E. J.; Wu, P.; Chong, G.; Ghement, I.; Singh, S.; Akl, E. A.; Eyawo, O.; Guyatt, G.; Berwanger, O.; Briel, M. Efficacy and Safety of Statin Treatment for Cardiovascular Disease: A Network Meta-Analysis of 170,255 Patients From 76 Randomized Trials. *QJM* **2011,** *104* (2), 109–124.
15. Tonelli, M.; Lloyd, A.; Clement, F.; Conly, J.; Husereau, D.; Hemmelgarn, B.; Klarenbach, S.; McAlister, F. A.; Wiebe, N.; Manns, B. Efficacy of Statins for Primary Prevention in People at Low Cardiovascular Risk: A Meta-Analysis. *CMAJ* **2011,** *183* (16), E1189–E1202.
16. Mills, E. J.; O'Regan, C.; Eyawo, O.; Wu, P.; Mills, F.; Berwanger, O.; Briel, M. Intensive Statin Therapy Compared With Moderate Dosing for Prevention of Cardiovascular Events: A Meta-Analysis of >40000 Patients. *Eur. Heart J.* **2011,** *32* (11), 1409–1415.
17. Chan, D. K.; O'Rourke, F.; Shen, Q.; Mak, J. C.; Hung, W. T. Meta-Analysis of the Cardiovascular Benefits of Intensive Lipid Lowering With Statins. *Acta Neurol. Scand.* **2011,** *124* (3), 188–195.

18. Taylor, F.; Huffman, M. D.; Macedo, A. F.; Moore, T. H.; Burke, M.; Davey Smith, G.; Ward, K.; Ebrahim, S. Statins for the Primary Prevention of Cardiovascular Disease. *Cochrane Database Syst. Rev.* **2013,** *1,* CD004816.
19. Ahn, C. H.; Choi, S. H. New Drugs for Treating Dyslipidemia: Beyond Statins. *Diabetes Metab. J.* **2015,** *39* (2), 87–94.
20. Fruchart, J. C.; Davignon, J.; Hermans, M. P.; Al-Rubeaan, K.; Amarenco, P.; Assmann, G.; Barter, P.; Betteridge, J.; Bruckert, E.; Cuevas, A.; Farnier, M.; Ferrannini, E.; Fioretto, P.; Genest, J.; Ginsberg, H. N.; Gotto, A. M., Jr.; Hu, D.; Kadowaki, T.; Kodama, T.; Krempf, M.; Matsuzawa, Y.; Nunez-Cortes, J. M.; Monfil, C. C.; Ogawa, H.; Plutzky, J.; Rader, D. J.; Sadikot, S.; Santos, R. D.; Shlyakhto, E.; Sritara, P.; Sy, R.; Tall, A.; Tan, C. E.; Tokgozoglu, L.; Toth, P. P.; Valensi, P.; Wanner, C.; Zambon, A.; Zhu, J.; Zimmet, P. Residual Macrovascular Risk in 2013: What Have We Learned? *Cardiovasc. Diabetol.* **2014,** *13,* 26.
21. Corrao, G.; Conti, V.; Merlino, L.; Catapano, A. L.; Mancia, G. Results of a Retrospective Database Analysis of Adherence to Statin Therapy and Risk of Nonfatal Ischemic Heart Disease in Daily Clinical Practice in Italy. *Clin. Ther.* **2010,** *32* (2), 300–310.
22. Joy, T. R.; Hegele, R. A. Narrative Review: Statin-Related Myopathy. *Ann. Intern. Med.* **2009,** *150* (12), 858–868.
23. Law, M.; Rudnicka, A. R. Statin Safety: A Systematic Review. *Am. J. Cardiol.* **2006,** *97* (8A), 52C–60C.
24. Fernandez, G.; Spatz, E. S.; Jablecki, C.; Phillips, P. S. Statin Myopathy: A Common Dilemma Not Reflected in Clinical Trials. *Cleve. Clin. J. Med.* **2011,** *78* (6), 393–403.
25. Maningat, P.; Breslow, J. L. Needed: Pragmatic Clinical Trials for Statin-Intolerant Patients. *N. Engl. J. Med.* **2011,** *365* (24), 2250–2251.
26. Taha, D. A.; De Moor, C. H.; Barrett, D. A.; Gershkovich, P. Translational Insight Into Statin-Induced Muscle Toxicity: From Cell Culture to Clinical Studies. *Transl. Res.* **2014,** *164* (2), 85–109.
27. Chatzizisis, Y. S.; Koskinas, K. C.; Misirli, G.; Vaklavas, C.; Hatzitolios, A.; Giannoglou, G. D. Risk Factors and Drug Interactions Predisposing to Statin-Induced Myopathy: Implications for Risk Assessment, Prevention and Treatment. *Drug Saf.* **2010,** *33* (3), 171–187.
28. Alfirevic, A.; Neely, D.; Armitage, J.; Chinoy, H.; Cooper, R. G.; Laaksonen, R.; Carr, D. F.; Bloch, K. M.; Fahy, J.; Hanson, A.; Yue, Q. Y.; Wadelius, M.; Maitland-van Der Zee, A. H.; Voora, D.; Psaty, B. M.; Palmer, C. N.; Pirmohamed, M. Phenotype Standardization for Statin-Induced Myotoxicity. *Clin. Pharmacol. Ther.* **2014,** *96* (4), 470–476.
29. Pirillo, A.; Catapano, A. L. Statin Intolerance: Diagnosis and Remedies. *Curr. Cardiol. Rep.* **2015,** *17* (5), 27.
30. Ridker, P. M. LDL Cholesterol: Controversies and Future Therapeutic Directions. *Lancet* **2014,** *384* (9943), 607–617.
31. Cannon, C. P.; Blazing, M. A.; Giugliano, R. P.; McCagg, A.; White, J. A.; Theroux, P.; Darius, H.; Lewis, B. S.; Ophuis, T. O.; Jukema, J. W.; De Ferrari, G. M.; Ruzyllo, W.; De Lucca, P.; Im, K.; Bohula, E. A.; Reist, C.; Wiviott, S. D.; Tershakovec, A. M.; Musliner, T. A.; Braunwald, E.; Califf, R. M. Ezetimibe Added to Statin Therapy After Acute Coronary Syndromes. *N. Engl. J. Med.* **2015,** *372* (25), 2387–2397.
32. Boden, W. E.; Probstfield, J. L.; Anderson, T.; Chaitman, B. R.; Desvignes-Nickens, P.; Koprowicz, K.; McBride, R.; Teo, K.; Weintraub, W. Niacin in Patients With Low HDL Cholesterol Levels Receiving Intensive Statin Therapy. *N. Engl. J. Med.* **2011,** *365* (24), 2255–2267.
33. HPS2-THRIVE Collaborative Group. HPS2-THRIVE Randomized Placebo-Controlled Trial in 25 673 High-Risk Patients of ER Niacin/Laropiprant: Trial Design, Pre-Specified Muscle and Liver Outcomes, and Reasons for Stopping Study Treatment. *Eur. Heart J.* **2013,** *34* (17), 1279–1291.
34. Keech, A.; Simes, R. J.; Barter, P.; Best, J.; Scott, R.; Taskinen, M. R.; Forder, P.; Pillai, A.; Davis, T.; Glasziou, P.; Drury, P.; Kesaniemi, Y. A.; Sullivan, D.; Hunt, D.; Colman, P.; d'Emden, M.; Whiting, M.; Ehnholm, C.; Laakso, M. Effects of Long-Term Fenofibrate Therapy on Cardiovascular Events in 9795 People With Type 2 Diabetes Mellitus (the FIELD Study): Randomised Controlled Trial. *Lancet* **2005,** *366* (9500), 1849–1861.
35. Ginsberg, H. N.; Elam, M. B.; Lovato, L. C.; Crouse, J. R., III; Leiter, L. A.; Linz, P.; Friedewald, W. T.; Buse, J. B.; Gerstein, H. C.; Probstfield, J.; Grimm, R. H.; Ismail-Beigi, F.; Bigger, J. T.; Goff, D. C., Jr.; Cushman, W. C.; Simons-Morton, D. G.; Byington, R. P. Effects of Combination Lipid Therapy in Type 2 Diabetes Mellitus. *N. Engl. J. Med.* **2010,** *362* (17), 1563–1574.
36. Wang, D. Q. Regulation of Intestinal Cholesterol Absorption. *Annu. Rev. Physiol.* **2007,** *69,* 221–248.
37. Wang, L. J.; Song, B. L. Niemann-Pick C1-Like 1 and Cholesterol Uptake. *Biochim. Biophys. Acta* **2012,** *1821* (7), 964–972.
38. Yu, L.; Bharadwaj, S.; Brown, J. M.; Ma, Y.; Du, W.; Davis, M. A.; Michaely, P.; Liu, P.; Willingham, M. C.; Rudel, L. L. Cholesterol-Regulated Translocation of NPC1L1 to the Cell Surface Facilitates Free Cholesterol Uptake. *J. Biol. Chem.* **2006,** *281* (10), 6616–6624.
39. Ge, L.; Wang, J.; Qi, W.; Miao, H. H.; Cao, J.; Qu, Y. X.; Li, B. L.; Song, B. L. The Cholesterol Absorption Inhibitor Ezetimibe Acts by Blocking the Sterol-Induced Internalization of NPC1L1. *Cell Metab.* **2008,** *7* (6), 508–519.
40. Temel, R. E.; Tang, W.; Ma, Y.; Rudel, L. L.; Willingham, M. C.; Ioannou, Y. A.; Davies, J. P.; Nilsson, L. M.; Yu, L. Hepatic Niemann-Pick C1-Like 1 Regulates Biliary Cholesterol Concentration and Is a Target of Ezetimibe. *J. Clin. Invest.* **2007,** *117* (7), 1968–1978.
41. Altmann, S. W.; Davis, H. R., Jr.; Zhu, L. J.; Yao, X.; Hoos, L. M.; Tetzloff, G.; Iyer, S. P.; Maguire, M.; Golovko, A.; Zeng, M.; Wang, L.; Murgolo, N.; Graziano, M. P. Niemann-Pick C1 Like 1 Protein Is Critical for Intestinal Cholesterol Absorption. *Science* **2004,** *303* (5661), 1201–1204.
42. Davis, H. R., Jr.; Hoos, L. M.; Tetzloff, G.; Maguire, M.; Zhu, L. J.; Graziano, M. P.; Altmann, S. W. Deficiency of Niemann-Pick C1 Like 1 Prevents Atherosclerosis in ApoE−/− Mice. *Arterioscler. Thromb. Vasc. Biol.* **2007,** *27* (4), 841–849.
43. Davies, J. P.; Scott, C.; Oishi, K.; Liapis, A.; Ioannou, Y. A. Inactivation of NPC1L1 Causes Multiple Lipid Transport Defects and Protects Against Diet-Induced Hypercholesterolemia. *J. Biol. Chem.* **2005,** *280* (13), 12710–12720.
44. Yamanashi, Y.; Takada, T.; Suzuki, H. Niemann-Pick C1-Like 1 Overexpression Facilitates Ezetimibe-Sensitive Cholesterol and Beta-Sitosterol Uptake in CaCo-2 Cells. *J. Pharmacol. Exp. Ther.* **2007,** *320* (2), 559–564.
45. Xie, P.; Zhu, H.; Jia, L.; Ma, Y.; Tang, W.; Wang, Y.; Xue, B.; Shi, H.; Yu, L. Genetic Demonstration of Intestinal NPC1L1 As a Major Determinant of Hepatic Cholesterol and Blood Atherogenic Lipoprotein Levels. *Atherosclerosis* **2014,** *237* (2), 609–617.
46. Stitziel, N. O.; Won, H. H.; Morrison, A. C.; Peloso, G. M.; Do, R.; Lange, L. A.; Fontanillas, P.; Gupta, N.; Duga, S.; Goel, A.; Farrall, M.; Saleheen, D.; Ferrario, P.; Konig, I.; Asselta, R.; Merlini, P. A.; Marziliano, N.; Notarangelo, M. F.; Schick, U.; Auer, P.; Assimes, T. L.; Reilly, M.; Wilensky, R.; Rader, D. J.; Hovingh, G. K.; Meitinger, T.; Kessler, T.; Kastrati, A.; Laugwitz, K. L.; Siscovick, D.; Rotter, J. I.; Hazen, S. L.; Tracy, R.; Cresci, S.; Spertus, J.; Jackson, R.; Schwartz, S. M.; Natarajan, P.; Crosby, J.; Muzny, D.; Ballantyne, C.; Rich, S. S.; O'Donnell, C. J.; Abecasis, G.; Sunyaev, S.; Nickerson, D. A.; Buring, J. E.; Ridker, P. M.; Chasman, D. I.; Austin, E.; Ye, Z.; Kullo, I. J.; Weeke, P. E.; Shaffer, C. M.; Bastarache, L. A.; Denny, J. C.; Roden, D. M.; Palmer, C.; Deloukas, P.; Lin, D. Y.; Tang, Z. Z.; Erdmann, J.; Schunkert, H.; Danesh, J.; Marrugat, J.; Elosua, R.; Ardissino, D.; McPherson, R.; Watkins, H.; Reiner, A. P.; Wilson, J. G.; Altshuler, D.; Gibbs, R. A.; Lander, E. S.; Boerwinkle, E.; Gabriel, S.; Kathiresan, S. Inactivating Mutations in NPC1L1 and Protection From Coronary Heart Disease. *N. Engl. J. Med.* **2014,** *371* (22), 2072–2082.
47. Davis, H. R.; Veltri, E. P. Zetia: Inhibition of Niemann-Pick C1 Like 1 (NPC1L1) to Reduce Intestinal Cholesterol Absorption and Treat Hyperlipidemia. *J. Atheroscler. Thromb.* **2007,** *14* (3), 99–108.
48. Hawes, B. E.; O'Neill, K. A.; Yao, X.; Crona, J. H.; Davis, H. R., Jr.; Graziano, M. P.; Altmann, S. W. In Vivo Responsiveness to Ezetimibe Correlates With Niemann-Pick C1 Like-1 (NPC1L1) Binding Affinity: Comparison of Multiple Species NPC1L1 Orthologs. *Mol. Pharmacol.* **2007,** *71* (1), 19–29.
49. Wang, J.; Chu, B. B.; Ge, L.; Li, B. L.; Yan, Y.; Song, B. L. Membrane Topology of Human NPC1L1, a Key Protein in Enterohepatic Cholesterol Absorption. *J. Lipid Res.* **2009,** *50* (8), 1653–1662.
50. Descamps, O. S.; De Sutter, J.; Guillaume, M.; Missault, L. Where Does the Interplay Between Cholesterol Absorption and Synthesis in the Context of Statin and/or Ezetimibe Treatment Stand Today? *Atherosclerosis* **2011,** *217* (2), 308–321.
51. Norata, G. D.; Ballantyne, C. M.; Catapano, A. L. New Therapeutic Principles in Dyslipidaemia: Focus on LDL and Lp(a) Lowering Drugs. *Eur. Heart J.* **2013,** *34* (24), 1783–1789.
52. Mikhailidis, D. P.; Sibbring, G. C.; Ballantyne, C. M.; Davies, G. M.; Catapano, A. L. Meta-Analysis of the Cholesterol-Lowering Effect of Ezetimibe Added to Ongoing Statin Therapy. *Curr. Med. Res. Opin.* **2007,** *23* (8), 2009–2026.
53. Catapano, A. L.; Davidson, M. H.; Ballantyne, C. M.; Brady, W. E.; Gazzara, R. A.; Tomassini, J. E.; Tershakovec, A. M. Lipid-Altering Efficacy of the Ezetimibe/Simvastatin Single Tablet Versus Rosuvastatin in Hypercholesterolemic Patients. *Curr. Med. Res. Opin.* **2006,** *22* (10), 2041–2053.

54. Catapano, A.; Brady, W. E.; King, T. R.; Palmisano, J. Lipid Altering-Efficacy of Ezetimibe Co-Administered With Simvastatin Compared With Rosuvastatin: A Meta-Analysis of Pooled Data From 14 Clinical Trials. *Curr. Med. Res. Opin.* **2005,** *21* (7), 1123–1130.
55. Morrone, D.; Weintraub, W. S.; Toth, P. P.; Hanson, M. E.; Lowe, R. S.; Lin, J.; Shah, A. K.; Tershakovec, A. M. Lipid-Altering Efficacy of Ezetimibe Plus Statin and Statin Monotherapy and Identification of Factors Associated With Treatment Response: A Pooled Analysis of Over 21,000 Subjects From 27 Clinical Trials. *Atherosclerosis* **2012,** *223* (2), 251–261.
56. Foody, J. M.; Toth, P. P.; Tomassini, J. E.; Sajjan, S.; Ramey, D. R.; Neff, D.; Tershakovec, A. M.; Hu, H.; Tunceli, K. Changes in LDL-C Levels and Goal Attainment Associated With Addition of Ezetimibe to Simvastatin, Atorvastatin, or Rosuvastatin Compared With Titrating Statin Monotherapy. *Vasc. Health Risk Manag.* **2013,** *9,* 719–727.
57. Sakamoto, K.; Kawamura, M.; Kohro, T.; Omura, M.; Watanabe, T.; Ashidate, K.; Horiuchi, T.; Hara, H.; Sekine, N.; Chin, R.; Tsujino, M.; Hiyoshi, T.; Tagami, M.; Tanaka, A.; Mori, Y.; Inazawa, T.; Hirano, T.; Yamazaki, T.; Shiba, T. Effect of Ezetimibe on LDL-C Lowering and Atherogenic Lipoprotein Profiles in Type 2 Diabetic Patients Poorly Controlled by Statins. *PLoS One* **2015,** *10* (9), e0138332.
58. Farnier, M. Ezetimibe/Statin Combination Therapy to Treat Patients With Type 2 Diabetes. *Atheroscler. Suppl.* **2015,** *17,* 2–8.
59. Kastelein, J. J.; Akdim, F.; Stroes, E. S.; Zwinderman, A. H.; Bots, M. L.; Stalenhoef, A. F.; Visseren, F. L.; Sijbrands, E. J.; Trip, M. D.; Stein, E. A.; Gaudet, D.; Duivenvoorden, R.; Veltri, E. P.; Marais, A. D.; de Groot, E. Simvastatin With or Without Ezetimibe in Familial Hypercholesterolemia. *N. Engl. J. Med.* **2008,** *358* (14), 1431–1443.
60. Villines, T. C.; Stanek, E. J.; Devine, P. J.; Turco, M.; Miller, M.; Weissman, N. J.; Griffen, L.; Taylor, A. J. The ARBITER 6-HALTS Trial (Arterial Biology for the Investigation of the Treatment Effects of Reducing Cholesterol 6-HDL and LDL Treatment Strategies in Atherosclerosis): Final Results and the Impact of Medication Adherence, Dose, and Treatment Duration. *J. Am. Coll. Cardiol.* **2010,** *55* (24), 2721–2726.
61. Meaney, A.; Ceballos, G.; Asbun, J.; Solache, G.; Mendoza, E.; Vela, A.; Meaney, E. The VYtorin on Carotid Intima-Media Thickness and Overall Arterial Rigidity (VYCTOR) Study. *J. Clin. Pharmacol.* **2009,** *49* (7), 838–847.
62. Bogiatzi, C.; Spence, J. D. Ezetimibe and Regression of Carotid Atherosclerosis: Importance of Measuring Plaque Burden. *Stroke* **2012,** *43* (4), 1153–1155.
63. Howard, B. V.; Roman, M. J.; Devereux, R. B.; Fleg, J. L.; Galloway, J. M.; Henderson, J. A.; Howard, W. J.; Lee, E. T.; Mete, M.; Poolaw, B.; Ratner, R. E.; Russell, M.; Silverman, A.; Stylianou, M.; Umans, J. G.; Wang, W.; Weir, M. R.; Weissman, N. J.; Wilson, C.; Yeh, F.; Zhu, J. Effect of Lower Targets for Blood Pressure and LDL Cholesterol on Atherosclerosis in Diabetes: The SANDS Randomized Trial. *JAMA* **2008,** *299* (14), 1678–1689.
64. Fleg, J. L.; Mete, M.; Howard, B. V.; Umans, J. G.; Roman, M. J.; Ratner, R. E.; Silverman, A.; Galloway, J. M.; Henderson, J. A.; Weir, M. R.; Wilson, C.; Stylianou, M.; Howard, W. J. Effect of Statins Alone Versus Statins Plus Ezetimibe on Carotid Atherosclerosis in Type 2 Diabetes: The SANDS (Stop Atherosclerosis in Native Diabetics Study) Trial. *J. Am. Coll. Cardiol.* **2008,** *52* (25), 2198–2205.
65. Masuda, J.; Tanigawa, T.; Yamada, T.; Nishimura, Y.; Sasou, T.; Nakata, T.; Sawai, T.; Fujimoto, N.; Dohi, K.; Miyahara, M.; Nishikawa, M.; Nakamura, M.; Ito, M. Effect of Combination Therapy of Ezetimibe and Rosuvastatin on Regression of Coronary Atherosclerosis in Patients With Coronary Artery Disease. *Int. Heart J.* **2015,** *56* (3), 278–285.
66. Habara, M.; Nasu, K.; Terashima, M.; Ko, E.; Yokota, D.; Ito, T.; Kurita, T.; Teramoto, T.; Kimura, M.; Kinoshita, Y.; Tsuchikane, E.; Asakura, Y.; Matsubara, T.; Suzuki, T. Impact on Optical Coherence Tomographic Coronary Findings of Fluvastatin Alone Versus Fluvastatin + Ezetimibe. *Am. J. Cardiol.* **2014,** *113* (4), 580–587.
67. Ballantyne, C. M.; Blazing, M. A.; King, T. R.; Brady, W. E.; Palmisano, J. Efficacy and Safety of Ezetimibe Co-Administered With Simvastatin Compared With Atorvastatin in Adults With Hypercholesterolemia. *Am. J. Cardiol.* **2004,** *93* (12), 1487–1494.
68. Baigent, C.; Landray, M. J.; Reith, C.; Emberson, J.; Wheeler, D. C.; Tomson, C.; Wanner, C.; Krane, V.; Cass, A.; Craig, J.; Neal, B.; Jiang, L.; Hooi, L. S.; Levin, A.; Agodoa, L.; Gaziano, M.; Kasiske, B.; Walker, R.; Massy, Z. A.; Feldt-Rasmussen, B.; Krairittichai, U.; Ophascharoensuk, V.; Fellstrom, B.; Holdaas, H.; Tesar, V.; Wiecek, A.; Grobbee, D.; de Zeeuw, D.; Gronhagen-Riska, C.; Dasgupta, T.; Lewis, D.; Herrington, W.; Mafham, M.; Majoni, W.; Wallendszus, K.; Grimm, R.; Pedersen, T.; Tobert, J.; Armitage, J.; Baxter, A.; Bray, C.; Chen, Y.; Chen, Z.; Hill, M.; Knott, C.; Parish, S.; Simpson, D.; Sleight, P.; Young, A.; Collins, R. The Effects of Lowering LDL Cholesterol With Simvastatin Plus Ezetimibe in Patients With Chronic Kidney Disease (Study of Heart and Renal Protection): A Randomised Placebo-Controlled Trial. *Lancet* **2011,** *377* (9784), 2181–2192.
69. Suzuki, H.; Watanabe, Y.; Kumagai, H.; Shuto, H. Comparative Efficacy and Adverse Effects of the Addition of Ezetimibe to Statin Versus Statin Titration in Chronic Kidney Disease Patients. *Ther. Adv. Cardiovasc. Dis.* **2013,** *7* (6), 306–315.
70. Kato, E. T.; Giugliano, R. P.; Blazing, M. A.; Bohula-May, E.; Guneri, S.; White, J. A.; Tershakovec, A. M.; Musliner, T.; Braunwald, E.; Cannon, C. P. Benefit and Safety of Adding Ezetimibe to Statin Therapy on Cardiovascular Outcomes in 4416 Women in the IMPROVE-IT Trial. *Circulation* **2015,** *132,* A17862.
71. Giugliano, R. P.; et al. For the IMPROVE-IT Investigators. Benefit of Adding Ezetimibe to Statin Therapy on Cardiovascular Outcomes and Safety in Patients With vs. Without Diabetes: The IMPROVE-IT Trial. Presented at ESC Congress 2015. London, England, UK. Abstract 1947.
72. Wiviott, S. D.; Giugliano, R. P.; Blazing, M. A.; Cannon, C. P.; Zhou, J.; Murphy, S. A.; Tershakovec, A. M.; Musliner, T.; Braunwald, E. Reduction in Non-hemorrhagic Stroke With Ezetimibe/Simvastatin Compared With Simvastatin Alone in the IMPROVE-IT Trial. *Circulation* **2015,** *132,* A19694.
73. Pisciotta, L.; Fasano, T.; Bellocchio, A.; Bocchi, L.; Sallo, R.; Fresa, R.; Colangeli, I.; Cantafora, A.; Calandra, S.; Bertolini, S. Effect of Ezetimibe Coadministered With Statins in Genotype-Confirmed Heterozygous FH Patients. *Atherosclerosis* **2007,** *194* (2), e116–e122.
74. Gagne, C.; Gaudet, D.; Bruckert, E. Efficacy and Safety of Ezetimibe Coadministered With Atorvastatin or Simvastatin in Patients With Homozygous Familial Hypercholesterolemia. *Circulation* **2002,** *105* (21), 2469–2475.
75. Kalogirou, M.; Tsimihodimos, V.; Elisaf, M. Pleiotropic Effects of Ezetimibe: Do They Really Exist? *Eur. J. Pharmacol.* **2010,** *633* (1–3), 62–70.
76. Avellone, G.; Di Garbo, V.; Guarnotta, V.; Scaglione, R.; Parrinello, G.; Purpura, L.; Torres, D.; Campisi, D. Efficacy and Safety of Long-Term Ezetimibe/Simvastatin Treatment in Patients With Familial Hypercholesterolemia. *Int. Angiol.* **2010,** *29* (6), 514–524.
77. Sahebkar, A.; Simental-Mendia, L. E.; Guerrero-Romero, F.; Golledge, J.; Watts, G. F. Effect of Statin Therapy on Plasma PCSK9 Concentrations: A Systematic Review and Meta-Analysis of Clinical Trials. *Diabetes Obes. Metab.* **2015,** *17,* 1042–1055.
78. Abifadel, M.; Elbitar, S.; El Khoury, P.; Ghaleb, Y.; Chemaly, M.; Moussalli, M. L.; Rabes, J. P.; Varret, M.; Boileau, C. Living the PCSK9 Adventure: From the Identification of a New Gene in Familial Hypercholesterolemia Towards a Potential New Class of Anticholesterol Drugs. *Curr. Atheroscler. Rep.* **2014,** *16* (9), 439.
79. Careskey, H. E.; Davis, R. A.; Alborn, W. E.; Troutt, J. S.; Cao, G.; Konrad, R. J. Atorvastatin Increases Human Serum Levels of Proprotein Convertase Subtilisin/Kexin Type 9. *J. Lipid Res.* **2008,** *49* (2), 394–398.
80. Dubuc, G.; Chamberland, A.; Wassef, H.; Davignon, J.; Seidah, N. G.; Bernier, L.; Prat, A. Statins Upregulate PCSK9, the Gene Encoding the Proprotein Convertase Neural Apoptosis-Regulated Convertase-1 Implicated in Familial Hypercholesterolemia. *Arterioscler. Thromb. Vasc. Biol.* **2004,** *24* (8), 1454–1459.
81. Navarese, E. P.; Kolodziejczak, M.; Schulze, V.; Gurbel, P. A.; Tantry, U.; Lin, Y.; Brockmeyer, M.; Kandzari, D. E.; Kubica, J. M.; D'Agostino, R. B., Sr.; Kubica, J.; Volpe, M.; Agewall, S.; Kereiakes, D. J.; Kelm, M. Effects of Proprotein Convertase Subtilisin/Kexin Type 9 Antibodies in Adults With Hypercholesterolemia: A Systematic Review and Meta-Analysis. *Ann. Intern. Med.* **2015,** *163* (1), 40–51.
82. Li, C.; Lin, L.; Zhang, W.; Zhou, L.; Wang, H.; Luo, X.; Luo, H.; Cai, Y.; Zeng, C. Efficiency and Safety of Proprotein Convertase Subtilisin/Kexin 9 Monoclonal Antibody on Hypercholesterolemia: A Meta-Analysis of 20 Randomized Controlled Trials. *J. Am. Heart Assoc.* **2015,** *4* (6), e001937.
83. Zhang, X. L.; Zhu, Q. Q.; Zhu, L.; Chen, J. Z.; Chen, Q. H.; Li, G. N.; Xie, J.; Kang, L. N.; Xu, B. Safety and Efficacy of Anti-PCSK9 Antibodies: A Meta-Analysis of 25 Randomized, Controlled Trials. *BMC Med.* **2015,** *13,* 123.
84. Langslet, G.; Emery, M.; Wasserman, S. M. Evolocumab (AMG 145) for Primary Hypercholesterolemia. *Expert. Rev. Cardiovasc. Ther.* **2015,** *13* (5), 477–488.
85. Koren, M. J.; Scott, R.; Kim, J. B.; Knusel, B.; Liu, T.; Lei, L.; Bolognese, M.; Wasserman, S. M. Efficacy, Safety, and Tolerability of a Monoclonal Antibody to Proprotein Convertase Subtilisin/Kexin Type 9 As Monotherapy in Patients With Hypercholesterolaemia (MENDEL): A Randomised, Double-Blind, Placebo-Controlled, Phase 2 Study. *Lancet* **2012,** *380* (9858), 1995–2006.

86. Koren, M. J.; Lundqvist, P.; Bolognese, M.; Neutel, J. M.; Monsalvo, M. L.; Yang, J.; Kim, J. B.; Scott, R.; Wasserman, S. M.; Bays, H. Anti-PCSK9 Monotherapy for Hypercholesterolemia: The MENDEL-2 Randomized, Controlled Phase III Clinical Trial of Evolocumab. *J. Am. Coll. Cardiol.* **2014,** *63* (23), 2531–2540.
87. Giugliano, R. P.; Desai, N. R.; Kohli, P.; Rogers, W. J.; Somaratne, R.; Huang, F.; Liu, T.; Mohanavelu, S.; Hoffman, E. B.; McDonald, S. T.; Abrahamsen, T. E.; Wasserman, S. M.; Scott, R.; Sabatine, M. S. Efficacy, Safety, and Tolerability of a Monoclonal Antibody to Proprotein Convertase Subtilisin/Kexin Type 9 in Combination With a Statin in Patients With Hypercholesterolaemia (LAPLACE-TIMI 57): A Randomised, Placebo-Controlled, Dose-Ranging, Phase 2 Study. *Lancet* **2012,** *380* (9858), 2007–2017.
88. Robinson, J. G.; Nedergaard, B. S.; Rogers, W. J.; Fialkow, J.; Neutel, J. M.; Ramstad, D.; Somaratne, R.; Legg, J. C.; Nelson, P.; Scott, R.; Wasserman, S. M.; Weiss, R. Effect of Evolocumab or Ezetimibe Added to Moderate- or High-Intensity Statin Therapy on LDL-C Lowering in Patients With Hypercholesterolemia: The LAPLACE-2 Randomized Clinical Trial. *JAMA* **2014,** *311* (18), 1870–1882.
89. Blom, D. J.; Hala, T.; Bolognese, M.; Lillestol, M. J.; Toth, P. D.; Burgess, L.; Ceska, R.; Roth, E.; Koren, M. J.; Ballantyne, C. M.; Monsalvo, M. L.; Tsirtsonis, K.; Kim, J. B.; Scott, R.; Wasserman, S. M.; Stein, E. A. A 52-Week Placebo-Controlled Trial of Evolocumab in Hyperlipidemia. *N. Engl. J. Med.* **2014,** *370* (19), 1809–1819.
90. Sullivan, D.; Olsson, A. G.; Scott, R.; Kim, J. B.; Xue, A.; Gebski, V.; Wasserman, S. M.; Stein, E. A. Effect of a Monoclonal Antibody to PCSK9 on Low-Density Lipoprotein Cholesterol Levels in Statin-Intolerant Patients: The GAUSS Randomized Trial. *JAMA* **2012,** *308* (23), 2497–2506.
91. Stroes, E.; Colquhoun, D.; Sullivan, D.; Civeira, F.; Rosenson, R. S.; Watts, G. F.; Bruckert, E.; Cho, L.; Dent, R.; Knusel, B.; Xue, A.; Scott, R.; Wasserman, S. M.; Rocco, M. Anti-PCSK9 Antibody Effectively Lowers Cholesterol in Patients With Statin Intolerance: The GAUSS-2 Randomized, Placebo-Controlled Phase 3 Clinical Trial of Evolocumab. *J. Am. Coll. Cardiol.* **2014,** *63* (23), 2541–2548.
92. Raal, F.; Scott, R.; Somaratne, R.; Bridges, I.; Li, G.; Wasserman, S. M.; Stein, E. A. Low-Density Lipoprotein Cholesterol-Lowering Effects of AMG 145, a Monoclonal Antibody to Proprotein Convertase Subtilisin/Kexin Type 9 Serine Protease in Patients With Heterozygous Familial Hypercholesterolemia: The Reduction of LDL-C With PCSK9 Inhibition in Heterozygous Familial Hypercholesterolemia Disorder (RUTHERFORD) Randomized Trial. *Circulation* **2012,** *126* (20), 2408–2417.
93. Raal, F. J.; Stein, E. A.; Dufour, R.; Turner, T.; Civeira, F.; Burgess, L.; Langslet, G.; Scott, R.; Olsson, A. G.; Sullivan, D.; Hovingh, G. K.; Cariou, B.; Gouni-Berthold, I.; Somaratne, R.; Bridges, I.; Wasserman, S. M.; Gaudet, D. PCSK9 Inhibition With Evolocumab (AMG 145) in Heterozygous Familial Hypercholesterolaemia (RUTHERFORD-2): A Randomised, Double-Blind, Placebo-Controlled Trial. *Lancet* **2015,** *385* (9965), 331–340.
94. Stein, E. A.; Honarpour, N.; Wasserman, S. M.; Xu, F.; Scott, R.; Raal, F. J. Effect of the Proprotein Convertase Subtilisin/Kexin 9 Monoclonal Antibody, AMG 145, in Homozygous Familial Hypercholesterolemia. *Circulation* **2013,** *128* (19), 2113–2120.
95. Raal, F. J.; Honarpour, N.; Blom, D. J.; Hovingh, G. K.; Xu, F.; Scott, R.; Wasserman, S. M.; Stein, E. A. Inhibition of PCSK9 With Evolocumab in Homozygous Familial Hypercholesterolaemia (TESLA Part B): A Randomised, Double-Blind, Placebo-Controlled Trial. *Lancet* **2015,** *385* (9965), 341–350.
96. Sabatine, M. S.; Giugliano, R. P.; Wiviott, S. D.; Raal, F. J.; Blom, D. J.; Robinson, J.; Ballantyne, C. M.; Somaratne, R.; Legg, J.; Wasserman, S. M.; Scott, R.; Koren, M. J.; Stein, E. A. Efficacy and Safety of Evolocumab in Reducing Lipids and Cardiovascular Events. *N. Engl. J. Med.* **2015,** *372* (16), 1500–1509.
97. Koren, M. J.; Giugliano, R. P.; Raal, F. J.; Sullivan, D.; Bolognese, M.; Langslet, G.; Civeira, F.; Somaratne, R.; Nelson, P.; Liu, T.; Scott, R.; Wasserman, S. M.; Sabatine, M. S. Efficacy and Safety of Longer-Term Administration of Evolocumab (AMG 145) in Patients With Hypercholesterolemia: 52-Week Results From the Open-Label Study of Long-Term Evaluation Against LDL-C (OSLER) Randomized Trial. *Circulation* **2014,** *129* (2), 234–243.
98. Stein, E. A.; Swergold, G. D. Potential of Proprotein Convertase Subtilisin/Kexin Type 9 Based Therapeutics. *Curr. Atheroscler. Rep.* **2013,** *15* (3), 310.
99. McKenney, J. M.; Koren, M. J.; Kereiakes, D. J.; Hanotin, C.; Ferrand, A. C.; Stein, E. A. Safety and Efficacy of a Monoclonal Antibody to Proprotein Convertase Subtilisin/Kexin Type 9 Serine Protease, SAR236553/REGN727, in Patients With Primary Hypercholesterolemia Receiving Ongoing Stable Atorvastatin Therapy. *J. Am. Coll. Cardiol.* **2012,** *59* (25), 2344–2353.
100. Roth, E. M.; McKenney, J. M.; Hanotin, C.; Asset, G.; Stein, E. A. Atorvastatin With or Without an Antibody to PCSK9 in Primary Hypercholesterolemia. *N. Engl. J. Med.* **2012,** *367* (20), 1891–1900.
101. Stein, E. A.; Gipe, D.; Bergeron, J.; Gaudet, D.; Weiss, R.; Dufour, R.; Wu, R.; Pordy, R. Effect of a Monoclonal Antibody to PCSK9, REGN727/SAR236553, to Reduce Low-Density Lipoprotein Cholesterol in Patients With Heterozygous Familial Hypercholesterolaemia on Stable Statin Dose With or Without Ezetimibe Therapy: A Phase 2 Randomised Controlled Trial. *Lancet* **2012,** *380* (9836), 29–36.
102. Kereiakes, D. J.; Robinson, J. G.; Cannon, C. P.; Lorenzato, C.; Pordy, R.; Chaudhari, U.; Colhoun, H. M. Efficacy and Safety of the Proprotein Convertase Subtilisin/Kexin Type 9 Inhibitor Alirocumab Among High Cardiovascular Risk Patients on Maximally Tolerated Statin Therapy: The ODYSSEY COMBO I Study. *Am. Heart J.* **2015,** *169* (6), 906–915. e13.
103. Cannon, C. P.; Cariou, B.; Blom, D.; McKenney, J. M.; Lorenzato, C.; Pordy, R.; Chaudhari, U.; Colhoun, H. M. Efficacy and Safety of Alirocumab in High Cardiovascular Risk Patients With Inadequately Controlled Hypercholesterolaemia on Maximally Tolerated Doses of Statins: The ODYSSEY COMBO II Randomized Controlled Trial. *Eur. Heart J.* **2015,** *36* (19), 1186–1194.
104. Kastelein, J. J.; Robinson, J. G.; Farnier, M.; Krempf, M.; Langslet, G.; Lorenzato, C.; Gipe, D. A.; Baccara-Dinet, M. T. Efficacy and Safety of Alirocumab in Patients With Heterozygous Familial Hypercholesterolemia Not Adequately Controlled With Current Lipid-Lowering Therapy: Design and Rationale of the ODYSSEY FH Studies. *Cardiovasc. Drugs Ther.* **2014,** *28* (3), 281–289.
105. Kastelein, J. J.; Ginsberg, H. N.; Langslet, G.; Hovingh, G. K.; Ceska, R.; Dufour, R.; Blom, D.; Civeira, F.; Krempf, M.; Lorenzato, C.; Zhao, J.; Pordy, R.; Baccara-Dinet, M. T.; Gipe, D. A.; Geiger, M. J.; Farnier, M. ODYSSEY FH I and FH II: 78 Week Results With Alirocumab Treatment in 735 Patients With Heterozygous Familial Hypercholesterolaemia. *Eur. Heart J.* **2015,** *36* (43), 2996–3003.
106. Robinson, J. G.; Colhoun, H. M.; Bays, H. E.; Jones, P. H.; Du, Y.; Hanotin, C.; Donahue, S. Efficacy and Safety of Alirocumab As Add-On Therapy in High-Cardiovascular-Risk Patients With Hypercholesterolemia Not Adequately Controlled With Atorvastatin (20 or 40 mg) or Rosuvastatin (10 or 20 mg): Design And Rationale of the ODYSSEY OPTIONS Studies. *Clin. Cardiol.* **2014,** *37* (10), 597–604.
107. Bays, H.; Gaudet, D.; Weiss, R.; Ruiz, J. L.; Watts, G. F.; Gouni-Berthold, I.; Robinson, J.; Zhao, J.; Hanotin, C.; Donahue, S. Alirocumab as Add-On to Atorvastatin Versus Other Lipid Treatment Strategies: ODYSSEY OPTIONS I Randomized Trial. *J. Clin. Endocrinol. Metab.* **2015,** *100* (8), 3140–3148.
108. Farnier, M.; Jones, P.; Severance, R.; Averna, M.; Steinhagen-Thiessen, E.; Colhoun, H. M.; Du, Y.; Hanotin, C.; Donahue, S. Efficacy and Safety of Adding Alirocumab to Rosuvastatin Versus Adding Ezetimibe or Doubling the Rosuvastatin Dose in High Cardiovascular-Risk Patients: The ODYSSEY OPTIONS II Randomized Trial. *Atherosclerosis* **2015,** *244,* 138–146.
109. Moriarty, P. M.; Thompson, P. D.; Cannon, C. P.; Guyton, J. R.; Bergeron, J.; Zieve, F.; Bruckert, E.; Jacobson, T. A.; Kopecky, S. L.; Baccara-Dinet, M. T.; Du, L.; Pordy, R.; Gipe, D. Efficacy and Safety of Alirocumab vs. Ezetimibe in Statin-Intolerant Patients, With a Statin Rechallenge Arm: The ODYSSEY ALTERNATIVE Randomized Trial. *J. Clin. Lipidol.* **2015,** *9* (6), 758–769.
110. Roth, E. M.; McKenney, J. M. ODYSSEY MONO: Effect of Alirocumab 75 mg Subcutaneously Every 2 Weeks As Monotherapy Versus Ezetimibe Over 24 Weeks. *Future Cardiol.* **2015,** *11* (1), 27–37.
111. Robinson, J. G.; Farnier, M.; Krempf, M.; Bergeron, J.; Luc, G.; Averna, M.; Stroes, E. S.; Langslet, G.; Raal, F. J.; El Shahawy, M.; Koren, M. J.; Lepor, N. E.; Lorenzato, C.; Pordy, R.; Chaudhari, U.; Kastelein, J. J. Efficacy and Safety of Alirocumab in Reducing Lipids and Cardiovascular Events. *N. Engl. J. Med.* **2015,** *372* (16), 1489–1499.
112. Schwartz, G. G.; Bessac, L.; Berdan, L. G.; Bhatt, D. L.; Bittner, V.; Diaz, R.; Goodman, S. G.; Hanotin, C.; Harrington, R. A.; Jukema, J. W.; Mahaffey, K. W.; Moryusef, A.; Pordy, R.; Roe, M. T.; Rorick, T.; Sasiela, W. J.; Shirodaria, C.; Szarek, M.; Tamby, J. F.; Tricoci, P.; White, H.; Zeiher, A.; Steg, P. G. Effect of Alirocumab, a Monoclonal Antibody to PCSK9, on Long-Term Cardiovascular Outcomes Following Acute Coronary Syndromes: Rationale and Design of the ODYSSEY Outcomes Trial. *Am. Heart J.* **2014,** *168* (5), 682–689.

113. Ballantyne, C. M.; Neutel, J.; Cropp, A.; Duggan, W.; Wang, E. Q.; Plowchalk, D.; Sweeney, K.; Kaila, N.; Vincent, J.; Bays, H. Results of Bococizumab, a Monoclonal Antibody Against Proprotein Convertase Subtilisin/Kexin Type 9, From a Randomized, Placebo-Controlled, Dose-Ranging Study in Statin-Treated Subjects With Hypercholesterolemia. *Am. J. Cardiol.* **2015,** *115* (9), 1212–1221.
114. Rader, D. J.; Kastelein, J. J. Lomitapide and Mipomersen: Two First-in-Class Drugs for Reducing Low-Density Lipoprotein Cholesterol in Patients With Homozygous Familial Hypercholesterolemia. *Circulation* **2014,** *129* (9), 1022–1032.
115. Crooke, S. T.; Geary, R. S. Clinical Pharmacological Properties of Mipomersen (Kynamro), a Second Generation Antisense Inhibitor of Apolipoprotein B. *Br. J. Clin. Pharmacol.* **2013,** *76* (2), 269–276.
116. Visser, M. E.; Witztum, J. L.; Stroes, E. S.; Kastelein, J. J. Antisense Oligonucleotides for the Treatment of Dyslipidaemia. *Eur. Heart J.* **2012,** *33* (12), 1451–1458.
117. Akdim, F.; Stroes, E. S.; Sijbrands, E. J.; Tribble, D. L.; Trip, M. D.; Jukema, J. W.; Flaim, J. D.; Su, J.; Yu, R.; Baker, B. F.; Wedel, M. K.; Kastelein, J. J. Efficacy and Safety of Mipomersen, an Antisense Inhibitor of Apolipoprotein B, in Hypercholesterolemic Subjects Receiving Stable Statin Therapy. *J. Am. Coll. Cardiol.* **2010,** *55* (15), 1611–1618.
118. Akdim, F.; Visser, M. E.; Tribble, D. L.; Baker, B. F.; Stroes, E. S.; Yu, R.; Flaim, J. D.; Su, J.; Stein, E. A.; Kastelein, J. J. Effect of Mipomersen, an Apolipoprotein B Synthesis Inhibitor, on Low-Density Lipoprotein Cholesterol in Patients With Familial Hypercholesterolemia. *Am. J. Cardiol.* **2010,** *105* (10), 1413–1419.
119. Kastelein, J. J.; Wedel, M. K.; Baker, B. F.; Su, J.; Bradley, J. D.; Yu, R. Z.; Chuang, E.; Graham, M. J.; Crooke, R. M. Potent Reduction of Apolipoprotein B and Low-Density Lipoprotein Cholesterol by Short-Term Administration of an Antisense Inhibitor of Apolipoprotein B. *Circulation* **2006,** *114* (16), 1729–1735.
120. McGowan, M. P.; Tardif, J. C.; Ceska, R.; Burgess, L. J.; Soran, H.; Gouni-Berthold, I.; Wagener, G.; Chasan-Taber, S. Randomized, Placebo-Controlled Trial of Mipomersen in Patients With Severe Hypercholesterolemia Receiving Maximally Tolerated Lipid-Lowering Therapy. *PLoS One* **2012,** *7* (11), e49006.
121. Raal, F. J.; Santos, R. D.; Blom, D. J.; Marais, A. D.; Charng, M. J.; Cromwell, W. C.; Lachmann, R. H.; Gaudet, D.; Tan, J. L.; Chasan-Taber, S.; Tribble, D. L.; Flaim, J. D.; Crooke, S. T. Mipomersen, an Apolipoprotein B Synthesis Inhibitor, for Lowering of LDL Cholesterol Concentrations in Patients With Homozygous Familial Hypercholesterolaemia: A Randomised, Double-Blind, Placebo-Controlled Trial. *Lancet* **2010,** *375* (9719), 998–1006.
122. Stein, E. A.; Dufour, R.; Gagne, C.; Gaudet, D.; East, C.; Donovan, J. M.; Chin, W.; Tribble, D. L.; McGowan, M. Apolipoprotein B Synthesis Inhibition With Mipomersen in Heterozygous Familial Hypercholesterolemia: Results of a Randomized, Double-Blind, Placebo-Controlled Trial to Assess Efficacy and Safety As Add-On Therapy in Patients With Coronary Artery Disease. *Circulation* **2012,** *126* (19), 2283–2292.
123. Akdim, F.; Tribble, D. L.; Flaim, J. D.; Yu, R.; Su, J.; Geary, R. S.; Baker, B. F.; Fuhr, R.; Wedel, M. K.; Kastelein, J. J. Efficacy of Apolipoprotein B Synthesis Inhibition in Subjects With Mild-to-Moderate Hyperlipidaemia. *Eur. Heart J.* **2011,** *32* (21), 2650–2659.
124. Visser, M. E.; Wagener, G.; Baker, B. F.; Geary, R. S.; Donovan, J. M.; Beuers, U. H.; Nederveen, A. J.; Verheij, J.; Trip, M. D.; Basart, D. C.; Kastelein, J. J.; Stroes, E. S. Mipomersen, an Apolipoprotein B Synthesis Inhibitor, Lowers Low-Density Lipoprotein Cholesterol in High-Risk Statin-Intolerant Patients: A Randomized, Double-Blind, Placebo-Controlled Trial. *Eur. Heart J.* **2012,** *33* (9), 1142–1149.
125. Yu, R. Z.; Geary, R. S.; Flaim, J. D.; Riley, G. C.; Tribble, D. L.; vanVliet, A. A.; Wedel, M. K. Lack of Pharmacokinetic Interaction of Mipomersen Sodium (ISIS 301012), a 2′-*O*-Methoxyethyl Modified Antisense Oligonucleotide Targeting Apolipoprotein B-100 Messenger RNA, With Simvastatin and Ezetimibe. *Clin. Pharmacokinet.* **2009,** *48* (1), 39–50.
126. Li, N.; Li, Q.; Tian, X. Q.; Qian, H. Y.; Yang, Y. J. Mipomersen is a Promising Therapy in the Management of Hypercholesterolemia: A Meta-Analysis of Randomized Controlled Trials. *Am. J. Cardiovasc. Drugs* **2014,** *14* (5), 367–376.
127. Panta, R.; Dahal, K.; Kunwar, S. Efficacy and Safety of Mipomersen in Treatment of Dyslipidemia: A Meta-Analysis of Randomized Controlled Trials. *J. Clin. Lipidol.* **2015,** *9* (2), 217–225.
128. Sahebkar, A.; Watts, G. F. New LDL-Cholesterol Lowering Therapies: Pharmacology, Clinical Trials, and Relevance to Acute Coronary Syndromes. *Clin. Ther.* **2013,** *35* (8), 1082–1098.
129. Toth, P. P. Emerging LDL Therapies: Mipomersen-Antisense Oligonucleotide Therapy in the Management of Hypercholesterolemia. *J. Clin. Lipidol.* **2013,** *7* (3 Suppl), S6–S10.
130. Hashemi, N.; Odze, R. D.; McGowan, M. P.; Santos, R. D.; Stroes, E. S.; Cohen, D. E. Liver Histology During Mipomersen Therapy for Severe Hypercholesterolemia. *J. Clin. Lipidol.* **2014,** *8* (6), 606–611.
131. Thomas, G. S.; Cromwell, W. C.; Ali, S.; Chin, W.; Flaim, J. D.; Davidson, M. Mipomersen, an Apolipoprotein B Synthesis Inhibitor, Reduces Atherogenic Lipoproteins in Patients With Severe Hypercholesterolemia at High Cardiovascular Risk: A Randomized, Double-Blind, Placebo-Controlled Trial. *J. Am. Coll. Cardiol.* **2013,** *62* (23), 2178–2184.
132. Santos, R. D.; Duell, P. B.; East, C.; Guyton, J. R.; Moriarty, P. M.; Chin, W.; Mittleman, R. S. Long-Term Efficacy and Safety of Mipomersen in Patients With Familial Hypercholesterolaemia: 2-Year Interim Results of an Open-Label Extension. *Eur. Heart J.* **2015,** *36* (9), 566–575.
133. Erqou, S.; Kaptoge, S.; Perry, P. L.; Di Angelantonio, E.; Thompson, A.; White, I. R.; Marcovina, S. M.; Collins, R.; Thompson, S. G.; Danesh, J. Lipoprotein(a) Concentration and the Risk of Coronary Heart Disease, Stroke, and Nonvascular Mortality. *JAMA* **2009,** *302* (4), 412–423.
134. Gurdasani, D.; Sjouke, B.; Tsimikas, S.; Hovingh, G. K.; Luben, R. N.; Wainwright, N. W.; Pomilla, C.; Wareham, N. J.; Khaw, K. T.; Boekholdt, S. M.; Sandhu, M. S. Lipoprotein(a) and Risk of Coronary, Cerebrovascular, and Peripheral Artery Disease: The EPIC-Norfolk Prospective Population Study. *Arterioscler. Thromb. Vasc. Biol.* **2012,** *32* (12), 3058–3065.
135. Kamstrup, P. R.; Tybjaerg-Hansen, A.; Steffensen, R.; Nordestgaard, B. G. Genetically Elevated Lipoprotein(A) and Increased Risk of Myocardial Infarction. *JAMA* **2009,** *301* (22), 2331–2339.
136. Kraft, H. G.; Lingenhel, A.; Raal, F. J.; Hohenegger, M.; Utermann, G. Lipoprotein(a) in Homozygous Familial Hypercholesterolemia. *Arterioscler. Thromb. Vasc. Biol.* **2000,** *20* (2), 522–528.
137. Lamon-Fava, S.; Diffenderfer, M. R.; Marcovina, S. M. Lipoprotein(a) Metabolism. *Curr. Opin. Lipidol.* **2014,** *25* (3), 189–193.
138. Santos, R. D.; Raal, F. J.; Catapano, A. L.; Witztum, J. L.; Steinhagen-Thiessen, E.; Tsimikas, S. Mipomersen, an Antisense Oligonucleotide to Apolipoprotein B-100, Reduces Lipoprotein(A) in Various Populations With Hypercholesterolemia: Results of 4 Phase III Trials. *Arterioscler. Thromb. Vasc. Biol.* **2015,** *35* (3), 689–699.
139. Kolski, B.; Tsimikas, S. Emerging Therapeutic Agents to Lower Lipoprotein (A) Levels. *Curr. Opin. Lipidol.* **2012,** *23* (6), 560–568.
140. Hooper, A. J.; Burnett, J. R.; Watts, G. F. Contemporary Aspects of the Biology and Therapeutic Regulation of the Microsomal Triglyceride Transfer Protein. *Circ. Res.* **2015,** *116* (1), 193–205.
141. Goldberg, A. C. Emerging Low-Density Lipoprotein Therapies: Microsomal Triglyceride Transfer Protein Inhibitors. *J. Clin. Lipidol.* **2013,** *7* (3 Suppl), S16–S20.
142. Wetterau, J. R.; Gregg, R. E.; Harrity, T. W.; Arbeeny, C.; Cap, M.; Connolly, F.; Chu, C. H.; George, R. J.; Gordon, D. A.; Jamil, H.; Jolibois, K. G.; Kunselman, L. K.; Lan, S. J.; Maccagnan, T. J.; Ricci, B.; Yan, M.; Young, D.; Chen, Y.; Fryszman, O. M.; Logan, J. V.; Musial, C. L.; Poss, M. A.; Robl, J. A.; Simpkins, L. M.; Slusarchyk, W. A.; Sulsky, R.; Taunk, P.; Magnin, D. R.; Tino, J. A.; Lawrence, R. M.; Dickson, J. K., Jr.; Biller, S. A. An MTP Inhibitor That Normalizes Atherogenic Lipoprotein Levels in WHHL Rabbits. *Science* **1998,** *282* (5389), 751–754.
143. Shiomi, M.; Ito, T. MTP Inhibitor Decreases Plasma Cholesterol Levels in LDL Receptor-Deficient WHHL Rabbits by Lowering the VLDL Secretion. *Eur. J. Pharmacol.* **2001,** *431* (1), 127–131.
144. Liao, W.; Hui, T. Y.; Young, S. G.; Davis, R. A. Blocking Microsomal Triglyceride Transfer Protein Interferes With apoB Secretion Without Causing Retention or Stress in the ER. *J. Lipid Res.* **2003,** *44* (5), 978–985.
145. Cuchel, M.; Bloedon, L. T.; Szapary, P. O.; Kolansky, D. M.; Wolfe, M. L.; Sarkis, A.; Millar, J. S.; Ikewaki, K.; Siegelman, E. S.; Gregg, R. E.; Rader, D. J. Inhibition of Microsomal Triglyceride Transfer Protein in Familial Hypercholesterolemia. *N. Engl. J. Med.* **2007,** *356* (2), 148–156.

146. Cuchel, M.; Meagher, E. A.; du Toit Theron, H.; Blom, D. J.; Marais, A. D.; Hegele, R. A.; Averna, M. R.; Sirtori, C. R.; Shah, P. K.; Gaudet, D.; Stefanutti, C.; Vigna, G. B.; Du Plessis, A. M.; Propert, K. J.; Sasiela, W. J.; Bloedon, L. T.; Rader, D. J. Efficacy and Safety of a Microsomal Triglyceride Transfer Protein Inhibitor in Patients With Homozygous Familial Hypercholesterolaemia: A Single-Arm, Open-Label, Phase 3 Study. *Lancet* **2013,** *381* (9860), 40–46.
147. Stefanutti, C.; Blom, D. J.; Averna, M. R.; Meagher, E. A.; Theron, H.; Marais, A. D.; Hegele, R. A.; Sirtori, C. R.; Shah, P. K.; Gaudet, D.; Vigna, G. B.; Sachais, B. S.; Di Giacomo, S.; du Plessis, A. M.; Bloedon, L. T.; Balser, J.; Rader, D. J.; Cuchel, M. The Lipid-Lowering Effects of Lomitapide Are Unaffected by Adjunctive Apheresis in Patients With Homozygous Familial Hypercholesterolaemia—A Post-Hoc Analysis of a Phase 3, Single-Arm, Open-Label Trial. *Atherosclerosis* **2015,** *240* (2), 408–414.
148. Averna, M.; Cefalu, A. B.; Stefanutti, C.; Di Giacomo, S.; Sirtori, C. R.; Vigna, G. Individual Analysis of Patients With HoFH Participating in a Phase 3 Trial With Lomitapide: The Italian Cohort. *Nutr. Metab. Cardiovasc. Dis.* **2016,** *26* (1), 36–44.
149. Raper, A.; Kolansky, D. M.; Sachais, B. S.; Meagher, E. A.; Baer, A. L.; Cuchel, M. Long-Term Clinical Results of Microsomal Triglyceride Transfer Protein Inhibitor Use in a Patient With Homozygous Familial Hypercholesterolemia. *J. Clin. Lipidol.* **2015,** *9* (1), 107–112.
150. Roeters van Lennep, J.; Averna, M.; Alonso, R. Treating Homozygous Familial Hypercholesterolemia in a Real-World Setting: Experiences With Lomitapide. *J. Clin. Lipidol.* **2015,** *9* (4), 607–617.
151. Sacks, F. M.; Stanesa, M.; Hegele, R. A. Severe Hypertriglyceridemia With Pancreatitis: Thirteen Years' Treatment With Lomitapide. *JAMA Intern. Med.* **2014,** *174* (3), 443–447.
152. Derosa, G.; D'Angelo, A.; Franzetti, I. G.; Ragonesi, P. D.; Gadaleta, G.; Scalise, F.; Ciccarelli, L.; Piccinni, M. N.; Cicero, A. F. Efficacy and Safety of Ezetimibe/Simvastatin Association on Non-Diabetic and Diabetic Patients With Polygenic Hypercholesterolemia or Combined Hyperlipidemia and Previously Intolerant to Standard Statin Treatment. *J. Clin. Pharm. Ther.* **2009,** *34* (3), 267–276.
153. Tuteja, S.; Duffy, D.; Dunbar, R. L.; Movva, R.; Gadi, R.; Bloedon, L. T.; Cuchel, M. Pharmacokinetic Interactions of the Microsomal Triglyceride Transfer Protein Inhibitor, Lomitapide, With Drugs Commonly Used in the Management of Hypercholesterolemia. *Pharmacotherapy* **2014,** *34* (3), 227–239.
154. Parini, P.; Rudel, L. L. Is There a Need for Cholesteryl Ester Transfer Protein Inhibition? *Arterioscler. Thromb. Vasc. Biol.* **2003,** *23* (3), 374–375.
155. Barter, P. J.; Caulfield, M.; Eriksson, M.; Grundy, S. M.; Kastelein, J. J.; Komajda, M.; Lopez-Sendon, J.; Mosca, L.; Tardif, J. C.; Waters, D. D.; Shear, C. L.; Revkin, J. H.; Buhr, K. A.; Fisher, M. R.; Tall, A. R.; Brewer, B. Effects of Torcetrapib in Patients at High Risk for Coronary Events. *N. Engl. J. Med.* **2007,** *357* (21), 2109–2122.
156. Forrest, M. J.; Bloomfield, D.; Briscoe, R. J.; Brown, P. N.; Cumiskey, A. M.; Ehrhart, J.; Hershey, J. C.; Keller, W. J.; Ma, X.; McPherson, H. E.; Messina, E.; Peterson, L. B.; Sharif-Rodriguez, W.; Siegl, P. K.; Sinclair, P. J.; Sparrow, C. P.; Stevenson, A. S.; Sun, S. Y.; Tsai, C.; Vargas, H.; Walker, M., III; West, S. H.; White, V.; Woltmann, R. F. Torcetrapib-Induced Blood Pressure Elevation Is Independent of CETP Inhibition and Is Accompanied by Increased Circulating Levels of Aldosterone. *Br. J. Pharmacol.* **2008,** *154* (7), 1465–1473.
157. Schwartz, G. G.; Olsson, A. G.; Abt, M.; Ballantyne, C. M.; Barter, P. J.; Brumm, J.; Chaitman, B. R.; Holme, I. M.; Kallend, D.; Leiter, L. A.; Leitersdorf, E.; McMurray, J. J.; Mundl, H.; Nicholls, S. J.; Shah, P. K.; Tardif, J. C.; Wright, R. S. Effects of Dalcetrapib in Patients With a Recent Acute Coronary Syndrome. *N. Engl. J. Med.* **2012,** *367* (22), 2089–2099.
158. Bloomfield, D.; Carlson, G. L.; Sapre, A.; Tribble, D.; McKenney, J. M.; Littlejohn, T. W., III; Sisk, C. M.; Mitchel, Y.; Pasternak, R. C. Efficacy and Safety of the Cholesteryl Ester Transfer Protein Inhibitor Anacetrapib As Monotherapy and Coadministered With Atorvastatin in Dyslipidemic Patients. *Am. Heart J.* **2009,** *157* (2), 352–360. e2.
159. Brousseau, M. E.; Schaefer, E. J.; Wolfe, M. L.; Bloedon, L. T.; Digenio, A. G.; Clark, R. W.; Mancuso, J. P.; Rader, D. J. Effects of an Inhibitor of Cholesteryl Ester Transfer Protein on HDL Cholesterol. *N. Engl. J. Med.* **2004,** *350* (15), 1505–1515.
160. Cannon, C. P.; Shah, S.; Dansky, H. M.; Davidson, M.; Brinton, E. A.; Gotto, A. M.; Stepanavage, M.; Liu, S. X.; Gibbons, P.; Ashraf, T. B.; Zafarino, J.; Mitchel, Y.; Barter, P. Safety of Anacetrapib in Patients With or at High Risk for Coronary Heart Disease. *N. Engl. J. Med.* **2010,** *363* (25), 2406–2415.
161. Millar, J. S.; Reyes-Soffer, G.; Jumes, P.; Dunbar, R. L.; deGoma, E. M.; Baer, A. L.; Karmally, W.; Donovan, D. S.; Rafeek, H.; Pollan, L.; Tohyama, J.; Johnson-Levonas, A. O.; Wagner, J. A.; Holleran, S.; Obunike, J.; Liu, Y.; Ramakrishnan, R.; Lassman, M. E.; Gutstein, D. E.; Ginsberg, H. N.; Rader, D. J. Anacetrapib Lowers LDL by Increasing ApoB Clearance in Mildly Hypercholesterolemic Subjects. *J. Clin. Invest.* **2015,** *125* (6), 2510–2522.
162. Davidson, M.; Liu, S. X.; Barter, P.; Brinton, E. A.; Cannon, C. P.; Gotto, A. M., Jr.; Leary, E. T.; Shah, S.; Stepanavage, M.; Mitchel, Y.; Dansky, H. M. Measurement of LDL-C After Treatment With the CETP Inhibitor Anacetrapib. *J. Lipid Res.* **2013,** *54* (2), 467–472.
163. Gotto, A. M., Jr.; Kher, U.; Chatterjee, M. S.; Liu, Y.; Li, X. S.; Vaidya, S.; Cannon, C. P.; Brinton, E. A.; Moon, J. E.; Shah, S.; Dansky, H. M.; Mitchel, Y.; Barter, P. Lipids, Safety Parameters, and Drug Concentrations After an Additional 2 Years of Treatment With Anacetrapib in the DEFINE Study. *J. Cardiovasc. Pharmacol. Ther.* **2014,** *19* (6), 543–549.
164. Brinton, E. A.; Kher, U.; Shah, S.; Cannon, C. P.; Davidson, M.; Gotto, A. M.; Ashraf, T. B.; McCrary Sisk, C.; Dansky, H.; Mitchel, Y.; Barter, P. Effects of Anacetrapib on Plasma Lipids in Specific Patient Subgroups in the DEFINE (Determining the Efficacy and Tolerability of CETP INhibition With AnacEtrapib) Trial. *J. Clin. Lipidol.* **2015,** *9* (1), 65–71.
165. Kastelein, J. J.; Besseling, J.; Shah, S.; Bergeron, J.; Langslet, G.; Hovingh, G. K.; Al-Saady, N.; Koeijvoets, M.; Hunter, J.; Johnson-Levonas, A. O.; Fable, J.; Sapre, A.; Mitchel, Y. Anacetrapib as Lipid-Modifying Therapy in Patients With Heterozygous Familial Hypercholesterolaemia (REALIZE): A Randomised, Double-Blind, Placebo-Controlled, Phase 3 Study. *Lancet* **2015,** *385* (9983), 2153–2161.
166. Nicholls, S. J.; Brewer, H. B.; Kastelein, J. J.; Krueger, K. A.; Wang, M. D.; Shao, M.; Hu, B.; McErlean, E.; Nissen, S. E. Effects of the CETP Inhibitor Evacetrapib Administered As Monotherapy or in Combination With Statins on HDL and LDL Cholesterol: A Randomized Controlled Trial. *JAMA* **2011,** *306* (19), 2099–2109.
167. Nicholls, S. J.; Lincoff, A.; Barter, P.; et al. The ACCELERATE Trial: Impact of the Cholesteryl Ester Transfer Protein Inhibitor Evacetrapib on Cardiovascular Outcome. Presented at the 65th Annual Scientific Session and Expo of the American College of Cardiology. April 2–4, 2016, Chicago, IL.
168. Ford, J.; Lawson, M.; Fowler, D.; Maruyama, N.; Mito, S.; Tomiyasu, K.; Kinoshita, S.; Suzuki, C.; Kawaguchi, A.; Round, P.; Boyce, M.; Warrington, S.; Weber, W.; van Deventer, S.; Kastelein, J. J. Tolerability, Pharmacokinetics and Pharmacodynamics of TA-8995, a Selective Cholesteryl Ester Transfer Protein (CETP) Inhibitor, in Healthy Subjects. *Br. J. Clin. Pharmacol.* **2014,** *78* (3), 498–508.
169. Hovingh, G. K.; Kastelein, J. J.; van Deventer, S. J.; Round, P.; Ford, J.; Saleheen, D.; Rader, D. J.; Brewer, H. B.; Barter, P. J. Cholesterol Ester Transfer Protein Inhibition by TA-8995 in Patients With Mild Dyslipidaemia (TULIP): A Randomised, Double-Blind, Placebo-Controlled Phase 2 Trial. *Lancet* **2015,** *386* (9992), 452–460.
170. Pinkosky, S. L.; Filippov, S.; Srivastava, R. A.; Hanselman, J. C.; Bradshaw, C. D.; Hurley, T. R.; Cramer, C. T.; Spahr, M. A.; Brant, A. F.; Houghton, J. L.; Baker, C.; Naples, M.; Adeli, K.; Newton, R. S. AMP-Activated Protein Kinase and ATP-Citrate Lyase Are Two Distinct Molecular Targets for ETC-1002, a Novel Small Molecule Regulator of Lipid and Carbohydrate Metabolism. *J. Lipid Res.* **2013,** *54* (1), 134–151.
171. Filippov, S.; Pinkosky, S. L.; Lister, R. J.; Pawloski, C.; Hanselman, J. C.; Cramer, C. T.; Srivastava, R. A.; Hurley, T. R.; Bradshaw, C. D.; Spahr, M. A.; Newton, R. S. ETC-1002 Regulates Immune Response, Leukocyte Homing, and Adipose Tissue Inflammation via LKB1-Dependent Activation of Macrophage AMPK. *J. Lipid Res.* **2013,** *54* (8), 2095–2108.
172. Ballantyne, C. M.; Davidson, M. H.; Macdougall, D. E.; Bays, H. E.; Dicarlo, L. A.; Rosenberg, N. L.; Margulies, J.; Newton, R. S. Efficacy and Safety of a Novel Dual Modulator of Adenosine Triphosphate-Citrate Lyase and Adenosine Monophosphate-Activated Protein Kinase in Patients With Hypercholesterolemia: Results of a Multicenter, Randomized, Double-Blind, Placebo-Controlled, Parallel-Group Trial. *J. Am. Coll. Cardiol.* **2013,** *62* (13), 1154–1162.
173. Gutierrez, M. J.; Rosenberg, N. L.; Macdougall, D. E.; Hanselman, J. C.; Margulies, J. R.; Strange, P.; Milad, M. A.; McBride, S. J.; Newton, R. S. Efficacy and Safety of ETC-1002, a Novel Investigational Low-Density Lipoprotein-Cholesterol-Lowering Therapy for the Treatment of Patients With Hypercholesterolemia and Type 2 Diabetes Mellitus. *Arterioscler. Thromb. Vasc. Biol.* **2014,** *34* (3), 676–683.
174. Thompson, P. D.; Rubino, J.; Janik, M. J.; MacDougall, D. E.; McBride, S. J.; Margulies, J. R.; Newton, R. S. Use of ETC-1002 to Treat Hypercholesterolemia in Patients With Statin Intolerance. *J. Clin. Lipidol.* **2015,** *9* (3), 295–304.
175. Morrison, A.; Hokanson, J. E. The Independent Relationship Between Triglycerides and Coronary Heart Disease. *Vasc. Health Risk Manag.* **2009,** *5* (1), 89–95.

176. Sarwar, N.; Danesh, J.; Eiriksdottir, G.; Sigurdsson, G.; Wareham, N.; Bingham, S.; Boekholdt, S. M.; Khaw, K. T.; Gudnason, V. Triglycerides and the Risk of Coronary Heart Disease: 10,158 Incident Cases Among 262,525 Participants in 29 Western Prospective Studies. *Circulation* **2007,** *115* (4), 450–458.
177. Labreuche, J.; Touboul, P. J.; Amarenco, P. Plasma Triglyceride Levels and Risk of Stroke and Carotid Atherosclerosis: A Systematic Review of the Epidemiological Studies. *Atherosclerosis* **2009,** *203* (2), 331–345.
178. Tenenbaum, A.; Klempfner, R.; Fisman, E. Z. Hypertriglyceridemia: A Too Long Unfairly Neglected Major Cardiovascular Risk Factor. *Cardiovasc. Diabetol.* **2014,** *13* (1), 159.
179. Watts, G. F.; Karpe, F. Triglycerides and Atherogenic Dyslipidaemia: Extending Treatment Beyond Statins in the High-Risk Cardiovascular Patient. *Heart* **2011,** *97* (5), 350–356.
180. Miller, M.; Stone, N. J.; Ballantyne, C.; Bittner, V.; Criqui, M. H.; Ginsberg, H. N.; Goldberg, A. C.; Howard, W. J.; Jacobson, M. S.; Kris-Etherton, P. M.; Lennie, T. A.; Levi, M.; Mazzone, T.; Pennathur, S. Triglycerides and Cardiovascular Disease: A Scientific Statement From the American Heart Association. *Circulation* **2011,** *123* (20), 2292–2333.
181. Scherer, J.; Singh, V. P.; Pitchumoni, C. S.; Yadav, D. Issues in Hypertriglyceridemic Pancreatitis: An Update. *J. Clin. Gastroenterol.* **2014,** *48* (3), 195–203.
182. Pirillo, A.; Catapano, A. L. Update on the Management of Severe Hypertriglyceridemia—Focus on Free Fatty Acid Forms of Omega-3. *Drug Des. Devel. Ther.* **2015,** *9,* 2129–2137.
183. Davidson, M. H.; Johnson, J.; Rooney, M. W.; Kyle, M. L.; Kling, D. F. A Novel Omega-3 Free Fatty Acid Formulation Has Dramatically Improved Bioavailability During a Low-Fat Diet Compared With Omega-3-Acid Ethyl Esters: The ECLIPSE (Epanova((R)) Compared to Lovaza((R)) in a Pharmacokinetic Single-Dose Evaluation) Study. *J. Clin. Lipidol.* **2012,** *6* (6), 573–584.
184. Offman, E.; Marenco, T.; Ferber, S.; Johnson, J.; Kling, D.; Curcio, D.; Davidson, M. Steady-State Bioavailability of Prescription Omega-3 on a Low-Fat Diet Is Significantly Improved With a Free Fatty Acid Formulation Compared With an Ethyl Ester Formulation: The ECLIPSE II Study. *Vasc. Health Risk Manag.* **2013,** *9,* 563–573.
185. Kastelein, J. J.; Maki, K. C.; Susekov, A.; Ezhov, M.; Nordestgaard, B. G.; Machielse, B. N.; Kling, D.; Davidson, M. H. Omega-3 Free Fatty Acids for the Treatment of Severe Hypertriglyceridemia: The EpanoVa for Lowering Very High Triglycerides (EVOLVE) Trial. *J. Clin. Lipidol.* **2014,** *8* (1), 94–106.
186. Davidson, M. H.; Maki, K. C.; Bays, H.; Carter, R.; Ballantyne, C. M. Effects of Prescription Omega-3-Acid Ethyl Esters on Lipoprotein Particle Concentrations, Apolipoproteins AI and CIII, and Lipoprotein-Associated Phospholipase A(2) Mass in Statin-Treated Subjects With Hypertriglyceridemia. *J. Clin. Lipidol.* **2009,** *3* (5), 332–340.
187. Maki, K. C.; Bays, H. E.; Dicklin, M. R.; Johnson, S. L.; Shabbout, M. Effects of Prescription Omega-3-Acid Ethyl Esters, Coadministered With Atorvastatin, on Circulating Levels of Lipoprotein Particles, Apolipoprotein CIII, and Lipoprotein-Associated Phospholipase A2 Mass in Men and Women With Mixed Dyslipidemia. *J. Clin. Lipidol.* **2011,** *5* (6), 483–492.
188. Kastelein, J. J. P.; Maki, K. C.; Susekov, A.; Ezhov, M.; Nordestgaard, B. G.; Kling, D.; Davidson, M. H. Management of Severe Hypertriglyceridemia With a Novel Omega-3 Free-Fatty Acid Formulation: Subgroups in the EVOLVE Trial. *J. Clin. Lipidol.* **2013,** *7* (3), 271–272.
189. Maki, K. C.; Orloff, D. G.; Nicholls, S. J.; Dunbar, R. L.; Roth, E. M.; Curcio, D.; Johnson, J.; Kling, D.; Davidson, M. H. A Highly Bioavailable Omega-3 Free Fatty Acid Formulation Improves the Cardiovascular Risk Profile in High-Risk, Statin-Treated Patients With Residual Hypertriglyceridemia (the ESPRIT Trial). *Clin. Ther.* **2013,** *35* (9), 1400–1411. e1-3.
190. https://www.clinicaltrials.gov/ct2/show/study/NCT02104817.
191. Scott, L. J. Alipogene Tiparvovec: A Review of Its Use in Adults With Familial Lipoprotein Lipase Deficiency. *Drugs* **2015,** *75* (2), 175–182.
192. Gaudet, D.; de Wal, J.; Tremblay, K.; Dery, S.; van Deventer, S.; Freidig, A.; Brisson, D.; Methot, J. Review of the Clinical Development of Alipogene Tiparvovec Gene Therapy for Lipoprotein Lipase Deficiency. *Atheroscler. Suppl.* **2010,** *11* (1), 55–60.
193. Stroes, E. S.; Nierman, M. C.; Meulenberg, J. J.; Franssen, R.; Twisk, J.; Henny, C. P.; Maas, M. M.; Zwinderman, A. H.; Ross, C.; Aronica, E.; High, K. A.; Levi, M. M.; Hayden, M. R.; Kastelein, J. J.; Kuivenhoven, J. A. Intramuscular Administration of AAV1-Lipoprotein Lipase S447X Lowers Triglycerides in Lipoprotein Lipase-Deficient Patients. *Arterioscler. Thromb. Vasc. Biol.* **2008,** *28* (12), 2303–2304.
194. Carpentier, A. C.; Frisch, F.; Labbe, S. M.; Gagnon, R.; de Wal, J.; Greentree, S.; Petry, H.; Twisk, J.; Brisson, D.; Gaudet, D. Effect of Alipogene Tiparvovec (AAV1-LPL(S447X)) on Postprandial Chylomicron Metabolism in Lipoprotein Lipase-Deficient Patients. *J. Clin. Endocrinol. Metab.* **2012,** *97* (5), 1635–1644.
195. Norata, G. D.; Tsimikas, S.; Pirillo, A.; Catapano, A. L. Apolipoprotein C-III: From Pathophysiology to Pharmacology. *Trends Pharmacol. Sci.* **2015,** *36* (10), 675–687.
196. Jorgensen, A. B.; Frikke-Schmidt, R.; Nordestgaard, B. G.; Tybjaerg-Hansen, A. Loss-of-Function Mutations in APOC3 and Risk of Ischemic Vascular Disease. *N. Engl. J. Med.* **2014,** *371* (1), 32–41.
197. Crosby, J.; Peloso, G. M.; Auer, P. L.; Crosslin, D. R.; Stitziel, N. O.; Lange, L. A.; Lu, Y.; Tang, Z. Z.; Zhang, H.; Hindy, G.; Masca, N.; Stirrups, K.; Kanoni, S.; Do, R.; Jun, G.; Hu, Y.; Kang, H. M.; Xue, C.; Goel, A.; Farrall, M.; Duga, S.; Merlini, P. A.; Asselta, R.; Girelli, D.; Olivieri, O.; Martinelli, N.; Yin, W.; Reilly, D.; Speliotes, E.; Fox, C. S.; Hveem, K.; Holmen, O. L.; Nikpay, M.; Farlow, D. N.; Assimes, T. L.; Franceschini, N.; Robinson, J.; North, K. E.; Martin, L. W.; DePristo, M.; Gupta, N.; Escher, S. A.; Jansson, J. H.; Van Zuydam, N.; Palmer, C. N.; Wareham, N.; Koch, W.; Meitinger, T.; Peters, A.; Lieb, W.; Erbel, R.; Konig, I. R.; Kruppa, J.; Degenhardt, F.; Gottesman, O.; Bottinger, E. P.; O'Donnell, C. J.; Psaty, B. M.; Ballantyne, C. M.; Abecasis, G.; Ordovas, J. M.; Melander, O.; Watkins, H.; Orho-Melander, M.; Ardissino, D.; Loos, R. J.; McPherson, R.; Willer, C. J.; Erdmann, J.; Hall, A. S.; Samani, N. J.; Deloukas, P.; Schunkert, H.; Wilson, J. G.; Kooperberg, C.; Rich, S. S.; Tracy, R. P.; Lin, D. Y.; Altshuler, D.; Gabriel, S.; Nickerson, D. A.; Jarvik, G. P.; Cupples, L. A.; Reiner, A. P.; Boerwinkle, E.; Kathiresan, S. Loss-of-Function Mutations in APOC3, Triglycerides, and Coronary Disease. *N. Engl. J. Med.* **2014,** *371* (1), 22–31.
198. Graham, M. J.; Lee, R. G.; Bell, T. A., III; Fu, W.; Mullick, A. E.; Alexander, V. J.; Singleton, W.; Viney, N.; Geary, R.; Su, J.; Baker, B. F.; Burkey, J.; Crooke, S. T.; Crooke, R. M. Antisense Oligonucleotide Inhibition of Apolipoprotein C-III Reduces Plasma Triglycerides in Rodents, Nonhuman Primates, and Humans. *Circ. Res.* **2013,** *112* (11), 1479–1490.
199. Brahm, A. J.; Hegele, R. A. Chylomicronaemia-Current Diagnosis and Future Therapies. *Nat. Rev. Endocrinol.* **2015,** *11* (6), 352–362.
200. Gaudet, D.; Brisson, D.; Tremblay, K.; Alexander, V. J.; Singleton, W.; Hughes, S. G.; Geary, R. S.; Baker, B. F.; Graham, M. J.; Crooke, R. M.; Witztum, J. L. Targeting APOC3 in the Familial Chylomicronemia Syndrome. *N. Engl. J. Med.* **2014,** *371* (23), 2200–2206.
201. Gaudet, D.; Alexander, V. J.; Baker, B. F.; Brisson, D.; Tremblay, K.; Singleton, W.; Geary, R. S.; Hughes, S. G.; Viney, N. J.; Graham, M. J.; Crooke, R. M.; Witztum, J. L.; Brunzell, J. D.; Kastelein, J. J. Antisense Inhibition of Apolipoprotein C-III in Patients With Hypertriglyceridemia. *N. Engl. J. Med.* **2015,** *373* (5), 438–447.
202. Yen, C. L.; Stone, S. J.; Koliwad, S.; Harris, C.; Farese, R. V., Jr. Thematic Review Series: Glycerolipids. DGAT Enzymes and Triacylglycerol Biosynthesis. *J. Lipid Res.* **2008,** *49* (11), 2283–2301.
203. Smith, S. J.; Cases, S.; Jensen, D. R.; Chen, H. C.; Sande, E.; Tow, B.; Sanan, D. A.; Raber, J.; Eckel, R. H.; Farese, R. V., Jr. Obesity Resistance and Multiple Mechanisms of Triglyceride Synthesis in Mice Lacking Dgat. *Nat. Genet.* **2000,** *25* (1), 87–90.
204. Stone, S. J.; Myers, H. M.; Watkins, S. M.; Brown, B. E.; Feingold, K. R.; Elias, P. M.; Farese, R. V., Jr. Lipopenia and Skin Barrier Abnormalities in DGAT2-Deficient Mice. *J. Biol. Chem.* **2004,** *279* (12), 11767–11776.
205. DeVita, R. J.; Pinto, S. Current Status of the Research and Development of Diacylglycerol *O*-Acyltransferase 1 (DGAT1) Inhibitors. *J. Med. Chem.* **2013,** *56* (24), 9820–9825.
206. Meyers, C. D.; Serrano-Wu, M.; Amer, A.; Chen, J.; Rocheford, E.; Commerford, R.; Hubbard, B. K.; Brousseau, M. E.; Li, L.; Meihui, P.; Chatelain, R.; Dardik, B. The DGAT1 Inhibitor Pradigastat Decreases Chylomicron Secretion and Prevents Postprandial Triglyceride Elevation in Humans. *J. Clin. Lipidol.* **2013,** *7* (3), 285.
207. Meyers, C. D.; Tremblay, K.; Amer, A.; Chen, J.; Jiang, L.; Gaudet, D. Effect of the DGAT1 Inhibitor Pradigastat on Triglyceride and apoB48 Levels in Patients With Familial Chylomicronemia Syndrome. *Lipids Health Dis.* **2015,** *14,* 8.
208. Kjems, L.; Meyers, C. D.; Thuren, T. Diacylglycerol Acyltransferase 1 (DGAT1) Inhibition as a Metabolic Regulator: Clinical Benefits of Pradigastat in Obese Patients With Type 2 Diabetes. *J. Clin. Lipidol.* **2014,** *8* (3), 301–302.

7.19 Drug Discovery in Tissue Fibrosis

S Pinto, M Hoek, Y Huang, P Costet, L Ma, and JE Imbriglio, Merck Research Laboratories, Kenilworth, NJ, United States

© 2017 Elsevier Ltd. All rights reserved.

Dedicated to Nanda Sinha, a great mentor and chemist, who passed away in 2016.

7.19.1	**General Overview**	695
7.19.2	**Idiopathic Pulmonary Fibrosis**	696
7.19.2.1	Introduction	696
7.19.2.2	Epidemiology	696
7.19.2.3	Pathophysiology	696
7.19.2.4	Experimental Animal Models	697
7.19.2.5	Current Treatment	697
7.19.2.6	Ongoing Clinical Trials	698
7.19.2.7	Emerging Biology and Therapeutic Treatment	698
7.19.2.8	Concluding Remarks	700
7.19.3	**Chronic Kidney Disease**	701
7.19.3.1	Introduction	701
7.19.3.2	Epidemiology	701
7.19.3.3	Pathophysiology	701
7.19.3.3.1	Features of renal fibrosis (anatomy, histology)	701
7.19.3.3.2	Evidence for role of fibrosis in CKD progression	701
7.19.3.4	Animal Models of Fibrotic Renal Disease	702
7.19.3.4.1	Unilateral ureteral obstruction	702
7.19.3.4.2	5/6th nephrectomy (5/6th Nx)	702
7.19.3.4.3	Puromycin aminonucleoside	702
7.19.3.4.4	AA injury	702
7.19.3.4.5	Alport syndrome	702
7.19.3.5	Current Treatment	702
7.19.3.6	Ongoing Clinical Trials	703
7.19.3.7	Emerging Biology and Therapeutic Treatment	704
7.19.3.8	Conclusions and Perspectives	705
7.19.4	**Liver Fibrosis**	705
7.19.4.1	Introduction	705
7.19.4.2	Epidemiology	705
7.19.4.3	Pathophysiology	706
7.19.4.4	Experimental Animal Models	707
7.19.4.5	Drugs Evaluated in Preclinical and Clinical Trials	707
7.19.4.6	Emerging Biology	708
7.19.4.7	Concluding Remarks	709
References		709

Abbreviations

ARB Angiotensin receptor blockers
BMP Bone morphogenetic proteins
CKD Chronic kidney disease
ECM Extracellular matrix
EMT Epithelial–mesenchymal transition
ESRD End-stage renal disease
GFR Glomerular filtration rate
HDAC Histone deacetylase
IPF Idiopathic pulmonary fibrosis
NAFLD Nonalcoholic fatty liver disease
NASH Nonalcoholic steatohepatitis
PAN Puromycin aminonucleoside
PPAR Peroxisome proliferator-activated receptor
ROS Reactive oxygen species
TGF-β Transforming growth factor beta
UUO Unilateral ureteral obstruction
α-SMA Alpha smooth muscle actin

7.19.1 General Overview

End-stage organ damage is typically associated with fibrosis. The fibrotic event leads to disruption of the normal architecture of a wide variety of tissues, which ultimately leads to organ dysfunction and failure. Fibrotic diseases pose one of the most serious health problems in current medicine and represent a series of economic burden to the health system. It has been estimated that as much as 45% of the mortality worldwide are attributed to fibrosis.[1] Multiple studies examining pathways and targets have grown over the years. However translation of these findings to clinical studies has remained a challenge in the area of pharmaceutical research. In this review we will provide an overview of the events leading to the fibrotic state in multiple tissues and end-stage organ damage. Several examples will be outlined in this article including fibrosis of the lung as in idiopathic pulmonary fibrosis (IPF); fibrosis of the liver as in nonalcoholic steatohepatitis (NASH) and liver cirrhosis; and fibrosis of the kidney characteristic of chronic kidney disease (CKD). Furthermore we will describe the underlying molecular pathways associated with these events as well as the multiple pharmacological agents identified for these targets currently at various stages of clinical development.

Although the etiology of fibrosis varies from organ to organ, similar pathology is observed across multiple tissues. As illustrated (Fig. 1), the cellular events that lead to the hallmark characterization of a fibrotic tissue are relatively well understood.[2] Fibrotic disorders are characterized by common, persistent, and chronic inflammation which is initiated by injury to the epithelium and the endothelium. Dysregulation of metabolic pathways including endoplasmic reticulum (ER) and cellular stress, and overproduction of reactive oxygen species (ROS) are some of the common causes of epithelium/endothelium injury. Regardless of the cause, persistent injury eventually leads to activation and migration of inflammatory cells such as T-cells, macrophages, and granulocytes to the site of injury. Production of cytokines and chemokines in turn further activates the macrophages and fibroblasts. The fibrotic event is characterized by increased and persistent production of extracellular matrix (ECM). The primary cells responsible for ECM productions are the alpha smooth muscle actin (α-SMA)-expressing myofibroblasts which are derived from local fibroblasts or from mesenchymal cells. Other cells that contribute to the formation of ECM include fibrocytes which are cells derived from bone marrow[3] as well as epithelial cells, which may undergo epithelial–mesenchymal transition (EMT).[4] The amount of collagen deposition is regulated by the rate of collagen synthesis and breakdown. The kinetics of collagen production is controlled by metalloproteases MMPs and MMP inhibitors (TIMPs). During a fibrotic event, the synthesis of new collagen by fibroblasts exceeds the rate at which it is degraded leading to increased collagen accumulation.[5] The most abundant collagen subtypes are collagen type I and collagen type III, although there are other subtypes which are involved in the process. The secreted collagen gets cross-linked by a family of enzymes called lysyl oxidases such as lysyl oxidase-like 2 (LOXL2) to form abnormal ECM. Deposition of ECM will lead to remodeling, disruption of the normal architecture, and eventually organ failure. This process of uncontrolled fibrosis is different from controlled repair occurring during normal wound healing.[6]

In the last couple of decades the pharmaceutical and biotech industries become increasingly interested in targeting key components in the fibrotic core pathways. One area of focus has been targeting the transforming growth factor beta (TGF-β), which is considered to be the main cytokine in all fibrotic events. Various approaches have been taken to target TGF-β either directly or

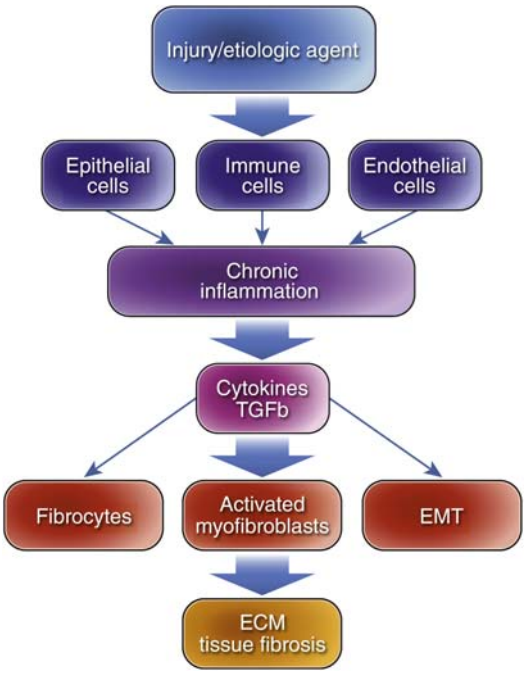

Fig. 1 Disease progression of tissue fibrosis.

indirectly by targeting pathways associated with its activation and regulation. TGF-βs are secreted cytokines, which are synthesized as part of a large molecule, the pro-TGF-β containing the latency-associated proteins. The release of TGF-β from the pro-TGF-β complex can be achieved through several processes.[7] The main process by which TGF-β is activated is thought to be through the RGD-containing integrins.[8] Other mechanisms include proteolytic activity by plasmin, matrix-metalloproteinases, treatment with mild acids,[9] or through the action of thrombospondin.[10] Once TGF-β is activated it can bind to its receptor TGF-β R2 and ALK5 (TGF-β receptor-1).[11] These are the type I and type II Ser/Thr kinase receptors which form a heterodimer upon ligand binding. Once the complex is formed, it propagates signaling by phosphorylating SMAD3 which then forms a complex with SMAD4. Upon dimerization, the complex translocates to the nucleus where it binds to key DNA response elements to transcriptionally control target genes involved in fibrogenesis.[11]

Although our understanding of the process and the mechanisms by which fibrosis is formed has grown, most chronic fibrotic diseases remain poorly treated. The very first approval of antifibrotic drugs pirfenidone and nintedanib in 2014 provided insight into clinical development path for IPF. Other pharmacological and biological agents discussed in this article are in various stages of preclinical and clinical development for multiple indications related to IPF and other fibrotic diseases. It is well accepted that diseases like IPF, NASH, CKD, etc. share common molecular pathways. This concept led to the speculation that IPF could serve as a clinical proof of concept (POC) and an entry point for other indications. The concept of targeting key core fibrotic pathways is reasonable; however, it has yet to be demonstrated that the same mechanisms have similar effect across tissues independent of the underlying injury. Furthermore, the notion that those pharmacological blockages of fibrosis pathways will be efficacious in preventing or slowing down end-stage organ failure remains to be proven in the clinic. In the next several years the field is anticipated to continue growing. Increased efforts in preclinical model development, pathway mining, and basic mechanistic work around cellular signaling will provide insight into the underlying biology of the fibrotic diseases. In addition, the outcome of multiple clinical development programs that are ongoing will shed light into some of these questions.

7.19.2 Idiopathic Pulmonary Fibrosis

7.19.2.1 Introduction

IPF is a life-threatening and devastating disease, and there is no cure available. The median survival is 3–5 years from the time of diagnosis.[12] IPF is the most severe form of interstitial lung disease (ILD) and occurs in 20–30% ILD patients,[13–15] predominantly in adults who are 50–85 years old. IPF patients universally develop dyspnea from progressive ventilatory restriction and hypoxia, and respiratory failure is the most common cause of death (~60%).[16,17] The disease course of IPF is unpredictable, and up to 20% IPF patients experience acute exacerbation, which results in a hospital mortality of at least 50%.[18,19]

7.19.2.2 Epidemiology

In the United States, the prevalence of IPF is 14.0–27.9 cases per 100,000 people, and the annual incidence is estimated to be 6.8–8.8 cases per 100,000 people. In Europe, the prevalence is 1.25–23.4 cases per 100,000 people, and the annual incidence is estimated to be 0.22–7.4 cases per 100,000 people. In Asia the prevalence is 1.7–4.9 cases per 100,000 people, and the annual incidence is 0.9–2.23 cases per 100,000 people.[13,19–31] Distribution of IPF across two genders is uneven, and more men than women are affected and the ratio is estimated to be 1.5:1.[32] Overall, evidences suggest that the prevalence and annual incidence of IPF are increasing, particularly among the elderly (>65 years old), with the estimation that 1 in 1000 will develop IPF.

Among all the IPF patients, 1–4% of IPF patients have a family history of IPF and the symptoms seem to present at younger ages.[33–36] Recent studies suggested that genetic factors, such as polymorphisms around the genes MUC5B, SPA, SPC, SPPL2C, TERT, and TOLLIP, are associated with IPF.[37–45] Environmental risk factors for IPF include cigarette smoking, exposure to organic and inorganic dusts, pharmacologic therapies, and microbial agents such as Epstein–Barr virus. Despite those reported genetic and nongenetic associations, the specific roles of those risk factors and how they interact with each other in the course of the disease are still largely unknown.

7.19.2.3 Pathophysiology

The exact cause of IPF is not completely understood. It was initially believed that inflammation was the leading cause of IPF, but with the failure of multiple trials involving immunosuppressive agents, particularly the PANTHER-IPF trial (prednisolone, azathioprine, and *N*-acetylcysteine combo therapy for IPF),[46] the focus has been shifted to fibrosis.

Histologically, IPF lungs show marked fibrosis with architectural distortion and honeycombing distributed along the inferior portions of the lobes with subpleural accentuation. Unlike other lung diseases, inflammation is very limited in IPF lungs. Epithelial damage is now thought to be the initiator of fibrogenesis in IPF. In a normal setting, alveolar type 2 lung epithelial cells come into injured site to repair lung epithelium once there is damage. However, if there is a recurrent or persistent damage to lung epithelial cells, these cells will initiate proliferation, migration, and activation of fibroblast cells or other fibrosis progenitor cells such as fibrocytes to the damage site.[47] Epithelial cells can also undergo a process called EMT and acquire a fibroblast-like phenotype, becoming mobile and expressing mesenchymal proteins and type I collagen while losing epithelial markers such as E-cadherin.[48] However, it still remains to be determined how much the EMT process contributes to the fibrotic process.[49] Activated

fibroblast cells or myofibroblast cells are responsible for excessive deposition of collagen and formation of fibrotic foci, a hallmark feature of IPF histology. Stiffening of lung tissue caused by accumulation/cross-linking of collagen and other ECM components will ultimately damage the delicate structure of the alveolar spaces and result in poor gas exchange and difficulty in breathing and death.[50]

At the molecular level, genetic mutations or exposure to environmental risk factors induce ER stress in lung epithelial cells, which triggers release of profibrotic factors, such as TGF-β1,[51,52] platelet-derived growth factor (PDGF),[53,54] connective tissue growth factor (CTGF),[55] and cytokines including interleukin-4 (IL-4) and interleukin-13 (IL-13).[56,57] TGF-β1 is thought to be the master regulator of fibrosis. Direct activation of fibroblast cells by TGF-β1 causes overexpression of ECM proteins as well as TGF-β1 itself. TGF-β1 can also induce EMT of epithelial cells, which serves as a feed-forward mechanism to activate more surrounding fibroblast cells. In contrast, secretion of PDGF by epithelial cells induces proliferation but not activation of fibroblast cells. In addition to these two major players, many other secreted factors, such as Wnt proteins,[58–60] have potential roles in IPF. It is currently well appreciated that IPF is caused by a cascade of events involving the crosstalk between epithelial cells and fibroblast cells through secreted factors. Other than the cell-secreted growth factors, chemokines, and cytokines, ECM components also contribute to fibrosis by modulating fibrotic signaling. It has been demonstrated that fibroblast cells are subject to regulation by mechanical cues. Stiffening of ECM due to excessive collagen deposition and cross-linking induces reorganization of cytoskeleton network in fibroblast cells through integrins, which then provides cues to transdifferentiate fibroblast cells into myofibroblast cells through mechanotransducers such as YAP and TAZ.[61] Other ECM components such as lumican, hyaluronan, or even endostatin, a breakdown product of collagen XVIII, are also implicated in modulation of fibroblast activation.[62] Overall, IPF is a result of complex interplay between multiple cell types engaging both intracellular and extracellular mechanisms.

7.19.2.4 Experimental Animal Models

The common animal models used for the study of IPF include chemically induced models, such as asbestos, bleomycin, silica, or fluorescein isothiocyanate-induced lung fibrosis models; irradiation-induced lung fibrosis model; age-dependent fibrosis models, genetically modified mouse lung fibrosis models; and humanized mouse models.

Among all the models, the bleomycin model has been the most commonly applied model over the past few decades, and intratracheal delivery of bleomycin is the most common delivery route. In this model, fibrosis happens in a short period of time (2–4 weeks). Disease progression in the bleomycin model can be separated into two phases, the inflammation phase and the fibrosis phase. In the inflammation phase, a bleomycin insult creates DNA damage, generates free radicals, and induces oxidative stress, which causes cell necrosis and apoptosis and ultimately tissue edema and inflammation, with elevation of cytokines such as tumor necrosis factor alpha (TNF-α) and interleukin 1 beta. After the first week, inflammation subsides and fibrosis starts its course, and by approximately day 14, the expression of TGF-β1 peaks and collagen deposits resembling IPF fibrosis becomes prominent.[63–65] Despite its popularity, bleomycin model using a single dose is not fully consistent with human IPF histologically due to the obvious lack of fibroblastic loci and epithelium hyperplasia. It was suggested that repetitive dosing of bleomycin induces histopathologic changes reminiscent of those seen in IPF patients. Nevertheless, efficacy of the FDA approved drugs pirfenidone (Esbriet) and nintedanib (Ofev) in rodent bleomycin models (mouse, rat, and hamster) has been successfully translated into clinic.

Each animal lung fibrosis model has its own advantages and disadvantages. When evaluating outcomes of any of the models, one must ensure that collagen deposition truly reflects fibrosis. Some appropriate assays include biochemical quantification of collagen using Sircol collagen assay, hydroxyproline assay, or Western blotting of fibrosis markers such as collagen and α-SMA, and histologic evaluation of total collagen or collagen subtypes and other markers such as α-SMA. Alternatively, isotope-guided analysis of newly synthesized ECM proteins can be applied to gain a closer look at the dynamics of fibrosis. To complement the biochemical and histologic measurement, lung mechanics can be measured, such as lung compliance values derived from pressure-volume loops. Nevertheless, with the successful translation from rodents to human for the two approved drugs pirfenidone and nintedanib, bleomycin-induced lung fibrosis model will remain as an anchor model for IPF drug development.

7.19.2.5 Current Treatment

Pirfenidone (Esbriet) and nintedanib (Ofev) (**Fig. 2**) are the first agents approved by FDA and other regulatory agencies for treatment of IPF.

Pirfenidone (5-methyl-1-phenyl-2-[1H]-pyridone) is developed as an oral drug. The exact antifibrotic molecular mechanisms of pirfenidone are not well understood. Preclinically, this molecule demonstrated both anti-inflammatory and anti-fibrotic activities in both in vitro and in vivo studies. In vitro, it inhibits the release of pro-inflammatory and pro-fibrotic cytokines and growth factors, as well as inhibiting the proliferation of fibroblasts and synthesis of ECM proteins from fibroblast cells in response to fibrotic growth factors such as PDGF and TGF-β. In vivo, it showed efficacy in multiple bleomycin lung fibrosis models, including mouse, rat, and hamster models.[66–68] Clinically, pirfenidone is indicated for mild and moderate IPF, and the treatment effect of Pirfenidone appears to begin immediately and persist through the course of therapy measured by vital capacity. More importantly, the use of pirfenidone is correlated with improved mortality in IPF patients.[69] The common side effects of pirfenidone include liver enzyme elevation, high photosensitivity, gastrointestinal disorders, nausea, and rash, with some patients having to discontinue treatment in the clinical trials due to severe side effects.

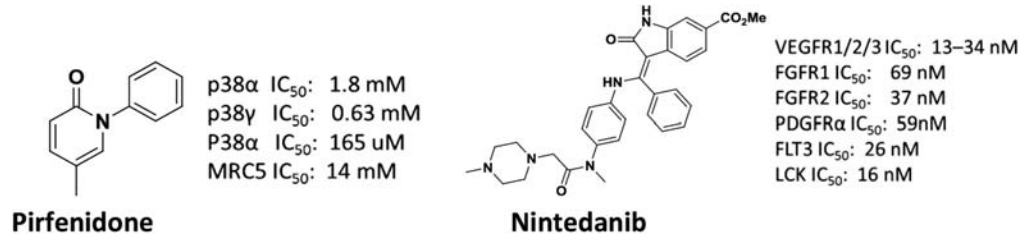

Fig. 2 Pirfenidone and nintedanib: structures and inhibitory activities.

Nintedanib (methyl (3*Z*)-3-{[(4-{methyl[(4-methylpiperazin-1-yl) acetyl]amino}phenyl) amino] (phenyl)methylidene}-2-oxo-2,3-dihydro-1*H*-indole-6-carboxylate) is a small molecule tyrosine kinase inhibitor that is administered orally. It was initially developed as an anticancer drug to treat nonsmall cell lung cancer due to its anti-angiogenesis activity. Nintedanib has inhibitory effect on multiple kinases, including VEGFR, PDGFR, FGFR, Flt-3, Lck, Lyn, and SRC by binding to their ATP binding pocket, and its efficacy on the first 3 kinases is believed to play a role in IPF. It was also shown to inhibit tyrosine phosphorylation of TGF-β receptor type II. Preclinically, nintedanib was able to decrease fibrosis scores, and expression of procollagen and TGF-β1 in both mouse and rat bleomycin lung fibrosis models.[70] Similar findings were reproduced in a silica-induced mouse lung fibrosis model.[70] Due to the broad activity against tyrosine kinases, it is not surprising that nintedanib has a spectrum of adverse effects such as elevation of liver enzymes, gastrointestinal disorders, headache, and weight loss. For nintedanib, there is no evidence to show reduced mortality in IPF patients.[30]

7.19.2.6 Ongoing Clinical Trials

Although pirfenidone and nintedanib have been approved for IPF, the goal of these two therapies is not to cure the disease, but rather stabilize the disease progression. IPF still remains a significant unmet medical need and there is obvious room to improve with respect to drug efficacy and side effects over the long-term treatment. Because of this many companies are spearheading clinical trials with new agents of different mechanisms. Those mechanisms are summarized in **Table 1**.

Other mechanisms being tested in clinical trials are antioxidants, stem cell therapy, immunoglobulin therapy, and others that are unspecified.

7.19.2.7 Emerging Biology and Therapeutic Treatment

Significant advances have been made in our understanding of the pathogenesis of IPF and fundamental biology in tissue fibrosis in the past decade. With this emerging biology, the number of potential targets for IPF has dramatically increased. Other than those

Table 1 Agents on clinical trials for IPF

Modality	*Drug*	*Target*	*Development status*	*Company*
Small molecules	BMS-986020	Lysophosphatidic acid receptor 1 (LPA1R)	Phase II	Bristol-Myers Squibb
	GSK2126458	PI3K–AKT pathway	Phase I	GlaxoSmithKline
	Riociguat	Soluble guanidine cyclase (sGC)	Phase II	Bayer
	TD139	Galectin-3	Phase I/II	Galecto/Bristol-Myers Squibb
Biologics	CNTO 888	CC-chemokine ligand 2 (CCL 2)	Phase II	Centocor
	FG-3019	CTGF	Phase II	FibroGen/Bristol-Myers Squibb
	IW001	Purified collagen V	Phase I	Immuneworks
	Lebrikizumab	Interleukin-13 (IL-13)	Phase II	Roche/Chugai
	Lecithinized superoxide dismutase	Lecithinized superoxide dismutase	Phase II	LTT Biopharma
	PRM-151	Fibrocytes	Phase I	Promedior
	SAR156597	Interleukin-4 (IL-4) and IL-13	Phase I/II	Sanofi
	Simtuzumab	Collagen and lysyl oxidase-like 2 (LOXL2)	Phase II	Gilead
	STX-100	αVβ6 integrin	Phase II	Biogen Idec
	Tralokinumab	IL-13	Phase II	AstraZeneca
Combo	Combined PEX, rituximab and steroids	Combined plasma exchange (PEX), rituximab, and conventional corticosteroid	Phase I/II	University of Pennsylvania

Table 2 Preclinical agents for IPF

Mechanism	*Compound*	*Preclinical validation*
FAK[71]	PF-562271	Bleomycin model
αVβ6[72]	CWHM 12	Bleomycin/CCl_4 model
αVβ1[73]	c8	Bleomycin/CCl_4 model
LOXL2[74]	β-Aminopropionitrile	Bleomycin model
PAR1[75]	SCH79797	Bleomycin/CCl_4 model
PAI1[76]	TM5275	Lung fibrosis model
Neutrophil elastase[77]	Sivelestat	Bleomycin model
EPRS[78]	Halofuginone	Bleomycin model
CXCR4[79]	AMD3100	Bleomycin model
WNT[80]	ICG-001	Bleomycin model
PTGER[81]	Butaprost	Bleomycin model
$P2X_7$[82]	A-438079	Interstitial fibrosis model
Galectin-3[83]	TD139	Bleomycin model
P38/MAPK[84]	SB239063	Bleomycin model
ATX[85]	GWJ-A-23	Bleomycin model
Relaxin[86]	Compound **8**	Bleomycin model
BET[87,88]	JQ-1	Bleomycin model
NR4A1[89]	Cytosporone B	Interstitial fibrosis model
Rho kinase[90]	Y-27632	Bleomycin model

that have already been tested in clinical trials, many more are being explored preclinically (Table 2), many of which can be put into the following categories:

1. TGF-β1 and fibrosis core pathways: TGF-β1 receptor/ALK5 inhibitor, αVβ6 integrin inhibitor, αVβ1 integrin inhibitor, and WNT/β-catenin signaling modulators.

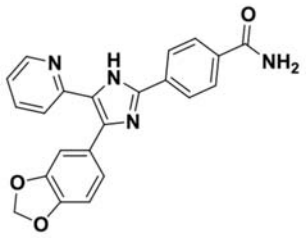

SB-431541 (ALK5 IC_{50}: 94 nM)

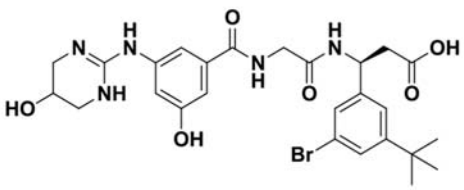

CWHM12 (αvβ6 IC_{50}: 1.5 nM)

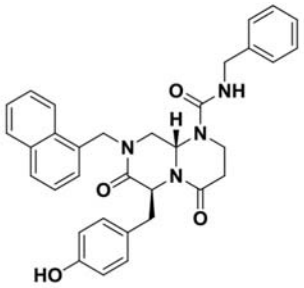

ICG-001 (β-catenin IC_{50}: 3.0 uM)

2. ROS pathway: NOX4 inhibitor and other antioxidants.

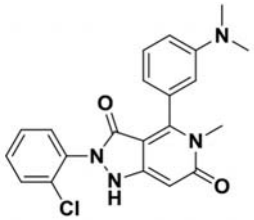

GKT - 137831 (NOX1/4 Ki: 100-150 nM)

3. Epigenetic regulation: miR-21, miR-31, other microRNAs, and BET inhibitor.

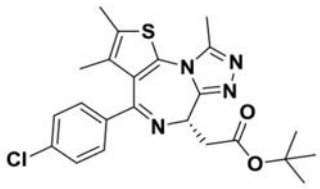

(+) JQ-1 (BRD4 IC_{50}: 33-77 nM)

4. Coagulation pathway: PAR-1 inhibitor and factor Xa inhibitor.

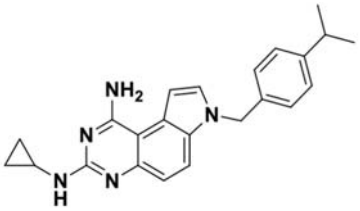

SCH 79797 (PAR1 IC_{50}: 70 nM)

5. Fibroblast/myofibroblast differentiation and migration: Rho kinase inhibitor, FAK inhibitor, TRPV4 inhibitor, Sonic-hedgehog pathway inhibitor, sphingosine kinase inhibitors, and sphingosine-1-phosphate receptor antagonist.

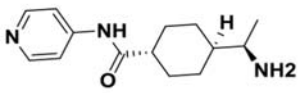

Y-27632 (ROCK1/2 Ki: 0.22/0.3 uM)

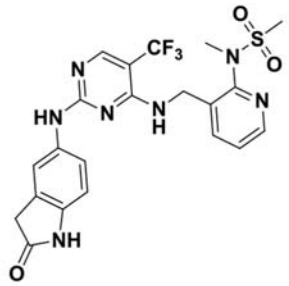

PF-562271 (FAK IC_{50}: 1.5 nM)

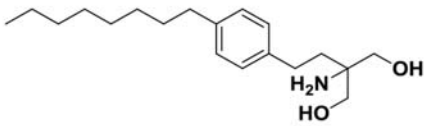

Fingolimod (S1PR1/3/4/5 EC_{50} ~ 7-8 nM)

6. Inflammation pathways: NLRP3 inhibitor, PAI1, prostaglandin E2 and EP2 receptor agonist.

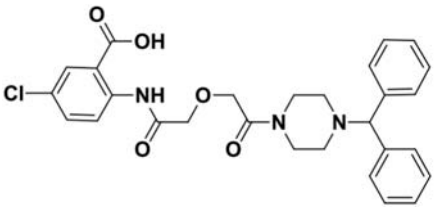

TM5275 (PAI1 IC_{50}: 6.95 uM)

7.19.2.8 Concluding Remarks

IPF remains a severe disease with poorer prognosis than most cancers, and no cure is currently available. However, failures of numerous trials focusing on immunosuppression and success of pirfenidone and nintedanib anchoring on antifibrosis have provided guidance for future development of IPF medicine. To date, more than a dozen IPF trials are being actively ongoing and many more novel mechanisms are being tested preclinically. It is to be hoped that in coming years the increased effort around IPF will lead to more choices for patients and physicians who are taking care of them.

7.19.3 Chronic Kidney Disease

7.19.3.1 Introduction

CKD is a major burden on healthcare systems world-wide and represents one of the most prevalent conditions where fibrotic processes are thought to play a pathophysiological role. Renal function is typically defined by glomerular filtration rate (GFR) which is usually estimated from serum concentrations of the freely filtered metabolite creatinine. Albuminuria is a commonly used secondary marker of renal dysfunction. Early stages of CKD (stages 1 and 2) are characterized by mild changes in GFR with attendant albuminuria, whereas later stages of CKD (stages 3 and 4) are associated with more severe decreases in GFR with or without albuminuria. Progression of CKD is typically slow in early stages, due to abundant renal reserve, and is more rapid in later stages. Key accelerants of CKD include diabetes, hypertension, and age, each of which contributes substantially to the risk of developing CKD and progression to end-stage renal disease (ESRD), where dialysis or transplant are required.

7.19.3.2 Epidemiology

In the United States, the overall prevalence of CKD of any stage is 15% of the general population, with 8% of the population at stage 3 or above (CDC website). The incidence rate of CKD stage 3 or above in the United States is estimated to be 10.38 per 1000 person years. Diabetes is the major risk factor for CKD and ESRD in the United States. Around 40% of all diabetics have CKD and diabetes is a contributor to ~40% of all cases of ESRD in the US population.[91] Hypertension was noted as a primary contributor to ~27% of ESRD cases and primary glomerular disease contributed to ~12% of ESRD cases (USRDS). CKD is a major risk factor for cardiovascular disease and patients with low GFR and albuminuria are at 3.2 fold greater risk of cardiovascular events compared to patients with normal renal function.[92] CKD is also a major burden on the healthcare systems, largely due to the high cost of dialysis or kidney transplants once patients progress to end-stage disease. CKD is estimated to cost the US ~$55 billion, and treatment costs for ESRD contribute to 7% of the entire Medicare budget (USRDS). Limited therapeutic options exist for CKD, with ACE inhibitor or angiotensin receptor blocker (ARB) therapy, the only proven treatments to slow the progression of diabetic or hypertensive CKD. Steroids and other immunosuppressive regimens are the primary modalities used to treat primary glomerular diseases such as nephrotic syndrome or focal segmental glomerular sclerosis (FSGS).

7.19.3.3 Pathophysiology

7.19.3.3.1 Features of renal fibrosis (anatomy, histology)

Renal fibrosis is the hallmark and the final common pathway of CKD, regardless of underlying etiology. The pathological finding of renal fibrosis is characterized by progressive tissue scarring including glomerulosclerosis, tubulointerstitial fibrosis, and loss of renal parenchyma (including tubular atrophy, loss of capillaries, and podocytes).[93] Indeed, diphtheria toxin-induced podocyte depletion in rats expressing human diphtheria toxin receptor causes glomerulosclerosis and is linked to progression of glomerular diseases.[94] Imbalance of ECM synthesis over degradation results in excessive accumulation of ECM proteins and fibrosis. Renal fibrogenesis is a dynamic and progressive process mediated by augmented injurious signals, such as profibrotic and proinflammatory pathways, as well as impairment of endogenous protective mechanisms in the kidney. TGF-β is a master regulator of fibrosis and is increased in fibrotic diseases. Cross talk among TGF-β, integrins, and the ECM is implicated in the development and progression of renal fibrosis.[8,95] Interestingly, intersection of profibrotic and metabolic pathways during the progress of renal fibrosis was suggested in a recent intriguing preclinical study, which demonstrated a role for TGF-β in the inhibition of fatty acid oxidation in renal tubular epithelial cells. Correction of defective fatty acid oxidation in tubular epithelial cells may lead to the development of novel therapeutic agents combating kidney fibrosis.[96]

7.19.3.3.2 Evidence for role of fibrosis in CKD progression

Progressive renal fibrosis ultimately leads to ESRD, a devastating disorder that demands new therapies. Preclinically, treatment with low doses of a pan-TGF-β mAb in puromycin aminonucleoside (PAN)-induced CKD model in rats improved renal fibrosis and renal function.[97] Whether antifibrotic mechanisms lead to improvement of renal function in the clinic is still in question. In a study in patients with lupus nephritis (313 patients, follow-up of 61.5 ± 34.9 months), tubulointerstitial fibrosis was found to be a significant independent risk factor predicting renal outcome (free of end-stage kidney disease or serum creatinine doubling).[98] Diabetic kidney disease was traditionally considered primarily a glomerular disease, but it is now accepted that the rate of renal function decline correlates best with the degree of renal tubulointerstitial fibrosis.[99,100] Surprisingly, Lilly's clinical trial testing a TGF-β1 specific antibody (LY2382770, ClinicalTrials.gov Identifier NCT01113801) in patients with diabetic kidney disease failed to show improvement of renal function, which may relate to a narrow therapeutic window or because only the TGF-β1 isoform was targeted (ASN annual meeting, 2014). Pirfenidone, which targets multiple pathways including TGF-β and TNF-α, was recently shown to improve renal function in a small cohort of patients with diabetic kidney disease, suggesting that targeting multiple pathophysiological pathways might increase the probability of clinical success in this patient population.[101]

7.19.3.4 Animal Models of Fibrotic Renal Disease

The common animal models used for the study of renal fibrosis include surgically induced models, such as unilateral ureteral obstruction (UUO) and 5/6th nephrectomy, chemically induced models such as PAN and the aristolochic acid model (AA), as well as genetic models of fibrotic renal disease such as the Col4a1/Alport disease model.

7.19.3.4.1 Unilateral ureteral obstruction

The model of UUO in the rodent produces progressive tubulointerstitial fibrosis, and is useful to examine mechanisms of tubulointerstitial fibrosis in vivo.[102] Complete UUO (by complete ligation of the urethra) initiates a series of pathophysiologic events in the obstructed kidney, resulting in marked renal hemodynamic change, interstitial inflammation (peak at 2–3 days), followed by tubular dilation, tubular atrophy, and progressive tubulointerstitial fibrosis within 2 weeks.[102] The advantages of this model include the following: (1) it can be induced in either rats or mice and shows no specific strain dependence; (2) it is highly reproducible; and (3) the contralateral kidney serves as a control. However, the UUO model in general is a very aggressive renal fibrosis model with the inability to measure changes in renal function. Despite these issues, many putative antifibrotic mechanisms have shown therapeutic potential in the UUO model. For example, deficiency of integrin β6, which locally activates TGF-β in injured tubular epithelial cells, markedly inhibited tubulointerstitial fibrosis in a UUO model.[103]

7.19.3.4.2 5/6th nephrectomy (5/6th Nx)

5/6th nephrectomy mimics the progressive renal failure after loss of renal mass in humans. Two different experimental approaches are used: uninephrectomy followed by either surgical excision of approximately half of the remaining tissue, or ligation of polar branches of the renal artery.[102] In mice, a combination of ligation and ablation model was used due to limited renal artery branching.[104] The 5/6th Nx model presents with proteinuria, glomerulosclerosis, tubulointerstitial fibrosis, and decline of renal function with time. The 5/6th Nx model induced by ligation is also associated with severe hypertension.[102,104] For compounds targeting antifibrotic mechanisms without hemodynamic effects, adequate BP control is required in this model. 5/6th Nx model in mice model is highly strain dependent. Mice on 129/Sv and Swiss-Webster background are among the few mouse strains susceptible to development of glomerulosclerosis after 5/6th Nx.[104] Treatment with high dose of ARBs or mineralocorticoid receptor antagonists not only slows down the progression of kidney injury but also induces regression of glomerulosclerosis in the 5/6th Nx model.[105,106]

7.19.3.4.3 Puromycin aminonucleoside

Single intravenous injection of PAN in rats induces podocyte injury and acute PAN nephrosis.[107] The peak of proteinuria and decline of renal function measured by serum creatinine usually occur between day 7 and 10 after PAN injection.[108] Expression of Nephrin A podocyte specific marker, was changed and showed a remarkable redistribution from the filtration slits to the podocyte plasma membrane.[108] Peroxisome proliferator-activated receptor gamma (PPARγ) agonists, when given at the time or after puromycin injection, reduced proteinuria and restored synaptopodin in the podocyte.[109] Multiple intraperitoneal injections of PAN plus uninephrectomy in rats induce chronic FSGS.[97] The chronic PAN model in rats has been used to evaluate antifibrotic mechanisms as well as mitochondrial dysfunction.[97,110]

7.19.3.4.4 AA injury

Tubulointerstitial fibrosis can be induced by multiple intraperitoneal injections of AA in mice or subcutaneous injections of AA in rats. The AA model is associated with an inflammatory infiltrate, tubulointerstitial fibrosis, and renal function decline.[111] The translational ability of this model is high since clinically AA induces Chinese herb nephropathy and Balkan endemic nephropathy.

7.19.3.4.5 Alport syndrome

Alport syndrome, caused by mutations in the genes encoding α3, α4, or α5 chains of type IV collagen (*COL4A3*, *COL4A4*, and *COL4A5*), is a genetic disorder characterized by progressive glomerulosclerosis associated with hearing loss and lens abnormalities.[112] A mouse model of Alport nephropathy was produced by introducing a null mutation of the α3 chain of collagen IV (Col4a3 −/−) in the 129X1/SvJ background. This model develops proteinuria with mild hematuria by 5 weeks after birth, severe glomerulosclerosis with subsequent tubulointerstitial fibrosis about 10 weeks of age, and progressive renal function decline and kidney failure by ∼11–14 weeks of age.[102] It was reported recently that anti-microRNA-21 oligonucleotides prevented Alport nephropathy progression by modulating metabolic pathways in this mouse model.[113]

7.19.3.5 Current Treatment

There are limited treatment options for patients with CKD. Blockers of the renin–angiotensin system (RAS) including ACE inhibitors and ARBs have been shown to slow the progression of CKD. This has been shown in diabetic kidney disease (IDNT, RENAAL) and in nondiabetic CKD (AASK).[114–116] Risk reduction in the composite renal/mortality endpoint in all these trials was around 20%.

RAS blockers are vasodilatory agents that act on the renal vasculature and induce a preferential dilation of the efferent arteriole. This results in a decrease in intraglomerular pressure and reduces hyperfiltration and stretch-induced glomerular injury.

Importantly, the renal hemodynamic effects of RAS blockers also acutely decrease renal blood flow and GFR, an effect that is clinically relevant.[116] Dual blockade of the RAS system has been shown in multiple clinical trials to increase the risk of acute kidney injury, an effect partially attributed to the hemodynamic effects of RAS blockade, and is currently contraindicated.[117] RAS blockers are also thought to have direct antifibrotic effects. The angiotensin II type 1 receptor (AT1R) receptor signals through ERK to activate noncanonical SMAD signaling and AngII is extremely profibrotic in multiple preclinical models. AngII levels are elevated in multiple tissues including the kidney in response to chronic tissue injury, and RAS blockade directly antagonizes the profibrotic effects of AngII in vitro and in multiple animal models.

In nephrotic syndrome, steroids are first-line treatment options with efficacy attributed to their anti-inflammatory effects, but they are not suitable for chronic management of disease due to multiple systemic side effects. Patients that do not respond to steroid therapy are often treated with other immuno-suppressive agents including calcineurin inhibitors and other disease-modifying antirheumatic drugs. RAS blockade is also part of the standard treatment paradigm for FSGS, a glomerular disease characterized by extensive glomerular scarring, though few trials have rigorously tested the efficacy of these agents in that disease.[118]

7.19.3.6 Ongoing Clinical Trials

A number of therapies with a primarily antifibrotic mechanism of action have recently been tested in various forms of CKD. Pirfenidone, an antifibrotic/antiinflammatory drug with a poorly understood mechanism of action, was tested in a small phase IIa trial in diabetic nephropathy in 2011.[101] Though there was no change in albuminuria, renal function as measured by GFR declined less precipitously in the low dose arm of that study, suggestive of potential benefit. However, there are no reported ongoing trials of pirfenidone for CKD though it was recently approved for the treatment of IPF (Roche/Intermune). Eli Lilly tested an anti-TGF-β1 specific antibody (LY2382770; ClinicalTrials.gov Identifier: NCT01113801) in a larger phase II trial in diabetic kidney disease. Multiple doses were tested, but no efficacy was observed on either urinary albumin or creatinine-based eGFR. A second anti-TGF-β antibody (fresolimumab, Genzyme/Sanofi) with broader specificity has recently been tested in 36 patients with FSGS. Overall efficacy on proteinuria was modest and not dose-dependent, but there was evidence of durable response in seven patients (ASN meeting, 2015). A Nox1/4 inhibitor from Genkyotex, GKT137831, also recently did not meet its primary endpoints in a phase IIa trial in diabetic nephropathy based on a statement posted on the company's website. There are thus mixed data on the effect of a variety of antifibrotic therapies in CKD.

Despite the equivocal results for antifibrotic therapies in renal disease, a number of other antifibrotic agents are currently in early clinical testing for CKD (listed in **Table 3**). FT-011, a derivative of the antiinflammatory/antifibrotic agent tranilast, is in clinical trials for diabetic nephropathy (**Fig. 3**). This agent has shown robust efficacy in numerous preclinical models of fibrotic disease and it will be interesting to see how these effects translate.[119,120] Of potential concern is the fact that the parental compound, tranilast, showed evidence of liver toxicity in a large phase III trial for the prevention of restenosis after percutaneous coronary intervention.[121]

ASK1 is a serine/threonine kinase, belonging to the MAP kinase-kinase-kinase family. Activation of ASK1 leads to activation of c-Jun N-terminal kinases and p38 MAPKs, inducing apoptosis of cells, inflammation, and fibrosis.[122] ASK1 plays important roles in many stress-related disease states, including renal fibrosis and diabetic nephropathy (**Fig. 4**).[123,124] Though this mechanism is less studied than others, ASK1 is thought to play a key role in integrating tissue injury signals such as ER stress and ROS with the fibrotic response. Gilead is the only company with an ASK1 inhibitor in clinical trials (GS-4997) for CKD, and they are pursuing this mechanism in combination with LOXL2 inhibitors for NASH.[125]

MiR-21 is a pro-fibrotic miRNA that has been implicated in liver and renal fibrosis. A recent preclinical study highlighted the therapeutic potential of blockade of miR-21 in both the mouse Alport syndrome model and the UUO model.[113] Based on the strength Regulus is currently contemplating initiating a trial with their miR-21 RG-012 inhibitor in Alport syndrome patients in early 2016.

La Jolla Therapeutics announced preliminary positive data in diabetic nephropathy with an anti-Galectin-3 preparation, but recently discontinued further work on this target to focus on other assets in their portfolio. Other antifibrotic mechanisms with recent clinical activity in CKD include CTGF antibodies (FG-3019, Fibrogen) and a small molecule antifibrotic PM-4050 (Prometic) with a poorly understood mechanism.

Table 3 Agents on clinical trials for kidney fibrosis

Compound	*Route of administration*	*Molecular target*
GKT-137831	Oral	NOX1/4 inhibitor
Pirfenidone	Oral	Multiple
GS-4997	Oral	ASK1
PBI-4050	Oral	Unknown MOA
FG-3019	Injection	CTGF
FT-011	Oral	Unknown MOA
RG-012	Injection	Anti-miR-21

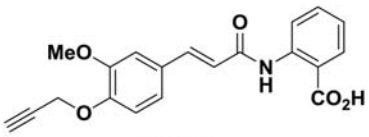

80-100% inhibition at 100 uM

Fig. 3 Inhibitory activity of FT011 on TGF-β stimulated production of collagen synthesis in cultured mesangial cells.

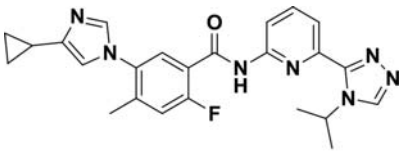

ASK1 inhibitor (GS-4997): IC_{50} 3 nM

Fig. 4 Inhibitory activity for GS-4997 in in vitro kinase assays.

7.19.3.7 Emerging Biology and Therapeutic Treatment

There has been some debate in the past decade over the role of EMT in renal fibrosis.[126–128] Much of this controversy has centered on whether epithelial cells contribute to the myofibroblast pool in fibrotic kidneys. Fate-mapping studies suggest this is not the case, though it is clear that injured renal epithelia play a critical role in the progressive injury response.[129] Recent proof of concept studies in transgenic rodent models provide strong support that interactions between injured tubular epithelial cells and interstitial fibroblasts are important in driving renal fibrosis.[130] Reactivation or deletion of Snail1 (encoding snail family zinc finger 1, known as Snail1) in mouse renal epithelial cells promoted or improved renal fibrosis.[131,132]

Emerging data support the concept that integrins in the kidney modulate not only podocytes adhesion to the glomerular basement membrane (GBM) and filtration barrier functions but also TGF-β activation and ECM balance.[95] Multiple RGD-binding integrins (αvβ1, αvβ3, αvβ5, αvβ6, and αvβ8) are implicated in fibrosis.[72,133] Integrin αvβ6 is preferentially expressed at sites of injured tubular epithelial cells, binding and activating latent precursor TGF-β locally.[134] Integrin αvβ6 is an attractive target for lung and kidney fibrosis. Robust preclinical validation has been performed using genetic integrin β6 KO mice and pharmacological neutralizing αvβ6 monoclonal antibodies in fibrosis models in lung and kidney as well as in Alport CKD model.[103,135,136] A humanized monoclonal antibody against αvβ6 integrin, STX-100, is currently under evaluation in a randomized, placebo-controlled phase II IPF trial (NCT01371305). In contrast to αvβ6, integrin αvβ1 is thought to be expressed specifically in the fibroblasts. Upregulation of integrin αv and β1 was reported in renal biopsy samples from human diabetic kidney disease.[137] A small molecule αvβ1 inhibitor was shown recently to reduce fibrosis in multiple rodent fibrosis models.[73]

Bone morphogenetic protein 7 (BMP7), which counteracts TGF-β signaling, protects against renal fibrosis.[126,138,139] Gremlin (Grem1), an endogenous antagonist of BMP, is involved in fibrotic process in the kidney.[140,141] Expression of Gremlin 1 is increased in several models of fibrosis and human diabetic kidney disease.[142] Gremlin aggravates hyperglycemia-induced podocyte injury by a TGF-β/Smad-dependent signaling pathway.[140] Overexpression of human Gremlin in proximal tubular epithelial cells in transgenic mice aggravates diabetic kidney injury.[141] Inhibition of Gremlin in Grem1 heterozygous mice attenuated diabetes-induced glomerular basement membrane thickening and microalbuminuria compared to wild type (WT) diabetic mice.[143] Gremlin may also exert BMP-independent responses, including the regulation of cell migration, angiogenesis in endothelial cells, and the activation of Smad signaling and related profibrotic effects in tubular epithelial cells.[144]

Facilitating ECM degradation may prove to be an attractive antifibrotic mechanism.[145,146] The human epididymis protein 4 (HE4) gene, which encodes a putative serine protease inhibitor, is highly expressed in kidney of patients with diabetic nephropathy, human and mouse fibrotic kidneys, and is elevated in the serum of patients with kidney fibrosis.[147] The profibrotic mechanism of HE4 may be related to its ability to suppress the activity of multiple proteases, including serine proteases and matrix metalloproteinases, resulting in a reduced capacity to degrade type I collagen. Treatment with an HE4-neutralizing antibody reduced renal fibrosis in multiple mouse models.[147] Whether inhibition of HE4 improves renal fibrosis and functions warrants further investigation.

In the last few years, a direct link between metabolic dysregulation in renal epithelial cells and fibrosis has begun to emerge. It has long been known that a variety of metabolic interventions such as adiponectin and PPARγ agonists ameliorate renal dysfunction in diabetic animal models, but the basis for these protective effects was often attributed to modulating the effects of gluco- or lipotoxicity. However, the beneficial effects of PPAR agonists and 5′ adenosine monophosphate-activated protein kinase (AMPK) activators in nondiabetic models of CKD hinted at a more pleiotropic mode of action for these agents.[148,149] These observations have been bolstered by recent data that have linked mitochondrial dysfunction and defects in fatty acid oxidation to kidney disease in both diabetic and nondiabetic kidney disease, based on perturbations in urinary tricarboxylic acid cycle (TCA) cycle metabolite

levels and changes transcriptional profiles from biopsies of diseased kidneys.[96,150,151] Further evidence of a primary role in mitochondrial dysfunction in fibrotic kidney disease comes from transcriptional profiles in the mouse model of Alport syndrome which is characterized by extensive renal fibrosis, in which deficits in oxidative phosphorylation and mitochondrial dysfunction pathways were seen.[113] Finally, inherited deficiencies in CoQ10 biosynthesis have been shown to cause rare forms of steroid-resistant nephrotic syndrome, highlighting a critical role for mitochondrial function in human glomerular dysfunction and scarring.[152]

The link between mitochondrial function and renal fibrosis appears to be direct. TGF-β acutely suppresses mitochondrial function in renal epithelial cells in vitro, and the profibrotic effects of TGF-β on pro-fibrotic gene expression can be reversed by PPARα agonists such as fenofibrate.[96] The pro-fibrotic miRNA miR-21 appears to act in part by suppressing genes involved in mitochondrial function, and anti-miR21 is effective in suppressing renal disease in both the Alport and UUO mouse models.[113] The effect in the UUO is PPARα dependent, again highlighting a link between fibrosis and metabolism. Finally, other high-level regulators of mitochondrial function such as AMPK activators and PPAR agonists have been reported to be effective in numerous models of renal dysfunction.[148,151,153]

As yet, a unifying hypothesis linking these observations is lacking, though it has long been known that fatty acids and glutamine are the main source of energy for renal epithelia. When mitochondrial function is impaired, renal epithelial cells could lack the metabolic flexibility to shift to other energy sources and then initiate an injury program that can be ameliorated by restoring the ability to utilize these carbon sources. This would imply that master regulators of fatty acid oxidation and mitochondrial function such as AMPK activators or PPAR agonists might be interesting targets that could directly impact renal fibrosis. Anti-miR-21 is currently being tested in Alport syndrome and this will provide an interesting POC for targeting metabolic regulators in renal disease.

Epigenetic regulators have prominent antifibrotic effects, though much of these data have been elaborated in nonrenal models.[154] Most interesting in this group of targets are miRNAs which are emerging as a class of targets that have pleiotropic—yet restricted effects. The potential role of miR-21 in fibrosis has already been discussed, but a number of other miRs such as miR-29 and miR-200 are also associated with fibrotic renal disease and might represent interesting targets. An interesting aspect of miRNA biology is their potential to act in an endocrine manner, by release from cells in exosomes.[155] A further understanding in this field has the potential to open up a number of novel pathways for intervention.

A number of nonspecific histone deacetylase (HDAC) inhibitors including vorinostat, valproic acid, and sodium butyrate ameliorate renal disease in diabetic and fibrotic models. Their effects have been attributed to modulation of the NO pathway as well as direct effects on fibrotic pathways through BMP7. Finally, knockouts in the histone methyltransferase EZH2 have recently been shown to be renoprotective in diabetic nephropathy models, which was attributed to modulation of endogenous antioxidant defenses through TxnIP induction.

7.19.3.8 Conclusions and Perspectives

There is abundant evidence that fibrosis is a key pathophysiological pathway in the progression of renal disease. Despite some recent clinical setbacks, fibrotic pathways still represent an attractive area for the development of disease-modifying therapies in an area with limited therapeutic options. Exciting advances in the understanding of key pathways driving fibrosis in the kidney, in particular around the link between metabolism and fibrosis and the emerging role of miRNAs as master regulators of fibrosis, hold promise for the next generation of antifibrotic therapies for kidney disease.

7.19.4 Liver Fibrosis

7.19.4.1 Introduction

Acute liver injury induces a transient process of wound healing. Upon chronic injuries such as viral hepatitis, metabolic imbalance, or alcohol consumption, fibrosis arises as an excess deposit of ECM. The accumulation of scar tissue leads to cirrhosis with changes in the relative abundance of hepatic cell types and the organ's vasculature. Ultimately these modifications—that can progress over decades—lead to portal hypertension, liver failure and death. Liver cancer also usually appears in the presence of cirrhosis. Recent therapies for hepatitis B and C proved that cirrhosis and fibrosis can be reversed, encouraging the search for new therapies.

7.19.4.2 Epidemiology

Chronic liver disease and cirrhosis are associated with 36,000 annual deaths in the United States.[156] Nonalcoholic fatty liver disease (NAFLD) is the most common liver disease and affects 70–80% of obese and diabetics.[157] NAFLD is characterized by a continuum of histological abnormalities, ranging from steatosis to NASH with fibrosis and may ultimately evolve into cirrhosis and end-stage liver disease.[158] Cirrhosis moved from the 18th to the 13th rank in all cause of death in the world from 1990 to 2013.[156] The disease progresses over decades and patients usually die in their 50's or 60's from complications such as portal hypertension. Liver cancer often occurs in the presence of cirrhosis and is responsible for 10,000 deaths per year.

7.19.4.3 Pathophysiology

Liver cirrhosis is defined histologically as an accumulation of scar tissue due to fibrosis and abnormal architecture of the vasculature.[159,160] The liver's parenchyma contains epithelial cells (hepatocytes) and endothelial cells that form fenestrated sinusoids (Fig. 5). Hepatic stellate cells (HSCs) and Kupffer cells reside in the space of Disse that separates the blood flow of the sinusoids from the hepatocytes. Fibrosis corresponds to the accumulation and modification of the ECM in the space of Disse that overcomes fibrolysis by collagen-degrading enzymes such a metalloproteinases. Fibril-forming collagen types I, II, and V, and basement membrane collagens (types IV, VI) together with the glycoconjugates such as fibronectin induce the loss of hepatocytes microvilli and the loss of fenestration in the sinusoids (capillarization). Development of a fibrous septa linking the central and portal veins shunts the parenchyma and the bidirectional plasma flow between hepatocytes and the sinusoids lumen and impairs the liver's function (Fig. 5). Alteration in the architecture of the vasculature ultimately leads to portal hypertension.

In the space of Disse, myofibroblasts are the source of ECM during fibrosis. Myofibroblasts are characterized by the expression of alpha smooth muscle cell actin and a contractile phenotype. They also produce cytokines that further enhance inflammation, proliferation, and propagation of fibrosis. Myofibroblasts are mainly derived from HSC. Quiescent, vitamin A storing HSC are activated upon initial injury, depleted of vitamin A and lead the way to fibrosis by becoming myofibroblasts if not eliminated by apoptosis during the normal wound healing process. Other cell types contribute to the pool of myofibroblasts such as portal fibroblasts, circulating fibrocytes, bone marrow derived cells, and epithelial cells through epithelial to mesenchymal transition.[161]

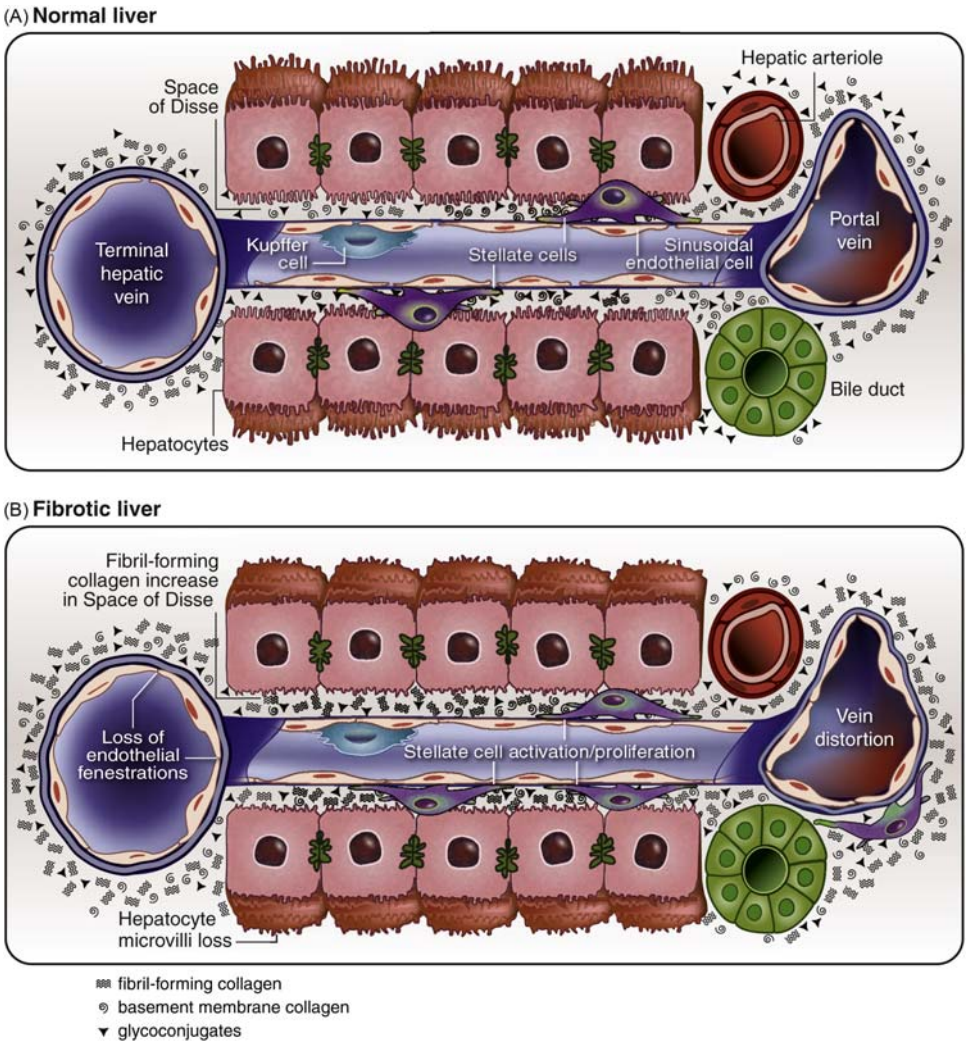

Fig. 5 Normal versus fibrotic liver. Reproduced from Hernandez-Gea, V.; Friedman, S. L. Pathogenesis of Liver Fibrosis. *Annu. Rev. Pathol.* **2011**, *6*, 425–456.

7.19.4.4 Experimental Animal Models

Rodents are the most commonly used species as models of liver injury.[162,163] These models can be classified according to the type of injury used: chemicals, cholestasis, autoimmune, and diet.[162] We will focus here on the models induced by carbon tetrachloride (CCl_4) or bile duct ligation, which are commonly used. CCl_4 is metabolized into the CCl_3 radical by cytochrome p450 2E1 present in perivenular hepatocytes. Necrosis in the centro-lobular area triggers wound healing and localized scar tissue. Repeated injuries prevent resolution of the wound healing and allows for progression into fibrosis. The model offers a window on the various steps of the disease with fibrosis at 2–4 weeks to severe bridging fibrosis at 5–7 weeks and cirrhosis at 8–9 weeks. Longer treatments induce micronodular cirrhosis, portal hypertension, and ascites. Note that compounds tested in this model can interfere with the extent of the disease if they modulate cyp2E1 expression and CCl_4 metabolism. Bile duct ligation is mostly performed in rats because they lack a gall bladder, contrary to mice.[163] This prevents some issues such as the risk of perforation of the gallbladder and death. After laparotomy, the bile duct is ligated above the pancreatic duct and below the junction of hepatic ducts and the segment in between both ligations is resected. The interruption of bile flow induces proliferation of the bile duct epithelial cells, portal inflammation. Portal fibrosis appears within weeks. Although portal hypertension and shunting of the portal to systemic circulation has been described within 6–8 weeks, the architectural defects typical of cirrhosis are usually not observed.

7.19.4.5 Drugs Evaluated in Preclinical and Clinical Trials

There is no current treatment approved for reducing fibrosis in the liver. Still, the regenerative nature of this organ makes it a good candidate for antifibrosis and even anti-cirrhosis therapy, as seen with treatments of chronic hepatitis B[164] and hepatitis C.[165]

Data from preclinical models suggest that multiple pathways could be targeted successfully.[166] We will mention four examples. First, by inhibiting TGFβ1 signaling pathway through impairment of TGF-β activation or its sensing by the cell, inhibitors of integrin improved hepatic fibrosis. Inhibitor of αVβ1 and αVβ6 integrins C8 and CWHM12 attenuated fibrosis in the CCl_4 mouse model (Fig. 6).[72,73]

Second, inhibitors of collagen accumulation also proved efficacious. HOE077 is an inhibitor of prolyl hydroxylase (proline is a major constituent of collagen) that prevents HSC activation and prevented pig serum-induced liver fibrosis in rats (Fig. 7).[167] Third, inhibitors of the RAS such as losartan were proven efficacious in preclinical models such as rat CCl_4.[168] Fourth, bile acid receptor activation improved fibrosis in farnesoid X receptor ligand obeticholic acid reduced fibrosis in CCl_4 or in bile duct ligation mice.[169,170] Thus there might be a broad spectrum of targets and pathways that are opportunities for new therapeutics.

Translation of these findings to humans remains a challenge. In fact, antifibrotic agents have largely failed at reducing liver fibrosis in the clinic. One example are the agonists of PPARγ that are antiinflammatory and reduce stellate cell activation, the antioxidant vitamin E, or colchicine that inhibit collagen secretion.[171] Still, there is a path forward as illustrated by the outcome of some recent clinical trials. Besides the anti-hepatitis C treatments that showed protective effects obeticholic acid improved fibrosis

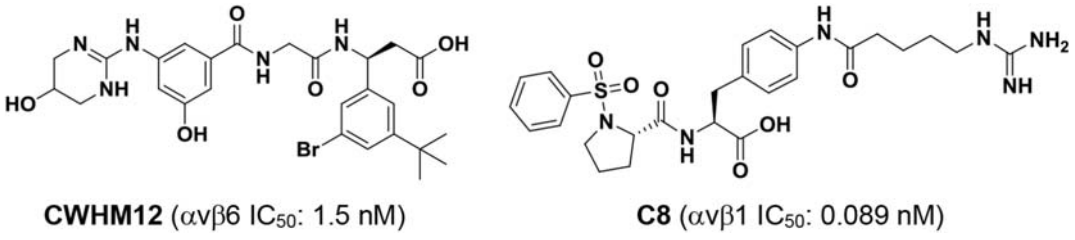

Fig. 6 Structure of CWHM12 and C8.

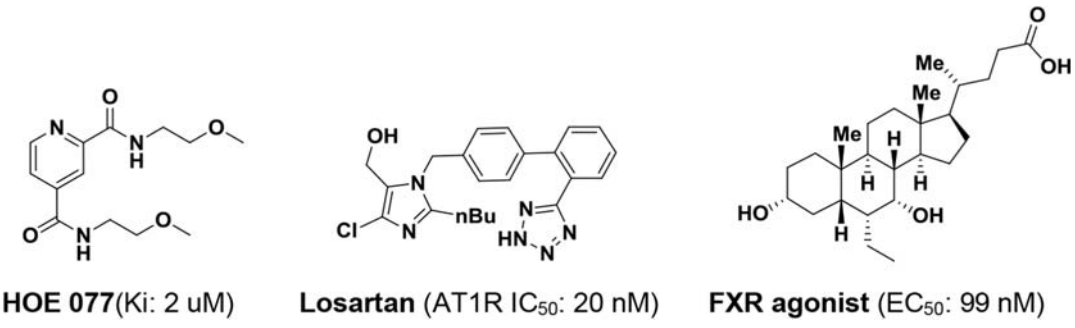

Fig. 7 Structure of HOE 077, losartan, obeticholic acid (INT-747).

in some patients with noncirrhotic, NASH (Fig. 7).[172] Candesartan, an AT1R blocking agent (ARB), aimed at reducing portal hypertension, did improve fibrosis in patients with alcoholic liver disease (Fig. 7).[173]

Table 4 lists small molecules in clinical trials for fibrosis. Biologics are also being evaluated. As an example, Simtuzumab is a monoclonal antibody raised against LOXL2 in phase II in HIV and/or hepatitis C-infected patients with hepatic fibrosis (clinical trial NCT01707472).

7.19.4.6 Emerging Biology

One major development in the field of hepatic fibrosis has been the identification of the main cell types contributing to the disease. The initial injury leading to hepatic fibrosis affects hepatocytes and biliary cells by enrolling multiple effector cells.[171] Dissecting the relative contribution of each cell type has been the subject of numerous studies but HSCs emerge as the main source of ECM after their transformation into myofibroblasts. By tracing cell expressing collagen 1A1 in CCl_4 and bile duct ligation mice models, Iwaisako et al. were able to show that HSCs represent >87% of myofibroblasts in the CCl_4 model.[184] Similar findings were made in the BDL model at day 14 and 20, although portal fibroblasts represented the majority of myofibroblasts in the early stage of fibrosis. Molecular profiling of these cell types instead of the whole tissue gives an unprecedented insight into the biology at play.[184] New targets specific to stellate cell activation could be identified.

Activation of HSCs by transcription factors-mediated modulation of gene expression has been well documented.[159] Epigenetic regulations are also at play, exemplified by DNA methylation, histone modification, or silencing by noncoding RNAs.[159] Histone deacetylation and acetylation modify the structure of chromatin by making it respectively more or less condensed. Trichostatin A is an inhibitor of class I, II, and IV HDAC and blocked the activation of rat HSC in vitro, including the upregulation of aSMA (Fig. 8).[185] Genome-wide analysis of DNA methylation revealed changes in quiescent versus activated HSCs.[186] Decitabine, an inhibitor of methyl-CpG-binding protein MeCP2 that accumulates in myofibroblasts, blocked transdifferentiation of HSC.[187] Noncoding RNA also alters gene expression in HSC (Fig. 8).[188] Overexpression of miRNA-150 and miRNA-194 inhibited SMA expression and collagen-I secretion in LX2 cells.[189] Future studies of how epigenetic affects liver fibrosis will deepen our understanding of the pathology and might identify new therapeutic targets.

Adaptative and immune systems do play a role in fibrosis. An interesting research area concerns the role of intestinal bacteria in liver disease. Much attention has been recently focused on the interaction between the gut's microbiome and metabolic diseases, including NASH. Changes in intestinal bacteria have been identified in models of liver disease.[190] Recent findings might explain how toll-like receptor 4 is a bridge between gut microbiome and fibrosis, since it is present on stellate cells, activated by bacterial lipopolysaccharides, and associated with portal inflammation in patients with fatty liver disease.[191]

Table 5 presents a list of small molecules that have been evaluated for their antifibrotic properties in liver. Elucidating the nature of the injury and the biological pathways that are responsible for stellate cell activation should lead to more therapeutics.

Table 4 Small molecules in clinical trials for liver fibrosis[120,174–183]

Compound	*Route of administration*	*Molecular target*
GKT-137831	Oral	NOX1/4 inhibitor
Bardoxolone	Oral	NRF2-KEAP1
Sirolimus	Oral	Allosteric mTOR inhibitor
Baricitinib	Oral	Dual JAK1/2 inhibitor
Beraprost	Oral	Prostacyclin mimetic
Bindarit	Oral	CCL2/7/8 inhibitor
FT-011	Oral	Unknown MOA

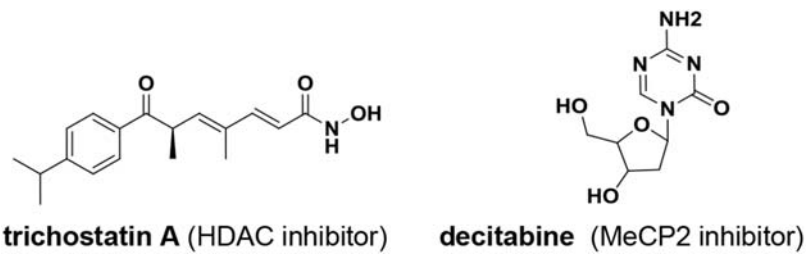

trichostatin A (HDAC inhibitor) **decitabine** (MeCP2 inhibitor)

Fig. 8 Structure of trichostatin A and decitabine.

Table 5 Emerging biology in treating liver fibrosis

Mechanism	*Compound*	*Preclinical validation*
C–C chemokine receptor type 5	Maraviroc	NAFLD model
Integrin αVβ6	CWHM 12	Bleomycin/CCL_4 model
Integrin αVβ1	C8	Bleomycin/CCL_4 model
Prolyl hydroxylase	HOE 077	Liver fibrosis model
Glutamyl-prolyl-tRNA synthetase (EPRS)	Halofuginone	Thioacetamide model
Pregnane X receptor (PXR)	Pregnenolone 16α carbonitrile	CCL_4 model
T-type Ca channel	Efonidipone	CCL_4 model
Protein kinase C δ (PKCδ)	Rottlerlin	NASH model
5-Hydroxytryptamine 2A/2B receptors 5-$HT_{2A/2B}$	Sarpogrelate	Cirrhosis model
Lopoxin A4 (LXA_4)	BML-111	CCL_4 model
Nuclear receptor subfamily 4 group A member 1 NR4A1	Cytosporone B	Interstitial fibrosis model
Galectin 3	GM-CT-01 and GR-MD-02	Streptozotocin + high fat diet

Small molecules validated in fibrosis preclinical models.[72,73,78,89,167,192–201]

7.19.4.7 Concluding Remarks

Liver fibrosis is a major health issue that can lead to cirrhosis and death. Much progress has been done in our understanding of the pathology. Although there is no specific treatment yet, the reversible nature of cirrhosis and fibrosis has been demonstrated with treatments of hepatitis. Identification of the relative contribution of effector cells and careful delineation of the pathways activated or repressed in these cells should lead to new targets and more specific treatments.

References

1. Wynn, T. A. Fibrotic Disease and the T(H)1/T(H)2 Paradigm. *Nat. Rev. Immunol.* **2004,** *4,* 583–594.
2. Friedman, S. L.; Sheppard, D.; Duffield, J. S.; Violette, S. Therapy for fibrotic diseases: nearing the starting line. *Sci. Transl. Med.* **2013,** *5* (167), 167.
3. Bellini, A.; Mattoli, S. The Role of the Fibrocyte, a Bone Marrow-Derived Mesenchymal Progenitor, in Reactive and Reparative Fibroses. *Lab. Investig.* **2007,** *87,* 858–870.
4. Thiery, J. P.; Acloque, H.; Huang, R. Y.; Nieto, M. A. Epithelial-Mesenchymal Transitions in Development and Disease. *Cell* **2009,** *139,* 871–890.
5. Laurent, G. J. Dynamic State of Collagen: Pathways of Collagen Degradation In Vivo and Their Possible Role in Regulation of Collagen Mass. *Am. J. Physiol.* **1987,** *252,* C1–C9.
6. Diegelmann, R. F.; Evans, M. C. Wound Healing: An Overview of Acute, Fibrotic and Delayed Healing. *Front. Biosci.* **2004,** *9,* 283–289.
7. Travis, M. A.; Sheppard, D. TGF-Beta Activation and Function in Immunity. *Annu. Rev. Immunol.* **2014,** *32,* 51–82.
8. Munger, J. S.; Sheppard, D. Cross Talk Among TGF-Beta Signaling Pathways, Integrins, and the Extracellular Matrix. *Cold Spring Harb. Perspect. Biol.* **2011,** *3,* a005017.
9. Lyons, R. M.; Keski-Oja, J.; Moses, H. L. Proteolytic Activation of Latent Transforming Growth Factor-Beta From Fibroblast-Conditioned Medium. *J. Cell Biol.* **1988,** *106,* 1659–1665.
10. Ribeiro, S. M.; Poczatek, M.; Schultz-Cherry, S.; Villain, M.; Murphy-Ullrich, J. E. The Activation Sequence of Thrombospondin-1 Interacts With the Latency-Associated Peptide to Regulate Activation of Latent Transforming Growth Factor-Beta. *J. Biol. Chem.* **1999,** *274,* 13586–13593.
11. Massague, J.; et al. TGF-Beta Receptors. *Mol. Reprod. Dev.* **1992,** *32,* 99–104.
12. Nathan, S. D.; et al. Long-Term Course and Prognosis of Idiopathic Pulmonary Fibrosis in the New Millennium. *Chest* **2011,** *140,* 221–229.
13. Travis, W. D.; et al. An Official American Thoracic Society/European Respiratory Society Statement: Update of the International Multidisciplinary Classification of the Idiopathic Interstitial Pneumonias. *Am. J. Respir. Crit. Care Med.* **2013,** *188,* 733–748.
14. Collard, H. R.; King, T. E., Jr. Demystifying Idiopathic Interstitial Pneumonia. *Arch. Intern. Med.* **2003,** *163,* 17–29.
15. Katzenstein, A. L.; Myers, J. L. Idiopathic Pulmonary Fibrosis: Clinical Relevance of Pathologic Classification. *Am. J. Respir. Crit. Care Med.* **1998,** *157,* 1301–1315.
16. Olson, A. L.; et al. Mortality From Pulmonary Fibrosis Increased in the United States From 1992 to 2003. *Am. J. Respir. Crit. Care Med.* **2007,** *176,* 277–284.
17. Panos, R. J.; Mortenson, R. L.; Niccoli, S. A.; King, T. E., Jr. Clinical Deterioration in Patients With Idiopathic Pulmonary Fibrosis: Causes and Assessment. *Am. J. Med.* **1990,** *88,* 396–404.
18. Simon-Blancal, V.; et al. Acute Exacerbation of Idiopathic Pulmonary Fibrosis: Outcome and Prognostic Factors. *Respiration* **2012,** *83,* 28–35.
19. Kim, D. S.; et al. Acute Exacerbation of Idiopathic Pulmonary Fibrosis: Frequency and Clinical Features. *Eur. Respir. J.* **2006,** *27,* 143–150.
20. Collard, H. R.; et al. Burden of Illness in Idiopathic Pulmonary Fibrosis. *J. Med. Econ.* **2012,** *15,* 829–835.
21. Fernandez Perez, E. R.; et al. Incidence, Prevalence, and Clinical Course of Idiopathic Pulmonary Fibrosis: A Population-Based Study. *Chest* **2010,** *137,* 129–137.
22. Gjonbrataj, J.; et al. Incidence of Idiopathic Pulmonary Fibrosis in Korea Based on the 2011 ATS/ERS/JRS/ALAT Statement. *Int. J. Tuberc. Lung Dis.* **2011,** *19,* 742–746.
23. Lai, C. C.; et al. Idiopathic Pulmonary Fibrosis in Taiwan—A Population-Based Study. *Respir. Med.* **2012,** *106,* 1566–1574.
24. Lee, A. S.; Mira-Avendano, I.; Ryu, J. H.; Daniels, C. E. The Burden of Idiopathic Pulmonary Fibrosis: An Unmet Public Health Need. *Respir. Med.* **2014,** *108,* 955–967.
25. Nalysnyk, L.; Cid-Ruzafa, J.; Rotella, P.; Esser, D. Incidence and Prevalence of Idiopathic Pulmonary Fibrosis: Review of the Literature. *Eur. Respir. Rev.* **2012,** *21,* 355–361.
26. Natsuizaka, M.; et al. Epidemiologic Survey of Japanese Patients With Idiopathic Pulmonary Fibrosis and Investigation of Ethnic Differences. *Am. J. Respir. Crit. Care Med.* **2014,** *190,* 773–779.
27. Ohno, S.; Nakaya, T.; Bando, M.; Sugiyama, Y. Idiopathic Pulmonary Fibrosis—Results From a Japanese Nationwide Epidemiological Survey Using Individual Clinical Records. *Respirology* **2008,** *13,* 926–928.
28. Raghu, G.; et al. An Official ATS/ERS/JRS/ALAT Statement: Idiopathic Pulmonary Fibrosis: Evidence-Based Guidelines for Diagnosis and Management. *Am. J. Respir. Crit. Care Med.* **2011,** *183,* 788–824.
29. Raghu, G.; Weycker, D.; Edelsberg, J.; Bradford, W. Z.; Oster, G. Incidence and Prevalence of Idiopathic Pulmonary Fibrosis. *Am. J. Respir. Crit. Care Med.* **2006,** *174,* 810–816.
30. Richeldi, L.; et al. Efficacy and Safety of Nintedanib in Idiopathic Pulmonary Fibrosis. *N. Engl. J. Med.* **2014,** *370,* 2071–2082.

31. Ryerson, C. J.; et al. Depression and Functional Status are Strongly Associated With Dyspnea in Interstitial Lung Disease. *Chest* **2011,** *139,* 609–616.
32. Selman, M.; King, T. E.; Pardo, A. Idiopathic Pulmonary Fibrosis: Prevailing and Evolving Hypotheses About Its Pathogenesis and Implications for Therapy. *Ann. Intern. Med.* **2001,** *134,* 136–151.
33. Allam, J. S.; Limper, A. H. Idiopathic Pulmonary Fibrosis: Is It a Familial Disease? *Curr. Opin. Pulm. Med.* **2006,** *12,* 312–317.
34. Lee, H. L.; et al. Familial Idiopathic Pulmonary Fibrosis: Clinical Features and Outcome. *Chest* **2005,** *127,* 2034–2041.
35. Steele, M. P.; et al. Clinical and Pathologic Features of Familial Interstitial Pneumonia. *Am. J. Respir. Crit. Care Med.* **2005,** *172,* 1146–1152.
36. Wahidi, M. M.; et al. Familial Pulmonary Fibrosis in the United States. *Chest* **2002,** *121,* 30S.
37. Ono, S.; et al. Surfactant Protein C G100S Mutation Causes Familial Pulmonary Fibrosis in Japanese Kindred. *Eur. Respir. J.* **2011,** *38,* 861–869.
38. Stock, C. J.; et al. Mucin 5B Promoter Polymorphism Is Associated With Idiopathic Pulmonary Fibrosis but Not With Development of Lung Fibrosis in Systemic Sclerosis or Sarcoidosis. *Thorax* **2013,** *68,* 436–441.
39. Peljto, A. L.; et al. Association Between the MUC5B Promoter Polymorphism and Survival in Patients With Idiopathic Pulmonary Fibrosis. *JAMA* **2013,** *309,* 2232–2239.
40. Lawson, W. E.; et al. Genetic Mutations in Surfactant Protein C are a Rare Cause of Sporadic Cases of IPF. *Thorax* **2004,** *59,* 977–980.
41. Willander, H.; et al. High-Resolution Structure of a BRICHOS Domain and Its Implications for Anti-Amyloid Chaperone Activity on Lung Surfactant Protein C. *Proc. Natl. Acad. Sci. U. S. A.* **2012,** *109,* 2325–2329.
42. Wang, Y.; et al. Genetic Defects in Surfactant Protein A2 Are Associated With Pulmonary Fibrosis and Lung Cancer. *Am. J. Hum. Genet.* **2009,** *84,* 52–59.
43. Cronkhite, J. T.; et al. Telomere Shortening in Familial and Sporadic Pulmonary Fibrosis. *Am. J. Respir. Crit. Care Med.* **2008,** *178,* 729–737.
44. Alder, J. K.; et al. Short Telomeres Are a Risk Factor for Idiopathic Pulmonary Fibrosis. *Proc. Natl. Acad. Sci. U. S. A.* **2008,** *105,* 13051–13056.
45. Armanios, M. Y.; et al. Telomerase Mutations in Families With Idiopathic Pulmonary Fibrosis. *N. Engl. J. Med.* **2007,** *356,* 1317–1326.
46. Behr, J.; et al. German Guideline for Diagnosis and Management of Idiopathic Pulmonary Fibrosis. *Pneumologie* **2013,** *67,* 81–111.
47. Andersson-Sjoland, A.; et al. Fibrocytes Are a Potential Source of Lung Fibroblasts in Idiopathic Pulmonary Fibrosis. *Int. J. Biochem. Cell Biol.* **2008,** *40,* 2129–2140.
48. Lomas, N. J.; Watts, K. L.; Akram, K. M.; Forsyth, N. R.; Spiteri, M. A. Idiopathic Pulmonary Fibrosis: Immunohistochemical Analysis Provides Fresh Insights Into Lung Tissue Remodelling With Implications for Novel Prognostic Markers. *Int. J. Clin. Exp. Pathol.* **2012,** *5,* 58–71.
49. Yamada, M.; et al. Dual-Immunohistochemistry Provides Little Evidence for Epithelial-Mesenchymal Transition in Pulmonary Fibrosis. *Histochem. Cell Biol.* **2008,** *129,* 453–462.
50. Suki, B.; Bates, J. H. Extracellular Matrix Mechanics in Lung Parenchymal Diseases. *Respir. Physiol. Neurobiol.* **2008,** *163,* 33–43.
51. Khalil, N.; et al. Increased Production and Immunohistochemical Localization of Transforming Growth Factor-Beta in Idiopathic Pulmonary Fibrosis. *Am. J. Respir. Cell Mol. Biol.* **1991,** *5,* 155–162.
52. Khalil, N.; et al. Enhanced Expression and Immunohistochemical Distribution of Transforming Growth Factor-Beta in Idiopathic Pulmonary Fibrosis. *Chest* **1991,** *99,* 65S–66S.
53. Nagaoka, I.; Trapnell, B. C.; Crystal, R. G. Upregulation of Platelet-Derived Growth Factor-A and -B Gene Expression in Alveolar Macrophages of Individuals With Idiopathic Pulmonary Fibrosis. *J. Clin. Invest.* **1990,** *85,* 2023–2027.
54. Antoniades, H. N.; et al. Platelet-Derived Growth Factor in Idiopathic Pulmonary Fibrosis. *J. Clin. Invest.* **1990,** *86,* 1055–1064.
55. Allen, J. T.; Knight, R. A.; Bloor, C. A.; Spiteri, M. A. Enhanced Insulin-Like Growth Factor Binding Protein-Related Protein 2 (Connective Tissue Growth Factor) Expression in Patients With Idiopathic Pulmonary Fibrosis and Pulmonary Sarcoidosis. *Am. J. Respir. Cell Mol. Biol.* **1999,** *21,* 693–700.
56. Furuie, H.; Yamasaki, H.; Suga, M.; Ando, M. Altered Accessory Cell Function of Alveolar Macrophages: A Possible Mechanism for Induction of Th2 Secretory Profile in Idiopathic Pulmonary Fibrosis. *Eur. Respir. J.* **1997,** *10,* 787–794.
57. Murray, L. A.; et al. Hyper-Responsiveness of IPF/UIP Fibroblasts: Interplay Between TGFbeta1, IL-13 and CCL2. *Int. J. Biochem. Cell Biol.* **2008,** *40,* 2174–2182.
58. Chilosi, M.; et al. Aberrant Wnt/Beta-Catenin Pathway Activation in Idiopathic Pulmonary Fibrosis. *Am. J. Pathol.* **2003,** *162,* 1495–1502.
59. Konigshoff, M.; et al. WNT1-Inducible Signaling Protein-1 Mediates Pulmonary Fibrosis in Mice and Is Upregulated in Humans With Idiopathic Pulmonary Fibrosis. *J. Clin. Invest.* **2009,** *119,* 772–787.
60. Konigshoff, M.; et al. Functional Wnt Signaling Is Increased in Idiopathic Pulmonary Fibrosis. *PLoS One* **2008,** *3,* e2142.
61. Liu, F.; et al. Mechanosignaling Through YAP and TAZ Drives Fibroblast Activation and Fibrosis. *Am. J. Physiol. Lung Cell. Mol. Physiol.* **2015,** *308,* L344–L357.
62. Yamaguchi, Y.; et al. A Peptide Derived From Endostatin Ameliorates Organ Fibrosis. *Sci. Transl. Med.* **2012,** *4,* 136ra71.
63. Collins, J. F.; McCullough, B.; Coalson, J. J.; Johanson, W. G., Jr. Bleomycin-Induced Diffuse Interstitial Pulmonary Fibrosis in Baboons. II. Further Studies on Connective Tissue Changes. *Am. Rev. Respir. Dis.* **1981,** *123,* 305–312.
64. McCullough, B.; Collins, J. F.; Johanson, W. G., Jr.; Grover, F. L. Bleomycin-Induced Diffuse Interstitial Pulmonary Fibrosis in Baboons. *J. Clin. Invest.* **1978,** *61,* 79–88.
65. Della Latta, V.; Cecchettini, A.; Del Ry, S.; Morales, M. A. Bleomycin in the Setting of Lung Fibrosis Induction: From Biological Mechanisms to Counteractions. *Pharmacol. Res.* **2015,** *97,* 122–130.
66. Iyer, S. N.; Hyde, D. M.; Giri, S. N. Anti-Inflammatory Effect of Pirfenidone in the Bleomycin-Hamster Model of Lung Inflammation. *Inflammation* **2000,** *24,* 477–491.
67. Mansoor, J. K.; Chen, A. T.; Schelegle, E. S.; Giri, S. Effect of Diet-Ingested Pirfenidone on Pulmonary Function, Cardiovasculature and Blood Gas Measurements in Rats. *Res. Commun. Mol. Pathol. Pharmacol.* **1999,** *103,* 260–268.
68. Oku, H.; et al. Antifibrotic Action of Pirfenidone and Prednisolone: Different Effects on Pulmonary Cytokines and Growth Factors in Bleomycin-Induced Murine Pulmonary Fibrosis. *Eur. J. Pharmacol.* **2008,** *590,* 400–408.
69. King, T. E., Jr.; et al. A Phase 3 Trial of Pirfenidone in Patients With Idiopathic Pulmonary Fibrosis. *N. Engl. J. Med.* **2014,** *370,* 2083–2092.
70. Wollin, L.; Maillet, I.; Quesniaux, V.; Holweg, A.; Ryffel, B. Antifibrotic and Anti-Inflammatory Activity of the Tyrosine Kinase Inhibitor Nintedanib in Experimental Models of Lung Fibrosis. *J. Pharmacol. Exp. Ther.* **2014,** *349,* 209–220.
71. Lagares, D.; et al. Inhibition of Focal Adhesion Kinase Prevents Experimental Lung Fibrosis and Myofibroblast Formation. *Arthritis Rheum.* **2012,** *64,* 1653–1664.
72. Henderson, N. C.; et al. Targeting of Alpha v Integrin Identifies a Core Molecular Pathway That Regulates Fibrosis in Several Organs. *Nat. Med.* **2013,** *19,* 1617–1624.
73. Reed, N. I.; et al. The Alphavbeta1 Integrin Plays a Critical in vivo Role in Tissue Fibrosis. *Sci. Transl. Med.* **2015,** *7,* 288ra79.
74. Riley, D. J.; et al. Beta-Aminopropionitrile Prevents Bleomycin-Induced Pulmonary Fibrosis in the Hamster. *Am. Rev. Respir. Dis.* **1982,** *125,* 67–73.
75. Sonin, D. L.; et al. Protease-Activated Receptor 1 Inhibition by SCH79797 Attenuates Left Ventricular Remodeling and Profibrotic Activities of Cardiac Fibroblasts. *J. Cardiovasc. Pharmacol. Ther.* **2013,** *18,* 460–475.
76. Huang, W. T.; Vayalil, P. K.; Miyata, T.; Hagood, J.; Liu, R. M. Therapeutic Value of Small Molecule Inhibitor to Plasminogen Activator Inhibitor-1 for Lung Fibrosis. *Am. J. Respir. Cell Mol. Biol.* **2012,** *46,* 87–95.
77. Taooka, Y.; Maeda, A.; Hiyama, K.; Ishioka, S.; Yamakido, M. Effects of Neutrophil Elastase Inhibitor on Bleomycin-Induced Pulmonary Fibrosis in Mice. *Am. J. Respir. Crit. Care Med.* **1997,** *156,* 260–265.
78. Bruck, R.; et al. Halofuginone to Prevent and Treat Thioacetamide-Induced Liver Fibrosis in Rats. *Hepatology* **2001,** *33,* 379–386.
79. Song, J. S.; et al. Inhibitory Effect of CXC Chemokine Receptor 4 Antagonist AMD3100 on Bleomycin Induced Murine Pulmonary Fibrosis. *Exp. Mol. Med.* **2010,** *42,* 465–472.
80. Henderson, W. R., Jr.; et al. Inhibition of Wnt/Beta-Catenin/CREB Binding Protein (CBP) Signaling Reverses Pulmonary Fibrosis. *Proc. Natl. Acad. Sci. U. S. A.* **2010,** *107,* 14309–14314.
81. Huang, S.; Wettlaufer, S. H.; Hogaboam, C.; Aronoff, D. M.; Peters-Golden, M. Prostaglandin E(2) Inhibits Collagen Expression and Proliferation in Patient-Derived Normal Lung Fibroblasts via E Prostanoid 2 Receptor and cAMP Signaling. *Am. J. Physiol. Lung Cell. Mol. Physiol.* **2007,** *292,* L405–L413.
82. Ding, W. Y.; et al. Prostaglandin F2alpha Facilitates Collagen Synthesis in Cardiac Fibroblasts via an F-Prostanoid Receptor/Protein Kinase C/Rho Kinase Pathway Independent of Transforming Growth Factor Beta1. *Int. J. Biochem. Cell Biol.* **2012,** *44,* 1031–1039.

83. Mackinnon, A. C.; et al. Regulation of Transforming Growth Factor-beta1-Driven Lung Fibrosis by Galectin-3. *Am. J. Respir. Crit. Care Med.* **2012,** *185,* 537–546.
84. Underwood, D. C.; et al. SB 239063, a p38 MAPK Inhibitor, Reduces Neutrophilia, Inflammatory Cytokines, MMP-9, and Fibrosis in Lung. *Am. J. Physiol. Lung Cell. Mol. Physiol.* **2000,** *279,* L895–L902.
85. Oikonomou, N.; et al. Pulmonary Autotaxin Expression Contributes to the Pathogenesis of Pulmonary Fibrosis. *Am. J. Respir. Cell Mol. Biol.* **2012,** *47,* 566–574.
86. Pini, A.; et al. Prevention of Bleomycin-Induced Pulmonary Fibrosis by a Novel Antifibrotic Peptide With Relaxin-Like Activity. *J. Pharmacol. Exp. Ther.* **2010,** *335,* 589–599.
87. Tang, X.; et al. Assessment of Brd4 Inhibition in Idiopathic Pulmonary Fibrosis Lung Fibroblasts and In Vivo Models of Lung Fibrosis. *Am. J. Pathol.* **2013,** *183,* 470–479.
88. Tang, X.; et al. BET Bromodomain Proteins Mediate Downstream Signaling Events Following Growth Factor Stimulation in Human Lung Fibroblasts and Are Involved in Bleomycin-Induced Pulmonary Fibrosis. *Mol. Pharmacol.* **2013,** *83,* 283–293.
89. Palumbo-Zerr, K.; et al. Orphan Nuclear Receptor NR4A1 Regulates Transforming Growth Factor-Beta Signaling and Fibrosis. *Nat. Med.* **2015,** *21,* 150–158.
90. Lee, A. H.; et al. Rho-Kinase Inhibitor Prevents Bleomycin-Induced Injury in Neonatal Rats Independent of Effects on Lung Inflammation. *Am. J. Respir. Cell Mol. Biol.* **2014,** *50,* 61–73.
91. Afkarian, M.; et al. Kidney Disease and Increased Mortality Risk in Type 2 Diabetes. *J. Am. Soc. Nephrol.* **2013,** *24,* 302–308.
92. Ninomiya, T.; et al. Albuminuria and Kidney Function Independently Predict Cardiovascular and Renal Outcomes in Diabetes. *J. Am. Soc. Nephrol.* **2009,** *20,* 1813–1821.
93. Liu, Y. Renal Fibrosis: New Insights Into the Pathogenesis and Therapeutics. *Kidney Int.* **2006,** *69,* 213–217.
94. Wharram, B. L.; Goyal, M.; Wiggins, J. E.; Sanden, S. K.; Hussain, S.; Filipiak, W. E.; Saunders, T. L.; Dysko, R. C.; Kohno, K.; Holzman, L. B.; Wiggins, R. C. Podocyte Depletion Causes Glomerulosclerosis: Diphtheria Toxin-Induced Podocyte Depletion in Rats Expressing Human Diphtheria Toxin Receptor Transgene. *J. Am. Soc. Nephrol.* **2005,** *16,* 2941–2952.
95. Pozzi, A.; Zent, R. Integrins in Kidney Disease. *J. Am. Soc. Nephrol.* **2013,** *24,* 1034–1039.
96. Kang, H. M.; et al. Defective Fatty Acid Oxidation in Renal Tubular Epithelial Cells Has a Key Role in Kidney Fibrosis Development. *Nat. Med.* **2014,** *21,* 37–46.
97. Ma, L. J.; et al. Divergent Effects of Low Versus High Dose Anti-TGF-Beta Antibody in Puromycin Aminonucleoside Nephropathy in Rats. *Kidney Int.* **2004,** *65,* 106–115.
98. Yu, F.; Wu, L. H.; Tan, Y.; Li, L. H.; Wang, C. L.; Wang, W. K.; Qu, Z.; Chen, M. H.; Gao, J. J.; Li, Z. Y.; Zheng, X.; Ao, J.; Zhu, S. N.; Wang, S. X.; Zhao, M. H.; Zou, W. Z.; Liu, G. Tubulointerstitial Lesions of Patients With Lupus Nephritis Classified by the 2003 International Society of Nephrology and Renal Pathology Society System. *Kidney Int.* **2010,** *77,* 820–829.
99. Mauer, S. M.; Steffes, M.; Ellis, E. N.; Sutherland, D. E.; Brown, D. M.; Goetz, F. C. Structural-Functional Relationships in Diabetic Nephropathy. *J. Clin. Invest.* **1984,** *74,* 1143–1155.
100. Bohle, A.; Wehrmann, M.; Bogenschütz, O.; Batz, C.; Müller, C. A.; Müller, G. A. The Pathogenesis of Chronic Renal Failure in Diabetic Nephropathy. Investigation of 488 Cases of Diabetic Glomerulosclerosis. *Pathol. Res. Pract.* **1991,** *187,* 251–259.
101. Sharma, K.; et al. Pirfenidone for Diabetic Nephropathy. *J. Am. Soc. Nephrol.* **2011,** *22,* 1144–1151.
102. Yang, H. C.; Zuo, Y.; Fogo, A. B. Models of Chronic Kidney Disease. *Drug Discov. Today Dis. Model.* **2010,** *7,* 13–19.
103. Ma, L. J.; et al. Transforming Growth Factor-Beta-Dependent and -Independent Pathways of Induction of Tubulointerstitial Fibrosis in Beta6(−/−) Mice. *Am. J. Pathol.* **2003,** *163,* 1261–1273.
104. Ma, L. J.; Fogo, A. B. Model of Robust Induction of Glomerulosclerosis in Mice: Importance of Genetic Background. *Kidney Int. Suppl.* **2003,** *64,* 350–355.
105. Ma, L. J.; et al. Regression of Glomerulosclerosis With High-Dose Angiotensin Inhibition Is Linked to Decreased Plasminogen Activator Inhibitor-1. *J. Am. Soc. Nephrol.* **2005,** *16,* 966–976.
106. Aldigier, J. C.; Kanjanbuch, T.; Ma, L. J.; Brown, N. J.; Fogo, A. B. Regression of Existing Glomerulosclerosis by Inhibition of Aldosterone. *J. Am. Soc. Nephrol.* **2005,** *16,* 3306–3314.
107. Grond, J.; Muller, E. W.; van Goor, H.; Weening, J. J.; Elema, J. D. Differences in Puromycin Aminonucleoside Nephrosis in Two Rat Strains. *Kidney Int.* **1988,** *33,* 524–529.
108. Luimula, P.; Ahola, H.; Wang, S. X.; Solin, M. L.; Aaltonen, P.; Tikkanen, I.; Kerjaschki, D.; Holthöfer, H. Nephrin in Experimental Glomerular Disease. *Kidney Int.* **2000,** *58,* 1461–1468.
109. Zuo, Y.; et al. Protective Effects of PPARgamma Agonist in Acute Nephrotic Syndrome. *Nephrol. Dial. Transplant.* **2012,** *27,* 174–181.
110. Hagiwara, M.; Yamagata, K.; Capaldi, R. A.; Koyama, A. Mitochondrial Dysfunction in Focal Segmental Glomerulosclerosis of Puromycin Aminonucleoside Nephrosis. *Kidney Int.* **2006,** *69,* 1146–1152.
111. Neelisetty, S.; et al. Renal Fibrosis Is Not Reduced by Blocking Transforming Growth Factor-Beta Signaling in Matrix-Producing Interstitial Cells. *Kidney Int.* **2015,** *88,* 503–514.
112. Katayama, K.; Nomura, S.; Tryggvason, K.; Ito, M. Searching for a Treatment for Alport Syndrome Using Mouse Models. *World J. Nephrol.* **2014,** *3,* 230–236.
113. Gomez, I. G.; et al. Anti-microRNA-21 Oligonucleotides Prevent Alport Nephropathy Progression by Stimulating Metabolic Pathways. *J. Clin. Invest.* **2015,** *125,* 141–156.
114. Brenner, B. M.; et al. Effects of Losartan on Renal and Cardiovascular Outcomes in Patients With Type 2 Diabetes and Nephropathy. *N. Engl. J. Med.* **2001,** *345,* 861–869.
115. Lewis, E. J.; et al. Renoprotective Effect of the Angiotensin-Receptor Antagonist Irbesartan in Patients With Nephropathy Due to Type 2 Diabetes. *N. Engl. J. Med.* **2001,** *345,* 851–860.
116. Wright, J. T., Jr.; et al. Effect of Blood Pressure Lowering and Antihypertensive Drug Class on Progression of Hypertensive Kidney Disease: Results From the AASK Trial. *JAMA* **2002,** *288,* 2421–2431.
117. Fried, L. F.; et al. Combined Angiotensin Inhibition for the Treatment of Diabetic Nephropathy. *N. Engl. J. Med.* **2013,** *369,* 1892–1903.
118. D'Agati, V. D.; Kaskel, F. J.; Falk, R. J. Focal Segmental Glomerulosclerosis. *N. Engl. J. Med.* **2011,** *365,* 2398–2411.
119. Gilbert, R. E.; et al. A Purpose-Synthesised Anti-Fibrotic Agent Attenuates Experimental Kidney Diseases in the Rat. *PLoS One* **2012,** *7,* e47160.
120. Zhang, Y.; et al. FT011, a New Anti-Fibrotic Drug, Attenuates Fibrosis and Chronic Heart Failure in Experimental Diabetic Cardiomyopathy. *Eur. J. Heart Fail.* **2012,** *14,* 549–562.
121. Holmes, D. R., Jr.; et al. Results of Prevention of REStenosis With Tranilast and Its Outcomes (PRESTO) Trial. *Circulation* **2002,** *106,* 1243–1250.
122. Kawarazaki, Y.; Ichijo, H.; Naguro, I. Apoptosis Signal-Regulating Kinase 1 as a Therapeutic Target. *Expert Opin. Ther. Targets* **2014,** *18,* 651–664.
123. Ma, F. Y.; Tesch, G. H.; Nikolic-Paterson, D. J. ASK1/p38 Signaling in Renal Tubular Epithelial Cells Promotes Renal Fibrosis in the Mouse Obstructed Kidney. *Am. J. Physiol. Ren. Physiol.* **2014,** *307,* F1263–F1273.
124. Tesch, G. H.; et al. ASK1 Inhibitor Halts Progression of Diabetic Nephropathy in Nos3-Deficient Mice. *Diabetes* **2015,** *64,* 3903–3913.
125. Lin, J. H.; Zhang, J. J.; Lin, S. L.; Chertow, G. M. Design of a Phase 2 Clinical Trial of an ASK1 Inhibitor, GS-4997, in Patients With Diabetic Kidney Disease. *Nephron* **2015,** *129,* 29–33.
126. Kalluri, R.; Neilson, E. G. Epithelial-Mesenchymal Transition and Its Implications for Fibrosis. *J. Clin. Invest.* **2003,** *112,* 1776–1784.
127. Liu, Y. Epithelial to Mesenchymal Transition in Renal Fibrogenesis: Pathologic Significance, Molecular Mechanism, and Therapeutic Intervention. *J. Am. Soc. Nephrol.* **2004,** *15,* 1–12.
128. Quaggin, S. E.; Kapus, A. Scar Wars: Mapping the Fate of Epithelial-Mesenchymal-Myofibroblast Transition. *Kidney Int.* **2011,** *80,* 41–50.
129. Duffield, J. S.; Lupher, M.; Thannickal, V. J.; Wynn, T. A. Host Responses in Tissue Repair and Fibrosis. *Annu. Rev. Pathol.* **2013,** *8,* 241–276.
130. Humphreys, B. D.; et al. Intrinsic Epithelial Cells Repair the Kidney After Injury. *Cell Stem Cell* **2008,** *2,* 284–291.
131. Lovisa, S.; et al. Epithelial-to-Mesenchymal Transition Induces Cell Cycle Arrest and Parenchymal Damage in Renal Fibrosis. *Nat. Med.* **2015,** *21,* 998–1009.
132. Grande, M. T.; Sánchez-Laorden, B.; López-Blau, C.; De Frutos, C. A.; Boutet, A.; Arévalo, M.; Rowe, R. G.; Weiss, S. J.; López-Novoa, J. M.; Nieto, M. A. Snail1-Induced Partial Epithelial-to-Mesenchymal Transition Drives Renal Fibrosis in Mice and Can Be Targeted to Reverse Established Disease. *Nat. Med.* **2015,** *21,* 989–997.
133. Henderson, N. C.; Sheppard, D. Integrin-Mediated Regulation of TGFbeta in Fibrosis. *Biochim. Biophys. Acta* **2013,** *1832,* 891–896.

134. Sheppard, D. Integrin-Mediated Activation of Latent Transforming Growth Factor Beta. *Cancer Metastasis Rev.* **2005,** *24,* 395–402.
135. Munger, J. S.; et al. The Integrin Alpha v Beta 6 Binds and Activates Latent TGF Beta 1: A Mechanism for Regulating Pulmonary Inflammation and Fibrosis. *Cell* **1999,** *96,* 319–328.
136. Hahm, K.; et al. Alpha v Beta6 Integrin Regulates Renal Fibrosis and Inflammation in Alport Mouse. *Am. J. Pathol.* **2007,** *170,* 110–125.
137. Jin, D. K.; Fish, A. J.; Wayner, E. A.; Mauer, M.; Setty, S.; Tsilibary, E.; Kim, Y. Distribution of Integrin Subunits in Human Diabetic Kidneys. *J. Am. Soc. Nephrol.* **1996,** *7,* 2636–2645.
138. Zeisberg, M.; et al. BMP-7 Counteracts TGF-Beta1-Induced Epithelial-to-Mesenchymal Transition and Reverses Chronic Renal Injury. *Nat. Med.* **2003,** *9,* 964–968.
139. Zeisberg, M.; Kalluri, R. Reversal of Experimental Renal Fibrosis by BMP7 Provides Insights Into Novel Therapeutic Strategies for Chronic Kidney Disease. *Pediatr. Nephrol.* **2008,** *23,* 1395–1398.
140. Li, G.; et al. Gremlin Aggravates Hyperglycemia-Induced Podocyte Injury by a TGFbeta/Smad Dependent Signaling Pathway. *J. Cell. Biochem.* **2013,** *114,* 2101–2113.
141. Marchant, V.; Droguett, A.; Valderrama, G.; Burgos, M. E.; Carpio, D.; Kerr, B.; Ruiz-Ortega, M.; Egido, J.; Mezzano, S. Tubular Overexpression of Gremlin in Transgenic Mice Aggravates Renal Damage in Diabetic Nephropathy. *Am. J. Physiol. Ren. Physiol.* **2015,** *309,* F559–F568.
142. Dolan, V.; Murphy, M.; Sadlier, D.; Lappin, D.; Doran, P.; Godson, C.; Martin, F.; O'Meara, Y.; Schmid, H.; Henger, A.; Kretzler, M.; Droguett, A.; Mezzano, S.; Brady, H. R. Expression of Gremlin, a Bone Morphogenetic Protein Antagonist, in Human Diabetic Nephropathy. *Am. J. Kidney Dis.* **2005,** *45,* 1034–1039.
143. Roxburgh, S. A.; Kattla, J. J.; Curran, S. P.; O'Meara, Y. M.; Pollock, C. A.; Goldschmeding, R.; Godson, C.; Martin, F.; Brazil, D. P. Allelic Depletion of Grem1 Attenuates Diabetic Kidney Disease. *Diabetes* **2009,** *58,* 1641–1650.
144. Kim, M.; Yoon, S.; Lee, S.; Ha, S. A.; Kim, H. K.; Kim, J. W.; Chung, J. Gremlin-1 Induces BMP-Independent Tumor Cell Proliferation, Migration, and Invasion. *PLoS One* **2012,** *7,* e35100.
145. Ma, L. J.; Fogo, A. B. Modulation of Glomerulosclerosis. *Semin. Immunopathol.* **2007,** *29,* 385–395.
146. Ma, L. J.; Fogo, A. B. PAI-1 and Kidney Fibrosis. *Front. Biosci. (Landmark Ed.)* **2009,** *14,* 2028–2041.
147. LeBleu, V. S.; Teng, Y.; O'Connell, J. T.; Charytan, D.; Müller, G. A.; Müller, C. A.; Sugimoto, H.; Kalluri, R. Identification of Human Epididymis Protein-4 as a Fibroblast-Derived Mediator of Fibrosis. *Nat. Med.* **2013,** *19,* 227–231.
148. Ma, L. J.; Marcantoni, C.; Linton, M. F.; Fazio, S.; Fogo, A. B. Peroxisome Proliferator-Activated Receptor-Gamma Agonist Troglitazone Protects Against Nondiabetic Glomerulosclerosis in Rats. *Kidney Int.* **2001,** *59,* 1899–1910.
149. Satriano, J.; Sharma, K.; Blantz, R. C.; Deng, A. Induction of AMPK Activity Corrects Early Pathophysiological Alterations in the Subtotal Nephrectomy Model of Chronic Kidney Disease. *Am. J. Physiol. Ren. Physiol.* **2013,** *305,* F727–F733.
150. Sharma, K.; et al. Metabolomics Reveals Signature of Mitochondrial Dysfunction in Diabetic Kidney Disease. *J. Am. Soc. Nephrol.* **2013,** *24,* 1901–1912.
151. Dugan, L. L.; et al. AMPK Dysregulation Promotes Diabetes-Related Reduction of Superoxide and Mitochondrial Function. *J. Clin. Invest.* **2013,** *123,* 4888–4899.
152. Ashraf, S.; et al. ADCK4 Mutations Promote Steroid-Resistant Nephrotic Syndrome Through CoQ10 Biosynthesis Disruption. *J. Clin. Invest.* **2013,** *123,* 5179–5189.
153. Kanjanabuch, T.; et al. PPAR-Gamma Agonist Protects Podocytes From Injury. *Kidney Int.* **2007,** *71,* 1232–1239.
154. Dwivedi, R. S.; Herman, J. G.; McCaffrey, T. A.; Raj, D. S. Beyond Genetics: Epigenetic Code in Chronic Kidney Disease. *Kidney Int.* **2011,** *79,* 23–32.
155. Montecalvo, A.; et al. Mechanism of Transfer of Functional microRNAs Between Mouse Dendritic Cells via Exosomes. *Blood* **2012,** *119,* 756–766.
156. GBD 2013 Mortality and Causes of Death Collaborators. Global, Regional, and National Age-Sex Specific All-Cause and Cause-Specific Mortality for 240 Causes of Death, 1990–2013: A Systematic Analysis for the Global Burden of Disease Study 2013. *Lancet* **2015,** *385* (9963), 117–171. http://dx.doi.org/10.1016/S0140-6736(14)61682-2.
157. Duseja, A.; Chalasani, N. Epidemiology and Risk Factors of Nonalcoholic Fatty Liver Disease (NAFLD). *Hepatol. Int.* **2013,** *7* (Suppl. 2), 755–764.
158. Musso, G.; Cassader, M.; Rosina, F.; Gambino, R. Impact of Current Treatments on Liver Disease, Glucose Metabolism and Cardiovascular Risk in Non-Alcoholic Fatty Liver Disease (NAFLD): A Systematic Review and Meta-Analysis of Randomised Trials. *Diabetologia* **2012,** *55,* 885–904.
159. Hernandez-Gea, V.; Friedman, S. L. Pathogenesis of Liver Fibrosis. *Annu. Rev. Pathol.* **2011,** *6,* 425–456.
160. Sharma, S.; Khalili, K.; Nguyen, G. C. Non-Invasive Diagnosis of Advanced Fibrosis and Cirrhosis. *World J. Gastroenterol.* **2014,** *20,* 16820–16830.
161. Lee, S. J.; Kim, K. H.; Park, K. K. Mechanisms of Fibrogenesis in Liver Cirrhosis: The Molecular Aspects of Epithelial-Mesenchymal Transition. *World J. Hepatol.* **2014,** *6,* 207–216.
162. Delire, B.; Starkel, P.; Leclercq, I. Animal Models for Fibrotic Liver Diseases: What We Have, What We Need, and What Is Under Development. *J. Clin. Transl. Hepatol.* **2015,** *3,* 53–66.
163. Starkel, P.; Leclercq, I. A. Animal Models for the Study of Hepatic Fibrosis. *Best Pract. Res. Clin. Gastroenterol.* **2011,** *25,* 319–333.
164. Marcellin, P.; et al. Regression of Cirrhosis During Treatment With Tenofovir Disoproxil Fumarate for Chronic Hepatitis B: A 5-Year Open-Label Follow-Up Study. *Lancet* **2013,** *381,* 468–475.
165. George, S. L.; et al. Clinical, Virologic, Histologic, and Biochemical Outcomes After Successful HCV Therapy: A 5-Year Follow-Up of 150 Patients. *Hepatology* **2009,** *49,* 729–738.
166. Nanthakumar, C. B.; et al. Dissecting Fibrosis: Therapeutic Insights From the Small-Molecule Toolbox. *Nat. Rev. Drug Discov.* **2015,** *14,* 693–720.
167. Matsumura, Y.; et al. Prolyl 4-Hydroxylase Inhibitor (HOE 077) Inhibits Pig Serum-Induced Rat Liver Fibrosis by Preventing Stellate Cell Activation. *J. Hepatol.* **1997,** *27,* 185–192.
168. Wei, H. S.; et al. Effects of AT1 Receptor Antagonist, Losartan, on Rat Hepatic Fibrosis Induced by CCl(4). *World J. Gastroenterol.* **2000,** *6,* 540–545.
169. Fickert, P.; et al. Farnesoid X Receptor Critically Determines the Fibrotic Response in Mice but Is Expressed to a Low Extent in Human Hepatic Stellate Cells and Periductal Myofibroblasts. *Am. J. Pathol.* **2009,** *175,* 2392–2405.
170. Verbeke, L.; et al. Obeticholic Acid, a Farnesoid X Receptor Agonist, Improves Portal Hypertension by Two Distinct Pathways in Cirrhotic Rats. *Hepatology* **2014,** *59,* 2286–2298.
171. Rockey, D. C.; Bell, P. D.; Hill, J. A. Fibrosis—A Common Pathway to Organ Injury and Failure. *N. Engl. J. Med.* **2015,** *373,* 96.
172. Neuschwander-Tetri, B. A.; et al. Farnesoid X Nuclear Receptor Ligand Obeticholic Acid for Non-Cirrhotic, Non-Alcoholic Steatohepatitis (FLINT): A Multicentre, Randomised, Placebo-Controlled Trial. *Lancet* **2015,** *385,* 956–965.
173. Kim, M. Y.; et al. Beneficial Effects of Candesartan, an Angiotensin-Blocking Agent, on Compensated Alcoholic Liver Fibrosis—A Randomized Open-Label Controlled Study. *Liver Int.* **2012,** *32,* 977–987.
174. Jha, J. C.; et al. Genetic Targeting or Pharmacologic Inhibition of NADPH Oxidase Nox4 Provides Renoprotection in Long-Term Diabetic Nephropathy. *J. Am. Soc. Nephrol.* **2014,** *25,* 1237–1254.
175. Hecker, L.; et al. Reversal of Persistent Fibrosis in Aging by Targeting Nox4-Nrf2 Redox Imbalance. *Sci. Transl. Med.* **2014,** *6,* 231ra47.
176. Aoyama, T.; et al. Nicotinamide Adenine Dinucleotide Phosphate Oxidase in Experimental Liver Fibrosis: GKT137831 as a Novel Potential Therapeutic Agent. *Hepatology* **2012,** *56,* 2316–2327.
177. de Zeeuw, D.; et al. Bardoxolone Methyl in Type 2 Diabetes and Stage 4 Chronic Kidney Disease. *N. Engl. J. Med.* **2013,** *369,* 2492–2503.
178. Pergola, P. E.; et al. Bardoxolone Methyl and Kidney Function in CKD With Type 2 Diabetes. *N. Engl. J. Med.* **2013,** *365,* 327–336.
179. Korfhagen, T. R.; et al. Rapamycin Prevents Transforming Growth Factor-Alpha-Induced Pulmonary Fibrosis. *Am. J. Respir. Cell Mol. Biol.* **2009,** *41,* 562–572.
180. Wu, M. J.; et al. Rapamycin Attenuates Unilateral Ureteral Obstruction-Induced Renal Fibrosis. *Kidney Int.* **2006,** *69,* 2029–2036.
181. Dees, C.; et al. JAK-2 as a Novel Mediator of the Profibrotic Effects of Transforming Growth Factor Beta in Systemic Sclerosis. *Arthritis Rheum.* **2012,** *64,* 3006–3015.
182. Takenaka, M.; et al. Effect of Beraprost Sodium (BPS) in a New Rat Partial Unilateral Ureteral Obstruction Model. *Prostaglandins Leukot. Essent. Fat. Acids* **2009,** *80,* 263–267.

183. Zhu, X. Y.; et al. The Chemokine Monocyte Chemoattractant Protein-1 Contributes to Renal Dysfunction in Swine Renovascular Hypertension. *J. Hypertens.* **2009,** *27,* 2063–2073.
184. Iwaisako, K.; et al. Origin of Myofibroblasts in the Fibrotic Liver in Mice. *Proc. Natl. Acad. Sci. U. S. A.* **2014,** *111,* E3297–E3305.
185. Niki, T.; et al. A Histone Deacetylase Inhibitor, Trichostatin A, Suppresses Myofibroblastic Differentiation of Rat Hepatic Stellate Cells in Primary Culture. *Hepatology* **1999,** *29,* 858–867.
186. Page, A.; et al. Hepatic Stellate Cell Transdifferentiation Involves Genome-Wide Remodeling of the DNA Methylation Landscape. *J. Hepatol.* **2016,** *64* (3), 661–673.
187. Mann, J.; et al. Regulation of Myofibroblast Transdifferentiation by DNA Methylation and MeCP2: Implications for Wound Healing and Fibrogenesis. *Cell Death Differ.* **2007,** *14,* 275–285.
188. Teng, K. Y.; Ghoshal, K. Role of Noncoding RNAs as Biomarker and Therapeutic Targets for Liver Fibrosis. *Gene Expr.* **2015,** *16,* 155–162.
189. Venugopal, S. K.; et al. Liver Fibrosis Causes Downregulation of miRNA-150 and miRNA-194 in Hepatic Stellate Cells, and Their Overexpression Causes Decreased Stellate Cell Activation. *Am. J. Physiol. Gastrointest. Liver Physiol.* **2010,** *298,* G101–G106.
190. Fouts, D. E.; Torralba, M.; Nelson, K. E.; Brenner, D. A.; Schnabl, B. Bacterial Translocation and Changes in the Intestinal Microbiome in Mouse Models of Liver Disease. *J. Hepatol.* **2014,** *56,* 1283–1292.
191. Vespasiani-Gentilucci, U.; et al. Hepatic Toll-Like Receptor 4 Expression Is Associated With Portal Inflammation and Fibrosis in Patients With NAFLD. *Liver Int.* **2015,** *35,* 569–581.
192. Ochoa-Callejero, L.; et al. Maraviroc, a CCR5 Antagonist, Prevents Development of Hepatocellular Carcinoma in a Mouse Model. *PLoS One* **2013,** *8*, e53992.
193. Perez-Martinez, L.; et al. Maraviroc, a CCR5 Antagonist, Ameliorates the Development of Hepatic Steatosis in a Mouse Model of Non-Alcoholic Fatty Liver Disease (NAFLD). *J. Antimicrob. Chemother.* **2014,** *69,* 1903–1910.
194. Sakaida, I.; et al. The Prolyl 4-Hydroxylase Inhibitor HOE 077 Prevents Activation of Ito Cells, Reducing Procollagen Gene Expression in Rat Liver Fibrosis Induced by Choline-Deficient L-Amino Acid-Defined Diet. *Hepatology* **1996,** *23,* 755–763.
195. Marek, C. J.; et al. Pregnenolone-16alpha-carbonitrile Inhibits Rodent Liver Fibrogenesis via PXR (Pregnane X Receptor)-Dependent and PXR-Independent Mechanisms. *Biochem. J.* **2005,** *387,* 601–608.
196. Sugano, N.; et al. T-Type Calcium Channel Blockade as a Therapeutic Strategy Against Renal Injury in Rats With Subtotal Nephrectomy. *Kidney Int.* **2008,** *73,* 826–834.
197. Lee, S. J.; et al. PKCdelta as a Regulator for TGFbeta1-Induced Alpha-SMA Production in a Murine Nonalcoholic Steatohepatitis Model. *PLoS One* **2013,** *8*, e55979.
198. Kim, D. C.; et al. 5-HT2A Receptor Antagonists Inhibit Hepatic Stellate Cell Activation and Facilitate Apoptosis. *Liver Int.* **2013,** *33,* 535–543.
199. Hamasaki, Y.; et al. A 5-Hydroxytryptamine Receptor Antagonist, Sarpogrelate, Reduces Renal Tubulointerstitial Fibrosis by Suppressing PAI-1. *Am. J. Physiol. Ren. Physiol.* **2013,** *305,* F1796–F1803.
200. Zhou, X. Y.; et al. BML-11, a Lipoxin Receptor Agonist, Protected Carbon Tetrachloride-Induced Hepatic Fibrosis in Rats. *Inflammation* **2013,** *36,* 1101–1106.
201. Traber, P. G.; Zomer, E. Therapy of Experimental NASH and Fibrosis With Galectin Inhibitors. *PLoS One* **2013,** *8*, e83481.

7.20 β_3-AR Agonists for the Treatment of Overactive Bladder

SD Edmondson, Merck Research Laboratories, Kenilworth, NJ, United States

© 2017 Elsevier Ltd. All rights reserved.

7.20.1	**Overactive Bladder**	715
7.20.1.1	Prevalence, Etiology, and Impact	715
7.20.1.2	Treatment of OAB: An Unmet Medical Need	715
7.20.2	**History of β_3-Adrenergic Receptors**	715
7.20.2.1	Discovery and Description of β_3-Adrenergic Receptors (Adrenoceptors)	715
7.20.2.2	Pharmacology of β_3-AR Agonists	717
7.20.2.2.1	Metabolic effects of β_3-ARs	717
7.20.2.2.2	Cardiovascular effects of β_3-ARs	717
7.20.2.2.3	The role of β_3-ARs in overactive bladder	718
7.20.3	**β_3-AR Agonists in Discovery and Development**	719
7.20.3.1	Overview of β_3-AR Agonists in the Literature	719
7.20.3.2	Potent Rat β_3-AR Agonists in Early Human Clinical Trials	721
7.20.3.3	Medicinal Chemistry of Human β_3-AR Agonists	721
7.20.3.3.1	Discovery of BMS-196085 and related analogs	721
7.20.3.3.2	Discovery of LY-377604 and related compounds	722
7.20.3.3.3	Discovery of rafabegron and related analogs	723
7.20.3.3.4	Discovery of an oxazole ring as an acid bioisostere	723
7.20.3.3.5	Discovery of amibegron and other cyclic β_3-AR agonists	723
7.20.3.3.6	Discovery of solabegron and related analogs	724
7.20.3.3.7	Discovery of ritobegron and related analogs	725
7.20.3.3.8	Discovery of MK-0634, vibegron, and related analogs	725
7.20.3.3.9	Discovery of mirabegron and a series of biphenyl acid β_3-AR agonists	727
7.20.4	**Summary**	729
References		730

Glossary/Abbreviations/Acronyms

AC adenylyl cyclase
AMs antimuscarinic agents; antimuscarinics; anticholinergics
API active pharmaceutical ingredient
ARs adrenergic receptors
ATP adenosine triphosphate
BAT brown adipose tissue
BID twice daily
BOO bladder outflow obstruction
cAMP cyclic adenosine monophosphate
CMG cystometrogram
CNS central nervous system
DO detrusor overactivity
eNOS endothelial nitric oxide synthase
F oral bioavailability
FFAs free fatty acids
GPCRs G protein-coupled receptors
hERG human ether-a-go-go
HRQoL health-related quality of life
HSL hormone-sensitive lipase
i.v. intravenous
ICS International Continence Society
IMI intramicturition interval
IP intellectual property
IVP intravesicular pressure
LHS left-hand side
LUTS lower urinary tract symptoms
NO nitric oxide
OAB overactive bladder
OCAS oral controlled absorption system
PD pharmacodynamic
PEAT phenylethanolaminotetraline
PK pharmacokinetic
PKA protein kinase A
PKG protein kinase G
QoL quality of life
RHS right-hand side
SAR structure–activity relationship(s)
SERT serotonin transporter
$T_{1/2}$ half-life
TGs triglycerides
UCP1 uncoupling protein 1
WAT white adipose tissue
α-ARs alpha adrenergic receptors, alpha adrenoceptors
β_1-ARs beta-1 adrenergic receptors; beta-1 adrenoceptors
β_2-ARs beta-2 adrenergic receptors; beta-2 adrenoceptors
β_3-ARs beta-3 adrenergic receptors; beta-3 adrenoceptors

7.20.1 Overactive Bladder

7.20.1.1 Prevalence, Etiology, and Impact

Overactive bladder (OAB) is a chronic and frequently debilitating syndrome resulting from lower urinary tract dysfunction that negatively impacts the quality of life (QoL) of 11–19% of the worldwide population.[1–5] Prevalence increases with age, and for those over the age of 65, the estimated prevalence is 30%.[5,6] With an increasingly aging world population, the overall prevalence of OAB is therefore expected to continue to increase in the coming years.

The International Continence Society (ICS) defines OAB as a group of lower urinary tract symptoms (LUTS) including "urgency, with or without urge incontinence, usually with increased frequency and nocturia."[7] The etiology of OAB has been linked to multiple factors including anatomical and tissue changes associated with aging, lifestyle choices, various comorbidities, and personal characteristics.[8–13] In addition to significantly impacting QoL, OAB has also been associated with a decline in overall health.[14,15] Symptoms such as urgency, urge incontinence, and incontinence episodes cause the most significant reduction in QoL, and consequently, these symptoms are frequently included as end points in clinical trials studying efficacy of pharmacotherapies aimed at treating OAB. Nocturia (multiple nighttime voiding episodes) has been associated with depression due to the interruption of sleep as well as an increase in bone fractures and subsequent mortality in elderly populations.[16,17] Although OAB is not life-threatening, patients who suffer from it experience a significant drop in their health-related QoL, their physical functioning, and their psychological well-being.[18] Moreover, OAB confers a substantial economic impact worldwide with an estimated cost of over $12 billion per year in the United States alone.[19,20]

7.20.1.2 Treatment of OAB: An Unmet Medical Need

OAB often goes undiagnosed due to the belief by patients that their symptoms are a normal part of aging or due to embarrassment to discuss their condition with physicians.[21] For similar reasons, a high percentage of patients that are diagnosed also go untreated.[22] Treatment options for patients suffering from OAB include behavior therapy, pharmacotherapy, and finally surgical therapy when the previous two options fail.[23] Behavioral approaches include bladder training, pelvic exercises, and education and application of lifestyle changes to mitigate the risk of some of the more detrimental symptoms of OAB.[6,24] When behavioral approaches fail, however, patients are often treated with the first-line pharmacotherapy of antimuscarinic agents (also known as anticholinergic agents).

Antimuscarinic (AM) agents are antagonists at the M_2 and/or M_3 muscarinic receptors, which are important for signaling contraction of the detrusor muscle that surrounds the urinary bladder.[25–28] AM agents have been the standard-of-care pharmacotherapy of OAB for more than 40 years, and improvements in urgency, frequency of micturition, and urge incontinence have been demonstrated with these drugs. Although efficacious, this drug class suffers from a number of undesirable effects that limit both patient and physician satisfaction. Muscarinic receptors exist in the brain where they play an important role in cognitive function. AM agents that penetrate the brain have been linked to cognitive impairment in elderly patients, and therefore, the selection of an AM agent with reduced potential for CNS penetration is recommended.[29] Additionally, nonselective blockade of the M_2/M_3 muscarinic receptors can lead to adverse effects such as dry mouth and constipation due to the presence of this receptor in salivary glands and the gastrointestinal tract, respectively.[28] Much attention has been focused on mitigating these side effects with some degree of success by using a strategy to reduce maximal plasma drug concentrations (C_{max}) using extended-release formulations. Additionally, alternate routes of administration and modification of the muscarinic receptor antagonist subtype selectivity are other strategies that have been pursued to reduce these tolerability concerns.[26,30] Nevertheless, more than 70% of patients discontinue therapy with AM agents because they are unsatisfied with the balance between efficacy and tolerability.[25,28–32] With this high discontinuation rate of the current first-line pharmacotherapy for OAB, it is clear that there is an unmet medical need for treatments with improved adherence that will translate to improved outcomes for patients that suffer from OAB.

7.20.2 History of β_3-Adrenergic Receptors

7.20.2.1 Discovery and Description of β_3-Adrenergic Receptors (Adrenoceptors)

The adrenergic receptors (ARs or adrenoceptors) are a class of G protein-coupled receptors (GPCRs) that have been known for decades as a rich source of pharmacology. Modulation of ARs by either activation or antagonism has resulted in many druggable targets for pharmaceutical intervention. Endogenous agonists of the ARs include naturally occurring catecholamines such as epinephrine (adrenaline, **1**) and norepinephrine (noradrenaline, **2**; Fig. 1). Distinct patterns of agonist and antagonist affinities are the basis for the further categorization of these ARs into α_1-, α_2-, β_1-, β_2-, and β_3-ARs.[33,34] At a high level, activation of the β-ARs at the cell surface catalyzes a cascade of events that results in stimulation of adenylyl cyclase and subsequent intracellular conversion of ATP to cAMP (Fig. 2), which in turn causes a broad range of physiological responses. Isoproterenol (isoprenaline, **3**) is an example of an agonist that is more selective for the β-ARs compared with the α-ARs, although it is not selective among the three β-receptor subtypes. Although the β_1- and β_2-ARs have been studied as early as the 1940s,[35] the existence of a third β_3-AR, sometimes called an "atypical β-adrenoceptor," was only confirmed in 1989 when it was first cloned and characterized.[36,37]

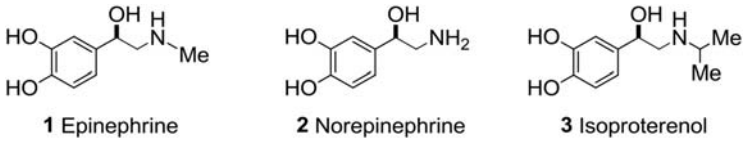

Fig. 1 Some nonselective β-AR agonists. Epinephrine and norepinephrine are endogenous ligands, and isoproterenol is a more stable nonselective agonist of β-AR receptors.

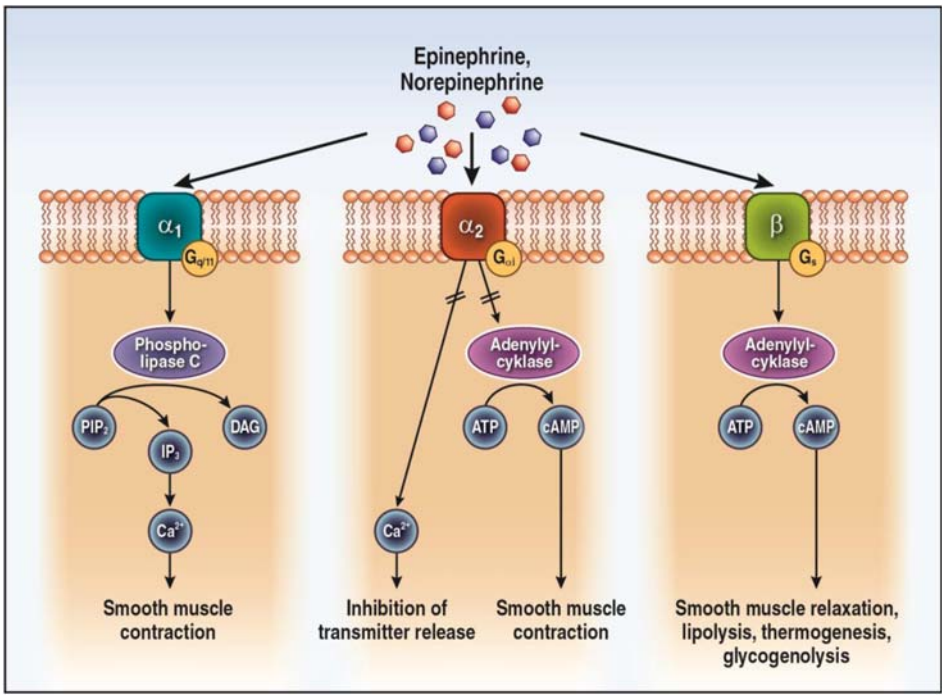

Fig. 2 Adrenergic receptor signaling pathways.

At that time, the β_3-AR was found to be present in rat adipose tissue where it was responsible for mediating metabolic effects such as thermogenesis and the lipolysis of triglycerides (TGs) into glycerol and free fatty acids (FFAs).

The structure of β_3-ARs consists of seven transmembrane (TM) amino acid domains composed of 22–28 amino acids each. Site-directed mutagenesis studies suggest that at least four of these TM domains are responsible for ligand binding, and this topic has been recently reviewed.[38] The gene for the β_3-AR is polymorphic, and extensive research has been applied to attempt to better understand the functional consequences of these polymorphisms, particularly with respect to potential genetic links to hypertension, diabetes, and obesity.[39–41] Sequence homology of β_3 across multiple species (mouse, rat, dog, cow, monkey, and human) is between 79 and 90% with higher homology between monkeys and humans than between rodents and humans.[42] These species disconnects contribute to potency disconnects between rodents and primates in many of the β_3-AR agonists reported in the 1980s and early 1990s.[42] Indeed, many early agonists such as BRL 37344 (**4**),[43] CGP 12177A (**5**),[44] and CL 316,243 (**6**)[45] that were discovered to be potent and selective rodent β_3-AR agonists are either less potent or less selective for human β_3-ARs (Fig. 3).[39] Across subtypes, the human β_3-AR possesses only ~50–70% sequence homology to β_1- and β_2-ARs, suggesting that installing selectivity for β_3-AR agonists is achievable provided that optimization is done with receptors expressed from the appropriate species.[39,46,47]

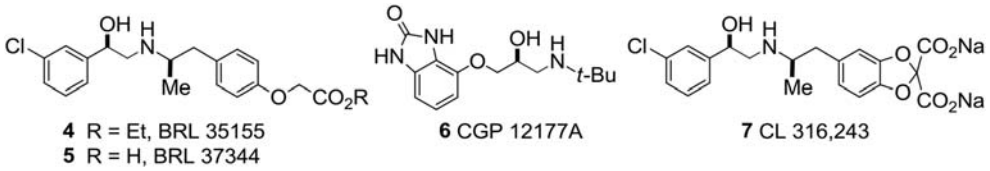

Fig. 3 Early rodent selective β_3-AR agonists frequently used in rodent pharmacology studies.

7.20.2.2 Pharmacology of β_3-AR Agonists

7.20.2.2.1 Metabolic effects of β_3-ARs

Although originally identified in white and brown adipose tissue, the β_3-AR receptor has now also been found in multiple tissue beds including the detrusor muscle that surrounds the urinary bladder, the urothelium, the gallbladder, the large and small intestines, the human heart, the brain, the colon, and the near-term myometrium.[38,48] Activation of β_3-ARs in adipocytes leads to thermogenesis (in brown adipose tissue or BAT) and/or lipolysis (in both BAT and white adipose tissue or WAT) through coupling with the Gs and Gi proteins followed by a cascade of signaling pathways triggered by increases in intracellular cAMP (through Gs)[49] and ERK1/2 (through Gi),[50] respectively (Fig. 4).

In BAT, activation of β_3-ARs triggers increased expression of uncoupling protein 1 (UCP1), which goes on to induce thermogenesis. Meanwhile, in WAT, activation of β_3-ARs induces hydrolysis of TGs and consequently an increase in circulating concentrations of FFAs. The FFAs released in WAT then undergo fatty acid oxidation in BAT through the increased expression of UCP1 in BAT. β_3-AR agonists therefore mobilize fat stores in preclinical species by inducing lipolysis in WAT, while the FFAs then further act as fuel for FFA oxidation and thermogenesis in BAT.[51] Taken together, this cascade of events translates into decreased body weight without food intake reduction, increased energy expenditure, and reduced body fat in preclinical models.[38] These actions of selective β_3-AR agonists have led to decades of investigations for the use of these compounds as a treatment of obesity.[51–55]

β_3-AR agonists have also been investigated for the treatment of diabetes.[51,56] Chronic treatment of the rat β_3-AR agonists **4** and **6** in various rodent diabetes models, for example, results in improved oral glucose tolerance, decreased plasma insulin levels, and/or improved insulin sensitization.[57–59] Although more needs to be understood about the mechanism of these effects, it has been proposed that β_3-AR agonists increase glucose utilization in skeletal muscle.[60] Another recent hypothesis is that some of these antidiabetic and antiobesity effects may be related to the browning of white adipose and/or the maintenance of BAT upon β_3-AR activation in these tissue beds.[56]

7.20.2.2.2 Cardiovascular effects of β_3-ARs

β_3-ARs in cardiomyocytes are linked to the Gi protein and their activation by agonists invokes a negative inotropic effect (Fig. 4). At a receptor expression level, β_3-ARs have been found in both normal and diseased hearts; however, their expression is upregulated

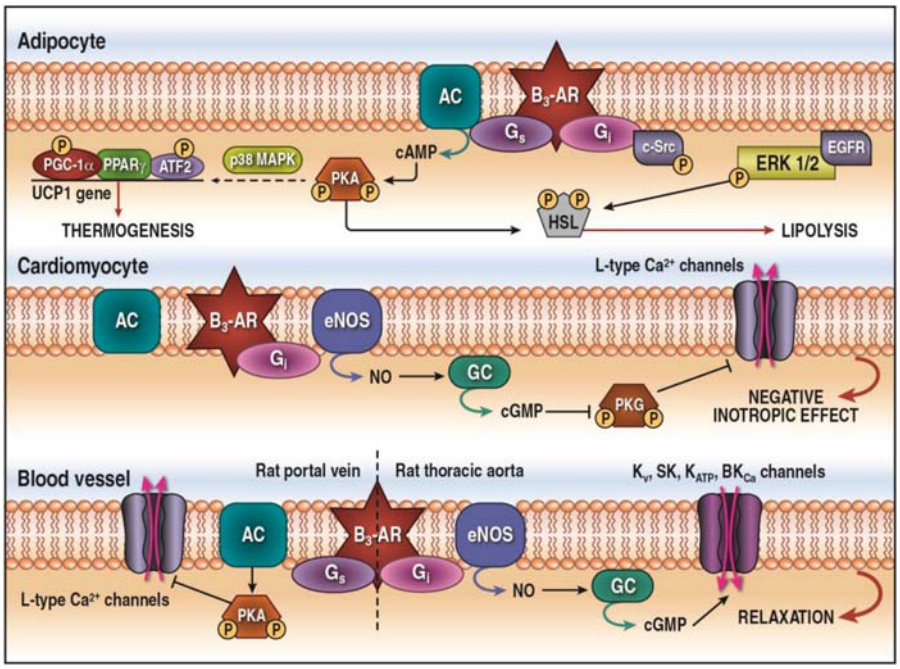

Fig. 4 Cardiometabolic tissue signaling pathways relevant to activation of the β_3-AR. (A) In adipocytes, the β_3-AR is coupled to the Gs protein that activates adenylyl cyclase (AC), which subsequently converts ATP to cAMP leading to activation of protein kinase A (PKA). Upon activation, protein kinase A (PKA) phosphorylates p38 MAP kinase, which then leads to thermogenesis through the action of the uncoupling protein 1 (UCP1) gene. PKA also phosphorylates hormone-sensitive lipase (HSL) leading to lipolysis of triglycerides to glycerol and free fatty acids. Alternatively, lipolysis can be induced through the Gi pathway via the action of ERK1/2 and subsequent phosphorylation of HSL. (B) In cardiomyocytes, the β_3-AR signals through the Gi pathway to activate endothelial nitric oxide synthase (eNOS), which then releases nitric oxide (NO). The increased intracellular NO then activates soluble guanylyl cyclase (GC) releasing cGMP, which then activates protein kinase G (PKG) leading to a negative inotropic effect through calcium ion efflux. (C) In the vasculature, the β_3-AR acts through the Gs signaling pathway to induce calcium efflux through L-type Ca^{2+} channels. In the rat aorta, β_3-ARs can act through the Gi signaling cascade to induce relaxation of blood vessels.

during ischemic and dilated cardiomyopathies in humans.[61] Consequently, it has been postulated that β_3-ARs may play a role in the treatment of heart failure, which has prompted recent investigations into the effects of β_3-AR agonists on cardiovascular pathophysiology. The specific role of β_3-AR agonists in heart failure has yet to be determined, however, and research continues in this potentially exciting area.[61–67]

In vasculature, the β_3-ARs are again coupled with either Gs or Gi proteins and activation of these receptors can lead to vasodilation and subsequent hypotension through two separate biochemical cascades (Fig. 4). Selective and potent rodent and dog β_3-AR agonists **4**, **5**, and **6** induce hypotension and peripheral vasodilation in mice, rats, and dogs but not in monkeys—likely due to their reduced potency at the monkey β_3-AR receptor.[68–72] In anesthetized rhesus monkeys, potent and selective rhesus β_3-AR agonists were shown to evoke peripheral vasodilation, facial flushing, and reflex tachycardia consistent with the effects reported in nonprimates.[73]

The profound vascular effects observed in dogs and monkeys were not observed, however, in humans. Early compounds taken into the clinic as β_3-AR agonists were generally nonselective over either the β_1- or β_2-ARs, which often translated into adverse cardiovascular effects consistent with these off-target activities.[51,74,75] Although some of the early β_3-AR agonists studied in humans induced tachycardia, more recent potent and selective human agonists studied in the clinic have exhibited acceptable cardiovascular safety profiles in humans. For example, no changes in systolic or diastolic blood pressure were observed in a 28-day clinical study upon treatment with a potent and selective human β_3-AR agonist.[76] Furthermore, a recent review of clinical data for mirabegron, a potent and selective human β_3-AR agonist, concluded that this compound possesses a good overall cardiovascular safety profile.[74]

7.20.2.2.3 The role of β_3-ARs in overactive bladder

β-AR activation has long been known to be an important contributor to relaxation of the detrusor muscle, thus enabling bladder compliance during the filling phase of the micturition cycle.[77] It wasn't until the latter half of the 1990s, however, that a series of studies using β_3-AR agonists such as **4**, **5**, and **6** revealed that the β_3-AR is a major functional contributor to β-AR-mediated bladder relaxation in multiple species (Fig. 5).[78–83] Since these early discoveries, a series of *ex vivo* studies demonstrated that potent and selective β_3-AR agonists from a broad range of structure classes can relax precontracted bladder muscle strips in a variety of species including humans.[84,85] In the detrusor muscle, the β_3-ARs are coupled with Gs proteins and their activation increases cAMP through the action of adenylyl cyclase. Subsequent signaling from cAMP then leads to bladder smooth muscle relaxation. In addition to this cAMP-dependent pathway to bladder relaxation, there is a potential contribution from a cAMP-independent pathway, but most studies suggest that the cAMP-dependent pathways play the more significant role in this process.[86] Finally, β_3-ARs were also found to play a functional role for urine storage in the urothelium tissue, which was once believed to serve only as an impenetrable barrier to protect blood and tissue from substances in urine.[87,88]

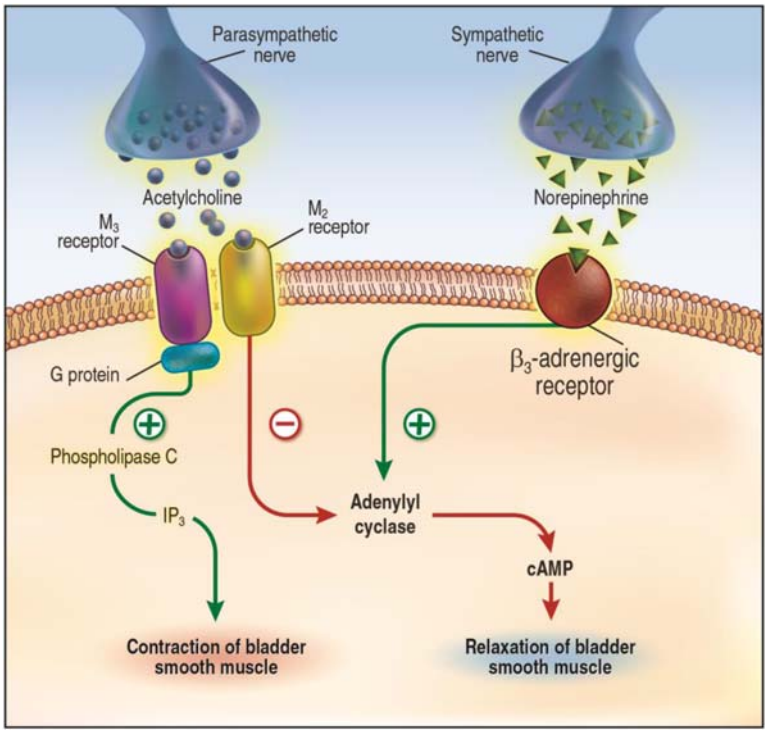

Fig. 5 Signaling pathways in the human detrusor muscle.

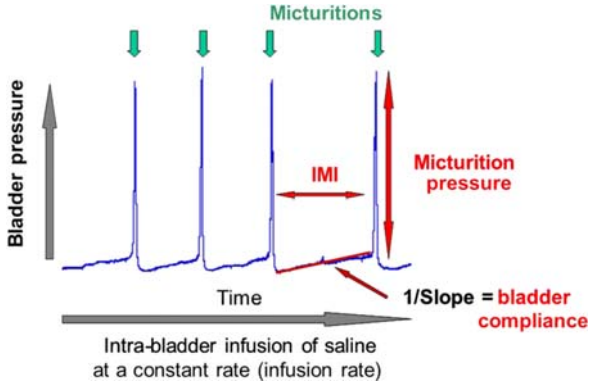

Fig. 6 Representative cystometrogram (CMG) from a preclinical cystometry study. Cystometry is a diagnostic procedure, often performed on anesthetized animals, that is used to evaluate urinary bladder function. A solution, typically saline, is infused into the bladder at a constant rate through a catheter. Pressure builds inside the bladder as it fills with fluid, and eventually, the bladder muscle contracts resulting in expulsion of the liquid in a micturition event denoted by green arrows. This event completes the micturition cycle and the bladder again fills with fluid to repeat the cycle. The measured time between two micturition events is defined as the intramicturition interval (IMI). Bladder capacity (maximum volume of fluid in the bladder) can be measured by multiplying the fluid infusion rate by the IMI. Micturition pressure is the difference in pressure between the highest pressure and the pressure trough after a micturition event. Bladder compliance is the inverse slope of the bladder pressure during the filling phase of the micturition cycle.

In multiple species, cystometry-based models have been used to measure the effects of β_3-AR agonists on bladder compliance and bladder function (Fig. 6).[89] In rat bladder hyperactivity models, for example, selective β_3-AR agonists such as compounds **4** and **6** increase bladder contraction (intramicturition) intervals while reducing contraction amplitude (force) and baseline pressure.[90,91] Mechanistic cystometry studies have also helped shed light into effects of β_3-AR agonists beyond detrusor muscle relaxation. For example, studies with compound **6** suggest a potential contribution of β_3-AR agonists to facilitate urine storage in rats by inhibiting bladder afferent neurotransduction.[92,93] Finally, a recent study demonstrated that intravesicular administration of selective rat β_3-AR agonists resulted in a decrease in micturition frequency as well as a decrease in contraction force in anesthetized rats, suggesting an active role for the urothelium in the effects of β_3-AR agonists.[94] These findings further suggest β_3-AR agonists may improve bladder function through multiple physiological pathways in addition to direct effects arising from detrusor muscle relaxation.[89] Overall, evidence from *in vitro* and *in vivo* studies suggests that β_3-AR agonists act on multiple cell types to regulate bladder function. Results from some of the more advanced mechanistic studies performed in rats with potent and selective rat β_3-AR agonists still need to be confirmed in humans, but the overwhelming evidence to date supports the use of β_3-AR agonists to treat symptoms related to OAB through multiple actions.[95,96]

Muscarinic receptors in the urinary bladder are known to increase smooth muscle tone, and β_3-AR activation has been shown to induce relaxation of smooth muscle as well as oppose muscarinic-mediated muscle contraction (Fig. 5). Each of these two receptor types is therefore important in the regulation of the micturition cycle, and their opposing actions suggest that combination therapies of AM agents with β_3-AR agonists may offer additional opportunities to improve symptoms of patients with OAB.[97] *In vitro* studies on human detrusor muscle demonstrated that the combination of an AM agent with a β_3-AR agonist results in further relaxation of bladder smooth muscle beyond that of either agent alone.[98] Furthermore, a recent rat cystometry study that evaluated the effects of an AM agent and a β_3-AR agonist on bladder capacity in a bladder hyperactivity model revealed that the combination of these two drugs results in a greater increase in bladder capacity compared with either agent alone.[99] Although the earlier rat studies demonstrate potentially additive effects between AMs and β_3-AR agonists on bladder function in rats, it nevertheless remains to be demonstrated in humans whether these combinations will translate into improved efficacy and/or tolerability. Moreover, the balance of antagonism between M_2 and M_3 may also affect the outcome of combination therapy with β_3-AR agonists due to differences between the biochemical effects of the M_2 and M_3 receptors in the detrusor muscle and other tissues involved in modulation of the micturition cycle such as afferent neurons and the urothelium. Clearly much remains to be learned but the future appears to be promising for the use of combination therapies with β_3-AR agonists in patients who suffer from OAB.[100–104]

7.20.3 β_3-AR Agonists in Discovery and Development

7.20.3.1 Overview of β_3-AR Agonists in the Literature

After the first publication of the cloning and expression of the human β_3-AR in 1989[36] and the subsequent reports that β_3-AR agonists evoke lipolysis and thermogenesis in rodents,[37] research publications describing biology, pharmacology, and ligands for the β_3-AR increased dramatically (Fig. 7). Indeed, the rich pharmacology associated with β_3-ARs has produced a steady stream of publications that continues to this day. Early reports of potent and selective *rodent* β_3-AR agonists gave way to reports of potent

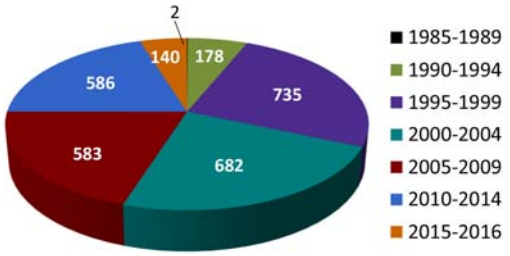

Fig. 7 A total of 2906 peer-reviewed scientific publications containing the text "beta-3 adrenergic" or "beta-3 adrenoceptor" were found between 1985 and 2016 using the Ex Libris Primo literature search tool.[105]

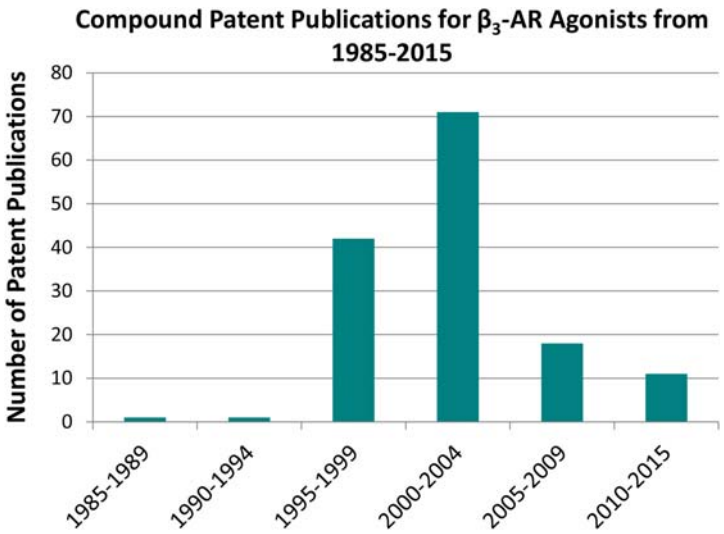

Fig. 8 A summary of β_3-AR modulator compound patent publications from 1985–2015 sorted by first publication date. A total of 144 patent publications were identified from a patent search using Thomson Reuters Cortellis software package from the search query terms "adrenoceptor" and "beta-3" to afford a comprehensive list of patent publications. Other synonymous search terms (eg, "adrenergic receptor" and "beta-3") yielded fewer results and were included in the former query. Three hundred seventy-one initial hits were further filtered by including product patents to afford 147 hits. Each patent publication was then evaluated, and three compound patents not covering β_3-AR receptor modulators were removed.

and selective *human* β_3-AR agonists. Scientists intent on optimization of these ligands developed newer and more sophisticated *in vitro* and *in vivo* models to evaluate novel β_3-AR-mediated pharmacology while also developing more advanced models to inform on selectivity over β_1- and β_2-AR-mediated pharmacology.

Patents describing ligands at the β_3-AR peaked in the decade between 1995 and 2005 (Fig. 8). Early patent publications described potent and selective ligands at the rodent β_3-AR, however, as the research field advanced agonists were later optimized for potency and selectivity at the human β_3-AR. General structural features for the majority of β_3-AR agonists are similar, with an ethanolamine moiety playing a central role as the minimum pharmacophore (Fig. 9).[46] The left-hand side (LHS) of β_3-AR agonists is frequently a minimally substituted aromatic ring designed to mimic catechols **1**–**3**. Typically, this is a phenyl or pyridyl ring attached to the alcohol-bearing carbon of the ethanolamine moiety either directly (X = nothing) or through a methanol ether linker (X = $-OCH_2-$). Aside from relatively simple substituents, the central ethanolamine region is largely conserved for all potent

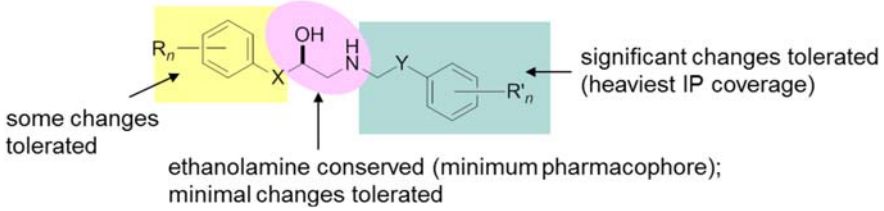

Fig. 9 General pharmacophore and SAR overview of β_3-AR agonists.

β_3-AR agonists, and elaborate changes to this region are not well tolerated. The right-hand side (RHS) of the ethanolamine tolerates the broadest structural variety, though there is usually an aromatic ring that is 2–3 linker atoms away from the secondary amine.

The first series of β_3-AR agonists contained a carboxylic acid moiety attached to the RHS aromatic ring through a short linker at R′ (Fig. 9). The acid was found to be important for both potency at β_3-AR and selectivity over β_1- and β_2-ARs; however, it also reduced permeability in these early ligands, and consequently, teams struggled to achieve oral bioavailability. As medicinal chemistry strategies matured, researchers succeeded at improving oral bioavailability either through a prodrug strategy (eg, esters) or through the use of acid bioisosteres. The large number of patent publications that describe β_3-AR agonists stemming from a single ethanolamine pharmacophore is testament to the creativity and perseverance of scientists working in the field. Several β_3-AR agonists progressed into human clinical trials, and the SAR and optimization strategies that were used to identify these clinical candidates are described in the following sections.

7.20.3.2 Potent Rat β_3-AR Agonists in Early Human Clinical Trials

The earliest generation of β_3-AR agonists was unsuccessful in the clinic as potential drugs for the treatment of obesity and/or diabetes.[106] Active metabolites of BRL 35155 (**4**) and BRL 26830 (**7**) were optimized as selective agonists using assays with rat β_1-, β_2-, and β_3-ARs, and these showed promising profiles in rodent models for obesity and diabetes (Fig. 8).[57,58,107] The reduced species homology between rat and human receptors, however, afforded either divergent potencies of these compounds between the rat and human β_3-ARs or modest selectivities over human β_1- and β_2-ARs or both.[39] Consequently, prodrugs such as **4** and **8** (Fig. 10) had little/no effect on thermogenesis or metabolism in humans,[108,109] although compound **8** was reported to increase insulin-simulated glucose uptake in humans in a glucose clamp study.[110] Additionally, compound **8** was able to induce thermogenesis and weight loss in calorie-restricted subjects; however, it was unclear whether these effects were due to activation of both β_2- and β_3-AR or to β_3-AR alone.[111] Moreover, adverse effects such as tremors and tachycardia were observed in humans with compound **8,** which were attributed to off-target effects at the β_1- or β_2-ARs.[101,112]

Modest effects in the clinic were also observed upon administration of CL 316,243 (**7**) including improvements on insulin action, increased fatty acid oxidation, and increased lipolysis of triglycerides to FFAs and glycerol.[113,114] No changes in energy expenditure or body weight were observed in humans and **7** did not induce tremors or cardiovascular changes.[113] This compound possesses poor oral bioavailability, however, and in humans, it only exhibits modest selectivity over the human β_2-AR.[39,51] Finally, ICI D7114 (**10**), a prodrug for its active metabolite compound **11**, and ZD 2079 both elicit profound metabolic effects and activation of BAT in preclinical species,[114,115] but neither compound demonstrated thermogenesis in humans (Fig. 10).[116,117]

7.20.3.3 Medicinal Chemistry of Human β_3-AR Agonists

By the mid-1990s, the failure of the first generation of potent rat β_3-AR agonists to achieve success in the clinic together with advances in cloning and expressing the human β_3-AR opened the door to a new era of agonists optimized for potency at human β_3-AR and selectivity over human β_1- and β_2-ARs. These medicinal chemistry advances coincided with additional advances in β_3-AR biology and the discovery of new potential therapeutic indications for these compounds.

In the meantime, the next generation of potent and selective human β_3-AR agonists was assessed as potential drugs to treat obesity/diabetes, but clinical data for these indications were again disappointing. Consequently, further efforts to pursue β_3-AR agonists for diabetes and/or obesity ended.[38,42] On the other hand, the second generation of potent and selective human β_3-AR agonists proved safer in humans than earlier agonists and were eventually repurposed for a variety of new potential indications including, but not limited to, OAB.

7.20.3.3.1 Discovery of BMS-196085 and related analogs

Medicinal chemistry reports from Bristol-Myers Squibb (BMS) focused on the progression of β_3-AR agonists for the treatment of obesity and/or diabetes. Replacement of the RHS phenyl ring of the standard β_3-AR agonist pharmacophore with heteroaromatics such as thiazole BMS-187257 (**13**; Fig. 11) was done in an effort to match or exceed the human β_3-AR potency and selectivity of **4**. Although **13** was similar to **4** in terms of potency, the selectivity over β_1- and β_2-ARs was not significantly improved. Moreover, the potent β_3-AR agonist activity of the thiazole heterocycle moiety did not transfer to the truncated series in which the phenoxy

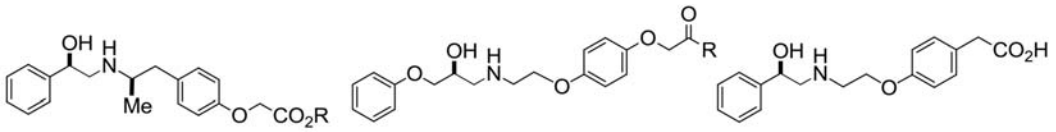

8 R = Me, BRL 26830 (racemate)
9 R = H, active drug

10 R = -NHCH$_2$CH$_2$OMe, ICI D7114
11 R = OH, active drug

12 ZD 2079

Fig. 10 Early representative rodent β_3-AR agonists evaluated in humans.

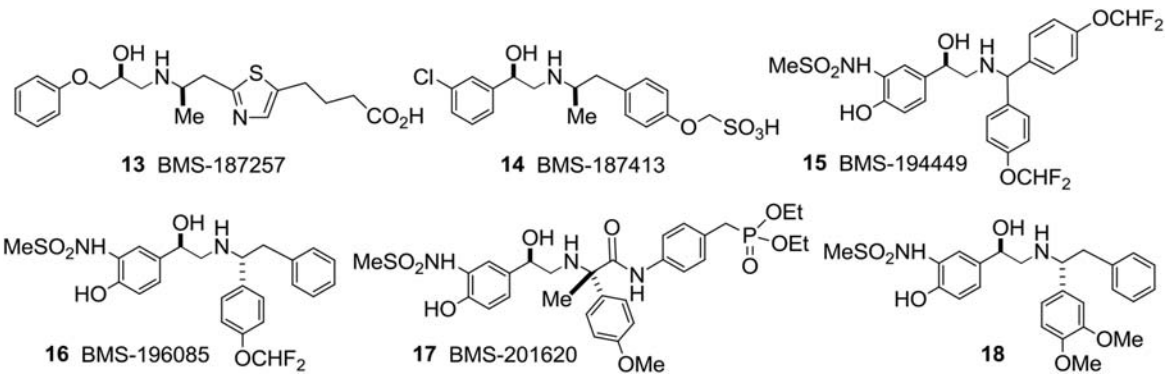

Fig. 11 Medicinal chemistry leading to the discovery of BMS-196085 (**16**) and beyond.

LHS was replaced by a directly connected phenyl group.[118] A new focus to modify the carboxylic acid group of **4** afforded sulfonic acid BMS-187413 (**14**), which was similar in potency and selectivity to **4** but with a distinct RHS acid moiety.[119]

A screening hit from the BMS sample collection identified a series of full β_3-AR agonists, which possessed 4-hydroxy-3-methanesulfonylanilides as bioisosteres for the LHS catechol moiety found in nonselective β-AR agonists. This series of agonists was also potent at the β_2-AR, however, and further optimization of the RHS yielded promising clinical candidates BMS-194449 (**15**)[120] and BMS-196085 (**16**)[121] as compounds with improved *in vitro* selectivity over β_1- and β_2-ARs. Both compounds exhibited poor oral bioavailability in preclinical species due to rapid glucuronidation of the alcohol moieties during first-pass metabolism. The *in vivo* selectivity of these compounds was evaluated in African green monkeys during dose–response studies where β_3-AR-mediated lipolysis (as measured by FFA increases) was compared with off-target effects mediated by β_1-AR (tachycardia) and β_2-AR (hypokalemia). Compounds **15** and **16** exhibited sufficient *in vivo* margins in monkeys to progress into development and subsequently the clinic where they were evaluated after i.v. dosing for their PD effects in humans. Despite promising *in vivo* selectivity in monkeys, **15** evoked lipolysis in a small group of healthy humans at a similar dose/exposure that caused QT prolongation, which was attributed to β_2-AR activation.[120] Compound **16**, on the other hand, evoked increases in FFAs in humans after an i.v. dose that did not effect any β_1- or β_2-AR-mediated side effects, thus supporting progression to multiple-day studies. Unfortunately, a 2-week continuous i.v. dose study with **16** in humans failed to produce any significant increases in metabolic rate up to doses that induced tachycardia, and consequently, further development of this compound was halted.[121]

Further improvements in selectivity over β_1- and β_2-ARs were realized with additional modification of the RHS region of this lead class resulting in the discovery of phosphate ester BMS-201620 (**17**).[122] Although its oral bioavailability in preclinical species was still poor, **17** was nevertheless progressed into humans based on its improved safety margin over off-target effects in the African green monkey models described in the preceding text. Once again, however, there was no difference between the onset of lipolysis resulting from i.v. administered **17** and QT prolongation in healthy volunteers, and so further clinical studies with **17** were terminated.[122] Although additional analogs with modified RHS regions (eg, compound **18**) were identified with improved overall PK profiles and similar *in vivo* margins for β_3-AR-mediated lipolysis compared with off-target effects mediated by β_1 and β_2, further progression of these compounds as potential clinical candidates ceased when compound **16** failed to demonstrate sustained increases in metabolic rate in humans after multiple days of dosing.[123]

7.20.3.3.2 Discovery of LY-377604 and related compounds

Lilly reported a series of highly selective human β_3-AR agonists more elaborated on the LHS region of the general β_3-AR pharmacophore. Urea LY-362884 (**19**) was reported as an early analog in this series that showed excellent *in vitro* β_3-AR potency and selectivity (Fig. 12). This compound also differentiated from earlier agonists by its reduced propensity to induce atrial tachycardia in rats, a PD effect believed to be mediated by a low-affinity state of the β_1-AR.[124,125] Although **19** increased energy expenditure in diet-induced obese rats, its poor oral bioavailability prompted additional optimization in this series. Further SAR demonstrated that excellent selectivity over rat atrial tachycardia was maintained with deletion of one of the urea H-bond donating groups to afford

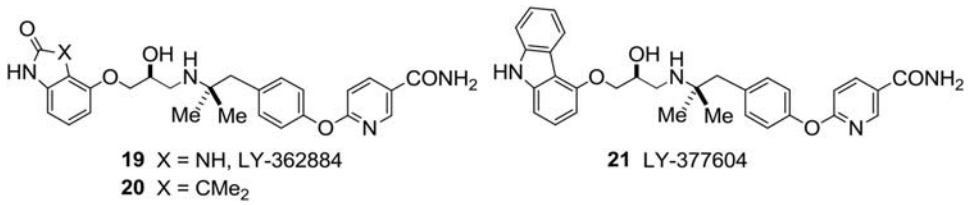

Fig. 12 A series of selective β_3-AR agonists more fully elaborated in the LHS region.

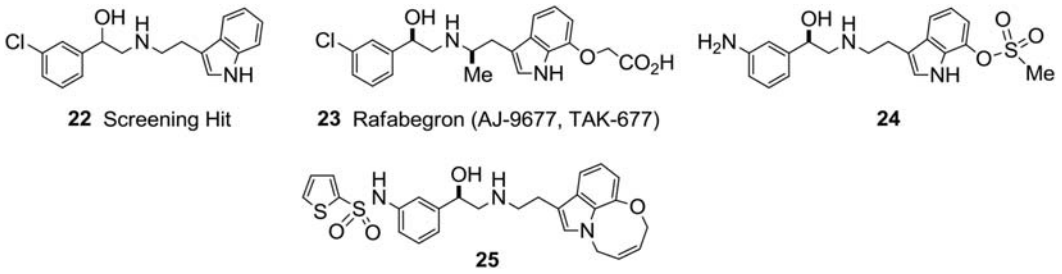

Fig. 13 Medicinal chemistry leading to the discovery of rafabegron (**23**) and beyond.

20, which also increased energy expenditure in rats. Only minimal improvement in rat oral bioavailability was observed with **20** (F = 10%),[126] however, and further elaboration of the LHS moiety afforded carboline LY-377604 (**21**), which was reported to have improved preclinical oral bioavailabilities.[127]

7.20.3.3.3 Discovery of rafabegron and related analogs

A screening hit (**22**) discovered at Dainippon in the early 1990s revealed that the phenyl ring typically present in the RHS portion of β_3-AR agonists can be replaced by an indole moiety (Fig. 13).[128,129] In *ex vivo* studies, **22** demonstrated an ability to inhibit rat colonic contraction while having minimal effect on the rat uterus and the guinea pig trachea indicating potential β_3-AR selective pharmacology.[128] Introduction of an acetic acid substituent to the indole ring and a chiral methyl group at the methylene carbon adjacent to the secondary amine together with resolution of the racemic alcohol resulted in significant improvements at both potency and selectivity for β_3-AR activation. The resulting optimized analog rafabegron (**23**, AJ-9677) demonstrated efficacy in diabetic and obese mouse and rat models.[129–131] Further SAR in this series was focused on (a) removing the chiral methyl group in **23** to facilitate synthesis and reduce the cost of API production and (b) replacement of the acid moiety to improve permeability. Compound **24**[132] was discovered to be a promising analog from this series, and further elaboration of the methyl sulfonate substituent on the RHS side to a cyclic derivative resulted in a series of non-acid-bearing β_3-AR agonists such as compound **25** with improved permeability and selectivity over β_1- and β_2-ARs.[133] Unfortunately, administration of rafabegron (**23**) in obese patients did not afford any significant changes in energy expenditure, body weight, fasting plasma glucose levels, FFA levels, or insulin levels leading to the discontinuation of this compound for further clinical studies.[134]

7.20.3.3.4 Discovery of an oxazole ring as an acid bioisostere

An early search for potent and selective human β_3-AR agonists at Pfizer led to the discovery of indole CP-331,679 (**26**), with a RHS carboxylic acid moiety that confers excellent selectivity (>100-fold) over β_1- and β_2-ARs (Fig. 14).[135] Not surprisingly, however, **26** as well as its ester prodrugs exhibited poor (<10%) oral bioavailability in rats. A renewed focus on improving physicochemical properties to increase oral absorption while maintaining potency and selectivity afforded sulfonylurea **27**. When dosed orally in rats at 30 mg/kg, compound **27** increases oxygen consumption (a surrogate for increased metabolic rate) at a similar magnitude as an intraperitoneal dose of 10 mg/kg, suggesting improved oral absorption of **27** relative to the previous compound **26**.[136] Importantly, compound **27** demonstrated that improved oral bioavailability may be achieved by deletion of the carboxylic acid moiety typically present in the RHS region. Further efforts to improve properties by reducing molecular weight and improving drug-like physicochemical properties resulted in identification of a series of heteroaryl acid bioisosteres in the RHS region culminating in the phenyloxazole **28**. Not only does **28** possess excellent β_3-AR potency and selectivity, but also it possesses high oral bioavailabilities in rats and dogs (F = 66 and 59%, respectively). Compound **28** demonstrated dose-dependent increases in oxygen consumption in rats with a minimal effect on heart rate increase, further proving its promise as an orally active β_3-AR agonist.[137]

7.20.3.3.5 Discovery of amibegron and other cyclic β_3-AR agonists

The crowded competitive environment around the key central pharmacophore of β_3-AR agonists has inspired innovative ways to maintain critical components of the pharmacophore while extending into new intellectual property (IP) space. Cyclization of the linker between the secondary amine and the RHS phenyl group afforded cyclohexane derivative GS-332 (**29**), which was

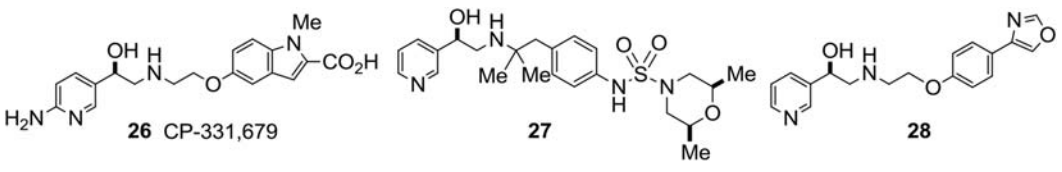

Fig. 14 Medicinal chemistry of β_3-AR agonists from Pfizer.

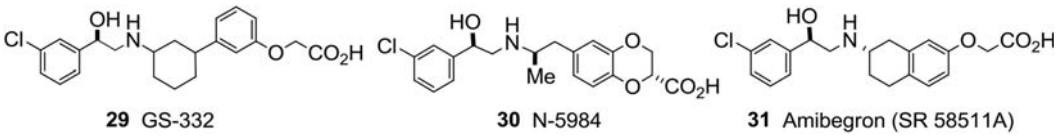

Fig. 15 Structure of novel cyclized pharmacophores and amibegron (**31**).

evaluated in a rat cystometry study where it evoked an increase in the bladder capacity relative to vehicle-treated rats (Fig. 15).[138] Chemists at Nisshin generated a novel cyclic RHS structure class by fusing a dioxane ring to the RHS phenyl moiety leading to the potent and selective β_3-AR agonist N-5984 (**30**).[139]

One of the earliest reported cyclic agonists to exhibit pharmacological differentiation from the first-generation rat β_3-AR agonists was Sanofi's amibegron (**31**) (Fig. 9). Amibegron possesses a novel phenylethanolaminotetraline (PEAT) RHS moiety that helps impart excellent β_3-AR selectivity. In a rat colon motility assay believed to be specific for β_3-AR pharmacology, amibegron inhibited motility in the rat colon without relaxing guinea pig trachea (a β_2-AR-mediated effect) or increasing atrial frequency (a β_1-AR-mediated effect).[140] Amibegron's potency at rat colon motility inhibition was similar to that of the nonselective β-AR agonist isoproterenol (**3**) but without the undesirable effects on trachea and atrial tissues that were attributed to a lack of selectivity over β_1- and β_2-AR agonism. Amibegron never progressed beyond early-phase clinical trials for the treatment of metabolic disorders,[38] however, as it was repurposed for the treatment of depression based on its antidepressant and antianxiolytic activities in rats together with reports that β_3-ARs are present in the brain.[141,142] More recently, however, research has appeared that suggests that the antidepressant activity of amibegron may be attributed to its blockade of serotonin reuptake at the serotonin receptors.[143,144] This compound has recently been shown to be in phase 3 clinical trials for the treatment of major depressive disorder.[38]

7.20.3.3.6 Discovery of solabegron and related analogs

Early research at SmithKline Beecham to identify potent human β_3-AR agonists focused on the introduction of various acidic moieties at the RHS side to improve selectivity over human β_1- and β_2-ARs. Phosphinic acid analog **32**, for example, was reported as a key discovery in this early SAR effort to dial out activity at the other β-AR subtypes (Fig. 16).[145] Parallel to this work, a team at Glaxo discovered an aniline linker between the secondary amine and the RHS phenyl ring that afforded potent human β_3-AR agonists with a chlorophenyl ring on the LHS side such as compound **33**. Improvements in selectivity over β_1- and β_2-ARs were achieved with the installment of a series of acid bioisosteres to afford selective β_3-AR agonists such as acylsulfonamide **34**.[146] To improve the dog pharmacokinetic (PK) profiles of analogs such as **34**, the team then screened a series of biaryl acid derivatives that were simplified by removal of the chiral methyl moiety to eventually identify the biaryl acid solabegron (**35**) as a promising analog with good overall half-lives and oral bioavailabilities in rats, dogs, and monkeys ($T_{1/2s}$ = 2.1, 3.3, and 4.5 h; F = 30, 43, and 46%, respectively).[147] Further optimization of this biaryl series led to the discovery of the structurally related analog **36,** which demonstrated even better potency and selectivity for the human β_3-AR with further improvements in its overall dog PK profile ($T_{1/2}$ = 6.1 h; F = 60%).

Solabegron was initially studied in db/db mice for its antidiabetic and thermogenesis properties,[148] but as attention shifted away from obesity/diabetes as indications for β_3-AR agonists, the compound was repositioned as a potential treatment for irritable bowel syndrome (IBS) and OAB. In addition to adipose tissue, cardiovascular tissue, and bladder smooth muscle, β_3-ARs are expressed in the human gastrointestinal tract.[149,150] In normal mice, rodent β_3-AR agonists have been shown to delay GI transit, while no effect was observed in β_3-AR-deficient mice.[151] In another study demonstrating the function of β_3-AR agonists in rodents, the selective rodent β_3-AR agonist **6** decreased fecal weight in a rat diarrhea model.[152] Finally, multiple teams have reported that β_3-AR agonists inhibit spontaneous human colon contractions in *ex vivo* studies using isolated human colon samples.[153–156] Solabegron was able to inhibit cholinergic contractions in isolated human colon samples; however, when it was tested in healthy human volunteers, there was no overall change in gastric, small bowel, or colonic transit after 7 days at 50 or 200 mg twice-daily doses.[157] In this study, solabegron was reported to be rapidly absorbed with a T_{max} that ranged from 1 to 3 h and a mean half-life ranging from 1.6 to 2.3 h.

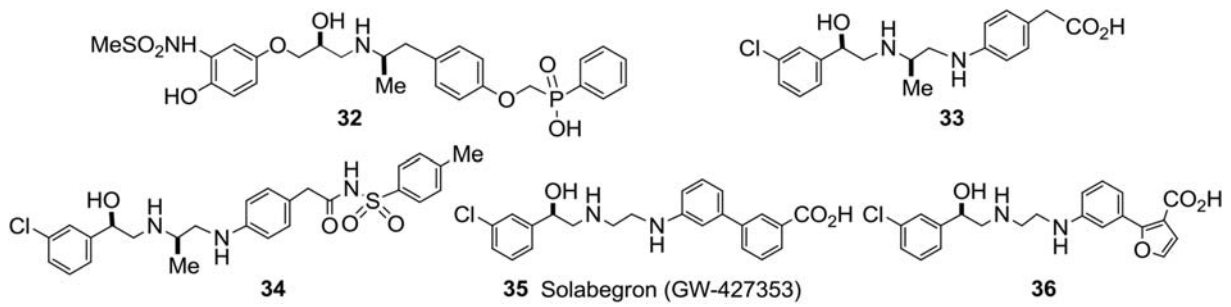

Fig. 16 Medicinal chemistry leading to the discovery of solabegron (**35**) and beyond.

Furthermore, the compound had no effect on bowel function during this study. Consequently, solabegron was not an effective treatment for IBS as it has no overall effect on gastrointestinal transit or bowel function.[157]

Solabegron was more successful as a treatment for OAB.[158] This compound demonstrated bladder smooth muscle relaxation in dog bladder strips as well as increased bladder capacity in a dog cystometry model.[159] Additionally, solabegron induced relaxation of precontracted isolated human bladder strips in an *ex vivo* study.[160] In a phase 2, double-blind placebo-controlled study in female OAB patients, solabegron reduced the number of incontinence episodes from baseline compared with placebo after 8 weeks of treatment at doses of 50 and 125 mg twice daily (BID).[161] Additionally, solabegron reduced the number of micturitions over 24 h from baseline compared with placebo at week 4 and week 8 as well as the number of urgency episodes over 24 h. A dose-dependent increase in voided volume in the same study suggests that solabegron also dose-dependently increases bladder capacity. With regard to tolerability, there was no difference between placebo group and drug treatment group in the incidence of dry mouth or constipation, two of the key tolerability issues that lead to discontinuation of AM therapies. On the other hand, a few patients receiving the 50 and 125 mg BID doses exhibited hypertension. Follow-up on cardiovascular parameters with 24 h blood pressure monitoring demonstrated no significant mean changes from baseline out to week 8 for ambulatory systolic or diastolic blood pressure, mean arterial pressure, or heart rate for each dose of solabegron tested.[161] Overall, the phase 2 study of solabegron in female OAB patients was promising; however, longer term phase 3 studies in a broader patient population would be needed to better inform on the potential of this drug to treat patients suffering from OAB.[158]

7.20.3.3.7 Discovery of ritobegron and related analogs

Early work from Kissei revealed that phenol derivatives such as ritodrine (**37**) possess potent β_2-AR and β_3-AR agonist activity (Fig. 17).[162] In an early report, they describe the use of a ferret detrusor muscle relaxation assay to help steer SAR toward potent β_3-AR agonists while maintaining high selectivity over β_1- and β_2-AR pharmacology using rat atria and rat uteri.[163] Further modifications of the LHS portion of this lead class afforded compounds that exhibited further improvements in β_3-AR agonism at the human receptor. The dimethylphenyl analog KUC 7322 (**39**) was selected for further development as its ethyl ester prodrug ritobegron (**38**) that improved oral exposures in rats by about an order of magnitude.[164] The active drug **39** is a potent and selective rat β_3-AR agonist and was shown to relax precontracted rat bladder muscle at a potency and efficacy comparable with rat β_3-AR agonists **3**, **4**, and **6**.[165] *In vivo*, the prodrug **38** dose-dependently decreases intravesicular pressure (IVP) in the rat bladder. In contrast to the nonselective β-AR agonist **3**, however, compound **39** showed much higher selectivity in rats for its effects on atrial rate and myometrial contraction, thus demonstrating improved selectivity with respect to *in vivo* PD effects.[165]

To demonstrate the effects of this drug in a primate, compounds **38** and **39** were evaluated in a series of cynomolgus monkey studies.[166] The acid **39** reduced resting tension in isolated cynomolgus bladder tissue at a potency and efficacy similar to **3** and **6**. In contrast to **3**, however, compound **39** was significantly more selective for its bladder effects compared with its effects on atrial rate (β_1-AR-mediated effect) and tracheal relaxation (β_2-AR-mediated effect). In anesthetized cynomolgus monkeys, intraduodenally administered **38** dose-dependently decreased intravesicular bladder pressure without having any effects on blood pressure or heart rate even at the highest dose tested (10 mg/kg). Moreover, the drug concentrations that induce bladder relaxation in the *in vitro* study correlated well with the efficacious plasma concentrations from the *in vivo* study, suggesting a potential *in vitro*/*in vivo* correlation that may help guide human PK targets. Ritobegron progressed into phase 3 clinical trials for the treatment of OAB; however, these trials were halted, and although the results have not been published, a press release from Kissei reported that the efficacy end points from this study were not achieved.[101]

7.20.3.3.8 Discovery of MK-0634, vibegron, and related analogs

A screening hit from Merck's sample collection (**40**) afforded a good starting point for a discovery program aimed at identifying selective human β_3-AR agonists (Fig. 18).[167] Instead of using animal tissue assays to identify selective human β_3-AR agonists, the cloned human β_3-AR *in vitro* assay was used to guide human β_3-AR agonist potency, and binding to β_1- and β_2-AR was used to guide selectivity over these subtypes.[167–169] The binding assay was critical because the active enantiomer of **40** showed potent binding to β_1- and β_2-ARs but very little functional agonist activity at these antitargets. A significant improvement in human β_3-AR selectivity was achieved by shortening the linker chain between the amine and the RHS phenyl group, removal of the chiral methyl substituent, and replacement of the methoxy substituent with a sulfonamide moiety such as **41**.[170] Further elaboration of the RHS bromide to a series of ureas culminated in the discovery of the potent human and rhesus β_3-AR agonist L-755,507 (**42**), which was more than 440-fold selective over binding to human β_1- and β_2-ARs.[170] When administered intravenously to rhesus monkeys, compound **42** increases lipolysis and metabolic rate dose-dependently, thus demonstrating β_3-AR-mediated PD effects

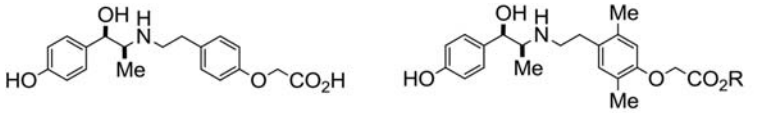

37 Ritodrine (KUL-7211)

38 R = Et, Ritobegron (KUC 7483)
39 R = H, KUC 7322 (active metabolite)

Fig. 17 Medicinal chemistry leading to the discovery of ritobegron (**38**).

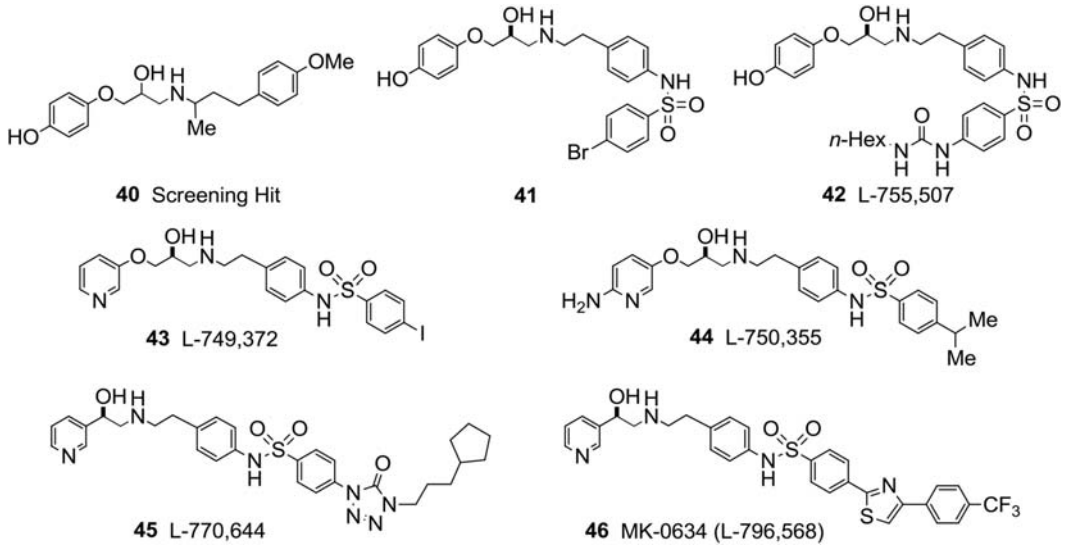

Fig. 18 Medicinal chemistry leading to the discovery of MK-0634 (**46**).

in a primate. Furthermore, only minimal increases in heart rate were observed, which further confirmed a high *in vivo* selectivity over β_1-AR.[171]

The promising PD effects of **42** in rhesus monkeys together with the poor oral PK profile of this compound in preclinical species prompted further investigation to improve the overall PK profile of this sulfonamide series. Further investigation in this series suggested that absorption could be achieved by replacement of the RHS urea, but oral bioavailability was still poor due to rapid glucuronidation of the LHS phenol moiety. Replacement of the phenol with either a pyridine ring or an aminopyridine ring helped address the first-pass metabolism liability, while replacement of the urea with more hydrophobic substituents such as iodine L-749,372 (**43**) and isopropyl L-750,355 (**44**) improved absorption. Although oral bioavailabilities for **43** and **44** were still somewhat low in rats (4% and 13%, respectively), they were significantly improved in dogs (41% and 47%, respectively). In the human β_3-AR *in vitro* assay, both of these compounds appeared to be partial agonists, although both demonstrated full lipolytic effects when administered to rhesus monkeys.[172] Further efforts to improve these compounds were focused on improving the overall PK properties while also improving *in vitro* selectivity over human β_1- and β_2-AR binding. Introduction of the arylethanolamine moiety instead of the aryloxy group on the LHS side[173] accompanied by further modification of the urea moiety of **42**[174,175] ultimately led to the discovery of L-770,664 (**45**), a potent and highly selective human β_3-AR agonist with moderate oral bioavailability in both rats and dogs (27% for both).[176] Compound **45** was investigated extensively in rhesus monkeys where in increased metabolic rate, lipolysis induces facial flushing and also tachycardia that was attributed to the vasodilation effects of β_3-AR agonism.[73,176]

To further improve the oral bioavailability of **45**, extensive investigation was performed to identify replacements of the aliphatic RHS "tail," which culminated in the discovery of MK-0634 (**46**). A wide range of fused heterocycles[177] and substituted biaryl groups[178–181] were tolerated in the RHS region; however, few demonstrated improved oral bioavailability or selectivity compared with **45**. A breakthrough was realized with the discovery and optimization of a thiazole benzenesulfonamide substituent that showed improvements in potency, selectivity, and oral bioavailability compared with previous analogs.[182–184] The compound with the best combination of potency, selectivity, and overall PK properties was the trifluoromethylphenyl-substituted benzene thiazole MK-0634 (**46**), which was selected for further *in vivo* evaluation.[183] Compound **46** evoked hyperglycerolemia (lipolysis) in dogs after oral dosing and dose-dependently in monkeys in sequential rising dose i.v. infusion studies. The ED_{50} for the expected β_3-AR-mediated lipolysis in monkeys (0.26 mg/kg) was substantially lower than the dose observed to modestly increase the heart rate with this compound ($ED_{15HR} = 10$ mg/kg).[183] Further development of compound **46** supported its advancement into human clinical trials. After a single-dose administration of **46** in obese men, this compound increased both metabolic rate and lipolysis as measured by increases in circulating plasma FFAs and glycerol.[185] Although the acute lipolysis and metabolic rate increases observed with **46** suggested β_3-AR target engagement was achieved in adipose tissue at the exposures studied, a 28-day study with **46** in obese men at matching drug exposures revealed that the lipolysis and metabolic rate increases were not sustained, and further study of this compound for obesity was discontinued.[70] Compound **46** was later repurposed for the treatment of OAB where it demonstrated reductions in the number of daily micturitions, total incontinence, urge incontinence, and strong urge after 8 weeks of dosing in OAB patients.[186] The efficacy of **46** from this study was comparable with similar reports using the AM agent Detrol LA at 12 weeks of treatment, but in contrast to Detrol LA, compound **46** showed a low rate of prevalence of dry mouth or constipation.[186,187] Unfortunately, further development of **46** for the treatment of OAB was stopped due to structure-based toxicity observed in preclinical safety studies. Moreover, compound **46** possessed additional structure-specific liabilities such as victim drug–drug interactions, phospholipidosis in preclinical species, and the formation of metabolites that circulate at high levels in preclinical species and

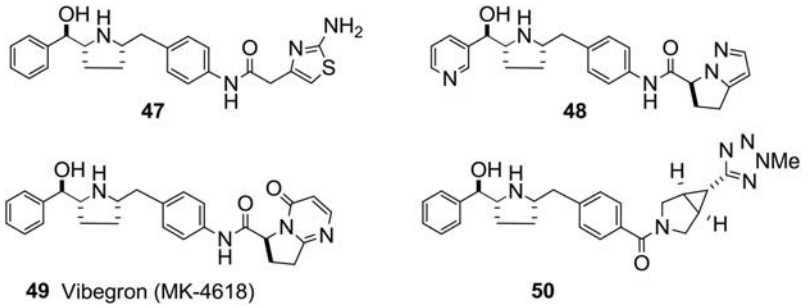

Fig. 19 Medicinal chemistry leading to the discovery of vibegron (**49**) and beyond.

humans.[186] Consequently, a new effort was initiated to identify a backup compound more suitable for long-term clinical development for the treatment of OAB.

One of the liabilities of **46** is related to oxidative metabolism that occurs around the secondary amine moiety and results in cleavage of the chain to form metabolites that accumulate in preclinical species and humans.[188,189] To reduce the risk of oxidative metabolism and the linker cleavage concern, a pyrrolidine ring was incorporated into the ethanolamine pharmacophore, thus introducing a second generation of β_3-AR agonists such as compound **47** (Fig. 19).[189] The aminothiazole **47** possessed poor oral bioavailability, however, which prompted evaluation of additional RHS groups. Some early SAR from a related anilide series revealed that the right balance between the LHS aromatic ring and the RHS anilide heterocycles could afford compounds with improved overall PK properties,[190] and application of these early discoveries to the pyrrolidine scaffold led to the discovery of compound **48**, which possessed modest to excellent oral bioavailabilities in rats, dogs, and monkeys (35%, 100%, and 11%, respectively) and excellent selectivity over β_1- and β_2-ARs.[191] Additionally, **48** decreases micturition pressure in a rat bladder hyperactivity model, thus confirming its PD effects in the tissue of interest. On the other hand, more extensive off-target screening demonstrated that **48** inhibited serotonin transport (SERT) and hERG, and the acetamide moiety underwent rapid hydrolysis in human plasma to afford the aniline. Although the resulting aniline was negative in an *in vitro* mutagenicity assay, this nevertheless suggested a risk for human-specific metabolites that would not be formed in preclinical species. Consequently, an improved overall profile was sought.

By changing the pyrazole of **48** to a pyrimidone and the LHS pyridine ring to a phenyl, the issues encountered with compounds **46**–**48** were solved. Vibegron (**49**) was selective over hERG, SERT, $\beta_{1/2}$-ARs, and a large panel of off-target assays. Additionally, the overall cross-species PK properties for **49** are excellent with oral bioavailabilities between 20 and 46% across three species and preclinical $T_{1/2s}$ ranging from 7 to 14 h. In contrast to **48**, compound **49** was stable in human plasma incubations, thus indicating a reduced risk for formation of human-specific metabolites.[186] Furthermore, the overall profile of **48** suggests a low risk for this compound to be a victim or a perpetrator of any drug–drug interactions. In rats, **49** dose-dependently decreased micturition pressure, increased functional bladder capacity, and increased lipolysis, thus demonstrating the effects of activation *in vivo*. Importantly, compound **49** demonstrated a reduced risk for phospholipidosis *in vitro*[192] as well as *in vivo*, and the overall preclinical safety profile of this compound supports long-duration phase 3 clinical trials. Vibegron (**49**) is currently in phase 3 clinical trials for the treatment of OAB.

More recently, the same team reported a benzamide series in the RHS region such as compound **50**.[193] This "reverse amide" series demonstrates that potent and selective β_3-AR agonists can be identified that lack the hydrogen-bond donor that is often present in this region. Although good oral bioavailabilities were achieved in rats and dogs (56% and 51%, respectively), the half-lives in these species were suboptimal, and further work in this series is needed to identify a compound with improved potential for QD dosing in humans.

7.20.3.3.9 Discovery of mirabegron and a series of biphenyl acid β_3-AR agonists

Inspired by the cyclic PEAT derivative **13**, a team at Fujisawa fused a cycloheptane ring to the RHS phenyl ring of the standard β_3-AR agonist pharmacophore to generate a new class of agonists. By hybridizing the fused seven-membered ring analog with early rat β_3-AR agonists **6** and **4**, novel analogs FR-165914 (**51**)[194] and FK-175 (**52**)[195] were generated (Fig. 20). Upon oral dosing in rodent models, FR-149175 demonstrates antiobesity and antidiabetic effects.[195,196] In obese Zucker fatty rats, compound **52** increased lipolysis and oxygen consumption (energy expenditure) dose-dependently in a rising single-dose study. Additionally, increased oxygen consumption was sustained during twice-daily oral dosing after two weeks of treatment with **52** in these rats demonstrating that the thermogenic pharmacodynamic effect is not attenuated upon multiple-day dosing.[195] In phase 1 clinical trials, compound **52** was well absorbed, but its human half-life and potency were insufficient to support once-daily dosing for OAB, and thus, the compound was discontinued.[197]

Further SAR in the PEAT class of β_3-AR agonists led to identification of tetralin **53** as a promising potent and highly selective β_3-AR agonist in this fused-ring class. In rats, dogs, and monkeys, **53** exhibited impressive oral bioavailabilities ($F > 60\%$) and half-lives (14, 14, and 8 h, respectively).[197] In a dog cystometry model that used carbachol to increase IVP in the bladder, i.v. administration of compound **53** resulted in a reduction of IVP similar to that observed for compound **52**, thus supporting its use as a potential therapeutic for the treatment of OAB. In a structurally related series of ring-opened derivatives, optimization around

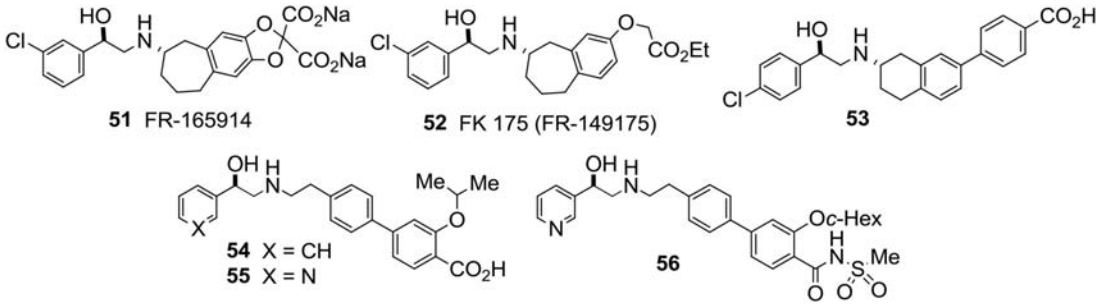

Fig. 20 Medicinal chemistry leading to the discovery of a series of biaryl acid-derived β_3-AR agonists and their acylsulfonamide bioisosteres.

the biaryl benzoic acid moiety led to identification of compound **54**, which exhibits excellent human β_3-AR potency and selectivity over human β_1- and β_2-ARs.[198] Further SAR on the LHS led to the identification of the related pyridine derivative **55**, which also possessed excellent potency and selectivity.[199] Both **54** and **55** showed good oral bioavailabilities in preclinical species ($F > 60\%$ and 25%, respectively), but the phenyl analog **54** had longer half-lives in rats, dogs, and monkeys ($T_{1/2} = 9.5$, 14.5, and 22 h, respectively) compared with pyridine **55** ($T_{1/2} = 3.5$, 9.9, and 2.2 h, respectively). Upon intraduodenal (i.d.) administration of these compounds into dogs, both **54** and **55** demonstrated excellent efficacy in the carbachol-induced IVP model, although the pyridine analogs generally outperformed the phenyl analogs.[198,199] The overall balance of potency, selectivity, and PK profile led the team to select compound **54** as a clinical candidate.[199]

In vitro metabolite identification studies with compounds such as **54** and **55** in hepatocytes revealed the presence of metabolites resulting from oxidative metabolism and cleavage at the carbon–nitrogen bond to the left of the secondary amine and acyl glucuronidation of the carboxylic acid moiety.[200] In order to reduce the risk of formation of potentially toxic metabolites, the team sought to replace the carboxylic acid moiety with acylsulfonamide acid bioisosteres such as compound **56**. Despite elimination of the carboxylic acid moiety, compound **56** maintains excellent β_3-AR potency and selectivity over β_1- and β_2-ARs. Moreover, compound **56** maintained good overall oral bioavailabilities in preclinical species ($F \geq 25\%$) but relatively short half-lives in rats, dogs, and monkeys ($T_{1/2} = 3.0$, 5.5, and 4.7 h, respectively).[200] In the dog carbachol cystometry model, a reduction in IVP was observed with a series of acylsulfonamides, although their IVP reduction was less than their acid counterparts likely due to the higher lipophilicity and therefore higher plasma protein binding of this series.

Inspired by the early sulfonamides such as **41** that were reported to be potent and selective human β_3-AR agonists,[167] a team of scientists at Astellas designed a series of RHS acetanilide-derived β_3-AR agonists to mimic the orientation of the two RHS aromatic groups of the sulfonamide series. 2-Pyridylacetanilide derivative **57** was identified as an early lead toward discovery of a selective β_3-AR agonist with roughly a 10-fold selectivity over β_1-AR agonism (**Fig. 21**).[201] A significant improvement in selectivity over β_1-AR was eventually achieved by introduction of a methyl group to the anilide nitrogen. Potency at β_3-AR was retained with removal of the phenol moiety and modification of the RHS to the benzyl-substituted imidazole **58**.[202] High selectivity over human β_1- and β_2-AR activation could also be achieved without methylation of the anilide by replacement of the imidazole ring with aminothiazoles such as compound **78**. Once-daily oral administration of compounds **58** and **59** for 4 days to diabetic KK mice resulted in a reduction in plasma glucose levels at doses of 30 and 3 mg/kg/day, respectively.[202,203] Next, replacement of the LHS phenoxymethylene group with a simple phenyl ring and removal of the phenyl ring from the aminothiazole afforded **60**, the most potent and selective β_3-AR agonist reported in the series.[204] Finally, removal of the methyl substituent on the thiazole ring afforded mirabegron (**61**, YM-178).[205,206]

Mirabegron is well characterized in various *in vitro* and *in vivo* models of bladder muscle relaxation and bladder dysfunction. *In vitro*, mirabegron induces concentration-dependent relaxation of isolated precontracted bladder strips from both normal rats and rats with partial bladder outflow obstruction (BOO).[206–208] Similarly, mirabegron relaxes precontracted bladder strips from healthy humans as well as patients with BOO due to benign prostate hyperplasia (BPH) both with and without detrusor overactivity (DO).[206,209] In anesthetized rats, the actions of mirabegron and oxybutynin, an AM agent, differ from each other. Both compounds

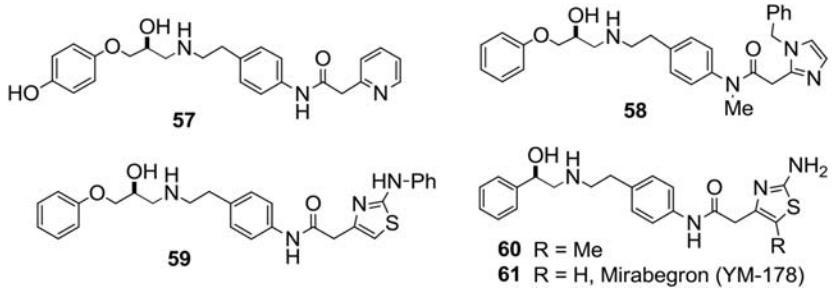

Fig. 21 Medicinal chemistry leading to the discovery of mirabegron (**61**).

are able to dose-dependently reduce the frequency of bladder contractions to improve urine storage, but only mirabegron was able to do so without affecting the contraction amplitude.[206] Additionally, mirabegron was able to reduce resting IVP in anesthetized rats, while AMs such as oxybutynin and tolterodine had no effect on IVP.[210] Finally, one recent cystometry study in rats demonstrated that mirabegron can inhibit mechanosensitive bladder afferent activity and that this is a potential mode of action for its effects on the reduction of bladder microcontractions.[211] In contrast, oxybutynin had no effect on the number bladder microcontractions in the same study.[211] Atherosclerosis can contribute to the symptoms of OAB when accompanied by bladder ischemia and subsequent DO. In a conscious rat model of chronic bladder ischemia, mirabegron increased bladder capacity, voiding volume, and micturition intervals, thus suggesting that the compound may have a protective effect on bladder function in patients with DO due to bladder ischemia.[212] In conscious cynomolgus monkeys, oral administration of mirabegron dose-dependently decreased micturition frequency and increased voiding volume per micturition.[213] Moreover, mirabegron also evoked concentration-dependent relaxation of precontracted monkey bladder strips.[213]

Results from preclinical safety assessment studies with mirabegron in rats and dogs have been summarized, and only effects consistent with β_3-AR activation in preclinical species were present near clinically relevant doses/exposures.[205] These effects typically include elevated heart rate in rats and dogs and a decrease in blood pressure in dogs consistent with the vasodilatory effects of β_3-AR agonists in this species.[69–72] At high exposure multiples, hepatotoxicity, neurotoxicity, cardiovascular toxicity, and reproductive effects were noted, although many of these effects were reversible and monitorable.[205] Mirabegron was neither genotoxic nor carcinogenic in the standard set of genotoxicity assays and from the 2-year rodent carcinogenicity studies, thus mitigating any concerns around the aniline substructure or the aminothiazole moiety.[205]

Mirabegron is formulated using an oral controlled absorption system (OCAS)[214] that serves to facilitate once-daily dosing in humans as well as to reduce the C_{max}. In humans, the oral bioavailability of mirabegron is about 24–53% and the terminal half-life from the extended-release formulation is around 50 h.[215] The compound is eliminated mostly as intact parent in both urine and feces, although metabolites were also detected in urine as well as in circulation. Circulating metabolites are inactive and possess shorter half-lives than parent; therefore, they all exhibit formation rate-limited kinetics. Major circulating metabolites are due to amide hydrolysis followed by glucuronidation followed by dealkylation around the secondary amine.[216] In renally impaired patients, mirabegron plasma concentrations are increased; therefore, a lower dose is recommended for this patient population.[217] Mirabegron is metabolized by both CYP3A and CYP2D6,[218] and it shows only a modest increase in drug levels in patients who are poor CYP2D6 metabolizers compared with patients who are extensive CYP2D6 metabolizers.[219] This compound is also a CYP2D6 inhibitor, and when co-dosed with drugs metabolized by CYP2D6, an increase in their systemic exposure was observed.[220] Consequently, care must be taken not to co-dose mirabegron with a drug metabolized by CYP2D6 that possesses a narrow therapeutic index.

The clinical safety of mirabegron has been reviewed extensively, and in general, the compound is safe and well tolerated at clinically relevant exposures.[205,221–223] An analysis of clinical data comparing patients treated with mirabegron with patients treated with AM agents revealed that mirabegron appears to be better tolerated with respect to gastrointestinal adverse events such as dry mouth, constipation, dyspepsia, and nausea.[222] The long history of cardiovascular effects associated with earlier, less selective β_3-AR agonists has led to careful evaluation of the cardiovascular effects of mirabegron in patients with OAB. At the clinically used dose of 50 mg QD, mirabegron causes small increases in blood pressure ($\leq$1 mm Hg) and pulse rate (1 bpm) compared with placebo.[223] Larger increases in pulse rate (5–6 bpm) were noted in the proof-of-concept study in OAB patients who were dosed with immediate-release mirabegron twice daily.[224] These small changes in pulse rate and/or blood pressure were not associated with any clinically significant increases in cardiovascular AEs. At therapeutic doses, mirabegron does not cause any increase in QTc or ventricular arrhythmia; however, at a supertherapeutic dose of 200 mg, a prolongation of the QTc interval was observed in women.[225] As a result of clinical trial exclusion criteria, mirabegron has not yet been studied in some high-risk populations such as patients with arrhythmia, uncontrolled hypertension, or heart failure.[223]

Multiple clinical trials have demonstrated the benefits of mirabegron in patients suffering from OAB syndrome, and the results of these studies have been summarized recently.[205,226,227] With regard to efficacy at treating symptoms of patients with OAB, mirabegron is as efficacious as most AMs including the market leader tolterodine ER. Compared with placebo, reductions in daily micturitions, voiding volume, daily episodes of urinary incontinence, and daily episodes of urge urinary incontinence were observed with daily treatment of mirabegron. Mirabegron also demonstrated improvement on subjective secondary end points compared with placebo as measured by quality-of-life questionnaires for patients with OAB. The overall tolerability profile of mirabegron is similar to placebo, whereas the rates of adverse effects are increased with AM agents relative to placebo. Although both 50 mg and 100 mg daily doses were studied in phase 3 clinical trials, it was determined that the higher dose does not offer any additional benefit to OAB patients, and thus, the current recommended dose is 50 mg for most patients and 25 mg for patients with severe renal insufficiencies or moderate hepatic failure. Importantly, mirabegron was efficacious in patients who discontinued AM therapy due to either lack of efficacy or poor tolerability.[228] In summary, mirabegron is the first-in-class β_3-AR agonist approved drug that is currently used for the treatment of patients who suffer from OAB. It is efficacious, safe, and well tolerated and is recommended as a treatment option for patients who either have discontinued AM therapy or are contraindicated for AM agents.

7.20.4 Summary

Valuable lessons that apply to the broader field of drug discovery can be gleaned from reviewing the history of β_3-AR agonists. For example, the disconnect between ligand SAR at rodent β_1-, β_2-, and β_3-ARs and the corresponding human receptors led to some early

clinical failures with β3-AR agonists due to either lack of efficacy, adverse effects, or both. Moreover, species differences in early ligand profiles made it difficult to discern whether the corresponding clinical failures were due to differences in β3-AR biology (ie, mechanism-based) or to the progression of suboptimal agonists into humans (ie, compound-based).[42,48] As greater biochemical and pharmacological rigor was applied to optimize potent and selective human β3-AR agonists, an improved understanding of both the preclinical and clinical pharmacology of selective β_3-AR agonists emerged.

After potency and selectivity were addressed, significant hurdles remained to identify safe and orally bioavailable β_3-AR agonists. The polar nature of the conserved ethanolamine pharmacophore limited passive permeability of early agonists, and this hurdle was overcome through the use of prodrugs, acid bioisosteres, and/or novel ways to present the acid moieties. Once oral bioavailability was achieved, however, there are reports of new safety challenges that emerged due to metabolites arising from the resulting compounds. Consequently, teams focused on removing the metabolic hot spots that may have contributed to safety concerns while also seeking to maintain acceptable oral bioavailability. Finally, more recent optimization efforts describe the importance of managing physicochemical properties to reduce toxicity risks.[229]

IP coverage around β_3-AR agonist chemical structures has largely focused around a single conserved ethanolamine pharmacophore derived from the receptors' endogenous ligands. As a result of this crowded competitive space, scientists working in the area were increasingly challenged to create novel structure classes through a variety of different strategies. For example, heteroatom incorporation into linkers or incorporation of heteroaromatic rings in the place of phenyls was frequently leveraged as a means to generate novel IP space. Likewise, innovative incorporation of saturated rings into the extended pharmacophore region often served as a launching point for novel IP while simultaneously improving selectivity of the resulting scaffolds. Finally, the need to improve oral bioavailability often led to the incorporation of SAR that also afforded novel IP space, thus underscoring the proverb that necessity is the mother of invention. Importantly, each successful new scaffold discovery required reoptimization of the remaining substituents to achieve adequate potency, selectivity, and physicochemical and ADMET properties for further development. Once optimized, the final clinical candidates possessed unique profiles with respect to advantages and liabilities, thus demonstrating that a common pharmacophore can ultimately yield optimized compounds with distinct profiles. Regardless of the impetus behind the discovery of these multiple novel scaffolds, it is a testimony to the creativity of the medicinal chemists working in this area that well over 100 patent publications have appeared around a single conserved pharmacophore.

The switch of therapeutic indication for β_3-AR agonists away from obesity and diabetes to OAB illustrates some of the opportunities and challenges that can be encountered when repurposing therapeutics. It is clear from early animal models used to characterize compounds that most organizations initiated β_3-AR agonist programs with the goal to develop a drug to treat either obesity or diabetes. As disappointing clinical data began to emerge, however, the search for new indications for these potent and selective β_3-AR agonists became apparent. Indeed, β_3-AR is expressed in multiple tissues, and agonists induce a broad range of measurable pharmacologies in preclinical species. Ultimately, the weight of evidence in favor of using β_3-AR agonists to treat symptoms of OAB gave way to reports of success in the clinic in OAB patients. Clearly, the availability of potent and selective β_3-AR agonists accelerated investigations into the new indication by facilitating the acquisition of supportive preclinical data in OAB animal models. Nevertheless, some of the challenges encountered in repurposing these agonists as new animal models were incorporated to guide optimization efforts.[96] Care must be exercised in bridging pharmacodynamic data from different tissues, however, as the effects of β_3-AR agonists in the bladder may not reflect their effects in adipose tissue, and translational PK/PD strategies needed to be further developed.[230,231] Evidence continues to accumulate for the use of β_3-AR agonists to treat a variety of additional disorders[38] such as heart failure[62–67] and preterm labor,[232–234] and some of the lessons learned from the transition between obesity and OAB may be applied for these new efforts.

β_3-AR agonists are emerging as one of the most promising new therapeutic options for the treatment of OAB.[235,236] A comparative cross analysis of published OAB efficacy and safety data comparing mirabegron data with data from six different AM agents revealed that the β_3-AR agonist exhibited similar efficacy but with an improved tolerability profile compared with the AM agents, especially with respect to dry mouth.[237] Additionally, a recent evaluation of patient and physician preferences for oral OAB medications revealed a patient preference for drugs exhibiting a profile that more closely resembles β_3-AR agonists than AM agents.[238] Further clinical comparisons are needed, however, to better inform on the risks and benefits of these two classes of medications. One promising direction for the future of OAB pharmacotherapy is the use of combinations of existing AM agents with β_3-AR agonists.[91–93,239] The two mechanisms may complement each other and offer even better options for patients who suffer from OAB.

In conclusion, research on β_3-AR agonists has provided not only a promising new therapeutic option for the treatment of OAB but also a valuable insight into the broader field of drug discovery. Early challenges to characterize the biological profile of β_3-AR agonists were solved but new challenges to optimize chemical matter arose. As the chemistry challenges were solved, focus shifted once again back to the biology of β_3-AR agonists and the search for an appropriate therapeutic indication. Ultimately, the successful discovery of the application of β_3-AR agonist to treat OAB is a testimony to the perseverance and innovation of the hundreds of scientists who have worked in this field throughout the past 27 years.

References

1. Haab, F. Chapter 1: The Conditions of Neurogenic Detrusor Overactivity and Overactive Bladder. *Neurourol. Urodyn.* **2014,** *33,* S2–S5.
2. Irwin, D. E.; Kopp, Z. S.; Agatep, B.; Milsom, I.; Abrams, P. Worldwide Prevalence Estimates of Lower Urinary Tract Symptoms, Overactive Bladder, Urinary Incontinence and Bladder Outlet Obstruction. *Br. J. Urol.* **2011,** *108* (7), 1132–1138.

3. Irwin, D. E.; Milsom, I.; Hunskaar, S.; Reilly, K.; Kopp, Z.; Herschorn, S.; Coyne, K.; Kelleher, C.; Hampel, C.; Artibani, W.; Abrams, P. Population-Based Survey of Urinary Incontinence, Overactive Bladder, and Other Lower Urinary Tract Symptoms in Five Countries: Results of the EPIC Study. *Eur. Urol.* **2006,** *50,* 1306–1314.
4. Omukwugha, E.; Zuckerman, I. H.; McNally, D.; Coyne, K. S.; Vats, V.; Mullins, C. D. The Total Economic Burden of Overactive Bladder in the United States: A Disease-Specific Approach. *Am. J. Manag. Care* **2009,** *15,* S90–S97.
5. Stewart, W. F.; Van Rooyen, J. B.; Cundiff, G. W.; Abrams, P.; Herzog, A. R.; Corey, R.; Hunt, T. L.; Wein, A. J. Prevalence and Burden of Overactive Bladder in the United States. *World J. Urol.* **2003,** *20,* 327–336.
6. Natalin, R.; Lorenzetti, F.; Dambros, M. Management of OAB in Those Over Age 65. *Curr. Urol. Rep.* **2013,** *14,* 379–385.
7. Abrams, P.; Cardozo, L.; Fall, M.; Griffiths, D.; Rosier, P.; Ulmsten, U.; Kerrebroeck, P. V.; Victor, A.; Wein, A. The Standardisation of Terminology of Lower Urinary Tract Function: Report from the Standardisation Sub-Committee of the International Continence Society. *Urology* **2003,** *61,* 37–49.
8. Schneider, T.; Marschall-Kehrel, D.; Hanisch, J. U.; Michel, M. C. Do Gender, Age, or Lifestyle Factors Affect Responses to Antimuscarinic Treatment in Overactive Bladder Patients? *Int. J. Clin. Pract.* **2010,** *64,* 1287–1293.
9. Hirayama, A.; Torimoto, K.; Mastusita, C.; Okamoto, N.; Morikawa, M.; Tanaka, N.; Fujimoto, K.; Yoshida, K.; Hirao, Y.; Kurumatani, N. Risk Factors for New-Onset Overactive Bladder in Older Subjects: Results of the Fujiwara-Kyo Study. *Urology* **2012,** *80,* 71–76.
10. Lowalekar, S. K.; Cristofaro, V.; Radisavljevic, Z. M.; Yalla, S. V.; Sullivan, M. P. Loss of Bladder Smooth Muscle Caveolae in the Aging Bladder. *Neurourol. Urodyn.* **2012,** *31,* 586–592.
11. Smith, P. P. Aging and the Underactive Detrusor: A Failure of Activity of Activation? *Neurourol. Urodyn.* **2010,** *29,* 408–412.
12. Andersson, K.-E.; Arner, A. Urinary Bladder Contraction and Relaxation: Physiology and Pathophysiology. *Physiol. Rev.* **2004,** *84,* 935–986.
13. Michel, M.; Barendrecht, M. M. Physiological and Pathological Regulation of the Autonomic Control of Urinary Bladder Contractility. *Pharmacol. Ther.* **2008,** *117,* 297–312.
14. Brown, J. S.; McGhan, W. F.; Chokroverty, S. Comorbidities Associated With Overactive Bladder. *Am. J. Manag. Care* **2000,** *6,* S574–S579.
15. Wagner, T. H.; Hu, T. W.; Bentkover, J.; LeBlanc, K.; Stewart, W.; Corey, R.; et al. Health-Related Consequences of Overactive Bladder. *Am. J. Manag. Care* **2002,** *8,* S598–S607.
16. Breyer, B. N.; Schindel, A. W.; Erickson, B. A.; Blaschko, S. D.; Steers, W. D.; Rosen, R. C. The Association of Depression, Anxiety, and Nocturia: A Systematic Review. *J. Urol.* **2013,** *190,* 953–957.
17. Nakagawa, H.; Niu, K.; Hozawa, A.; Ikeda, Y.; Kaiho, Y.; Ohmori-Matsuda, K.; Nakaya, N.; Kuriyama, S.; Ebihara, S.; Nagatomi, R.; Tsuji, I.; Arai, Y. Impact of Nocturia on Bone Fracture and Mortality in Older Individuals: A Japanese Longitudinal Cohort Study. *J. Urol.* **2010,** *184,* 1413–1418.
18. Keheller, C. J.; Cardozo, L. D.; Khullar, V.; Salvatore, S. A New Questionairre to Assess the Quality of Life of Urinary Incontinent Women. *Br. J. Obstet. Gynaecol.* **1997,** *104,* 1374–1379.
19. Irwin, D. E.; Mungapen, L.; Milsom, I.; Kipp, Z.; Reeves, P.; Kelleher, C. The Economic Impact of Overactive Bladder Syndrome in Six Western Countries. *BJU Int.* **2009,** *103,* 202–209.
20. Hu, T. W.; Wagner, T. H.; Bentkover, J. D.; LeBlanc, K.; Piancentini, A.; Stewart, W. F.; Corey, R.; Zhou, S. Z.; Hunt, T. L. Estimated Economic Costs of Overactive Bladder in the United States. *Urology* **2003,** *61,* 1123–1128.
21. Abrams, P.; Kelleher, C. J.; Kerr, L. A.; Rogers, R. G. Overactive Bladder Significantly Affects Quality of Life. *Am. J. Manag. Care* **2000,** *6,* S580–S590.
22. Helfand, B. T.; Evans, R. M.; McVary, K. T. A Comparison of the Frequencies of Medical Therapies for Overactive Bladder in Men and Women: Analysis of More Than 7.2 Million Aging Patients. *Eur. Urol.* **2010,** *57,* 586–591.
23. Ouslander, J. G. Management of Overactive Bladder. *N. Eng. J. Med.* **2004,** *350,* 786–799.
24. Gormley, E. A.; Lightner, D. J.; Burgio, K. L.; Chai, T. C.; Clemens, J. Q.; Culkin, D. J.; Das, A. K.; Foster, H. E.; Scarpero, H. M.; Tessier, C. D.; Vasavada, S. P. Diagnosis and Treatment of Overactive Bladder (Non-Neurogenic) in Adults: AUA/SUFU Guideline. *J. Urol.* **2012,** *188,* 2455–2463.
25. Robinson, D.; Cardozo, L. Antimuscarinic Drugs to Treat Overactive Bladder. *Br. Med. J.* **2012,** *344,* e2130.
26. Smith, A. L.; Wein, A. J. Recent Advances in the Development of Antimuscarinic Agents for Overactive Bladder. *Trends Pharmacol. Sci.* **2010,** *31,* 470–475.
27. Chapple, C. R.; Khullar, V.; Gabriel, Z.; Muston, D.; Bitoun, C. E.; Weinstein, D. The Effects of Antimuscarinic Treatments in Overactive Bladder: An Update of a Systematic Review and Meta-Analysis. *Eur. Urol.* **2008,** *54,* 543–562.
28. Abrams, P.; Andersson, K. E. Muscarinic Receptor Antagonists for Overactive Bladder. *BJU Int.* **2007,** *100,* 987–1006.
29. Chancellor, M.; Boone, T. Anticholinergics for Overactive Bladder: Central Nervous System Effects. *CNS Neurosci. Ther.* **2012,** *18,* 167–174.
30. Dmochowski, R. R. Improving the Tolerability of Anticholinergic Agents in the Treatment of Overactive Bladder. *Drug Saf.* **2005,** *28,* 583–600.
31. Chancellor, M. B.; Migliaccio-Walle, K.; Bramley, T. J.; Chaudhari, S. L.; Corbell, C.; Globe, D. Long-Term Patterns of Use and Treatment Failure with Anticholinergic Agents for Overactive Bladder. *Clin. Ther.* **2013,** *35,* 1744–1751.
32. Sexton, C. C.; Notte, S. M.; Maroulis, C.; Dmochowski, R. R.; Cardozo, L.; Subramanian, D.; Coyne, K. S. Persistence and Adherence in the Treatment of Overactive Bladder Syndrome with Anticholinergic Therapy: A Systematic Review of the Literature. *Int. J. Clin. Pract.* **2011,** *65,* 567–585.
33. Hieble, J. P. Subclassification and Nomenclature of α- and β-Adrenoceptors. *Curr. Top. Med. Chem.* **2007,** *7,* 129–134.
34. Bylund, D. B.; Eikenberg, D. C.; Hieble, J. P.; Langer, S. Z.; Lefkowitz, R. J.; Minneman, K. P.; Molinoff, P. B.; Ruffolo, R. R.; Trendelenburg, U. International Union of Pharmacology Nomenclature of Adrenoceptors. *Pharmacol. Rev.* **1994,** *46,* 121–136.
35. Ahlquist, R. P. A Study of the Adrenotropic Receptors. *Am. J. Physiol.* **1948,** *153,* 586–600.
36. Emorine, L. J.; Marullo, S.; Briend-Sutren, M. M.; Patey, G.; Tata, K.; Delavier-Klutchko, C.; Strosberg, A. D. Molecular Characterization of the Human β_3-Adrenergic Receptor. *Science* **1989,** *245,* 1118–1121.
37. Arch, J. R. S.; Kaumann, A. J. β_3 and Atypical β_3-Adrenoceptors. *Med. Res. Rev.* **1993,** *13* (6), 663–729.
38. Ursino, M. G.; Vasina, V.; Raschi, E. The β_3-Adrenoceptor as a Therapeutic Target: Current Perspectives. *Pharmacol. Res.* **2009,** *59,* 221–234.
39. Cernecka, H.; Sand, C.; Michel, M. C. The Odd Sibling: Features of β_3-Adrenoceptor Pharmacology. *Br. J. Pharmacol.* **2010,** *160,* 1048–1061.
40. Masuo, K. Adrenoceptor Polymorphisms in Hypertension and Diabetes With Obesity—Update in 2013. *Curr. Hypertens. Rev.* **2013,** *9* (4), 246–256.
41. Masuo, K.; Lambert, G. W. Relationships of Adrenoceptor Polymorphisms With Obesity. *J. Obes.* **2011,** *2011,* 1–10. Article ID 609485.
42. Arch, J. R. S. Challenges in β_3-Adrenoceptor Agonist Drug Development. *Ther. Adv. Endocrinol. Metab.* **2011,** *2* (2), 59–64.
43. Arch, J. R. S.; Ainsworth, A. T.; Cawthorne, M. A.; Piercy, V.; Sennitt, M. V.; Thody, V. E.; Wilson, C.; Wilson, S. A. Atypical β-Adrenoceptor on Brown Adipocytes as Target for Anti-Obesity Drugs. *Nature* **1984,** *309,* 163–165.
44. Staehelin, M.; Simons, P.; Jaeggi, K.; Wigger, N. CGP-12177: A Hydrophilic Beta-Adrenergic Receptor Radioligand Reveals High Affinity Binding of Agonists to Intact Cells. *J. Biol. Chem.* **1983,** *258,* 3496–3502.
45. Dolan, J. A.; Muenkel, H. A.; Burns, M. G.; Pellegrino, S. M.; Fraser, C. M.; Pietri, F.; Strosberg, A. D.; Largis, E. E.; Dutia, M. D.; Bloom, J. D.; Bass, A. S.; Tankella, T. K.; Cobuzzi, A.; Lai, F. M.; Claus, T. H. Beta-3 Adrenoceptor Selectivity of the Dioxolane Dicarboxylate Phenethanolamines. *J. Pharmacol. Exp. Ther.* **1994,** *269,* 1000–1006.
46. Perrone, M. G.; Scilimati, A. β_3-Adrenoceptor Ligand Development History Through Patent Review. *Expert Opin. Ther. Pat.* **2011,** *21* (4), 505–536.
47. Strosberg, A. D. Structure and Function of the β_3-Adrenergic Receptor. *Annu. Rev. Pharmacol. Toxicol.* **1997,** *37,* 421–450.
48. Michel, M. C.; Ochodnicky, P.; Summers, R. J. Tissue Functions Mediated by β_3-Adrenoceptors—Findings and Challenges. *Naunyn Schmiedebergs Arch. Pharmacol.* **2010,** *382,* 103–108.
49. Soeder, K. J.; Snedden, S. K.; Cao, W.; La Rocca, G. J.; Daniel, K. W.; Luttrell, L. M.; Collins, S. The β_3-Adrenergic Receptor Activates Mitogen-Activated Protein Kinase in Adipocytes Through a Gi-Dependent Mechanism. *J. Biol. Chem.* **1999,** *274,* 12017–12022.

50. Cao, W.; Luttrell, L. M.; Medvedev, A. V.; Pierce, K. L.; Daniel, K. W.; Dixon, T. M.; Lefkowitz, R. J.; Collins, S. Direct Binding of Activated c-Src to the β_3-Adrenergic Receptor is Required for MAP Kinase Activation. *J. Biol. Chem.* **2000,** *275,* 38131–38134.
51. Weyer, C.; Gautier, J. F.; Danforth, E. Development of Beta3-Adrenoceptor Agonists for the Treatment of Obesity and Diabetes—An Update. *Diabetes Metab.* **1999,** *25,* 11–21.
52. Collins, S.; Cao, W.; Robidoux, J. Learning New Tricks From Old Dogs: β-Adrenergic Receptors Teach New Lessons on Firing Up Adipose Tissue Metabolism. *Mol. Endocrinol.* **2004,** *18* (9), 2123–2131.
53. Arch, J. R. S. The Discovery of Drugs for Obesity, the Metabolic Effects of Leptin and Variable Receptor Pharmacology: Perspectives From β_3-Adrenoceptor Agonists. *Naunyn Schmiedebergs Arch. Pharmacol.* **2008,** *378,* 225–240.
54. Sammons, M. F.; Price, D. A. Modulation of Adipose Tissue Thermogenesis as a Method for Increasing Energy Expenditure. *Bioorg. Med. Chem. Lett.* **2014,** *24,* 425–429.
55. Weber, A. E. β_3-Adrenergic Receptor Agonists for the Treatment of Obesity. *Annu. Rep. Med. Chem.* **1998,** *33,* 193–202.
56. Lee, Y.-H.; Mottillo, E. P.; Granneman, J. G. Adipose Tissue Plasticity from WAT to BAT and in Between. *Biochim. Biophys. Acta* **2014,** *1842,* 358–369.
57. Cawthorne, M. A.; Sennitt, M. V.; Arch, J. R.; Smith, S. A. BRL 35135, A Potent and Selective Atypical Beta-Adrenoceptor Agonist. *Am. J. Clin. Nutr.* **1992,** *55,* 252S–257S.
58. Liu, Y. L.; Cawthorne, M. A.; Stock, M. J. Biphasic Effects of the Beta-Adrenoceptor agonist, BRL 37344, on Glucose Utilization in Rat Isolated Skeletal Muscle. *Br. J. Pharmacol.* **1996,** *117,* 1355–1361.
59. de Souza, C. J.; Hirshman, M. F.; Horton, E. S. CL-316,243, A Beta3-Specific Adrenoceptor Agonist, Enhances Insulin-Stimulated Glucose Disposal in Nonobese Rats. *Diabetes* **1997,** *46,* 1257–1263.
60. Yoshida, T.; Sakane, N.; Wakabayashi, Y.; Umekawa, T.; Kondo, M. Anti-obesity and Anti-diabetic Effects of CL 316,243, A Highly Specific Beta 3-Adrenoceptor Agonist, in Yellow KK Mice. *Life Sci.* **1994,** *54,* 491–498.
61. Moniotte, S.; Kobzik, L.; Feron, O.; Trochu, J. N.; Gauthier, C.; Balligand, J. L. Upregulation of Beta3-Adrenoceptors and Altered Contractile Response to Inotropic Amines in Human Failing Myocardium. *Circulation* **2001,** *59,* 135–163.
62. Rozec, B. Gauthier, β_3-Adrenoceptors in the Cardiovascular System: Putative Roles in Human Pathologies. *Pharmacol. Ther.* **2006,** *111,* 652–673.
63. Dessy, C.; Balligand, J.-L. Beta$_3$-Adrenergic Receptors in Cardiac and Vascular Tissues: Emerging Concepts and Therapeutic Perspectives. *Adv. Pharmacol.* **2010,** *59,* 135–163.
64. Bhadada, S. V.; Patel, B. M.; Mehta, A. A.; Goyal, R. K. β_3 Receptors: Role in Cardiometabolic Disorders. *Ther. Adv. Endocrinol. Metab.* **2011,** *2* (2), 65–79.
65. Michel, M. C.; Harding, S. E.; Bond, R. A. Are there Functional β_3-Adrenoceptors in the Human Heart? *Br. J. Pharmacol.* **2011,** *162,* 817–822.
66. Gauthier, C.; Rozec, B.; Manoury, B.; Balligand, J.-L. Beta-3 Adrenoceptors as New Therapeutic Targets for Cardiovascular Pathologies. *Curr. Heart Fail. Rep.* **2011,** *8,* 184–192.
67. Balligand, J.-L. Beta3-Adrenoreceptors in Cardiovascular Disease: New Roles for an "Old" Receptor. *Curr. Drug Deliv.* **2013,** *10,* 64–66.
68. Mohrer, D. K.; Chruscinski, A.; Schauble, E. H.; Bernstein, D.; Kobilka, B. K. Cardiovascular and Metabolic Alterations in Mice Lacking Both β_1- and β_2-Adrenergic Receptors. *J. Biol. Chem.* **1999,** *274,* 16701–16708.
69. Shen, Y.-T.; Cervoni, P.; Claus, T.; Vatner, S. F. Differences in β_3-Adrenergic Receptor Cardiovascular Regulation in Conscious Primates, Rats and Dogs. *J. Pharmacol. Exp. Ther.* **1996,** *278,* 1435–1443.
70. Shen, Y.-T.; Zhang, H.; Vatner, S. F. Peripheral Vascular Effects of Beta-3 Adrenergic Receptor Stimulation in Conscious Dogs. *J. Pharmacol. Exp. Ther.* **1994,** *268,* 466–473.
71. Tavernier, G.; Galitzky, J.; Bousquet-Melou, A.; Montastruc, J. L.; Berlan, M. The Positive Chronotrophic Effect Induced by BRL 37344 and CGP 12177, Two *Beta*-3 Adrenergic Agonists, Does Note Involve Cardiac *Beta* Adrenoceptors but Baroreflex Mechanisms. *J. Pharmacol. Exp. Ther.* **1992,** *263,* 1083–1090.
72. Berlan, M.; Galitzky, J.; Bousquet-Melou, A.; Lafontan, M.; Montastruc, J. L. Beta-3 Adrenoceptor-Mediated Increase in Cutaneous Blood Flow in the Dog. *J. Pharmacol. Exp. Ther.* **1994,** *268,* 1444–1451.
73. Hom, G. J.; Forrest, M. J.; Bach, T. J.; Brady, E.; Candelore, M. R.; Cascieri, M. A.; Fletcher, D. J.; Fisher, M. H.; Iliff, S. A.; Mathvink, R.; Metzger, J.; Pecore, V.; Saperstein, R.; Shih, T.; Weber, A. E.; Wyvratt, M.; Zafian, P.; Macintyre, D. E. β_3-Adrenoceptor Agonist-Induced Increases in Lipolysis, Metabolic Rate, Facial Flushing, and Reflex Tachycardia in Anesthetized Rhesus Monkeys. *J. Pharmacol. Exp. Ther.* **2001,** *297,* 299–307.
74. Rosa, G. M.; Ferrero, S.; Nitti, V. W.; Wagg, A.; Saleem, T.; Chapple, C. R. Cardiovascular Safety of β_3-Adrenoceptor Agonists for the Treatment of Patients With Overactive Bladder Symptoms. *Eur. Urol.* **2016,** *69,* 311–323.
75. Baker, J. G. The Selectivity of β-adrenoceptor Agonists at the Human β_1, β_2, and β_3 Adrenoceptors. *Br. J. Pharmacol.* **2010,** *160,* 1048–1061.
76. Larsen, T. M.; Toubro, S.; van Baak, M. A.; Gottesdiener, K. M.; Larson, P.; Saris, W. H. M.; Astrup, A. Effects of a 28-d Treatment With L-796568, A Novel β_3-Adrenergic Receptor Agonist, On Energy Expenditure and Body Composition in Obese Men. *Am. J. Clin. Nutr.* **2002,** *76,* 780–788.
77. Andersson, K.-E. Pharmacology of the Lower Urinary Tract Smooth Muscles and Penile Erectile Tissues. *Pharmacol. Rev.* **1993,** *45,* 253–308.
78. Yamazaki, Y.; Takeda, H.; Akahane, M.; Igawa, Y.; Nishizawa, O.; Ajisawa, Y. Species Differences in the Distribution of β-Adrenoceptor Subtypes in Bladder Smooth Muscle. *Br. J. Pharmacol.* **1998,** *124,* 593–599.
79. Igawa, Y.; Yamazaki, Y.; Takeda, H.; Akahane, M.; Ajisawa, Y.; Yoneyama, T.; Nishizawa, O. Possible β_3-Adrenoceptor-Mediated Relaxation of the Human Detrusor. *Acta Physiol. Scand.* **1998,** *164,* 117–118.
80. Seguchi, H.; Nishimura, J.; Zhou, Y.; Niiro, N.; Kumazawa, J.; Kanaide, H. Expression of β_3-Adrenoceptors in Rat Detrusor Muscle. *J. Urol.* **1998,** *159,* 2197–2201.
81. Fujimura, T.; Tamura, K.; Tsutsumi, T.; Yamamoto, T.; Nakamura, K.; Koibuchi, Y.; Kobayashi, M.; Yamaguchi, O. Expression and Possible Functional Role of the β_3-Adrenoceptor in Human and Rat Detrusor Muscle. *J. Urol.* **1999,** *161,* 680–685.
82. Igawa, Y.; Yamazaki, Y.; Takeda, H.; Hayakawa, K.; Akahane, M.; Ajisawa, Y.; Yoneyama, T.; Nishizawa, O.; Andersson, K.-E. Functional and Molecular Biological Evidence for a Possible β_3-Adrenoceptor in the Human Detrusor Muscle. *Br. J. Pharmacol.* **1999,** *126,* 819–825.
83. Takeda, M.; Obara, K.; Mizusawa, T.; Tomita, Y.; Arai, K.; Tsutsui, T.; Hatano, A.; Takahashi, K.; Nomura, S. Evidence for β_3-Adrenoceptor Subtypes in Relaxation of the Human Urinary Bladder Detrusor: Analysis by Molecular Biological and Pharmacological Methods. *J. Pharmacol. Exp. Ther.* **1999,** *288,* 1367–1373.
84. Michel, M. C.; Vrydag, W. α_1-, α_2-, and β-Adrenoceptors in the Urinary Bladder, Urethra, and Prostate. *Br. J. Pharmacol.* **2006,** *147,* S88–S119.
85. Gillespi, J. I.; Rouget, C.; Palea, S.; Granato, C.; Korstanje, C. Beta Adrenergic Modulation of Spontaneous Microcontractions and Electrical Field-Stimulated Contractions in Isolated Strips of Rat Urinary Bladder from Normal Animals and Animals With Partial Bladder Outflow Obstruction. *Naunyn Schmiedebergs Arch. Pharmacol.* **2015,** *388,* 719–726.
86. Yamaguchi, O.; Chapple, C. R. β_3-Adrenoceptors in Urinary Bladder. *Neurourol. Urodyn.* **2007,** *26,* 752–756.
87. Otsuka, A.; Shinbo, H.; Matsumoto, R.; Kurita, Y.; Ozono, S. Expression and Functional Role of β-Adrenoceptors in the Human Urinary Bladder Urothelium. *Naunyn Schmiedebergs Arch. Pharmacol.* **2008,** *377,* 473–481.
88. Tyagi, P.; Thomas, C. A.; Yoshimura, N.; Chancellor, M. B. Investigations into the Presence of Functional β_1, β_2, and β_3 Adrenoceptors in Urothelium and Detrusor of Human Bladder. *Int. Braz J Urol* **2009,** *35,* 76–82.
89. Michel, M. C.; Ochodnicky, P.; Homma, Y.; Igawa, Y. β-Adrenoceptor Agonist Effects in Experimental Models of Bladder Dysfunction. *Pharmacol. Ther.* **2011,** *11,* 40–49.
90. Woods, M.; Carson, N.; Norton, N. W.; Sheldon, J. H.; Argentieri, T. M. Efficacy of the β_3-Adrenergic Receptor Agonist CL-316243 on Experimental Bladder Hyperreflexia and Detrusor Instability in the Rat. *J. Urol.* **2001,** *166,* 1142–1147.
91. Kullmann, F. A.; Limberg, B. J.; Artim, D. E.; Shah, M.; Downs, T. R.; Contract, D.; Wos, J.; Rosenbaum, J. S.; de Groat, W. C. Effects of β_3-Adrenergic Receptor Activation on Rat Urinary Bladder Hyperactivity Induced by Ovariectomy. *J. Pharmacol. Exp. Ther.* **2009,** *330,* 704–717.
92. Aizawa, N.; Igawa, Y.; Nishizawa, O.; Wyndaele, J.-J. Effects of CL316,243, A β_3-Adrenoceptor Agonist, and Intravesical Prostaglandin E_2 on the Primary Bladder Afferent Activity of the Rat. *Neurourol. Urodyn.* **2010,** *29,* 771–776.

93. Nagabukuro, H.; Degenhardt, A.; Villa, K. L.; Mistry, S. L.; Gichuru, L.; Jochnowitz, N.; Abbadie, C. Correlation Between Pharmacologically-Induced Changes in Cystometric Parameters and Spinal c-Fos Expression in Rats. *Auton. Neuroscience. Bas. Clin.* **2010,** *156,* 19–26.
94. Kullmann, F. A.; Downs, T. R.; Atrim, D. E.; Limberg, B. J.; Shah, M.; Contract, D.; de Groat, W. C.; Rosenbaum, J. S. Urothelial Beta-3 Adrenergic Receptors in the Rat Bladder. *Neurourol. Urodyn.* **2011,** *30,* 144–150.
95. Andersson, K.-E.; Martin, N.; Nitti, V. Selective β_3-Adrenoceptor Agonists for the Treatment of Overactive Bladder. *J. Urol.* **2013,** *190,* 1173–1180.
96. Michel, M. C.; Korstanje, C. β_3-Adrenoceptor Agonists for Overactive Bladder Syndrome: Role of Translational Pharmacology in a Repositioning Clinical Drug Development Project. *Pharmacol. Ther.* **2016,** *159,* 66–82.
97. Dale, P. R.; Cernecka, H.; Schmidt, M.; Dowling, M. R.; Charlton, S. J.; Pieper, M. P.; Michel, M. C. The Pharmacological Rationale for Combining Muscarinic Receptor Antagonists and β_3-Adrenoceptor Agonists in the Treatment of Airway and Bladder Disease. *Curr. Opin. Pharmacol.* **2014,** *16,* 31–42.
98. Otsuka, A.; Matsumoto, R.; Suzuki, T.; Yoshikawa, S.; Kobayashi, R.; Kanie, S.; Shinbo, H.; Kurita, Y.; Ozono, S. Combination Effect of β_3-Adrenoceptor Agonist and Muscarinic Receptor Antagonist on Human Detrusor Muscle Relaxation In Vitro. *Neurourol. Urodyn.* **2012,** *31,* 894–895.
99. Akira, F.; Shoji, K.; Yusuke, K.; Shin, E.; Yasuyuki, S.; Naoki, Y. Combination Therapy With β_3-Adrenoceptor Agonists and Muscarinic Acetylcholine Receptor Antagonists: Efficacy in Rats with Bladder Overactivity. *Int. J. Urol.* **2016.** http://dx.doi.org/10.1111/iju.13066.
100. Sacco, E.; Bientinesi, R. Innovative Pharmacotherapies for Women With Overactive Bladder: Where Are We Now and What Is in the Pipeline? *Int. Urogynecol. J.* **2015,** *26,* 629–640.
101. Giarenis, I.; Robinson, D.; Cardosa, L. Overactive Bladder and the β_3-Adrenoceptor Agonists: Current Strategy and Future Prospects. *Drugs* **2015,** *72,* 1707–1713.
102. Michel, M. C. Therapeutic Modulation of Urinary Bladder Function: Multiple Targets at Multiple Levels. *Annu. Rev. Pharmacol. Toxicol.* **2015,** *55,* 269–287.
103. Igawa, Y.; Michel, M. C. Pharmacological Profile of β_3-Adrenoceptor Agonists in Clinical Development for the Treatment of Overactive Bladder Syndrome. *Naunyn Schmiedebergs Arch. Pharmacol.* **2013,** *386,* 177–183.
104. Andersson, K.-E. β_3-Receptor Agonists for Overactive Bladder—New Frontier or More of the Same? *Curr. Urol. Rep.* **2013,** *14,* 435–441.
105. The Search Searches a Collection of Scientific Publication Databases Including the Science Citation Index Expanded (Web of Science), MEDLINE/PubMed (NLM), Scopus (Elsevier), SciVerse ScienceDirect (Elsevier), and Wiley Online Library. Duplicate Publications Between the Databases and the Search Terms Were Removed.
106. Granneman, J. G. β_3 Adrenergic Receptors as a Therapeutic Target for Obesity. In *Obesity: Pathology and Therapy;* Lockwood, D. H., Heffner, T. G., Eds.; Springer-Verlag: Berlin, Heidelberg, 2000; p 343.
107. Savontaus, E.; Rouru, J.; Boss, O.; Huupponen, R.; Koulu, M. Differential Regulation of Uncoupling Proteins by Chronic Treatments with β_3-Adrenergic Agonist BRL 35135 and Metformin in Obese fa/fa Zucker Rats. *Biochem. Biophys. Res. Commun.* **1998,** *246,* 899–904.
108. Mitchell, T. H.; Ellis, R. D. M.; Smith, S. A.; Robb, G.; Cawthorne, M. A. Effects of BRL 35135, a β-Adrenoceptor Agonist With Novel Selectivity, on Glucose Tolerance and Insulin Sensitivity in Obese Subjects. *Int. J. Obes.* **1989,** *13,* 757–766.
109. Connacher, A. A.; Bennet, W. M.; Jung, R. T.; Rennie, M. J. Metabolic Effects of Three Weeks Administration of the β_3-Adrenoceptor Agonist BRL 26830A. *Int. J. Obes.* **1992,** *16,* 685–694.
110. Smith, S. A.; Cawthorne, M. A.; Fay, L. C.; McCullough, D. A.; Mitchell, T. H. Effect of a Novel β-Adreneoceptor Agonist on Insulin Sensitivity in Lean Healthy Male Volunteers (Abstract). *Diabetologia* **1994,** *37,* 15A.
111. Connacher, A. A.; Lakie, M.; Powers, N.; Elton, R. A.; Walsh, E. G.; Jung, R. T. Temor and the Anti-Obesity Drug BRL 26830A. *Br. J. Pharmacol.* **1990,** *30,* 613–615.
112. Wheeldon, N. M.; McDevitt, D. G.; Lipworth, B. J. Cardiac Effects of the $Beta_3$-Adrenoceptor Agonist BRL 26830A. *Br. J. Pharmacol.* **1994,** *7,* 363–369.
113. Weyer, C.; Tataranni, P. A.; Snitker, S.; Danforth, E.; Ravussin, E. Increase in Insulin Action and Fat Oxidation Following Treatment with CL 316,243, A Highly Selective $Beta_3$-Adrenoceptor Agonist in Humans. *Diabetes* **1998,** *47,* 1555–1561.
114. Calles-Escandon, J.; Steiner, K.; Danforth, E. Increased Lipolysis in Obese Insulin Resistant Individuals After 3 Month Treatment with a Highly-Selective β_3-Adrenergic Receptor (Abstract). *Obes. Res.* **1997,** *5,* 018; Holloway, B.; Howe, R.; Rao, B. S.; Stribling, D.; Mayers, R. M.; Briscoe, M. G.; Jackson, J. M. ICI D7114 A Novel Selective β-Adrenoceptor Agonist Selectively Stimulates Brown Fat and Increases Whole-Body Oxygen Consumption. *Br. J. Pharmacol.* **1991,** *104,* 97–104.
115. Need Preclinical Ref for Efficacy in Rats or Mice or Other Preclin Species for ZD 2079.
116. Goldberg, G.; Prentice, A. M.; Murgatroyed, P. R.; Tuersley, M. D. Effects of Metabolic Rate and Fuel Selection of a Selective β_3 Agonist (ICI D7114) in Healthy Lean Men. *Int. J. Obes.* **1995,** *19,* 625–631.
117. Toubro, S.; Astrup, A. The Selective β_3 Agonist ZD 2079 Stimulates 24-Hour Energy Expenditure Through Increased Fidgeting. A 14 Day, Randomized Placebo-Controlled Study in Obese Subjects. *Int. J. Obes.* **1995,** *19,* 070. Abstract.
118. Fisher, L. G.; Sher, P. M.; Skwish, S.; Michel, I. M.; Seiler, S. M.; Dickinson, K. E. J. BMS-187257, A Potent, Selective, and Novel Heterocyclic β_3 Adrenergic Receptor Agonist. *Bioorg. Med. Chem. Lett.* **1996,** *6,* 2253–2258.
119. Sher, P. M.; Mathur, A.; Fisher, L. G.; Wu, G.; Skwish, S.; Michel, I. M.; Seiler, S. M.; Dickinson, K. E. J. Carboxyl-Promoted Enhancement of Selectivity for the β_3 Adrenergic Receptor. Negative Charge of the Sulfonic Acid BMS-187413 Introduces β_3 Binding Selectivity. *Bioorg. Med. Chem. Lett.* **1997,** *7,* 1583–1588.
120. Washburn, W. N.; Sher, P. M.; Poss, K. M.; Girotra, R. N.; McCann, P. J.; Gavai, A. V.; Mikkilineni, A. B.; Mathur, A.; Cheng, P.; Dejneka, T. C.; Sun, C. Q.; Wang, T. C.; Harper, T. W.; Russell, A. D.; Slusarchyk, A.; Skwish, S.; Allen, G. T.; Hillyer, D. E.; Frohlich, B. H.; Abboa-Offei, B. E.; Cap, M.; Waldron, T. L.; George, R. J.; Tesfamariam, B.; Ciosek, C. P.; Ryono, D.; Young, D. A.; Dickinson, K. E.; Seymour, A. A.; Arbeeny, C. M.; Gregg, R. E. Beta 3 Agonists. Part 1: Evolution From Inception to BMS-194449. *Bioorg. Med. Chem. Lett.* **2001,** *11,* 3035–3039.
121. Gavai, A. V.; Sher, P. M.; Mikkilineni, A. B.; Poss, K. M.; McCann, P. J.; Girotra, R. N.; Fisher, L. G.; Wu, M. S.; Bednarz, A.; Mathur, T. C.; Wang, C.; Sun, Q.; Slusarchyk, D. A.; Skwish, S.; Allen, G. T.; Hillyer, D. E.; Frohlich, B. H.; Abboa-Offei, B. E.; Cap, M.; Waldron, T. L.; George, R. J.; Tesfamariam, B.; Harper, T. W.; Ciosek, C. P.; Young, D. A.; Dickinson, K. E.; Seymour, A. A.; Arbeeny, C. M.; Washburn, W. N. BMS-196085: A Potent and Selective Full Agonist of the Human β3 Adrenergic Receptor. *Bioorg. Med. Chem. Lett.* **2001,** *11,* 3041–3044.
122. Washburn, W. N.; Sun, Q.; Bisacchi, G.; Wu, G.; Gavai, A. V.; Cheng, P. T.; Sher, P. M.; Ryono, D.; Gavai, A. V.; Poss, K.; Girotra, R. N.; McCann, P. J.; Mikkilineni, A. B.; Dejneka, T. C.; Wang, T. C.; Merchant, Z.; Morella, M.; Arbenny, C. M.; Harper, T. W.; Slusarchyk, D. A.; Skwish, S.; Russell, A. D.; Allen, G. T.; Tesfamariam, B.; Frohlich, B. H.; Abboa-Offei, B. E.; Cap, M.; Waldron, T. L.; George, R. J.; Ciosek, C. P.; Young, D.; Dickinson, K. E.; Seymour, A. A. BMS-201620: A Selective β3 Agonist. *Bioorg. Med. Chem. Lett.* **2004,** *14,* 3525–3529.
123. Washburn, W. N.; Harper, T. W.; Wu, G.; Godfrey, J. D.; McCann, P.; Girotra, R.; Shao, C.; Zhang, H.; Gavai, A.; Mikkilineni, A.; Dejneka, T.; Ahmed, S.; Caringal, Y.; Hangeland, J.; Zhang, M.; Cheng, P. T. W.; Russell, A. D.; Skwish, S.; Slusarchyk, D. A.; Allen, G. T.; Frohlich, B. H.; Abboa-Offei, B. E.; Cap, M.; Waldron, T. L.; George, R. J.; Tesfamariam, B.; Dickinson, K. E.; Seymour, A. A.; Sher, P. M. Arylpropanolamines: Selective β3 Agonists Arising From Strategies to Mitigate Phase 1 Metabolic Transformations. *Bioorg. Med. Chem. Lett.* **2007,** *17,* 4290–4296.
124. Finley, D. R.; Bell, M. G.; Borel, A. G.; Bloomquist, W. E.; Cohen, M. L.; Heiman, M. L.; Kriauciunas, A.; Matthews, D. P.; Miles, T.; Neel, D. A.; Rito, C. J.; Sall, D. J.; Shuker, A. J.; Stephens, T. W.; Tinlsey, F. C.; Winter, M. A.; Jesudason, C. D. Potent Benzimidazolone Based Human β_3 Adrenergic Receptor Agonists. *Bioorg. Med. Chem. Lett.* **2006,** *16,* 5691–5694.
125. Cohen, M. L.; Bloomquist, W.; Kriauciunas, A.; Shuker, A.; Calligaro, D. Aryl Propanolamines: Comparison of Actiivty at Human β_3 Receptors, Rat β_3 Receptors, and Rat Atrial Receptors Mediating Tachycardia. *Br. J. Pharmacol.* **1999,** *126,* 1018–1024.
126. Stevens, F. C.; Bloomquist, W. E.; Borel, A. G.; Cohen, M. L.; Droste, C. A.; Heiman, M. L.; Kriauciunas, A.; Sall, D. J.; Tinsley, F. C.; Jesudason, C. D. Potent Oxindole Based Human β_3 Adrenergic Receptor Agonists. *Bioorg. Med. Chem. Lett.* **2007,** *17,* 6270–6273.

127. Jesudason, C. D.; Bell, M. G.; Crowell, T. A.; Droste, C. A.; Jones, C. D.; Kim, G.; Matthews, D. P.; Neel, D. A.; Rito, C. J.; Shuker, A. J.; Winter, M. A.; Bryant, R. D.; Fisher, J. W.; Peters, M. K.; Trankle, W. G.; Heiman, M. L.; Kriauciunas, A. V.; Tinsley, F. C.; Dananberg, J.; Miller, J. W. 220th ACS National Meeting, Washington D.C. MEDI-300.
128. Harada, H.; Hirokawa, Y.; Suzuki, K.; Hiyama, Y.; Oue, M.; Kawashima, H.; Yoshida, N.; Furutani, Y.; Kato, S. Novel and Potent Human and Rat β_3-Adrenergic Receptor Agonists Containing Substituted 3-Indolylalkylamines. *Bioorg. Med. Chem. Lett.* **2003,** *13,* 1301–1305.
129. Harada, H.; Hirokawa, Y.; Suzuki, K.; Hiyama, Y.; Oue, M.; Kawashima, H.; Kato, H.; Yoshida, N.; Furutani, Y.; Kato, S. Discovery of a Novel and Potent Human and Rat β_3-Adrenergic Receptor Agonist, [3-[(2*R*)-[[(2*R*)-(3-Chlorophenyl)-2-Hydroxyethyl]amino]propyl]-1*H*-Indol-7-yloxy]Acetic Acid. *Chem. Pharm. Bull.* **2005,** *53,* 184–198.
130. Kato, H.; Ohue, M.; Kato, K.; Nomura, A.; Toyosawa, K.; Furutani, Y.; Kimura, S.; Kadowaki, T. Mechanism of Amelioration of Insulin Resistance by β_3-Adrenoceptor Agonist AJ-9677 in the KK-Ay/Ta Diabetic Obese Mouse Model. *Diabetes* **2001,** *50,* 113–122.
131. Sugimoto, T.; Ogawa, W.; Kasuga, M.; Yokoyama, Y. Chronic Effects of AJ-9677 on Energy Expenditure and Energy Source Utilization in Rats. *Eur. J. Pharmacol.* **2005,** *519,* 135–145.
132. Sawa, M.; Tateishi, H.; Mizuno, K.; Harada, H.; Oue, M.; Tsujiuchi, H.; Furutani, Y.; Kato, S. Tryptamine—Based Human β_3-Adrenergic Receptor Agonists. Part 2: SAR of the Methylene Derivatives. *Bioorg. Med. Chem. Lett.* **2004,** *14,* 5963–5966.
133. Mizuno, K.; Sawa, M.; Harada, H.; Taoka, I.; Yamashita, H.; Oue, M.; Tsujiuchi, H.; Arai, Y.; Suzuki, S.; Furutani, Y.; Kato, S. Discovery of 1,7-Cyclized Indoles as a New Class of Potent and Highly Selective Human β_3-Adrenergic Receptor Agonists With High Cell Permeability. *Bioorg. Med. Chem.* **2005,** *13,* 855–868.
134. Redman, L. M.; de Jonge, L.; Fang, X.; Gamlin, B.; Recker, D.; Greenway, F. L.; Smith, S. R.; Ravussin, E. Lack of an Effect of a Novel β_3-Adrenoceptor Agonist, TAK-677, on Energy Metabolism in Obese Individuals: A Double-Blind, Placebo-Controlled Randomized Study. *J. Endocrinol. Metab.* **2007,** *92,* 527–531.
135. Dow, R. L. β_3-Adrenergic Agonists: Potential Therapeutics for Obesity. *Expert. Opin. Invest. Drugs* **1997,** *6,* 1811–1825.
136. Dow, R. L.; Paight, E. S.; Schneider, S. R.; Hadcock, J. R.; Hargrove, D. M.; Martin, K. A.; Maurer, T. S.; Nardone, N. A.; Tess, D. A.; DaSilfa-Jardine, P. Potent and Selective, Sulfamide-Based Human β_3-Adrenergic Receptor Agonists. *Bioorg. Med. Chem. Lett.* **2004,** *14,* 3235–3240.
137. Lafontaine, J. A.; Day, R. F.; Dibrino, J.; Hadcock, J. R.; Hargrove, D. M.; Linhares, M.; Martin, K. A.; Maurer, T. S.; Nardone, N. A.; Tess, D. A.; DaSilva-Jardine, P. Discovery of Potent and Orally Bioavailable Heterocycle-Based β_3-Adrenergic Receptor Agonists, Potential Therapeutics for the Treatment of Obesity. *Bioorg. Med. Chem. Lett.* **2007,** *17,* 5245–5250.
138. Iizuki, H.; Osaka, Y.; Kondo, S.; Morita, T. Effect of an Atypical Adrenergic β_3-Agonist, GS-332: Sodium (2*R*)-[3-[3-[2-(3-Chorophenyl)-2-Hydroxyethylamino]Cyclohexyl] Phenoxy] Acetate, on Urinary Bladder Function in Rats. *J. Smooth Muscle Res.* **1998,** *34,* 139–149.
139. Yanagisawa, T.; Sato, T.; Yamada, H.; Sukegawa, J.; Nunoki, K. Selectivity and Potency of Agonists for the Three Subtypes of Cloned Human β-Adrenoceptors Expressed in Chinese Hamster Ovary Cells. *J. Exp. Med.* **2000,** *192,* 181–193.
140. Bianchetti, A.; Manara, L. In Vitro Inhibition of Intestinal Motility by Phenylethanolaminotetralines: Evidence of Atypical β-Adrenoceptors in Rat Colon. *Br. J. Pharmacol.* **1990,** *100,* 831–839.
141. Tamburella, A.; Micale, V.; Leggio, G. M.; Drago, F. The β_3 Adrenoceptor Agonist, Amibegron (SR58611A) Counteracts Stress-Induced Behavioral and Neurochemical Changes. *Eur. Neuropsychopharmacol.* **2010,** *20,* 704–713.
142. For an overview of β3-AR localization and potential function in the CNS, see Ghanemi, A.; Hu, X. Elements Toward Novel Therapeutic Targeting of the Adrenergic System. *Neuropeptides* **2015,** *49,* 25–35.
143. Tanyeri, P.; Buyokokuroglu, M. E.; Mutlu, O.; Ulak, G.; Akar, F. Y.; Celikurt, I. K.; Erden, B. F. Involvement of Serotonin Receptor Subtypes in the Antidepressant-Like Effect of Beta Receptor Agonist Amibegron (SR 58611A): An Experimental Study. *Pharmacol. Biochem. Behav.* **2013,** *105,* 12–16.
144. Tanyeri, P.; Buyokokuroglu, M. E.; Mutlu, O.; Ulak, G.; Akar, F. Y.; Celikurt, I. K.; Erden, B. F. Evidence That the Anxiolytic-Like Effects of the Beta3 Receptor Agonist Amibegron Involve Serotoninergic Receptor Activity. *Pharmacol. Biochem. Behav.* **2013,** *110,* 27–32.
145. Beeley, L. J.; Berge, J. M.; Chapman, H.; Dean, D. K.; Kelly, J.; Lowden, K.; Kotecha, N. R.; Morgan, H. K. A.; Rami, H. K.; Thompson, M.; Vong, A. K. K.; Ward, R. W. A Simplified Template Approach Towards the Synthesis of a Potent Beta-3 Adrenoceptor Agonists at the Human Receptor. *Bioorg. Med. Chem. Lett.* **1997,** *7,* 219–224.
146. Uehling, D. E.; Donaldson, K. H.; Deaton, D. N.; Hyman, C. E.; Sugg, E. E.; Barrett, D. G.; Hughes, R. G.; Reitter, B.; Adkinson, K. K.; Lancaster, M. E.; Lee, F.; Hart, R.; Paulik, M. A.; Sherman, B. W.; True, T.; Cowan, C. Synthesis and Evaluation of Potent and Selective β_3 Adrenergic Receptor Agonists Containing Acylsulfonamide, Sulfonylsulfonamide, and Sulfonylurea Carboxylic Acid Isosteres. *J. Med. Chem.* **2002,** *45,* 567–583.
147. Uehling, D. E.; Shearer, B. G.; Donaldson, K. H.; Chao, E. Y.; Deaton, D. N.; Adkinson, K. K.; Brown, K. K.; Cariello, N. F.; Faison, W. L.; Lancaster, M. E.; Lin, J.; Hart, R.; Milliken, T. O.; Paulik, M. A.; Sherman, B. W.; Sugg, E. E.; Cowan, C. Biarylaniline Phenethanolamines as Potent and Selective β_3 Adrenergic Receptor Agonists. *J. Med. Chem.* **2006,** *49,* 2758–2771.
148. Shearer, B. G.; Chao, E. Y.; Uehling, D. E.; Deaton, D. N.; Cowan, C.; Sherman, B. W.; Milliken, T. O.; Faison, W.; Brown, K. K.; Adkinson, K. K.; Lee, F. Synthesis and Evaluation of Potent and Selective β_3 Adrenergic Receptor Agonists Containing Heterobiaryl Carboxylic Acids. *Bioorg. Med. Chem. Lett.* **2007,** *17,* 4670–4677.
149. Krief, S.; Lonnqvist, F.; Raimbault, S.; Baude, B.; Van Spronsen, A.; Arner, P.; Strosberg, A. G.; Ricquier, D.; Emorine, L. J. Tissue Distribution of β_3-Adrenergic Receptor mRNA in Man. *J. Clin. Invest.* **1993,** *91,* 344–349.
150. Anthony, A.; Schepelmann, S.; Guillaume, J. L.; Strosberg, A. D.; Dhillon, A. P.; Pounder, R. E.; Wakefield, A. J. Localization of the β_3-Adrenoceptor in the Human Gastrointestinal Tract: an Immunohistochemical Study. *Aliment. Pharmacol. Ther.* **1998,** *12,* 519–525.
151. Fletcher, D. S.; Candelore, M. R.; Grujic, D.; Lowell, B. B.; Luell, S.; Susulic, V. S.; Macintyre, D. E. Beta-3 Adrenergic Receptor Agonists Cause an Increase in Gastrointestinal Transit Time in Wild-Type Mice, but Not in Mice Lacking the Beta-3 Adrenergic Receptor. *J. Pharmacol. Exp. Ther.* **1998,** *287,* 720–724.
152. Cellek, S.; Thangiah, R.; Bassil, A. K.; Campbell, C. A.; Gray, K. M.; Stretton, J. L.; Lalude, O.; Vivekanandan, S.; Wheeldon, A.; Winchester, W. J.; Sanger, G. J.; Schemann, M.; Lee, K. Demonstration of Functional Neuronal β_3-Adrenoceptors Within the Enteric Nervous System. *Gastroenterology* **2007,** *133,* 175–183.
153. De Ponti, F.; Gibelli, G.; Croci, T.; Arcidiaco, M.; Crema, F.; Manara, L. Functional Evidence of Atypical Beta 3-Adrenoceptors in the Human Colon Using the Beta 3-Selective Adrenoceptor Antagonist, SR 59230A. *Br. J. Pharmacol.* **1996,** *117,* 1374–1376.
154. Bardou, M.; Dousset, B.; Deneux-Tharaux, C.; Smadja, C.; Naline, E.; Chaput, J. C.; Naveau, S.; Manara, L.; Croci, T.; Advenier, C. In Vitro Inhibition of Human Colonic Motility With SR 59119A and SR 59104A: Evidence of a β_3-Adrenoceptor-Mediated Effect. *Eur. J. Pharmacol.* **1998,** *353,* 281–287.
155. De Ponti, F.; Modini, C.; Gibelli, G.; Crema, F.; Frigo, G. Atypical Betaadrenoceptors Mediating Relaxation in the Human Colon: Functional Evidence for β_3-Rather Than β_4-Adrenoceptors. *Pharmacol. Res.* **1999,** *39,* 345–348.
156. Manara, L.; Croci, T.; Aureggi, G.; Guagnini, F.; Maffrand, J. P.; Le Fur, G.; Mukenge, S.; Ferla, G. Functional Assessment of Beta Adrenoceptor Subtypes in Human Colonic Circular and Longitudinal (Taenia Coli) Smooth Muscle. *Gut* **2000,** *47,* 337–342.
157. Grudell, A. B. M.; Camilleri, M.; Jensen, K. L.; Foxx-Orenstein, A. E.; Burton, D. D.; Ryks, M. D.; Baxter, K. L.; Cox, D. S.; Dukes, G. E.; Kelleher, D. L.; Zinsmeister, A. R. Dose–response Effect of a β_3-Adrenergic Receptor Agonist, Solabegron, on Gastrointestinal Transit, Bowel Function, and Somatostatin Levels in Health. *Am. J. Physiol. Gastrointest. Liver Physiol.* **2008,** *294,* G1114–G1119.
158. Ellsworth, P.; Fantasia, J. Solabegron: A Potential Future Addition to the β_3 Adrenoceptor Agonist Armamentarium for the Management of Overactive Bladder. *Expert Opin. Invest. Drugs* **2015,** *24,* 413–419.
159. Hicks, A.; McCafferty, G. P.; Riedel, E.; Aiyar, N.; Pullen, M.; Evans, C.; Luce, T. D.; Coatney, R. W.; Rivera, G. C.; Westfall, T. D.; Hieble, J. P. GW427353 (Solabegron), A Novel, Selective β_3-Adrenergic Receptor Agonist, Evokes Bladder Relaxation and Increases Micturition Reflex Threshold in the Dog. *J. Pharmacol. Exp. Ther.* **2007,** *323,* 202–209.
160. Biers, S. M.; Reynard, J. M.; Brading, A. F. The Effects of a New Selective b3-Adrenoceptor Agonist (GW427353) on Spontaneous Activity and Detrusor Relaxation in Human Bladder. *BJU Int.* **2006,** *98,* 1310–1314.

161. Ohlstein, E. H.; von Keitz, A.; Michel, M. C. A Multicenter, Double-Blind, Randomized, Placebo-Controlled Trial of the β_3-Adrenoceptor Agonist Solabegron for Overactive Bladder. *Eur. Urol.* **2012,** *62,* 834–840.
162. Tanaka, N.; Tamai, T.; Mukaiyama, H.; Hirabayashi, A.; Muranaka, H.; Akahane, S.; Mitaya, H.; Akahane, M. J. *Med. Chem.* **2001,** *44,* 1436–1445.
163. Takeda, H.; Igawa, Y.; Komatsu, Y.; Yamazaki, Y.; Akahane, M.; Nishizawa, O.; Ajisawa, Y. Characterization of β-Adrenoceptor Subtypes in the Ferret Urinary Bladder *In Vitro* and *In Vivo*. *Eur. J. Pharmacol.* **2000,** *403,* 147–155.
164. Abe, Y.; Ota, E.; Endo, T.; Murakami, M.; Kobayashi, M. Absorption, Disposition, Metabolism, and Excretion of Ritobegron (KUC-7483), A Novel Selective β_3-Adrenoceptor Agonist, in Rats. *Pharmazie* **2014,** *69,* 881–888.
165. Maruyama, I.; Goi, Y.; Tatemichi, S.; Maruyama, K.; Hoyano, Y.; Yamakazi, Y.; Kusama, H. Bladder Selectivity of the Novel β_3-Agonist Ritobegron (KUC-7483) Explored by *In Vitro* and *In Vivo* Studies in the Rat. *Naunyn Schmiedebergs Arch. Pharmacol.* **2012,** *385,* 845–852.
166. Maruyama, I.; Tatemichi, S.; Goi, Y.; Maruyama, K.; Hoyano, Y.; Yamazaki, Y.; Kusama, H. Effects of Ritobegron (KUC-7483), A Novel Selective β_3-Adrenoceptor Agonist, on Bladder Function in Cynomolgus Monkey. *J. Pharmacol. Exp. Ther.* **2012,** *342,* 163–168.
167. Weber, A. E.; Mathvink, R. J.; Perkins, L.; Hutchins, J. E.; Candelore, M. R.; Tota, L.; Strader, C. D.; Wyvratt, M. J.; Fisher, M. H. Potent, Selective Benzenesulfonamide Agonists of the Human β_3 Adrenergic Receptor. *Bioorg. Med. Chem. Lett.* **1998,** *8,* 1101–1106.
168. Granneman, J. G.; Lahners, K. N.; Rao, D. D. Expression of Beta 3-Adrenoceptor mRNA in Rat Tissues. *Mol. Pharmacol.* **1992,** *42,* 964–970.
169. Liggett, S. B. Functional Properties of the rat and Human β_3-Adrenergic Receptors: Differential Agonist Activation of Recombinant Receptors in Chinese Hamster Ovary Cells. *Mol. Pharmacol.* **1992,** *42,* 634–637.
170. Parmee, E. R.; Ok, H. O.; Candelore, M. R.; Tota, L.; Deng, L.; Strader, C. D.; Wyvratt, M. J.; Fisher, M. H.; Weber, A. E. Discovery of L-755,507: A Subnanomolar Human β_3 Adrenergic Receptor Agonist. *Bioorg. Med. Chem. Lett.* **1998,** *8,* 1107–1112.
171. Fisher, M. H.; Amend, A. M.; Bach, T. J.; Barker, J. M.; Brady, E. J.; Candelore, M. R.; Carroll, D.; Cascieri, M. A.; Chiu, S.-H. L.; Deng, L.; Forrest, M. J.; Hegarty-Friscino, B.; Guan, X.-M.; Hom, G. J.; Hutchins, J. E.; Kelly, L. J.; Mathvink, R. J.; Metzger, J. M.; Miller, R. R.; Ok, H. O.; Parmee, E. R.; Saperstein, R.; Strader, C. D.; Stearns, R. A.; Thompson, G. M.; Tota, L.; Vicario, P. P.; Weber, A. E.; Woods, J. W.; Wyvratt, M. J.; Zafian, P. T.; MacIntyre, D. E. A Selective Human β3 Adrenergic Receptor Agonist Increases Metabolic Rate in Rhesus Monkeys. *J. Clin. Invest.* **1998,** *101,* 2387–2393.
172. Weber, A. E.; Ok, H. O.; Alvaro, R. F.; Candelore, M. R.; Cascieri, M. A.; Chiu, S.-H. L.; Deng, L.; Forrest, M. J.; Hom, G. J.; Hutchins, J. E.; Kao, J.; MacIntyre, D. E.; Mathvink, R. J.; McLoughlin, D.; Miller, R. R.; Newbold, R. C.; Olah, T. V.; Parmee, E. R.; Perkins, L.; Stearns, R. A.; Strader, C. D.; Szumiloski, J.; Tang, Y. S.; Tota, L.; Vicario, P. P.; Wyvratt, M. J.; Fisher, M. H. 3-Pyridyloxypropanolamine Agonists of the β3 Adrenergic Receptor With Improved Pharmacokinetic Properties. *Bioorg. Med. Chem. Lett.* **1998,** *8,* 1107–1112.
173. Naylor, E. M.; Colandrea, V. J.; Candelore, M. R.; Cascieri, M. A.; Colwell, L. F.; Deng, L.; Feeney, W. P.; Forrest, M. J.; Hom, G. J.; MacIntyre, D. E.; Strader, C. D.; Tota, L.; Wang, P.-R.; Wyvratt, M. J.; Fisher, M. H.; Weber, A. E. 3-Pyridylethanolamines: Potent and Selective Human β_3 Adrenergic Receptor Agonists. *Bioorg. Med. Chem. Lett.* **1998,** *8,* 3087–3092.
174. Parmee, E. R.; Naylor, E. M.; Perkins, L.; Colandrea, V. J.; Ok, H. O.; Candelore, M. R.; Cascieri, M. A.; Deng, L.; Feeney, W. P.; Forrest, M. J.; Hom, G. J.; MacIntyre, D. E.; Miller, R. R.; Stearns, R. A.; Strader, C. D.; Tota, L.; Wyvratt, M. J.; Fisher, M. H.; Weber, A. E. Human β_3 Adrenergic Receptor Agonists Containing Cyclic Ureidobenzenesulfonamides. *Bioorg. Med. Chem. Lett.* **1999,** *9,* 749–754.
175. Naylor, E. M.; Parmee, E. R.; Colandrea, V. J.; Perkins, L.; Brockunier, L.; Candelore, M. R.; Cascieri, M. A.; Colwell, L. F.; Deng, L.; Feeney, W. P.; Forrest, M. J.; Hom, G. J.; MacIntyre, D. E.; Strader, C. D.; Tota, L.; Wang, P.-R.; Wyvratt, M. J.; Fisher, M. H.; Weber, A. E. Human β_3 Adrenergic Receptor Agonists Containing Imidazolidinone and Imidazolone Benzenesulfonamides. *Bioorg. Med. Chem. Lett.* **1999,** *9,* 755–758.
176. Shih, T. L.; Candelore, M. R.; Cascieri, M. A.; Chiu, S.-H. L.; Colwell, L. F.; Deng, L.; Feeney, W. P.; Forrest, M. J.; Hom, G. J.; MacIntyre, D. E.; Miller, R. R.; Stearns, R. A.; Strader, C. D.; Tota, L.; Wyvratt, M. J.; Fisher, M. H.; Weber, A. E. L-770,644: A Potent and Selective Human β_3 Adrenergic Receptor Agonist With Improved Bioavailability. *Bioorg. Med. Chem. Lett.* **1999,** *9,* 1251–1254.
177. Mathvink, R. J.; Barritta, A. M.; Candelore, M. R.; Cascieri, M. A.; Deng, L.; Tota, L.; Strader, C. D.; Wyvratt, M. J.; Fisher, M. H.; Weber, A. E. Potent, Selective Human β_3 Adrenergic Receptor Agonists Containing a Substituted Indoline-5-Sulfonamide Pharmacophore. *Bioorg. Med. Chem. Lett.* **1999,** *9,* 1869–1874.
178. Feng, D. D.; Biftu, T.; Candelore, M. R.; Cascieri, M. A.; Colwell, L. F.; Deng, L.; Feeney, W. P.; Forrest, M. J.; Hom, G. J.; MacIntyre, D. E.; Miller, R. R.; Stearns, R. A.; Strader, C. D.; Tota, L.; Wyvratt, M. J.; Fisher, M. H.; Weber, A. E. Discovery of an Orally Bioavailable Alkyl Oxadiazole β_3 Adrenergic Receptor Agonist. *Bioorg. Med. Chem. Lett.* **2000,** *10,* 1427–1429.
179. Biftu, T.; Feng, D. D.; Liang, G.-B.; Kuo, H.; Qian, X.; Naylor, E. M.; Colandrea, V. J.; Candelore, M. R.; Cascieri, M. A.; Colwell, L. F.; Forrest, M. J.; Hom, G. J.; MacIntyre, D. E.; Stearns, R. A.; Strader, C. D.; Wyvratt, M. J.; Fisher, M. H.; Weber, A. E. Synthesis and SAR of Benzyl and Phenoxymethylene Oxadiazole Benzenesulfonamides as Selective β_3 Adrenergic Receptor Agonist Antiobesity Agents. *Bioorg. Med. Chem. Lett.* **2000,** *10,* 1431–1434.
180. Ok, H. O.; Reigle, L. B.; Candelore, M. R.; Cascieri, M. A.; Colwell, L. F.; Deng, L.; Feeney, W. P.; Forrest, M. J.; Hom, G. J.; MacIntyre, D. E.; Strader, C. D.; Tota, L.; Wang, P.; Wyvratt, M. J.; Fisher, M. H.; Weber, A. E. Substituted Oxazole Benzenesulfonamides as Potent Human β_3 Adrenergic Receptor Agonists. *Bioorg. Med. Chem. Lett.* **2000,** *10,* 1531–1534.
181. Brockunier, L. L.; Parmee, E. R.; Ok, H. O.; Candelore, M. R.; Cascieri, M. A.; Colwell, L. F.; Deng, L.; Feeney, W. P.; Forrest, M. J.; Hom, G. J.; MacIntyre, D. E.; Tota, L.; Wyvratt, M. J.; Fisher, M. H.; Weber, A. E. Human β_3 Adrenergic Receptor Agonists Containing 1,2,3-Triazole-Substituted Benzenesulfonamides. *Bioorg. Med. Chem. Lett.* **2000,** *10,* 2111–2114.
182. Mathvink, R. J.; Tolman, J. S.; Chitty, D.; Candelore, M. R.; Cascieri, M. A.; Colwell, L. F.; Deng, L.; Feeney, W. P.; Forrest, M. J.; Hom, G. J.; MacIntyre, D. E.; Tota, L.; Wyvratt, M. J.; Fisher, M. H.; Weber, A. E. Potent, Selective 3-Pyridylethanolamine β_3 Adrenergic Receptor Agonists Possessing a Thiazole Benzenesulfonamide Pharmacophore. *Bioorg. Med. Chem. Lett.* **2000,** *10,* 1971–1973.
183. Mathvink, R. J.; Tolman, J. S.; Chitty, D.; Candelore, M. R.; Cascieri, M. A.; Colwell, L. F.; Deng, L.; Feeney, W. P.; Forrest, M. J.; Hom, G. J.; MacIntyre, D. E.; Miller, R. R.; Stearns, R. A.; Tota, L.; Wyvratt, M. J.; Fisher, M. H.; Weber, A. E. Discovery of a Potent, Orally Bioavailable β_3 Adrenergic Receptor Agonist, (R)-N-[4-[2-[[2-Hydroxy-2-(3-pyridinyl)ethyl]amino]ethyl]phenyl]-4-[4-[4-(trifluoromethyl)phenyl]thiazol-2-yl]benzenesulfonamide. *J. Med. Chem.* **2000,** *43,* 3832–3836.
184. Stearns, R. A.; Miller, R. R.; Tang, W.; Kwei, G. Y.; Tang, F. S.; Mathvink, R. J.; Naylor, E. M.; Chitty, D.; Colandrea, V. J.; Weber, A. E.; Colletti, A. E.; Strauss, J. R.; Keohane, C. A.; Feeney, W. P.; Iliff, S. A.; Chiu, S.-H. L. The Pharmacokinetics of a Thizaole Benzenesulfonanamide β_3 Adrenergic Receptor Agonist and Its Analogs in Rats, Dogs, and Monkeys: Improving Oral Bioavailability. *Drug Metab. Dispos.* **2002,** *30,* 771–777.
185. van Baak, M. A.; Hul, G. B. J.; Toubro, S.; Astrup, A.; Gottesdiener, K. M.; DeSmet, M.; Saris, W. H. M. Acute Effect of L-796568, A Novel β_3 Adrenergic Receptor Agonist, On Energy Expenditure in Obese Men. *Clin. Pharmacol. Ther.* **2002,** *71,* 272–279.
186. Edmondson, S. D.; Zhu, C.; Kar, N. F.; Di Salvo, J.; Nagabukuro, H.; Sacre-Salem, B.; Dingley, K.; Berger, R.; Goble, S. D.; Morriello, G.; Harper, B.; Moyes, C. R.; Shen, D.-M.; Wang, L.; Ball, R.; Fitzmaurice, A.; Frenkl, T.; Gichuru, L. N.; Ha, S.; Hurley, A. L.; Jochnowitz, N.; Levorse, D.; Mistry, S.; Miller, R. R.; Ormes, J.; Salituro, G. M.; Sanfiz, A.; Stevenson, A. S.; Villa, K.; Zamlynny, B.; Green, S.; Struthers, M.; Weber, A. E. Discovery of Vibegron: A Potent and Selective β3 Adrenergic Receptor Agonist for the Treatment of Overactive Bladder. *J. Med. Chem.* **2016,** *59,* 609–623.
187. Zinner, N. R.; Mattiasson, A.; Stanton, S. L. Efficacy, Safety, and Tolerability of Extended-Release Once-Daily Tolterodine Treatment for Overactive Bladder in Older versus Younger Patients. *J. Am. Geriatr. Soc.* **2002,** *50,* 799–807.
188. Tang, W.; Stearns, R. A.; Miller, R. R.; Ngui, J. S.; Mathvink, R. J.; Weber, A. E.; Kwei, G. Y.; Strauss, J. R.; Keohane, C. A.; Doss, G. A.; Chiu, S. H.; Baillie, T. A. Metabolism of a Thiazole Benzenesulfonamide Derivative, a Potent and Selective Agonist of the Human β_3-Adrenergic Receptor, in Rats: Identification of a Novel Isethionic Acid Conjugate. *Drug Metab. Dispos.* **2002,** *30,* 778–787.

189. Morriello, G. J.; Wendt, H. R.; Bansal, A.; Di Salvo, J.; Feighner, S.; He, J.; Hurley, A. L.; Hreniuk, D. L.; Salituro, G. M.; Reddy, M. V.; Galloway, S. M.; McGettigan, K. K.; Laws, G.; McKnight, C.; Doss, G. A.; Tsou, N. N.; Black, R. M.; Morris, J.; Ball, R. G.; Sanfiz, A. T.; Streckfuss, E.; Struthers, M.; Edmondson, S. D. Design of a Novel Pyrrolidine Scaffold Utilized in the Discovery of Potent and Selective Human β3 Adrenergic Receptor Agonists. *Bioorg. Med. Chem. Lett.* **2011,** *21,* 1865–1870.
190. Goble, S. D.; Wang, L.; Howell, K. L.; Bansal, A.; Berger, R.; Brockunier, L.; DiSalvo, J.; Feighner, S.; Harper, B.; He, J.; Hurley, A.; Hreniuk, D.; Parmee, E.; Robbins, M.; Salituro, G.; Sanfiz, A.; Streckfuss, E.; Watkins, E.; Weber, A. E.; Struthers, M.; Edmondson, S. D. Heterocyclic Acetamide and Benzamide Derivatives as Potent and Selective Human β_3-Adrenergic Receptor Agonists With Improved Rodent Pharmacokinetic Profiles. *Bioorg. Med. Chem. Lett.* **2010,** *20,* 1895–1899.
191. Moyes, C. R.; Berger, R.; Goble, S. D.; Harper, B.; Shen, D.-M.; Wang, L.; Bansal, A.; Brown, P. N.; Chen, A. S.; Dingley, K. H.; Di Salvo, J.; Fitzmaurice, A.; Gichuru, L. N.; Hurley, A. L.; Jochnowitz, N.; Miller, R. R.; Mistry, S.; Nagabukuro, H.; Salituro, G. M.; Sanfiz, A.; Stevenson, A. S.; Villa, K.; Zamlynny, B.; Struthers, M.; Weber, A. E.; Edmondson, S. D. Design, Synthesis, and Evaluation of Conformationally Restricted Acetanilides as Potent and Selective β3 Adrenergic Receptor Agonists for the Treatment of Overactive Bladder. *J. Med. Chem.* **2014,** *57,* 1437–1453.
192. Bhandari, N.; Figueroa, D. J.; Lawrence, J. W.; Gerhold, D. L. Phospholipidosis Assay in HepG2 Cells and Rat or Rhesus Hepatocytes Using Phospholipid Probe NBD-PE. *Assay Drug Dev. Technol.* **2008,** *6,* 407–420.
193. Zhu, C.; Kar, N. F.; Li, B.; Costa, M.; Dingley, K. H.; Di Salvo, J.; Ha, S. N.; Hurley, A. L.; Li, X.; Miller, R. R.; Salituro, G. M.; Struthers, M.; Weber, A. E.; Hale, J. J.; Edmondson, S. D. Discovery of Benzamides as Potent Human β_3-Adrenergic Receptor Agonists. *Bioorg. Med. Chem. Lett.* **2016,** *26,* 55–59.
194. Hattori, K.; Nagano, M.; Kato, T.; Nakanishi, I.; Imai, K.; Kinoshita, T.; Sakane, K. Asymmetric Synthesis of FR165914: A Novel β_3-Adrenergic Agonist With a Benzocycloheptene Structure. *Bioorg. Med. Chem. Lett.* **1995,** *5,* 2821–2824.
195. For a lead reference, see Yamamoto, H.; Takakura, S.; Yamamoto, T.; Satoh, H.; Higaki, M.; Tomoi, M.; Shimomura, K. FR149175, A β_3-Adrenoceptor-Selective Agonist, is a Possible Therapeutic Agent for Non-Insulin Dependent Diabetes Mellitus. *Jpn. J. Pharmacol.* **1997,** *74,* 109–112.
196. Hatakeyama, Y.; Sakata, Y.; Takakura, S.; Manda, Y.; Mutoh, S. Acute and Chronic Effects of FR-149175, A β_3-Adrenergic Receptor Agonist, on Energy Expenditure in Zucker Fatty Rats. *Am. J. Physiol. Regul. Integr. Comp. Physiol.* **2004,** *287,* R336–R341.
197. Imamishi, M.; Nakajima, Y.; Tomishima, Y.; Hamashima, H.; Washizuka, K.; Sakurai, M.; Matsui, S.; Imamura, E.; Ueshima, K.; Yamamoto, T.; Yamamoto, N.; Ishikawa, H.; Nakano, K.; Unami, N.; Hamada, K.; Matsumura, Y.; Takamura, F.; Hattori, K. Discovery of a Novel Series of Benzoic Acid Derivatives as Potent and Selective Human β3-Adrenergic Receptor Agonists With Good Oral Bioavailability. 3. Phenylethanolaminotetraline (PEAT) Skeleton Containing Biphenyl or Biphenyl Ether Moiety. *J. Med. Chem.* **2008,** *51,* 4804–4822.
198. Imamishi, M.; Tomishima, Y.; Itou, S.; Hamashima, H.; Nakajima, Y.; Washizuka, K.; Sakurai, M.; Matsui, S.; Imamura, E.; Ueshima, K.; Yamamoto, T.; Yamamoto, N.; Ishikawa, H.; Nakano, K.; Unami, N.; Hamada, K.; Matsumura, Y.; Takamura, F.; Hattori, K. Discovery of a Novel Series of Biphenyl Benzoic Acid Derivatives as Potent and Selective Human β_3-Adrenergic Receptor Agonists With Good Oral Bioavailability. Part I. *J. Med. Chem.* **2008,** *51,* 1925–1944.
199. Imamishi, M.; Itou, S.; Washizuka, K.; Hamashima, H.; Nakajima, Y.; Araki, T.; Tomishima, Y.; Sakurai, M.; Matsui, S.; Imamura, E.; Ueshima, K.; Yamamoto, T.; Yamamoto, N.; Ishikawa, H.; Nakano, K.; Unami, N.; Hamada, K.; Matsumura, Y.; Takamura, F.; Hattori, K. Discovery of a Novel Series of Biphenyl Benzoic Acid Derivatives as Highly Potent and Selective Human β_3-Adrenergic Receptor Agonists With Good Oral Bioavailability. Part II. *J. Med. Chem.* **2008,** *51,* 4002–4020.
200. Hattori, K.; Toda, S.; Imamishi, M.; Itou, S.; Nakajima, Y.; Washizuka, K.; Araki, T.; Hamashima, H.; Tomishima, Y.; Sakurai, M.; Matsui, S.; Imamura, E.; Ueshima, K.; Yamamoto, T.; Yamamoto, N.; Ishikawa, H.; Nakano, K.; Unami, N.; Hamada, K.; Matsumura, Y.; Takamura, F. Discovery of a Highly Potent and Selective Biphenylacylsulfonamide-Based β3-Adrenergic Receptor Agonists and Evaluation of Physical Properties as Potential Overactive Bladder Therapies. Part 5. *J. Med. Chem.* **2009,** *52,* 3063–3072.
201. Maruyama, T.; Onda, K.; Hayakawa, M.; Matsui, T.; Takasu, T.; Ohta, M. Discovery of Novel Acetanilide Derivatives as Potent and Selective β_3-Adrenergic Receptor Agonists. *Eur. J. Med. Chem.* **2009,** *44,* 2533–2543.
202. Maruyama, T.; Onda, K.; Hayakawa, M.; Seki, N.; Takahashi, T.; Moritomo, H.; Suzuki, T.; Matsui, T.; Takasu, T.; Nagase, I.; Ohta, M. Synthesis and Evaluation of Novel Phenoxypropanolamine Derivatives Containing Acetanilides as Potent and Selective β_3-Adrenergic Receptor Agonists. *Bioorg. Med. Chem.* **2009,** *17,* 3283–3294.
203. Maruyama, T.; Onda, K.; Suzuki, T.; Hayakawa, M.; Takahashi, T.; Matsui, T.; Takasu, T.; Nagase, I.; Ohta, M. Synthesis and Evaluation of N-Phenyl-(2-Aminothiazol-4-yl) acetamides With Phenoxypropanolamine Moiety as Selective β_3-Adrenergic Receptor Agonists. *Chem. Pharm. Bull.* **2012,** *60,* 647–658.
204. Maruyama, T.; Onda, K.; Hayakawa, M.; Suzuki, T.; Kimizuka, T.; Matsui, T.; Takasu, T.; Nagase, I.; Hamada, N.; Ohta, M. Synthesis and Evaluation of Novel Phenylethanolamine Derivatives Containing Acetanilides as Potent and Selective β_3-Adrenergic Receptor Agonists. *Chem. Pharm. Bull.* **2010,** *58,* 533–545.
205. Sacco, E.; Bientinesi, R.; Tienforti, D.; Racioppi, M.; Gulino, G.; D'Agostino, D.; Vittori, M.; Bassi, P. Discovery History and Clinical Development of Mirabegron for the Treatment of Overactive Bladder and Urinary Incontinence. *Expert Opin. Drug Discovery* **2014,** *9,* 433–448.
206. Takasu, T.; Ukai, M.; Sato, S.; Matsui, T.; Nagase, I.; Maruyama, T.; Sasamata, M.; Miyata, K.; Uchida, H.; Yamaguchi, O. Effect of (*R*)-2-(2-Aminothiazol-4-yl)-4′-{2-[(2-Hydroxy-2-Phenylethyl)Amino]ethyl} Acetanilide (YM178), a Novel Selective β_3 Adrenoceptor Agonist, on Bladder Function. *J. Pharmacol. Exp. Ther.* **2007,** *321,* 642–647.
207. Hatanaka, T.; Ukai, M.; Watanabe, M.; Someya, A.; Ohtake, A.; Suzuki, M.; Ueshima, K.; Sato, S.; Sasamata, M. *In Vitro* and *In Vivo* Pharmacological Profile of the Selective β_3-Adrenoceptor Agonist Mirabegron in Rats. *Naunyn Schmiedebergs Arch. Pharmacol.* **2013,** *386,* 247–253.
208. Gillespie, J. J.; Rouget, C.; Palea, S.; Granato, C.; Korstanje, C. Beta Adrenergic Modulation of Spontaneous Microcontractions and Electrical Field-Stimulated Contractions in Isolated Strips of Rat Urinary Bladder From Normal Animals and Animals With Partial Bladder Outflow Obstruction. *Naunyn Schmiedebergs Arch. Pharmacol.* **2015,** *388,* 719–726.
209. Svale, J.; Nordling, J.; Bouchelouche, K.; Andersson, K.-E.; Korstanje, C.; Bouchelouche, P. The Novel β_3-Adrenoceptor Agonist Mirabegron Reduces Carbachol-Induced Contractile Activity in Detrusor Tissue From Patients With Bladder Outflow Obstruction With or Without Detrusor Overactivity. *Eur. J. Pharmacol.* **2013,** *699,* 101–105.
210. Hatanaka, T.; Ukai, M.; Watanabe, M.; Someya, A.; Ohtake, A.; Suzuki, M.; Ueshima, K.; Kaku, S. Effect of Mirabegron, a Novel β_3-Adrenoceptor Agonist, on Bladder Function During Storage Phase in Rats. *Naunyn Schmiedebergs Arch. Pharmacol.* **2013,** *386,* 71–78.
211. Aizawa, N.; Homma, Y.; Igawa, Y. Effects of Mirabegron, a Novel β_3-Adrenoceptor Agonist, on Primary Bladder Afferent Activity and Bladder Microcontractions in Rats Compared With the Effects of Oxybutynin. *Eur. Urol.* **2012,** *62,* 1165–1173.
212. Sawada, N.; Nomiya, M.; Hood, B.; Koslov, D.; Zarifpour, M.; Andersson, K.-E. Protective Effect of a β_3-Adrenoceptor Agonist on Bladder Function in a Rat Model of Chronic Bladder Ischemia. *Eur. Urol.* **2013,** *64,* 664–671.
213. Hatanaka, T.; Ukai, M.; Watanabe, M.; Someya, A.; Ohtake, A.; Suzuki, M.; Ueshima, K.; Sato, S.; Masuda, N. Pharmacological Profile of the Selective β_3-Adrenoceptor Agonist Mirabegron in Cynomolgus Monkeys. *Naunyn Schmiedebergs Arch. Pharmacol.* **2013,** *386,* 1001–1008.
214. Nokhodchi, A.; Raja, S.; Patel, P.; Asare-Addo, K. The Role of Oral Controlled Release Matrix Tablets in Drug Delivery Systems. *BioImpacts* **2012,** *2,* 175–187.
215. Krauwinkel, W.; van Dijk, J.; Schaddelee, M.; Eltink, C.; Meijer, J.; Strabach, G.; van Marle, S.; Kerbusch, V.; van Gelderen, M. Pharmacokinetic Properties of Mirabegron, a β_3-Adrenoceptor Agonist: Results From Two Phase I, Randomized, Multiple-Dose Studies in Healthy Young and Elderly Men and Women. *Clin. Ther.* **2012,** *34,* 2144–2160.
216. Takusagawa, S.; van Lier, J. J.; Suzuki, K.; Nagata, M.; Meijer, J.; Krauwinkel, W.; Schaddelee, M.; Sekiguchi, M.; Miyashita, A.; Iwatsubo, T.; van Gelderen, M.; Usui, T. Absorption, Metabolism and Excretion of [^{14}C]Mirabegron (YM178), a Potent and Selective β_3-Adrenoceptor Agonist, After Oral Administration to Healthy Male Volunteers. *Drug Metab. Dispos.* **2012,** *40,* 815–824.
217. Dickinson, J.; Lewand, M.; Sawamoto, T.; Krauwinkel, W.; Schaddelee, M.; Keirns, J.; Kerbusch, V.; Moy, S.; Meijer, J.; Kowalski, D.; Morton, R.; Lasseter, K.; Riff, D.; Kupcova, V.; Gelderen, M. Effect of Renal or Hepatic Impairment on the Pharmacokinetics of Mirabegron. *Clin. Drug Investig.* **2012,** *33,* 11–23.
218. Takusagawa, S.; Yajima, K.; Miyashita, A.; Uehara, S.; Iwatsubo, T.; Usui, T. Identification of Human Cytochrome P450 Isoforms and Esterases Involved in the Metabolism of Mirabegron, a Potent and Selective β_3-Adrenoceptor Agonist. *Xenobiotica* **2012,** *42,* 957–967.
219. Lee, J.; Moy, S.; Meijer, J.; Krauwinkel, W.; Sawamoto, T.; Kerbusch, V.; Kowalski, D.; Roy, M.; Marion, A.; Takusagawa, S.; van Gelderen, M.; Keirns, J. Role of Cytochrome P450 Isoenzymes 3A and 2D6 in the *In Vivo* Metabolism of Mirabegron, a β_3-Adrenoceptor Agonist. *Clin. Drug Investig.* **2013,** *33,* 429–440.

220. Takusagawa, S.; Miyashita, A.; Iwatsubo, T.; Usui, T. *In Vitro* Inhibition and Induction of Human Cytochrome P450 Enzymes by Mirabegron, a Potent and Selective β_3-Adrenoceptor Agonist. *Xenobiotica* **2012,** *42,* 1187–1196.
221. Tyagi, P.; Tyagi, V. Mirabegron, a β_3-Adrenoceptor Agonist for the Potential Treatment of Urinary Frequency, Urinary Incontinence or Urgency Associated With Overactive Bladder. *IDrugs* **2010,** *13,* 713–722.
222. Tyagi, P.; Tyagi, V.; Chancellor, M. Mirabegron: A Safety Review. *Expert. Opin. Drug Saf.* **2011,** *10,* 287–294.
223. Rosa, G. M.; Ferrero, S.; Nitti, V. W.; Wagg, A.; Saleem, T.; Chapple, C. R. Cardiovascular Safety of β_3-Adrenoceptor Agonists for the Treatment of Patients with Overactive Bladder Syndrome. *Eur. Urol.* **2016,** *69,* 311–323.
224. Chapple, C. R.; Amarenco, G.; Aramburu, M. A. L.; Everaert, K.; Liehne, J.; Lucas, M.; Vik, V.; Ridder, A.; Snijder, R.; Yamaguchi, O. A Proof-of-Concept Study: Mirabegron, a New Therapy for Overactive Bladder. *Neurourol. Urodyn.* **2012,** *32,* 1116–1122.
225. Malik, M.; van Gelderen, E. M.; Lee, J. H.; Kowalski, D. L.; Yen, M.; Goldwater, R.; Mujais, S. K.; Schaddelee, M. P.; de Koning, P.; Kaibara, A.; Moy, S. S.; Kierns, J. J. Proarrhythmic Safety of Repeat Doses of Mirabegron in Healthy Subjects: A Randomized, Double-Blind, Placebo-, and Active-Controlled Thorough QT Study. *Clin. Pharmacol. Ther.* **2012,** *92,* 696–706.
226. Vij, M.; Drake, M. J. Clinical Use of the β_3 Adrenoceptor Agonist Mirabegron in Patients With Overactive Bladder Syndrome. *Ther. Adv. Urol.* **2015,** *7,* 241–248.
227. Thiagamoorthy, G.; Kotes, S.; Zacche, M.; Cardozo, L. The Efficacy and Tolerability of Mirabegron, a β_3 Adrenoceptor Agonist, in Patients With Symptoms of Overactive Bladder. *Ther. Adv. Urol.* **2016,** *8,* 38–46.
228. Khullar, V.; Cambronero, J.; Angulo, J. C.; Wooning, M.; Blauwet, M. B.; Dorrepaal, C.; Martin, N. E. Efficacy of Mirabegron in Patients With and Without Prior Antimuscarinic Therapy for Overactive Bladder: A Post hoc Analysis of a Randomized European-Australian Phase 3 Trial. *BMC Urol.* **2013,** *13,* 45.
229. Meanwell, N. A. Improving Drug Candidates by Design: A Focus on Physicochemical Properties as a Means of Improving Compound Disposition and Safety. *Chem. Res. Toxicol.* **2011,** *24,* 1420–1456.
230. Morgan, P.; Van Der Graaf, P. H.; Arrowsmith, J.; Feltner, D. E.; Drummond, K. S.; Wegner, C. D.; Street, S. D. A. Can the Flow of Medicines be Improved? Fundamental Pharmacokinetic and Pharmacological Principles Toward Improving Phase II Survival. *Drug Discov. Today* **2012,** *17,* 419–424.
231. Cook, D.; Brown, D.; Alexander, R.; March, R.; Morgan, P.; Satterthwaite, G.; Pangalos, M. N. Lessons Learned From the Fate of AstraZeneca's Drug Pipeline: A Five-Dimensional Framework. *Nat. Rev. Drug Discov.* **2014,** *13,* 419–431.
232. Rouget, C.; Bardou, M.; Breuiller-Fouche, M.; Loustalot, C.; Qi, H.; Naline, E.; Croci, T.; Carbol, D.; Advenier, C.; Leroy, M. J. β_3-Adrenoceptor Is the Predominant β-Adrenoceptor Subtype in Human Myometrium and its Expression Is up-Regulated in Pregnancy. *J. Clin. Endocrinol. Metab.* **2005,** *90,* 1644–1650.
233. Croci, T.; Cecchi, R.; Marini, P.; Rouget, C.; Viviani, N.; Germain, G.; Guagnini, F.; Fradin, Y.; Descamps, L.; Pascal, M.; Advenier, C.; Breuiller-Fouche, M.; Leroy, M.-J.; Bardou, M. *In Vitro* and *In Vivo* Pharmacological Characterization of Ethyl-4-{trans-4-[((2S)-2-Hydroxy-3-{4-Hydroxy-3[(Methylsulfonyl)amino]-Phenoxy}propyl) Amino]cyclohexyl}benzoate Hydrochloride (SAR150640), A New Potent and Selective Human β3-Adrenoceptor Agonist for the Treatment of Preterm Labor. *J. Pharmacol. Exp. Ther.* **2007,** *321,* 1118–1126.
234. Bardou, M.; Rouget, C.; Breuiller-Fouche, M.; Loustalot, C.; Naline, E.; Sagot, P.; Frydman, R.; Morcillo, E. J.; Advenier, C.; Leroy, M.-J.; Morrison, J. J. Is the beta3-Adrenoceptor (ADRB3) a Potential Target for Uterorelaxant drugs? *BMC Pregnancy Childbirth* **2007,** *7,* S14.
235. Shvarts, G. Y.; Shvarts, P. G.; Plotnikov, A. N.; Savvin, D. Y. Drugs for the Treatment of Overactive Bladder Syndrome: Present and Future (Review). *Pharm. Chem. J.* **2013,** *46* (12), 3–10.
236. Karmarkar, R.; Khullar, V. Emerging Drugs for Overactive Bladder. *Expert Opin. Emerg. Drugs* **2015,** *20,* 613–624.
237. Maman, K.; Aballea, S.; Nazir, J.; Desroziers, K.; Neine, M.-E.; Siddiqui, E.; Odeyemi, I.; Hakimi, Z. Comparative Efficacy and Safety of Medical Treatments for the Management of Overactive Bladder: A Systematic Literature Review and Mixed Treatment Comparison. *Eur. Urol.* **2014,** *65,* 755–765.
238. Heisen, M.; Baeten, S. A.; Verheggen, B. G.; Stoelzel, M.; Hakimi, Z.; Ridder, A.; van Maanen, R.; Stolk, E. A. Patient and Physician Preferences for Oral Pharmacotherapy for Overactive Bladder: Two Discrete Choice Experiments. *Curr. Med. Res. Opin.* **2016,** *32,* 787–796.
239. De Nunzio, C.; Presicce, F.; Pirozzi, L.; Castellan, P.; Schips, L.; Cindolo, L.; Lombardo, R.; Tubaro, A. The Current Indications and the Benefits of Combining a β_3-Agonist with an Anticholinergic for the Treatment of OAB. *Curr. Drug Targets* **2015,** *16,* 1198–1206.

This page intentionally left blank

COMPREHENSIVE MEDICINAL CHEMISTRY III

This page intentionally left blank

COMPREHENSIVE MEDICINAL CHEMISTRY III

EDITORS-IN-CHIEF

Samuel Chackalamannil
Rutgers University, Piscataway, NJ, United States

David Rotella
Montclair State University, Montclair, NJ, United States

Simon E. Ward
University of Sussex, Brighton, United Kingdom

VOLUME 8

CASE HISTORIES IN RECENT DRUG DISCOVERY

VOLUME EDITOR

Joerg Holenz
R&D Neurosciences TAU, GSK, PA, United States

ELSEVIER

Elsevier
Radarweg 29, PO Box 211, 1000 AE Amsterdam, The Netherlands
The Boulevard, Langford Lane, Kidlington, Oxford OX5 1GB, United Kingdom
50 Hampshire Street, 5th Floor, Cambridge, MA 02139, United States

Copyright © 2017 Elsevier Ltd. All rights reserved

No part of this publication may be reproduced or transmitted in any form or by any means, electronic or mechanical, including photocopying, recording, or any information storage and retrieval system, without permission in writing from the publisher. Details on how to seek permission, further information about the Publisher's permissions policies and our arrangements with organizations such as the Copyright Clearance Center and the Copyright Licensing Agency, can be found at our website: www.elsevier.com/permissions.

This book and the individual contributions contained in it are protected under copyright by the Publisher (other than as may be noted herein).

Notices
Knowledge and best practice in this field are constantly changing. As new research and experience broaden our understanding, changes in research methods, professional practices, or medical treatment may become necessary.

Practitioners and researchers may always rely on their own experience and knowledge in evaluating and using any information, methods, compounds, or experiments described herein. In using such information or methods they should be mindful of their own safety and the safety of others, including parties for whom they have a professional responsibility.

To the fullest extent of the law, neither the Publisher nor the authors, contributors, or editors, assume any liability for any injury and/or damage to persons or property as a matter of products liability, negligence or otherwise, or from any use or operation of any methods, products, instructions, or ideas contained in the material herein.

Library of Congress Cataloging-in-Publication Data
A catalog record for this book is available from the Library of Congress

British Library Cataloguing-in-Publication Data
A catalogue record for this book is available from the British Library

ISBN 978-0-12-803200-8

For information on all publications visit our website at
http://store.elsevier.com

Working together
to grow libraries in
developing countries
www.elsevier.com • www.bookaid.org

Publisher: Oliver Walter
Acquisition Editor: Rachel Gerlis
Content Project Manager: Gemma Tomalin
Associate Content Project Manager: Marise Willis
Designer: Mark Rogers

Printed and bound in the United Kingdom

PREFACE

Previous editions of *Comprehensive Medicinal Chemistry*, published in 1990 and 2006, provided an integrated reference source that encompassed all major aspects of drug discovery research. The third edition follows this tradition and considerably expands its scope and content.

The trailblazing scientific discoveries of the 21st century have brought new opportunities for drug discovery research. The discipline of medicinal chemistry continues to evolve as it adapts to these new opportunities and strives to solve new challenges. Covered in the new edition are not only the breakthrough therapies of the past decade in cancer, hepatitis C, heart failure, dyslipidemia, cystic fibrosis, multiple sclerosis, HIV, etc., but also extensive discussion of new business models in drug discovery research, shifting industry demographics, emerging technologies, *in silico* drug discovery tools, experimental ADME and toxicology, and biologics medicine. The tone of this edition is prospective in which contributors identify outstanding issues and paths forward in their area of expertise. The aim is to provide drug discovery scientists in industry, government, academia, and research organizations with a contemporary global perspective on the field that includes a look ahead in selected areas.

The eight individual volumes fulfill these objectives and include extensive discussion of biomolecular therapeutics, drug targeting and delivery, development of chemical biology tools, data collection and analysis, *in silico* models as predictors for biological properties, identification/validation of new targets, approaches to quantify target engagement, new methods for synthesis of drug candidates such as green chemistry, development of novel scaffolds for drug discovery, and the role of regulatory agencies in drug discovery.

The individual volume editors have done an outstanding job to identify topics and contributors to meet these goals and we thank them for their hardwork and diligence. In volume 1, Ana Martinez and Carmen Gil recruited an international group of contributors who provide chapters on the emerging role of organizations other than traditional pharmaceutical companies in drug discovery, the evolving science of chemical biology, and new organic chemistry contributions to the discipline. In volume 2, Helmut Buschmann, Norbert Handler, and Andrea Wolkerstorfer have accomplished a seemingly impossible task and attracted world-leading experts across the wide field of drug discovery enabling technologies, covering contemporary thinking in a wide range of key disciplines that enable modern medicinal chemistry and drug discovery and development. The computational enabling technologies are the focus of volume 3, in which Andy Davis and Colin Edge have assembled chapters covering both ligand-based and protein structure–based advances as well as exciting new methodologies and case studies exploiting these. Alan Wilson identified experts in the fields of pharmacokinetics and toxicology who describe a wide range of contemporary advances in prediction and analysis of pharmaceutical properties and drug safety in volume 4. In volume 5, Ian Collins, Louis Lombardo, and Will Watkins have assembled leading experts to discuss high impact drug discovery accomplishments over the past decade in cancer chemotherapeutics, immunology and inflammation, and infectious diseases therapeutic areas. Ved Srivastava edited volume 6 on biologic medicines, a significant and rapidly evolving area where medicinal chemistry plays an important role. The chapters in this volume provide timely information on not only protein-based drugs, such as monoclonal antibodies and therapeutic proteins, but also peptides and nucleic acid–based therapeutics. Volume 7, edited by Adrian Hall, Santhosh Neelamkavil, and Rob Jones, presents a detailed account of the major advances in CNS, metabolic, and cardiovascular fields over the past decade and the promising new opportunities. Joerg Holenz edited volume 8 that presents case histories of successful drug discovery and strategic differentiation that have resulted in commercialized drugs and candidates in advanced clinical trials.

We are truly grateful to the publishing team at Elsevier that includes Gemma Tomalin, Rachel Gerlis, Marise Willis, and Sean Simms for their assistance and support throughout the process. With their expertise, this project became what we believe is a noteworthy and valuable resource for the discipline of medicinal chemistry. We look forward to the response and feedback of our colleagues who will use this information in their own work.

Samuel Chackalamannil, David P. Rotella, and Simon E. Ward

EDITORS-IN-CHIEF: BIOGRAPHIES

Dr. Samuel Chackalamannil

Dr. Chackalamannil obtained his PhD in chemistry from Yale University in 1984 and subsequently worked in drug discovery research at Schering-Plough Corporation and Merck Research Laboratories, where he was a distinguished fellow when he left in 2011. Since then, he has been teaching at Ernest Mario School of Pharmacy, Rutgers University, New Jersey.

Dr. Chackalamannil has significant accomplishments in the discovery of new medicines. He led the discovery of vorapaxar (Zontivity®), an FDA-approved antiplatelet drug for the prevention of heart attack and stroke. His group also discovered a PDE-5 inhibitor clinical candidate dasantafil and an adenosine A2a antagonist clinical candidate for the treatment of Parkinson's disease. Altogether, he was responsible for the discovery of nine development candidates in cardiovascular, central nervous system, and metabolic disease areas.

Dr. Chackalamannil is a coinventor of 62 allowed US patents and numerous patent applications worldwide. He has published 81 peer-reviewed articles and has coauthored a book. He has also given numerous lectures at international meetings and academic institutions.

Dr. Chackalamannil is a two-time recipient of the Thomas Alva Edison Award for Emerging Technology Patent and a two-time recipient of the Presidential Award for Discovery at Schering-Plough Research Institute. He has chaired several sessions at American Chemical Society national meetings and Gordon Research Conference on Medicinal Chemistry and was an organizer for Chemistry as a Life Science Symposium.

Dr. David Rotella

Dr. Rotella earned a PhD in medicinal chemistry from The Ohio State University and carried out postdoctoral research in organic chemistry at Penn State University. He joined the faculty at Montclair State University in July 2011 as the Margaret and Herman Sokol Professor of medicinal chemistry after a successful career in the pharmaceutical industry. He is an expert in the discovery and optimization of small molecule drug candidates for use in metabolic, cardiovascular, cancer, and central nervous system diseases. His current research is focused on discovering new lead compounds for use in parasitic and central nervous system diseases. He has coedited the seventh edition of *Burger's Medicinal Chemistry* and is a senior editor for the Royal Society of Chemistry's Drug Discovery book series. He has authored over 40 peer-reviewed articles, is an inventor on 8 issued US patents, and has contributed 10 book chapters.

Simon E. Ward

Simon Ward has an MA in natural sciences and PhD in synthetic organic chemistry from Cambridge University, UK. He has a wide-ranging experience of drug discovery in both large and small companies (GlaxoSmithKline, Knoll Pharmaceuticals, Vernalis, Chiroscience, BioCrea) and specialist experience of discovering and developing drugs for central nervous system indications. He has led multidisciplinary project teams and medicinal chemistry groups from target identification through to early clinical studies, delivering multiple clinical development candidates across indications. He is a fellow of the Royal Society of Chemistry. He is currently a professor of medicinal chemistry at the University of Sussex, UK, and the director of the Sussex Drug Discovery Centre, which he established within the University of Sussex in 2010.

This page intentionally left blank

CONTRIBUTORS TO VOLUME 8

W Albrecht
c-a-i-r biosciences GmbH, Ulm, Germany

A Ali
Rahway, NJ, United States

D J Anderson
Cleave Biosciences, Burlingame, CA, United States

S M Bauer
Eberhard Karls University, Tuebingen, Germany

A Blaukat
Merck KGaA, Darmstadt, Germany

A A Boezio
Amgen Inc., Cambridge, MA, United States

M H Bolli
Actelion Pharmaceuticals Ltd, Allschwil, Switzerland

C Boss
Actelion Pharmaceuticals Ltd, Allschwil, Switzerland

D C Brookings
UCB Pharma, Slough, United Kingdom

J N Burrows
Medicines for Malaria Venture, Geneva, Switzerland

S A Charman
Monash University, Parkville, VIC, Australia

B L Chenard
Neurogen Corporation, a subsidiary of Ligand Pharmaceuticals, Branford, CT, United States; and Chenab LLC, Waterford, CT 08385

J Ciavarri
Takeda Pharmaceuticals International Co., Cambridge, MA, United States

J N Cumming
Merck & Co., Inc., Kenilworth, NJ, United States

D Doller
Neurogen Corporation, a subsidiary of Ligand Pharmaceuticals, Branford, CT, United States; and Alcyoneus/ScienceWorks, Sparta, NJ, United States

J Duffy
Rahway, NJ, United States

K Edman
AstraZeneca, Gothenburg, Sweden

M R V Finlay
AstraZeneca, Cambridge, United Kingdom

Y R Freund
Anacor Pharmaceuticals, Inc., Palo Alto, CA, United States

J Gatfield
Actelion Pharmaceuticals Ltd, Allschwil, Switzerland

F Giordanetto
D E Shaw Research LLC, New York, NY, United States

T Hansson
AstraZeneca, Gothenburg, Sweden

J-C Harmange
Amgen Inc., Cambridge, MA, United States; and Third Rock Ventures, Boston, MA, United States

M P Hay
The University of Auckland, Auckland, New Zealand

K O Hicks
The University of Auckland, Auckland, New Zealand

K J Hodgetts
Neurogen Corporation, a subsidiary of Ligand Pharmaceuticals, Branford, CT, United States; and Brigham and Women's Hospital and Harvard Medical School, Cambridge, MA, United States

M Iglarz
Actelion Pharmaceuticals Ltd, Allschwil, Switzerland

R T Jacobs
Anacor Pharmaceuticals, Inc., Palo Alto, CA, United States

H Kawasaki
Central Pharmaceutical Research Institute, Japan Tobacco, Takatsuki, Japan

J E Krause
Neurogen Corporation, a subsidiary of Ligand Pharmaceuticals, Branford, CT, United States; and Alcyoneus/ScienceWorks, Sparta, NJ, United States

S Langston
Takeda Pharmaceuticals International Co., Cambridge, MA, United States

S A Laufer
Eberhard Karls University, Tuebingen, Germany

J O Link
Gilead Sciences, Inc., Foster City, CA, United States

J Mathias
Worldwide Medicinal Chemistry, Pfizer Worldwide Research and Development, Cambridge, United States

D Matthews
Medicines for Malaria Venture, Geneva, Switzerland

S Nomura
Mitsubishi Tanabe Pharma Corporation, Toda, Japan

Alexander Pasternak
Merck & Co., Inc., Kenilworth, NJ, United States

E A Peterson
Amgen Inc., Cambridge, MA, United States; and Biogen, Cambridge, MA, United States

D Pettersen
AstraZeneca Mölndal, Mölndal, Sweden

M A Phillips
University of Texas Southwestern Med Center, Dallas, TX, United States

K G Pike
AstraZeneca Oncology Chemistry, Cambridge, United Kingdom

P K Rathod
University of Washington, Seattle, WA, United States

M Rolfe
Cleave Biosciences, Burlingame, CA, United States

T Rueckle
Medicines for Malaria Venture, Geneva, Switzerland

O Schadt
Merck KGaA, Darmstadt, Germany

J D Scott
Merck & Co., Inc., Kenilworth, NJ, United States

P Sjö
AstraZeneca, Gothenburg, Sweden

M J Sofia
Arbutus Biopharma, Inc., Doylestown, PA, United States

A W Stamford
Merck & Co., Inc., Rahway, NJ, United States

C O Strickland
Merck & Co., Inc., Kenilworth, NJ, United States

J Tarrant
Neurogen Corporation, a subsidiary of Ligand Pharmaceuticals, Branford, CT, United States; and Harding University, Searcy, AR, United States

A Treiber
Actelion Pharmaceuticals Ltd, Allschwil, Switzerland

S Venkatraman
Merck Research Laboratories, Kenilworth, NJ, United States

R A Ward
AstraZeneca, Cambridge, United Kingdom

W R Wilson
The University of Auckland, Auckland, New Zealand

D J Wustrow
Cleave Biosciences, Burlingame, CA, United States

L Xing
Worldwide Medicinal Chemistry, Pfizer Worldwide Research and Development, Cambridge, United States

T Yamaguchi
Central Pharmaceutical Research Institute, Japan Tobacco, Takatsuki, Japan

B K S Yeung
Novartis Institute for Tropical Diseases, Singapore

Y-K Zhang
Anacor Pharmaceuticals, Inc., Palo Alto, CA, United States

H-J Zhou
Cleave Biosciences, Burlingame, CA, United States

CONTENTS OF VOLUME 8

Preface *v*

Editors-in-Chief: Biographies *vii*

Contributors to Volume 8 *ix*

Editorial Board *xiii*

Introduction *xv*

8.01 Medicinal Chemistry Case History: Osimertinib (AZD9291) 1
R A Ward and M R V Finlay

8.02 Trametinib 33
H Kawasaki and T Yamaguchi

8.03 Discovery of the Hypoxia-Activated Prodrug SN30000 58
M P Hay, K O Hicks, and W R Wilson

8.04 The Discovery of First-in-Class Inhibitors of the Nedd8-Activating Enzyme (NAE) and the Ubiquitin-Activating Enzyme (UAE) 95
J Ciavarri and S Langston

8.05 The Discovery of p97 Inhibitors 113
D J Wustrow, D J Anderson, M Rolfe, and H-J Zhou

8.06 Discovery of AMG 337: Using Structure Guided Scaffold Hybridization to Optimize Physicochemical Properties and Target Coverage of a MET Kinase Inhibitor 138
A A Boezio, E A Peterson, and J-C Harmange

8.07 Discovery of AZD0156: The First Potent and Selective Inhibitor of ATM Kinase for Clinical Evaluation 161
K G Pike

8.08 Tepotinib 178
O Schadt and A Blaukat

8.09 Verubecestat 204
A W Stamford, J N Cumming, J D Scott, and C O Strickland

8.10 The Discovery of Macitentan—A Standard Medicinal Chemistry Program? 252
M H Bolli, C Boss, J Gatfield, M Iglarz, and A Treiber

8.11 Case Histories: Anacetrapib 284
A Ali and J Duffy

8.12 Discovery of ROMK Inhibitor MK-7145: A Novel Mechanism Diuretic 308
Alexander Pasternak

8.13 Fragment-Based Discovery of AZD2716: A Novel, Potent Secreted Phospholipase A_2 ($sPLA_2$) Inhibitor for the Treatment of Coronary Artery Disease 339
F Giordanetto and D Pettersen

8.14 Canagliflozin 349
S Nomura

8.15 The Discovery and Development of *Seletalisib*: A Potent and Selective PI3Kδ Inhibitor for Inflammatory Diseases 366
D C Brookings

8.16 Medicinal Chemistry Case History: Structure-Based Drug Design of Oral and Inhaled p38 MAP Kinase Inhibitors as Clinical Candidates 408
L Xing and J Mathias

8.17 Are Two Better Than One in Rheumatoid Arthritis? Development of Dual p38α MAPK/PDE-4 Inhibitors for Treatment of TNFα-Driven Diseases 431
W Albrecht, S M Bauer, and S A Laufer

8.18 The Discovery of Potent and Selective Nonsteroidal Glucocorticoid Receptor Modulators AZD5423 and AZD7594, for the Inhaled Treatment of Respiratory Diseases 450
P Sjö, T Hansson, and K Edman

8.19 The Discovery of the MCH-1 Receptor Antagonist NGD-4715 for the Potential Treatment of Obesity 488
J Tarrant, K J Hodgetts, B L Chenard, J E Krause, and D Doller

8.20 Case History: AN5568 (SCYX-7158) 516
Y-K Zhang, Y R Freund, and R T Jacobs

8.21 KAE609 (Cipargamin): Discovery of Spiroindolone Antimalarials 529
B K S Yeung

8.22 Medicinal Chemistry Case History: Discovery of the Dihydroorate Dehydrogenase Inhibitor DSM265 as an Antimalarial Drug Candidate 544
M A Phillips, P K Rathod, T Rueckle, D Matthews, J N Burrows, and S A Charman

8.23 Harvoni: A Combination Therapy for Curing HCV 558
M J Sofia and J O Link

8.24 Discovery of Boceprevir and Narlaprevir: Ketoamide-Derived HCV NS3 Serine Protease Inhibitors for the Treatment of Chronic Hepatitis C 583
S Venkatraman

Index 609

EDITORIAL BOARD

EDITORS-IN-CHIEF

Samuel Chackalamannil
Rutgers University, Piscataway, NJ, United States

David Rotella
Montclair State University, Montclair, NJ, United States

Simon E. Ward
University of Sussex, Brighton, United Kingdom

VOLUME 1
GENERAL PERSPECTIVE - THE FUTURE OF DRUG DISCOVERY

VOLUME EDITORS

Ana Martinez
Centro de Investigaciones Biologicas-CSIC, Madrid, Spain

Carmen Gil
Centro de Investigaciones Biologicas-CSIC, Madrid, Spain

VOLUME 2
DRUG DISCOVERY TECHNOLOGIES

VOLUME EDITORS

Helmut Buschmann
Savira Pharmaceuticals GmbH, Vienna, Austria

Norbert Handler
Savira Pharmaceuticals GmbH, Vienna, Austria

Andrea Wolkerstorfer
Baxalta Innovations GmbH — Now part of Shire, Vienna, Austria

VOLUME 3
IN SILICO DRUG DISCOVERY TOOLS

VOLUME EDITORS

Andrew M. Davis
AstraZeneca R&D Gothenburg, Gothenburg, Sweden

Colin Edge
GlaxoSmithKline Medicines Research Centre, Stevenage, United Kingdom

VOLUME 4
EXPERIMENTAL ADME AND TOXICOLOGY

VOLUME EDITOR

Alan G. E. Wilson
Lexicon Pharmaceuticals, The Woodlands, TX, United States

VOLUME 5
CANCER, IMMUNOLOGY AND INFLAMMATION, AND INFECTIOUS DISEASE

VOLUME EDITORS

Ian Collins
The Institute of Cancer Research, London, United Kingdom

William Watkins
Gilead Sciences, Foster City, CA, United States

Louis J. Lombardo
Bristol-Myers Squibb Research and Development, Princeton, NJ, United States

VOLUME 6
BIOLOGICS MEDICINE

VOLUME EDITOR

Ved Srivastava
Intarcia Therapeutics, Durham, NC, United States

VOLUME 7
CNS, PAIN, METABOLIC SYNDROME, CARDIOVASCULAR, TISSUE FIBROSIS AND URINARY INCONTINENCE

VOLUME EDITORS

Adrian Hall
UCB BioPharma SPRL, Brussels, Belgium

Santhosh Neelamkavil
Merck Research Laboratories, Kenilworth, NJ, United States

Rob Jones
BlackThorn Therapeutics, San Francisco, CA, United States

VOLUME 8
CASE HISTORIES IN RECENT DRUG DISCOVERY

VOLUME EDITOR

Joerg Holenz
R&D Neurosciences TAU, GSK, PA, United States

INTRODUCTION

For Claudia

Challenged by the decrease in productivity mainly due to high clinical attrition rates, pharmaceutical research, and development has fundamentally changed within the recent years. Disease understanding and target validation based on genetic evidence have significantly improved and lay the ground for testing selective modulation of relevant pathological pathways in stratified patient populations in the clinic. To name a few examples, advances in biology such as the ready availability of inducible pluripotent stem cells (iPSCs) along with gene editing (CRISPR-CAS9) have revolutionized phenotypic high content screening, and Chemical Biology has emerged as an important discipline for generating novel target hypotheses to selectively modulate disease relevant phenotypes.

These major drug discovery paradigm changes, but also the increased advances in the field of biological drugs (vaccines, antibodies, or cell-and-gene therapy), have put enormous pressure on Medicinal Chemistry to innovate itself and respond by demonstrating not only that chemical entities can be successfully developed for demanding targets but also that those drugs offer significant advantages in areas of high unmet medical need.

In this volume, I am very proud to present 24 powerful "answers" of distinguished Medicinal Chemists to the challenge of how to tackle the increasing demands for candidate drugs with respect to quality, disease relevance, and translatability successfully. Case histories have always represented a fascinating opportunity for the reader to learn: from "tips and tricks" how to solve a specific problem to best Medicinal Chemistry practices and strategies. At all major conferences, Medicinal Chemistry success stories are among the keynote lectures to attract and inspire audiences and to jointly celebrate learnings. I have been very fortunate to work with such an outstanding team of authors from academia, biotech, and big pharma to deliver what I believe is a very substantial, comprehensive, and up-to-date reference for successful applied Medicinal Chemistry.

Special thanks go to my series editor Samuel Chackalamannil, David P. Rotella, and the entire Elsevier team for their continuous support and their trust in my concept.

Joerg Holenz
Head of Neuroscience Virtual Proof-of-Concept DPU
R&D Neurosciences TAU, GSK, Collegeville,
Pennsylvania, 19426-0989, United States

This page intentionally left blank

PERMISSION ACKNOWLEDGMENTS

The following material is reproduced with kind permission of Taylor & Francis

Scheme 2 Cellular Imaging in Drug Discovery: Biomolecular Imaging and Informatics (HCS, HCA, HCI)
Figure 2 Past Present Future
Figure 5 Past Present Future
Figure 6 Past Present Future
www.taylorandfrancisgroup.com

The following material is reproduced with kind permission of Oxford University press

Table 1 Targeting G-quadruplex Nucleic Acids for Cancer Therapy
Table 2 Targeting G-quadruplex Nucleic Acids for Cancer Therapy
Figure 1 Protein Structure Prediction and Homology Modelling
www.oup.com

The following material is reproduced with kind permission of American Association for the Advancement of Science

Figure 3b,c Cellular Imaging in Drug Discovery: Biomolecular Imaging and Informatics (HCS, HCA, HCI)
www.aaas.org

The following material is reproduced with kind permission of Nature Publishing Group

Table 4 Use of Stem Cells in Toxicology
Table 6 Use of Stem Cells in Toxicology
Figure 17 Strategy and Tactics for Designing Analogs; Biochemical Characterization of the Large Molecules
Figure 30 Strategy and Tactics for Designing Analogs; Biochemical Characterization of the Large Molecules
Figure 2 Cellular Imaging in Drug Discovery: Biomolecular Imaging and Informatics (HCS, HCA, HCI)
Figure 3a Cellular Imaging in Drug Discovery: Biomolecular Imaging and Informatics (HCS, HCA, HCI)
Figure 4 Cellular Imaging in Drug Discovery: Biomolecular Imaging and Informatics (HCS, HCA, HCI)
Figure 5a Cellular Imaging in Drug Discovery: Biomolecular Imaging and Informatics (HCS, HCA, HCI)
Figure 9a Cellular Imaging in Drug Discovery: Biomolecular Imaging and Informatics (HCS, HCA, HCI)
Figure 20 Epigenetics: Novel Therapeutics Targeting Epigenetics
Figure 1 UCB5857
Figure 6 Empirical and Physics Based Calculations of Physical Properties
Figure 4 Progress and Challenges in the Development if PET Ligands to Aid CNS Drug Discovery
http://www.nature.com

8.01 Medicinal Chemistry Case History: Osimertinib (AZD9291)

RA Ward and MRV Finlay, AstraZeneca, Cambridge, United Kingdom

© 2017 Elsevier Ltd. All rights reserved.

8.01.1	**The Role of Epidermal Growth Factor Receptor (EGFR) Biology in Nonsmall Cell Lung Cancer (NSCLC)**	1
8.01.2	**The Discovery of Osimertinib (AZD9291)**	2
8.01.2.1	EGFR Mutant-Selective Hypothesis	2
8.01.2.2	Identification of a Mutant-Selective Lead Series	4
8.01.2.3	Lead Optimization to the Discovery of Osimertinib	11
8.01.3	**Emerging Clinical Data of Osimertinib**	23
8.01.4	**Current Progress of EGFR-Mutant Inhibitors**	24
8.01.5	**Learnings, Future Challenges, and Opportunities**	26
Acknowledgments		30
References		30

Abbreviations

DM Double mutant
EGFR Epidermal growth factor receptor
GSH Glutathione
LC-MS Liquid chromatography–mass spectrometry
LLE Ligand lipophilicity efficiency
NSCLC Nonsmall cell lung cancer
PK Pharmacokinetics
QSPR Quantitative structure property relationship
SAR Structure–activity relationships
SM Single mutant
TKI Tyrosine kinase inhibitor
WT Wild-type

8.01.1 The Role of Epidermal Growth Factor Receptor (EGFR) Biology in Nonsmall Cell Lung Cancer (NSCLC)

Ligand induced activation of receptor tyrosine kinases such as the EGFR promotes activation of downstream pathways, driving proproliferative and survival cellular signals.[1] In a subset of NSCLC, the tumor is characterized by EGFR activating mutations (AMs) such as an exon-19 deletion (eg, E746-A750) or an L858R single point mutation, which largely renders the receptor constitutively activated even in the absence of ligand binding.[2] This results in sustained hyper-activation of signaling pathways downstream of EGFR such as protein kinase B and extracellular signal-regulated kinase, and promotes oncogenic dependency of the cell on these proproliferative and survival drives from the mutated EGFR. Therefore, abrogation of activated EGFR signaling using small molecule inhibitors results in a pronounced tumor cell apoptosis and inhibition of tumor growth through the prevention of signaling and therefore reduced oncogenic drive.

"First-generation" EGFR tyrosine kinase inhibitors (TKIs), such as gefitinib and erlotinib, are now National Comprehensive Cancer Network recommended therapies in NSCLC patients with AMs in EGFR.[3,4] Approximately 70% of patients respond to these drugs with significant tumor shrinkage but eventually develop resistance within 10–16 months. In up to two-thirds of these patients, disease progression appears to be driven by the emergence of a secondary acquired mutation T790M (ie, threonine changed to a methionine), in exon-20 of EGFR gene (typically referred to as the "gatekeeper mutation"), and in combination with an activating sensitizing mutation in the same protein.[5] This TKI-resistant form of mutant EGFR is therefore commonly referred to as the "double mutant" (DM) form.

The mechanism by which these AMs of EGFR exert their effect is not proven but in vitro studies on the L858R mutation have shown there to be a decreased affinity to Adenosine triphosphate (ATP) (**Fig. 1**),[7] thereby increasing the potency of compounds such as gefitinib (**1**)[8] and erlotinib (**2**).[9] It has been proposed that the AMs may bias the equilibrium toward active conformation of the kinase to which a number of inhibitors may bind (**Fig. 2**).[9,10] Further reports suggest additional mechanisms, including the differential ability of the mutants to sample the active and inactive conformations[11,12] and impact on release of ADP. However, the acquired mutation T790M has been shown to increase the affinity of the kinase for ATP,[7,13] substantially reducing the cellular activity of ATP-competitive inhibitors such as gefitinib and erlotinib toward EGFR T790M. T790 is known as the "gatekeeper residue" and it is positioned at the entrance of what is typically referred to as the "back pocket"[14] of the kinase, the nature of this residue impacts on which compounds are tolerated in this region of the protein. It is also likely that there is a steric component to the resistance mechanism against early EGFR inhibitors, which have a preference for threonine gatekeeper as this is the target to which they were initially identified.

A number of additional EGFR-TKIs were subsequently developed based on the anilinoquinazoline template of gefitinib/erlotinib, often referred to as second-generation inhibitors. Unlike gefitinib and erlotinib, these inhibitors contain an acrylamide functionality that covalently bonds to C797 (ie, cysteine at position 797).[15,16] Such compounds reported include afatinib, **3**;[17]

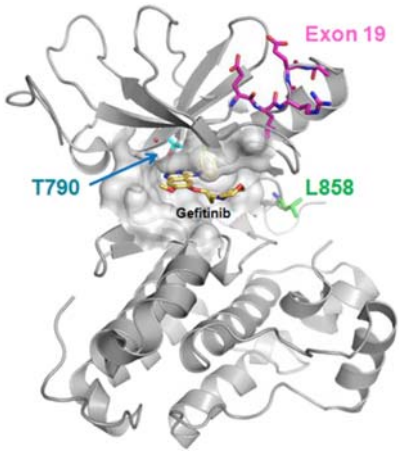

Fig. 1 EGFR crystal structure highlighting location of activating (L858R and Exon 19 deletion) and acquired mutation (T790M) in the kinase domain of EGFR (pdb code 2ITY[6]). Reprinted (adapted) with permission from Ward et al., *J. Med. Chem.* **2013**, *56* (17), 7025–7048. Copyright (2013) American Chemical Society.

canertinib, **4**;[18] and dacomitinib, **5**[19] shown in **Fig. 2**. The formation of this covalent bond apparently makes these inhibitors irreversible and thus able to overcome the increase in ATP affinity of the DM resulting in increased activity in cellular models compared to their reversible counterparts. C797, however, is present in all these forms of EGFR; therefore not only do these second-generation compounds have increased activity against the activating and resistant mutations but also against the wild-type (WT) enzyme. Inhibition of WT EGFR is not thought to significantly contribute to clinical efficacy in patients with EGFR mutation-positive advanced NSCLC but is thought to be responsible for the most commonly observed clinical side effects such as skin rash and diarrhea.[20] As these side effects are typically dose limiting in patients, it appears the WT activity of these inhibitors limits achievable activity against the T790M mutation in a clinical setting. Afatinib was approved by the Food and Drug Administration (FDA) for use in patients with activating EGFR mutations, and in addition, the reversible EGFR inhibitor icotinib **6** has been approved in NSCLC by the China Food and Drug Administration (CFDA) in China.

8.01.2 The Discovery of Osimertinib (AZD9291)

The discovery of osimertinib is described in three sections. The first section describes the specific activity profile, we aimed for, with a novel small molecule, which would be required to show clinical efficacy against the emerging T790M mutation. The second section reports our lead generation strategy, which rapidly identified the lead series using focused compound biochemical testing and structure-based design. We then report our lead optimization work to overcome some key challenges around the template, which ultimately resulted in the discovery of osimertinib.

8.01.2.1 EGFR Mutant-Selective Hypothesis

Our hypothesis behind the initiation of this work was that to successfully target the acquired T790M mutation in a clinical setting an inhibitor needed to be able to not only show potent cellular activity against the T790M form but that a "mutant-selective" profile was required where an optimal compound had reduced activity against the WT form of EGFR.[21] Ideally, an appropriate inhibitor would also show potent cellular activity against the AMs of EGFR (**Table 1**). First-generation inhibitors such as gefitinib and erlotinib had been demonstrated to be ineffective due to limited activity against the L858R/T790M and Exon19-del/T790M DM forms in vitro, in vivo, and in a clinical setting. Although compounds such as afatinib are reported to show in vitro activity against the T790M DMs it was not clear they had an appropriate profile due to their potent activity against WT EGFR. Central to our design hypothesis was the direct exploitation of T790M mutation to leverage selectivity against the WT form of EGFR. When we initiated this work at AstraZeneca, there were no examples of small molecule inhibitors with such a profile reported in the literature (**Fig. 3**).

To confirm our understanding of first- and second-generation inhibitor cellular profiles, we measured the cellular activity of a number of known inhibitors against the different forms of EGFR (**Table 2**) using assays detecting phosphorylation endpoints. These included the WT enzyme with a human LoVo cell line and the Exon-19del activating mutant (AM) using a PC9 cell line. Activity against the L858R/T790M DM enzyme was measured in a NCI-H1975 cell line. Although much of this dataset had been published by a number of different groups, we believed it was useful to measure compound activities in consistent assays to allow an accurate comparison of their biological profile.

Gefitinib and erlotinib were confirmed to be active against WT EGFR, with greater activity against the AM and significantly reduced cellular activity against DM EGFR (3.3 and 7.6 μM respectively). Afatinib (**3**) and dacomitinib (**5**) had increased activity

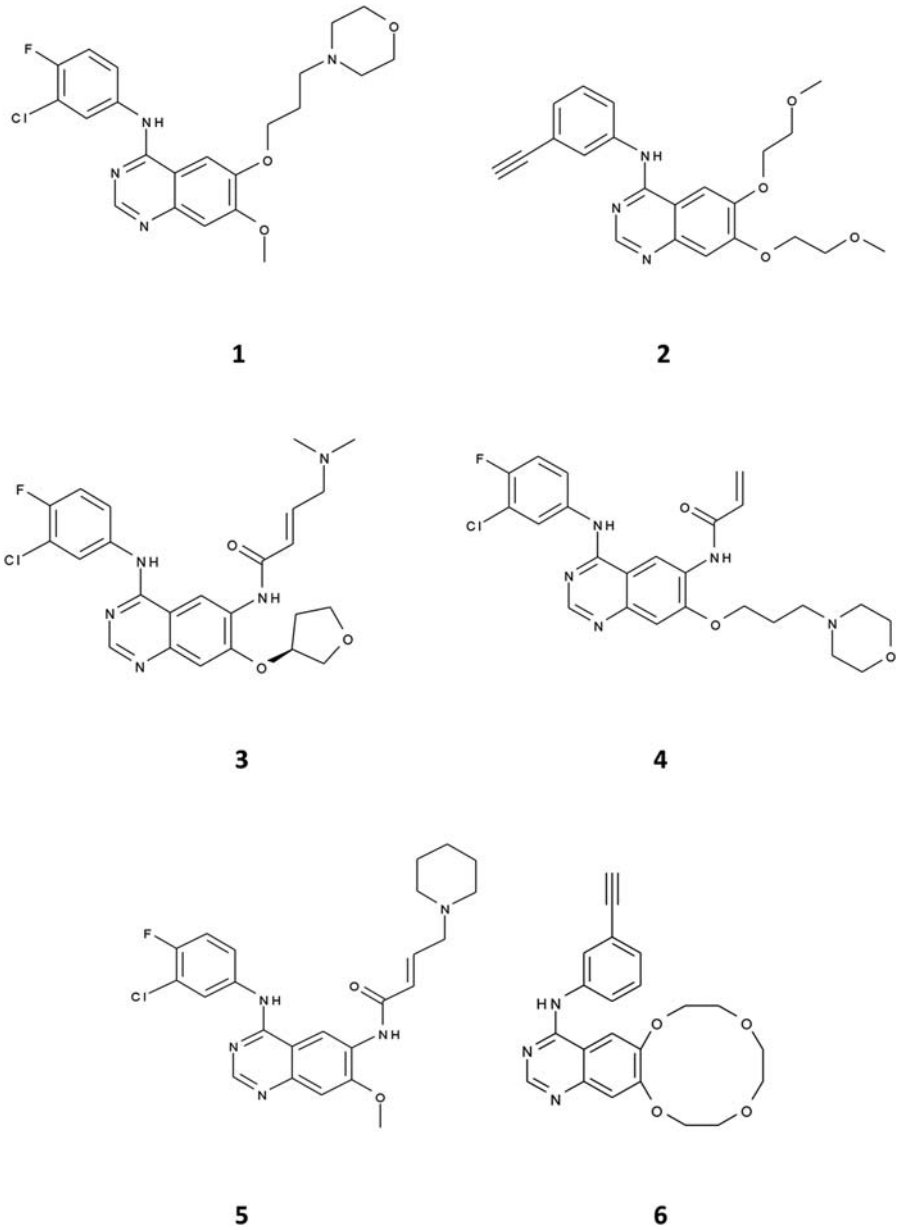

Fig. 2 Selection of first (**1**, **2**, and **6**) and second (**3**–**5**) generation EGFR inhibitors disclosed in the literature.

Table 1 Representation of first- and second-generation EGFR inhibitor profiles compared to our hypothesized "mutant-selective" profile

Compounds	*Generation*	*EGFR activating mutations (Exon19del/L858R)*	*EGFR double mutations (Exon19del/T790M and L858R/T790M)*	*EGFR wild-type*
Gefitinib/erlotinib	First	Active	Inactive	Active
Afatinib/dacomitinib	Second	Active	Active	Active
Unmet medical need	T790M mutant-Selective	Active	Active	Margin

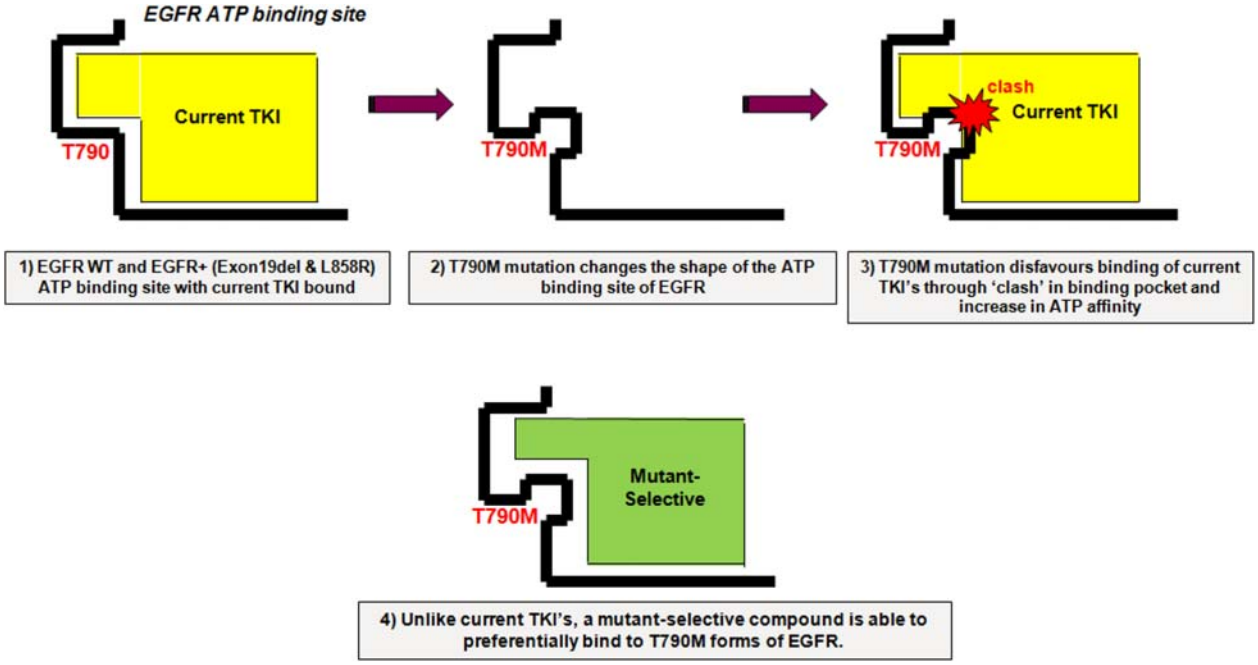

Fig. 3 Structural rationale for EGFR T790 mutant-selective inhibitor hypothesis.

Table 2 Cellular activity profile of published EGFR inhibitors against the double mutant (DM), activating mutant (AM), and wild-type (WT) enzymes

Compound	*DM cell (μM)*	*AM cell (μM)*	*WT cell (μM)*	*DM/WT margin*
Gefitinib (**1**)	3.3	0.0087	0.062	0.02
Erlotinib (**2**)	7.6	0.0059	0.077	0.01
Afatinib (**3**)	0.023	0.00057	0.012	0.53
Dacomitinib (**5**)	0.042	0.00063	0.011	0.27

[a]Activity data quoted as the geometric mean IC_{50} of at least three independent measurements. DM/WT margin is calculated by dividing the mean wild-type IC_{50} by mean double mutant IC_{50}.
Reprinted (adapted) with permission from Ward et al. *J. Med. Chem.* **2013**, *56* (17), 7025–7048. Copyright (2013) American Chemical Society.

against WT and AM EGFR, along with increased activity against the DM compared to gefitinib and erlotinib. Importantly, the potency of these compounds against the DM is lower than the potency against WT EGFR (ie, DM to WT margin of <1). These data confirmed our rationale for the clinical opportunity for a novel T790M mutant-selective inhibitor series.

8.01.2.2 Identification of a Mutant-Selective Lead Series

The rationale we followed was to identify a DM selective template, through exploitation of differences in properties of the threonine and methionine gatekeeper residues. We hypothesized that exploiting the hydrophobic nature of the methionine gatekeeper residue to leverage increased potency might lead to a profile in which the compounds are active against the DM enzyme, but with reduced activity against WT EGFR. Ideally, compounds would also show greater activity toward the activating EGFR mutations than WT, but this was not specifically considered at this stage as part of our design hypothesis.

Subsequently, a set of 40 compounds was tested in EGFR WT and DM biochemical enzyme assays at an external contract research organization,[22] Fig. 4, to inform our hypothesis around exploitation of the gatekeeper residue. This set included reversible EGFR inhibitors from our corporate compound collection (red) and a selection of published irreversible EGFR inhibitors (yellow). Additional compounds from our collection were added that had shown activity against kinases with methionine gatekeepers during historic internal drug discovery projects (blue). The reversible EGFR inhibitors showed higher activity against the WT form compared to the DM. The irreversible anilinoquinazoline-based EGFR inhibitors (including **3**, **4**, and **5**) showed significant activity in both assays, consistent with an increase in activity from the formation of the covalent bond. However, it is difficult to accurately compare the relative potencies of the reversible versus irreversible compounds in these assays due to their different mechanism of action, irreversible inhibitors often demonstrating time-dependent inhibition.[23,24] This aside, the subset of compounds that was of particular relevance for our efforts to target EGFR T790M were the aforementioned examples from internal AstraZeneca projects.

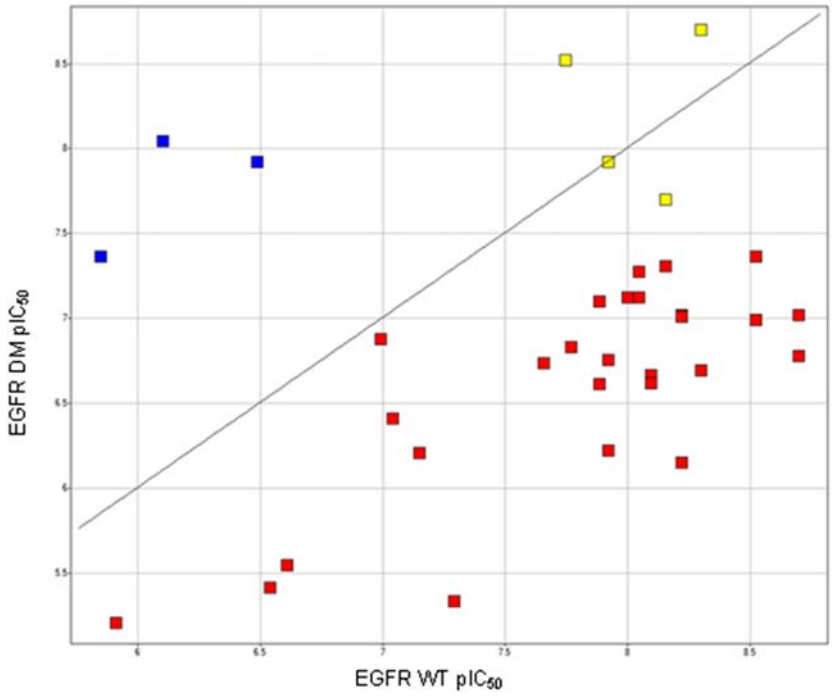

Fig. 4 EGFR wild-type (*WT*) and T790M/L858R (*DM*) biochemical assay data on a subset of compounds. *Red points* are reversible EGFR inhibitors, *yellow points* are covalent EGFR inhibitors, *blue points* are selected compounds from internal AstraZeneca projects. Reprinted (adapted) with permission from Ward et al., *J. Med. Chem.* **2013**, *56* (17), 7025–7048. Copyright (2013) American Chemical Society.

Importantly, these compounds showed promising activity against DM EGFR with selectivity over WT. Example **7** (Table 3) contains an indole "head-group" on a mono-anilino-pyrimdine (MAP) core with IC_{50} 0.009 μM against the DM enzyme and 88-fold selectivity over WT. Although compound **7** was active in this biochemical DM assay, a large enzyme to cell drop-off of around 90-fold was observed when tested in our H1975 DM cellular assay (IC_{50} 0.77 μM). This drop-off is likely driven by the high ATP affinity of this enzyme and the high ATP concentration present in the cellular environment.[25] We then directed our efforts to convert **7** into an (irreversible) covalent inhibitor to lessen the impact of the increased affinity of ATP for the mutant kinase, while maintaining selectivity over the WT EGFR.

A modeled binding mode of compound **7** was generated using protein–ligand docking software[26] and a public domain crystal structure of the EGFR-T790M mutation (PDB code 2JIT[7]).

Our hypothesis from the molecular modeling (MM) was that a hydrogen bond acceptor on the pyrimidine core formed a hydrogen bond to the kinase hinge, specifically to the backbone hydrogen bond donor of Met-793 (Fig. 5). A key feature of this binding mode is that the chlorine substituent is directed toward the methionine gatekeeper, supporting our rationale to target this region of the pocket through lipophilic interactions compared to the more hydrophilic WT threonine. The indole group is

Table 3 Identified double mutant (DM)-selective reversible EGFR inhibitor

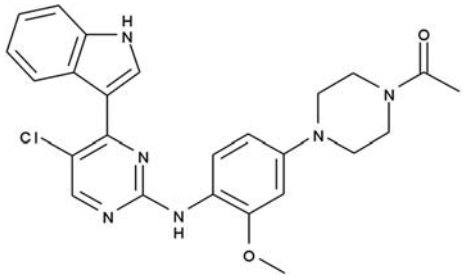

Compound	*DM enzyme (μM)*	*WT enzyme (μM)*	*DM/WT selectivity*	*DM cell (μM)*
7	0.009	0.79	88	0.77

Reprinted (adapted) with permission from (Ward et al. *J. Med. Chem.* **2013**, *56* (17), 7025–7048). Copyright (2013) American Chemical Society.

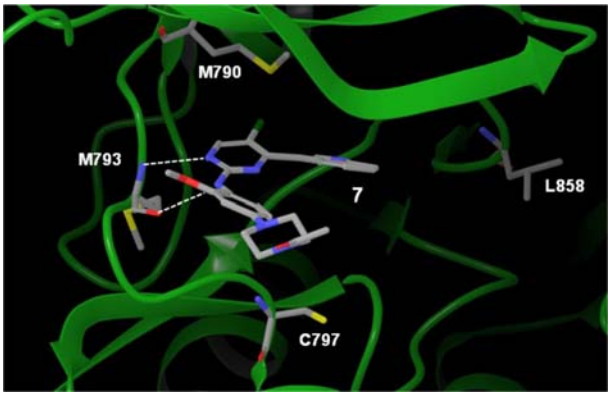

Fig. 5 Modeled binding mode of compound **7** in published EGFR crystal structure (PDB code 2JIT), which contains a T790M mutation. Reprinted (adapted) with permission from Ward et al., *J. Med. Chem.* **2013**, *56* (17), 7025–7048. Copyright (2013) American Chemical Society.

positioned adjacent to the region of the kinase referred to as the "back pocket." The anilino group of the inhibitor is oriented toward solvent and was also predicted to provide a hydrogen bond donor to interact with the hinge region. We subsequently attempted to design compounds with a reactive substituent positioned in a manner that would enable targeting C797 via the formation of a covalent bond based on this binding mode. The *meta*-position of the aniline appeared to be the most suitable location and such examples were prioritized. A range of potential substituents were modeled and from this work we decided to incorporate an acrylamide-based side chain. A particular example of interest from our synthesis efforts was compound **8**, which showed improved cellular activity in the DM cell assays with selectivity over WT (**Table 4**). Also of great interest was that this compound also showed promising (and surprising) activity in our PC9 (Exon19-del) AM cell assay.

Additional examples were then synthesized, including an example with an *ortho*-methoxy group at R_1 (compound **9**), which showed increased activity and improved broader kinase selectivity. Further examples were synthesized with the acrylamide attached to different regions of the molecule. Interestingly, moving the acrylamide to the *para*-position, which is also likely to be positioned near Cys-797, appears not to result in covalent inhibition. This compound showed only moderate activity in the DM biochemical assay (0.3 μM) and minimal activity in cellular assays.

To gain confidence that these compounds were able to form the desired covalent bond, **9** was prioritized for crystallization in an EGFR WT structural system.[27] The binding mode of compound **9** was subsequently solved (PDB code 4LI5), shown in **Fig. 6**, showing covalent bond formation to Cys-797. In this case, the binding mode of this template in the EGFR receptor was consistent with the binding mode found in our earlier modeling work.

One of the key issues with these early compounds was high lipophilicity ($LogD_{7.4} > 4.3$). Excessive lipophilicity can often translate into both poor physicochemical properties and pharmacokinetics (PK) and may hinder subsequent development of a series.[28,29] A primary aim of the evolution of this series was to reduce the overall lipophilicity, indicated in subsequent tables by experimental $LogD_{7.4}$ measurements, while retaining (ideally further increasing) EGFR potency and the favorable WT selectivity profile. The primary activity and WT selectivity of subsequent compounds were measured using in-house cellular assays as we felt that the additional data from biochemical assays would have limited impact.

Table 4 Activity data for inhibitors targeting C797

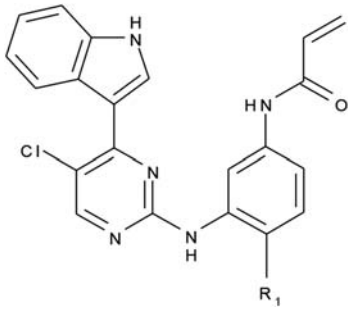

Compound	*R_1*	*DM enzyme (μM)*	*SM cell (μM)*	*DM cell (μM)*	*WT cell (μM)*	*DM/WT selectivity*	*$LogD_{7.4}$*
8	H	0.053	0.27	0.081	3.5	43	>4.3
9	OMe	0.0063	0.029	0.022	0.55	25	>4.3

Reprinted (adapted) with permission from (Ward et al. *J. Med. Chem.* **2013**, *56* (17), 7025–7048). Copyright (2013) American Chemical Society.

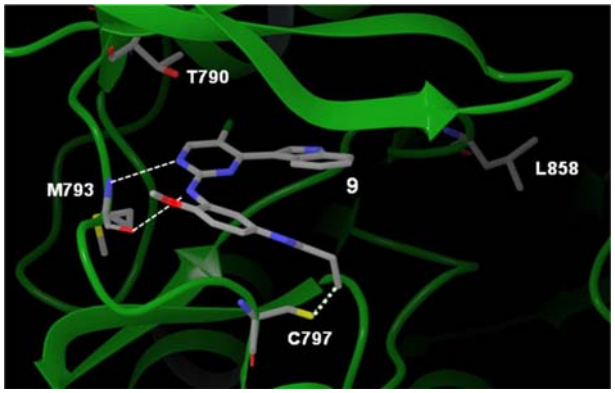

Fig. 6 Protein crystal structure of compound **9** bound in wild-type EGFR. The described covalent bond to Cys-797 is shown. (PDB code: 4LI5). Reprinted (adapted) with permission from Ward et al., *J. Med. Chem.* **2013**, *56* (17), 7025–7048. Copyright (2013) American Chemical Society.

In an attempt to improve the physical properties of compounds, we decided to modify the indole group, or what we referred to as the "head-group." In addition, we assessed the effect of the addition of a basic functionality to the acrylamide (Table 5). The pyrazolopyridine (compound **10**) was an interesting head-group that we had previously utilized in our IGF1R project, maintaining satisfactory potency in our double and single mutant cell assays (IC_{50} 0.033 and 0.15 μM) with an improved margin to WT EGFR (390-fold). Furthermore, the basic acrylamide-based side chains of template B (examples **11** and **12**) showed a small decrease in activity of two- to threefold compared to the neutral equivalents, but with a marked reduction in $LogD_{7.4}$. Based on the overall potency, selectivity and physical property profile of **12** this compound was selected as a key in vivo probe compound for this template. These compounds also began to populate a more favorable area of physicochemical property space, with a ligand lipophilicity efficiency (LLE) of 3.4 for example **12** using the DM cell assay and experimental $LogD_{7.4}$.

Our modeling work predicted that the 5-position of our template would be located adjacent to the "gatekeeper residue"; we therefore surmised that varying this position may have some interesting effects on the primary potency and WT selectivity of compounds. Our initial compound contained a chlorine atom at this position, which is relatively lipophilic and therefore changes here offered the potential for compound lipophilicity to be reduced.[30] A range of 5-substituted compounds were subsequently synthesized and assessed across our in-house cellular assays (Table 6).

The range of substituents investigated varied in both size and lipophilicity. Interestingly, although compound potency varied in the DM cell assay, the LLE (using the DM cell data) remained constant at around 3.4-3.5 except for R_1=H where it was increased to 4. This was an interesting result as removing the chlorine of compound **12** (giving compound **13**) reduced $LogD_{7.4}$ by an order of magnitude (3.6 compared to 2.6) and might enable physicochemical properties of this series to be improved. Although the DM activity was reduced for compound **13**, compared to **12** (0.25 vs. 0.096 μM), the activity against the AM was broadly unchanged (0.39 vs. 0.40 μM). The DM selectivity of **13** was reduced to 80-fold, from 237-fold for compound **12**, rationalized by chlorine interacting more effectively with the methionine gatekeeper residue. Our collective data across these compounds suggested that it might be possible to achieve reasonable potency in the EGFR double and AMs, while leveraging selectivity over WT, without a chlorine in the 5-position to enable improved compound properties.

The potency of covalent inhibitors is impacted by both reversible binding properties to the protein (K_i) and their ability to covalently bind to the active site (k_{inact}). It is therefore important to aim for compounds of sufficient chemical reactivity toward an active site residue (in this example cysteine), while balancing against off-target binding, which could lead to idiosyncratic toxicity.[31] One method of optimizing covalent compounds in this way is through the measurement of k_{inact}/K_i values. This approach, however, proved technically challenging using our assays so we were unable to exploit it for driving structure–activity relationships (SAR) routinely,[23] although progress has been made more recently in this area.[32] The alternative approach we used was to establish a suitable "reactivity window" for our compounds and to develop an understanding of how to synthesize compounds that were likely to fall within the intended range. As a measure of thiol reactivity we have used an assay based on determining the second order rate constant (k_{GSH}) for the reaction of our compounds with glutathione (GSH).[33–35]

In an attempt to determine the structural and electronic features that influenced the chemical reactivity of our compounds, a set of 6-membered aromatic ring acrylamide-containing "models" were investigated in the GSH assay (Table 7). These "model" acrylamides have relatively good aqueous solubility and thus avoided any complication of reaction kinetics that might have arisen due to compound precipitation. All compounds were stable in phosphate buffer alone at pH 7.4. In the presence of GSH a simple addition reaction (Scheme 1) was observed, generating the more polar GSH adduct, seen by liquid chromatography–mass spectrometry (LC-MS) as a mass increase of 307 units.

The Hammett plots in Fig. 7 enabled a quantitative understanding of the relationship between the electronic effects exerted through the R_1 position of the acrylamide, expressed as sigma values, and reactivity. This knowledge was then applied to design elaborated compounds, which sit in the desired reactivity window, using appropriate R_1 sigma values. From our results set, the rate of the reaction appeared to be dependent upon the electron withdrawing ability of groups in the R_1 position (Fig. 7) of the

Table 5 Activity and lipophilicity data for compounds targeting an improved physicochemical property space

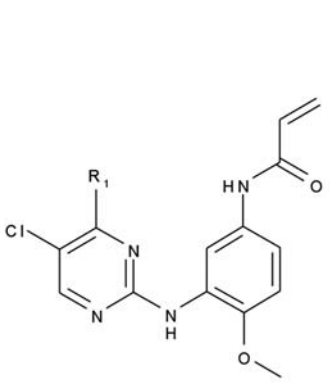

A

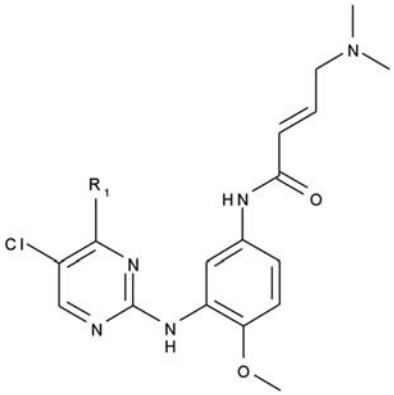

B

Compound	*Template*	*R_1*	*AM cell (μM)*	*DM cell (μM)*	*WT cell (μM)*	*DM/WT selectivity*	*$LogD_{7.4}$*	*LLE[a] (DM)*
9	A	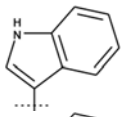	0.029	0.022	0.55	25	>4.3	<3.4
10	A	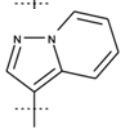	0.15	0.033	12.8	390	>4.3	<3.2
11	B	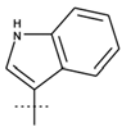	0.085	0.053	1.55	29	4.1	3.2
12	B	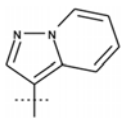	0.40	0.096	23	240	3.6	3.4

[a]LLE (DM) = pIC50 DM (Cell)—$LogD_{7.4}$.
Reprinted (adapted) with permission from (Ward et al. *J. Med. Chem.* **2013**, *56* (17), 7025–7048). Copyright (2013) American Chemical Society.

Table 6 Activity and lipophilicity data of compounds exploring the effect of the 5-substituent position (R_1) on the pyrimidine

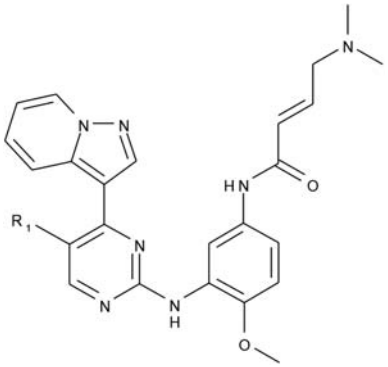

Compound	*R_1*	*AM cell (μM)*	*DM cell (μM)*	*WT cell (μM)*	*DM/WT selectivity*	*$LogD_{7.4}$*	*LLE (DM)*
12	Cl	0.40	0.096	23	237	3.6	3.4
13	H	0.39	0.25	20	80	2.6	4
14	F	0.38	0.22	19	85	3.3	3.4
15	Me	0.25	0.29	24	82	3	3.5
16	S(=O)Me	1.3	15.2	>30	>2	1.3	3.5

Reprinted (adapted) with permission from (Ward et al. *J. Med. Chem.* **2013**, *56* (17), 7025–7048). Copyright (2013) American Chemical Society.

Table 7 Glutathione (GSH) reactivity of 6-membered ring aromatic "model" compounds

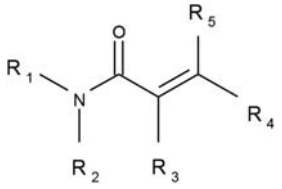

ID	*GSH* $t_{1/2}$ *(min)*	*Log* k_{GSH} [a] $(M^{-1} s^{-1})$	R_1	R_2	R_3	R_4	R_5	R_1 σ_{meta}	R_1 σ_I
17	816	−2.51	4-Aminophenyl	H	H	H	H	−0.006	0.052
18	323	−2.11	4-Fluorophenyl	H	H	H	H	0.12	0.13
19	2940	−3.07	Benzyl	H	H	H	H	−0.08	0
20	436	−2.24	Phenyl	C	H	H	H	0.06	0.12
21	299	−2.08	Phenyl	H	H	H	H	0.06	0.12
22	428	−2.23	2-Methylphenyl	H	H	H	H	0.07	0.119
23	524	−2.32	4-Methoxyphenyl	H	H	H	H	0.05	0.11
24	37.2	−1.17	2-Cyanophenyl	H	H	H	H	0.18	0.194
25	145	−1.76	3-Fluorophenyl	H	H	H	H	0.15	0.16
26	361	−2.16	4-Methylphenyl	H	H	H	H	0.06	0.1
27	22	−0.94	2-Pyridyl	H	H	H	H	0.33	0.25
28	32.9	−1.12	4-Cyanophenyl	H	H	H	H	0.221	0.175
29	>8640	≤3.54	*tert*-Butyl-phenyl	H	C	H	H	−0.043	0.05
30	>10,000	≤3.60	Phenyl	H	C	H	H	0.06	0.12
31	>10,000	≤3.60	Phenyl	H	H	C	C	0.06	0.12
32	>10,000	≤3.60	Phenyl	H	H	C	H	0.06	0.12

Sigma values determined using ACD/Labs software (version 12.01).
All compounds with an absolute rate constant showed a more polar product peak of mass parent +307 except example **22** where no products were observed (reflects much slower reaction compared to other compounds coupled to detection limits of LC-MS).
[a]Note rate constant *k* derived using [GSH] 4.61 mM.
Reprinted (adapted) with permission from Ward et al., *J. Med. Chem.* **2013**, *56* (17), 7025–7048. Copyright (2013) American Chemical Society.

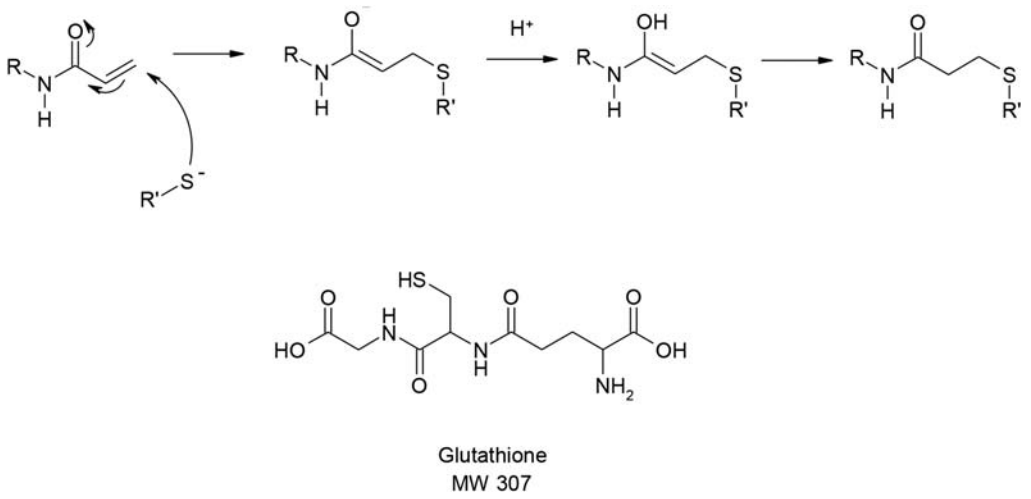

Scheme 1 Addition reaction of model compounds with glutathione.

acrylamide. In particular, the inductive effect of the R_1 group (represented either as σ_{meta} or σ_{ind}) was seen to determine thiol reactivity with ρ values of 5.56 and 9.23, respectively. The addition of further electronic descriptors such as σ_{para} or σ_{meso} to the Hammett equations and in Fig. 7 did not appear to be significant. Such inductive electron withdrawal at the R_1 position would be consistent with enhanced polarization of the alkene bond via carbonyl conjugation and also serve to stabilize the enolic transition state. The introduction of methyl groups on to either the α or β carbon of the "model" acrylamides (R_3 and R_4) resulted in no reaction being observed with GSH, removing these substituents as options on elaborated compounds. A similar decrease in thiol reactivity following methylation at the α and β carbon has been observed by other workers in their investigations with α,β-unsaturated

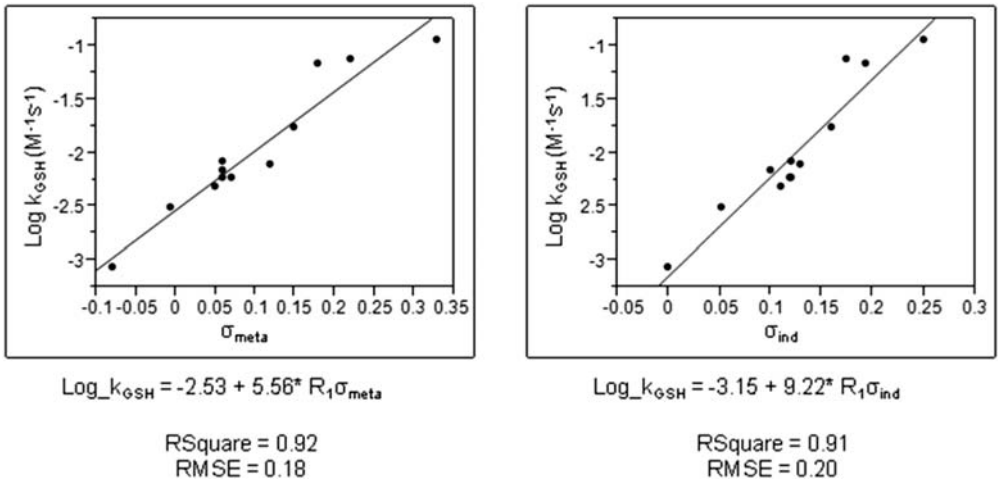

Fig. 7 Hammett plot of σ_{meta} and σ_{ind} properties versus compound reactivity (Log k_{GSH}) across the "model" compound set. Reprinted (adapted) with permission from Ward et al., *J. Med. Chem.* **2013**, *56* (17), 7025–7048. Copyright (2013) American Chemical Society.

aldehydes, ketones, esters, acids, and amides.[36–39] Engels et al. calculated via quantum mechanical/MM an increased energy barrier to methyl thiolate attack on α,β-unsaturated phenyl ketones with an elevated energy of the enolate intermediate upon methylation at the α and β positions, suggesting steric effects as a possible reason for such a reactivity change.[38] While other workers have similarly suggested steric effects as an explanation for decreased reactivity for α and β-methylation,[36] Kerske et al. argue that reactant stabilization by hyperconjugation of α and β methyls and not steric hindrance is the reason for the lowered reactivity.[39]

This SAR and the equations based on these Hammett plots more generally were used to try and predict compound reactivity of more elaborated compounds through further optimization of the series. In seeking to define a suitable "reactivity window," elaborated project compounds studied for GSH reactivity were also tested in the DM cell assay. **Fig. 8** reveals the relationship between cellular potency and GSH reactivity for a subset of compounds. As hoped, there is not a strong correlation since initial target noncovalent binding (K_i) will play a key part in defining potency (R^2 0.52 and RMSE 0.53). Noncovalent contribution to the binding is essential for driving the selectivity of these compounds over other proteins with potentially accessible cysteine residues. There is, however, a general trend toward more reactive compounds showing increased activity and compounds with pIC_{50} values >7 for the most part tend to have GSH half lives <400 min. As such we took a GSH half-life of 400 min as a guide for a suitable lower limit of reactivity. Afatinib (**3**) is now an FDA approved clinical agent and reported clinical side effects of the compound appear to be linked to the inhibition of WT EGFR rather than off-target effects due to covalent binding. For this reason, this seemed an appropriate compound to benchmark in our GSH assay generating a half-life of 25 min. We therefore used a half-life of 25 min as the higher limit to the window of reactivity we aimed to work within.

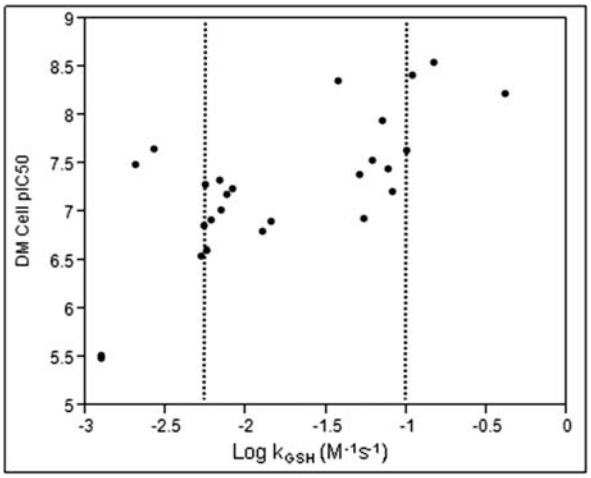

Fig. 8 Compound reactivity measured by Log k_{GSH} ($M^{-1}s^{-1}$) plotted against EGFR double mutant (DM) cellular pIC_{50} for the elaborated compounds reported in this article. *Dashed lines* indicate the "reactivity window" in which the design of novel compounds was subsequently focused. Reprinted (adapted) with permission from Ward et al., *J. Med. Chem.* **2013**, *56* (17), 7025–7048. Copyright (2013) American Chemical Society.

Compound **12** was identified as a suitable in vivo proof of concept (POC) compound from our early lead generation work (Table 8). To build further confidence in the covalent mechanism of action, the equivalent nonreactive propionamide was synthesized, which showed significantly reduced cellular activity (2.3 μM). Although not the most potent (or WT selective) example synthesized, the overall balance of properties identified **12** as having an acceptable combination of activity and PK properties (Table 12). In addition, **12** demonstrated encouraging antiproliferative activity when tested in our H1975 (DM), PC9 (AM), and Calu3 (WT) cell lines with an EC_{50} of 0.099, 0.14, and 1.78 μM, respectively. This profile is consistent with the described cellular activity using phosphorylation endpoints showing significant activity in the double and single mutants with selectivity over the EGFR WT. **12** was orally dosed in an in vivo efficacy study using an H1975 DM xenograft model in immune-compromised mice. Tumor growth was measured from start of treatment and assessed by comparison of the mean change in tumor volume for the control and treated groups, and represented as tumor growth inhibition (where >100% total growth inhibition, TGI is a regression from start size). Compound **12** showed significant efficacy of 105% TGI of the tumors after 7 days at an oral dose of 60 mg kg^{-1} day^{-1} (formulated as the mesylate salt to improve solubility and PK properties).

Compound **12** was also administered in an efficacy study in a PC9 AM cell line and a WT A431 cell line in immunocompromised mice. The activity against the PC9 xenograft model at the same dose (134% TGI, resulting in tumor regression) was encouraging and compound **12** showed reduced activity against the A431 xenograft model (46% TGI), as compared to the PC9 and H1975 studies, reflecting the WT margin demonstrated from the in vitro cellular profile (Table 9).

In comparison, an oral dose of gefitinib of 6.25 mg kg^{-1} day^{-1} (representative of the clinically relevant human dose) showed 142% TGI in the PC9 xenograft model and 79% TGI in the A431 xenograft model after 7 days (Table 13). Gefitinib showed little activity in the H1975 xenograft model, as an oral dose of 100 mg $kg^{-1}day^{-1}$ resulted in 8% TGI after 7 days.

To assess the broader kinase selectivity of our series, we routinely submitted key compounds to a panel of >70 diverse kinases at the University of Dundee,[40] testing at a concentration of 1 μM in biochemical assays. Compound **12** showed >75% inhibition in 10 kinases, which were IGF1R, insulin receptor (IR), CAMKKbeta, CHK2, PBK, FLT1, MAP3K11, smMLCK, BTK, and MELK. However, out of these kinases only BTK has a cysteine in the same position as EGFR so the mode of inhibition is likely to be via a reversible mechanism in the majority of these targets. Consequently, we believed that such covalent inhibitors such as compound **12** would have increased selectivity versus those off-targets in a cellular setting.

8.01.2.3 Lead Optimization to the Discovery of Osimertinib

Our aim was to further increase the potency of our series by exploiting additional interactions with the protein, along with the learning from our exploration of compound reactivity.[41] As part of this, we synthesized a set of compounds with a piperazine substituent on the *para*-position of the aniline, which we hoped would be tolerated from compounds such as **7** (Table 10). We expected that the addition of the piperazine adjacent to the acrylamide would impact the conformation and geometry of both substituents so we were keen to assess whether this combination was compatible with good potency on our template. We combined this change with 5-position SAR described in the previous section, using both our indole and pyrazolopyridine "head-groups."

Table 8 Overview of activity, physicochemical, and PK data of compound **12**

Compound	*AM cell (μM)*	*DM cell (μM)*	*WT cell (μM)*	*Solubility (μM)* [a]	*PPB %Free (M/R/H)* [b]	*Human Heps (μL $min^{-1} \times 10^6$)*	*Rat Heps (μL $min^{-1} \times 10^6$)*	*hERG (μM)*	*Rat PK CL/F* [c]
12	0.40	0.096	23	1.6	1.2/1.2/0.8	<3	18	4.2	8.1/45%

[a]Solubility performed under thermodynamic conditions using crystalline solid.
[b]Plasma protein binding (PPB) was assessed by equilibrium dialysis in the appropriate species (mouse/rat/human) at 37°C. Free and bound concentrations were quantified by LC-MS.
[c]Intravenous clearance (mL min^{-1} kg^{-1}) in male Han Wistar rats when dosed with a 3 μmol kg^{-1} solution. Oral bioavailability observed with a 6 μmol kg^{-1} solution dosed to male Han Wistar Rats.
Reprinted (adapted) with permission from (Ward et al. *J. Med. Chem.* **2013**, *56* (17), 7025–7048). Copyright (2013) American Chemical Society.

Table 9 Summary of efficacy data from xenograft studies on compound **12** compared to gefitinib (**1**)

Compound	*Oral dose (mg $kg^{-1}day^{-1}$)*	*H1975 (% TGI)*	*PC9 (% TGI)*	*A431 (% TGI)*
12	60	105 ($\rho < 0.001$)	134 ($\rho < 0.01$)	46 ($\rho < 0.05$)
Gefitinib (**1**)	6.25	8[a] ($\rho <$ NS)	142 ($\rho < 0.001$)	79 ($\rho < 0.001$)

Statistical significance (ρ values in brackets) was calculated from compound treated and vehicle groups using a one-tailed *t*-test, "NS" indicates %TGI was not significantly different from vehicle.
[a]Data from 100 mg $kg^{-1}day^{-1}$ oral dose of gefitinib.
Reprinted (adapted) with permission from Ward et al., *J. Med. Chem.* **2013**, *56* (17), 7025–7048. Copyright (2013) American Chemical Society.

Table 10 Activity and lipophilicity data on compounds with the addition of a piperazine group

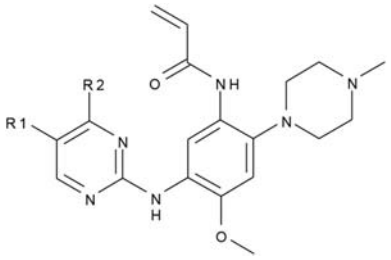

Compound	R_1	R_2	*AM cell (μM)*	*DM cell (μM)*	*WT cell (μM)*	*DM/WT selectivity*	*LogD$_{7.4}$*	*LLE(DM)*
33	Cl	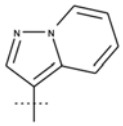	0.14	0.019	12	620	4.1	4.1
34	H	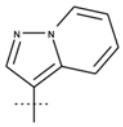	0.14	0.071	19	270	NT	-
35	Cl	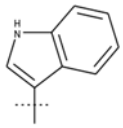	0.023	0.0056	0.77	140	3.7	4.6
36	H	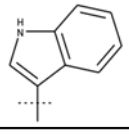	0.017	0.068	1.3	19	3.4	3.7

Reprinted (adapted) with permission from Ward et al. *J. Med. Chem.* **2013**, *56* (17), 7025–7048. Copyright (2013) American Chemical Society.

The emerging data suggested a general improvement in potency with the addition of the piperazine substituent (**Table 11**). Compound **33** is more potent than **12** in both primary cell assays (0.14 vs. 0.4 μM in the single mutant and 0.019 vs. 0.096 μM in the DM assays), while maintaining good selectivity for the DM over WT. There is a small increase in reactivity against GSH for compound **33** ($t_{1/2}$ 188 min) compared to 352 min for compound **12,** which is consistent with the small increase in electron withdrawing ability of the group attached to the acrylamide nitrogen (σ_{meta} 0.09 compared to sig σ_{meta} 0.07). A number of factors could influence this increase in compound activity including the preference for a basic group in this region of the protein, the increased compound reactivity along with the effect on acrylamide geometry. The LLE of these compounds is improved with **33** showing an increased LLE of 4.1, compared to 3.4 for **12**. Removal of the chlorine (compound **34**) showed a reduction in DM cellular activity, 0.071 μM compared to 0.019 μM, but minimal impact on single mutant activity as observed previously. The transferring of this learning back to the indole "head-group" identified compounds that were significantly more potent against the single and DM. Example **35** is a particularly potent compound, with an LLE = 4.6. The data on these compounds is consistent with the early data on this head-group with the indole-containing compounds showing a reduced margin with WT EGFR (140-fold and 19-fold for **35** and **36,** respectively), albeit with greater absolute DM activity. These more recent compounds were then profiled more broadly to assess the impact of the piperazine group on nonefficacy properties.

At this stage, we began to monitor IGF1R actively more routinely, driven by the knowledge that our initial lead compound was synthesized within our internal IGF1R drug discovery program. While compound **36** showed broadly similar DM potency to **12**, it had reduced IGF1R activity and increased AM activity with no increase in lipophilicity, which was of significant interest, albeit with a slightly reduced WT margin. Broader kinase selectivity for these inhibitors, as judged by profiling in a kinase selectivity screen,[10] also appeared to be good. Compound **33** appeared to offer superior selectivity for the mutant forms of the receptor, although **36**, as mentioned above, did carry significantly less activity against IGF1R, which also has a methionine gatekeeper. Although a lipophilic group at the pyrimidine 5-position appeared to offer a favorable interaction with the methionine in both IGF1R and the EGFR DM we speculated that covalent binding to EGFR would help drive selectivity over IGF1R, where the binding was noncovalent. While IGF1R inhibitors have been employed in a clinical setting, their lack of selectivity with respect to inhibition of IR signaling has in some instances led to dose limiting toxicity and monitoring these effects can complicate study designs[11] and more recently such effects have been observed with CO-1686 (rociletinib) from an active metabolite.[42] However, **33** in contrast to **36** did offer modest exposure when dosed orally at 50 mg kg^{-1} in SCID mice so we focused further work around this compound.

Table 11 Structures and selected properties of piperazine-substituted compounds compared to compound **12**

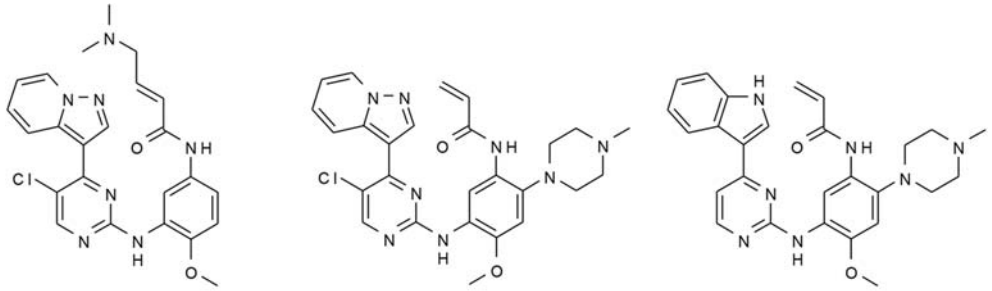

12 **33** **36**

	12	*33*	*36*
DM cell IC_{50} (μM)[a]	0.091	0.019	0.063
AM cell IC_{50} (μM)[a]	0.388	0.14	0.015
WT cell IC_{50} (μM)[a]	>20	12	1.2
$LogD_{7.4}$	3.6	3.6	3.4
LLE (DM cell)[b]	3.4	4.1	3.8
Nude mouse PO 50 mg kg^{-1} (C_{max} μM, AUC μM h)	5.8, 67	2.7, 13.4	0, 0
Mouse Heps Cl_{int} (μL min^{-1} 10^6cells^{-1})	35	-	53
Solubility, pH 7.4 (μM)[c]	1	>973	828
hERG IC_{50} (μM)	4.2	7.1	9.1
IGF1R (enz) IC_{50} (μM)	0.004 (n=1)	0.002	0.813 (n=1)
Kinase panel[d] hits (>90% inhibition at 1 μM)	CHK2 (90%) CAMKKbeta (94%) IGF1R (98%) INSR (97%)	CAMKKbeta (92%) IGF1R (97%)	Not tested

[a]Inhibition of EGFR phosphorylation. All cell IC_{50} measurements reported are the geometric mean of at least two independent measurements unless otherwise indicated. The standard error of the mean (SEM) is not shown, as all three assays were found to be highly reproducible on repeat testing (pIC_{50} SEM typically $_{50}$ values are time dependent and are quoted as measured following an incubation period of 2 h. Double mutant (DM) cell line: H1975. Activating mutant exon 19 del (AM) cell line: PC9. Wild type (WT) cell line: LoVo.
[b]Ligand lipophilicity efficiency (LLE) is calculated from DM cell pIC_{50} – log $D_{7.4}$.
[c]Aqueous solubility measurement was performed under thermodynamic conditions using solid material.
[d]MRC protein phosphorylation unit at the University of Dundee.
Reprinted (adapted) with permission from (Finlay et al. *J. Med. Chem.* **2014**, *57* (20), 8249–8267). Copyright (2014) American Chemical Society.

One early avenue we explored as part of this work was around a piperazine-amide subset of compounds (Fig. 9). While a number of these compounds offered reasonable profiles, we stopped working on such compounds due to the moderate cellular potency and greater progress of other avenues. A number of other carbon and oxygen linked basic side chains were also examined, but they offered little advantage in terms of potency, physical properties, or oral exposure when compared to the nitrogen linked systems described earlier.

One area of most interest to us was around compounds where the piperazine group had been replaced with particular basic side chains, producing a number of examples with exquisite cellular potency and three key examples are shown here (Table 12). Of additional interest was that this increase in potency did not come with the addition of further lipophilicity (as also noted for **33** and **36**), in contrast to some of our earlier SAR in regions of the molecule such as the 5-position of the pyrimidine. Encouraged by these data, we further made and tested a range of compounds from this subseries. The compounds showed excellent cellular potency against both mutants in phosphorylation (and phenotypic antiproliferation assays) with selectivity over WT EGFR. Compound LogD was around 3 along with modest aqueous solubility in pH 7.4 buffer being evident. In addition, they also showed good overall kinase selectivity, apparently improved from earlier compounds and the GSH reactivity also fitted into our understanding of a suitable "reactivity window." However, these compounds showed moderate affinity for the hERG channel and potent IGF1R activity in a similar fashion to earlier examples. The in vitro intrinsic clearance of the compounds was relatively high but, encouraged by the overall profile of the series, we elected to investigate the exposure of the compounds when dosed orally in the SCID mouse. Compounds were prioritized for in vivo work based on cell potency, free fraction, and aqueous solubility.

Compound **37** was well tolerated at a 50 mg kg^{-1} once daily oral dose and excellent exposure was observed. Plasma levels achieved were substantial and well in excess of the concentrations needed to achieve free cover over the cellular IC_{50} values. As a consequence, for subsequent compounds in the series, we reduced to 10 mg kg^{-1} as an initial dose. At this lower dose, multiples of free cover were still achieved for compounds **38** and **39** and these inhibitors were selected for evaluation in a pharmacodynamic (PD) study. A single dose of compounds **37**, **38**, and **39** were administered orally in SCID mice at 10 mg kg^{-1}, and the percentage knockdown of EGFR phosphorylation in H1975 (DM) and PC9 (AM) xenografts was measured compared to control (Tables 13 and 14 and Figs. 10 and 11). These compounds showed a profound effect on the PD biomarker. In the PC9 tumor cell line, **39** and **38**

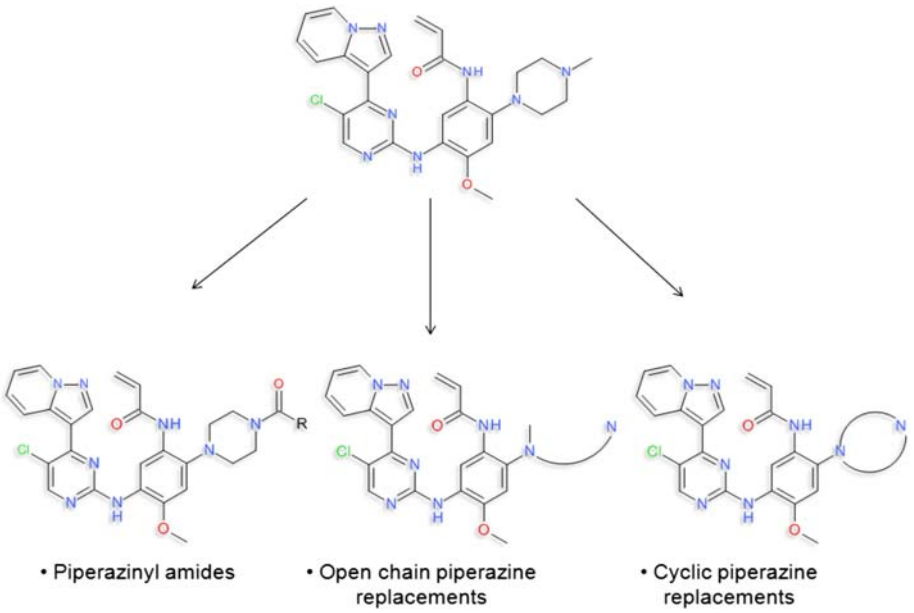

Fig. 9 Summary of modifications to the piperazine region.

showed broadly similar effects with maximal inhibition (85% and 83%, respectively) at the 6 h time point. Compound **37** showed slightly less biomarker modulation at 6 h but in contrast to the other two compounds continued to show sustained inhibition at the 24 h time point. In contrast, in the H1975 PD study, all three compounds showed sustained biomarker inhibition out to 24 h, although **38** now showed the most marked effect. By the 30 h time point, **39** inhibitory effects seemed to have been reduced whereas **38** still displayed a significant level of biomarker modulation. Given these data, the three compounds were selected for further evaluation in antitumor efficacy studies.

As with our earlier efficacy study on compound **12**, in vivo xenograft models representing the drug-resistant, DM (H1975), AM (PC9), and WT (A431) were selected. Compounds were dosed orally once a day for 7 days (Fig. 12).

At 10 mg $kg^{-1}day^{-1}$, all three compounds showed pronounced tumor growth inhibition in the two mutant models (Fig. 12), with regression being achieved in each case, while having relatively little impact on the A431 WT model. With this encouraging data, we elected to more fully characterize the PK properties of these compounds in rat and dog, where good cross-species PK was observed.

As the incorporation of the basic side chains described earlier in **37**, **38**, and **39** had brought significant benefits relative to the early lead compound **12**, we elected to further explore the indole head-group using this learning. Although we had previously moved away from the indole head-group due to its more modest oral PK properties and lower WT margin,[7] the enhanced potency available from this novel basic side chain SAR prompted us to reexamine this subseries. Thus we decided to explore a matrix of compounds where we would incorporate favored groups at the 5-position of the pyrimidine core, along with the indole head-group with the basic side chain SAR. Leading examples from this work are shown in Table 15.

It can be seen that incorporation of the newly identified basic side chain delivered high cellular potency across all the examples shown (Table 15). However, the presence (or indeed absence) of a substituent at the 5-position of the pyrimidine ring also had a differential effect on DM potency (and therefore EGFR WT selectivity), IGF1R potency, and hERG binding. From the data generated, it reinforced the earlier observation that a 5-substituent had a beneficial impact on EGFR DM cell potency, possibly driven by interaction with the methionine gatekeeper residue although in the case of the more polar cyano 5-substituent, the conformational effect on the indole group may be important. A similar pattern is observed for IGF1R activity, although it should be noted that the potency increase imparted by the 5-Cl was generally of a greater magnitude for IGF1R than any of the EGFR mutants or WT receptor. The presence or absence of a methyl group on the indole 1-position nitrogen also had an impact on IGF1R activity. Analysis of the broader data suggested that the removal of the methyl group generally results in increased cell potency against all three Epidermal growth factor (EGF) forms, with human Ether-à-go-go Related Gene (hERG) potency having no discernible trend. However, the NH indole analogs showed increased IGF1R potency. The SAR for WT selectivity is also interesting, with DM selectivity over WT showing a trend to be greater for the N-methylated compounds. When profiled in the Millipore kinase selectivity panel,[10] it became evident that for the two 5-H compounds tested, in addition to reducing IGF1R and INSR activity, we had also maintained the high broader kinase selectivity of our above-described inhibitors. In summary the 5-Cl group appeared to bring benefits to DM cellular potency and WT selectivity, but issues around IGF1R and hERG activity. The 5-H equivalents showed reduced potency and WT selectivity, but reduced IGF1R and hERG activity. However, the cellular activity of the 5-H equivalents could be recovered to some extent by the inclusion of the indole head-group with indole alkylation allowing increased WT selectivity.

Table 12 Structures and selected properties of compounds **37**, **38**, and **39**

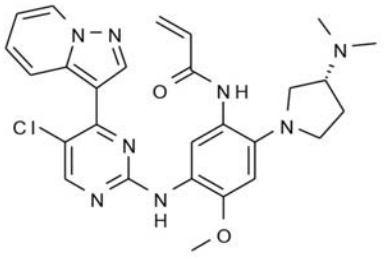

37

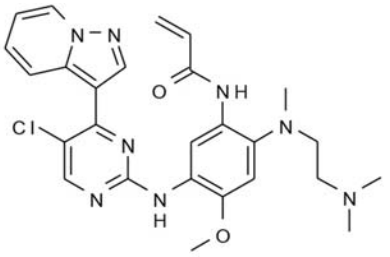

38

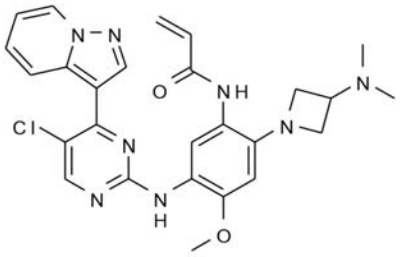

39

	37	*38*	*39*
DM cell IC_{50} (nM)	2	0.6	4
AM cell IC_{50} (nM)	16	2	21
WT cell IC_{50} (nM)	357	145	938
DM anti proliferative cell GI_{50} (nM)	7	3	17
AM anti proliferative cell GI_{50} (nM)	10	4	19
WT anti proliferative cell GI_{50} (nM)	384	180	846
$LogD_{7.4}$	3.1	2.8	3.3
LLE (DM cell)	5.6	6.4	5.1
Min sol pH 7.4 (μM)	28 (Xtl)	222 (Xtl)	43 (Xtl)
Rat % free[a]	7.1	6.4	5.1
Human % free	2.7	3.2	2.5
Nude mouse % free	7.8	3.2	5.0
Rat Heps Cl_{int}	20	59	27
Human Heps Cl_{int} (μL $min^{-1}10^6cells^{-1}$)	<3	14	5.2
Mouse Heps Cl_{int} (μL $min^{-1}10^6cells^{-1}$)	19	60	22
hERG IC_{50} (μM)	5.6	6.7	4.0
IGF1R (enz) IC_{50} (μM)	0.007	0.006	0.026
GSH mean t ½ (min)	140	90	257
pK_a (measured)	8.1	9	7.2
Kinase panel hits ($>$90% inhibition at 1 μM)	IGF1R (98%) INSR (98%)	IGF1R (97%) INSR (99%)	IGF1R (97%) INSR (98%)

[a]Plasma protein binding was assessed by equilibrium dialysis in the appropriate species at 37°C in 10% plasma and extrapolated to 100% with a single site binding model. Free and bound concentrations were quantified by LC-MS.
Reprinted (adapted) with permission from (Finlay et al. *J. Med. Chem.* **2014**, *57* (20), 8249–8267). Copyright (2014) American Chemical Society.

Table 13 % inhibition of p-EGFR (measured by R&D Systems ELISA kits, not site specific and expressed as ratio of phosphorylated/total) in mice bearing PC9 tumors following 10 mg kg^{-1} oral dose of compounds **37**, **38**, and **39**

Compound	*1 h*	*6 h*	*16 h*	*24 h*	*30 h*
37	–	76*	–	68*	–
38	30	83***	60**	38	10
39	57**	85**	52*	19	–

Statistical significance (*p*-values) was calculated by comparing compound treated and vehicle groups using a two-tailed *t*-test, unequal variance; *p*-values are indicated as follows: * <0.05, ** <0.01, *** <0.001. See supporting information for further detail.
Reprinted (adapted) with permission from (Finlay et al. *J. Med. Chem.* **2014**, *57* (20), 8249–8267). Copyright (2014) American Chemical Society.

Table 14 % inhibition of p-EGFR in mice bearing H1975 tumors following 10 mg kg^{-1} oral dose of compounds **37**, **38**, and **39**

Compound	*1 h*	*6 h*	*16 h*	*24 h*	*30 h*
37	–	94***	–	88***	–
38	89***	100***	94**	93**	80***
39	37	99***	82***	79***	50**

P-values are indicated as follows: * <0.05, ** <0.01, *** <0.001.
Reprinted (adapted) with permission from (Finlay et al. *J. Med. Chem.* **2014**, *57* (20), 8249–8267). Copyright (2014) American Chemical Society.

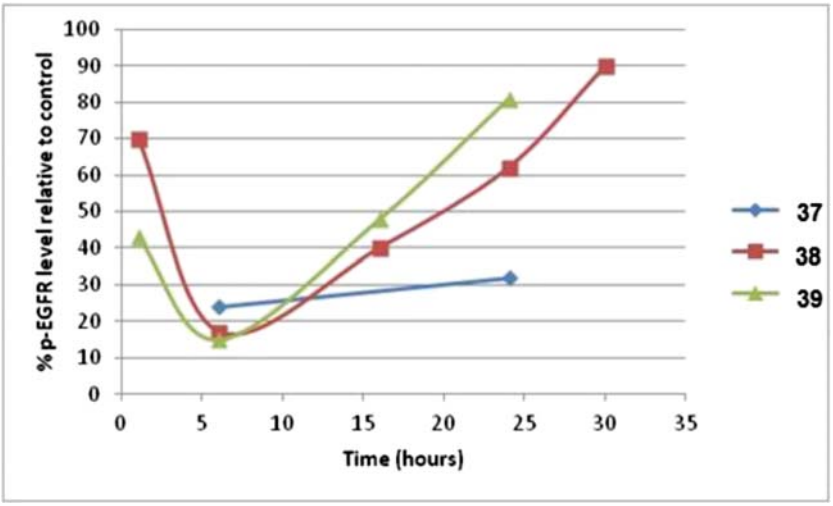

Fig. 10 p-EGFR inhibition time course profile in PC9 (sensitizing mutant) xenograft bearing mice following 10 mg kg^{-1} oral dose of compounds **37**, **38**, and **39**. Reprinted (adapted) with permission from Finlay et al., *J. Med. Chem.* **2014**, *57* (20), 8249–8267. Copyright (2014) American Chemical Society.

Examining the data for this matrix of compounds in more detail, the profile of most of the compounds was broadly similar to our earlier examples described above. However, Compound **44** demonstrated improved rat PK, reduced hERG affinity, and improved IGF1R margins relative to the previously described compounds and was selected for further investigation. Compound **44** also offered an additional degree of broader chemical and profile diversity when compared to the previously described lead compounds. Upon dosing **44** in our three efficacy models, we observed comparable efficacy at relatively low doses (10 mg $kg^{-1}day^{-1}$, Fig. 13). Intriguingly, excellent efficacy was also observed when **44** was dosed at 5 mg $kg^{-1}day^{-1}$ and this unprecedented level of activity combined with its previously mentioned attractive attributes added to our interest in this compound, despite the slightly lower WT selectivity. Given the significant free cover of earlier compounds, it seems difficult to explain how this level of efficacy could be achieved with the relatively modest exposure achieved with **44** (free $C_{max} = 13$ nM, 0.9-fold free cover over DM cell IC_{50}), but further understanding did become apparent with additional studies.

Our focus subsequently turned to the investigation of the in vivo toxicological profile of our preferred compounds. With our observation around the IGF1R activity of some compounds, we designed bespoke rat toxicology studies to explore whether reversible inhibition of IGF1R/INSR would lead to hyperglycemia or impaired insulin signaling in vivo. Rats received a single oral dose of 200 mg kg^{-1} of each compound with assessment of blood glucose and insulin concentrations over a 24 h period. While all compounds were broadly tolerated well, a single oral dose of **38** and **37** led to marked hyperglycemia and hyperinsulinemia

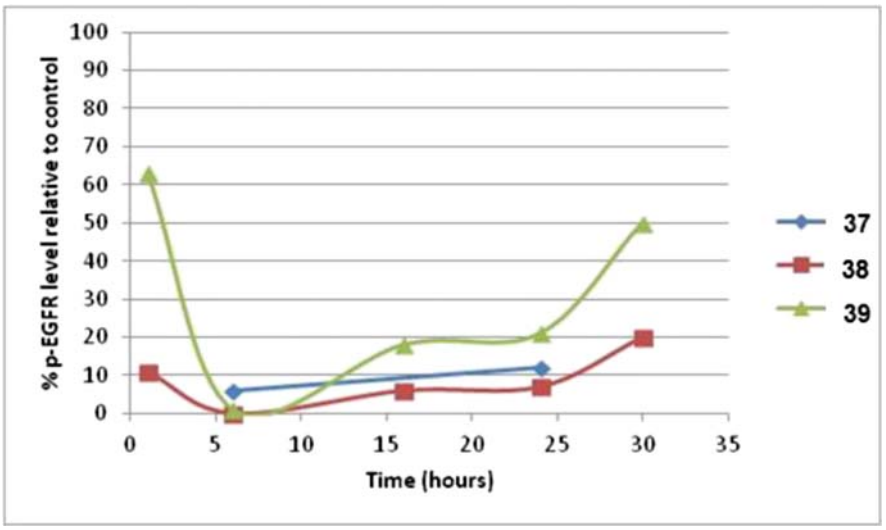

Fig. 11 p-EGFR inhibition time course profile in H1975 (double mutant) xenograft bearing mice following 10 mg kg^{-1} oral dose of compounds **37**, **38**, and **39**. Reprinted (adapted) with permission from Finlay et al., *J. Med. Chem.* **2014**, *57* (20), 8249–8267. Copyright (2014) American Chemical Society.

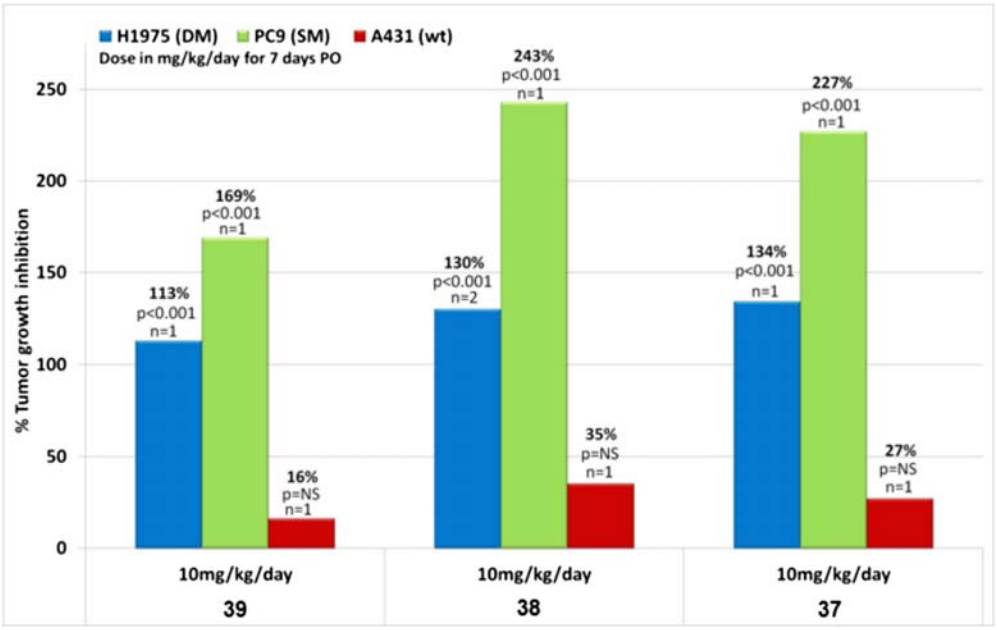

Fig. 12 In vivo efficacy of **37**, **38**, and **39** when dosed orally in tumor bearing immune-compromised mice at 10 mg $kg^{-1}day^{-1}$ QD. H1975 efficacy is represented in *blue*, with PC9 data in *green*, and A431 in *red*. Statistical significance (*p*-values) was calculated by comparing compound treated and vehicle groups using a one-tailed *t*-test, "NS" indicates %TGI was not significant from vehicle. Reprinted (adapted) with permission from Finlay et al., *J. Med. Chem.* **2014**, *57* (20), 8249–8267. Copyright (2014) American Chemical Society.

(Figs. 14 and 15), whereas at the same dose, **39** did not cause significant changes in blood glucose levels, but insulin levels were clearly increased, consistent with insulin being a more sensitive marker for perturbation of the glucose/insulin axis. Compound **44**, however, did not impact measured levels of glucose or insulin. This is consistent with the observation that **44** did not inhibit IGF1R or INSR with significant potency. For compound **44**, pharmacological cover over the INSR IC_{50} and perturbation of the insulin-glucose axis was therefore considered extremely unlikely.

Although IGF1R inhibitors have been studied clinically in an oncology setting, hyperglycemia can be dose limiting.[11] Inhibition of IGF1R and INSR signaling and its associated pharmacology had the potential to limit maximal tolerated doses in the NSCLC EGFR sensitive patient setting. Furthermore, it could affect patient exclusion criteria and require additional monitoring during

Table 15 Structure and selected data for indole compounds **40–45**

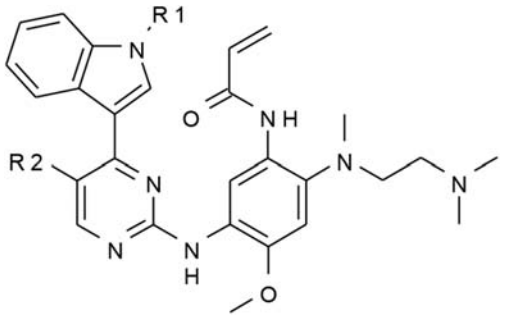

	40	*41*	*42*	*43*	*44*	*45*
R_1/R_2	Me/CN	Me/Cl	H/Cl	Me/Me	Me/H	H/H
DM cell IC_{50} (nM)	0.9	2	0.2	1	15	2
AM cell IC_{50} (nM)	1	2	0.6	2	17	2
WT cell IC_{50} (nM)	46	58	11	71	480	33
DM anti proliferative cell GI_{50} (nM)	2 ($n=1$)	4 ($n=1$)	2 ($n=1$)	4 ($n=1$)	24	16
AM anti proliferative cell GI_{50} (nM)	0.8 ($n=1$)	3 ($n=1$)	2 ($n=1$)	2 ($n=1$)	23	21
WT anti proliferative cell GI_{50} (nM)	101 ($n=1$)	192 ($n=1$)	144 ($n=1$)	970 ($n=1$)	264	58
IGF1R IC_{50} (nM)	38 ($n=1$)	40 ($n=1$)	7 ($n=1$)	196 ($n=1$)	2900	263
hERG IC_{50} (μM)	4.3	7.4	14.8	15.6	16.2	17.5
$LogD_{7.4}$	2.7	3.3	3.3	2.8	3.4	2.9
Min sol pH 7.4 (μM)	57	759	75	576	7	79
Rat HW % free	11	–	7.5	–	3.2	16
Human % free	8.9	2.3	3.6	7.5	2.9	7.5
Mouse % free	–	–	–	–	3.4	13.4
Rat Heps Cl_{int} (μL $min^{-1}10^6cells^{-1}$)			88		27	27
Human Heps Cl_{int} (μL $min^{-1}10^6cells^{-1}$)	10	10	<3	5.6	3.4	<3
Rat HW IV Cl (mL $min^{-1}kg^{-1}$)	62	27	12	–	45	–
Rat HW PO F (%)	6	7	1	–	45	–
Mouse AUC/C_{max} (μM h μM^{-1}) 10 mg kg^{-1} PO	0.28/0.11	1.3/0.31	3.3/1.2	0/0	1.4/0.38	0.203/0.047
GSH mean t ½ (min)	–	–	136	123	121	191

Reprinted (adapted) with permission from (Finlay et al. *J. Med. Chem.* **2014**, *57* (20), 8249–8267). Copyright (2014) American Chemical Society.

clinical trials. In light of these findings it was decided to focus remaining efforts on **44** and **39,** which had no or minimal effects on the IGF1R-INSR axis, respectively.

We subsequently performed a preliminary cardiovascular safety evaluation on compounds **44** and **39**. The compounds were assessed in an in vivo guinea pig model[15] to explore the effect of the compounds on hemodynamic, ECG, and contractility parameters. Comparison of the cardiovascular profile revealed a major difference in the compounds with respect to QT prolongation. In contrast to **44**, **39** was associated with a pronounced QT prolongation at free C_{max} concentrations <30-fold predicted human free C_{max}. These data were consistent with the in vitro data for both compounds with **39** having a greater affinity for the hERG ion channel than **44** (Ionworks hERG IC_{50} for **39** and **44** is 4.3 and 16.2 μM, respectively). In view of the data package, as a whole, **44** was considered to have a desirable profile and ultimately selected as clinical candidate AZD9291,[43] subsequently given the generic name osimertinib.

In addition to the relatively short 7-day antitumor models previously described, longer term studies were subsequently carried out with compound **44** resulting in long-term sustainable efficacy[43] at a dose of 5 mg $kg^{-1}day^{-1}$ in the H1975 DM model (**Fig. 16**). At the same dose in the AM PC9 model compound **44** showed increased efficacy when compared to a 6.25 mg $kg^{-1}day^{-1}$ dose of gefitinib, matching clinical exposure as previously with our compound **12** study (**Table 9**).

The selectivity profile of **44** as determined in the Millipore kinase panel[16] of 270 kinases is shown in **Fig. 17**, and it can be seen that the compound displays an excellent overall profile with the majority of more active hits being other tyrosine kinases.

Although we had not been able to generate an X-ray crystal structure of **44** bound to an EGFR T790M mutant, we were able to utilize a published structure (pdb code 3IKA)[8] to model the binding mode, as shown in **Fig. 13**. Notable features include the covalent bond formed to C797, the hinge interaction at M793, and the orientation of the indole. This binding mode was also consistent with the binding mode of the earlier compounds, which we crystallized in WT EGFR (**Fig. 18**).

Fig. 19 summarizes in detail the key differences between the binding mode of **44** into EGFR T790M and first-generation inhibitors such as gefitinib or erlotinib. As discussed previously, a key difference is the scaffold of the inhibitor, osimertinib containing a monoanilinopyrimidine core as opposed to an anilinoquinazoline core. This monoanilinopyrimidine scaffold enables osimertinib to interact with the T790M gatekeeper mutation more favorably than gefitinib or erlotinib, reflected in the T790M

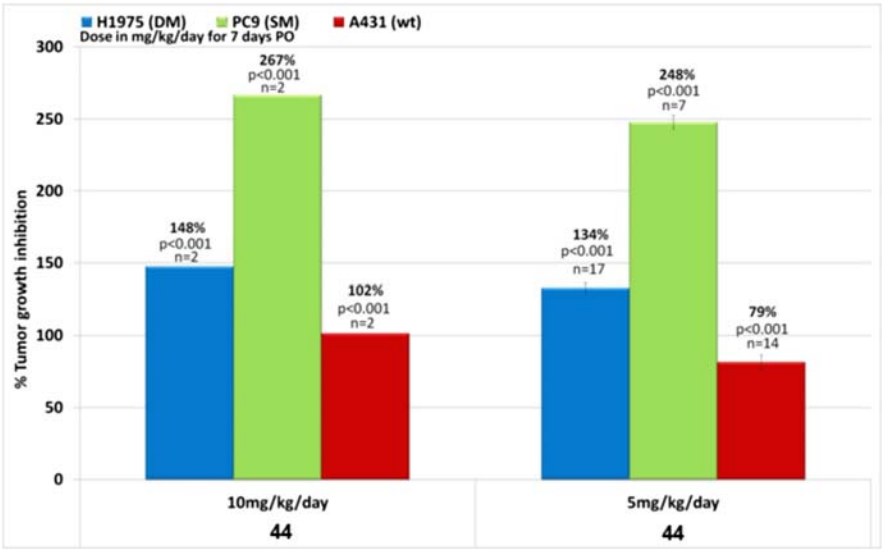

Fig. 13 In vivo xenograft activity of **44** when dose orally in tumor bearing immune-compromised mice at 10 and 5 mg kg^{-1} QD. Reprinted (adapted) with permission from Finlay et al., *J. Med. Chem.* **2014**, *57* (20), 8249–8267. Copyright (2014) American Chemical Society.

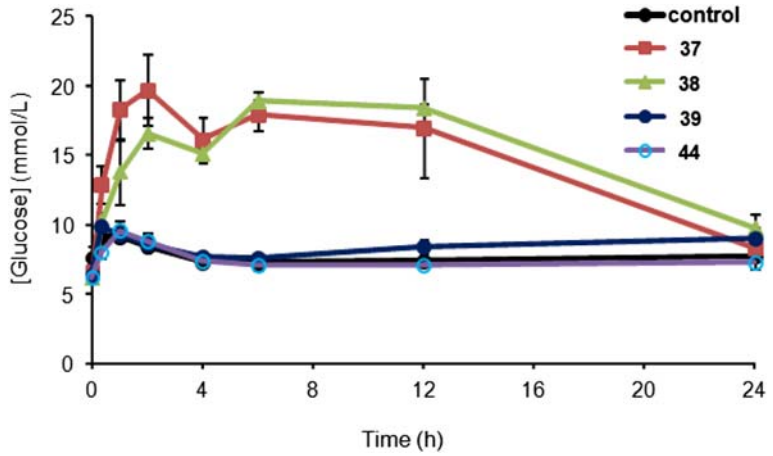

Fig. 14 Compound effects of blood glucose levels in the rat following a single 200 mg kg^{-1} oral dose of compounds **37**, **38**, **39**, and **44**. Reprinted (adapted) with permission from Finlay et al., *J. Med. Chem.* **2014**, *57* (20), 8249–8267. Copyright (2014) American Chemical Society.

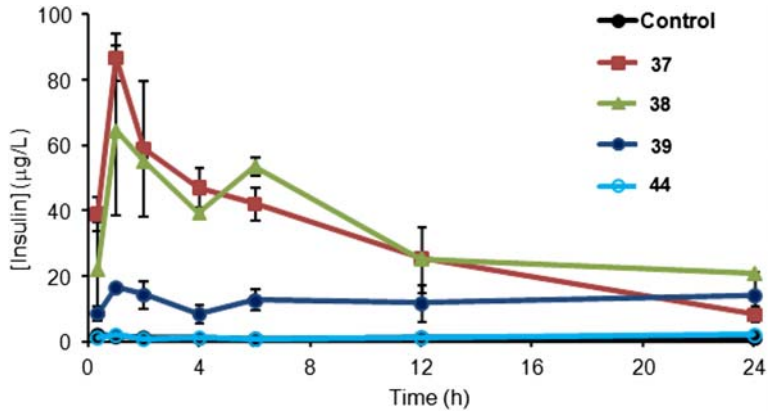

Fig. 15 Compound effects of blood insulin levels in the rat following a single 200 mg kg^{-1} oral dose of compounds **37**, **38**, **39**, and **44**. Reprinted (adapted) with permission from Finlay et al., *J. Med. Chem.* **2014**, *57* (20), 8249–8267. Copyright (2014) American Chemical Society.

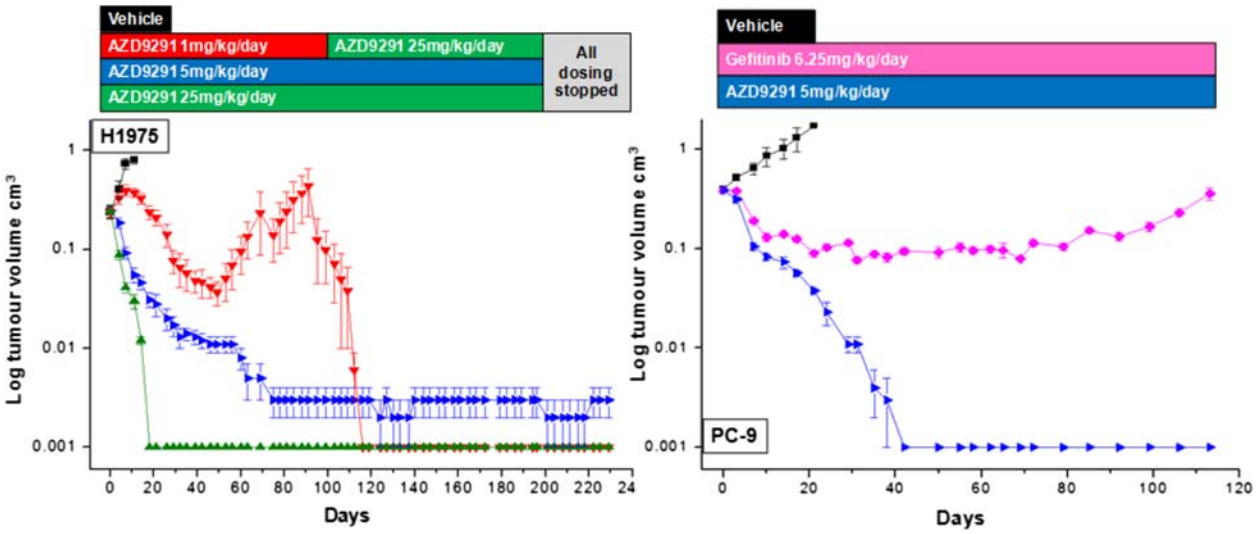

Fig. 16 Long-term antitumor studies in H1975 double mutant and PC9 activating mutant xenograft models for compound **44**. Figure adapted from Cross et al., *Cancer Discov.* **2014**, *4*, 1046–1061.

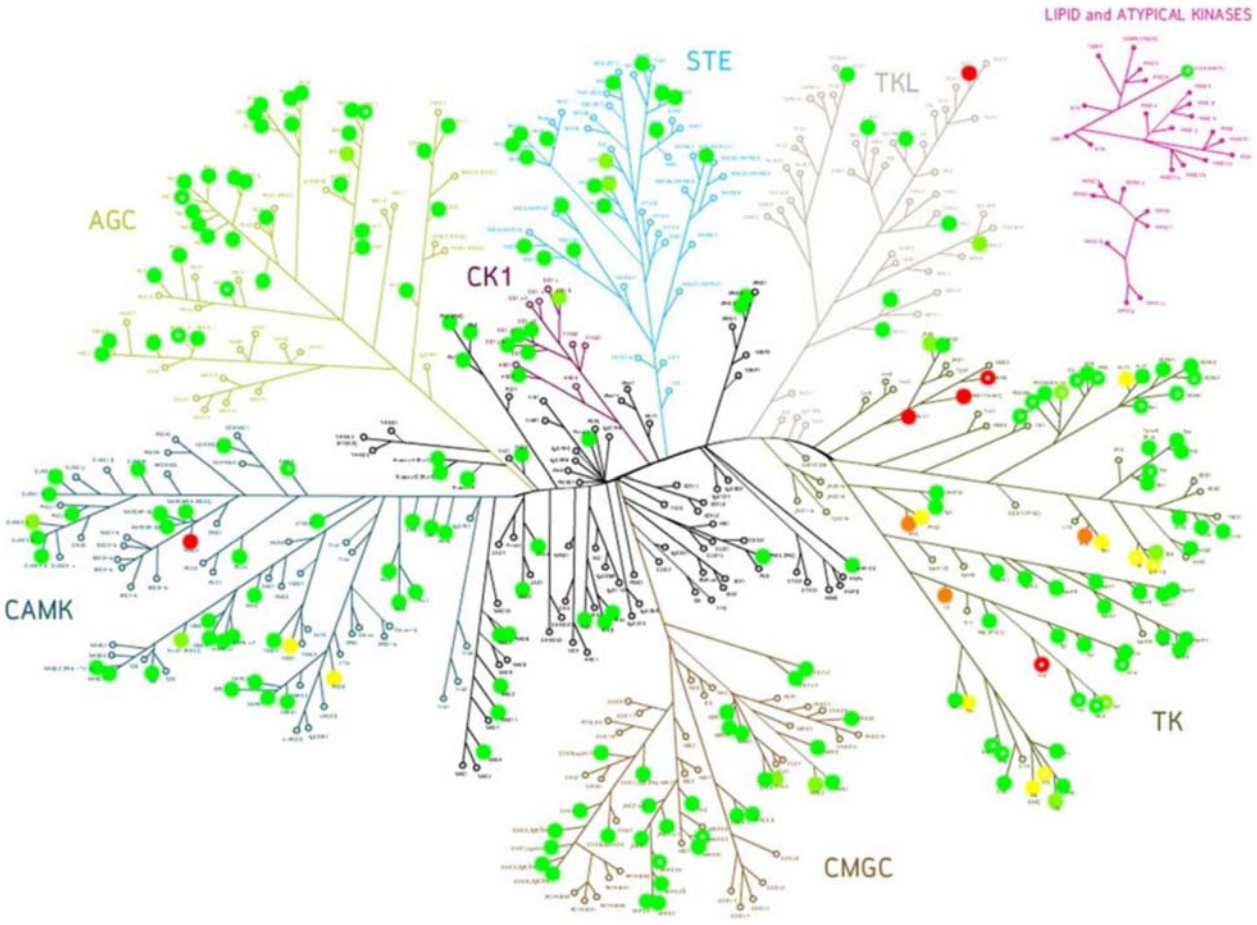

Fig. 17 Millipore kinase selectivity profile for compound **44**. Colors are indicative of % inhibition at 1 μM as follows; *dark green* = 0-20% of control, *light green* = 20-40% of control, *yellow* = 40-60% of control, *orange* = 60-80% of control, and *red* = 80-100% of control. Full % inhibition data is listed in the supporting information including IC_{50} data for those kinases with an analogs cysteine to C797. Reprinted (adapted) with permission from Finlay et al., *J. Med. Chem.* **2014**, *57* (20), 8249–8267. Copyright (2014) American Chemical Society.

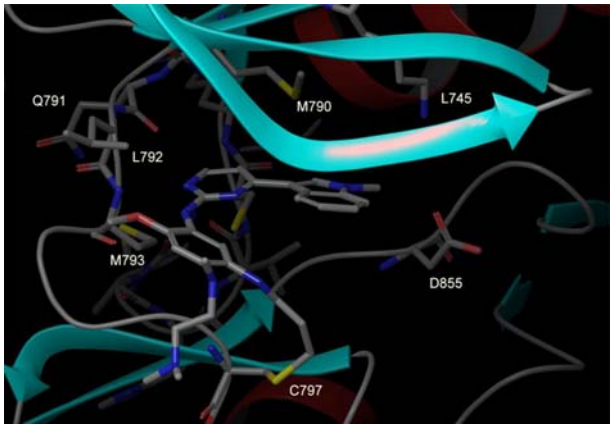

Fig. 18 Modeled binding mode of **44**. See supporting information for further details. Adapted from the American Association for Cancer Research: Cross D.A.E. et al., AZD9291, an Irreversible EGFR TKI, Overcomes T790M-Mediated Resistance to EGFR Inhibitors in Lung Cancer. *Cancer Discov.* **2014**, *4*, 1046–1061.

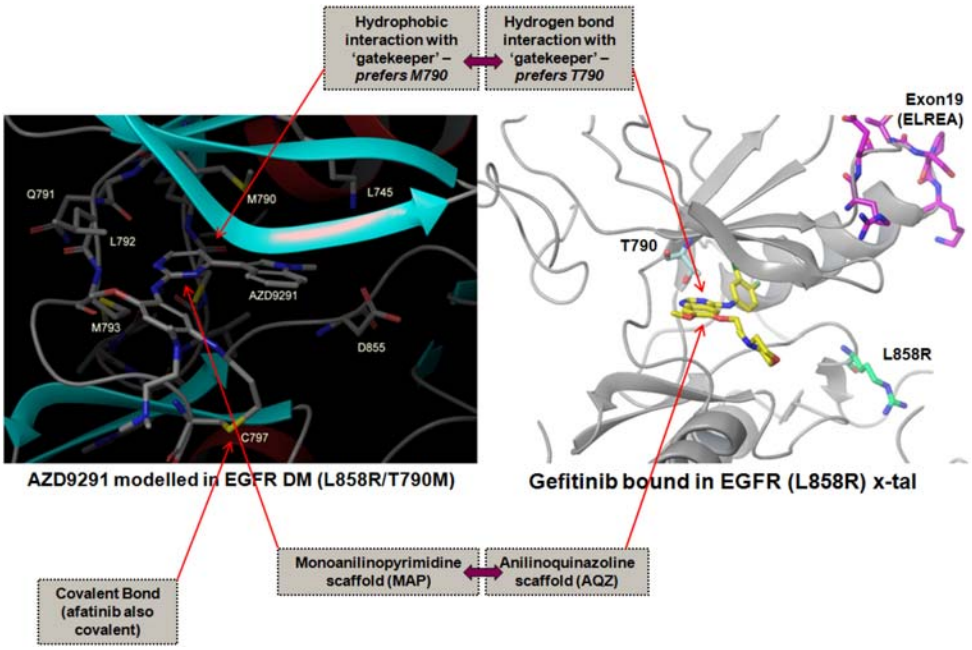

Fig. 19 Comparison of the predicted binding mode of **44** (osimertinib) and EGFR T790M compared to first-generation EGFR inhibitors.

mutant-selective profile of osimertinib. Osimertinib is also a covalent inhibitor through the formation of a covalent bond to C797S, which enables the compound to inhibit the T790M protein in cellular concentrations of ATP.

Our subsequent focus was to further understand the metabolic fate of compound **44** in vivo. Previously, when investigating in vivo metabolism in rat bile samples, minimal metabolism had been evident apart from GSH conjugation to the acrylamide portion of the molecule. In contrast, when in vivo plasma samples from rat and mouse were assessed in more detail, it became evident that loss of the indole *N*-methyl group occurred, leading to small quantities of compound **45** (AZ5104), Fig. 20. In addition, dealkylation was also seen to occur to a small extent in the *N,N,N′*-trimethylethylenediamine side chain of **8**, yielding **46**. A small amount of the side chain *N*-oxide was also evident at low levels.

Highlighted in Fig. 15 are the total levels for **44**, **45**, and **46** over a 12 h period following a 25 mg kg^{-1} oral dose in the nude mouse. Compound **46** appeared to offer a broadly similar potency and selectivity profile to the parent compound. In contrast, we had previously prepared and profiled **45** (see Table 15), but despite its impressive double and AM potency, we had not progressed the compound further, partly due to its slightly reduced in vitro WT margin. In addition, oral dosing of **44** in the mouse led to only modest levels of exposure and low levels of free cover over the cellular IC_{50} values (Fig. 21).

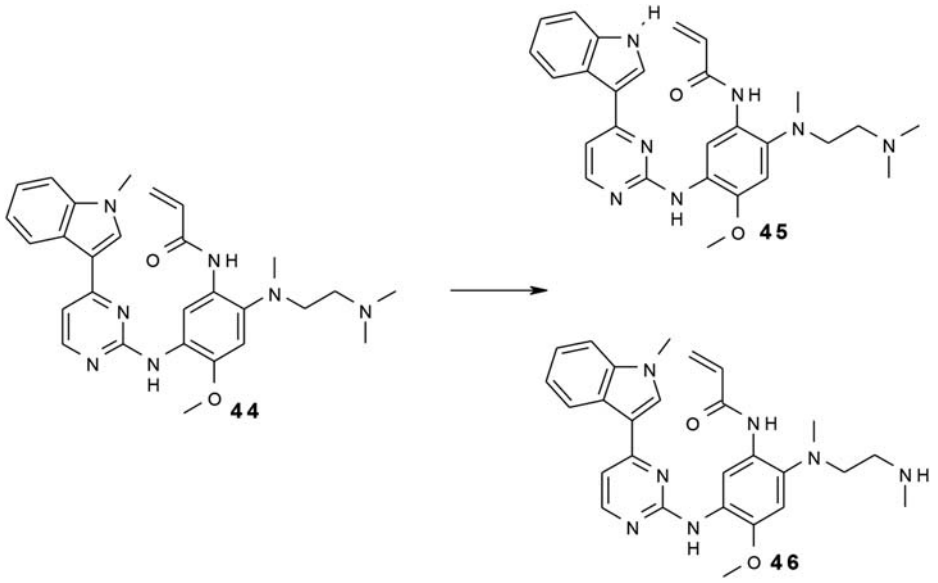

Fig. 20 Compound **44** and identified circulating metabolites **45** and **46**.

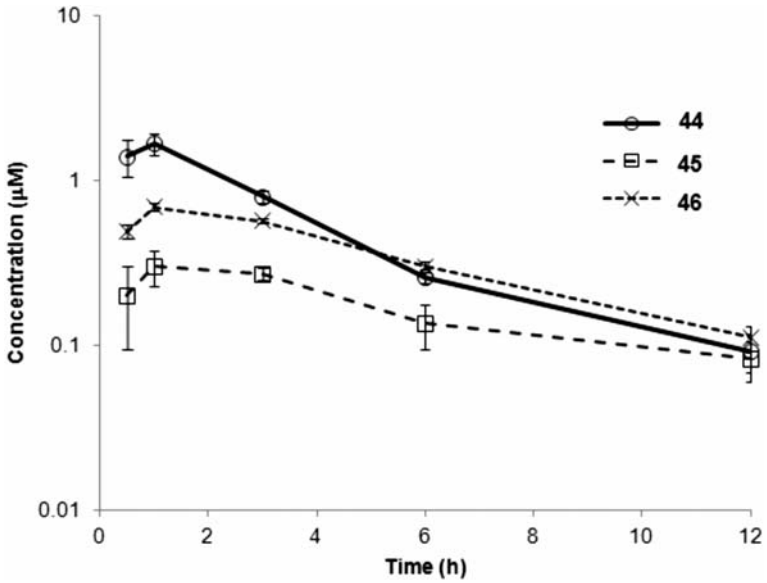

Fig. 21 Total levels for **44**, **45**, and **46** over a 12 h period following a 25 mg kg^{-1} oral dose of **44** in the nude mouse. The markers are mean values ± SEM. Reprinted (adapted) with permission from Finlay et al., *J. Med. Chem.* **2014**, *57* (20), 8249–8267. Copyright (2014) American Chemical Society.

Nevertheless, there was an intriguing prospect that a degree of the observed efficacy in vivo for 44 was enhanced by the generation of metabolite 45. While 45 is present at lower concentrations in vivo than 44, the higher cellular potency and lower protein binding equate to broadly similar free cover in vivo. A number of experiments were undertaken to try and establish the in vivo efficacy of 44 in the absence of 45. These included codosing mice with 44 and the pan cytochrome P-450 inhibitor benzotriazol-1-amine[17,18] in an attempt to reduce oxidative metabolism of the indole *N*-methyl group to give 45. In addition, we undertook the preparation of an isotopically labeled version of 44, where the indole *N*-methyl group was replaced by the $^{13}CD_3$ equivalent. Our hypothesis here was that the kinetic isotope effect[19] might slow the deuterium atom extraction process relative to the corresponding hydrogen atom reaction and thus suppress formation of 45, but neither of these measures were able to completely prevent the in vivo formation of 45.

To understand the implications of the presence of the metabolite 45 in vivo, we elected to dose 45 in the previously described antitumor models. These studies (Fig. 22) suggested that while substantial double and AM efficacy is apparent, the level of WT efficacy was also significant, reflecting the narrower in vitro margin as predicted from the in vitro cellular potency. It is also noteworthy

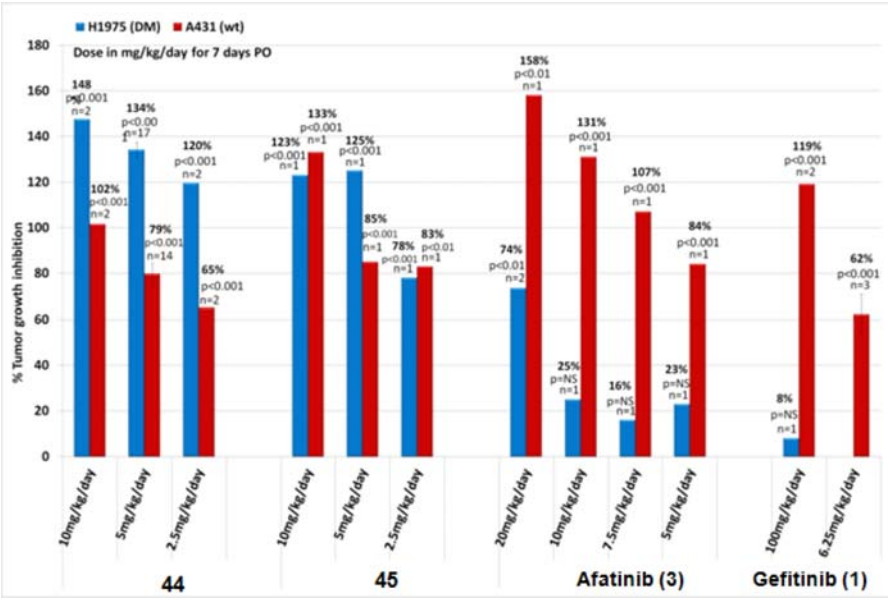

Fig. 22 In vivo efficacy profiles (% tumor growth inhibition) of **44**, **45**, afatinib (**3**), and gefitinib (**1**). Reprinted (adapted) with permission from Finlay et al., *J. Med. Chem.* **2014**, *57* (20), 8249–8267. Copyright (2014) American Chemical Society.

that in the case of **45**, only very modest cover over the free cell IC_{50} is needed to achieve significant efficacy. This is also apparent for **44**, but the presence of **45** in vivo perhaps makes this observation simpler to rationalize.

Comparison of the efficacy profiles between the two compounds revealed significant differences, and while it is likely that **45** contributes to the observed in vivo efficacy of **44**, the parent compound has a large influence. It is apparent from Fig. 16 that the efficacy profiles of **44** and **45** are quite different from both the reversible inhibitor gefitinib (**1**), and the irreversible EGFR inhibitor afatinib (**4**) and that mutant-selective inhibitors **44** and **45** offer a superior efficacy profile than these earlier agents. Clearly, the extent of formation of **45** in human patients would be a pivotal piece of information, as while its absence could potentially reduce the efficacy of the agent, more substantial levels could potentially lead to diminished margins to EGFR driven WT toxicity. Upon dosing patients in a clinical setting, however, this risk appeared reduced, vide infra. Predicting an efficacious dose in patients for this agent therefore presented challenges as estimating the levels of metabolite exposure in humans would be important along with the irreversible mode of action also needing consideration. The full details of these studies have been reported elsewhere, but basing human PK estimations on a metabolite **45** formation rate of 25% of parent (formation of **46** could not be quantified in vitro), the predicted efficacious dose in patients based on data from the H1975 DM model was approximately 10 mg, with a 20 mg predicted dose based on the PC9 AM model.

In silico modeling of human absorption[20] showed that **44** should not be solubility limited at clinically relevant doses with Fabs $>50\%$ up to 330 mg. Although the free base properties of **44** were considered to offer a low biopharmaceutical risk, the mesylate salt was selected for further work due to manufacturing risks around the physical form of the free base. In vivo studies established that the PK of **44**-mesylate were largely comparable to those of the free base.

We have described herein the rapid evolution of a chemical series from lead selection through to candidate nomination and the emerging clinical findings with this novel agent. From start of the project in early 2009, we were able to deliver clinical candidate AZD9291 in Mar. 2012 (first synthesized 9 Jun. 2011), for first time in man, studies commencing in Mar. 2013. During the course of this work, a number of key challenges were addressed including off-target kinase selectivity and cardiovascular safety. AZD9291 offered a number of advantages over earlier EGFR TKI agents including high cellular potency, superior efficacy in relevant disease models, and selectivity over the WT form of the receptor. To date, reproducible drug exposure has been achieved in humans, and of particular significance was the early evidence of tumor responses in patients who had previously progressed on earlier treatments, accompanied by good tolerability. Full synthetic procedures for all the highlighted EGFR inhibitors from our drug discovery program can be found in our two J. Med. Chem publications from 2013[21] and 2014.[41]

8.01.3 Emerging Clinical Data of Osimertinib

The mesylate salt of **44** was first dosed in Mar. 2013 to patients with EGFRm + advanced NSCLC, who had disease progression following treatment with an EGFR TKI (including **1** or **2**). Based on our preclinical data, the initial dose selected for oral administration to patients was 20 mg, once a day. Initial PK data from this cohort of six patients is shown further.[21] It can be seen that after a single dose, 7-day washout and then 8 days of once daily dosing, exposure to **44**, **45**, and **46** was observed. It is also evident that

the formation rate of the **45** metabolite is largely consistent with the predicted levels, and that inter patient variability is low (Fig. 23). Clearly these data discharge to some extent the aforementioned potential risks around the presence or absence of **45**.

Clinical testing with osimertinib showed encouraging efficacy in NSCLC patients from the first patient dosed. Specific data from two patients have been reported[21,22] from the AURA Phase I study and are presented here (NCT01802632). Serial computerised tomography (CT) scans from two patients who received **44** at a 20 mg once daily dose are shown (Figs. 24 and 25). Prior to commencing dosing, both patients' tumors were known to exhibit T790M mutations as well as EGFR sensitizing mutations. The first patient was a 57-year-old East Asian female from South Korea, diagnosed with stage IV EGFR mutant (Exon 19 deletion) NSCLC in May 2011. Tumor shrinkage on treatment with **44** was 39.7% at RECIST 1.1 (response evaluation criteria in solid tumors)[23] scan 1, 48.3% by scan 2 (Fig. 18), remained at 48.3% at both scan 3 and scan 4, and was 51.7% at scan 5 (data not shown).

The second subject[21] was a 57-year-old white female from the United Kingdom, diagnosed with Stage IV lung adenocarcinoma in Dec. 2010. At the cycle 1 day 15 assessments on **44**, the patient reported full resolution of preexisting persistent nocturnal cough. Tumor shrinkage was 38% at RECIST 1.1 scan 1, 39.3% by scan 2, 56.7% by scan 3 (Fig. 19), 62% by scan 4, and 59.3% by scan 5 (data not shown). By Cycle 7 day 1, the patient reported significant improvement in preexisting hair and eyelash abnormalities, which had developed during the immediately prior gefitinib therapy. Both patients had a duration of response of approximately 9 months and were progression-free on 20 mg day^{-1} of compound **44** mesylate salt for approximately 11 months until disease progression by RECIST 1.1. No significant aberration of blood glucose levels were noted in either patient during the study.

Osimertinib was approved by the US FDA on 13 Nov. 2015, with a recent disclosure showing an overall response rate of 66.1% in T790M positive patients (Fig. 26).[44] This approval was based on data from the preplanned analysis of both AURA (NCT01802632) and AURA2 (NCT02094261) clinical trials at the 80 mg QD dose.

Further disclosures from this analysis demonstrated a median progression-free survival of 9.7 months (maturity 39%). Additional emerging data of osimertinib in first-line treatment of advanced EGFRm NSCLC treatment from the Phase 1 AURA study have also been very positive, showing that 72% of patients were alive and progression-free at 12 months, with an overall confirmed response rate of 75%.[44] In addition, osimertinib has also demonstrated clinical activity in cases of EGFR-mutant NSCLC with brain metastases and leptomeningeal disease.[45] In support of this, positron emission tomography imaging demonstrated that osimertinib is highly distributed into cynomolgus monkey brain. In all patients treated with osimertinib at all doses, diarrhea and rash were the most reported adverse events; these were however primarily low grade as hoped from the mutant-selective profile. Along with the rapid discovery phase this has been one of the fastest development journeys for a drug in history. From the dosing of the first patient to approval of osimertinib by the US FDA, the process took only 2 years and 8 months.

8.01.4 Current Progress of EGFR-Mutant Inhibitors

Since we initiated our efforts to identify compounds with this preferred selectivity profile, other compounds have been reported exploiting similar principles (Table 16). An early example published was from the Dana-Farber Cancer Institute (WZ-4002, **47**),[54]

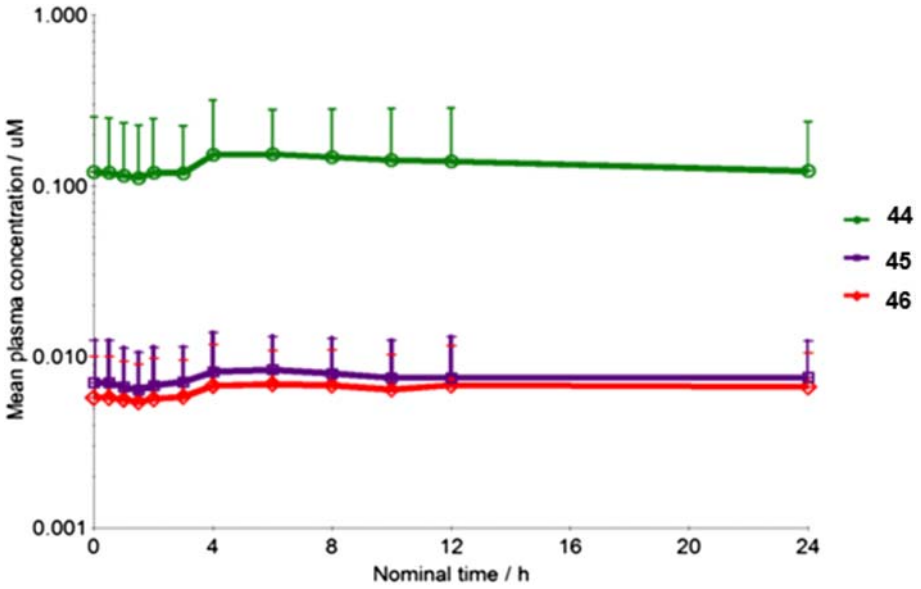

Fig. 23 Preliminary plasma concentration versus time plots (mean + SD) of **44**, **45**, and **46** after 8 days of once daily 20 mg oral doses of **44** to patients with advanced EGFRm + NSCLC in AURA Phase 1 study (NCT01802632) ($n = 6$). Adapted from the American Association for Cancer Research: Cross D.A.E. et al., AZD9291, an Irreversible EGFR TKI, Overcomes T790M-Mediated Resistance to EGFR Inhibitors in Lung Cancer. *Cancer Discov.* **2014**, *4*, 1046–1061.

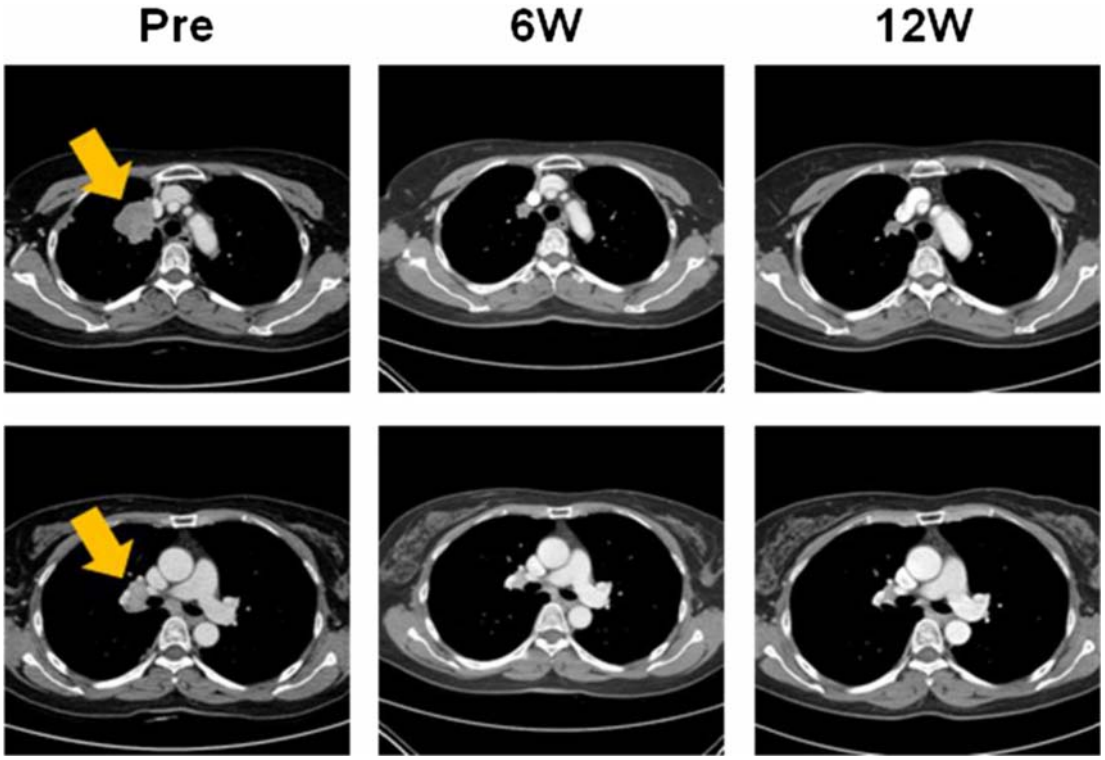

Fig. 24 Serial computed tomography scans of the chest from patients before and after treatment with **8** in a phase I trial. Images from a 57-year-old Korean female patient diagnosed with Stage IV nonsmall cell lung cancer in May 2011. Adapted from the American Association for Cancer Research: Cross D.A.E. et al., AZD9291, an Irreversible EGFR TKI, Overcomes T790M-Mediated Resistance to EGFR Inhibitors in Lung Cancer. *Cancer Discov.* **2014**, *4*, 1046–1061.

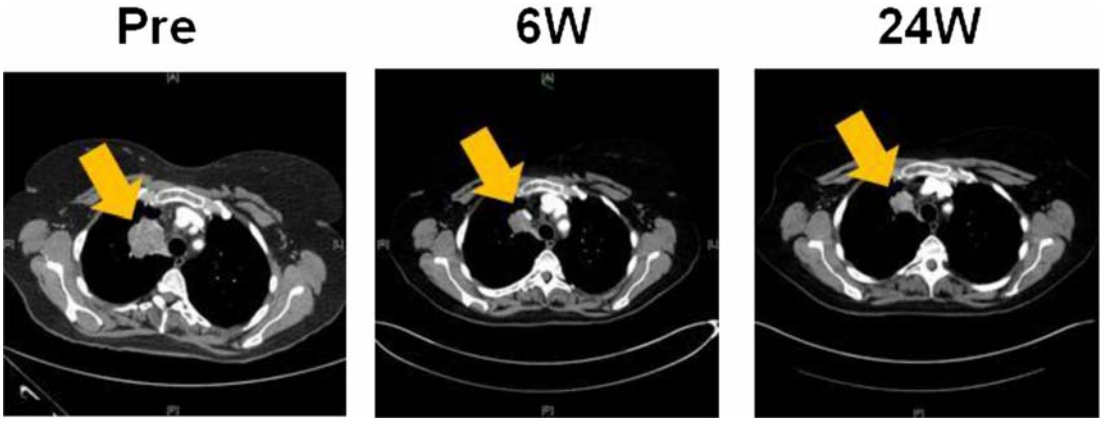

Fig. 25 Serial computed tomography scans of the chest from patients before and after treatment with **44** in a phase I trial. Images from a 57-year-old British female never smoker diagnosed with Stage IV lung adenocarcinoma in Dec. 2010. Adapted from the American Association for Cancer Research: Cross D.A.E. et al., AZD9291, an Irreversible EGFR TKI, Overcomes T790M-Mediated Resistance to EGFR Inhibitors in Lung Cancer. *Cancer Discov.* **2014**, *4*, 1046–1061.

based on a pyrimidine template along with additional covalent inhibitors from Clovis Oncology (CO-1686/rociletinib, **48**), and Hanmi Pharmaceuticals (HM61713) have been reported to be in clinical studies. More recently, reports have emerged of additional covalent inhibitors targeting EGFR T790M include ASP8273 (Astellas), EGF-816 **49** (Novartis), AC0010 (ACEA Biosciences), TAS-121 (Taiho), and PF-06747775 **50** (Pfizer). Also reported is the reversible anaplastic lymphoma kinase inhibitor (AP26113/brigatinib) from Ariad, with reported activity against the T790M DM form of EGFR.

Although clinical data from a number of the more recent inhibitors has been disclosed at meetings such as the American Association for Cancer Research and American Society of Clinical Oncology, clear comparisons of their clinical efficacy and side-effect

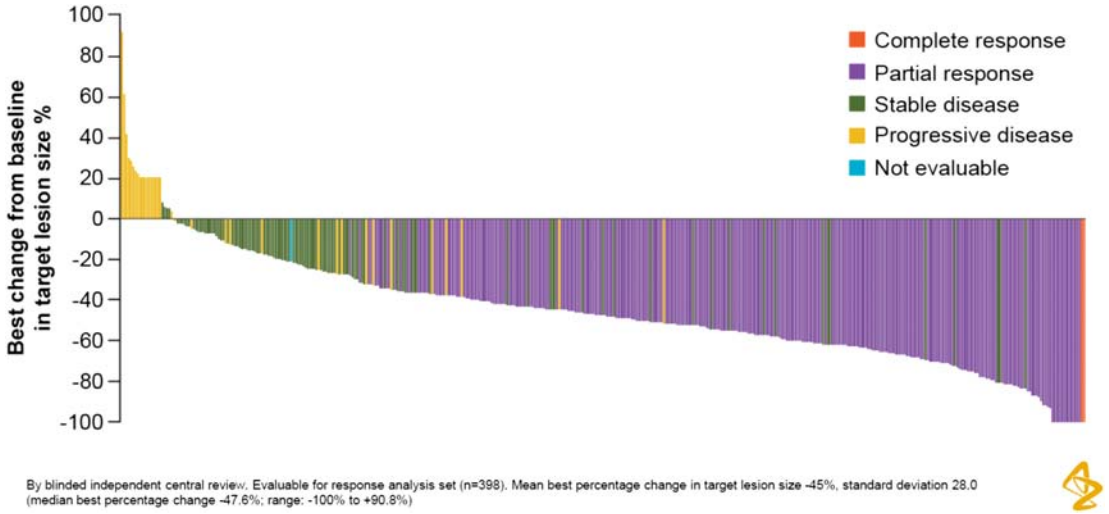

Fig. 26 AZD9291 in pretreated patients with T790M positive advanced nonsmall cell lung cancer (NSCLC): pooled analysis. By blinded independent central review. Evaluable for response analysis set ($n=398$). Mean best percentage change in target lesion size -45%, standard deviation 28.0 (median best percentage change -47.6%; range: -100% to $+90.8\%$).[44] Adapted from a presentation by Goss G.D. ECC 2015 European Cancer Congress.

profiles are challenging due to limited data. A significant number of preclinical compounds have been disclosed including covalent and noncovalent inhibitors.[55–57] It is beyond the scope of this article to attempt to summarize all of these, but the area continues to attract significant interest from the pharmaceutical industry and academia.

8.01.5 Learnings, Future Challenges, and Opportunities

As clinical data emerges on patients treated with osimertinib, and the subsequent approval by the US FDA in Nov. 2015 and positive Commission for Health Improvement (CHIMP) recommendation in Dec. 2015, it is perhaps timely to reflect on the potential learning's from our drug discovery program and also a chance to look forward to additional opportunities and challenges. A number of publications highlight the significant ongoing challenges pharmaceutical companies face in delivering new drugs to the market, in response to this a recent AstraZeneca publication sought to identify key attributes of drug discovery projects, which appeared important to successful delivery.[58] These factors were summarized in a "5Rs framework," which considers the right target, right tissue, right safety, right patients, and right commercial potential of a drug discovery program (Fig. 27). Although this framework was not developed when the drug discovery project that delivered osimertinib was initiated, many of the strengths of the drug discovery program are reflected in these areas. In terms of "right target" EGFR biology is relatively well understood with a clear idea of the primary target (EGFR DM) being a key driver of tumor growth. An additional benefit to the project was that suitable in vitro and in vivo models (with clear disease linkage) could be rapidly deployed in-house to enable novel compounds to be tested against disease-relevant models. In particular the availability of the DM resistant H1975 and PC9 AM cell lines enabled early access to relevant cellular assays and in vivo models. For "right tissue," in addition to have compounds with good PK properties, it was important to have access to reliable PK/PD models to ensure accurate dose predictions, especially important with the impact of active metabolites. In terms of "right safety" a number of potential off-targets were suspected upfront and therefore closely monitored, such as EGFR WT in particular, which was a key part of the compound profile. Activity against IGF1R/INSR and hERG was also monitored as possible risks with suitable in vivo models available to assess this. The "right patient" aspect was also strong with this drug discovery program as the initial focus would be on patients, who have failed on current TKIs and therefore readily identifiable, in addition to progress being made to detect the presence of the T790M mutation from patient samples. The "right commercial potential" of such an agent was perhaps more difficult to estimate with confidence at such an early stage of the project. However, it was felt that if a compound with the specific "mutant-selective" profile could be identified, it would show significant clinical benefit to a number of NSCLC patients with limited treatment options.

Other publications have also assessed emerging targets for drug discovery projects. A publication from Pfizer summarized "The four pillars of cell-based target validation." The aim of their work was by applying the four principles to new projects one could be more confident between the link between target perturbation and disease-relevant pharmacological modulation. The pillars highlight the importance of cellular penetration, target engagement, and selectivity along with the expression of functional pharmacology and relevant phenotype. Again, these themes could be considered as being particular strengths of our internal drug discovery program for identifying mutant-selective EGFR inhibitors.

Table 16 Selection of EGFR T790M targeting inhibitors which have been tested in human clinical trials

Compound	*Structure*	*Company*	*Clinical phase*
Osimertinib (44) (AZD9291)	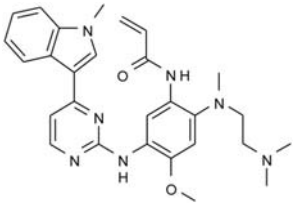	AstraZeneca	Approved by FDA (Nov. 2015)
WZ-4002 (47)	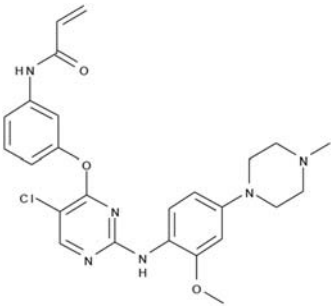	Dana-Farber Cancer Institute/Gatekeeper Pharmaceuticals, Inc	–
Rociletinib[46] **(48) (CO-1686)**	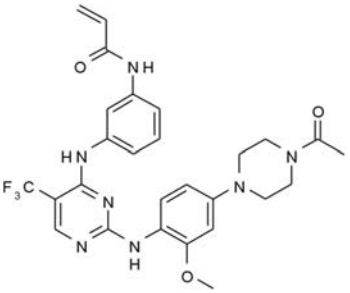	Clovis Oncology (originally discovered by Avila Therapeutic, acquired by Celgene)	Phase III
AP26113[47]	Structure not disclosed	Ariad Pharmaceuticals	Phase II
HM61713[48]	Structure not disclosed	Hanmi Pharmaceutical/Boehringer Ingelheim	Phase II
ASP8273[49]	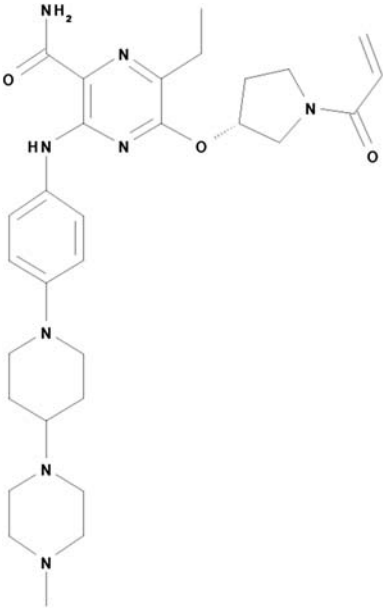	Astellas Pharma	Phase I

(Continued)

Table 16 Selection of EGFR T790M targeting inhibitors which have been tested in human clinical trials—cont'd

Compound	*Structure*	*Company*	*Clinical phase*
EGF816[50] **(49)**	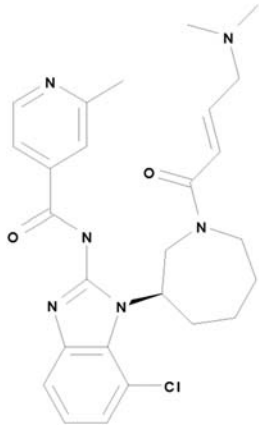	Novartis	Phase I
AC0010[51] **(Avitinib)**	Structure not disclosed	ACEA Biosciences	Phase I
TAS-121[52]	Structure not disclosed	Taiho (now Otsuka)	Phase I
PF-06747775[53] **(50)**	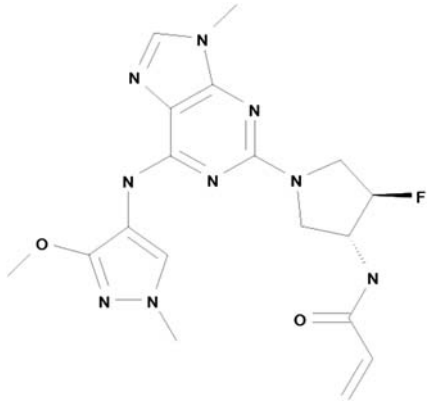	Pfizer	Phase I

With respect to the medicinal chemistry optimization strategy there are also some reflections that are useful to consider. The broad timelines for the key stages of the project are captured in Fig. 28 and show rapid progress of the drug discovery and clinical phase.

One early decision within our drug discovery program was to fully commit to a covalent strategy to overcome the issues with the significant enzyme cell drop-off due to high ATP affinity of the EGFR T790M DM. Although covalent inhibitors are currently being reported relatively frequently, in the early phase of our drug discovery there were relatively few specifically designed covalent inhibitors and prosecuting such a strategy faced some resistance. This focus on a covalent strategy enabled internal work to de-risk covalent compounds using in vitro approaches such as our GSH reactivity assay. A second important decision was to use compound **12** as an early in vivo probe to benchmark against gefitinib as an important POC of the approach. Although this compound had some issues and was therefore not likely to be a clinical candidate (moderate potency, poor properties, and hERG activity) the data generated was invaluable as it enabled understanding of what levels of potency and PK cover might be required for a clinical candidate. This was especially important due to the lack of previous experiences in-house with testing covalent inhibitors in vitro and in vivo. Finally, another important decision to the drug discovery program was made when short-list compounds **37**, **38**, and **39** had been evaluated. These compounds appeared of high quality and one option was to stop chemistry at that stage and ultimately select one of these as a clinical candidate. However, internal AstraZeneca chemistry continued to target compounds of reduced IGF1R and hERG activity, which we had flagged as potential risks with these early compounds. This continued chemistry, in combination with targeted prenomination toxicity work to look at effects on glucose/insulin and hERG resulted in **37**, **38**, and **39** being discontinued and **44** (osimertinib) being identified as a replacement to those compounds with minimal delay in the final selection of a clinical candidate. Therefore, one reflection here might be that chemistry should continue until enough confidence is generated in the potential clinical candidate that no further chemistry is required as once chemistry has stopped, there can be significant delay in restarting and reestablishing a suitable compound testing cascade.

Right target/ efficacy	▪ Strong link between target and disease ▪ Differentiating efficacy ▪ Available and predictive biomarkers
Right tissue/ right exposure	▪ Adequate bioavailability and tissue exposure ▪ Human PK / PD prediction, PD biomarkers ▪ Drug-drug interaction
Right safety	▪ Differentiating safety ▪ Predicted margin – secondary pharmacology ▪ Reactive metabolites, Gentox, drug-drug interactions ▪ Target liability
Right patients	▪ Scientific evidence in lead indication ▪ Risk / benefit stratification of patient population
Right commercial	▪ Differentiated value proposition vs. future standard of care ▪ Invest to win/priority areas – DTPP / CDTP ▪ Market access/payor/provider focus ▪ PHC strategy including diagnostic/biomarkers

Fig. 27 The 5Rs framework developed for project assessment.

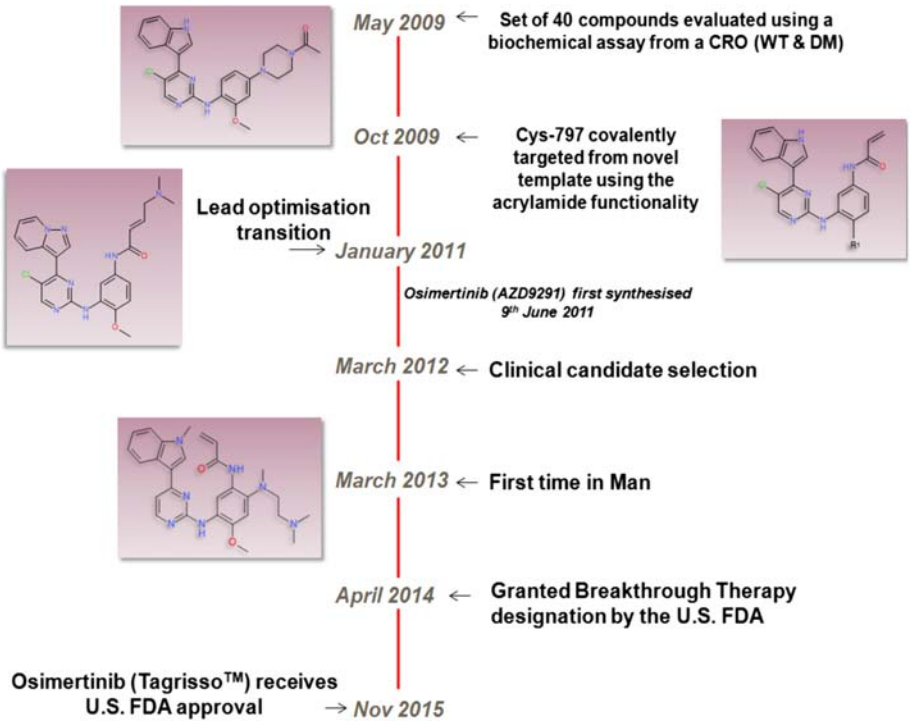

Fig. 28 Drug discovery and clinical phases of the osimertinib drug discovery project.

The recently emerging clinical data from osimertinib also reinforces the challenges and potential limitations with small molecule kinase inhibitors around issues with emerging resistance mechanism. In the same way as the T790M mutation emerges when patients are dosed with gefitinib or erlotinib, early data suggests a subset of patients become resistant to osimertinib via a C797S mutation.[59] In previous work at AstraZeneca, this mutation had been speculated as a potential mechanism of resistance to covalent EGFR inhibitors more broadly, as this amino acid is the residue to which osimertinib (and compounds such as CL-1033 and afatinib) covalently binds to.[60] Emerging mechanisms of resistance have also recently been disclosed for CO-1686 (rociletinib),[61] which includes emergence of EGFR T790 WT clones in vivo and additional point mutations in vitro.[62] There is therefore likely to be an ongoing requirement for additional therapies that circumvent various mechanisms of resistance as they emerge in the clinical setting. As inhibitors are developed targeting other kinases within the kinome, a similar story may develop against a number of these, therefore learning from these experiences with EGFR could have great benefit in oncology more broadly than EGFR and NSCLC. A significant challenge moving forward in kinase drug discovery appears to be how these acquired mutations

and resistance mechanisms are addressed. An aspect of this is how such mutations will inevitably lead to smaller, more fragmented patient populations, leading to challenges in identifying mutation status using next generation sequencing approaches. Although as these patient populations become fragmented thought has to be given to the feasibility of targeting each emerging mutation with additional novel, mutant-specific compounds. In future being able to reliably predict such emerging resistance mechanisms preclinically, ideally in vitro, would be of great benefit to direct such ongoing drug discovery efforts.

In addition to the monotherapy clinical studies for the various T790M directed inhibitors in the clinic, a number of combinations of clinical trials are also underway for osimertinib, rociletinib, and EGF-816, among others. This includes combination studies with MEK and MET small molecule kinase inhibitors and anti-PD-L1 antibodies.[63,64] Such combination approaches may also be an effective way to target potential emerging resistance mechanisms. It is likely that combination strategies with approved and novel agents will be extremely important to find the most effective therapeutic options for NSCLC patients.

Acknowledgments

We would like to thank all of our colleagues who were involved in this work, of which there are many, in what was an interdisciplinary team. We would also like to take this opportunity to thank all of our collaborators who have worked with us through the discovery, development, and clinical phases. Most of all we would like to thank all the patients who have taken part in a clinical trial of osimertinib to which we are extremely grateful.

References

1. Normanno, N.; De Luca, A.; Bianco, C.; Strizzi, L.; Mancino, M.; Maiello, M. R.; Carotenuto, A.; De Feo, G.; Caponigro, F.; Salomon, D. S. Epidermal Growth Factor Receptor (EGFR) Signaling in Cancer. *Gene* **2006,** *366,* 2–16.
2. Sharma, S. V.; Bell, D. W.; Settleman, J.; Haber, D. A. Epidermal Growth Factor Receptor Mutations in Lung Cancer. *Nat. Rev. Cancer* **2007,** *7,* 169–181.
3. Pao, W.; Chmielecki, J. Rational, Biologically Based Treatment of EGFR-Mutant Non-Small-Cell Lung Cancer. *Nat. Rev. Cancer* **2010,** *10,* 760–774.
4. Maemondo, M.; Inoue, A.; Kobayashi, K.; Sugawara, S.; Oizumi, S.; Isobe, H.; Gemma, A.; Harada, M.; Yoshizawa, H.; Kinoshita, I.; Fujita, Y.; Okinaga, S.; Hirano, H.; Yoshimori, K.; Harada, T.; Ogura, T.; Ando, M.; Miyazawa, H.; Tanaka, T.; Saijo, Y.; Hagiwara, K.; Morita, S.; Nukiwa, T. Gefitinib or Chemotherapy for Non-Small-Cell Lung Cancer With Mutated EGFR. *N. Engl. J. Med.* **2010,** *362,* 2380–2388.
5. Kobayashi, S.; Boggon, T. J.; Dayaram, T.; Jaenne, P. A.; Kocher, O.; Meyerson, M.; Johnson, B. E.; Eck, M. J.; Tenen, D. G.; Halmos, B. EGFR Mutation and Resistance of Non-Small-Cell Lung Cancer to Gefitinib. *N. Engl. J. Med.* **2005,** *352,* 786–792.
6. Yun, C.; Boggon, T. J.; Li, Y.; Woo, M. S.; Greulich, H.; Meyerson, M.; Eck, M. J. Structures of Lung Cancer-Derived EGFR Mutants and Inhibitor Complexes: Mechanism of Activation and Insights Into Differential Inhibitor Sensitivity. *Cancer Cell* **2007,** *11,* 217–227.
7. Yun, C.; Mengwasser, K. E.; Toms, A. V.; Woo, M. S.; Greulich, H.; Wong, K.; Meyerson, M.; Eck, M. J. The T790M Mutation in EGFR Kinase Causes Drug Resistance by Increasing the Affinity for ATP. *Proc. Natl. Acad. Sci. U. S. A.* **2008,** *105,* 2070–2075.
8. Maemondo, M.; Inoue, A.; Kobayashi, K.; Sugawara, S.; Oizumi, S.; Isobe, H.; Gemma, A.; Harada, M.; Yoshizawa, H.; Kinoshita, I.; Fujita, Y.; Okinaga, S.; Hirano, H.; Yoshimori, K.; Harada, T.; Ogura, T.; Ando, M.; Miyazawa, H.; Tanaka, T.; Saijo, Y.; Hagiwara, K.; Morita, S.; Nukiwa, T. Gefitinib or Chemotherapy for Non-Small-Cell Lung Cancer With Mutated EGFR. *N. Engl. J. Med.* **2010,** *362,* 2380–2388.
9. Shepherd, F. A.; Pereira, J. R.; Ciuleanu, T.; Tan, E. H.; Hirsh, V.; Thongprasert, S.; Campos, D.; Maoleekoonpiroj, S.; Smylie, M.; Martins, R.; van Kooten, M.; Dediu, M.; Findlay, B.; Tu, D.; Johnston, D.; Bezjk, A.; Clark, G.; Santabarbara, P.; Seymour, L. Erlotinib in Previously Treated Non-Small-Cell Lung Cancer. *N. Engl. J. Med.* **2005,** *353,* 123–132.
10. Zhang, Z.; Stiegler, A. L.; Boggon, T. J.; Kobayashi, S.; Halmos, B. EGFR-Mutated Lung Cancer: A Paradigm of Molecular Oncology. *Oncotarget* **2010,** *1,* 497–514.
11. Sogabe, S.; Kawakita, Y.; Igaki, S.; Iwata, H.; Miki, H.; Cary, D. R.; Takagi, T.; Takagi, S.; Ohta, Y.; Ishikawa, T. Structure-Based Approach for the Discovery of Pyrrolo[3,2-d] pyrimidine-Based EGFR T790M/L858R Mutant Inhibitors. *ACS Med. Chem. Lett.* **2013,** *4,* 201–205.
12. Gajiwala, K. S.; Feng, J.; Ferre, R.; Ryan, K.; Brodsky, O.; Weinrich, S.; Kath, J. C.; Stewart, A. Insights Into the Aberrant Activity of Mutant EGFR Kinase Domain and Drug Recognition. *Structure (Oxford, U. K.)* **2013,** *21,* 209–219.
13. Yun, C.; Woo, M. S.; Greulich, H.; Meyerson, M.; Eck, M. J.; Wong, K. In *In Structural and Mechanistic Studies of Lung Cancer Mutations in the EGFR Kinase Reveal a Novel Mechanism of Drug Resistance;* 2008. pp. COMP-373.
14. Davis, M. I.; Hunt, J. P.; Herrgard, S.; Ciceri, P.; Wodicka, L. M.; Pallares, G.; Hocker, M.; Treiber, D. K.; Zarrinkar, P. P. Comprehensive Analysis of Kinase Inhibitor Selectivity. *Nat. Biotechnol.* **2011,** *29,* 1046–1051.
15. Lovly, C. M.; Horn, L. Strategies for Overcoming EGFR Resistance in the Treatment of Advanced-Stage NSCLC. *Curr. Treat. Options Oncol.* **2012,** *13* (4), 516–526.
16. Ou, S. I. Second-Generation Irreversible Epidermal Growth Factor Receptor (EGFR) Tyrosine Kinase Inhibitors (TKIs): A Better Mousetrap? A Review of the Clinical Evidence. *Crit. Rev. Oncol. Hematol.* **2012,** *83,* 407–421.
17. Miller, V. A.; Hirsh, V.; Cadranel, J.; Chen, Y.; Park, K.; Kim, S.; Zhou, C.; Su, W.; Wang, M.; Sun, Y.; Heo, D. S.; Crino, L.; Tan, E.; Chao, T.; Shahidi, M.; Cong, X. J.; Lorence, R. M.; Yang, J. C. Afatinib Versus Placebo for Patients With Advanced, Metastatic Non-Small-Cell Lung Cancer After Failure of Erlotinib, Gefitinib, or Both, and One or Two Lines of Chemotherapy (LUX-Lung 1): A Phase 2b/3 Randomised Trial. *Lancet Oncol.* **2012,** *13,* 528–538.
18. Allen, L. F.; Eiseman, I. A.; Fry, D. W.; Lenehan, P. F. CI-1033, an Irreversible Pan-erbB Receptor Inhibitor and Its Potential Application for the Treatment of Breast Cancer. *Semin. Oncol.* **2003,** *30,* 65–78.
19. Kalous, O.; Conklin, D.; Desai, A. J.; O'Brien, N. A.; Ginther, C.; Anderson, L.; Cohen, D. J.; Britten, C. D.; Taylor, I.; Christensen, J. G.; Slamon, D. J.; Finn, R. S. Dacomitinib (PF-00299804), an Irreversible Pan-HER Inhibitor, Inhibits Proliferation of HER2-Amplified Breast Cancer Cell Lines Resistant to Trastuzumab and Lapatinib. *Mol. Cancer Ther.* **2012,** *11,* 1978–1987.
20. Johnston, J. B.; Navaratnam, S.; Pitz, M. W.; Maniate, J. M.; Wiechec, E.; Baust, H.; Gingerich, J.; Skliris, G. P.; Murphy, L. C.; Los, M. Targeting the EGFR Pathway for Cancer Therapy. *Curr. Med. Chem.* **2006,** *13,* 3483–3492.
21. Ward, R. A.; Anderton, M. J.; Ashton, S.; Bethel, P. A.; Box, M.; Butterworth, S.; Colclough, N.; Chorley, C. G.; Chuaqui, C.; Cross, D. A.; Dakin, L. A.; Debreczeni, J. E.; Eberlein, C.; Finlay, M. R.; Hill, G. B.; Grist, M.; Klinowska, T. C.; Lane, C.; Martin, S.; Orme, J. P.; Smith, P.; Wang, F.; Waring, M. J. Structure- and Reactivity-Based Development of Covalent Inhibitors of the Activating and Gatekeeper Mutant Forms of the Epidermal Growth Factor Receptor (EGFR). *J. Med. Chem.* **2013,** *56,* 7025–7048.
22. Merck Millipore www.millipore.com.
23. Singh, J.; Petter, R. C.; Baillie, T. A.; Whitty, A. The Resurgence of Covalent Drugs. *Nat. Rev. Drug Discov.* **2011,** *10,* 307–317.
24. Rauh, D. In *In Targeting Protein Kinases With Irreversible Inhibitors;* 2011. pp. MEDI-157.

25. Singh, J.; Evans, E.; Hagel, M.; Labinski, M.; Dubrovskiy, A.; Nacht, M.; Petter, R. C.; Prasad, A.; Sheets, M.; St Martin, T.; Tjin Tham Sjin, R.; Westlin, W.; Zhu, Z. Superiority of a Novel EGFR Targeted Covalent Inhibitor Over Its Reversible Counterpart in Overcoming Drug Resistance. *MedChemComm* **2012,** *3,* 780–783.
26. Friesner, R. A.; Banks, J. L.; Murphy, R. B.; Halgren, T. A.; Klicic, J. J.; Mainz, D. T.; Repasky, M. P.; Knoll, E. H.; Shelley, M.; Perry, J. K.; Shaw, D. E.; Francis, P.; Shenkin, P. S. Glide: A New Approach for Rapid, Accurate Docking and Scoring. 1. Method and Assessment of Docking Accuracy. *J. Med. Chem.* **2004,** *47,* 1739–1749.
27. Proteros biostructures www.proteros.de.
28. Edwards, M. P.; Price, D. A. Role of Physicochemical Properties and Ligand Lipophilicity Efficiency in Addressing Drug Safety Risks. *Annu. Rep. Med. Chem.* **2010,** *45,* 381–391.
29. Leeson, P. D.; Springthorpe, B. The Influence of Drug-Like Concepts on Decision-Making in Medicinal Chemistry. *Nat. Rev. Drug Discov.* **2007,** *6,* 881–890.
30. Leach, A. G.; Jones, H. D.; Cosgrove, D. A.; Kenny, P. W.; Ruston, L.; MacFaul, P.; Wood, J. M.; Colclough, N.; Law, B. Matched Molecular Pairs as a Guide in the Optimization of Pharmaceutical Properties; a Study of Aqueous Solubility, Plasma Protein Binding and Oral Exposure. *J. Med. Chem.* **2006,** *49,* 6672–6682.
31. Johnson, D. S.; Weerapana, E.; Cravatt, B. F. Strategies for Discovering and Derisking Covalent, Irreversible Enzyme Inhibitors. *Future Med. Chem.* **2010,** *2,* 949–964.
32. Schwartz, P. A.; Kuzmic, P.; Solowiej, J.; Bergqvist, S.; Bolanos, B.; Almaden, C.; Nagata, A.; Ryan, K.; Feng, J.; Dalvie, D.; Kath, J. C.; Xu, M.; Wani, R.; Murray, B. W. Covalent EGFR Inhibitor Analysis Reveals Importance of Reversible Interactions to Potency and Mechanisms of Drug Resistance. *Proc. Natl. Acad. Sci. U. S. A.* **2014,** *111,* 173–178.
33. Clarke, E. D.; Greenhow, D. T.; Adams, D. Metabolism-Related Assays and Their Application to Agrochemical Research: Reactivity of Pesticides With Glutathione and Glutathione Transferases. *Pestic. Sci.* **1998,** *54,* 385–393.
34. MacFaul, P. A.; Morley, A. D.; Crawford, J. J. A Simple In Vitro Assay for Assessing the Reactivity of Nitrile Containing Compounds. *Bioorg. Med. Chem. Lett.* **2009,** *19,* 1136–1138.
35. Schwobel, J. A. H.; Madden, J. C.; Cronin, M. T. D. Examination of Michael Addition Reactivity Towards Glutathione by Transition-State Calculations. *SAR QSAR Environ. Res.* **2010,** *21,* 693–710.
36. Esterbauer, H.; Zollner, H.; Scholz, N. Reaction of Glutathione With Conjugated Carbonyls. *Z. Naturforsch. C* **1975,** *30,* 466–473.
37. Bohme, A.; Thaens, D.; Paschke, A.; Schuurmann, G. Kinetic Glutathione Chemoassay to Quantify Thiol Reactivity of Organic Electrophiles-Application to Î±, Î2-Unsaturated Ketones, Acrylates, and Propiolates. *Chem. Res. Toxicol.* **2009,** *22,* 742–750.
38. Paasche, A.; Schiller, M.; Schirmeister, T.; Engels, B. Mechanistic Study of the Reaction of Thiol-Containing Enzymes With α, β-Unsaturated Carbonyl Substrates by Computation and Chemoassays. *ChemMedChem* **2010,** *5,* 869–880.
39. Krenske, E. H.; Petter, R. C.; Zhu, Z.; Houk, K. N. Transition States and Energetics of Nucleophilic Additions of Thiols to Substituted α, β-Unsaturated Ketones: Substituent Effects Involve Enone Stabilization, Product Branching, and Solvation. *J. Org. Chem.* **2011,** *76,* 5074–5081.
40. Bain, J.; Plater, L.; Elliott, M.; Shpiro, N.; Hastie, C. J.; McLauchlan, H.; Klevernic, I.; Arthur, J. S. C.; Alessi, D. R.; Cohen, P. The Selectivity of Protein Kinase Inhibitors: A Further Update. *Biochem. J.* **2007,** *408,* 297–315.
41. Finlay, M. R.; Anderton, M.; Ashton, S.; Ballard, P.; Bethel, P. A.; Box, M. R.; Bradbury, R. H.; Brown, S. J.; Butterworth, S.; Campbell, A.; Chorley, C.; Colclough, N.; Cross, D. A.; Currie, G. S.; Grist, M.; Hassall, L.; Hill, G. B.; James, D.; James, M.; Kemmitt, P.; Klinowska, T.; Lamont, G.; Lamont, S. G.; Martin, N.; McFarland, H. L.; Mellor, M. J.; Orme, J. P.; Perkins, D.; Perkins, P.; Richmond, G.; Smith, P.; Ward, R. A.; Waring, M. J.; Whittaker, D.; Wells, S.; Wrigley, G. L. Discovery of a Potent and Selective EGFR Inhibitor (AZD9291) of Both Sensitizing and T790M Resistance Mutations That Spares the Wild Type Form of the Receptor. *J. Med. Chem.* **2014,** *57,* 8249–8267.
42. Clovis. AACR Annual Meeting. April 18–22, 2015 Philadelphia, PA.
43. Cross, D. A.; Ashton, S. E.; Ghiorghiu, S.; Eberlein, C.; Nebhan, C. A.; Spitzler, P. J.; Orme, J. P.; Finlay, M. R.; Ward, R. A.; Mellor, M. J.; Hughes, G.; Rahi, A.; Jacobs, V. N.; Red Brewer, M.; Ichihara, E.; Sun, J.; Jin, H.; Ballard, P.; Al-Kadhimi, K.; Rowlinson, R.; Klinowska, T.; Richmond, G. H.; Cantarini, M.; Kim, D. W.; Ranson, M. R.; Pao, W. AZD9291, an Irreversible EGFR TKI, Overcomes T790M-Mediated Resistance to EGFR Inhibitors in Lung Cancer. *Cancer Discov.* **2014,** *4,* 1046–1061.
44. (a) Goss, G. D. ECC 2015 European Cancer Congress; (b) Ramalingamat, S. S. World Conference on Lung Cancer 2015. *J. Thorac. Oncol.* **2015,** *10* (9, Suppl2), S319. abstract Mini 16.07.
45. (a) Kim, D. W.; et al. Preclinical Evidence and Clinical Cases of AZD9291 Activity in EGFR-Mutant Non-Small Cell Lung Cancer (NSCLC) Brain Metastases (BM). Presented at European Society for Medical Oncology (ESMO) Annual Meeting, Madrid; 26–30 September 2014; (b) Lee, D. AACR-NCI-EORTC Congress, 5–9 November 2015; abstract PR07.
46. Walter, A. O.; Sjin, R. T. T.; Haringsma, H. J.; Ohashi, K.; Sun, J.; Lee, K.; Dubrovskiy, A.; Labenski, M.; Zhu, Z.; Wang, Z.; Sheets, M.; St. Martin, T.; Karp, R.; van Kalken, D.; Chaturvedi, P.; Niu, D.; Nacht, M.; Petter, R. C.; Westlin, W.; Lin, K.; Jaw-Tsai, S.; Raponi, M.; Van Dyke, T.; Etter, J.; Weaver, Z.; Pao, W.; Singh, J.; Simmons, A. D.; Harding, T. C.; Allen, A. Discovery of a Mutant-Selective Covalent Inhibitor of EGFR that Overcomes T790M-Mediated Resistance in NSCLC. *Cancer Discov.* **2013,** *3,* 1404–1415.
47. Nguyen, K. S.; Neal, J. W.; Wakelee, H. Review of the Current Targeted Therapies for Non-Small-Cell Lung Cancer. *World J. Clin. Oncol.* **2014,** *5,* 576–587.
48. Stinchcombe, T. E. Recent Advances in the Treatment of Non-Small Cell and Small Cell Lung Cancer. *F1000Prime Rep.* **2014,** *6,* 117. eCollection 2014.
49. Two Drugs Beat Back Lung Tumors. *Cancer Discov.* **2015,** *5,* 100.
50. Novartis. AACR Annual Meeting. April 18–22, 2015. Philadelphia, PA.
51. AC-0010, https://clinicaltrials.gov/ct2/show/NCT02448251, 2015.
52. Taiho. AACR Annual Meeting. April 18–22, 2015. Philadelphia, PA. 2015.
53. Planken, S.; Nair, S. K.; Kath, J. C.; Lafontaine, J.; Weinrich, S.; Cheng, H. K.; Sutton, S. C.; Johnson, T. O.; Zientek, M.; Nagata, A.; Gajiwala, K.; Solowiej, J.; Murray, B. W.; Yin, M.; Hemkens, M. In *In Discovery and Development of a Series of Irreversible EGFR_T790M 7H-pyrrolo[2, 3-d]pyrimidine Inhibitors With High Selectivity Over EGFR Wild Type;* 2015. pp. MEDI-320.
54. Cheng, H.; Nair, S. K.; Murray, B. W.; Almaden, C.; Bailey, S.; Baxi, S.; Behenna, D.; Cho-Schultz, S.; Dalvie, D.; Dinh, D. M.; Edwards, M. P.; Feng, J. L.; Ann Ferre, R.; Gajiwala, K. S.; Hemkens, M. D.; Jackson-Fisher, A.; Jalaie, M.; Johnson, T. O.; Kania, R. S.; Kephart, S.; Lafontaine, J.; Lunney, B.; Liu, K. K. -C.; Liu, Z.; Matthews, J.; Nagata, A.; Niessen, S.; Ornelas, M. A.; Orr, S. T. M.; Pairish, M.; Planken, S.; Ren, S.; Richter, D.; Ryan, K.; Sach, N.; Shen, H.; Smeal, T.; Solowiej, J.; Sutton, S.; Tran, K.; Tseng, E.; Vernier, W.; Walls, M.; Wang, S.; Weinrich, S. L.; Xin, S.; Xu, H.; Yin, M. -J.; Zientek, M.; Zhou, R.; Kath, J. C. Discovery of 1-{(3R,4R)-3-[({5-Chloro-2-[(1-methyl-1H-pyrazol-4-yl)amino]-7H-pyrrolo[2,3-d]pyrimidin-4-yl}oxy)methyl]-4-methoxypyrrolidin-1-yl}prop-2-en-1-one (PF-06459988), a Potent, WT Sparing, Irreversible Inhibitor of T790M-Containing EGFR Mutants. *J. Med. Chem.* **2016**, *59* (5), 2005–2024.
55. Hanan, E. J.; Eigenbrot, C.; Bryan, M. C.; Burdick, D. J.; Chan, B. K.; Chen, Y.; Dotson, J.; Heald, R. A.; Jackson, P. S.; La, H.; Lainchbury, M. D.; Malek, S.; Purkey, H. E.; Schaefer, G.; Schmidt, S.; Seward, E. M.; Sideris, S.; Tam, C.; Wang, S.; Yeap, S. K.; Yen, I.; Yin, J.; Yu, C.; Zilberleyb, I.; Heffron, T. P. Discovery of Selective and Noncovalent Diaminopyrimidine-Based Inhibitors of Epidermal Growth Factor Receptor Containing the T790M Resistance Mutation. *J. Med. Chem.* **2014,** *57,* 10176–10191.
56. Bryan, M. C.; Chan, B.; Diederich, F.; Dotson, J.; Hanan, E.; Heffron, T.; Lainchbury, M.; Heald, R.; Seward, E. M. Patent Application Country: Application: WO; WO; Priority Application Country: US Patent WO2014210354, 2014.
57. Bryan, M. C.; Burdick, D.; Chan, B.; Chen, Y.; Dotson, J.; Eigenbrot, C.; Hanan, E. J.; Heald, R.; Heffron, T. P.; Jackson, P.; La, H.; Lainchbury, M.; Malek, S.; Mann, S. E.; Purkey, H.; Schaefer, G.; Schmidt, S.; Seward, E.; Sideris, S.; Wang, S.; Yen, I.; Yu, C. In *Pyridones as Highly Selective, Reversible Inhibitors of T790M Double-Mutants of EGFR. ACS Med. Chem. Lett.;* 2016. *7*(1),100–104.
58. Cook, D.; Brown, D.; Alexander, R.; March, R.; Morgan, P.; Satterthwaite, G.; Pangalos, M. N. Lessons Learned From the Fate of AstraZeneca's Drug Pipeline: A Five-Dimensional Framework. *Nat. Rev. Drug Discov.* **2014,** *13,* 419–431.

59. Thress, K. S.; Paweletz, C. P.; Felip, E.; Cho, B. C.; Stetson, D.; Dougherty, B.; Lai, Z.; Markovets, A.; Vivancos, A.; Kuang, Y.; Ercan, D.; Matthews, S. E.; Cantarini, M.; Barrett, J. C.; Janne, P. A.; Oxnard, G. R. Acquired EGFR C797S Mutation Mediates Resistance to AZD9291 in Non-Small Cell Lung Cancer Harboring EGFR T790M. *Nat. Med.* **2015,** *21,* 560–562.
60. Avizienyte, E.; Ward, R. A.; Garner, A. P. Comparison of the EGFR Resistance Mutation Profiles Generated by EGFR-Targeted Tyrosine Kinase Inhibitors and the Impact of Drug Combinations. *Biochem. J.* **2008,** *415,* 197–206.
61. Piotrowska, Z.; Niederst, M. J.; Mino-Kenudson, M.; Hata, A. N.; Digumarthy, S.; Muzikansky, A.; Dias-Santagata, D.; Iafrate, A. J.; Shaw, A. T.; Engelman, J. A.; Sequist, L. V.; Karlovich, C. A.; Raponi, M.; Allen, A. R.; Wakelee, H. A.; Neal, J. W.; Fulton, L.; Lockerman, E. L.; Kalsy, A.; Garcia, A. R.; Mulvey, H. E.; Parks, M. K.; DiCecca, R. H. Heterogeneity Underlies the Emergence of EGFRT790 Wild-Type Clones Following Treatment of T790M-Positive Cancers With a Third-Generation EGFR Inhibitor. *Cancer Discov.* **2015,** *5,* 713–722.
62. Ercan, D.; Choi, H. G.; Yun, C. H.; Capelletti, M.; Xie, T.; Eck, M. J.; Gray, N. S.; Janne, P. A. EGFR Mutations and Resistance to Irreversible Pyrimidine Based EGFR Inhibitors. *Clin. Cancer Res.* **2015,** *21,* 3913–3923.
63. https://clinicaltrials.gov/ct2/show/NCT02143466, 2015.
64. Eberlein, C. A.; Stetson, D.; Markovets, A. A.; Al-Kadhimi, K. J.; Lai, Z.; Fisher, P. R.; Meador, C. B.; Spitzler, P.; Ichihara, E.; Ross, S. J.; Ahdesmaki, M. J.; Ahmed, A.; Ratcliffe, L. E.; O'Brien, E. L.; Barnes, C. H.; Brown, H.; Smith, P. D.; Dry, J. R.; Beran, G.; Thress, K. S.; Dougherty, B.; Pao, W.; Cross, D. A. Acquired Resistance to the Mutant-Selective EGFR Inhibitor AZD9291 Is Associated With Increased Dependence on RAS Signaling in Preclinical Models. *Cancer Res.* **2015,** *75,* 2489–2500.

8.02 Trametinib

H Kawasaki and T Yamaguchi, Central Pharmaceutical Research Institute, Japan Tobacco, Takatsuki, Japan

© 2017 Elsevier Ltd. All rights reserved.

8.02.1	**Introduction**	33
8.02.2	**Concept**	34
8.02.3	**Lead Compound Identification**	35
8.02.4	**SAR Study-1**	38
8.02.5	**SAR Study-2**	44
8.02.6	**Mechanism of Action and Pharmacological Characterization**	46
8.02.6.1	Target Identification of Trametinib	46
8.02.6.2	MEK Inhibitory Activity of Trametinib	49
8.02.6.3	Pharmacological Characterization of Trametinib	50
8.02.7	**Polymorphism Study**	53
8.02.8	**Synthetic Studies**	54
8.02.9	**Addendum**	55
8.02.10	**Conclusion**	55
References		56

8.02.1 Introduction

Trametinib (**1**) is an orally available MEK1/MEK2 inhibitor with high potency and high selectivity possibly due to its allosteric binding mode to MEK protein.[1–3] This compound was originally discovered by our group in 2004, and then its clinical trials were conducted by a GlaxoSmithKline group.[4,5] MEK1, MEK2 are protein kinases that play a central role in the MAPK pathway, which is comprised of ras, c-Raf/B-Raf, MEK1/MEK2, and ERK1/ERK2. In human malignant tumors, the Raf–MEK–ERK pathway is often hyperactivated through aberrant activation of the receptor tyrosine-kinases or gain-of-function mutations in the Ras or B-Raf gene.[6] Therefore, in the last two decades, manipulation of this pathway has been of much interest as a molecular targeting antitumor therapy. However, despite the promise of the preclinical evidence, previous MEK inhibitors have proven to be less efficacious for patients.[7,8] In 2013, an open-label international Phase III study demonstrated a statistically significant increase in progression free survival (PFS) in the trametinib treatment group compared with the chemotherapy group in unresectable or metastatic melanoma patients with BRAF V600E or V600K mutation.[4] From this result, trametinib, as the first MEK1/MEK2 inhibitor, has been approved as a single-agent oral treatment for unresectable or metastatic melanoma in adult patients with BRAF V600E or V600K mutations by the US Food and Drug Administration (FDA) in 2013. In addition to this, a combination therapy of trametinib with the BRAF inhibitor dabrafenib has been evaluated in clinical trials, comparing this dual drug strategy with single-agent therapy of another BRAF inhibitor vemurafenib[9] or with single-agent therapy with dabrafenib.[10] Each of these studies demonstrated a significant increase in PFS in patients treated with trametinib as compared to active comparators. Particularly in the study comparing trametinib with vemurafenib, the overall survival rate, a primary endpoint, was increased in combination therapy group with statistical significance. Also in the study compared with single-agent treatment of dabrafenib, the combination of trametinib with dabrafenib tends to yield a statistically significant increase in overall survival rate. It should be noted that this combination therapy showed much benefit for the patients by reducing the incidence of new cutaneous squamous-cell carcinoma that is often observed as an adverse effect in dabrafenib-treated patients. From these results, the combination treatment of trametinib with dabrafenib has been approved in the United States in 2014,[11] and the EU in 2015.[12] In Japan, the submission documents for an approval of trametinib and dabrafenib has been completed and approved in 2016 (**Fig. 1**).[13]

In the present chapter, the development story of trametinib, a unique compound that opened a new horizon in melanoma treatment, will be reviewed with a focus on its lead identification and subsequent medicinal chemistry campaign. Interestingly, this compound was not discovered from pursuing MEK inhibitory activities. Instead, the lead compound was identified by a phenotypic cellular high-throughput screening (HTS) assay. The HTS campaign, leading to the lead identification of trametinib, was designed as a screening of a compound with the ability to induce the expression level of $p15^{INK4b}$, an endogenous cyclin-dependent kinase (CDK) inhibitor protein. This methodology resulted in the discovery of compound **2** as a lead compound.[1,14] Extensive medicinal chemistry efforts were undertaken for this lead structure (**2**), by improving the antiproliferative effect on cancer cells as well as various drug-like properties, and trametinib was selected as a clinical candidate. Although the molecular target of trametinib was unknown until the time that trametinib was synthesized, a chemical biological technique revealed that MEK1/MEK2 were the binding proteins of trametinib. Possibly due to this unique development process, trametinib has a distinct core structure compared with other MEK inhibitors. This core structure may provide the ADME profile with low Cmax/trough ratio, which is ideal for antitumor agents with a narrow therapeutic window. The most stable crystal form of trametinib identified through

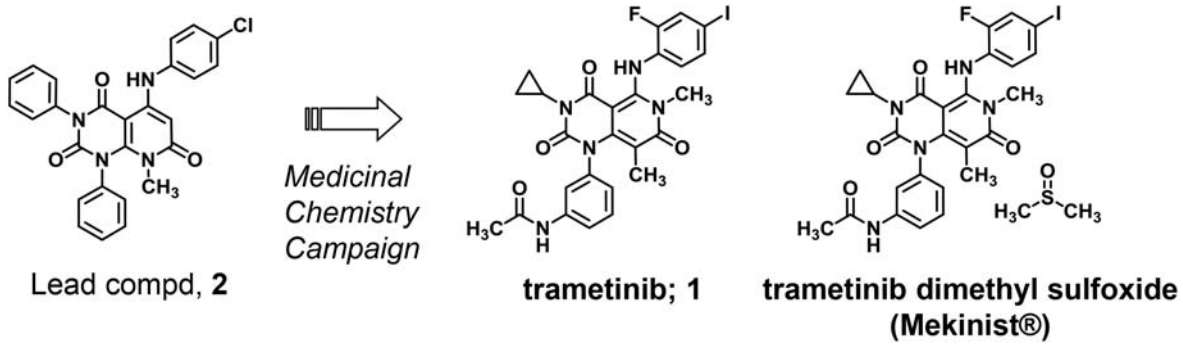

Fig. 1 Trametinib developed from lead compound **2**.

polymorphism study lost its oral exposure. This issue was solved by searching for a stable solvate instead of salts. Thus, we found trametinib DMSO, the first FDA approved drug of this solvate. The practical synthetic route to trametinib featuring its unusual rearrangement reaction is highly efficient and suitable for large scale production.

8.02.2 Concept

The lead compound (**2**) was identified by a phenotypic screening for its ability to induce the expression of a cell cycle regulatory protein, $p15^{INK4b}$, which inhibits CDK4 and CDK6, important proteins for the progression of the cell cycle from G1 phase to S phase.[1,14] Subsequently, trametinib was discovered by extensive medicinal chemistry efforts and its binding proteins were found and proven to be MEK1 and MEK2.[15] Disruption of cell cycle control, reported in numerous tumor cells, is thought to be one of the primary causes of malignant transformation.[16] CDK are key regulators that function in a phase-specific manner during cell cycle progression (Fig. 2). Cyclin D–CDK4/CDK6 and cyclin E–CDK2 play important roles in the G1 to S phase transition of the cell cycle by phosphorylating the tumor suppressor retinoblastoma protein (pRb), which forms a complex with E2F. The phosphorylation of pRb by CDKs causes release and activation of E2F, allowing transcription of genes necessary for the progression to S phase (Fig. 2).[16,17]

The loss of G1/S transition control in tumor cells often arises from aberrant activation of cell-proliferative signaling pathways or inactivation of cell cycle-regulating proteins. Of these pathways, the Ras–MAPK pathway has been investigated extensively. The classical MAPK cascade, comprising c-Raf or B-Raf, MEK1/MEK2, and ERK1/ERK2, is constitutively activated in various malignant tumors, often through gain-of-function mutation of Ras and Raf family members. These activating mutations cause increased expression level of cyclin D, leading to CDK activation and aberrant cell proliferation.[18,19] The cell cycle progression through cyclin–CDK activation is negatively regulated by CDK inhibitors (CKIs). Two families of CKI have been identified in mammalian cells: One includes $p21^{WAF1}$ and $p27^{KIP1}$, each of which inhibits cyclin E/A–CDK2 complexes. The other family, referred to as the INK4 family, is comprised of $p16^{INK4a}$, $p15^{INK4b}$, $p18^{INK4c}$, and $p19^{INK4d}$, which inhibit cyclin D–CDK4/6. $p16^{INK4a}$ is known to function as a tumor suppressor (Fig. 2). Mutation or inactivation of $p16^{INK4a}$ has been detected in many human malignant tumors,[20] and mice deficient in $p16^{INK4a}$ are highly susceptible to malignant tumors.[21,22] $p15^{INK4b}$ has similar functions to $p16^{INK4a}$ with regard to the suppression of CDK4/CDK6, leading to cell cycle arrest at the G1 phase. TGFβ inhibits cell proliferation at the G1 phase and induces the expression of $p15^{INK4b}$ ~30-fold in human keratinocyte HaCaT cells, suggesting that $p15^{INK4b}$ may act as an effector of TGFβ-mediated cell cycle arrest.[23] It has also been demonstrated that the overexpression of $p15^{INK4b}$ in cancer

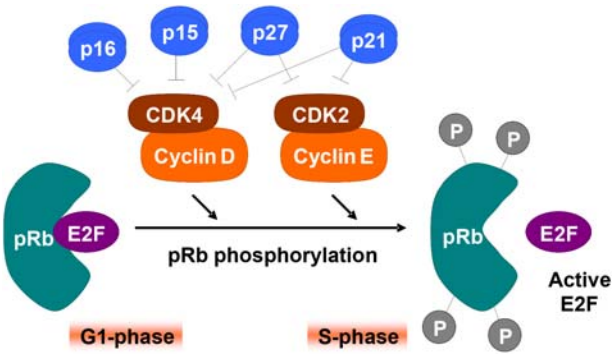

Fig. 2 Cell cycle regulation.

cells induced cell cycle arrest at the G1 phase.[24,25] These observations imply that $p15^{INK4b}$ may function as a replacement for $p16^{INK4a}$, and that agents with the ability to induce $p15^{INK4b}$ may provide new strategies for the prevention or therapy of malignancies, especially against tumors that lack $p16^{INK4a}$ function.[26] Therefore, we conducted a HTS campaign with our chemical library to find a compound that had the ability to increase the expression level of $p15^{INK4b}$. This screening assay was designed as a phenotypic type of screening,[14] and the lead compound was successfully identified in this assay. The first MEK1/MEK2 inhibitor, trametinib, was discovered from this lead structure by subsequent extensive medicinal chemistry efforts.

8.02.3 Lead Compound Identification

A phenotypic type of screening assay was employed for the HTS assay and its primary index was set as the ability of the compound to increase the expression level of $p15^{INK4b}$. To establish a robust screening assay, several cell lines, including mainly melanoma cell lines, were evaluated by whether $p15^{INK4b}$ was constitutively expressed and its expression was induced upon TGFβ stimulation as a potential positive control for the screening assay. However, among these cell lines, none of them demonstrated upregulation of $p15^{INK4b}$ by TGFβ stimulation. Therefore, we decided to use HaCaT cells, which are immortalized human keratinocytes. These cells have been reported to upregulate $p15^{INK4b}$ expression when the cells are stimulated by TGFβ.[23] Three readouts, $p15^{INK4b}$ mRNA quantification, $p15^{INK4b}$ protein quantification, or reporter gene assay using $p15^{INK4b}$ promoter region, were investigated and compared. The quantification of mRNA by q-PCR and the quantification of protein by Western blot method had a problem of low throughput, whereas mRNA quantification of the branched-DNA method and the reporter gene assay did not have such problems. Finally, we employed $p15^{INK4b}$ mRNA quantification by the branched-DNA method for our HTS phenotypic screening assay, since this method gave us a robust window of signal/noise ratio and reproducible results.[14]

By applying this HTS phenotypic screening assay for our chemical library, hit compounds were selected if $p15^{INK4b}$ mRNA was upregulated more than 50% from the basal level by treatment with a single dose of a compound at 10 μM. Then, 22 compounds were selected from those hit compounds after reproducibility assay and the dose-dependency study (Fig. 3, data only shown for the three lead candidates).

The 22 compounds were categorized into seven groups by similarity of core structure, and seven representative compounds were further investigated to determine if the compound had an ability to induce $p15^{INK4b}$ protein in cancer cells since HaCaT cells were not tumor cells. A part of the NCI60 cell lines were screened and 16 cell lines were selected by the following criteria: the expression of $p15^{INK4b}$ was detected by mRNA level and protein level and the promoter of $p15^{INK4b}$ was not inactivated by the methylation. Using those 16 cell lines, $p15^{INK4b}$ induction was evaluated after the treatment of those seven lead candidate compounds. A human renal cancer cell line, ACHN, exhibited relatively high sensitivity to the lead candidates; some compounds induced the expression of $p15^{INK4b}$ in the ACHN cells. Among them, compounds **2**, **3**, and **4**, which showed robust and reproducible $p15^{INK4b}$ induction (Fig. 4), were further confirmed as the cell cycle was arrested after the compound treatment. Compounds **3** and **4** share the adenine-like core structure employed in various tyrosine kinase inhibitors. Since gefitinib (**15**) was a representative compound among these inhibitors around that time, the phosphorylation of EGFR upon EGF stimulation was investigated in ACHN cells after the treatment of compounds **3** and **4**. Compound **4** clearly inhibited EGFR phosphorylation. In addition, we found that gefitinib also had the ability to induce $p15^{INK4b}$ expression and to arrest the cell cycle at G1 phase in our assay system (Fig. 4).[27]

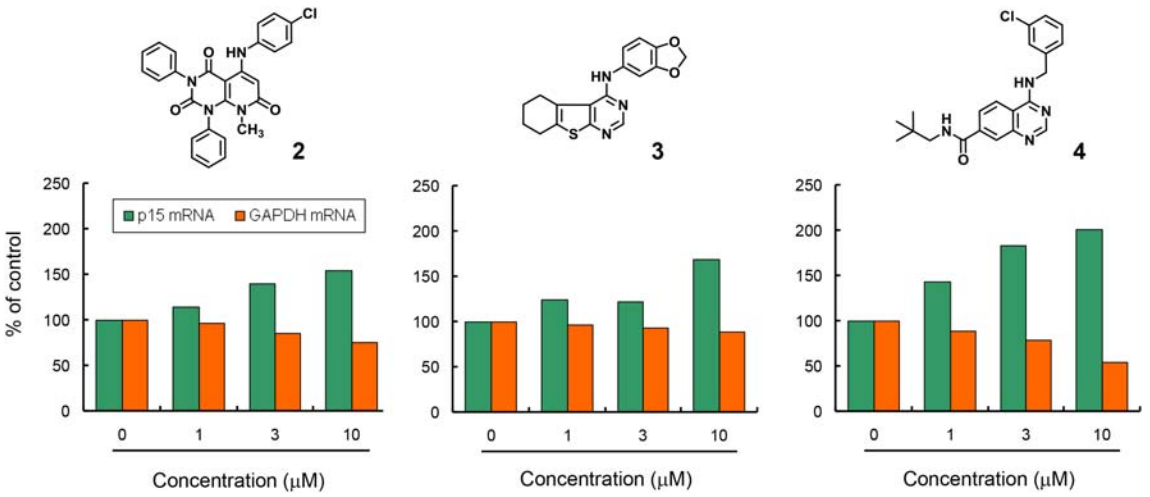

Fig. 3 $p15^{INK4b}$ induction by lead candidates. HaCaT cells were treated with 1, 3, 10 μM of compound **2**, **3**, and **4** for 24 h, then the expression level of $p15^{INK4b}$ mRNA was determined by branched-DNA methods. The housekeeping gene GAPDH mRNA was also measured. The values are indicated as % of control (ratio with respect to mRNA levels in vehicle (DMSO) treated cells).

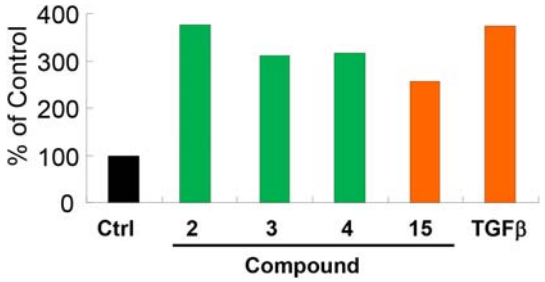

Fig. 4 p15^{INK4b} protein expression in ACHN cells treated with lead candidates. Cells from a renal cancer cell line, ACHN cells were treated with 10 μM of compound **2**, **3**, **4**, gefitinib (**15**) or TGFβ for 24 h, then the expression level of p15^{INK4b} protein was determined by Western blotting. The values are indicated as % of control (ratio to vehicle (DMSO) treated cells).

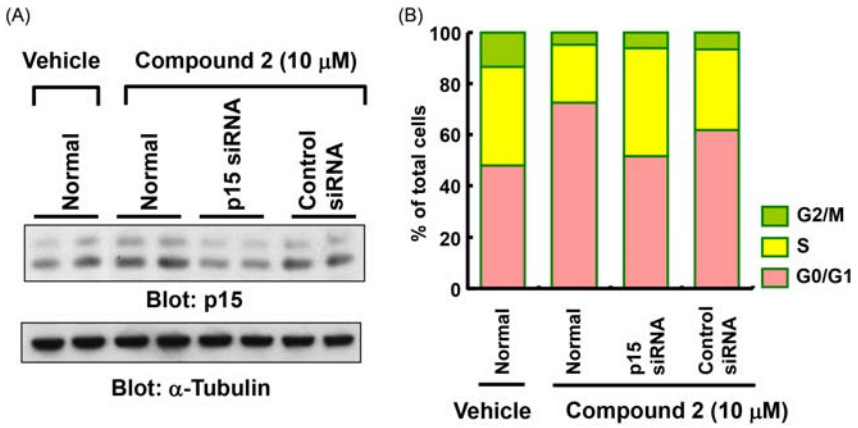

Fig. 5 p15^{INK4b} expression and cell cycle analysis in p15^{INK4b}-siRNA treated cells. Effect of p15^{INK4b} siRNA on cell cycle arrest by compound **2** in human renal carcinoma cell line ACHN. The expression levels of p15^{INK4b} were determined by Western blot (A). Cell cycle analysis was performed in compound **2**-treated ACHN cells after p15^{INK4b} siRNA transfection (B). The representative data was shown from 2 to 3 independent experiments.

Further confirmation studies were conducted with compounds **2**, **3**, and **4** to evaluate if p15^{INK4b} induction was involved in the cell cycle arrest effect, using p15^{INK4b} knockdown cells by the siRNA method. As a result, the G1-cell cycle arrest by the compounds was attenuated in p15^{INK4b} siRNA treated cells (Fig. 5, results only shown about compound **2**), suggesting that p15^{INK4b} at least contributes to the growth arrest effect of the lead candidate compounds. To clarify compound effects on the growth of normal cells, a colony formation assay was carried out using normal human bone marrow cells. All of the lead candidates (**2**, **3**, **4**) and gefitinib (**15**) had no effect on colony formation up to 10 μM, suggesting that p15^{INK4b} inducer compounds have minimal effect on the cell growth of normal cells (Fig. 6).

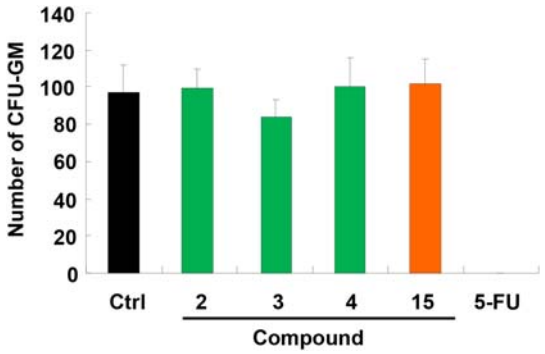

Fig. 6 Colony formation assay using human bone marrow cells. Normal human bone marrow cells were treated with 10 μM of compound **2**, **3**, **4**, **15** or 5-fluorouracil (5-FU), and cultured in the presence of several cytokines. The number of granulocyte/macrophage colonies (CFU-GM) was counted 7 days after the start of treatment.

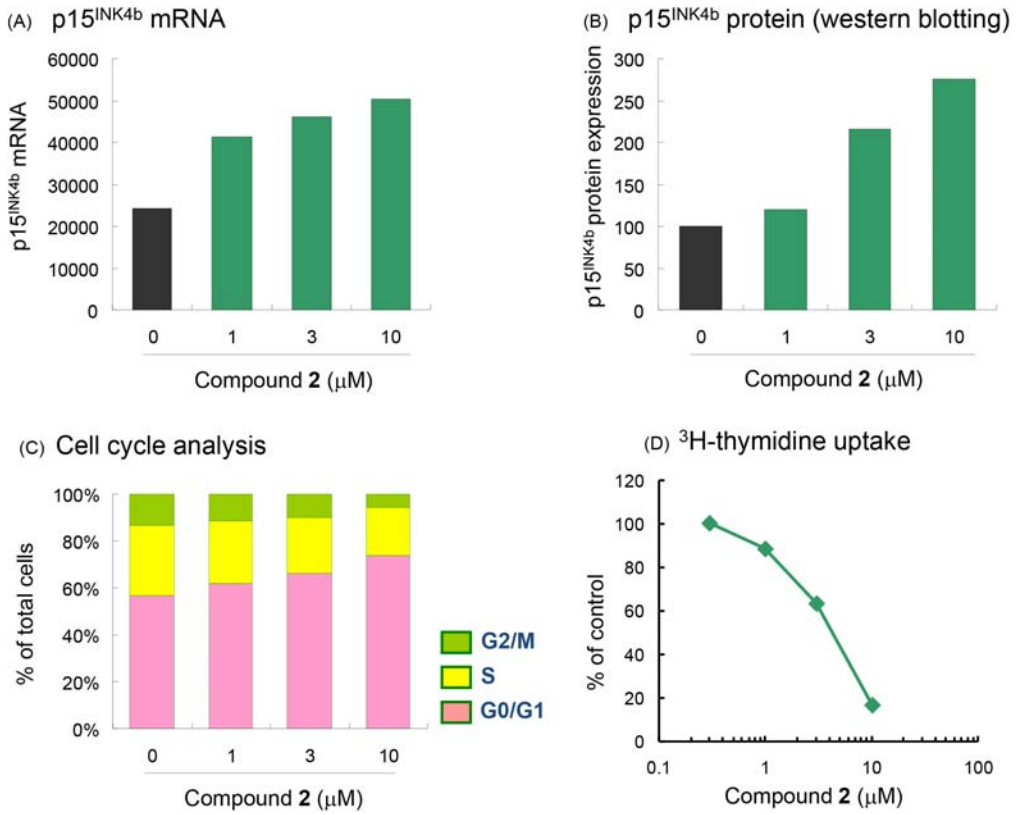

Fig. 7 p15^{INK4b} induction, G1-arrest, cell growth inhibition by compound **2**. ACHN cells were treated with 1, 3, 10 μM of compound **2** for 24 h, then the expression level of p15^{INK4b} mRNA and protein were determined by q-PCR (A), and Western blotting (B), respectively. The cell cycle arrest was examined by the cell cycle analysis with flow cytometry (C) and the cell growth activity was determined by ^{3}H-thymidine uptake study (D).

The lead candidates, compounds **2**, **3**, and **4**, were nominated as described above. At that time of 2002–03, investigators in this field considered the discovery of a highly selective kinase inhibitor still to be a great scientific challenge. Indeed, our lead candidate, compound **4**, exhibited suppression activity of EGFR phosphorylation in the cells after stimulation by EGF, for example. Since unfavorable adverse effects due to low selectivity of the compound should be circumvented in this project as well, we selected compound **2** with distinct structural features as an antitumor drug, but not compounds **3** and **4**, which have substructures that could potentially interact with the hinge region of protein kinases. As shown in Fig. 7, lead compound **2** induced the expression of p15^{INK4b} mRNA and protein in ACHN cells in a concentration dependent manner, resulting in cell cycle arrest at G1 phase and growth inhibition over the same concentration range. The IC_{50} values of this compound (**2**) for growth inhibitory activity were determined as 4800 nM in ACHN cells (a human renal cancer cell line) and 990 nM in HT-29 cells (a human colon cancer cell line) (Fig. 8). The medicinal chemistry effort of lead optimization was initiated for this compound **2**, looking at cell growth inhibition activity as the index of SAR.

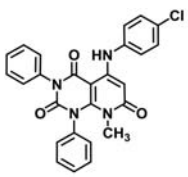

Lead compd, **2**

- p15 protein inductive ability
  - 2-3 fold (at 10000 nM)
- Cancer Cell Lines Growth Inhibition (IC_{50})
  - ACHN 4800 nM (renal adenocarcinoma)
  - HT-29 990 nM (colorectal adenocarcinoma)
- Physical Property
  - ClogP 6.3
  - Solubility: very low

Fig. 8 Lead compound.

8.02.4 SAR Study-1

Variations in the substituents at the 1- and 3-positions of the pyridopyrimidine core were first examined. As indicated by the increase in the IC_{50} values (Table 1), these modifications (**5a–5g**) were not well tolerated.

Next we explored substitution on the aniline ring. Chloro-substitution was tolerated at all positions, but 2- and 3-homologs were twofold less active than **2** (Table 2). Accordingly, we investigated substitution at the 4-position as shown in Table 3. The simple phenyl analog (**7a**) was less active than **2**, as were other alkyl analogs (**7b–7d**). Methyl (**7b**) and ethyl (**7c**) (one carbon extension) equally showed weak potency. However, substitution with a halogen atom was more sensitive. Replacement of the chlorine with the bromine atom (**7f**) improved potency by twofold.

Compounds synthesized thus far had three aromatic rings on the pyrimidine core and their hydrophobicity was very high (ClogP > 6). In addition, they formed very stable crystals and thus had low solubility. We often had difficulties in measuring their NMR spectra even in DMSO-d_6. These features made them unattractive starting points for further optimization. In an effort to reduce hydrophobicity, we next systematically replaced each of the three benzene rings with less lipophilic small alkyl groups.

Replacement of the 1-phenyl substituent (**8a–8c**) or the phenyl group of the 5-aniline moiety with alkyl groups (**9b**, **9c**) resulted in a decrease in potency as shown in Tables 4 and 5.

We modified the remaining phenyl ring at the 3-position (Table 6). Compounds (**10a–10d**), which contain simple alkyl chains, were found to be less active. Cyclic alkyl groups such as cyclopentyl (**10f**) and cyclohexyl (**10g**) also gave no improvement. However, the compound **10e**, possessing a cyclopropyl group, showed similar potency to **2**.

Table 1 Substitution at the 1- and 3-positions SAR

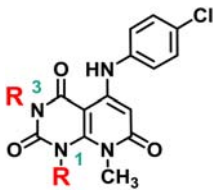

		IC_{50} (nM)	
Compound	*R*	*ACHN*	*HT-29*
2	Ph	4800	990
5a	2-Me-Ph	>10,000	
5b	3-Me-Ph	>10,000	
5c	4-Me-Ph	>10,000	
5d	4-F-Ph	9700	
5e	4-Cl-Ph	>1000	
5f	4-MeO-Ph	>10,000	
5g	3-Thienyl	7450	

Table 2 Substitution at the 5-position SAR-1

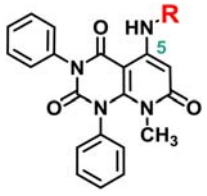

		IC_{50} (nM)	
Compound	*R*	*ACHN*	*HT-29*
2	4-Cl-Ph	4800	990
6a	3-Cl-Ph	9300	
6b	2-Cl-ph	8950	

Table 3 Substitution at the 4-position of aniline SAR-1

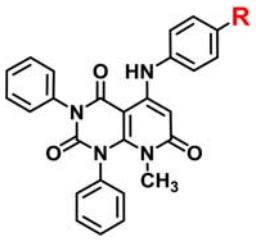

		IC_{50} (nM)	
Compound	*R*	*ACHN*	*HT-29*
7a	H	>10,000	
7b	Me	8200	
7c	Et	9900	
7d	Ph	>10,000	
7e	F	>10,000	
2	Cl	4800	990
7f	Br	2850	

Table 4 Substitution at the 1-position SAR

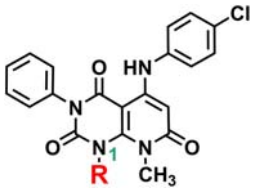

		IC_{50} (nM)	
Compound	*R*	*ACHN*	*HT-29*
2	Ph	4800	990
8a	Me	>10,000	
8b	cPr	>10,000	
8c	iBu	>10,000	

Table 5 Substitution at the 5-position SAR-2

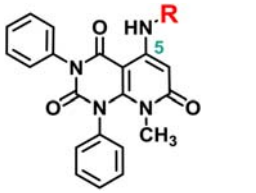

		IC_{50} (nM)	
Compound	*R*	*ACHN*	*HT-29*
2	4-Cl-Ph	4800	990
9a	4-Cl-Bn	>10,000	
9b	cHex	>10,000	
9c	neoPen	>10,000	

Table 6 Substitution at the 3-position SAR-1

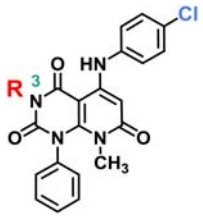

		IC_{50} (nM)	
Compound	*R*	*ACHN*	*HT-29*
2	Ph	4800	990
10a	Me	>10,000	
10b	Et	9900	
10c	Pr	>10,000	
10d	iPr	>10,000	
10e	cPr	5950	
10f	cPen	>10,000	
10g	cHex	>10,000	

We also examined the same modification in the bromo-series (Table 7). We were delighted to find that **11b**, which contained the cyclopropyl group at the 3-position and the *para* bromo substituent at the aniline ring, improved potency by twofold. Moreover the hydrophobicity of **11b** was reduced as expected (ClogP 5). Interestingly, compound **11c** with the cyclobutyl group showed weak potency. Only the cyclopropyl group among other cycloalkyls gave a modest improvement in potency. Compound **11b** displayed a poor pharmacokinetic (PK) profile (low %*F* of 11%, mouse). Still, we tested this compound in an HT-29 human tumor xenograft model. Encouragingly, **11b** showed the first sign of antitumor effect in this model, although high dosing of **11b** was needed (30 mg/kg, bid, p.o., 43% tumor growth inhibition). It took seven months for us to obtain this compound. One might think that this small improvement was not significant, but this finding fueled further exploration by keeping our morale high.

We next introduced a small substituent (e.g., methyl, halogen, methoxy, etc.) at the 2- or 3-position on the aniline ring. Alkyl analogs (**12a**, **12b**) and oxygen-containing substituent (**12e**, **12f**) attenuated potency (Table 8). Introduction of a halogen atom at the 2-position (**12c**, **12d**) resulted in an increase in potency. Compound **12c** with a fluorine atom showed a fourfold improvement compared to **11b**. However, 3-substitution (**13a**, **13b**) was not well tolerated (Table 9). These results indicated that analogs with the 2,4-disubstituted pattern were promising inhibitors.

Having an improved compound (**12c**), we revisited exploration of the substitution at the 4-position on the aniline ring. Representative examples are shown in Table 10. We found that as the size of the substituent increased from hydrogen (**14a**) to ethyl (**14c**), the compounds became more potent. However, lengthening the carbon chain to 3 in the propyl derivative (**14d**) resulted in

Table 7 Substitution at the 3-position SAR-2

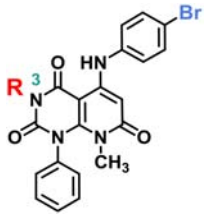

		IC_{50} (nM)	
Compound	*R*	*ACHN*	*HT-29*
7f	Ph	2850	
11a	Et	4600	290
11b	cPr	1270	100
11c	cBu	>10,000	2200
11d	$cPrCH_2$	5700	1200
11e	CF_3CH_2	5100	1300

Table 8 Substitution at the 2-position of aniline SAR

		IC_{50} (nM)	
Compound	*R*	*ACHN*	*HT-29*
11b	H	1270	100
12a	Me	1900	445
12b	Et	>10,000	>3000
12c	F	325	15
12d	Cl	755	65
12e	OH	>10,000	>3000
12f	OMe	4400	870

a slight loss in activity. However, cyclopropyl (**14e**) restored potency to the level of **14c**. This outcome indicated the existence of a small pocket on the target protein that recognizes the *para*-substituents. Introduction of a halogen substituent improved potency as the size of the substituent increased from fluoro (**14f**) to bromo (**12c**). In the end, compound **12c** with a bromo substituent was the most potent, and no additional improvement on potency was noted.

Having come to an impasse, we decided to consult structures of anticancer agents from other companies. In those days, gefitinib (**15**) and erlotinib (**16**) were lionized as promising molecularly targeted drugs in many articles (Fig. 9). However, we realized that we could not apply other substitution pattern on the aniline ring of gefitinib because compounds **6a** (3-Cl) and **14f** (4-F) were not potent. Erlotinib with an ethynyl group on its aniline ring attracted our attention. Although the position of the ethynyl was 3- instead of 4- in erlotinib, we tried it anyway. We synthesized compound **14i** with the ethynyl substituent by Sonogashira reaction of synthetic intermediate **14l** having an iodo substituent. Capable medicinal chemists usually avoid synthesizing compounds with iodo substituent as drug candidates. However, I noticed one of my colleagues put both **14i** and **14l** into a list of compounds for biological assays. I thought "poverty dulls the wit," but I didn't bother to cross iodo-compound **14l** off the list with weary sigh. The next week, we were astonished to hear the news. Biologists rushed into our room and told us both compounds were the most potent synthesized to date and IC_{50} values for HT-29 were less than 30 nM with complete growth inhibition at this dose! The IC_{50} values turned out to be 5.9 nM for ethynyl (**14i**), and most excitingly, 1.5 nM for iodo (**14l**). This iodo-compound was 500-fold more potent than lead compound **2**.

Table 9 Substitution at the 3-position of aniline SAR

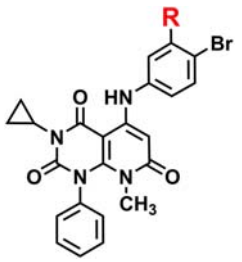

		IC_{50} (nM)	
Compound	*R*	*ACHN*	*HT-29*
11b	H	1270	100
13a	Me	8350	2200
13b	F	5150	925

Table 10 Substitution at the 4-position of aniline SAR-2

Compound	R	IC_{50} (nM)	
		ACHN	HT-29
14a	H	10,000	1300
14b	Me	1300	110
14c	Et	185	27
14d	Pr	2100	230
14e	cPr	290	39
14f	F	>3000	>1000
14g	Cl	4600	102
12c	Br	325	15
14h	vinyl	104	15
14i	C≡CH	42	5.9
14j	C≡C-Me	>3000	>1000
14k	CN	>10,000	1600
14l	I	13	1.5

Compounds **14h** and **14i**, which bear unsaturated carbon substituents, were more potent than the saturated ethyl (**14c**). However, lengthening the carbon chain to three (**14j**) again reduced potency. Interestingly, the cyano variant (**14k**), of almost the same size as the ethynyl, only showed weak potency.

Caco2 permeabilities for compounds **14c** and **14h** were relatively high (Caco2 permeability (cm/s 10^{-6}): **14c**, 30.3; **14h**, 19.5), however, highly potent compounds such as **14i**, **12c**, and **14l** exhibited very low permeability of less than 0.1. These compounds also showed very low aqueous solubility and high hydrophobicity (ClogP **14l**, 5.5). We set out to investigate introduction of hydrophilic groups on the 1-phenyl ring of **12c** and **14l** as a means to improve physicochemical properties. We also expected some increase in potency. Early results of the incorporation of a methoxy group into the phenyl ring at the 1-position revealed that substitution was tolerated at the *meta*-position of the phenyl in terms of potency (data not shown). Representative results of *meta*-substitution on the phenyl are summarized in Table 11. We first examined the incorporation of amine or carboxyl group, which are suitable for salt formation, into compound **12c**. Amino group analogs (**17a**, **17b**) retained potency, while carboxylic groups (**17c**, **17d**) attenuated their activity dramatically. We were delighted to observe that some of the neutral hydrophilic groups gave satisfactory results. An acetamide analog (**17f**) and a sulfonamide (**17i**) gave two to threefold improvement in potency. Sulfamide (**17j**) exhibited further improvement in potency, but this compound was labile to metabolism (in vitro). The same modification to iodo-compound **14l** afforded highly potent compounds (**18a**, **18b**). Compound **18b** exhibited IC_{50} values of 3.9 and 0.37 nM for ACHN and HT-29, respectively. These two compounds reduced their hydrophobicity (ClogP **18a**, 4.5; **18b**, 4.3) and exhibited improved permeability (Caco2 permeability (cm/s 10^{-6}) **18a**, 28.4; **18b**, 18.1). With all these promising data, we believed we had succeeded in obtaining a candidate compound for development. However, unexpected experimental results forced us to give up all the compounds synthesized so far. (Details will be discussed in "SAR Study-2" section.)

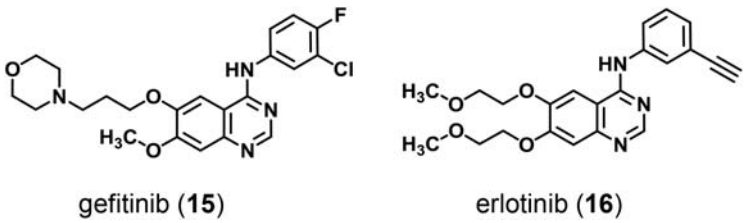

Fig. 9 Structures of gefitinib and erlotinib.

Table 11 Polar group substitution SAR-1

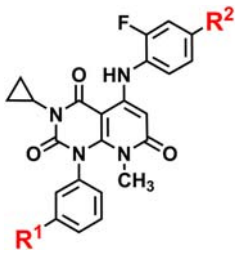

Compound	R^1	R^2	IC_{50} (nM)	
			ACHN	*HT-29*
12c	H	Br	325	15
17a	Morpholino	Br	250	11
17b	OCH_2CH_2morpholino	Br	970	57
17c	COOH	Br	>3000	>1000
17d	CH_2CH_2COOH	Br	>3000	250
17e	CONHMe	Br	1550	64
17f	NHCOMe	Br	167	6.2
17g	NHCOOEt	Br	630	34
17h	NHCONHEt	Br	845	38
17i	$NHSO_2Me$	Br	80	4.5
17j	$NHSO_2NMe_2$	Br	35	2.3
17k	SO_2NMe_2	Br	150	8.4
14l	H	I	13	1.5
18a	NHCOMe	I	13	0.66
18b	$NHSO_2Me$	I	3.9	0.37

The general syntheses of the compounds discussed thus far are outlined in Fig. 10. Treatment of **22** with methyl amine afforded key intermediate **23** in 96% yield. Chlorination of **21** proceeded with poor regioselectivity and needed to be improved. The introduction of different aryl groups at the 5-position in the final step was accomplished by thermal reaction of the tosylate **25** with appropriate aromatic amines and afforded good yields of the target compounds **26**. However, compounds bearing the

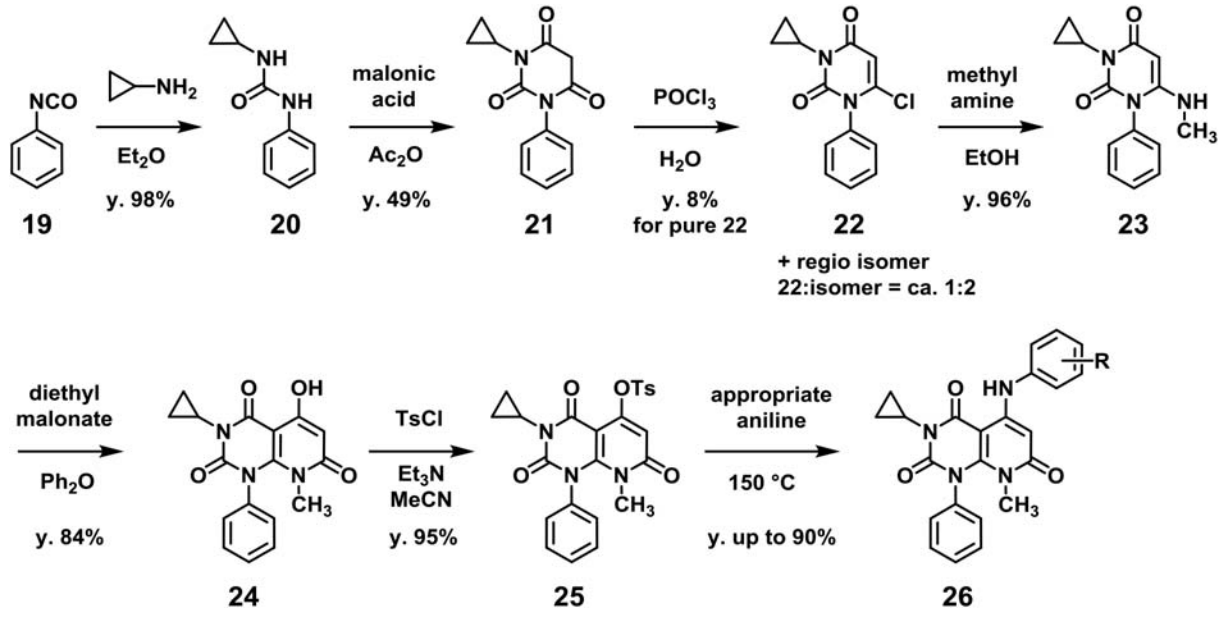

Fig. 10 Syntheses of **26** (**10e**, **11b**, **12**–**14**).

iodo substituent in the aniline ring (e.g., **18b**) were prepared in only c.30% yield due to the deiodination of iodo-aniline caused by employing a high temperature reaction condition. We addressed these issues rigorously in the synthesis stated above. We will discuss these in "Synthetic Studies" section.

8.02.5 SAR Study-2

We succeeded in obtaining a very potent compound (**18b**) starting from lead compound **2**. Analogs (**2**–**18b**) detailed in the previous section possessed the pyrido[2,3-*d*]pyrimidine core. But, unfortunately, the compounds with this pyrido[2,3-*d*]pyrimidine core proved to be unstable under weakly basic conditions as shown in Fig. 11. In the basic desilylation step of the precursor of **14i**, one of my associates noticed the formation of a side-product having the same MW as the target molecule **14i**. The side-product was assigned as compound **27** having the pyrido[4,3-*d*]pyrimidine core. After a few weeks, we determined the structure of **27** by careful analyses by two-dimensional NMR. We assumed that this new core was generated through the opening of the pyrimidinedione ring by the attack of a nucleophile (in this case methanol) at the C-2 carbonyl and subsequent ring-closure reaction gave another pyrimidinedione by the attack of the neighboring nitrogen atom of the other aniline.

Although compound **18b** exhibited a promising activity profile, we decided not to pursue **18b** and its analogs as suitable candidate for development due to their chemical instability. On the other hand, the newly formed pyrido[4,3-*d*]core was chemically stable. Compound **11b** provided the rearranged product **28** under basic conditions in the same way as illustrated in Fig. 11. And this rearranged **28** was very weak in potency (Fig. 12). However, we noticed compounds **11b** and **28** shared very similar chemical motifs, the spatial arrangement of two benzene and cyclopropane rings and three carbonyls on two heterocyclic cores was almost identical and only the positions of the nitrogen were swapped. We hypothesized that placement of appropriate substituents on the rearranged scaffold might afford chemically stable and highly potent compounds.

First, we transposed the bromine atom from the lower left position of **28** to the upper right position to afford **29**. But the potency was not restored. Next, we introduced a methyl substituent at the 8-position of **29**. Compound **30** had activity comparable to the parent **11b**. We reasoned that this was due to a potential effect of the methyl substituent on the orientation of the neighboring phenyl ring. Finally, introduction of the 2-F,4-I aniline moiety to give **31a** provided the substantial boost in potency that we sought. Compound **31a** exhibited the highly potent activity similar to **14l**.

Caco2 permeability for compound **31a** was good (Caco2 permeability (cm/s 10^{-6}) was 14), however, this compound was highly hydrophobic (ClogP 5.96). Although we asked our PK-specialists to measure the in vivo PK on **31a**, they politely turned it down due to the poor physicochemical profile of this compound. So, we set out to investigate introduction of hydrophilic groups on the 1-phenyl ring, the lower left, as a means to enhance hydrophilicity and hopefully improve the antiproliferative activity (the same strategy as mentioned before applied for the conversion from compound **14l** to **18a**,**b**).

Among the various functional groups that we examined, amides and sulfonamides were the preferred substituents in terms of potency (Table 12). Especially, compounds **31b** and **31d** substituted at the 3-position improved potency by threefold. On the other hand, a compound substituted at the 4-position such as **31c** resulted in an attenuation in potency by 10-fold. Compounds **31b** and

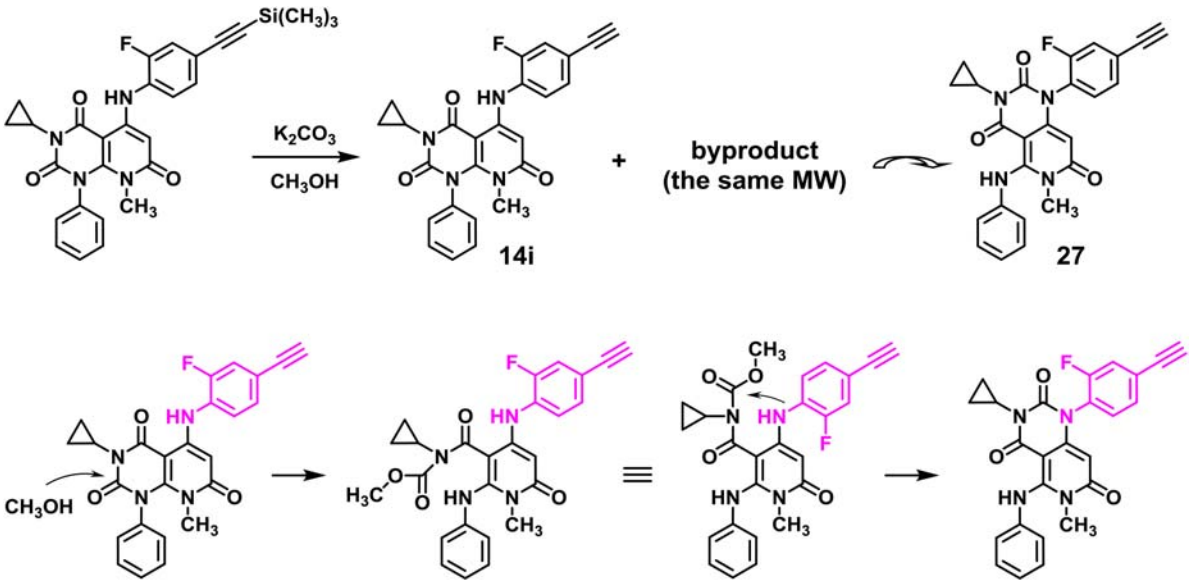

Fig. 11 Lability of pyrido[2,3-*d*]pyrimidine core.

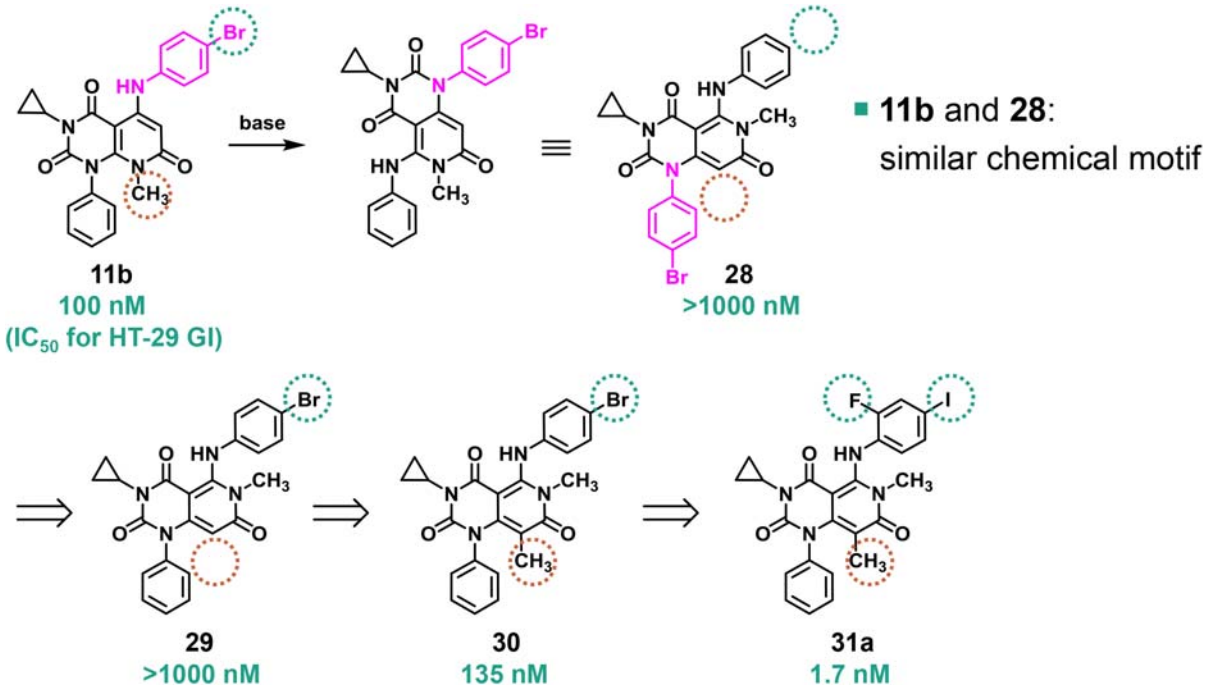

Fig. 12 Optimization of newly found core.

31d reduced their hydrophobicity (ClogP **31b**, 4.99; **31d**, 4.77) and retained good permeability (Caco2 permeability (cm/s 10^{-6}) **31b**, 17; **31d**, 26) (Table 13). Moreover, this modification resulted in a reasonable improvement in solubility. These compounds had an acceptable oral bioavailability of 30–60%.

To confirm the in vivo efficacy of compounds **31b** and **31d**, we evaluated the antitumor effect in the nude mouse xenograft model. HT-29 cells were inoculated subcutaneously into the right flank of nude mice, and compound **31b** or **31d** was administered orally once daily for 14 days starting from 5 days after the inoculation. Both 0.3 mg/kg and 1 mg/kg of compound **31b** were effective in inhibiting the HT-29 xenograft growth, and 1 mg/kg of compound **31b** blocked the tumor increase almost completely (Fig. 13).[2] In contrast, the antitumor effect of compound **31d** was ~10-fold weaker than that of compound **31b** on a dose-dependency basis. No significant changes in body weight of nude mice were observed after treatment of compounds **31b** or **31d**, suggesting that both compounds had sufficient efficacy of antitumor effect with lower dose range than the maximum tolerance doses. (The maximum tolerance dose was determined later as 3 mg/kg for compound **31b** and 30 mg/kg for compound **31d**.) We

Table 12 Polar group substitution SAR-2

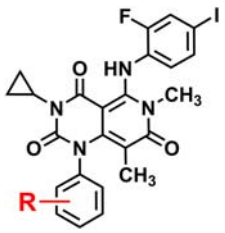

		IC_{50} (nM)	
Compound	*R*	*ACHN*	*HT-29*
31a	H	25	1.7
31b	3-NHCOMe	9.8	0.57
31c	4-NHCOMe	195	14
31d	3-$NHSO_2Me$	6.4	0.52
31e	4-$NHSO_2Me$	22	1.4

Table 13 PK related parameters

Compound	*ClogP*	*Solubility (PBS) (μM)*	*Caco2 permeability (cm/s 10^{-6})*	*AUC (μMh)*	*%F*
31a	6.0	<0.2	14		
31b	5.0	5.3	26	88	30
31d	4.8	3.3	17	59	59
31e	4.8	3.0	18	64	19

AUC and %*F* were determined after dosing orally mice at 30 mg/kg in 0.5% methyl cellulose suspension.

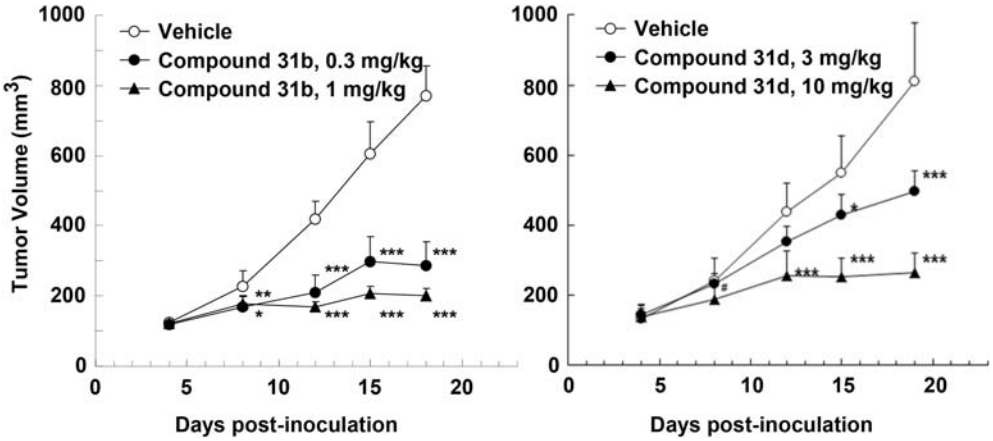

Fig. 13 Antitumor effect of **31b** and **31d** in nude mice bearing HT-29 xenografts. HT-29 cells were inoculated subcutaneously into the right flank of nude mice, and compound **31b**, **31d**, or vehicle (10% PEG400, 10% cremophor EL) was administered orally once daily for 14 days starting from 5 days after the inoculation. Tumor volumes were measured twice a week. The results are expressed as mean ± SD ($n=6$). $^{*}P<.05$, $^{**}P<.01$, $^{***}P<.001$ versus vehicle (Dunnett's test).

also evaluated PD0325901 (**34**, Fig. 19) in this model, and found that 30 mg/kg of PD0325901 (**34**) showed comparable efficacy of 1 mg/kg for compound **31b**.

The pharmacokinetic profiles in mouse for **31b** and **31d** are presented in Fig. 14. The compounds were administered intravenously to mice at 1 mg/kg. Compound **31b** showed longer mean residence time (MRT) and higher blood concentrations than **31d**. These features of **31b** might contribute to the superior in vivo activity of this compound (Fig. 13). The PK profile of **31b** was studied in three preclinical species (mouse, rat, and dog) as shown in Fig. 15. The compound showed low blood clearance and a long half-life, especially in dog. These features might translate into sustained plasma drug concentrations and narrow "peak/trough" ratio in human studies.

We selected compound **31b** (JTP-74057, GSK1120212, trametinib) as a candidate for further development based on the results of these in vivo xenograft model and PK studies.

8.02.6 Mechanism of Action and Pharmacological Characterization

8.02.6.1 Target Identification of Trametinib

During the discovery process of trametinib, we carried out the HTS screening campaign with the index of $p15^{INK4b}$ induction. Lead optimization was performed with the index of antiproliferative activity in ACHN and HT-29 cells, in vivo PK profile, and in vivo efficacy in the mouse xenograft model.[1,14] However, the molecular target of trametinib was still unknown at the time of discovery of this compound. Therefore, we undertook a search for the binding partner of trametinib by precise pharmacological and biological profiling. The $p15^{INK4b}$ upregulation was considered to be still involved in the antiproliferative effect of trametinib, since the relationship was found to be very reasonable between $p15^{INK4b}$ protein expression and antiproliferative activity during the course of lead optimization to trametinib (Table 14).

To clarify the mechanism of $p15^{INK4b}$ induction by trametinib, we examined the direct effect of trametinib on the $p15^{INK4b}$ promoter and the effect on degradation of $p15^{INK4b}$ mRNA, but these studies did not afford significant insights, leaving the mechanism of action of trametinib an enigma. On the other hand, an analysis of the expression levels of cell cycle related proteins revealed that trametinib can increase the expression of $p27^{KIP1}$ and decrease the expression of cyclin A and cyclin D1 while also affecting the $p15^{INK4b}$ induction activities (Fig. 16). In addition to this, the decrease in the phosphorylation of pRb can be seen in trametinib treated cells, indicating that those changes are related to the G1 cell cycle arrest effect of trametinib

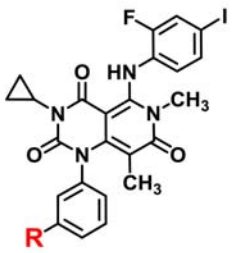

31b: R = NHCOMe
31d: R = $NHSO_2Me$
(31b: trametinib)

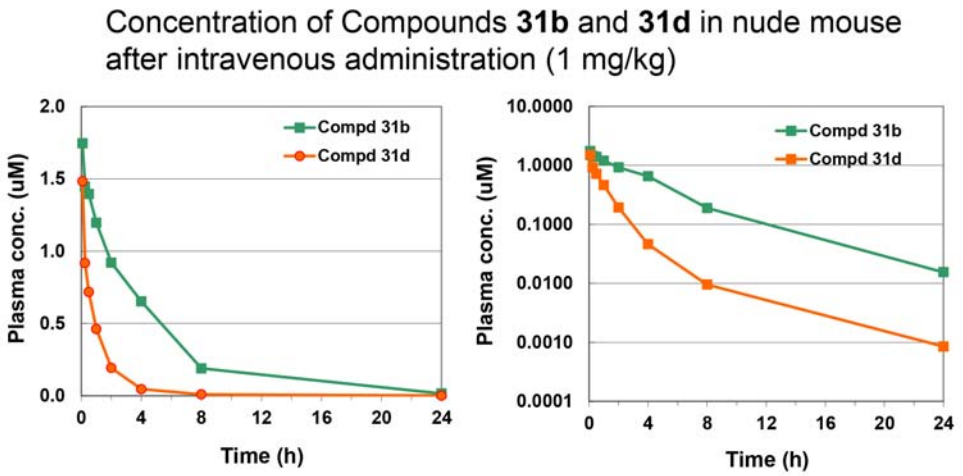

Compd	C_{5min}	$t_{1/2\alpha}$	$t_{1/2\beta}$	AUC_{0-inf}	CLtot	Vdss	MRT_{0-inf}
	(uM)	(h)	(h)	(uM·h)	(L/h/kg)	(L/kg)	(h)
31b	1.7	0.57	3.7	7.7	0.21	0.9	4.4
31d	1.5	0.41	3.7	1.6	0.97	1.7	1.7

Fig. 14 PK parameters (iv) in nude mice. Concentration of compounds **31b** and **31d** in nude mouse after intravenous administration (1 mg/kg).

(Fig. 16).[14] c-Myc was found to be the earliest gene that is affected by trametinib treatment (data not shown here).[14] The expression of c-Myc rapidly decreased within 2 h after starting the trametinib treatment. This rapid effect led us to speculate that the molecular target of trametinib might exist in the growth signaling pathway(s).

The drug-affinity chromatography technique using chemical probes was utilized for the molecular target exploration of trametinb.[15] As a starting point, we selected and synthesized compounds for the chemical probe. We had successfully incorporated a hydrophilic moiety into the 1-position in the benzene ring of **31a** during the SAR process, so we considered that the linker moiety to the resin (Sepharose) could be incorporated into this region. Compound **32** was prepared as a most potent probe and **33** was

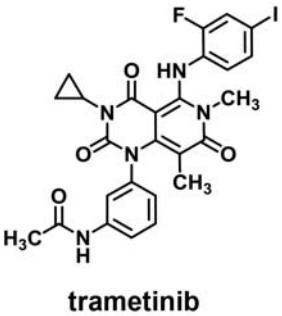

trametinib

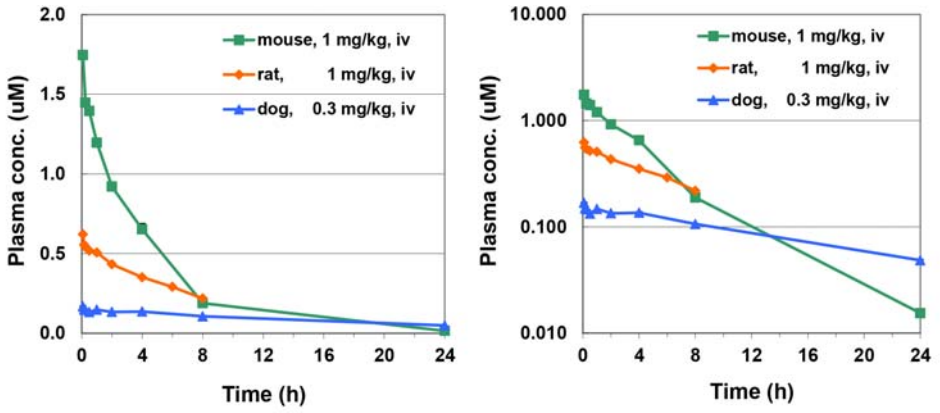

species	C_{5min}	$t_{1/2\alpha}$	$t_{1/2\beta}$	AUC_{0-inf}	CLtot	Vdss	MRT_{0-inf}
	(uM)	(h)	(h)	(uM·h)	(L/h/kg)	(L/kg)	(h)
mouse	1.73	0.57	3.7	7.7	0.21	0.9	4.4
rat	0.62	0.71	6.1	4.9	0.34	2.9	8.7
dog	0.17	0.55	14.5	3.3	0.15	3.0	20.2

Fig. 15 PK parameters (iv) of trametinib.

Table 14 Relationship between cell growth inhibition and $p15^{INK4b}$ protein expression

	Cell growth inhibition (IC_{50}; μM)		*$p15^{INK4b}$ protein induction (ACHN; μM)*							
Compound	*ACHN*	*HT-29*	*0.001*	*0.01*	*0.03*	*0.1*	*0.3*	*1*	*3*	*10*
2	4.6	1.1						+	+	++
11b	1.5	0.11				−	+/++	+/++	++	
12c	0.19	0.023			+	++	++	++		
1	0.0098	0.00057	−	+/++	+/++					
25	>10	>3								−

ACHN or HT-29 cells were treated with test compounds for 24 h, then cell growth activity was determined by ^{3}H-thymidine uptake assay. The results were shown as IC_{50} values. In addition, the expression level of $p15^{INK4b}$ protein in ACHN cells was examined by Western blotting after the treatment with various concentrations of test article for 24 h. (−); no induction, (+); weak induction, (++); strong induction of $p15^{INK4b}$ protein.

prepared as a less potent probe. Compounds **32** and **33** themselves showed very weak antiproliferative activity, but its pentanoyl derivative on the primary amine, which demonstrated the Sepharose-immobilized chemical probe status, exhibited the IC_{50} values of 2.1 and 840 nM for **32** and **33** in the HT-29 cell growth assay, respectively (**Fig. 17**).[15]

Taken together, compounds **32** and **33** were considered to be useful for the chemical probes in the drug-affinity chromatography. To identify specific binding targets, we prepared three chemical affinity resins. The first was unconjugated and used as a negative control, the second was conjugated with compound **33**, and the third was conjugated with the most potent compound **32**, which shared most of the structure to trametinib. HT-29 cell lysates were incubated with the individual resins and the bound proteins were extracted by pull-down assays. Specific binding proteins, including a dominant 46 kDa protein, accumulated in the compound-conjugated resins (**Fig. 18**).

To confirm that the resin conjugated with **32** was specifically bound to the 46 kDa protein, we performed competitive binding analyses using the free active compound (**18b**). As a result, the addition of the free form of compound **18b** into the HT-29 lysate clearly competed with the **32**-immobilized resin for the binding to the 46 kDa protein (**Fig. 18**). The bound 46 kDa proteins were then subjected to LC/MS/MS analysis as the specific binding partner of trametinib. MEK1 and MEK2 were the major proteins bound to **32**, with less extensive binding to **33**, and negligible binding to the negative control resin.[15] Western blot analysis using anti-MEK antibody also revealed that MEK1 and MEK2 proteins were strongly detected at the 46 kDa position in the pull-down extract of the **32**-conjugated resin. Further evidence that trametinib specifically binds to MEK1 and MEK2 and that its binding pocket was the same as PD0325901 (**34**) (**Fig. 19**) was provided by experiments using PD0325901 (**34**); **34** competed with **32**-immobilized resin for the binding to MEK1 and MEK2.[15] PD0325901 is an allosteric MEK1/2 inhibitor discovered by Pfizer, which was in Phase 2 clinical trials at the time of our studies.[28]

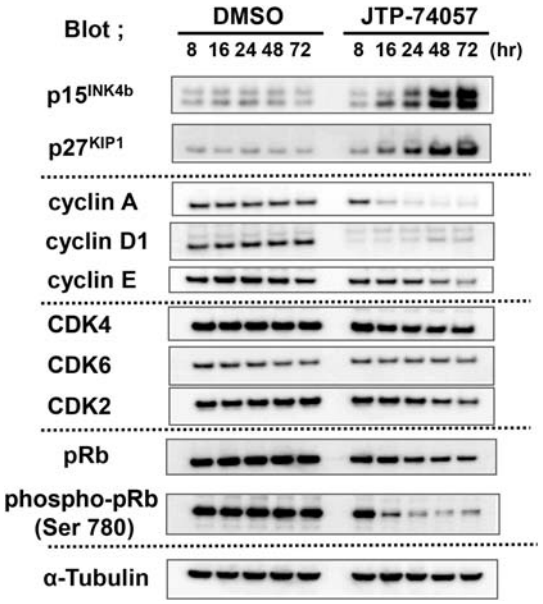

Fig. 16 Effect of trametinib (**1**) on cell-cycle-related protein expression in HT-29 cells. Expression levels of various cell-cycle-related proteins with 10 nM trametinib (**1**, JTP-74057) treatment were assessed by Western blot analysis. DMSO was used as a control. The representative data was shown from 2 to 3 independent experiments.

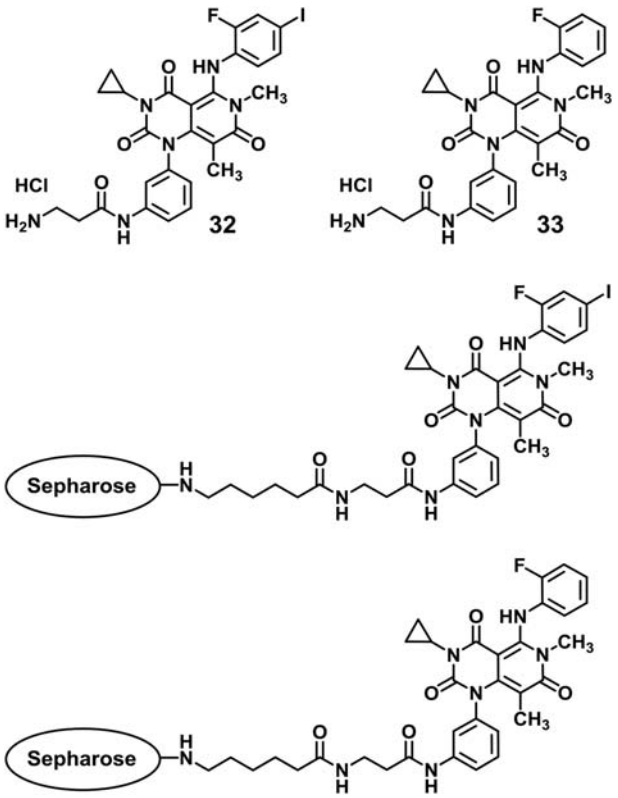

Fig. 17 Structures of trametinib derivatives and chemical affinity probes.

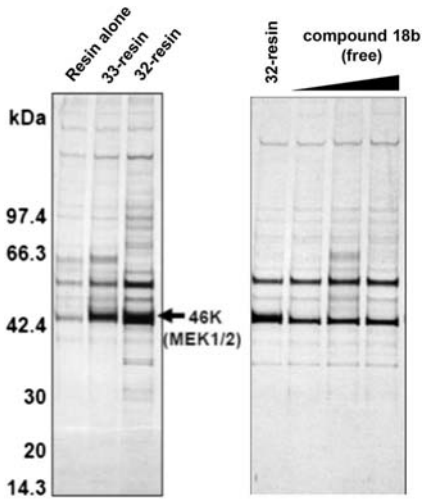

Fig. 18 Drug-affinity chromatography. HT-29 cell lysates were incubated with negative control resin (resin alone), **33**-conjugated resin, or **32**-conjugated resin and the bound proteins were extracted by pull-down assays, then subjected to SDS-PAGE analysis (left). The 46 kDa protein was competed by adding increasing concentrations of free compound **18b** (right).

8.02.6.2 MEK Inhibitory Activity of Trametinib

Once we had identified MEK1 and MEK2 as the binding target of trametinib (**1**), we examined the inhibitory activity of trametinib (**1**) against MEK1/MEK2 kinase activity. The inhibitory activity of trametinib (**1**) was determined by measuring the phosphorylation of ERK2, substrate of MEK, by phosphorylated MEK1 or MEK2. Unexpectedly, the IC_{50} value of trametinib (**1**) in this assay platform was 290 nM, unreasonably weak compared with the cell growth inhibitory activity, which was in the subnanomolar concentration range (Fig. 20). The same discrepancy was seen for PD0325901(**34**), whose IC_{50} value was determined as 120 nM (cell growth

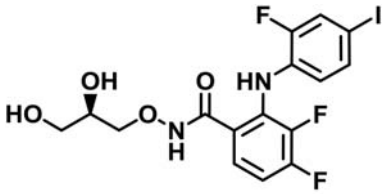

PD0325901 (**34**)

Fig. 19 Structure of PD0325901.

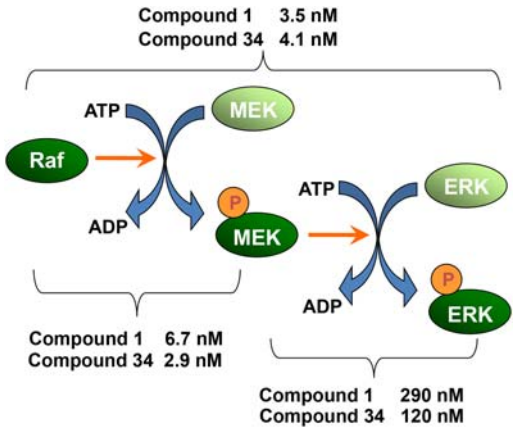

Fig. 20 Inhibitory activities (IC_{50} values) in Raf, MEK single kinase assay or Raf/MEK/ERK cascade kinase assay.

inhibition IC_{50} was 3.4 nM) (Fig. 20). Then, we employed a cascade kinase assay, which consist of active Raf, unphosphorylated (i.e., inactivated) MEK1 or MEK2 and unphosphorylated ERK2.[15] Under these conditions, trametinib (**1**)'s IC_{50} value was determined as 3.5 nM in the B-Raf–MEK1–ERK2 cascade kinase assay (Fig. 20). The IC_{50} value of PD0325901 (**34**) was 4.1 nM in the same cascade assay. Further analysis revealed that trametinib (**1**) and PD0325901 (**34**) inhibited MEK1 phosphorylation by active Raf with the IC_{50} values of 6.7 and 2.9 nM, respectively.[15] Taken together, our results demonstrated that trametinib (**1**) favorably binds to unphosphorylated MEK1/MEK2, resulting in the block of phosphorylation and activation by upstream molecule Raf. Trametinib (**1**) also had an ability to inhibit kinase activity of phosphorylated MEK1/MEK2 even though its activity was considered to be weaker than blockade of activation of MEK1/MEK2 protein by Raf.

Selectivity of trametinib (**1**) over several kinases was examined using a kinase panel study. Trametinib (**1**) did not show inhibitory activity up to 10 μM over the other 98 kinases examined (Table 15). We also retrospectively examined the kinase inhibitory activity of the lead compound (**2**) using a subset of the kinase panel. However, the lead compound (**2**) did not show MEK1 inhibitory activity even at 10 μM because of using phosphorylated MEK1 in this platform, implying that we would not have been able to identify this lead structure if we had conducted our HTS screening campaign using the phosphorylated MEK1 kinase assay platform. The choice of phenotypic screening might be considered an example of serendipity in this trametinib discovery story.

8.02.6.3 Pharmacological Characterization of Trametinib

Trametinib (**1**) is the MEK1/MEK2 selective inhibitor with a nanomolar or subnanomolar range of activity. Here, we provide a summary of the pharmacological activity of trametinib (**1**). Table 16 shows the antiproliferative effects of trametinib (**1**) using 10 human colorectal cancer cell lines. Trametinib (**1**) exhibited strongest IC_{50} values against HT-29 and COLO205 cells, which are known to bear the gain-of-function mutation in B-Raf protein. The cell lines bearing a K-Ras mutation showed a wide range of sensitivity to trametinib. In contrast, COLO320 DM cells, bearing the wild-type gene in both B-Raf and K-Ras, were found to be resistant to trametinib even at 10,000 nM.[2] Trametinib (**1**) also inhibited the growth of normal human lung fibroblasts (NHLF) with the IC_{50} values of 31 nM, which is more than 50-fold weaker than the IC_{50} values in B-Raf mutant, HT-29 and COLO205 cells. 5-Fluorouracil (5-FU), a standard-of-care colon cancer drug, inhibited within a narrow range of IC_{50} values regardless of the mutation status of cell line, whereas the antitumor effect of trametinib seemed to be highly dependent on the mutation status of cell line. Consistent with this, Western blot analysis of the phosphorylation level of ERK1/2 revealed that constitutive ERK phosphorylation was detected in all cell lines except of COLO320 DM and it was inhibited by trametinib treatment (Fig. 21).

Table 15 Effect of trametinib (**1**) on various kinase activities at 10 μM

Kinase	*% of control*	*Kinase*	*% of control*	*Kinase*	*% of control*	*Kinase*	*% of control*
Abl	95	EphB2	107	MKK6	70	PKCθ	114
Abl (T3151)	112	EphB4	124	MKK7β	109	PKCζ	102
ALK	166	ErbB4	101	MSK1	111	PKD2	98
Arg	111	Fes	95	MST2	94	Plk3	91
Aurora-A	124	FGFR3	98	NEK2	119	PRAK	91
Axl	114	Fgr	86	p70S6K	104	PRK2	98
Bmx	93	Flt3	107	PAK2	96	Ret	109
BTK	104	Fms	128	PAR-1Bα	116	ROCK-II	99
CaMKIV	97	Fyn	101	PDGFRα	111	Ros	107
CDK1/cyclin B	104	GSK3α	99	PDGFRβ	111	Rse	112
CDK2/cyclin A	101	GSK3β	98	PDK1	107	Rsk1	116
CDK2/cyclin E	104	IGF-1R	95	Pim-1	94	Rsk2	94
CDK3/cyclin E	101	IKKα	123	PKA	98	Rsk3	102
CDK5/p35	102	IKKβ	111	PKBα	107	SAPK2a	84
CDK6/cyclin D3	107	IR	129	PKBβ	103	SAPK2b	104
CDK7/cyclin H/MAT1	106	JNK1α1	104	PKBγ	109	SAPK3	97
CHK1	113	JNK2α2	97	PKCα	101	SAPK4	109
CHK2	98	JNK3	76	PKCβI	108	SGK	114
CK1δ	105	Lck	110	PKCβII	102	Syk	74
CK2	101	Lyn	95	PKCγ	107	Tie2	103
c-Raf	108	MAPK1(ERK1)	86	PKCδ	97	TrkA	59
CSK	97	MAPK2(ERK2)	108	PKCε	103	TrkB	120
cSRC	82	MAPKAP-K2	109	PKCη	107	Yes	104
EGFR	104	**MEK1**	28	PKCι	83	ZAP-70	111
EphA2	93	Met	150	PKCμ	111		

Results are shown as % of control, where the vehicle control is represented as 100%.

Table 16 In vitro growth inhibitory activities of trametinib (**1**) and 5-FU against human colorectal cancer cell lines and normal lung fibroblasts

		Growth inhibition (IC_{50} value)	
Cell line	*Mutation status*	*Compound **1**(trametinib) (nM)*	*5-FU (μM)*
COLO205	B-Raf	0.52 ± 0.02	1.7 ± 0.6
HT-29	B-Raf	0.48 ± 0.06	3.8 ± 0.04
HCT-15	K-Ras	174 ± 73	2.5 ± 0.2
HCT 116	K-Ras	5.7 ± 0.9	3.0 ± 0.4
LS-174T	K-Ras	4.1 ± 0.7	9.2 ± 1.0
SW480	K-Ras	8.5 ± 4.5	17.6 ± 3.4
SW620	K-Ras	2.3 ± 0.8	15.1 ± 0.5
T84	K-Ras	36 ± 13	18.8 ± 14.4
LoVo	K-Ras	2.2 ± 0.02	5.7 ± 1.0
COLO320 DM	WT	> 10,000	3.8 ± 0.3
NHLF	Normal cell	31 ± 9.8	6.7 ± 2.1

Various human colorectal cancer cell lines or human normal lung fibroblasts (NHLF) were treated with various concentrations of trametinib (**1**) or 5-FU for 72 h. Viable cell number was determined by sulforhodamine B assay.

As mentioned in the earlier section, trametinib induced the expression of CDK inhibitors $p15^{INK4b}$ and $p27^{KIP1}$, and we examined the expression level of $p15^{INK4b}$ and $p27^{KIP1}$ in these cell lines after treatment with trametinib. As shown in Fig. 21, both $p15^{INK4b}$ and $p27^{KIP1}$ were upregulated in the HT-29, COLO205, HCT-15, HCT116, and LoVo cells, whereas either $p15^{INK4b}$ or $p27^{KIP1}$ was upregulated in the LS-174T, SW480, SW620, and T84 cells. Most importantly, the resistant cell line, COLO320 DM cells, showed no induction of $p15^{INK4b}$ or $p27^{KIP1}$ by trametinib treatment, suggesting that upregulation of either $p15^{INK4b}$ or $p27^{KIP1}$ is a prerequisite for growth inhibition by trametinib.[2] Also, our phenotypic HTS campaign leading to the discovery of trametinib was considered to be the assay monitoring a potential pharmacodynamic biomarker of an MEK inhibitor; fortunately, we selected appropriate cells in which $p15^{INK4b}$ can be upregulated as a consequence of MEK inhibition.

In vivo antitumor efficacy of trametinib (**1**) was determined using a nude mouse xenograft model as mentioned earlier. Single oral dosing of trametinib at 1 mg/kg was administered to nude mice bearing HT-29 xenografts. The phosphorylation of ERK1/2 was completely inhibited in the established tumor within 1 h after the dosing, and this effect was diminished by 24 h after the dosing.[2]

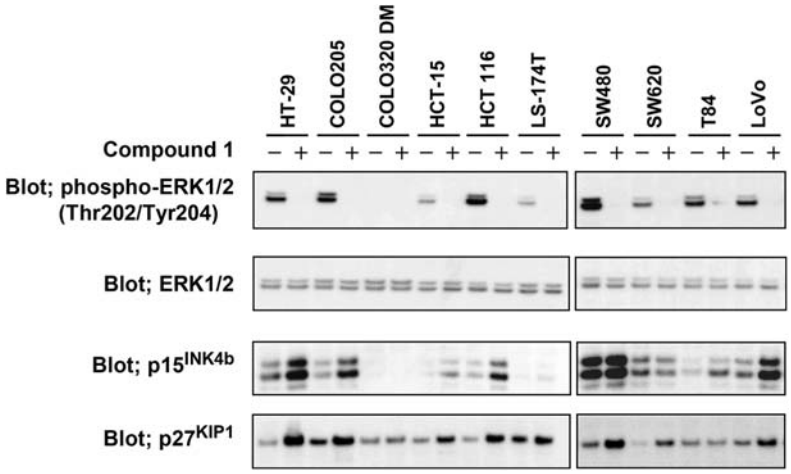

Fig. 21 Effect of trametinib (**1**) on phosphorylation of ERK1/2 and expression of $p15^{INK4b}$, and $p27^{KIP1}$ in various colorectal cancer cell lines. Ten colorectal cancer cell lines were treated with or without compound **1** at 100 nM (in case of HT-29, 10 nM). After 2 h (ERK1/2) or 24 hours ($p15^{INK4b}$, $p27^{KIP1}$), cells were lysed and phospho-ERK1/2, ERK1/2, $p15^{INK4b}$ or $p27^{KIP1}$ were detected by Western blot. The representative data are shown from 2 to 3 independent experiments.

As shown in Fig. 13, administration of 1 mg/kg of trametinib resulted in complete suppression of tumor growth in the HT-29 xenograft model. The antitumor effect of trametinib was also evaluated in another B-Raf mutant cell line, the COLO205 xenograft model. In this case, complete tumor regression was observed in 4 out of 6 mice in which the tumor degenerated to the point that tumor volume was not measurable at a dose of 1 mg/kg, where only complete growth suppression of tumor was observed in the HT-29 xenografts (Fig. 22).[2]

Despite the fact that trametinib inhibited the proliferation of HT-29 and COLO205 cells with comparable IC_{50} values in vitro, COLO205 tumors were much more sensitive to trametinib treatment than HT-29 tumors in vivo. To address this issue, apoptosis induction by trametinib was analyzed in vitro using HT-29 and COLO205 cells. Although trametinib induced apoptosis both in HT-29 and COLO205 cells, COLO205 cells were found to be more sensitive to trametinib than HT-29 in terms of apoptosis induction (data not shown).[2] Since it has been reported that HT-29 cells, but not COLO205 cells, have a mutation in PIK3CA, encoding a catalytic subunit (p100α) of phosphatidylinositol 3-kinase (PI3K) in addition to B-Raf mutation, excess activation of the PI3K–Akt pathway would occur in HT-29 cells concomitantly with MAPK pathway activation. Indeed, a combination treatment of trametinib with an Akt inhibitor, API-2, effectively induced apoptosis at lower concentrations in HT-29 cells (data not shown).[2]

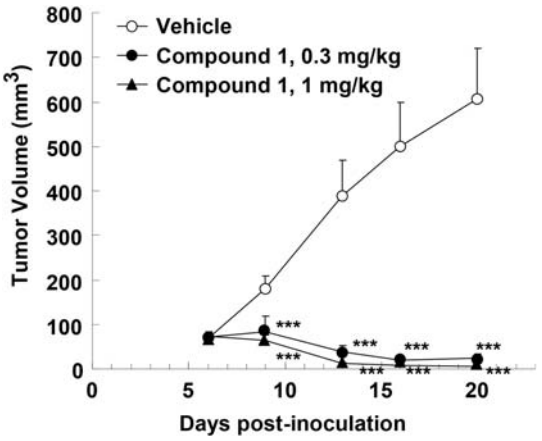

Fig. 22 Antitumor effect of trametinib (**1**) in nude mice bearing COLO205 xenografts. COLO205 cells were inoculated subcutaneously into the right flank of nude mice, and compound **1** or vehicle (10% PEG400, 10% cremophor EL) was administered orally once daily for 14 days starting from 7 days after the inoculation. Tumor volumes were measured twice a week. The results are expressed as mean ± SD ($n=6$). $^{***}P<.001$ versus vehicle (Dunnett's test).

8.02.7 Polymorphism Study

Next we performed the crystalline polymorphism study on trametinib. Several initial batches of trametinib had a melting point (mp) of 180°C and showed acceptable oral bioavailability. However, a new crystal form emerged unexpectedly after several preparations of this compound. This form had a very high mp of 300°C, and exhibited almost no oral exposure. (This polymorph proved to be the most stable after thorough polymorphism study.) In this kind of situation, one of the strategies commonly employed is preparing salts with different molecular packing motifs from that of a parent molecule. One can expect the increase of aqueous solubility. However, we were trapped in a difficult situation because this compound was almost neutral and did not form stable salts with hydrochloric acid or sulfuric acid, for example. The sodium salt could be obtained utilizing weakly acidic NH proton, however, this salt immediately turned into the parent free form upon contact with water. We next searched for stable solvates. Trametinib formed a variety of solvates with Class 3 solvents. For example, solvates with ethanol, 1-propanol, 2-propanol, formic acid, and acetic acid were easily prepared by recrystallization conditions. Although most solvates partially desolvated under reduced pressure, no desolvation occurred in the case of the acetic acid solvate under reduced pressure at 60°C for 3 h. We confirmed the ratio of trametinib to acetic acid to be 1:1 by NMR, elemental analysis, and X-ray. We prepared several lots of acetic acid solvates for biological testing. Our biologist colleagues told us this solvate smelled strong upon opening the lid of a vial. We checked the stability once again and found under more rigorous conditions this solvate had lost acetic acid partially (reduced pressure, 60°C, 48 h, 8% loss; 80°C, 60 h, 60% loss). We abandoned further work with the acetic acid solvate and were in a deadlock once again. One day, my colleagues brought me an NMR spectrum and said "Might this be the one we are looking for?" That was a DMSO solvate. The NMR spectrum clearly showed the ratio of trametinib to DMSO was exactly 1:1. Although data had been collected before the polymorphism study of trametinib had been performed, my coworker hesitated because none of us had ever heard of a "DMSO solvate" as a drug substance. Due to the high boiling point of DMSO (b.p. DMSO, 189°C; AcOH, 118°C) desolvation of this solvate had not been observed even under rigorous drying conditions. We were delighted to observe that the DMSO solvate of trametinib also passed the stability test (80°C, open air, 3 days; 60°C, 75% RH, 3 weeks, etc.). As shown in the X-ray crystal structure in Fig. 23, the unit cell contains two molecules of both trametinib and DMSO, and a hydrogen bond is formed between the oxygen atom of DMSO and the nitrogen of the acetamide moiety of trametinib. Oral exposure was restored as expected. DMSO is a Class 3 solvent, so there's no safety concern. We selected trametinib DMSO for development. Later, trametinib DMSO became the first FDA approved drug of this solvate.

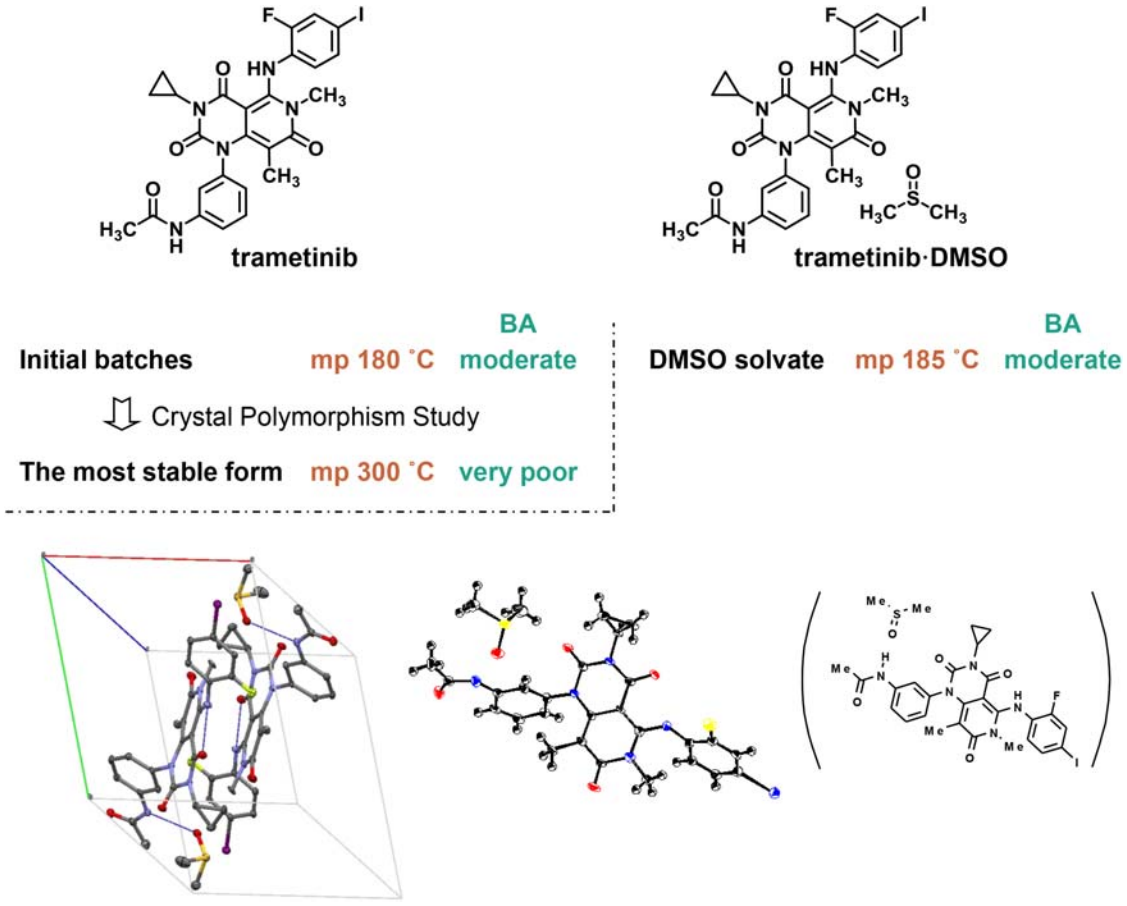

Fig. 23 Crystal polymorphism study of trametinib.

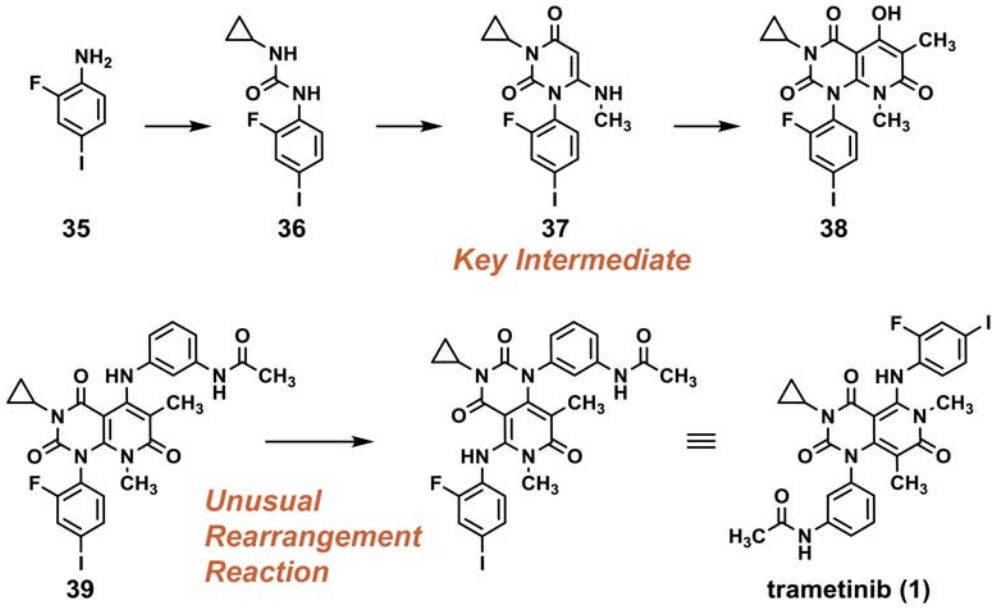

Fig. 24 Synthetic plan of trametinib.

8.02.8 Synthetic Studies

The synthetic plan for trametinib is outlined in Fig. 24. We employed the unusual rearrangement reaction mentioned earlier for the final step. The synthesis of the key intermediate **37** regioselectively without chromatographic purification was an important issue.

Key intermediate **37** could be conveniently prepared if the chloride **41** was obtained regioselectively (Fig. 25). However chlorination of **40** with phosphoryl chloride produced a mixture of the two regioisomeric chlorides **41** and **42**, with a predominant formation of undesired **42**. We tried to vary the reaction conditions by changing the amount of added water or base. But the ratio of **41** and **42** was always c.1:2. When we separated pure chlorides **41** and **42**, and reacted each of them separately under the chlorination conditions, both pure **41** and **42** gave a mixture of **41** and **42** in the same ratio. This outcome clarified that this chlorination reaction proceeded under thermodynamic control, and we abandoned this approach.

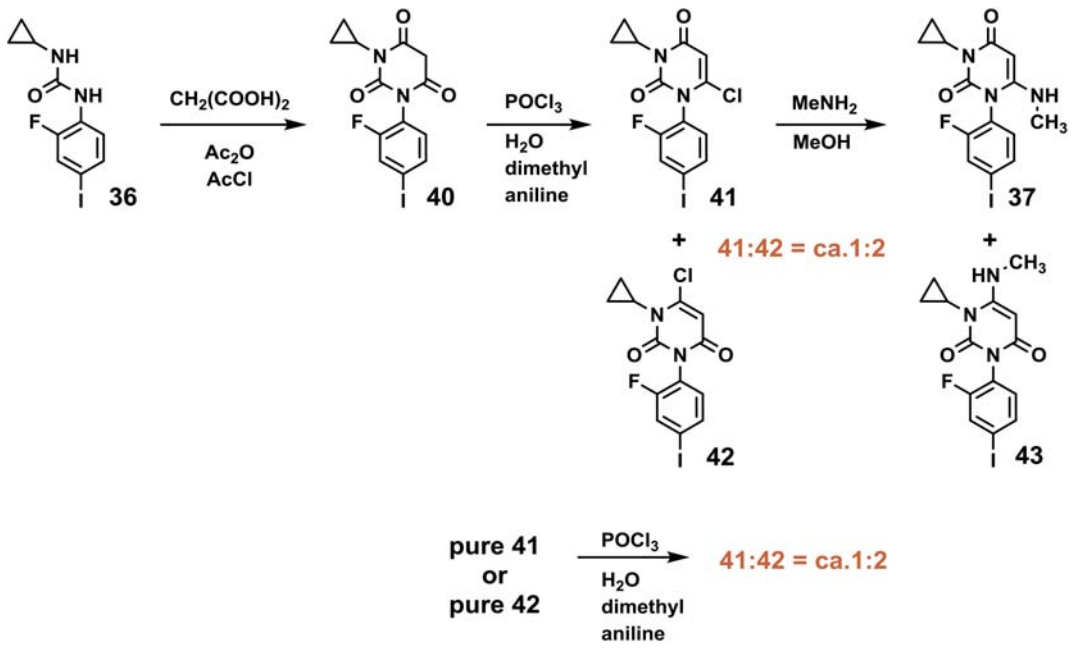

Fig. 25 Preparation of key intermediate-1.

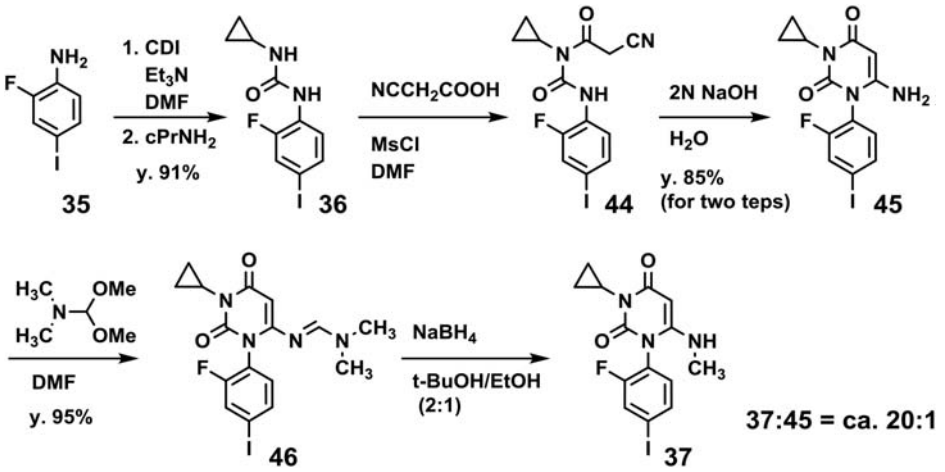

Fig. 26 Preparation of key intermediate-2.

We next investigated an alternative route to synthesize key intermediate **37**, which employed the reduction of the amidine **46** as a key step (Fig. 26). Urea **36** was obtained in high yield by treatment of 2-fluoro-4-iodoaniline (**35**) subsequently with carbonyldiimidazole and cyclopropyl amine. In this reaction, the issue of deiodination of iodo-aniline mentioned before ("SAR Study-1" section) was not present, because this reaction did not require high temperature. Condensation of urea **36** with cyanoacetic acid to give **44** was accomplished using mesyl chloride as an activating reagent. This reaction also proceeded by using acetic anhydride, acetyl chloride, or tosyl chloride, but mesyl chloride gave the best results. Ring-closure reaction of **44** to give **45** smoothly proceeded in a warm alkaline solution in good yield. Direct mono-methylation of the primary amine in **45** was not possible due to the enamine-like character of this compound. However, amine **45** reacted with *N*,*N*-dimethylformamide dimethyl acetal on the primary nitrogen, and gave a high yield of the amidine **46**. Reduction of **46** with sodium borohydride gave the desired mono-methylated **37** and reduction side-product **45**.[29,30] Ratio of **37**:**45** was sensitive to the solvent system employed for reduction reaction. For example, reduction of **46** in methanol gave undesired **45** as a major product (**37**:**45** = 1:1.3). We finally found that the best solvent system for this reduction reaction was *tert*-butanol/ethanol = 2:1, which gave the key intermediate in high selectivity of **37**:**45** = c.20:1.

Subsequent ring-closure reaction of **37** with methylmalonic acid gave **38** in good yield by using **37** purified by column chromatography (Fig. 27). However, crude **37** gave various yields of **38** depending on the lot used. A closer look clarified that the reaction yield was very low when the reduction was quenched by acetic acid whereas quenching with citric acid gave high yield. We speculated that crude **37** contained boric acid (or its derivatives) and quenching the reaction with acetic acid interfered the next ring-closure reaction. This kind of small finding might not seem important, but was a real enjoyment for us chemists when working on the large scale process development. Tosylation of **38** afforded **47**. Thermal reaction of **47** with the substituted aniline gave a high yield of **39**. Finally, trametinib was obtained employing the unusual rearrangement reaction of **39** as mentioned before.

The synthetic route to trametinib is summarized in Fig. 27. The 10-step sequence required no chromatography, and resulted in an overall yield of 34% of trametinib. The unusual rearrangement reaction to trametinib proceeded in very high yield. One of the desirable features of this route is only the final compound is biologically highly active, so the other compounds do not require special handling. This synthetic route was refined at GSK and was performed conveniently on a 40 kg scale.

8.02.9 Addendum

MEK inhibitors such as Pfizer's compound are known to bind an allosteric pocket adjacent to the ATP-binding pocket. And these compounds are classified as type III inhibitors.[31–33] We speculate that trametinib also binds the same allosteric pocket (see "Target Identification of Trametinib" section).[15]

The compounds with an iodo-substituent on the aniline ring exhibited high potency as explained in the text. This is due to halogen bonding between iodine and the backbone carbonyl of the enzyme, and has been reviewed.[34]

8.02.10 Conclusion

In conclusion, starting from an initial lead **2** identified by a cellular high-throughput screen to identify the compounds that increase $p15^{INK4b}$ and SAR studies to improve antiproliferative activity against cancer cells culminated in the discovery of **1**, trametinib (JTP-74057, GSK1120212), a highly potent, selective, and orally active MEK inhibitor. Trametinib displays remarkable potency

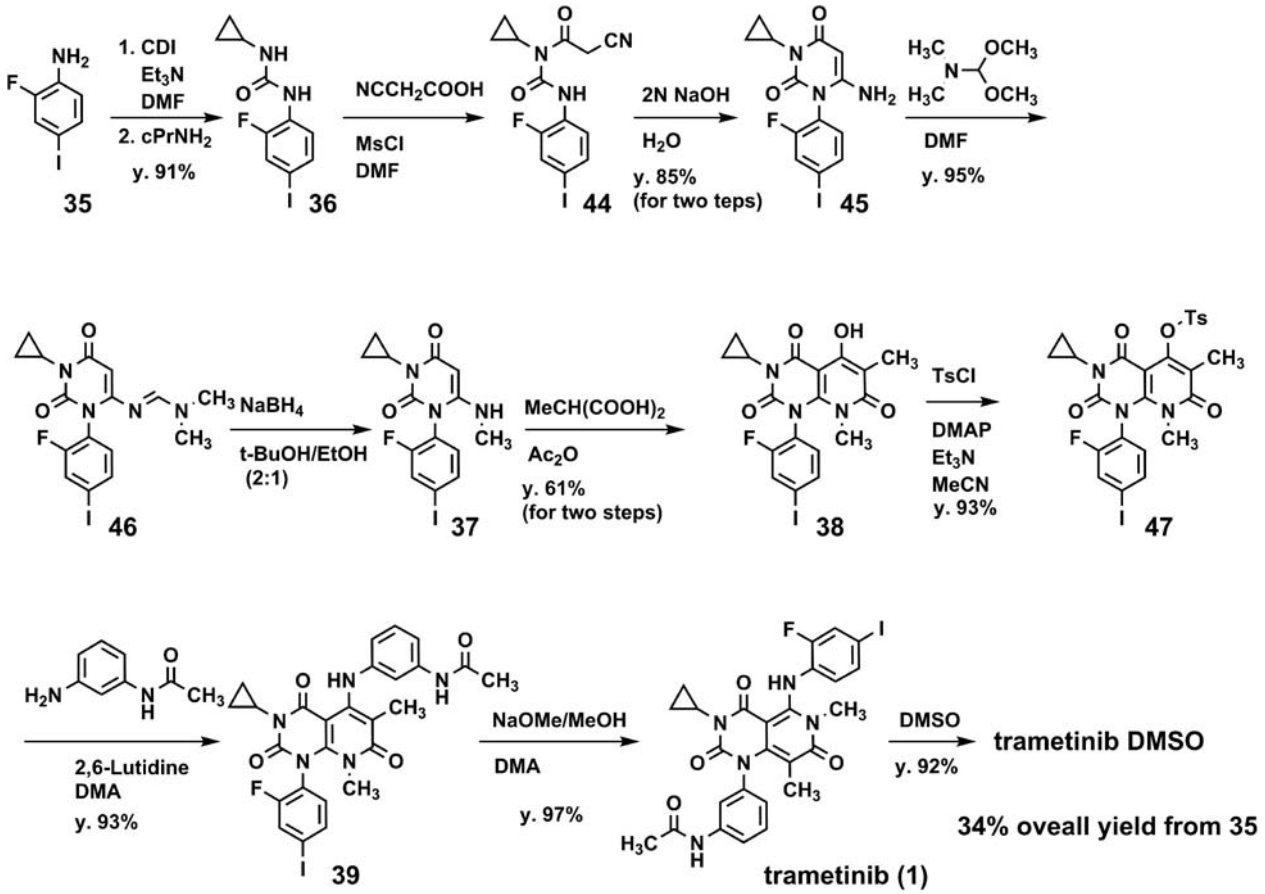

Fig. 27 Synthetic route to trametinib.

in antiproliferative cellular assays and excellent in vivo activity. Trametinib is a new structural class of MEK inhibitor possessing the unique pyrido[4,3-*d*]pyrimidine core. The synthetic route to trametinib featuring unusual rearrangement reaction is concise and highly efficient. Inhibition of the MEK–ERK pathway offers a very promising therapeutic strategy for cancers with activating mutants Ras and Raf. Trametinib is now widely available for use as a single-agent or in combination with the Raf inhibitor, dabrafenib, in the treatment of patients with unresectable or metastatic melanoma with a BRAF V600E or V600K mutation. The research and development of trametinib is still being extensively continued, including not only the melanoma therapy in combination with novel immunotherapies targeting the activation of antitumor immune response, but also the treatment options for the other solid tumors and leukemia. As of Oct. 2015, around 300 references in the literature could be found in PubMed regarding the research on trametinib/GSK1120212/JTP-74057, and over 100 clinical trials for trametinib, both active and completed studies, are listed in the ClinicalTrials.gov. Trametinib, discovered by a unique strategy of the phenotypic screening followed by extensive medicinal chemistry and the target identification by chemical biology methods, has opened up a new horizon for melanoma therapeutic options as well as for a combination therapeutic strategy for malignant tumors using more than two molecular targeting drugs.

References

1. Abe, H.; Kikuchi, S.; Hayakawa, K.; Iida, T.; Nagahashi, N.; Maeda, K.; Sakamoto, J.; Matsumoto, N.; Miura, T.; Matsumura, K.; Seki, N.; Inaba, T.; Kawasaki, H.; Yamaguchi, T.; Kakefuda, R.; Nanayama, T.; Kurachi, H.; Hori, Y.; Yoshida, T.; Kakegawa, J.; Watanabe, Y.; Gilmartin, A. G.; Richter, M. C.; Moss, K. G.; Laquerre, S. G. Discovery of a Highly Potent and Selective MEK Inhibitor: GSK1120212 (JTP-74057 DMSO Solvate). *ACS Med. Chem. Lett.* **2011,** *2* (4), 320–324.
2. Yamaguchi, T.; Kakefuda, R.; Tajima, N.; Sowa, Y.; Sakai, T. Antitumor Activities of JTP-74057 (GSK1120212), a Novel MEK1/2 Inhibitor, on Colorectal Cancer Cell Lines In Vitro and In Vivo. *Int. J. Oncol.* **2011,** *39* (1), 23–31.
3. Gilmartin, A. G.; Bleam, M. R.; Groy, A.; Moss, K. G.; Minthorn, E. A.; Kulkarni, S. G.; Rominger, C. M.; Erskine, S.; Fisher, K. E.; Yang, J.; Zappacosta, F.; Annan, R.; Sutton, D.; Laquerre, S. G. GSK1120212 (JTP-74057) is an Inhibitor of MEK Activity and Activation with Favorable Pharmacokinetic Properties for Sustained In Vivo Pathway Inhibition. *Clin. Cancer Res.* **2011,** *17* (5), 989–1000.
4. Flaherty, K. T.; Robert, C.; Hersey, P.; Nathan, P.; Garbe, C.; Milhem, M.; Demidov, L. V.; Hassel, J. C.; Rutkowski, P.; Mohr, P.; Dummer, R.; Trefzer, U.; Larkin, J. M.; Utikal, J.; Dreno, B.; Nyakas, M.; Middleton, M. R.; Becker, J. C.; Casey, M.; Sherman, L. J.; Wu, F. S.; Ouellet, D.; Martin, A. M.; Patel, K. Improved Survival with MEK Inhibition in BRAF-Mutated Melanoma. *N. Engl. J. Med.* **2012,** *367* (2), 107–114.

5. http://www.gsk.com/en-gb/media/press-releases/2013/two-new-gsk-oral-oncology-treatments-braf-inhibitor-tafinlar-dabrafenib-capsules-and-the-first-mek-inhibitor-mekinist-trametinib-tablets-approved-by-fda-as-single-agent-therapies/.
6. Sebolt-Leopold, J. S.; Herrera, R. Targeting the Mitogen-Activated Protein Kinase Cascade to Treat Cancer. *Nat. Rev. Cancer* **2004,** *4* (12), 937–947.
7. Rinehart, J.; Adjei, A. A.; LoRusso, P. M.; Waterhouse, D.; Hecht, J. R.; Natale, R. B.; Hamid, O.; Varterasian, M.; Asbury, P.; Kaldjian, E. P.; Gulyas, S.; Mitchell, D. Y.; Herrera, R.; Sebolt-Leopold, J. S.; Meyer, M. B. Multicenter Phase II Study of the Oral MEK Inhibitor, CI-1040, in Patients with Advanced non-Small-Cell Lung, Breast, Colon, and Pancreatic Cancer. *J. Clin. Oncol.* **2004,** *22* (22), 4456–4462.
8. Haura, E. B.; Ricart, A. D.; Larson, T. G.; Stella, P. J.; Bazhenova, L.; Miller, V. A.; Cohen, R. B.; Eisenberg, P. D.; Selaru, P.; Wilner, K. D.; Gadgeel, S. M. A Phase II Study of PD-0325901, an Oral MEK Inhibitor, in Previously Treated Patients with Advanced non-Small Cell Lung Cancer. *Clin. Cancer Res.* **2010,** *16* (8), 2450–2457.
9. Robert, C.; Karaszewska, B.; Schachter, J.; Rutkowski, P.; Mackiewicz, A.; Stroiakovski, D.; Lichinitser, M.; Dummer, R.; Grange, F.; Mortier, L.; Chiarion-Sileni, V.; Drucis, K.; Krajsova, I.; Hauschild, A.; Lorigan, P.; Wolter, P.; Long, G. V.; Flaherty, K.; Nathan, P.; Ribas, A.; Martin, A. M.; Sun, P.; Crist, W.; Legos, J.; Rubin, S. D.; Little, S. M.; Schadendorf, D. Improved Overall Survival in Melanoma with Combined Dabrafenib and Trametinib. *N. Engl. J. Med.* **2015,** *372* (1), 30–39.
10. Long, G. V.; Stroyakovskiy, D.; Gogas, H.; Levchenko, E.; de Braud, F.; Larkin, J.; Garbe, C.; Jouary, T.; Hauschild, A.; Grob, J. J.; Chiarion Sileni, V.; Lebbe, C.; Mandalà, M.; Millward, M.; Arance, A.; Bondarenko, I.; Haanen, J. B.; Hansson, J.; Utikal, J.; Ferraresi, V.; Kovalenko, N.; Mohr, P.; Probachai, V.; Schadendorf, D.; Nathan, P.; Robert, C.; Ribas, A.; DeMarini, D. J.; Irani, J. G.; Casey, M.; Ouellet, D.; Martin, A. M.; Le, N.; Patel, K.; Flaherty, K. Combined BRAF and MEK Inhibition Versus BRAF Inhibition Alone in Melanoma. *N. Engl. J. Med.* **2014,** *371* (20), 1877–1888.
11. http://www.gsk.com/en-gb/media/press-releases/2014/gsk-gains-accelerated-fda-approval-for-combination-use-of-mekinist-trametinib-and-tafinlar-dabrafenib/.
12. https://www.novartisoncology.com/news/media-releases/novartis-receives-EU-approval-for-tafinlar%C2%AE-and-mekinist%C2%AE%2C-first-combination-approved-for-patients-with-aggressive-form-of-melanoma.
13. http://www.novartis.co.jp/news/2016/pr20160328_01.html.
14. Yamaguchi, T.; Yoshida, T.; Kurachi, R.; Kakegawa, J.; Hori, Y.; Nanayama, T.; Hayakawa, K.; Abe, H.; Takagi, K.; Matsuzaki, Y.; Koyama, M.; Yogosawa, S.; Sowa, Y.; Yamori, T.; Tajima, N.; Sakai, T. Identification of JTP-70902, a p15INK4b-Inductive Compound, as a Novel MEK1/2 Inhibitor. *Cancer Sci.* **2007,** *98* (11), 1809–1816.
15. Yoshida, T.; Kakegawa, J.; Yamaguchi, T.; Hantani, Y.; Okajima, N.; Sakai, T.; Watanabe, Y.; Nakamura, M. Identification and Characterization of a Novel Chemotype MEK Inhibitor Able to Alter the Phosphorylation State of MEK1/2. *Oncotarget* **2012,** *3* (12), 1533–1545.
16. Sherr, C. J. Mammalian G1 Cyclins. *Cell* **1993,** *73* (6), 1059–1065.
17. Dowdy, S. F.; Hinds, P. W.; Louie, K.; Reed, S. I.; Arnold, A.; Weinberg, R. A. Physical Interaction of the Retinoblastoma Protein with Human D Cyclins. *Cell* **1993,** *73* (3), 499–511.
18. Roovers, K.; Assoian, R. K. Integrating the MAP Kinase Signal into the G1 Phase Cell Cycle Machinery. *Bioessays* **2000,** *22* (9), 818–826.
19. Mercer, K. E.; Pritchard, C. A. Raf Proteins and Cancer: B-Raf is Identified as a Mutational Target. *Biochim. Biophys. Acta* **2003,** *1653* (1), 25–40.
20. Ruas, M.; Peters, G. The p16INK4a/CDKN2A Tumor Suppressor and its Relatives. *Biochim. Biophys. Acta* **1998,** *1378* (2), F115–F177.
21. Serrano, M.; Lee, H.; Chin, L.; Cordon-Cardo, C.; Beach, D.; DePinho, R. A. Role of the INK4a Locus in Tumor Suppression and Cell Mortality. *Cell* **1996,** *85* (1), 27–37.
22. Sharpless, N. E.; Bardeesy, N.; Lee, K. H.; Carrasco, D.; Castrillon, D. H.; Aguirre, A. J.; Wu, E. A.; Horner, J. W.; DePinho, R. A. Loss of p16Ink4a with Retention of p19Arf Predisposes Mice to Tumorigenesis. *Nature* **2001,** *413* (6851), 86–91.
23. Hannon, G. J.; Beach, D. p15INK4B is a Potential Effector of TGF-β-Induced Cell Cycle Arrest. *Nature* **1994,** *371* (6494), 257–261.
24. Stone, S.; Dayananth, P.; Jiang, P.; Weaver-Feldhaus, J. M.; Tavtigian, S. V.; Cannon-Albright, L.; Kamb, A. Genomic Structure, Expression and Mutational Analysis of the P15 (MTS2) Gene. *Oncogene* **1995,** *11* (5), 987–991.
25. Thullberg, M.; Bartkova, J.; Khan, S.; Hansen, K.; Rönnstrand, L.; Lukas, J.; Strauss, M.; Bartek, J. Distinct Versus Redundant Properties Among Members of the INK4 Family of Cyclin-Dependent Kinase Inhibitors. *FEBS Lett.* **2000,** *470* (2), 161–166.
26. Matsuzaki, Y.; Sakai, T. INK4 Family—A Promising Target for 'Gene-Regulating chemoprevention' and 'Molecular-Targeting prevention' of Cancer. *Environ. Health Prev. Med.* **2005,** *10* (2), 72–77.
27. Koyama, M.; Matsuzaki, Y.; Yogosawa, S.; Hitomi, T.; Kawanaka, M.; Sakai, T. ZD1839 Induces p15INK4b and Causes G1 Arrest by Inhibiting the Mitogen-Activated Protein Kinase/Extracellular Signal-Required Kinase Pathway. *Mol. Cancer Ther.* **2007,** *6* (5), 1579–1587.
28. Trujillo, J. I. MEK Inhibitors: A Patent Review 2008–2010. *Expert Opin. Therap. Patents* **2011,** *21* (7), 1045–1069.
29. Kelley, J. L.; McLean, E. W. Synthesis of 9-(2-Fluorobenzyl)-6-Methylamino-9H-Purine. *J. Heterocycl. Chem.* **1986,** *23* (4), 1189–1193.
30. Zhang, J.; Chang, H.-M.; Kane, R. R. Reductive Monoalkylation of Aromatic Amines via Amidine Intermediates. *Synlett* **2001,** *2001* (5), 643–645.
31. Ohren, J. F.; Chen, H.; Pavlovsky, A.; Whitehead, C.; Zhang, E.; Kuffa, P.; Yan, C.; McConnell, P.; Spessard, C.; Banotai, C.; Mueller, W. T.; Delaney, A.; Omer, C.; Sebolt-Leopold, J.; Dudley, D. T.; Leung, I. K.; Flamme, C.; Warmus, J.; Kaufman, M.; Barrett, S.; Tecle, H.; Hasemann, C. A. Structures of Human MAP Kinase Kinase 1 (MEK1) and MEK2 Describe Novel Noncompetitive Kinase Inhibition. *Nat. Struct. Mol. Biol.* **2004,** *11* (12), 1192–1197.
32. Wallace, E. M.; Lyssikatos, J.; Blake, J. F.; Seo, J.; Yang, H. W.; Yeh, T. C.; Perrier, M.; Jarski, H.; Marsh, V.; Poch, G.; Livingston, M. G.; Otten, J.; Hingorani, G.; Woessner, R.; Lee, P.; Winkler, J.; Koch, K. Potent and Selective Mitogen-Activated Protein Kinase Kinase (MEK) 1,2 Inhibitors. 1. 4-(4-Bromo-2-fluorophenylamino)-1-methylpyridin-2(1*H*)-ones. *J. Med. Chem.* **2006,** *49* (2), 441–444.
33. Dong, Q.; Dougan, D. R.; Gong, X.; Halkowycz, P.; Jin, B.; Kanouni, T.; O'Connell, S. M.; Scorah, N.; Shi, L.; Wallace, M. B.; Zhou, F. Discovery of TAK-733, a Potent and Selective MEK Allosteric Site Inhibitor for the Treatment of Cancer. *Bioorg. Med. Chem. Lett.* **2011,** *21* (5), 1315–1319.
34. Wilcken, R.; Zimmermann, M. O.; Lange, A.; Joerger, A. C.; Boeckler, F. M. Principles and Applications of Halogen Bonding in Medicinal Chemistry and Chemical Biology. *J. Med. Chem.* **2013,** *56* (4), 1363–1388.

8.03 Discovery of the Hypoxia-Activated Prodrug SN30000

MP Hay, KO Hicks, and WR Wilson, The University of Auckland, Auckland, New Zealand

© 2017 Elsevier Ltd. All rights reserved.

8.03.1	**Introduction**	58
8.03.1.1	Preamble	58
8.03.1.2	Hypoxia	58
8.03.1.3	Drug Development in the Context of Hypoxia	60
8.03.1.4	Tirapazamine	61
8.03.2	**Building a Toolset for Bioreductive Drug Discovery**	63
8.03.2.1	Introductory Remarks	63
8.03.2.2	Structure–Activity Toolset	63
8.03.2.3	Measuring Extravascular Drug Transport	64
8.03.2.4	Developing a Spatially Resolved-PK–PD Model	67
8.03.3	**Drug Discovery Campaign to Identify a Second-Generation TPZ Analog**	68
8.03.3.1	Design Criteria	68
8.03.3.2	DNA Targeting	69
8.03.3.3	BTOs With Improved EVT	70
8.03.3.4	Exploring 3-Alkyl BTOs: Role of H Bonding on EVT	74
8.03.3.5	Designing Novel Analogs	76
8.03.3.6	Summary	79
8.03.4	**Characterization of SN30000**	80
8.03.4.1	Preamble	80
8.03.4.2	Synthesis Optimization	81
8.03.4.3	SN30000 Is an Improved TPZ Analog	83
8.03.4.4	Mechanism of DNA Damage	85
8.03.4.5	Predictive Biomarkers and Response Biomarkers for SN30000	86
8.03.5	**Summary**	87
Acknowledgments		88
References		88

8.03.1 Introduction

8.03.1.1 Preamble

Tumor hypoxia (deprivation of oxygen in tumor cells) is arguably one of the best validated targets for oncology drug development.[1] Tumor hypoxia has been demonstrated to occur in a wide range of human tumors and is a driver of tumor progression through adaptive responses and resistance to therapy through reduction in proliferation and failure to fix radiation-induced DNA damage. Despite being the subject of drug discovery efforts for over four decades, hypoxia is one of the least successfully drugged oncology targets. In this age of "targeted therapy," why have we failed to capitalize on this opportunity? In this article, we background the case for targeting hypoxic tumor cells and explore a recent drug discovery campaign to develop a drug targeted against hypoxic cells in solid tumors. We aim to give insight into the difficulties presented by this ubiquitous target and how specific tools have been developed to increase the chances of success.

8.03.1.2 Hypoxia

Tumor hypoxia arises as a result of an imbalance between supply and demand for oxygen. The supply of oxygen is diffusion limited in small, avascular tumors, and in larger tumors, oxygen supply is compromised by disordered and dysfunctional tumor vasculature.[2,3] This deficiency is exacerbated by increased metabolic demand within tumors, and collectively, this imbalance results in pathophysiological hypoxia. However, the target is not a simple binary proposition. The depth of hypoxia varies greatly, and the spatial and temporal distribution of hypoxia is highly heterogeneous, both within individual tumors and between tumors of the same type, even in the same patient (**Fig. 1A**).[8] This complexity has been complicated by considerable ambiguity in the literature around definitions of "normoxia" and "hypoxia." This ambiguity stems from the various measurement systems used to report hypoxia and semantic variations (**Fig. 1B**).[9] Three commonly used units for oxygen concentration are shown on the *x*-axis of **Fig. 1B**. While normoxic conditions used in most cell culture experiments have around 20% oxygen (measured in the humidified gas phase and assumed to be in equilibrium with culture medium), the level of oxygen in peripheral "normal" tissues is considerably lower, typically in the range of 3–7%. Fine-needle measurements of oxygen tension in tumor tissue made using an Eppendorf oxygen electrode

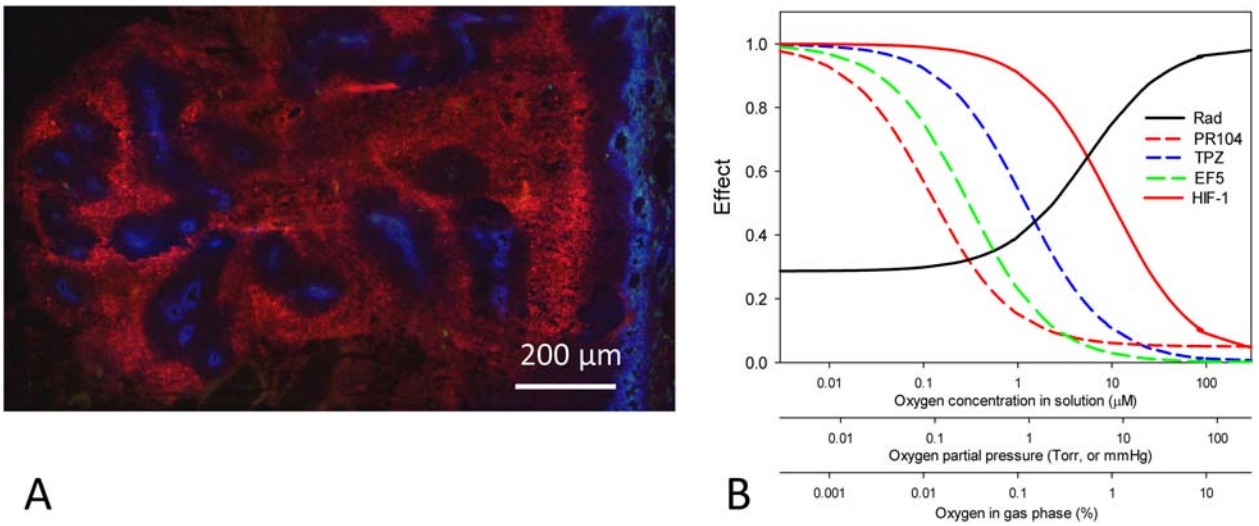

Fig. 1 (A) Detection of hypoxic cells in a SiHa human cervical carcinoma xenograft grown subcutaneously in nude mice. Hypoxic marker EF5 (60 mg kg^{-1}) was administrated intraperitoneally 1.5 h, and blood vessel perfusion marker Hochest33342 (40 mg kg^{-1}) was administered intravenously 2 min before the mice were euthanized. Frozen sections (8 μm) were immunostained for the hypoxic marker (EF5, *red*) and perfused blood vessels identified by Hochest33342 fluorescence (*blue*). (B) Oxygen detection and response. Schematic representation of quantitative oxygen dependencies for ionizing radiation, bioreductive activation of prodrugs and imaging agents, and biological responses to hypoxia. The curves are based on representative oxygen sensitivity parameters for clonogenic cell killing by ionizing radiation (Rad),[4] tirapazamine (TPZ),[5] and PR-104A.[6] Also shown is the binding of 2-nitroimidazole etanidazole pentafluoride (EF5) to intracellular proteins.[7] Biological responses to hypoxia are time and cell type dependent; an indicative relationship shown here is based on acute stabilization of HIF1 in HT1080 cells.[7] Modified and redrawn from Wilson, W. R.; Hay, M. P. Targeting Hypoxia in Cancer Therapy. *Nature Rev. Cancer* **2011**, *11*, 393–410.

are regarded as the gold standard and have identified a wide range of oxygen tensions within solid tumors.[8] The oxygen concentration for half-maximal effect (K_{O_2}) for radiation-induced cell killing is ~4 μM,[10] and cells below ~1 μM (0.1%) (Fig. 1) are considered radiobiologically resistant. Nitroimidazole-based probes[11] are activated at relatively low oxygen tensions with K_{O_2} values ~0.5 μM (0.05%) and report radiobiological hypoxia (Fig. 1). In contrast, the identification of the role of hypoxia-inducible factor-1 (HIF-1)[12] in the cellular response to low oxygen tensions has provided another measure of hypoxia where HIF-mediated response has a higher K_{O_2} of ~10 μM (1%).[7] A variety of endogenous markers, such as carbonic anhydrase IX (CA IX)[13] and osteopontin,[14] that are regulated by HIF-1 report this higher range of oxygen tension. Hypoxia also varies in temporal sense with "cycling hypoxia"[15] resulting changes in vessel perfusion on a timescale from minutes to hours.[16,17] Cycling hypoxia is considered to be of particular importance in the development of an aggressive phenotype.[18]

The identification of the molecular signaling pathways mediated by HIF-1 and their roles in the adaptive response to hypoxia have increased understanding of the role of hypoxia in tumor progression.[12,19] Hypoxia plays a role in the suppression of cell death responses[20,21] including immune suppression,[22,23] initiation of angiogenesis[24] and vasculogenesis,[25] and activation of a glycolytic shift in metabolism,[26,27] and hypoxia enhances invasion[28] and metastasis.[29–31] Hypoxia also promotes genomic instability through increased production of reactive oxygen species (ROS)[32] and suppression of DNA repair processes.[33,34]

Despite the expansive growth in our understanding of the molecular consequences of hypoxia in the last decade and the consequent implications for therapy, most of the initial understanding of the impact of hypoxia came from radiotherapy studies. While early clinical studies demonstrated radiosensitivity was influenced by blood flow,[35,36] it was not until the work of Gray that hypoxia was implicated in radioresistance.[37,38] Studies using Eppendorf oxygen electrodes in accessible tumors, such as head and neck squamous cell carcinoma (HNSCC) and cervical carcinoma, revealed a significant incidence of hypoxia in these tumors.[8] These studies indicated hypoxia could be related to resistance to radiotherapy impacting on local tumor control and overall survival.[39–42] Further evidence that hypoxia impacts treatment outcomes is accruing, not only particularly in the head and neck cancer setting where radiotherapy or chemoradiotherapy is the definitive treatment[43–46] but also in other tumor sites.[21,46–49] The pathophysiological conditions present in tumors that lead to hypoxia such as poor perfusion, large and variable distances between capillaries,[3] and high interstitial pressures[50] can also limit the diffusion of chemotherapeutic agents.[51] In addition, these physiological responses to hypoxia can promote chemoresistance,[52,53] although it should be noted that, in some instances, these changes may result in increased sensitivity to chemotherapy.[1]

The high incidence of tumor hypoxia, its influence on tumor progression, and treatment outcome clearly implicate hypoxia as a validated prospect for a "targeted therapy" approach. However, drug development targeting hypoxia has an extensive and somewhat checkered history.

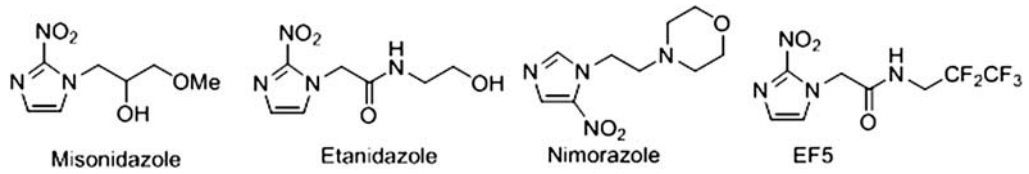

Fig. 2 Nitroimidazole oxygen-mimetic radiation sensitizers and imaging agents.

8.03.1.3 Drug Development in the Context of Hypoxia

Initial efforts to ameliorate the impact of tumor hypoxia on therapy focused on the modification of tumor oxygen levels. Fractionated radiation schedules allowed partial reoxygenation between fractions,[54] while increased oxygen delivery to tumors was achieved with hyperbaric oxygen[55] or carbogen breathing.[56–58] Drug discovery efforts based on small-molecule oxygen mimetics have an extensive history.[59] Electron-affinic nitroimidazoles were intended to mimic oxygen and "fix" radiation damage in hypoxic tumor cells.[59–61] Leading candidates such as misonidazole[62] and etanidazole[63] (Fig. 2) were trialed extensively with fractionated radiotherapy but were ultimately unsuccessful.[64–66] A less electron-affinic 5-nitroimidazole radiosensitizer, nimorazole, was shown to be well tolerated.[67,68] Nimorazole has shown activity in combination with radiotherapy for head and neck cancer[69] and is in clinical use in Denmark. Although the clinical experience with these modalities has provided mixed results, when taken together in a meta-analysis, these interventions to modify hypoxia have been shown to provide benefit,[70] further strengthening the case for the therapeutic targeting of hypoxia. Importantly, retrospective analysis of hypoxia in these tumors, based on a hypoxic gene expression signature, showed that benefit is restricted to patients with more hypoxic tumors.[43] This points to the importance of stratifying patients based on tumor hypoxia in the clinical development of hypoxia-targeted agents.[71] Prospective trials evaluating nimorazole in conjunction with hypoxia markers are currently in progress (ClinialTrials.gov identifiers, NCT01880359 and NCT01950689).

Theoretically, these attempts to modify hypoxia could restore tumor radiosensitivity of fully oxygenated cells. A new approach evolved where hypoxia-activated prodrugs (HAPs) were designed to directly kill hypoxic tumor cells.[1,72–75] This approach also had the potential to leverage the presence of hypoxic cells to release cytotoxins that could diffuse to adjacent tumor cells and lead to increased tumor cell kill.

From a design perspective, HAPs may be characterized as containing a bioreductive trigger unit that deactivates or masks a cytotoxic effector unit through a physical or electronic linker unit.[76] This concept covers a large number of chemically diverse prodrugs linked by a common mechanism of activation (Fig. 3A). One-electron reduction of the bioreductive trigger unit by reductase enzymes may be reversed in the presence of oxygen leading to the formation of superoxide and the parent prodrug.[77] This redox cycling is relatively nontoxic because of detoxification of the superoxide by superoxide dismutase and reduction of the resulting H_2O_2 by catalase, glutathione peroxidase, and peroxiredoxins. In the absence of oxygen, the initial radical may then rearrange or fragment to a reactive species that mediates cytotoxicity or may be further reduced to activate the effector molecule. This concept has been the subject of extensive drug design efforts producing a wide range of exploratory HAPs, and these can be categorized in six chemical classes: nitroaryl, nitroheteroaryl, quinone, metal complex, aliphatic N-oxide, and heteroaryl N-oxide compounds (Fig. 3B).[1,74] It is worthwhile to note that most, if not all, of the HAP compounds violate structural alert rules generally espoused within the drug development community.[78] Furthermore, the idea that metabolism is necessary for activity requires special consideration and needs to be explicitly addressed in drug design in this context (section "Measuring Extravascular Drug Transport").

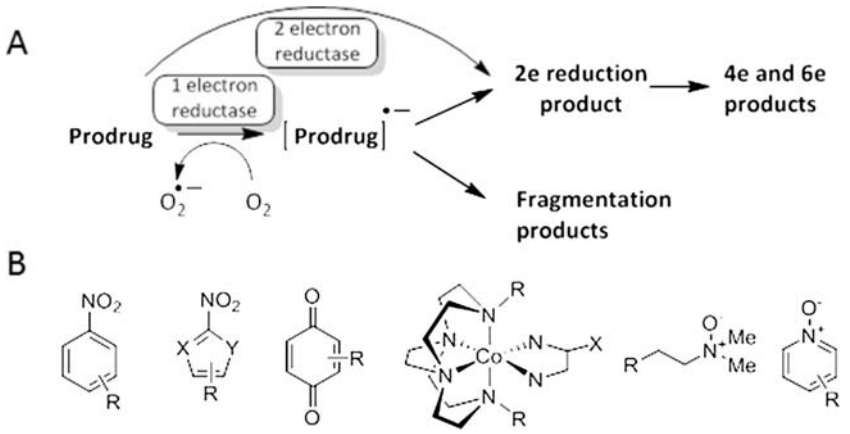

Fig. 3 (A) A general mechanism of activation for HAPs. (B) Chemical classes explored as HAPs.

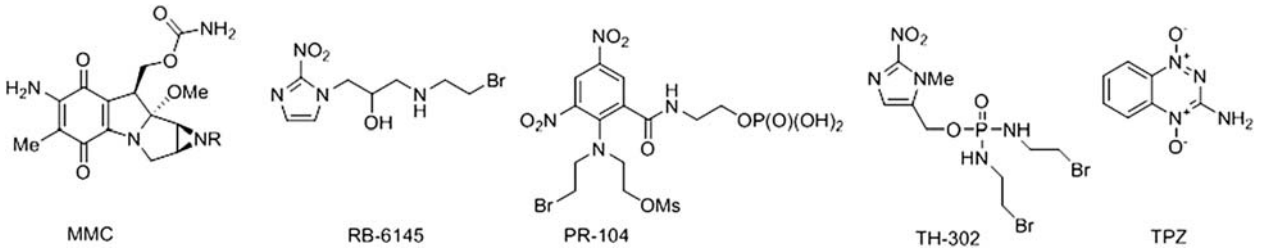

Fig. 4 Hypoxia-activated prodrugs.

The earliest demonstration of a potential HAP approach came with the observation that mitomycin C (Fig. 4) was activated by bioreduction[79,80] and that one-electron reduction of quinones could result in redox cycling in the presence of oxygen.[81,82] Although mitomycin C and related quinones (porfiromycin, apazaquinone)[83,84] can act as HAPs, they are also susceptible to two-electron activation that compromises their hypoxic selectivity and, in the case of apazaquinone (aka EO9) that is activated by the two electron reductase DT-diaphorase,[85] this provides a therapeutic targeting strategy.[86]

Evolving from known electron-affinic radiosensitizers such as misonidazole,[62] a variety of nitroimidazoles and related nitroheterocycles were explored as HAPs[87–91] culminating in the identification of RB-6145.[92] Unfortunately, preclinical development was curtailed by the observation of induced blindness in animal studies that was related to ablation of hypoxic tissue within the retina.[93]

Early work identifying nitroreduction as an electronic switch leading to the activation of nitrogen mustards[94–96] led to a structure–activity exploration of dinitrobenzamide mustards[95,97–100] culminating in the identification of PR-104 that is the phosphate prodrug of HAP PR-104A.[101] Nitroreduction of PR-104A to hydroxylamine and amine compounds, which can be catalyzed by P450 oxidoreductase (POR)[102] and other diflavin reductases[103] under hypoxia, results in the activation of the mixed bromomesylate mustard to generate DNA cross-links.[104] PR-104 demonstrated single-agent activity and synergistic activity in combination with radiation and chemotherapy in multiple xenograft models.[101] Observations of single-agent activity in some xenografts suggested unexpected activation under aerobic conditions.[105,106] The aldo-keto reductase isoform 1C3 (AKR1C3) was identified as the enzyme responsible for aerobic (oxygen-insensitive) activation of PR-104A activation.[105] Phase I clinical trials demonstrated dose-limiting hematologic toxicity,[107,108] with enteritis and liver failure also observed at the very high doses achievable in leukemia patients.[109] AKR1C3 expression in myeloid progenitor cells was suggested as a contributor to toxicity.[110] Preclinical studies suggest possible utility in cancers with high AKR1C3 expression,[111–113] although these also suggest that AKR1C3 is not the sole determinant of monotherapy activity and that a broader understanding of predictive biomarkers would thus be required for further clinical development.

A similar approach is being pursued by Threshold Pharmaceuticals in their development of TH-302 (evofosfamide). Based on early work on nitroheterocyclic prodrugs of phosphoramidate mustards,[114,115] a nitroimidazole prodrug of bromoisophosphoramide mustard was identified as a HAP.[116] Reduction of the nitroimidazole trigger unit initiates fragmentation and release of the phosphoramide.[117] TH-302 displays marked hypoxic selectivity *in vitro*[116–118] and impressive preclinical activity as a single agent[119] or in combination studies in a variety of tumor xenograft models.[117,120] Unfortunately, positive indications from two phase II clinical studies[121,122] were not replicated in phase III trials in pancreatic cancer in combination with gemcitabine (NCT01746979) and in sarcoma with docetaxel (NCT01440088).

8.03.1.4 Tirapazamine

Tirapazamine (3-amino-benzotriazine 1,4-dioxide, TPZ, **1**) was identified from an antimicrobial collection prepared by Bill Lee at Stanford Research Institute International (Palo Alto, CA) and characterized as a HAP by Martin Brown at Stanford University.[123] It was the first example of an N-oxide HAP and has been the subject of extensive research for three decades.[124–126] TPZ displays considerable hypoxic selectivity *in vitro*, typically from 50- to 300-fold when measured by either clonogenic survival or inhibition of proliferation.[127–129] TPZ undergoes bioreductive metabolism by one-electron reductases, for example, POR,[130,131] inducible nitric oxide synthase,[132] and undefined nuclear reductases,[133] to generate relatively nontoxic 1-oxide **2** and minor amounts of nor-oxide **3** (Fig. 5). Direct two-electron reduction to 1-oxide **2** or four-electron reduction to nor-oxide **3** does not contribute to cytotoxicity. An intermediate radical **4** was proposed to act as the oxygen sensor and to mediate cytotoxicity.[134,135] In the absence of oxygen, the reducing radical **4** may undergo protonation (**5**) and subsequent rearrangement to produce an oxidizing radical.[136,137] The identity of this radical species has been the subject of considerable debate with the formation of hydroxyl radical benzotriazinyl (BTZ) radical **6** or aryl radical **7** proposed. Kent Gates and colleagues have proposed the formation of hydroxyl radical[136] and demonstrated a fingerprint of DNA damage by TPZ that mimics that seen for hydroxyl radical.[138] In isotope-labeling studies of a related but considerably more electron-affinic benzotriazine dioxide (BTO) analog of TPZ, they present evidence for the formation of hydroxyl radical.[139] In contrast, Bob Anderson and colleagues at the University of Auckland have used pulse radiolysis and electron paramagnetic resonance (EPR) studies to explore possible radical species generated after the protonation of the initial oxidizing radical **4**. They have demonstrated the presence of several species including an oxidizing BTZ radical **6**[137,140] and minor contributions from aryl radical proposed as **7**.[141] Critically, they did not observe evidence for the production of hydroxyl radical from TPZ.

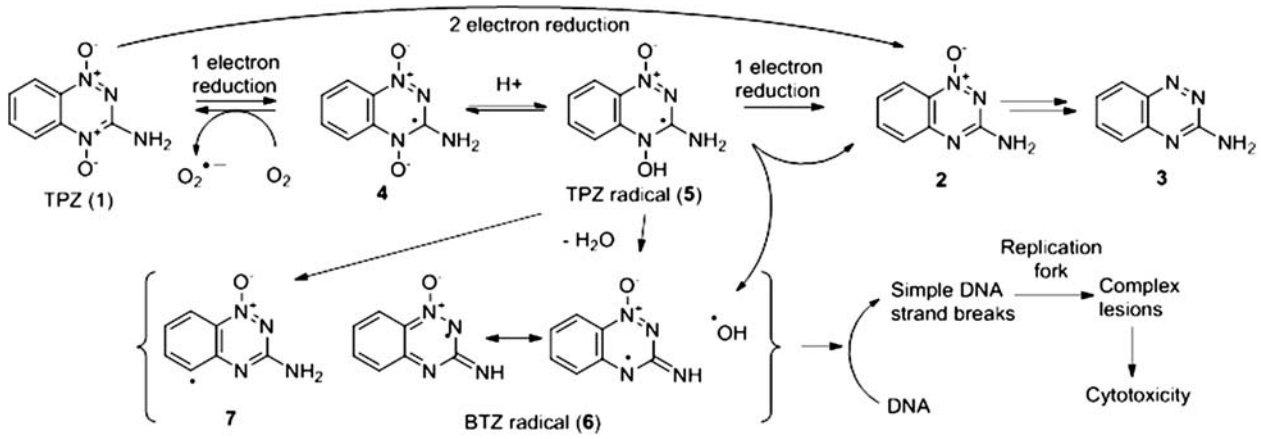

Fig. 5 Bioreductive mechanism of TPZ activation.

Analog studies with a variety of 3-substituted BTO analogs demonstrated that a variety of radical species are produced after rearrangement of the initial reducing radical and that the product distribution is subject to electronic influences,[141] while EPR studies with related quinoxaline 1,4-dioxides show formation of hydroxyl radical is promoted by increased electron affinity.[142] While discussion on the exact nature of the radicals that mediate TPZ cytotoxicity is ongoing,[143,144] this had not hindered the advancement of TPZ or the pursuit of improved analogs.

A distinctive feature of TPZ and other members of the class is the oxygen sensitivity of the initial radical. The K_{O_2} of TPZ is approximately 1–3 μM[5] and this is approximately 10- to 30-fold higher than nitroaryl and nitroimidazole HAPs (**Fig. 1B**).[128] It has been suggested that this oxygen sensitivity complements the oxygen dependence of external beam radiotherapy[5] and allows N-oxide HAPs such as TPZ to kill hypoxic cells at intermediate oxygen concentrations, thus targeting the most important subpopulation of radioresistant tumor cells.[4,5]

Bioreduction results in complex DNA damage as observed by using comet assay[145,146] or γH2AX induction[147,148] and includes clustered DNA single-strand breaks, double-strand breaks, and covalently bound topoisomerase complexes.[149] Consequently, this damage is repaired by multiple repair processes including homologous recombination repair (HRR) of replication fork-associated double-strand breaks.[150,151]

TPZ demonstrated additional cell killing in tumor xenograft models in combination with both single-dose radiation[152] and fractionated radiation.[153,154] In preclinical studies, TPZ displayed synergistic activity in combination with cisplatin[155,156] through hypoxia-dependent inhibition of the repair of cisplatin-induced DNA cross-links.[157] Preclinical pharmacology studies revealed TPZ was converted predominantly to the corresponding 1-oxide **2** and small amount of the nor-oxide **3** after i.p. or i.v. injection.[158,159] Large single doses of TPZ induced weight loss, hyperactivity, and tremors, while myelotoxicity was observed with fractionated daily dosing.[160]

TPZ has been the subject of extended clinical investigation with variable results. Evidence of activity was seen in early-stage trials, and this has validated the concept of hypoxia targeting to some degree. However, disappointing results in phase III trials have compromised TPZ's advance to registration.[126,161,162] Initial trials revealed TPZ was well tolerated up to 390–450 mg m^{-2} as a single agent.[163] Dose reductions were required in combination with chemotherapy, and TPZ was used at 260 mg m^{-2} in combination with cisplatin.[164] TPZ induced nausea and vomiting, diarrhea, weight loss and muscle cramps, reversible hearing loss, and tinnitus.[126,162] Clinical evaluation has focused on non-small cell lung cancer (NSCLC),[165–168] cervical carcinoma,[169–174] and HNSCC and more recently on the potentiation of chemoradiotherapy, particularly cisplatin and radiation.[175,176] Indications of activity in the randomized phase III CATAPULT I trial in advanced NSCLC where TPZ, in combination with cisplatin, provided significant increases in response rates and overall survival compared with cisplatin alone[167] were supplanted by a superior combination of etoposide and cisplatin in the NSCLC CATAPULT II trial.[166] In the head and neck setting, a phase II trial suggested that TPZ, in combination with cisplatin chemoradiotherapy, was efficacious with a trend in favor of the TPZ arm for increased locoregional control and failure-free survival over 5-fluorouracil (5-FU) plus chemoradiotherapy.[175] However, this effect was only seen in patients with hypoxic tumors as defined by ^{18}F-misonidazole PET imaging, and the converse was also seen; the 5-FU–chemoradiotherapy combination was considerably less effective for patients with hypoxic tumors.[46,177] Unfortunately, TPZ did not significantly improve overall survival or local tumor control in a large, randomized phase III trial[176] where poor radiotherapy quality control[178] and failure to select patients with hypoxic tumors for TPZ treatment reduced the power of the study. A retrospective analysis of treatment compliance identified a trend in favor of TPZ for time to locoregional failure (HR 0.74, 95% CI 0.53–1.04, $P=0.067$).[178] Further analysis of the hypoxia imaging data from the phase I and II trials also considered the impact of human papillomavirus (HPV) status and suggested further stratification on the basis of HPV p16 status, with hypoxic, p16-negative patients most likely to benefit from the addition of TPZ to chemoradiation therapy.[179] Unfortunately, this observation came too late to influence the conduct of the phase III TPZ trials, and TPZ development has been halted (personal communication, Prof. J. M. Brown).

8.03.2 Building a Toolset for Bioreductive Drug Discovery

8.03.2.1 Introductory Remarks

In 2003, we entered into collaboration with Prof. Martin Brown at Stanford University on an NIH-funded program grant to develop a second-generation BTO analog of TPZ. By this time, TPZ was well advanced in clinical evaluation and, although positive clinical results were documented, a series of problems that limited the activity of TPZ as a HAP were becoming apparent. TPZ had relatively low aqueous solubility and required extended infusion times in the initial monotherapy study.[159,163] TPZ demonstrated significant toxicities that limited its therapeutic ratio. Perhaps the most significant limitation was that TPZ was substantially less selective for hypoxic cells in three-dimensional culture models[180] or tumor xenografts[181] than for those in monolayer cell culture. These observations provided real opportunities for the development of an improved analog as a "fast follower." This campaign was run in an academic drug discovery environment with emphasis on development of improved tools for lead optimization rather than "brute-force" screening of analogs.

8.03.2.2 Structure–Activity Toolset

As we embarked on the discovery program for a second-generation TPZ analog, we turned to the literature to understand the scope of existing structure–activity relationships (SAR). TPZ had been identified from a library of antimicrobial agents, but we were surprised at the limited number of BTOs evaluated,[123,127,182,183] given the extensive preclinical and clinical studies on TPZ. Even the patent literature on the class was relatively terse.[184] Initial studies had demonstrated that increased electron affinity gave increased hypoxic cytotoxicity *in vitro* and increased toxicity *in vivo* and that *in vitro* hypoxic selectivity was maximal for TPZ itself.[123,127] Addition of strongly basic diethylaminoalkyl side chains linked through the 3-amino position (**8**; **Fig. 6**) provided increases in hypoxic cytotoxicity and selectivity *in vitro*, but did not translate into increased activity against hypoxic cells *in vivo*, at least in part due to reduced drug exposure (reduced drug half-life at maximum tolerated dose (MTD)).[182] In a subsequent study, the use of electron-withdrawing substituents at the 7-position to increase electron affinity, and consequently hypoxic cytotoxicity, was combined with solubilizing dialkylaminoalkyl side chains to provide BTO analogs (e.g., **9**) with increased *in vitro* hypoxic potency relative to TPZ but reduced hypoxic selectivity and reduced *in vivo* activity. Notably, several analogs bearing 3-alkyl substituents (**10**, **11**) displayed improved potency and selectivity *in vitro*, and this translated to comparable efficacy to TPZ *in vivo* in a fractionated radiation model.[183]

Our first objective was to prepare a toolset of compounds that would allow us to more closely define the SAR for cytotoxicity and hypoxic selectivity and understand the possibilities and limitations around BTO synthesis. To this end, we prepared a set of 34 3-amino BTOs **12** with a variety of substituents on the benzo ring (X = NEt_2, NMe_2, OMe, Me, F, Cl, CF_3, $MeSO_2$, and *n*-$BuSO_2$) that provided compounds spanning a wide range of electron affinity and steric interaction and a modest range of lipophilicity.[129] We utilized a two-step synthesis starting from appropriately substituted nitroanilines **13** (**Fig. 7**). These were condensed with cyanamide under acidic conditions to form the intermediate guanidines that were then cyclized under strongly basic conditions in an Arndt cyclization[185] to produce the corresponding benzotriazine 1-oxides **14**.[186] This process was conducted as a melt and produced a significant exotherm to drive the reaction to completion. Although effective for a wide range of analogs, this sequence is really only suitable on a millimolar scale. These 1-oxides **14** could be oxidized to the corresponding 1,4-dioxides **12** in modest yields. We surveyed a range of oxidants and found that peracetic acid or, preferably, pertrifluoroacetic acid provided the best conversion to products. This reaction was always a compromise with extensive conversion being associated with complex by-product mixtures and difficult chromatographic separations. In practice, we settled for lower conversion and a relatively simple purification of starting material and product. Preparation of 5-substituted compounds has been proved to be difficult with compounds only ever isolated in very low yields, presumably due to steric interference at the peri N-4 position. Although the two-step procedure was less efficient than the direct condensation[187] that provides 1,4-dioxide **12** directly from nitrofuroxan **19** (benzo[*c*][1,2,5]oxadiazole 1-oxide), it provides access to a wider range of compounds, including monosubstituted analogs with unequivocal regioisomeric identification. In addition, this route also provides the corresponding 1-oxides **14** that are the primary metabolites in this class and thus useful as standards in mechanistic and pharmacological studies. We were also able to convert 3-amino-1-oxides **14** to the corresponding chlorides **15** and install 3-aminoalkyl side chains (e.g., **17**) (section "BTOs With Improved EVT"). Alternately, we could convert **14** to iodides **16** and use Pd-mediated cross-coupling reactions[188,189] to access 3-alkyl BTOs and 3-aryl BTOs **18** in subsequent studies (section "Exploring 3-Alkyl BTOs: Role of H bonding on EVT"). This was more efficient than the alternative Bamberger triazine synthesis of 3-alkyl triazines **23**,[190] which still required a difficult oxidation step to give triazine dioxides **18**.[183]

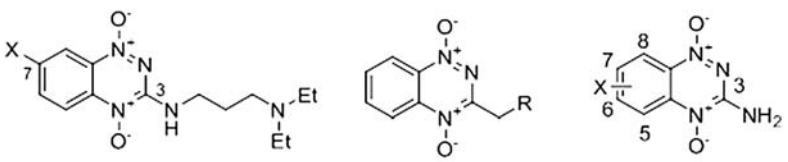

Fig. 6 TPZ and related BTO analogs.

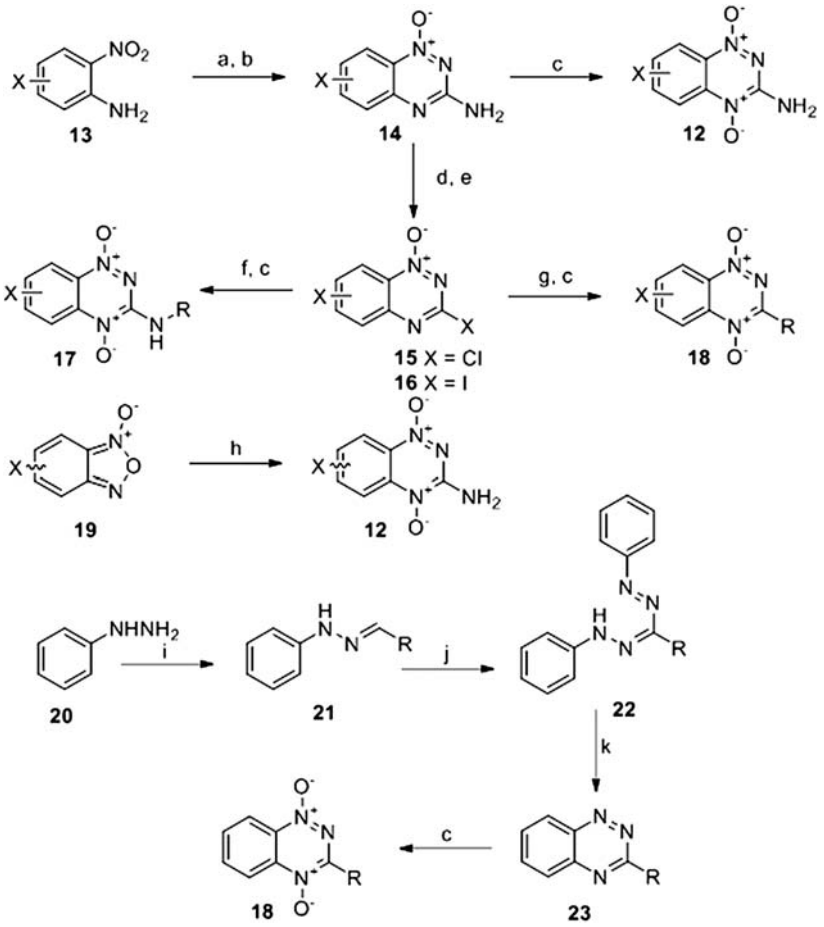

Fig. 7 Synthesis of BTO analogs. Reagents: (a) NH_2CN, HCl; (b) aq. NaOH; (c) CH_3CO_3H or CF_3CO_3H, DCM; (d) $NaNO_2$, CF_3CO_2H; (e) DMF, $POCl_3$; (f) RNH_2, DME; (g) Stille or Suzuki reaction; (h) Na_2NCN, MeOH; (i) RCHO, EtOH; (j) Aniline, $NaNO_2$, HCl, HOAc; (k) $BF_3 \cdot HOAc$.

We determined the lipophilicity of a subset of 12 compounds as octanol/water partition coefficients (P) at pH 7.4 and were able to train predictive software (Advanced Chemistry Development Inc., Toronto, Canada) to reliably predict the lipophilicity as ($\log P$) of BTO compounds going forward. The SAR set spanned a limited range of $\log P$ from -1.38 to 0.84. These BTOs were generally less soluble than TPZ, and this did preclude determination of aerobic cytotoxicity for some compounds, but otherwise did not limit the study. The compounds spanned a wide range of electron affinity with one-electron reduction potentials [$E(1)$], measured by pulse radiolysis, covering the range from -671 to -240 mV. This spans the zone of electron affinity for efficient bioreduction by mammalian enzymes (approximately –450 to -300 mV). We found $E(1)$ values correlated with the Hammett sigma substituent parameter with 5- and 8-substituted BTOs best described by σ_m and 6- and 7-substituted BTOs described by σ_p. The electron affinity correlated with aerobic, but not hypoxic, toxicity as determined by clonogenic survival of murine SCCVII tumor cells consistent with increased aerobic metabolism and cytotoxicity mediated by ROS formed by redox cycling of the radical anion. This toolset of BTOs also allowed us to confirm that the sulforhodamine B proliferation-based assay of cytotoxicity was a suitable surrogate for the "gold standard" clonogenic survival assay with excellent correlation of IC_{50} (drug concentration over 4 h exposure to reduce cell density of either murine SCC VII or human HT29 colon carcinoma cells to 50% of controls) against C_{10} (drug concentration over 1 h exposure to reduce clonogenic survival by one log). This provided a considerable streamlining of the discovery campaign.

8.03.2.3 Measuring Extravascular Drug Transport

The next component required to underpin our campaign was an *in vitro* system to evaluate extravascular drug transport (EVT). Early evidence for the limited EVT of TPZ had been gathered in multicellular tumor spheroids (MTS)[180] or tumor xenografts.[181] MTS are 3-D cell cultures that grow as spheres with many features of the extravascular compartment of tumors including diffusion-limited hypoxia and gradients of nutrients, pH, and proliferation as a function of distance from their boundary.[191–193] In order to investigate TPZ transport further, we used multicellular layer (MCL) cultures (Fig. 8A), an alternative *in vitro* 3-D model of the extravascular compartment developed in our laboratory.[194,195] Cells are grown on a semipermeable support membrane to a thickness of ~100–400 μm, which is approximately the distance between the capillaries in many tumors. MCLs are used in diffusion chambers

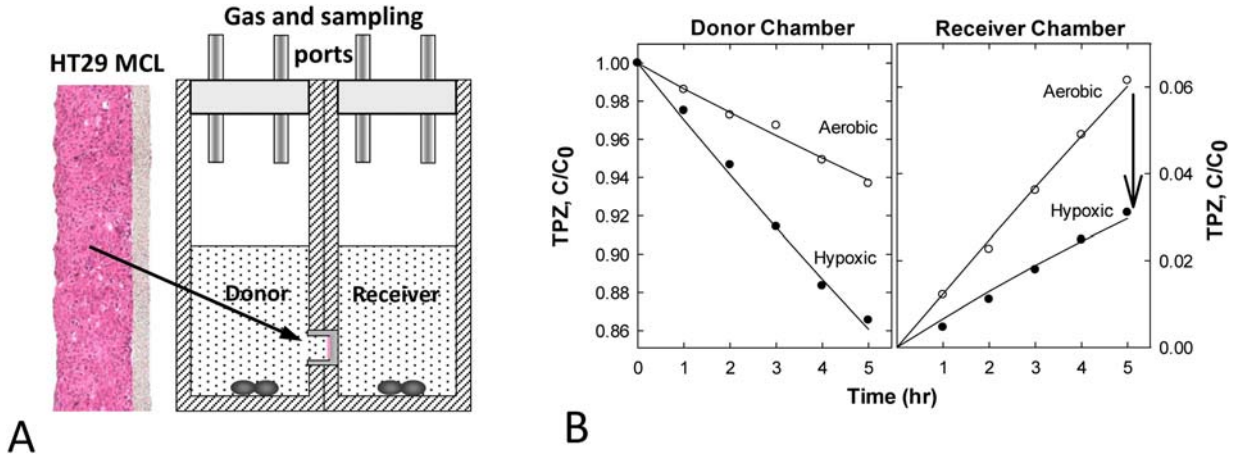

Fig. 8 (A) MCL cultures and diffusion chamber apparatus. Drug is introduced to the donor chamber and measured in both chambers as a function of time. (B) Measured TPZ concentrations in donor and receiver chambers. Clear demonstration that TPZ penetration is lower under hypoxia is shown by decreased concentrations (normalized to the initial concentration, C_0) in the receiver chamber (indicated by *arrow*). The lower concentrations in the donor chamber under hypoxia reflect metabolic consumption in the MCLs, which limit penetration. Adapted and redrawn from Pruijn, F. B.; Patel, K.; Hay, M. P.; Wilson, W. R.; Hicks, K. O. Prediction of Tumour Tissue Diffusion Coefficients of Hypoxia-Activated Prodrugs from Physicochemical Parameters. *Aust. J. Chem.* **2008**, *61*, 687–693.

(Fig. 8A) to study the rate of drug transport by measuring drug concentrations in culture medium on each side of the MCL using compound-specific analytic techniques such as high-performance liquid chromatography (HPLC) and liquid chromatography/mass spectrometry. We, and others, had previously used MCLs to demonstrate that TPZ transport under anoxia is hindered by rapid bioreductive metabolism (Fig. 8B).[196–198] In addition, these studies enable quantitation of the key parameters that determine drug transport in tumor tissue: the diffusion coefficient and rates of cellular uptake, binding, and irreversible metabolism.

Parameters are fitted using a reaction–diffusion equation to describe transport in the MCL:

$$\frac{\partial C}{\partial t} = D\frac{\partial^2 C}{\partial x^2} - M \tag{1}$$

where C is the free drug concentration, x is the distance diffused through the MCL, t is time, M is the rate of drug reaction, and D is the drug diffusion coefficient. M generally has the form

$$M = k_{\text{met}}C + k_{\text{f}}C - k_{\text{r}}C_{\text{b}} + \cdots \tag{2}$$

where k_{met} is the rate constant for first-order metabolism and k_{f} and k_{r} are forward and reverse rate constants for first-order binding (e.g., reversible binding to macromolecules when binding sites are in excess). Other terms including higher-order reaction can be added as required[195,199] as can explicit intracellular and extracellular compartments.[200]

For BTO analogs, D may be estimated using aerobic MCLs to suppress bioreductive metabolism and the parameters for M estimated using hypoxic MCLs, either directly or by scaling k_{met} determined in single-cell suspensions to MCL cell density[198] (see section "Developing a Spatially Resolved-PK–PD Model" and Ref. 201 for further details).

We were able to measure the diffusion coefficients for a training set of structurally diverse BTOs and to develop an algorithm to predict D in MCLs (D_{mcl}) from physicochemical parameters: MW, log$P$ 7.4, and number of H-bond donors (HD) and acceptors (HA).[202,203]

$$\log(D_{\text{mcl}}) = a + b\log\text{MW} + \frac{c}{1+\exp\left(\frac{\log P_{7.4} - x + y\cdot\text{HD} + z\cdot\text{HA}}{w}\right)} \tag{3}$$

These parameters can be interpreted using simple expressions in 1-D geometries to predict concentrations in the effect compartment (i.e., cells distant from the drug source) with high spatial and temporal resolution. Particularly useful in the drug development context are the T_{90} and the penetration half distance ($X_{1/2}$) in a plane region (Fig. 9). The T_{90} is the time to reach 90% concentration at a distance of L from the source in a slab of thickness $2L$:[204]

$$T_{90} = 0.9\frac{L^2}{D} \tag{4}$$

(which is related to the characteristic diffusion time for compounds that undergo no reaction). $X_{1/2}$ for compounds that are consumed by first-order metabolism is given by

$$X_{1/2} = \ln(2)\sqrt{\frac{D}{k_{\text{met}}}} \tag{5}$$

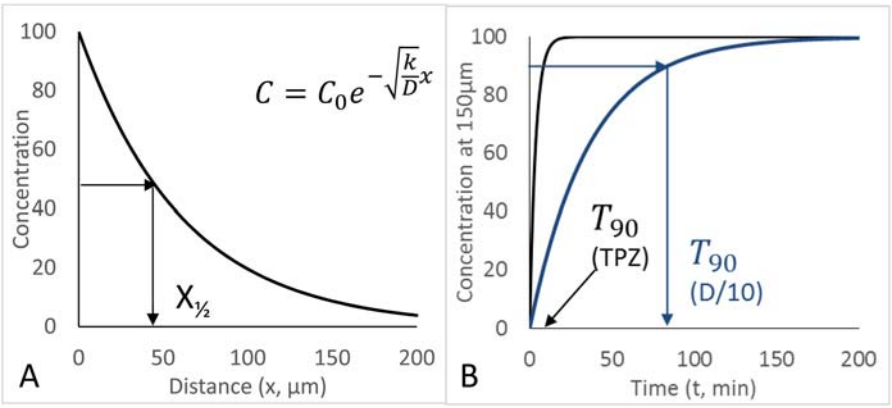

Fig. 9 Representations of drug EVT. (A) Penetration half distance ($X_{1/2}$) for TPZ in anoxic HT29 tumor tissue ($D=4\times10^{-7}$ cm^{2}s^{-1}, $k=0.58$ s^{-1}) is 45 μm. (B) The T_{90} for TPZ in well-oxygenated tissue at a distance $L=150$ μm is 8.4 min. The T_{90} for a compound with 10-fold lower effective diffusion coefficient is also shown in *blue* ($D=4\times10^{-8}$ cm^{2}s^{-1}).

where k_{met} is derived directly at tissue cell density from MCL studies. Other useful derived transport parameters such as the penetration distance for compounds that undergo near-zero-order consumption (e.g., O_2) can also be calculated.[38,205,206]

Generally, the diffusion coefficients of most low-MW drugs are sufficient to allow rapid equilibration in the extravascular compartment unless they react intra- or extracellularly. Taken alone, irreversible metabolism will generally limit drug penetration distance with little effect on the time to reach steady state, while reversible uptake or binding will substantially increase the equilibration time,[195,207] which can be estimated by T_{90}. For example, TPZ is expected to reach peak concentrations rapidly in hypoxic tissue but at a substantially lower concentration than in plasma. The relatively low diffusion coefficient of TPZ in HT29 MCLs (4.0×10^{-7}cm^2 s^{-1}) results in $T_{90}=8.4$ min at 150 μm under aerobic conditions but when combined with high rate of bioreductive metabolism ($k_{met}=0.58$ min^{-1} at HT29 MCL cell density) results in a predicted $X_{1/2}$ of 45 μm at steady state for planar diffusion into hypoxic tissue (Fig. 9).

The importance of distinguishing the mechanisms of drug consumption leading to reduced penetration or delayed equilibration is further outlined by simple simulations of free drug concentrations in the effect compartment (150 μm from a blood vessel where drug plasma concentration decays with a half-life of 30 min) (Fig. 10). The flux of drug through MCLs can be described well by three different EVT models: simple diffusion, diffusion with metabolism, and diffusion with reversible binding (Fig. 10A). However, the predicted concentration–time profiles at a distance of 150 μm into a plane tissue slab are very different for the three EVT models (Fig. 10B).

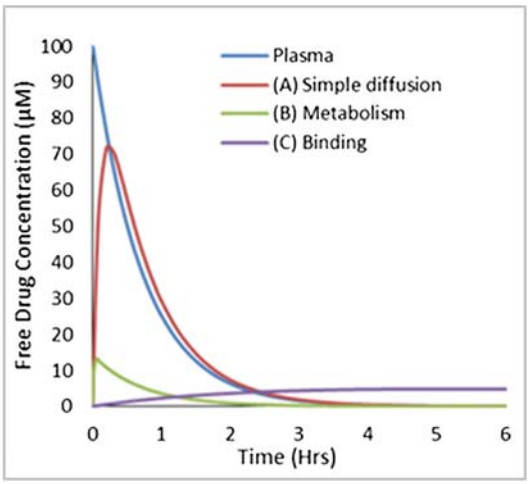

Fig. 10 Simulation of free drug concentrations at 150 μm from a blood vessel for a drug with a plasma half-life of 30 min illustrates how diffusion kinetics differ depending on the mode of drug consumption. Transport parameters were derived from the three models fitted to a single set of hypothetical MCL data. The intercapillary region is approximated by diffusion into a plane slab from both sides, and this is intermediate between radial inward and radial outward diffusions. The cases are simple diffusion ($D=2.5\times10^{-7}$ cm^{2}s^{-1}), irreversible metabolism ($D=5\times10^{-7}$ cm^{2}s^{-1}, $k_{met}=0.95$ s^{-1}), and reversible binding ($D=5\times10^{-7}$ cm^{2}s^{-1}, $k_f/k_r=200$). Modified and redrawn from Wilson, W. R.; Hicks, K. O. Measurement of Extravascular Drug Diffusion in Multicellular Layers. *Br. J. Cancer* **1999**, *79*, 1623–1626.

The earlier-mentioned transport models can generally be distinguished by fitting the concentration–time profile in the donor and the receiver chamber. This approach clearly demonstrated that for TPZ, the EVT impediment for anoxic MCLs compared with that for oxic MCLs is due to metabolic consumption, rather than a change in D under anoxia. Therefore, EVT could be modeled for subsequent analogs by measuring D in oxic MCLs and the kinetics of metabolic consumption in single-cell suspensions under anoxia and scaling the derived metabolism rate constant (k_{met}) to MCL cell density using MCL flux data. The latter strategy enabled sampling of the cell population over time to determine clonogenicity and hence development of pharmacokinetic/pharmacodynamic (PK–PD) models relating exposure to cytotoxicity (see section "Developing a Spatially Resolved-PK–PD Model").

In view of these considerations, it was hypothesized that improving the transport properties of BTOs had potential to improve *in vivo* activity and selectivity. This could be achieved by either increasing the drug diffusion coefficient (D) or decreasing bioreductive metabolism (k_{met}). However, the difficulty with the latter approach is that reductive drug metabolism in tumor cells is essential for hypoxic cytotoxicity. Consequently, the challenge for BTO analog development is to optimize the rate of metabolism, rather than minimize it.

8.03.2.4 Developing a Spatially Resolved-PK–PD Model

To achieve this optimization, we developed a detailed spatially-resolved (SR)-PK–PD model for TPZ transport, metabolism, and cytotoxicity[5,198,208] in tumor tissue. The cytotoxicity of TPZ could be related to its metabolism as a function of drug concentration and time of HT29 cells.[198] Drug concentrations in the extracellular medium were measured by HPLC, and cell survival (clonogenicity) was measured by plating cells from the same sample. Using a simple chemical kinetic scheme, cell killing was related to the intracellular concentration of cytotoxic metabolite that is in turn related to the rate of metabolism of parent drug. In general, this gives the form

$$\log \text{cell kill} = -\log \text{SF} = \gamma k_{met} C^m T^n \tag{6}$$

where SF is the cell surviving fraction and γ, m, and n are fitted parameters. The transport and PD models were then used to predict the concentration, and hence cell killing, at each point in hypoxic MCLs, and good agreement between measured and predicted average cell killings was observed.[198] From this equation, useful parameters for drug development may be calculated—the CT_{10} that is the area under the concentration–time curve providing 1 log cell kill and the M_{10} ($=k_{met} \times CT_{10}$) that is the amount of metabolism required to produce 1 log cell kill and is a measure of the efficiency by which bioreductive BTO metabolism produces cytotoxicity.

While a penetration problem was confirmed to result in decreased cell kill for large hypoxic 3-D cultures, it was not immediately obvious that this would translate to an analogous problem in HT29 tumor xenografts used for drug screening, where there is a continuous gradient of oxygen concentration. Hypoxia most commonly occurs in tumors as small focal regions at large distances from the capillaries (**Fig. 1A**). It follows from Fick's first law with reaction that distance can exacerbate the penetration problem for a fixed-size metabolic sink. In addition, both oxygen and drug concentrations in tumors can be affected by known aspects of tumor structure and function such as heterogeneity in intercapillary distances, vessel diameters, blood flow rates, and extraction of compound from the tortuous, leaky microvascular network.[209] We developed an *in silico* SR-PK–PD model for TPZ in a mapped microvascular network using Green's function method that had been used for simulating oxygen distribution (**Fig. 11**).[201,208–211]

To simulate bioreductive drug action, additional parameters for TPZ PK–PD were included (see Ref. 201 for details): the oxygen dependence of metabolism and cytotoxicity described by the oxygen concentration required for half-maximal suppression of TPZ activity ($K_{O_2} \sim 1.2$ μM O_2)[5]and TPZ plasma pharmacokinetics in mice that was generally first order at high doses for TPZ and BTO analogs.[208] The distribution of TPZ in this microvascular network was simulated with the free drug concentration in mouse plasma (determined by PK of total drug and estimation of free fraction by equilibrium dialysis) as the input[208] allowing the calculation of surviving fraction at each point. The model predicted heterogeneous distribution for TPZ due to the complex 3-D structure with a range of intercapillary distances and oxygen concentrations (**Fig. 11**). The model clearly predicted less cell killing in the microregion than the theoretical maximum attainable if TPZ was homogenously distributed at the same concentration as in plasma (see Refs. 201,208 for more details). Simulating improved transport over a realistic range of diffusion coefficients indicated a five- to sixfold increase in hypoxic cell kill in addition to radiation alone, and a similar increase in hypoxic selectivity compared to that for well-oxygenated zone was possible (**Fig. 12**).

By using tumor cell survival in Green's function model as the efficacy endpoint, the predictions of the model could be directly compared with the results of the clonogenic survival assays after tumors were excised from mice treated with TPZ combined with radiation (see Refs. 201,208,212 for methodology). Good agreement was seen between predicted and observed hypoxic cell killings for TPZ. We extended this SR-PK–PD evaluation to a set of 15 structurally diverse BTO analogs and found there was a strong correlation between model-predicted and measured hypoxic cell killings ($R^2 = 0.89$), but a poor correlation when the model did not include EVT ($R^2 = 0.32$). This result provided the confirmation that explicit consideration of EVT was vital for a BTO analog discovery campaign and further that the model would allow us to efficiently identify BTO analogs with improved *in vivo* activity. We have gone on to extend the correlation as more compounds have become available in the program (**Fig. 13**), and it is gratifying to note that the correlation has not changed significantly. We have also developed a modified model for TPZ in a second tumor xenograft (SiHa cervical carcinoma).[6]

With these considerations in mind, we designed an analog screening algorithm with additional decision points based on parameters derived from 3-D cultures and SR-PK–PD modeling (**Fig. 14**).

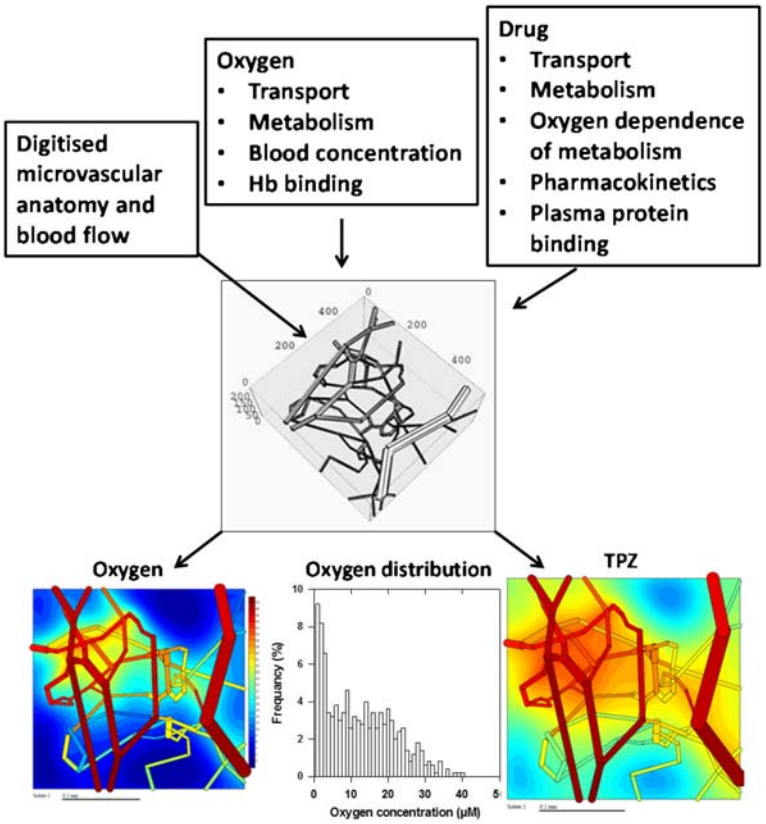

Fig. 11 Simulation of oxygen and TPZ distribution in the 3-D SR-PK–PD model in the digitized, mapped rat R3230Ac microvascular network from Ref. 209. The lower images show the simulated oxygen and TPZ concentrations for an input of 50 μM of each. This model reproduced key features of the dysfunctional vasculature in tumors resulting in oxygen distributions typical of tumors. Predictions of cell killing based on simulated drug distributions are shown in **Fig. 12**. Modified and redrawn from Hicks, K. O. Introducing Drug Transport Early in the Design of Hypoxia Selective Anticancer Agents Using a Mathematical Modelling Approach. In *New Challenges for Cancer Systems Biomedicine*; D'Onofrio, A., Cerrai, P., Gandolfi, A., Eds.; Springer: Italy, 2012; pp 337–354.

8.03.3 Drug Discovery Campaign to Identify a Second-Generation TPZ Analog

8.03.3.1 Design Criteria

Having assembled the tools to conduct our campaign, we defined our objectives based on the limitations that impaired TPZ activity and the requirements to advance a second-generation BTO into clinical development:

- Increased aqueous solubility relative to potency
- Improved EVT
- Improved hypoxic selectivity *in vivo*
- Improved therapeutic index in preclinical models
- An unencumbered patent position

TPZ has only modest aqueous solubility (9 mM in phosphate-buffered saline) necessitating lengthy infusions, so BTOs with increased solubility and/or potency would be advantageous.

Metabolism in hypoxic cells had been demonstrated to limit the EVT and hypoxia-selective cytotoxicity of TPZ in tumors as discussed earlier. Thus, BTOs with improved EVT would be expected to display increased hypoxic selectivity *in vivo*, and we hypothesized these compounds should also display an improved therapeutic index. We considered normal tissue toxicity to be less affected by poor EVT, and so any improvement in EVT was likely to improve the therapeutic index of a BTO through increased tumor cell killing. Patents held by Sanofi Winthrop covered the core benzotriazine 1,4-dioxide motif with a considerable range of substituents on the benzo ring and amino, alkyl, and aryl substituents at the 3-position. We adopted two strategies to secure a patent position: a selection invention approach based on the identification of generically defined BTOs with unexpectedly good activity and a search for BTO structures outside the definitions of the Sanofi Winthrop patents.[184] We limited our exploration to benzotriazines because the obvious isostere strategy around 2-cyano-quinoxaline 1,4-dioxides had been explored.[213–215]

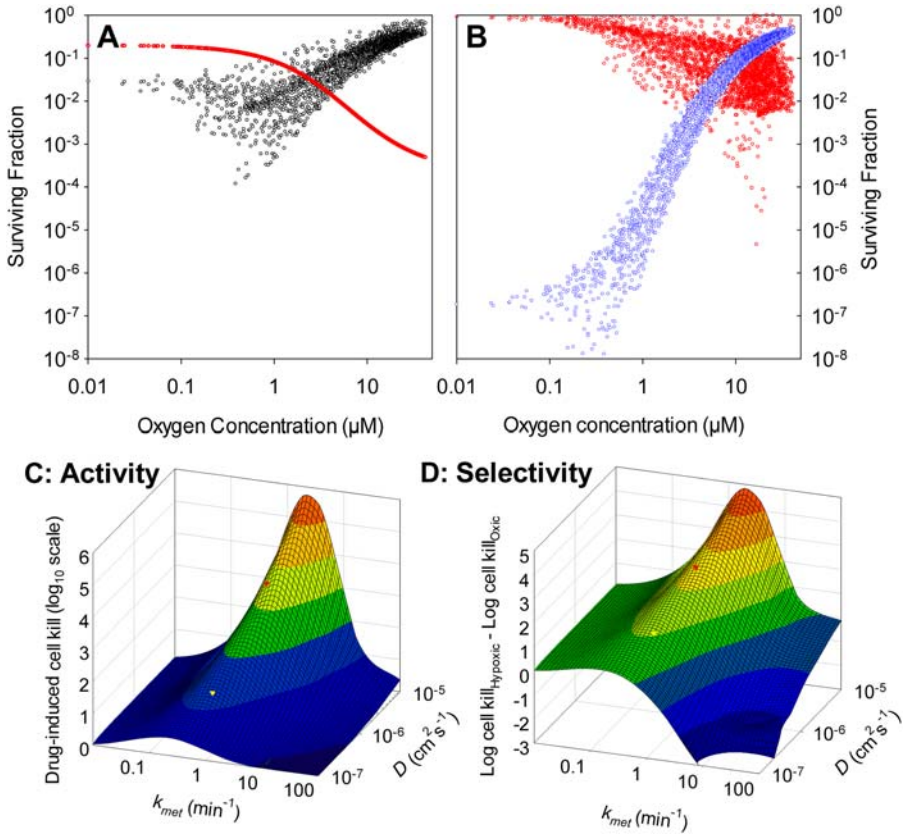

Fig. 12 (A) Predicted cell kill by TPZ (*black*) and radiation (*red*) plotted as a function of oxygen concentration simulated in the microvascular network model. (B) A hypothetical BTO analog with a fivefold higher *D* (*blue*) shows improved cell killing in the hypoxic region, while a fivefold increase in k_{met} (*red*) results in little killing of hypoxic cells and a loss of hypoxic selectivity. Lower graphs show drug-induced hypoxic cell kill in addition to radiation (C) and hypoxia selectivity (D) for hypothetical BTO analogs over a wide range of diffusion coefficients with the same relationship between cell kill and bioreductive metabolism as for TPZ. The figures show that for each diffusion coefficient, there is an optimum rate of metabolism above which tumor penetration becomes limiting and below which potency is lost. Modified and redrawn from Hicks, K. O.; Pruijn, F. B.; Secomb, T. W.; Hay, M. P.; Hsu, R.; Brown, J. M.; Denny, W. A.; Dewhirst, M. W.; Wilson, W. R. Use of Three-Dimensional Tissue Cultures to Model Extravascular Transport and Predict *in vivo* Activity of Hypoxia-Targeted Anticancer Drugs. *J. Natl. Cancer Inst.* **2006**, *98*, 1118–1128.

8.03.3.2 DNA Targeting

While we were developing the methodology for the PK–PD model, we took the opportunity to explore a DNA-targeting approach to improve the activity of a TPZ analog. TPZ had been demonstrated to kill tumor cells by causing a variety of DNA damage including base damage, single-strand breaks, and double-strand breaks.[136,216] Evidence from Martin Brown's lab suggested that only the fraction of TPZ activated by nuclear reductases contributed to hypoxic cell killing[133,217] and that cytoplasmic activation was unproductive metabolism. Further, it was hypothesized that this unproductive metabolism, especially in the mitochondria,[218] was responsible for observed clinical toxicities such as tinnitus, reversible hearing loss, and muscle cramping[162] through redox cycling and the formation of ROS. This evidence, in conjunction with previous reports of DNA targeting of bioreductive agents,[219–221] suggested that such a targeting approach might provide solutions to several of the design criteria. We expected the DNA-targeted BTOs to be more potent than TPZ and increasing the production of toxic radicals close to the target (DNA) might improve the therapeutic index of BTO analogs. We prepared a prototype, SN26955 (**24**) (Fig. 15), which linked a 9-aminoacridine unit to TPZ via the 3-amino group to explore this hypothesis.[222] BTO **24** was a moderately strong DNA binder ($K_{DNA} = 14.3 \times 10^4\ M^{-1}$) and displayed increased formation of single- and double-strand breaks leading to increased hypoxic cytotoxicity *in vitro* compared to TPZ while retaining similar hypoxic selectivity. However, this increased activity *in vitro* did not translate into hypoxic cell killing *in vivo*, and this was postulated to result from poor EVT.

Concern that the DNA binding of SN29655 might be limiting its diffusion[223] led us to design a series of analogs of SN29655 in which we modulated the DNA-binding affinity though modification of the chromophore or the basicity of the amine side chain.[224] We hypothesized that a "minimal" DNA chromophore would provide improved EVT characteristics[207] while retaining increased hypoxic potency and selectivity. We prepared a series of BTO analogs linked by amines of varying basicity to 4-quinoline, 1-phenazine, and 4-acridine carboxamides. The DNA-binding affinity of the compounds ranged over 5200-fold and correlated strongly with hypoxic cytotoxicity, but not selectivity. All compounds were selectively cytotoxic against hypoxic cells with several

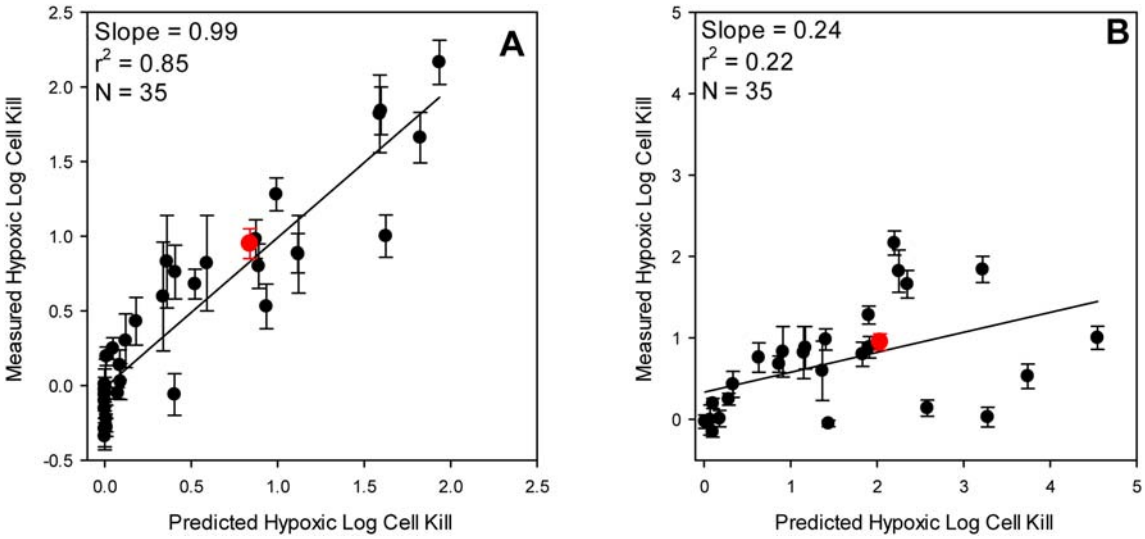

Fig. 13 (A) Correlation between hypoxic cell killings predicted by the SR-PK–PD model in the tumor microvascular network and cell killing observed in HT29 tumor xenografts for all analogs tested. (B) A similar correlation with cell kill predicted using the microvascular network with the same oxygen gradient but assuming the extravascular compartment has a homogenous drug concentration (tissue drug concentrations equal to those in plasma). Hypoxic log cell kill is defined as in the text. This updates the previously reported correlation[208] with the addition of 19 further compounds. TPZ is in *red*. Adapted and redrawn from Hicks, K. O. Introducing Drug Transport Early in the Design of Hypoxia Selective Anticancer Agents Using a Mathematical Modelling Approach. In *New Challenges for Cancer Systems Biomedicine*; D'Onofrio, A., Cerrai, P., Gandolfi, A., Eds.; Springer: Italy, 2012; pp 337–354.

acridine 4-carboxamides (e.g., **25** and **26**; Fig. 15) with reduced DNA-binding affinity ($K_{DNA} = 0.75$ and 3.3×10^4 M^{-1}, respectively) displaying excellent hypoxic selectivity (HCR, 87 and 124, respectively). The 4-acridine carboxamide BTO **26** was demonstrated to increase the free radical-induced production of both single- and double-strand breaks under hypoxia compared with TPZ itself.[225] Plasmid DNA was damaged by hydroxyl radicals generated from the radiolysis of water, and potentiation of single- and double-strand breakages was measured in the presence of TPZ and DNA-targeted BTO analogs. BTO **26** was able to increase single-strand breaks by 18-fold, and double-strand breaks were increased by 110-fold. In addition, targeting a 1-oxide BTO was seen to potentiate single-strand breakage, but not double-strand breakage, compared to TPZ. This study supported the hypothesis that nuclear localization increases productive metabolism and hypoxic potency. While DNA targeting of BTO analogs demonstrated increased hypoxic potency and selectivity, it became apparent that even with a moderate DNA-binding unit, metabolism would compromise EVT. The impact of a binding component on the model for diffusion can be seen in Fig. 9B. We attempted to offset this metabolic liability by preparing less-electron-affinic BTO analogs (e.g., **27**), and although addition of the 6-Me group halved k_{met}, this was still some ninefold higher than for TPZ.[208] Thus, metabolism and diffusion liabilities found in DNA targeting dominated the micro-pharmacokinetic properties of these BTOs that were predicted to be inactive *in vivo*, defeating this approach to increasing the therapeutic index of BTO analogs.[208]

These early studies provided additional insight into the requirements for successful bioreductive drug design and demonstrated the power of using an integrated screening model to include diffusion and metabolism parameters along with *in vitro* cytotoxicity, allowing early predictions of *in vivo* hypoxic selectivity.

8.03.3.3 BTOs With Improved EVT

Our next endeavor was to expand upon previous SAR studies from Martin Brown's group where a 3-amino-linked side chain bearing a basic amine was used to increase aqueous solubility.[182,183] As noted in section "Structure–Activity Toolset," strongly basic diethylaminoalkyl side chains (e.g., **8**) increased solubility, hypoxic toxicity, and selectivity *in vitro*, but did not translate into increased activity against hypoxic cells *in vivo*. Further increases in *in vitro* hypoxic potency were obtained by adding electron-withdrawing substituents at the 7-position (e.g., **9**) to increase electron affinity; however, these analogs displayed reduced hypoxic selectivity *in vitro* and reduced *in vivo* activity.[183] We had previously observed the addition of an electron-donating 6-methyl substituent had provided a BTO analog **12** (X = 6-Me) with reduced *in vitro* hypoxic potency and similar hypoxic selectivity to TPZ[129] but which had demonstrated a dramatic fourfold increase in killing hypoxic cells *in vivo* compared to TPZ,[208] despite extremely low aqueous solubility. We sought to build on this observation while directly addressing EVT in our design criteria and exploring the SAR around EVT (Fig. 16).

We prepared a series of 6-substituted BTO analogs bearing a variety of 3-aminoalkylamines to explore the impact of lipophilicity and amine pK_a on EVT. The electron-donating 6-substituents were designed to offset the increase in electron affinity due to the 3-

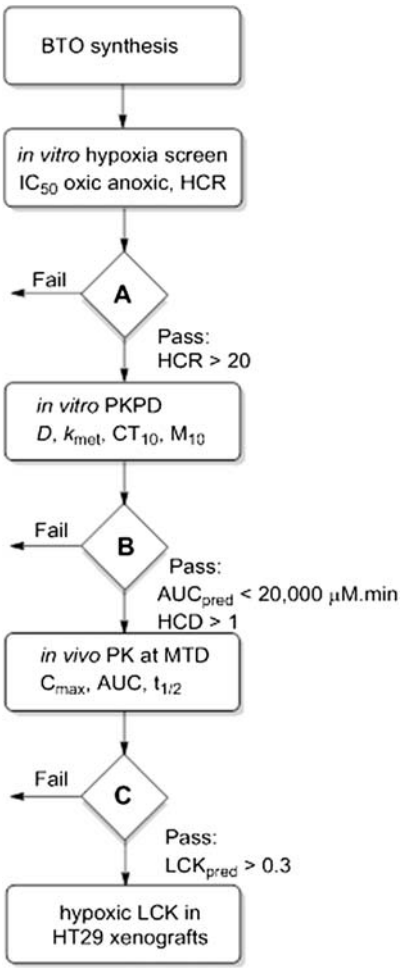

Fig. 14 SR-PK–PD model-guided algorithm for bioreductive drug design. Definitions: HCR, hypoxic cytotoxicity ratio, IC_{50}(oxic)/IC_{50}(anoxic); D, tissue diffusion coefficient (see Eq. 3); k_{met}, first-order rate constant for metabolism in anoxic cell suspensions scaled to cell density in MCLs; CT_{10}, the area under the concentration–time curve providing 10% surviving fraction; M_{10}, amount of drug metabolized for 10% surviving fraction; AUC_{pred}, predicted area under the plasma concentration–time curve required to give 1 log cell kill of HT29 tumors in addition to that produced by a single 20 Gy dose of gamma radiation (μM min); HCD, *in vivo* hypoxic cytotoxicity differential = $LKC_{hypoxic}/LCK_{oxic}$, [log cell kill in the radiobiologically hypoxic region (< 4 μM O_2)]/[log cell kill in aerobic region (> 30 μM O_2)]; MTD, maximum tolerated dose of drug given i.p. to CD-1 nu/nu mice (μmol kg^{-1}); C_{max}, maximum plasma drug concentration (μM); AUC, area under the plasma drug concentration–time curve (μM min); $t_{1/2}$, terminal drug half-life (min); LCK_{pred}, predicted log cell kill of hypoxic tumor cells in addition to radiation; drug given at 75% of MTD 5 min after irradiation of HT29 tumors; hypoxic cell killing was determined as [log(clonogens/g of tumor for radiation only)] − [log(clonogens/g of tumor for radiation plus drug)].

aminoalkylamino group and so optimize the rates of bioreductive metabolism in hypoxic tissue (Fig. 16). The 43 BTO analogs prepared were evaluated using our screening strategy based on the SR-PK–PD model (sections "Measuring Extravascular Drug Transport" and "Developing a Spatially Resolved-PK–PD Model"). We measured, or estimated by calculation, the key *in vitro* PK–PD parameters (D, k_{met}, CT_{10}, and M_{10}) (see Fig. 14 for definitions) for HT29 cells and used the model to calculate the AUC_{pred} required

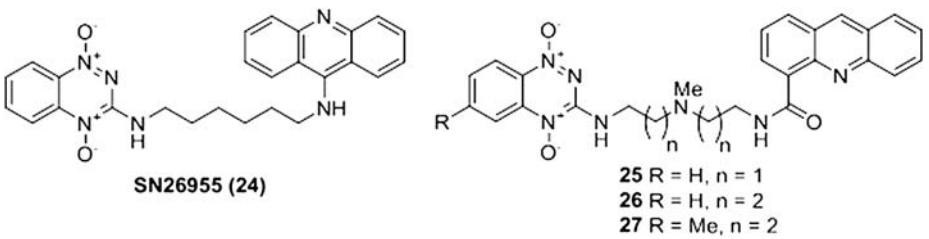

Fig. 15 DNA targeting of BTOs.

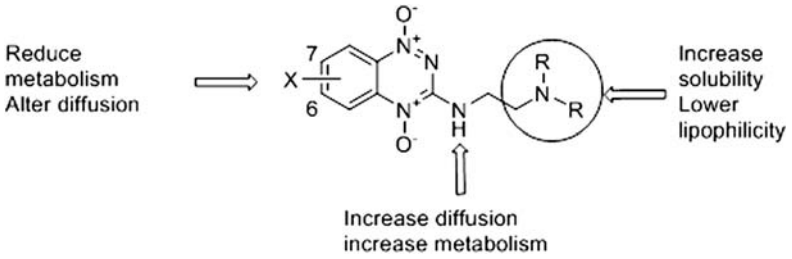

Fig. 16 Structural influences on EVT.

to give 1 log hypoxic cell kill in tumors and the HCD where HCD = [LCK (hypoxic)]/[LCK (oxic)]. These parameters were used to prioritize compounds for initial *in vivo* evaluation of toxicity and pharmacokinetic profile to obtain plasma AUC, C_{max}, and $t_{1/2}$ values that were used in the PK–PD model to calculate the log hypoxic cell killing (LCK_{pred}) predicted in HT29 xenografts. We selected those compounds for which the LCK_{pred} was >0.5. We also used the one-dimensional EVT parameter $X_{1/2}$ to provide a convenient indicator of EVT.

It became readily apparent that the addition of the solubilizing side chain compromised EVT primarily through increased electron affinity, shown by an increase in the $E(1)$ values of 60 mV for **30** (−396 mV)[226] over TPZ (−456 mV),[129] and a consequent elevation of k_{met}. Thus, BTO analogs bearing side chains with pK_a values of 8.5 and higher (**28**–**30**) showed increased hypoxic potency while maintaining *in vitro* hypoxic selectivity as a consequence of significantly increased hypoxic metabolism (k_{met}) (Table 1). Only the near-neutral morpholide **31** displayed lower hypoxic potency and hypoxic metabolism compared to TPZ. Whereas the more basic analogs had much lower $X_{1/2}$ values, the morpholide was similar to TPZ. When translated into AUC_{pred}, only morpholide **31** gave a similar value to TPZ with the more basic amines requiring much higher AUC_{pred} values, and a similar pattern was observed with the predicted hypoxic selectivity parameter HCD. This clearly suggested that simply adding solubilizing side chains would compromise EVT and that this needed to be offset by a reduction in electron affinity and/or an increase in lipophilicity. We sought to explore both arms of this hypothesis.

Addition of electron-donating 6-methyl substituents lowered electron affinity (the $E(1)$ of **32** (−440 mV)[226] was 44 mV lower than **30**) and generally increased $X_{1/2}$ values through reduced hypoxic metabolism (lower k_{met} values), but again, only examples with weakly basic morpholine side chains, for example, **33**, had improved $X_{1/2}$ relative to TPZ. Although more lipophilic alkyl substituents (Et, iPr, and tBu) did increase lipophilicity and diffusion coefficients within a homologous series, modest gains were accompanied by compromised aqueous solubility. This prompted us to consider 6-alkoxy BTO analogs where a stronger

Table 1 In vitro and modeling parameters for selected 6-substituted BTOs

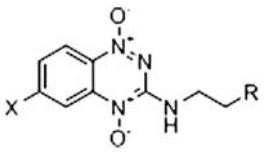

BTO	*X*	*R*	*pK$_a$*[a]	*Anoxic IC$_{50}$ (μM)*	*HCR*[b]	D *calculated*[c]	k$_{met}$[d] *(min)*	X$_{1/2}$[e] *(μm)*	*AUC$_{pred}$*[f] *(μM min)*	*HCD*[g]
TPZ	H	na	na	5.1	71	4.17	0.58	45	10,300	4.1
28	H	CH_2NMe_2	9.3	3.4	49	2.40	1.8	18	50,300	0.3
29	H	N-pyrrole	9.5	0.6	70	2.77	7.9	10	22,000	0.3
30	H	NMe_2	8.5	0.7	80	3.38	9.1	10	19,200	0.5
31	H	N-morpholine	6.6	17.3	34	3.58	0.55	44	12,400	5.7
32	Me	NMe_2	8.5	1.9	159	3.78	1.5	28	4280	3.3
33	Me	CH_2N-morpholine	7.3	15.5	25	5.56	0.38	66	13,900	6.7
34	MeO	NMe_2	8.5	7.7	89	2.87	0.54	35	13,800	2.7
35	MeO	CH_2N-morpholine	7.4	18.0	52	3.79	0.11	120	32,600	9.7

[a]Calculated using ACD pK_a.
[b]Hypoxic cytotoxicity ratio.
[c]Diffusion coefficients in HT29 MCLs $\times 10^{-7}$ cm^2 s^{-1}.
[d]First-order rate constant for metabolism in anoxic HT29 cell suspensions, scaled to cell density in MCLs.
[e]Penetration half distance in anoxic HT29 tumor tissue.
[f]Predicted area under the plasma concentration–time curve required to give 1 log cell kill of HT29 tumors in addition to that produced by a single 20 Gy dose of γ radiation.
[g]In vivo hypoxic cytotoxicity differential = $LKC_{hypoxic}/LCK_{oxic}$.
Source: Hay, M. P.; Hicks, K. O.; Pruijn, F. B.; Pchalek, K.; Siim, B. G.; Wilson, W. R.; Denny, W. A. Pharmacokinetic/Pharmacodynamic Model-Guided Identification of Hypoxia-Selective 1,2,4-Benzotriazine 1,4-Dioxides With Antitumor Activity: The Role of Extravascular Transport. *J. Med. Chem.* **2007**, *50*, 6392–6404.

electronic influence was expected to dampen hypoxic metabolism. Indeed, the $E(1)$ of **34** was down to -500 mV,[226] and this reduced electron affinity was reflected in lowered hypoxic potencies relative to 6-H (**30**) and 6-alkyl analogs (**32**). The more polar alkoxy substituents lowered lipophilicity and gave lower diffusion coefficients. This was balanced by low rates of hypoxic metabolism and generally resulted in similar or improved EVT properties compared to TPZ, for example, **34** and **35**. However, in examples where a weakly basic amine was present, for example, **35**, the rates of hypoxic metabolism were so low that they compromised hypoxic potency, leading to a high required drug AUC_{pred}.

The application of the screening algorithm (Fig. 14) predicted that, with the exception of the morpholide **31**, the unsubstituted BTO analogs would likely be inactive at decision point B (AUC_{pred} values over 20,000 μM min and HCD values significantly less than those for TPZ). The addition of the 6-Me group improved the AUC_{pred} and HCD values for all analogs resulting in most passing the criteria for advancement to *in vivo* testing, with the exception of several weak bases where a loss in potency compromised the AUC_{pred}. A similar pattern emerged for other 6-alkyl and 6-alkoxy analogs explored with excellent EVT being compromised by very low potency in the case of weak bases, for example, **35**, leading to a very high AUC_{pred} requirement in these instances.

Although a total of 18 compounds passed the threshold at decision point B, we elected to triage 11 lipophilic analogs because of close structural similarity to analogs that failed because of high *in vivo* toxicity. We determined the MTD and plasma PK data for the remaining seven BTOs and found they were better tolerated than TPZ, but within homologous series, increases in lipophilicity and electron affinity were accompanied by increased toxicity. Although half of the analogs gave increased AUC values compared to TPZ, when compared as a ratio of injected dose, the AUC values ranged from 70% to 200% of that for TPZ. In particular, more lipophilic amines with strongly basic side chains displayed a considerable PK liability. The plasma PK data were used in the SR-PK–PD model to predict active compounds ($LCK_{pred} > 0.5$), and these BTOs were evaluated against HT29 xenografts. A single dose of BTO was given i.p. 5 min after a high dose (20 Gy) of radiation, which was designed to sterilize the oxic compartment of the tumor. Drug activity was assessed by an *ex vivo* clonogenic survival assay comparing drug alone, radiation alone, and the combination. The additional cell kill observed over radiation alone represents the killing of hypoxic tumor cells (LCK) for the BTO (Fig. 17). All BTOs were sufficiently soluble to administer as solutions, and none displayed any single-agent activity as expected on mechanistic grounds. We had included several BTOs predicted to fail on the basis of low LCK_{pred} values to confirm the robustness of the SR-PK–PD model, and these did not display any activity. Six of six compounds predicted to be active on the basis of LCK_{pred} did in fact display significant hypoxic cell killing *in vivo* with two compounds **33** and **34** displaying superior activity to TPZ, while of three BTOs with borderline LKC_{pred}, two were inactive and one was active.

Overall, there was good agreement between LCK_{pred} and the LCK observed in HT29 tumors (correlation coefficient, $R^2 = 0.78$, $P < 0.001$). This was a gratifying confirmation of the previous model validation conducted with a different set of BTO analogs.[208] Perhaps of more significance was the observation that three of the six active BTOs identified would not have been selected for *in vivo* evaluation if the usual criteria of increasing *in vitro* hypoxic potency ($IC_{50} < 5$ μM) and selectivity (HCR > 71) compared with those for TPZ had been applied. Conversely, if these *in vitro* selection criteria had been applied to the 43 BTOs in the study, then only 14 of 43 candidates would have qualified but, based on PK–PD modeling, only three would have been found to be active against hypoxic cells *in vivo*. This exercise provides further evidence for the value of optimizing EVT parameters *in vitro* and combining these data with PK data using the PK–PD modeling to identify active compounds for *in vivo* evaluation. The structural evolution of the BTOs through this EVT optimization (Fig. 18) demonstrates that relatively small structural changes have a dramatic effect and that improving EVT is necessary, but not sufficient, for improved *in vivo* activity. With further validation of the SR-PK–PD and the identification of two BTOs **33** and **34** with superior activity to TPZ against hypoxic cells *in vivo*, we moved to a lead optimization phase where we wished to increase the potency of the BTOs and secure a composition-of-matter intellectual property position.

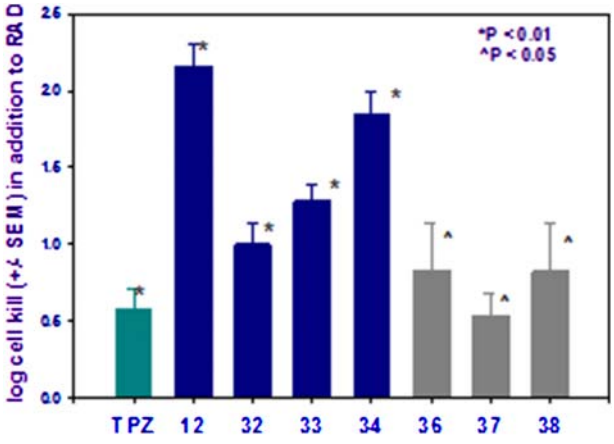

Fig. 17 Activity of representative 3-amino alkyl BTOs against hypoxic cells in HT29 tumor xenografts in CD-1 nude mice by *ex vivo* clonogenic assay. Drugs were administered i.p. at 75% of MTD 5 min after 20 Gy of radiation. Significance compared to LCK for RAD alone. Compound 12 (6-Me-BTO).

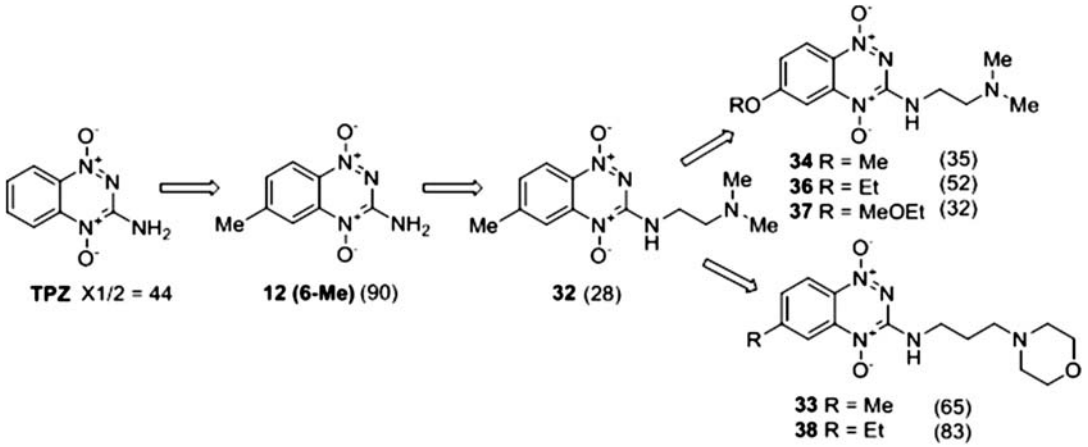

Fig. 18 Influence of structure on EVT (as $X_{1/2}$) for 3-aminoalkyl BTOs.

8.03.3.4 Exploring 3-Alkyl BTOs: Role of H Bonding on EVT

During our initial exploration of a series of solubilized BTO analogs, much of the gains in *in vivo* activity could be ascribed to increased drug plasma concentrations at equivalent toxicity rather than clear increases in EVT compared to TPZ (e.g., **34**). Hence, we sought to build on early BTOs[183] where the 3-amino group was replaced with a 3-alkyl substituent.[227] These analogs would allow us to further explore the impact of the H-bond donors (HD) on EVT with an expectation, based on the strong dependence of diffusion coefficient on HD described earlier (section "Measuring Extravascular Drug Transport"), that removing HD would increase EVT. We fully expected that a balancing act would be required with the influences of each structural modification having multiple consequences (Fig. 19).

Rather than using the low-yielding Bamberger condensation of 3-alkyl diphenylformazans **22** (Fig. 7)[190] and oxidation of the resultant 3-alkyltriazines **23**,[183] we elected to use palladium-mediated cross-coupling reactions to install alkyl and aryl groups at the 3-position. Thus, conversion of 3-NH_2-BTO 1-oxides to the corresponding chlorides **15** provided key intermediates to access 3-alkyl- and aryl-substituted BTOs **18** using Pd-mediated Stille and Suzuki reactions, respectively (Fig. 7).[188,189,227] Modification of a 3-allyl side chain using ozonolysis with a reductive workup provided access to a series of alcohols that could be further elaborated with solubilizing basic amine side chains. Based on the relatively weak electron donation of alkyl substituents ($\sigma_p = -0.17$) compared to 3-NH_2 ($\sigma_p = -0.66$), we anticipated 3-alkyl BTOs would also demonstrate increased hypoxic metabolism and potency. Consequently, we also prepared a series of 3-ethyl BTO analogs bearing an electron-donating alkyl or alkoxy side chain at the 6- or 7-position to modulate the electron affinity of the BTO and to provide a handle for solubilizing functionality. We processed the 43 analogs prepared through the PK–PD model as described in the preceding text. While simple 3-alkyl BTOs (e.g., **10** and **11**; Table 2) did show dramatically improved diffusion coefficients, this positive effect on EVT was negated by strong increases in hypoxic metabolism driven by elevated electron affinity; $E(1)$ values ranged from -376 to -327 mV compared with -456 mV for TPZ. BTOs **10** and **11** did display improved EVT, but $X_{1/2}$ values for other analogs were generally lower than for TPZ, and this translated into predictions of poor *in vivo* activity. BTOs **10** (SR4895) and **11** (SR4941) had been previously identified as active *in vivo*,[183] and we confirmed **10** and **11** as having similar activity to TPZ against hypoxic cells in HT29 tumor xenografts (Fig. 21). The addition of electron-donating side chains at the 6- and 7-positions resulted in lowered electron affinity and hypoxic metabolism with the 6-position being more influential (e.g., **42** vs. **44**; Table 2). The consequent reduction in hypoxic metabolism, combined with increased diffusion provided by the 3-ethyl substituent, provided a series of compounds (e.g., **40**, **41**, **42**, and **44**) with generally improved EVT ($X_{1/2}$: 42–156) compared to TPZ ($X_{1/2}$: 45). However, the aqueous solubility of these neutral analogs was no better than for TPZ. We added a variety of basic amine side chains that provided increased aqueous solubility at the expense of EVT due to

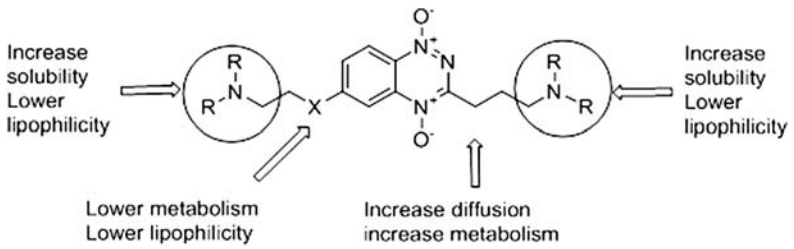

Fig. 19 Design for increasing potency and diffusion.

Table 2 In vitro and modeling parameters for selected 3-alkyl substituted BTOs

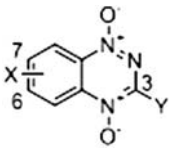

BTO	*X*	*Y*	*pK$_a$*[a]	*Anoxic IC$_{50}$ (μM)*	*HCR*[b]	D *calculated*[c]	k$_{met}$[d] *(min)*	X$_{1/2}$[e] *(μm)*	*AUC$_{pred}$*[f] *(μM min)*	*HCD*[g]
TPZ	H	-NH$_2$	na	5.1	71	4.2	0.58	45	10,300	4.1
10	H	-Et	na	6.8	54	28.3	1.90	63	7450	8.2
11	H	-EtOMe	na	3.5	49	19.2	2.00	55	5400	6.2
39	H	-PrNmorph	8.9	0.39	71	7.3	6.78	18	80,600	0.3
40	6-Me-	-Et	na	11.4	63	28.6	0.66	112	8970	8.1
41	6-MeO-	-Et	na	16.8	73	25.0	0.30	156	8720	10.8
42	6-HOPrO-	-Et	na	17.0	54	9.1	0.13	140	13,000	10.5
43	6-MorphNPrO-	-Et	7.3	6.8	153	12.4	0.53	64	7600	6.5
44	7-HOPrO-	-Et	na	6.9	146	6.4	0.44	65	6330	6.0
45	7-MorphNPrO-	-Et	7.3	3.0	147	9.1	0.73	60	3090	6.0

[a]Calculated using ACD pK_a.
[b]Hypoxic cytotoxicity ratio.
[c]Diffusion coefficients in HT29 MCLs $\times 10^{-7}$ cm^{2}s^{-1}.
[d]First-order rate constant for metabolism in anoxic HT29 cell suspensions, scaled to cell density in MCLs.
[e]Penetration half distance in anoxic HT29 tumor tissue.
[f]Predicted area under the plasma concentration–time curve required to give 1 log cell kill of HT29 tumors in addition to that produced by a single 20 Gy dose of γ radiation.
[g]In vivo hypoxic cytotoxicity differential = LKC$_{hypoxic}$/LCK$_{oxic}$.
Source: Hay, M. P.; Pchalek, K.; Pruijn, F. B.; Hicks, K. O.; Siim, B. G.; Anderson, R. F.; Shinde, S. S.; Phillips, V.; Denny, W. A.; Wilson, W. R. Hypoxia-Selective 3-Alkyl 1,2,4-Benzotriazine 1,4-Dioxides: The Influence of Hydrogen Bond Donors on Extravascular Transport and Antitumor Activity. *J. Med. Chem.* **2007**, *50*, 6654–6664.

increased hypoxic metabolism. A compromise was found where the near-neutral morpholine side chains (e.g., **43** and **45**) gave adequate aqueous solubility with minimal impact on hypoxic metabolism, leading to increased EVT relative to TPZ. Interestingly, the morpholides **43** and **45** had larger diffusion coefficients compared to the corresponding alcohols, **42** and **44**, respectively, despite being less lipophilic, emphasizing the strong, negative influence of HD on diffusion.

A total of 14 out of 43 3-alkyl BTOs qualified for *in vivo* evaluation, but eight neutral analogs were triaged because of poor aqueous solubility. While improving EVT is necessary to identify improved TPZ analogs, the additional requirement for BTOs to display good macro PK characteristics is clearly illustrated in the analog series in Fig. 20. Although these compounds possess excellent EVT characteristics and were predicted to be active on the basis of their AUC$_{pred}$ and HCD, the negative effect of increasing lipophilicity and amine pK_a on both host toxicity and AUC acts to undermine the potential efficacy of **47**.

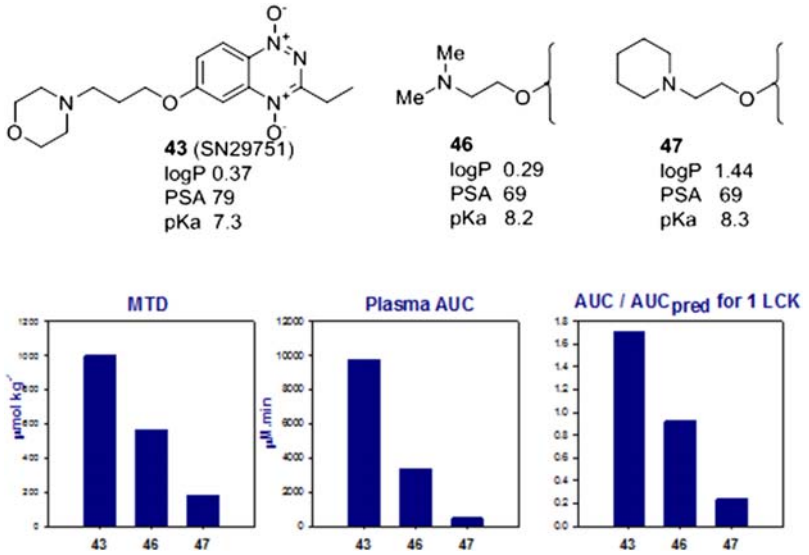

Fig. 20 Influence of amine lipophilicity and pK_a on host toxicity and drug exposure. MTDs were determined for single i.p. injections of drug to CD-1 nude mice and were defined as the highest dose that did not cause drug-related deaths, body weight loss of more than 15%, or severe morbidity in a group of six animals over 28 days. PK measurements were determined at 75% of MTD for each BTO.

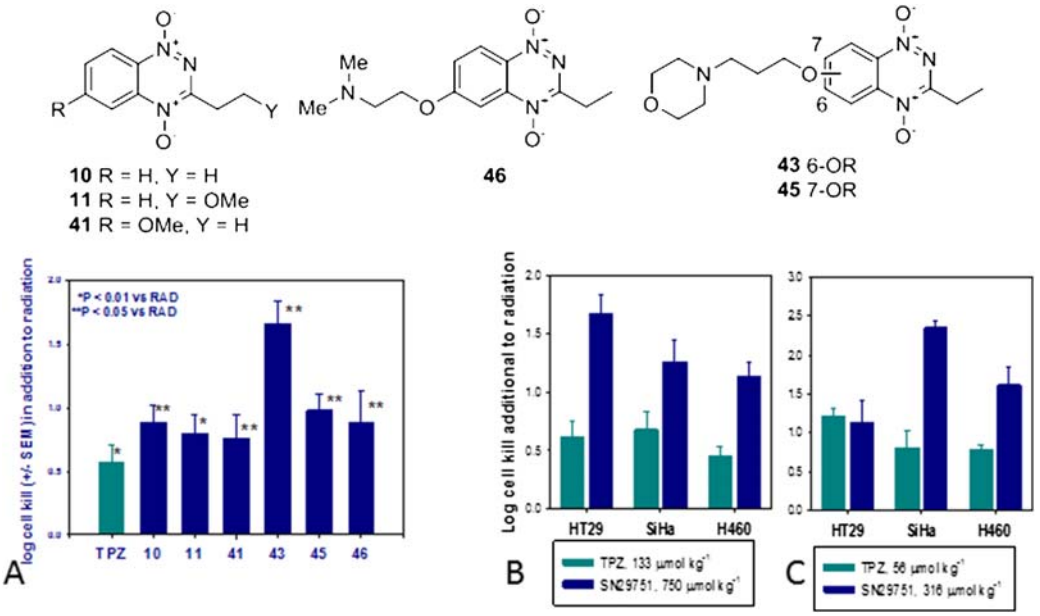

Fig. 21 (A) Activity of representative 3-alkyl BTOs against hypoxic cells in HT29 tumor xenografts in CD-1 nude mice by *ex vivo* clonogenic assay. Drugs were administered i.p. at 75% of MTD 5 min after 20 Gy of radiation. Significance compared to LCK for radiation alone. (B) Single-dose radiation (15 Gy for SiHa, 20 Gy for HT29, and H460 tumor xenografts), with compounds administered 5 min after irradiation. (C) Fractionated radiation (8×2.5 Gy), with compounds administered 30 min before each radiation dose.

All compounds predicted to be active on the basis of the full PK–PD prediction were found to show similar or improved activity against hypoxic cells in HT29 tumor xenografts (Fig. 21), demonstrating the predictive power of the SR-PK–PD modeling approach. In particular, BTO **43** (aka SN29751) demonstrated approximately threefold greater log cell kill of hypoxic cells than TPZ.

One can rationalize the design elements that led to increased EVT and increased *in vivo* activity of **43** (Fig. 22). Replacement of the 3-NH_2 group of TPZ with a 3-ethyl group (**10**) leads to a higher tissue diffusion coefficient and reflects the importance of minimizing HD for improved EVT. The concomitant increase in electron affinity and thus bioreductive metabolism would preclude efficient tissue penetration, but this is offset by the electron-donating 6-alkoxy side chain (**41**), which provides further significant increase in EVT. However, the low aqueous solubility of **41** suggested the addition of a weakly basic morpholine group (**43**) that increases aqueous solubility, albeit with a reduction in EVT due to reduced diffusion.

Further *in vivo* evaluation of SN29751 demonstrated impressive activity against SiHA and H460 tumor xenografts in combination with single dose of radiation (Fig. 21B) and modest activity against HT29 tumor xenografts and excellent activity against SiHa and H460 xenografts in combination with fractionated radiation (Fig. 21C).[212] The exceptional activity of BTO **43** led us to successfully pursue a selection invention patent strategy to protect BTO **43**.[228] This patent provided coverage of BTO **43**, but was not broad enough to be commercially appealing so we continued exploring the patent landscape around TPZ.

8.03.3.5 Designing Novel Analogs

Having demonstrated that the combination of chemical design and an SR-PK–PD model-guided approach could deliver BTOs with significantly superior killing of hypoxic tumor cells *in vivo* compared to TPZ, we tried to identify an intellectual property position that did not overlap with patents from Sanofi Winthrop around benzotriazine 1,4-dioxides[184] and AstraZeneca around isosteric 2-cyanoquinoxaline 1,4 dioxides.[215] Careful examination of the Sanofi Winthrop patents revealed an opportunity to exploit; no account had been made for an extended central chromophore with an alicyclic ring system fused to the benzotriazine core, despite

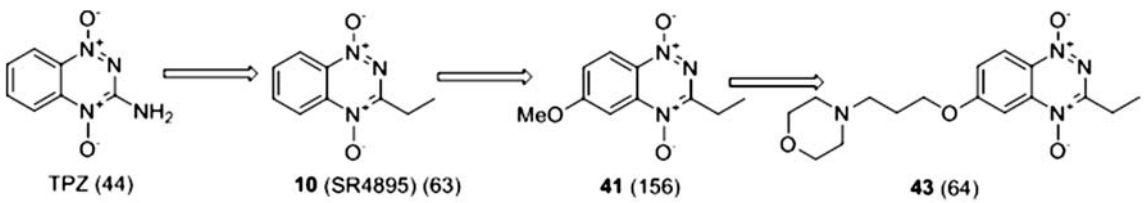

Fig. 22 Influence of structure on EVT (as $X_{1/2}$) for 3-alkyl BTOs.

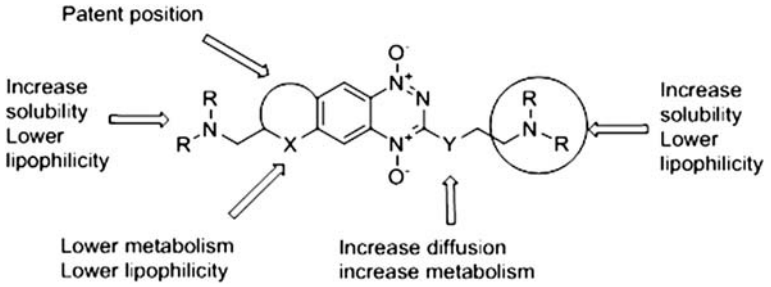

Fig. 23 Design for novel TTO analogs.

fused aryl and heteroaryl cores and cycloalkyl substituents being generically covered. This provided an opportunity to exploit, and we set out to explore the potential of such fused chromophore systems using our SR-PK–PD model-guided approach. The potential for the alicyclic ring to contribute to increases in EVT through increased lipophilicity and reduced electron affinity was countered by recognition that the extended ring system would reduce aqueous solubility, thus requiring a solubilizing group (Fig. 23). With this balancing act constraining design, we sought to explore a wide range of tricyclic systems (tricyclic triazine 1,4-dioxides (TTOs)) that could provide compounds with improved *in vivo* efficacy.

Our first step was to prepare a simple example of a TTO to validate the concept. This example consisted of a fused cyclopentyl ring system (7,8-dihydro-6*H*-indeno[5,6-*e*][1,2,4]triazine). 5-Indanamine was readily converted to the corresponding 6-nitro-5-indanamine and further elaborated using our methodology developed for benzotriazine analogs (Fig. 24). Condensation of the appropriate nitroaniline **48** with cyanamide and Arndt cyclization under strongly basic conditions provided triazine 1-oxides **49**. Diazotization in trifluoroacetic acid followed by chlorination of the intermediate phenol provided triazine 3-chlorides **50**. Displacement of the chloride with various amines installed a series of 3-aminoalkyl side chains, and 1-oxides **52** were oxidized to TTOs **53** with pertrifluoroacetic acid with an excess of trifluoroacetic acid to prevent oxidation of aliphatic amine side chains.

Our prototypical TTO (**61**) looked a promising candidate based on *in vitro* data and demonstrated that the fused alkyl ring could act to lower electron affinity and provide increased lipophilicity, offsetting the impact of the polar, solubilizing side chain to give improved EVT compared to TPZ (Table 3). Modeling predictions based on *in vitro* data suggested a modest PK requirement and potentially a selective compound *in vivo*. However, **61** proved to be relatively toxic *in vivo* and displayed low AUC (988 μmol min) (Fig. 26); PK–PD modeling predicted no *in vivo* activity and the compound was shelved. Although a disappointing result, **61** did provide a starting point for further optimization (Fig. 25).

Our first task was to improve on the PK profile of **61**. We explored a variety of solubilizing amine side chains to vary the pK_a and lipophilicity in order to further define an SAR for *in vivo* toxicity and to increase the *in vivo* drug exposure, that is, to maximize AUC_{actual}/AUC_{pred}. We prepared a series of 20 analogs of **61** with side chain variations that provided wide range of pK_a and lipophilicity. Again, weakly basic amines such as morpholine (e.g., **62**) provided the best EVT, primarily due to low hypoxic metabolism and

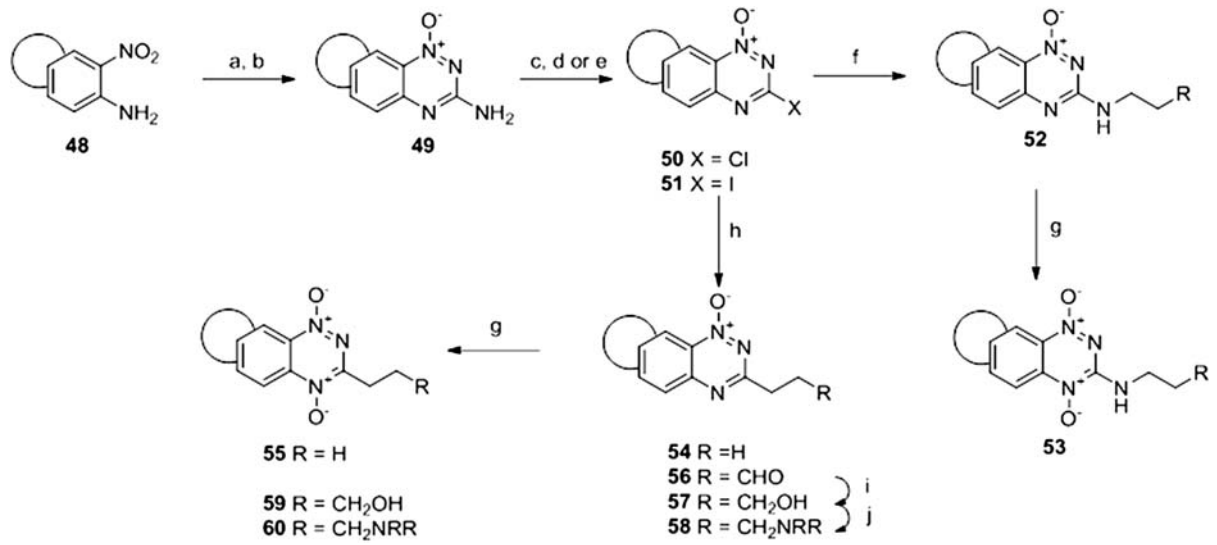

Fig. 24 Synthesis of tricyclic triazine dioxides. Reagents: (a) NH_2CN, HCl; (b) aq. NaOH; (c) $NaNO_2$, CF_3CO_2H; (d) DMF, $POCl_3$; (e) *t*BuONO, CH_2I_2, CuI, THF; (f) RNH_2, DME; (g) CH_3CO_3H or CF_3CO_3H, DCM; (h) Stille or Heck reaction; (i) $NaCNBH_3$, EtOH; (j) MsCl, Et_3N, DCM, then Amine, DMF.

Table 3 In vitro and modeling parameters for selected TTOs

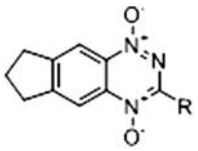

BTO	*R*	E*(1) (mV)*	*pK$_a$*[a]	*Anoxic IC$_{50}$ (μM)*	*HCR*[b]	D *calculated*[c]	k$_{met}$[d] *(min)*	X$_{1/2}$[e] *(μm)*	*AUC$_{pred}$*[f] *(μM min)*	*HCD*[g]
TPZ	NH_2	−456	na	5.1	71	4.2	0.58	45	10,300	4.1
61	$NH(CH_2)_2NMe_2$	−486	8.5	2.5	145	5.9	0.44	62	6731	6.4
62	$NH(CH_2)_3$Nmorph	na	7.4	21.4	20	9.6	0.19	119	9860	9.9
63	$NH(CH_2)_2$Nazepane	na	8.7	1.4	52	12.1	1.98	42	7530	3.6
64	$(CH_2)_3$Nmorph	401	7.1	2.4	135	15.1	0.80	74	3554	7.0
65	7-Me; $(CH_2)_3$Nmorph	na	7.1	2.9	72	21.0	0.96	80	4960	5.8
66	$(CH_2)_3NMe_2$	na	8.9	0.54	386	17.1	2.13	48	5392	2.3

[a]Calculated using ACD pK_a.
[b]Hypoxic cytotoxicity ratio.
[c]Diffusion coefficients in HT29 MCLs $\times 10^{-7}$ cm^{2}s^{-1}.
[d]First-order rate constant for metabolism in anoxic HT29 cell suspensions, scaled to cell density in MCLs.
[e]Penetration half distance in anoxic HT29 tumor tissue.
[f]Predicted area under the plasma concentration–time curve required to give 1 log cell kill of HT29 tumors in addition to that produced by a single 20 Gy dose of γ radiation.
[g]In vivo hypoxic cytotoxicity differential = LKC$_{hypoxic}$/LCK$_{oxic}$.
Source: Hay, M. P.; Hicks, K. O.; Pchalek, K.; Lee, H. H.; Blaser, A.; Pruijn, F. B.; Anderson, R. F.; Shinde, S. S.; Wilson, W. R.; Denny, W. A. Tricyclic [1,2,4]Triazine 1,4-Dioxides as Hypoxia Selective Cytotoxins. *J. Med. Chem.* **2008**, *51*, 6853-6865.

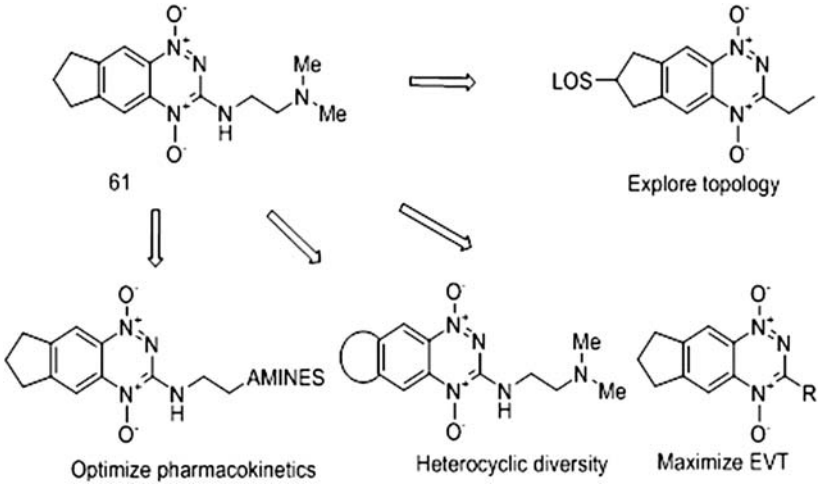

Fig. 25 Exploration of SAR for TTOs.

modest impact on diffusion (Table 3). More lipophilic amines (e.g., **63**) did not always provide improvements in EVT because of increased hypoxic metabolism. We advanced 12 TTO analogs into MTD testing and found a similar relationship between pK_a and lipophilicity and *in vivo* toxicity and PK parameters to that observed with earlier BTOs (Fig. 26). The reduction in AUC for the more lipophilic analogs undermined any increases in potency and resulted in PK–PD model predictions of inactivity. In summary, from the group of 20 TTOs, we were able to predict and confirm *in vivo* activity in 2/2 TTOs, both of which carried a morpholine side chain. However, the *in vivo* hypoxic LCK was modest (**62**, LCK 0.68 ± 0.14) and provided no benefit over TPZ (LCK 0.59 ± 0.15), so further exploration was required.

We explored the diversity of the fused ring substituents where the heteroatoms would further modulate the electron affinity of the TTOs (Fig. 25). We expanded the range of tricyclic variants with the fused ring selected from simple cycloalkyl (e.g., cyclopentyl, cyclohexyl, and cycloheptyl) and substituted cyclopentyl to isomeric dihydrofurans, tetrahydropyrans, dioxolane, and substituted pyrrolidine and piperidine rings fused at either the 6,7- or 7,8-position (Fig. 24).[229] We combined these ring systems with neutral 3-aminoalkyl or weakly basic pK_a 3-aminoalkylamine substituents (pK_a 7.4–8.5) to reduce the impact of the amine side chain on EVT. In general terms, the cycloalkyl–TTO analogs displayed increased lipophilicity, and the position of the fused ring did not alter its influence of the ring on EVT parameters. In the case of fused oxygen or nitrogen containing rings, the position of the heteroatom was important with a stronger influence on electron affinity and consequently hypoxic

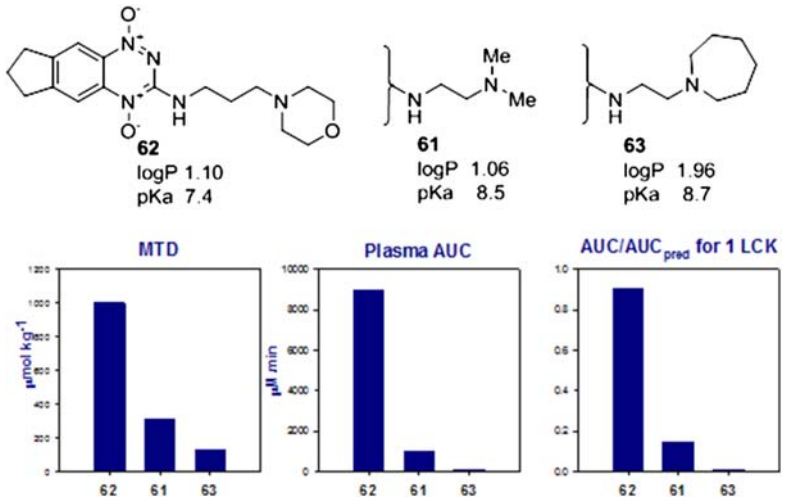

Fig. 26 Influence of amine lipophilicity and pK_a on host toxicity and drug exposure. MTDs were determined for single i.p. injections of drug to CD-1 nude mice and were defined as the highest dose that did not cause drug-related deaths, body weight loss of more than 15%, or severe morbidity in a group of six animals over 28 days. PK measurements were determined at 75% of MTD for each BTO.

potency and metabolism, when at the "6" position rather than the "7" or "8" positions (BTO ring numbering). The heteroatom also reduced lipophilicity significantly, and this factor dominated corresponding reductions in hypoxic metabolism resulting in a negative impact on EVT across the board. The low hypoxic potency and metabolism contributed to high AUC_{pred} values, and the modest diffusion parameters contributed to low predicted *in vivo* hypoxic selectivity (HCD). While this was disappointing, we consoled ourselves with the wide array of novel compounds that provided strategic support for the composition-of-matter patent needed to secure the TTOs.

In an effort to increase hypoxic potency without compromising EVT, we next explored 3-alkyl substituents combined with a limited number of fused chromophores (cyclopentyl, dihydrofuran, and piperidine) (Fig. 25). 3-Amino triazine 1-oxides **49** were converted to 3-iodides **51** by diazotization with *tert*-butyl nitrite in THF followed by iodination with diiodomethane (Fig. 24). Stille reactions of various triazine 3-iodides **51** gave the corresponding 3-ethyl analogs **54**, while Heck reactions with allyl alcohol provide a series of 3-propanals **56** that were further elaborated to tricyclic 1-oxides bearing 3-propanols **57** and various 3-propylamine side chains **58** that were oxidized to the corresponding TTOs **59** and **60**, respectively.

We explored different topologies with the solubilizing functionality attached via either the 3-alkyl substituent or the fused ring (Fig. 25). The fused rings were selected to best balance the effect of the 3-alkyl substituents on electron affinity. These compounds were generally more lipophilic and displayed higher diffusion coefficients than TPZ with only the polar influence of the dihydrofuran ring outweighing the removal of the 3-NH bond donor on diffusion. The greatest effect on EVT was seen for compounds with a fused cyclopentyl ring and an amine side chain linked via a 3-alkyl substituent. Compounds bearing weakly basic amines (e.g., **64** and **65**) displayed exceptionally high diffusion coefficients (Table 3), which more than offset accompanying increases in hypoxic metabolism. PK–PD modeling predicted modest AUC_{pred} requirements and increased *in vivo* hypoxic selectivity. In contrast, the presence of a more basic, more lipophilic amine (e.g., **66**) compromised EVT through strongly increased hypoxic metabolism, and this undermined the PK–PD predictions with a reduction in expected hypoxic selectivity *in vivo*, despite exceptional hypoxic selectivity *in vitro*. We investigated the animal toxicity of a series of these promising TTOs and again found a trend between lipophilicity, amine pK_a, and MTD and consequently AUC (Fig. 27). The weakly basic morpholide **64** displayed the least host toxicity and best AUC and increasing lipophilicity (**65**), and amine pK_a (**66** and **67**) increased host toxicity resulting in drastically reduced drug exposures. The predicted activity of **64** was confirmed with a hypoxic LCK of 1.4, approximately 2.5-fold greater than TPZ.

The combination of the lipophilic, electron-donating cyclopentyl ring with a 3-aminoalkylamino side chain in BTO **61** provided modestly increased EVT and excellent hypoxic selectivity, which suggested excellent *in vivo* potential (Fig. 28). However, the combination of increased lipophilicity with a moderately basic amine side chain undermined this potential, and BTO **61** was predicted inactive on the basis of the very low AUC achieved. Reducing the amine pK_a provided increased diffusion and a reduction in hypoxic metabolism to suggest excellent EVT. However, the potential was only partially realized with **62** displaying modest hypoxic cell killing *in vivo* due to relatively low potency. By increasing the potency and diffusion through removal of the 3-NH- group (**64**), a modest decrease in EVT was observed, but the increased metabolism led to increased hypoxic cell killing with **64** showing excellent *in vivo* activity (see section "Mechanism of DNA Damage").

8.03.3.6 Summary

In total, we prepared 281 BTO and TTO analogs, including 43 low-solubility compounds for the SAR "toolset" study (Fig. 29). Fifty-six compounds were immediately triaged because they were not sufficiently soluble to allow the determination of their HCR. We

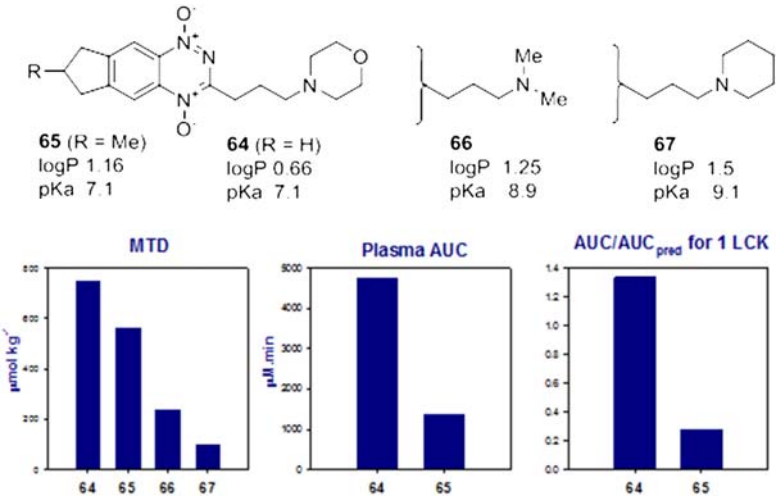

Fig. 27 Influence of amine lipophilicity and pK_a on host toxicity and drug exposure. MTDs were determined for single i.p. injections of drug to CD-1 nude mice and were defined as the highest dose that did not cause drug-related deaths, body weight loss of more than 15%, or severe morbidity in a group of six animals over 28 days. PK measurements were determined at 75% of MTD for each BTO.

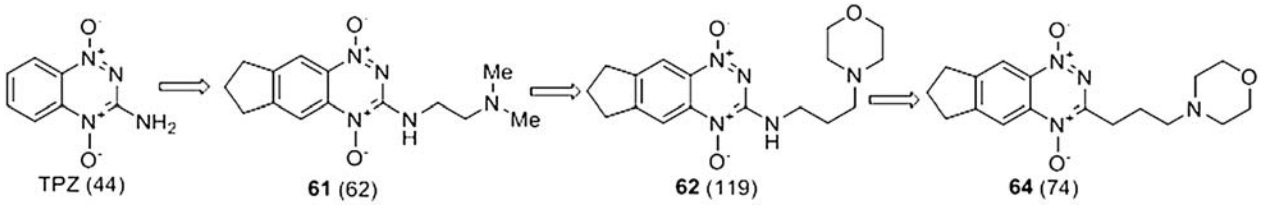

Fig. 28 Influence of structure on EVT (as $X_{1/2}$) for TTOs.

had set a relatively low threshold to advancement through checkpoint A (HRC > 20 in both HT29 and SiHa cells), and a majority of compounds (182) passed through this checkpoint. We evaluated 173 of these compounds for clonogenic survival and metabolic consumption in HT29 cells under anoxic conditions to determine the first-order rate constant for metabolism, k_{met}. The tissue diffusion coefficients were calculated from physicochemical properties (MW, log *D*, and the number of HD and HA) using an established relationship for a "training" set of BTOs measured in 3-D MCLs.[203] These values were used in the PK–PD model to calculate the *in vivo* HCD and the AUC required to achieve a hypoxic LCK of 0.5 at checkpoint B. The filters used at this checkpoint required compounds to have an HCD > 1 and AUC_{pred} of less than 20,000 μM min, twice that of TPZ at its MTD in CD-1 nude mice. We determined the PK at 75% of MTD for 123 compounds; 115 actives and eight compounds predicted to be inactive that were to act as negative controls. These PK data were then used in a second iteration of the PK–PD model to identify compounds with LCK_{pred} greater than 0.3. As noted earlier, a number of lipophilic, basic amines, which passed the checkpoint for LCK_{pred}, were rejected on the basis of low MTD values precluding attainment of the requisite AUCs. Eighteen BTOs, which were predicted active, along with 12 of 32 compounds predicted inactive, were evaluated against HT29 tumor xenografts in combination with radiation. Sixteen of eighteen were found to have statistically significant activity, and one of the false positives had a statistically insignificant hypoxic LCK of 0.60 ± 0.36. In contrast, 12/12 compounds predicted to be inactive were found to be inactive, despite displaying appreciable hypoxic selectivity *in vitro*. Analysis showed that neither *in vitro* hypoxic potency as IC_{50} ($r^2 = 0.07$ and $P = 0.16$) nor selectivity as $\log_{10}$ HCR ($r^2 = 0.02$ and $P = 0.47$) correlated with hypoxic LCK.[212] This campaign efficiently identified active BTOs and TTOs by explicitly considering micro-PK parameters along with systemic PK relative to toxicity with SN29751 (**43**) designated as a lead BTO and SN30000 (**64**) as a lead TTO.

8.03.4 Characterization of SN30000

8.03.4.1 Preamble

The identification of SN30000 as a lead analog of TPZ based on its ability to kill hypoxic tumor cells in an *ex vivo* clonogenic assay brought us into a new phase of the discovery campaign. We sought to characterize the activity of SN30000 in comparison with TPZ to confirm it for clinical development.

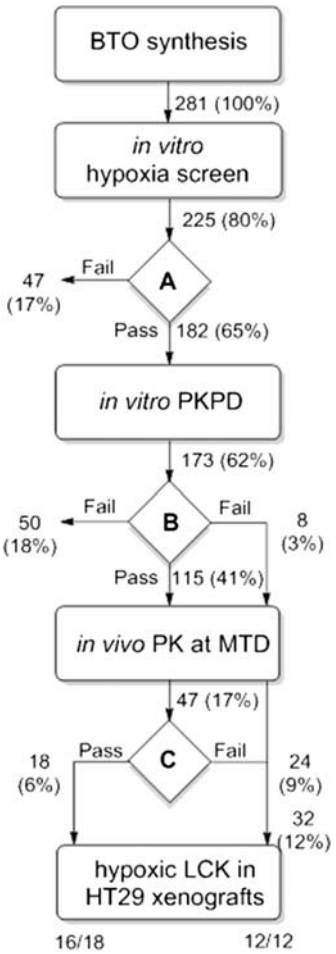

Fig. 29 PK–PD-guided lead optimization of BTO analogs.

8.03.4.2 Synthesis Optimization

We needed to prepare gram quantities of SN30000 to support a more in-depth biological evaluation, and this provided an opportunity to optimize the synthesis before transferring to the pilot plant for Chemistry, Manufacturing and Controls (CMC) development.

Our initial synthesis of SN30000 started from the commercially available 5-aminoindane **68** that was protected as the acetamide **69** and nitrated with KNO_3 in H_2SO_4 (Fig. 30). These initial nitration conditions gave all possible nitro isomers, which could be separated by column chromatography. Although producing both 6-nitro and 4-nitro isomers **70** and **71**, which could be elaborated to linear and angular TTOs, respectively, the modest yield (~25%) of the desired 6-nitro-5-acetamide **70** was unsatisfactory. Optimization of the nitration conditions identified milder conditions as a viable alternative. The use of $cHNO_3$ in acetic acid with careful temperature control gave an excellent yield of **70** with only ~9% of **71** after an aqueous workup. Rather than isolate the 6-nitro isomer at this stage, we carried the mixture through hydrolysis of the acetamides and crystallized 6-nitro-5-aminoindane **72** in 73% yield for the two steps. The original condensation of **72** with excess cyanamide was carried out as a melt with addition of cHCl initiating an exothermic reaction to generate the intermediate guanidine. This could be cyclized in the presence of 7 M NaOH to give indanotriazine 1-oxide **73** that was purified using column chromatography. Although we could carry out this procedure on a 100 g scale, concerns about controlling the exothermic reaction led us to develop a milder condensation procedure. We conducted the reaction using 4 M HCl in dioxane added slowly to a solution of **72** in dioxane with a fourfold excess of cyanamide at 80°C giving **72** in a final concentration of 0.5 M. The reaction proceeded smoothly and went to completion in ~1 h at 100°C. The mixture was cooled, petroleum ether added, and the mixture stood at room temperature overnight before the solvent was decanted from the resulting precipitate. After washing with ether, the solid was dried under a stream of nitrogen and then suspended in water, treated with 7 M NaOH and stirred at 100°C for several hours. On completion of the reaction, the mixture was cooled and diluted with water and the resulting precipitate filtered to provide 1-oxide **73** in yields of 92–94%. The anhydrous Sandmeyer reaction was initially carried out with diiodomethane, but this was replaced with iodine when we scaled this reaction up. Diazotization of **73** with *tert*-butyl nitrite in the presence of CuI and iodine gave the 3-iodide **74** in moderate to good yields (58–79%) after an aqueous

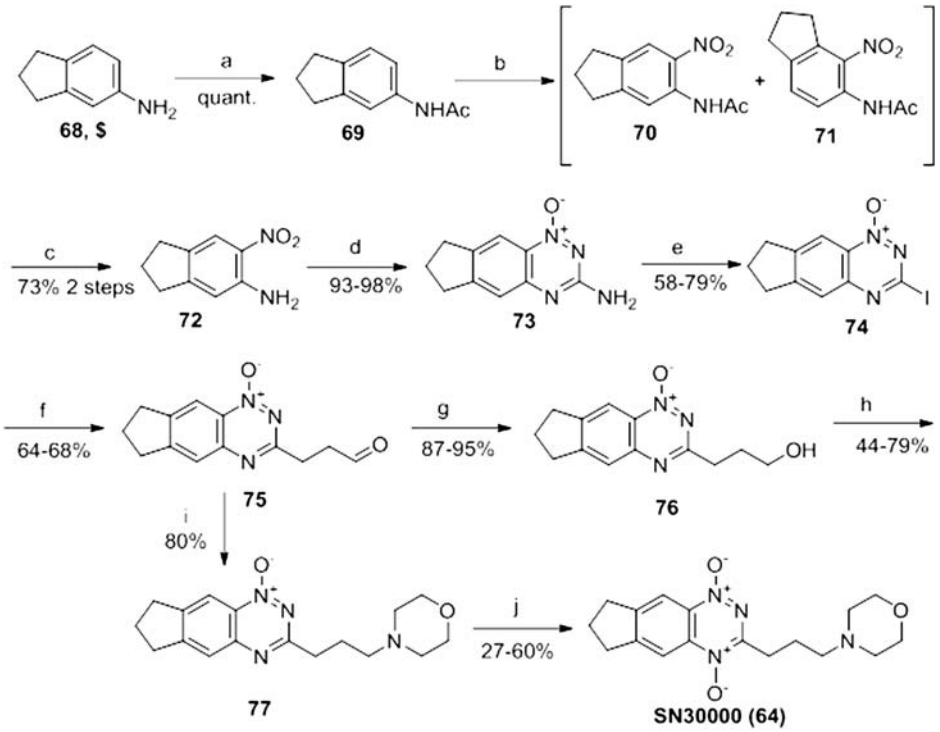

Fig. 30 Synthesis of SN30000. Reagents: (a) Ac_2O, dioxane; (b) $cHNO_3$, HOAc; (c) aq. HCl; (d) NH_2CN, HCl in dioxane, then aq. NaOH; (e) tBuONO, I_2, CuI, THF; (f) allylOH, $Pd(OAc)_2$, $Bu_4N^+Cl^-$, $NaHCO_3$, THF; (g) $NaCNBH_3$, EtOH; (h) MsCl, Et_3N, DCM, then morpholine; (i) $NaBH(OAc)_3$, morpholine, DCM, EtOH; (j) 70% H_2O_2, $(CF_3CO)_2O$, DCM.

workup and filtration of the organic fraction through a short plug of alumina. Careful control of reaction time and temperature and exclusion of moisture eliminated the formation of 3-H and 3-OH by-products. Standard Heck conditions were used to install the alkyl side chain to provide aldehyde **75** in moderate yields (64–68%) with only an aqueous workup and filtration through a plug of silica required for purification. Installation of the terminal morpholine could be accomplished either directly, via a reductive amination to give **77**, or stepwise by reduction to the alcohol **76**, mesylation and displacement with morpholine. In our hands, the stepwise approach was more convenient with $NaCNBH_3$-mediated reduction proceeding well (87–95%), and the subsequent conversion to the morpholide using standard conditions provided the morpholide **77** that was purified by crystallization as the HCl salt in moderate yields (47–79%). The direct reductive amination of **75** using $NaCNBH_3$ was accomplished in poor to low yields (15–52%) on a small scale, and we elected not to pursue this reaction for scale-up. The critical step in the synthesis was the final oxidation of 1-oxide **77** to 1,4-dioxide SN30000. Over several years, we had explored a wide range of oxidants and conditions to oxidize a wide variety of BTOs. We had settled on the oxidation with preformed pertrifluoroacetic acid added to a solution of 1-oxide in dichloromethane at room temperature as the most effective. BTOs with aliphatic amine side chains were protected by addition of trifluoroacetic acid, and reactions were only run to partial completion to avoid the complex mixtures that were produced if more forcing conditions were used. In our initial synthesis of SN30000, we typically isolated ~10% recovered starting 1-oxide and ~50% of SN30000. Obviously, this necessitated a chromatographic purification, and although we could isolate SN30000 in high purity and moderate yields (47–60%) at a 10 g scale, we sought to eliminate the chromatographic step. Despite our best efforts, we were unable to identify conditions to drive reactions to completion or to isolate SN30000 products without chromatography. When we used an acid/base partitioning step, followed by filtration of the organic fraction through an alumina plug, and crystallization of the hydrochloride salt, we suffered from lower yields (~27–56%) of SN30000 with significant levels (1–7%) of the starting 1-oxide **77** present.

We transferred the synthesis to our CMC contractor at Onyx Scientific Ltd, Sunderland, the United Kingdom, and were gratified that the scale-up was achieved without major changes to the synthetic route. The first five steps were scaled without note to provide 5 kg quantities of iodide **74**. However, several key modifications were made in the pilot plant to achieve a robust, scalable Good Manufacturing Practice (GMP) synthesis. The first of these was to use the reductive amination of aldehyde **75** with $NaBH(OAc)_3$ that provided **77** directly in 80% yield. An optimized oxidation procedure was defined using preformed pertrifluoroacetic acid added to a solution of 1-oxide **77** in DCM/HOAc, and the mixture was stirred for up to 4 days to effect maximum conversion to the product. Extensive crystallization trials were conducted on SN30000 to establish a purification process. In the final analysis, a relatively simple crystallization from EtOAc with subsequent slurrying of the precipitate in EtOAc gave the free base of **64** in acceptable purity with the major contaminant being the starting 1-oxide **77**. Further crystallization of the hydrochloride salt from EtOAc provided GMP grade SN30000.

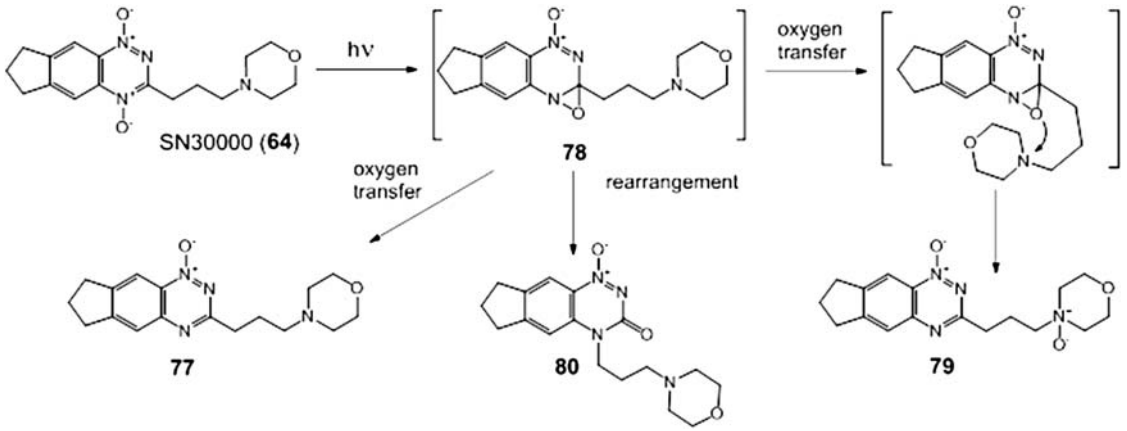

Fig. 31 Photolytic rearrangement of SN30000.

Some of the difficulties encountered in the purification and isolation of SN30000 were ascribed to the instability of the compound. SN30000 was found to unstable during silica gel chromatography. Although the compound did display an exothermic decomposition by differential scanning calorimetry, extensive testing for explosivity concluded that SN30000 was not an explosion risk. However, SN30000 did display significant photosensitivity, decomposing under ambient light to produce several products. Photolysis of solutions of SN30000 under UV or visible light produced predominantly the side chain N-oxide **79** via intramolecular oxygen transfer from the intermediate oxaziridine **78** (Fig. 31).[230] A small amount of a rearrangement product 3-keto BTO **80** and traces of 1-oxide **77** were also detected, presumably from intermolecular oxygen transfer. The photolysis products were shown to be less cytotoxic *in vitro* and less toxic to mice than SN30000.[230] The practical resolution of this problem was to store and formulate SN30000 and solutions in amber vials, and this has proved to be satisfactory.

8.03.4.3 SN30000 Is an Improved TPZ Analog

SN30000, while mechanistically similar to TPZ, is a quantitatively improved analog where the optimization of physicochemical parameters leads to improved micro and systemic pharmacokinetic properties and results in increased activity against hypoxic cells both *in vitro* and *in vivo*. Although SN30000 has a higher MW, it has an approximately fivefold increase in aqueous solubility by virtue of a weakly basic amine side chain (Table 4). Elevation of electron affinity [$E(1)$] raises the rate of hypoxic metabolism (k_{met}) and hypoxic potency, while removal of HD increases diffusion (D) (Fig. 32), producing improved EVT ($X_{1/2}$) compared to TPZ. SN30000 is more potent than TPZ under anoxia as measured by IC_{50} (proliferation assay) against a panel of eight cell lines (Fig. 33A). SN30000 is also more selective for anoxia than is TPZ in both the proliferation assay (Fig. 33B) and by clonogenic survival (Fig. 33C). Importantly, the potencies of SN30000 and TPZ were highly correlated in this panel,[212] supporting the view

Table 4 Physicochemical properties of TPZ and SN30000 and PK–PD parameters for prediction of hypoxic cell killing in HT29 xenografts in CD-1 male nude mice at 75% of MTD

Parameter (units)	*TPZ*	*SN30000*
Physicochemical properties		
MW (Da)	178	367
Solubility (mM) Culture medium (37°C)	8.9	48.5
E(1) (mV)	-456 ± 8	-401 ± 8
Log *P*, pH 7.4	-0.34 ± 0.02	0.50 ± 0.05
pK_a (Calculated)	NA	7.1
HD, HA	2, 6	0, 7
PK–PD parameters		
k_{met} (min^{-1})	1.30 ± 0.04 (74)	1.53 ± 0.21 (8)
D ($\times 10^{-6}$ $cm^2 s^{-1}$)	0.40 ± 0.02 (12)	1.26 ± 0.11 (6)
$X_{1/2}$	45	74
Dose (75% of MTD) (μmol kg^{-1})	133	562
C_{max} (μM)	61.7 ± 0.1	85.1 ± 7.8
$AUC_{p\infty}$ (μM h)	49	79
$t_{1/2}$ (min)	27.9	32.1

Values are means and SEM (number of determinations in parentheses).

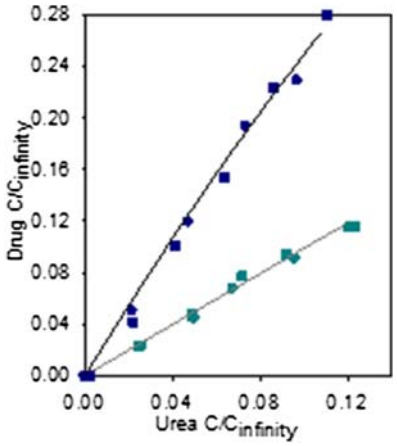

Fig. 32 Diffusion of TPZ (*cyan symbols*) and SN30000 (*blue symbols*) through HT29 MCLs. *Symbols* represent the drug concentration in the receiver compartment after diffusion through the MCL. Concentrations are expressed as fractions of the expected concentration at equilibrium and plotted against the ^{14}C-urea internal standard (instead of time) to account for differences in MCL thickness. Two replicate experiments are shown (with different symbols) for each compound. Redrawn from Hicks, K. O.; Siim, B. G.; Jaiswal, J. K.; Pruijn, F. B.; Fraser, A. M.; Patel, R.; Hogg, A.; Liyanage, H. D. S.; Dorie, M. J.; Brown, J. M.; Denny, W. A.; Hay, M. P.; Wilson, W. R. Pharmacokinetic/Pharmacodynamic Modeling Identifies SN30000 and SN29751 as Tirapazamine Analogues With Improved Tissue Penetration and Hypoxic Cell Killing in Tumors. *Clin. Cancer Res.* **2010**, *16*, 4946–4957.

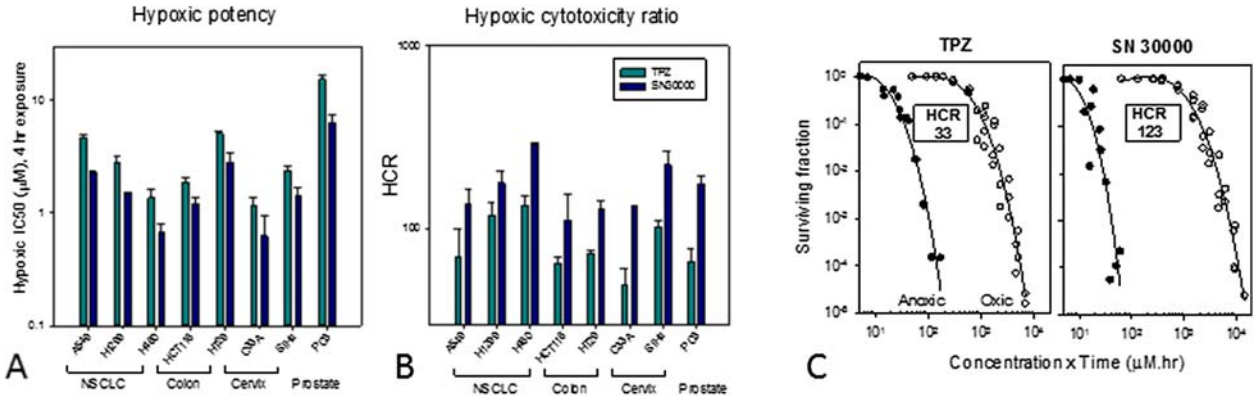

Fig. 33 Activity of TPZ and SN30000 against anoxic cells *in vitro*. (A) Hypoxic cytotoxicity to various human tumor cells by proliferation assay with a 4 h drug exposure. (B) Hypoxic selectivity [HCR = IC_{50}(oxic)/IC_{50}(anoxic)]. (C) Hypoxic selectivity by clonogenic assay. Modified and redrawn from Hicks, K. O.; Siim, B. G.; Jaiswal, J. K.; Pruijn, F. B.; Fraser, A. M.; Patel, R.; Hogg, A.; Liyanage, H. D. S.; Dorie, M. J.; Brown, J. M.; Denny, W. A.; Hay, M. P.; Wilson, W. R. Pharmacokinetic/Pharmacodynamic Modeling Identifies SN30000 and SN29751 as Tirapazamine Analogues With Improved Tissue Penetration and Hypoxic Cell Killing in Tumors. *Clin. Cancer Res.* **2010**, *16*, 4946–4957.

that the two compounds have a common mechanism of action. In addition, both show a similar DNA repair profile in a panel of repair mutant lines.[151]

When administered to mice as a single i.p. dose, SN30000 was better tolerated than TPZ, gave increased peak plasma concentrations, and had an increased plasma half-life (Table 4).[212] When administered as a single dose at 75% of the MTD, SN30000 gave increased hypoxic cell kill in combination with a single dose of radiation determined by *ex vivo* clonogenic survival (Fig. 34A). This effect was consistent in three xenograft models (HT29, SiHa cervical carcinoma, and H460, non-small cell lung carcinoma), and a similar, but somewhat attenuated, response was seen in a fractionated radiation experiment where radiation and drug were given twice daily for 4 days in the same xenograft models (Fig. 34B). No activity was seen with SN30000 alone in any of the xenograft models, and this is consistent with selective killing of the hypoxic subpopulation. SN30000 also showed significant activity in combination with fractionated radiation in a growth delay endpoint at doses of 176 or 263 μmol kg^{-1} ($P = 0.0058$ and 0.0004, respectively, log-rank test) (Fig. 34C). SN30000 in combination with radiation also provided a significant growth delay of H460 tumor xenografts compared to radiation alone in nude rats.[231]

It is important to note that SN30000 is not universally active in all tumor models. It did not provide significant additional clonogenic cell killing in DLD-1 breast cancer xenografts when combined with radiation.[118] This points to the importance of identifying predictive biomarkers to support its clinical development.

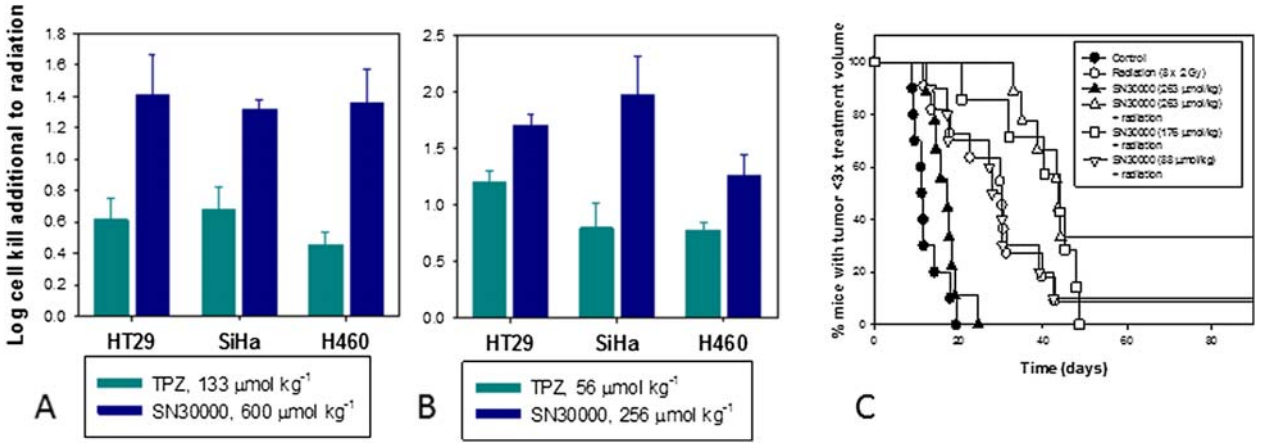

Fig. 34 Activity of TPZ and SN30000 against hypoxic cells in human tumor xenografts in combination with radiation. Comparison of cell killing by tumor excision and clonogenic assay 18 h after the end of treatment (mean and SEM for five mice). (A) Single-dose radiation (15 Gy for SiHa, 20 Gy for HT29, and H460 tumor xenografts), with compounds administered 5 min after irradiation. (B) Fractionated radiation (8×2.5 Gy), with compounds administered 30 min before each radiation dose. (C) SN30000 alone and 30 min before each dose of fractionated radiation (8×2 Gy) against SiHa xenografts by tumor regrowth assay. Modified and redrawn from Hicks, K. O.; Siim, B. G.; Jaiswal, J. K.; Pruijn, F. B.; Fraser, A. M.; Patel, R.; Hogg, A.; Liyanage, H. D. S.; Dorie, M. J.; Brown, J. M.; Denny, W. A.; Hay, M. P.; Wilson, W. R. Pharmacokinetic/Pharmacodynamic Modeling Identifies SN30000 and SN29751 as Tirapazamine Analogues With Improved Tissue Penetration and Hypoxic Cell Killing in Tumors. *Clin. Cancer Res.* **2010**, *16*, 4946–4957.

Building on studies demonstrating that SN30000 and pentafluorinated etanidazole (EF5) were reduced by the same reductases[148], PET imaging studies in H460 xenografts in rats also suggested that ^{18}F-EF5 was a suitable biomarker for hypoxia (see section "Predictive Biomarkers and Response Biomarkers for SN30000").[231]

8.03.4.4 Mechanism of DNA Damage

SN30000 qualitatively displays the same mechanism of activation and interaction with DNA as TPZ. It is reduced by POR to form a radical anion **81** (Fig. 35) that is reducing in nature and cannot oxidize DNA. In the presence of oxygen, this radical anion is oxidized back to SN30000 with concomitant formation of superoxide. The radical anion may be protonated (**82**), and elimination of water provides an oxidizing radical, which mediates DNA damage with production of 1-oxide **77**. Pulse radiolysis and EPR studies have identified the benzodiazinyl (BDZ) radical **83** (equivalent to the BTZ radical **6** for TPZ (Fig. 5)) as the main radical species involved in the oxidation of DNA, although formation of a minor amount of a more potent aryl radical **84** was also observed.[232] Notably, no evidence was seen for the formation of hydroxyl radical that has been proposed[136] as the main species

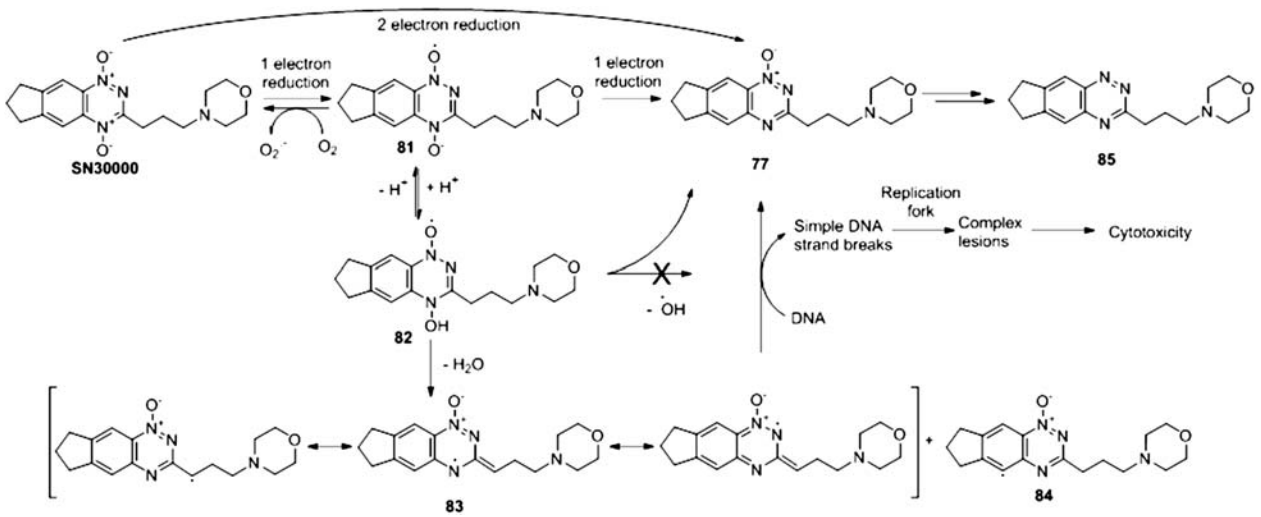

Fig. 35 Bioreductive activation of SN30000.

effecting DNA damage for TPZ (see section "Tirapazamine"). The BDZ radical **83**, formed by one-electron oxidation of 1-oxide **77** with selenite radical, was shown to react with 2-deoxyribose at a greater rate than TPZ. SN30000 was also shown to cause double-strand breaks in DNA plasmids after reduction by POR at approximately twice the rate of TPZ. This increased reactivity was ascribed to the higher reduction potential of the BDZ radical formed from SN30000 compared with the corresponding BTZ radical **6** derived from TPZ and also from a contribution to DNA damage from the highly reactive aryl radical **84**.[232] SN30000 and TPZ were not metabolized under oxic conditions, but metabolism of both was highly correlated ($r^2 = 0.87$ and $P < 0.001$) across a diverse panel of 14 tumor cell lines under anoxia.[148] Manipulation of POR levels resulted in similar changes in SN30000 and TPZ metabolism and DNA damage as measured by γH2AX formation. Small amounts of the nor-oxide **85** have been observed *in vitro* and *in vivo*, mimicking the bioreduction of TPZ.[148,212]

8.03.4.5 Predictive Biomarkers and Response Biomarkers for SN30000

A central issue for clinical development of SN30000, as for other HAPs, is the identification of predictive biomarkers (companion diagnostics) that can be used to enrich for potentially responsive tumor subtypes in early-phase clinical trials; once clinically validated, these biomarkers could ultimately be used for identification of individual tumors in a personalized medicine context. Discovery and validation of predictive biomarkers for HAPs are challenging given that determinants of sensitivity are multifactorial, encompassing hypoxia, expression of the one-electron reductases that activate the prodrug, and intrinsic (cell-autonomous) sensitivity to the active cytotoxin.

An interesting possibility is that 2-nitroimidazole probes that bind covalently in hypoxic cells, such as pimonidazole and EF5, might be activated by the same one-electron reductases as SN30000 and might thereby act as dual reporters of hypoxia and SN30000 reductases. In support of this hypothesis, metabolic activation of SN30000 (and TPZ) strongly correlated with covalent binding of EF5 in a genetically diverse panel of 14 human tumor cell lines under anoxia.[148] The same study varied hypoxic fraction in HCT116 xenografts by manipulating the respiratory gas and demonstrated that EF5 binding (assessed by flow cytometry) predicted sensitivity of individual tumors to SN30000-induced DNA damage (γH2AX formation). Further evidence that EF5 and SN30000 are activated by the same reductases was provided by a subsequent study in which overexpression of members of the diflavin reductase family (POR, MTRR, NOS3A, and NDOR) resulted in similar activation of both substrates under anoxia.[233] It is noteworthy that binding of EF3, a close analog of EF5, showed differences in maximal binding within small fragments from HNSCC biopsies incubated under hypoxia,[234] suggesting that interpatient variations in one-electron reductase activity may be important. The reported association between avidity for the PET probe ^{18}F-FMISO and sensitivity to TPZ in HNSCC[46,179] may thus reflect the ability of 2-nitroimidazole PET probes to act as dual reporters for both hypoxia and activity of BTO-activating reductases. These observations suggest PET imaging with ^{18}F-labeled 2-nitroimidazole probes currently in clinical use such as FMISO, FAZA, and HX4[235] can provide a mechanistically well-matched companion diagnostic for clinical development of SN30000. However, new hypoxia imaging modalities such as oxygen-enhanced MRI[236] may also have utility if variation in reductase expression emerges as less important than variation in the extent and depth of hypoxia between tumors.

While functional imaging clearly has potential for identifying SN30000-responsive tumors, profiling of molecular determinants of sensitivity offers a complementary approach with the flexibility to explore all three classes of biomarkers (hypoxia, reductases, and intrinsic sensitivity). Expression of a hypoxia-responsive mRNA expression signature has been shown in a retrospective study to identify HNSCC patients who benefit from the hypoxia-selective radiosensitizer nimorazole (**3**) in combination with radiotherapy.[43] If validated in prospective studies currently in progress, this will provide strong motivation for the use of gene expression signatures to identify hypoxic tumors in other settings. Multiplexing with mRNAs for SN30000 reductases would be a logical extension but will obviously require identification of the reductases involved. The well-studied one-electron reductase POR was the first enzyme shown to be capable of metabolic activation of SN30000 when overexpressed in hypoxic tumor cell lines.[148,237] As noted earlier, other members of the diflavin reductase family (MTRR, NOS2A, and NDOR1) also activate SN30000 when overexpressed.[233] The endoplasmic reticulum-associated flavoreductase FOXRED2 also reduces both SN30000 and TPZ in a hypoxia-dependent manner.[238] However, such studies do not establish a role for these reductases at endogenous levels of expression in human tumors. In fact, knockout of *POR* with zinc finger nucleases in two human tumor cell lines (HCT116 and SiHa) had little effect on their ability to metabolize SN30000 to its 1-oxide **77**, its anti-proliferative activity, or clonogenic cell killing under anoxia,[237] suggesting the existence of additional reductases.

As a first step toward identifying the reductases involved, we recently used genome-wide lentiviral short hairpin (sh) RNA libraries (82,017 barcoded shRNAs targeting 16,019 genes) to knock down expression of genes that confer SN30000 sensitivity.[239] Surprisingly, screening for SN30000 resistance by deep sequencing of shRNA barcodes in surviving populations identified *POR* as the only gene consistently selected in a HCT116 cell line with a single copy of the *POR* gene. Specificity was confirmed by demonstrating a correlation between the extent of selection of the four POR shRNAs and the extent of knockdown by lentiviruses expressing each shRNA. Further, no such enrichment of these shRNAs was found when the screen was repeated using a *POR*-null (biallelic knockout) HCT116 clone. Further screens using a focused shRNA library encompassing all flavoreductase genes, with high clonal representation, also identified POR as the sole screening hit in both PANC-1 and HT29 cells, again with no such selection of POR shRNAs in the *POR* null line. The shRNA screens thus identified POR as the most important single determinant of SN30000 sensitivity in hypoxic human tumor cell lines. The same study examined the quantitative relationship between POR expression and SN30000 activation, both in a series of HCT116 clones and in a diverse panel of human cell lines. This demonstrated a substantial non-POR contribution, suggesting nonspecific "leakage" of electrons from multiple flavoreductases that individually make too

small a contribution to be enriched in the screens. What is not yet clear is whether this background activation is sufficient to provide hypoxic-selective killing in tumors. This study[239] also extended a previous immunohistochemical (IHC) evaluation of POR expression in human tumors,[103] demonstrating wide variance in expression between individual HNSCC tumors. Importantly, it was also shown that POR expression is more spatially homogenous than the endogenous hypoxia marker CA IX, suggesting that POR is relatively uniformly expressed in hypoxic and oxic zones. Thus, the sampling problems that confound assessment of tumor hypoxia by IHC[240,241] are likely to be less of a constraint in evaluating POR expression. These findings identify POR as requiring evaluation as a predictive biomarker in clinical trials of SN30000 and other HAPs. Although specificity of the POR antibody used in these studies has been thoroughly validated,[103,239] it is noteworthy that a quantitative targeted proteomic assay for POR proteotypic peptides is also available.[237] Given the potential for multiplexing large numbers of proteotypic targets by mass spectrometry, this platform presents a further attractive option for biomarker evaluation in the clinic.

The third class of predictive biomarkers, namely, the gene products that influence intrinsic sensitivity to the free radical cytotoxin(s) arising from one-electron reduction of SN30000, may be more difficult to identify using forward genetic screens (such as shRNA libraries) in a bulk culture format given that the most likely pathways (e.g., DNA damage response/repair and free radical detoxification) are likely to confer sensitivity rather than resistance when knocked down. Such genes are difficult to identify by deep sequencing of bulk cultures because of stochastic loss of shRNAs at low surviving fraction, even if they are neutral with respect to drug sensitivity. Studies with cell lines in which HRR genes such as *BRCA1*, *BRCA2*, *PALB2*, *XRCC3*, and *Rad51d* are mutated, knocked out, or knocked down demonstrate that this pathway is important in the repair of DNA lesions induced by TPZ and SN30000.[118,150,151] In addition, HRR is suppressed by chronic hypoxia through multiple mechanisms,[34] so it may play a role in enhancing SN30000 sensitivity in hypoxic tumor cells. However, the synthetic lethality induced by HRR loss is less pronounced for TPZ and SN30000 than for HAPs of DNA cross-linking agents such as PR-104A and TH-302,[118,151] so it is not yet clear whether HRR status will be an important determinant of sensitivity. A more complete view of determinants of intrinsic sensitivity may require use of arrayed RNA interference reagents or more powerful forward genetic screens in bulk cultures such as high-representation CRISPR/Cas9 libraries able to quantify loss of fitness[242] and resistance. In addition, CRISPR libraries that use Cas9 constructs engineered to drive gene expression[243] have exciting potential for gain-of-function genetic screens to identify pathways that modulate intrinsic sensitivity.

Although current SN30000 biomarker development is in the discovery phase, any predictive biomarker (or set of biomarkers) will ultimately need to be validated in phase II/III clinical studies. In the absence of that validation, the choice of tumor types for initial exploration of SN30000 in the clinic needs to be driven by evidence that hypoxia limits outcomes with the current standard of care and information about potential determinants of sensitivity at a population level. The case is perhaps strongest for combination with (chemo)radiotherapy for the treatment of advanced HNSCC where there is compelling evidence that hypoxia determines outcome.[42,43,70] Recent evidence identifies the HPV-negative subset as a distinct molecular subtype[244] with relatively poor chemoradiation outcomes[245] and evidence shows improved local tumor control when TPZ is combined with cisplatin and radiotherapy for treatment of hypoxic tumors.[179] Increased hypoxia in recurrent tumors within the radiation field because of suppression of angiogenesis[246] also suggests possible applications in the treatment of recurrent squamous cell carcinomas and brain tumors (the latter potentially exploiting the high blood–brain barrier permeability of SN30000).

During clinical development, response biomarkers that provide early readout of clinical activity also have high value. This aspect of SN30000 development has not yet been explored thoroughly. Hypoxia- and reductase-dependent inductions of γH2AX by SN30000 have been documented[148] and would assist in confirming mechanism, although the requirement for sampling the tumor post-treatment would limit utility. A small but significant reduction in ^{18}F-EF5 specific uptake values was observed 24 h after SN30000 treatment of H460 tumors in athymic rats, accompanied by increased apoptosis in regions distant from the blood vessels,[231] although it is not clear whether the loss of metabolic viability of hypoxic cells will typically be fast enough post-SN30000 for this to be a useful early response marker in the clinic. The distinction between predictive and response biomarkers becomes blurred when one considers use of hypoxia imaging during fractionated radiotherapy to assess residual hypoxia and thus determine whether administration of HAP should be continued. Preclinical studies to address this question would be highly informative.

8.03.5 Summary

We have successfully conducted a drug discovery campaign to identify an improved TPZ analog SN30000, and a backup compound SN29751, using an SR-PK–PD model-guided approach. The use of the PK–PD modeling in our discovery algorithm allowed us to ignore the misdirection provided by *in vitro* hypoxic potency and selectivity data and to successfully and efficiently predict compounds with increased *in vivo* hypoxic selectivity compared to TPZ. A key focus during this investigation was the improvement in EVT through optimization of diffusion and metabolism properties of the BTOs. We have also uncovered, although not completely defined, the SAR for *in vivo* toxicity and AUC for BTO analogs, at least in murine models. In this campaign, we have predicted and confirmed the activity of 16 BTO analogs from a pool of 280 BTO compounds with only one incorrect prediction.

We have demonstrated that SN30000 has the improved properties we sought as design targets at the outset of our campaign. In particular, we have improved both solubility and potency with SN30000 being approximately fivefold more soluble than TPZ and having increased hypoxic potency against a panel of human tumor cell lines. SN30000 displays improved EVT compared to TPZ as a consequence of increased diffusion, which more than offsets a small increase in hypoxic metabolism. These properties translate to

increased predicted hypoxic selectivity *in vivo* that, when combined with the lower toxicity of SN30000, results in SN30000 displaying increased killing of hypoxic cells *in vivo* in a range of human tumor xenograft models in combination with radiation.

SN30000 has undergone preclinical development including CMC studies where a GMP synthesis has been developed and preclinical formulation and toxicology studies in rats have been completed. SN30000 and its backup compound SN29751 are both protected by patents. The search for suitable biomarkers for hypoxia and competent reductases is well advanced, and SN30000 is ready to advance to clinical evaluation.

Acknowledgments

The authors would like to acknowledge the team who contributed to the discovery and development of SN30000. At the Auckland Cancer Society Research Centre (ACSRC), we thank Dr. Robert Anderson, Dr. Adrian Blaser, Dr. Swarna Gamage, Dr. Francis Hunter, Dr. Ho Lee, Dr. Karin Pchalek, Dr. Frederik Pruijn, Dr. Sujata Shinde, Dr. Bronwyn Siim, Dr. Jingli Wang, Dr. Shanjing Yang, Jane Botting, Annie Fraser, Alison Hogg, Sisira Kumar, Sarath Liyanage, and Rita Patel for their contributions to the design, synthesis, and evaluation of the compounds. We would particularly like to acknowledge Prof. Bill Denny (ACSRC), Prof. Martin Brown (Stanford University), and Dr. Thorsten Melcher (J&J Innovation) for their strong support of the program. We thank Prof. Timothy Secomb (University of Arizona) for his continuing developmental support of Green's function PK–PD modeling capabilities and Prof. Secomb and Prof. Mark Dewhirst (Duke University) for the use of the digitized tumor networks. We also would like to thank the Cancer Research UK Centre for Drug Development, and their contractors, for major contributions to GMP synthesis of SN30000 (Dr. Nigel Westwood and the team at Onyx Scientific Ltd, Sunderland, the United Kingdom), formulation (Prof. Gavin Halbert and the Cancer Research UK Formulation Unit at Strathclyde), and GLP toxicology (Dr. David Edwards and Sequani Ltd, Ledbury, the United Kingdom).

References

1. Wilson, W. R.; Hay, M. P. Targeting Hypoxia in Cancer Therapy. *Nat. Rev. Cancer* **2011,** *11,* 393–410.
2. Vaupel, P.; Mayer, A. Hypoxia in Cancer: Significance and Impact on Clinical Outcome. *Cancer Metastasis Rev.* **2007,** *26,* 225–239.
3. Dewhirst, M. W.; Cao, Y.; Moeller, B. Cycling Hypoxia and Free Radicals Regulate Angiogenesis and Radiotherapy Response. *Nat. Rev. Cancer* **2008,** *8,* 425–437.
4. Wouters, B. G.; Brown, J. M. Cells at Intermediate Oxygen Levels Can Be More Important Than the "Hypoxic Fraction" in Determining Tumor Response to Fractionated Radiotherapy. *Radiat. Res.* **1997,** *147,* 541–550.
5. Hicks, K. O.; Siim, B. G.; Pruijn, F. B.; Wilson, W. R. Oxygen Dependence of the Metabolic Activation and Cytotoxicity of Tirapazamine: Implications for Extravascular Transport and Activity in Tumors. *Radiat. Res.* **2004,** *161,* 656–666.
6. Hicks, K. O.; Myint, H.; Patterson, A. V.; Pruijn, F. B.; Siim, B. G.; Patel, K.; Wilson, W. R. Oxygen Dependence and Extravascular Transport of Hypoxia-Activated Prodrugs: Comparison of the Dinitrobenzamide Mustard PR-104A and Tirapazamine. *Int. J. Radiat. Oncol. Biol. Phys.* **2007,** *69,* 560–571.
7. Tuttle, S. W.; Maity, A.; Oprysko, P. R.; Kachur, A. V.; Ayene, I. S.; Biaglow, J. E.; Koch, C. J. Detection of Reactive Oxygen Species via Endogenous Oxidative Pentose Phosphate Cycle Activity in Response to Oxygen Concentration. *J. Biol. Chem.* **2007,** *282,* 36790–36796.
8. Vaupel, P.; Hockel, M.; Mayer, A. Detection and Characterization of Tumor Hypoxia Using pO_2 Histography. *Antioxid. Redox Signal.* **2007,** *9,* 1221–1235.
9. McKeown, S. R. Defining Normoxia, Physoxia and Hypoxia in Tumours-Implications for Treatment Response. *Br. J. Radiol.* **2014,** *87,* 20130676.
10. Whillans, D. W.; Hunt, J. W. A Rapid-Mixing Comparison of the Mechanisms of Radiosensitization by Oxygen and Misonidazole in CHO Cells. *Radiat. Res.* **1982,** *90,* 126–141.
11. Horsman, M. R.; Mortensen, L. S.; Petersen, J. B.; Busk, M.; Overgaard, J. Imaging Hypoxia to Improve Radiotherapy Outcome. *Nat. Rev. Clin. Oncol.* **2012,** *9,* 674–687.
12. Semenza, G. L. Targeting HIF-1 for Cancer Therapy. *Nat. Rev. Cancer* **2003,** *3,* 721–732.
13. Koukourakis, M. I.; Bentzen, S. M.; Giatromanolaki, A.; Wilson, G. D.; Daley, F. M.; Saunders, M. I.; Dische, S.; Sivridis, E.; Harris, A. L. Endogenous Markers of Two Separate Hypoxia Response Pathways (Hypoxia Inducible Factor 2 Alpha and Carbonic Anhydrase 9) Are Associated With Radiotherapy Failure in Head and Neck Cancer Patients Recruited in the CHART Randomized Trial. *J. Clin. Oncol.* **2006,** *24,* 727–735.
14. Overgaard, J.; Eriksen, J. G.; Nordsmark, M.; Alsner, J.; Horsman, M. R. Danish Head and Neck Cancer Study Group Plasma Osteopontin, Hypoxia, and Response to the Hypoxia Sensitiser Nimorazole in Radiotherapy of Head and Neck Cancer: Results From the DAHANCA 5 Randomised Double-Blind Placebo-Controlled Trial. *Lancet Oncol.* **2005,** *6,* 757–764.
15. Brown, J. M. Evidence for Acutely Hypoxic Cells in Mouse Tumours, and a Possible Mechanism of Reoxygenation. *Br. J. Radiol.* **1979,** *52,* 650–656.
16. Chaplin, D. J.; Durand, R. E.; Olive, P. L. Acute Hypoxia in Tumors: Implications for Modifiers of Radiation Effects. *Int. J. Radiat. Oncol. Biol. Phys.* **1986,** *12,* 1279–1282.
17. Chaplin, D. J.; Olive, P. L.; Durand, R. E. Intermittent Blood Flow in a Murine Tumor: Radiobiological Effects. *Cancer Res.* **1987,** *47,* 597–601.
18. Lee, C. T.; Boss, M. K.; Dewhirst, M. W. Imaging Tumor Hypoxia to Advance Radiation Oncology. *Antioxid. Redox Signal.* **2014,** *21,* 313–337.
19. Semenza, G. L. Hypoxia and Cancer. *Cancer Metastasis Rev.* **2007,** *26,* 223–224.
20. Graeber, T. G.; Osmanian, C.; Jacks, T.; Housman, D. E.; Koch, C. J.; Lowe, S. W.; Giaccia, A. J. Hypoxia-Mediated Selection of Cells With Diminished Apoptotic Potential in Solid Tumours. *Nature* **1996,** *379,* 88–91.
21. Erler, J. T.; Cawthorne, C. J.; Williams, K. J.; Koritzinsky, M.; Wouters, B. G.; Wilson, C.; Miller, C.; Demonacos, C.; Stratford, I. J.; Dive, C. Hypoxia-Mediated Down-Regulation of Bid and Bax in Tumors Occurs via Hypoxia-Inducible Factor 1-Dependent and -Independent Mechanisms and Contributes to Drug Resistance. *Mol. Cell. Biol.* **2004,** *24,* 2875–2889.
22. Yotnda, P.; Wu, D.; Swanson, A. M. Hypoxic Tumours and Their Effect on Immune Cells and Cancer Therapy. *Methods Mol. Biol.* **2010,** *651,* 1–29.
23. Labiano, S.; Palazon, A.; Melero, I. Immune Response Regulation in the Tumor Microenvironment by Hypoxia. *Semin. Oncol.* **2015,** *42,* 378–386.
24. Gnarra, J. R.; Zhou, S.; Merrill, M. J.; Wagner, J. R.; Krumm, A.; Papavassiliou, E.; Oldfield, E. H.; Klausner, R. D.; Linehan, W. M. Post-Transcriptional Regulation of Vascular Endothelial Growth Factor mRNA by the Product of the VHL Tumor Suppressor Gene. *Proc. Natl. Acad. Sci. U. S. A.* **1996,** *93,* 10589–10594.
25. Kioi, M.; Vogel, H.; Schultz, G.; Hoffman, R. M.; Harsh, G. R.; Brown, J. M. Inhibition of Vasculogenesis, but Not Angiogenesis, Prevents the Recurrence of Glioblastoma After Irradiation in Mice. *J. Clin. Invest.* **2010,** *120,* 694–705.
26. Semenza, G. L. HIF-1: Upstream and Downstream of Cancer Metabolism. *Curr. Opin. Genet. Dev.* **2010,** *20,* 51–56.
27. Cairns, R. A.; Harris, I. S.; Mak, T. W. Regulation of Cancer Cell Metabolism. *Nat. Rev. Cancer* **2011,** *11,* 85–95.
28. Pennacchietti, S.; Michieli, P.; Galluzzo, M.; Mazzone, M.; Giordano, S.; Comoglio, P. M. Hypoxia Promotes Invasive Growth by Transcriptional Activation of the Met Proto-oncogene. *Cancer Cell* **2003,** *3,* 347–361.
29. Hill, R. P.; Marie-Egyptienne, D. T.; Hedley, D. W. Cancer Stem Cells, Hypoxia and Metastasis. *Semin. Radiat. Oncol.* **2009,** *19,* 106–111.

30. Chang, Q.; Jurisica, I.; Do, T.; Hedley, D. W. Hypoxia Predicts Aggressive Growth and Spontaneous Metastasis Formation From Orthotopically Grown Primary Xenografts of Human Pancreatic Cancer. *Cancer Res.* **2011,** *71,* 3110–3120.
31. Mujcic, H.; Hill, R. P.; Koritzinsky, M.; Wouters, B. G. Hypoxia Signaling and the Metastatic Phenotype. *Curr. Mol. Med.* **2014,** *14,* 565–579.
32. Guzy, R. D.; Hoyos, B.; Robin, E.; Chen, H.; Liu, L.; Mansfield, K. D.; Simon, M. C.; Hammerling, U.; Schumacker, P. T. Mitochondrial Complex III Is Required for Hypoxia-Induced ROS Production and Cellular Oxygen Sensing. *Cell Metab.* **2005,** *1,* 401–408.
33. Bristow, R. G.; Hill, R. P. Hypoxia, DNA Repair and Genetic Instability. *Nat. Rev. Cancer* **2008,** *8,* 180–192.
34. Scanlon, S. E.; Glazer, P. M. Multifaceted Control of DNA Repair Pathways by the Hypoxic Tumor Microenvironment. *DNA Repair* **2015,** *32,* 180–189.
35. Schwarz, G. About the Desensitisation Against X-Ray and Radium Rays. *Munch. Med. Wochenschr.* **1909,** *24,* 1217–1219.
36. Mottram, J. C. A Factor of Importance in the Radio Sensitivity of Tumours. *Br. J. Radiol.* **1936,** *9,* 606–614.
37. Gray, L. H.; Conger, A. D.; Ebert, M.; Hornsey, S.; Scott, O. C. Concentration of Oxygen Dissolved in Tissues at the Time of Irradiation as a Factor in Radiotherapy. *Br. J. Radiol.* **1953,** *26,* 638–648.
38. Thomlinson, R. H.; Gray, L. H. The Histological Structure of Some Human Lung Cancers and Possible Implications for Radiotherapy. *Br. J. Cancer* **1955,** *9,* 539–549.
39. Brizel, D. M.; Scully, S. P.; Harrelson, J. M.; Layfield, L. J.; Bean, J. M.; Prosnitz, L. R.; Dewhirst, M. W. Tumor Oxygenation Predicts for the Likelihood of Distant Metastases in Human Soft Tissue Sarcoma. *Cancer Res.* **1996,** *56,* 941–943.
40. Movsas, B.; Chapman, J. D.; Hanlon, A. L.; Horwitz, E. M.; Greenberg, R. E.; Stobbe, C.; Hanks, G. E.; Pollack, A. Hypoxic Prostate/Muscle pO_2 Ratio Predicts for Biochemical Failure in Patients With Prostate Cancer: Preliminary Findings. *Urology* **2002,** *60,* 634–639.
41. Fyles, A.; Milosevic, M.; Hedley, D.; Pintilie, M.; Levin, W.; Manchul, L.; Hill, R. P. Tumor Hypoxia Has Independent Predictor Impact Only in Patients With Node-Negative Cervix Cancer. *J. Clin. Oncol.* **2002,** *20,* 680–687.
42. Nordsmark, M.; Bentzen, S. M.; Rudat, V.; Brizel, D.; Lartigau, E.; Stadler, P.; Becker, A.; Adam, M.; Molls, M.; Dunst, J.; Terris, D. J.; Overgaard, J. Prognostic Value of Tumor Oxygenation in 397 Head and Neck Tumors After Primary Radiation Therapy. An International Multi-Center Study. *Radiother. Oncol.* **2005,** *77,* 18–24.
43. Toustrup, K.; Sorensen, B. S.; Nordsmark, M.; Busk, M.; Wiuf, C.; Alsner, J.; Overgaard, J. Development of a Hypoxia Gene Expression Classifier With Predictive Impact for Hypoxic Modification of Radiotherapy in Head and Neck Cancer. *Cancer Res.* **2011,** *71,* 5923–5931.
44. Kaanders, J. H.; Wijffels, K. I.; Marres, H. A.; Ljungkvist, A. S.; Pop, L. A.; van den Hoogen, F. J.; de Wilde, P. C.; Bussink, J.; Raleigh, J. A.; van der Kogel, A. J. Pimonidazole Binding and Tumor Vascularity Predict for Treatment Outcome in Head and Neck Cancer. *Cancer Res.* **2002,** *62,* 7066–7074.
45. Evans, S. M.; Du, K. L.; Chalian, A. A.; Mick, R.; Zhang, P. J.; Hahn, S. M.; Quon, H.; Lustig, R.; Weinstein, G. S.; Koch, C. J. Patterns and Levels of Hypoxia in Head and Neck Squamous Cell Carcinomas and Their Relationship to Patient Outcome. *Int. J. Radiat. Oncol. Biol. Phys.* **2007,** *69,* 1024–1031.
46. Rischin, D.; Hicks, R. J.; Fisher, R.; Binns, D.; Corry, J.; Porceddu, S.; Peters, L. J. Trans-Tasman Radiation Oncology Group Prognostic Significance of [18F]-Misonidazole Positron Emission Tomography-Detected Tumor Hypoxia in Patients With Advanced Head and Neck Cancer Randomly Assigned to Chemoradiation With or Without Tirapazamine: A Substudy of Trans-Tasman Radiation Oncology Group Study 98.02. *J. Clin. Oncol.* **2006,** *24,* 2098–2104.
47. Buffa, F. M.; Harris, A. L.; West, C. M.; Miller, C. R. Large Meta-Analysis of Multiple Cancers Reveals a Common, Compact and Highly Prognostic Hypoxia Metagene. *Br. J. Cancer* **2010,** *102,* 428–435.
48. van Malenstein, H.; Gevaert, O.; Libbrecht, L.; Daemen, A.; Allemeersch, J.; Nevens, F.; Van Cutsem, E.; Cassiman, D.; De Moor, B.; Verslype, C.; van Pelt, J. A Seven-Gene Set Associated With Chronic Hypoxia of Prognostic Importance in Hepatocellular Carcinoma. *Clin. Cancer Res.* **2010,** *16,* 4278–4288.
49. Tan, E. Y.; Yan, M.; Campo, L.; Han, C.; Takano, E.; Turley, H.; Candiloro, I.; Pezzella, F.; Gatter, K. C.; Millar, E. K.; O'Toole, S. A.; McNeil, C. M.; Crea, P.; Segara, D.; Sutherland, R. L.; Harris, A. L.; Fox, S. B. The Key Hypoxia Regulated Gene CAIX Is Upregulated in Basal-Like Breast Tumours and Is Associated With Resistance to Chemotherapy. *Br. J. Cancer* **2009,** *100,* 405–411.
50. Heldin, C. H.; Rubin, K.; Pietras, K.; Ostman, A. High Interstitial Fluid Pressure—An Obstacle in Cancer Therapy. *Nat. Rev. Cancer* **2004,** *4,* 806–813.
51. Minchinton, A. I.; Tannock, I. F. Drug Penetration in Solid Tumours. *Nat. Rev. Cancer* **2006,** *6,* 583–592.
52. Rohwer, N.; Cramer, T. Hypoxia-Mediated Drug Resistance: Novel Insights on the Functional Interaction of HIFs and Cell Death Pathways. *Drug Resist. Updat.* **2011,** *14,* 191–201.
53. Warfel, N. A.; El-Deiry, W. S. HIF-1 Signaling in Drug Resistance to Chemotherapy. *Curr. Med. Chem.* **2014,** *21,* 3021–3028.
54. Kallman, R. F.; Dorie, M. J. Tumor Oxygenation and Reoxygenation During Radiation Therapy: Their Importance in Predicting Tumor Response. *Int. J. Radiat. Oncol. Biol. Phys.* **1986,** *12,* 681–685.
55. Bennett, M. H.; Feldmeier, J.; Smee, R.; Milross, C. Hyperbaric Oxygenation for Tumour Sensitisation to Radiotherapy. *Cochrane Database Syst. Rev.* **2012,** *4.* http://dx.doi.org/10.1002/14651858.CD005007.pub3. Art. No.: *CD005007.*
56. Saunders, M.; Dische, S. Clinical Results of Hypoxic Cell Radiosensitisation From Hyperbaric Oxygen to Accelerated Radiotherapy, Carbogen and Nicotinamide. *Br. J. Cancer* **1996,** *27,* S271–S278.
57. Kaanders, J. H.; Pop, L. A.; Marres, H. A.; Bruaset, I.; van den Hoogen, F. J.; Merkx, M. A.; van der Kogel, A. J. ARCON: Experience in 215 Patients With Advanced Head-and-Neck Cancer. *Int. J. Radiat. Oncol. Biol. Phys.* **2002,** *52,* 769–778.
58. Janssens, G. O.; Rademakers, S. E.; Terhaard, C. H.; Doornaert, P. A.; Bijl, H. P.; van den Ende, P.; Chin, A.; Marres, H. A.; de Bree, R.; van der Kogel, A. J.; Hoogsteen, I. J.; Bussink, J.; Span, P. N.; Kaanders, J. H. Accelerated Radiotherapy With Carbogen and Nicotinamide for Laryngeal Cancer: Results of a Phase III Randomized Trial. *J. Clin. Oncol.* **2012,** *30,* 1777–1783.
59. Wardman, P. Chemical Radiosensitizers for Use in Radiotherapy. *Clin. Oncol.* **2007,** *19,* 397–417.
60. Dische, S. Chemical Sensitisers for Hypoxic Cells: A Decade of Experience in Clinical Radiotherapy. *Radiother. Oncol.* **1985,** *3,* 97–115.
61. Overgaard, J. Clinical Evaluation of Nitroimidazoles as Modifiers of Hypoxia in Solid Tumors. *Oncol. Res.* **1994,** *6,* 509–518.
62. Adams, G. E.; Dische, S.; Fowler, J. F.; Thomlinson, R. H. Hypoxic Cell Sensitisers in Radiotherapy. *Lancet* **1976,** *1,* 186–188.
63. Brown, J. M.; Yu, N. Y.; Brown, D. M.; Lee, W. W. SR-2508: A 2-Nitroimidazole Amide Which Should Be Superior to Misonidazole as a Radiosensitizer for Clinical Use. *Int. J. Radiat. Oncol. Biol. Phys.* **1981,** *7,* 695–703.
64. Grigsby, P. W.; Winter, K.; Wasserman, T. H.; Marcial, V.; Rotman, M.; Cooper, J.; Keys, H.; Asbell, S. O.; Phillips, T. L. Irradiation With or Without Misonidazole for Patients With Stages IIIB and IVA Carcinoma of the Cervix: Final Results of RTOG 80-05. Radiation Therapy Oncology Group. *Int. J. Radiat. Oncol. Biol. Phys.* **1999,** *44,* 513–517.
65. Eschwege, F.; Sancho-Garnier, H.; Chassagne, D.; Brisgand, D.; Guerra, M.; Malaise, E. P.; Bey, P.; Busutti, L.; Cionini, L.; N'Guyen, T.; Romanini, A.; Chavaudra, J.; Hill, C. Results of a European Randomized Trial of Etanidazole Combined With Radiotherapy in Head and Neck Carcinomas. *Int. J. Radiat. Oncol. Biol. Phys.* **1997,** *39,* 275–281.
66. Lee, D. J.; Cosmatos, D.; Marcial, V. A.; Fu, K. K.; Rotman, M.; Cooper, J. S.; Ortiz, H. G.; Beitler, J. J.; Abrams, R. A.; Curran, W. J. Results of an RTOG Phase III Trial (RTOG 85-27) Comparing Radiotherapy Plus Etanidazole With Radiotherapy Alone for Locally Advanced Head and Neck Carcinomas [comment]. *Int. J. Radiat. Oncol. Biol. Phys.* **1995,** *32,* 567–576.
67. Overgaard, J.; Overgaard, M.; Nielsen, O. S.; Pedersen, A. K.; Timothy, A. R. A Comparative Investigation of Nimorazole and Misonidazole as Hypoxic Radiosensitizers in a C3H Mammary Carcinoma In Vivo. *Br. J. Cancer* **1982,** *46,* 904–911.
68. Overgaard, J.; Overgaard, M.; Timothy, A. R. Studies of the Pharmacokinetic Properties of Nimorazole. *Br. J. Cancer* **1983,** *48,* 27–34.
69. Overgaard, J.; Hansen, H. S.; Overgaard, M.; Bastholt, L.; Berthelsen, A.; Specht, L.; Lindelov, B.; Jorgensen, K. A. A Randomized Double-Blind Phase III Study of Nimorazole as a Hypoxic Radiosensitizer of Primary Radiotherapy in Supraglottic Larynx and Pharynx Carcinoma. Results of the Danish Head and Neck Cancer Study (DAHANCA) Protocol 5-85. *Radiother. Oncol.* **1998,** *46,* 135–146.
70. Overgaard, J. Hypoxic Modification of Radiotherapy in Squamous Cell Carcinoma of the Head and Neck—A Systematic Review and Meta-Analysis. *Radiother. Oncol.* **2011,** *100,* 22–32.

71. Toustrup, K.; Sorensen, B. S.; Lassen, P.; Wiuf, C.; Alsner, J.; Overgaard, J. Gene Expression Classifier Predicts for Hypoxic Modification of Radiotherapy With Nimorazole in Squamous Cell Carcinomas of the Head and Neck. *Radiother. Oncol.* **2012,** *102,* 122–129.
72. Brown, J. M.; Wilson, W. R. Exploiting Tumor Hypoxia in Cancer Treatment. *Nat. Rev. Cancer* **2004,** *4,* 437–447.
73. Stratford, I. J.; Williams, K. J.; Cowen, R. L.; Jaffar, M. Combining Bioreductive Drugs and Radiation for the Treatment of Solid Tumors. *Semin. Radiat. Oncol.* **2003,** *13,* 42–52.
74. Chen, Y.; Hu, L. Design of Anticancer Prodrugs for Reductive Activation. *Med. Res. Rev.* **2009,** *29,* 29–64.
75. Sartorelli, A. C. Therapeutic Attack of Hypoxic Cells of Solid Tumors: Presidential Address. *Cancer Res.* **1988,** *48,* 775–778.
76. Denny, W. A.; Wilson, W. R.; Hay, M. P. Recent Developments in the Design of Bioreductive Drugs. *Br. J. Cancer* **1996,** *74,* S32–S38.
77. Mason, R. P.; Holtzman, J. L. The Role of Catalytic Superoxide Formation in the O_2 Inhibition of Nitroreductase. *Biochem. Biophys. Res. Commun.* **1975,** *67,* 1267–1274.
78. Nelson, S. Metabolic Activation and Drug Toxicity. *J. Med. Chem.* **1982,** *25,* 753–765.
79. Schwartz, H. S.; Sodergren, J. E.; Philips, F. S. Mitomycin C: Chemical and Biological Studies on Alkylation. *Science* **1963,** *142,* 1181–1183.
80. Iyer, V. N.; Szybalski, W. Mitomycins and Porfiromycins: Chemical Mechanism of Activation and Cross-Linking of DNA. *Science* **1964,** *145,* 55–58.
81. Bachur, N. R.; Gordon, S. L.; Gee, M. V. A General Mechanism for Microsomal Activation of Quinone Anticancer Agents to Free Radicals. *Cancer Res.* **1978,** *38,* 1745–1750.
82. Kennedy, K. A.; Rockwell, S.; Sartorelli, A. C. Preferential Activation of Mitomycin C to Cytotoxic Metabolites by Hypoxic Tumor Cells. *Cancer Res.* **1980,** *40,* 2356–2360.
83. Lin, A. J.; Cosby, L. A.; Shanky, C. W.; Sartorelli, A. C. Potential Bioreductive Alkylating Agents. I. Benzoquinone Derivatives. *J. Med. Chem.* **1972,** *15,* 1247–1252.
84. Phillips, R. M.; Hendriks, H. R.; Peters, G. J. EO9 (Apaziquone): From the Clinic to the Laboratory and Back Again. *Br. J. Pharmacol.* **2013,** *168,* 11–18.
85. Bailey, S. M.; Wyatt, M. D.; Friedlos, F.; Hartley, J. A.; Knox, R. J.; Lewis, A. D.; Workman, P. Involvement of DT-Diaphorase (EC 1.6.99.2) in the DNA Cross-Linking and Sequence Selectivity of the Bioreductive Anti-Tumour Agent EO9. *Br. J. Cancer* **1997,** *76,* 1596–1603.
86. van der Heijden, A. G.; Moonen, P. M.; Cornel, E. B.; Vergunst, H.; de Reijke, T. M.; van Boven, E.; Barten, E. J.; Puri, R.; van Kalken, C. K.; Witjes, J. A. Phase II Marker Lesion Study With Intravesical Instillation of Apaziquone for Superficial Bladder Cancer: Toxicity and Marker Response. *J. Urol.* **2006,** *176,* 1349–1353.
87. Naylor, M. A.; Stephens, M. A.; Stratford, I. J.; Keohane, A.; O'Neill, P.; Threadgill, M. D.; Webb, P.; Fielden, E. M.; Adams, G. E. Aziridinyl Nitropyrroles and Nitropyrazoles as Hypoxia-Selective Cytotoxins and Radiosensitizers. *Anticancer Drug Des.* **1991,** *6,* 151–167.
88. Jenkins, T. C.; Naylor, M. A.; O'Neill, P.; Threadgill, M. D.; Cole, S.; Stratford, I. J.; Adams, G. E.; Fielden, E. M.; Suto, M. J.; Stier, M. A. Synthesis and Evaluation of Alpha-[[(2-haloethyl)amino]methyl]-2-nitro-1H-imidazole-1-ethanols as Prodrugs of Alpha-[(1-aziridinyl)methyl]-2-nitro-1H-imidazole-1-ethanol (RSU-1069) and Its Analogues Which Are Radiosensitizers and Bioreductively Activated Cytotoxins. *J. Med. Chem.* **1990,** *33,* 2603–2610.
89. Naylor, M. A.; Threadgill, M. D.; Webb, P.; Stratford, I. J.; Stephens, M. A.; Fielden, E. M.; Adams, G. E. 2-Nitroimidazole Dual-Function Bioreductive Drugs: Studies on the Effects of Regioisomerism and Side-Chain Structural Modifications on Differential Cytotoxicity and Radiosensitization by Aziridinyl and Oxiranyl Derivatives. *J. Med. Chem.* **1992,** *35,* 3573–3578.
90. Naylor, M. A.; Threadgill, M. D.; Showalter, H. D.; Stratford, I. J.; Stephens, M. A.; Fielden, E. M.; Adams, G. E. Synthesis of the Enantiomers of the Bioreductively-Activated Cytotoxin RSU-1069 and Its Prodrug RB6145 and Lack of Stereoselectivity in Their Cytotoxicity and Radiosensitization In Vitro. *Drug Des. Discov.* **1993,** *10,* 249–255.
91. Threadgill, M. D.; Webb, P.; O'Neill, P.; Naylor, M. A.; Stephens, M. A.; Stratford, I. J.; Cole, S.; Adams, G. E.; Fielden, E. M. Synthesis of a Series of Nitrothiophenes With Basic or Electrophilic Substituents and Evaluation as Radiosensitizers and as Bioreductively Activated Cytotoxins. *J. Med. Chem.* **1991,** *34,* 2112–2120.
92. Suto, M. J.; Stier, M. A.; Werbel, L. M. Dual-Function Radiosensitizers. Alpha-[[(2-bromoethyl)amino]methyl]-2-nitro-1H-imidazole-1-ethanol and Related Compounds: Preparation via an Aziridine Equivalent. *J. Med. Chem.* **1991,** *34,* 1207–1209.
93. Lee, A. E.; Wilson, W. R. Hypoxia-Dependent Retinal Toxicity of Bioreductive Anticancer Prodrugs in Mice. *Toxicol. Appl. Pharmacol.* **2000,** *163,* 50–59.
94. Denny, W. A.; Wilson, W. R. Considerations for the Design of Nitrophenyl Mustards as Agents With Selective Toxicity for Hypoxic Tumor Cells. *J. Med. Chem.* **1986,** *29,* 879–887.
95. Palmer, B. D.; Wilson, W. R.; Pullen, S. M.; Denny, W. A. Hypoxia-Selective Antitumor Agents. 3. Relationships Between Structure and Cytotoxicity Against Cultured Tumor Cells for Substituted *N,N*-Bis(2-chloroethyl)anilines. *J. Med. Chem.* **1990,** *33,* 112–121.
96. Palmer, B. D.; Wilson, W. R.; Denny, W. A. Nitro Analogues of Chlorambucil as Potential Hypoxia-Selective Anti-Tumour Drugs. *Anticancer Drug Des.* **1990,** *5,* 337–349.
97. Palmer, B. D.; Wilson, W. R.; Cliffe, S.; Denny, W. A. Hypoxia-Selective Antitumor Agents. 5. Synthesis of Water-Soluble Nitroaniline Mustards With Selective Cytotoxicity for Hypoxic Mammalian Cells. *J. Med. Chem.* **1992,** *35,* 3214–3222.
98. Palmer, B. D.; Wilson, W. R.; Atwell, G. J.; Schultz, D.; Xu, X. Z.; Denny, W. A. Hypoxia-Selective Antitumor Agents. 9. Structure-Activity Relationships for Hypoxia-Selective Cytotoxicity Among Analogues of 5-[*N,N*-Bis(2-chloroethyl)amino]-2,4-dinitrobenzamide. *J. Med. Chem.* **1994,** *37,* 2175–2184.
99. Palmer, B. D.; van Zijl, P.; Denny, W. A.; Wilson, W. R. Reductive Chemistry of the Novel Hypoxia-Selective Cytotoxin 5-[*N, N*-Bis(2-chloroethyl)amino]-2,4-dinitrobenzamide. *J. Med. Chem.* **1995,** *38,* 1229–1241.
100. Palmer, B. D.; Wilson, W. R.; Anderson, R. F.; Boyd, M.; Denny, W. A. Hypoxia-Selective Antitumor Agents. 14. Synthesis and Hypoxic Cell Cytotoxicity of Regioisomers of the Hypoxia-Selective Cytotoxin 5-[*N,N*-Bis(2-chloroethyl)amino]-2,4-dinitrobenzamide. *J. Med. Chem.* **1996,** *39,* 2518–2528.
101. Patterson, A. V.; Ferry, D. M.; Edmunds, S. J.; Gu, Y.; Singleton, R. S.; Patel, K.; Pullen, S. M.; Hicks, K. O.; Syddall, S. P.; Atwell, G. J.; Yang, S.; Denny, W. A.; Wilson, W. R. Mechanism of Action and Preclinical Antitumor Activity of the Novel Hypoxia-Activated DNA Crosslinking Agent PR-104. *Clin. Cancer Res.* **2007,** *13,* 3922–3932.
102. Guise, C. P.; Wang, A.; Thiel, A.; Bridewell, D.; Wilson, W. R.; Patterson, A. V. Identification of Human Reductases That Activate the Dinitrobenzamide Mustard Prodrug PR-104A: A Role for NADPH:Cytochrome P450 Oxidoreductase Under Hypoxia. *Biochem. Pharmacol.* **2007,** *74,* 810–820.
103. Guise, C. P.; Abbattista, M. R.; Tipparaju, S. R.; Lambie, N. K.; Su, J.; Li, D.; Wilson, W. R.; Dachs, G. U.; Patterson, A. V. Diflavin Oxidoreductases Activate the Bioreductive Prodrug PR-104A Under Hypoxia. *Mol. Pharmacol.* **2012,** *81,* 31–40.
104. Singleton, R. S.; Guise, C. P.; Ferry, D. M.; Pullen, S. M.; Dorie, M. J.; Brown, J. M.; Patterson, A. V.; Wilson, W. R. DNA Crosslinks in Human Tumor Cells Exposed to the Prodrug PR-104A: Relationships to Hypoxia, Bioreductive Metabolism and Cytotoxicity. *Cancer Res.* **2009,** *69,* 3884–3891.
105. Guise, C. P.; Abbattista, M.; Singleton, R. S.; Holford, S. D.; Connolly, J.; Dachs, G. U.; Fox, S. B.; Pollock, R.; Harvey, J.; Guilford, P.; Donate, F.; Wilson, W. R.; Patterson, A. V. The Bioreductive Prodrug PR-104A Is Activated Under Aerobic Conditions by Human Aldo-Keto Reductase 1C3. *Cancer Res.* **2010,** *70,* 1573–1584.
106. Houghton, P. J.; Lock, R.; Carol, H.; Morton, C. L.; Phelps, D.; Gorlick, R.; Kolb, E. A.; Keir, S. T.; Reynolds, C. P.; Kang, M. H.; Maris, J. M.; Wozniac, A. W.; Gu, Y.; Wilson, W. R.; Smith, M. A. Initial Testing of the Hypoxia Activated Prodrug PR-104 by the Pediatric Preclinical Testing Program. *Pediatr. Blood Cancer* **2011,** *57,* 443–453.
107. Jameson, M. B.; Rischin, D.; Pegram, M.; Gutheil, J.; Patterson, A. V.; Denny, W. A.; Wilson, W. R. A Phase I Trial of PR-104, a Nitrogen Mustard Prodrug Activated by Both Hypoxia and Aldo-Keto Reductase 1C3, in Patients With Solid Tumors. *Cancer Chemother. Pharmacol.* **2010,** *65,* 791–801.
108. McKeage, M. J.; Gu, Y.; Wilson, W. R.; Hill, A.; Amies, K.; Melink, T. J.; Jameson, M. B. A Phase I Trial of PR-104, a Pre-Prodrug of the Bioreductive Prodrug PR-104A, Given Weekly to Solid Tumour Patients. *BMC Cancer* **2011,** *11,* 432.
109. Konopleva, M.; Thall, P. F.; Arana, Y. C.; Borthakur, G.; Coveler, A.; Bueso-Ramos, C.; Benito, J.; Konoplev, S.; Gu, Y.; Ravandi, F.; Jabbour, E.; Faderl, S.; Thomas, D.; Cortes, J.; Kadia, T.; Kornblau, S.; Daver, N.; Pemmaraju, N.; Nguyen, H. Q.; Feliu, J.; Lu, H.; Wei, C.; Wilson, W. R.; Melink, T. J.; Gutheil, J. C.; Andreeff, M.; Estey, E. H.; Kantarjian, H. Phase I/II Study of the Hypoxia-Activated Prodrug PR104 in Refractory/Relapsed Acute Myeloid Leukemia and Acute Lymphoblastic Leukemia. *Haematologica* **2015,** *100,* 927–934.
110. Down, J.; Parmar, K.; D'Andrea, A. D.; Donate, F.; Patterson, A. V.; Wilson, W. R. Aldo-Keto Reductase 1C3 as a Novel Target for the Aerobic Activation of the Prodrug PR-104A in Human Hematopoietic Cells. Proceedings of 56th Annual Meeting Radiation Research Society, Maui, Hawaii, September 25–29, 2010; PS7.95.
111. Abbattista, M. R.; Jamieson, S. M.; Gu, Y.; Nickel, J. E.; Pullen, S. M.; Patterson, A. V.; Wilson, W. R.; Guise, C. P. Pre-Clinical Activity of PR-104 as Monotherapy and in Combination With Sorafenib in Hepatocellular Carcinoma. *Cancer Biol. Ther.* **2015,** *16,* 610–622.

112. Jamieson, S. M.; Gu, Y.; Manesh, D. M.; El-Hoss, J.; Jing, D.; MacKenzie, K. L.; Guise, C. P.; Foehrenbacher, A.; Pullen, S. M.; Benito, J.; Smaill, J. B.; Patterson, A. V.; Mulaw, M. A.; Konopleva, M.; Bohlander, S. K.; Lock, R. B.; Wilson, W. R. A Novel Fluorometric Assay for Aldo-Keto Reductase 1C3 Predicts Metabolic Activation of the Nitrogen Mustard Prodrug PR-104A in Human Leukaemia Cells. *Biochem. Pharmacol.* **2014,** *88,* 36–45.
113. Manesh, D. M.; El-Hoss, J.; Evans, K.; Richmond, J.; Toscan, C. E.; Bracken, L. S.; Hedrick, A.; Sutton, R.; Marshall, G. M.; Wilson, W. R.; Kurmasheva, R. T.; Billups, C.; Houghton, P. J.; Smith, M. A.; Carol, H.; Lock, R. B. AKR1C3 Is a Biomarker of Sensitivity to PR-104 in Preclinical Models of T-Cell Acute Lymphoblastic Leukemia. *Blood* **2015,** *126,* 1193–1202.
114. Borch, R. F.; Liu, J.; Schmidt, J. P.; Marakovits, J. T.; Joswig, C.; Gipp, J. J.; Mulcahy, R. T. Synthesis and Evaluation of Nitroheterocyclic Phosphoramidates as Hypoxia-Selective Alkylating Agents. *J. Med. Chem.* **2000,** *43,* 2258–2265.
115. Borch, R. F.; Liu, J.; Joswig, C.; Baggs, R. B.; Dexter, D. L.; Mangold, G. L. Antitumor Activity and Toxicity of Novel Nitroheterocyclic Phosphoramidates. *J. Med. Chem.* **2001,** *44,* 74–77.
116. Duan, J. X.; Jiao, H.; Kaizerman, J.; Stanton, T.; Evans, J. W.; Lan, L.; Lorente, G.; Banica, M.; Jung, D.; Wang, J.; Ma, H.; Li, X.; Yang, Z.; Hoffman, R. M.; Ammons, W. S.; Hart, C. P.; Matteucci, M. Potent and Highly Selective Hypoxia-Activated Achiral Phosphoramidate Mustards as Anticancer Drugs. *J. Med. Chem.* **2008,** *51,* 2412–2420.
117. Meng, F.; Evans, J. W.; Bhupathi, D.; Banica, M.; Lan, L.; Lorente, G.; Duan, J. X.; Cai, X.; Mowday, A. M.; Guise, C. P.; Maroz, A.; Anderson, R. F.; Patterson, A. V.; Stachelek, G. C.; Glazer, P. M.; Matteucci, M. D.; Hart, C. P. Molecular and Cellular Pharmacology of the Hypoxia-Activated Prodrug TH-302. *Mol. Cancer Ther.* **2012,** *11,* 740–751.
118. Hunter, F. W.; Hsu, H. L.; Su, J.; Pullen, S. M.; Wilson, W. R.; Wang, J. Dual Targeting of Hypoxia and Homologous Recombination Repair Dysfunction in Triple-Negative Breast Cancer. *Mol. Cancer Ther.* **2014,** *13,* 2501–2514.
119. Sun, J. D.; Liu, Q.; Wang, J.; Ahluwalia, D.; Ferraro, D.; Wang, Y.; Duan, J. X.; Ammons, W. S.; Curd, J. G.; Matteucci, M. D.; Hart, C. P. Selective Tumor Hypoxia Targeting by Hypoxia-Activated Prodrug TH-302 Inhibits Tumor Growth in Preclinical Models of Cancer. *Clin. Cancer Res.* **2012,** *18,* 758–770.
120. Liu, Q.; Sun, J. D.; Wang, J.; Ahluwalia, D.; Baker, A. F.; Cranmer, L. D.; Ferraro, D.; Wang, Y.; Duan, J. X.; Ammons, W. S.; Curd, J. G.; Matteucci, M. D.; Hart, C. P. TH-302, a Hypoxia-Activated Prodrug With Broad *in vivo* Preclinical Combination Therapy Efficacy: Optimization of Dosing Regimens and Schedules. *Cancer Chemother. Pharmacol.* **2012,** *69,* 1487–1498.
121. Chawla, S. P.; Cranmer, L. D.; Van Tine, B. A.; Reed, D. R.; Okuno, S. H.; Butrynski, J. E.; Adkins, D. R.; Hendifar, A. E.; Kroll, S.; Ganjoo, K. N. Phase II Study of the Safety and Antitumor Activity of the Hypoxia-Activated Prodrug TH-302 in Combination With Doxorubicin in Patients With Advanced Soft Tissue Sarcoma. *J. Clin. Oncol.* **2014,** *32,* 3299–3306.
122. Borad, M. J.; Reddy, S. G.; Bahary, N.; Uronis, H. E.; Sigal, D.; Cohn, A. L.; Schelman, W. R.; Stephenson, J., Jr.; Chiorean, E. G.; Rosen, P. J.; Ulrich, B.; Dragovich, T.; Del Prete, S. A.; Rarick, M.; Eng, C.; Kroll, S.; Ryan, D. P. Randomized Phase II Trial of Gemcitabine Plus TH-302 Versus Gemcitabine in Patients With Advanced Pancreatic Cancer. *J. Clin. Oncol.* **2015,** *33,* 1475–1481.
123. Zeman, E. M.; Brown, J. M.; Lemmon, M. J.; Hirst, V. K.; Lee, W. W. SR-4233: A New Bioreductive Agent With High Selective Toxicity for Hypoxic Mammalian Cells. *Int. J. Radiat. Oncol. Biol. Phys.* **1986,** *12,* 1239–1242.
124. Brown, J. M. SR 4233 (Tirapazamine): A New Anticancer Drug Exploiting Hypoxia in Solid Tumours. *Br. J. Cancer* **1993,** *67,* 1163–1170.
125. Brown, M.; Henry, S. Kaplan Distinguished Scientist Award Lecture 2007. The Remarkable Yin and Yang of Tumour Hypoxia. *Int. J. Radiat. Biol.* **2007,** *2010* (86), 907–917.
126. Ghatage, P.; Sabagh, H. Is There a Role for Tirapazamine in the Treatment of Cervical Cancer? *Expert Opin. Drug Metab. Toxicol.* **2012,** *8,* 1589–1597.
127. Zeman, E. M.; Baker, M. A.; Lemmon, M. J.; Pearson, C. I.; Adams, J. A.; Brown, J. M.; Lee, W. W.; Tracy, M. Structure-Activity Relationships for Benzotriazine Di-N-Oxides. *Int. J. Radiat. Oncol. Biol. Phys.* **1989,** *16,* 977–981.
128. Koch, C. J. Unusual Oxygen Concentration Dependence of Toxicity of SR-4233, a Hypoxic Cell Toxin. *Cancer Res.* **1993,** *53,* 3992–3997.
129. Hay, M. P.; Gamage, S. A.; Kovacs, M. S.; Pruijn, F. B.; Anderson, R. F.; Patterson, A. V.; Wilson, W. R.; Brown, J. M.; Denny, W. A. Structure-Activity Relationships of 1,2,4-Benzotriazine 1,4-Dioxides as Hypoxia-Selective Analogues of Tirapazamine. *J. Med. Chem.* **2003,** *46,* 169–182.
130. Fitzsimmons, S. A.; Lewis, A. D.; Riley, R. J.; Workman, P. Reduction of 3-Amino-1,2,4-benzotriazine-1,4-di-N-oxide (Tirapazamine, WIN 59075, SR 4233) to a DNA-Damaging Species: A Direct Role for NADPH:Cytochrome P450 Oxidoreductase. *Carcinogenesis* **1994,** *15,* 1503–1510.
131. Patterson, A. V.; Saunders, M. P.; Chinje, E. C.; Talbot, D. C.; Harris, A. L.; Stratford, I. J. Overexpression of Human NADPH:Cytochrome *c* (P450) Reductase Confers Enhanced Sensitivity to Both Tirapazamine (SR 4233) and RSU 1069. *Br. J. Cancer* **1997,** *76,* 1338–1347.
132. Chinje, E. C.; Cowen, R. L.; Feng, J.; Sharma, S. P.; Wind, N. S.; Harris, A. L.; Stratford, I. J. Non-Nuclear Localized Human NOSII Enhances the Bioactivation and Toxicity of Tirapazamine (SR4233) In Vitro. *Mol. Pharmacol.* **2003,** *63,* 1248–1255.
133. Evans, J. W.; Yudoh, K.; Delahoussaye, Y. M.; Brown, J. M. Tirapazamine Is Metabolized to Its DNA-Damaging Radical by Intranuclear Enzymes. *Cancer Res.* **1998,** *58,* 2098–2101.
134. Baker, M. A.; Zeman, E. M.; Hirst, V. K.; Brown, J. M. Metabolism of SR 4233 by Chinese Hamster Ovary Cells: Basis of Selective Hypoxic Cytotoxicity. *Cancer Res.* **1988,** *48,* 5947–5952.
135. Laderoute, K.; Wardman, P.; Rauth, A. M. Molecular Mechanisms for the Hypoxia-Dependent Activation of 3-Amino-1,2,4-benzotriazine-1,4-dioxide (SR 4233). *Biochem. Pharmacol.* **1988,** *37,* 1487–1495.
136. Daniels, J. S.; Gates, K. S. DNA Cleavage by the Antitumor Agent 3-Amino-1,2,4-benzotriazine 1,4-Dioxide (SR4233): Evidence for Involvement of Hydroxyl Radical. *J. Am. Chem. Soc.* **1996,** *118,* 3380–3385.
137. Anderson, R. F.; Shinde, S. S.; Hay, M. P.; Gamage, S. A.; Denny, W. A. Activation of 3-Amino-1,2,4-benzotriazine 1,4-Dioxide Antitumor Agents to Oxidizing Species Following Their One-Electron Reduction. *J. Am. Chem. Soc.* **2003,** *125,* 748–756.
138. Chowdhury, G.; Junnotula, V.; Daniels, J. S.; Greenberg, M. M.; Gates, K. S. DNA Strand Damage Product Analysis Provides Evidence That the Tumor Cell-Specific Cytotoxin Tirapazamine Produces Hydroxyl Radical and Acts as a Surrogate for O_2. *J. Am. Chem. Soc.* **2007,** *129,* 12870–12877.
139. Shen, X.; Rajapakse, A.; Gallazzi, F.; Junnotula, V.; Fuchs-Knotts, T.; Glaser, R.; Gates, K. S. Isotopic Labeling Experiments That Elucidate the Mechanism of DNA Strand Cleavage by the Hypoxia-Selective Antitumor Agent 1,2,4-Benzotriazine 1,4-di-N-oxide. *Chem. Res. Toxicol.* **2014,** *27,* 111–118.
140. Shinde, S. S.; Hay, M. P.; Patterson, A. V.; Denny, W. A.; Anderson, R. F. Spin Trapping of Radicals Other Than the ·OH Radical Upon Reduction of the Anticancer Agent Tirapazamine by Cytochrome P450 Reductase. *J. Am. Chem. Soc.* **2009,** *131,* 14220–14221.
141. Shinde, S. S.; Maroz, A.; Hay, M. P.; Patterson, A. V.; Denny, W. A.; Anderson, R. F. Characterization of Radicals Formed Following Enzymatic Reduction of 3-Substituted Analogues of the Hypoxia-Selective Cytotoxin 3-Amino-1,2,4-benzotriazine 1,4-Dioxide (Tirapazamine). *J. Am. Chem. Soc.* **2010,** *132,* 2591–2599.
142. Yadav, P.; Marshall, A. J.; Reynisson, J.; Denny, W. A.; Hay, M. P.; Anderson, R. F. Fragmentation of the Quinoxaline N-Oxide Bond to the OH Radical Upon One-Electron Bioreduction. *Chem. Commun.* **2014,** *50,* 13729–13731.
143. Yin, J.; Glaser, R.; Gates, K. S. Electron and Spin-Density Analysis of Tirapazamine Reduction Chemistry. *Chem. Res. Toxicol.* **2012,** *25,* 620–633.
144. Yin, J.; Glaser, R.; Gates, K. S. On the Reaction Mechanism of Tirapazamine Reduction Chemistry: Unimolecular N-OH Homolysis, Stepwise Dehydration, or Triazene Ring-Opening. *Chem. Res. Toxicol.* **2012,** *25,* 634–645.
145. Olive, P. L.; Vikse, C. M.; Banath, J. P. Use of the Comet Assay to Identify Cells Sensitive to Tirapazamine in Multicell Spheroids and Tumors in Mice. *Cancer Res.* **1996,** *56,* 4460–4463.
146. Siim, B. G.; van Zijl, P. L.; Brown, J. M. Tirapazamine-Induced DNA Damage Measured Using the Comet Assay Correlates With Cytotoxicity Towards Hypoxic Tumour Cells In Vitro. *Br. J. Cancer* **1996,** *73,* 952–960.
147. Olive, P. L.; Banath, J. P.; Sinnott, L. T. Phosphorylated Histone H2AX in Spheroids, Tumors, and Tissues of Mice Exposed to Etoposide and 3-Amino-1,2,4-benzotriazine-1,3-dioxide. *Cancer Res.* **2004,** *64,* 5363–5369.

148. Wang, J.; Foehrenbacher, A.; Su, J.; Patel, R.; Hay, M. P.; Hicks, K. O.; Wilson, W. R. The 2-Nitroimidazole EF5 Is a Biomarker for Oxidoreductases That Activate Bioreductive Prodrug CEN-209 Under Hypoxia. *Clin. Cancer Res.* **2012,** *18,* 1684–1695.
149. Peters, K. B.; Brown, J. M. Tirapazamine: A Hypoxia-Activated Topoisomerase II Poison. *Cancer Res.* **2002,** *62,* 5248–5253.
150. Evans, J. W.; Chernikova, S. B.; Kachnic, L. A.; Banath, J. P.; Sordet, O.; Delahoussaye, Y. M.; Treszezamsky, A.; Chon, B. H.; Feng, Z.; Gu, Y.; Wilson, W. R.; Pommier, Y.; Olive, P. L.; Powell, S. N.; Brown, J. M. Homologous Recombination Is the Principal Pathway for the Repair of DNA Damage Induced by Tirapazamine in Mammalian Cells. *Cancer Res.* **2008,** *68,* 257–265.
151. Hunter, F. W.; Wang, J.; Patel, R.; Hsu, H. L.; Hickey, A. J.; Hay, M. P.; Wilson, W. R. Homologous Recombination Repair-Dependent Cytotoxicity of the Benzotriazine di-N-oxide CEN-209: Comparison With Other Hypoxia-Activated Prodrugs. *Biochem. Pharmacol.* **2012,** *83,* 574–585.
152. Zeman, E. M.; Hirst, V. K.; Lemmon, M. J.; Brown, J. M. Enhancement of Radiation-Induced Tumor Cell Killing by the Hypoxic Cell Toxin SR 4233. *Radiother. Oncol.* **1988,** *12,* 209–218.
153. Brown, J. M.; Lemmon, M. J. Potentiation by the Hypoxic Cytotoxin SR 4233 of Cell Killing Produced by Fractionated Irradiation of Mouse Tumors. *Cancer Res.* **1990,** *50,* 7745–7749.
154. Brown, J. M.; Lemmon, M. J. SR 4233: A Tumor Specific Radiosensitizer Active in Fractionated Radiation Regimes. *Radiother. Oncol.* **1991,** *20* (S1), 151–156.
155. Dorie, M. J.; Brown, J. M. Tumor-Specific, Schedule-Dependent Interaction Between Tirapazamine (SR 4233) and Cisplatin. *Cancer Res.* **1993,** *53,* 4633–4636.
156. Dorie, M. J.; Brown, J. M. Potentiation of the Anticancer Effect of Cisplatin by the Hypoxic Cytotoxin Tirapazamine. In *Tumor Oxygenation;* Vaupel, P. W., Kelleher, D. K., Gunderoth, M., Eds.; Fischer-Verlag: Stuttgart, New York, 1994; pp 125–135.
157. Kovacs, M. S.; Hocking, D. J.; Evans, J. W.; Siim, B. G.; Wouters, B. G.; Brown, J. M. Cisplatin Anti-Tumour Potentiation by Tirapazamine Results From a Hypoxia-Dependent Cellular Sensitization to Cisplatin. *Br. J. Cancer* **1999,** *80,* 1245–1251.
158. Walton, M. I.; Workman, P. Pharmacokinetics and Bioreductive Metabolism of the Novel Benzotriazine di-N-oxide Hypoxic Cell Cytotoxin Tirapazamine (WIN 59075; SR 4233; NSC 130181) in Mice. *J. Pharmacol. Exp. Ther.* **1993,** *265,* 938–947.
159. Graham, M. A.; Senan, S.; Robin, H., Jr.; Eckhardt, N.; Lendrem, D.; Hincks, J.; Greenslade, D.; Rampling, R.; Kaye, S. B.; von Roemeling, R.; Workman, P. Pharmacokinetics of the Hypoxic Cell Cytotoxic Agent Tirapazamine and Its Major Bioreductive Metabolites in Mice and Humans: Retrospective Analysis of a Pharmacokinetically Guided Dose-Escalation Strategy in a Phase I Trial. *Cancer Chemother. Pharmacol.* **1997,** *40,* 1–10.
160. Spiegel, J. F.; Spear, M. A.; Brown, J. M. Toxicology of Daily Administration to Mice of the Radiation Potentiator SR 4233 (WIN 59075). *Radiother. Oncol.* **1993,** *26,* 79–81.
161. McKeown, S. R.; Cowen, R. L.; Williams, K. J. Bioreductive Drugs: From Concept to Clinic. *Clin. Oncol.* **2007,** *19,* 427–442.
162. Reddy, S. B.; Williamson, S. K. Tirapazamine: A Novel Agent Targeting Hypoxic Tumor Cells. *Expert Opin. Investig. Drugs* **2009,** *18,* 77–87.
163. Senan, S.; Rampling, R.; Graham, M. A.; Wilson, P.; Robin, H., Jr.; Eckardt, N.; Lawson, N.; McDonald, A.; von Roemeling, R.; Workman, P.; Kaye, S. B. Phase I and Pharmacokinetic Study of Tirapazamine (SR 4233) Administered Every Three Weeks. *Clin. Cancer Res.* **1997,** *3,* 31–38.
164. Johnson, C. A.; Kilpatrick, D.; von Roemeling, R.; Langer, C.; Graham, M. A.; Greenslade, D.; Kennedy, G.; Keenan, E.; O'Dwyer, P. J. Phase I Trial of Tirapazamine in Combination With Cisplatin in a Single Dose Every 3 Weeks in Patients With Solid Tumors. *J. Clin. Oncol.* **1997,** *15,* 773–780.
165. Sandler, A. B.; Nemunaitis, J.; Denham, C.; von Pawel, J.; Cormier, Y.; Gatzemeier, U.; Mattson, K.; Manegold, C.; Palmer, M. C.; Gregor, A.; Nguyen, B.; Niyikiza, C.; Einhorn, L. H. Phase III Trial of Gemcitabine Plus Cisplatin Versus Cisplatin Alone in Patients With Locally Advanced or Metastatic Non-Small-Cell Lung Cancer. *J. Clin. Oncol.* **2000,** *18,* 122–130.
166. Shepherd, F.; Koschel, G.; von Pawel, J.; Gatzmeier, U.; van Zandwiyk, N.; Woll, P.; van Klavren, R.; Krasko, P.; Desimone, P.; Nicolson, M.; Pieters, W.; Bigelow, R.; Rey, A.; Biallet, J.; Loh, E. Comparison of Tirazone (Tirapazamine) and Cisplatin vs. Etoposide and Cisplatin in Advanced Non-Small Cell Lung Cancer (NSCLC): Final Results of the International Phase III CATAPULT II Trial. *Lung Cancer* **2000,** *29* (S1), 28. Abstract 87.
167. von Pawel, J.; von Roemeling, R.; Gatzemeier, U.; Boyer, M.; Elisson, L. O.; Clark, P.; Talbot, D.; Rey, A.; Butler, T. W.; Hirsh, V.; Olver, I.; Bergman, B.; Ayoub, J.; Richardson, G.; Dunlop, D.; Arcenas, A.; Vescio, R.; Viallet, J.; Treat, J. Tirapazamine Plus Cisplatin Versus Cisplatin in Advanced Non-Small-Cell Lung Cancer: A Report of the International CATAPULT I Study Group. Cisplatin and Tirapazamine in Subjects With Advanced Previously Untreated Non-Small-Cell Lung Tumors. *J. Clin. Oncol.* **2000,** *18,* 1351–1359.
168. Williamson, S. K.; Crowley, J. J.; Lara, P. N., Jr.; McCoy, J.; Lau, D. H.; Tucker, R. W.; Mills, G. M.; Gandara, D. R. Phase III Trial of Paclitaxel Plus Carboplatin With or Without Tirapazamine in Advanced Non-Small-Cell Lung Cancer: Southwest Oncology Group Trial S0003. *J. Clin. Oncol.* **2005,** *23,* 9097–9104.
169. Aghajanian, C.; Brown, C.; O'Flaherty, C.; Fleischauer, A.; Curtin, J.; Roemeling, R.; Spriggs, D. R. Phase I Study of Tirapazamine and Cisplatin in Patients With Recurrent Cervical Cancer. *Gynecol. Oncol.* **1997,** *67,* 127–130.
170. Craighead, P. S.; Pearcey, R.; Stuart, G. A Phase I/II Evaluation of Tirapazamine Administered Intravenously Concurrent With Cisplatin and Radiotherapy in Women With Locally Advanced Cervical Cancer. *Int. J. Radiat. Oncol. Biol. Phys.* **2000,** *48,* 791–795.
171. Covens, A.; Blessing, J.; Bender, D.; Mannel, R.; Morgan, M. A Phase II Evaluation of Tirapazamine Plus Cisplatin in the Treatment of Recurrent Platinum-Sensitive Ovarian or Primary Peritoneal Cancer: A Gynecologic Oncology Group Study. *Gynecol. Oncol.* **2006,** *100,* 586–590.
172. Maluf, F. C.; Leiser, A. L.; Aghajanian, C.; Sabbatini, P.; Pezzulli, S.; Chi, D. S.; Wolf, J. K.; Levenback, C.; Loh, E.; Spriggs, D. R. Phase II Study of Tirapazamine Plus Cisplatin in Patients With Advanced or Recurrent Cervical Cancer. *Int. J. Gynecol. Cancer* **2006,** *16,* 1165–1171.
173. Rischin, D.; Narayan, K.; Oza, A. M.; Mileshkin, L.; Bernshaw, D.; Choi, J.; Hicks, R.; McClure, B.; Fyles, A. Phase 1 Study of Tirapazamine in Combination With Radiation and Weekly Cisplatin in Patients With Locally Advanced Cervical Cancer. *Int. J. Gynecol. Cancer* **2010,** *20,* 827–833.
174. DiSilvestro, P. A.; Ali, S.; Craighead, P. S.; Lucci, J. A.; Lee, Y. C.; Cohn, D. E.; Spirtos, N. M.; Tewari, K. S.; Muller, C.; Gajewski, W. H.; Steinhoff, M. M.; Monk, B. J. Phase III Randomized Trial of Weekly Cisplatin and Irradiation Versus Cisplatin and Tirapazamine and Irradiation in Stages IB2, IIA, IIB, IIIB, and IVA Cervical Carcinoma Limited to the Pelvis: A Gynecologic Oncology Group Study. *J. Clin. Oncol.* **2014,** *32,* 458–464.
175. Rischin, D.; Peters, L.; Fisher, R.; Macann, A.; Denham, J.; Poulsen, M.; Jackson, M.; Kenny, L.; Penniment, M.; Corry, J.; Lamb, D.; McClure, B. Tirapazamine, Cisplatin, and Radiation Versus Fluorouracil, Cisplatin, and Radiation in Patients With Locally Advanced Head and Neck Cancer: A Randomized Phase II Trial of the Trans-Tasman Radiation Oncology Group (TROG 98.02). *J. Clin. Oncol.* **2005,** *23,* 79–87.
176. Rischin, D.; Peters, L. J.; O'Sullivan, B.; Giralt, J.; Fisher, R.; Yuen, K.; Trotti, A.; Bernier, J.; Bourhis, J.; Ringash, J.; Henke, M.; Kenny, L. Tirapazamine, Cisplatin, and Radiation Versus Cisplatin and Radiation for Advanced Squamous Cell Carcinoma of the Head and Neck (TROG 02.02, HeadSTART): A Phase III Trial of the Trans-Tasman Radiation Oncology Group. *J. Clin. Oncol.* **2010,** *28,* 2989–2995.
177. Hicks, R. J.; Rischin, D.; Fisher, R.; Binns, D.; Scott, A. M.; Peters, L. J. Utility of FMISO PET in Advanced Head and Neck Cancer Treated With Chemoradiation Incorporating a Hypoxia-Targeting Chemotherapy Agent. *Eur. J. Nucl. Med. Mol. Imaging* **2005,** *32,* 1384–1391.
178. Peters, L. J.; O'Sullivan, B.; Giralt, J.; Fitzgerald, T. J.; Trotti, A.; Bernier, J.; Bourhis, J.; Yuen, K.; Fisher, R.; Rischin, D. Critical Impact of Radiotherapy Protocol Compliance and Quality in the Treatment of Advanced Head and Neck Cancer: Results From TROG 02.02. *J. Clin. Oncol.* **2010,** *28,* 2996–3001.
179. Trinkaus, M. E.; Hicks, R. J.; Young, R. J.; Peters, L. J.; Solomon, B.; Bressel, M.; Corry, J.; Fisher, R.; Binns, D.; McArthur, G. A.; Rischin, D. Correlation of p16 Status, Hypoxic Imaging Using [18F]-Misonidazole Positron Emission Tomography and Outcome in Patients With Loco-Regionally Advanced Head and Neck Cancer. *J. Med. Imaging Radiat. Oncol.* **2014,** *58,* 89–97.
180. Durand, R. E.; Olive, P. L. Evaluation of Bioreductive Drugs in Multicell Spheroids. *Int. J. Radiat. Oncol. Biol. Phys.* **1992,** *22,* 689–692.
181. Durand, R. E.; Olive, P. L. Physiologic and Cytotoxic Effects of Tirapazamine in Tumor-Bearing Mice. *Radiat. Oncol. Investig.* **1997,** *5,* 213–219.
182. Minchinton, A. I.; Lemmon, M. J.; Tracy, M.; Pollart, D. J.; Martinez, A. P.; Tosto, L. M.; Brown, J. M. Second-Generation 1,2,4-Benzotriazine 1,4-di-N-oxide Bioreductive Anti-Tumor Agents: Pharmacology and Activity In Vitro and In Vivo. *Int. J. Radiat. Oncol. Biol. Phys.* **1992,** *22,* 701–705.
183. Kelson, A. B.; McNamara, J. P.; Pandey, A.; Ryan, K. J.; Dorie, M. J.; McAfee, P. A.; Menke, D. R.; Brown, J. M.; Tracy, M. 1,2,4-Benzotriazine 1,4-Dioxides. An Important Class of Hypoxic Cytotoxins With Antitumor Activity. *Anticancer Drug Des.* **1998,** *13,* 575–592.

184. Lee, W. W.; Brown, J. M.; Grange, E. W.; Martinez, A. P.; Tracy, M.; Pollart, D. J. 1,2,4 Benzotriazine Oxides as Radiosensitizers and Selective Cytotoxic Agents. U.S. Patent 5,624,925, April 29, 1997.
185. Arndt, F. Ring Closing Reactions Between Nitro and Amino Groups Forming Triazines. *Chem. Ber* **1913,** *46,* 3522–3529.
186. Mason, J. C.; Tennant, G. Heterocyclic N-Oxides. Part VI. Synthesis and Nuclear Magnetic Resonance Spectra of 3-Aminobenzo-1,2,4-Triazines and Their Mono- and Di-N-Oxides. *J. Chem. Soc. (B)* **1970,** 911–916.
187. Seng, F.; Ley, K. Simple Synthesis of 3-Amino-1,2,4-benzotriazine 1,4-Dioxide. *Angew. Chem. Int. Ed. Engl.* **1972,** *11,* 1009–1010.
188. Hay, M. P.; Denny, W. A. New and Versatile Synthesis of 3-Alkyl- and 3-Aryl-1,2,4-benzotriazine 1,4-Dioxides: Preparation of the Bioreductive Cytotoxins SR4895 and SR4941. *Tetrahedron Lett.* **2002,** *43,* 9569–9571.
189. Pchalek, K.; Hay, M. P. Stille Coupling Reactions in the Synthesis of Hypoxia-Selective 3-Alkyl-1,2,4-benzotriazine 1,4-Dioxide Anticancer Agents. *J. Org. Chem.* **2006,** *71,* 6530–6535.
190. Atallah, R. H.; Nazer, M. Z. Oxides of 3-Methyl 1,2,4-Benzotriazine. *Tetrahedron* **1982,** *38,* 1793–1796.
191. Durand, R. E. Chemosensitivity Testing in V79 Spheroids: Drug Delivery and Cellular Microenvironment. *J. Natl. Cancer Inst.* **1986,** *77,* 247–252.
192. Sutherland, R. M. Cell and Environment Interactions in Tumor Microregions: The Multicell Spheroid Model. *Science* **1988,** *240,* 177–184.
193. Hirschhaeuser, F.; Menne, H.; Dittfeld, C.; West, J.; Mueller-Klieser, W.; Kunz-Schughart, L. A. Multicellular Tumor Spheroids: An Underestimated Tool Is Catching Up Again. *J. Biotechnol.* **2010,** *148,* 3–15.
194. Cowan, D. S.; Hicks, K. O.; Wilson, W. R. Multicellular Membranes as an *in vitro* Model for Extravascular Diffusion in Tumours. *Br. J. Cancer* **1996,** *27,* S28–S31.
195. Hicks, K. O.; Ohms, S. J.; van Zijl, P. L.; Denny, W. A.; Hunter, P. J.; Wilson, W. R. An Experimental and Mathematical Model for the Extravascular Transport of a DNA Intercalator in Tumours. *Br. J. Cancer* **1997,** *76,* 894–903.
196. Hicks, K. O.; Fleming, Y.; Siim, B. G.; Koch, C. J.; Wilson, W. R. Extravascular Diffusion of Tirapazamine: Effect of Metabolic Consumption Assessed Using the Multicellular Layer Model. *Int. J. Radiat. Oncol. Biol. Phys.* **1998,** *42,* 641–649.
197. Kyle, A. H.; Minchinton, A. I. Measurement of Delivery and Metabolism of Tirapazamine to Tumour Tissue Using the Multilayered Cell Culture Model. *Cancer Chemother. Pharmacol.* **1999,** *43,* 213–220.
198. Hicks, K. O.; Pruijn, F. B.; Sturman, J. R.; Denny, W. A.; Wilson, W. R. Multicellular Resistance to Tirapazamine Is Due to Restricted Extravascular Transport: A Pharmacokinetic/Pharmacodynamic Study in HT29 Multicellular Layer Cultures. *Cancer Res.* **2003,** *63,* 5970–5977.
199. Kuiper, C.; Vissers, M. C.; Hicks, K. O. Pharmacokinetic Modeling of Ascorbate Diffusion Through Normal and Tumor Tissue. *Free Radicals Biol. Med.* **2014,** *77,* 340–352.
200. Foehrenbacher, A.; Patel, K.; Abbattista, M.; Guise, C. P.; Secomb, T. W.; Wilson, W. R.; Hicks, K. O. The Role of Bystander Effects in the Antitumor Activity of the Hypoxia-Activated Prodrug PR-104. *Front. Oncol.* **2013,** *3,* 263.
201. Hicks, K. O. Introducing Drug Transport Early in the Design of Hypoxia Selective Anticancer Agents Using a Mathematical Modelling Approach. In *New Challenges for Cancer Systems Biomedicine;* D'Onofrio, A., Cerrai, P., Gandolfi, A., Eds.; Springer: Italy, 2012; pp 337–354.
202. Pruijn, F. B.; Patel, K.; Hay, M. P.; Wilson, W. R.; Hicks, K. O. Prediction of Tumour Tissue Diffusion Coefficients of Hypoxia-Activated Prodrugs From Physicochemical Parameters. *Aust. J. Chem.* **2008,** *61,* 687–693.
203. Pruijn, F. B.; Sturman, J. R.; Liyanage, H. D. S.; Hicks, K. O.; Hay, M. P.; Wilson, W. R. Extravascular Transport of Drugs in Tumor Tissue: Effect of Lipophilicity on Diffusion of Tirapazamine Analogs in Multicellular Layer Cultures. *J. Med. Chem.* **2005,** *48,* 1079–1087.
204. Wilson, W. R.; Denny, W. A. DNA-Binding Nitroheterocycles as Hypoxia-Selective Cytotoxins. In *Radiation Research, a Twentieth-Century Perspective;* Dewey, W. C., Edington, M., Fry, R. J. M., Hall, E. J., Whitmore, G. F., Eds.; 2nd ed.; Academic Press: San Diego, 1992; pp 796–801.
205. Tannock, I. F. Oxygen Diffusion and the Distribution of Cellular Radiosensitivity in Tumours. *Br. J. Radiol.* **1972,** *45,* 515–524.
206. Carlson, D. J.; Keall, P. J.; Loo, B. W., Jr.; Chen, Z. J.; Brown, J. M. Hypofractionation Results in Reduced Tumor Cell Kill Compared to Conventional Fractionation for Tumors With Regions of Hypoxia. *Int. J. Radiat. Onc. Biol. Phys.* **2011,** *79,* 1188–1195.
207. Hicks, K. O.; Pruijn, F. B.; Baguley, B. C.; Wilson, W. R. Extravascular Transport of the DNA Intercalator and Topoisomerase Poison *N*-[2-(Dimethylamino)ethyl]acridine-4-carboxamide (DACA): Diffusion and Metabolism in Multicellular Layers of Tumor Cells. *J. Pharmacol. Exp. Ther.* **2001,** *297,* 1088–1098.
208. Hicks, K. O.; Pruijn, F. B.; Secomb, T. W.; Hay, M. P.; Hsu, R.; Brown, J. M.; Denny, W. A.; Dewhirst, M. W.; Wilson, W. R. Use of Three-Dimensional Tissue Cultures to Model Extravascular Transport and Predict In Vivo Activity of Hypoxia-Targeted Anticancer Drugs. *J. Natl. Cancer Inst.* **2006,** *98,* 1118–1128.
209. Secomb, T. W.; Hsu, R.; Braun, R. D.; Ross, J. R.; Gross, J. F.; Dewhirst, M. W. Theoretical Simulation of Oxygen Transport to Tumors by Three-Dimensional Networks of Microvessels. *Adv. Exp. Med. Biol.* **1998,** *454,* 629–634.
210. Hsu, R.; Secomb, T. W. A Green's Function Method for Analysis of Oxygen Delivery to Tissue by Microvascular Networks. *Math. Biosci.* **1989,** *96,* 61–78.
211. Secomb, T. W.; Hsu, R.; Park, E. Y.; Dewhirst, M. W. Green's Function Methods for Analysis of Oxygen Delivery to Tissue by Microvascular Networks. *Ann. Biomed. Eng.* **2004,** *32,* 1519–1529.
212. Hicks, K. O.; Siim, B. G.; Jaiswal, J. K.; Pruijn, F. B.; Fraser, A. M.; Patel, R.; Hogg, A.; Liyanage, H. D. S.; Dorie, M. J.; Brown, J. M.; Denny, W. A.; Hay, M. P.; Wilson, W. R. Pharmacokinetic/Pharmacodynamic Modeling Identifies SN30000 and SN29751 as Tirapazamine Analogues With Improved Tissue Penetration and Hypoxic Cell Killing in Tumors. *Clin. Cancer Res.* **2010,** *16,* 4946–4957.
213. Monge, A.; Palop, J. A.; Lopez, D. C.; Senador, V.; Martinez-Crespo, F. J.; Sainz, Y.; Narro, S.; Garcia, E.; de Miguel, C.; Gonzalez, M. Hypoxia-Selective Agents Derived From Quinoxaline 1,4-Di-N-oxides. *J. Med. Chem.* **1995,** *38,* 1786–1792.
214. Monge, A.; Martinez-Crespo, F. J.; Lopez, D. C.; Palop, J. A.; Narro, S.; Senador, V.; Marin, A.; Sainz, Y.; Gonzalez, M.; Hamilton, E. Hypoxia-Selective Agents Derived From 2-Quinoxalinecarbonitrile 1,4-Di-N-oxides. 2. *J. Med. Chem.* **1995,** *38,* 4488–4494.
215. Barker, D. D.; Monge, A.; Hamilton, E. Cytotoxic Quinoxaline 1,4-Dioxides. U.K. Patent Appl. GB2,297,089 A, 24 June, 1996.
216. Wang, J.; Biedermann, K. A.; Brown, J. M. Repair of DNA and Chromosome Breaks in Cells Exposed to SR 4233 Under Hypoxia or to Ionizing Radiation. *Cancer Res.* **1992,** *52,* 4473–4477.
217. Delahoussaye, Y. M.; Evans, J. W.; Brown, J. M. Metabolism of Tirapazamine by Multiple Reductases in the Nucleus. *Biochem. Pharmacol.* **2001,** *62,* 1201–1209.
218. Wouters, B. G.; Delahoussaye, Y. M.; Evans, J. W.; Birrell, G. W.; Dorie, M. J.; Wang, J.; MacDermed, D.; Chiu, R. K.; Brown, J. M. Mitochondrial Dysfunction After Aerobic Exposure to the Hypoxic Cytotoxin Tirapazamine. *Cancer Res.* **2001,** *61,* 145–152.
219. Denny, W. A.; Roberts, P. B.; Anderson, R. F.; Brown, J. M.; Phil, D.; Wilson, W. R. NLA-1: A 2-Nitroimidazole Radiosensitizer Targeted to DNA by Intercalation. *Int. J. Radiat. Oncol. Biol. Phys.* **1992,** *22,* 553–556.
220. Cowan, D. S.; Matejovic, J. F.; McClelland, R. A.; Rauth, A. M. DNA-Targeted 2-Nitroimidazoles: In Vitro and In Vivo Studies. *Br. J. Cancer* **1994,** *70,* 1067–1074.
221. Papadopoulou, M. V.; Ji, M.; Rao, M. K.; Bloomer, W. D. 4-[3-(2-Nitro-1-imidazolyl)propylamino]-7-chloroquinoline Hydrochloride (NLCQ-1), a Novel Bioreductive Agent as Radiosensitizer In Vitro and In Vivo: Comparison With Tirapazamine. *Oncol. Res.* **2001,** *12,* 325–333.
222. Delahoussaye, Y. M.; Hay, M. P.; Pruijn, F. B.; Denny, W. A.; Brown, J. M. Improved Potency of the Hypoxic Cytotoxin Tirapazamine by DNA-Targeting. *Biochem. Pharmacol.* **2003,** *65,* 1807–1815.
223. Siim, B. G.; Hicks, K. O.; Pullen, S. M.; van Zijl, P. L.; Denny, W. A.; Wilson, W. R. Comparison of Aromatic and Tertiary Amine N-Oxides of Acridine DNA Intercalators as Bioreductive Drugs. Cytotoxicity, DNA Binding, Cellular Uptake, and Metabolism. *Biochem. Pharmacol.* **2000,** *60,* 969–978.
224. Hay, M. P.; Pruijn, F. B.; Gamage, S. A.; Liyanage, H. D.; Kovacs, M. S.; Patterson, A. V.; Wilson, W. R.; Brown, J. M.; Denny, W. A. DNA-Targeted 1,2,4-Benzotriazine 1,4-Dioxides: Potent Analogues of the Hypoxia-Selective Cytotoxin Tirapazamine. *J. Med. Chem.* **2004,** *47,* 475–488.
225. Anderson, R. F.; Harris, T. A.; Hay, M. P.; Denny, W. A. Enhanced Conversion of DNA Radical Damage to Double Strand Breaks by 1,2,4-Benzotriazine 1,4-Dioxides Linked to a DNA Binder Compared to Tirapazamine. *Chem. Res. Toxicol.* **2003,** *16,* 1477–1483.

226. Shinde, S. S.; Anderson, R. F.; Hay, M. P.; Gamage, S. A.; Denny, W. A. Oxidation of 2-Deoxyribose by Benzotriazinyl Radicals of Antitumor 3-Amino-1,2,4-benzotriazine 1,4-Dioxides. *J. Am. Chem. Soc.* **2004,** *126,* 7865–7874.
227. Hay, M. P.; Pchalek, K.; Pruijn, F. B.; Hicks, K. O.; Siim, B. G.; Anderson, R. F.; Shinde, S. S.; Phillips, V.; Denny, W. A.; Wilson, W. R. Hypoxia-Selective 3-Alkyl 1,2,4-Benzotriazine 1,4-Dioxides: The Influence of Hydrogen Bond Donors on Extravascular Transport and Antitumor Activity. *J. Med. Chem.* **2007,** *50,* 6654–6664.
228. Denny, W. A.; Hay, M. P.; Hicks, K. O.; Pruijn, F. B.; Wilson, W. R.; Pchalek, K. Novel 1,2,4-Benzotriazine-1,4-dioxides. U.S. Patent 7,816,521, 19 October, 2010.
229. Hay, M. P.; Hicks, K. O.; Pchalek, K.; Lee, H. H.; Blaser, A.; Pruijn, F. B.; Anderson, R. F.; Shinde, S. S.; Wilson, W. R.; Denny, W. A. Tricyclic [1,2,4]triazine 1,4-Dioxides as Hypoxia Selective Cytotoxins. *J. Med. Chem.* **2008,** *51,* 6853–6865.
230. Gu, Y.; Jaiswal, J. K.; Wang, J.; Hicks, K. O.; Hay, M. P.; Wilson, W. R. Photodegradation of the Benzotriazine 1,4-Di-N-oxide Hypoxia-Activated Prodrug SN30000 in Aqueous Solution. *J. Pharm. Sci.* **2014,** *103,* 3464–3472.
231. Chitneni, S. K.; Bida, G. T.; Yuan, H.; Palmer, G. M.; Hay, M. P.; Melcher, T.; Wilson, W. R.; Zalutsky, M. R.; Dewhirst, M. W. 18F-EF5 PET Imaging as an Early Response Biomarker for the Hypoxia-Activated Prodrug SN30000 Combined With Radiation Treatment in a Non-Small Cell Lung Cancer Xenograft Model. *J. Nucl. Med.* **2013,** *54,* 1339–1346.
232. Anderson, R. F.; Yadav, P.; Patel, D.; Reynisson, J.; Tipparaju, S. R.; Guise, C. P.; Patterson, A. V.; Denny, W. A.; Maroz, A.; Shinde, S. S.; Hay, M. P. Characterisation of Radicals Formed by the Triazine 1,4-Dioxide Hypoxia-Activated Prodrug SN30000. *Org. Biomol. Chem.* **2014,** *12,* 3386–3392.
233. Wang, J.; Guise, C. P.; Dachs, G. U.; Phung, Y.; Hsu, A. H.; Lambie, N. K.; Patterson, A. V.; Wilson, W. R. Identification of One-Electron Reductases That Activate Both the Hypoxia Prodrug SN30000 and Diagnostic Probe EF5. *Biochem. Pharmacol.* **2014,** *91,* 436–446.
234. Evans, S. M.; Hahn, S.; Pook, D. R.; Jenkins, W. T.; Chalian, A. A.; Zhang, P.; Stevens, C.; Weber, R.; Weinstein, G.; Benjamin, I.; Mirza, N.; Morgan, M.; Rubin, S.; McKenna, W. G.; Lord, E. M.; Koch, C. J. Detection of Hypoxia in Human Squamous Cell Carcinoma by EF5 Binding. *Cancer Res.* **2000,** *60,* 2018–2024.
235. Kumar, P.; Bacchu, V.; Wiebe, L. I. The Chemistry and Radiochemistry of Hypoxia-Specific, Radiohalogenated Nitroaromatic Imaging Probes. *Semin. Nucl. Med.* **2015,** *45,* 122–135.
236. Linnik, I. V.; Scott, M. L.; Holliday, K. F.; Woodhouse, N.; Waterton, J. C.; O'Connor, J. P.; Barjat, H.; Liess, C.; Ulloa, J.; Young, H.; Dive, C.; Hodgkinson, C. L.; Ward, T.; Roberts, D.; Mills, S. J.; Thompson, G.; Buonaccorsi, G. A.; Cheung, S.; Jackson, A.; Naish, J. H.; Parker, G. J. Noninvasive Tumor Hypoxia Measurement Using Magnetic Resonance Imaging in Murine U87 Glioma Xenografts and in Patients With Glioblastoma. *Magn. Reson. Med.* **2014,** *71,* 1854–1862.
237. Su, J.; Gu, Y.; Pruijn, F. B.; Smaill, J. B.; Patterson, A. V.; Guise, C. P.; Wilson, W. R. Zinc Finger Nuclease Knockout of NADPH:Cytochrome P450 Oxidoreductase (POR) in Human Tumour Cell Lines Demonstrates That Hypoxia-Activated Prodrugs Differ in POR Dependence. *J. Biol. Chem.* **2013,** *288,* 37138–37153.
238. Hunter, F. W.; Jaiswal, J. K.; Hurley, D. G.; Liyanage, H. D. S.; MacManaway, S. P.; Gu, Y.; Richter, S.; Wang, J.; Tercel, M.; Print, C. G.; Wilson, W. R.; Pruijn, F. B. The Flavoprotein FOXRED2 Reductively Activates Nitro-Chloromethylbenzindolines and Other Hypoxia-Targeting Prodrugs. *Biochem. Pharmacol.* **2014,** *89,* 224–235.
239. Hunter, F. W.; Young, R. J.; Shalev, Z.; Vellanki, R. N.; Wang, J.; Gu, Y.; Joshi, N.; Sreebavan, S.; Weinreb, I.; Goldstein, D. P.; Moffat, J.; Ketela, T.; Brown, K. R.; Koritzinsky, M.; Solomon, B.; Rischin, D.; Wilson, W. R.; Wouters, B. G. Identification of P450 Oxidoreductase as a Major Determinant of Sensitivity to Hypoxia-Activated Prodrugs. *Cancer Res.* **2015,** *75,* 4211–4223.
240. Iakovlev, V. V.; Pintilie, M.; Morrison, A.; Fyles, A. W.; Hill, R. P.; Hedley, D. W. Effect of Distributional Heterogeneity on the Analysis of Tumor Hypoxia Based on Carbonic Anhydrase IX. *Lab. Invest.* **2007,** *87,* 1206–1217.
241. Dhani, N. C.; Serra, S.; Pintilie, M.; Schwock, J.; Xu, J.; Gallinger, S.; Hill, R. P.; Hedley, D. W. Analysis of the Intra- and Intertumoral Heterogeneity of Hypoxia in Pancreatic Cancer Patients Receiving the Nitroimidazole Tracer Pimonidazole. *Br. J. Cancer* **2015,** *113,* 864–871.
242. Wang, T.; Birsoy, K.; Hughes, N. W.; Krupczak, K. M.; Post, Y.; Wei, J. J.; Lander, E. S.; Sabatini, D. M. Identification and Characterization of Essential Genes in the Human Genome. *Science* **2015,** *350,* 1096–1101. http://dx.doi.org/10.1126/science.aac7041.
243. Konermann, S.; Brigham, M. D.; Trevino, A. E.; Joung, J.; Abudayyeh, O. O.; Barcena, C.; Hsu, P. D.; Habib, N.; Gootenberg, J. S.; Nishimasu, H.; Nureki, O.; Zhang, F. Genome-Scale Transcriptional Activation by an Engineered CRISPR-Cas9 Complex. *Nature* **2015,** *517,* 583–588.
244. The Cancer Genome Atlas Network. Comprehensive Genomic Analysis of Head and Neck Squamous Cell Carcinomas. *Nature* **2015,** *517,* 576–582.
245. Swick, A. D.; Chatterjee, A.; De Costa, A. M.; Kimple, R. J. Modulation of Therapeutic Sensitivity by Human Papillomavirus. *Radiother. Oncol.* **2015,** *116,* 342–345.
246. Brown, J. M. Vasculogenesis: A Crucial Player in the Resistance of Solid Tumours to Radiotherapy. *Br. J. Radiol.* **2014,** *87,* 20130686.

8.04 The Discovery of First-in-Class Inhibitors of the Nedd8-Activating Enzyme (NAE) and the Ubiquitin-Activating Enzyme (UAE)

J Ciavarri and S Langston, Takeda Pharmaceuticals International Co., Cambridge, MA, United States

© 2017 Elsevier Ltd. All rights reserved.

8.04.1	The Ubiquitin Proteasome System	95
8.04.2	UAE and NAE	96
8.04.3	The Discovery of Pevonedistat (MLN4924/TAK-924)	97
8.04.4	Pevonedistat In Vitro and In Vivo Evaluation	100
8.04.5	The Discovery of TAK-243 (MLN7243)	104
8.04.6	Selection of the Development Candidate	108
8.04.7	Profile of the Clinical Candidate	109
References		111
Relevant Websites		112

8.04.1 The Ubiquitin Proteasome System

Protein homeostasis is the dynamic process by which a cell regulates protein turnover to maintain the balance of protein levels required for proper growth and development.[1,2] While early work implicated lysosomal degradation as largely responsible for this function, it was later shown to be insufficient in explaining variations in protein stability or degradation rates under changing physiological conditions. Further work showed that, along with lysosomal activity, a significant subset of protein turnover is regulated by the collection of enzymes and proteases of the ubiquitin proteasome system (UPS).[3] The ground-breaking work of Ciechanover[4] and Wilkinson[5] identified the role of ubiquitin (Ub), a 76 amino acid protein of unknown function when originally isolated, as a post-translational modifier of proteins which plays a critical role in the quality control mechanism of the UPS. Mediated by a series of enzymes (E1, E2, E3), a Ub chain is covalently linked to a substrate which enables recognition by the proteasome, the large proteolytic complex responsible for protein degradation.[6,7] Following removal of the Ub chain, the protein is processed by the proteolytic core of the proteasome and the resulting peptide fragments are available for use in the synthesis of new protein (**Fig. 1**).[8]

The UPS plays a key role in a diverse array of cellular functions from cell cycle control and transcription to development[9–12] and aberrations within this pathway have been implicated in a number of diseases.[3] Moreover, cancer cells exist in a heightened state of cellular stress and rely on the machinery of the UPS to a greater extent than normal cells making this an area of focus for therapeutic intervention.[10,13] Early efforts to impact targets within this pathway focused on inhibition of the proteasome. Validation of this approach was realized with the approval of the small molecule proteasome inhibitor bortezomib (VELCADE®, Millennium Pharmaceuticals, Inc. a wholly owned subsidiary of Takeda Pharmaceuticals, Ltd.) as an effective treatment for multiple myeloma and mantle cell lymphoma.[8,10,12,14,15] Further work in this area resulted in the approval of the proteasome inhibitors carfilzomib (Kyprolis®, Amgen)[16–18] and the orally bioavailable ixazomib (NINLARO®, Takeda).[16,19] These molecules act by disrupting protein homeostasis and increasing proteotoxic stress within the cell which results in the induction of apoptosis.[10,13] The effectiveness of this treatment in multiple myeloma may be due to the fact that the myeloma cells express increased levels of the pro-survival transcription factor NF-kB and proteasome inhibition stabilizes the endogenous inhibitor of NF-kB (Ik-B).[10,11,20] Further research, however, suggests a greater contribution from activation of the unfolded protein response (UPR) and the induction of pro-apoptotic UPR genes.[21] While transformative for the treatment of multiple myeloma and mantle cell lymphoma, therapeutic application of proteasome inhibitors has so far only been approved in these particular cancer types while showing no success in the solid tumor setting.[10,22] Targeting other components within the UPS is a potential strategy to improve outcomes across a wider variety of tumor types and many of these targets have been the subject of extensive reviews.[9,10,12] This article will describe our efforts toward the identification of inhibitors of two targets within this pathway: the Nedd8-activating enzyme (NAE) and the ubiquitin-activating enzyme (UAE).

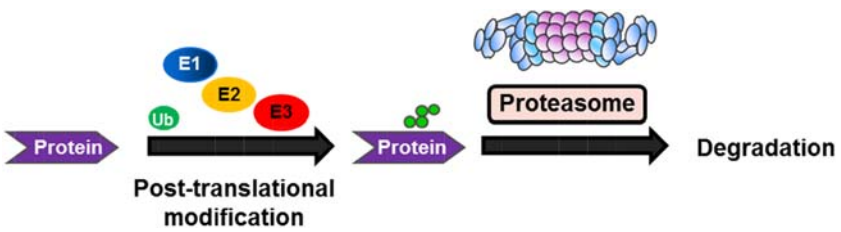

Fig. 1 Overview of the ubiquitin proteasome system (UPS).

8.04.2 UAE and NAE

Within the UPS, E1-activating enzymes initiate the process of modifying a protein with Ub or a ubiquitin-like (Ubl) modifier. In the context of the UAE pathway, activation of Ub occurs in an ATP-dependent fashion by way of a three-step mechanism (Fig. 2).[23] In Step 1, ATP and Ub bind UAE and react to form an adenylate between the C-terminal glycine of Ub and the adenosine monophosphate (AMP) of ATP. The resulting AMP-Ub adduct undergoes nucleophilic attack by the catalytic cysteine of UAE to form a Ub-Cys thioester (Step 2) after which an additional adenylation step occurs and a second equivalent of AMP-Ub binds UAE (Step 3).

The resulting ternary complex is now poised to transfer Ub from the catalytic cysteine of the E1 to one of its corresponding E2-conjugating enzymes (aka Ubc, Ub-conjugating enzyme) (Fig. 3).[24]

Transfer of Ub (as the single protein or as a poly-Ub chain) to a lysine residue of a substrate is mediated by an E3 Ub-protein ligase[12,23,25] whose function is to bring the protein in close proximity to the E2-Ub species (Fig. 4). The manner in which Ub transfer occurs is dependent on the class of E3 ligase involved in the process. For HECT-domain E3 ligases, Ub is first transferred to a conserved cysteine residue of the E3 and then to the substrate. Other E3s (U-box proteins, monomeric RING finger E3s, and multisubunit E3 complexes that contain a RING finger protein) mediate transfer directly from the E2 to the substrate protein.[12,26] Proteins tagged with a poly-Ub chain linked through lys-48 (K48) on Ub are targeted for degradation by the proteasome. In addition to this function, the UAE pathway plays a role in a variety of other cellular signaling processes including DNA repair, autophagy, histone function, receptor internalization, and protein localization.[3,11,27] These different functions are dependent upon whether a protein is mono- or poly-ubiquitinated along with which amino acid residue ubiquitination occurs. Poly-ubiquitination at Lys48 (K48) of the Ub protein results in degradation of the substrate by the proteasome. Poly-ubiquitination at an alternate lysine residue (i.e., Lys63) or mono-ubiquitination manifests in one or more of the aforementioned cellular functions.[3,9,11]

Subsequent to the discovery of UAE, seven other E1-activating enzymes were identified which share a similar homology and employ similar activation mechanisms to that described earlier. Importantly, however, each E1 employs different components within their corresponding activation pathways to impart specificity of function to modified substrates.[28] Of these, the pathway initiated by NAE is responsible for modifying the cullin family of proteins[29] with the Ubl modifier nedd8 (neural precursor cell-expressed, developmentally downregulated protein 8).[30] The cullin proteins act as a core scaffold for a subclass of Ub E3's, the cullin-RING ligases (CRLs) and posttranslational modification of the cullins with nedd8 is required for ligase activity (Fig. 5). Numbering in the hundreds, this set of E3 ligases is involved in regulating the ubiquitination of proteins which have important

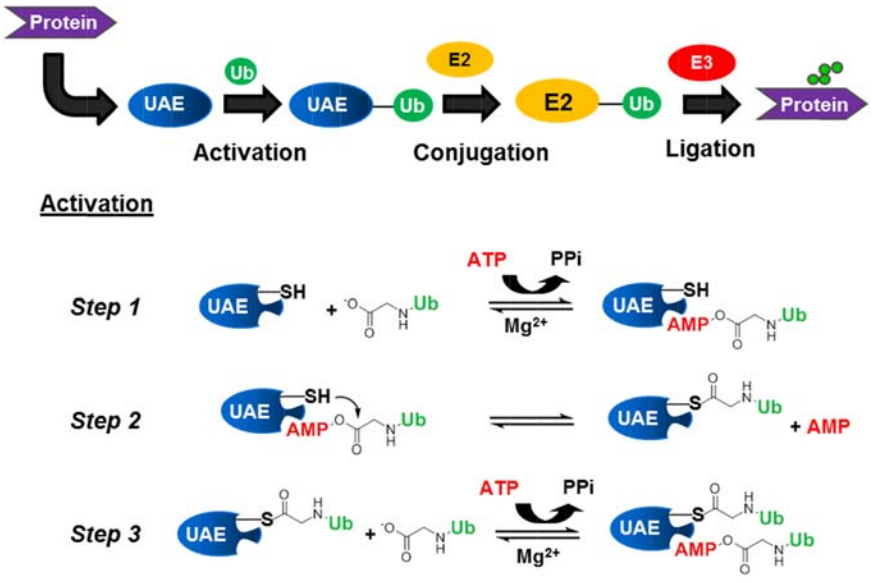

Fig. 2 The mechanism of E1 activation exemplified by the ubiquitin-activating enzyme (UAE).

Fig. 3 Transfer of an "activated" ubiquitin molecule to an E2-conjugating enzyme.

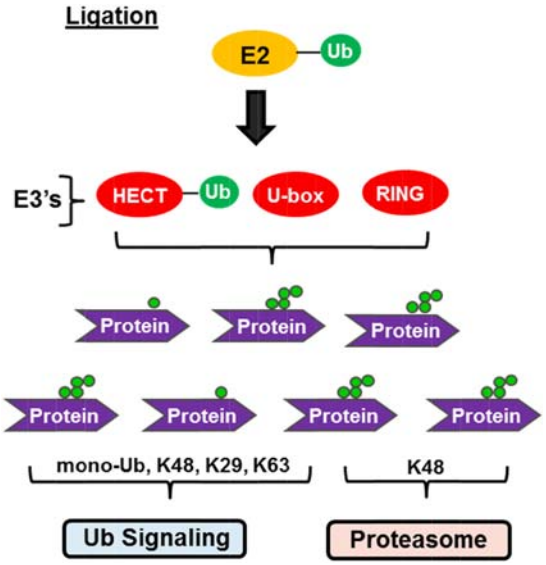

Fig. 4 E3-mediated transfer of ubiquitin from an E2-conjugating enzyme to a substrate.

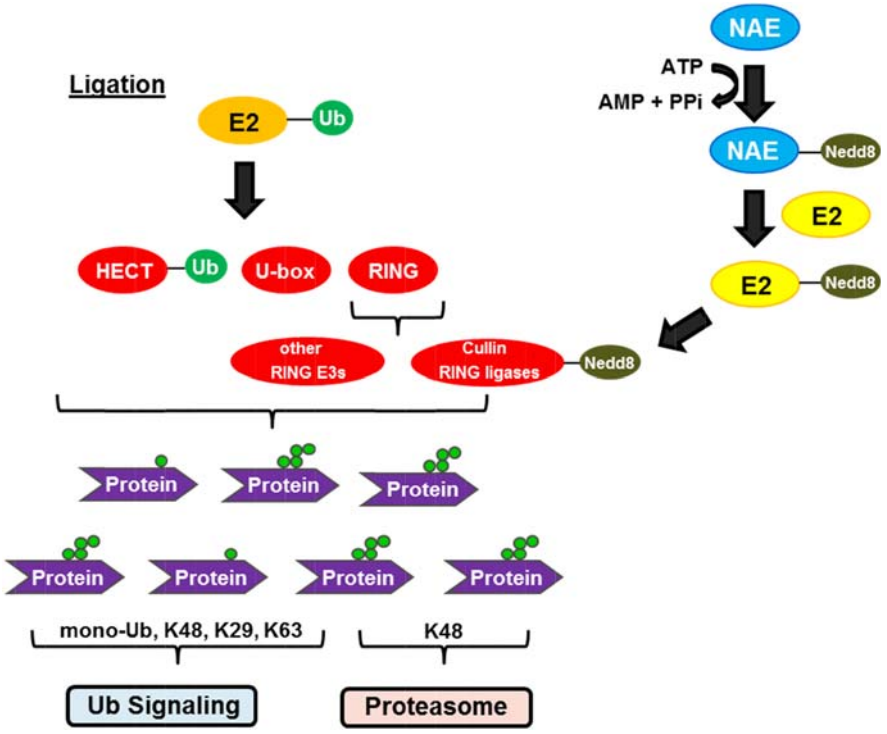

Fig. 5 The Nedd8-activating enzyme (NAE) pathway.

roles in cellular processes associated with cancer cell growth and survival pathways.[15,26] As a target upstream of the proteasome, inhibition of NAE would be expected to disrupt cancer cell protein homeostasis more selectively than inhibition of proteasome activity with potential differences in clinical efficacy.[15]

8.04.3 The Discovery of Pevonedistat (MLN4924/TAK-924)

Efforts toward a small-molecule inhibitor of NAE began with a high-throughput screen from which a series of N-6 substituted adenosine derivatives was obtained as weak, micromolar inhibitors of NAE. Following up on this, a diverse set of N6 (purine numbering

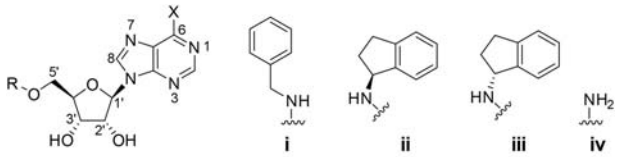

Compound	R	X	NAE IC_{50} (nM)
1	H	i	15,000
2	H	ii	1600
3	H	iii	38,000
4 (AMP)	$(OH)_2P=O$	iv	13,000
5	$(OH)_2P=O$	ii	120

Fig. 6 Early SAR: follow-up of a high-throughput screen.

system) amine analogs was generated where SAR indicated a preference for benzyl amine substituents (Fig. 6). In particular (*S*)-1-aminoindane provided one of the most active inhibitors (**2**), albeit with low micromolar activity, against the target. Recognizing that AMP (**4**) is known to be a weak inhibitor of NAE as a result of product inhibition,[31] a 5′-*O*-phosphate group was appended to compound **2** to provide the first submicromolar inhibitor of NAE within this series (**5**).

While potent in a biochemical assay, compound **5** showed no activity when evaluated in a cellular assay measuring NFκB activity, a transcription factor and downstream substrate of the NAE pathway. As alluded to in the Introduction, the protein IκB is the endogenous inhibitor of NFκB[32] and IκB protein levels are dependent on the NAE activation pathway (Fig. 7). Upon stimulation of cells by the cytokine TNFα, IκB is phosphorylated by the IκB kinase (IKK). Downstream of NAE, the neddylated CRLs SCF-βTRCP is the E3 responsible for ubiquitination of phospho-IκB resulting in its subsequent degradation by the proteasome.[33] By blocking the degradation of IkB, NAE inhibition prevents the NFκB transcription factor from entering the cell nucleus and exerting its activity.

Medicinal chemistry efforts to address cell potency revealed that replacement of the phosphate with the neutral sulfamate group greatly improved biochemical potency and yielded the first cell active compounds (compounds **6** and **7**, Fig. 8). Despite favorable enzyme and cell potency, however, a screen against other E1's showed that these adenosine sulfamate derivatives lacked desirable selectivity over UAE and the SUMO-activating enzyme (SAE).

Furthermore, compounds of this type exhibited an inherent chemical instability wherein the sulfamate moiety was displaced by intramolecular cyclization with N3 of the adenine ring (Fig. 9). Mitigating this degradation event and improving selectivity over other E1s were initial SAR goals within this series.

Initial attempts were made to reduce the leaving group ability of the sulfamate via replacement with either a sulfamide (**8**) or sulfonamide (**9**). While this afforded compounds with greater chemical stability and improved selectivity over UAE and SAE, compounds of this type generally resulted in a decrease in on-target cellular potency (Fig. 10).

Alternatively, attempts were made to reduce the nucleophilicity of the adenine N3 by substituting at N6 with electron withdrawing groups (e.g., acyl (**10**), sulfonamide (**11**), and urea (**12**)). This resulted in diminished selectivity over other E1's along with a reduction in cellular potency (Fig. 11). Replacement of the electron donating nitrogen linkage with carbon (phenethyl

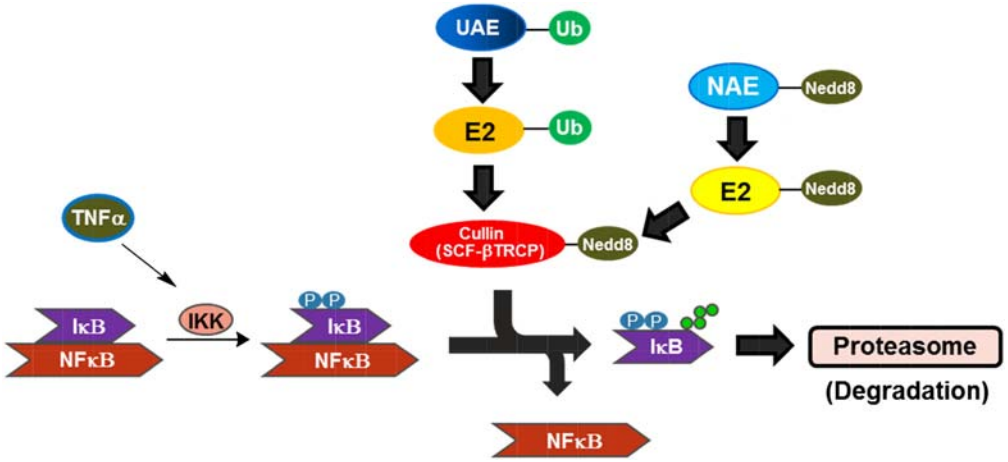

Fig. 7 Basis for the NFκB cellular assay: inhibition of NAE prevents the degradation of phospho-IκB which results in a decrease in NFκB activity.

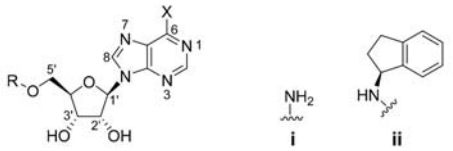

Compound	R	X	NAE IC_{50} (nM)	UAE IC_{50} (nM)	SAE IC_{50} (nM)	NFκB IC_{50} (nM)
4 (AMP)	$(OH)_2P=O$	i	13,000	780	1900	>50,000
6	SO_2NH_2	i	0.5	10*	6	100
5	$(OH)_2P=O$	ii	120	>1000	1800	>50,000
7	SO_2NH_2	ii	0.5	2	10	38

*mouse UAE

Fig. 8 5′-Sulfamate compounds show improved potency compared with the corresponding 5′-phosphate analogs. For some compounds, mouse-derived UAE was used in the biochemical assay and is noted with an asterisk (*). All other compounds evaluated against human-derived UAE. *Mouse UAE.

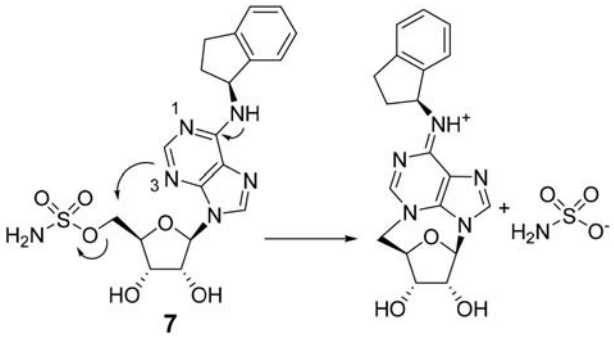

Fig. 9 Undesired degradation of compound **7**.

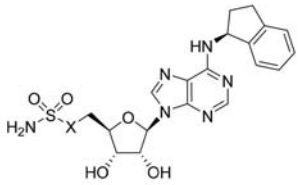

Compound	X	NAE IC_{50} (nM)	UAE IC_{50} (nM)	SAE IC_{50} (nM)	NFκB IC_{50} (nM)
7	O	0.5	2	10	38
8	NH	2	450	1800	180
9	CH_2	12	>1000	>100,000	370

Fig. 10 Investigation of sulfamate replacements.

compound **13**) mitigated the cyclization event and afforded a compound with very good biochemical/cell potency. While this molecule exhibited excellent selectivity over SAE, it displayed only modest selectivity over UAE. Variations on this theme in the form of the conformationally rigidified phenethylene (**14**) and phenylacetylene (**15**) were potent but not selective.

In addition to exploring side-chain modifications, SAR around the adenine ring was investigated in order to address selectivity/stability (Fig. 12). While removal of the N3 nitrogen (imidazo-pyrimidine **16**), resulted in a compound with diminished cellular potency, the corresponding pyrrolo-pyrimidine **17** (N7 removal) displayed excellent activity against NAE and afforded an improvement in selectivity over both UAE and SAE. Separately, the impact of the removal of the hydroxyl groups on the ribose moiety was explored. From this effort, it was found that the 3′-OH was required for potency (**20**) whereas 2′-deoxy compounds retained potency and showed improved selectivity (**19**, **21**). Replacement of the ribose moiety with the cyclopentane also afforded potent analogs (**18**, **22**) and eliminated the anomeric center within the molecule. In particular, the combined removal of N7 and the 2′-OH with the cyclopentane modification afforded compound **23** which was potent, selective, and cell active. However, the molecule was still prone to internal cyclization.

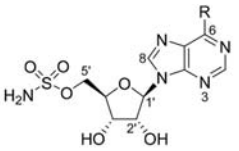

Compound	R	NAE IC_{50} (nM)	UAE IC_{50} (nM)	SAE IC_{50} (nM)	NFκB IC_{50} (nM)
7	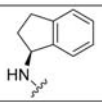	0.5	2	10	38
10	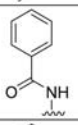	1	2	180	910
11	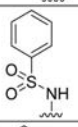	4	44,000*	140	5800
12	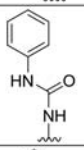	13	2	120	6200
13	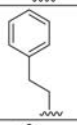	5	93	730	100
14	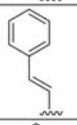	1	4	26	62
15		0.3	0.3	3	35

*mouse UAE

Fig. 11 Efforts to mitigate undesired cyclization: N6 modification. *Mouse UAE.

Another approach to address the cyclization event was to prevent alignment of the leaving group and the nucleophile. The "nonnatural" anti configuration of the cyclopentane ring was explored by generating the methylene sulfamate epimer at the 4′-position of compound **23** (compound **24**, Fig. 13). It was not known whether compounds with an anti configuration would retain activity. Surprisingly, this stereoisomer maintained excellent potency and, gratifyingly, the anti configuration prevented the internal cyclization between the sulfamate moiety and the purine-like base.

Importantly, these compounds unexpectedly proved potent in both biochemical and cell assays and exhibited very good selectivity over UAE and SAE (Fig. 14). A survey of N-6 substituents (**25–30**) confirmed that the compound substituted with the (*S*)-aminoindane was preferred over, for example, benzyl, α-methylbenzyl, and the opposite (*R*)-amino indane isomer (Fig. 14). Compound **24** was ultimately selected as the clinical candidate (pevonedistat).

8.04.4 Pevonedistat In Vitro and In Vivo Evaluation

The selectivity of pevonedistat within a cellular setting is demonstrated by Western blot analysis. A dose titration of the inhibitor in HCT116 cells prevented the formation of the thioester formed between the E2-conjugating enzyme (Ubc12) associated with NAE and the Nedd8 protein whereas thioesters associated with either UAE (Ubc10-Ub) or SAE (Ubc9-SUMO) activity remain uninhibited at up to 3 μM of compound throughout a 24-h incubation period (Fig. 15A). Further evidence of target engagement was observed with the corresponding decrease in neddylated cullin proteins following a similar dose response. Over the same time frame, substrates of CRLs were stabilized (e.g., NRF2, CDT-1, and p27), and markers of apoptosis (cleaved caspase and cleaved

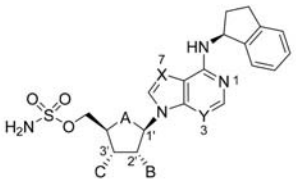

Compound	X,Y A,B,C	NAE IC_{50} (nM)	UAE IC_{50} (nM)	SAE IC_{50} (nM)	NFκB IC_{50} (nM)
7	X = N, Y = N A = O, B = C = OH	0.5	2	10	38
16	X = N, Y = CH A = O, B = C = OH	8	6	>1000	460
17	X = CH, Y = N A = O, B = C = OH	1	45	750	16
18	X = N, Y = N A = CH_2, B = C = OH	2	3	31	38
19	X = N, Y = N A = O, B = H, C = OH	1	140	180	20
20	X = N, Y = N A = O, B = OH, C = H	230	>100,000	>100,000	4400
21	X = CH, Y = N A = O, B = H, C = OH	5	>1000	4800	60
22	X = N, Y = N A = CH_2, B = H, C = OH	9	>1000	180	44
23	X = CH, Y = N A = CH_2, B = H, C = OH	24	6700*	3000	84

*mouse UAE

Fig. 12 Efforts to mitigate undesired cyclization: scaffold and ribose modifications. *Mouse UAE.

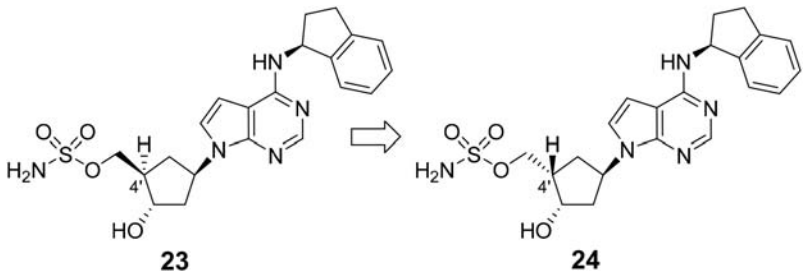

Fig. 13 A compound epimeric at the 4′-position does not undergo internal cyclization.

poly (ADP-ribose) polymerase (PARP)) were evident (Fig. 15B). This is consistent with average cell viability LD_{50} in an ATPLite assay of approximately 80 nM in HCT116 cells at 72 h.

To illustrate activity in vivo, nude mice bearing HCT116 xenografts were given a single subcutaneous injection of pevonedistat (Fig. 16). A dose-dependent pharmacodynamic response was observed with a decrease in levels of neddylated cullins with a maximal response around 2 h and returning toward baseline at 24 h. The converse is observed with levels of substrate, such as CDT1 and NRF2, increasing and giving a maximum response between 2 and 5 h and returning toward baseline at 24 h.[15]

To evaluate the effect on tumor growth, nude mice bearing subcutaneous xenografts derived from human HCT116 tumor cells were administered pevonedistat by subcutaneous injection on a variety of schedules and doses (Fig. 17).[15] Tumor growth inhibition was assessed by measuring tumor volume and comparing with control. Antitumor activity was similarly assessed in severe combined immunodeficient (SCID) mice bearing LY10 human tumor xenografts.[34] These and additional studies demonstrated that pevonedistat effectively suppressed tumor growth at doses and schedules that were well tolerated and supported advancement into human clinical trials.[35,36]

One of the most intriguing aspects of the NAE effort which required extensive follow-up was the stark difference in potency observed upon replacement of the phosphate moiety with a sulfamate. A crystal structure of pevonedistat bound to NAE in the presence of the Nedd8 protein suggested no clear interaction that could explain this dramatic potency shift (Fig. 18A). A breakthrough

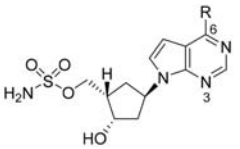

Compound	R	NAE IC_{50} (nM)	UAE IC_{50} (nM)	SAE IC_{50} (nM)	NFκB IC_{50} (nM)
24 (pevonedistat)	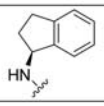	3	620	16,000	16
25		3	750*	190	98
26	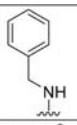	12	43,000*	39,000	120
27	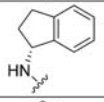	6	71,000*	>100,000	54
28	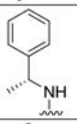	69	86,000*	>100,000	4100
29	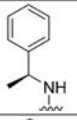	30	53,000*	>100,000	210
30	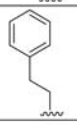	8	17,000*	26,000	90

*mouse UAE

Fig. 14 Investigation of C6 SAR. *Mouse UAE.

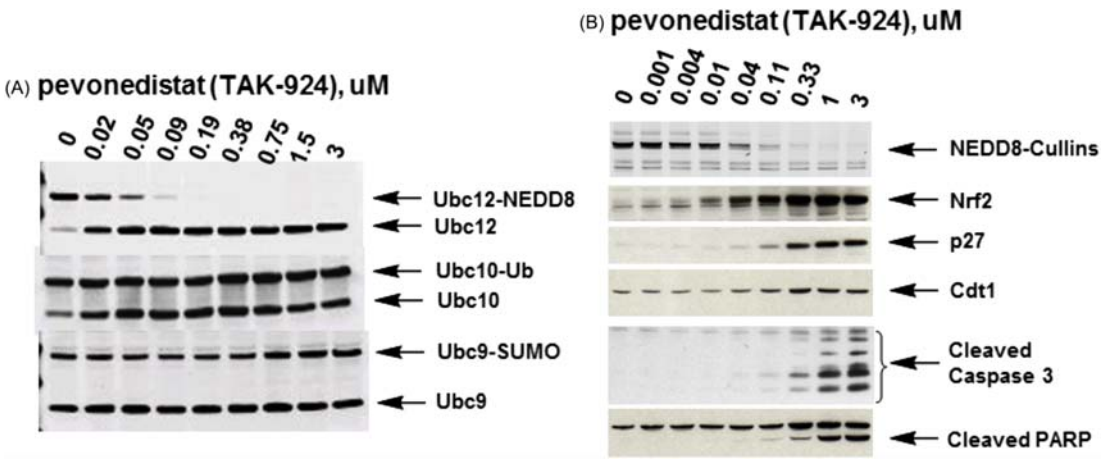

Fig. 15 HCT116 cells treated with pevonedistat for 24 h. (A) Pevonedistat selectively inhibits NAE over the related activating enzymes SAE and UAE. (B) Pevonedistat causes stabilization of cullin-RING ligase substrates and induces apoptosis.

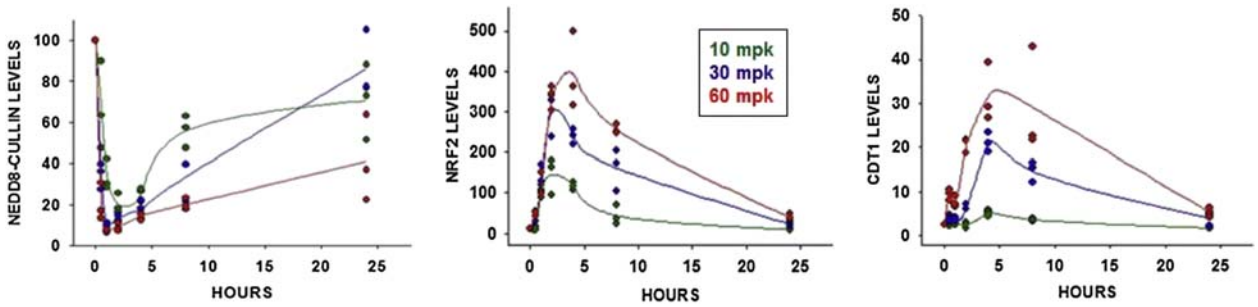

Fig. 16 Pevonedistat caused depletion of neddylated cullins and accumulation of CRL substrates (NRF2 and CDT1) in tumor xenografts. Protein levels of tumor lysate were measured by quantitative immunoblot analysis.

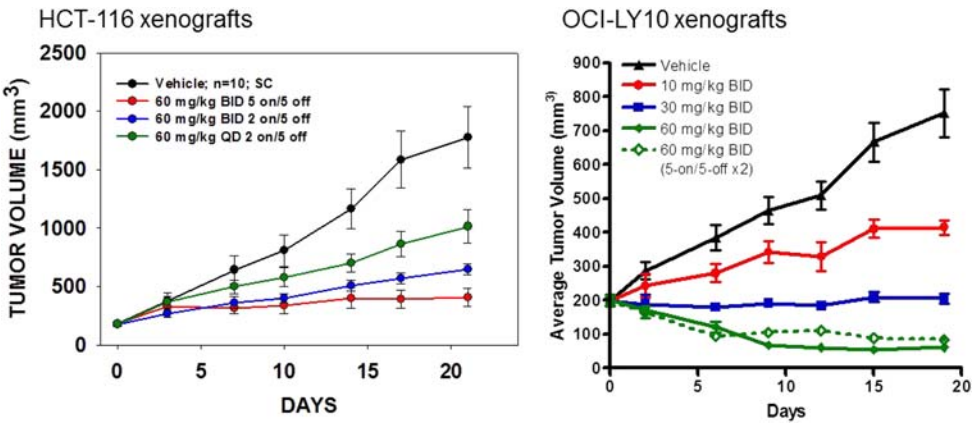

Fig. 17 Pevonedistat exhibits antitumor activity in several xenograft models in a dose-dependent manner. Activity is also observed on various dosing schedules. All dosing regimens shown were well tolerated.

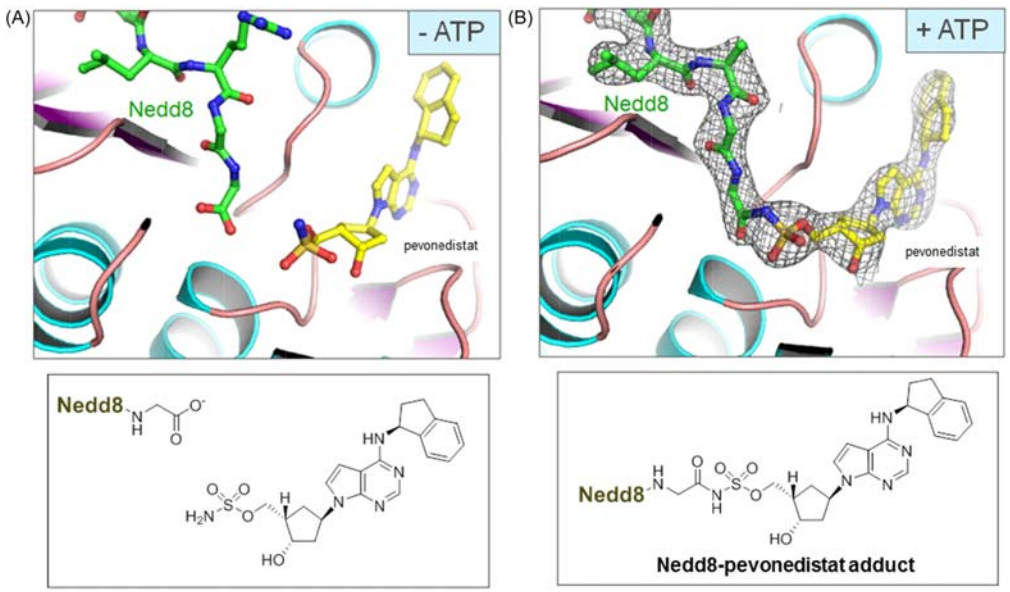

Fig. 18 (A) Crystal structure of pevonedistat/Nedd8/NAE without ATP. (B) Crystal structure of pevonedistat/Nedd8/NAE with ATP showing the formation of a covalent bond between the inhibitor and the Nedd8 protein.

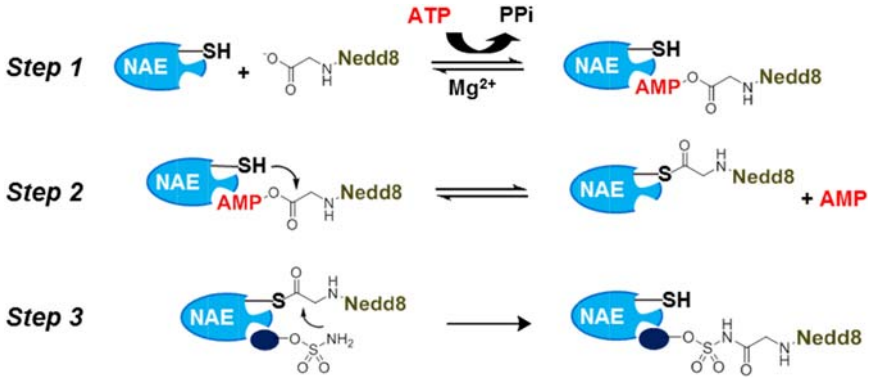

Fig. 19 The mechanism of "substrate-assisted inhibition."

observation was realized when a crystal structure was obtained in the presence of ATP: cocrystallization of MLN4924 with NAE/Nedd8/ATP revealed continuous electron density between the nitrogen of the sulfamate and the C-terminus of the Nedd8 protein showing that a *covalent bond had formed between the inhibitor and the Ubl* (Fig. 18B).[14] This covalent adduct, incorporating all the recognition elements intrinsic to the Nedd8 protein, binds noncovalently to the adenylation active site normally occupied by ATP and Nedd8 and acts as an inhibitor of the enzyme.[14,37]

Termed "substrate-assisted inhibition," the extensive set of experiments performed to elucidate the mechanism of adduct formation are described by Soucy[15] and Brownell.[14] From this work, it was determined that the first two steps of the activation pathway take place to form the singly loaded NAE-Nedd8 thioester (Fig. 19). At this point, instead of formation of the subsequent ternary complex, the inhibitor effectively competes for the ATP-binding site (Step 3) whereupon Nedd8 is transferred to the nitrogen nucleophile of the sulfamate resulting in a stable adduct that is tightly bound to the enzyme.

8.04.5 The Discovery of TAK-243 (MLN7243)

With the success of the NAE program and the knowledge gained from elucidating the mechanism of action of pevonedistat, attention was turned toward investigating UAE as a potential oncology target. Since UAE is upstream of the proteasome and impacts a greater number of substrates than NAE, it is hypothesized that inhibition should result in distinct biological outcomes thereby warranting clinical investigation.

Compounds from the adenosine sulfamate series provided an attractive starting point for the UAE program. As exemplified by **7** and **15** (Fig. 20), this chemotype displayed excellent biochemical potency against multiple E1s. Initial efforts were focused on obtaining UAE selective inhibitors and it was observed that substitution with an indole (**31**) diminished activity against SAE. Furthermore, the change from nitrogen to carbon linkage at the C6 position significantly mitigated the cyclization event that was problematic early on in the NAE campaign.

SAR exploration around the indole ring with electron-withdrawing and electron-donating groups afforded a set of UAE inhibitors with varying degrees of selectivity over NAE and SAE. From these data (Fig. 21), substitution at the six position on the indole moiety afforded compounds with optimal potency and selectivity albeit with some limitation to the size of substituent that could be accommodated (compare potency of **33** with **35**).

During the course of SAR exploration, it was realized that certain compounds within this series inhibited protein synthesis (as determined by incorporation of [(**35**)*S*]-methionine into proteins within cells). A change from ribose to cyclopentane eliminated

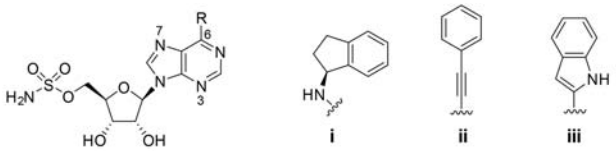

Compound	R	NAE IC_{50} (nM)	UAE IC_{50} (nM)	SAE IC_{50} (nM)
7	i	0.5	2	10
15	ii	0.3	0.3	3
31	iii	500	7	>1000

Fig. 20 Starting points for the UAE program (biochemical assay).

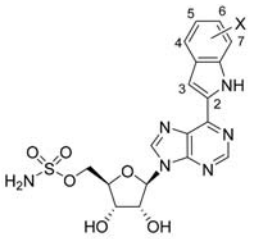

Compound	X	UAE IC50 (nM)	NAE IC50 (nM)	SAE IC50 (nM)
31	-	7	500	>1000
32	7-OMe	110	270	>1000
33	6-OMe	4	960	NA
34	4-OiPr	23	240	>1000
35	6-OiPr	22	>1000	1300
36	6-CF3	4	>1000	4900
37	6-Cl	3	700	7100

Fig. 21 Indole analogs within the adenosine sulfamate series provided selective UAE inhibitors.

this undesired activity with little variation in the overall SAR (data not disclosed). From this effort, compound **38**, which displayed comparable biochemical potency and a similar selectivity profile to its corresponding ribose derivative, was selected as a tool molecule to probe in vivo effects of UAE inhibition (Fig. 22). In addition to excellent enzyme potency, compound **38** displayed reasonable on-target cellular activity (Ubc10-Ub: 520 nM). The Ubc10-Ub assay monitors the formation of the thioester formed between the catalytic cysteine of one of the E2 enzymes associated with UAE (Ubc10) and Ub and therefore provides a direct readout of UAE inhibition. Despite favorable on-target in vitro activity, the compound failed to have meaningful impact on pharmacodynamic markers in vivo (i.e., inhibition of polyubiquitination and subsequent stabilization of substrate proteins in vivo).

In light of this, an effort was made to identify alternative chemotypes suitable for evaluating the in vivo impact of UAE inhibition. A variety of scaffolds which placed N9 of the adenosine sulfamate series exo to the ring system was investigated (Fig. 23). Synthesis of several different 5,6 and 6,6 ring systems resulted in compounds with excellent potency against the target. An overlay of the crystal structures of compound **39** and the pyrazolo-pyrimidine **40** illustrates the conservation of key hydrogen bond interactions and the position of the hydrophobic moieties between the two scaffolds. The hydroxyl substituents on the cyclopentane rings of both compounds interact with an aspartic acid residue (Asp470) in the active site. In addition, a hydrogen bond to the backbone nitrogen of Val520 is maintained in both structures. While SAR around several different chemotypes was extensively explored, the pyrazolo-pyrimidine scaffold (as represented by compound **40**) became the main focus of the program and the remainder of this article will detail efforts around this particular scaffold.

Structure–activity relationships around the adenosine sulfamate series showed that both the 2′- and 3′-hydroxyl groups on a cyclopentane were optimal for potency against UAE. This trend was further explored within the pyrazolo-pyrimidine series. In the example where Ar = Ph (Fig. 24, compounds **40–42**), SAR showed that the 2′-hydroxyl group is required for optimum biochemical potency against UAE. Compounds with larger hydrophobic groups (**43–49**) resulted in greater potency against both UAE and NAE relative to their unsubstituted phenyl counterparts. In general, compounds with a 2′-hydroxyl group showed better cellular potency than those without this functional group as evaluated in an assay measuring the inhibition of protein polyubiquitination (K48 cell assay). As discussed in the introduction, UAE catalyzes the reaction that appends a chain of Ub molecules (linked through the lys48 (K48) residue of the Ub protein) to a substrate. An inhibitor's ability to prevent this from taking place provides a downstream readout of UAE target engagement. Overall, compounds within the pyrazolo-pyrimidine series showed excellent selectivity over SAE while selectivity over NAE proved more challenging.

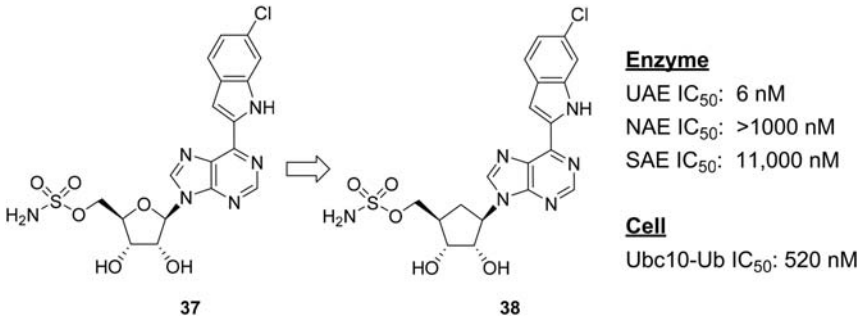

Fig. 22 UAE selective inhibitor from the 'adensosine-sulfamate' AS series as a tool molecule for in vivo evaluation.

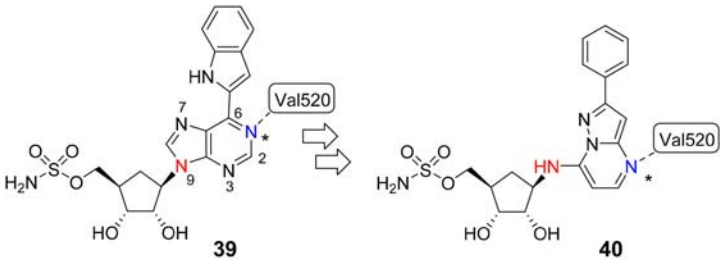

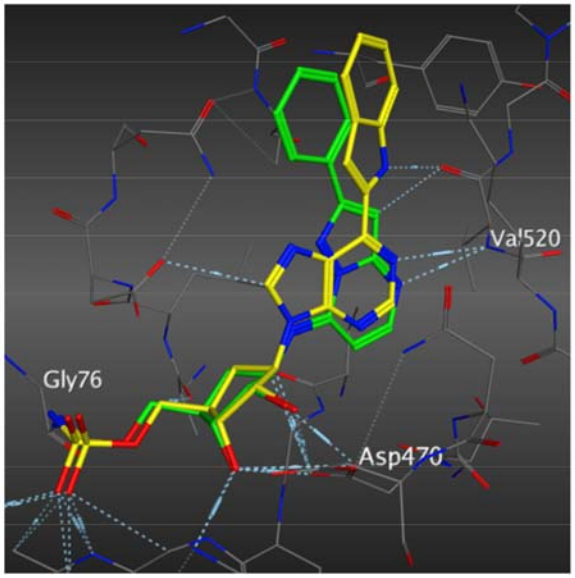

Fig. 23 Overlay of X-ray crystal structures of adenosine-sulfamate **39** and pyrazolo-pyridine **40** bound to UAE.

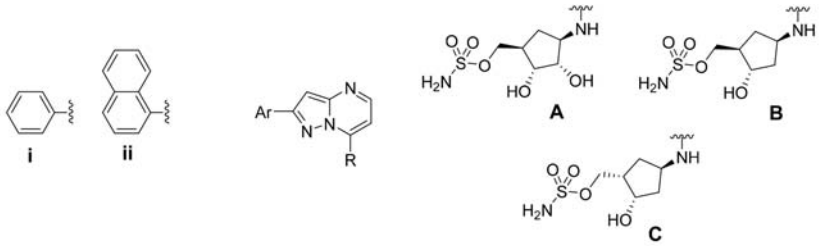

Compound	Ar	R	UAE IC_{50} (nM)	NAE IC_{50} (nM)	SAE IC_{50} (nM)	K48 (cell) IC_{50} (nM)
40	i	A	12	66	1400	NA
41	i	B	640	380	3300	9800
42	i	C	150	820	>50,000	NA
43	ii	A	1	2	440	55
44	ii	B	9	24	3900	1100
45	ii	C	26	110	>50,000	3900

Fig. 24 Varying hydrophobic and cyclopentane substitution within the pyrazolo-pyrimidine scaffold.

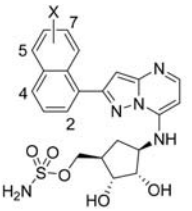

Compound	X	UAE IC_{50} (nM)	NAE IC_{50} (nM)	K48 IC_{50}(nM)
43	-	1	2	55
46	4-F	1	3	69
47	5-F	0.4	1	21
48	6-CHF2	0.4	0.4	22
49	4-Cl	1	1	31
50	4-Me	0.4	0.3	23
51	2,4-dichloro	14	370	730
52	2-Me	4	37	350

Fig. 25 SAR around naphthyl ring substitution.

Following up on the improvement in potency observed with the increase in aryl hydrophobicity, SAR of variously substituted naphthyl derivatives on the pyrazolo-pyrimidine scaffold was explored (Fig. 25). Substitution with fluorine at either C4 (**46**) or C5 (**47**) of the naphthyl substituent afforded excellent biochemical and cellular potency as did a CHF_2 group at C6 (**48**). A chlorine substituted at C4 provided a compound with activity similar to its fluorinated counterpart (compare compounds **46** and **49**) as did switching to an electron donating methyl group (**50**). While these examples illustrated that substitution at most positions around the naphthyl ring was well tolerated, substitution at the 2-position deviated from this trend. The 2-methyl derivative **52** and the 2,4-dichloro compound **51** showed greatly diminished cellular potency. Interestingly, these compounds displayed a meaningful difference in potency between UAE and NAE and provided a path forward to explore selectivity over NAE within this series.

Toward this end, a series of substituted naphthyl derivatives was synthesized with increasing steric bulk at the 2-position (Fig. 26). In particular, the isopropoxy substituted naphthyl compound **55** afforded a molecule that was still quite potent against UAE (3 nM) in the biochemical assay but was not active against NAE (>1000 nM). The favorable impact on selectivity appeared to be specific to the naphthyl group. 2-Methoxynaphthyl compound **54** showed >100-fold selectivity over NAE where the effect was not nearly as pronounced for the corresponding 2-methoxyphenyl compound (**56**, ~fivefold selective in the biochemical assay).

Despite favorable selectivity, compounds such as **55** showed dramatically diminished cellular activity and, while further refinement could have overcome this, the question was raised as to whether or not selectivity over NAE was necessary to identify a suitable clinical candidate. As discussed in the Introduction, there is an overlap in the function of NAE and UAE. NAE controls a subset of E3 ligases (the CRLs)[26] that are directly involved in ubiquitination (which, of course, requires UAE activity). Inhibition of UAE prevents the activation of Ub and obviates the function of all E3's including cullin-dependent E3's. Therefore, it was hypothesized that the phenotype of a *dual* UAE/NAE inhibitor would be identical to that of a UAE *selective* inhibitor. The phenotype of NAE selective inhibition, established during the NAE program with pevonedistat, exhibited DNA re-replication and the accumulation of cells in the

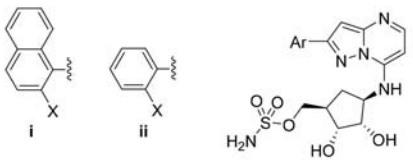

Compound	Ar	X	UAE IC_{50} (nM)	NAE IC_{50} (nM)	K48 IC_{50}(nM)
43	i	H	1	2	55
53	i	Me	4	37	350
54	i	OMe	1	160	160
55	i	OiPr	3	>1000	450
56	ii	OMe	3	16	210

Fig. 26 Increasing size of 2-substituent on the naphthyl ring improved selectivity for UAE over NAE.

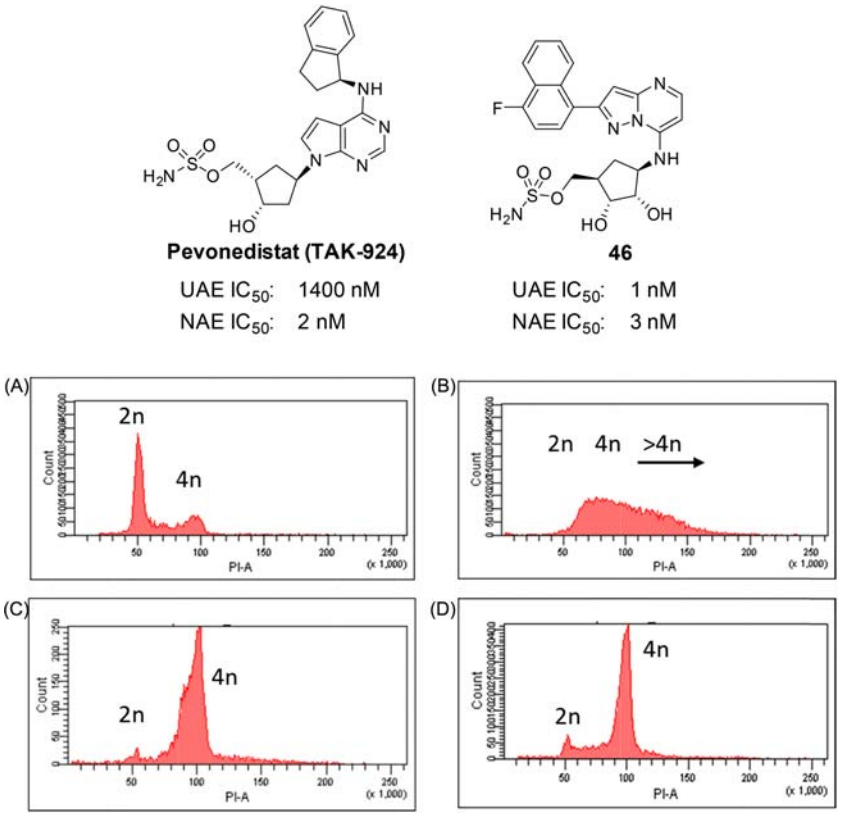

Fig. 27 FACS analysis of dual NAE/UAE and UAE selective inhibitors and comparison with the selective NAE inhibitor pevonedistat in HCT116 cells. (A) DMSO (control). (B) Pevonedistat. (C) Selective UAE inhibitor (compound not shown). (D) Dual UAE/NAE inhibitor (compound **46**).

S-phase of the cell cycle as observed by fluorescence-activated cell sorting (FACS) analysis (Fig. 27B).[15] Inhibition and phenotype analysis with a *selective* UAE inhibitor (compound not shown) resulted in cell cycle arrest in the G2 phase (Fig. 27C). A *dual* UAE/NAE inhibitor (compound **46**) exhibited this same G2 arrest phenotype (Fig. 27D) and confirmed the dominant UAE phenotype of inhibition over that of NAE inhibition.

A possible explanation for the difference in phenotype lies in the substrates which are modified within each pathway. The replication licensing factor CDT1, following DNA replication, is ultimately ubiquitinated and degraded in an NAE (CRL)-dependent manner to ensure replication occurs only once within a cell cycle. When NAE is inhibited CDT1 cannot be degraded and remains active thereby inducing the DNA re-replication phenotype observed. Presumably, this would occur upon UAE inhibition as well since there is an overlap in function of NAE and UAE which should also lead to the stabilization of CDT1. However, UAE inhibition also results in the stabilization of the protein geminin, the endogenous inhibitor of CDT1. Stabilization of both geminin and CDT1 would prevent the cellular imbalance observed resulting from NAE inhibition and therefore prevent the re-replication phenotype.[38] To summarize this observation: An NAE inhibitor inhibits only NAE activity. A UAE inhibitor inhibits both UAE and NAE function regardless of its activity against NAE.

8.04.6 Selection of the Development Candidate

Having established the dominant UAE phenotype, selectivity for UAE over NAE was not considered critical to moving forward and focus was directed toward in vivo evaluation of potent UAE inhibitors regardless of NAE inhibition. Along with exploration of SAR around the naphthyl moiety, considerable effort was focused on other variously substituted aryl and heteroaryl substituents. This work identified a clear preference for compounds with meta-substituted phenyl substituents as exemplified by a comparison of compound **61** (which was ultimately selected as the clinical candidate) with the corresponding ortho (**62**) and para (**63**) compounds that showed diminished biochemical and cellular potency (Fig. 28).

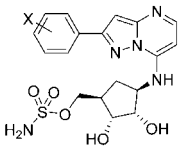

Compound	X	UAE IC_{50} (nM)	NAE IC_{50} (nM)	K48 IC_{50}(nM)
57*	*m*-N-pyrrolidine	1	24	40
58*	*m*-OCF3	2	320	140
59*	*m*-TMS	2	38	160
60*	*m*-Br	5	24	250
61 (TAK-243)	*m*-SCF3	1	25	76
62	*o*-SCF3	40	420	6100
63	*p*-SCF3	35	180	2900

*racemic compound

Fig. 28 Exploration of *m*-substituted phenyl compounds.

8.04.7 Profile of the Clinical Candidate

Compounds that displayed potent on-target cellular activity were further profiled in vitro in advance of in vivo evaluation. In addition to excellent activity in the K48 polyubiquitination assay, TAK-243 (**61**) displayed excellent cytotoxicity as determined in an ATPlite assay in HCT116 cells (Fig. 29A). Furthermore, the compound inhibited the formation of the Ubc10-ubiquitin thioester adduct with an IC_{50} of 50 nM thereby preventing the downstream transfer of Ub to protein substrates. This leads to the stabilization of short-lived proteins such as c-jun and c-myc and the induction of ER (endoplasmic reticulum) stress as indicated by the stabilization of ATF and GADD34 (Fig. 29B). The accumulation of cleaved PARP signified the induction of an apoptotic response (Fig. 29C). A crystal structure of TAK-243 bound to UAE (in the presence of Ub and ATP) revealed the formation of a covalent adduct formed between the sulfamate moiety of the compound and C-terminal glycine of Ub (Fig. 29D).

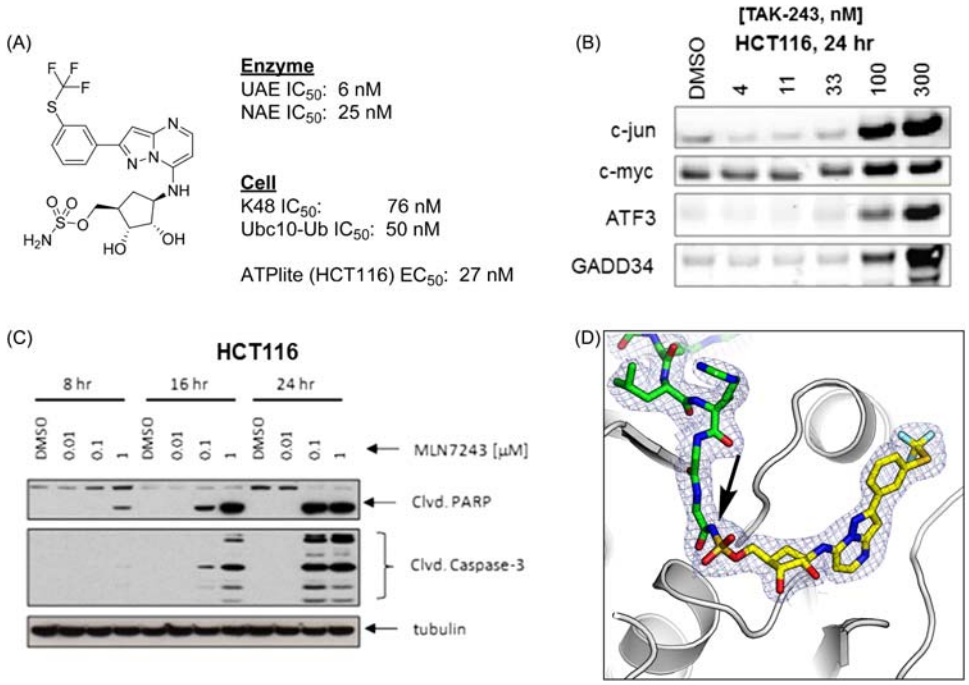

Fig. 29 (A) In vitro profile of TAK-243. (B) Western blot analysis of proteins stabilized as a result of UAE inhibition. (C) Western blot analysis of apoptotic markers cleaved PARP (HCT116 cells). (D) Crystal structure of TAK-243 (*arrow* indicates the bond between the sulfamate of the inhibitor and ubiquitin).

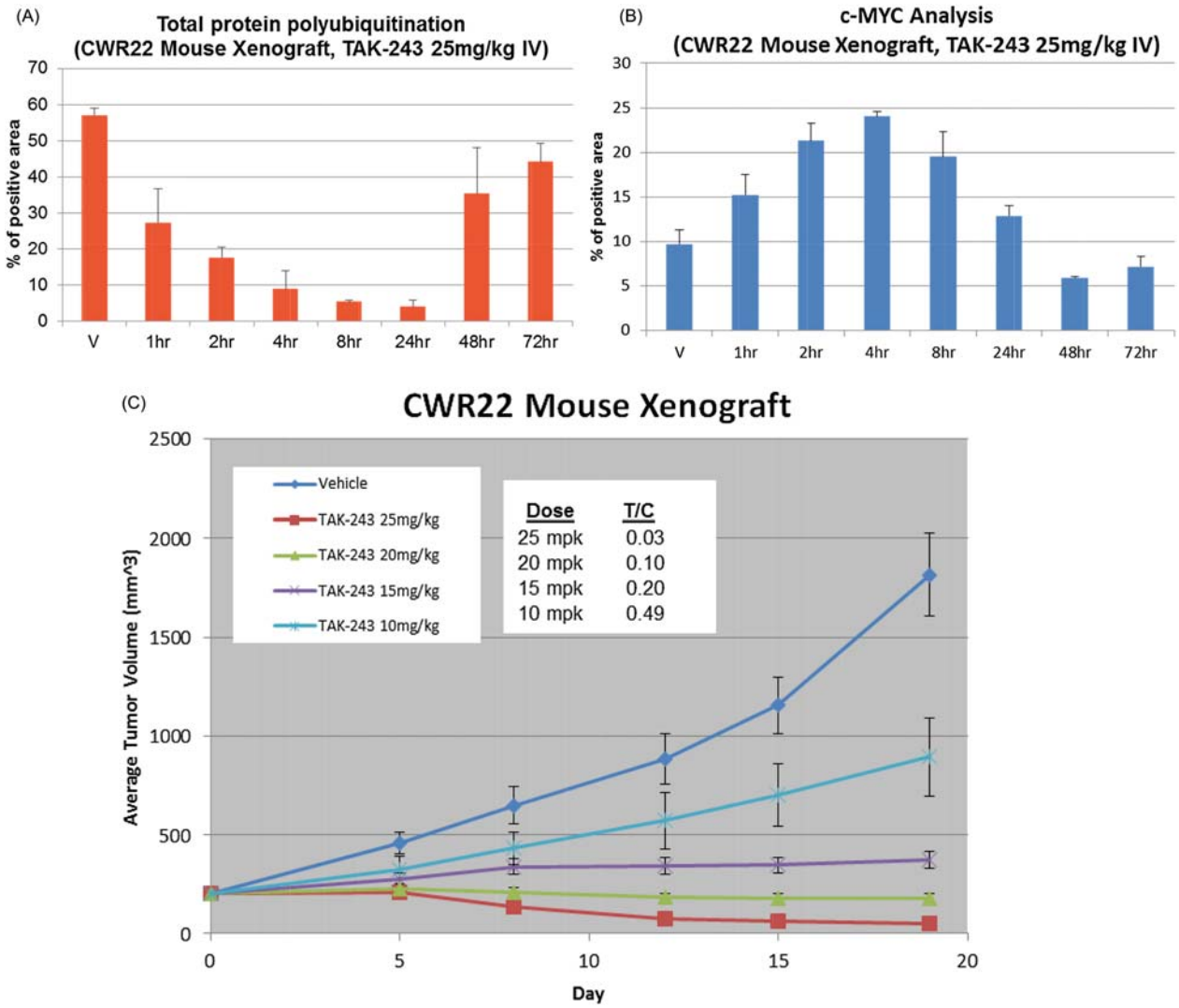

Fig. 30 (A) PD response in CWR22 tumor samples: levels of polyubiquitinated protein conjugates decreases over time. (B) Accumulation of c-Myc as a result of UAE inhibition. (C) 21-day efficacy study in CWR22 mouse xenografts (IV dose, twice weekly, MTD is 25 mpk).

In vivo, TAK-243 displayed a robust and durable pharmacodynamic response. For example, immunohistochemistry analysis of tumor samples from a cell-line-derived CWR-22 xenograft (prostate cancer model) showed a very good correlation between the loss of poly-ubiquitinated proteins (Fig. 30A) and the stabilization of the protein c-myc that persisted out to 24 h (Fig. 30B). This translated into excellent antitumor activity in the same model treated with TAK-243 on a clinically relevant twice weekly dosing schedule (Fig. 30C).

TAK-243 also showed antitumor activity in a patient-derived colon adenocarcinoma model following the same twice weekly dosing schedule (Fig. 31A) and tumor samples from both treated and untreated animals were analyzed by immunohistochemistry. The clear presence of inhibitor-Ub adduct (Fig. 31B) and the loss of polyubiquinated proteins (Fig. 31C) in treated samples provided confidence that tumor growth inhibition was driven by target engagement. In addition to the nonclinical efficacy studies described herein, TAK-243 exhibited broad antitumor activity across a variety of cell-line derived and primary tumor xenograft models. These data supported the initiation of a phase I dose escalation clinical trial (C33001) in solid tumors.

The clinical success of proteasome inhibition afforded validation that disruption of the UPS is a valid approach to the treatment of cancer. Building on this knowledge, attention was turned to other targets within the UPS in order to impact protein quality control in a different and potentially more selective fashion. TAK-924 and TAK-243 represent the first E1-activating enzyme inhibitors to enter the clinic. These mechanism-based inhibitors form a covalent adduct in situ that is tight-binding, ATP competitive, and reversible. The adduct takes advantage of the strong protein–protein interactions native to the E1 and its corresponding Ub or Ubl to bind noncovalently to the enzyme. This leads to durable pharmacodynamic responses and broad in vivo efficacy in nonclinical models. In addition to potential clinical benefit, intervention with small molecules affords tools to better understand the molecular mechanisms and interactions involved in the complex array of processes within the UPS and enable development of the next generation of chemotherapeutic agents.

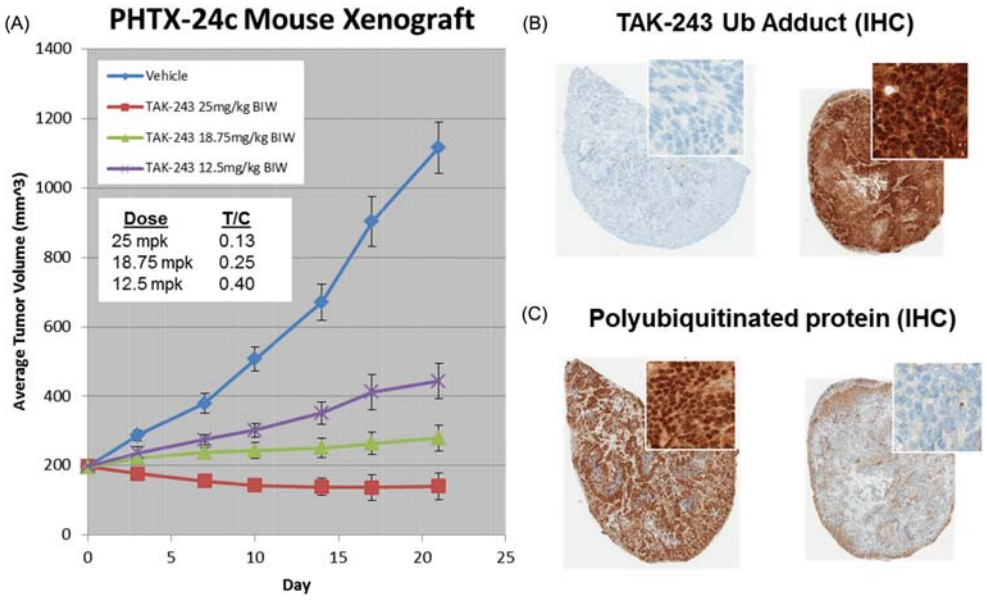

Fig. 31 (A) Twenty-one day efficacy study in PHTX-132Lu xenografts (IV dose, twice weekly). Efficacious response was seen at the maximum tolerated dose of the compound (25 mpk), at ¾ MTD (18.75 mpk) and at ½ MTD (12.5 mpk). (B) and (C) IHC (immunohistochemistry) analysis of treated tumor samples (PHTX-24c, 16 h post-single IV dose of 25 mpk) showing the detection of inhibitor-Ub adduct (B) and the loss of polyubiquinated proteins (C).

References

1. Balch, W. E.; Morimoto, R. I.; Dillin, A.; Kelly, J. W. Adapting Proteostasis for Disease Intervention. *Science* **2008,** *319,* 916–919.
2. Powers, E. T.; Morimoto, R. I.; Dillin, A.; Kelly, J. W.; Balch, W. E. Biological and Chemical Approaches to Diseases of Proteostasis Deficiency. *Annu. Rev. Biochem.* **2009,** *78,* 959–991.
3. Ciechanover, A. Intracellular Protein Degradation: From a Vague Idea Thru the Lysosome and the Ubiquitin-Proteasome System and Onto Human Diseases and Drug Targeting. *Cell Death Differ.* **2005,** *12,* 1178–1190.
4. Hershko, A.; Ciechanover, A.; Heller, H.; Haas, A. L.; Rose, I. A. Proposed Role of ATP in Protein Breakdown: Conjugation of Protein With Multiple Chains of the Polypeptide of ATP-Dependent Proteolysis. *Proc. Natl. Acad. Sci. U. S. A.* **1980,** *77,* 1783–1786.
5. Wilkinson, K. D.; Urban, M. K.; Haas, A. L. Ubiquitin Is the ATP-Dependent Proteolysis Factor I of Rabbit Reticulocytes. *J. Biol. Chem.* **1980,** *255,* 7529–7532.
6. Etlinger, J. D.; Goldberg, A. L. A Soluble ATP-Dependent Proteolytic System Responsible for the Degradation of Abnormal Proteins in Reticulocytes. *Proc. Natl. Acad. Sci. U. S. A.* **1977,** *74,* 54–58.
7. Peters, J. M.; Franke, W. W.; Kleinschmidt, J. A. Distinct 19 S and 20 S Subcomplexes of the 26 S Proteasome and Their Distribution in the Nucleus and the Cytoplasm. *J. Biol. Chem.* **1994,** *269,* 7709–7718.
8. Molineaux, S. M. Molecular Pathways: Targeting Proteasomal Protein Degradation in Cancer. *Clin. Cancer Res.* **2011,** *18,* 15–20.
9. Nalepa, G.; Rolfe, M.; Harper, J. W. Drug Discovery in the Ubiquitin-Proteasome System. *Nat. Rev. Drug Discov.* **2006,** *5,* 596–613.
10. Deshaies, R. J. Proteotoxic Crisis, the Ubiquitin-Proteasome System, and Cancer Therapy. *BMC Biol.* **2014,** *12,* 94.
11. Popovic, D.; Vucic, D.; Dikic, I. Ubiquitination in Disease Pathogenesis and Treatment. *Nat. Med.* **2014,** *20,* 1242–1253.
12. Bedford, L.; Lowe, J.; Dick, L. R.; Mayer, R. J.; Brownell, J. E. Ubiquitin-Like Protein Conjugation and the Ubiquitin-Proteasome System as Drug Targets. *Nat. Rev. Drug Discov.* **2011,** *10,* 29–46.
13. Luo, J.; Solimini, N. L.; Elledge, S. J. Principles of Cancer Therapy: Oncogene and Non-Oncogene Addiction. *Cell* **2009,** *136,* 823–837.
14. Brownell, J. E.; Sintchak, M. D.; Gavin, J. M.; Liao, H.; Bruzzese, F. J.; Bump, N. J.; et al. Substrate-Assisted Inhibition of Ubiquitin-Like Protein-Activating Enzymes: The NEDD8 E1 Inhibitor MLN4924 Forms a NEDD8-AMP Mimetic in Situ. *Mol. Cell* **2010,** *37,* 102–111.
15. Soucy, T. A.; Smith, P. G.; Milhollen, M. A.; Berger, A. J.; Gavin, J. M.; Adhikari, S.; et al. An Inhibitor of NEDD8-Activating Enzyme as a New Approach to Treat Cancer. *Nature* **2009,** *458,* 732–736.
16. Ocio, E. M.; Mateos, M. V.; San-Miguel, J. F. Novel Agents Derived From the Currently Approved Treatments for MM: Novel Proteasome Inhibitors and Novel IMIDs. *Expert Opin. Investig. Drugs* **2012,** *21,* 1075–1087.
17. Moreau, P. The Emerging Role of Carfilzomib Combination Therapy in the Management of Multiple Myeloma. *Expert Rev. Hematol.* **2014,** *7,* 265–290.
18. Vij, R.; Siegel, D. S.; Jagannath, S.; Jakubowiak, A. J.; Stewart, A. K.; McDonagh, K.; et al. An Open-Label, Single-Arm, Phase 2 Study of Single-Agent Carfilzomib in Patients With Relapsed and/or Refractory Multiple Myeloma Who Have Been Previously Treated With Bortezomib. *Br. J. Haematol.* **2012,** *158,* 739–748.
19. Shah, N.; Biran, N.; Vesole, D. H. Ixazomib: An Oral Proteasome Inhibitor for the Treatment of Multiple Myeloma. *Expert Opin. Orphan Drugs* **2015,** *4,* 105–113.
20. Chen, J. J.; Tsu, C. A.; Gavin, J. M.; Milhollen, M. A.; Bruzzese, F. J.; Mallender, W. D.; et al. Mechanistic Studies of Substrate-Assisted Inhibition of Ubiquitin-Activating Enzyme by Adenosine Sulfamate Analogues. *J. Biol. Chem.* **2011,** *286,* 40867–40877.
21. Obeng, E. A.; Carlson, L. M.; Gutman, D. M.; Harrington, W. J., Jr.; Lee, K. P.; Boise, L. H. Proteasome Inhibitors Induce a Terminal Unfolded Protein Response in Multiple Myeloma Cells. *Blood* **2006,** *107,* 4907–4916.
22. Johnson, D. E. The Ubiquitin-Proteasome System: Opportunities for Therapeutic Intervention in Solid Tumors. *Endocr. Relat. Cancer* **2015,** *22,* T1–T17.
23. Hershko, A.; Heller, H.; Elias, S.; Ciechanover, A. Components of Ubiquitin-Protein Ligase System. Resolution, Affinity Purification, and Role in Protein Breakdown. *J. Biol. Chem.* **1983,** *258,* 8206–8214.
24. van Wijk, S. J.; Timmers, H. T. The Family of Ubiquitin-Conjugating Enzymes (E2s): Deciding Between Life and Death of Proteins. *FASEB J.* **2010,** *24,* 981–993.
25. Hershko, A.; Ciechanover, A. The Ubiquitin System. *Annu. Rev. Biochem.* **1998,** *67,* 425–479.

26. Petroski, M. D.; Deshaies, R. J. Function and Regulation of Cullin-RING Ubiquitin Ligases. *Nat. Rev. Mol. Cell Biol.* **2005,** *6,* 9–20.
27. Kristariyanto, Y. A.; Abdul Rehman, S. A.; Campbell, D. G.; Morrice, N. A.; Johnson, C.; Toth, R.; et al. K29-Selective Ubiquitin Binding Domain Reveals Structural Basis of Specificity and Heterotypic Nature of k29 Polyubiquitin. *Mol. Cell* **2015,** *58,* 83–94.
28. Schulman, B. A.; Harper, J. W. Ubiquitin-Like Protein Activation by E1 Enzymes: The Apex for Downstream Signalling Pathways. *Nat. Rev. Mol. Cell Biol.* **2009,** *10,* 319–331.
29. Pan, Z. Q.; Kentsis, A.; Dias, D. C.; Yamoah, K.; Wu, K. Nedd8 on Cullin: Building an Expressway to Protein Destruction. *Oncogene* **2004,** *23,* 1985–1997.
30. Gong, L.; Yeh, E. T. Identification of the Activating and Conjugating Enzymes of the NEDD8 Conjugation Pathway. *J. Biol. Chem.* **1999,** *274,* 12036–12042.
31. Haas, A. L.; Rose, I. A. The Mechanism of Ubiquitin Activating Enzyme. A Kinetic and Equilibrium Analysis. *J. Biol. Chem.* **1982,** *257,* 10329–10337.
32. Ghosh, S.; Baltimore, D. Activation In Vitro of NF-Kappa B by Phosphorylation of Its Inhibitor I Kappa B. *Nature* **1990,** *344,* 678–682.
33. Read, M. A.; Brownell, J. E.; Gladysheva, T. B.; Hottelet, M.; Parent, L. A.; Coggins, M. B.; et al. Nedd8 Modification of cul-1 Activates SCF(Beta(TrCP))-Dependent Ubiquitination of IkappaBalpha. *Mol. Cell. Biol.* **2000,** *20,* 2326–2333.
34. Milhollen, M. A.; Traore, T.; Adams-Duffy, J.; Thomas, M. P.; Berger, A. J.; Dang, L.; et al. MLN4924, a NEDD8-Activating Enzyme Inhibitor, Is Active in Diffuse Large B-Cell Lymphoma Models: Rationale for Treatment of NF- B-Dependent Lymphoma. *Blood* **2010,** *116,* 1515–1523.
35. Bhatia, S.; Pavlick, A. C.; Boasberg, P.; Thompson, J. A.; Mulligan, G.; Pickard, M. D.; et al. A Phase I Study of the Investigational NEDD8-Activating Enzyme Inhibitor Pevonedistat (TAK-924/MLN4924) in Patients With Metastatic Melanoma. *Investig. New Drugs* **2016,** *34,* 439–449.
36. Swords, R. T.; Erba, H. P.; DeAngelo, D. J.; Bixby, D. L.; Altman, J. K.; Maris, M.; et al. Pevonedistat (MLN4924), a First-in-Class NEDD8-Activating Enzyme Inhibitor, in Patients With Acute Myeloid Leukaemia and Myelodysplastic Syndromes: A Phase 1 Study. *Br. J. Haematol.* **2015,** *169,* 534–543.
37. Walden, H.; Podgorski, M. S.; Huang, D. T.; Miller, D. W.; Howard, R. J.; Minor, D. L., Jr.; et al. The Structure of the APPBP1-UBA3-NEDD8-ATP Complex Reveals the Basis for Selective Ubiquitin-Like Protein Activation by an E1. *Mol. Cell* **2003,** *12,* 1427–1437.
38. Ballabeni, A.; Zamponi, R.; Moore, J. K.; Helin, K.; Kirschner, M. W. Geminin Deploys Multiple Mechanisms to Regulate Cdt1 Before Cell Division Thus Ensuring the Proper Execution of DNA Replication. *Proc. Natl. Acad. Sci.* **2013,** *110,* E2848–E2853.

Relevant Websites

http://www.cellsignal.com/common/content/content.jsp?id=pathways-ubiquitin—An overview of the Ubiquitin Proteasome System with relevant references.
https://clinicaltrials.gov/ct2/results?term=MLN7243&Search=Search—Clinical trial with TAK-243.
https://clinicaltrials.gov/ct2/results?term=pevonedistat&Search=Search—Clinical trials with pevonedistat.
http://www.deshaieslab.com—Research in the Deshais lab is focused on understanding the link between defects in protein homeostasis and disease.
http://www.drugbank.ca/drugs/DB00188—An overview of bortezomib.
https://harper.hms.harvard.edu—The Harper lab is a recognized leader in the field of protein homeostasis and ubiquitin signaling.
https://www.stjude.org/directory/s/brenda-schulman.html—The Schulman lab is focused on understanding the mechanism and impact of Ubl transfer in the post-translational modification of substrate proteins.

8.05 The Discovery of p97 Inhibitors

DJ Wustrow[a], **DJ Anderson, M Rolfe, and H-J Zhou,** Cleave Biosciences, Burlingame, CA, United States

© 2017 Elsevier Ltd. All rights reserved.

8.05.1	**Introduction**	113
8.05.1.1	Rationale for p97 Inhibition as a Cancer Target	113
8.05.1.1.1	Nononcogene addiction pathways	113
8.05.1.1.2	p97 and protein homeostasis	113
8.05.1.2	Mass Screening and Initial Hit to Lead Efforts	114
8.05.1.2.1	HTS screen and hit triage	114
8.05.1.2.2	Hit to lead investigations	115
8.05.2	**Discovery of CB-5083**	118
8.05.2.1	Lead Development Efforts	118
8.05.2.1.1	Changes in p97 biochemical assay	118
8.05.2.1.2	Alternative synthesis of ML240	119
8.05.2.1.3	Guiding principles used in lead development of 26 (ML240)	119
8.05.2.1.4	Investigation to changes of the *N*-benzyl substituent of ML240	120
8.05.2.1.5	Benzimidazole analogs	121
8.05.2.1.6	Exploration of other fused pyrimidine cores	121
8.05.2.1.7	Evidence of p97 inhibition in cellular assays and in vivo	125
8.05.2.2	Candidate Seeking Efforts	126
8.05.3	**Further Evaluations of CB-5083 and Analogs**	132
8.05.3.1	LipE and Cell Penetration	132
8.05.4	**Summary of p97 Inhibitors Reported From Competitors' Efforts**	132
8.05.4.1	2-(Cyclohexylmethylamino)pyrimidines	132
8.05.4.2	Alkylsulfanyl Triazoles	134
8.05.4.3	Compounds Discovered by U. Pittsburgh/UCSF Collaboration	135
8.05.4.3.1	5-*N*-(3-(1H-indol-2yl)-phenyl-piperidines	135
8.05.4.3.2	*N*-5-indolyl-carboxamides	135
8.05.5	**Summary and Future Directions**	135
Acknowledgments		136
References		136

8.05.1 Introduction

8.05.1.1 Rationale for p97 Inhibition as a Cancer Target

8.05.1.1.1 Nononcogene addiction pathways

The occurrence of oncogenic mutations that either hyper-activate tumor cell growth pathways or inactivate tumor suppression pathways is a key step in the conversion of healthy tissue to a malignant lesion. Several oncogenic driver mutations have been successfully targeted to produce antitumor therapies but these therapies suffer from short response duration and rapid development of resistance. Tumor cells exist in a highly stressed environment and frequently become dependent upon a number of fundamental biological pathways in order to adapt to the stress of the tumor environment, and dependence on these pathways is called nononcogene addiction (**Fig. 1**).[1] Recently these pathways have become interesting targets for anticancer therapy. One reason to target these nononcogenic pathways is the recognition of heterogeneity in the oncogenic driver mutations within individual tumors that can rapidly render individual oncogene targeted therapies inactive (**Fig. 1**).[2] By targeting the underlying nononcogenic addiction pathways one could provide effective therapies where the number or heterogeneity of oncogenic mutations has caused the tumor mass to become resistant to targeted therapies. One key nononcogenic pathway cancer cells rely on is the control of protein homeostasis. Many tumor cell types require high levels of proteasome activity and efficient mechanisms for dealing with unwanted, incorrectly translated or misfolded proteins to prevent lethal levels of proteotoxic stress from accumulating.[1b]

8.05.1.1.2 p97 and protein homeostasis

The highly abundant protein p97, also called Valosin-containing protein (VCP) or cdc48 in yeast, serves multiple cellular functions through interaction with a variety of cofactor proteins. One main function of p97 is to act as a key regulator of protein homeostasis by sitting at the junction of two important pathways that cells use to deal with proteotoxic stress, the ubiquitin proteasome pathway

[a]Current address: FLX Bio, South San Francisco, CA, United States.

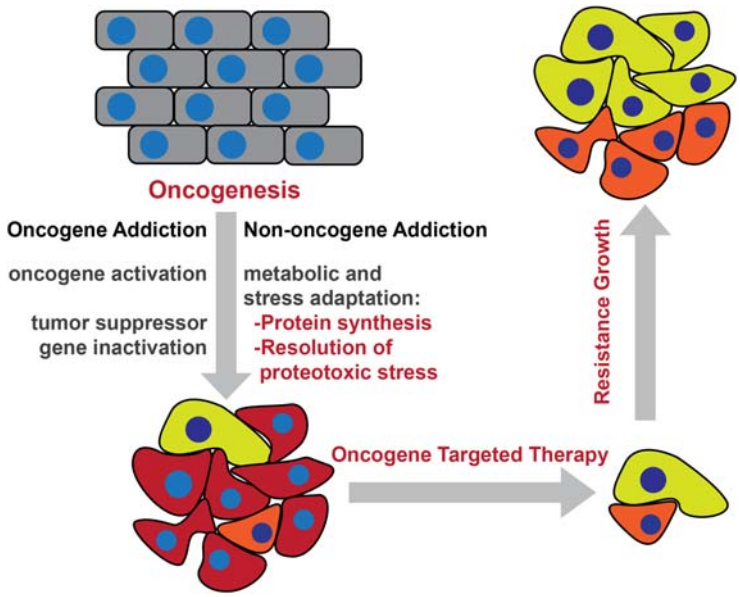

Fig. 1 Interaction of oncogenic and nononcogenic factors in the transformation of normal tissue to cancerous lesions that are heterogeneous and susceptible to targeted agent resistance.

Fig. 2 Domains of p97 protein.

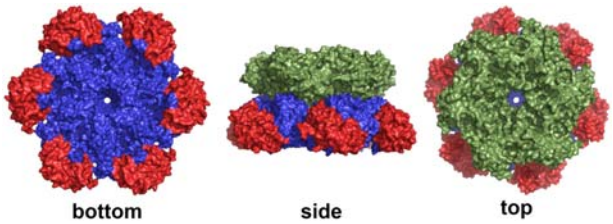

Fig. 3 Cryo-electron microscopy images of the p97 hexamer.[5]

and the autophagy lysosome pathway.[3] The protein p97 is a member of the AAA+ family of ATPases. This a heterogeneous group of ATPases that act as mechanoenzymes by converting the chemical energy of ATP to generate force that is used to translocate and remodel protein/protein, protein/nucleic acid, or protein/membrane complexes.[4] Six p97 protein monomers with each monomer containing three protein subdomains (Fig. 2) combine to form a homohexamer (Fig. 3). Recently a cryo-electron microscopic image of the hexamer has been published.[5]

The N-terminal domain is responsible for binding cofactor proteins which help to direct p97 to different processes within the cell. The D1 domain binds tightly to ADP and interactions between D1 sites on adjacent monomers are important for hexamer formation. The D2 domain is responsible for the majority of the ATP hydrolysis activity of p97.[6] An important function of p97 is to extract polyubiquitinated (poly-Ub) proteins from the endoplasmic reticulum (ER) and other organelles and deliver them to the 26S proteasome for degradation (Fig. 4). Previous work has shown that knockdown of p97 interrupts this process leading to increases in poly-ubiquitinated proteins and buildup of mis-folded proteins in the ER which leads to an induction of the unfolded protein response (UPR) resulting in apoptotic cell death.[7] Given p97's critical role in protein homeostasis, inhibition of its ATPase activity was hypothesized to result in preferential killing of cancer cells that have a high protein synthesis burden.[8] Therefore, several groups have put forth efforts in discovering small molecule inhibitors of p97. This review will cover published medicinal chemistry efforts directed at finding new inhibitors of the ATPase activity of p97.

8.05.1.2 Mass Screening and Initial Hit to Lead Efforts

8.05.1.2.1 HTS screen and hit triage

To better understand the role of p97 cellular functions, there was a desire to discover a compound that could rapidly block the ATPase activity of p97 and enable the study of the downstream effects of this inhibition. A robust biochemical assay was developed

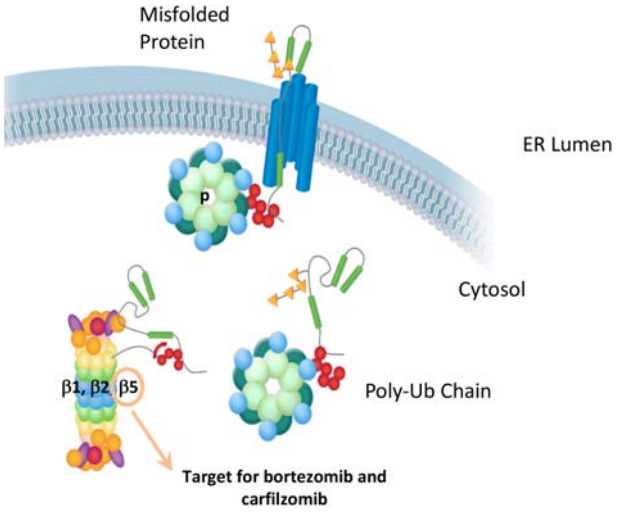

Fig. 4 Role of p97 in processing of misfolded proteins.

that measured recombinant p97 ATPase activity via a luminescent readout of ADP generated from hydrolysis of ATP.[9] This assay was used to screen over 234,000 compounds from two compound libraries (Maybridge HitFinder Collection and the National Institutes of Health Molecular Libraries Small Molecule Repository) at concentrations of 8–10 μM. From the initial 959 mass screen hits (hit rate of 0.4%), 759 hits were retested in triplicate yielding 333 active compounds of which 54 compounds inhibited p97 ATPase activity by more than 50% at $\leq$8 μM. Retesting of these compounds in a 10-point titration yielded only 5 compounds with IC_{50} values under 10 μM. Subsequent retesting of selected compounds resulted in a group of 28 compounds with measurable IC_{50}s in the ATPase assay, several with IC_{50} concentrations in the single-digit micromolar range. This collection of 28 compounds was assessed in a cellular assay that measured the ability of compounds to inhibit the p97 dependent degradation of a fluorescently labeled protein substrate (Ub^{G76V}-GFP).[7] Results from this assay were used to prioritize a group of the 10 most potent compounds (**1**–**10**) for assessment of the selectivity of their interactions with p97 in cells vs. other AAA+ ATPases and other enzymes involved in the UPS (Table 1). This was accomplished by comparing the compounds' ability to inhibit Ub^{G76V}-GFP degradation to that of two luciferase labeled proteins whose degradation was known to be independent of p97; ODD-Luc (oxygen-dependent degradation domain of HIF1a which requires ubiquitination but not p97 activity) and Luc-ODC (luciferase fused to the ubiquitin-independent degradation domain of ornithine decarboxylase) whose degradation is proteasome dependent but ubiquitin and p97 independent. Of the molecules assessed, compounds **1** (DBeQ) and **2** were 10-fold weaker at inhibiting the p97 independent degradation of Luc-ODC or Luc-ODD than the p97 dependent degradation of Ub^{G76V}-GFP (Table 1).

It is interesting to note that many of these compounds determined to have nonselective activity at the cellular level also contained reactive functionality or other structural features found in compounds that often are identified as hits in HTS. Such compounds sometimes referred to as pan assay interfering compounds[10] generally have a poor track record in hit to lead efforts. These include structures such as ketones, chloro-ketones (**3**, **4**, **6**, **8**), Michael acceptor functionality (**7**, **9**), and hydrazine functionality (**10**).

Subsequent biochemical studies determined that **1** was a reversible and competitive inhibitor at the ATPase D2 site of p97 with an IC_{50} of 2.3 μM while only weakly inhibiting the closely related ATPase NSF (<25% inhibition at 100 μM). On the basis of these findings of selective p97 inhibition in both biochemical and cellular contexts, **1** was chosen as the lead molecule from this mass screening effort. Although the previously described p97 inhibitor Eeyarestatin (**11**)[11] inhibited the degradation of the p97 reporter Ub^{G76V}-GFP it did not inhibit the ATPase activity of purified p97. Although compound **11** has been shown to interact with p97 with μM affinity through surface plasmon resonance, gene expression data suggest that it lacks cellular specificity.[12] Furthermore, compound **11** has also been shown to interact with ataxin 3 [11]and Sec61.[13] Analogs of the 2-anilino-thiazole class such as 3-(2-((4-hydroxyphenyl)amino)thiazol-4-yl)phenol (compound **12**) with submicromolar p97 inhibitory potency had also previously been described in the literature (Fig. 5).[14] However, this series of compounds has also been reported to be active against other enzymes, such as neuropeptide Y5 receptor and sphingosine kinase with a similar potency. Despite its advantage in biochemical selectivity, DBeQ was hampered by its micromolar inhibitory potency and poor physicochemical properties including very low aqueous solubility.

8.05.1.2.2 Hit to lead investigations

To discover improved inhibitors of p97 structure activity relationship (SAR) studies were initiated in a joint effort between the University of Kansas and Cal Tech. These efforts focused on both DBeQ (**1**) and the somewhat weaker 2-aryl quinazoline analog (**2**) that had also been identified in the HTS. Changes to the 2 and 4 substituents on the quinazoline core as well as the addition of substituents on the phenyl ring of the quinazoline were investigated.[15] Using an "analog by catalog" approach, commercially

Table 1 Top 10 hits form p97 HTS and triage

Structure	*Compound*	*p97 IC_{50} (μM)*	*UbG76V-GFP IC_{50} (μM)*	*ODD-Luc IC_{50} (μM)*	*LUC-ODC IC_{50} (μM)*
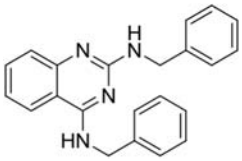	**1 DBeQ**	1.5	2.6	56	45
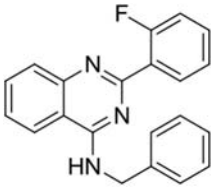	**2**	3	9	43	>30
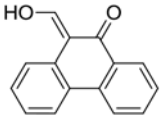	**3**	0.26	1.1	4.4	NM
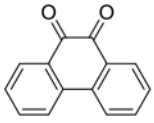	**4**	3.5	1.3	3.3	ND
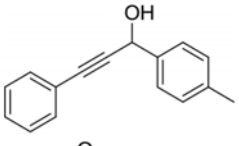	**5**	0.2	3.4	5.2	11
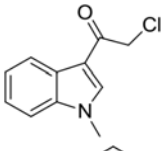	**6**	1.3	3.6	18	NM
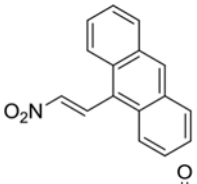	**7**	0.8	5.0	17	NM
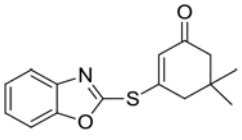	**8**	6.1	6.6	NM	NM
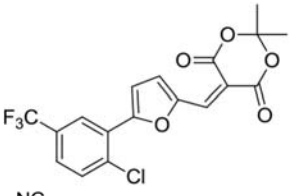	**9**	13	7.5	NM	NM
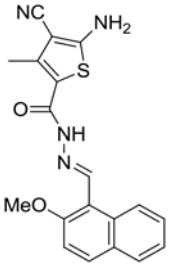	**10**	2	10	NM	NM

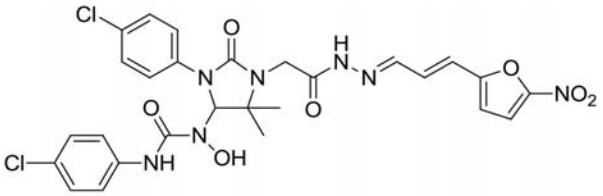

11 Eeyarestatin

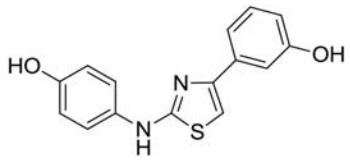

12 Myriad Inhibitor

Fig 5 Compounds previously reported to be p97 inhibitors.

Table 2 DeBQ quinazoline analogs demonstrating initial SAR[15]

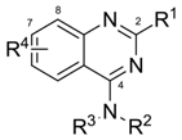

Compound	R^1	R^2	R^3	R^4	*ATPase*	Ub^{G76A} *GFP*
13	2-Chlorophenyl	Benzyl	H	H	1.2	8
14	3-Nitrophenyl	Benzyl	H	H	5.9	4
15	Phenyl	Benzyl	H	7-Cl	70	12
16	*p*-Tolyl	Benzyl	H	7-Cl	39	24
17	Piperidinyl	Benzyl	H	H	26	7.3
18	Morpholinyl	Benzyl	H	H	23	36
19	Phenyl	Benzyl	Me	H	49	17
20	*N*-aminophenyl	Phenyl	H	H	2.6	7.2
21	*N*-aminophenyl	Benzyl	H	H	2.3	3.1
22	*N*-amino(3-chlorophenyl)	Benzyl	H	H	0.48	7.8
23	*N*-amino(3-chlorophenyl)	4-Fluorobenzyl	H	H	1.5	5.7
24	*N*-amino(4-methoxyphenyl)	Benzyl	H	H	3	1.3
25	*N*-aminobenzyl	Benzyl	H	OMe	0.6	10

available quinazoline analogs were assayed for their ability to block p97 ATPase activity in both the biochemical and cell-based assays described above (Table 2). A few compounds were found with modestly improved biochemical potency, but their cell-based potency was less than that of DBeQ. Importantly, this early effort showed that the SAR was not flat and identified a number of molecules with substantially reduced potency. Methylation of the 4-*N*-benzyl nitrogen (**19**) resulted in a significant loss of activity. Compounds having a 7-chloro substituent (**15** and **16**) showed significantly decreased potency while compound **25** with an 8-methoxy substituent had improved biochemical potency. Overall none of the commercially available analogs tested showed a significant improvement over **1**. Directed synthesis of analogs investigated a range of amino-aromatic functionality at the 2-position of the quinazoline (P2). The best of these functionalities were combined with small changes to the quinazoline core. These compounds were prepared by a simple two-step procedure as shown in Scheme 1. The 4-position amine could be selectively introduced through reaction of the desired amine of dichloroquinazolines or analogous tetrahydroquinazoline. Subsequent reaction of the aminochloroquinazoline with a second amine under microwave conditions resulted in the target compounds. Substitution of the P2 position with bicyclic heterocycles with the 1-N linked benzimidazole and benzomorpholino ring systems is the most potent. Compounds **26** (ML-240) and **27** (ML-241) were identified as probe compounds because they both had biochemical ATPase IC_{50}s of approximately 0.1 μM. However **26** was more potent than **27** at inhibiting p97 activity within cells as evidenced by the cellular Ub^{G76V}-GFP assay (IC_{50} 0.9 vs. 3.5 μM). This difference translated into more potent effects in inducing tumor cell death. Substitution of the benzimidazole aromatic ring of **26** resulted in some compounds such as **28** with improved biochemical potency but decreased cell-based potency. Explorations of other heterocyclic functionality (i.e., **29** to **31**) at the P2 position failed to yield superior analogs and were not pursued further.

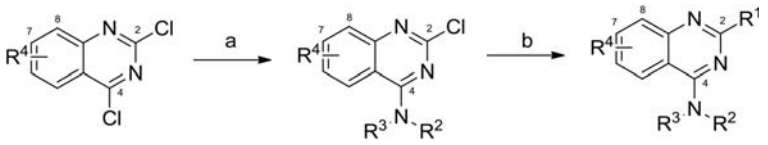

Scheme 1 General synthetic route to DBeQ analogs. Conditions: (a) R_2R_3NH, Et_3N, MeCN, rt 16 h; (b) R_4R_5NH, MeCN microwave irradiation, 180°C, 1 h.

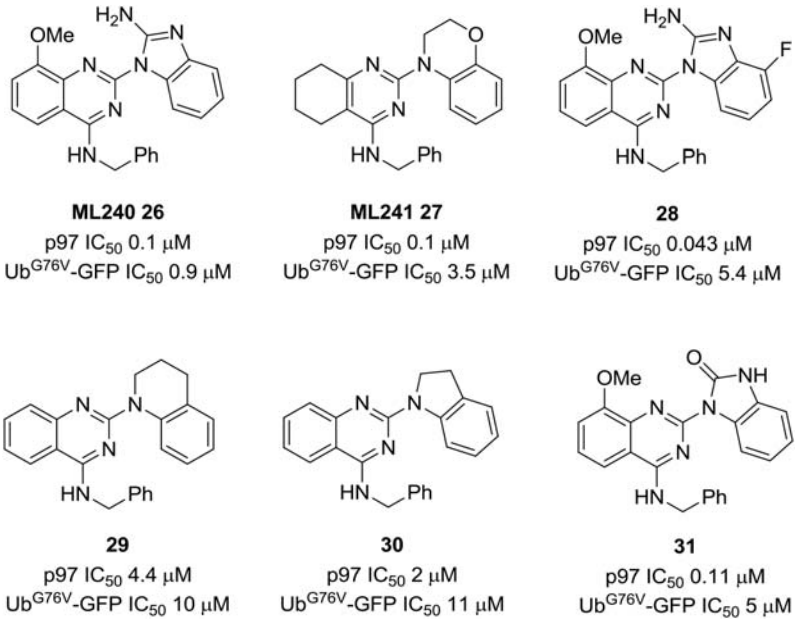

Like compound **1**, **26** was shown to inhibit p97 in an ATP-competitive manner. The selectivity of ML240 against 174 kinase ATP sites was assessed by measuring their ability to inhibit the binding of a reactive ATP acyl phosphate probe (Kinative assay, ActivX, San Diego, CA) (Fig. 8). Compound **26** inhibited labeling of only three of 170 kinase domains by greater than 50% when tested at 20 μM: PIP5K3, JAK1 JH2, and DNAPK.[16] ML240 was also assessed against 43 CNS relevant targets and found to be inactive at all except for 5HT5a with an affinity of 2.5 μM.

Despite being the most potent p97 inhibitor so far reported, **26** had low aqueous solubility (0.32 μg/mL) at pH 6.2 in aqueous PIONS buffer, high plasma protein binding in both human and mouse (>99.6% in a high throughput dialysis assay) and low stability in mouse hepatocytes (<1% remaining at 1 h). Together, these properties decreased the likelihood that it would be useful for establishing an in vivo proof of concept (POC) for a p97 inhibitor in mouse tumor models.

8.05.2 Discovery of CB-5083

8.05.2.1 Lead Development Efforts

8.05.2.1.1 Changes in p97 biochemical assay

As efforts got underway at Cleave Biosciences to discover more potent and drug-like p97 inhibitors a new version of the p97 biochemical ATPase assay was instituted. The new assay used a lower p97 protein concentration relative to the ATP concentration used in the earlier version of the assay.[17] These changes had two desirable effects: (1) use of less p97 protein per assay well and (2) increasing the dynamic range of the assay to allow differentiation of more potent inhibitors of p97. The changes in concentrations and IC_{50}s of DBeQ and ML240 are listed in Table 3. These changes in the assay allowed for the differentiation of more potent compounds.

Table 3 Comparison of p97 ATPase biochemical assays

ATPase assay reference	*p97 Conc. (μM)*	*ATP conc. (μM)*	*Rel ATP/p97 ratio*	*DBeQ (**1**) IC_{50} (μM)*	*ML240 (**26**) IC_{50} (μM)*
Chou[15]	0.25	100	400	1.6	0.11
Anderson[17]	0.020	20	1,000	7.0	0.82

8.05.2.1.2 Alternative synthesis of ML240

Compound **26** was prepared by condensation of chloro-pyrimidine **32** with 2-aminobenzimidazole **33**. However, it was never unambiguously determined whether the coupling took place on the nitrogen of the imidazole or on the 2-amino group which would produce compound **34**. An alternative synthesis of **26** was carried out by condensation of chloropyrimidine **32** with 2,3-diaminopyrimidine **35** using Hartwig–Buchwald conditions, followed by condensation of **36** with cyanuric bromide and resulted in the unambiguous production of **26** validating the original structural assignment.[15,18]

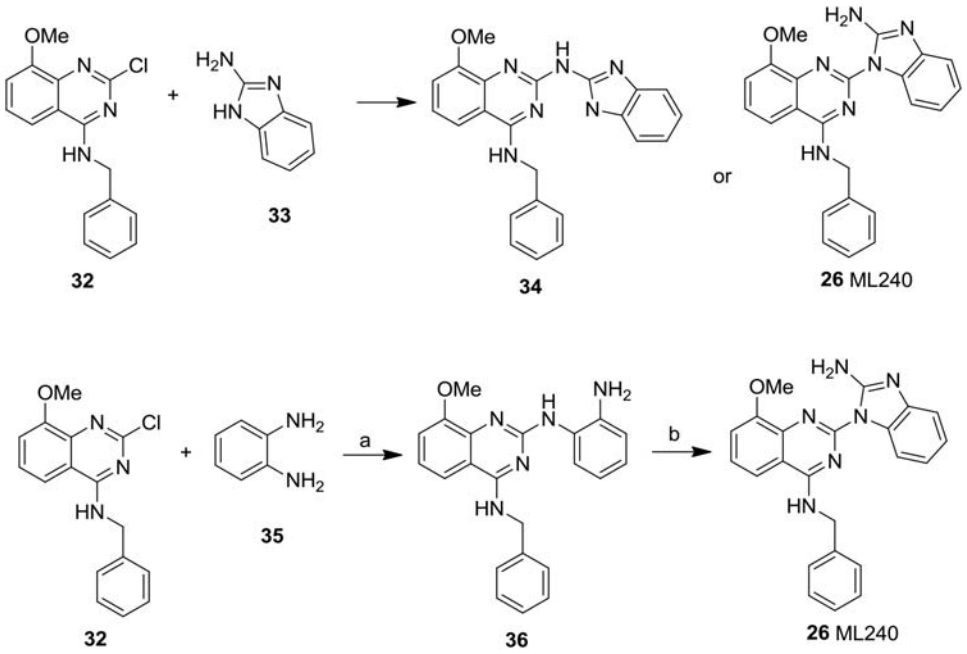

Reagents and conditions: (A). $Pd(OAc)_2$, BINAP, Cs_2CO_3, dioxane, 100°C; (B). BrCN, MeCN, H_2O, rt.

8.05.2.1.3 Guiding principles used in lead development of 26 (ML240)

Throughout the work leading to CB-5083, significant attention was paid to changes that led to both improvements in biochemical potency and improvements in physical properties. A guiding principle was to focus on those changes that resulted in increases in biochemical potency without disproportionately increasing calculated log P (cLogP). One way to quantify the contribution of lipophilicity to increases in target potency is the metric lipophilicity efficiency (LipE).[19] This is calculated by the equation $LipE = pIC_{50} - cLogP$. Analysis of the hit to lead work that produced ML240 determined that significant improvements in p97 biochemical potency could be achieved while simultaneously decreasing cLogP as evidenced by increased LipE (**Scheme 2**).

Since p97 is a highly expressed intracellular target it stands to reason that efficient cellular penetration of inhibitors is needed for good cellular activity. Control of polar surface area (PSA) would also play a role making p97 inhibitors with good cellular potency.

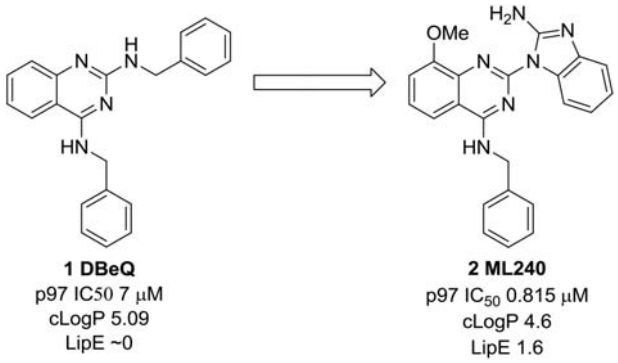

Scheme 2 Improvement in both potency and physical properties.

8.05.2.1.4 Investigation to changes of the N-benzyl substituent of ML240

Investigation of the importance of the 4-*N*-benzyl functionality found in ML240 was undertaken. A variety of synthetic methods were used to assess alternatives to this functionality (Scheme 3). Various amines were regioselectively added to the 4-position of the 2,4-dichloroquinazoline **37** producing the corresponding 4-amino-2-chloro quinazolines 38a-c which were converted in two steps to the target compounds **40**–**42**. Similarly the dichloroquinazoline **37** could be reacted with ammonia and the resulting 4-aminoquinazoline was acylated and converted to target **46**. Target **49** was prepared by substituting the benzyl alcohol anion for the amine. Coupling of compound **37** and boronic acid **50** resulted in **51** which was converted in three steps to target compound

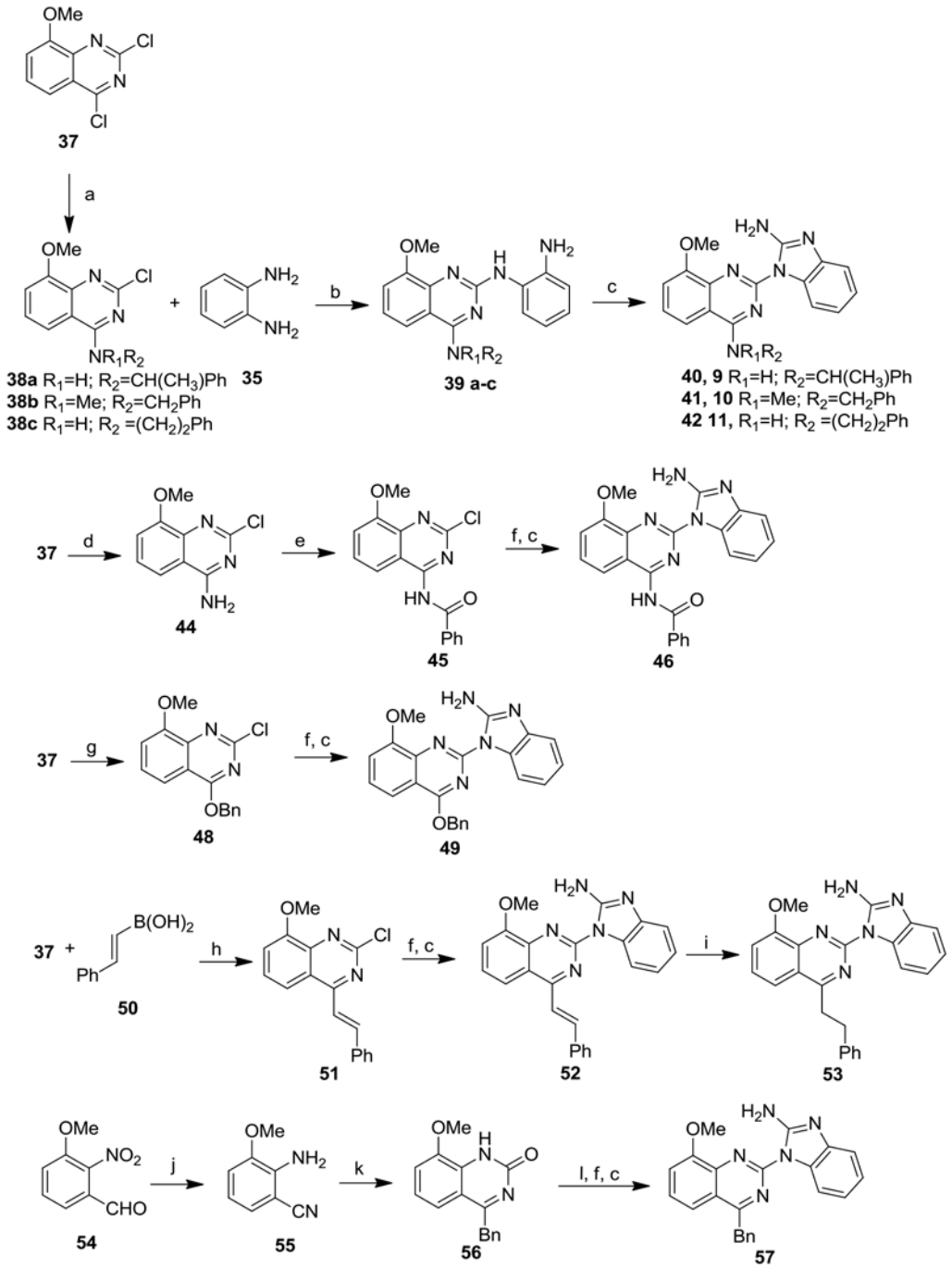

Scheme 3 Generalized routes to synthesize ML240 *N*-benzyl analogs. Reagents and conditions: (a) HNR_1R_2, MeCN, rt; (b) $Pd(OAc)_2$, BINAP, Cs_2CO_3, dioxane, 100°C; (c) BrCN, MeCN, H_2O, rt; (d) NH_3, dioxane, rt; (e) PhCOCl, NaH, DMF, 0°C; (f) **35**, $Pd(OAc)_2$, BINAP, Cs_2CO_3, dioxane, 100°C; (g) BnOH, NaH, DMF, −20°C; (h) $Pd(PPh_3)_4$, K_3PO_4, dioxane, H_2O, 100°C; (i) Pd/C, H_2, MeOH, rt; (j) (1) I_2, NH_3, H_2O, rt, (2) Fe, AcOH, rt; (k) (1) $PhCH_2MgBr$, Et_2O, reflux, (2) $ClCO_2Me$, THF, 0°C; (l) $POCl_3$, $PhNMe_2$, reflux.

Table 4 SAR expansion on the 4-positions of quinazoline

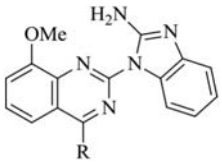

Compound	*R*	*p97i IC_{50} (μM)*	*CLogP*
26	NHBn	0.815	4.6
40	NHCH(Me)Ph	>5.0	5.0
41	N(Me)CH_2Ph	>5.0	5.3
42	$NHCH_2CH_2Ph$	>5.0	4.9
46	NHCOPh	>5.0	4.3
49	OCH_2Ph	>5.0	4.8
53	CH_2CH_2Ph	>5.0	5.0
57	CH_2Ph	>5.0	4.6

53. Addition of the phenyl Grignard reagent to compound **53**, pyrimidine formation, and addition of the 2-amino-benzimidazole resulted in target compound **57**. All of the changes to the *N*-benzyl group resulted in complete loss of p97 inhibitory activity consistent with the earlier studies that this group was absolutely crucial for activity. Substitution on the aromatic ring also led to a loss in the binding activity. Taken together these findings discouraged further exploration in this region of the molecule and efforts were focused on other regions of the molecule (Table 4).

8.05.2.1.5 Benzimidazole analogs

The lack of toleration to changes to the 4-*N*-benzyl substituent shifted focus to the 2-benzimidazole functionality found in ML240. A systematic survey of simple changes to the 2-substituents on the benzimidazole, the necessity of the phenyl ring of the benzimidazole system, and the nature of the linkage to the 4-*N*-benzyl pyrimidine system was investigated.

The syntheses of these analogs are outlined in Schemes 4 and 5. Selective acylation at the 2-amino position of **58** (Scheme 4) and coupling resulted in compound **59**, the N-acylated version of **ML-240**. The *N*-monomethyl and *N*,*N*-dimethylated derivatives **60** and **61**, respectively could be prepared from key intermediate **36** as could the 2-hydroxy derivative **62** which also likely exists in solution as its tautomer, the 2-benzimidazolone. The cyclohexyl-imidazole analog was prepared in three steps from 2-chlorocyclohexanone **64** by condensation with acetyl-guanidine, condensation of the resulting *N*-acyl imidazole, and removal of the acetyl group resulted in the desired cyclohexyl imidazole analog **65**. The dimethyl-imidazole analog **68** was prepared in a similar way. Taking advantage of the known procedure to selectively prepare 1-*N*-BOC-benzimidazole allowed the preparation of compound **70** whose spectroscopic properties were distinct from **26** (ML-240) and consistent with the symmetry of the molecule.

The C-linked benzimidazole **74** could be prepared via the 2-bromomethyl-pyrimidine derivative **72** followed by coupling with the benzimidazole and installation of the 4-*N*-benzyl group. The two substituent analogs **76a** and **76b** could be simply prepared by coupling the readily available 2-substituted benzimidazoles with key intermediate **32** using palladium-catalyzed conditions.

Introduction of the acetyl group on the 2-position nitrogen of **26** led to a complete loss of potency, however introduction of one or two methyl groups to this nitrogen resulted in compounds **60** and **61** with somewhat improved potency, albeit with increases in cLogP over 5. This was a direction that was not further explored. However it was found that introduction of a replacement of the 2-amino functionality of the benzimidazole with a hydroxyl group (compound **62**) led to a loss in potency. Presence of only a hydrogen at the two position of the benzimidazole led to a complete loss of activity. However introduction of a methyl substituent (compound **76a**) or methoxy substituent (compound **76d**) led to compounds with p97 biochemical IC_{50}s under 200 nM while maintaining or somewhat increasing LipE compared to **26**. Interestingly the 2-ethyl-substituted benzimidazole derivative **76c** was completely inactive. Replacement of the phenyl ring of the benzimidazole of **26** with either a cyclohexyl ring as in compound **65** or 4,5-dimethyl substituents (compound **68**) resulted in a complete loss of activity as did connecting to the pyrimidine ring through the 2-nitrogen of the benzimidazole (compound **70**) or a C-linkage to the 1-nitrogen of the benzimidazole (compound **74**) (Table 5).

8.05.2.1.6 Exploration of other fused pyrimidine cores

In parallel with attempts to improve potency through manipulation of the substituent at the 2-position of the benzimidazole, efforts were underway to explore pyrimidine cores with reduced lipophilicity and/or aromaticity. Introduction of additional polar functionality through the 8-alkoxy substituent of the quinazoline ring and replacement of the phenyl ring of the quinazoline with heterocyclic or saturated carbocyclic functionality on the quinazoline ring were studied. A variety of these alternative fused 4-*N*-benzyl-2-chloro pyrimidines were prepared as outlined in Scheme 6. These intermediates were used to prepare final

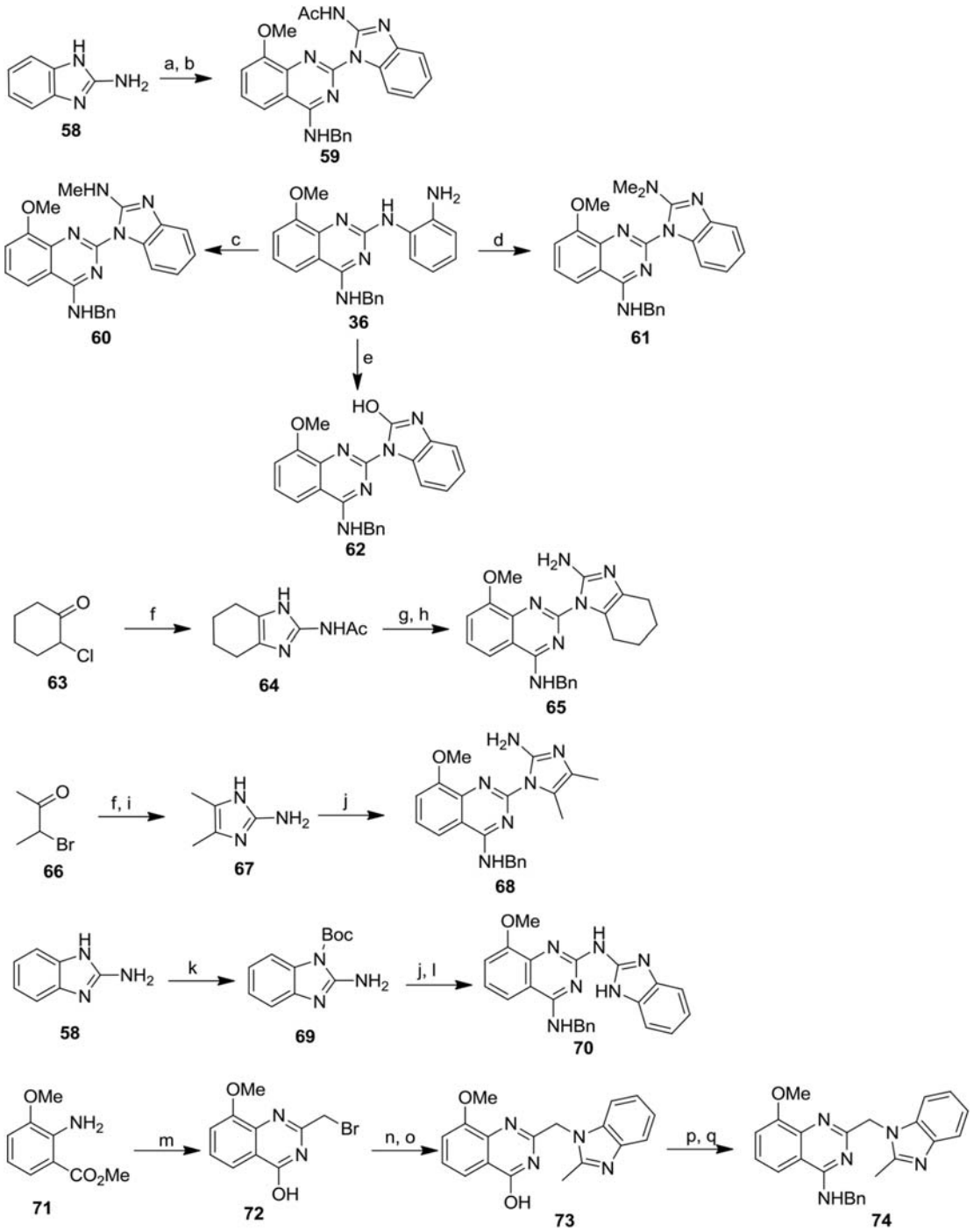

Scheme 4 Synthesis of initial benzimidazole analogs. Reagents and conditions: (a) Ac_2O, TEA, THF, 0°C; (b) **32**, $Pd(dba)_3$, X-Phos, Cs_2CO_3, dioxane, 100°C; (c) (1). MeNCS, Et_2O, rt, (2). MeI, EtOH, rt; (d) (1) $Me_2N^+=C(Cl)NMe_2.Cl^-$, $CHCl_3$, −30°C, (2). xylene, reflux; (e) CDI, dioxane, 100°C; (f) $MeCONHC(NH_2)=NH$, MeCN, reflux; (g) **32**, $Pd(dba)_3$, *t*-BuPhos, *t*-BuOK, dioxane, 100°C; (h) NH_2NH_2, EtOH, H_2O, 70°C; (i) H_2SO_4, MeOH, H_2O, 70°C; (j) 32, $Pd(OAc)_2$, BINAP, Cs_2CO_3, dioxane, 100°C; (k) $(Boc)_2O$, TEA, DMF, rt; (l) TFA, DCM, rt; (m) $BrCH_2CN$, HCl (aq.), reflux; (n) 2-methybenzimidazole, K_2CO_3, MeCN, 50°C; (o) $MeC(OMe)_3$, EtOH, rt; (p) $POCl_3$, $PhNMe_2$, reflux; (q) $BnNH_2$, MeCN, rt.

compounds with P2 benzimidazole substituents having either amino, methyl, or methoxy at the 2-position of the benzimidazole ring system by methods outlined previously.

An attempt was made to decrease lipophilicity by introducing polar functionality to the 8-alkoxy substituent on the pyrimidine ring. Removal of the methyl group from compound **32** followed by introduction of methoxy-ethyl functionality gave intermediate **78**. The pyrimidine diols **79a**[20] and **79b**[21] were converted to their respective dichlorides which were converted

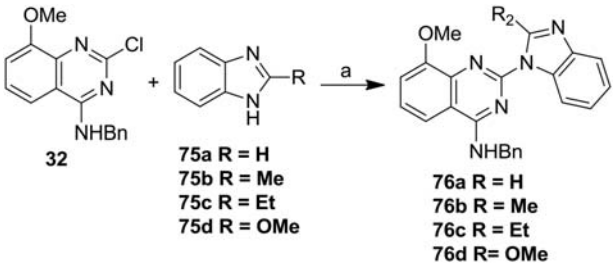

Scheme 5 Synthesis of 2-methoxy and 2-methyl benzimidazole analogs. Reagents and conditions: (a) $Pd_2(dba)_3$, X-Phos, Cs_2CO_3, dioxane, 100°C.

Table 5 SAR expansion on the 2-position of the quinazoline

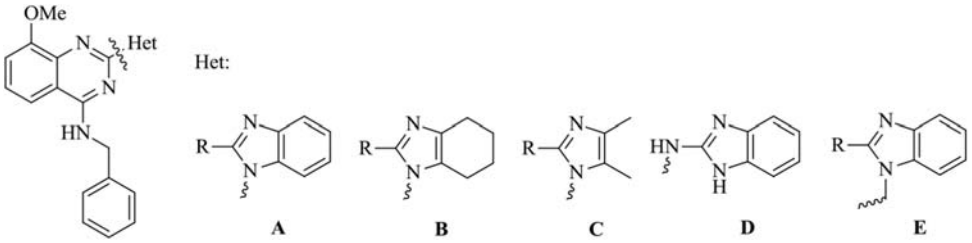

Compound	*Het*	*R*	*p97i IC_{50} (μM)*	*CLogP*	*LipE*
59	A	NHAc	>5.0	4.7	
60	A	NHMe	0.233	5.0	1.6
61	A	NMe_2	0.227	5.7	0.9
62	A	OH	1.068	4.6	1.3
65	B	NH_2	>5.0	3.9	
68	C	NH_2	>5.0	3.3	
76a	A	H	>5.0	4.5	
76b	A	Me	0.152	4.8	2.0
76c	A	Et	>5.0	5.4	
76d	A	OMe	0.145	5.2	1.6
70	D	—	>5.0	5.2	
74	E	Me	>5.0	5.1	

Notes: All experiments to determine IC_{50} values were run with at least duplicates at each compound dilution and all IC_{50} values were averaged when determined in two or more independent experiments.

to their respective 4-*N*-benzyl-2-chloro derivatives **80a** and **80b**. The cyclohexanone carboxylate **81** was used to readily prepare the tetrahydroquinazoline **82**, which was selectively converted to compound **83**.

The *N*-benzyl-4-pyridinone **84** was readily converted to the pyrimidine dichloride **85**. To avoid the problem of selectively removing the *N*-benzyl group of the fused piperidine nitrogen at the end of the sequence in the presence of the *N*-benzyl group at the 4-position of the pyrimidine, a protecting group switch was implemented on **85**. Reaction of **85** with acetyl chloride effected removal of the *N*-benzyl group which was quickly replaced with the Boc protecting group giving compound **86** which was converted to the 4-*N*-benzyl-2-chloropyrimidine **87**. The 2-chloropyrimidine derivatives were converted to the 2-benzimidazole-pyrimidine target compounds **88–98** using the methodology previously described.

A variety of pyrimidinyl-benzimidazoles with small substituents in the 2-position of the benzimidazole were evaluated (Table 6). The introduction of the methoxy-ethoxy group at the 8-position of the quinazoline ring system (compounds **88–90**) led to decreases in potency for all 2-benzimidazole substituents that were assessed. Replacement of the 8-methoxy-phenyl ring of the quinazoline of ML240 resulted in a significant decrease in potency. Replacement of the phenyl ring of the quinazoline with a thiophene resulted in compound **91** with a significant decrease in potency, whereas replacement with a thiazole ring system resulted in compound **92** with only slightly decreased potency and a cLogP of 4.5 one of the lowest so far calculated. However replacement of the methoxy-substituted phenyl ring with a fused cyclohexyl ring resulted in our first compounds with potency below 100 nM. Compound **94** with a 2-methyl-benzimidazolyl or compound **95** with a 2-methoxybenzimidazolyl substituent in the two position of the tetrahydroquinazoline had p97 IC_{50}s of 98 and 76 nM, respectively. Introduction of a nitrogen atom into the saturated ring resulted in significant losses of potency across compounds **96–98**. Twenty percent to fifty percent improvements in LipE values were observed for some compounds. Although compound **92** was somewhat less potent than **26**, reductions in

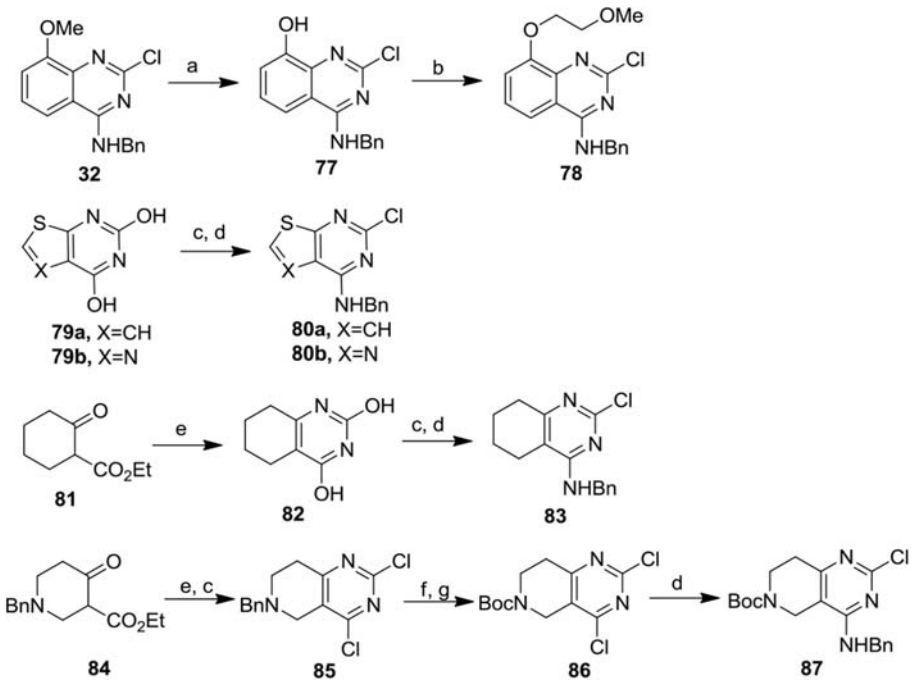

Scheme 6 Generalized routes to synthesize benzylamino-substituted cores. Reagents and conditions: (a) BBr_3, DCM, 0°C; (b) $MeO(CH_2)_2Br$, DCM, 0°C; (c) $POCl_3$, $PhNMe_2$ or DIPEA, reflux; (d) $BnNH_2$, MeCN, rt; (e) urea, NaOMe, MeOH, reflux; (f) $MeCH(Cl)OCOCl$, $Cl(CH_2)_2Cl$, reflux; (g) Boc_2O, Et_3N, DCM, rt.

Table 6 Assessment of alternative fused pyrimidine cores

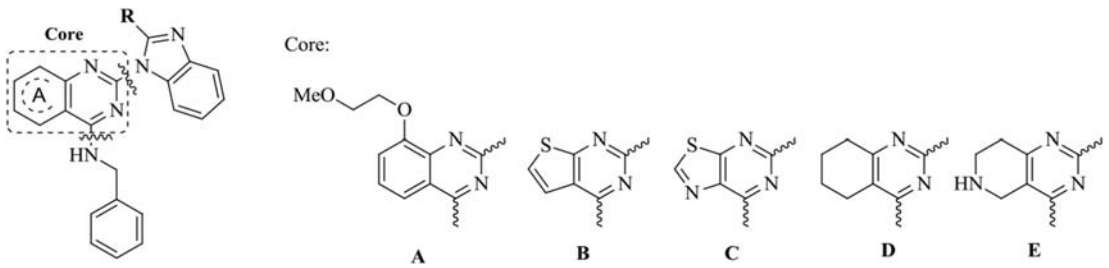

Compound	*Core*	*R*	*p97i IC_{50} (μM)*	*CLogP*	*LipE*
88	A	NH_2	0.907	4.4	1.6
89	A	Me	0.304	4.6	1.9
90	A	OMe	0.370	5.0	1.4
91	B	NH_2	3.000	4.7	0.8
92	C	OMe	0.180	4.5	2.2
93	D	NH_2	0.425	4.6	1.8
94	D	Me	0.098	4.8	2.2
95	D	OMe	0.076	5.2	1.9
96	E	NH_2	>5.0	3.1	
97	E	Me	>5.0	3.2	
98	E	OMe	3.134	3.6	1.9

Notes: All experiments to determine IC_{50} values were run with at least duplicates at each compound dilution and all IC_{50} values were averaged when determined in two or more independent experiments.

CLogP led to increased LipE values. While this was a promising trend it was also recognized that **92** had five aromatic rings. It has been noted that increased numbers of aromatic rings correlate with decreased solubility.[22] For this reason focus shifted to compounds **93–98** having a nonaromatic ring fused to the pyrimidine core. The tetrahydropyrimidines **94** and **95** represented the first compounds under 100 nM in the p97 biochemical assay. Although these compounds suffered from modest increases in cLogP, they also had somewhat increased LipE values. Compound **98** having a piperidine ring fused to the pyrimidine ring resulted in a compound with reduced potency but also significantly reduced cLogP which also led to a modest increase in LipE. Compound **95** was the first compound we had made that had a p97 inhibitory potency significantly under 100 nM and so was selected for more detailed study.

8.05.2.1.7 Evidence of p97 inhibition in cellular assays and in vivo

Expected consequences of p97 inhibition would be a buildup of polyubiquitinated proteins as they are not chaperoned by p97 to the 26S proteasome and hence they are not degraded. In addition the buildup of mis-folded proteins in the ER causes accumulation of C/EBP homologous protein (CHOP), a protein associated with activation of the UPR. Immunofluorescence assays were developed to look for changes to intracellular levels of both of these proteins.[17] Treatment of cells with compound **95** resulted in a dose-dependent increase in both of these cellular markers of p97 inhibition (Fig. 6).

Poly-UB and CHOP accumulation occurred after treatment of A549 tumor cells with varying concentration of compound **95**. These elevations occurred at similar concentration which led to cell death at 72 h (IC_{50} 3.9 μM) suggesting that this mechanism was the route of cellular toxicity. The dose–response curve for CHOP was shifted to the right compared to the 6 h accumulation numbers for poly-UB. This is consistent with the fact that CHOP accumulation occurs as a consequence of poly-ubiquitinated proteins accumulating in the ER. After oral administration (300 mg/kg) to mice bearing A549 tumors increases in poly-UB in tumor lysates were observed by a western blot assay (Fig. 7A). Repeated treatment with compound **95** (300 mg/kg) over 32 days caused a 79% inhibition in tumor growth similar to that caused by the maximum tolerated dose regimen of taxol (Fig. 7B).

The specificity of the interaction of compound **95** with the D2 ATPase site of p97 was assessed using an ATP probe which was attached to a biotin label (ActivX, San Diego, CA) (ref). The probe irreversibly labels lysines in the ATP binding sites found in kinases and ATPases. After trypsin digestion of a lysate from A549 cells the peptide fragments were passed through a streptavidin column to capture those peptide fragments from the ATP sites labeled with biotin. The abundance of the labeled versus unlabeled sites was quantified by mass spectral detection (Fig. 8). Labeling of the proteins existing in the cellular lysates of A549 tumor cells in the presence or absence of **95** was assessed by measuring the abundance of labeled peptide signals after tryptic digest and purification. Compound **95** selectively inhibited labeling at the D2 site of p97 by 65% but did not prevent the labeling of any other ATPase sites from >130 different ATPases including the p97 D1 site. This specific interaction with the D2 domain of p97 is consistent with its ability to inhibit the ATPase activity of p97 since the D2 region has been shown to be primarily responsible for the ATPase activity of p97.

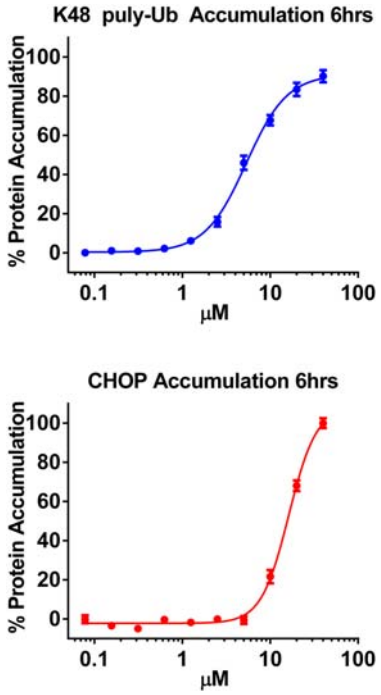

Fig. 6 Accumulation of Poly-Ub and CHOP caused by compound **95**.

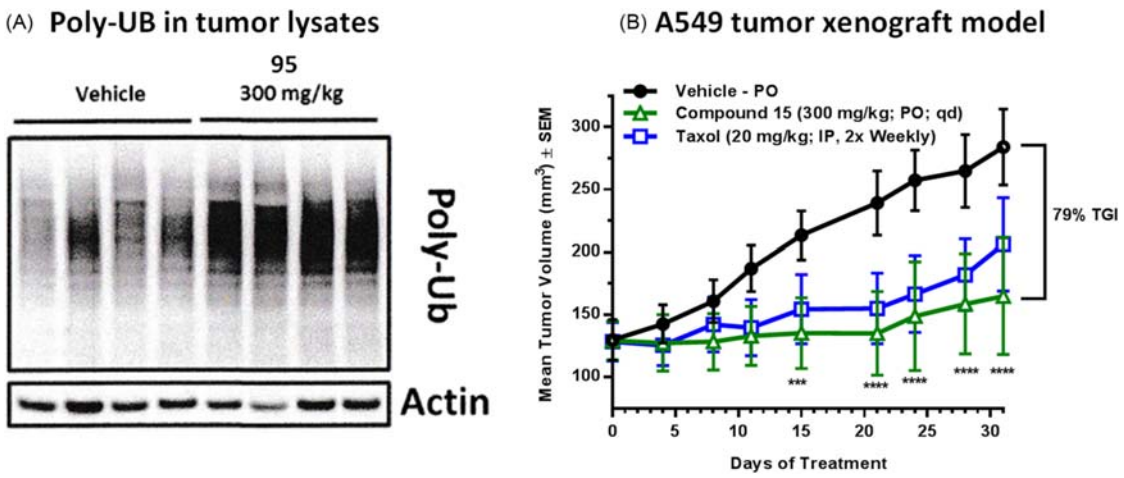

Fig. 7 In vivo effects of compound **95** (A) Poly-UB in tumor lysates (B) A549 tumor xenograft model.

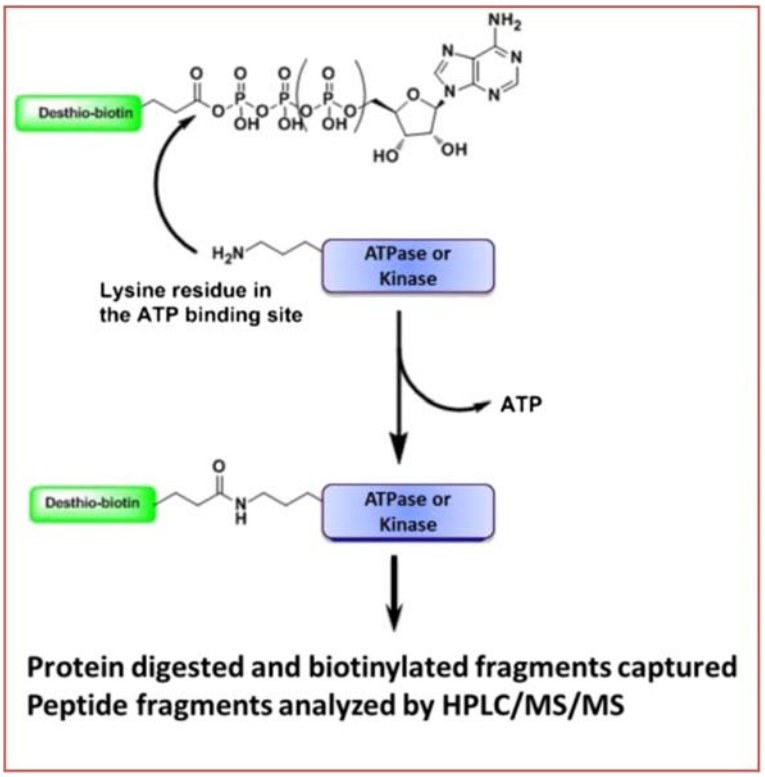

Fig. 8 Mechanism of ATP site labeling and detection.

Together these studies demonstrated that blockade of p97 ATPase activity at the D2 site could cause significant increases in poly-ubiquitinated proteins and markers of ERAD induction and prevent tumor growth increases at a tolerable dose in mice. The data provided to our knowledge the first in vivo validation of the p97 D2 site as a potentially druggable anticancer target. While compound **95** provided the first in vivo POC for p97 it was also realized that additional improvements in potency would be needed in order to produce a viable drug candidate.

8.05.2.2 Candidate Seeking Efforts

Next attention was turned to constructing molecules that replaced the benzimidazole with other 5–6 heterocyclic systems attached to saturated fused pyrimidine cores. A variety of 2-substituted 5,6 ring heterocycles that could be obtained commercially or be prepared as in Scheme 7 were assessed.

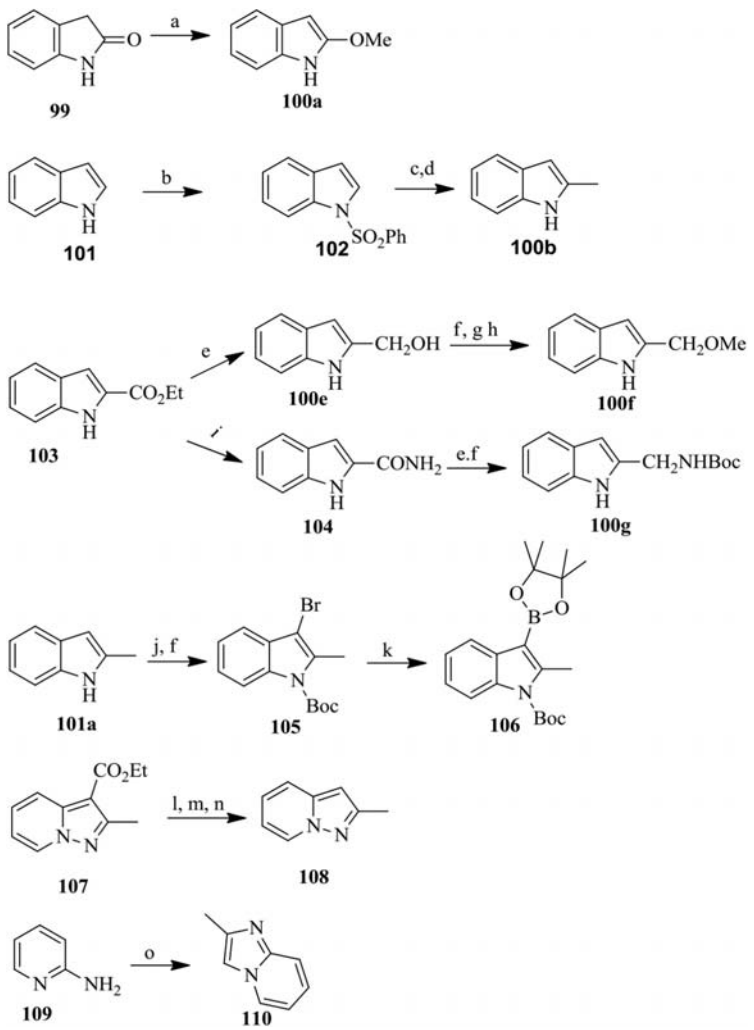

Scheme 7 Synthesis of 2-substituted 5,6 heterocyclic systems. Reagents and conditions: (a) $PhSO_2Cl$, NaH, THF; (b) n-BuLi, MeI, THF, −40°C; (c) NaOH; H_2O, EtOH, 40°C; (d) Me_3OBF_4, $CHCl_3$, rt; (e) $LiAlH_4$, THF, 0°C; (f) $(Boc)_2O$, DAMP, TEA, DCM, rt; (g) MeI, NaH, THF, 0°C; (h) TFA, DCM, 0°C; (i) NH_3, THF, rt; (j) Br_2, DMF; (k) 2-isopropoxy-4,4,5,5-tetramethyl-1,3,2-dioxaborolane, *n*-BuLi, THF, −78°C; (l) NaOH, MeOH, H_2O, reflux; (m) NBS, $NaHCO_3$, DMF, 0°C; (n) *n*-BuLi, THF, −78°C; (o) $MeCOCH_2Br$, EtOH, dioxane.

Methylation of the oxindole **99** by trimethyl tetrafluoroborate gave the 2-methoxy indole **100a**. Lithiation of the sulfonamide-indole **102** with *n*-butyl lithium occurred at the two position of the indole to ultimately produce 2-methylindole **101a** after removal of the sulfonamide group. Reduction of ester **103** to 2-hydroxymethyl indole **100c** and methylation of this compound gave 2-methoxymethyl indole **100f**. Conversion of ester **103** to the amide followed by reduction and Boc protection resulted in **100g**. To facilitate coupling at the indole at the three position the 2-methyl, 3-boronate protected indole **106** was prepared by bromination of indole **101a** followed by protection to give **105**. Halogen lithium exchange was affected by *n*-butyl-Li and the anion at the three position of the indole was quenched with the diborolane ester which gave the 3-indolyl boronate ester **106**. The known ester **107** was converted to bromide which was lithiated and then protonated to give the 2-methyl imidazopyridine **108**. 2-Amino-pyridine (**109**) was condensed with bromoacetone to produce the methyl-imidazopyridine **110**.

The indole **100** could be efficiently coupled to chloropyrimidine **83** via Pd-mediated Hartwig–Buchwald-type coupling. It was necessary to use cesium carbonate as the base for efficient coupling. Suzuki coupling between chloropyrimidine **83** and the 3-indolyl boronate ester **106** gave compound **119**. Palladium-catalyzed Heck-type coupling of **108** and **110** with **83** gave target compounds **120** and **121**. Condensation of the protected dihydropyridine fuses pyrimidine **87** with 2-methyl indole (**100b**) followed by deprotection to give target compound **122**.

Replacement of the indole analog **112** where the 3-nitrogen of compound **95** was replaced with a CH resulted in a twofold improvement in p97 inhibitor potency. Not surprisingly this compound suffered from acid instability due to the enolic nature of the methyl ether. Subsequently it was found that an indole having methyl group in this position as in compound **113** imparted similar potency. Compound **113** had similar LipE suggesting that the increase in potency was largely due to increased lipophilicity. Further elaboration of these two positions of the indole did not lead to further improvement in potency or physical properties

Table 7 Alternative 5,6 P2 heterocycles

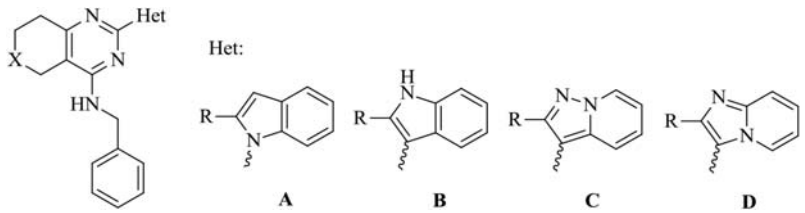

Compound	*X*	*Het*	*R*	*p97i IC_{50} (μM)*	*A549 CTG IC_{50} (μM)*	*CLogP*	*LipE*
112	CH_2	A	OMe	0.043	7.11	5.1	2.3
113	CH_2	A	Me	0.047	6.53	5.4	1.9
114	CH_2	A	Et	0.445	ND	5.9	0.5
115	CH_2	A	CF_3	0.651	>40	6.1	0.1
116	CH_2	A	CH_2OH	0.068	8.4	4.3	2.9
117	CH_2	A	CH_2OMe	0.795	>40.0	4.9	1.2
118	CH_2	A	CH_2NH_2	0.153	4.7	4.3	2.5
119	CH_2	B	Me	0.149	15.84	5.9	0.9
120	CH_2	C	Me	0.367	25	5.5	0.9
121	CH_2	D	Me	0.248	18.21	4.7	1.9
122	NH	A	Me	0.192	8.64	3.9	2.8

(compounds **114–118**). Investigation of alternative 5,6-heterocyclic cores (compounds **119–121**) resulted in compounds having reduced potency. To explore the effect of the introduction of a heteroatom into the saturated ring of the fused pyrimidine the tetrahydro-pyridine **122** was prepared. Although this compound had reduced potency compared to the tetrahydro-quinazoline **113** it also had significantly decreased cLogP resulting in an increase in LipE. This compound also had the best mouse bioavailability properties so far seen ($F = 44\%$). Because of this a more detailed investigation of substitution on the six-membered ring of the indole was undertaken (**Table 7**).

The target compounds in **Table 8** were prepared by condensation of the substituted indoles with fused pyrimidine **87** as previously described. Attempts to couple seven-substituted indoles using the Buchwald-type conditions were unsuccessful likely due to steric issues. As shown in **Table 8** substituents at the 5 or 6 position of the indole nucleus resulted in an almost complete loss of activity. However substituents at the 4 position were better tolerated with the 4-cyano substituted indole derivative **134** having slightly better potency compared to the unsubstituted derivative **122**. Although with a slightly lower cLogP the 4-nitrile imparted a slightly higher cLogP relative to the unsubstituted compound and thus compound **134** also enjoyed a slightly higher LipE value (3.3 vs. 2.9) compared to **122**. Given that the 4-halogen-substituted analogs **131** and **132** were tolerated but had decreased potency and that the trifluoromethyl analog **133** had decreased potency, we hypothesized that the increased potency of **134** was due to the carbonyl-like nature of the nitrile rather than solely to its electron withdrawing effect. To further explore this possibility the nitrile in the 4 position of the indole of **134** was replaced with a carboxylic acid giving **135** which had both increased potency and decreased lipophilicity giving an LipE of 6.6. However unlike compound **134**, which had modest activity in the cell titer glow viability assay, compound **135** as well as the 4-tetrazole isostere **136** were completely inactive in the cellular assay. A possible explanation for this is that the zwitterionic nature of **135** and **136** inhibited efficient cellular penetration preventing activity. However when an amide was placed in the 4 position of the indole (compound **137**) both biochemical and cellular potency were significantly increased and a good LipE was achieved. However substitution of the amide nitrogen (compounds **138**, **139**, and **140**) resulted in significant decreases in biochemical and cellular potency. Based on the good profile of the 4-amido-2-methyl indole analog **137**, investigation of this P2 substituent on a variety of other fused pyrimidine cores was undertaken.

Additional fused pyrimidine cores with nitrogen and oxygen in alternative positions of the ring fused to the pyrimidine were prepared as shown in **Scheme 8**. Reaction of *N*-benzyl pyrimidinone ester **141** with urea under basic conditions resulted in pyrimidine diol **142**. Chlorination and removal of the benzyl protecting group resulted in **143**. Protection of the basic amino group with the BOC group and selective addition of the methyl phenyl group to the four position of the pyrimidine gave compound **144**. Attempts to make tetrahydropyrano pyrimidines were complicated by the fact that the pyran would not survive the forcing conditions used to form the pyrimidine diol. In a milder two-step procedure vinylogous carbamates **146** were formed and treated with trichloro acetyl isocyanate, and cyclization with ammonia in methanol resulted in pyrimidine diols **147**. Chlorination and installation of the aminomethyl phenyl functionality produced the pyrano pyrimidines **148** (**Scheme 9**).

Attempted coupling of 4-amido-2-methylindole with chloropyrimidines resulted in a mixture of products from coupling through both the amide and indole nitrogens. As shown in **Scheme 10**, target compounds **149–153** could more efficiently be prepared by first coupling 4-cyano-2-methylindole with the fused 2-chloropyrimidines followed by conversion of the cyano functionality to the amide. In the case of piperidino-pyrimidines the Boc protecting group was removed before conversion of the nitrile

Table 8 Substitution on phenyl ring of the indole

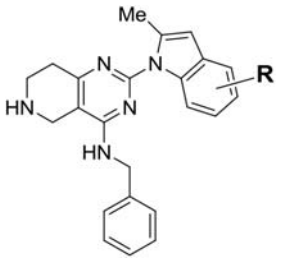

Compound	*R*	*p97i IC_{50} (μM)*	*A549 CTG IC_{50} (μM)*	*CLogP*	*LipE*
123	5-Me	>5.0	ND	4.3	
124	5-OMe	>5.0	ND	3.6	
125	5-CN	>5.0	ND	3.7	
126	6-Me	3.860	ND	4.3	1.1
127	6-OMe	>5.0	ND	3.6	
128	6-CN	8.908	ND	3.7	1.4
129	4-Me	0.648	7.85	4.3	1.9
130	4-OMe	2.075	ND	3.6	2.1
131	4-F	0.342	6.28	4.0	2.5
132	4-Cl	0.632	7.24	4.4	1.8
133	4-CF_3	3.912	ND	4.7	0.7
134	4-CN	0.144	8.92	3.7	3.1
135	4-CO_2H	0.095	>40.0	0.4	6.6
136	4-(5-tetrazolyl)	0.015	>40.0	1.2	6.6
137	4-$CONH_2$	0.040	2.33	2.5	4.9
138	4-CONHMe	0.215	6.03	2.8	3.9
139	4-$CONMe_2$	>5.0	ND	3.0	
140	4-$CONHCHMe_2$	4.832	ND	3.5	1.8

Notes: All experiments to determine IC_{50} values were run with at least duplicates at each compound dilution and all IC_{50} values were averaged when determined in two or more independent experiments.

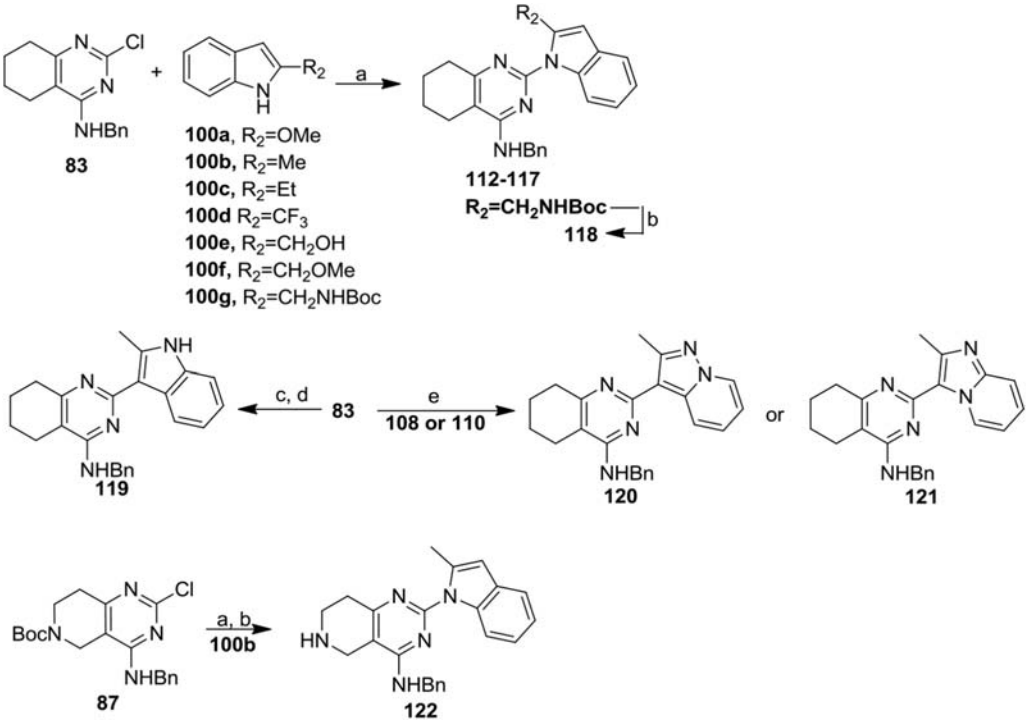

Scheme 8 Generalized routes to synthesize the target molecules **112–122**. Reagents and conditions: (a) $Pd_2(dba)_3$, X-Phos, Cs_2CO_3, dioxane, 100°C; (b) TFA, DCM, rt; (c) 106, $Pd(PPh_3)_4$, K_3PO_4, dioxane, H_2O, 100°C; (d) HCl, MeOH, rt; (e) $Pd(PPh_3)_4$, KOAc, DMA, 150°C.

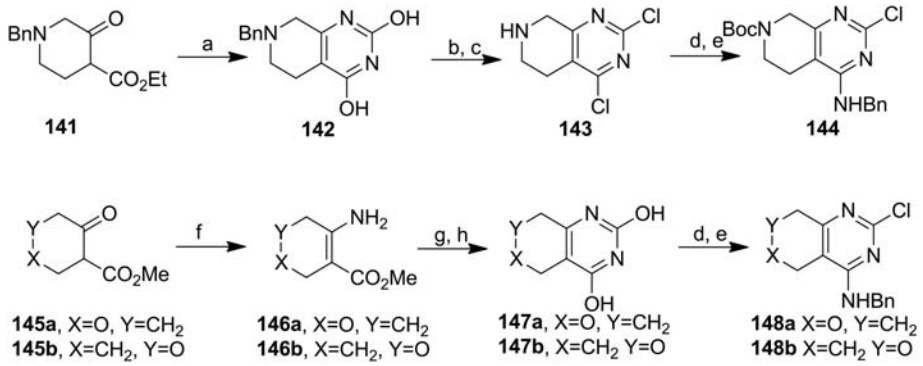

Scheme 9 Synthesis of alternative fused pyrimidine analogs Reagents and conditions: (a) urea, NaOMe, MeOH, reflux; (b) $POCl_3$, $PhNMe_2$ or DIPEA, reflux; (c) $MeCH(Cl)OCOCl$, $Cl(CH_2)_2Cl$, reflux; (d) Boc_2O, Et_3N, DCM, rt; (e) $BnNH_2$, MeCN, rt; (f) NH_4OAc, MeOH, rt; (g) $Cl_3CCONCO$, MeCN, rt; (h) NH_3, MeOH, rt.

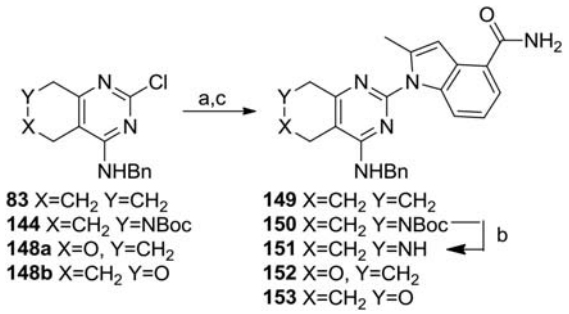

Scheme 10 Preparation of compounds **148–153**. Reagents and conditions: (a) 4-cyan- 2-methylindole, $Pd_2(dba)_3$, X-Phos, Cs_2CO_3, dioxane, 100°C; (b) TFA, DCM, rt; (c) $Pd(OAc)_2$, Ph_3P, MeC = NOH.

to the amine. The regiochemical assignment of the *N*-benzyl and indole positions at the 4 and 2 position of the pyrimidine was confirmed by X-ray crystallography of the dihydrate of compound **152** (Fig. 9).

Of the 4-amido-2-methylindole analogs prepared, the tetrahydroquinazoline analog **149** had the greatest inhibitory potency (IC_{50} of 6 nM) against the ATPase activity of p97. However this compound had an increased cLogP resulting in a reduced LipE relative to the piperidino analog **137**. Likely because of its improved biochemical potency compound **149** was the first compound we observed that had activity against A549 cancer cells in the submicromolar range. The 7-aza-fused piperidine analog **151** was weaker than the 6-aza analog **137** in both the biochemical and cellular assays. The 6-oxo-pyrano-pyrimidine analog **152** had good

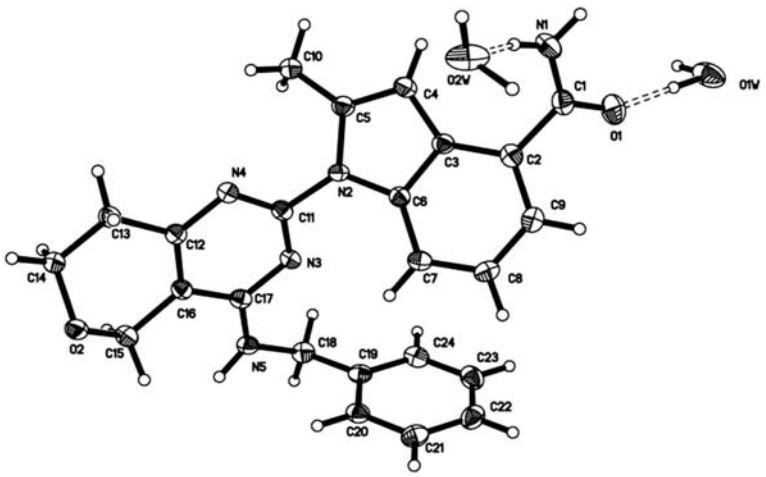

Fig. 9 X-ray crystal structure of the dihydrate of compound **152**.

Table 9 Exploration of fused ring substituents[18]

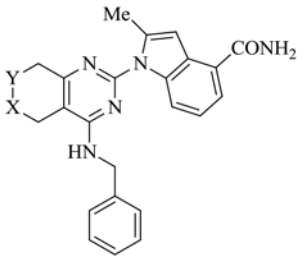

Compound	*X*	*Y*	*p97i IC_{50} (μM)*	*A549 viability IC_{50} (μM)*	*CLogP*	*LipE*
149	CH_2	CH_2	0.006	0.59	4.1	4.1
151	CH_2	NH	0.071	2.44	2.6	4.6
152	O	CH_2	0.011	0.68	2.7	5.2
153	CH_2	O	0.023	1.07	2.8	4.9

Table 10 Physical and pharmaceutical properties of compounds **149** and **152**

Compound	*Solubility pH 1.2 (μg/mL)*	*Solubility pH 7.4 (μg/mL)*	*Caco2 A to B P_{app} (10^{-6} cm/s)*	*Caco2 AB/BA ratio*	*Mouse microsomes T1/2 min*
149	915	4	68	0.8	44
152	1233	32	52	0.7	122

biochemical potency and had submicromolar IC_{50} in the cellular assay. Its combination of good in vitro potency and reduced cLogP resulted in the highest lipE (5.2) observed in this effort. Compound **152** showed both greater biochemical and cellular potency than the 7-oxo analog **153** with compound **152** showing similar submicromolar cellular potency to **149** (Table 9).

The pharmaceutical properties of the two most potent p97 inhibitors **149** and **152** are compared in Table 10. Both compounds exhibited good solubility in acidic aqueous media (pH 2 as found in the stomach) while compound **152** is somewhat more soluble at the slightly higher pH as found in the lower intestinal tract where most drug absorption occurs. Both compounds showed good Caco2 intestinal cell permeability with favorable AB/BA asymmetry suggesting good absorption after oral dosing with little likelihood of the inhibition of uptake from the intestine by efflux transporters. Both compounds showed reasonable stability in mouse liver microsomes.

With these favorable in vitro ADME characteristics both compounds were taken into in vivo PK/PD studies. Both compounds were administered orally as a suspension in 0.5% methylcellulose at a dose of 150 mg/kg; plasma and tumor samples at multiple time points (2, 6, 16, and 24 h) were harvested for PK/PD analysis (Fig. 10). **152** had an approximately twofold higher exposure in both plasma and tumor compared to **149**. Compound **152** also achieved a more sustained PD effect of polyubiquitin accumulation in tumor, especially at later time points. Anti-tumor activity of the two compounds was assessed in an HCT116 tumor xenograft model at their maximum tolerated doses and schedules. Oral administration of **152** was administered every day (qd), whereas **149** was administered every other day (q2d). Both **152** and **149** showed anti-tumor activity in this study (Fig. 11).

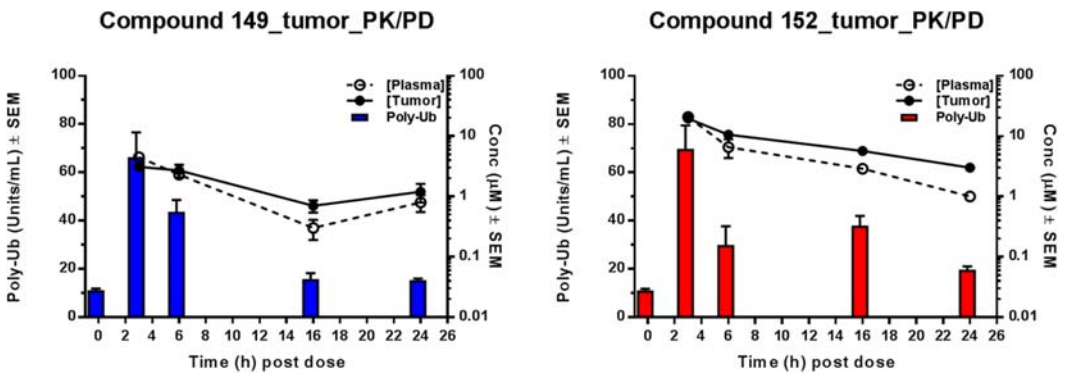

Fig. 10 PK/PD comparison of **149** and **152**.

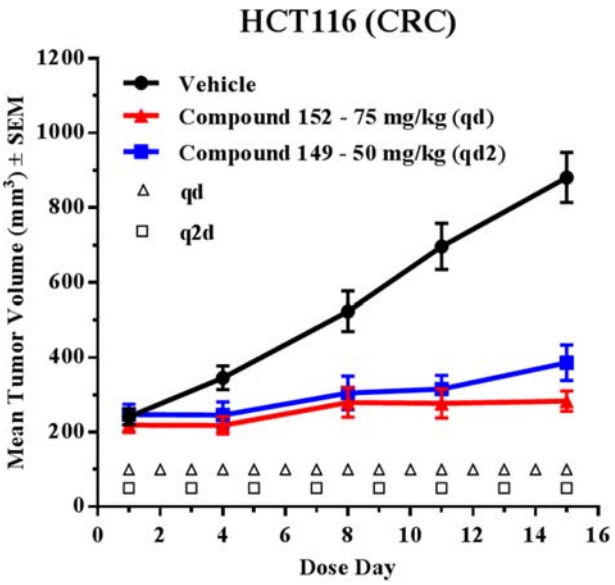

Fig. 11 Comparison of maximum tolerated doses of compounds **149** and **152** in a tumor xenograft study.

Selectivity of **152** for other ATPase and kinase sites was assessed using the irreversible ATP probe as shown in Fig. 8.[16] Compound **152** inhibited 97% of probe binding to the D2 ATPase region of p97 in cellular lysates of A549 tumor cells while not interacting with the D1 ATPase region or the ATPase region of over 135 other ATPase sites. In addition **152** was assessed against 387 kinases (Proqinase Screen) at 5 μM concentration. Only three kinases had >50% inhibition at this concentration and only DNAPK had significant activity at concentrations under 1 μM (IC_{50} 0.519 μM).No DNAPK cellular effects were observed. In addition **152** had no significant interactions with 77 GPCRs and ion channels.

Based on its good biochemical selectivity, as well as its PK and tolerability profile compound **152** (CB-5083) was selected for further preclinical development and is currently being evaluated in clinical trials.

8.05.3 Further Evaluations of CB-5083 and Analogs

8.05.3.1 LipE and Cell Penetration

An important part of the optimization process leading to the discovery of **CB-5083** was improvement in cellular potency. As shown in Fig. 12 in the early part of the program p97 biochemical potency increased and there was a general trend to increased cellular potency. However as the biochemical potency increased beyond 30 nM there was a less pronounced increase in cellular potency with increasing biochemical potency. Previously we had hypothesized that poor cellular permeability owing to the zwitterionic nature of biochemically potent analogs **135** and **136** was responsible for their lack of cellular activity. This led us to explore the relationship between LipE and cellular potency.

The LipE metric allowed plotting of a value derived from a combination of biochemical potency and cLogP against cellular potency. In Fig. 13 the pEC_{50} of A549 cell viability against LipE of p97 analogs under 30 nM is plotted. This reveals a parabolic relationship wherein all of the most potent analogs ($pEC_{50}>6$) were concentrated in the LipE range between approximately 4 and 5.5. Those analogs having a LipE value less than 4 and having a higher cLogP relative to their biochemical potency were challenged to exhibit good cellular potency because of poorer solubility in cellular media. Alternatively for compounds with LipE values greater than 5.5 all had cLogP values below 2.5. This greater polarity likely inhibited good cellular penetration required to achieve intracellular compound levels sufficient to effectively inhibit abundant p97 protein. Many of the compounds with lower cellular potency having LipE between 4 and 5.5 had PSA's ≥ 110 A^2 which also likely would inhibit there efficient penetration into the cell.

8.05.4 Summary of p97 Inhibitors Reported From Competitors' Efforts

8.05.4.1 2-(Cyclohexylmethylamino)pyrimidines

The alkylsulfanylpyrimidine **154** was discovered through a mass screening effort at Nerviano pharmaceuticals, and a medicinal chemistry program was set up to identify the key structural features responsible for activity and to improve the biological profile of this class of compounds.[23] Extensive SAR studies produced the amide **155** with improved p97 biochemical potency. However

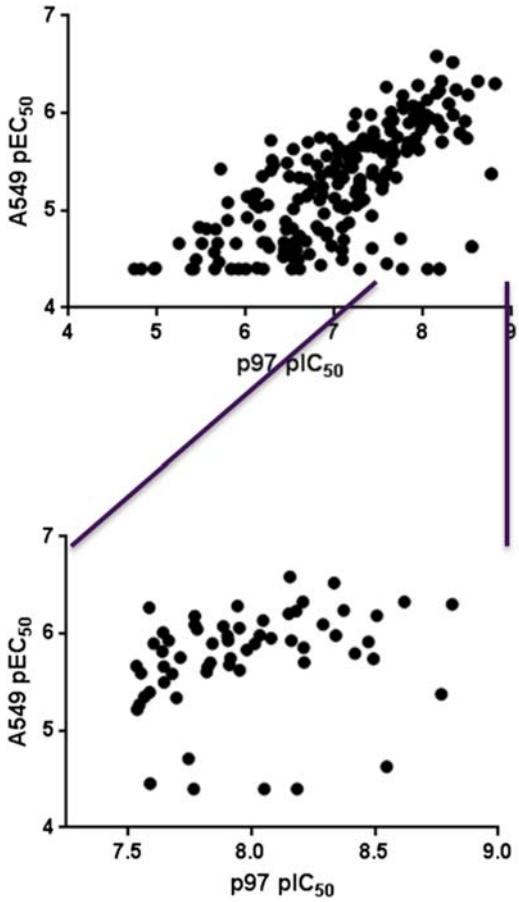

Fig. 12 Correlation of biochemical and cellular potency.

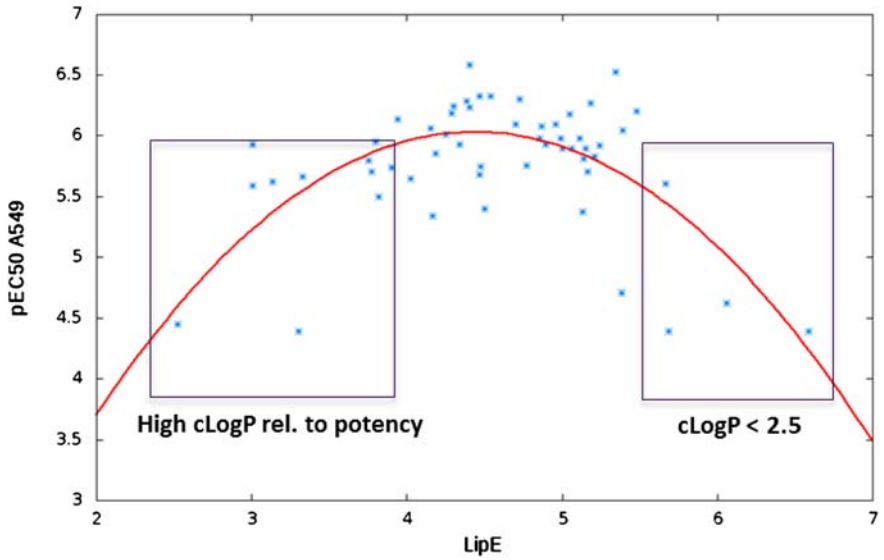

Fig. 13 Correlation of LipE with A549 pEC_{50}.

compound **155** had only modest potency in an HCT116 cellular assay but did show evidence of p97 inhibition in these cells through increases in poly-UB and CHOP protein biomarkers.

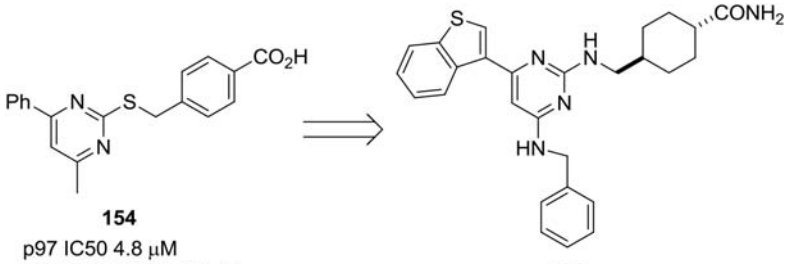

154
p97 IC50 4.8 μM
HCT-116 IC50 > 20 μM

155
p97 IC50 0.074μM
HCT-116 IC50 5.4 μM

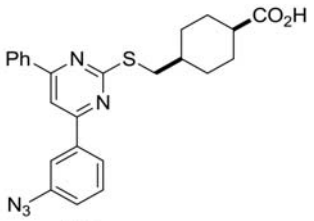

156
p97 IC50 0.879 μM

As part of these efforts compound **156** was prepared as a photoaffinity label. It was found to label Asp479 which is near the D2 site of p97 consistent with the competitive nature of these inhibitors.

8.05.4.2 Alkylsulfanyl Triazoles

A group at Nerviano and Genentech used HTS of over 1 million compounds to identify the 1,2,4-alkylsulfanyl 1,2,4-triazole **157**.[24] It was able to inhibit p97 ATPase activity with an IC_{50} of 2.69 μM but was devoid of antiproliferative effects up to a concentration of 20 μM. The biochemical potency was unaffected by altering ATP concentration in assay conditions suggesting a mechanism of noncompetitive inhibition with respect to this substrate. Moreover, serial dilution experiments and mass spectrometric analysis of p97 upon incubation with a molar excess of the inhibitor indicated that it possesses reversible binding properties.

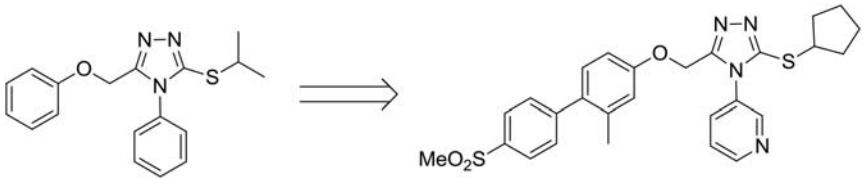

157 **158**

A comprehensive investigation of the SAR of this series led to the discovery of **158** with improved biochemical potency and submicromolar cellular potency (p97 IC_{50} 0.024 μM; HCT-116 IC_{50} 0.38 μM).

Compound **158** (NMS-873) was shown to be selective against a handful of other AAA ATPases (NSF, SPATA5, VPS4B, and cdc6), HSP90, as well as a panel of 50 kinases. No activity was detected at concentrations up to 10 μM. Like the original lead **157** the potency of p97 inhibition by compound **158** was not affected by increased ATP concentration. The compound was shown to be rapidly cleared by human liver microsomes (Cl_{int} = 422 mL/min/kg) and showed only modest exposure and bioavailbility after oral dosing in mice. Perhaps this explains why no in vivo activity has been reported with this compound (**Table 11**).

It has been hypothesized that noncompetitive or allosteric inhibitors of p97 would be advantageous because they would be less affected by the high intracellular concentration of ATP. However a comparison of biochemcial and cellular potency between the competitive inhibitor compound **152** and the allosteric inhibitor **158** suggests this may not be the case. In both cases there is an approximate fivefold shift between biochemical potency and cell viability for both compounds and similar shifts for the CHOP and Poly-UB markers of activity. These results do not suggest an advantage for the allosteric modulator over the competitive inhibitor in terms of activity under cellular conditions.

Table 11 Comparison of competitive and noncompetitive p97 ATPase inhibitor

				HCT116 cellular data		
ID	*p97 ATPase inhibition*	*p97 IC_{50} (μM)*	*LipE*	*Viability EC_{50} (μM)*	*CHOP IC_{50} (μM)*	*K48 IC_{50} (μM)*
152[18]	Competitive at D2	0.011	5.2	0.67	0.77	0.19
158[24]	Allosteric at D1/D2	0.055	3.3	2.68	4.69	1.86

8.05.4.3 Compounds Discovered by U. Pittsburgh/UCSF Collaboration

A collaboration led by groups at the University of Pittsburgh and the University of California, San Francisco has recently reported the discovery of two other series of p97 inhibitors.

8.05.4.3.1 5-N-(3-(1H-indol-2yl)-phenyl-piperidines

The 5-trifluoromethyl indole derivative **159** was identified as a p97 inhibitor with modest potency.[25] A number of analogs were prepared to invesitgate the effect of changes to the 5-position substituent on the indole. The most potent analog in a p97 biochemical assay was a 5-nitro compound **160**. Interestingly the authors found that the pentafluorosulfanyl group (compound **164**) was not a good replacement for the trifluoromethyl group found in the original lead. Somewhat surprisingly the trifluoromethoxy group (compound **163**) was found to be a superior replacement for the trifluoromethyl group. No cellular activity is reported for these compounds. Recently a cryo-electron microscopy derived image of the 5-fluoro derivative **165** bound between the D1 and D2 ATPase regions in p97 has been published.[5] This structure may be useful for further optimization of this series (Table 12).

8.05.4.3.2 N-5-indolyl-carboxamides

The indolyl-pyrazine carboxamide **166** was discovered in the same mass screen as the previous series.[26] A small series of analogs was prepared as shown in Table 13. The most potent of these was the pyridine carboxamide **166**. Other changes to the aminopyrizine core or the 2-indolyl substituent led to a loss of potency. Compound **166** appears to be an allosteric modulator as its potency appears to increase with higher ATP concentrations.

8.05.5 Summary and Future Directions

Several lines of evidence point to the AAA+ ATPase, p97, as a potenitally interesting target for the development of novel anticancer therapies. Mass screening of an NIH compound library against p97 ATPase activity and subsequent hit triage identified DeBQ (**1**) as the most promising hit from this effort. Subsequent hit to lead efforts identified **26** (ML240) as a compound with submicromolar potency. Further lead development and candidate seeking efforts identified **152** (CB-5083) as a first-in-class potent and selective

Table 12 Indolyl-phenyl piperidine p97 inhibitors[25]

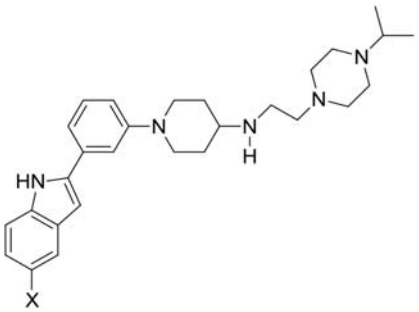

Compound	*X*	*p97 ADP Glo IC_{50} (μM)*
159	CF_3	4.7
160	NO_2	0.05
161	CH_3	0.24
162	OCH_3	0.71
163	OCF_3	0.31
164	SF_5	21.5
165	F	0.027

Table 13 *N*-5-indolyl heterocyclic amides[26]

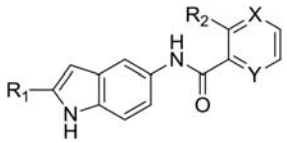

#	R1	R2	X	Y	P97 IC_{50} 20 μM ATP (IC_{50} μM)	P97 IC_{50} 100 μM ATP (IC_{50} μM)
166	Me	NH_2	N	N	11.5	3.5
167	Me	NH_2	CH	N	>50	
168	Me	NH_2	N	CH	2.6	0.5
169	Me	H	N	N	>50	
170	H	NH_2	N	N	>50	

p97 inhibitor which is currently in clinical development. Key to the success of these efforts was attention to molecular changes that caused increases in potency while maintaining or decreasing lipophilicity using increase in LipE as a tracking mechanism.

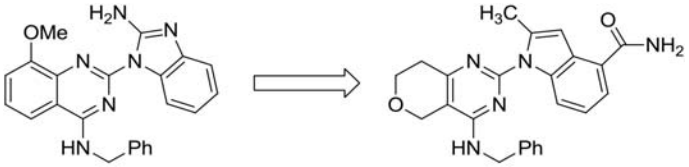

26 ML-240
p97 IC_{50} 0.815 μM
cLogP 4.6
LipE 1.6

152 CB-5083
p97 IC_{50} 0.011 μM
cLogP 2.7
LipE 5.2

Potency and LipE were also shown to play a role in determining cellular potency likely by influencing target affinity and cell permeability. Other efforts have resulted in the discovery of an additional series of competitive inhibitors (i.e., **155**) and a related photoaffinity label suggested a binding mode for these compounds. Three series of allosteric modulators have also been explored (i.e., **158** (NMS-873), **165**, and **167**). An image of **165** bound to p97 derived using cryo-EM techniques produced a structure that may be useful for further optimization of this series of allosteric modulators.

Most of the efforts to optimize p97 inhibitors so far published have measured ATPase inhibiton of the protein in the absense of cofactor proteins that are known to play a key role in mediating the translocation of various substrates. Recently Chou and coworkers have demonstrated that the ATPase inhibitory potency is differentially affected by various p97 cofactor proteins.[27] Since these cofactor proteins influence the substrates affected by the mechanical activity of p97, identifying compounds that can selectively inhibit specific p97-cofactor complexes could be an important new direction in the search for p97 inhibitors with differential cellular and therapeutic effects.

Acknowledgments

The authors would like to acknowledge Ronan LeMoine for leading the in vivo pharmacology efforts and providing the reported xengraft and PK/PD data. We would also like to acknowledge Ray Deshaies for his leadership in the p97 field as well as helpful discussions and Laura Shawver for her helpful comments on this manuscript.

References

1. (a) Galluzzi, L.; Vitale, I.; Kroemer, G. Past, Present, and Future of Molecular and Cellular Oncology. *Front. Oncol.* **2011,** *1,* 1; (b) Luo, J.; Solimini, N. L.; Elledge, S. J. Principles of Cancer Therapy: Oncogene and Non-Oncogene Addiction. *Cell* **2009,** *136* (5), 823–837.
2. (a) Swanton, C. Intratumor Heterogeneity: Evolution Through Space and Time. *Cancer Res.* **2012,** *72* (19), 4875–4882; (b) Renovanz, M.; Kim, E. L. Intratumoral Heterogeneity, Its Contribution to Therapy Resistance and Methodological Caveats to Assessment. *Front. Oncol.* **2014,** *4,* 142.
3. Barthelme, D.; Sauer, R. T. Origin and Functional Evolution of the Cdc48/p97/VCP AAA+ Protein Unfolding and Remodeling Machine. *J. Mol. Biol.* **2016**, *8,* 1861.
4. Sauer, R. T.; Bolon, D. N.; Burton, B. M.; Burton, R. E.; Flynn, J. M.; Grant, R. A.; Hersch, G. L.; Joshi, S. A.; Kenniston, J. A.; Levchenko, I.; Neher, S. B.; Oakes, E. S. C.; Siddiqui, S. M.; Wah, D. A.; Baker, T. A. Sculpting the Proteome With AAA+ Proteases and Disassembly Machines. *Cell* **2004,** *119* (1), 9–18.
5. Banerjee, S.; Bartesaghi, A.; Merk, A.; Rao, P.; Bulfer, S. L.; Yan, Y.; Green, N.; Mroczkowski, B.; Neitz, R. J.; Wipf, P.; Falconieri, V.; Deshaies, R. J.; Milne, J. L. S.; Huryn, D.; Arkin, M.; Subramaniam, S. 2.3 Å Resolution Cryo-EM Structure of Human p97 and Mechanism of Allosteric Inhibition. *Science* **2016,** *351* (6275), 871–875.

6. Song, C.; Wang, Q.; Li, C. C. ATPase Activity of p97-Valosin-Containing Protein (VCP). D2 Mediates the Major Enzyme Activity, and D1 Contributes to the Heat-Induced Activity. *J. Biol. Chem.* **2003,** *278* (6), 3648–3655.
7. Wójcik, C.; Rowicka, M.; Kudlicki, A.; Nowis, D.; McConnell, E.; Kujawa, M.; DeMartino, G. N. Valosin-Containing Protein (p97) Is a Regulator of Endoplasmic Reticulum Stress and of the Degradation of N-End Rule and Ubiquitin-Fusion Degradation Pathway Substrates in Mammalian Cells. *Mol. Biol. Cell* **2006,** *17* (11), 4606–4618.
8. Radhakrishnan, S. K.; den Besten, W.; Deshaies, R. J. p97-Dependent Retrotranslocation and Proteolytic Processing Govern Formation of Active Nrf1 Upon Proteasome Inhibition. *eLife* **2014,** *3*, e01856.
9. Chou, T. F.; Brown, S. J.; Minond, D.; Nordin, B. E.; Li, K.; Jones, A. C.; Chase, P.; Porubsky, P. R.; Stoltz, B. M.; Schoenen, F. J.; Patricelli, M. P.; Hodder, P.; Rosen, H.; Deshaies, R. J. Reversible Inhibitor of p97, DBeQ, Impairs Both Ubiquitin-Dependent and Autophagic Protein Clearance Pathways. *Proc. Natl. Acad. Sci. U. S. A.* **2011,** *108* (12), 4834–4839.
10. Baell, J. B.; Holloway, G. A. New Substructure Filters for Removal of pan Assay Interference Compounds (PAINS) from Screening Libraries and for Their Exclusion in Bioassays. *J. Med. Chem.* **2010,** *53* (7), 2719–2740.
11. Wang, Q.; Li, L.; Ye, Y. Inhibition of p97-Dependent Protein Degradation by Eeyarestatin I. *J. Biol. Chem.* **2008,** *283* (12), 7445–7454.
12. Wang, Q.; Shinkre, B. A.; Lee, J. G.; Weniger, M. A.; Liu, Y.; Chen, W.; Wiestner, A.; Trenkle, W. C.; Ye, Y. The ERAD Inhibitor Eeyarestatin I Is a Bifunctional Compound With a Membrane-Binding Domain and a p97/VCP Inhibitory Group. *PLoS ONE* **2010,** *5* (11), e15479.
13. Cross, B. C.; McKibbin, C.; Callan, A. C.; Roboti, P.; Piacenti, M.; Rabu, C.; Wilson, C. M.; Whitehead, R.; Flitsch, S. L.; Pool, M. R.; High, S.; Swanton, E. Eeyarestatin I Inhibits Sec61-Mediated Protein Translocation at the Endoplasmic Reticulum. *J. Cell Sci.* **2009,** *122* (Pt 23), 4393–4400.
14. Bursavich, M. G.; Parker, D. P.; Willardsen, J. A.; Gao, Z. H.; Davis, T.; Ostanin, K.; Robinson, R.; Peterson, A.; Cimbora, D. M.; Zhu, J. F.; Richards, B. 2-Anilino-4-Aryl-1,3-Thiazole Inhibitors of Valosin-Containing Protein (VCP or p97). *Bioorg. Med. Chem. Lett.* **2010,** *20* (5), 1677–1679.
15. Chou, T. F.; Li, K.; Frankowski, K. J.; Schoenen, F. J.; Deshaies, R. J. Structure-Activity Relationship Study Reveals ML240 and ML241 as Potent and Selective Inhibitors of p97 ATPase. *Chem. Med. Chem.* **2013,** *8* (2), 297–312.
16. Patricelli, M. P.; Szardenings, A. K.; Liyanage, M.; Nomanbhoy, T. K.; Wu, M.; Weissig, H.; Aban, A.; Chun, D.; Tanner, S.; Kozarich, J. W. Functional Interrogation of the Kinome Using Nucleotide Acyl Phosphates. *Biochemistry* **2007,** *46* (2), 350–358.
17. Anderson, D. J.; Le Moigne, R.; Djakovic, S.; Kumar, B.; Rice, J.; Wong, S.; Wang, J.; Yao, B.; Valle, E.; Kiss von Soly, S.; Madriaga, A.; Soriano, F.; Menon, M. K.; Wu, Z. Y.; Kampmann, M.; Chen, Y.; Weissman, J. S.; Aftab, B. T.; Yakes, F. M.; Shawver, L.; Zhou, H. J.; Wustrow, D.; Rolfe, M. Targeting the AAA ATPase p97 as an Approach to Treat Cancer Through Disruption of Protein Homeostasis. *Cancer Cell* **2015,** *28* (5), 653–665.
18. Zhou, H. J.; Wang, J.; Yao, B.; Wong, S.; Djakovic, S.; Kumar, B.; Rice, J.; Valle, E.; Soriano, F.; Menon, M. K.; Madriaga, A.; Kiss von Soly, S.; Kumar, A.; Parlati, F.; Yakes, F. M.; Shawver, L.; Le Moigne, R.; Anderson, D. J.; Rolfe, M.; Wustrow, D. Discovery of a First-in-Class, Potent, Selective, and Orally Bioavailable Inhibitor of the p97 AAA ATPase (CB-5083). *J. Med. Chem.* **2015,** *58* (24), 9480–9497.
19. Leeson, P. D.; Springthorpe, B. The Influence of Drug-Like Concepts on Decision-Making in Medicinal Chemistry. *Nat. Rev. Drug Discov.* **2007,** *6* (11), 881–890.
20. Odingo, J.; O'Malley, T.; Kesicki, E. A.; Alling, T.; Bailey, M. A.; Early, J.; Ollinger, J.; Dalai, S.; Kumar, N.; Singh, R. V.; Hipskind, P. A.; Cramer, J. W.; Ioerger, T.; Sacchettini, J.; Vickers, R.; Parish, T. Synthesis and Evaluation of the 2,4-Diaminoquinazoline Series as Anti-Tubercular Agents. *Bioorg. Med. Chem.* **2014,** *22* (24), 6965–6979.
21. Childress, S. J.; McKee, R. L. Thiazolopyrimidines. *J. Am. Chem. Soc.* **1951,** *73* (8), 3862–3864.
22. Ritchie, T. J.; Macdonald, S. J.; Young, R. J.; Pickett, S. D. The Impact of Aromatic Ring Count on Compound Developability: Further Insights by Examining Carbo- and Hetero-Aromatic and -Aliphatic Ring Types. *Drug Discov. Today* **2011,** *16* (3–4), 164–171.
23. Cervi, G.; Magnaghi, P.; Asa, D.; Avanzi, N.; Badari, A.; Borghi, D.; Caruso, M.; Cirla, A.; Cozzi, L.; Felder, E.; Galvani, A.; Gasparri, F.; Lomolino, A.; Magnuson, S.; Malgesini, B.; Motto, I.; Pasi, M.; Rizzi, S.; Salom, B.; Sorrentino, G.; Troiani, S.; Valsasina, B.; O'Brien, T.; Isacchi, A.; Donati, D.; D'Alessio, R. Discovery of 2-(Cyclohexylmethylamino)pyrimidines as a New Class of Reversible Valosine Containing Protein Inhibitors. *J. Med. Chem.* **2014,** *57* (24), 10443–10454.
24. Polucci, P.; Magnaghi, P.; Angiolini, M.; Asa, D.; Avanzi, N.; Badari, A.; Bertrand, J.; Casale, E.; Cauteruccio, S.; Cirla, A.; Cozzi, L.; Galvani, A.; Jackson, P. K.; Liu, Y.; Magnuson, S.; Malgesini, B.; Nuvoloni, S.; Orrenius, C.; Sirtori, F. R.; Riceputi, L.; Rizzi, S.; Trucchi, B.; O'Brien, T.; Isacchi, A.; Donati, D.; D'Alessio, R. Alkylsulfanyl-1,2,4-Triazoles, a New Class of Allosteric Valosine Containing Protein Inhibitors. Synthesis and Structure-Activity Relationships. *J. Med. Chem.* **2013,** *56* (2), 437–450.
25. Alverez, C.; Arkin, M. R.; Bulfer, S. L.; Colombo, R.; Kovaliov, M.; LaPorte, M. G.; Lim, C.; Liang, M.; Moore, W. J.; Neitz, R. J.; Yan, Y.; Yue, Z.; Huryn, D. M.; Wipf, P. Structure–Activity Study of Bioisosteric Trifluoromethyl and Pentafluorosulfanyl Indole Inhibitors of the AAA ATPase p97. *ACS Med. Chem. Lett.* **2015,** *6* (12), 1225–1230.
26. Alverez, C.; Bulfer, S. L.; Chakrasali, R.; Chimenti, M. S.; Deshaies, R. J.; Green, N.; Kelly, M.; LaPorte, M. G.; Lewis, T. S.; Liang, M.; Moore, W. J.; Neitz, R. J.; Peshkov, V. A.; Walters, M. A.; Zhang, F.; Arkin, M. R.; Wipf, P.; Huryn, D. M. Allosteric Indole Amide Inhibitors of p97: Identification of a Novel Probe of the Ubiquitin Pathway. *ACS Med. Chem. Lett.* **2016,** *7* (2), 182–187.
27. Gui, L.; Zhang, X.; Li, K.; Frankowski, K. J.; Li, S.; Wong, D. E.; Moen, D. R.; Porubsky, P. R.; Lin, H. J.; Schoenen, F. J.; Chou, T.-F. Evaluating p97 Inhibitor Analogues for Potency Against p97–p37 and p97–Npl4–Ufd1 Complexes. *ChemMedChem* **2016,** *11* (9), 953–957.

8.06 Discovery of AMG 337: Using Structure Guided Scaffold Hybridization to Optimize Physicochemical Properties and Target Coverage of a MET Kinase Inhibitor

AA Boezio, Amgen Inc., Cambridge, MA, United States
EA Peterson, Amgen Inc., Cambridge, MA, United States; and Biogen, Cambridge, MA, United States
J-C Harmange, Amgen Inc., Cambridge, MA, United States; and Third Rock Ventures, Boston, MA, United States

© 2017 Elsevier Ltd. All rights reserved.

8.06.1 Introduction 138
8.06.2 Discussion 138
8.06.3 Conclusion 158
Acknowledgments 158
References 158

Abbreviations

CYP cytochrome P450
DEAD diethyl azodicarboxylate
DMSO dimethyl sulfoxide
GST glutathione *S*-transferase
GSH glutathione
HATU 2-(1H-7-Azabenzotriazol-1-yl)-1,1,3,3-tetramethyl uronium hexafluorophosphate
HGF hepatocyte growth factor
HLM human liver microsomes
HPMC hydroxypropyl methyl cellulose
MET mesenchymal epithelial transition factor
MsLM mouse liver microsomes
NADPH nicotinamide adenine dinucleotide phosphate
PBS phosphate-buffered saline
RLM rat liver microsomes
SIF simulated intestinal fluid
SGF simulated gastric fluid
TDI time-dependent inhibition

8.06.1 Introduction

The receptor tyrosine kinase mesenchymal epithelial transition factor (MET) and its endogenous ligand, hepatocyte growth factor (HGF), are implicated in cellular processes relevant to cancer such as cell proliferation, survival, motility, migration, and invasion.[1] Amplification of the MET gene, overexpression of MET, activating mutations, and cross-talk are some of the mechanisms of deregulation that have been found in human cancers.[2] The strong association between the amplification of signaling via the MET/HGF pathway in some human cancers makes it an ideal target for the development of corrective therapeutics targeting both its growth factor, HGF, and the kinase activity of the MET receptor.[3]

Several monoclonal antibodies directed against HGF are currently at different stages of clinical development.[4] Although anti-HGF monoclonal antibodies have been shown to reduce tumor burden in animal models and in early clinical trials, their use will likely be limited to HGF-driven cancers. Ligand-independent activation of the MET/HGF pathway represents another important mechanism of tumorigenesis; therefore, direct inhibition of MET kinase activity should provide a more general approach, addressing both ligand-dependent and ligand-independent MET deregulation.[5] Toward this objective, several small molecule inhibitors of the MET receptor kinase with different binding modes (classes Ia, Ib, II, and other) have been described and have progressed to the clinic.[6] This chapter will outline our contribution to the discovery and the preclinical development of a best-in-class MET kinase inhibitor, **AMG 337** (Fig. 1).[7]

8.06.2 Discussion

The first effort toward the discovery of an MET receptor kinase inhibitor at Amgen resulted in the evaluation of **AMG 458** (Fig. 1) as a potential development candidate.[8] **AMG 458** is representative of a class II-type kinase inhibitor, which adopts an extended conformation, projecting past the gatekeeper residue into a distal hydrophobic pocket.[9] Although this compound displayed good enzymatic inhibition, it was only marginally selective[10] over off-target kinases,[11] confounding the evaluation of its pharmacological activities (Fig. 2). Furthermore, it exhibited a pronounced loss of potency when evaluated in a cellular assay that measured

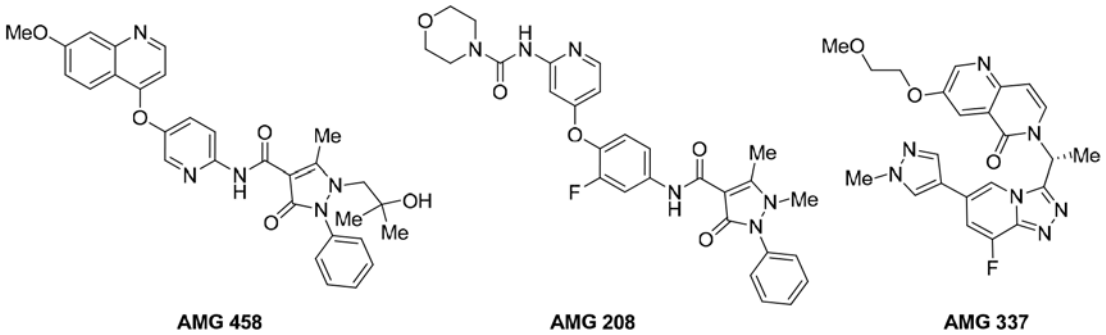

Fig. 1 Class Ib and II MET inhibitors nominated as clinical candidates by Amgen.

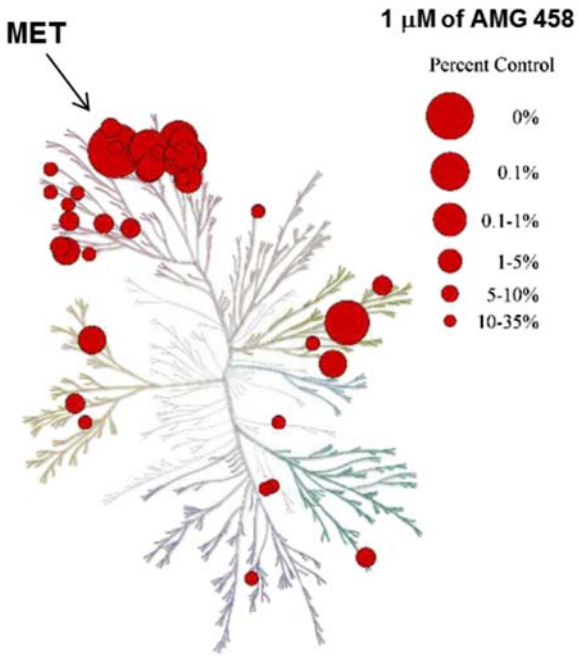

Fig. 2 KINOMEscan of **AMG 458**.

inhibition of MET autophosphorylation (Table 1). **AMG 458** achieved good oral exposure and displayed moderate unbound clearance in rodent, resulting in >50% target inhibition (HGF-induced phosphorylation of MET in mouse liver) for up to 12 h at a single oral dose of 30 mg/kg (Table 1). Ultimately, **AMG 458** was evaluated in a MET-dependent xenograft model, the NIH-3 T3/TPR-Met model derived from NIH3T3 cells transfected with human TPR-Met, an oncogenic form of MET.[12] When administered orally q.d. or b.i.d., **AMG 458** induced dose-dependent tumor growth inhibition with approximate ED_{50} of 12 mg/kg and an ED_{90} of 34 mg/kg. Unfortunately, preclinical analysis of the metabolic fate of **AMG 458** identified the formation of methoxyquinoline thioether glutathione adducts in vitro and in vivo, which halted its further development.[13]

In an attempt to mitigate the concerning metabolic fate of **AMG 458** and improve its overall properties the hinge binder moiety was targeted first. This effort led to the identification of **AMG 208** (Fig. 1), another class II MET inhibitor that progressed into Phase I clinical trials.[14] Although **AMG 208** exhibited evidence of antitumor activity in humans with manageable toxicity,[15] the identification of more potent and selective[16] inhibitors was desirable to fully harness the potential of MET inhibition.

This objective, coupled with a report from Sugen Inc. in 2005[17] describing several potent, selective low molecular weight MET inhibitors (Fig. 3), provided an alternative path to design selective inhibitors with the requisite properties to maintain prolonged inhibition of MET (>50% inhibition for 12–24 h) in a mouse PD model to achieve robust antitumor activity at low doses in MET-driven xenograft models.[18]

To evaluate this new family of MET inhibitors, three novel analogs (**2**–**4**) were prepared and evaluated for their inhibition of MET kinase activity.[19] Since compound **2** had the greatest activity and showed complete selectivity (>25 μM) over a panel of 25 kinases,[20] it was investigated further (Table 2).

Table 1 First-generation MET inhibitor: **AMG 458**

MET IC_{50}	*AMG 458*
Biochemical[a]	2 nM
Cellular[b]	60 nM
LipE[c] (cLogP)	5.9 (2.9)
Rat pharmacokinetics[d]	
Cl[e] [Cl_u][f]	0.38 L/h/kg [34]
$T_{1/2}$	3.6 h
F%[g]	100
Mouse liver PD response[h]	
Dose	30 mg/kg
Last time pt > 50% inhibition	up to 6 h
Plasma C_u at time pt	109 nM
TGI in mouse NIH-3 T3/TPR-Met Xenograft[i]	
ED_{50} of 12 mg/kg	ED_{90} of 34 mg/kg

[a]Inhibition of MET kinase activity, $n \geq 2$.
[b]Inhibition of HGF-mediated MET phosphorylation in PC3 cells, $n \geq 2$.
[c]LipE = pIC_{50} − cLogP.
[d]In vivo experiments were carried out using male Sprague-Dawley rats $n = 3$.
[e]*iv*, 0.5 mg/kg (DMSO).
[f]Plasma unbound fraction (f_u) was measured using equilibrium dialysis; concentration = 5 μg/mL.
[g]*po*, 2 mg/kg (1% Tween 80, 2% HPMC in water, pH 2.2 adjusted with hydrochloric acid).
[h]See Ref. 8 for the mouse liver PD response.
[i]Approximated values. See Ref. 8 for the TGI in mouse NIH-3 T3/TPR-Met xenograft.

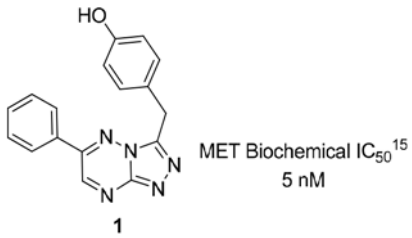

Fig. 3 Reported MET inhibitor (**1**).

Table 2 Novel class Ib MET inhibitors

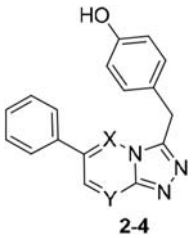

Compound	*X*	*Y*	*Biochemical MET IC_{50} (nM)*[a]	*LipE*[b] *(cLogP)*
2	N	CH	120	4.0 (2.9)
3	CH	N	610	3.5 (2.7)
4	CH	CH	2100	2.1 (3.6)

[a]Inhibition of MET kinase activity, $n \geq 2$.
[b]LipE = pIC_{50} − cLogP.

In order to understand the origin of the potency and selectivity of this series, compound **2** was co-crystallized with MET (Fig. 4).[21] Contrary to **AMG 458**, which extended deep into the hydrophobic pocket behind the gatekeeper residue typical of a class II inhibitor, compound **2** presented a different binding mode. This class Ib binding mode only occurs with movement of the activation loop, allowing the inhibitor to wrap around Met1211. Additionally, the inhibitor interacted with the hinge residue (Met1160) of the kinase via the phenol portion of the molecule. The core had a favorable pi-stacking interaction between

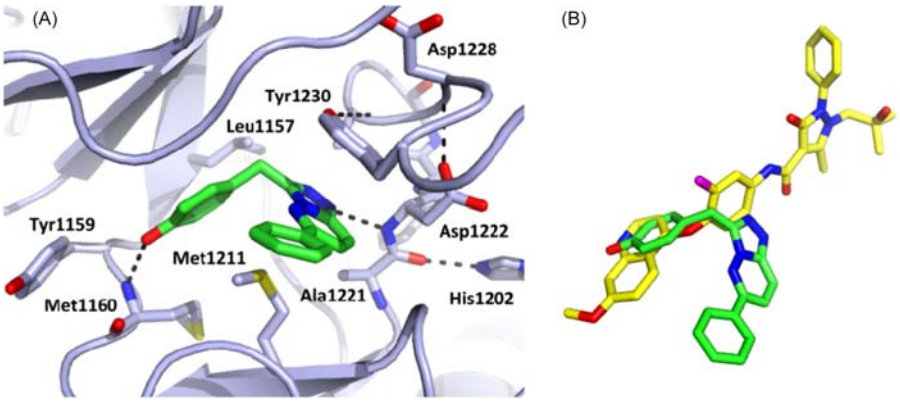

Fig. 4 (A) Co-crystal structures of triazolopyridazine **2** *(green)* and MET. (B) overlay with **AMG 458** analog *(yellow)*.

Tyr1230 and the triazolopyridazine portion of the inhibitor. Although compound **2** represented an attractive starting point, this compound exhibited moderate to high intrinsic clearance (RLM $Cl_{int} = 160$ μL/min/mg and HLM $Cl_{int} = 63$ μL/min/mg).

The overlay of the structures of a close analog of **AMG 458**[22] and compound **2** bound to the catalytic domain of MET revealed an overlap between the *p*-hydroxyphenyl moiety of compound **2** and the quinoline ether portion of **AMG 458** (Fig. 4B). Based on this analysis, hybrid compound **5** was prepared, replacing the phenolic structural alert[23] of **2** with the methoxyquinoline of **AMG 458**.[19]

Compound **5**, a member of the "*O*-linked series," displayed excellent biochemical and cellular potencies and importantly, an attractive selectivity profile comparable to compound **2**.[24] Compound **5** was co-crystalized with MET to confirm its binding mode.[25] As shown in Fig. 5, the predicted binding conformation was verified, with the methoxyquinoline of compound **5** bound to the hinge region and the triazolopyridazine moiety pi-stacking with Tyr1230.

While compound **5** represented a step in the right direction, its microsomal clearance across species was also moderate to high (RLM $Cl_{int} = 416$ μL/min/mg and HLM $Cl_{int} = 88$ μL/min/mg). In order to address this issue, metabolite identification studies were performed. The studies revealed that the C6-phenyl ring was prone to metabolism (Fig. 6). Incubation of triazolopyridazine **5** with rat and human liver microsomes in the presence of NADPH qualitatively yielded C6-phenylarene oxidation product as one of the major metabolites. Also identified in the study were metabolites arising from oxidative cleavage at the benzylic ether carbon (**7** and **8**).

Guided by analysis of the co-crystal structure, various groups were introduced onto the C6 arene in an attempt to mitigate the oxidative liability observed at the C-6 position of the triazolopyridazine.

Introduction of fluorine on the phenyl ring was investigated in an effort to block the observed metabolic activation and to modulate π-stacking interactions[26] with the anticipation of increased potency (Table 3). Both *para* and *meta* substitutions (**10** and **11**) were potent in the enzyme assay with ~3× shift in the cellular assay. The *ortho*-substituted fluorine analogue **12** was not as well tolerated, presumably due to the steric interaction with the triazolopyridazone core, which would rotate the C6-aryl group out of the optimal planar arrangement. In addition, both the 3,4-difluoro (**13**) and the 3,5-difluoro (**14**) analogs were potent against MET kinase activity, but again showed a reduced potency in the cellular assay. Interestingly, the trifluoro analogue **15** was potent in the biochemical and cellular assay with $IC_{50} < 10$ nM. The co-crystal structure of **5** also indicated that the *para*-position of the C-6 phenyl substituent projected toward solvent; therefore, polar functionality could be incorporated at this position to improve physicochemical properties. The introduction of a methylcarboxamide in compound **16** afforded a compound with improved cellular

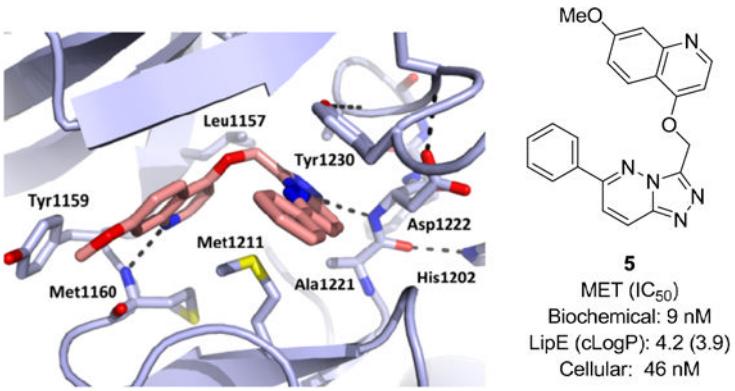

Fig. 5 Co-crystal structure of triazolopyridazine **5** and MET.

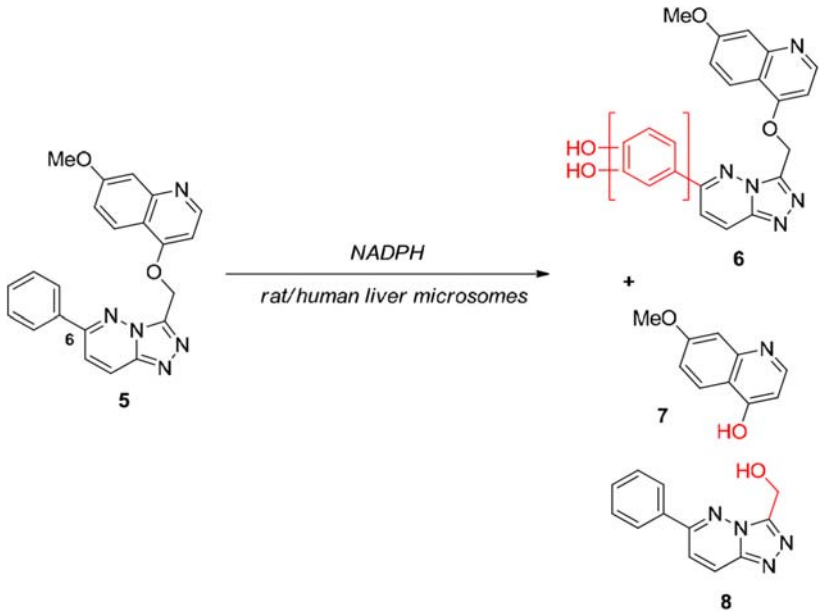

Fig. 6 Identification of metabolic liabilities.

potency compared to compound **5**. The cellular potency of **16** could be further improved by incorporation of a fluorine atom *ortho* to the amide with compound **17**. In addition to substituted phenyl rings, five-membered heterocycles were also explored. Methylisothiazole **21** and *N*-methylpyrazole **23** were found to be optimal groups that led to desirable pharmacokinetic properties while maintaining 1 and 5 nM cellular activity, respectively.

Selected analogs from Table 3 were evaluated in rat pharmacokinetic studies (Table 4). Compound **5**, trifluoro analog **15**, methylisothiazole **21**, and the methyl pyrazole **23** demonstrated low in vivo clearance and moderate oral bioavailability. Both fluorobenzamide analog **17** and methylthiophene **20** were rapidly cleared in vivo and were not pursued further (data not shown).[19]

Although compounds such as **15** and **23** represented valuable leads based on their respective unbound clearance, this series suffered from significant CYP 3A4 time-dependent inhibition (TDI).[27] The absence of a corrective effect on TDI upon introduction of fluorine on the C6 phenyl (compounds **13** and **14**) or a heterocycle (compound **21**) was indicative of a different mechanism of inactivation (Table 5).[28] Therefore, the second major metabolic pathway observed with this series, yielding the formation of hydroxyquinoline **7** and alcohol **8** (Fig. 6) was considered as an alternative mechanism. While increasing the steric hindrance around the ether moiety did not reduce TDI (**24** and **25**), converting the oxygen tether to a nitrogen atom proved to be beneficial, as evidenced by compound **26**. Unfortunately, this change also led to a much weaker inhibition of MET.

Examination of the co-crystal structure of compound **5** revealed that the bent geometry of the tether was critical to allow the inhibitor to properly wrap around Met1211. This favored conformation would be disrupted in compound **26** with a repulsive clash between the −NH of the tether and the hydrogen present on the quinoline at C5 (represented in *red* in Fig. 7). It was hypothesized that the proper binding conformation could be restored by replacing the C5−CH of the quinoline with a nitrogen, as shown with naphthyridine **27**. This change restored the potent inhibition of MET kinase activity and led to the "*N*-linked triazolopyridazine series" described in Table 6.[28]

As anticipated, compound **27** showed improved potency compared to **26** and furthermore, compound **27** showed reduced TDI liability (Table 6). The SAR observed previously at the C6 position in the *O*-linked series translated well to the *N*-linked scaffold, leading to compound **30**. Also, compounds in this series showed reduced unbound clearance when compared to the *O*-linked analogues (Table 7).

To evaluate the properties of this series in vivo, compound **30** was dosed in a mouse PD model. Compound **30** was administered at 30 mg/kg by oral gavage and HGF-induced MET phosphorylation was quantified at various time points thereafter. Sustained inhibition of MET was achieved, with > 50% of inhibition measured 12 h after a single oral dose. Based on this encouraging profile, compound **30** was further characterized; however, low aqueous solubility (HCl/PBS/SIF: > 200/3/13 μg/mL) and the associated dose limiting absorption hampered its progression.

While compound **30** represented a significant overall improvement compared to **AMG 458** with regard to potency and selectivity, the structural and physicochemical properties of this series were not optimal for solubility. To address this limitation while maintaining the remarkable potency and selectivity of these class Ib inhibitors, polarity was introduced and efforts were made to reduce the sp2 character of the compounds. In the process of identifying heterocyclic replacements of the triazolpyridazine and the naphthyridine, optimization of the tether to the hinge binder was explored.

Table 3 SAR of the *O*-linked triazolopyridazine series

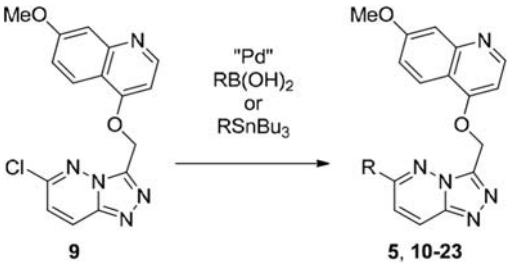

9 **5, 10-23**

Compound	*R*	*Biochemical IC_{50} (nM)*[a]	*Cellular IC_{50} (nM)*[b]	*LipE*[c] *(cLogP)*
5		9	46	4.2 (3.9)
10	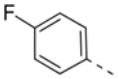	12	42	3.9 (4.0)
11	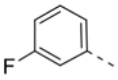	7	20	4.1 (4.0)
12	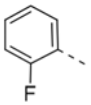	67	398	3.2 (4.0)
13	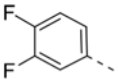	9	26	4.0 (4.1)
14	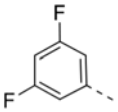	7	14	4.0 (4.1)
15	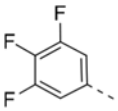	4	7	4.2 (4.2)
16	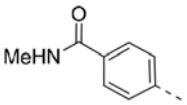	6	16	5.6 (2.6)
17	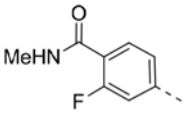	3	3	5.9 (2.5)
18		2	6	5.0 (3.7)
19	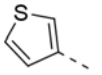	4	29	4.9 (3.5)
20	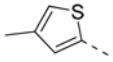	1	2	4.8 (4.2)
21	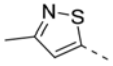	3	1	5.3 (3.3)
22		29	132	4.3 (3.2)
23	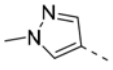	7	5	6.2 (2.0)

[a]Inhibition of MET kinase activity, $n \geq 2$.
[b]Inhibition of HGF-mediated MET phosphorylation in PC3 cells, $n \geq 2$.
[c]$LipE = pIC_{50} - cLogP$.

Table 4 In vitro and in vivo PK properties of *O*-linked triazolopyridazines **5**, **15**, **21**, and **23**

Compound	*5*	*15*	*21*	*23*
RLM Cl_{int}[a] (μL/min/mg)	416	119	353	94
MsLM Cl_{int}[a] (μL/min/mg)	122	208	173	29
HLM Cl_{int}[a] (μL/min/mg)	88	14	79	<14
Plasma f_u rat	0.005[b]	0.001[b]	<0.001[b]	0.012[b]
Mouse	0.017[b]	0.005[b]	0.037[c]	0.141[b]
Human	0.009[b]	0.004[b]	0.003[c]	0.057[b]
Rat pharmacokinetics[d]				
Cl (L/h/kg)	0.37[e]	0.06[f]	0.24[g]	0.36[h]
Cl_u (L/h/kg)	75	58	>244	30
V_{ss} (L/kg)	0.38	0.15	0.35	0.25
$T_{1/2}$ (h)	1.0	3.5	1.1	1.2
F (%)	43[i]	22[i]	59[i]	124[i]

[a]In vitro (*RLM*, rat liver microsomes; *MsLM*, mouse liver microsomes; *HLM*, human liver microsomes).
[b]Plasma unbound fraction (f_u) was measured using equilibrium dialysis; concentration = 5 μg/mL.
[c]Plasma unbound fraction (f_u) was measured using ultrafiltration; concentration = 10 μg/mL.
[d]In vivo experiments were carried out using male Sprague-Dawley rats $n = 3$.
[e]*iv*, 0.5 mg/kg (20% captisol in water, pH 3.5 adjusted with methanesulfonic acid).
[f]*iv*, 0.3 mg/kg (DMSO).
[g]*iv*, 0.25 mg/kg (DMSO).
[h]*iv*, 0.25 mg/kg (20% hydroxypropyl beta-cyclodextrin in water, pH 3.5 adjusted with methanesulfonic acid).
[i]*po*, 2 mg/kg (100% OraPlus).
[j]*po*, 2 mg/kg (1% Tween 80, 2% HPMC in water, pH 2.2 adjusted with hydrochloric acid).

Table 5 *O*-linked triazolopyridazines; MET potency and time-dependent inhibition of CYP3A4

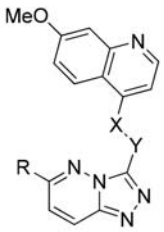

5, 13, 14, 21, 24, 25, 26

Compound	*R*	X–Y	*Biochemical IC_{50} (nM)*[a]	*CYP3A4 IC_{50}/IC_{50} (w/Preinc.) (μM)*[b]
5			9	32/4
13	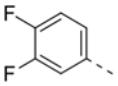		9	>50/6
14	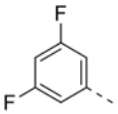		7	>50/8
21	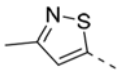		3	17/5
24			100	14/4
25			240	18/9
26			1400	>50/50

[a]Inhibition of MET kinase activity, $n \geq 2$.
[b]Inhibition of CYP3A4 (midazolam 10-hydroxylation) is represented by IC_{50} shift with and without preincubation of the compound in the presence of NADPH.

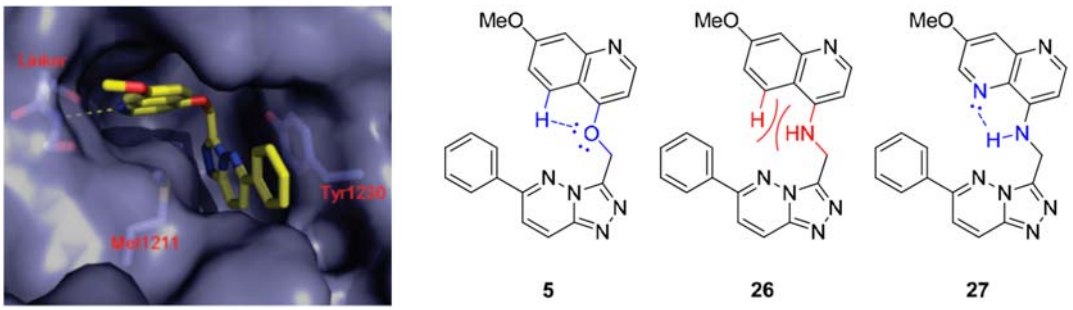

Fig. 7 Favored binding mode conformation of compound **5**.

Table 6 SAR of the *N*-linked triazolopyridazine series

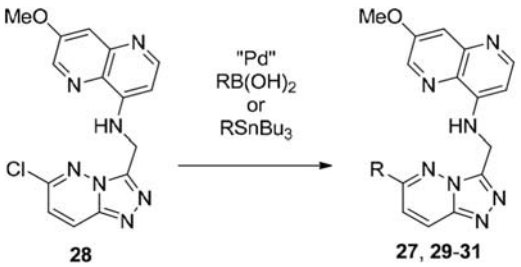

Compound	*R*	*Biochemical IC_{50} (nM)*[a]	*Cellular IC_{50} (nM)*[b]	*LipE*[c] *(cLogP)*	*CYP3A4 IC_{50}/IC_{50} (w/Preinc.) (μM)*[d]
27		17	14	4.6 (3.2)	>50/41
29	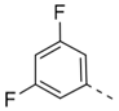	5	3	4.8 (3.5)	>50/29
30	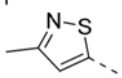	6	3	5.6 (2.6)	>50/26
31	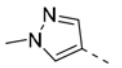	13	3	6.6 (1.3)	>50/40

[a]Inhibition of MET kinase activity, $n \geq 2$.
[b]Inhibition of HGF-mediated MET phosphorylation in PC3 cells, $n \geq 2$.
[c]LipE = pIC_{50} − cLogP.
[d]Inhibition of CYP3A4 (midazolam 1′-hydroxylation) IC_{50} shift with and without preincubation of the compound in the presence of NADPH.

Table 7 In vitro and in vivo PK parameters of *N*-linked triazolopyridazine **23–26**

Compound	*27*	*29*	*30*	*31*
RLM Cl_{int}[a] (μL/min/mg)	74	53	59	<14
MsLM Cl_{int}[a] (μL/min/mg)	78	49	60	13
HLM Cl_{int}[a] (μL/min/mg)	22	47	24	<14
Plasma f_u[b] rat	0.004	0.002	0.007	0.015
Mouse	0.024	0.023	0.064	0.120
Human	0.009	0.008	0.025	0.089
Rat pharmacokinetics[c]				
Cl (L/h/kg)	0.13[d]	0.043[d]	0.19[e]	0.29[e]
Cl_u (L/h/kg)	32	21	26	20
V_{ss} (L/kg)	0.42	0.20	0.30	0.31
$T_{1/2}$ (h)	4.2	3.8	1.8	1.0
F (%)[f]	31	62	53	38

[a]In vitro (*RLM*, rat liver microsomes; *MsLM*, mouse liver microsomes; *HLM*, human liver microsomes).
[b]Plasma unbound fraction (f_u) was measured using equilibrium dialysis; concentration = 5 μg/mL.
[c]In vivo experiments were carried out using male Sprague-Dawley rats $n = 3$.
[d]*iv*, 0.25 mg/kg (DMSO).
[e]*iv*, 0.25 mg/kg (20% hydroxypropyl beta-cyclodextrin in water, pH 3.5 adjusted with methanesulfonic acid).
[f]*po*, 2 mg/kg (1% Tween 80, 2% HPMC in water, pH 2.2 adjusted with hydrochloric acid).

As evidenced by the dramatic improvement in potency moving from **26** to **27**, the two heterocyclic systems that comprise the class Ib inhibitors form a close interaction that can either enforce the desired binding conformation or disrupt it. With this knowledge, the tether and the two heterocyclic systems were optimized in concert to maximize, through favorable intramolecular contact, a conformation similar to the bound conformation. The replacement of the triazolopyridazine with a more polar and less saturated triazolopyridone provided **32**.[29] While this change preserved key features of the triazolopyridazine, both the tether and the hinge binding moiety needed to be altered to obtain the optimal conformation. Guided by structure-based design, a simple methylene tether was incorporated, projecting an unsubstituted quinoline toward the hinge residue in a manner reminiscent of earlier compounds (**2**, **3**, and **4**). The encouraging potency (610 nM) and improved solubility (HCl/PBS/SIF: $>200/>200/60$ μg/mL) of compound **32** warranted further optimization (**Table 8**).

Efforts to improve the potency of the triazolopyridone scaffold were informed by the SAR developed during the optimization of the *O*- and *N*-linked series described above. As mentioned previously, the coplanar arrangement of the C6 substituent and the heterocyclic core was crucial for maintaining potency through the pi-stacking interaction with Tyr1230. For the triazolopyridone scaffold, a methylisothiazole substituent was anticipated to be uniquely suited to provide the required planarity due to a nonbonding intramolecular interaction of the isothiazole sulfur atom with the proximal carbonyl of the triazolopyridone.[30] Indeed, the introduction of the methylisothiazole as in compound **33** provided an increased potency in the biochemical assay (21 nM); however, greater improvement in potency was still required.

As shown in **Fig. 8A**, the inhibitor also interacted with the carbonyl of Arg1208 with dual hydrogen bonding interaction and possessed the desired pi-stacking interaction with Tyr1230. However, the sp3 hybridized carbons present in the triazolopyridone **33** would likely not be optimal and thus unsaturation was re-introduced to test this hypothesis (**34**). Although the introduction of the methyl isothiazole (**33**) and the unsaturated core (**34**) imparted enhanced potency in comparison to **32**, both changes led to a dramatic decrease in solubility (HCl/PBS/SIF for compound **33**: $43/2/<1$ μg/mL) and **34**: $80/<1/5$ μg/mL).

Further exploration of this scaffold, informed by the co-crystal structure, led to the introduction of a methyl group on the tether that was intended to fill the small lipophilic pocket defined by the side chains of Val1092, Leu1157, Ala1226, and Lys1110 (**35**). Although the substitution of the benzylic position did not drastically increase potency or solubility, it was hypothesized that introduction of a chiral center would be beneficial for selectivity and could reduce oxidative metabolism of the benzylic carbon through increased steric bulk. Lastly, the addition of the methoxy group on the quinoline (see 8B for overlay) gave **36**, which maintained potency while providing a handle for the introduction of solubilizing groups as represented by compound **37** (HCl/PBS/SIF: 37/9/40 μg/mL). Combining previously described SAR with the discovery of the optimal C6-methylisothiazole, the potency of the triazolopyridone scaffold was improved >1000-fold from the initial compound (**32**), with the synthesis of only 35 compounds in this series.

Concurrent to efforts focused on replacement of the triazolopyridazine with a triazolopyridone core, a second replacement was also investigated. As learned through inhibitors **2** and **4**, removal of the N5 atom ($X=N \rightarrow X=CH$) led to a significant loss in potency (**Table 2**). However, the introduction of a fluorine atom at the C8 position, potentially filling a small cleft within the active site,[32] increased the potency as evidenced upon comparison of compounds **38** and **39**.[33] This new series, which contained an 8-fluorotriazolopyridine moiety tethered via a methylene unit to a quinoline, afforded a molecule with encouraging inhibitory activity.

The 8-fluorotriazolopyridine series underwent rapid optimization, incorporating the same set of C6-heterocycles as described previously. As shown in **Table 9**, a coplanar pyrazole (**40**) or isoxazole (**41–43**) was beneficial for proper binding. A bis-fluoro group (**40–41**) or a methyl substituent (**42–43**) at the benzylic position was tolerated and filled the same small lipophilic pocket described previously. Geminal dimethyl, cyclopropyl, and ethyl substituents were not tolerated in this space and the stereochemistry of the methyl substituent required the (*S*)-enantiomer for good potency. Lastly, the combinations of chiral substitutions, the planar C6 ring, and the methoxy side chain improved the potencies to 2 nM in our biochemical assay and 3 and 6 nM in our cellular assay, respectively, shown by compounds **42** and **43**.

In order to understand the clearance mechanism for this series, metabolic profiling experiments were conducted. The major metabolic pathway for these compounds was mediated by glutathione *S*-transferase (GST), displacing the aromatic fluorine at the C8 position with glutathione (GSH). Metabolism by GSH conjugation as the primary clearance mechanism for a drug can be problematic due to the existence of multiple GST isoforms in the human population as well as for the potential of GSH depletion leading to oxidative stress if the drug is dosed at high and/or repeated doses.[34] As a means to triage compounds before progressing them into more resource intensive studies, an in vitro assessment was conducted to determine the extent of GSH conjugation.[35]

Using the in vitro GSH conjugation assay, it was observed that two remote components of the core were playing an important role in affecting the reactivity with GSH (**Fig. 9**). For compound **41**, the electron-withdrawing nature of the fluorines on the benzylic carbon, combined with the electron deficiency of the methylisoxazole, acted to increase the amount of GSH conjugation significantly. The electron donating capability of the heterocycle attached at the C6 position modulated the extent of GSH displacement, with the more electron-donating pyrazole group showing reduced incorporation of GSH even in combination with the benzylic fluorines (**40**).[36] The extent of GSH displacement was greatly decreased with removal of the fluorines present on the bridging carbon (**41** → **42** → **43**).

Since inhibitor **43** showed the best overall profile with respect to potency and GSH conjugation, its metabolic fate was further investigated by incubation with NADPH in liver microsomes. Analysis by LC–MS revealed that **43** displayed differing metabolic profiles across species, which could present complications for further advancement (**Fig. 10A**). Incubation of **43** in monkey and human liver microsomes showed oxidation of the tether methyl group (M4) as the major pathway of biotransformation; however,

Table 8 SAR of triazolopyridinone series

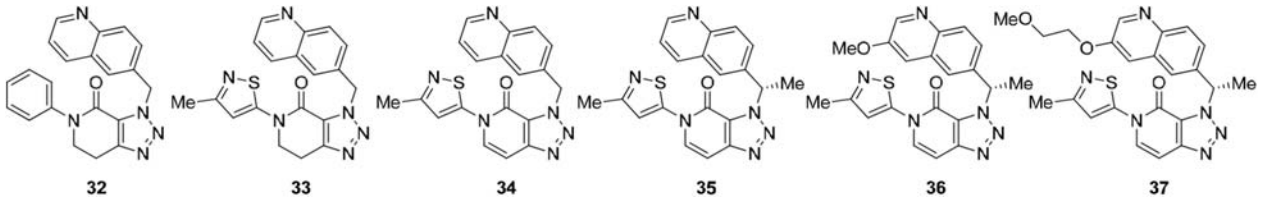

Compound	*32*	*33*	*34*	*35*	*36*	*37*
Biochemical IC_{50} (nM)[a]	612	21	3	2	1	0.6
Cellular IC_{50} (nM)[b]	–	62	5	3	2	2
LipE[c] (cLogP)	4.4 (1.8)	6.4 (1.3)	6.4 (2.2)	6.3 (2.5)	6.1 (2.9)	6.4 (2.8)

[a]Inhibition of MET kinase activity, $n \geq 2$.
[b]Inhibition of HGF-mediated MET phosphorylation in PC3 cells, $n \geq 2$.
[c]$LipE = pIC_{50} - cLogP$.

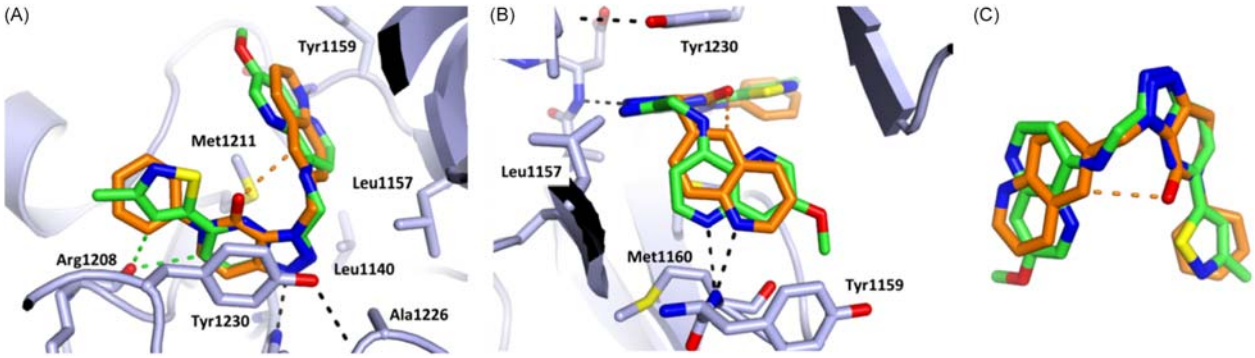

Fig. 8 Overlay of **30** *(green)* and **32** *(orange)* in the active site of MET.[31]

this metabolite was below the detection limit in mouse, dog, and rat liver microsomes. The major metabolite in mouse liver microsomes was demethylation of the methoxyquinoline (M1). This metabolite was also present in rat and dog liver microsomes in addition to metabolites resulting from oxidation of the methylisoxazole (M2) and the triazolopyridine ring (M3). While it was certainly possible to progress this compound forward, the complication of predicting human PK in light of the observed species differences in metabolism made compound **43** less desirable.

One hypothesis for potentially altering the metabolism of **43** was to introduce an alternative metabolic soft spot. Thus inhibitor **44**, bearing an ethoxymethoxy solubilizing group on the quinoline, was synthesized and showed similar potency to compound **43** (Table 10). Compound **44** was also incubated with NADPH in the presence of the liver microsome panel. The introduction of the ethoxymethoxy solubilizing chain provided an alternative site of metabolism that was the major site in all species. The primary metabolites formed after incubation of **44** with mouse, rat, dog, monkey, and human liver microsomes were demethylation of the ethoxymethoxy side chain (M6) and subsequent oxidation to acid M7 (Fig. 10B).

The parallel lead optimization efforts on the triazolopyridone and 8-fluorotriazolopyridine scaffolds culminated in compounds **37** and **44** (Table 10). These two compounds demonstrated single-digit nanomolar potency in both biochemical and cellular assays. Their favorable rat PK showed that both compounds could achieve robust exposure levels above the measured IC_{50} in the cellular assay since the PK in mouse was generally similar to rat.[37] The promising potency and PK attributes of **37** and **44** led to their characterization in a mouse PD model.

Despite only modest improvement in solubility from naphthyridine **30**, compound **37** showed outstanding efficacy and extended coverage in a mouse PD model. It displayed >90% inhibition of HGF-induced phosphorylation of MET at 10 mg/kg up to 12 h, with an associated unbound plasma concentration of 20 nM, providing 11-fold coverage of the cellular IC_{50}. Furthermore, it also achieved unbound coverage of the cellular IC_{50} for up to 24 h. 8-Fluorotriazolopyridine **44**, while demonstrating excellent in vitro potency, excellent solubility, and nearly identical PK to **37**, did not show the same extended inhibition of MET activity in the PD model. As mentioned previously, extended inhibition of MET in a mouse PD model was required for robust tumor growth inhibition. The more robust PD response provided by **37** made this molecule seem more attractive at the outset, but upon further investigation, it was determined that the triazolopyridone scaffold exhibited TDI of CYP3A4 and undesirable solubility. Compound **44** did not exhibit TDI liabilities, but as stated above, did not meet the efficacy requirements for advancement. Thus the team devised a means to combine these two scaffolds in order to identify a molecule that fulfilled the potency and efficacy requirements without the risk of TDI.

In order to merge sustained efficacy with mitigated TDI liability, two key design elements derived from **37** to **44** were hybridized to afford compound **45**. First, it was hypothesized that the superior efficacy of compound **37** in the PD time-course model was a result of the favorable U-shaped binding mode that is reinforced by a key intramolecular interaction between the carbonyl of the pyridone (in *orange*) and the hydrogen of the quinoline as shown in Fig. 11A. The second consideration was eliminating the CYP3A4 TDI while maintaining the superior efficacy of compound **37**. Upon juxtaposition of **37** and **44**, the CYP3A4 TDI activity was attributed to the triazolopyridinone ring of **37**, since both series shared the quinoline hinge-binding element. Accordingly, the 8-fluorotriazolopyridine portion of **44** (in *green*, Fig. 11C) was combined with a naphthyridinone ring system to afford **45**, in which the direction of the internal H-bond interaction, exhibited by **37**, had been reversed (in *orange*, Fig. 11B). This new scaffold was found to maintain single-digit nanomolar inhibition of MET phosphorylation (MET biochemical IC_{50} 3 nM, cellular IC_{50} 9 nM) and furthermore did not show TDI.

A co-crystal of **45** within the catalytic domain of unphosphorylated MET was obtained[38] indicating that the inhibitor adopts the desired U-shaped binding mode around Met1211 (Fig. 12A and B). Furthermore, the hypothesis that the naphthyridinone carbonyl and H-5′ of the 8-fluorotriazolopyridine ring would participate in an intramolecular H-bond to reinforce the optimal binding mode was confirmed by the 3.3 Å distance between these two moieties. The naphthyridinone nitrogen atom N-1 participates in a single-point hydrogen bond with linker residue Met1160, while N-1′ of the 8-fluorotriazolopyridine interacts with the backbone −NH of Asp 1222. Additionally, a face-to-face π-stacking interaction is observed between Tyr1230 and the 8-fluorotriazolopyridine ring system. A two-point binding contact between hydrogens on C-7′ and C-4″ and the lone pairs of the Arg1208 carbonyl group is also apparent. Confirmation that the (*R*)-enantiomer is preferred by the protein was demonstrated by the methyl substituent filling

Table 9 SAR of triazolopyridine series

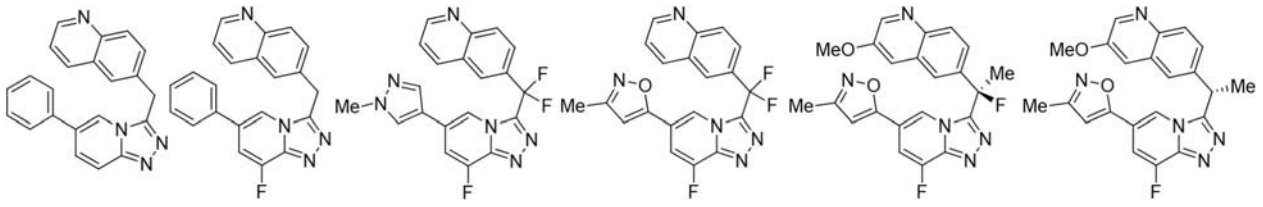

38 39 40 41 42 43

Compound	*38*	*39*	*40*	*41*	*42*	*43*
Biochemical IC_{50} (nM)[a]	211	61	22	9	2	2
Cellular IC_{50} (nM)[b]	–	–	15	9	3	6
LipE (cLogP)[c]	2.5 (4.2)	3.2 (4.1)	5.6 (2.1)	5.6 (2.5)	5.5 (3.2)	5.1 (3.6)

[a]Inhibition of MET kinase activity, $n \geq 2$.
[b]Inhibition of HGF-mediated MET phosphorylation in PC3 cells, $n \geq 2$.
[c]$LipE = pIC_{50} - cLogP$.

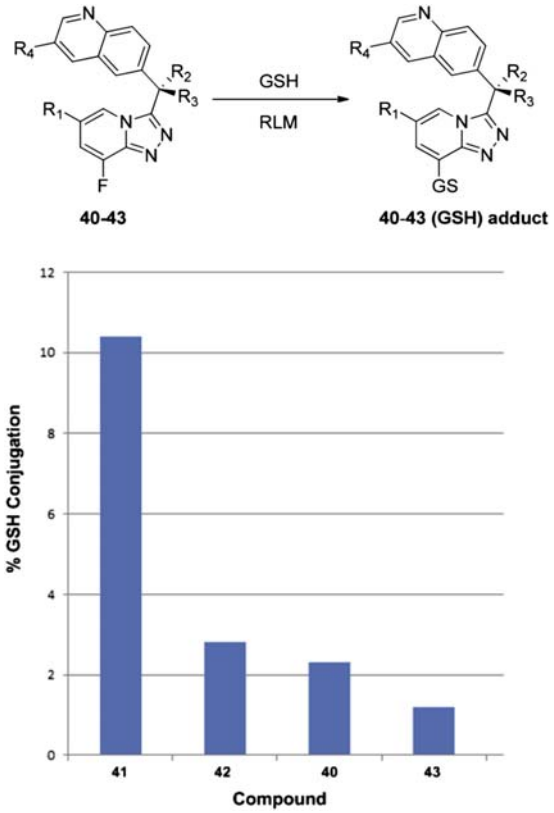

Fig. 9 Effect of substituents on the extent of glutathione conjugation.

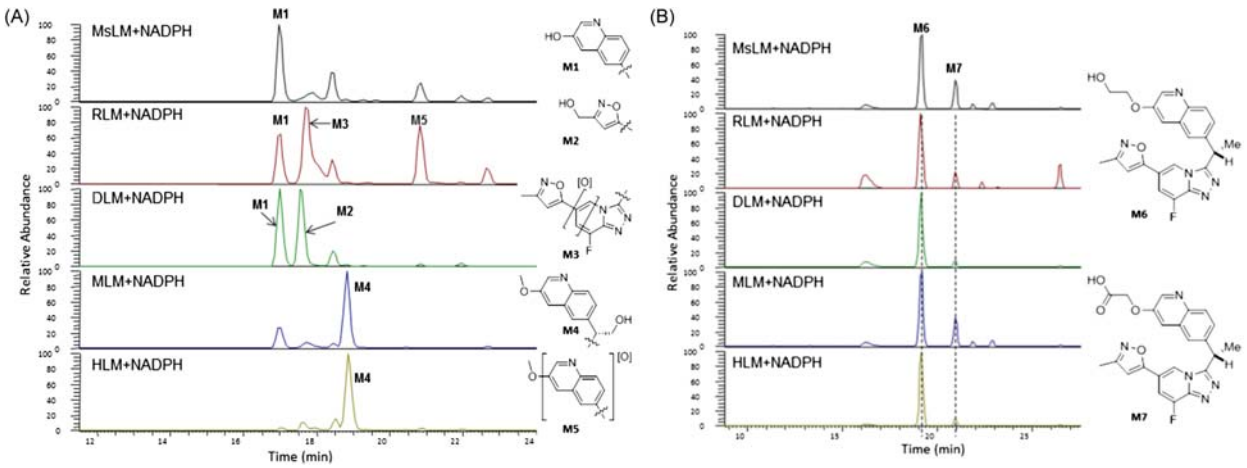

Fig. 10 Multiple species metabolite profile of **43** and **44** after incubation with liver microsomes and NADPH. *MsLM*, mouse liver microsomes; *RLM*, rat liver microsomes; *DLM*, dog liver microsomes; *MLM*, monkey liver microsomes; *HLM*, human liver microsomes.

a small, lipophilic pocket in MET, defined by the side chains of Val1092, Leu1157, Ala1226, and Lys1110.[39] Finally, the fluorine atom at the 8′-position fills a small cleft within the active site, where it sits perpendicular to the backbone carbonyl of Asn1209.[40]

The synthesis of **45** required the individual construction of coupling partners **49a** and **53a** (Scheme 1). Stille cross-coupling of 5-chloro-2,3-difluoropyridine (**46a**) and commercially available isoxazole stannane **47** yielded intermediate **48a**, which was treated with hydrazine to form pyridyl hydrazine **49a**. Coupling partner **53a** was prepared as a racemic mixture in two steps from naphthyridinone **50a** through alkylation with ethyl 2-bromopropanoate (**51**) followed by hydrolysis of the resultant ester (**52a**) under acidic conditions. Acid **53a** underwent HATU-mediated amide coupling with hydrazine **49a**, after which cyclization under dehydrative conditions provided the racemic 8-fluorotriazolopyridine product in 52% yield over two steps. Finally, separation of racemic **45** by chiral chromatography afforded the active (*R*)-enantiomer of **45**.[41]

Table 10 Representative MET compounds (**30**, **37**, and **44**) from three distinct series

Compound	*30*	*37*	*44*
MET IC_{50}			
Biochemical[a]	6 nM	0.6 nM	1 nM
Cellular[b]	3 nM	2 nM	5 nM
LipE[c] (cLogP)	5.6 (2.6)	6.4 (2.8)	5.4 (3.5)
Solubility			
0.01 N HCl/PBS/SIF (μg/mL)	>200/3/13	37/9/40	>200/52/126
CYP3A4 TDI[d]			
IC_{50}/IC_{50} (w/Preinc.) (μM)	>50/26	21/1.5	>50/>50
In vitro ADME			
RLM Cl_{int}[e] (μL/min/mg)	59	89	31
MsLM Cl_{int}[e] (μL/min/mg)	60	68	53
HLM Cl_{int}[e] (μL/min/mg)	24	84	32
Plasma f_u[f] rat	0.007	0.018	0.022
Mouse	0.064	0.027	0.146
Human	0.025	0.012	0.053
Rat pharmacokinetics[g]			
Cl (L/h/kg)	0.19[h]	0.56[i]	0.57[i]
Cl_u (L/h/kg)	26	31	26
$T_{1/2}$ (h)	1.8	3.4	4.2
F (%)	44[j]	43[k]	46[k]
Liver PD response[l]			
Dose (mg/kg)	30	10	10
Last time pt >50% inhibition	12 h	24 h	9 h
Plasma C_u at time pt	4 nM	6 nM	10 nM

[a]Inhibition of MET kinase activity, $n \geq 2$.
[b]Inhibition of HGF-mediated MET phosphorylation in PC3 cells, $n \geq 2$.
[c]LipE = pIC_{50} − cLogP.
[d]Inhibition of CYP3A4 (midazolam 1′-hydroxylation) IC_{50} shift with and without preincubation of the compound in the presence of NADPH.
[e]In vitro (*RLM*, rat liver microsomes; *MsLM*, mouse liver microsomes; *HLM*, human liver microsomes).
[f]Plasma unbound fraction (f_u) was measured using equilibrium dialysis; concentration = 5 μg/mL.
[g]In vivo experiments were carried out with male Sprague-Dawley rats $n = 3$.
[h]*iv*, 0.25 mg/kg (20% hydroxypropyl beta-cyclodextrin in water, pH 3.5 adjusted with methanesulfonic acid).
[i]*iv*, 0.25 mg/kg (DMSO).
[j]*po*, 2 mg/kg (1%Tween 80, 2% HPMC, pH 2.2 adjusted with hydrochloric acid).
[k]*po*, 2 mg/kg (1%Tween 80, 2% HPMC, pH 2.2 adjusted with methansulfonic acid).
[l]See Refs.[28,29,33] for PD measurements.

Alternatively, an enantioselective synthesis of compound **45** was achieved via preparation of a chiral acid coupling partner **55** (Scheme 2).[42] Mitsunobu reaction between naphthyridinone **50a** and (*S*)-methyl lactate (**54**), followed by ester hydrolysis afforded compound **55** in high yield and >95% *ee*.[43] HATU-mediated amide coupling of **49a** with **55**, followed by cyclization under dehydrative conditions yielded **45** in high yield and with complete retention of enantiomeric excess.

Having identified a structurally unique scaffold with nanomolar inhibition of MET phosphorylation without TDI liability, compound **45** was further characterized. The solubility of **45** (0.01 N HCl, PBS, SIF: 172, 34, 55 μg/mL) was superior to compounds **30** and **37** and the associated plasma-free fraction (f_u) was high across species relative to compounds **30**, **37**, and **44** (Table 12). Naphthyridone **45** demonstrated low intrinsic clearance in rat, mouse, and human liver microsomes, consistent with the low to moderate in vivo clearance observed in male Sprague-Dawley rats. While **45** showed similar total clearance (Cl) to compounds **30**, **37**, and **44** in rat, i.e., 0.38 L/h/kg vs. 0.19, 0.57, and 0.56 L/h/kg, respectively, the unbound clearance (Cl_u) was significantly improved for **45** compared to **30**, **37**, and **44**. The unbound clearance for compound **45** was 1.9 L/h/kg, vs. 26, 26, 31 L/h/kg for compounds **30**, **37**, and **44**, respectively, which could be advantageous for lowering human dose requirements. Furthermore, compound **45** demonstrated both a reasonable bioavailability and half-life for further in vivo testing. In the mouse PD assay,

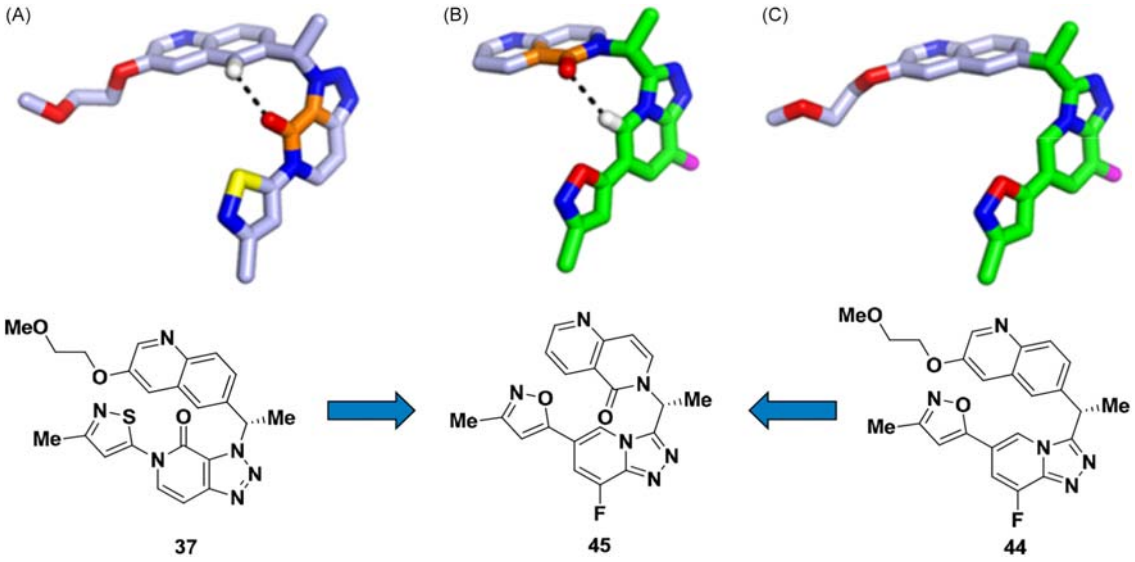

Fig. 11 Origin of the naphthyridinone series, represented by hybrid **45**.

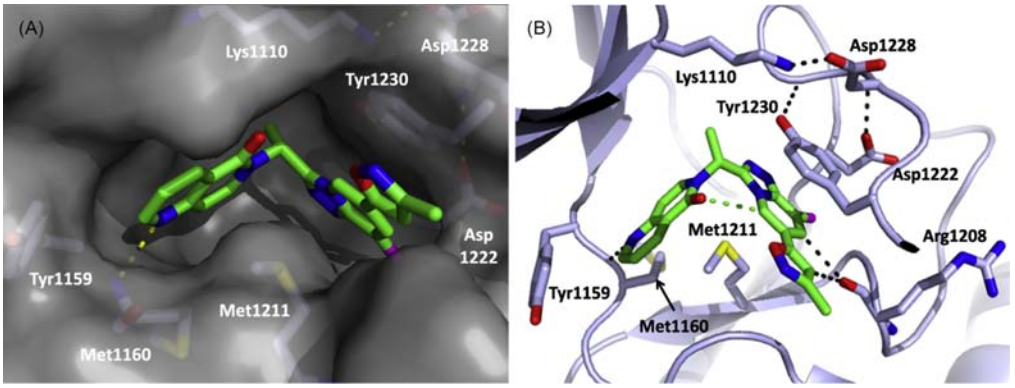

Fig. 12 Co-crystal structure of MET and naphthyridinone **45**.

compound **45** was dosed orally at 10 mg/kg and showed 91% inhibition of MET phosphorylation for 9 h with an associated unbound plasma concentration of 193 nM, covering both the cellular IC_{50} and IC_{90} (Fig. 13). Despite the improvements in solubility and the lack of TDI for compound **45**, a more efficacious molecule was necessary in order to achieve the required >50% inhibition of MET at the 24 h time point in the mouse PD assay.

In order to further explore the SAR around lead compound **45**, a general synthetic method was developed to allow for rapid preparation of naphthyridinone analogs substituted at the C-3 position. Substitution at this position had proved pivotal for improving physicochemical properties, metabolism, and potency in compounds **37** and **44**. In addition, variation at the C-6′ position was also important; since both the 3-methylisoxazole and the *N*-methyl pyrazole were good partners with the 8-fluorotriazolopyridine core (Table 9). Finally, since removal of the fluorine substituent at the 8-position had not been investigated with the more potent naphthyridone scaffold, variation of this substituent was also included in the SAR.

The modified synthesis of naphthyridinone analogs began with a Suzuki reaction between 5-chloro-2,3-difluoropyridine (**46a**) or 5-bromo-2-fluoropyridine (**46b**) and 3-methyl-5-(tributylstannyl)isoxazole (**47**) or a Stille reaction with 1-methyl-4-(4,4,5,5-tetramethyl-1,3,2-dioxaborolan-2-yl)-1H-pyrazole (**60**), yielding fluoropyridine intermediates **48b–d** (Scheme 3). **48b–d** were combined with hydrazine in *i*-PrOH and warmed to afford hydrazines **49b–d**. Naphthyridinones substituted at the C-3 position were derived through an annulation reaction between commercially available ethyl 5-bromo-2-methylnicotinate (**56**) and 1,3,5-triazine (**57** under basic conditions producing 3-bromo-1,6-naphthyridin-5(6*H*)-one (**58**) in 91% yield).[44] Substitution of bromine was achieved by heating with NaOMe/MeOH or $MeOCH_2CH_2ONa/MeOCH_2CH_2OH$ in the presence of 3,4,7,8-tetramethyl-1,10-phenanthroline and CuI as catalysts to provide naphthyridinones intermediates **50b,c**. Exposure of **50b,c** and (±)-ethyl 2-iodopropanoate (**59**) to Cs_2CO_3 in THF at elevated temperature generated racemic ethyl esters **52b,c**, which were converted to the corresponding carboxylic acids **53b,c** through treatment with an aqueous solution of HCl. HATU-mediated coupling of the carboxylic acids **53a–c** with hydrazines **49a–d** yielded the hydrazide intermediates, which underwent dehydrative cyclization with DEAD, $TMSN_3$, and PPh_3 to give triazolopyridines **45**, **61–68** after chiral separation.[45]

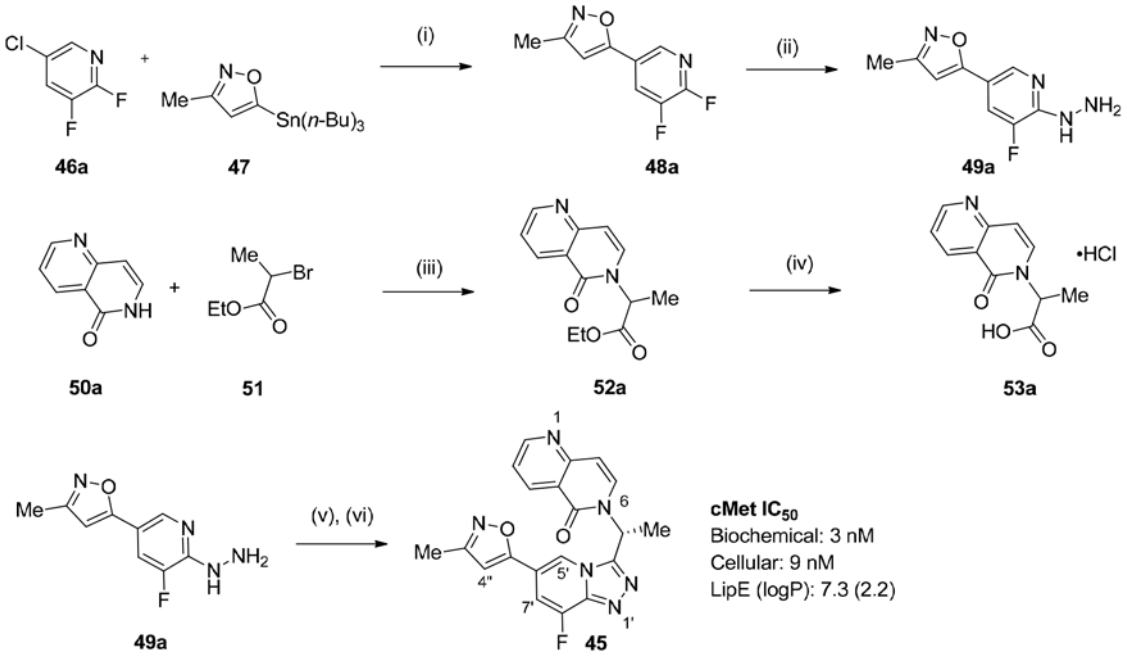

Scheme 1 Synthesis of naphthyridinone **45**. [a]Reagents and conditions: (i) $Pd(OAc)_2$, X-Phos, 1,4-dioxane/water, 100°C, 18 h, 60%; (ii) NH_2NH_2, *i*-PrOH, 65°C, 3 h, 90%; (iii) Cs_2CO_3, THF, 60°C, 3 h, quantitative; (iv) aq. HCl, 60°C, 7 h; (v) **53a**, HATU, Hunig's base, DMF, 23°C, 3 h; (vi) PPh_3, $TMSN_3$, DEAD, THF, 23°C, 3 h, 52% over two steps, then chiral separation.

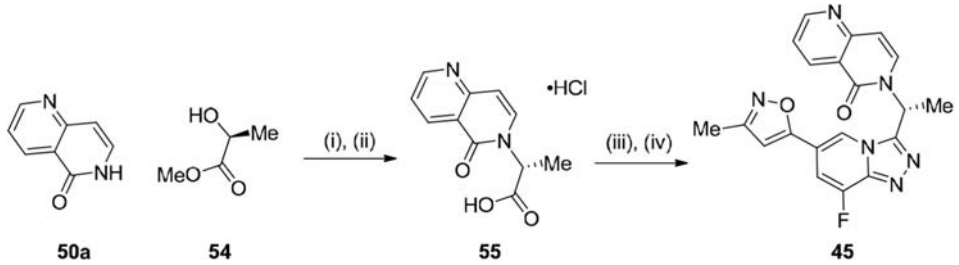

Scheme 2 Enantioselective synthesis of naphthyridinone **45**. [a]Reagents and conditions: (i) PPh_3, DEAD, THF, 0–23°C, 10 h; (ii) aq. HCl, THF, 75°C, 10 h, 67% over two steps; (iii) **49a**, HATU, Hunig's base, MeCN, 0°C, 30 min, 77%; (iv) PPh_3, $TMSN_3$, DEAD, THF, 20°C, 1 h, 83%.

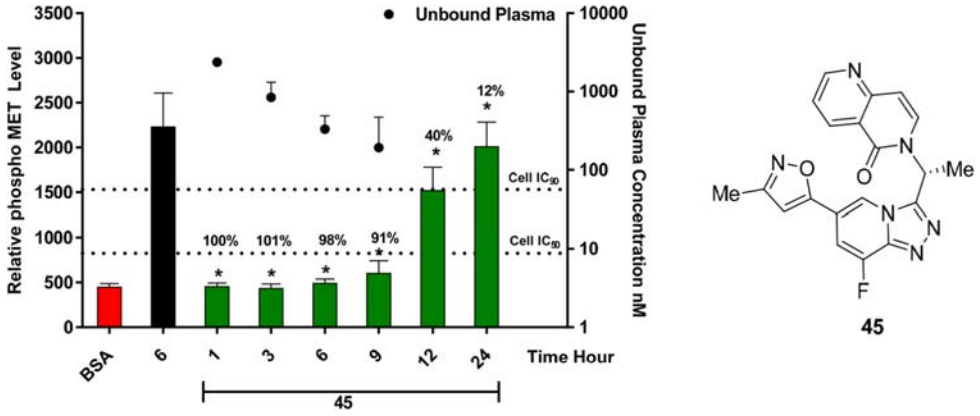

Fig. 13 Compound **45** inhibited HGF-induced phosphorylation of MET over time in the mouse liver PD assay after oral administration at 10 mg/kg (10 mL/kg dose volume, formulated in 2% hydroxypropyl methylcellulose 1% Tween 80 in water, pH 2.2 adjusted with methanesulfonic acid). Data represent the mean ± standard deviation ($n = 3$ mice per group). Statistical significance was determined by ANOVA followed by Bonferroni/Dunn post hoc test. $^*p < 0.0001$ compared to HGF control. *Red circles* represent the mean terminal unbound concentration of **45** in the plasma ± standard deviation ($n = 3$ mice per group).

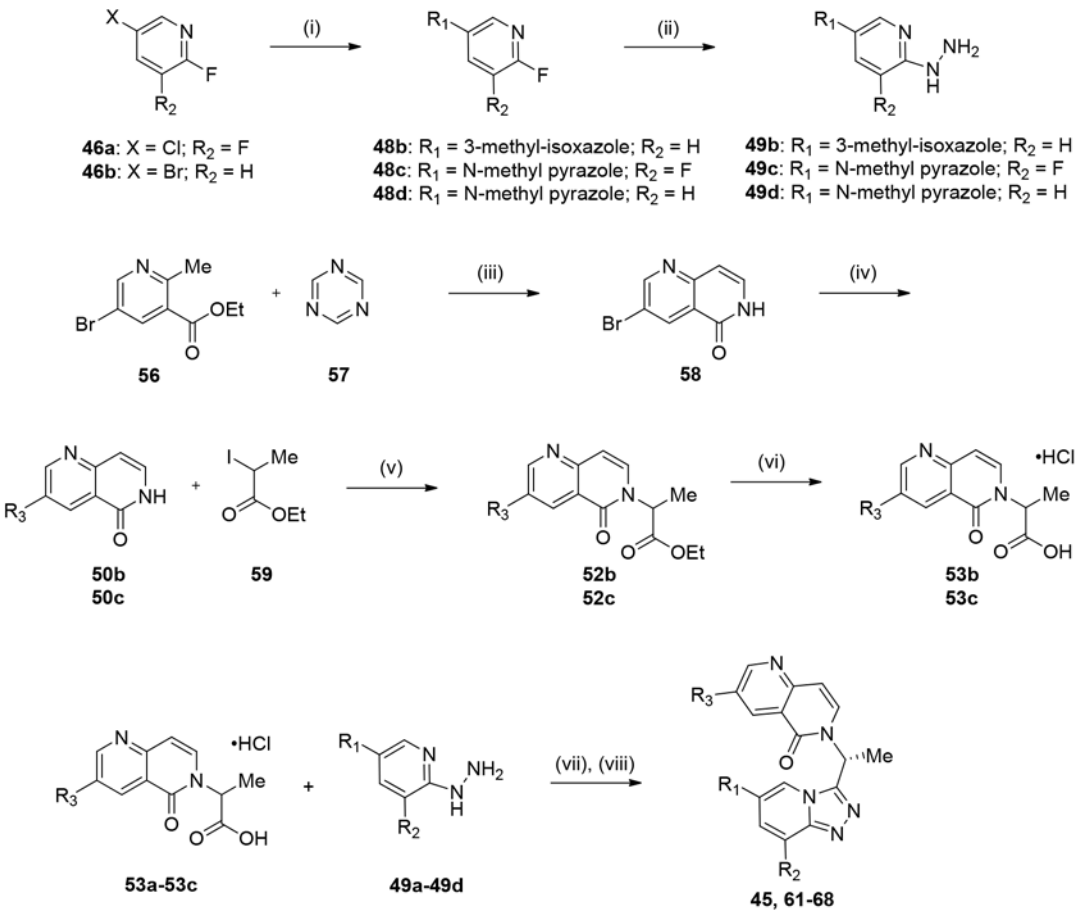

Scheme 3 Synthesis of naphthyridinones (**45**, **61**–**68**). [a]Reagents and conditions: (i) for **48b**: 3-methyl-5-(tributylstannyl)isoxazole (**47**), $Pd_2(dba)_3$, $P(t\text{-}Bu)_3{\bullet}BF_4$, CsF, 1,4-dioxane, 90°C, 12 h, 66%; for **48c**: 1-methyl-4-(4,4,5,5-tetramethyl-1,3,2-dioxaborolan-2-yl)-1*H*-pyrazole (**60**), $Pd(OAc)_2$, X-Phos, K_3PO_4, 1,4-dioxane/water, 100°C, 45 min, 81%; for **48d**: 1-methyl-4-(4,4,5,5-tetramethyl-1,3,2-dioxaborolan-2-yl)-1*H*-pyrazole (**60**), $PdCl_2$(dppf), Cs_2CO_3, 1,4-dioxane/water, 90°C, 3 h, 87%; (ii) NH_2NH_2, *i*-PrOH, for **49b**: 60°C, 2 h, 96%; for **49c**: 65°C, 3 h, 97%; for **49b**: 60°C, 48 h, 98%; (iii) *t*-BuOK, DMSO, 80°C, 1 h, 91%; (iv) 3,4,7,8-tetramethyl-1,10-phenanthroline, CuI, for **50b**: MeONa, MeOH, 130°C, 24 h, 89% (75% pure); for **50c**: *t*-BuONa, $MeOCH_2CH_2OH$, 124°C, 21 h, 85% (v) Cs_2CO_3, THF, for **52b**: DMF, 70°C, 18 h, 40%; **52c**: THF, 60°C, 90 min, 53%; (vi) aq. HCl, for **53b**: 80°C, 10 h, 85%; for **53c**: THF, 65°C, 4 h, 78%; (vii) for HATU, Hunig's base, MeCN or DMF, 23°C, 1–3 h, 23–92%; (viii) PPh_3, $TMSN_3$, DEAD, THF, 23°C, 1–3 h, 20–73%; then chiral separation.

Modification of the C6′ position with a variety of heterocycles provided SAR consistent with that observed for the scaffolds represented by **30** and **44**. Biochemical and cellular potencies were maintained across multiple variations made within the naphthyridinone series with LipE[46] values ranging from 7.0 to 7.9 (Table 11). C-6′ substitution with methylisoxazole (**45**, **61**–**63**) and methylpyrazole (**64**–**68**) appeared interchangeable with respect to potency. The addition of methoxy (**61**, **65**, and **67**) or methoxyethoxy (**62**, **63**, **66**, and **68**) groups at the C-3 position of the naphthyridinone, installed for the purposes of improving solubility, was also well tolerated and maintained or slightly increased the potency (2–3 ×) in the biochemical assay when compared to the unsubstituted naphthyridinones **45** or **64**. Finally, replacement of the C8 fluorine with hydrogen showed a slight decrease in potency (4–6 ×), but only in the analogs containing a pyrazole at C6′ (**65** vs. **67** and **66** vs. **68**).

The metabolic stability and pharmacokinetic properties of **45**, **61**–**68** were evaluated and low microsomal clearance was observed across species for all compounds (Table 12). The free fraction in rat, mouse, and human plasma was relatively high, consistent with data collected for compound **45**. No obvious differentiation was observed based upon respective unbound clearance (Cl_u) and oral bioavailability (%F) for the inhibitors shown in Table 12. One consideration was the consistent cross-species metabolism demonstrated by inhibitors containing a methoxyethoxy group (**62**, **63**, and **66**) in contrast to inhibitors with an undecorated naphthyridine or a methoxy group. When inhibitors **63** and **66** were incubated with NADPH in the presence of liver microsomes, their metabolic profiles were relatively consistent across species, showing demethylation of the $MeOCH_2$-CH_2O-side chain and subsequent oxidation to the acid.[47] Consequently, compounds **62**, **63**, and **66** were selected for advancement into a PD time-course study as a means to determine which of these promising compounds would provide extended duration of coverage over the IC_{50} for MET inhibition.

Table 11 Representative naphthyridinones **45**, **61–68**

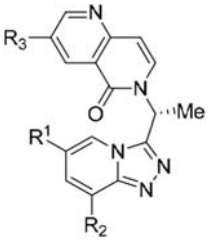

Compound	R^1	R^2	R^3	*Biochemical IC_{50} (nM)*[a]	*Cellular IC_{50}(nM)*[b]	*LipE*[c]	*cLogP*
45	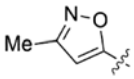	F	H	3	9	7.3	1.2
61		F	MeO	2	5	7.2	1.6
62		F	$MeOCH_2CH_2O$	1	7	7.5	1.5
63		H	$MeOCH_2CH_2O$	2	7	7.4	1.3
64	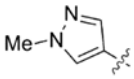	F	H	2	8	7.8	0.9
65		F	MeO	1	6	7.6	1.3
66		F	$MeOCH_2CH_2O$	1	5	7.9	1.1
67		H	MeO	9	11	7.0	1.1
68		H	$MeOCH_2CH_2O$	3	8	7.5	1.0

[a]Inhibition of MET kinase activity, $n \geq 2$.
[b]Inhibition of HGF-mediated MET phosphorylation in PC3 cells, $n \geq 2$.
[c]LipE = pIC_{50} − cLogP.

Table 12 In vitro and in vivo PK parameters of naphthyridinones **45**, **61–68**

Compound	*45*	*61*	*62*	*63*	*64*	*65*	*66*	*67*	*68*
RLM Cl_{int}[a] (μL/min/mg)	8	–	16	9	8	12	6	9	<5
MsLM Cl_{int}[a] (μL/min/mg)	<5	–	14	23	<5	7	8	7	7
HLM Cl_{int}[a] (μL/min/mg)	14	–	20	7	<5	<5	9	<5	8
Plasma f_u[b] rat	0.196	–	0.080	0.190	0.271	0.139	0.174	0.206	0.296
Mouse	0.245	–	0.317	0.435	0.376	0.353	0.366	0.409	0.424
Human	0.320	–	0.409	0.338	0.478	0.309	0.419	0.286	0.498
Rat pharmacokinetics[c]									
Cl (L/h/kg)[d]	0.38	0.46	0.20	0.29	0.28	0.12	0.27	0.65	0.70
Cl_u (L/h/kg)	1.9	–	2.4	1.5	1.0	0.9	1.6	3.2	2.4
V_{ss} (L/kg)	0.4	0.5	0.7	1.0	0.7	0.5	0.9	1.2	1.3
$T_{1/2}$ (h)	0.8	1.1	2.9	2.4	4.0	3.6	3.0	1.7	1.8
F (%)[e]	44	31	54	59	31	43	30	36	25

[a]In vitro (*RLM*, rat liver microsomes; *MsLM*, mouse liver microsomes; *HLM*, human liver microsomes).
[b]Plasma unbound fraction (f_u) were measured using equilibrium dialysis; Concentration = 5 μg/mL.
[c]In vivo experiments with male Sprague-Dawley rats (n=3).
[d]*iv*, 0.25 mg/kg (DMSO).
[e]*po*, 2 mg/kg (2% HPMC 1% Tween 80 in water, pH 2.2 adjusted with methanesulfonic acid).

Unlike compounds **45** and **62**, compounds **63** and **66** exhibited extended inhibition of MET activity in mice, achieving >90% inhibition of HGF-induced phosphorylation of MET for at least 12 h at a dose of 10 mg/kg (Fig. 14). Furthermore, compounds **63** and **66** maintained approximately 50% inhibition over a 24 h period.[48] Based on these results, **63** and **66** were selected as structurally diverse candidates for PK profiling in a second preclinical species.

Compounds **63** and **66** showed low clearance and moderate volumes of distribution at steady-state, with comparable half-lives following IV administration to beagle dogs (Table 13). After oral dosing at 10 and 30 mg/kg, the exposure increased proportionally to dose for both inhibitors and the oral bioavailability for **63** and **66** was also comparable. Overall, both compounds had reasonable dog *iv* and *po* PK properties.

Ultimately, **66** was advanced and evaluated in an MET-dependent xenograft model (Fig. 15). Following oral administration (*q.d.*) of **66** at 0.1, 0.3, 1, 3, and 10 mg/kg over 22 days, dose-dependent tumor growth inhibition was observed with an ED_{50} of 0.3 mg/kg and an ED_{90} of 0.8 mg/kg with no adverse effect on body weight.[49] This represents a more than 40–43 × improvement over the tumor growth inhibition (ED_{50} and ED_{90}) results provided by the original clinical candidate **AMG 458**.

Illustrated by the graph of unbound plasma concentration of **66** over time, doses covering the cellular IC_{90} for at least 12 h (3 and 10 mg/kg) resulted in >90% tumor growth inhibition. Compound **66** did not suffer from CYP3A4 TDI, exhibited good solubility in its hydrate form (0.01 N HCl/PBS/SIF: 174/77/>200 μg/mL) and displayed exquisite selectivity against a panel of 402 tyrosine and serine/threonine kinases (Fig. 16).[50] These attributes, when coupled with its long half-life in rat and dog, its predictable metabolism and good human dose projection, led to the selection of compound **66** as the clinical candidate designated **AMG 337**.

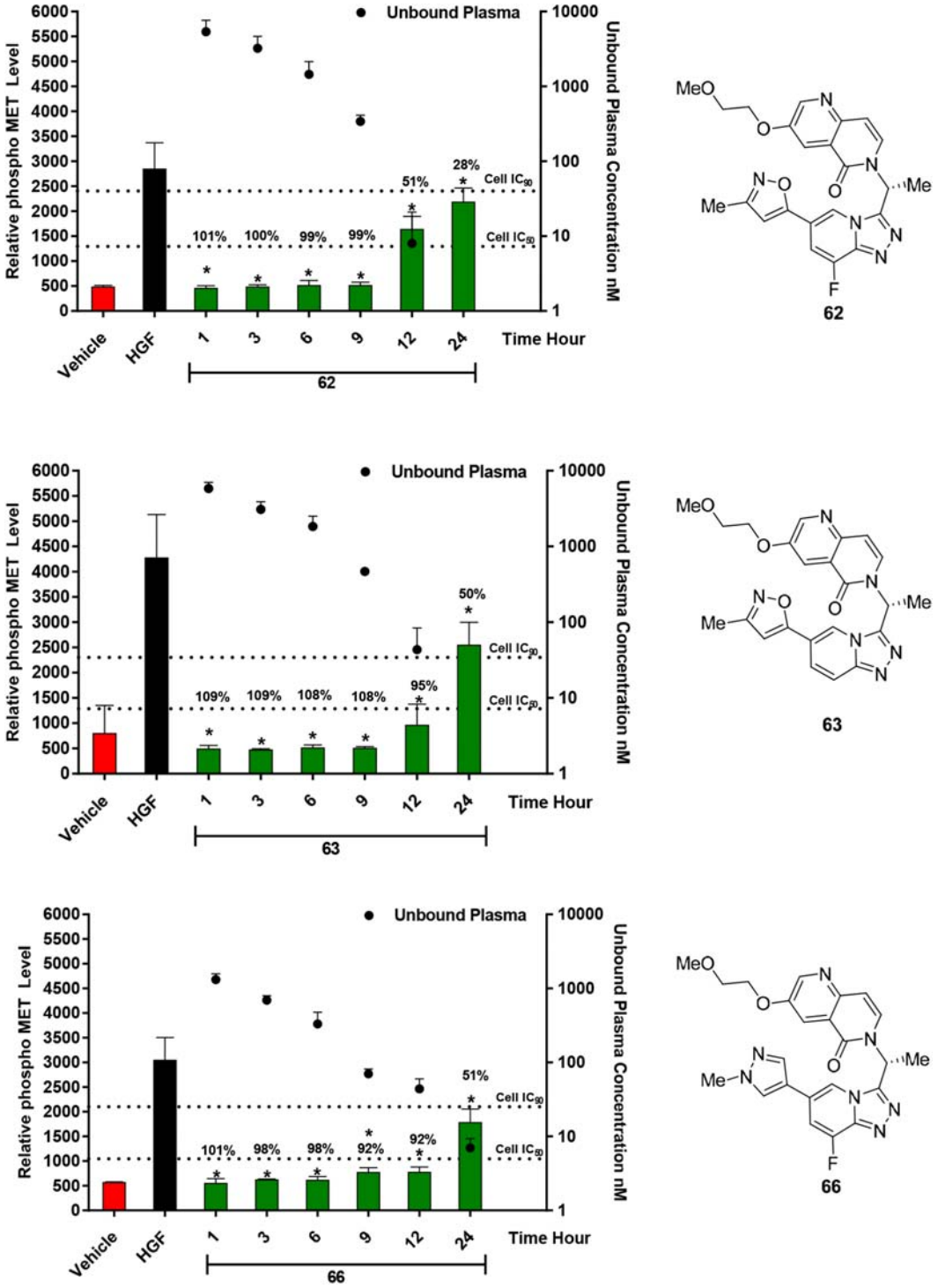

Fig. 14 The effect of **62**, **63**, and **66** on HGF-induced phosphorylation of MET over time in the mouse liver PD assay after oral administration at 10 mg/kg (10 mL/kg dose volume, formulated in 2% hydroxypropyl methylcellulose 1% Tween 80 in water, pH 2.2 adjusted with methanesulfonic acid). Data represent the mean ± standard deviation ($n=3$ mice per group). Statistical significance was determined by ANOVA followed by Bonferroni/Dunn post hoc test. *$p<0.0001$ compared to HGF control. *Red circles* represent the mean terminal unbound concentration of compound **62**, **63**, or **66** in the plasma ± standard deviation ($n=3$ mice per group).

AMG 337 was dosed once daily in patients with advanced solid tumor, escalating from 25 to 400 mg to access safety, tolerability, and PK. No accumulation was observed over the 28 days of dosing, and the observed half-life ranged from 4.6 to 6.9 h, supporting a QD dosing regimen with a median T max of 2–3 h. For all doses, the cellular IC_{50} and IC_{90} were covered for up to 24 h. The MTD was determined to be 300 mg.[51]

Table 13 Dog PK parameters for **63** and **66**

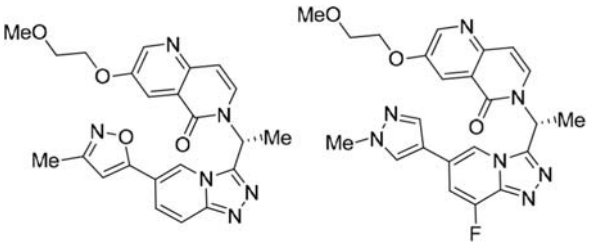

Compound	*63*	*66*
Dog pharmacokinetics[a]		
Cl (L/h/kg)	0.30[b]	0.23[c]
Cl_u (L/h/kg)[d]	0.68	0.46
V_{ss} (L/kg)	1.4	1.1
$T_{1/2}$ (h)	4.3	5.9
10 mg/kg $AUC_{0\rightarrow\infty}$ ($\mu g \times h/L$)	19,300	21,000
F (%)	53[e]	49[e]
30 mg/kg $AUC_{0\rightarrow\infty}$ ($\mu g \times h/L$)	94,100	82,600
F (%)	87[e]	64[e]

[a]In vivo experiments with male beagle dogs ($n=3$).
[b]*iv*, 0.425 mg/kg (20% hydroxypropyl beta-cyclodextrin in water).
[c]*iv*, 0.713 mg/kg (20% hydroxypropyl beta-cyclodextrin in water, pH 3.5 adjusted with methanesulfonic acid).
[d]Unbound fraction (f_u) were measured using equilibrium dialysis; Concentration = 5 μg/mL.
[e]*po*, (2% HPMC 1% Tween 80 in water, pH 2.0 adjusted with methanesulfonic acid).

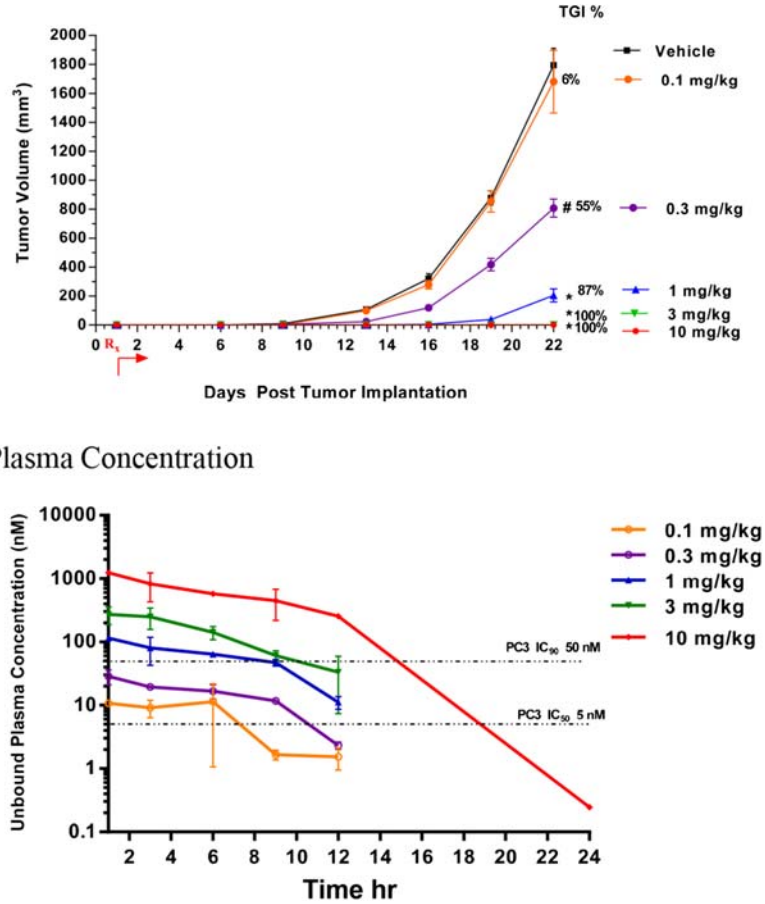

Fig. 15 Effect of compound **66** on tumor growth in the NIH-3 T3/TPR-Met xenograft model. Compound **60** was administered by oral gavage once per day beginning 24 h post-tumor cell implantation (10 mL/kg dose volume, formulated in 20% hydroxypropyl beta-cyclodextrin in water, pH 3.5 adjusted with methanesulfonic acid). Results are expressed as mean ± standard error ($n=12$ per group). Asterisk denotes $p<0.0005$ compared to treatment with vehicle. Vehicle: 20% HPBCD, pH 3.5 adjusted with methanesulfonic acid).

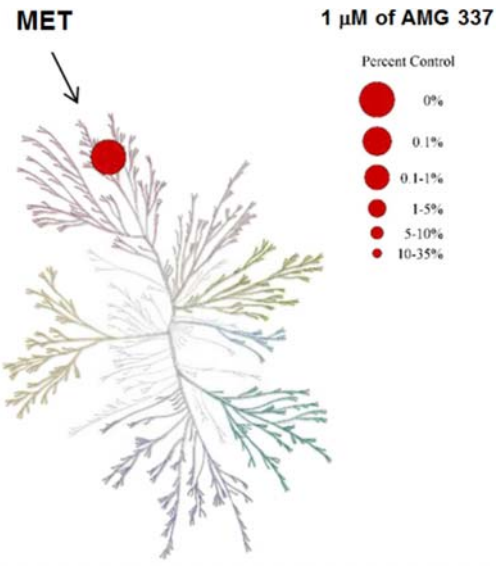

Fig. 16 KINOMEscan of **AMG 337**.

8.06.3 Conclusion

A thorough analysis of the bound structures of our inhibitors throughout the optimization process enabled the selection of ideal scaffolds and substitutions leading to two advanced series of MET receptor kinase inhibitors, represented by compounds **37** and **44**. The combination of both series, guided by the exploitation of an intramolecular hydrogen bond to favor the active conformation, and a careful analysis of metabolism across species led to the discovery of **AMG 337 (66)**. This exquisitely potent and selective MET inhibitor, demonstrated a sustained inhibition of MET phosphorylation in a mouse liver pharmacodynamic model and strong tumor growth inhibition in an MET-dependent mouse efficacy model. The favorable clinical pharmacokinetics and tolerability of **AMG 337** warranted its progression into Phase II trials.

Acknowledgments

Albrecht, B. K.; Amore, B.; Bak, A.; Baker, D.; Bauer, D.; Beaupre, D. M.; Bellon, S.; Berry, L.; Bio, M. M.; Boezio, C.; Booker, S.; Broome, M. A.; Burgess, T. L.; Caenepeel, S.; Caudillo, I.; Chen, A.; Choquette, D.; Chu-Moyer, M; Clausen, A.; Colletti, A. E.; Copeland, K. W.; Coxon, A.; D'Amico, E.; Damore, M. A.; Deng, H.; Dominguez, C.; Dussault, I.; Fang, Y.-Q.; Fridrich, C.; Fu S.; Hansen, K. B.; Hamid, O.; Hirai, S.; Hoffman, D.; Hollis, L. S. Hong, D. S.; Huang, L.; Hughes, P. E.; Hungate, R. W.; Hwang, Y. C.; Janku, F.; Kendall, R.; Khan, R.; Kaplan-Lefko, P.; Kha, H. T.; Kim, T.-S.; Kittaneh, M.; Kurzrock, R.; Kwak, E. L.; Larrow, J. F.; Lee, M.; Lewis, R. T.; Lin, M.-H. J.; Liu, L.; Loberg, R. D.; Lockhart, A. C.; Lohman, J.; Long, A. M.; LoRusso, P.; Mattson, B.; Milne, J. E.; Moriguchi, J.; Ngarmchamnanrith, G.; Norman, M. H.; O'Connor, A.; Osgood, T.; Potashman, M.; Potter, M. S.; Radinsky, R.; Reese, M.; Rex, K.; K. Romero, K.; Rosen P.; Santostefano, M.; Siegmund, A. C.; Shah, K.; Shimanovich, R.; Springer, S.; Stec, M.; Tang, R.; Teffera, Y.; Vaida, K. R.; Werner, J.; Wilsily, A.; Wiedemann, S.; Whittington, D. A.; Xi, N.; Yang, K.; Zhang, Y.; Zhao, Z.; & ASCO.

See also: 8.08. Tepotinib.

References

1. Giordano, S.; Ponzetto, C.; Di Renzo, M. F.; Cooper, C. S.; Comoglio, P. M. Tyrosine kinase receptor indistinguishable from the c-met protein. *Nature* **1989,** *339*, 155–156.
2. Dharmawardana, P. G.; Giubellino, A.; Bottaro, D. P. Hereditary papillary renal carcinoma type I. *Curr. Mol. Med.* **2004,** *4*, 855–868.
3. Gherardi, E.; Birchmeier, W.; Birchmeier, C.; Vande Woude, G. Targeting MET in cancer: rationale and progress. *Nat. Rev. Cancer* **2012,** *12*, 89–103.
4. Zhang, Y.; Jain, R. K.; Zhu, M. Recent Progress and advances in HGF/MET-targeted therapeutic agents for cancer treatment. *Biogeosciences* **2015,** *3*, 149–181.
5. Porter, J. Small molecule c-Met kinase inhibitors: a review of recent patents. *Expert Opin. Ther. Pat.* **2010,** *20*, 159–177.
6. Cui, J. J. Targeting receptor tyrosine kinase MET in cancer: small molecule inhibitors and clinical progress. *J. Med. Chem.* **2014,** *57*, 4427–4453.

7. (a) Bio, M.; Fang, E.; Milne, J. E.; Wiedemann, S.; Wilsily, A. Method for the Preparation of (1,2,4)-Triazolo[4,3-a]Pyridines. PCT Int. Appl. December 31, 2014, WO 2014210042 A2 20141231;(b) Albrecht, B. K.; Bauer, D.; Bellon, S.; Bode, C. M.; Booker, S.; Boezio, A.; Choquette, D.; D'Amico, E.; Harmange, J.-C.; Hirai, S.; Hungate, R. W.; Kim, T.-S.; Lewis, R. T.; Liu, L.; Lohman, J.; Norman, M. H.; Potashman, M.; Siegmund, A. C.; Springer, S.; Stec, M.; Xi, N.; Yang, K.; Peterson, E. A.; Romero, K.; Copeland, K. W. Fused Heterocyclic Derivatives and Method of Use as c-Met Inhibitors. PCT Int. Appl. July 23, 2009, WO 2009091374 A2 20090723;
(c) Boezio, A. A.; Copeland, K. W.; Rex, K.; Albrecht, K. B.; Bauer, D.; Bellon, S. F.; Boezio, C.; Broome, M. A.; Choquette, D.; Coxon, A.; Dussault, I.; Hirai, S.; Lewis, R.; Lin, M.-H. J.; Lohman, J.; Liu, J.; Peterson, E. A.; Potashman, M.; Shimanovich, R.; Teffera, Y.; Whittington, D. A.; Vaida, K. R.; Harmange, J.-C. Discovery of (R)-6-(1-(8-Fluoro-6-(1-methyl-1H-pyrazol-4-yl)-[1,2,4]triazolo[4,3-a]pyridin-3-yl)ethyl)-3-(2-methoxyethoxy)-1,6-naphthyridin-5(6H)-one (AMG 337), a Potent and Selective Inhibitor of MET with High Unbound Target Coverage and Robust In Vivo Antitumor Activity. *J. Med. Chem.* **2016,** *59,* 2328–2342.
8. Liu, L.; Siegmund, A.; Xi, N.; Kaplan-Lefko, P.; Rex, K.; Chen, A.; Lin, J.; Moriguchi, J.; Berry, L.; Huang, L.; Teffera, Y.; Yang, Y.; Zhang, Y.; Bellon, S. F.; Lee, M.; Shimanovich, R.; Bak, A.; Dominguez, C.; Norman, M. H.; Harmange, J.-C.; Dussault, I.; Kim, T.-S. Discovery of a potent, selective, and orally bioavailable c-Met inhibitor: 1-(2-hydroxy-2-methylpropyl)-N-(5-(7-methoxyquinolin-4-yloxy)pyridin-2-yl)-5-methyl-3-oxo-2-phenyl-2,3-dihydro-1H pyrazole-4-carboxamide (AMG 458). *J. Med. Chem.* **2008,** *51,* 3688–3691.
9. PDB deposition code number for the crystal structure of MET + **AMG 458** close analog is 5T3Q.
10. A characteristic of class II Met inhibitor (see reference 6 for more detail).
11. AMG 458 was > 2000-fold selective over VEGFR-2 and IGF-1R, see: Liu, L.; Norman, M. H.; Lee, L.; Xi, N.; Siegmund, A.; Boezio, A. B.; Booker, S.; Choquette, D.; D'Angelo, N. D.; Germain, J.; Yang, K.; Yang, Y.; Zhang, Y.; Bellon, S. F.; Whittington, D. A.; Harmange, J.-C.; Dominguez, C.; Kim, T.-S.; Dussault, I. Structure-based design of novel class II c-Met inhibitors: 2. SAR and kinase selectivity profiles of the pyrazolone series *J. Med. Chem.* **2012,** *55,* 1868–1897.
12. (a) Zhang, Y.; Kaplan-Lefko, P. J.; Rex, K.; Yang, Y.; Moriguchi, J.; Osgood, T.; Mattson, B.; Coxon, A.; Reese, M.; Kim, T.-S.; Lin, J.; Chen, A.; Burgess, T. L.; Dussault, I. Identification of a novel recepteur d'origine Nantais/c-Met small-molecule kinase inhibitor with antitumor activity in vivo. *Cancer Res.* **2008,** *68,* 6680–6687; (b) Park, M.; Dean, M.; Cooper, C. S.; Schmidt, M.; O'Brien, S. J.; Blaire, D. G.; Vande Woude, G. F. Mechanism of met oncogene activation. *Cell* **1986,** *45,* 895–904.
13. Teffera, Y.; Colletti, A. E.; Harmange, J.-C.; Hollis, L. S.; Albrecht, B. K.; Boezio, A. A.; Liu, J.; Zhao, Z. Chemical reactivity of methoxy 4-O-aryl quinolines: Identification of glutathione displacement products in vitro and in vivo. *Chem. Res. Toxicol.* **2008,** *21,* 2216–2222.
14. (a) https://clinicaltrials.gov/ct2/show/NCT00813384?term%20=%20amg%20+%20208&rank%20=%201; (b) http://wwwext.amgen.com/~/media/amgen/full/www-amgen-com/downloads/investors/2014_annual_report_and_10-k.ashx?la%20=%20en. (c) Additional detail will be published in due course. Manuscripts in preparation.
15. Hong, D. S.; Rosen, P.; Lockhart, A. C.; Fu, S.; Janku, F.; Kurzrock, R.; Khan, R.; Amore, B.; Caudillo, I.; Deng, H.; Hwang, Y. C.; Loberg, R.; Ngarmchamnanrith, G.; Beaupre, D. M.; Lee, P. A first-in-human study of AMG 208, an oral MET inhibitor, in adult patients with advanced solid tumors. *Oncotarget* **2015,** *6,* 18693–18706.
16. With an IC_{50} of 5 nM for MET, at higher concentrations, AMG 208 inhibited other kinases, such as VEGF receptor 2 (VEGF-R2, IC_{50} = 112 nM).
17. Zhang, F.-J.; Vojkovsky, T.; Huang, P.; Liang, C.; Do, S. H.; Koenig, M.; Cui, J. Preparation of Triazolotriazines as c-Met Modulators for Treating Cancer. *PCT Int. Appl.* **2005,** WO2005010005.
18. For a discussion of the relationship between MET target coverage and tumor growth inhibition, see: Yamazaki, S.; Skaptason, J.; Romero, D.; Lee, J. H.; Zou, H. Y.; Christensen, J. G.; Koup, J. R.; Smith, B. J.; Koudriakova, T. Pharmacokinetic-pharmacodynamic modeling of biomarker response and tumor growth inhibition to an orally available cMet kinase inhibitor in human tumor xenograft mouse models *Drug Metab. Dispos.* **2008,** *36,* 1267–1274.
19. Albrecht, B. K.; Harmange, J.-C.; Bauer, D.; Berry, L.; Bode, C.; Boezio, A. A.; Chen, A.; Choquette, D.; Dussault, I.; Fridrich, C.; Hirai, S.; Hoffman, D.; Larrow, J. F.; Kaplan-Lefko, P.; Lin, J.; Lohman, J.; Long, A. M.; Moriguchi, J.; O'Connor, A.; Potashman, M. H.; Reese, M.; Rex, K.; Siegmund, A.; Shah, K.; Shimanovich, R.; Springer, S. K.; Teffera, Y.; Yang, Y.; Zhang, Y.; Bellon, S. Discovery and optimization of triazolopyridazines as potent and selective inhibitors of the c-Met kinase. *J. Med. Chem.* **2008,** *51,* 2879–2882.
20. An internal kinase panel was used as a first point of selectivity triage, the panel included KDR, IGF1R, Tie2, Lck, Jak3, BTK, p38R, PKBR, PKAR, Aur1/2, Abl among others.
21. PDB deposition code number for the crystal structure of MET + **2** is 3CCN.
22. Compound 58e in reference 11: N-(3-fluoro-4-((7-(methyloxy)-4-quinolinyl)oxy)phenyl)-1-(2-hydroxy-2-methylpropyl)-5-methyl-3-oxo-2-phenyl-2,3-dihydro-1H-pyrazole-4-carboxamide.
23. Stepan, A. F.; Walker, D. P.; Bauman, J.; Price, D. A.; Baillie, T. A.; Kalgutkar, A. S.; Aleo, M. D. Structural alert/reactive metabolite concept as applied in medicinal chemistry to mitigate the risk of idiosyncratic drug toxicity: A perspective based on the critical examination of trends in the top 200 drugs marketed in the united states. *Chem. Res. Toxicol.* **2011,** *24,* 1345–1410.
24. 25 μM in internal kinase panel including KDR, IGF1R, Tie2, Lck, Jak3, BTK, p38R, PKBR, PKAR, Aur1/2, Abl among others.
25. PDB deposition code number for the crystal structure of MET + 5 is 3CD8.
26. Wheeler, S. E. Local nature of substituent effects in stacking interactions. *J. Am. Chem. Soc.* **2011,** *133,* 10262–10274.
27. Zhou, S.; Chan, S. Y.; Goh, B. C.; Chan, E.; Duan, W.; Huang, M.; McLeod, H. L. Mechanism-based inhibition of cytochrome P450 3A4 by therapeutic drugs. *Clin. Pharmacokinet.* **2005,** *44,* 279–304.
28. Boezio, A. A.; Berry, L.; Albrecht, B. K.; Bauer, D.; Bellon, S. F.; Bode, C.; Chen, A.; Choquette, D.; Dussault, I.; Hirai, S.; Kaplan-Lefko, P.; Larrow, J. F.; Lin, M. H.; Lohman, J.; Potashman, M. H.; Rex, K.; Santostefano, M.; Shah, K.; Shimanovich, R.; Springer, S. K.; Teffera, Y.; Yang, Y.; Zhang, Y.; Harmange, J.-C. Discovery and optimization of potent and selective triazolopyridazine series of c-Met inhibitors. *Bioorg. Med. Chem. Lett.* **2009,** *19,* 6307–6312.
29. Bode, C. M.; Boezio, A. A.; Albrecht, B. K.; Bellon, S. F.; Berry, L.; Broome, M. A.; Choquette, D.; Dussault, I.; Lewis, R. T.; Lin, M.-H. J.; Rex, K.; Whittington, D. A.; Yang, Y.; Harmange, J.-C. Discovery and optimization of a potent and selective triazolopyridinone series of c-Met inhibitors. *Bioorg. Med. Chem. Lett.* **2012,** *22,* 4089–4093.
30. Beno, B. R.; Yeung, K.-S.; Bartberger, M. D.; Pennington, L. D.; Meanwell, N. A. A Survey of the Role of Noncovalent Sulfur Interactions in Drug Design. *J. Med. Chem.* **2015,** *58,* 4383–4438.
31. PDB deposition code number for the crystal structure of MET + **30** is 4DEG and **32** is 4DEH.
32. Perpendicular to the backbone carbonyl of Asn1209.
33. Peterson, E. A.; Teffera, Y.; Albrecht, B. K.; Bauer, D.; Bellon, S. F.; Boezio, A.; Boezio, C.; Broome, M. A.; Choquette, D.; Copeland, K. W.; Dussault, I.; Lewis, R.; Lin, M.-H. J.; Lohman, J.; Liu, J.; Potashman, M.; Rex, K.; Shimanovich, R.; Whittington, D. A.; Vaida, K. R.; Harmange, J.-C. Discovery of potent and selective 8-fluorotriazolopyridine c-□Met inhibitors. *J. Med. Chem.* **2015,** *58,* 2417–2430.
34. Hinson, J. A.; Roberts, D. W.; James, L. P. Adverse Drug Reactions. In *Handbook of experimental pharmacology,* Uetrecht, J., Ed.; Vol. 196, Springer: New York, 2010.
35. After 2 h of incubation, the ratio of GSH conjugate to remaining parent was measured by LC − MS. (see reference 13 for more details).
36. For an analysis of electronic properties of various five membered heterocycles, see the following: Katritzky, A. R.; Pozharskii, A. F. *Handbook of Heterocyclic Chemistry,* 2nd ed.; Amsterdam: Pergamon, 2000, 378.
37. Microsomal turnover was the main driver for clearance and their intrinsic clearance were similar.
38. PDB deposition code number for the crystal structure of MET + **45** is 5EYC. Additional, PDB deposition code number for the crystal structure of MET + **66** is 5EYD).
39. The absolute stereochemistry was assigned by crystallization of enantiopure **45** with unphosphorylated MET and confirmed from chiral synthesis (see Scheme 2).
40. Müller, K.; Faeh, C.; Diederich, F. Fluorine in pharmaceuticals: looking beyond intuition. *Science* **2007,** *317,* 1881–1886.
41. Potency of the (*S*)-enantiomer (MET Biochemical IC_{50}: 963 nM, Cellular IC_{50}: 2630 nM).
42. For alternative route of synthesis of **55**, see: Fang, Y.-Q.; Bio, M. M.; Hansen, K. B.; Potter, M. S.; Clausen, A. Magnesium coordination-directed *N*-selective stereospecific alkylation of 2-pyridones, carbamates, and amides using α-halocarboxylic acids *J. Am. Chem. Soc.* **2010,** *132,* 15525–15527.

43. Although this exact asymmetric synthesis was efficient, other derivatives often led to degradation of *ee* upon amide coupling.
44. Balogh, M.; Hermecz, I.; Naray-Szabo, G.; Simon, K.; Meszaros, Z. Studies on naphthyridines. An unexpected product in Hantzsch pyridine synthesis. *J. Chem. Soc. Perkin Trans.* **1986,** *1,* 753–757.
45. The stereochemistry of **61**-**68** was made based on potency and in analogy to the known potent enantiomer of **45**.
46. Lipophilic-efficiency metrics are reported for purpose of retrospective analysis of this work.
47. Same as the triazolopyridine series.
48. Compounds **63** and **65** maintained also approximately 50% inhibition over 24 h.
49. Hughes, P. E.; Rex, K.; Caenepeel, S.; Yang, T.; Zhang, Y.; Broome, M. A.; Kha, H. T.; Burgess, T. L.; Amore, B.; Kaplan-Lefko, P. J.; Moriguchi, J.; Werner, J.; Damore, M. A.; Baker, D.; Choquette, D. M.; Harmange, J.-C.; Radinsky, R.; Kendall, R.; Dussault, I.; Coxon, A. In Vitro and In Vivo Activity of AMG 337, a Potent and Selective MET Kinase Inhibitor, in MET-Dependent Cancer Models. *Mol. Cancer Ther.* **2016,** *15,* 1568–1579.
50. *KINOMEscan*™. At a concentration of 1 μM, compound **23** binds to MET (3.1% POC) and no other kinases $<$ 50% POC).
51. Hong, D. S.; LoRusso, P.; Hamid, O.; Beaupre, D. M.; Janku, F.; Khan, R.; Kittaneh, M.; Loberg, R. D.; Amore, B.; Caudillo, I.; Hwang, Y. C.; Tang, R.; Ngarmchamnanrith, G.; Kwak, E. L. First-in-human study of AMG 337, a highly selective oral inhibitor of MET, in adult patients (pts) with advanced solid tumors. In ASCO Annual Meeting 2508; 2014.

8.07 Discovery of AZD0156: The First Potent and Selective Inhibitor of ATM Kinase for Clinical Evaluation

KG Pike, AstraZeneca Oncology Chemistry, Cambridge, United Kingdom

© 2017 Elsevier Ltd. All rights reserved.

8.07.1	**Introduction**	161
8.07.1.1	The DNA Damage Response	161
8.07.1.2	Ataxia-Telangiectasia Mutated Kinase	162
8.07.1.3	Inhibitors of ATM Kinase	162
8.07.2	**Discovery of Novel, Potent, and Selective ATM Inhibitors With Oral Bioavailability**	164
8.07.3	**The Importance of Predicting Dose to Man and Maximum Absorbable Dose**	167
8.07.4	**The Discovery of AZD0156: A First in Class Potent, Selective and Orally Available ATM Inhibitor Suitable for Clinical Evaluation**	169
8.07.4.1	Identification of a Scaffold With Increased Permeability	169
8.07.4.2	Achieving ATM Selectivity With Imidazo[5,4-c]quinolin-2-one Based Compounds	170
8.07.4.3	Optimization of Basic Imidazo[5,4-c]quinolin-2-ones	170
8.07.4.4	Profile of AZD0156	171
8.07.5	**Conclusion**	174
Acknowledgments		175
References		175

Abbreviations

DDR DNA damage response
DMPK Drug metabolism and pharmacokinetic properties
DSB Double strand break
hERG Human ether-a-go-go related gene
HRR Homologous recombination repair
IR Ionizing radiation
LLE Lipophilic ligand efficiency
mTOR Mammalian target of rapamycin
NHEJ Nonhomologous end-joining
PARP Poly(ADP-ribose) polymerase
PBPK Physiologically based pharmacokinetic
PI3K Phosphatidylinositol 3-kinase
PIKK Phosphatidylinositol 3-kinase (PI3K)-related kinase
SSB Single-strand break

8.07.1 Introduction

8.07.1.1 The DNA Damage Response

The DNA within our cells is constantly under attack from endogenous sources, environmental mutagens, and carcinogens with tens of thousands of DNA damage events occurring every day.[1,2] Many different mechanisms have evolved to deal with the different forms of DNA damage thus evoking different repair mechanisms and signaling pathways which include cell-cycle arrest, regulation of DNA replication, and the repair or bypass of DNA damage.[3] The collective term for these various responses is DNA damage response (DDR). Five major repair pathways exist within human cells: base excision repair which repairs the DNA single-strand breaks (SSBs) primarily generated from the processing of modified bases and abasic sites[4]; homologous recombination repair (HRR) which is a relatively efficient and accurate repair pathway for DNA double-strand breaks (DSBs) but which relies upon the presence of undamaged sister chromatid DNA[5]; nonhomologous end-joining (NHEJ) which also repair DNA DSBs but are not dependent on the presence of replicated DNA[6]; nucleotide excision repair which deals with modified nucleotides and UV-induced damage[7]; and mismatch repair which deals with replication errors such as mismatch base-pairing and nucleotide insertions/deletions.[8] Whilst DNA SSBs are the most common form of DNA damage with an estimated 20,000 events at least per cell per day, the less common DNA DSBs are the most cytotoxic lesions due to the issues associated with accurate chromosome segregation during cell division. The formation of DNA DSBs is the primary driver for cytotoxicity for ionizing radiation (IR) and a number of approved cancer chemotherapies, such as topoisomerase I and II inhibitors (e.g., camptothecin, irinotecan, etoposide, doxorubicin, etc.), and can also be induced by targeting specific DDR pathways (such as inhibition of poly(ADP-ribose) polymerase (PARP) with the approved drug olaparib). The increased number of DNA DSBs induced by these therapies results in a pause of the cell cycle to allow repair of the accumulated damage; however, should this damage reach a sufficient threshold, or persist for long enough, programmed cell death (apoptosis) is triggered. Cells in the S-phase, that is, during DNA synthesis, are more sensitive to DNA damaging agents due to the vulnerable structure of DNA. Opportunities to interfere with the repair of DNA DSBs may,

therefore, result in increased levels and/or duration of DNA damage and consequently may potentiate the cytotoxicity of DSB inducing agents. The DDR of cancer cells differ in three important aspects to those of normal cells.[9] Firstly, most (if not all) cancer cells will have lost one or more DDR pathways thereby resulting in an increased dependency on those remaining pathways. Secondly, cancer cells have increased levels of replication stress compared with normal cells as a result of oncogenic drivers, loss of cell-cycle checkpoints, and increased levels of intrinsic reactive oxygen species (ROS).[10,11] Finally, cancer cells have increased levels of endogenous DNA damage as a result of factors associated with increased proliferation, such as increased transcription and increased metabolic and replication stress. These key differences between cancer cells and normal cells mean that cancer cells are more sensitive to exogenous DNA damage and support the hypothesis that targeting DDR pathways may cause greater effects in cancer cells thus providing a therapeutic margin to exploit in the clinic.

8.07.1.2 Ataxia-Telangiectasia Mutated Kinase

Ataxia-telangiectasia mutated (ATM) kinase is a member of the phosphatidylinositol 3-kinase (PI3K)-related kinase (PIKK) family of atypical serine/threonine protein kinases (also comprising ATR, DNAPKcs, mammalian target of rapamycin (mTOR), SMG1, and the nonenzymatic TRRAP)[12] and plays a central role in the DDR by regulating the detection and repair of DNA DSBs.[13,14] ATM derives its name from a rare human autosomal recessive disorder ataxia-telangiectasia (A-T) that results from mutations in the *ATM* gene. A-T patients suffer a variety of symptoms amongst which are immunodeficiency, extreme radiosensitivity, and a predisposition to cancer. Cells from A-T patients have been shown to have abnormal cell-cycle arrest in the G_1, S, and G_2 phases, and show hypersensitivity to IR.[15] Like other PIKK family members, ATM is a large protein (350 kDa) comprising 3056 residues and containing a kinase domain with a relatively high degree of similarity to the lipid kinase PI3K.[16] Recruitment of the inactive dimeric form of ATM to the site of a DNA DSB is mediated by the DNA-end tethering MRE11-RAD50-NBS1 (MRN) complex and results in the autophosphorylation of ATM on serine 1981.[17,18] This autophosphorylation event activates ATM leading to dimer dissociation and subsequent phosphorylation of nearby histone variant H2AX on serine 139 (γH2AX) thereby initiating the assembly of DDR components at the breakage site to facilitate DNA repair, cell-cycle arrest, and/or cell death.[19,20] ATM directly phosphorylates p53 on serine 15, Mdm2, and Chk2 thus stabilizing p53 by preventing its Mdm2-mediated ubiquitinylation and degradation.[21–23] Upon activation and accumulation in the nucleus, p53 acts as transcription factor to drive the expression of genes involved in G_1/S cell cycle checkpoint activation and apoptosis.[24] ATM-mediated Chk2 phosphorylation induces degradation of the phosphatase Cdc25A which would otherwise promote S-phase progression through activation of Cdk2 that is needed for DNA synthesis.[25] In addition, hundreds of substrates are phosphorylated in an ATM-dependent manner, demonstrating the complexity of the ATM-mediated DDR pathways.[26] Loss of ATM activity has been shown to increase the sensitivity of virtually all cells to IR whereas upregulation of ATM signaling has been observed in different cancers leading to both chemoresistance and radioresistance.[27–29] Small molecule inhibitors of ATM have been shown to recapitulate the phenotype of A-T cells thus affecting the ability of the cells to mount a cytoprotective response to DNA damage and mouse models in which ATM has been knocked out have also been shown to have increased radiosensitivity and a predisposition to developing cancer.[30] In addition to its key role in coordinating the DDR response to DNA DSBs, growing evidence suggests a role for ATM in signaling and protecting against oxidative stress through its activation by surface cysteine residue oxidation.[31] This activity has been linked to ATM's vascular-protecting function at regions of highly fluctuating oxidative conditions during pathoneoangiogenesis.[32] The central role of ATM in coordinating repair pathways in response to induced DNA DSBs highlights this protein as a highly attractive pharmacological target to sensitize tumor cells to both chemotherapy and radiotherapy.[33,34] The benefit of ATM inhibition may not only reside in the enhancement of DNA DSB cytotoxicity but there may also be the opportunity to exploit the concept of synthetic lethality.[35,36]

8.07.1.3 Inhibitors of ATM Kinase

The promise of ATM inhibition to provide a potentially meaningful treatment for cancer patients has resulted in the identification and disclosure of a number of ATM inhibitors with differing profiles and properties (Fig. 1).[16,37] Wortmannin (**1**) was the first reported inhibitor of ATM enzyme ($IC_{50} = 0.15\ \mu M$) although it also inhibits a number of other PIKK enzymes (DNAPK $IC_{50} = 0.016\ \mu M$, ATR $IC_{50} = 1.8\ \mu M$) and its primary activity resides against PI3K ($IC_{50} = 0.003\ \mu M$). Wortmannin (**1**) sensitizes cells to IR but concentrations above those required to inhibit ATM are required for optimal radiosensitization. A549 lung

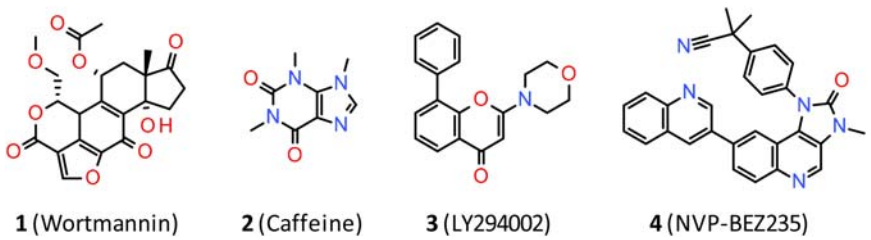

Fig. 1 Structures of nonselective ATM inhibitors in the public domain.

adenocarcinoma cells treated with both wortmannin (**1**) and IR displayed S-phase and G_2-phase abnormalities observed with ATM deficient cells.[38] Caffeine (**2**) has also been reported as a relatively weak and nonspecific ATM inhibitor with an in vitro IC_{50} of 200 μM against the ATM enzyme and weak activity against a number of PIKK enzymes (ATR $IC_{50}=1100$ μM, DNAPK $IC_{50}=10{,}000$ μM).[39] The discovery of LY294002 (**3**), developed by Eli Lilly from the naturally occurring flavonoid quercetin, provided a significant step forward in the understanding of the PIKK enzymes.[40] LY294002 (**3**) is an ATP competitive inhibitor with modest potency against a variety of PI3K and PIKK enzymes (PI3Kα,β,γ,δ $IC_{50}=0.55$, 16, 12, and 1.6 μM, respectively; mTOR $IC_{50}=2.5$ μM; DNAPK $IC_{50}=2.5$ μM); however, activity against ATM is surprisingly limited.[41] Crystallographic studies of LY294002 (**3**) bound to the ATP-binding site of PI3Kγ have revealed that the inhibitor forms a key interaction from the oxygen of the morpholine unit to the hinge region of the kinase.[42] More recently the dual PI3K/mTOR inhibitor NVP-BEZ235 (**4**), taken into clinical studies by Novartis, has been shown to inhibit ATM and a number of other PIKKs in addition to PI3K and mTOR (ATM $IC_{50}=0.007$ μM; DNAPK $IC_{50}=0.005$ μM; PI3Kα,β,γ,δ $IC_{50}=0.004$, 0.075, 0.005, and 0.007 μM, respectively; mTOR $IC_{50}=0.021$ μM).[43] The ability of NVP-BEZ235 (**4**) to block both the HRR and NHEJ DSB repair pathways through simultaneous inhibition of both ATM and DNAPK has been shown to result in the radiosensitization of a number of cancer cells; however, its clinical development appears to have been halted.[44,45]

Whilst the identification of pan PI3K/PIKK inhibitors has undoubtedly advanced the biological understanding of these important targets, the development of selective agents has allowed researchers to further probe the biology of individual proteins (Fig. 2). KU-55933 (**5**) was one of the first potent and selective inhibitors of ATM to be reported and was developed following the extensive structure–activity relationship (SAR) studies performed on chemical scaffolds related to the pan-PI3K and pan-PIKK inhibitor LY294002 (**3**).[46] KU-55933 (**5**) is an ATP-competitive, potent inhibitor of ATM enzyme ($IC_{50}=0.013$ μM) with impressive selectivity over the closely related enzymes DNAPK ($IC_{50}=2.5$ μM), ATR ($IC_{50}>100$ μM), mTOR ($IC_{50}=9.3$ μM), and PI3K ($IC_{50}=16.6$ μM).[47] Whilst structural data for ATM is not currently available, docking simulations using homology models of ATM combined with observed SAR suggest that KU-55933 (**5**) binds to ATM in an analogous fashion to that observed for LY294002 (**3**) in PI3Kγ (i.e., the morpholine oxygen binding to the kinase hinge). KU-55933 (**5**) was shown to sensitize HeLa cells to the cytotoxic effects of topoisomerase I and II inhibitors and to IR; however, the utility of KU-55933 (**5**) in vivo has been limited by its poor physicochemical properties, in particular low aqueous solubility and low oral bioavailability. Optimization of KU-55933 (**5**) has resulted in the discovery of second generation ATM inhibitors, such as KU-60019 (**6**) and KU-59403 (**7**), in which polar substituents have been appended to tricyclic core resulting in moderately improved potency and aqueous solubility.[48,49] KU-60019 (**6**) and KU-59403 (**7**) are potent inhibitors of ATM enzyme ($IC_{50}=0.006$ μM and 0.003 μM, respectively) whilst retaining high selectivity over ATR, DNAPK, mTOR, and PI3K (>270-fold and >300-fold, respectively). Cellular potency was also improved with KU-60019 (**6**) and KU-59403 (**7**) giving effective chemosensitization at a concentrations of 3 μM and 1 μM, respectively, whereas concentrations of 10 μM were required to observe similar effects with KU-55933 (**5**). When dosed at 50 mg kg^{-1} i.p., KU-59403 (**7**) showed tumor concentrations considered above those required to deliver effective chemosensitization for 4 h. Whilst administration of KU-59403 (**7**) alone did not result in any significant antitumor efficacy, when dosed at either 12.5 or 25 mg kg^{-1} i.p. bis in die, twice daily (BID) for 5 days, in combination with etoposide, a dose-dependent increase in tumor growth delay was observed. A similar dosing schedule combining KU-59403 (**7**) with irinotecan has also been shown to be effective without any obvious unacceptable adverse effects on the animals (as measured by body weight loss). KU-60019 (**6**) has been reported to radiosensitize human glioma cells in vitro and significantly reduce migration, invasion, and growth.[50] Glioblastoma multiforme (GBM) is the most common and lethal primary brain tumor in adults where current treatment (surgery followed by fractionated radiotherapy and treatment with temozolomide) provides a median survival of just 12–15 months.[51] The poor survival is attributed to an intrinsic radioresistance and chemoresistance with around one third of GBM tumors containing p53 mutations

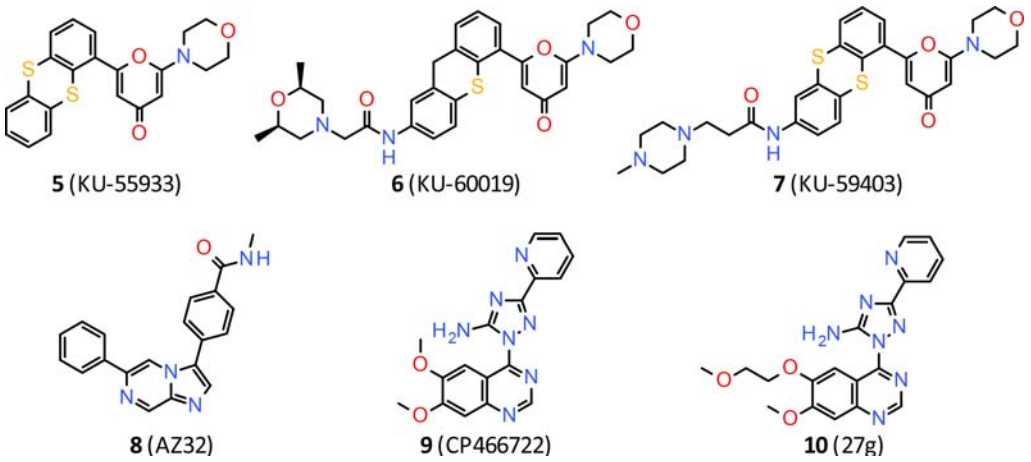

Fig. 2 Structures of selective ATM inhibitors in the public domain.

and ~80% harboring other cell-cycle checkpoint deficits. The clear unmet medical need for treating GBM combined with the potential for ATM inhibitors to radiosensitize GBM cells makes this an exciting opportunity to demonstrate the clinical benefit of small molecule ATM inhibition. KU-60019 (**6**) has low blood–brain barrier (BBB) penetration and therefore only low concentrations of compound are observed in brain tissue following systemic administration; however, when dosed intercranially (through the use of minipumps) and combined with radiation, KU-60019 (**6**) has shown a significant increase in the survival of mice bearing human orthotopic gliomas.[52] More recently, AstraZeneca has disclosed AZ32 (**8**), a specific inhibitor of ATM possessing good BBB penetration in mouse. AZ32 (**8**) is a potent inhibitor of ATM enzyme ($IC_{50} < 0.006$ μM) with moderate potency against ATM in cell ($IC_{50} = 0.31$ μM) and good selectivity over ATR (ATR cell $IC_{50} > 23$ μM) whilst also possessing high permeability in MDCK cell lines overexpressing MDR1 (P_{app} A–B $= 33.7 \times 10^{-6}$ cm s^{-1}, efflux ratio = 0.4).[53] Following an oral dose of 200 mg kg^{-1} in mice AZ32 (**8**) achieves free brain concentrations in excess of the cellular IC_{50} for approximately 22 h. When combined with IR, this dose of AZ32 (**8**) results in a significant increase in survival of mice bearing orthotopic gliomas. The quinazoline CP466722 (**9**) was identified following a screen of 1500 compounds from the Pfizer compound library and shown to be a moderately potent inhibitor of ATM in cells ($IC_{50} = 0.37$ μM). CP466722 (**9**) does show activity against a number of additional kinases including PI3K and PIKK enzymes (significant activity against 106 out of 451 kinases when tested at 3 μM); however, little activity against either ATR or DNAPK was observed in cells.[54] CP466722 (**9**) has low aqueous solubility (28 μM) and high clearance with a short half-life in mice (CL = 160 mL h^{-1}, $t_{1/2} = 1$ h) and was, therefore, unsuited for further in vivo assessment. Optimization of this scaffold identified 27 g (**10**) which although showing slightly reduced ATM potency ($IC_{50} = 1.2$ μM), displays increased selectivity when tested against a panel of diverse kinases (significant activity against 41 out of 451 kinases when tested at 3 μM), reduced propensity for oxidative metabolism and improved in vivo pharmacokinetics in mouse ($t_{1/2} = 19$ h).[55] Similar efficacy was observed for both CP466722 (**9**) and 27 g (**10**) when evaluated at 10 μM in a clonogenic assay in which MCF7 cells were treated with compound and irradiated with increasing doses of IR (0, 2, and 4 Gy).

Despite the emergence of small molecule inhibitors of ATM with encouraging selectivity profiles there remains a clear need to develop molecules with increased potency and selectivity combined with physiochemical and pharmacokinetic properties suitable for in vivo target validation. Such developments in compound activity and properties will be vital to provide compounds suitable for the clinical evaluation of ATM inhibition.

8.07.2 Discovery of Novel, Potent, and Selective ATM Inhibitors With Oral Bioavailability

A directed screen of approximately 15,000 compounds from the AstraZeneca compound collection was initiated to identify compounds with the ability to inhibit the phosphorylation of ATM on serine 1981 in HT29 cells following irradiation. Analysis of the data generated identified the quinoline carboxamide hit **11** (Fig. 3A) as a moderately potent inhibitor of ATM in cells ($IC_{50} = 0.82$ μM) but with selectivity for ATM over ATR, as measured by inhibition of pCHK1 in HT29 cells following treatment with 4-nitroquinoline 1-oxide ($IC_{50} = 4.4$ μM). Compound **11** was shown to be a potent inhibitor of ATM enzyme ($IC_{50} = 0.008$ μM) with moderate to good selectivity over closely related enzymes (>10-fold selective for ATM over DNAPK and PI3Kα and >100-fold selective over mTOR, PI3Kβ, and PI3Kγ).[56] Compound **11** also showed encouraging selectivity when assessed

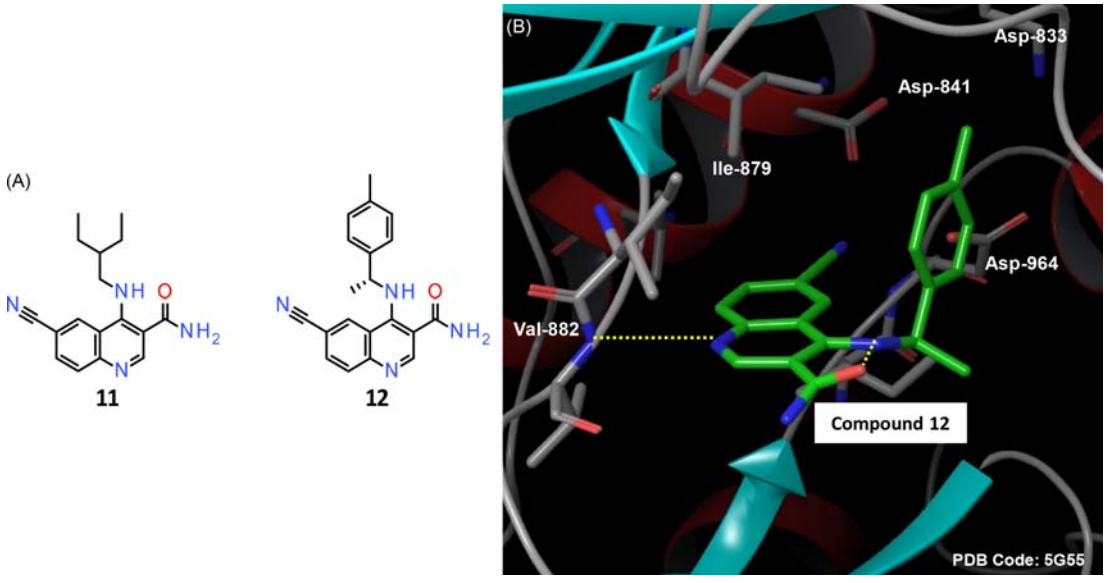

Fig. 3 (A) Structure of screening hit **11** and closely related PI3K inhibitor **12**. (B) X-ray structure of **12** bound into PI3Kγ (PDB code: 5G55).

against a diverse panel of kinases with only 8 of the 124 kinases tested showing >50% inhibition when tested at 1 μM. Despite the encouraging selectivity profile, the physicochemical properties of **11** were considered suboptimal with low aqueous solubility (19 μM), high intrinsic clearance (CL_{int}) in hepatocytes (rat $CL_{int}=74$ μL min^{-1} 10^6 $cells^{-1}$, human $CL_{int}=74$ μL min^{-1} 10^6 $cells^{-1}$), and activity against the hERG (human ether-a-go-go related gene) ion channel ($IC_{50}=2.3$ μM) all requiring optimization.[57,58] However, it was considered that the relatively high lipophilicity of this hit ($\log D_{7.4}=3.5$) may, in part, be responsible for these properties and, therefore, an optimization campaign was undertaken with the goal of increasing ATM cellular potency and selectivity whilst simultaneously optimizing physicochemical and pharmacokinetic parameters.

The use of X-ray crystal structure data to inform the optimization of small molecule kinase inhibitors is well documented but unfortunately no crystal structure of ATM exists; however, structural data is available for the closely related kinases PI3Kγ and mTOR.[59] Examination of existing near neighbors of **11** within the AstraZeneca collection highlighted compound **12** (Fig. 3A) a closely related compound with known activity against PI3K (PI3Kα enzyme $IC_{50}=0.0055$ μM). Structural data for **12** bound into the active site of PI3Kγ exists and, given the relatively high levels of homology between the ATP-binding sites of ATM and PI3K, it was felt that this data may be informative. Close inspection of the structure (Fig. 3B) shows the quinoline nitrogen forming a key interaction with the hinge region of the kinase as well as suggesting an opportunity to build out from both the C4 and C6 positions of this scaffold, thereby offering the potential to position substituents deeper into the binding pocket in an attempt to pick up additional constructive interactions with the protein surface. An internal hydrogen bonding interaction between the 4-amino substituent and the 3-carboxamide substituent can also be observed, presumably helping to organize the molecule in a bioactive conformation. Although **12** does not have appreciable activity against ATM in cells ($IC_{50}>30$ μM) we hypothesized that a similar binding mode may be adopted by **11** when bound into ATM and as such the optimization of both the 4-amino and 6-cyano susbstituents was prioritized.

SAR exploration quickly established that significant improvements in both ATM cellular potency and selectivity could be achieved by replacing the 6-cyano substituent with an aromatic group, in particular the 3-pyridyl isomer exemplified in **13** (Table 1). The positioning of the pyridine nitrogen appears key to maintain potency and selectivity with closely related analogs showing a significant reduction in both parameters; however, the lipophilic nature of **13** results in poor physicochemical properties, in particular, poor aqueous solubility and high turnover in hepatocyte incubations. Substitution on the pyridyl ring was tolerated when *para* to the quinoline core and it was appreciated that this might provide an opportunity to modulate lipophilicity through

Table 1 SAR for quinoline carboxamide scaffold

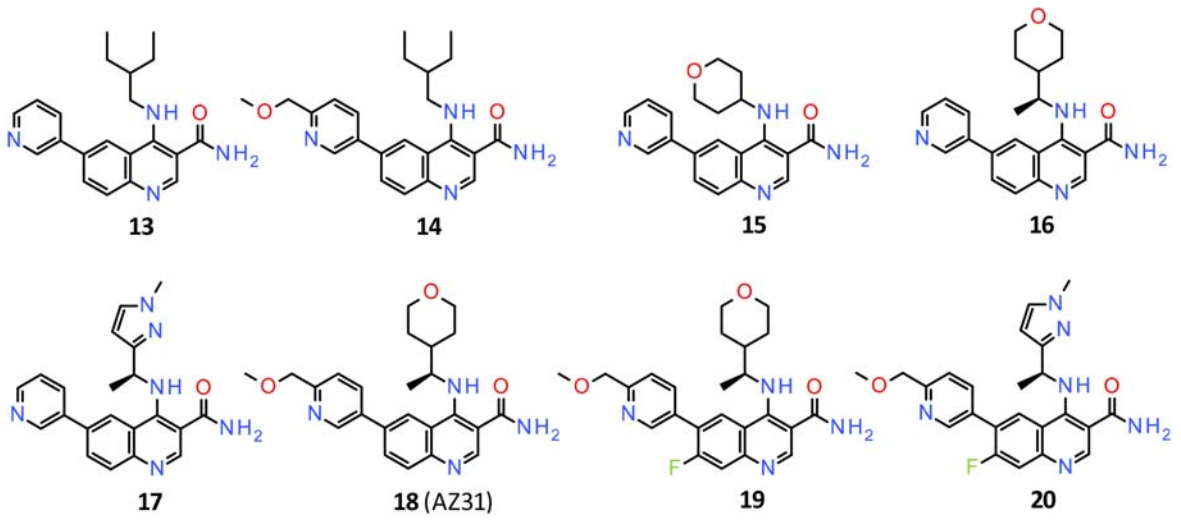

Entry	*ATM cell IC_{50} (μM)*	*ATR cell IC_{50} (μM)*	*log$D_{7.4}$*	*Solubility (μM)*	*Human/rat hep CL_{int} (μL min^{-1} 10^6 $cells^{-1}$)*	*hERG IC_{50} (μM)*	*LLE*
13	0.073	>11	4.0	4	43/140	0.67	3.1
14	0.045	>30	>4.3	3	<6.8/110	2.5	<3.0
15	0.95	3.1	1.9	>610	<4.2/8.5	2.1	4.1
16	0.17	>14	2.5	>1340	14/38	3.6	4.3
17	0.12	0.64	2.5	230	10/31	11	4.4
18 (AZ31)	0.046	>30	2.5	590	<2.6/<5.3	4.5	4.8
19	0.052	>30	2.8	18	<2.7/5.4	8.9	4.5
20	0.033	>19	2.7	69	<1.5/5.3	22	4.8

the introduction of small polar functionality. Unfortunately, those substituents that retained the desired potency and selectivity profile, such as the methoxymethyl substituent present in **14**, had little observed impact on the physicochemical properties or on hERG affinity, although some improvements in metabolic stability were observed.

In parallel with the optimization of the 6-substituent, high throughput chemistry approaches were utilized to vary the 4-amino substituent with the intent of reducing the lipophilicity of the molecule. Such a design strategy resulted in the identification of **15** which, although showing a slight reduction in potency and selectivity when compared to **13**, shows a highly significant reduction in lipophilicity ($\Delta \log D_{7.4} = 2.1$) (Table 1). The concept of lipophilic ligand efficiency (LLE) has been widely reported in the literature and is routinely used within the Medicinal Chemistry community as a measure of compound quality to limit the optimization of less productive lipophilicity-driven interactions between inhibitor and protein.[60,61] When comparing the LLE (ATM Cell pIC_{50}–$\log D_{7.4}$) of **13** and **15**, a clear improvement is observed. The reduced lipophilicity of **15** results in dramatically improved physicochemical properties (i.e., increased metabolic stability and improved aqueous solubility) thereby validating the design strategy. Interestingly, the reduction in lipophilicity appears to have little impact on hERG affinity suggesting that reducing lipophilicity per se will not be sufficient to remove this potential liability. A range of bespoke chiral amines with metabolically stable functionality and relatively low lipophilicity is available within AstraZeneca as a result of a forward-looking Strategic Reagent Initiative program and the incorporation of such amines into the quinoline carboxamide scaffold resulted in the identification of compounds such as **16** and **17**.[62] Whilst the incorporation of these specific chiral amines has resulted in a slight increase in lipophilicity compared to **15**, this is more than compensated by an increase in ATM potency thus resulting in an improved LLE. The impact of this increased lipophilicity on both solubility and metabolic stability has been relatively minor resulting in compounds with a more attractive balance of properties. Whilst there still appears to be little correlation between lipophilicity and hERG affinity in this series it is interesting to note that the chiral pyrazole containing amine incorporated into **17** does appear to reduce hERG activity. The chirality of these amines is important for the biological activity with the majority of the ATM potency appearing to reside in a single enantiomer; however, the exact stereochemistry of the preferred enantiomer was found to vary depending on the amine introduced. Docking simulations utilizing an homology model of ATM were unable to adequately rationalize this observation. The combination of SAR understanding from both the 4-amino and the 6-substituent resulted in the identification of compound **18**, a potent and selective ATM inhibitor with promising physicochemical properties although still possessing activity against hERG. Compound **18** was selected for further profiling and given the external identifier of AZ31.

AZ31 (**18**) is a potent inhibitor of ATM enzyme ($IC_{50} = < 0.0012$ μM) with excellent selectivity over closely related enzymes (>500-fold selective over DNAPK and PI3Kα and >1000-fold selective over mTOR, PI3Kβ, and PI3Kγ). When tested against a diverse range of kinase targets AZ31 (**18**) inhibited 0 out of 126 kinases by >50% when tested at 1 μM. Assessment of permeability using Caco2 cells showed AZ31 (**18**) to have reasonable permeability (P_{app} A–B $= 5.2 \times 10^{-6}$ cm s^{-1}) and in vivo pharmacokinetic evaluation showed the compound to have low to moderate clearance combined with reasonable bioavailability in both rat and dog (CL = 18 and 50 mL $min^{-1}kg^{-1}$, $F = 46\%$ and 31% in rat and dog, respectively). AZ31 (**18**) showed good exposure in mice with an oral dose of 100 mg kg^{-1} quaque, once a day (QD) of AZ31 (**18**) giving unbound plasma exposures in excess of the ATM cell IC_{50} for approximately 24 h. The efficacy of AZ31 (**18**) was assessed in HT29 tumor-bearing immunocompromised mice following oral administration at 100 mg kg^{-1} QD, in combination with IR (2 Gy delivered on each of days 1–5 of the study) (Fig. 4A). Whilst AZ31 (**18**) treatment alone gave no benefit and IR alone gave only a modest benefit, the combination of AZ31 (**18**) and IR produced a significant reduction of tumor growth highlighting the radiosensitizing effect of ATM inhibition in this in vivo model. The ability for AZ31 (**18**) to potentiate the effect of DNA DSB inducing chemotherapy was also assessed in an SW620 (colorectal cancer cell line) xenograft model. Significant reduction in tumor growth was observed following oral administration of AZ31 (**18**) at 100 mg kg^{-1} QD combined with irinotecan dosed at 50 mg kg^{-1} Q7D i.p. (Fig. 4B). Interestingly in this model the regrowth of tumors was observed following the cessation of treatment; however, a second round of combination treatment again drives tumor regression. No monotherapy effect was seen in this model for AZ31 (**18**) and monotherapy efficacy for irinotecan was modest.

Brief examination of the SAR at other positions around the quinoline core uncovered that the incorporation of a fluorine into the 7-position reduces hERG affinity whilst having only a minor reduction of ATM potency, exemplified by **19** (Table 1). However, solubility was reduced in this instance. Substituents larger than fluorine appeared to result in a much more significant reduction in ATM potency; however, combination of the 7-fluoro with the pyrazole containing 4-amino substituent gave rise to compounds such as **20** which are potent, selective ATM inhibitors with significantly reduced hERG affinity when compared with AZ31 (**18**). Substitution at either the 2- or 8-positions was not tolerated, which is consistent with such groups disrupting the hydrogen bond between the quinoline nitrogen and the hinge region of the kinase. Substitution at the 5-position also leads to a significant reduction in potency and it was postulated that this substitution pattern will interfere with the internal hydrogen bond formed between the 4-amino and 3-carboxamide motifs. The importance of this internal hydrogen bond was also supported by the observation that potency is significantly reduced, or completely removed, when replacing the 4-amino substituent with a 4-alkoxy substituent, or when removing the 3-carboxamide motif. These observations support the original hypothesis concerning the similar binding mode of the quinoline carboxamide scaffold in ATM and PI3K.

Compound **20** retains the excellent enzyme potency and selectivity observed for AZ31 (**18**) (**20**: ATM enzyme $IC_{50} = < 0.0006$ μM with >500-fold selectivity over DNAPK and PI3Kα and >1000-fold selective over mTOR, PI3Kβ, and PI3Kγ) with 3 out of 386 kinases inhibited by >50% when tested at 1 μM against a diverse panel of kinases. The permeability of **20** was good (Caco-2 P_{app} A–B $= 14 \times 10^{-6}$ cm s^{-1}) and reasonable in vivo pharmacokinetic profiles were observed in rat and dog (CL = 13 and 13 mL $min^{-1}kg^{-1}$, $F = 29\%$ and 71%, respectively). Good oral exposure in mouse was observed with a dose of 50 mg kg^{-1} BID of **20** giving unbound plasma exposures in excess of the ATM cell IC_{50} for approximately 24 h. The

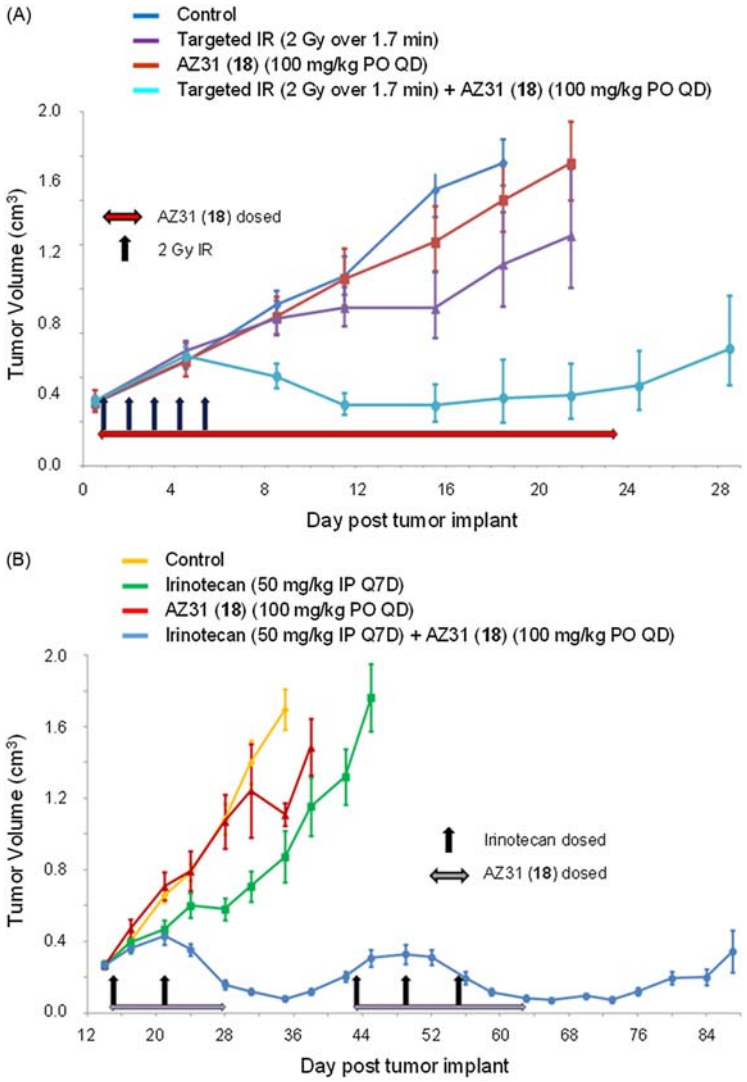

Fig. 4 (A) AZ31 (**18**) potentiates the efficacy of IR in an HT29 xenograft model. (B) AZ31 (**18**) potentiates the efficacy of irinotecan in an SW620 xenograft model.

efficacy of **20** was explored in SW620 tumor-bearing immunocompromised mice following oral administration at 50 mg kg^{-1} BID (dosed on days 2–4 of a weekly cycle) in combination with irinotecan dosed at 50 mg i.p. Q7D (Fig. 5). This combination schedule was tolerated and gave a significant tumor growth reduction following a 3-week regimen which was found to be statistically significant and greater than the reduction observed with irinotecan treatment alone and highlights that continuous inhibition of ATM is not required for efficacy in this model. This observation may allow the opportunity to further increase the therapeutic margin of an ATM inhibitor, combined with a DNA DSB inducing agent, in the clinic through the careful selection of an appropriate schedule.

8.07.3 The Importance of Predicting Dose to Man and Maximum Absorbable Dose

The failure of candidate drugs during clinical trials as a result of unsuitable drug metabolism and pharmacokinetic properties (DMPK) has been highlighted as one of the major reasons for attrition within the clinical development of new therapies and as a result significant attention is placed on these parameters during candidate optimization and final selection.[63–65] One of the key parameters to consider during candidate selection is the predicted dose required to achieve the clinical exposures necessary to elicit a desired biological response. Many methods of predicting clinical doses exist including the method described by McGinnity et al. which takes into account the human pharmacokinetic parameters of clearance and volume of distribution as well as protein binding, gut absorption, bioavailability, and dosing interval. This method has been validated using a number of marketed drugs

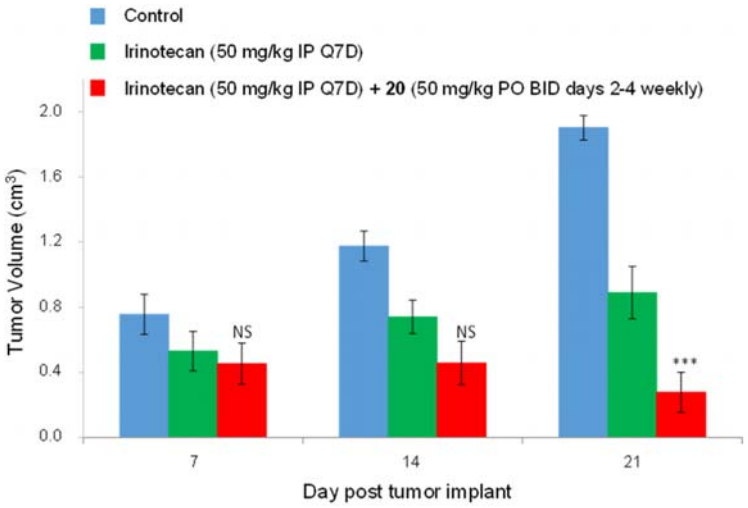

Fig. 5 Compound **20** potentiates the efficacy of irinotecan in an SW620 xenograft model.

and assumes that efficacy will be observed if unbound plasma concentrations exceed a defined threshold (defined by in vitro or in vivo measures of biological potency) for a defined period.[66] As a result many companies, including AstraZeneca, routinely use predicted clinical dose as an optimization parameter and to assist candidate selection.[67] In addition to identifying candidate drugs with low predicted clinical dose, it is important to understand the developability of the selected candidate. Oral administration remains the preferred route of administration for many new therapies due to ease of use for the intended patients, but poor absorption characteristics for an orally administered candidate will require significant investment in formulation approaches thus adding significant cost and time to the clinical development program; for such compounds the developability would be considered low. In extreme cases poor absorption characteristics may actually prevent the candidate from achieving sufficient clinical exposure to properly test the intended biological hypothesis. One of the parameters that has recently come to prominence when looking to assess the developability of a compound is the maximum absorbable dose (D_{abs}).[68–70] Values for D_{abs} can be predicted using computational simulation software such as GastroPlus from easily measured in vitro parameters, such as aqueous solubility and permeability, combined with knowledge of intestinal surface area and transit times. D_{abs} has been shown to correlate well with in vivo bioavailability for cases where solubility is moderate to good. For compounds with poor aqueous solubility it is important to assess solubility in media which better mimics the small intestinal lumen. In order to minimize the risk of being unable to test a biological hypothesis in the clinic and to simplify clinical development, where possible AstraZeneca has adopted the approach of selecting compounds with a low predicted clinical dose (<50 mg) and a significant margin between the predicted clinical dose and the D_{abs} ($D_{abs} > 10$ times the clinical dose).

Several methods exist for the prediction of human pharmacokinetics and subsequent predicted clinical efficacious dose including allometry-based methods and more complex physiologically based pharmacokinetic (PBPK) models.[71,72] The use of PBPK modeling for AZ31 (**18**) predicted relatively low clearance in human; however, the relatively modest volume of distribution predicted for this neutral compound resulted in only a modest predicted half-life ($\sim$6 h). This, when combined with other key parameters, predicted that a dose of 430 mg QD would be required to achieve a free plasma concentration in excess of the determined ATM IC_{50} for 24 h (thereby replicating the level and duration of target engagement observed at efficacious doses in the preclinical efficacy studies). It was also appreciated that these predicted parameters would result in relatively narrow margin for AZ31 (**18**) between predicted maximum concentration (C_{max}), when corrected for protein binding, and hERG affinity which could also introduce further risk during development. An analogous modeling approach suggests that despite a low predicted clearance for **20**, the low volume of distribution will result in a half-life of $\sim$4 h. This relatively short half-life means that a dose of either 700 mg QD or 88 mg BID would be required to deliver the duration and extent of target engagement believed necessary for clinical efficacy. Whilst successful candidates have progressed with higher clinical doses than these, the relatively low differential between the predicted doses and the predicted D_{abs} (AZ31 (**18**) $D_{abs} = 2000$ mg; **20** $D_{abs} = 530$ mg) was a cause of concern and highlighted the potential for further optimization to identify a candidate with lower predicted efficacious clinical dose and an increased margin between predicted dose and predicted D_{abs}. When considering the factors important in predicting both human pharmacokinetics and clinical doses it is important to realize that different parameters can have a greater or lesser impact; for example, whilst increasing potency (once corrected for protein binding changes) will always reduce dose predictions in a proportional manner, the increase of predicted half-life can have a much more profound influence (especially in those cases where the predicted half-life is significantly shorter than the required duration of biological target engagement). Compounds AZ31 (**18**) and **20** are predicted to have relatively short half-lifes in man and therefore, when considering opportunities to reduce the predicted clinical dose of these compounds, the optimization of human half-life was considered a promising strategy. The relatively low metabolic turnover of these compounds suggests that a strategy to increase the volume of distribution (V_{ss}) would constitute

a more profitable strategy for increasing predicted half-life than one of further reducing clearance. Many studies have been reported in an attempt to accurately describe the molecular properties that influence V_{ss} and one of the more dominant parameters is often ionization state, with acid compounds tending to show low V_{ss}, neutral compounds showing moderate values, and bases often showing significantly higher values.[73] Therefore, a strategy to incorporate basic substituents into an ATM inhibitor could be regarded as a sensible strategy to reduce human dose predictions.

8.07.4 The Discovery of AZD0156: A First in Class Potent, Selective and Orally Available ATM Inhibitor Suitable for Clinical Evaluation

8.07.4.1 Identification of a Scaffold With Increased Permeability

Thorough SAR exploration of both the 4- and 6-substituents of the quinoline carboxamide scaffold has resulted in a wealth of data to aid SAR understanding and a detailed retrospective analysis of the data highlighted the potential to incorporate a basic substituent in 6-position, exemplified by **21** (Fig. 6). Compound **21** is a highly potent inhibitor of ATM in cells ($IC_{50} = 0.0086$ μM) with excellent selectivity over ATR ($IC_{50} > 30$ μM) and provides evidence that a basic substituent in this region can provide a constructive interaction with the protein. However, despite the promising levels of potency and selectivity observed, the permeability of **21** was low and a significant efflux liability was observed (MDCK-MDR1 P_{app} A–B $= 0.8 \times 10^{-6}$ cm s^{-1}, efflux ratio = 28). Given the reasonably high lipophilicity of **21** ($\log D_{7.4} = 2.8$), the low permeability was presumed to be driven by a combination of the number of hydrogen bonding groups (in particular hydrogen bond donating groups) and the presence of a basic center. These data suggest that it would be a significant challenge to identify a basic compound from the quinoline carboxamide scaffold that would have the required permeability profile without increasing lipophilicity to a level likely to severely compromise aqueous solubility and metabolic stability (i.e., $\log D_{7.4} > 3$); therefore, it was considered essential that a new, inherently more permeable scaffold be found to facilitate continued optimization.

Examples in which aromatic rings have been removed from a template and replaced with a "pseudo-ring" system constrained by internal hydrogen bonding are well known and indeed this is a commonly used strategy when looking to "scaffold hop" to different templates or to reduce either the lipophilicity or aromatic content of a scaffold.[74] However, it was appreciated that the quinoline carboxamide scaffold already contains such a "pseudo-ring" between the 4-amino substituent and the 3-carboxamide substituent, and that the contribution of these motifs to the overall number of hydrogen bond donors is likely to contribute significantly to the relatively poor permeability of this scaffold. Therefore, we proposed a strategy in which the "pseudo-ring" is replaced by an appropriate covalently bonded cyclic system that would ensure the substituents are correctly positioned to maintain potency whilst simultaneously reducing the hydrogen bond donor count. A number of possible tricyclic systems with the potential to fulfill these desired criteria can be conceived but knowledge gained from the screening of existing internal equity suggested that the imidazo[5,4-c]quinolin-2-one scaffold, such as that present in **22**, was both synthetically tractable and known to have activity against related PIKK kinases (Fig. 6). Indeed, the dual PI3K/mTOR inhibitor NVP-BEZ235 (**4**), which is also known to be a potent inhibitor of a number of PIKK enzymes including ATM, contains this same imidazo[5,4-c]quinolin-2-one scaffold thus providing further evidence of the ability of this scaffold to inhibit ATM, whilst at the same time highlighting the challenge of achieving the required level of selectivity.

Comparison of quinoline carboxamide **15** with the analogous imidazo[5,4-c]quinolin-2-one **22** shows that ATM potency is broadly maintained (**15**: ATM cell $IC_{50} = 0.95$ μM, **22**: ATM cell $IC_{50} = 0.36$ μM); however, the selectivity of **22** against closely related kinases is significantly reduced and indeed **22** appears to have greater affinity for ATR than for ATM (**22**: ATR cell $IC_{50} = 0.087$ μM). Pleasingly, imidazo[5,4-c]quinolin-2-one **22** does show the anticipated increase in permeability, alongside a concomitant reduction in efflux, when compared to quinoline carboxamide analog **15** (**22**: MDCK-MDR1 P_{app} A–B $= 30 \times 10^{-6}$ cm s^{-1}, efflux ratio = 1.5, Caco2 P_{app} A–B $= 60 \times 10^{-6}$ cm s^{-1}, efflux ratio = 0.6; **15**: MDCK-MDR1 P_{app} A–B $= 4.8 \times 10^{-6}$ cm s^{-1}, efflux ratio = 10, Caco2 P_{app} A–B $= 15 \times 10^{-6}$ cm s^{-1}, efflux ratio = 4.5). This improved permeability is achieved with only a modest increase in lipophilicity ($\Delta \log D_{7.4} = 0.3$) thus supporting the hypothesis that the imidazo[5,4-c]quinolin-2-one is an inherently more permeable scaffold whilst also highlighting the key role that the number of hydrogen bond donors plays in limiting permeability for the quinoline carboxamide scaffold. Despite the subtle increase in lipophilicity, **22** retains good stability in hepatocyte incubations (rat $CL_{int} = 9.4$ μL min^{-1} 10^6 $cells^{-1}$, human $CL_{int} < 4.9$ μL min^{-1} 10^6 $cells^{-1}$), although aqueous solubility is reduced (12 μM) and some affinity for hERG is still apparent ($IC_{50} = 11$ μM).

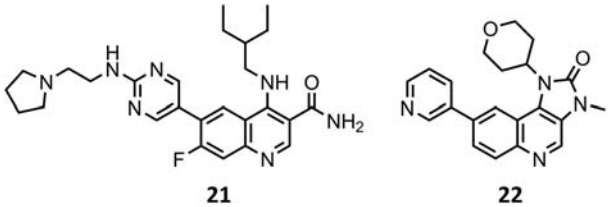

Fig. 6 Structures of **21** and **22**.

Table 2 SAR for the imidazo[5,4-c]quinolin-2-one scaffold

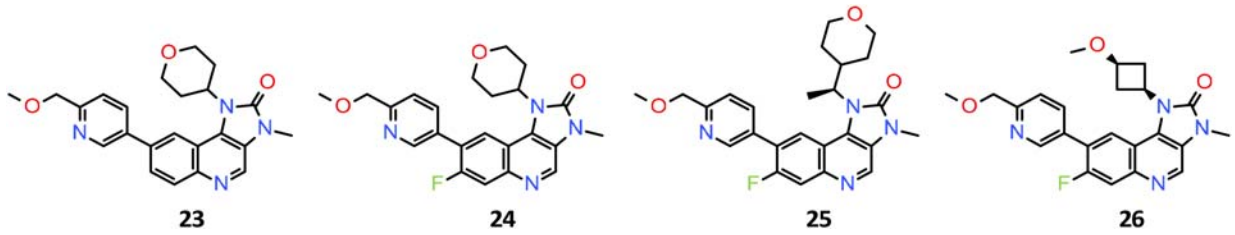

Entry	ATM cell IC_{50} (μM)	ATR cell IC_{50} (μM)	log$D_{7.4}$	Solubility (μM)	Human/rat hep CL_{int} ($\mu L\ min^{-1}\ 10^6\ cells^{-1}$)	hERG IC_{50} (μM)	MDCK P_{app} A–B (10^{-6} cm s^{-1})/efflux ratio	LLE
23	0.372	>12.9	2.3	19	<3/63	>33	31.8/1.4	4.1
24	0.447	>20	2.4	99	<4/7.5	27	42.5/0.8	3.9
25	0.488	>30	2.7	>1000	22/1.6	15	27.3/0.8	3.6
26	0.104	>30	2.7	37	8.8/4.5	9.0	37.8/0.4	4.3

8.07.4.2 Achieving ATM Selectivity With Imidazo[5,4-c]quinolin-2-one Based Compounds

Initial SAR exploration of this new scaffold highlighted a high degree of similarity between the 8-position of the imidazo[5,4-c]quinolin-2-one core and the analogous 6-position in the quinoline carboxamide scaffold. This observation is exemplified by **23** in which the introduction of the methoxymethyl substituted pyridine motif in the 8-position has both improved ATM potency and importantly reestablished a high level of selectivity for ATM over ATR (Table 2). Compound **23** remains stable in human hepatocyte incubations and continues to show high levels of permeability and low levels of efflux. The aqueous solubility of **23** remains low. The incorporation of a fluorine in the 7-position of the imidazo[5,4-c]quinolin-2-one scaffold, **24**, again highlights similarity in the SAR between this scaffold and the quinoline carboxamides with a slight reduction in potency observed but, in this instance, an improvement in aqueous solubility. However, divergent SAR was observed when comparing the 4-amino substituent of the quinoline carboxamide scaffold with the analogous 1-position of the imidazo[5,4-c]quinolin-2-one core. The introduction of previously optimized chiral substituents into the imidazo[5,4-c]quinolin-2-one scaffold, exemplified by **25**, failed to deliver the anticipated improvement in potency and a reduction in LLE was observed. Following a detailed exploration of this position it was found that small cyclic alkyl groups, such as the methoxycyclobutyl motif in **26**, are amongst the most favored substituents. Compound **26** showed good pharmacokinetic properties in rat with good bioavailability (>100%) and low to moderate clearance (22.5 mL min^{-1} kg^{-1}); however, as anticipated for a neutral compound the V_{ss} was relatively low (0.98 L kg^{-1}) and therefore resulted in a modest half-life (2.7 h). Compound **26** provides a relatively potent and highly selective start point with excellent permeability from which to explore the introduction of basic substituents intended to increase pharmacokinetic half-life through the modulation of V_{ss}.

8.07.4.3 Optimization of Basic Imidazo[5,4-c]quinolin-2-ones

Combining the newly acquired SAR understanding of the imidazo[5,4-c]quinolin-2-one scaffold with the detailed understanding of the quinoline carboxamide SAR resulted in the design of compound **27** containing a basic chain similar to that contained in **21**. Compound **27** shows a significant increase in ATM potency again suggesting that a basic center in this region is able to form a constructive interaction with the protein; furthermore, **27** displays excellent levels of selectivity for ATM over ATR (Table 3). The incorporation of a polar, ionizable group results in a large reduction in log $D_{7.4}$ and a dramatic increase in aqueous solubility but has a negative impact on permeability. However, the inherently more permeable nature of the imidazo[5,4-c]quinolin-2-one scaffold means that despite this impact the permeability of **27** remains moderate. Compound **27** is stable in hepatocyte incubations and has only modest activity against the hERG ion channel. The reduced lipophilicity of **27**, combined with the increased ATM potency, results in a clear improvement in compound quality (as measured by LLE). The influence of hydrogen bond donors on permeability has already been established and so a further improvement in permeability was sought through the removal of the NH linking the basic chain to the core. A range of different linkers were investigated with the replacement of the NH by oxygen (exemplified by **28**) found to be well tolerated and give a significant improvement in permeability. Although the LLE for **28** is considerably lower than that for **27** the overall balance of properties was considered advantageous. Further exploration of oxygen linked basic chains highlighted the importance of the linker length with the three carbon chain present in **29** proving optimal; in addition, the reduced hERG activity and high aqueous solubility of basic compounds such as **29** negates any benefit offered by the incorporation of the 7-fluoro substituent thus allowing its removal and thereby providing an additional increase in ATM potency. Compound **29** is an extremely potent and selective inhibitor of ATM with good solubility, moderate turnover in human

Table 3 SAR of imidazo[5,4-c]quinolin-2-one compounds containing basic substituents

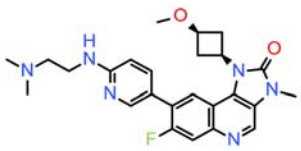

27

28

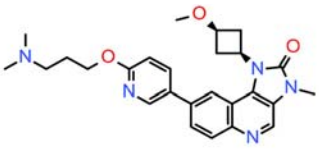

29

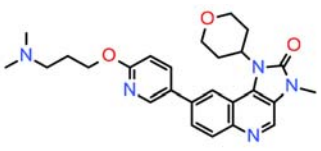

30 (AZD0156)

Entry	*ATM cell IC_{50} (μM)*	*ATR cell IC_{50} (μM)*	*log$D_{7.4}$*	*Solubility (μM)*	*Human/rat hep CL_{int} ($\mu L\ min^{-1}\ 10^6\ cells^{-1}$)*	*hERG IC_{50} (μM)*	*MDCK P_{app} A–B (10^{-6} cm s^{-1})/efflux ratio*	*LLE*
27	0.006	>30	1.7	>1000	2.8/9.6	24	3.4/11	6.5
28	0.023	>30	2.0	>1000	8.3/12	>33	16/1.6	5.6
29	0.00025	>30	1.6	540	8.7/5.1	>33	7.8/3.0	8.0
30 (AZD0156)	0.00058	6.2	1.4	>800	3.3/5.7	>33	6.6/5.1	7.9

hepatocytes, and moderate to good permeability. Pharmacokinetic evaluation of **29** in rat showed low to moderate clearance (19.5 mL $min^{-1}kg^{-1}$) and good bioavailability (50%). Pleasingly, the basic nature of **29** had the desired impact by increasing V_{ss} (5.7 L kg^{-1}) and therefore gave an increased half-life (~5 h). The higher V_{ss} predicted for **29** in man offsets the predicted moderate to high predicted clearance resulting in a predicted half-life of ~15 h. The longer predicted half-life of **29**, combined with the much improved potency means that the predicted clinically efficacious dose is now extremely low (<10 mg) with a large margin to the predicted D_{abs} (>3000 mg). This dramatic reduction of predicted dose and large differential between predicted dose and D_{abs} means that compounds such as **29** can be considered to carry a significantly reduced risk, when compared to compounds such as AZ31 (**18**) or **20**, if progressed to the clinic. Significant exploration of the basic substituent highlighted the ability to replace the dimethylamino motif with other simple bases, such as azetidine, pyrrolidine, and piperidine; however, closely related bases such as morpholine were largely inactive highlighting the restricted nature of the SAR in this position.

In the quinoline carboxamide series the SAR for different regions of the molecule was found to be broadly additive, to establish if the same might be true in the imidazo[5,4-c]quinolin-2-one scaffold a number of compounds were designed which combined preferred groups identified in different regions. These studies showed the SAR to again be broadly additive in nature thereby helping inform future design and resulted in the identification of a number of potent and selective molecules with encouraging physicochemical properties. Amongst these compounds, **30** was identified as a subnanomolar inhibitor of ATM in cells, with >10,000-fold selectivity over ATR, good solubility, and low turnover in human hepatocytes. Compound **30** was considered to possess an extremely attractive balance of properties and was consequently selected for further profiling and given the internal/external identifier AZD0156.[75]

8.07.4.4 Profile of AZD0156

AZD0156 (**30**) is an exceptionally potent inhibitor of ATM with excellent selectivity over closely related targets in both enzyme and cell based assays (Table 4). When screened at 1 μM against a panel of 397 kinases AZD0156 (**30**) showed excellent general kinome selectivity with activity above 65% inhibition observed for only 5 kinases (HASPIN: 67%; JAK1(JH2domain-pseudokinase): 67%; LRRK2: 87%; mTOR: 93%; PIK4CB: 70%). A stable crystalline form of AZD0156 (**30**) was identified and shown to have good aqueous solubility. AZD0156 (**30**) has high levels of unbound drug in rat, dog, and human plasma, is permeable with good pharmacokinetics in both rat and dog, and does not inhibit any of the five major isoforms of human cytochrome p450 at the

Table 4 Potency and selectivity data for AZD0156 (**30**)

Target	*Enzyme IC_{50} (μM)*	*Cell IC_{50} (μM)*
ATM	0.00004[a]	0.00058
ATR	–	6.2
DNAPK	0.14	–
mTOR	0.20	0.61
PI3Kα	0.32	1.4
PI3Kβ	1.8	–
PI3Kγ	1.1	–
PI3Kδ	0.27	–

[a]IC_{50} value corrected for tight binding.

Table 5 Physicochemical and pharmacokinetic properties of AZD0156 (**30**)

	*AZD0156 (**30**)*
Crystalline solubility	$>800\ \mu M$
% free (rat, dog, human)	11.4%, 40.9%, 29.0%
MDCK P_{app} A–B/efflux ratio	6.6×10^{-6} cm s^{-1}/5.1
Caco2 P_{app} A-B/efflux ratio	5.6×10^{-6} cm s^{-1}/8.5
Hepatocyte CL_{int} (rat, dog, human)	3.3, 3.3, 5.7, $\mu L\ min^{-1}\ 10^6\ cells^{-1}$
Rat PK (CL, V_{ss}, F)	15.5 mL $min^{-1} kg^{-1}$, 4.3 L kg^{-1}, 57%
Dog PK (CL, V_{ss}, F)	33.3 mL $min^{-1} kg$, 17.6 L kg^{-1}, 54%
CYP inhibition (3A4, 2D6, 2C9, 1A2, 2C19)	$IC_{50}>30\ \mu M$

concentrations tested (Table 5). Detailed in vitro metabolite identification studies have suggested that the major route of metabolism in man will be FMO mediated *N*-oxidation of the basic dimethylamino moiety. Independent synthesis of this *N*-oxide has allowed detailed profiling and shown it to be a potent and selective ATM inhibitor (ATM cell $IC_{50}=0.005\ \mu M$, ATR cell $IC_{50}=10\ \mu M$), albeit significantly less potent that AZD0156 (**30**). Whilst the potential for this metabolite to contribute to efficacy is appreciated, metabolic conversion of AZD0156 (**30**) to the *N*-oxide in hepatocyte incubations is relatively low ($\leq 10\%$ in rat, dog, and human hepatocytes), and only low levels were detected in rat and dog in in vivo studies ($<10\%$ of parent by AUC).

The ability of AZD0156 (**30**) to potentiate the efficacy of DNA DSB inducing agents was assessed in vitro by combining with either SN-38 (the active agent of the topoisomerase I inhibitor irinotecan) or olaparib (a PARP inhibitor which indirectly induces DNA DSBs by trapping PARP on DNA).[76] In SW620 cells the IC_{50} for SN-38 is reduced when combined with AZD0156 (**30**) (Fig. 7A) thereby showing that AZD0156 (**30**) can potentiate the efficacy of SN-38. A similar effect was observed on the IC_{50} of olaparib when combined with AZD0156 (**30**) in FaDu cells (Fig. 7B) demonstrating that AZD0156 (**30**) can potentiate the efficacy of olaparib. AZD0156 (**30**) shows good exposure in mice thereby allowing the in vivo assessment of ATM inhibition in mouse xenograft models. When combined with irinotecan dosed at 50 mg kg^{-1} i.p. Q7D, AZD0156 (**30**) dosed orally at 20 mg kg^{-1} QD (on days 2–4 of a weekly cycle) showed clear synergy and caused tumor regression in an SW620 xenograft model in immunocompromised mice (Fig. 8A). No appreciable efficacy was observed in this model when AZD0156 (**30**) was dosed as a monotherapy. The addition of AZD0156 (**30**), dosed orally at 5 mg kg^{-1} QD (on days 1–3 of a weekly cycle), to olaparib, dosed orally at

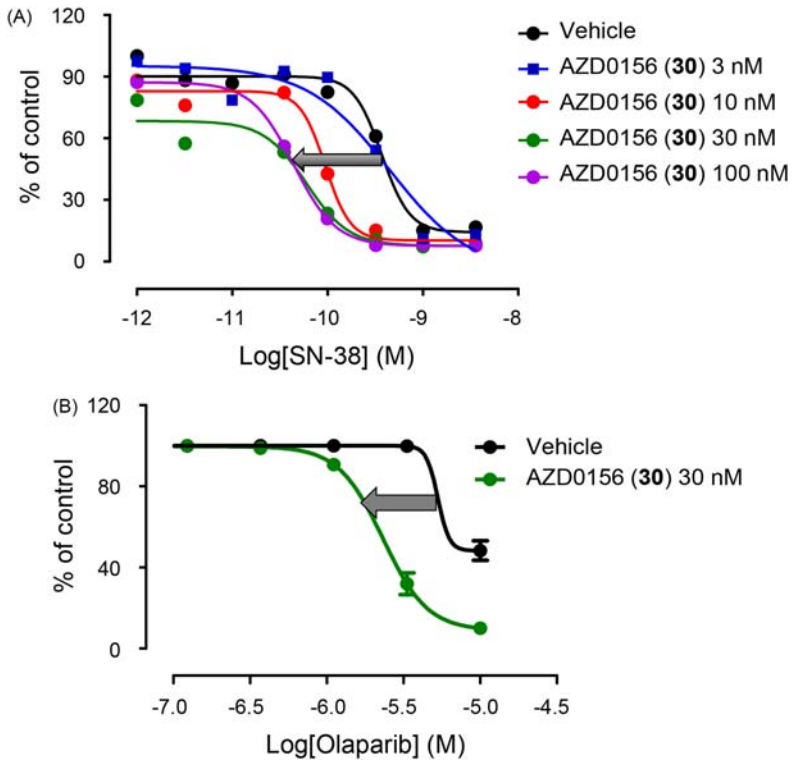

Fig. 7 (A) AZD0156 (**30**) potentiates the in vitro efficacy of SN-38 (IC_{50} shift on addition of AZD0156 (**30**) highlighted by *gray arrow*). (B) AZD0156 (**30**) potentiates the in vitro efficacy of olaparib (IC_{50} shift on addition of AZD0156 (**30**) highlighted by *gray arrow*).

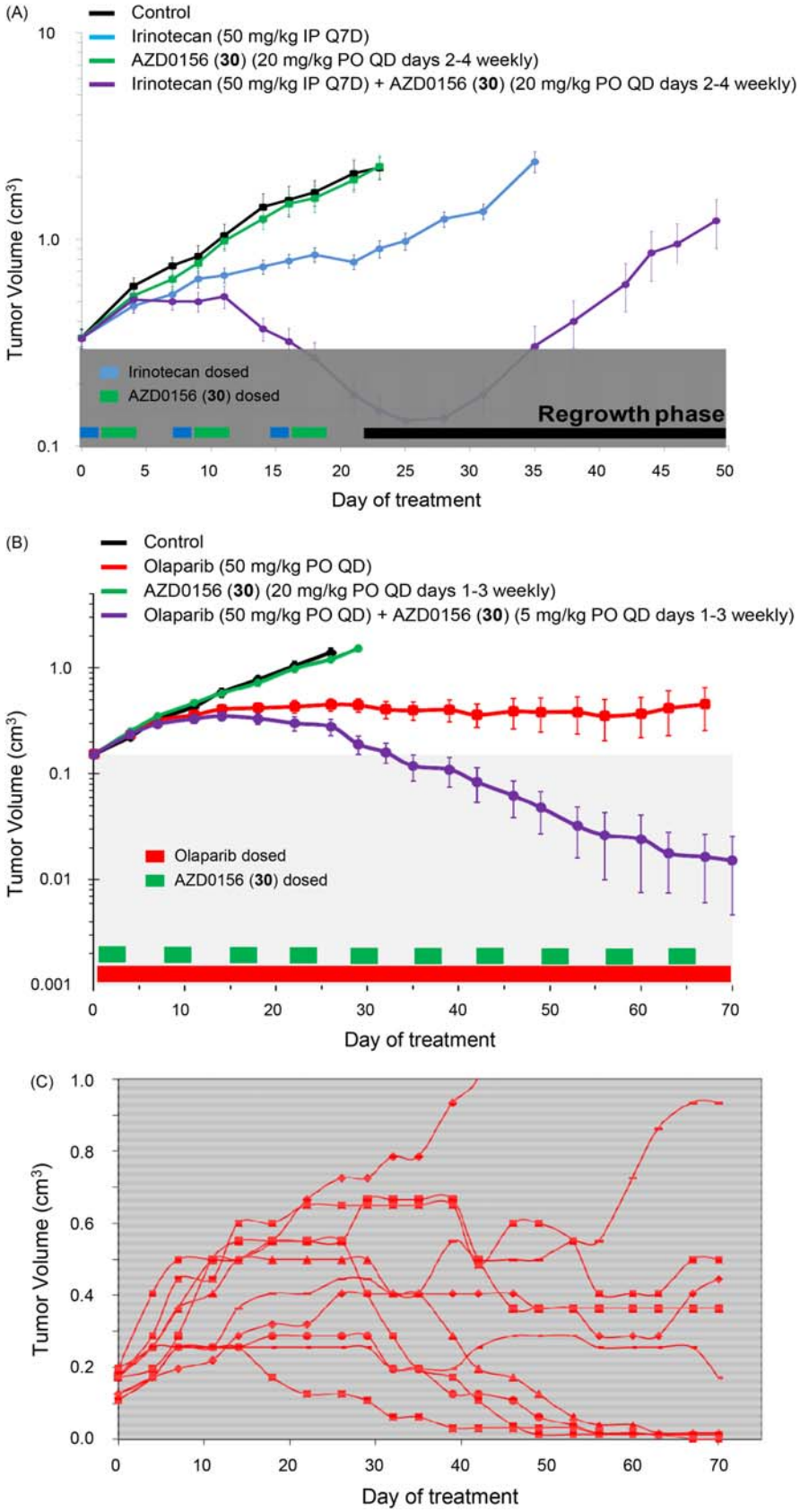

Fig. 8 (A) AZD0156 (**30**) potentiates the efficacy of irinotecan in an SW620 xenograft model. (B) AZD0156 (**30**) potentiates the efficacy of olaparib in a HBCx-10 patient derived tumor xenograft model. (C) 4 out of 10 mice show tumor regressions in a HBCx-10 patient derived tumor xenograft model following treatment with olaparib (50 mg kg^{-1} PO QD). (D) 9 out of 10 mice show tumor regressions in a HBCx-10 patient derived tumor xenograft model following treatment with olaparib (50 mg kg^{-1} PO QD) and AZD0156 (**30**) (5 mg kg^{-1} PO QD days 1–3 weekly).

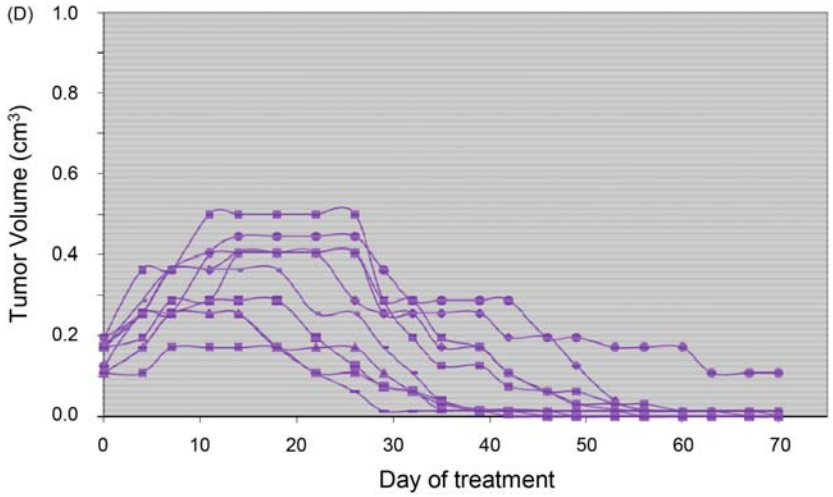

Fig. 8 (*continued*).

50 mg kg^{-1} QD, also resulted in clear synergy and tumor regression when examined in immunocompromised mice bearing HBCx-10 patient derived tumors (Fig. 8B). HBCx-10 is a ductal adenocarcinoma with mutated Brca2, mutated TP53, no HER2 overexpression and no PR/ERα overexpression (i.e., it is triple-negative) which is sensitive to monotherapy treatment with olaparib when used as a mouse xenograft model.[77] The impact of the combination is arguably more apparent when examining the tumor growth in individual animals from the study. For mice treated with olaparib alone a range of effects were observed with 4 out of 10 mice showing tumor regression (Fig. 8C). However, 9 out of 10 mice treated with a combination of AZD0156 (**30**) and olaparib showed tumor regression clearly highlighting the ability of ATM inhibition to sensitize tumors to olaparib treatment (Fig. 8D).

PBPK based modeling suggests that AZD0156 (**30**) is likely to have a half-life of ~10 h in man and is predicted to give good oral bioavailability. Early estimates of the efficacious clinical dose, based on achieving unbound concentrations in excess of the cellular ATM IC_{50} for 24 h, are low (<10 mg) and show an excellent margin to the predicted D_{abs} (>4000 mg), thereby suggesting that AZD0156 (**30**) has a relatively low risk of being unable to achieve concentrations in the clinic suitable to test the biological hypothesis. Toxicological evaluation of AZD0156 (**30**) in both rats and dogs supported progression to the clinic and AZD0156 (**30**) is currently being evaluated in a Phase I clinical trial in combination with olaparib.

8.07.5 Conclusion

Targeting the DDR of cancer cells provides an exciting opportunity to treat cancer by exploiting the inherent differences between cancerous and normal cells. As a key regulator of the response and repair of cytotoxic DNA DSBs, ATM provides an attractive pharmacological target. Previous disclosed ATM inhibitors have hinted at the potential for ATM inhibition to enhance the efficacy of both radiotherapy and DSB-inducing chemotherapies but limitations in either their potency, selectivity, or pharmacokinetic properties have restricted their utility. A focused screen of compounds in the AstraZeneca compound collection, followed by an iterative optimization campaign, resulted in the identification of novel, potent, selective, and orally available ATM inhibitors such as AZ31 (**18**) and **20**. Such compounds have played an important role in helping to validate the potential of ATM inhibition to potentiate both IR and chemotherapy in disease relevant in vivo models. Candidate selection strategies focused on identifying compounds with a low predicted clinically efficacious dose and high developability, highlighted opportunities to further improve compound profiles to reduce DMPK risks. In particular, the potential to increase pharmacokinetic half-life, thereby significantly reducing clinical dose, was appreciated and a strategy of increasing V_{ss} was adopted. To allow the successful optimization of V_{ss} a more permeable scaffold was required and knowledge of the likely bioactive conformation, alongside an understanding of the molecular properties contributing to permeability, resulted in the discovery of potent and selective compounds from an imidazo[5,4-c]quinolin-2-one scaffold. Introduction of basic substituents to this permeable scaffold led to further improvements in potency and pharmacokinetic properties resulting in compounds with low predicted dose and high predicted developability. The discovery of AZD0156 (**30**), an extremely potent and selective ATM inhibitor with good physicochemical properties and preclinical pharmacokinetics, has allowed more detailed in vivo target validation and has now entered clinical trials.

One of the key challenges facing the successful clinical development of ATM inhibitors will be to understand how best to combine with the variety of DSB inducing agents, and which patients will respond best to such combinations. As the use of AZD0156 (**30**) further develops our understanding of the biology and potential of ATM inhibition additional opportunities for

rational combinations, or even for monotherapy treatment, may well emerge.[78] The potential for ATM inhibition to combine with radiotherapy is also an area of active research and the importance of the BBB in the potential to treat patients with brain tumors (such as GBM) will need to be established to ensure that clinical agents with suitable profiles can be developed. The biology of ATM is known to include its activation by ROS and the emergence of high-quality ATM inhibitors will allow more detailed investigations into these areas and may uncover the potential for ATM inhibition outside of cancer therapies. For example, recent publications suggest that ATM inhibition may have therapeutic potential in Huntingdon's disease.[79]

The identification and subsequent clinical development of AZD0156 (**30**) will provide a significant step forward in the understanding of targeting both ATM and the DDR in general and has the potential to provide a therapy that will make a significant improvement in the life of patients.

Acknowledgments

The author would like to acknowledge the contributions of all the members of the project team responsible for the discovery and profiling of AZD0156 (**30**) and in particular the contributions of Bernard Barlaam, Nicola Colclough, Elaine Cadogan, Richard Ducray, Giles Ouvry, Philip MacFaul, Gareth Hughes, Phil Jewsbury, and Martin Pass.

References

1. Jackson, S. P.; Bartek, J. The DNA Damage Response in Human Biology and Disease. *Nature* **2009,** *461,* 1071–1078.
2. Ciccia, A.; Elledge, S. J. The DNA Damage Response: Making It Safe to Play With Knives. *Mol. Cell* **2010,** *40,* 179–204.
3. Hoeijmakers, J. H. Genome Maintenance Mechanisms for Preventing Cancer. *Nature* **2001,** *411,* 366–374.
4. Caldecott, K. W. DNA Single-Strand Break Repair. *Exp. Cell Res.* **2014,** *329,* 2–8.
5. Shibata, A.; Jeggo, P. A. DNA Double-Strand Break Repair in a Cellular Context. *Clin. Oncol.* **2014,** *26,* 243–249.
6. Radhakrishnan, S. K.; Jette, N.; Lees-Miller, S. P. Non-Homologous End Joining: Emerging Themes and Unanswered Questions. *DNA Repair (Amst.)* **2014,** *17,* 2–8.
7. Hoeijmakers, J. H. DNA Damage, Aging and Cancer. *N. Engl. J. Med.* **2009,** *361,* 1475–1485.
8. Jiricny, J. The Multifaceted Mismatch-Repair System. *Nat. Rev. Mol. Cell Biol.* **2006,** *7,* 335–346.
9. O'Connor, M. J. Targeting the DNA Damage Response. *Mol. Cell Rev.* **2016,** *60,* 547–560.
10. Macheret, M.; Halazonetis, T. D. DNA Replication Stress as a Hallmark of Cancer. *Annu. Rev. Pathol.* **2015,** *10,* 425–448.
11. Sabharwal, S. S.; Schumacker, P. T. Mitochondrial ROS in Cancer: Initiators, Amplifiers or an Achilles' Heel. *Nat. Rev. Cancer* **2014,** *14,* 709–721.
12. Fruman, D. A.; Meyers, R. E.; Cantley, L. C. Phosphoinositide Kinases. *Annu. Rev. Biochem.* **1998,** 481–507.
13. Abraham, R. T. Cell Cycle Checkpoint Signaling Through the ATM and ATR Kinases. *Genes Dev.* **2001,** *15,* 2177–2196.
14. Shiloh, Y. ATM and Related Protein Kinases: Safeguarding Genome Integrity. *Nat. Rev. Cancer* **2003,** *3,* 155–168.
15. Shiloh, Y. Ataxia-Telangiectasia and the Nijmegen Breakage Syndrome: Related Disorders but Genes Apart. *Annu. Rev. Genet.* **1997,** *31,* 635–662.
16. Andrs, M.; Korabecny, J.; Nepovimova, E.; Jun, D.; Hodny, Z.; Moravcova, S.; Hanzlikova, H.; Kuca, K. The Development of Ataxia Telandiectasia Mutated Kinase Inhibitors. *Mini Rev. Med. Chem.* **2014,** *14,* 805–811.
17. Lee, J. H.; Paull, T. T. ATM Activation by DNA Double-Strand Breaks Through the Mre11-Rad50-Nbs1 Complex. *Science* **2005,** *308* (5721), 551–554.
18. Bakkenist, C. J.; Kastan, M. B. DNA Damage Activates ATM Through Intermolecular Autophosphorylation and Dimer Dissociation. *Nature* **2003,** *421,* 499–506.
19. Burma, S.; Chen, B. P.; Murphy, M.; Kurimasa, A.; Chen, D. J. ATM Phosphorylates Histone H2AX in Response to DNA Double-Strand Breaks. *J. Biol. Chem.* **2001,** *276* (45), 42462–42467.
20. Scully, R.; Xie, A. Double Strand Break Repair Functions of Histone H2AX. *Mutat. Res.* **2013,** *750* (1–2), 5–14.
21. Banin, S.; Moyal, I.; Shieh, S.-Y.; Taya, Y.; Anderson, C. W.; Chessa, L.; Smorodinsky, N. I.; Prives, C.; Reiss, Y.; Shiloh, Y.; Ziv, Y. Enhanced Phosphorylation of p53 by ATM in Response to DNA Damage. *Science* **1998,** *281* (5383), 1674–1677.
22. Matsuoka, S.; Huang, M.; Elledge, S. J. Linkage of ATM to Cell Cycle Regulation by the Chk2 Protein Kinase. *Science* **1998,** *282* (5395), 1893–1896.
23. Marine, J.-C.; Lozano, G. Mdm2-Mediated Ubiquitylation: p53 and Beyond. *Cell Death Differ.* **2010,** *17* (1), 93–102.
24. Sullivan, K. D.; Gallant-Behm, C. L.; Henry, R. E.; Fraikin, J. L.; Espinosa, J. M. The p53 Circuit Board. *Biochim. Biophys. Acta* **2012,** *1825* (2), 229–244.
25. Falck, J.; Mailand, N.; Syljuasen, R. G.; Bartek, J.; Lukas, J. The ATM-Chk2-Cdc25A Checkpoint Pathway Guards Against Radioresistant DNA Synthesis. *Nature* **2001,** *410* (6830), 842–847.
26. Bennetzen, M. V.; Larsen, D. H.; Bunkenborg, J.; Bartek, J.; Lukas, J.; Anderson, J. S. Site-Specific Phosphorylation Dynamics of the Nuclear Proteome During the DNA Damage Response. *Mol. Cell. Proteomics* **2010,** *9* (6), 1314–1323.
27. Kastan, M. Ataxia-Telangiectasia-Broad Implications for a Rare Disorder. *N. Engl. J. Med.* **1995,** *333,* 622–663.
28. Moding, E. J.; Kastan, M. B.; Kirsch, D. G. Strategies for Optimizing the Response of Cancer and Normal Tissues to Radiation. *Nat. Rev. Drug Discov.* **2013,** *12,* 526–542.
29. Cremona, C. A.; Behrens, A. ATM Signaling and Cancer. *Oncogene* **2014,** *33* (26), 3351–3360.
30. Barlow, C.; Hirostune, S.; Paylor, R.; Liyanage, M.; Eckhaus, M.; Collins, F.; Shiloh, Y.; Crawley, J. N.; Ried, T.; Tagle, D.; Wynshaw-Boris, A. Atm-deficient mice:a paradigm of ataxia telangiectasia. *Cell* **1996,** *86* (1), 159–171.
31. Guo, Z.; Kozlov, S.; Lavin, M. F.; Person, M. D.; Paull, T. T. ATM Activation by Oxidative Stress. *Science* **2010,** *330* (6003), 517–521.
32. Ditch, S.; Paull, T. T. The ATM Protein Kinase and Cellular Redox Signaling: Beyond the DNA Damage Response. *Trends Biochem. Sci.* **2012,** *37* (1), 15–22.
33. Sarkaria, J. N.; Eshleman, J. S. ATM as a Target for Novel Radiosensitizers. *Semin. Radiat. Oncol.* **2001,** *11,* 316–327.
34. Zhu, Y.; Hu, J.; Hu, Y.; Liu, W. Targeting DNA Repair Pathways: A Novel Approach to Reduce Cancer Therapeutic Resistance. *Cancer Treat. Rev.* **2009,** *35,* 590–596.
35. Kaelin, W. G., Jr. The Concept of Synthetic Lethality in the Context of Anticancer Therapy. *Nat. Rev. Cancer* **2005,** *5,* 689–698.
36. O'Connor, M. J.; Martin, N. M.; Smith, G. C. Targeted Cancer Therapies Based on the Inhibition of DNA Strand Break Repair. *Oncogene* **2007,** *26,* 7816–7824.
37. Vecchio, D.; Frosina, G. Targeting the Ataxia Telangiectasia Mutated Protein in Cancer Therapy. *Curr. Drug Targets* **2016,** *17,* 139–153.
38. Sarkaria, J. N.; Busby, E. C.; Tibbetts, R. S.; Kennedy, A. P.; Hill, D. E.; Abraham, R. T. Inhibition of Phosphoinositide 3-Kinase Related Kinases by the Radiosensitizing Agent Wortmannin. *Cancer Res.* **1998,** *58* (19), 4375–4382.

39. Sarkaria, J. N.; Busby, E. C.; Tibbetts, R. S.; Roos, P.; Taya, Y.; Karnitz, L. M.; Abraham, R. T. Inhibition of ATM and ATR Kinase Activities by the Radiosensitizing Agent, Caffeine. *Cancer Res.* **1999,** *59* (17), 4375–4382.
40. Vlahos, C. J.; Matter, W. F.; Hui, K. Y.; Brown, R. F. A Specific Inhibitor of Phosphatidylinositol 3-Kinase, 2-(4-Morpholinyl)-8-Phenyl-4H-1-Benzopyran-4-one. *J. Biol. Chem.* **1994,** *269,* 5241–5248.
41. Andrs, M.; Korabecny, J.; Jun, D.; Hodny, Z.; Bartek, J.; Kuca, K. Phosphatidylinositol 3-Kinase (PI3K) and Phosphatidylinositol 3-Kinase-Related Kinase (PIKK) Inhibitors: Importance of the Morpholine Ring. *J. Med. Chem.* **2015,** *58,* 41–71.
42. Walker, E. H.; Pacold, M. E.; Perisic, O.; Stephens, L.; Hawkins, P. T.; Wymann, M. P.; Williams, R. L. Structural Determinants of Phosphoinositide 3-Kinase Inhibition by Wortmannin, LY294002, Quercetin, Myricetin, and Staurosporine. *Mol. Cell* **2000,** *6,* 909–919.
43. Maria, S. M.; Stauffer, F.; Brueggen, J.; Furet, P.; Schnell, C.; Fritsch, C.; Brachmann, S.; Chene, P.; De Pover, A.; Schoemaker, K.; Fabbro, D.; Gabriel, D.; Simonen, M.; Murphy, L.; Finan, P.; Sellers, W.; García-Echeverría, C. Identification and Characterization of NVP-BEZ235, a New Orally Available Dual Phosphatidylinositol 3-Kinase/Mammailian Target of Rapamycin Inhibitor With Potent In Vivo Antitumor Activity. *Mol. Cancer Ther.* **2008,** *7* (7), 1851–1863.
44. Gil del Alcazar, C. R.; Hardebeck, M. C.; Mukherjee, B.; Tomimatsu, N.; Gao, X.; Yan, J.; Xie, X.-J.; Bachoo, R.; Li, L.; Habib, A. A.; Habib, S. B. Inhibition of DNA Double-Strand Break Repair by the Dual PI3K/mTOR Inhibitor NVP-BEZ235 as a Strategy for Radiosensitization of Glioblastoma. *Clin. Cancer Res.* **2014,** *20* (5), 1235–1248.
45. Mukherjee, B.; Tomimatsu, N.; Amancherla, K.; Camacho, C. V.; Pichamoorthy, N.; Burma, S. The Dual PI3K/mTOR Inhibitor NVP-BEZ235 Is a Potent Inhibitor of ATM- and DNA-PKcs-Mediated DNA Damage Responses. *Neoplasia* **2012,** *14,* 34–43.
46. Hollick, J. J.; Rigoreau, L. J. M.; Cano-Soumillac, C.; Cockcroft, X.; Curtin, N. J.; Frigerio, M.; Golding, B. T.; Guiard, S.; Hardcastle, I. R.; Hickson, I.; Hummersone, M. G.; Menear, K. A.; Martin, N. M. B.; Matthews, I.; Newell, D. R.; Ord, R.; Richardson, C. J.; Smith, G. C. M.; Griffin, R. J. Pyranone, Thiopyranone, and Pyridone Inhibitors of Phosphatidylinositol 3-Kinase Related Kinases. Structure-Activity Relationships for DNA-Dependent Protein Kinase Inhibition, and Identification of the First Potent and Selective Inhibitor of the Ataxia Telangiectasia Mutated Kinase. *J. Med. Chem.* **2007,** *50,* 1958–1972.
47. Hickson, I.; Zhao, Y.; Richardson, C. J.; Green, S. J.; Martin, N. M. B.; Orr, A. I.; Reaper, P. M.; Jackson, S. P.; Curtin, N. J.; Smith, G. C. M. Identification and Characterization of a Novel and Specific Inhibitor of the Ataxia-Telangiectasia Mutated Kinase ATM. *Cancer Res.* **2004,** *64,* 9152–9159.
48. Golding, S. E.; Rosenberg, E.; Valerie, N.; Hussaini, I.; Frigerio, M.; Cockcroft, X. F.; Chong, W. Y.; Hummersone, M.; Rigoreau, L.; Menear, K. A.; O'Connor, M. J.; Povirk, L. F.; van Meter, T.; Valerie, K. Improved ATM Kinase Inhibitor KU-60019 Radiosensitizes Glioma Cells, Compromises Insulin, AKT and ERK Prosurvival Signaling, and Inhibits Migration and Invasion. *Mol. Cancer Ther.* **2009,** *8* (10), 2894–2902.
49. Batey, M. A.; Zhao, Y.; Kyle, S.; Richardson, C.; Slade, A.; Martin, N. M.; Lau, A.; Newell, D. R.; Curtin, N. J. Preclinical Evaluation of a Novel ATM Inhibitor, KU-59403, In Vitro and In Vivo in p53 Functional and Dysfunctional Models of Human Cancer. *Mol. Cancer Ther.* **2013,** *12* (6), 959–967.
50. Golding, S. E.; Rosenberg, E.; Adams, B. R.; Wignarajah, S.; Beckta, J. M.; O'Connor, M. J.; Valerie, K. Dynamic Inhibition of ATM Kinase Provides a Strategy for Glioblastoma Multiforme Radiosensitization and Growth Control. *Cell Cycle* **2012,** *11* (6), 1167–1173.
51. Stupp, R.; Hegi, M. E.; Gilbert, M. R.; Chakravarti, A. Chemoradiotherapy in Malignant Glioma: Standard of Care and Future Directions. *J. Clin. Oncol.* **2007,** *25,* 4127–4136.
52. Biddlestone-Thorpe, L.; Sajjad, M.; Rosenberg, E.; Beckta, J. M.; Valerie, N. K. C.; Tokarz, M.; Adams, B. R.; Wagner, A. F.; Khalil, A.; Gilfor, D.; Golding, S. E.; Deb, S.; Temesi, D. G.; Lau, A.; O'Connor, M. J.; Choe, K. S.; Parada, L. F.; Lim, S. K.; Mukhopadhyay, N. D.; Valerie, K. ATM Kinase Inhibition Preferentially Sensitizes p53-Mutant Glioma to Ionizing Radiation. *Clin. Cancer Res.* **2013,** *19* (12), 3189–3200.
53. Karlin, J.; Allen, J.; Odedra, R.; Hughes, G.; Farrington, P.; Ducray, R.; Ouvry, G.; Degorce, S.; Wilson, J.; Smith, A.; Patel, B.; Thomason, A.; Vincent, J.; Colclough, N.; Ahmad, S. F.; Beckta, J. M.; Tokarz, M.; Mukhopadhyay, N. D.; Barlaam, B.; Pike, K. G.; Cadogan, E.; Pass, M.; Valerie, K.; Durant, S. Blood-Brain Barrier Penetrating ATM Inhibitor Radio-Sensitizes Intracranial Gliomas in Mice, AACR 2016 (abstract #3041).
54. Rainey, M. D.; Charlton, M. E.; Stanton, R. V.; Kastan, M. B. Transient Inhibition of ATM Kinase is Sufficient to Enhance Cellular Sensitivity to Ionizing Radiation. *Cancer Res.* **2008,** *68* (18), 7466–7474.
55. Min, J.; Guo, K.; Suryadevara, P. K.; Zhu, F.; Holbrook, G.; Chen, Y.; Feau, C.; Young, B. M.; Lemoff, A.; Connelly, M. C.; Kastan, M. B.; Guy, R. K. Optimization of a Novel Series of Ataxia-Telangiectasia Mutated Kinase Inhibitors as Potential Radiosensitizing Agents. *J. Med. Chem.* **2016,** *59,* 559–577.
56. Degorce, S. L.; Barlaam, B.; Cadogan, E.; Dishington, A.; Ducray, R.; Glossop, S. C.; Hassall, L. A.; Lach, F.; Lau, A.; McGuire, T. M.; Nowak, T.; Ouvry, G.; Pike, K. G.; Thomason, A. G. Discovery of Novel 3-Quinline Carboxamides as Potent, Selective and Orally Bioavailable Inhibitors of Ataxia Telangiectasia Mutated (ATM) Kinase. *J. Med. Chem.* **2016,** *59,* 6281–6292.
57. Redfern, W. S.; Carlsson, L.; Davis, A. S.; Lynch, W. G.; MacKenzie, I.; Palethorpe, S.; Siegl, P. K. S.; Strang, I.; Sullivan, A. T.; Wallis, R.; Camm, A. J.; Hammond, T. G. Relationships Between Preclinical Cardiac Electrophysiology, Clinical QT Interval Prolongation and Torsade de Pointes for a Broad Range of Drugs: Evidence for a Provisional Safety Margin in Drug Development. *Cardiovasc. Res.* **2003,** *58,* 32–45.
58. Waring, M. J.; Johnstone, C.; McKerrecher, D.; Pike, K. G.; Robb, G. Matrix-Based Multiparameter Optimisation of Glucokinase Activators: The Discovery of AZD1092. *Med. Chem. Commun.* **2011,** *2,* 775–779.
59. Yang, H.; Rudge, D. G.; Koos, J. D.; Vaidialingham, B.; Yang, H. J.; Pavletich, N. P. mTOR Kinase Structure, Mechanism and Regulation. *Nature* **2013,** *497* (7448), 217–223.
60. Tarcsay, A.; Nyiri, K.; Keseru, G. M. Impact of Lipophilic Efficiency on Compound Quality. *J. Med. Chem.* **2012,** *55,* 1252–1260.
61. Murray, C. W.; Erlanson, D. A.; Hopkins, A. L.; Keseru, G. M.; Leeson, P. D.; Rees, D. C.; Reynolds, C. H.; Richmond, N. J. Validity of Ligand Efficiency Metrics. *Med. Chem. Lett.* **2014,** *5,* 616–618.
62. Goldberg, F. W. Design of Novel Reagent Sets to Enhance Drug Discovery, 247th ACS National Meeting, 2014 (Abstract #MEDI-29).
63. Pammolli, F.; Magazzini, L.; Riccaboni, M. The Productivity Crisis in Pharmaceutical R&D. *Nat. Rev. Drug Discov.* **2011,** *10,* 428–438.
64. Kola, I.; Landis, J. Can the Pharmaceutical Industry Reduce Attrition Rates? *Nat. Rev. Drug Discov.* **2004,** *3,* 711–718.
65. Summerfield, S.; Jeffrey, P. Discovery DMPK: Changing Paradigms in the Eighties, Nineties and Noughties. *Expert Opin. Drug Discov.* **2009,** *4,* 207–218.
66. McGinnity, D. F.; Collington, J.; Austin, R. P.; Riley, R. J. Evaluation of Human Pharmacokinetics, Therapeutic Dose and Exposure Predictions Using Marketed Oral Drugs. *Curr. Drug Metab.* **2007,** *8,* 463–479.
67. Page, K. M. Validation of Early Human Dose Prediction: A Key Metric for Compound Progression in Drug Discovery. *Mol. Pharm.* **2016,** *13* (2), 609–620.
68. Johnson, K. C.; Swindell, A. C. Guidance in the Setting of Drug Particle Size Specification to Minimize Variability in Absorption. *Pharm. Res.* **1996,** *3,* 1795–1798.
69. Hilgers, A. R.; Smith, D. P.; Biermacher, J. J.; Day, J. S.; Jensen, J. L.; Sims, S. M.; Adams, W. J.; Friis, J. M.; Palandra, J.; Hosley, J. D.; Shobe, E. M.; Burton, P. S. Predicting Oral Absorption of Drugs: A Case Study With a Novel Class of Antimicrobial Agents. *Pharm. Res.* **2003,** *20* (8), 1149–1155.
70. Ding, X.; Rose, J. P.; Van Gelder, J. Developability Assessment of Clinical Drug Products With Maximum Absorbable Doses. *Int. J. Pharm.* **2012,** *427* (2), 260–269.
71. Leahy, D. E.; Arundel, P. A.; Blakey, G. E.; Rowland, M. Physiologic Based Pharmacokinetic Modeling and QSAR. *Bioact. Compd. Des.* **1996,** 147–151.
72. Nestorov, I. A.; Aarons, L. J.; Arundel, P. A.; Rowland, M. Lumping of Whole-Body Physiologically Based Pharmacokinetic Models. *J. Pharmacokinet. Biopharm.* **1998,** *26* (1), 21–46.
73. Smith, D. A.; Beaumont, K.; Maurer, T. S.; Di, L. Volume of Distribution in Drug Design. *J. Med. Chem.* **2015,** *58,* 5691–5698.
74. Furet, P.; Caravatti, G.; Guagnano, V.; Lang, M.; Meyer, T.; Schoepfer, J. Entry Into a New Class of Protein Kinase Inhibitors by Pseudo Ring Design. *Bioorg. Med. Chem. Lett.* **2008,** *18,* 897–900.
75. Pike, K. G.; Barlaam, B.; Colclough, N.; McGuire, T. M.; Cadogan, E.; Pass, M.; Hassall, L. A.; Hawkins, J.; Holmes, J.; Dishington, A.; Robb, G.; Ducray, R.; Ouvry, G.; Degorce, S. L.; Lau, A.; MacFaul, P.; Hughes, G. Identifying High Quality, Potent and Selective Inhibitors of ATM Kinase: Discovery of AZD0156, AACR Annual Meeting 2016; Poster #4859.

76. Cadogan, E. Discovery and Preclinical Pharmacology of AZD0156: A First in Class Potent and Selective Inhibitor of Ataxia Telangiectasia Mutated (ATM) Kinase, AACR Annual Meeting 2016, Presented as Part of the New Drugs on the Horizon Session.
77. Ellison, G.; Huang, S.; Carr, H.; Wallace, A.; Ahdesmaki, M.; Bhaskar, S.; Mills, J. A Reliable Method for the Detection of *BRCA1* and *BRCA2* Mutations in Fixed Tumour Tissue Utilizing Multiplex PCR-Based Targeted Next Generation Sequencing. *BMC Clin. Pathol.* **2015,** *15,* 1–14.
78. Morgado-Palacin, I.; Day, A.; Murga, M.; Lafarga, V.; Anton, M. E.; Tubbs, A.; Chen, H.; Ergan, A.; Anderson, R.; Bhandoola, A.; Pike, K. G.; Barlaam, B.; Cadogan, E.; Wang, X.; Pierce, A. J.; Hubbard, C.; Armstrong, S. A.; Nussenzweig, A.; Fernandez-Capetillo, O. Targeting ATR and ATM Kinase Activities in MLL-Rearranged AML. *Sci. Signal.* **2016,** *9* (445), ra91.
79. Lu, X.-H.; Mattis, V. B.; Wang, N.; Al-Ramahi, I.; van den Berg, N.; Fratantoni, S. A.; Waldvogel, H.; Greiner, E.; Osmand, A.; Elzein, K.; Xiao, J.; Dijkstra, S.; De Pril, R.; Vinters, H. V.; Faull, R.; Signer, E.; Kwak, S.; Marugan, J. J.; Botas, J.; Fischer, D. F.; Svendsen, C. N.; Munoz-Sanjuan, I.; Yang, X. W. Targeting ATM Ameliorates Mutant Huntingtin Toxicity in Cell and Animal Models of Huntingdon's Disease. *Sci. Transl. Med.* **2014,** *6* (268), 1–12.

8.08 Tepotinib

O Schadt and A Blaukat, Merck KGaA, Darmstadt, Germany

© 2017 Elsevier Ltd. All rights reserved.

8.08.1	**Introduction**	178
8.08.2	**Discussion**	179
8.08.2.1	Optimization of Aryl Substitution Pattern: Reduction of PDE Activity	182
8.08.2.2	Identification of Bioisosteric Core Replacements: Address Chemical Instability	182
8.08.2.3	Final Optimization, Selection, and Characterization of a Putative Clinical Candidate	184
8.08.2.4	Back to the Bench! Identification of Bioisosteric Carbamate Replacements	187
8.08.2.5	Optimization of Pyrimidine Substituents: Introduction of Solubility	187
8.08.2.6	Fine-Tuning of the Phenyl Pyridazinone Substitution Pattern	190
8.08.2.7	Final Selection of the Solubilizing Anchor Led to the Identification of Tepotinib	190
8.08.3	**Characterization of Tepotinib**	192
8.08.4	**Pharmacokinetic Characterization of Tepotinib**	195
8.08.5	**Pharmacodynamic Characterization of Tepotinib**	195
8.08.6	**Summary and Conclusion**	200
8.08.7	**Supplementary Material**	201
Acknowledgment		202
References		202

8.08.1 Introduction

The c-Met oncoprotein is a kinase and belongs to the receptor tyrosine kinase (RTK) superfamily activated by its physiological ligand hepatocyte growth factor (HGF).[1] HGF binding results in a dimerization of the c-Met followed by consecutive autophosphorylation, which in turn activates multiple signaling cascades involved in cell survival, motility, migration, proliferation, and angiogenesis (e.g., the PI3K/Akt and MAPK/ERK pathways).[2] During embryonic development, c-Met activation followed by mesenchymal–epithelial transition is of utmost importance for cell motility and, as a consequence, organ morphogenesis. Therefore, it is not surprising that knockout of c-Met or its physiological ligand HGF is embryonically lethal.[3,4]

c-Met is typically expressed in a variety of epithelial tissues, and HGF expression is predominantly detected on tissues of mesenchymal origin.[5]

The physiological role of c-Met is not completely understood, but it was reported that following tissue damage, upregulation of both c-Met and HGF is associated with cell motility and tissue regeneration.[6,7]

Under physiological conditions, c-Met is strictly regulated during embryonic development and tissue homeostasis with physiologically relevant expression levels in differentiated tissue like liver and lung.

Molecular analyses of cancer patient samples revealed different dysregulations of c-Met function, as a result of overexpression, mutational activation, or amplification.[8] These alterations are observed in many types of cancer, including liver and lung cancer.[9] In addition, activating point mutations of c-Met are ultimately responsible for certain forms of hereditary and sporadic papillary renal carcinoma.[10] Furthermore, c-Met activation by its various mechanisms is associated with rapid tumor growth, metastasis, invasiveness, and induction of angiogenesis. Retrospective studies indicated a correlation between poor patient prognosis and overexpression of c-Met or HGF.[11]

c-Met was initially described in 1984 by Copper et al.[12], but it took almost two decades to realize the relevance as a promising target in oncology and identify suitable modulators of this important oncogene. Besides monoclonal antibodies against the physiological ligand (HGF) or the c-Met receptor, multiple small-molecule c-Met inhibitors are described in the literature.[13] In principle, two different types of c-Met inhibitors are described in the literature: highly selective c-Met inhibitors and inhibitors where c-Met is only a component in a more polypharmacological profile. Though many spectrum-selective kinase inhibitors provide a pharmacologically relevant c-Met component like staurosporine, XL-880, and XL-184, the polypharmacological nature of these inhibitors is often regarded as a double-edged sword. On the one hand, there is certainly a beneficial pharmacological component associated to the inhibition of multiple cancer-related kinases, but on the other hand, the applicability of multispecific kinase inhibitors like staurosporine is often hampered by the simultaneous interaction with toxicologically relevant targets, ultimately leading to an unacceptably narrow therapeutic index.

The first reasonably selective c-Met inhibitor described in the literature was crizotinib back in 2006. Since the first publications of crizotinib (PF-02341066),[14] many scientists became interested and tried to identify proprietary ligands for this highly relevant proto-oncogene. As a result, highly potent and selective c-Met inhibitors like PF-04217903,[15] SGX-523,[16] and JNJ-38877605[17] were identified (Fig. 1).

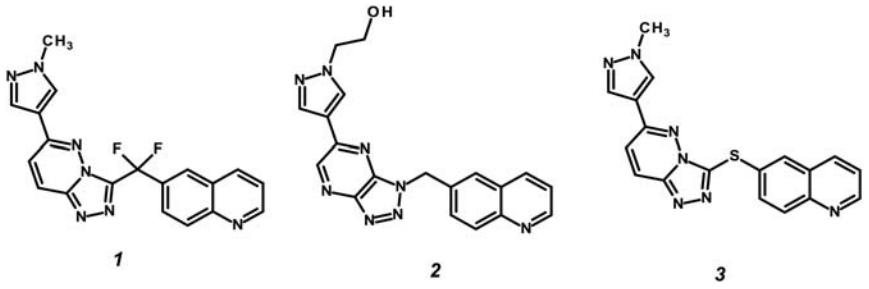

Fig. 1 Monospecific c-Met inhibitors: (**1**) JNJ-38877605, (**2**) PF-04217903, and (**3**)SGX-523.

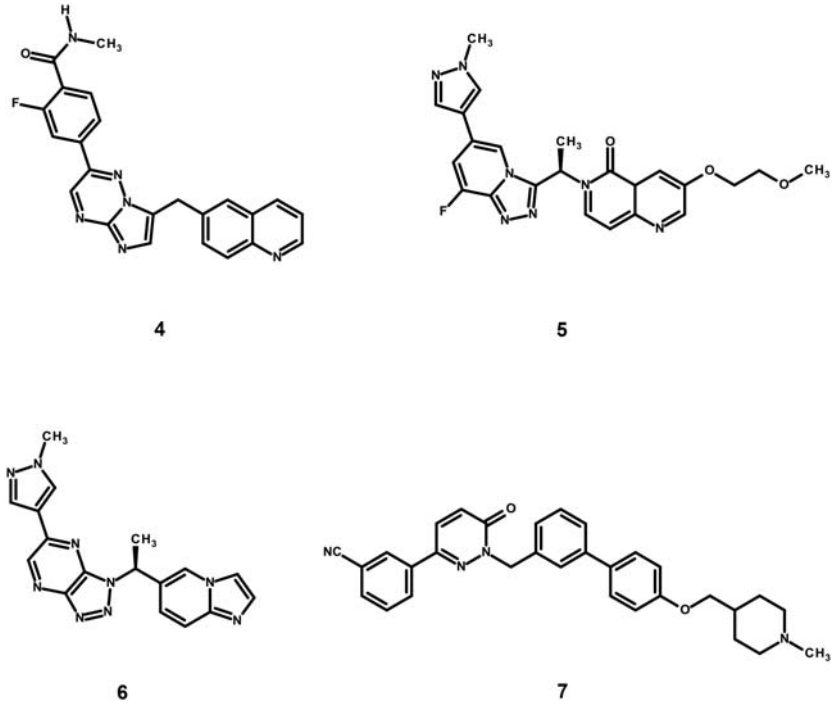

Fig. 2 Monospecific c-Met inhibitors: (**4**) capmatinib (INCB-28060), (**5**) AMG-337, (**6**) savolitinib (AZD6094), (**7**) and tepotinib (MSC2156119/EMD 1214063).

A number of clinical studies were performed to evaluate the safety and efficacy profile of agents inhibiting c-Met activity. These agents span a panel of diverse therapeutic modalities and include ligand-dependent activation of c-Met (monoclonal antibodies binding against HGF like ficlatuzumab (SCH-900105/AV-299)[18] or rilotumumab (AMG102))[19] and ligand-dependent c-Met activation by monoclonal one-armed antibodies against the c-Met receptor like onartuzumab[20] and selective small-molecule tyrosine kinase inhibitors like savolitinib (AZD6094),[21] AMG-337,[22] capmatinib (INCB-28060),[23] or tepotinib (MSC2156119)[24] shown in Fig. 2.

8.08.2 Discussion

Our c-Met program started with an internal high-throughput screening campaign of approximately 350 k compounds against the kinase domain of the c-Met receptor (hit rate ~ 0.5 %). Besides multiple well-known and spectrum-selective kinase inhibitors, thiadiazinone **8** (Fig. 3) was identified as an uncommon structural class. This HTS hit, originally synthesized for a phosphodiesterase

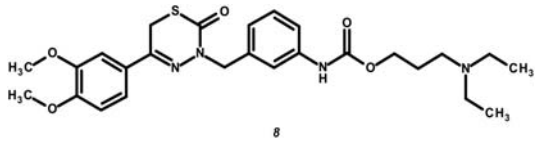

Fig. 3 Initial hit molecule, thiadiazinone **8**.

Table 1 PDE activities of two representative carbamates

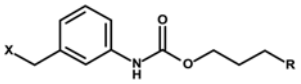

Cpd	*X*	*R*	*c-Met biochemIC_{50} (nM)*	*PDE3 IC_{50} (nM)*	*PDE4 IC_{50} (nM)*
8	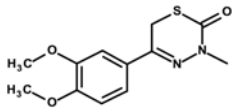	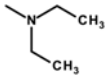	35	1500	63
12	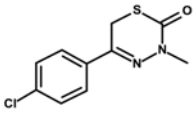		90	1%inh.@10 μM	49%inh.@10 μM

inhibitor project, was identified as a potent inhibitor of c-Met (*in vitro* IC_{50} (c-Met) = 35 nM and cellular IC_{50} (c-Met) = 795 nM, Table 1).

Supportive x-ray structures of c-Met in complex with multiple thiadiazinones incl. compound **8** were rapidly available (Fig. 4—PDB-ID: 4R1Y). Details from these x-ray structures revealed the essential binding interactions and guided the subsequent compound optimization process. Similar to other selective c-Met kinase inhibitors like JNJ-38877605, PF-04217903, AZD6094 (volitinib), or AMG-337, thiadiazinone **8** is bound in the ATP pocket of c-Met in a U-shaped binding mode. The most important structural features are the interaction of the carbamate carbonyl with the backbone nitrogen of Met1160 within the hinge region, the benzylic bend, which arranges the residues, and a carbonyl interaction of the pyridazinone to Asp 1222 of the DFG motif, which probably contributes to the overall potency and selectivity of the ligand. Another H-bond is formed to a side chain of Asn1164, and

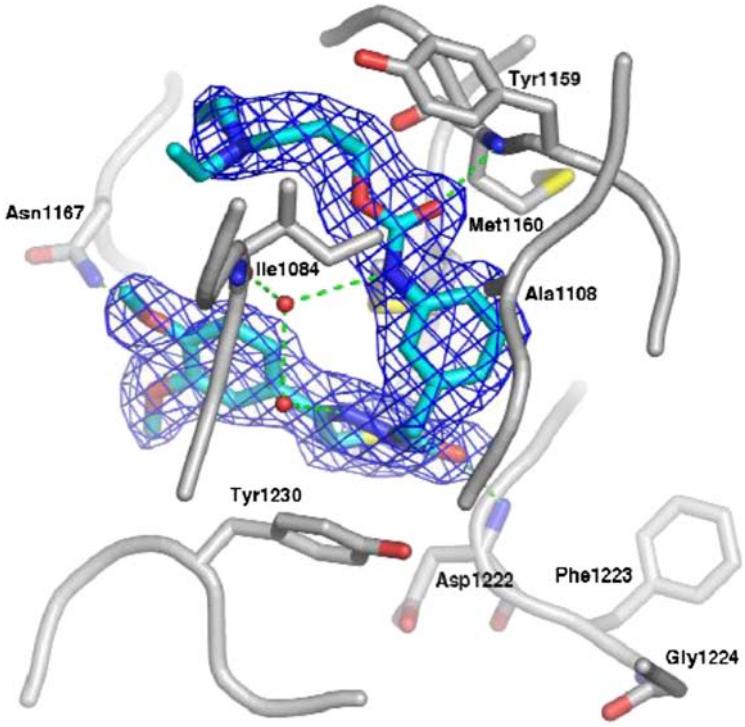

Fig. 4 The x-ray structure of the binding pocket of c-Met kinase in complex with thiadiazinone **8** with at 2.0 Å resolution (PDB-ID: 4R1Y). The inhibitor and neighboring protein side chains are depicted as stick model, colored according to the chemical type ($C_{(inhibitor)}$, cyan; $C_{(protein)}$, gray; O, red; N, blue; S, yellow). Hydrogen bonds are indicated as green dotted lines.

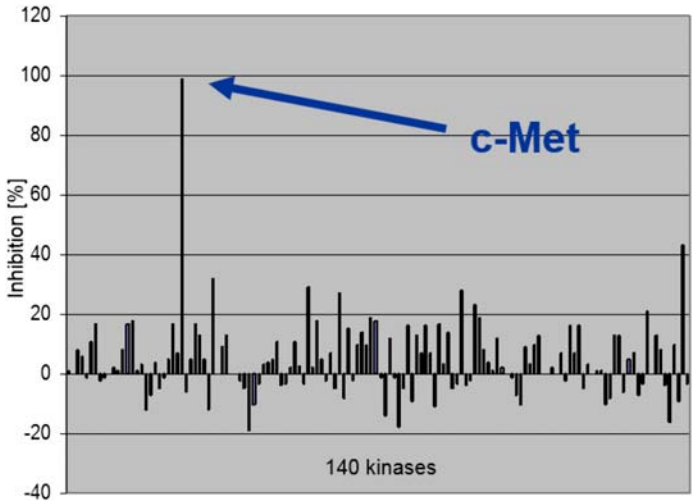

Fig. 5 Kinase profiling of thiadiazinone 8 against 140 kinases at 10 μM.

there are additional hydrophilic interactions from the carbamate NH group, bridged by a water molecule, to the main chain carbonyl of Ile1084 (from the glycine-rich loop). In addition, one of the methoxy groups of the 3,4 dimethoxy phenyl moiety is in close proximity to Asn1167, potentially contributing to the overall potency of the ligand. Furthermore, the binding of thiadiazinone **8** is supported by hydrophobic interactions involving Ala1108, Tyr1159, Met1211, and Tyr1230 (Fig. 4).

In addition to promising enzymatic and cellular c-Met potency, the physicochemical parameters of thiadiazinone **8** are within acceptable ranges including solubility of more than 100 μg ml^{-1} and a logD of 2.5. Kinase profiling activities, depicted in Fig. 5, revealed that thiadiazinone **8** is a highly selective c-Met inhibitor; however, unwanted off-target activities, that is, phosphodiesterase inhibition, were observed (PDE3 $IC_{50} \sim 1500$ nM, PDE4 $IC_{50} \sim 60$ nM)[25].

Subsequent evaluation of the pharmacokinetic profile of **8** revealed an oral bioavailability of less than 5% and a clearance of larger than 6 l h^{-1} kg^{-1}, which is considered to be suboptimal and focus of improvement. Retrospectively, one could argue based on binding efficiency considerations that the molecular weight was slightly too high to qualify thiadiazinone 8 (514.7 g mol^{-1} with a BEI value of 14.5) as an attractive starting point for an optimization program. However, it quickly became evident that molecules with reduced molecular weight, like thiadiazinone **13** (429.5 g mol^{-1} with a BEI value of 17.8), provided a comparable activity profile with an improved PK profile (Table 2).

Table 2 Properties of carbamates

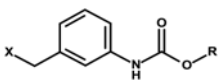

Cpd	*X*	*R*	*c-Met biochemIC$_{50}$ (nM)*[a]	*c-Met cell IC$_{50}$ (nM)*[b]	*Mouse PK*[c]		*BEI*
8	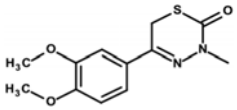	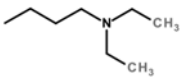	35	795	CL (L h^{-1} kg^{-1}) 6	F (%) <5	14.5
13	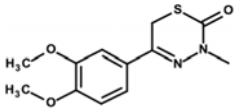	CH_2CH_3	22	3400	1.5	~30	17.8
14	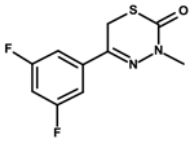	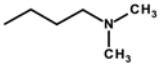	6	340	3.4	~25	17.8

[a]Off-chip mobility shift assay using GST-His_6-tagged recombinant human c-Met kinase domain and FITC-labeled Srctide as substrate. For details, please see the supplementary data of Bioorg. Med. Chem. Lett. 2015.[24a]
[b]Cellular activity in HGF-stimulated A549 (human carcinoma) cell determination by electrochemiluminescence (ECL) assay. Phospho c-Met was detected using a capture antibody specific for the c-Met extracellular domain and antiphosphotyrosine antibodies for detection. For details, please see the supplementary data of Bioorg. Med. Chem. Lett. 2015.[24a]
[c]Screening (cocktail) PK study (please see supplementary data of Bioorg. Med. Chem. Lett. 2015[24a] for further details)

Table 3 Influence of aryl substitution pattern on c-Met activity of thiadiazinone carbamates

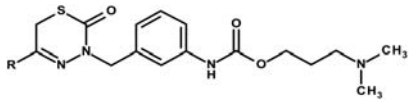

Cpd	*R*	*c-Met biochemIC$_{50}$ (nM)*	*c-Met cell IC$_{50}$(nM)*	*clogP*	*BEI*
9	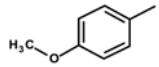	9	1200	3.38	17.6
10	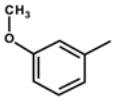	15	1100	3.38	17.1
11	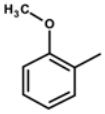	72	5400	3.38	15.6

8.08.2.1 Optimization of Aryl Substitution Pattern: Reduction of PDE Activity

Approximately 30 different aromatic substitution patterns covering electron donating and electron withdrawing substituents and different heterocycles and sterically demanding residues were synthesized[26] and tested. The resulting structure–activity relationship, in line with the binding model built from the cocrystal structure, suggested that a wide variety of substitution patterns and heterocycles are tolerated without significantly impacting biochemical activity. One caveat is that the coplanarity of the aryl moiety with the thiadiazinone ring cannot be compromised. For example, ortho substituents like the exemplified compound **11** are considerably less potent compared with meta- or parasubstitution patterns of compounds **9** and **10** (Table 3).

One of our first optimization efforts was to remove the unwanted off-target, PDE activity. According to literature, methoxy phenyl but especially the 3,4 dimethoxy phenyl residue present in compounds **8** and **13** were described as well-known PDE recognition motives.[27] Based on initial reassuring data that, for example, 4-chloro phenyl **12** demonstrated a significantly reduced PDE activity, our first optimization effort was dedicated to the identification of alternative substituents preferably in the meta- or paraposition without significant PDE activity.

Contribution of the observed interaction between one of the methoxy groups of **8** and Asn1167 to the overall binding was not mandatory to maintain affinity. On the contrary, there was a slight tendency toward an improved affinity for the monosubstituted methoxy phenyl derivatives **9** and **10**. However, the goal to identify a potent c-Met inhibitor without a pronounced PDE activity on any of the PDE isoenzymes was achieved by replacing the 3,4-dimethoxyphenyl substituent by a 3,5-difluorophenyl residue, which resulted in cpd **14** with an increased biochemical and cellular potency. The overall improvement is immediately evident by calculating molecular descriptors of the overall compound quality like the binding efficiency index (BEI). This simple optimization of the substitution pattern improved the BEI value from 14.5 to 17.8 and in addition provided a compound with a comparable or even reduced IV clearance and increased oral bioavailability in mice compared with thiadiazinone **8**.

8.08.2.2 Identification of Bioisosteric Core Replacements: Address Chemical Instability

Despite the improvements in potency, the thiadiazinone series was limited due to chemical instability. Repeated evidence showed that under harsh conditions (high temperatures or anhydrous acidic conditions), the thiadiazinone ring decomposes potentially liberating CSO. This chemical instability negatively affects not only chemical accessibility and the synthetic yields but also shelf life and may cause potential issues in long-term assays. Therefore, the strategy was to identify suitable bioisosteres[28] as potential thiadiazinone replacements with high priority. With the exception of the acylpyrazolines, which were already identified as additional hit matter in the high-throughput screening, approximately 20 additional five- and six-membered heterocycles and annelated bicyclic ring systems were synthesized. The properties of the four most active bioisosteres are described in Table 4.

c-Met cocrystal structures of representatives of every lead structure class could be obtained, which provided valuable insights into the binding conformation of the bioisosteric thiadiazinone replacements. All four thiadiazinone core replacements, namely, pyridazinones[29] **15**, acylpyrazolines[30] **16**, benzoxazolones[31] **17**, and thiadiazolinones **18**, share the already-discussed essential pharmacophoric features like a hydrogen bond acceptor in a defined orientation and a coplanar extended aromatic moiety in the ribose pocket. As anticipated, the core replacements also show a comparable and overlapping structure–activity relationship in our enzymatic assay (Table 4).

Table 4 Selection of bioisosteric thiadiazinone replacements

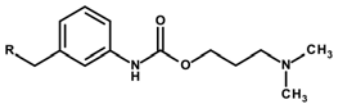

Cpd	R	c-Met biochem IC_{50} (nM)	c-Met cell IC_{50}(nM)	Stability PBS buffer pH 7.4	Stability SGF pH 1.2	Stability human plasma	BEI
15	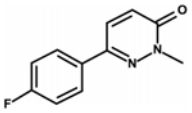	14	400	89	88	100	18.5
16	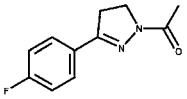	165	3100	73	91	46	15.9
17	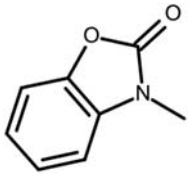	110	2500	100	87	87	18.8
18	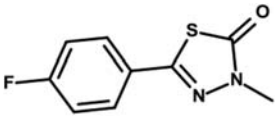	43	1300	100	85	83	17.1

Despite its slightly reduced potency, one particularly interesting modification from a bioisosteric point of view is the compound class of acylpyrazolines **16**. This compound class was initially identified during the HTS run and was elaborated in parallel to the optimization activities around the thiadiazinone class. The compound class of the acylpyrazolines provides all required pharmacophoric features. The reduction of the ring size and insertion of the carbonyl into the side chain (Fig. 6), which forms the important Asp 1222 interaction to the c-Met protein, result in a comparable binding mode and structure–activity relationship.

The structure–activity relationship on c-Met for all bioisosteric compound classes was assessed to be widely comparable to the parental thiadiazinones and could therefore easily transferred from one compound class to the other. Extended stability tests in standard media were done for all potential bioisosteric core replacements. These stability tests revealed a significant plasma instability for the series of acylpyrazolines around compound **16** (Table 4). Although the decomposition product was not elucidated, it was hypothesized that amidases present in the plasma might be responsible for the clearance of the amide bond. This instability in combination with a suboptimal pharmacokinetic behavior *in vitro* and *in vivo* profile led to the decision to deprioritize the acylpyrazoline series. The most promising bioisosteric replacement, pyridazinone **15**, turned out to be equipotent in the biochemical and cellular c-Met potency (14 and 400 nM, respectively) compared with the thiadiazinone **14** (6 and 340 nM, respectively). In addition, based on a slightly more favorable ratio between enzyme and cell potency, the decision was made to focus our optimization efforts on this novel compound class.

The chemical accessibility for pyridazinones is excellent and offers the opportunity to independently optimize the different moieties of this scaffold in acceptable overall yields. Starting from the commercially available benzaldehydes, the synthesis followed a four-step synthetic protocol where the pyridazinone ring is formed by condensing the respective benzaldehyde with glyoxylic acid in the presence of hydrazine. The regioselectivity between oxygen and nitrogen alkylation of the following benzylation step was

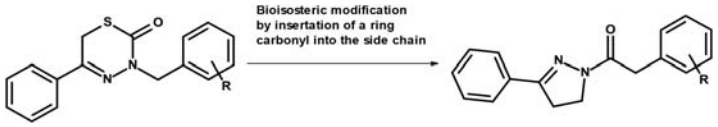

Fig. 6 Bioisosteric modification.

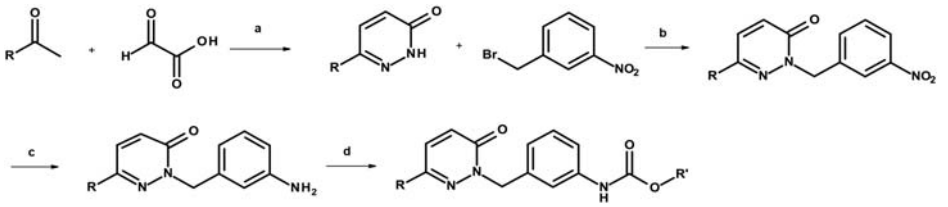

Scheme 1 Synthesis of carbamate derivatives. Reagents and conditions: (A) hydrazine hydrate, AcOH, 95 °C, (B) K_2CO_3, acetonitrile, 80 °C; (C) H_2, RaNi, THF; (D) ClCOOR', pyridine, dichloromethane, rt.

highly dependent on the base that is used. The use of potassium carbonate allows for the regioselectivity to favor nitrogen alkylation and only traces of the undesired benzylether could be detected under these conditions. The subsequent hydrogenation of the aryl nitro moiety does not affect the core fragment but could potentially interfere with sensitive substituents in the R residue. The final carbamate formation was performed under standard conditions in high yields. The whole synthesis including specific protocols has been published recently (**Scheme 1**).[24.a]

This versatile synthetic route allows for the optimization of the solubilizing moiety in the last step of the synthesis via *in situ* generation of a suitable chloroformate followed by the preparation of the respective carbamate. In contrast to the thiadiazinones, which were regularly found to decompose under anhydrous HCl conditions during hydrochloride salt formation, the pyridazinones turned out to be stable under acidic conditions and allow for the more convenient purification method of hydrochloride salt crystallization.

The influence on enzymatic potency of modifications in the solubilizing anchor is marginal, but this part of the molecule was exploited to optimize secondary parameters like solubility.

8.08.2.3 Final Optimization, Selection, and Characterization of a Putative Clinical Candidate

With the exception of compounds containing rigidified modifications like piperidine **25**, significant reduction of biochemical c-Met potency and BEI value was not observed for a variety of solubilizing anchor moieties (**Table 5**). The binding efficiency index turned out to be in a comparable range between 17.5 and 20.5. However, the c-Met activity of compounds bearing a basic amine turned out

Table 5 Influence of different carbamates on activity and solubility

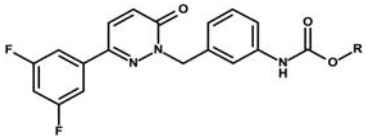

Cpd	*R*	*c-Met biochemIC$_{50}$ (nM)*	*c-Met cell IC$_{50}$(nM)*	*Solubility S$_{kin}$ (μM)*	*BEI*
19	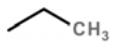	4	620	9.3	21.8
20	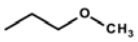	3	170	21	20.5
21	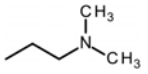	11	1900	139	18.6
22	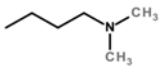	2	130	163	19.7
23	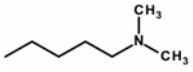	10	190	136	17.5
24	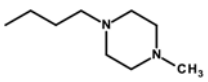	2	53	150	17.5
25	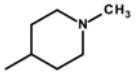	120	4900	135	15.2

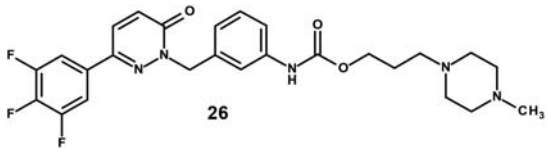

Fig. 7 Structure of pyridazinone carbamate 26.

to be superior compared to neutral modifications like compound **19** or **20**. In particular, derivatives with three methylene units between the carbamate and the basic center represent the optimum in biochemical and cellular c-Met potency in particular (**22** and **24**). Besides the cellular potency, the compound selection for further optimization was mainly driven by solubility considerations.

The optimization of the linker and solubility anchor followed by fine-tuning of the substitution pattern of the aryl residue attached to the pyridazinone ring led to the introduction of a third fluorine atom in the paraposition and finally to the identification of carbamate **26** (Fig. 7), which provided a favorable physicochemical and pharmacodynamic *in vitro* profile.

Carbamate **26** is a highly potent inhibitor of c-Met with IC_{50}'s in the single-digit nanomolar range on the isolated enzyme and 50 nM in A549 cells. Kinase profiling of **26** on a panel of 80 kinases revealed that the compound is a highly selective c-Met inhibitor, which seems to be a conserved feature of this compound class expected to stabilize an inactive conformer of the c-Met protein.

In addition to the pharmacological profiling (Table 6) and structural information provided by cocrystal structures, valuable additional biophysical insights like binding constants and residence times were provided by surface plasmon resonance (SPR) measurements. The residence time of the piperazine carbamate **26** on the c-Met receptor was measured to be 12.6 min with a Kd of 0.5 nM (Table 16). The overall quality of this particular c-Met inhibitor is underlined by a favorable physchem profile of solubility and stability (Table 7). The favorable overall *in vitro* profile justified a more in-depth *in vivo* characterization of compound **26**. Therefore, a broader pharmacokinetic and pharmacodynamics *in vivo* profiling of carbamate **26** and initial safety assays were performed in parallel.

The *in vitro* and *in vivo* PK profile of **26** is summarized in Tables 8 and 9, respectively. The intrinsic clearance in human hepatocytes is lower than 0.28 l h^{-1} kg^{-1}. There are no concerning CYP inhibition data, although this compound is mainly metabolized by the same CYP that it is inhibiting (CYP3A4). The compound showed reasonable plasma protein binding in the range of 98 % and some residual PgP substrate properties. No reactive metabolites have been found by glutathione adduct trapping. In mice, the compound is sufficiently stable, and no hints of instability have been observed in dog, monkey, or human plasma. Interestingly, for unknown reasons, the compound seems to be highly unstable in rat plasma. With the exception of rats, the *in vivo* PK profiles in three different species showed good to very good clearance, half-life values, and oral bioavailability. Allometric scaling based on these results predicts that **26** will be a low-clearance drug in humans with a long half-life and a good oral bioavailability.

Table 6 Pharmacological profile of pyridazinone carbamate **26**

Cpd	*c-Met biochemIC_{50} (nM)*	*c-Met cell IC_{50}(nM)*	*Kinases profiling at 1 μM*	*BEI*	*Kd (nM)*	*Residence time (min)*
26	5.2	51	0/80	16.1	0.5	12.6

Table 7 Physchem and stability data of pyridazinone carbamate **26**

Cpd	*clogP*	*clogD*	*tPSA*	*Thermodynamic solubility PBS pH 7.4 (μg ml^{-1})*	*Stability pH 8.5[a] (%)*	*Stability pH 1.2 (SGF)[a] (%)*	*Stability human plasma[a] (%)*
26	3.1	2.4	77.5	0.197	100	100	>99

[a]% remaining after 2 h

Table 8 *In vitro* ADME data of pyridazinone carbamate 26

Cpd	*Cl_{int} (human) (microsomes) (L h^{-1} kg^{-1})*	*Cl_{int} (human) (hepatocytes) (L h^{-1} kg^{-1})*	*CYP inhibition*	*CYP metabolism*	*Protein binding (human)*	*Caco-2 permeability (10^6 cm s^{-1})*	*Reactive metabolites*	*Plasma stability[a] rat/mouse/human*
26	1.41	<0.28	≥5.6 μM	CYP3A4 (major) CYP2D6 (minor)	97.2–98.5 % (conc. dep.)	14	No GSH adducts	<5 / ~80 / >99

[a]Stability measured at 37 °C (24 h incubation) expression as (% remaining)

Table 9 *In vivo* ADME data of pyridazinone carbamate **26**

In vivo *profile*					*Predicted PK*
Species	Mouse	Rat	Monkey	Dog	Human
CL (L h^{-1} kg^{-1})	1.5	>4	0.03	0.43	0.01–0.04
Vss (L kg^{-1})	12.2	20.2	0.44	8.9	1.0
t1/2 (h)	6.5	2.5	13.7	16.0	14–70
F (%)	58	15	65	75	>60

PK/PD studies using compound **26** were performed to demonstrate a dose-dependent target engagement *in vivo* (Fig. 8) and to guide the optimal dosing and scheduling regimes. These PK/PD studies indicated that a single application of 50 mg kg^{-1} of compound **26** is sufficient to inhibit the kinase activity of c-Met almost completely for 2 days *in vivo*, whereas doses of 25 mg kg^{-1} resulted in a transient and incomplete target engagement (Fig. 8).

In addition to these PK/PD studies, an *in vivo* efficacy testing in a xenograft model using HS746T, a c-Met amplified gastric cancer cell line, was performed in CD1 mice (Fig. 9). Compound **26** was given orally once daily at doses of 25, 50, and 100 mg/kg. Impressively, in line with the expectations based on the target coverage in the PK/PD studies, complete regression could be achieved in this gastric cancer model by using 50 mg/kg/d or higher doses of cpd. 26. The durability of the response is reflected by the fact that no tumor regrowth was observed, for at least 20 days, even when the treatment was stopped. Comparable activities could be achieved by using autocrine c-Met-dependent tumor cell lines like U87MG glioblastoma cells or mouse fibroblasts transfected with the clinically relevant fusion protein TPR-Met.

In parallel to the extensive pharmacokinetic and pharmacodynamic characterization, piperazine **26** was characterized in the first set of relevant safety assays. Unfortunately, it turned out that the compound showed a significant hERG activity of ~50 nM in our cellular patch clamp assay. The *in vitro* hERG activity was also visible in a ventricular wedge assay where piperazine 26 significantly increased the refractory period and reduced the force of contraction at physiologically relevant concentrations. In addition to a significant risk for QT prolongation (delayed ventricular repolarization), the piperazine **26** also showed a dose-dependent, direct, and inverse cardiovascular side effect on heart rate and blood pressure. Furthermore, based on histological studies, it became evident that compound **26** induced phospholipidosis in rats in various tissues like liver and lung, and after intravenous application, a dose-dependent hemolysis was observed. This effect might be due to the amphiphilic nature of this particular compound, induced

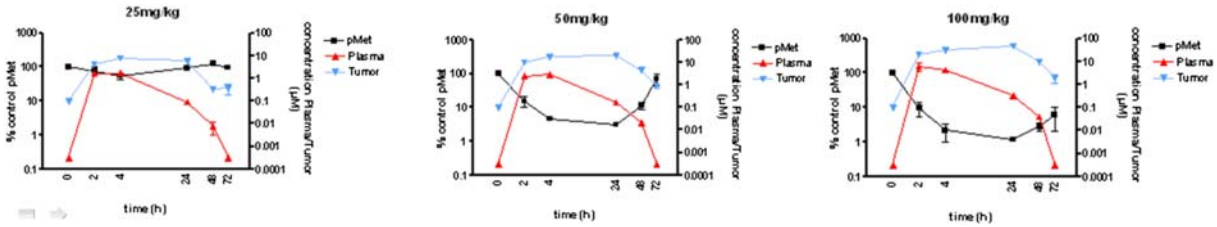

Fig. 8 Concentration/time curves and degree of target coverage after single application of 25 mg kg^{-1}, 50 mg kg^{-1}, and 100 mg kg^{-1} of carbamate **26** in a PK/PD experiment (cell line).

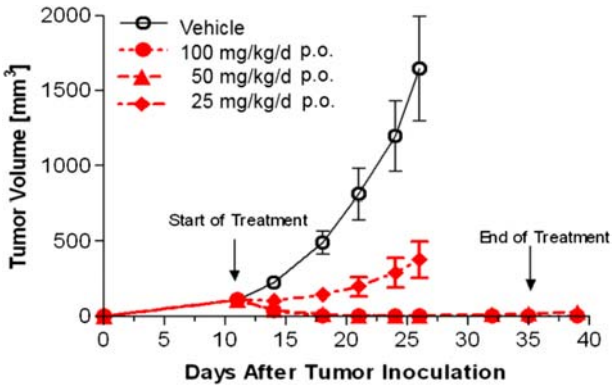

Fig. 9 Xenograft model using HS746T, a c-Met-amplified gastric cancer cell line, in CD1 mice applying orally 25, 50, and 100 mg kg^{-1} d^{-1} of carbamate **26**.

by a strong basic head group (calculated bpKa of 8.1) in combination with a rather lipophilic residual structure on the one hand forming micelles and on the other hand potentially interfering with membrane integrity. Compound **26** also induces the formation of micronuclei in the presence of metabolic activation by S9 mix (genotoxicity potential). The capability of alkyl carbamates to induce micronuclei, by the formation of an epoxide as a reactive intermediate after metabolic activation, is described in the literature for some carbamates like ethyl carbamates. [32] Taken altogether, these findings led to the disappointing conclusion that the therapeutic safety index of this compound does not justify further development and the optimization of the pyridazinones had to be continued with a focus on safety aspects.

8.08.2.4 Back to the Bench! Identification of Bioisosteric Carbamate Replacements

It was suspected that some of the undesired safety-related properties of the compound, that is, the positive micronucleus test, QT prolongation, and observed hemolysis could be attributed to the carbamate/linker/solubility anchor region of the molecule. Therefore, a broad screen for alternative groups that could act as potential carbamate replacements was conducted.

Initially, closely related linear bioisosteric analogs, like amides, retroamides, ureas, and retrocarbamates, were synthesized, but it quickly became evident that these analogs share the same liabilities and may even add additional complications. For example, urea derivatives led to reduced permeability due to an increased number of hydrogen bond donors.

Therefore, another approach was evaluated where several five-membered heterocycles, with a hydrogen bond acceptor as the hinge-binding element, were designed and docked into the pyridazinone carbamate cocrystal structure. In alignment with the docking results, it became evident that the nitrogen acceptor that interacts with Met1160 has to be located in the 2-position of the heterocyclic carbamate bioisostere. Interestingly, one of the first compounds synthesized, a 5-methyl-[1,2,4]oxadiazol-3-yl derivative, demonstrated a significant inhibition of c-Met (IC_{50}: 23 nM), which is comparable to the corresponding alkyl carbamates **19** and **27** (c-Met IC_{50} of 4 and 7 nM, respectively). Unfortunately, oxadiazole pyridazinone **28** lacked cellular potency, which fostered the decision to discontinue the oxadiazole series. As expected by our virtual docking results, the isomeric oxadiazole **29** was less active in the biochemical and cellular assay, probably because the nitrogen in the 2-position, serving as the hinge-binding element, was absent or sterically shielded by the methyl group, potentially causing a repulsive steric interaction of the methyl substituent with the hinge region of the c-Met protein, which consequently led to a nonoptimal positioning of the donor nitrogen. Additional evidence for this hypothesis was derived from the matched molecular pair of the two thiazole isomers **32** and **33** and their inverted isomer **34**. Although the biochemical activity of thiazole **32** was already in a reasonable range of 20 nM, the search for alternative ring systems was continued in order to avoid potential metabolic liabilities of thiazoles. Based on thiazole **32** and by applying the well-known bioisosterism of sulfur, C=C and N=C bonds,[33] six-membered ring compounds **35**, **36**, and **37** were prepared. It became evident that, besides the obligatory hydrogen bond acceptor and its acceptor qualities, a certain coplanarity was found to be essential for an optimal interaction of the hydrogen bond acceptor with the backbone N-H of Met1160. Based on the available cocrystal structures of all five- and six-membered heterocycles, the presence of a CH-π interaction between the H-atom next to the hinge acceptor pointing toward the π-system of Tyr1159 was identified as an additional ligand/receptor interaction, contributing to the overall affinity. The lacking CH-π interaction is the anticipated explanation for the reduced affinity of only 4200 nM for pyridazine **37**.

In addition to biarylic modifications, a few annelated heterobicyclic systems were synthesized, providing a hydrogen bond acceptor and a polarizable C-H donor. As an example, quinoline **38** depicted in Fig. 10 was found to be a reasonably potent c-Met inhibitor. The biochemical c-Met activity of quinoline **38** (45 nM) was comparable to phenyl oxadiazole **28**, phenyl thiadiazole **32**, or even phenyl pyrimidine **36**. The properties of quinolines, however, are controversially discussed in the literature. Even severe side effects like a potential risk of neurotoxicity, mutagenicity, and a tendency to form reactive metabolites are described in the literature. Especially in the absence of superiority in any particular property, these considerations in combination with a limited access to versatile building blocks led to the deprioritization of this particular class.

From a holistic perspective,[34] parasubstituted phenyl pyrimidines demonstrated the best overall profile including biochemical and cellular potency and physicochemical properties, providing all necessary pharmacophoric features like a near coplanarity of the six-membered heterocycle with the phenyl group and the presence of a polarized hydrogen alpha to the nitrogen in close proximity to Met1160. Therefore, pyrimidine derivative **36** was chosen as the most promising inhibitor for further derivatization.

8.08.2.5 Optimization of Pyrimidine Substituents: Introduction of Solubility

In the next optimization cycle, different smaller and more sterically demanding substituents including acids, bases, and additional aromatic systems were introduced to the paraposition of the pyrimidine ring. All compounds tested so far suffered from a significant

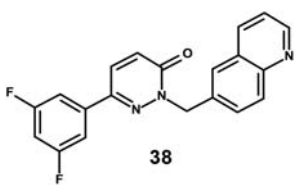

38

Fig. 10 Quinoline **38** as exemplified heterobicyclic hinge binder.

split between the biochemical and the cellular autophosphorylation assay of about a factor of 100. In the majority of the cases, the limited aqueous solubility (<1 μg ml^{-1} in a PBS buffer at pH 7.4 for methylpyrimidine derivative **36**) was expected to be the reason for the rather weak activity in the cellular A549 assay ($IC_{50} \sim 0.55$ μM).

The BEI values (approximately 21) for pyrimidine derivatives bearing a small substituent like methyl (compound **36**) or amino (compound **39**) were assessed to be reasonably attractive. Small substituents in the paraposition of the pyrimidine like alkyl, amino, hydroxyl, halogen, or carboxylic acids (**36** and **39–42**) did not show a significant improvement in cellular activity (**Table 10**). Sterically more demanding aromatic substituents like methyl pyrazole or smaller modified chains like cpds **43–47** demonstrated a significantly improved cellular potency and a reduced drop-off between the biochemical and the cellular assay of ~ 10. In analogy to the structure–property relationships in the carbamate class around compound **26**, the introduction of a basic anchor fragment, attached to the pyrimidine, increased the solubility and the amphiphilic character of the inhibitor, which ultimately led to an improved cellular potency and reduces the split between the biochemical and cellular assay. In addition to a larger set of

Table 10 Bioisosteric replacements of carbamate by various five- and six-membered heterocycles

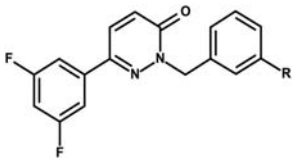

Cpd	*R*	*c-Met biochemIC_{50} (nM)*	*c-Met cellularIC_{50} (nM)*	*Solubility S_{kin} (μM)*	*BEI*
27	$NHCOOCH_3$	7	1200	3.0	22.0
19	$NHCOOCH_2CH_3$	4	620	9.3	21.8
28	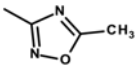	23	10000	<2.6	20.1
29	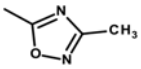	315	n.d.	n.d.	17.1
30	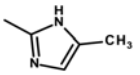	530	12000	45	16.6
31	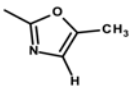	8	2400	<2,6	21.3
32	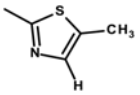	20	2100	<2.6	19.5
33	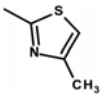	96	4700	<2.6	17.7
34	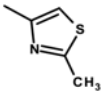	390	n.d.	<2.6	16.2
35	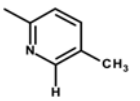	150	520	<2.6	17.5
36	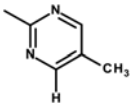	5	550	<2.6	21.3
37	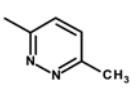	1300	>30000	4.1	15.1

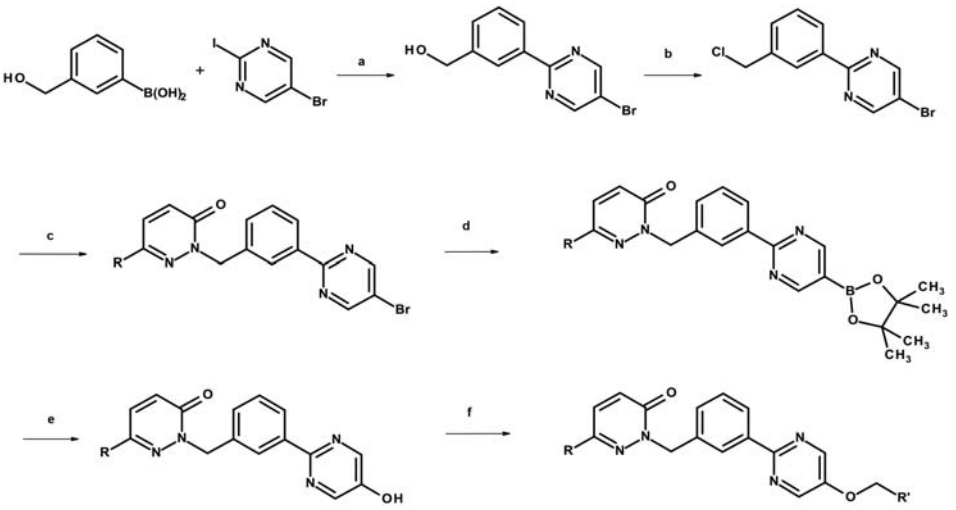

Scheme 2 Synthesis of pyrimidine derivatives via route A (detailed synthetic procedures are described in reference 24a and 24d). Reagents and conditions: (A) 1 mol % $PdCl_2(PPh_3)_2$, 2 eq. Na_2CO_3, toluene/water/ethanol (1:1:2), 80 °C; (B) $SOCl_2$, 30 °C; (C) 6-aryl-2H-pyridazin-3-one, 1 eq. Cs_2CO_3, DMF, 40 °C or 1 eq. K_2CO_3, NMP, 80 °C; (D) 1.2 eq. bis(pinacolato)diboron, 3 eq. KOAc, 3 mol % $PdCl_2(PPh_3)_2$, DMF, 70 °C; (E) 1.5 eq. sodium perborate, THF/water, rt; (F) R'CH_2OH, triphenylphosphine, diisopropyl azodicarboxylate, THF, rt.

parasubstituted pyrimidines, a significantly lower number of metasubstituted pyrimidines were synthesized and tested for their ability to inhibit the activity of the c-Met kinase. Although meta- and paramodified aminoalkoxy pyrimidines offered the advantage of a lower drop-off between the cellular and biochemical activity values, the parasubstituted aminoalkoxy pyrimidine **47** demonstrated a superior biochemical and cellular potency compared with the corresponding isomer **46**.

A reasonable potency and a favorable physicochemical profile are regarded as a prerequisite for an attractive lead structure. However, the main complication for the discontinued carbamate series including compound **26** was the unfavorable safety profile incl. hERG activity and *in vitro* formation of micronuclei in the presence of metabolic activation by S9 mix. In order to get the first impression of the safety profile of the pyrimidine series, a set of representative compounds were tested in the micronucleus test assay and in the cellular hERG patch clamp assay. As expected, pyrimidines did not induce the formation of micronuclei in general. The inherent hERG activity of nonsubstituted pyrimidines was negligible, but depending on the lipophilicity and basicity of the solubilizing anchor, compounds like diaminopropyloxy pyrimidine **47** showed a residual hERG activity in the patch clamp assay[35] of around 6 μM. In contrast to the initially elaborated carbamate **26**, which turned out to be equipotent in the cellular c-Met autophosphorylation and the hERG patch clamp assay (both IC_{50}'s ~ 50 nM), even pyrimidines containing a basic anchor like **47** provided an initial hERG safety window of ~100 on a cellular level.

Based on these results and despite the fact that the clogP value of the cellular active compounds **43–47**, ranging between 3.8 and 4.1, is still regarded to be tendentially on the higher side, it was concluded that amino alkyloxy pyrimidines including compound **47** provided a more balanced profile. These modifications are offering a reasonable cellular potency in combination with an acceptable physicochemical and safety profile and therefore should be regarded as a blueprint for further derivatives. Multiple synthetic routes offer the access to para-alkoxy-substituted pyrimidinyl pyridazinones and are extensively described in the literature. One exemplified approach to access pyrimidine derivatives with a basic solubility anchor connected to the pyrimidine nucleus by an ether bridge is shown in **Scheme 2**.

Synthetic route A offered the advantage that the diversification step for the introduction of alkyl ethers was designed to be the ultimate step. The synthetic sequence and the involved chemistry came with certain flexibility as described in **Scheme 3** for the synthesis route B and allowed for multiple rearrangements in order to perform the diversifying step in the aryl pyridazinone part in the penultimate or ultimate step (**Scheme 3**). An additional advantage of this flexible synthesis was that the route could be adopted according to the prerequisites and limitations of the compounds to be synthesized. This especially became important for rather harsh synthetic conditions in the presence of labile substituents in the phenyl pyridazinone moiety.

N,*N*-dimethylamino-propoxy pyrimidine **47** had significantly improved cellular activity (**Table 11**) compared with pyrimidines without a basic moiety like alkyl, amino, hydroxyl, halogen, or carboxylic acids (**36** and **39–42**). This compound was regarded as an advanced lead and therefore extensively profiled in physicochemical and DMPK-related assays. The favorable overall physicochemical and stability profile of compound **47** is summarized in **Table 12**. Despite the relatively high clogP value of 4.1, the *N*,*N*-dimethylamino-propoxy pyrimidine **47** is surprisingly soluble.

The overall *in vitro* PK profile of pyrimidine **47** is summarized in **Table 13** and does not reveal any significant liabilities. Although the *in vitro* microsomal clearance in rodents is regarded suboptimal (**Table 13**), the intrinsic clearance in human hepatocytes and human microsomes is lower than 0.28 l h^{-1} kg^{-1} and lower than 10 μl min^{-1} mg^{-1}, respectively. CYP inhibition studies for compound **47** showed that only CYP2C9 was inhibited with an IC_{50} of 6.7 μM, whereas all other CYP isoenzymes (2C19, 1A2,

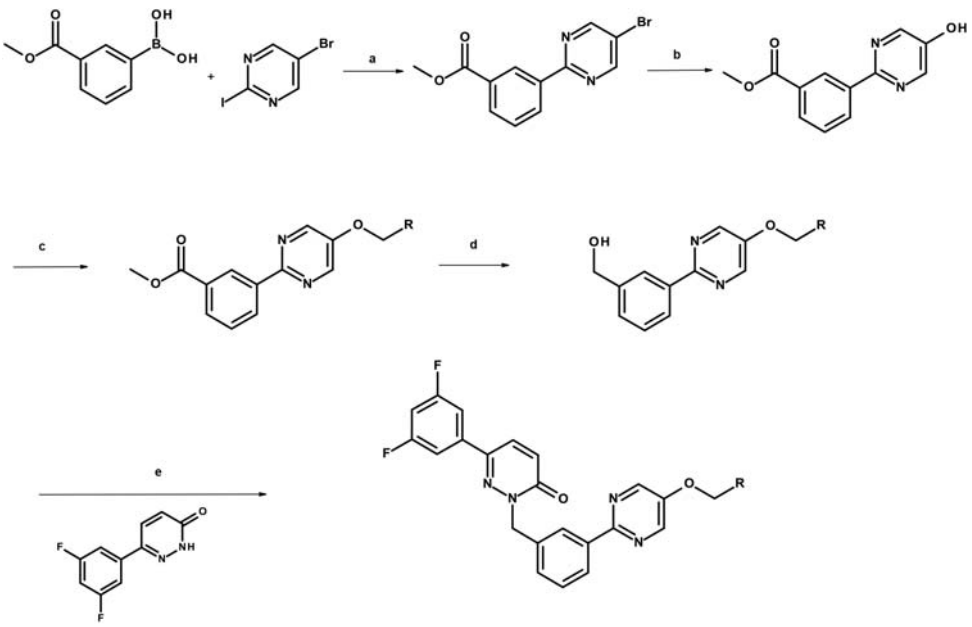

Scheme 3 Synthesis of pyrimidine derivatives via route B (detailed synthetic procedures are described in reference 24a and 24d). Reagents and conditions: (A) 1 mol % $PdCl_2(PPh_3)_2$, $KHCO_3$, toluene/water/methanol (1:1:2), 80 °C; (B) 1.2 eq. bis(pinacolato)diboron, 3 eq. KOAc, 3 mol % $PdCl_2(PPh_3)_2$, DMF, 70 °C; 1.5 eq. sodium perborate, THF/water, rt; (C) , triphenylphosphine, diisopropyl azodicarboxylate, THF, rt. (D) DIBAH, toluene, THF (E) , triphenylphosphine, diisopropyl azodicarboxylate, THF, rt.

2D6, and 3A4) are inhibited with IC_{50} values higher than 20 μM. Plasma protein binding in human plasma was concentration dependent and measured in a range of 97.4–99.06% at concentrations of 0.3 and 10 μM. The highly permeable pyridazinone **47** does not form reactive metabolites, which was tested by glutathione adduct trapping,[36] and in contrast to the observations for carbamate **26** in our plasma stability assay, pyrimidine **47** turned out to be stable in plasma of all species.

8.08.2.6 Fine-Tuning of the Phenyl Pyridazinone Substitution Pattern

Although the overall profile of the difluorophenyl pyridazinone **47** was reassuring, the relatively high lipophilicity in combination with a pronounced amphiphilic character reminded us of the phospholipidosis and hemolysis issue observed for the highly lipophilic carbamate with a pronounced molecular dipole. In order to further understand the SAR and reduce the safety risk, 40 additional molecules were synthesized with different substitution patterns and aryl/heteroaryl variations of the pyridazinone were synthesized with the focus of significantly reducing calculated logP/logD. This set of compounds was not only fully characterized with a special focus on the biochemical and cellular potency but also keeping an eye on the respective physicochemical and DMPK profile. A representative set of compounds including some key parameters are summarized in Table 14. Compared to the initial difluorophenyl residues, the majority of the modifications did not result in an improved biochemical or cellular potency (as in **48**, **49**, and **50**). The only compounds, combining a reduced lipophilicity with an improved biochemical and cellular activity, were 4-cyanophenyl- or 3-cyanophenyl pyridazinones **51** and **52** offering a factor of 3 in cellular and biochemical potency while lowering the measured logD value by 0.6. One potential explanation for the significantly improved potency of the cyano isomers **51** and especially for **52** could be derived from the integration of the cyano group into the water network interacting with multiple water molecules in the x-ray structure depicted in Fig. 11.

4-Cyanophenyl- and 3-cyanophenyl-derived pyridazinones **51** and **52** seem equally qualified for further optimization. While there was no striking difference to rationally favor one cyano substitution pattern over the other, due to the limited pharmacological and physicochemical profile, the metasubstituted compound was picked for further derivatization merely because of a slightly more favorable *in vitro* DMPK profile.

8.08.2.7 Final Selection of the Solubilizing Anchor Led to the Identification of Tepotinib

The last optimization cycle was dedicated to the identification and final selection of an appropriate solubilizing anchor for the 3-cyano phenyl substitution, balancing the need for a pronounced solubility and potency against a pronounced amphiphilic nature, its potential safety implications, and the associated pharmacokinetic profile of the respective compounds. Only a small set of meta-cyanophenyl-derived pyrimidines were synthesized based on our experience accumulated during the optimization of the solubilizing anchor in the carbamate series. Along with a small set of additional modifications not discussed in this communication,

Table 11 Introduction of substituents in the paraposition of the pyrimidine ring and their influence on *in vitro* c-Met potency and solubility

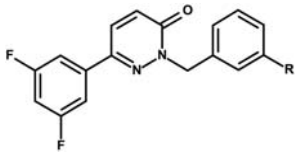

Cpd	*R*	*c-Met biochemIC$_{50}$ (nM)*	*c-Met cellularIC$_{50}$ (nM)*	*Kinetic solubility PBS pH 7.4 (μM)*	*clogP*	*BEI*
36	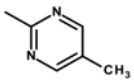	5	550	<2.6	3.6	21.3
39	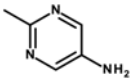	8	350	<2.6	2.5	20.7
40	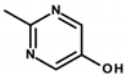	92	3800	34	3.3	17.9
41	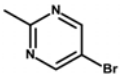	26	300	<2.2	4.2	16.7
42	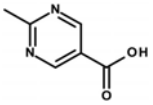	260	n.d.	>200	3.6	15.7
43	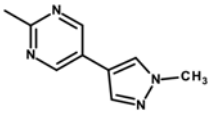	8	35	<2.2	3.8	17.7
44	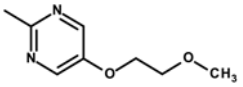	4	41	<2[a]	3.9	18.6
45	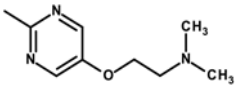	7	90	102	4.0	17.6
46	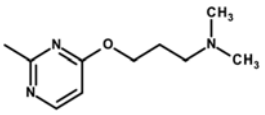	220	3800	n.d.	4.1	13.9
47	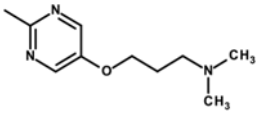	8	56	81	4.1	17.0

Table 12 Physchem and stability data of pyrimidine 47

Cpd	*clogP*	*clogD*	*tPSA*	*Thermodynamic solubility PBS pH 7.4 (μg ml^{-1})*	*Stability pH 8.5[a] (%)*	*Stability pH 1.2 (SGF)[a] (%)*	*Stability human plasma[a] (%)*
47	4.1	2.6	70.9	625	100	100	100

[a]% remaining after 2 h

Table 13 *In vitro* ADME data of pyridazinone **47**

Cpd	*Microsomal Cl_{int} (mouse/rat/human) ($\mu l\ min^{-1}\ mg^{-1}$)*	*Cl_{int} (human) (hepatocytes) ($L\ h^{-1}\ kg^{-1}$)*	*CYP inhibition*	*Protein binding (human)*	*Caco-2 permeability ($10^6\ cm\ s^{-1}$)*	*Reactive metabolites*
47	296 / 82 / < 10	<0.227	≥6.7 μM	97.4–99.06 % (conc. dep.)	14	No GSH adducts

Table 14 Fine tuning of aryl substitution pattern

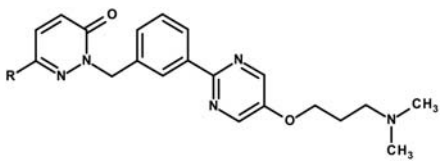

Cpd	R	*c-Met biochem IC_{50} (nM)*	*c-Met cell IC_{50}(nM)*	*$logD_{meas}$*	*Kinetic solubility PBS pH 7.4 (μM)*	*BEI*
47	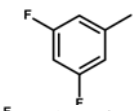	8	56	3.0	81	17.0
48	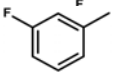	16	53	2.6	121	17.0
49		60	63	1.4	n.d.	16.3
50	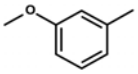	59	510	2.6	106	15.3
51	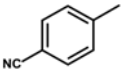	3	14	n.d.	142	18.3
52	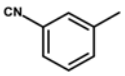	6	15	2.4	131	17.6

the main focus was on morpholines and piperidines described in Table 15. The dimethylaminopropyl-derived compound **52** already had acceptable pharmacokinetic properties in mice; the morpholino derivative **53** demonstrated an improved clearance but had somewhat lower cellular potency. Finally, the methylpiperidine derivative **7** (MSC2156119, also known as EMD 1214063 or tepotinib) combined very high biochemical and cellular potency of <1 nM and 6 nM, respectively, with suitable pharmacokinetic properties. The relatively high BEI values of more than 18.3 and the measured logD value of 1.4 were even more reassuring and increased the confidence that **7** should be regarded as a clinical candidate.

Shortly after the structure-guided rational design and the final selection of tepotinib **7**, selected compounds, representing important milestones or decisions in the compound optimization process, were selected and tested for their biophysical binding characteristics (k_{on}, k_{off}, and residence time) by solid plasmon resonance (SPR)[37]. Their key characteristics are summarized in Table 16.

It turned out that the residence time of tepotinib **7** was prolonged by orders of magnitude compared with even structurally closely related compounds, and serendipitously, a compound with a very long residence time of >1000 min was picked.

8.08.3 Characterization of Tepotinib

One of the very first characterizations after the final selection of tepotinib **7** was to confirm the anticipated binding conformation by solving a cocrystal structure of **7** in complex with c-Met. The resulting complex had a resolution of 1.2 Å (Fig. 11, PDB-ID: 4R1V), proving the assumed U-shaped binding mode, and was well in line with our expectations based on earlier cocrystal structures and our in-depth understanding of the underlying structure–activity relationship of this particular pyridazinone compound class.

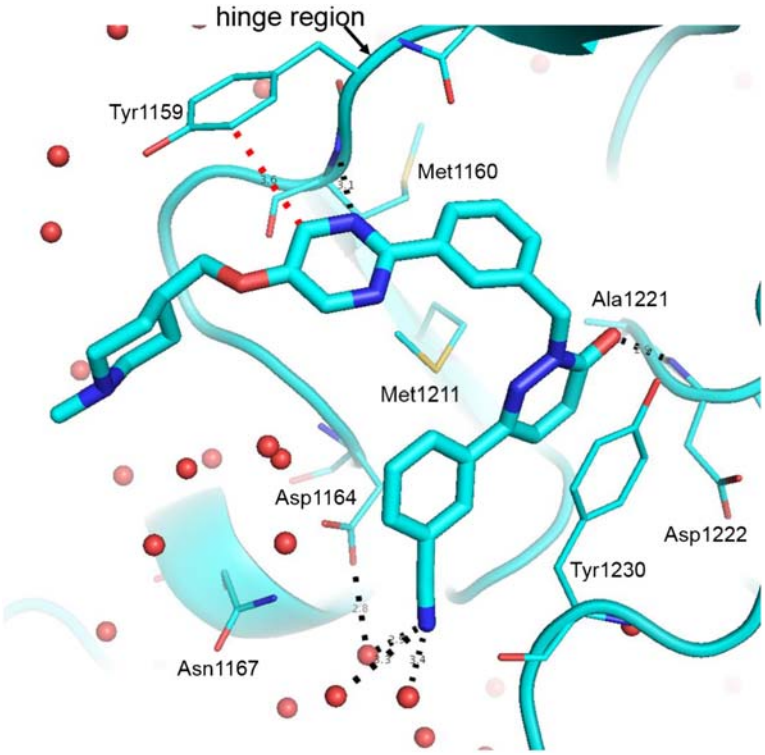

Fig. 11 The x-ray structure of the binding pocket of c-Met kinase in complex with tepotinib 7 with at 1.2. Å resolution (PDB-ID: 4R1V). Important ligand/protein interactions are shown as dashed lines, namely, the interaction between the pyrimidine nitrogen and the backbone of Met1160 (black), the pyridazinone O-atom and Asp1222 (black), and multiple interactions from the cyano group of the cyano phenyl toward different water molecules building a water cluster (black). Another potentially important interaction is calculated with the software tool ViewContacts[34] and visualized as dashed red line describing a close proximity (3.6 Å) and potential interaction of a CH–π interaction between the pyrimidine 3-CH-atom and the side chain of Tyr1159.

Table 15 Final selection of solubilizing anchor

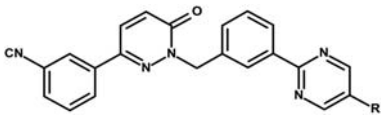

Cpd	*R*	*c-Met biochem IC_{50} (nM)*	*c-Met cell IC_{50}(nM)*	*clogD*	*BEI*	*Mouse PK*[a]	
						CL (L/h/kg)	*F (%)*
52	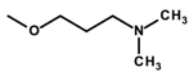	6	15	2.4	17.6	6.1	~32
53	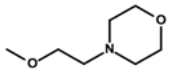	1	34	3.4	18.2	2.1	~35
7[b]	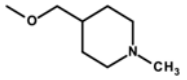	<1	6	1.4	>18.3	4.0	~41

[a]Screening (cocktail) PK study (please see the supplementary data of Bioorg. Med. Chem. Lett. 2015[24])
[b]For synthesis of cpd **7**, please see the supplementary data of Bioorg. Med. Chem. Lett. 2015[24a]

Table 16 Residence time

Cpd	*KD (M)*	k_{off} (s^{-1})	k_{on} (Ms^{-1})	*Residence time (min)*
26	4.54E-10	1.32E-03	2.90E+06	12.6
47	4.90E-10	5.91E-04	1.21E+06	28.2
51	3.64E-10	9.49E-04	2.61E+06	17.6
52	2.46E-10	1.14E-03	4.64E+06	14.6
7	n.m.[a]	n.m.[a]	n.m.[a]	>1000

[a]not reliably measurable due to the very long residence time. KD for tepotinib **7** is estimated to be < 100 pM

As expected, tepotinib is a class I ATP competitive inhibitor bound in the already-known binding mode to c-Met with the pyrimidine nitrogen as a hinge binder toward Met1160 and a nonclassical CH-π interaction between the pyrimidine and Tyr1159. In addition, the interaction between the pyridazinone O-atom and Asp1222 was visible and potentially contributes to the overall selectivity of this particular compound class. Although one could have expected a direct interaction between the cyano group of the meta cyano phenyl residue and Asn1167, the recognized interaction is water mediated by a cluster of three water molecules embedded into the overall water network and connected to Asp1164. These contacts may serve as an explanation for the significantly improved biochemical activities of the cyano-substituted phenyl residues compared with other substituents like fluoro or chloro. In summary, the following residues can be found in the vicinity of the ligand with a maximum distance of 3.9 A: Ile1084, Ala1108, Leu1140, Leu1157, Pro1158, Tyr1159, Met1160, Lys1161, Gly1163, Asp1164, Arg1208, Met1211, Ala1221, Asp1222, Ala1226, and Tyr1230.

A broad kinase profiling of tepotinib **7** was conducted at concentrations of 100 nM and 10000 nM. At a concentration of 100 nM (Fig. 12), **7** was not able to inhibit more than 30% of the activity of any kinase (besides c-Met) out of 284 kinases tested. In a second screening campaign at 10 μM (more than 1000-fold above the c-Met IC_{90} of MSC2156119), only 5 out of 242 kinases were

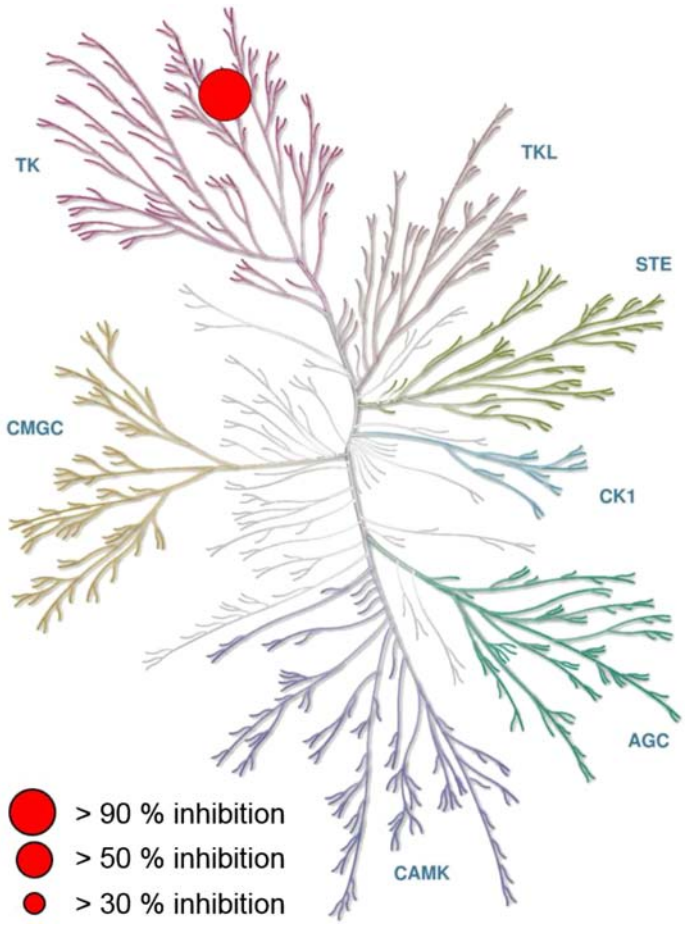

Fig. 12 Graphic representation of a percentage of inhibition of 284 kinases at a concentration of 100 nM of **tepotinib 7**.

inhibited by tepotinib with more than 50% (IRAK4, TrkA, Axl, IRAK1, and Mer). The IC_{50} determinations for the 5 kinases resulted in values ranging from 615 to 2272 nM. These activities are considered not to be relevant, because it is unlikely that MSC2156119 will achieve the pharmacologically relevant inhibitory free concentration of these kinases *in vivo*.

8.08.4 Pharmacokinetic Characterization of Tepotinib

The overall pharmacokinetic *in vitro* profile of tepotinib is summarized in Table 17. As it is symptomatic for this compound class, the microsomal clearance in rodents is pronounced, whereas **7** (MSC2156119) only showed a negligible intrinsic clearance in human microsomes and hepatocytes with $<10\ \mu l\ min^{-1}\ mg^{-1}$ and $<0.28\ L\ h^{-1}\ kg^{-1}$, respectively. All CYP P450 inhibition IC50s are equal or higher than 30 μM, and the CYP phenotyping revealed that tepotinib is mainly metabolized by CYP 3A4 without any evidence for reactive metabolites or metabolic intermediates evaluated by glutathione adduct trapping. **7** showed a human plasma protein binding of about 94% and was stable in plasma of mice, rats, dogs, and humans. According to CaCo2 studies, tepotinib can be considered as a highly permeable compound.

The *in vivo* pharmacokinetic properties of **7** were determined in regulatory (mono) PK studies in 4 preclinical species using solutions in solutol HS15/ethanol/water and suspensions in 0.25% aqueous methocel for *IV* and *PO* administration, respectively (Table 18). The *IV* clearance (CL) was moderate to high, in part even exceeding the liver blood flow in the respective species. The results may suggest elimination of **7** via hepatic *and* extrahepatic pathways at least in rats and dogs. The considerably lower clearance in monkeys is assumed to be due to a lower contribution of extrahepatic elimination. The volume of distribution at steady state (V_{ss}) was consistently high across all species indicative of pronounced distribution of **7** into organs and tissues. The *IV* plasma half-life ($t_{1/2}$) was moderate in rodents and longer in nonrodents. The oral bioavailability (F) from methocel suspension ranged from slightly more than 20% in dogs and monkeys up to 55% in rats despite the high clearance of **7** in the latter species. This is, however, well in line with the aforementioned assumption of extrahepatic elimination pathways.

Taken altogether, tepotinib **7** exhibits an overall acceptable pharmacokinetic profile with intermediate to high clearances, large volumes of distribution, medium to long plasma half-lives, and moderate oral bioavailability in the preclinical species tested. Based on various allometric scaling approaches (also considering, e.g., *in vitro* CL_{int} values as correction factors), a moderate clearance, a high volume of distribution, and consequently a long plasma half-life were predicted for humans.

8.08.5 Pharmacodynamic Characterization of Tepotinib

As described previously in the literature[24.b,24.c], the c-Met-related pharmacology of tepotinib was extensively studied *in vitro* and *in vivo*. First of all, cellular activity of tepotinib was investigated in HGF-stimulated A549 lung cancer cells using a capture ELISA assay format. Cells were serum-starved for 12 hto reduce background tyrosine phosphorylation, preincubated with test compounds for 30–45 min, and then stimulated with 100 ng ml^{-1} recombinant human HGF (R&D Systems) for 5 min. Reactions were stopped on ice by adding detergent-containing lysis buffer including a protease and phosphatase inhibitor cocktail. c-Met was captured on white ELISA plates using an antibody against its extracellular domain (R&D Systems), and total tyrosine phosphorylation was detected with a biotin-coupled version of the antiphosphotyrosine antibody pY99 (Santa Cruz), streptavidin-HRP (Amersham

Table 17 *In vitro* ADME data of pyridazinone pyrimidine **7**

Cpd	*Microsomal Cl_{int} (mouse/rat/human) ($\mu l\ min^{-1}\ mg^{-1}$)*	*Cl_{int} (human) (hepatocytes) ($L\ h^{-1}\ kg^{-1}$)*	*CYP inhibition*	*Protein binding (human)*[a]	*Caco-2 permeability ($10^6\ cm\ s^{-1}$)*	*Reactive metabolites*
7	131 / 52 / < 10	<0.28	≥30 μM	93.7%	11	No GSH adducts

[a]Stability measured at 37 °C (24 h incubation) expression as (% remaining)

Table 18 Pharmacokinetic data for compound **7** in preclinical species

Parameter[a]	*Mouse*	*Rat*	*Monkey*	*Dog*
Dose, mg kg^{-1} (*IV*/*PO*)	2 / 5	3 / 6	2 / 5	2 / 5
CL (*IV*), L $h^{-1}\ kg^{-1}$	4.0	4.7	0.73	3.3
V_{ss} (*IV*), L kg^{-1}	8.2	20	9.6	26
$t_{½}$ (*IV*), h	2.1	3.2	10	7.6
C_{max} (*PO*), ng mL^{-1}	62.2	66.0	55.5	22.4
F (*PO*), %	~41	~55	~25	~22

[a]Mean PK parameters in three female animals (mono PK studies)

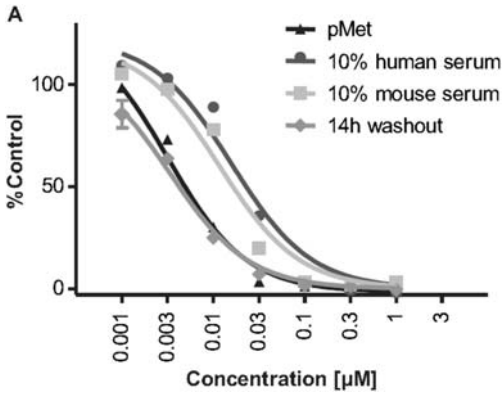

Fig. 13 Inhibition of HGF-induced c-Met phosphorylation by tepotinib **7** in A459 cells testing different conditions (triangles: standard (serum-free) conditions, squares: in the presence of 10% mouse serum, circles: in the presence of 10% human plasma, diamonds: standard (serum-free) conditions), after removal of tepotinib by 3x washing and 14 hrs incubation in fresh serum-free medium.

Biosciences), and a subsequent chemiluminescence reaction. Under these conditions, tepotinib inhibited the HGF-induced c-Met tyrosine phosphorylation with an IC_{50} of 6 nM and an efficacy of 100% (Fig. 13: triangles).

To address the effect of serum protein binding and metabolizing enzymes in serum on the activity of tepotinib, a similar cellular c-Met phosphorylation assay was conducted in the presence of 10% mouse serum or 10% human serum. Higher serum concentrations could not be used as they suppressed the HGF-induced c-Met phosphorylation, likely by binding of the added HGF to serum proteins or HGF inactivation by serum proteases. In the presence of murine or human serum, the IC_{50} values of tepotinib **7** were only shifted by a factor of ~2–5 as compared with serum-free conditions, likely reflecting the impact of serum protein binding on the effective free inhibitor concentration. This 2–5-fold IC_{50} shift was less dramatic than expected, based on the 96.9% plasma protein binding of tepotinib.

The sustainability of cellular c-Met inhibition was assessed by removing the tepotinib-containing supernatant after 30–45 min of incubation and washing cells. After a period of ~14 hrs in serum-free medium without inhibitor, HGF-induced c-Met tyrosine phosphorylation was measured using the capture ELISA assay. Despite the removal of the inhibitor-containing supernatant and extensive washing of the cells, a short incubation period with tepotinib was sufficient to block HGF-induced c-Met phosphorylation for at least 14 hrs reflected by unchanged IC_{50} values suggesting cellular retention and long-lasting activity of tepotinib. This observation supports the assumption that tepotinib has sustained pharmacological activity due to an extended residence time on c-Met. These effects were confirmed in additional models with high ligand-independent c-Met activation by c-Met gene copy number amplification and/or exon 14 skipping, like MKN-45 or Hs746T gastric cancer cells (data not shown).

Additional evidence for the long-lasting pharmacological effects of tepotinib came from autoradiograms of tumor-bearing mice after single oral dose application of ^{14}C-labeled tepotinib depicted in Fig. 14. Even after 24 and 48 h, the radioactivity is still detectable in target-expressing tissues like liver or the subcutaneously grafted tumor (Hs746T) suggestion, a long residence time of tepotinib, and a sustained c-Met inhibition.

The correlation between drug concentrations in plasma and tumor at various time points after a single application of tepotinib was studied in an *in vivo* PK/PD experiment (Fig. 15). In addition, a number of biomarkers downstream of the c-Met signaling pathway were analyzed to further characterize the mode of action (Fig. 16).

For these preclinical PK/PD studies, the levels of tyrosine phosphorylated c-Met in Hs746T gastric cancer xenografts were evaluated after a single oral application of tepotinib either by Western blotting or by immunohistochemistry with a phosphorylation site-specific antibody (Y^{1234}/Y^{1235}). The degree of target inhibition was then correlated with plasma and tumor levels of tepotinib.

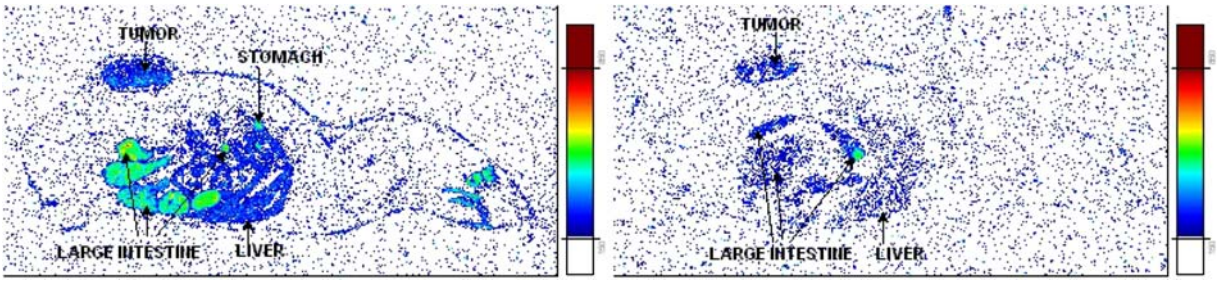

Fig. 14 Distribution of drug-related [^{14}C] radioactivity after single oral administration of 6 mg/kg [^{14}C]-tepotinib to tumor-bearing (Hs746T) nude mice (left 24 hrs and right 48 hrs).

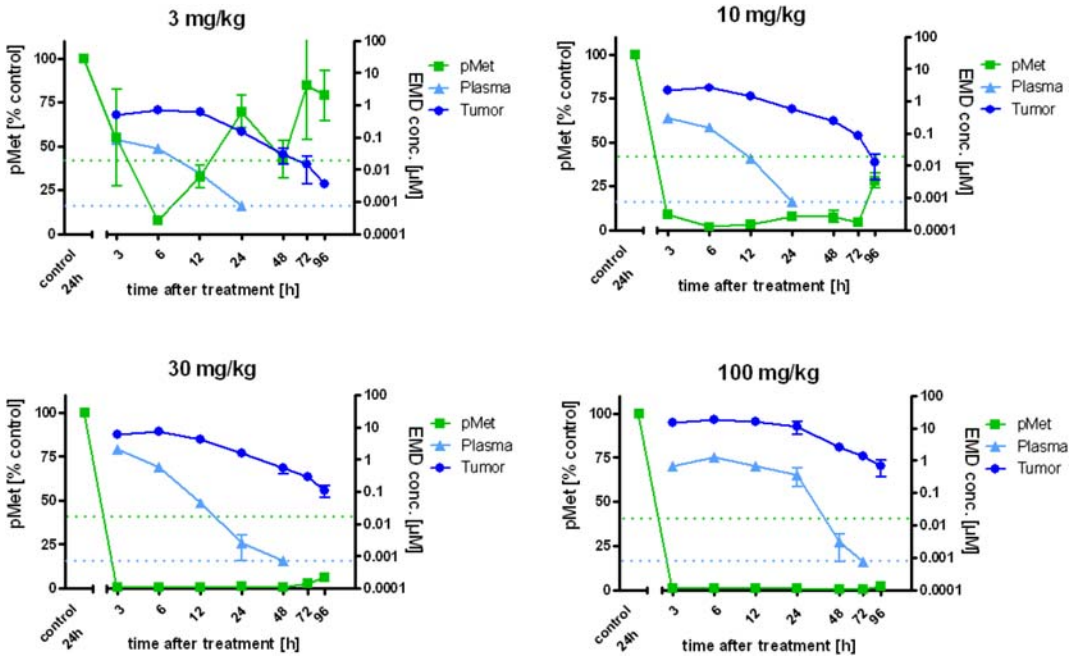

Fig. 15 Correlation of c-Met tyrosine phosphorylation (green squares) and drug concentrations in plasma (blue triangles) and tumor tissue (blue circles) following a single administration of 3, 10, 30, and 100 mg kg^{-1} of tepotinib. The dotted blue line indicates the detection limit for tepotinib, and the dotted green line marks the cellular IC_{50} of tepotinib for the inhibition of c-Met tyrosine phosphorylation in the presence of serum proteins.

In agreement with the PK study results, the relatively high volume of distribution (V_{ss} (mouse) ~ 8.2) of tepotinib led to compound concentrations in tumor tissue always higher than the corresponding plasma concentrations and remaining well above the cellular IC_{50} for considerable amount of time. The oral application of 30 and 100 mg kg^{-1} of tepotinib resulted in tumor concentrations of ≥ 100 nM and almost undetectable levels of phospho-c-Met for at least 4 days (Fig. 15). Even a daily dose of 10 mg kg^{-1} was sufficient to inhibit c-Met more than 90% for up to 3 days. Only a dose of 3 mg kg^{-1} was not able to block c-Met autophosphorylation for a sustained period of time. Altogether, the quantitative PK/PD data confirmed the sustained presence of tepotinib in the target tissue and a strong, long-lasting inhibition of c-Met *in vivo*.

Immunohistochemical studies utilizing tumor samples from PK/PD experiments confirmed a time- and dose-dependent inhibition of c-Met phosphorylation and suggest a tepotinib-induced cell cycle arrest and induction of apoptosis in Hs746T xenografts judged by decreased expression of cyclin D1 and increased levels of p27 and cleaved caspase-3 (Fig. 17).

Additional studies using targeted proteomic approaches and mRNA gene expression analysis aimed to identify pharmacodynamic biomarkers that could be detected in plasma and would therefore not require sequential tumor biopsies that are difficult to obtain in a clinical setting. Among several candidate biomarkers, the inhibition of IL-8 and VEGF secretion from tumor cells by tepotinib was considered most robust and worth to explore in the clinic.

Considering the strong constitutive activation of c-Met signaling in tumor cells with a c-Met gene amplification, the working hypothesis discussed in the literature (poster AACR 2006)[38] was that a sustained target coverage of greater than 90% is required to induce a therapeutically meaningful effect. Based on the generated PK/PD data, this would translate to an expected minimal efficacious dose of 3–10 mg kg^{-1} d^{-1} PO for c-Met-amplified tumor models, like Hs746T gastric or EBC-1 lung cancer xenografts.

Based on this hypothesis, c-Met-amplified human Hs746T and EBC-1 tumors were grafted onto mice and, depending on the cell line, treated with different daily doses of tepotinib, which should lead to a sustained > 90% target inhibition throughout the treatment period. As expected, in case of HS746T tumor-bearing mice, a daily dose of 10 mg kg^{-1} tepotinib **7** for 10 days resulted in an impressive complete response rate of 80% (tumors not detectable anymore in 8/10 animals) (Fig. 18), without any impact on body weights. In general, oral daily doses of up to 200 mg/kg tepotinib were well tolerated without any body weight changes, confirming the clean off-target profile of tepotinib and suggesting that even sustained c-Met inhibition is not associated with any acute toxicity in mice.

To assess the durability of response, c-Met amplified EBC-1 lung tumor xenografts were treated with doses of 6 and 15 mg kg^{-1} for 5 days followed by 2 days of drug holiday. This schedule was chosen for convenience reasons, only.

When the vehicle-treated control group reached the predefined maximal tumor volume at day 32, the treatment was stopped for all animals with the purpose to determine tumor growth delay. In the 6 mg kg^{-1} dose group, tumor growth reduction was observed during the treatment period, but 20 days after discontinuing the tepotinib treatment, tumors nearly reached the predefined maximal volume. In contrast, the 15 mg kg^{-1} dose of tepotinib applied PO using the 5 days on/2 days off schedule did result in an

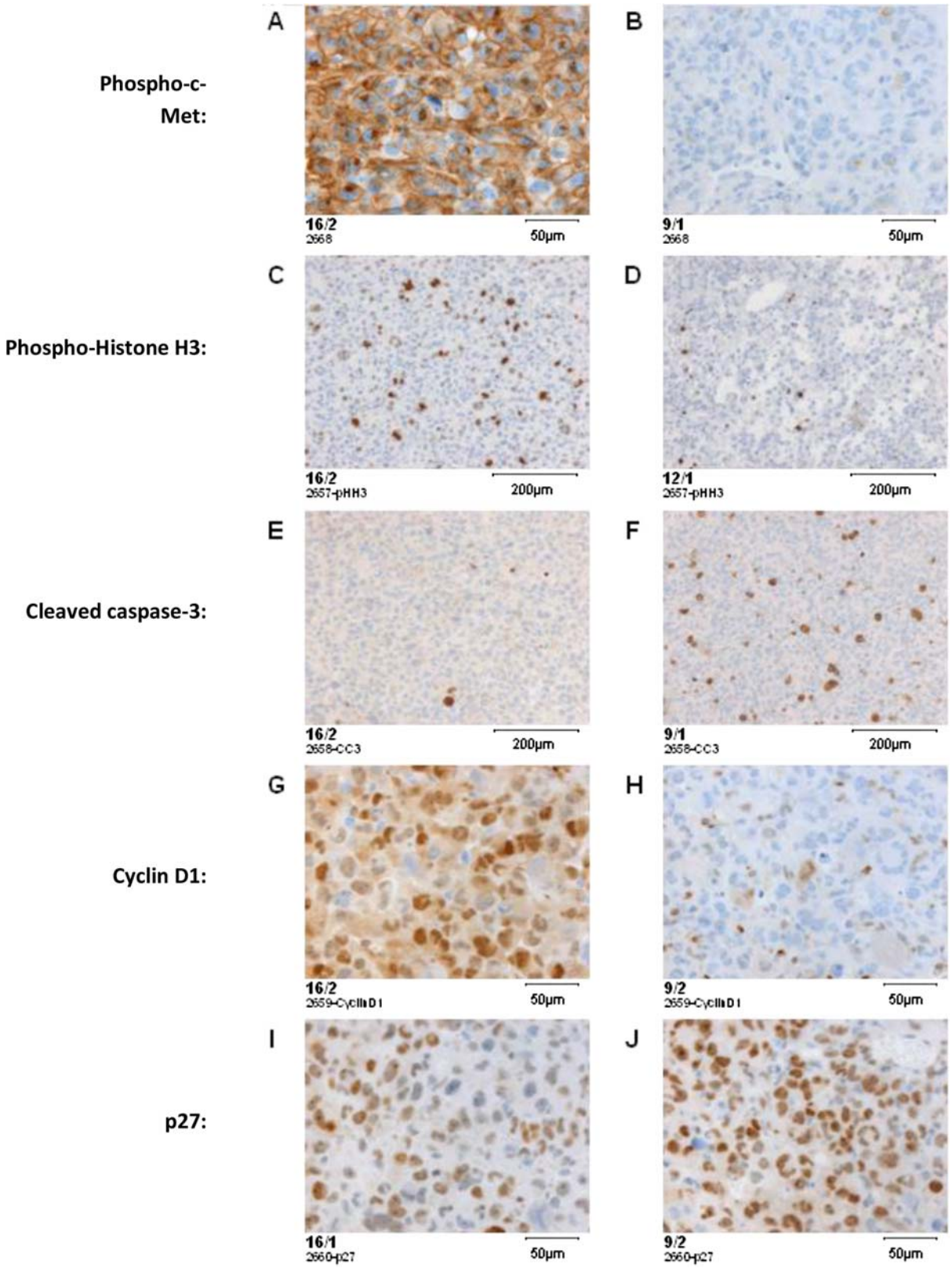

Fig. 16 Immunohistochemical analysis of phospho-Met (A, B)(Y^{1234}/Y^{1235}), phospho-histone H3 (C, D), cleaved caspase-3 (E, F), cyclin D1 (G, H), and p27 (I, J) levels in Hs746T xenografts treated for 24 (B, F, H, J) or 48 hrs (D) with vehicle (A, C, E, G, I) or 30 mg/kg of tepotinib as a single dose.

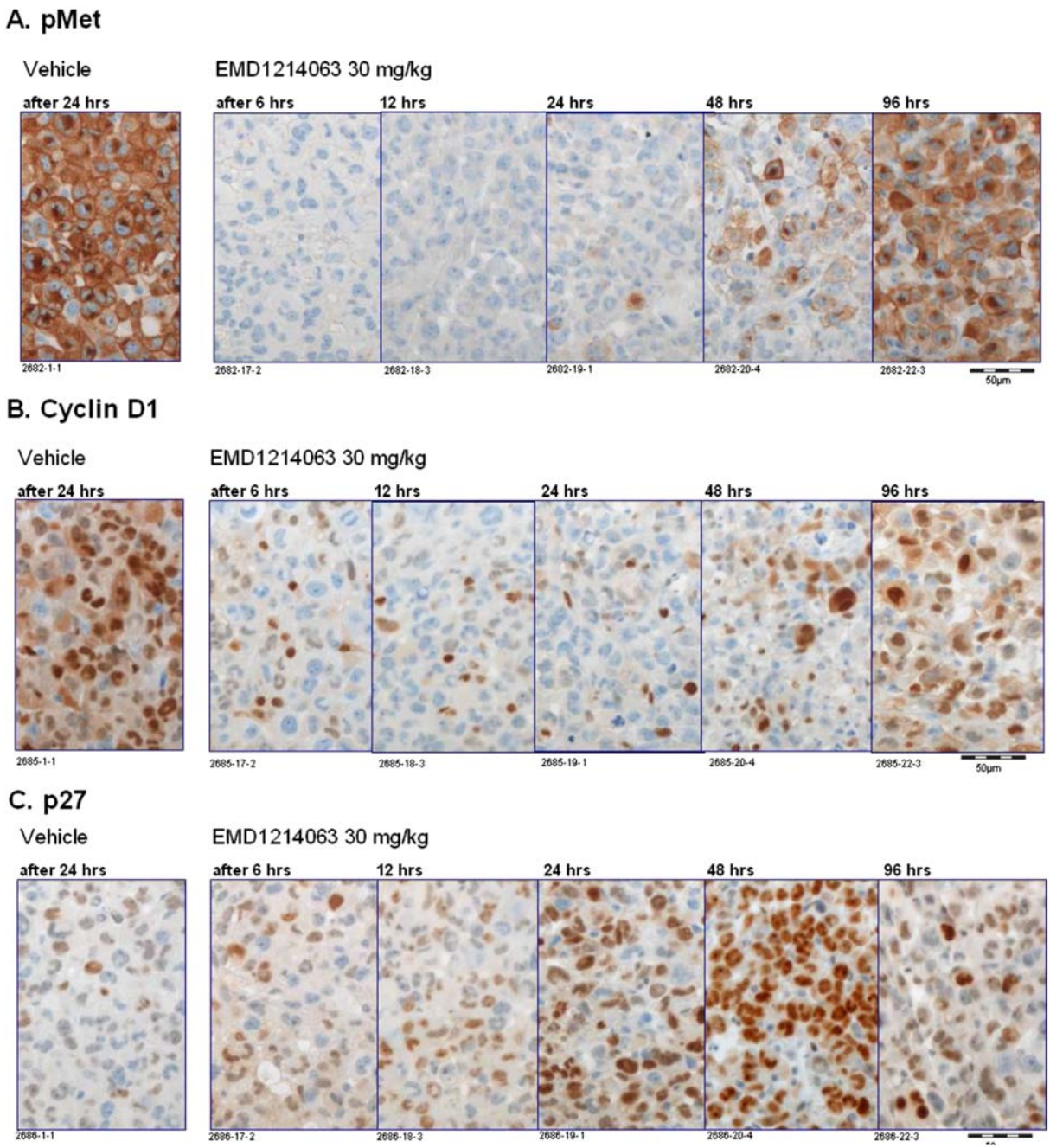

Fig. 17 Immunohistochemical analysis of phospho-Met (A), cyclin D1 (B), and p27 (C) levels in Hs746T xenografts different times after treatment with a single dose of 30 mg/kg of tepotinib (EMD1214063).

impressive complete response rate of 100% during the entire observation period of 84 days, well beyond the tepotinib treatment period of 32 days (Fig. 19). Again, all treatment regimens were well tolerated in mice without any body-weight changes.

In addition to highly oncogene addicted c-Met amplified tumor models, tepotinib was also very efficacious in autocrine models like KP-4 pancreatic tumors that secrete large amounts of HGF that permanently activate the coexpressed c-Met receptor and in genetically engineered murine tumors that express the constitutively active intracellular TPR-Met fusion protein (data not shown). The fact that murine HGF does not fully cross-react with human c-Met has initially limited further characterization of tepotinib in models where c-Met is activated by paracrine HGF stimulation. Therefore, genetically engineered mice were generated that express human HGF and allowed to study a larger variety of human tumor models that do express c-Met.

Based on its good preclinical safety profile, tepotinib could be well combined with standard of care chemotherapy and other targeted therapies, like small-molecule EGFR or PI3K pathway inhibitors (data not shown).

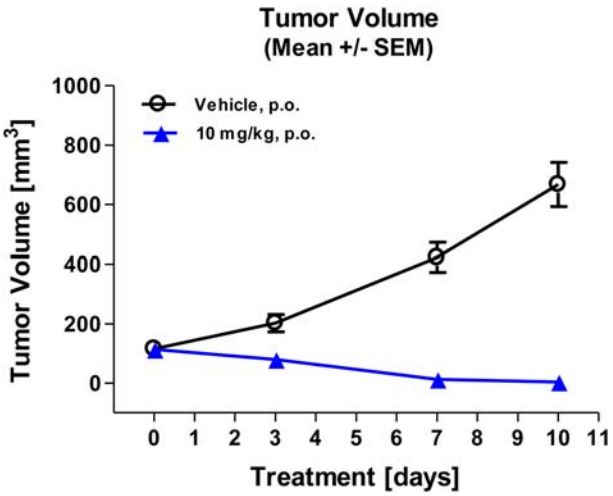

Fig. 18 Inhibition of the growth of Hs746T gastric cancer xenografts by a 10-d oral treatment with 10 mg kg^{-1} d^{-1} tepotinib.

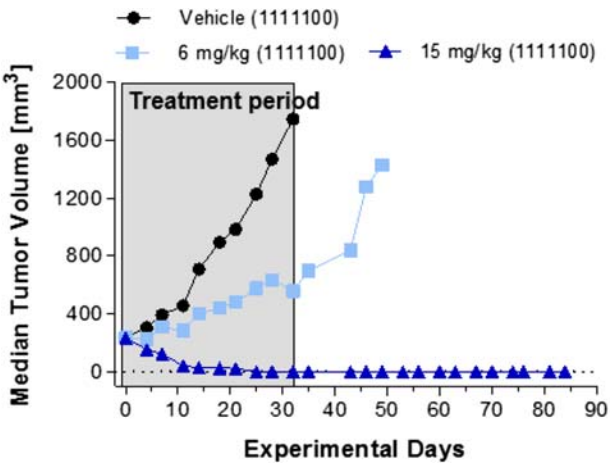

Fig. 19 Tumor growth inhibition of EBC-1 lung xenografts in nude mice treated with 6 and 15 mg kg^{-1} PO using a 5 days on/2 days off schedule. The treatment period is highlighted by a gray box.

In preclinical studies, high c-Met expression, c-Met gene amplification, exon 14 skipping, and c-Met and HGF coexpression were identified as a potentially predictive biomarker for the response of tepotinib.

Together with more extensive PK/PD studies in other tumor models, a comprehensive set of efficacy studies in regular xenografts and patient-derived primary tumor models, more detailed PK characterizations, and a robust preclinical safety package formed the basis for the human dose prediction and combined with phase I data for a selection of an optimal biologically active dose for phase II studies.

8.08.6 Summary and Conclusion

In summary (Fig. 20), the rationally guided compound optimization of our internal c-Met inhibitor program, started from an attractive singleton identified in a HTS run of 350 k compounds and led to the identification of tepotinib (**7**). The interesting thiadiazinone carbamates chemical series came from an internal phosphodiesterase program and demonstrated a high degree of kinase selectivity in combination with a significant inhibitory activity on c-Met kinase activity of around 30 nM. Though the binding efficiency index was only 14.5, the compound had a reasonable physicochemical profile and good solubility. Evaluating the biochemical and cellular structure–activity relationship that was regularly supported by cocrystal structures of c-Met in complex with various compounds from different classes, led to the identication of pyridazinone carbamates as a first generation of pharmacologically active and apparently attractive c-Met inhibitors. While this class of first-generation inhibitors including compound **26** had to be discontinued because of their unfavorable toxicological profile (phospholipidosis, QT prolongation, and direct cardiovascular side effects), the structural insights and the accumulated understanding of the pharmacological and toxicological structure–

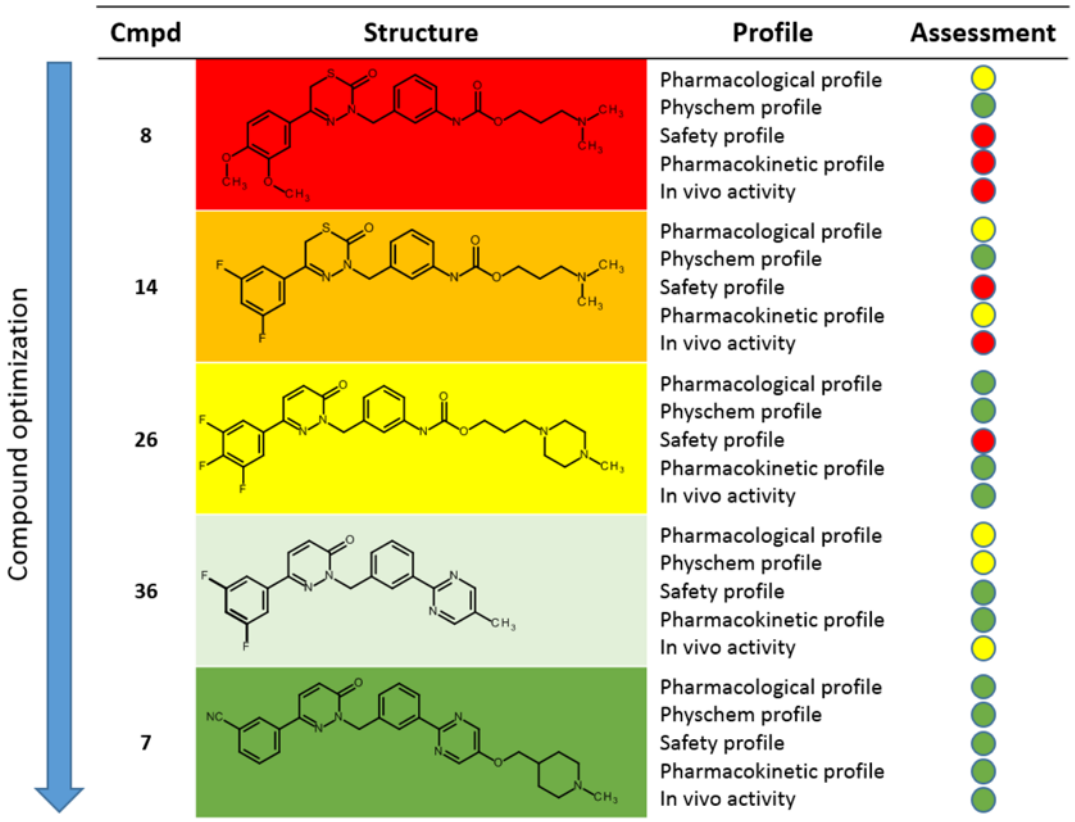

Fig. 20 A simplified graphic representation of the compound optimization process and some profile considerations.

activity relationship paved the way for a more holistic and finally successful compound optimization approach. The first milestone on the journey from an initial HTS hit toward a clinical candidate was the optimization of the substitution pattern of the aryl ring in order to diminish the residual PDE activity, followed by the switch from the chemically somewhat labile thiadiazinones toward the chemically more stable pyridazinones. The most valuable modification was the identification of the pyrimidine hinge binder as a potent and superior bioisostere of the toxicologically questionable alkyl carbamate. This modification is retrospectively regarded as the major breakthrough in the overall optimization process. This observation and the associated profile of the compounds are again underlining the reputation of pyrimidines as one of the preferred heterocycles used regularly in medicinal chemistry.[39] Subsequent fine-tuning of the solubilizing anchor and the aryl substitution pattern seems somehow trivial, but it was guided by the general compound quality considerations to identify a compound providing a balanced drug profile. Though many compounds consisting of combinations of different substructural motives, like pyridazinones, thiadiazinones, benzoxazolones, or carbamates, oxadiazoles and pyrimidines demonstrated significant *in vitro* potency on the c-Met kinase in combination with a reasonable pharmacokinetic and physicochemical profile; the most impressive *in vivo* efficacy was achieved by combining the pyridazinone core with pyrimidine moieties.

Tepotinib **7** demonstrated outstanding *in vivo* activity in multiple HGF-dependent and HGF-independent xenograft models, which may potentially be explained by the extraordinary residence time of more than 15 hoin combination with a pronounced PK/PD disconnect initially observed in cellular washout experiments. This explanation is also supported by a long-lasting target inhibition in our PK/PD *in vivo* experiments and by the sustained tumor concentration observed in autoradiographic *in vivo* experiments using tumor-bearing mice. Tepotinib offers a promising pharmacological *in vitro* and *in vivo* profile including the significant modulation of relevant downstream markers in combination with a favorable toxicological profile without the aforementioned concerning safety signals seen for the pyridazinone carbamate around compound **26**. Tepotinib **7** (MSC2156119) is an exquisitely selective and highly potent c-Met inhibitor with a reassuring pharmacokinetic and pharmacodynamic profile. Tepotinib **7** is currently evaluated in clinical phase II proof-of-concept studies in EGFR-inhibitor-resistant, c-Met overexpressing NSCLC and in c-Met overexpressing hepatocellular cancer in order to evaluate the potential of monospecific c-Met inhibitors in these particular oncological applications.

8.08.7 Supplementary Material

Experimental details including assay protocols and synthetic procedures are mainly described in references (24a–d) and (29)–(31).

Acknowledgment

We would like to thank Dieter Dorsch, Frank Stieber, Doris Weidenkopf-Look, Winfried Hofmann, Daniela Radtki, Claudio Ritzert, Amandine Bouhelier, Christoph Goeldner, Beate Opelt, Corinna Rettig, Cornelia Manderscheid, Peter Wendel, Markus Woissyk, Georg Stoehr, and Andreas Werner for synthetic support; Lukas Roth, Irina Onofrei, Iris Mannberger, Ralf Emmerich, Friedhelm Bladt, Manja Friese-Hamim, Christine Knuehl, and Ulrich Pehl for supervising and conducting biological assays and experiments; Michael Meyring for pharmacokinetic support; Ulrich Graedler for refining and providing the cocrystal structures; Joerg Bomke and Daniel Schwarz for providing the SPR data; and Bayard Huck, Dieter Dorsch, and Dirk Finsinger for reviewing the manuscript.

See also: 8.06. Discovery of AMG 337: Using Structure Guided Scaffold Hybridization to Optimize Physicochemical Properties and Target Coverage of a MET Kinase Inhibitor.

References

1. Eder, J. P.; Vande Woude, G. F.; Boerner, S. A.; LoRusso, P. M. Novel therapeutic inhibitors of the c-Met signaling pathway in cancer. *Clin. Cancer Res.* **2009,** *15,* 2207–2214.
2. Birchmeier, C.; Birchmeier, W.; Gherardi, E.; Vande Woude, G. F. Met, metastasis, motility and more. *Nat. Rev. Mol. Cell Biol.* **2003,** *4,* 915–925.
3. Bladt, F.; Riethmacher, D.; Isenmann, S.; Aguzzi, A.; Birchmeier, C. Essential role for the c-met receptor in the migration of myogenic precursor cells into the limb bud. *Nature* **1995,** *376,* 768–771.
4. Schmidt, C.; Bladt, F.; Goedecke, S.; Brinkmann, V.; Zschiesche, W.; Sharpe, M.; et al. Scatter factor / hepato-cyte growth factor is essential for liver development. *Nature* **1995,** *373,* 699–702.
5. Di Renzo, M. F.; Narsimhan, R. P.; Olivero, M.; Bretti, S.; Giordano, S.; Medico, E.; Gaglia, P.; Zara, P.; Comoglio, P. M. *Oncogene* **1991,** *6,* 1997.
6. Liu, Y.; Tolbert, E. M.; Lin, L.; Thursby, M. A.; Sun, A. M.; Nakamura, T.; et al. Up-regulation of hepatocyte growth factor receptor: an amplification and targeting mechanism for hepatocyte growth factor action in acute renal failure. *Kidney Int.* **1999,** *55,* 442–453.
7. Xian, C. J.; Couper, R.; Howarth, G. S.; Read, L. C.; Kallincos, N. C. Increased expression of HGF and c-Met in rat small intestine during recovery from methotrexate-induced mucositis. *Br. J. Cancer* **2000,** *82,* 945–952.
8. Goetsch, L.; Caussanel, V. Selection criteria for c-Met-targeted therapies: emerging evidence for biomarkers. *Biomark. Med* **2010,** *4,* 149–170.
9. (a) Gherardi, E.; Birchmeier, W.; Birchmeier, C.; Vande Woude, G. *Nat. Rev. Cancer* **2012,** *12,* 89; (b) Goyal, L.; Muzumdar, M. D.; Zhu, A. X. *Clin. Cancer Res.* **2013,** *19,* 2310; (c) Turke, A. B.; Zejnullahu, K.; Wu, Y. L.; Song, Y.; Dias-Santagata, D.; Lifshits, E.; Toschi, L.; Rogers, A.; Mok, T.; Sequist, L.; Lindeman, N. I.; Murphy, C.; Akhavanfard, S.; Yeap, B. Y.; Xiao, Y.; Capelletti, M.; Iafrate, A. J.; Lee, C.; Christensen, J. G.; Engelman, J. A.; Jänne, P. A. *Cancer Cell* **2010,** *17,* 77.
10. Schmidt, L.; Duh, F. M.; Chen, F.; Kishida, T.; Glenn, G.; Choyke, P.; et al. Germline and somatic mutations in the tyrosine kinase domain of the MET proto-oncogene in papillary renal carcinomas. *Nat. Genet.* **1997,** *16,* 68–73.
11. (a) Gherardi, E.; Birchmeier, W.; Birchmeier, C.; Vande Woude, G. *Nat. Rev. Cancer* **2012,** *12,* 89. Erratum in Nat. Rev. Cancer; Graveel, C. R.; Tolbert, D.; Vande Woude, G. F. *Cold Spring Harb. Perspect. Biol.* **2013,** *5* (7).
12. Cooper, C. S.; Park, M.; Blair, D. G.; Tainsky, M. A.; Huebner, K.; Croce, C. M.; Vande Woude, G. F. *Nature* **1984,** *311* (5981), 29–33.
13. (a) Cecchi, F.; Rabe, D. C.; Bottaro, D. P. *Expert Opin. Ther. Targets* **2012,** *16,* 553; (b) Smyth, E. C.; Sclafani, F.; Cunningham, D. *Onco Targets Ther.* **2014,** *7,* 1001.
14. (a) Kim, S.-E.; Shi, Z.-D.; Peach, M.; Giubellino, A.; Nicklaus, M. C.; Bottaro, D.; Burke, T. R. Design and synthesis of c-met kinase inhibitors based on an in silico screen-derived lead. From Abstracts of Papers, 234th ACS National Meeting, Boston, MA, United States, August 19-23, 2007; (b) Zou Helen, Y.; Qiuhua, Li; Lee Joseph, H.; Arango Maria, E.; McDonnell Scott, R.; Shinji, Yamazaki; Koudriakova Tatiana, B.; Gordon, Alton; Cui Jingrong, J.; Pei-Pei, Kung.; et al. An orally available small-molecule inhibitor of c-Met, PF-2341066, exhibits cytoreductive antitumor efficacy through antiproliferative and antiangiogenic mechanisms. *Cancer Res.* **2007,** *67* (9), 4408–4417; (c) Christensen, James G.; Zou Helen, Y.; Arango Maria, E.; Qiuhua, Li; Lee Joseph, H.; McDonnell Scott, R.; Shinji, Yamazaki; Alton Gordon, R.; Barbara, Mroczkowski; Gerrit, Los. Cytoreductive antitumor activity of PF-2341066, a novel inhibitor of anaplastic lymphoma kinase and c-Met, in experimental models of anaplastic large-cell lymphoma. *Mol. Cancer Ther.* **2007,** *6* (12 Pt 1), 3314–3322.
15. Cui, J. J.; McTigue, M.; Nambu, M.; Tran-Dube, M.; Pairish, M.; Shen, H.; Jia, L.; Cheng, H.; Hoffman, J.; Le, P.; et al. Discovery of a Novel Class of Exquisitely Selective Mesenchymal-Epithelial Transition Factor (c-MET) Protein Kinase Inhibitors and Identification of the Clinical Candidate 2-(4-(1-(Quinolin-6-ylmethyl)-1H-[1,2,3]triazolo[4,5-b] pyrazin-6-yl)-1H-pyrazol-1-yl)ethanol (PF-04217903) for the Treatment of Cancer. *J. Med. Chem.* **2012,** *55* (18), 8091–8109.
16. Buchanan, S. G.; Hendle, J.; Lee, P. S.; Smith, C. R.; Bounaud, P. Y.; Jessen, K. A.; et al. SGX523 is an exquisitely selective, ATP-competitive inhibitor of the MET receptor tyrosine kinase with antitumor activity in vivo. *Mol. Cancer Ther.* **2009,** *8,* 3181–3190.
17. (a) Underiner, T. L.; Herbertz, T.; Miknyoczki, S. *J. Anti-Cancer Agents Med. Chem.* **2010,** *10,* 7; (b) Lu, T.; Alexander, R.; Connors, R. W.; Cummings, M. D.; Galemmo, R. A.; Hufnagel, H. R.; Johnson, D. L.; Khalil, E.; Leonard, K. A.; Markotan, T. P.; Maroney, A. C.; Sechler, J. L.; Travins, J. M.; Tuman, R. W. *PCT Int. Appl.* **2007**. WO2007075567.
18. (a) Meetze, A. K.; Boudrow, A.; Connoly, K.; et al. Anti-tumor activity of SCH 900105 (AV299), an anti-HGF antibody in non-small cell lung cancer models. AACR-NCI-EORTC—international conference—molecular target and cancer therapeutics, 2009; p p. C173; (b) Meetze, A. K.; Connoly, K.; Boudrow, A.; et al. Preclinical efficacy and pharmacodynamics of SCH 900105 (AV-299) and anti-HGF antibody in an intracranial glioblastoma. AACR-NCI-EORTC—international conference—molecular target and cancer therapeutics**;** 2009; p p. C181; (c) Ramanathan, R. K.; Paymo, C. F.; Papadopoulos, P. K.; et al. A phase 1 first-in-human study of SCH 900105, an antihepatocyte growth factor (HGF) monoclonal antibody, in subjects with advanced solid cancer, AACR, 2009; Abstract A100; 2009; (d) Patnaik, A.; Weiss, G. J.; Papadopoulos, K. P.; et al. Phase I ficlatuzumab monotherapy or with erlotinib for refractory advanced solid tumours and multiple myeloma. *Br. J. Cancer* **2014,** *111* (2), 272; (e) Tabernero, J.; Elez, M. E.; Herranz, M.; et al. A pharmacodynamic/pharmacokinetic study of ficlatuzumab in patients with advanced solid tumors and liver metastases. *Clin. Cancer Res.* **2014,** *20* (10), 2793.
19. Zhang, Y.; Doshi, S.; Zhu, M. Pharmacokinetics and pharmacodynamics of rilotumumab: A decade of experience in preclinical and clinical cancer research. *Br. J. Clin. Pharmacol.* **2015,** *80* (5), 957.
20. (a) Morley, R.; Cardenas, A.; Hawkins, P.; et al. PLoS ONE, Safety of onartuzumab in patients with solid tumors: Experience to date from the onartuzumab clinical trial program. *PLoS ONE* **2015,** *10* (10), e0139679; (b) Jin, H.; Yang, R.; Zheng, Z.; Romero, M.; Ross, J.; Bou-Reslan, H.; et al. MetMAb, the one-armed 5D5 anti-c-Met antibody, inhibits orthotopic pancreatic tumor growth and improves survival. *Cancer Res.* **2008,** *68,* 4360–4368.
21. Schuller, A. G.; Barry, E. R.; Jones, R. D.; et al. The MET inhibitor AZD6094 (Savolitinib, HMPL-504) induces regression in papillary renal cell carcinoma patient-derived xenograft models. *Clin. Cancer Res.* **2015,** *21* (12), 2811.
22. Boezio, A.; Albrecht, B.; Bauer, D.; et al. Discovery of AMG 337, a potent and selective inhibitor of c-Met with high unbound exposure and robust, extended in vivo antitumor activity. 250th Am Chem Soc (ACS) Natl Meet (August 16-20, Boston) 2015. Abst MEDI 344.
23. Liu, X.; Wang, Q.; Yang, G.; Marando, C.; Koblish, H. K.; Hall, L. M.; et al. A novel kinase inhibitor, INCB28060, blocks c-MET-dependent signaling, neoplastic activities, and cross-talk with EGFR and HER-3. *Clin. Cancer Res.* **2011,** *17,* 7127–7138.

24. (a) Dorsch, D.; Schadt, O.; Stieber, F.; et al. Identification and optimization of pyridazinones as potent and selective c-Met kinase inhibitors. *Bioorg. Med. Chem. Lett.* **2015,** *25* (7), 1597; (b) Bladt, F.; Faden, B.; Friese-Hamim, M.; Knuehl, C.; Wilm, C.; Fittschen, C.; Grädler, U.; Meyring, M.; Dorsch, D.; Jaehrling, F.; Pehl, U.; Stieber, F.; Schadt, O.; Blaukat, A. *Clin. Cancer Res.* **2013,** *19,* 2941; (c) Bladt, F.; Friese-Hamim, M.; Ihling, C.; Wilm, C.; Blaukat, A. *Cancers* **2014,** *6,* 1736; (d) Dorsch, D.; Stieber, F.; Schadt, O.; Blaukat, A. *PCT Int. Appl.* **2009**. WO2009006959.
25. Bender, A. T.; Beavo, J. A. PDE3 inhibition can lead to ventricular arrhythmias, PDE4 inhibitors may promote emesis. *Pharmacol. Rev.* **2006,** *58,* 488.
26. Synthesis described in Jonas, R.; Wolf, M.; Klockow, M., Eur. Pat. Appl. EP 723962 A1 and Jonas, R.; Wolf, M.; Beier, N., Ger. Offen. (1997), DE 19604388 A1.
27. (a) Kodimuthali, A.; Jabaris, S. S. L.; Pal, M. *J. Med. Chem.* **2008,** *51,* 5471; (b) Kümmerle, A. E.; Schmitt, M.; Cardozo, S. V. S.; Lugnier, C.; Villa, P.; Lopes, A. B.; Romeiro, N. C.; Justiniano, H.; Martins, M. A.; Fraga, C. A. M.; Bourguignon, J.-J.; Barreiro, E. *J. Med. Chem.* **2012,** *55,* 7525.
28. Meanwell, N. A. Synopsis of Some Recent Tactical Application of Bioisosteres in Drug Design. *J. Med. Chem.* **2011,** *54,* 2529–2591.
29. Dorsch, D.; Schadt, O.; Blaukat, A. *PCT Int. Appl* **2007**. WO2007065518.
30. Dorsch, D.; Schadt, O.; Blaukat, A. *PCT Int. Appl.* **2007**. WO2007019933.
31. Dorsch, D.; Stieber, F.; Schadt, O.; Blaukat, A. *PCT Int. Appl.* **2008**. WO2008148449.
32. Shimkin, M. B.; Wieder, R.; McDonough, M.; Fishbein, L.; Swern, D. *Cancer Res.* **1969,** *29,* 2184.
33. Zavod, R. M.; Knittel, J. J. In *Foye's Principles of Medicinal Chemistry;* Lemke, T. L., Williams, D. A., Eds., 7th ed.; Lippincott Williams and Wilkins: Baltimore, 2013; p 53.
34. Kuhn, B.; Fuchs, J. E.; Reutlinger, M.; Stahl, M.; Taylor, N. R. *J. Chem. Inf. Model.* **2011,** *51,* 3180.
35. Danker, T.; Moeller, C. Early identification of hERG liabilites in drug discovery programs by automated patch clamp. *Front. Pharmacol.* **2014,** *5,* 203.
36. (a) Grillo, M. Detecting reactive drug metabolites for reducing the potential for drug toxicity. *Expert Opin. Drug Metab. Toxicol.* **2015,** *11* (8), 1281–1302; (b) Lassila, T.; Rousu, T.; Mattila, S.; Chesné, C.; Pelkonen, O.; Turpeinen, M.; Tolonen, A. Formation of GSH-trapped reactive metabolites in human livermicrosomes, S9 fraction, HepaRG-cells, and human hepatocytes. *J. Pharm. Biomed. Anal.* **2015,** *115,* 345–351.
37. Huber, W. A new strategy for improved secondary screening and lead optimization using high-resolution SPR characterization of compound–target interactions. *J. Mol. Recognit.* **2005,** *18,* 273–281.
38. Zou, H. Y.; Li, Q.; Arango, M.; McDonnell, S. R.; Dusell, C.; Stempniak, M.; Yamazaki, S.; Koudriakova, T.; Alton, G.; Cui, J.; Tran-Dube, M.; Kung, P. P.; Nambu, M.; Los, G.; Bender, S.; Mroczkowski, B.; Christensen, J. *Identification and Characterization of an Orally Bioavailable Small Molecule Inhibitor of c-Met Kinase with Cytoreductive Antitumor Properties In Vivo, Poster 4596, Abstract LB-273, AACR,* 2006.
39. Ritchie, T. J.; Macdonald, S. J. F.; Peace, S.; Pickett, S. D.; Luscombe, C. N. The developability of heteroaromatic and heteroaliphatic rings—do some have a better pedigree as potential drug molecules than others? *Med. Chem. Commun.* **2012,** *3,* 1062–1069.

8.09 Verubecestat

AW Stamford, Merck & Co., Inc., Rahway, NJ, United States
JN Cumming, JD Scott, and CO Strickland, Merck & Co., Inc., Kenilworth, NJ, United States

© 2017 Elsevier Ltd. All rights reserved.

8.09.1	**Introduction**	204
8.09.2	**BACE1 Characteristics and Drug Discovery Challenges**	206
8.09.3	**BACE1 Inhibitor Lead-Finding Strategies**	207
8.09.3.1	Overview	207
8.09.3.2	BACE1 and CatD in vitro Assays	208
8.09.3.3	Hydroxyethylamine-Based Peptidomimetic Inhibitors	208
8.09.3.4	Fragment Screening: Discovery of New Inhibitor Chemotypes	210
8.09.3.4.1	Fragment screening and hit triage	210
8.09.3.4.2	Iminoheterocycle scaffold design and validation	212
8.09.3.4.3	Iminohydantoin hit-to-lead prosecution	214
8.09.4	**Lead Optimization**	219
8.09.4.1	Iminohydantoins: S3 Occupancy	219
8.09.4.2	Iminohydantoins: Advanced Lead Optimization	221
8.09.4.3	Core Modification: Ring Expansion to Iminopyrimidinone	223
8.09.4.4	In Vivo Validation and Development of a High-Throughput Rat PD Assay	226
8.09.4.5	Iminopyrimidinones: Advanced Optimization of the P1-P3 Biaryl Series	229
8.09.4.6	Structural Differentiation: Occupancy of S2′	231
8.09.4.7	From Acyl Guanidines to Sulfonyl Guanidines: Discovery of Iminothiadiazinane Dioxides	235
8.09.5	**Discovery of Verubecestat**	237
8.09.5.1	S1–S3 Spanning Diaryl Amides: Rationale	237
8.09.5.2	Verubecestat Cocrystal Structure, in vitro Profile, and Key SAR	238
8.09.5.3	Verubecestat Synthesis	240
8.09.5.4	PK/PD Profile of Verubecestat in Preclinical Species	241
8.09.5.5	Human Dose and PK/PD Projections	242
8.09.6	**Clinical Evaluation**	243
8.09.7	**Conclusions**	245
References		246
Relevant Websites		251

8.09.1 Introduction

Alzheimer's disease (AD) is a chronic, progressive, ultimately fatal neurodegenerative disease, and is the most common cause of dementia.[1] Predominantly a disease of the elderly, AD is a leading cause of death in the United States[2] and is increasing in incidence globally as the population ages.[3] In 2015, there were an estimated 46 million patients with dementia worldwide, and the estimated cost for caring for these individuals was US$ 818 billion.[4] By 2050 the global incidence of AD is projected to nearly triple,[4] and estimates place the annual cost of patient care at >US$ 1 trillion in the United States alone,[5] creating an unsustainable healthcare burden.

Initial symptoms of AD usually manifest as short-term memory loss. As the disease progresses there is a worsening of cognitive function, decreased ability to perform activities of daily living, and profound personality and behavioral disturbances.[1] In the latter stages of the disease patients typically require constant care, placing a significant burden on family members and caregivers. Current treatments—the acetylcholinesterase inhibitors and the *N*-methyl-D-aspartate receptor antagonist memantine—provide modest, temporary symptomatic benefit but do not impact the underlying disease pathogenesis.[6] Consequently, there is an urgent need to develop disease-modifying therapies that alleviate the profound patient, caregiver, and socioeconomic burden of the disease.

Invariant histopathological hallmarks in postmortem AD patient brains are extracellular neuritic plaques composed primarily of aggregated amyloid β (Aβ) peptides and intracellular neurofibrillary tangles composed primarily of hyperphosphorylated tau protein.[7] The disease progresses over the course of decades with the occurrence of pathological changes in the brain antecedent to the emergence of cognitive symptoms. The temporal relationship between biomarkers of AD pathophysiology—amyloid positron emission tomography (PET) imaging, tau PET imaging, cerebrospinal fluid (CSF) $A\beta_{42}$, CSF Tau, and structural MRI—suggests that amyloid accumulation occurs early in the disease process while accumulation of Tau tangles occurs later and correlates more closely with neuron loss and clinical symptoms of cognitive decline.[8,9]

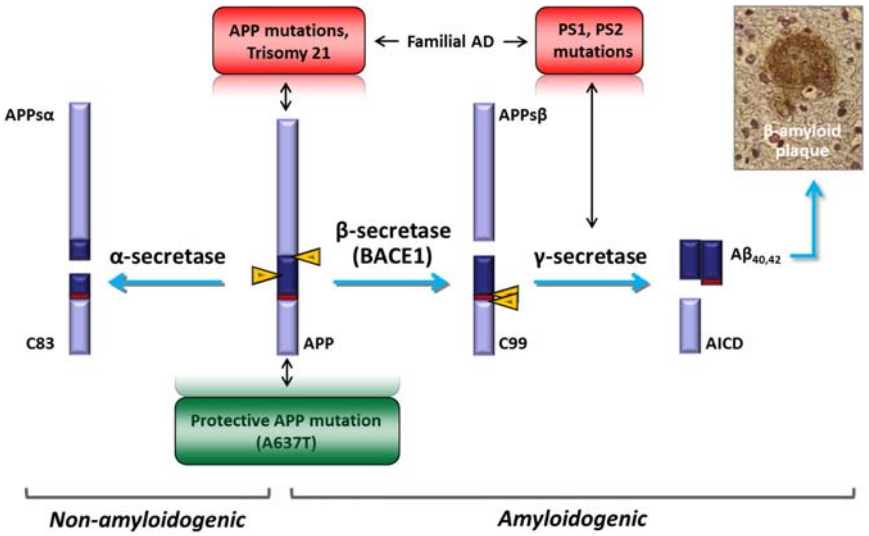

Fig. 1 Schematic representation of the amyloidogenic and nonamyloidogenic pathways of amyloid precursor protein (APP) processing. In the amyloidogenic pathway, APP is cleaved by BACE1 to produce soluble APPβ (APPsβ) and C99. The C99 fragment is further cleaved by γ-secretase to release amyloid β fragments, primarily $A\beta_{40}$ but also $A\beta_{42}$, which is highly prone to aggregation, and the APP intracellular domain (AICD). In the nonamyloidogenic pathway, APP is cleaved by α-secretase to produce soluble APPα (APPsα) and C83, which itself is subsequently cleaved by γ-secretase to produce nonaggregating species.

According to the amyloid hypothesis of AD, the aberrant accumulation of Aβ peptides, particularly $A\beta_{42}$, either as soluble oligomeric species or as plaques, is causative of the impaired neurotransmission, neuroinflammation, neuronal cell death, and ultimately dementia that is characteristic of the disease.[10–12] The Aβ peptides are produced from the transmembrane amyloid precursor protein (APP) by two sequential proteolytic cleavages that constitute a minor APP processing pathway (Fig. 1).[13] The first committed step in Aβ peptide synthesis is the cleavage of APP at its β-site by β-site APP cleaving enzyme 1 (BACE1), also known as β-secretase, resulting in shedding of the APP ectodomain APPsβ. The remaining membrane-bound C-terminal fragment C99 is subsequently processed by γ-secretase (GS), affording not only multiple isoforms of the Aβ peptides, predominantly $A\beta_{40}$, but also minor amounts of the $A\beta_{42}$ isoform that is highly prone to aggregation[14] and is the principal component of the neuritic plaques characteristic of AD.[15] The majority of APP is processed by α-secretase-mediated cleavage within the Aβ domain yielding a membrane-bound C-terminal fragment that is subsequently processed by GS leading to nonamyloidogenic products.

Although aspects of the etiology of AD remain poorly understood, several lines of genetic, biochemical, and biomarker evidence support the amyloid hypothesis.[16–18] Early-onset autosomal dominant familial AD is associated with mutations in APP and in the GS components presenilin-1 and -2, and all of these mutations increase total Aβ and/or the proportion of Aβ species with a greater propensity to aggregate. APP gene trisomy as occurs in Down syndrome is associated with increased Aβ production, amyloid deposition, and AD. Conversely, a rare APP mutation (A673T) was recently identified that is associated with reduced risk of developing AD and with improved cognitive function in the elderly (see below).[19] The highest known risk factor for late-onset sporadic AD is the presence of the APOE gene allele APOE4, which is associated with increased amyloid accumulation.[20] Finally, recent studies support reduced levels of $A\beta_{42}$ in the CSF, indicative of reduced $A\beta_{42}$ clearance, and the presence of amyloid aggregates in the brain as prognostic biomarkers for AD.[8,9]

Inhibition of BACE1 is widely regarded as the most promising therapeutic approach for development of a disease-modifying AD therapy.[21,22] First cloned and characterized in 1999, BACE1 is a transmembrane aspartyl protease.[23–27] In the brain, BACE1 is preferentially expressed in neurons which produce the majority of Aβ in the CNS,[23,24,28] and BACE1 expression and activity is increased in the brains of AD patients.[29–31] The enzyme is highly expressed in the nervous system early in development, and is subsequently downregulated.[32] In mature animals there is broad, low level BACE1 expression and secretion of Aβ across a variety of cell types and tissues.

Validation of BACE1 as a prime therapeutic target for AD has been provided by extensive genetic studies performed in mice. Bace1 knockout (KO) mice do not produce Aβ confirming that BACE1 is the major enzyme responsible for Aβ production in vivo.[33] Furthermore, Bace1 heterozygous mice obtained by crossing Bace1 KO mice with transgenic mice that overexpress human APP harboring familial AD mutations have reduced plaque deposition and improved cognitive function compared to Bace1 homozygous APP transgenic mice.[34–36] The rare protective APP mutation A673T mentioned above provides human genetic validation of BACE1 as an important AD therapeutic target.[19] This mutation occurs two amino acid residues C-terminal to the BACE1 cleavage site, reduces the rate of BACE1-mediated APP processing and Aβ peptide production by 40%,[19] and results in Aβ species that are less prone to aggregation compared to Aβ derived from wild-type APP.[37,38] The presence of the A673T variant is associated with five- to sevenfold reduced risk of developing AD and improved cognitive function in the elderly.[19] Conversely, the APP mutation A673V

that occurs at the position identical to the A673T variant leads to increased BACE1-mediated APP processing and Aβ production, and individuals homozygous for this mutation develop early-onset AD.[39]

Despite the progression of multiple drug candidates into long-term clinical trials, amyloid-centric approaches have failed to provide clear clinical benefit to date, and this has been cited as evidence against the validity of the amyloid hypothesis.[40] However, limitations of the drug candidates tested, of their mechanisms of action, or of clinical trial designs confound this viewpoint. The majority of these agents targeted Aβ synthesis with small molecule GS inhibitors or modulators, or targeted Aβ directly with antibodies, but in clinical trials they produced at best modest effects on CSF Aβ levels or brain amyloid plaques due to dose-limiting side effects and/or inadequate target engagement.[41] In one such trial, although the Aβ antibody solanezumab failed to meet its Phase 3 clinical endpoints, prespecified post-hoc analyses demonstrated that patients with mild AD had a modest but significant slowing of cognitive decline.[42] In the same trials, patients with moderate AD showed no benefit. These results suggest that intervention earlier in the disease process may be beneficial, and additional Phase 3 trials with solanezumab are currently underway to test this hypothesis.

BACE1 inhibitors are among the newer agents to target amyloid reduction as a therapeutic approach to AD, and they appear capable, with proper design and safety profiling, of effecting a more profound lowering of CNS Aβ than earlier approaches. The most advanced agent targeting this mechanism is verubecestat (MK-8931), currently in Phase 3 clinical trials in patients with mild-to-moderate AD and in patients with early stage, prodromal AD. Beginning with initiation of our BACE1 inhibitor program and chronicling a number of strategies and approaches, this article describes the discovery of verubecestat, which is uniquely positioned to provide a robust test of the amyloid hypothesis.

8.09.2 BACE1 Characteristics and Drug Discovery Challenges

Mature BACE1 is a 501 amino acid single transmembrane domain aspartyl protease that belongs to the pepsin family of proteases.[43] The catalytic domain contains two signature hexapeptide motifs each bearing an aspartic acid residue that forms a catalytic dyad intimately involved in substrate proteolysis. An additional structural aspect of BACE1 is a β-hairpin loop that forms a mobile flap over the active site. A crystal structure of the BACE1 apo protein (**Fig. 2**) shows a water molecule bound to the catalytic aspartates and the flap in a partially closed conformation.[44]

BACE1 is initially synthesized as a zymogen that is converted to its mature form through the action of furin convertases in the Golgi. During maturation BACE1 undergoes several posttranslational modifications and its intracellular localization is influenced by a number of regulatory proteins. Posttranslational modifications of BACE1 include disulfide cross-linking, glycosylation, acetylation, phosphorylation, and palmitoylation; the regulatory roles of many of these modifications are not well understood.[23,43] The transmembrane domain of BACE1 orients the catalytic domain to project into the lumen of intracellular organelles, proximal to the APP β-cleavage site. Typical of most aspartyl proteases, an acidic pH near 5 is optimal for BACE1 catalytic activity.[24] Accordingly, the majority of APP processing by BACE1 occurs in endosomes and in the trans-Golgi network where the lumenal pH is maintained in the acidic range (pH 5–6).[43]

At the outset of our discovery program there were two major considerations that had the potential to pose significant obstacles. Since there was no precedent for the development of brain-permeable inhibitors of aspartyl proteases, first was the need to discover inhibitors sufficiently small and with suitable physicochemical properties to be brain penetrant in order to inhibit brain BACE1, and hence directly lower brain-derived Aβ levels. Precedent for aspartyl protease inhibitor drug development was established by the marketed HIV protease inhibitors and the renin inhibitor aliskiren.[45,46] However, these agents tend to be large peptidomimetic structures with physicochemical properties that confer poor permeability and P-glycoprotein (Pgp) efflux susceptibility that limits oral bioavailability and brain penetration.

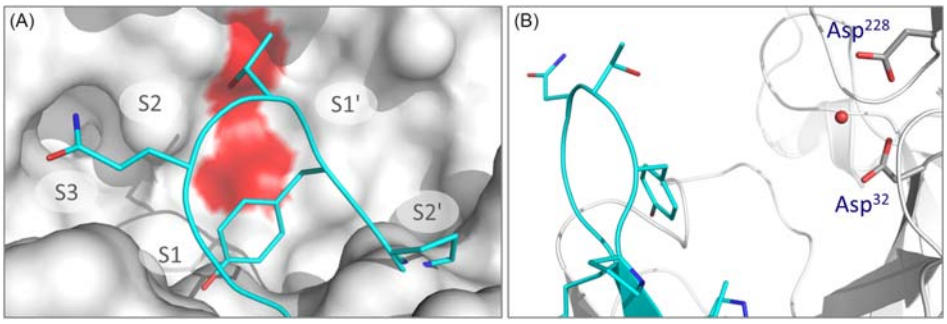

Fig. 2 (A) X-ray structure of the active site of the BACE1 apo protein showing the surface of the protein in *gray* with the surface of the two catalytic aspartates in *red*. A β-hairpin loop, shown as a *blue ribbon* with side chains, forms a flap in front of the aspartates; unless explicitly stated, the flap is omitted from X-ray views for clarity. (B) View of the active site of BACE1 apo structure from the prime side showing that the two catalytic aspartates are bound to a water molecule.

The second challenge was to achieve adequate selectivity over other human aspartyl proteases with relatively small, low molecular weight (MW) BACE1 inhibitors. Analysis of the substrate specificity of BACE1 versus the aspartyl proteases cathepsin D (CatD), cathepsin E (CatE), pepsin, renin, and napsin A suggested that the challenge of achieving selectivity over these enzymes might be readily surmountable.[47] In particular, we considered sufficient selectivity for BACE1 over the lysosomal enzyme CatD to be paramount since loss of function of this aspartyl protease had been shown to cause neurodegeneration, blindness, and postnatal lethality in mice.[48] Given those findings, new compounds that we prepared during lead optimization were routinely counterscreened against CatD. At the outset of our program, we implemented a selectivity criterion of >100-fold for BACE1 over CatD based on K_i values to be acceptable for compound advancement. After the discovery of verubecestat, reports emerged of CatD-mediated toxicity in animals with competitors' BACE1 inhibitors that highlighted the importance of achieving adequate selectivity for BACE1 over CatD.[49–51] Notably, inhibitor pK_a has been shown to be a key determinant of CatD-mediated toxicity, whereby basic inhibitors have lower selectivity in cells due to lysosomal accumulation compared to that measured in cell-free enzyme assays.[51] During the course of the work described herein, preclinical safety data generated from chronic animal studies with a number of our weakly basic lead compounds that had BACE1/CatD selectivity ratios in the hundreds of fold and CatD affinity in the single digit micromolar range were devoid of findings that were ascribed to CatD inhibition. Based on these internal observations, and lacking knowledge of the CatD-mediated toxicity of competitors' inhibitors prior to the discovery of verubecestat, we did not significantly modify the CatD selectivity criterion that remained in place for the duration of the work described in this article.

Shortly after BACE1 was discovered, a close homolog designated as BACE2 was also identified.[52,53] Unlike BACE1, BACE2 is expressed mainly in the periphery and has very low expression levels in the CNS. In addition, heterologous expression studies indicate that the preferred sites of APP cleavage by BACE2 are 19–20 residues C-terminal to the BACE1 cleavage site, affording distinct cleavage products.[54–56] Consequently BACE2 does not significantly contribute to Aβ production in vivo. This was confirmed by studies of brain tissue or cultured neurons derived from Bace1 KO mice in which Aβ production is almost completely suppressed, and by the demonstration that Bace2 KO mice produce normal levels of Aβ.[33,57,58] At the outset of our efforts, the effects of BACE2 loss of function had not been reported. Recent studies have established a role of BACE2 in pigmentation in rodents. BACE2 processes the melanosome structural protein PMEL17 and Bace2 KO mice display fur hypopigmentation.[58] Additionally, BACE2 has been shown to process the pancreatic β-cell proteins Tmem27 and islet amyloid polypeptide, and inhibition of BACE2-mediated processing of these substrates has been proposed to be of benefit in Type 2 diabetes.[59,60] At the commencement of our drug discovery efforts it was anticipated that selectivity for BACE1 over BACE2 would be very difficult to achieve due to the high active site sequence homology between the two enzymes.[47,52,53] This was indeed the case, and as our program evolved, the relatively benign or possibly beneficial phenotypes related to BACE2 loss of function that emerged mitigated concerns related to lack of inhibitor selectivity for BACE1 over BACE2.

At the time BACE1 was first characterized, it was reported that Bace1 KO mice were viable, healthy, and lacked an overtly negative phenotype, thus mitigating concerns of toxicity mediated by BACE1 inhibition.[33,57] This view has evolved as more recent data generated with Bace1 KO mice and/or BACE1 pharmacological inhibition has revealed potential adverse consequences of inhibiting BACE1-mediated processing of substrates unrelated to APP.[21,28,61] The best characterized of these substrates are members of the neuregulin 1 (NRG1) family, NRG1 type I and NRG1 type III. Bace1 KO mice show reductions in peripheral nerve myelination[32,62] and in muscle spindle formation,[63] which has been ascribed to loss of BACE1-mediated processing of NRG1 type III and NRG1 type I, respectively. Importantly, these as well as other phenotypes observed in homozygous Bace1 KO mice are not seen in Bace1 heterozygous mice, and are not recapitulated in adult wild-type mice administered BACE1 inhibitors, thus supporting a greater impact of BACE1 activity in early development and the need to achieve substantial (>50%) inhibition of BACE1 for these phenotypes to manifest even in early development. This latter assertion is further supported by the observation that Bace1 is expressed at markedly higher levels in the developing mouse CNS relative to adult mice.[32]

In sum, while appropriate safety monitoring of clinical trials is essential, the available data does not preclude the possibility that substantial long-term pharmacological BACE1 inhibition in AD patients could be a safe approach to disease modification. A recent review of the known BACE1 biology emphasized that BACE1 inhibitor clinical trials not only need to address the degree of BACE1 inhibition required for disease modification in AD, but also balance this with achieving a safe therapeutic window to potential BACE1-mediated adverse effects.[61]

8.09.3 BACE1 Inhibitor Lead-Finding Strategies

8.09.3.1 Overview

We assigned high priority to development of BACE1 inhibitors for disease modification, and from the outset we invested significant resources in support of multiple hit finding approaches to identify tractable inhibitor lead series. Like most organizations in this highly competitive area, we conducted high-throughput screening (HTS), and we also pursued parallel synthesis and screening of targeted libraries. Unfortunately, neither of these approaches delivered viable leads. In addition, we were able to leverage substantial capabilities and expertise in the areas of protein X-ray crystallography, structure-based design, and fragment screening which were established at Schering-Plough during the 1990s. Accordingly, shortly after the initial reports of the characterization of BACE1 had appeared in the literature, we commenced BACE1 protein production and crystallization efforts. This positioned us to conduct a fragment screen and characterization of screening hit binding modes by X-ray crystallography in 2001–2002. These

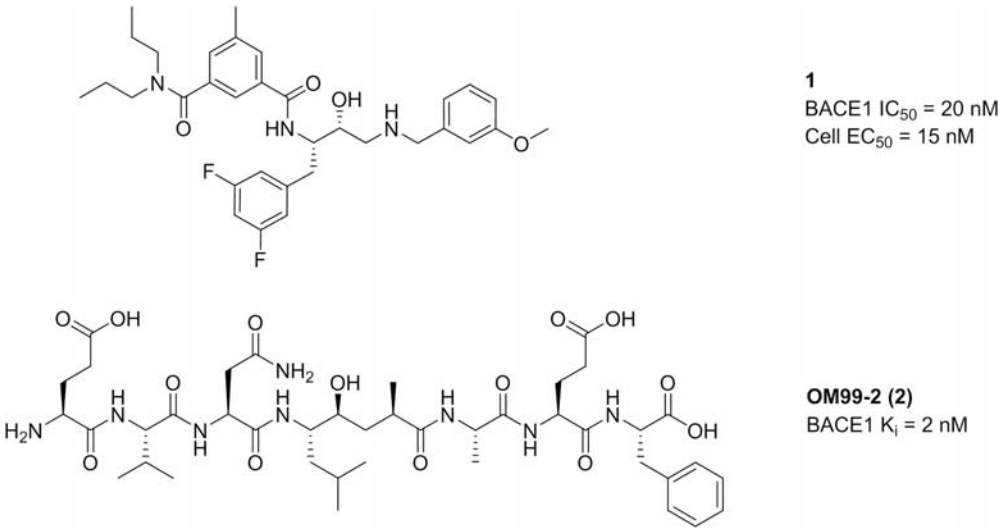

Fig. 3 Structures of hydroxyethylamine peptidomimetic BACE inhibitor **1**,[64,65] and of substrate-based peptidomimetic inhibitor OM99-2.[66,67]

fragment screening hits were of critical importance to the success of the program and their discovery and early structure-driven optimization efforts are described in Section "Fragment Screening: Discovery of New Inhibitor Chemotypes."

Also at about this time, the first potent inhibitors containing the hydroxylethylamine (HEA) peptidomimetic transition state isostere were published in the patent literature, exemplified by **1** from Elan/Pharmacia (Fig. 3).[64,65] These structures followed publication by Ghosh and Tang in 2000 of an X-ray structure of a peptidomimetic substrate-based inhibitor, the homostatine OM99-2 (**2**), bound to BACE1, which established that the enzyme was amenable to crystallography and structure-based design.[66,67] An attractive property of HEA analogs such as **1**, in addition to their high BACE1 affinity, was their cell potency indicative of their intrinsic cell penetration properties.[65] Consequently, to jump-start our program, we employed a scaffold-hopping approach to the development of novel inhibitors as described in Section "Hydroxyethylamine-Based Peptidomimetic Inhibitors," in parallel with our fragment-based approach.

8.09.3.2 BACE1 and CatD in vitro Assays

Throughout our program two key in vitro assays that we used to evaluate the BACE1 potency of inhibitors were variants of a cell-free enzymatic assay, and a cell-based functional assay that measured inhibition of $A\beta_{40}$ secretion in response to a BACE1 inhibitor. The initial enzymatic assay utilized a soluble form of BACE1 and an 18mer peptide substrate possessing the familial AD Swedish mutation (KM → NL).[68] A refined version of the assay that was used to determine K_i values employed a lower BACE1 enzyme concentration and a 12mer substrate that retained the KM → NL substitution (BACE1 $K_m = 8\ \mu M$).[69] Both peptide substrates were fluorescently labeled to enable measurement of BACE1-mediated substrate hydrolysis in the presence of a BACE1 inhibitor through time-resolved fluorescence resonance energy transfer (HTRF) methods.

The cell-based assay employed HEK-293 cells stably transfected to express human APP containing the familial AD Swedish (K670N/M671L) and London (V717I) mutations.[68] These mutations result in increased APP processing and increased secretion of $A\beta_{40}$ and $A\beta_{42}$ into the culture medium. Quantification of Aβ peptide secretion in response to a BACE1 inhibitor was determined by Aβ antibody capture methods and the potency of an inhibitor to reduce Aβ secretion was expressed as an IC_{50}.

The CatD enzymatic counterscreen assay employed human liver CatD and a fluorogenic 12mer peptide substrate to measure proteolytic activity in the presence of an inhibitor by fluorescence resonance energy transfer methods.[69]

8.09.3.3 Hydroxyethylamine-Based Peptidomimetic Inhibitors

Using **1**[64,65] as a starting point, our initial goal was to develop brain penetrant, patentable inhibitors that lowered CNS Aβ levels following systemic administration to rodents. Inhibitor **1** engages in a number of specific interactions with BACE1 (Fig. 4), and our initial approach was to minimize disruption of these interactions to avoid significant loss of affinity. In addition to hydrogen bonding interactions between the HEA transition state isostere and the catalytic dyad, the amine hydrogen of **1** is within hydrogen bonding distance of the Gly^{34} carbonyl and the hydrophobic S2′ pocket is occupied by the methoxyphenyl group. In the nonprime region, the difluorophenyl group makes hydrophobic contacts with the S1 pocket and the amide hydrogen engages in a hydrogen bond with Gly^{230}. The isophthalamide spans the S2 and S3 pockets with its distal amide carbonyl picking up a hydrogen bond to Thr^{232}. Docking studies based on an X-ray cocrystal structure of **1** bound to BACE1 suggested that the enzyme could accommodate the steric demand of a cyclic amine motif formed through introduction of a two- or three-atom bridge linking the methylene

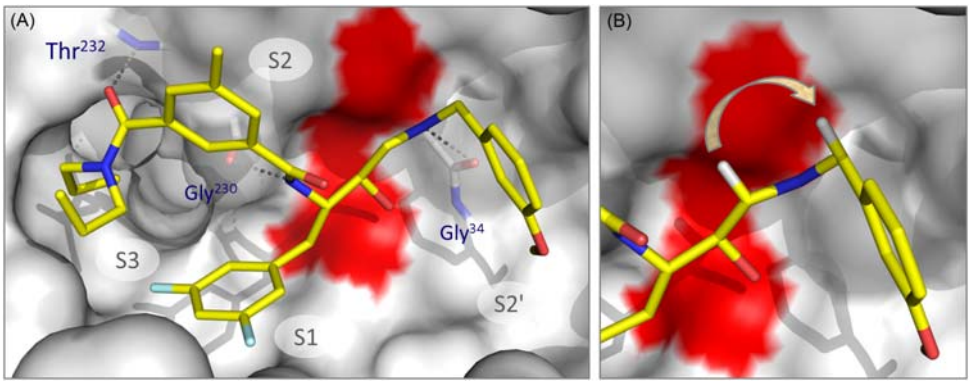

Fig. 4 (A) X-ray structure of hydroxyethylamine **1** bound to BACE1 showing key interactions of the structure with the enzyme. (B) Close-up view of hydroxyethylamine portion of **1** showing the potential for cyclization around the amine.

carbons flanking the secondary amine nitrogen. Furthermore, modeling suggested that conformational constraint imposed by such a cyclic amine would not disrupt the key interactions of the HEA transition state isostere with the catalytic dyad and might provide an ideal vector into the S2′ pocket.

Implementation of this design strategy by Cumming et al. and by Iserloh et al. proved to be successful, with potent piperazine- and pyrrolidine-based inhibitors such as **3** and **4** (Fig. 5A) identified through this approach.[70–73] The piperazine core in particular was useful not just for SAR development, but also for generation of high specific activity radiolabeled material for ex vivo studies, for example, compound ^{35}S-**5**. X-ray cocrystal structures of these inhibitors confirmed that their binding mode relative to **1** was highly conserved, as shown for **3** in Fig. 5B. In addition, the sulfonyl group of the piperazine sulfonamide of **3** was engaged in a hydrogen bond with the backbone amide NH of Thr^{72} in the flap that was not present with **1** (Fig. 5C).[70]

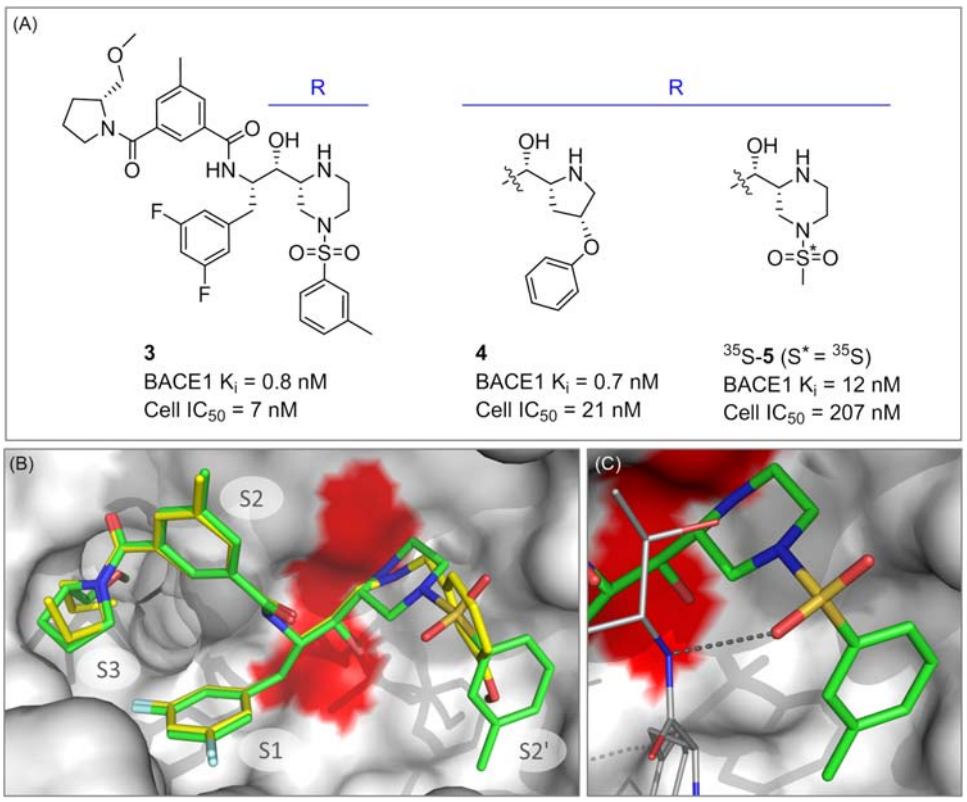

Fig. 5 (A) Structures of optimized cyclic amine peptidomimetic BACE inhibitors **3** and **4** and of radioligand ^{35}S-**5**. (B) Overlay of the X-ray structures of acyclic hydroxyethylamine **1** (*yellow*) and piperazine sulfonamide **3** (*green*) showing their well-conserved binding modes. (C) Close-up view of the hydrogen bonding interaction between one of the sulfonyl oxygens of piperazine sulfonamide **3** and backbone NH of Thr^{72} in the flap.

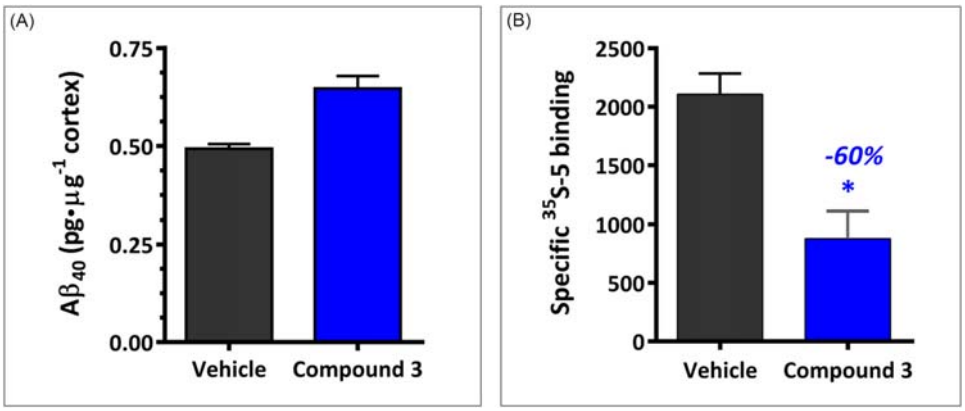

Fig. 6 (A) Lack of effect of subchronic administration of piperazine sulfonamide **3** (300 mg kg^{-1} SC, BID, 5 days) on brain $A\beta_{40}$ levels in TgCRND8 mice. Plasma levels of $A\beta_{40}$ were completely suppressed. (B) Ex vivo binding of ^{35}**S-5** to brain slices from TgCRND8 mice following subchronic treatment with piperazine sulfonamide **3**.

Of the novel cyclic amine containing HEA inhibitors that were identified, **3** was among the most potent in regard to its activity in the cell-based assay and was assessed for its potential to lower Aβ levels in vivo.[70] The in vivo model we initially employed was transgenic CRND8 mice (TgCRND8), which overexpress the human APP gene containing the Swedish (K670N/M671L) and Indiana (V717F) familial AD mutations. These mice produce high levels of Aβ peptides and develop very aggressive plaque pathology in the brain accompanied by deficits in learning and memory acquisition commencing at approximately 3 months of age.[74] Disappointingly, acute subcutaneous administration of **3** at doses of 30–300 mg kg^{-1} to TgCRND8 mice had no effect on cortex $A\beta_{40}$ levels, although profound inhibition of plasma $A\beta_{40}$ levels was observed at each dose. While compound **3** is a substrate for Pgp, which would be expected to limit its CNS exposure, brain binding studies of **3** by equilibrium dialysis of mouse brain homogenates were consistent with unbound levels of **3** in the brain being at or above its cell IC_{50} value. Subchronic administration of **3** to TgCRND8 mice (subcutaneous doses of 300 mg kg^{-1} twice daily for 5 days) completely suppressed plasma Aβ levels but did not cause reduction of brain Aβ levels (Fig. 6A).[70] Brain slices from these mice were subjected to ex vivo binding studies with the labeled inhibitor ^{35}**S-5**, which indicated that approximately 60% BACE1 occupancy had been achieved during the study (Fig. 6B). The lack of brain Aβ inhibition after subchronic administration of **3** was particularly striking, leading us to conclude that high brain BACE1 occupancy was necessary to elicit brain Aβ reduction (see Section "In Vivo Validation and Development of a High-Throughput Rat PD Assay").

From these experiments and from additional SAR exploration with peptidomimetic cyclic amines, we concluded that the challenges to achieve adequate oral bioavailability and brain penetration with an HEA inhibitor were likely insurmountable. At about the time these results were generated, prosecution of the fragment-derived iminoheterocycle series had provided tool compounds that inhibited centrally derived Aβ production in vivo as described in Section "In Vivo Validation and Development of a High-Throughput Rat PD Assay," and we abandoned our efforts on the HEA series in order to focus exclusively on the fragment-derived series.

8.09.3.4 Fragment Screening: Discovery of New Inhibitor Chemotypes

8.09.3.4.1 Fragment screening and hit triage

Soon after the purification and cloning of BACE1 was reported in the literature, an efficient *E. coli* expression and protein refolding system were developed in-house by Wang et al. that provided large quantities of the purified BACE1 catalytic domain for inhibitor cocrystallization studies.[75] To enable protein NMR-based fragment screening, Wang et al. adapted this expression system to generate homogenously ^{15}N-labeled BACE1 catalytic domain for detection of weak binders by ^{1}H-^{15}N HSQC NMR spectroscopy.[75,76] A virtually complete assignment of backbone NMR resonances corresponding to the catalytic domain of human BACE1 was determined to facilitate a detailed analysis of fragment hit binding.[77] At this early stage, gram amounts of purified BACE1 protein were produced to ensure that screening by NMR and structural studies to inform hit triage and optimization would not be limited by protein availability.

NMR screening of a 10,000-member fragment library was conducted in the laboratory of Wang et al. by screening compounds as mixtures of 10 against ^{15}N-labeled BACE1.[76] Active mixtures were deconvoluted by NMR to identify the active single compound(s), which were confirmed by repeating the NMR experiment with a compound solution freshly prepared from solid sample. This campaign required several months to complete and afforded active site-directed weak binders from multiple distinct chemical classes represented by structures **6–11** in Fig. 7. By comparing their BACE1 chemical shift perturbations with those induced by OM99-2, it was confirmed that each of these hits bound in the BACE1 active site. Affinity of these hits was in the micromolar to millimolar range as determined by NMR titration experiments.[76] Hit follow-up was conducted through efforts to generate X-ray cocrystal structures with the initial hits, and by NMR screening of near neighbors to identify additional candidates for X-ray

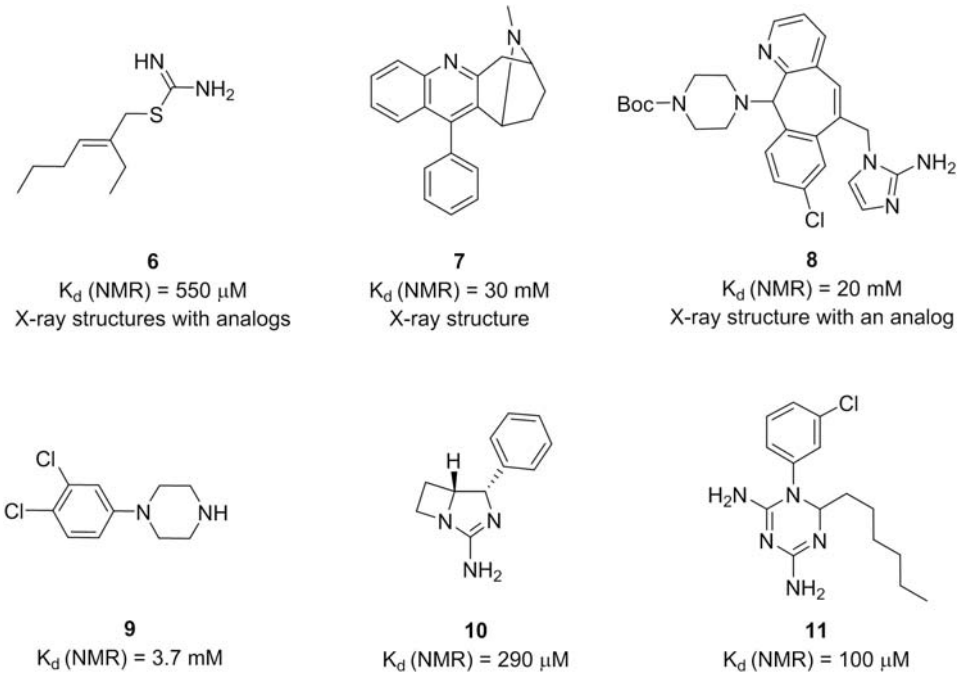

Fig. 7 Structures of representative active site-directed weak binders of BACE1 identified through ^{1}H-^{15}N HSQC NMR screening of a 10,000-member fragment library.[76]

crystallography. Of the initial structural classes that were discovered by Wang et al.,[76] three of these afforded X-ray cocrystal structures, either with the initial hits—isothiourea **6**, tropylquinoline **7**, and fused azatricycle **8**—or with analogs thereof. Enabled by detailed information on their binding modes, synthetic chemistry effort was applied to each of these chemotypes; however, it was the isothiourea class that provided a path to a viable lead series.

Chemical shift changes in the HSQC NMR spectra of isothiourea **6** indicated that this ligand interacted with the catalytic dyad as well as with Ile^{118} and Gly^{230} in S1 and Gly^{34} in S1′.[76] Due to the potentially attractive nature of its binding interactions that were similar to those of OM99-2, this hit was prioritized for additional follow up. To identify a higher affinity analog, a high concentration biochemical assay and NMR spectroscopy were employed in tandem to screen about 200 isothioureas that were available in our compound collection.[76] Screening of these isothioureas at high concentrations in the enzymatic assay resulted in the identification of analog **12** as a weak BACE1 inhibitor (IC_{50} approximately 200 μM) that had higher affinity than initial screening hit **6** as determined by NMR titration experiments (NMR K_d 15 μM vs. 550 μM). Chemical shift perturbations were consistent with binding of **12** to the catalytic dyad, and to the S1 and S3 pockets (Fig. 8).

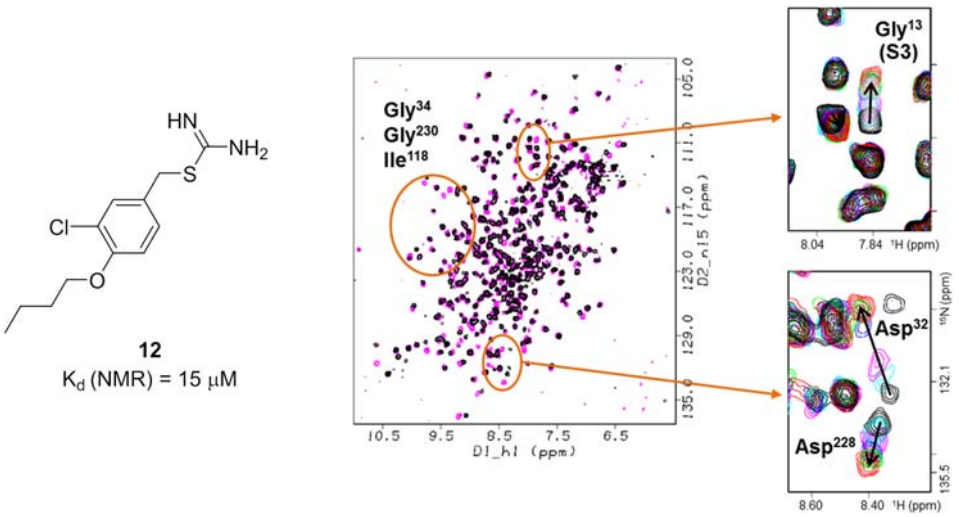

Fig. 8 Concentration-dependent HSQC NMR chemical shift perturbations observed in ^{15}N-labeled BACE1 induced by binding of isothiourea **12** to the active site.

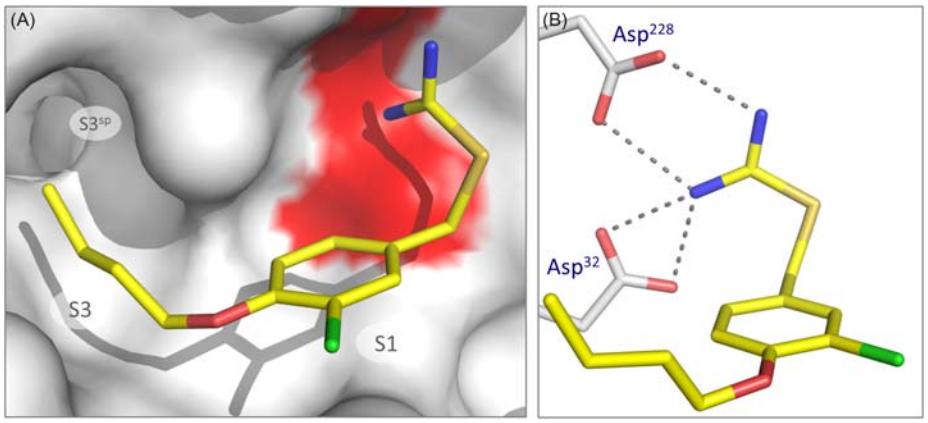

Fig. 9 (A) X-ray cocrystal structure of isothiourea **12** bound to BACE1. (B) Detailed view highlighting the unique hydrogen bonding network of the amidine moiety with the catalytic dyad.

Details of this binding mode were confirmed by a high-resolution X-ray cocrystal structure (Fig. 9) in which the amidine of **12** was engaged in a hydrogen bonding network directly with the active site Asp^{228} and Asp^{32} residues, an interaction that was at the time unprecedented for an aspartyl protease.[76] This binding mode was also unique among the other fragment chemical classes for which we were able to generate X-ray structures in BACE1, with tropylquinoline **7** and an analog of fused azatricycle **8** each interacting with the aspartates through one or two bridging water molecules. In addition to direct interactions with the catalytic dyad, the phenyl and butoxy groups of **12** made hydrophobic contacts with the S1 and S3 pockets, respectively, with the butyl group extending toward a narrow channel near S3, termed the $S3^{sp}$ subsite.

In addition to providing the initial high-resolution X-ray cocrystal structure of **12** that was inspirational for inhibitor design efforts described below, the ability to generate cocrystals of **12** with BACE1 was critical for rapid generation of crystal structures of new inhibitors through soaking experiments. This allowed crystal structures of inhibitors bound to BACE1 to be solved with cycle times synchronous with data generated from the NMR and enzymatic activity assays, enabling structural information to inform inhibitor design and SAR development in real time. This was especially critical for interpreting SAR in the early stages of the project when multiple binding modes were observed.

8.09.3.4.2 Iminoheterocycle scaffold design and validation

With detailed knowledge of the binding mode of **12** in hand, careful consideration was given to its development into a progressible lead series. At the outset we sought to replace the isothiourea moiety itself due to concerns related to its potential toxicity and hydrolytic instability. To achieve this, two approaches were pursued in parallel. The first approach employed by Wang et al. involved targeted NMR screening of low MW heterocyclic isosteres that contain an amidine moiety required for interaction with the catalytic dyad.[76] This effort identified planar aromatic heterocycles such as 2-aminopyridine **13** as low affinity BACE1 inhibitors (Fig. 10A). The X-ray cocrystal structure of **13** bound to BACE1 confirmed the hydrogen bonding network between the aminopyridine and the

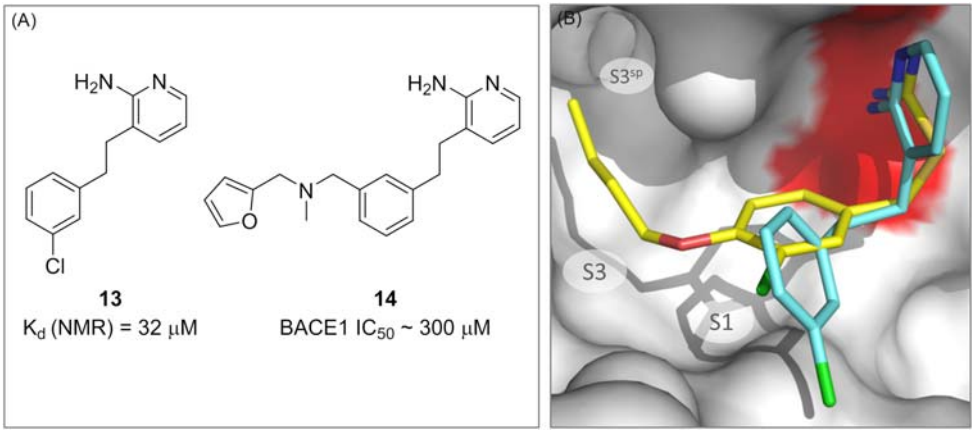

Fig. 10 (A) Structures of low affinity 2-aminopyridine BACE1 inhibitors **13** and **14**. (B) Overlay of X-ray crystal structures of isothiourea **12** (*yellow*) and 2-aminopyridine **13** (*blue*) bound to BACE1 confirming that the aminopyridine moiety of **13** recapitulates the catalytic aspartate interactions seen with isothiourea **12**.[76]

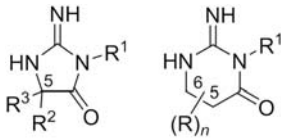

Fig. 11 Generic structures of cyclic acyl guanidines **15** and **16** designed from isothiourea fragment screening hit **12**.[69]

catalytic dyad, and revealed that the chlorophenyl group was positioned near the S1 pocket but oriented roughly perpendicular to the corresponding phenyl group of **12** (Fig. 10B). Enabled by this structural information, we conducted a focused SAR exploration designed to gain affinity by exploiting interactions in the S1–S3 region. Identification of more potent analogs with measurable biochemical activity proved challenging, with **14** being notable in that it displayed weak enzymatic inhibitory activity (Fig. 10A). An X-ray cocrystal structure of **14** bound to BACE1 confirmed that the phenyl group bound in S1 and that the furanyl group bound deep in $S3^{sp}$.[76]

In the second approach Zhu et al. pursued de novo design of heterocyclic scaffolds that preserved key features of the isothiourea **12** necessary for its BACE1 affinity.[69] We hypothesized that the basicity of the isothiourea ($pK_a \sim 9$) was important for driving enthalpic interactions with the catalytic dyad. Computational analysis suggested that the catalytic dyad is doubly deprotonated when bound to the protonated amidine of **12**. This led Zhu et al. to propose that the pK_a value of a designed inhibitor should be greater than the endosomal compartment (pH ~5-6), the native environment of active BACE1 in vivo. In addition to presenting the amidine motif in its protonated form, modulating the pK_a of the inhibitor in a weakly basic range was also expected to enhance blood–brain barrier permeability through interconversion of the protonated and unprotonated forms. A second design criterion was to restrict the number of hydrogen bond donors in the unprotonated form of the scaffold to the two essential for interaction with the catalytic dyad, as the number of hydrogen bond donors is inversely correlated with brain penetration.[78] These lines of reasoning led Zhu et al. to consider the 5-membered cyclic acyl guanidine **15** and its 6-membered congener **16** (Fig. 11) that were expected to possess pK_a values in the desirable range. For **15**, the importance of disubstitution of C5 was appreciated at the outset to prevent tautomerization to an aromatic system and substantial loss of basicity, a concern that does not attend the 6-membered analog **16**, which offers two sp^3 carbons for potential substitution.[69]

Zhu et al. initially focused on the 5-membered iminohydantoins due to their synthetic accessibility.[69] Regioisomeric iminohydantoins **17** and **18**, differing in which ring nitrogen is substituted, were both considered to be potentially viable scaffolds (Fig. 12A). Docking experiments on the des-chloro versions of these designed putative ligands yielded binding poses similar to that of isothiourea **12**, with the amidine motif of the core hydrogen bonded to the catalytic dyad and the chlorophenyl substituent placed in the S1 pocket (Fig. 12B), and both prototype scaffolds were prioritized for synthesis. Once in hand, NMR experiments revealed that the N3-substituted isomers **17** and **19** produced significant BACE1 chemical shift perturbations, whereas the N1-substituted isomers **18** and **20** did not. We were initially surprised by this result, but pK_a measurements demonstrated that the N1-substituted analog **20** is substantially less basic (pK_a 4.2) than the N3-substituted variant **19** (pK_a 7.2), with the latter possessing a weakly basic pK_a in a desirable range for a CNS-active drug.[69]

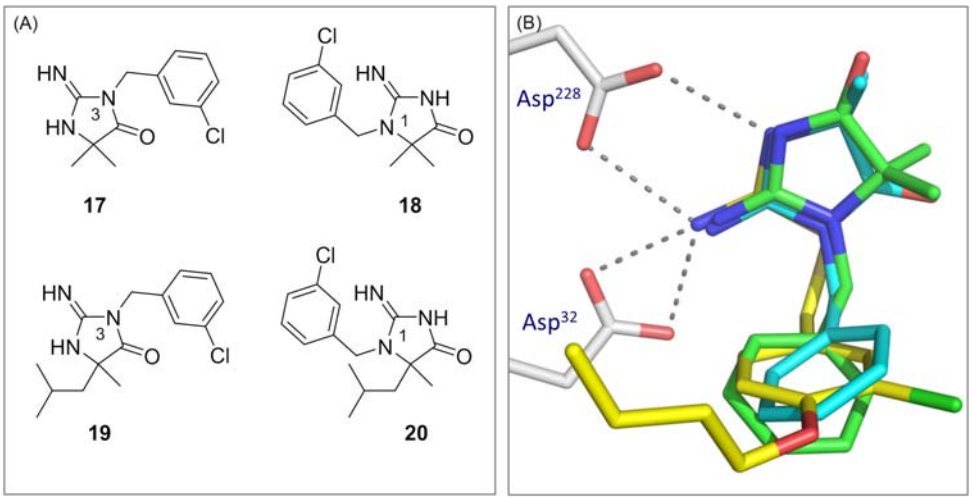

Fig. 12 (A) Structures of designed N3- and N1-substituted iminohydantoins **17**–**20**. (B) Models of the des-chloro analogs of **17** (*blue*) and **18** (*green*) overlaid with isothiourea **12** (*yellow*) showing conservation of the hydrogen bonding network with the catalytic dyad and consistency of binding in S1.

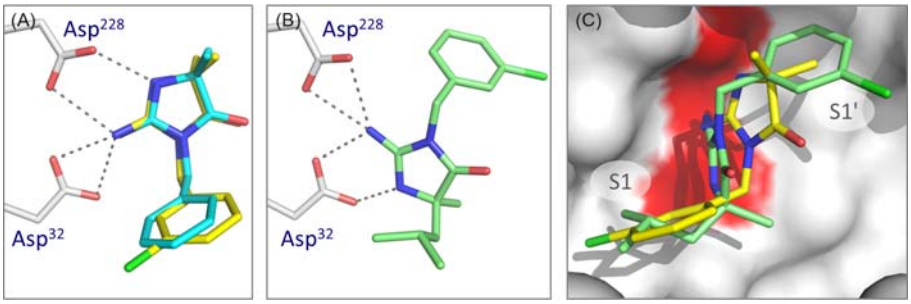

Fig. 13 X-ray crystal structures of designed iminohydantoin fragments bound to BACE1. (A) Overlay showing the excellent agreement between the structure of compound **17** (*yellow*) and of the docked conformation of the des-chloro analog used for modeling (*blue*). (B) Binding of compound **19** to the catalytic dyad. (C) Compounds **17** (*yellow*) and **19** (*green*) overlayed showing 180 degree flip of binding modes.

Gratifyingly, an X-ray cocrystal structure of N3-substituted iminohydantoin **17** confirmed the predicted binding mode (Fig. 13A).[69] This structure revealed the extensive hydrogen-bonding network between the amidine and the catalytic dyad, with the ligand participating in a bidentate interaction with Asp^{228}, similar to that of isothiourea **12**, and the chlorophenyl substituent occupying the S1 pocket. Interestingly, however, an X-ray cocrystal structure of the other N3-substituted iminohydantoin **19** revealed that the modest change of methyl to isobutyl at C5 resulted in a binding mode in which the iminohydantoin core is flipped 180 degree in the active site (Fig. 13B and C). In this binding mode, the hydrogen-bonding requirements of the ligand amidine motif and the catalytic dyad remain satisfied but with the Asp^{32} now engaged in the bidentate interaction, while the chlorophenyl substituent occupies S1′ and the isobutyl group projects into S1.[69] The flipped binding modes of **17** and **19** reinforced early on the challenges of prosecuting fragments, and highlighted the importance of timely X-ray cocrystal structures for interpretation of emerging SAR and for informing prospective modeling studies.

Comparison of the binding modes of iminohydantoins **17** and **19** with aminopyridine **14** highlighted a perceived key advantage of the nonplanar iminohydantoin scaffold. The sp^3 center of the iminohydantoin ring provides direct, favorable trajectories toward the prime and nonprime pockets adjacent to the catalytic dyad. On the other hand, the planar aminopyridine scaffold defines vectors that are perpendicular to the enzyme specificity pockets and thus requires incorporation of additional rotatable bonds to orient the substituents toward these pockets. This is shown clearly in an overlay of the X-ray structures of iminohydantoin **19** and of aminopyridine **14** bound to BACE1 (Fig. 14). Whereas there is only one rotatable bond from the iminohydantoin core to the S1 substituent, there are three from the 2-aminopyridine core. Based on this analysis the iminohydantoin scaffold was considered an inherently more efficient design, and given the limited resources available at the time, the aminopyridine series was deprioritized.

8.09.3.4.3 Iminohydantoin hit-to-lead prosecution

Having accomplished biophysical validation of the designed iminohydantoin scaffold as a novel aspartyl protease binding motif, the team was faced with the daunting prospect of developing this scaffold into potent, selective BACE1 inhibitors with CNS drug-like properties. Both binding modes displayed by **17** and **19** presented opportunities for affinity gains based on the disposition of the 3- and 5-substituents in the active site. However, the unpredictability of binding modes coupled with reliance on NMR for SAR development posed significant challenges. To advance the program as rapidly as possible, Zhu et al. adopted a strategy of targeting a relatively large number of analogs through parallel synthesis and identifying promising structural modifications by medium-throughput BACE1 NMR chemical shift perturbation analysis.[69] Promising analogs were further triaged in the enzymatic

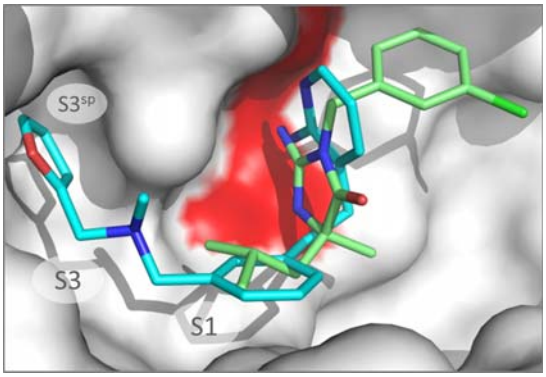

Fig. 14 Overlay of the X-ray structures of iminohydantoin **19** (*green*) and of 2-aminoypyridine **14** (*blue*) bound to BACE1, showing the additional rotatable bonds required to reach the S1 pocket required by the nonoptimal, planar aminopyridine scaffold.

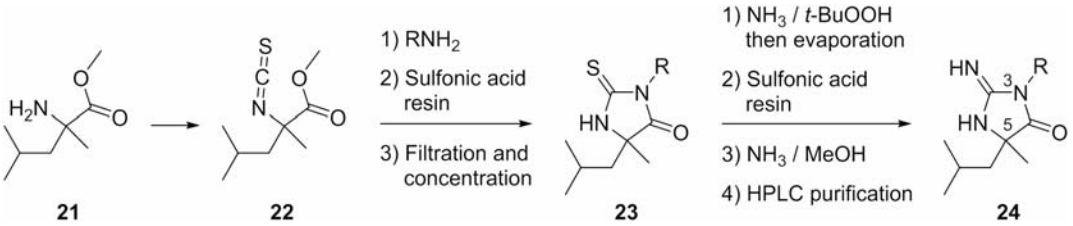

Fig. 15 Parallel synthetic method for rapid expansion of SAR in N3-substituted iminohydantoin series. Synthesis of analogs **24** proceeded via isothiocyanate **22** and thiohydantoin **23**.

HTRF assay and through determination of BACE1 cocrystal structures, with the initial goal of identifying functionally active BACE1 inhibitors with well-understood binding characteristics.

Starting from α,α-disubstituted amino acids like **21**, parallel synthesis chemistry allowed ready access to N3-modified analogs of the core while incorporating more targeted modifications at the 5-position represented by **24** (Fig. 15). Influenced by the structure of OM99-2 bound to BACE1 in which the inhibitor P1 leucine side chain binds in a position similar to the isobutyl group of **19**, the 5-isobutyl group was selected as a preferred substituent for our parallel synthesis libraries. Fig. 16 highlights the most important hits that were identified via this strategy, represented by benzyl ureas **25** and **26**[69] and piperidine analogs **27** and **28**.[79] The benzyl urea series preceded the piperidine series and was the focus of our early optimization efforts; its evolution will be discussed in depth.

NMR experiments allowed us to quickly determine that analogs of **19** in which the phenyl group bore a variety of substituents at the meta and para positions consistently produced BACE1 chemical shift perturbations. Moreover, para-substituted benzyl ureas exemplified by **25** and **26** emerged as the first inhibitors with micromolar potency in the enzymatic assay. Generally phenyl ureas were up to an order of magnitude more potent than the corresponding alkyl ureas as shown by the comparison of **25** and **26**.[69]

X-ray crystallography again revealed how structural changes influence binding modes in unpredictable ways, with the BACE1 cocrystal structures of **25** and **26** showing very different binding modes (Fig. 17). Analogous to the original iminohydantoin

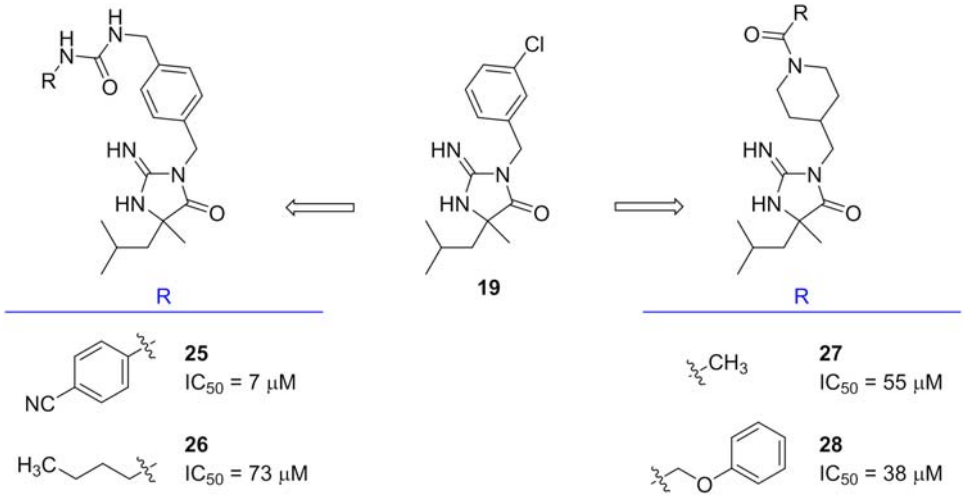

Fig. 16 Structures of N3-modified iminohydantoins **25**–**28** identified through parallel synthesis as modifications of the original designed ligand **19**.

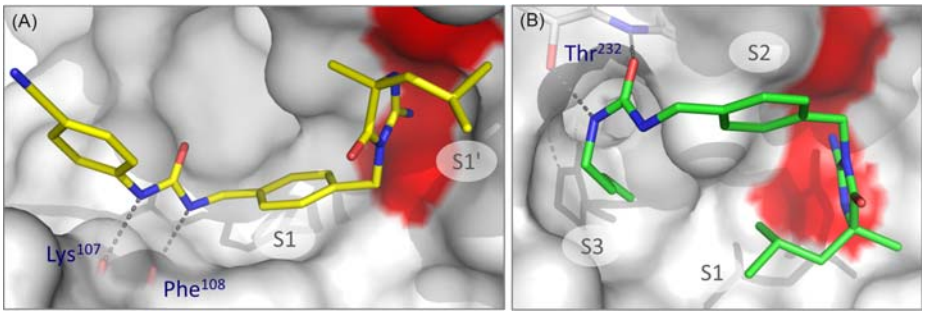

Fig. 17 X-ray crystal structures of N3-benzyl urea-substituted iminohydantoins bound to BACE1 showing the 180 degree flip seen in their binding poses as well as key interactions each makes with the enzyme. (A) Bound structure of compound **25**. (B) Bound structure of compound **26**.

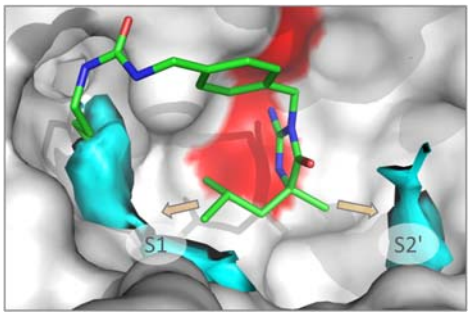

Fig. 18 Hydrophobic surface map of the BACE1 active site (*blue*) with iminohydantoin **26** bound showing trajectories from the C5 substituents into and toward the lipophilic S1 and S2′ subsites.

inhibitors **17** and **19**, the two structures were flipped by 180 degree depending on their substituents. In the X-ray cocrystal structure of the more potent phenyl urea **25**, the isobutyl group occupies the S1′ pocket and the benzyl moiety binds near S1 with the cyanophenyl substituent projecting toward the protein surface (Fig. 17A). The two urea hydrogens participate in hydrogen bonding interactions with backbone carbonyls of Lys[107] and Phe[108]. On the other hand, the cocrystal structure of the less potent analog **26** shows that the isobutyl group occupies the S1 pocket and the benzyl group projects toward the nonprime sites, with the urea participating in two hydrogen bonding interactions with Thr[232] and providing a vector for the butyl group to penetrate into the S3 pocket (Fig. 17B).[69]

Careful consideration of the two binding modes led Zhu et al. to deprioritize phenyl urea **25** for further SAR studies. Despite having greater potency, its reliance on the urea hydrogen bonding interactions for affinity was considered a liability for CNS penetration, and a path for designing out this undesirable feature seemed unclear. Instead, Zhu et al. decided to focus on optimization of the binding mode represented by butyl urea **26**.[69] The binding mode afforded by **26** not only possessed one fewer essential hydrogen bond donor but also offered opportunities for optimization of the isobutyl group in S1 and by building from the 5-methyl substituent to capitalize on binding in S2′. Both of these subsites are relatively hydrophobic (Fig. 18), and a significant portion of our optimization effort utilized lipophilic groups to reach these regions.

Iterative design cycles based on this strategy resulted in cyclic urea **29** that provided our first iminoheterocyclic BACE1 inhibitor with affinity under 100 nM (Fig. 19).[69] This result was important because it demonstrated that it was possible to generate potent BACE1 inhibitors based on the iminoheterocyclic scaffold. On the other hand, the focus on structure-based affinity-driven optimization had introduced a number of drawbacks, including a high MW, a high c log *P*, a potency shift in the cellular assay relative to intrinsic affinity, poor oral pharmacokinetic (PK) properties, and lack of selectivity over the related aspartyl protease CatD. The poor properties of **29** were also reflected by the modest ligand efficiency (LE) value of 0.25, which was essentially identical to the optimized examples in the peptidomimetic series.

The deficiencies in the profile of **29** prompted us to reevaluate our strategy. To identify a more lead-like starting point Zhu et al. pursued a minimum pharmacophore approach with the intent of defining less lipophilic, lower MW, more highly ligand efficient

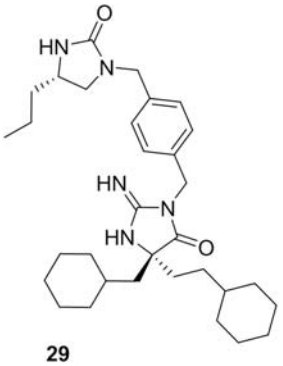

29
BACE1 K_i = 71 nM (LE 0.25)
Cell IC_{50} = 695 nM
CatD / BACE1 = 0.4
Rat AUC = 0.6 μM•h (10 mg•kg^{-1} PO)
Mouse plasma f_u < 0.1%
cLogP = 7.5

Fig. 19 Structure and profile of optimized N3-elaborated iminohydantoin **29**.

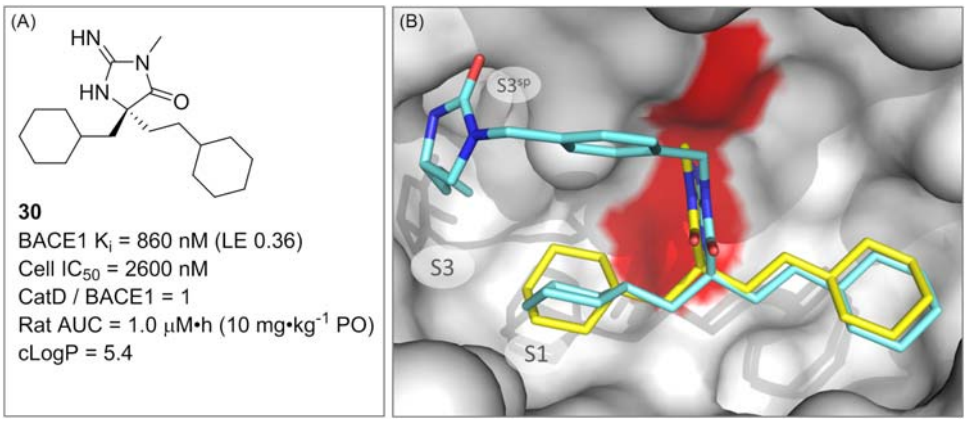

Fig. 20 (A) Structure of truncated N3-methyl iminohydantoin **30**. (B) Overlay of X-ray structures of N3-elaborated iminohydantoin **29** (*blue*) and the racemate of N3-methyl iminohydantoin **30** (*yellow*) bound to BACE1.

scaffolds that could subsequently be reoptimized with control of physicochemical parameters into more desirable property space. Toward this end, it was apparent from the crystal structures of **29** and its analogs that the phenylene motif did not engage in productive interactions with BACE1, but merely served to link the N3-position of the iminohydantoin core to the urea moiety that bound in the S3 pocket. The suboptimal nature of this N3-substituent was confirmed by its truncation to a methyl group in compound **30** (Fig. 20A), which showed only a relatively modest loss of affinity with a substantial increase in LE (LE 0.39) and a significant reduction of c log*P* and cellular potency shift.[69] The conserved binding mode of **30** relative to **29** presented the opportunity to reoccupy the S3 pocket from the substituent residing in S1 in a more efficient manner by exploiting the contiguity of the S1 and S3 pockets (Fig. 20B). This strategy was attractive due to the relative hydrophobicity of this region of the enzyme, and was reminiscent of the approach that was successfully applied to the discovery of the renin inhibitor Aliskiren.[46]

Initial forays in this area by Caldwell et al. resulted in the identification of inhibitors exemplified by **31**, which were bound as intended with the cyclopentyl group extending into the S3 pocket (Fig. 21A).[80] However, while CatD selectivity was significantly increased, improvement of BACE1 affinity was difficult to achieve. A more potent subclass of inhibitors represented by aminoquinoline **32** was discovered by derivatizing the S1 amino group with hydrogen bond acceptor-containing groups. We were surprised to find that in the binding mode of **32** and related amides and ureas, the S3 subsite was unoccupied, and the nitrogen substituent instead occupied a narrow hydrophobic surface extending from S1 toward a solvent-exposed region defined by Lys^{107}, Phe^{108} (which forms a hydrogen bond between its carbonyl and **32**), and Ile^{110} (Fig. 21B).[80] While inhibitors such as **32** had improved affinity and selectivity over CatD, they remained highly lipophilic and deficient with respect to cellular potency and PK properties, and therefore, efforts on this subseries were abandoned.

While the S1–S3 approach applied directly to **30** failed to provide a progressible path to more optimized inhibitors, we were simultaneously exploring direct replacement of the cyclohexylmethyl and cyclohexylethyl substituents of this scaffold. Major emphasis was placed not only on further reduction of lipophilicity, but also on decreasing the number of rotatable bonds to achieve entropically driven affinity gains and improvement of oral PK properties. In the course of these efforts, a series of analogs was generated in which the alkyl substituents were replaced by phenyl directly attached to the iminohydantoin core. In addition to satisfying the design criteria above, our interest in a phenyl substituent was further bolstered by a structure-based rationale arising from comparison of the flap configurations of BACE1 seen in X-ray structures with peptidic inhibitor OM99-2 and with the racemate of **30** (Fig. 22). With OM99-2, the flap is in a relatively closed conformation and places the aryl side chain of Tyr^{71} toward the prime side of the enzyme. With iminohydantoin **30**, the flap position is more reminiscent of the BACE1 apo structure in that it is more open with the Tyr^{71} side chain residue oriented toward the nonprime side of the enzyme. This leaves a relatively open space more proximal to the aspartates than S2′, which we subsequently termed the F′ subsite.

Based on this analysis, we reasoned that replacement of the prime-side binding cyclohexylethyl group of **30** with a phenyl moiety directly attached to the C5 position of the iminohydantoin core would project that group into the F′ site. To that end, we synthesized racemic C5-phenyl iminohydantoins **33–36** and prochiral diphenyl iminohydantoin **37** (Fig. 23A). With the exception of C5-benzyl analog **36**, these variants retained a similar level of micromolar affinity for BACE1 versus the racemic version of **30** (BACE1 $K_i = 1.4$ μM). To our surprise, however, when racemic **33** was soaked with BACE1, the (*S*)-enantiomer with the phenyl group in F′ was not observed in the X-ray structure as designed; instead the (*R*)-enantiomer was observed with the phenyl group bound in S1 (Fig. 23B). In addition, there was a notable and unexpected shift of the iminohydantoin core itself, with the C5 position moving 1.4 Å toward the nonprime side to place the S1 phenyl group in a position corresponding to that of the cyclohexyl group of **30**. For each of the other racemic analogs **34–36**, binding of the (*R*)-enantiomer was observed exclusively, placing the phenyl group in the S1 pocket in the same region as **33**. Prochiral diphenyl analog **37** also bound with its core and pro-(*R*) phenyl group was similarly positioned.[69] This profound preference for S1 phenyl occupancy and accompanying unpredicted shift in binding pose of the core again highlights the importance of X-ray crystallography for key insights into inhibitor binding.

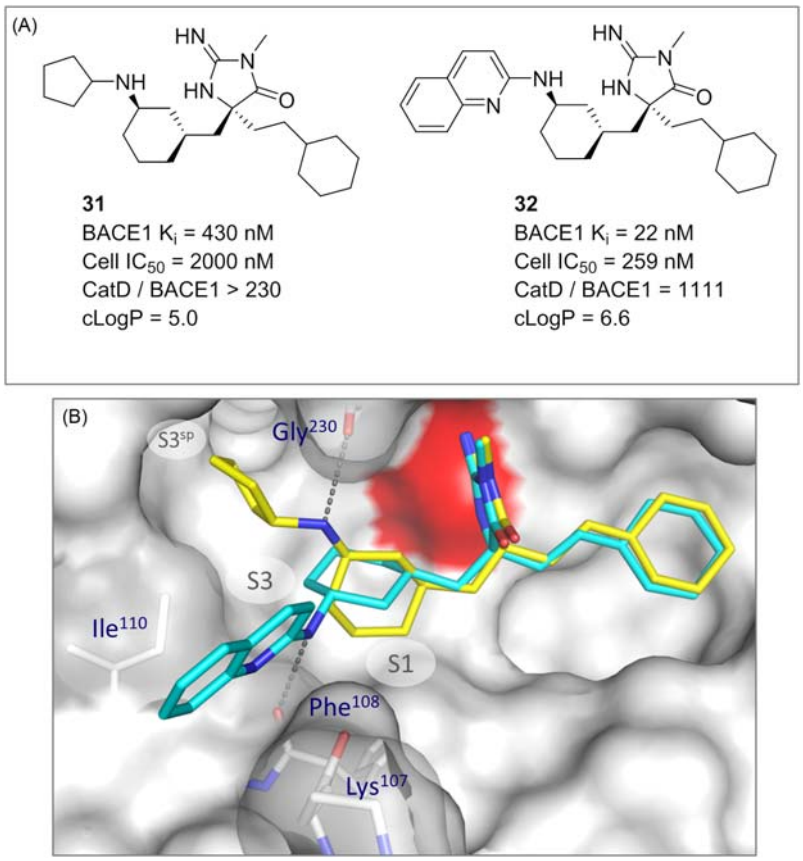

Fig. 21 (A) Structures of S1 aminocyclohexane-derived iminohydantoins **31** and **32**. (B) Overlay of X-ray structures of **31** (*yellow*) and **32** (*blue*) bound to BACE1 showing the different trajectory induced by derivatization of the S1 aminocyclohexane with a hydrogen bond acceptor group as in **32**.

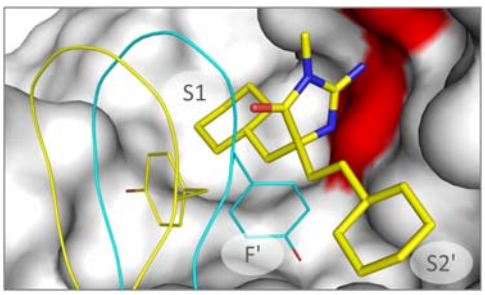

Fig. 22 Comparison of the flap positions in X-ray structures of the racemate of iminohydantoin **30** (*yellow*) and of OM99-2 (*not shown*) bound to BACE1. The flaps are represented as ribbons with their Tyr^{71} side chains displayed, and they are colored by compound—the flap from the iminohydantoin X-ray is *yellow* and the flap from OM99-2 is *blue*. In the OM99-2 structure, the flap is in a relatively closed position with Tyr^{71} oriented on the prime side. In the iminohydantoin structure, the flap is in a more open conformation with the Tyr^{71} side chain moved to the nonprime side. We termed the open space left by that flap movement in the iminohydantoin structure as the F' subsite.

The discovery of diphenyl iminohydantoin **37** by Zhu et al. was a key breakthrough for our program.[69] This low MW compound, of MW just slightly less than of the original isothiourea hit **12**, had single digit micromolar affinity and retained high LE (Fig. 24A). Its c log*P* of 1.9 was much more favorable in comparison with **30;** it had a minimal shift in cellular potency and displayed greater than 20-fold selectivity over CatD. The compound also achieved high plasma exposures and was brain penetrant following oral administration to rats. The X-ray cocrystal structure of **37** demonstrates that the pro-(*R*) phenyl occupies the S1 pocket in analogy to the racemic C5-phenyl iminohydantoins above. In addition, the flap is in a well-organized, partially closed conformation with the Tyr^{71} aromatic ring providing an edge–face interaction with the S1 phenyl group of **37** and the phenol of Tyr^{71} donating a hydrogen bond to the carbonyl of Lys^{107} (Fig. 24B). The pro-(*S*) phenyl substituent projects toward but does not occupy the

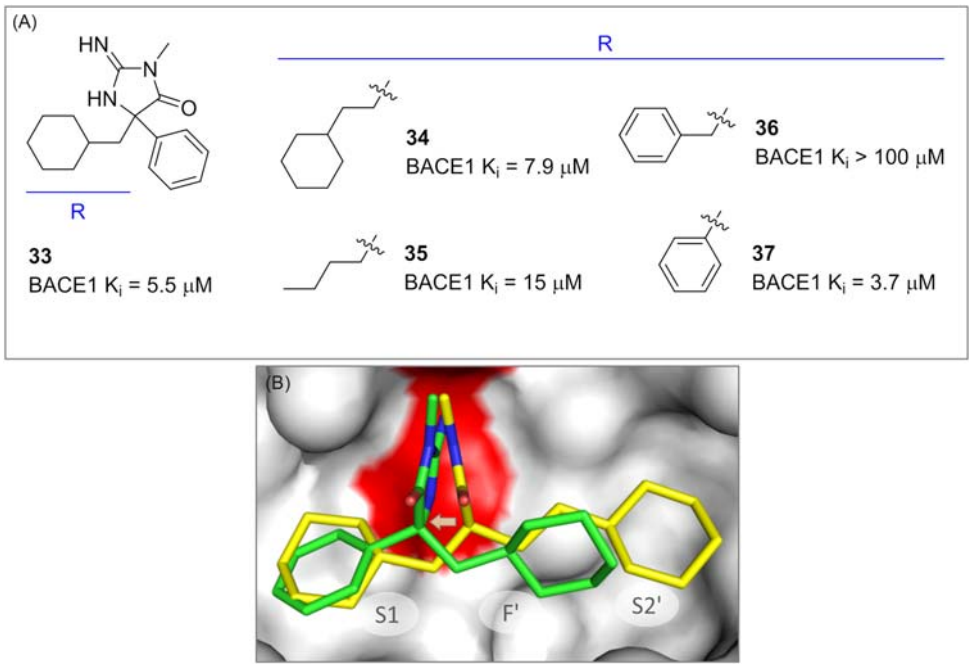

Fig. 23 (A) Structures of C5-phenyl iminohydantoins **33**–**37**. (B) Overlay of the X-ray structures of racemic C5-phenyl iminohydantoin **33** (*green*) and the racemate of C5-bis(cyclohexylalkyl) iminohydantoin **30** (*yellow*) bound to BACE1 showing the C5-phenyl group of **33** in S1 and the resulting 1.4 Å shift in its core binding pose.

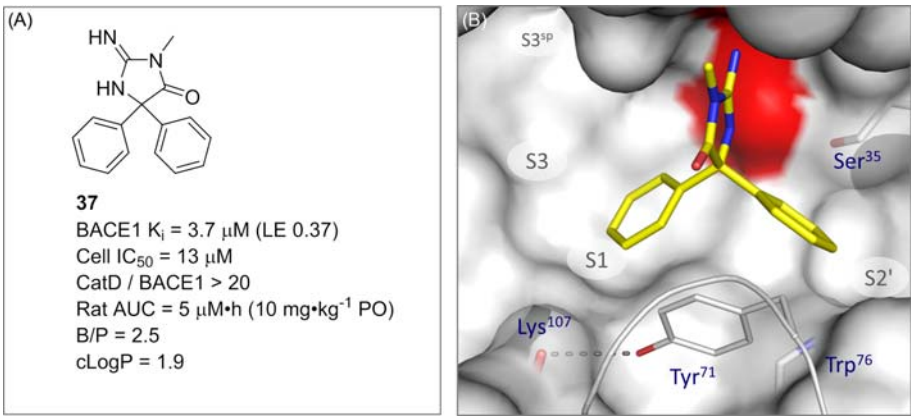

Fig. 24 (A) Structure and profile of C5-diphenyl iminohydantoin **37**. (B) Key aspects from the X-ray structure of **37** bound to BACE1 showing the pro-(*R*) phenyl group in the S1 pocket.

S2′ pocket, and instead engages in hydrophobic interactions with the Ser^{35}, Trp^{76}, and Tyr^{71} of the flap. Remarkably, scientists at Wyeth independently discovered **37**, which we learned upon publication of their patent application a few months after our disclosure[81] of the structure of **37** in a patent application. A subsequent publication by the Wyeth group confirmed that they discovered **37** via HTS in contrast to our fragment-based approach.[82]

8.09.4 Lead Optimization

8.09.4.1 Iminohydantoins: S3 Occupancy

With compound **37** in hand as an attractive lead-like starting point the team considered approaches to higher affinity analogs while maintaining desirable overall properties. In silico docking experiments suggested that the meta positions of either the pro-(*R*) or

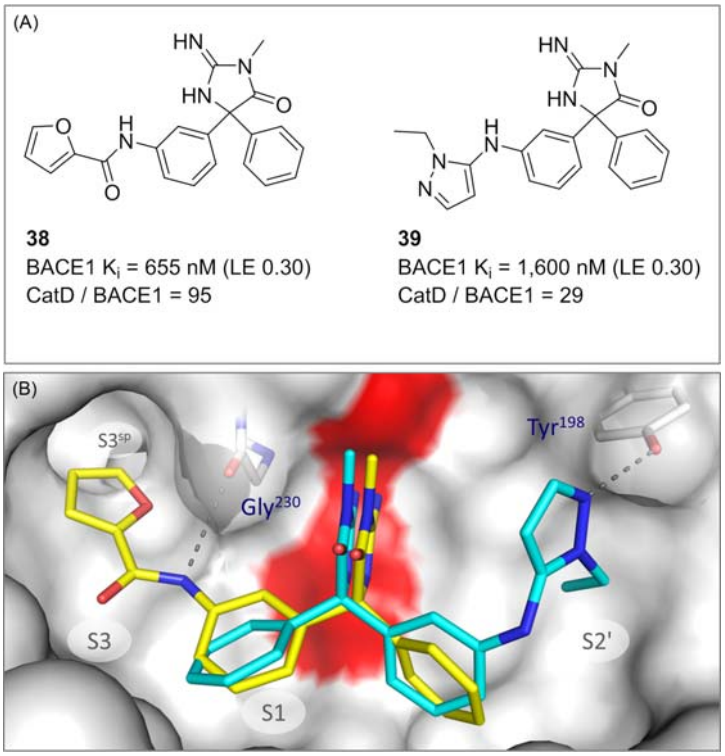

Fig. 25 (A) Structures of racemic *meta*-amino-substituted diphenyl iminohydantoins **38** and **39**. (B) Overlay of X-ray structures of **38** (*yellow*) and **39** (*blue*) bound to BACE1 showing their occupancy of S1/S3 and S1/S2′, respectively.

pro-(*S*) phenyl groups of **37** provided favorable vectors toward S3 and S2′, respectively, and multiple structural motifs were prioritized for evaluation. One of these incorporated a nitrogen linker at the meta position as exemplified by furan carboxamide **38**[83] and diarylamine **39**[84] (Fig. 25A). Both of these compounds afforded affinity gains, and X-ray cocrystal structures with BACE1 showed that the binding modes of **38** and **39** were distinct, binding in S3 and S2′, respectively, in general support of our binding hypotheses (Fig. 25B). Furan carboxamide **38** bound with the furanyl group occupying the S3 pocket and the amide hydrogen engaged in a hydrogen bond with the Gly^{230} carbonyl. On the other hand, pyrazole derivative **39** bound with the pyrazole ethyl group in S2′ and with a pyrazole nitrogen accepting a hydrogen bond from Tyr^{198}. Neither of these N-linked chemotypes received further resourcing due to the emergence of the more promising biaryl series (vide infra), although knowledge of the binding mode of **38** later proved to be pivotal to the discovery of our lead clinical candidate verubecestat as discussed in Section "Discovery of Verubecestat."

In a second structural presentation that was prioritized for synthesis, Cumming et al. incorporated an aryl group directly attached to the meta position of the pro-(*R*) phenyl of **37** to form a 3-biaryl motif that reached into S3 and potentially $S3^{sp}$.[85] Introduction of an additional phenyl substituent as in **40** increased c log*P* by approximately two log units, but this could be mitigated by substitution of the biaryl motif with polar groups or by incorporation of a more polar heterocycle in place of phenyl (Fig. 26A). Pursuit of this approach paid immediate dividends. 3-Pyridyl derivative **41** and 3-methoxyphenyl analog **42** showed substantial gains in affinity over **37** with maintenance of good LE, which was in contrast to biphenyl analog **40** which showed essentially no gain in affinity. In the X-ray cocrystal structure of **41**, the (*R*)-enantiomer in fact bound with the pyridyl group in S3 (Fig. 26B),[85] which was an important confirmation of our design as we had considered that the (*S*)-enantiomer could have bound with the biaryl group displayed in S2′ as observed for **39**. The nitrogen of the S3 pyridyl in **41** was positioned at the entrance of $S3^{sp}$ within hydrogen bonding distance of an ordered water molecule. The X-ray cocrystal structure of the more potent methoxyphenyl analog **42**[86] was virtually superimposable with that of **41**, the only significant difference being occupancy of $S3^{sp}$ by the methoxy group with accompanying displacement of the ordered water molecule, clearly highlighting the benefit of $S3^{sp}$ occupancy to affinity. A more extensive scan of substituted aryl and heteroaryl groups in S3 reinforced these findings, namely that analogs bearing an S3 moiety that hydrogen bond to or displace the water molecule in $S3^{sp}$ showed gains in affinity over the simple C5-diphenyl parent **37**, whereas those that cannot (e.g., analogs **43** and **44** of **41** and **42**, respectively, Fig. 26A), showed essentially no benefit to affinity.[85] These results were an early highlight of the importance of optimal interactions in $S3^{sp}$ that again became important later as part of the discovery of verubecestat.

At this stage, optimization efforts continued in two complementary directions—further optimization of substitution about the iminohydantoin core while simultaneously expanding our effort into development of additional new iminoheterocycle cores.

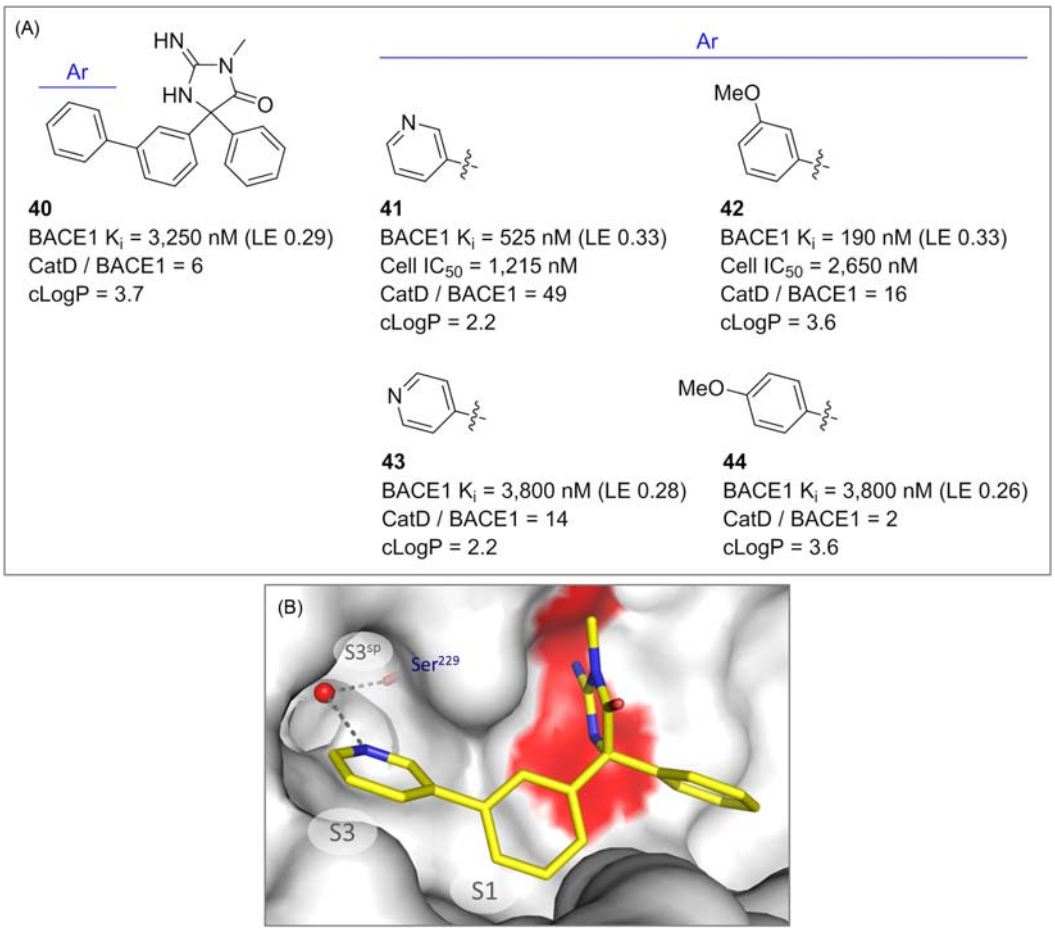

Fig. 26 (A) Structures of racemic biaryl substituted iminohydantoins **40–44**. (B) X-ray structure of biaryl analog **41** showing binding of the (*R*)-enantiomer and hydrogen bonding interaction between the pyridyl nitrogen and an ordered water in $S3^{sp}$.[85]

8.09.4.2 Iminohydantoins: Advanced Lead Optimization

Further optimization of the iminohydantoin series by Cumming et al. examined potential replacements for the phenyl group bound in F′ in the analogs above, with the intent of identifying alternative moieties with lower MW and/or c log*P*.[87] As part of this effort, we were able to successfully incorporate structural information gleaned from earlier SAR development around N3-piperidine-substituted iminohydantoins **27** and **28** (Fig. 16). In that effort, we explored C5 variations in combination with a nonoptimized C5-butyl group to allow this core to find its own optimized pose, for example, general structure **45** (Fig. 27A). This approach was informed by the multiple binding modes observed within the active site during our preliminary exploration of the iminohydantoins (Section "Fragment Screening: Discovery of New Inhibitor Chemotypes"). With the N3-piperidine series, a small sampling of aromatic, heteroaromatic, and saturated cyclic C5 variants in combination with the C5 *n*-butyl group all showed generally flat SAR with affinities in the 1–5 μM range. To understand any changes in binding that had occurred, we obtained crystal structures of a number of these analogs bound to BACE1. While in most cases the compounds bound with the (*R*) configuration, as seen earlier for N-methyl analogs **33–36** (Fig. 23), C5-cyclopropyl analog **46** unexpectedly bound in the (*S*) configuration to display the cyclopropyl group in the F′ subsite (Fig. 27B).[87] Most interestingly, overlay of **46** and the S1-binding C5-phenyl analog **47** in this subseries suggested that the combination of these two C5 modifications should be favorable in the context of S1–S3 biaryl subseries.

Cumming et al. returned to the N3-methyl iminohydantoin core to test this hypothesis, and gratifyingly the first analogs **48** and **49** (Fig. 28A) showed slightly improved or similar BACE1 affinity and cell Aβ lowering potency versus the analogous F′ phenyl analogs **41** and **42** (Fig. 26A).[85] An overlay of the X-ray structures of S3 methoxyphenyl analogs **42** and **49** showed that the inhibitor binding modes with C5-phenyl and C5-cyclopropyl were well conserved. The flap maintained the same conformation as well, but moved in closer to the C5-cyclopropyl analog, with the Tyr^{71} side chain shifting by 1.3 Å between the two structures (Fig. 28B). A more extensive set of F′ analogs showed that, among a fairly broad set of variants, including other cycloalkyl groups as well as alkyl and heteroaryl moieties, the cyclopropyl was unique in imparting the improved potency.[85] Given the half-log improvement in LE due to the lower MW of the F′-cyclopropyl analogs, we continued significant optimization of this scaffold.

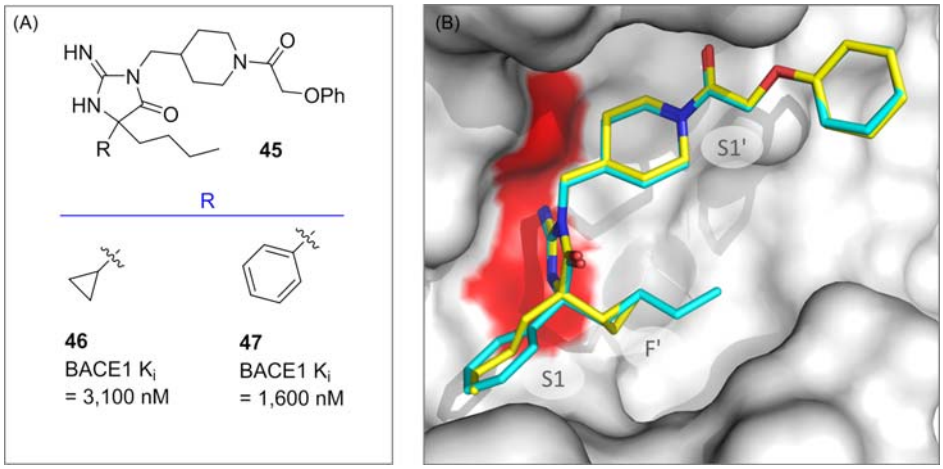

Fig. 27 (A) General structure of C5 variants in the N3-piperidinyl iminohydantoin series **45** and structures of C5-cyclopropyl and C5-phenyl analogs **46** and **47**. (B) Overlay of X-ray structures of **46** (*yellow*) and **47** (*blue*) bound to BACE1 suggesting that phenyl and cyclopropyl cosubstitution at C5 should be favorable.[87]

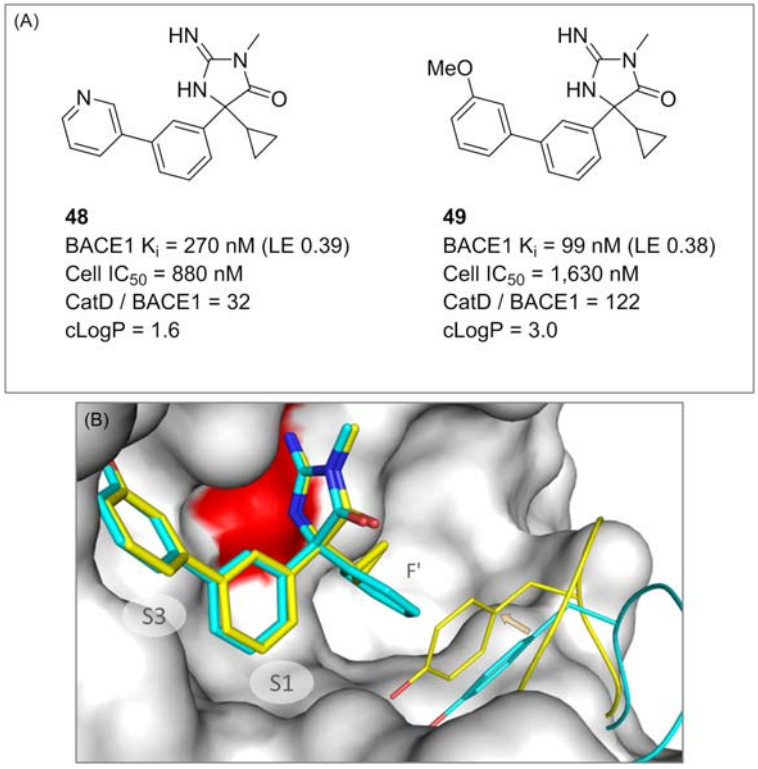

Fig. 28 (A) Structures of early C5-cyclopropyl, C5-biaryl iminohydantoins **48** and **49**. (B) Overlay of the X-ray structures of F'-cyclopropyl analog **49** (*yellow*) and F'-phenyl analog **42** (*blue*) bound to BACE1 showing the conserved binding mode between the modifications as well as movement of the flap (ribbon, colored to match inhibitor structure) with Tyr^{71} 1.3 Å closer to F'-cyclopropyl analog **49**.

A scan of S3 substituents with the cyclopropyl iminohydantoin core clearly revealed the direct relationship between c log*P* and cell potency shift, with a c log*P* of 2.5 or less required for a cellular potency shift versus enzymatic K_i of less than 10-fold. In most cases, control of c log*P* was achieved with a substituted pyridyl moiety as the S3 group, the impact of which is clearly seen when comparing 3-chlorophenyl analog **50** (c log*P* 3.8, cell shift 40-fold) with 3-chloro-5-pyridyl analog **51** (c log*P* 2.4, cell potency shift sevenfold) (Fig. 29). Based on this analysis, we fixed the S3 substituent as 3-pyridyl and next sought to examine the effects of occupancy deeper into the relatively narrow $S3^{sp}$ pocket given that our earlier SAR showed that the organized water in that pocket could be displaced by methoxy, as well as by chloro and cyano, all of which were essentially equipotent. To that end, a larger, linear

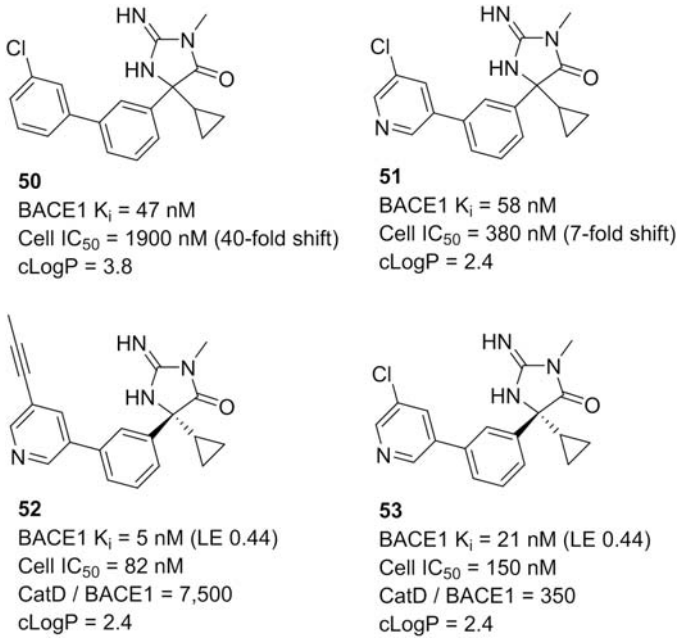

Fig. 29 Structures of C5-cyclopropyl iminohydantoins with substituted pyridyl groups in S3 with analog **52** showing the benefit to BACE1 affinity and selectivity over CatD imparted by deeper occupancy of $S3^{sp}$.[85]

propynyl group on as S3 pyridyl moiety using resolved core provided **52**, which showed a fourfold improvement in BACE1 affinity and a 20-fold improvement in selectivity over CatD versus the corresponding resolved chloro analog **53** (Fig. 29).[85] Both of these resolved analogs possessed excellent LE.

An X-ray crystal structure of **52** bound to BACE1 showed that the propynyl group projected deeper into $S3^{sp}$ as designed where it engaged in a favorable hydrophobic interaction with Ala^{335} (Fig. 30).[85] In CatD, this residue is replaced with a larger and more polar aspartate residue that would not be expected to accommodate the propynyl group. This difference in residues is reflected in the significant increase in selectivity seen with **52**, which is achieved both through improved BACE1 affinity and through decreased affinity for CatD. Propynyl analog **52** represented our most optimized iminohydantoin BACE inhibitor; it was one of the only compounds in that series to have cellular potency less than 100 nM, although it was still 16-fold shifted from its potency against purified enzyme, and it possessed excellent plasma exposure ($AUC_{0-6h} = 18$ μM h) following a single 10 mg kg^{-1} oral dose in a rat PK screen, albeit with only modest CNS exposure.

8.09.4.3 Core Modification: Ring Expansion to Iminopyrimidinone

In parallel with optimization of the S1–S3 and F′ substituents in the iminohydantoin series, we also sought to design and explore other novel iminoheterocycle cores that could similarly engage the BACE1 catalytic dyad while simultaneously opening additional

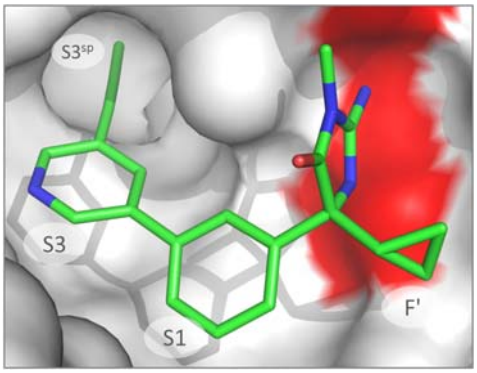

Fig. 30 X-ray structure of optimized iminohydantoin **52** bound to BACE1. In the $S3^{sp}$ site of CatD, there is an Asp residue in place of the Ala^{335} of BACE1, resulting in both steric and electrostatic differences that are less favorable to binding of the propynyl group of **52**.

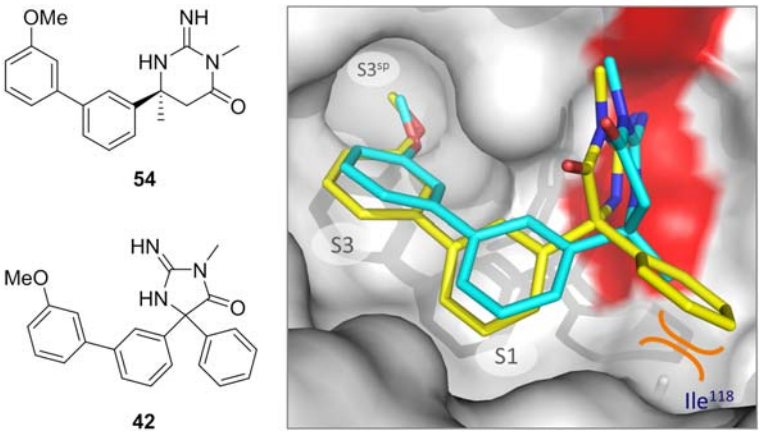

Fig. 31 Overlay of the modeled docking pose of iminopyrimidinone **54** (*blue*) versus the X-ray structure of iminohydantoin **42** (*yellow*) bound to BACE1 showing the difference in trajectory toward the prime side of the enzyme and the potential for close contact with Ile^{118} from larger C5-substituents on the iminopyrimidinone core.[86]

SAR opportunities and potentially offering unique physicochemical properties. To that end, one direction we pursued early in our program was ring expansion of the five-membered iminohydantoin core to a six-membered iminopyrimidinone ring (e.g., general structure **16**, Fig. 11).[86] This new core offered two important points of differentiation. First, in terms of SAR, incorporation of a second sp^3 center not only provided an additional site for exploration, but modeling suggested that this change would introduce nonplanarity into the ring in contrast to the planar iminohydantoin, and this change in molecular shape would potentially alter the trajectories of substituents into both the prime and nonprime sides. Particularly noteworthy for prospectively docked iminopyrimidinone **54** was the prime-side facing substituent pointing more directly to the protein backbone versus iminohydantoin **42** (Fig. 31), suggesting a preference for smaller substituents at that position, while changes to the conformation of the S1–S3 biaryl were more subtle. The second change induced by ring expansion was to increase the basicity of the amidine center of the iminopyrimidinone, which could be beneficial in reducing the cellular potency shift seen with the iminohydantoins since more basic analogs could favor increased partitioning into acidic endosomal compartments where BACE1 processes APP. Since this was an endemic issue with the iminohydantoins, the change was particularly attractive.[86]

Analogs **54–59** (Fig. 32A) were among the earliest examples made in this series to test the design elements described above, with the C6 methyl and phenyl groups designed to plumb the effects of trajectory changes toward the nonprime side, and the biaryl substituents to enable facile comparison with the iminohydantoin series.[86] As anticipated by modeling, the C6-methyl iminopyrimidinones were significantly more potent than their C6-phenyl counterparts and, importantly for this novel core, were roughly equipotent to the analogous iminohydantoins (cf. iminohydantoins **41** and **42**, Fig. 26). An X-ray crystal structure of compound **54** bound to BACE1 agreed well with the modeling result above (Fig. 32B). Notably, the C6-methyl group was positioned 3.6 Å from Ile^{118}, favorable for a hydrophobic interaction but a distance that would not tolerate the larger phenyl substituent without significant perturbation of the binding mode. In terms of effects of core basicity, when comparing matched sets of biaryl substituents, the increased basicity of the iminopyrimidinone core translated to substantially lower or no cell potency shift versus the corresponding iminohydantoins (e.g., threefold for S3 methoxyphenyl iminopyrimidinone **54** vs. 14–16-fold for the analogous iminohydantoins **42** and **52**) despite similar or higher c log*P* values for the iminopyrimidinones.[86] It is worth noting that we later learned that the iminopyrimidinone core was independently identified by the Astex/AstraZeneca collaboration through their fragment-based discovery and hit optimization approach.[88]

A rat PK screen on these initial iminopyrimidinone analogs described by Stamford et al. clearly identified the 3-cyanophenyl substituent of **58** as preferred for further SAR development, with a single oral 10 mg kg^{-1} dose producing a plasma of $AUC_{0\text{-}6h}$ of 8.6 μM h, versus a dose-matched AUC_{0-6h} of less than 1 μM h with the other two S3 analogs.[86] Fixing the distal cyanophenyl substituent, we examined a large number of mono- and bicyclic heteroaryl groups (Fig. 33) as replacements for the proximal phenyl group, from which several SAR trends stand out. First, thienyl variants, and in particular the 2,4- and 2,5-isomers **60** and **61**, respectively, were the only modifications that improved on the affinity conferred by phenyl while maintaining essentially no cellular potency shift as well as imparting similar selectivities over CatD.[86] Many heteroaryl groups conferred affinity similar to that of phenyl, though those whose heteroatoms would face the carbonyl of Gly^{230} in the S1 pocket (e.g., 2,6-pyridyl **62** and 2,5-furanyl **63**) were significantly less potent. Several benzothienyl modifications **64–66** were also examined that afforded alternate trajectories into S3 and/or differentiated filling of the open S1–S3 pockets. While at best slightly more potent than P1 phenyl, they offered no advantage given their increased MW, reflected in lower LE, and in fact they showed increased cell potency shifts due to their higher c log*P* values.[89]

With the 2,4- and 2,5-thienyl regioisomers identified as conferring the most affinity in the initial biaryl iminopyrimidinone analogs, and seeking further affinity and cell potency gains, we turned our attention to modifications in S3. The most profound improvements in affinity and cell potency were obtained by replacement of the cyanophenyl moiety by the

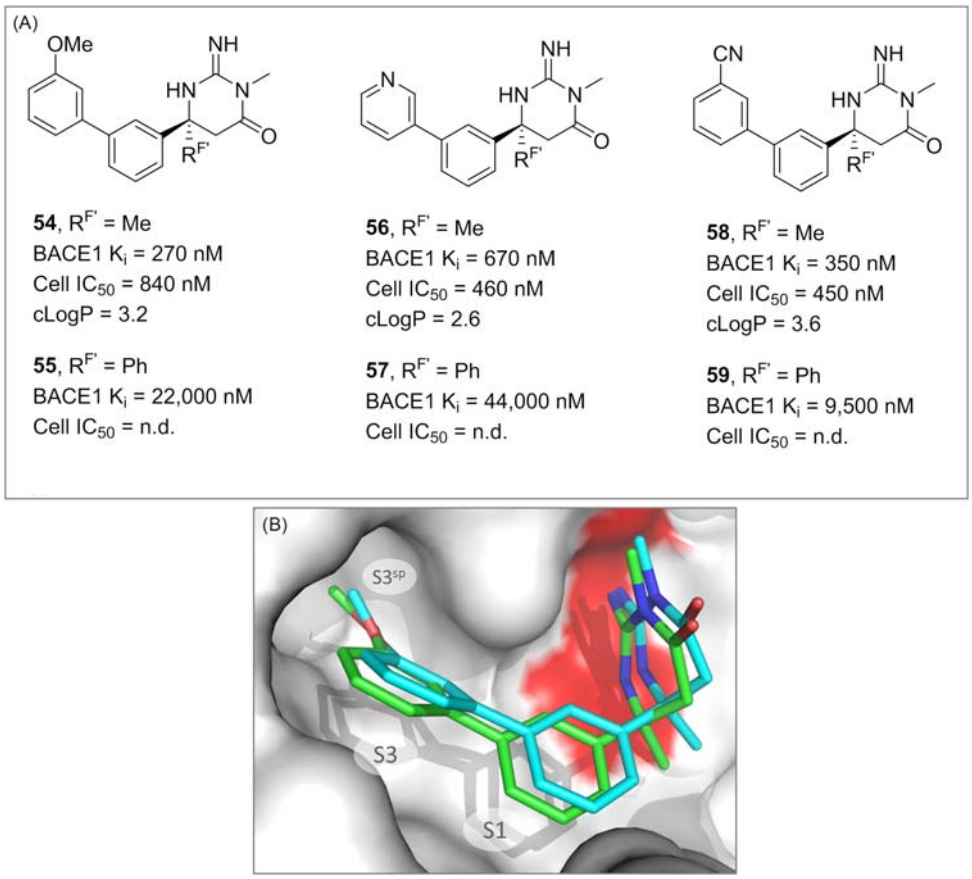

Fig. 32 (A) Structures of S1 phenyl S1–S3 biaryl iminopyrimidinones **54**–**59**. (B) Overlay of the modeled docking pose (*blue*) and X-ray crystal structure (*green*) of iminopyrimidinone **54** bound to BACE1.

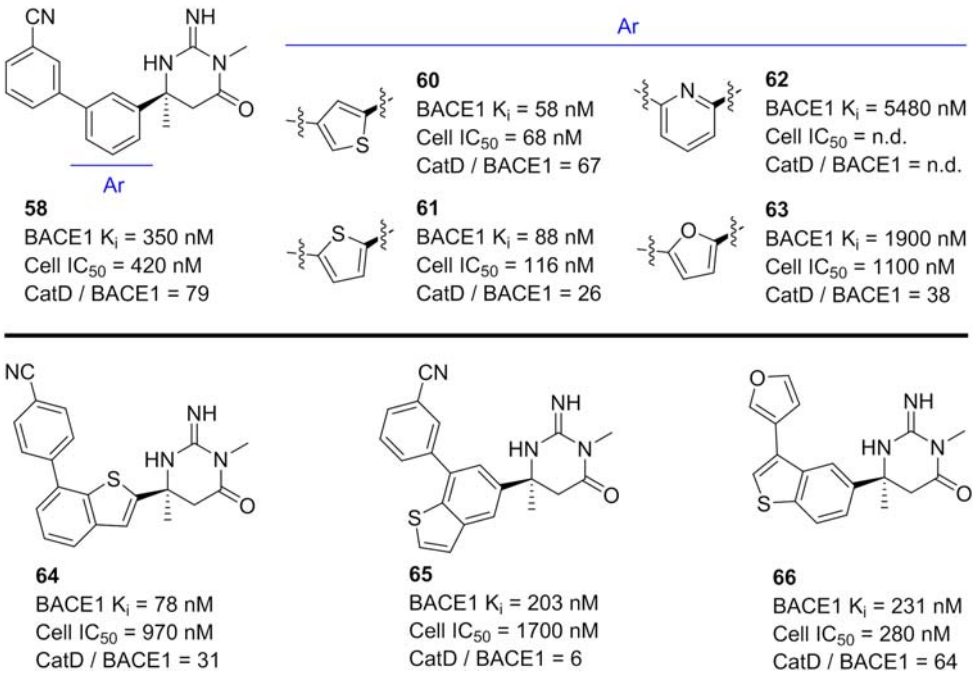

Fig. 33 Key elements of SAR in the S1–S3 biaryl iminopyrimidinone series exemplified by compounds **58** and **60**–**66**.

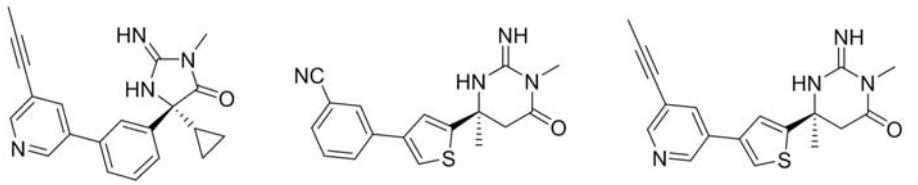

52
BACE1 K_i = 5 nM (LE 0.44)
Cell IC_{50} 82 nM
CatD / BACE1 = 7,500
Caco-2 efflux ratio = 2.6
permeability = 185 nm•s^{-1}
Rat plasma f_u = 4%
Mouse plasma f_u = 4%
cLogP = 2.4
PSA = 69 Å^2

60
BACE1 K_i = 58 nM (LE 0.43)
Cell IC_{50} = 68 nM
CatD / BACE1 = 67
Caco-2 efflux ratio = 2.4
permeability = 174 nm•s^{-1}
Rat plasma f_u = 15%
Mouse plasma f_u = 17%
cLogP = 3.2
PSA = 80 Å^2

67
BACE1 K_i = 8 nM (LE 0.46)
Cell IC_{50} = 13 nM
CatD / BACE1 = 129
Caco-2 efflux ratio = 3.5
permeability = 144 nm•s^{-1}
Rat plasma f_u = 6%
Mouse plasma f_u = 12%
cLogP = 2.2
PSA = 69 Å^2

Fig. 34 Detailed profiles of key inhibitors used in development of an in vivo PD assay.

3-propyn-1-yl-5-pyridyl moiety, affording analog **67** (Fig. 34).[86] In particular, **67**, with single digit nanomolar affinity and comparable cell potency, proved to be an important tool compound as described in the next section. In fact this compound, along with its progenitors iminopyrimidinone **60** and iminohydantoin **52**, helped to establish a new paradigm for characterizing in vivo pharmacodynamic (PD) effects for our program.

8.09.4.4 In Vivo Validation and Development of a High-Throughput Rat PD Assay

The discovery of **52**, **60**, and **67** over the course of a few months marked a watershed for the program. These compounds proved to be critical tools for characterizing inhibitor-mediated in vivo pharmacology and paved the way for the development of a high-throughput PD assay that drove optimization of the in vivo properties of subsequent generations of inhibitors.

Upon discovery of **60** as the first inhibitor in the series with a K_i value less than 100 nM combined with essentially equipotent cell activity, high Caco-2 permeability, oral bioavailability, and reasonable brain penetration, this compound was profiled in the TgCRND8 mouse model. As was discussed in the context of peptidomimetic inhibitor **3** in Section "Hydroxyethylamine-Based Peptidomimetic Inhibitors," an advantage of this model is that large amounts of Aβ are produced in the brains of these mice and it was well established that orally administered GS inhibitors caused profound reductions of brain Aβ levels in these mice.[90] Single acute oral doses of **60** up to 200 mg kg^{-1} in TgCRND8 mice failed to elicit significant reduction of cortex $Aβ_{40}$ levels despite causing complete ablation of plasma $Aβ_{40}$ levels, a result that was reminiscent of studies with peptidomimetic **3**. Notably, mouse brain homogenate binding studies suggested that free brain levels of roughly 70 nM were attained at the 200 mg kg^{-1} dose, a value similar to the in vitro potency of the compound. Gratifyingly, subchronic administration of **60** (200 mg kg^{-1} PO, 5 days, BID) resulted in somewhat higher exposure and a modest 30% reduction of brain $Aβ_{40}$ levels (Fig. 35). This was important as it was

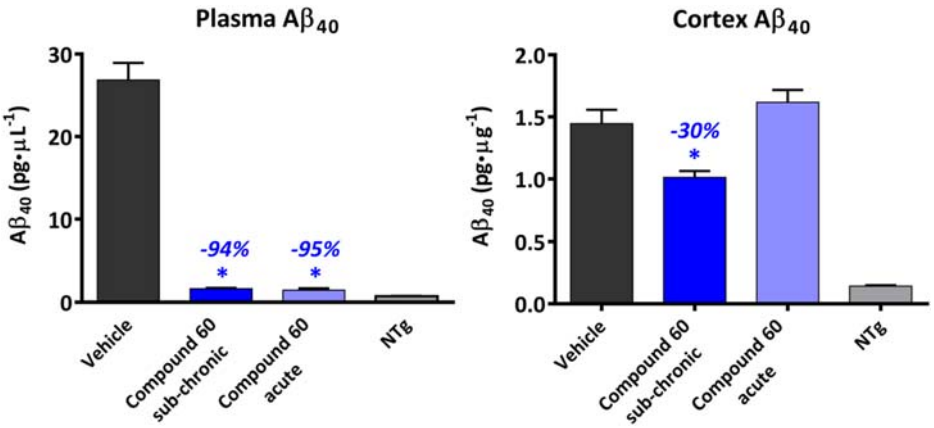

Fig. 35 Comparison of the effects on $Aβ_{40}$ in plasma and cortex in TgCRND8 mice following subchronic (5 days, BID) and acute, single dose administration of 200 mg kg^{-1} PO of compound **60**. The $Aβ_{40}$ levels in plasma and cortex of nontransgenic mice (NTg) are included for comparison.

the first demonstration of brain Aβ lowering by a BACE1 inhibitor in our program, and furthermore at that time there were no reports from any source of inhibitors that lowered brain Aβ despite the intensive efforts of many groups over several years.

Given the challenges that we had experienced in developing inhibitors with potent central activity up to this point, and having identified **60** as novel, nonpeptidic inhibitor with favorable drug-like attributes including central activity after subchronic oral dosing, it was of interest to assess its impact on disease modification upon chronic dosing in TgCRND8 mice. Hyde et al. therefore designed a study to determine the effects of **60** (100 mg kg^{-1} day^{-1}) formulated in diet on total brain Aβ levels, amyloid plaque deposition, and cognitive function in TgCRND8 mice.[91] Dosing was commenced in preplaque animals at 6 weeks of age and continued for 6 months. At multiple time points during dosing, independent groups of mice that received **60** had statistically significant reductions in cortical $Aβ_{40}$ and $Aβ_{42}$ levels of 26-37% relative to age-matched vehicle controls (Fig. 36A). At the 6-month time point, a 35% reduction in mature plaque density as defined by Thioflavin S positive area was also observed in the cortex of treated mice. In the Morris water maze, a model of learning and memory, mice treated with **60** for 6 months did not show benefit to their efficiency of finding the hidden platform; however, evidence of improved performance relative to age-matched controls and performance similar to that of age-matched nontransgenic controls was evident in the probe trial component of the water maze (Fig. 36B). Moreover, through the duration of the study, **60** was well tolerated and no overt compound-related safety concerns were identified at the termination of the study. These results were exciting because they were the first demonstration that partial chronic BACE1 inhibition via pharmacological intervention could realize disease modification in an AD model.[91]

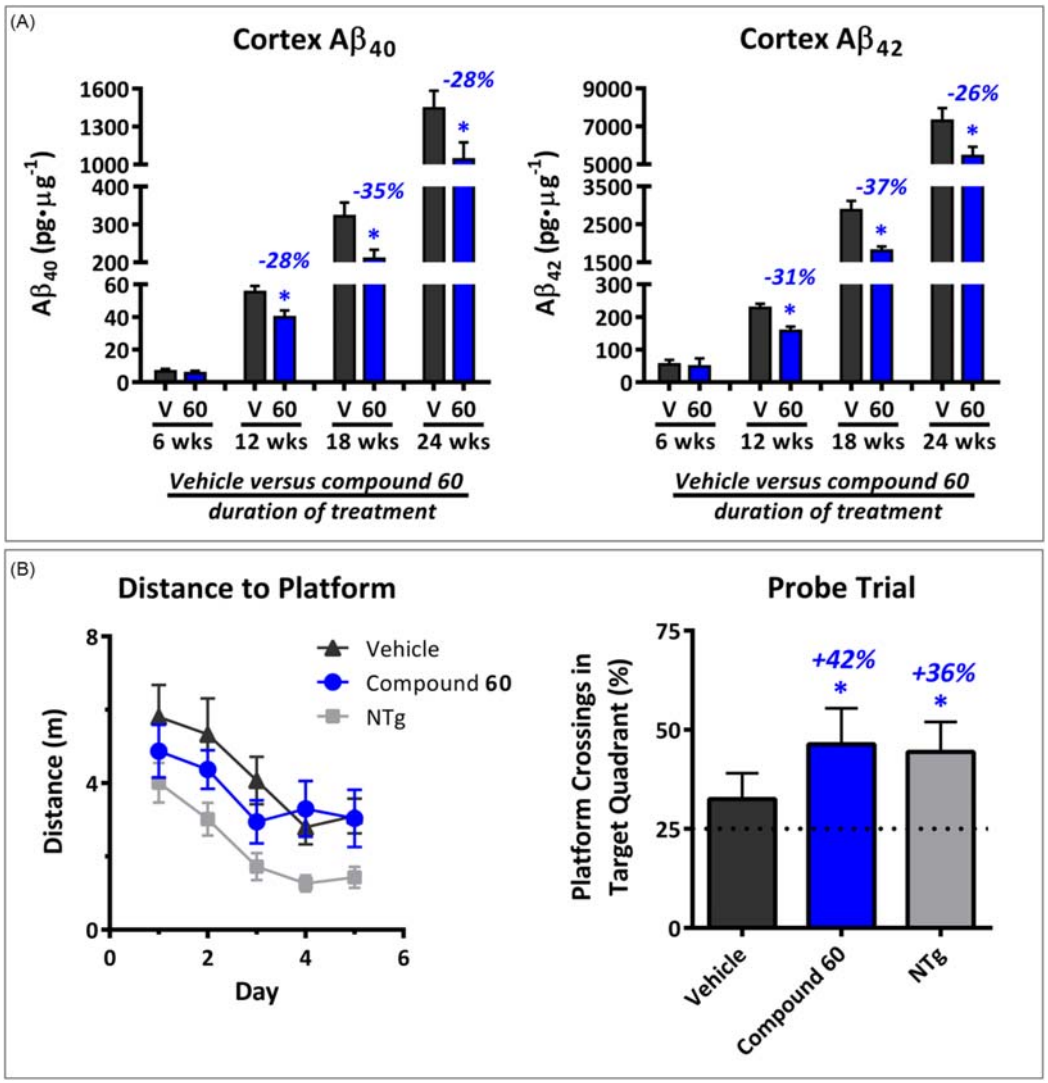

Fig. 36 (A) Effects on cortical $Aβ_{40}$ and $Aβ_{42}$ in TgCRND8 mice over time as a result of chronic dosing with 100 mg kg^{-1} day^{-1} in diet of compound **60**. (B) Performance of TgCRND8 mice in the Morris water maze cognition model following 6 months of treatment with 100 mg kg^{-1} day^{-1} in diet of compound **60** relative to age-matched TgCRND8 and nontransgenic (NTg) controls treated with vehicle.[91]

While the positive outcome of the chronic study conducted by Hyde et al. provided tremendous impetus to the program, the lack of potency of **60** and related inhibitors with respect to acute cortex Aβ reduction in TgCRND8 mice, as well as the low throughput of the assay, presented significant obstacles for SAR development. The striking differential potency between the plasma and central compartments in TgCRND8 mice could not be explained by differences in potency between peripheral and CNS BACE1; a number of inhibitors including **60** were essentially equipotent in reducing Aβ production by cultured TgCRND8 mouse neuronal cells and HEK293 cells. At this stage we pursued two parallel avenues that significantly shaped our strategy to identify more centrally potent inhibitors. First we sought to understand fundamental parameters of BACE1 in vivo biology that may be contributing to the weak central potency. Second, concerned that the weak central potency may be dependent on the overexpression of the human FAD APP-Swedish mutant gene in TgCRND8 mice, we invested in the development of an acute PD assay in nontransgenic rats.

As a framework to investigate the first avenue, we advanced the hypothesis that BACE1 may be rate limiting for Aβ production in the periphery, but not in the CNS; therefore higher enzyme inhibition in the brain relative to the periphery might be required to achieve central Aβ reduction. To interrogate this hypothesis, Hyde et al. determined brain Aβ levels and inhibitor activity were determined in wild-type Bace1 heterozygous (Bace1 HET) mice which have 50% of the BACE1 levels of wild-type mice.[92] Interestingly, Bace1 HET mice showed approximately 50% reduction of $A\beta_{40}$ in the plasma consistent with a 50% reduction of peripheral enzyme activity. In contrast, no significant reduction in brain or CSF Aβ levels was observed in Bace1 HET mice in comparison with Bace1 wild-type mice (**Fig. 37A**). This suggests that BACE1 is rate limiting for Aβ production in the periphery but not in the CNS, possibly because BACE1 in the brain is not saturated with its substrate APP. This observation is also consistent with the hypothesis that a higher degree of brain BACE1 inhibition is required to reduce brain Aβ levels relative to the degree of peripheral BACE1 inhibition required to reduce peripheral Aβ. Moreover, oral administration of doses at or above 100 mg kg^{-1} of compound **67** to Bace1 HET

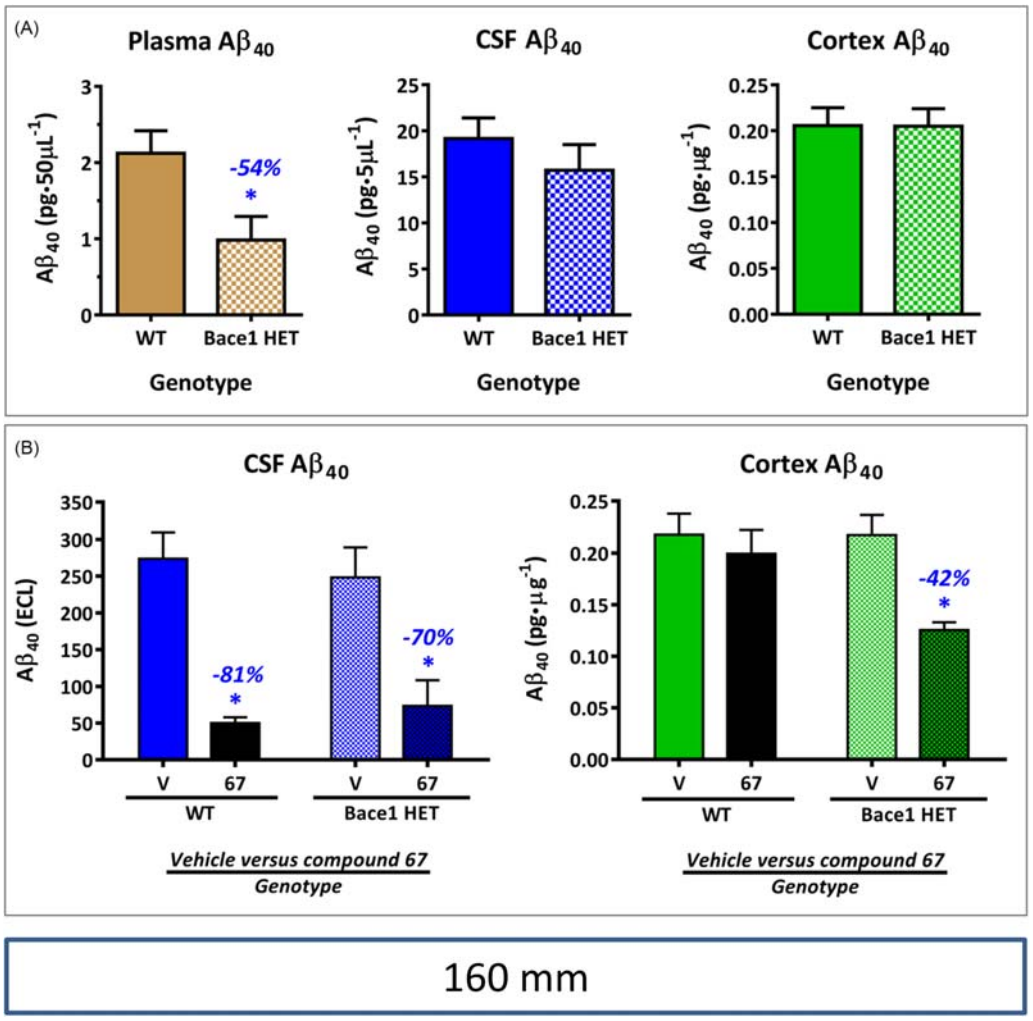

Fig. 37 (A) Levels of $A\beta_{40}$ in plasma, CSF, and cortex in wild-type (WT) and Bace1 heterozygous mice (Bace1 HET). (B) Effects of acute treatment with 200 mg kg^{-1} PO of compound **67** on $A\beta_{40}$ levels in CSF (expressed as electrochemiluminescence, ECL) and cortex of wild-type and of Bace1 heterozygous mice.

mice elicited significant reduction of cortex $A\beta_{40}$ (cf. Fig. 37B for 200 mg kg^{-1} dose of **67**), presumably due to combined genetic and pharmacological ablation of BACE1 activity, whereas no cortex $A\beta_{40}$ reduction was observed in Bace1 wild-type mice treated with the same doses of **67**. From these studies it was inferred that very high BACE1 occupancy (much greater than 50%) is necessary to achieve significant acute brain Aβ reduction. This conclusion was also supported by subchronic studies with the peptidomimetic inhibitor **3** described in Section "Hydroxyethylamine-Based Peptidomimetic Inhibitors."

In pursuit of the second avenue that impacted program strategy, that is, development of a PD assay in nontransgenic rats, sensitive immunoassays were developed to quantify Aβ levels in rats. In addition to our concern that the TgCRND8 mouse may be inherently less sensitive to BACE1 inhibition, the dynamics of Aβ production and turnover in nontransgenic rats was more likely to be similar to Aβ dynamics in the human sporadic AD population. Due to their larger size compared with mice, use of rats would also enable reliable, routine sampling of CSF to determine changes in CSF Aβ levels in response to BACE1 inhibitor treatment, providing a surrogate for brain Aβ inhibition that could be translated into human clinical studies as a primary biomarker for proof of activity. Use of CSF Aβ levels as a surrogate biomarker for brain Aβ inhibition was also supported by studies with GS inhibitors in Tg mice overexpressing APP[93,94] and in non-Tg rodent species[95,96] that published contemporaneously with our ongoing efforts.

In assessing our tool compounds in nontransgenic rats, Hyde et al. showed that acute oral administration of **60** at doses up to 100 mg kg^{-1} caused a dose-dependent reduction in CSF Aβ levels but, in contrast, did not affect cortex $A\beta_{40}$ levels across this dose range (Fig. 38A).[92] Plasma $A\beta_{40}$ levels were profoundly reduced at each dose tested. The higher affinity analogs **52** and **67** had similar profiles—they were more potent in reducing CSF Aβ levels across a similar dose range, but failed to elicit significant brain Aβ reduction after a single oral dose. Gratifyingly, multiple oral doses of **67** (as few as three doses of 100 mg kg^{-1} separated by 12 h) elicited robust cortical $A\beta_{40}$ reduction possibly related to the accumulation (~twofold) of **67** that was observed under the multiple dosing conditions (Fig. 38B).[92] Contrastingly, the structurally similar pyrazole analog **68** (Fig. 38C),[97] which has properties comparable to those of **60**, failed to impact CSF Aβ levels following a single oral dose, despite essentially complete ablation of plasma $A\beta_{40}$ levels, demonstrating that dramatic changes to the plasma Aβ pool occurred independently of the CSF Aβ pool in rats (Fig. 38D). Combined with the observation of direct brain activity of **67**, this result provided confidence that changes in CSF Aβ levels were a sensitive measure of changes in brain-derived Aβ in response to a BACE1 inhibitor, consistent with conclusions drawn from studies with GS inhibitors.

The outcomes of these studies conducted in the laboratory of Hyde et al.[92] had significant implications for our medicinal chemistry program. The profiles of optimized inhibitors identified to date highlighted the challenges of achieving free brain concentrations sufficient to drive the high degree of brain BACE1 inhibition necessary for significant brain Aβ inhibition. Inspection of the in vitro potency, permeability, and physicochemical properties profiles of these leads failed to provide insight into a set of parameters that could predict robust brain activity at acceptable doses to guide further SAR development. While Caco-2 cell efflux ratios of these leads were modest, it was later unambiguously determined that in a cell line overexpressing Pgp the compounds are Pgp efflux substrates which likely restricted their brain exposure and PD activity. Nevertheless, we were encouraged that inhibitors such as **67** had demonstrated significant brain activity given that at the time of these discoveries, 6-7 years after the discovery of BACE1, there remained no reports in the public domain of centrally active BACE1 inhibitors despite enormous industry-wide efforts. Consequently, new target synthesis continued to be guided by structure-based design and directed to ligand efficient inhibitors that occupied properties space (c log*P*, PSA, MW) represented by the current leads. In addition, an acute rat CSF Aβ screen was implemented early in our compound evaluation protocol to provide a rapid read on central PD activity for multiple compounds per week to identify compounds of high interest and to guide future optimization efforts.

8.09.4.5 Iminopyrimidinones: Advanced Optimization of the P1-P3 Biaryl Series

With an eye toward further improvement of the profile of the biaryl iminopyrimidinones, Stamford et al. pursued additional SAR around the S1 2,5-thienyl moiety. In analogy to the 2,4-thienyl series, in which introduction of an S3 propynylpyridine substituent imparted benefits in BACE1 affinity and cell-based potency, we prepared the analogous 2,5-thienyl regioisomer **69** (Fig. 39).[86] While this compound showed slightly less affinity for BACE1 than 2,4-isomer **67**, it offered the opportunity for introduction of small, flap-facing substituents at the 3-position of the thiophene to potentially impart affinity gains. To that end, 3-chlorothienyl analog MBi-1 (**70**) showed significant improvements in affinity and cellular activity, with only a modest increase in cell potency shift despite its higher c log*P*. In the acute rat CSF screen established as discussed above, MBi-1 inhibited CSF $A\beta_{40}$ by 66% 3 h after a single 10 mg kg^{-1} oral dose, an effect similar to that of the positive control **67** dosed at 30 mg kg^{-1} orally in the same experiment. Based on this potent CSF $A\beta_{40}$ PD response, MBi-1 was subjected to more in-depth profiling.[86]

MBi-1 showed favorable PK properties in rats with oral bioavailability of 69%, a plasma terminal half-life of 3 h, and an average brain/plasma ratio of 3. These results were anticipated by its good permeability and low efflux ratio in Caco-2 cells (P_{app} 153 nm s^{-1}, AP/BL 2.4) as well as its low intrinsic clearance in rat hepatocytes (4.9 μL min^{-1}million $cells^{-1}$). CSF and cortex $A\beta_{40}$ levels were reduced in a dose-dependent manner 3 h after rats were administered single oral doses of MBi-1 across the dose range of 0.3–30 mg kg^{-1}, with ED_{50} values for CSF and cortex of 4 and 6 mg kg^{-1}, respectively. The unbound plasma concentration of 15 nM at the ED_{50} was significantly lower than that of **67** (~200 nM), and the substantially improved acute CSF and cortical $A\beta_{40}$ potency of MBi-1 may be due to a combination of intrinsically higher BACE1 affinity and improved brain uptake.[86]

In an X-ray structure of compound MBi-1 bound to BACE1, the chlorinated thienyl group caused the flap to move into a more closed conformation relative to the isomeric thienyl analog **67** with Tyr^{71} of the flap repositioned toward the prime side and in proximity with the iminopyrimidinone C5 methylene group, inducing a pocket to accommodate the chloro group (Fig. 40).

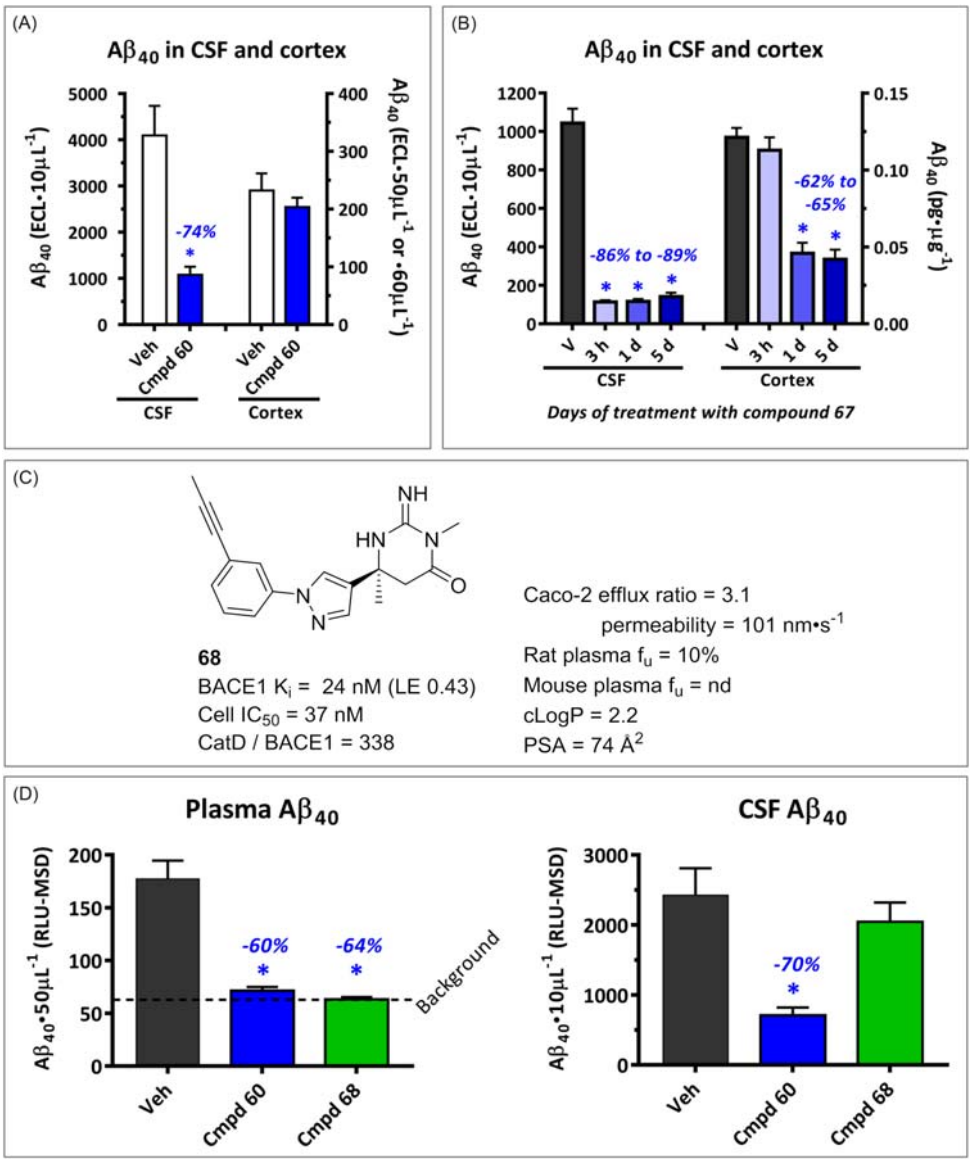

Fig. 38 In vivo studies in nontransgenic rats. (A) Effects of single dose treatment with 100 mg kg^{-1} PO of compound **60** on CSF and cortex $A\beta_{40}$ levels; plasma $A\beta_{40}$ levels were also profoundly reduced. (B) Effects of single and multiple dose (BID) treatment with 100 mg kg^{-1} PO of compound **67** on CSF and cortex $A\beta_{40}$. (C) Structure and profile of pyrazole tool compound **68**. (D) Comparison of the effects of single doses of compounds **60** (100 mg kg^{-1} PO) and **68** (80 mg kg^{-1} PO) on plasma and CSF $A\beta_{40}$ levels (expressed as relative luminescence units—mesoscale diagnostics, RLU-MSD), clearly demonstrating that effects in these two pools are distinct.

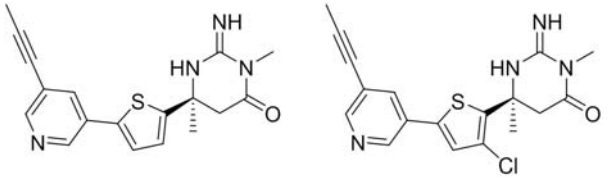

69
BACE1 K_i = 33 nM (LE 0.42)
Cell IC_{50} = 42 nM
CatD / BACE1 = 47
cLogP = 2.5

MBi-1 (70)
BACE1 K_i = 2 nM (LE 0.48)
Cell IC_{50} = 10 nM
CatD / BACE1 = 21
cLogP = 3.2

Fig. 39 Structures of S1 2,5-thienyl biaryl iminopyrimidinones **69** and MBi-1 (**70**).

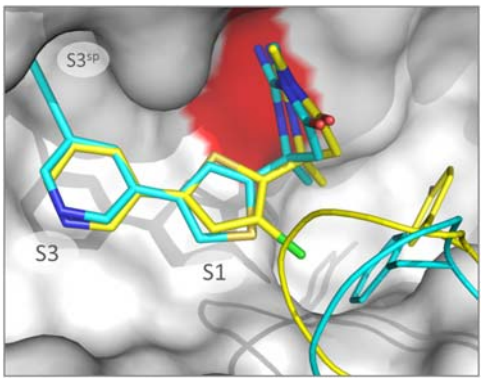

Fig. 40 Overlay of X-ray crystal structures of S1 thienyl biaryl iminopyrimidinone **67** (*blue*) and MBi-1 (*yellow*) showing the dramatic change in flap conformations (shown as ribbons, colored to match inhibitors) induced by the 3-chloro substituent of MBi-1.

While the selectivity of MBi-1 over CatD was similar to that of its des-chloro precursor **69**, its selectivity over a number of other human aspartyl proteases (pepsin, CatE, and renin) was moderate to high (260-, 350-, and >10,000-fold, respectively). Typical of compounds in this series, compound MBi-1 was not selective over BACE2 ($K_i < 1$ nM).[86]

While the profile of MBi-1 represented a high point of discovery in the S1–S3 binding class of inhibitors with respect to its PK/PD profile, the compound was considered unsuitable for progression. Despite its improved in vivo potency on an exposure basis, its CatD affinity and selectivity were considered to be inadequate. Furthermore, the propynyl pyridine moiety was susceptible to oxidative metabolism and formation of glutathione adducts, raising potential safety concerns. Nevertheless, the discovery of MBi-1 validated our molecular design and compound triaging strategy. The molecular properties of MBi-1, including MW (373), log*D* (1.8), and pK_a (7.5), all fall well within those considered optimal for CNS drugs. Substantial advances in addressing CatD selectivity and metabolism concerns were later achieved through more profound structural changes to the S1–S3 binding biaryl motif, leading to the discovery of verubecestat as discussed in Section "Discovery of Verubecestat."

8.09.4.6 Structural Differentiation: Occupancy of S2′

Beyond the S1–S3 filling approaches, we also sought to identify more structurally differentiated approaches to development of BACE inhibitors to derisk unforeseen structure-based toxicity or other issues that might arise as endemic in the S1–S3 biaryl series. From the crystal structures of **60** and other biaryl iminopyrimidinones, we had clearly seen that the biaryl moiety adopted a pseudoaxial conformation (Fig. 41A). Mandal et al. hypothesized that stabilization of this presumably higher energy bioactive conformation might offer an avenue for further structural modification of the iminopyrimidinone core, particularly if done in combination with occupancy of S2′, which we had not significantly reinvestigated since our earlier work with the cyclohexylalkyl substituents.[98] By analyzing the X-ray structures of **60** and analogs Mandal et al. also recognized that there was sufficient room in the active site for ring fusion at the C5-C6 of the iminopyrimidinone core that could enable occupancy of S2′ (Fig. 41B). Combining those observations, energetic calculations with a five-membered ring fused to C5-C6 of **60** predicted a modest 0.9 kcal mol^{-1} stabilization of the pseudoaxial conformation, and further modeling suggested that the nitrogen atom of a 3,4-fused pyrrolidine (e.g., general structure **71**, Fig. 41C) would offer a favorable vector for facile SAR development in S2′.[98] It should be noted that there

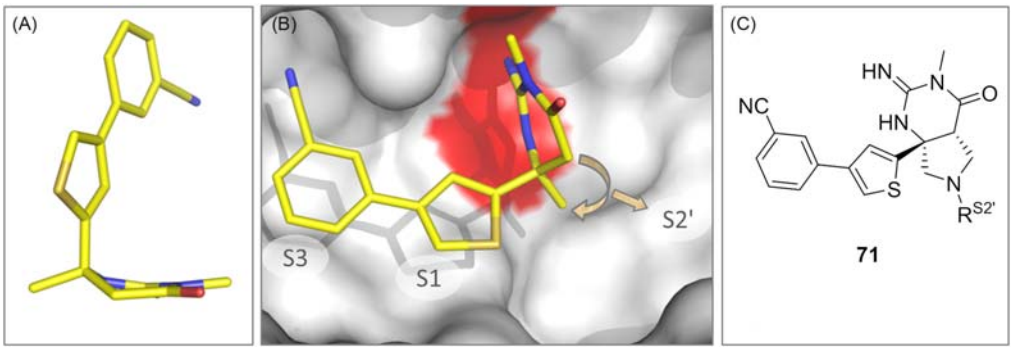

Fig. 41 (A) Structure of biaryl iminopyrimidinone **60** oriented to highlight the pseudoaxial conformation of the core biaryl substituent. (B) X-ray cocrystal structure of **60** and BACE1 showing potential to fuse a ring to the core and grow into the S2′ subsite. (c) Generic structure of designed fused pyrrolidine iminopyrimidinone **71**.

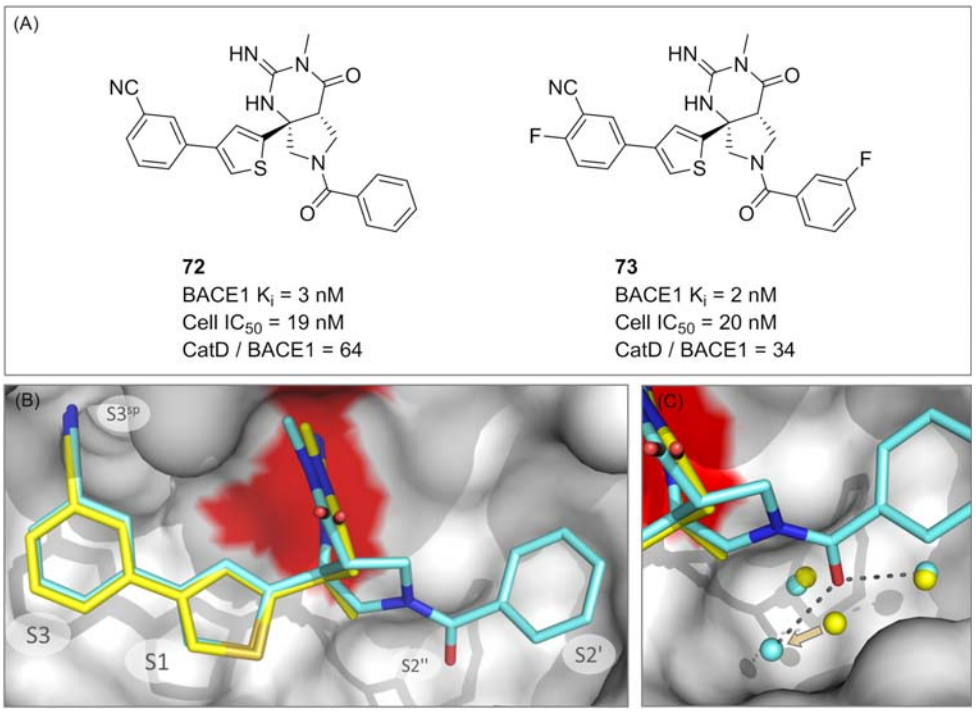

Fig. 42 (A) Structures of early fused pyrrolidine analogs bearing benzamide substituents. (B) Overlay of X-ray structures of fused pyrrolidine **72** (*blue*) and its prime-side unsubstituted progenitor **60** (*yellow*) bound to BACE1 showing the highly conserved binding mode of the nonprime side and core after introduction of the fused pyrrolidine ring. (C) Close-up view of the prime side subsites showing the 1.8 Å difference in the position of one of the waters in the S2″ pocket upon binding of benzamide **72**. Waters are colored to match the inhibitors.

are several conserved water molecules in this subsite that are part of a hydrogen bonding network with the protein backbone, and the effects of occupancy of this region were unknown when we initiated these efforts.

To our satisfaction, we found that benzamide **72** and several close analogs, for example, fluorinated compound **73**, showed a more than 10-fold improvement in intrinsic affinity over **60** with a modest improvement in cellular activity and retention of selectivity over CatD (Fig. 42A). The X-ray structure of **72** bound to BACE1 showed that the binding mode of the core and biaryl nonprime side of the molecule was highly conserved with that of **60** and that the benzamide projected into S2′ as designed (Fig. 42B). Interestingly, whereas modeling suggested that one of the conserved water molecules in a pocket near the S2′ subsite, termed the S2″ pocket, might be displaced by the benzamide carbonyl, the water instead rearranged to accommodate a hydrogen bond to that carbonyl (Fig. 42C). Unfortunately, while these initial examples validated the design of the fused pyrrolidine imino-pyrimidinones in terms of their potency and selectivity, their PK properties in rat were substantially eroded from their nonfused precursor. This may be due to their relatively high rat hepatocyte clearance and/or susceptibility to Pgp efflux as manifested by analog **73** (rat hepatocyte clearance = 46 μL $min^{-1}10^6$ $cells^{-1}$, Caco-2 efflux ratio = 17).[98]

To mimic interactions of the carbonyl oxygen with the conserved water in the S2″ site while replacing the benzamide moiety, which were hypothesized to be detrimental to the PK properties in the series, Mandal et al. explored a series of N2-pyridyl and N2-pyrimidinyl analogs.[98] These modifications, in combination with small substituents around the heteroaryl rings as exemplified by analogs **74**–**76** (Fig. 43A), were generally well tolerated and recapitulated the affinity, cell potency shift, and CatD selectivity profile of the benzamides. An X-ray structure of 3-methoxypyridyl analog **74** bound to BACE1 showed that the pyridyl nitrogen did in fact replicate the hydrogen bonding interaction of benzamide **72** with a water in the S2″ site (Fig. 43B). Unexpectedly and in contrast, introduction of a methoxy group at the 6-position of the pyridine in analog **75** caused a large shift of the pyridine ring of more than 1 Å toward S2″, embedding the methoxy group deep in that subpocket and displacing two of the conserved water molecules from that region (Fig. 43C). This modification was accompanied by high BACE1 affinity and similar CatD selectivity. This change in binding pose was replicated with *N*-pyrimidine analogs, with 5-fluoro-6-methoxypyrimidine analog **76** also showing promising affinity, cell potency, and CatD selectivity.[98]

Unfortunately, **76** showed only modest activity in the rat CSF assay, lowering Aβ levels by 45% following a 30 mg kg^{-1} oral dose, and was similar to many of the analogs in this series.[98] This inferior in vivo PD response relative to the earlier nonfused pyrrolidine lead MBi-1 is driven at least in part by its poor CNS penetration, to which the relatively high MW and PSA values for these compounds (e.g., MW = 478 and PSA = 117 $Å^2$ for **76**) likely contributed. In addition, like many related structures in this initial effort, **76** showed time-dependent inhibition of CYP3A4, which was likely due to bioactivation of the heteroaryl ring and generation of a reactive intermediate which we had observed for a related analog.[98]

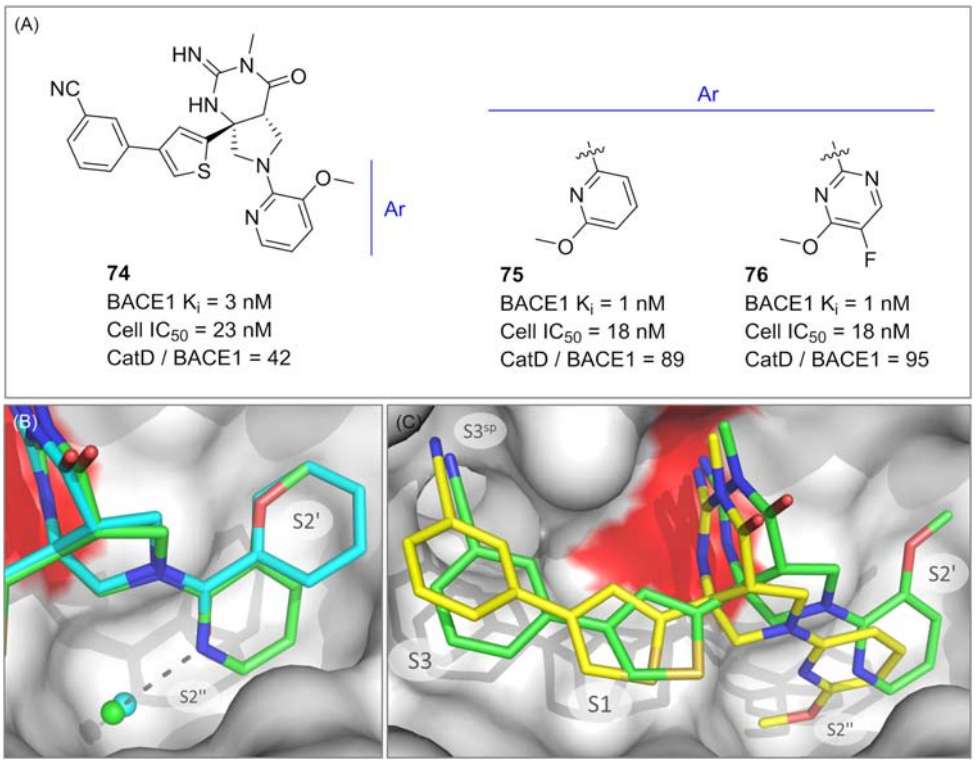

Fig. 43 (A) Structures of N-heteroaryl fused pyrrolidine analogs **74**–**76**. (B) Detail of the S2″ region from an overlay of the X-ray crystal structures of benzamide **72** (*blue*) and N-pyridyl analog **74** (*green*) bound to BACE1 showing that the pyridine nitrogen of **74** recapitulated the positioning and hydrogen bonding interactions with a conserved water in that subsite. Waters are colored to match inhibitors. (C) Overlay of the X-ray crystal structures of N-pyridyl analogs **74** (*green*) and **75** (*yellow*) showing the significant change in pose induced by binding of the 6-methoxy group deep into S2″ with analog **75**.

Given our interest in the structural diversity represented by this new series, Mandal et al. pursued a strategy to rescue the profile of these molecules.[99] First, this involved truncation of the S3 cyanophenyl to reduce the relatively high MW of in the series. The anticipated loss of affinity could then be addressed through further modification of the S1 and S2″ binding motifs. In parallel, to mitigate time-dependent CYP3A4 inhibition, we examined fully substituting the pyrimidine ring as a route to block oxidation of the pyrimidine and/or direct the metabolic pathway to the newly introduced substituent itself. Gratifyingly, the combination of these two modifications in cyanothiophene **77** provided an analog with only a modest loss in affinity, albeit with an increase in LE over its biaryl predecessor due to its lower molecule weight (Fig. 44). In addition, truncated cyanothiophene **77** possessed a modest cellular potency shift, only a slight erosion of CatD selectivity, and importantly, a significantly attenuated time-dependent inhibition of CYP3A4 (preincubation $IC_{50} = 18$ μM vs. 2 μM for **76**). Though lower in MW, the cyano group on the S1 thienyl of **77** contributed to a PSA that was equivalent to the biaryl analogs, and the compound showed a similar level of CSF Aβ40 lowering activity (−47%) in the acute rat PD screen following an orally administered dose of 30 mg kg^{-1}. Although we examined additional SAR beyond methyl at the four-position of the pyrimidine ring, other modifications offered no benefit or eroded the potency and selectivity of the resulting analogs.[99]

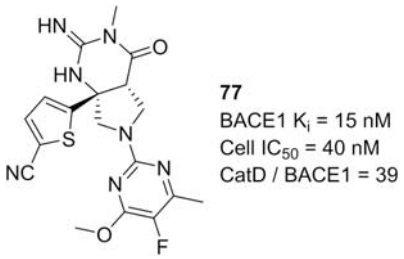

Fig. 44 Structure of unoptimized truncated fused pyrrolidine iminopyrimidinone **77**.

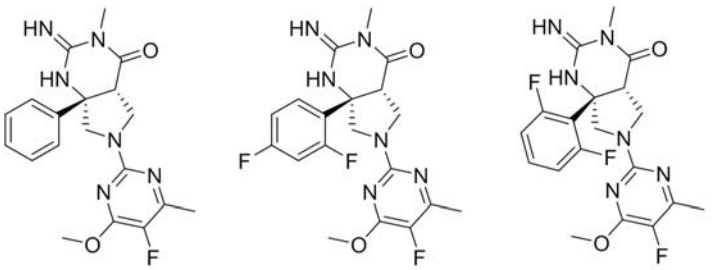

Fig. 45 Structures of S1 phenyl fused pyrrolidine iminopyrimidinone analogs **78**, MBi-4 (**79**), and **80**.

Along with optimizing the S2″ binding substituent, Mandal et al. also reexamined SAR in the S1 pocket in the truncated subseries since we anticipated there would be no particular benefit to keeping the S1 thiophene that had been incorporated as the best moiety to properly display S3 substituents in the S1–S3 biaryl iminopyrimidinone series. To that end, we initially returned to an S1 phenyl group as well as a set of its fluorinated variants (Fig. 45), all of which possessed roughly 20 Å^2 lower PSA than the S1 cyanothiophene. The unsubstituted baseline phenyl analog **78** was roughly equipotent to cyanothiophene analog **77**, and introduction of an *ortho*- or *para*-fluorine to the phenyl ring, or combination thereof as in 2,4-difluorophenyl analog MBi-4 (**79**), resulted in a several-fold improvement in affinity to give single-digit nanomolar BACE1 inhibitors. Interestingly, introduction of a second ortho fluorine as in 2,6-difluoro analog **80** completely ablated any gain in affinity, with this and other analogs containing the bis-*ortho*-fluorophenyl at best equipotent to the unsubstituted analog **77**.[99]

To understand these subtle differences in SAR, X-ray structures of selected compounds were again useful. The crystal structure of 2,4-difluorophenyl analog MBi-4 bound to BACE1 indicated that the improvement in affinity for the 2-fluoro and 4-fluoro bearing analogs could be due to electrostatic interactions with Tyr^{71} of the flap and/or with Trp^{115} in the distal part of S1 (Fig. 46A). It is interesting to note that the 2,4-difluoro moiety avoided a flipped conformation in which the *ortho*-fluoro pointed not toward the flap but instead toward the backbone of the protein. That it did not bind in that latter conformation presaged a potential reason for the reduced affinity of the 2,6-difluoro-substituted analog **80**. In the X-ray obtained of the racemate of compound **80** bound to BACE, the second *ortho*-fluorine is oriented toward the protein backbone and is only 3.1 Å from the Gly^{230} carbonyl, potentially representing a weakly negative interaction (Fig. 46B). Also from these crystal structures, regardless of fluorine substitution on the S1 phenyl, the binding mode of the molecules is well conserved with excellent overlap of the S2″ pyrimidine and fused iminopyrimidinone core.[99]

Encouragingly, all of these initial S1 phenyl and fluorophenyl analogs were slightly to significantly more selective over CatD than cyanothiophene **77**, and they all showed only a slight or no time-dependent inhibition of CYP3A4.[99] We explored some additional expansion of the S1 SAR to include 2-chlorophenyl analogs such as **81**, in analogy to the chlorothiophene present in MBi-1, as well as benzothiophene **82** (Fig. 47). The 2-chloro analogs offered no benefit in in vitro profile over their 2-fluoro counterparts and in fact demonstrated inferior oral PK profiles in rats. The S1 benzothiophene analog **82** had equal affinity with other high affinity

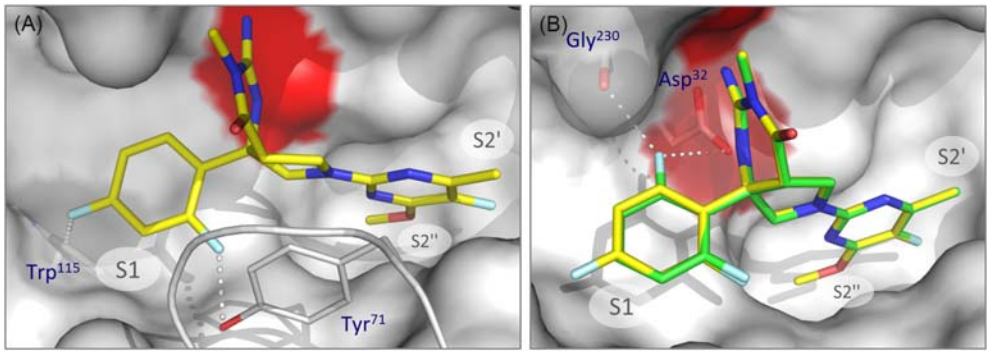

Fig. 46 (A) X-ray crystal structure of S1 2,4-difluorophenyl-fused pyrrolidine iminopyrimidinone MBi-4 (*yellow*) bound to BACE1 showing interactions of the ortho and para fluoro substituents that may be beneficial to affinity. (B) Overlay of X-ray structures of S1 2,6-difluorophenyl fused pyrrolidine analog **80** (*green*) and MBi-4 (*yellow*) showing the well-conserved binding modes and showing interactions of the additional ortho fluoro substituent in **80** that may be deleterious to affinity.

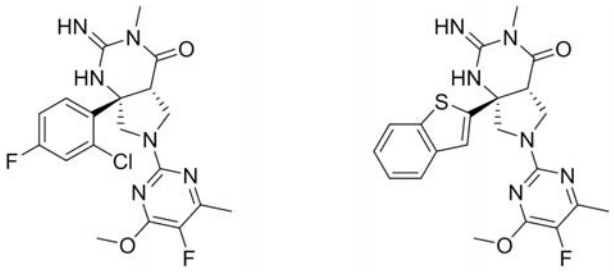

Fig. 47 Structures of S1 2-chlorophenyl and S1 benzothiophene fused pyrrolidine iminopyrimidinones **81** and **82**.

analogs against BACE1, but showed a much larger cellular potency shift owing to the significantly higher c log*P* (e.g., 3.3 for **82** vs. 2.6 for 2,4-difluorophenyl analog MBi-4). In addition, CatD selectivity attained with the benzothiophene modification was much lower than that of the other S1 modifications.

Ultimately, 2,4-difluorophenyl analog MBi-4 was chosen for more in-depth characterization given its excellent overall balance of affinity, cell potency, and selectivity. This compound exhibited high clearance and low-to-moderate oral bioavailability in rats, dogs, and monkeys, which was attributed to high hepatic extraction and plasma instability of the compound in these species. In contrast, MBi-4 had low intrinsic clearance in human hepatocytes and was stable in human plasma, supporting a prediction of once-daily dosing in humans.[99]

In addition to its lack of CYP3A4 inhibition, MBi-4 did not inhibit or induce cytochrome P450 enzymes involved in xenobiotic metabolism, suggesting a low risk for perpetrating drug-drug interactions. The compound is a potent inhibitor of BACE2 (K_i 2.7 nM) and in a patch clamp assay inhibited the hERG channel with an IC_{50} of 1.9 μM. Additionally MBi-4 did not have significant activity against a diverse panel of receptors, enzymes, and ion channels with the exception of weak affinity for the histamine H2, melatonin MT1, and motilin receptors with K_i values in the micromolar range.[99]

In the rat PD assay, MBi-4 lowered $A\beta_{40}$ levels in the CSF and cortex with ED_{50} values of 5 and 13 mg kg^{-1}, respectively, which compared favorably with the nonfused pyrrolidine biaryl iminopyrimidinone lead MBi-1. Importantly, the similar $A\beta_{40}$ ED_{50} values were achieved with comparable unbound plasma concentrations—the unbound plasma EC_{50} values for CSF $A\beta_{40}$ for MBi-4 and MBi-1 were 30 and 15 nM, respectively. The PK/PD profile of MBi-4 was also determined in nonhuman primates. In cynomolgus monkeys, $A\beta_{40}$ lowering was achieved in the CSF (35%) and cortex (58%) 4 h after a single 10 mg kg^{-1} oral dose. This was an important result as it showed that changes in CSF Aβ levels were indicative of effects in the cortex in a primate species and thus built confidence that CSF $A\beta_{40}$ would be an effective biomarker of brain Aβ inhibition in patients in a clinical setting. Interestingly, the PD effect in cortex was more pronounced than in CSF. This is not unexpected in an acute dose setting since levels in the cortex are a direct measure in the compartment where $A\beta_{40}$ is produced, whereas levels of $A\beta_{40}$ in the CSF are in part dependent on the kinetics of its transit to the CSF compartment. This temporal effect was confirmed in a dose–response time course study of CSF Aβ lowering in cisterna magna ported monkeys with maximal CSF $A\beta_{40}$ inhibition occurring at 12–24 h after a single oral dose, which was significantly delayed relative to the timing of peak plasma and CSF concentrations of MBi-4.[99]

As the culmination of research in the fused pyrrolidine series, MBi-4 represented an advanced lead that was structurally differentiated from the S1–S3 spanning biaryl iminopyrimidinone represented by MBi-1. Compound MBi-4 was positioned for clinical development, supported by its preclinical safety profile and favorable human dose projections derived from PK/PD data in preclinical species to achieve significant central Aβ reduction at steady state under a QD dosing regimen. However, further development of this series was suspended in light of the emergence of a superior inhibitor class, namely the iminothiadiazinane dioxide diaryl amide series described in Section "Discovery of Verubecestat." Compounds from this new series, which ultimately delivered verubecestat, were substantially more potent in vivo and offered the potential for a lower dose and a superior therapeutic window to enable testing of a much greater dose–response range for central Aβ inhibition in the clinic.

8.09.4.7 From Acyl Guanidines to Sulfonyl Guanidines: Discovery of Iminothiadiazinane Dioxides

MBI-1 and MBi-4 represented successful optimization efforts that followed from our overarching strategy to balance improvements in potency and profile against unproductive increases in MW, number of rotatable bonds, PSA, or other characteristics that can erode the overall drug-like nature of molecules and result in issues later in development. These two structurally differentiated iminopyrimidinones were important lead compounds for the program. However, both structures were highly engineered, and small alterations to their structure often resulted in significant erosion to different aspects of their profiles, whether be it cell potency, selectivity, off-target, or PD activity.

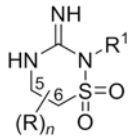

83

Fig. 48 Generic structure of the novel iminothiadiazinane dioxide core **83**.

While we continued to explore SAR of the iminopyrimidinone series, we simultaneously pursued the discovery of novel catalytic dyad binding motifs. To that end Scott et al. and Gilbert et al. sought to replace the iminopyrimidinone acyl group with a sulfonyl group as in the unprecedented iminothiadiazinane dioxide core **83** (Fig. 48).[100,101] Beyond the subtle, possibly beneficial effects on inhibitor profiles that this change could bring, such as we had observed in the progression from iminohydantoin to iminopyrimidinone, we were attracted to the novel intellectual property space offered by the iminothiadiazinane dioxide motif. This had become a priority as we anticipated increased competition in this chemical space in the years since the initial disclosure of cyclic acylguanidines in 2005–2006 by us and others.

The iminothiadiazinane dioxide motif was evaluated in the context of both the S1–S3 biaryl presentation exemplified by **84** and **85** and the fused pyrrolidine S1-S2′ display as in analogs **86** and **87** (Fig. 49).[100,101] With respect to calculated properties in comparison with the corresponding iminopyrimidinones, replacement of the carbonyl group by the sulfonyl group imparted somewhat higher PSA and lower c log*P* values, although these remained within CNS drug-like ranges. We also anticipated that introduction of the sulfonyl group would result in reduced basicity relative to identically substituted iminopyrimidinones, although the unreliability of calculated pK_a values created uncertainty in predicting the magnitude of this effect, and the impact on inhibitor profiles was unclear. In addition, the change to an sp^3 sulfonyl from an sp^2 carbonyl would make the monocyclic iminothiadiazinane core of **84** and **85** less rigid, and importantly, modeling simulations suggested that the bioactive pseudoaxial disposition of the biaryl motif was close to the minimum energy conformation. Furthermore, in silico docking experiments suggested that the increased

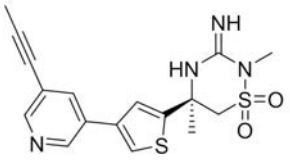

84
BACE1 K_i = 6 nM (LE 0.45)
Cell IC_{50} = 35 nM
CatD / BACE1 = 350
Caco-2 efflux ratio = 2.6
permeability = 149 nm•s^{-1}
pKa = 7.3
Rat CSF $A\beta_{40}$ (10 mg•kg^{-1} PO) = -61%
$Plasma_{3h,u}$ (B/P) = 120 nM (0.4)

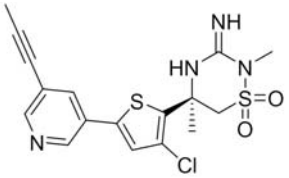

85
BACE1 K_i = 2.4 nM (LE 0.45)
Cell IC_{50} = 55 nM
CatD / BACE1 = 47
Caco-2 efflux ratio = 1.6
permeability = 278 nm•s^{-1}
pKa = 6.6
Rat CSF, cortex $A\beta_{40}$ (10 mg•kg^{-1} PO) = -82%, -53%
$Plasma_{3h,u}$ (B/P) = 7 nM (2.3)

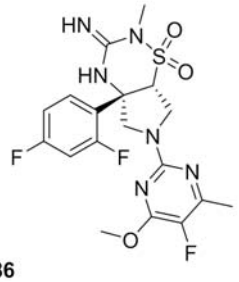

86
BACE1 K_i = 30 nM (LE 0.33)
Cell IC_{50} = 222 nM
CatD / BACE1 = 78
pKa = 6.2

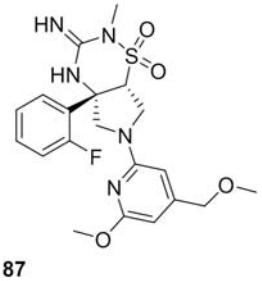

87
BACE1 K_i = 7 nM (LE 0.36)
Cell IC_{50} = 13 nM
CatD / BACE1 > 138

Fig. 49 Structures of thiadiazinane dioxide S1–S3 biaryl analogs **84** and **85** and S1-S2″ fused pyrrolidine analogs **86** and **87**.

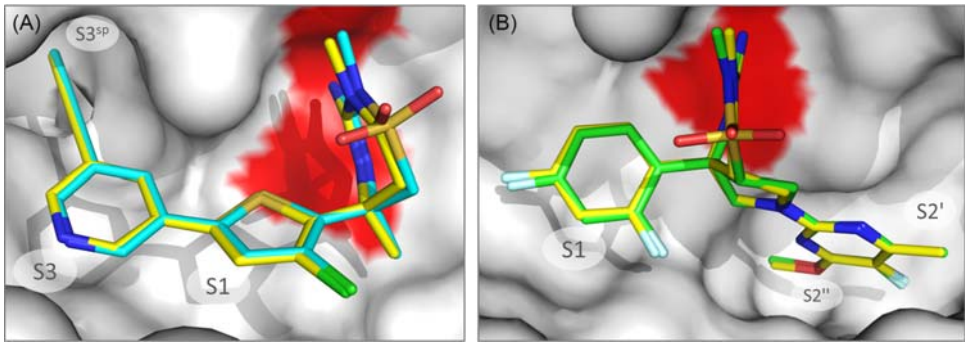

Fig. 50 (A) Overlay of X-ray structures of S1–S3 biaryl iminothiadiazinane dioxide **85** (*blue*) and of iminopyrimidinone MBi-1 (*yellow*) bound to BACE1. (B) Overlay of X-ray structures of S1-S2′ fused pyrrolidine iminothiadiazinane dioxide **86** (*green*) and of iminopyrimidinone MBi-4 (*yellow*) bound to BACE1. Both sets of overlays show excellent conservation of binding modes between the iminothiadiazinane dioxide and iminopyrimidinone cores.

steric demand of the sulfonyl group in both the monocyclic and fused bicyclic cores would not cause unfavorable interactions with BACE1.[100]

Upon synthesis and testing of the biaryl thiadiazinane dioxide analogs **84** and **85**, we were gratified to find that they possessed single-digit nanomolar BACE1 binding affinities that compared favorably to the corresponding iminopyrimidinone analogs (i.e., **67** and MBi-1 with BACE1 K_i values of 8 and 2 nM, respectively). Notably, the X-ray cocrystal structure of **85** bound to BACE1 confirmed that the thiadiazinane dioxide core was a good surrogate for the iminopyrimidinone as the overlay with MBi-1 showed that the two inhibitors were virtually superimposable (**Fig. 50A**). Introduction of the tetrahedral sulfonyl group did not cause a significant change in the conformation of the core nor did it alter the trajectory of the biaryl substituent into the S1-S3-S3^{sp} pockets. Generally with respect to BACE1 affinity and CatD selectivity, the iminothiadiazinane dioxide and iminopyrimidinone biaryl analogs exhibited very similar SAR.[100] On the other hand, fused pyrrolidine iminothiadiazinane dioxide **86** prepared by Gilbert et al. had about a 10-fold lower affinity than MBi-4 despite a similarly near-superimposable binding mode in an X-ray structure with BACE1 (**Fig. 50B**).[101]

The measured pK_a values for **85** and **86** were significantly less basic than those of the corresponding iminopyrimidinones, and this probably accounts for the magnified cellular potency shifts observed for these analogs. In the case of the fused pyrrolidine subseries explored by Gilbert et al., affinity and, to some extent, cell potency could be rescued by modification of the pyrimidinyl substituent to the (methoxymethyl)pyridyl group present in **87**. Despite the ability to achieve such improvements, the pyrrolidino-fused analogs displayed weak central PD activity in rats when screened with oral doses up to 30 mg kg^{-1} even though they possessed high cell permeability and brain penetration, and achieved unbound plasma concentrations similar to their iminopyrimidinone counterparts.[101] Although we lack understanding of the reasons for the poor PD activity of the fused pyrrolidine analogs, it is possible that their reduced basicity alters their intracellular distribution leading to reduced BACE1 inhibition in vivo.

In a comparison of the iminothiadiazinane biaryl analogs **84** and **85** it is important to note that the magnitude of the pK_a and related cell shifts was highly dependent on the 6-aryl substituent with the chlorothienyl analog **85** (pK_a 6.6) having the weaker basicity and greater shift between its K_i and cell IC_{50} values. Despite the reduced cellular potency, **85** robustly reduced $A\beta_{40}$ levels in the CSF and cortex of rats by 82% and 53%, respectively after a single oral dose of 10 mg kg^{-1}. On an exposure basis comparing unbound plasma concentrations of **84** and **85** for the observed PD activity in that study, the latter compound was substantially more potent (120 nM for **84** vs. 7 nM for **85**). This is presumably due to its enhanced CNS penetration imparted by its increased permeability and reduced susceptibility to efflux relative to **84** as indicated by a comparison of their permeabilities and efflux ratios in the Caco-2 bidirectional assay. Not only did the greater potency of the chlorothienyl analog **85** relative to **84** recapitulate the rank order of potency for the thiophene isomers in the iminopyrimidinone series (i.e., MBi-1 >**67**), but **85** was also appreciably more potent in vivo than its iminopyrimidinone counterpart MBi-1. The superior in vivo potency of **85** clearly validated the iminothiadiazine dioxide catalytic dyad binding motif as a viable scaffold with superior properties to the iminopyrimidinone, and also served to highlight the profound and unpredictable impact on in vivo activity that subtle changes in physicochemical properties such as pK_a, PSA, and log D can impart. In addition, representative iminothiadiazinane dioxide analogs showed enhanced hydrolytic stability under weakly basic conditions compared to analogous iminopyrimidinone derivatives, highlighting an additional advantage of the iminothiadiazinane dioxide core.[100]

8.09.5 Discovery of Verubecestat

8.09.5.1 S1–S3 Spanning Diaryl Amides: Rationale

While the increased potency of **85** relative to MBi-1 was an advantage, it nonetheless did not meet criteria for advancement due to deficiencies it had in common with MBi-1 such as inadequate CatD selectivity (47-fold) and concerns about the metabolic lability

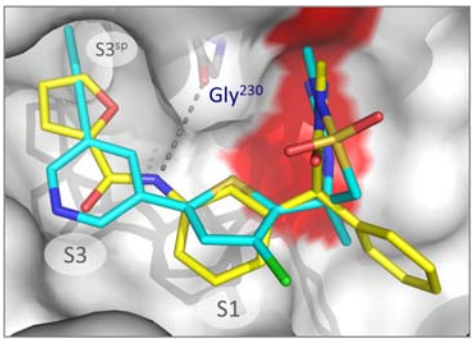

Fig. 51 Overlay of the X-ray cocrystal structures of diaryl iminohydantoin **38** (*yellow*) and biaryl iminothiadiazinane **85** (*blue*) bound to BACE1.

of the propynyl pyridine moiety. To remedy these deficiencies, Scott et al. pursued more profound structural variations of the S1–S3 spanning biaryl motif.[100] Among those explored was a series of diaryl carboxamide analogs inspired by iminohydantoin **38** (Fig. 25) which, despite its weak BACE1 affinity, caught our attention because it possessed some intrinsic selectivity for BACE1 over CatD. Overlay of the X-ray structures of **38** and of **85** bound to BACE1 showed that the furanyl moiety of **38** was positioned deeply in $S3^{sp}$, not dissimilar to the propynyl moiety of **85** (Fig. 51). In addition, the amide hydrogen of **38** was within hydrogen bonding distance of the Gly^{230} carbonyl of the enzyme.[100]

Recognizing that the trajectory of the carboxamide substituent into the S1–S3 pockets from the iminohydantoin core of **38** may not have been optimal and could contribute to the weak BACE1 affinity of this compound, Scott et al. prepared a series of iminopyrimidinone and iminothiadiazinane dioxide diaryl amides, exemplified by **88** and verubecestat (**89**, MK-8931), respectively (Fig. 52). To our satisfaction, both compounds were high affinity BACE1 inhibitors with potent cell-based activity. Surprisingly, these analogs were extremely selective for BACE1 over CatD, exhibiting selectivity ratios of $>10{,}000$-fold. Consistent with the trend observed with the biaryl analogs **85** and MBi-1, the iminothiadiazinane analogs were significantly less basic than the corresponding iminopyrimidinones, manifesting in this case as unexpectedly large differences in their permeabilities, efflux ratios, and in vivo profiles. The iminothiadiazinane verubecestat had much greater permeability and a lower efflux ratio than the iminopyrimidinone **88**, and this translated into a substantial difference in in vivo potency. In rats, verubecestat potently reduced $A\beta_{40}$ levels in the CSF and cortex with ED_{50} values of $<10\ mg\ kg^{-1}$ 3 h after oral administration, corresponding to unbound plasma EC_{50} values of <100 nM. In contrast, the CSF and cortex $A\beta_{40}$ ED_{50}s of **88** were $\geq 30\ mg\ kg^{-1}$ 3 h following oral administration, which corresponded to unbound plasma levels of ≥ 190 nM.[100]

8.09.5.2 Verubecestat Cocrystal Structure, in vitro Profile, and Key SAR

In the X-ray cocrystal structure of verubecestat bound to BACE1 (Fig. 53), the S1–S3 phenyl picolinamide group projects pseudoaxially from the iminothiadiazinane core, with the fluorophenyl group occupying the S1 pocket. The flap-facing fluoro substituent is accommodated in a region created by positioning of the flap Tyr^{71} toward the prime side allowing the flap to be in a well-defined, rather closed position similar to the MBi-1 cocrystal structure with BACE1. The fluoropyridyl moiety occupies the S3 pocket and extends into $S3^{sp}$. As was observed with the iminohydantoin analog **38**, the amide NH of the inhibitor is within hydrogen bonding

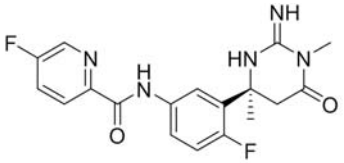

88
BACE1 K_i = 4 nM
Cell IC_{50} = 5 nM
CatD / BACE1 > 10,000X
Rat CSF, cortex $A\beta_{40}$ $ED_{50} \geq 30\ mg{\cdot}kg^{-1}$
$Plasma_u$ ($30\ mg{\cdot}kg^{-1}$) = 190 nM
Caco-2 efflux ratio = 11
permeability = $22\ nm{\cdot}s^{-1}$
pKa = 8.3

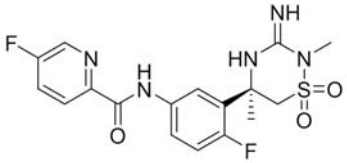

verubecestat (89, MK-8931)
BACE1 K_i = 2 nM
Cell IC_{50} = 2 nM
CatD / BACE1 > 10,000X
Rat CSF, cortex $A\beta_{40}$ $ED_{50} < 10\ mg{\cdot}kg^{-1}$
$Plasma_u$ ($10\ mg{\cdot}kg^{-1}$) = 100 nM
Caco-2 efflux ratio = 2.4
permeability = $128\ nm{\cdot}s^{-1}$
pKa = 7.5

Fig. 52 Structure of verubecestat and its iminopyrimidinone analog **88**.

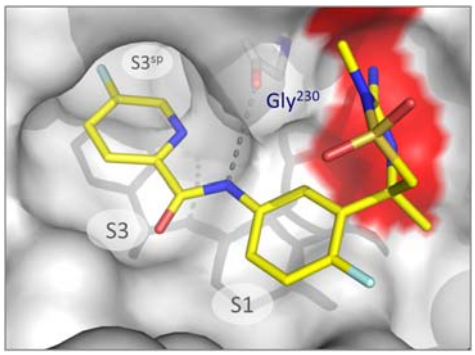

Fig. 53 X-ray structure of verubecestat bound to BACE1.

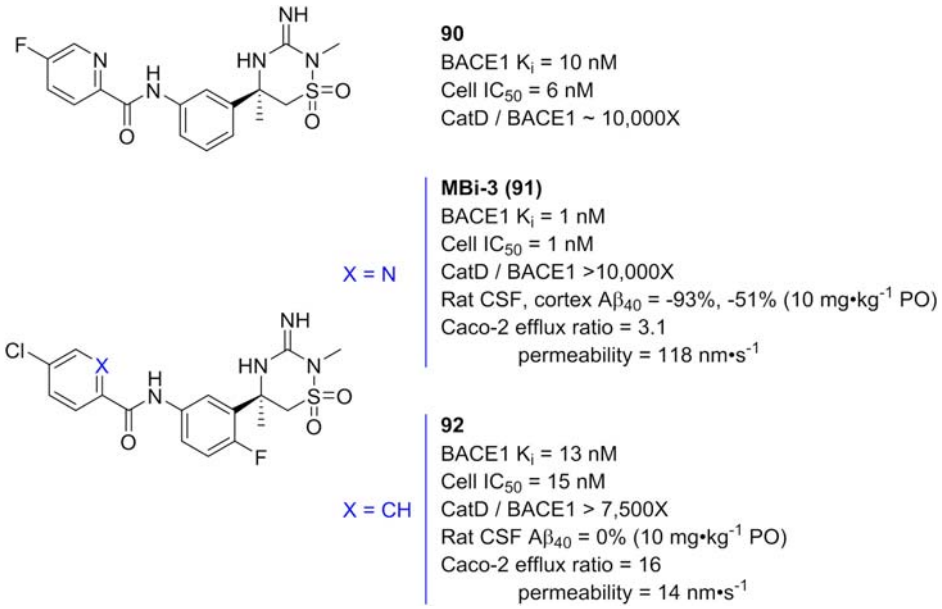

Fig. 54 Structures of analogs **90**, MBi-3 (**91**), and **92** showing key S1 and S3 SAR around verubecestat.

distance of the Gly^{230} carbonyl oxygen. The two aryl rings of the inhibitor are in a trans, near-coplanar configuration with the pyridyl nitrogen *syn* to the amide hydrogen.[100]

Key SAR highlights related to verubecestat are shown in Fig. 54. The 6-desfluoro analog **90** is about fivefold less potent, demonstrating that the fluoro substituent on the S1 phenyl group of verubecestat provides enhancement of affinity similar to that observed for the similarly positioned chloro substituent of **85**. Replacement of the pyridyl group in the diaryl carboxamide by phenyl results in about a 10-fold loss of affinity (e.g., MBi-3 (**91**) vs. **92**), which we attributed to a change in the conformational bias about the pyridyl—carbonyl bond caused by loss of the internal hydrogen bond between the pyridyl nitrogen and the amide NH. The absence of the internal hydrogen bond also has a significant impact on permeability and efflux susceptibility in Caco-2 cells, again underscored by comparison of MBi-3 and **92**, presumably due to the impact of unmasking of the amide hydrogen bond donor on solvation and recognition by Pgp. The combination of these effects had a dramatic impact on the ability of the compounds to lower CNS $A\beta_{40}$ in the rat PD assay, with MBi-3 having a very similar profile as verubecestat but **92** having no effect on $A\beta_{40}$ at a matched dose. It should be noted that with all of the aforementioned modifications, selectivity over CatD remained high; all of the analogs in Fig. 54 had selectivities for BACE1 versus CatD of >7500-fold.[100]

The high selectivity of verubecestat and its analogs for BACE1 over CatD can be ascribed to differences between the S1, S3, and $S3^{sp}$ pockets of the two enzymes. In particular, the S3 and $S3^{sp}$ pockets of CatD are smaller than the corresponding pockets of BACE1. Overlay of a CatD crystal structure with the verubecestat/BACE1 cocrystal structure reveals that the fluoropyridine moiety of verubecestat is too large to occupy the smaller S3 and $S3^{sp}$ pockets of CatD (Fig. 55). Presumably, rotation of the pyridyl group of verubecestat to alleviate these steric clashes within S3 and $S3^{sp}$ of CatD would be disfavored due to the disruption of the preferred near-planar picolinamide conformation of the inhibitor.[100]

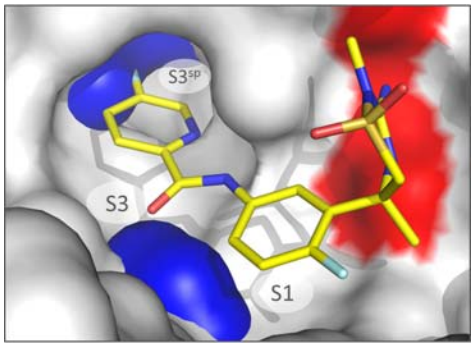

Fig. 55 X-ray cocrystal structure of verubecestat in BACE1 overlayed with CatD X-ray structure with CatD residues Phe[131] in S1, and Ala[13] and Asp[323] in S3/S3[sp] highlighted in *blue*.

In addition to its lack of CatD inhibition, verubecestat was essentially inactive against the human aspartyl proteases CatE and pepsin with K_i values greater than 100 μM and was a weak inhibitor of renin ($K_i = 38$ μM). Not surprisingly, verubecestat was a potent inhibitor of the BACE1 homolog BACE2 ($K_i = 0.38$ nM) which, based on the known biology of BACE2 and the lack of overt issues associated with BACE2 inhibition on chronic dosing, did not preclude development of the compound. Verubecestat had no significant activity when screened against a diverse panel of enzymes, receptors, ion channels, and transporters. Verubecestat is not an inhibitor or inducer of cytochrome P450 isozymes 3A4, 2D6, 2C9, or 2C19 and is not expected to elicit drug-drug interactions in a therapeutic setting. The compound is an inhibitor of the I_{KR} channel encoded by hERG ($IC_{50} = 2.2$ μM); this was shown to be of no consequence in Phase 1 clinical trials at supratherapeutic doses.[100]

8.09.5.3 Verubecestat Synthesis

The discovery synthesis of verubecestat developed by Scott et al. is shown in Fig. 56.[100] The route installed the S1 substituent in the first step through diastereoselective addition to the ketimine and allowed for extensive SAR exploration in S3 since that substituent was introduced in the penultimate step through amide coupling.

The synthesis began with addition of the conjugate base of sulfonamide **93** to ketimine **94** to afford the chiral amino sulfonamide **95** with good diastereoselectivity and moderate yield, establishing the lone stereocenter of verubecestat. Following a two-step deprotection of the sulfinamide and *para*-methoxybenzyl groups under acidic conditions to afford **96**, the iminothiadiazinane

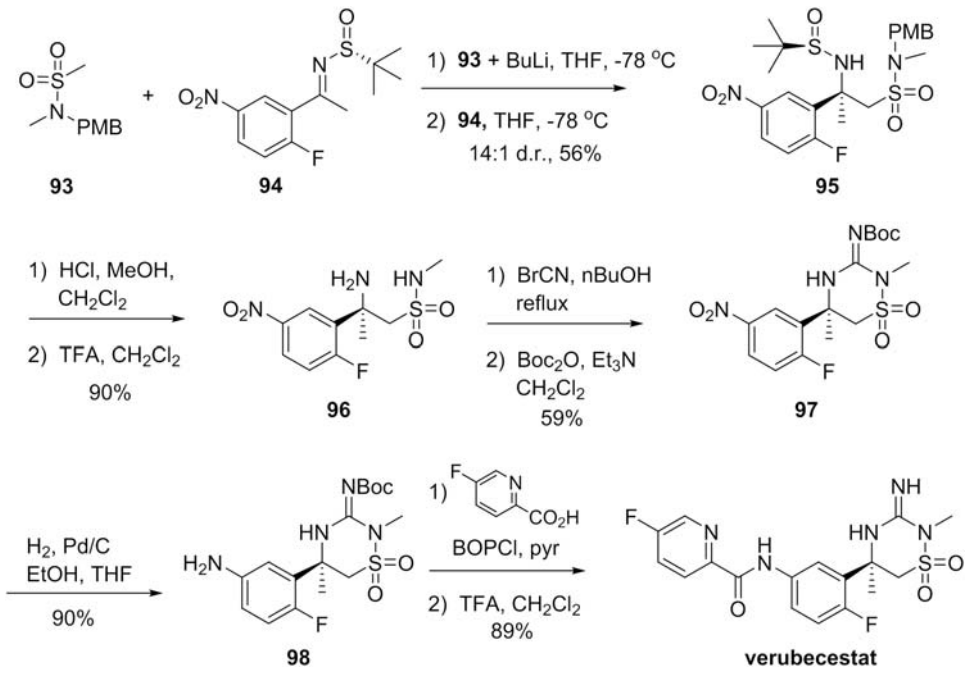

Fig. 56 Discovery synthesis of verubecestat.

dioxide core was formed using cyanogen bromide and the imino group was protected as a *tert*-butyl carbamate to afford **97**. Reduction of the nitrophenyl moiety to the corresponding aniline **98** was followed by amide coupling with 5-fluoropyridine carboxylic acid and removal of the imino protecting group to afford verubecestat which was crystallized as the free base, the physical form selected as the development form.

8.09.5.4 PK/PD Profile of Verubecestat in Preclinical Species

Preclinical PK parameters of verubecestat were determined in rats, dogs, and monkeys. Verubecestat had moderate oral bioavailability of 45% in rats and high bioavailability of $\geq$95% in dogs and monkeys. Across the preclinical species, total clearance was low to moderate and the volume of distribution was moderate to high. This translated to terminal half-lives of verubecestat of 2, 5, and 10 h in rats, monkeys, and dogs, respectively. Allometric scaling of PK parameters from the three preclinical species was consistent with once-per-day dosing in humans. In vitro, verubecestat had high permeability of 28.6×10^{-6} cm s^{-1} in LLC-PK-1 cells and was demonstrated to be a Pgp substrate with an efflux ratio of 11 in the same cell line overexpressing human MDR-1. Human plasma protein binding was relatively low (55%) and was similar to that observed in preclinical species (50-64%). Verubecestat also had low turnover in human hepatocytes, building confidence that a once-per-day dosing regimen would be supported in humans.[100]

The PK/PD profile of verubecestat was determined as described by Kennedy et al. in rats and monkeys.[102] Single oral doses of verubecestat were administered to rats to define the duration and dose dependence of its effects on plasma, CSF, and cortex Aβ_{40} levels. Acute oral administration of verubecestat (10 or 30 mg kg^{-1}) to rats elicited substantial CSF and cortical Aβ_{40} reduction, with peak effects on Aβ_{40} levels occurring 3–6 h after dosing and diminishing rapidly thereafter. The maximal reduction of CSF and cortical Aβ_{40} was delayed relative to the peak total concentrations of verubecestat in plasma, brain, and CSF, which were observed $\leq$1 h after dosing.[92] This lag is likely attributable to multiple factors (e.g., the time required for turnover of preexisting Aβ) and is consistent with previous studies.[49,103]

Oral administration of verubecestat across the dose range of 1–100 mg kg^{-1} to rats caused dose-dependent reductions in plasma, CSF, and cortical Aβ_{40} (**Fig. 57**), and additional doses as low as 0.03 mg kg^{-1} were effective in lowering Aβ_{40} in plasma. Maximal Aβ_{40} reductions of >90% were achieved in all three compartments. The ED_{50} values for reduction of plasma, CSF, and cortical Aβ_{40} were 0.03, 5, and 8 mg kg^{-1}, respectively, corresponding to unbound plasma EC_{50} values of 1, 48, and 78 nM, in the respective compartments. The enhanced potency in the periphery relative to the CSF and brain is consistent with the combined effects of BACE1 being rate limiting for Aβ production in the periphery but not in the CNS, and the Pgp efflux susceptibility of the compound restricting its CNS exposure.[102]

To establish the PK/PD response of verubecestat in nonhuman primates, Kennedy et al. determined a time course of the acute effects of verubecestat on plasma and CSF Aβ_{40} levels in cisterna magna cannulated cynomolgus monkeys via serial sampling over 24 h (**Fig. 58A**).[102] Single oral doses of verubecestat (3 or 10 mg kg^{-1}) reduced CSF Aβ_{40} with peak reductions of 72% and 81%, respectively observed 12 h postdose. The reduction of CSF Aβ_{40} was sustained at near-maximal levels for 24 h. Verubecestat elicited similar effects on CSF sAPPβ levels in this study. Plasma Aβ_{40} levels were inhibited to the limit of detection of the assay at 24 h at both dose levels. Consistent with the PK/PD relationship observed in rats, peak effects on CSF Aβ_{40} levels significantly lagged verubecestat peak plasma and CSF concentrations. The duration of the PD effect in cynomolgus monkeys is also consistent with the sustained plasma and CSF levels over the time course of the experiment; at 24 h unbound plasma and CSF levels were 24 and 14 nM, respectively, for the 3 mg kg^{-1} dose and thus exceeded the in vitro K_i value. The CSF-to-unbound plasma concentration of verubecestat was significantly less than unity at each time point of the serial sampling in accord with the observation that in vitro and in vivo verubecestat is a Pgp substrate.[100,102] In a separate study in cynomolgus monkeys, verubecestat elicited a profound 72% reduction in cortex Aβ_{40} 4 h after an oral dose of 10 mg kg^{-1} (**Fig. 58B**). CSF Aβ_{40} levels were reduced by 60% in this study, an effect similar in magnitude to that seen in the serial CSF sampling studies.[102] The observation that the potency of verubecestat for cortical versus CSF Aβ reduction was minimally shifted in rats and not shifted in monkeys despite the efflux susceptibility of the compound

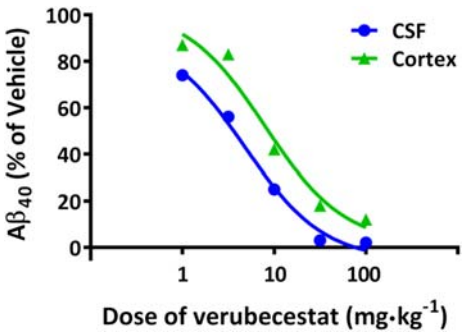

Fig. 57 Acute CSF and cortex Aβ_{40} dose–response study of verubecestat in Sprague–Dawley rats (3 h after 1, 3, 10, 30, or 100 mg kg^{-1} PO administration).

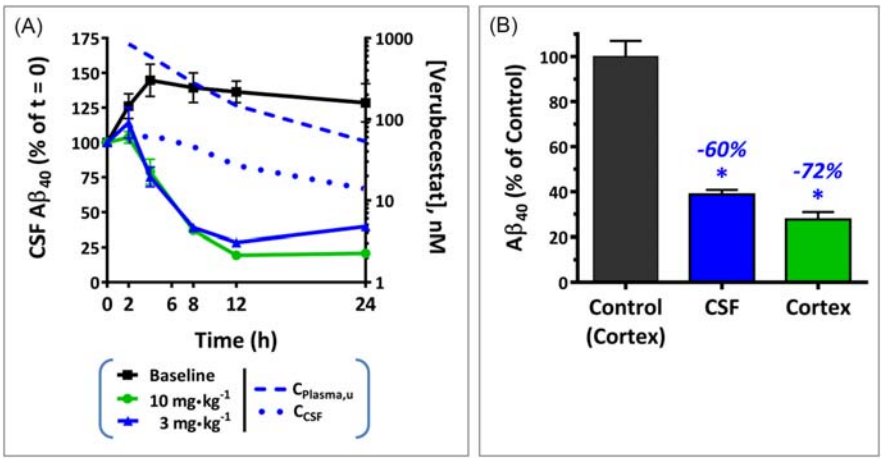

Fig. 58 (A) Time course of CSF $A\beta_{40}$ levels in cynomolgus monkeys orally dosed with 3 and 10 mg kg^{-1} of verubecestat. Unbound plasma and CSF concentrations of verubecestat are indicated for the 3 mg kg^{-1} dose. (B) Acute effect of verubecestat (10 mg kg^{-1} PO) on CSF and cortex $A\beta_{40}$ in cynomolgus monkeys.

was important because it provided added confidence that in the clinic CSF Aβ biomarkers would be a reliable measure of brain Aβ inhibition.

Inhibition of brain and CSF Aβ under conditions of chronic verubecestat administration was also investigated. Once-daily oral doses of verubecestat administered to monkeys at the suprapharmacological doses of 10, 30, and 100 mg kg^{-1} for 9 months afforded substantial (up to >90%) reductions of CSF $A\beta_{40}$, $A\beta_{42}$, and sAPPβ levels and cortex $A\beta_{40}$ and sAPPβ levels, demonstrating that the acute effects of verubecestat on central Aβ biomarkers were maintained after chronic administration. Similar effects were observed in rats under chronic dosing conditions, with profound reductions of cortex $A\beta_{40}$ observed after 3 months of once-daily oral doses of 25, 75, and 200 mg kg^{-1}.[102]

8.09.5.5 Human Dose and PK/PD Projections

Allometric scaling of PK parameters from rats, dogs, and monkeys in conjunction with data from PD studies in cynomolgus monkeys was used to generate human dose projections. The human target steady-state trough plasma concentration was set to the level required to produce 75% lowering of the clinical biomarker CSF $A\beta_{40}$, which projected to a once-daily oral dose of 35 mg. The relatively low QD dose reflected the favorable projected half-life (11 h) and oral bioavailability (75%).[100,102] The physical properties of the crystalline free base form of the compound that was selected for development were highly favorable. Verubecestat has aqueous solubility of 1.6 mM and at the projected human dose of 35 mg was classified as a BCS class 1 substance.[100]

It should be noted that the targeted 75% reduction of CSF $A\beta_{40}$ was not arbitrary, but rather it reflected significant consideration of the magnitude of Aβ lowering that could be both required and practically achieved to affect disease modification in symptomatic or prodromal AD patients. On the lower end of inhibition, chronic administration of **60** to young, preplaque TgCRND8 mice modestly reduced Aβ levels (~30%), yet produced some evidence of cognitive changes (Section "**In Vivo Validation and Development of a High-Throughput Rat PD Assay**").[91] Similarly, experiments that crossed Bace1 KO mice with TgPDAPP mice (Section "**Introduction**") showed that 20% lowering of central Aβ was safe, inhibited plaque deposition, and improved the cognitive phenotype relative to Bace1 homozygous wild-type/TgPDAPP mice.[34–36] The report of the human APP mutation A673T that partially inhibits Aβ production (~40% reduced Aβ) and protects against AD was published early in the verubecestat development program and was timely in that it provided human validation of the benefit of lifelong modest Aβ inhibition against a backdrop of failed amyloid-based clinical trials.[19] We recognized, however, that the modest levels of Aβ inhibition in subjects with this mutation were present from conception and might not reflect the degree of Aβ inhibition required for disease modification through pharmacological intervention in clinical settings of established disease in adults.

Considering the upper end of central Aβ inhibition, as indicated from chronic dosing in rats and monkeys, the preclinical safety profile of verubecestat offered the potential to interrogate a broad dose–response range for Aβ lowering. Practically, the clinical target of 75% CSF Aβ reduction at steady state represented the upper end of the dose–response curve; modeling predicted that disproportional increases in doses would be required to achieve statistically greater levels of Aβ reduction. Therefore, given our desire to balance maximizing the probability of efficacy with the need to guard against any mechanism-based issues that might attend a high degree of chronic BACE1 inhibition in humans, we ultimately focused on 75% inhibition as a robust level of Aβ lowering prior to the initiation of clinical trials, with the intention of also targeting a lower dose that would test a more modest degree of CSF Aβ reduction.[102] The ability to interrogate essentially a full dose–response curve for Aβ inhibition with verubecestat was in stark contrast to the GS inhibitors and anti-Aβ antibodies where dose-limiting side effects in the clinic limited the degree of Aβ lowering that could be tested.

8.09.6 Clinical Evaluation

Design of clinical trials for disease-modifying therapies for AD evolved significantly since iminoheterocycle BACE inhibitors were first disclosed in 2005. In fact, at the end of that same year, the Alzheimer's Association Roundtable hosted a conference with attendees from academia, industry, and the FDA, as well as patients and caregivers, to discuss on how best to clinically assess disease modification.[104] Compounds discussed at that meeting were a GS inhibitor (semagacestat, Eli Lilly),[105] a GS modulator (*R*-flurbuprophen, Myriad),[106] a monoclonal antibody (AB001, a second generation version of AN1792, Elan),[107] and an agent to promote Aβ clearance (Alzemed, Neurochem).[108] At that time, all of the well-characterized BACE1 inhibitors in the literature were of peptidic or peptidomimetic origin and, as discussed in Section "**Hydroxyethylamine-Based Peptidomimetic Inhibitors**," did not have profiles that offered promise for clinical development. Significant focus at that meeting was on the use of CSF Aβ and phosphorylated tau as biomarkers, and on the potential of amyloid imaging with PET tracers to be a more sensitive biomarker than MRI measurements of brain volume for detecting early stages of AD.[104]

To that point, researchers have long believed that earlier intervention could be more beneficial to patients, though the infrastructure to properly diagnose and recruit people with mild cognitive impairment and presymptomatic (prodromal) AD has only recently been in place and is still developing.[109–112] In particular, a longitudinal study reported in 2010 by Avid Radiopharmaceuticals definitively connected amyloid imaging using their tracer AV-45 with postmortem presence of plaque in the brain.[113] This study, in conjunction with an additional longitudinal study and earlier reports,[8,114] led to FDA approval of AV-45 the following year. Also, in 2010, Jack et al. published a hypothetical model of biomarker changes in the context of disease progression, later refined in 2013 (**Fig. 59**).[9] This model codified the perspective that changes in Aβ significantly precede both changes in other biomarkers and functional decline, supported by amyloid imaging using another agent, Pittsburgh compound B.[8]

To build the foundation for long-term verubecestat Phase 3 outcome trials, an extensive series of Phase 1 studies to assess safety, PK, and resulting Aβ PD effect of verubecestat was conducted in healthy volunteers and AD patients. In healthy volunteers, single oral doses up to 550 mg and multiple oral doses up to 250 mg once per day for 14 days elicited dose-dependent reductions of the three BACE1-dependent biomarkers, CSF $A\beta_{40}$, $A\beta_{42}$, and sAPPβ, with >90% maximal reductions achieved at the top doses in both of the studies (**Fig. 60**).[102] The compound was generally well tolerated, and concentrations in both plasma and CSF were increased in a dose-proportional manner. As had been observed preclinically in monkeys, CSF levels of verubecestat were lower than the unbound plasma concentrations, consistent with its susceptibility to Pgp-mediated efflux.

In patients with mild-to-moderate AD, oral doses of 12, 40, and 60 mg once per day for 7 days were also generally well tolerated and once again resulted in dose-dependent reductions of the three biomarkers. Maximal reduction of CSF $A\beta_{40}$ and $A\beta_{42}$ of >80% was observed at both the 40 and 60 mg doses (**Fig. 61**). Importantly, the PD activity of verubecestat was consistent between the healthy volunteers and AD patients, showing that there was no dramatic effect of the presence of disease on safety or on the ability of BACE1 inhibition to lower central Aβ.[102]

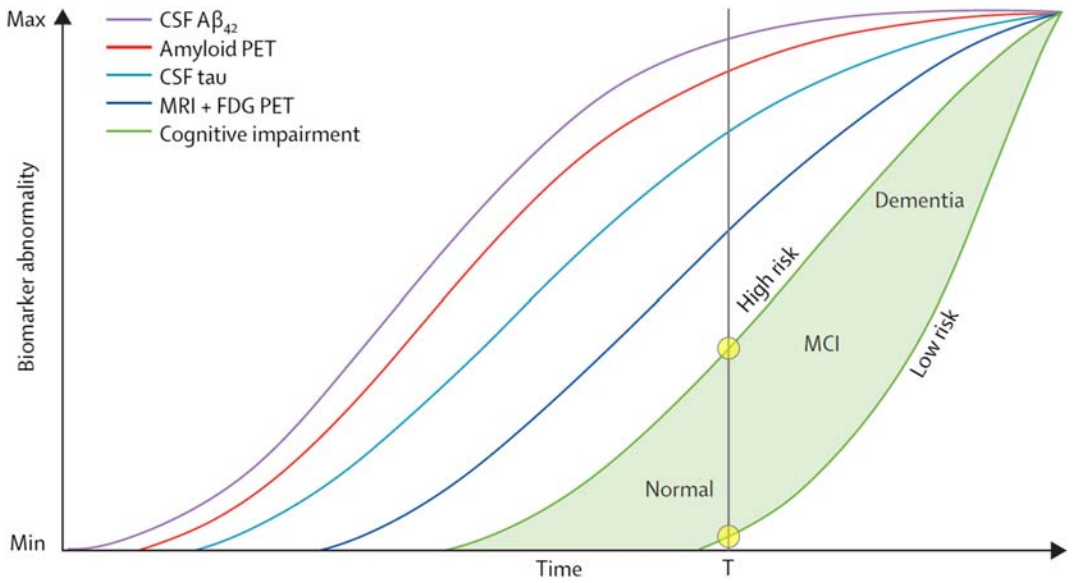

Fig. 59 Hypothetical model developed by Jack et al. of biomarker changes over time in Alzheimer's disease onset and progression.[9] The *y*-axis reflects the severity of the biomarker abnormality. CSF Aβ42 (*purple*) is the earliest biomarker to show abnormalities, followed by amyloid PET imaging (*red*), CSF tau (*light blue*), and finally MRI and fluorodeoxyglucose (FDG) PET imaging (*dark blue*). Actual cognitive impairment is represented as a range (*green*) between those at high risk and at low risk based on genetic factors, comorbidities, or lifestyle. The *vertical gray line* represents the expected degree of biomarker changes and the risk for manifestation of cognitive impairment at a particular point in time.

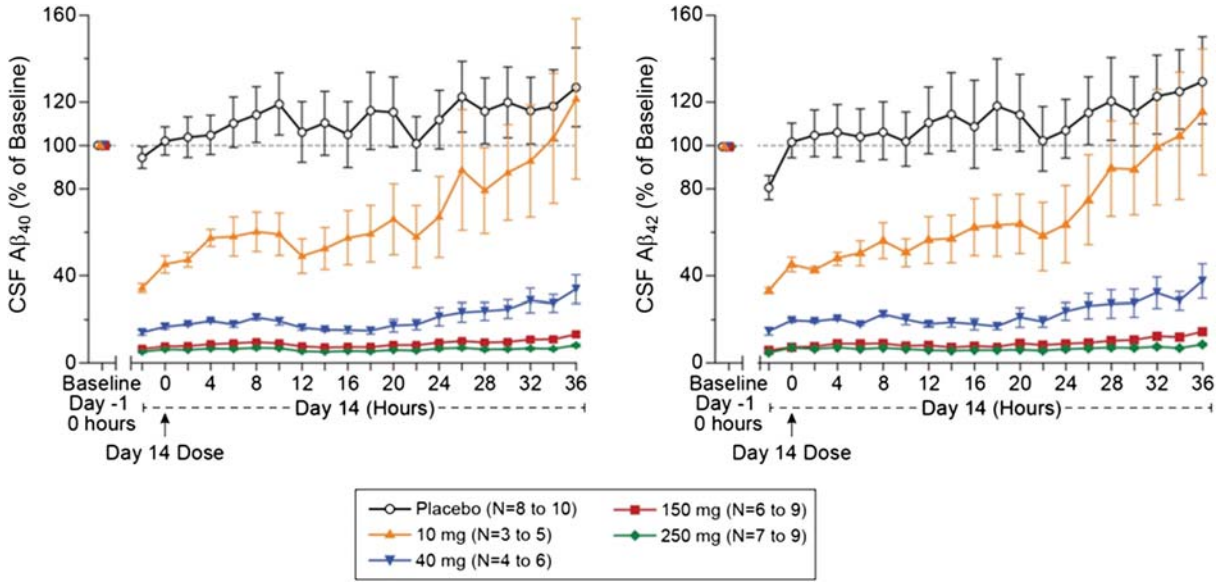

Fig. 60 Dose-dependent reduction of CSF $A\beta_{40}$ and $A\beta_{42}$ in healthy, nonelderly adults following 14 days of once-daily oral doses of 10, 40, or 150 or 250 mg of verubecestat. Day 14 CSF samples were obtained every 2 h from an indwelling lumbar catheter starting 2 h before the last dose. Baseline levels of CSF $A\beta_{40}$ and $A\beta_{42}$ were determined from a sample collected via lumbar puncture prior to the start of verubecestat treatment.

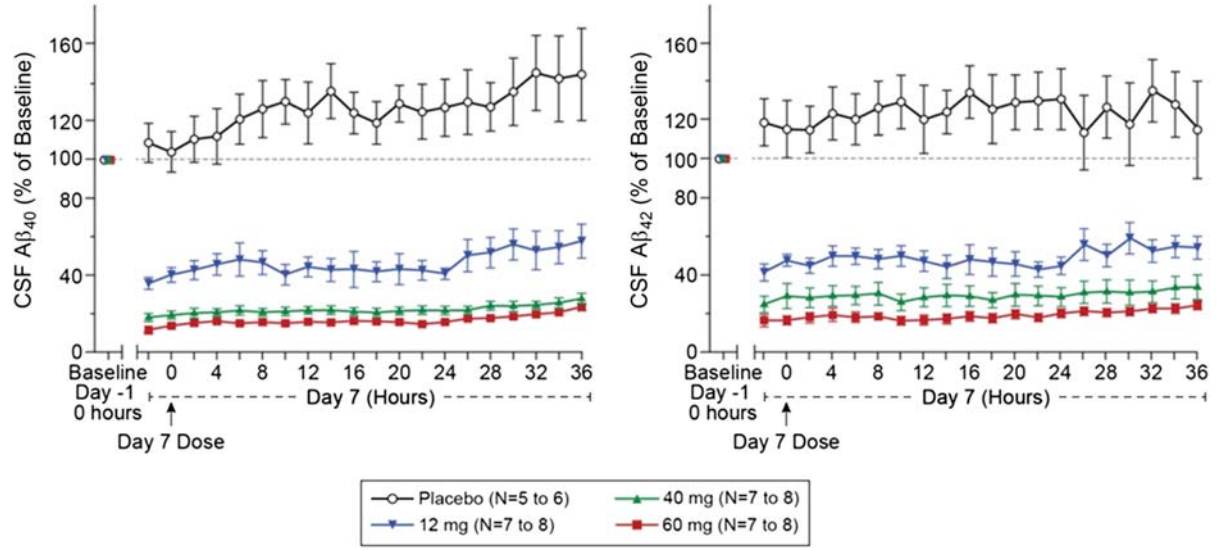

Fig. 61 Dose-dependent reduction of CSF $A\beta_{40}$ and $A\beta_{42}$ in Alzheimer's patients following 7 days of once-daily oral doses of 12, 40, or 60 mg of verubecestat. Day 7 CSF samples were obtained every 2 h from an indwelling lumbar catheter starting 2 h before the last dose. Baseline levels of CSF $A\beta_{40}$ and $A\beta_{42}$ were determined from a sample collected via lumbar puncture prior to the start of verubecestat treatment.

Verubecestat was advanced into two Phase 3 trials, the first BACE inhibitor to reach this milestone, and each study is enrolling patients at a different stage of the disease. One of the trials, designated EPOCH (NCT01739348),[115] is investigating verubecestat in mild-to-moderate AD. The second trial, known as APECS (NCT01953601),[116] is investigating verubecestat in earlier stage prodromal AD patients. As part of its adaptive design, the EPOCH trial included an initial Phase 2 arm in which a cohort of 400 patients was evaluated for 3 months to test the safety of verubecestat and enable initiation of the longer term Phase 3 trials. The doses for this cohort—12, 40, and 60 mg—mirrored those used in the Phase 1 study in AD patients described above. Ultimately, the 12 and 40 mg doses were selected for continuation into the two Phase 3 trials supported by modeling of the extensive Phase 1 data set, which projected that 95% of the patients receiving the 12 mg dose would have CSF $A\beta_{40}$ reductions in the 50–75% range and that 95% of those on the 40 mg dose would have 80–90% CSF $A\beta_{40}$ lowering. Importantly, these two patient populations would be largely nonoverlapping, with one testing partial and the other testing near full inhibition.[102]

The EPOCH trial is a randomized, placebo controlled, double-blind efficacy, and safety trial of verubecestat in approximately 1960 subjects with mild-to-moderate AD. The duration of the trial is 18 months with cognitive and functional primary outcome measures. Cognitive function will be assessed as change from baseline in the Alzheimer's Disease Assessment Scale Cognitive Subscale score,[117] while functional outcome will be measured via the Alzheimer's Disease Cooperative Study—Activities of Daily Living score.[118] Secondary outcome measures include additional functional and cognitive assessments [change from baseline scores in Clinical Dementia Rating Scale-Sum of Boxes (CDR-SB),[119] Mini Mental State Examination,[120] and Neuropsychiatric Inventory[121]] and biomarker changes comprising changes in brain amyloid load, CSF total tau, and hippocampal volume. EPOCH was fully enrolled by late 2015, and primary trial completion is scheduled for Jul. 2017 with a 4-year extension phase.

The APECS trial is a Phase 3, randomized, placebo-controlled, double-blind clinical trial to study the efficacy and safety of verubecestat in approximately 1500 subjects with prodromal AD. An inclusion criterion for the trial is a positive amyloid imaging PET scan using [^{18}F]flutemetamol tracer or positive CSF tau/Aβ42 ratio. This trial is 24 months in duration with the primary efficacy outcome measure of change from baseline in the CDR-SB score. As with the EPOCH trial, secondary outcome measures include additional cognitive and functional assessments, and changes from baseline in total hippocampal volume and CSF total tau. The estimated primary completion date of the APECS trial is Jul. 2019.

With no disease-modifying therapy of any mechanism yet approved by the FDA or other health agencies, the regulatory landscape continues to evolve even as clinical trials of verubecestat and other agents are in progress. In 2013, the FDA issued guidance that improved cognition and daily function would be required for regulatory approval of disease modification for early-stage disease.[122] Interestingly, Eli Lilly recently announced that, in an ongoing Phase 3 trial in mild AD patients with the anti-Aβ monoclonal antibody solanezumab, measures of cognition will be the sole primary endpoint, with functional changes specified as secondary endpoints.[123] The reason for this change was not clear, but has a logical basis since function is largely intact and changes slowly in the early stages of the disease. Thus drug effects on function may be difficult to detect. Despite FDA guidance to the contrary, this change may also reflect a gambit that it will be difficult to deny approval to a compound that shows significant improvements in cognition even in the absence of significant effects on functional outcome. If successful, this precedent could have broad implications for the development of disease-modifying agents in the AD field.

8.09.7 Conclusions

The discovery of verubecestat was the pinnacle of our BACE inhibitor discovery program, and it was achieved through the confluence of many factors. Key among these were access to novel starting chemical matter from the use of emerging screening technologies, early adoption of structure-based drug design, a strategy focused on optimization of drug-like properties beneficial for CNS penetration, placement of a high-throughput in vivo assay high in the research funnel, and, more generally, close collaboration between the many functions that drive drug discovery. An important facet of our medicinal chemistry strategy was repeated innovation around the aspartyl protease binding motif as well as around exploration of the adjacent binding sites, coupled with a willingness to walk away from potency in favor of overall properties of the molecules. The 12-year pathway from the start of the program to initiation of Phase 3 featured many avenues of exploration, some more fruitful than others, as well as a number of unexpected discoveries. In this article, we have attempted to capture a number of these aspects of our efforts and especially our decision making at key points. Taken together, they highlight the importance of risk-taking and perseverance in prosecution of the most challenging of drug targets.

Verubecestat entered Phase 3 in 2013, the first BACE inhibitor to achieve this milestone, and is one of only two compounds that have advanced to this stage in the clinic. In 2016 Eli Lilly and AstraZeneca announced the progression of the inhibitor LY3314814/AZD3293, which was discovered at AstraZeneca (**99**, Fig. 62), representing the second Phase 3 entrant.[124,125] In retrospect, beyond these two molecules, it is striking that all of the disclosed structures of BACE inhibitors that have entered the clinic or have demonstrated robust preclinical Aβ lowering in large animal species contain iminoheterocycle-based aspartyl protease binding motifs (additional representative examples **100–105** are shown in Fig. 62). In addition to the shared amidine moiety that makes the key interactions with the catalytic dyad, these structures all possess an aryl group that occupies the S1 subsite. To that end, while all of these structures have additional substituents that occupy either the S3 subsite, the S2′ subsite, or both, benzyl amidine **106** is a representation of a common structural element contained in all of the depicted compounds.

The privileged nature of substructure **106** embodied in inhibitors, first disclosed by Schering-Plough, Wyeth, and AstraZeneca/Astex in 2005–2006, is reflected in the patent analysis in Fig. 63.[132,133] A search on this key structural element shows that beginning in 2009, several years after those initial disclosures, there were an increasingly large number of research groups employing this structural element. At the peak from 2011 through 2014, there were 20–40 applications per year claiming BACE1 inhibitors containing this structural motif. It is a remarkable coalescence around a single structural element, and reflects the complexity and difficulty in obtaining high-quality chemical matter for this target. Ultimately, our efforts and those of everyone in the field are directed to improving the lives of patients. Verubecestat and iminoheterocycle BACE inhibitors in general represent a breakthrough in the ability to target BACE1, definitively test the amyloid hypothesis, and, most importantly, offer patients hope for development of a disease-modifying therapy for AD.

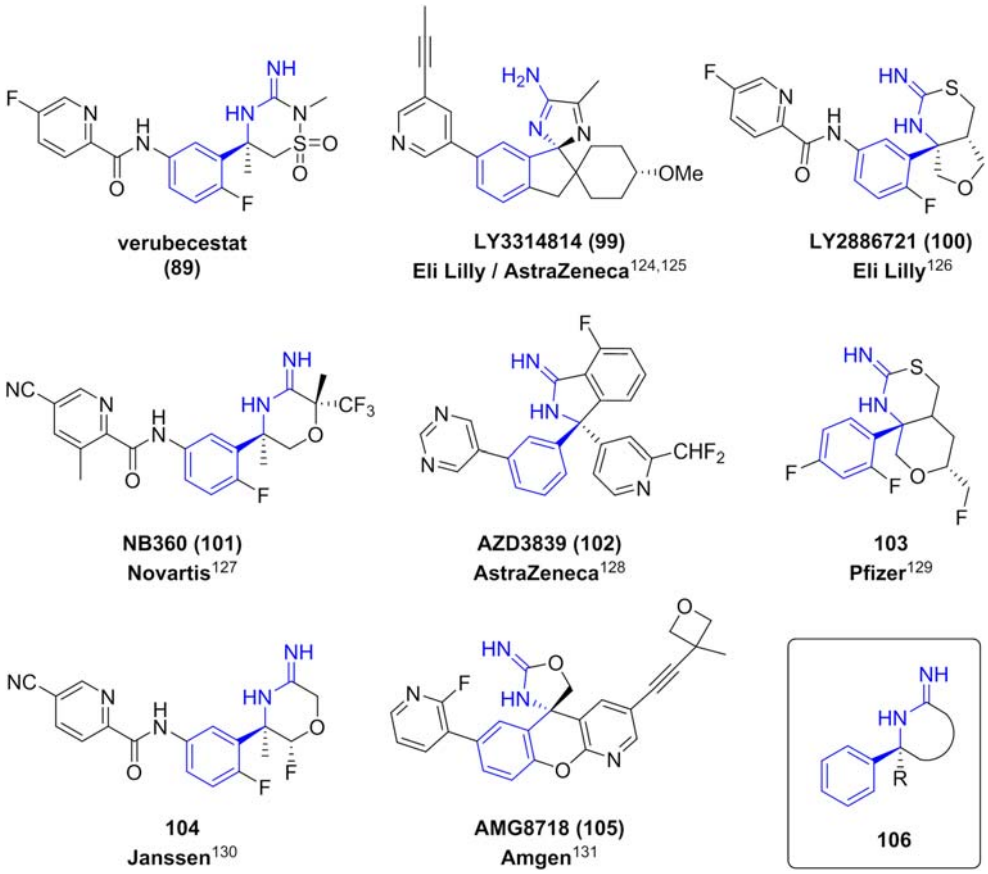

Fig. 62 Structures of the two BACE inhibitors that have progressed to Phase 3 clinical trials, verubecestat and LY3314814 (**99**), as well as a representative selection of structurally diverse compounds **100**–**105**[126–131] from other companies that have entered clinical or advanced preclinical development. The common structural element **106** is present in all of these compounds and is highlighted in *blue* within each structure.

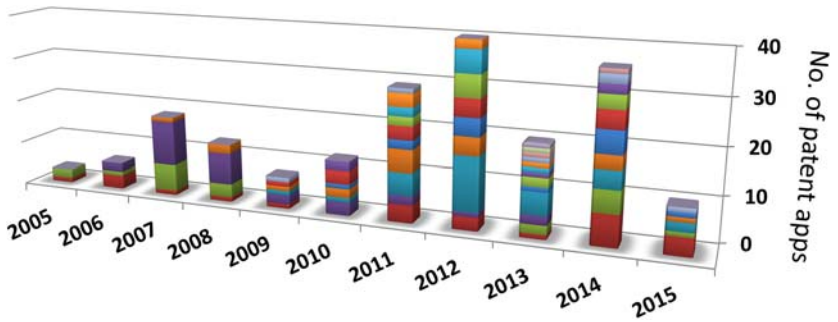

Fig. 63 Number of patent applications that claim BACE inhibitors containing key structural element **106** beginning from first disclosure of the iminoheterocycle binding motif in 2005 through 2015. In each year, the columns are colored by research group.

See also: 7.08. Targeting β-Secretase (BACE) for the Treatment of Alzheimer's Disease.

References

1. Cummings, J. L. Alzheimer's Disease. *N. Engl. J. Med.* **2004,** *351,* 56–67.
2. James, B. D.; Leurgans, S. E.; Hebert, L. E.; Scherr, P. A.; Yaffe, K.; Bennett, D. A. Contribution of Alzheimer Disease to Mortality in the United States. *Neurology* **2014,** *82,* 1045–1050.

3. Prince, M.; Bryce, R.; Albanese, E.; Wimo, A.; Ribeiro, W.; Ferri, C. P. The Global Prevalence of Dementia: A Systematic Review and Metaanalysis. *Alzheimers Dement.* **2013,** *9,* 63–75.
4. Alzheimer's Disease International. *World Alzheimer Report 2015*, http://www.alz.co.uk/research/WorldAlzheimerReport2015.pdf.
5. Alzheimer's Association. *2016 Alzheimer's Disease Facts and Figures*, http://www.alz.org/documents_custom/2016-facts-and-figures.pdf.
6. Aisen, P. S.; Cummings, J.; Schneider, L. S. Symptomatic and Nonamyloid/tau Based Pharmacologic Treatment for Alzheimer Disease. *Cold Spring Harb. Perspect. Med.* **2011,** *2,* a006395.
7. Braak, H.; Thal, D. R.; Ghebremedhin, E.; Tredici, K. D. Stages of the Pathologic Process in Alzheimer Disease: Age Categories From 1 to 100 Years. *J. Neuropathol. Exp. Neurol.* **2011,** *70,* 960–969.
8. Jack, C. R.; Knopman, D. S.; Jagust, W. J.; Shaw, L. M.; Aisen, P. S.; Weiner, M. W.; Petersen, R. C.; Trojanowski, J. Q. Hypothetical Model of Dynamic Biomarkers of the Alzheimer's Pathological Cascade. *Lancet Neurol.* **2010,** *9,* 119–128.
9. Jack, C. R.; Knopman, D. S.; Jagust, W. J.; Petersen, R. C.; Weiner, M. W.; Aisen, P. S.; Shaw, L. M.; Vemuri, P.; Wiste, H. J.; Weigand, S. D.; Lesnick, T. G.; Pankratz, V. S.; Donohue, M. C.; Trojanowski, J. Q. Tracking Pathophysiological Processes in Alzheimer's Disease: An Updated Hypothetical Model of Dynamic Biomarkers. *Lancet Neurol.* **2013,** *12,* 207–216.
10. Hardy, J.; Selkoe, D. J. The Amyloid Hypothesis of Alzheimer's Disease: Progress and Problems on the Road to Therapeutics. *Science* **2002,** *297,* 353–356.
11. Hardy, J. The Amyloid Hypothesis for Alzheimer's Disease: A Critical Reappraisal. *J. Neurochem.* **2009,** *110,* 1129–1134.
12. Selkoe, D. J.; Hardy, J. The Amyloid Hypothesis of Alzheimer's Disease at 25 Years. *EMBO Mol. Med.* **2016,** *8,* 595–608.
13. De Strooper, B. Proteases and Proteolysis in Alzheimer Disease: A Multifactorial View on the Disease Process. *Physiol. Rev.* **2010,** *90,* 465–494.
14. Selkoe, D. J. Soluble Oligomers of the Amyloid Beta-Protein Impair Synaptic Plasticity and Behavior. *Behav. Brain Res.* **2008,** *192,* 106–113.
15. Jarrett, J. T.; Berger, E. P.; Lansbury, P. T. The Carboxy Terminus of the β Amyloid Protein is Critical for the Seeding of Amyloid Formation: Implications for the Pathogenesis of Alzheimer's Disease. *Biochemistry* **1993,** *32,* 4693–4697.
16. Musiek, E. S.; Holtzman, D. M. Three Dimensions of the Amyloid Hypothesis: Time, Space and 'Wingmen'. *Nat. Neurosci.* **2015,** *18,* 800–806.
17. Van Cauwenberghe, C.; Van Broeckhoven, C.; Sleegers, K. The Genetic Landscape of Alzheimer Disease: Clinical Implications and Perspectives. *Genet. Med.* **2016,** *18,* 421–430.
18. Karch, C. M.; Cruchaga, C.; Goate, A. M. Alzheimer's Disease Genetics: From the Bench to the Clinic. *Neuron* **2014,** *83,* 11–26.
19. Jonsson, T.; Atwal, J. K.; Steinberg, S.; Snaedal, J.; Jonsson, P. V.; Bjornsson, S.; Stefansson, H.; Sulem, P.; Gudbjartsson, D.; Maloney, J.; Hoyte, K.; Gustafson, A.; Liu, Y.; Lu, Y.; Bhangale, T.; Graham, R. R.; Huttenlocher, J.; Bjornsdottir, G.; Andreassen, O. A.; Jönsson, E. G.; Palotie, A.; Behrens, T. W.; Magnusson, O. T.; Kong, A.; Thorsteinsdottir, U.; Watts, R. J.; Stefansson, K. A Mutation in APP Protects Against Alzheimer's Disease and Age-Related Cognitive Decline. *Nature* **2012,** *488,* 96–99.
20. Yu, J. T.; Tan, L.; Hardy, J. Apolipoprotein E in Alzheimer's Disease: An Update. *Annu. Rev. Neurosci.* **2014,** *37,* 79–100.
21. Vassar, R.; Kuhn, P. H.; Haass, C.; Kennedy, M. E.; Rajendran, L.; Wong, P. C.; Lichtenthaler, S. F. Function, Therapeutic Potential and Cell Biology of BACE Proteases: Current Status and Future Prospects. *J. Neurochem.* **2014,** *130,* 4–28.
22. Yan, R.; Vassar, R. Targeting the β Secretase BACE1 for Alzheimer's Disease Therapy. *Lancet Neurol.* **2014,** *13,* 319–329.
23. Vassar, R.; Bennett, B. D.; Babu-Khan, S.; Kahn, S.; Mendiaz, E. A.; Denis, P.; Teplow, D. B.; Ross, S.; Amarante, P.; Loeloff, R.; Luo, Y.; Fisher, S.; Fuller, J.; Edenson, S.; Lile, J.; Jarosinski, M. A.; Biere, A. L.; Curran, E.; Burgess, T.; Louis, J. C.; Collins, F.; Treanor, J.; Rogers, G.; Citron, M. Beta-Secretase Cleavage of Alzheimer's Amyloid Precursor Protein by the Transmembrane Aspartic Protease BACE. *Science* **1999,** *286,* 735–741.
24. Sinha, S.; Anderson, J. P.; Barbour, R.; Basi, G. S.; Caccavello, R.; Davis, D.; Doan, M.; Dovey, H. F.; Frigon, N.; Hong, J.; Jacobson-Croak, K.; Jewett, N.; Keim, P.; Knops, J.; Lieberburg, I.; Power, M.; Tan, H.; Tatsuno, G.; Tung, J.; Schenk, D.; Seubert, P.; Suomensaari, S. M.; Wang, S.; Walker, D.; Zhao, J.; McConlogue, L.; John, V. Purification and Cloning of Amyloid Precursor Protein Beta-Secretase From Human Brain. *Nature* **1999,** *402,* 537–540.
25. Yan, R.; Bienkowski, M. J.; Shuck, M. E.; Miao, H.; Tory, M. C.; Pauley, A. M.; Brashier, J. R.; Stratman, N. C.; Mathews, W. R.; Buhl, A. E.; Carter, D. B.; Tomasselli, A. G.; Parodi, L. A.; Heinrikson, R. L.; Gurney, M. E. Membrane-Anchored Aspartyl Protease With Alzheimer's Disease β-Secretase Activity. *Nature* **1999,** *402,* 533–537.
26. Lin, X.; Koelsch, G.; Wu, S.; Downs, D.; Dashti, A.; Tang, J. Human Aspartic Protease Memapsin 2 Cleaves the β-Secretase Site of β-Amyloid Precursor Protein. *Proc. Natl. Acad. Sci. U. S. A.* **2000,** *97,* 1456–1460.
27. Hussain, I.; Powell, D.; Howlett, D. R.; Tew, D. G.; Meek, T. D.; Chapman, C.; Gloger, I. S.; Murphy, K. E.; Southan, C. D.; Ryan, D. M.; Smith, T. S.; Simmons, D. L.; Walsh, F. S.; Dingwall, C.; Christie, G. Identification of a Novel Aspartic Protease (Asp 2) as β-Secretase. *Mol. Cell. Neurosci.* **1999,** *14,* 419–427.
28. Dominguez, D.; Tournoy, J.; Hartmann, D.; Huth, T.; Cryns, K.; Deforce, S.; Serneels, L.; Camacho, I. E.; Marjaux, E.; Craessaerts, K.; Roebroek, A. J.; Schwake, M.; D'Hooge, R.; Bach, P.; Kalinke, U.; Moechars, D.; Alzheimer, C.; Reiss, K.; Saftig, P.; De Strooper, B. Phenotypic and Biochemical Analyses of BACE1- and BACE2-Deficient Mice. *J. Biol. Chem.* **2005,** *280,* 30797–30806.
29. Fukumoto, H.; Cheung, B. S.; Hyman, B. T.; Irizarry, M. D. β-Secretase Protein and Activity Are Increased in the Neocortex in Alzheimer Disease. *Arch. Neurol.* **2002,** *59,* 1381–1389.
30. Yang, L.-B.; Lindholm, K.; Yan, R.; Citron, M.; Xia, W.; Yang, X.-L.; Beach, T.; Sue, L.; Wong, P.; Price, D.; Li, R.; Shen, Y. Elevated β-Secretase Expression and Enzymatic Activity Detected in Sporadic Alzheimer Disease. *Nat. Med.* **2003,** *9,* 3–4.
31. Li, R.; Lindholm, K.; Yang, L.-B.; Yue, X.; Citron, M.; Yan, R.; Beach, T.; Sue, L.; Sabbagh, M.; Cai, H.; Wong, P.; Price, D.; Shen, Y. Amyloid β Peptide Load Is Correlated With Increased β-Secretase Activity in Sporadic Alzheimer's Disease Patients. *Proc. Natl. Acad. Sci. U. S. A.* **2004,** *101,* 3632–3637.
32. Willem, M.; Garratt, A. N.; Novak, B.; Citron, M.; Kaufmann, S.; Rittger, A.; De Strooper, B.; Saftig, P.; Birchmeier, C.; Haass, C. Control of Peripheral Nerve Myelination by the β-Secretase BACE1. *Science* **2006,** *314,* 664–666.
33. Luo, Y.; Bolon, B.; Kahn, S.; Bennett, B. D.; Babu-Khan, S.; Denis, P.; Fan, W.; Kha, H.; Zhang, J.; Gong, Y.; Martin, L.; Louis, J. C.; Yan, Q.; Richards, W. G.; Citron, M.; Vassar, R. Mice Deficient in BACE1, the Alzheimer's Beta-Secretase, Have Normal Phenotype and Abolished Beta-Amyloid Generation. *Nat. Neurosci.* **2001,** *4,* 231–232.
34. Ohno, M.; Chang, L.; Tseng, W.; Oakley, H.; Citron, M.; Klein, W. L.; Vassar, R.; Disterhoft, J. F. Temporal Memory Deficits in Alzheimer's Mouse Models: Rescue by Genetic Deletion of BACE1. *Eur. J. Neurosci.* **2006,** *23,* 251–260.
35. Ohno, M.; Cole, S. L.; Yasvoina, M.; Zhao, J.; Citron, M.; Berry, R.; Disterhoft, J. F.; Vassar, R. BACE1 Gene Deletion Prevents Neuron Loss and Memory Deficits in 5XFAD APP/PS1 Transgenic Mice. *Neurobiol. Dis.* **2007,** *26,* 134–145.
36. McConlogue, L.; Buttini, M.; Anderson, J. P.; Brigham, E. F.; Chen, K. S.; Freedman, S. B.; Games, D.; Johnson-Wood, K.; Lee, M.; Zeller, M.; Liu, W.; Motter, R.; Sinha, S. Partial Reduction of BACE1 Has Dramatic Effects on Alzheimer Plaque and Synaptic Pathology in APP Transgenic Mice. *J. Biol. Chem.* **2007,** *282,* 26326–26334.
37. Benilova, I.; Gallardo, R.; Ungureanu, A.-A.; Cano, V. C.; Snellinx, A.; Ramakers, M.; Bartic, C.; Rousseau, F.; Schymkowitz, J.; Strooper, B. D. The Alzheimer Disease Protective Mutation A2T Modulates Kinetic and Thermodynamic Properties of Amyloid-β (Aβ) Aggregation. *J. Biol. Chem.* **2014,** *289,* 30977–30989.
38. Maloney, J. A.; Bainbridge, T.; Gustafson, A.; Zhang, S.; Kyauk, R.; Steiner, P.; Brug, M. V. D.; Liu, Y.; Ernst, J. A.; Watts, R. J.; Atwal, J. K. Molecular Mechanisms of Alzheimer Disease Protection by the A673T Allele of Amyloid Precursor Protein. *J. Biol. Chem.* **2014,** *289,* 30990–31000.
39. Di Fede, G.; Catania, M.; Morbin, M.; Rossi, G.; Suardi, S.; Mazzoleni, G.; Merlin, M.; Giovagnoli, A. R.; Prioni, S.; Erbetta, A.; Falcone, C.; Gobbi, M.; Colombo, L.; Bastone, A.; Beeg, M.; Manzoni, C.; Francescucci, B.; Spagnoli, A.; Cantu, L.; Del Favero, E.; Levy, E.; Salmona, M.; Tagliavini, F. A Recessive Mutation in the APP Gene With Dominant-Negative Effect on Amyloidogenesis. *Science* **2009,** *323,* 1473–1477.
40. Herrup, K. The Case for Rejecting the Amyloid Cascade Hypothesis. *Nat. Neurosci.* **2015,** *18,* 794–799.
41. Karran, E.; Hardy, J. A Critique of the Drug Discovery and Phase 3 Clinical Programs Targeting the Amyloid Hypothesis for Alzheimer Disease. *Ann. Neurol.* **2014,** *76,* 185–205.

42. Doody, R. S.; Thomas, R. G.; Farlow, M.; Iwatsubo, T.; Vellas, B.; Joffe, S.; Kieburtz, K.; Raman, R.; Sun, X.; Aisen, P. S.; Siemers, E.; Liu-Seifert, H.; Mohs, R. Phase 3 Trials of Solanezumab for Mild-to-Moderate Alzheimer's Disease. *N. Engl. J. Med.* **2014,** *370,* 311–321.
43. Vassar, R.; Kovacs, D. M.; Yan, R.; Wong, P. C. The β-Secretase Enzyme BACE in Health and Alzheimer's Disease: Regulation, Cell Biology, Function, and Therapeutic Potential. *J. Neurosci.* **2009,** *29,* 12787–12794.
44. Hong, L.; Tang, J. Flap Position of Free Memapsin 2 (β-Secretase), a Model for Flap Opening in Aspartic Protease Catalysis. *Biochemistry* **2004,** *43,* 4689–4695.
45. Eder, J.; Hommel, U.; Cumin, F.; Martoglio, B.; Gerhartz, B. Aspartic Proteases in Drug Discovery. *Curr. Pharm. Des.* **2007,** *13,* 271–285.
46. Wood, J. M.; Maibaum, J.; Rahuel, J.; Grütter, M. G.; Cohen, N.-C.; Rasetti, V.; Rüger, H.; Göschke, R.; Stutz, S.; Fuhrer, W.; Schilling, W.; Rigollier, P.; Yamaguchi, Y.; Cumin, F.; Baum, H.-P.; Schnell, C. R.; Herold, P.; Mah, R.; Jensen, C.; O'Brien, E.; Stanton, A.; Bedigian, M. P. Structure-Based Design of Aliskiren, a Novel Orally Effective Renin Inhibitor. *Biochem. Biophys. Res. Commun.* **2003,** *308,* 698–705.
47. Grüninger-Leitch, F.; Schlatter, D.; Küng, E.; Nelböck, P.; Döbeli, H. Substrate and Inhibitor Profile of BACE (β-Secretase) and Comparison With Other Mammalian Aspartic Proteases. *J. Biol. Chem.* **2001,** *277,* 4687–4693.
48. Koike, M.; Nakanishi, H.; Saftig, P.; Ezaki, J.; Isahara, K.; Ohsawa, Y.; Schulz-Schaeffer, W.; Watanabe, T.; Waguri, S.; Kametaka, S.; Shibata, M.; Yamamoto, K.; Kominami, E.; Peters, C.; von Figura, K.; Uchiyama, Y. Cathepsin D Deficiency Induces Lysosomal Storage With Ceroid Lipofuscin in Mouse CNS Neurons. *J. Neurosci.* **2000,** *20,* 6898–6906.
49. May, P. C.; Dean, R. A.; Lowe, S. L.; Martenyi, F.; Sheehan, S. M.; Boggs, L. N.; Monk, S. A.; Mathes, B. M.; Mergott, D. J.; Watson, B. M.; Stout, S. L.; Timm, D. E.; Smith Labell, E.; Gonzales, C. R.; Nakano, M.; Jhee, S. S.; Yen, M.; Ereshefsky, L.; Lindstrom, T. D.; Calligaro, D. O.; Cocke, P. J.; Greg Hall, D.; Friedrich, S.; Citron, M.; Audia, J. E. Robust Central Reduction of Amyloid-β in Humans With an Orally Available, Non-Peptidic β-Secretase Inhibitor. *J. Neurosci.* **2011,** *31,* 16507–16516.
50. Fielden, M. R.; Werner, J.; Jamison, J. A.; Coppi, A.; Hickman, D.; Dunn, R. T., II; Trueblood, E.; Zhou, L.; Afshari, C. A.; Lightfoot-Dunn, R. Retinal Toxicity Induced by a Novel β-Secretase Inhibitor in the Sprague–Dawley Rat. *Toxicol. Pathol.* **2015,** *43,* 581–592.
51. Riddell, D.; Zuhl, A. M.; Nolan, C.; Atchison, A.; Ambroise, C.; Beck, E. M.; Niessen, S.; Hou, X.; am Ende, C. S.; O'Neill, B.; Brodney, M. A.; Johnson, D. S. Lysosomotropism of Basic BACE1 Inhibitors Contributes to Increased Cellular Potency Against Cathepsin D and Ocular Toxicity. *Neurodegener. Dis.* **2015,** *15* (Suppl. 1), 730.
52. Bennett, B. D.; Babu-Khan, S.; Loeloff, R.; Louis, J.-C.; Curran, E.; Citron, M.; Vassar, R. Expression Analysis of BACE2 in Brain and Peripheral Tissues. *J. Biol. Chem.* **2000,** *275,* 20647–20651.
53. Farzan, M.; Schnitzler, C. E.; Vasilieva, N.; Leung, D.; Choe, H. BACE2, a β-Secretase Homolog, Cleaves at the β Site and Within the Amyloid-β Region of the Amyloid-β Precursor Protein. *Proc. Natl. Acad. Sci. U. S. A.* **2000,** *97,* 9712–9717.
54. Yan, R.; Munzner, J. B.; Shuck, M. E.; Bienkowski, M. J. BACE2 Functions As an Alternative α-Secretase in Cells. *J. Biol. Chem.* **2001,** *276,* 34019–34027.
55. Fluhrer, R.; Capell, A.; Westmeyer, G.; Willem, M.; Hartung, B.; Condron, M. M.; Teplow, D. B.; Haass, C.; Walter, J. A. Non-Amyloidogenic Function of BACE-2 in the Secretory Pathway. *J. Neurochem.* **2002,** *81,* 1011–1020.
56. Cai, H.; Wang, Y.; McCarthy, D.; Wen, H.; Borchelt, D. R.; Price, D. L.; Wong, P. C. BACE1 is the Major β-Secretase for Generation of Aβ Peptides by Neurons. *Nat. Neurosci.* **2001,** *4,* 233–234.
57. Roberds, S. L.; Anderson, J.; Basi, G.; Bienkowski, M. J.; Branstetter, D. G.; Chen, K. S.; Freedman, S. B.; Frigon, N. L.; Games, D.; Hu, K.; Johnson-Wood, K.; Kappenman, K. E.; Kawabe, T. T.; Kola, I.; Kuehn, R.; Lee, M.; Liu, W.; Motter, R.; Nichols, N. F.; Power, M.; Robertson, D. W.; Schenk, D.; Schoor, M.; Shopp, G. M.; Shuck, M. E.; Sinha, S.; Svensson, K. A.; Tatsuno, G.; Tintrup, H.; Wijsman, J.; Wright, S.; McConlogue, L. BACE Knockout Mice Are Healthy Despite Lacking the Primary β-Secretase Activity in Brain: Implications for Alzheimer's Disease Therapeutics. *Hum. Mol. Genet.* **2001,** *10,* 1317–1324.
58. Shimshek, D. R.; Jacobson, L. H.; Kolly, C.; Zamurovic, N.; Balavenkatraman, K. K.; Morawiec, L.; Kreutzer, R.; Schelle, J.; Jucker, M.; Bertschi, B.; Theil, D.; Heier, A.; Bigot, K.; Beltz, K.; Machauer, R.; Brzak, I.; Perrot, L.; Neumann, U. Pharmacological BACE1 and BACE2 Inhibition Induces Hair Depigmentation by Inhibiting PMEL17 Processing in Mice. *Sci. Rep.* **2016,** *6,* 21917.
59. Esterházy, D.; Stützer, I.; Wang, H.; Rechsteiner, M. P.; Beauchamp, J.; Döbeli, H.; Hilpert, H.; Matile, H.; Prummer, M.; Schmidt, A.; Lieske, N.; Boehm, B.; Marselli, L.; Bosco, D.; Kerr-Conte, J.; Aebersold, R.; Spinas, G. A.; Moch, H.; Migliorini, C.; Stoffel, M. BACE2 Is a β Cell-Enriched Protease That Regulates Pancreatic β Cell Function and Mass. *Cell Metab.* **2011,** *14,* 365–377.
60. Rulifson, I. C.; Cao, P.; Miao, L.; Kopecky, D.; Huang, L.; White, R. D.; Samayoa, K.; Gardner, J.; Wu, X.; Chen, K.; Tsuruda, T.; Homann, O.; Baribault, H.; Yamane, H.; Carlson, T.; Wiltzius, J.; Li, Y. Identification of Human Islet Amyloid Polypeptide As a BACE2 Substrate. *PLoS One* **2016,** *11* (2), e0147254.
61. Barão, S.; Moechars, D.; Lichtenthaler, S. F.; De Strooper, B. BACE1 Physiological Functions May Limit Its Use As Therapeutic Target for Alzheimer's Disease. *Trends Neurosci.* **2016,** *39,* 158–169.
62. Hu, X.; Hicks, C. W.; He, W.; Wong, P.; Macklin, W.; Trapp, B. D.; Yan, Y. BACE1 Modulates Myelination in the Central and Peripheral Nervous System. *Nat. Neurosci.* **2006,** *9,* 1520–1525.
63. Cheret, C.; Willem, M.; Fricker, F. R.; Wende, H.; Wulf-Goldenberg, A.; Tahirovic, S.; Nave, K.-A.; Saftig, P.; Haass, C.; Garratt, A. N.; Bennett, D. L.; Birchmeier, C. Bace1 and Neuregulin-1 Cooperate to Control Formation and Maintenance of Muscle Spindles. *EMBO J.* **2013,** *32,* 2015–2028.
64. Maillaird, M.; Hom, C.; Gailunas, A.; Jagodzinska, B.; Fang, L.Y.; John, V.; Freskos, J.N.; Pulley, S.R.; Beck, J.P.; Tenbrink, R.E. Preparation of Substituted Amines to Treat Alzheimer's Disease. WO2002002512, 2002.
65. Maillard, M. C.; Hom, R. K.; Benson, T. E.; Moon, J. B.; Mamo, S.; Bienkowski, M.; Tomasselli, A. G.; Woods, D. D.; Prince, D. B.; Paddock, D. J.; Emmons, T. L.; Tucker, J. A.; Dappen, M. S.; Brogley, L.; Thorsett, E. D.; Jewett, N.; Sinha, S.; John, V. Design, Synthesis, and Crystal Structure of Hydroxyethyl Secondary Amine-Based Peptidomimetic Inhibitors of Human β-Secretase. *J. Med. Chem.* **2007,** *50,* 776–781.
66. Hong, L.; Koelsch, G.; Lin, X.; Wu, S.; Terzyan, S.; Ghosh, A. K.; Zhang, X. C.; Tang, J. Structure of the Protease Domain of Memapsin 2 (β-Secretase) Complexed With Inhibitor. *Science* **2000,** *290,* 150–153.
67. Ghosh, A. K.; Shin, D.; Downs, D.; Koelsch, G.; Lin, X.; Ermolieff, J.; Tang, J. Design of Potent Inhibitors for Human Brain Memapsin 2 (β-Secretase). *J. Am. Chem. Soc.* **2000,** *122,* 3522–3523.
68. Kennedy, M. E.; Wang, W.; Song, L.; Lee, J.; Zhang, L.; Wong, G.; Wang, L.; Parker, E. Measuring Human β-Secretase (bace1) Activity Using Homogeneous Time-Resolved Fluorescence. *Anal. Biochem.* **2003,** *319,* 49–55.
69. Zhu, Z.; Sun, Y.; Ye, Y.; Voigt, J.; Strickland, C.; Smith, E. M.; Cumming, J.; Wang, L.; Wong, J.; Wang, Y. S.; Wyss, D. F.; Chen, X.; Kuvelkar, R.; Kennedy, M. E.; Favreau, L.; Parker, E.; McKittrick, B. A.; Stamford, A.; Czarniecki, M.; Greenlee, W.; Hunter, J. C. Discovery of Cyclic Acylguanidines As Highly Potent and Selective β-Site Amyloid Cleaving Enzyme (BACE) Inhibitors: Part I—Inhibitor Design and Validation. *J. Med. Chem.* **2010,** *53,* 951–965.
70. Cumming, J.; Babu, S.; Huang, Y.; Carrol, C.; Chen, X.; Favreau, L.; Greenlee, W.; Guo, T.; Kennedy, M.; Kuvelkar, R.; Le, T.; Li, G.; McHugh, N.; Orth, P.; Ozgur, L.; Parker, E.; Saionz, K.; Stamford, A.; Strickland, C.; Tadesse, D.; Voigt, J.; Zhang, L.; Zhang, Q. Piperazine Sulfonamide BACE1 Inhibitors: Design, Synthesis, and in vivo Characterization. *Bioorg. Med. Chem. Lett.* **2010,** *20,* 2837–2842.
71. Cumming, J. N.; Le, T. X.; Babu, S.; Carroll, C.; Chen, X.; Favreau, L.; Gaspari, P.; Guo, T.; Hobbs, D. W.; Huang, Y.; Iserloh, U.; Kennedy, M. E.; Kuvelkar, R.; Li, G.; Lowrie, J.; Mchugh, N. A.; Ozgur, L.; Pan, J.; Parker, E. M.; Saionz, K.; Stamford, A. W.; Strickland, C.; Tadesse, D.; Voigt, J.; Wang, L.; Wu, Y.; Zhang, L.; Zhang, Q. Rational Design of Novel, Potent Piperazinone and Imidazolidinone BACE1 Inhibitors. *Bioorg. Med. Chem. Lett.* **2008,** *18,* 3236–3241.
72. Iserloh, U.; Pan, J.; Stamford, A. W.; Kennedy, M. E.; Zhang, Q.; Parker, E. M.; McHugh, N. A.; Favreau, L.; Strickland, C.; Voigt, J. Discovery of an Orally Efficacious 4-Phenoxypyrrolidine-Based BACE1 Inhibitor. *Bioorg. Med. Chem. Lett.* **2008,** *18,* 418–422.
73. Iserloh, U.; Wu, Y.; Cumming, J. N.; Pan, J.; Wang, L. Y.; Stamford, A. W.; Kennedy, M. E.; Kuvelkar, R.; Chen, X.; Parker, E. M.; Strickland, C.; Voigt, J. Potent Pyrrolidine and Piperidine-Based BACE-1 Inhibitors. *Bioorg. Med. Chem. Lett.* **2008,** *18,* 414–417.

74. Chishti, M. A.; Yang, D. S.; Janus, C.; Phinney, A. L.; Horne, P.; Pearson, J.; Strome, R.; Zuker, N.; Loukides, J.; French, J.; Turner, S.; Lozza, G.; Grilli, M.; Kunicki, S.; Morissette, C.; Paquette, J.; Gervais, F.; Bergeron, C.; Fraser, P. E.; Carlson, G. A.; St. George-Hyslop, P.; Westaway, D. Early-Onset Amyloid Deposition and Cognitive Deficits in Transgenic Mice Expressing a Double Mutant Form of Amyloid Precursor Protein 695. *J. Biol. Chem.* **2001,** *276,* 21562–21570.
75. Wang, Y.-S.; Beyer, B. M.; Senior, M. M.; Wyss, D. F. Characterization of Autocatalytic Conversion of Precursor BACE1 by Heteronuclear NMR Spectroscopy. *Biochemistry* **2005,** *44,* 16594–16601.
76. Wang, Y.-S.; Strickland, C.; Voigt, J. H.; Kennedy, M. E.; Beyer, B. M.; Senior, M. M.; Smith, E. M.; Nechuta, T. L.; Madison, V. S.; Czarniecki, M.; Mckittrick, B. A.; Stamford, A. W.; Parker, E. M.; Hunter, J. C.; Greenlee, W. J.; Wyss, D. F. Application of Fragment-Based NMR Screening, X-ray Crystallography, Structure-Based Design, and Focused Chemical Library Design to Identify Novel μM Leads for the Development of nM BACE-1 (β-Site APP Cleaving Enzyme 1) Inhibitors. *J. Med. Chem.* **2010,** *53,* 942–950.
77. Liu, D.; Wang, Y.-S.; Gesell, J. J.; Wilson, E.; Beyer, B. M.; Wyss, D. F. Backbone Resonance Assignments of the 45.3 kDa Catalytic Domain of Human BACE1. *J. Biomol. NMR* **2004,** *29,* 425–426.
78. Mahar Doan, K. M.; Humphreys, J. E.; Webster, L. O.; Wring, S. A.; Shampine, L. J.; Serabjit-Singh, C. J.; Adkison, K. K.; Polli, J. W. Passive Permeability and p-Glycoprotein-Mediated Efflux Differentiate Central Nervous System (CNS) and Non-CNS Marketed Drugs. *J. Pharmacol. Exp. Ther.* **2002,** *303,* 1029–1037.
79. Smith, E.; Iserloh, U.; Pan, J.; Huang, Y.; Li, G.; Cumming, J.; Wang, L.; Voigt, J.; Strickland, C.; Kennedy, M. E.; Chen, X.; Kuvelkar, R.; Favoreau, L.; Zhu, Z.; McKittrick, B.; Stamford, A.; Czarniecki, M.; Parker, E.; Hunter, J.; Greenlee, W. Optimization of the Iminohydantoin Series of BACE-1 Inhibitors. Part 5: Exploration of the S1' and S2-S3 Binding Sites. Abstracts of Papers, 238th American Chemical Society National Meeting, Washington, DC, United States, August 16–20, 2009. MEDI-267.
80. Caldwell, J. P.; Mazzola, R. D.; Durkin, J.; Chen, J.; Chen, X.; Favreau, L.; Kennedy, M. E.; Kuvelkar, R.; Lee, J.; McHugh, N. A.; Mckittrick, B. A.; Orth, P.; Stamford, A.; Strickland, C.; Voigt, J.; Wang, L.; Zhang, L.; Zhang, Q.; Zhu, Z. Discovery of Potent Iminoheterocycle BACE1 Inhibitors. *Bioorg. Med. Chem. Lett.* **2014,** *24,* 5455–5459.
81. Zhu, Z.; McKittrick, B.; Sun, Z.-Y.; Ye, Y.; Voigt, J.; Strickland, C.; Smith, E.; Stamford, A.; Greenlee, W.; Wu, Y.; Iserloh, U.; Mazzola, R.; Caldwell, J.; Cumming, J.; Wang, L.; Guo, T.; Le, T.X.H.; Saionz, K.W.; Babu, S.D.; Hunter, R.C. Preparation of Heterocyclic Aspartyl Protease Inhibitors for Treating Various Diseases. WO2005058311, 2005.
82. Nowak, P.; Cole, D. C.; Aulabaugh, A.; Bard, J.; Chopra, R.; Cowling, R.; Fan, K. Y.; Hu, B.; Jacobsen, S.; Jani, M.; Jin, G.; Lo, M.-C.; Malamas, M. S.; Manas, E. S.; Narasimhan, R.; Reinhart, P.; Robichaud, A. J.; Stock, J. R.; Subrath, J.; Svenson, K.; Turner, J.; Wagner, E.; Zhou, P.; Ellingboe, J. W. Discovery and Initial Optimization of 5,5′-Disubstituted Aminohydantoins As Potent β-Secretase (BACE1) Inhibitors. *Bioorg. Med. Chem. Lett.* **2010,** *20,* 632–635.
83. Zhu, Z.; McKittrick, B.A.; Sun, Z.-Y.; Ye, Y.C.; Voigt, J.H.; Strickland, C.; Smith, E.M.; Stamford, A.; Greenlee, W.J.; Mazzola, R.; Caldwell, J.; Cumming, J.N.; Wang, L.; Wu, Y.; Iserloh, U.; Guo, T.; Le, T.X.H.; Saionz, K.W.; Babu, S.D.; Hunter, R.C.; Morris, M.L.; Gu, H.; Qian, G.; Tadesse, D. Heterocyclic Aspartyl Protease Inhibitors. US20060111370, 2006.
84. Zhu, Z.; McKittrick, B.A.; Sun, Z.-Y.; Ye, Y.C.; Voigt, J.H.; Strickland, C.; Smith, E.M.; Stamford, A.; Greenlee, W.J.; Mazzola, R.; Caldwell, J.; Cumming, J.N.; Wang, L.; Wu, Y.; Iserloh, U.; Liu, X.; Guo, T.; Le, T.X.H.; Saionz, K.W.; Babu, S.D.; Hunter, R.C.; Morris, M.L.; Gu, H.; Qian, G.; Tadesse, D.; Huang, Y.; Li, G.; Pan, J.; Misiaszek, J.; Lai, G.; Duo, J.; Qu, C.; Shao, Y. Heterocyclic Aspartyl Protease Inhibitors. US20080200445, 2008.
85. Cumming, J. N.; Smith, E. M.; Wang, L.; Misiaszek, J.; Durkin, J.; Pan, J.; Iserloh, U.; Wu, Y.; Zhu, Z.; Strickland, C.; Voigt, J.; Chen, X.; Kennedy, M. E.; Kuvelkar, R.; Hyde, L. A.; Cox, K.; Favreau, L.; Czarniecki, M. F.; Greenlee, W. J.; Mckittrick, B. A.; Parker, E. M.; Stamford, A. W. Structure Based Design of Iminohydantoin BACE1 Inhibitors: Identification of an Orally Available, Centrally Active BACE1 Inhibitor. *Bioorg. Med. Chem. Lett.* **2012,** *22,* 2444–2449.
86. Stamford, A. W.; Scott, J. D.; Li, S. W.; Babu, S.; Tadesse, D.; Hunter, R.; Wu, Y.; Misiaszek, J.; Cumming, J. N.; Gilbert, E. J.; Huang, C.; McKittrick, B. A.; Hong, L.; Guo, T.; Zhu, Z.; Strickland, C.; Orth, P.; Voigt, J. H.; Kennedy, M. E.; Chen, X.; Kuvelkar, R.; Hodgson, R.; Hyde, L. A.; Cox, K.; Favreau, L.; Parker, E. M.; Greenlee, W. J. Discovery of an Orally Available, Brain Penetrant BACE1 Inhibitor That Affords Robust CNS Aβ Reduction. *ACS Med. Chem. Lett.* **2012,** *3,* 897–902.
87. Cumming, J.; Wang, L.; Smith, E.; Chen, X.; Czarniecki, M.; Favreau, L.; Greenlee, W.; Hunter, J.; Kennedy, M.; Kuvelkar, R.; Madison, V.; McKittrick, B.; Parker, E.; Stamford, A.; Strickland, C.; Sun, Z.-Y.; Voigt, J.; Zhu, Z. Optimization of the Iminohydantoin Series of BACE1 Inhibitors. Part 4: Exploration of the F' Subsite in the C5-Aryl Series. Abstracts of Papers, 238th American Chemical Society National Meeting, Washington, DC, United States, August 16–20, 2009. MEDI-268.
88. Edwards, P. D.; Albert, J. S.; Sylvester, M.; Aharony, D.; Andisik, D.; Callaghan, O.; Campbell, J. B.; Carr, R. A.; Chessari, G.; Congreve, M.; Frederickson, M.; Folmer, R. H. A.; Geschwindner, S.; Koether, G.; Kolmodin, K.; Krumrine, J.; Mauger, R. C.; Murray, C. W.; Olsson, L.-L.; Patel, S.; Spear, N.; Tian, G. Application of Fragment-Based Lead Generation to the Discovery of Novel, Cyclic Amidine β-Secretase Inhibitors With Nanomolar Potency, Cellular Activity, and High Ligand Efficiency. *J. Med. Chem.* **2007,** *50,* 5912–5925.
89. Cumming, J. N.; Misiaszek, J.; Iserloh, U.; Babu, S.; Mazzola, R. D., Jr.; Caldwell, J.; Chen, X.; Czarniecki, M.; Duo, J.; Durkin, J.; Greenlee, W. J.; Gu, H.; Guo, T.; Huang, Y.; Hunter, R.; Kennedy, M. E.; Kuvelkar, R.; Madison, V.; McKittrick, B. A.; Le, T.; Meng, T.; Pan, J.; Li, G.; Parker, E. M.; Qian, G.; Saionz, K.; Stamford, A. W.; Strickland, C.; Tadesse, D.; Sun, Z.-Y.; Voigt, J.; Wang, L.; Wong, J.; Hyde, L.; Leach, P.; Wu, Y.; Zhang, L.; Zhang, Q.; Zhao, J.; Zhu, Z.; Favreau, L. Novel Iminopyrimidinone β-Secretase Inhibitors: Part 1. P1-P3 SAR. Abstracts of Papers, 239th American Chemical Society National Meeting, San Francisco, CA, United States, March 21–25, 2010. MEDI-531.
90. Josien, H.; Bara, T.; Rajagopalan, M.; Clader, J. W.; Greenlee, W. J.; Favreau, L.; Hyde, L. A.; Nomeir, A. A.; Parker, E. M.; Song, L.; Zhang, L.; Zhang, Q. Novel Orally Active Morpholine *n*-Arylsulfonamides γ-Secretase Inhibitors With Low CYP 3A4 Liability. *Bioorg. Med. Chem. Lett.* **2009,** *19,* 6032–6037.
91. Hyde, L. A.; Del Vecchio, R. A.; Kazdoba, T. M.; Manning, R.; Terracina, G.; Zhang, Q.; Babu, S.; Guo, T.; Tadesse, D.; Zhang, L.; Parker, E. M.; Stamford, A.; Kennedy, M. E. Chronic Administration of a Novel BACE Inhibitor Reduced Brain Aβ Levels and Mature Plaques and Modestly Improved Cognition in Transgenic CRND8-APP$^{swe/ind}$ Mice. *Alzheimers Dement.* **2010,** *6,* S539.
92. Hyde, L. A.; Leach, P. T.; Zhang, Q.; Terracina, G.; Werner, B. J.; Hodgson, R. A.; Cantu, C.; Chen, X.; Chen, M.; Misiaszek, J.; Wu, Y.; Babu, S.; Guo, T.; Tadesse, D.; Zhang, L.; Parker, E. M.; Stamford, A.; Kennedy, M. E. Discovery of Novel, Potent BACE Inhibitors With Central Activity for the Treatment of Alzheimer's Disease. *Alzheimers Dement.* **2010,** *6,* S592.
93. Lanz, T. A.; Hosley, J. D.; Adams, W. J.; Merchant, K. P. Studies of Aβ Pharmacodynamics in the Brain, Cerebrospinal Fluid, and Plasma in Young (Plaque-Free) Tg2576 Mice Using the γ-Secretase Inhibitor N2-[(2S)-2-(3,5-Difluorophenyl)-2-hydroxyethanoyl]-N1-[(7S)-5-methyl-6-oxo-6,7-dihydro-5H-dibenzo[b,d]azepin-7-yl]-l-alaninamide (LY-411575). *J. Pharmacol. Exp. Ther.* **2004,** *309,* 49–55.
94. Barten, D. M.; Guss, V. L.; Corsa, J. A.; Loo, A.; Hansel, S. B.; Zheng, M.; Munoz, B.; Srinivasan, K.; Wang, B.; Robertson, B. J.; Polson, C. T.; Wang, J.; Roberts, S. B.; Hendrick, J. P.; Anderson, J. J.; Loy, J. K.; Denton, R.; Verdoorn, T. A.; Smith, D. W.; Felsenstein, K. M. Dynamics of β-Amyloid Reductions in Brain, Cerebrospinal Fluid, and Plasma of β-Amyloid Precursor Protein Transgenic Mice Treated With a γ-Secretase Inhibitor. *J. Pharmacol. Exp. Ther.* **2005,** *312* (2), 635–643.
95. Best, J. D.; Jay, M. T.; Otu, F.; Ma, J.; Nadin, A.; Ellis, S.; Lewis, H. D.; Pattison, C.; Reilly, M.; Harrison, T.; Shearman, M. S.; Williamson, T. L.; Atack, J. R. Quantitative Measurement of Changes in Amyloid-β(40) in the Rat Brain and Cerebrospinal Fluid Following Treatment With the γ-Secretase Inhibitor LY-411575 [N2-[(2S)-2-(3,5-Difluorophenyl)-2-hydroxyethanoyl]-N1-[(7S)-5-methyl-6-oxo-6,7-dihydro-5H-dibenzo[b,d]azepin-7-yl]-l-alaninamide]. *J. Pharmacol. Exp. Ther.* **2005,** *313,* 902–908.
96. Best, J. D.; Jay, M. T.; Otu, F.; Churcher, I.; Reilly, M.; Morentin-Gutierrez, P.; Pattison, C.; Harrison, T.; Shearman, M. S.; Atack, J. R. In Vivo Characterization of Aβ(40) Changes in Brain and Cerebrospinal Fluid Using the Novel γ-Secretase Inhibitor *N*-[*cis*-4-[(4-Chlorophenyl)sulfonyl]-4-(2,5-difluorophenyl)cyclohexyl]-1,1,1-trifluoromethanesulfonamide (MRK-560) in the Rat. *J. Pharmacol. Exp. Ther.* **2006,** *317,* 786–790.
97. Iserloh, U.; Cumming, J. N.; Mazzola, R. D., Jr.; Babu, S.; Caldwell, J.; Chen, X.; Czarniecki, M.; Duo, J.; Durkin, J.; Greenlee, W. J.; Gu, H.; Guo, T.; Hunter, R.; Kennedy, M. E.; Kuvelkar, R.; Madison, V.; McKittrick, B. A.; Le, T.; Meng, T.; Pan, J.; Misiaszek, J.; Parker, E. M.; Qian, G.; Saionz, K.; Stamford, A. W.; Strickland, C.; Tadesse, D.; Voigt, J.; Wang, L.; Wong, J.; Wu, Y.; Zhao, J.; Zhu, Z.; Sun, G.; Hyde, L.; Leach, P.; Zhang, L.; Zhang, Q.; Li, G.; Huang, Y.; Favreau, L.; Misiaszek, J.; Sun, Z.-Y. Novel Iminopyrimidinone β-Secretase (BACE1) Inhibitors: Part 2. P1-Azoles. Abstracts of Papers, 239th American Chemical Society National Meeting, San Francisco, CA, United States, March 21–25, 2010. MEDI-532.

98. Mandal, M.; Zhu, Z.; Cumming, J. N.; Liu, X.; Strickland, C.; Mazzola, R. D.; Caldwell, J. P.; Leach, P.; Grzelak, M.; Hyde, L.; Zhang, Q.; Terracina, G.; Zhang, L.; Chen, X.; Kuvelkar, R.; Kennedy, M. E.; Favreau, L.; Cox, K.; Orth, P.; Buevich, A.; Voigt, J.; Wang, H.; Kazakevich, I.; McKittrick, B. A.; Greenlee, W.; Parker, E. M.; Stamford, A. W. Design and Validation of Bicyclic Iminopyrimidinones As Beta Amyloid Cleaving Enzyme-1 (BACE1) Inhibitors: Conformational Constraint to Favor a Bioactive Conformation. *J. Med. Chem.* **2012,** *55,* 9331–9345.
99. Mandal, M.; Cumming, J. N.; Caldwell, J. P.; Zhu, Z.; Wu, Y.; Misiaszek, J.; Liu, X.; Strickland, C.; Mazzola, R. D.; Leach, P.; Grzelak, M.; Hyde, L.; Zhang, Q.; Terracina, G.; Zhang, L.; Chen, X.; Kuvelkar, R.; Kennedy, M. E.; Michener, M.; Smith, B.; Favreau, L.; Cox, K.; Orth, P.; Buevich, A.; Voigt, J.; Wang, H.; Kazakevich, I.; McKittrick, B. A.; Greenlee, W.; Parker, E. M.; Stamford, A. W. Structure-Based Design of an Iminoheterocyclic BACE1 Inhibitor That Lowers Central Aβ in Non-Human Primates. *J. Med. Chem.* **2016,** *59,* 3231–3248.
100. Scott, J.D.; Li, S.W.; Brunskill, A.P.J.; Chen, X.; Cox, K.; Cumming, J.N.; Forman, M.; Gilbert, E.J.; Hodgson, R.A.; Hyde, L.A.; Jiang, Q.; Iserloh, U.; Kazakevich, I.; Kuvelkar, R.; Mei, H.; Meredith, J.; Misiaszek, J.; Orth, P.; Rossiter, L.M.; Slater, M.; Stone, J.; Strickland, C.; Voigt, J.H.; Wang, G.; Wang, H.; Wu, Y.; Greenlee, W.J.; Parker, E.M.; Kennedy, M.E.; Stamford, A.W. Discovery of the 3-Imino-1,2,4-thiadiazinane 1,1-dioxide Derivative Verubecestat (MK-8931)—A β-Site Amyloid Precursor Protein Cleaving Enzyme 1 Inhibitor for the Treatment of Alzheimer's Disease. *J. Med. Chem.* accepted for publication. DOI: 10.1021/acs.jmedchem.6b00307.
101. Gilbert, E.; Huang, C.; Stamford, A.; Cumming, J.; Greenlee, W.; Kennedy, M.; Parker, E.; Kuvelkar, R.; Cox, K.; Voigt, J.; Strickland, C.; Palamanda, J. Pyrrolidine-Fused Iminoheterocycles As BACE1 Inhibitors for the Treatment of Alzheimer's Disease. Abstracts of Papers, 244th ACS National Meeting & Exposition, Philadelphia, PA, United States, August 19–23, 2012. MEDI 101.
102. Kennedy, M.E.; Stamford, A.W.; Chen, X.; Cox, K.; Cumming, J.N.; Dockendorf, M.F.; Egan, M.; Ereshefsky, L.; Hodgson, R.A.; Hyde, L.A.; Jhee, S.; Kleijn, H.J.; Kuvelkar, R.; Li, W.; Mattson, B.A.; Mei, H.; Palcza, J.; Scott, J.D.; Tanen, M.; Troyer, M.D.; Tseng, J.; Stone, J.A.; Parker, E.M.; Forman, M. Discovery of Verubecestat (MK-8931), a BACE1 Inhibitor That Dramatically Reduces CNS Aβ Levels in Alzheimer's Disease Patients. *Sci. Transl. Med.* **2016**, accepted for publication.
103. Lu, Y.; Barton, H. A.; Leung, L.; Zhang, L.; Hajos-Korcsok, E.; Nolan, C. E.; Liu, J.; Becker, S. L.; Wood, K. M.; Robshaw, A. E.; Taylor, C. K.; O'Neill, B. T.; Brodney, M. A.; Riddell, D. Cerebrospinal Fluid β-Amyloid Turnover in the Mouse, Dog, Monkey and Human Evaluated by Systematic Quantitative Analyses. *Neurodegener. Dis.* **2013,** *12,* 36–50.
104. Mohs, R. C.; Kawas, C.; Carrillo, M. C. Optimal Design of Clinical Trials for Drugs Designed to Slow the Course of Alzheimer's Disease. *Alzheimers Dement.* **2006,** *2,* 131–139.
105. Siemers, E.; Skinner, M.; Dean, R. A.; Gonzales, C.; Satterwhite, J.; Farlow, M.; Ness, D.; May, P. C. Safety, Tolerability, and Changes in Amyloid β Concentrations After Administration of a γ-Secretase Inhibitor in Volunteers. *Clin. Neuropharmacol.* **2005,** *28,* 126–132.
106. Gasparini, L.; Ongini, E.; Wilcock, D.; Morgan, D. Activity of Flurbiprofen and Chemically Related Anti-Inflammatory Drugs in Models of Alzheimer's Disease. *Brain Res. Rev.* **2005,** *48,* 400–408.
107. Gilman, S.; Koller, M.; Black, R. S.; Jenkins, L.; Griffith, S. G.; Fox, N. C.; Eisner, L.; Kirby, L.; Rovira, M. B.; Forette, F.; Orgogozo, J. M. Clinical Effects of Aβ Immunization (AN1792) in Patients With AD in an Interrupted Trial. *Neurology* **2005,** *64,* 1553–1562.
108. Aisen, P. S. The Development of Anti-Amyloid Therapy for Alzheimer's Disease: From Secretase Modulators to Polymerisation Inhibitors. *CNS Drugs* **2005,** *19,* 989–996.
109. Cummings, J. L. Controversies in Alzheimer's Disease Drug Development. *Int. Rev. Psychiatry* **2008,** *20,* 389–395.
110. Sperling, R. A.; Aisen, P. S.; Beckett, L. A.; Bennett, D. A.; Craft, S.; Fagan, A. M.; Iwatsubo, T.; Jack, C. R., Jr.; Kaye, J.; Montine, T. J.; Park, D. C.; Reiman, E. M.; Rowe, C. C.; Siemers, E.; Stern, Y.; Yaffe, K.; Carrillo, M. C.; Thies, B.; Morrison-Bogorad, M.; Wagster, M. V.; Phelps, C. H. Toward Defining the Preclinical Stages of Alzheimer's Disease: Recommendations From the National Institute on Aging-Alzheimer's Association Workgroups on Diagnostic Guidelines for Alzheimer's Disease. *Alzheimers Dement.* **2011,** *7,* 280–292.
111. Jack, C. R., Jr.; Albert, M. S.; Knopman, D. S.; McKhann, G. M.; Sperling, R. A.; Carrillo, M. C.; Thies, B.; Phelps, C. H. Introduction to the Recommendations From the National Institute on Aging-Alzheimer's Association Workgroups on Diagnostic Guidelines for Alzheimer's Disease. *Alzheimers Dement.* **2011,** *7,* 257–262.
112. Vassar, R. BACE1 Inhibitor Drugs in Clinical Trials for Alzheimer's Disease. *Alzheimers Res. Ther.* **2014,** *6,* 89. http://alzres.biomedcentral.com/articles/10.1186/s13195-014-0089-7 (accessed 15 May 2016).
113. Clark, C. M.; Schneider, J. A.; Mintun, M. M. A.; Bedell, B. J.; Beach, T. G.; Sadowsky, C. H.; Doraiswamy, P. M.; Gamez, J.; Sabbagh, M. N.; Fleisher, A. S.; Schaerf, F.; Waseem, M.; Pontecorvo, M. J.; Hefti, F. F.; Skovronsky, D. M. Phase III Trial Results for the Amyloid PET Imaging Agent Florbetapir F 18 (^{18}F-AV-45): Imaging to Histopathologic Correlations in an End-of-Life Human Subject Study. *Alzheimers Dement.* **2010,** *6,* S71.
114. Clark, C. M.; Schneider, J. A.; Bedell, B. J.; Beach, T. G.; Bilker, W. B.; Mintun, M. A.; Pontecorvo, M. J.; Hefti, F.; Carpenter, A. P.; Flitter, M. L.; Krautkramer, M. J.; Kung, H. F.; Coleman, R. E.; Doraiswamy, P. M.; Fleisher, A. S.; Sabbagh, M. N.; Sadowsky, C. H.; Reiman, E. P.; Reiman, P. E. M.; Zehntner, S. P.; Skovronsky, D. M. Use of Florbetapir-PET for Imaging Beta-Amyloid Pathology. *JAMA* **2011,** *305,* 275–283.
115. An Efficacy and Safety Trial of Verubecestat (MK-8931) in Mild to Moderate Alzheimer's Disease (P07738) (EPOCH). https://clinicaltrials.gov/ct2/show/NCT01739348 (accessed 19 May 2016).
116. Efficacy and Safety Trial of Verubecestat (MK-8931) in Participants With Prodromal Alzheimer's Disease (MK-8931-019) (APECS). https://clinicaltrials.gov/ct2/show/NCT01953601 (accessed 19 May 2016).
117. Rosen, W. G.; Mohs, R. C.; Davis, K. L. A New Rating Scale for Alzheimer's Disease. *Am. J. Psychiatry* **1984,** *141,* 1356–1364.
118. Galasko, D.; Bennett, D.; Sano, M.; Ernesto, C.; Thomas, R.; Grundman, M.; Ferris, S. An Inventory to Assess Activities of Daily Living for Clinical Trials in Alzheimer's Disease (the Alzheimer's Disease Cooperative Study). *Alzheimer Dis. Assoc. Disord.* **1997,** *11* (Suppl 2), S33–S39.
119. Berg, L.; Miller, P. J.; Storandt, M.; Duchek, J.; Morris, J. C.; Rubin, E. H.; Burke, W. J.; Coben, L. A. Mild Senile Dementia of the Alzheimer Type: 2. Longitudinal Assessment. *Ann. Neurol.* **1988,** *23,* 477–484.
120. Folstein, M. F.; Folstein, S. E.; McHugh, P. R. A Practical Method for Grading the Cognitive State of Patients for the Clinician. *J. Psychiatr. Res.* **1975,** *12,* 189–198.
121. Cummings, J. L.; Mega, M.; Gray, K.; Rosenberg-Thompson, S.; Carusi, D. A.; Gornbein, J. The Neuropsychiatric Inventory: Comprehensive Assessment of Psychopathology in Dementia. *Neurology* **1994,** *44,* 2308–2314.
122. United States Food and Drug Administration. Guidance for Industry Alzheimer's Disease: Developing Drugs for the Treatment of Early Stage Disease (FDA-2013-D-0077) DRAFT. http://www.fda.gov/downloads/Drugs/GuidanceComplianceRegulatoryInformation/Guidances/UCM338287.pdf (accessed 15 May 2016).
123. Eli Lilly Newsroom—Product News. Lilly Announces Change to Primary Endpoint of EXPEDITION3 Study. https://investor.lilly.com/releasedetail.cfmReleaseID=960661 (accessed 15 May 2016).
124. May, P. C.; Willis, B. A.; Lowe, S. L.; Dean, R. A.; Monk, S. A.; Cocke, P. J.; Audia, J. E.; Boggs, L. N.; Borders, A. R.; Brier, R. A.; Calligaro, D. O.; Day, T. A.; Ereshefsky, L.; Erickson, J. A.; Gevorkyan, H.; Gonzales, C. R.; James, D. E.; Jhee, S. S.; Komjathy, S. F.; Li, L.; Lindstrom, T. D.; Mathes, B. M.; Martényi, F.; Sheehan, S. M.; Stout, S. L.; Timm, D. E.; Vaught, G. M.; Watson, B. M.; Winneroski, L. L.; Yang, Z.; Mergott, D. J. The Potent BACE1 Inhibitor LY2886721 Elicits Robust Central Aβ Pharmacodynamic Responses in Mice, Dogs, and Humans. *J. Neurosci.* **2015,** *35,* 1199–1210.
125. Neumann, U.; Rueeger, H.; Machauer, R.; Veenstra, S. J.; Lueoend, R. M.; Tintelnot-Blomley, M.; Laue, G.; Beltz, K.; Vogg, B.; Schmid, P.; Frieauff, W.; Shimshek, D. R.; Staufenbiel, M.; Jacobson, L. H. A Novel BACE Inhibitor NB-360 Shows a Superior Pharmacological Profile and Robust Reduction of Amyloid-β and Neuroinflammation in APP Transgenic Mice. *Mol. Neurodegener.* **2015,** *10,* 44.
126. Swahn, B.-M.; Kolmodin, K.; Karlström, S.; von Berg, S.; Söderman, P.; Holenz, J.; Berg, S.; Lindström, J.; Sundström, M.; Turek, D.; Kihlström, J.; Slivo, C.; Andersson, L.; Pyring, D.; Rotticci, D.; Öhberg, L.; Kers, A.; Bogar, K.; von Kieseritzky, F.; Bergh, M.; Olsson, L.-L.; Janson, J.; Eketjäll, S.; Georgievska, B.; Jeppsson, F.; Fälting, J. Design and Synthesis of β-Site Amyloid Precursor Protein Cleaving Enzyme (BACE1) Inhibitors With in vivo Brain Reduction of β-Amyloid Peptides. *J. Med. Chem.* **2012,** *55,* 9346–9361.

127. Butler, C. R.; Brodney, M. A.; Beck, E. M.; Barreiro, G.; Nolan, C. E.; Pan, F.; Vajdos, F.; Parris, K.; Varghese, A. H.; Helal, C. J.; Lira, R.; Doran, S. D.; Riddell, D. R.; Buzon, L. M.; Dutra, J. K.; Martinez-Alsina, L. A.; Ogilvie, K.; Murray, J. C.; Young, J. M.; Atchison, K.; Robshaw, A.; Gonzales, C.; Wang, J.; Zhang, Y.; O'Neill, B. T. Discovery of a Series of Efficient, Centrally Efficacious BACE1 Inhibitors Through Structure-Based Drug Design. *J. Med. Chem.* **2015,** *58,* 2678–2702.
128. Rombouts, F. J. R.; Tresadern, G.; Delgado, O.; Martinez-Lamenca, C.; Van Gool, M.; Garcia-Molina, A.; Alonso de Diego, S. A.; Oehlrich, D.; Prokopcova, H.; Alonso, J. M.; Austin, N.; Borghys, H.; Van Brandt, S.; Surkyn, M.; De Cleyn, M.; Vos, A.; Alexander, R.; Macdonald, G.; Moechars, D.; Gijsen, H.; Trabanco, A. A. 1,4-Oxazine β-Secretase 1 (BACE1) Inhibitors: From Hit Generation to Orally Bioavailable Brain Penetrant Leads. *J. Med. Chem.* **2015,** *58,* 8216–8235.
129. Dineen, T. A.; Chen, K.; Cheng, A. C.; Derakhchan, K.; Epstein, O.; Esmay, J.; Hickman, D.; Kreiman, C. E.; Marx, I. E.; Wahl, R. C.; Wen, P. H.; Weiss, M. M.; Whittington, D. A.; Wood, S.; Fremeau, R. T.; White, R. D.; Patel, V. F. Inhibitors of β-Site Amyloid Precursor Protein Cleaving Enzyme (BACE1): Identification of (*S*)-7-(2-Fluoropyridin-3-yl)-3-((3-methyloxetan-3-yl)ethynyl)-5'H-spiro[chromeno[2,3-b]pyridine-5,4'-oxazol]-2'-amine (AMG-8718). *J. Med. Chem.* **2014,** *57,* 9811–9831.
130. Eli Lilly Newsroom—Product News. Eli Lilly and Company and AstraZeneca Announce Continuation of Pivotal Clinical Trial for People With Early Alzheimer's Disease. https://investor.lilly.com/releasedetail.cfmReleaseID=960661 (accessed 19 May 2016).
131. Eketjäll, S.; Janson, J.; Kaspersson, K.; Bogstedt, A.; Jeppsson, F.; Fälting, J.; Budd Haeberlein, S.; Kugler, A. R.; Alexander, R. C.; Cebers, G. AZD3293: A Novel, Orally Active BACE1 Inhibitor With High Potency and Permeability and Markedly Slow Off-Rate Kinetics. *J. Alzheimers Dis.* **2016,** *50,* 1109–1123.
132. Stamford, A.; Strickland, C. Inhibitors of BACE for Treating Alzheimer's Disease: A Fragment-Based Drug Discovery Story. *Curr. Opin. Chem. Biol.* **2013,** *17,* 320–328.
133. Wyss, D. F.; Cumming, J. N.; Strickland, C. O.; Stamford, A. W. BACE Inhibitors. In *Fragment-Based Drug Discovery: Lessons and Outlook;* Erlanson, D. A., Jahnke, W., Erlanson, D. A., Jahnke, W., Eds.; vol. 67; Wiley: Hoboken, NJ, 2016; pp 329–353.

Relevant Websites

http://www.alz.org/—Website of the Alzheimer's Association whose mission is to advance research to end Alzheimer's and dementia while enhancing care for those living with the disease.

http://www.alz.co.uk/—Website of Alzheimer's Disease International whose mission is to strengthen and support Alzheimer associations, to raise awareness about dementia worldwide, to make dementia a global health priority, to empower people with dementia and their care partners, and to increase investment in dementia research.

https://alzres.biomedcentral.com/articles/10.1186/s13195-014-0089-7—A review of BACE1 Biology and BACE1 inhibitor drugs in clinical trials for Alzheimer's disease.

https://clinicaltrials.gov/ct2/resultsterm=mk-8931—Information on the verubecestat Phase 3 clinical trials.

http://www.merck.com/clinical-trials/infographics/8931-019.html—Information on the verubecestat Phase 3 clinical trials.

8.10 The Discovery of Macitentan—A Standard Medicinal Chemistry Program?

MH Bolli, C Boss, J Gatfield, M Iglarz, and A Treiber, Actelion Pharmaceuticals Ltd, Allschwil, Switzerland

© 2017 Elsevier Ltd. All rights reserved.

8.10.1	**Introduction**	253
8.10.1.1	Biology and Pharmacology of the ET System	253
8.10.1.2	Project Goals	254
8.10.1.3	Compound Profiling and Selection Cascade	254
8.10.1.4	Identifying Starting Points for Our Discovery Program	254
8.10.1.5	Competition, Structures of Known ERAs	255
8.10.1.5.1	Peptidomimetic ERAs	255
8.10.1.5.2	Small molecule ERAs	256
8.10.2	**Medicinal Chemistry Efforts Leading to the Discovery of Macitentan**	261
8.10.2.1	Selected Starting Points	261
8.10.2.2	Progress of the Project	262
8.10.3	**Preclinical Properties of Macitentan**	267
8.10.3.1	From Physicochemistry to Primary Cell Pharmacology: The Distinct Profile of Macitentan	268
8.10.3.1.1	Distinct physicochemical and conformational properties of macitentan	268
8.10.3.1.2	Distinct receptor interaction forces for macitentan as compared to other ERAs	268
8.10.3.1.3	From a distinct binding mode to sustained target blockade and higher antagonistic efficacy in primary human target cells	269
8.10.3.2	Tissue Distribution in Animal Models of PAH	270
8.10.3.3	In Vivo Efficacy and Comparison With Other ERAs	271
8.10.4	**Macitentan in Humans**	271
8.10.4.1	Pharmacokinetics	273
8.10.4.2	Metabolism	274
8.10.4.3	Liver Safety	274
8.10.4.4	Drug–Drug Interactions	275
8.10.4.5	Macitentan for the Treatment of PAH	276
8.10.5	**Conclusions**	276
Acknowledgment		277
References		278

Abbreviations

ABC Area between curves
AUC Area under the curve
BSEP Bile salt excretion pump
CHO Chinese hamster ovary
CL_{int} Intrinsic clearance
CYP Cytochrome P450
Dahl-S Dahl salt-sensitive
DOCA Deoxycorticosterone acetate
ERA Endothelin receptor antagonists
ET Endothelin
ET-1 Endothelin-1
FDA Food and Drug Administration
HR Heart rate
MAP Mean arterial pressure
MCT Monocrotaline
NMR Nuclear magnetic resonance
NTCP Sodium (Na^+) taurocholate cotransporting polypeptide
OATP Organic anion-transporting polypeptide
PAH Pulmonary arterial hypertension
PASMC Pulmonary arterial smooth muscle cell
PBPK Physiology-based pharmacokinetic
PK Pharmacokinetics
SAR Structure–activity relationship
SD Standard deviation
SERAPHIN Study with an endothelin receptor antagonist in pulmonary arterial hypertension

8.10.1 Introduction

The present case study summarizes key aspects of the drug discovery program that led to the discovery of macitentan (Opsumit®, ACT-064992, Fig. 1), a potent, orally active dual endothelin receptor antagonist (ERA) that is an approved long-term treatment for patients with pulmonary arterial hypertension (PAH). Starting from the structure of known ERAs, we focused on optimizing three key properties: in vitro potency on both endothelin (ET) receptors, in vivo efficacy in hypertensive Dahl salt-sensitive (Dahl-S) rats, and in vivo liver safety in a rat model of bile salt transport interference. The results and processes outlined later illustrate how our approach may be successfully applied to other drug discovery programs.

8.10.1.1 Biology and Pharmacology of the ET System

Discovered in 1988, endothelin-1 (ET-1) is a 21-amino acid peptide produced by endothelial and other cells, which is considered one of the most potent vasoconstrictors known. ET-1 release by endothelial cells is polarized toward the tissue, where it acts in a paracrine/autocrine fashion on neighboring cells. In addition to causing vasoconstriction, ET-1 stimulates cell proliferation, fibrosis and inflammation, smooth muscle and cardiomyocyte hyperplasia and hypertrophy, extracellular matrix deposition, and aldosterone and catecholamine production.[1–3]

ET-1 binds to two homologous G protein-coupled receptors, ET_A and ET_B. Both receptor subtypes activate Gq protein-mediated signaling pathways causing phospholipase Cβ activation and protein kinase C activation, which lead to increases in cytosolic calcium levels. In vascular smooth muscle cells the activation of ET receptors followed by increases in cytosolic calcium promotes cytoskeletal contraction and cellular proliferation as seen in pulmonary arteries of patients suffering from PAH, a devastating disease characterized by increased pulmonary endothelial ET-1 release.[4–6]

Under physiological conditions, ET_A receptors predominate on vascular smooth muscle cells and mediate vasoconstriction, whereas endothelial ET_B receptors may mediate vasodilation, through nitric oxide release, and hemodilution.[7,8] In various cardiovascular diseases, we and others have observed that endothelial ET_B-mediated vasodilation is lost, while ET_B receptors are upregulated in the smooth muscle cell layers of blood vessels and contribute to vasoconstriction.[9,10] Therefore, in pathology both ET_A and ET_B receptors mediate the detrimental effects of ET-1, be it vasoconstriction or cell proliferation and inflammation.[2,9,11,12]

These observations suggest that dual ET receptor antagonism might provide superior efficacy and safety compared to ET_A-selective receptor antagonism. Indeed, in animal models of pulmonary hypertension and models of chronic heart failure, dual receptor antagonism was necessary to significantly increase survival.[1,13,14] Safety might also be improved with dual ERAs, as chronic stimulation of unantagonized ET_B receptors could explain some secondary effects of ET_A-selective antagonists, such as increased cell proliferation[15] and exaggerated fluid retention.[16,17] Clinical trials have showed increased clinical worsening in idiopathic pulmonary fibrosis in patients treated with an ET_A-selective antagonist but not with dual ERAs.[18–20]

As mentioned earlier, the key role of ET-1 in the pathophysiology of PAH was suggested by extensive preclinical research, and dual ET receptor blockade was first validated as a therapeutic strategy by the positive clinical trials of bosentan **2** in PAH patients (Fig. 7).[13] Since then, other ERAs have been approved for this indication: sitaxentan **26** (Fig. 6, IC_{50} ET_A 1.4 nM, ET_B 9.8 μM, voluntarily withdrawn in 2010 based on the observation of a risk of potentially life-threatening idiosyncratic liver injury),[21,22] ambrisentan **19** (Fig. 5, K_i ET_A 1 nM, ET_B 195 nM),[23] and macitentan **1** (Fig. 1). PAH and the major etiologies of PAH are associated with elevated ET-1 synthesis or elevated plasma ET-1 concentrations.[1,24] In idiopathic or secondary PAH, increased ET-1 immunostaining was seen in the plexiform lesions and the endothelial cells of pulmonary arteries characterized by medial thickening.[4] ET receptors, ET_B receptors in particular, were upregulated in the interstitium and the media of pulmonary arteries in different forms of pulmonary hypertension.[25,26] Overexpression of ET-1 was also observed in the right ventricle of rats with pulmonary hypertension, suggesting a local effect of endogenous ET-1 on cardiac remodeling.[27]

Therefore, contribution of both ET_A and ET_B receptors to the remodeling effects of ET-1 (including inflammation, proliferation, hypertrophy, fibrosis) combined with the wide tissue distribution of the ET system, its upregulation in pathological situations, and its local autocrine/paracrine activity, make the tissue ET system an important factor in promoting pulmonary vascular structural damage and cardiac hypertrophy. These key features of the ET system were the basis for compound profiling as we wanted a compound exhibiting a better efficacy and safety profile compared to existing ERAs.

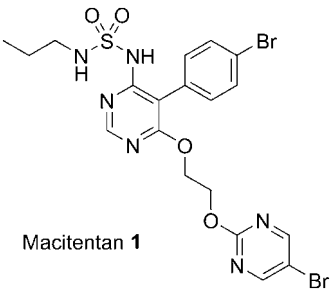

Macitentan **1**

Fig. 1 The structure of macitentan **1**.

8.10.1.2 Project Goals

The ERA program was the first drug discovery project initiated at Actelion Pharmaceuticals Ltd after its foundation in December 1997. The goal of this project was to discover and develop a more potent and efficacious ERA that would not be limited by the safety signals observed with bosentan. With receptor binding IC_{50} values of 45 and 202 nM at ET_A and ET_B, respectively, bosentan **2** markedly reduced the arterial blood pressure in animal models of hypertension. In Phase II and Phase III clinical trials, bosentan was best dosed at 125 mg twice daily. At this dose, however, about 11% of patients treated with bosentan **2** showed a transient, dose-dependent increase in serum liver aminotransferase levels of >3 times the upper limit of normal.[28–30] In view of these data, we aimed at identifying a novel dual ERA for the treatment of patients with PAH that was more potent and more efficacious than bosentan **2**, could be administered to patients once daily, and had no liver liability.

8.10.1.3 Compound Profiling and Selection Cascade

The assays that served to specifically assess the key properties of potency, in vivo efficacy, and liver safety formed the cornerstones of our compound profiling cascade (Table 1). In vitro assessment of ET_A and ET_B blockade was performed by measuring the inhibition of binding of ^{125}I-labeled ET-1 to membranes of Chinese hamster ovary (CHO) cells expressing the human recombinant ET_A or ET_B receptor.[32,33] As mentioned earlier, bosentan showed IC_{50} values of 45 and 202 nM at ET_A and ET_B, respectively. The potency on ET_A and ET_B was further assessed in an ex vivo functional inhibition assay using isolated aorta and trachea rings, respectively.[34] In these tests, bosentan showed pA_2 values of 6.78 and 6.47. As animal and human data suggested that optimal efficacy on blood pressure reduction and safety with respect to edema formation is obtained with dual ERAs[1,2,9,11–14,16,17] we prioritized compounds with the ability to block both ET_A and ET_B receptors.

Beyond this classical in vitro assessment, compounds more potent than bosentan were tested in vivo in hypertensive rats to assess the efficacy profile of the new chemical structures. We selected the Dahl-S rat model, which is a model of systemic hypertension associated with increased vascular ET production and hence a good responder to ET receptor blockade.[35,36] Selected compounds were administered orally at a dose of 3 mg kg^{-1} to hypertensive Dahl-S rats, and arterial blood pressure and heart rate (HR) were recorded using a telemetry device implanted in the animal. The area between curves (ABC) calculated between the period before and after the treatment served as efficacy measure and was compared to that of bosentan.

In this model, both ET receptors contribute to the maintenance of elevated blood pressure, with a predominant role of ET_A receptors. To confirm ET_B receptor blockade in vivo, we also tested the effect of selected compounds on plasma levels of ET-1, which is a biomarker for ET_B receptor engagement as these receptors, within the pulmonary circulation, mediate clearance of ET-1.[31,37,38]

In parallel, compounds with an in vivo efficacy superior to that of bosentan were also tested in vivo in a model relevant for hepatic safety. Mechanistic studies by Fattinger et al.[39] suggested that the hepatotoxicity observed in patients treated with bosentan is mediated by its ability to inhibit the hepatic bile salt excretion pump (BSEP) leading to intrahepatic cholestasis, and proposed increases in plasma bile salt concentrations as a marker for in vivo hepatic BSEP inhibition. Therefore we screened in vivo in rats for compounds that did not increase plasma bile salts, as a surrogate for hepatotoxicity.

Thus the pharmacological characterization of the compounds was designed to encompass the desired properties of a new ERA: dual blockade of ET receptors, high efficacy, and improved liver safety in vivo.

8.10.1.4 Identifying Starting Points for Our Discovery Program

In view of the large number of known ERAs,[40–46] we decided to start our drug discovery program from a selection of published ERAs rather than to search for novel scaffolds with a high-throughput screening campaign. We therefore tried to categorize the various

Table 1 Key experiments of the compound profiling and selection cascade

Property	*Activity*	*Experiment*
Potency	ET_A receptor blockade in vitro	Receptor binding on CHO cell membranes
	ET_B receptor blockade in vitro	Receptor binding on CHO cell membranes
	⇩	
	ET_A receptor blockade ex vivo	Inhibition of ET-1-induced rat aorta constriction[31]
	ET_B receptor blockade ex vivo	Inhibition of sarafotoxin S6c-induced rat trachea constriction[31]
	⇩	
Efficacy	ET_A receptor blockade in vivo	Blood pressure reduction in Dahl-S rats
	ET_B receptor blockade in vivo	Plasma ET-1 level increase in the rat
	⇩	
Safety	Standard safety assessment in vitro	eg, P450 inhibition, hERG channel blockade
	Liver safety assessment in vivo	Plasma bile salt levels in the rat

ERAs according to their structures and analyze the existing data on potency and efficacy as a preparation for the selection of viable starting points. Our analysis of the known ERAs is briefly sketched in the following paragraphs.

8.10.1.5 Competition, Structures of Known ERAs

Based on the importance and the ubiquity of the ET system in the body,[47] ERAs were expected to be effective treatment options for a large variety of cardiovascular diseases, such as hypertension,[48–50] heart failure,[51] renal failure,[52,53] myocardial infarction, subarachnoid hemorrhage, and cerebral vasospasm as well as proliferative diseases such as fibrosis[25] and cancer.[54] These attractive opportunities triggered a vast number of activities throughout the pharmaceutical industry and academia to identify small molecule ERAs with diverse selectivity profiles. The majority of industrial programs focused on the discovery of either ET_A-selective or dual ET_A/ET_B receptor antagonists, and only a limited number of publications disclose ET_B-selective compounds.[40–46]

In the following paragraphs, some of the most prominent approaches leading to ERAs are summarized to reveal the basis of our own efforts that culminated in the discovery of macitentan. While a few of the early projects involved peptidomimetic approaches, the majority of discovery programs focused on identifying small molecule ERAs.

8.10.1.5.1 Peptidomimetic ERAs

Fig. 2 summarizes the peptide-based ERAs. All of these molecules were studied in vivo following parenteral administration. From the early efforts to optimize cyclic peptides that were isolated from *Streptomyces misakiensis* that inhibited the ET receptors, two prominent analogs, BQ-123 **3**[55] and BQ-788 **4**[56] emerged (Fig. 2). While the cyclic peptide **3** is a highly potent and selective antagonist of the ET_A receptor, the linear tripeptide **4** specifically blocks the ET_B receptor. Over the years, both molecules have been used in a number of pharmacological studies in animals and humans.[57–69]On the other hand, the cyclic peptide TAK-044 **6** represents a dual ERA that has also been studied in humans as a potential i.v. drug in indications such as hypertension, myocardial infarction, and acute renal failure.[70–73] The peptidomimetic IRL3630 **5** was discovered by elaborating a rational approach that identified key amino acids of the natural ligand ET-1 responsible for its high receptor affinity. Studies in guinea pigs showed that bolus injections of **5** were able to suppress the respiratory resistance changes induced by ET-1.[74–77]

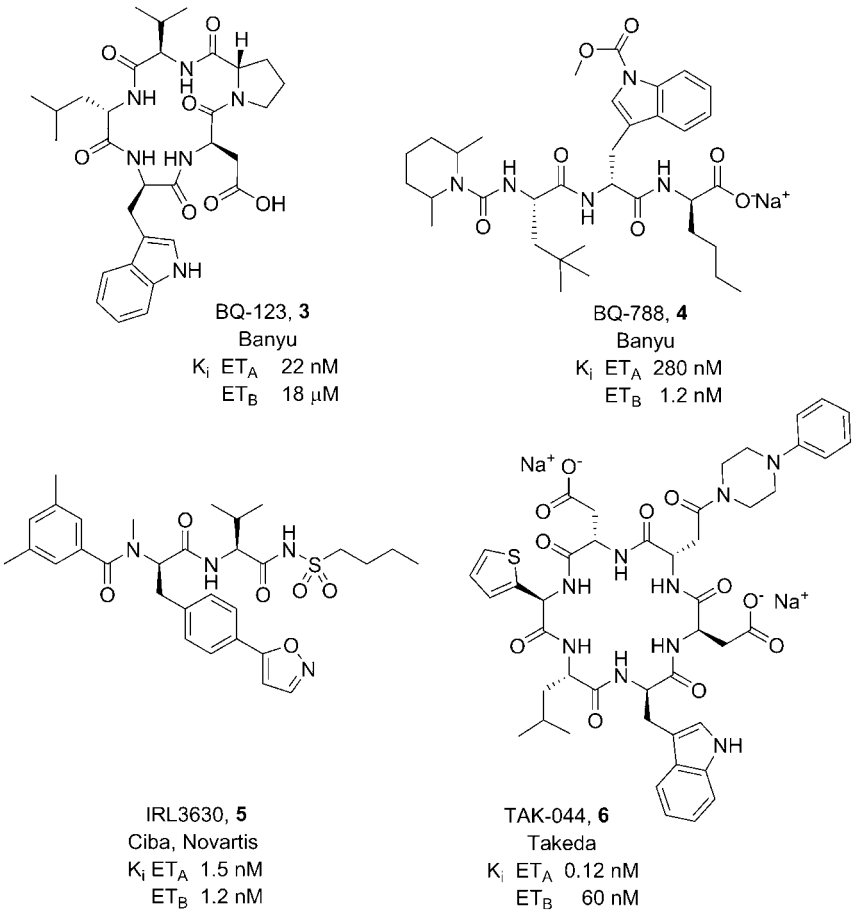

Fig. 2 Structure of peptidic and peptidomimetic ERAs.

8.10.1.5.2 Small molecule ERAs

A quick inspection of the structures of the known small molecule ERAs suggests that an acidic function is mandatory to obtain high affinity. In addition, a general structure of ERAs can be drawn as depicted in Fig. 3.[42] Depending on the nature of the acidic function and the core, this generalized scheme allows the small molecule ERAs to be subdivided into three classes. In the first class of compounds, a carboxylic acid is attached to a 5 to 10 membered heterocyclyl or heteroaryl template, which is further substituted with two aromatic rings and an optional substituent (eg, enrasentan **7**, atrasentan **9**, fadosentan **17**). In the second class of ERAs the carboxylic acid is attached to an alkoxy chain that bears aromatic substituents (eg, ambrisentan **19**). A third class of ERAs is characterized by an acidic aryl sulfonamide bound to a more linear core structure such as an acetic acid or a biphenyl moiety (eg, sitaxentan **26**). Finally, a fourth class of ERAs consists of acidic aryl sulfonamides that are attached to a pyrimidine bearing up to three additional substituents (eg, bosentan **2**).

8.10.1.5.2.1 Carboxylic acids bound to a cyclic core

Examples of the first class of ERAs are shown in Fig. 4. It is interesting to note that although the structures in Fig. 4 are closely related, they were discovered by several independent approaches.

Scientists at SmithKline Beecham worked on the indane carboxylic acids such as enrasentan **7**.[41,78,79] Enrasentan showed IC_{50} values of 1 and 111 nM on ET_A and ET_B, respectively, and was studied in Phase II clinical trials in patients with chronic heart failure (ENCOR study) and in patients with left ventricular systolic dysfunction.[80,81] A close analog of enrasentan, the di-acid **8**, showed a similar potency profile and was particularly suitable for i.v. administration.[82–84]

Abbott's design of ERAs was based on replacing the indane moiety of enrasentan by a pyrrolidine.[85,86] This allowed for a much easier structure–activity relationship (SAR) investigation of the space opposite to the carboxylic acid. Hence, exploring the substituent attached to the pyrrolidine nitrogen led to the identification of the ET_A-selective atrasentan **9** (IC_{50} ET_A 0.31 nM, IC_{50} ET_B 191 nM)[85,86] as well as a number of highly ET_B-selective antagonists such as **10**.[87,88] Atrasentan **9** was well tolerated in healthy subjects and Phase II and III clinical studies focused on its use in diabetes and chronic kidney disease[53,89] as well as prostate cancer.[90,91]

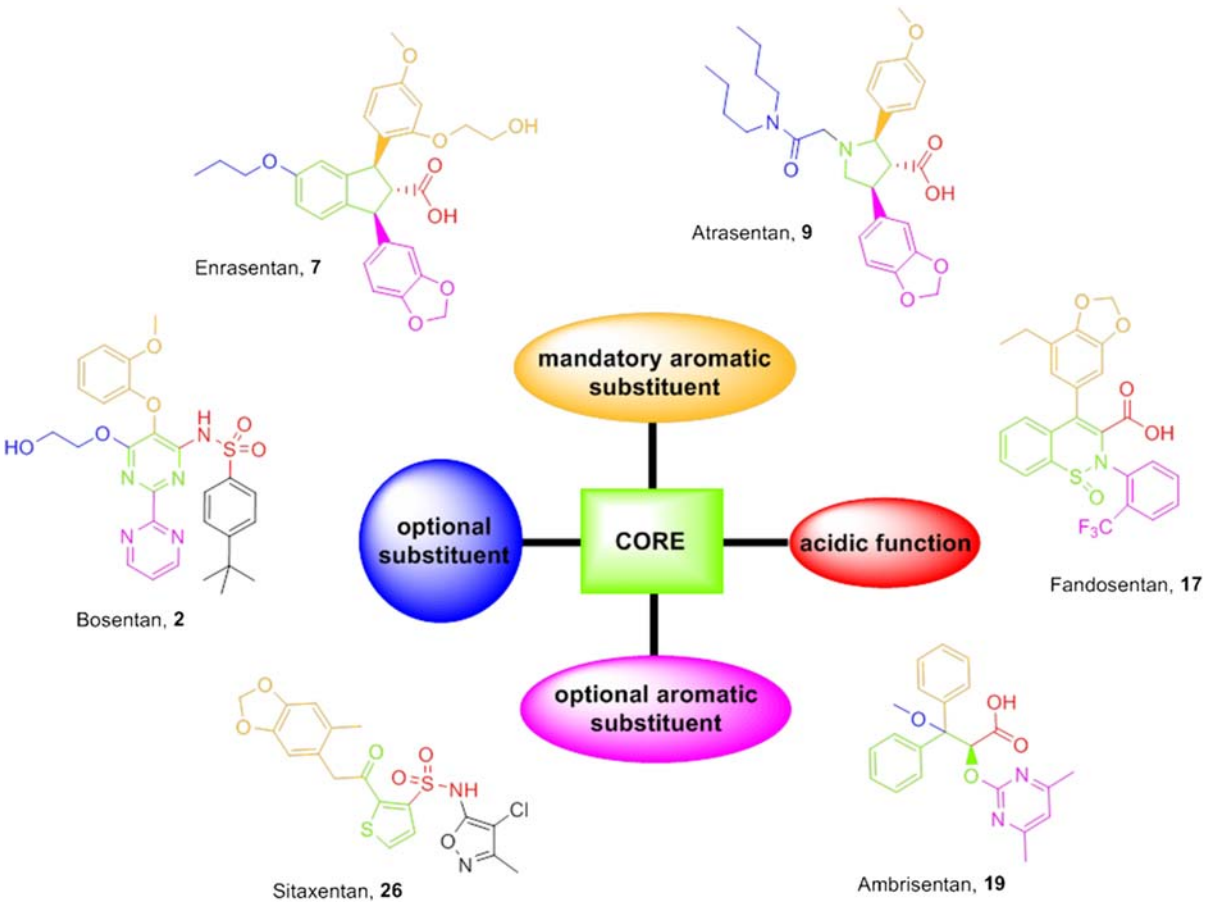

Fig. 3 General structure of endothelin receptor antagonists and a few structures of ERAs for illustration. For a superposition of the structure of ambrisentan **19** with the scaffold of enrasentan **7** see Riechers et al.[23]

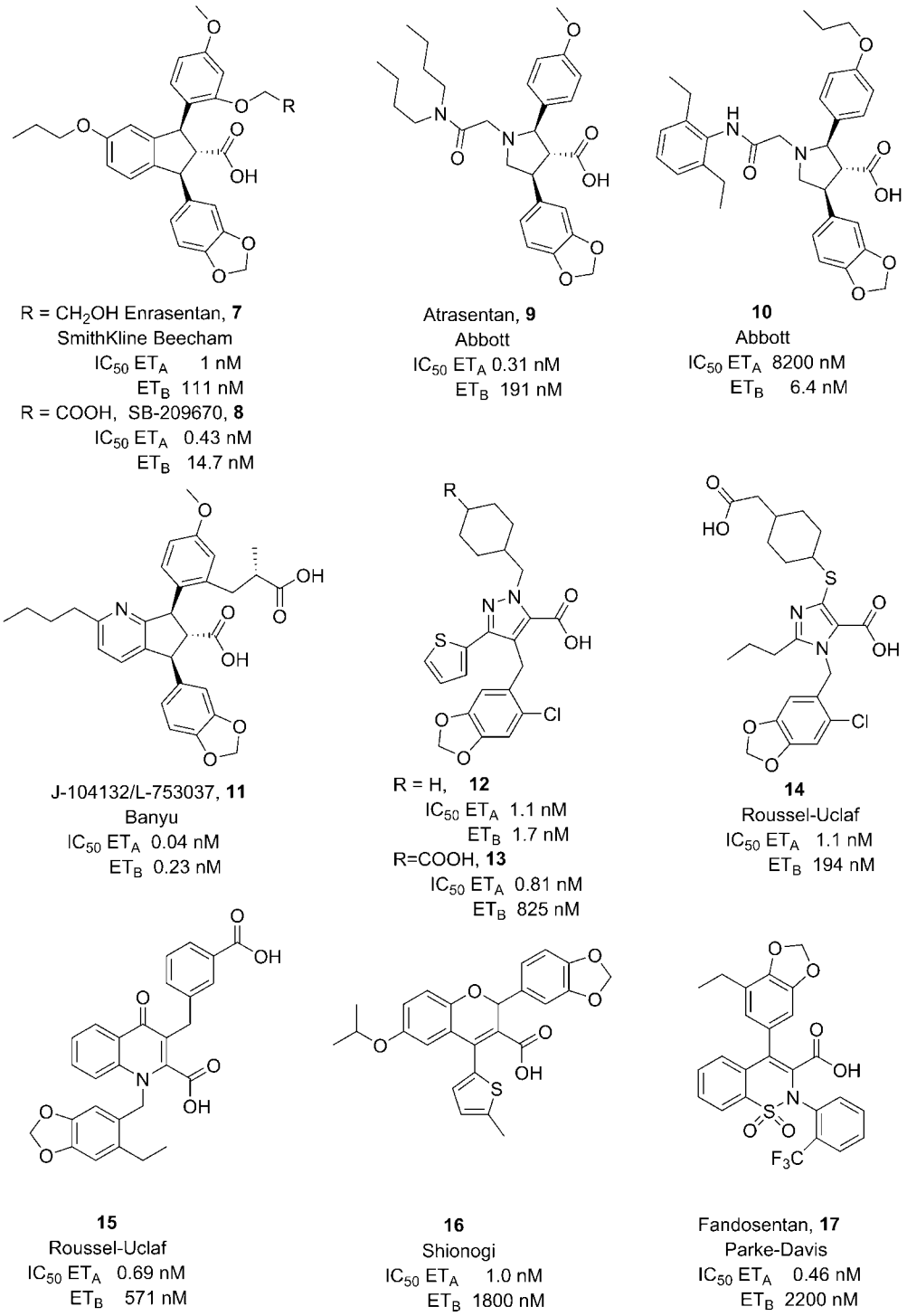

Fig. 4 Structures of ERAs containing a carboxylic acid attached to an aliphatic or aromatic ring.

Efforts by a research team at Banyu Pharmaceuticals were aimed at reducing the lipophilicity of enrasentan. Introduction of a nitrogen to the indane scaffold furnished highly potent ERAs such as J-104132/L-753037 **11**.[92] Interestingly, in contrast to the related di-acid **8**, this compound was well suited for oral dosing.[93] As part of a collaboration with Merck & Co., the cyclopentanopyridine **11** was studied in patients with congestive heart failure.[94]

Researchers at Hoechst Marion Roussel discovered highly potent ET_A-selective (eg, **13**) and dual ERAs (eg, **12**) by optimizing a series of pyrazol-5-ols that were identified by screening their in-house compound library for ET receptor binding.[95,96] Further

investigations led to imidazole-5-carboxylic acid derivatives such as **14**, which showed efficacy in blocking the ET-1 induced pressor response in the rat.[97] In the same high-throughput screening, a series of 6-substituted quinolones was found to be active on ET_A and ET_B. Superposition of these quinolones with **8** led to the design of compounds such as **15**, a potent and orally active selective ET_A receptor antagonist.[98]

Based on the observation that angiotensin II receptor blockers and ERAs share structural features, scientists at Shionogi modified their chromene-based angiotensin II receptor antagonists to yield highly potent orally available ET_A-selective ERAs such as **16**.[99]

The benzothiazine-3-carboxylic acid fandosentan **17**, discovered by Parke-Davis, represents one of the last examples of ERAs consisting of a carboxylic acid attached to a hetero-aromatic core structure. Fandosentan was characterized as a potent ET_A receptor-selective antagonist with good oral bioavailability in rat and dog and promising pharmacological effects in hypoxia induced pulmonary hypertension in the lamb.[100] However, no clinical data have been reported.

8.10.1.5.2.2 Carboxylic acids attached to an acyclic core

Representatives of the second class of small molecule ERA are shown in **Fig. 5**. Important contributions by BASF/Knoll started from a high-throughput screening hit originally designed as an herbicide and resulted in the discovery of the diphenylpropionic acid derivatives darusentan **18** and ambrisentan **19**.[23] While darusentan did not meet the primary endpoints in Phase III clinical trials for the treatment of patients with resistant systolic hypertension, and was discontinued for the treatment of hypertension, myocardial infarction, and congestive heart failure,[101–105] ambrisentan **19** is an approved treatment for PAH (marketed in the United States by Gilead as Letairis® and in Europe by GlaxoSmithKline as Volibris®).[106]

Rhône-Poulenc Rorer's phenoxyphenylacetic acid derivative **20** was discovered by optimizing two lead structures identified in-house. Although this potent and orally active compound was selected as a development candidate, no clinical data are available.[107]

8.10.1.5.2.3 Arylsulfonamides bound to a biphenyl or acetic acid core

The selection of compounds compiled in **Fig. 6** illustrates the third class of small molecule ERAs wherein an aryl sulfonamide is attached to either a biphenyl or an acetic acid core. Several of these aryl sulfonamides are based on benzene sulfonamide **21**, which was identified as a 69 μM screening hit at Bristol-Myers Squibb. First SAR studies led to the identification of the orally active dansyl sulfonamide **22**, which showed an ET_A-binding IC_{50} value of 150 nM.[108] Replacing the central naphthaline by a biphenyl moiety followed by further optimization culminated in the discovery of the two highly potent and selective ET_A receptor antagonists BMS193884 **23** and edonentan **24**,[109,110] which were both studied in Phase II clinical trials with congestive heart failure patients.[111]

Zeneca's approach to optimize the dansyl sulfonamide **22** ultimately furnished zibotentan (ZD-4054) **25**,[112,113] an ET_A-selective antagonist that was primarily investigated for the treatment of prostate cancer.[114–117]

Medicinal chemists at Immuno Pharmaceuticals, a subsidiary of Texas Biotechnology Corporation, based their discovery program on replacing the benzene sulfonamide in **7** by a thiophene sulfonamide.[118] Extensive preclinical studies eventually led to selecting sitaxentan (TBC 11251) **26** for clinical development in heart failure and pulmonary hypertension.[21,119,120] The compound is a highly ET_A-selective antagonist with IC_{50} values of 1.4 nM and 9.8 μM at ET_A and ET_B, respectively, exhibited excellent bioavailability of 60–100% in rats and dogs and prevented acute hypoxia-induced pulmonary hypertension in rats at 15 mg kg^{-1} p.o. dosing. Sitaxentan was marketed as Thelin®, but was voluntarily withdrawn in 2010 based on the observation of a potentially life-threatening risk of idiosyncratic liver injury.[22] Meanwhile, drug discovery efforts continued and TBC3711 **27** was selected for clinical development on the basis of its high potency and ET_A selectivity, and its carefully optimized pharmacokinetics (PK) properties. TBC3711 **27** is among the most selective ET_A receptor antagonists tested in humans, was well tolerated, and showed an oral bioavailability of $>80\%$ and a half-life of 6–7 h in healthy volunteers.[121]

Detailed SAR studies aimed at improving the weak affinity that α-phenoxyphenylacetic acid-based angiotensin II receptor antagonists showed for the ET receptors led to the discovery of L-754142 **28**. This most prominent representative, wherein an arylsulfonamide is bound to an acetic acid core antagonized both ET receptors with high potency, and in the rat inhibited the big-ET-1

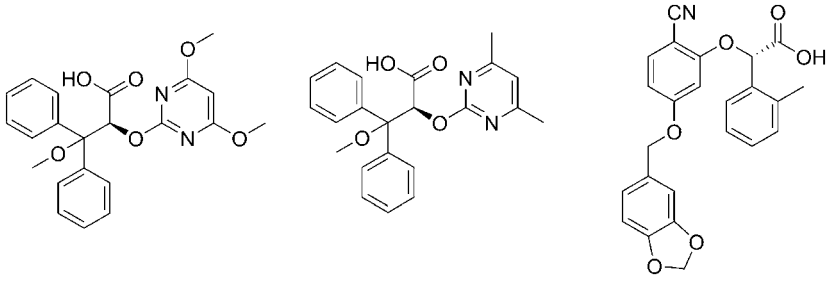

Darusentan, **18**
Knoll/BASF
K_i ET_A 6 nM
ET_B 371 nM

Ambrisentan, **19**
Knoll/BASF
K_i ET_A 1 nM
ET_B 195 nM

RPR118031A, **20**
Rhône-Poulenc Rorer
IC_{50} ET_A 6.7 nM

Fig. 5 ERAs consisting of a carboxylic acid attached to a further decorated alkoxy chain.

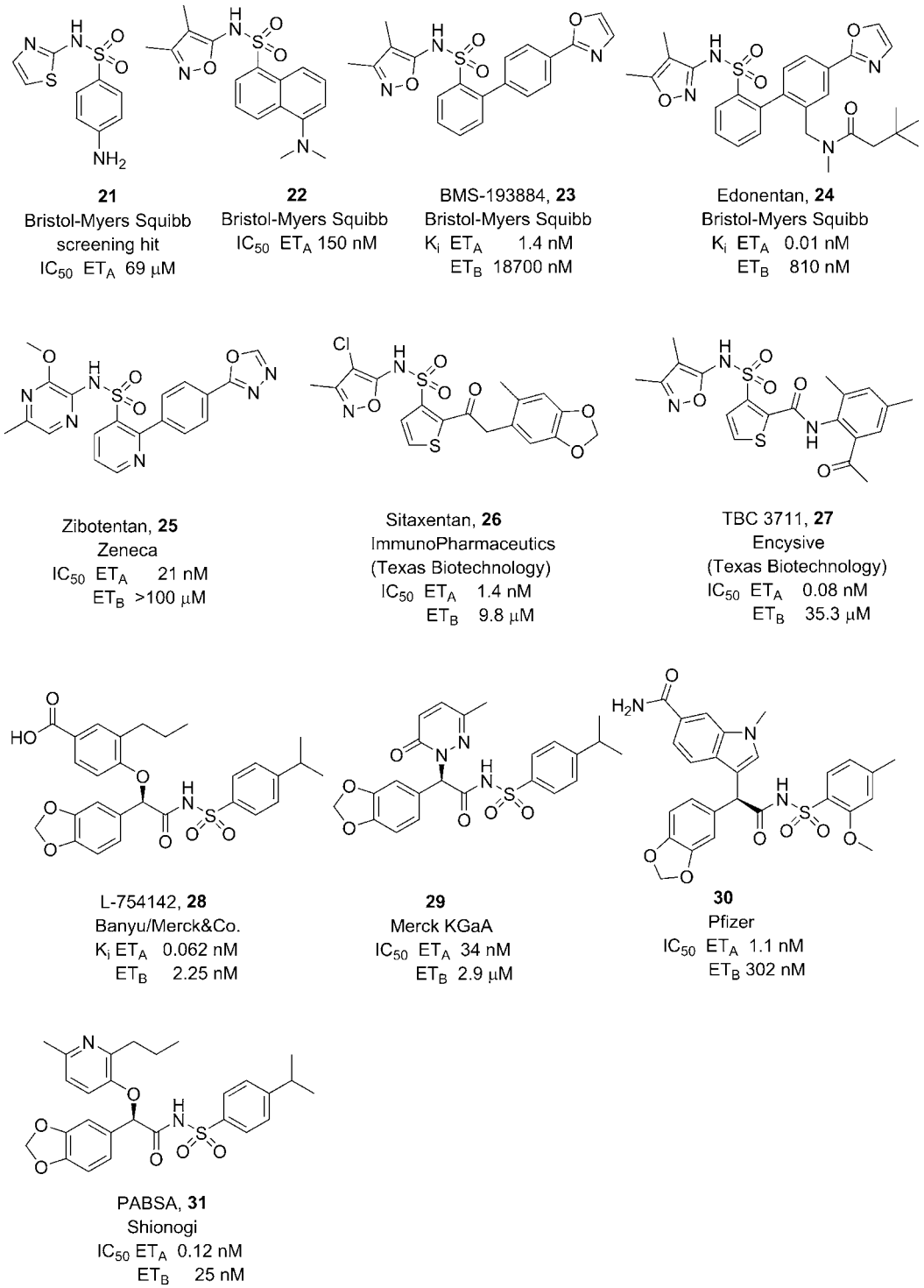

Fig. 6 A third class of ERAs incorporating an aryl sulfonamide bound to an carboxylic acid or a (bis)-aryl moiety.

induced pressor response with an ED_{50} of 0.56 mg kg^{-1} p.o. and a long duration of action.[122,123] Compounds related to **28** have been reported by Merck KGaA (**29**),[124] Pfizer (**30**),[125] and Shionogi (PABSA, **31**).[126]

8.10.1.5.2.4 Arylsulfonamides bound to a pyrimidine core

A few examples of ERAs incorporating an aryl sulfonamide attached to a pyrimidine core are compiled in **Fig. 7**. Researchers at Roche discovered that compound **32**, prepared in the context of an antidiabetic program, inhibited ET receptors in vitro and

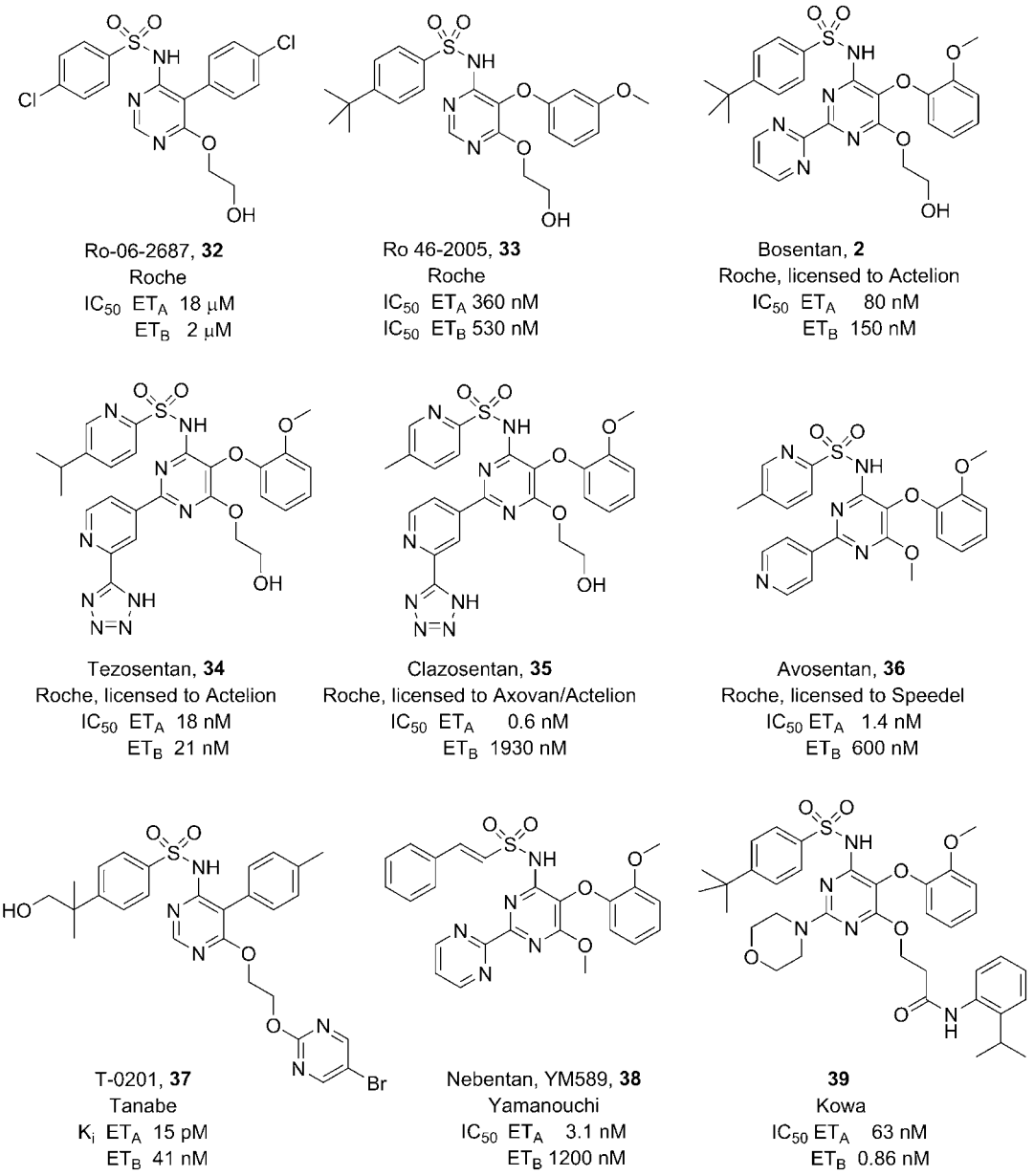

Fig. 7 Structures of ERA incorporating an aryl sulfonamide attached to a pyrimidine.

antagonized the ischemia-induced renal vasoconstriction in the rat. Preliminary optimization of this lead structure led to the identification of Ro 46-2005 **33**, the first orally available small molecule dual ERA.[32,127] In-depth SAR work performed at Roche resulted in the discovery of several compounds with reported clinical history. The orally available dual ERA bosentan **2**[34,128] was studied in a number of cardiovascular and fibrosis indications and was approved under the tradename Tracleer® for the treatment of PAH.[29,30,129,130] The ET_A-selective avosentan **36**[131,132] underwent clinical testing in patients with diabetic nephropathy but was stopped due to intolerable side effects (fluid retention).[133] The 5-isopropyl-2-pyridine sulfonamide tezosentan **34**[134] is a highly potent dual ERA designed for i.v. application. Phase III clinical studies in acute heart failure patients were discontinued due to low probability of achieving significant efficacy.[135–137] Interestingly, the 5-methyl-2-pyridine analog clazosentan **35** is highly selective for the ET_A receptor[138] In patients with aneurysmal subarachnoid hemorrhage, clazosentan reduced the risk of angiographic vasospasm and occurrence of rescue therapy but did not affect new cerebral infarction and mortality.[139,140] Basing their drug discovery efforts on the structure of pyrimidine **33**, additional proprietary ERAs were found by research teams at Tanabe, Yamanouchi, and Kowa. Although promising preclinical data have been published for T-0201 **37**,[141–143] nebentan **38**,[144–146] and Kowa's morpholine derivative **39**,[147] no clinical development has been reported for these three compounds.

8.10.2 Medicinal Chemistry Efforts Leading to the Discovery of Macitentan

8.10.2.1 Selected Starting Points

As a result of our analysis of known ERAs, we decided to select one lead structure from each of the five sub-classes outlined in section "Competition, Structures of Known ERAs" as starting points for our medicinal chemistry efforts. The five lead compounds were selected on the basis of their ability to block both the ET_A and the ET_B receptor and their efficacy in vivo, eg, blockade of the ET-1-induced pressor response. Hence, the structures of IRL3630 **5**,[76] pyrazole **12**,[96,148] ambrisentan **19**,[23] L-754142 **28**,[123] and bosentan **2**[34] (Fig. 8) were considered attractive representatives for a peptidomimetic, a carboxylic acid attached to a heterocycle, a carboxylic acid attached to an alkyl scaffold, an aryl sulfonamide attached to an acetic acid core, and an aryl sulfonamide attached to a pyrimidine, respectively.

In the following paragraph we briefly summarize our strategies to modify the five selected compounds to discover novel ERAs. We also show how results from first analogs we prepared influenced a further shortlisting of the approaches.

To get rid of the peptide-like nature of compound **5**, an approach similar to the one reported for substance P antagonists was undertaken.[149,150] Hence, a set of IRL3630 (**5**, Fig. 8) analogs was prepared wherein, eg, a malonic acid (**40**), an amino-piperidine moiety (**41**), or an aromatic ring (**42**) replaced part of the lead compound's peptide backbone (Fig. 9). Unfortunately, all prepared examples showed considerably lower in vitro potency when compared to the original IRL series. In addition, the synthesis of some of these analogs turned out to be much more cumbersome than expected. Similarly, attempts to modify the scaffolds of compounds **12** and **28** led to analogs with significantly lower affinity for the ET receptors. For instance, corresponding analogs of compound **28** incorporating a sulfonylurea scaffold rather than a sulfonylamide showed IC_{50} values >1 μM at both ET_A and ET_B. On the other hand, analogs of pyrazole **12** that were based on alternative heteroaromatic core structures showed IC_{50} values >10 μM. In the series of ambrisentan **19** analogs, our approach was based on introducing a ring between the carbon of the methoxy group and one of the phenyl rings to rigidify the compound's scaffold (Fig. 10). In addition, patent literature around **19**[151] suggested that the oxygen of the methoxy group could be replaced with a nitrogen. These two modifications led to the general structure **43** as a proposal for novel ERAs. Compound **44** (as racemate), which was among the very first examples prepared in this novel class, showed IC_{50} values of 12 and 184 nM at ET_A and ET_B, respectively, and reduced the mean arterial blood pressure (MAP) after oral administration of 30 mg kg^{-1} to hypertensive Dahl-S rats. These observations confirmed the viability of this approach. A comparison of the structures of bosentan **2** with that of Tanabe's clinical candidate **37** (Fig. 11) prompted us to attach the 5-bromo-pyrimidine moiety present in **37** to the ethylene glycol side chain of bosentan. Although the resulting compound **45** was rather large (Mw = 707), its high affinity for both the ET_A and ET_B receptors (Fig. 11) made this approach very attractive for further exploration.

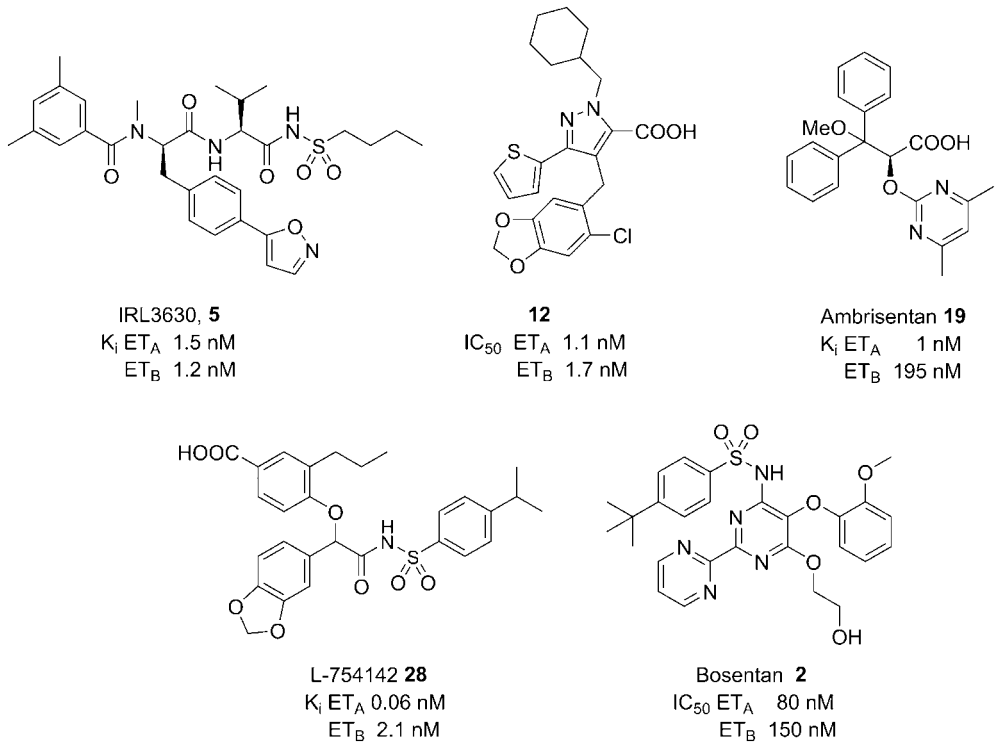

Fig. 8 Structures and published potencies of the ERAs IRL3630 **5**,[76] pyrazole **12**,[96] ambrisentan **19**,[23] L-754142 **28**,[123] and bosentan **2**[128] selected as starting points for our medicinal chemistry program.

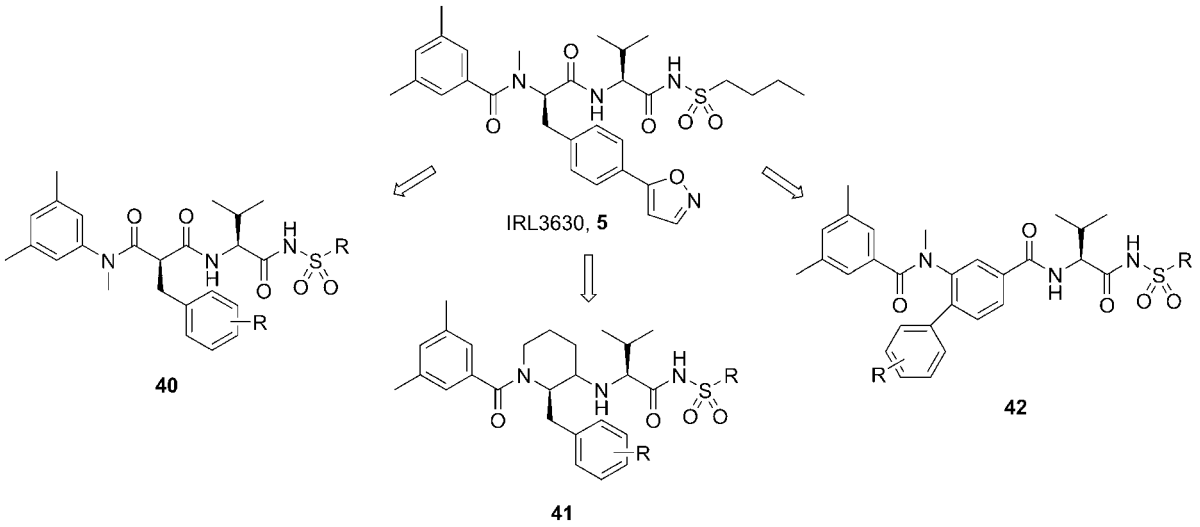

Fig. 9 Proposed analogs of IRL3630 **5**.

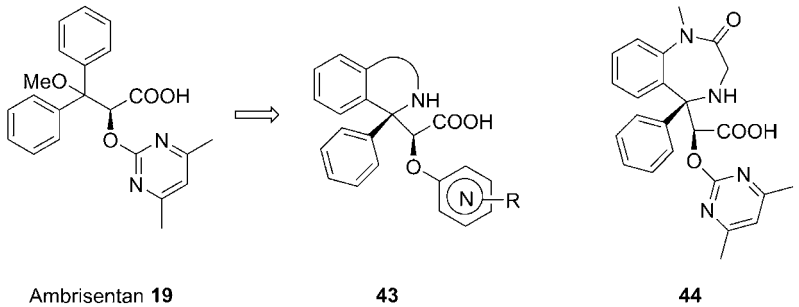

Fig. 10 Introducing an additional ring to the structure of ambrisentan **19** delivered novel ERAs such as tetrahydro-benzo[e][1,4]diazepin-2-one **44**.

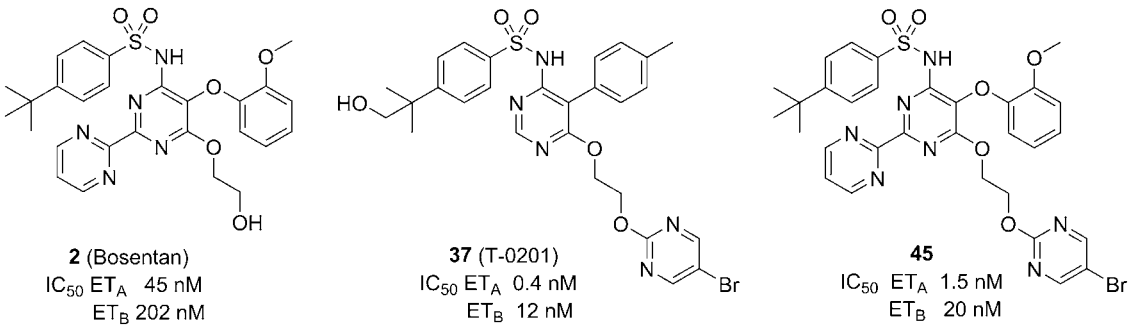

Fig. 11 Structure and in vitro activity of bosentan **2**, T-0201 **37** and a first bosentan analog **45** incorporating the 5-bromo-pyrimidine moiety of **37**.

As a result of these early evaluations, further investigation of analogs of compounds **2** and **19** clearly appeared warranted, while additional efforts to explore compound **5**, **12**, and **28** analogs seemed less attractive and were therefore suspended.

8.10.2.2 Progress of the Project

Optimization of the pyrimidine and the benzodiazepinone series occurred in parallel and followed an analogous approach. These efforts culminated in the discovery of macitentan **1** (Fig. 1) and compound **46** (Fig. 12) as best representatives of the pyrimidine and benzodiazepinone series, respectively. For both compound classes, detailed SAR analyses have been published previously[33,152] and the following discussion, therefore, focuses on the discovery process from a more conceptual perspective using exemplary SAR data only.

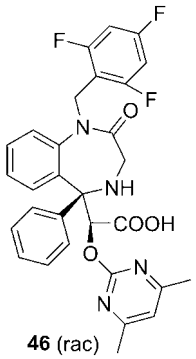

46 (rac)

Fig. 12 Structure of compound **46**, one of the best benzodiazepinone derivatives. This compound showed IC_{50} values of 17 nM and 565 nM on ET_A and ET_B, respectively, and was efficacious in vivo.[152]

Close to 2000 pyridimine and about 400 benzodiazepine derivatives were prepared in the course of our medicinal chemistry program. ET-1 binding competition IC_{50} values on ET_A and ET_B were measured for each of these compounds. About 400 compounds were at least as potent as bosentan and were thus characterized in the functional assays using rat aorta and trachea rings. As shown in Fig. 13, plotting aorta pA_2-values against ET_A IC_{50} values showed a clear relationship between the two parameters (Spearman correlation coefficient $\rho = 0.66$) demonstrating that functional potency obtained from rat tissue correlates with the binding affinity measured on the human ET_A receptor. As expected, the aorta pA_2 values did not correlate with the compound's potency at the ET_B receptor ($\rho < 0.1$), confirming that the endothelium-denuded aorta responds to ET_A receptor modulation only. Analogous results were obtained when trachea pA_2 values were compared with ET_A ($\rho = 0.2$, negligible correlation) and ET_B ($\rho = 0.48$, relationship, Fig. 14) IC_{50} values. However, for both the pyrimidine and the benzodiazepinone class the correlation between the pA_2 and the corresponding IC_{50} value showed significant scattering and a considerable number of compounds deviate more than a factor of three from the correlation line. Unfortunately, there is not enough data available to allow us to determine whether the observed scattering is due to differences in the affinity of our compounds for the rat and human ET receptors. In addition, although we suspected that physicochemical properties of the compound influence its functional potency, we were unable to identify any specific physicochemical parameter that explained the observed behavior. For instance, plotting aorta pA_2 values against clog*P* or clog $D_{7.4}$ (data not shown) did not reveal any relationship between the two parameters ($\rho < 0.1$). As a consequence, we applied the thresholds for the IC_{50} and pA_2 values for compound advancement more leniently as we progressed with our discovery program.

For about 300 of the 400 compounds tested on aorta and trachea rings, the functional potency on ET_A was at least as high as that of bosentan (pA_2 value > 6.8). These compounds were further profiled in vivo by measuring their effect on blood pressure in hypertensive Dahl-S rats. For illustration, the MAP and HR recordings after oral administration of 3 mg kg^{-1} of bosentan and macitentan

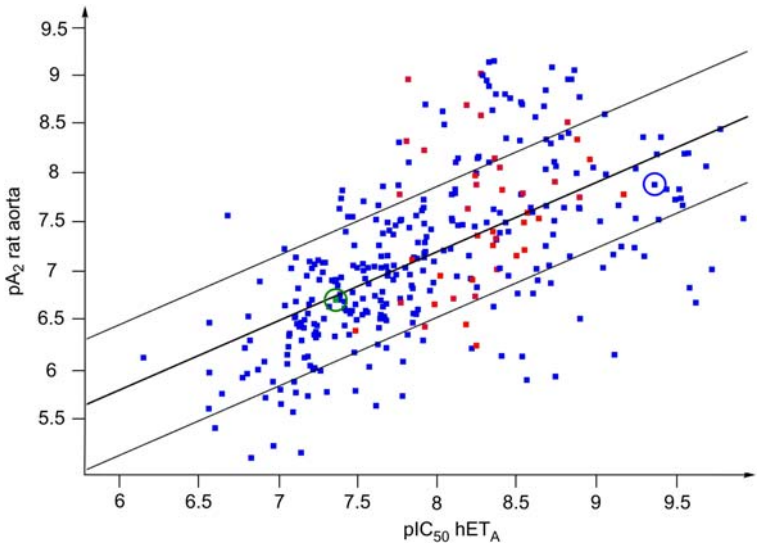

Fig. 13 Correlation of ET_A pIC_{50} and aorta pA_2 values of pyrimidine derivatives (*blue*), benzodiazepinone derivatives (*red*), bosentan **2** (*green circle*), and macitentan **1** (*blue circle*); linear correlation with standard deviation is shown.

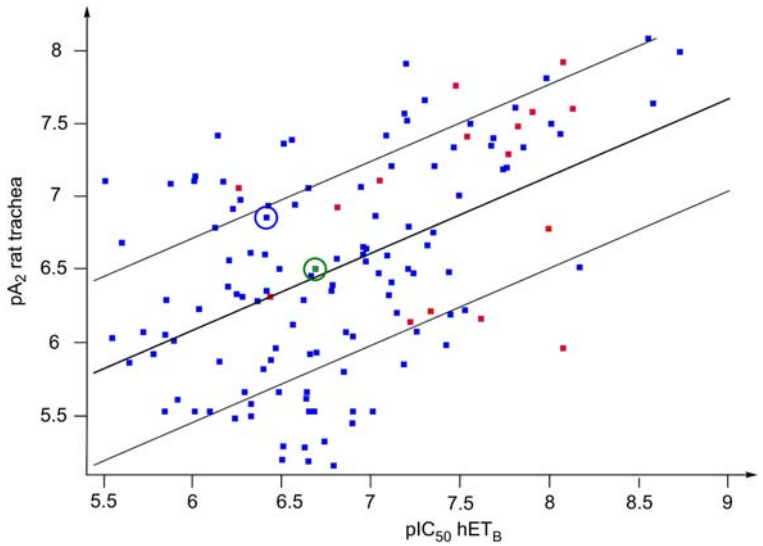

Fig. 14 Correlation of ET_A pIC_{50} and trachea pA_2 values of pyrimidine derivatives (*blue*), benzodiazepinone derivatives (*red*), bosentan **2** (*green circle*), and macitentan **1** (*blue circle*); linear correlation with standard deviation is shown.

are shown in Fig. 15. None of the tested compounds showed an effect on HR. A quick glance at the MAP recordings in Fig. 15 is sufficient to note that macitentan is significantly more efficacious than bosentan in this model of hypertension. A more accurate ranking of the compounds was based on the calculated ABC values of the MAP recordings. Most of the highly efficacious compounds (ABC $\geq$500 mmHg h) displayed a pA_2 value greater than that of bosentan. The data also demonstrated that a high pA_2 value is necessary but not sufficient for a compound to show oral activity. This observation came as no surprise, as oral activity depends, of course, not only on the functional potency but is influenced by many more factors such as compound dissolution, absorption, metabolic stability, tissue distribution, clearance, etc. Hence, while the pA_2 values helped to prioritize compounds for in vivo testing in the beginning, the overall progress of the project was clearly driven by the emerging in vivo efficacy data.

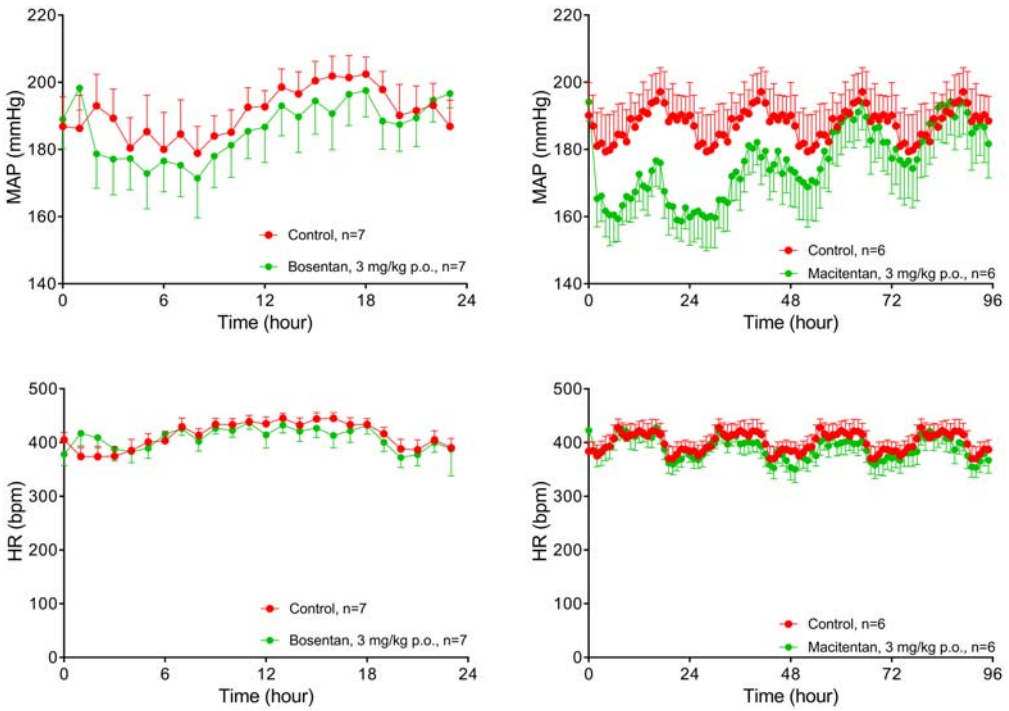

Fig. 15 MAP (*top*) and HR (*bottom*) recordings before and after oral administration of 3 mg kg^{-1} of bosentan **2** (*left*) and macitentan **1** (*right*) to hypertensive Dahl-S rats. Please note the different ranges of the *X*-axis for bosentan (24 h) and macitentan (96 h).

Table 2 In vitro SAR of the sulfonamide moiety

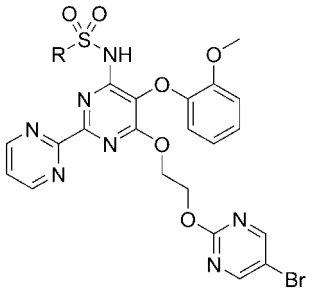

Compound	*R*	*IC_{50} ET_A (nM)*	*IC_{50} ET_B (nM)*	*Mw*	*ABC[a] (mmHg h)*
Bosentan 2	(*tert*-Butyl–phenyl) Structure see **Fig. 7**	45	200	551	−88
45	4-*tert*-Butyl–phenyl	1.5	20	707	n.d.
47	Phenyl	10	340	652	Inactive
48	Methyl	110	1150	590	n.d.
49	*n*-Propyl	9.4	570	618	−177
50	*n*-Propyl-NH	3.8	320	633	n.d.
51	*n*-Butyl-NH	1.7	170	647	−232

[a]3 mg kg^{-1} p.o. to conscious hypertensive Dahl-S rats (n=5–8).

The examples compiled in Tables 2–8 illustrate the observed in vivo SAR and demonstrate how the early availability of in vivo data shaped the discovery process.

As mentioned in section "Selected Starting Points," compound **45**, which combined the structure of bosentan with the 5-bromopyrimidine moiety of T-0201 **37**, showed high potency at the ET_A and ET_B receptor. However, with a molecular weight of 707 this compound is rather large. First efforts therefore aimed at reducing the molecule's size while keeping its favorable potency profile. To this end, stepwise reduction of the sulfonamide moiety was investigated. While removing the *tert*-butyl group at the benzene sulfonamide to give compound **47** (Table 2) led to a moderate decrease in affinity, a further reduction of this moiety to a methyl group (compound **48**) not unexpectedly resulted in a more pronounced potency loss. To our surprise, however, a rather short alkyl chain such as a propyl group (compound **49**) largely restored the compounds' affinity, in particular for the ET_A receptor. Inserting a nitrogen between the alkyl chain and the sulfur to yield sulfamide derivatives further improved the potency on both ET receptors (eg, compounds **50** and **51**). Most importantly, compounds **50** and **51**, incorporating a much smaller sulfonamide/sulfamide moiety when compared to bosentan clearly displayed superior in vivo efficacy. The two compounds showed an ABC of −177 and −232 mmHg h, respectively, while bosentan at the same dose reached an ABC of −88 mmHg h only. Based on

Table 3 In vitro and in vivo SAR of the 2-substituent at the core pyrimidine

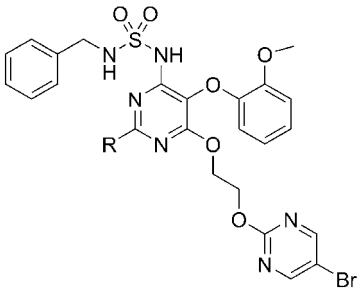

Compound	*R*	*IC_{50} ET_A (nM)*	*IC_{50} ET_B (nM)*	*Mw*	*ABC[a] (mmHg h)*
52	2-Pyrimidinyl	1.9	150	681	−160
53	4-Pyridyl	3.4	560	680	−100
54	4-Morpholinyl	1.4	190	688	−38
55	Methoxy	40	2490	633	n.d.
56	H	6.9	530	603	−100

[a]3 mg kg^{-1} p.o. to conscious hypertensive Dahl-S rats (n=5–8).

Table 4 In vivo and in vitro SAR of the 5-substituent at the core pyrimidine

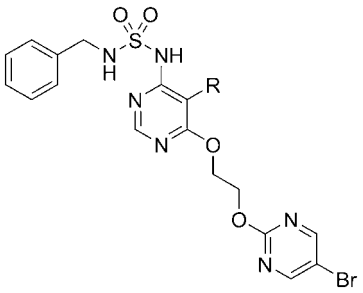

Compound	*R*	*IC_{50} ET_A (nM)*	*IC_{50} ET_B (nM)*	*Mw*	*ABC*[a] *(mmHg h)*
56	2-Methoxy-phenoxy	6.9	530	603	−100
57	3-Methoxy-phenoxy	1.0	460	603	−245
58	3-Methoxy-6-chloro-phenoxy	1.4	710	637	−639
59	4-Chlorophenyl	1.4	510	591	−593
60	4-Bromophenyl	1.6	460	636	−445

[a]3 mg kg^{-1} p.o. to conscious hypertensive Dahl-S rats (n=5–8).

Table 5 In vitro and in vivo SAR of the substituent at the second pyrimidine

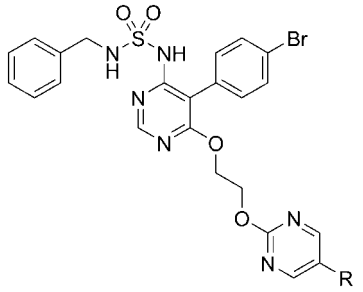

Compound	*R*	*IC_{50} ET_A (nM)*	*IC_{50} ET_B (nM)*	*pA_2 aorta*	*Mw*	*ABC*[a] *(mmHg h)*
60	Br	1.6	460	8.4	636	−445
61	Cyclopropyl	0.9	280	8.03	597	−23
62	OCH_3	1.7	260	n.d.	587	−85
63	SCH_3	0.4	60	8.4	603	−506

[a]3 mg kg^{-1} p.o. to conscious hypertensive Dahl-S rats (n=5–8).

Table 6 Physicochemical and target interaction profiles of macitentan **1**, bosentan **2**, and ambrisentan **19**[31,153,154]

Property	*Macitentan 1*	*Bosentan 2*	*Ambrisentan 19*
Antagonistic potency K_b (PASMC) (nM)	0.14	1.1	0.12
pK_a	6.2	5.1	3.5
log $D_{7.4}$	2.9	1.3	−0.4
Charge–charge interaction with Arg^{326} in ET_A	No	Yes	Yes
Receptor occupancy half-life (PASMC) (min)	17	1	<1
Insurmountability of antagonism (PASMC)	Yes	No	No

PASMC, pulmonary arterial smooth muscle cells.

the in vivo efficacy of sulfamide **51** and the more general observation that the sulfamides showed higher potency on ET_B when compared to the corresponding sulfonamide analogs, the sulfamide class was explored in more detail.

The series of benzyl sulfamide derivatives compiled in Table 3 illustrate the optimization of the 2-substituent at the core pyrimidine. As evident from compounds **53** and **54**, replacing the pyrimidine in **52** by a pyridine or a morpholine, respectively, delivered potent compounds but brought no advantage with respect to molecular weight and in vivo efficacy. On the other hand, replacing

Table 7 The effect of bosentan, macitentan, and its metabolite M6 on plasma bile salts after intravenous administration at a dose of 25 mg kg^{-1}

	Δ Plasma bile salts[a]		
Compound	*10 min (μM)*	*45 min (μM)*	*120 min (μM)*
Vehicle [b]	0.4 ± 3.4	−2.0 ± 5.7	−0.5 ± 5.9
Bosentan	18 ± 13	1.1 ± 5.1	−1.6 ± 3.1
Macitentan	3.7 ± 4.4	1.8 ± 4.1	3.5 ± 4.8
M6	2.5 ± 6.7	−4.3 ± 11	−2.0 ± 13

[a]Results are calculated as individual differences from pre-dose values and presented as mean ± SD (standard deviation) of $n = 6$.
[b]0.5% methylcellulose in water.

Table 8 Serum bile salts in the multiple ascending dose study with macitentan in healthy subjects

Dose (mg)	*Bile salts (μM)*[a] *day 1*	*Bile salts (μM)*[a] *day 10*
Placebo	10.7 ± 2.4	12.2 ± 4.0
1	9.8 ± 1.7	10.8 ± 1.2
3	9.8 ± 1.4	11.1 ± 1.6
10	11.8 ± 1.2	14.8 ± 2.7
30	11.8 ± 2.7	13.3 ± 1.4

[a]Bile salts in serum were determined before dosing on both dosing days, results are expressed as mean ± SD of $n = 6$–8.

the pyrimidine in position 2 by a methoxy group (compound **55**) not only reduced the molecular weight but also the affinity of the compound for the ET receptors. Interestingly, however, omitting the 2-substituent completely to give compound **56** largely maintained its potency on the ET receptors as well as its in vivo efficacy.

The examples given in Table 4 exemplify the in vitro and in vivo SAR of the 5-substituent at the core pyrimidine. The 3-methoxyphenoxy analog **57** of compound **56** was not only more potent on ET_A but also more efficacious in the Dahl-S rat hypertension model. Adding a chloro substituent in position 6 of the phenol moiety (compound **58**) or replacing the 3-methoxy-phenoxy substituent with a 4-chloro- (**59**) or 4-bromo- (**60**) phenyl ring did not affect the potency on ET_A but further improved the compound's in vivo efficacy.

The compounds in Table 5 have been selected to shed light on the in vivo SAR of the 5-substituent attached to the pyrimidine at the ethylene glycol. Even though all four compounds in Table 5 have comparable affinities for the ET_A and the ET_B receptor and similarly high aorta pA_2 values, their efficacy in reducing the MAP in hypertensive Dahl-S rats is clearly different. At an oral dose of 3 mg kg^{-1}, the derivatives incorporating a bromine (**60**) or a methylthio substituent (**63**) were significantly more active than bosentan, while the nearly equipotent cyclopropyl (**61**) and methoxy (**62**) analogs had only a small effect.

Taken together, the compounds in Tables 2–5 demonstrate that in cases where the in vitro potency profiling did not allow compounds to be distinguished, the in vivo efficacy data served as a valuable basis for SAR development and compound prioritization and thus contributed to a rapid progress of the discovery program.

As a last key profiling step, the potential to change plasma bile salt concentrations in Wistar rats was assessed after i.v. administration of those approximately 40 compounds that were clearly more efficacious than bosentan in the Dahl-S rat hypertension model (ABC $\geq$ 500). Due to the limited number of compounds tested in this assay, no detailed SAR could be established. Nevertheless, while all of the tested benzodiazepine derivatives induced changes in plasma bile salt levels, several pyrimidine derivatives showed no activity in this assay (Fig. 16). This observation and the fact that the benzodiazepines often had to be dosed 10 times higher to achieve an in vivo efficacy comparable to that obtained with pyrimidine derivatives, reduced the attractiveness of the benzodiazepinone derivatives. Based on the results of the bile salt experiment, the data of additional standard safety assessments, as well as the properties outlined in section "Preclinical Properties of Macitentan" later, macitentan was eventually selected as a preclinical candidate.

8.10.3 Preclinical Properties of Macitentan

Macitentan was selected based on its potent dual ET_A and ET_B receptor antagonism, its high in vivo efficacy, and, when compared to bosentan **2**, its reduced risk of interaction with bile salt transport. This section summarizes the results of more detailed physicochemical and mechanistic studies and shows how structural properties translated into in vivo efficacy. Macitentan will be compared with the two other ERAs approved for the therapy of PAH, bosentan **2** and ambrisentan **19**.

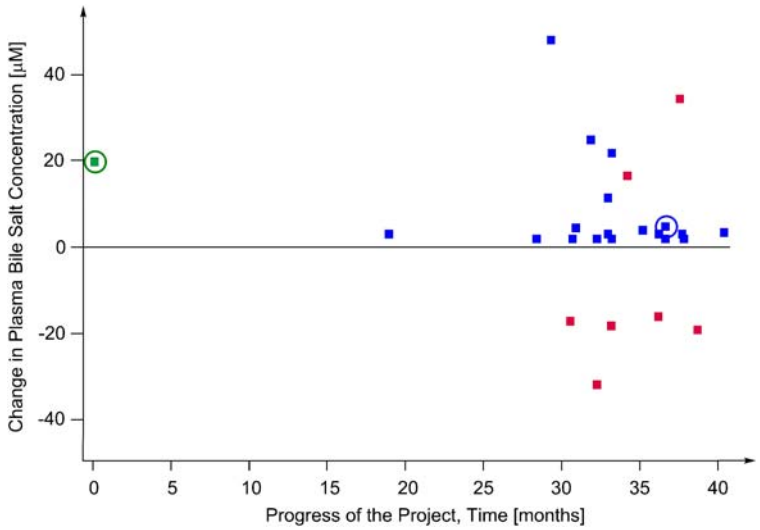

Fig. 16 Plasma bile salt concentrations after i.v. administration of 25 mg kg^{-1} of benzodiazepinone (*red*), or pyrimidine (*blue*) derivatives, bosentan **2** (*green circle*) and macitentan **1** (*blue circle*) to Wistar rats.

8.10.3.1 From Physicochemistry to Primary Cell Pharmacology: The Distinct Profile of Macitentan

Macitentan's in vivo efficacy in hypertensive Dahl-S rats was clearly superior to that of bosentan **2** (see previous section and Refs. 33,155) and ambrisentan **19**.[9,152] To explain this marked difference a series of physicochemical, molecular, and cell biological studies comparing macitentan **1**, bosentan **2**, and ambrisentan **19** were carried out. These studies uncovered a distinct profile for macitentan in terms of acidity, lipophilicity, conformational flexibility, binding mode, target dissociation kinetics, and antagonistic efficacy.[31,153,154,156] In the following sections we describe how the physicochemical and conformational profile of macitentan affects binding mode and binding kinetics, and leads to increased antagonistic efficacy despite a target affinity similar to those of bosentan **2** and ambrisentan **19**.

8.10.3.1.1 Distinct physicochemical and conformational properties of macitentan

Key structural and physicochemical properties of macitentan **1**, bosentan **2**, and ambrisentan **19** are compiled in Table 6. Macitentan and its sulfamide analogs have pK_a values of around 6.2. This weak acidity is unique among the known ERAs, which being either carboxylic acids or aryl sulfonamides have pK_a values at least one unit lower, as is the case for ambrisentan ($pK_a = 3.5$) and bosentan ($pK_a = 5.1$). In fact, the acidic function in ERAs had so far been thought to be essential for target binding, allowing for a charge–charge interaction with positively charged Arg^{326} (ET_A) or Arg^{343} (ET_B), as shown for bosentan.[157] Also its high lipophilicity distinguishes macitentan ($\log D_{7.4} = 2.9$) from bosentan ($\log D_{7.4} = 1.3$) and ambrisentan ($\log D_{7.4} = -0.4$). Thus early on in the development of macitentan, its low acidity and high lipophilicity suggested a potentially different receptor binding mode involving different binding forces.

Molecular modeling of ERAs binding to their target requires a notion of the relevant antagonist conformation. In the cases of bosentan **2** and ambrisentan **19**, molecular flexibility is low and conformational variation is therefore limited. This is in contrast to macitentan, whose structure allows considerable conformational variation. Nuclear magnetic resonance (NMR) studies in aqueous solution performed to elucidate the conformation of macitentan under physiological conditions indicated that macitentan is present in a compact conformation characterized by pyrimidine π–π-stacking (Fig. 17). This conformation allows an unparalleled and precise occupation of a hydrophobic pocket in the modeled ET_A receptor.[154]

8.10.3.1.2 Distinct receptor interaction forces for macitentan as compared to other ERAs

Comparison of macitentan **1** and bosentan **2** binding to a common ERA binding site in the ET_A receptor using molecular modeling suggested potentially different binding modes of the two molecules, characterized by the differential involvement of three amino acids (Fig. 18). Site-directed mutagenesis of these three proposed key interaction amino acid residues (Arg^{326}Gln, Leu^{322}Ala, and Ile^{355}Ala) affected macitentan and bosentan binding in opposing ways.[154]

Macitentan binding was not affected after exchanging charged Arg^{326} for an uncharged Gln residue, while bosentan and ambrisentan binding was essentially lost. The exchange of Leu^{322} for Ala abolished macitentan binding, but had no effect on bosentan and ambrisentan binding. Mutating Ile^{355} to Ala abolished bosentan binding, but not macitentan binding. In conjunction with the ET_A model, these data suggest that macitentan in its compact conformation binds via a tight hydrophobic fit (Leu^{322}) to a subpocket within the ET binding site without necessity for charge–charge interaction (Arg^{326}) and without contact to the peripheral Ile^{355}. The more extended bosentan molecule uses obligatory charge–charge interactions (Arg^{326}) and does not fully occupy this subpocket (no contact to Leu^{322}), but protrudes from it (Ile^{355}-interaction). Also ambrisentan requires the electrostatic interaction with Arg^{326}

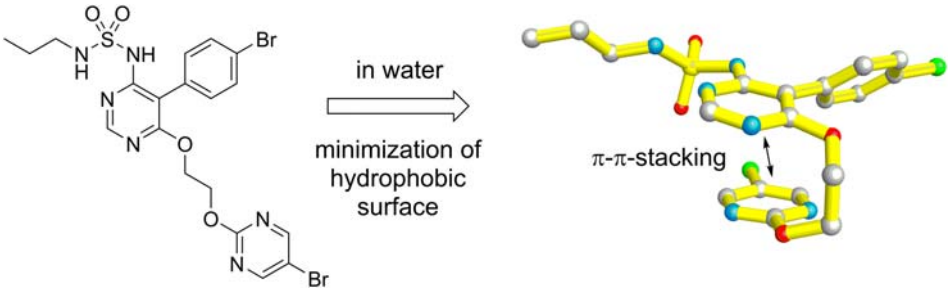

Fig. 17 Conformation of macitentan in water. Compact conformation of macitentan in aqueous solution as proposed by molecular modeling and corroborated by 2D NMR spectroscopy. Ball colors are: carbon, *gray*; nitrogen, *blue*; oxygen, *red*; sulfur, *yellow*; bromine, *green*. Hydrogens have been omitted for reason of clarity.

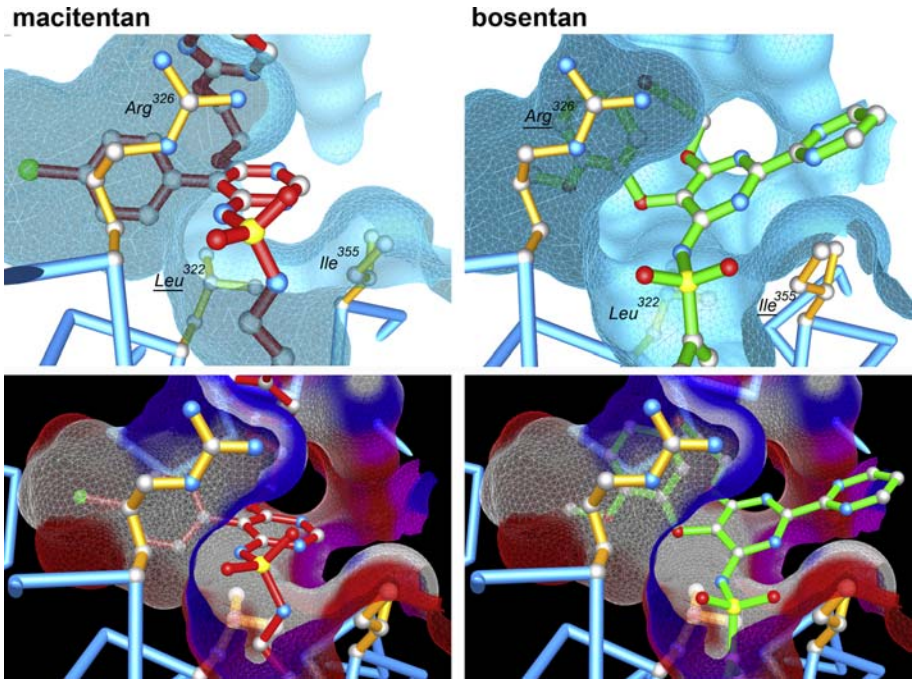

Fig. 18 Macitentan (*left*) and bosentan (*right*) interacting with the ET_A receptor as proposed by mutational experiments and molecular modeling. Three amino acids, Leu^{322}, Arg^{326}, and Ile^{355}, differentially contribute to macitentan and bosentan interaction, causing a hydrophobic and an electrostatic interaction mode, respectively. The same perspectives of the complexes are shown, one of them including polar surface distribution (*red*: H–bond acceptor; *blue*: H–bond donor; *pink*: H–bond acceptor and donor; *white*: lipophilic). Amino acid residues essential for ERA binding are underlined. Reproduced from Gatfield, J.; Mueller Grandjean, C.; Bur, D.; Bolli, M. H.; Nayler, O. Distinct ETA Receptor Binding Mode of Macitentan as Determined by Site Directed Mutagenesis. *PLoS One* **2014**, *9*, e107809.

for binding, indicating similar charge-dependent binding forces for the acidic ambrisentan and bosentan molecules but not for the less acidic macitentan molecule. In conclusion, the macitentan binding mode is characterized by a good hydrophobic fit and a lack of charge–charge interaction at the target receptor and therefore is distinct from that of other more acidic ERAs.

8.10.3.1.3 From a distinct binding mode to sustained target blockade and higher antagonistic efficacy in primary human target cells

It is increasingly realized that in vivo efficacy depends not only on (1) antagonist affinity for the target and (2) in vivo exposure but also on (3) the ability of the antagonist to avoid direct competition with the sometimes highly concentrated natural agonist for target binding. Most (70%) of the newly Food and Drug Administration (FDA)-approved antagonists avoid competition by a variety of mechanisms,[158,159] and probably the most prominent mechanism is slow kinetics of dissociation from the target. Slow target dissociation and thus long receptor occupancy half-life lead to insurmountable antagonism, ie, the inability of the natural agonist, even at very high concentrations, to activate an antagonist-occupied receptor.[160] The evolution of angiotensin II receptor blockers

over the past 20 years illustrates that an increase in receptor occupancy half-life and insurmountability is paralleled by an increase in clinical efficacy.[159,161,162]

Different binding modes of antagonists can affect ligand–receptor binding kinetics and several examples are known where a tight hydrophobic fit between ligand and a receptor pocket leads to increases in receptor occupancy time,[163,164] while charge–charge interactions in ligand–receptor pairs with less tight fit are associated with rapid dissociation kinetics.[165] Therefore, we performed second messenger signaling studies with human primary pulmonary arterial smooth muscle cells (PASMC) to determine the dissociation kinetics and the surmountability profiles of macitentan, bosentan, and ambrisentan. All three compounds were highly potent antagonists of ET-1 signaling at low ET-1 concentrations ($K_b = 0.1–1$ nM; see **Table 6**). Interestingly, however, their receptor occupancy half-lives, as determined by washout assays, were very different. Bosentan and ambrisentan displayed very short half-lives (1 min) at ET receptors in PASMCs. In contrast, macitentan displayed a ~20-fold increased receptor occupancy half-life of 17 min, which is probably sufficient to withstand a locally released wave of the highly unstable para/autocrine ET-1 peptide. The extremely short receptor occupancy half-lives observed for ambrisentan and bosentan are typical of diffusion-controlled drug–target interaction, which occurs (i) in the absence of conformational changes in target or drug and (ii) for binding events with rapid solvation/desolvation of target and drug.[166]

Since many antagonists with longer receptor occupancy half-lives display higher antagonist efficacy,[158,161,162,164,167] ie, insurmountability, we performed curve shift assays to assess competitivity profiles of macitentan, ambrisentan, and bosentan (**Fig. 19**). The distinctly slower target dissociation of macitentan indeed translated into an insurmountable mode of antagonism as evidenced by the inability of even very high ET-1 concentrations to efficiently activate the macitentan-blocked ET receptors in PASMCs, the relevant therapeutic cell type. This more efficient mode of antagonism places macitentan, in contrast to bosentan and ambrisentan, into the class of modern and efficacious drugs that are resistant to competition by the natural ligand.

In summary, based on its specific structure and conformation and its unique physicochemical properties, macitentan displays a distinct binding mode, which leads to slow target dissociation kinetics and, most importantly, to highly efficacious insurmountable antagonism of ET-1 signaling in PASMCs.

8.10.3.2 Tissue Distribution in Animal Models of PAH

Macitentan possesses physicochemical properties (eg, log $D_{7.4}$) that favor partitioning into tissue more than other ERAs, such as bosentan and ambrisentan.[31] Such properties, in addition to its binding mode, could explain the greater efficacy achieved in vivo, as macitentan could access more receptors in the cardiovascular tissue. We therefore investigated its tissue distribution using microautoradiography. We were interested in two aspects: first, the difference in distribution between a healthy animal and a diseased one (for this we selected the bleomycin rat model of pulmonary fibrosis associated with pulmonary hypertension) and second, we wanted to compare the distribution of macitentan with that of bosentan. We first observed that administration of radiolabeled ^{14}C-macitentan showed a greater distribution of drug into the lung of bleomycin-treated rats as compared to healthy rats. This might be attributed to a greater permeability of the damaged lung. Second, we observed that the distribution of labeled macitentan into the general lung tissue of pulmonary hypertensive rats was superior to that of ^{14}C-bosentan.[156] This greater pulmonary distribution was confirmed by quantitative tissue analysis using high-pressure liquid chromatography. We also observed a greater distribution of macitentan compared to bosentan in the right ventricle, the target organ in pulmonary hypertension, on which ERAs can exert direct antihypertrophic activity.

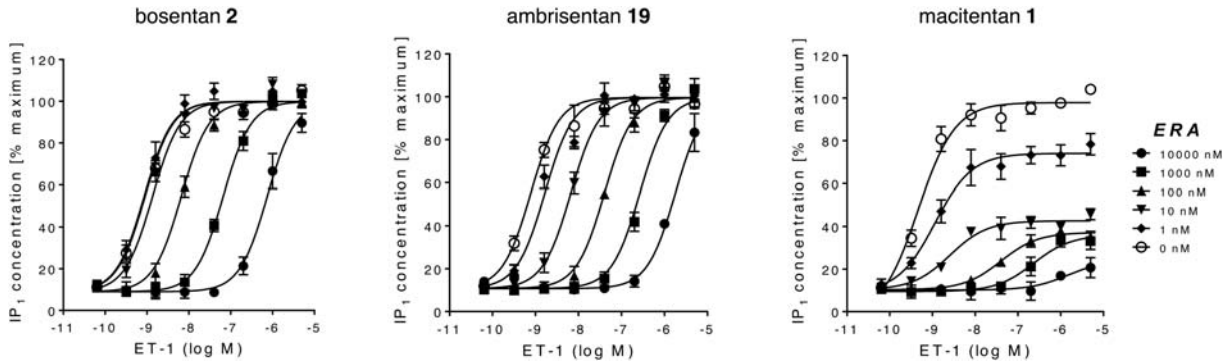

Fig. 19 Effect of bosentan 2, ambrisentan 19, and macitentan 1 on ET-1-induced IP_1 accumulation in human PASMC. Cells were pre-incubated with dilution series of antagonists followed by the addition of a dilution series of ET-1. After 20 min of stimulation, cells were lysed and the IP_1 content was determined. Raw data from four independent experiments were normalized, and average values ±SEM are shown. IP_1, inositol-1-phosphate. Reproduced from Gatfield, J.; Mueller Grandjean, C.; Sasse, T.; Clozel, M.; Nayler, O. Slow Receptor Dissociation Kinetics Differentiate Macitentan from Other Endothelin Receptor Antagonists in Pulmonary Arterial Smooth Muscle Cells. *PLoS One* **2012**, *7*, e47662.

8.10.3.3 In Vivo Efficacy and Comparison With Other ERAs

In vivo data generated during the drug discovery phase showed that single-dose administration of macitentan in conscious hypertensive rats equipped with telemetry triggered a long-lasting decrease in blood pressure, which was superior in terms of amplitude and duration of action to that achieved with bosentan. We confirmed this efficacy profile in rat models of pulmonary hypertension using double telemetry technology to simultaneously measure systemic and pulmonary arterial blood pressure. Macitentan dose-dependently induced a long-lasting decrease in pulmonary blood pressure without increasing HR and, importantly, without decreasing systemic blood pressure (Fig. 20).

This highlights one of the beauties of dual ET receptor antagonism: only vascular beds where the ET system is activated will respond to an ERA. Hence, in healthy vessels, where no dysregulation of the ET system is found, no vascular response occurs, reflecting the minor role of ET in the regulation of vascular tone in physiology. Consequently, in normotensive rats with no activation of the ET system, macitentan, like bosentan,[168] had no effect on systemic blood pressure up to the highest dose tested. On the other hand, macitentan was able to reduce systemic arterial blood pressure in hypertensive Dahl-S and DOCA-salt rats because both Dahl-S and DOCA-salt rats have increased expression of vascular ET-1.[49] In the monocrotaline model of pulmonary hypertension, pulmonary dysregulation of the vascular ET system is observed,[169] and associated with an increase of local pulmonary pressure, whereas the systemic blood pressure of these animals remains in the physiological range.[31] Likewise, in patients with PAH during the phase III study, macitentan decreased pulmonary vascular resistance while no noticeable effect on systemic blood pressure was observed.[170]

The sustained duration of action of macitentan (eg, up to 48 h at a dose of 10 mg kg^{-1}) in hypertensive rats was attributed to its pharmacokinetic properties, including a half-life of 2–5 h, and the formation of the active metabolite M6 (also known as ACT-132577, Scheme 1) with an even longer half-life of 8.4 h in the rat.[31] Metabolite M6 is also a dual ERA, approximately eightfold less potent than macitentan on ET_A and twofold less potent on ET_B receptors. On the basis of these characteristics, M6 may contribute to the in vivo efficacy of macitentan.[31]

To investigate whether macitentan was able to achieve a greater pharmacological effect than other ERAs, a study was designed in which Dahl-S hypertensive rats were given a maximally effective dose of macitentan on top of maximally effective doses of either ambrisentan (used as an ET_A-selective receptor antagonist) or bosentan (dual ET_A/ET_B receptor antagonist).[155] In both cases, macitentan was able to further decrease blood pressure when given on top of the other ET receptor antagonist; conversely, these compounds were not able to cause additional blood pressure reduction when given on top of macitentan. The add-on effect of macitentan on top of bosentan (Fig. 21) or ambrisentan suggests that macitentan is able to achieve a more effective blockade of ET-1-mediated effects in vivo, probably by additional blockade of ET_B receptors (vs. ambrisentan), superior tissue distribution, and an increased receptor occupancy half-life (vs. ambrisentan and bosentan).[9,155]

Finally, chronic studies were initiated to investigate the effect of macitentan on pulmonary artery and cardiac remodeling in rat models of pulmonary hypertension. Chronic administration of macitentan dose-dependently inhibited pulmonary vascular and right ventricular remodeling and, in contrast to bosentan, prolonged survival (Fig. 22). Indeed, we observed that in rats treated with doses of antagonists exerting similar hemodynamic effects on the pulmonary vasculature, macitentan was superior to bosentan in preventing remodeling of the right ventricle.[9] Therefore the improvement of survival observed with macitentan could be attributed to a superior cardiac protection compared to bosentan. These results were indeed encouraging and supported a clinical program aimed at demonstrating an effect of macitentan on hard endpoints such as morbidity and mortality.

8.10.4 Macitentan in Humans

The following sections illustrate how preclinical properties translated into efficacy and safety in humans. To clearly outline the advances made with macitentan, key observations with the benchmark bosentan are summarized at the beginning of the following sections, where appropriate.

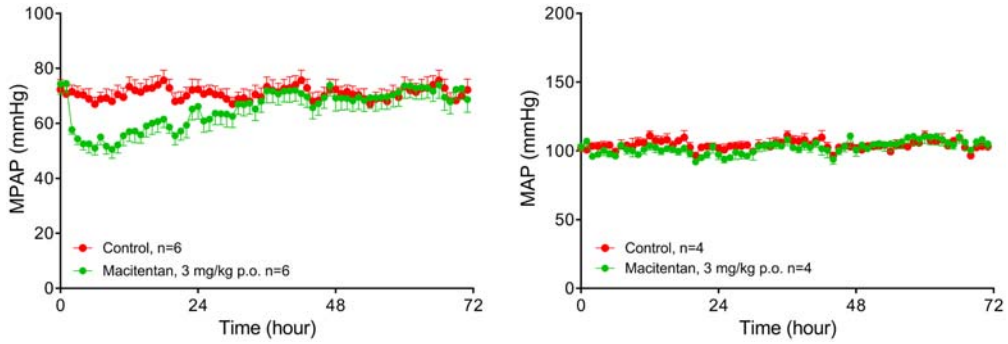

Fig. 20 Concomitant telemetry traces showing mean pulmonary arterial pressure (MPAP, *left*) and systemic arterial pressure (MAP, *right*) in conscious pulmonary hypertensive rats (Sugen/hypoxia model). Single oral administration of macitentan is followed by a selective and sustained decrease in pulmonary pressure without significant change in systemic pressure.

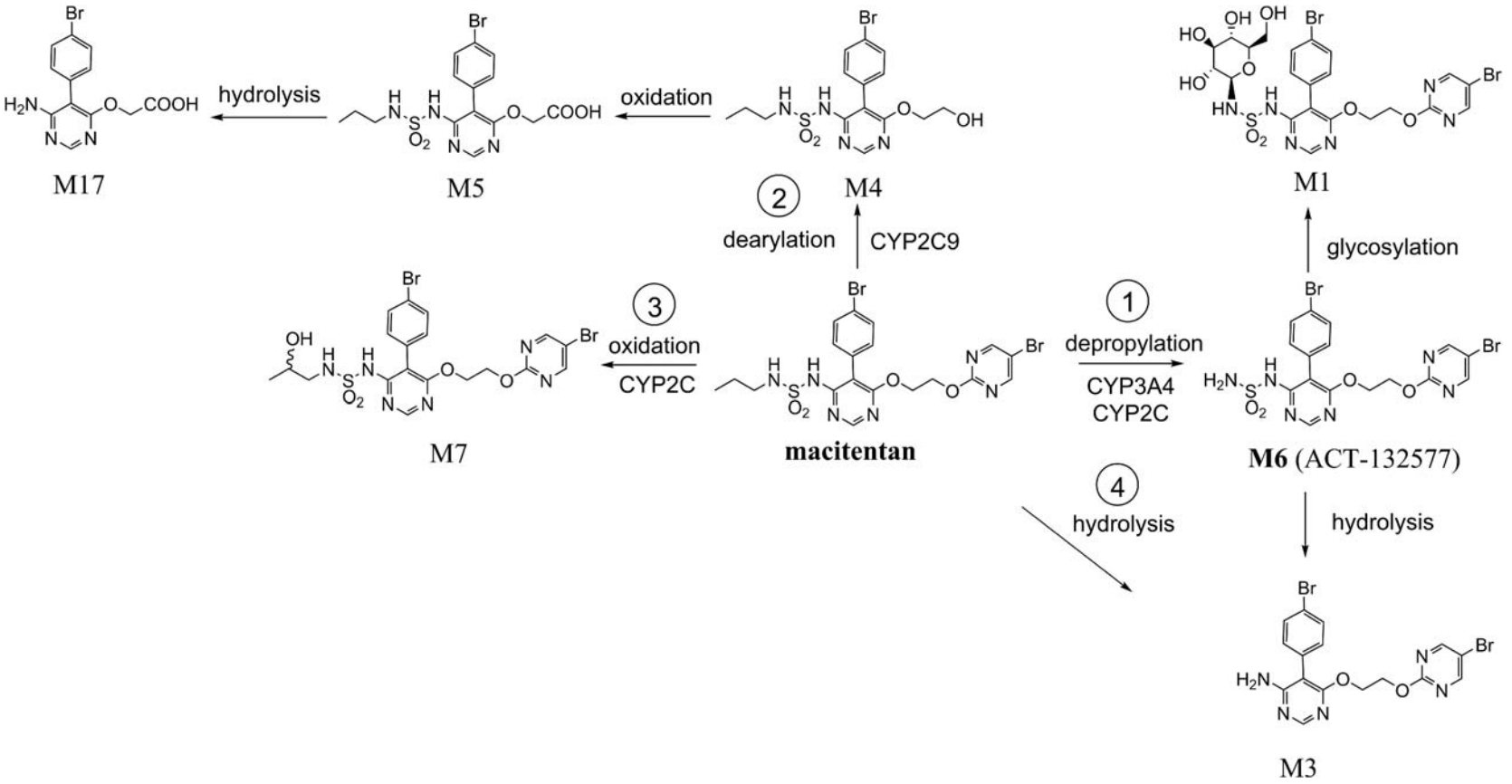

Scheme 1 The four metabolic pathways of macitentan in humans. Metabolite M6 is pharmacologically active with similar potency to macitentan. Metabolites M3 and M4 are significantly less active, while M5 is inactive.[171] Pharmacological activity of M1, M7, and M17 was not determined.

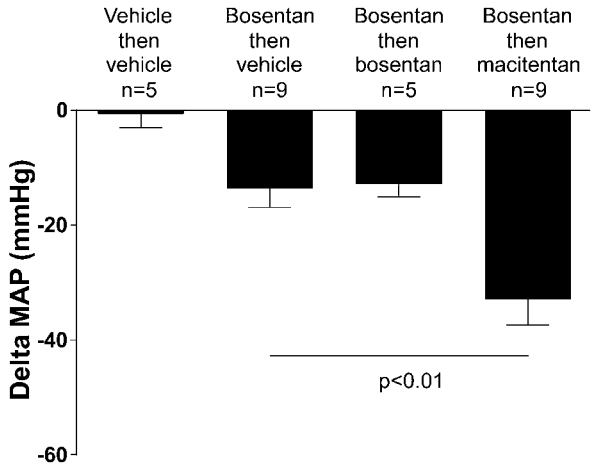

Fig. 21 Effect on mean arterial pressure (Delta MAP) after oral administration of either macitentan (30 mg kg^{-1}) or bosentan (100 mg kg^{-1}) on top of a maximally effective dose of bosentan (100 mg kg^{-1}) to hypertensive Dahl-S rats. Reproduced from Iglarz, M.; Bossu, A.; Wanner, D.; Bortolamiol, C.; Rey, M.; Hess, P.; Clozel, M. Comparison of Pharmacological Activity of Macitentan and Bosentan in Preclinical Models of Systemic and Pulmonary Hypertension. *Life Sci.* **2014**, *118*, 333–339.

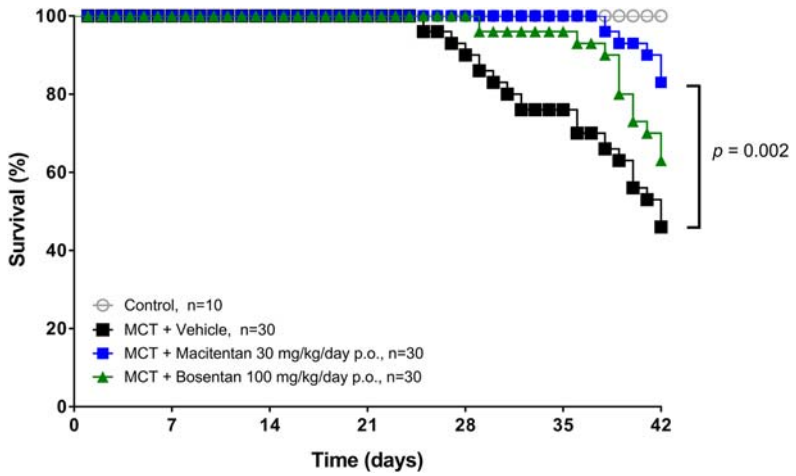

Fig. 22 Survival curve of control and monocrotaline (MCT)-induced pulmonary hypertensive rats ($n=30$/group except $n=10$ in control). Rats were treated with macitentan, bosentan, or vehicle just after MCT administration. Only macitentan significantly improved survival ($p<0.002$ vs. vehicle-treated MCT on day 42).

8.10.4.1 Pharmacokinetics

The maintenance dose of bosentan for the treatment of PAH is 125 mg b.i.d. Bosentan is rapidly absorbed after oral dosing and reaches peak plasma concentrations of 1317 ng mL^{1} within 3 h after a single dose.[172] Steady-state is reached after 3–5 days and plasma concentrations are then about 50% compared to single-dose data, likely because bosentan induces its own metabolism. Its volume of distribution at steady-state is 30 L, ie, approximately body water volume, indicating reasonable penetration into tissues. Hepatic disposition is mediated by OATP1B1 and OATP1B3 as evidenced by the sensitivity of bosentan PK to concomitant organic anion-transporting polypeptide (OATP) inhibitors.[173] Bosentan plasma exposure was increased by about 30- to 48-fold in the presence of cyclosporine A[174] or lopinavir/ritonavir.[175] In contrast, inhibition of metabolism by the CYP3A4 inhibitor ketoconazole led to an only about twofold increase in bosentan exposure.[176] OATP-mediated hepatic uptake is therefore considered the rate-limiting step in overall clearance. Despite a fairly low plasma clearance of 17 Lh^{-1}, bosentan has a terminal half-life of only 5.4 h and needs to be given twice daily. Bosentan undergoes extensive metabolism catalyzed by CYP3A4 and CYP2C9 to yield three metabolites, one of which retains activity on ET receptors and may contribute to about 20% to the overall pharmacological effect. Bosentan metabolites are mostly excreted via the bile while renal elimination is a minor excretion pathway.[177]

Conceptually, pharmacokinetic optimization of a drug can be achieved in several ways. Drug clearance could be reduced either by increasing the drug's stability toward metabolizing enzymes and/or by modifying its hepatic disposition profile, ie, by decreasing

drug concentrations in liver cells. Bosentan exhibits an intrinsic metabolic clearance (CL_{int}) with human liver microsomes of only 15 μL min^{-1} mg and thus offered little room for improvement. The corresponding value for macitentan is in fact about 150 μL min^{-1} mg and macitentan, therefore, is not an obviously superior candidate over bosentan. Decreasing OATP affinity was another option to reduce drug clearance by limiting entry into hepatocytes. This approach, however, created a dilemma as it was believed that ET receptor binding relies on the interaction of a negative charge of the antagonist with Arg326.[157] In the case of ambrisentan, this negative charge is provided by a carboxylic acid while bosentan contains an aromatic sulfonamide. The negative charge makes them, however, candidate substrates for anion transporters, and interactions with OATP transport proteins have indeed been described for several members of the class.[173,178,179] Key structural changes in macitentan versus bosentan constitute the replacement of the sulfonamide by a sulfamide moiety leading to an increase in pK_a from 5.1 to 6.2,[31] and an increase in overall lipophilicity. The octanol/water partition coefficient log $D_{7.4}$ of macitentan is 2.9, while it is only 1.3 for bosentan. Reduced acidity and increased lipophilicity both facilitate membrane permeability and consequently shift the balance driving liver disposition from OATP transport to passive diffusion. Intrahepatic macitentan concentration is therefore determined by the free concentration in blood. As a result of this optimization, oral clearance of macitentan in human is 1.74 Lh^{-1}. Considering the estimated oral bioavailability of 74%,[180] this leads to a systemic clearance of 2.3 Lh^{-1}, ie, about 10 times lower than the corresponding value of 30 Lh^{-1} for bosentan.[172] Macitentan consequently qualified for a once-a-day dosing regimen at a marketed dose of 10 mg for the treatment of PAH.[170] The increased lipophilicity, however, was at the expense of solubility, and macitentan's low solubility in the gut is the likely reason for its slow oral absorption, as median T_{max} is reached after 8 h. Peak plasma concentrations and plasma exposure (AUC_t) at a single dose of 10 mg are 106 ng mL^{-1} and 1722 ng $(mL\,h)^{-1}$, respectively.[181] Drug levels decline with an apparent terminal elimination half-life of 16 h.[181] As a consequence of its long half-life, macitentan accumulates by about 1.74-fold after multiple dosing. The pharmacologically active metabolite M6 (also known as ACT-132577) is slowly formed in man and reaches peak plasma concentrations only about 9 h after macitentan administration. Plasma half-life of M6 is about 43 h, leading to an accumulation of 7.1-fold after multiple dosing. M6 exposure at steady-state exceeds that of parent macitentan by 2.9-fold.[181,182]

8.10.4.2 Metabolism

Metabolic disposition of macitentan in man was investigated in healthy subjects after a single 10 mg dose of ^{14}C-labeled macitentan.[182] Macitentan was extensively metabolized prior to excretion into urine and feces to an about equal extent. Macitentan metabolism in man is characterized by four distinct pathways (**Scheme 1**), ie, (1) oxidative depropylation of the sulfamide group to M6, mainly catalyzed by CYP3A4 and a minor contribution of the CYP2C family; (2) oxidative dearylation of the ethylene glycol to M4 catalyzed by CYP2C9. M4 then undergoes oxidation to the acid M5 followed by hydrolysis to M17; (3) hydroxylation of the propyl chain to form M7, catalyzed by CYP2C enzymes; and (4) hydrolysis of macitentan and M6 to form M3. M17 was the most prominent metabolite detected in human urine, followed by the glucose conjugate M1, the hydrolysis product M3 and the acid M5. Metabolites M3, M5, and M17 were also observed in human feces, accompanied by smaller amounts of M6 and M7. Metabolism studies in bile duct-cannulated rats and dogs showed that all four primary pathways present in humans were also evident in animals.[171]

8.10.4.3 Liver Safety

During clinical development of bosentan, elevated ALT levels were observed in 16% of chronic heart failure patients at 500 mg bosentan twice daily[183] and in 11% of PAH patients[28,30]at 125 mg bosentan twice daily, compared to 4% and 2% on placebo, respectively. Dose-dependent increases in plasma bile salts and alkaline phosphatase were observed alongside changes in liver transaminases. Mechanistically, inhibition of the bile salt export pump BSEP by bosentan and its metabolites has been identified as the likely reason for the observed changes in plasma transaminases.[39] BSEP is an ATP-dependent transport protein located at the canalicular domain of hepatocytes and mediates the rate-limiting step in bile salt secretion from blood into bile.[184,185] In canalicular rat liver membrane vesicles and in Sf9 vesicles overexpressing rat bsep, bosentan and its metabolites inhibited taurocholate transport in vitro. In rats, plasma bile salts increased in a dose-dependent manner after intravenous dosing of bosentan.[39] These rat findings were later substantiated with human BSEP.[186] Moreover, bosentan itself accumulates in liver cells as it is a substrate of OATP transport proteins.[173] Both elements together led to the hypothesis that bosentan treatment might initially disrupt bile salt homeostasis through blockade of BSEP-mediated bile salt excretion into bile. As the accumulating bile salts are cytotoxic at high concentrations, the observed liver transaminase elevations in man are likely the result of secondary bile salt toxicity in hepatocytes. This hypothesis is supported by observations in PAH patients receiving concomitant HIV protease inhibitors like Kaletra® (lopinavir/ritonavir), a potent inhibitor of both CYP3A4 and OATP. Bosentan trough plasma concentrations were increased by 48-fold in this subpopulation.[175]

The effects of macitentan and its active metabolite M6 on bile salt homeostasis were tested at a single-dose in the above-mentioned rat model developed by Fattinger et al.[39] Macitentan and M6 were individually tested at an intravenous dose of 25 mg kg^{-1}, and the change in plasma bile salts measured at 10, 45, and 120 min after dosing. Bosentan as well as a vehicle control were included into the design (**Table 7**). In agreement with literature data,[39] bosentan increased plasma bile salts by 18 ± 13 μM at 10 min post-dose, which then returned to pre-dose values within 45 min after dosing. Under the same conditions, plasma bile salt changes after 10 min were 3.7 ± 4.4 μM for macitentan and 2.5 ± 6.7 μM for M6, and thus not different from vehicle (0.4 ± 3.4 μM).

Bile salt changes upon chronic macitentan treatment were monitored in the toxicology program in the rat and dog.[187] Rats were treated for 4 weeks at doses up to 1500 mg kg^{-1}, and for 26 weeks at up to 250 mg kg^{-1}. No difference between dose groups was noted in any of the rat studies. Steady-state plasma exposures for macitentan and M6 in male rats at 250 and 1500 mg kg^{-1} were about 23- to 212-fold and 42- to 183-fold, respectively, above human exposure at the approved dose of 10 mg. Top doses in the 4- and 39-week studies in the dog were 250 and 100 mg kg^{-1}, respectively. There was no difference between dose groups treated with macitentan and vehicle in any of the three chronic toxicity studies in the dog. Plasma exposures of macitentan and M6 at 100 and 250 mg kg^{-1} were about 18- to 26-fold and 187- to 500-fold, respectively, above human exposure at 10 mg. Serum bile salt concentrations monitored in the multiple-ascending dose study in healthy male subjects at macitentan doses of 1–30 mg for 10 days were in a narrow range from 7.7 to 19 μM and showed no discernible trend toward increased levels at any dose (**Table 8**).[188]

From a more mechanistic perspective, inhibition of bile salt transport was investigated at the level of the transport proteins responsible for hepatic bile salt trafficking, ie, the sodium-dependent taurocholate cotransporting polypeptide (NTCP) and the bile salt export pump (BSEP). NTCP (SLC10A1) and BSEP (ABCG2) are the major transport proteins responsible for moving bile salts from blood into liver cells.[184,185,189] The results of these inhibition experiments are summarized in **Table 9**.

NTCP was equally inhibited by macitentan and M6 with IC_{50} values in the range of 14–18 μM, whereas BSEP was inhibited with IC_{50} ranging from 18 to 60 μM. These in vitro data are thus not different from those of bosentan with reported IC_{50} values on BSEP and NTCP of 25–77 μM and 24–30 μM, respectively. From a drug discovery perspective, it is a fair question whether an isolated view on BSEP inhibition would have been an appropriate approach to identify follow-up compounds devoid of cholestatic potential. It is important to conceptionalize that toxicity is not only a function of (off-)target affinity but also of drug concentrations at the target site. A complete assessment, therefore, also needs due consideration of local drug concentrations. As outlined in the section on macitentan PK, hepatic disposition differs significantly between bosentan and macitentan. Bosentan uptake into liver cells is largely dependent on OATP transport.[173] In contrast, the increased lipophilicity of macitentan allows it to enter liver cells by passive diffusion, while OATP transport only contributes about 20% to overall cellular uptake.[187,193] These mechanistic considerations were substantiated using a physiology-based pharmacokinetic (PBPK) model for macitentan and M6.[180] For a human 10 mg dose, this PBPK model projected total macitentan concentrations at steady-state in plasma, portal vein, and liver of 400 nM, 419 nM, and 72 nM, respectively, while the corresponding values for M6 were 1722 nM for plasma/portal vein and 159 nM for liver. Even without correction for plasma protein binding, these concentrations are significantly below those observed in the bile salt transport experiments described earlier. Based on this more physiological view, it is obvious why macitentan's liver safety profile is much superior to that of bosentan despite a similar inhibitory potency on BSEP and NTCP.

8.10.4.4 Drug–Drug Interactions

The drug–drug interaction potential of bosentan is mostly driven by its P450 induction potential. Biochemically, bosentan shows a classical P450 induction pattern as it activates the PXR nuclear receptor and induces CYP2C9 and CYP3A4 in human hepatocytes.[194] Clinically, concomitant bosentan at 125 mg b.i.d. reduces drug levels of a number of comedications dependent on these enzymes including cyclosporine A,[174] simvastatin,[195] and warfarin[196] by about 50%. Its dependency on OATP-mediated hepatic uptake leads to marked, up to 48-fold increases in bosentan plasma levels when given together with rifampicin, cyclosporine, or ritonavir/lopinavir.[175]

The inhibition potential of macitentan and its active metabolite M6 on a panel of P450 enzymes and drug transporters was characterized in vitro (**Table 10**).[180,197]

While macitentan and M6 showed no inhibition of CYP1A2, CYP2A6, CYP2B6, CYP2C19, CYP2D6, and CYP2E1 ($IC_{50} > 50$ μM), they showed weak to moderate inhibition of CYP2C8, CYP2C9, and CYP3A4. Macitentan and M6 are P450 inducers in vitro.[180] Both compounds increased CYP3A4 expression in human hepatocytes, while no relevant changes in CYP1A2 or CYP2C9 expression were observed.[180] Upregulation of CYP3A4 is likely mediated via PXR, as both compounds activated the nuclear receptor in a reporter-gene assay with EC_{50} values of 1.2 and 8.0 μM, respectively. Macitentan is a substrate of CYP3A4 and CYP2C enzymes.[180] Moreover, macitentan as well as M6 are weak substrates of OATP1B3 but not OATP1B1.[198]

The relevance of these in vitro studies was investigated in a series of clinical drug–drug interaction studies with macitentan at a dose of 10 mg. Sildenafil and warfarin were chosen as CYP3A4 and CYP2C9 substrates to assess the P450 inhibition potential clinically, as both are important comedications in the treatment of PAH. Concomitant macitentan caused a minor, not clinically relevant increase in exposure to sildenafil.[199] The anticoagulant warfarin is marketed as a racemic mixture of which the R-

Table 9 Inhibition of BSEP- and NTCP-mediated taurocholate transport by the endothelin receptor antagonists bosentan, macitentan, and macitentan metabolite M6

Compound	*BSEP IC_{50} (μM)*	*NTCP IC_{50} (μM)*	*References*
Bosentan	25–77	24–30	186,190–192
Macitentan	18 ± 5	18 ± 2	187
M6	60 ± 14	14 ± 2	187

Table 10 IC_{50} values of macitentan and M6 on a panel of human P450 enzymes and drug transporters

P450 enzyme	*Macitentan (μM)*	*M6 (μM)*	*Transporter*	*Macitentan (μM)*	*M6 (μM)*
CYP1A2	>50	>50	P-gp	>100	~100
CYP2A6	>50	>100	OATP1B1	6.9	21
CYP2B6	>50	>100	OATP1B3	14	56
CYP2C8	21	23	OAT1	3.7	4.7
CYP2C9	5.6	31	OAT3	0.7	1.5
CYP2C19	>50	15	OCT1	>100	>100
CYP2D6	>50	>100	OCT2	>100	>100
CYP2E1	>50	>100	MATE1	30	>100
CYP3A4	24–37	7.3–11	BCRP	1.0	5.7

enantiomer is a sensitive CYP2C9 substrate. No interaction was observed when warfarin was concomitantly administered with macitentan.[200] The lack of P450 induction was confirmed in a recent drug–drug interaction study with the oral contraceptive Trinovum® (ethinyl estradiol/norethisterone).[201] These studies indicate that macitentan at a dose of 10 mg is neither an inhibitor nor an inducer of P450 enzymes.

Interaction studies with ketoconazole, rifampicin, and cyclosporine A were conducted to quantify the dependence of macitentan clearance on CYP3A4 and OATP transporters. Macitentan exposure increased by about twofold in the presence of the strong CYP3A4 inhibitor ketoconazole, given at a once daily dose of 400 mg, while the exposure to metabolite M6 was reduced by 26%.[202] The CYP3A4 inducer rifampicin reduced exposure to macitentan by approximately 80% but had no effect on M6 concentrations in plasma.[198] Both studies confirm the important role of CYP3A4 in the clearance of macitentan as indicated by the in vitro studies. PBPK modeling suggested that CYP3A4 contributes about 60% to total clearance.[180] The sensitivity of macitentan PK to OATP inhibition was probed in a clinical interaction study with cyclosporine A.[198] Concomitant cyclosporine A had only a marginal effect on macitentan drug levels. This is a marked difference to the 30-fold increased trough levels observed in the corresponding interaction study with bosentan,[174] confirming the role of passive diffusion, a consequence of increased lipophilicity, in the hepatic disposition of macitentan.

8.10.4.5 Macitentan for the Treatment of PAH

The research efforts leading to the discovery and development of macitentan culminated in a landmark Phase III clinical trial, the Study with an Endothelin Receptor Antagonist in Pulmonary Arterial Hypertension to Improve Clinical Outcome (SERAPHIN). SERAPHIN was an ambitious study, and differed from previous clinical trials of PAH treatments in several important ways. Whereas in previous trials the primary endpoint was change in the 6-min walk distance, a measure of exercise tolerance, SERAPHIN, in an event-driven design, used a composite endpoint of time to first morbidity or mortality event as a direct measure of disease progression. Furthermore, previous trials were relatively small—enrolling less than 200 patients—and, with 12–24 weeks of treatment, of relatively short duration.[203,204] SERAPHIN enrolled 742 patients, who were treated for up to 3.6 years, with a median exposure time of about 2 years.[170]

Macitentan 10 mg significantly reduced the risk of morbidity and mortality by 45% as compared to placebo ($p < 0.001$), confirming the expectations raised by the preclinical efficacy profile not only in terms of hemodynamics but also with regard to reversal of vascular and cardiac remodeling.[170,205] The effect on the primary endpoint was driven mainly by a decrease in worsening of PAH and consistent across disease severity and patient populations receiving macitentan as monotherapy or in combination with other PAH-specific therapies. There was also a significant decrease in the risk for PAH-related death or hospitalization, a secondary endpoint.[170] Significant improvements were observed for several additional parameters including exercise capacity as measured with the 6-min walk test, World Health Organization functional class, and health-related quality of life. Macitentan was generally well tolerated in this long-term study, and, especially important, the incidence of elevated liver enzymes was not different in the macitentan-treated groups compared to the placebo group, validating our screening efforts to improve the liver safety profile.

In 2013, in part on the basis of SERAPHIN, the US FDA approved macitentan 10 mg once daily for the treatment of PAH to delay disease progression and to reduce PAH related hospitalizations.[206] It was the first time that an oral PAH medication was approved for this indication based on a morbidity/mortality endpoint. In contrast to bosentan, for which liver monitoring is required, for macitentan liver monitoring is recommended and should be performed as clinically indicated. A benefit of macitentan on top of concomitant-specific PAH treatments was recognized. By the end of 2014, macitentan had been launched in 18 countries worldwide. In the EU, macitentan was granted orphan drug status based on the data from SERAPHIN.[207]

8.10.5 Conclusions

The goal of our drug discovery efforts was to identify a novel dual ERA for the treatment of patients with PAH that is devoid of the shortcomings of bosentan, ie, is more potent and more efficacious, can be administered to patients once a day only, and, in

particular, has no liver liability. In view of the large number of known ERAs, we decided to start our own drug discovery efforts from the structure of published ERAs rather than to perform a high-throughput screening. A careful analysis of the structures of these ERAs suggested that they could be divided into five structural classes, and we selected one prototypical structure from each of these categories for further optimization. In the course of our medicinal chemistry program, close to 2000 final compounds were prepared based on a core pyrimidine, about 400 represented benzodiazepinone derivatives, and another 100 compounds consisted of analogs of peptidomimetic **5**, pyrazole **12**, and *N*-acetylsulfonamide **28**. Of the about 2500 compounds tested in ET-1 binding assays, around 400 showed IC_{50} values of <20 nM and <400 nM on ET_A and ET_B, respectively, and were therefore tested for their functional potency ex vivo in rat aorta and trachea constriction experiments. About 300 compounds passed the in vitro and ex vivo potency criteria and were directly tested in an in vivo efficacy model. Nearly 40 compounds were clearly superior to bosentan in reducing the MAP in hypertensive Dahl-S rats and were therefore shortlisted for the in vivo liver safety assessment. A handful of compounds showed no effect on plasma bile salt levels after i.v. administration to Wistar rats and macitentan was finally selected among those compounds that passed additional standard safety tests.

This approach offered several attractive features that had a clear impact on the speed and the way the discovery project progressed. The use of telemetered conscious hypertensive Dahl-S rats allowed relatively easy, fast, and reliable hemodynamic monitoring and under the experimental settings chosen, the compound consumption for in vivo characterization was so little (10 mg) that the first batch of a compound usually delivered sufficient material for in vivo testing. The relatively high throughput of the in vivo experiment enabled us to base our SAR analyses to a large extent on efficacy data. As a consequence, we did not follow a more "classical" stepwise approach by characterizing the compounds in in vitro and in vivo DMPK assays prior to in vivo efficacy testing.

Macitentan's outstanding in vivo efficacy is accompanied if not caused by a target receptor interaction mode distinct from other ERAs: its low acidity and very compact conformation in aqueous solution allow macitentan to bind to a small subpocket within its target receptor using hydrophobic rather than charge–charge interaction forces. This tight hydrophobic fit is the likely basis for the distinctly slow target dissociation kinetics and insurmountable antagonism of macitentan, which place it among the number of modern and efficacious antagonists that resist competition with the natural agonist by a kinetic mechanism. This property, together with a superior tissue distribution, allows for a more complete inhibition of ET_A and ET_B receptors. Indeed, macitentan showed superior in vivo pharmacological activity versus other ERAs; not only acutely on hemodynamics but also in chronic models of pulmonary hypertension. Its ability to reduce vascular and right ventricular hypertrophy translated into a significant improvement in survival in rats, demonstrating its potential for long-term benefit.

The obvious result of macitentan's pharmacokinetic optimization is its significantly lower daily human dose of 10 mg and its more convenient once-a-day dosing regimen, compared to the bosentan dose of 125 mg given twice daily. Macitentan's superior drug–drug interaction and liver safety profile is not obvious from basic pharmacokinetic data, as bioavailability of both compounds is in the range of 50–70%, and drug exposures at steady state only differ by about 2.5-fold. From a biochemical perspective, the liabilities of bosentan originate from its dependence on OATP transport, induction of P450 enzymes, and inhibition of BSEP. From a more physiological view, all three issues have a common denominator, ie, the high drug concentrations in the liver. The increased lipophilicity of macitentan leads to a significant change in hepatic disposition by shifting the driving force for tissue penetration from active OATP transport to passive diffusion. As a consequence, intrahepatic macitentan concentrations are determined by and limited to the unbound drug concentrations in plasma. Unbound drug concentrations in the liver are therefore expected to be in the nanomolar range and thus markedly below those concentrations associated with P450 induction or BSEP inhibition in vitro. It is unclear with hindsight whether macitentan would have been selected in a classical lead optimization approach based on preclinical safety readouts, as neither its BSEP inhibition nor its PXR activation profile in vitro offer obvious advantages over bosentan. This highlights the concept that lead optimization needs to consider physiological parameters as much as biochemical data early in the discovery process to identify the most promising drug candidates. The early use of PK/pharmacodynamics modeling should be considered to properly integrate physicochemical and biological data in a comprehensive manner. The outcome of this approach was validated in clinical trials in which the absence of P450 induction as well as the superior liver safety profile of macitentan was finally demonstrated. Clinical outcome favorably translated into the labels of Opsumit® (macitentan 10 mg).[206,208]

Bosentan, the first ERA to be approved and the first oral therapy for PAH, was unquestionably a major breakthrough in the treatment of PAH. Macitentan, discovered through the rational targeted approach described here, represents an optimized ERA. In the landmark SERAPHIN trial, macitentan significantly reduced the risk of morbidity and mortality (composite endpoint) and of PAH related hospitalizations, and was effective in combination with other PAH therapies. In addition to excellent efficacy, macitentan showed an improved safety profile and was not associated with excess peripheral edema or liver enzyme elevations. Taking all these aspects into consideration, macitentan represents a genuine advance in the care of patients with PAH.

Acknowledgment

The authors gratefully acknowledge the medical writing support and editorial advice of Susan Flores as well as technical support of Markus Rey to produce Figs. 15 and 20–22.

References

1. Michel, R. P.; Langleben, D.; Dupuis, J. The Endothelin System in Pulmonary Hypertension. *Can. J. Physiol. Pharmacol.* **2003,** *81,* 542–554.
2. Iglarz, M.; Clozel, M. At the Heart of Tissue: Endothelin System and End-Organ Damage. *Clin. Sci. (Lond.)* **2010,** *119,* 453–463.
3. Shao, D.; Park, J. E.; Wort, S. J. The Role of Endothelin-1 in the Pathogenesis of Pulmonary Arterial Hypertension. *Pharmacol. Res.* **2011,** *63,* 504–511.
4. Giaid, A.; Yanagisawa, M.; Langleben, D.; Michel, R. P.; Levy, R.; Shennib, H.; Kimura, S.; Masaki, T.; Duguid, W. P.; Stewart, D. J. Expression of Endothelin-1 in the Lungs of Patients with Pulmonary Hypertension. *N. Engl. J. Med.* **1993,** *328,* 1732–1739.
5. Bouallegue, A.; Daou, G. B.; Srivastava, A. K. Endothelin-1-Induced Signaling Pathways in Vascular Smooth Muscle Cells. *Curr. Vasc. Pharmacol.* **2007,** *5,* 45–52.
6. Galie, N.; Hoeper, M. M.; Humbert, M.; Torbicki, A.; Vachiery, J. L.; Barbera, J. A.; Beghetti, M.; Corris, P.; Gaine, S.; Gibbs, J. S.; Gomez-Sanchez, M. A.; Jondeau, G.; Klepetko, W.; Opitz, C.; Peacock, A.; Rubin, L.; Zellweger, M.; Simonneau, G. Guidelines for the Diagnosis and Treatment of Pulmonary Hypertension: The Task Force for the Diagnosis and Treatment of Pulmonary Hypertension of the European Society of Cardiology (ESC) and the European Respiratory Society (ERS), Endorsed by the International Society of Heart and Lung Transplantation (ISHLT). *Eur. Heart J.* **2009,** *30,* 2493–2537.
7. Takayanagi, R.; Kitazumi, K.; Takasaki, C.; Ohnaka, K.; Aimoto, S.; Tasaka, K.; Ohashi, M.; Nawata, H. Presence of non-Selective Type of Endothelin Receptor on Vascular Endothelium and Its Linkage to Vasodilation. *FEBS Lett.* **1991,** *282,* 103–106.
8. Filep, J. G.; Fournier, A.; Foldes-Filep, E. Effects of the ETA/ETB Receptor Antagonist, Bosentan on Endothelin-1-Induced Myocardial Ischaemia and Oedema in the Rat. *Br. J. Pharmacol.* **1995,** *116,* 1745–1750.
9. Iglarz, M.; Steiner, P.; Wanner, D.; Rey, M.; Hess, P.; Clozel, M. Vascular Effects of Endothelin Receptor Antagonists Depends on Their Selectivity for ET_A vs. ET_B Receptors and on the Functionality of Endothelial ETB Receptors. *J. Cardiovasc. Pharmacol.* **2015,** *66,* 332–337.
10. Black, S. M.; Mata-Greenwood, E.; Dettman, R. W.; Ovadia, B.; Fitzgerald, R. K.; Reinhartz, O.; Thelitz, S.; Steinhorn, R. H.; Gerrets, R.; Hendricks-Munoz, K.; Ross, G. A.; Bekker, J. M.; Johengen, M. J.; Fineman, J. R. Emergence of Smooth Muscle Cell Endothelin B-Mediated Vasoconstriction in Lambs with Experimental Congenital Heart Disease and Increased Pulmonary Blood Flow. *Circulation* **2003,** *108,* 1646–1654.
11. Kakoki, M.; Hirata, Y.; Hayakawa, H.; Tojo, A.; Nagata, D.; Suzuki, E.; Kimura, K.; Goto, A.; Kikuchi, K.; Nagano, T.; Omata, M. Effects of Hypertension, Diabetes Mellitus, and Hypercholesterolemia on Endothelin Type B Receptor-Mediated Nitric Oxide Release from Rat Kidney. *Circulation* **1999,** *99,* 1242–1248.
12. Clozel, M.; Flores, S. Endothelin Receptors as Drug Targets in Chronic Cardiovascular Diseases: The Rationale for Dual Antagonism. *Drug Dev. Res.* **2006,** *67,* 825–834.
13. Mulder, P.; Richard, V.; Derumeaux, G.; Hogie, M.; Henry, J. P.; Lallemand, F.; Compagnon, P.; Mace, B.; Comoy, E.; Letac, B.; Thuillez, C. Role of Endogenous Endothelin in Chronic Heart Failure: Effect of Long-Term Treatment with an Endothelin Antagonist on Survival, Hemodynamics, and Cardiac Remodeling. *Circulation* **1997,** *96,* 1976–1982.
14. Yang, L. L.; Gros, R.; Kabir, M. G.; Sadi, A.; Gotlieb, A. I.; Husain, M.; Stewart, D. J. Conditional Cardiac Overexpression of Endothelin-1 Induces Inflammation and Dilated Cardiomyopathy in Mice. *Circulation* **2004,** *109,* 255–261.
15. Hocher, B.; Kalk, P.; Slowinski, T.; Godes, M.; Mach, A.; Herzfeld, S.; Wiesner, D.; Arck, P. C.; Neumayer, H. H.; Nafz, B. ETA Receptor Blockade Induces Tubular Cell Proliferation and Cyst Growth in Rats with Polycystic Kidney Disease. *J. Am. Soc. Nephrol.* **2003,** *14,* 367–376.
16. Kohan, D. E.; Rossi, N. F.; Inscho, E. W.; Pollock, D. M. Regulation of Blood Pressure and Salt Homeostasis by Endothelin. *Physiol. Rev.* **2011,** *91,* 1–77.
17. Vercauteren, M.; Strasser, D.; Vezzali, E.; Stalder, A.; Iglarz, M.; Hess, P.; Clozel, M. Vasopressin is Involved in Endothelin Receptor Antagonist-Induced Fluid Retention in Rat. Differential Effect of Selective ETA and Dual ETA/ETB Receptor Antagonists. *Eur. Respir. J.* **2012,** *40,* 716s.
18. King, T. E., Jr.; Brown, K. K.; Raghu, G.; du Bois, R. M.; Lynch, D. A.; Martinez, F.; Valeyre, D.; Leconte, I.; Morganti, A.; Roux, S.; Behr, J. BUILD-3: A Randomized, Controlled Trial of Bosentan in Idiopathic Pulmonary Fibrosis. *Am. J. Respir. Crit. Care Med.* **2011,** *184,* 92–99.
19. European Medicines Agency, Volibris, http://www.ema.europa.eu/ema/index.jsp?curl=pages/medicines/human/medicines/000839/human_med_001151.jsp&mid=WC0b01ac058001d124 (accessed October 2, 2015).
20. Raghu, G.; Behr, J.; Brown, K. K.; Egan, J. J.; Kawut, S. M.; Flaherty, K. R.; Martinez, F. J.; Nathan, S. D.; Wells, A. U.; Collard, H. R.; Costabel, U.; Richeldi, L.; de Andrade, J.; Khalil, N.; Morrison, L. D.; Lederer, D. J.; Shao, L.; Li, X.; Pedersen, P. S.; Montgomery, A. B.; Chien, J. W.; O'Riordan, T. G. Treatment of Idiopathic Pulmonary Fibrosis with Ambrisentan: A Parallel, Randomized Trial. *Ann. Intern. Med.* **2013,** *158,* 641–649.
21. Wu, C.; Chan, M. F.; Stavros, F.; Raju, B.; Okun, I.; Mong, S.; Keller, K. M.; Brock, T.; Kogan, T. P.; Dixon, R. A. Discovery of TBC11251, a Potent, Long Acting, Orally Active Endothelin Receptor-A Selective Antagonist. *J. Med. Chem.* **1997,** *40,* 1690–1697.
22. Thomson Reuters Drug News. Pfizer Withdraws Thelin from Market and Halts Clinical Trials. *Daily Drug News* **2010**, December 14. http://drugnews.thomson-pharma.com/ddn/article.do?id=107166 (accessed June 2016).
23. Riechers, H.; Albrecht, H. P.; Amberg, W.; Baumann, E.; Bernard, H.; Bohm, H. J.; Klinge, D.; Kling, A.; Muller, S.; Raschack, M.; Unger, L.; Walker, N.; Wernet, W. Discovery and Optimization of a Novel Class of Orally Active Nonpeptidic Endothelin-A Receptor Antagonists. *J. Med. Chem.* **1996,** *39,* 2123–2128.
24. Klings, E. S.; Farber, H. W. The Pathogenesis of HIV-Associated Pulmonary Hypertension. *Adv. Cardiol.* **2003,** *40,* 71–82.
25. Abraham, D. J.; Vancheeswaran, R.; Dashwood, M. R.; Rajkumar, V. S.; Pantelides, P.; Xu, S. W.; du Bois, R. M.; Black, C. M. Increased Levels of Endothelin-1 and Differential Endothelin Type A and B Receptor Expression in Scleroderma-Associated Fibrotic Lung Disease. *Am. J. Pathol.* **1997,** *151,* 831–841.
26. Bauer, M.; Wilkens, H.; Langer, F.; Schneider, S. O.; Lausberg, H.; Schäfers, H.-J. Selective Upregulation of Endothelin B Receptor Gene Expression in Severe Pulmonary Hypertension. *Circulation* **2002,** *105,* 1034–1036.
27. Miyauchi, T.; Yorikane, R.; Sakai, S.; Sakurai, T.; Okada, M.; Nishikibe, M.; Yano, M.; Yamaguchi, I.; Sugishita, Y.; Goto, K. Contribution of Endogenous Endothelin-1 to the Progression of Cardiopulmonary Alterations in Rats with Monocrotaline-Induced Pulmonary Hypertension. *Circ. Res.* **1993,** *73,* 887–897.
28. Gabbay, E.; Fraser, J.; McNeil, K. Review of Bosentan in the Management of Pulmonary Arterial Hypertension. *Vasc. Health Risk Manag.* **2007,** *3,* 887–900.
29. Dhillon, S. Bosentan—A Review of Its Use in the Management of Digital Ulcers Associated with Systemic Sclerosis. *Drugs* **2009,** *69,* 2005–2024.
30. Dhillon, S.; Keating, G. M. Bosentan—A Review of Its Use in the Management of Mildly Symptomatic Pulmonary Arterial Hypertension. *Am. J. Cardiovasc. Drugs* **2009,** *9,* 331–350.
31. Iglarz, M.; Binkert, C.; Morrison, K.; Fischli, W.; Gatfield, J.; Treiber, A.; Weller, T.; Bolli, M. H.; Boss, C.; Buchmann, S.; Capeleto, B.; Hess, P.; Qiu, C.; Clozel, M. Pharmacology of Macitentan, an Orally Active Tissue-Targeting Dual Endothelin Receptor Antagonist. *J. Pharmacol. Exp. Ther.* **2008,** *327,* 736–745.
32. Breu, V.; Loffler, B. M.; Clozel, M. In Vitro Characterization of Ro 46-2005, a Novel Synthetic non-Peptide Endothelin Antagonist of ETA and ETB Receptors. *FEBS Lett.* **1993,** *334,* 210–214.
33. Bolli, M. H.; Boss, C.; Binkert, C.; Buchmann, S.; Bur, D.; Hess, P.; Iglarz, M.; Meyer, S.; Rein, J.; Rey, M.; Treiber, A.; Clozel, M.; Fischli, W.; Weller, T. The Discovery of N-[5-(4-Bromophenyl)-6-[2-[(5-Bromo-2-Pyrimidinyl)oxy]Ethoxy]-4-Pyrimidinyl]-N′-p Ropylsulfamide (Macitentan), an Orally Active, Potent Dual Endothelin Receptor Antagonist. *J. Med. Chem.* **2012,** *55,* 7849–7861.
34. Clozel, M.; Breu, V.; Gray, G. A.; Kalina, B.; Loffler, B. M.; Burri, K.; Cassal, J. M.; Hirth, G.; Muller, M.; Neidhart, W.; et al. Pharmacological Characterization of Bosentan, a New Potent Orally Active Nonpeptide Endothelin Receptor Antagonist. *J. Pharmacol. Exp. Ther.* **1994,** *270,* 228–235.
35. Hess, P.; Clozel, M.; Clozel, J. P. Telemetry Monitoring of Pulmonary Arterial Pressure in Freely Moving Rats. *J. Appl. Physiol. (1985)* **1996,** *81,* 1027–1032.
36. Rey, M.; Weber, E. W.; Hess, P. D. Simultaneous Pulmonary and Systemic Blood Pressure and ECG Interval Measurement in Conscious, Freely Moving Rats. *J. Am. Assoc. Lab. Anim. Sci.* **2012,** *51,* 231–238.
37. Löffler, B. M.; Breu, V.; Clozel, M. Effect of Different Endothelin Receptor Antagonists and of the Novel non-Peptide Antagonist Ro 46-2005 on Endothelin Levels in Rat Plasma. *FEBS Lett.* **1993,** *333,* 108–110.

38. Dupuis, J.; Goresky, C. A.; Fournier, A. Pulmonary Clearance of Circulating Endothelin-1 in Dogs In Vivo: Exclusive Role of ETB Receptors. *J. Appl. Physiol. (1985)* **1996,** *81,* 1510–1515.
39. Fattinger, K.; Funk, C.; Pantze, M.; Weber, C.; Reichen, J.; Stieger, B.; Meier, P. J. The Endothelin Antagonist Bosentan Inhibits the Canalicular Bile Salt Export Pump: A Potential Mechanism for Hepatic Adverse Reactions. *Clin. Pharmacol. Ther.* **2001,** *69,* 223–231.
40. Jarvis, B.; Duff, R.; Elkinson, S. Endothelin Receptor Antagonists and Cardiovascular Disease. *Drugs R D* **1999,** *2,* 13–16.
41. Clark, W. M. Synthetic Approaches to Endothelin Receptor Antagonists in Clinical Development. *Curr. Opin. Drug Discov. Devel* **1999,** *2,* 565–577.
42. Boss, C.; Bolli, M.; Weller, T. Endothelin Receptor Antagonists: Structures, Synthesis, Selectivity and Therapeutic Applications. *Curr. Med. Chem.* **2002,** *9,* 349–383.
43. Dasgupta, F.; Mukherjee, A. K.; Gangadhar, N. Endothelin Receptor Antagonists—An Overview. *Curr. Med. Chem.* **2002,** *9,* 549–575.
44. Wu, C.; Holland, G. W.; Brock, T. A.; Dixon, R. A. F. Recently Discovered Sulfonamide-, Acyl Sulfonamide- and Carboxylic Acid-Based Endothelin Antagonists. *IDrugs* **2003,** *6,* 232–239.
45. Iqbal, J.; Sanghi, R.; Das, S. K. Endothelin Receptor Antagonists: An Overview of Their Synthesis and Structure–Activity Relationship. *Mini-Rev. Med. Chem.* **2005,** *5,* 381–408.
46. Houde, M.; Labonté, J.; D'Orléans-Juste, P. Peptide and Non-Peptide Antagonists Targeting Endothelin Receptors in Physiology and Pathology. *Curr. Pharm. Des.* **2011,** *17,* 2613–2625.
47. Webb, M. L.; Meek, T. D. Inhibitors of Endothelin. *Med. Res. Rev.* **1997,** *17,* 17–67.
48. Goddard, J.; Webb, D. J. Endothelin Receptor Antagonists. Promising new Agents in the Management of Cardiovascular Disorders. *Drugs R&D* **1999,** *2,* 1–12.
49. Schiffrin, E. L. Role of Endothelin-1 in Hypertension and Vascular Disease. *Am. J. Hypertens.* **2001,** *14,* 83S–89S.
50. Kim, N. H. S.; Rubin, L. J. Endothelin in Health and Disease: Endothelin Receptor Antagonists in the Management of Pulmonary Artery Hypertension. *J. Cardiovasc. Pharmacol. Ther.* **2002,** *7,* 9–19.
51. Suresh, D. P.; Lamba, S.; Abraham, W. T. New Developments in Heart Failure: Role of Endothelin and the Use of Endothelin Receptor Antagonists. *J. Card. Fail.* **2000,** *6,* 359–368.
52. Pollock, D. M. Endothelin Antagonists in the Treatment of Renal Failure. *Curr. Opin. Investig. Drugs* **2001,** *2,* 513–520.
53. Kohan, D. E.; Pollock, D. M. Endothelin Antagonists for Diabetic and Non-Diabetic Chronic Kidney Disease. *Br. J. Clin. Pharmacol.* **2013,** *76,* 573–579.
54. Nelson, J.; Bagnato, A.; Battistini, B.; Nisen, P. The Endothelin Axis: Emerging Role in Cancer. *Nat. Rev. Cancer* **2003,** *3,* 110–116.
55. Ishikawa, K.; Fukami, T.; Nagase, T.; Fujita, K.; Hayama, T.; Niiyama, K.; Mase, T.; Ihara, M.; Yano, M. Cyclic Pentapeptide Endothelin Antagonists with High ETA Selectivity. Potency- and Solubility-Enhancing Modifications. *J. Med. Chem.* **1992,** *35,* 2139–2142.
56. Ishikawa, K.; Ihara, M.; Noguchi, K.; Mase, T.; Mino, N.; Saeki, T.; Fukuroda, T.; Fukami, T.; Ozaki, S.; Nagase, T.; et al. Biochemical and Pharmacological Profile of a Potent and Selective Endothelin B-Receptor Antagonist, BQ-788. *Proc. Natl. Acad. Sci. U. S. A.* **1994,** *91,* 4892–4896.
57. Moreland, S. BQ-123, a Selective Endothelin ETA Receptor Antagonist. *Cardiovasc. Drug Rev.* **1994,** *12,* 48–69.
58. Okada, M.; Nishikibe, M. BQ-788, a Selective Endothelin ET(B) Receptor Antagonist. *Cardiovasc. Drug Rev.* **2002,** *20,* 53–66.
59. Sakai, S.; Miyauchi, T.; Kobayashi, M.; Yamaguchi, I.; Goto, K.; Sugishita, Y. Inhibition of Myocardial Endothelin Pathway Improves Long-Term Survival in Heart Failure. *Nature* **1996,** *384,* 353–355.
60. Goddard, J.; Strachan, F. E.; Maccallum, H.; Cumming, A. D.; Rankin, A. J.; Webb, D. J. Selective ET_A Endothelin Receptor Antagonism Is as Effective in Reducing Blood Pressure and Vascular Resistance as Combined $ET_{A/B}$ Receptor Antagonism in both Healthy Volunteers and Patients with Chronic Renal Failure. *Circulation* **2000,** *102,* 417. Abst. 2030.
61. Bohm, F.; Pernow, J.; Lindstrom, J.; Ahlborg, G. ET_A Receptors Mediate Vasoconstriction Whereas ET_B Receptors Clear Endothelin-1 in the Splanchnic and Renal Circulation of Healthy Men. *Eur. Heart J.* **2002,** *23* (Suppl.). Abst. 3254.
62. Sharaf, H. A.; Wilkinson, I. B.; McEniers, C. M.; Foo, R.; Kuc, R.; Ashby, M.; Brown, M. J. The Effect of BQ788 on Hemodynamics and Aldosterone Levels in Healthy Volunteers. *J. Hypertens.* **2002,** *20* (Suppl. 4). Abst P0131.
63. Apostolopoulou, S. C.; Rammos, S.; Kyriakides, Z. S.; Webb, D. J.; Johnston, N. R.; Cokkinos, D. V.; Kremastinos, D. T. Acute Endothelin A Receptor Antagonism Improves Pulmonary and Systemic Haemodynamics in Patients with Pulmonary Arterial Hypertension That Is Primary or Autoimmune and Related to Congenital Heart Disease. *Heart* **2003,** *89,* 1221–1226.
64. Tripathi, D.; Therapondos, G.; Ferguson, J. W.; Webb, D. J.; Newby, E. E.; Hayes, P. C. Role of Endothelin-1 in the Maintenance of Systemic and Portal Haemodynamics in Patients with Cirrhosis: A Randomised Double Blind Placebo-Controlled Haemodynamic Study of Endothelin-A and Endothelin-B Receptor Antagonism. *Gut* **2004,** *53* (Suppl. 3). Abst 046.
65. Mitchell, A.; Detmer, N.; Rushentsova, U.; Philipp, T. Effects of ET-1 Antagonism on ET-1-Mediated Vasoconstriction in the Skin Microcirculation of Obese Patients with Atherosclerosis. *J. Hypertens.* **2006,** *24* (Suppl. 4). Abst. P12.186.
66. Dhaun, N.; Macintyre, I. M.; Melville, V.; Lilitkarntakul, P.; Johnston, N. R.; Goddard, J.; Webb, D. J. Blood Pressure-Independent Reduction in Proteinuria and Arterial Stiffness After Acute Endothelin-A Receptor Antagonism in Chronic Kidney Disease. *Hypertension* **2009,** *54,* 113–119.
67. Wexberg, P.; Sperker, W.; Morgenthaler, N. G.; Heinzl, H.; Adlbrecht, C.; Plass, C.; Glogar, H. D.; Lang, I. M.; Neunteufl, T. Inhomogeneous Vasomotor Effects of Moderate Selective and Non-Selective Endothelin-Receptor Blockade in Stable Coronary Artery Disease. *Heart* **2009,** *95,* 1258–1264.
68. Cardillo, C.; Schinzari, F.; Melina, D.; Mores, N.; Bosello, S.; Peluso, G.; Zoli, A.; Ferraccioli, G. Improved Endothelial Function After Endothelin Receptor Blockade in Patients with Systemic Sclerosis. *Arthritis Rheum.* **2009,** *60,* 1840–1844.
69. Bruno, R. M.; Sudano, I.; Ghiadoni, L.; Masi, L.; Taddei, S. Interactions Between Sympathetic Nervous System and Endogenous Endothelin in Patients with Essential Hypertension. *Hypertension* **2011,** *57,* 79–84.
70. Kikuchi, T.; Ohtaki, T.; Kawata, A.; Imada, T.; Asami, T.; Masuda, Y.; Sugo, T.; Kusumoto, K.; Kubo, K.; Watanabe, T.; et al. Cyclic Hexapeptide Endothelin Receptor Antagonists Highly Potent for both Receptor Subtypes ETA and ETB. *Biochem. Biophys. Res. Commun.* **1994,** *200,* 1708–1712.
71. Watanabe, T.; Awane, Y.; Ikeda, S.; Fujiwara, S.; Kubo, K.; Kikuchi, T.; Kusumoto, K.; Wakimasu, M.; Fujino, M. Pharmacology of a Non-Selective ETA and ETB Receptor Antagonist, TAK-044 and the Inhibition of Myocardial Infarct Size in Rats. *Br. J. Pharmacol.* **1995,** *114,* 949–954.
72. Masuda, Y.; Sugo, T.; Kikuchi, T.; Kawata, A.; Satoh, M.; Fujisawa, Y.; Itoh, Y.; Wakimasu, M.; Ohtaki, T. Receptor Binding and Antagonist Properties of a Novel Endothelin Receptor Antagonist, TAK-044 [Cyclo[D-Alpha-Aspartyl-3-[(4-Phenylpiperazin-1-yl) Carbonyl]-L-Alanyl-L-Alpha-Aspartyl-D-2-(2-Thienyl) Glycyl-L-Leucyl-D-Tryptophyl]Disodium Salt], in Human EndothelinA and EndothelinB Receptors. *J. Pharmacol. Exp. Ther.* **1996,** *279,* 675–685.
73. Adis R&D Profile. TAK 044. *Drugs R&D* **1999**, *2*, 35–37.
74. Früh, T.; Saika, H.; Svensson, L.; Pitterna, T.; Sakaki, J.; Okada, T.; Urade, Y.; Oda, K.; Fujitani, Y.; Takimoto, M.; Yamamura, T.; Inui, T.; Makatani, M.; Takai, M.; Umemura, I.; Teno, N.; Toh, H.; Hayakawa, K.; Murata, T. IRL 2500: A Potent ET_B Selective Antagonist. *Bioorg. Med. Chem. Lett.* **1996,** *6,* 2323–2328.
75. Sakaki, J.; Murata, T.; Yuumoto, Y.; Nakamura, I.; Trueh, T.; Pitterna, T.; Iwasaki, G.; Oda, K.; Yamamura, T.; Hayakawa, K. Discovery of IRL 3461: A Novel and Potent Endothelin Antagonist with Balanced ETA/ETB Affinity. *Bioorg. Med. Chem. Lett.* **1998,** *8,* 2241–2246.
76. Sakaki, J.; Murata, T.; Yuumoto, Y.; Nakamura, I.; Hayakawa, K. Stereoselective Synthesis of a Novel and Bifunctional Endothelin Antagonist, IRL 3630. *Bioorg. Med. Chem. Lett.* **1998,** *8,* 2247–2252.
77. Makatani, M.; Fujitani, Y.; Takimoto, M.; Oda, K.; Sasaki, Y.; Hori, S.; Inui, T.; Sakaki, J.; Okada, T.; Hoshiko, K.; Yamamura, T. Effect of a Novel Bifunctional Endothelin Receptor Antagonist, IRL 3630A, on Guinea Pig Respiratory Mechanics. *Eur. J. Pharmacol.* **2000,** *406,* 139–147.
78. Ohlstein, E. H.; Nambi, P.; Lago, A.; Hay, D. W.; Beck, G.; Fong, K. L.; Eddy, E. P.; Smith, P.; Ellens, H.; Elliott, J. D. Nonpeptide Endothelin Receptor Antagonists. VI: Pharmacological Characterization of SB 217242, a Potent and Highly Bioavailable Endothelin Receptor Antagonist. *J. Pharmacol. Exp. Ther.* **1996,** *276,* 609–615.

79. Abraham, W. T.; Ascheim, D.; Demarco, T.; Klapholz, M.; Kukin, M.; Miller, A.; Yellen, L.; Holclslaw, T. L.; Packer, M. Effects of Enrasentan, a Nonselective Endothelin Receptor Antagonist, in Class II to III Heart Failure: Results of the Enrasentan Cooperative Randomized (ENCOR) Evaluation. *J. Am. Cardiol. Coll.* **2001,** *38,* 612.
80. Cosenzi, A. Enrasentan, an Antagonist of Endothelin Receptors. *Cardiovasc. Drug Rev.* **2003,** *21,* 1–16.
81. Prasad, S. K.; Dargie, H. J.; Smith, G. C.; Barlow, M. M.; Grothues, F.; Groenning, B. A.; Cleland, J. G.; Pennell, D. J. Comparison of the Dual Receptor Endothelin Antagonist Enrasentan with Enalapril in Asymptomatic Left Ventricular Systolic Dysfunction: A Cardiovascular Magnetic Resonance Study. *Heart* **2006,** *92,* 798–803.
82. Ohlstein, E. H.; Nambi, P.; Douglas, S. A.; Edwards, R. M.; Gellai, M.; Lago, A.; Leber, J. D.; Cousins, R. D.; Gao, A.; Frazee, J. S.; et al. SB 209670, a Rationally Designed Potent Nonpeptide Endothelin Receptor Antagonist. *Proc. Natl. Acad. Sci. U. S. A.* **1994,** *91,* 8052–8056.
83. Elliott, J. D.; Lago, M. A.; Cousins, R. D.; Gao, A.; Leber, J. D.; Erhard, K. F.; Nambi, P.; Elshourbagy, N. A.; Kumar, C.; Lee, J. A.; et al. 1,3-Diarylindan-2-Carboxylic Acids, Potent and Selective Non-Peptide Endothelin Receptor Antagonists. *J. Med. Chem.* **1994,** *37,* 1553–1557.
84. Shennib, H.; Lee, A. G.; Kuang, J. Q.; Yanagisawa, M.; Ohlstein, E. H.; Giaid, A. Efficacy of Administering an Endothelin-Receptor Antagonist (SB209670) in Ameliorating Ischemia-Reperfusion Injury in Lung Allografts. *Am. J. Respir. Crit. Care Med.* **1998,** *157,* 1975–1981.
85. Winn, M.; von Geldern, T. W.; Opgenorth, T. J.; Jae, H. S.; Tasker, A. S.; Boyd, S. A.; Kester, J. A.; Mantei, R. A.; Bal, R.; Sorensen, B. K.; Wu-Wong, J. R.; Chiou, W. J.; Dixon, D. B.; Novosad, E. I.; Hernandez, L.; Marsh, K. C. 2,4-Diarylpyrrolidine-3-Carboxylic Acids—Potent ETA Selective Endothelin Receptor Antagonists. 1. Discovery of A-127722. *J. Med. Chem.* **1996,** *39,* 1039–1048.
86. Jae, H. S.; Winn, M.; von Geldern, T. W.; Sorensen, B. K.; Chiou, W. J.; Nguyen, B.; Marsh, K. C.; Opgenorth, T. J. Pyrrolidine-3-Carboxylic Acids as Endothelin Antagonists. 5. Highly Selective, Potent, and Orally Active ET(A) Antagonists. *J. Med. Chem.* **2001,** *44,* 3978–3984.
87. Liu, G.; Kozmina, N. S.; Winn, M.; von Geldern, T. W.; Chiou, W. J.; Dixon, D. B.; Nguyen, B.; Marsh, K. C.; Opgenorth, T. J. Design, Synthesis, and Activity of a Series of Pyrrolidine-3-Carboxylic Acid-Based, Highly Specific, Orally Active ET(B) Antagonists Containing a Diphenylmethylamine Acetamide Side Chain. *J. Med. Chem.* **1999,** *42,* 3679–3689.
88. von Geldern, T. W.; Tasker, A. S.; Sorensen, B. K.; Winn, M.; Szczepankiewicz, B. G.; Dixon, D. B.; Chiou, W. J.; Wang, L.; Wessale, J. L.; Adler, A.; Marsh, K. C.; Nguyen, B.; Opgenorth, T. J. Pyrrolidine-3-Carboxylic Acids as Endothelin Antagonists. 4. Side Chain Conformational Restriction Leads to ET(B) Selectivity. *J. Med. Chem.* **1999,** *42,* 3668–3678.
89. Andress, D. L.; Coll, B.; Pritchett, Y.; Brennan, J.; Molitch, M.; Kohan, D. E. Clinical Efficacy of the Selective Endothelin A Receptor Antagonist, Atrasentan, in Patients with Diabetes and Chronic Kidney Disease (CKD). *Life Sci.* **2012,** *91,* 739–742.
90. Schulman, C. Atrasentan: The First Endothelin Receptor Antagonist for Hormone-Refractory Prostate Cancer. *Eur. Urol. Suppl.* **2003,** *2,* 20–27.
91. Nelson, J. B.; Love, W.; Chin, J. L.; Saad, F.; Schulman, C. C.; Sleep, D. J.; Qian, J.; Steinberg, J.; Carducci, M. Phase 3, Randomized, Controlled Trial of Atrasentan in Patients with Nonmetastatic, Hormone-Refractory Prostate Cancer. *Cancer* **2008,** *113,* 2478–2487.
92. Niiyama, K.; Mase, T.; Takahashi, H.; Naya, A.; Katsuki, K.; Nagase, T.; Ito, S.; Hayama, T.; Hisaka, A.; Ozaki, S.; Ihara, M.; Yano, M.; Fukuroda, T.; Noguchi, K.; Nishikibe, M.; Ishikawa, K. 6-Carboxy-5,7-Diarylcyclopenteno[1,2-b]Pyridine Derivatives: A Novel Class of Endothelin Receptor Antagonists. *Bioorg. Med. Chem.* **2002,** *10,* 2461–2470.
93. Nishikibe, M.; Ohta, H.; Okada, M.; Ishikawa, K.; Hayama, T.; Fukuroda, T.; Noguchi, K.; Saito, M.; Kanoh, T.; Ozaki, S.; Kamei, T.; Hara, K.; William, D.; Kivlighn, S.; Krause, S.; Gabel, R.; Zingaro, G.; Nolan, N.; O'Brien, J.; Clayton, F.; Lynch, J.; Pettibone, D.; Siegl, P. Pharmacological Properties of J-104132 (L-753,037), a Potent, Orally Active, Mixed ETA/ETB Endothelin Receptor Antagonist. *J. Pharmacol. Exp. Ther.* **1999,** *289,* 1262–1270.
94. O'Rourke, S. T. J-104132 Banyu. *Curr. Opin. Cardiovasc. Pulm. Renal Investig. Drugs* **2000,** *2,* 51–54.
95. Zhang, J.; Didierlaurent, S.; Fortin, M.; Lefrancois, D.; Uridat, E.; Vevert, J. P. Nonpeptide Endothelin Antagonists: From Lower Affinity Pyrazol-5-ols to Higher Affinity Pyrazole-5-Carboxylic Acids. *Bioorg. Med. Chem. Lett.* **2000,** *10,* 1351–1355.
96. Zhang, J.; Didierlaurent, S.; Fortin, M.; Lefrancois, D.; Uridat, E.; Vevert, J. P. Potent Nonpeptide Endothelin Antagonists: Synthesis and Structure–Activity Relationships of Pyrazole-5-Carboxylic Acids. *Bioorg. Med. Chem. Lett.* **2000,** *10,* 2575–2578.
97. Heckmann, B.; Jouquey, S.; Vevert, J.-P.; Zhang, J. Novel Imidazole N-Benzyldioxol Derivatives, Methods for Preparing the Same, Resulting Intermediates, Pharmaceutical Compositions and Use of Said Derivatives as Endothelin Antagonists. WO199717339, May 15, 1997.
98. Haesslein, J. L.; Baholet, I.; Fortin, M.; Iltis, A.; Khider, J.; Periers, A. M.; Pierre, C.; Vevert, J. P. 1,3-Disubstituted-2-Carboxy Quinolones: Highly Potent and Selective Endothelin A Receptor Antagonists. *Bioorg. Med. Chem. Lett.* **2000,** *10,* 1487–1490.
99. Ishizuka, N.; Matsumura, K.; Sakai, K.; Fujimoto, M.; Mihara, S.; Yamamori, T. Structure–Activity Relationships of a Novel Class of Endothelin-A Receptor Antagonists and Discovery of Potent and Selective Receptor Antagonist, 2-(Benzo[1,3]Dioxol-5-yl)-6-Isopropyloxy-4-(4-Methoxyphenyl)-2H-Chromene-3-Carbox Ylic Acid (S-1255). 1. Study on Structure–Activity Relationships and Basic Structure Crucial for ET(A) Antagonism. *J. Med. Chem.* **2002,** *45,* 2041–2055.
100. Coe, Y.; Haleen, S. J.; Welch, K. M.; Coceani, F. The Endothelin-A-Receptor Antagonist PD 180988 (Cl-1034) Selectively Reverses the Pulmonary Vasoconstrictor Response to Hypoxia in the Lamb. *J. Cardiovasc. Pharmacol.* **2000,** *36,* S331–S333.
101. Philipp, S.; Monti, J.; Pagel, I.; Langenickel, T.; Notter, T.; Ruschitzka, F.; Luscher, T.; Dietz, R.; Willenbrock, R. Treatment with Darusentan Over 21 Days Improved cGMP Generation in Patients with Chronic Heart Failure. *Clin. Sci. (Lond.)* **2002,** *103* (Suppl. 48), 249S–253S.
102. Luscher, T. F.; Enseleit, F.; Pacher, R.; Mitrovic, V.; Schulze, M. R.; Willenbrock, R.; Dietz, R.; Rousson, V.; Hurlimann, D.; Philipp, S.; Notter, T.; Noll, G.; Ruschitzka, F. Hemodynamic and Neurohumoral Effects of Selective Endothelin A (ET(A)) Receptor Blockade in Chronic Heart Failure: The Heart Failure ET(A) Receptor Blockade Trial (HEAT). *Circulation* **2002,** *106,* 2666–2672.
103. Anand, I.; McMurray, J.; Cohn, J. N.; Konstam, M. A.; Notter, T.; Quitzau, K.; Ruschitzka, F.; Luscher, T. F. Long-Term Effects of Darusentan on Left-Ventricular Remodelling and Clinical Outcomes in the EndothelinA Receptor Antagonist Trial in Heart Failure (EARTH): Randomised, Double-Blind, Placebo-Controlled Trial. *Lancet* **2004,** *364,* 347–354.
104. Black, H. R.; Bakris, G. L.; Weber, M. A.; Weiss, R.; Shahawy, M. E.; Marple, R.; Tannoury, G.; Linas, S.; Wiens, B. L.; Linseman, J. V.; Roden, R.; Gerber, M. J. Efficacy and Safety of Darusentan in Patients with Resistant Hypertension: Results from a Randomized, Double-Blind, Placebo-Controlled Dose-Ranging Study. *J. Clin. Hypertens. (Greenwich)* **2007,** *9,* 760–769.
105. Weber, M. A.; Black, H.; Bakris, G.; Krum, H.; Linas, S.; Weiss, R.; Linseman, J. V.; Wiens, B. L.; Warren, M. S.; Lindholm, L. H. A Selective Endothelin-Receptor Antagonist to Reduce Blood Pressure in Patients with Treatment-Resistant Hypertension: A Randomised, Double-Blind, Placebo-Controlled Trial. *Lancet* **2009,** *374,* 1423–1431.
106. Frampton, J. E. Ambrisentan. *Am. J. Cardiovasc. Drugs* **2011,** *11,* 215–226.
107. Astles, P. C.; Brealey, C.; Brown, T. J.; Facchini, V.; Handscombe, C.; Harris, N. V.; McCarthy, C.; McLay, I. M.; Porter, B.; Roach, A. G.; Sargent, C.; Smith, C.; Walsh, R. J. Selective Endothelin A Receptor Antagonists. 3. Discovery and Structure–Activity Relationships of a Series of 4-Phenoxybutanoic Acid Derivatives. *J. Med. Chem.* **1998,** *41,* 2732–2744.
108. Stein, P. D.; Hunt, J. T.; Floyd, D. M.; Moreland, S.; Dickinson, K. E.; Mitchell, C.; Liu, E. C.; Webb, M. L.; Murugesan, N.; Dickey, J.; et al. The Discovery of Sulfonamide Endothelin Antagonists and the Development of the Orally Active ETA Antagonist 5-(Dimethylamino)-N-(3,4-Dimethyl-5-Isoxazolyl)-1-Naphthalenesulfonamide. *J. Med. Chem.* **1994,** *37,* 329–331.
109. Murugesan, N.; Gu, Z.; Stein, P. D.; Spergel, S.; Mathur, A.; Leith, L.; Liu, E. C.; Zhang, R.; Bird, E.; Waldron, T.; Marino, A.; Morrison, R. A.; Webb, M. L.; Moreland, S.; Barrish, J. C. Biphenylsulfonamide endothelin Receptor Antagonists. 2. Discovery of 4′-Oxazolyl Biphenylsulfonamides as a New Class of Potent, Highly Selective ET(A) Antagonists. *J. Med. Chem.* **2000,** *43,* 3111–3117.
110. Murugesan, N.; Gu, Z.; Spergel, S.; Young, M.; Chen, P.; Mathur, A.; Leith, L.; Hermsmeier, M.; Liu, E. C.; Zhang, R.; Bird, E.; Waldron, T.; Marino, A.; Koplowitz, B.; Humphreys, W. G.; Chong, S.; Morrison, R. A.; Webb, M. L.; Moreland, S.; Trippodo, N.; Barrish, J. C. Biphenylsulfonamide Endothelin Receptor Antagonists. 4. Discovery of N-[[2′-[[(4,5-Dimethyl-3-Isoxazolyl)Amino]Sulfonyl]-4-(2-Oxazolyl)[1,1′-Biphenyl]—2-yl]Methyl]-N,3,3-Trimethylbutanamide (BMS-207940), a Highly Potent and Orally Active ET(A) Selective Antagonist. *J. Med. Chem.* **2003,** *46,* 125–137.

111. Hulpke-Wette, M.; Buchhorn, R. BMS-193884 and BMS-207940 Bristol-Myers Squibb. *Curr. Opin. Investig. Drugs* **2002,** *3,* 1057–1061.
112. Bradbury, R. H.; Butlin, R. J.; James, R. M. N-Heteroaryl-pyridinesulfonamide Derivatives and Their Use as Endothelin Antagonists. WO1996040681, Dec 19, 1996.
113. Mortlock, A. A.; Bath, C.; Butlin, R. J.; Heys, C.; Hunt, S. J.; Reid, A. C.; Sumner, N. F.; Tang, E. K.; Whiting, E.; Wilson, C.; Wright, N. D. N-Methyl-2-[4-(2-Methylpropyl) Phenyl]-3-(3-Methoxy-5-Methylpyrazin-2-Ylsulfamoyl)Benzamide; One of a Class of Novel Benzenesulphonamides Which Are Orally-Active, ET_A-Selective Endothelin Antagonists. *Bioorg. Med. Chem. Lett.* **1997,** *7,* 1399–1402.
114. James, N. D.; Caty, A.; Payne, H.; Borre, M.; Zonnenberg, B. A.; Beuzeboc, P.; McIntosh, S.; Morris, T.; Phung, D.; Dawson, N. A. Final Safety and Efficacy Analysis of the Specific Endothelin A Receptor Antagonist Zibotentan (ZD4054) in Patients with Metastatic Castration-Resistant Prostate Cancer and Bone Metastases Who Were Pain-Free or Mildly Symptomatic for Pain: A Double-Blind, Placebo-Controlled, Randomized Phase II Trial. *BJU Int.* **2010,** *106,* 966–973.
115. Dawson, N.; Payne, H.; Battersby, C.; Taboada, M.; James, N. Health-Related Quality of Life in Pain-Free or Mildly Symptomatic Patients with Metastatic Hormone-Resistant Prostate Cancer Following Treatment with the Specific Endothelin A Receptor Antagonist Zibotentan (ZD4054). *J. Cancer Res. Clin. Oncol.* **2011,** *137,* 99–113.
116. Schelman, W. R.; Liu, G.; Wilding, G.; Morris, T.; Phung, D.; Dreicer, R. A Phase I Study of Zibotentan (ZD4054) in Patients with Metastatic, Castrate-Resistant Prostate Cancer. *Invest. New Drugs* **2011,** *29,* 118–125.
117. Nelson, J. B.; Fizazi, K.; Miller, K.; Higano, C.; Moul, J. W.; Akaza, H.; Morris, T.; McIntosh, S.; Pemberton, K.; Gleave, M. Phase 3, Randomized, Placebo-Controlled Study of Zibotentan (ZD4054) in Patients with Castration-Resistant Prostate Cancer Metastatic to Bone. *Cancer* **2012,** *118,* 5709–5718.
118. Raju, B.; Wu, C.; Castillo, R.; Okun, I.; Stavros, F.; Chan, M. F. 2-Aryloxycarbonylthiophene-3-Sulfonamides: Highly Potent and ET_A Selective Endothelin Receptor Antagonists. *Bioorg. Med. Chem. Lett.* **1997,** *7,* 2093–2098.
119. Graul, A.; Leeson, P. A.; Castañer, J. Sitaxsentan Sodium. *Drugs Future* **2000,** *25,* 159–164.
120. Wu-Wong, J. R. Sitaxsentan (ICOS-Texas Biotechnology). *Curr. Opin. Investig. Drugs* **2001,** *2,* 531–536.
121. Wu, C.; Decker, E. R.; Blok, N.; Bui, H.; You, T. J.; Wang, J.; Bourgoyne, A. R.; Knowles, V.; Berens, K. L.; Holland, G. W.; Brock, T. A.; Dixon, R. A. Discovery, Modeling, and Human Pharmacokinetics of N-(2-Acetyl-4,6-Dimethylphenyl)-3-(3,4-Dimethylisoxazol-5-Ylsulfamoyl)Thiophene-2-Carboxamide (TBC3711), a Second Generation, ETA Selective, and Orally Bioavailable Endothelin Antagonist. *J. Med. Chem.* **2004,** *47,* 1969–1986.
122. Walsh, T. F.; Fitch, K. J.; Williams, D. L., Jr.; Murphy, K. L.; Nolan, N. A.; Pettibone, D. J.; Chang, R. S. L.; O'Malley, S. S.; Clineschmidt, B. V.; Veber, D. F.; Greenlee, W. J. Potent Dual Antagonists of Endothelin and Angiotensin II Receptors Derived from α-Phenoxyphenylacetic Acids (Part III). *Biorg. Med. Chem. Lett.* **1995,** *5,* 1155–1158.
123. Williams, D. L., Jr.; Murphy, K. L.; Nolan, N. A.; O'Brien, J. A.; Pettibone, D. J.; Kivlighn, S. D.; Krause, S. M.; Lis, E. V., Jr.; Zingaro, G. J.; Gabel, R. A.; et al. Pharmacology of L-754,142, a Highly Potent, Orally Active, Nonpeptidyl Endothelin Antagonist. *J. Pharmacol. Exp. Ther.* **1995,** *275,* 1518–1526.
124. Dorsch, D.; Mederski, W. W. K. R.; Osswald, M.; Devant, R. M.; Schmitges, C.-J.; Christadler, M.; Wilm, C. Pyridazinones with a Pendant Acylsulfonamide Moiety as Endothelin Receptor Antagonists. *Bioorg. Med. Chem. Lett.* **1997,** *7,* 275–280.
125. Rawson, D. J.; Dack, K. N.; Dickinson, R. P.; James, K. The Design and Synthesis of a Novel Series of Indole Derived Selective ET_A Antagonists. *Bioorg. Med. Chem. Lett.* **2002,** *12,* 125–128.
126. Iwasaki, T.; Mihara, S.; Shimamura, T.; Kawakami, M.; Hayasaki-Kajiwara, Y.; Naya, N.; Fujimoto, M.; Nakajima, M. Pharmacological Characterization of PABSA, an Orally Active and Highly Potent Endothelin-Receptor Antagonist. *J. Cardiovasc. Pharmacol.* **1999,** *34,* 139–147.
127. Clozel, M.; Breu, V.; Burri, K.; Cassal, J.-M.; Fischli, W.; Gray, G. A.; Hirth, G.; Löffler, B.-M.; Müller, M.; Neidhart, W.; Ramuz, H. Pathophysiological Role of Endothelin Revealed by the First Orally Active Endothelin Receptor Antagonist. *Nature* **1993,** *365,* 759–761.
128. Neidhart, W.; Breu, V.; Bur, D.; Burri, K.; Clozel, M.; Hirth, G.; Müller, M.; Wessel, H. P.; Ramuz, H. The Discovery of Nonpeptide Endothelin Receptor Antagonists. Progression Towards Bosentan. *Chimia* **1996,** *50,* 519–524.
129. Mealy, N. E.; Bayes, M.; del Fresno, M. Bosentan. *Drugs Future* **2001,** *26,* 1149–1154.
130. Hoette, S.; O'Callaghan, D. S.; Jardim, C.; Souza, R. Dual Receptor Blockade by Bosentan: Clinical Experience in Treatment of Pulmonary Hypertension. *J. Receptor Ligand Channel Res.* **2010,** *3,* 113–121.
131. Breu, V.; Coassolo, P.; Neidhart, W.; Roux, S.; Weiss, P. Preparation of N-(pyridylpyrimidinyl)heterocyclysulfonamides as endothelin receptor antagonists. WO2000052007, Feb 28, 2000.
132. Dutzler, R.; Ernstb, B.; Hediger, M. A.; Keppler, D.; Mohr, P.; Neidhart, W.; Marki, H. P. Channels and Transporters. Mini-Symposium of the Division of Medicinal Chemistry (DMC) of the Swiss Chemical Society (SCS) at the Department of Chemistry, University of Basel, May 27, 2010. *Chimia (Aarau)* **2010,** *64,* 662–666.
133. Mann, J. F.; Green, D.; Jamerson, K.; Ruilope, L. M.; Kuranoff, S. J.; Littke, T.; Viberti, G. Avosentan for Overt Diabetic Nephropathy. *J. Am. Soc. Nephrol.* **2010,** *21,* 527–535.
134. Clozel, M.; Ramuz, H.; Clozel, J. P.; Breu, V.; Hess, P.; Loffler, B. M.; Coassolo, P.; Roux, S. Pharmacology of Tezosentan, New Endothelin Receptor Antagonist Designed for Parenteral Use. *J. Pharmacol. Exp. Ther.* **1999,** *290,* 840–846.
135. Tovar, J. M.; Gums, J. G. Tezosentan in the Treatment of Acute Heart Failure. *Ann. Pharmacother.* **2003,** *37,* 1877–1883.
136. Teerlink, J. R.; McMurray, J. J.; Bourge, R. C.; Cleland, J. G.; Cotter, G.; Jondeau, G.; Krum, H.; Metra, M.; O'Connor, C. M.; Parker, J. D.; Torre-Amione, G.; Van Veldhuisen, D. J.; Frey, A.; Rainisio, M.; Kobrin, I. Tezosentan in Patients with Acute Heart Failure: Design of the Value of Endothelin Receptor Inhibition with Tezosentan in Acute Heart Failure Study (VERITAS). *Am. Heart J.* **2005,** *150,* 46–53.
137. McMurray, J. J.; Teerlink, J. R.; Cotter, G.; Bourge, R. C.; Cleland, J. G.; Jondeau, G.; Krum, H.; Metra, M.; O'Connor, C. M.; Parker, J. D.; Torre-Amione, G.; van Veldhuisen, D. J.; Lewsey, J.; Frey, A.; Rainisio, M.; Kobrin, I. Effects of Tezosentan on Symptoms and Clinical Outcomes in Patients with Acute Heart Failure: The VERITAS Randomized Controlled Trials. *JAMA* **2007,** *298,* 2009–2019.
138. Roux, S.; Breu, V.; Giller, T.; Neidhart, W.; Ramuz, H.; Coassolo, P.; Clozel, J. P.; Clozel, M. Ro 61-1790, a New Hydrosoluble Endothelin Antagonist: General Pharmacology and Effects on Experimental Cerebral Vasospasm. *J. Pharmacol. Exp. Ther.* **1997,** *283,* 1110–1118.
139. Wang, X.; Li, Y. M.; Li, W. Q.; Huang, C. G.; Lu, Y. C.; Hou, L. J. Effect of Clazosentan in Patients with Aneurysmal Subarachnoid Hemorrhage: A Meta-Analysis of Randomized Controlled Trials. *PLoS One* **2012,** *7,* e47778.
140. Macdonald, R. L.; Higashida, R. T.; Keller, E.; Mayer, S. A.; Molyneux, A.; Raabe, A.; Vajkoczy, P.; Wanke, I.; Bach, D.; Frey, A.; Marr, A.; Roux, S.; Kassell, N. Clazosentan, an Endothelin Receptor Antagonist, in Patients with Aneurysmal Subarachnoid Haemorrhage Undergoing Surgical Clipping: A Randomised, Double-Blind, Placebo-Controlled Phase 3 Trial (CONSCIOUS-2). *Lancet Neurol.* **2011,** *10,* 618–625.
141. Hoshino, T.; Yamauchi, R.; Kikkawa, K.; Yabana, H.; Murata, S. Pharmacological Profile of T-0201, a Highly Potent and Orally Active Endothelin Receptor Antagonist. *J. Pharmacol. Exp. Ther.* **1998,** *286,* 643–649.
142. Morimoto, H.; Ohashi, N.; Shimadzu, H.; Kushiyama, E.; Kawanishi, H.; Hosaka, T.; Kawase, Y.; Yasuda, K.; Kikkawa, K.; Yamauchi-Kohno, R.; Yamada, K. Potent and Selective ET-A Antagonists. 2. Discovery and Evaluation of Potent Water Soluble N-(6-(2-Aryloxy)Ethoxy)-4-Pyrimidinyl)Sulfonamide Derivatives. *J. Med. Chem.* **2001,** *44,* 3369–3377.
143. Takahashi, M.; Taniguchi, T.; Tanaka, T.; Kanamaru, H.; Okada, K.; Muramatsu, I. Pharmacological Characterization of TA-0201, an Endothelin Receptor Antagonist, with Recombinant and Human Prostate Endothelin Receptors. *Eur. J. Pharmacol.* **2003,** *467,* 185–189.
144. Harada, H.; Kazami, J.; Watanuki, S.; Tsuzuki, R.; Sudoh, K.; Fujimori, A.; Sanagi, M.; Orita, M.; Nakahara, H.; Shimaya, J.; Tsukamoto, S.; Tanaka, A.; Yanagisawa, I. Ethenesulfonamide and Ethanesulfonamide Derivatives, a Novel Class of Orally Active Endothelin-A Receptor Antagonists. *Bioorg. Med. Chem.* **2001,** *9,* 2955–2968.
145. Yuyama, H.; Fujimori, A.; Sanagi, M.; Koakutsu, A.; Noguchi, Y.; Sudoh, K.; Sasamata, M.; Miyata, K. A Novel and Selective Endothelin ET(A) Receptor Antagonist YM598 Prevents the Development of Chronic Hypoxia-Induced Pulmonary Hypertension in Rats. *Vascul. Pharmacol.* **2005,** *43,* 40–46.
146. Sugimoto, K.; Tsuruoka, S.; Fujimura, A. Renal Protective Effect of YM598, a Selective Endothelin ET(A) Receptor Antagonist, Against Diabetic Nephropathy in OLETF Rats. *Eur. J. Pharmacol.* **2002,** *450,* 183–189.

147. Hirata, M.; Deushi, T.; Takahashi, Y.; Tamura, M.; Ohshima, T.; Oda, T.; Ishikawa, T. Pyrimidine Derivatives. WO199709318, Mar 13, 1997.
148. Fortin, M.; Zhang, J. Novel Pyrazole and Pyrazolone Derivatives for Use as Endothelin Receptor Antagonists. WO199612706, May 2, 1996.
149. Mah, R.; Gerspacher, M.; von Sprecher, A.; Stutz, S.; Tschinke, V.; Anderson, G. P.; Bertrand, C.; Subramanian, N.; Ball, H. A. Biphenyl Derivatives as Novel Dual NK(1)/NK(2)-Receptor Antagonists. *Bioorg. Med. Chem. Lett.* **2002,** *12,* 2065–2068.
150. Gerspacher, M.; von Sprecher, A.; Mah, R.; Anderson, G. P.; Bertrand, C.; Subramanian, N.; Hauser, K.; Ball, H. A. N-[(R, R)-(E)-1-(4-Chloro-Benzyl)-3-(2-oxo-Azepan-3-Ylcarbamoyl)-Allyl]-N-Methyl-3,5-bis-Trifluoromethyl-Benzamide: An Orally Active Neurokinin NK1/NK2 Antagonist. *Bioorg. Med. Chem. Lett.* **2000,** *10,* 1467–1470.
151. Amberg, W.; Kling, A.; Klinge, D.; Riechers, H.; Hergenröder, S.; Raschack, M.; Unger, L. New β-Amino and β-Azidocarboxylic Acid Derivatives, the Production Thereof and the Use thereof as Endothelin Receptor Antagonists. WO9858916, Dec 30, 1998.
152. Bolli, M. H.; Marfurt, J.; Grisostomi, C.; Boss, C.; Binkert, C.; Hess, P.; Treiber, A.; Thorin, E.; Morrison, K.; Buchmann, S.; Bur, D.; Ramuz, H.; Clozel, M.; Fischli, W.; Weller, T. Novel Benzo[1,4]Diazepin-2-One Derivatives as Endothelin Receptor Antagonists. *J. Med. Chem.* **2004,** *47,* 2776–2795.
153. Gatfield, J.; Mueller Grandjean, C.; Sasse, T.; Clozel, M.; Nayler, O. Slow Receptor Dissociation Kinetics Differentiate Macitentan from Other Endothelin Receptor Antagonists in Pulmonary Arterial Smooth Muscle Cells. *PLoS One* **2012,** *7,* e47662.
154. Gatfield, J.; Mueller Grandjean, C.; Bur, D.; Bolli, M. H.; Nayler, O. Distinct ETA Receptor Binding Mode of Macitentan As Determined by Site Directed Mutagenesis. *PLoS One* **2014,** *9,* e107809.
155. Iglarz, M.; Bossu, A.; Wanner, D.; Bortolamiol, C.; Rey, M.; Hess, P.; Clozel, M. Comparison of Pharmacological Activity of Macitentan and Bosentan in Preclinical Models of Systemic and Pulmonary Hypertension. *Life Sci.* **2014,** *118,* 333–339.
156. Iglarz, M.; Landskroner, K.; Bauer, Y.; Vercauteren, M.; Rey, M.; Renault, B.; Studer, R.; Vezzali, E.; Freti, D.; Hadana, H.; Schlapfer, M.; Cattaneo, C.; Bortolamiol, C.; Weber, E.; Whitby, B. R.; Delahaye, S.; Wanner, D.; Steiner, P.; Nayler, O.; Hess, P.; Clozel, M. Comparison of Macitentan and Bosentan on Right Ventricular Remodeling in a Rat Model of Non-Vasoreactive Pulmonary Hypertension. *J. Cardiovasc. Pharmacol.* **2015,** *66* (5), 457–467.
157. Breu, V.; Hashido, K.; Broger, C.; Miyamoto, C.; Furuichi, Y.; Hayes, A.; Kalina, B.; Loffler, B. M.; Ramuz, H.; Clozel, M. Separable Binding Sites for the Natural Agonist Endothelin-1 and the Non-Peptide Antagonist Bosentan on Human Endothelin-A Receptors. *Eur. J. Biochem.* **1995,** *231,* 266–270.
158. Swinney, D. C. Biochemical Mechanisms of New Molecular Entities (NMEs) Approved by United States FDA During 2001–2004: Mechanisms Leading to Optimal Efficacy and Safety. *Curr. Top. Med. Chem.* **2006,** *6,* 461–478.
159. Swinney, D. C.; Haubrich, B. A.; Liefde, I. V.; Vauquelin, G. The Role of Binding Kinetics in GPCR Drug Discovery. *Curr. Top. Med. Chem.* **2015,** *15,* 2504–2522.
160. Kenakin, T.; Jenkinson, S.; Watson, C. Determining the Potency and Molecular Mechanism of Action of Insurmountable Antagonists. *J. Pharmacol. Exp. Ther.* **2006,** *319,* 710–723.
161. Le, M. T.; Pugsley, M. K.; Vauquelin, G.; Van Liefde, I. Molecular Characterisation of the Interactions Between Olmesartan and Telmisartan and the Human Angiotensin II AT1 Receptor. *Br. J. Pharmacol.* **2007,** *151,* 952–962.
162. Gradman, A. H. AT(1)-Receptor Blockers: Differences That Matter. *J. Hum. Hypertens.* **2002,** *16* (Suppl. 3), S9–S16.
163. Zhang, C.; Srinivasan, Y.; Arlow, D. H.; Fung, J. J.; Palmer, D.; Zheng, Y.; Green, H. F.; Pandey, A.; Dror, R. O.; Shaw, D. E.; Weis, W. I.; Coughlin, S. R.; Kobilka, B. K. High-Resolution Crystal Structure of Human Protease-Activated Receptor 1. *Nature* **2012,** *492,* 387–392.
164. Swinney, D. C. Molecular Mechanism of Action (MMoA) in Drug Discovery. *Ann. Rep. Med. Chem.* **2011,** *46,* 301–317.
165. Granier, S.; Manglik, A.; Kruse, A. C.; Kobilka, T. S.; Thian, F. S.; Weis, W. I.; Kobilka, B. K. Structure of the Delta-Opioid Receptor Bound to Naltrindole. *Nature* **2012,** *485,* 400–404.
166. Lu, H.; Tonge, P. J. Drug-Target Residence Time: Critical Information for Lead Optimization. *Curr. Opin. Chem. Biol.* **2010,** *14,* 467–474.
167. Copeland, R. A. The Drug-Target Residence Time Model: A 10-Year Retrospective. *Nat. Rev. Drug Discov.* **2016,** *15,* 87–95.
168. Verma, S.; Bhanot, S.; McNeill, J. H. Effect of Chronic Endothelin Blockade in Hyperinsulinemic Hypertensive Rats. *Am. J. Physiol.* **1995,** *269,* H2017–H2021.
169. Sauvageau, S.; Thorin, E.; Villeneuve, L.; Dupuis, J. Change in Pharmacological Effect of Endothelin Receptor Antagonists in Rats with Pulmonary Arterial Hypertension: Role of ET_B-Receptor Expression Levels. *Pulm. Pharmacol. Ther.* **2009,** *22,* 311–317.
170. Pulido, T.; Adzerikho, I.; Channick, R. N.; Delcroix, M.; Galie, N.; Ghofrani, H. A.; Jansa, P.; Jing, Z. C.; Le Brun, F. O.; Mehta, S.; Mittelholzer, C. M.; Perchenet, L.; Sastry, B. K.; Sitbon, O.; Souza, R.; Torbicki, A.; Zeng, X.; Rubin, L. J.; Simonneau, G. Macitentan and Morbidity and Mortality in Pulmonary Arterial Hypertension. *N. Engl. J. Med.* **2013,** *369,* 809–818.
171. Treiber, A.; Miraval, T.; Bolli, M. H.; Funel, J.-A.; Segrestaa, J.; Seeland, S. The Metabolism of the Dual Endothelin Receptor Antagonist Macitentan in Rat and Dog. *Xenobiotica* **2016,** *46,* 253–267.
172. Dingemanse, J.; van Giersbergen, P. L. Clinical Pharmacology of Bosentan, a Dual Endothelin Receptor Antagonist. *Clin. Pharmacokinet.* **2004,** *43,* 1089–1115.
173. Treiber, A.; Schneiter, R.; Hausler, S.; Stieger, B. Bosentan Is a Substrate of Human OATP1B1 and OATP1B3: Inhibition of Hepatic Uptake as the Common Mechanism of Its Interactions with Cyclosporin A, Rifampicin, and Sildenafil. *Drug Metab. Dispos.* **2007,** *35,* 1400–1407.
174. Binet, I.; Wallnofer, A.; Weber, C.; Jones, R.; Thiel, G. Renal Hemodynamics and Pharmacokinetics of Bosentan with and Without Cyclosporine A. *Kidney Int.* **2000,** *57,* 224–231.
175. Dingemanse, J.; van Giersbergen, P. L.; Patat, A.; Nilsson, P. N. Mutual Pharmacokinetic Interactions Between Bosentan and Lopinavir/Ritonavir in Healthy Participants. *Antivir. Ther.* **2010,** *15,* 157–163.
176. van Giersbergen, P. L.; Halabi, A.; Dingemanse, J. Single- and Multiple-Dose Pharmacokinetics of Bosentan and Its Interaction with Ketoconazole. *Br. J. Clin. Pharmacol.* **2002,** *53,* 589–595.
177. Weber, C.; Gasser, R.; Hopfgartner, G. Absorption, Excretion, and Metabolism of the Endothelin Receptor Antagonist Bosentan in Healthy Male Subjects. *Drug Metab. Dispos.* **1999,** *27,* 810–815.
178. Katz, D. A.; Carr, R.; Grimm, D. R.; Xiong, H.; Holley-Shanks, R.; Mueller, T.; Leake, B.; Wang, Q.; Han, L.; Wang, P. G.; Edeki, T.; Sahelijo, L.; Doan, T.; Allen, A.; Spear, B. B.; Kim, R. B. Organic Anion Transporting Polypeptide 1B1 Activity Classified by SLCO1B1 Genotype Influences Atrasentan Pharmacokinetics. *Clin. Pharmacol. Ther.* **2006,** *79,* 186–196.
179. Spence, R.; Mandagere, A.; Richards, D. B.; Magee, M. H.; Dufton, C.; Boinpally, R. Potential for Pharmacokinetic Interactions Between Ambrisentan and Cyclosporine. *Clin. Pharmacol. Ther.* **2010,** *88,* 513–520.
180. de Kanter, R.; Sidharta, P. N.; Delahaye, S.; Gnerre, C.; Segrestaa, J.; Buchmann, S.; Kohl, C.; Treiber, A. Physiologically-Based Pharmacokinetic Modeling of Macitentan: Prediction of Drug–Drug Interactions. *Clin. Pharmacokinet.* **2016,** *55,* 369–380.
181. Sidharta, P. N.; Treiber, A.; Dingemanse, J. Clinical Pharmacokinetics and Pharmacodynamics of the Endothelin Receptor Antagonist Macitentan. *Clin. Pharmacokinet.* **2015,** *54,* 457–471.
182. Bruderer, S.; Hopfgartner, G.; Seiberling, M.; Wank, J.; Sidharta, P. N.; Treiber, A.; Dingemanse, J. Absorption, Distribution, Metabolism, and Excretion of Macitentan, a Dual Endothelin Receptor Antagonist, in Humans. *Xenobiotica* **2012,** *42,* 901–910.
183. Packer, M.; McMurray, J.; Massie, B. M.; Caspi, A.; Charlon, V.; Cohen-Solal, A.; Kiowski, W.; Kostuk, W.; Krum, H.; Levine, B.; Rizzon, P.; Soler, J.; Swedberg, K.; Anderson, S.; Demets, D. L. Clinical Effects of Endothelin Receptor Antagonism with Bosentan in Patients with Severe Chronic Heart Failure: Results of a Pilot Study. *J. Card. Fail.* **2005,** *11,* 12–20.
184. Gerloff, T.; Stieger, B.; Hagenbuch, B.; Madon, J.; Landmann, L.; Roth, J.; Hofmann, A. F.; Meier, P. J. The Sister of P-Glycoprotein Represents the Canalicular Bile Salt Export Pump of Mammalian Liver. *J. Biol. Chem.* **1998,** *273,* 10046–10050.
185. Stieger, B.; Fattinger, K.; Madon, J.; Kullak-Ublick, G. A.; Meier, P. J. Drug- and Estrogen-Induced Cholestasis Through Inhibition of the Hepatocellular Bile Salt Export Pump (Bsep) of Rat Liver. *Gastroenterology* **2000,** *118,* 422–430.

186. Mano, Y.; Usui, T.; Kamimura, H. Effects of Bosentan, an Endothelin Receptor Antagonist, on Bile Salt Export Pump and Multidrug Resistance-Associated Protein 2. *Biopharm. Drug Dispos.* **2007,** *28,* 13–18.
187. Treiber, A.; Aanismaa, P.; de Kanter, R.; Delahaye, S.; Treher, M.; Hess, P.; Sidharta, P. Macitentan Does Not Interfere with Hepatic Bile Salt Transport. *J. Pharmacol. Exp. Ther.* **2014,** *350,* 130–143.
188. Sidharta, P. N.; van Giersbergen, P. L.; Dingemanse, J. Safety, Tolerability, Pharmacokinetics, and Pharmacodynamics of Macitentan, an Endothelin Receptor Antagonist, in an Ascending Multiple-Dose Study in Healthy Subjects. *J. Clin. Pharmacol.* **2013,** *53,* 1131–1138.
189. Doring, B.; Lutteke, T.; Geyer, J.; Petzinger, E. The SLC10 Carrier Family: Transport Functions and Molecular Structure. *Curr. Top. Membr.* **2012,** *70,* 105–168.
190. Dawson, S.; Stahl, S.; Paul, N.; Barber, J.; Kenna, J. G. In Vitro Inhibition of the Bile Salt Export Pump Correlates with Risk of Cholestatic Drug-Induced Liver Injury in Humans. *Drug Metab. Dispos.* **2012,** *40,* 130–138.
191. Warner, D. J.; Chen, H.; Cantin, L. D.; Kenna, J. G.; Stahl, S.; Walker, C. L.; Noeske, T. Mitigating the Inhibition of Human Bile Salt Export Pump by Drugs: Opportunities Provided by Physicochemical Property Modulation, in Silico Modeling, and Structural Modification. *Drug Metab. Dispos.* **2012,** *40,* 2332–2341.
192. Leslie, E. M.; Watkins, P. B.; Kim, R. B.; Brouwer, K. L. Differential Inhibition of rat and Human Na+-Dependent Taurocholate Cotransporting Polypeptide (NTCP/SLC10A1)by Bosentan: A Mechanism for Species Differences in Hepatotoxicity. *J. Pharmacol. Exp. Ther.* **2007,** *321,* 1170–1178.
193. Weiss, J.; Theile, D.; Spalwisz, A.; Burhenne, J.; Riedel, K. D.; Haefeli, W. E. Influence of Sildenafil and Tadalafil on the Enzyme- and Transporter-Inducing Effects of Bosentan and Ambrisentan in LS180 Cells. *Biochem. Pharmacol.* **2013,** *85,* 265–273.
194. van Giersbergen, P. L.; Treiber, A.; Schneiter, R.; Dietrich, H.; Dingemanse, J. Inhibitory and Inductive Effects of Rifampin on the Pharmacokinetics of Bosentan in Healthy Subjects. *Clin. Pharmacol. Ther.* **2007,** *81,* 414–419.
195. Dingemanse, J.; Schaarschmidt, D.; van Giersbergen, P. L. Investigation of the Mutual Pharmacokinetic Interactions Between Bosentan, a Dual Endothelin Receptor Antagonist, and Simvastatin. *Clin. Pharmacokinet.* **2003,** *42,* 293–301.
196. Weber, C.; Banken, L.; Birnboeck, H.; Schulz, R. Effect of the Endothelin-Receptor Antagonist Bosentan on the Pharmacokinetics and Pharmacodynamics of Warfarin. *J. Clin. Pharmacol.* **1999,** *39,* 847–854.
197. Actelion Pharmaceuticals Ltd. Data on file.
198. Bruderer, S.; Äänismaa, P.; Homery, M.-C.; Häusler, S.; Landskroner, K.; Sidharta, P. N.; Treiber, A.; Dingemanse, J. Effect of Cyclosporine and Rifampin on the Pharmacokinetics of Macitentan, a Tissue-Targeting Dual Endothelin Receptor Antagonist. *Am. Assoc. Pharm. Sci. J.* **2012,** *14,* 68–78.
199. Sidharta, P. N.; van Giersbergen, P. L.; Wolzt, M.; Dingemanse, J. Investigation of Mutual Pharmacokinetic Interactions Between Macitentan, a Novel Endothelin Receptor Antagonist, and Sildenafil in Healthy Subjects. *Br. J. Clin. Pharmacol.* **2014,** *78,* 1035–1042.
200. Sidharta, P. N.; Dietrich, H.; Dingemanse, J. Investigation of the Effect of Macitentan on the Pharmacokinetics and Pharmacodynamics of Warfarin in Healthy Male Subjects. *Clin. Drug Investig.* **2014,** *34,* 545–552.
201. Hurst, N.; Pellek, M.; Dingemanse, J.; Sidharta, P. N. Lack of Pharmacokinetic Interactions Between Macitentan and a Combined Oral Contraceptive in Healthy Female Subjects. *J. Clin. Pharmacol.* **2016,** *56,* 669–674.
202. Atsmon, J.; Dingemanse, J.; Shaikevich, D.; Volokhov, I.; Sidharta, P. N. Investigation of the Effects of Ketoconazole on the Pharmacokinetics of Macitentan, a Novel Dual Endothelin Receptor Antagonist, in Healthy Subjects. *Clin. Pharmacokinet.* **2013,** *52,* 685–692.
203. Savarese, G.; Paolillo, S.; Costanzo, P.; D'Amore, C.; Cecere, M.; Losco, T.; Musella, F.; Gargiulo, P.; Marciano, C.; Perrone-Filardi, P. Do Changes of 6-Minute Walk Distance Predict Clinical Events in Patients with Pulmonary Arterial Hypertension? *J. Am. Coll. Cardiol.* **2012,** *60,* 1192–1201.
204. Preston, I. R.; Suissa, S.; Humbert, M. New Perspectives in Long-Term Outcomes in Clinical Trials of Pulmonary Arterial Hypertension. *Eur. Respir. Rev.* **2013,** *22,* 495–502.
205. Vercauteren, M.; Hadana, H.; Cattaneo, C.; Kramberg, M.; Bortolamiol, C.; Rey, M.; Renault, B.; Bauer, Y.; Steiner, P.; Iglarz, M.; Vezzali, E.; Weber, E.; Strasser, D.; Studer, R.; Mulder, P.; Nayler, O.; Hess, P.; Richard, V.; Clozel, M. Therapeutic Effect of Macitentan, a Novel Dual Endothelin Receptor Antagonist, on Right Ventricular Structure and Function in Pulmonary Arterial Hypertensive Rats. *Am. J. Respir. Crit. Care Med.* **2015,** *191,* A1953.
206. Food and Drug Administration, OPSUMIT—Macitentan Tablet, Film Coated, http://www.accessdata.fda.gov/spl/data/a5b4a23d-735c-40a0-ba90-ab51eaa34656/a5b4a23d-735c-40a0-ba90-ab51eaa34656.xml (accessed October 2015).
207. European Medicines Agency, Public Summary of Opinion on Orphan Designation: Macitentan for the Treatment of Pulmonary Arterial Hypertension, EU/3/11/909, http://www.ema.europa.eu/ema/index.jsp?curl=pages/medicines/human/orphans/2011/10/human_orphan_000970.jsp&mid=WC0b01ac058001d12b (accessed September 2015).
208. European Medicines Agency, Opsumit, http://www.ema.europa.eu/ema/index.jsp?curl=pages/medicines/human/medicines/002697/human_med_001717.jsp&mid=WC0b01ac058001d124 (accessed October 2015).

8.11 Case Histories: Anacetrapib

A Ali and J Duffy, Rahway, NJ, United States

© 2017 Elsevier Ltd. All rights reserved.

8.11.1	**Introduction**	284
8.11.1.1	The HDL Hypothesis and CETP	284
8.11.1.2	Pharmacodynamic Validation with Early CETP Inhibitors	285
8.11.2.	**Structure Activity Studies and the Discovery of Anacetrapib**	286
8.11.3.	**Early Clinical Evaluation of Anacetrapib**	292
8.11.4	**Torcetrapib Termination and the Safety Analysis of CETP Inhibition**	295
8.11.5	**Further Preclinical Safety Evaluation of CETP Inhibition**	295
8.11.6	**Return to the Clinic: The *DEFINE* Study**	296
8.11.7	**Adipose Distribution Studies with Anacetrapib**	297
8.11.8	**Preclinical Efficacy Support for Reverse Cholesterol Transport**	298
8.11.9	**The Re-Emergent Importance of CETP Inhibitor-Induced Lowering of LDL-C**	300
8.11.10	**Clinical Outcomes Trials of CETP Inhibitors: The *REVEAL* Study**	300
8.11.11	**Conclusion**	302
Acknowledgments		303
References		303
Relevant Websites		307

8.11.1 Introduction

The discovery and development of anacetrapib provides insight into the intense feedback loop that drives biopharmaceutical research. The preclinical discovery program provided a compound with significant therapeutic potential. The clinical development program revealed features of the compound and the target that triggered additional preclinical research, which in turn influenced the clinical development plan. This ongoing process has been correctly characterized by Jordan elsewhere in this series as "a conversation between the laboratory and the clinic."[1] This case history illustrates the dynamic nature in which the discovery and development of anacetrapib has progressed in light of a continual flow of new information. Importantly, the account also demonstrates how the discovery team is called upon throughout the clinical program to address new developments as they arise.

8.11.1.1 The HDL Hypothesis and CETP

Heart disease is the leading cause of death in both low and high income countries, and over half of all deaths from heart disease in the United States are due to coronary artery disease.[2,3] The analysis of the Framingham Heart Study established that high levels of low-density lipoprotein cholesterol (LDL-C) and very low-density lipoprotein cholesterol (VLDL-C) were associated with higher mortality from coronary heart disease (CHD). This epidemiological study provided an even stronger inverse correlation associating high levels of high-density lipoprotein cholesterol (HDL-C) and lower CHD mortality.[4,5] Indeed, from this and other population-based studies, it is apparent that each 1 mg dL^{-1} decrease in plasma VLDL-C/LDL-C is associated with a 1% decrease in CHD risk, and that each 1 mg dL^{-1} increase in plasma HDL-C is associated with a 2–3% decrease in CHD risk.[6] This epidemiology correlation led to the cholesterol hypotheses of intervention that CHD mortality risk could be reduced by the pharmacologic lowering of VLDL-V/LDL-C and the pharmacologic elevation of HDL-C.

The intervention hypothesis for lowering of LDL-C has been thoroughly validated by clinical data, whereas the benefit of HDL-C elevation is not yet established. Since the publication of these epidemiology findings, a variety of LDL-C lowering agents have proven to be effective in reducing the risk of CHD mortality. The primary therapy for LDL-C reduction includes the HMG Co-A reductase inhibitors (statins) that inhibit the biosynthesis of cholesterol in the liver. Aggressive intervention therapy with statins can significantly reduce plasma LDL-C and reduce CHD event risk by 30–40%.[7] A further reduction in LDL-C has been achieved by the addition of the cholesterol absorption inhibitor ezetimibe, and this has provided a further risk reduction in patients with acute coronary syndrome (ACS).[8] Very recently, data have emerged from therapy with inhibitory antibodies to proprotein convertase subtilisin-kexin type 9 (PCSK9) that additionally indicate the mortality benefit of further reduction in LDL-C, although cardiovascular outcome studies are ongoing with this therapy.[9]

Despite the impressive 30–40% reduction in CHD mortality risk from lowering LDL-C, considerable residual risk remains. It is possible that additional pharmacologic intervention to concomitantly elevate HDL-C would provide a further CHD mortality risk reduction. Niacin and fibrates have been utilized for modest elevation of HDL-C (5–25%), but niacin therapy induces side effects such as flushing that makes high-dose use intolerable for many. In addition, a recent meta-analysis of clinical results for existing

HDL-C raising drugs did not demonstrate a reduction in cardiovascular mortality associated with the level of HDL-C elevation available from these therapies.[10]

A mechanism that more aggressively elevates HDL-C was needed to more conclusively test the HDL-C intervention hypothesis. In 1985, Koizumi, Mabuchi, and colleagues published a study of a Japanese population of healthy individuals with a genetic deficiency in cholesteryl ester transfer protein (CETP).[11] These individuals exhibited 300–600% increase in plasma HDL-C, and decreased incidence of CHD as compared to the general population. Subsequent studies of multiple CETP-deficient subject groups have generally validated the elevation of circulating HDL-C in this population. However, conflicting and even contradictory data have been reported on the influence of CETP deficiency for CHD risk for these individuals, possibly due to small sample sizes and varying methodology.[12]

CETP is a plasma glycoprotein that is physically associated with HDL particles in circulation.[13] The primary function of CETP involves the transfer of cholesterol esters (CE) and triglycerides (TG) between particles of VLDL/LDL and HDL to promote concentration equilibrium (Fig. 1). The mechanism for CETP transfer was originally proposed as a shuttle between lipoprotein fractions, where CETP carried a cargo of cholesterol ester (CE) and/or triglycerides (TG) in a central channel of the protein.[14] However, recent cryo-electron microscopy studies support the function of CETP as a conduit tunnel in a ternary complex with two lipoprotein particles for CE and TG exchange.[15] The conduit tunnel mechanism has been questioned, as CE transfer was demonstrated in vitro in the presence of selective antibodies that bind either end of the central channel of CETP.[16]

Pharmacologically, CETP is critically involved in the reverse cholesterol transport pathway for cholesterol excretion through the liver. As illustrated in Fig. 1, ApoA1 containing HDL particles are a primary vehicle for hepatic excretion of cholesterol. In this mechanism excess cholesterol ester is removed from macrophage foam cells in vascular tissue by nascent, preβ-HDL and HDL particles through the action of ATP-binding cassette transfer proteins such as ABCA1 and ABCG1. The HDL particle transports the cholesterol ester to the liver for uptake by the hepatic scavenger receptor B1 (SR-B1) for excretion to the bile. In this way, the extraction of cholesterol from vascular tissue by HDL leads to cholesterol-enriched HDL particles for excretion, providing an overall antiatherogenic effect. This process may be circumvented by CETP, which transfers CE from HDL to more CE-deficient ApoB containing LDL and VLDL particles, and conversely transfers triglycerides from VLDL/LDL to HDL. These LDL particles may similarly facilitate hepatic CE removal via uptake by the LDL receptor, as a parallel cholesterol disposal route. However, LDL particles may also be absorbed beyond the epithelium of vascular wall where they become oxidized, releasing CE into macrophages and contributing to atherosclerotic plaque formation.

Inhibition of CETP blocks the transfer of CE from HDL to VLDL/LDL, and blocks the transfer of TG from VLDL/LDL to HDL. This inhibition is anticipated to maintain the CE-rich HDL for liver-mediated cholesterol disposal and facilitate a net increase in reverse cholesterol transport and cholesterol efflux. The fundamental hypothesis of CETP inhibition therapy is that inhibiting the transfer of CE from HDL particles to LDL particles will result in net increased efflux of CE from the arterial wall to the bile, thus preventing progression of atherosclerotic occlusion.

8.11.1.2 Pharmacodynamic Validation with Early CETP Inhibitors

Preclinical studies published in the 1990s and early 2000s supported the proposal that CETP inhibition would have an antiatherogenic effect. Several species, including mice, rats, and dogs, express little or no plasma CETP. These species exhibit a significantly higher fraction of total cholesterol in HDL-C as compared to species that express CETP, such as cynomolgus monkeys, hamsters,

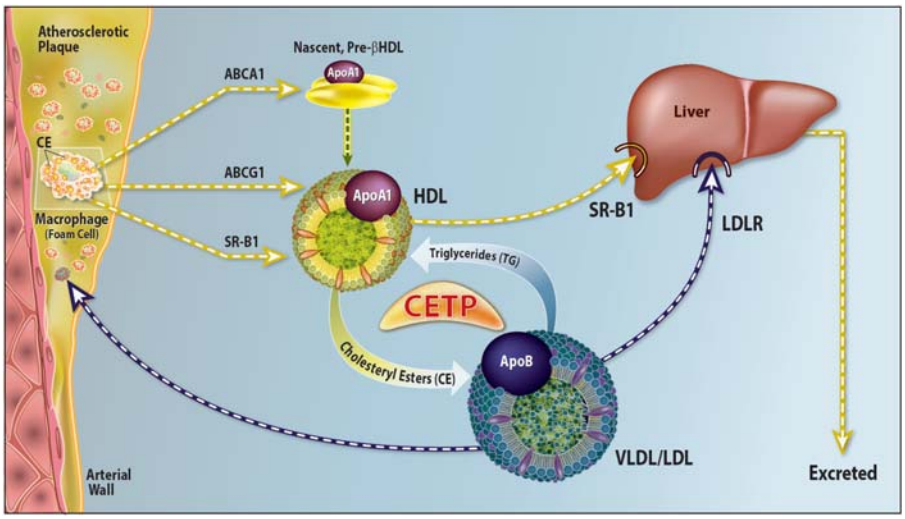

Fig. 1 The role of CETP in reverse cholesterol transport.

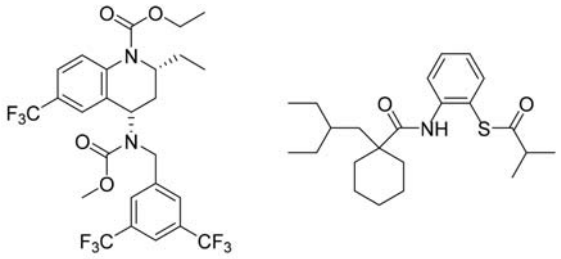

Fig. 2 Early clinical CETP inhibitors

and rabbits.[17] Researchers were further intrigued by the characterization of transgenic C57B6 mice that express cynomolgus[18] or human[19] CETP protein and display a more atherogenic lipoprotein profile, with significantly reduced HDL-C/LDL-C ratio, relative to their wild-type counterparts.

In conjunction with these preclinical genetic studies in the 1990s, several research groups reported the first small molecule CETP inhibitors.[20] The field accelerated considerably in the early 2000s with the publication of potent and reversible CETP inhibitors from Pfizer in the patent literature,[21] followed by their description of these CETP inhibitors, including CP-529,414 (torcetrapib **1**, Fig. 2) in scientific meetings.[22] During the same period, Japan Tobacco had reported less potent covalent thioester-containing CETP inhibitors including JTT-705 (dalcetrapib **2**, Fig. 2).[23] Importantly, Japan Tobacco had also reported the first administration of a CETP inhibitor in healthy volunteers and established that a 4-week treatment with 900 mg JTT-705 resulted in a 37% decrease in CETP activity and a 34% increase in total HDL-C.[24]

Based on preclinical studies and the early clinical data, it became apparent that CETP inhibition could elevate HDL-C levels by an unprecedented magnitude. In order to harness this powerful mechanism, a discovery research team was assembled at Merck that included a significant medicinal chemistry effort. The team initiated a drug discovery program for potent and selective CETP inhibitors in 2002 using a dual approach. They searched for lead compounds that would provide novel chemical matter for SAR investigations, and they examined CETP inhibitors that were being reported in the literature for insights into the pharmacophore properties of the compounds and in vitro pharmacology of the biological pathway.

8.11.2. Structure Activity Studies and the Discovery of Anacetrapib

The search for novel CETP inhibitors was enabled by the development and miniaturization of a fluorescence-based assay system utilizing a BODIPY fluorescence CE label that provided a significantly improved signal-to-noise ratio over prior CETP assays.[25] This optimization allowed the assay to be successfully miniaturized to 3456-well assay plate format, enabling the successful high-throughput screening campaign.

The screen of the entire Merck sample collection resulted in the identification of the 2-aryl benzoxazole **3** (Fig. 3). The compound represented a reasonable starting point for the program with CETP inhibitory potency IC_{50} of 1.1 μM, but it was highly lipophilic and contained undesirable structural characteristics such as an aniline moiety. Remarkably, the chemistry team learned during the course of lead optimization that this compound was not unique to Merck. Benzoxazole **3** had been similarly identified as a screening hit by scientists at Bristol Myers Squibb.[26] This compound was the focus of intense optimization efforts at Merck, which included varying substituents on the benzoxazole ring,[27] phenoxyl replacement,[28,29] the incorporation of structural constraints,[30] and the replacement of the embedded aniline substituent.[31] Each of these lines of investigation led to compounds of moderate intrinsic potency. Additionally, some of the compounds exhibited modest pharmacodynamic (PD) activity in the in vivo assay with the elevation of HDL-C in transgenic mice expressing cynomolgus CETP.[18] However, despite extensive efforts, the lead compounds in this series remained constrained by poor solubility, low oral exposure, and/or prohibitive off-target activity.

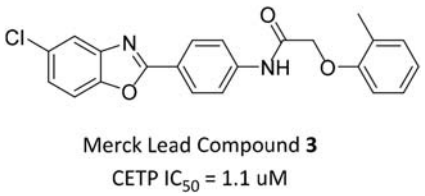

Fig. 3 Merck lead compound for CETP inhibition.

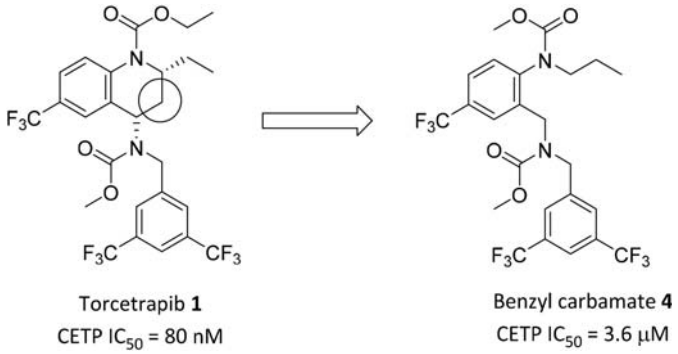

Fig. 4 Arylbenzoxazole and benzyl carbamate CETP leads.

In a parallel effort, attention was focused on other CETP inhibitors that had been reported in the literature, including Pfizer's CETP inhibitor torcetrapib **1** (Fig. 2). The goal was the design of novel, proprietary lead structures with unique properties and fresh directions for further optimization. The chemistry team approached this activity with the hypothesis that the substituents responsible for the potency and efficacy of known CETP inhibitors might be constrained using alternative scaffolds to impart novel and more favorable characteristics. Several lines of research were pursued, taking inspiration from substituents contained in several disclosed CETP inhibitors. The progress in some of these additional investigations has been published.[32] However, the most fruitful line of research would ultimately lead to the discovery of anacetrapib, and that account is presented here in detail.

The early investigations included novel compounds that open the ring of the central dihydroquinoline core of torcetrapib **1**, which yielded a proprietary acyclic scaffold as illustrated in Fig. 4. The resulting benzyl carbamate **4** was approximately 50-fold less potent than torcetrapib in the in vitro CETP inhibition assay, exhibiting an IC_{50} of 3.6 μM. Early SAR efforts were focused on elaboration of the phenyl carbamate and benzylic substituents, and cyclization of the phenyl carbamate. These efforts were largely unsuccessful. In the search for a nontraditional isostere for the phenylcarbamate substituent, the team reasoned that a biphenyl substituent might occupy the same pharmacophore space with readily accessible chemistry. A series of molecules relying on simple Suzuki coupling reactions was designed and executed to interrogate this idea. This work afforded a meaningful advance in the series with the synthesis of the prototype biphenyl CETP inhibitor **5**, which was twofold more potent than the lead carbamate **4** (Fig. 5).[33] Based on this encouraging result, a number of biphenyl analogs were prepared to probe their impact on potency in vitro

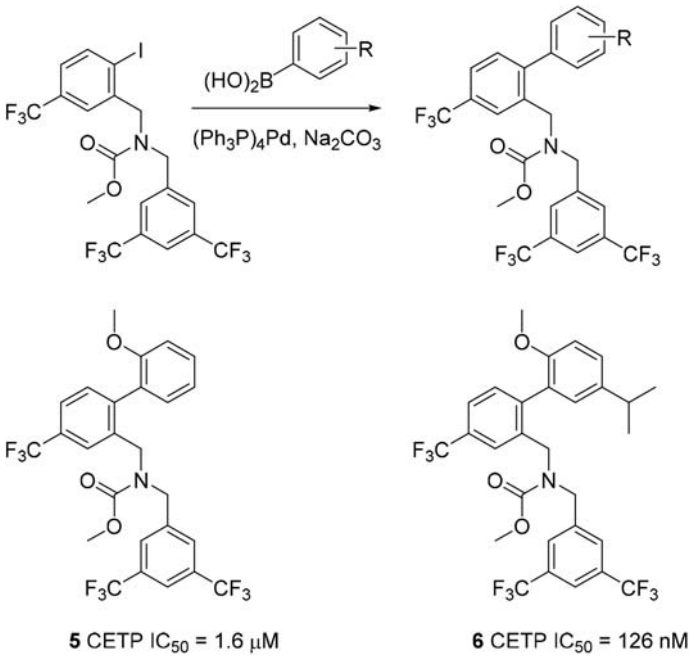

Fig. 5 Prototype biphenyl CETP inhibitors.

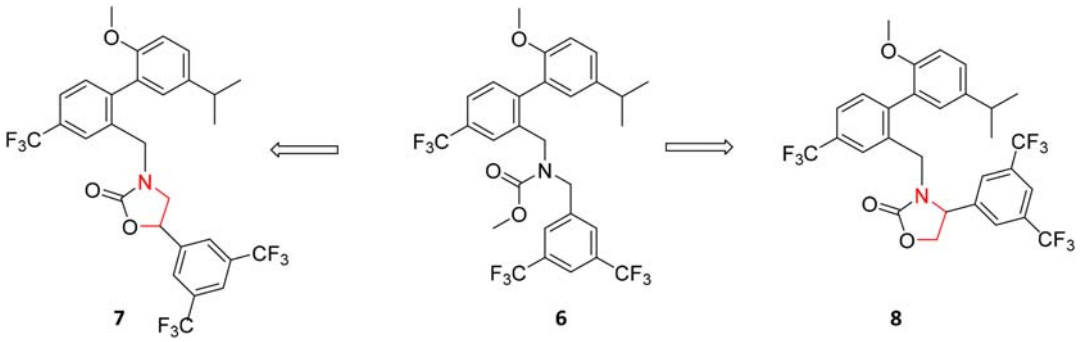

Fig. 6 Proposal of oxazolidinone constrained biphenyl CETP inhibitors.

and in vivo. It quickly became apparent that the optimal substitution pattern on the distal phenyl ring would be 2-methoxy, 5-isopropyl as in **6**, which exhibited another 15-fold improvement in intrinsic CETP inhibitory potency as compared to **5**. Indeed this substitution pattern on the biphenyl substituent would ultimately be retained in anacetrapib.

Compound **6** was an early benchmark compound for the program due to its potent inhibitory activity against CETP ($IC_{50}=126$ nM). It exhibited significant pharmacodynamic (PD) activity in an assay utilizing the CETP B6 transgenic mouse model.[34] The PD assay was optimized using compound **6** to provide maximal HDL-C elevation as a means to standardize in vivo testing of subsequent compounds. The ideal protocol involved use of a 24-h BID dosing regimen. A prebleed plasma sample was taken followed by dosing of the test compound at $t=0$ h, $t=7$ h and a terminal bleed at $t=24$ h to examine the change in HDL-C due to compound administration. The benchmark compound **6** administered at 10 mg kg^{-1} BID exhibited a moderate PD response affording elevation of 10 mg dL^{-1} in HDL-C (+54%). However, significant liabilities with **6** still needed to be addressed. The compound was rapidly metabolized when incubated in liver microsomes from rats or humans, and **6** exhibited low oral bioavailability in mouse pharmacokinetic (PK) studies of $<10\%$.

The chemistry team focused on improving the potency and efficacy of lead candidates, and a number of conformationally constrained analogs were prepared to probe their impact on in vitro and in vivo potency. Among these were the oxazolidinone regioisomers **7** and **8** (Fig. 6).[35] The chemistry team reasoned that a structural constraint around the remaining carbamate functionality might secure the carbamate and bis-trifluoromethyl phenyl substituent in an active conformation for CETP inhibition.

Regioisomer **7** was prepared by reaction of the epoxide **9** with benzylamine **10** to yield the corresponding amino alcohol **11**, which was then cyclized to the corresponding oxazolidinone using triphosgene (Scheme 1). Regioisomer **8** was prepared by alkylation of benzylamine **10** with bromide **12** affording intermediate **13**. This ester was then reduced to the desired amino alcohol **14** with $LiAlH_4$. Cyclization with triphosgene led to the racemic oxazolidinone **8**. Regioisomer **8** was disappointingly weak as an inhibitor of CETP ($IC_{50}=14$ μM). Gratifyingly, regioisomer **7** was a potent CETP inhibitor as the racemic mixture ($IC_{50}=133$ nM). Stereochemistry appeared to be important to potency, as chiral resolution of **7** provided the (4*S*)-oxazolidinone enantiomer ($IC_{50}=93$ nM) and the (4*R*)-oxazolidinone, which afforded significantly weaker inhibitory potency. Unfortunately, the incorporation of an oxazolidinone conformational constraint did not improve the PK of the series, as (*S*)-**7** exhibited low oral bioavailability in mice ($<5\%$) and no significant PD effect in the transgenic mouse assay.

It was possible that further improvements in PK and potency could be achieved from the oxazolidinone scaffold by building additional rotational constraints on the substituents. The chemistry team reasoned that the 5-methylene position on the oxazolidinone ring of **7** could be investigated using commercially available chiral oxazolidinones derived from norephedrine.[36] Indeed, the preparation of **15** and **16** (Table 1) demonstrated that introduction of a stereospecific methyl group on the oxazolidinone ring resulted in substantial boost of in vitro potency for **15** ($IC_{50}=39$ nM). This improvement was also accompanied by increased PD activity in the CETP transgenic mouse model. Interestingly, the majority of the biological activity was found to reside in the (+) *cis* enantiomers (**15** and **22**) rather than the (−) *cis* isomers (**16** and **19**) and *trans* isomers (**17**, **18**, and **21**), which were substantially less active (Table 1). Importantly, this work established that the (*S*)- and (*R*)-stereochemistries at the 4-and 5-positions, respectively, afforded significantly more potent CETP inhibition. Substitution of the oxazolidinone at the 4-position was further investigated by the synthesis of the ethyl derivatives **21** and **22**, the gem-dimethyl derivatives **25** and **26**, and spiro-cyclopropyl derivatives **27** and **28;** however, none of these structural modifications led to further improvements in in vivo activity.

The in vitro potency and PD efficacy of **15** inspired the incorporation of the 3,5-bis-trifluoromethyl substituents on the phenyl ring, as in **7** and **8**. This combination afforded **20**, which exhibited further improvement in intrinsic potency, and provided the highest PD activity that had been observed on the program. The compound had modest mouse PK, with oral bioavailability of 15%, and poor physical properties ($\log D=7.1$), but it also afforded reduced activity on ancillary ion channels (IK_r, $Na_v1.5$, $Ca_v1.2$) and metabolic enzymes. As such, the compound became an important benchmark for the program.

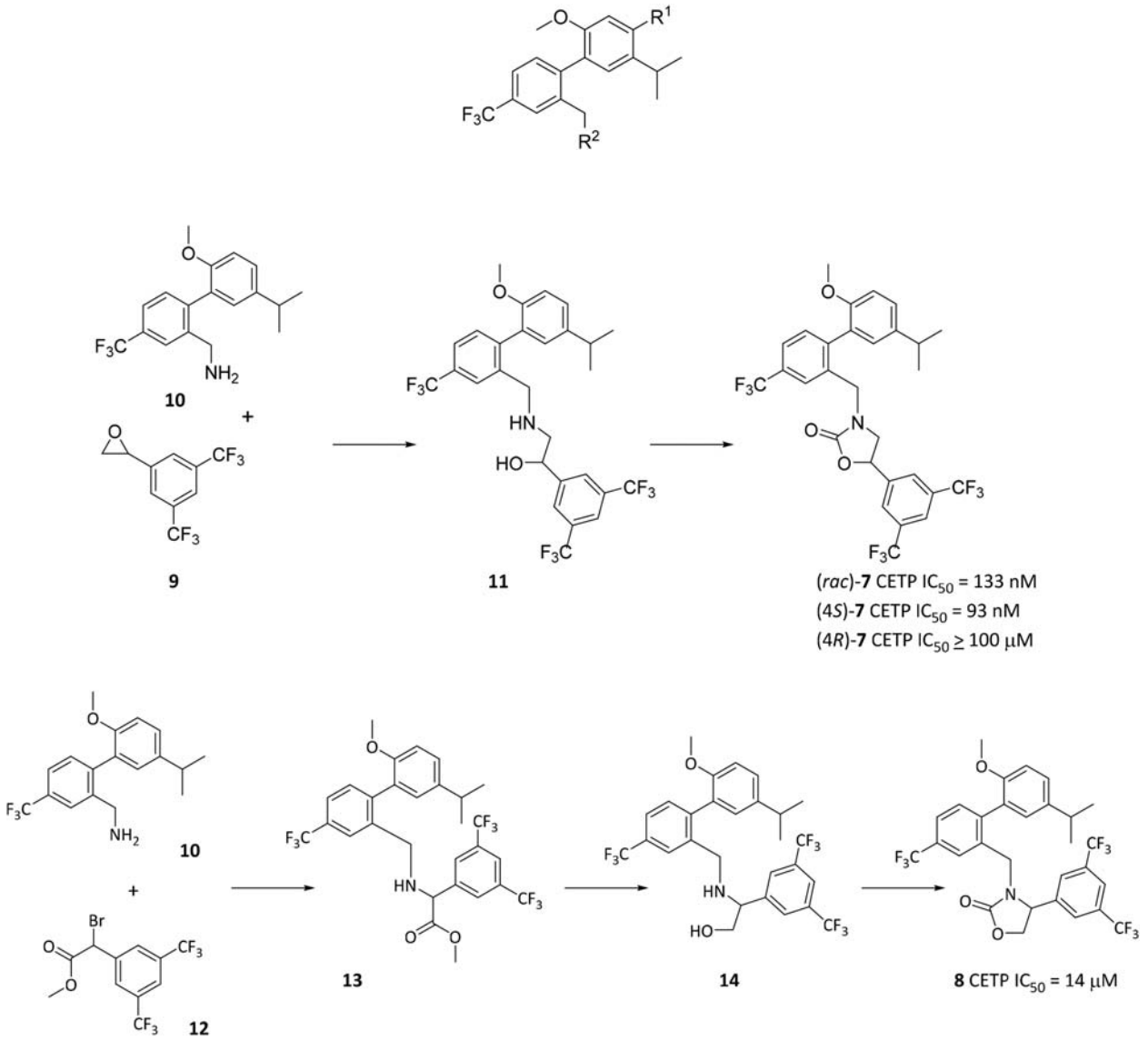

Scheme 1 Synthetic routes to oxazolidinone CETP inhibitors **7** and **8**.

Table 1 Selected SAR of substituted biphenyl oxazolidinones CETP inhibitors

			CE transfer inhibition		*Δ↑HDL-C*
Compound	*R^1*	*R^2*	*IC_{50} (nM)*	*% max (10 μM)*	*(mg mL^{-1} @ 10 mg kg^{-1} PO)*[a]
6	H	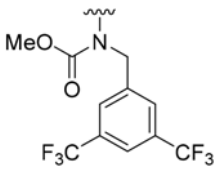	126	87	10
(S)-**7**	H	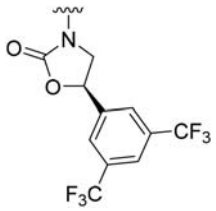	93	93	No effect

(Continued)

Table 1 Selected SAR of substituted biphenyl oxazolidinones CETP inhibitors—cont'd

			CE transfer inhibition		*Δ↑HDL-C*
Compound	*R^1*	*R^2*	*IC_{50} (nM)*	*% max (10 μM)*	*(mg mL^{-1} @ 10 mg kg^{-1} PO)*[a]
15	H	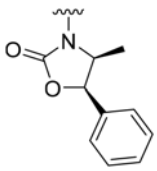	39	94	6.3
16	H	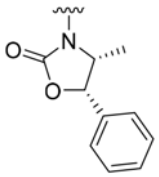	5.67×10^3	90	n.m.[c]
17	H	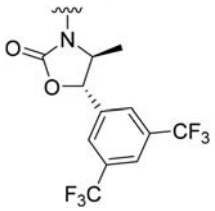	n.d.[b]	20	n.m.[c]
18	H	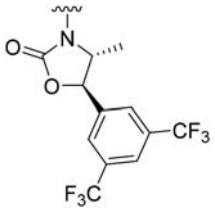	266	90	n.m.[c]
19	H	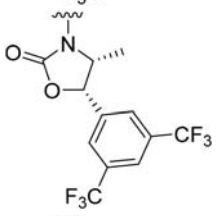	n.d.[b]	8	n.m.[c]
20	H	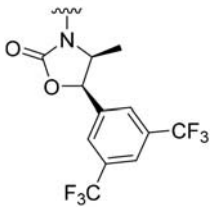	15	94	22
21	H	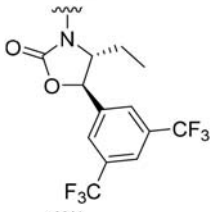	n.d.[b]	49	n.m.[c]
22	H	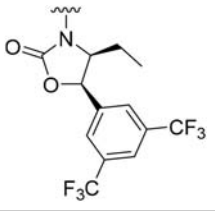	268	87	n.m.[c]

Table 1 Selected SAR of substituted biphenyl oxazolidinones CETP inhibitors—cont'd

Compound	R^1	R^2	CE transfer inhibition		Δ↑HDL-C
			IC_{50} (nM)	% max (10 μM)	(mg mL^{-1} @ 10 mg kg^{-1} PO)[a]
23	F	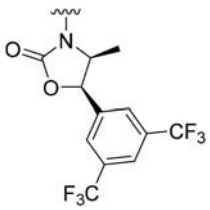	17	94	28
24	F	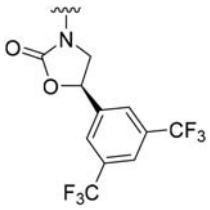	26	97	6.3
25	F	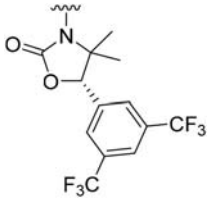	n.d.[b]	21	n.m.[c]
26	F	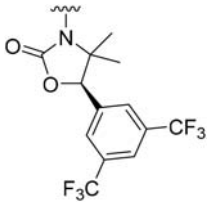	18	94	17
27	F	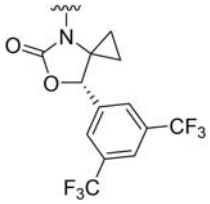	n.d.[b]	25	n.m.[c]
28	F	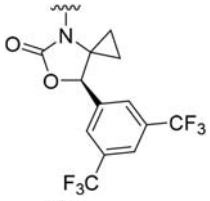	18	96	5.2
29	F	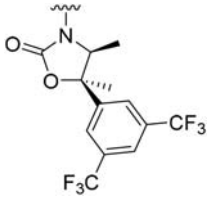	n.d.[b]	46	n.m.[c]

[a]Mean increase in HDL cholesterol in B6-Tg(CETP) mice following BID doses, 10 mg kg^{-1} PO.
[b]n.d.: not determined; IC_{50} values not reported in cases where % max ≤ 50% at 10 μM.
[c]n.m.: not measured.

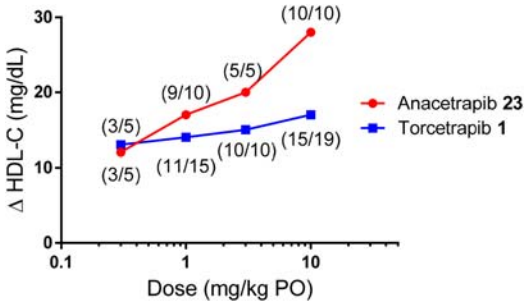

Fig. 7 Dose titration of anacetrapib (**23**) and torcetrapib (**1**) in B6-Tg(CETP) mice. Mean increase in HDL cholesterol in B6-Tg(CETP) mice with the # of mice responding/# of mice tested shown in parentheses.

Table 2 Mean Pharmacokinetic Parameters of anacetrapib **23** in preclinical species

Parameter [a]	*Mouse*	*Rat*	*Dog*	*Rhesus*
Cl_p (mL min^{-1} kg^{-1})	11	9.3	2.7	0.8
V_d (L kg^{-1})	2.0	4.2	0.9	1.5
$T_{1/2}$ (h)	3.6	12	8	33
AUCN (μM·h·kg mg^{-1})	0.35	0.66	1.86	12
C_{max} (μM)	0.28	0.12	0.5	1.2
T_{max} (h)	1.0	3.3	2.0	4.0
F_{oral} (%) [b]	15	24	23	27

[a] Cl_p, plasma clearance (blood clearance for mice); V_d, volume of distribution; $T_{1/2}$, terminal half-life; AUCN, IV normalized area under curve; C_{max}, observed maximal plasma concentration following oral dosing; T_{max}, time to reach the C_{max}; F_{oral}, oral bioavailability.
[b] The IV doses were formulated in DMSO:PEG400:water (10:55:35. v/v/v) and injected at 0.6 mg kg^{-1} to male C57BL/6 mice, and were formulated in PEG300:water (70:30, v/v) and injected at 0.4 mg kg^{-1} to male Sprague–Dawley rats and 0.1 mg kg^{-1} to male Beagle dogs and rhesus monkeys. The oral doses were formulated in DMSO:Cremophor:Saline (2:4:94, v/v/v) and given at 2 mg kg^{-1} to mice, and were formulated in Imwitor:Tween80 (1:1, w/w) and given at 1 mg kg^{-1} to rats, dogs, and monkeys.

In-depth characterization of the metabolism of **20** and related analogues revealed a metabolic liability due to glutathione addition to the biphenyl ring. In an interesting development, fluorine substitution of the biphenyl ring reduced glutathione conjugation relative to the des-fluoro analog. Despite the reluctance of the chemists to introduce the tenth fluorine substituent into the lead candidate, this modification was ultimately adopted owing to the decreased propensity of in vivo reactive metabolite formation and a safer projected overall toxicological profile.[37] The addition of the 4-fluoro substituent to **20** afforded the biphenyl oxazolidinone **23**, which was further characterized as a potential development candidate. Compound **23** consistently increased HDL-C levels in a dose-dependent manner at doses of 1, 3, and 10 mg kg^{-1} respectively in the B6-Tg(CETP) mouse model with an effect comparable to or better than torcetrapib (Fig. 7). The pharmacokinetic profile of **23** was characterized in multiple species (Table 2). Although **23** did not provide significantly greater exposure in mice than the des-fluoro analogue **20**, it was possible that the decreased likelihood of a reactive metabolite would improve the long-term safety profile of the compound. The compound exhibited a good pharmacokinetic profile across species with moderate oral bioavailabilities, low clearances, and long half-lives consistent with likely QD dosing in humans. Additional derivatives of the oxazolidinone lead class were thoroughly investigated,[38] but these modifications did not provide compounds superior to **23**.

Based on its favorable in vitro and in vivo properties, compound **23** was selected as a development candidate for the CETP inhibitor program. The compound was subjected to a standard battery of preclinical safety characterization tests, including Ames assays, cardiovascular studies in mice, dogs, and rhesus monkeys, and dose-limiting toxicity studies in mice and rhesus monkeys. The results validated the development potential for compound **23** as a novel agent for lipid therapy. The compound was redesignated as MK-0859 for development, and ultimately designated as anacetrapib.

8.11.3. Early Clinical Evaluation of Anacetrapib

On the basis of the positive preclinical safety and pharmacodynamic evidence developed above, anacetrapib was advanced to phase I clinical studies. The single rising dose studies established the effect of food, age, gender, and obesity on compound exposure and plasma CETP inhibition.[39] Anacetrapib was found to be safe and well tolerated at single doses from 2 to 1000 mg, with nonlinear dose-dependent increase in exposure that was similar among demographic groups. However, systemic exposure was significantly enhanced when anacetrapib was administered with a high-fat meal, affording a 3.7-fold increase in the oral $AUC_{0-\infty}$ of the

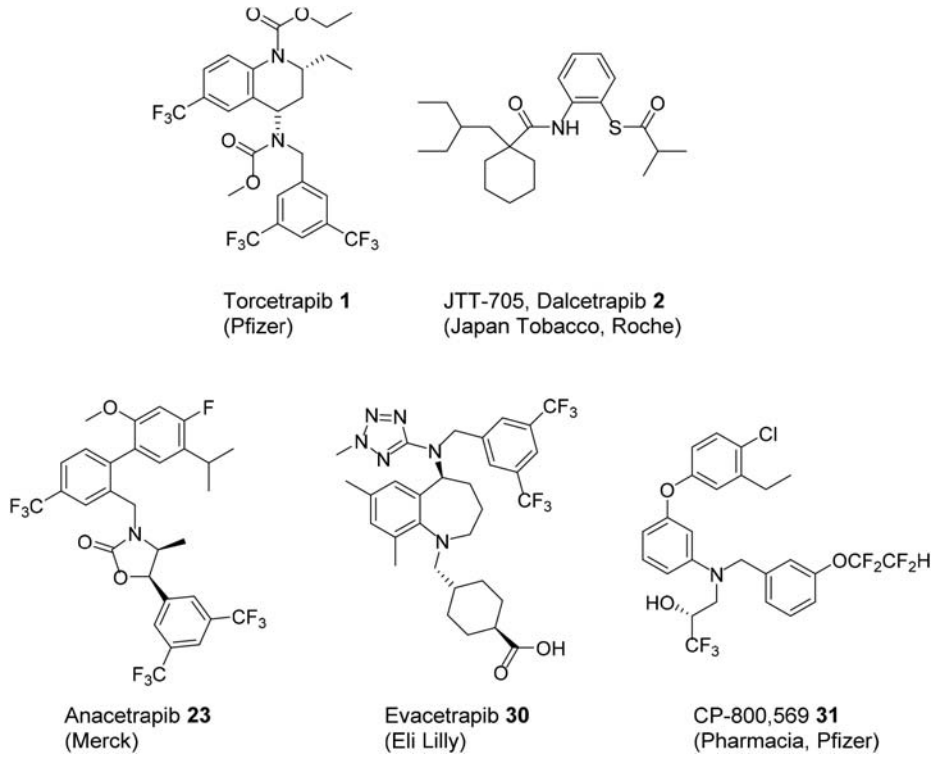

Fig. 8 Clinically investigated CETP inhibitors with disclosed structures.

compound following a 25-mg dose. Furthermore, anacetrapib was found to be primarily metabolized by the CYP3A4 enzyme, as coadministration with the CYP3A inhibitor ketoconazole led to a four- to sixfold increase in exposure.[40]

The multiple ascending dose studies provided further insight on the food effect, as well as the target engagement and pharmacodynamic effects of anacetrapib when administered alone.[41] Healthy volunteers were administered anacetrapib at once daily doses of 20–800 mg for 14 days, and the food effect was found to be more prevalent after steady-state exposure had been achieved (day 7). The oral AUC of a 200-mg dose of the compound increased from 1 to 2 $\mu M \cdot h\ L^{-1}$ following an overnight fast to 38 $\mu M \cdot h\ L^{-1}$ when administered with a high-fat meal. Plasma CETP activity was maximally inhibited to ~90% within 4 h of the first dose, and this inhibition was attenuated by day 14 to 80–85% inhibition at peak and 40–60% inhibition at trough (24 h post dose). The decreased inhibitory activity with anacetrapib over 2 weeks was accompanied by over twofold increase in circulating CETP protein. This study also provided evidence establishing the lipid-altering effects of anacetrapib. Maximal lipid effects were noted following a 200-mg dose after a high-fat meal, afforded a 123% increase in HDL-C and a 56% decrease in LDL-C. Higher doses did not further alter lipids, regardless of the higher exposure achieved. This observation was important to the further study of anacetrapib, in the conclusion that the compound had achieved the maximum possible pharmacodynamic effects available through this mechanism.

The Phase I studies also provided evidence of the biphasic pharmacokinetic elimination profile of anacetrapib. Although the compound exhibited an effective half-life of ~20 h, a longer terminal elimination phase of ~60–80 h was observed. This profile was best described by a two-compartment pharmacokinetic model with clearance occurring from a low-volume central compartment, accompanied by a slower clearance, high volume peripheral compartment.[39]

During the discovery and development program for anacetrapib, the team closely monitored the safety and efficacy profile that was being reported by Pfizer for torcetrapib. Eight-week phase II studies of torcetrapib in a small number of dyslipidemic subjects revealed elevations in both systolic and diastolic blood pressure when torcetrapib was dosed either alone[42] or in addition to atorvastatin.[43] The incidence of blood pressure elevation was low in each of these trials and was not dose-dependent or consistent over time. It was noted with interest, however, that Pfizer advanced to phase III trials testing a submaximal 60 mg fixed dose of torcetrapib with atorvastatin in imaging trials (ILLUSTRATE,[44] RADIANCE 1, and RADIANCE 2[45]) and an outcomes trial (ILLUUMINATE[46]). This dose was below the 90 mg dose that afforded the highest elevation in HDL-C and greatest decrease in LDL-C in their phase II studies, and the Merck team speculated that the lower development dose of torcetrapib may have been selected in an attempt to mitigate blood pressure effects.

Fig. 8 and **Table 3** provide the structures of CETP inhibitors and full names of clinical trials, respectively, mentioned by name in this case history.[47] The chemical structure for TA-8995 (Dezima, Amgen) (**Table 4**) has not yet been disclosed.

As a result of the reported observations with torcetrapib, a clinical trial was initiated in Jul., 2006 with anacetrapib to investigate the effect on 24-h ambulatory blood pressure in healthy individuals.[48] The results from this study established that anacetrapib had

Table 3 Acronyms and full names of efficacy trials for CETP inhibitors

CETP Inhibitor	*Sponsor*	*Trial (Identifier)*	*Name*
Anacetrapib	Merck	DEFINE (NCT00685776)	Determining the Efficacy and Tolerability of CETP Inhibition with Anacetrapib
		REALIZE (NCT01524289)	Randomized Evaluation of Anacetrapib Lipid-Modifying Therapy in Patients with Heterozygous Familial Hypercholesterolemia
		REVEAL (NCT01252953)	Randomized Evaluation of the Effects of Anacetrapib through Lipid-Modification
Dalcetrapib	Roche	dal-ACCUTE (NCT01323153)	A Study of Dalcetrapib in Patients Hospitalized For An Acute Coronary Syndrome
		dal-PLAQUE 1/2 (NCT00655473) (NCT01059682)	Safety and Efficacy of Dalcetrapib on Atherosclerotic Disease Using Novel Non-Invasive Multimodality Imaging
		dal-VESSEL (NCT00655538)	Effect of RO4607381 (dalcetrapib) on Vascular Function in Patients With Coronary Heart Disease (CHD) or CHD-Risk Equivalent Patients
		dal-OUTCOMES (NCT006585515)	A Randomized, Double-blind, Placebo-controlled Study Assessing the Effect of Dalcetrapib on Cardiovascular Mortality in Clinically Stable Patients With a Recent Acute Coronary Syndrome
Evacetrapib	Eli Lilly	ACCELERATE (NCT01687998)	Assessment of the Clinical Effects of Cholesteryl Ester Transfer Protein Inhibition with Evacetrapib in Patients at High-Risk for Vascular Outcomes
TA-8995[a] (AMG-899)	Dezima (Amgen)	TULIP (NCT01970215)	TA-8995: Its Use in Patients With Mild Dyslipidaemia
Torcetrapib	Pfizer	ILLUSTRATE (NCT00134173)	Investigation of Lipid Level Management Using Coronary Ultrasound to Assess Reduction of Atherosclerosis by CETP Inhibition and HDL Elevation
		RADIANCE 1/2 (NCT00136981) (NCT00134238)	Rating Atherosclerotic Disease Change by Imaging with a New CETP Inhibitor
		ILLUMINATE (NCT00134264)	Investigation of Lipid Level Management to Understand its Impact in Atherosclerotic Events

[a]The structure of TA-8995 has not been disclosed.

Table 4 Cardiovascular events during the treatment phase of the DEFINE trial.

	Anacetrapib N = *808* n *(%)*	*Placebo* N = *804* n *(%)*
Pre-specified adjudicated CV safety endpoint	16 (2.0)	21 (2.8)
Cardiovascular death	4 (0.5)	1 (0.1)
Nonfatal MI	6 (0.7)	9 (1.1)
Unstable angina	1 (0.1)	6 (0.7)
Nonfatal stroke	5 (0.6)	5 (0.6)
Death from any cause	11 (1.4)	8 (1.0)
Revascularization	8 (1.0)	28 (3.5)
Death or major CV event	27 (3.3)	43 (5.3)

no significant effect on ambulatory blood pressure as compared to placebo. This supported the development team's conclusion that the blood pressure effects observed with torcetrapib in human subjects and preclinical species were compound-specific to torcetrapib, and not mediated by CETP inhibition.

Concurrent with the ambulatory blood pressure study outlined above, Merck launched a phase II placebo-controlled dose ranging study of anacetrapib administered as monotherapy and coadministered with atorvastatin in 589 patients with primary hypercholesterolemia or mixed hyperlipidemia.[49] In this 8-week study, patients were randomized to receive either placebo or daily doses of anacetrapib at 10, 40, 150, or 300 mg, with or without 20 mg of atorvastatin. The study was designed to provide the critical pharmacodynamic data needed to perform a large cardiovascular outcomes trial that would be required to establish the benefit of CETP inhibitors in addition to statins for the management of cardiovascular risk. The final patient completed this study on Friday, Dec. 1, 2006, providing a complete and closed data set for analysis of primary and secondary endpoints. The timing and duration of this study would turn out to be a remarkable and fortuitous coincidence for Merck.

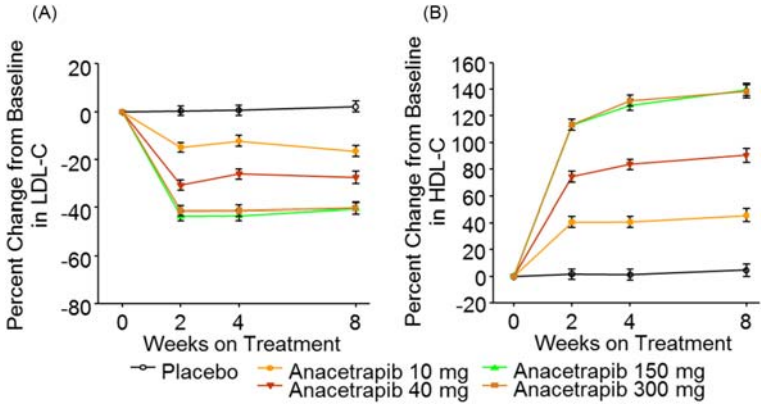

Fig. 9 Changes from baseline in LDL-C (A) or HDL-C (B) over time for anacetrapib administration at the indicated dose versus placebo.

8.11.4 Torcetrapib Termination and the Safety Analysis of CETP Inhibition

On Saturday, Dec. 2, 2006, Pfizer announced that the ILLUMINATE trial of torcetrapib was being halted prematurely for safety reasons by recommendation from the independent data and safety monitoring board (DSMB).[46] The ILLUMINATE trial had enrolled over 15,000 patients with a history of cardiovascular disease, with half receiving an optimized dose of atorvastatin (10–80 mg) and half receiving atorvastatin plus 60 mg of torcetrapib. The data monitoring board had noted a significant 25% increased risk of cardiovascular events and 58% increase in death from any cause in patients receiving torcetrapib as compared to placebo. The announced termination of the ILLUMINATE trial caused an immediate precautionary suspension of further developmental activities for anacetrapib until significant additional data could be gathered. The Merck team sought to fully examine the data from the ILLUMINATE trial, to analyze the internal anacetrapib clinical data for any similar safety signal, to examine both compounds extensively in preclinical safety models to differentiate their profile, and to develop additional safety steps in the development plan to proceed with anacetrapib clinical investigation.

In light of the torcetrapib termination, the efficacy and safety data from the anacetrapib phase II study outlined above were carefully analyzed. The results supported the further clinical development of the compound.[49] Following 8 weeks of drug administration as monotherapy, anacetrapib resulted in a dose-dependent increase in HDL-C of maximally 139% and a maximal reduction in LDL-C of 40% (Fig. 9). The results from coadministration with 20 mg of atorvastatin afforded a similar maximal elevation in HDL-C and an additive reduction in LDL-C to 70% reduction as compared to baseline. Additional dose-related effects included a reduction in apolipoprotein B ($\leq$30%), an increase in apolipoprotein A1 ($\leq$47%), an increase in apolipoprotein E ($\leq$40%), reduction in lipoprotein(a) ($\leq$50%), and no change in total cholesterol, total triglycerides, or c-reactive protein. These plasma biomarkers were further supportive of the potential for anacetrapib to provide an antiatherogenic effect. As is evident from Fig. 9, the efficacy was similar for the 150 mg and 300 mg doses, indicating that maximal efficacy could be achieved following $\leq$150 mg dose of the compound. The maximal changes in lipid profile were greater than those achieved with torcetrapib (HDL-C = +72%, LDL-C = −25% at 60 mg)[46] or dalcetrapib (JTT-705) (HDL-C = +30–40% at 600 mg)[24] indicating that greater CETP inhibition had been achieved with anacetrapib than in comparator clinical studies. Importantly, anacetrapib was safe and well tolerated at all doses. The data demonstrated that anacetrapib had no effect on blood pressure while achieving a CETP-mediated lipid response greater than torcetrapib.

8.11.5 Further Preclinical Safety Evaluation of CETP Inhibition

The clinical safety findings with torcetrapib inspired the research team to a deeper preclinical safety evaluation of CETP inhibition. The details from the ILLUMINATE trial of suggested several avenues to investigate the safety pharmacology of torcetrapib as compared to other CETP inhibitors. The ILLUMINATE researchers noted that after 12 months of treatment with torcetrapib, patients exhibited decreased plasma potassium, increased sodium, and increased bicarbonate as compared to the placebo group.[46] This cluster of biomarkers suggested to the clinical researchers that a potential mineralocorticoid excess was associated with the blood pressure elevation. A post hoc evaluation of patient plasma from the ILLUMINATE trial supported this hypothesis, showing increased aldosterone levels in the torcetrapib group following 3 months of dosing with torcetrapib. The findings of elevated plasma aldosterone and electrolyte changes were further supported by pooled analysis of plasma from the RADIANCE imaging trials of torcetrapib.[50]

Biopharmaceutical research teams from several organizations began intensive study of torcetrapib to identify the mechanism of ancillary pharmacology, and these studies have been reviewed.[51] A research team at Merck embarked on a significant preclinical safety evaluation of several CETP inhibitors to more fully derisk the mechanism of CETP inhibition before further clinical

progression of this target. The Merck team focused first on the significant increase in systolic blood pressure in the ILLUMINATE trial (~4 mmHg) among patients taking torcetrapib as compared to placebo.[46] In preclinical studies, torcetrapib infusion produced a significant elevation of mean arterial pressure in both B6-CETP transgenic mice and wild-type B6 mice that lack CETP.[52] Additionally, torcetrapib was found to increase mean arterial pressure in anesthetized rats, anesthetized dogs, and conscious rhesus monkeys. These experiments indicated that the blood pressure effects of torcetrapib were evident in the absence of circulating CETP (B6 mice and rats) or in the presence of CETP (B6-CETP mice, dogs, and rhesus monkeys), and therefore are not mediated by CETP inhibition. None of this ancillary pharmacology was exhibited by anacetrapib.

The possible mechanism of the blood pressure effect of torcetrapib was also investigated in these experiments.[52] Torcetrapib had no direct effect on isolated rat vascular smooth muscle, eliminating vascular contraction as a likely cause. The potential for a central nervous system mechanism was also eliminated, as torcetrapib produced an identical increase in blood pressure in both control and pithed rats. The involvement of the sympathetic nervous system was eliminated, as mean arterial pressure elevation by torcetrapib was not affected by coadministration with an angiotensin II blocker or a mixed endothelin A/B antagonist. The team did note, however, that an intravenous infusion of torcetrapib to conscious rats produced a significant elevation in the plasma of the adrenal stress hormones aldosterone and corticosterone. This effect was not observed with a similar infusion of anacetrapib. Notably, the blood pressure effect of torcetrapib was not evident in adrenalectomized rats, indicating an adrenal origin for the mean arterial pressure increase. However, blood pressure elevation by torcetrapib in rats remained during coadministration of an α_1-adrenoreceptor antagonist or a β_1-adrenoreceptor antagonist. Additionally, the torcetrapib-mediated aldosterone and corticosterone release was prevented by coadministration with a 3β-hydroxysteroid dehydrogenase inhibitor, but the mean arterial pressure increase was not affected. These results indicated that the blood pressure increase due to torcetrapib is related to the adrenal gland, but not in direct response to aldosterone or corticosterone release.

The unique preclinical toxicity profile of torcetrapib was further validated by elegant pharmacology experiments from several teams that included scientists from Pfizer, Roche, Eli Lilly, Abbott, Johnson and Johnson, and numerous academic institutions. Particularly noteworthy among these studies was careful ancillary SAR experiments of the torcetrapib lead class reported by scientists at Pfizer.[53,54] Their studies revealed that the reversal of a single (2*S*)-ethyl stereocenter in torcetrapib to the (2*R*)-stereochemistry eliminated the BP elevation in rats in the dihydroquinoline series.[55] The results of these collective investigations by several research groups have recently been reviewed.[51] The experiments conclusively established that the preclinical BP elevation and hormone release associated with torcetrapib were not associated with the mechanism of CETP inhibition, and were not shared by structurally differentiated CETP inhibitors such as anacetrapib.

8.11.6 Return to the Clinic: The *DEFINE* Study

The preclinical and clinical safety biomarkers discovered for torcetrapib were not evident in the analysis of clinical patient samples from other CETP inhibitors. The phase II study of anacetrapib showed no changes in electrolytes or aldosterone following 8 weeks of dosing up to 300 mg.[49] Similarly, the reported studies of dalcetrapib indicated no change in electrolytes or aldosterone following 48 weeks of dosing at up to 900 mg.[56]

Based on the analysis of the clinical biomarkers and safety data from the anacetrapib trials, along with extensive preclinical safety assessment investigations, Merck proceeded with the clinical development program of anacetrapib. The development team had achieved full confidence that anacetrapib lacked the blood pressure effects of torcetrapib, and that it did not induce the changes in plasma aldosterone and serum electrolytes that had been identified in post hoc analyses of plasma from torcetrapib clinical studies. In light of these positive comparator biomarker data, the development team designed a study to establish with predictive probability that treatment with anacetrapib is not associated with the rate of adverse cardiovascular effects reported with torcetrapib.

Since maximal lipid-altering effects were achieved at submaximal exposure of anacetrapib, it was important to determine the minimum dose required for maximal efficacy. The development team utilized a population pharmacokinetics model-based approach to determine the appropriate dose for phase III development studies.[57] There were multiple variables that had been identified in the phase I and phase II trials that were incorporated into the pharmacodynamic model of anacetrapib. These included nonlinear pharmacokinetics, accumulation to steady-state exposure, variable exposure due to fasting, low-fat or high-fat meal consumption, the potential for differential exposure in healthy volunteers versus dyslipidemic patients, and the different formulations utilized in the early clinical studies. Additionally, the complex two-compartment elimination profile was incorporated into the model to calculate the degree of plasma CETP activity at both peak and trough drug concentrations that would afford the maximal response in HDL-C and LDL-C. This complex model was then utilized in computational clinical trial simulations to select the final dose and formulation for phase III development and registration. The simulation analysis resulted in a prediction that a 100-mg dose formulated as a hot-melt extrusion would provide the minimum dose necessary to provide the maximum pharmacologic effect. These recommendations were utilized in the subsequent phase III studies.

The development team sought to determine the likelihood that the 25% increase in CV events observed in the ILLUMINATE trial of torcetrapib would not be observed in larger patient populations using anacetrapib therapy. The DEFINE trial (**Table 1**) was designed as an extensive phase III safety study, and was significantly overpowered to establish lipid effects.[58] This study randomized over 1600 patients who had a history or risk of coronary heart disease and who were receiving statin treatment to maintain their LDL-C levels between 50–100 mg dL^{-1} and with HDL-C levels <60 mg dL^{-1}. Study subjects were administered 100 mg of anacetrapib or placebo for 18 months, followed by a 3-month study follow-up. The primary endpoints included both LDL-C reduction

from baseline and prespecified clinical safety parameters, such as cardiovascular death, myocardial infarction, stroke, and hospitalization for unstable angina. Only a small number of cardiovascular events were anticipated from this sample size and study duration, but the DEFINE study was powered using a Bayesian probability approach to provide statistical confidence that a cardiovascular safety signal similar to that seen with the torcetrapib ILLUMINATE trial would not likely be observed in larger anacetrapib outcomes studies.

The DEFINE trial achieved its primary endpoints.[59] In the final analysis of 1623 patients, a 100 mg dose led to an increase of 138% in circulating HDL-C and a reduction of almost 40% in LDL-C beyond that achieved with statin therapy by 24 weeks. This is precisely the degree of lipid modification that was predicted by the computational modeling effort outlined previously.[57] These lipid effects were sustained throughout the 18-month treatment period. It must be noted that the LDL-C levels reported for the DEFINE study were derived using the Friedewald equation, which is commonly used in clinical practice and relies on an assumption of the ratio of TG to very low-density cholesterol (VDL-C).[60] This ratio is actually altered during the course of treatment with a CETP inhibitor, as transfer of TG from LDL fractions is inhibited. Indeed, a post hoc analysis of a subset of serum samples from DEFINE revealed that the actual magnitude of LDL-C reduction may have been closer to 25–35% when samples were reanalyzed using the more resource intensive β-quantification method.[61]

Importantly, the DEFINE study established the safety of anacetrapib therapy, and by inference the safety of aggressive CETP inhibition. In contrast to torcetrapib, anacetrapib had no effect on plasma electrolyte levels, circulating aldosterone levels, or blood pressure. The prespecified adjudicated clinical safety endpoints of death or major CV events are provided in **Table 4**. These endpoints were observed in 16 patients receiving anacetrapib and in 21 patients receiving placebo. Based on the Bayesian analysis prespecified for this trial, the results provided a 94% predictive probability of dismissing the likelihood of a 25% (torcetrapib-like) increase in CV events in larger outcomes studies with anacetrapib.

Further extension of the DEFINE trial provided additional information on the efficacy, safety, and pharmacokinetics of anacetrapib. A 2-year extension study was completed for 803 patients from the DEFINE study ($n=370$ on anacetrapib, $n=433$ on placebo).[62] This extension provided similar exposure and efficacy to the treatment period of the DEFINE trial, and further validated the safety of exposure to anacetrapib for up to 58 months. Additionally, a wash-out study was completed to determine the residual levels of anacetrapib in plasma, as well as residual effects on lipid parameters.[63] At 12 weeks following the last dose of anacetrapib, the mean plasma concentration was approximately 45% of the mean trough concentration while on treatment. There was continued evidence of anacetrapib pharmacodynamic effect on lipid parameters at the end of the wash-out period as well, with a mean 20% reduction from baseline LDL-C (Friedewald equation method) and 79% elevation in HDL-C. A further evaluation of patients from earlier phase II studies of anacetrapib found that residual drug levels of 7–8% of mean trough concentration could still be detected in plasma up to 4 years following the cessation of dosing of anacetrapib. Therefore, it is apparent that anacetrapib does have complex elimination kinetics, with a terminal half-life for anacetrapib that is significantly longer than was estimated from earlier phase I studies.

8.11.7 Adipose Distribution Studies with Anacetrapib

It was evident from the residual elimination data from the DEFINE trial that additional preclinical and clinical characterization of anacetrapib biodistribution would be helpful to further understand the half-life of anacetrapib, and so an effort was undertaken to fully characterize the disposition of the compound in vivo. Anacetrapib is a poly-fluorinated lipophilic compound ($\log D=7.1$), raising the possibility that the compound accumulates in adipose tissue during the treatment phase with slow release following the cessation of dosing. Additionally, CETP itself could function as a depot for bound anacetrapib, as CETP is expressed in multiple tissues including adipose.[64] To fully investigate this distribution, the preclinical research team performed a dose-accumulation and wash-out study in four groups of mice: wild type (WT) lean and WT with diet-induced obesity (DIO) mice that naturally lack CETP, and transgenic NFR-lean and NFR-DIO mice that express human CETP.[65] Anacetrapib exposure and distribution were analyzed during 6 weeks of dosing at 10 mg kg^{-1} in feed, to approximate the human exposure from the daily 100 mg dose, and during a 35-week washout period. The study confirmed the central role of white adipose tissue in the accumulation and retention of anacetrapib, as well as the contribution of this tissue to the long terminal elimination phase in DIO mice. CETP expression afforded higher blood concentration during the treatment phase of the study, but had a diminished impact on drug retention during the elimination phase. There was significantly lower accumulation of anacetrapib in brown adipose tissue, and the compound did not exhibit appreciable accumulation in the mouse brain.

The clinical team similarly examined adipose biopsy tissue from healthy human subjects who received 100 mg day^{-1} for up to 16 weeks, followed by a 52-week recovery phase.[66] During and after the dosing regimen, blood and adipose tissue were analyzed for concentrations of anacetrapib. The concentration of anacetrapib in plasma reached a plateau by ~4 weeks of dosing, but the concentration in adipose tissue continued to accumulate to levels ~64-fold higher than plasma by 16 weeks of dosing. During the recovery phase, concentrations of anacetrapib in adipose tissue remain stable for at least 1 year after cessation of dosing. These studies established that anacetrapib accumulates in adipose tissue, with the slow release from adipose hypothesized to contribute to the observed long terminal plasma half-life. Similar to all other clinical studies of anacetrapib, there were no safety findings of note in this investigation.

8.11.8 Preclinical Efficacy Support for Reverse Cholesterol Transport

The DEFINE trial had firmly established the safety of CETP inhibition by anacetrapib, and had affirmed the pharmacodynamic effect of CETP inhibition on HDL-C and LDL-C. However, the clinical team remained intrigued by the lack of meaningful benefit of torcetrapib in the ILLUMINATE trial despite achieving robust lipid effects. It was possible that the beneficial effect of torcetrapib therapy was overwhelmed by ancillary safety pharmacology. Post hoc analyses of phase III trials of torcetrapib provided some supporting evidence for this hypothesis. The imaging trials using intravascular ultrasonography did not meet the primary endpoints of reduced progression in the change of atheroma volume[67] (ILLUSTRATE trial) or reduced yearly rate of change of carotid intima-media thickness (RADIANCE 1 trial[68] or RADIANCE 2[69] trial). However, a post hoc analysis of the ILLUSTRATE trial results revealed a possible signal of efficacy. An inverse relationship was observed between the increase in HDL-C due to torcetrapib administration, and the progression of atherosclerosis. Patients in the highest quartile of HDL-C elevation achieved an actual regression of percent atheroma volume as compared to continued progression for other quartiles in the torcetrapib group and the entire placebo group.[70] While this observation was encouraging, it was not definitive.

An alternative hypothesis for the lack of clinical efficacy of torcetrapib continues to be investigated, which is that the subfraction of HDL that is enhanced by CETP inhibition is less effective as a vehicle for reverse cholesterol transport than the HDL produced by other means such as lifestyle changes (weight loss, increased exercise, dietary restrictions, and smoking cessation). As illustrated in Fig. 1, CETP mediates the transfer of CE and TG between HDL and VLDL/LDL particles (heterotypic transfer). However, it may also mediate the transfer of CE and TG among the various subfractions of HDL (homotypic transfer). These HDL subfractions include (in increasing size) preβ-HDL, HDL_3, HDL_2, and apoE-rich HDL, as illustrated in Fig. 10. By inhibiting homotypic transfer of CE and TG, CETP inhibition would alter the relative population of these HDL subclasses. In this way, it would be possible that CETP inhibitors promote the formation of HDL particles that are suboptimal for reverse cholesterol transport. Indeed, in an early phase II trial, the addition of torcetrapib (120 mg QD for 4 weeks) to atorvastatin therapy resulted in almost 10-fold higher increase in larger HDL_2-C than smaller HDL_3-C.[71] The distinctions among HDL subclasses are not trivial. Different subclasses have been proposed to have differing correlative benefit for protection against coronary heart disease, although conflicting results have been found for the relative importance of HDL_3-C and HDL_2-C from prospective studies.[72] As such, a hypothesis has developed that the magnitude of HDL-C elevation is not as important as the efficiency of the resultant HDL in promoting cholesterol efflux capacity through reverse cholesterol transport. The importance of cholesterol efflux capacity was recently supported in an analysis of the Dallas Heart Study.[73] In this prospective study of almost 3000 adults over 9 years, subjects in the highest quartile of cholesterol efflux capacity maintained a 67% reduction in cardiovascular risk over the lowest quartile, whereas overall HDL-C level was not associated with cardiovascular risk.

In light of this hypothesis, biopharmaceutical researchers including those at Merck and Roche embarked on a major effort to investigate the impact of CETP inhibitors on cholesterol efflux, and whether different inhibitors had unique attributes for reverse cholesterol transport. Among the CETP inhibitors investigated in the clinic, dalcetrapib from Roche has a unique biochemical mechanism of action. Dalcetrapib inhibits CETP by forming a labile covalent disulfide bond with Cys13 of the protein.[74] Dalcetrapib

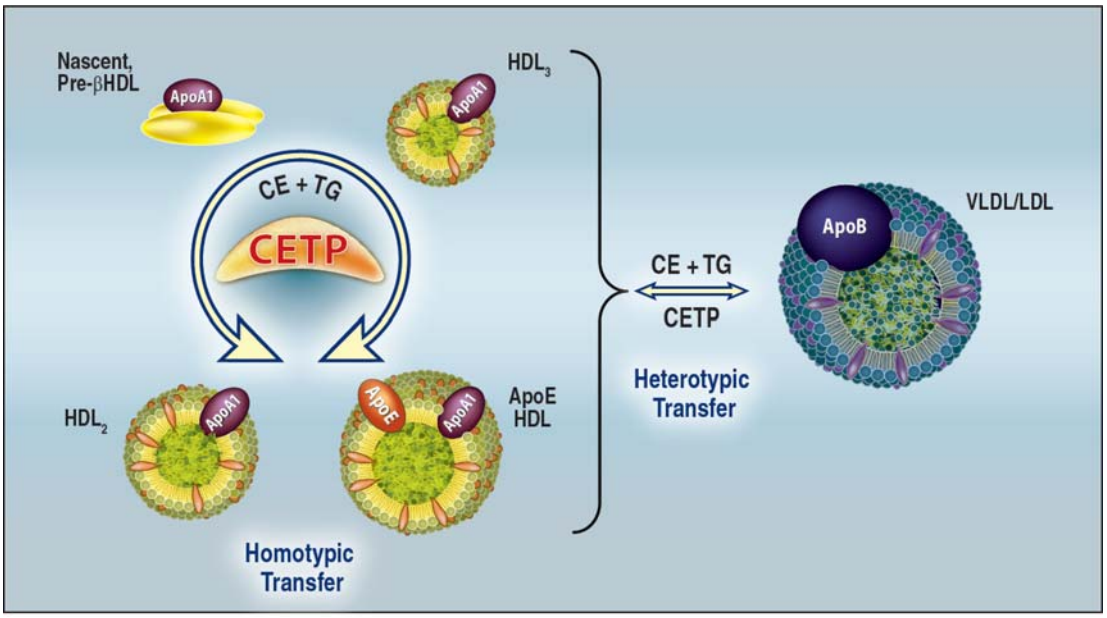

Fig. 10 Homotypic and heterotypic transfer of CE and TG by CETP.

inhibition is time dependent with the intrinsic potency (IC_{50}) increasing 26-fold following a 24-h incubation of dalcetrapib with CETP, while anacetrapib and torcetrapib are reversible and show no such time dependence.[75]

Scientists at both Roche and Merck intensively investigated whether the covalent modification of CETP by dalcetrapib conferred unique efficacy as compared to the reversible CETP inhibitors anacetrapib and torcetrapib. These studies lead to divergent and in some cases contradictory results. Functionally, the three compounds share several features of in vitro pharmacology.[75] All three of the compounds inhibited the transfer of both CE and TG between HDL and LDL particles, and all three compounds induced the formation of a stable CETP–HDL complex in vitro. All three compounds were found to displace radiolabeled anacetrapib or torcetrapib with binding potencies equivalent to their functional potencies, indicating a common active site for inhibition. Subsequently, the X-ray crystal structure of the CETP–torcetrapib complex was solved by scientists at Pfizer, confirming the binding of torcetrapib in the direct vicinity of the Cys13 residue of CETP required for dalcetrapib inhibition.[76] This observation provided evidence of a conserved binding site in CETP for dalcetrapib and torcetrapib, and by inference anacetrapib.

However, the nature of the functional inhibition may be different between dalcetrapib and anacetrapib. Scientists at Roche were the first to propose this distinction with in vitro studies measuring the transfer of [^{3}H]cholesteryl ester between HDL subfractions.[77] They found that anacetrapib and torcetrapib inhibited the transfer of CE from HDL_3-C to HDL_2-C, whereas dalcetrapib did not inhibit homotypic transfer of CE among HDL subfractions. This distinction was not observed by the Merck team, who found that all three compounds inhibited homotypic transfer from HDL_3-C to HDL_2-C in vitro.[78] The Roche team also found that incubation of human plasma with anacetrapib and torcetrapib actually decreased the level of preβ-HDL at concentrations of 1–10 μM, whereas incubation with dalcetrapib increased the level of preβ-HDL (at 10 μM only).[77] It is generally recognized that small preβ-HDL is critical as an early component of reverse cholesterol transport.[79] These distinctions led the Roche team to classify dalcetrapib as a CETP modulator, as opposed to the CETP inhibitors anacetrapib and torcetrapib.

The Merck team further investigated the inhibition of HDL_3-C to HDL_2-C homotypic transfer by anacetrapib both in vitro (human plasma) and in vivo in NFR-CETP transgenic mice.[78] Both anacetrapib and dalcetrapib were shown to moderately inhibit homotypic transfer of [^{3}H]cholesterol from HDL_3 to HDL_2 in vitro, with maximal inhibition of $\leq$50% despite further increases in inhibitor concentration. In vivo, transgenic mice were treated with anacetrapib at 100 mg kg^{-1} day^{-1} for 5 days, then injected with [$^2H_6$]-cholesterol labeled HDL_3. The radiolabeled cholesterol appeared almost immediately in HDL_2, similar to vehicle-treated mice during the first hour, and then accumulated more rapidly in HDL_2 than vehicle-treated mice over the next six hours, in direct contrast to the in vitro studies. The appearance of labeled cholesterol was significantly reduced in LDL or VLDL particles ($\leq$30% in anacetrapib-treated mice as compared to vehicle). The experiments provided a puzzling contrast between the in vitro inhibition of homotypic transfer and the in vivo appearance of CE homotypic transfer. It remains possible that CETP inhibition blocks homotypic transfer of CE among HDL subfractions in vivo, and that alternate mechanisms are available for HDL remodeling such as particle maturation from HDL_3 to HDL_2.

The researchers at Roche also studied the in vivo effects of the three inhibitors in normolipidemic (lean) golden Syrian hamsters, which naturally express CETP.[77] Following a 7-day treatment of dalcetrapib (100 mg kg^{-1} BID), torcetrapib (30 mg kg^{-1} QD) or anacetrapib (30 mg kg^{-1} QD), the hamsters were injected with [^{3}H]cholesterol-labeled macrophages. The fecal excretion of [^{3}H] total sterols was monitored for the next ten days to measure the efficiency of reverse cholesterol transport from macrophages to feces for the radiolabeled cholesterol. The Roche team found that dalcetrapib and torcetrapib significantly increased fecal excretion of [^{3}H]sterols, whereas anacetrapib afforded no significant effect despite affording the largest relative increase in HDL-C levels. The authors proposed that the clinical outcome of a CETP modulator such as dalcetrapib may be distinct from CETP inhibitors such as anacetrapib in the reduction of CVD risk, and that the relative magnitude of overall HDL-C elevation between the compounds may not be fully relevant for the prediction of clinical efficacy.

To the contrary, the Merck team subsequently demonstrated effective anacetrapib-mediated reverse cholesterol transport in golden Syrian hamsters that were made dyslipidemic by a high-fat diet.[80] Following treatment with anacetrapib for 14 days in feed (60 mg kg^{-1}), [^{3}H]cholesterol-loaded macrophages were injected into the hamsters and fecal excretion was monitored for 48 h. The team found significant increases in [^{3}H]cholesterol by 90% and [^{3}H]bile acids by 57% relative to vehicle. The difference between the Roche and Merck observations with anacetrapib could be ascribed to important methodological differences in the experiments, including the use of normolipidemic versus dyslipidemic hamsters, differences in dose and duration of anacetrapib treatment, and differences in collection period for feces. In fact, a subsequent study of anacetrapib and dalcetrapib in hamsters indicated that this was indeed the case. At doses that provide equal levels of CETP inhibition in vivo, only dalcetrapib stimulated HDL-derived cholesterol fecal excretion in normolipidemic hamsters, whereas only anacetrapib promoted macrophage-derived cholesterol fecal excretion in dyslipidemic hamsters.[81]

Similar to the Roche investigators, the Merck team found that anacetrapib inhibited the generation of preβ-HDL when incubated in human plasma in vitro, whereas dalcetrapib did not inhibit or increase preβ-HDL (up to 10 μM).[82] However, the effect was quite different in vivo. In dyslipidemic golden Syrian hamsters, treatment with anacetrapib for 14 days (60 mg kg^{-1} QD) showed a significant elevation of preβ-HDL, whereas treatment with dalcetrapib (200 mg kg^{-1} BID) produced no such elevation. The divergent results between the two compounds might be ascribed to differences in intrinsic potency, but the results indicate that CETP inhibition in vivo does not decrease levels of preβ-HDL, at least in dyslipidemic hamsters.

The multiple complex experiments outlined above illustrate the sophisticated preclinical tools that are used for the evaluation of CETP-mediated reverse cholesterol transport, as well as the difficulty in translating the results to human cardiovascular disease. In order to identify the optimal translational pharmacology system for lipid research, the Merck researchers coordinated an exhaustive lipidomics analysis of 24 experimental pharmacology models.[83] By examining five primate species (including humans), six mouse

strains, and six other nonprimate species, the team found that nonhuman primate models demonstrated the closest overall match to dyslipidemic humans. Based on these findings, anacetrapib was examined in lean rhesus macaques at a dose of 150 mg kg^{-1} for 10 days.[84] The compound afforded similar effects on plasma lipids as those found clinically in humans, with an elevation of HDL-C of 110% and reduction of LDL-C of 65–79%. The rhesus studies have also featured analysis of the inhibition of TG transfer as well as CE by anacetrapib.[85] This species may enable preclinical RCT experiments that are more fully translational to clinical observations.

A single clinical trial has examined the effect of CETP inhibition on cholesterol efflux. The dal-ACUTE study administered 600 mg of dalcetrapib or placebo to patients within 1 week of acute coronary syndrome (myocardial infarction or unstable angina) for 24 weeks of treatment.[86] The researchers found that dalcetrapib elevated HDL-C by 32% with no significant change in LDL-C. An ex vivo analysis of patient plasma revealed no change in preβ-HDL. Notably, serum from patients in the treatment group exhibited a significant 9.5% improvement in ex vivo capacity for cholesterol efflux capacity a macrophage-derived cell line assay.[87] Whether this improvement was sufficient to improve cardiac outcome would be independently determined in the dal-OUTCOMES study.

8.11.9 The Re-Emergent Importance of CETP Inhibitor-Induced Lowering of LDL-C

There remained an intriguing aspect of dalcetrapib, which was the only clinically investigated CETP inhibitor to afford elevation of HDL-C with no significant reduction of LDL-C. Before proceeding with a large-scale outcomes study for anacetrapib, the Merck team examined the clinical data supporting a hypothesis that HDL-C and LDL-C levels might be independently modified by different CETP inhibitors.[88] An analysis of all of the published phase II data for monotherapy with CETP inhibitors suggests that a common functional mechanism is operative for all CETP inhibitors. A graphical representation of the phase II studies for anacetrapib (Merck),[49] evacetrapib (Eli Lilly),[89] CP-800,569 (Pfizer),[90] Torcetrapib (Pfizer),[91] dalcetrapib (Roche),[92] and including the recently reported data from the TULIP trial for TA-8995 (Dezima/Amgen)[93] is provided in Fig. 11. It is apparent from this graphical examination of the clinical data that all CETP inhibitors have similar relative effects on the elevation of circulating HDL-C and reduction of circulating LDL-C. This linear relationship in pharmacodynamic effect supports a common pharmacologic mechanism among the CETP inhibitors, including anacetrapib and dalcetrapib, and indicates they do not afford unique profiles for HDL-C effects or LDL-C effects.

An emergent line of research into the effects of CETP inhibition regards the importance of inhibitor-mediated lowering of LDL-C, and the decreased number of LDL particles as an additional contributor to cardiovascular disease risk reduction. Treatment with anacetrapib changes the distribution balance of CE from LDL to HDL particles (Fig. 1), which is hypothesized to have an atheroprotective effect. However, anacetrapib has recently been shown to afford a significant decrease in the number of LDL particles in both healthy individuals and dyslipidemic patients, as measured by plasma ApoB protein concentration.[94,95] The clinical team further investigated the kinetics of ApoB clearance in dyslipidemic patients treated with anacetrapib either with or without atorvastatin for 4 weeks.[96] Anacetrapib was found to reduce the ApoB pool by significantly increasing the clearance rate of LDL-ApoB without affecting the production rate.

8.11.10 Clinical Outcomes Trials of CETP Inhibitors: The *REVEAL* Study

The clinical safety profile established by the DEFINE study for anacetrapib indicated that ancillary safety pharmacology would not hinder the analysis of clinical outcomes data. Furthermore, the preclinical efficacy experiments performed on anacetrapib and other CETP inhibitors supported the likelihood that CETP inhibition would facilitate reverse cholesterol transport, which may provide an overall antiatherogenic effect. However, it was clear following the experience with Pfizer's torcetrapib in the ILLUMINATE trial that

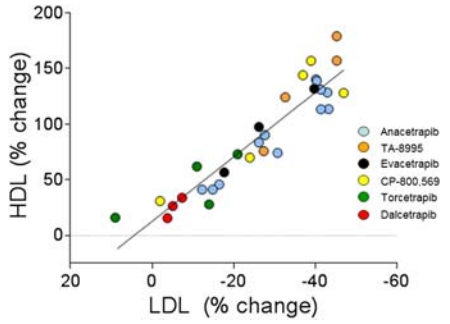

Fig. 11 Comparison of the relative low- and high-density lipoprotein cholesterol changes observed in phase II studies with CETP inhibitors at multiple dose levels for each compound. Adapted with permission from Johns, D. G.; Duffy, J. L.; Fisher, T.; Hubbard, B. K.; Forrest, M. J. On- and Off-Target Pharmacology of Torcetrapib: Current Understanding and Implications for the Structure Activity Relationships (SAR), Discovery and Development of Cholesteryl Ester Transfer Protein (CETP) Inhibitors. *Drugs* **2012**, *72*, 491–507.

a large outcomes study would be required to establish a significant reduction in cardiovascular disease risk for CETP inhibitors to provide value.

As the development team contemplated the design of the outcomes study for anacetrapib, they were aware that dalcetrapib was under broad investigation by Roche in several late-stage clinical trials listed in Table 3 and known collectively as the dal-HEART (DALcetrapib HDL Evaluation, Atherosclerosis and Reverse cholesterol Transport) program. The largest of these, the dal-OUTCOMES trial, initiated in April, 2008 and was designed to randomize $\geq$15,600 patients who had been hospitalized for acute coronary syndrome within 4–12 weeks prior to initiating treatment.[97] Patients received either placebo or 600 mg dalcetrapib for a minimum of 2 years, with the primary efficacy measurement as first occurrence to acute myocardial infarction, unstable angina requiring hospitalization, atherothrombotic stroke, or coronary heart disease mortality. The trial was to proceed until $\geq$1600 primary events had been registered, which was anticipated to conclude in 2013. The research program also included three surrogate endpoint trials. The dal-PLAQUE trial examined high-risk cardiovascular disease patients on dalcetrapib or placebo for 24 months for differences in progression of vascular wall thickness and plaque burden as assessed by MRI and PET/CT techniques.[98] The dal-PLAQUE 2 study examined coronary artery disease patients for the effect of dalcetrapib or placebo on carotid intima-media thickness by ultrasonography.[99] The dal-VESSAL study examined the effect of dalcetrapib versus placebo in coronary heart disease or coronary artery disease patients for brachial flow-mediated dilation by ultrasound techniques, as well as 24-h ambulatory blood pressure.[100]

While the dal-OUTCOMES study was underway, Merck initiated the REVEAL cardiovascular outcomes trial in June, 2011 (Table 4).[101] The study is ongoing and is anticipated to conclude in early 2017, once a median follow-up time of 4 years has been achieved for patients on treatment. As of the time of submission for this case history, REVEAL has completed enrollment with 30,450 patients randomized to receive 100 mg anacetrapib or placebo in addition to atorvastatin therapy. Rather than focus on recent acute coronary syndrome patients as had been examined in dal-OUTCOMES, the REVEAL trial enrolled patients with established coronary artery disease, with a history of myocardial infarction, cardiovascular disease, peripheral artery disease, or diabetes mellitus with other evidence of coronary heart disease. Patients in the study are evaluated for the primary endpoints of coronary mortality, myocardial infarction, or coronary revascularization procedure. A companion study of anacetrapib in patients with heterozygous familial hypercholesterolemia was also launched in February of 2012. The REALIZE study (Table 1) evaluated the efficacy of anacetrapib when added to other lipid modifying agents in this difficult to treat patient population.[102]

Important developments have occurred among studies of comparator CETP inhibitors while the REVEAL study has been underway. On May 7, 2012, after the initiation of the REVEAL trial, Roche announced the early termination of the dal-OUTCOMES trial due to a lack of clinically meaningful efficacy based on the second interim analysis by the independent data safety monitoring board.[103] All ongoing studies in the dal-HEART program were also terminated. In their analysis, over 70% of the primary end-point events had occurred with no significant difference between the dalcetrapib group and the placebo group on the composite or individual endpoints.[104] During the median dosing period of 31 months, HDL-C levels were elevated by 31 to 40% by the administration of dalcetrapib, with no significant effect on LDL-C. There was no dalcetrapib-mediated change in systolic blood pressure, plasma aldosterone, or circulating electrolytes. However, the interim analysis established that there was only 1.1% likelihood that a risk reduction of $\geq$10% would be observed among the entire study population if the trial was completed.

At the time of early termination for the dal-HEART program, two of the surrogate endpoint trials had fully completed. The dal-VESSEL trial showed no improvement or impairment in flow-mediated dilation over 3 months, and also showed no change in ambulatory blood pressure.[105] However, the dal-PLAQUE trial indicated that dalcetrapib may decrease inflammation and total vessel area over 6–24 months of treatment as measured by MRI and PET/CT.[106] A recent post hoc analysis of PET data from dal-PLAQUE indicated that dalcetrapib treatment had no effect on the progression of vascular calcification over 6 months of treatment.[107]

It must be noted that a preliminary post hoc pharmacogenomic analysis of dal-OUTCOMES data has provided some indication of efficacy for a subgroup of patients in the study. A team of researchers, including several involved in the dal-OUTCOMES trial, have identified a specific polymorphism in the *ADCY9* gene that is associated with a 39% risk reduction in primary endpoints for patients in the dalcetrapib treatment group, and this correlation was supported by further pharmacogenomic analysis of patients, the smaller dal-PLAQUE-2 study.[108] This polymorphism is present in 20% of the general population, which potentially identifies a sizable group of acute coronary syndrome patients that could receive benefit from dalcetrapib therapy. Based on these results, DalCor Pharmaceuticals was formed to continue development of dalcetrapib in patients with this polymorphism. They have announced a plan to return to the clinic to evaluate dalcetrapib in this subgroup in 2016.[109]

Following the termination of the dal-OUTCOMES trial, in October, 2012, Eli Lilly initiated an outcomes trial with evacetrapib called ACCELERATE (Table 3).[110] In this study, 12,092 patients were randomized to receive 130 mg of evacetrapib or placebo in addition to standard medical treatment for a minimum of 1.5 years. Similar to the dal-OUTCOMES enrollment, patients were enrolled in ACCELERATE if they had experienced acute coronary syndrome within the preceding 4–52 weeks. Patients were also enrolled if they had peripheral vascular disease, transient ischemic stroke, or diabetes with coronary artery disease. The primary efficacy endpoints were similar to dal-OUTCOMES (coronary mortality, myocardial infarction, or coronary revascularization). The trial was designed to proceed until $\geq$1670 patients reached the primary end point.

However, on Oct. 12, 2015, Eli Lilly announced the early termination of the ACCELERATE trial due to lack of clinically meaningful efficacy based on an interim analysis by the independent data safety monitoring board.[111] Eli Lilly noted that the study was not being stopped for safety reasons, but rather based on the low probability that the study would achieve its primary endpoints based on the interim results. As of the submission of this case history, the full results of the interim analysis of the ACCELERATE trial have not been reported.

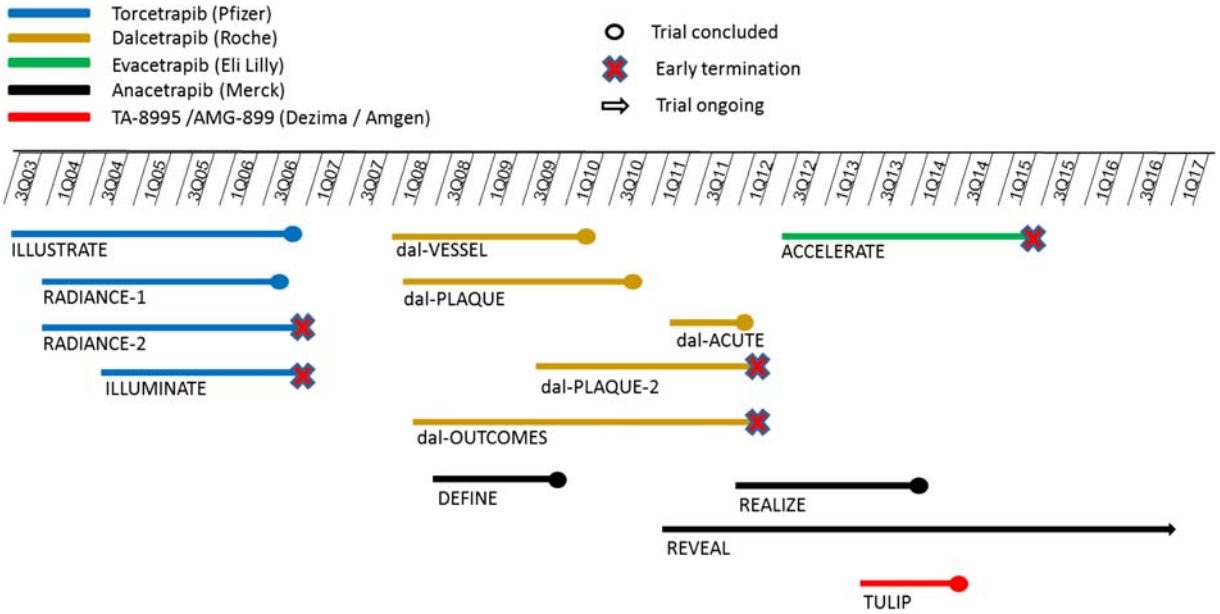

Fig. 12 Timeline of efficacy clinical trials for CETP inhibitors

The trial terminations described above leave only the REVEAL outcomes study for anacetrapib ongoing to completion. A prespecified interim analysis was performed in Nov., 2015 by the independent data monitoring committee, who recommended that the REVEAL trial continue to completion.[112] Their analysis included both a safety analysis and a futility analyses. The timelines associated with the CETP clinical trials above are illustrated in Fig. 12.[113] The details and summary results of each of these trials are summarized in Table 5.

8.11.11 Conclusion

The outcomes studies on three CETP inhibitors have been terminated during interim analysis by their respective monitoring committees for either safety (torcetrapib) or futility (dalcetrapib, evacetrapib). Anacetrapib has completed the final interim analysis by the independent data safety monitoring board, and it remains the sole CETP inhibitor under investigation in a clinical outcomes trial. The data from the completed REVEAL study are expected in 2017. Contrary to torcetrapib, anacetrapib has established a positively differentiated safety profile in both preclinical and clinical studies that will facilitate the completion of the outcomes trial. Contrary to dalcetrapib, anacetrapib has established significantly greater pharmacodynamic effect in the elevation of HDL-C and reduction of LDL-C that would indicate that anacetrapib would afford a more robust test of the CETP inhibition hypothesis. By comparison with evacetrapib, however, anacetrapib shares a similar efficacy pharmacodynamics and safety profile at the dose administered.

Differences between the design of the ACCELERATE trial of evacetrapib and the REVEAL trial of anacetrapib could provide insight into the possibility that different results will be observed with these two compounds. The ACCELERATE trial was terminated following a median follow-up time of ~2 years, which may not have provided enough time for evacetrapib to exert a beneficial effect. Prior studies of statins have demonstrated a lag in efficacy ranging from 6 months to 2 years. For example, a ~1-year lag in outcome efficacy was observed in the IMPROVE-IT trial of ezetimibe added to simvastatin, in which over 18,000 patients with acute coronary syndrome were treated for a median follow-up of 6 years to identify an additional 2% absolute reduction in cardiovascular disease risk.[114] By contrast, the REVEAL trial will maintain 4 years median follow-up. Additionally, the patient populations for ACCELERATE included subjects 1–12 months following acute coronary syndrome, who may be more prone to early cardiovascular events as opposed to a more chronic vascular disease population for REVEAL. Improved reverse cholesterol transport, achieved through CETP inhibition, may be more beneficial in the chronic cardiovascular disease population in REVEAL. Finally, the ACCELERATE trial enrolled over 12,000 patients as compared to over 30,000 patients in the REVEAL study. This larger sample size of REVEAL, coupled with the longer follow-up for the completed interim analysis (~3 years), may allow for the detection of a smaller effect size that passed interim futility analysis as compared to the interim analysis of ACCELERATE.

The utility of CETP inhibition to reduce cardiovascular risk is the subject of considerable debate in the scientific community. As such, the continued investigation of CETP inhibition has been alternately referred to in editorial analyses as either a "strategy to reduce cardiovascular risk"[115] or the "suspension of disbelief."[116] The debate will be significantly informed by the results of the REVEAL clinical investigation, which is anticipated in 2017.

Table 5 Summary of CETP inhibitor advanced safety and efficacy trials

Compound (dose)	*Trial*	*Patient population*	*Efficacy measure*	*↑HDL-C/ ↓LDL-C*	*Outcome*	*Ref.*
Torcetrapib (60 mg)	ILLUMINATE	15,067 High CV risk	CV death, MI, stroke, UA outcomes	70-80%/ 20–30%	Interim analysis early termination: ↑CV end point and all-cause mortality.	46
	RADIANCE 1	Familial hypercholesterolemia or atherogenic dyslipidemia	Progression of carotid intima-medial thickening via ultrasonography	54%/ 20%	Negative	68
	ILLUSTRATE	1188 CAD	Progression of coronary atherosclerosis via intravascular ultrasound	61%/ 20%	Negative	67
Dalcetrapib (600 mg)	dal-OUTCOMES	15,871 ACS (within 4–12 weeks of MI)	CV death, MI, stroke, UA outcomes	30–40%/ 0–7%	Interim analysis early termination in 2012: Clinical futility.	104
	dal-ACUTE	300 ACS (within 1 week of MI or UA)	% HDL-C change at 24 weeks	32%/0%	Increased total cholesterol efflux 9%, no change in preβ-HDL	86
	dal-PLAQUE	130 High CV risk	Progression of vascular wall thickness and plaque burden by MRI and PET/CT	31%/0%	Slight decrease in total vessel area and inflammation	106
	dal-VESSEL	476 High CV risk	Improvement in flow-mediated dilation by ultrasound	31%/0%	No improvement or impairment	105
	dal-PLAQUE 2	931 CAD	Progression of coronary atherosclerosis via intravascular ultrasound		Early termination, data not available	108
Evacetrapib (130 mg)	ACCELERATE	12,092 ACS (within 4–52 weeks of MI) or high CV risk	CV death, MI, stroke, UA, coronary revascularization outcomes	130%/ 40%	Interim analysis early termination in 2015: Clinical futility	111
Anacetrapib (100 mg)	DEFINE			130–140%/ 30–40%	Safe and well tolerated	59
	REALIZE	306 Heterozygous familial hypercholesterolemia	% LDL-C change at 52 weeks	102%/ 40%	Safe and well tolerated	102
	REVEAL	30,624 CAD	CV death, MI, stroke via outcomes		Interim analysis recommended continuation in 2015, anticipated conclusion in 2017	112
TA-8995/ AMG-899 ($\leq$10 mg)	TULIP	364 Mild dyslipidemia	% LDL-C and % HDL-C change at 12 weeks	$\leq$179%/ $\leq$45%	Safe and well tolerated	93

Acknowledgments

The authors are indebted to Dr. Doug Johns of Merck Research Labs for his valuable assistance in the preparation of this manuscript.

See also: 7.18. Advances in Hypercholesterolemia.

References

1. Jordan, V. C. Tamoxifen. In *Comprehensive Medicinal Chemistry II,* vol. 8, Taylor, J. B., Triggle, D. J., Taylor, J. B., Triggle, D. J., Eds.; Elsevier: New York, 2007.
2. Mathers, C. D.; Lopez, A. D.; Murray, C. J. L. The Burden of Disease and Mortality by Condition: Data, Methods, and Results for 2001. In *Global Burden of Disease and Risk Factors;* Lopez, A. D., Mathers, C. D., Ezzati, M., Jamison, D. T., Murray, C. J. L., Eds.; World Bank: Washington, DC, 2006; pp 45–93.

3. Mozaffarian, D.; Benjamin, E. J.; Go, A. S.; Arnett, D. K.; Blaha, M. J.; Cushman, M.; de Ferranti, S.; Despres, J.-P.; Fullerton, H. J.; Howard, V. J.; Huffman, M. D.; Judd, S. E.; Kissela, B. M.; Lackland, D. T.; Lichtman, J. H.; Lisabeth, L. D.; Liu, S.; Mackey, R. H.; Matchar, D. B.; McGuire, D. K.; Mohler, E. R.; Moy, C. S.; Munter, P.; Mussolino, M. E.; Nasir, K.; Neumar, R. W.; Nichol, G.; Palaniappan, L.; Pandey, D. K.; Reeves, M. J.; Rodriguez, C. J.; Sorlie, P. D.; Stein, J.; Towfighi, A.; Turan, T. N.; Virani, S. S.; Willey, J. Z.; Woo, D.; Yeh, R. W.; Turner, M. B. Heart Disease and Stroke Statistics—2015 Update. *Circulation* **2015,** *131,* e254–e268.
4. Gordon, T.; Castelli, W. P.; Hjortland, M. C.; Kannel, W. B.; Dawber, T. R. High Density Lipoprotein as a Protective Factor Against Coronary Heart Disease. *Am. J. Med.* **1977,** *62,* 707–714.
5. Castelli, W. P. Cholesterol and Lipids in the Risk of Coronary Artery Disease—The Framingham Heart Study. *Can. J. Cardiol.* **1988,** *4* (Suppl. A), 5A–10A.
6. Gordon, D. J.; Basil, M. R. High-Density Lipoprotein—The Clinical Implications of Recent Studies. *N. Engl. J. Med.* **1989,** *321,* 1311–1316.
7. Cholesterol Treatment Trialists' Collaboration. Efficacy and Safety of More Intensive Lowering of LDL Cholesterol: A Meta-Analysis of Data From 170,000 Participants in 26 Randomised Trials. *Lancet* **2010,** *376,* 1670–1681.
8. Cannon, C. P.; Blazing, M. A.; Giugliamo, R. P.; McGragg, A.; White, J. A.; Theroux, P.; Darius, H.; Lewis, B. S.; Ophuis, T. O.; Jukema, W.; De Ferrari, G. M.; Ruzyllo, W.; De Lucca, P.; Im, K.; Bohula, E. A.; Reist, C.; Wiviott, S. D.; Tershakovec, A. M.; Musliner, T. A.; Braunwald, E.; Califf, R. M. Ezetimibe Added to Statin Therapy After Acute Coronary Syndromes. *N. Engl. J. Med.* **2015,** *372,* 2387–2397.
9. Doggrell, S. A.; Lynch, K. A. Is There Enough Evidence With Evolocumab and Alirocumab (Antibodies to Proprotein Convertase Substilisin-Kexin Type, PCSK9) on Cardiovascular Outcomes to Use Them Widely? *Expert. Opin. Biol. Ther.* **2015,** *15,* 1671–1675.
10. Kaur, N.; Pandey, A.; Negi, H.; Shafiq, N.; Reddy, N.; Reddy, S.; Kaur, H.; Chadha, N.; Malhotra, S. Effect of HDL-Raising Drugs on Cardiovascular Outcomes: A Systematic Review and Meta-Regression. *PLoS One* **2014,** *9,* e94585.
11. Koizumi, J.; Mabuchi, H.; Yoshimura, A.; Michishita, I.; Takeda, M.; Itoh, H.; Sakai, Y.; Sakai, T.; Ueda, K.; Takeda, R. Deficiency of Serum Cholesteryl-Ester Transfer Activity in Patients With Familial Hyperphalipoproteinaemia. *Atherosclerosis* **1985,** *58,* 175–186.
12. Mabuchi, H.; Nohara, A.; Inazu, A. Cholesteryl Ester Transfer Protein (CETP) Deficiency and CETP Inhibitors. *Mol. Cells* **2014,** *37,* 777–784.
13. Pattnaik, N. M.; Zilversmit, D. B. Interaction of Cholesteryl Ester Exchange Protein With Human Plasma Lipoproteins and Phospholipid Vesicles. *J. Biol. Chem.* **1979,** *254,* 2782–2786.
14. Barter, P. J.; Jones, M. E. Kinetic Studies of the Transfer of Esterified Cholesterol Between Human Plasma Low and High Density Lipoproteins. *J. Lipid Res.* **1980,** *21,* 238–249.
15. Zhang, L.; Yan, F.; Zhang, S.; Lei, D.; Charles, M. A.; Cavigiolio, G.; Oda, M.; Krauss, R. M.; Weisgraber, K. H.; Rye, K.-A.; Pownall, H. J.; Qiu, X.; Ren, G. Structural Basis of Transfer Between Lipoproteins by Cholesteryl Ester Transfer Protein. *Nat. Chem. Biol.* **2012,** *8,* 342–349.
16. Lauer, M. E.; Graff-Meyer, A.; Rufer, A. C.; Maugeais, C.; von der Mark, E.; Matile, H.; D'Arcy, B.; Magg, C.; Ringler, P.; Muller, S. A.; Scherer, S.; Dernick, G.; Thoma, R.; Hennig, M.; Niesor, E. J.; Stahlberg, H. Cholesterol Ester Transfer Between Lipoproteins Does Not Require a Ternary Tunnel Complex With CETP. *J. Struct. Biol.* **2016,** *194,* 191–198.
17. Tsutsumi, K.; Hagi, A.; Inoue, Y. The Relationship Between Plasma High Density Lipoprotein Cholesterol Levels and Cholesteryl Ester Transfer Protein Activity in Six Species of Healthy Experimental Animals. *Biol. Pharm. Bull.* **2001,** *24,* 579–581.
18. Marotti, K. R.; Castle, C. K.; Murray, R. W.; Rehberg, E. F.; Polites, H. G.; Melchior, G. W. The Role of Cholesteryl Ester Transfer Protein in Primate Apolipoprotein A-I Metabolism. Insights From Studies With Transgenic Mice. *Arterioscler. Thromb. Vasc. Biol.* **1992,** *12,* 736–744.
19. Plump, A. S.; Masucci-Magoulas, L.; Bruce, C.; Bisgaier, C. L.; Breslow, J. L.; Tall, A. R. Increased Atherosclerosis in ApoE and LDL Receptor Gene Knock-Out Mice as a Result of Human Cholesteryl Ester Transfer Protein Transgene Expression. *Arterioscler. Thromb. Vasc. Biol.* **1999,** *19,* 1105–1110.
20. Sikorski, J. A.; Glenn, K. C. Cholesteryl Ester Transfer Protein as a Potential Therapeutic Target to Improve the HDL to LDL Cholesterol Ratio. In *Annual Reports in Medicinal Chemistry,* vol. 35, Doherty, A. M., Ed.; Elsevier: New York, 2000; pp 251–260.
21. Deninno, M. P.; Magnus-Arytey, G. T.; Ruggeri, R. B.; Wester, R. T. 2000 4-Carboxyamino-2-Substituted-1,2,3,4-tetrahydroquinolines as CETP Inhibitors. WO 2000017164, May 30, 2000.
22. Ruggeri, R. B.; Wester, R. T.; Magnus-Aryitey, G. Abstracts of Papers. 225th National Meeting of the American Chemical Society, New Orleans, LA, March 23–27, 2003; American Chemical Society: Washington, DC, 2003. MEDI-156.
23. Shinkai, H.; Maeda, K.; Yamasaki, T.; Okamoto, H.; Uchida, I. Bis(2-(Acylamino)phenyl) disulfides, 2-(acylamino)benzenethiols, and *S*-(2-(acylamino)phenyl) alkanethioates as Novel Inhibitors of Cholesteryl Ester Transfer Protein. *J. Med. Chem.* **2000,** *43,* 3566–3572.
24. De Grooth, G. J.; Kuivenhven, J. A.; Stalenhoef, A. F. H.; de Graaf, J.; Zwinderman, A. H.; Posma, J. L.; van Tol, A.; Kastelein, J. J. P. Efficacy and Safety of a Novel Cholesteryl Ester Transfer Protein Inhibitor, JTT-705, in Humans: A Randomized Phase II Dose–Response Study. *Circulation* **2002,** *105,* 2159–2165.
25. Eveland, S. S.; Milot, D. P.; Guo, Q.; Chen, Y.; Hyland, S. A.; Peterson, L. B.; Jezequel-Sur, S.; O'Donnell, G. T.; Zuck, P. D.; Ferrer, M.; Strulovici, B.; Laterza, B.; Wagner, J. A.; Tanaka, W. K.; Sparrow, C. P.; Anderson, M. S. A High-Precision Fluorogenic Cholesteryl Ester Transfer Protein Assay Compatible With Animal Serum and 3456-Well Assay Technology. *Anal. Biochem.* **2007,** *368,* 239–249.
26. Harikrishnan, L. S.; Kamau, M. G.; Herpin, T. F.; Morton, G. C.; Liu, Y.; Cooper, C. B.; Salvati, M. E.; Qiao, J. X.; Wang, T. C.; Adam, L. P.; Taylor, D. S.; Chen, A. Y. A.; Yin, X.; Seethala, R.; Peterson, T. L.; Nirschl, D. S.; Miller, A. V.; Weigelt, C. A.; Appiah, K. K.; O'Connell, J. C.; Lawrence, R. M. 2-Arylbenzoxazoles as Novel Cholesteryl Ester Transfer Protein Inhibitors: Optimization via Array Synthesis. *Bioorg. Med. Chem. Lett.* **2008,** *18,* 2640–2644.
27. Smith, C. J.; Ali, A.; Chen, L.; Hammond, M. L.; Anderson, M. S.; Chen, Y.; Eveland, S. S.; Guo, Q.; Hyland, S. A.; Milot, D. P.; Sparrow, C. P.; Wright, S. D.; Sinclair, P. J. 2 Arylbenzoxazoles as CETP Inhibitors: Substitution of the Benzoxazole Moiety. *Bioorg. Med. Chem. Lett.* **2010,** *20,* 346–349.
28. Hunt, J. A.; Gonzalez, S.; Kallashi, F.; Hammond, M. L.; Pivnichny, J. V.; Tong, X.; Xu, S. S.; Anderson, M. S.; Chen, Y.; Eveland, S. S.; Hyland, S. A.; Milot, D. P.; Sparrow, C. P.; Wright, S. D.; Sinclair, P. J. 2-Arylbenzoxazoles as CETP Inhibitors: Substitution and Modification of the α-Alkoxyamide Moiety. *Bioorg. Med. Chem. Lett.* **2010,** *20,* 1019–1022.
29. Kallashi, F.; Kim, D.; Kowalchick, J.; Park, Y. J.; Hunt, J. A.; Ali, A.; Smith, C. J.; Hammond, M. L.; Pivnichny, J. V.; Tong, X.; Xu, S. S.; Anderson, M. S.; Chen, Y.; Eveland, S. S.; Guo, Q.; Hyland, S. A.; Milot, D. P.; Cumiskey, A. M.; Latham, M.; Peterson, L. B.; Rosa, R.; Sparrow, C. P.; Wright, S. D.; Sinclair, P. J. 2-Arylbenzoxazoles as CETP Inhibitors. Raising HDL-C in cynoCETP Transgenic Mice. *Bioorg. Med. Chem. Lett.* **2011,** *21,* 558–561.
30. Sweis, R. F.; Hunt, J. A.; Kallashi, F.; Hammond, M. L.; Chen, Y.; Eveland, S. S.; Guo, Q.; Hyland, S. A.; Milot, D. P.; Cumiskey, A. M.; Latham, M.; Rosa, R.; Peterson, L.; Sparrow, C. P.; Wright, S. D.; Anderson, M. S.; Sinclair, P. J. 2-(4-Carbonylphenyl)benzoxazole Inhibitors of CETP: Scaffold Design and Advancement in HDL-c Raising Efficacy. *Bioorg. Med. Chem. Lett.* **2011,** *21,* 1890–1895.
31. Sweis, R. F.; Hunt, J. A.; Sinclair, P. J.; Chen, Y.; Eveland, S. S.; Guo, Q.; Hyland, S. A.; Milot, D. P.; Cumiskey, A. M.; Latham, M.; Rosa, R.; Peterson, L.; Sparrow, C. P.; Wright, S. D.; Rosa, R.; Peterson, L.; Sparrow, C. P.; Wright, S. D.; Anderson, M. S. 2-(4-Carbonylphenyl)benzoxazole Inhibitors of CETP: Attenuation of hERG Binding and Improved HDL-c Raising Efficacy. *Bioorg. Med. Chem. Lett.* **2011,** *21,* 2597–2600.
32. Wilson, J. E.; Kurukulasuriya, R.; Reibarkh, M.; Reiter, M.; Zwicker, A.; Zhao, K.; Zhang, F.; Anand, R.; Colandrea, V. J.; Cumiskey, A.-M.; Crespo, A.; Duffy, R. A.; Murphy, B. A.; Mitra, K.; Johns, D. G.; Duffy, J. L.; Vachal, P. Discovery of Novel Indoline Cholesterol Ester Transfer Protein Inhibitors (CETP) Through a Structure-Guided Approach. *ACS Med. Chem. Lett.* **2016,** *7,* 261–265.
33. Lu, Z.; Napolitano, J. B.; Theberge, A.; Ali, A.; Hammond, M. L.; Tan, E.; Tong, X.; Xu, S. S.; Latham, M. J.; Peterson, L. B.; Anderson, M. S.; Eveland, S. Z.; Guo, Qiu; Hyland, S. A.; Milot, D. P.; Chen, Y.; Sparrow, C. P.; Wright, S. D.; Sinclair, P. J. Design of a Novel Class of Biphenyl CETP Inhibitors. *Bioorg. Med. Chem. Lett.* **2010,** *20,* 7469–7747.
34. Hayek, T.; Chajek-Shaul, T.; Walsh, A.; Agellon, L. B.; Moulin, P.; Tall, A. R.; Breslow, J. L. An Interaction Between the Human Cholesteryl Ester Transfer Protein (CETP) and Apolipoprotein A-1 Genes in Transgenic Mice Results in a Profound CETP-Mediated Depression of High Density Lipoprotein Cholesterol Levels. *J. Clin. Invest.* **1992,** *90,* 505–510.

35. Thompson, C. F.; Ali, A.; Quraishi, N.; Lu, Z.; Hammond, M. L.; Sinclair, P. J.; Anderson, M. S.; Eveland, S. Z.; Guo, Q.; Hyland, S. A.; Milot, D. P.; Sparrow, C. P.; Wright, S. D. Discovery of Substituted Biphenyl Oxazolidinone Inhibitors of Cholesteryl Ester Transfer Protein. *ACS Med. Chem. Lett.* **2011,** *2,* 424–427.
36. Smith, C. J.; Ali, A.; Hammond, M. L.; Li, H.; Lu, Z.; Napolitano, J. B.; Taylor, G. E.; Thompson, C. F.; Anderson, M. S.; Chen, Y.; Eveland, S. S.; Guo, Q.; Hyland, S. A.; Milot, D. P.; Sparrow, C. P.; Wright, S. D.; Cumiskey, A. M.; Latham, M. J.; Peterson, L. B.; Rosa, R.; Pivnichny, J. V.; Tong, X.; Xu, S. S.; Sinclair, P. J. Biphenyl Substituted Oxazolidinones as Cholesteryl Ester Transfer Protein Inhibitors: Modifications of the Oxazolidinone Ring Leading to the Discovery of Anacetrapib. *J. Med. Chem.* **2011,** *54,* 4880–4895.
37. Kumar, S.; Mitra, K.; Kassahun, T.; Bailie, T. A. Approaches for Minimizing Metabolic Activation of New Drug Candidates in Drug Discovery. In *Adverse Drug Reactions;* Uetrecht, J., Ed.; *Handbook of Experimental Pharmacology*; Springer: New York, 2009; pp 511–544.
38. Lu, Z.; Chen, Y.-H.; Napolitano, J. B.; Taylor, G.; Ali, A.; Hammond, M. L.; Deng, Q.; Tan, E.; Tong, X.; Xu, S. S.; Lantham, M. J.; Peterson, L. B.; Anderson, M. S.; Eveland, S. S.; Guo, Q.; Hyland, S. A.; Milot, D. P.; Chen, Y.; Sparrow, C. P.; Wright, S. D.; Sinclair, P. J. SAR Studies on the Central Phenyl Ring of Substituted Biphenyl Oxazolidinone Potent CETP Inhibitors. *Bioorg. Med. Chem. Lett.* **2012,** *22,* 199–203.
39. Krishna, R.; Garg, A.; Panebianco, D.; Cote, J.; Bergman, A. J.; Van Hoydonck, P.; Laesthem, T.; Van Dyck, K.; Chen, J.; Chavez-Eng, C.; Archer, L.; Lutz, R.; Hilliard, D.; Snyder, K.; Jin, B.; Van Bortel, L.; Lasseter, K. C.; Al-Huniti, N.; Dykstra, K.; Gottesdiener, K.; Wagner, J. A. Single-Dose Pharmacokinetics and Pharmacodynamics of Anacetrapib, a Potent Cholesteryl Ester Transfer Protein (CETP) Inhibitor, in Healthy Subjects. *Br. J. Clin. Pharmacol.* **2009,** *68,* 535–545.
40. Krishna, R.; Bergman, A. J.; Jin, B.; Garg, A.; Roadcap, B.; Chiou, R.; Dru, J.; Cote, J.; Laethem, T.; Wang, R. W.; Didolkar, V.; Vets, E.; Gottesdiener, K.; Wagner, J. A. Assessment of the CYP3A4-Mediated Drug Interaction Potential of Anacetrapib, a Potent Cholesteryl Ester Transfer Protein (CETP) Inhibitor, in Healthy Volunteers. *J. Clin. Pharmacol.* **2009,** *49,* 80–87.
41. Krishna, R.; Bergman, A. J.; Jin, B.; Fallon, M.; Cote, J.; Van Hoydonck, P.; Laethem, T.; Gendrano, I. N.; Van Dyck, K.; Hilliard, D.; Laterza, O.; Snyder, K.; Chavez-Eng, C.; Lutz, R.; Chen, J.; Bloomfield, D. M.; De Smet, M.; Van Bortel, L. M.; Gutierrez, M.; Al-Huniti, N.; Dykstra, K.; Gottesdiener, K. M.; Wagner, J. A. Multiple-Dose Pharmacodynamics and Pharmacokinetics of Anacetrapib, a Potent Cholesteryl Ester Transfer Protein (CETP) Inhibitor, in Healthy Subjects. *Clin. Pharmacol. Ther.* **2008,** *84,* 679–683.
42. Davidson, M. H.; McKenney, J. M.; Shear, C. L.; Revkin, J. H. Efficacy and Safety of Torcetrapib, a Novel Cholesteryl Ester Transfer Protein Inhibitor, in Individuals With Below-Average High-Density Lipoprotein Cholesterol Levels. *J. Am. Coll. Cardiol.* **2006,** *48,* 1774–1781.
43. McKenney, J. M.; Davidson, M. H.; Shear, C. L.; Revkin, J. H. Efficacy and Safety of Torcetrapib, a Novel Cholesteryl Ester Transfer Protein Inhibitor, in Individuals With Below-Average High-Density Lipoprotein Cholesterol Levels on a Background of Atorvastatin. *J. Am. Coll. Cardiol.* **2006,** *48,* 1782–1790.
44. Nissen, S. E.; Tardif, J.-C.; Nicholls, S. J.; Revkin, J. H.; Shear, C. L.; Duggan, W. T.; Ruzyllo, W.; Bachinsky, W. B.; Lasala, G. P.; Tuzcu, E. M. Effect of Torcetrapib on the Progression of Coronary Atherosclerosis. *N. Engl. J. Med.* **2007,** *356,* 1304–1316.
45. Kastelein, J. J. P.; van Leuven, S. I.; Evans, G. W.; Riley, W. A.; Revkin, J. H.; Shear, C. L.; Bots, M. L. Designs of RADIANCE 1 and 2: Carotid Ultrasound Studies Comparing the Effects of Torcetrapib/Atorvastatin With Atorvastatin Alone on Atherosclerosis. *Curr. Med. Res. Opin.* **2007,** *23,* 885–894.
46. Barter, P. J.; Caufield, M.; Eriksson, M.; Grundy, S. M.; Kastelein, J. J. P.; Komaja, M.; Lopez-Sendon, J.; Mosca, L.; Tardif, J.-C.; Waters, D. D.; Shear, C. L.; Revkin, J. H.; Buhr, K. A.; Fisher, M. R.; Tall, A. R.; Brewer, J. H. Effects of Torcetrapib in Patients at High Risk for Coronary Events. *N. Engl. J. Med.* **2007,** *357,* 2109–2122.
47. www.clinicaltrials.gov—Trial identifiers are available from United States National Institutes of Health.
48. Krishna, R.; Anderson, M. S.; Bergman, A. J.; Jin, B.; Fallon, M.; Cote, J.; Rosko, K.; Chavez-Eng, C.; Lutz, R.; Bloomfield, D. M.; Gutierrez, M.; Doherty, J.; Bueberdorf, F.; Chadakewitz, J.; Gottesdiener, K. M.; Wagner, J. A. Effect of the Cholesteryl Ester Transfer Protein Inhibitor, Anacetrapib, on Lipoproteins in Patients With Dyslipidemia and on 24-Hour Ambulatory Blood Pressure in Healthy Individuals: Two Double-Blind, Randomized Placebo-Controlled Phase I Studies. *Lancet* **2007,** *370,* 1907–1914.
49. Bloomfield, D.; Carlson, G. L.; Sapre, A.; Tribble, D.; McKenney, J. M.; Littlejohn, T. W.; McCrary Sisk, C.; Mitchel, Y.; Pasternak, R. C. Efficacy and Safety of the Cholesteryl Ester Transfer Protein Inhibitor Anacetrapib as Monotherapy and Coadministered With Atorvastatin in Dyslipidemic Patients. *Am. Heart J.* **2009,** *157,* 352–360.
50. Vergeer, M.; Bots, M. L.; van Leuven, S. I.; Basart, D. C.; Sijbrands, E. J.; Evans, G. W.; Grobbee, D. E.; Visseren, F. L.; Stalenhoef, A. F.; Stroes, E. D.; Kastelein, J. J. P. Cholesterol Ester Transfer Protein Inhibitor Torcetrapib and Off-Target Toxicity: A Pooled Analysis of the Rating Atherosclerotic Disease Change by Imaging With a New CETP Inhibitor (RADIANCE) Trials. *Circulation* **2008,** *118,* 2515–2522.
51. Johns, D. G.; Duffy, J.; Fisher, T.; Hubbard, B. K.; Forrest, M. J. On- and Off-Target Pharmacology of Torcetrapib: Current Understanding and Implications for the Structure Activity Relationships (SAR), Discovery and Development of Cholesteryl Ester-Transfer Protein (CETP) Inhibitors. *Drugs* **2012,** *72,* 491–507.
52. Forrest, M. J.; Bloomfield, D.; Briscoe, R. J.; Brown, P. N.; Cumiskey, A.-M.; Ehrhart, J.; Hershey, J. C.; Keller, W. J.; Ma, X.; McPherson, H. E.; Messina, E.; Peterson, L. B.; Sharif-Rodriguez, W.; Siegl, P. K. S.; Sinclair, P. J.; Sparrow, C. P.; Stevenson, A. S.; Sun, A.-Y.; Tsai, C.; Vargas, H.; Walker, M., III; West, S. H.; White, V.; Woltmann, R. F. Torcetrapib-Induced Blood Pressure Elevation Is Independent of CETP Inhibition and Is Accompanied by Increased Circulating Levels of Aldosterone. *Br. J. Pharmacol.* **2008,** *154,* 1465–1473.
53. Blasi, E.; Bamberger, M.; Knight, D.; Engwall, M.; Wolk, R.; Winter, S.; Betts, A.; John-Baptiste, A.; Keiser, J. Effects of CP-532,623 and Torcetrapib, Cholesteryl Ester Transfer Protein Inhibitors, on Arterial Blood Pressure. *J. Cardiovasc. Pharmacol.* **2009,** *53,* 507–516.
54. Hu, X.; Dietz, J. D.; Xia, C.; Knight, D. R.; Loging, W. T.; Smith, A. H.; Yuan, H.; Perry, D. A.; Keiser, J. Torcetrapib Induces Aldosterone and Cortisol Production by an Intracellular Calcium-Mediated Mechanism Independently of Cholesteryl Ester Transfer Protein Inhibition. *Endocrinology* **2009,** *150,* 2211–2219.
55. DePasquale, M.; Cadelina, G.; Knight, D.; Loging, W.; Winter, S.; Blasi, E.; Perry, D.; Keiser, J. Mechanistic Studies of Blood Pressure in Rats Treated With a Series of Cholesteryl Ester Transfer Protein Inhibitors. *Drug Dev. Res.* **2009,** *70,* 35–48.
56. Stein, E. A.; Roth, E. M.; Rhyne, J. M.; Burgess, T.; Kallend, D.; Robinson, J. G. Safety and Tolerability of Dalcetrapib (RO4607381/JTT-705): Results From a 48-Week Trial. *Eur. Heart J.* **2010,** *31,* 480–488.
57. Krishna, R.; Bergman, A. J.; Green, M.; Dockendorf, M. F.; Wagner, J. A.; Dykstra, K. Model-Based Development of Anacetrapib, a Novel Cholesteryl Ester Transfer Protein Inhibitor. *AAPS J.* **2011,** *13,* 179–190.
58. Cannon, C. P.; Dansky, H. M.; Davidson, M.; Gotto, A. M.; Brinton, E. A.; Gould, A. L.; Stepanavage, M.; Liu, S. X.; Shah, S.; Rubino, J.; Gibbons, P.; Hermanowski-Vosatka, A.; Binkowitz, B.; Mitchel, Y.; Barter, P. Design of the DEFINE Trial Determining the Efficacy and Tolerability of CETP Inhibition With Anacetrapib. *Am. Heart J.* **2009,** *158,* 513–519.e3.
59. Cannon, C. P.; Shah, S.; Dansky, H. M.; Davidson, M.; Brinton, E. A.; Gotto, A. M.; Stepanavage, M.; Liu, S. X.; Gibbons, P.; Ashraf, T. B.; Zafarino, J.; Mitchel, Y.; Barter, P. Safety of Anacetrapib in Patients With or at Risk for Coronary Heart Disease. *N. Engl. J. Med.* **2010,** *363,* 2406–2415.
60. Friedewald, W. T.; Levy, R. I.; Fredrickson, D. S. Estimation of the Concentration of Low-Density Lipoprotein Cholesterol in Plasma, Without Use of the Preparative Ultracentrifuge. *Clin. Chem.* **1972,** *18,* 499–502.
61. Davidson, M.; Liu, S. X.; Barter, P.; Brinton, E. A.; Cannon, C. P.; Gotto, A. M.; Leary, E. T.; Shah, S.; Stepavage, M.; Mitchel, Y.; Danskey, H. M. Measurement of LDL-C After Treatment With the CETP Inhibitor Anacetrapib. *J. Lipid Res.* **2013,** *54,* 467–472.
62. Gotto, A. M.; Kher, U.; Chatterjee, M. S.; Liu, Y.; Li, X. S.; Vaidya, S.; Cannon, C. P.; Brinton, E. A.; Moon, J. E.; Shah, S.; Dansky, H. M.; Mitchel, Y.; Barter, P. Lipids, Safety Parameters, and Drug Concentrations After an Additional 2 Years of Treatment With Anacetrapib in the DEFINE Study. *J. Cardiovasc. Pharmacol. Ther.* **2014,** *19,* 543–549.
63. Gotto, A. M.; Cannon, C. P.; Li, X. S.; Vaidya, S.; Ker, U.; Brinton, E. A.; Davidson, M.; Moon, J. E.; Shah, S.; Dansky, H. M.; Mitchel, Y.; Barter, P. Evaluation of Lipids, Drug Concentration, and Safety Parameters Following Cessation of Treatment With the Cholesteryl Ester Transfer Protein Inhibitor Anacetrapib in Patients With or at High Risk for Coronary Heart Disease. *Am. J. Cardiol.* **2014,** *113,* 76–83.
64. Radeau, T. P.; Lau, M.; Robb, M.; McDonnel, M.; Ailhaud, G.; McPherson, R. Cholesteryl Ester Transfer Protein (CETP) mRNA Abundance in Human Adipose Tissue: Relationship to Cell Size and Membrane Cholesterol Content. *J. Lipid Res.* **1995,** *36,* 2552–2561.

65. Hartman, G.; Kumar, S.; Johns, D.; Giheyas, F.; Guystein, D.; Shen, X.; Burton, A.; Lederman, H.; Lutz, R.; Jackson, T.; Chavez-Eng, C.; Mitra, K. Disposition Into Adipose Tissue Determines Accumulation and Elimination Kinetics of the Cholesteryl Ester Transfer Protein Inhibitor Anacetrapib in Mice. *Drug Metab. Dispos.* **2016,** *44,* 428–434.
66. Gutstein, D.; Krishna, R.; Johns, D.; Mitra, K.; Hartman, G.; Hammilton, V.; Cote, J.; Ferdous, G.; Shah, S.; Mitchel, Y. Observed Long Plasma Terminal Half-Life of Anacetrapib (ANA) Is Associated With Adipose Deposition: Characterization of Plasma and Adipose Pharmacokinetics (PK) in Mice and Humans. Abstracts of Papers, ACPT 2015 Annual Meeting, New Orleans, LA, March 3–7, American Society for Clinical Pharmacology and Therapeutics: Alexandria, VA, PI-05, 2015.
67. Nissen, S. E.; Tardif, J. C.; Nicholls, S. J.; Revkin, J. H.; Shear, C. L.; Duggan, W. T.; Ruzyllo, W.; Bachinsky, W. B.; Lasala, G. P.; Tuzcu, E. M. Effect of Torcetrapib on the Progression of Coronary Atherosclerosis. *N. Engl. J. Med.* **2007,** *356,* 1304–1316.
68. Kastelein, J. J. P.; van Leuven, S. I.; Burgess, L.; Evans, G. W.; Kuivenhoven, J. A.; Barter, P. J.; Revkin, J. H.; Grobbee, D. E.; Riley, W. A.; Shear, C. L.; Duggan, W. T.; Bots, M. L. Effect of Torcetrapib on Carotid Atherosclerosis in Familial Hypercholesterolemia. *N. Engl. J. Med.* **2007,** *356,* 1620–1630.
69. Bots, M. L.; Visseren, F. L.; Evans, G. W.; Riley, W. A.; Revkin, J. H.; Tegeler, C. H.; Shear, C. L.; Duggan, W. T.; Vicari, R. M.; Grobbee, D. E.; Kastelein, J. J. Torcetrapib and Carotid Intima-Media Thickness in Mixed Dyslipidaemia (RADIANCE 2 Study): A Randomized, Double-Blind Trial. *Lancet* **2007,** *370,* 153–160.
70. Nicholls, S. J.; Tuzcu, M.; Brennan, D. M.; Tardif, J.-C.; Nissen, S. E. Cholesteryl Ester Transfer Protein Inhibition, High-Density Lipoprotein Raising, and Progression of Coronary Atherosclerosis: Insights From ILLUSTRATE (Investigation of Lipid Level Management using Coronary Ultrasound to Assess Reduction of Atherosclerosis by CETP Inhibition and HDL Elevation). *Circulation* **2008,** *118,* 2506–2514.
71. Brousseau, M. E.; Schaefer, E. J.; Wolfe, M. L.; Bloedon, L. T.; Digenio, A. G.; Clark, R. W.; Mancuso, J. P.; Rader, D. J. Effects of an Inhibitor of Cholesteryl Ester Transfer Protein on HDL Cholesterol. *N. Engl. J. Med.* **2004,** *350,* 1505–1515.
72. Joshi, P. H.; Toth, P. P.; Lirette, S. T.; Griswold, M. E.; Masaro, J. M.; Martin, S. S.; Blaha, M. J.; Kulkami, K. R.; Khokhar, A. A.; Correa, A.; D'Agustino, R. D.; Johnes, S. R. Association of High-Density Lipoprotein Subclass and Incident Coronary Heart Disease: The Jacksonville Heart and Framingham Offspring Cohort Studies. *Eur. J. Prev. Cardiol.* **2016,** *23,* 41–49.
73. Rohatgi, A.; Khera, A.; Berry, J.; Givens, E. G.; Ayers, C. R.; Wedin, K. E.; Neeland, I. J.; Yuhanna, I. S.; Rader, D. R.; de Lemos, J. A.; Shaul, P. W. HDL Cholesterol Efflux Capacity and Incident of Cardiovascular Events. *N. Engl. J. Med.* **2014,** *371,* 2383–2393.
74. Okamoto, H.; Yonemori, F.; Koreklyo, W.; Minowa, T.; Maeda, K.; Shinkai, H. A Cholesterol Ester Transfer Protein Inhibitor Attenuates Atherosclerosis in Rabbits. *Nature* **2000,** *406,* 203–207.
75. Ranalletta, M.; Bierilo, K. H.; Chen, Y.; Milot, D.; Chen, Q.; Tung, E.; Houde, C.; Elowe, N. H.; Garcia-Calvo, M.; Porter, G.; Eveland, S.; Frantz-Wattley, B.; Kavana, M.; Addona, G.; Sinclair, P.; Sparrow, C.; O'Neill, E. A.; Koblan, K.; Sitlani, A.; Hubbard, B.; Fisher, T. S. Biochemical Characterization of Cholesteryl Ester Transfer Protein Inhibitors. *J. Lipid Res.* **2010,** *51,* 2739–2752.
76. Liu, S.; Mistry, A.; Reynolds, J. M.; Lloyd, D. B.; Griffor, M. C.; Perry, D. A.; Ruggeri, R. B.; Clark, R. W.; Qiu, X. Crystal Structures of Cholesteryl Ester Transfer Protein in Complex With Inhibitors. *J. Biol. Chem.* **2012,** *287,* 37321–37329.
77. Niesor, E. J.; Magg, C.; Ogawa, N.; Okamoto, H.; von der Mark, E.; Matile, H.; Schmid, G.; Clerc, R. G.; Chaput, E.; Blum-Kaelin, D.; Huber, W.; Thoma, R.; Pflieger, P.; Kakutani, M.; Takahashi, D.; Dernick, G.; Maugeais, C. Modulating Cholesteryl Ester Transfer Protein Activity Maintains Efficient Pre-β-HDL Formation and Increases Reverse Cholesterol Transport. *J. Lipid Res.* **2010,** *51,* 3443–3454.
78. Johns, D. J.; Chen, Y.; Wang, S.-P.; Castro-Perez, J.; Previs, S. F.; Roddy, T. P. Inhibition of Cholesteryl Ester Transfer Protein Increases Cholesteryl Ester Content of Large HDL Independently of HDL-to-HDL Homotypic Transfer: In Vitro vs In Vivo Comparison Using Anacetrapib and Dalcetrapib. *Eur. J. Pharmacol.* **2015,** *762,* 256–262.
79. Hutchins, P. M.; Heinecke, J. W. Cholesterol Efflux Capacity, Macrophage Reverse Cholesterol Transport and Cardioprotective HDL. *Curr. Opin. Lipidol.* **2015,** *26,* 388–393.
80. Castro-Perez, J.; Briand, F.; Gagen, K.; Wang, S.-P.; Chen, Y.; McLaren, D. G.; Shah, V.; Vreeken, R. J.; Hankemeier, T.; Sulpice, T.; Roddy, T. P.; Hubbard, B. K.; Johns, D. J. Anacetrapib Promotes Reverse Cholesterol Transport and Bulk Cholesterol Excretion in Syrian Golden Hamsters. *J. Lipid Res.* **2011,** *52,* 1965–1973.
81. Briand, F.; Thieblemont, Q.; Muztte, E.; Burr, N.; Urbain, I.; Sulpice, T.; Johns, D. G. Anacetrapib and Dalcetrapib Differently Alters HDL Metabolism and Macrophage-to-Feces Reverse Cholesterol Transport at Similar Levels of CETP Inhibition in Hamsters. *Eur. J. Pharmacol.* **2014,** *740,* 135–143.
82. Wang, S.-P.; Daniels, E.; Chen, Y.; Castro-Perez, J.; Zhou, H.; Akinsanya, K. O.; Previs, S. F.; Roddy, S. P.; Johns, D. G. In Vivo Effects of Anacetrapib on preb HDL: Improvement in HDL Remodeling Without Effects on Cholesterol Absorption. *J. Lipid Res.* **2013,** *54,* 2858–2865.
83. Yin, W.; Carballo-Jane, E.; McLaren, D. G.; Mendoza, V. H.; Gagen, K.; Geoghagan, N. S.; McNamara, L. A.; Gorski, J. N.; Eiermann, G. J.; Petrov, A.; Wolff, M.; Tong, X.; Wilsie, L.; Akiyama, T. E.; Chen, J.; Thankappan, A.; Xue, J.; Ping, X.; Andrews, G.; Wickham, L. A.; Gai, C. L.; Trinh, T.; Kulick, A. A.; Donnelly, M. J.; Voronin, G. O.; Rosa, R.; Cumiskey, A.-M.; Bekkari, K.; Mitnaul, L. J.; Puig, O.; Chen, F.; Raubertas, R.; Wong, P. H.; Hansen, B. C.; Koblan, K. S.; Roddy, T. P.; Hubbards, B. K.; Strack, A. M. Plasma Lipid Profiling Across Species for the Identification of Optimal Animal Models of Human Dyslipidemia. *J. Lipid Res.* **2012,** *53,* 51–65.
84. Roddy, T. P.; McLaren, D. G.; Chen, Y.; Xie, D.; Dunn, K.; Kulik, A.; Szeto, D.; Forrest, G.; Albanese, K.; Donnelly, M.; Gai, C.; Gewain, A.; Lederman, H.; Jensen, K. K.; Ai, X.; Vachal, P.; Akinsanya, K. O.; Cleary, M. A.; Previs, S. F.; Dansky, H. M.; Johns, D. G. Effects of Anacetrapib on Plasma Lipids, Apolipoproteins and PCSK9 in Healthy, Lean Rhesus Macaques. *Eur. J. Pharmacol.* **2014,** *740,* 410–416.
85. McLaren, D. G.; Previs, S. F.; Phair, R. D.; Stout, S. J.; Xie, D.; Chen, Y.; Salituro, G. M.; Xu, S. S.; Castro-Perez, J. M.; Opiteck, G. J.; Akinsanya, K. O.; Cleary, M. A.; Dansky, H. M.; Johns, D. G.; Roddy, T. P. Evaluation of Cholesteryl Ester Transfer Protein Activity In Vivo Under Non-Steady State Conditions: Influence of Anacetrapib on High Density Lipoprotein Triglyceride Flux. *J. Lipid Res.* **2016,** *57,* 398–409.
86. Ray, K. K.; Ditmarsch, M.; Kallend, D.; Niesor, E. J.; Suchankova, G.; Upmanyu, R.; Anzures-Cabrera, J.; Lehnert, V.; Pauly-Evers, M.; Holme, I.; Stasek, J.; van Hessen, M. W. J.; Jones, P. The Effect of Cholesteryl Ester Transfer Protein Inhibition on Lipids, Lipoproteins, and Markers of HDL Function After an Acute Coronary Syndrome: The dal-ACUTE Randomized Trial. *Eur. Heart J.* **2014,** *35,* 1792–1800.
87. Khera, A. V.; Cuchel, M.; de la Llera-Moya, M.; Rodrigues, A.; Burke, M. F.; Jafri, K.; French, B. C.; Phillips, J. A.; Mucksavage, M. L.; Wilensky, R. L.; Mohler, E. R.; Rothblat, G. H.; Rader, D. J. Cholesterol Efflux Capacity, High-Density Lipoprotein Function, and Atherosclerosis. *N. Engl. J. Med.* **2011,** *364,* 127–135.
88. Niesor, E. J. Different Effects of Compounds Decreasing Cholesteryl Ester Transfer Protein Activity on Lipoprotein Metabolism. *Curr. Opin. Lipidol.* **2011,** *22,* 288–295.
89. Nichols, S. J.; Brewer, H. B.; Kastelein, J. J. P.; Krueger, K. A.; Wang, M.-D.; Shao, M.; Hu, B.; McErlean, E.; Nissen, S. E. Effects of the CETP Inhibitor Evacetrapib Administered as Monotherapy or in Combination With Statins on HDL and LDL Cholesterol. *JAMA* **2011,** *306,* 2099–2109.
90. Wolk, R.; Chen, D.; Clark, R. W.; Mancuso, J.; Barclay, P. L. Pharmacokinetic, Pharmacodynamics, and Safety Profile of a New Cholesteryl Ester Transfer Protein Inhibitor in Healthy Human Subjects. *Nature* **2009,** *86,* 430–437.
91. Clark, R. W.; Sutfin, T. A.; Ruggeri, R. B.; Willauer, A. T.; Sugarman, E. D.; Magnus-Aryitet, G.; Cosgrove, P. G.; Sand, T. M.; Wester, R. T.; Williams, J. A.; Perlman, M. E.; Bamberger, M. J. Raising High-Density Lipoprotein in Humans Through Inhibition of Cholesteryl Ester Transfer Protein: An Initial Multidose Study of Torcetrapib. *Arterioscler. Thromb. Vasc. Biol.* **2004,** *24,* 490–497.
92. Stein, E. A.; Stroes, E. S. G.; Steiner, G.; Buckley, B. M.; Capponi, A. M.; Burgess, T.; Neisor, E. J.; Kallend, D.; Kastelein, J. J. P. Safety and Tolerability of Dalcetrapib. *Am. J. Cardiol.* **2009,** *104,* 82–91.
93. Hovingh, G. K.; Kastelein, J. J. P.; van Deventer, S. J. H.; Round, P.; Ford, J.; Saleheen, D.; Rader, D. J.; Brewer, H. B.; Barter, P. J. Cholesterol Ester Transfer Protein Inhibition by TA-8995 in Patients With Mild Dyslipidemia (TULIP): A Randomized, Double-Blind, Placebo-Controlled Phase 2 Trial. *Lancet* **2015,** *386,* 452–460.
94. Krauss, R. M.; Wojnooski, K.; Orr, J.; Geaney, J. C.; Pinto, C. A.; Liu, Y.; Wagner, J. A.; Luk, J. M.; Johnson-Levonas, A. O.; Anderson, M. S.; Dansky, H. M. Changes in Lipoprotein Subfraction Concentration and Composition in Healthy Individuals Treated With the CETP Inhibitor Anacetrapib. *J. Lipid Res.* **2012,** *53,* 540–547.
95. Krauss, R. M.; Pinto, C. A.; Liu, Y.; Johnson-Levonas, A. O.; Dansky, H. M. Changes in LDL Particle Concentrations After Treatment With the Cholesteryl Ester Transfer Protein Inhibitor Anacetrapib Alone or in Combination With Atorvastatin. *J. Clin. Lipidol.* **2015,** *9,* 93–102.

96. Millar, J. S.; Reyes-Soffer, G.; Jumes, P.; Dunbar, R.; deGoma, E. M.; Baer, A. L.; Karmally, W.; Donovan, D. S.; Rafeek, H.; Pollan, L.; Tohyama, J.; Johnson-Levonas, A. O.; Wagner, J. A.; Holleran, S.; Obunike, J.; Liu, Y.; Ramakrishnan, R.; Lassman, M. E.; Gutstein, D. E.; Ginsberg, H. N.; Rader, D. J. Anacetrapib Lowers LDL by Increasing ApoB Clearance in Mildly Hypercholesterolemic Subjects. *J. Clin. Invest.* **2016,** *125,* 2510–2522.
97. Schwartz, G. G.; Olsson, A. G.; Ballantyne, C. M.; Barter, P. J.; Holme, I. M.; Kallend, D.; Leiter, L. A.; Leitersdorf, E.; McMurray, J. J. V.; Shah, P. K.; Tardif, J.-C.; Chaitman, B. R.; Duttinger-Maddux, R.; Mathieson, J. Rationale and Design of the dal-OUTCOMES Trial: Efficacy and Safety of Dalcetrapib in Patients With Recent Acute Coronary Syndrome. *Am. Heart J.* **2009,** *158,* 896–901.e3.
98. Fayad, Z. A.; Mani, V.; Woodward, M.; Kallend, D.; Bansilal, S.; Pozza, J.; Burgess, T.; Fuster, V.; Rudd, J. H. F.; Tawakol, A.; Farkouh, M. E. Rationale and Design of dal-PLAQUE: A Study Assessing Efficacy and Safety of Dalcetrapib on Progression or Regression of Atherosclerosis Using Magnetic Resonance Imaging and 18F-Fluorodeoxyglucose Positron Emission Tomography/Computed Tomography. *Am. Heart J.* **2011,** *2011* (162), 214–221.
99. United States National Institutes of Health www.clinicaltrials.gov trial identifier: NCT01059682.
100. Kastelein, J. J. P.; Duivenvoorden, R.; Deanfield, J.; de Groot, E.; Jukema, J. W.; Kaski, J.-C.; Munzel, T.; Taddei, S.; Lehnert, V.; Burgess, T.; Kallend, D.; Luscher, T. F. Rationale and Design of dal-VESSEL: A Study to Assess the Safety and Efficacy of Dalcetrapib on Endothelial Function Using Brachial Artery Flow-Mediated Vasodilatation. *Curr. Med. Res. Opin.* **2011,** *27,* 141–150.
101. United States National Institutes of Health www.clinicaltrials.gov trial identifier: NCT01252953.
102. Kastelein, J. J. P.; Besseling, J.; Shah, S.; Bergeron, J.; Langslet, G.; Hovingh, G. K.; Al-Saady, N.; Koeijvoets, M.; Hunter, J.; Johnson-Levonas, A. O.; Fable, J.; Sapre, A.; Mitchel, Y. Anacetrapib as Lipid-Modifying Therapy in Patients With Heterozygous Familial Hypercholesterolaemia (REALIZE): A Randomized, Double-Blind, Placebo-Controlled, Phase 3 Study. *Lancet* **2015,** *385,* 2153–2161.
103. Roche Press Release May 7, 2012, http://www.roche.com/media/store/releases/med-cor-2012-05-07.htm (accessed January 11, 2016)
104. Schwartz, G. G.; Olsson, A. G.; Abt, M.; Ballabtyne, C. M.; Barter, P. J.; Brumm, J.; Chaitman, B. R.; Holme, I. M.; Kallend, D.; Leiter, L. A.; Leitersdorf, E.; McMurray, J. J. V.; Mundl, H.; Nicholls, S. J.; Shah, P. K.; Tardif, J.-C.; Wright, R. S. Effects of Dalcetrapib in Patients With a Recent Acute Coronary Syndrome. *N. Engl. J. Med.* **2012,** *367,* 2089–2099.
105. Luscher, T. F.; Taddei, S.; Kaski, J.-C.; Jukema, J. W.; Kallend, D.; Munzel, T.; Kastelein, J. J. P.; Deanfield, J. E. Vascular Effects and Safety of Dalcetrapib in Patients With or at Risk of Coronary Heart Disease: The dal-VESSEL Randomized Clinical Trial. *Eur. Heart J.* **2012,** *33,* 857–865.
106. Fayad, Z. A.; Venkatesh, M.; Kallend, D.; Abt, M.; Burgess, T.; Fuster, V.; Ballantyne, C. M.; Stein, E. A.; Tardiff, J.-C.; Rudd, J. H. F.; Farkouh, M. E.; Tawakol, A. Safety and Efficacy of Dalcetrapib on Atherosclerotic Disease Using Novel Non-Invasive Multimodality Imaging (dal-PLAQUE): A Randomized Clinical Trial. *Lancet* **2011,** *378,* 1547–1559.
107. Joshi, F. R.; Rajani, N. K.; Abt, M.; Woodward, M.; Bucerius, J.; Mani, V.; Tawakol, A.; Kallend, D.; Fayad, Z. A.; Rudd, J. H. F. Does Vascular Calcification Accelerate Inflammation? A Substudy of the dal-PLAQUE Trial. *J. Am. Coll. Cardiol.* **2016,** *67,* 70–78.
108. Tardif, J.-C.; Rheaume, E.; Perreault, L.-P. L.; Gregoire, J. C.; Zada, Y. F.; Asselin, G.; Provost, S.; Barhdadi, A.; Rhainds, D.; L'Allier, P. L.; Ibrahim, R.; Upmanyu, R.; Niesor, E. J.; Benghozi, R.; Suchankova, G.; Laghrissi-Thode, F.; Guertin, M.-C.; Olsson, A. G.; Mongrain, I.; Schwartz, G. G.; Dube, M.-P. Pharmacogenomic Determinants of the Cardiovascular Effects of Dalcetrapib. *Circ. Cardiovasc. Genet.* **2015,** *8,* 372–382.
109. United States National Institutes of Health www.clinicaltrials.gov trial identifier: NCT02525939.
110. Nichols, S. J.; Lincoff, A. M.; Barter, P. J.; Brewer, H. B.; Fox, K. A. A.; Gibson, C. M.; Grainger, C.; Menon, V.; Montalescot, G.; Rader, D.; Tall, A. R.; McErlean, E.; Riesmeyer, J.; Vangerow, B.; Ruotolo, G.; Weerakkody, G. J.; Nissen, S. E. Assessment of the Clinical Effects of Cholesteryl Ester Transfer Protein Inhibition With Evacetrapib in Patients at High-Risk for Vascular Outcomes: Rationale and Design of the ACCELERATE Trial. *Am. Heart J.* **2015,** *170,* 1061–1106.
111. Eli Lilly Press Release Oct. 12, 2015, https://investor.lilly.com/releasedetail.cfm?ReleaseID=936130 (accessed January 9, 2016).
112. Merck/MSD Press Release Nov. 13, 2015, http://www.mercknewsroom.com/news-release/research-and-development-news/merck-provides-update-reveal-outcomes-study (accessed January 11, 2016).
113. Study start dates and completion dates are available at United States National Institutes of Health www.clinicaltrials.gov.
114. Cannon, C. P.; Blazing, M. A.; Giugliano, R. P.; McCagg, A.; White, J. A.; Theroux, P.; Darius, H.; Lewis, B. S.; Ophuis, T. O.; Jukema, W.; De Ferrari, G. M.; Ruzyllo, W.; De Licca, P.; Im, K. A.; Bohula, E. A.; Reist, C.; Wiviott, S. D.; Tershakovec, A. M.; Musliner, T. A.; Braunwald, E.; Califf, R. M. Ezetimibe Added to Statin Therapy After Acute Coronary Syndromes. *N. Engl. J. Med.* **2015,** *372,* 2387–2397.
115. Barter, P. J.; Nicholls, S. J.; Kastelein, J. J. P.; Rye, K. A. CETP Inhibition as a Strategy to Reduce Cardiovascular Risk: The Pro Case. *Circulation* **2015,** *132,* 423–432.
116. Hovingh, G. K.; Ray, K. K.; Boekholdt, S. M. CETP As a Target to Lower CVD Risk: Suspension of Disbelief? *Circulation* **2015,** *132,* 433–440.

Relevant Websites

www.clinicaltrials.gov.
http://www.cdc.gov/cholesterol/index.htm.

8.12 Discovery of ROMK Inhibitor MK-7145: A Novel Mechanism Diuretic

Alexander Pasternak, Merck & Co., Inc., Kenilworth, NJ, United States

© 2017 Elsevier Ltd. All rights reserved.

8.12.1	Introduction	308
8.12.2	Hit Identification	309
8.12.3	Program Assays	310
8.12.4	Hit to Lead	311
8.12.5	Parallel Discovery of the 2-(4-(1*H*-Tetrazol-1-yl)phenyl)-1-(piperazin-1-yl)ethan-1-one Scaffold	312
8.12.6	First Proof of Biology: Diuresis and Natriuresis Efficacy With a Neutral Potassium Excretion Profile	315
8.12.7	Mechanism of ROMK Inhibition by Compound 25	316
8.12.8	Efforts to Enhance ROMK Selectivity Over the hERG Channel	317
8.12.9	Scaffold Modification Toward Improving ROMK Inhibitor Pharmacokinetic Properties	319
8.12.10	ROMK Inhibitors Reduce Blood Pressure in Spontaneously Hypertensive Rats	321
8.12.11	Parallel SAR Evolution of the Original Piperazine Series	322
8.12.12	Selection of Compound 57 as the Clinical Compound MK-7145	328
8.12.13	MK-7145 Displays Additive or Synergistic Blood Pressure Lowering Efficacy in Combination With Candesartan and HCTZ	330
8.12.14	Backup Efforts Focused on Longer Preclinical Half-Lives and Structural Diversity: The Dibasic Piperazine Series	331
8.12.15	Effects of ROMK Inhibitor 61 in Dahl Salt-Sensitive Rats	333
8.12.16	Backup Efforts Focused on Longer Preclinical Half-Lives and Structural Diversity, Efforts Involving Alternative Scaffolds	334
8.12.17	MK-7145 Clinical Trials	335
8.12.18	Conclusions	336
References		337

8.12.1 Introduction

Renal outer medullary potassium (ROMK) was the first identified member[1] of the inwardly rectifying family of potassium (K_{ir}) channels, which include seven subfamilies ($K_{ir}1$–7) that differ in tissue distribution, strength of rectification, and in their regulation.[2] K_{ir} channels are tetramers comprising four identical or related subunits, each containing two transmembrane helices, which form a central conduction pathway.[3] ROMK expression is highly restricted to the kidney, where it plays a critical role in the regulation of electrolyte and extracellular fluid-volume homeostasis.[4] Importantly, ROMK is expressed on the apical membrane of epithelial cells lining multiple segments of the nephron, including the thick ascending loop of Henle (TALH), the collecting tubule (CT), and the cortical collecting duct (CCD).[5–7] At the TALH, ROMK participates in potassium recycling across the apical membrane, providing the substrate K^+ ions necessary for NaCl reabsorption by the Na^+–K^+–$2Cl^-$ co-transporter, the rate-limiting step for sodium reabsorption in this part of the nephron and the target for loop diuretics such as furosemide (Fig. 1). Approximately 30% of the total filtered NaCl is reabsorbed in the TALH, with accompanying osmotic water reabsorption contributing to concentration of urine along the nephron. Since the potassium concentration in the tubular fluid is much less than that of sodium or chloride, ROMK secretion of potassium is critically required for NaCl reabsorption by the Na^+–K^+–$2Cl^-$ co-transporter. Thus, ROMK inhibitors should provide indirect inhibition of the

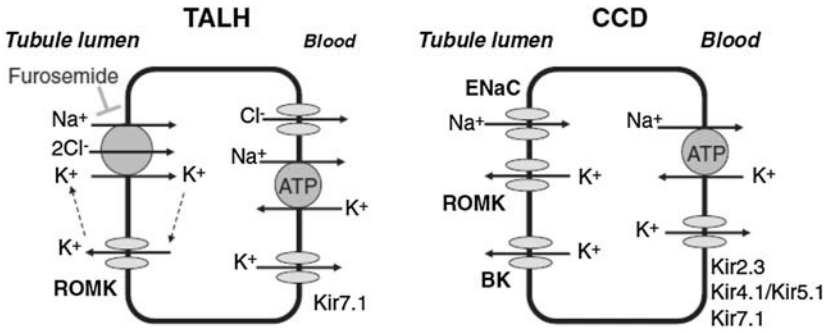

Fig. 1 Physiological role of ROMK in the thick ascending limb of Henle (TALH) and the cortical collecting duct (CCD) segments of the nephron. From Garcia, M. L.; Kaczorowski, G. J. *Curr. Opin. Pharmacol.* **2014**, *15*, 1–6.

Na^+–K^+–$2Cl^-$ co-transporter, evoking diuresis and natriuresis comparable to a loop diuretic. In the CT and CCD, ROMK represents a key potassium secretory pathway, critical for maintaining potassium homeostasis. In the CCD, potassium secretion by ROMK shifts the luminal membrane potential, thereby increasing the electrochemical driving force for sodium reabsorption via the amiloride-sensitive epithelial sodium channel, ENaC, the rate-limiting step for sodium reabsorption in the CCD (Fig. 1). Inhibition of ROMK in the CCD is therefore expected to counter the potassium loss and hypokalemia associated with loop and thiazide diuretics. In addition, the coupling of ROMK to ENaC in the CCD may provide additional natriuresis efficacy. Thus, selective inhibition of ROMK along multiple segments of the nephron may provide a greater cumulative efficacy with reduced potassium loss compared to loop and thiazide diuretics, which target transport pathways in only a single segment of the nephron.

The impetus for Merck's interest in developing ROMK inhibitors was twofold: First, available thiazide and loop diuretics remain key drug classes for treating hypertension and heart failure, respectively[8]; however, they are dose and efficacy limited,[9] in part due to safety issues such as hypokalemia, a decrease in plasma potassium levels which can trigger dangerous cardiac arrhythmias. In addition, they typically have short half-lives, leading to rebound sodium reabsorption, which blunts efficacy. In the case of loop diuretics such as furosemide, diuretic resistance[10] leads to loss of efficacy, particularly as heart failure or renal function worsens. Thus, there is a need for next-generation diuretics, which can provide improved efficacy without the liabilities of the current standards of care. Second, there is compelling human and rodent genetic validation for ROMK as a novel mechanism diuretic target. Notably, patients with Bartter syndrome type II have autosomal recessive loss-of-function mutations in the KCNJ1 gene, with a clinical presentation that includes renal salt wasting, polyuria, hypotension, mild hypokalemia, and metabolic alkalosis.[11] Moreover, Lifton and colleagues have reported that heterozygous carriers of loss-of-function KCNJ1 mutations, identified in the Framingham Heart Study, have lower blood pressure, a reduced risk of stroke, and are protected from developing hypertension by age 60; however, they otherwise do not present with the clinical features of Bartter syndrome.[12] ROMK knockout mice[13] recapitulate the Bartter syndrome type II phenotype. Finally, Zhou and colleagues at Merck have shown that Dahl salt-sensitive rats with heterozygous ROMK disruption display reduced blood pressure compared to wild-type rats when challenged with a 4% salt diet. Taken together, the genetic evidence, coupled with the expression and role of ROMK in the nephron, suggests that ROMK inhibitors will represent a new class of diuretics with the potential for improved efficacy and reduced risk of hyperkalemia compared to standard-of-care thiazide and loop diuretics.

The initial program goal was to identify a tractable lead series that could be optimized for selectivity over the cardiac voltage-gated potassium channel hERG and related K_{ir} channel family subtypes. In particular, a key requirement was for development of ROMK inhibitors with excellent selectivity over the related strong inward rectifier $K_{ir}2.1$ cardiac channel, which is associated with life-threatening long QTc syndrome.[14,15] In addition, we sought a lead series with suitable pharmacokinetic properties to enable proof of biology in pharmacodynamic models, and to permit eventual optimization for qd dosing in humans.

8.12.2 Hit Identification

In contrast to other ion channel families, the pharmacology of K_{ir} family channels is relatively unexplored.[16] Garcia and Kaczorowski noted that HTS campaigns directed toward K_{ir} family targets have yielded few interesting or chemically tractable hits, impeding discovery of selective inhibitors and potential drug development.[17] At the time that the ROMK program at Merck was initiated there were no known small molecule-selective ROMK inhibitors. Tertiapin (TPN), a bee venom peptide, was the only previously described ROMK inhibitor, demonstrating potent inhibition of the rat channel[18] but significantly weaker inhibition of the human isoform.[19] Later, Denton and coworkers at Vanderbilt University described the discovery of ROMK inhibitors **VU590** and **VU591** (Fig. 2). Inhibitor **VU590** was discovered directly through a high-throughput screening (HTS) campaign and was shown to inhibit both ROMK (IC_{50} 290 nM)[20] and $K_{ir}7.1$. Medicinal chemistry modification of another hit from the same screening campaign afforded inhibitor **VU591** (IC_{50} 240 nM), which demonstrated selectivity over the $K_{ir}7.1$ channel (no inhibition at 10 μM).[21] Unfortunately, **VU591** did not induce diuresis in rats,[22] possibly due to high plasma protein binding[21] or poor pharmacokinetic and physicochemical properties. In addition, efforts to replace the two nitro substituents were unsuccessful for these inhibitors.

An HTS campaign of Merck's internal sample collection of ~1.5 million compounds using a membrane potential-based fluorescent assay[23] identified very few attractive hits. The largest cluster of related hits originated from Merck's abandoned hERG channel

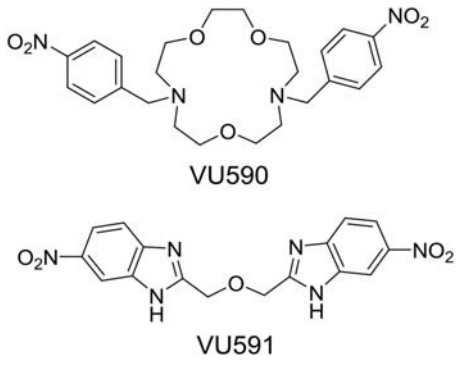

Fig. 2 ROMK inhibitors discovered by Vanderbilt University researchers.

blocker antiarrhythmic program from the late 1980s, and these hits displayed picomolar hERG inhibition and relatively weak ROMK inhibitory activity (>1 μM). Based on the low probability of success for converting these highly potent hERG blockers to selective ROMK inhibitors, we chose not to pursue these hits. On surveying our hit package we observed that there were several structurally unrelated weak hits bearing a nitrophenyl group. One of these was the simple and low molecular weight fragment hit, 1-(4-nitrophenethyl)piperazine **1**. Compound **1** displayed moderate inhibitory potency on ROMK, IC_{50} 5.2 μM, in a functional $^{86}Rb^{+}$ efflux assay from CHO cells stably expressing the human ROMK channel, but showed ~30-fold greater potency on the outward delayed rectifier potassium channel (Kv11.1, human ether-a-go-go-related gene, hERG). Importantly, compound **1** demonstrated excellent selectivity over the related cardiac $K_{ir}2.1$ channel. Surprisingly, when compound **1** was subjected to HPLC purification and resubmitted for assay, all of the ROMK inhibitory activity was lost (**Fig. 3**). A careful examination of the HPLC–MS data from the original sample showed good overall purity, but a minor peak, integrating to about 1% abundance, was visible and corresponded to a molecular weight of 384. We wondered whether this minor impurity could possibly account for all of the ROMK activity seen for the screening hit **1**. Based on the molecular weight, we hypothesized that a likely structure for the impurity could be the symmetrical 1,4-bis(4-nitrophenethyl)piperazine, **2**. We independently synthesized compound **2** and confirmed in our assays that, indeed, all of the activity of the original hit must be derived from this impurity.[24] Consistent with this, the inhibition of ROMK (IC_{50} 0.052 μM) and hERG (IC_{50} 0.005 μM) was approximately two orders of magnitude more potent; fortunately the potency on $K_{ir}2.1$ remained negligible (IC_{50} > 100 μM). It is noteworthy that two independent screening campaigns of unique sample collections (one by Vanderbilt University researchers and the other by Merck) each led to the discovery of symmetrical bis(nitrophenyl) containing lead scaffolds, suggesting the privileged role of the nitrophenyl pharmacophore for interactions with ROMK and provoking the speculation that these compounds may be binding in a symmetrical fashion or in a way such that each nitrophenyl forms a similar interaction with two of the identical or similar tetrameric subunits within the channel, which itself displays quasi-C4 symmetry. Based on mutagenesis studies and computational analysis of binding of **VU591** to a homology model of ROMK, Denton proposed a V-shaped or folded conformation with the nitrophenyl pharmacophores of **VU591** interacting near identical asparagine residues on adjacent tetramer subunits.[25]

Clearly there were concerns about compound **2** as a program starting point. The nitro groups were viewed as a potential toxicity liability[26] and would need to be replaced as a first order of business. Compound **2** had poor pharmacokinetic properties in rats with high clearance (261 mL/min/kg) and was 10-fold more potent on hERG than on ROMK. The selectivity would need to be inverted and significantly improved. Further, there was concern that the "privileged" piperazine scaffold could lead to promiscuous off-target activity.

8.12.3 Program Assays

The ROMK functional assays that drove SAR development in the Merck program have been previously described in detail by Felix and coworkers.[27] Early in the program the team employed a functional assay in CHO cells stably expressing human $K_{ir}1.1$, where efflux of the $^{86}Rb^{+}$ isotope was monitored as our primary assay. A key advantage of this assay was that measurements could be made in the absence and presence of increasing concentrations of human serum (up to 100%), helping to assess, in a high-throughput fashion, the impact of protein binding to the potency of ROMK inhibitors. Spot checking of plasma protein binding indicated a good correlation of serum shift with measured plasma protein binding. As a secondary medium-throughput assay, we employed

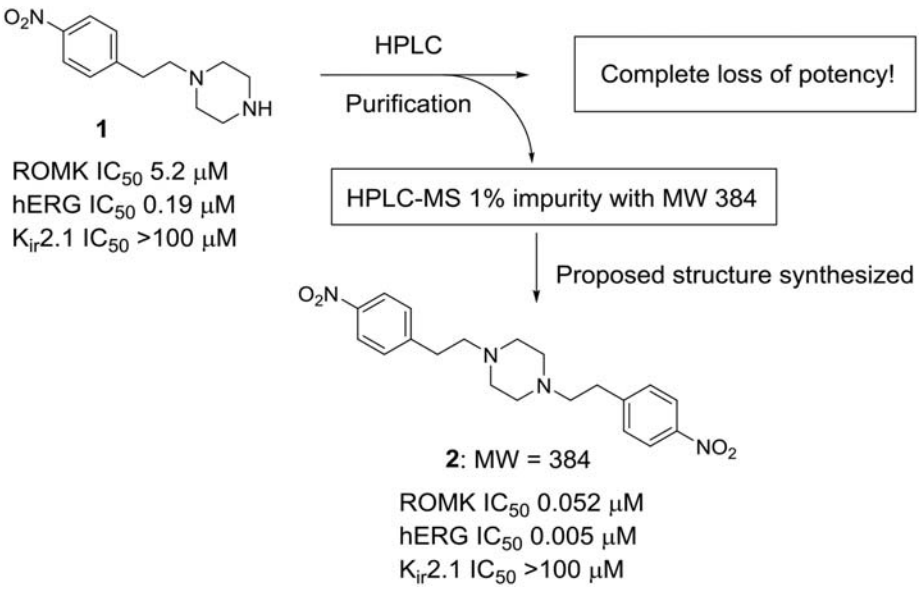

Fig. 3 Discovery of a viable ROMK hit from a 1% impurity detected in an otherwise inactive screening hit.

a functional electrophysiology (voltage clamp) assay in CHO cells stably expressing Kir1.1 channels using the IonWorks automated electrophysiology platform (molecular devices). As the program progressed the team developed an alternative primary screen, a high-throughput functional thallium flux fluorescence assay measuring the ability of thallium to permeate through $K_{ir}1.1$ channels, employing HEK293 cells stably transfected with $hK_{ir}1.1$ or $rK_{ir}1.1$, or MDCK cells stably transfected with $rK_{ir}1.1$.

hERG activity was assessed initially by measuring displacement of ^{35}S MK-499 from HEK-293 cells stably expressing hERG.[28] Functional hERG activity was measured by electrophysiology studies employing QPatch (Biolin Scientific) or PatchXpress (Molecular Devices) platforms. In general, correlation between hERG binding potency and functional activity was good, but there were exceptions where significant potency shifts were observed (~10% of the time); therefore, the hERG functional electrophysiology assay was used as a routine secondary assay for compounds prioritized for advancement down the program's research operating plan (ROP). Counterscreening versus $K_{ir}2.1$ was measured using a functional fluorescence assay that measures the ability of thallium to permeate through open $K_{ir}2.1$ channels stably expressed in HEK293 cells.

8.12.4 Hit to Lead

Tang and coworkers have described initial SAR efforts to define the optimal scaffold dimensions and identify bioisosteres for ROMK hit **2**.[24] Extension or contraction of one of the ethyl linkers between the piperazine core and a nitrophenyl pharmacophore (not shown) led to significant reductions in potency (IC_{50} 3.8 and >10 μM, respectively), establishing that the dimensions of hit **2** are optimal with the two carbon linker on each side of the piperazine core and a total atom count of 8 atoms between nitrophenyl pharmacophores. Nitro groups are capable of forming hydrogen bonding and other interactions,[29] and when present on aromatic rings, nitro groups polarize the aromatic π-system. Relatively few nitrophenyl group bioisosteres have been described, with examples including pyridyl, benzoate, and difluorophenyl.[30] As described in Table 1, both nitro groups present in compound **2** are absolutely necessary for maintaining ROMK potency; elimination of one nitro group by replacing with hydrogen (**3**) led to a complete loss of potency (>10 μM). Numerous potential nitrophenyl bioisosteres were surveyed systematically (Table 1). These included alternative substituted phenyl or fused bicyclic systems capable of acting as hydrogen bond acceptors, and/or alternative electron-withdrawing substituents. Previously described nitrophenyl bioisosteres, benzoate (**11**) and pyridyl (not shown, IC_{50} >30 μM) led to complete loss of potency. 4-Substitution of phenyl with ester (**10**), trifluoromethyl (**14**), halogen (**12**, **13**), methoxy (**15**), methyl sulfone (**16**)/sulfoxide, and heterocycles (**7**, **8**) all led to significant or complete loss of potency; however, 4-cyanophenyl (**4**), 5-benzo(2,1,3-oxadiazole) (**6**), and 4-phthalide (**9**) pharmacophores retained comparable activity to

Table 1 The search for nitrophenyl group isosteres[24]

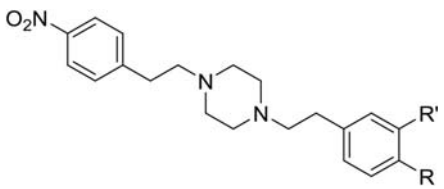

Compound	R, R′	IC_{50} (μM)	
		ROMK[a]	hERG[b]
2	$-NO_2$, –H	0.052	0.005
3	–H, –H	>10	ND[c]
4	–CN, –H	0.079	0.009
5	–H, –CN	3.8	0.022
6[d]	5-Benzo(2,1,3-oxadiazole)	0.17	0.025
7	2-Oxazole, –H	4.3	0.047
8	5-Pyrimidine, –H	>10	ND
9[d]	4-Phthalide	0.089	0.15
10	$-CO_2Et$, –H	2.9	0.019
11	$-CO_2H$, –H	>30	ND
12	–F, –H	3.1	0.023
13	–Cl, –H	>10	ND
14	$-CF_3$, –H	>10	ND
15	–OMe, –H	4.6	0.007
16	$-SO_2Me$, –H	9.4	0.15

[a]ROMK activity is from the $^{86}Rb^+$ efflux functional assay.
[b]hERG activity is from the ^{35}S MK-499 displacement binding assay.
[c]ND, no data.
[d]R, R′, and phenyl together represent the named fused bicyclic ring.

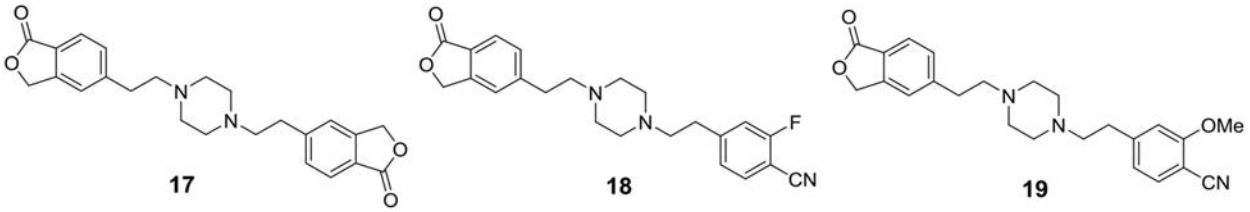

Fig. 4 Mixing and matching nitrophenyl bioisosteres provide ROMK leads without nitro groups.

nitrophenyl. Of particular interest was the 4-phthalide (**9**) pharmacophore, which in addition to retaining ROMK potency, also demonstrated slightly weaker hERG potency (30-fold weaker compared to compound **2**). It is also noteworthy that the 4-phthalide group displayed good ROMK activity while related acyclic 4-substituted esters were significantly less potent, possibly suggesting a tight binding fit without space for acyclic extended esters.

Having identified three nitrophenyl bioisosteres the next step was to mix and match these groups, eliminating all nitro groups in the series. Through this exercise and some follow-on SAR work, Tang and coworkers identified compounds **17**–**19** (Fig. 4), which displayed comparable potency to hit **2** in the $^{86}Rb^{+}$ efflux functional assay (Table 2). Compounds **17**–**19** also demonstrated similar high ROMK potency to hit **2** in a follow-up electrophysiology assay. When assessed in the ^{35}S MK-499 displacement binding assay, all three compounds provided reduced hERG potencies, leading to some of the first examples of ROMK inhibitors that were selective over hERG. In particular, compounds **17** and **19** demonstrated 73- and 37-fold selectivity windows for ROMK over hERG. Moreover, compounds **17** and **18** were assessed for off-target K_{ir} channel activity and were shown to display no significant inhibition of the $K_{ir}2.1$, $K_{ir}2.3$, $K_{ir}4.1$, and $K_{ir}7.1$ channels (all >100 μM).

ROMK inhibitor **17** was assessed for its pharmacokinetic properties in rats, where it demonstrated a significantly improved profile compared to hit **2** (Table 3), supporting the tractability of this lead series for identification of analogs with pharmacokinetic properties suitable for conduct of proof-of-biology studies in pharmacodynamic models.

8.12.5 Parallel Discovery of the 2-(4-(1*H*-Tetrazol-1-yl)phenyl)-1-(piperazin-1-yl)ethan-1-one Scaffold

During the search for nitrophenyl bioisosteres an intermediate **20** leading to the synthesis of analog **21** was submitted to the program assays and found to display better ROMK potency as the acylpiperazine **20** than as the reduced dibasic target analog **21** (Fig. 5).[31] In addition, the resulting ROMK inhibitor **20** had balanced ROMK/hERG potency, representing a 10-fold improvement in ROMK selectivity compared to the starting point **2**. Thus, the phenyl tetrazole pharmacophore added to our list of nitrophenyl bioisosteres. Encouraged, we prepared a series of analogs with a variety of small heterocycles to further expand our options; surprisingly, no other heteroaryl, even the closely related tetrazoles and triazoles, provided comparable ROMK potency (Fig. 6).

Table 2 ROMK and hERG potency of ROMK inhibitors **17**, **18**, and **19**[24]

	IC_{50} (μM)			
Compound	*ROMK $^{86}Rb^{+}$ efflux*	*ROMK EP[a]*	*hERG[b]*	*Ratio hERG[b]/ROMK EP*
2	0.052	0.024	0.005	0.21
17	0.089	0.026	1.9	73
18	0.049	0.030	0.17	5.7
19	0.089	0.043	1.6	37

[a]ROMK electrophysiology using the IonWorks platform.
[b]hERG activity is from the ^{35}S MK-499 displacement binding assay.

Table 3 Comparison of rat pharmacokinetic properties[a] of hit **2** and lead **18**[24]

	Compound	
	2	*18*
Cl (L/kg)	261	59
AUCNpo (μM h kg/mg)	0.023	0.46
Half-life (h)	1.9	1.5
F_{po} (%)	14	64

[a]1 mg/kg iv and 2 mg/kg po doses.

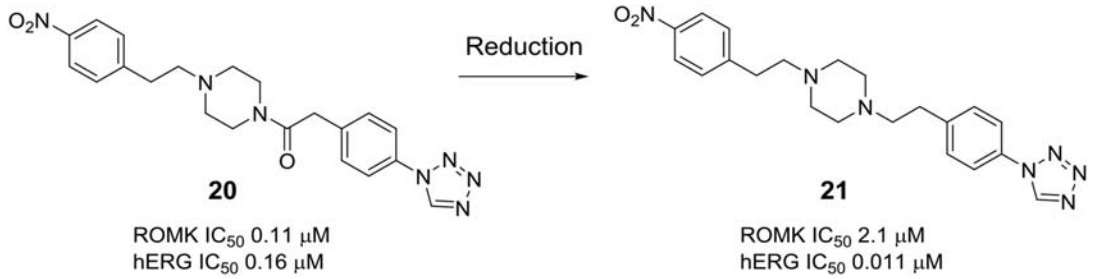

Fig. 5 Serendipitous discovery of the 2-(4-(1*H*-tetrazol-1-yl)phenyl)-1-(piperazin-1-yl)ethan-1-one scaffold. ROMK potency is measured by $^{86}Rb^{+}$ efflux functional assay, hERG potency is from binding assay.

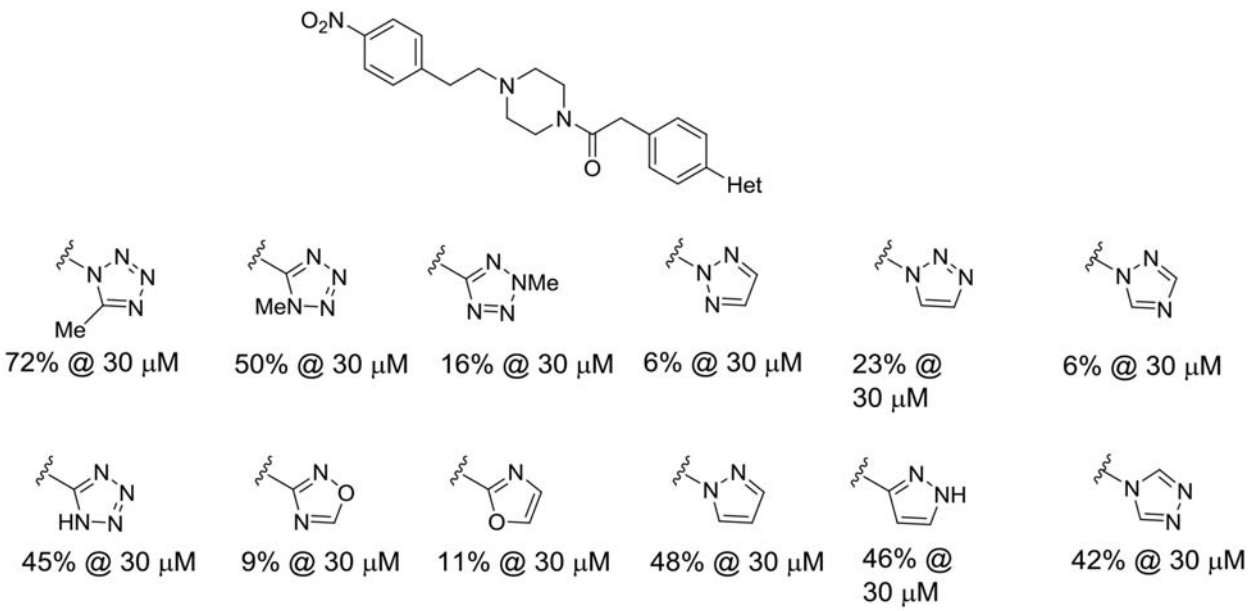

Fig. 6 Heterocycle replacements attempted for the phenyl tetrazole ($^{86}Rb^{+}$ efflux % inhibition at 30 μM).[31]

One interpretation of this observation is that the tetrazole may engage in multiple interactions with involvement of more than one nitrogen; substitution is not tolerated due to steric/space requirements and/or possible change in the angle between phenyl and tetrazole, which may prefer to be planar rather than twisted.

With the modified scaffold and a new nitrophenyl bioisostere in hand we again paired these features with the other available isosteres and further probed SAR, providing the compounds described in Table 4. The analog bearing the 4-phthalide pharmacophore (**25**) provided the best ROMK potency and an ~100-fold selectivity window for ROMK over hERG. The regioisomeric phthalide **26** displayed significantly weaker ROMK potency; however the ring expanded isochroman-1-one **30** gave comparable ROMK potency to **25** with excellent selectivity over the hERG channel (~200-fold). Notably, conversion of compound **25** to the corresponding benzolactam **27**, or removal of one of the lactone oxygen atoms to give **28** or **29**, led to complete or partial loss of ROMK potency. This suggests that, like the phenyl tetrazole, it may be that the lactone moiety is engaging in more than one hydrogen bonding acceptor interactions and that this may be a required feature for optimal interaction with ROMK.

Having established the phthalide pharmacophore in compound **25** as a preferred one, Tang and coworkers explored substitution around the phthalide ring system (Table 5). Small groups such as methyl (**31**) and fluoro (**34**) were tolerated at the 4-position, giving comparable potency to the unsubstituted parent **25**, and in the case of fluoro, a slightly improved selectivity over hERG (hERG/ROMK 282-fold). Unfortunately, 4-fluoro substitution generally led to higher clearance in rat PK studies (not shown), possibly by making the phthalide more susceptible to lactone ring opening. Increasing the 4-substituent size led to erosion of ROMK potency (**32**, **33**, **35**, and **36**). Substitution at the 6- and 7-positions of the phthalide system uniformly led to loss of potency.

Compounds **25**, **30**, and **31** were further assessed in ROMK and hERG electrophysiology assays as shown in Table 6. All three compounds provided good ROMK potency and selectivity for ROMK over hERG of 70-fold for compound **25**, 295-fold for compound **30**, and 181-fold for compound **31**. As a general observation, the isochroman-1-one and 4-methylphthalide pharmacophores present in **30** and **31** generally give improved selectivity over hERG by two- to threefold, and reduced clearance in pharmacokinetic studies compared to the parent unsubstituted phthalide pharmacophore.

Table 4 Paired nitrophenyl bioisosteres and structure–activity relationships[31]

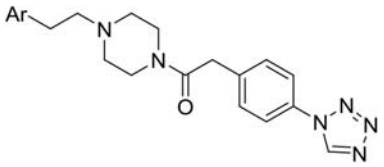

Compound	*Ar*	*ROMK IC_{50}*[a]	*hERG IC_{50}*[b]
22	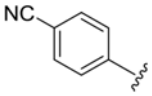	0.92	0.42
23	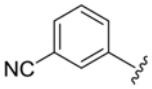	0.47	2.7
24	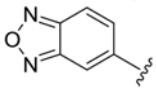	0.16	1.3
25	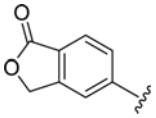	0.11	14
26	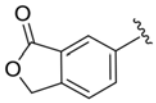	7.1	32
27	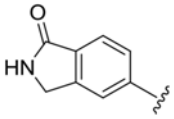	>32	ND
28	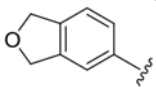	1.3	2.5
29	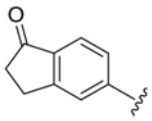	1.2	6.5
30	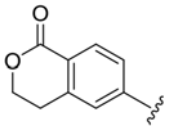	0.24	43

[a]ROMK potency determined using the functional $^{86}Rb^{+}$ efflux assay.
[b]hERG activity measured using the ^{35}S MK-499 displacement binding assay.

Compound **25** was evaluated in functional assays for several related inward rectifier channels and demonstrated excellent selectivity for ROMK ($K_{ir}2.1$ and $K_{ir}2.3$ IC_{50}'s >50 μM, $K_{ir}4.1$ and $K_{ir}7.1$ IC_{50}'s >10 μM).[32] Compound **25** also gave excellent selectivity over the cardiac channels Nav1.5 (>30 μM) and Cav1.2 (>100 μM). Compound **25** was further assessed for off-target activity in a panel of 166 enzymes and radioligand binding assays run by MSD Pharma Services; when tested at 10 μM, **25** inhibited only the serotonin transporter with an IC_{50} of 9.1 μM. Compound **25** was shown to have comparable activity against the rat ROMK channel using the $^{86}Rb^{+}$ efflux assay (0.113 μM), making it amenable for in vivo studies in rats.

ROMK inhibitor **25** was assessed in pharmacokinetic studies in Sprague–Dawley (SD) rats and in dogs, where it demonstrated good oral bioavailabilities with moderate oral exposures and short half-lives (Table 7).[32] In a rat bile duct cannulated rat study using ^{3}H-**25**, the primary metabolites identified were the lactone ring opened acid (>parent, urine and bile), and to a lesser extent a metabolite resulting from oxidation of the phthalide system (urine).[33] The parent compound was also eliminated intact in urine and bile.

Table 5 Substitution SAR studies of the phthalide pharmacophore

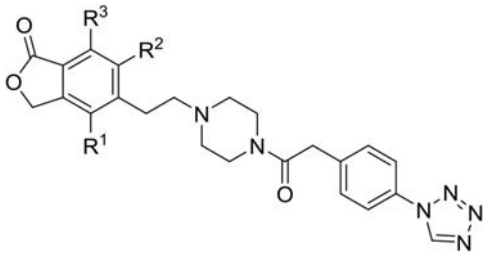

Compound	*R^1*	*R^2*	*R^3*	*ROMK IC_{50}[a] (μM)*	*hERG IC_{50}[b] (μM)*
25	–H	–H	–H	0.11	14
31	–Me	–H	–H	0.19	20
32	–Et	–H	–H	0.30	27
33	–c-Pr	–H	–H	0.43	12
34	–F	–H	–H	0.11	31
35	–Cl	–H	–H	0.25	17
36	–OMe	–H	–H	1.4	40
37	–H	–Me	–H	0.46	14
38	–H	–F	–H	0.46	26
39	–H	–OMe	–H	1.5	5.6
40	–H	–H	–Me	1.1	10
41	–H	–H	–F	0.44	13
42	–H	–H	–Cl	0.83	3.4

[a]ROMK potency determined using the functional $^{86}Rb^+$ efflux assay.
[b]hERG activity measured using the ^{35}S MK-499 displacement binding assay.
Adapted from: Tang, H.; de Jesus, R. K.; Walsh, S. P.; Zhu, Y.; Yan, Y.; Priest, B. T.; Swensen, A. M.; Alonso-Galicia, M.; Felix, J. P.; Brochu, R. M.; Bailey, T.; Thomas-Fowlkes, B.; Zhou, X.; Pai, L.-Y.; Hampton, C.; Hernandez, M.; Ownes, K.; Roy, S.; Kaczorowski, G. J.; Yang, L.; Garcia, M.; Pasternak, A. *Bioorg. Med. Chem. Lett.* **2013**, *23*, 5829–5832.

Table 6 ROMK and hERG functional potency of compounds **25** and **30** determined in electrophysiology assays[31]

Compound	*25*	*30*	*31*
ROMK EP (μM)	0.064	0.061	0.072
hERG EP (μM)	4.5	18	13
hERG/ROMK EP IC_{50} ratio	70	295	181

Table 7 Pharmacokinetic properties of compound **25** in rat and dog[32]

Compound	*Rat[a]*	*Dog[a]*
Cl (L/kg)	40	36
Vds (mL/min/kg)	0.66	1.9
AUCNpo (μM h kg/mg)	0.34	0.88
Half-life (h)	0.62	1.4
F_{po} (%)	33	80

[a]1 mg/kg iv, $n=2$; 2 mg/kg po, $n=3$.

8.12.6 First Proof of Biology: Diuresis and Natriuresis Efficacy With a Neutral Potassium Excretion Profile

With a selective and orally bioavailable ROMK inhibitor now available in **25**, the next step was to assess pharmacodynamic activity in animal models. The acute diuretic, natriuretic, and kaliuretic activity of compound **25** was assessed in conscious, volume-loaded SD rats, with the clinically used thiazide diuretic hydrochlorothiazide (HCTZ) employed as a positive control (Fig. 7).[32] Oral administration of compound **25** at 1, 3, 10, and 50 mg/kg doses evoked dose-dependent increases in urine output and sodium excretion in the 4 h post saline load compared to the vehicle-treated group, while potassium excretion remained unchanged at all doses. A maximal diuretic and natriuretic effect was observed at the 10 mg/kg dose. As expected, HCTZ also provided dose-dependent

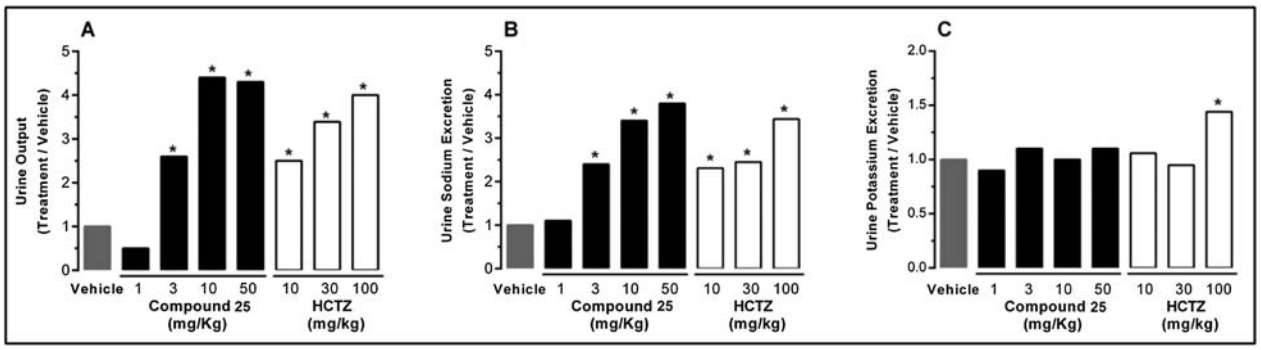

Fig. 7 Effect of compound **25** and HCTZ on urinary output and sodium and potassium excretion rates in SD rats. Adult male SD rats ($n=5$–6 per treatment) were dosed by oral gavage with indicated doses of either compound **25** or HCTZ. After 30 min, voiding was induced by giving each animal a saline load. Urine collection took place over the next 4 h and was analyzed for volume (A) and for sodium (B) and potassium (C) content. Data are presented as fold change relative to values obtained in the vehicle-treated animals. $^*p<.05$ vs. vehicle. This figure is taken with permission from Garcia, M. L.; Priest, B. T.; Alonso-Galicia, M.; Zhou, X.; Felix, J. P.; Brochu, R. M.; Bailey, T.; Thomas-Fowlkes, B.; Liu, J.; Swensen, A.; Pai, L.-Y.; Xiao, J.; Hernandez, M.; Hoagland, K.; Ownes, K.; Tang, H.; de Jesus, R. K.; Roy, S.; Kaczorowski, G. J.; Pasternak, A. *J. Pharmacol. Exp. Ther.* **2014**, *348*, 153–164.

elevations in urine output and sodium excretion at 10, 30, and 100 mg/kg doses, with its maximum effect observed at 100 mg/kg; however, in contrast to compound **25**, at the maximally efficacious dose HCTZ significantly elevated potassium excretion. Both compounds provided similar magnitudes of diuresis and natriuresis at their maximally efficacious doses. Similarly, diuresis and electrolyte excretion of **25** and HCTZ were assessed in conscious, euvolemic dogs, where compound **25** at 10 and 50 mg/kg produced dose-dependent natriuresis and diuresis reaching a similar magnitude to that of an approximately efficacious dose of HCTZ (data not shown).[32] Again, in dogs, compound **25** did not increase potassium excretion in urine, while HCTZ did at an equally natriuretic dose. Taken together, the pharmacodynamic data in rats and dogs provided a first proof of biology that ROMK inhibitors will be new mechanism diuretic agents with a reduced propensity for potassium loss in urine compared to standard-of-care diuretics.

8.12.7 Mechanism of ROMK Inhibition by Compound 25

With potent and selective ROMK inhibitors in hand we sought to better understand the mechanism of inhibition. To inform on the potential binding site of compound **25** several site-directed ROMK mutants were generated, with a focus on residues facing the ion conduction pore that differed between ROMK and $K_{ir}2.1$, which our compounds do not significantly inhibit.[32] These residues were selected using homology models generated based on the crystal structure of the chicken $K_{ir}2.2$ channel.[3] Amino acid residues in ROMK were mutated individually to the corresponding residues from $K_{ir}2.1$ and all mutants were transiently expressed in TsA-201 cells and examined by whole cell voltage clamp. Of the seven mutant constructs generated (M81L, L128F, S130A, Q152E, L166V, V168C, N171D), five generated measurable currents (all but S130A and L166V). Of these five constructs, four were potently inhibited by compound **25** ($IC_{50}<100$ nM); however, the mutant resulting from replacement of asparagine 171 (N171) in ROMK with aspartate (found in $K_{ir}2.1$) led to a reduced inhibition by compound **25** by two orders of magnitude (**Table 8**). Based on the significant reduction in inhibitor potency evoked by addition of a charged amino acid, we prepared a second mutant construct, N171Q, replacing the asparagine with a still neutral related glutamine. This also resulted in a shift to weaker inhibition potency by about one order of magnitude. These data suggest that N171, which faces the pore within the transmembrane region of the channel below the selectivity filter, may contribute to potent inhibition of ROMK by compound **25**. This is consistent with site-directed mutagenesis and patch clamp data generated by Denton and colleagues with ROMK inhibitor **VU591**, which also showed a dependence of channel block on pore residue N171.[25] We have explored potential docking poses of compound **25** and other ROMK inhibitors. Both horizontal and vertical poses within the pore, wherein the N171 residue can interact through hydrogen bonds with two or one of the terminal pharmacophores, respectively, seem possible. We favor the horizontal pose which would allow similar interactions between the terminal pharmacophores to adjacent or opposite transmembrane tetrameric subunits; this would nicely account for the favorable inhibition profiles of symmetrical ROMK inhibitors.

Table 8 Loss of inhibitor **25** potency in ROMK N171 mutants by whole cell voltage clamp[32]

$hK_{ir}1.1$ construct	*IC_{50} (nM)*
WT ROMK	81
N171D	~7100
N171Q	~720

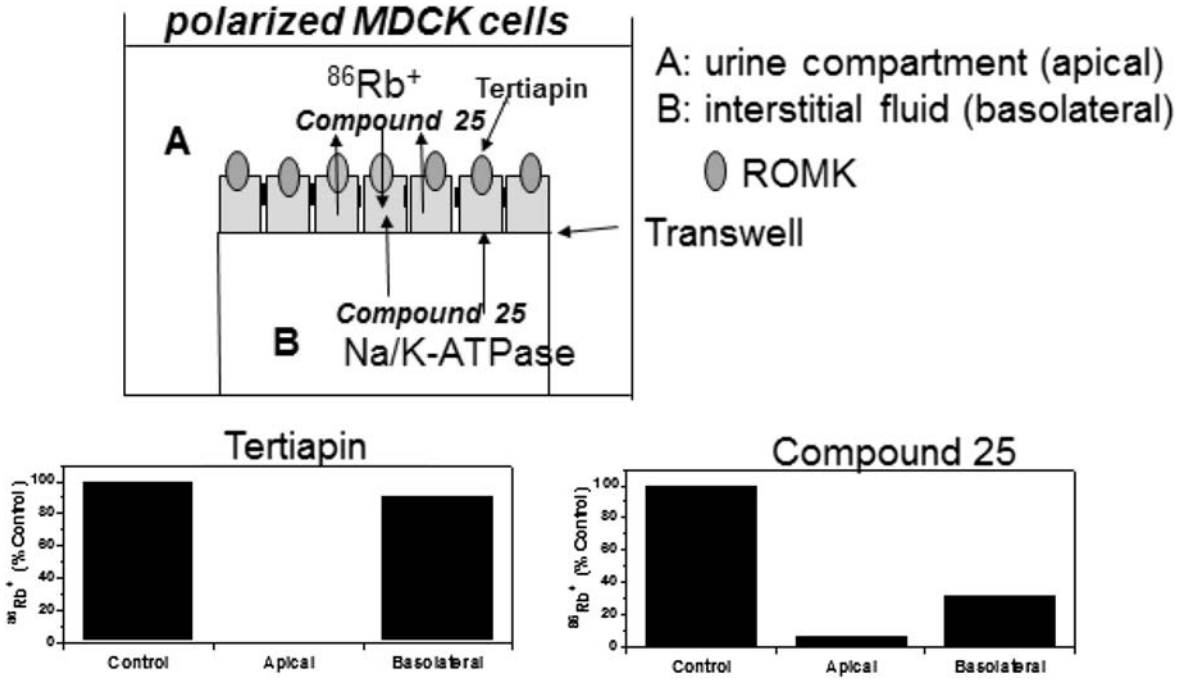

Fig. 8 Inhibition of ROMK stably expressed in polarized MDCK cells on permeable Transwell supports. Tertiapin inhibits ROMK only when applied to the apical side, while compound **25** inhibits when applied from either the apical or basolateral sides. Adapted from: Garcia, M. L.; Priest, B. T.; Alonso-Galicia, M.; Zhou, X.; Felix, J. P.; Brochu, R. M.; Bailey, T.; Thomas-Fowlkes, B.; Liu, J.; Swensen, A.; Pai, L.-Y.; Xiao, J.; Hernandez, M.; Hoagland, K.; Ownes, K.; Tang, H.; de Jesus, R. K.; Roy, S.; Kaczorowski, G. J.; Pasternak, A. *J. Pharmacol. Exp. Ther.* **2014**, *348*, 153–164.

Most diuretics, including thiazide and loop diuretics, access their targets from the apical (luminal) side of the epithelial cells lining the nephron.[34] In order to do this, loop and thiazide diuretics are actively transported into the tubular lumen by organic anion or cation transporters. Because of this, patients with renal insufficiency are susceptible to reduced efficacy of diuretic treatment, requiring dose escalation to maintain efficacy. Garcia and colleagues explored access of compound **25** to ROMK using MDCK-rK_{ir}1.1 cells grown as a monolayer on permeable Transwell supports. This model provides a polarized system with apical and basolateral membranes separated by an impermeable barrier due to the tight cell junctions (Fig. 8).[32] Inhibition of ROMK was determined by measuring inhibition of efflux of $^{86}Rb^+$ from the basolateral compartment to the apical side. Application of the impermeable peptide ROMK inhibitor tertiapin to both the apical and basolateral compartments led to ROMK inhibition only from the apical face, supporting that ROMK is exclusively expressed at the apical surface of the MDCK-rK_{ir}1.1 cells, that tertiapin only blocks the channel from the apical face, and that there is not leakage of tertiapin through the cell monolayer. In contrast, compound **25** inhibited efflux of $^{86}Rb^+$ whether applied to the apical or basolateral compartments, indicating that compound **25** accesses the channel from the cytoplasm which can be reached from either the apical (urine) or basolateral (blood) compartments, presumably due to the high cell permeability of compound **25** (Papp 23×10^{-6} cm/s in LLC-PK1 cells). This feature differentiates ROMK inhibitors from loop and thiazide diuretics, which generally have poor permeability, and only access their targets from the apical face.

Denton and colleagues at Vanderbilt University have used compound **25** in studies to elucidate the sites of action of ROMK inhibitors in the nephron.[35] In these studies compound **25** was administered to volume-loaded rats alone and in combination with diuretics acting in the TALH (bumetanide), the distal tubule (HCTZ), and in the CCD (amiloride and benzamil). Compound **25** was shown to produce diuresis and natriuresis without loss of potassium in urine when dosed alone. Additive effects on diuresis and natriuresis were observed when compound **25** was combined with HCTZ, amiloride, and benzamil, but not with bumetanide. Based on this, the Vanderbilt team concluded that, as expected, the major diuretic site of action of ROMK inhibitors is in the TALH and CCD. Since additive effects were seen when combining compound **25** with the ENaC inhibitors amiloride and benzamil, the authors concluded that blockade of ROMK in the CCD does not completely inhibit sodium reabsorption by ENaC. Finally the Vanderbilt team observed that compound **25** blocked the potassium loss in urine caused by the loop diuretic bumetanide, which they attributed to inhibition of potassium secretion by ROMK in the TALH and CCD.

8.12.8 Efforts to Enhance ROMK Selectivity Over the hERG Channel

Despite the ~100-fold selectivity of compound **25** for ROMK over the hERG channel, the team sought to further enhance the ROMK/hERG selectivity window. It is now well established that inhibition of hERG is associated with QT prolongation, which

can trigger torsade de pointes and possible degeneration into life-threatening ventricular fibrillation.[36] Walsh and Tang described a number of approaches that were explored to improve selectivity of **25** for ROMK over hERG.[37,38] Lipophilic amines are a common feature of many hERG channel blockers; consequently, a common strategy for dialing out hERG activity is to reduce amine basicity.[39] To probe the role of the basic amine in **25**, neutral compound **31** in which the basic amine is replaced by CH was targeted (Fig. 9). While elimination of the basic amine was tolerated (only a twofold loss of ROMK potency), this modification did not provide any enhancement in selectivity over hERG. In a related approach, addition of carboxylic acid groups in various positions (unpublished, not shown) to generate neutral zwitterionic analogs uniformly led to loss of ROMK activity in parallel with decreased hERG activity. Hydroxy and fluoro substituents were installed onto the phthalide benzylic linker position since these were expected to reduce basicity of the piperazine. Both modifications led to significant reductions in hERG potency and improvements in the hERG/ROMK selectivity ratio. Hydroxy analog **45**, while twofold more selective over hERG, lost potency on ROMK. The fluoro analog **46** retained ROMK potency and demonstrated a 1000-fold selectivity over hERG. Unfortunately, compound **46** provided a short half-life in rat pharmacokinetic studies (half-life 0.35 h). Interestingly, compound **44** with a benzylic methyl substituent also improved ROMK selectivity over hERG, and in this case, this effect cannot be attributed to reduced basicity of the piperazine, suggesting that conformational factors may also be playing a role.

Since small molecule inhibition of hERG is thought to be enhanced by π-stacking and hydrophobic interactions with aromatic residues in the hERG pore, common approaches to improve selectivity over hERG include reducing log *P* and modifying aromatic rings to be more electron deficient, for example by replacing with electron-deficient heterocycles like pyridyl.[39] Walsh and colleagues described testing this approach in the Merck ROMK inhibitor series by making a variety of analogs in which the phthalide and phenyl tetrazole pharmacophore phenyl groups were replaced with heterocycles such as pyridyl (Fig. 10).[37] Aza-phthalide analogs **47** and **48** both resulted in loss of ROMK potency; however, right-side pyridyl tetrazole analogs retained ROMK potency. Of the two regioisomers, compound **50** demonstrated better potency and selectivity over hERG (500-fold, by ROMK $^{86}Rb^{+}$ efflux and hERG ^{35}S MK-499 displacement binding assay). When compound **50** was assessed in ROMK and hERG electrophysiology assays it demonstrated excellent potency on ROMK (IC_{50} 20 nM) and very good selectivity over hERG (hERG EP IC_{50} 17 μM, 850-fold selectivity). Compound **50** was assessed in an anesthetized vagotomized cardiovascular dog model ($n=3$)[40] to confirm that the high selectivity for ROMK over hERG would ensure CV safety in vivo. Following a rising dose IV infusion of compound **50** at a cumulative 10 mg/kg dose (average peak unbound plasma concentration 21 μM), no changes were observed in the QT interval. In an acute diuresis model in Sprague–Dawley rats, compound **50** at 10 mg/kg provided robust diuresis and natriuresis (4-fold and 2.8-fold increase compared to vehicle-treated rats, respectively), exceeding that of 10 mg/kg of HCTZ (2.8-fold and 2.2-fold increase compared to vehicle-treated rats, respectively). Unfortunately, compound **50** had short half-lives across preclinical species presumably due to high clearance resulting from elimination by intact renal clearance and metabolism, similar to that observed with compound **25**. In addition, compound **50** had poor bioavailability in rhesus monkeys (Table 9).[37] Therefore, **50** was not selected for further advancement.

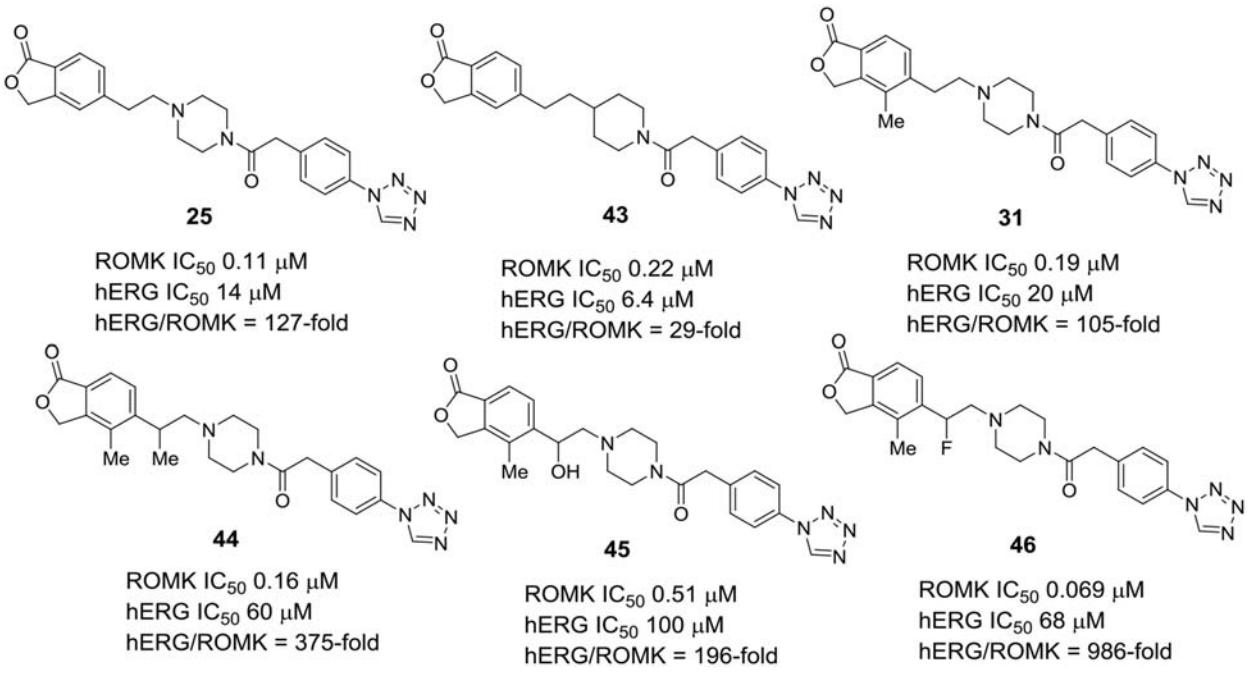

Fig. 9 Efforts to improve selectivity over hERG by substitution and modulation of basicity.

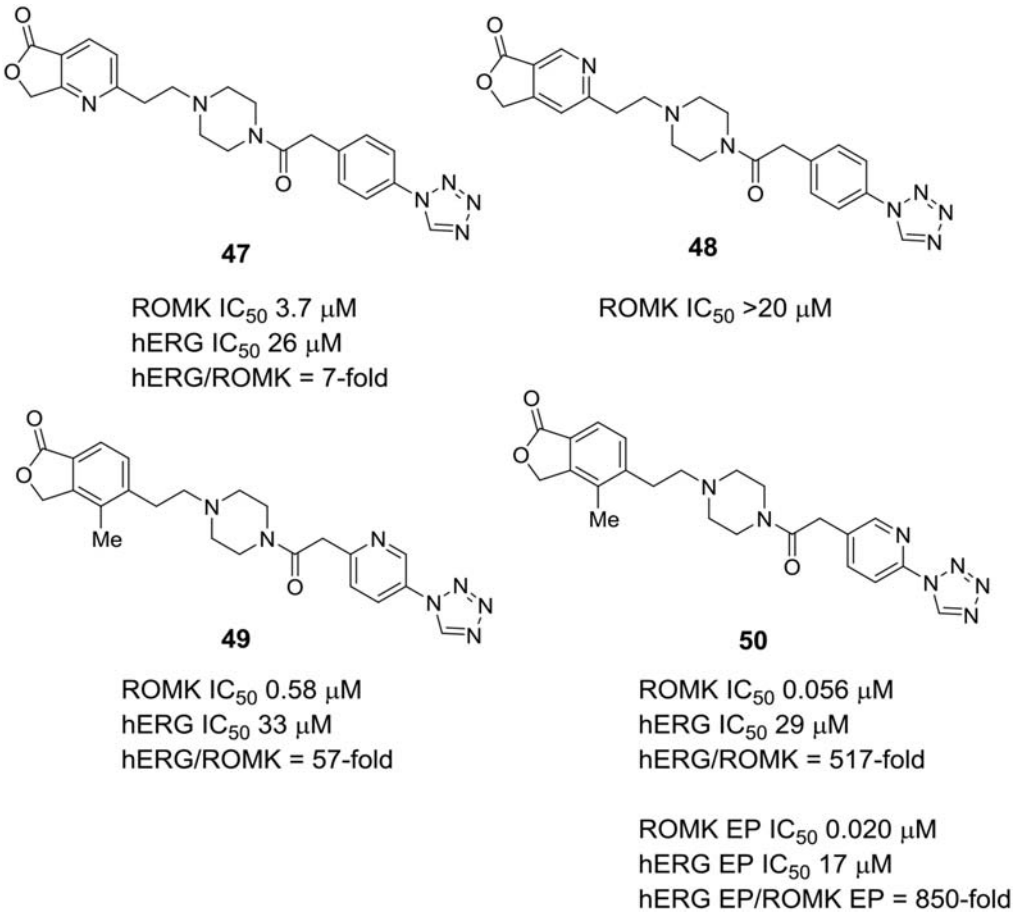

Fig. 10 Incorporation of pyridyl into phthalide and phenyl tetrazole pharmacophores.

Table 9 Pharmacokinetic properties of **50** in rat, dog, and rhesus monkey

Species	*Dose IV (po) mg/kg*	*Cl (L/kg)*	*AUCNpo (μM h kg/mg)*	*Half-life (h)*	F_{po} *(%)*
SD rat	1 (2)	45	0.84	0.44	38
Dog	0.5 (–)	4.6	–	1.3	–
Rhesus	0.25 (0.5)	63	0.001	1.1	<1

8.12.9 Scaffold Modification Toward Improving ROMK Inhibitor Pharmacokinetic Properties

Loop diuretics such as furosemide are viewed as less efficacious blood pressure lowering agents than thiazide diuretics; this has been attributed to their short durations of action followed by rebound sodium reabsorption, due in part to short half-lives and lack of sustained target engagement.[41,42] As part of the program's SAR efforts we explored many different conformationally constrained analogs in which a variety of saturated and unsaturated ring systems were incorporated by tethering from the ethyl linkers either to the terminal pharmacophores or to the central piperazine ring (Fig. 11). Many of these cyclized analogs retained good ROMK potency (e.g., all of the scaffolds shown in Fig. 11 provided active ROMK inhibitors), demonstrating the remarkable tolerance for core scaffold modification, which is in contrast to modifications of the terminal pharmacophores, where we found SAR to be very narrow and unforgiving. A more thorough description of the scope and profiles of some the scaffolds explored can be found in a ROMK patent review by Martelli and coauthors.[43]

While many of the resulting analogs demonstrated good ROMK potency and in some cases improved pharmacokinetic properties, these modifications frequently reduced selectivity over the hERG channel. An exception to this trend was recently reported by Zhu and coworkers who described the discovery of conformationally constrained ROMK inhibitor analogs in which the central piperazine ring is fused to morpholine, thiomorpholine, and piperazine rings.[44] The rationale was to (1) modulate basicity of the piperazine nitrogen to probe effects on hERG selectivity; (2) introduce rigidity which we hoped would help to make the

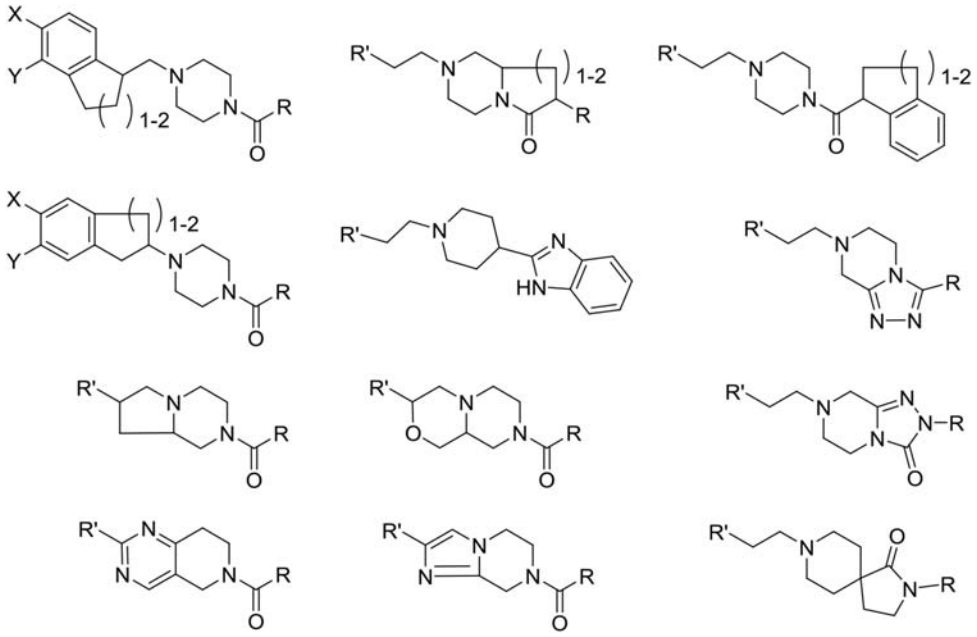

Fig. 11 ROMK scaffolds incorporating cyclic conformation constraints.

resulting analogs less susceptible to CYP enzyme-mediated oxidative metabolism; (3) incorporate substitution at the pharmacophore benzylic position which we had observed could modestly reduce clearance in pharmacokinetic studies (e.g., benzylic methyl substitution). While fused ring systems incorporating morpholine, thiomorpholine, and piperazine rings all led to active ROMK inhibitors, the morpholine-fused (octahydropyrazino[2,1-c][1,4]oxazine)-based analogs provided the best overall profiles. Key compounds highlighted by Zhu and coworkers are shown in Fig. 12. Direct cyclization from compound **50** led to four diastereomers, all retaining potency on ROMK, with the most potent isomer being compound **52**. The lack of a strong preference for a single diastereomer, or especially for *trans* or *cis* relative stereochemistry, was surprising. A general observation was that with analogs in which the terminal pharmacophore was more sterically encumbered (such as with ortho-methyl) there was not a strong preference

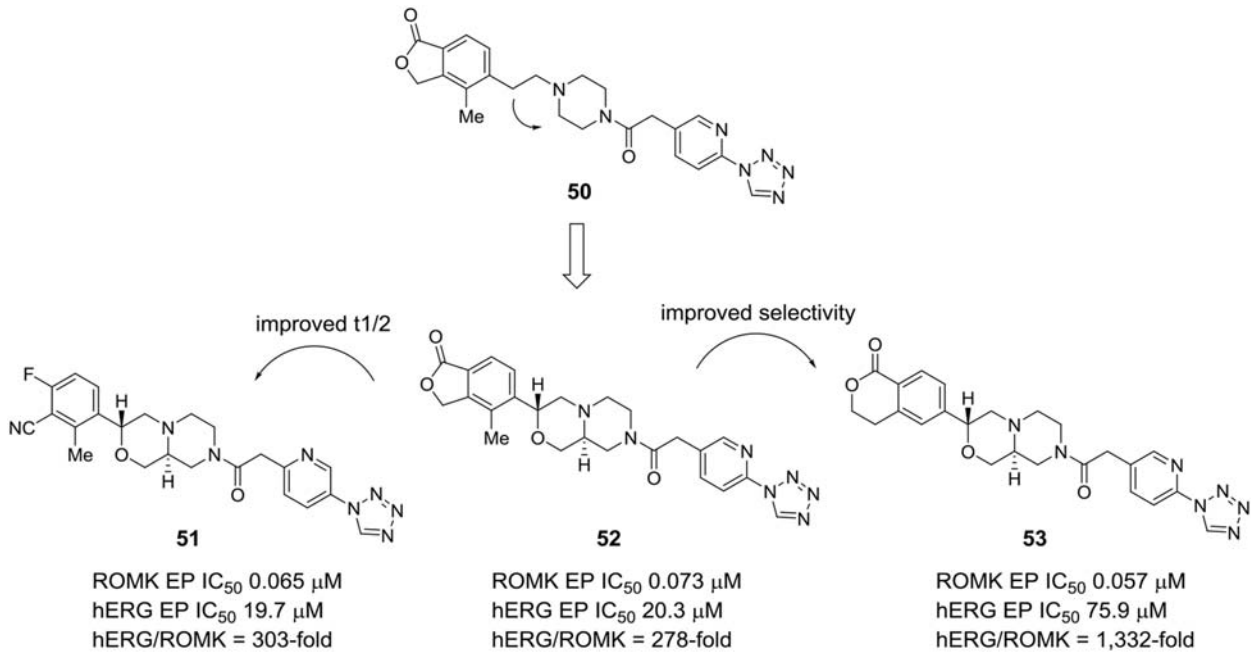

Fig. 12 Lead compounds from the conformationally constrained octahydropyrazino[2,1-c][1,4]oxazine scaffold. ROMK and hERG data are from electrophysiology studies (EP). Reduced clearance rate is associated with significantly diminished in vitro turnover in microsomes.

between *trans* versus *cis* relative stereochemistry, possibly because of more facile flipping between the morpholine boat and chair conformations (less energy difference between them with hindered pharmacophores). On the other hand, smaller terminal pharmacophores (such as that of **53**) led to a greater preference for the *trans* relative stereochemistry, which favors a more extended, rather than bent scaffold arrangement.

Following the discovery of compound **52**, further mix and match combinations of left- and right-side pharmacophores led to compounds **51** and **53**. Compound **53** demonstrated good functional ROMK potency and excellent (improved) selectivity over the hERG channel. Compound **53** was assessed in an anesthetized vagotomized cardiovascular dog model ($n=3$) where no changes were observed in the QT interval or other cardiovascular parameters up to the maximally achieved peak total plasma concentration 82 μM (dog plasma-free fraction, Fu = 22%). Incorporation of the 2-fluoro-6-methylbenzonitrile pharmacophore in compound **51** was associated with improved pharmacokinetic properties while maintaining ROMK potency and ~300-fold selectivity over the hERG channel. Compound **51** was assessed in an anesthetized cardiovascular guinea pig model ($n=3$) where no changes were observed in the QT interval up to the maximally achieved average peak unbound plasma concentration of 59 μM. Compounds **51** and **53** demonstrated excellent selectivity for ROMK. Both compounds were selective against the related inwardly rectifying cardiac $K_{ir}2.1$ channel ($IC_{50} > 100$ μM), as well as the Cav1.2, Nav1.5, and Iks cardiac channels (all $IC_{50} > 30$ μM). Compounds **51** and **53** were assessed in a panel of 115 and 164 assays, respectively, at MDS Pharma Services. Compound **51** had only one hit at < 10 μM (somatostatin subtype 2, IC_{50} 4.1 μM). Compound **53** had only one hit at < 10 μM (endothelin converting enzyme, IC_{50} 9.7 μM). Neither **51** nor **53** demonstrated significant inhibition against a panel of CYP enzymes (3A4, 2D6, and 2C9, all $IC_{50} > 50$ μM). Both compounds showed low plasma protein binding across species (e.g., %Fu for compound **51**: rat 48%, dog 52%, monkey 60%, human 58%). Both compounds had excellent cell permeability measured in LLC-PK1 cells: **51** Papp 28; **53** Papp 25.

A comparison of the rat pharmacokinetic properties of octahydropyrazino[2,1-c][1,4]oxazine analogs **51**, **52**, and **53** in comparison to the parent acyclic compounds **25** and **50** is shown in **Table 10**. The fused bicyclic analogs all demonstrated reduced clearance and improved half-lives compared to their acyclic precursor compounds. All three analogs showed good oral bioavailability. The reduced clearance seen for compounds **51–53** correlates with significantly lower turnover in microsome and hepatocyte incubation studies compared to the parent acyclic analogs.[45] As an example, when compound **51** was incubated with rat, dog, rhesus, and human hepatocytes for 90 min the % parent remaining was 61%, 96%, 91%, and 99%, respectively. A ^{14}C-**51** bile duct cannulated dog study confirmed that the compound is eliminated primarily as intact parent in urine and bile, and is by far the major component in plasma. **Table 11** shows the pharmacokinetic properties of compounds **51** and **53** in dogs and rhesus monkeys. Compound **53** had relatively short half-lives in dog and monkey; however compound **51** had long half-lives, significantly differentiating from earlier program compounds. Both compounds were considered as potential clinical candidate compounds (see later).

8.12.10 ROMK Inhibitors Reduce Blood Pressure in Spontaneously Hypertensive Rats

Compounds **51** and **53** were assessed for blood pressure lowering, diuresis, and natriuresis efficacy in conscious telemetered spontaneously hypertensive rats (SHR) housed in metabolism cages.[46] Compound **51**, when dosed by oral gavage, provided robust

Table 10 Rat pharmacokinetic properties of octahydropyrazino[2,1-c][1,4]oxazine leads compared to parent acyclic analogs

	Compounds				
Rat pharmacokinetics	*25*	*50*	*51*	*52*	*53*
Dose iv/po (mg/kg)	1/2	1/2	1/2	0.5/1	0.5/1
Cl (L/kg)	40	45	21	14	17
AUCN (μM h kg/mg)	0.34	0.84	0.79	2.1	1.4
Half-life (h)	0.62	0.44	1.5	1.0	0.85
F_{po} (%)	33	38	46	82	65

Table 11 Pharmacokinetics of compounds **51** and **53** in dogs and rhesus monkeys (iv/po doses 1 and 2 mg/kg)

	51		*53*	
	Dog	*Rhesus*	*Dog*	*Rhesus*
Cl (L/kg)	2.5	4.0	7.9	13.9
AUCN (μM h kg/mg)	16.7	6.0	7.6	0.93
Half-life (h)	17.3	5.0	1.6	1.6
F_{po} (%)	100	67	100	37

Table 12 Blood pressure efficacy in telemetered spontaneously hypertensive rats (SHR)

Compound	*51*	*51*	*53*	*53*	*HCTZ*[a]
Dose (mg/kg)	3	10	3	10	25
Day 1 24 h diuresis (fold increase)[b]	1.4	1.6	1.1	1.2	1.1
δSBP[c] by Day 3 (mmHg)	−9	−16	−1	−3	−12
4 h plasma exposure (μM)[d]	0.03	1.9	0.21	0.98	–
0–4 h urine concentration (μM)	0.87	5.9	3.3	11.2	–

[a]HCTZ, hydrochlorothiazide.
[b]Compared to vehicle; $n=5$.
[c]SBP, systolic blood pressure.
[d]From parallel pharmacokinetic sampling.

blood pressure lowering at 3 and 10 mg/kg doses (Table 12), comparable or exceeding that of hydrochlorothiazide at a 25 mg/kg dose (approximately the maximally efficacious dose in this model based on a prior full dose–response study). This demonstrates that beyond inducing diuresis and natriuresis, ROMK inhibitors are able to reduce blood pressure in preclinical models, as expected based on the human and rodent genetics. Surprisingly, compound **53** provided minimal blood pressure lowering, which correlated to a reduced 24-h diuretic effect compared to compound **53**. Based on the comparable in vitro potency of the two compounds (Fig. 12) and the similar or higher exposure levels in plasma and urine for compound **53** compared to **51**, it is difficult to explain the discrepancy in the 24 h diuresis and blood pressure lowering effects. Considering the rat pharmacokinetic studies, the rat half-life of compound **51** is nearly twofold that of compound **53**, suggesting the possibility that compound **51** engages ROMK for a longer period of time; if trough exposures contribute to driving efficacy, then this might explain the superior efficacy of compound **51**. In any case, the team learned that the SHR model can provide key differentiation between compounds enabling prioritization of the compounds that will provide the greatest in vivo efficacy. Moreover, the SHR model could be used as a tool to gain a better understanding of the pharmacokinetic–pharmacodynamic relationships.

8.12.11 Parallel SAR Evolution of the Original Piperazine Series

As SAR in the acylpiperazine lead series was diverging from the original piperazine hit series, the Merck team continued in parallel to develop the SAR in the latter series. In some cases SAR between the two series corresponded well and was transferable, and in others SAR diverged, leading to greater structural differentiation between the two subseries. Similar to the acylpiperazine series, Walsh and coworkers demonstrated that installation of a phthalide 4-methyl substituent led to retained or improved ROMK potency and an incremental improvement in hERG selectivity (Fig. 13 and Table 13).[47]

As described earlier, installation of a benzylic hydroxyl group in the acylpiperazine lead series led to a significant reduction of hERG inhibitory potency; however this was accompanied by a corresponding drop in ROMK potency, so the net improvement in selectivity over hERG was only twofold (see compounds **31** and **45** in Fig. 9). When this same modification was explored in the original piperazine series the resulting SAR diverged from that in the acylpiperazine series (Fig. 14 and Table 14). For example,

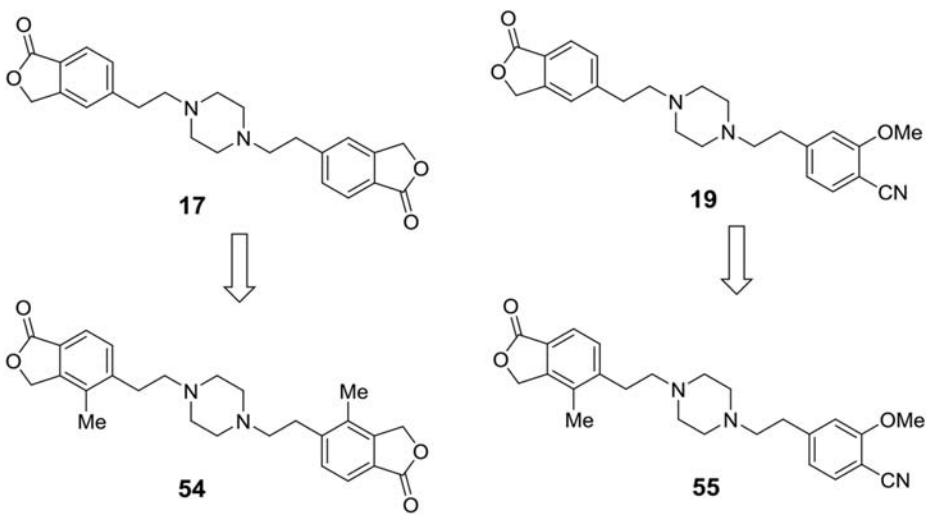

Fig. 13 Incorporation of phthalide 4-methyl provides incremental improvements in hERG selectivity.

Table 13 ROMK and hERG potency of analogs **17**, **19**, **54**, and **55**

Compound	*ROMK IC_{50} (μM)*[a]	*hERG IC_{50} (μM)*[b]	*hERG/ROMK ratio*
17	0.078	1.9	24
19	0.089	1.6	18
54	0.076	3.0	39
55	0.035	2.1	60

[a]ROMK potency determined using the functional $^{86}Rb^{+}$ efflux assay.
[b]hERG activity measured using the ^{35}S MK-499 displacement binding assay.

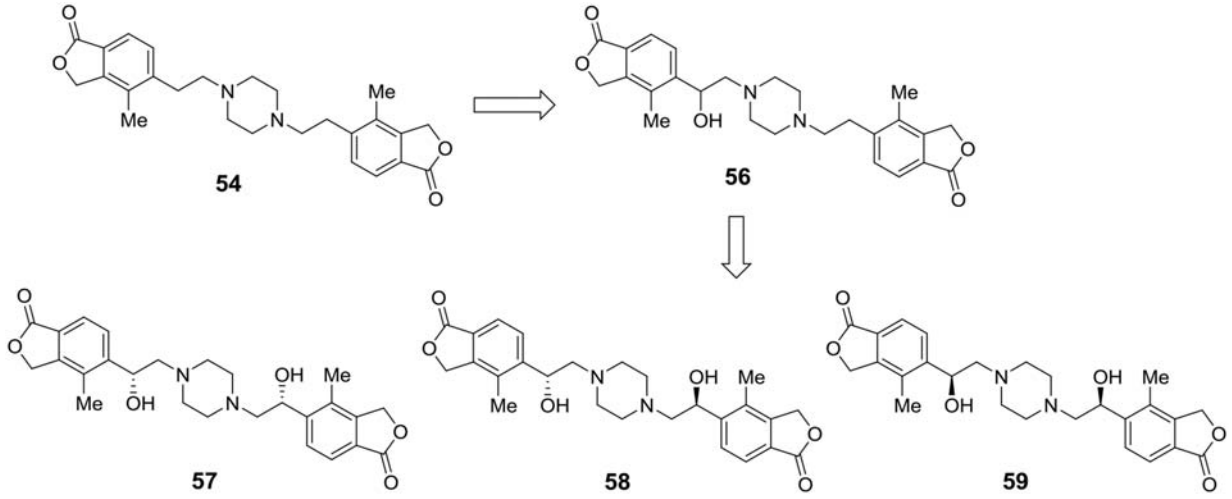

Fig. 14 Installation of hydroxyl groups improves selectivity ove the hERG channel.

Table 14 ROMK and hERG potency of **54**, and **56–59**, measured by electrophysiology

Compound	*ROMK EP IC_{50} (μM)*	*hERG EP IC_{50} (μM)*	*Ratio hERG EP/ROMK EP*
54	0.009	3.0[a]	333[a]
56	0.013	8.3	624
57	0.009	22	2444
58	0.009	>30	>3333
59	0.012	22	1833

[a]hERG activity for compound **54** was measured in the ^{35}S MK-499 displacement binding assay.

installation of a single hydroxyl group into symmetrical analog **54**, provided **56**, which retained ROMK potency and still demonstrated a twofold improvement in selectivity over hERG (as a mixture of two enantiomers).[38] Encouraged, a second benzylic hydroxyl group was installed, leading to three single diastereomers analogs (*R,R*; *meso*; *S,S*; **57–59**, respectively). Amazingly, not only did these analogs retain excellent functional inhibition potency on ROMK, but selectivity over hERG also dramatically improved (1800- to >3300-fold, Table 14), affording some of the most potent and selective compounds identified in the program. The *meso* compound **58** had poor solubility and was challenging to isolate, while the *R,R* and *S,S*-isomers had much better solubility.

Compounds **57** and **59** had comparable PK profiles; however the *meso*-isomer **58** demonstrated somewhat higher clearance and a shorter half-life (Table 15). Based on its physicochemical properties, pharmacokinetic characteristics and inferior *in vivo* diuresis profile in volume-loaded SD rats, *vide infra*, the *meso*-isomer **58** was not advanced further.[38]

Compounds **57–59** were assessed in an acute volume-loaded SD rat diuresis model (described in reference 32).[38] Adult male SD rats were dosed by oral gavage with the indicated doses of compounds. After 30 min, voiding was induced by giving each animal a saline load. Urine collection took place over the next 4 h and was analyzed for volume and electrolyte content. Data are presented as fold change relative to values obtained in the vehicle-treated animals (Table 16). The *R,R*-isomer **57** provided the most robust diuretic and natriuretic effect, with the *S,S*-isomer **59** giving intermediate efficacy and the *meso*-isomer giving relatively modest efficacy. Even at the 0.3 mg/kg dose compound **57** provided greater efficacy than compounds **58** and **59** at 10-fold higher (3 mg/kg) doses. Although the exact reason for these differences in not clear, the shorter half-life of **58** may account for its weaker efficacy.

Table 15 Rat pharmacokinetic properties of compounds **57–59**[38]

Compound	*57*	*58*	*59*
Dose IV/po (mg/kg)	1/2	0.5/1	0.5/1
Cl (mL/min/kg)	56	82	54
Vdss (L/kg)	3.8	5.8	4.5
$AUCN_{po}$ (μM h kg/mg)	0.14	0.13	0.30
Half-life (h)	1.1	0.86	1.4
F%	21	45	44

Table 16 Acute (4 h) diuresis and natriuresis profiles[a] of diastereomers **57–59** following oral dosing[38]

Compound	*Dose (mg/kg)*	*Diuresis fold increase*[b]	*Natriuresis fold increase*[b]
57	0.3	6.4*	6.2*
57	1	8.6*	8.6*
57	3	9.0*	8.0*
57	10	9.4*	8.5*
58	0.3	1.3	1.4
58	1	1.6	1.5
58	3	1.9	2.2
59	1	3.5*	3.7*
59	3	4.5*	4.1*

[a] $n=5$ per group.
[b] Compared to vehicle.
* $p<.05$ vs. vehicle.

Other factors that could impact the relative efficacy of the diastereomers might be differential urinary exposure at the site of action in the tubular lumen and/or differing ROMK channel dissociation rates. On the basis of the in vivo data, compound **57** was selected for further profiling.

In an assay that measures the ability of thallium to permeate through open hROMK channels stably expressed in HEK293 cells, compound **57** blocks the thallium-induced fluorescence signal with an IC_{50} value of 6.6 ± 1.9 nM ($n=9$), in good correspondence with the potency observed by automated IonWorks electrophysiology (9 nM).[46] In MDCK cells stably expressing the rat ROMK channel, thallium flux is inhibited by compound **57** with an IC_{50} value of 6.3 ± 1.7 nM ($n=4$). In manual electrophysiological recordings of HEK-rKir1.1, HEK-dKir1.1, or rhesus Kir1.1 channels transiently transfected into TsA-201 cells, **57** provided estimated IC_{50} values of 4.9, 8.8, and 8.6 nM, for rat, rhesus or dog Kir1.1, respectively, indicating little species differences. To determine the off rate of compound **57** from rat ROMK channels, stable recordings of rat ROMK currents were established, compound was applied and equilibrated (100 nM), at which point compound was removed from the bath solution and recovery of the rat ROMK current was monitored. Compound **57** demonstrated a slow recovery of current [off rate (time constant, τ_{off}) >40 min.]. This distinguishes it from its diastereomers **58** and **59** which when tested in a similar fashion had estimated off rates of 22 and 4 min, respectively. It also distinguishes it from acylpiperazine analog **53** which had an estimated off rate of 19 min. The long off rate of compound **57** may play a role in its superior diuretic efficacy at matched doses compared to these other analogs by extending target engagement.

Compound **57** did not demonstrate significant inhibition of other K_{ir} family channels screened (IC_{50} $K_{ir}2.1$ and $K_{ir}2.3$, >100 μM; IC_{50} $K_{ir}4.1$ and $K_{ir}7.1$ >30 μM), nor did it significantly inhibit other cardiac channels such as Cav1.2 and Nav1.5 (both with IC_{50} >30 μM); in electrophysiology assays with I_{Ks}, I_{Na}, and L-type I_{Na} channels, no inhibition was observed (<5%) at the highest tested concentration of 30 μM. In a broad counterscreening panel of 166 enzymes and radioligand binding assays performed at MSD Pharma Services, compound **57** demonstrated good overall selectivity, showing inhibition of 50% or greater at 10 μM for only three assays: acetyl cholinesterase, ACES, $IC_{50}=9.94$ μM, human serotonin transporter, SERT, $IC_{50}=0.12$ μM, and somatostatin subtype 1, sst1, IC_{50} 2.63 μM. In a functional assay using HEK293 cells stably transfected with human SERT, compound **57** inhibited uptake of ^{3}H-serotonin with an IC50 value of 2.40 ± 0.32 μM ($n=5$). Somatostatin subtype 1 activity was assessed in an internal binding assay measuring displacement of ^{125}I-somatostatin-14 where it demonstrated an IC_{50} of 14.5 μM. In a functional assay using cAMP in agonist mode in CHO K1 cells stably expressing sst1 performed at Multispan compound **57** did not display significant agonist activity (EC_{50} >30 μM). Based on the ~300-fold selectivity for ROMK over SERT, the low plasma exposures required for efficacy in diuresis and blood pressure models, and the observation that compound **57** is a Pgp substrate (human Mdr1 B–A/A–B ratio = 12), we concluded that there should be sufficient margins against any adverse CNS effects related to SERT inhibition.[38] It should be noted that based on PET tracer studies using ^{11}C-DASB, the efficacy of SERT inhibitors is believed to require ≥80% SERT occupancy at trough in humans.[48]

Table 17 Pharmacokinetic properties of compound **57** in dogs and rhesus monkeys

Species	*Dog*	*Rhesus*
Cl (mL/min/kg)	56	29
Vdss (L/kg)	7.5	6.7
$AUCN_{po}$ (μM h kg/mg)	0.32	0.30
Half-life (h)	1.7	4.0
F%	51	25

Compound **57** was assessed in an anesthetized vagotomized cardiovascular dog model ($n=3$)[40] to confirm that the high selectivity for ROMK over hERG would ensure CV safety in vivo. Following a rising dose IV infusion of compound **57** at a cumulative 10 mg/kg dose (average peak plasma concentration 11.6 μM), no changes were observed in heart rate, mean arterial pressure, or in the QT interval and other electrocardiographic parameters.

ROMK inhibitor **57** was evaluated in pharmacokinetic studies in dogs and rhesus monkeys where it demonstrated moderate clearance rates (**Table 17**).[38] Compound **57** had a short half-life in dog and a moderate half-life in monkey. In a bile duct cannulated rat study with ^{3}H-**57**, the major clearance mechanisms were oxidative metabolism by CYP3A4 and urinary excretion of unchanged parent; minor metabolism pathways included glucuronidation and lactone hydrolysis.[49] The major circulating component was parent. ROMK inhibitor **57** was not a potent reversible inhibitor of human CYP3A4, CYP2C9, or CYP2D6 ($IC_{50}>50$ μM) and was not a time-dependent inhibitor of CYP3A4 at 10 and 50 μM. Inhibitor **57** was not a potent hPXR activator ($EC_{50}>30$ μM; 5% activation at 30 μM). Compound **57** had low plasma protein binding across species (%Fu rat 57%, dog 62%, rhesus monkey 67%, and human 29%), differentiating from standard-of-care loop and thiazide diuretics which typically have high plasma protein binding. The projected human half-life of compound **57** was estimated to be ~5 h based upon a combination of in vitro to in vivo correlation and allometric scaling from preclinical species. Inhibitor **57** had good permeability in LLC-PK1 cells (Papp: 20×10^{-6} cm/s) and demonstrated significant colonic absorption in dogs with an $AUC_{0-24\ h}$ ratio of colonic to oral exposure of 0.36.[49] This supported the possibility that compound **57** could be formulated for extended release if the human half-life should prove to be inconsistent with qd dosing.

Hampton and coworkers have described the acute renal excretory function of compound **57** in conscious female mongrel dogs.[46] In this model restrained mongrel dogs were fitted with catheters inserted into the urinary bladder to permit timed urine collections and maintained with a continuous intravenous saline-based infusion (1 mL/min) via venous catheter. Following a 60-min equilibration period, dogs were dosed orally with compound **57** and comparator diuretics and urine and blood samples were collected for 180 min. **Fig. 15** shows the natriuretic dose response for compound **57** in this model in comparison to an approximately maximally efficacious dose of HCTZ.

The acute diuretic and electrolyte excretion responses of **57** (0.1, 0.3, 1, or 3 mg/kg) is compared with HCTZ (10 mg/kg) and furosemide (1, 3, 10, or 25 mg/kg) in **Table 18**. Compound **57** evoked dose-dependent increases in diuresis and natriuresis. At the 0.3-mg/kg dose the magnitude of diuresis and natriuresis was greater than that obtained with HCTZ at its maximally efficacious dose in this model, and equivalent to that obtained at 3 mg/kg of furosemide. The maximal effect of **57** was achieved at 1 mg/kg; no further significant response was obtained at 3 mg/kg. Similarly, the maximal effect of furosemide was achieved at 10 mg/kg as no further increase in diuresis or natriuresis was observed at 25 mg/kg. Kaliuresis in compound **57**-treated animals was comparable to that of vehicle-treated animals whereas an approximately twofold increase was observed in animals that received HCTZ. Consequently, the U_K/U_{Na} excretion ratio was more favorable for ROMK inhibitor **57** than for HCTZ. Similarly, furosemide at 3 mg/kg also elicited increased kaliuresis relative to vehicle, again leading to a more favorable U_K/U_{Na} excretion ratio for ROMK inhibitor **57** at 0.3 mg/kg compared to furosemide at 3 mg/kg, doses at which both compounds gave similar natriuresis. This observation is consistent with expectations based on the expression of ROMK in the CCD, where it plays a critical role in potassium homeostasis

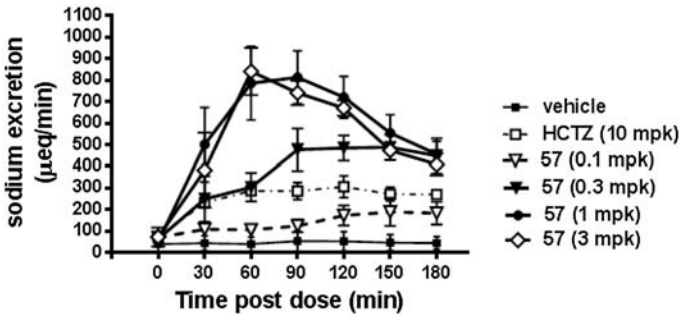

Fig. 15 Acute natriuretic response of compound **57** and HCTZ in mongrel dogs.

Table 18 Comparison of the efficacy of **57** with furosemide and HCTZ in the acute renal dog model

	Vehicle	*Furosemide*				*57*				*HCTZ*
	Dose: 0 (mg/kg)	*Dose: 1 (mg/kg)*	*Dose: 3 (mg/kg)*	*Dose: 10 (mg/kg)*	*Dose: 25 (mg/kg)*	*Dose: 0.1 (mg/kg)*	*Dose: 0.3 (mg/kg)*	*Dose: 1.0 (mg/kg)*	*Dose: 3.0 (mg/kg)*	*Dose: 10 (mg/kg)*
Diuresis: mL (fold change[a])	67	225 (3.4)	531 (7.9)	990 (14.8)	1050 (15.7)	138 (2.1)	447 (6.7)	739 (11)	656 (9.8)	264 (3.9)
Natriuresis: mequiv. (fold change[a])	9.4	42 (4.5)	84 (8.9)	132 (14)	134 (14.2)	27 (2.9)	75 (8.0)	115 (12.2)	106 (11.3)	49 (5.2)
Chloride: mequiv. (fold change[a])	7.9	45 (5.7)	87 (11)	141 (17.8)	147 (18.6)	21 (2.7)	75 (9.5)	113 (14.3)	109 (13.8)	52 (6.6)
Kaliuresis: mequiv. (fold change[a])	3.9	6 (1.5)	9 (2.3)	18 (4.6)	21 (5.4)	2.4 (0.6)	4.5 (1.2)	6 (1.5)	7.7 (2)	6.7 (1.7)
Calciuresis: total (fold change[a])	2.0	18.9 (9.5)	36 (18)	66 (33)	69 (34.5)	4.3 (2.2)	33.4 (16.7)	58 (29)	55 (27.5)	2.1 (1)
Urinary magnesium: total (fold change[a])	6.5	10.7 (1.6)	18 (2.8)	30 (4.6)	45 (6.9)	9.7 (1.5)	18 (2.8)	36 (5.5)	25 (3.8)	5.7 (0.9)

[a]Fold change is calculated relative to vehicle.

and suggests that ROMK inhibitors may have a reduced risk of inducing hypokalemia compared to thiazide and loop diuretics. Both compound **57** and furosemide increased calcium and magnesium excretion to a similar extent at equinatriuretic doses, while HCTZ did not. Loop diuretics such as furosemide are known to increase calcium and magnesium excretion since they attenuate the transepithelial potential which establishes the driving force for paracellular uptake of calcium and magnesium ions. Mechanistically, ROMK inhibitors would be expected to act in the same way as they also (indirectly) block sodium reabsorption through the Na^+–K^+–$2Cl^-$ co-transporter. Glomerular filtration rate (GFR) was not changed in animals that received **57** in this acute setting.

In addition to monitoring the response to acute treatment, both **57** (0.3 mg/kg/day) and HCTZ (10 mg/kg/day) were dosed po, for 7 days and urinary and plasma electrolytes, as well as compound levels, were monitored at 30 min intervals for 3 h post dosing on Days 1 and 7.[46] The dose of compound **57** was selected based on its equinatriuretic potency to the 10 mg/kg dose of HCTZ. The acute diuretic and natriuretic response to compound **57** was maintained upon 7-day dosing whereas both responses were diminished in dogs dosed with HCTZ for 7 days (data not shown). Plasma potassium levels were not significantly altered by compound **57** treatment at the 0.3 mg/kg dose, whereas a marked decrease was observed at day 7 in HCTZ-treated dogs (Fig. 16). Compared to vehicle-treated group, chronic dosing with **57** had no effect on plasma glucose, calcium, magnesium, sodium, chloride, uric acid, or blood urea nitrogen levels (data not shown). However, bicarbonate levels were found to be elevated after 6 days of dosing with MK-7145, consistent with metabolic alkalosis associated with loop diuretics. In the 3 h post dosing plasma and urine concentrations of **57** were very similar on days 1 and 7 with ~30- to 60-fold higher exposures in urine compared to plasma. As an example exposure on day 7 in plasma and urine for the 150–180-min time interval was 0.060 and 1.81 μM, respectively. Since ROMK is expressed on the apical face of epithelial cells lining the tubular lumen of the nephron, it is possible that urinary exposure may play a key role in driving efficacy.

The BP lowering and diuretic activity of compound **57** (0.3, 1, 3, 10, and 30 mg/kg/day, po) administered daily for 4 days was assessed in male SHR using radiotelemetry.[46] ROMK inhibitor **57** evoked dose-dependent decreases in systolic blood pressure (SBP) (Fig. 17, panel A) and diastolic blood pressure (DBP). Maximal lowering of SBP (~20 mmHg) was observed by day 2 at both the 10

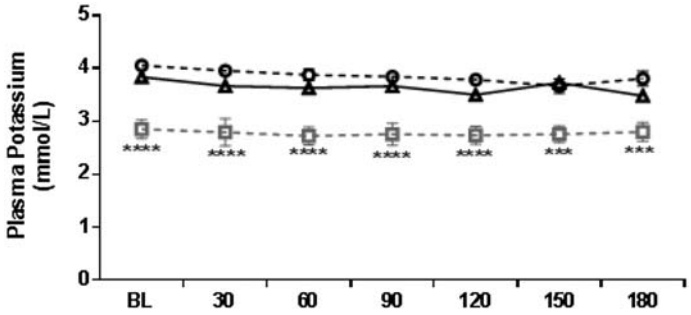

Fig. 16 Plasma potassium levels were not significantly altered by **57** (▽), whereas a marked decrease was observed at Day 7 in HCTZ (□) versus vehicle (○)-treated dogs. ***$p<.001$, ****$p<.0001$ vs. vehicle. Adapted from: Hampton, C.; Zhou, X.; Felix, J. P.; Priest, B. T.; Thomas-Fowlkes, B.; Pai, L.-Y.; Alonso-Galicia, M.; Xiao, J.; Corona, A.; Price, O.; Hernandez, M.; Gill, C.; Shah, K.; Rasa, C.; Hoagland, K.; Owens, K.; Tang, H.; Tong, V.; Roy, S.; Sullivan, K.; Kaczorowski, G. J.; Metzger, J. M.; Pasternak, A.; Garcia, M. L. *J. Pharmacol. Exp. Ther.* **2016**, published ahead of print July 18, 2016, http://dx.doi.org/10.1124/jpet.116.235150.

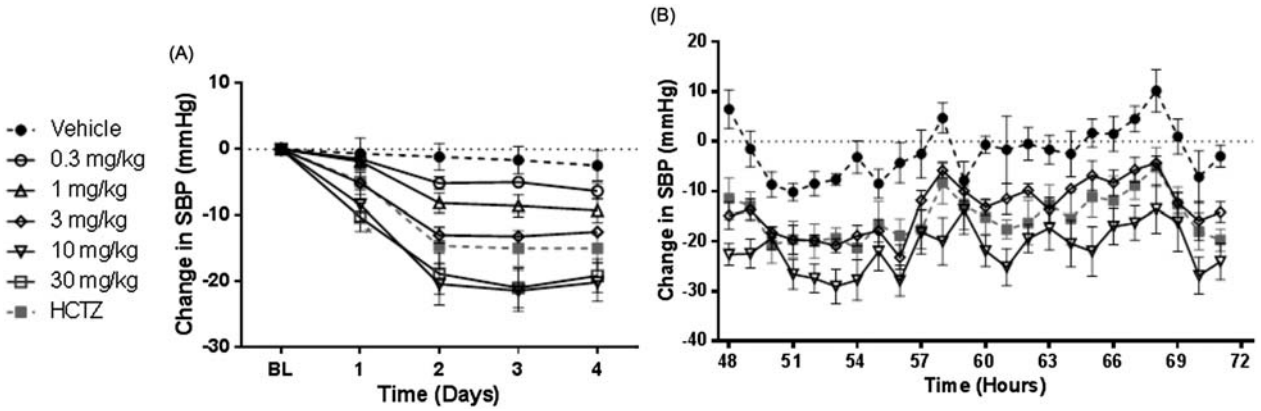

Fig. 17 Compound **57** dose response in spontaneously hypertensive rats. Panel A: daily mean systolic blood pressure lowering; Panel B: average hourly SBP during Day 3 of treatment. Adapted from: Hampton, C.; Zhou, X.; Felix, J. P.; Priest, B. T.; Thomas-Fowlkes, B.; Pai, L.-Y.; Alonso-Galicia, M.; Xiao, J.; Corona, A.; Price, O.; Hernandez, M.; Gill, C.; Shah, K.; Rasa, C.; Hoagland, K.; Owens, K.; Tang, H.; Tong, V.; Roy, S.; Sullivan, K.; Kaczorowski, G. J.; Metzger, J. M.; Pasternak, A.; Garcia, M. L. *J. Pharmacol. Exp. Ther.* **2016**, published ahead of print July 18, 2016, doi:10.1124/jpet.116.235150.

Table 19 Plasma and urine exposures of compound **57** from a parallel PK study with dose-associated systolic blood pressure lowering

	Plasma levels (μM) Day 4 Time point post qd dose					
*Compound **57***	*1 h*	*4 h*	*8 h*	*0–4 h total urine levels (μM) Day 4*	*4–24 h total urine levels (μM) Day 4*	*SBP △ Day 4 (mmHg)*
0.3	0.011	LOQ	LOQ	0.20	0.19	−6
1	0.028	0.014	0.009	0.57	0.36	−9
3	0.11	0.047	0.040	1.6	0.79	−12
10	0.52	0.18	0.080	9.3	3.5	−20
30	4.1	1.1	0.34	24	9.6	−19

and 30 mg/kg/day doses. At the 3 mg/kg dose of compound **57**, the magnitude of BP lowering (∼12 mmHg) was similar to that achieved with HCTZ (25 mg/kg/day) at its approximately maximally efficacious dose based on a prior dose range study. Importantly, in comparison to the blood pressure efficacy seen for earlier ROMK inhibitors **51** and **53** (Table 12, earlier) compound **57** produced a greater magnitude of blood pressure lowering at the same doses and produced efficacy at lower doses and at lower plasma exposures (Table 19). For example, compound **51** lowered systolic blood pressure by 16 mmHg at a 10 mg/kg dose, while compound **57** provided comparable blood pressure lowering at the 3 mg/kg dose. Despite the short half-life of compound **57** in rats, the extent of BP lowering was maintained throughout day 3 in all treatment groups (Fig. 17, panel B). Parallel pharmacokinetic studies established that at the maximally efficacious (10 mg/kg) dose of compound **57**, trough unbound plasma levels (∼0.003 μM) are below the compound's IC_{50} on the rat channel. However, late urine collection near trough (20–24 h) indicated that urine exposures are ∼100-fold higher than plasma exposures at trough,[49] suggesting the possibility that urine exposure helps to maintain target engagement throughout the full 24 h dosing interval.

Analysis of the correlation between blood pressure lowering efficacy and diuresis and natriuresis indicated that blood pressure efficacy is not correlated to acute peak effects (not shown), but instead to day 1 net 24 h diuresis and natriuresis (Fig. 18, panels A and B, respectively). Typically, ROMK inhibitor-mediated acute diuretic and natriuretic effects in rats are very robust and return to baseline after about 2 h post dose. In some cases, there is a rebound sodium and water retention which diminishes the overall net 24 h diuretic and natriuretic effect. Thus, the more potent ROMK inhibitors in lowering blood pressure or the doses at which blood pressure lowering is observed are those that are able to sustain a net 24 h diuretic and natriuretic response (Fig. 19); this ability may be linked to the ROMK inhibitor half-life, trough urine, and plasma exposure, in vitro potency, and possibly to the channel off rate. Note from Fig. 19 that diuresis efficacy is maintained through all days of the study and this is associated with increased water intake by the rats (not shown).

Urine samples were also analyzed to determine the magnitude of calcium excretion relative to vehicle. During the 4 h postdose, compound **57** at all doses led to an increased calcium excretion rate compared to vehicle (three- to sixfold, data not shown). During the subsequent 20 h (4- to 24-h interval) calcium excretion became less pronounced, with only the 10 and 30 mg/kg doses of **57** giving a 1.5- to 3-fold increase in calcium excretion rate. This calciuretic effect is consistent with observations in dogs, *vide supra*, and is also associated with the profile of clinically used loop diuretics such as furosemide.

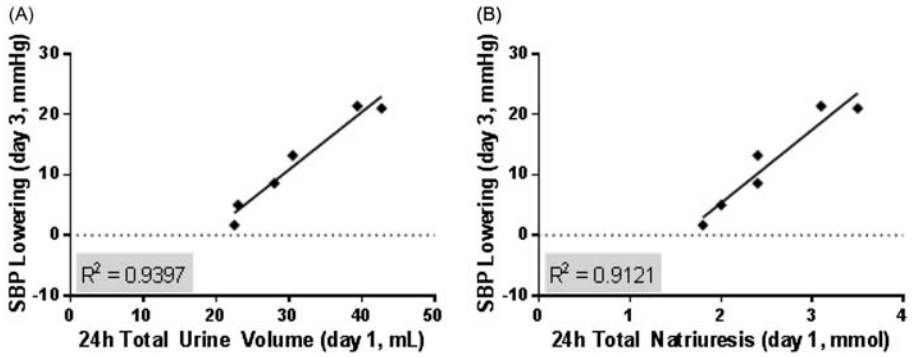

Fig. 18 Blood pressure lowering in SHR by compound **57**. Panel A: correlation of blood pressure lowering with 24 h urine volume; Panel B: correlation of blood pressure lowering with 24 h natriuresis. Adapted from: : Hampton, C.; Zhou, X.; Felix, J. P.; Priest, B. T.; Thomas-Fowlkes, B.; Pai, L.-Y.; Alonso-Galicia, M.; Xiao, J.; Corona, A.; Price, O.; Hernandez, M.; Gill, C.; Shah, K.; Rasa, C.; Hoagland, K.; Owens, K.; Tang, H.; Tong, V.; Roy, S.; Sullivan, K.; Kaczorowski, G. J.; Metzger, J. M.; Pasternak, A.; Garcia, M. L. *J. Pharmacol. Exp. Ther.* **2016**, published ahead of print July 18, 2016, doi:10.1124/jpet.116.235150.

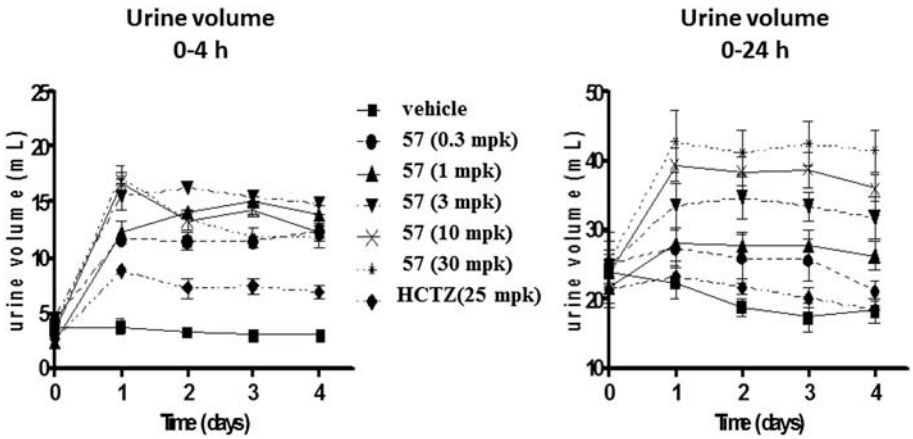

Fig. 19 Comparison of acute and 24 h diuretic effects for compound **57** in SHR rats.

In light of the short half-life of compound **57** in rats, 3 mg/kg and 10 mg/kg qd and 3 mg/kg bid po doses were compared in a 4-day study in SHR to probe the pharmacokinetic (PK)–pharmacodynamic (PD) correlation of **57**.[50] The bid doses were at 12 h intervals. The results (Fig. 20 and Table 20) illustrate that 3 mg/kg bid dosing confers superior systolic blood pressure lowering (−23 mmHg on Day 4) to either 3 or 10 mg/kg qd dosing (−12 and −17 mmHg, respectively). These results, together with exposure data from a parallel bid versus qd PK study, suggest that trough, but not peak exposure, correlates better with BP lowering efficacy of the compound in SHR. Despite the lower total dose, 3 mg/kg bid dosing provides a higher trough plasma exposure and an equivalent 12–24 h urine exposure compared to the 10 mpk qd dosing paradigm. This prolonged exposure correlates to a more prolonged diuretic effect (Table 21). In a parallel pharmacokinetic study, the 10 mg/kg qd and 3 mg/kg bid dose regimens give the same 24 h diuresis fold change versus vehicle when averaged over 3 days; however, the 3 mg/kg bid dose regimen gives greater diuresis than the 10 mg/kg dose from 12–24 h (1.9-fold compared to 1.5-fold change compared to vehicle, respectively). Because both qd and bid dosing conferred full 24-h systolic blood pressure reduction compared to vehicle, bid dosing improves the magnitude of blood pressure lowering, but is not required for maintaining the 24-h duration of efficacy. Taken together, these data suggest that ROMK inhibitors with longer half-lives and reduced peak-to-trough ratios will provide improved efficacy.

Finally, to test the durability of blood pressure lowering by ROMK inhibitors, a 14-day study in SHR evaluating compound **57** at 1 and 3 mg/kg doses was conducted. Blood pressure lowering was maintained throughout the course of the study, indicating that the pharmacodynamic effects are sustained and do not wane over time.[46]

8.12.12 Selection of Compound 57 as the Clinical Compound MK-7145

Starting from the program initial lead **2**, two quite distinct subclasses of potent and selective ROMK inhibitors were developed (Fig. 21). From these two subclasses, compounds **51**, **53**, and **57** were milestone compounds that were profiled as potential clinical

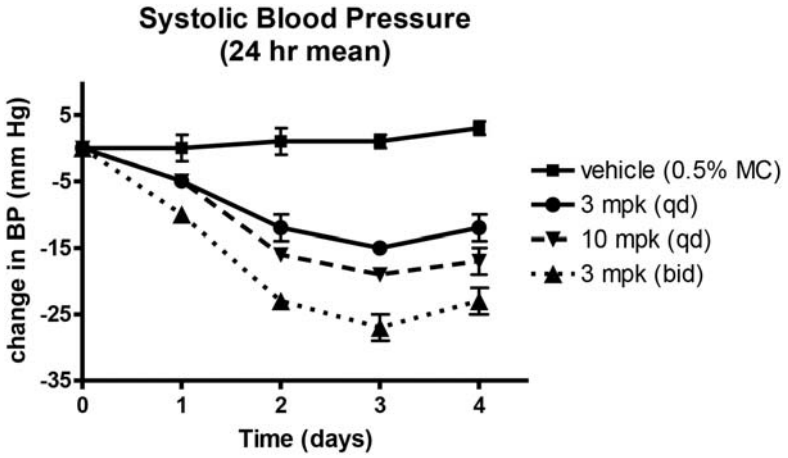

Fig. 20 Blood pressure lowering efficacy of 3 and 10 mg/kg qd vs. 3 mg/kg bid dosing of **57** in SHR (bid doses are at 12 h intervals).

Table 20 Relationship between plasma and urine drug levels following 10 mg/kg qd and 3 mg/kg bid po dosing of **57** in SHR

	Drug levels at Day 4					
	Plasma (nM)			*Urine (nM)*		
MK-7145 dose	*Time: 4 h*	*Time: 12 h*	*Time: 24 h*	*Time: 0–4 h*	*Time: 4–12 h*	*Time: 12–24 h*
3 mg/kg qd	39	5	4	1790	1450	530
3 mg/kg bid	21	14	7	2350	1100	1270
10 mg/kg qd	96	8	$<$LOQ	9550	3610	1340

Table 21 Comparison of 0–24 h and 12–24 h days 1–3 average diuresis for compound **57** dosed at 3 and 10 mg/kg qd and 3 mg/kg bid (fold change compared to vehicle)

	Days 1–3 averaged diuresis[a]	
Dose	*0–24 h*	*12–24 h*
3 mg/kg qd	1.5	1.0
10 mg/kg qd	2.0	1.5
3 mg/kg bid	2.0	1.9

[a]Fold change compared to vehicle, $n=5$–6/dose group.

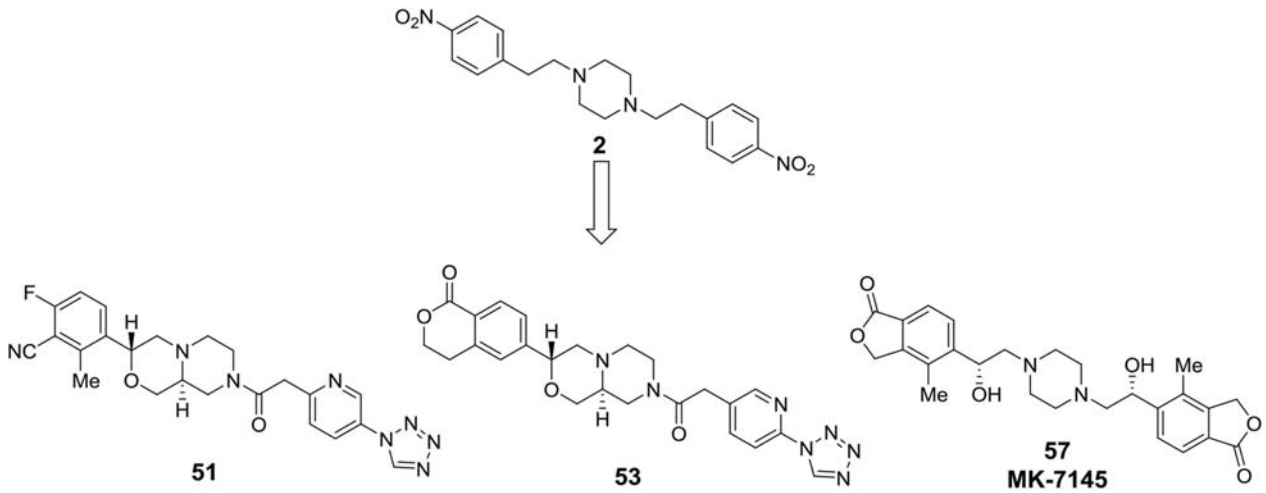

Fig. 21 Potent and selective ROMK inhibitors in two distinct lead series originating from the same original hit.

Table 22 Comparison of key features of **51**, **53**, and **57**

Compound	*51*	*53*	*57*
ROMK EP IC_{50} (nM)	65	57	9
hERG EP IC_{50} (μM)	19.7	75.9	22.0
Rat, dog, rhesus $t_{1/2}$ (h)	1.5, 17.3, 5	0.85, 1.6, 1.6	1.1, 1.7, 4
δSBP (mmHg) at Day 3 in SHR at 3, 10 mg/kg	−9, −16	−1, −3	−13, −22

development compounds (Table 22). All three compounds demonstrated good selectivity over the hERG channel and good margins in cardiovascular safety models. Based on allometric scaling of preclinical PK and in vitro–in vivo correlation studies, compound **51** had the longest projected human half-life (10 h), followed by compound **57** (5 h). However, compound **57** consistently demonstrated robust efficacy at lower doses in all pharmacodynamic models assessed compared to other available compounds. Therefore, compound **57** was selected as the clinical development compound and was designated MK-7145. The main perceived risk associated with MK-7145 was that its human half-life might not be compatible with qd dosing. As discussed previously, MK-7145 has good cell permeability and demonstrated acceptable colonic absorption in a dog model. Therefore, MK-7145 was deemed a candidate for development of an extended release formulation should the human half-life be determined to be insufficient. In addition, identification of backup clinical candidates would focus on identification of longer half-life compounds in addition to structural differentiation versus MK-7145. In this regard, compound **51** was viewed as a potential backup compound in that it provided good structural differentiation and improved preclinical half-lives compared to MK-7145. Ultimately, additional modifications to compound **51** would further improve preclinical half-lives and efficacy in spontaneously hypertensive rats and lead to a structurally differentiated backup molecule.

8.12.13 MK-7145 Displays Additive or Synergistic Blood Pressure Lowering Efficacy in Combination With Candesartan and HCTZ

Combination therapy with two or more antihypertensive drugs is required for most patients with hypertension in order to reach target blood pressure.[51] Combination therapy can provide improved blood pressure control and may offer improved tolerability compared to higher dose monotherapy. For example, Lacourciere and coworkers reported improved responder rates in patients with stage 2 and stage 3 systolic hypertension by combination of angiotensin receptor blocker valsartan with HCTZ compared to valsartan monotherapy; this was achieved without significant effect on tolerability.[52] Similarly, it is likely that ROMK inhibitors could be used clinically in combination with other antihypertensive agents with a potential to provide superior combination effects compared to standard-of-care thiazide and loop diuretics used in treatment of hypertension and heart failure, respectively.

To explore the combination therapy potential of ROMK inhibitors with angiotensin receptor blockers, the effect of combined treatment of MK-7145 with candesartan on blood pressure was evaluated in SHR.[46] MK-7145 (10 mg/kg/day, po), HCTZ (25 mg/kg/day, po), or vehicle was administered for 7 days to achieve a stable level of BP reduction. Subsequently, all animals received a submaximal dose of candesartan (0.1 mg/kg/day, po) for 2 days. In agreement with the dose–response study, MK-7145 (10 mg/kg) reduced systolic blood pressure (~20 mmHg) by day 2 which was sustained for the duration of the 7 day treatment. The magnitude of blood pressure lowering with HCTZ (25 mg/kg) was 10–15 mmHg. Addition of candesartan to the vehicle group (0.1 mg/kg) lowered blood pressure in by ~15 mmHg. In animals previously administered HCTZ, the addition of candesartan provided an additional 15–20 mmHg reduction in systolic blood pressure. However, candesartan when administered in combination with MK-7145 provided an additional 20–30 mmHg reduction in BP (Table 23), demonstrating a greater than additive effect on blood pressure and a greater overall magnitude of efficacy compared to the HCTZ/candesartan combination. Additional combination studies with submaximal and maximal doses of candesartan (0.1 and 1 mg/kg, respectively), using a range of doses of MK-7145 (1, 3, and 10 mg/kg), consistently provided greater than additive blood pressure lowering for all combinations tested (data not shown). Consequently, the combination of MK-7145 with angiotensin receptor blockers may provide an attractive option for treatment of hypertension.

To identify whether there is potential synergy between MK-7145 and HCTZ and to evaluate the ability of HCTZ to block the calciuretic response elicited by MK-7145, two combination studies were performed in SHR.[46] Minimally (study 1) and maximally (study 2) effective doses of HCTZ (10 and 25 mg/kg, respectively) were combined with doses of MK-7145 which produce a minimal (1 mg/kg) and maximal (10 mg/kg) calciuretic effect. MK-7145 and HCTZ were also dosed alone at these doses. The results demonstrate that the blood pressure lowering efficacy achieved is at least additive at each combination tested (Table 24), supporting that the two diuretics lower blood pressure by distinct additive mechanisms.

In the first of the two combination studies, the 10 mpk dose of HCTZ was able to block the small calciuretic effect seen with 1 mg/kg of MK-7145 and reduce the calciuretic effect of the 10 mpk dose of MK-7145 by ~50% (Table 25). In the second study (with 25 mg/kg HCTZ), the higher dose of HCTZ was able to reduce the calciuretic effect of MK-7145 by ~80% (data not shown). Taken together, the combination of ROMK inhibitors with hydrochlorothiazide provides additive blood pressure lowering while providing a more calcium neutral excretion profile.

Table 23 Systolic blood pressure (24 h mean) in spontaneously hypertensive rats before Day 7 and after Days 1 and 2 of dosing with 0.1 mg/kg candesartan

	Mean 24 h SBP		
	Monotherapy (7 days)	*+0.1 mg/kg candesartan*	
	Δ Day 7 (mmHg)	*Δ Day 1 (mmHg)*	*Δ Day 2 (mmHg)*
Vehicle	2	−12	−16
MK-7145 (10 mg/kg)	−18	−38	−47
HCTZ (25 mg/kg)	−10	−24	−32

Table 24 Systolic blood pressure (24 h mean) in spontaneously hypertensive rats after Day 4 of dosing MK-7145 with hydrochlorothiazide (HCTZ)

	δSBP Day 4 (mmHg)
Vehicle	3
HCTZ (10 mg/kg)	−7
HCTZ (25 mg/kg)	−11
MK-7145 (1 mg/kg)	−13
MK-7145 (10 mg/kg)	−20
MK-7145 (1 mg/kg) + HCTZ (10 mg/kg)	−22
MK-7145 (10 mg/kg) + HCTZ (10 mg/kg)	−27
MK-7145 (10 mg/kg) + HCTZ (25 mg/kg)	−39

Table 25 HCTZ coadministration diminishes the calciuretic response elicited by MK-7145 (study 1)

	0–24 h urinary calcium (mg)		
	Day 3	*Day 4*	*Day 5*
Vehicle	0.25 ± 0.19	0.37 ± 0.21	0.30 ± 0.25
10 mpk HCTZ	−1.82 ± 0.4	−1.75 ± 0.42	−1.72 ± 0.5
1 mpk MK-7145	1.08 ± 0.24	1.2 ± 0.32	1.32 ± 0.39
1 mpk MK-7145 + 10 mpk HCTZ	0.1 ± 0.28	0.1 ± 0.26	−0.03 ± 0.28
10 mpk MK-7145	2.92 ± 0.89	2.8 ± 0.75	2.08 ± 0.71
10 mpk MK-7145 + HCTZ	1.5 ± 0.31	1.27 ± 0.45	1.57 ± 0.56

8.12.14 Backup Efforts Focused on Longer Preclinical Half-Lives and Structural Diversity: The Dibasic Piperazine Series

Following the discovery of MK-7145, a similar SAR approach was explored on the unsymmetrical hybrid dibasic piperazine analogs. Consistent with the trend seen in Fig. 14, installation of two hydroxyl groups into analogs **60** and **55** led to potent analogs with improved selectivity over the hERG channel. Incorporation of cyanopyridyl in place of cyanophenyl further enhanced selectivity over hERG, leading to potent ROMK inhibitors, **61** and **63**, both with excellent selectivity over the hERG channel (Fig. 22 and Table 26).[47] Interestingly, in this case there were more profound differences between diastereomers in terms of ROMK potency. For example, of four possible diastereomers of **61**, the *R,S*-isomer (shown) provided the best ROMK potency (ROMK EP IC_{50} 0.018 μM), followed by the *R,R*-isomer (ROMK EP IC_{50} 0.090 μM) and the much weaker *S,S* and *R,R*-isomers (ROMK EP IC_{50} both >1 μM). As shown previously, installation of an ortho-methoxy group onto the cyanophenyl (and here also cyanopyridyl) pharmacophores provided better selectivity over hERG (**63** compared to **61**). Similar to **61**, the optimal absolute stereochemistry of **63** was *R,S*. Preparation of the three possible diastereomers of the symmetrical methoxypyridylnitrile pharmacophore type provided compound **64** as the most potent single diastereomer (undetermined absolute stereochemistry, but presumed to be *S,S* based on analogy to other analogs); however, this compound, while potent on ROMK, demonstrated significantly reduced selectivity over the hERG channel, indicating that at least one phthalide pharmacophore is required for optimal selectivity over hERG.[49] Interestingly, as a general observation, the cyanopyridyl pharmacophores provide improved pharmacokinetic profiles compared to the phthalide pharmacophores, but this comes at the price of hERG selectivity. By striking a balance, with one phthalide and one cyanopyridyl pharmacophore, we hoped to achieve improved pharmacokinetic properties, while retaining sufficient hERG

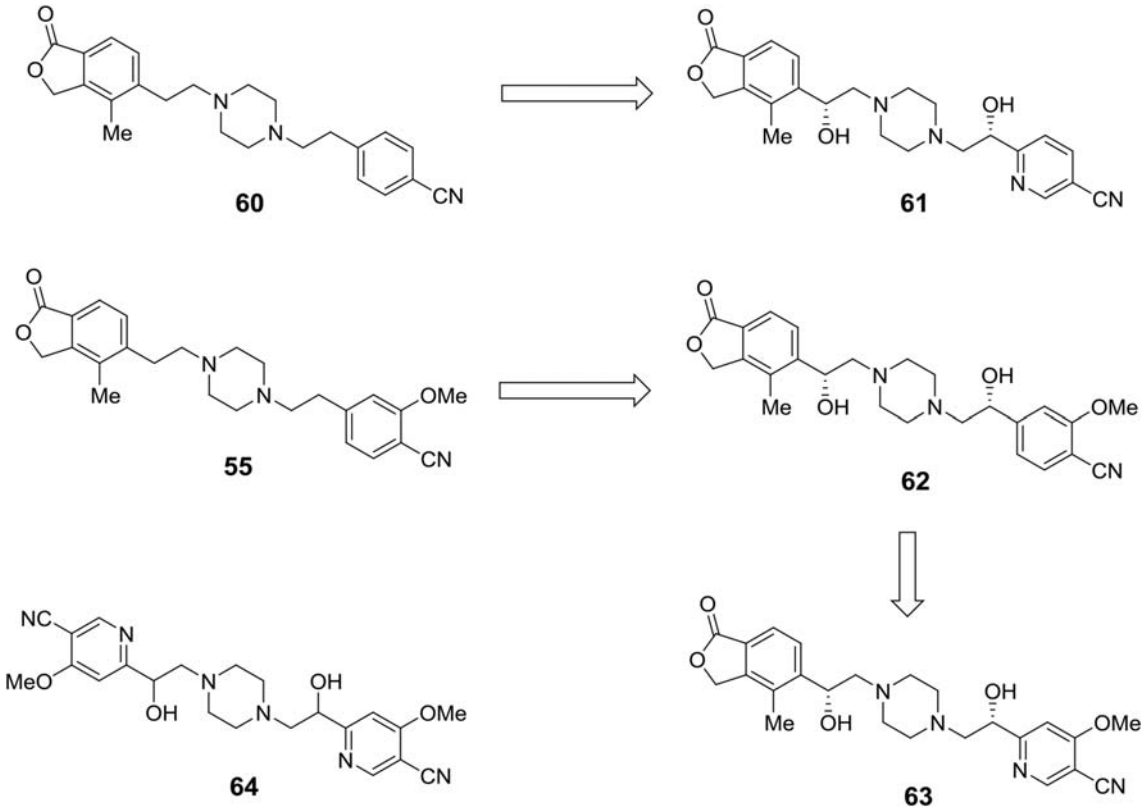

Fig. 22 Incorporation of benzylic hydroxyl groups and cyanopyridine in unsymmetrical dibasic piperazine lead series.

Table 26 ROMK and hERG potency of **60**, **61**, **55**, **62**, **63**, and **64** measured by electrophysiology

Compound	*ROMK EP IC_{50} (μM)*	*hERG EP IC_{50} (μM)*	*Ratio hERG EP/ROMK EP*
60	0.30[a]	0.43[b]	1.4[a,b]
61	0.018	12	667
55	0.087	86%@10 μM	–
62[c]	0.033	5.1[b]	155[b]
63	0.027	33	1222
64[d]	0.050	3.5[e]	70[e]

[a]ROMK potency for **60** was determined using the functional $^{86}Rb^{+}$ efflux assay.
[b]hERG activity for **60** and **62** was measured using the ^{35}S MK-499 displacement binding assay.
[c]Absolute stereochemistry at cyanophenyl benzylic position is not confirmed, but presumed as *R* since it is the more potent of the two single diastereomers.
[d]Single diastereomer with undetermined absolute stereochemistry; most potent of three stereoisomers. By analogy, stereochemistry presumed to be *S,S*.
[e]hERG activity for **64** was measured using a hERG thallium flux functional assay in HEK 293 cells.

selectivity. In fact, both compounds **61** and **63** had attractive pharmacokinetic properties in rats, with good oral bioavailability, reduced clearance rates, and longer half-lives compared to the symmetrical analogs such as **57** (Table 27).

Compound **63** was further assessed in dog and monkey pharmacokinetic studies, where it similarly demonstrated good oral bioavailability and good half-lives (Table 28). ROMK inhibitor **63** was not an inhibitor of CYP3A4, 2D6, 2C9 (IC_{50} all >50 μM), but showed weak inhibition of CYP2C8 (IC_{50} 8.2 μM). Compound **63** had low plasma protein binding across species (%Fu rat 43%, dog 83%, rhesus 63%, and human 58%) and had good permeability measured in LLC-PK1 cells (Papp 23×10^{-6} cm/s). The projected human half-life of compound **63** determined from allometric scaling of preclinical PK was estimated to be 10 h, significantly longer than commonly used loop diuretics such as furosemide and longer than the projected human half-life of MK-7145 (~5 h). Compound **63** demonstrated robust diuretic and natriuretic efficacy without loss of potassium in urine (kaliuresis) in both volume-loaded SD rats and in female mongrel dogs (data not shown).[47]

ROMK inhibitor **63** demonstrated comparable functional potency in thallium flux assays for rat and dog ROMK (0.014 and 0.042 μM, respectively). Like other members of this class of ROMK inhibitors, **63** had good selectivity over other members of

Table 27 Rat pharmacokinetic properties of compounds **61** and **63** (1 mg/kg iv, 2 mg/kg po)

SD rat PK (1 mg/kg iv, 2 mg/kg po)	*61*	*63*
Cl (mL/min/kg)	23	31
$AUCN_{po}$ (μM h kg/mg)	1.6	0.84
Half-life (h)	2.0	1.6
F %	96	65

Table 28 Dog and monkey pharmacokinetic properties of compound **63**

Species	*Dose iv/po (mg/kg)*	*Cl (L/kg)*	*AUCN (μM h kg/mg)*	t½ *(h)*	F_{po} *(%)*
Dog	0.5/1	5.6	5.6	5.9	84
Rhesus	1/2	25	0.51	7.2	30

Table 29 Blood pressure efficacy of **63** in spontaneously hypertensive rats (SHR)

Compound	*63*				*HCTZ*[a]
Dose (mg/kg)	0.3	1	3	10	25
Day 1–3 avg 24 h diuresis (fold increase)[b]	1.5	1.8	1.8	2.3	1.2
Day 1 24 h natriuresis (fold increase)[b]	1.0	1.6	1.4	1.8	1.3
δSBP[c] by Day 3 (mmHg)	−10	−18	−25	−34	−15
4 h plasma exposure (μM)[d]	0.03	0.08	0.24	1.7	–
0–4 h urine concentration (μM)	5.7	23.2	109.5	727.6	–

[a]HCTZ, hydrochlorothiazide.
[b]Compared to vehicle; $n=5$.
[c]SBP, systolic blood pressure.
[d]From parallel pharmacokinetic sampling.

the K_{ir} channel family ($K_{ir}2.3$, $K_{ir}2.1$, >100 μM; $K_{ir}4.1$ and $K_{ir}7.1>10$ μM) and over the cardiac channels screened (Nav1.2 and Cav2.1, both >30 μM). In a panel of 115 assays conducted by Ricerca Biosciences, compound **62** had no activities identified at ≤ 10 μM. Thus, inhibitor **63** has excellent selectivity for ROMK.

Compound **63** was assessed for blood pressure lowering, dieresis, and natriuresis efficacy using conscious spontaneously hypertensive rats[46] (SHR) equipped with telemetry devices and held in metabolism cages (Table 29). ROMK inhibitor **63** provided dose-dependent and robust blood pressure lowering by day 3, at least equivalent to that provided by MK-7145 (**57**). At a 1 mg/kg dose compound **63** reduced systolic blood pressure by 18 mmHg, comparable to an approximately maximally efficacious 25 mg/kg dose of hydrochlorothiazide which lowered systolic blood pressure by 15 mmHg. The magnitude of blood pressure lowering correlated well with both day 1 24 h natriuresis fold increase and the average 24 h diuresis fold increase from days 1–3.

Based on its overall profile, compound **63** was positioned as a structurally related potential backup clinical development compound with longer projected human half-life in the event that the lead compound **57** (MK-7145) should have an inadequate human half-life for qd dosing. Ultimately, MK-7145 demonstrated a longer human half-life than predicted in human clinical trials in healthy male subjects (~13 h), and the decision was made to focus on identifying a long half-life more structurally differentiated backup to mitigate risk of a potential tolerability issue occurring at some later time during development. Nonetheless, compounds **61** and **63** were used as tool compounds and surrogates to MK-7145 for numerous studies to further characterize ROMK inhibitors, explore mechanism of action, and determine points of differentiation from standard-of-care thiazide and loop diuretics.

8.12.15 Effects of ROMK Inhibitor 61 in Dahl Salt-Sensitive Rats

The Dahl salt-sensitive hypertensive rat (Dahl SS) is a well-established rodent model of salt-sensitive hypertension and progressive kidney injury. Dahl rats fed a high salt diet rapidly develop hypertension and reduced renal function with increased proteinuria, and exhibit other features common with hypertension in humans.[53] Zhou and coworkers recently described studies examining systemic hemodynamic, renal function and structure, vascular function, and cardiac structure in Dahl salt-sensitive rats on a high salt diet employing tool ROMK inhibitor **61** and comparing to HCTZ.[54] Zhou conducted two studies, one a therapeutic study in which Dahl rats had been maintained on a high salt (4% salt) diet for 5 weeks to establish a hypertensive state followed by treatment with **61** and HCTZ for 4 weeks, and a second prophylactic study where diuretic treatment was initiated after only 1 week on a high salt diet and

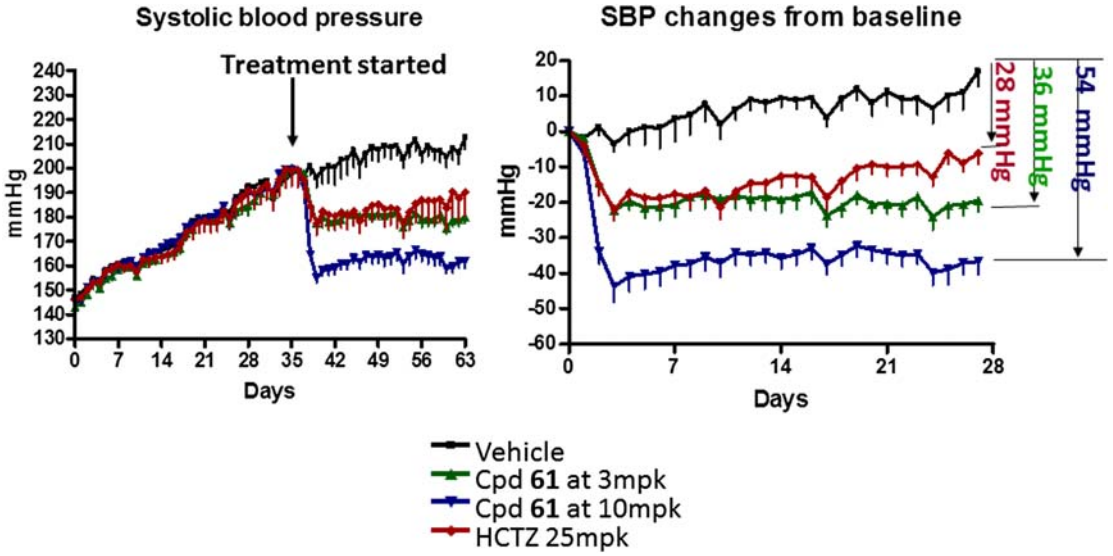

Fig. 23 Therapeutic treatment of Dahl salt-sensitive rats previously maintained on a 4% salt diet for 5 weeks with compound **61** (3 and 10 mg/kg) and HCTZ (25 mg/kg). From Zhou, X.; Forrest, M. J.; Sharif-Rodriguez, W.; Forrest, G.; Szeto, D.; Zhu, Y.; Cui, Y.; Pan, Y.; Urosevic-Price, O.; Wang, L.; Stevenson, A. S.; Zhou, Y.; Stribling, S.; Dajee, M.; Zhao, H.; Ormes, J. D.; Pasternak, A.; Walsh, S. P.; Roy, S.; Sullivan, K. A. *Hypertension* (submitted for publication).

prevention of development of hypertension compared to the vehicle group was monitored over the following 8 weeks. In the therapeutic study (Fig. 23), 4-week treatment of the resulting hypertensive rats with 3 and 10 mg/kg/day doses of **61** and a 25 mg/kg/day dose of HCTZ lead to decreased systolic blood pressure for all treated groups, with a continued rise in blood pressure observed in the vehicle group. By the end of the 4-week treatment period, compound **61** at both doses provided greater blood pressure lowering compared to HCTZ at 25 mg/kg/day. At the 10 mg/kg/day dose, compound **61** reduced blood pressure to nearly baseline levels prior to salt feeding. Moreover, blood pressure lowering efficacy was maintained throughout the 4 weeks of treatment.

In the prophylactic study (not shown), both doses of **61** lowered systolic blood pressure to approximately presalt feeding baseline levels and prevented development of hypertension for the full 8 weeks of treatment.[54] HCTZ also lowered blood pressure and maintained reduced blood pressure throughout the 8 weeks of treatment; however there was a gradual erosion of efficacy such that there was only a 44 mmHg decrease compared to the vehicle-treated animals at the study end, while there was a 62 and 70 mmHg reduction compared to vehicle for the 3 and 10 mg/kg/day dose groups of compound **61**.

In addition to superior blood pressure lowering efficacy compared to HCTZ, compound **61** reduced proteinuria, a marker of kidney injury, in both studies with a greater benefit for compound **61** at the 10 mg/kg/day dose compared to HCTZ at 25 mg/kg/day. Both compound **61** and HCTZ reduced biomarkers for kidney injury (LPN, KIM-1) compared to the vehicle-treated group. Compound **61** also preserved vascular function, decreased kidney and heart weight changes, and improved kidney and heart histopathological scoring compared to the vehicle-treated groups.

8.12.16 Backup Efforts Focused on Longer Preclinical Half-Lives and Structural Diversity, Efforts Involving Alternative Scaffolds

As indicated previously, analogs such as **51**, based on the octahydropyrazino[2,1-c][1,4]oxazine scaffold, represented a structurally distinct subclass of ROMK inhibitors showing improved preclinical pharmacokinetic profiles compared to MK-7145. Future publications will detail additional SAR studies following from compound **51**, and leading to analogs with even longer preclinical half-lives and culminating in the identification of the first backup ROMK clinical compound. Other scaffold modifications to the original dibasic piperazine core compounds also proved fruitful. Chobanian and coworkers recently reported on the discovery of potent ROMK inhibitors with good selectivity over hERG based upon a spirocyclic core scaffold (Fig. 24).[55] Very potent ROMK inhibitors could be generated from this scaffold. Importantly, from an SAR perspective, the spiropyrolidine could be used for C—N coupling reactions, allowing much more rapid pharmacophore SAR exploration, including by parallel synthesis techniques. This resulted in identification of several novel pharmacophores, providing structural differentiation from the limited selection of previously known left- or right-side pharmacophores. In some cases, the new pharmacophores were only useful when incorporated into these spirocyclic scaffolds. Compound **65** represents a milestone compound with good ROMK potency and selectivity over hERG, and favorable overall preclinical pharmacokinetic properties (half-lives in rat 2.1 h, dog 8.6 h, rhesus 1.8 h). Future communications will detail subsequent modification of compound **65**, providing improved compounds, including a second backup clinical development compound.

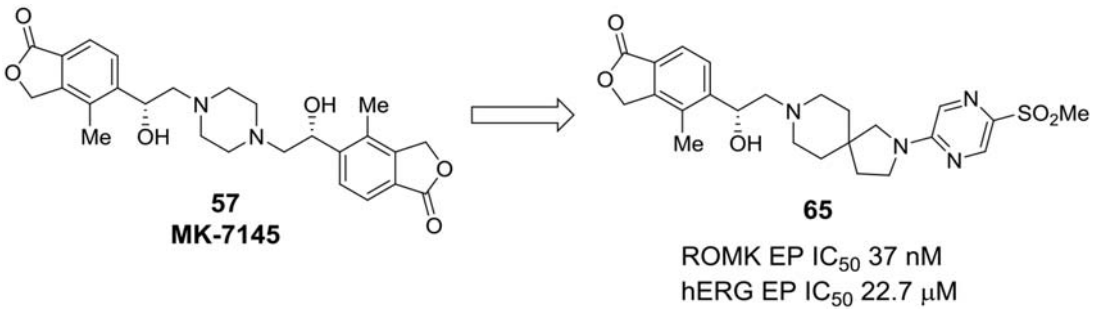

Fig. 24 Scaffold hopping leads to potent spirocyclic ROMK inhibitors.

8.12.17 MK-7145 Clinical Trials

At the time of writing this manuscript, data from clinical trials with MK-7145 have not been disclosed. A search of ClinicalTrials.gov lists two clinical trials conducted with MK-7145. One study is entitled "A Phase Ib, Randomized, Double-Blind, 4-Treatment, 2-Period Incomplete Block Study to Evaluate the Multiple Dose Effects of MK-7145 and Hydrochlorothiazide Compared to Placebo on Blood Pressure in Male Patients With Hypertension" (ClinicalTrials.gov Identifier: NCT01370655). The described purpose of this study was to evaluate the antihypertensive efficacy and tolerability of MK-7145 in comparison to HCTZ in participants with mild-to-moderate hypertension. The 28-day study's listed primary endpoints included, (1) time-weighted average over 24 h post dose decrease in systolic blood pressure with MK-7145 at 6 mg/day versus placebo; (2) time-weighted average over 24 h post dose decrease in systolic blood pressure with MK-7145 6 mg versus hydrochlorothiazide; and (3) urinary sodium excretion (UNaV) for MK-7145 at 6 mg/day versus placebo (24 h post dose on Day 1). This study enrolled 46 male patients with essential hypertension between the ages of 18 and 75. Daily doses of MK-7145 were 3 mg/kg/day and 6 mg/kg/day and doses of HCTZ were 25 mg/kg/day. This study was indicated to be completed in Jan. of 2012.

The second study listed at the ClinicalTrials.gov (described as terminated) is entitled, "A Two Part, Open-label, Phase I Study to Evaluate the Safety, Tolerability, Pharmacokinetics and Pharmacodynamics of MK-7145 in Patients With Renal Insufficiency (Part I) and Heart Failure With Renal Insufficiency (Part II)" (ClinicalTrials.gov Identifier: NCT01558674). Part I is described as a 3-period, active comparator-controlled, fixed sequence study to evaluate the safety, tolerability, pharmacokinetics, and pharmacodynamics of MK-7145 compared to furosemide in participants with moderate-to-severe renal insufficiency without heart failure. The primary hypothesis for Part I was that at least one well-tolerated dose of MK-7145 will produce a greater 24 h urinary excretion of sodium on the 1st day of MK-7145 dosing than 80 mg furosemide (on the 1st day of furosemide dosing) in participants with moderate-to-severe renal insufficiency. If MK-7145 was shown safe at natriuretic doses in renal insufficiency in Part I of this study, MK-7145 would then be investigated in participants with heart failure and renal insufficiency (Part II). Part II was planned as a 4-period, fixed sequence, active comparator-controlled (in Period 1), titration (in Periods 2, 3, and 4) study to evaluate the safety, tolerability, pharmacokinetics, and pharmacodynamics of a titration regimen of MK-7145 compared to an optimized stable maintenance regimen of furosemide or torsemide in participants with New York Heart Association (NYHA) Class II and III heart failure and moderate or severe renal insufficiency. The primary hypothesis for Part II was that at least one dose of MK-7145, titrated according to a fixed dose titration regimen, will be associated with a reduction in N-terminal pro-brain natriuretic peptide (NT-proBNP) compared to furosemide or torsemide (at 24 h postdose on the last dosing day of each period) in participants with NYHA class II/III HF with moderate or severe renal insufficiency. The doses of MK-7145 are listed as 2 and 8 mg/day and the dose of the comparator furosemide was 80 mg/day. The study's primary endpoints are indicated as, (1) change from baseline in first 24 h UNa (Part I) [Time Frame: Baseline (Day 3 predose) and 0–24 h postdose on Day 4 (first day of active treatment) of each treatment period (Treatments A, B, and C)]; and (2) NT-proBNP values at 24 h post last dose (Part II) [Time Frame: Day 14 for Periods 1–3 (Treatments D, E, and F); Day 28 of Period 4. Twelve patients were enrolled for this study. Inclusion criteria for part I included a requirement for estimated creatinine clearance of $\leq$45 mL/min. Inclusion criteria for part II included a requirement for estimated creatinine clearance of $\leq$45 mL/min and the designation of Class II or III heart failure as specified by the New York Heart Association (NYHA) functional classification for heart failure with NT-proBNP $\geq$1000 pg/mL on clinically optimized therapy with a stable dose (for at least 2 weeks) of furosemide or torsemide.

Considering that these two trials are listed for patients with hypertension and renal insufficiency, one may surmise that MK-7145 must have been safe and well tolerated and provided adequate exposures and overall pharmacokinetic properties in initial first-in-human single ascending and multiple ascending dose studies in healthy subjects. In addition, one would expect that initial indications of diuresis and natriuresis efficacy would have warranted further studies in patient populations. Moreover it is noteworthy that the doses in these two trials ranged from 2 to 8 mg/day, suggesting that efficacy was anticipated at low doses. The details of these and other clinical studies will be reported in due course.

8.12.18 Conclusions

Thiazide and loop diuretics remain important and widely used therapeutic agents in the management of hypertension and heart failure, respectively; however, no new diuretic agents have been introduced for decades, despite the opportunities for improvements over existing standard-of-care diuretics.

Hypertension is a primary risk factor for cardiovascular morbidity and mortality. It is a leading cause of end-stage renal disease, and is a risk factor for myocardial infarction, heart failure, stroke, and dementia. Hypertension affects an estimated 30% of the adult US population (>72 million people) and has a prevalence of >65% in people older than 60 years.[56] Despite the large number of medications available, blood pressure remains largely uncontrolled, with almost half of the hypertensive population remaining suboptimally controlled.[57] Clinicians frequently need to use combination therapies for achieving target blood pressure levels. Even then, ~14% of patients are categorized as having resistant hypertension, defined as inadequate blood pressure control even when adhering to a combination of at least three optimally dosed antihypertensive agents of different classes, with one ideally being a diuretic.[58] Moreover, certain hypertensive patient segments are underserved by available treatments, including patients with hypertension and diabetes, hypertension and chronic kidney disease, and heart failure with preserved ejection fraction.[56] Within the diuretic class, thiazides, such as HCTZ, are the most widely prescribed and are used as first line therapy to treat uncomplicated hypertension, or as a component of combination therapy. Hypokalemia (serum potassium concentration <3.5 mequiv./L) and elevations in fasting blood glucose are the major liabilities associated with thiazides and limit the doses used clinically to those that are suboptimal for natriuresis and blood pressure lowering. No new diuretics are known to be in development for hypertension, but an ideal novel diuretic should be potassium neutral, provide blood pressure efficacy ≥25 mg HCTZ, and be suitable for combination therapy. In addition, advantages in treating underserved patient segments such as patients with hypertension and diabetes or hypertension and chronic kidney disease would provide additional value.

Heart failure is a worldwide healthcare problem, with more than one million hospitalizations in the United States for acute heart failure per year. About one third of acute heart failure patients are rehospitalized with congestive symptoms within 6–12 months. By the year 2030 the prevalence of heart failure in the United States is projected to be 2.97%, with >8 million Americans living with heart failure.[59] Loop diuretics are the preferred agents used to treat the symptoms and signs of congestion; however, they appear to be suboptimal in preventing heart failure-related rehospitalization. In addition, loop diuretics typically have short half-lives, leading to rebound sodium reabsorption, which blunts overall efficacy. Loop diuretics such as furosemide are also subject to diuretic resistance,[10] leading to progressive loss of efficacy, particularly as heart failure or renal function worsens. Dose-dependent adverse events associated with loop diuretics include disruptions in plasma electrolyte levels, including hypokalemia, as well as deafness. An ideal new diuretic for heart failure would provide improved efficacy, a reduced incidence of hypokalemia, a smoother more sustained and tolerable diuresis profile, immunity to diuretic resistance, and improved efficacy when renal function is impaired.

In this article, the medicinal chemistry story leading to the development of ROMK inhibitors as new mechanism diuretics was reviewed, tying together work described in a series of publications over recent years. The story started with discovery of the program lead from a screening hit minor impurity, then continued with identification of nitrophenyl pharmacophore isosteres and the SAR steps leading to incremental, step-wise improvements in selectivity over hERG and improvements in pharmacokinetic properties. The review concluded with a detailed description of the Merck clinical compound MK-7145 along with its pharmacology in preclinical species. Overall, these efforts led to the discovery of several structurally differentiated subclasses of potent and ROMK inhibitors, all originating from the common initial hit. Proof of biology in rat and dog diuresis models and in SHR and Dahl salt-sensitive rat hypertension models was described, confirming expectations based on human and rodent genetics that ROMK inhibitors should be potent diuretics with a neutral potassium excretion profile. Importantly, MK-7145 and other ROMK inhibitors demonstrated superior blood pressure lowering compared to hydrochlorothiazide in preclinical hypertension models. These effects were additive or synergistic in combination with angiotensin receptor blockers and with thiazide diuretics. The combination of MK-7145 at 3 and 10 mg/kg/day doses with candesartan provided synergistic blood pressure lowering of a greater magnitude than that observed with the combination of 25 mg/kg/day of hydrochlorothiazide with candesartan. ROMK inhibitors further differentiate from thiazide and loop diuretics in that they can access their target from both the apical and basolateral faces of the epithelial cells lining the tubular lumen (standard-of-care loop diuretics and thiazides access their targets only from the apical face). This offers the potential that ROMK inhibitors could demonstrate improved efficacy in patients with renal insufficiency compared to loop diuretics like furosemide which has reduced delivery to the tubular lumen in the presence of renal dysfunction. The ROMK inhibitors described here project to, or have been shown to have significantly longer half-lives in humans compared to loop diuretics such as furosemide and torsemide, which may improve the time course of diuresis and limit rebound sodium reabsorption effects. Taken together, ROMK inhibitors such as MK-7145 represent the first new mechanism diuretics to be discovered in decades, and offer the possibility of providing improved outcomes in the treatment of hypertension or heart failure.

See also: 7.17. Treatments for Heart Failure.

References

1. Ho, K.; Nichols, C. G.; Lederer, W. J.; Lytton, J.; Vassilev, P. M.; Kanazirska, M. V.; Hebert, S. C. *Nature* **1993,** *362,* 31–38.
2. Nichols, C. G.; Lopatin, A. N. *Annu. Rev. Physiol.* **1997,** *59,* 171–191.
3. Tao, X.; Avalos, J. L.; Chen, J.; MacKinnon, R. *Science* **2009,** *326,* 1668–1674.
4. Welling, P. A.; Ho, K. *Am. J. Physiol. Renal Physiol.* **2009,** *297,* F849–F863.
5. Xu, J. Z.; Hall, A. E.; Peterson, L. N.; Bienkowski, M. J.; Eessalu, T. E.; Hebert, S. C. *Am. J. Physiol.* **1997,** *273* (5, Part 2), F739–F748.
6. Palmer, L. G.; Choe, H.; Frindt, G. *Am. J. Physiol.* **1997,** *273* (3, Part 2), F404–F410.
7. Lu, M.; Wang, T.; Yan, Q.; Yang, X.; Dong, K.; Knepper, M. A.; Wang, W.; Giebisch, G.; Shull, G. E.; Hebert, S. C. *J. Biol. Chem.* **2002,** *277,* 37881–37887.
8. Roush, G. C.; Kaur, R.; Ernst, M. E. *J. Cardiovasc. Pharmacol. Ther.* **2014,** *19* (1), 5–13.
9. Flack, J. M.; Cushman, W. C. *Am. J. Med.* **1996,** *101* (Suppl. 3A), 53S–60S.
10. Ellison, D. H. *Cardiology* **2001,** *96,* 132–143.
11. Simon, D. B.; KAret, F. E.; Rodriguez-Soriano, J.; Hamdan, J. H.; DiPietro, A.; Trachtman, H.; Sanjad, S. A.; Lifton, R. P. *Nat. Genet.* **1996,** *14,* 152–156.
12. Ji, W.; Foo, J. N.; O'Roak, B. J.; Zhao, H.; Larson, M. G.; Simon, D. B.; Newton-Cheh, C.; State, M. W.; Levy, D.; Lifton, R. P. *Nat. Genet.* **2008,** *40,* 592–599.
13. Lorenz, J. N.; Baird, N. R.; Judd, L. M.; Noonan, W. T.; Andringa, A.; Doetschman, T.; Manning, P. A.; Liu, L. H.; Miller, M. L.; Shull, G. E. *J. Biol. Chem.* **2002,** *277,* 37871–37880.
14. Hibino, H.; Inanobe, A.; Furutani, K.; Murukami, S.; Findlay, I.; Kurachi, Y. *Physiol. Rev.* **2010,** *90,* 291–366.
15. Preisig-Muller, R.; Schlichthorl, G.; Goerge, T.; Heinen, S.; Bruggemann, A.; Rajan, S.; Derst, C.; Veh, R. W.; Daut, J. *Proc. Natl. Acad. Sci. U. S. A.* **2002,** *99,* 7774–7779.
16. Swale, D. R.; Kharade, S. V.; Denton, J. S. *Curr. Opin. Pharmacol.* **2014,** *15,* 7–15.
17. Garcia, M. L.; Kaczorowski, G. J. *Curr. Opin. Pharmacol.* **2014,** *15,* 1–6.
18. Jin, W.; Lu, Z. *Biochemistry* **1998,** *37,* 13291–13299.
19. Felix, J. P.; Liu, J.; Schmalhofer, W. A.; Bailey, T.; Bednarek, M. A.; Kinkel, S.; Weinglass, A. B.; Kohler, M.; Kaczorowski, G. J.; Priest, B. T.; Garcia, M. L. *Biochemistry* **2006,** *45,* 10129–10139.
20. Lewis, L. M.; Bhave, G.; Chauder, B. A.; Banerjee, S.; Lornsen, K. A.; Redha, R.; Fallen, K.; Lindsley, C. W.; Weaver, C. D.; Denton, J. S. *Mol. Pharmacol.* **2009,** *76,* 1094–1103.
21. Bhave, G.; Chauder, B. A.; Liu, W.; Dawson, E. S.; Kadakia, R.; Nguyen, T. T.; Lewis, L. M.; Meiler, J.; Weaver, C. D.; Satlin, L. M.; Lindsley, C. W.; Denton, J. S. *Mol. Pharmacol.* **2011,** *79,* 42–50.
22. Kharade, S. V.; Flores, D.; Lindsley, C. W.; Satlin, L. M.; Denton, J. S. *Am. J. Physiol. Renal Physiol.* **2016,** *310,* F732–F737.
23. Solly, K.; Cassaday, J.; Felix, J. P.; Garcia, M. L.; Ferrer, M.; Strulovici, B.; Kiss, L. *Assay Drug Dev. Technol.* **2008,** *6* (2), 225–234.
24. Tang, H.; Walsh, S. P.; Yan, Y.; de Jesus, R. K.; Shahripour, A.; Teumelsan, N.; Zhu, Y.; Ha, S.; Owens, K.; Thomas-Fowlkes, B. S.; Felix, J. P.; Liu, J.; Kohler, M.; Priest, B. T.; Bailey, T.; Brochu, R.; Alonso-Galicia, M.; Kaczorowski, G. J.; Roy, S.; Yang, L.; Mills, S. G.; Grcia, M. L.; Pasternak, A. *ACS Med. Chem. Lett.* **2012,** *3,* 367–372.
25. Swale, D. R.; Sheehan, J. H.; Banerjee, S.; Husni, A. S.; Nguyen, T. T.; Meiler, J.; Denton, J. S. *Biophys. J.* **2015,** *108,* 1094–1103.
26. Purohit, V.; Basu, A. K. *Chem. Res. Toxicol.* **2000,** *13* (8), 673–692.
27. Felix, J. P.; Priest, B. T.; Solly, K.; Bailey, T.; Brochu, R. M.; Liu, C. J.; Kohler, M. G.; Kiss, L.; Alonso-Galicia, M.; Tang, H.; Pasternak, A.; Kaczorowski, G. J.; Garcia, M. L. *Assay Drug Dev. Technol.* **2012,** *10* (5), 417–431.
28. Wang, J.; Della Penna, K.; Wang, H.; Karczewski, J.; Connolly, T. M.; Koblan, K. S.; Bennett, P. B.; Salata, J. J. *Am. J. Phys.* **2003,** *284,* 256.
29. Taylor, R.; Mullaley, A.; Mullier, G. W. *Pestic. Sci.* **1990,** *29,* 197–213.
30. Meanwell, N. A. *J. Med. Chem.* **2011,** *54,* 2529–2591.
31. Tang, H.; de Jesus, R. K.; Walsh, S. P.; Zhu, Y.; Yan, Y.; Priest, B. T.; Swensen, A. M.; Alonso-Galicia, M.; Felix, J. P.; Brochu, R. M.; Bailey, T.; Thomas-Fowlkes, B.; Zhou, X.; Pai, L.-Y.; Hampton, C.; Hernandez, M.; Ownes, K.; Roy, S.; Kaczorowski, G. J.; Yang, L.; Garcia, M.; Pasternak, A. *Bioorg. Med. Chem. Lett.* **2013,** *23,* 5829–5832.
32. Garcia, M. L.; Priest, B. T.; Alonso-Galicia, M.; Zhou, X.; Felix, J. P.; Brochu, R. M.; Bailey, T.; Thomas-Fowlkes, B.; Liu, J.; Swensen, A.; Pai, L.-Y.; Xiao, J.; Hernandez, M.; Hoagland, K.; Ownes, K.; Tang, H.; de Jesus, R. K.; Roy, S.; Kaczorowski, G. J.; Pasternak, A. J. *Pharmacol. Exp. Ther.* **2014,** *348,* 153–164.
33. Unpublished data.
34. Breyer, J.; Jacobsen, H. R. *Annu. Rev. Med.* **1990,** *41,* 265–275.
35. Kharade, S. V.; Flores, D.; Lindsley, C. W.; Satlin, L. M.; Denton, J. S. *Am. J. Physiol. Renal Physiol.* **2015,** *310,* 732–737.
36. Cavero, I.; Mestre, M.; Guillon, J.-M.; Crumb, W. *Expert Opin. Pharmacother.* **2000,** *1,* 947.
37. Walsh, S. P.; Shahripour, A.; Tang, H.; de Jesus, R. K.; Teumelsan, N.; Zhu, Y.; Frie, J.; Priest, B.; Swensen, A. M.; Alonso-Galicia, M.; Felix, J. P.; Brochu, R. M.; Bailey, T.; Thomas-Fowlkes, B.; Zhou, X.; Pai, L.-Y.; Hampton, C.; Hernandez, M.; Owens, K.; Ehrhart, J.; Roy, S.; Kaczorowski, G. J.; Yang, L.; Garcia, M. L.; Pasternak, A. *Bioorg. Med. Chem. Lett.* **2016,** *26* (9), 2339–2343.
38. Tang, H.; Zhu, Y.; Teumelsan, N.; Walsh, S. P.; Shahripour, A.; Priest, B. T.; Swensen, A. M.; Felix, J. P.; Brochu, R. M.; Bailey, T.; Thomas-Fowlkes, B.; Pai, L.-Y.; Hampton, C.; Hernandez, M.; Metzger, J.; Forrest, M.; Zhou, X.; Owens, K.; Tong, V.; Parmee, E.; Roy, S.; Kaczorowski, G. J.; Yang, L.; Alonso-Galicia, M.; Garcia, M.; Pasternak, A. *ACS Med. Chem. Lett.* **2016,** *7* (7), 697–701.
39. Jamieson, C.; Moir, E. M.; Rankovic, Z.; Wishart, G. *J. Med. Chem.* **2006,** *49* (17), 529–546.
40. Tashibu, H.; Miyazaki, H.; Aoki, K.; Akie, Y.; Yamamoto, K. *J. Pharmacol. Sci. (Tokyo, Japan)* **2005,** *99,* 473.
41. Tamargo, J.; Segura, J.; Ruilope, L. M. *Expert Opin. Pharmacother.* **2014,** *15* (5), 605–621.
42. Ellison, D. H. *Semin. Nephrol.* **1999,** *19* (6), 581–597.
43. Martelli, A.; Testai, L.; Breschi, M. C.; Calderone, V. *Expert Opin. Ther. Patents* **2015,** *25* (9), 1035–1051.
44. Zhu, Y.; de Jesus, R. K.; Tang, H.; Walsh, S. P.; Jiang, J.; Gu, X.; Teumelsan, N.; Shahripour, A.; Pio, B.; Ding, F.-X.; Ha, S.; Priest, B. T.; Swensen, A. M.; Alonso-Galicia, M.; Felix, J. P.; Brochu, R. M.; Bailey, T.; Thomas-Fowlkes, B.; Zhou, X.; Pai, L.-Y.; Hampton, C.; Hernandez, M.; Owens, K.; Ehrhart, J.; Roy, S.; Kaczorowski, G. J.; Yang, L.; Parmee, E. R.; Sullivan, K.; Garcia, M. L.; Pasternak, A. *Bioorg Med. Chem. Lett.* **2016**. http://dx.doi.org/10.1016/j.bmcl.2016.10.064.
45. Unpublished results.
46. Hampton, C.; Zhou, X.; Felix, J. P.; Priest, B. T.; Thomas-Fowlkes, B.; Pai, L.-Y.; Alonso-Galicia, M.; Xiao, J.; Corona, A.; Price, O.; Hernandez, M.; Gill, C.; Shah, K.; Rasa, C.; Hoagland, K.; Owens, K.; Tang, H.; Tong, V.; Roy, S.; Sullivan, K.; Kaczorowski, G. J.; Metzger, J. M.; Pasternak, A.; Garcia, M. L. *J. Pharmacol. Exp. Ther.* **2016,** *359,* 194–206.
47. Walsh, S. P.; Shahripour, A.; Tang, H.; Teumelsan, N.; Frie, J.; Zhu, Y.; Priest, B. T.; Swensen, A. M.; Liu, J.; Margulis, M.; Visconti, R.; Weinglass, A.; Felix, J. P.; Brochu, R. M.; Bailey, T.; Thomas-Fowlkes, B.; Alonso-Galicia, M.; Zhou, X.; Pai, L.-Y.; Corona, A.; Hampton, C.; Hernandez, M.; Bently, R.; Chen, J.; Shah, K.; Metzger, J.; Forrest, M.; Owens, K.; Tong, V.; Ha, S.; Roy, S.; Kaczorowski, G. J.; Yang, L.; Parmee, E.; Garcia, M. L.; Sullivan, K.; Pasternak, A. *ACS Med. Chem. Lett.* **2015,** *6,* 747–752.
48. Meyer, J. H.; Wilson, A. A.; Sagrati, S.; Hussey, D.; Carella, A.; Potter, W. Z.; Ginovart, N.; Spencer, E. P.; Cheok, A.; Houle, S. *Am. J. Psychiatry* **2004,** *161* (5), 826–835.
49. Unpublished data.
50. As of this manuscript preparation, unpublished work by Corona, A.; Pai, L.-Y.; Tong, V.; Miller, R. R.; Alonso-Galicia, M.; Garcia, M. L.; Metzger, J.; Zhou, X.; Pasternak, A.
51. Frank, J. *Am. Fam. Physician* **2008,** *77* (9), 1279–1286.
52. Lacourciere, Y.; Poirer, L.; Hebert, D.; Assouline, L.; Stolt, P.; Rehel, B.; Khyder, Y. *Clin. Ther.* **2005,** *27* (7), 1013–1021.

53. Rapp, J. P. *Hypertension* **1982,** *4* (6), 753–763.
54. Zhou, X.; Forrest, M. J.; Sharif-Rodriguez, W.; Forrest, G.; Szeto, D.; Zhu, Y.; Cui, Y.; Pan, Y.; Urosevic-Price, O.; Wang, L.; Stevenson, A. S.; Zhou, Y.; Stribling, S.; Dajee, M.; Zhao, H.; Ormes, J. D.; Pasternak, A.; Walsh, S. P.; Roy, S.; Sullivan, K. A. *Hypertension* (submitted for publication).
55. Chobanian, H. R.; Guo, Y.; Pio, B.; Tang, H.; Teumelsan, N.; Clements, M.; Frie, J.; Ferguson, R.; Guo, Z.; Thomas-Fowlkes, B. S.; Felix, J. P.; Liu, J.; Kohler, M.; Priest, B.; Hampton, C.; Pai, L.-Y.; Corona, A.; Metzger, J.; Tong, V.; Joshi, E. M.; Xu, L.; Owens, K.; Maloney, K.; Sullivan, K.; Pasternak, A. *Bioorg Med. Chem. Lett.* **2016**. http://dx.doi.org/10.1016/j.bmcl.2016.10.032.
56. Kovell, L. C.; Ahmed, H. M.; Misra, S.; Whelton, S. P.; Prokopowicz, G. P.; Blumenthal, R. S.; McEvoy, J. W. *J. Am. Heart Assoc.* **2015,** *4* (12), 1–11.
57. Nwankwo, T.; Yoon, S.; Burt, V.; Gu, Q. *Natl. Center Health Stat.* **2013,** *133,* 1–8.
58. Rossignol, P.; Massy, Z. A.; Aziz, M.; Bakris, G.; Ritz, E.; Covic, A.; Goldsmith, D.; Heine, G. H.; Jager, K. J.; Kanbay, M.; Mallamaci, F.; Ortiz, A. *Lancet* **2015,** *386,* 1588–1598.
59. Heidenreich, P. A.; Albert, N. M.; Allen, L. A.; Bluemke, D. A.; Butler, J.; Fonarow, G. C.; Ikonomidis, J. S.; Khavjou, O.; Konstam, M. A.; Maddox, T. M.; Nichol, G.; Pham, M.; Pina, I. L.; Trogdon, J. G. *Circ. Heart Fail.* **2013,** *6,* 606–619.

8.13 Fragment-Based Discovery of AZD2716: A Novel, Potent Secreted Phospholipase A_2 ($sPLA_2$) Inhibitor for the Treatment of Coronary Artery Disease

F Giordanetto, D E Shaw Research LLC, New York, NY, United States
D Pettersen, AstraZeneca Mölndal, Mölndal, Sweden

© 2017 Elsevier Ltd. All rights reserved.

8.13.1	Introduction	339
8.13.2	Medicinal Chemistry Strategy	340
8.13.3	Results	340
References		347

8.13.1 Introduction

Phospholipase A_2 (PLA_2) is a diverse family of lipolytic enzymes that hydrolyze the acyl ester bond at the *sn*-2 position of glycerophospholipids to yield free fatty acids and lysophospholipids.[1] Among the various classes of PLA_2s insofar described, secreted PLA_2s ($sPLA_2$s) are characterized by low molecular mass (13–18 kDa), a histidine–aspartic acid catalytic dyad, and are dependent on Ca^{2+} for their catalytic function.[2] As their hydrolytic activity is directed to substrates with micellar and surfactant properties, $sPLA_2$'s biological function is a complex result of subtle interfacial kinetics of enzyme–substrate recognition, partitioning, and subsequent catalysis.[3] A total of 11 different $sPLA_2$ isoforms (group Ib, IIa, IIc, IId, IIe, IIf, III, V, X, XIIa, and XIIb) have been reported in mammals.[4,5] The different $sPLA_2$ isoforms display unique tissue and cellular distributions, and enzymatic properties, suggesting diverse, tissue-specific contributions in various pathophysiological phenomena. For instance, four $sPLA_2$ isoforms (IIA, III, V, and X) have been detected in human atherosclerotic lesions.[6] Among these, group IIA, V, and X $sPLA_2$s have been independently associated with disease progression, due to their direct implication in several proatherogenic actions in the arterial wall.[7–9] The enzymatic action of $sPLA_2$s rapidly degrades lipoproteins' phospholipids. As such, $sPLA_2$s induce the accumulation of bioactive lipids in the vessel wall and promote significant lipoprotein modifications, which in turn alter their function. The products of $sPLA_2$s' catalysis significantly activate macrophages and directly contribute to foam cell formation.[5,7,9,10] Additionally, as arachidonic acid is one of the most frequent fatty acids esterified at the *sn*-2 position of phospholipids, $sPLA_2$s are de facto affecting the rate-limiting step in eicosanoid production.[11] Overall, $sPLA_2$s' action triggers the release and accumulation of several pro-inflammatory stimuli and mediators in atherosclerotic lesions.[5,7,9,10] Furthermore, epidemiological analyses have indicated that increased levels of $sPLA_2$ mass and activity are significantly related to increased occurrence of cardiovascular events, prevalence, and progression of atherosclerosis and may constitute independent risk factors.[12]

Due to the crucial importance of $sPLA_2$s in modulating the function of lipids and lipoproteins, as well as controlling several mechanisms directly related to inflammation, $sPLA_2$s seem well poised to influence atherogenesis. Accordingly, $sPLA_2$ inhibitors could be useful for the treatment of atherosclerosis. Interestingly, the historical $sPLA_2$ inhibitor varespladib methyl (Fig. 1), developed by scientists at Eli-Lilly as an early example of structure-based optimization,[13,14] has been evaluated in short duration (12–16 weeks) clinical trials for the treatment of rheumatoid arthritis and acute coronary syndrome (ACS) with negative results.[15,16] The clinical failure in ACS has been ascribed to the limited duration of treatment in a severely impaired patient population, where the postulated beneficial lipid-altering effects of $sPLA_2$ inhibition could not be realized fully. These results prompted for a different clinical strategy addressing an alternative patient segment.

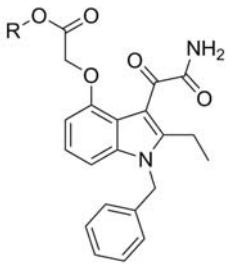

R = H, **varespladib**; $clogD_{7.4}$: -0.6
R = Me, **varespladib methyl**; $clogD_{7.4}$: 2.9

Fig. 1 Archetypal $sPLA_2$ inhibitors: varespladib and its methyl ester prodrug, varespladib methyl. Relevant log *D* values at pH 7.4 have been calculated with ChemAxon.

Atherogenesis is a dynamic process resulting from lengthy and complex physiological modifications along multiple axes (e.g., lipid metabolism, inflammation, and cardiac function). Specifically, we were interested to more thoroughly investigate the lipoprotein modifying effects[17–19] of $sPLA_2$ inhibition on cardiovascular disease alongside its anti inflammatory properties. As part of AstraZeneca' cardiovascular and metabolic disorders portfolio, we therefore started a research program directed to the identification of a novel $sPLA_2$ inhibitor to be evaluated in long-term clinical studies in a coronary artery disease patient population.

8.13.2 Medicinal Chemistry Strategy

The competitive situation in which we operated prompted for a very pragmatic approach. Varespladib methyl provided a useful benchmark for evaluating our progress and defining the sought target product profile. Varespladib is a potent $sPLA_2$ inhibitor whose marked polar character is optimized by the use of a prodrug (varespladib methyl) to enable sufficient intestinal absorption during oral administration. Importantly, the glyoxamide and carboxylate functionalities of varespladib that are responsible for its low lipophilicity are essential pharmacophoric features for chelating the catalytic Ca^{2+} ion in the $sPLA_2$ binding site.[13,14] As dosing to a large patient population over a long therapeutic regimen was required in a coronary artery disease setting, the use of a prodrug was judged to be inappropriate for our intended clinical candidate due to the potential interpatient variability at a pharmacokinetic (PK) level and pharmacodynamics (PDs) implications. Anticipating a common pharmacophore to varespladib, the polar character of the series should have been compatible with once daily oral administration, as a further requirement in a patient population which is already exposed to multiple concomitant therapies as standard of care. Lipophilicity was therefore understood as a critical optimization parameter as it influences cellular membrane permeability.[20] While in this case high lipophilicity would be advantageous for intestinal absorption and partitioning into phospholipids and lipoproteins with a view to access the $sPLA_2$ binding site, it could also be counterproductive when critical development parameters such as aqueous solubility, metabolic stability, and toxicology are concerned.[20] For these reasons, we envisioned a structure-based fragment approach with strong monitoring of ligand efficiency parameters in order to maximize the odds of combining chemical matter novelty, lipophilicity control, and developability.[21]

Cheminformatics analysis of $sPLA_2$-centered biological data in combination with available structural data as from apo and ligand-bound $sPLA_2$ crystal structures[13,14] highlighted the effectiveness of primary carboxamides in interacting with the $sPLA_2$ catalytic pocket. Specifically, their carbonyl atom is coordinating the Ca^{2+} ion as well as establishing a hydrogen bond with the protein, while the amide nitrogen atom is hydrogen bonded to two additional sites on $sPLA_2$. We therefore compiled a selection of primary aromatic amide-containing fragments (heavy atom count ≥ 10 and ≤ 18) by triaging our corporate database for (a) fit to the $sPLA_2$ binding site using molecular docking, (b) biochemical inhibition of $sPLA_2$-IIa, as the most widely expressed $sPLA_2$ isoform in humans,[22] and (c) functional inhibition of $sPLA_2$ activity in human plasma, as assessed using an established protocol.[23] The last step was of critical importance in ensuring translatability to a clinical setting as plasma $sPLA_2$ activity inhibition represented the mode-of-action biomarker to be used in future clinical trials. While $sPLA_2$-IIa is the most widely expressed $sPLA_2$ isoform, additional $sPLA_2$ isoforms will likely contribute to total plasma $sPLA_2$ activity. For these reasons, and considering their role in lipoprotein modulation,[17–19] inhibition of $sPLA_2$-V and $sPLA_2$-X was also monitored as part of the screening cascade. Lastly, the lipophilic profile of the compounds was projected against passive permeability, metabolic stability, and solubility as in vitro signposts before a more thorough assessment of their PK and PD profiles in vivo. Here, multispecies PK analyses were used to preliminary gauge dosing estimates for preclinical toxicological studies and clinical development. Nonhuman primates were instead utilized to minimize translational differences in $sPLA_2$-related biology and lipoprotein profiles, thereby providing a measure of the PD effect.

8.13.3 Results

The results of the initial hit identification process previously described are summarized in Table 1. Three fragment hits were singled out from the triaging workflow as potential starting points for future chemical exploration. These include benzamide, anthranilic amide, and imidazopyridine carboxamide derivatives **1**–**3** (Table 1). While all three fragments displayed significant $sPLA_2$-IIa inhibition (IC_{50}: 2.1–24 μM) and adequate ligand efficiency parameters (LE: 0.35–0.39), the reduction of human plasma $sPLA_2$ activity represented a major discriminant among them. Here, only compound **1** was able to potently inhibit plasma $sPLA_2$ activity in a concentration-dependent fashion with an unbound IC_{50} value of 0.9 μM, probably because of its enhanced solubility compared to **2** and **3**. In an effort to evaluate whether plasma $sPLA_2$ inhibition of **2** and **3** could be brought on par with the more efficient fragment **1**, nearest neighbor analysis and screening was employed to explore the structure–activity relationships of **2** and **3** (data not shown). Unfortunately, this exercise did not highlight any immediate potency gain opportunities. Instead, it revealed a consistent low aqueous solubility profile for fragment hit **3** and analogs. As this liability also prevented successful cocrystallization of $sPLA_2$ and **3**, we turned our attention to the most potent fragment hit **1** insofar identified.

Resolving the molecular complex between **1** and $sPLA_2$-X using X-ray crystallography highlighted the high-quality interactions established by the carboxamide function of **1**, as shown in Fig. 2. Here, the amide group engaged $sPLA_2$-X with three hydrogen bonds to G28, H46, and D47 (corresponding to $sPLA_2$-IIa G29, H47, and D48) and one additional coordination bond to the catalytic Ca^{2+} ion in the binding pocket. Furthermore, the 4-benzyl side chain was accommodated in a lipophilic cleft consisting of residues I2, L5, A6, V9, P17, I18, and M21 (corresponding to L2, F5, H6, I9, A17, A18, and G22 in $sPLA_2$-IIa, Fig. 2). It is noteworthy to mention

Table 1 Hit identification results

Entry	*Structure*	*sPLA$_2$-IIa (− X) IC$_{50}$ (μM)*	*Plasma IC$_{u,50}$ (μM)*[a]	F$_u$ *(%)*	*LE/LLE* [b]
Varespladib		0.028 (0.041)	0.008	12.5	0.37/7.2
1	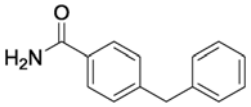	24 (2.2)	0.9	1.8	0.39/2.2
2	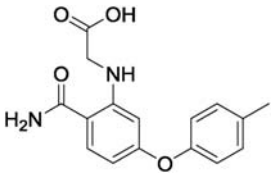	2.1 (ND)	3.9	2.7	0.35/2.7
3	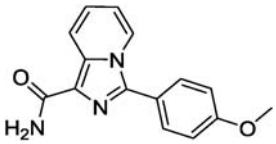	2.3 (ND)	5.0	2.8	0.37/2.3

[a]Calculated as human plasma sPLA$_2$ IC$_{50}$ (μM) × compound's unbound fraction in human plasma (F_u)/100.
[b]Ligand efficiency, LE (kcal/mol/HAC), calculated as − RTln(sPLA$_2$-IIa IC$_{50}$)/heavy atom count. Ligand lipophilicity efficiency (LLE) calculated as pIC$_{50}$ (sPLA$_2$-IIa)–log *D*.
Salient properties for the top 3 fragment hits are listed.

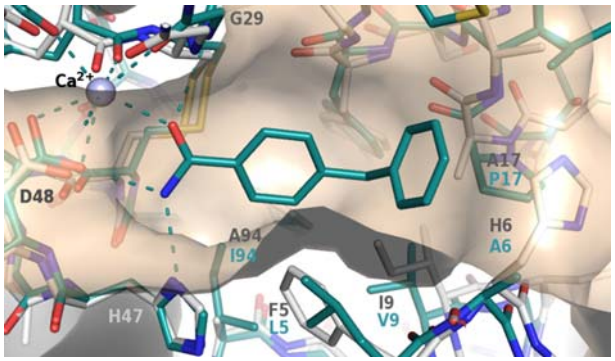

Fig. 2 Superposition of the crystal structure of **1** bound to sPLA$_2$-X (*cyan*) and a crystal structure of sPLA$_2$-IIa (*gray*). Residues that differ between the two proteins are labeled in *cyan* and *gray*, respectively. The calcium ion is depicted as a *purple sphere* and hydrogen bonds are displayed as *dashed lines*. The surface is generated from the sPLA$_2$-IIa crystal structure.

that the catalytic sites of sPLA$_2$-IIa and sPLA$_2$-X are identical in the amide coordinating amino acids and display similar lipophilic character in the side lipophilic pocket. Overlay of the available sPLA$_2$-IIa and sPLA$_2$-X crystal structures indicated that the 4-benzyl group of **1** could establish an adequate, although not optimal, steric fit to the slightly less voluminous sPLA$_2$-IIa pocket, as suggested by the lower affinity for such isoform (cf. 2.2 and 24 μM, **Table 1**). Based on the biochemical and structural data generated, **1** represented an ideal starting point for a structure-based, medicinal chemistry exploration. The limited size of the fragment hit coupled with its significant human plasma sPLA$_2$ inhibition and the presence of several exit vectors on its structure for further chemical manipulation offered adequate potential for its optimization. Moreover, the benzamide moiety also appeared favorable from an intellectual property perspective, as prior art analysis indicated no chemical precedents in the sPLA$_2$ field, which has been historically dominated by indole-containing chemotypes.[13,14] Based on the binding mode of **1**, we then hypothesized an optimization strategy aimed at establishing a second coordination bond between the inhibitor and the catalytic Ca^{2+} ion in the sPLA$_2$ binding site. This was driven by (a) a potential affinity and functional inhibition increase as a result of a bidentate Ca^{2+} chelate and additional van der Waals contact with the sPLA$_2$ enzymes, and (b) to afford an overall less lipophilic inhibitor considering that the additional Ca^{2+} interacting element would have required the introduction of a carboxylic acid functionality in its structure. Due to structure-based constraints, the ortho position of the benzamide ring was identified as an adequate growth vector for extending toward the Ca^{2+} ion. Using iterative molecular modeling and pragmatic forecasting of affinity increments using ligand efficiencies isovalues, we synthesized an initial set of compounds, **4**–**8**, to test the validity of our strategy. As described in **Scheme 1**, bromo benzonitrile was benzylated using a Neghishi coupling protocol with benzylzinc bromide in 80% yield. The directing capacity of the cyano group was then used to *ortho* lithiate the obtained 4-benzyl-benzonitrile using the bulky lithium 2,2,6,6-tetramethylpiperidide (LTMP).[24] Quenching of the obtained lithium

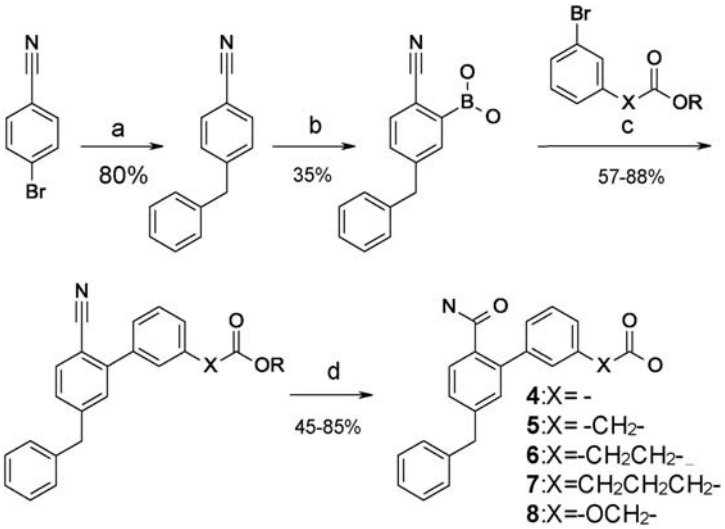

Scheme 1 Synthetic approach to compounds **4–8**. Reagents and conditions: (A) benzylzinc bromide, $Pd(Ph_3)_4$, THF, 60°C. (B) 1. nBuLi, tetramethylpiperidine 2. $B(OiPr)_3$, THF −78°C. (C) 3-Bromophenyl carboxylic acid **A**, $Pd(dppf)Cl_2$, Cs_2CO_3, DMF, 90°C. (D) *n*-Propanol:H_2O (10:1), KOH (10 equiv.), 80–100°C.

anion by triisopropylborate ($B(OiPr)_3$) generated the key boronic acid intermediate. Suzuki–Miyaura coupling of the corresponding ester-containing bromides was performed under anhydrous conditions in order to avoid ester hydrolysis. This gave the corresponding benzonitrile esters in generally moderate-to-high yields (57–88%). Compounds **4–8** were then obtained by simultaneous hydrolysis of the nitrile and ester functionalities to the corresponding carboxamide and carboxylic acid, respectively, with yields typically in the range of 45–85%. Here, in order to minimize hydrolysis of the formed primary amide, we use excess KOH in *n*-propanol and water at elevated temperatures ($\sim 80-100°C$) over 0.5–3 h. The use of lower aliphatic alcohols (e.g., methanol) resulted in faster hydrolysis of the nitriles but also increased formation of the corresponding di-carboxylic acid byproducts and was not deemed suitable.

The potential for further derivatization of the chosen ortho position on the benzamide scaffold was confirmed by derivatives **4–8,** which displayed improved $sPLA_2$-IIa inhibition compared to the unsubstituted parent compound (Table 2). Here, introduction of a 3-benzoic acid moiety (**4**) was the least favored with an IC_{50} of 0.91 μM for the $sPLA_2$-IIa isoform. By progressively increasing the distance between the carboxylic acid group and the phenyl ring via the insertion of methylene units (**5–7**), a parabolic effect on potency was observed. Specifically, the best compromise was afforded by the phenylpropionic acid side chain (**6**) over the phenylacetic acid (**5**) and phenylbutanoic acid (**7**) counterparts. When the benzylic methylene was replaced by an oxygen atom, a greater than 10-fold decrease in $sPLA_2$-II inhibition was observed (cf. **6** and **8**, Table 2). This result indicated a precise conformational requirement for the carboxylic acid-containing side chain (see in the following section). Derivative **6** offered submicromolar IC_{50} values against all the $sPLA_2$ isoforms tested, being most potent on $sPLA_2$-IIa (IC_{50}: 0.012 μM). The measured potencies were consistent with favorable efficiency parameters, both in terms of size (ligand efficiency, LE: 0.4) as well as lipophilicity (ligand lipophilicity efficiency, LLE: 6.4). Gratifyingly, the measured inhibition at the recombinant protein level translated to significant inhibition of human plasma $sPLA_2$ activity, with compound **7** displaying comparable inhibition to varespladib ($IC_{u,50}$: 0.007 and 0.008 μM, respectively). We succeeded in obtaining the cocrystal structure of **6** bound to $sPLA_2$-IIa and were able to evaluate the validity of our structure-based hypotheses. The bound conformation of **6** confirmed the sought ligand-mediated calcium chelation, as shown in Fig. 3. In an analogous manner to that observed for the original fragment hit **1**, the carbonyl oxygen atom of the amide group of **4** established the first coordination bond to the Ca^{2+} ion and three additional hydrogen bonds to G29, H47, and D48. Furthermore, the carboxylate moiety of **6** established the second coordination bond to the catalytic Ca^{2+} ion (interatomic distance: 2.8 Å) and an additional hydrogen bond to the backbone amide group of G31, as shown in Fig. 3. The 4-benzylbenzamide part of **6** was observed bound in a similar orientation, rotameric state, and interactions pattern as in **1**, while the additional phenyl ring substituting the carboxamide scaffold in its ortho position engaged significant van der Waals contacts with the aliphatic side chains of L2 and V30 and the backbone methylene of G29.

Compound **6** demonstrated a broad $sPLA_2$ potency profile coupled with significant plasma $sPLA_2$ inhibition ability and favorable size and lipophilicity efficiency. This prompted a widespread characterization campaign in order to verify any potential limitations for further development. The main concern was the combination of lipophilicity and unsubstituted phenyl rings. Despite the carboxamide and carboxylate functionalities, **6** demonstrated a relatively high experimental log *D* (1.5) and its lipophilicity had to be related to typical in vitro parameters as PK and safety surrogates. Furthermore, several positions on three phenyl rings would have been available for oxidative metabolism, adding to potential phase II metabolism targeting the carboxylic acid group. Table 3 summarizes the findings from such an investigation.

Table 2 Profile for the initial exploration set comprising compounds **2**–**6**

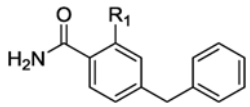

Entry	*R*	*sPLA$_2$-IIa IC$_{50}$ (μM)*	*sPLA$_2$-V IC$_{50}$ (μM)*	*sPLA$_2$-X IC$_{50}$ (μM)*	*Plasma IC$_{u,50}$ (μM)*[a]	*LE/LLE*[b]
Varespladib		0.028	0.12	0.041	0.008	0.37/7.2
1		24	NA[c]	2.2	0.9	0.39/2.2
4	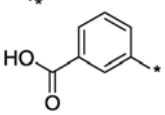	0.91	>10	NA[c]	NA[c]	0.33/4.9
5	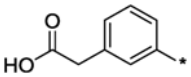	0.07	1.4	1.1	0.04	0.38/5.9
6	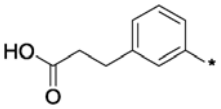	0.012	0.36	0.28	0.007	0.4/6.4
7	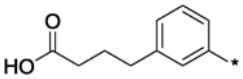	0.11	4.1	5.4	0.03	0.34/5
8	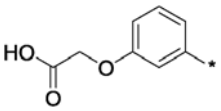	0.19	3.7	3.7	ND[d]	0.34/5.4

[a]Calculated as human plasma sPLA$_2$ IC$_{50}$ (μM) × compound's unbound fraction in human plasma (F_u)/100.
[b]Ligand efficiency, LE (kcal/mol/HAC), calculated as $-$RTln(sPLA$_2$-IIa IC$_{50}$)/heavy atom count. Ligand lipophilicity efficiency (LLE) calculated as pIC$_{50}$ (sPLA$_2$-IIa)–log *D*.
[c]Not active at maximum tested concentration (25 μM).
[d]Not determined.

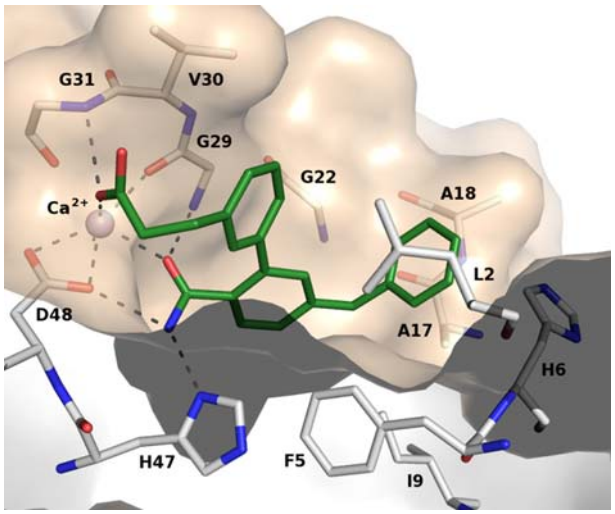

Fig. 3 Cocrystal structure of **6** bound to sPLA$_2$-IIa. The calcium ion is depicted as a *purple sphere*, and relevant hydrogen bonds are displayed as *dashed lines*.

Compound **6** was found to be soluble in the Hank's Balanced Salt Solution (HBSS), endowed with high passive diffusion in Caco-2 cells without any significant efflux, and metabolically stable when incubated in human cryopreserved hepatocytes. These positive attributes were further confirmed by in vivo PK analysis using two different species, rat and dog. Here, high bioavailabilities, low systemic clearances, and distribution volumes were observed. At the highest tested concentration, compound **6** did not inhibit any of the major human cytochrome P450 enzymes or ion channels which are of special relevance to cardiac function. Nevertheless, **6** inhibited the uptake of pitavastatin in HEK293 cells transfected with the human organic anionic transporter polypeptide 1B1

Table 3 Experimental profile of compound **6**

	6	
Solubility (pH 7.4) (μM)[a]		98
P_{app} (10^{-6} cm/s)[b]		40.1
HEP Cl_{int} (μL/min/10^{-6} cells)[c]		5.2
hERG, $Na_v1.5$, IKs, $K_v4.3$, $Ca_v3.2$, $Ca_v1.2$ IC_{50} (μM)[d]		>33.3
"Worst" CYP450 IC_{50} (μM)[e]		>20
OATP1B1 IC_{50} (μM)[f]		2.2
PK[g]	*Rat*	*Dog*
Dose i.v./p.o. (μmol/kg)	2/4	1/2
CL (mL/min/kg)	1	0.3
V_{ss} (L/kg)	0.22	0.26
F (%)	81	82

[a]DMSO/HBSS solubility measured at pH 7.4.
[b]Permeability measured in Caco-2 cells in the A to B direction, pH 6.5.
[c]Intrinsic clearance of test compounds after incubation with human hepatocytes.
[d]Patch clamp assay using IONWORKS™ technology in CHO cells expressing the relevant human ion channel.
[e]Inhibition of metabolic degradation of the corresponding substrate by human recombinant cytochrome P450s (3A4, 2C9, 2C19, 2D6, 1A2, and 2C8) at 37°C. The percent inhibition is determined at five different concentrations and reported as IC_{50}.
[f]Inhibition of pivastatin uptake to HEK293 cells transfected with human OATP1B1.
[g]Pharmacokinetic parameters calculated from noncompartmental analysis concentrations in fasted Sprague Dawley rats and Beagle dogs (i.v./p.o. N = 2).

(OATP1B1) with an estimated IC_{50} of 2.2 μM. This finding was of specific relevance since the OATP1B1 transporter is mechanistically required for statin's hypocholesterolemic action. In fact OATP1B1 mediates the access of statins to the liver compartment where they can then inhibit the function of their target enzyme 3-hydroxy-3-methylglutaryl-coenzyme A (HMG-CoA) reductase.[25–27] Considering that an eventual $sPLA_2$ inhibitor for the treatment of coronary artery disease will have to be co-administered with statin and additional medications, as established standard of care, it was important to try and minimize the risk for such clinically relevant drug–drug interaction. OATP1B1 has a preference for anionic compounds such as statins. Given that the anionic nature of our compound was also part of the established $sPLA_2$ pharmacophore due to the second coordination bond to the Ca^{2+}, complete removal of the carboxylate group was initially not deemed feasible. Instead, we resorted to the notion that modification of the molecular environment around the carboxylic acid of **6** might have been sufficient to perturb its interaction with OATP1B1 while being compatible with the $sPLA_2$ binding pocket environments. More specifically, substitution of the carbon atom in alpha to the carboxylic acid was of special appeal. This was postulated to (a) provide a steric impediment to the interaction with OATP1B1 and (b) enhance $sPLA_2$ potency through a conformational "freezing" of the carboxylic acid side chain due to gauche-like effects. Based on structure-based constraints in the $sPLA_2$ pocket and atomic economy considerations with a view to minimize the impact on compound lipophilicity, we opted to install mono and diatomic substituents on compound **6**. Accordingly, we synthesized compounds **7**–**9**, following **Scheme 2**. Here, the appropriately 2-substituted-dimethyl malonate was alkylated using 3-bromo benzylbromide, followed by a three-step telescoped sequence to the propionic methyl ester derivative. This consisted of (1) hydrolysis of the malonate derivative using NaOH, (2) decarboxylation in an oil bath at 140°C using acetic acid as medium, and (3) re-esterification to afford the relevant methyl ester derivative (75–90%). The subsequent boronylation step was accomplished using $(Bpin)_2$, Pd-106 in the presence of potassium acetate as base to yield, after column chromatography, the corresponding boronic pincacol esters (46–76%). These could then be used directly without further purification in the successive Suzuki–Miyaura coupling step with 4-benzyl-2-chlorobenzonitrile, which was prepared via Negishi coupling analogously to the route depicted in **Scheme 1**. Finally, racemic **9**–**11** were obtained by hydrolysis using KOH in *n*-propanol, as previously described in **Scheme 1**. Separation of enantiomers for racemic mixture **9** using chiral stationary HPLC-phases afforded (*R*)-**9** in 34% overall yield over nine operational steps. This general synthetic route has proven very practical in a discovery setting and was scaled to yield up to >10 g of title compound (*R*)-**9**. Nevertheless, a more robust, scalable, and enantioselective synthetic approach was developed in our laboratories to support early development activities for (*R*)-**9**. The route hinged on an elegant asymmetric hydrogenation step and has been recently described in detail.[28]

As shown in **Table 4**, the introduction of a methyl group in alpha to the carboxylate (**9**) demonstrated an isoform-specific effect on potency: it was neutral at $sPLA_2$-IIa, while it significantly increased inhibition of $sPLA_2$-V and reduced that of $sPLA_2$-X. As a result, the plasma $sPLA_2$ inhibition profile of **9** was superior to that of **4** ($IC_{u,50}$: 0.001 and 0.007 μM, respectively). Remarkably, the structural modification of the carboxylic acid surroundings by an alpha-methyl group yielded the sought-after effect at the statin transporter level, and **9** did not show any significant inhibition of OATP1B1 at the maximum tested concentration (25 μM). Interestingly, ethyl and cyclopropyl substitutions (**10**, **11**) were not as effective when considering the added size and lipophilicity, possibly highlighting suboptimal van der Waals contacts with the $sPLA_2$. More importantly, they showed a deteriorating effect on metabolic stability in human hepatocytes (cf. **10**, **11**, and **9**, **Table 4**), which was not regarded to be compatible with further progression.

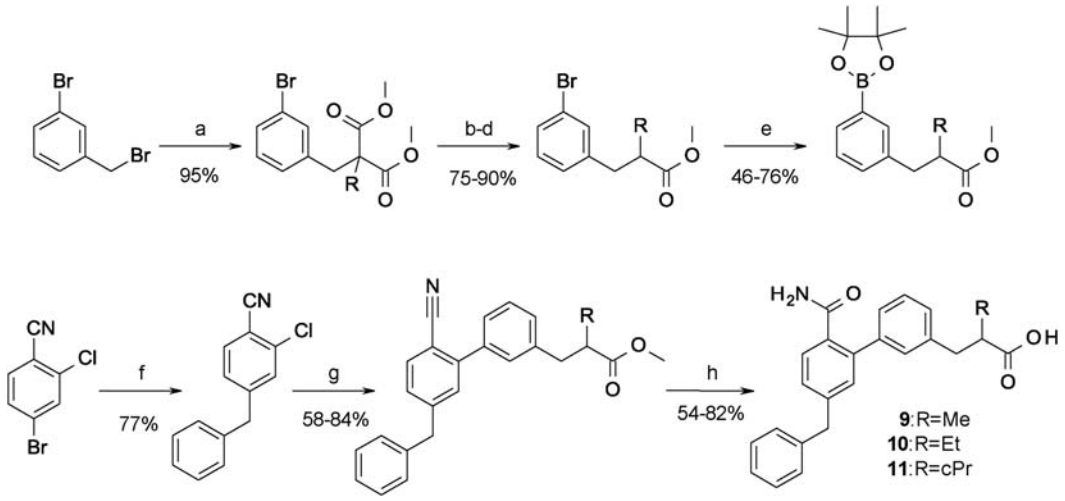

Scheme 2 Synthetic approach to compounds **9**–**11**. Reagents and conditions: (A) dimethylmalonate, Cs_2CO_3, DMF, 70°C, 2 h. (B) NaOH (4 equiv.), H_2O:MeOH 3:1 80°C 2 h. (C) HOAc (3 M), reflux. (D) HCl, MeOH 60°C, 2.5 h. (E) $(Bpin)_2$ (1.3 equiv.), KOAc (2.5 equiv.), $Pd(dppf)Cl_2$ (6.5 mol%), dioxane, 90°C. (F) BnZnBr (1.5 equiv., 0.5 M in THF), $Pd(PPh_3)_4$ (5 mol%), THF, 60°C, 2 h. (G) **B**, $Pd(dbpf)Cl_2$ (5 mol%), Cs_2CO_3, DMF, 90°C, 1.5 h. (H) *n*-propanol, H_2O (10:1), KOH (10 equiv.), 80–100°C.

Table 4 $sPLA_2$ potency and optimization parameters for compounds **4**–**11**

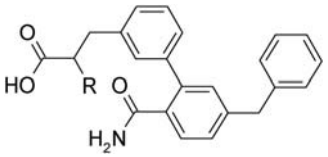

Entry	*R*	*$sPLA_2$-IIa IC_{50} (μM)*[a]	*$sPLA_2$-V IC_{50} (μM)*[a]	*$sPLA_2$-X IC_{50} (μM)*[a]	*Plasma $IC_{u,50}$ (μM)*[b]	*HEP Cl_{int} ($\mu L/min/10^{-6}$ cells)*[c]	*OATP1B1 IC_{50} (μM)*[d]
4	H	0.012	0.36	0.28	0.007	5.2	2.2
9	Me	0.011	0.07	0.75	0.001	9.6	NA[e]
10	Et	0.021	0.07	0.43	0.0008	25	ND[f]
11	CyPr	0.018	0.25	0.58	0.0009	21	ND[f]
(*S*)-9	(*S*)-Me	0.038	1.2	3.8	ND	9.3	ND[f]
(*R*)-9	(*R*)-Me	0.010	0.04	0.4	0.0001	12	NA[e]

[a]Results are mean of at least two experiments. Experimental errors within 20% of value.
[b]Calculated as Plasma $sPLA_2$ IC_{50} (μM) × compound's unbound fraction in human plasma (F_u)/100.
[c]Intrinsic clearance of test compounds after incubation with human hepatocytes.
[d]Inhibition of pivastatin uptake to HEK293 cells transfected with human OATP1B1.
[e]Not active at maximum tested concentration (25 μM).
[f]Not determined.

The racemic mixture 9 displayed a substantial improvement in key optimization properties in the current compound series. We therefore proceeded to separate and characterize the two enantiomers to verify individual compound's contributions to the properties of interest. In line with expectations informed by the structural biology framework in which we operated, $sPLA_2$ inhibition was profoundly affected by stereochemistry. Here, the *R* enantiomer proved to be the most active, half-maximally inhibiting $sPLA_2$-IIa, -V and -X at 10, 40, and 400 nM, respectively (Table 4). As a result, (*R*)-9 was the most potent human plasma $sPLA_2$ inhibitor in this study ($IC_{u,50}$: 0.1 nM) and maintained no OATP1B1 inhibitory activity at the highest tested concentration. Despite a higher metabolic turnover in human hepatocytes compared to previous analogs in the series (cf. (*R*)-9 and **4**, Table 4), the combination of excellent potency and minimized risk for drug–drug interactions with statins triggered additional profiling of its PDs and PK properties.

$sPLA_2$ activity in human plasma has shown relevant correlations to the risk of developing cardiovascular events and associated mortality.[12] Nevertheless, we were also interested to assess inhibition of $sPLA_2$ activity beyond the plasma compartment. As atherosclerotic lesions are complex matrix environments with a marked cellular context, we first evaluated cellular $sPLA_2$ activity inhibition using a HepG2 cell line as a cellular model system. Here, (*R*)-9 effectively inhibited $sPLA_2$ activity with an IC_{50} of less than 14 nM. It is noteworthy that, in the same experiment, (*R*)-9 also suppressed the production of $sPLA_2$-IIa (IC_{50}: 176 ± 28 nM) via a mechanism

Table 5 PK parameters of compound (*R*)-**9**

PK observable[a]	*Mouse*	*Rat*	*Dog*	*Cynomolgus*
N i.v./p.o.	2/2	2/2	2/2	2/2
Dose i.v./p.o. (μmol/kg)	10/50	2/8	1/3	5/15.8
Oral AUC_{0-inf} (μM × h)	69.7	70	284.1	71.3
CL (mL/min/kg)	9.2	1	0.2	2.8
V_{ss} (L/kg)	2.8	0.21	0.15	1.1
F (%)	76.3	84	91	81

[a]Pharmacokinetic parameters calculated from noncompartmental analysis concentrations in fasted animals.

not yet elucidated, probably involving paracrine feedback loops.[8] We then proceeded to verify the $sPLA_2$ inhibitory ability of (*R*)-**9** in a more pathological setting. To this end, we homogenated atherosclerotic plaques obtained from carotid endarterectomy of coronary artery disease patients ($N=7$).[29] When (*R*)-**9** was incubated in this disease-relevant milieu, it inhibited $sPLA_2$ activity with an IC_{50} of 56 ± 10 nM, thus confirming a broad spectrum $sPLA_2$ inhibitory profile, which is independent of the biological compartment considered.

In vivo PK analysis of (*R*)-**9** generally reflected the in vitro characteristics previously highlighted, as summarized in **Table 5**. Across multiple species absorption was rapid and T_{max} was reached in less than 2 h resulting in consistently high bioavailabilities (76.3–91%). Despite the moderate intrinsic clearance recorded in hepatocytes across different animal species, in vivo systemic clearance was overall low and enabled significant, sustained compound exposure over time ($AUC_{0\text{-}inf}$: 69.7–284.1 μM × h).

Building on the observed PK parameters, and the in vitro $sPLA_2$ inhibition measured in cynomolgus monkey plasma ($IC_{u,50}$: 1 nM), we resolved to evaluate the in vivo $sPLA_2$ inhibitory effect of (*R*)-**9** in an effort to delineate PK–PD relationships and assist further allometry-based dose predictions. PK–PD modeling indicated that a 30 mg dose of (*R*)-**9** would have been enough to maintain half maximal $sPLA_2$ inhibition over a 24 h period (data not shown). (*R*)-**9** was thus orally administered to cynomolgus monkeys ($N=2$) and sampling of plasma at different time points was used to simultaneously analyze the compound concentration and $sPLA_2$ activity. An appropriate vehicle correction using a 30 mg bolus of aqueous suspending vehicle (the formulation used for dosing (*R*)-**9**) was applied to quantify $sPLA_2$ activity inhibition, as summarized in **Fig. 4**. A concentration-dependent inhibition of $sPLA_2$ activity in plasma ($IC_{u,80}$: 13 ± 3 nM) was observed and this reflected very well the time course of (*R*)-**9**'s exposure profile

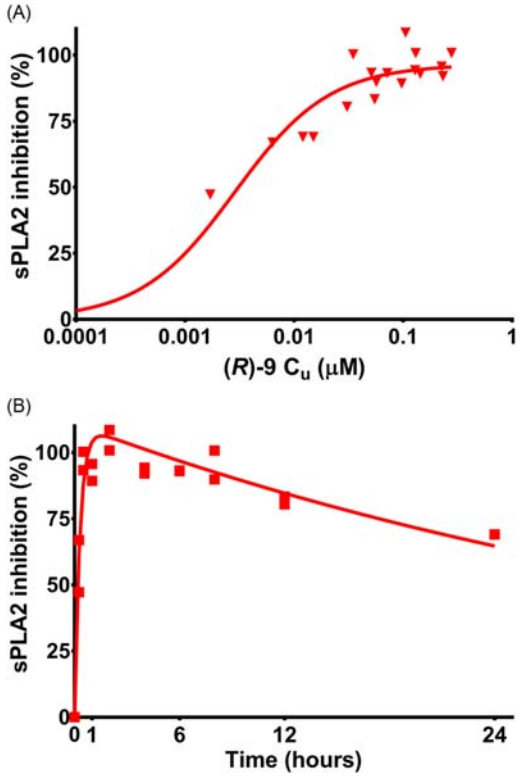

Fig. 4 Vehicle-corrected plasma $sPLA_2$ activity inhibition, corresponding PK–PD relationship (A) and time course (B) following oral administration of 30 mg (*R*)-**9** to cynomolgus monkeys ($N=2$).

(Fig. 4). These results further corroborated the sPLA$_2$ inhibitory potential of (*R*)-**9**. The compounds also displayed a favorable toxicological profile, as from standard 1 week to 1 month maximum tolerated dose protocols, in three different preclinical species (i.e., Wistar rat, beagle dog, and cynomolgus monkey). Overall, the experimental evidence accumulated indicated sufficient potential for further clinical development of (*R*)-**9**.

The aim of the project was to deliver inhibitors of sufficient quality to be used in long-term clinical studies focusing on carotid artery disease patients, where the combination of antiinflammatory and lipoprotein modifying effects deriving from sPLA$_2$ inhibition was postulated to deliver maximum therapeutic benefits. Due to the high stringency requirements in terms of efficacy, PK, and safety of the target patient population, we wanted to access the best possible chemical starting points with the greatest potential for successful optimization. We therefore initiated a fragment-based project to bias our chemical matter selection process on small and highly efficient compounds. We therefore used a triaging process focused on sPLA$_2$ inhibition and X-ray crystallography. Of special importance was the integration of a clinically relevant functional endpoint as part of the fragment selection process, in order to minimize translational uncertainties. This resulted in the identification of 4-benzylbenzamide (**1**) as an initial fragment hit fulfilling our requirements. Two design cycles based on structural information, ligand efficiency reasoning, physicochemical property control, and medicinal chemistry tactics rapidly optimized key developmental properties such as potency, PK, and risk for drug–drug interactions. In this context, the importance of readily available, relevant experimental data cannot be overemphasized enough. These activities culminated in the design of (*R*)-**9** (**AZD2716**), a novel, potent sPLA$_2$ inhibitor with excellent PK properties, sustained in vivo target engagement and minimized risk for drug–drug interactions. Based on the available results, **AZD2716** was selected as a clinical candidate for the treatment of coronary artery disease. One sentence on current status?

See also: 8.11. Case Histories: Anacetrapib.

References

1. Arita, H.; Nakano, T.; Hanasaki, K. Thromboxane A$_2$: Its Generation and Role in Platelet Activation. *Prog. Lipid Res.* **1989,** *28* (4), 273–301.
2. Six, D. A.; Dennis, E. A. The Expanding Superfamily of Phospholipase A(2) Enzymes: Classification and Characterization. *Biochim. Biophys. Acta* **2000,** *1488* (1–2), 1–19.
3. Singer, A. G.; Ghomashchi, F.; Le Calvez, C.; Bollinger, J.; Bezzine, S.; Rouault, M.; Sadilek, M.; Nguyen, E.; Lazdunski, M.; Lambeau, G.; Gelb, M. H. Interfacial Kinetic and Binding Properties of the Complete Set of Human and Mouse Groups I, II, V, X, and XII Secreted Phospholipases A$_2$. *J. Biol. Chem.* **2002,** *277* (50), 48535–48549.
4. Kudo, I.; Murakami, M. Phospholipase A$_2$ Enzymes. *Prostaglandins Other Lipid Mediat.* **2002,** *68–69,* 3–58.
5. Murakami, M.; Sato, H.; Miki, Y.; Yamamoto, K.; Taketomi, Y. A New Era of Secreted Phospholipase A$_2$. *J. Lipid Res.* **2015,** *56* (7), 1248–1261.
6. Hurt-Camejo, E.; Camejo, G.; Peilot, H.; Öörni, K.; Kovanen, P. Phospholipase A$_2$ in Vascular Disease. *Circ. Res.* **2001,** *89* (4), 298–304.
7. Rosenson, R. S.; Gelb, M. H. Secretory Phospholipase A$_2$: A Multifaceted Family of Proatherogenic Enzymes. *Curr. Cardiol. Rep.* **2009,** *11* (6), 445–451.
8. Rosenson, R. S.; Hurt-Camejo, E. Phospholipase A$_2$ Enzymes and the Risk of Atherosclerosis. *Eur. Heart J.* **2012,** *33* (23), 2899–2909.
9. Mallat, Z.; Lambeau, G.; Tedgui, A. Lipoprotein-Associated and Secreted Phospholipases A$_2$ in Cardiovascular Disease: Roles as Biological Effectors and Biomarkers. *Circulation* **2010,** *122* (21), 2183–2200.
10. Shridas, P.; Webb, N. R.; Shridas, P.; Webb, N. R. Diverse Functions of Secretory Phospholipases A$_2$, Diverse Functions of Secretory Phospholipases A$_2$. *Adv. Vasc. Med.* **2014,** *2014* (2014), e689815.
11. Pernas, P.; Masliah, J.; Olivier, J.-L.; Salvat, C.; Rybkine, T.; Bereziat, G. Type II Phospholipase A$_2$ Recombinant Overexpression Enhances Stimulated Arachidonic Acid Release. *Biochem. Biophys. Res. Commun.* **1991,** *178* (3), 1298–1305.
12. Lind, L.; Simon, T.; Johansson, L.; Kotti, S.; Hansen, T.; Machecourt, J.; Ninio, E.; Tedgui, A.; Danchin, N.; Ahlström, H.; Mallat, Z. Circulating Levels of Secretory- and Lipoprotein-Associated Phospholipase A$_2$ Activities: Relation to Atherosclerotic Plaques and Future All-Cause Mortality. *Eur. Heart J.* **2012,** *33* (23), 2946–2954.
13. Draheim, S. E.; Bach, N. J.; Dillard, R. D.; Berry, D. R.; Carlson, D. G.; Chirgadze, N. Y.; Clawson, D. K.; Hartley, L. W.; Johnson, L. M.; Jones, N. D.; McKinney, E. R.; Mihelich, E. D.; Olkowski, J. L.; Schevitz, R. W.; Smith, A. C.; Snyder, D. W.; Sommers, C. D.; Wery, J. P. Indole Inhibitors of Human Nonpancreatic Secretory Phospholipase A$_2$. 3. Indole-3-Glyoxamides. *J. Med. Chem.* **1996,** *39* (26), 5159–5175.
14. Schevitz, R. W.; Bach, N. J.; Carlson, D. G.; Chirgadze, N. Y.; Clawson, D. K.; Dillard, R. D.; Draheim, S. E.; Hartley, L. W.; Jones, N. D.; Mihelich, E. D. Structure-Based Design of the First Potent and Selective Inhibitor of Human Non-Pancreatic Secretory Phospholipase A$_2$. *Nat. Struct. Biol.* **1995,** *2* (6), 458–465.
15. Bradley, J. D.; Dmitrienko, A. A.; Kivitz, A. J.; Gluck, O. S.; Weaver, A. L.; Wiesenhutter, C.; Myers, S. L.; Sides, G. D. A Randomized, Double-Blinded, Placebo-Controlled Clinical Trial of LY333013, a Selective Inhibitor of Group II Secretory Phospholipase A$_2$, in the Treatment of Rheumatoid Arthritis. *J. Rheumatol.* **2005,** *32* (3), 417–423.
16. Nicholls, S. J.; Kastelein, J. J. P.; Schwartz, G. G.; Bash, D.; Rosenson, R. S.; Cavender, M. A.; Brennan, D. M.; Koenig, W.; Jukema, J. W.; Nambi, V.; Wright, R. S.; Menon, V.; Lincoff, A. M.; Nissen, S. E. VISTA-16 Investigators. Varespladib and Cardiovascular Events in Patients with an Acute Coronary Syndrome: The VISTA-16 Randomized Clinical Trial. *JAMA* **2014,** *311* (3), 252–262.
17. Hanasaki, K.; Yamada, K.; Yamamoto, S.; Ishimoto, Y.; Saiga, A.; Ono, T.; Ikeda, M.; Notoya, M.; Kamitani, S.; Arita, H. Potent Modification of Low Density Lipoprotein by Group X Secretory Phospholipase A$_2$ Is Linked to Macrophage Foam Cell Formation. *J. Biol. Chem.* **2002,** *277* (32), 29116–29124.
18. Ishimoto, Y.; Yamada, K.; Yamamoto, S.; Ono, T.; Notoya, M.; Hanasaki, K. Group V and X Secretory Phospholipase A(2)s-Induced Modification of High-Density Lipoprotein Linked to the Reduction of Its Antiatherogenic Functions. *Biochim. Biophys. Acta* **2003,** *1642* (3), 129–138.
19. de Beer, F. C.; Connell, P. M.; Yu, J.; de Beer, M. C.; Webb, N. R.; van der Westhuyzen, D. R. HDL Modification by Secretory Phospholipase A$_2$ Promotes Scavenger Receptor Class B Type I Interaction and Accelerates HDL Catabolism. *J. Lipid Res.* **2000,** *41* (11), 1849–1857.
20. Waring, M. J. Lipophilicity in Drug Discovery. *Expert Opin. Drug Discovery* **2010,** *5* (3), 235–248.
21. Erlanson, D. A. Introduction to Fragment-Based Drug Discovery. *Top. Curr. Chem.* **2012,** *317,* 1–32.
22. Lambeau, G.; Gelb, M. H. Biochemistry and Physiology of Mammalian Secreted Phospholipases A$_2$. *Annu. Rev. Biochem.* **2008,** *77,* 495–520.
23. Petrovic, N.; Grove, C.; Langton, P. E.; Misso, N. L.; Thompson, P. J. A Simple Assay for a Human Serum Phospholipase A$_2$ That is Associated With High-Density Lipoproteins. *J. Lipid Res.* **2001,** *42* (10), 1706–1713.
24. Kristensen, J.; Lysén, M.; Vedsø, P.; Begtrup, M. Synthesis of Ortho Substituted Arylboronic Esters by In Situ Trapping of Unstable Lithio Intermediates. *Org. Lett.* **2001,** *3* (10), 1435–1437.

25. Hsiang, B.; Zhu, Y.; Wang, Z.; Wu, Y.; Sasseville, V.; Yang, W. P.; Kirchgessner, T. G. A Novel Human Hepatic Organic Anion Transporting Polypeptide (OATP2). Identification of a Liver-Specific Human Organic Anion Transporting Polypeptide and Identification of Rat and Human Hydroxymethylglutaryl-CoA Reductase Inhibitor Transporters. *J. Biol. Chem.* **1999,** *274* (52), 37161–37168.
26. Mizuno, N.; Niwa, T.; Yotsumoto, Y.; Sugiyama, Y. Impact of Drug Transporter Studies on Drug Discovery and Development. *Pharmacol. Rev.* **2003,** *55* (3), 425–461.
27. Shitara, Y.; Horie, T.; Sugiyama, Y. Transporters as a Determinant of Drug Clearance and Tissue Distribution. *Eur. J. Pharm. Sci.* **2006,** *27* (5), 425–446.
28. Karlsson, S.; Sörensen, H.; Andersen, S. M.; Cruz, A.; Ryberg, P. An Enantioselective Hydrogenation of an Alkenoic Acid as a Key Step in the Synthesis of AZD2716. *Org. Process. Res. Dev.* **2016,** *20* (2), 262–269.
29. Hurt-Camejo, E.; Andersen, S.; Standal, R.; Rosengren, B.; Sartipy, P.; Stadberg, E.; Johansen, B. Localization of Nonpancreatic Secretory Phospholipase A_2 in Normal and Atherosclerotic Arteries. Activity of the Isolated Enzyme on Low-Density Lipoproteins. *Arterioscler. Thromb. Vasc. Biol.* **1997,** *17* (2), 300–309.

8.14 Canagliflozin

S Nomura, Mitsubishi Tanabe Pharma Corporation, Toda, Japan

© 2017 Elsevier Ltd. All rights reserved.

8.14.1	**Introduction**	349
8.14.2	**Concept for Novel Antidiabetic Agents**	350
8.14.3	**The First Oral SGLT2 Inhibitor**	350
8.14.3.1	Discovery of T-1095	350
8.14.3.2	Efficacy and Pharmacokinetic Issues of T-1095	351
8.14.4	**Discovery of Canagliflozin**	353
8.14.4.1	Exploration of *C*- and *N*-glucosides Bearing a Heteroaromatic Ring	353
8.14.4.2	Syntheses of *C*-glucosides Bearing a Heteroaromatic Ring	354
8.14.4.3	SAR of the Typical *C*-glucosides With a Heteroaromatic Ring	355
8.14.4.4	The Synthesis of Canagliflozin	357
8.14.4.5	Canagliflozin: A Selective SGLT2 Inhibitor	357
8.14.4.6	Efficacy of Canagliflozin	360
8.14.5	**Clinical Outcomes**	361
8.14.5.1	Mechanism of Action of SGLT2 Inhibitors	361
8.14.5.2	24-Week Phase 3 Study in Japanese Patients	361
8.14.5.3	Phase 3 CANTATA Trials	363
8.14.5.4	Improvement of β-Cell Function	363
8.14.6	**Conclusion**	363
References		364
Relevant Websites		365

Abbreviations

ADOPT a diabetes outcome progression trial
AGE advanced glycation end product
CHOK Chinese hamster ovary-K
DPP4 dipeptidyl peptidase IV
FPG fasting plasma glucose
GI gastrointestinal
GLP-1 glucagon-like peptide-1
GLUT facilitating glucose transporter
HbA1c hemoglobin A1c
MMTT mixed-meal tolerance test
OGTT oral glucose tolerance test
PK pharmacokinetic
PYY peptide YY
RT_G renal threshold for glucose
SAR structure–activity relationship
SD Sprague Dawley
SGLT sodium glucose cotransporter
SHR-cp spontaneously hypertensive corpulent congenic rat
STZ streptozotocin
T2DM type 2 diabetes mellitus
UGE urinary glucose excretion
ZDF Zucker diabetic fatty

8.14.1 Introduction

Humans have acquired many physiological systems through evolution to maintain blood glucose homeostasis. Blood glucose levels are under the control of several hormones, such as glucagon, adrenaline, and cortisol, and are additionally controlled via absorption by sodium glucose co-transporters (SGLTs). However, dietary changes, satiation, and sedentary lifestyle in recent years have increased the number of patients with type 2 diabetes (T2DM).[1]

In 1990, Rossetti put forward a hypothesis of glucose toxicity,[2] stating that continuous hyperglycemia induces insulin resistance and impaired insulin secretion. Further, glucose reacts as an aldehyde with the amine portion of proteins to produce denatured proteins, called advanced glycation end products (AGEs). AGE deposition induces microangiopathy and causes diabetic complications. Therefore, despite being the essential energy source, glucose ironically acts as a toxic substance when in chronic excess.

Most of the currently available diabetes treatments are aimed at improving either insulin secretion or insulin sensitivity via targeting insulin-dependent mechanisms.[3,4] However, treatment with such agents is often accompanied by secondary failure in efficacy and adverse events, including hypoglycemia or weight gain. Furthermore, in a diabetes outcome progression trial (ADOPT) study, which evaluated the long-term therapeutic effects of oral agents, those operating via insulin-dependent mechanisms, including

rosiglitazone, metformin, and glyburide, increased hemoglobin A1c (HbA1c) levels several years later.[5] This suggests that pancreatic β-cell dysfunction progresses with long-term treatment of drugs with an insulin-dependent mechanism of action.

8.14.2 Concept for Novel Antidiabetic Agents

In 1996, we, for the first time, asked whether it is possible to discharge excessive glucose from the body through medication. An agent capable of mediating such effects could normalize energy balance, and the induced decrease in blood glucose levels would cancel glucose toxicity to alleviate impaired insulin secretion, insulin resistance, and diabetic complications. We began to research into this concept with an aim to identify prototypic compounds that could enhance urinary glucose excretion (UGE).[6]

Glucose homeostasis is mainly regulated by hormones, such as insulin and glucagon, and by the autonomic nervous system. Plasma glucose levels fluctuate in response to the absorption of glucose in the intestines and utilization and production in peripheral tissues, including the liver and skeletal muscles.[7] In the kidney, glucose is filtered through the glomerulus, with glucose concentration in the filtrate at the glomerulus being the same as that in plasma. Filtered glucose is reabsorbed in the proximal tubules from the lumen to prevent the loss of calories.

Glucose reabsorption in renal epithelial cells is predominantly mediated by SGLT2, a low-affinity, high-capacity SGLT located in the early S1 segment of the proximal tubules. Glucose reabsorption is also, to a lesser extent, mediated by SGLT1, a high-affinity, low-capacity SGLT distributed in the more distal S3 segment of the proximal tubules (Fig. 1).[8–10] Reabsorbed glucose is then transferred to the basolateral extracellular space by the function of facilitating glucose transporters (GLUTs). In normoglycemic states, glucose levels in the filtrate are below the maximum transport capacity of tubular SGLTs. All glucose is, therefore, transported from the tubular lumen to the blood, and no UGE is detected. In contrast, when the glucose levels in the filtrate exceed the tubular SGLT's maximum transport capacity, the reabsorption process is saturated, and nonreabsorbed glucose is excreted in the urine. Under such hyperglycemic conditions, UGE increases in proportion to the blood glucose concentration above the threshold level.[11]

Although SGLT2 is located solely in the kidney, SGLT1 is distributed in the intestine and heart besides the kidney. In the small intestine, luminal glucose is absorbed through SGLT1 located on the luminal surface of epithelial cells. Therefore, SGLT2 mainly mediates renal glucose reabsorption, and SGLT1 mediates both intestinal glucose absorption and renal glucose reabsorption. SGLT2 expression is increased in patients with T2DM compared with that in nondiabetic subjects, and renal glucose uptake is enhanced in T2DM patients.[12] It is, therefore, likely that enhanced glucose reabsorption may contribute to the maintenance of hyperglycemia. Whereas mutations of SGLT1 are associated with intestinal glucose/galactose malabsorption, individuals with gene mutations in SGLT2 have persistent renal glycosuria in normoglycemia without any serious symptoms.[13–15] Thus, although the elimination of excess plasma glucose in the urine is a physiologically reasonable strategy to reduce plasma glucose levels and body calories, SGLT2 had never been considered as a drug target before the discovery of the oral SGLT2 inhibitor, T-1095.[16]

8.14.3 The First Oral SGLT2 Inhibitor

8.14.3.1 Discovery of T-1095

It has been reported that parenteral administration of phlorizin (**1**, Fig. 2), a natural glucoside derived from the bark of apple and pear trees, prevents renal glucose reabsorption through SGLT inhibition and promotes renal glycosuria.[17–21] Isolated by French chemists in 1835, phlorizin is well known for a long time to induce glycosuria. After the cloning of SGLT1 and SGLT2 in the

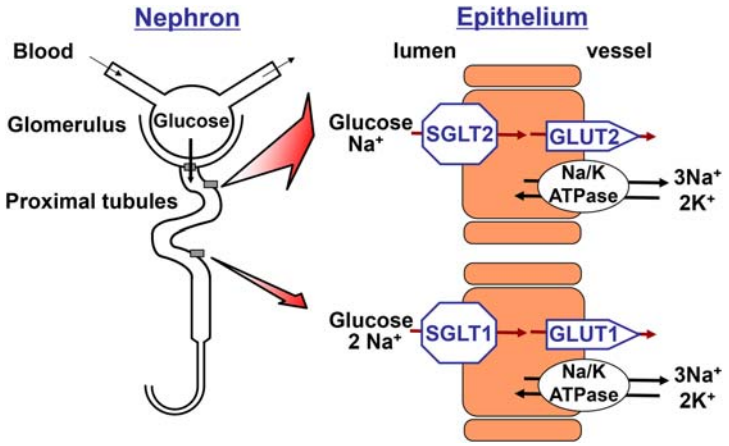

Fig. 1 Renal glucose reabsorption by sodium glucose cotransporters (SGLTs). Modified from Nomura, S. Renal Sodium-Dependent Glucose Cotransporter 2 (SGLT2) Inhibitors for New Anti-Diabetic Agent. *Curr. Top. Med. Chem.* **2010**, *10* (4), 411–418.

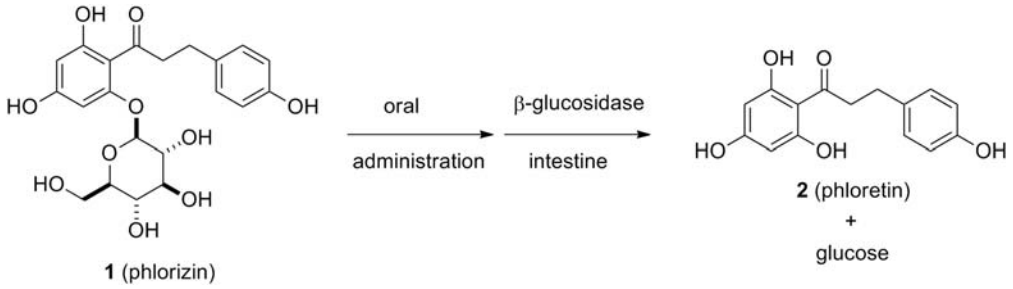

Fig. 2 Hydrolysis of **1** (phlorizin) by β-glucosidase in the intestine. Modified from Nomura, S. Renal Sodium-Dependent Glucose Cotransporter 2 (SGLT2) Inhibitors for New Anti-Diabetic Agent. *Curr. Top. Med. Chem.* **2010**, *10* (4), 411–418.

1990s, it became clear that phlorizin specifically and competitively inhibits both SGLT1 and SGLT2. Based on this knowledge, we pioneered the revolutionary idea of treating T2DM with an agent that enhances the excretion of glucose in the urine. The effect of phlorizin is, however, markedly reduced when administered orally because intestinal β-glucosidase hydrolyzes this compound into phloretin (**2**) and glucose (Fig. 2). Phlorizin had also been reported to induce renal impairment.[21] Hence, there had been no attempt to use phlorizin as an antidiabetic agent.

We explored the structure–activity relationship (SAR) of phlorizin derivatives to inhibit rat kidney SGLT activity and to increase UGE by oral administration in Sprague Dawley (SD) rats (Fig. 3). Removal of the 4′-hydroxyl group on the B ring of phlorizin provided resistance to β-glucosidase on oral treatment,[6] and the use of bicyclic benzofuran as the A ring showed superior UGE activity.[23] Finally, introduction of a methyl group on the B ring resulted in a selective human SGLT2 (hSGLT2) inhibitor, **3** (T-1095A). Further exploration of prodrugs to improve in vivo activity led to the discovery of the methoxycarbonyl prodrug **4** (T-1095) with enhanced resistance to β-glucosidase.[16,24] T-1095 induced UGE, following oral administration, and lowered blood glucose levels in diabetic animal models independent of insulin action. T-1095 is the first orally active SGLT2 inhibitor. Proof of concept for SGLT2 inhibitors, using T-1095, was published in 1999.[25]

8.14.3.2 Efficacy and Pharmacokinetic Issues of T-1095

Orally administered prodrug T-1095 is absorbed in the small intestine and converted to its active form, T-1095A, by the liver esterase. T-1095A then inhibits SGLT2 located in the proximal tubules (Fig. 4). Single oral administration of T-1095 dose-dependently

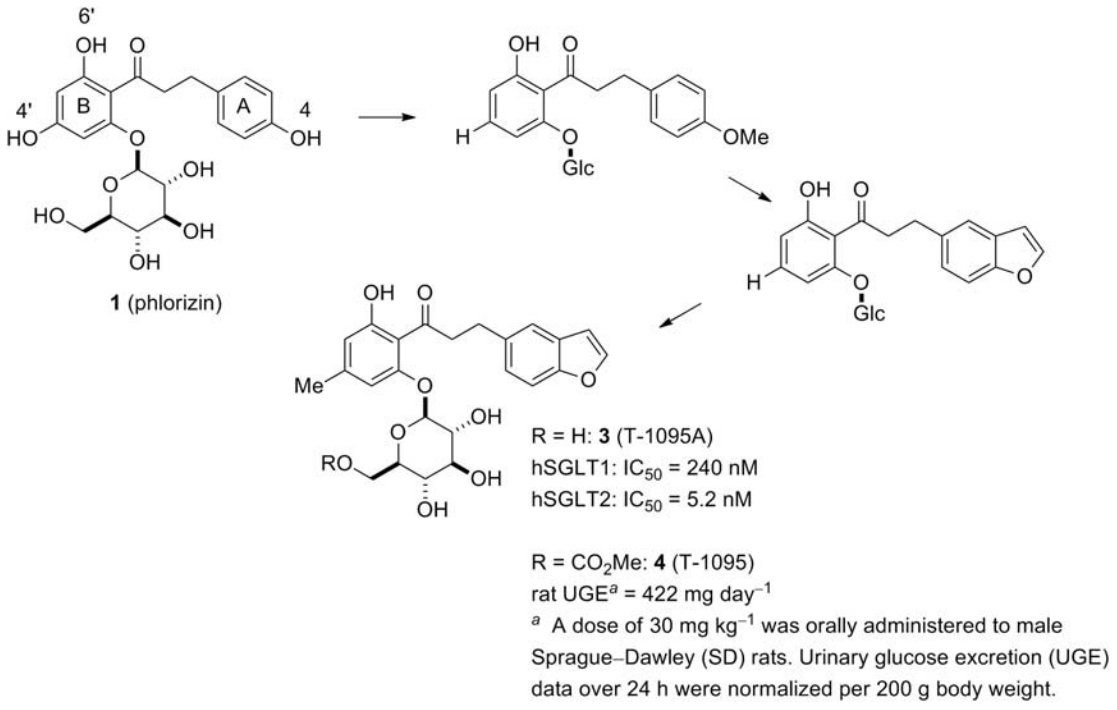

Fig. 3 Discovery of **4** (T-1095), the first orally active SGLT2 inhibitor. Data from Nomura et al.[22]

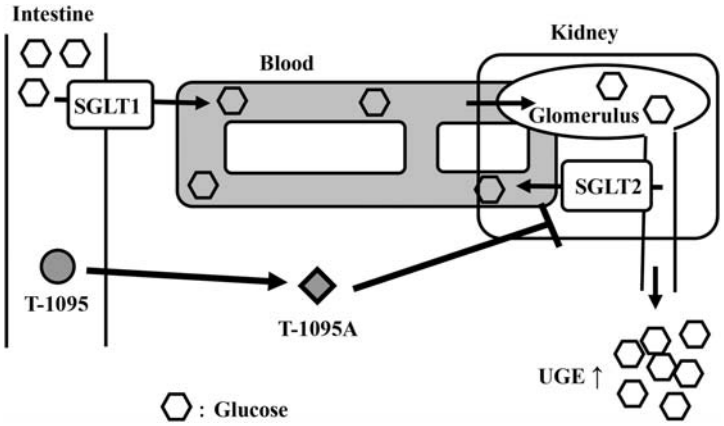

Fig. 4 Action of T-1095. Modified from Nomura, S. Renal Sodium-Dependent Glucose Cotransporter 2 (SGLT2) Inhibitors for New Anti-Diabetic Agent. *Curr. Top. Med. Chem.* **2010**, *10* (4), 411–418.

increased UGE in neonatally streptozotocin (STZ)-treated (n-STZ) rats, a nonobese rat model of T2DM. A concomitant significant reduction in blood glucose levels was also seen in this model. In contrast, T-1095 only slightly increased UGE, and blood glucose levels were only slightly affected in normoglycemic rats even at 100 mg kg^{-1} (Figs. 5 and 6).[26] This showed that the inhibition of renal SGLT2 does not significantly reduce blood glucose levels in normoglycemic ranges, suggesting the risk of hypoglycemia induction is low in contrast to insulin secretagogues, such as sulfonylureas and glinides.

Since increase in UGE by SGLT2 inhibition is dependent on the glomerular filtration of glucose, SGLT2 inhibition was expected to reduce blood glucose levels in any model of hyperglycemia. Single oral administration of T-1095 reduced blood glucose levels dose-dependently in a type 1 diabetic rat model produced by treatment with STZ at 6 or 7 weeks of age. Since these rats lack β-cell function, the results demonstrate that T-1095 exerts antihyperglycemic effects in an insulin-independent fashion (Fig. 7).[27] The antihyperglycemic effect of T-1095 was demonstrated in various T2DM rodent models, including Goto–Kakizaki rats,[28] Zucker diabetic fatty (ZDF) rats,[29,30] KKAy mice,[25] and db/db mice.[31] Taken together, the findings from these models have demonstrated that SGLT inhibition reduces hyperglycemia but hardly causes hypoglycemia below the normoglycemic range.

In addition to the acute reduction of hyperglycemia, long-term treatment with T-1095 controlled glucose levels and reduced fasting glucose and HbA1c levels in various animal models of hyperglycemia. After 4-week treatment with T-1095 in n-STZ rats, an oral glucose tolerance test (OGTT) revealed that an elevated glucose excursion in hyperglycemic animals was reduced and concomitant insulin release was restored. A hyperinsulinemic glucose clamp study in ZDF rats revealed that 4-week treatment with T-1095 reduced insulin resistance in peripheral tissues, including the liver and skeletal muscles.[29,30] In db/db mice, the progression of hyperglycemia and hyperinsulinemia was suppressed, and the exhaustion of pancreatic β-cells was prevented.[31] As hyperglycemia was controlled over a 4-week period in db/db mice, the improvement of insulin secretion and insulin sensitivity in hyperglycemic

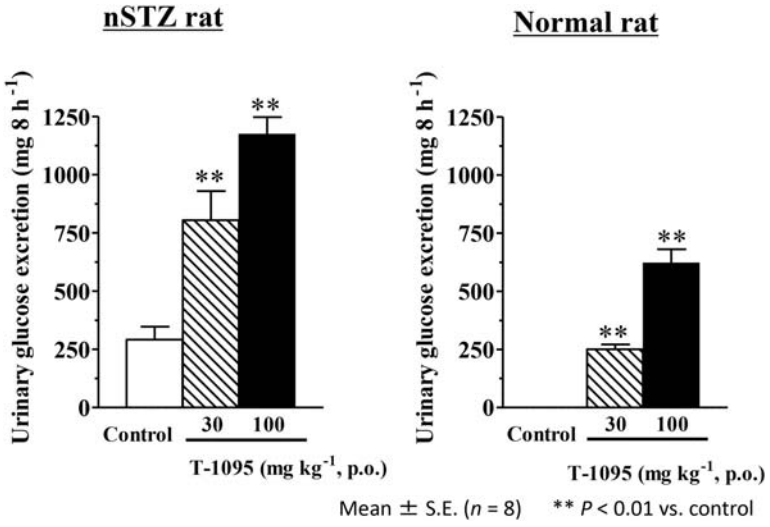

Fig. 5 T-1095 enhances urinary glucose excretion (UGE) more markedly in hyperglycemic than that in normoglycemic states. Data from Oku et al.[26]

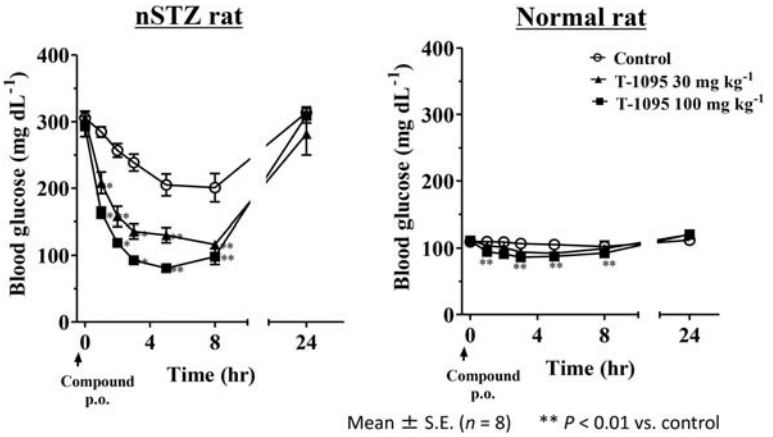

Fig. 6 T-1095 lowers blood glucose more markedly in hyperglycemic than that in normoglycemic states. Data from Oku et al.[26]

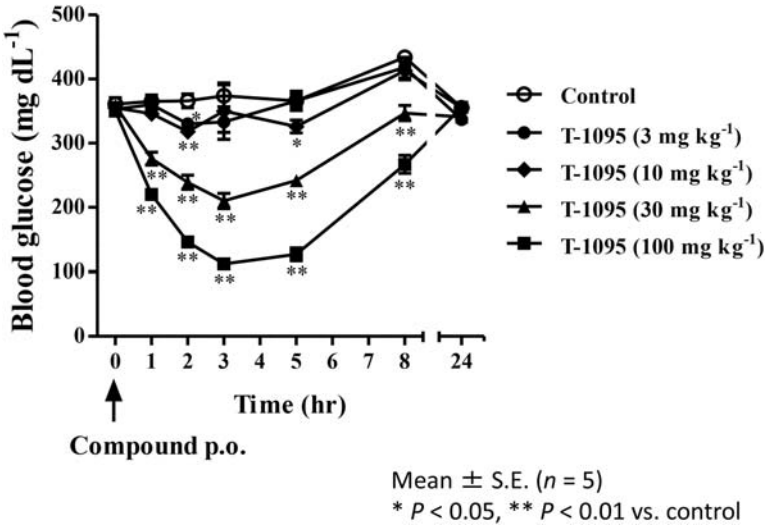

Fig. 7 T-1095 lowers blood glucose in streptozotocin-induced diabetic rats (STZ rats), a type 1 diabetes model. Data from Oku et al.[27]

animals was believed to be due to the alleviation of glucose toxicity. Furthermore, renal impairment in hyperglycemic animals was mitigated by long-term treatment with T-1095. These results indicated that a long-term inhibition of SGLT2 controls hyperglycemia and restores insulin secretion and insulin sensitivity through the alleviation of glucose toxicity, thus having the potential to relieve diabetic complications.

The aforementioned results provided a proof of principle for SGLT2 inhibition as a novel antidiabetic strategy with potential to control hyperglycemia, glucose toxicity, and complications. However, it was found that the *O*-glucoside portion of T-1095 is to some extent hydrolyzed to its aglycon in vivo in preclinical studies (Fig. 8). We, therefore, explored novel backup compounds that are more metabolically stable than T-1095.

8.14.4 Discovery of Canagliflozin

8.14.4.1 Exploration of *C*- and *N*-glucosides Bearing a Heteroaromatic Ring

After the reporting of T-1095-related compounds, several pharmaceutical companies began investigation into SGLT inhibitors (Fig. 9). Oral administration of nonglucoside pyrazole derivative **5** (WAY-123783) was reported to increase glycosuria in mice.[32] Later, WAY-123783 was speculated to be converted to an active metabolite pyrazole-*O*-glucoside, such as **6**, which inhibits SGLT activity and induces UGE in rats, following intravenous administration.[33] However, the compound **6** had already been patented by Kissei Pharmaceutical Co. (Kissei) in 2001.[34] Simplified benzylbenzene *O*-glucoside **7** was disclosed by Kissei[35] and Bristol-Myers Squibb (BMS)[36] in 2001. In addition, Kotobuki Seiyaku Co.[37] and BMS[38] unveiled the *C*-glucosides dihydrochalcone **8**

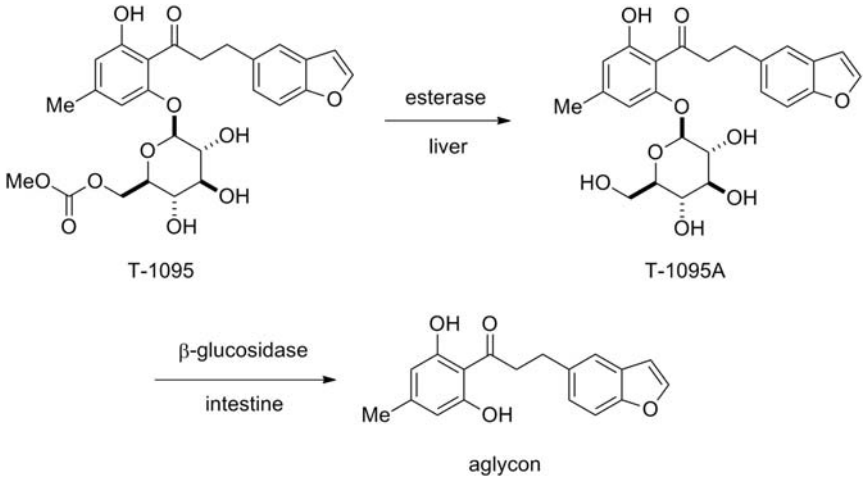

Fig. 8 Pharmacokinetic issues of T-1095.

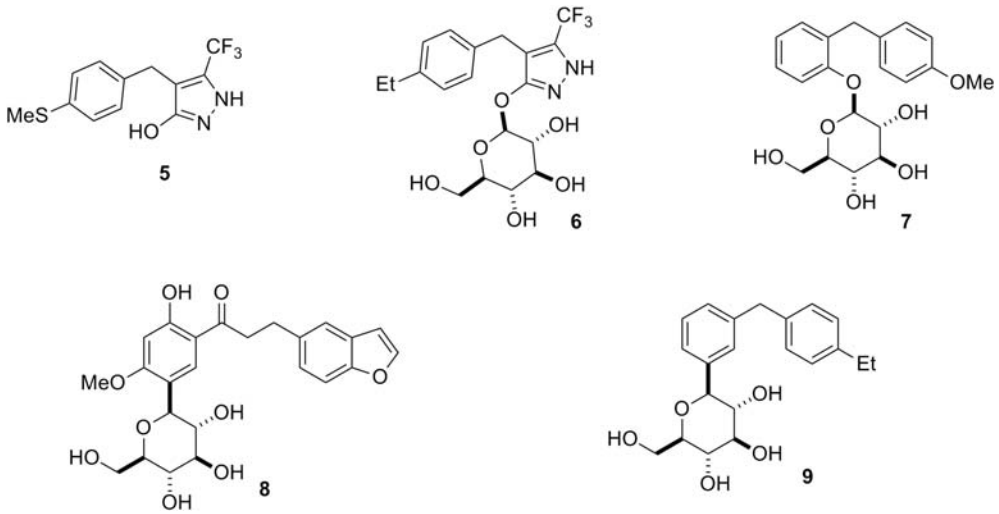

Fig. 9 Synthetic approach based on T-1095.

and benzylbenzene **9**, respectively, in the same year. We focused on the modification of *C*-glucosides because they are metabolically more stable than *O*-glucosides.

We explored *C*-glucosides and *N*-glucosides from scratch, with an aim to deliver compounds superior to previously published ones (Fig. 10). Benzylbenzyl *C*-glucoside **10** showed a weak inhibitory activity. In contrast, benzylaniline *N*-glucoside **11** possessed a strong inhibitory activity in vitro, although this aniline *N*-glucoside was metabolically unstable.[39,40] We, therefore, synthesized and evaluated a series of aromatic *C*-glucosides and aza-aromatic *N*-glucosides **12** bearing a heteroaromatic ring as the A or B ring. Exploration of aromatic *C*-glucosides **12** bearing a heteroaromatic ring as the A or B ring resulted in a series of *C*-glucosides **13** with a heteroaromatic B ring, which were more potent in vitro and in vivo than those with a heteroaromatic A ring (Fig. 11).[22] Optimization of these *C*-glucosides **13** led to the discovery of canagliflozin that has a substituted thiophene ring. The SAR of the representative compounds is shown in section "SAR of the Typical C-glucosides With a Heteroaromatic Ring." In addition, novel indole *N*-glucosides **14** were found among aza-aromatic *N*-glucosides **12** (Fig. 11).[39,41]

8.14.4.2 Syntheses of *C*-glucosides Bearing a Heteroaromatic Ring

The synthetic route for *C*-glucosides is outlined in Scheme 1.[22] As an aglycon part, arylbromides **15** were treated with *n*-butyllithium or *tert*-butyllithium to generate the corresponding aryllithium, followed by coupling with trimethylsilylated gluconolactone **16**. The resulting lactols directly led to desilylated methyl ethers **17** by the addition of methanesulfonic acid and methanol. Finally, *C*-glucoside derivatives **13** were obtained by the stereoselective reduction of **17** with a combination of triethylsilane and boron trifluoride etherate. The stereochemistry of *C*-glucosides **13** was determined as β-configuration based on the coupling constant of ~9.5 Hz between

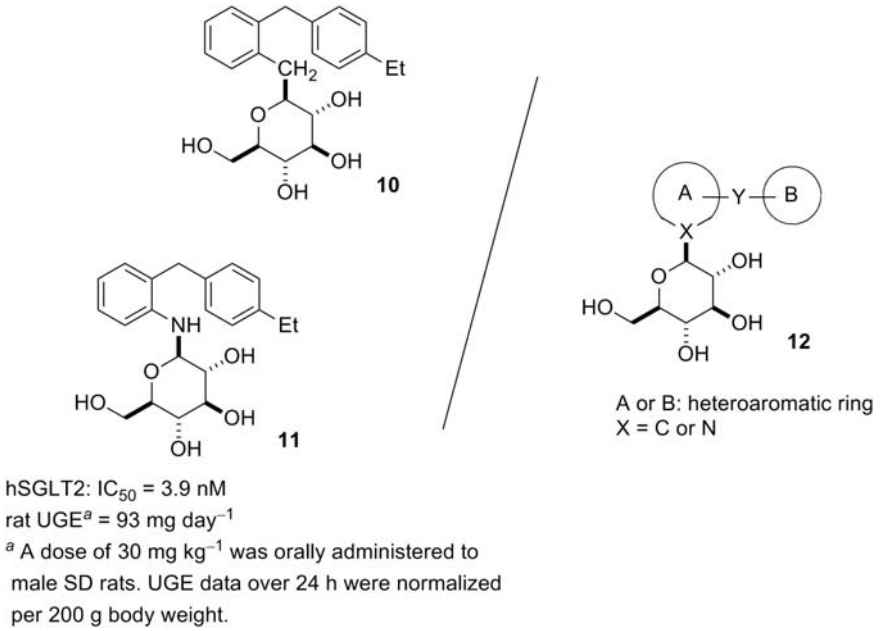

Fig. 10 Exploration of *C*- and *N*-glucosides. Data from Yamamoto et al.[39]

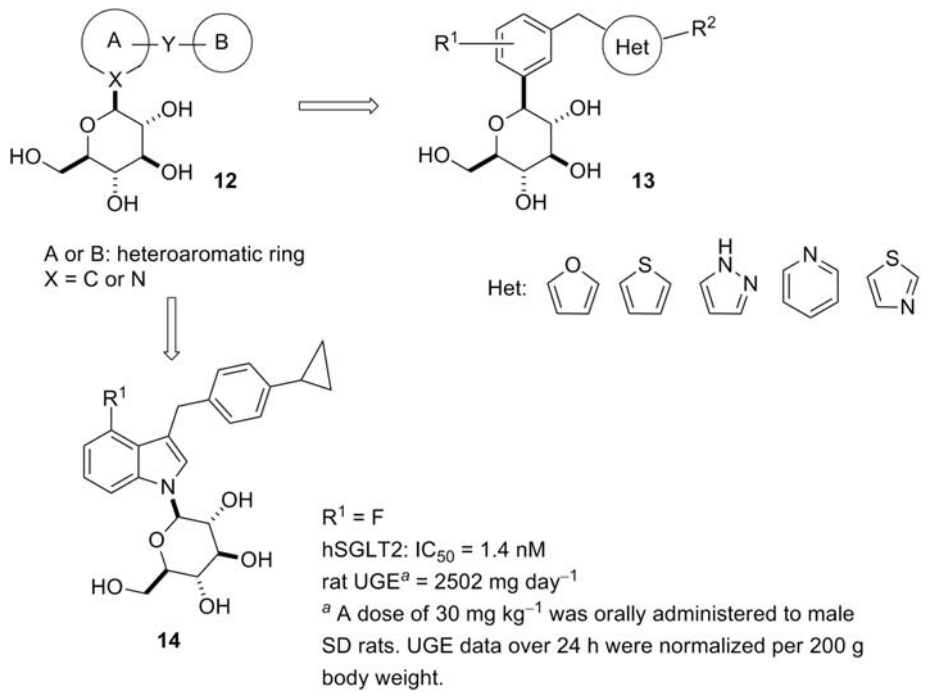

Fig. 11 Exploration of *C*- and *N*-glucosides bearing a heteroaromatic ring. Data from Nomura et al.[41]

anomeric proton and adjacent proton in the proton NMR spectrum. Aglycons represented by **15** were prepared via Friedel–Crafts acylation or by coupling reaction with heteroaryllithium followed by the reduction of ketone or carbinol. To provide thiazole derivatives, the corresponding ketoamides were cyclized using Lawesson's reagent (Scheme 2).[22]

8.14.4.3 SAR of the Typical *C*-glucosides With a Heteroaromatic Ring

The SAR of the typical *C*-glucoside compounds is shown in Table 1.[22] Effects of furan, thiophene, pyrazole, pyridine, and thiazole derivatives **13** were evaluated for hSGLT2 activity and for UGE in male SD rats per 200 g of body weight over 24 h. Ethylthiophene derivative **19** showed higher hSGLT2 inhibitory potency compared with ethylfuran **18** or ethylpyridine **23** derivatives.

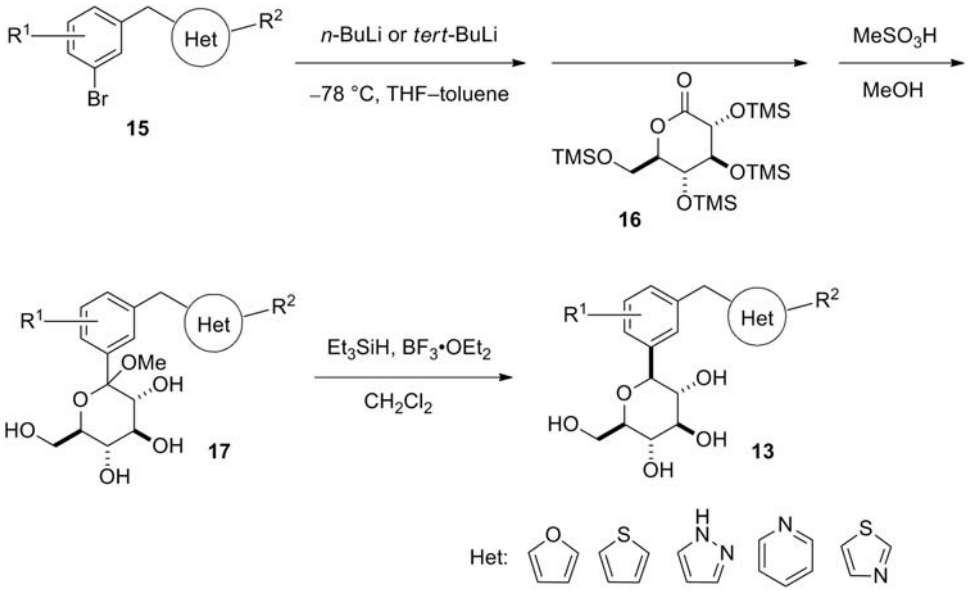

Scheme 1 Syntheses of **13**. Modified from Nomura, S.; Sakamaki, S.; Hongu, M.; Kawanishi, E.; Koga, Y.; Sakamoto, T.; Yamamoto, Y.; Ueta, K.; Kimata, H.; Nakayama, K.; Tsuda-Tsukimoto, M., Discovery of Canagliflozin, A Novel C-Glucoside with Thiophene Ring, as Sodium-Dependent Glucose Cotransporter 2 Inhibitor for the Treatment of Type 2 Diabetes Mellitus. *J. Med. Chem.* **2010**, *53* (17), 6355–6360.

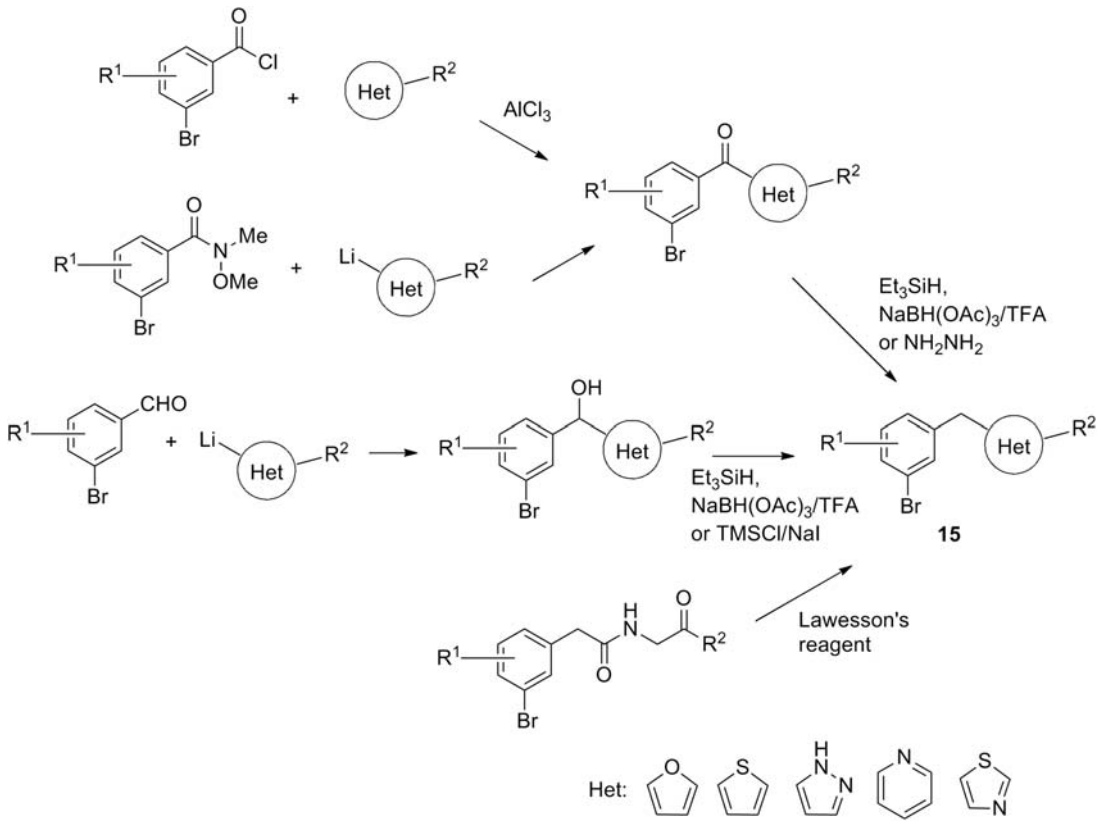

Scheme 2 Syntheses of aglycons **15**. Modified from Nomura, S.; Sakamaki, S.; Hongu, M.; Kawanishi, E.; Koga, Y.; Sakamoto, T.; Yamamoto, Y.; Ueta, K.; Kimata, H.; Nakayama, K.; Tsuda-Tsukimoto, M., Discovery of Canagliflozin, A Novel C-Glucoside with Thiophene Ring, as Sodium-Dependent Glucose Cotransporter 2 Inhibitor for the Treatment of Type 2 Diabetes Mellitus. *J. Med. Chem.* **2010**, *53* (17), 6355–6360.

Table 1 Structure–activity relationship (SAR) of the typical *C*-glucosides with a heteroaromatic ring

	Compound	R^1	Het-R^2	hSGLT2 IC_{50}(nM)	UGE[a] (mg day^{-1})
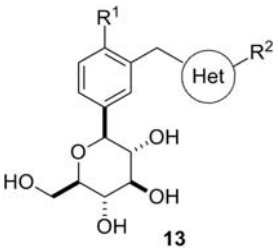 13	**18**	H	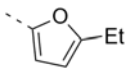	920	ND[b]
	19	H	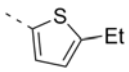	17	373
	20	Cl	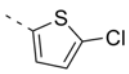	2.4	2495
	21	Me	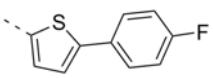	2.2	3696
	22	Cl	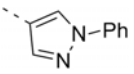	32	ND[b]
	23	Cl	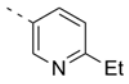	28	ND[b]
	24	Me	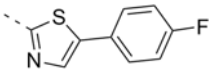	8.1	1277

[a]Each compound was orally administered at a dose of 30 mg kg^{-1} to male SD rats. UGE data over 24 h were normalized per 200 g body weight.
[b]*ND*, not determined.
Data from Nomura et al.[22]

Phenylthiophene derivative **21** also exhibited higher hSGLT2 inhibitory activity and higher UGE than phenylpyrazole **22** or phenylthiazole **24** derivatives. Thiophene derivatives showed the highest potency among these *C*-glucosides. For R^1 substituents, the halogeno (chloro of **20**) or lower alkyl (methyl of **21**) group provided higher in vitro potency than proton (**19**). Regarding in vivo potency and chemical stability, a substituted aryl (4-fluorophenyl of **21**) group was more preferable to alkyl (ethyl of **19**) or halogeno (chloro of **20**) groups in the R^2 substituent position. From these thiophene derivatives, **21** (canagliflozin, TA-7284/JNJ-28431754) was selected as a clinical candidate.

8.14.4.4 The Synthesis of Canagliflozin

An alternative synthetic route was evaluated (Scheme 3).[42] Aryl iodide **25** was treated with 2-butylmagnesium chloride–lithium chloride complex to generate arylmagnesium salt, followed by coupling with acetylated gluconolactone **26** at −35°C to −40°C. The resulting lactol was directly converted to **27** by reduction with silane. Finally, canagliflozin was obtained by the hydrolysis of **27**. Lemaire et al. reported a short and efficient stereoselective synthesis of canagliflozin (Scheme 4).[43] Aryl iodide **25** was treated with *n*-butyllithium to generate aryllithium, followed by the addition of zinc bromide–lithium bromide complex. The resulting transmetallated Ar–Zn–Ar was coupled with glucosyl bromide **28** at 90–100°C to produce the β-arylated glucoside **29** in 75% yield. The highly stereoselective cross coupling reaction was achieved via anomeric oxonium ion **30** due to the neighboring effect of a pivaloyl group. Finally, canagliflozin was obtained by the hydrolysis of **29**.

8.14.4.5 Canagliflozin: A Selective SGLT2 Inhibitor

The IC_{50} values of T-1095A and canagliflozin were 240 and 910 nM, respectively, for hSGLT1 and 5.2 and 2.2 nM, respectively, for SGLT2 in assays using Chinese hamster ovary-K (CHOK) cells stably expressing either hSGLT1 or hSGLT2. GLUT1 conducts the uptake of glucose in almost all tissues. Neither compound inhibited GLUT1 activity in L6 myoblast cells up to 10 μM (Table 2).[22] In addition, canagliflozin showed only weak inhibition of other SGLTs and GLUTs (Table 3).[44,45] Based on this data, canagliflozin is a highly potent and selective inhibitor of hSGLT2. Single oral administration of either T-1095 or canagliflozin at 30 mg kg^{-1} to male SD rats induced UGE over a 24 h period of 422 and 3696 mg, respectively, per 200 g body weight (Table 2).[22]

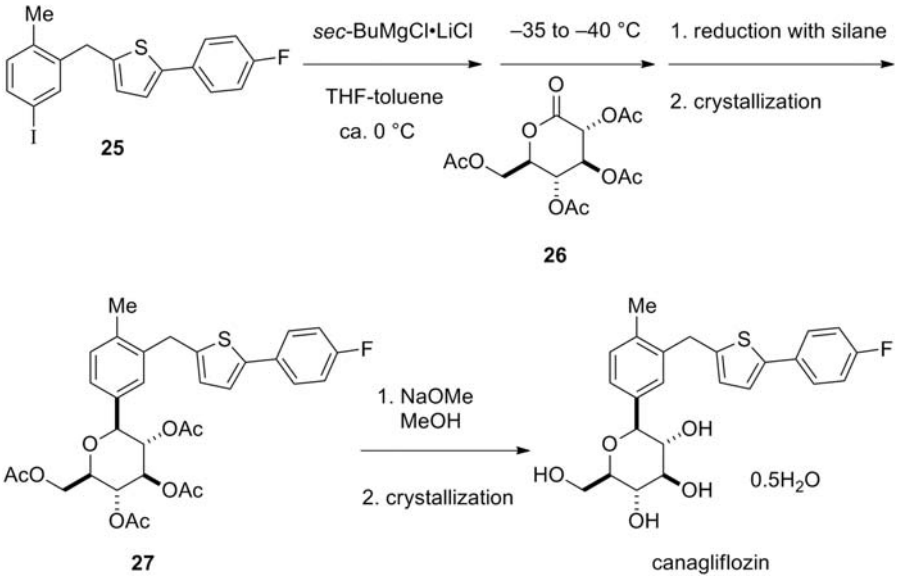

Scheme 3 Additional synthetic route for canagliflozin.

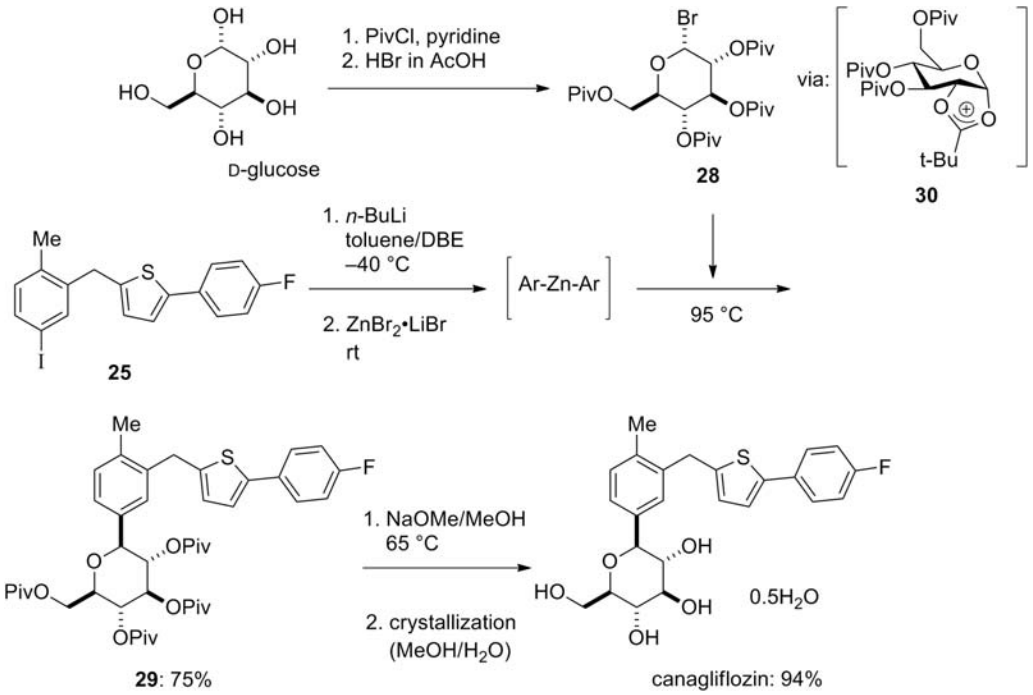

Scheme 4 Stereoselective synthesis of canagliflozin. Modified from Lemaire, S.; Houpis, I. N.; Xiao, T.; Li, J.; Digard, E.; Gozlan, C.; Liu, R.; Gavryushin, A.; Diène, C.; Wang, Y.; Farina, V.; Knochel, P., Stereoselective C-Glycosylation Reactions with Arylzinc Reagents. *Org. Lett.* **2012**, *14* (6), 1480–1483.

Pharmacokinetic (PK) studies revealed a much higher exposure of canagliflozin compared with T-1095 following oral administration at 10 mg kg^{-1} in male SD rats (Table 4) with $AUC_{0-inf,po}$ 35,980 ng h mL^{-1}, $t_{1/2,po}$ 5.2 h, and oral bioavailability of 85%.[22] At 24 h after oral administration of 3 mg kg^{-1} canagliflozin, unbound plasma concentration was similar to the IC_{50} value for SGLT2.[44] These studies demonstrate that the plasma level of canagliflozin is sufficient to inhibit SGLT2 in the renal tubules after oral dosing. The notable UGE most likely reflects superior PK properties of canagliflozin and highly potent SGLT2 inhibition in vivo.

Table 2 Effects of T-1095A, T-1095, and canagliflozin on hSGLT1, hSGLT2, facilitating glucose transporter 1 (GLUT1), and UGE

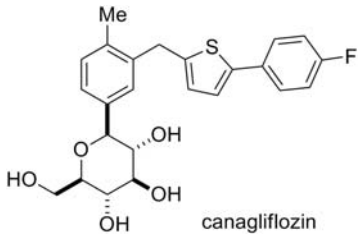

canagliflozin

IC_{50} (nM)				
Compound	*hSGLT1*	*hSGLT2*	*GLUT1*	*UGE*[a] *(mg day^{-1})*
T-1095A	240	5.2	>10,000	
T-1095[b]				422
Canagliflozin	910	2.2	>10,000	3696

[a]Compound T-1095 or canagliflozin was orally administered at a dose of 30 mg kg^{-1} to male SD rats. UGE data over 24 h were normalized per 200 g body weight.
[b]An ester prodrug T-1095 is rapidly converted to active metabolite T-1095A in vivo; thus, in vitro hSGLT inhibitory activities of T-1095 are not shown.
Data from Nomura et al.[22]

Table 3 Selectivity of canagliflozin over other SGLTs and GLUTs

	IC_{50} (μM)[a]				
Compound	*hSGLT3*	*hSGLT4*	*hSGLT6*	*hSGLT5 (from Ref. 45)*	*hSMIT1*
Canagliflozin	>10	>10	3.1	1.7	>10

	IC_{50} (μM)[b]
Rat skeletal muscle myoblast (expressing GLUT1)	>10
HepG2 cells (expressing GLUT1 and GLUT2)	>50
Human primary adipocytes (with insulin)	6.8±2.6
CHO cells expressing human GLUT5	>20

[a]IC_{50} values are expressed as means.
[b]IC_{50} values are expressed as means±S.D.
Data from Kuriyama et al.[44] and Grempler et al.[45]

Table 4 Pharmacokinetic (PK) parameters of T-1095A and canagliflozin in male Sprague Dawley (SD) rats following intravenous and oral administrations

Compound	*T-1095A*	*T-1095*[a]	*Canagliflozin*	
Dose (mg kg^{-1})	1	10	3	10
Route	iv	po	iv	po
C_{max} (ng mL^{-1})	–	80	–	2513
t_{max} (h)	–	1.3	–	5.0
AUC_{0-inf} (ng h mL^{-1})	153	304	12,703	35,980
$t_{1/2}$ (h)	1.3	2.2	5.0	5.2
CL_{tot} (mL h^{-1} kg^{-1})	7506	–	236	–
Vd_{ss} (mL kg^{-1})	11,390	–	1357	–
F (%)	–	20	–	85

[a]Because a prodrug T-1095 is very rapidly converted to T-1095A in vivo, PK parameters of T-1095A are shown.
Data from Nomura et al.[22]

8.14.4.6 Efficacy of Canagliflozin

Single oral administration of canagliflozin smoothly and continuously reduced blood glucose levels in ZDF rats over 24 h. Conversely, canagliflozin hardly affected blood glucose levels in normoglycemic rats (Fig. 12).[44] Whereas at 24 h after oral administration of 3 mg kg^{-1} canagliflozin, unbound plasma concentration was similar to the IC_{50} value for SGLT2, and the C_{max} value was much lower than the IC_{50} value for SGLT1 even after treatment with 30 mg kg^{-1} canagliflozin. Although UGE is increased after treatment with canagliflozin, 24 h accumulated UGE was not significantly different between canagliflozin- and vehicle-treated ZDF rats. This is because the plasma glucose levels of ZDF rats are higher than the renal threshold for glucose (RT_G), and UGE is detected in nontreated ZDF rats. After treatment with canagliflozin, glucose reabsorption is temporarily inhibited due to SGLT2 inhibition, and reduction in plasma glucose levels and renal glucose filtration is observed. Due to reduced glucose levels in the glomerular filtrate, UGE is reduced compared with that in nontreated hyperglycemic ZDF rats. As glucose excretion is reduced along with reduction of hyperglycemia, it is likely that the control of hyperglycemia with canagliflozin would be accompanied with a low risk of hypoglycemia.

Table 5 shows the result of 4-week treatment of canagliflozin in ZDF rats. ZDF rats develop hyperglycemia and hyperinsulinemia from 5 to 12 weeks of age, and plasma insulin levels decrease thereafter, while hyperglycemia persists. Fed plasma glucose and HbA1c levels decreased markedly following canagliflozin treatment. Chronic canagliflozin treatment also alleviated reduction in plasma insulin levels after 12 weeks of age via continuous control of hyperglycemia. In addition, canagliflozin treatment reduced blood glucose excursion and improved impaired insulin secretion following glucose challenge in an OGTT.[46] Histochemical analysis also revealed the preservation of pancreatic β-cells. Thus, it was demonstrated that canagliflozin improves pancreatic β-cell function through canceling glucose toxicity.

Effects of treatment with a combination of canagliflozin and dipeptidyl peptidase IV (DPP4) inhibitors were evaluated in ZDF rats.[47,48] A single oral treatment of canagliflozin and teneligliptin suppressed plasma glucose elevation in an OGTT in

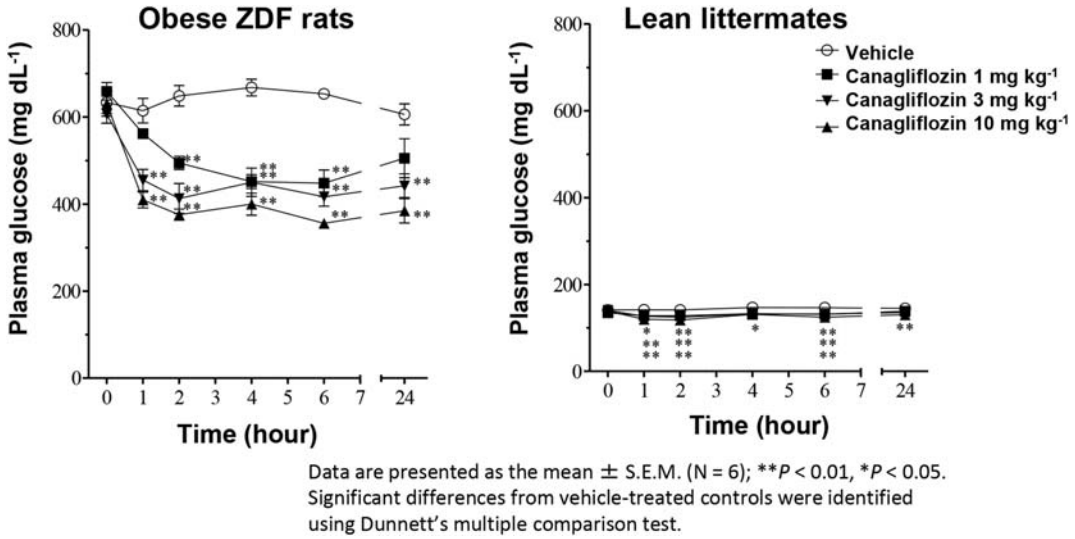

Fig. 12 Blood glucose-lowering effects in Zucker diabetic fatty (ZDF) rats. Data from Kuriyama et al.[44]

Table 5 Effects of a 4-week treatment of canagliflozin on blood glucose and insulin levels in ZDF rats

	Vehicle	*3 mg kg^{-1}*	*10 mg kg^{-1}*	*30 mg kg^{-1}*
Fed plasma glucose (mg dL^{-1})	598.2 ± 18.0	248.0 ± 13.5*	182.0 ± 7.1*	199.9 ± 14.7*
HbA1c (%)	11.5 ± 0.3	7.1 ± 0.3*	5.6 ± 0.3*	5.5 ± 0.3*
Insulin (ng mL^{-1})	5.2 ± 0.4	7.9 ± 0.1*	7.9 ± 0.1*	7.8 ± 0.1*
OGTT	–	–	–	–
Blood glucose ($AUC_{0–120\ min}$, mg dL^{-1} min)	70,704 ± 1289	27,883 ± 1806*	23,989 ± 1881*	16,549 ± 822*
Plasma insulin ($AUC_{0–120\ min}$, ng mL^{-1} min)	221 ± 13	342 ± 27*	403 ± 33*	288 ± 34
Ratio of insulin AUC/glucose AUC	0.003 ± 0.000	0.013 ± 0.002*	0.017 ± 0.002*	0.018 ± 0.002*

ZDF rats were treated with different doses of canagliflozin or vehicle for 4 weeks. Fed plasma glucose levels, HbA1c, and plasma insulin were determined at the end of this study. In addition, an OGTT was conducted. Blood glucose, plasma insulin, and urine glucose excretion were measured during OGTT. Data are presented as mean ± SEM ($n = 8$). *AUC*, area under the curve; *HbA1c*, glycated hemoglobin; *OGTT*, oral glucose tolerance test; *ZDF*, Zucker diabetic fatty.
*$p < 0.05$ compared with vehicle-treated group.
Data from Liang et al.[46]

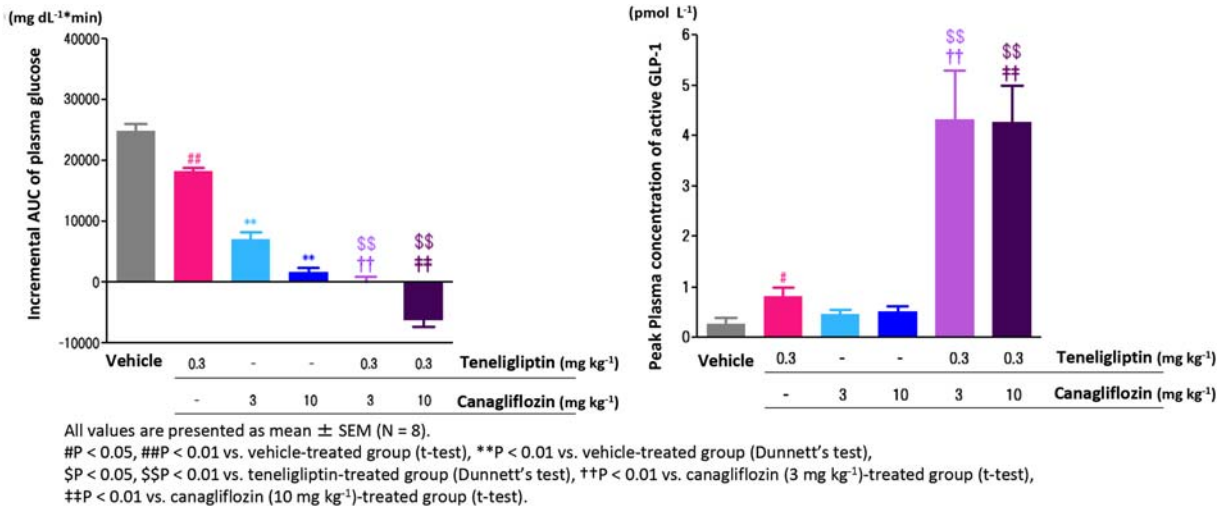

All values are presented as mean ± SEM (N = 8).
#P < 0.05, ##P < 0.01 vs. vehicle-treated group (t-test), **P < 0.01 vs. vehicle-treated group (Dunnett's test),
$P < 0.05, $$P < 0.01 vs. teneligliptin-treated group (Dunnett's test), ††P < 0.01 vs. canagliflozin (3 mg kg^{-1})-treated group (t-test),
‡‡P < 0.01 vs. canagliflozin (10 mg kg^{-1})-treated group (t-test).

Fig. 13 Effects of treatment with a combination of canagliflozin and dipeptidyl peptidase IV (DPP4) inhibitor teneligliptin during an oral glucose tolerance test (OGTT) in ZDF rats. Data from Oguma et al.[47]

13-week-old ZDF rats. The combined treatment further improved glucose intolerance and elevated plasma active glucagon-like peptide-1 (GLP-1) in a synergistic manner compared with single treatment of canagliflozin or teneligliptin (Fig. 13).[47] Because there were no PK interaction of the drugs and no further inhibition of plasma DPP4 activity compared with that in the teneligliptin-treated animals, it was suggested that canagliflozin promoted the meal-induced secretion of GLP-1 in intestinal cells.

SGLT1 mediates glucose absorption in intestinal epithelial cells. Although canagliflozin is an SGLT2 inhibitor, it also inhibits SGLT1 at a concentration 150 times higher than that for SGLT2 inhibition.[44] When canagliflozin is administered by oral gavage, intraluminal concentration in the upper small intestine is believed to be sufficient for SGLT1 inhibition. It was suggested that glucose absorption is partly suppressed and that intraluminal glucose concentration is temporarily increased through intestinal SGLT1 inhibition. Increase in intraluminal glucose stimulates secretion of GLP-1 in the distal part of small intestine. Detailed analysis of the combined use of canagliflozin and the DPP4 inhibitor sitagliptin showed close correlations between SGLT1 inhibition and elevation of plasma GLP-1 levels. It was, therefore, concluded that canagliflozin inhibits SGLT1 and suppresses glucose excursion in an OGTT through the suppression of glucose absorption in the upper small intestine and an increased glucose stimulates secretion of GLP-1 in the lower small intestine (Fig. 14).[48]

Hypertension and T2DM are often comorbid with obesity, and patients with comorbidity of these diseases have high risk of cardiovascular and cerebrovascular incidents. Spontaneously hypertensive corpulent congenic rats (SHR-cp) develops hypertension, obesity, hyperglycemia, and hyperlipidemia. A preliminary study indicated that canagliflozin reduces the development of hyperglycemia, hypertension, and hyperlipidemia in these animals. It was suggested that these effects were mediated by diuresis and calorie loss due to enhanced UGE and subsequent body weight reduction.[49]

8.14.5 Clinical Outcomes

8.14.5.1 Mechanism of Action of SGLT2 Inhibitors

The term "RT_G" defines the plasma glucose concentration at which tubular reabsorption of glucose reaches saturation; therefore, when glucose concentrations are above this threshold, UGE increases linearly. RT_G in healthy subjects is ~180 mg dL^{-1}, while RT_G in patients with T2DM rises to ~240 mg dL^{-1}. This higher value appears to be due to increased SGLT2 expression in patients as previously mentioned.[12] Canagliflozin lowers RT_G to 70–90 mg dL^{-1} in patients with T2DM. This value is safely above the plasma glucose levels causing symptomatic hypoglycemia. Therefore, a low risk of hypoglycemia is expected during treatment with canagliflozin. The inhibition of renal glucose reabsorption by canagliflozin decreases RT_G, enhances UGE, and consequently reduces blood glucose levels in patients with T2DM (Fig. 15).[50,51]

8.14.5.2 24-Week Phase 3 Study in Japanese Patients

Efficacy and safety of canagliflozin monotherapy were determined in patients with T2DM, with decreases in HbA1c and fasting plasma glucose (FPG) levels as the primary endpoints. In a phase 3 study, T2DM patients, who were inadequately controlled by diet and exercise, received 100 mg or 200 mg canagliflozin or placebo orally once per day for 24 weeks. The change in HbA1c at the end of the treatment period was −1.03% in the 100 mg canagliflozin group, this being a statistically significant reduction compared with that in the placebo group. The decrease in HbA1c in the canagliflozin group was evident by week 4 and reached

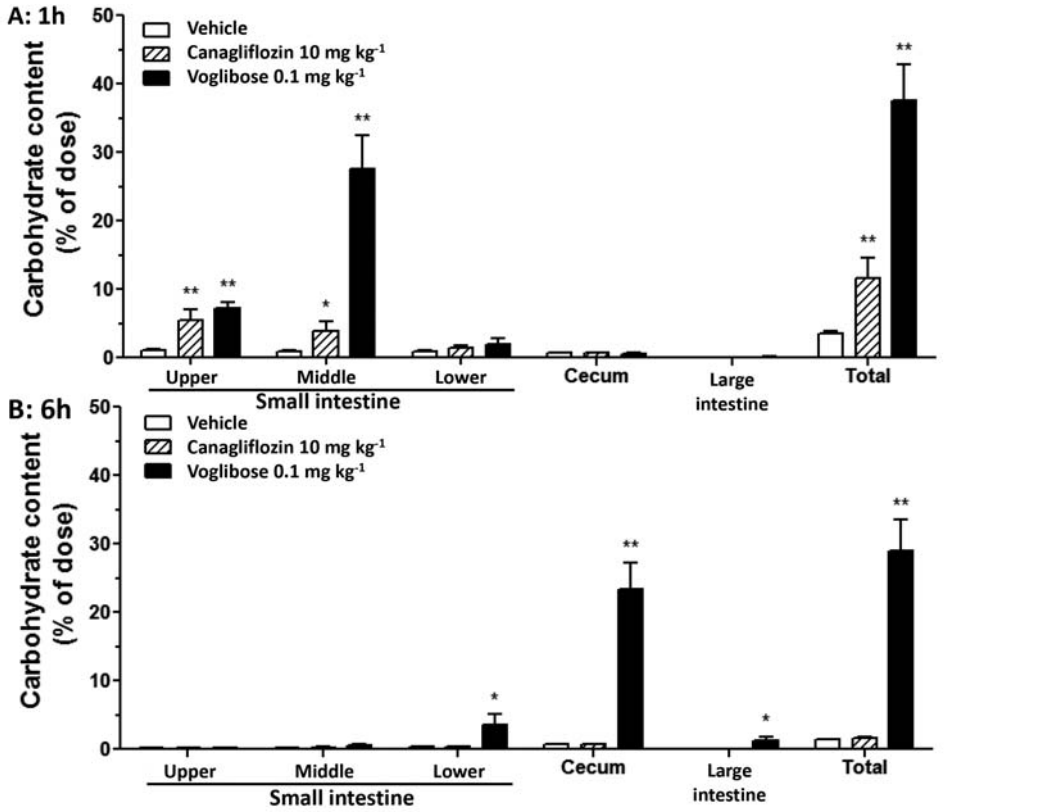

Carbohydrate content in upper SI, middle SI, lower SI, cecum, LI, and total segment of intestine 1-h (A) or 6-h (B) after sucrose-loading. Canagliflozin (10 mg kg^{-1}) or voglibose (0.1 mg kg^{-1}) and sucrose solution (2.5 g kg^{-1}) were simultaneously administered to SD rats by oral gavage. Intestinal contents were collected from GI tract divided into five parts. Data are presented as the mean ± S.E.M. (N = 6); *P < 0.05, **P < 0.01, Significant differences from vehicle treated groups were identified using Student's t-test.

Fig. 14 Effects of canagliflozin on carbohydrate absorption in the gastrointestinal (GI) tract in sucrose-loaded SD rats. Data from Oguma et al.[48]

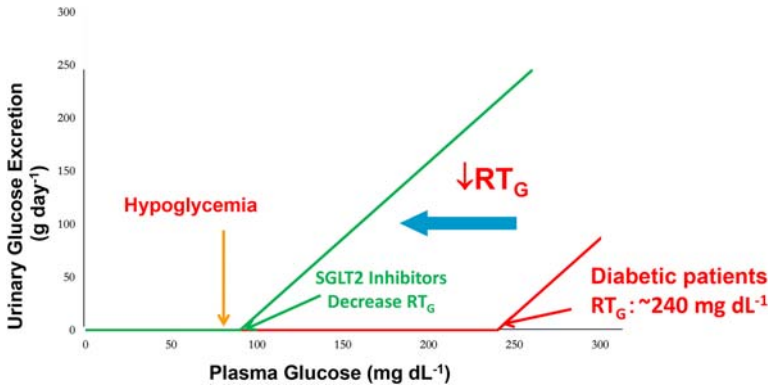

Fig. 15 SGLT inhibition lowers the renal threshold for glucose reabsorption (RT_G).

a plateau at around 12 weeks. Along with this change in HbA1c, FPG decreased over time in the canagliflozin group. In addition, plasma glucose excursion decreased significantly in the canagliflozin group in an OGTT conducted at week 24. The proinsulin/C-peptide ratio decreased, and HOMA-β increased significantly in the canagliflozin group. This result demonstrates that the 24-week treatment with canagliflozin improves pancreatic β-cell function and controls plasma glucose levels in a long-term period. Canagliflozin was generally well tolerated with a low incidence of hypoglycemia.[52]

In addition to the favorable improvement in the glycemic control, canagliflozin at 100 mg decreased body weight over time, with a change of −3.00% at 24 weeks. It is believed that continuous calorie loss due to glucose excretion in the urine induces weight reduction. Furthermore, systolic blood pressure was reduced significantly in the 100 mg canagliflozin group compared with that in

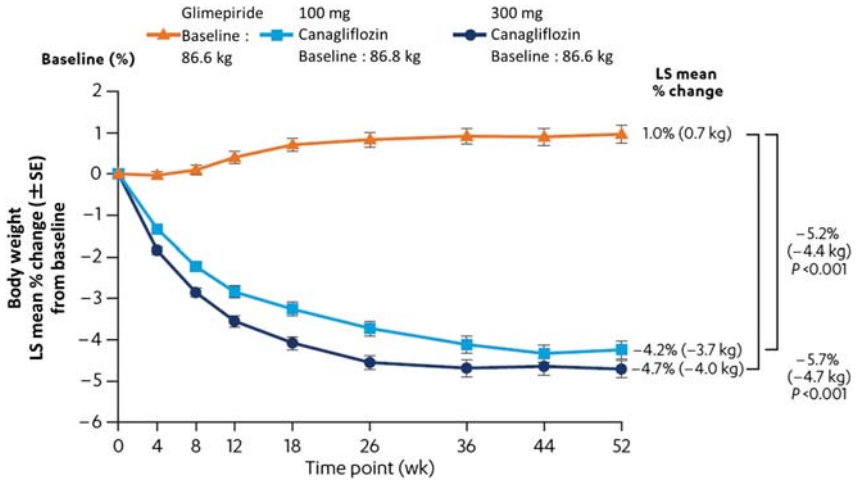

Fig. 16 CANTATA-SU trial: reduction in body weight. Data from Cefalu et al.[53]

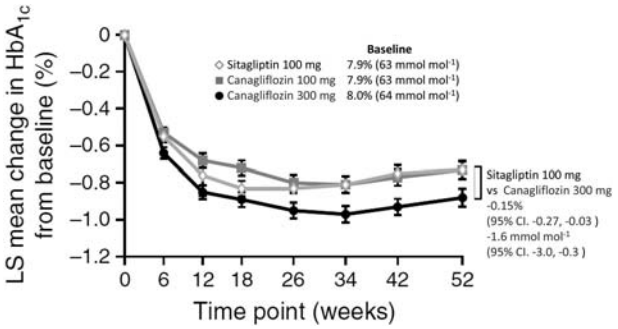

Fig. 17 CANTATA-D trial: reduction in HbA1c. Data from Lavalle-González et al.[54]

the placebo group, by 5.16 mmHg at the end of the treatment period. The reduction in systolic blood pressure may have been due to weight loss and osmotic diuresis.[52]

8.14.5.3 Phase 3 CANTATA Trials

The efficacy for lowering of HbA1c was similar between canagliflozin (100 mg) and sulfonylurea glimepiride (5.6 mg) in patients with T2DM at 52 weeks in the phase 3 CANTATA-SU trial. Canagliflozin significantly reduced body weight at week 52, whereas a slight increase was shown with glimepiride (Fig. 16). In the canagliflozin group, roughly two-thirds of the reduction in body weight was due to the loss of fat mass, and reduction in visceral fat was slightly greater than that in subcutaneous adipose tissues.[53] The efficacy for lowering HbA1c of 100 mg canagliflozin was noninferior to sitagliptin, and that of 300 mg canagliflozin was superior to sitagliptin (100 mg) in the phase 3 CANTATA-D trial in subjects with T2DM at 52 weeks of treatment (Fig. 17).[54]

8.14.5.4 Improvement of β-Cell Function

Phase 3 trials have also shown that in mixed-meal tolerance tests (MMTTs), postprandial plasma glucose excursion is reduced, and glucose-induced insulin secretion is enhanced in canagliflozin-treated T2DM patients.[55] In addition, postprandial GLP-1 and peptide YY (PYY) levels were elevated.[56] These results suggested that canagliflozin delays glucose absorption immediately after oral treatment and improves pancreatic β-cell function over long-term treatment.

8.14.6 Conclusion

Researchers at the Mitsubishi Tanabe Pharma Corporation discovered and developed SGLT2 inhibitors T-1095 and canagliflozin based on the revolutionary idea for treating T2DM with drugs that induce the excretion of excess glucose in the urine. The inhibition of renal glucose reabsorption enhances UGE and improves hyperglycemia. A long-term control of hyperglycemia reduces glucose

toxicity and preserves pancreatic β-cell function. Moreover, calorie loss due to enforced glucose disposal is associated with weight loss and reduction in blood pressure.[57] With its highly effective antidiabetic properties and strong safety profile, we expect canagliflozin to provide an innovative new approach to diabetic therapy.

See also: 7.13. Sodium–Glucose Cotransporters.

References

1. International Diabetes Federation. *IDF Diabetes Atlas,* 6th ed.; International Diabetes Federation: Brussels, 2013. http://www.idf.org/diabetesatlas.
2. Rossetti, L.; Giaccari, A.; DeFronzo, R. A. Glucose Toxicity. *Diabetes Care* **1990,** *13* (6), 610–630.
3. Inzucchi, S. E.; Bergenstal, R. M.; Buse, J. B.; Diamant, M.; Ferrannini, E.; Nauck, M.; Peters, A. L.; Tsapas, A.; Wender, R.; Matthews, D. R. Management of Hyperglycaemia in Type 2 Diabetes, 2015: A Patient-Centred Approach. Update to a Position Statement of the American Diabetes Association and the European Association for the Study of Diabetes. *Diabetologia* **2015,** *58,* 429–442.
4. Inzucchi, S. E.; Bergenstal, R. M.; Buse, J. B.; Diamant, M.; Ferrannini, E.; Nauck, M.; Peters, A. L.; Tsapas, A.; Wender, R.; Matthews, D. R. Management of Hyperglycaemia in Type 2 Diabetes, 2015: A Patient-Centred Approach. Update to a Position Statement of the American Diabetes Association and the European Association for the Study of Diabetes. *Diabetes Care* **2015,** *38,* 140–149.
5. Kahn, S. E.; Haffner, S. M.; Heise, M. A.; Herman, W. H.; Holman, R. R.; Jones, N. P.; Kravitz, B. G.; Lachin, J. M.; O'Neill, M. C.; Zinman, B.; Viberti, G. Glycemic Durability of Rosiglitazone, Metformin, or Glyburide Monotherapy. *N. Engl. J. Med.* **2006,** *355* (23), 2427–2443.
6. Tsujihara, K.; Hongu, M.; Saito, K.; Inamasu, M.; Arakawa, K.; Oku, A.; Matsumoto, M. Na^+-Glucose Cotransporter Inhibitors as Antidiabetics. I. Synthesis and Pharmacological Properties of 4′-Dehydroxyphlorizin Derivatives Based on a New Concept. *Chem. Pharm. Bull. (Tokyo)* **1996,** *44* (6), 1174–1180.
7. Chao, E. C.; Henry, R. R. SGLT2 Inhibition—A Novel Strategy for Diabetes Treatment. *Nat. Rev. Drug Discov.* **2010,** *9,* 551–559.
8. Wright, E. M. Renal Na^+-Glucose Cotransporters. *Am. J. Physiol. Renal Physiol.* **2001,** *280,* F10–F18.
9. Mackenzie, B.; Loo, D. D. F.; Panayotova-Heiermann, M.; Wright, E. M. Biophysical Characteristics of the Pig Kidney Na^+/Glucose Cotransporter SGLT2 Reveal a Common Mechanism for SGLT1 and SGLT2. *J. Biol. Chem.* **1996,** *271* (51), 32678–32683.
10. Kanai, Y.; Lee, W.-S.; You, G.; Brown, D.; Hediger, M. A. The Human Kidney Low Affinity Na^+/Glucose Cotransporter SGLT2. Delineation of the Major Renal Reabsorptive Mechanism for D-Glucose. *J. Clin. Invest.* **1994,** *93,* 397–404.
11. Deetjen, P.; Baeyer, H. V.; Drexel, H. Renal Handling of D-Glucose and Other Sugars. In *Textbook of Nephrology;* Massry, S. G., Glassock, R. J., Eds., 3rd ed.; Vol. 1; Williams & Wilkins Press: Baltimore, MD, 1995; pp 90–94.
12. Rahmoune, H.; Thompson, P. W.; Ward, J. M.; Smith, C. D.; Hong, G.; Brown, J. Glucose Transporters in Human Renal Proximal Tubular Cells Isolated from the Urine of Patients with Non-Insulin-Dependent Diabetes. *Diabetes* **2005,** *54,* 3427–3434.
13. Abdul-Ghani, M. A.; DeFronzo, R. A. Inhibition of Renal Glucose Reabsorption: A Novel Strategy for Achieving Glucose Control in Type 2 Diabetes Mellitus. *Endocr. Pract.* **2008,** *14* (6), 782–790.
14. Scholl-Bürgi, S.; Santer, R.; Ehrich, J. H. H. Long-Term Outcome of Renal Glucosuria Type 0: The Original Patient and His Natural History. *Nephrol. Dial. Transplant.* **2004,** *19* (9), 2394–2396.
15. Oemar, B. S.; Byrd, D. J.; Brodehl, J. Complete Absence of Tubular Glucose Reabsorption: A New Type of Renal Glucosuria (Type 0). *Clin. Nephrol.* **1987,** *27* (3), 156–160.
16. Tsujihara, K.; Hongu, M.; Saito, K.; Kawanishi, H.; Kuriyama, K.; Matsumoto, M.; Oku, A.; Ueta, K.; Tsuda, M.; Saito, A. Na^+-Glucose Cotransporter (SGLT) Inhibitors as Antidiabetic Agents. 4. Synthesis and Pharmacological Properties of 4′-Dehydroxyphlorizin Derivatives Substituted on the B Ring. *J. Med. Chem.* **1999,** *42* (26), 5311–5324.
17. Ehrenkranz, J. R. L; Lewis, N. G.; Kahn, C. R.; Roth, J. Phlorizin: A Review. *Diabetes Metab. Res. Rev.* **2005,** *21,* 31–38.
18. Toggenburger, G.; Kessler, M.; Semenza, G. Phlorizin as a Probe of the Small-Intestinal Na^+, D-Glucose Cotransporter. A Model. *Biochim. Biophys. Acta* **1982,** *688,* 557–571.
19. Alvarado, F.; Crane, R. K. Studies on the Mechanism of Intestinal Absorption of Sugars. VII. Phenylglycoside Transport and Its Possible Relationship to Phlorizin Inhibition of the Active Transport of Sugars by the Small Intestine. *Biochim. Biophys. Acta* **1964,** *93,* 116–135.
20. Alvarado, F.; Crane, R. K. Phlorizin as a Competitive Inhibitor of the Active Transport of Sugars by Hamster Small Intestine, In Vitro. *Biochim. Biophys. Acta* **1962,** *56,* 170–172.
21. McKee, F. W.; Hawkins, W. B. Phlorhizin Glucosuria. *Physiol. Rev.* **1945,** *25,* 255–280.
22. Nomura, S.; Sakamaki, S.; Hongu, M.; Kawanishi, E.; Koga, Y.; Sakamoto, T.; Yamamoto, Y.; Ueta, K.; Kimata, H.; Nakayama, K.; Tsuda-Tsukimoto, M. Discovery of Canagliflozin, a Novel *C*-Glucoside with Thiophene Ring, as Sodium-Dependent Glucose Cotransporter 2 Inhibitor for the Treatment of Type 2 Diabetes Mellitus. *J. Med. Chem.* **2010,** *53* (17), 6355–6360.
23. Hongu, M.; Tanaka, T.; Funami, N.; Saito, K.; Arakawa, K.; Matsumoto, M.; Tsujihara, K. Na^+-Glucose Cotransporter Inhibitors as Antidiabetic Agents. II. Synthesis and Structure–Activity Relationships of 4′-Dehydroxyphlorizin Derivatives. *Chem. Pharm. Bull. (Tokyo)* **1998,** *46* (1), 22–33.
24. Hongu, M.; Funami, N.; Takahashi, Y.; Saito, K.; Arakawa, K.; Matsumoto, M.; Yamakita, H.; Tsujihara, K. Na^+-Glucose Cotransporter Inhibitors as Antidiabetic Agents. III. Synthesis and Pharmacological Properties of 4′-Dehydroxyphlorizin Derivatives Modified at the OH Groups of the Glucose Moiety. *Chem. Pharm. Bull* **1998,** *46* (10), 1545–1555.
25. Oku, A.; Ueta, K.; Arakawa, K.; Ishihara, T.; Nawano, M.; Kuronuma, Y.; Matsumoto, M.; Saito, A.; Tsujihara, K.; Anai, M.; Asano, T.; Kanai, Y.; Endou, H. T-1095, An Inhibitor of Renal Na^+-Glucose Cotransporters, May Provide a Novel Approach to Treating Diabetes. *Diabetes* **1999,** *48,* 1794–1800.
26. Oku, A.; Ueta, K.; Nawano, M.; Arakawa, K.; Kano-Ishihara, T.; Matsumoto, M.; Saito, A.; Tsujihara, K.; Anai, M.; Asano, T. Antidiabetic Effect of T-1095, An Inhibitor of Na^+-Glucose Cotransporter, in Neonatally Streptozotocin-Treated Rats. *Eur. J. Pharmacol.* **2000,** *391,* 183–192.
27. Oku, A.; Ueta, K.; Arakawa, K.; Kano-Ishihara, T.; Matsumoto, M.; Adachi, T.; Yasuda, K.; Tsuda, K.; Saito, A. Antihyperglycemic Effect of T-1095 Via Inhibition of Renal Na^+-Glucose Cotransporters in Streptozotocin-Induced Diabetic Rats. *Biol. Pharma. Bull.* **2000,** *23* (12), 1434–1437.
28. Ueta, K.; Ishihara, T.; Matsumoto, Y.; Oku, A.; Nawano, M.; Fujita, T.; Saito, A.; Arakawa, K. Long-Term Treatment with the Na^+-Glucose Cotransporter Inhibitor T-1095 Causes Sustained Improvement in Hyperglycemia and Prevents Diabetic Neuropathy in Goto-Kakizaki Rats. *Life Sci.* **2005,** *76,* 2655–2668.
29. Nawano, M.; Ueta, K.; Oku, A.; Arakawa, K.; Saito, A.; Funaki, M.; Anai, M.; Kikuchi, M.; Oka, Y.; Asano, T. Hyperglycemia Impairs the Insulin Signaling Step Between PI 3-Kinase and Akt/PKB Activations in ZDF Rat Liver. *Biochem. Biophys. Res. Commun.* **1999,** *266,* 252–256.
30. Nawano, M.; Oku, A.; Ueta, K.; Umebayashi, I.; Ishirahara, T.; Arakawa, K.; Saito, A.; Anai, M.; Kikuchi, M.; Asano, T. Hyperglycemia Contributes Insulin Resistance in Hepatic and Adipose Tissue But Not Skeletal Muscle of ZDF Rats. *Am. J. Physiol. Endocrinol. Metab.* **2000,** *278,* E535–E543.
31. Arakawa, K.; Ishihara, T.; Oku, A.; Nawano, M.; Ueta, K.; Kitamura, K.; Matsumoto, M.; Saito, A. Improved Diabetic Syndrome in C57BL/KsJ-db/db Mice by Oral Administration of the Na^+-Glucose Cotransporter Inhibitor T-1095. *Br. J. Pharmacol.* **2001,** *132,* 578–586.
32. Kees, K. L.; Fitzgerald, J. J.; Steiner, K. E.; Mattes, J. F.; Mattes, J. F.; Mihan, B.; Tosi, T.; Tosi, T.; Mondoro, D.; McCaleb, M. L. New Potent Antihyperglycemic Agents in db/db Mice: Synthesis and Structure–Activity Relationship Studies of (4-Substituted Benzyl)(Trifluoromethyl)Pyrazoles and -Pyrazolones. *J. Med. Chem.* **1996,** *39* (20), 3920–3928.

33. Ohsumi, K.; Matsueda, H.; Hatanaka, T.; Hirama, R.; Umemura, T.; Oonuki, A.; Ishida, N.; Kageyama, Y.; Maezono, K.; Kondo, N. Pyrazole-*O*-Glucosides as Novel Na^+-Glucose Cotransporter (SGLT) Inhibitors. *Bioorg. Med. Chem. Lett.* **2003,** *13,* 2269–2272.
34. Fujikura, H.; Nishimura, T.; Katsuno, K.; Hiratochi, M.; Iyobe, A.; Fujioka, M.; Isaji, M. Glucopyranosyloxypyrazole Derivatives, Medicinal Compositions Containing the Same and Intermediates in the Production Thereof. PCT Int. Appl. WO 01/16147, 2001.
35. Fujikura, H.; Fushimi, N.; Nishimura, T.; Tatani, K.; Katsuno, K.; Hiratochi, M.; Tokutake, Y.; Isaji, M. Glucopyranosyloxy Benzylbenzene Derivatives, Medicinal Compositions Containing the Same and Intermediates for the Preparation of the Derivatives. PCT Int. Appl. WO 01/68660, 2001.
36. Washburn, W. N.; Sher, P. M.; Wu, G. O-Aryl Glucoside SGLT2 Inhibitors and Method. PCT Int. Appl. WO 01/74834, 2001.
37. Tomiyama, Y.; Kobayashi, Y.; Noda, A.; Tomiyama, I.; Tomiyama, T. C-Glycoside, Method for Producing the Same and Medicine Containing the Same. Jpn. Kokai Tokkyo Koho, JP2001288178, 2001.
38. Ellsworth, B.; Washburn, W. N.; Sher, P. M.; Wu, G.; Meng, W. C-Aryl Glucoside SGLT2 Inhibitors. PCT Int. Appl. WO 01/27128, 2001.
39. Yamamoto, Y.; Kawanishi, E.; Koga, Y.; Sakamaki, S.; Sakamoto, T.; Ueta, K.; Matsushita, Y.; Kuriyama, C.; Tsuda-Tsukimoto, M.; Nomura, S. *N*-Glucosides as Human Sodium-Dependent Glucose Cotransporter 2 (hSGLT2) Inhibitors. *Bioorg. Med. Chem. Lett.* **2013,** *23,* 5641–5645.
40. Nomura, S. Renal Sodium-Dependent Glucose Cotransporter 2 (SGLT2) Inhibitors for New Anti-Diabetic Agent. *Curr. Top. Med. Chem.* **2010,** *10* (4), 411–418.
41. Nomura, S.; Yamamoto, Y.; Matsumura, Y.; Ohba, K.; Sakamaki, S.; Kimata, H.; Nakayama, K.; Kuriyama, C.; Matsushita, Y.; Ueta, K.; Tsuda-Tsukimoto, M. Novel Indole-*N*-Glucoside, TA-1887 as a Sodium Glucose Cotransporter 2 Inhibitor for Treatment of Type 2 Diabetes. *ACS Med. Chem. Lett.* **2014,** *5,* 51–55.
42. Filliers, W. F. M.; Broeckx, R. L. M.; Nieste, P. H. J.; Hatsuda, M.; Yoshinaga, M.; Yada, M.; Teleha, C. Process for the Preparation of Compounds Useful as Inhibitors of SGLT. PCT Int. Appl. WO 10/043682, 2010.
43. Lemaire, S.; Houpis, I. N.; Xiao, T.; Li, J.; Digard, E.; Gozlan, C.; Liu, R.; Gavryushin, A.; Diène, C.; Wang, Y.; Farina, V.; Knochel, P. Stereoselective C-Glycosylation Reactions with Arylzinc Reagents. *Org. Lett.* **2012,** *14* (6), 1480–1483.
44. Kuriyama, C.; Xu, J. Z.; Lee, S. P.; Qi, J.; Kimata, H.; Kakimoto, T.; Nakayama, K.; Watanabe, Y.; Taniuchi, N.; Hikida, K.; Matsushita, Y.; Arakawa, K.; Saito, A.; Ueta, K.; Shiotani, M. Analysis of the Effect of Canagliflozin on Renal Glucose Reabsorption and Progression of Hyperglycemia in Zucker Diabetic Fatty Rats. *J. Pharmacol. Exp. Ther.* **2014,** *351,* 423–431.
45. Grempler, R.; Thomas, L.; Eckhardt, M.; Himmelsbach, F.; Sauer, A.; Sharp, D. E.; Bakker, R. A.; Mark, M.; Klein, T.; Eickelmann, P. Empagliflozin, A Novel Selective Sodium Glucose Cotransporter-2 (SGLT-2) Inhibitor: Characterization and Comparison with Other SGLT-2 Inhibitors. *Diabetes Obes. Metab.* **2012,** *14* (1), 83–90.
46. Liang, Y.; Arakawa, K.; Ueta, K.; Matsushita, Y.; Kuriyama, C.; Martin, T.; Du, F.; Liu, Y.; Xu, J.; Conway, B.; Conway, J.; Polidori, D.; Ways, K.; Demarest, K. Effect of Canagliflozin on Renal Threshold for Glucose, Glycemia, and Body Weight in Normal and Diabetic Animal Models. *PLoS ONE* **2012,** *7* (2), e30555.
47. Oguma, T.; Kuriyama, C.; Nakayama, K.; Matsushita, Y.; Yoshida, K.; Kiuchi, S.; Ikenaga, Y.; Nakamaru, Y.; Hikida, K.; Saito, A.; Arakawa, K.; Oka, K.; Ueta, K.; Shiotani, M. The Effect of Combined Treatment with Canagliflozin and Teneligliptin on Glucose Intolerance in Zucker Diabetic Fatty Rats. *J. Pharmacol. Sci.* **2015,** *127,* 456–461.
48. Oguma, T.; Nakayama, K.; Kuriyama, C.; Matsushita, Y.; Yoshida, K.; Hikida, K.; Obokata, N.; Tsuda-Tsukimoto, M.; Saito, A.; Arakawa, K.; Ueta, K.; Shiotani, M. Intestinal Sodium Glucose Cotransporter 1 Inhibition Enhances Glucagon-Like Peptide-1 Secretion in Normal and Diabetic Rodents. *J. Pharmacol. Exp. Ther.* **2015,** *354,* 279–289.
49. Matsushita, Y.; Kuriyama, C.; Ueta, K.; Arakawa, K.; Shiotani, M. *J. Jpn. Diabetes Soc.* **2014,** *57* (Suppl.), S-173.
50. Devineni, D.; Curtin, C. R.; Polidori, D.; Gutierrez, M. J.; Murphy, J.; Rusch, S.; Rothenberg, P. L. Pharmacokinetics and Pharmacodynamics of Canagliflozin, a Sodium Glucose Co-transporter 2 Inhibitor, in Subjects with Type 2 Diabetes Mellitus. *J. Clin. Pharmacol.* **2013,** *53* (6), 601–610.
51. Polidori, D.; Sha, S.; Sarich, T.; Devineni, D.; Rothenberg, P. L. Canagliflozin Lowers the Renal Threshold for Glucose Excretion in Lean, Obese and Type 2 Diabetic Subjects. *Diabetologia* **2010,** *53* (Suppl. 1), S350.
52. Inagaki, N.; Kondo, K.; Yoshinari, T.; Takahashi, N.; Susuta, Y.; Kuki, H. Efficacy and Safety of Canagliflozin Monotherapy in Japanese Patients with Type 2 Diabetes Inadequately Controlled with Diet and Exercise: A 24-Week, Randomized, Double-Blind, Placebo-Controlled, Phase III Study. *Expert Opin. Pharmacother.* **2014,** *15* (11), 1501–1515.
53. Cefalu, W. T.; Leiter, L. A.; Yoon, K.-H.; Arias, P.; Niskanen, L.; Xie, J.; Balis, D. A.; Canovatchel, W.; Meininger, G. Efficacy and Safety of Canagliflozin Versus Glimepiride in Patients with Type 2 Diabetes Inadequately Controlled with Metformin (CANTATA-SU): 52 Week Results from a Randomised, Double-Blind, Phase 3 Non-Inferiority Trial. *Lancet* **2013,** *382,* 941–950.
54. Lavalle-González, F. J.; Januszewicz, A.; Davidson, J.; Tong, C.; Qiu, R.; Canovatchel, W.; Meininger, G. Efficacy and Safety of Canagliflozin Compared with Placebo and Sitagliptin in Patients with Type 2 Diabetes on Background Metformin Monotherapy: A Randomized Trial. *Diabetologia* **2013,** *56* (12), 2582–2592.
55. Polidori, D.; Mari, A.; Ferrannini, E. Canagliflozin, A Sodium Glucose Co-Transporter 2 Inhibitor, Improves Model-Based Indices of Beta Cell Function in Patients with Type 2 Diabetes. *Diabetologia* **2014,** *57,* 891–901.
56. Polidori, D.; Sha, S.; Mudaliar, S.; Ciaraldi, T. P.; Ghosh, A.; Vaccaro, N.; Farrell, K.; Rothenberg, P.; Henry, R. R. Canagliflozin Lowers Postprandial Glucose and Insulin by Delaying Intestinal Glucose Absorption in Addition to Increasing Urinary Glucose Excretion. *Diabetes Care* **2013,** *36,* 2154–2161.
57. Idris, I.; Donnelly, R. Sodium-Glucose Co-transporter-2 Inhibitors: An Emerging New Class of Oral Antidiabetic Drug. *Diabetes Obes. Metab.* **2009,** *11,* 79–88.

Relevant Websites

http://www.medscape.com/viewarticle/777503—FDA Advisory Panel Supports Diabetes Drug Canagliflozin.

http://www.fda.gov/NewsEvents/Newsroom/PressAnnouncements/ucm345848.htm—FDA approves Invokana to treat type 2 diabetes. First in a new class of diabetes drugs.

http://www.fda.gov/downloads/AdvisoryCommittees/CommitteesMeetingMaterials/Drugs/EndocrinologicandMetabolicDrugsAdvisoryCommittee/UCM334550.pdf—FDA Briefing Document—Food and Drug Administration.

http://www.fda.gov/Drugs/DrugSafety/ucm461449.htm—FDA Drug Safety Communication: FDA Revises Label of Diabetes Drug Canagliflozin (Invokana, Invokamet) to Include Updates on Bone Fracture Risk and New Information on Decreased Bone Mineral Density.

http://www.investor.jnj.com/releasedetail.cfm?releaseid=827412—Janssen Initiates CREDENCE Study in Patients with Type 2 Diabetes and Diabetic Nephropathy. Trial Seeks to Examine the Effects of INVOKANA® on the Progression of Diabetic Nephropathy.

https://clinicaltrials.gov/ct2/show/NCT02065791—Evaluation of the Effects of Canagliflozin on Renal and Cardiovascular Outcomes in Participants with Diabetic Nephropathy (CREDENCE).

http://www.jnj.com/news/all/phase-3-canvas-trial-show-canagliflozin-as-add-on-therapy-to-insulin-lowered-blood-sugar-levels-in-patients-with-type-2-diabetes-at-an-elevated-risk-for-cardiovascular-disease—First Results from Phase 3 CANVAS Trial Show Canagliflozin as Add-on Therapy to Insulin Lowered Blood Sugar Levels in Patients with Type 2 Diabetes at an Elevated Risk for Cardiovascular Disease. Canagliflozin Also Shown Effective and Generally Well-Tolerated in Patients with Type 2 Diabetes Aged 55 to 80 in Separate Phase 3 Study.

https://clinicaltrials.gov/ct2/show/NCT01032629—CANVAS, CANagliflozin cardioVascular Assessment Study.

http://www.drugs.com/history/invokana.html—Invokana Approval History.

https://www.invokanahcp.com/prescribing-information.pdf—Invokana PDR.

8.15 The Discovery and Development of *Seletalisib*: A Potent and Selective PI3Kδ Inhibitor for Inflammatory Diseases

DC Brookings, UCB Pharma, Slough, United Kingdom

© 2017 Elsevier Ltd. All rights reserved.

8.15.1	**Introduction**	366
8.15.1.1	The Rationale for Selectively Targeting PI3Kδ to Treat Inflammatory Disease	367
8.15.1.2	Implementation of a Screening Cascade and Description of Key Assays	368
8.15.1.2.1	Description of in vitro potency assays	369
8.15.1.2.2	The in vivo pharmacology screening cascade	370
8.15.2	**The Medicinal Chemistry Program**	371
8.15.2.1	Initial Approaches to PI3Kδ Selective Inhibitors	371
8.15.2.1.1	Looking for a new approach—Identification of a novel scaffold	371
8.15.2.2	Development of the Structure Activity Relationship	372
8.15.2.2.1	Early SAR development	373
8.15.2.3	*First Generation* PI3Kδ Inhibitors: Scope and Limitations	378
8.15.2.4	Driving Improvement of ADMET Parameters Through Physicochemical Modification	379
8.15.2.4.1	Replacement of the C2 phenyl with acyclic amines	379
8.15.2.4.2	Replacement of the C2 phenyl with cyclic amines	380
8.15.2.5	Development and Pharmacological Characterization of Triazinyl-Piperazinones	383
8.15.2.5.1	Potency and ADMET characterization of triazinyl-piperazinones	383
8.15.2.5.2	Metabolite ID studies with compound **54**	383
8.15.2.5.3	Pharmacological assessment of compound **54**	385
8.15.2.5.4	Off-target and ancillary profiling of compound **54**	386
8.15.2.6	In Vitro Genotoxicity Screening	387
8.15.2.7	*Second Generation Inhibitors*: Development of the 3-Pyridyl *N*-Oxides	387
8.15.2.7.1	Identification of 3-pyridyl *N*-oxide as an effective bioisostere of a carbonyl group	387
8.15.2.7.2	Characterization of compound **67**	389
8.15.2.7.3	General metabolic profile of the quinoline C2 pyridyl *N*-oxides	393
8.15.2.7.4	Metabolite identification studies with compound **67**	397
8.15.2.7.5	Optimizing the PK profile of compound **67**	398
8.15.2.8	Identification and Characterization of *Seletalisib*	400
8.15.2.8.1	Impact of the CF_3 Group 1: In vitro biology comparison between compounds **67** and **86**	400
8.15.2.8.2	Impact of the CF_3 Group 2: Comparison of PK parameters between compounds **67** and **86**	402
8.15.2.8.3	Metabolic profile of compound **86**	403
8.15.2.8.4	Pharmacological evaluation of compound **86**	403
8.15.3	**Preclinical Development**	404
8.15.4	**Clinical Data and Status**	404
8.15.5	**Conclusion**	405
Acknowledgments		405
References		405

8.15.1 Introduction

In this article, we describe the medicinal chemistry program that led to the identification and clinical development of the potent and selective PI3Kδ inhibitor *seletalisib*, currently in a Phase 2 trial for Sjögren's syndrome.[1,2] The therapeutic rationale for selective PI3K inhibition in inflammatory diseases will be discussed followed by a detailed description of the medicinal chemistry campaign. Highlights include the use of a virtual library of heterocycles[3] coupled with electrostatic modeling to identify novel chemical starting points, the optimization of physicochemical parameters to achieve drug-like properties, the use of in vitro genotoxicity screening in drug discovery, and the successful application of a pyridine *N*-oxide as a bioisostere of a amide. It is hoped that the story of our research will enlighten and inform current and future generations of medicinal chemists as we discuss the highs and lows of our program and the many lessons learnt upon the ultimately successful journey to *seletalisib*.

8.15.1.1 The Rationale for Selectively Targeting PI3Kδ to Treat Inflammatory Disease

The Class 1 phosphoinositide 3-kinase enzymes are a well characterized family of lipid kinases that catalyze the phosphorylation of phosphatidylinositol 4,5 bisphosphate (PIP_2) to the key signaling molecule phosphatidylinositol 3,4,5 trisphosphate (PIP_3) which in turn triggers a wide range of downstream biological events impacting diverse functions including cell growth, proliferation, chemotaxis, differentiation, and survival.[4,5] The Class I subset of PI3K comprises four isoforms of the catalytic p110 subunit, the Class 1A isoforms p110α, β, and δ, and the Class 1B isoform, p110γ (**Fig. 1**). The fundamental role of the Class 1 PI3Ks in a wide range of critical cellular events has made them attractive targets for therapeutic intervention.[6–8] The PI3Kα and PI3Kβ isoforms are ubiquitously expressed, whereas PI3Kγ and PI3Kδ are expressed more highly in leukocytes than in other cell types, implying a more specific and important role in leukocyte development and function.[4,9,10] PI3Kδ is also expressed in endothelial cells, synoviocytes, osteoclasts, and stromal cells.[11,12]

Although PI3Kγ and PI3Kδ have a similar cellular distribution, they are differentially coupled in specific cells. PI3Kγ is generally coupled to G protein-coupled receptors, including leukotriene and chemokine receptors, and plays a particularly important role in chemokine-mediated cell recruitment and the activation of innate immune cells at sites of inflammation.[4,11] In contrast, PI3Kδ is required for signaling downstream of several tyrosine kinase immune receptors, including the T-cell receptor (TCR), the B-cell receptor (BCR), and the Fc epsilon receptor 1 (FcεR1), thereby playing a key role in the acquired immune response.[13,14]

The selective expression and function of PI3Kδ in leukocytes provides a rationale for exploring this isoform as a therapeutic target for diseases featuring pathological activation of the PI3K pathway in hematopoietic cells, including B-cell malignancies and immune disorders.[15,16] Indeed in genetically modified mice that either lack p110δ or express the kinase inactive mutant, $p110\delta^{D910A/D910A}$, phenotypes, including lymphocyte developmental defects, attenuated signaling by antigen receptors, B-cell functional defects, and decreased T-cell-dependent responses, are observed while the mice remain viable and fertile.[17–19]

The ubiquitous expression of the PI3Kα and PI3Kβ isoforms has consequently limited their therapeutic utility to the field of oncology, however in contrast the enriched expression of the PI3Kδ and PI3Kγ isoforms to leukocytes and the revelation of their functional effects have led to the hypothesis that selective inhibition of these two isoforms will provide an opportunity to target inflammatory and autoimmune disease.[7]

The crucial role of the PI3K kinases in multiple physiological functions has ensured that they have long been a favored target of the medicinal chemistry community.[20,21] To date that research has culminated in the successful delivery of multiple classes of potent and selective PI3K inhibitors into clinical development (**Fig. 2**).[7,8] Isoform-selective PI3K inhibitors include those that selectively target p110α (BYL-719, INK-1117), p110β (AZD6482), p110δ (e.g., AMG 319, GSK2269557,[22] idelalisib [CAL-101]), p110α/p110δ (e.g., copanlisib, pictilisib, AZD8835), p110β/p110δ (e.g., acalisib, AZD8186), and p110δ/p110γ (e.g., duvelisib [IPI-145, INK1197], Tenalisib [RP-6530], RV-1729).[6,7]

The most clinically advanced PI3Kδ inhibitor *idelalisib* (Zydelig) has been approved by the FDA in combination with rituximab for the treatment of adult patients with chronic lymphocytic leukemia.[23,24] The current limitation of *idelalisib* to hematological malignancies is presumed to be due to the tolerability of the molecule and side effect profile. Interestingly although *idelalisib* is described as a PI3Kδ selective inhibitor, the fold-selectivity against the gamma isoform compared to the delta isoform in biochemical kinase assays is relatively modest (α 328-fold, β 226-fold, and γ 35-fold).[25] Additionally the PI3Kδ/γ dual selective inhibitor *duvelisib* (α 640-fold, β 34-fold, and γ 11-fold) has recently failed to meet the primary endpoint in a Phase 2 trial of rheumatoid arthritis when dosed at 0.5, 1, and 5 mg twice a day. Clinical trials with *duvelisib* are still ongoing in hematological cancers at higher doses (25 mg twice a day) potentially indicating a tolerability issue limiting dose in the arthritis clinical trial and thereby impacting

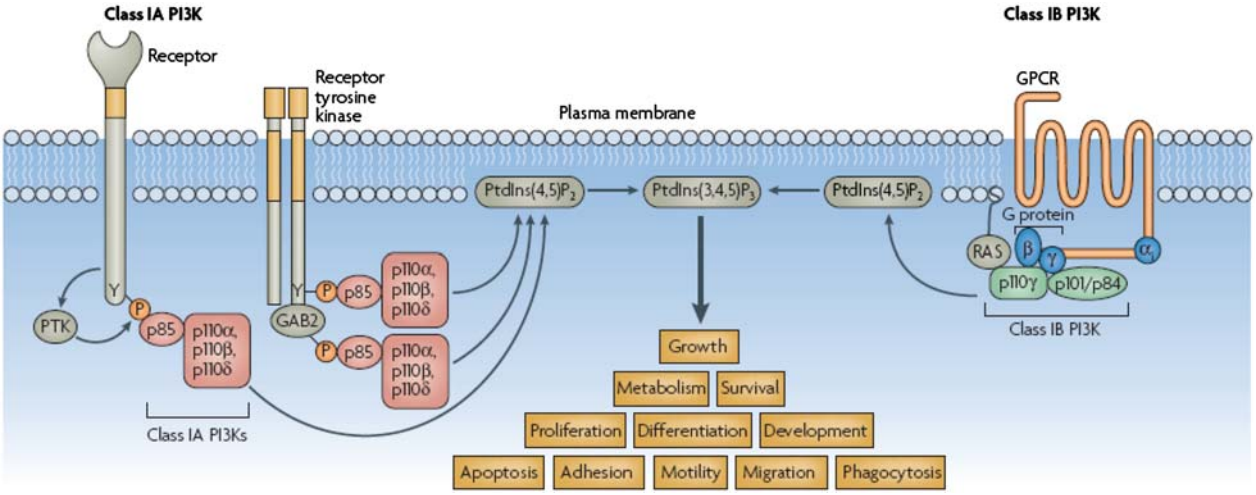

Fig. 1 The Class 1 PI3 kinases. Reproduced from Rommel, C.; Camps, M.; Ji, H. PI3K Delta and PI3K Gamma: Partners in Crime in Inflammation in Rheumatoid Arthritis and Beyond? *Nat. Rev. Immunol.* **2007**, *7* (3), 191–201.

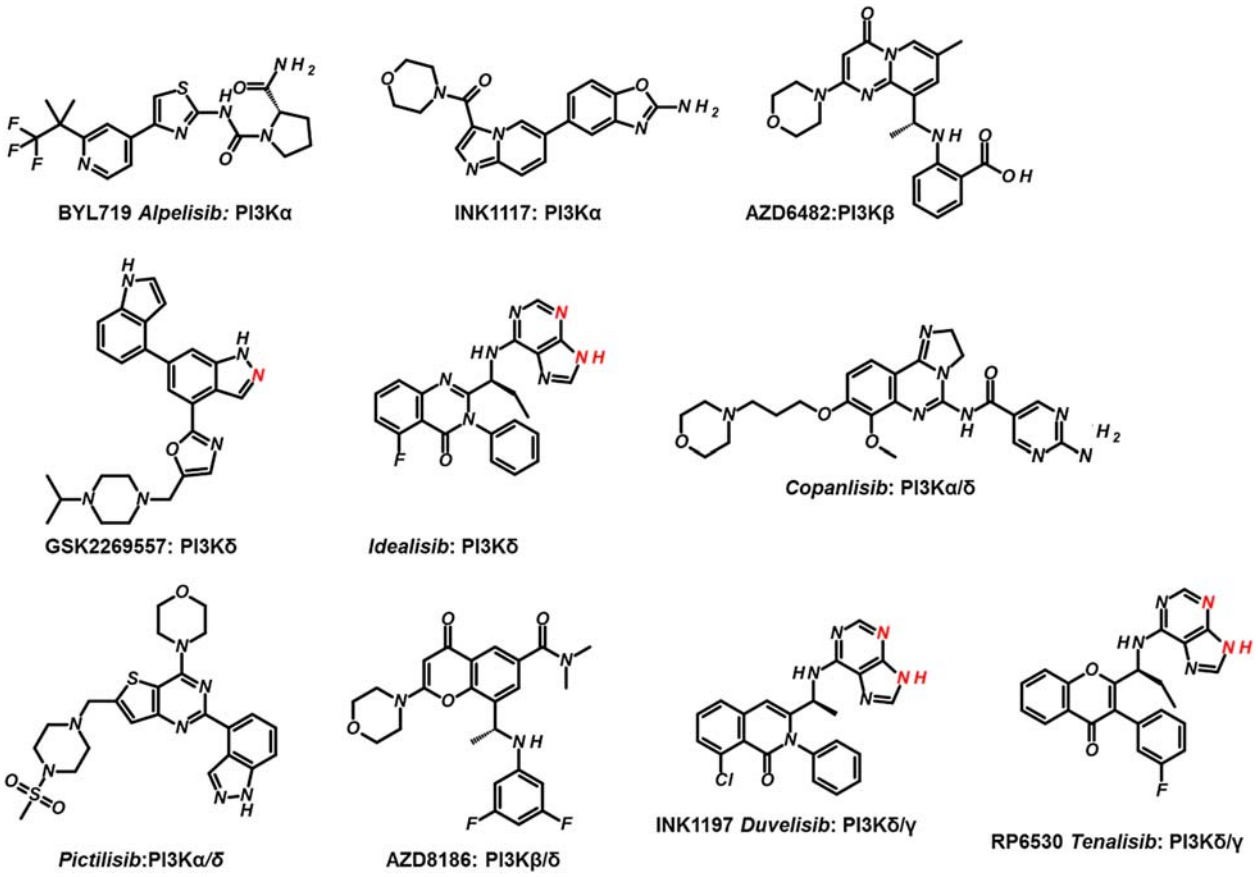

Fig. 2 Structures of representative ATP competitive and isoform-selective PI3K inhibitors currently in clinical development. Compounds are grouped by their isoform selectivity profiles. The key hydrogen bond interactions with the hinge region of the PI3K kinase are shown in *red* where known.

efficacy. While both the delta and gamma isoforms have been implicated in the proinflammatory pathways involved in rheumatoid arthritis, it is not clear that inhibition of both isoforms is necessary for clinical benefit.[11] It can be postulated that exquisitely selective PI3Kδ inhibitors *without* gamma isoform activity could provide additional tolerability benefit and hence open up the potential for clinical efficacy in inflammatory and immunological diseases.

In summary, there is evidence to conclude that the therapeutic utility of Class 1 PI3K inhibitors in inflammatory disease would be best accomplished by an isoform-selective inhibitor targeting PI3Kδ for those diseases with a significant B- and T-cell involvement. Certainly selectivity against the PI3K alpha and beta isoforms would be an absolute requirement for any PI3K inhibitor targeting inflammatory disease with selectivity against the gamma isoform also potentially providing additional tolerability benefit.

With this information in mind, we established our medicinal chemistry program to discover selective PI3Kδ inhibitors.

8.15.1.2 Implementation of a Screening Cascade and Description of Key Assays

One of the most fundamental aspects of any medicinal chemistry program is the establishment of a robust screening cascade. The first objective is to establish the potency and efficacy of the molecules in a range of pharmacological models, from primary enzyme activity and selectivity, through cellular assays to confirm target engagement and functional effect, and ultimately into animal models of disease. Concurrently, a range of drug-like properties are assessed, to ensure that the molecules possess the desired physicochemical and ADMET properties. The screening cascade established for our program is presented in Fig. 3.

In a screening paradigm typical of many small molecule drug discovery projects, the screening cascade is arranged in a series of tiers whereby compounds progress from initial assessment of in vitro potency in *Tier 1* through progressively more complex and resource intensive assays designed to establish the PI3Kδ potency, efficacy, and specificity in cellular assays (*Tier 2*) and finally in vivo pharmacology (*Tier 4*). In parallel, the ADMET and PK characteristics of the compounds are also assessed to establish the suitability of the compounds both for preclinical testing and their likely predicted human PK profile (*Tiers 2 and 3*). Given the large number of small molecules synthesized in a typical small molecule drug discovery program (in our case ~3000), a key requirement of the cascade is to filter out compounds which do not meet preset criteria in the high-throughput assays to ensure that only compounds with the desired profile progress to the later assays.

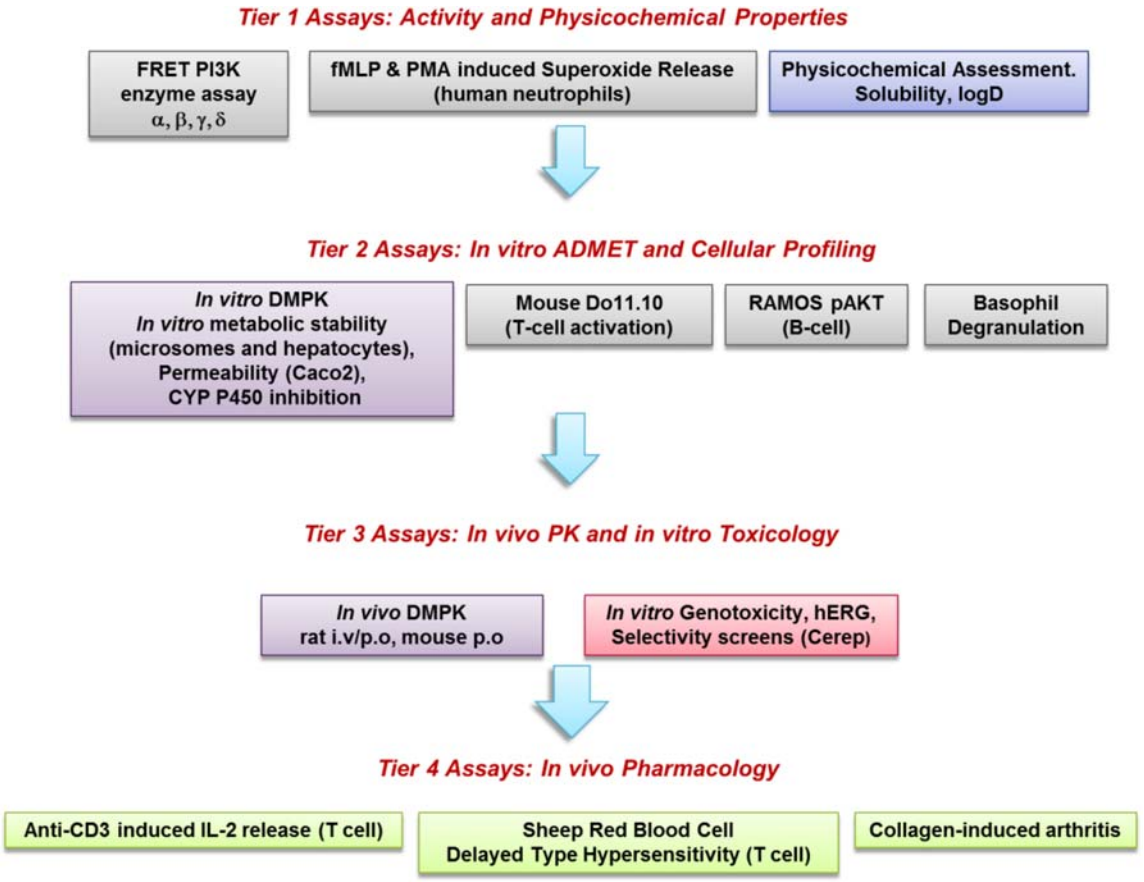

Fig. 3 The screening cascade established for our PI3Kδ program. In vitro potency assays are shown in *gray* boxes, physicochemical property assays shown in *blue* boxes, ADMET and PK assays shown in *purple* boxes, safety assays shown in *red* boxes, and in vivo pharmacology assays shown in *green* boxes.

These criteria are typically defined by a target product profile (TPP) which outlines the desired biological profile of a molecule. In our case, the critical aspects of the TTP were >500-fold-selectivity against the α, β, and γ isoforms, <100 nM cellular potency, efficacy in PI3Kδ driven pharmacology models, and a predicted human PK profile consistent with a once-daily oral dosing regimen. Clearly the critical assays for our program were therefore PI3K isoform enzymatic selectivity, potency in a functional PI3K specific cellular assay (fMLP-stimulated superoxide release), and finally proof of efficacy and potency in the in vivo disease model (murine CIA).

8.15.1.2.1 Description of in vitro potency assays

Initially newly synthesized molecules were assessed for activity and isoform selectivity in a enzymatic inhibition assay using a homogeneous time resolved fluorescence[26] PI3 kinase enzymatic assay (Millipore) with either p110 α, β, and δ (Millipore), or p110γ (produced in-house). Compounds with sufficient activity against PI3Kδ and isoform selectivity were then assessed for cellular activity in a range of secondary assays. Fig. 3 describes four critical cellular assays: the fMLP and PMA induced superoxide release assay in primary human neutrophils, the phospho-AKT assay in the RAMOS B-cell line, the D0.11.10 T-cell proliferation assay and the human whole blood basophil degranulation assay. Each assay and their function in the screening cascade are briefly described here.

8.15.1.2.1.1 The fMLP/PMA superoxide release assay in neutrophils

The fMLP-stimulated superoxide release neutrophil assay was established as the primary functional assay to demonstrate the cellular activity and selectivity of the compounds. Superoxide release by human neutrophils in response to fMLP stimulation has a time-dependent requirement for PI3Kδ signaling.[27] Critically the use of differential stimuli (fMLP vs. PMA) allowed the selectivity of the biological response to be established. Superoxide release via fMLP stimulation is regulated by the PI3K pathway, while in contrast PMA-stimulated superoxide release is regulated via PKC and is therefore not PI3K dependent. By establishing the selectivity of the cellular response through the PMA *counterscreen*, we could rapidly establish that the cellular activity generated was due to inhibition of the PI3K pathway and not potential off-target activities. Due to the ability to deploy the fMLP- and

PMA-stimulated cellular assay in a high-throughput plate format, we were able to establish this assay as our frontline cellular assay and screen >50 compounds a week.

8.15.1.2.1.2 The D0.11.10 proliferation assay

The key in vivo mechanistic and disease pharmacology studies were performed in murine models and consequently we needed to confirm functional activity against mouse PI3Kδ. To characterize the functional activity of our PI3Kδ inhibitors in a mouse system, and as TCR signaling is PI3Kδ-dependent,[13] a murine TCR-dependent cellular assay was established. T-cells from the D011.10 mouse express a transgenic TCR which recognizes a peptide from ovalbumin.[28] In response to OVA peptide stimulation, the T-cells from D011.10 mice are activated and subsequently proliferate. Selective inhibition of murine PI3Kδ can therefore be expected to inhibit the proliferation of these cells and formed the basis of the assay. The D011.10 proliferation assay served to confirm the activity of our compounds against mouse PI3Kδ ahead of screening in the pharmacology cascade.

8.15.1.2.1.3 The pAKT assay in RAMOS cells

While the high-throughput superoxide release assay provided confirmation of a PI3K-dependent functional effect in human cells, we also wished to establish a cellular readout of mechanistic target engagement. The development of a robust target engagement assay requires the identification of a downstream biological event that is (a) selectively driven by, and is proximal to, PI3Kδ and (b) can be effectively measured in a readily accessible and robust way. The phosphorylation of AKT following activation of the BCR is a selective event mediated by PI3Kδ[4] (Fig. 4).

Activation of the BCR in Ramos cells was achieved by cross-linking with anti-IgM. Cellular phosphorylated AKT ($pSer^{473}$) was detected using the Meso Scale Discovery pAKT assay protocol. Selective PI3Kδ inhibitors can therefore be expected to inhibit the production of pAKT and thus provide evidence of target engagement in cells.

8.15.1.2.1.4 The basophil degranulation assay

In addition to the high-throughput cellular assays established for screening of new molecules and the target engagement assay, the project also required a functional cellular assay which would provide a potential ex vivo biomarker for PI3Kδ inhibition in clinical studies. Such an assay would require the following properties: (a) a functional readout dependant on PI3Kδ inhibition, (b) an assay compatible with testing human whole blood, and (c) suitable sensitivity and robustness to enable use in a clinical setting.

Basophils are circulating granulocytes that play a key role in allergic hypersensitivity reactions. FcεRI-induced degranulation of basophils has been shown to be PI3Kδ-dependent and therefore provides a mechanistic readout for activity of PI3Kδ inhibition.[29] Upon degranulation, CD63 is expressed on the cell surface when granule membranes containing CD63 fuse with the plasma membrane and this marker was used to determine the activity of compounds in human whole blood by flow cytometry. Establishment of a robust basophil degranulation assay provided a measure of target engagement and PI3Kδ-mediated functional inhibition that was successfully deployed as a clinical biomarker in the Phase 1 clinical studies with *seletalisib*.

8.15.1.2.2 The in vivo pharmacology screening cascade

Compounds with suitable potency and selectivity in the in vitro assays and appropriate exposure in mouse following oral dosing were subsequently assessed in a range of in vivo pharmacology models briefly described here:

8.15.1.2.2.1 Anti-CD3-induced IL2 release model

The first pharmacology model assessed the inhibition of IL2 release following intravenous administration of anti-CD3 antibody to male Balb/c mice. The anti-CD3 antibody activates the TCR via cross-linking and IL-2, a key T-cell growth factor, is the first cytokine produced. PI3Kδ plays a pivotal role in the signaling cascade downstream of the TCR (Fig. 4) and thus PI3Kδ inhibitors can be

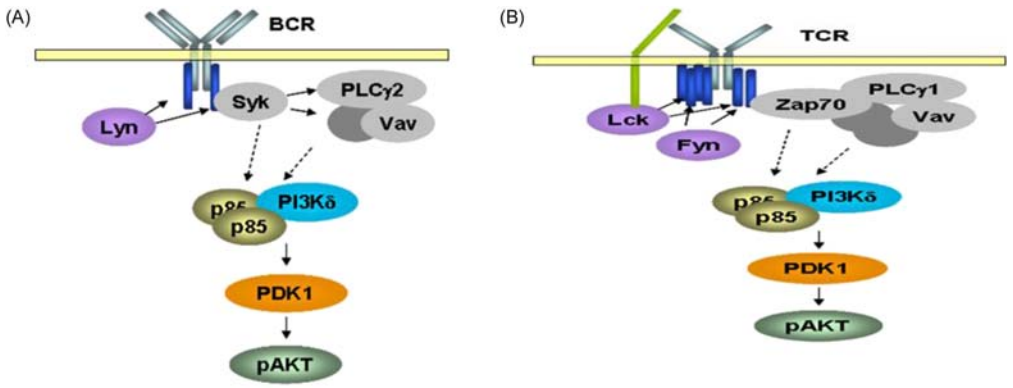

Fig. 4 PI3Kδ mediated signaling downstream of the (A) B-cell receptor and (B) T-cell receptor showing the location of PI3Kδ and AKT in the signaling cascade.

expected to inhibit this model. The anti-CD3-induced IL2 release model provides our first in vivo assessment of PI3Kδ inhibition on T-cells and requires only short-term (2 h) exposure in mouse.

8.15.1.2.2.2 Sheep red blood cell delayed type hypersensitivity model

The sheep red blood cell delayed type hypersensitivity (SRBC DTH) model is a classical Type IV hypersensitivity reaction. Male Balb/c mice are sensitized by intravenous administration of SRBCs and subsequently challenged with additional SRBC to the footpad 4 days later. This results in an antigen-specific footpad swelling that is dependent upon CD4+ T (compared to a group of mice which are nonsensitized but received the footpad challenge with SRBCs, thus providing a baseline level of nonantigen specific footpad swelling). PI3Kδ inhibitors are administered orally throughout the study duration with the first dose prior to sensitization. Data are shown as the change in footpad swelling compared to prechallenge levels and plotted as the mean.

8.15.1.2.2.3 Murine collagen-induced arthritis model

In order to establish the functional efficacy of our PI3Kδ inhibitors in a model of human inflammatory disease, we deployed the murine collagen-induced arthritis model (CIA).[30,31] Male DBA/1 mice are immunized by intradermal injection of type II Collagen (CII) in Complete Freund's adjuvant on day 0 and then in Incomplete Freund's adjuvant on day 14. Body weights and clinical scores are recorded daily using the following scoring system for each individual paw; 0 = normal, 1 = ankle/wrist swollen, 2 = ankle/wrist and pad swollen, and 3 = ankle/wrist and pad and digits swollen. The maximum score per paw is three with each mouse scoring a maximum of 12. Total scores per animal are used to calculate the group mean score per day and data is shown as mean ± SE. Compounds are administered orally and dosing is either initiated prior to immunization (prophylactically) or on the day of disease onset (therapeutically).

8.15.2 The Medicinal Chemistry Program

8.15.2.1 Initial Approaches to PI3Kδ Selective Inhibitors

Our initial approach to PI3Kδ selective inhibitors derived from an earlier internal program dedicated to the discovery of pan selective PI3K inhibitors for oncology indications[32] (Fig. 5). From a series of substituted thiazolylmorpholines, we noticed that 3-substituted thiophenes displayed emerging selectivity for the delta isoform, further development of this series led to the compound **UCB1412727** which displayed excellent PI3Kδ selectivity and importantly efficacy in the murine CIA model when dosed prophylactically. Unfortunately development of **UCB1412727** proved problematic due to its poor physicochemical properties and solubility. In preclinical toxicology **UCB1412727** demonstrated an unacceptable safety profile and further development was therefore halted.

Encouraged by the pharmacological proof of principal demonstrated by **UCB1412727** that selective PI3Kδ inhibitors could inhibit the mouse CIA model, but keen to identify a different chemotype devoid of the toxicity issues, we turned our attention to a structurally differentiated back-up series that we had been developing in parallel.

8.15.2.1.1 Looking for a new approach—Identification of a novel scaffold

During our development of **UCB1412727** several Class 1 PI3K inhibitors were reported with promising isoform selectivity profiles: PIK-39 (**1**) and IC87114[33,34] (**2**). The cocrystal structure of PIK-39 in PI3Kδ was reported[35] revealing the structural basis of selectivity for this novel molecular class (Fig. 6). The structure revealed that the compounds were able to selectively inhibit PI3Kδ due to the formation of a ligand induced allosteric "specificity pocket," not present in the apo-structure, caused by the movement of the Met^{752} and Trp^{760} residues. The 3*H* quinazolin-4-one core of **1** and **2** occupy this hydrophobic "specificity pocket" sandwiched between Trp^{760} and Ile^{777} on one side and Met^{752} and Pro^{758} on the other. In PI3Kδ these residues are inherently more flexible

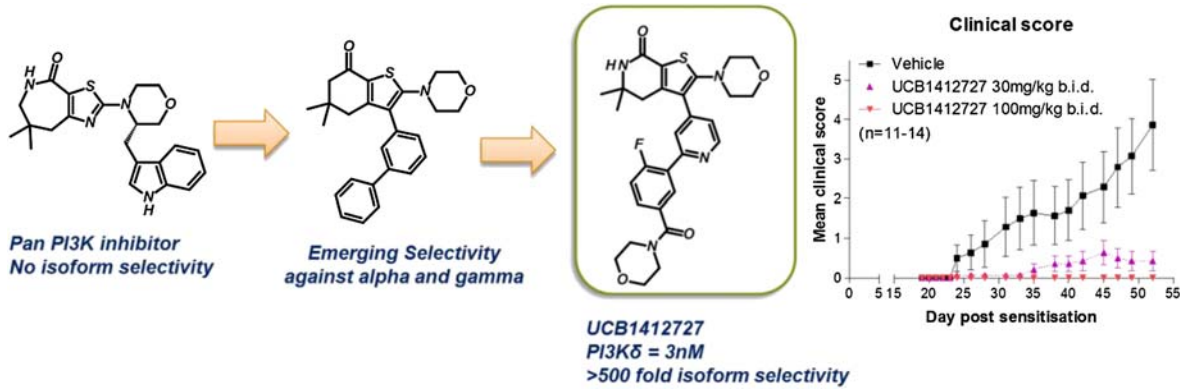

Fig. 5 The development of **UCB1412727** and efficacy in the murine cAIA model of arthritis.

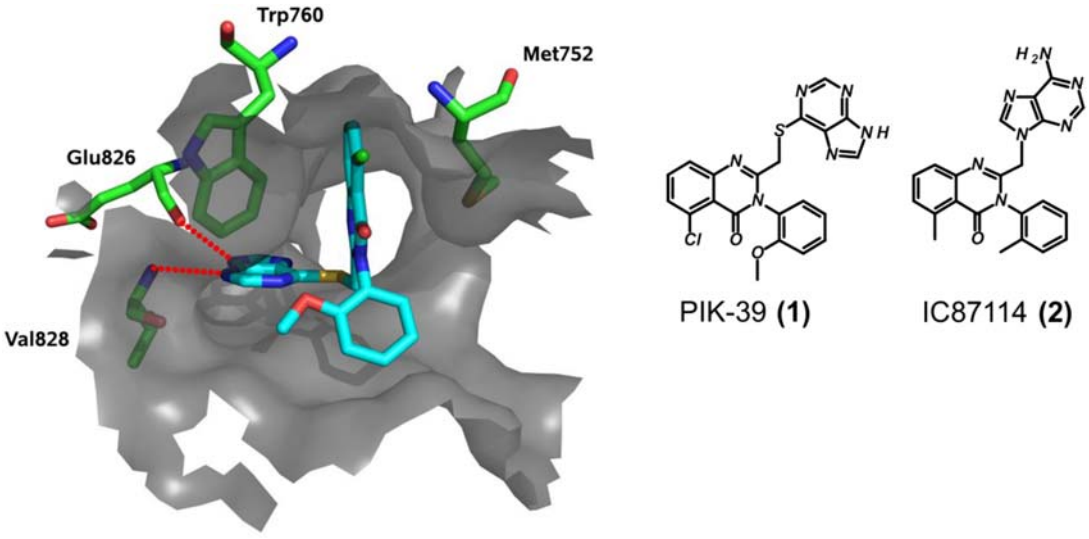

Fig. 6 Cocrystal structure of PIK-39 (**1**) in PI3Kδ (PDB code 2wxf). The *ligand induced selectivity pocket* is formed by the movement of Met752 and Trp760 residues to accommodate the 3*H*-quinazolin-4-one core. The purine hinge-binding group forms a bidentate hydrogen bond interaction (shown in *red*) to the backbone residues Val^{828} (NH) and Glu^{826} (C=O) in the hinge region of the kinase. The *ortho* methoxy group points toward the mouth of the pocket over a hydrophobic region.

than in the other isoforms and thus the formation of the selectivity pocket is tolerated and the key 3*H* quinazolin-4-one core accommodated. The *ligand induced selectivity pocket* present in PI3Kδ is thought to be the primary basis of the PI3Kδ isoform selectivity of this class of compounds. The other key-binding features were revealed to be a bidentate hydrogen bonding interaction between a hydrogen bond acceptor on the purine and the amide NH of the backbone Val^{828} and a complementary hydrogen bond donor (NH) of the purine to the carbonyl group of the Glu^{826} residue. These residues are located in the hinge region of the kinase and thus the motifs which interact with these residues are commonly known as *hinge-binding groups*. The *ortho*-substituted phenyl rings of **1** and **2** sit in a hydrophobic region pointing toward the mouth of the pocket and ultimately to solvent, thus providing a potential area of the molecule to introduce polar functionality and modify physicochemical properties.

With both PIK-39 and IC87114 reliant on a substituted 3*H* quinazolin-4-one core, we wished to develop novel series of inhibitors taking advantage of the induced Met^{752}/Trp^{760} selectivity pocket but based on alternative heterocyclic core structures. Initially we examined conservative structural variations and moved a nitrogen in the 3*H* quinazolin-4-one to give the regioisomeric pyrido [1,2-*a*]pyrimidin-4-one (**3**). We were surprised to find that (**3**) possessed no quantifiable activity against any PI3K isoform (**Table 1**). Clearly a simplistic attempt to mimic the core by synthesis of topologically close analogs was unlikely to prove successful and we realized that other properties, in particular the electronics of the ring systems, would need to be evaluated.

Concurrently we had developed a propriety virtual database containing a complete set of all feasible heterocyclic ring systems Virtual Exploratory Heterocyclic Library (VEHICLe).[3] A potential application of this database was scaffold-hopping by facilitating the in silico comparison of heterocyclic ring systems based on a range of calculated parameters, including electrostatic potential (ESP). We reasoned that this approach would be ideally suited to identifying potential replacements of the 3*H*-quinazolin-4-one core of (**1**). Analysis of the ESP of the core of **1** (Core A) compared to the inactive regioisomer **3** (Core B) allowed us to rationalize this loss of potency in terms of the comparably low electronegativity (electron richness) of the pyridyl ring in Core B (**Fig. 7**) compared to the benzo ring in Core A. This part of the ligand sits within the induced *selectivity pocket* and may indicate a preference for electron-rich aromatic rings in the pocket. After calculating the ESP of a large number of heterobicyclic systems in VEHICLe, the quinoxaline (Core C) was selected on the basis of its ESP similarity to 3*H*-quinazolin-4-one (Core A) and synthetic tractability.

We were delighted to observe that synthesis of the quinoxaline and then the quinolone derivatives provided potent PI3Kδ inhibitors with promising selectivity profiles (compounds **4** and **5**, **Table 1**). The inactivity of compound **3** compared to the quinoline matched pair **6** highlights the criticality of electrostatic analysis in successfully identifying novel scaffolds for this inhibitor class. Our use of VEHICLe allowed rapid identification of novel core scaffolds and the establishment of a series of selective PI3Kδ inhibitors. This technique can conceivably find productive application in any small molecule medicinal chemistry program.

8.15.2.2 Development of the Structure Activity Relationship

With novel quinoxaline and quinoline scaffolds in hand we embarked on a campaign to rapidly define the structure activity relationship (SAR). Guided by the crystal structure of PIK-39, we envisaged that potency would be determined by substitution of the core and the nature of the hinge-binding group. The aryl substituent in the C2-position meanwhile could serve as a handle to

Table 1 Replacements of the *3H*-quinazolin-4-one from ESP analysis of the VEHICLe database[3]

Compounds	*Structure*	*PI3Kδ IC_{50} (μM)*	*PI3Kα IC_{50} (μM)*	*PI3Kβ IC_{50} (μM)*	*PI3Kγ IC_{50} (μM)*
3	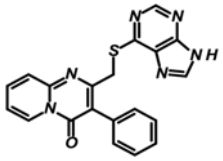	>30	>30	>30	>30
4	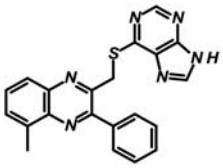	0.3	>30	>30	12
5	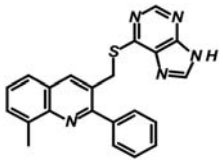	0.15	21	12	5.2
6	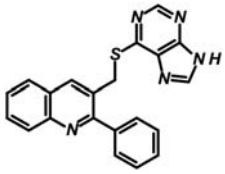	0.37	>30	>30	16

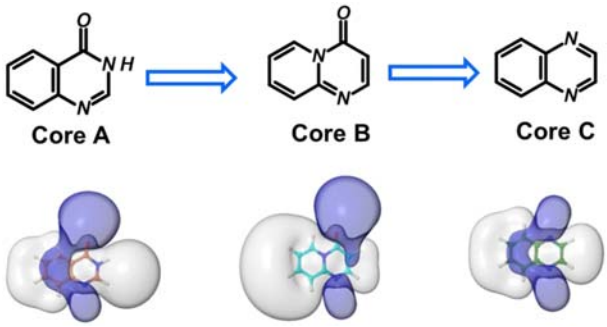

Fig. 7 QM calculated electrostatic potential surfaces of heterocycles to identify suitable replacements of the (A) 3*H*-quinazolin-4-one, (B) pyrido [1,2-*a*]pyrimidin-4-one, and (C) quinoxaline. The *blue areas* represent electronegative potential (electron rich) while the *white* denote electropositive potential (electron deficient).

modify the physicochemical properties of the molecule without impacting potency due to its orientation out of the enzyme pocket and toward solvent.

8.15.2.2.1 Early SAR development

8.15.2.2.1.1 Quinoline core substitutions and C2 aryl SAR

Following the identification of the quinoxaline and quinoline inhibitors **4** and **5** we focused our efforts on the quinoline **5** due to the synthetic tractability of the scaffold and initially established the SAR on the quinoline core (Table 2) and C2 aryl group (Table 3).

Notably a methyl scan of the quinoline core confirmed that substitution in the 6- and 7-positions eroded potency but substitution in the 8-position (**9**) modestly increased potency by approximately threefold. In the C2-position, substitution of the phenyl ring produced a detrimental effect on potency in the *meta* or *para* positions (**11** and **12**) but was tolerated in the *ortho* position (**10**).

Table 2 Quinoline core SAR: Substitution in the 8-position increases potency

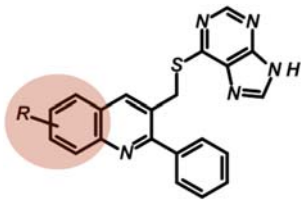

Compounds	*R*	*PI3Kδ IC_{50} (μM)*	*PI3Kα IC_{50} (μM)*	*PI3Kβ IC_{50} (μM)*	*PI3Kγ IC_{50} (μM)*
6	H	0.37	>30	>30	15.8
7	6-CH_3	3.4	>30	>30	>30
8	7-CH_3	8.2	>30	>30	>30
9	**8-CH_3**	0.12	21	9.1	5.0

Table 3 Initial C2 aryl SAR

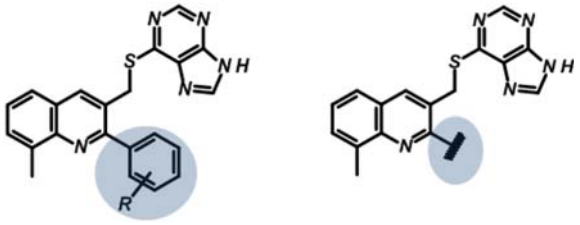

Compounds	*R*	*Aryl*	*PI3Kδ IC_{50} (μM)*	*PI3Kα IC_{50} (μM)*	*PI3Kβ IC_{50} (μM)*	*PI3Kγ IC_{50} (μM)*
10	2-CH_3	–	0.12	18.4	9.6	1.6
11	3-CH_3	–	0.59	12.7	7.0	8.4
12	4-CH_3	–	2.6	–	7.5	15.9
13	2-Cl	–	0.33	17.7	6.9	6.1
14	2-OCH_3		0.26	>30	7.5	3.0
15	4-F		0.72	–	8.9	3.0
16	–		0.2			
17	–		0.4			
18	–		0.3			

Both electron withdrawing (**13**) and electron donating groups (**14**) were accommodated in the *ortho* position. Importantly replacement of the phenyl ring by a range of 5- or 6-membered heterocycles was also possible; the 3-pyridyl group in particular would play a pivotal role in the eventual identification of *seletalisib*.

8.15.2.2.1.2 SAR of the linker between the quinoline and hinge-binding group

Our initial inhibitors were based on a thioether linkage between the quinoline core and the hinge-binding group. Benzylic thioethers are well-known metabolic liabilities due to the oxidation of the sulfur atom and the adjacent methylene group (Fig. 8). In our case, oxidation of the benzylic methylene led to a hydrolytically unstable thioacetal (**A**) and subsequent loss of the purine hinge-binding group, while oxidation of the sulfur to a sulfoxide or sulfone leaving group (**B**) resulted in the formation of an electrophilic center and a potentially reactive metabolite.[36]

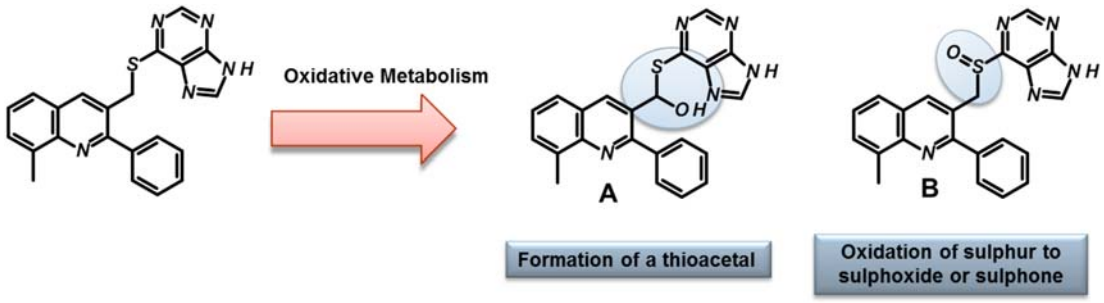

Fig. 8 Putative metabolic pathways and formation of potential reactive metabolites associated with the benzylic thioether.

Given the limitations of the thioether, we first investigated alternative linking atoms and also substitution on the methylene carbon (Fig. 9). Two key modifications produced exceptional increases in potency, namely the incorporation of a methyl group onto the benzylic methylene of **9** which resulted in a 10-fold increase in potency against PI3Kδ (compound **19**) and the replacement of the sulfur atom in **9** with an NH group providing an additional 20-fold increase in potency (compound **20**).

Critically combination of these two productive modifications led to compound **22** which delivered our first single digit nanomolar PI3Kδ inhibitor with an IC_{50} of 7 nM and a 53-fold increase in potency compared to the original thioether **9**. Promising isoform selectivity was observed against PI3Kα (~500-fold) and PI3Kβ (~200-fold), but optimization of the selectivity over PI3Kγ (20-fold) was clearly necessary.

The stereochemistry of the methyl group was critical with the *S* enantiomer demonstrating a eudismic ratio of ~40-fold over the *R* enantiomer (**23**). The preference for the *S* enantiomer was demonstrated in a number of matched pairs and is a consistent feature of the SAR. A tentative explanation for the stereochemical preference is suggested in Fig. 10. Docking of compounds **22** and **23** into the PI3Kδ crystal structure confirms that both molecules, as expected, make the crucial bidentate hydrogen bond interactions with the hinge residues with the 8-methyl quinoline occupying the induced selectivity pocket. The chiral methyl group occupies different environments depending on the stereochemistry. For the more active *S* enantiomer (**22**), the methyl group is directed toward the

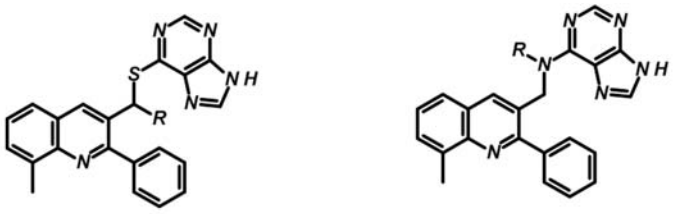

R	Cmpd	PI3Kδ IC_{50} μM
H	**9**	0.37
CH_3	**19**	**0.04**

R	Cmpd	PI3Kδ IC_{50} μM
H	**20**	0.02
CH_3	**21**	**2.4**

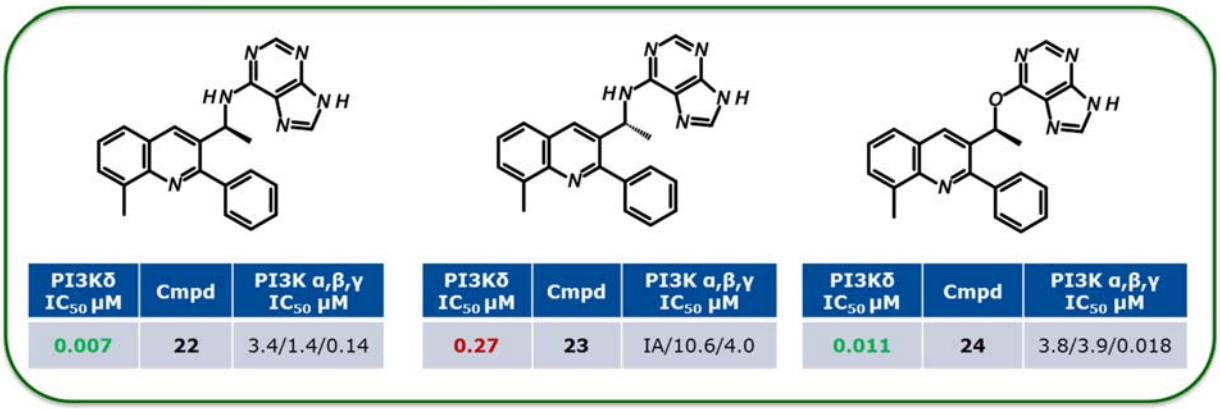

PI3Kδ IC_{50} μM	Cmpd	PI3K α,β,γ IC_{50} μM
0.007	**22**	3.4/1.4/0.14

PI3Kδ IC_{50} μM	Cmpd	PI3K α,β,γ IC_{50} μM
0.27	**23**	IA/10.6/4.0

PI3Kδ IC_{50} μM	Cmpd	PI3K α,β,γ IC_{50} μM
0.011	**24**	3.8/3.9/0.018

Fig. 9 Development of chiral alpha methyl benzylamine linkers.

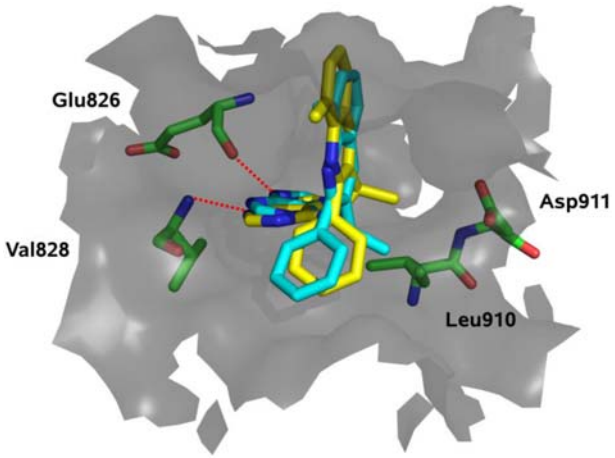

Fig. 10 Docking of compound **22** *S* enantiomer *(cyan)* and compound **23** *R* enantiomer *(yellow)* into the PI3Kδ crystal structure 2WXF (PIK-39). The docking pose indicates that **22** directs its methyl group toward Leu^{910} forming a more favorable hydrophobic contact while **23** potentially directs its methyl group toward Asp^{911} forming a less favorable hydrophobic/polar clash with the carboxylic acid side chain.

side chain of Leu^{910} making a favorable hydrophobic interaction. In contrast when the methyl group is in the *R* configuration, it is directed toward the side chain of Asp^{91}, a highly polar carboxylate residue potentially resulting in unfavorable interactions.

Crystal structures would be necessary to unequivocally prove the hypothesis, but SAR developed in the series consistently showed that lipophilic groups were preferred on the benzylic position with a strong preference for the *S* enantiomer, consistent with our hypothesis.

Replacement of the amine with an oxygen atom (**24**) while maintaining excellent potency against PI3Kδ ($IC_{50} = 11$ nM) possessed inferior selectivity against the gamma isoform (PI3Kγ $IC_{50} = 18$ nM). Crucially these O-linked compounds proved to be hydrolytically unstable which precluded their further utility. Methylation of the benzylic amine (compound **21**) was not tolerated resulting in a 100-fold reduction in activity compared to **20**.

8.15.2.2.1.3 SAR of the hinge-binding group

With a highly optimized and potent α methyl-benzylamine linker in hand, our attention next turned to the nature of the heterocyclic hinge-binding group. In our first generation of inhibitors, the purine motif provided a bidentate interaction with Val^{828} and Glu^{826}. Purines, however, are ubiquitous scaffolds in a wide variety of pharmacologically active compounds and we were wary of the potential off-target activities and associated toxicology that this structural motif could bring. We therefore assessed a number of alternative hinge-binding groups (>50 examples) with a selection of these described in **Table 4**.

The regioisomeric pyrazolo[1,5-*a*]pyrimidine where the NH hydrogen bond donor (HBD) is eliminated (**25**) established that the bidentate hydrogen bond was not necessary for activity. The critical requirement for effective binding was a hydrogen bond acceptor *para* to the linking nitrogen, (the HBA highlighted in red in **Table 4**). Compounds lacking this feature such as **32** had greatly diminished activity compared to the molecular matched pair (MMP) **31**. A wide range of heterocycles provided effective hinge-binding groups including 6,6, 6,5, and 5,6 bicyclic ring systems and also monocyclic groups with the triazine **33** proving the most efficient monocycle. Interestingly, incorporation of an exocyclic amino group into the purine compound **20** to provide **27** retained activity against PI3Kδ but also introduced significant activity against the PI3Kγ isoform ($IC_{50} = 65$ nM). Similar incorporation of the exocyclic amine into the pyrazolo[1,5-*a*]pyrimidine **25** did not result in a compound with dual δ/γ activity (compound **26**), suggesting that the gamma activity relied on the potential tridentate hydrogen bond donor/acceptor/donor motif in the 2-aminopurinyl hinge-binding group. Somewhat surprisingly the profile of **26** was consistent with dual PI3K δ/α inhibitors (PI3Kα $IC_{50} = 15$ nM).

The importance of the 2-amino exocyclic amine as a HBD for activity is supported by the observation that replacing the amine in **26** with a methyl to give **28** resulted in a significant reduction in potency across the Class IA isoforms especially PI3Kα although interestingly the potency of the Class 1B isoform PI3Kγ was not significantly affected. These observations highlight the dramatic effects on isoform selectivity that small structural changes of the hinge-binding group can induce. The SAR illustrates the potential of this molecular class to access alternative PI3K isoform selectivity profiles.

Although dual PI3Kδ/γ selective compounds were not the focus of our project, we were keen to determine if the initial observation that 2-aminopurinyl groups increase PI3Kγ activity (and concomitantly reduce δ/γ selectivity) was consistent across a range of molecules. To explore these phenomena we analyzed a set of MMPs. MMP analysis is a powerful method of interpreting and analyzing SAR[37,38] by comparing data between pairs of molecules that differ by a single and consistent structural change. We compared eight identical pairs of molecules (**Fig. 11**) where the pairs differed only in the nature of the 2-purinyl substituent ($R = H$ vs. $R = NH_2$).

Table 4 Development of the hinge-binding group

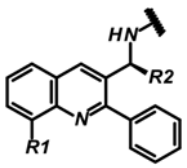

Compounds	*Hinge binder*	*R1*	*R2*	*PI3Kδ IC_{50}*	*PI3Kα IC_{50}*	*PI3Kβ IC_{50}*	*PI3Kγ IC_{50}*
25	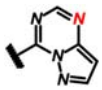	CH_3	CH_3	3 nM	2452 nM	1510 nM	120 nM
26	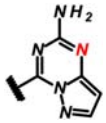	CH_3	CH_3	11 nM	15 nM	805 nM	1240 nM
27	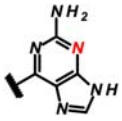	CH_3	H	9 nM	>10 μM	5600 nM	65 nM
28	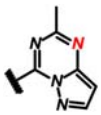	CH_3	CH_3	200 nM	>10 μM	6200 nM	580 nM
29	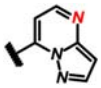	CH_3	CH_3	0.2 nM	630 nM	350 nM	19 nM
30	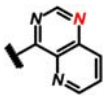	Cl	CH_3	0.16 nM	330 nM	245 nM	5 nM
31	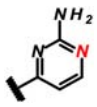	CH_3	H	500 nM	>30 μM	>10 μM	>10 μM
32	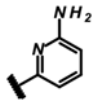	CH_3	H	>10 μM	>30 μM	>10 μM	>30 μM
33	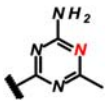	CH_3	CH_3	16 nM	6170 nM	2344 nM	64 nM

Comparison of these matched pairs demonstrated that the 2-amino group consistently delivered compounds with improved PI3Kγ activity by 5- to 50-fold. Furthermore the analysis clearly demonstrated that the 2-amino compounds possessed reduced selectivity against gamma (compared to the delta activity).

For our program PI3Kγ activity was not desired, however the observation demonstrates how, through the SAR fieldwork demanded by medicinal chemistry, new selectivity opportunities can be developed and furthermore illustrates the power of MMP analysis in confirming empirical observations made initially with single compounds.

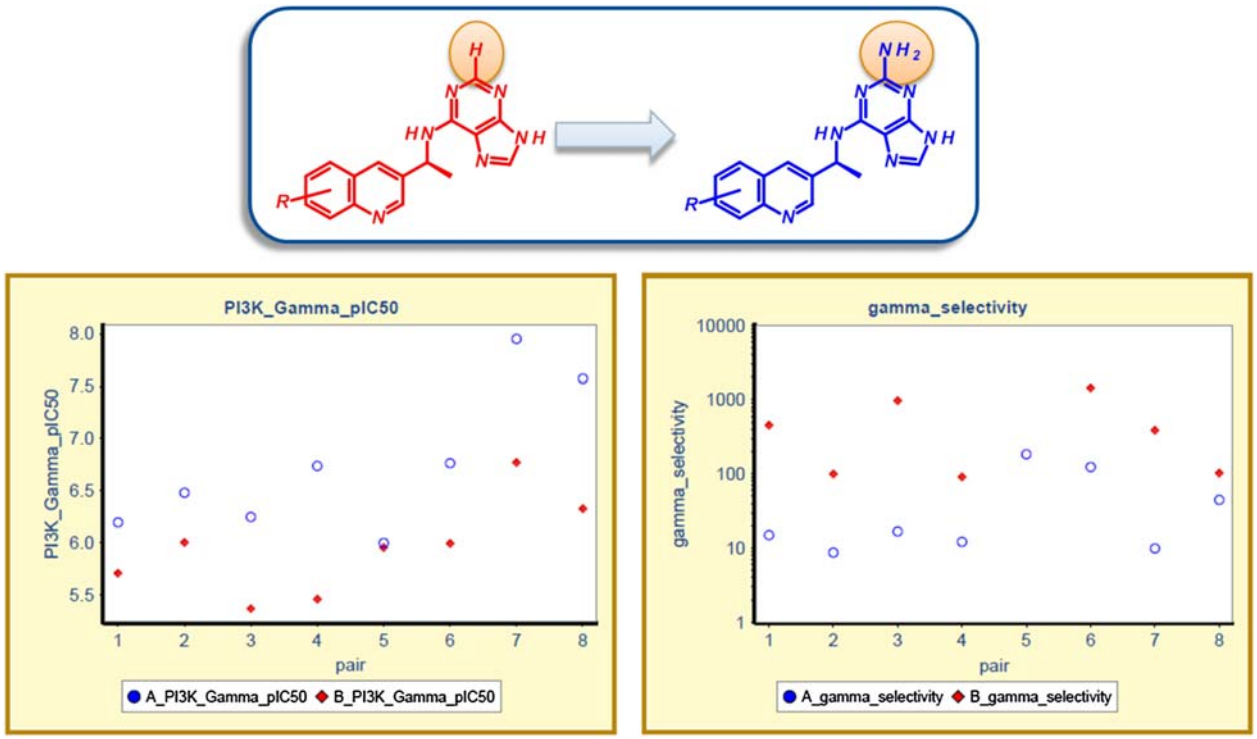

Fig. 11 Molecular matched pair analysis of 2-amino purine (in *blue*) versus purine (in *red*) containing PI3K inhibitors demonstrating consistent increased PI3Kγ activity and reduced selectivity against PI3Kδ.

8.15.2.3 *First Generation* PI3Kδ Inhibitors: Scope and Limitations

Our initial SAR drive allowed us to replace the metabolically compromised thioether with a highly potent and stable alpha methyl benzylamine. A wide range heterocycles were able to act as effective hydrogen bond acceptors for the crucial hinge-binding interaction replacing the initial purine group. Combining these SAR insights led to a number of highly potent PI3Kδ inhibitors with good selectivity against the alpha and beta isoforms, a representative selection of which are described in Table 5.

Exquisite potency against PI3Kδ could be achieved with primary enzyme potency <1 nM for compounds **30** and **29** translating into good activity in the primary cellular fMLP-stimulated superoxide release assay ($IC_{50}<20$ nM). Importantly the compounds were inactive in the PMA counter screen confirming that the cellular activity was driven solely through the PI3K pathway. While the selectivity against the Class 1A PI3K isoforms (α and β) was excellent, typically >1000-fold, selectivity against PI3Kγ was modest ranging from only 4- to 30-fold despite the significant changes to the hinge-binding group. We hypothesized that the poor selectivity against the Class 1B PI3Kγ isoform was linked to the presence of the C2 aryl group as it had been a common feature of the molecules synthesized at that time.

The physicochemical properties of the molecules were poor with high lipophilicity ($\log D$ generally >3) translating into poor aqueous solubility and high metabolic clearance as measured in both the human liver microsome and rat hepatocyte in vitro incubations. These characteristics unsurprisingly led to poor in vivo PK properties. Compound **22**, a representative example of the *First Generation* compounds, possessed high clearance equivalent to liver blood flow (i.v. $CL_b = 88$ mL min^{-1} kg^{-1}) and consequently poor bioavailability in rat consistent with high in vitro metabolic instability.

In particular, compound **29** characterized the challenge with these molecules. Despite exquisite enzyme and cellular potency, the high lipophilicity ($\log D$ 3.8) led to unacceptably high in vitro metabolic instability in both human and rat systems. Gratifyingly replacement of the pyrazolo[1,5-*a*]pyrimidine in **29** with the methyl amino1,3,5-triazine to give **33** led to the expected reduction in lipophilicity ($\log D$ 2.1), providing a significant increase in both in vitro metabolic stability (in human liver microsomes) and aqueous solubility. Unfortunately **33** lost ~10-fold in cellular potency compared to **29** and still possessed an unacceptably poor PI3Kγ selectivity profile. However it had been clearly demonstrated that reduction in global lipophilicity could provide the desired improvement in the in vitro metabolic stability and solubility. The challenge presented was to achieve this without compromising the nanomolar PI3Kδ activity and at the same time improving the selectivity profile against PI3Kγ.

While we had established a highly potent molecular platform for selective PI3Kδ inhibition, a number of significant challenges remained. Optimization of the drug-like properties[39] of the molecules was necessary to establish in vivo exposure and pharmacological activity. In addition, to achieve our ideal candidate profile, the selectivity against PI3Kγ required drastic improvement.

Table 5 First generation potent and selective PI3Kδ inhibitors

Compounds	*30*	*34*	*29*	*33*
PI3Kδ IC_{50}	0.16 nM	45 nM	0.2 nM	16 nM
PI3K α/β/γ selectivity	×2000/×1500/×**30**	×350/×160/×**20**	>1000/>1000/×**20**	×380/×140/×**4**
fMLP IC_{50}	6 nM	250 nM	17 nM	136 nM
PMA CS	IA	IA	IA	IA
HLM CL_{int}[a]	15	26	141	10
Rat Hep CL_{int}[b]	33	–	580	–
log *D*	ND	3.6	3.8	2.1
Aq. Sol. (pH 7.4)	1 μM	37 μM	32 μM	>350 μM
PSA	64	79	55	90
LLE[#]	–	3.7	5.2	5.1

[a]Human liver microsomal CL_{int} μL $min^{-1}mg^{-1}$ protein.
[b]Rat hepatocyte CL_{int} μL $min^{-1}10^{-6}$ cells.
[#]LLE = lipophilic ligand efficiency (pIC_{50} − log *D*).
ND, not determined.

8.15.2.4 Driving Improvement of ADMET Parameters Through Physicochemical Modification

The insights gleaned from the X-ray structure suggested that the C2-position of the quinoline would be ideally placed as a handle to modify the physicochemical properties of the molecules due to its proximity to solvent and lack of obvious interactions with the protein. Furthermore, the highly lipophilic substituted phenyl moieties that had been utilized to date were obvious targets for replacement due to the poor PI3Kγ selectivity and physicochemical properties of the *First Generation Molecules* and therefore this is where our attention turned.

8.15.2.4.1 Replacement of the C2 phenyl with acyclic amines

If, as we supposed, the C2 group was not making any significant interactions with the protein, we envisaged that replacement of the phenyl ring with smaller and more polar groups should be accommodated. Initially we replaced the C2 phenyl moiety with a simple *N*-methyl amine (Table 6) and discovered that compound **35** maintained reasonable PI3Kδ potency of 43 nM representing only an approximately fivefold drop in potency from the analogous C2 phenyl-substituted compound. Furthermore compound **35** presented a unique selectivity profile compared to the *First Generation* C2 aryl compounds in that the selectivity over the Class 1B PI3Kγ isoform was greater (100-fold) than the selectivity against the Class 1A isoforms (α 80-fold and β 12-fold). Intrigued by this surprising selectivity profile, we synthesized a range of acyclic amine analogs a selection of which are presented in Table 6.

As expected a wide range of polar functionality was tolerated with alcohols (**37**), amides (**38–40**), ethers (**36**), and bases (**41** and **42**), all providing potent molecules. The differentiated selectivity profile suggested by **35** was maintained with typically the selectivity against PI3Kγ exceeding the selectivity against the alpha and beta isoforms. Up to 1000-fold-selectivity against gamma could be achieved for the imidazole substituted compound **41** with good (>300-fold) selectivity against alpha and beta. The initial SAR conducted on the purine hinge-binding group was transferable to the other potent hinge-binding groups previously identified illustrated by the exceptional potency of **42**.

Replacing the phenyl ring by polar acyclic amines led to a reduction in lipophilicity by at least 1 log unit. Gratifyingly this brought the expected benefits to the drug-like properties of these molecules with improved solubility (all compounds in Table 6 >350 μM in the kinetic aqueous solubility assay) and improved stability in in vitro microsomal incubations. Notably the potency against PI3Kδ matched or exceeded the C2 phenyl analogs with compound **41** <1 nM in the enzyme assay and 5 nM in the fMLP cell-based assay. The compounds were also inactive in the PMA counter screen, confirming that the exceptional cellular potency was driven through the PI3K pathway. The increasing potency in parallel with reduced lipophilicity resulted in markedly improved lipophilic ligand efficiency[40] with values for these molecules typically >5.

Improvement in in vitro drug-like properties is only valuable if that improvement translates to robust in vivo PK properties, and, in particular, oral exposure in appropriate preclinical species. We took compound **39** into in vivo rat PK studies, and the PK parameters are summarized in Table 7.

Disappointingly **39** suffered from high clearance, equivalent to liver blood flow and no oral bioavailability. The high in vivo clearance was not predicted from the in vitro hepatocyte data, indicating that **39** was a substrate for active transporter-mediated

Table 6 Quinoline C2 SAR: Replacement of C2 phenyl with alicyclic amines

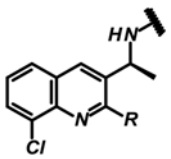

Compounds	*Hinge binder*	*R*	*PI3Kδ IC_{50} (nM)*	*Isoform selectivity α/β/γ*	*fMLP IC_{50}*	*In vitro CL_{int}*	*log* D
35	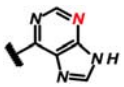		43	×80/×12/×100	83 nM	11[a]	3.1
36	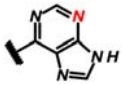	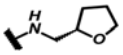	(*S*) 58 (*R*) 12	×100/×40/×120[a]	117 nM[a]	27[a,b]	3.2
37	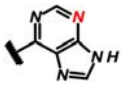	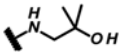	10	×74/×30/×100	32 nM	20[a]	3.1
38	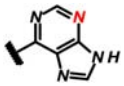	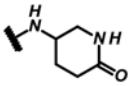	17	×120/×70/×160	30 nM	–	2.5
39	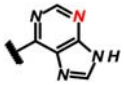	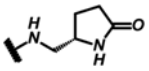	4	×240/×76/×450	24 nM	12[a]	2.6
40	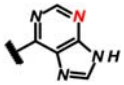	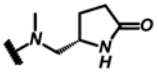	15	×300/×110/×230	–	200[c]	–
41	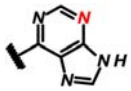	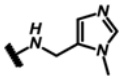	<1	×600/×330/×1100	5 nM	19[c]	2.6
42	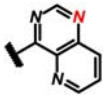	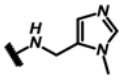	1	×125/×420/×660	18 nM	40[c]	3.1

[a]Human liver microsomal CL_{int} μL min^{-1} mg^{-1} protein.
[b]Data for the (*R*) enantiomer.
[c]Rat hepatocyte CL_{int} μL $min^{-1}10^6$ cells.

clearance. The Caco-2 data revealed that **39** was indeed a strong efflux substrate (ER = 500). In order to determine the mechanisms of clearance more precisely, we conducted a rat bile duct cannulated (BDC) study with **39**. Anesthetized rats were dosed i.p. with compound and plasma, bile and urine sampled over 2 h. We discovered that 40% of the dose was excreted as parent in the bile, confirming that active transport of parent was the major clearance pathway in vivo. Typically high HBD count is strongly correlated with propensity for efflux and active transport.[41] We sought to reduce the HBD count by methylation of the C2 amine to give **40** (Table 6). This resulted in a potent compound with improved Caco-2 profile, however the methyl group proved to be a metabolic weakness and the in vitro metabolic instability precluded in vivo assessment.

High metabolic clearance driven by dealkylation continued to plague compounds such as **41**, where we had removed one HBD. Furthermore, the imidazole function despite providing exceptional potency proved to be a liability, displaying potent cytochrome P450 inhibition.

8.15.2.4.2 Replacement of the C2 phenyl with cyclic amines

Based on the emerging data, it was clear that tertiary amines at C2 provided a basis to balance the improved physicochemical properties, solubility, and metabolic stability of the secondary amines with reduced efflux potential by reducing the HBD count. Cyclic

Table 7 PK parameters of selected C2 aliphatic amine substituted quinolines

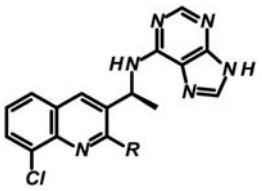

Compounds	*R*	*Caco-2* P_{app} *(nms*$^{-1}$*)*	*Efflux ratio*	*CYP 3A4* IC_{50} *(μM)*	*Rat hepatocyte* CL_{int}	*Rat* CL_b *1 mg kg*$^{-1}$ *i.v.*	*Rat %* F *3 mg kg*$^{-1}$ *p.o*
39	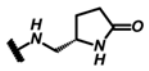	25	500	17	17	86 mL min^{-1}kg^{-1}	0%
41	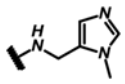	ND	ND	<5	78	ND	ND

Rat hepatocyte CL_{int} μL min$^{-1}10^{-6}$ cells, Rat Cl_b mL/min/kg.
ND, not determined.

tertiary amines were an obvious strategy to avoid the ubiquitous metabolic dealkylation pathways plaguing the acyclic analogs and it was here we next focused our attention. An illustrative selection of the SAR is described in Table 8.

The initial cyclic amine is exemplified by the morpholine **43** which displayed moderate potency against PI3Kδ (IC_{50} = 37 nM) but significantly eroded selectivity against the gamma isoform. Substitution at the 3-position (**44**) led to a reduction of potency. We next synthesized a number of 4-substituted piperidine and piperazine analogs in order to place polar substituents toward the solvent exposed "neck" of the binding pocket in accordance with the previously described structural data. Similar to the SAR described for the acyclic amines, a wide range of polar substituents encompassing both HBD and acceptor groups could be tolerated.

In particular, the *N*-acetyl piperazine **45** produced a significant potency boost and combined with the potent pyrido[3,2-*d*]pyrimidine hinge-binding group (**48**) provided unprecedented PI3Kδ potency of 60pM and good isoform selectivity (>500-fold). Pleasingly the exceptional potency in the enzymatic assay also translated into high potency in the fMLP cellular assay (2 nM). The key carbonyl functionality could also be extended further out into the pocket as exemplified by the dimethyl amide **47** which provided a potent molecule but suffered from high metabolic clearance due to dealkylation of the piperazine and the terminal amide group. Interestingly the carboxylic acid **46** maintained enzymatic potency (PI3Kδ IC_{50} 65 nM), however in contrast to the neutral compounds the acid lacked cellular activity probably due to poor cellular permeability of the carboxylic acid. The isoform selectivity of **46** showed an unexpected profile with significant PI3Kβ activity. Importantly this was not due to a broad loss of isoform selectivity, the molecule retained good selectivity against the alpha and gamma isoforms but a specific increase in PI3Kβ potency. A similar profile was apparent in compound **49** with a hydroxylethyl piperazine C2 substituent. We hypothesized empirically that the increased beta activity was due to the presence of a HBD in the C2-position. While activity against the beta isoform was intolerable for our program, we were alert to the potential opportunities in oncology for differentially *dual* selective PI3K inhibitors such as these. These empirical observations similar to the dual δ/γ selectivity described for the aminopurines earlier again highlight the additional selectivity opportunities provided by an extensive interrogation of the SAR.

We realized that although the *N*-acetyl piperazine substituted quinolines such as **48** provided exceptional potency, the rapid metabolism by deacetylation prevented their further development. Wishing to explore the topological requirements of the carbonyl hydrogen bond acceptor and to incorporate it into the molecule in a metabolically robust fashion, we synthesized the piperazinone analogs **50** and **53**. We were delighted to find that the piperazinones retained the exceptional potency displayed by the *N*-acetyl piperazines but with reduced lipophilicity and improved metabolic stability. Synthesis of the *N*-methyl analog **51** resulted in an ~10-fold reduction of potency demonstrating the importance of the amide NH and suggesting additional interactions with the protein. Ring expansion to the homopiperazinone **52** also led to a reduction of potency.

Our successful campaign to replace the metabolically vulnerable phenyl ring with amines resulted in compounds where the exceptional enzymatic and cellular potency achieved in the *First Generation* inhibitors was maintained but importantly, the global reduction in lipophilicity drove a significant improvement in solubility and metabolic stability.

Serendipitously we found that the C2 amino compounds also improved the selectivity over PI3Kγ and we were able to maintain this selectivity as we developed the SAR. Cyclic tertiary amines allowed us to address issues with active transport and poor permeability and we identified that a strategically positioned amide function within the piperazinone ring could combine the desired potency with metabolic stability as exemplified by compounds **50** and **53**. Having alighted on the piperazinone as an optimal

Table 8 Quinoline C2 SAR: Replacement of the C2 phenyl with cyclic amines

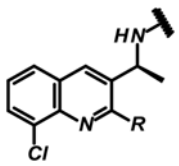

Compounds	*Hinge binder*	*R*	*PI3Kδ pIC50 (nM)*	*Isoform selectivity α/β/γ*	*fMLP IC50*	*Hu in vitro CL_{int}*	*log D pH 7.4*
43	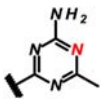		37	×200/×55/×**12**	–	–	
44	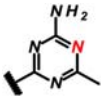		228	×50/×16/×**7**	–	–	–
45	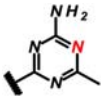	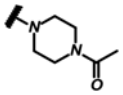	6	×3500/×1300/×62	32 nM	6[a]	2.9
46	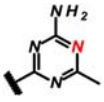	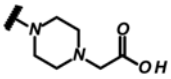	65	×500/×**5**/×58	>5 μM	5[a]	0.81
47	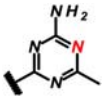	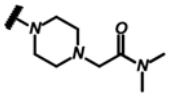	3	>1000/×140/×690	12 nM	52[a]	2.7
48	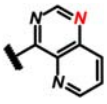	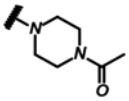	0.06	×6300/×2800/×780	2 nM	20[a]	3.7
49	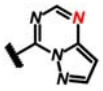	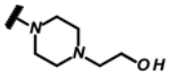	16	>1000/×**9**/>1000	–	–	–
50	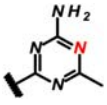	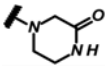	6	×640/×35/×110	30 nM	11[a] 5[b]	2.6
51	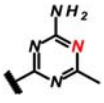	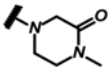	74	×200/×36/×31	200 nM	10[a]	2.9
52	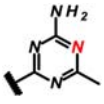	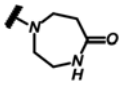	26	×930/×56/×10	162 nM	10[a]	2.5
53	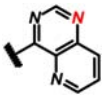	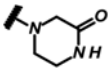	<0.1	>1000/>200/>100	1.2 nM	16[b]	2.8

[a]Microsomal CL_{int} μL min^{-1} mg^{-1} protein.
[b]Hepatocyte CL_{int} μL min^{-1} 10^{-6} cells.

C2 substituent in combination with the triazinyl or pyrido[3,2-*d*]pyrimidine hinge binder, our attention next turned to establishing the in vivo exposure and subsequent pharmacological activity of these molecules.

8.15.2.5 Development and Pharmacological Characterization of Triazinyl-Piperazinones

8.15.2.5.1 Potency and ADMET characterization of triazinyl-piperazinones

We combined the piperazinone with triazinyl and pyrido[3,2-*d*]pyrimidine hinge-binding groups to provide a panel of compounds which were subjected to a broader panel of in vitro potency (Table 9) and ADEMT assays (Table 10) in order to identify compounds suitable for in vivo assessment.

The pyrimidopyridine compound **53** exhibited the most potent activity in cell assays but was compromised by the high in vitro metabolic clearance in rat hepatocytes and human microsomes, while also exhibiting potent CYP inhibition activity especially against the 2C9 isoform. Pleasingly, replacement of the pyrimidopyrimidine with triazinyl hinge-binding groups (compounds **50** and **54–56**) provided compounds with good stability in human hepatocytes and an improved CYP inhibition profile. In terms of potency, the 8-Cl substituted compounds **50** and **54** maintained better cellular potency in the fMLP and D0.11.10 assays than the 8-CH_3 substituted quinolines. In particular **54** exhibited excellent potency in the target engagement pAKT RAMOS assay (IC_{50} 8 nM). The presence of the 5-methyl triazine in **50** reduced selectivity against the PI3Kβ isoform 10-fold compared to the 5H triazine **54** although improved the CYP inhibition profile especially against the 2C9 isoform (13 μM vs. 0.7 μM). The thermodynamic aqueous solubility at neutral pH of these compounds was promising and compound **54** showed good permeability and low efflux in the Caco-2 assay. Based on these encouraging in vitro data, we assessed these compounds in rat PK studies with the data presented in Table 11.

The compounds displayed low to moderate in vivo clearance and good oral bioavailability. In contrast to earlier compounds such as **39**, the in vivo clearance values were well predicted from the in vitro clearance data, indicating that the nonmetabolic active transport mediated clearance which prevented the progression of earlier compounds had been overcome.

8.15.2.5.2 Metabolite ID studies with compound 54

With compound **54** displaying an encouraging profile, we sought to identify the major metabolites from in vitro hepatocyte and microsomal incubations and the in vivo PK studies. A summary of the main metabolic pathways identified are summarized in Fig. 12, with the metabolites identified from human hepatocyte incubations described in Table 12.

In human hepatocytes the major metabolite identified was oxidation of the triazine hinge-binding group. Lower levels of piperazinone metabolism were seen, either hydrolysis or low levels of direct glucuronidation thought to occur on the secondary amide.

Table 9 In vitro enzymatic and cellular potency data for selected piperazinones

					Cellular activity IC_{50}			
Compounds	*Hinge binder*	*R*	*PI3Kδ IC_{50}*	*Isoform selectivity α/β/γ*	*fMLP (nM)*	*PMA (μM)*	*RAMOS pAKT*	*D0.11.10 proliferation*
53	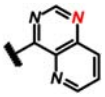	8-Cl	0.1	>1000/>200/>100	1.2	>10	–	–
50	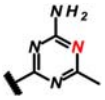	8-Cl	6	×640/×**35**/×110	30	>10	–	40 nM
54	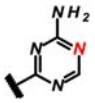	8-Cl	7	>1000/×330/×700	30	>10	8 nM	70 nM
55	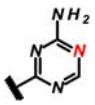	8-CH_3	12	×2000/×520/×580	180	>10	–	170 nM
56	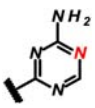	7-F, 8-CH_3	12	×490/×650/×275	190	>10	–	–

Table 10 In vitro ADMET data for selected piperazinones

			Hepatocyte CL_{int}		CYP inhibition IC_{50}			Caco-2		
Compounds	*Hinge binder*	*R*	*Hu*	*Rat*	*3A4 (μM)*	*2D6 (μM)*	*2C9 (μM)*	P_{app}	*ER*	*Thermo sol pH 7.4*
53	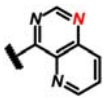	8-Cl	16[a]	125	8.5	12	0.5	–	–	–
50	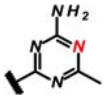	8-Cl	5	23	30	>50	13	–	–	115 μM
54	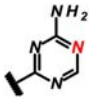	8-Cl	4	17	9	>50	0.7	37	9	88 μM
55		8-CH_3	4	10	>50	>50	9			ND
56	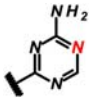	7-F, 8-CH_3	7	6	14	>50	4			ND

[a]Data for human microsomes. microsomal CL_{int} μL min^{-1} mg^{-1} protein; hepatocyte CL_{int} μL min^{-1} 10^{-6} cells.

Table 11 In vivo PK plasma data in male Han Wistar rats

		1 mg kg^{-1} *i.v.*			*3 mg* kg^{-1} *p.o.*		
Compounds	*R*	*CL (mL min* kg^{-1}*)*	*Vss (L* kg^{-1}*)*	$T_{1/2}$	C_{max} *(ng* mL^{-1}*)*	*AUC (ng h* mL^{-1}*)*	*%F*
50	8-Cl	30	2.1	0.9	249	832	54
54	8-Cl	19	2.2	1.9	233	966	42
55	8-CH_3	13	2.2	1.1	703	2407	62
56	7-F, 8-CH_3	36	2.1	2.2	207	454	52

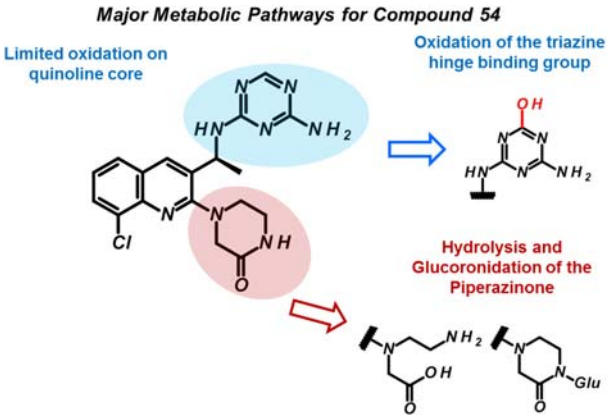

Fig. 12 The main metabolic pathways with proposed structures of metabolites identified for lead triazinyl-piperazinone **54**.

Table 12 Compound **54** metabolite ID from human hepatocyte incubations

Human hepatocytes	m/z	*Mass shift*	t_R *(min)*	*Level*	*Location*
Compound **54**	399.1446	0.0000	5.03		
+O	415.1394	15.9948	4.37	Major	Triazine
Hydrolysis	417.1550	18.0105	4.20	Minor	Piperazinone
+Gluc	575.1765	176.0319	5.17	Minor	Piperazinone

In human in vitro systems no metabolism of the quinoline core was observed, however in rodent systems, both in vitro and in vivo, metabolism of the quinoline core is observed albeit with the triazine and piperazinone metabolic pathways still predominating.

8.15.2.5.3 Pharmacological assessment of compound 54

To support pharmacological evaluation of **54**, we conducted an oral PK study in Balb–c mice at 10 mg kg^{-1} (Fig. 13). Excellent exposure was achieved with a C_{max} of 11.2 μM and AUC_{last} of 41.2 μM h. The free concentration (total concentration corrected for plasma protein binding) of **54** at 1 and 7 h was 170 and 33 nM, respectively. These free concentrations exceeded the cellular IC_{50} activities in the fMLP and D0.11.10 assays at 1 h and both the enzymatic PI3Kδ and RAMOS pAKT activity over the measured 7 h period demonstrating that **54** was suitable for assessment of the dose and exposure relationship in in vivo models.

Overall **54** exhibited an excellent in vitro and in vivo profile and the best balance of properties in the triazinyl-piperazinone class. The in vivo efficacy of this molecule was assessed in a range of immune mechanistic models.

*8.15.2.5.3.1 Assessment of **54** in the anti-CD3 IL-2 release assay*

In order to demonstrate mechanistic inhibition of PI3Kδ in vivo, we first determined the activity of **54** in a short-term model, the inhibition of IL-2 release following anti-CD3 antibody administration in Balb/c mice (Fig. 14). Pretreatment with **54** (0.1–30 mg kg^{-1} p.o.) 30 min before anti-CD3 antibody administration produced a dose-dependent inhibition of IL-2 levels (Fig. 11). The relationship between the total compound concentration in blood and effect (% inhibition of IL-2 release) was analyzed using an I_{MAX} model. The relationship was described by an IC_{50} value of 201 nM (95% CL of 152–266 nM) and an I_{MAX} value of 92 ± 3%. Taking into account the protein binding of the compound, this equates to an unbound IC_{50} value of 4 nM which was in good agreement with both the PI3Kδ enzymatic activity (IC_{50} 7 nM) and the inhibition of pAKT in RAMOS cells (IC_{50} 8 nM), providing confidence that the observed pharmacological effect was driven by PI3Kδ inhibition.

While the activity in the mechanistic anti-CD3 IL-2 release assay provided evidence of target engagement in vivo, we wished to demonstrate a functional effect in a more complex model. To this end we took **54** into the SRBC DTH model.

*8.15.2.5.3.2 Assessment of compound **54** in the SRBC DTH model*

Sensitization and challenge with SRBC resulted in an antigen-specific footpad swelling. **54** was administered orally once daily from prior to sensitization at 3, 10, and 30 mg kg^{-1}. All dose levels significantly inhibited footpad swelling such that the magnitude of residual footpad swelling was comparable to the negative control group (Fig. 15). The total compound concentration in blood was determined 1 h postdose on the final day of dosing, for the 3 mg kg^{-1} dose a free concentration of 32 ± 8 nM was obtained which correlated with the enzyme potency activity of **54**.

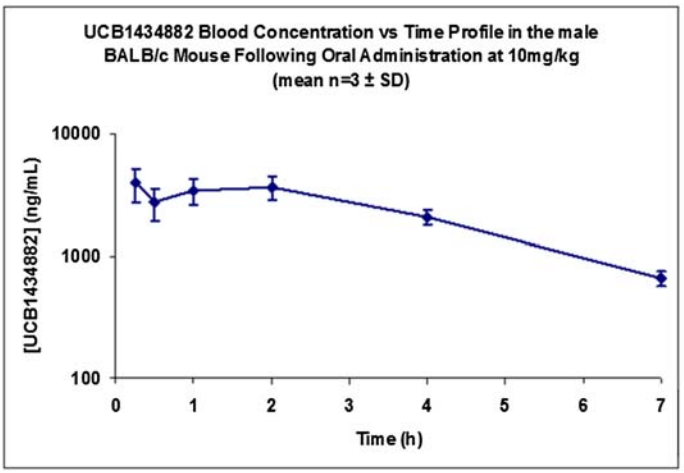

Parameter	
C_{max}	11.2μM
AUC_{last}	41.2 μM.hr
Free conc @ 1 hour	170nM
Free conc @ 7 hours	33nM

Fig. 13 PK profile of compound **54** in Balb–c mice at 10 mg kg^{-1} following oral administration.

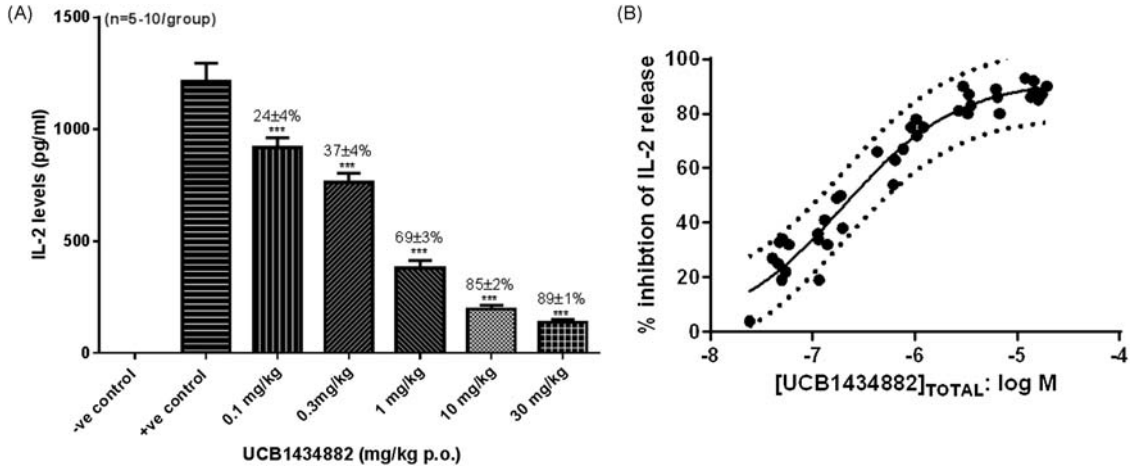

Fig. 14 Inhibition of anti-CD3 antibody-induced IL-2 release in vivo. Vehicle and **54** in 1% methylcellulose (400 cps) was administered 30 min prior to anti-CD3 antibody (0.01 mg kg^{-1} i.v.), which activated T-cells. Mice were sacrificed 90 min later. Dose (A) and concentration (B) response relationships are shown. Statistical significance is denoted as follows, $***p < 0.001$ compared to positive control group (Dunnets multiple comparison test).

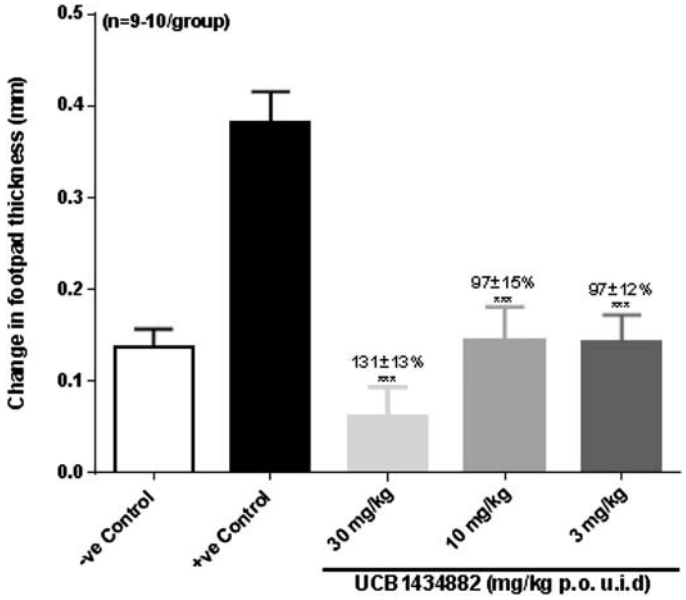

Fig. 15 Inhibition of the SRBC DTH model in vivo. Vehicle and compound **54** in 1% methylcellulose (400 cps) was administered orally once daily throughout the study. Animals were sensitized (i.v.) and challenged (i.pl.) with SRBC to elicit an antigen-specific footpad swelling. Mice were sacrificed 60 min after the last compound dose and 24 h post footpad challenge. Dose-dependent inhibition of footpad swelling was obtained. Statistical significance is denoted as follows, $***p < 0.001$ compared to positive control group (Dunnets multiple comparison test).

The efficacy and potency of compound **54** in both the anti-CD3 and SRBC DTH assays provided validation of our in vivo cascade and importantly, validation of the quinoline chemotype in PI3Kδ driven models. Furthermore, the good correlation of the in vivo activity with the in vitro PI3Kδ potency provided additional confidence that the effects observed were driven by on target activity.

8.15.2.5.4 Off-target and ancillary profiling of compound 54

Following the promising pharmacological activity demonstrated by **54**, we next profiled the compound in a range of in vitro toxicology screens in order to evaluate suitability for further preclinical development. The screening included initial in vitro genotoxicity assessment, activity against the hERG channel, and an off-target screen against a variety of biological targets (performed at Cerep and Invitrogen). The significant off-target activities are shown in Table 13.

Compound **54** proved remarkably clean in a panel of approximately 200 kinases, enzyme, and receptor targets, the only significant activities ($IC_{50} < 10$ μM) were observed against Aurora A (0.48 μM) and FGR kinase (2.1 μM). To assess the potential cardiovascular safety, we screened compound **54** against the hERG ion channel as activity against this ion channel is commonly associated

Table 13 Selected ancillary profile of compound **54**

Invitrogen kinase selectivity		*In vitro genotoxicity*		*In vitro cardiac toxicity*
Aurora A IC_{50}	FGR IC_{50}	AMES test	HGS	hERG IC_{50}
0.48 μM	2.1 μM	−ve	+ve	17.5 μM

with the risk of QTc prolongation in the clinic.[42,43] Gratifyingly, we saw only modest activity against the hERG channel. The critical issue with compound **54** was the positive activity in the genotoxicity assays, in particular the Human Greenscreen (HGS), an assay measuring induction of the DNA repair enzymes.[44,45] Close analogs of compound **54** also induced micronucleus formation in in vitro assays.[46] The potential for genotoxicity highlighted by these in vitro screens coupled with the micromolar inhibition of the cytochrome P450 enzymes described previously led us to conclude that compound **54** was not suitable for further development. Furthermore, the genotoxicity issues seen with **54** turned out to be a class wide liability with the triazinyl-piperazinones and therefore a fundamental redesign of our leading chemical matter was necessary.

In the following section, the genotoxicty screening process we used at the time of the program and the extent of the issue we faced will be outlined before describing how we reengineered the lead series to overcome the genotoxicity issues, leading ultimately, to the identification of *seletalisib*.

8.15.2.6 In Vitro Genotoxicity Screening

The genotoxicity screening cascade, we used consisted of firstly, the HGS assay[44,45] to assess the potential for DNA damage, followed by confirmation in an in vitro micronucleus test[46] measuring the formation of micronuclei in Chinese hamster ovary cells. In parallel, an AMES mpf[47] test for mutagenesis potential was also conducted.

We quickly identified that compound **54** and other representative leading triazine molecules were positive in the HGS assay. Crucially we found that molecules positive in the HGS assay were also positive in the in vitro micronucleus assay, confirming that the propensity for DNA damage translated into undesired functional effect (formation of micronuclei in vitro). Broadly the compounds tended to be inactive in the AMES mutagenicity tests. A representative selection of the SAR observed in the HGS assay is provided in **Table 14**.

Crucially we observed positives in the HGS assay both in the presence and absence of the rat microsomal fraction S9, indicating that we were dealing with two potential genotoxic mechanisms; intrinsic ability to interact with and damage DNA (−S9) and also via the production of genotoxic metabolites (+S9) possibly involving reactive intermediates. With these mechanisms in mind, analysis of the emerging SAR led to some key empirical observations. Firstly we observed that the amino triazinyl (compounds **58**, **61**, and **62**) and amino purinyl (data not shown) hinge-binding groups tended to have a high hit rate in the HGS in the absence of S9, indicating a propensity for intrinsic genotoxicity. Additionally a similar profile, suggesting an increased potential for intrinsic genotoxicity, was apparent for piperazinones and *N*-acyl piperazines C2 substituents (compounds **53**, **58**, **48**, and **60**). Although certain combinations with the C2 piperazinone could provide a clean in vitro profile such as **63**, this particular molecule suffered from high metabolic clearance and it was clear that the potentially genotoxic functionality (piperazinone and triazine) limited the scope of the SAR to address other drug-like properties.

For compounds that were HGS positive in the presence of S9 (+S9), it appeared that electron-rich quinolines had a greater propensity for genotoxicity as illustrated by the positives for compounds with the 8-CH_3 substituents (**57** and **58**) compared to the 8-Cl substituted quinolines where no HGS hits in the presence of S9 were observed. We had shown through metabolite ID studies (see section "**General metabolic profile of the quinoline C2 pyridyl *N*-oxides**") that the quinoline ring could be oxidatively activated to an aryl epoxide (a well-known metabolic pathway for quinolines[48,49]) and furthermore we had demonstrated glutathione conjugation through the quinoline epoxidation pathway from the in vitro metabolic studies. The potential for this reactive metabolite pathway to lead to DNA damage, or other adverse drug reactions was evident. Clearly addressing this problematic metabolic pathway in future molecules would be desirable.

The broad conclusions from the genotoxicity screening are summarized in **Fig. 16**.

These empirical observations led us to conclude that in order to address the genotoxicity issues with confidence, we would need to accomplish three key goals:

(1) Replace the triazinyl hinge-binding group
(2) Design a replacement for the C2 piperazinone which maintained the advantageous potency and physicochemical properties but was devoid of genotoxic liabilities
(3) Focus on electron deficient quinolines to reduce or eliminate the potential for metabolism via the epoxidation pathway

8.15.2.7 *Second Generation Inhibitors*: Development of the 3-Pyridyl *N*-Oxides

8.15.2.7.1 Identification of 3-pyridyl N*-oxide as an effective bioisostere of a carbonyl group*

Armed with these new objectives, we initially turned our attention to replacement of the C2 piperazinone group, as we had already established a large number of potent hinge-binding group alternatives to the aminotriazine (see **Table 4**).

Table 14 Representative genotoxicity data generated on lead molecules in the HGS and AMES mpf assays

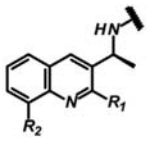

Compounds	Hinge binder	R1	R2	PI3Kδ IC_{50} (nM)	Human Greenscreen +S9	Human Greenscreen −S9	AMES mpf assay
57	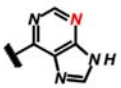	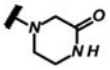	8-CH_3	0.7			
53	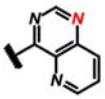	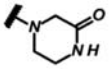	8-Cl	<1			
58	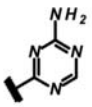	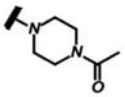	8-CH_3	50			
48	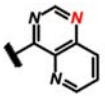	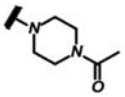	8-Cl	0.06			
59	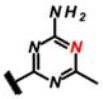	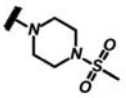	8-Cl	34			
60	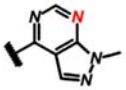	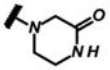	8-Cl	15			
61	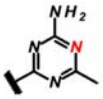		8-Cl	10			
62	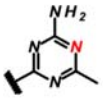	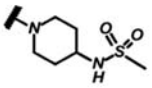	8-Cl	32			
63	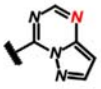	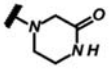	8-Cl	0.3			

Red indicates a positive result in the assay (genotoxicity flag) while *green* represents a negative result (no genotoxicity flag).

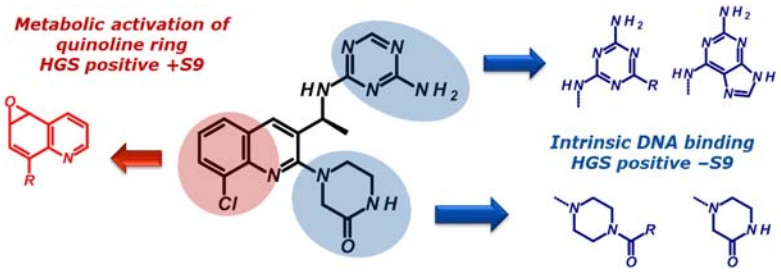

Fig. 16 Summary of the two genotoxic mechanisms identified. (i) Metabolic activation of the quinoline ring and (ii) intrinsic ability to induce DNA damage.

Having established that the presence of a hydrogen bond acceptor in C2 was critical to high potency, we reasoned that a 3-pyridyl or pyridone could prove potent alternatives to the piperzinone carbonyl (Table 15).

The 3-pyridyl group (**66**) proved to be a potent replacement but suffered from high metabolic clearance and unacceptable inhibition of cytochrome P450 enzymes. We reasoned that the 3-pyridone could overcome these limitations and were delighted to find that **64** provided a potent compound without the CYP inhibition liabilities. However **64** suffered from unacceptably high metabolic clearance in human hepatocyte incubations. We reasoned that the high metabolic clearance in human hepatocytes was primarily driven by glucuronidation of the pyridone functionality based on metabolite identification studies on close analogs. Attempts to eliminate the potential for glucuronidation by methylation to give **65** unfortunately eroded PI3Kδ potency 100-fold. Encouraged by the potency of **64**, we further reasoned that replacement of the pyridone with a 3-pyridyl-*N*-oxide would maintain the desired hydrogen bond acceptor functionality but remove the potential for glucuronidation and improve metabolic stability.

We were pleased to find that, as expected, the pyridine *N*-oxide **67** resulted in a potent compound with promising selectivity against the alpha and beta isoforms. Importantly the CYP liabilities associated with the analogous pyridyl compound were eliminated and metabolic stability in hepatocyte incubations improved. Most importantly compound **67**, in contrast to the triazinyl-piperazinones, was clean in the in vitro HGS assay. Further genotoxicity screening in the in vitro micronucleus and AMES testing confirmed that compound **67** was not genotoxic. Combination of the 3-pyridyl-*N*-oxide with the aminotriazinyl hinge-binding group to give **68** provided a compound free of the genotoxicity flags associated with previous triazine analogs but the reduced PI3Kδ and cellular activity discouraged further investigation.

Interestingly moving the position of the *N*-oxide from the 3- to the 4-position to provide compound **69** resulted in a dramatic and substantial loss of potency and selectivity especially against the PI3Kα isoform. It is unclear from the known binding mode of these compounds why such a modest change would induce a profound loss of selectivity. The pyridyl *N*-oxide sits toward solvent and a small change in the regiosiomer should leave the key interaction with the induced selectivity pocket intact. One potential explanation is that the molecules undergo a fundamental change in binding mode such that the classic "selectivity pocket" formed by the movement of Met^{752} and Trp^{760} is not induced. Unfortunately crystallographic data to substantiate this tentative hypothesis was unobtainable, however the example serves to illustrate once again how seemingly small structural changes in molecules can change selectivity profiles in unexpected ways and open up potential for other therapeutic opportunities.

The discovery of the 3-pyridyl-*N*-oxide group as an effective replacement of the piperazinone was a vital strategic breakthrough in the medicinal chemistry program. The *N*-oxide provided a solution to the genotoxicity flags associated with the piperazinone and in combination with the pyrido[3,2-*d*]pyrimidine hinge-binding group provided highly potent inhibitors exemplified by compound **67**. Furthermore incorporation of the polar pyridine *N*-oxide provided compounds with good solubility, metabolic stability in human and rat hepatocyte incubations and that were devoid of cytochrome P450 inhibition.

8.15.2.7.2 Characterization of compound 67

8.15.2.7.2.1 Comparison of UCB1434882 and UCB1442243

As compound **67** solved the genotoxicity issues associated with our previous lead molecule **54**, we next fully characterized **67**, Table 16 describes the comparative data between **67** and our previous lead triazinyl-piperazinone **54**.

The comparative data presented in Table 16 highlights how the key structural changes, namely the replacement of the C2 piperazinone with the 3-pyridyl-*N*-oxide and replacement of the triazinyl hinge-binding group with the pyrido[3,2-*d*]pyrimidine, resolved the ancillary issues that prevented the development of the triazinyl-piperazinones. Notably compound **67** was devoid of the genotoxicity, kinase activity, and cytochrome P450 inhibition that blighted **54**. Excellent enzymatic and cellular potency was maintained, although typically for C2 aryl groups we observed suboptimal selectivity against the PI3Kγ and β isoforms.

Comparing the ADMET properties of these molecules, the in vitro metabolic stability in human hepatocytes was encouraging and greatly improved from the earlier highly lipophilic C2 phenyl analogs. Compound **67** displayed a reasonable oral rat PK profile; despite a relatively high in vivo clearance (equivalent to approximately 2/3 of liver blood flow) oral bioavailability of 29% was achieved due to the excellent permeability and aqueous solubility (426 μM @ pH 7.4) of compound **67**. Although the rat PK of **67** was suitable for preclinical development and would support achieving the exposures required for the rat toxicology program,

Table 15 Development of the 3-pyridyl-*N*-oxide as a bioisostere of the piperazinone

	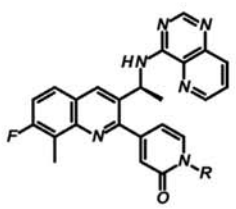		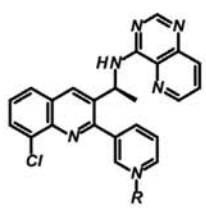		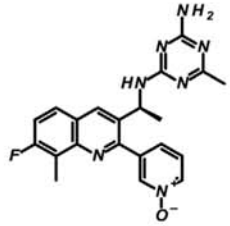	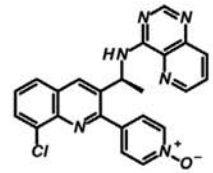
R	*H*	*CH_3*	*Pyridine*	N-*Oxide*	–	–
Compounds	***64***	***65***	***66***	***67***	***68***	***69***
PI3Kδ IC_{50}	0.6 nM	62 nM	<1 nM	5 nM	18 nM	57 nM
PI3K α/β/γ selectivity	×730/×400/×400	×235/×400/×**23**	>1000/ >1000/×60	×880/×194/×71	>1000/>1000/×60	×**3**/×**8**/×**0.5**
fMLP IC_{50}	5 nM	341 nM	5 nM	10 nM	50 nM	12 nM
Hu in vitro CL_{int}	23[a]	10[b]	14[b]	7[a]	9[a]	9[b]
Rat in vitro CL_{int}	19[b]	20[b]	43[a]	13[a]	8[a]	2[a]
CYP inhibition	>30 μM, all isoforms	ND	3A4 2 μM	>30 μM, all isoforms	>25 μM, all isoforms	>30 μM, all isoforms
Human Greenscreen		ND				ND
PSA	93	93	76	89	115	89

[a]Hepatocyte clearance CL_{int} μL $min^{-1}10^{-6}$ cells.
[b]Microsomal clearance CL_{int} μL $min^{-1}mg^{-1}$ protein.

Table 16 Comparison of triazine **54** and 3-pyridyl-*N*-oxide **67**

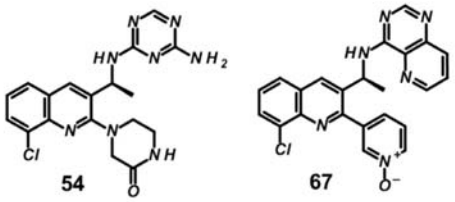

54 **67**

	54	*67*		*54*	*67*
PI3Kδ IC_{50}	7 nM	5 nM	Hu Hep CL_{int}	4	7.5
PI3K sel α/β/γ	×1000/×330/×700	×880/×194×71	Rat hepatocyte CL_{int}	17	13
RAMOS pAKT IC_{50}	8 nM	12 nM	Caco-2: P_{app} (nms^{-1})/ER	34/9	35/24
D0.11.10 IC_{50}	70 nM	44 nM	Rat i.v. 1 mg kg^{-1}. Cl	19 mL $min\ kg^{-1}$	43 mL $min^{-1}\,kg^{-1}$
Aurora B IC_{50}	0.48 μM	>30 μM	Rat p.o. 3 mg kg^{-1} %*F*	42%	29%
hERG IC_{50}	17.5 μM	>30 μM	CYP inhibition	2C9 0.7 μM	>20 μM all isoforms
Genotoxicity					

we felt that there was room to further improve the in vivo PK profile of **67** in addition to the improvement necessary in the selectivity against PI3Kγ and β isoforms.

8.15.2.7.2.2 X-ray structure of UCB1442243 in PI3Kγ

We obtained a cocrystal structure of compound **67** with PI3Kγ (Fig. 17) which confirmed that the compound adopted the classical binding mode with the pyrido[3,2-*d*]pyrimidine hinge-binding group making a key hydrogen bond with the NH of Val^{882} and the 8-Cl quinoline positioned in the induced selectivity pocket.

*8.15.2.7.2.3 In vivo efficacy assessment of compound **67***

We assessed the pharmacological activity of **67** in a similar manner to triazinyl-piperazinone **54**. The data from the anti-CD3-induced IL2 release assay is presented in Fig. 18 and the SRBC DTH model in Fig. 19.

8.15.2.7.2.3.1 Anti-CD3-induced IL2 release model

Pretreatment with **67** (0.3–30 mg kg^{-1} p.o.) produced a dose-dependent inhibition of IL-2 levels (Fig. 18). As previously mentioned, the relationship between the total compound concentration in blood and effect was analyzed using an I_{MAX} model.

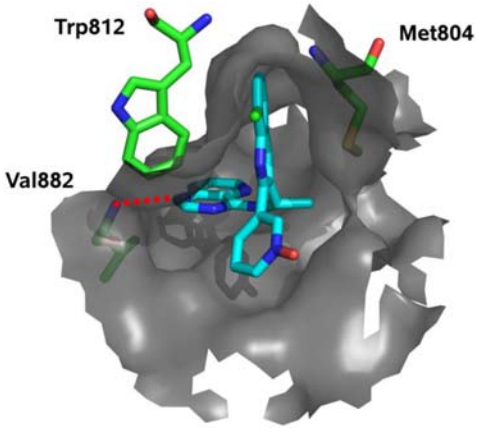

Fig. 17 Cocrystal structure of compound **67** with PI3Kγ. The pyrido[3,2-*d*]pyrimidine hinge-binding group forms a monodentate hydrogen bond with Val^{882} backbone NH (shown in *red*) while the 8-Cl quinoline core sits in the *induced selectivity pocket* formed by movement of Met^{804} and Trp^{812}. The 3-pyridyl-*N*-oxide is orientated toward solvent and makes no obvious interactions with the protein.

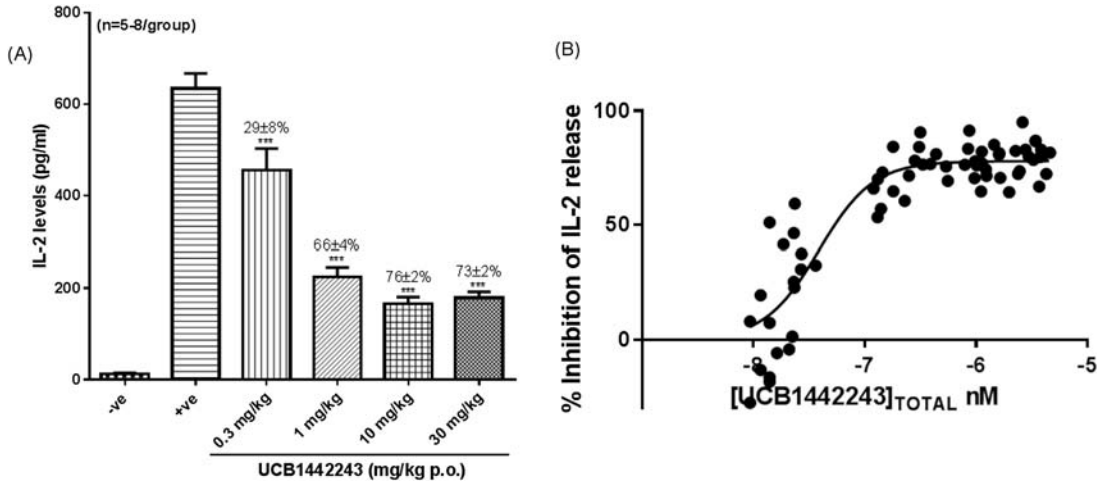

Fig. 18 Inhibition of anti-CD3-induced IL-2 release in vivo. Vehicle and compound **67** in 1% methylcellulose (400 cps) was administered 30 min prior to anti-CD3 (0.01 mg kg^{-1} i.v.), mice were sacrificed 90 min later. Dose (A) and concentration (B) response relationships are shown. Statistical significance is denoted as follows, $***p < 0.001$ compared to positive control group (Dunnets multiple comparison test).

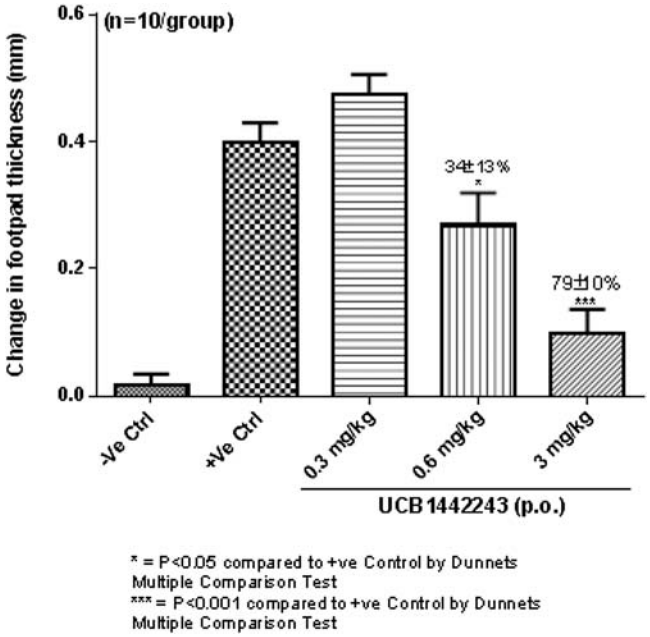

Fig. 19 Inhibition of the SRBC DTH model in vivo. Vehicle and compound **67** in 1% methylcellulose (400 cps) was administered orally once daily throughout the study. Animals were sensitized (i.v.) and challenged (i.pl.) with SRBC to elicit an antigen-specific footpad swelling. Mice were sacrificed 60 min after the last compound dose and 24 h post footpad challenge. Dose-dependent inhibition of footpad swelling was obtained. Statistical significance is denoted as follows, $*p < 0.05$ and $***p < 0.001$ compared to the positive control group (Dunnets multiple comparison test).

The relationship was described by an IC_{50} value of 39 nM (95% CL of 27–55 nM). Taking into account the plasma protein binding of the compound, this equated to an unbound IC_{50} value of 10 nM which was consistent with the in vitro enzyme potency of **67**.

8.15.2.7.2.3.2 Sheep red blood cell delayed type hypersensitivity

Sensitization and challenge with SRBC resulted in an antigen-specific footpad swelling. Compound **67** was administered orally once daily from prior to sensitization over the dose range 0.3–3 mg kg^{-1}. Dose-dependent inhibition of footpad swelling was obtained at 0.6 and 3 mg kg^{-1} (Fig. 19).

Overall compound **67** demonstrated a very similar pharmacological profile to the lead triazinyl-piperazinone **54**, confirming that the reengineering of the lead molecules to avoid the genotoxicity issues had not compromised the in vivo potency and efficacy of our initial series of compounds.

8.15.2.7.3 General metabolic profile of the quinoline C2 pyridyl N-oxides

While the C2 pyridyl *N*-oxide class of quinolines exemplified by **67** had resolved a number of issues with the triazinyl-piperazinone class of inhibitors, we wished to optimize the PK profile of these compounds by further reducing metabolism. In order to construct rational medicinal chemistry strategies, a detailed knowledge of the metabolic pathways across species coupled with identification of the metabolic weak spots was required. In the following section, we will describe the global metabolic understanding we developed on the quinoline C2 pyridyl *N*-oxides illustrated by specific metabolite identification. Finally we will show how we applied this knowledge to the optimization of compound **67**.

8.15.2.7.3.1 Metabolism of the quinoline core

The major metabolic pathways identified on the quinoline core fell into two broad subclasses:

(1) Oxidative Phase 1 metabolism of the quinoline ring to a reactive, electrophilic aryl epoxide intermediate followed by a number of different fates, including glucuronidation or glutathione trapping dependant on the nature of the rest of the molecule
(2) Oxidation of metabolically labile quinoline substituents, most notably the 8-methyl group

8.15.2.7.3.1.1 Phase 1 and Phase 2 metabolism of the quinoline core via an aryl epoxide

The susceptibility of quinolines to suffer metabolic oxidation through the formation of aryl epoxide intermediates is well known.[49] These aryl epoxides are reactive electrophiles which are not isolated but are opened by nucleophilic addition of either water (Pathway A) or glutathione (GSH) (Pathway B) (Fig. 20). The hydroxylated products (phenols), in certain cases, became a handle for further Phase 2 glucuronidation.

In our case the general 2,3 substitution pattern of the quinolines meant that epoxidation can be expected to occur on the benzo ring in the 5,6; 6,7; or 7,8-positions. Metabolite screening across a wide range of quinolines identified two major metabolic pathways from this reactive epoxide intermediate (Fig. 20):

(i) *Pathway A* oxidation followed by subsequent hydrolysis of the epoxide intermediate to a diol, elimination to a phenol, and finally (in most cases) Phase 2 glucuronidation (+OGlu)
(ii) *Pathway B* oxidation followed by nucleophilic addition of glutathione to the common reactive intermediate epoxide (+GSH and H_2O)

High levels of glutathione trapping can potentially be an issue in drug development as it indicates a propensity for the formation of reactive metabolites, and thus increased potential for toxicity.[50,51] Therefore, in addition to the metabolite identification studies, we also screened key compounds in reactive metabolite screens, microsomal (S9) incubations with added glutathione or KCN to examine reactive metabolite potential.

As part of our SAR development and to reduce the susceptibility of the quinoline ring to oxidative metabolism, we had prepared a number of halogenated analogs with fluorine or chlorine substituents on the aromatic ring. Incorporation of these leaving groups led to changes in metabolic fate that allowed us to define more precisely the regiochemistry of oxidation and also led to the observation of a unique metabolic pathway in dog.

Specifically fluorinated analogs presented metabolites with a mass gain of +303 consistent with addition of glutathione, oxygen, and loss of fluorine. The proposed pathway for this metabolism is described in Fig. 21. Formation of the aryl epoxide intermediate

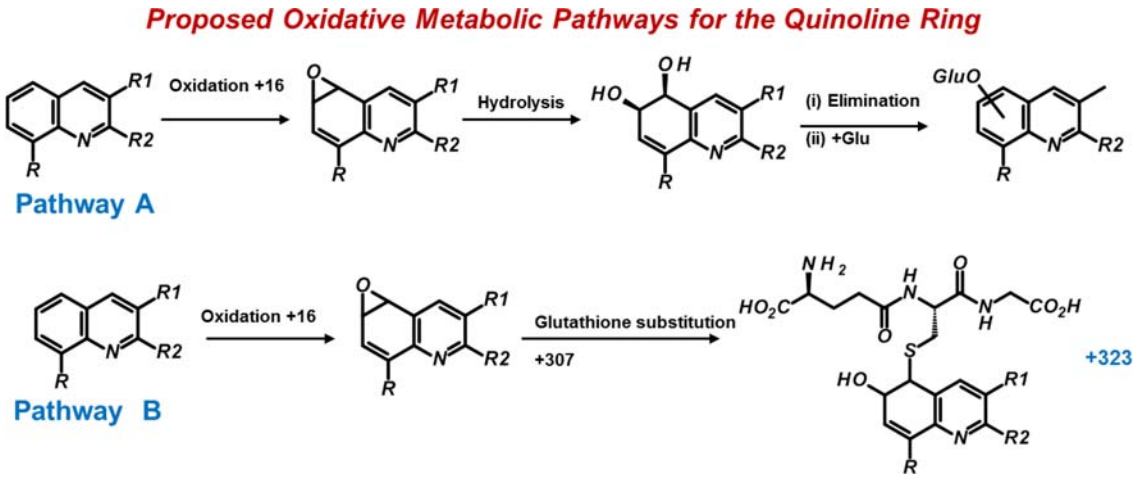

Fig. 20 General scheme for the oxidative activation of the quinoline core through an aryl epoxide intermediate and subsequent trapping by water or glutathione nucleophiles.

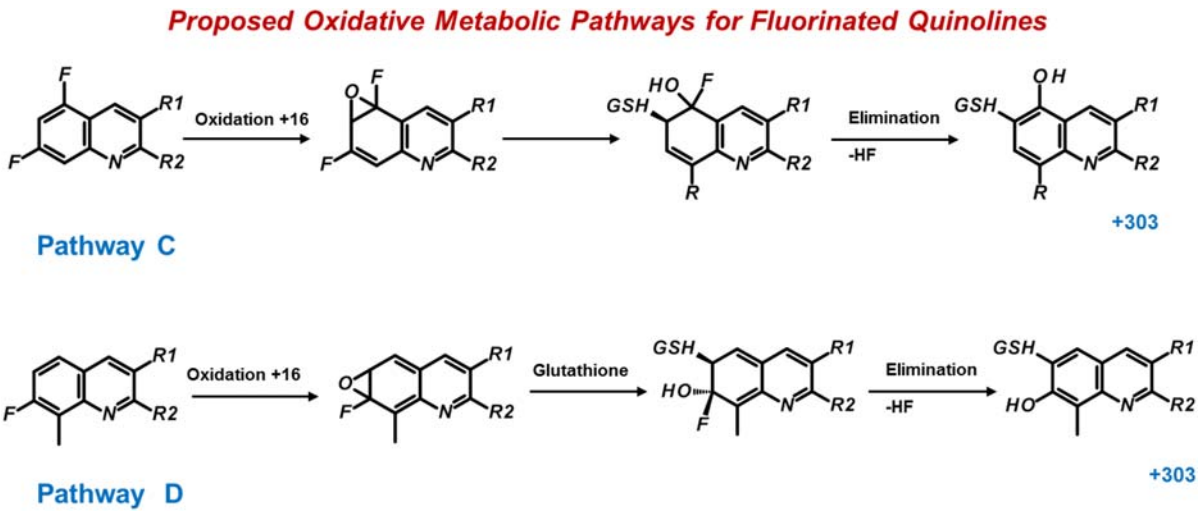

Fig. 21 Addition elimination metabolic pathway for 5, 7, and 7 fluorinated quinolines.

next to the aromatic fluoride provides an alternative metabolic fate after the addition of glutathione, namely elimination of hydrogen fluoride with concomitant aromatization of the quinoline ring.

The addition/elimination pathway was initially observed for the 5,7 difluro substituted quinolines (*Pathway C*), in this case the precise regiochemistry of the formed metabolite cannot be certain (elimination of either the 5F or 7F can be envisaged). However in the case of the 7F,8Me core (*Pathway D*), confirmation of the +OGSH, −F metabolite (+303) allows a more certain postulation of the likely regiochemistry. Elimination of the 7F must occur, with likely epoxidation occurring at the least sterically hindered 6,7-position with subsequent glutathione addition postulated to occur at the least sterically encumbered 6-position on the quinoline. Unequivocal assignment of the metabolite structure would require isolation of the metabolite or independent synthesis and subsequent NMR analysis, a significant effort beyond the scope of these molecules. However, the example serves to illustrate how metabolite identification through mass spectrometry coupled with mechanistic reasoning can allow structural assignment of metabolites with a reasonable degree of confidence.

A strategically important quinoline substitution pattern was the 8-Cl, as it was well represented in leading molecules including **54** and **67**. Metabolism of quinolines containing the 8-Cl substituent is illustrated in Fig. 22.

Interestingly compound **70** demonstrated a different metabolic pathway in human and rat systems compared to dog. In rat and human hepatocytes, *Pathway E* provided a +OGSH –Cl metabolite consistent with epoxidation at the 7,8-position followed by opening of the aryl epoxide intermediate by glutathione and elimination of HCl (in analogy to the pathways described for fluorinated quinolines). In contrast, dog microsomal incubations produced a major +O metabolite (*Pathway F*). The postulated

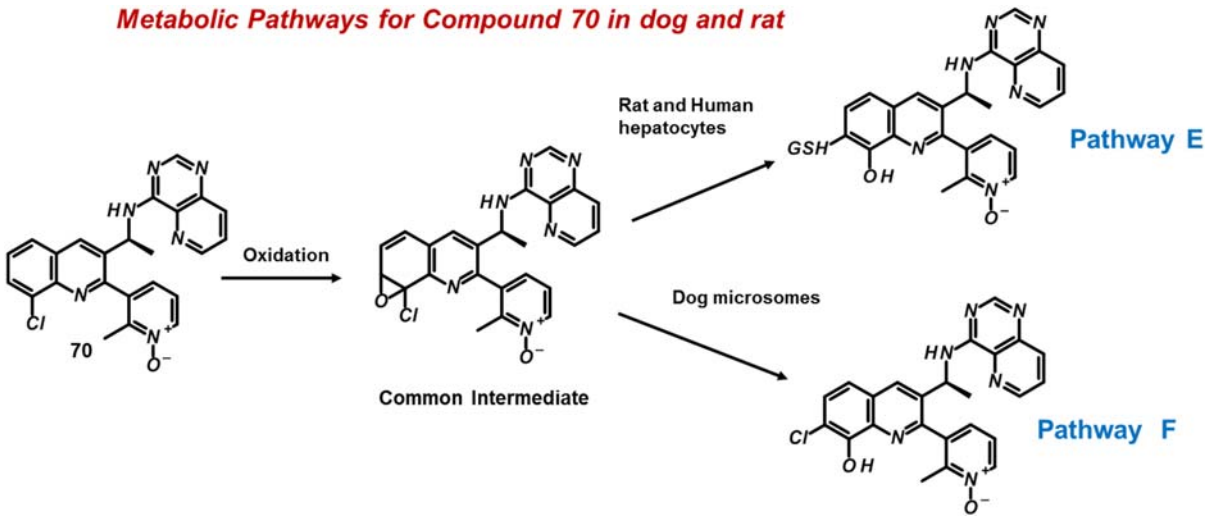

Fig. 22 Metabolic pathways observed for compound **70** a representative 8-Cl quinoline. Of note is the dog-specific chlorine migration pathway the "NIH" shift.

metabolic pathway involves formation of the same common aryl epoxide intermediate but, in this case, rather than reaction with glutathione the epoxide opening is accompanied by migration of the chlorine atom to the 7-position. This migratory pathway was seen in other closely related analogs where the regiochemistry was unambiguously confirmed by independent chemical synthesis of the metabolite. The hydroxylation induced migration of a halogen, commonly known as the "NIH" shift after the *National Institute of Health* was first reported in 1967[52] and furthermore similar dog-specific "NIH" shift metabolism has been previously reported.[53] The involvement of the chlorine atom in both metabolic pathways provided evidence that epoxidation occurs in the 7,8-position as shown.

8.15.2.7.3.1.2 Oxidation of quinoline substituents

While the predominant metabolic fate of the quinoline core was arene oxidation, where metabolically vulnerable groups such as methyl were present specific hydroxylation could occur on the substituents as opposed to the quinoline core itself. In the following section, the metabolic profile of compound **68** will be discussed. The elucidation of the metabolic profile of **68** also illustrates the utility of ^{1}H NMR in the unequivocal identification of metabolites and the occasional discrepancy between in vitro and in vivo metabolic clearance values.

Compound **68** (Table 15) possessed low in vitro clearance in both rat (hepatocyte $Cl_{int} = 8$) and human (microsome $Cl_{int} = 3$) systems with low levels of a single minor +O metabolite, *Metabolite A*. However when dosed in rat **68** demonstrated surprisingly high CL_b (77 mL min^{-1} kg^{-1}) and low oral exposure ($AUC_{inf} = 273$ ng h mL^{-1}). To understand the high clearance, which was not predicted from the in vitro hepatocyte data, a BDC rat study was performed. Based on the relatively high efflux ratio seen in Caco-2 cells (ER 26), we expected to see high levels of parent excreted in the bile consistent with a nonmetabolic clearance pathway. To our surprise, only a relatively small amount of parent was seen in the bile with ~90% of the dose present as one major +O metabolite. Fig. 23 shows the LC-UV trace for the bile from the rat BDC study. The metabolite profile was consistent with *Metabolite A*; however, the levels seen from the in vivo study greatly exceeded those seen from the in vitro incubation explaining the unexpectedly high in vivo clearance. The disconnect between the in vitro and in vivo clearance data highlights the importance of obtaining confirmatory in vivo data and not relying exclusively on in vitro measurements.

In order to unequivocally identify the major metabolite, rat bile was harvested from the study and the metabolite isolated by preparative reverse phase HPLC. Sufficient quantity was isolated to obtain ^{1}H NMR spectra of the major metabolite (Fig. 24). By comparison to the spectra of the parent molecule, which had been fully structurally assigned, it can be clearly seen by the downfield shift of the protons of carbon 8 (from 2.7 to 5.3 ppm) and the appearance of the OH (signal 9) at ~5 ppm, that the major metabolite was the oxidation of the quinoline 8-CH_3 group to the corresponding benzylic alcohol.

The benefit of ^{1}H NMR is that it allows unequivocal structural assignment to be made. However unless in vitro or in vivo studies are designed specifically to generate enough metabolite for ^{1}H NMR studies, there is often insufficient concentration of metabolite to provide meaningful ^{1}H spectra. The relatively low sensitivity and the ubiquitous presence of hydrogen in endogenous molecules necessitate the concentration and purification of samples from biological matrices. The use of ^{19}F NMR, however, can provide highly selective spectra, with very good signal to noise sensitivity from unpurified samples due to the very low natural abundance of fluorine in biological matrices. While ^{19}F NMR does not facilitate structural assignment as comprehensively as ^{1}H NMR, it is a powerful technique for monitoring levels of metabolite from biological samples.[54] As **68** contained a fluorine atom we wished to evaluate the utility of ^{19}F NMR in monitoring the metabolite levels directly from rat bile. Fig. 25 shows the ^{19}F NMR spectra of a sample of unprocessed rat bile showing a clear single peak for the benzylic alcohol metabolite. Clearly ^{19}F NMR would be an excellent tool for monitoring the metabolic turnover of compounds such as **68** especially as the peaks for parent and metabolite are clearly distinguished and are directly proportional to each other in quantitative terms.

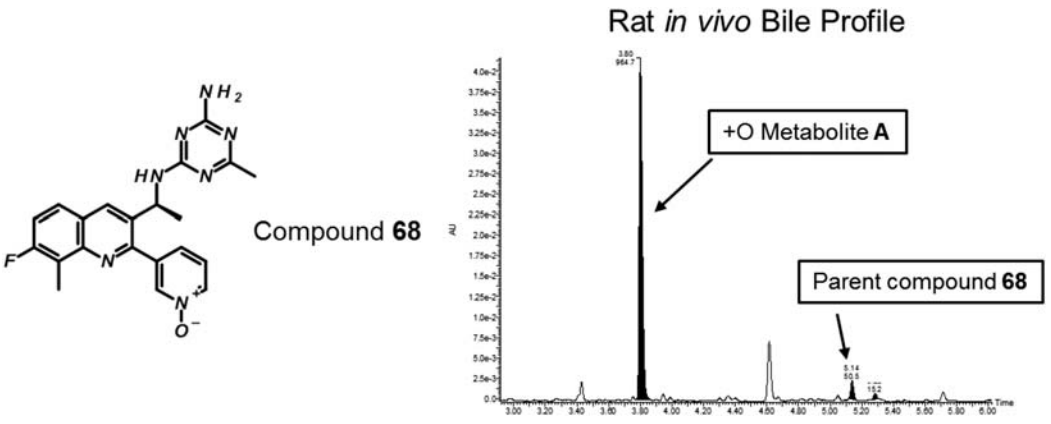

Fig. 23 LC-UV trace of **68** and metabolite A in rat bile.

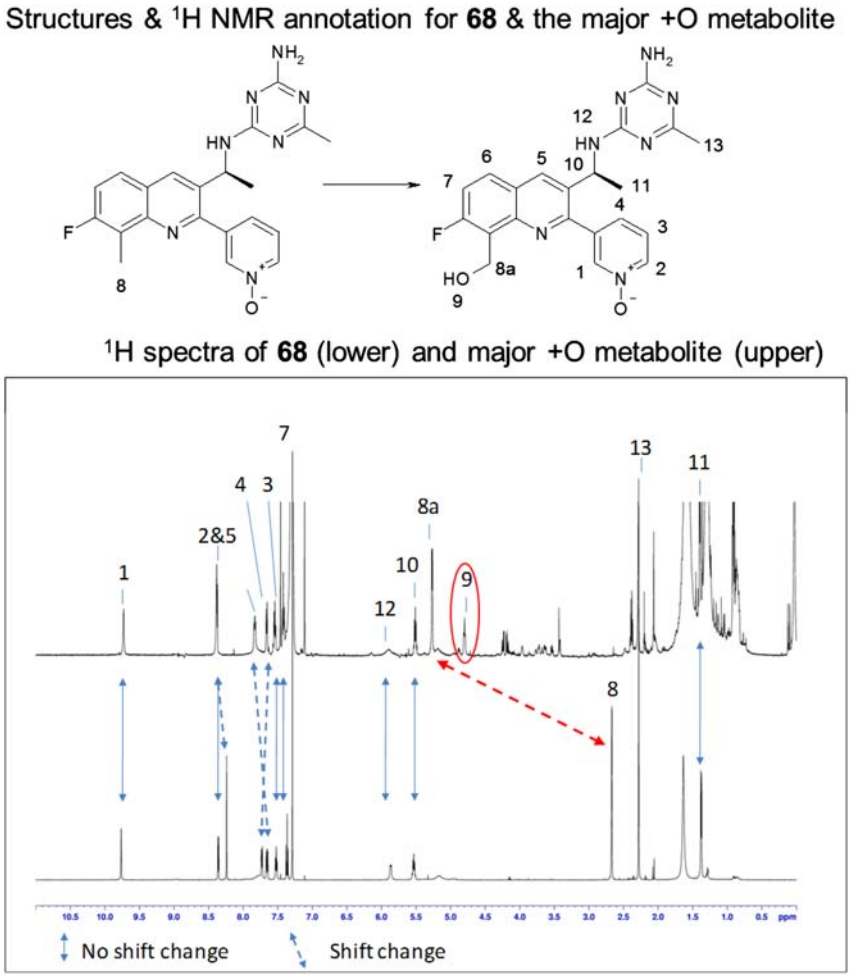

Fig. 24 ^{1}H NMR and structural assignment of **68** and the +O metabolite isolated from rat bile. Key signals are highlighted in *red*.

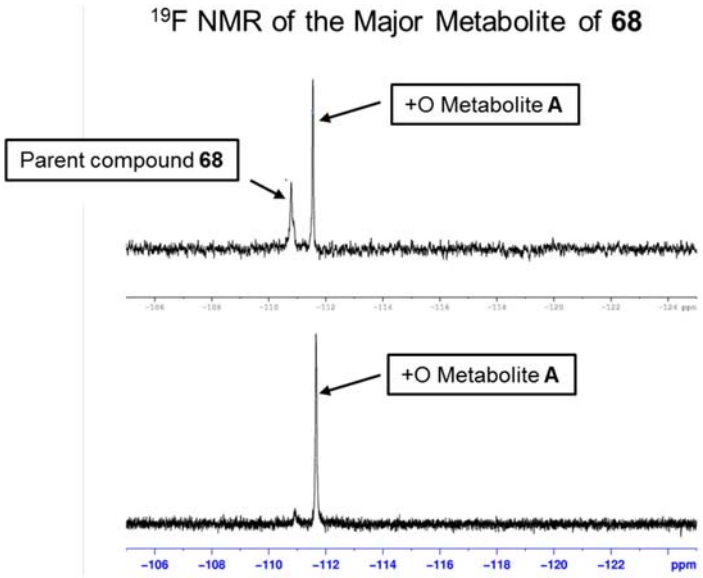

Fig. 25 ^{19}F NMR of (*top*) a sample of unprocessed rat bile containing the major +O metabolite of **68** spiked with parent compound and (*bottom*) ^{19}F NMR of unprocessed rat bile with no added **68** showing the quantitative abundance of the metabolite over the parent.

8.15.2.7.3.2 Metabolism of the pyrido[3,2-d]pyrimidine hinge-binding group

The pyrido[3,2-*d*]pyrimidine hinge-binding group was subject to a variety of phase 1 oxidative metabolism resulting in either *N*-oxidation or oxidation on the carbon between the two nitrogen atoms on the pyrimidine ring (Fig. 26). Typically in human in vitro systems, metabolism of the hinge-binding group was a significant metabolic pathway compared to the oxidation of the quinoline core, whereas conversely in rat quinoline core oxidation predominated. The species difference in relative metabolic pathways is not atypical and, in our case, it reiterated the need to address both potential sites of metabolism in order to improve the PK profile in rat (to support preclinical toxicology), and ultimately reduce human metabolism to achieve the desired once-daily dosing drug profile.

8.15.2.7.3.3 Metabolism of the pyridyl-N-oxide

The C2 pyridyl-*N*-oxide predominantly suffered from reduction to the parent pyridine with little or no observable direct oxidation of the heterocyclic ring itself. Metabolite ID studies of parent pyridines typically revealed the potential for oxidation of the pyridine to the *N*-oxide so the potential for a reduction/oxidation recycling of 3-pyridyl-*N*-oxide compounds could be envisaged. In our case the production of the pyridine as a significant metabolite necessitated full profiling of the parent pyridines both in terms of their intrinsic PI3Kδ potency (potential formation of active metabolites), inhibitory potential with the CYP 450 cytochromes, and other ancillary profiles.

8.15.2.7.4 Metabolite identification studies with compound 67

Specific metabolite identification studies with **67** from both in vitro incubations and in vivo studies revealed the main metabolic pathways for this molecule summarized in Fig. 27.

The main metabolite identified from human hepatocyte incubations was reduction of the pyridine *N*-oxide to the pyridine **66** with additional minor oxidation products both on the pyrido[3,2-*d*]pyrimidine hinge-binding group and the quinoline core (via the epoxidation mechanisms described in the previous section). In rat in vivo studies, a glutathione adduct was also observed suggesting that quinoline core oxidation was the major metabolic pathway in rat. Although human in vitro data provided no direct evidence of glutathione conjugation (Table 17), the levels of glutathione adducts produced in in vitro systems were generally low and as such could well be below the limits of detection of the LCMS system. Certainly the possibility of glutathione metabolites being generated in vivo could not be entirely discounted based on the in vitro data.

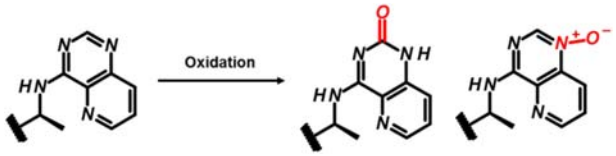

Fig. 26 Proposed primary oxidative metabolites of the pyrido[3,2-*d*]pyrimidine hinge-binding group shown in *red*.

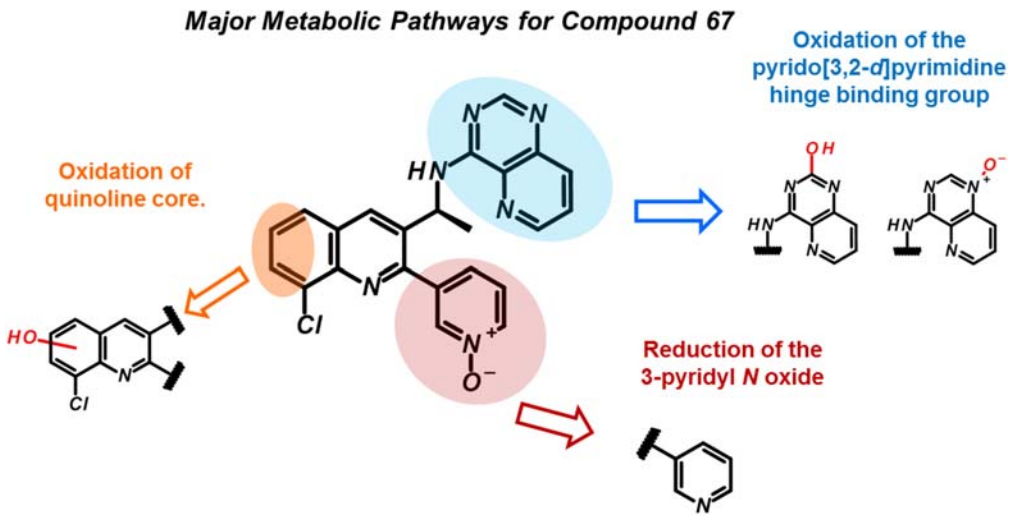

Fig. 27 The main metabolic pathways identified for lead pyrido[3,2-*d*]pyrimidine 3-pyridyl-*N*-oxide **67**.

Table 17 Compound **67** Metabolite ID from human hepatocyte incubations

Human hep	m/z	*Mass shift*	t_R *(min)*	*Level*	*Location*
Compound **67**	429.1225	0.0000	4.52		
−O	413.1276	−15.9949	5.02	Major	Pyridine
Hydrolysis	447.1331	18.0106	3.03	Minor	
+O	445.1174	15.9949	4.83	Minor	Quinoline or hinge-binding group
+O	445.1174	15.9949	5.40	Minor	

8.15.2.7.5 Optimizing the PK profile of compound 67

8.15.2.7.5.1 SAR and impact on metabolism of quinoline substitution

The metabolite ID studies with **67** and broader metabolite ID studies with related quinolines highlighted oxidation of the quinoline ring and pyrido[3,2-*d*]pyrimidine hinge-binding group as significant metabolic pathways with potential for formation of reactive metabolites. From a medicinal chemistry point of view, the introduction of electron withdrawing groups into strategic positions on the molecule was an attractive tactic to reduce the metabolic clearance of compound **67**. We wished to further explore the possibilities of other electron withdrawing groups on the quinoline ring and set about exploring the SAR.

The effect of introducing electron withdrawing groups into the quinoline ring on PI3Kδ activity and metabolic stability is summarized in **Table 18**. The electron-rich 8-CH_3 quinoline **71** suffers from very high metabolic clearance in rat hepatocytes and a positive genotoxicity flag. Introducing a simple electron withdrawing substituent such as a fluorine into the 7-position, (compound **72**), results in a substantial increase in metabolic stability in rat hepatocytes, despite an increase in lipophilicity. The observation highlighted the sensitivity of metabolic clearance to the electronic nature of the quinoline ring. The PI3Kδ activity of **72** was maintained in the key cellular assays. Replacement of the metabolically vulnerable 8 methyl group with chlorine to give **67** also resulted in a substantial increase in metabolic stability especially in human hepatocytes.

In order to reduce the metabolic clearance of **67**, we sought to incorporate strongly electron withdrawing groups into the 8-position. Incorporation of a CF_3 group (**75**) resulted in an increase in rat hepatocyte stability, but no significant effect on human hepatocyte stability; perhaps consistent with the observation that quinoline oxidation is the major metabolic pathway in rat. The modest effect on metabolic stability could be attributed to the fact that while electron density on the quinoline ring was reduced compared to **67**, the lipophilicity was increased (log *D* 1.8 to log *D* 2.5) potentially producing opposing influences on metabolic stability. Synthesis of the tri-fluoro substituted analog **78** provided an electron deficient quinoline but with a log *D* similar to **67**. Pleasingly the metabolic stability in human hepatocytes was greatly enhanced, demonstrating the ability of the multifluorinated aromatic ring to eliminate oxidative metabolism. Unfortunately, the compound was ~100-fold less potent than **67** thought to be due to the sensitivity of substitution on the 6-position as compounds **73** and **74** demonstrated that 5-position substitution was well tolerated. Synthesis of the 8-CN (**76**) and 8-SO_2Me (**77**) analogs provided compounds that were both potent against PI3Kδ in the enzymatic assay and metabolically stable in both human and rat hepatocytes. The increased metabolic stability was

Table 18 Quinoline SAR and the effect of electron withdrawing groups on metabolic stability and PI3Kδ IC_{50} activity

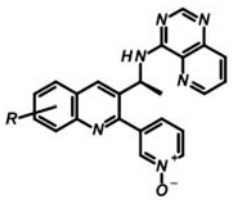

			Hepatocyte CL_{int}		*Cell activity*		
R	*Compounds*	*PI3Kδ* IC_{50} *(nM)*	*Human*	*Rat*	*fMLP (nM)*	*D0.11.10 (nM)*	*log* D
8-CH_3	**71**	4	ND	132	7	–	2.2
7-F, 8-CH_3	**72**	2	18	17	5	98	2.5
8-Cl	**67**	5	7.5	17	10	44	1.8
5-CN, 8-CH_3	**73**	2	ND	33	4	–	1.5
5,8 di Cl	**74**	5	10	11	24	–	2.6
8-CF_3	**75**	9	10	6	28	51	2.5
8-CN	**76**	17	3	8	332	417	1.0
8-SO_2CH_3	**77**	4	<3	3	278	270	0.6
5,6,8 tri F	**78**	521	<3	14	958	–	1.6

driven by both the reduced electron density on the quinoline core and the greatly reduced lipohilicity. However the low log *D* values resulted in poor cellular activity for both compounds, approximately 10-fold less potent than **67** in both the fMLP and D0.11.10 proliferation assays. We hypothesized that the loss of cellular potency was due to poor cellular permeability, and it appeared that a log *D* value of between 1.5 and 2.0 would result in the ideal balance of cellular potency and metabolic stability.

An alternative approach to reducing electron density in the quinoline ring could be envisaged by introducing a nitrogen to provide the corresponding napthyridine ring systems (Fig. 28). If the quinoline ring could be replaced by a napthyridine, we could anticipate that the epoxidation and glutathione conjugation metabolic pathways could be eliminated.

We synthesized a selection of napthyridine analogs, however the PI3Kδ activity was severely impaired. While the 1,5-napthyridine proved the most promising in terms of activity (PI3Kδ $IC_{50} = 120$ nM) and further improvements in activity could be anticipated by introduction of an 8 substituent and resolution of the enantiomers, the lack of potency compared to our lead molecules led us to abandon this particular approach.

Overall, despite extensive modifications to the quinoline core, the 8-Cl substituent and hence compound **67** remained the leading molecule based on in vitro data. We therefore turned our attention to other chemical modifications which could result in the desired reduction of electron density and oxidative metabolism.

8.15.2.7.5.2 Methyl to trifluoromethyl switch: Effects on PK and selectivity profile

Although our attempts to improve the profile of **67** by modification of the quinoline core had not proved successful, two key lessons could be taken from the process. Firstly that reducing electron density could improve metabolic stability but secondly reduction of log *D* below 1.5 led to significant and unacceptable loss of cellular activity. With these lessons in mind, we reasoned that apart from the quinoline C8-position, the only two other positions on the quinoline core amenable to modification were the C2- and C3-positions. As previously discussed, although the C2-position is tolerant of a wide range of substitution we had already alighted on a well-balanced and highly optimized substituent in the 3-pyridyl-*N*-oxide and felt that further modification here would prove unproductive. In contrast, the C3-position provided an opportunity to introduce a strongly electron withdrawing group if we replaced the chiral methyl group in **67** with a trifluoromethyl group (Fig. 29).

The introduction of fluorine into lead molecules is a commonly employed tactic in medicinal chemistry.[55,56] In this case, the strongly electron withdrawing effect of the trifluoromethyl could be expected not only to reduce the electron density on the quinoline core but also to have a significant impact on the ESP of the pyrido[3,2-*d*]pyrimidine hinge-binding group. We would expect that the basicity of the amino heterocycle would be reduced and the lipophilicity of the molecule increased (calculated log *P* increase of 0.6). We therefore reasoned that incorporation of the trifluoromethyl group in such a strategically sensitive point would have a beneficial impact in terms of reducing electron density across the whole molecule compared to the C8 substituents previously explored where the impact would be restricted primarily to the quinoline ring. Furthermore, as the CF_3 group is more lipophilic than a methyl group we could avoid compromising the global physicochemical properties of the molecule and retain cellular potency.

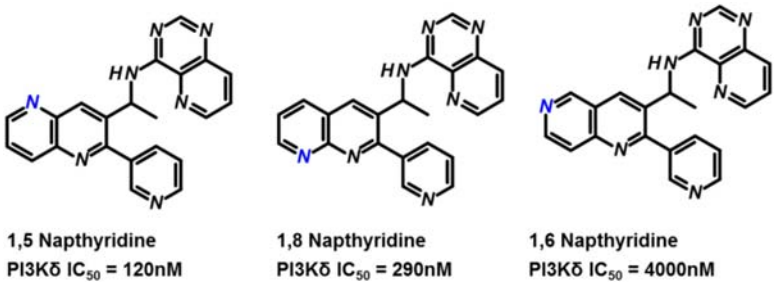

Fig. 28 Napthyridine replacements of the quinoline ring result in reduced PI3K activity.

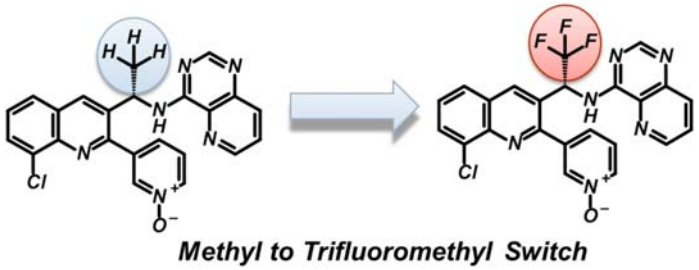

Fig. 29 Replacement of the chiral benzylic methyl group with trifluoromethyl.

We synthesized a number of MMPs where we replaced the chiral methyl group with a trifluoromethyl substituent (Table 19). We also conducted a methyl scan of the 3-pyridyl-*N*-oxide group with the intention of introducing steric bulk in the flanking positions *ortho* to the *N*-oxide. We reasoned that steric bulk in these positions could reduce the rate of pyridine *N*-oxide metabolism and also reduce the CYP inhibition potential of any resultant pyridine metabolites.

Replacement of the chiral methyl with a trifluoromethyl group pleasingly did not erode PI3Kδ potency and across the matched pairs a small improvement in in vitro human hepatocyte stability was observed despite the expected increase in lipohilicity (~0.5 log *D* increase for the $CH_3 \rightarrow CF_3$ switch). Interestingly comparing compound **79** to the trifluoromethyl analog **81** suggested that the trifluoromethyl group significantly improved selectivity against PI3Kγ; the >1000-fold-selectivity with **81** was the highest we had observed for a C2 aryl.

Substitution of the pyridine ring with a methyl groups in the 6-position reduced potency ~10-fold (**80** compared to **67**), but a methyl group in the 2-position was well tolerated (compounds **70** and **82**). The rationale for incorporating the 2-methyl substituent was to reduce the rate of pyridyl-*N*-oxide metabolic reduction and also reduce the CYP inhibition profile of the analogous pyridines. Metabolite ID studies in rat and human hepatocytes and metabolite analysis of rat bile confirmed that no pyridine *N*-oxide reduction was observed for compounds **70** and **82**, confirming that a methyl substituent in the 2-position of the pyridyl *N*-oxide was a suitable strategy for preventing *N*-oxide reduction.

Encouraged by the apparent improvement in the in vitro metabolic stability, we sought to establish if the increased stability translated into improved in vivo PK properties. Fig. 30 compares the in vitro and in vivo profile of compounds **84** and **85**. The trifluoromethyl analog **85** possessed an improved metabolic stability profile in rat hepatocytes that translated into lower in vivo clearance in rat and a markedly improved oral PK profile, with significantly increased exposure and oral bioavailability.

In summary, through our attempts to improve the metabolic stability of the first C2 pyridine-*N*-oxide **67**, we discovered that replacement of the chiral methyl group with a trifluoromethyl conferred greatly improved oral PK properties in rat, partly attributable to the improved in vitro metabolic stability. Furthermore in some analogs, the selectivity against the gamma isoform was markedly improved, a profile that was not easily accomplished in the C2 aryl subseries. We had also established that the 8-Cl quinoline substituent was optimal and that substitution of the pyridyl ring provided only limited benefit. With these observations in mind, the trifluoromethyl analog of **67** was clearly a key molecule demanding synthesis. As will be described in the following section, the profile of this molecule met our target criteria and ultimately led to the development of the compound as our clinical candidate *seletalisib*.

8.15.2.8 Identification and Characterization of *Seletalisib*

8.15.2.8.1 Impact of the CF_3 Group 1: In vitro biology comparison between compounds 67 and 86

The in vitro potency and selectivity profile of compounds **67** and **86** are presented in Table 20.

Notably the trifluoromethyl group conferred markedly improved selectivity against both the beta and gamma isoforms (approximately 10-fold). While the precise reasons behind the improved selectivity profile are unclear, it is significant as the selectivity profile for compound **86** (*seletalisib*) is highly competitive compared to the reported selectivity for the clinical PI3Kδ inhibitors *idelalisib*[25] and *duvelisib*[57] (Table 21). To the best of our knowledge, seletalisib represents the most selective PI3Kδ inhibitor reported to date.

Table 19 Properties of chiral methyl and trifluoromethyl quinolines

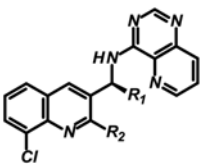

R1	CH_3			CF_3		
R2	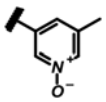	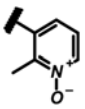	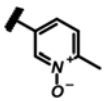	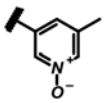	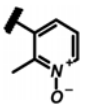	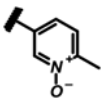
Compounds	**79**	**70**	**80**	**81**	**82**	**83**
PI3Kδ IC_{50}	12 nM	1 nM	**31** nM	3 nM	4 nM	**73** nM
Selectivity α/β/γ	×795/×280/×95	>1000/>1000×55	×620/×87/×62	>1000/>1000>1000	>1000/>1000×170	×274/×480/×123
fMLP IC_{50}	78 nM	36 nM	–	49 nM	27 nM	248 nM
D0.11.10 IC_{50}	95 nM	–	430 nM	–	23 nM	–
Hu hepatocyte CL_{int}	9	6	14	7	7	11
Rat hepatocyte CL_{int}	9	5	2	9	3	13
log *D*	1.9	1.8	2.0	2.5	2.4	2.7

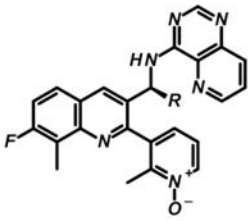

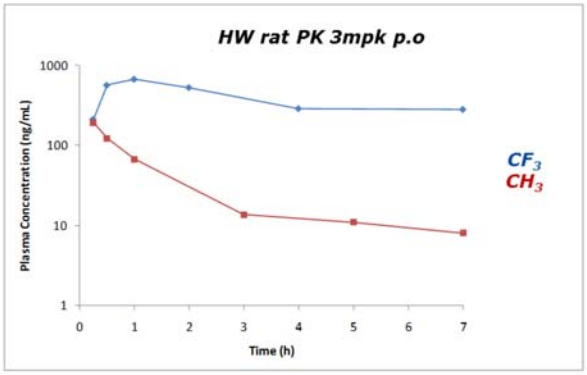

R	CH_3	CF_3
Compound	**84**	**85**
PI3Kδ IC_{50}	6nM	2nM
Selectivity α/β/γ	x900/>1000/ x20	>1000/>1000 x230
D0.11.10 IC_{50}	28nM	30nM
Rat Hep CL_{int}	21	9

R	CH_3	CF_3
Compound	**84**	**85**
Rat 1mg/kg i.v CL_b	43 mL/min/kg	20 mL/min/kg
Rat 3mg/kg p.o AUC_{inf}	334 ng.hr/mL	2834 ng.hr/mL
%F	29%	83%

Fig. 30 Comparison of the in vitro and in vivo profile of compounds **84** and **85** demonstrating the improved oral PK parameters conferred by the $CH_3 \rightarrow CF_3$ switch.

Table 20 Selected in vitro potency, selectivity, and physicochemical properties of compounds **67** and **86**

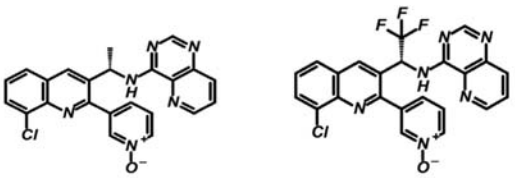

Compounds	***67***	***86***
PI3Kδ IC_{50}	5 nM	1.1 nM
Selectivity α/β/γ	×880/×194/×71	×3960/×2330/×819
fMLP IC_{50}	10 nM	16 nM
PMA counterscreen	IA	IA
RAMOS pAKT IC_{50}	12 nM	15 nM
D0.11.10 proliferation	44 nM	125 nM
Basophil degranulation IC_{50}	–	35 nM
Cerep profiling	–	No activity >50% @ 10 μM 55 receptor/enzyme panel
Kinase screen	–	No activity >50% @ 10 μM 239 kinases
In vitro micronucleus		
AMES mpf		
hERG IC_{50}	>30 μM	>30 μM
log *D*	1.8	2.45

Table 21 *idelalisib*[25] and *duvelisib*[57] data are taken from the biomedical literature and presented for comparison with *seletalisib*

PI3K isoform	Seletalisib *IC_{50} nM (fold-selectivity for PI3Kδ)*	Idelalisib *IC_{50} nM (fold-selectivity for PI3Kδ)*	Duvelisib *IC_{50} nM (fold-selectivity for PI3Kδ)*
PI3Kδ	1.1 (–)	2.5 (–)	2.5 (–)
PI3Kγ	900 (818×)	89 (35×)	27 (11×)
PI3Kβ	2563 (2330×)	565 (226×)	85 (34×)
PI3Kα	4356 (3960×)	820 (328×)	1602 (640×)

Specifically *seletalisib* displays at least a 10-fold-selectivity improvement against all the PI3K isoforms compared to the current clinical candidates. Against PI3Kγ and PI3Kβ, the selectivity is markedly improved and it will be intriguing to see if this improved isoform selectivity profile translates into improved tolerability in a clinical setting.

Compound **86** as expected displayed excellent cellular potency in a range of B-cell and T-cell driven assays [Ref. UCB JPET Biol Paper]. The selective inhibition of PI3Kδ is demonstrated by the potent inhibition of the fMLP driven superoxide release assay in neutrophils (IC_{50} 16 nM) and inactivity in the same assay when stimulated by the non-PI3K-dependant ligand PMA. Potent inhibition of downstream signaling from the BCR was demonstrated in the pAKT assay in RAMOS cells with an IC_{50} of 15 nM. In order to be able to measure directly the inhibition of PI3Kδ in a clinical setting, we had developed a whole blood basophil degranulation assay (described in Section "**The basophil degranulation assay**"). Compound **86** potently inhibited this assay with an IC_{50} of 35 nM.

The wider selectivity of **86** was also assessed in in vitro receptor binding and enzyme assays across a broad range of target classes, demonstrating that **86** is highly selective for PI3Kδ. Specifically when screened against a panel of 239 kinases, **89** showed no inhibitory activity against any targets >50% @ 10 μM. Wider screening against nonkinase enzymes, ion channels, and receptors revealed no significant activity. As expected, **86** maintained the clean profile in the early in vitro genotoxicity screens and hERG assays established by the methyl analog **67**.

In summary, replacement of the methyl in **67** with trifluoromethyl resulted in **86** which retained the excellent e*nzymatic and cellular* potency of **67** but with markedly improved selectivity against the gamma and beta isoforms. Importantly compound **86** is the most selective PI3Kδ inhibitor reported to date with a differentiated selectivity profile compared to the current PI3Kδ inhibitors in clinical development *idealisib* and *duvelisib*.

8.15.2.8.2 Impact of the CF_3 Group 2: Comparison of PK parameters between compounds 67 and 86

Given the promising biochemical and cellular profile of **86**, we investigated the PK parameters of this molecule. **Tables 22** and **23** disclose the comparative in vitro ADMET and in vivo PK data for compounds **67** and **86**.

The in vivo clearance data for rat and dog clearly illustrate that the trifluoromethyl analog **86** has approximately twofold lower in vivo clearance that the methyl compound **67**. The in vitro hepatocyte data in dog, rat, and human also suggest greater metabolic stability for the trifluoromethyl analog **86** compared to the methyl analog **67**. In the case of rat, the oral bioavailability is markedly improved from 29% to 98%. The Caco-2 data suggests an improved efflux ratio and intrinsic permeability for **86** which, together with the greater metabolic stability may explain the improved oral PK parameters for both trifluoromethyl analogs **86** and **85** compared to their methyl counterparts. Although the precise reasons for the improved in vivo intrinsic clearance and bioavailability for the trifluoromethyl compounds are not entirely clear, the consistent and significant positive impact of the chiral trifluoromethyl modification on the PK parameters is not in doubt.

Table 22 In vivo PK parameters of compounds **67** and **86** in rat, dog, cynomolgus monkey, and mouse

Study	*Parameter*	*Compound **67***	*Compound **86***
Rat	CL_b (mL $min^{-1}kg^{-1}$)	43	24
1 mg kg^{-1} i.v., 3 mg kg^{-1} p.o.	Vss (L kg^{-1})	1.4	2.3
	F (%)	29	98
	% in bile (BDC)	13	10
Dog	CL_b (mL $min^{-1}kg^{-1}$)	17	6
1 mg kg^{-1} i.v., 3 mg kg^{-1} p.o.	Vss (L kg^{-1})	0.5	0.8
	F (%)	37	26
Cyno	CL_b (mL $min^{-1}kg^{-1}$)	–	8.2
1 mg kg^{-1} i.v., 1.5 mg kg^{-1} p.o.	Vss (L kg^{-1})	–	2.9
	F (%)	–	40
Mouse 1 mg kg^{-1} i.v., 3 mg kg^{-1} p.o.	CL_b (mL $min^{-1}kg^{-1}$)	–	3.5
	Vss (L kg^{-1})	–	0.6
	F (%)	–	59
Mouse 10 mg kg^{-1} p.o.	CL/F (mL $min^{-1}kg^{-1}$)	9	6

Table 23 Selected in vitro ADMET parameters of compounds **67** and **86**

Parameter		*Compound **67***	*Compound **86***
Hepatocyte CL_{int} ($\mu L\ min^{-1}10^{-6}$ cells)	Rat	17	4.4
	Dog	23	13
	Cyno		2.9
	Human	7.5	5.6
Caco-2	A2B (nms^{-1})	35	170
	ER	24	4.5
CYP inhibition	Competitive	>10 μM all isoforms	>10 μM all isoforms
	TDI	>10 μM all isoforms	>10 μM all isoforms
CYP induction			Minor

Pleasingly compound **86** did not display any CYP P450 induction or inhibition liabilities, suggesting a low potential for drug/drug interactions in the clinic.

The in vivo PK profile of compound **86** in a range of preclinical species (rat, dog, and cyno), characterized by low to moderate intrinsic clearance and good bioavailability, supported progression to the necessary preclinical toxicology studies.

8.15.2.8.3 Metabolic profile of compound 86

The metabolic profile of **86** was determined in in vitro human, rat, dog, cynomolgus monkey hepatocytes, and microsomes, with the major human metabolites identified presented in Fig. 31. As expected, the metabolic profile was very similar to the methyl analog **67** with the major metabolic pathway in human and cynomolgus monkey hepatocytes being reduction to the pyridine (*Metabolite **A***) with further oxidation of the pyrido[3,2-*d*]pyrimidine hinge-binding group to *Metabolite **B***. In human microsomes, direct oxidation of the hinge-binding group was also seen (*Metabolite **C***). Importantly the metabolite profile in cynomolgus monkey hepatocytes and microsomes closely mirrored the human profile both in the metabolites produced and their relative levels.

Identification of the major metabolites across species is critical to the selection of the preclinical toxicology species to ensure that the metabolites produced in human systems are reproduced in the preclinical toxicology studies. In our case, the fact that cynomolgus monkey produced a metabolite profile that closely resembled the human results made it a promising candidate for the non-rodent toxicology species.

In summary, the metabolite profiling of **86** across species in vitro confirmed that, similar to the profile of compound **67**, the major metabolic pathway in human was reduction of the pyridyl *N*-oxide. Secondary pathways involved oxidation of the pyrido[3,2-*d*]pyrimidine hinge-binding group with the metabolic profile very similar in cynomolgus monkey.

8.15.2.8.4 Pharmacological evaluation of compound 86

Compound **86** was evaluated in our pharmacology cascade, as expected the compound demonstrated good efficacy and potency in the anti-CD3-induced IL2 assay and SRBC DTH assay similar to the data presented with compound **67**. We wished to determine the

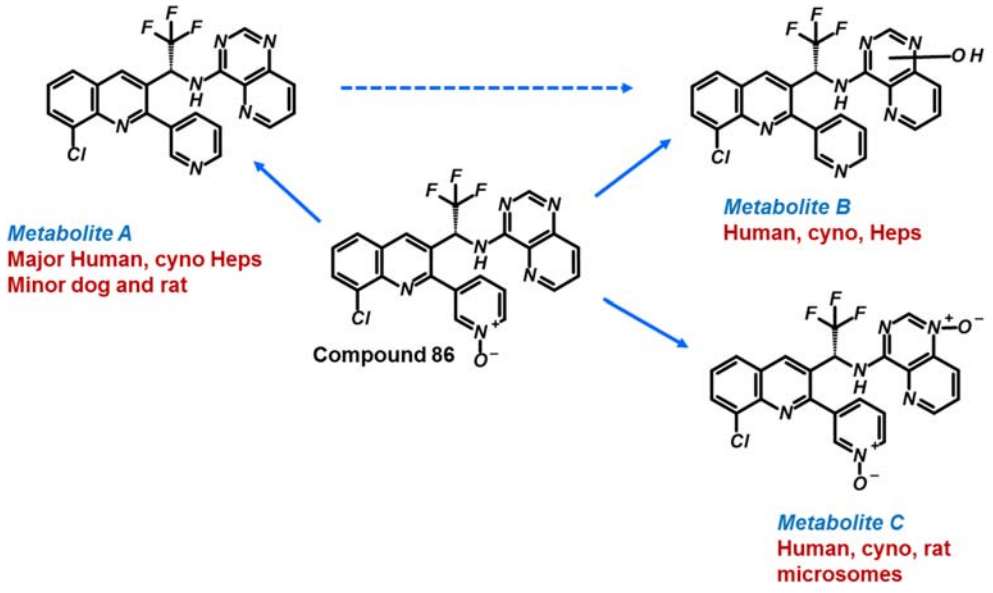

Fig. 31 Major metabolites of compound **86** identified from human in vitro hepatocyte and microsomal incubations.

efficacy of **86** in models of inflammatory disease and evaluated the compound in the mouse CIA (Fig. 32). Compound **86** was dosed at 10 mg kg^{-1} u.i.d. therapeutically (from disease onset) and significantly reduced clinical score over time with statistically significant difference from day 14. A reduction of AUC of the clinical score of $64 \pm 12\%$ compared to the vehicle control group was achieved.

The profound inhibition of the CIA model combined with the optimized potency, class leading PI3K isoform selectivity, and good in vivo PK profile led us to nominate compound **86** as a candidate for preclinical toxicology studies. The outline of these studies and the ultimate progression of compound **86** into the clinic as *seletalisib* are described in the next sections.

8.15.3 Preclinical Development

Preliminary repeat dose toxicity studies with *seletalisib* were performed in rats (5 days and 2 weeks) and monkeys (2 weeks). In light of the results of these studies, a GLP package was conducted to support clinical use and included a standard genotoxicity battery, 4-week repeat dose toxicity studies in rats and monkeys, and safety pharmacology studies assessing the respiratory, cardiovascular, and CNS functions. A brief summary of this GLP package is provided here.

Seletalisib was negative in in vitro (Ames test and Mouse lymphoma mutation assay) and in vivo (micronucleus induction assay in rat bone marrow erythrocytes) genotoxicity tests.

No adverse effects were observed on respiratory function or on general behavior.

In the hERG assay, *seletalisib* displayed an IC_{50} value of 52 μM, indicating a potential liability for blockade of the human-encoded IKr potassium channel only at high concentrations compared to the pharmacological activity. Indeed, 52 μM represents around 56,000-fold the free concentration inhibiting by 90% (IC_{90}) the PI3K delta enzymatic activity in vitro. In the pivotal GLP telemetry study conducted in conscious monkeys, *seletalisib* did not induce relevant QTc prolongation when administered at oral doses as high as 100 mg kg^{-1}, corresponding to c. 2585-fold the in vitro IC_{90} from the PI3K delta enzymatic activity assay. These data allowed us to conclude that *seletalisib* presented a low risk of proarrhythmia potential.

When administered orally once a day for 4 weeks to monkeys and rats, *seletalisib* induced similar histopathological findings in both species, mainly characterized by lymphoid tissue atrophy and inflammatory changes in the large intestine. In both monkeys and rats, these lymphoid tissue and intestinal findings showed reversibility after a 4-week treatment-free period and provided sufficient safety margin and confidence that *seletalisib* could be safely tested in humans.

8.15.4 Clinical Data and Status

Seletalisib entered first in man studies in Aug. 2013 successfully completing two combined single ascending dose/multiple ascending dose studies in healthy volunteers and mild-to-moderate psoriatic subjects (PS0001/NCT02303509: UP0021/NCT02207595) to evaluate its safety, tolerability, pharmacokinetic, and pharmacodynamic profile.

Seletalisib was well tolerated at doses ≤15 mg (PS0001) and ≤45 mg QD (UP0021) for 14 days. No safety concerns or dose-limiting toxicities were identified (PS0001). Incidence of gastrointestinal-related adverse events (AEs) was not dose related but higher incidences of skin rash AEs were associated with higher-dose *seletalisib* (UP0021).

Mean *seletalisib* plasma concentration-time profiles increased with increasing doses after single and multiple dosing, with no major deviations from dose proportionality and apparent $T_{1/2}$ values were supportive of once-daily dosing. Pharmacodynamic findings demonstrated ex vivo inhibition of basophil degranulation and identified improvements in histological assessment of skin biopsies and other markers of psoriatic biology with evidence of target engagement in psoriatic skin tissue.

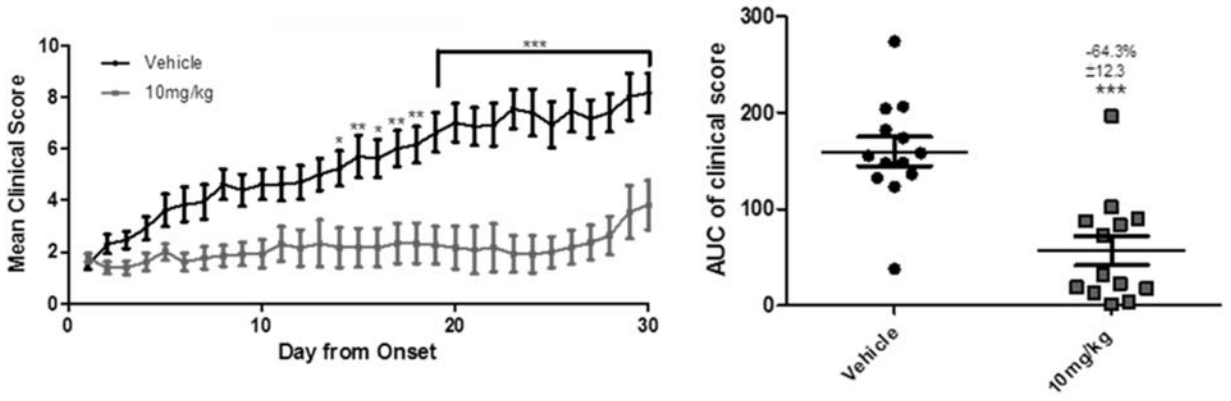

Fig. 32 Inhibition of collagen-induced arthritis in vivo. Vehicle and compound **86** in 1% methylcellulose (400cps) was administered orally once daily from day of disease onset. Animals were immunized with CII in CFA (i.d.) on day 0 and boosted with CII in IFA (i.d.) on day 14. Clinical score was assessed daily and mice were sacrificed 30 days after disease onset. Statistical significance is denoted as follows, $*p<0.05$, $**p<0.01$, and $***p<0.0001$ compared to positive control group (ANOVA with Bonferroni's post test).

The results of both PS0001 and UP0021 demonstrated a manageable safety and tolerability profile of *seletalisib*, provided PK results supportive of once-daily dosing, showed evidence of biological effect, and provided data supportive of exploration of efficacy in proof-of-concept studies.

On these bases, *seletalisib* has been progressed into a proof of concept (PoC) study in primary Sjögren's Syndrome (NCT02610543).

8.15.5 Conclusion

In this article, we have described the medicinal chemistry program leading to the discovery and development of *seletalisib*, which is, to our knowledge, the most selective PI3Kδ inhibitor yet reported. We began our journey with the hypothesis that inhibition of only the delta isoform of PI3 kinase would bring an optimal balance of clinical efficacy and tolerability for chronic use in inflammatory and autoimmune diseases. Through the efforts described in this article, we have successfully delivered *seletalisib* to the clinic in order to test that proposal.

As with any medicinal chemistry program, the experience has provided many valuable lessons which we hope the reader will find as instructive as we have. Of note has been the successful use of a virtual database of heterocyclic rings (VEHICLe[3]) and in silico electrostatic modeling to generate new scaffolds, an approach that can be applied to any medicinal chemistry program. Our exploration of the SAR led to the emergence of several unexpected selectivity profiles which could not be easily explained from our structural understanding. These empirical selectivity observations proved critical to the ultimate development of compounds with high selectivity against PI3Kγ and highlight the importance of thorough and comprehensive SAR "fieldwork" fully exploring the chemical diversity of the scaffold. The crucial gamma selectivity breakthroughs, both the C2 amines and the benzylic trifluoromethyl group, came indirectly from attempts to optimize physicochemical properties and PK. Crucial to the identification of this serendipitous gamma isoform selectivity was our early PI3K isoform selectivity screens and confirms that in medicinal chemistry "fortune favors the prepared screening cascade."

Our medicinal chemistry strategy focused on rapidly developing highly potent inhibitors and then subsequently optimizing the physicochemical and DMPK properties. We have shown how metabolite identification and developing a good mechanistic understanding of the major routes of metabolism can inform and guide a successful medicinal chemistry program in optimizing PK profiles.

The realization of the genotoxic potential of the triazinyl-piperazinones was a significant setback for the program and necessitated a major, but ultimately successful, redesign of the molecules. Access to a number of parallel in vitro genotoxicity assays to eliminate the possibility of false positives and negatives was crucial to be able to rapidly identify chemical space devoid of the genotoxicity risk. Our successful redesign of the molecules was based on the deployment of a 3-pyridyl-*N*-oxide as a bioisostere of a carbonyl group. In our case, the pyridyl-*N*-oxide also brought greatly improved metabolic stability and solubility to our molecules and, as shown in this article, is a valuable functional group in the medicinal chemist's armory.

The replacement of the benzylic methyl group with trifluoromethyl proved to be final piece in the *seletalisib* puzzle. It is one example of many in the medicinal chemistry literature[55] where judicious incorporation of fluorine results in improved PK properties. In our case, the in vitro ADMET data suggested marginal improvement and it was only when the compounds were taken into in vivo PK studies that the full benefit of the *trifluoromethyl switch* became apparent, highlighting the importance of in vivo experimentation to fully understand and interpret in vitro ADMET data.

Seletalisib completed preclinical toxicology and has successfully progressed into clinical studies. *Seletalisib* is currently undergoing a PoC study in primary Sjögren's syndrome where it will been seen if selective PI3Kδ inhibition can provide relief to patients suffering from chronic inflammatory and autoimmune diseases.

Acknowledgments

The author would like to acknowledge the many colleagues and functions that are a crucial part of any successful drug discovery program. In particular, thanks to the medicinal chemistry, DMPK, pharmacology, primary pharmacology, and nonclinical development teams at UCB.
The medicinal chemistry program was conducted in close collaboration with BioFocus DPI who provided medicinal chemistry support and expertise to the UCB project team. The author would like to thank the members of the BioFocus medicinal chemistry team who played a crucial role in the successful identification of *seletalisib* through a highly productive and enjoyable collaboration. Finally the comments, opinions, and statements in this article are entirely the authors own and do not represent those of UCB or any other party.

See also: 5.15. Lupus and Lupus Overlap Diseases: Emerging Therapies.

References

1. Goules, A. V.; Tzioufas, A. G. Primary Sjogren's Syndrome: Clinical Phenotypes, Outcome and the Development of Biomarkers. *Autoimmun Rev.* **2016,** *15* (7), 695–703.
2. Jonsson, R.; Bolstad, A. I.; Brokstad, K. A.; Brun, J. G. Sjogren's Syndrome—A Plethora of Clinical and Immunological Phenotypes With a Complex Genetic Background. *Ann. N. Y. Acad. Sci.* **2007,** *1108,* 433–447.

3. Pitt, W. R.; Parry, D. M.; Perry, B. G.; Groom, C. R. Heteroaromatic Rings of the Future. *J. Med. Chem.* **2009,** *52* (9), 2952–2963.
4. Okkenhaug, K. Rules of Engagement: Distinct Functions for the Four Class I PI3K Catalytic Isoforms in Immunity. *Ann. N. Y. Acad. Sci.* **2013,** *1280,* 24–26.
5. Okkenhaug, K. Signaling by the Phosphoinositide 3-Kinase Family in Immune Cells. *Annu. Rev. Immunol.* **2013,** *31,* 675–704.
6. Akinleye, A.; Avvaru, P.; Furqan, M.; Song, Y.; Liu, D. Phosphatidylinositol 3-Kinase (PI3K) Inhibitors as Cancer Therapeutics. *J. Hematol. Oncol.* **2013,** *6* (1), 88.
7. Stark, A. K.; Sriskantharajah, S.; Hessel, E. M.; Okkenhaug, K. PI3K Inhibitors in Inflammation, Autoimmunity and Cancer. *Curr. Opin. Pharmacol.* **2015,** *23,* 82–91.
8. Zhang, X.; Li, X. R.; Zhang, J. Current Status and Future Perspectives of PI3K and mTOR Inhibitor as Anticancer Drugs in Breast Cancer. *Curr. Cancer Drug Targets* **2013,** *13* (2), 175–187.
9. Ji, H.; Rintelen, F.; Waltzinger, C.; Bertschy Meier, D.; Bilancio, A.; Pearce, W.; Hirsch, E.; Wymann, M. P.; Ruckle, T.; Camps, M.; Vanhaesebroeck, B.; Okkenhaug, K.; Rommel, C. Inactivation of PI3Kgamma and PI3Kdelta Distorts T-Cell Development and Causes Multiple Organ Inflammation. *Blood* **2007,** *110* (8), 2940–2947.
10. Banham-Hall, E.; Clatworthy, M. R.; Okkenhaug, K. The Therapeutic Potential for PI3K Inhibitors in Autoimmune Rheumatic Diseases. *Open Rheumatol. J.* **2012,** *6,* 245–258.
11. Rommel, C.; Camps, M.; Ji, H. PI3K Delta and PI3K Gamma: Partners in Crime in Inflammation in Rheumatoid Arthritis and Beyond? *Nat. Rev. Immunol.* **2007,** *7* (3), 191–201.
12. Bartok, B.; Boyle, D. L.; Liu, Y.; Ren, P.; Ball, S. T.; Bugbee, W. D.; Rommel, C.; Firestein, G. S. PI3 Kinase Delta Is a Key Regulator of Synoviocyte Function in Rheumatoid Arthritis. *Am. J. Pathol.* **2012,** *180* (5), 1906–1916.
13. Okkenhaug, K.; Ali, K.; Vanhaesebroeck, B. Antigen Receptor Signalling: A Distinctive Role for the p110delta Isoform of PI3K. *Trends Immunol.* **2007,** *28* (2), 80–87.
14. Okkenhaug, K.; Turner, M.; Gold, M. R. PI3K Signaling in B Cell and T Cell Biology. *Front. Immunol.* **2014,** *5,* 557.
15. Foster, J. G.; Blunt, M. D.; Carter, E.; Ward, S. G. Inhibition of PI3K Signaling Spurs New Therapeutic Opportunities in Inflammatory/Autoimmune Diseases and Hematological Malignancies. *Pharmacol. Rev.* **2012,** *64* (4), 1027–1054.
16. Somoza, J. R.; Koditek, D.; Villasenor, A. G.; Novikov, N.; Wong, M. H.; Liclican, A.; Xing, W.; Lagpacan, L.; Wang, R.; Schultz, B. E.; Papalia, G. A.; Samuel, D.; Lad, L.; McGrath, M. E. Structural, Biochemical, and Biophysical Characterization of Idelalisib Binding to Phosphoinositide 3-Kinase Delta. *J. Biol. Chem.* **2015,** *290* (13), 8439–8446.
17. Clayton, E.; Bardi, G.; Bell, S. E.; Chantry, D.; Downes, C. P.; Gray, A.; Humphries, L. A.; Rawlings, D.; Reynolds, H.; Vigorito, E.; Turner, M. A Crucial Role for the p110delta Subunit of Phosphatidylinositol 3-Kinase in B Cell Development and Activation. *J. Exp. Med.* **2002,** *196* (6), 753–763.
18. Jou, S. T.; Carpino, N.; Takahashi, Y.; Piekorz, R.; Chao, J. R.; Carpino, N.; Wang, D.; Ihle, J. N. Essential, Nonredundant Role for the Phosphoinositide 3-Kinase p110delta in Signaling by the B-Cell Receptor Complex. *Mol. Cell. Biol.* **2002,** *22* (24), 8580–8591.
19. Okkenhaug, K.; Bilancio, A.; Farjot, G.; Priddle, H.; Sancho, S.; Peskett, E.; Pearce, W.; Meek, S. E.; Salpekar, A.; Waterfield, M. D.; Smith, A. J.; Vanhaesebroeck, B. Impaired B and T Cell Antigen Receptor Signaling in p110delta PI 3-Kinase Mutant Mice. *Science (New York, N.Y.)* **2002,** *297* (5583), 1031–1034.
20. Workman, P.; Clarke, P. A.; Raynaud, F. I.; van Montfort, R. L. Drugging the PI3 Kinome: From Chemical Tools to Drugs in the Clinic. *Cancer Res.* **2010,** *70* (6), 2146–2157.
21. Norman, P. Selective PI3Kdelta Inhibitors, a Review of the Patent Literature. *Expert Opin. Ther. Pat.* **2011,** *21* (11), 1773–1790.
22. Down, K.; Amour, A.; Baldwin, I. R.; Cooper, A. W.; Deakin, A. M.; Felton, L. M.; Guntrip, S. B.; Hardy, C.; Harrison, Z. A.; Jones, K. L.; Jones, P.; Keeling, S. E.; Le, J.; Livia, S.; Lucas, F.; Lunniss, C. J.; Parr, N. J.; Robinson, E.; Rowland, P.; Smith, S.; Thomas, D. A.; Vitulli, G.; Washio, Y.; Hamblin, J. N. Optimization of Novel Indazoles as Highly Potent and Selective Inhibitors of Phosphoinositide 3-Kinase Delta for the Treatment of Respiratory Disease. *J. Med. Chem.* **2015,** *58* (18), 7381–7399.
23. Furman, R. R.; Sharman, J. P.; Coutre, S. E.; Cheson, B. D.; Pagel, J. M.; Hillmen, P.; Barrientos, J. C.; Zelenetz, A. D.; Kipps, T. J.; Flinn, I.; Ghia, P.; Eradat, H.; Ervin, T.; Lamanna, N.; Coiffier, B.; Pettitt, A. R.; Ma, S.; Stilgenbauer, S.; Cramer, P.; Aiello, M.; Johnson, D. M.; Miller, L. L.; Li, D.; Jahn, T. M.; Dansey, R. D.; Hallek, M.; O'Brien, S. M. Idelalisib and Rituximab in Relapsed Chronic Lymphocytic Leukemia. *N. Engl. J. Med.* **2014,** *370* (11), 997–1007.
24. Graf, S. A.; Gopal, A. K. Idelalisib for the Treatment of Non-Hodgkin Lymphoma. *Expert. Opin. Pharmacother.* **2016,** *17* (2), 265–274.
25. Lannutti, B. J.; Meadows, S. A.; Herman, S. E.; Kashishian, A.; Steiner, B.; Johnson, A. J.; Byrd, J. C.; Tyner, J. W.; Loriaux, M. M.; Deininger, M.; Druker, B. J.; Puri, K. D.; Ulrich, R. G.; Giese, N. A. CAL-101, A p110delta Selective Phosphatidylinositol-3-Kinase Inhibitor for the Treatment of B-Cell Malignancies, Inhibits PI3K Signaling and Cellular Viability. *Blood* **2011,** *117* (2), 591–594.
26. Degorce, F.; Card, A.; Soh, S.; Trinquet, E.; Knapik, G. P.; Xie, B. HTRF: A Technology Tailored for Drug Discovery—A Review of Theoretical Aspects and Recent Applications. *Curr. Chem. Genomics* **2009,** *3,* 22–32.
27. Condliffe, A. M.; Davidson, K.; Anderson, K. E.; Ellson, C. D.; Crabbe, T.; Okkenhaug, K.; Vanhaesebroeck, B.; Turner, M.; Webb, L.; Wymann, M. P.; Hirsch, E.; Ruckle, T.; Camps, M.; Rommel, C.; Jackson, S. P.; Chilvers, E. R.; Stephens, L. R.; Hawkins, P. T. Sequential Activation of Class IB and Class IA PI3K Is Important for the Primed Respiratory Burst of Human but Not Murine Neutrophils. *Blood* **2005,** *106* (4), 1432–1440.
28. Murphy, K. M.; Heimberger, A. B.; Loh, D. Y. Induction by Antigen of Intrathymic Apoptosis of CD4 + CD8 + TCRlo Thymocytes in Vivo. *Science (New York, N.Y.)* **1990,** *250* (4988), 1720–1723.
29. Ali, K.; Bilancio, A.; Thomas, M.; Pearce, W.; Gilfillan, A. M.; Tkaczyk, C.; Kuehn, N.; Gray, A.; Giddings, J.; Peskett, E.; Fox, R.; Bruce, I.; Walker, C.; Sawyer, C.; Okkenhaug, K.; Finan, P.; Vanhaesebroeck, B. Essential Role for the p110delta Phosphoinositide 3-Kinase in the Allergic Response. *Nature* **2004,** *431* (7011), 1007–1011.
30. Pietrosimone, K. M.; Jin, M.; Poston, B.; Liu, P. Collagen-Induced Arthritis: A Model for Murine Autoimmune Arthritis. *Bio Protoc.* **2015,** *5* (20), 1626.
31. Hirose, J.; Tanaka, S. Animal Models for Bone and Joint Disease. CIA, CAIA Model. *Clin. Calcium* **2011,** *21* (2), 253–259.
32. Alexander, R.; Balasundaram, A.; Batchelor, M.; Brookings, D.; Crepy, K.; Crabbe, T.; Deltent, M. F.; Driessens, F.; Gill, A.; Harris, S.; Hutchinson, G.; Kulisa, C.; Merriman, M.; Mistry, P.; Parton, T.; Turner, J.; Whitcombe, I.; Wright, S. 4-(1,3-Thiazol-2-yl)morpholine Derivatives as Inhibitors of Phosphoinositide 3-Kinase. *Bioorg. Med. Chem. Lett.* **2008,** *18* (15), 4316–4320.
33. Puri, K. D.; Doggett, T. A.; Douangpanya, J.; Hou, Y.; Tino, W. T.; Wilson, T.; Graf, T.; Clayton, E.; Turner, M.; Hayflick, J. S.; Diacovo, T. G. Mechanisms and Implications of Phosphoinositide 3-Kinase Delta in Promoting Neutrophil Trafficking into Inflamed Tissue. *Blood* **2004,** *103* (9), 3448–3456.
34. Sadhu, C.; Masinovsky, B.; Dick, K.; Sowell, C. G.; Staunton, D. E. Essential Role of Phosphoinositide 3-Kinase Delta in Neutrophil Directional Movement. *J. Immunol. (Baltimore, Md.: 1950)* **2003,** *170* (5), 2647–2654.
35. Berndt, A.; Miller, S.; Williams, O.; Le, D. D.; Houseman, B. T.; Pacold, J. I.; Gorrec, F.; Hon, W. C.; Liu, Y.; Rommel, C.; Gaillard, P.; Ruckle, T.; Schwarz, M. K.; Shokat, K. M.; Shaw, J. P.; Williams, R. L. The p110 Delta Structure: Mechanisms for Selectivity and Potency of New PI(3)K Inhibitors. *Nat. Chem. Biol.* **2010,** *6* (2), 117–124.
36. Yang, Y.; Qiu, F.; Josephs, J. L.; Humphreys, W. G.; Shu, Y. Z. Bioactivation of 2-(Alkylthio)-1,3,4-Thiadiazoles and 2-(Alkylthio)-1,3-Benzothiazoles. *Chem. Res. Toxicol.* **2012,** *25* (12), 2770–2779.
37. Sushko, Y.; Novotarskyi, S.; Korner, R.; Vogt, J.; Abdelaziz, A.; Tetko, I. V. Prediction-Driven Matched Molecular Pairs to Interpret QSARs and Aid the Molecular Optimization Process. *J. Cheminf.* **2014,** *6* (1), 48.
38. Weber, J.; Achenbach, J.; Moser, D.; Proschak, E. VAMMPIRE: A Matched Molecular Pairs Database for Structure-Based Drug Design and Optimization. *J. Med. Chem.* **2013,** *56* (12), 5203–5207.
39. Leeson, P. D.; Springthorpe, B. The Influence of Drug-Like Concepts on Decision-Making in Medicinal Chemistry. *Nat. Rev. Drug Discov.* **2007,** *6* (11), 881–890.
40. Hopkins, A. L.; Keseru, G. M.; Leeson, P. D.; Rees, D. C.; Reynolds, C. H. The Role of Ligand Efficiency Metrics in Drug Discovery. *Nat. Rev. Drug Discov.* **2014,** *13* (2), 105–121.
41. Varma, M. V.; Chang, G.; Lai, Y.; Feng, B.; El-Kattan, A. F.; Litchfield, J.; Goosen, T. C. Physicochemical Property Space of Hepatobiliary Transport and Computational Models for Predicting Rat Biliary Excretion. *Drug Metab. Dispos.* **2012,** *40* (8), 1527–1537.
42. Gintant, G. A.; Su, Z.; Martin, R. L.; Cox, B. F. Utility of hERG Assays as Surrogate Markers of Delayed Cardiac Repolarization and QT Safety. *Toxicol. Pathol.* **2006,** *34* (1), 81–90.
43. Hancox, J. C.; McPate, M. J.; El Harchi, A.; Zhang, Y. H. The hERG Potassium Channel and hERG Screening for Drug-Induced Torsades de Pointes. *Pharmacol. Ther.* **2008,** *119* (2), 118–132.

44. Hastwell, P. W.; Webster, T. W.; Tate, M.; Billinton, N.; Lynch, A. M.; Harvey, J. S.; Rees, R. W.; Walmsley, R. M. Analysis of 75 Marketed Pharmaceuticals Using the GADD45a-GFP 'GreenScreen HC' Genotoxicity Assay. *Mutagenesis* **2009,** *24* (5), 455–463.
45. Birrell, L.; Cahill, P.; Hughes, C.; Tate, M.; Walmsley, R. M. GADD45a-GFP GreenScreen HC Assay Results for the ECVAM Recommended Lists of Genotoxic and Non-Genotoxic Chemicals for Assessment of New Genotoxicity Tests. *Mutat. Res.* **2010,** *695* (1–2), 87–95.
46. Tilmant, K.; Gerets, H. H.; De Ron, P.; Cossu-Leguille, C.; Vasseur, P.; Dhalluin, S.; Atienzar, F. A. The Automated Micronucleus Assay for Early Assessment of Genotoxicity in Drug Discovery. *Mutat. Res.* **2013,** *751* (1), 1–11.
47. Fluckiger-Isler, S.; Kamber, M. Direct Comparison of the Ames Microplate Format (MPF) Test in Liquid Medium With the Standard Ames Pre-Incubation Assay on Agar Plates by Use of Equivocal to Weakly Positive Test Compounds. *Mutat. Res.* **2012,** *747* (1), 36–45.
48. Saeki, K.; Takahashi, K.; Kawazoe, Y. Metabolism of Mutagenicity-Deprived 3-Fluoroquinoline: Comparison With Mutagenic Quinoline. *Biol. Pharm. Bull.* **1993,** *16* (3), 232–234.
49. Reigh, G.; McMahon, H.; Ishizaki, M.; Ohara, T.; Shimane, K.; Esumi, Y.; Green, C.; Tyson, C.; Ninomiya, S. Cytochrome P450 Species Involved in the Metabolism of Quinoline. *Carcinogenesis* **1996,** *17* (9), 1989–1996.
50. Hinson, J. A.; Pumford, N. R.; Nelson, S. D. The Role of Metabolic Activation in Drug Toxicity. *Drug Metab. Rev.* **1994,** *26* (1–2), 395–412.
51. Zhou, S.; Chan, E.; Duan, W.; Huang, M.; Chen, Y. Z. Drug Bioactivation, Covalent Binding to Target Proteins and Toxicity Relevance. *Drug Metab. Rev.* **2005,** *37* (1), 41–213.
52. Guroff, G.; Daly, J. W.; Jerina, D. M.; Renson, J.; Witkop, B.; Udenfriend, S. Hydroxylation-Induced Migration: The NIH Shift. Recent Experiments Reveal an Unexpected and General Result of Enzymatic Hydroxylation of Aromatic Compounds. *Science (New York, N.Y.)* **1967,** *157* (37), 1524–1530.
53. Sakamoto, K.; Nakamura, Y.; Aikoh, S.; Baba, T.; Perregaard, J.; Pedersen, H.; Moltzen, E. K.; Mulford, D. J.; Yamaguchi, T. Metabolism of Sertindole: Identification of the Metabolites in the Rat and Dog, and Species Comparison of Liver Microsomal Metabolism. *Xenobiotica* **1995,** *25* (12), 1327–1343.
54. Mutlib, A.; Espina, R.; Atherton, J.; Wang, J.; Talaat, R.; Scatina, J.; Chandrasekaran, A. Alternate Strategies to Obtain Mass Balance Without the Use of Radiolabeled Compounds: Application of Quantitative Fluorine (19F) Nuclear Magnetic Resonance (NMR) Spectroscopy in Metabolism Studies. *Chem. Res. Toxicol.* **2012,** *25* (3), 572–583.
55. Gillis, E. P.; Eastman, K. J.; Hill, M. D.; Donnelly, D. J.; Meanwell, N. A. Applications of Fluorine in Medicinal Chemistry. *J. Med. Chem.* **2015,** *58* (21), 8315–8359.
56. Shah, P.; Westwell, A. D. The Role of Fluorine in Medicinal Chemistry. *J. Enzyme Inhib. Med. Chem.* **2007,** *22* (5), 527–540.
57. Winkler, D. G.; Faia, K. L.; DiNitto, J. P.; Ali, J. A.; White, K. F.; Brophy, E. E.; Pink, M. M.; Proctor, J. L.; Lussier, J.; Martin, C. M.; Hoyt, J. G.; Tillotson, B.; Murphy, E. L.; Lim, A. R.; Thomas, B. D.; Macdougall, J. R.; Ren, P.; Liu, Y.; Li, L. S.; Jessen, K. A.; Fritz, C. C.; Dunbar, J. L.; Porter, J. R.; Rommel, C.; Palombella, V. J.; Changelian, P. S.; Kutok, J. L. PI3K-Delta and PI3K-Gamma Inhibition by IPI-145 Abrogates Immune Responses and Suppresses Activity in Autoimmune and Inflammatory Disease Models. *Chem. Biol.* **2013,** *20* (11), 1364–1374.

8.16 Medicinal Chemistry Case History: Structure-Based Drug Design of Oral and Inhaled p38 MAP Kinase Inhibitors as Clinical Candidates

L Xing and J Mathias, Worldwide Medicinal Chemistry, Pfizer Worldwide Research and Development, Cambridge, United States

© 2017 Elsevier Ltd. All rights reserved.

8.16.1	**Inflammatory Diseases**	408
8.16.1.1	Synthetic DMARDS	409
8.16.1.2	Biological DMARDs	409
8.16.2	**The p38 MAPK Pathway**	410
8.16.2.1	Small-Molecule p38 Clinical Candidates for Inflammatory Indications	410
8.16.3	**Approaches to the Discovery of p38 MAPK Inhibitors**	413
8.16.3.1	Structure-Based Drug Design	413
8.16.3.2	First-Generation Pyrazole-Based Inhibitors	414
8.16.3.3	Second-Generation Pyridinone-Based Inhibitors	414
8.16.3.4	Structural Hypothesis of Human Kinome Selectivity	415
8.16.3.5	Structure-Guided Lead Optimization	416
8.16.3.6	PH-797804 is the More Potent Atropisomer	416
8.16.4	**Characterizations of PH-797804**	418
8.16.4.1	*In Vitro* Activity	418
8.16.4.2	Kinase Selectivity Screening	418
8.16.4.3	Crystal Structure of PH-797804 Bound in p38α Kinase	418
8.16.4.4	Rotational Barrier, Chemical Stability, and Pharmaceutical Properties	419
8.16.4.5	Pharmacokinetic Properties of PH-797804	419
8.16.4.6	*In Vivo* Efficacy of PH-797804	420
8.16.5	**Designing Inhaled Inhibitors of p38α**	420
8.16.5.1	DFG-Out Conformation of p38	421
8.16.5.2	Design to Target the DFG-Out Conformation of p38	421
8.16.5.3	Lead Optimization of DFG-out Binders	422
8.16.5.4	Design Phase I Metabolism	423
8.16.5.5	Design Phase II Metabolism	423
8.16.5.6	Identification of PF-3715455	424
8.16.6	**Highlights of Clinical Data for PH-797804 and PF-3715455**	426
8.16.7	**Conclusions**	427
Acknowledgment		427
References		427

Abbreviations

MAPK Mitogen-activated protein kinase
RA Rheumatoid arthritis
COPD Chronic obstructive pulmonary disease
MDS Myelodysplastic syndrome
DMARDs Disease-modifying antirheumatic drugs
TNF-α Tumor necrosis factor-α
IL Interleukin
NF-kB Nuclear factor-kB
hWB Human whole blood
LPS Lipopolysaccharide
mCIA Mouse collagen-induced arthritis
SCW Strep cell wall
hs-CRP High-sensitivity C-reactive protein
HSP27 Heat shock protein 27
SPR Surface plasmon resonance
PBMC Peripheral blood mononuclear cell
SLF Simulated lung fluid

8.16.1 Inflammatory Diseases

Inflammation and immunity form the bases of many physiological and pathological processes. While of benefit during infection, excessive inflammation can contribute substantially to the pathogenesis of many chronic diseases, in which the immune system erroneously targets the body's own cells, tissues, and organs.[1,2]

Rheumatoid arthritis, inflammatory bowel disease, psoriasis, lupus, and multiple sclerosis are all autoimmune diseases, conditions in which the immune system loses its ability to differentiate the self from the foreign and directs an attack against healthy cells and tissues.[3] In rheumatoid arthritis (RA), the immune system attacks the synovium (tissue lining the joint capsule) causing local inflammation. It affects the lining of the joints, causing pain, swelling, and reduced mobility for the patient. This inflammatory response ultimately results in the destruction of ligaments, tendons, and muscles that support the joint.[4,5] Patients with severe joint damage are subject to surgical options. Systemic inflammation is also involved in the pathogenesis of chronic obstructive pulmonary disease (COPD).[6–8] Reduced lung function is associated with increased levels of systemic inflammatory markers, which may have important pathophysiological and therapeutic implications for subjects with stable COPD.

8.16.1.1 Synthetic DMARDS

As clinicians strive to achieve and maintain remission of symptoms and preserve joint function in patients, disease-modifying antirheumatic drugs (DMARDs) are introduced in early treatment of RA to limit joint damage from the outset. Methotrexate (MTX) is the most frequently used first-line DMARD due to its efficacy and low cost.[9–11] As an antifolate, it has multiple mechanisms of action in RA. However, it is often associated with serious side effects. Hepatotoxicity, fibrosis, and cirrhosis after prolonged use and liver enzyme elevations are frequently seen. Patients who take methotrexate need to be monitored regularly for liver and kidney function. It is also associated with potentially fatal opportunistic infections, especially *Pneumocystis* pneumonia. The adverse effects of methotrexate have prompted the search for safer and more efficacious new treatments.

8.16.1.2 Biological DMARDs

Several preeminent biologics have been approved for treatment of RA by the Food and Drug Administration (FDA). Treatment with infliximab (Remicade), adalimumab (Humira), etanercept (Enbrel), abatacept (Orencia), and rituximab (Rituxan) reduces joint pain and swelling and retards progression of bone loss in patients whose disease is unsatisfactorily controlled by conventional DMARDs.[12–15] A large number of the biological agents act as inhibitors of tumor necrosis factor (TNF), a monocyte-derived cytokine that has a wide variety of functions. The leading anti-TNF products (infliximab, adalimumab, and etanercept) have been shown to be effective in slowing down the signs and symptoms of rheumatoid arthritis, inhibiting the progression of structural damage, and improving physical function in patients with moderately to severely active rheumatoid arthritis.[16,17] The TNF inhibitors are intended chiefly to antagonize TNF-α, an inflammatory cytokine produced by activated monocytes, macrophages, and T cells in the synovium. Of the currently available anti-TNF therapies, etanercept is the only biologic that also blocks TNF-β, or lymphotoxin, as both infliximab and adalimumab block only TNF-α.

The main limitation with anti-TNF treatment is that large populations of patients do not respond to the drugs.[18,19] Clinical data show that between 59% and 75% of patients achieved an American College of Rheumatology 20 (ACR20) level of improvement, the minimum improvement expected and a common clinical trial primary endpoint. That leaves between 25% and 41% of patients who stop taking the anti-TNF drugs due to inadequate responses.

Rituximab (Rituxan) is a chimeric monoclonal antibody against CD20 that is primarily expressed on the cell surface of the mature B cells.[20] It is approved to treat diseases that are characterized by excessive numbers of B cells, overactive B cells, or dysfunctional B cells. By depleting the CD20 B cells, rituximab has been approved to treat autoimmune diseases including rheumatoid arthritis. In combination with methotrexate, rituximab has been shown to reduce signs and symptoms in adult patients with moderately to severely active RA who have had an inadequate response to one or more anti-TNF therapies.

Orencia (abatacept) is a T cell costimulation modulator that was approved for the RA treatment by the FDA in 2005 and by the European Commission in 2007.[21,22] The drug is a fully humanized soluble fusion protein that consists of the extracellular domain of cytotoxic T lymphocyte antigen-4 (CTLA4) linked to the Fc portion of human IgG1. It allays inflammation by interfering with the interaction between CD80/86 on antigen-presenting cells and CD28 on T cells, thus preventing T cell activation. It is labeled for reducing the signs and symptoms of RA, slowing the progression of structural damage, and improving physical function in adults who have had an inadequate response to one or more DMARDs.

In addition, other biological agents have been explored to complement the existing inhibitors. Among them, the IL-1 receptor antagonist anakinra (Kineret), the IL-6 antagonist tocilizumab (Actemra), the IL-15 antagonist AMG-714, and the adhesion molecule blockers (e.g., anti-CD20 antibody ocrelizumab) have emerged.[21–23]

The more targeted biologic therapies have not entirely reduced the side effects of traditional DMARDs and are sometimes associated with additional common effects, usually due to the disruption of the immune response and injection site reactions.[24] Despite the fact that these side effects are usually less harsh than traditional DMARDs, it is an area for improvement in new treatments. However, since the majority of biological DMARDs are used in practice in combination with methotrexate, their side effects are in addition to those mentioned earlier.

In general, the biological agents are limited due to requirement for parenteral administration, difficulty in dose titration, poor reversibility, induction of host neutralizing antibody response, high production costs, and a significant population of patients who are refractory to the treatment. Therefore, given the great successes of anti-TNF agents and advances made in understanding the molecular basis of their efficacy surrounding the role of TNF in the innate immune system, small-molecule targeted therapies remain a major goal of pharmaceutical research.

8.16.2 The p38 MAPK Pathway

Excessive production of TNF-α and other proinflammatory cytokines is involved in the pathogenesis of rheumatoid arthritis, Crohn's disease, inflammatory bowel disease, psoriasis, and COPD.[25,26] In an innate immune response, mitogen-activated protein kinase (MAPK) and nuclear factor-kB (NF-kB) are activated by pattern recognition receptors (PRRs) upon binding of the pathogen-associated molecular patterns (PAMPs). The 14 MAPKs discovered in mammalian cells are crucial to generating immune responses. Among them, extracellular signal-regulated kinase (ERK), p38, and Jun N-terminal kinase (JNK) have been extensively studied in the context of innate immunity.[27–30] Altogether, they play pivotal roles in the MAPK signal transduction pathway that cells use to adapt to inflammatory and stressful conditions. At the center of regulating a broad spectrum of inflammatory activities, the p38 kinase controls the biosynthesis of key proinflammatory cytokines at both the transcriptional and translational levels. As depicted in Fig. 1, pathogens or inflammatory stimuli initiate a phosphorylation cascade mediated by p38 kinase that leads to the transcription and translation of inflammatory response-associated genes that encode proteins such as TNF-α, IL-1β, IL-6, and IL-8.[28,31] TNF-α, IL-1β, and IL-6 are macrophage- and fibroblast-derived proteins that induce expression of inflammatory mediators such as COX-2, inducible nitric oxide synthase, adhesion molecules, and metalloproteinases, resulting in synovial inflammation and associated cartilage and bone destruction. In addition, the expression of cytokines and chemokines during an innate immune response could lead to subsequent induction of the adaptive immune response, further intensifying the amplitude and duration of an inflammatory reaction. The increased gene expressions of immune signaling molecules are vital to the magnitude and perpetuation of inflammatory mediators, causing chronic autoimmune disorders.

Inhibition of p38 MAPK has the potential of blocking the production of these cytokines and the subsequent amplification of the inflammatory cascade. Modulation of p38 by ATP-competitive small molecules has led to the generation of a variety of novel p38 inhibitors as potential therapeutics for the treatment of inflammatory conditions including Crohn's disease, COPD, psoriasis, and RA.[31–35]

The p38 MAP kinase family belongs to serine/threonine protein kinases and consists of four isoforms: α, β, γ, and δ. These kinases show a high degree of sequence homology, with 60–75% overall sequence identity and > 90% within the kinase domain.[36] The p38β kinase is the closest structural homologue to p38α, sharing 75% overall sequence identity, and close to 90% in the ATP-binding site. In general, p38 α and β kinase inhibition values parallel each other, and both isoforms are ubiquitously expressed. The α-isoform, however, is better characterized in terms of its role in inflammation.

Activation of the p38 MAPK signaling pathway also leads to the production of anti-inflammatory cytokines such as IL-10, activation of negative feedback loops initiated by the phosphorylation of transforming growth factor β-activated kinase-1-binding protein, and upregulation of MAP kinase phosphatases that dephosphorylate and inactivate p38 kinase, ERK, and JNK.[37–39] These multiple positive and negative pathway components highlight the complex feedback mechanisms that could limit MAPK activation to prevent excessive inflammation.[30]

8.16.2.1 Small-Molecule p38 Clinical Candidates for Inflammatory Indications

In the past two decades, the pharmaceutical industry has invested tremendous resources into research and development for p38 MAPK inhibitors resulted in the discovery of a variety of inhibitor classes with diverse molecular architecture.[32,34,40] A wide variety

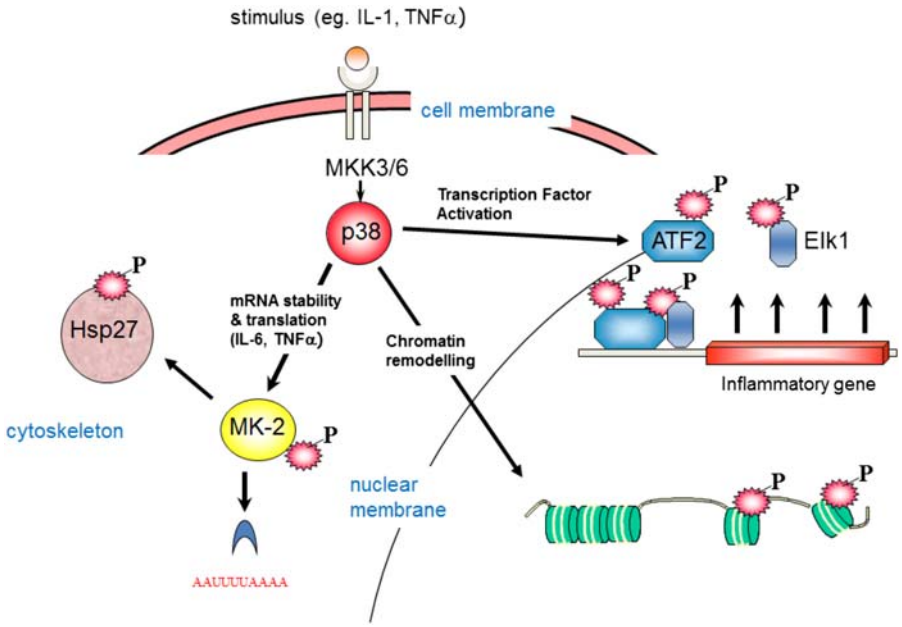

Fig. 1 The p38 MAPK as a central locus in inflammatory pathways.

of autoimmune disease treatments were attempted in clinical setting including rheumatoid arthritis, inflammatory bowel disease, psoriasis, systemic lupus erythematosus (SLE), and other indications like chronic obstructive pulmonary disease (COPD) that are characterized by chronic inflammation. Herein, we review the major advancement into human clinical studies in the field of p38 inhibition (Fig. 2) alongside the discovery of the most recent clinical p38 inhibitors within Pfizer.

The pyrimido-pyridazinone (VX-745) and pyridinyl-urea (VX-702)-based compounds were discovered by Vertex Pharmaceuticals.[41,42] In human whole blood, a cellular system that mimics the physiological *in vivo* milieu, LPS-stimulated TNF-α and IL-1β

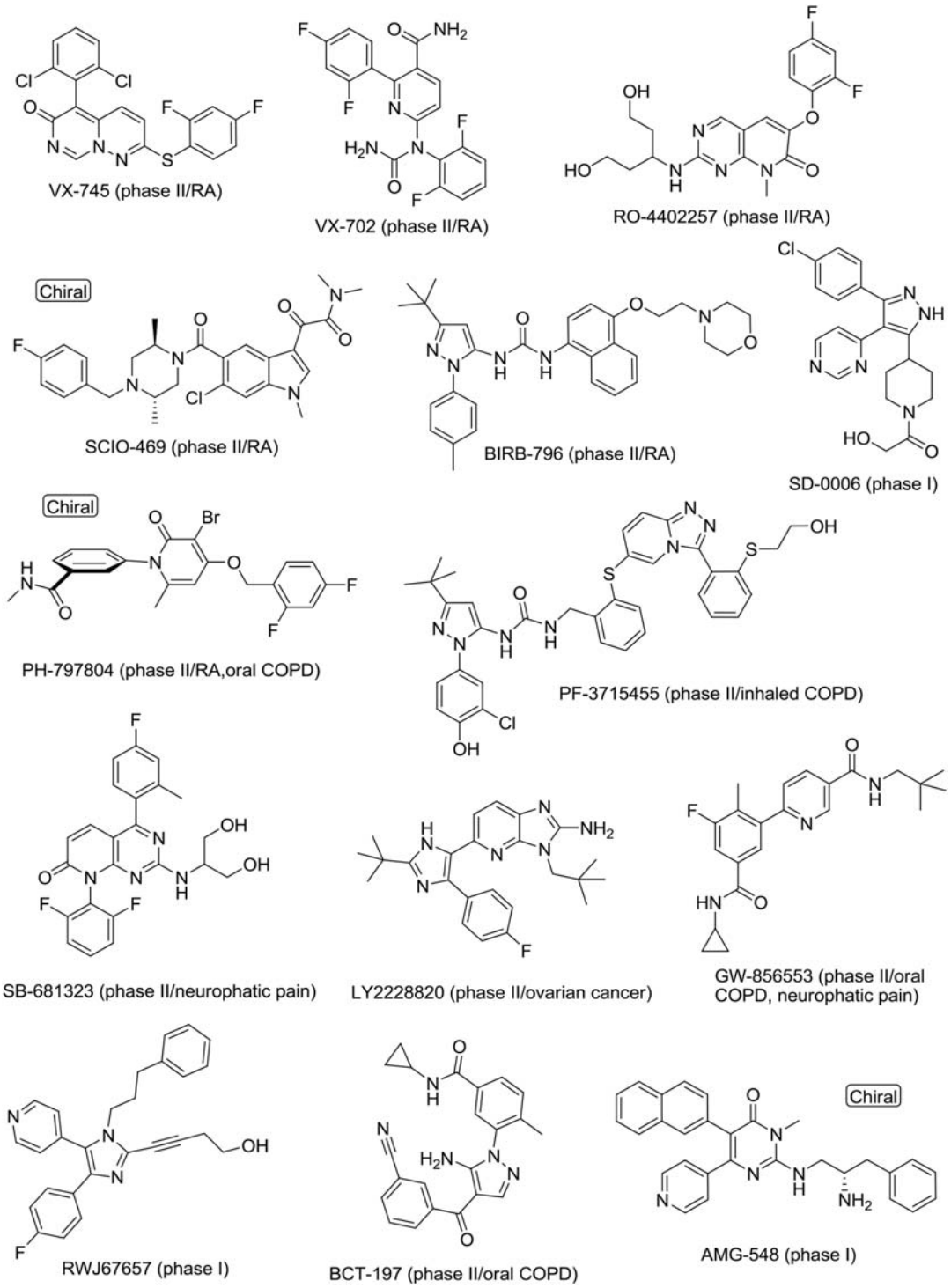

Fig. 2 Clinical candidates of p38 MAPK inhibitors along with their intended indications.

production were measured. VX-745 inhibits p38α and LPS-TNF-α in human whole blood (hWB) at IC_{50}'s of 5.0 nM and 700 nM, respectively. In RA patients, VX-745 was well tolerated and produced significantly higher ACR20 response rate than placebo (43% vs. 8%). However, further trials were suspended after neurological effects were observed in dogs. With much lower penetration of the blood–brain barrier, VX-702 was chosen as a backup to VX-745.[43] Two clinical trials were completed in the third quarter of 2007, one with VX-702 as a single agent in RA patients and the other phase II study as a once daily (QD) medicine in combination with methotrexate for three months.[44] In both studies, the ACR20 response rates among patients did not reach statistical significance. Reductions in the levels of C-reactive protein were observed as early as week 1, but the levels rapidly returned to baseline values by week 4.

SCIO-469 (talmapimod) was advanced to phase II human clinical trials for the treatment of rheumatoid arthritis, myelodysplastic syndrome (MDS), and acute dental pain.[45–49] It is a selective p38α inhibitor with >1000-fold selectivity versus ERK2, JNK1, and LCK. It potently inhibits p38α at enzyme level (IC_{50}: 9 nM) and moderately inhibits LPS-induced TNF-α production in human whole blood (IC_{50}: 300 nM).[50,51] Oral SCIO-469 administered at doses ranging from 90 to 360 mg daily was tolerated with common adverse events in MDS patients. Bone marrow and cytogenetic responses were rare, suggesting low likelihood of SCIO-469 at the tested dose levels having any disease-altering activity. In RA patients dosed at 30, 60, and 100 mg daily, no significant differences in ACR20 responses were found between SCIO-469 and placebo. Declines in C-reactive protein (CRP) and erythrocyte sedimentation rate during early treatment did not persist. Pharmacokinetic analysis demonstrated no statistically significant correlation in SCIO-469 average plasma trough concentrations with change in CRP values.

While most inhibitors of p38α bind only in the purine site, with p38α remaining in a "DFG-in" conformation, BIRB-796 binds at a site that extends into a "selectivity pocket," that is not used by ATP, displacing the Asp168-Phe169-Gly170 (DFG) motif at the start of the activation loop and promoting a "DFG-out" conformation.[52]

An inhibition in solution assay (ISA) measured K_D of BIRB-796 for nonactivated p38α to be <0.8 nM.[53] DFG-out compounds associate with p38α over 30-fold more slowly than purine site compounds (k_{on}: $0.85 \times 10^5\ s^{-1}\ M^{-1}$, k_{off}: $8.3 \times 10^{-6}\ s^{-1}$), apparently due to low abundance of the DFG-out conformation. At concentrations that inhibit cellular production of an inflammatory cytokine, TNF-α, selectivity pocket compounds decrease levels of phosphorylated p38α and β. In the *in vitro* and *in vivo* experiments, BIRB-796 inhibits all p38 MAPK isoforms.[54] By binding to a different conformation of the enzyme, compounds that prevent activation were believed to offer an alternative approach to modulation of p38α.

Out of a series of diaryl pyrazole-based inhibitors, SD-0006 was identified as a potent and selective compound for p38α and b MAP kinases over 50 other kinases screened including p38γ and p38δ.[55,56] In the mouse collagen-induced arthritis (mCIA) model, equivalent efficacy was shown to anti-TNF antibody treatment.[57] SD-0006 demonstrated good oral anti-inflammatory efficacy and cross species correlation between the rat, cynomolgus monkey, and human. Its development has been discontinued after phase I study in human healthy volunteers.

RO-4402257 (pamapimod) is a selective inhibitor of the α-isoform of p38. It inhibited p38α and p38β enzymatic activity, with IC_{50} values of 14 and 0.48nM, respectively, but showed no activity against p38δ or p38γ isoforms.[58] In murine collagen-induced arthritis, RO-4402257 reduced clinical signs of inflammation and bone loss at 50 mg/kg or greater. In a clinical study in patients with active RA, RO-4402257 was administrated as monotherapy in comparison with methotrexate (MTX).[59] After 12 weeks of daily therapy at one of the three doses (50, 150, or 300 mg), no clear evidence of efficacy was demonstrated. Intriguingly, the level of C-reactive protein (CRP) initially declined in the 300-mg patient group but rapidly returned to baseline at the second week and remained over the rest of the study period. Typical adverse findings are liver enzyme elevation and/or skin rash.[59,60]

In a randomized, placebo-controlled study in chronic obstructive pulmonary disease (COPD) patients, SB-681323 (dilmapimod) was given orally at single doses of 7.5 and 25 mg and shown to inhibit the p38 MAPK pathway via biomarker pHSP27 measurement and the TNF-α production.[61] In a separate trial, to evaluate the effect of dilmapimod on neuropathic pain symptoms and signs following nerve injury, 43 patients received twice daily doses at 15 mg/day for two weeks. Dilmapimod was well tolerated, with no clinically relevant safety findings. The average daily pain score was reduced with statistical significance during the second week of treatment among patients compared to placebo.[62]

GW-856553 (losmapimod) is a potent p38 MAPK inhibitor of both α (Ki: 8.1 nM)- and β (Ki: 7.6 nM)-isoforms.[63] A post hoc analysis based on a 6-month clinical study demonstrated reduction of exacerbations with the 15 mg twice daily dose in the subgroup of COPD patients with blood eosinophils 2% at baseline.[64] To fully support further clinical development, the findings need to be explored in a prospectively designed study in a COPD population. Identification of a subgroup of patients more likely to respond to treatment is a step toward personalized medicine by offering effective therapy to specific populations of high unmet need. GW-856553 was also evaluated in patients with chronic neuropathic pain, but the analgesic efficacy was not clinically meaningful.[65] Additionally, GW-856553 suppressed inflammation in patients with cardiovascular disease and improved vascular function.[66–68]

BCT-197 (acumapimod) is being developed by Novartis as an oral agent for COPD. From patent application, the compound inhibits p38α with an IC_{50} value of less than 1 μM.[69,70] In COPD patients, BCT-197 was evaluated at single dose of 20 and 75 mg with and/or without prednisone. The ongoing development is expected for regulatory filings in 2018. No further clinical trials in COPD patients have yet been disclosed. A phase II study was also performed in acute renal patients undergoing cardiac surgery, but development for that indication appears to have been terminated.

Using p38α immunoprecipitated from LPS-activated human monocytes, the IC_{50} of RWJ67657 was measured at 30 nM.[71] The compound inhibited the production of TNF-α and IL-1β by LPS-stimulated human PBMCs, with IC_{50} values of 3 and 11 nM, respectively. In the single-dose first-in-human (FIH) study, the terminal half-life of RWJ67657 was determined to be in the range of 5.1 to 7.7 hours.[72] The apparent clearance was proportional and decreased with increasing doses. The inhibition of

TNF-α, IL-6, and IL-8 was reported in a dose-dependent manner.[73] At the maximum dose of 1400 mg, reduction in peak serum levels of the proinflammatory cytokines exceeded 90%. Furthermore, RWJ67657 demonstrated potential in treating endocrine-resistant breast cancer.[74] Utilizing well-established xenograft tumor models, RWJ67657 exhibited potent antitumor properties, markedly decreasing tamoxifen-resistant tumor growth.

Following on to SD-0006, the lead generation and optimization efforts led to the identification of a novel pharmacophore **PH-797804** as a clinical candidate for RA and COPD.[75–79] First identified by molecular modeling and subsequently confirmed by chiral chromatography, **PH-797804** is the more potent atropisomer (aS) of a racemic pair.[75] In biochemical assays and other assays, **PH-797804** demonstrated high potency ($K_i = 5.8$ nM) and superior selectivity across broad human kinase genome.

In addition to treating autoimmune and the related disorders, LY2228820 dimesylate (Ralimetinib) is being investigated in a clinical trial in patients with ovarian cancer. The compound potently inhibited p38 α- and β-isoforms *in vitro* (IC_{50}: 5.3 and 3.2 nM, respectively) and produced significant tumor growth delay in multiple animal cancer models.[80]

Several additional compounds were evaluated clinically for the treatment of chronic inflammatory disorders. These included BMS-582949, ARRY-797, and AMG-548.[81–83] Either their structures were not disclosed or there were very little clinical data reported.

8.16.3 Approaches to the Discovery of p38 MAPK Inhibitors

8.16.3.1 Structure-Based Drug Design

Structural information of p38α kinase is rich with more than a hundred published structures generated by x-ray crystallography over the past two decades. Besides a small number of unphosphorylated, apo structures, most of the three-dimensional structures are binary complexes of p38α kinase and small-molecule inhibitors that compete for binding with cellular ATP.[55,84–92] The kinase hinge recognition elements predominantly involve a hydrogen bond with the Met109 backbone NH group. Some inhibitors engage an additional hydrogen bond with the upstream residue His107 via its backbone carbonyl, strictly mimicking the donor–acceptor pattern of the nucleoside interaction of ATP.[93]

The ATP-binding pocket is situated at the folding cleft of the N- and C-lobes of the kinase, which are connected by the hinge region. Interactions are formed with the hinge backbone through potentially two hydrogen bonds: The adenine N1 of ATP is an acceptor pairing with the backbone NH of Met109, and the 6-amino group is a donor to the backbone Leu108 downstream of the gatekeeper residue Thr106. Effective interaction in the ATP-binding pocket that complements the topological and the electrostatic characteristics of the kinase hinge is essential for potent inhibition of protein kinases.[94,95] Such canonical p38α kinase conformation is represented by the apo p38α crystal structure in Fig. 3A.

In addition to the catalytically active conformations, the DFG-out arrangement constitutes one of the frequently encountered inactive kinase conformations.[96,97] When the specific classes of inhibitor molecules bind, the conserved Asp168-Phe169-Gly170 (DFG) motif at the beginning of the activation loop rotates out of the ATP-binding site, creating a new pocket that is inaccessible in the active kinase conformation. By exploiting the induced pocket, submicromolar p38α kinase inhibitors were achieved, sparing the conventional hinge interaction entirely.[93] BIRB-796 exploits this catalytically incompetent conformation of the p38 kinase, which was envisioned to afford its high degree of selectivity against other protein kinases.[52] The urea moiety of BIRB-796 forms bidentate hydrogen bonds with the catalytic Glu71, and the naphthalene group occupies the p38α hydrophobic pocket (Fig. 3B). Both interactions facilitate the DFG-out conformation.

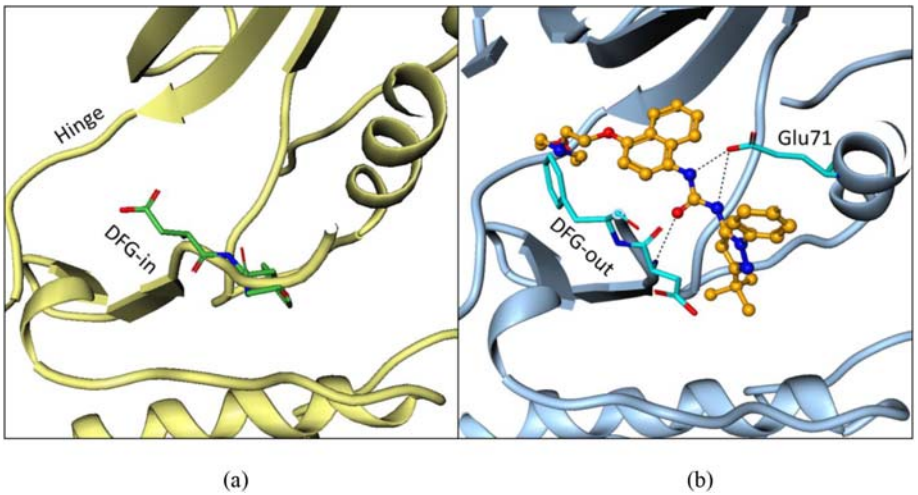

Fig. 3 The p38α kinase crystal structures. (A) Apo p38α showing DFG-in (Asp168-Phe169-Gly170) (PDB code: 1p38); (B) BIRB-796 binds to the DFG-out conformation of p38α kinase (PDB code: 1KV2).

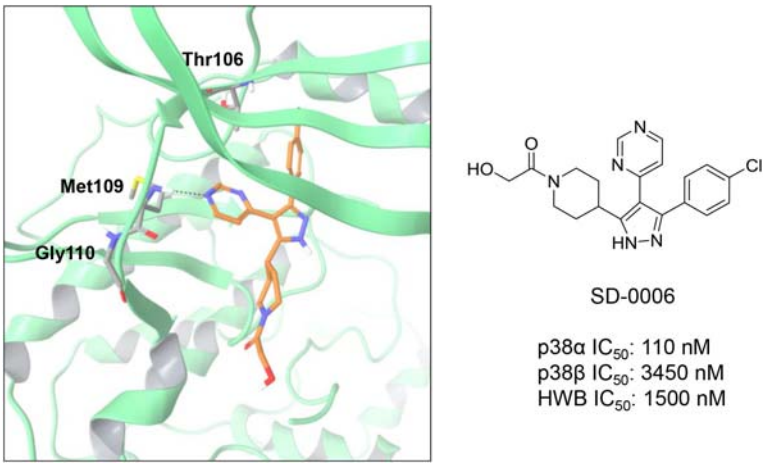

Fig. 4 Crystal structure of SD-0006 in p38α MAP kinase (PDB code: 3HL7).

8.16.3.2 First-Generation Pyrazole-Based Inhibitors

From high-throughput screening (HTS), a novel series of C(5)-substituted diarylpyrazoles were identified.[55] Following on, lead optimization identified pyrimidine to switch out the original pyridine at the C(4) position. The structure–activity relationships of the series were extensively explored with a focus on the various substituents at the C(5) position.[55,56] As this vector points to the opening cleft of ATP-binding site, it provided a handle to modulate the physicochemical properties of the compounds. SD-0006 was discovered out of the efforts. The pharmacokinetic experiments in both dog and rat indicated desirable properties in terms of half-life (rat and dog $t_{1/2} = 5–6$ hours) and bioavailability (>80% in both species).

The pyrazole group of SD-0006 serves as a central framework that helps to optimally position the two aromatic groups in the ATP-binding site of p38α kinase (Fig. 4). Crystal structure represented by SD-0006 has revealed a number of binding elements. One edge of the pyrazole moiety is stabilized by interactions with the flexible glycine flap that contains the consensus GXGXXG motif. One of the nitrogen atoms of the pyrazole ring directly interacts with the carboxylate side chain of Asp168. The 4-pyrimidine overlaps with adenine of ATP binding and forms conserved hydrogen bond with the hinge of p38α via Met109. The 4-chlorophenyl group binds in the lipophilic pocket of p38α. Overall, the binding of SD-0006 did not in any significant way perturb the native conformation of the apo p38α structure.[84,85]

8.16.3.3 Second-Generation Pyridinone-Based Inhibitors

The N-benzylpyridinone template was identified as a key feature for novelty and selectivity from the high-throughput screening hit SC-25028.[76] While its activity against p38α kinase was modest ($IC_{50} \sim 0.7$ μM), an early evaluation of selectivity against a panel of 48 kinases revealed that SC-25028 was very selective for p38, with less than 30% inhibition at 10 μM against the entire panel.

The crystal structure of SC-25028 bound to p38α kinase highlighted the key structural features associated with its binding mode.[76] In comparison with the earlier biaryl pyrazole-based structure, SC-25028 not only retained the conserved elements of binding to p38α kinase in the conventional kinase inhibition mode but also demonstrated unique structural features (Fig. 5).

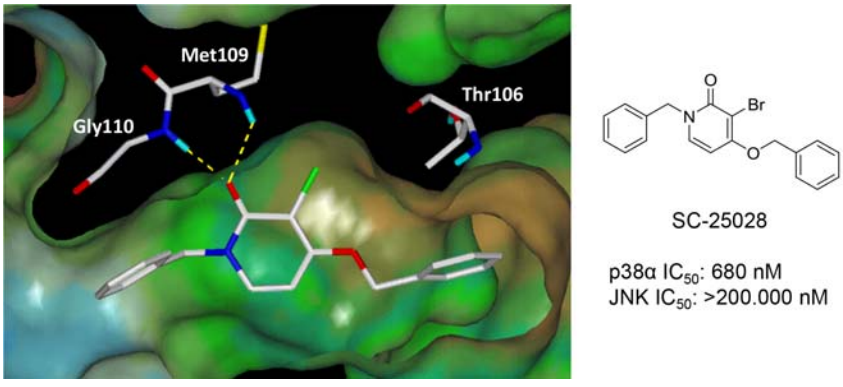

Fig. 5 Crystal structure of SC-25028 in complex with p38α kinase (PDB code: 3HP2).

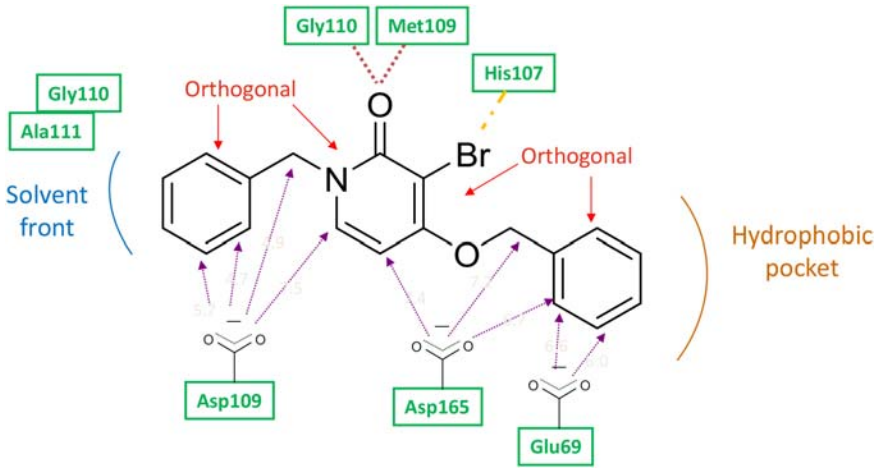

Fig. 6 Ligand–protein interaction map of SC-25028 chemical series.

A dual hydrogen bond to the backbones of Met109 and Gly110 was observed, which requires a peptide bond flip of Gly110. Devoid of a side chain, Gly110 uniquely furnishes the required flexibility for the conformational switch. The bromine atom uniquely forms a favorable halogen bond interaction (3.1 Å) with the backbone carbonyl of His107. The benzyloxyl group occupied the lipophilic pocket, and the N-benzyl group was directed toward the opening of the folding cleft. The two-dimensional schematic of the protein–ligand interaction pharmacophores of the chemical series represented by SC-25028 is delineated in Fig. 6.

8.16.3.4 Structural Hypothesis of Human Kinome Selectivity

Despite modest p38α activity of the initial hit, we postulated that the pyridinone class of compounds exhibits superior selectivity for p38 MAP kinase over other kinases, thanks to the TXXXG sequence motif on the kinase hinge. This was derived from the two characteristics of the binding interactions: (i) The hydrophobic encapsulation in a pocket that is distinct from phosphate binding of ATP, gated by Thr106, (ii) and the bidentate hydrogen bonds with Met109 and Gly110 requiring a peptide bond flip into the conformation that is only available for a glycine residue. The backbone flip occurs in p38α due to the presence of the glycine in the hinge region, which has no side chain and consequently affords necessary structural flexibility to be induced for a conformational flip. The flipped backbone conformation is prohibited by any residues other than a glycine due to their side chain presence.

Thr106 sits at the gatekeeping position that circumscribes access to the p38α aryl pocket. Its important role was substantiated by a number of site-directed mutagenesis studies.[98–100] Residues bearing side chains larger than threonine would temper the access to the aryl pocket. We mined the TXXXG motif in the human genome consisting of 518 protein kinase complements. The sequence profiles at the equivalent positions of Thr106 and Gly110 of p38α were plotted in Fig. 7. The analysis reveals

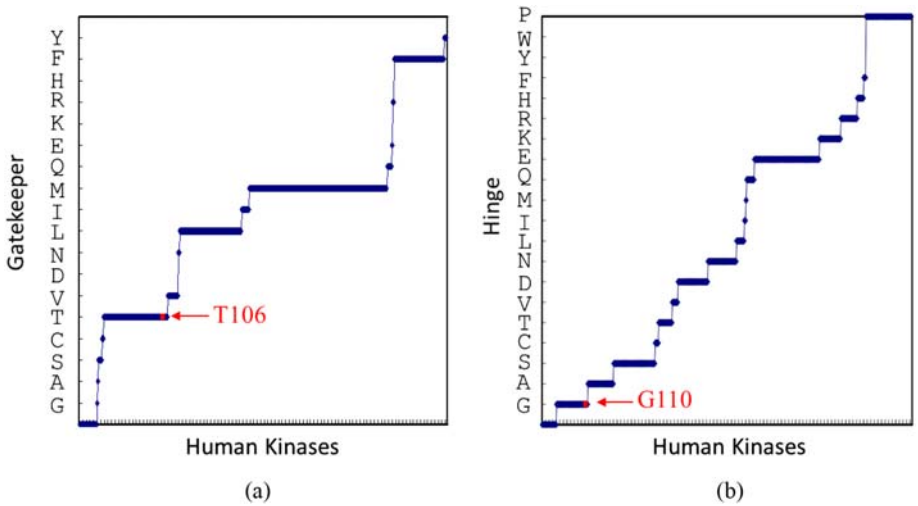

Fig. 7 Amino acid frequencies of the human kinome at positions corresponding to p38α kinase Thr106 (a) and Gly110 (b).

that 99 kinases or 20% of the kinome have threonine or an equivalent residue (cysteine, serine, alanine, and glycine) of similar or smaller side chain in place of Thr106. Likewise, 44 kinases share a glycine residue at the position corresponding to Gly110, which constitute 9% of the human kinase genome. The combined TXXXG motif is sparingly conserved in three kinases, p38α, p38β, and Myt-1 specifically. We thus derive a structural rationale for the observed high level of selectivity. Myt-1 is a mixed serine/threonine and tyrosine kinase upstream of CDKs. Its kinase domain is merely 23% identical to p38α in primary structure. Cross-reactivity is not anticipated for the pyridinone class of compounds due to the remote evolutionary relationship between Myt-1 and p38α kinase. Understanding the implication of such structural features to the desirable potency and specificity that can be achieved by a drug-like small molecule has paramount importance for targeting p38α kinase as a therapy for many chronic autoimmune disorders.

8.16.3.5 Structure-Guided Lead Optimization

Metabolic stability of SC-25028 was recognized as a primary liability as revealed by the human liver microsomal assay,[98–100] with only 52% of the parent compound being detected after incubation of 45 minutes. We believed that the two unsubstituted aromatic rings were most likely to be the site of oxidative metabolism. Efforts to increase metabolic stability were focused on halogen substitution to reduce the electron density in the rings, which also provides a steric block at certain positions. This strategy produced 10-fold potency improvement, largely owing to the augmented hydrophobic interaction via the 2,4-difluorobenzyloxy group in the deep selectivity pocket of p38α (compound 1, Fig. 8). Based on the SAR of halo substituted benzyloxy groups, it was concluded that the 2,4-difluorobenzyloxy group was optimal for potency.[76] In addition, N-debenzylation could be a potential contributor to the observed high clearance. In order to block oxidative cleavage of the C-N bond of N-benzyl moiety, the N-phenyl group was attempted. A series of N-phenyl pyridinone derivatives were prepared and evaluated for their activity, selectivity, *in vitro* stability, and pharmacokinetic profiles. The investigation led to the generation of 2 (Fig. 8), a potent and selective p38 kinase inhibitor that is stable in both the human and rat liver microsomal assays. Its ligand efficiency (LE) is comparable to SC-25028. JNK2 activities were measured as a tool to evaluate the potential for kinase selectivity. Consistent with the selectivity hypothesis, the compounds of the series remained inactive against JNK2.

Molecular modeling comparing the binding conformations using the overlaid models revealed that the N-benzyl and N-phenyl moieties superimposed closely in three-dimensional space (Fig. 9). Both aryl systems aligned in a parallel orientation to the peptide bond connecting residues Gly110 and Ala111. In such organization, the aryl rings are oriented in an orthogonal conformation with respect to the pyridinone to favor the ligand–protein interaction. Based on this observation, it was anticipated that rigidifying N-phenylpyridinone in its unbound state would reduce the entropic loss and yield a net gain in binding free energy. This was accomplished by installing orthosubstituents on both the phenyl and the pyridinone rings.[78] Further optimization produced the highly selective and potent clinical candidate **PH-797804**.

8.16.3.6 PH-797804 is the More Potent Atropisomer

Guided by the strategy of introducing orthogonality into the N-phenylpyridinone template, two methyl groups were installed onto the orthopositions. Due to steric constraints imposed by the pyridinone carbonyl and the 6,6′-methyl substituents, the rotation

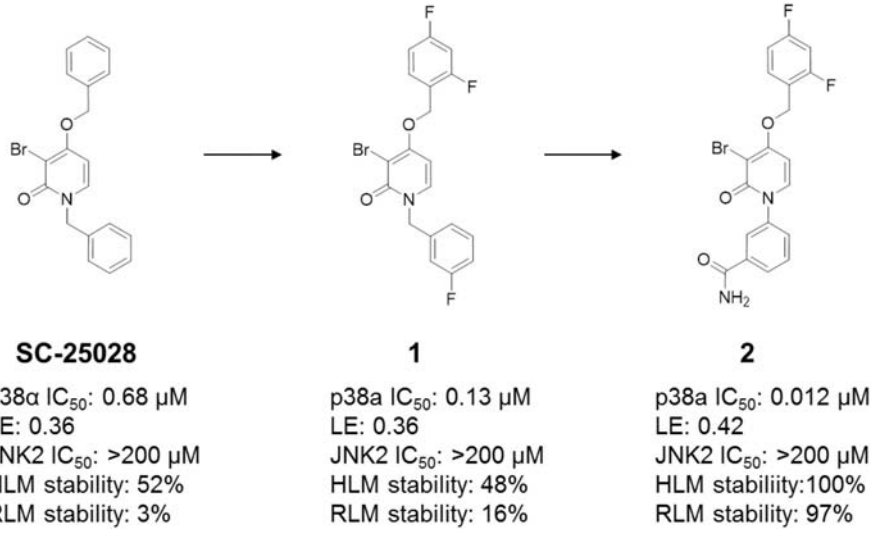

Fig. 8 Progression of lead optimization upon initial HTS hit.

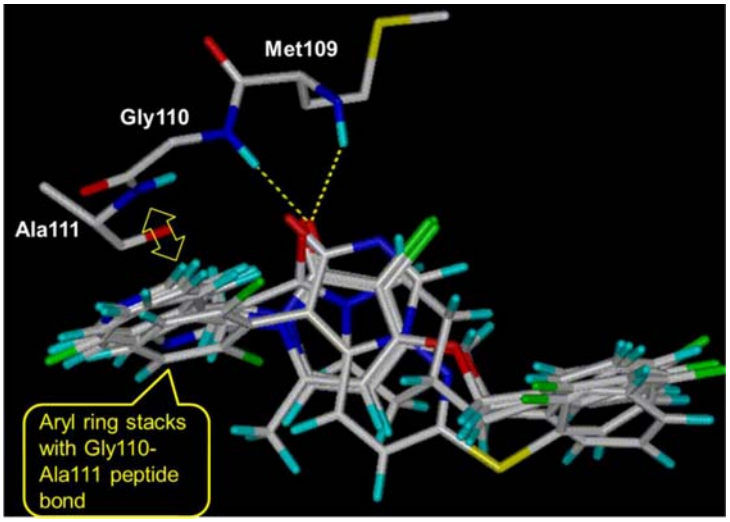

Fig. 9 An overlay model of p38 compounds showing consistent stacking interaction between the aryl ring of ligands of different chemotypes and the amide moiety of Gly110-Ala111.

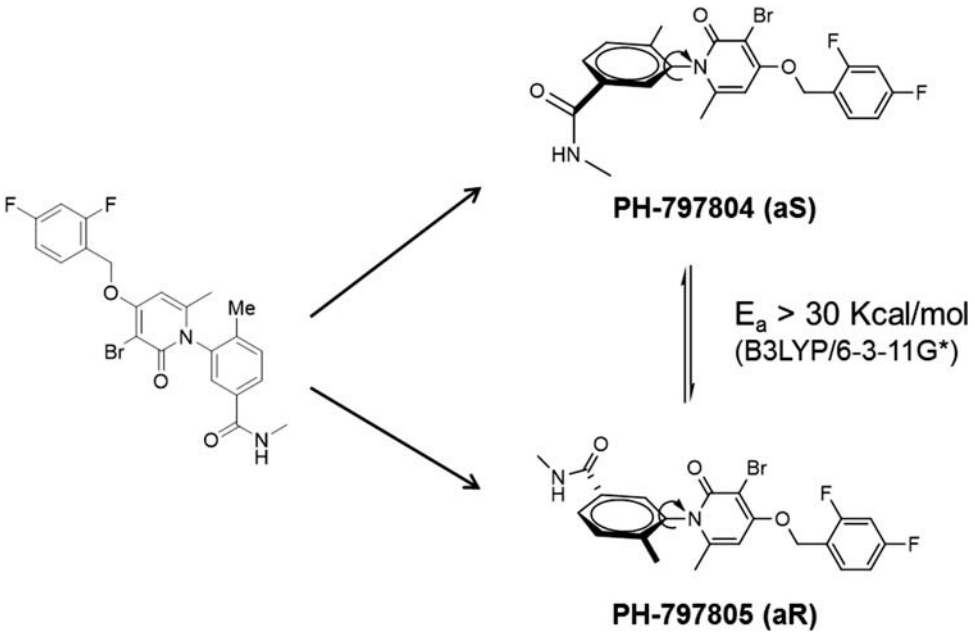

Fig. 10 **PH-797804** and **PH-797805** are the atropisomers of a racemic pair.

around the connecting bond of the pyridinone and the N-phenyl ring is restricted. This gives rise to discrete conformational spaces of N-phenyl pyridinone group, and as a result, two atropisomers do not interconvert under ambient conditions (Fig. 10). Molecular modeling predicted that the two isomers should differ in their binding affinity to p38α kinase. Whereas the atropic S isomer (aS) binds favorably, the opposite aR isomer incurs significant steric interferences with the p38α kinase.[79] Subsequently, chiral chromatography identified and separated the two isomers. Upon chiral separation and small-molecule x-ray diffraction experiment, it was confirmed that the more potent atropisomer (**PH-797804**) is the aS isomer of the racemic pair. The IC_{50} values from the p38α enzyme assay confirmed that **PH-797804** is 26 nM, whereas the off-isomer PH-797805 is more than 100-fold less potent (IC_{50}: 1800 nM). MAP kinase-modulated cytokine production (LPS-stimulated TNF-α and IL-1β) in whole blood was inhibited with comparable 26-fold differences in IC_{50} values by **PH-797804** (85 nM) and PH-797805 (4600 nM). Taking into account the inhibitor protein binding in the whole blood, the cellular potency of **PH-797804** correlates well with its inhibition of recombinant enzyme activity.[79] Extensive pharmacological characterization corroborates that **PH-797804** carries most activity *in vitro* and *in vivo* and possess high level of specificity across the broad human kinase genome.

8.16.4 Characterizations of PH-797804

8.16.4.1 *In Vitro* Activity

The average enzymatic competitive inhibition constant (K_i) of **PH-797804** for p38α kinase is 5.8 nM. Determined by ligand exchange reaction, the on-rate (K_{on}) and off-rate (K_{off}) values for **PH-797804** are 1.53x107 $M^{-1} \cdot s^{-1}$ and 0.058 s^{-1}, respectively, demonstrating reversibility along with rapid association and dissociation kinetics. The corresponding $t_{1/2}$ value for dissociation was 12.6 s.[101]

In monocytes, LPS-stimulated production of both TNF-α and IL-1β was inhibited by **PH-797804** in a concentration-dependent manner, with an IC_{50} value 3.4 nM for each cytokine. In human monocytic U937 cell line, LPS-stimulated TNF-α production was inhibited with an IC_{50} value of 5.9 nM. The p38 kinase activity was inhibited with an IC_{50} of 1.1 nM as measured by immune complex kinase assay of the downstream kinase MK-2. In contrast, no inhibitory effect was observed on either the JNK pathway (c-Jun phosphorylation) or ERK pathway (ERK phosphorylation) in U937 cells at concentrations up to 1 M.[75]

In addition to modulating inflammatory cytokine production, **PH-797804** also regulates COX-2 induction and PGE2 production. After treating with **PH-797804,** complete concentration-dependent inhibition of PGE2 production with RASF stimulation was observed (IC_{50}: 1.5 nM).[101]

8.16.4.2 Kinase Selectivity Screening

PH-797804 was extensively tested against several kinase screening panels for its off-target activities.[75] Over a hundred kinases have been screened, and **PH-797804** was found completely selective with no off-target signal.

The selectivity windows are greater than 500-fold compared with the primary target p38α kinase. In cellular assays, **PH-797804** demonstrated superior potency and selectivity consistent with biochemical measurements.[75] In addition, from our kinome mining, Myt-1 was identified as one of the three kinases that conserve the TXXXG motif. Myt-1 is a mixed serine/threonine and tyrosine kinase upstream of CDKs. Despite its low sequence identity to p38α, **PH-797804** was measured in an enzymatic assay developed at Pfizer. A marginal inhibition of 14% at 10 μM concentration confirmed the exceptional selectivity of **PH-797804**.

8.16.4.3 Crystal Structure of PH-797804 Bound in p38α Kinase

Fig. 11 illustrates binding interactions of **PH-797804** that are consistent with the other analogs of the pyridinone series.[75] The pyridinone carbonyl oxygen of **PH-797804** forms two hydrogen bonds, one with the amide nitrogen of Met109 and the other with the backbone NH group of Gly110. The 2,4-difluorophenyl group of **PH-797804** is encapsulated in a lipophilic pocket of p38α kinase, completely shielded from the solvent. The contour of the pocket appears to be thoroughly complementary to the halogenated phenyl ring of the inhibitor, from which a major portion of the binding free energy is derived as suggested by modeling studies. This hydrophobic pocket, unoccupied by ATP, appears to be the anchor point for the positioning and orientation of p38α kinase inhibitors of diverse chemical scaffolds. The gatekeeper residue Thr106, sitting at the entrance, thus controlling the access to the pocket, therefore is of essential importance to the binding affinity of p38α inhibitors.

In **PH-797804**, the 6,6′-methyl substituents and the pyridinone carbonyl together render the N-phenyl ring orthogonal to the pyridinone core. The density functional theory (DFT) calculation yielded a torsion angle of 76.2 upon full optimization (B3LYP/3-21G*), which suggests that in the minimum-energy state, the 6′-methyl derived from the N-phenyl ring is tilted slightly toward the pyridinone carbonyl. Upon binding to p38α kinase, **PH-797804** demonstrates a dihedral angle of 103.2, with the 6′-methyl tilting toward the 6-methyl off the pyridinone. The orthogonality of the N-phenyl pyridinone appears to be instrumental

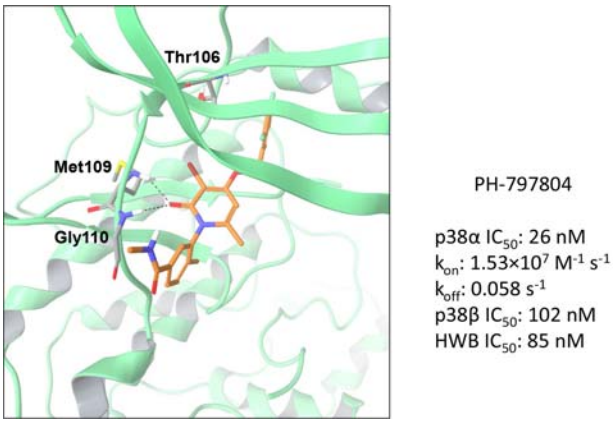

Fig. 11 Crystal structure of **PH-797804** bound in p38α kinase (PDB code: 3HLL).

to the inhibitory activity against p38α kinase, which strengthened the hydrogen bond acceptor of pyridinone oxygen and the stacking interaction with the p38α kinase hinge.

8.16.4.4 Rotational Barrier, Chemical Stability, and Pharmaceutical Properties

The interconversion rate of the atropisomers is an important consideration for the pharmaceutical development of a single enantiomer as a clinical candidate. Quantum mechanics theory was applied early on to determine the rotational energy barrier between the atropisomers. In the torsional scan experiments, the rotation around the bond connecting the pyridinone group and the N-phenyl ring was driven in both forward and backward directions to reveal possible hysteresis. The complete torsional profile was obtained by B3LYP/LACV3P level of theory, exhibiting two lowest energy conformers corresponding to **PH-797804** and PH-797805 (Fig. 12). Strain energies increase as the bond torsion deviates from the lowest energy states. The activation energy of isomeric interconversion is predicted to be greater than 31 kcal/mol, predicting a half-life of more than 100 years at ambient conditions for **PH-797804**.

At elevated temperatures, the relative amounts of each isomer were measured by HPLC in aqueous media and various solvents including dimethylfuran and toluene. Very little interconversion, typically $<1\%$, was observed over a period of two to four days. The highest interconversion was detected at 110 °C in toluene: $\sim 6\%$ after two days. Additional stability measurements were conducted in aqueous media for comparison of temperature effects. Two samples were taken from the single fraction collection in the preparation of PH-797805, characterized with a purity of $>99\%$. One sample was heated at 79 °C with a 90 °C bath. After 55 hours, it showed 97.1% enantiomeric excess, corresponding to $<1\%$ conversion into **PH-797804**. The other sample was maintained at 37 °C, and no change was detected after the same period of time. It is therefore concluded that racemization does not occur under the conditions tested.

The separate atropisomers are stable at ambient conditions during storage. The compounds were stored either in the solid state or as solutions in ethanol or acetonitrile. No loss in optical purity was observed at room temperature for at least three weeks. Furthermore, in preclinical pharmacokinetic studies and in *in vivo* efficacy models using various animal species, no isomeric conversion of **PH-797804** has been observed.

Consistent with the theoretical prediction, extensive pharmaceutical characterization has established the chemical stability of the conformationally restricted p38α inhibitor **PH-797804**. As a result, a chiral process was developed to support the preclinical and clinical development of **PH-797804**.

8.16.4.5 Pharmacokinetic Properties of PH-797804

The solubility of **PH-797804** was measured at <5 μg/ml in pH 7.0 phosphate buffer at room temperature. The intrinsic solubility remained the same given that no ionization in the physiological pH range was detected. The permeability of **PH-797804** was measured in Caco-2 studies from the apical to basolateral phase, ranging from 10×10^{-6} cm/s at 1 μM to 25×10^{-6} cm/s at 100 μM. **PH-797804** was determined to be a weak substrate of P-gp at projected clinical doses (efflux ratios <2.5).

Nonclinical pharmacokinetic studies of **PH-797804** were conducted in male Sprague–Dawley rat, male beagle dog, and male cynomolgus monkey, and all studies were conducted using crystalline compound. Based on these studies, **PH-797804**

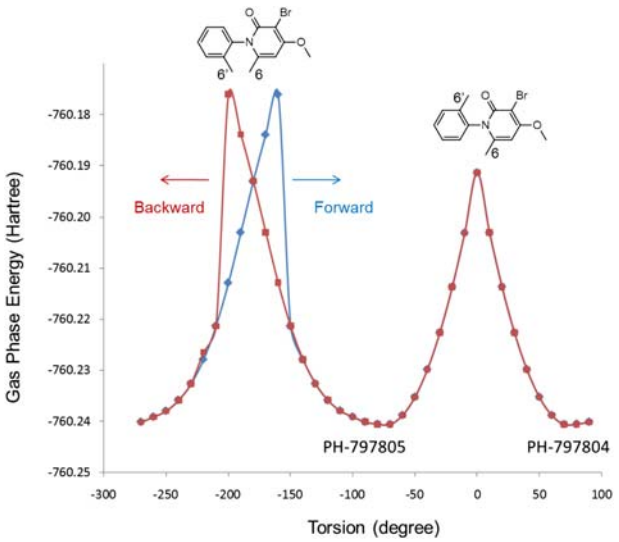

Fig. 12 Rotational profile of the model system by DFT B3LYP/LACV3P theory. Separate drives in forward and backward directions revealed hysteresis in transition along the 6,6'-Me phase.

has low plasma clearance and low to moderate volume of distribution resulting in half-lives of 2.60–3.86 h in rat and 11.4 and 3.93 h in dog and monkey, respectively. Moderate oral bioavailability was observed in monkey (23.2%) and rat (35.7–40.5%) when **PH-797804** was dosed orally as a milled suspension. Bioavailability in monkey increased to 36.2% after an oral solution dose, and the bioavailability of an oral solution dose in dog was 59.6%. Bioavailability in rat increased to 80.4% and >100% when **PH-797804** was dosed at 15 and 2 mg/kg, respectively, as oral solutions, which was consistent with dissolution limited absorption.

8.16.4.6 *In Vivo* Efficacy of PH-797804

The dose–response analysis demonstrated disparate efficacies for the two atropisomers in the acute *in vivo* model. LPS-induced TNF-α production in rats allowed evaluation of oral efficacy for inhibition of an acute inflammatory response.[101] Treatment of rats with **PH-797804** resulted in dose-dependent inhibition of LPS-induced TNF-α production, yielding an ED_{80} value of 0.3 mg/kg. In comparison, the ED_{80} for PH-797805 is greater than 10 mg/kg. **PH-797804** and PH-797805 have essentially the same pharmacokinetic properties (95% remaining in the rat metabolic stability assay); hence, the difference observed *in vivo* can be primarily attributed to translation from their *in vitro* activities.

The ability to suppress chronic inflammation was evaluated in an inflammatory arthritis model in rats induced by streptococcal cell wall (SCW) extract. The SCW model is characterized by an acute phase of inflammation from day 1 to day 5, followed by a more severe and chronic phase of bone destruction that occurs from day 10 to day 21. A role for TNF-α and IL-1β in the chronic phase has been demonstrated with neutralizing TNF-α and IL-1 antibodies. **PH-797804** was highly effective in attenuating SCW-induced inflammation. Untreated control rats exhibited profound joint inflammation from day 10 to day 21. **PH-797804** treatment resulted in dose-dependent inhibition of paw swelling when administered daily with an $ED_{50}$of 0.186 mg/kg. In comparison, PH-797805 required a daily dose of about 40 mg/kg to produce the half maximal efficacy. The potency and efficacy demonstrated by **PH-797804** provided sufficient rationale to advance it as a viable human drug candidate.

8.16.5 Designing Inhaled Inhibitors of p38α

In contrast to the requirements for successful oral drugs, highlighted in the discovery of **PH-797804**, delivery by inhalation requires a compound to demonstrate features that should deliver high local efficacy, allied to high systemic clearance and low oral bioavailability.[102–104]

These include (i) high potency to drive a low inhaled total dose, as current delivery options limit practical delivery of doses to approximately 1 mg of active pharmaceutical ingredient, (ii) low oral absorption and high clearance of any swallowed component to minimize systemic exposure, (iii) multiple routes of clearance to mitigate the risk of significantly increased exposure due to drug–drug interactions (DDIs), and (iv) physical characteristics suitable for a dry powder formulation, which includes crystallinity, melting point greater than 125 °C to allow for successful milling, and compatibility with lactose as the most commonly used inhaled excipient.

In addition to minimizing systemic exposure, features that facilitate an extended pharmacodynamic duration of action (DoA) in the lung, such as slow pharmacological dissociation (k_{off}) from the target, may be beneficial to drive local efficacy for inhaled drugs (Fig. 13).

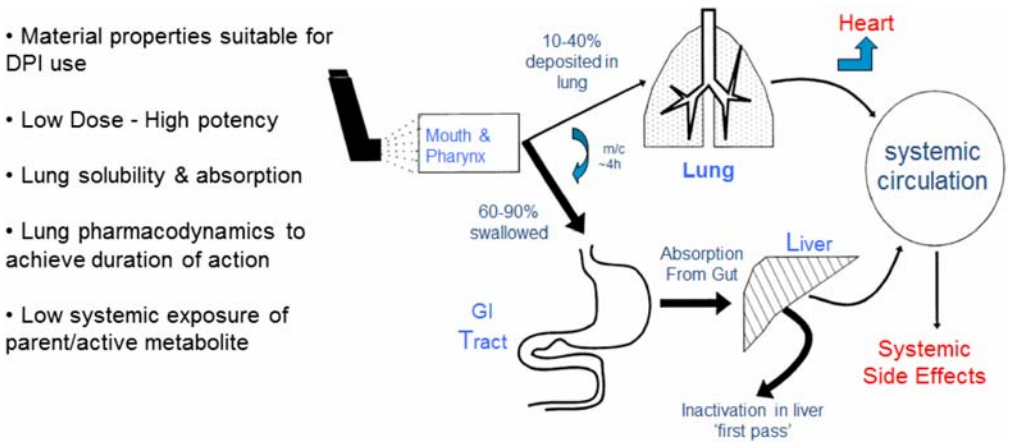

Fig. 13 Features associated with 'inhalation by design'.

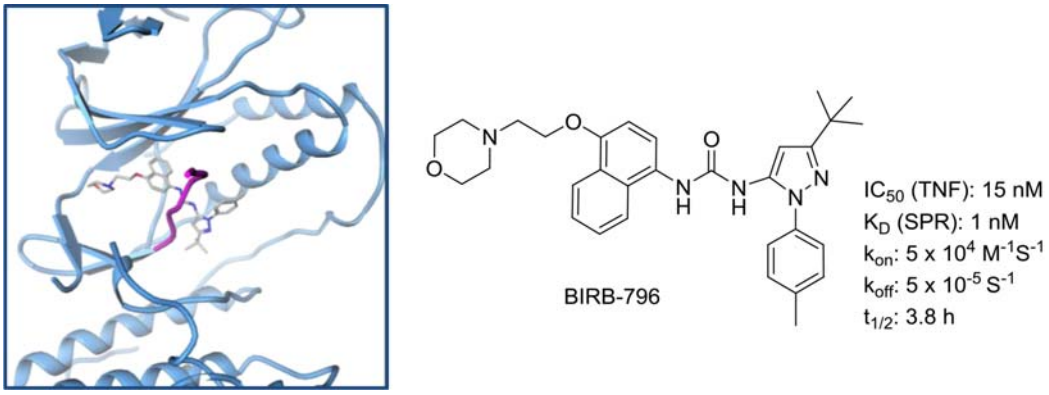

Fig. 14 BIRB-796 bound to p38α and kinetic binding parameters determined by SPR.

8.16.5.1 DFG-Out Conformation of p38

The reports of the oral p38 inhibitor **BIRB-796**[105] and, most importantly, its (then) novel mode of binding to p38 in a DFG-out conformation (Fig. 14), resulting in a slow onset/slow offset binding profile, suggested that leveraging this feature could deliver novel p38α inhibitors with excellent properties for inhalation through structure-based drug design.

The slow k_{on} and slow k_{off} rates observed with **BIRB-796** could be rationalized on the basis of the x-ray crystallography structure. For **BIRB-796** to bind to p38α, the activation loop (highlighted) containing the residues Asp168 (**D**)-Phe169 (**F**)-Gly170 (**G**) must undergo a movement of ~10 Å. The kinetics of this loop movement, allied to the affinity for the binding site thus created, dictate the rates of association and dissociation between the enzyme and inhibitor in this DFG-out binding mode.

Once the DFG-out conformation is obtained, a large lipophilic pocket is created, which can accommodate the arylpyrazole moiety of **BIRB-796**, driving a high affinity lipophilic interaction. The slow k_{off} then requires the DFG loop to move again and dissociation of the high affinity ligand.

8.16.5.2 Design to Target the DFG-Out Conformation of p38

Targeting the DFG-out conformation, therefore, appeared to be a very attractive strategy for the design of potent, lipophilic, long-acting p38α inhibitors for inhalation.[104]

Intriguingly, analogs containing an ATP-binding moiety allied to a urea substituent, exemplified by compound **CE-159167** (Fig. 15), had been identified from one of our oral p38α inhibitor programs and have been cocrystallized in p38α in the DFG-in conformation. In keeping with this binding mode, these compounds had been shown to display fast k_{on} and k_{off} rates, as determined by surface plasmon resonance (SPR).[104]

The overlay of a DFG-in structure of **CE-159167** with the DFG-out structure of **BIRB-796** in p38α (Fig. 15) highlighted several intriguing features including the following: (i) The urea groups of **CE-159167** and BIRB-796 are aligned perfectly, (ii) the N-2 and N-3 of the triazolopyridine group in **CE-159167** stabilize the unusual Gly110 flip in the hinge region of the ATP hinge site, and (iii)

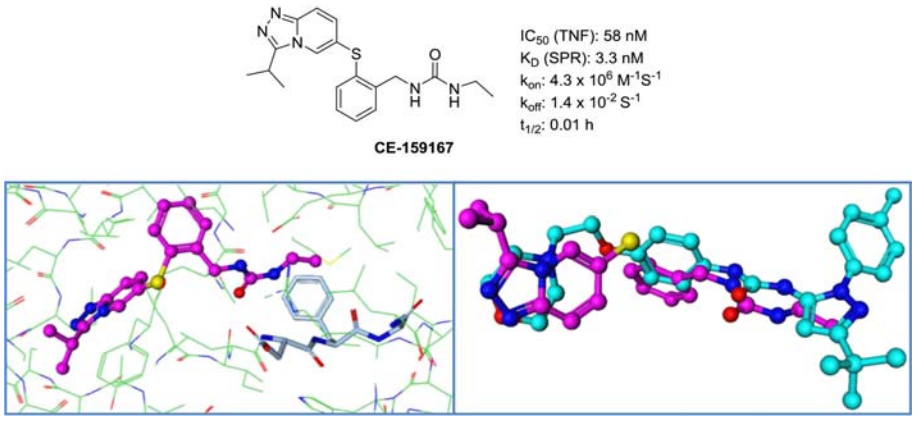

Fig. 15 Hybridization potential of a Pfizer DFG-in lead **CE-159167** (magenta) with BIRB-796 (cyan) in its DFG-out conformation.

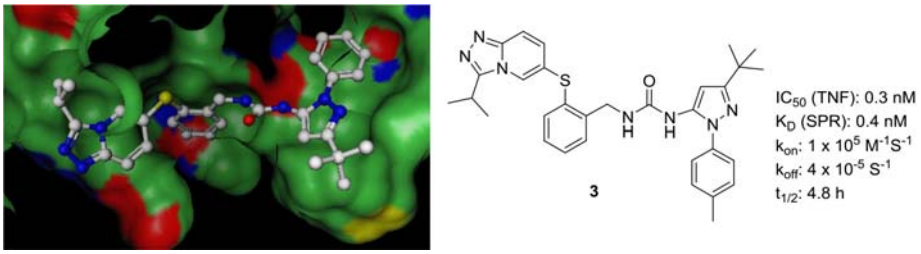

Fig. 16 Structure, binding kinetics, and crystal structure of lead 3 in p38α kinase.

the phenyl ring of **CE-159167** interacts with the gatekeeper residue (Thr106) and overlays with the naphthalene ring system of **BIRB-796**.

This overlay suggested that a hybrid between compounds **CE-159167** and **BIRB-796** could deliver a novel DFG-out binding inhibitor of p38α that would simultaneously engage the hinge, gatekeeper, and DFG-out pockets, displaying a similar slow k_{on}/slow k_{off} enzyme binding profile to that of BIRB-796. The hybrid compound **3** (Fig. 16) did, indeed, prove to be a very potent p38α inhibitor with slow k_{on}/k_{off} binding kinetics akin to those of BIRB-796.[104]

To obviate any issues from the slow k_{on} and k_{off} rates in our primary screening data, we used a cell-based assay, with a preincubation period, to profile target compounds for their ability to inhibit TNF-α production from LPS-stimulated human isolated peripheral blood mononuclear cells (PBMCs).

8.16.5.3 Lead Optimization of DFG-out Binders

With a promising lead (**3**) in hand, we sought to optimize the pharmacokinetic and pharmaceutical properties for inhalation while maintaining the high levels of potency and selectivity achieved.

Targeting high hepatic clearance, by multiple clearance pathways, was important for minimizing systemic exposure following absorption through the lung and absorption from the gut for any swallowed component of the dose. Ensuring that any metabolites produced lacked significant activity versus p38α was also a major design consideration.

While oxidative phase I metabolism was a clear design focus, we also sought to mitigate any potential for increased systemic exposures driven by CyP450-mediated drug–drug interaction (DDI) potential, by introducing handles for phase II, conjugation-based metabolism. Glucuronidation is a well-characterized phase II metabolic pathway that has high capacity and provides rapid drug inactivation via the polar glucuronide metabolites produced.[106]

The cocrystal structure of compound **3** in p38α (Fig. 17) highlighted several opportunities to incorporate suitable functionality to facilitate both phase I and phase II metabolism in order to achieve our desired clearance profile.

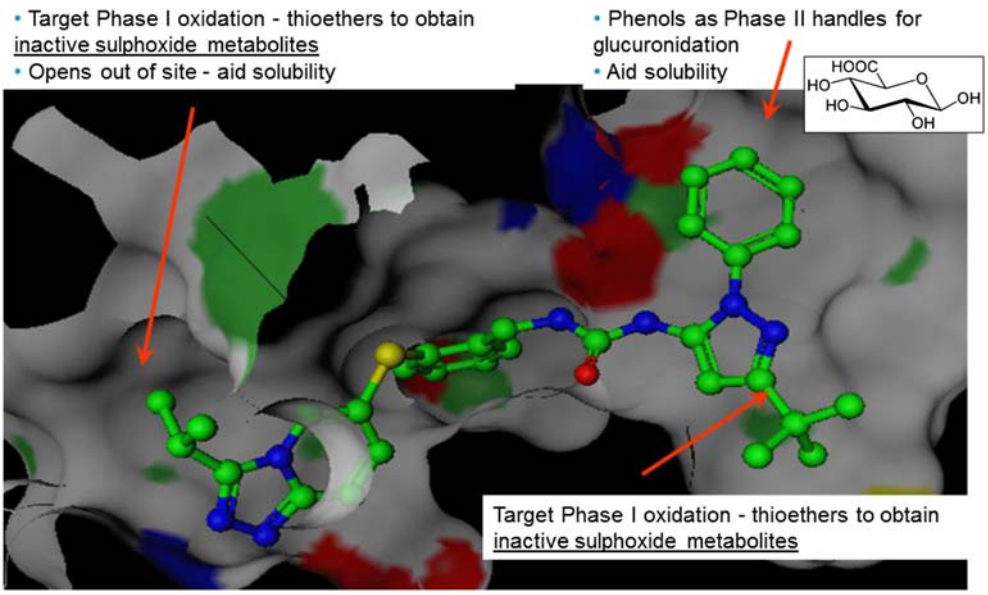

Fig. 17 Specific targeting of sites for metabolic soft spot design.

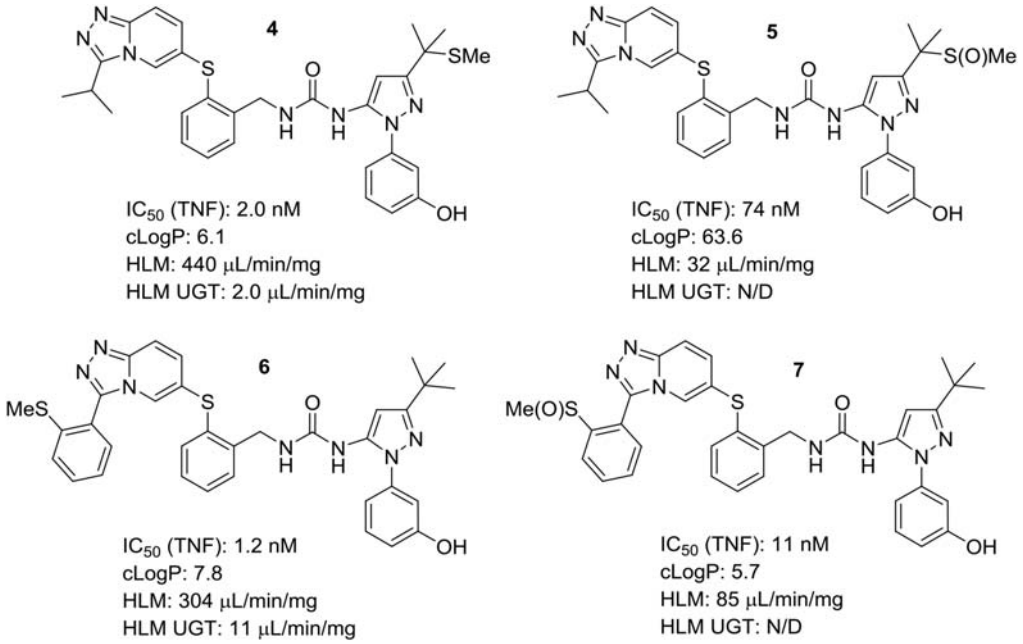

Fig. 18 Thioether-derived inhibitors of p38α targeting phase I metabolism.

8.16.5.4 Design Phase I Metabolism

Both the tert-butyl pyrazole and triazolopyridine isopropyl substituents in **3** occupy very lipophilic portions of the binding pocket. Introduction of a substituent vulnerable to phase I oxidative metabolism within these regions should direct metabolism toward the production of a more polar metabolite at these sites, with significantly reduced affinity for p38α.

The central thioether linkage already present in **3** could have also served this purpose effectively, as the likely polar sulfoxide and sulfone derivatives in the position were completely inactive versus p38α. The highly hindered nature of the linkage, however, completely obviated metabolism at this position in any of our *in vitro* hepatic systems.

As depicted in Fig. 18, introduction of a thiomethyl group into the tert-butyl pyrazole motif led to compound **4**, which demonstrated good potency and further increases in phase I metabolic liability. Moreover, the sulfoxide primary metabolite (**5**) displayed a significant (>30-fold) reduction in activity versus p38α.

Similarly, introducing a thiomethyl group into the triazolopyridine isopropyl substituent led to compound **6**. Again, compound **6** demonstrated good potency and high levels of phase I metabolic liability. The sulfoxide primary metabolite (**7**) also displayed > 10-fold reduction in activity versus p38α.

8.16.5.5 Design Phase II Metabolism

Weakly acidic phenols are well documented to undergo rapid glucuronidation.[106] The N-phenyl ring of the arylpyrazole moiety in **3** binds into an open and hydrated area of the DGF pocket and, therefore, seemed a suitable place to introduce phenolic substituents, with confidence that binding potency could be maintained.

Indeed, the introduction of phenol substituents in both the para- and metapositions of the N-aryl group, in **8** and **9**, respectively, retained potency, relative to **3**, and high levels of phase I metabolism were demonstrated in HLM systems by both compounds (Fig. 19).

When we assessed the phase II glucuronidation profile of both **8** and **9**, however, in HLM (by including the cofactor UDPGA and excluding the cytochrome P450-dependent cofactor NADPH), we did not observe appreciable levels of turnover, suggesting that both compounds were only substrates for phase I metabolic pathways. The acidity of the phenol groups was increased by approximately two units by flanking with an orthochlorine atom, leading to compounds **10** and **11** with pK_a values of 7.6 and 7.5, respectively. In both cases, potency versus p38α was enhanced slightly, relative to the analogous phenols. Moreover, high levels of metabolism were demonstrated both in *in vitro* HLM and HLM-UGT systems, indicating good potential for high clearance by phase I and phase II pathways from these orthochlorophenol derivatives.

In addition to exploring the structure-based incorporation of metabolic handles, we also used the cocrystal structure of **3** as the basis to explore whether we could incorporate flexible groups at the triazolopyridine isopropyl substituent in order to break up crystalline packing and improve solubility. Toward this end, compounds like **12** were prepared and demonstrated equivalent

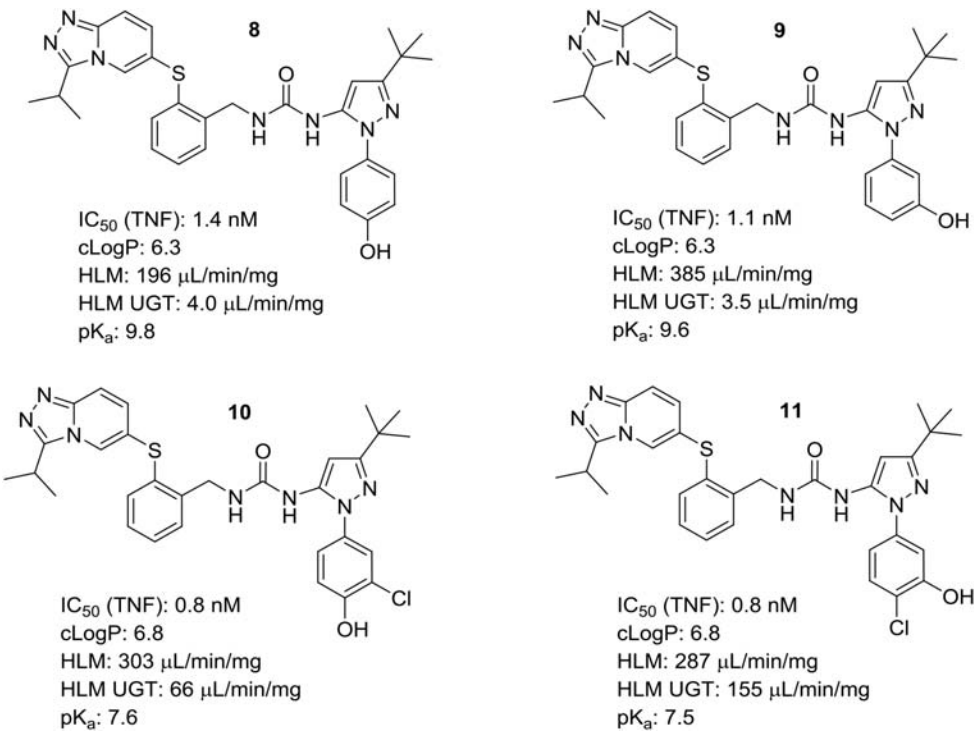

Fig. 19 Phenol-derived inhibitors of p38α targeting phase I metabolism.

potency and metabolic profiles while also increasing solubility in simulated lung fluid (SLF), relative to direct analog compound **6**, into the range of 1.0 μg/mL (which was comparable to that of our benchmark, the inhaled corticosteroid fluticasone).

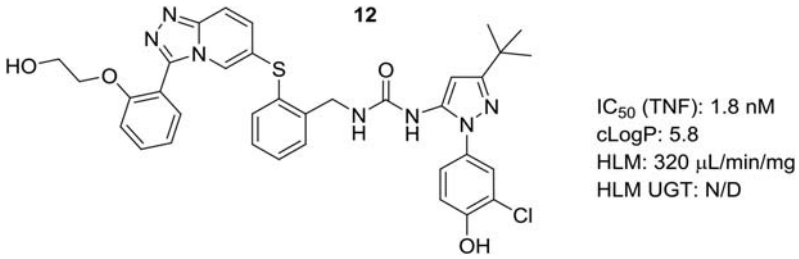

8.16.5.6 Identification of PF-3715455

Combining these features for potency, phase I and II metabolism and the enhanced SLF solubility increased solubility led to the discovery of our inhaled p38 inhibitor clinical agent **PF-3715455 (13)** (Fig. 20). Protein cocrystallization confirmed that compound **13** bound in the DFG-out mode in p38α as expected (Fig. 21).

Compound **13** is a very potent and selective inhibitor for the p38α enzyme, which translates into potent inhibition of proinflammatory cytokine release in whole cells relevant to COPD. Activity of **13** in the PBMC TNF assay (preincubation time of 1 h) was 1.7 nM, with the primary phase I sulfoxide metabolite (**14**) losing approximate 50-fold potency (no attempt was made to separate/identify sulfoxide stereochemistry in **14**).

The binding kinetics of **13** were determined versus the inactive/nonphosphorylated form of human p38α using SPR. The k_{on} and k_{off} kinetic parameters were observed, which suggested a K_D of approximately 1 pM and a half-life of approximately 80 h for binding to the inactive form of p38α. The mismatch between K_D generated for **13** from SPR binding kinetics and the biochemical IC_{50} from our PBMC assays likely reflects the fact that the cellular assay has not achieved equilibrium at the maximum 1 h time point that we used. These data suggest that **13** should provide optimal binding kinetics to overcome competition with high cellular levels of ATP and drive an extended cellular pharmacodynamics response following delivery to the lung.

Broad kinome profiling confirmed that **13** displays high selectivity, with IC_{50} at enzyme K_m for ATP of <1 μM for only 15 enzymes of the 205 recombinant kinases screened.[104]

Whole cell assays demonstrated that no whole cell activity was observed for three of these kinases, leaving p38β (SPR K_D: 23nM). This level of selectivity over p38β was not seen as a concern regarding potential for efficacy or to represent a safety liability.

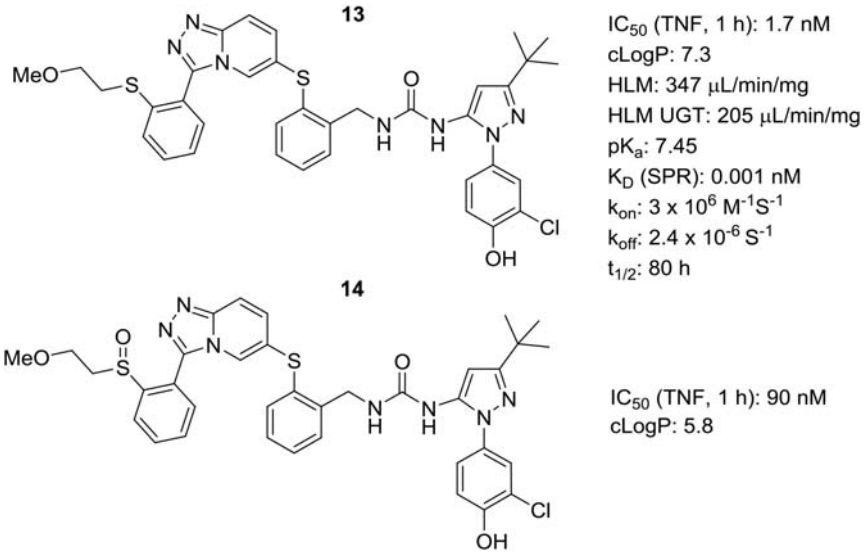

Fig. 20 **PF-3715455** (**13**) and its primary oxidative metabolite (**14**).

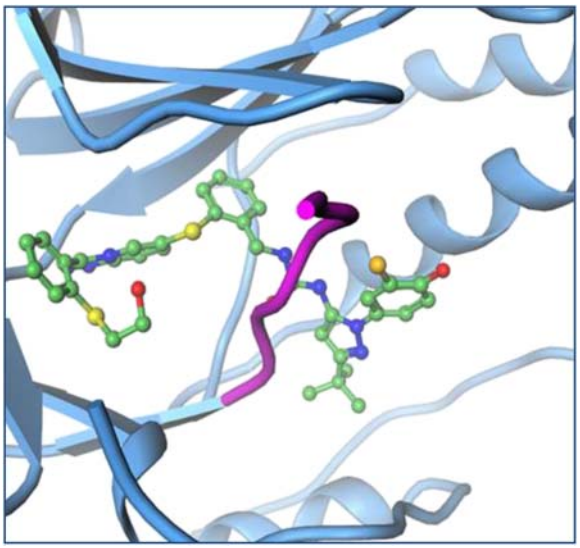

Fig. 21 Crystal structure of **PF-3715455** bound to p38α kinase.

In spite of their high molecular weight and very lipophilic nature, the crystallinity of compounds in this series had been confirmed by PXRD on a regular basis throughout optimization, and the pharmaceutical properties for **13** (clogP = 7.3, log D > 4.1) including crystallinity and stability on lactose were all assessed and considered suitable for dry powder inhalation.

Notably, solubility in simulated lung fluid (3.0 μg/mL) had been enhanced from previous members of the series through the inclusion of (i) the weakly acidic orthochloro phenol group and (ii) the flexible methoxy thioether substituent.

Key elements from the *in vitro* and *in vivo* pharmacokinetic analysis for **13** included (i) metabolite profiling from human hepatocytes to suggest that the glucuronide resulting from transfer to the chlorophenol is the major metabolite; (ii) coadministration of 2 μM ketoconazole (CYP3A4 inhibitor) in human hepatocytes, which did not lead to any significant reduction in intrinsic clearance, over the control incubations, suggesting that 13 should not be a victim of a DDI; and (iii) extremely high unbound clearance values of 33 and 15 mL/min/kg, following IV administration in rat and dog, respectively.

These data support our projections of low oral bioavailability in humans following any swallowed dose, coupled with very high intrinsic clearance for compound **13**. As such, any drug that reaches the systemic compartment would be expected to be cleared rapidly through conversion to inactive metabolites by both oxidative (phase I) and conjugation (phase II) pathways.

Finally, the preclinical safety profile of compound **13** suggests it would be tolerated in humans at clinically relevant inhaled doses.[104]

8.16.6 Highlights of Clinical Data for PH-797804 and PF-3715455

Historically, orally administered p38 MAPK inhibitors have been poorly tolerated in the clinic, eliciting side effects such as liver toxicity.[47] This is thought to be due, at least in part, to off-target polypharmacology driven by inhibitory effects on other closely related kinases.

The advent of highly selective oral p38α MAPK inhibitors, such as **PH-797804** and losmapimod, along with selective inhaled agents such as **PF-3715455**, which do not access the systemic compartment, is providing greater insight on the toleration and efficacy of p38 inhibitors in the clinic.

Lipopolysaccharide (LPS) inhalation in healthy subjects causes p38 activation in bronchial epithelial cells,[107] leading to the release of chemokines such as CXCL8 that promote neutrophil chemotaxis[108] and an influx of inflammatory cells into the airways of healthy subjects. The subsequent increase in the proportion of neutrophils observed in induced sputum should, therefore, be attenuated by drugs that inhibit p38 activation.

In three recent clinical trials, single doses of **PH-797804** (oral) and **PF-3715455** (inhalation) were administered to healthy subjects to explore the effect on neutrophilic lung inflammation in response to an inhaled LPS challenge. These studies aimed to provide mechanistic insights into the effectiveness of oral and inhaled p38 inhibitors in a human model of neutrophilic lung inflammation that is poorly responsive to current COPD medications such as corticosteroids. The effects of a single dose of an ICS (fluticasone propionate) in this model were also explored.[109]

Each study was a randomized, double-blind, placebo-controlled, single-dose crossover design. Study 1 used a 30 mg oral dose of **PH-797804**. Study 2 used a 30 mg oral dose of **PH-797804** with a 20 mg inhaled dose of **PF-3715455**. Study 3 used a 500 μg inhaled dose of fluticasone propionate. In each study, a baseline sputum sample was obtained within 14 days of the first dosing period when subjects were administered a single dose of randomized treatment. LPS challenge was administered 24 h after dosing with **PH-797804**/placebo in study 1. In study 2, inhaled LPS was administered either 24 h after dosing with **PH-797804** or 30 min after **PF-3715455**. In study 3, inhaled LPS was administered 30 min after dosing with fluticasone/placebo.

In studies 1 and 2, sputum supernatants were analyzed for interleukin 6 (IL-6), myeloperoxidase (MPO), monocyte chemotactic protein-1 (MCP-1), and macrophage inflammatory protein-1β (MIP-1 β). In study 3, sputum supernatants were analyzed for IL-6, MCP-1, and MIP-1β.

There was a statistically significant inhibition of the sputum neutrophil percentage post-LPS challenge caused by **PH-797804** compared to placebo in studies 1 and 2 ($p = 0.0096$ and 0.0001, respectively), with 15.1 and 15.3% reduction in mean sputum neutrophil percentage representing approximately 50% attenuation of the modeled LPS response. Study 2 also showed significant inhibition of sputum neutrophil percentage post-LPS challenge after administration of **PF-3715455** of 8.0%, which was approximately 25% attenuation of the modeled LPS response ($p = 0.031$). Sputum neutrophil percentage post-LPS challenge was not changed significantly by fluticasone propionate ($p = 0.55$).

Sputum supernatant cytokine levels were generally increased by LPS challenge in the placebo treatment period in all three studies. In study 1, **PH-797804** did not significantly inhibit cytokine levels compared with placebo, but there was evidence of trends toward significance for MCP-1 and MPO. In study 2, **PH-797804** significantly reduced IL-6, MPO, MCP-1, and MIP-1β levels compared with placebo. **PF-3715455** and fluticasone propionate had no effects on sputum cytokine measurements.

Efficacy has been achieved by **PH-797804** in moderate-to-severe COPD patients in proof-of-concept studies. The first phase II study of **PH-797804** demonstrated a clinically significant improvement in pulmonary function and dyspnea in 230 moderate-to-severe COPD patients.[110] In the double-blinded, parallel-group, multicenter trial, patients were randomized to orally receive placebo, 0.5, 3, 6, or 10 mg **PH-797804** once daily and treated for 6 weeks following a 2-week run-in. Compared with placebo, **PH-797804** showed statistically significant improvement in trough forced expiratory volume in 1 second (FEV_1) at 3 and 6 mg dosing regimens at week 6. **PH-797804** 3 mg and 6 mg also demonstrated improvement in the baseline dyspnea index/transition dyspnea index total focal score. An extended study evaluated **PH-797804** on top of salmeterol/fluticasone background.[111] Patients on stable does of ICS/LABA combination were randomized to receive either 6 mg of oral **PH-797804** or placebo once daily for 12 weeks. At 12 week, **PH-797804** demonstrated statistically significant improvement in trough FEV1 and the transitional dyspnea index. The hs-CRP level was consistently reduced throughout the dosing period.

In subjects with rheumatoid arthritis who are also taking methotrexate at stable dosage of 12.5-25 mg, **PH-797804** was evaluated for its safety, pharmacokinetic profile, and efficacy. The randomized, placebo-controlled study used 1 mg and 5 mg **PH-797804** orally administered once daily for 4 weeks.[112] Efficacy was demonstrated initially but was not sustained after two weeks. The decline of C-reactive protein (CRP) levels was also transient during the initial weeks of oral administration.

The difference in sustained efficacy that appears to be observed between the RA and COPD indications may reflect the different nature of the inflammatory response in the two diseases and continues to suggest that oral p38 inhibitors may yet deliver a medicine to treat COPD.

A number of competitive p38 kinase inhibitors have been reported to show anti-inflammatory efficacy in phase IIa studies of rheumatoid arthritis over the years, but their development has been terminated by the dose-limiting side effects of liver enzyme elevation and/or skin rash. **PH-797804** and **PF-3715455** are differentiated from the other p38 MAPK inhibitors by being generally safe and well tolerated in healthy volunteers, supported by their high level of potency, selectivity, biochemical efficiency, and/or extended lung retention. More importantly, in patients **PH-797804** was safe with a relatively low incidence of liver enzyme elevations (< 0.5%) and skin rash (< 10%). These observations are on the basis of five phase I studies and three proof-of-concept studies in rheumatoid arthritis, post-herpetic neuralgia, and/or COPD.

8.16.7 Conclusions

For the treatment of chronic diseases, small-molecule kinase inhibitors have to be highly specific in order to avoid unwanted effects caused by off-target inhibition. This is a high hurdle considering that the human kinome contains over 500 protein kinases sharing varying degrees of sequence homology. Structural insights into the unique p38 binding mechanism have guided discovery of several highly selective inhibitors. They advantageously engage the selectivity prerequisite encoded by the TXXXG sequence motif of p38α kinase. For **PH-797804**, its superior kinome selectivity is predicted by structural bioinformatics analysis and corroborated by large panels of screening assays.

The oral agent **PH-797804** was designed to be potent and selective for p38α, with an emphasis on (i) excellent selectivity, (ii) good pharmacokinetic parameters, and (iii) very low peak-to-trough exposure ratios, in order to deliver efficacy with a minimum potential for mechanism-driven side effects. The inhaled agent **PF-3715455** was designed to be potent and selective for p38α, with an emphasis on (i) slow enzyme association/dissociation kinetics to deliver prolonged lung inhibition of p38α allied to (ii) pharmacokinetic properties tuned to deliver very low oral bioavailability and (iii) pharmaceutical properties such as solid-form stability and crystallinity to ensure compatibility with a dry powder formulation for inhalation.

Both **PH-797804** and **PF-3715455** reduced neutrophilic airway inflammation after LPS challenge in healthy subjects. In contrast, inhaled fluticasone propionate at a dose of 500 μg had no effect. While inhaled delivery is often favored for respiratory drugs, as it increases lung compared with systemic exposure with the aim of increasing therapeutic pulmonary effects relative to systemic side effects, it appears that the increased systemic exposure of orally administered **PH-797804** provided superior pulmonary anti-inflammatory effects in these studies.[109]

Several compounds of different scaffolds blocking the p38 MAPK pathway have entered phase II clinical trials for RA patients.[46,59] They failed to demonstrate significant efficacy, showing early suppression of C-reactive protein (CRP) that was not sustained and often reversed by 2–4 weeks into the study. This suggests that other inflammatory pathways may have been upregulated in response to p38 blockade in RA.

The modest clinical efficacy and the transient suppression of biomarkers of inflammation observed in multiple studies suggest that p38 MAPK inhibition may not provide meaningful, sustained suppression of the chronic inflammation seen in RA. Inflammation acts along complex and overlapping pathways. Although p38α was originally proposed to carry predominantly proinflammatory functions, increasing evidence suggested that it also has crucial roles in tuning down inflammatory responses in specific cell types. It remains unknown whether compensatory upregulation of redundant or parallel pathways or autoactivation of the p38 signaling system may attenuate potential benefit of the investigational anti-inflammatory therapeutics.[113] Most of the clinical p38 programs have been terminated due to the lack of prolonged efficacy during the trial period of several months. They showed early suppression of C-reactive protein (CRP) that was not sustained and often reversed by 2–4 weeks into the study, hence failing to demonstrate statistically significant efficacy. The results suggest that other inflammatory pathways may have been upregulated in response to prolonged p38 blockade. The modest clinical efficacy and the transient suppression of biomarkers of inflammation observed in multiple studies suggest that p38 MAPK inhibition may not provide meaningful, sustained suppression of the chronic inflammation. It remains debatable whether it is preferable to combine inhibition of p38 with other targets in parallel inflammatory signaling pathways to achieve the desired efficacy in chronic inflammatory diseases. A mechanistic understanding of the clinical phenomenon would help direct efforts toward next generation of potentially promising therapies.

Acknowledgment

We acknowledge the work of colleagues on the p38 program teams over many years on the discovery and development of Pfizer p38 inhibitor clinical candidates. Compound **PH-797804** is commercially available via Sigma-Aldrich (catalog no. PZ0259).

See also: 5.13. Small Molecule Immunosuppressants in Inflammatory Disease. 8.17. Are Two Better than One in Rheumatoid Arthritis? Development of Dual p38α MAPK/PDE-4 Inhibitors for Treatment of TNFα-Driven Diseases.

References

1. Cotsapas, C.; Hafler, D. A. Immune-Mediated Disease Genetics: The Shared Basis of Pathogenesis. *Trends Immunol.* **2013,** *34,* 22–26.
2. Bresnihan, B. Pathogenesis of Joint Damage in Rheumatoid Arthritis. *J. Rheumatol.* **1999,** *26,* 717–719.
3. Rose, N. R.; Bona, C. Defining Criteria for Autoimmune Diseases (Witebsky's Postulates Revisited). *Immunol. Today* **1993,** *14,* 426–430.
4. Lacaille, D.; Anis, A. H.; Guh, D. P.; Esdaile, J. M. Gaps in Care for Rheumatoid Arthritis: A Population Study. *Arthritis Rheum.* **2005,** *53,* 241–248.
5. Olsen, N. J.; Stein, C. M. New Drugs for Rheumatoid Arthritis. *N. Engl. J. Med.* **2004,** *350,* 2167–2179.
6. Gan, W. Q.; Man, S. F.; Senthilselvan, A.; Sin, D. D. Association Between Chronic Obstructive Pulmonary Disease and Systemic Inflammation: A Systematic Review and a Meta-Analysis. *Thorax* **2004,** *59,* 574–580.
7. Agusti, A.; MacNee, W.; Donaldson, K.; Cosio, M. Hypothesis: Does COPD Have an Autoimmune Component? *Thorax* **2003,** *58,* 832–834.
8. Barnes, P. J. Chronic Obstructive Pulmonary Disease. *N. Engl. J. Med.* **2000,** *343,* 269–280.
9. Gaffo, A.; Saag, K. G.; Curtis, J. R. Treatment of Rheumatoid Arthritis. *Am. J. Health Syst. Pharm.* **2006,** *63,* 2451–2465.

10. Choi, H. K.; Hernan, M. A.; Seeger, J. D.; Robins, J. M.; Wolfe, F. Methotrexate and Mortality in Patients With Rheumatoid Arthritis: A Prospective Study. *Lancet* **2002,** *359,* 1173–1177.
11. Moreland, L. W.; Weinblatt, M. E.; Keystone, E. C.; Kremer, J. M.; Martin, R. W.; Schiff, M. H.; Whitmore, J. B.; White, B. W. Etanercept Treatment in Adults With Established Rheumatoid Arthritis: 7 Years of Clinical Experience. *J. Rheumatol.* **2006,** *33,* 854–861.
12. Okamoto, H.; Hoshi, D.; Kiire, A.; Yamanaka, H.; Kamatani, N. Molecular Targets of Rheumatoid Arthritis. *Inflamm. Allergy Drug Targets* **2008,** *7,* 53–66.
13. Kievit, W.; Fransen, J.; Oerlemans, A.; Kuper, H.; van der Laar, M.; de Rooij, D.; De Gendt, C.; Ronday, K.; Jansen, T.; van Oijen, P.; Brus, H.; Adang, E.; van Riel, P. The Efficacy of Anti-TNF in Rheumatoid Arthritis, a Comparison Between Randomised Controlled Trials and Clinical Practice. *Ann. Rheum. Dis.* **2007,** *66,* 1473–1478.
14. St Clair, E. W.; van der Heijde, D. M.; Smolen, J. S.; Maini, R. N.; Bathon, J. M.; Emery, P.; Keystone, E.; Schiff, M.; Kalden, J. R.; Wang, B.; Dewoody, K.; Weiss, R.; Baker, D. Active-Controlled Study of Patients Receiving Infliximab for the Treatment of Rheumatoid Arthritis of Early Onset Study, G. Combination of Infliximab and Methotrexate Therapy for Early Rheumatoid Arthritis: A Randomized, Controlled Trial. *Arthritis Rheum.* **2004,** *50,* 3432–3443.
15. Weinblatt, M. E.; Keystone, E. C.; Furst, D. E.; Kavanaugh, A. F.; Chartash, E. K.; Segurado, O. G. Long Term Efficacy and Safety of Adalimumab Plus Methotrexate in Patients With Rheumatoid Arthritis: ARMADA 4 Year Extended Study. *Ann. Rheum. Dis.* **2006,** *65,* 753–759.
16. Breedveld, F. C.; Weisman, M. H.; Kavanaugh, A. F.; Cohen, S. B.; Pavelka, K.; van Vollenhoven, R.; Sharp, J.; Perez, J. L.; Spencer-Green, G. T. The PREMIER Study: A Multicenter, Randomized, Double-Blind Clinical Trial of Combination Therapy With Adalimumab Plus Methotrexate Versus Methotrexate Alone or Adalimumab Alone in Patients With Early, Aggressive Rheumatoid Arthritis Who Had Not Had Previous Methotrexate Treatment. *Arthritis Rheum.* **2006,** *54,* 26–37.
17. Genovese, M. C.; Cohen, S.; Moreland, L.; Lium, D.; Robbins, S.; Newmark, R.; Bekker, P.; Study, G. Combination Therapy With Etanercept and Anakinra in the Treatment of Patients With Rheumatoid Arthritis who Have Been Treated Unsuccessfully With Methotrexate. *Arthritis Rheum.* **2004,** *50,* 1412–1419.
18. Hider, S. L.; Buckley, C.; Silman, A. J.; Symmons, D. P.; Bruce, I. N. Factors Influencing Response to Disease Modifying Antirheumatic Drugs in Patients With Rheumatoid Arthritis. *J. Rheumatol.* **2005,** *32,* 11–16.
19. Hyrich, K. L.; Lunt, M.; Watson, K. D.; Symmons, D. P.; Silman, A. J.; British Society for Rheumatology Biologics Register. Outcomes After Switching From One Anti-Tumor Necrosis Factor Alpha Agent to a Second Anti-Tumor Necrosis Factor Alpha Agent in Patients With Rheumatoid Arthritis: Results From a Large UK National Cohort Study. *Arthritis Rheum.* **2007,** *56,* 13–20.
20. Shaw, T.; Quan, J.; Totoritis, M. C. B Cell Therapy for Rheumatoid Arthritis: The Rituximab (Anti-CD20) Experience. *Ann. Rheum. Dis.* **2003,** *62* (Suppl. 2), ii55–ii59.
21. Emery, P.; Kosinski, M.; Li, T.; Martin, M.; Williams, G. R.; Becker, J. C.; Blaisdell, B.; Ware, J. E., Jr.; Birbara, C.; Russell, A. S. Treatment of Rheumatoid Arthritis Patients With Abatacept and Methotrexate Significantly Improved Health-Related Quality of Life. *J. Rheumatol.* **2006,** *33,* 681–689.
22. Moreland, L.; Bate, G.; Kirkpatrick, P. Abatacept. *Nat. Rev. Drug Discov.* **2006,** *5,* 185–186.
23. Maini, R. N.; Taylor, P. C.; Szechinski, J.; Pavelka, K.; Broll, J.; Balint, G.; Emery, P.; Raemen, F.; Petersen, J.; Smolen, J.; Thomson, D.; Kishimoto, T.; Charisma Study Group. Double-Blind Randomized Controlled Clinical Trial of the Interleukin-6 Receptor Antagonist, Tocilizumab, in European Patients With Rheumatoid Arthritis Who Had an Incomplete Response to Methotrexate. *Arthritis Rheum.* **2006,** *54,* 2817–2829.
24. Bongartz, T.; Sutton, A. J.; Sweeting, M. J.; Buchan, I.; Matteson, E. L.; Montori, V. Anti-TNF Antibody Therapy in Rheumatoid Arthritis and the Risk of Serious Infections and Malignancies: Systematic Review and Meta-Analysis of Rare Harmful Effects in Randomized Controlled Trials. *JAMA* **2006,** *295,* 2275–2285.
25. Choy, E. H. S.; Panayi, G. S. Cytokine Pathways and Joint Inflammation in Rheumatoid Arthritis. *N. Engl. J. Med.* **2001,** *344,* 907–916.
26. Waetzig, G. H.; Seegert, D.; Rosenstiel, P.; Nikolaus, S.; Schreiber, S. p38 Mitogen-Activated Protein Kinase is Activated and Linked to TNF-Alpha Signaling in Inflammatory Bowel Disease. *J. Immunol.* **2002,** *168,* 5342–5351.
27. Raingeaud, J.; Gupta, S.; Rogers, J. S.; Dickens, M.; Han, J.; Ulevitch, R. J.; Davis, R. J. Pro-Inflammatory Cytokines and Environmental Stress Cause p38 Mitogen-Activated Protein Kinase Activation by Dual Phosphorylation on Tyrosine and Threonine. *J. Biol. Chem.* **1995,** *270,* 7420–7426.
28. Adams, J. L.; Badger, A. M.; Kumar, S.; Lee, J. C. p38 MAP Kinase: Molecular Target for the Inhibition of Pro-Inflammatory Cytokines. *Prog. Med. Chem.* **2001,** *38,* 1–60.
29. Schieven, G. L. The Biology of p38 Kinase: A Central Role in Inflammation. *Curr. Top. Med. Chem.* **2005,** *5,* 921–928.
30. Arthur, J. S.; Ley, S. C. Mitogen-Activated Protein Kinases in Innate Immunity. *Nat. Rev. Immunol.* **2013,** *13,* 679–692.
31. Kumar, S.; Boehm, J.; Lee, J. C. p38 MAP Kinases: Key Signalling Molecules as Therapeutic Targets for Inflammatory Diseases. *Nat. Rev. Drug Discov.* **2003,** *2,* 717–726.
32. Saklatvala, J. The p38 MAP Kinase Pathway as a Therapeutic Target in Inflammatory Disease. *Curr. Opin. Pharmacol.* **2004,** *4,* 372–377.
33. Peifer, C.; Wagner, G.; Laufer, S. New Approaches to the Treatment of Inflammatory Disorders Small Molecule Inhibitors of p38 MAP Kinase. *Curr. Top. Med. Chem.* **2006,** *6,* 113–149.
34. Pettus, L. H.; Wurz, R. P. Small Molecule p38 MAP Kinase Inhibitors for the Treatment of Inflammatory Diseases: Novel Structures and Developments During 2006–2008. *Curr. Top. Med. Chem.* **2008,** *8,* 1452–1467.
35. Goldstein, D. M.; Kuglstatter, A.; Lou, Y.; Soth, M. J. Selective p38alpha Inhibitors Clinically Evaluated for the Treatment of Chronic Inflammatory Disorders. *J. Med. Chem.* **2010,** *53,* 2345–2353.
36. Kumar, S.; McDonnell, P. C.; Gum, R. J.; Hand, A. T.; Lee, J. C.; Young, P. R. Novel Homologues of CSBP/p38 MAP Kinase: Activation, Substrate Specificity and Sensitivity to Inhibition by Pyridinyl Imidazoles. *Biochem. Biophys. Res. Commun.* **1997,** *235,* 533–538.
37. Chanteux, H.; Guisset, A. C.; Pilette, C.; Sibille, Y. LPS Induces IL-10 Production by Human Alveolar Macrophages via MAPKinases- and Sp1-Dependent Mechanisms. *Respir. Res.* **2007,** *8,* 71.
38. Wadgaonkar, R.; Pierce, J. W.; Somnay, K.; Damico, R. L.; Crow, M. T.; Collins, T.; Garcia, J. G. Regulation of c-Jun N-Terminal Kinase and p38 Kinase Pathways in Endothelial Cells. *Am. J. Respir. Cell Mol. Biol.* **2004,** *31,* 423–431.
39. Shin, M. S.; Shinghirunnusorn, P.; Sugishima, Y.; Nishimura, M.; Suzuki, S.; Koizumi, K.; Saiki, I.; Sakurai, H. Cross Interference With TNF-Alpha-Induced TAK1 Activation via EGFR-Mediated p38 Phosphorylation of TAK1-Binding Protein 1. *Biochim. Biophys. Acta* **2009,** *1793,* 1156–1164.
40. Buhler, S.; Laufer, S. A. p38 MAPK Inhibitors: A Patent Review (2012–2013). *Expert Opin. Ther. Pat.* **2014,** *24,* 535–554.
41. Fiebich, B. L.; Mueksch, B.; Boehringer, M.; Hull, M. Interleukin-1beta Induces Cyclooxygenase-2 and Prostaglandin E(2) Synthesis in Human Neuroblastoma Cells: Involvement of p38 Mitogen-Activated Protein Kinase and Nuclear Factor-kappaB. *J. Neurochem.* **2000,** *75,* 2020–2028.
42. Duffy, J. P.; Harrington, E. M.; Salituro, F. G.; Cochran, J. E.; Green, J.; Gao, H.; Bemis, G. W.; Evindar, G.; Galullo, V. P.; Ford, P. J.; Germann, U. A.; Wilson, K. P.; Bellon, S. F.; Chen, G.; Taslimi, P.; Jones, P.; Huang, C.; Pazhanisamy, S.; Wang, Y. M.; Murcko, M. A.; Su, M. S. The Discovery of VX-745: A Novel and Selective p38alpha Kinase Inhibitor. *ACS Med. Chem. Lett.* **2011,** *2,* 758–763.
43. Ding, C. Drug Evaluation: VX-702, a MAP Kinase Inhibitor for Rheumatoid Arthritis and Acute Coronary Syndrome. *Curr. Opin. Investig. Drugs* **2006,** *7,* 1020–1025.
44. Damjanov, N.; Kauffman, R. S.; Spencer-Green, G. T. Efficacy, Pharmacodynamics, and Safety of VX-702, a Novel p38 MAPK Inhibitor, in Rheumatoid Arthritis: Results of Two Randomized, Double-Blind, Placebo-Controlled Clinical Studies. *Arthritis Rheum.* **2009,** *60,* 1232–1241.
45. Nikas, S. N.; Drosos, A. A. SCIO-469 Scios Inc. *Curr. Opin. Investig. Drugs* **2005,** *5,* 1205–1212.
46. Genovese, M. C.; Cohen, S. B.; Wofsy, D.; Weinblatt, M. E.; Firestein, G. S.; Brahn, E.; Strand, V.; Baker, D. G.; Tong, S. E. In *A Randomized, Double-Blind, Placebo-Controlled Phase 2 Study of an Oral p38a MAPK Inhibitor, SCIO-469, in Patients With Active Rheumatoid Arthritis (Abstract); Proceedings of the American College of Rheumatology 2008 Annual Meeting, San Francisco, CA, Oct 24–29, 2008;* American College of Rheumatology: Atlanta, GA: San Francisco, CA, 2008.
47. Genovese, M. C.; Cohen, S. B.; Wofsy, D.; Weinblatt, M. E.; Firestein, G. S.; Brahn, E.; Strand, V.; Baker, D. G.; Tong, S. E. A 24-Week, Randomized, Double-Blind, Placebo-Controlled, Parallel Group Study of the Efficacy of Oral SCIO-469, a p38 Mitogen-Activated Protein Kinase Inhibitor, in Patients With Active Rheumatoid Arthritis. *J. Rheumatol.* **2011,** *38,* 846–854.
48. Sokol, L.; Cripe, L.; Kantarjian, H.; Sekeres, M. A.; Parmar, S.; Greenberg, P.; Goldberg, S. L.; Bhushan, V.; Shammo, J.; Hohl, R.; Verma, A.; Garcia-Manero, G.; Li, Y. P.; Lowe, A.; Zhu, J.; List, A. F. Randomized, Dose-Escalation Study of the p38alpha MAPK Inhibitor SCIO-469 in Patients With Myelodysplastic Syndrome. *Leukemia* **2013,** *27,* 977–980.

49. Tong, S. E.; Deniels, S. E.; Montano, T.; Chang, S.; Desjardins, P. Scio-469, a Novel p38a MAPK Inhibitor, Provides Efficacy in Acute Post-Surgical Dental Pain. *Clin. Pharmacol. Ther.* **2004,** *75,* 3.
50. Murali Dhar, T. G.; Wrobleski, S. T.; Lin, S.; Furch, J. A.; Nirschl, D. S.; Fan, Y.; Todderud, G.; Pitt, S.; Doweyko, A. M.; Sack, J. S.; Mathur, A.; McKinnon, M.; Barrish, J. C.; Dodd, J. H.; Schieven, G. L.; Leftheris, K. Synthesis and SAR of p38alpha MAP Kinase Inhibitors Based on Heterobicyclic Scaffolds. *Bioorg. Med. Chem. Lett.* **2007,** *17,* 5019–5024.
51. Laufer, S.; Lehmann, F. Investigations of SCIO-469-Like Compounds for the Inhibition of p38 MAP Kinase. *Bioorg. Med. Chem. Lett.* **2009,** *19,* 1461–1464.
52. Pargellis, C.; Tong, L.; Churchill, L.; Cirillo, P. F.; Gilmore, T.; Graham, A. G.; Grob, P. M.; Hickey, E. R.; Moss, N.; Pav, S.; Regan, J. Inhibition of p38 MAP Kinase by Utilizing a Novel Allosteric Binding Site. *Nat. Struct. Biol.* **2002,** *9,* 268–272.
53. Sullivan, J. E.; Holdgate, G. A.; Campbell, D.; Timms, D.; Gerhardt, S.; Breed, J.; Breeze, A. L.; Bermingham, A.; Pauptit, R. A.; Embrey, K. J.; Read, J.; VanScyoc, W. S.; Ward, W. H. J. Prevention of MKK6-Dependent Activation by Binding to p38alpha MAP Kinase. *Biochemistry* **2005,** *44,* 16475–16490.
54. Kuma, Y.; Sabio, G.; Bain, J.; Shpiro, N.; Marquez, R.; Cuenda, A. BIRB796 Inhibits All p38 MAPK Isoforms in vitro and In Vivo. *J. Biol. Chem.* **2005,** *280,* 19472–19479.
55. Graneto, M. J.; Kurumbail, R. G.; Vazquez, M. L.; Shieh, H. S.; Pawlitz, J. L.; Williams, J. M.; Stallings, W. C.; Geng, L.; Naraian, A. S.; Koszyk, F. J.; Stealey, M. A.; Xu, X. D.; Weier, R. M.; Hanson, G. J.; Mourey, R. J.; Compton, R. P.; Mnich, S. J.; Anderson, G. D.; Monahan, J. B.; Devraj, R. Synthesis, Crystal Structure, and Activity of Pyrazole-Based Inhibitors of p38 Kinase. *J. Med. Chem.* **2007,** *50,* 5712–5719.
56. Walker, J. K.; Selness, S. R.; Devraj, R. V.; Hepperle, M. E.; Naing, W.; Shieh, H.; Kurambail, R.; Yang, S.; Flynn, D. L.; Benson, A. G.; Messing, D. M.; Dice, T.; Kim, T.; Lindmark, R. J.; Monahan, J. B.; Portanova, J. Identification of SD-0006, a Potent Diaryl Pyrazole Inhibitor of p38 MAP Kinase. *Bioorg. Med. Chem. Lett.* **2010,** *20,* 2634–2638.
57. Burnette, B. L.; Selness, S.; Devraj, R.; Jungbluth, G.; Kurumbail, R.; Stillwell, L.; Anderson, G.; Mnich, S.; Hirsch, J.; Compton, R.; De Ciechi, P.; Hope, H.; Hepperle, M.; Keith, R. H.; Naing, W.; Shieh, H.; Portanova, J.; Zhang, Y.; Zhang, J.; Leimgruber, R. M.; Monahan, J. SD0006: A Potent, Selective and Orally Available Inhibitor of p38 Kinase. *Pharmacology* **2009,** *84,* 42–60.
58. Hill, R. J.; Dabbagh, K.; Phippard, D.; Li, C.; Suttmann, R. T.; Welch, M.; Papp, E.; Song, K. W.; Chang, K. C.; Leaffer, D.; Kim, Y. N.; Roberts, R. T.; Zabka, T. S.; Aud, D.; Dal Porto, J.; Manning, A. M.; Peng, S. L.; Goldstein, D. M.; Wong, B. R. Pamapimod, a Novel p38 Mitogen-Activated Protein Kinase Inhibitor: Preclinical Analysis of Efficacy and Selectivity. *J. Pharmacol. Exp. Ther.* **2008,** *327,* 610–619.
59. Cohen, S. B.; Cheng, T. T.; Chindalore, V.; Damjanov, N.; Burgos-Vargas, R.; Delora, P.; Zimany, K.; Travers, H.; Caulfield, J. P. Evaluation of the Efficacy and Safety of Pamapimod, a p38 MAP Kinase Inhibitor, in a Double-Blind, Methotrexate-Controlled Study of Patients With Active Rheumatoid Arthritis. *Arthritis Rheum.* **2009,** *60,* 335–344.
60. Genovese, M. C. Inhibition of p38: Has the Fat Lady Sung? *Arthritis Rheum.* **2009,** *60,* 317–320.
61. Singh, D.; Smyth, L.; Borrill, Z.; Sweeney, L.; Tal-Singer, R. A Randomized, Placebo-Controlled Study of the Effects of the p38 MAPK Inhibitor SB-681323 on Blood Biomarkers of Inflammation in COPD Patients. *J. Clin. Pharmacol.* **2010,** *50,* 94–100.
62. Anand, P.; Shenoy, R.; Palmer, J. E.; Baines, A. J.; Lai, R. Y.; Robertson, J.; Bird, N.; Ostenfeld, T.; Chizh, B. A. Clinical Trial of the p38 MAP Kinase Inhibitor Dilmapimod in Neuropathic Pain Following Nerve Injury. *Eur. J. Pain* **2011,** *15,* 1040–1048.
63. Aston, N. M.; Bamborough, P.; Buckton, J. B.; Edwards, C. D.; Holmes, D. S.; Jones, K. L.; Patel, V. K.; Smee, P. A.; Somers, D. O.; Vitulli, G.; Walker, A. L. p38alpha Mitogen-Activated Protein Kinase Inhibitors: Optimization of a Series of Biphenylamides to Give a Molecule Suitable for Clinical Progression. *J. Med. Chem.* **2009,** *52,* 6257–6269.
64. Marks-Konczalik, J.; Costa, M.; Robertson, J.; McKie, E.; Yang, S.; Pascoe, S. A Post-hoc Subgroup Analysis of Data From a Six Month Clinical Trial Comparing the Efficacy and Safety of Losmapimod in Moderate-Severe COPD Patients With $</=2\%$ and $>2\%$ Blood Eosinophils. *Respir. Med.* **2015,** *109,* 860–869.
65. Ostenfeld, T.; Krishen, A.; Lai, R. Y.; Bullman, J.; Green, J.; Anand, P.; Scholz, J.; Kelly, M. A Randomized, Placebo-Controlled Trial of the Analgesic Efficacy and Safety of the p38 MAP Kinase Inhibitor, Losmapimod, in Patients With Neuropathic Pain From Lumbosacral Radiculopathy. *Clin. J. Pain* **2015,** *31,* 283–293.
66. Cheriyan, J.; Webb, A. J.; Sarov-Blat, L.; Elkhawad, M.; Wallace, S. M.; Maki-Petaja, K. M.; Collier, D. J.; Morgan, J.; Fang, Z.; Willette, R. N.; Lepore, J. J.; Cockcroft, J. R.; Sprecher, D. L.; Wilkinson, I. B. Inhibition of p38 Mitogen-Activated Protein Kinase Improves Nitric Oxide-Mediated Vasodilatation and Reduces Inflammation in Hypercholesterolemia. *Circulation* **2011,** *123,* 515–523.
67. Elkhawad, M.; Rudd, J. H.; Sarov-Blat, L.; Cai, G.; Wells, R.; Davies, L. C.; Collier, D. J.; Marber, M. S.; Choudhury, R. P.; Fayad, Z. A.; Tawakol, A.; Gleeson, F. V.; Lepore, J. J.; Davis, B.; Willette, R. N.; Wilkinson, I. B.; Sprecher, D. L.; Cheriyan, J. Effects of p38 Mitogen-Activated Protein Kinase Inhibition on Vascular and Systemic Inflammation in Patients With Atherosclerosis. *JACC Cardiovasc. Imaging* **2012,** *5,* 911–922.
68. Newby, L. K.; Marber, M. S.; Melloni, C.; Sarov-Blat, L.; Aberle, L. H.; Aylward, P. E.; Cai, G.; de Winter, R. J.; Hamm, C. W.; Heitner, J. F.; Kim, R.; Lerman, A.; Patel, M. R.; Tanguay, J. F.; Lepore, J. J.; Al-Khalidi, H. R.; Sprecher, D. L.; Granger, C. B.; The Solstice Investigators. Losmapimod, a Novel p38 Mitogen-Activated Protein Kinase Inhibitor, in Non-ST-Segment Elevation Myocardial Infarction: A Randomised Phase 2 Trial. *Lancet* **2014,** *384,* 1187–1195.
69. Novartis, A. *Use of a Pyrazole Derivative in the Treatment of Acute Exacerbations of Chronic Obstructive Pulmonary Disease.* US2013.
70. Novartis, A. *5-Membered Heterocycle-Based p38 Kinase Inhibitors.* US2012.
71. Wadsworth, S. A.; Cavender, D. E.; Beers, S. A.; Lalan, P.; Schafer, P. H.; Malloy, E. A.; Wu, W.; Fahmy, B.; Olini, G. C.; Davis, J. E.; Pellegrino-Gensey, J. L.; Wachter, M. P.; Siekierka, J. J. RWJ 67657, a Potent, Orally Active Inhibitor of p38 Mitogen-Activated Protein Kinase. *J. Pharmacol. Exp. Ther.* **1999,** *291,* 680–687.
72. Parasrampuria, D. A.; de Boer, P.; Desai-Krieger, D.; Chow, A. T.; Jones, C. R. Single-Dose Pharmacokinetics and Pharmacodynamics of RWJ 67657, a Specific p38 Mitogen-Activated Protein Kinase Inhibitor: A First-in-Human Study. *J. Clin. Pharmacol.* **2003,** *43,* 406–413.
73. Fijen, J. W.; Zijlstra, J. G.; De Boer, P.; Spanjersberg, R.; Tervaert, J. W.; Van Der Werf, T. S.; Ligtenberg, J. J.; Tulleken, J. E. Suppression of the Clinical and Cytokine Response to Endotoxin by RWJ-67657, a p38 Mitogen-Activated Protein-Kinase Inhibitor, in Healthy Human Volunteers. *Clin. Exp. Immunol.* **2001,** *124,* 16–20.
74. Antoon, J. W.; Bratton, M. R.; Guillot, L. M.; Wadsworth, S.; Salvo, V. A.; Elliott, S.; McLachlan, J. A.; Burow, M. E. Pharmacology and Anti-Tumor Activity of RWJ67657, a Novel Inhibitor of p38 Mitogen Activated Protein Kinase. *Am. J. Cancer Res.* **2012,** *2,* 446–458.
75. Xing, L.; Shieh, H. S.; Selness, S. R.; Devraj, R. V.; Walker, J. K.; Devadas, B.; Hope, H. R.; Compton, R. P.; Schindler, J. F.; Hirsch, J. L.; Benson, A. G.; Kurumbail, R. G.; Stegeman, R. A.; Williams, J. M.; Broadus, R. M.; Walden, Z.; Monahan, J. B. Structural Bioinformatics-Based Prediction of Exceptional Selectivity of p38 MAP Kinase Inhibitor PH-797804. *Biochemistry* **2009,** *48,* 6402–6411.
76. Selness, S. R.; Devraj, R. V.; Monahan, J. B.; Boehm, T. L.; Walker, J. K.; Devadas, B.; Durley, R. C.; Kurumbail, R.; Shieh, H.; Xing, L.; Hepperle, M.; Rucker, P. V.; Jerome, K. D.; Benson, A. G.; Marrufo, L. D.; Madsen, H. M.; Hitchcock, J.; Owen, T. J.; Christie, L.; Promo, M. A.; Hickory, B. S.; Alvira, E.; Naing, W.; Blevis-Bal, R. Discovery of N-Substituted Pyridinones as Potent and Selective Inhibitors of p38 Kinase. *Bioorg. Med. Chem. Lett.* **2009,** *19,* 5851–5856.
77. Selness, S. R.; Devraj, R. V.; Devadas, B.; Walker, J. K.; Boehm, T. L.; Durley, R. C.; Shieh, H.; Xing, L.; Rucker, P. V.; Jerome, K. D.; Benson, A. G.; Marrufo, L. D.; Madsen, H. M.; Hitchcock, J.; Owen, T. J.; Christie, L.; Promo, M. A.; Hickory, B. S.; Alvira, E.; Naing, W.; Blevis-Bal, R.; Messing, D.; Yang, J.; Mao, M. K.; Yalamanchili, G.; Vonder Embse, R.; Hirsch, J.; Saabye, M.; Bonar, S.; Webb, E.; Anderson, G.; Monahan, J. B. Discovery of PH-797804, a Highly Selective and Potent Inhibitor of p38 MAP Kinase. *Bioorg. Med. Chem. Lett.* **2011,** *21,* 4066–4071.
78. Selness, S. R.; Boehm, T. L.; Walker, J. K.; Devadas, B.; Durley, R. C.; Kurumbail, R.; Shieh, H.; Xing, L.; Hepperle, M.; Rucker, P. V.; Jerome, K. D.; Benson, A. G.; Marrufo, L. D.; Madsen, H. M.; Hitchcock, J.; Owen, T. J.; Christie, L.; Promo, M. A.; Hickory, B. S.; Alvira, E.; Naing, W.; Blevis-Bal, R.; Devraj, R. V.; Messing, D.; Schindler, J. F.; Hirsch, J.; Saabye, M.; Bonar, S.; Webb, E.; Anderson, G.; Monahan, J. B. Design, Synthesis and Activity of a Potent, Selective Series of N-Aryl Pyridinone Inhibitors of p38 Kinase. *Bioorg. Med. Chem. Lett.* **2011,** *21,* 4059–4065.
79. Xing, L.; Devadas, B.; Devraj, R. V.; Selness, S. R.; Shieh, H.; Walker, J. K.; Mao, M.; Messing, D.; Samas, B.; Yang, J. Z.; Anderson, G. D.; Webb, E. G.; Monahan, J. B. Discovery and Characterization of Atropisomer PH-797804, a p38 MAP Kinase Inhibitor, as a Clinical Drug Candidate. *ChemMedChem* **2012,** *7,* 273–280.

80. Campbell, R. M.; Anderson, B. D.; Brooks, N. A.; Brooks, H. B.; Chan, E. M.; De Dios, A.; Gilmour, R.; Graff, J. R.; Jambrina, E.; Mader, M.; McCann, D.; Na, S.; Parsons, S. H.; Pratt, S. E.; Shih, C.; Stancato, L. F.; Starling, J. J.; Tate, C.; Velasco, J. A.; Wang, Y.; Ye, X. S. Characterization of LY2228820 Dimesylate, a Potent and Selective Inhibitor of p38 MAPK With Antitumor Activity. *Mol. Cancer Ther.* **2014,** *13,* 364–374.
81. BMS Homepage. http://ctr.bms.com/OneBmsCtd/InitTrialDetailAction.do?pnum=IM119-015 (accessed Oct 16, 2015).
82. Array Homepage. http://investor.arraybiopharma.com/phoenix.zhtml?c=123810&p=irol-newsArticle&ID=1305781&highlight= (accessed Oct 16, 2015).
83. Amgen Homepage. http://wwwext.amgen.com/media/media_pr_detail.jsp?year=2003&releaseID=514785 (accessed Oct 16, 2015).
84. Wang, Z.; Harkins, P. C.; Ulevitch, R. J.; Han, J.; Cobb, M. H.; Goldsmith, E. J. The Structure of Mitogen-Activated Protein Kinase p38 at 2.1-A Resolution. *Proc. Natl. Acad. Sci. U. S. A.* **1997,** *94,* 2327–2332.
85. Wilson, K. P.; Fitzgibbon, M. J.; Caron, P. R.; Griffith, J. P.; Chen, W.; McCaffrey, P. G.; Chambers, S. P.; Su, M. S. Crystal Structure of p38 Mitogen-Activated Protein Kinase. *J. Biol. Chem.* **1996,** *271,* 27696–27700.
86. Fitzgerald, C. E.; Patel, S. B.; Becker, J. W.; Cameron, P. M.; Zaller, D.; Pilounis, V. B.; O'Keefe, S. J.; Scapin, G. Structural Basis for p38alpha MAP Kinase Quinazolinone and Pyridol-Pyrimidine Inhibitor Specificity. *Nat. Struct. Biol.* **2003,** *10,* 764–769.
87. Shewchuk, L.; Hassell, A.; Wisely, B.; Rocque, W.; Holmes, W.; Veal, J.; Kuyper, L. F. Binding Mode of the 4-Anilinoquinazoline Class of Protein Kinase Inhibitor: X-ray Crystallographic Studies of 4-Anilinoquinazolines Bound to Cyclin-Dependent Kinase 2 and p38 Kinase. *J. Med. Chem.* **2000,** *43,* 133–138.
88. Wang, Z.; Canagarajah, B. J.; Boehm, J. C.; Kassisa, S.; Cobb, M. H.; Young, P. R.; Abdel-Meguid, S.; Adams, J. L.; Goldsmith, E. J. Structural Basis of Inhibitor Selectivity in MAP Kinases. *Structure* **1998,** *6,* 1117–1128.
89. Tong, L.; Pav, S.; White, D. M.; Rogers, S.; Crane, K. M.; Cywin, C. L.; Brown, M. L.; Pargellis, C. A. A Highly Specific Inhibitor of Human p38 MAP Kinase Binds in the ATP Pocket. *Nat. Struct. Biol.* **1997,** *4,* 311–316.
90. Stelmach, J. E.; Liu, L.; Patel, S. B.; Pivnichny, J. V.; Scapin, G.; Singh, S.; Hop, C. E.; Wang, Z.; Strauss, J. R.; Cameron, P. M.; Nichols, E. A.; O'Keefe, S. J.; O'Neill, E. A.; Schmatz, D. M.; Schwartz, C. D.; Thompson, C. M.; Zaller, D. M.; Doherty, J. B. Design and Synthesis of Potent, Orally Bioavailable Dihydroquinazolinone Inhibitors of p38 MAP Kinase. *Bioorg. Med. Chem. Lett.* **2003,** *13,* 277–280.
91. Trejo, A.; Arzeno, H.; Browner, M.; Chanda, S.; Cheng, S.; Comer, D. D.; Dalrymple, S. A.; Dunten, P.; Lafargue, J.; Lovejoy, B.; Freire-Moar, J.; Lim, J.; McIntosh, J.; Miller, J.; Papp, E.; Reuter, D.; Roberts, R.; Sanpablo, F.; Saunders, J.; Song, K.; Villasenor, A.; Warren, S. D.; Welch, M.; Weller, P.; Whiteley, P. E.; Zeng, L.; Goldstein, D. M. Design and Synthesis of 4-Azaindoles as Inhibitors of p38 MAP Kinase. *J. Med. Chem.* **2003,** *46,* 4702–4713.
92. Goldstein, D. M.; Alfredson, T.; Bertrand, J.; Browner, M. F.; Clifford, K.; Dalrymple, S. A.; Dunn, J.; Freire-Moar, J.; Harris, S.; Labadie, S. S.; La Fargue, J.; Lapierre, J. M.; Larrabee, S.; Li, F.; Papp, E.; McWeeney, D.; Ramesha, C.; Roberts, R.; Rotstein, D.; San Pablo, B.; Sjogren, E. B.; So, O. Y.; Talamas, F. X.; Tao, W.; Trejo, A.; Villasenor, A.; Welch, M.; Welch, T.; Weller, P.; Whiteley, P. E.; Young, K.; Zipfel, S. Discovery of S-[5-Amino-1-(4-Fluorophenyl)-1H-Pyrazol-4-yl]-[3-(2,3-Dihydroxypropoxy)ph Enyl] Methanone (RO3201195), an Orally Bioavailable and Highly Selective Inhibitor of p38 MAP Kinase. *J. Med. Chem.* **2006,** *49,* 1562–1575.
93. Gill, A. L.; Frederickson, M.; Cleasby, A.; Woodhead, S. J.; Carr, M. G.; Woodhead, A. J.; Walker, M. T.; Congreve, M. S.; Devine, L. A.; Tisi, D.; O'Reilly, M.; Seavers, L. C. A.; Davis, D. J.; Curry, J.; Anthony, R.; Padova, A.; Murray, C. W.; Carr, R. A. E.; Jhoti, H. Identification of Novel p38alpha MAP Kinase Inhibitors Using Fragment-Based Lead Generation. *J. Med. Chem.* **2005,** *48,* 414–426.
94. Xing, L.; Rai, B.; Lunney, E. A. Scaffold Mining of Kinase Hinge Binders in Crystal Structure Database. *J. Comput. Aided Mol. Des.* **2014,** *28,* 13–23.
95. Xing, L.; Klug-Mcleod, J.; Rai, B.; Lunney, E. A. Kinase Hinge Binding Scaffolds and Their Hydrogen Bond Patterns. *Bioorg. Med. Chem.* **2015,** *23,* 6520–6527.
96. Huse, M.; Kuriyan, J. The Conformational Plasticity of Protein Kinases. *Cell* **2002,** *109,* 275–282.
97. Jacobs, M. D.; Caron, P. R.; Hare, B. J. Classifying Protein Kinase Structures Guides Use of Ligand-Selectivity Profiles to Predict Inactive Conformations: Structure of Lck/Imatinib Complex. *Proteins* **2008,** *70,* 1451–1460.
98. Eyers, P. A.; Craxton, M.; Morrice, N.; Cohen, P.; Goedert, M. Conversion of SB 203580-Insensitive MAP Kinase Family Members to Drug-Sensitive Forms by a Singel Amino-Acid Substitution. *Chem. Biol.* **1998,** *5,* 321–328.
99. Wilson, K. P.; McCaffrey, P. G.; Hsiao, K.; Pazhanisamy, S.; Galullo, V.; Bemis, G. W.; Fitzgibbon, M. J.; Caron, P. R.; Murcko, M. A.; Su, M. S. The Structural Basis for the Specificity of Pyridinylimidazole Inhibitors of p38 MAP Kinase. *Chem. Biol.* **1997,** *4,* 423–431.
100. Lisnock, J.; Tebben, A.; Frantz, B.; O'Neill, E. A.; Croft, G.; O'Keefe, S. J.; Li, B.; Hacker, C.; de Laszlo, S.; Smith, A.; Libby, B.; Liverton, N.; Hermes, J.; LoGrasso, P. Molecular Basis for p38 Protein Kinase Inhibitor Specificity. *Biochemistry* **1998,** *37,* 16573–16581.
101. Hope, H. R.; Anderson, G. D.; Burnette, B. L.; Compton, R. P.; Devraj, R. V.; Hirsch, J. L.; Keith, R. H.; Li, X.; Mbalaviele, G.; Messing, D. M.; Saabye, M. J.; Schindler, J. F.; Selness, S. R.; Stillwell, L. I.; Webb, E. G.; Zhang, J.; Monahan, J. B. Anti-Inflammatory Properties of a Novel N-Phenyl Pyridinone Inhibitor of p38 Mitogen-Activated Protein Kinase: Preclinical-to-Clinical Translation. *J. Pharmacol. Exp. Ther.* **2009,** *331,* 882–895.
102. Glossop, P. A.; Lane, C. A.; Price, D. A.; Bunnage, M. E.; Lewthwaite, R. A.; James, K.; Brown, A. D.; Yeadon, M.; Perros-Huguet, C.; Trevethick, M. A.; Clarke, N. P.; Webster, R.; Jones, R. M.; Burrows, J. L.; Feeder, N.; Taylor, S. C.; Spence, F. J. Inhalation by Design: Novel Ultra-Long-Acting Beta(2)-Adrenoreceptor Agonists for Inhaled Once-Daily Treatment of Asthma and Chronic Obstructive Pulmonary Disease That Utilize a Sulfonamide Agonist Headgroup. *J. Med. Chem.* **2010,** *53,* 6640–6652.
103. Millan, D. S. What is the Potential for Inhaled p38 Inhibitors in the Treatment of Chronic Obstructive Pulmonary Disease? *Future Med. Chem.* **2011,** *3,* 1635–1645.
104. Millan, D. S.; Bunnage, M. E.; Burrows, J. L.; Butcher, K. J.; Dodd, P. G.; Evans, T. J.; Fairman, D. A.; Hughes, S. J.; Kilty, I. C.; Lemaitre, A.; Lewthwaite, R. A.; Mahnke, A.; Mathias, J. P.; Philip, J.; Smith, R. T.; Stefaniak, M. H.; Yeadon, M.; Phillips, C. Design and Synthesis of Inhaled p38 Inhibitors for the Treatment of Chronic Obstructive Pulmonary Disease. *J. Med. Chem.* **2011,** *54,* 7797–7814.
105. Regan, J.; Capolino, A.; Cirillo, P. F.; Gilmore, T.; Graham, A. G.; Hickey, E.; Kroe, R. R.; Madwed, J.; Moriak, M.; Nelson, R.; Pargellis, C. A.; Swinamer, A.; Torcellini, C.; Tsang, M.; Moss, N. Structure-Activity Relationships of the p38alpha MAP Kinase Inhibitor 1-(5-Tert-Butyl-2-p-Tolyl-2H-Pyrazol-3-yl)-3-[4-(2-Morpholin-4-yl-Ethoxy)Naph-Thalen-1-yl]Urea (BIRB 796). *J. Med. Chem.* **2003,** *46,* 4676–4686.
106. Fisher, M. B.; Paine, M. F.; Strelevitz, T. J.; Wrighton, S. A. The Role of Hepatic and Extrahepatic UDP-Glucuronosyltransferases in Human Drug Metabolism. *Drug Metab. Rev.* **2001,** *33,* 273–297.
107. Roos-Engstrand, E.; Wallin, A.; Bucht, A.; Pourazar, J.; Sandstrom, T.; Blomberg, A. Increased Expression of p38 MAPK in Human Bronchial Epithelium After Lipopoly-saccharide Exposure. *Eur. Respir. J.* **2005,** *25,* 797–803.
108. Ovrevik, J.; Lag, M.; Holme, J. A.; Schwarze, P. E.; Refsnes, M. Cytokine and Chemokine Expression Patterns in Lung Epithelial Cells Exposed to Components Characteristic of Particulate Air Pollution. *Toxicology* **2009,** *259,* 46–53.
109. Singh, D.; Siew, L.; Christensen, J.; Plumb, J.; Clarke, G. W.; Greenaway, S.; Perros-Huguet, C.; Clarke, N.; Kilty, I.; Tan, L. Oral and Inhaled p38 MAPK Inhibitors: Effects on Inhaled LPS Challenge in Healthy Subjects. *Eur. J. Clin. Pharmacol.* **2015,** *71,* 1175–1184.
110. MacNee, W.; Allan, R. J.; Jones, I.; De Salvo, M. C.; Tan, L. F. Efficacy and Safety of the Oral p38 Inhibitor PH-797804 in Chronic Obstructive Pulmonary Disease: A Randomised Clinical Trial. *Thorax* **2013,** *68,* 738–745.
111. Fogel, R.; Shields, K.; Christensen, J.; Ribbing, J.; Perros-Huguet, C.; Clarke, N. A Phase II, Randomised, Placebo Controlled Trial of 12 Weeks Treatment With an Oral p38 Inhibitor in Patients With COPD on a Background of ICS/LABA. European Respiratory Society Annual Congress, Barcelona, September 7–11, 2013; Barcelona.
112. A study to evaluate the safety and pharmacokinetic profile of a p38 inhibitor (PH-79804) in subjects with rheumatoid arthritis who are also taking methotrexate. In Available from: https://clinicaltrials.gov/ct2/show/NCT00620685.
113. Cohen, P. Targeting Protein Kinases for the Development of Anti-Inflammatory Drugs. *Curr. Opin. Cell Biol.* **2009,** *21,* 317–324.

8.17 Are Two Better Than One in Rheumatoid Arthritis? Development of Dual p38α MAPK/PDE-4 Inhibitors for Treatment of TNFα-Driven Diseases

W Albrecht, c-a-i-r biosciences GmbH, Ulm, Germany
SM Bauer and SA Laufer, Eberhard Karls University, Tuebingen, Germany

© 2017 Elsevier Ltd. All rights reserved.

8.17.1	**Introduction**	431
8.17.1.1	Selective p38α MAPK Inhibition May Be Not Sufficient for Therapy of Inflammatory Disorders	432
8.17.1.1.1	The p38 MAPK cascade	432
8.17.1.1.2	Phosphodiesterase 4 (PDE-4)	433
8.17.2	**Chemistry: 1,2,4,5-Tetra-Substituted 2-Thioimidazoles: Preferred Templates to Target the ATP-Site of Protein Kinases**	434
8.17.2.1	In Vitro and In Vivo Pharmacodynamics	435
8.17.3	**Discovery of Dual p38α MAPK and PDE4 Inhibitors: Promising Compounds for Treatment of Inflammatory Disorders**	437
8.17.3.1	Chemistry of CBS-3595	439
8.17.3.1.1	Profiling of CBS-3595	439
8.17.4	**From in vitro Experiments Into Phase-I Clinical Trial: CBS-3595, a Dual Inhibitor of p38α MAPK/PDE-4**	439
8.17.4.1	Nonclinical Evaluation of CBS-3595 and Its Metabolite CBS-3728	440
8.17.4.1.1	IC_{50} determination in in vitro kinase activity assays	440
8.17.4.1.2	Investigation of kinome selectivity and other potential off-targets	440
8.17.4.1.3	Metabolism studies	441
8.17.4.1.4	Effect of CBS-3595 on leukotriene B_4 (LTB_4) release in LPS/fMLP-stimulated human whole blood	441
8.17.4.1.5	Effect of CBS-3595 on TNFα release in the rat following LPS-challenge	441
8.17.4.1.6	Effect of orally administered CBS-3595 on TNFα release in ex vivo-stimulated whole blood in Cynomolgus monkeys	442
8.17.4.1.7	Efficacy in hTNF-transgenic mice	443
8.17.4.1.8	CBS-3595 in a complete Freund's adjuvant (CFA) arthritis model using male Wistar rats	443
8.17.4.1.9	Safety pharmacology studies	444
8.17.4.1.10	Toxicological studies	445
8.17.4.2	Phase I: First-Use-in-Human Study of CBS-3595	446
8.17.4.2.1	Pharmacodynamic results	446
8.17.4.2.2	Pharmacokinetic results	446
8.17.5	**Conclusion and Lessons Learned in Retrospect**	447
8.17.6	**Perspective and Outlook**	448
References		449

8.17.1 Introduction

Rheumatoid arthritis (RA) is an inflammatory and degenerative autoimmune disease which affects approximately 1% of the adult population. All conventional concepts of therapy provided until now can influence the inflammation processes only in an inadequate manner and are linked to adverse side effects.

Biological agents (i.e., Infliximab (IFX), Adalimumab, Golimumab, Certolizumab, and Etanercept) that recognize and neutralize the inflammatory mediator tumor necrosis factor alpha (TNFα), also referred to as TNFα blockers, are also regarded as promising drugs for the treatment of other inflammatory diseases such as Crohn's disease, plaque psoriasis, psoriatic arthritis, and ankylosing spondylitis. However, these therapeutic strategies do not work successfully in some patients and moreover, these drugs are not administrable orally.

For other chronic inflammatory diseases such as asthma and chronic obstructive pulmonary disease (COPD), anticytokine treatment with, for example, IFX, has remained unsuccessful at doses that correspond to those applied for treatment of RA. The significantly higher costs are a significant disadvantage for the healthcare system when compared to the conventional concepts of therapy.

Based on both the safety issues and the extremely high costs of anti-TNFα therapy, we considered the significant advantages related to the development of orally active, small molecule drugs that target the specific signaling and synthesis pathways for TNFα by, for example, inhibition of p38α mitogen-activated protein kinase (MAPK) or phosphodiesterase 4 (PDE-4).

Available evidence suggests that additional benefits may be gained by combining the overlapping and complementary effects of p38α MAPK and PDE-4 inhibition in a single molecule, thereby offering the opportunity of a remarkably broad spectrum of multitargeted antiinflammatory activities.

8.17.1.1 Selective p38α MAPK Inhibition May Be Not Sufficient for Therapy of Inflammatory Disorders

Identified in the 1990s as a key enzyme for the regulation and expression of proinflammatory cytokines, such as TNFα, the protein kinase p38α MAPK has emerged as a treatment of inflammatory joint diseases as well as for other indications such as inflammatory bowel disease.

The family of p38 MAPKs, also known as stress-activated protein kinases, consists of four isoforms (α, β, γ, and δ), which are serine/threonine kinases with a molecular weight of 38 kDa being expressed in a tissue-specific manner. In general, there are three major signal transduction pathways involving MAPKs: the so-called extracellular signal-regulated kinase (ERK), the c-Jun N-terminal kinase (JNK), and the p38 MAPK pathway.

The p38 MAPK pathway regulates the synthesis of TNFα and IL-1β at both the transcriptional and the translational levels. In addition to the prevention of TNFα and IL-1β synthesis, inhibitors of p38α MAPK have been demonstrated to inhibit the production of nitric oxide as well as the expression of cyclooxygenase-2 and IL-6.

Furthermore, p38α MAPK has also been implicated in the regulation of IL-12 and interferon-γ, IL-4, and IL-10 gene transcription.[1]

Consequently, several drug candidates demonstrating potent inhibition of p38α MAPK in vitro also achieved significant antiinflammatory effects in various animal models. However, more than a dozen candidates failed in human phase II studies, for example, due to lack (or successive loss) of efficacy.

8.17.1.1.1 The p38 MAPK cascade

Under the effect of extracellular stimuli (e.g., mechanical stress, UV-radiation, oxidative stress, osmotic shock, hypoxia, proinflammatory cytokines such as IL-1/TNFα and lipopolysaccharide (LPS)), a concerted kinase cascade is set off, consisting of four hierarchically arranged levels (Fig. 1). The stimulus is relayed to an intracellular activator which, in turn, activates the MAP-kinasekinasekinases (MAP3Ks), such as ASK1, DLK1, TAK1, TAO, TPL2, MLK3, MEKK3/4, and ZAK. The MAP3Ks then activate the MAP-kinasekinases (MAP2Ks), such as MKK 3, 4, 6, and 7.

The p38 MAPKs are activated by the MAP2Ks via dual phosphorylation of the activation loop sequence Thr-Gly-Tyr. While both the MAP2Ks MKK3 and MKK6 are responsible for the activation of all four p38 MAPK isoforms, MKK4 specifically activates the isoforms 1 and 2 of the family of JNKs. Once being activated, the p38 MAPKs allow a swift and amplified response by activating a plethora of transcription factors and, in turn, activate downstream protein kinases and transcription factors that finally result in an increase of cytokine production, induction of apoptosis, leukocyte migration inflammatory responses, oxidative bursts, and degranulation. This complex signaling pathway allows redundancy and the development of escape mechanisms following chronic p38 MAPK inhibition.[1]

8.17.1.1.1.1 First generation antiinflammatory drugs

The p38α MAPK substrates MK2 and MK3 are particularly important in this inflammation pathway. This idea was demonstrated with knock-out mice which were insensitive to collagen-induced arthritis and much less sensitive to oxazolone-induced skin inflammation.

Encouraged by the idea of a possible decrease in the occurrence of adverse effects with simultaneously improved clinical safety, several companies initiated discovery programs for inhibitors with targets downstream of p38α MAPK. However, a recent review of publicly available data revealed no MK2 inhibitors involved in advanced stages of clinical development.[2]

In both in vitro models as well as in experimental in vivo arthritis models, p38α MAPK inhibitors effectively reduced or even completely suppressed the inflammatory events. Based on this knowledge, extensive research was undertaken for evaluation of new lead structures, identification of new target molecules, and for exploration of new synthetic strategies. Researchers at SmithKline Beecham (SKB) identified the mechanism of action of antiinflammatory pyridinylimidazoles as cytokine-suppressive

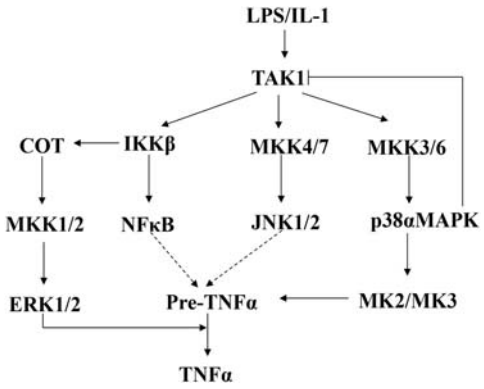

Fig. 1 Three major pathways lead to the activation of TNFα.[1]

antiinflammatory drugs and the resulting first prototype selective p38α MAPK inhibitor, SB203580 facilitated the experimental elucidation of various biological functions. However, clinical studies of this first generation p38α inhibitor revealed a dose limiting hepatotoxicity that may be due to interactions with the cytochrome P450 system.

8.17.1.1.1.2 Second generation antiiinflammatory drugs: Large variations in effectiveness against RA

The rationale for selecting p38α MAPK as a target for pharmacological intervention was based on the elucidation of its key role in the regulation of proinflammatory cytokine expression, the observations that p38α MAPK is highly activated in inflamed tissue from patients suffering from RA, inflammatory bowel disease, or COPD and on the demonstrated antiinflammatory efficacy of p38α MAPK inhibitors in experimental disease models which were associated with cytokine suppression.

Unfortunately, all p38α MAPK inhibitors that were advanced to clinical trials showed no effects that were superior to that of the placebo. Although the exact molecular mechanism behind this unexpected outcome has not yet been elucidated, p38α MAPK is generally no longer considered as a valid target for treatment of chronic inflammatory diseases.[2]

Highly potent and selective p38α MAPK inhibition could not provide efficacy and the treatment of chronic inflammatory diseases using p38α MAPK inhibitors remained unsuccessful. Despite excellent scientific rationale, it was shown that selective p38α MAPK inhibition was not sufficient for substantial long term TNFα inhibition due to the presence of various shunt or escape mechanisms.[1,3,4]

The failure of 22 p38α MAPK inhibitors in phase II/III RA studies demonstrated impressively the unforeseen lack of efficacy despite promising preclinical results.[5]

As described by Genovese: " … Finally, perhaps the most interesting science yet to be done will be that which yields a better understanding of why inhibition of this enzyme results in only a transient reduction in inflammation. Elucidating the cause of this phenomenon may yet help us understand how new classes of intracellular enzyme inhibitors may perform when they are evaluated in studies of inflammatory diseases."[6]

New approaches for the applicability of p38α MAPK inhibitors aim at indications that differ from RA, as well as distinct routes of administration, for example, treatment of COPD with an inhalative p38α MAPK inhibitor in contrast to the initial oral administration for RA treatment. Furthermore, in a shift of focus, the targets of p38α MAPK inhibitors have moved away from treatment of inflammation and toward the field of cancer. Recent research shows impressive results for the combination of Sorafenib with a selective p38α MAPK inhibitor in order to bypass the Sorafenib resistance of hepatocellular carcinoma which may be caused by an escape mechanism of the tumor via the p38α MAPK cascade.[7]

Additional approaches to overcome the aforementioned shunt or escape mechanisms that have developed out of p38α MAPK inhibition have been proposed. The cross-talk between the p38 MAPKs and the JNK or ERK-1/-2 pathway (**Fig. 1**) may offer a potential pathway of investigation. Both the JNKs and p38 MAPKs lead to the production of proinflammatory cytokines and thus enhance the inflammatory processes. One shunt and escape mechanism with reasonable impact on the failure of p38α MAPK inhibitors in clinical development is based on the overactivation of TAK1 which causes an overactivation of JNK pathways.[1–4]

Blockage of the p38 MAPK pathways leads to a positive feedback mechanism for JNK pathways. The intention to inhibit these bypasses gave rise to the idea that multitarget drugs inhibiting both key drivers of inflammatory processes may exhibit additive or even synergistic effects in vivo. Consequently, dual inhibitors of p38α MAPK and JNKs were developed and investigated. Deactivation of JNK3 and p38α MAPK provided neuroprotective effects as it resulted in complete rescue of primary striatal neurons from polyglutamine-expanded htt toxicity. Therefore, the design of dual JNK3/p38α MAPK inhibitors may be a promising strategy for treatment of, for example, Huntington's disease.[8]

In general, there has been a certain trend toward polypharmacology, even beyond the field of kinase inhibitors. In the words of Frantz, "Forget drugs carefully designed to hit one target, … a better way of treating complex diseases … may be to aim for several targets at once."[9]

8.17.1.1.2 Phosphodiesterase 4 (PDE-4)

The family of PDE-4 is cyclic adenosine phosphate (cAMP) hydrolyzing enzymes consisting of at least four subtypes (PDE-4 A, PDE-4 B, PDE-4 C, and PDE-4 D) which are primarily expressed in immune cells. They are involved in the regulation of a variety of cellular processes. The PDE pathway represents one of the most prominent mechanisms of degradation of cAMP, an important cellular second messenger. High intracellular concentration of the second messenger cAMP causes antiinflammatory signaling and thus, PDE-4 inhibition results in elevated intracellular cAMP levels which provide the antiinflammatory properties of PDE-4 inhibitors.

PDE-4 A and PDE-4 B are the predominant subtypes involved in inflammation. The role of PDE-4 C, with its very low expression levels, is unclear. The correlation of PDE-4 D inhibition with emesis is consistent with its expression in the brain and with knockout mouse studies that showed reduced or no emetic potential. Unfortunately, subtype selectivity for clinical PDE-4 inhibitors has not been reported by independent groups, thereby leaving a high level of uncertainty for the validity of this target.

Inhibitors of both p38α MAPK and PDE-4 have originally been considered as promising drugs for treatment of inflammatory disorders. In animal models PDE-4 inhibitors provided both bronchodilator and antiinflammatory effects. However, only a few PDE-4 inhibitors have reached approval with the most prominent examples being Roflumilast (Daxas EU, Daliresp US) in the treatment of a special subgroup of COPD affected patients and Apremilast (Otezla EU, US) in the treatment of psoriatic arthritis and severe plaque psoriasis.

Promising results from in vitro studies and experimental murine arthritis models suggested that Apremilast may also be effective for treatment of RA.[10]

In a phase II study, however, when Apremilast was administered at dose levels, which were efficacious in patients with psoriasis and psoriatic arthritis (20 mg b.i.d. and 30 mg b.i.d.) on top of a stable methotrexate treatment to patients with RA, no superior effect compared with placebo was achieved.[11]

As mentioned earlier, achievement of subtype selectivity of PDE-4 inhibitors has been a difficult task and thus, application of PDE-4 inhibitors is associated with nausea and emesis as major side effects. So far, for most of the developed PDE-4 inhibitors, the therapeutic window has not been large enough to achieve a significant clinical benefit at tolerated doses.[2]

In patients with asthma and COPD, TNFα, IL-1β, and IL-6 are found in increased amounts in the sputum and Bronchoalveolar lavage (BAL) fluid. Directly increasing the contractile response, TNFα acts directly on human airway smooth muscle. Furthermore, these cytokines amplify inflammation, in part through the activation of NF-κB, which leads to the increased expression of a number of inflammatory genes. However, treatment with biological TNFα blockers, such as IFX, produced relief in asthma patients, while COPD patients, in contrast, did not benefit from treatment with IFX when administrated at the doses that are effective in individuals with RA. An innovative and alternative strategy for treatment of airway inflammation is the application of small molecules with specific anticytokine action which interfere in cell signaling and thereby modulate the release of several cytokines.

In experimental models on airway inflammation, p38α MAPK inhibitors showed a significant effect whereas the results of in vitro experiments, which addressed the direct effect of the p38α MAPK inhibitors on the release of different cytokines were ambiguous. However, stimulation of macrophages from lung tissue and isolated monocytes from peripheral blood with LPS, p38α MAPK inhibitors significantly reduced expression and release of TNFα.[2]

Due to their lack of efficacy in RA and their emetogenic potential respectively, neither p38α MAPK inhibitors nor PDE-4 inhibitors met the high expectations as therapeutic targets for treatment of inflammatory disorders, when administered as monotherapy. However, the combination of PDE-4 inhibition with the antiinflammatory properties of p38α MAPK inhibition may be a successful approach. The conclusion that inhibition of p38α MAPK is not a valid strategy in chronic inflammation such as RA is based on the results of clinical phase II studies, in which the p38α MAPK inhibitor was administered either alone or in combination with Methotrexate (MTX). Surprisingly, except for a very few in vitro studies, the potential of p38α MAPK inhibition, when combined with a second mode of action, has never been systematically investigated.

This article reports the discovery of CBS-3595, a dual p38α MAPK/PDE4 inhibitor as well as the results of its evaluation in preclinical and phase I studies to elucidate this potentially synergistic antiinflammatory effect of dual inhibition of these two enzymes.

8.17.2 Chemistry: 1,2,4,5-Tetra-Substituted 2-Thioimidazoles: Preferred Templates to Target the ATP-Site of Protein Kinases

Starting from SKF-86002, initially reported as early as 1988, the reference compound SB203580 was developed as the prototypic p38α MAPK inhibitor with major off-target activity in the JNKs. This series of compounds were extremely valuable as tools and chemical probes, but suffered from CYP-450 interactions.[5] Fig. 2 shows the development of SB203580 and the tetrasubstituted 2-thioimidazoles from the early dihydrothiazoline-derived lead compound SKF-86002.

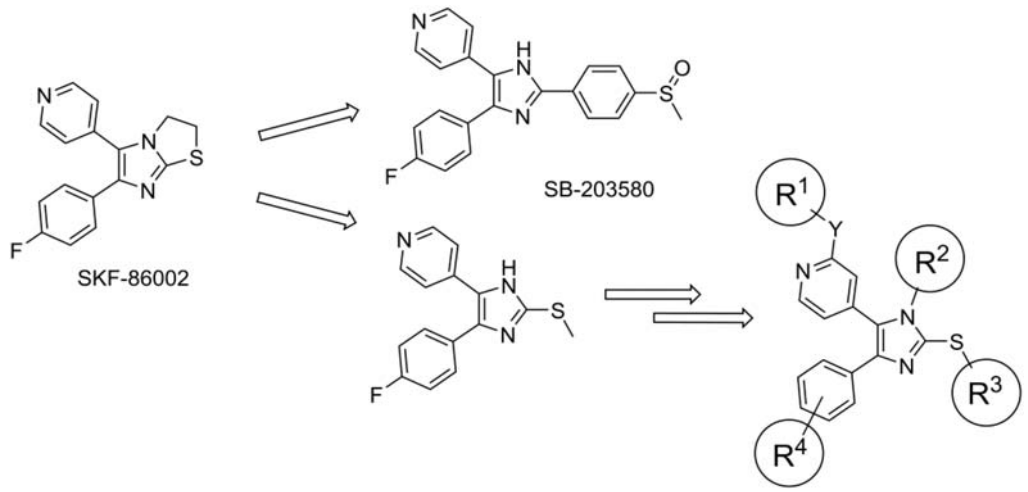

Fig. 2 Template development of tetrasubstituted 2-thioimidazoles from the Laufer Group.

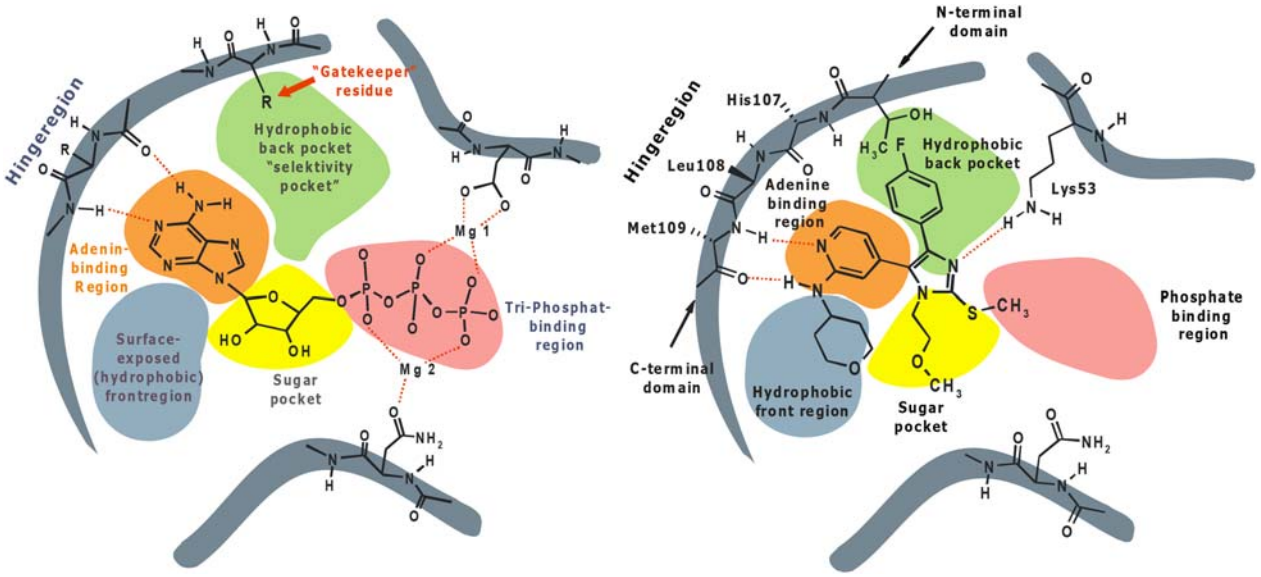

Fig. 3 Schematic binding modes of ATP (according to the Traxler model) and a tetrasubstituted 2-thioimidazole inhibitor to the ATP binding pocket according to Ref. 13.

Still maintaining the SKF-86002-derived pyridinyl-imidazole scaffold as the core structure, we cleaved the thiazole-ring of SKF-862002 in a manner that kept the sulfur atom at position 2 of the imidazole ring. Depending on the substitution pattern of these 2-thioimidazoles, the CYP-450 interactions could be reduced substantially.[12]

Tetrasubstituted 2-thioimidazoles are a perfect template to address the ATP binding site of protein kinases as shown in Fig. 3. In various research programs targeting, for example, p38 MAPKs, JNKs, Creatine kinase (CK), and Epidermal growth factor receptor (EGFR) we have synthesized more than 2500 compounds over the years. The synthetic strategies are extremely flexible and allow regioselective synthesis of a wide range of tri- and tetrasubstituted derivatives. For a general sketch, see Fig. 4. The outcome of this work is described in patents (WO 2002066458, WO 2004018458, WO 2006089798, and WO 2008023066) and numerous publications.

This compound collection (CBS library) with distinct substitution patterns (R^1–R^4) covers a broad range of specific interactions at the ATP binding site. Fig. 5 gives an overview.

1. Hydrophobic substituents at the pyrimidine ring (R^1)
2. Substitution of the imidazole ring (R^2)
3. Substitution of the sulfur atom in position C-2 for different substituents (R^3)
4. Substitution of the phenyl moiety (R^4)

Modification of the substituents at these four locations allows the regulation of selectivity and potency toward p38α MAPK, JNKs, CKs, EGFRs, and others.

Fig. 3 illustrates the binding interactions between the amino acids of the ATP-binding pocket of p38α MAPK and ATP as well as for one of our inhibitor molecules. The main interactions, as, for example, hydrogen bonds which are essential for the inhibitor's affinity, are shown.

Analyzing the Structure–activity relationships (SARs) within the CBS library comprising 2500 compounds, we could postulate for, for example, p38α MAPK: optimal interactions with the enzyme requires the tetra-substituted2-thioimidazoles to possess a 4-pyridinyl moiety, a 4-fluorophenyl group, and an unsubstituted N-atom in the imidazole ring adjacent to the 4-fluorophenyl group.

The nitrogen atom of 4-pyridinyl moiety interacts with the backbone amide-NH of Met109 located in the hinge region via a hydrogen bond. The 4-fluorophenyl ring is buried in the hydrophobic region I (selectivity pocket), which is limited by the so-called gatekeeper amino acid Thr106. The imidazole N-3 accepts a hydrogen bond from the ε-amino group of the Lys53 side chain.[8]

For the JNKs and CKs, some SARs could be derived as well; for other hits, for example, for EGFRs, were more random.

8.17.2.1 In Vitro and In Vivo Pharmacodynamics

In in vitro assays employing the isolated enzymes, the tetrasubstituted 2-thioimidazoles showed potent inhibition on p38α and JNK3 with IC_{50} values within the low nanomolar range and good kinome selectivity (for details, see synthesis references 8,12,13,15,17–29 and patents).

Furthermore, these compounds effectively prevented the release of TNFα and IL-1β from human Peripheral blood mononuclear cells (PBMCs) and human whole blood in vitro. Unfortunately, there was only a poor correlation between the enzyme data and data

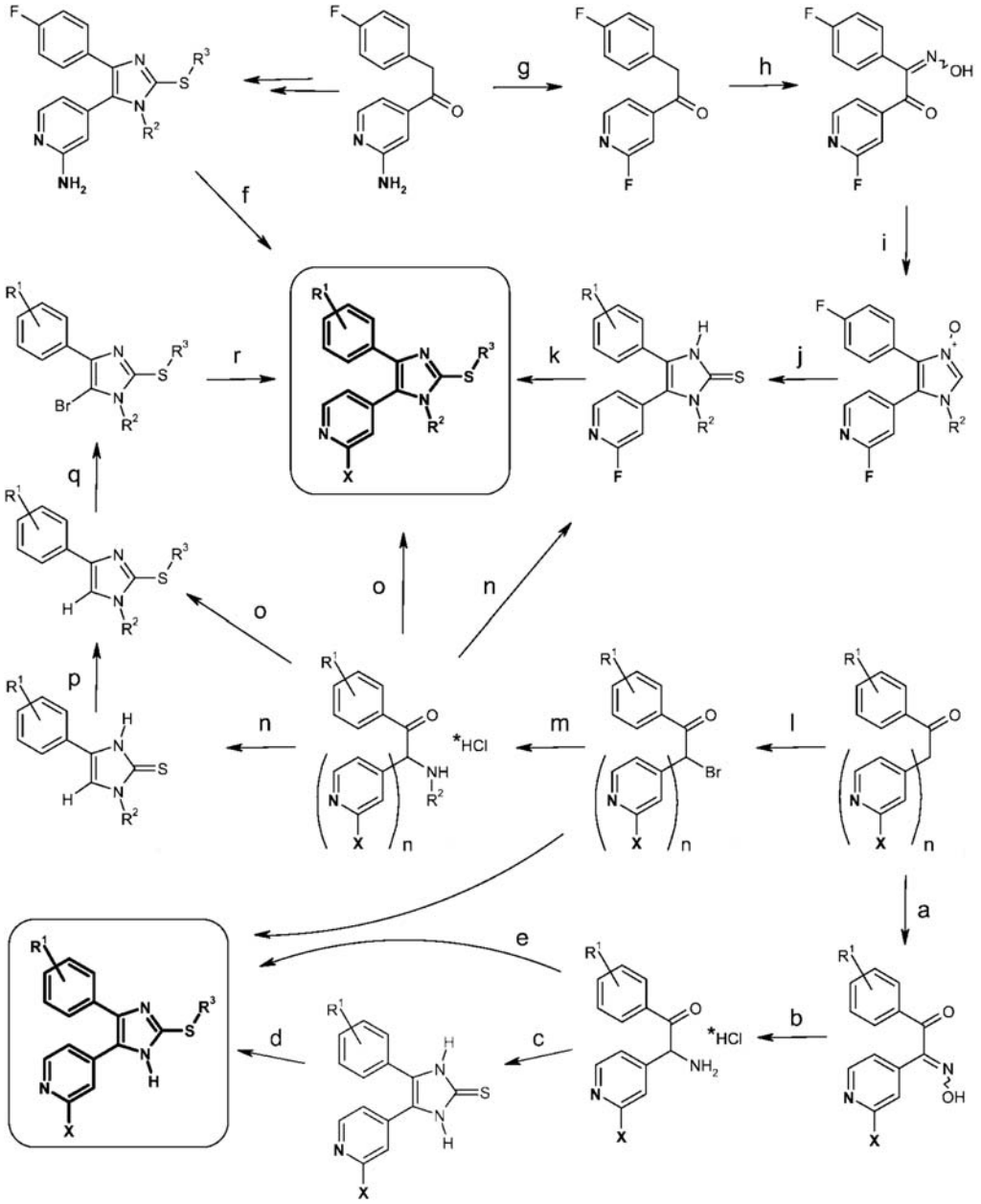

Fig. 4 Synthetic strategy to address all four substitution positions regioselectively; about 2500 compounds have been synthesized (CBS library). This overview was modified from Refs. 13–15. Reagents and conditions: (A) $NaNO_2$, AcOH, room temperature; (B) H_2, Pd/C, 1 atm, HCl in iPrOH, room temperature; (C) N,N-Dimethylformamide (DMF), Potassium thiocyanate (KSCN), reflux; (D) MeI, EtOH/THF, reflux, see also Ref. 12; (E) DMF, methyl-/ethyl-/benzylthiocyanate, reflux; see also Ref. 16; (F) 50% HBF_4 (aq), $NaNO_2$, 0-45°C; (G) $NaNO_2$, 70% HF in pyridine (Olah's reagent), −15 to −10°C to room temperature; (H) $NaNO_2$, AcOH, room temperature; (I) $(H_2CNR^2)_3$, EtOH, reflux; (J) 2,2,4,4-tetramethylcyclobutane-1,3-dithione, Dichloromethane (DCM), room temperature; (K) Hal-R^3, K_2CO_3, MeOH, room temperature; (L) Br_2, AcOH, room temperature; (M) excess H_2N-R^2, DCM, −5 to 0°C, then HCl in EtOH, Et_2O/acetone; (N) KSCN, DMF, reflux; (O) R^3-SCN, DMF = N,N-Dimethylformamide, reflux; (P) Hal-R^3, K_2CO_3, MeOH, room temperature; (Q) 1-Bromo-2,5-pyrrolidinedione (NBS), CCl_4, 0°C to room temperature; (R) $Pd(PPh_3)_4$ or $Pd(PPh_3)_2Cl_2$/PPh_3, Na_2CO_3 or K-OAc, toluene or DMF, 80-120°C. Parentheses: n=1: 4-pyridinyl- or n=0: hydrogen.

from pharmacologically more complex models as, for example, whole blood data. Thus, neither p38α MAPK inhibition, nor JNK3 inhibition, nor a combination of both correlated sufficiently with TNFα release from human whole blood, a complex but very predictive test system for in vivo models.

To evaluate their in vivo efficacy, inhibition of TNFα release was determined in an LPS/Galactosamine (D-Gal) mouse model after p.o. administration of a p38α MAPK selective compound (CBS-3408) and a dual p38α MAPK/JNK3 inhibitor (CBS-3435), both derived from the CBS library (Fig. 5).

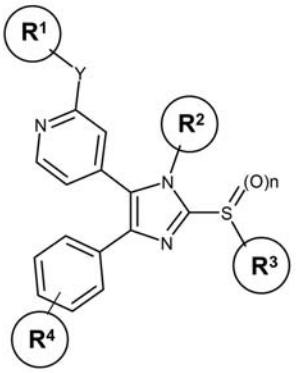

CBS #	R^1	R^2	R^3	R^4	n
3403	$NHCHCH_3Ph$	H	CH_3	4-F	0
3408	NHAc	CH_3	CH_3	4-F	0
3435	NHPh	H	CH_3	4-F	0
3595	NHAc	CH_3	CH_3	4-F	1
3728	NH_2	CH_3	CH_3	4-F	1

Fig. 5 Examples of pyridinyl-imidazole core structure substitution generating compounds of the CBS library.

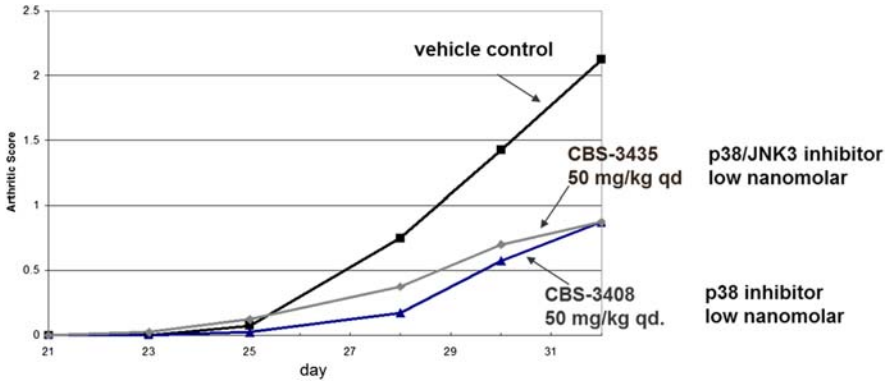

Fig. 6 Effect of CBS-3408 and CBS-3435 on collagen-induced arthritis in DBA/1 mice.

In the well-established collagen-induced arthritis in DBA/1 mice, a superior activity of the dual inhibitor was assumed, but even if the dual inhibitor CBS-3435 showed a slightly earlier onset. Surprisingly, both compounds reached the same arthritic score after 32 days. Also other compounds with inhibitory activities shifted to either one or the other enzyme and did not allow a correlation between in vivo activity and p38/JNK3 balance (Fig. 6).

8.17.3 Discovery of Dual p38α MAPK and PDE4 Inhibitors: Promising Compounds for Treatment of Inflammatory Disorders

The p38 MAPK inhibitors of the chemical class of pyridinylimidazoles have been intensely investigated and since the discovery of SB203580, many derivatives have shown substantially improved kinase selectivity and reduced liver toxicity potential (Fig. 7).

CBS-3408 is a low nanomolar p38α MAPK selective inhibitor. When applying CBS-3408 in an animal toxicology study, the compound was very well tolerated by rodents and gave clean in vitro toxicology outcomes. However, administration of CBS-3408 showed in the *Cynomolgus* monkey gender specific pharmacokinetics. Parallel metabolic studies discovered sulfoxidation as one pathway of metabolism (Fig. 8).[29]

Stimulated by these findings, a series of sulfoxides and sulfones were synthesized, finally leading to CBS-3595. This compound, having only moderate activity on both p38α MAPK and PDE-4 (around 200 nM), showed excellent in vitro and in vivo activities in various models of TNFα-driven inflammation.

At first glance, this sulfoxidation was considered as unfavorable, as its kinetics differed significantly between male and female animals in pharmacokinetic studies. Providing pro-chiral features, oxidation of the sulfur atom of the imidazole-S-alkyl-group may lead to two distinct enantiomers. Nevertheless, the dual inhibitory properties of CBS-3595 toward p38α MAPK and PDE-4 were verified in a variety of screening approaches. These approaches included in vitro characterization of the inhibitory potency on the isolated enzymes and kinome selectivity. Ex vivo experiments were performed to evaluate the compound's ability to reduce TNFα release from LPS-stimulated whole blood from human, rat, and monkey.

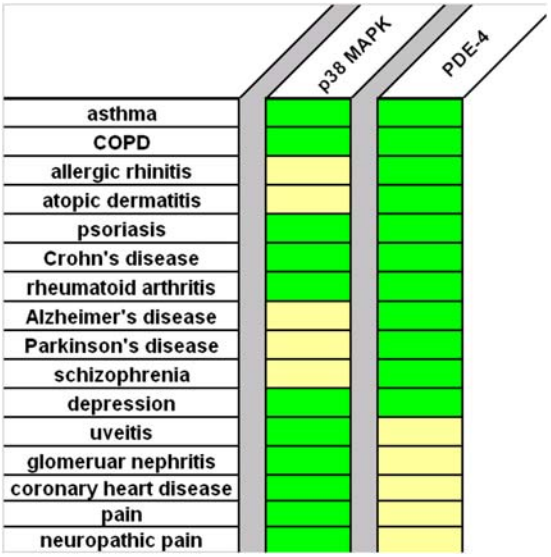

Fig. 7 Potential indications of p38α MAPK and PDE-4 inhibitors based on nonclinical experimental models and clinical studies according to Ref. 2. There is a substantial overlap with a chance of synergism by dual inhibition.

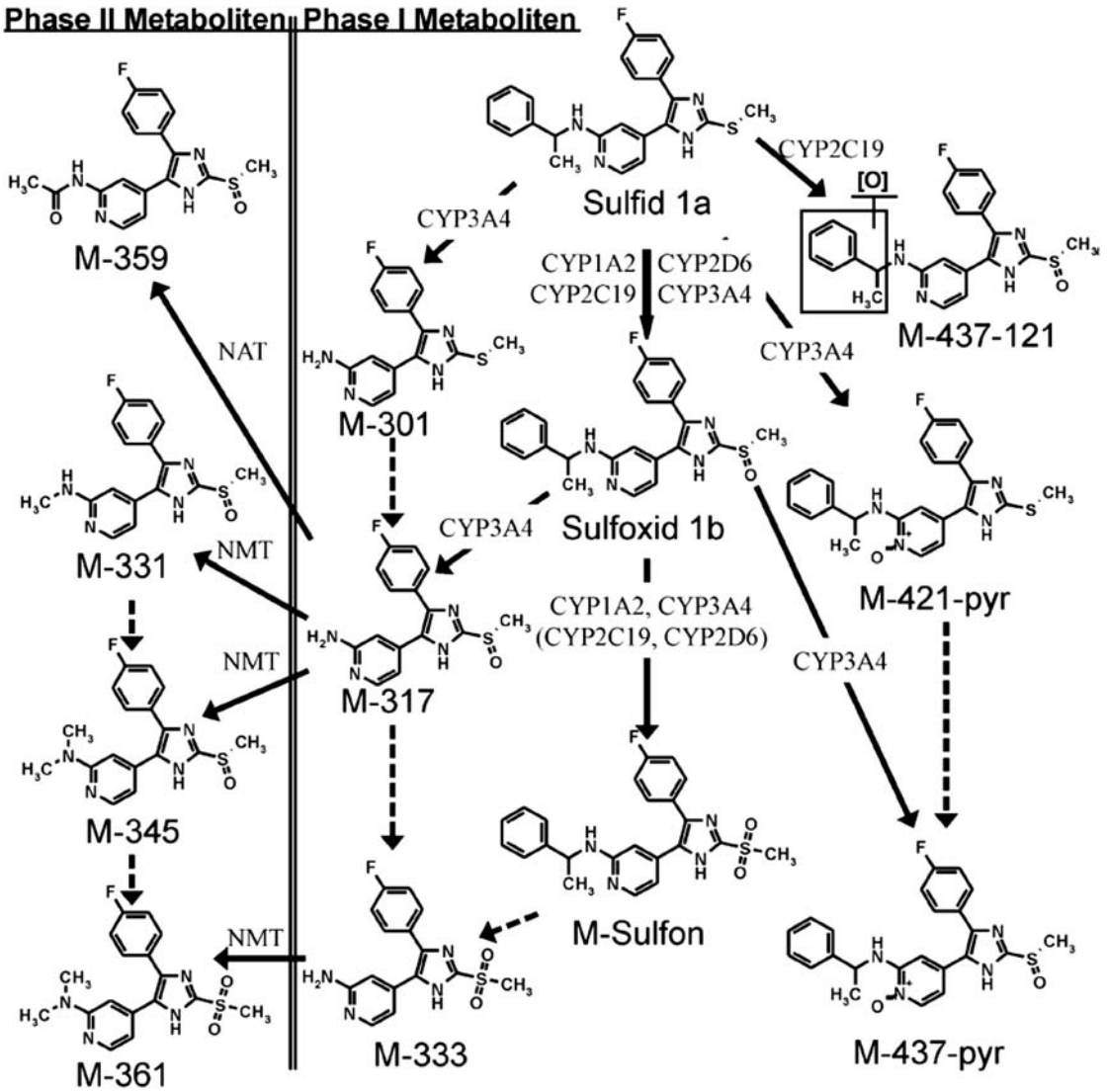

Fig. 8 Metabolic pathways of 2-thioimidazoles according to Ref. 29.

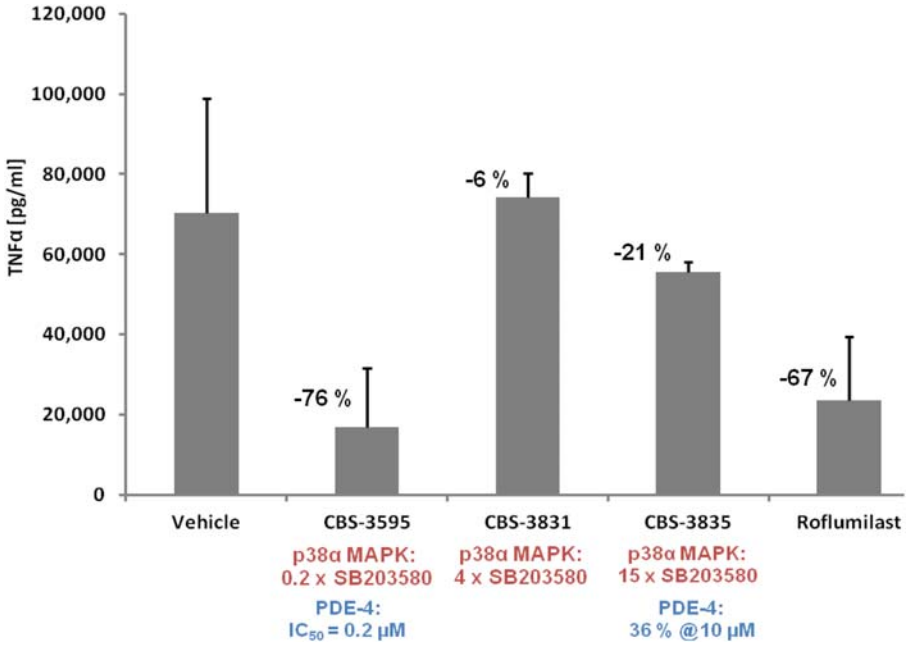

Fig. 9 Comparison of dual p38α MAPK/PDE-4 inhibitors bearing the tetrasubstituted imidazoles core with distinct inhibitory potencies with regard to their inhibition of TNFα release. Inhibition of TNFα release in Wistar rats following LPS-challenge.

Pharmacokinetic evaluations for determination of achieved plasma levels and relationship between dose and plasma concentrations were carried out in rats, dogs, and primates and also the metabolism of CBS-3595 was characterized.

CBS-3595, a dual p38α MAPK/PDE-4 inhibitor, was discovered by coincidence during preclinical experiments with CBS-3408, which is a selective and highly potent p38α MAPK inhibitor. In contrast, CBS-3595 shows only moderate, but well-balanced IC_{50} values of 100-500 nM and 200 nM for p38α MAPK and PDE-4, respectively. Sulfoxidation during metabolism of CBS-3408 yielded CBS-3595, which featured increased affinity toward the PDE-4 enzyme. Like p38α MAPK, PDE-4 represents an attractive target for treatment of chronic inflammatory diseases. Consequently, this specific class of dual inhibitors could result in the establishment of a new class of antiinflammatory drugs.

The inhibition of both p38α MAPK and PDE-4 seems to be synergistic. Neither p38α MAPK alone nor PDE-4 shows a similar effect on, for example, TNFα release in vivo. Even very potent p38α MAPK inhibitors such as CBS-3835 (15 times more potent than reference compound SB 203580) or Roflumilast, a registered PDE-4 inhibitor with an IC_{50} of 200 nM, feature similar performance as CBS-3595 (Fig. 9).

8.17.3.1 Chemistry of CBS-3595

The common synthetic route of CBS-3595 yielded the compound as racemic mixture. Single enantiomers are accessible via an enantioselective sulfoxidation in a good yield of 77% and an excellent optical purity of 98% ee, as described in Ref. 18 in more detail (Fig. 10).

8.17.3.1.1 Profiling of CBS-3595

R-CBS-3595 is one metabolite (sulfoxide) of CBS-3408 and due to its PDE-4 inhibition, is considered to account for the emetic side effects in monkeys when given in very high doses. This p38α MAPK/PDE4 inhibitor (100-500 nM/200 nM) is somewhat balanced in the middle nanomolar range.

Only the *R*-enantiomer is formed in vivo. This enantiomer is 10 times more active against PDE-4. In contrast, *S*/*R* enantiomers are equally active against p38α MAPK.

8.17.4 From in vitro Experiments Into Phase-I Clinical Trial: CBS-3595, a Dual Inhibitor of p38α MAPK/PDE-4

In a series of in vitro, ex vivo, and in vivo experiments, the potency of CBS-3595, its systemically available and pharmacologically active metabolite CBS-3728 and the reference compound SB203580 to suppress the production of the proinflammatory cytokine TNFα was demonstrated. These data indicated that CBS-3595 is a promising clinical candidate for treatment of human immune diseases which relate to the overproduction of TNFα.

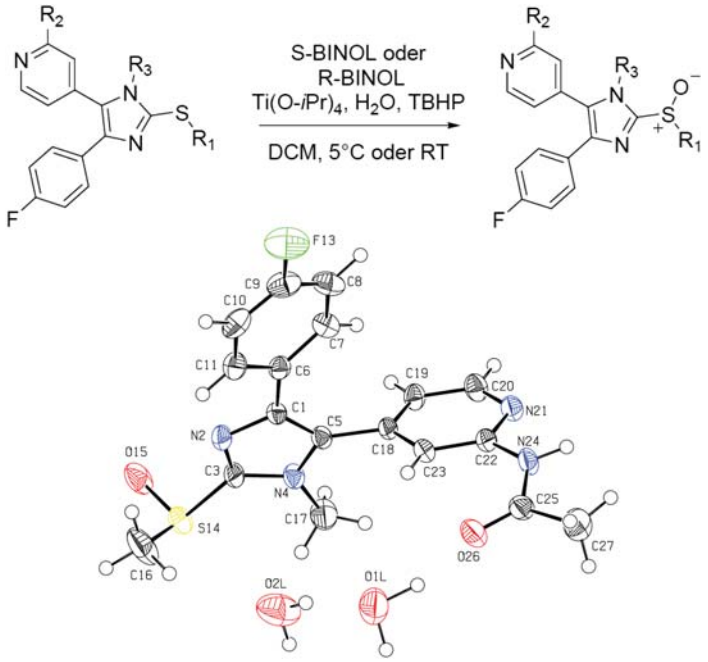

Fig. 10 Enantioselective synthesis of CBS-3595 and crystallographic confirmation of the R-conformer according to Ref. 18. Stereochemistry confirmed by x-ray single crystal analysis. CBS-3595 substitution: $R_1 = CH_3$; $R_2 = NHAc$; $R_3 = CH_3$.

Experiments for evaluation of the safety profile of CBS-3595 included acute toxicity and dose-finding studies as well as a 4 week toxicity study in the rat including a 2 week recovery phase. Moreover, the maximum tolerated dose was studied in Cynomolgus monkeys and also a 4 week toxicity study in Cynomolgus monkeys including a 2 week recovery phase was performed.

Above that, the mutagenic and carcinogenic potency was evaluated with an AMES test and also cytogenetic assay in human lymphocytes and an in vivo micronucleus test in mice.

The in vivo efficacy of CBS-3595 was first investigated in a polyarthritis rat model and a transgenic mouse model before the first clinical human use study was carried out in 44 volunteers for investigation of safety, tolerability, and pharmacokinetics and ex vivo pharmacodynamics of CBS-3595.

8.17.4.1 Nonclinical Evaluation of CBS-3595 and Its Metabolite CBS-3728

8.17.4.1.1 IC_{50} determination in in vitro kinase activity assays

Surface plasmon resonance studies with CBS-3595 and SB203580, an ATP-competitive, 4-(4-fluorphenyl)-5-pyridyl-imidazole p38α MAPK inhibitor, suggested that CBS-3595 was also an ATP-competitive p38α MAPK inhibitor.

The activity of recombinant p38α MAPK was inhibited with an IC_{50} of 4.19 ± 1.08 μM (mean ± SEM; $n = 8$) by CBS-3595 and 4.12 ± 1.45 μM (mean ± SEM; $n = 3$) for CBS-3728. The IC_{50} value for the reference compound SB203580 determined in this experiment was 0.45 ± 0.15 μM (mean ± SEM; $n = 12$). The activity in various p38α MAPK phosphorylation assays ranged between 200 and 500 nM.

PDE-4 expressed in U937 cells was inhibited by CBS-3595 and CBS-3728 with IC_{50} values of 0.2-0.4 μM and 1.98 μM, respectively.

8.17.4.1.2 Investigation of kinome selectivity and other potential off-targets

For evaluation of its kinome selectivity, a concentration of 10 μM of CBS-3595, corresponding to a concentration which was achieved in vivo during toxicological studies, was tested against a panel of 134 kinases (radiometric screening technology KinaseProfiler, Upstate, United Kingdom). Other p38 MAPK isoforms were inhibited by 18% (p38β), 0% (p38γ), and 35% (p38δ). JNK2α2 and JNK3 were inhibited by 51% and 76%, respectively.

Relevant off-target hits were JNK2α2, JNK3, and CK1δ (51%, 76%, and 94% of inhibition at 10 μM). Furthermore, the adenosine A_1 receptor was influenced to a lesser extent by CBS-3595 and CBS-3728 (50% and 40% of inhibition at 10 μM, respectively).

Apart from the above results, a set of 39 other G-protein coupled receptors remained unaffected after incubation with 10 μM of CBS-3595 and CBS-3728, as evaluated by a radioligand binding assay (MDS Pharma Services, Profiling Assays, Taiwan).

Additionally, the PDE isoforms PDE-3 and PDE-5 remained unaffected at a concentration of 10 μM of both CBS-3595 and CBS-3728.

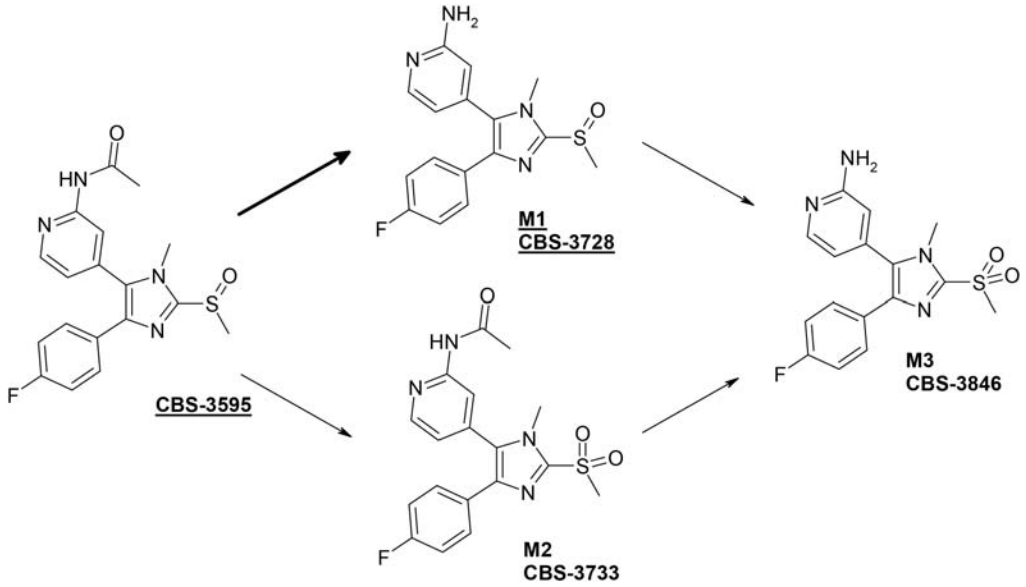

Fig. 11 Metabolic pathways of CBS-3595. http://emboj.embopress.org/content/22/21/5793.

8.17.4.1.3 Metabolism studies

In vitro absorption studies with Caco-2 cells indicated good membrane permeability and that CBS-3595 was not a substrate of P-glycoprotein. In vivo efficacy studies show excellent plasma levels after oral administration.

In vitro metabolism studies performed with liver microsomes from humans, rats, and monkeys as well as with human hepatocytes, demonstrated moderate to high metabolic stability of CBS-3595.

Two metabolites were identified: cleavage of the *N*-acetyl bond leading to the pharmacologically active metabolite M1 (CBS-3728) and oxidation to the sulfone leading to M2 (CBS-3733) as shown in Fig. 11.

However, it is unknown if the two enantiomers of CBS-3595 differ in metabolism and rates.

CBS-3595 had a low affinity toward plasma proteins. The unbound fraction varied between 78.1% and 90.0% in human, 63.1-86.3% in rat, and 58.3-66.7% in monkey plasma.

In vivo pharmacokinetic data were generated from the rat, dog, and Cynomolgus monkey. Despite the lack of pharmacokinetic data following intravenous drug administration, the extent of drug absorption of CBS-3595 appears to be similar in all species. After C_{max} was reached, a monophasic decline of plasma concentrations was observed in dogs, rats, and monkeys. Elimination half-lives of approximately 4 h in mongrel dogs, 8 h in beagle dogs, 1.8-2.2 h in rats, and 4-6 h in monkeys were determined. Therefore, the systemic elimination appears to be more rapid in rats when compared to dogs and monkeys. In all species, systemic exposure increased with the administered dose. In monkeys, no gender-specific pharmacokinetics was observed. Systemic exposure to CBS-3728 was much lower in monkeys compared to rats and dogs.

The metabolites of CBS-3408 were further characterized and it was found that mainly the *R*-enantiomer (*R*-CBS-3595) is formed in vivo. As mentioned earlier, the stereochemistry was confirmed by x-ray single crystal analysis. However, for synthesis of larger amounts of *R*-CBS-3595, methods allowing an enantioselective oxidation had to be developed, as the conventional chemical oxidation resulted in a racemic mixture of both enantiomers.

With regard to inhibitory activity against PDE-4, *R*-CBS-3595 showed a 10-fold higher potency, while both the *S*-enantiomer and the *R*-enantiomer of CBS-3595 were equally active toward p38α MAPK.

8.17.4.1.4 Effect of CBS-3595 on leukotriene B_4 (LTB_4) release in LPS/fMLP-stimulated human whole blood

In this assay, the reduction of the fMLP/LPS-triggered release of the eicosanoid lipid mediator LTB_4 from human whole blood was evaluated for CBS-3595 and Roflumilast was determined. Both compounds were able to reduce the levels of LTB_4 in a concentration-dependent manner. However, Roflumilast was more potent when compared to CBS-3595 which correlates with stronger inhibition of PDE-4. The p38 MAPK reference inhibitor SB203580 served as the negative control and, as expected, had no effect in this assay.

8.17.4.1.5 Effect of CBS-3595 on TNFα release in the rat following LPS-challenge

The in vivo efficacy of CBS-3595 was investigated in the rat model of LPS-induced TNFα release. In the first study using Sprague Dawley rats, a clear dose-response relationship was observed and ED_{50} and ED_{80}-values of 1 and 3 mg kg^{-1} p.o., respectively were calculated. These values correlated well with the determined serum concentrations of CBS-3595. These findings were later confirmed in additional studies with Lewis rats and Balb/c mice.

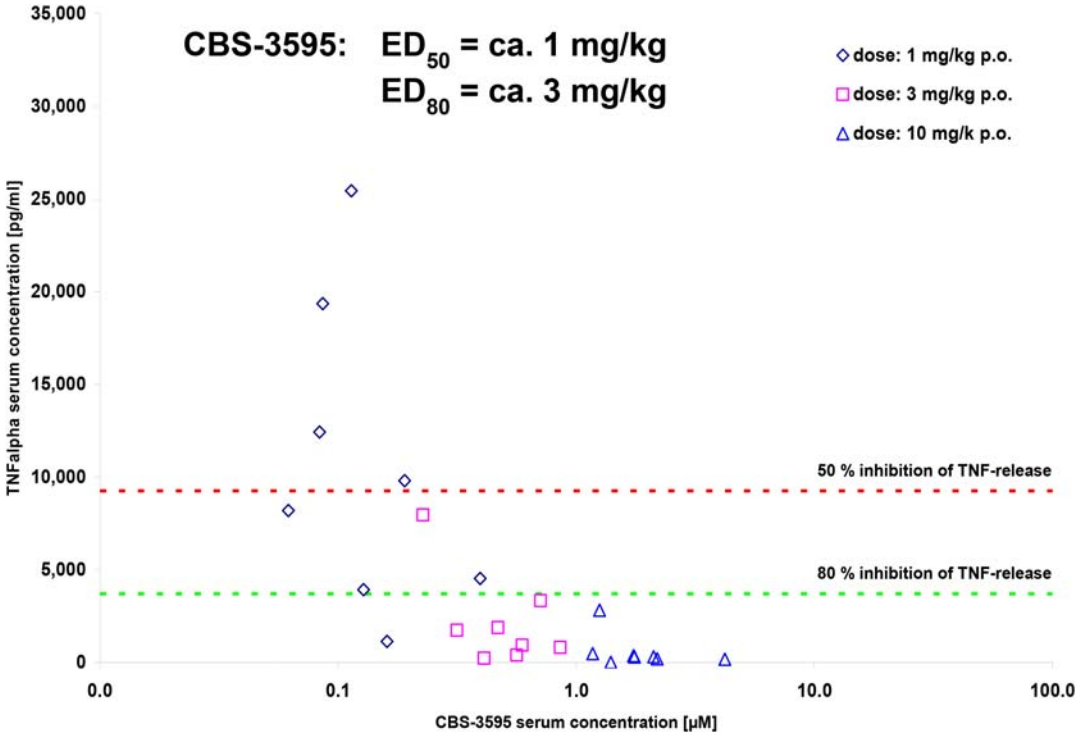

Fig. 12 Relationship between individual CBS-3595 serum concentrations, determined 2 h post LPS-challenge (3 h postdose) and TNFα release.

In detail, administration of 1, 3, and 10 mg kg^{-1} CBS-3595 led to a more effective inhibition of TNFα release of 43%, 88%, and 96%, respectively, while 3 mg kg^{-1} of SB203580 only led to a mean inhibition of TNFα release of 37%. This compares to a no-adverse-effect-level of 15 mg kg^{-1} day^{-1} p.o. as determined in the 4 weeks toxicity study in Sprague Dawley rats.

Thus, CBS-3595 is more potent in reduction of TNFα release when compared to the reference compound SB203580 and at least as effective as Roflumilast in these experiments. In TNF-transgenic mice, which develop a chronic inflammatory and destructive polyarthritis, CBS-3595 demonstrated beneficial effects on paw swelling, synovitis, erosion, and cartilage damage during 4 weeks of treatment.

The relationship between drug concentrations, determined 2 h post LPS-challenge (i.e., 3 h postdose) and TNFα release is illustrated in Fig. 12.

In seven out of eight animals dosed with 3 mg kg^{-1}, the TNFα concentrations were below the value which corresponds to an 80% inhibition. After administration of 10 mg kg^{-1}, the TNFα concentrations in all animals were below this 80% limit.

A second study clearly demonstrated that the extent of TNFα release depends on the time point of dosing. The closer the time of dosing to LPS-challenge, the higher the plasma concentrations at 1.5 h postdose, and the higher the inhibition of TNFα release. The comparison of data obtained with male and female animals indicated the absence of gender-specific differences in pharmacokinetics or efficacy. As already demonstrated in the first study, CBS-3595 was more effective than the reference compound SB203580 in blocking TNFα release (see Fig. 13).

When compared to Roflumilast in a head-to-head setting, both CBS-3595 and Roflumilast exhibited comparable effects toward the inhibition of TNFα release, with mean inhibition values of 8% and 67%, respectively.

8.17.4.1.6 Effect of orally administered CBS-3595 on TNFα release in ex vivo-stimulated whole blood in Cynomolgus monkeys

As part of the 4 week toxicity study in *Cynomolgus* monkeys, toxicokinetic blood sampling was also used to investigate the effect of orally administered CBS-3595 on TNFα release in ex vivo stimulated whole blood. In this study, a dose- and time-dependent inhibition of TNFα release was demonstrated. Following the first dose, a clear dose-dependent effect was observed. At the end of the 4 week treatment period, the highest efficacy was observed at the intermediate (males) and low dose levels (females).

Animals were treated with vehicle (five males, five females), 6 mg kg^{-1} day^{-1} (three males, three females), 12 mg kg^{-1} (three males, three females), and 20 mg kg^{-1} (five males, five females).

After 2 weeks of treatment, the high dose was increased to 25 mg kg^{-1}. On day 1 and day 27, blood samples were taken 1, 4, and 8 h postdose (on day 27 also 24 h postdose), for ex vivo stimulation with LPS. After 4 h of incubation at 37°C, plasma was harvested and TNFα concentrations were determined by ELISA.

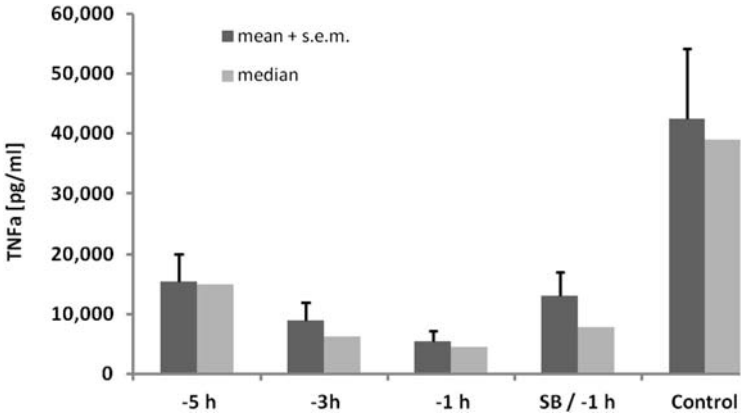

Fig. 13 Influence of time point of dosing with CBS-3595 on the inhibition of TNFα release in rats after LPS challenge and correlation with plasma concentrations.

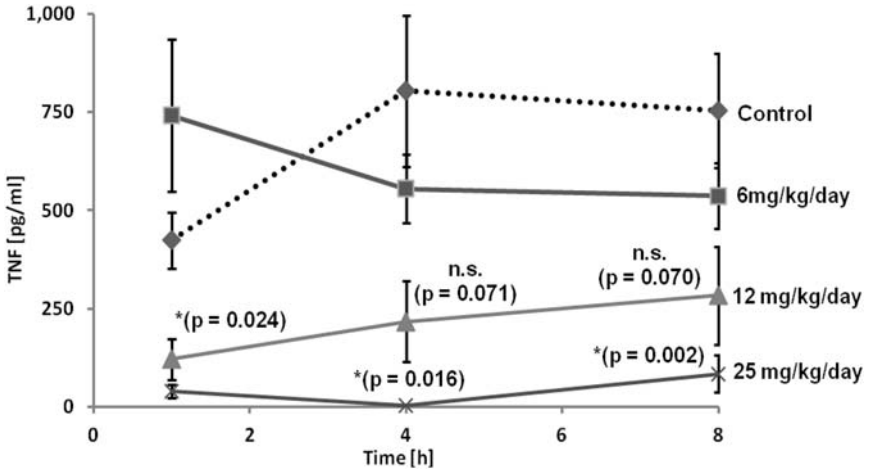

Fig. 14 Effect of orally administered CBS-3595 on TNFα synthesis in ex vivo LPS-stimulated whole blood from Cynomolgus monkeys.

In control animals, TNFα concentrations determined at 1 h postdose were substantially lower compared to the values determined at later time points. This result suggests that stress associated with repeated toxicokinetic blood sampling may have induced an endogenous TNFα production or may have increased the susceptibility to ex vivo added LPS.

Furthermore, it could be demonstrated that oral administration of CBS-3595 led to a substantial reduction of TNFα levels following ex vivo stimulation. The effect of orally administered CBS-3595 on TNFα release in ex vivo-stimulated whole blood was investigated in *Cynomolgus* monkeys.

In Fig. 14, TNFα levels determined in male and female animals on day 1 are illustrated demonstrating inhibition of TNFα after administration of CBS-3595 compared to vehicle.

8.17.4.1.7 Efficacy in hTNF-transgenic mice

A very challenging model for RA is human TNF (hTNF)-transgenic mice as only few highly active compounds show activity.[30] Even very potent p38α MAPK inhibitors from the structural class of pyridinyl imidazole from Roche and Aventis, Ro-4399249 and AVE-8677, gave moderate results even at a high dose of 100 mg kg^{-1} qd.[30]

In contrast, CBS-3595, at a dose of 20 mg kg^{-1} yielded similar activity to IFX, the current gold standard in RA after 10 days of treatment, showing again superior activity of dual p38α MAPK/PDE-4 inhibition (Fig. 15).

8.17.4.1.8 CBS-3595 in a complete Freund's adjuvant (CFA) arthritis model using male Wistar rats

A study comparing the efficacy of p38α MAPK inhibition of CBS-3595 versus ML3403, a known potent p38α MAPK inhibitor was conducted, the desired outcome being the decrease in TNFα plasma levels in a CFA arthritis model using male Wistar rats.

The reduction of TNFα levels after 21 days in the CBS-3595 group was significantly lower than in the ML3403 group (see Fig. 16). These results indicated that the decrease of TNFα levels could not be accounted for solely by p38α MAPK inhibition.[31]

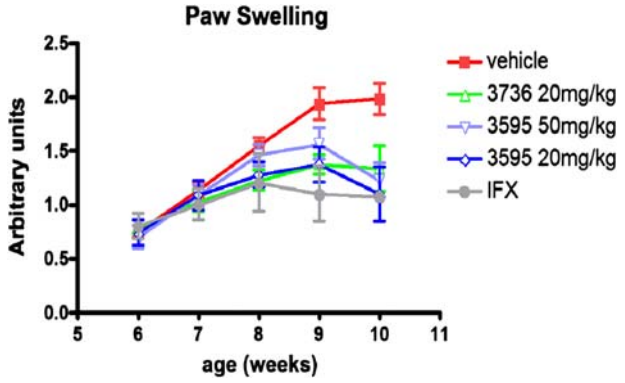

Fig. 15 Efficacy of CBS-3595 in hTNF-transgenic mice in comparison to Infliximab (IFX).

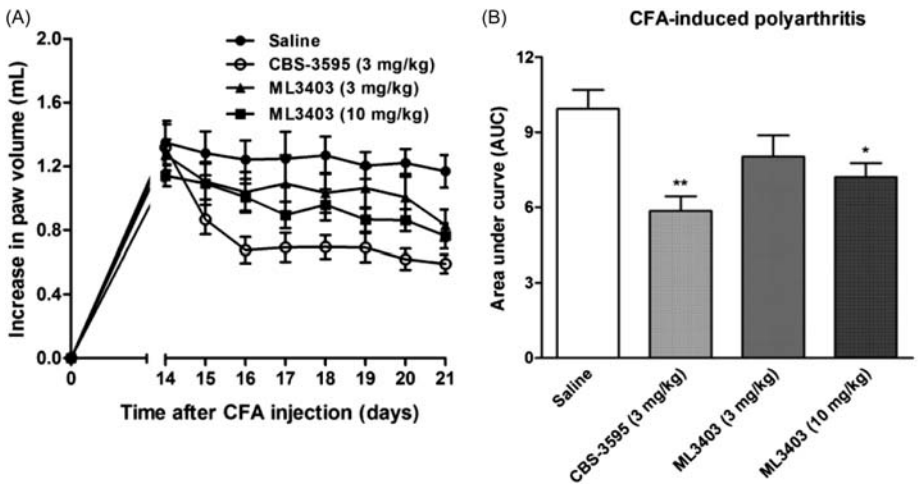

Fig. 16 Rheumatoid arthritis model and results for CBS-3595.

Similar results were claimed but not fully published for CGH2466 (Fig. 17), which proved to be a dual inhibitor of p38α MAPK and PDE-4 as well.

8.17.4.1.9 Safety pharmacology studies

The effects of CBS-3595 on vital functions, that is, CNS, respiratory tract, and cardiovascular system were investigated in vivo. In addition, the effect of the compound on the hERG channel was tested in an electrophysiological in vitro assay. However, based on expected maximum plasma concentrations in the range below 10 μM, the observed inhibition (IC_{50} = 213 μM) is without any safety relevance.

The effect of CBS-3595 on CNS activity was investigated after a single oral administration to conscious rats. Besides the observation of excessive defecation and soft feces after treatment with the test item at the dose levels of 30 and 300 mg kg^{-1}, loud breathing and excessive salivation were also noted on some occasions after treatment with CBS-3595 at the dose level of 300 mg kg^{-1}. No modifications in the reactivity to manipulation and stimuli associated with administration of CBS-3595 were reported at any of the dose levels tested. Thus, it was concluded that CBS-3595 had no major effects on the central nervous system at any of the tested dose levels.

The effects of CBS-3595 on cardiovascular function and cardiac electrophysiology were investigated after a single oral administration of 6, 12, and 20 mg kg^{-1} to conscious *Cynomolgus* monkeys with implanted telemetric devices. As the only clinical sign of this study, traces of whitish vomiting were reported for some animals at all dose levels of CBS-3595.

When compared to the control group, CBS-3595 induced tachycardia from 30 min after dosing until the end of the recording period at all the dose levels tested in the study. No modifications of systolic, diastolic, or mean blood pressure were reported after dosing with CBS-3595 at any dose level.

Decreases in the PQ and QT interval durations were reported after dosing with CBS-3595 at all dose levels, from 15 min after dosing until the end of the recording period and until 180 min after treatment. This was probably related to the concomitant increase in heart rate. When compared to the vehicle group, no significant modifications of corrected QT duration (QTf

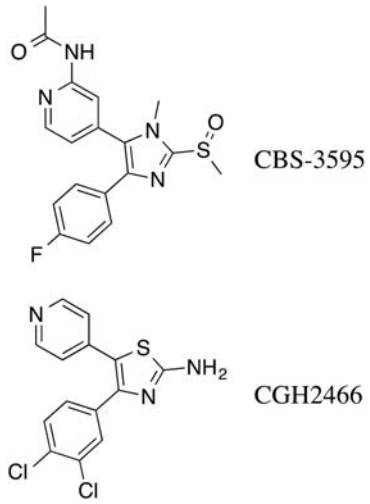

Fig. 17 Structures of CBS-3595 and CGH2466.

and QTv) were reported after dosing with CBS-3595 at any dose level. No modifications of QRS interval duration were observed after dosing with CBS-3595 at any of the dose levels tested in this study. In addition, periods of sinusal brady-arrhythmias were reported. These observations were dose-related and can possibly be a consequence of deep inspiration or nausea (this is consistent with the vomiting observed in the study). However, such periods of brady-arrhythmia were also reported before dosing on the third day of treatment. Premature ventricular complexes were also observed in two animals treated with CBS-3595.

To evaluate the potential modifications in respiratory function caused by CBS-3595, respiratory parameters were measured by whole body plethysmography following single doses of 0 (vehicle), 30, 100, and 300 mg kg^{-1} CBS-3595. Respiratory rate, peak flow times, enhanced pause, minute and tidal volume, were measured until 6 h postdosing. An increase in the minute volume, consecutive to an increase in the peak inspiratory flow, was observed after dosing with CBS-3595 at the dose-level of 300 mg kg^{-1}.

8.17.4.1.10 Toxicological studies

To investigate the acute toxicity of CBS-3595, five male and five female Sprague Dawley rats received a single oral (gavage) dose of 2000 mg kg^{-1} and the effects were observed for a period of 14 days. No mortalities were observed. As clinical signs, piloerection, hypoactivity, and dyspnea were noted on days 1 and 2. No clinical signs were noted from day 3.

In the sub-acute dose range finding study in the rat doses of 0 (vehicle), 50, 150, or 450 mg kg^{-1} day^{-1} were administered for a period of 7 days. There were no premature deaths during the study. Based on treatment-related and dose-dependent clinical signs such as hunched posture, piloerection, and ptyalism as well as effects on blood cells, a dosing schedule for the 4 week toxicity study was concluded.

The 4 week toxicity study was performed at dose levels of 0 (vehicle), 15, 50, and 150 mg kg^{-1}. After termination of the 28-day treatment period, animals of the control and high dose group were observed for a further 2 week treatment-free period. For toxicokinetic analysis, satellite animals were included. This study was conducted in compliance with Good laboratory practice (GLP) regulations.

There were no unscheduled deaths during this study. No treatment-related clinical signs were noted in the group receiving 15 mg kg^{-1}. In the intermediate and high dose groups, mild adverse effects were observed and a No-observed-effect level (NOEL) of 15 mg kg^{-1} day^{-1} was concluded.

In the 4 week toxicity study, the effect of CBS-3595 was investigated at doses of 0 (vehicle), 6, 12, and 20 mg kg^{-1}. After 2 weeks of treatment, the high dose was increased to 25 mg kg^{-1}. After termination of the 28-day treatment period, two male and female animals of the control and high dose group each were observed for a further 2 week treatment-free period. This study was conducted in compliance with GLP-regulations. There were no unscheduled deaths during this study. Except for occasional liquid feces, observed in a male animal of each treatment group, no treatment-related findings were observed. There was no significant difference in body weight between treatment groups and controls.

Under the conditions of this study, a NOEL could not be established for males or females, and is considered to be lower than 6 mg kg^{-1} day^{-1}. However, as none of the observed changes were considered to be adverse or of toxicological importance, the No Observable Adverse Effect Level is considered to be greater than 25 mg kg^{-1} day^{-1}.

To investigate the genotoxicity of CBS-3595, the following studies were performed: Ames test, in vivo micronucleus test in the mouse and a cytogenetic test in human lymphocytes. In the Ames test, CBS-3595 gave a negative, that is, nonmutagenic response in all *S. typhimurium* and *E. coli* strains investigated, in both the presence and absence of S9-mix.

The mouse bone marrow micronucleus test demonstrated that CBS-3595 was not clastogenic. In the cytogenetic assay with cultured human lymphocytes, CBS-3595 was not clastogenic in vitro in either the presence or absence of S9-mix.

8.17.4.2 Phase I: First-Use-in-Human Study of CBS-3595

As described, CBS-3595 shows a clearly superior pharmacodynamic profile compared with selective p38α MAPK inhibitors and has been widely investigated:

- PK data available from studies in rats, dogs, and primates, rapid absorption after oral administration of CBS-3595;
- low variability;
- very low plasma protein binding ($\ll$50%);
- in rats (LPS-model), very good correlation of plasma concentration with the observed inhibition of TNFα release;
- one pharmacologically less active major metabolite;
- no inhibition of Cytochrome P450s (CYPs) (1A2, 2C9, 2C19, 2D6, and 3A4) at 10 μM;
- dose-proportional pharmacokinetics;
- no critical findings in nonclinical studies to investigate the genotoxicity and the effect on the central nervous, respiratory, and cardiovascular system;
- dose-dependent safety profile in general toxicity studies in rodents and Cynomolgus monkeys.

A clinical study to investigate the safety, tolerability, pharmacokinetics, and ex vivo pharmacodynamics of CBS-3595 was therefore conducted.

The study was designed as a placebo-controlled, single-blind, randomized, consecutive dosing study. Based on nonclinical findings, a starting dose of 10 mg was selected and in case of absence of adverse events, 50 mg was chosen as next dose level. The dose of 10 mg was tolerated well but after administration of 50 mg CBS-3595, all four subjects reported nausea and malaise and some vomiting events were recorded. In a subsequent setting, doses of 20 and 30 mg were applied, which confirmed a clear relationship between dose and adverse events which were characteristic for PDE4-inhibitors.

To investigate the pharmacokinetics of CBS-3595 and its major metabolite CBS-3728, blood samples were analyzed by a validated Liquid chromatography–mass spectrometry (LC MS)/MS method. Noncompartmental analysis of concentration versus time profiles was applied to determine main pharmacokinetic parameters (C_{max}, T_{max}, $t_{½}$, AUC_{0-t}, and $AUC_{0-\infty}$) and urine samples were analyzed to determine the cumulative excretion of parent compound and metabolites. Additional blood samples were taken and treated with bacterial LPS, which induced the formation of the proinflammatory cytokine TNFα. To determine the ex vivo pharmacodynamics of CBS-3595, TNFα concentrations versus time profiles were generated.

8.17.4.2.1 Pharmacodynamic results

In placebo-treated subjects, the TNFα release did not remain constant during the observation period. Compared to the predose activity, which was set to 100% by definition, a trend toward increasing TNFα production was observed. Compared to placebo data, in subjects treated with CBS-3595, a clear inhibition of TNFα release was achieved.

8.17.4.2.2 Pharmacokinetic results

Determination of plasma concentrations of the parent drug CBS-3595 and the metabolite CBS-3728 suggests that CBS-3595 is readily absorbed from the gastro-intestinal tract. The absorption profile of CBS-3728 indicates an efficient presystemic metabolism of CBS-3595.

Mean peak plasma concentrations of CBS-3595 were in the range of 2-3 h postdosing. Afterwards, the parent drug is eliminated from systemic circulation with a half-life of approximately 3 h. In contrast, for the metabolite CBS-3728 an elimination half-life of 9-11 h was determined. Mean pharmacokinetic parameters of CBS-3595 (parent drug) and CBS-3728 (metabolite) are summarized in the table below:

CBS-3595 *CBS-3595 dose*	*Period* n	T_{max} *(h)*	C_{max} *(ng mL^{-1})*	AUC_{0-t} *(ng h mL^{-1})*	$T_{½}$ *(h)*	$AUC_{0-\infty}$ *(ng h mL^{-1})*
10 mg	I	2.20	75.9	355.4	2.7	388.0
	n=6	±1.30	±22.3	±115.0	±0.5	±129.1
50 mg	I	1.50	218.1	1264.8	3.2	1335.1
	n=4	±0.70	±30.8	±198.8	±0.9	±191.9
10 mg (fasting)	II	3.30	51.8	270.8	2.8	303.9
	n=6	±1.60	±12.5	±93.2	±0.4	±91.9
10 mg (fed)	II	3.70	50.9	295.8	2.8	329.4
	n=6	±1.40	±8.7	±70.8	±0.4	±87.5
20 mg	III	2.90	116.9	741.4	3.3	835.3
	n=6	±0.80	±33.2	±186.4	±0.4	±219.3
30 mg	III	2.30	173.0	986.2	3.4	1135.5
	n=2	N/A	N/A	N/A	N/A	N/A

CBS-3728 CBS-3728 dose	*Period* n	T_{max} *(h)*	C_{max} *(ng mL^{-1})*	AUC_{0-t} *(ng h mL^{-1})*	$T_{½}$ *(h)*	$AUC_{0-\infty}$ *(ng h mL^{-1})*
10 mg	I	4.70	61.3	976.0	9.5	1133.7
	n=6	±2.40	±15.6	±451.3	±3.0	±557.4
50 mg	I	5.00	196.9	2885.2	9.0	3104.5
	n=4	±1.20	±39.9	±519.8	±0.5	±541.8
10 mg (fasting)	II	6.00	50.9	930.9	11.3	1088.4
	n=6	±2.40	±9.4	±282.4	±2.0	±340.3
10 mg (fed)	II	6.70	47.1	859.6	10.7	1015.2
	n=6	±2.00	±10.8	±298.2	±2.4	±361.4
20 mg	III	5.00	119.9	2107.9	10.9	2370.2
	n=6	±1.10	±21.7	±87.3	±1.6	±98.3
30 mg	III	6.00	139.7	2436.0	11.3	2825.8
	n=2	N/A	N/A	N/A	N/A	N/A

Periods: I = prematurely interrupted part of study; II = cross-over part of study; III = 20 mg, 30 mg s.d. part of study.

In summary, 44 volunteers completed the study. After single oral dosing of a tolerated dose (10, 20 mg s.d.), inhibition of TNFα release in ex vivo stimulated blood samples reached approximately 50-80%.

A representative profile of the determined pharmacokinetics, pharmacodynamics, and time course of TNFα levels are shown in Figs. 18 and 19.

8.17.5 Conclusion and Lessons Learned in Retrospect

It was demonstrated that in both in vitro and animal models that combined dual p38α MAPK/PDE-4 inhibition is clearly superior for inhibition of biosynthesis and release of TNFα with regard to sheer TNFα release as well as for treatment of RA.

Pharmacokinetic criteria are often more important than pure activity. Even moderate inhibition of p38α MAPK and PDE-4 in the higher nanomolar range was observed, but with excellent kinetic properties and low plasma protein binding results with excellent efficacy in humans. A single 10-20 mg oral dose yielded 50-80% TNFα suppression ex vivo.

An unanswered question remains: why did vomiting occur in humans at much lower doses that provoked the same response in monkeys? One explanation could be differences in metabolism which are difficult to predict. In humans, the major metabolite CBS-3728 occurred in much higher doses than predicted by in vitro studies, even with human enzymes and microsomes as well as with animal in vivo studies, including monkeys.

A retrospective analysis of PDE-4 subtype inhibition showed that the metabolite CBS-3728 inhibited the isoform PDE-4 D3 much more strongly than the parent drug CBS-3595 (Fig. 20). Meanwhile, this isoform PDE-4 D3 is considered to be mainly responsible for the vomiting and nausea side effects of PDE-4 inhibitors.

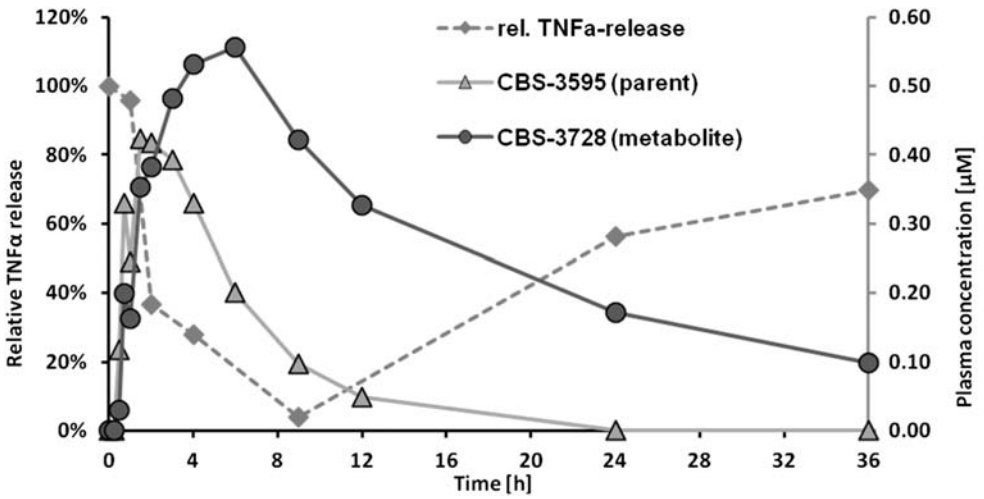

Fig. 18 Time course of TNFα release and plasma concentrations of CBS-3595 and its metabolite CBS-3728.

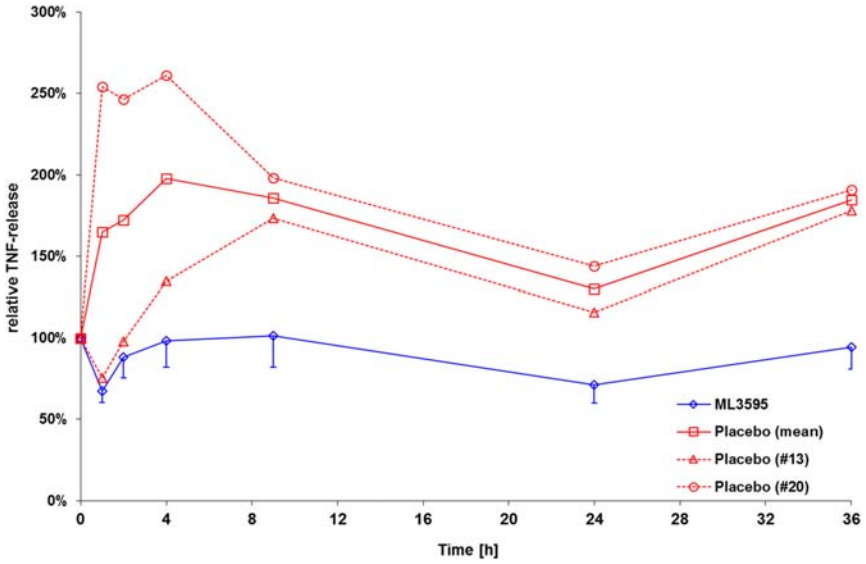

Fig. 19 Impact of CBS-3595 on TNFα release (ex vivo stimulation) in comparison with placebo.

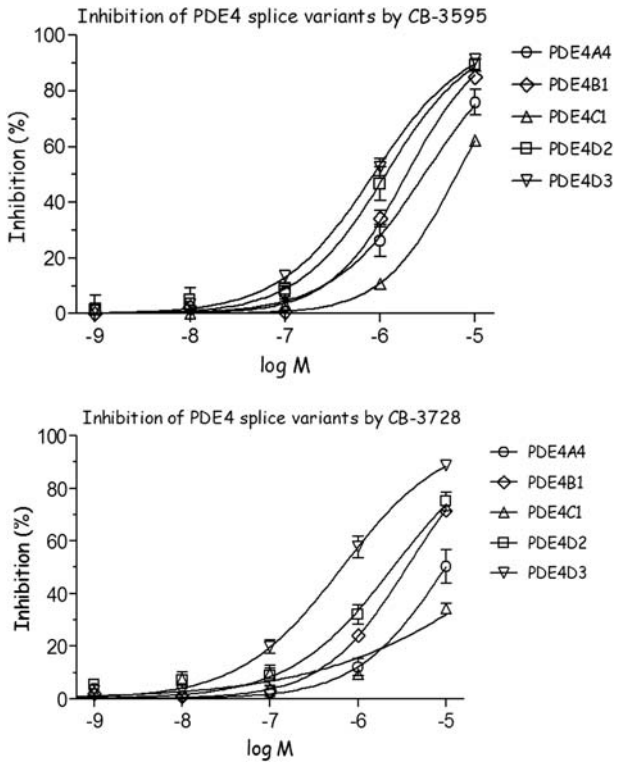

Fig. 20 PDE-4 isoform inhibition by CBS-3595 and its major human metabolite CBS-3728.

8.17.6 Perspective and Outlook

As of today, predicting isoform selectivity as applicable to rational design of inhibitors is still not possible. Even the contribution of the various isoforms to both activity and side effects is still unclear and has prevented many candidates from being further developed. Changing the route of application and systemic exposure seems to be a possible avenue to pursue. Besides RA, COPD and psoriasis are other indications for dual p38α MAPK/PDE-4 inhibitors. Both COPD and psoriasis allow topical/local application and therefore, allow low systemic exposure.

Follow up candidates of CBS-3595 for oral dosing may be selected by their isoform selectivity and metabolic stability. For topical/local application, one might vary the p38α MAPK/PDE-4 ratio and the metabolic stability.

To evaluate the effectiveness of CBS-3595 for treatment of COPD after inhalative application, ADME and physicochemical properties might be reconsidered. As CBS-3595 was selected for oral application, probably other candidates of the CBS library might be more suitable for topical or inhalative application.

See also: 5.12. Evolution of Small-Molecule Immunology Research—Changes Since CMC II. 5.13. Small Molecule Immunosuppressants in Inflammatory Disease. 5.15. Lupus and Lupus Overlap Diseases: Emerging Therapies.

References

1. Cheung, P. C. F.; et al. Feedback Control of the Protein Kinase TAK1 by SAPK2a/p38 Alpha. *EMBO J.* **2003,** *22* (21), 5793–5805.
2. Albrecht, W.; Laufer, S. Dual Inhibition of Phosphodiesterase-4 and p38 MAP Kinase: A Strategy for Treatment of Chronic Inflammatory Diseases. *Anti-Inflamm. Drug Discov.* **2012,** *26,* 137–157.
3. Mendoza, H.; et al. Roles for TAB1 in Regulating the IL-1-Dependent Phosphorylation of the TAB3 Regulatory Subunit and Activity of the TAK1 Complex. *Biochem. J.* **2008,** *409* (3), 711–722.
4. Wang, Y. J.; et al. Tumor Necrosis Factor-Induced Toxic Liver Injury Results From JNK2-Dependent Activation of Caspase-8 and the Mitochondrial Death Pathway. *J. Biol. Chem.* **2006,** *281* (22), 15258–15267.
5. Dominguez, C.; Powers, D. A.; Tamayo, N. p38 MAP Kinase Inhibitors: Many Are Made, but Few Are Chosen. *Curr. Opin. Drug Discov. Devel.* **2005,** *8* (4), 421–430.
6. Genovese, M. C. Inhibition of p38: Has the Fat Lady Sung. *Arthritis Rheum.* **2009,** *60* (2), 317–320.
7. Rudalska, R.; et al. In Vivo RNAi Screening Identifies a Mechanism of Sorafenib Resistance in Liver Cancer. *Nat. Med.* **2014,** *20* (10), 1138–1146.
8. Muth, F.; et al. Tetra-Substituted Pyridinylimidazoles as Dual Inhibitors of p38 Alpha Mitogen-Activated Protein Kinase and c-Jun N-Terminal Kinase 3 for Potential Treatment of Neurodegenerative Diseases (vol 58, pg 443, 2015). *J. Med. Chem.* **2015,** *58* (5), 2567.
9. Frantz, S. Drug Discovery: Playing Dirty. *Nature* **2005,** *437* (7061), 942–943.
10. McCann, F. E.; et al. Apremilast, a Novel PDE4 Inhibitor, Inhibits Spontaneous Production of Tumour Necrosis Factor-Alpha From Human Rheumatoid Synovial Cells and Ameliorates Experimental Arthritis. *Arthritis Res. Ther.* **2010,** *12* (3), R107.
11. Genovese, M. C.; et al. Apremilast in Patients With Active Rheumatoid Arthritis: A Phase II, Multicenter, Randomized, Double-Blind, Placebo-Controlled, Parallel-Group Study. *Arthritis Rheum.* **2015,** *67* (7), 1703–1710.
12. Laufer, S. A.; et al. Novel Substituted Pyridinyl Imidazoles as Potent Anticytokine Agents With Low Activity Against Hepatic Cytochrome P450 Enzymes. *J. Med. Chem.* **2003,** *46* (15), 3230–3244.
13. Laufer, S. A.; et al. Design, Synthesis, and Biological Evaluation of Novel Tri- and Tetrasubstituted Imidazoles as Highly Potent and Specific ATP-Mimetic Inhibitors of p38 MAP Kinase: Focus on Optimized Interactions With the Enzyme's Surface-Exposed Front Region. *J. Med. Chem.* **2008,** *51* (14), 4122–4149.
14. Laufer, S.; Wagner, G.; Kotschenreuther, D. Ones, Thiones, and N-Oxides: An Exercise in Imidazole Chemistry. *Angew. Chem. Int. Ed.* **2002,** *41* (13), 2290–2293.
15. Laufer, S. A.; Zimmermann, W.; Ruff, K. J. Tetrasubstituted Imidazole Inhibitors of Cytokine Release: Probing Substituents in the N-1 Position. *J. Med. Chem.* **2004,** *47* (25), 6311–6325.
16. Laufer, S. A.; Liedtke, A. J. A Concise and Optimized Four-Step Approach Toward 2-(Aryl-)alkylsulfanyl-, 4(5)-Aryl-, 5(4)-heteroaryl-Substituted Imidazoles Using Alkyl- or Arylalkyl Thiocyanates. *Tetrahedron Lett.* **2006,** *47* (40), 7199–7203.
17. Dimova, D.; et al. Assessing the Target Differentiation Potential of Imidazole-Based Protein Kinase Inhibitors. *J. Med. Chem.* **2012,** *55* (24), 11067–11071.
18. Buhler, S.; et al. Chiral Sulfoxides as Metabolites of 2-Thioimidazole-Based p38alpha Mitogen-Activated Protein Kinase Inhibitors: Enantioselective Synthesis and Biological Evaluation. *J. Med. Chem.* **2011,** *54* (9), 3283–3297.
19. Laufer, S.; et al. Tri- and Tetrasubstituted Imidazoles as p38alpha Mitogen-Activated Protein Kinase Inhibitors. *Bioorg. Med. Chem. Lett.* **2010,** *20* (22), 6671–6675.
20. Koch, P.; Laufer, S. Unexpected Reaction of 2-Alkylsulfanylimidazoles to Imidazol-2-ones: Pyridinylimidazol-2-ones as Novel Potent p38alpha Mitogen-Activated Protein Kinase Inhibitors. *J. Med. Chem.* **2010,** *53* (12), 4798–4802.
21. Bracht, C.; et al. Synthesis and Biological Testing of N-Aminoimidazole-Based p38alpha MAP Kinase Inhibitors. *ChemMedChem* **2010,** *5* (7), 1134–1142.
22. Ziegler, K.; et al. 2-Acylaminopyridin-4-ylimidazoles as p38 MAP Kinase Inhibitors: Design, Synthesis, and Biological and Metabolic Evaluations. *ChemMedChem* **2009,** *4* (11), 1939–1948.
23. Peifer, C.; et al. 3,4-Diaryl-isoxazoles and -imidazoles as Potent Dual Inhibitors of p38alpha Mitogen Activated Protein Kinase and Casein Kinase 1Delta. *J. Med. Chem.* **2009,** *52* (23), 7618–7630.
24. Pierre, K.; et al. Targeting the Ribose and Phosphate Binding Site of p38 Mitogen-Activated Protein (MAP) Kinase: Synthesis and Biological Testing of 2-Alkylsulfanyl-, 4(5)-Aryl-, 5(4)-Heteroaryl-Substituted Imidazoles. *J. Med. Chem.* **2008,** *51* (18), 5630–5640.
25. Laufer, S.; Koch, P. Towards the Improvement of the Synthesis of Novel 4(5)-Aryl-5(4)-heteroaryl-2-thio-Substituted Imidazoles and Their p38 MAP Kinase Inhibitory Activity. *Org. Biomol. Chem.* **2008,** *6* (3), 437–439.
26. Laufer, S. A.; Striegel, H. G.; Wagner, G. K. Imidazole Inhibitors of Cytokine Release: Probing Substituents in the 2 Position. *J. Med. Chem.* **2002,** *45* (21), 4695–4705.
27. Laufer, S. A.; Wagner, G. K. From Imidazoles to Pyrimidines: New Inhibitors of Cytokine Release. *J. Med. Chem.* **2002,** *45* (13), 2733–2740.
28. Abu Thaher, B.; et al. Role of the Hydrogen Bonding Heteroatom-Lys53 Interaction Between the p38alpha Mitogen-Activated Protein (MAP) Kinase and Pyridinyl-Substituted 5-Membered Heterocyclic Ring Inhibitors. *J. Med. Chem.* **2009,** *52* (8), 2613–2617.
29. Kammerer, B.; et al. Pharmacokinetics of ML3403 ({4-[5-(4-Fluorophenyl)-2-methylsulfanyl-3H-imidazol-4-yl]-pyridin-2-yl}-(1-phenylethyl)-amine), a 4-Pyridinylimidazole-Type p38 Mitogen-Activated Protein Kinase Inhibitor. *Drug Metab. Dispos.* **2007,** *35* (6), 875–883.
30. Zwerina, J.; et al. Activation of p38 MAPK is a Key Step in Tumor Necrosis Factor-Mediated Inflammatory Bone Destruction. *Arthritis Rheum.* **2006,** *54* (2), 463–472.
31. Koch, D. A.; et al. Efficacy and Gastrointestinal Tolerability of ML3403, a Selective Inhibitor of p38 MAP Kinase and CBS-3595, a Dual Inhibitor of p38 MAP Kinase and Phosphodiesterase 4 in CFA-Induced Arthritis in Rats. *Rheumatology (Oxford)* **2014,** *53* (3), 425–432.

8.18 The Discovery of Potent and Selective Nonsteroidal Glucocorticoid Receptor Modulators AZD5423 and AZD7594, for the Inhaled Treatment of Respiratory Diseases

P Sjö, T Hansson, and K Edman, AstraZeneca, Gothenburg, Sweden

© 2017 Elsevier Ltd. All rights reserved.

8.18.1	**Introduction**	450
8.18.1.1	Inhaled Glucocorticoids for the Treatment of Respiratory Diseases	450
8.18.1.2	The Glucocorticoid Receptor	452
8.18.1.3	Nonsteroidal Glucocorticoid Modulators	452
8.18.1.4	Structure of the Glucocorticoid Receptor	453
8.18.2	**Project Objective, Screening Cascade, and Compound Target Profile**	454
8.18.3	**Inhaled Drug Design and Challenges**	455
8.18.4	**Lead Identification**	456
8.18.5	**Lead Optimization Leading to AZD5423, Inhaled SGRM CD1**	462
8.18.6	**Lead Optimization Leading to AZD7594, Inhaled SGRM CD2**	468
8.18.6.1	Synthesis of AZD5423 and AZD7594	471
8.18.6.2	Physical Chemical Properties of Drug Candidates	473
8.18.6.3	Metabolism, Major Deactivation Pathways	474
8.18.6.3.1	AZD5423 metabolic profile	475
8.18.6.3.2	AZD7594 metabolic profile	476
8.18.6.3.3	Assessment of PK based drug–drug interaction potential	477
8.18.6.3.4	Prediction of human pharmacokinetics	477
8.18.6.4	In Vitro Pharmacology Assessment	478
8.18.6.4.1	Receptor binding and steroid NHR selectivity	478
8.18.6.5	In Vivo Pharmacology Assessment	479
8.18.6.5.1	Potency and mechanistic side effects in the rat Sephadex model	479
8.18.6.6	Predicted Therapeutic Dose	479
8.18.6.7	Mechanistic Side Effects	479
8.18.6.8	Duration of Effect	480
8.18.6.9	Functional Measurements in the Rat Sephadex Model	480
8.18.6.10	Efficacy in a "Disease-Like" Setting (Ovalbumin Model)	481
8.18.6.11	Acute Mouse LPS Model	481
8.18.6.12	Acute LPS Model—Lung Function Changes and MRI Imaging	482
8.18.6.13	Acute Cigarette Smoke Model	482
8.18.7	**Progression of AZD5423 and AZD7594 Into Development**	483
8.18.7.1	Progression of AZD5423	483
8.18.7.2	Progression of AZD7594	484
8.18.8	**Summary**	484
References		485

8.18.1 Introduction

8.18.1.1 Inhaled Glucocorticoids for the Treatment of Respiratory Diseases

Glucocorticoids represent the most potent antiinflammatory drugs available today and allow successful treatment of cancer, several chronic inflammatory, and autoimmune diseases.[1] This also includes the treatment of respiratory diseases, such as asthma and chronic obstructive pulmonary disease (COPD), where inhaled glucocorticoids (IGCs) used alone or in combination with bronchodilators are the mainstay of clinical therapy.[2]

There are a number of IGCs approved for the treatment of respiratory diseases, either alone or in combination with a long-acting inhaled β2-agonist (LABA). The most well-known IGCs are budesonide, fluticasone propionate, fluticasone furoate, beclometasone dipropionate, ciclesonide, mometasone furoate, and flunisolide (**Fig. 1**).

Asthma is a chronic disease that affects 235 million sufferers worldwide with ~250,000 annual deaths attributed to the disease. Prevalence is in the range of 4–11% across countries and is increasing due to western lifestyle and urbanization. An additional 100 million patients are estimated worldwide by 2025 (http://www.who.int/respiratory/asthma/en/). Asthma is characterized by

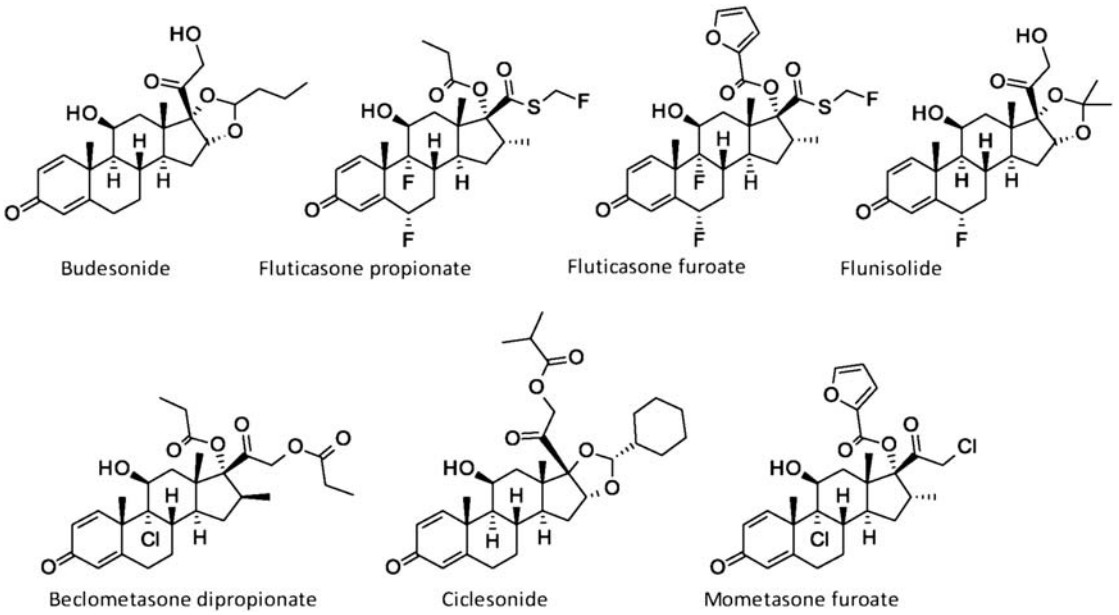

Fig. 1 Inhaled glucocorticoids used in the treatment of respiratory diseases.

varying, reversible airflow limitation, the airway narrowing causes symptoms such as wheezing, shortness of breath, chest tightness, and coughing. During periods of asthma exacerbations massive variability in lung function is seen, and this causes disruption in patients' lives and can even be life threatening. Today IGCs form the base of prophylactic asthma therapy in the Western world. Early intervention with IGCs has been shown to improve asthma control, normalizes lung function, and may also prevent irreversible airway damage. The combination of IGCs and LABAs represents a further improvement in the therapy of asthma, efficient in the treatment of the mild-to-moderate disease segment.[3]

Globally, COPD is a major cause of morbidity and disability, according to the latest estimates from the WHO 64 million people are suffering from COPD leading to 3 million annual deaths, COPD is by 2030 estimated to be the third leading cause of death in the world (http://www.who.int/respiratory/copd/en/). The cost to society caused by COPD in 2010 has been estimated to be $32BN in the United States alone and is expected to rise to $49BN by 2020.[4] Numbers aside, the devastating effect of the disease to the quality of life for the patients suffering from COPD must be remembered.[5] Smoking is shown to be the dominating risk factor in the industrialized world leading to the development of COPD, and it is estimated that 5–10% of the population is affected in most countries. The disease is progressive, leading to an irreversible airflow limitation, with a subsequent decrease in lung function that is characterized by recurrent episodes of cough, sputum production, and breathlessness. Most patients with COPD suffer from exacerbations, which may vary in severity and duration. Frequent exacerbations result in an accelerated lung function decline, decreased quality of life, and drives mortality. Current drug therapy is largely based on bronchodilators and GCs.[6] In spite of the impressive clinical efficacy of IGCs and IGC/LABA combinations observed in asthma, these effects do not fully translate to COPD. IGCs and IGC/LABA combinations have proven clinical efficacy on several patient outcomes in moderate to severe COPD, especially on preventing and treating exacerbations. Clinical efficacy has also been shown by IGS in reducing the overall mortality, as well as slowing down the rate of decline in quality of life of patients.[7] The IGC/LABA combination salbutamol–fluticasone furoate did show a significant reduction CD8 positive T cells, whilst it did not significantly change neutrophils and eosinophils numbers compared to placebo.[8] Emerging data on combining tiotropium with IGC/LABA fixed dose combinations suggest an even further improved potential for reducing COPD exacerbations, improving lung function, and quality of life.[9]

Despite the clinical efficacy of IGCs, it is clear that there is still a significant unmet medical need in the treatment of both diseases, particularly in COPD and severe asthma disease segments.

In patients whose disease is well controlled, IGCs are associated with a low frequency of systemic glucocorticoid-related side effects. However, target-related adverse effects have been reported in the literature, and the long-term use of high-dose IGCs therapy has the potential to cause systemic side effects associated with glucocorticoid-driven pharmacology. Side effects reported include: growth velocity decrease in children,[10] osteoporosis resulting from altered bone metabolism,[11] effects on the hypothalamic–pituitary–adrenal (HPA) axis,[12] and altered diabetic control (glucose mobilization, lipid metabolism).[13] Local side effects in the respiratory tract are also commonly associated with IGCs, including oropharyngeal candidiasis, dysphonia, reflex cough, bronchospasm, and pharyngitis.[14]

For the above reasons, highly selective glucocorticoid receptor (GR) modulators with an improved safety profile and improved therapeutic index (TI) are highly desirable and besides leading to overall improved safety profile. Such a compound also has a potential for further dose escalation leading to generate greater efficacy without compromising safety, ultimately leading to improved disease control in patients.

It is well known that adherence to asthma and COPD medication often is poor and is a significant contributor to poor treatment outcome.[15] Once daily inhaled dosing is envisioned as a strategy to improve compliance and ultimately health outcome. For this reason, developing new inhaled GR modulators, it is highly desirable to achieve duration of action that allows for a once daily dosing regimen for the use in all levels of asthma severity. Long-acting, inhaled GCs combined with once daily bronchodilators in a fixed-dose combination is envisioned to provide the basis for future improved inhaled treatments of asthma and COPD.[16]

8.18.1.2 The Glucocorticoid Receptor

Glucocorticoids exert their function through binding to the intracellular GR.[17] GR is a ligand-activated transcription factor that belongs to the nuclear hormone receptor (NHR) superfamily. Together with the mineralocorticoid receptor (MR), the progesterone receptor (PR), the androgen receptor (AR), and the estrogen receptors (ERα and ERβ) GR forms the steroid receptor subfamily. Phylogenetic analysis shows that GR, MR, PR, and AR are further distinct from the estrogen receptors and are referred to as the 3-ketosteroid receptors.[18]

GR is present in nearly all mammalian cells and is involved in a broad range of fundamental physiological functions spanning from metabolism and the immune response to skeletal growth and cognition. GR is activated by the glucocorticoid hormones cortisol in humans and corticosterone in rodents. These hormones are derived from cholesterol and are synthesized in an endocrine fashion.

Upon stimulus, the hypothalamus releases corticotrophin-releasing hormone, which triggers the anterior pituitary gland to produce adrenocorticotropic hormone (ACTH). ACTH, in turn, stimulates the adrenal cortex to synthesize and release cortisol. The cortisol levels are under circadian control, but the hormone can also be released in response to stress. To ensure that the magnitude of the functional response is appropriate, plasma concentration of cortisol is further adjusted by a negative feedback mechanism governed by GR occupancy in hypothalamus and the pituitary gland.[19]

GR is a modular protein comprising three domains: the N-terminal domain (NTD), the DNA-binding domain (DBD), and the C-terminal ligand-binding domain (LBD). In the resting state, GR predominantly resides in the cytoplasm in complex with several chaperone (hsp70, hsp90, and p23) and co-chaperone (FKBP51, FKBP52, Hop, and Tpr2) proteins. This assembly maintains both receptor stability and ensures hormone sensitivity.[20] Hormone binding to the LBD leads to a partial release of the chaperone complex and to nuclear translocation.[21] In the nucleus, GR binds to both DNA response elements and various coregulator proteins in a highly dynamic fashion.[22] These complexes can directly modify chromatin structure and will ultimately impact on the activity of the gene transcription apparatus. While the DBD governs the interactions to the DNA, the interactions between GR and the coregulators are primarily mediated by the activation functions on the NTD (AF-1) and the LBD (AF-2).[23] GR is an extremely versatile receptor, and several genomic modes of action have been described. The commonly accepted mechanism is transactivation (TA) where a GR dimer binds to the consensus glucocorticoid response element (GRE) leading to an upregulation of the gene transcript.[24] However, GR can also interfere with other transcription factors such as AP-1 or NF-κB in a process called transrepression (TR). In this instance, GR either tethers directly onto the other transcription factor or binds on an adjacent DNA element to repress the corresponding gene product.[25] In addition, a negative glucocorticoid response element (nGRE) where GR mediates direct repression of the target genes has been described.[26] Structural studies reveal that GR binding to the nGRE prevents DNA-mediated dimerization and illustrates how DNA sequences can directly influence the receptor arrangement and the polarity of the transcriptional response.[27]

The functional response to any specific glucocorticoid will depend both on the availability of the DNA response elements and the relative expression levels of the coregulator proteins. In addition, alternative splicing of the GR transcripts and different translation initiation sites gives rise to multiple GR isoforms, and several studies reveal that they exhibit distinct functional profiles.[28] The activity of each receptor isoform can be further modulated by a range of posttranslational modifications.[29] Ultimately, these factors will be integrated on the cellular, tissue, organ, and organism level delivering a pharmacological response.

8.18.1.3 Nonsteroidal Glucocorticoid Modulators

Modulation of GR receptor activity with nonsteroidal ligands, through differential coregulator recruitment, is envisioned as a route to develop GR ligands with improved efficacy and safety margins compared to conventional steroids-based GR ligands.[30] This idea is supported by related work in the field of nonsteroidal ligands acting on the estrogen and ARs.[31] During the last decade nonsteroidal GR ligands have been identified by several groups, a number of reviews are available that describe these efforts.[30,32] The aim for the majority of these programs has been to develop differentiated GR modulators aimed at oral administration (**Fig. 2**). Early examples of nonsteroidal selective GR modulators (SGRMs) include AL-438 (**1**) by Abbott/Ligand,[33] ZK 216348 (**2**) by Bayer Pharma AG,[34] and the *N*-arylpyrazolo derivative (**3**) by Merck.[35] More recent examples are BI 653048 (**4**) by Boehringer Ingelheim,[36] the trifluorocarbinol derivative **5** by GSK,[37] and the benzoxepine (**6**) by Lilly.[38] Two examples of compounds that are reported to have entered clinical trials are mapracorat (**7**) studied for topical treatment of inflammatory skin and ocular disorders[39] and fosdagrocorat (**8**) undergoing studies for the treatment of rheumatoid arthritis.[40] It should be noted that several of these nonsteroidal GR ligands contain the trifluoromethylcarbinol moiety (**2**, **4**, **5**, and **7**). A similar motif was studied in the discovery of the androgen antagonist bicalutamide (**Fig. 7**), and this will be discussed further in this account.[41]

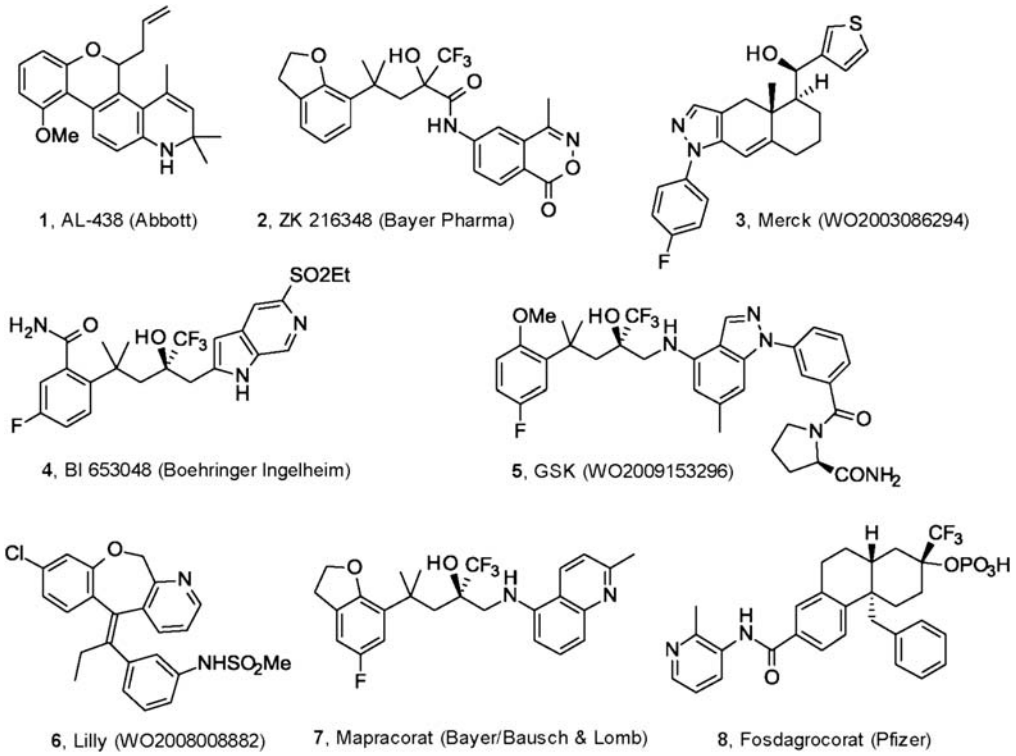

Fig. 2 Examples of nonsteroidal GR modulators reported in the literature.

8.18.1.4 Structure of the Glucocorticoid Receptor

It was realized at an early stage within the project, that access to high-quality experimental GR structure data would be a key success factor for the progression of the project allowing for an in-depth understanding of the structure–activity relationships (SARs) for the individual series. Furthermore it was envisioned that the structural data would form the basis for any computationally guided design efforts able to formulate and address complex hypotheses linking changes of the receptor structure to ligand-dependent changes in the pharmacological responses.

The first in-house X-ray structure obtained of the GR LBD confirmed the canonical nuclear receptor three-layered alpha helical sandwich fold previously reported (Fig. 3A).[42] Furthermore the structure showed how dexamethasone binds in the fully enclosed ligand-binding pocket in the receptor domain (Fig. 3B).

The interaction between the ligand and the receptor provides the basis for ligand potency and allosteric modulation of auxiliary surfaces, primarily AF-2 and the dimerization surface, directing functional response. As the ligand is completely surrounded by the receptor protein, nearly all atoms of dexamethasone are in contact with the surface of the ligand-binding pocket. While the bulk of the interactions is hydrophobic in nature, dexamethasone also forms the typical key hydrogen bond interactions with helices 3, 5, and 11. Specifically, the A-ring ketone moiety (Fig. 3C) makes direct interactions to the gatekeeper residues Gln570 and Arg611 from helices 3 and 5, respectively. The conformation of the gatekeeper residues is further stabilized by several conserved water molecules. A number of studies have highlighted that the helix 3–helix 5 interface is crucial for receptor activation, and all steroid hormones contain an A-ring functionality to exploit this agonist trigger.[43] At the opposite end of the ligand-binding pocket, Asn564 in helix 3 makes direct interactions to both the C11 and C21 hydroxy groups of dexamethasone. Asn564 is an important anchoring point for the ligands, this residue is fully conserved among the oxosteroid receptors, and the corresponding residue in the estrogen receptor is threonine. Looking at the second shell interactions, the asparagine residue is part of an extended hydrogen-bonding network that extends to the backbone carbonyl of a glutamate residue in the loop in between helices 11 and 12.[44] In close proximity to Asn564, Thr739 in helix 11 makes a direct interaction to the dexamethasone C20 ketone oxygen. However, in a number of subsequent complex structures of GR and different steroid-based ligands the threonine residue adopts different rotamer conformations, slightly changing the interaction pattern of this region and highlighting the versatility of ligand binding.[45] Nevertheless, the threonine residue is fully conserved among all steroid receptors where the endogenous hormone has a C20 ketone group (GR, MR, and PR). Taken together, the direct interactions to Asn564 and Thr739 have important roles in both ligand recognition and receptor activation through stabilization of the active helix 12 conformation. Finally, looking beneath the plane of the steroid ligand, the dexamethasone C17α hydroxyl makes a direct interaction to Gln642 in helix 7. This residue is a distinct feature of the GR-binding pocket. While AR also has a glutamine residue at the corresponding amino acid position in the protein sequence, a structural comparison reveals that it is further removed from the ligand.[44b]

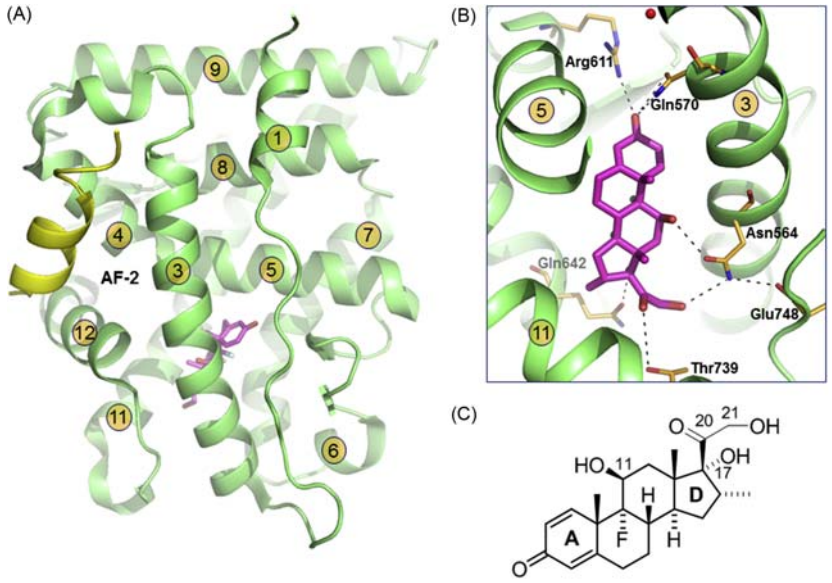

Fig. 3 (A) The GR LBD (*green*) with a TIF-2 peptide (*yellow*) and dexamethasone (*magenta*) binding at the receptor core. The structure comprises three helix layers; helices, 6, 7, and 10/11 at the back; 4, 5, 8, and 9 at the center; and 1, 3 at the front. The ligand-binding pocket is fully enclosed in the receptor delineated by helices 3, 5, 7, 11, and 12. (B) Details of the interaction in between dexamethasone and key residues of the ligand-binding pocket. Putative hydrogen bond interactions are shown as dashed lines. (C) The chemical structure and annotation of dexamethasone.

While the structure of GR in complex with dexamethasone provides a static view of the interactions in between the ligand and the receptor, a large numbers of complex structures with a range of different steroidal and nonsteroidal ligands have been published since.[37,45,46] Together, the ensemble of structures builds a more comprehensive appreciation of plasticity of the GR receptor and provides an emerging understanding of the underlying molecular drivers for different pharmacological responses.

8.18.2 Project Objective, Screening Cascade, and Compound Target Profile

In 2003, AstraZeneca launched a project with the aim to develop novel-inhaled SGRMs with improved efficacy and safety margin compared to existing IGCs aiming for once-daily treatment of Asthma and COPD. In 2005, AstraZeneca entered into a joint, 4 year, research collaboration with Bayer Pharma AG. The program included a joint discovery programs for discovery and development of inhaled, oral, and topically administrated GR modulators aiming at addressing a broad range of disease indications. However, the key focus for AstraZeneca was to progress inhaled GR modulators for the treatment of respiratory diseases which will be the focus for this article.

To progress the discovery program a set of biochemical and cellular assays was established. This included GR-binding assays using two different formats to measure receptor affinity, either in a competitive receptor-binding scintillation proximity assay using full-length human GR and radiolabeled dexamethasone. The second assay was a fluorescence polarization-binding assay (FP) using full-length GR measuring the displacement of a fluorescence labeled GR ligand.[47] NHR receptor selectivity for the PR, MR, AR, ERα, and ERβ receptors was determined using FP-based competitive receptor-binding assays. Receptor selectivity was determined as the ratio between receptor potencies in the different FP assays.

The functional GR activity was determined using an array of different cell assays. To determine the functional pharmacological effect, a reporter gene assay system was established allowing for both gene TR and TA to be measured. The TR activity was determined in Chago K1 cells stably transfected with a construct containing several TRE sites (AP-1 pathway) in front of a LacZ reporter gene. The TA activity was determined in Chago K1 cells, stably transfected with a plasmid construct where the MMTV promoter containing several GREs was inserted up-stream of the LacZ reporter gene. The antiinflammatory effects in primary cells were measured in peripheral blood mononuclear cells (PBMCs), measuring the inhibition of the release of tumor necrosis factor-α (TNF-α) in response to lipopolysaccharide (LPS) stimulation. The PBMC assay was established for both human and rat to allow for species cross-over estimates in a primary functional assay. Finally, an assay measuring the inhibition of TNF-α release from LPS-stimulated whole blood was established for both human and rat (Fig. 4).

Although various cellular models were used to describe the pharmacological effects of different compounds, the final differentiation versus IGCs ultimately relied on a direct comparison in in vivo models. To evaluate potency, duration, functional responses, mechanistic side effects, and the effects in "disease-like" scenarios in vivo, a range of animal models was used. In the studies described later, compounds were administered to the animals either using the intratracheal instillation or through inhalation.

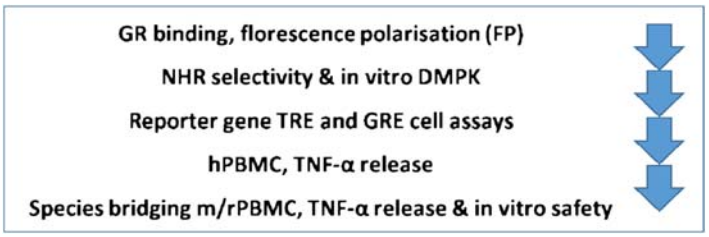

Fig. 4 Inhaled SGRM screening cascade, key in vitro assays used for compound progression.

Compound potency and mechanistic side effects were measured in the rat Sephadex model.[48] Male Sprague–Dawley rats were challenged via intratracheal instillation of Sephadex beads, and due to the inborn hypersensitivity of the rats toward dextran, an eosinophilic-driven inflammation develops over time in the lungs. The inflammatory response can be monitored by following the increase in lung weight (edema), which peaks at 24–48 h and is maintained for more than 7 days after provocation. GR-dependent effects on thymus weight were used to provide an estimate of the TI compared to IGCs.[49]

Effects on neutrophils and cytokine release were studied using the rat or mouse LPS models. As the exposure to significant levels of LPS is reported to be associated with the development and/or progression of many types of lung disease. In addition, human LPS studies have been used in several programs as the proof of principle model to progress compounds for further studies in COPD patients. The effects of following LPS simulation may be characterized by inflammatory processes in the lung, including neutrophilic inflammation and the increase in levels of cytokines.

Antiinflammatory responses were also studied in the acute cigarette smoke mouse model. In this model, female Balb/C mice were exposed to cigarette smoke twice daily for 4 days to induce a local inflammatory response in the lung, reflected by an increase in the number of neutrophils. Cigarette smoke is the main risk factor for developing COPD in humans.

Criteria for the project were defined including the following key criteria (candidate drug target profile):

- Potency in human peripheral blood mononuclear cells (hPBMCs), $IC_{50} < 1$ nM
- High clearance; >70% liver blood flow
- Nonhygroscopic, stable crystalline polymorph

In vivo differentiation assed in the rat Sephadex model showing improved therapeutic ratio versus ref IGCs.

8.18.3 Inhaled Drug Design and Challenges

Inhalation is the preferred route of administration for glucocorticoids for several reasons, but most importantly in order to reduce systemic GR-related side effects. This became evident though the successful introduction of beclomethasone dipropionate in 1972, the first IGC with a targeted delivery into the lung to achieve pulmonary effects with reduced systemic side effects compared to oral administration of the GR ligands.[50] Inhalation of drugs is based on a nonequilibrium concept where improvements in dose potency and safety of the administered drug are related to the ability to achieve high local concentrations while maintaining a low systemic exposure. Key properties targeted for compounds in the project were high pulmonary deposition and rapid systemic clearance. High pulmonary deposition may be achieved either via dissolution-dependent retention of the drug to the lung, such as seen for existing IGCs, or by basic compounds having a high degree of tissues distribution, reflected in large terminal volume of distribution (Vz) such as seen in LABAs. At the initiation of the project it was assumed that lung retention would be achieved using a slow dissolution rate approach, since GR is known to prefer binding to neutral ligands, while no examples were found of acidic or basic ligands showing any significant affinity to the receptor.

Compounds were tested in animal models either through dry powder inhalation or alternatively administered directly into the trachea of intubated animals, intratracheal (i.t.) instillation. There are pros and cons with each of the two methods: Generally, administration via inhalation to animals is regarded to be more relevant for the human clinical situation, since conscious animals are used and more uniform distribution in the lung is achieved. For this reason inhalation was used to obtain more precise measurements of compound pharmacology and also used for dose to man predictions. A significant disadvantage using this method is that crystalline compound is required to conduct the studies. The experimental procedure available also requires rather large amounts, ~2 g, of compound to prepare the tablet used to generate the powder flowing into the inhalation towers (Fig. 5).

A constraint of the inhaled dry powder administration is the limited dose that can be delivered to the patients' lung. The limitations of the dosage leads to that the predicted daily human dose (delivered to the lung) needs to be well below 100 $\mu g\,kg^{-1}$ or 3500 μg total daily dose assuming twice daily dosing (BID). Compared to oral dosing this limit may seem quite restrictive but reviewing inhaled compounds currently in clinical use, and most are efficacious at doses below 500 μg (~14 $\mu g\,kg^{-1}\,day^{-1}$). To achieve this level of potency provided a significant challenge to the SGRM project. While, for example, the endogenous hormone adrenaline meets this potency criterion binding to the β2-receptor, cortisol the natural hormone of the GR does not. IGCs such as budesonide and fluticasone propionate are several orders of magnitude more potent than cortisol. The following rule of thumb was

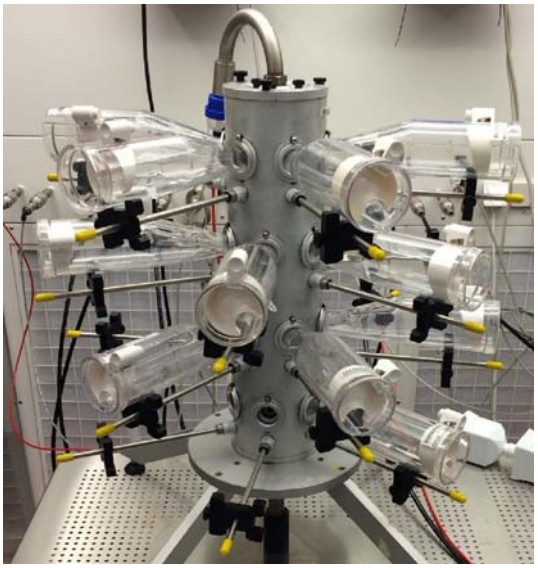

Fig. 5 Inhalation tower used in the dry powder inhalation (DPI) in vivo studies.

used in the project: to progress a compound into the primary in vivo studies, the potency in the PBMC assay needed to be equal or higher than that of budesonide, meaning that an IC_{50} of <1 nM was used as progression criteria.

In order to minimize systemic GR-dependent side effects, rapid metabolic deactivation was desired. There are a number of potential strategies to achieve this, such as esterase-mediated cleavage or via hepatic oxidative deactivation. Hepatic deactivation has many advantages and was preferred by the project. Preclinical in vitro models using microsomes and hepatocytes generally predict in vivo clearance well and are available for many species, e.g., human, rodent, dog. Furthermore, deactivation of existing IGCs relies on hepatic oxidative clearance, proving the viability of this principle also in the clinical setting. As systemic deactivation of ligands is of high importance to minimize systemic GR-dependent side effects, metabolite identification, synthesis of metabolites, and pharmacological evaluation of these became an integral part of the discovery project make-test cycle.

8.18.4 Lead Identification

A broad spectrum of lead generation methods was considered at the initiation of the project; however the early success of high-throughput screening (HTS) delivering workable chemical starting points prompted the project to fully focus the efforts to progress these screening hits.

The AstraZeneca, 660 k HTS compound collection was screened using a competitive GR fluorescence polarization assay leading to 5575 retest actives with $>50\%$ inhibition at 10 μM. A selection of retest actives (2409 DMSO solutions) was submitted for LC/MS purity and identity confirmation. Remaining compounds were clustered based on their chemical structure, and 435 cluster members were retested using freshly prepared DMSO solutions. This resulted in that 14 structurally diverse series and a number of structural singletons were selected for in-depth characterization including in vitro DMPK, physicochemical properties, selectivity over related steroid hormone receptors (PR, MR, ERα/β), and cell cytotoxicity providing the basis for prioritization (Fig. 6). Two hit series, exemplified by structures **9**–**12**, were selected as starting points for the Hit-to-Lead chemistry program. An additional set of compounds based on the three series exemplified by compounds **13**–**15** were retained within the program considered as back-up series. These series were all viewed as novel and potent GR binders, displaying binding potencies in the nM range. The most potent compound **11** had a GR-binding potency of IC_{50} 14 nM. In addition, most compounds showed high degree of selectivity toward other steroid hormone receptors tested.

The functional cellular activity was determined for all series using a reporter gene assay system run in agonistic mode, determining gene TR activity. The results revealed that all compounds tested showed low or no functional activity and were therefore considered to be antagonists. This was confirmed by screening compounds in the TR cellular assay in antagonistic mode using dexamethasone (10 nM) as agonistic substrate. Under these test conditions, at 10 μM concentration, compounds **9** and **11** showed 85% and 50% downregulation of the reporter gene signal, respectively. Thus, an initial key objective for the project was to introduce functional agonism in the series. It has previously been shown that limited structural changes to the structure of nonsteroidal ligands binding to steroid hormone receptors may change functional activity from antagonism to agonism and vice versa.[41] In the original report by Tucker et al., describing the discovery of the androgen antagonist bicalutamide, it was noted that matched pair, methyl congeners **16**, **18**, and **20** displayed no agonistic activity, while the trifluoromethyl analogues **17**, **19**, and **21** all exhibited high level of functional agonism. Though it was assumed that the increased acidity of the hydroxyl proton induced by the electron-withdrawing

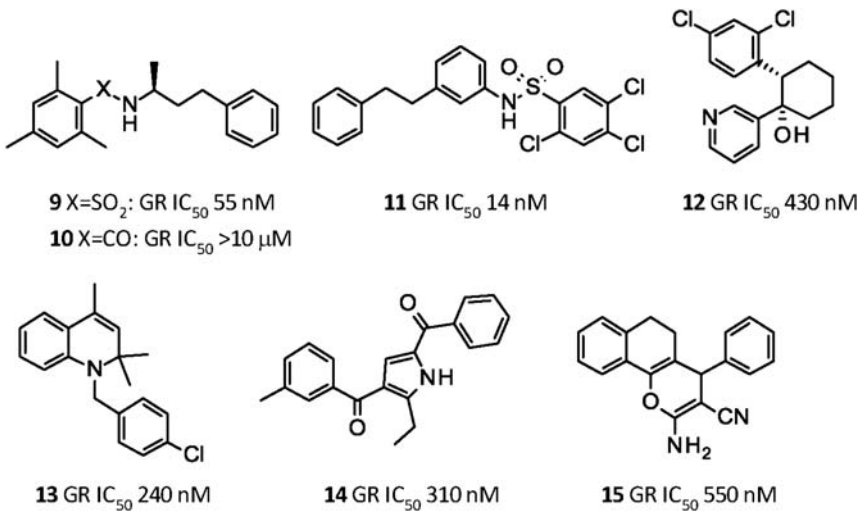

Fig. 6 HTS hits selected based on follow-up screening of primary actives. Compounds **9**–**12** were chosen for progression into the Hit-to-Lead chemistry program.

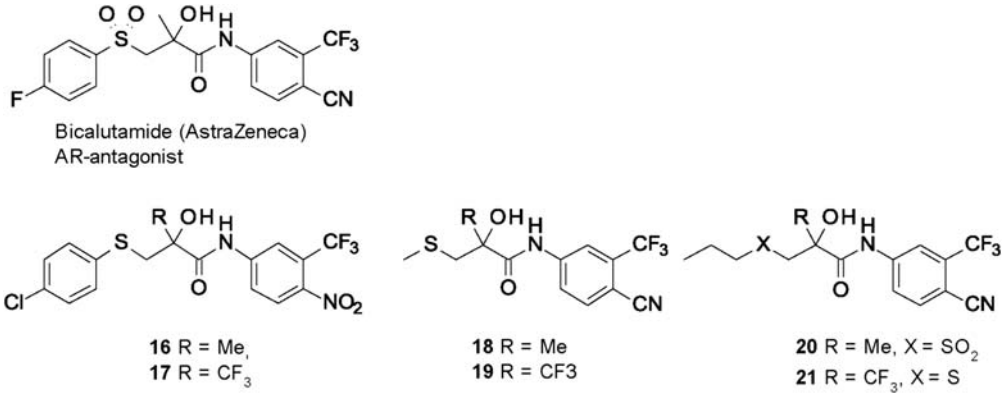

Fig. 7 Bicalutamide and bicalutamide analogues showing different antagonist–agonist receptor pharmacology. Compounds **16**, **18**, and **20** show no agonistic activity, while **17**, **19**, and **21** all displayed functional agonism.

trifluoromethyl group was driving agonism, lack of structural understanding of ligand–receptor interaction prevented a structure-based mechanistic understanding (Fig. 7). The publication of the first X-ray crystal structure of the W741L mutant AR LBD bound to *R*-bicalutamide in 2005 showed the interaction of the bicalutamide hydroxyl group with Asn705 in helix 3 and thus pointed to the importance of this interaction and stabilization of helix 3 as key structural drivers for functional agonism.[51]

The cyclohexanol-based series originated from the HTS singleton **12** showed nanomolar potency in the GR-binding assay, excellent NHR selectivity, but as previously mentioned displayed antagonism in the cellular TR reporter gene assay. A series of analogues to **12** was prepared aimed to improve the overall property profile and to explore the introduction of agonist triggers. However, the efforts to improve properties by reducing lipophilicity resulted in reduced biochemical GR potency, and as a result this series was parked.

The most promising hit series, the sulphonamides, included several compounds that displayed nanomolar potency in the GR-binding assay as well as a high degree of NHR selectivity as exemplified by compound **9**. This easily accessible compound was particular attractive based on the synthetic scope as it could be synthesized in one-step from commercially available starting materials. However, as previously mentioned all members of this series displayed functional antagonism. An initial key objective was therefore to introduce functional agonism in this series. The metabolic and physical–chemical properties also needed to improve during the initial phase of the project.

Early expansion of the sulphonamide HTS hit **9** included the synthesis of corresponding carboxamide **10**; however this resulted in complete loss of binding affinity to the GR receptor. The introduction of a heteroatom (N, O) in the benzylic position of compound **22** improved the synthetic scope now allowing parallel chemistry to be used in the initial exploitation of the series. A study of the activity of various aryl ethers and anilines was then initiated, using a synthetic route that enabled preparation of ethers (entry **23**) and amines (entries **26**–**29**) as single enantiomers starting from (*S*)-2-Amino-1-propanol.

Table 1 GR binding and activity in TR reporter gene assay for selected compounds

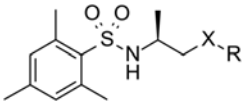

Compound	X	R	GR[a] IC_{50} (nM)	TR[a] IC_{50} (μM)	TR[a] Eff. (%)[b]
22	C	Phenyl	55	NA	–
23	O	4-Indole	23	NA	–
24	O	5-Isoquiniline	18	NA	–
25	O	5-Quinoline	240	0.96	71
26	NH	4-Indazole	42	0.76	57
27	NH	5-Quinoline	75	1.8	88
28	NH	6-Quinoline	10,000	NA	–
29	NN	6-Isoquinoline	10,000	NA	–

[a]Values are means of at least two experiments.
[b]% of dexamethasone at 10^{-6} M.

For several of the analogues the affinity to the receptor was retained or improved compared to compound **9** (Table 1). Interestingly, the attachment point to the heterocycle demonstrated a steep SAR. For example, the quinoline (**25**) linked through the 5-position has an affinity to the GR of 75 nM, whereas affinity is completely abolished for the 6-linked quinoline derivatives (**28–29**). This observation is supported by modeling studies in which the elongated ligand-binding pocket in the receptor strictly dictates size and shape of substituents allowed. From Table 1 it is also clear that the positioning of aromatic heteroatoms plays an important role for the functional activity. While the 5-isoquinoline (**24**) is more potent than the 5-quinoline (**25**) in the binding assay, only the 5-quinoline (**25**) is an agonist in the cellular TR assay. Modeling studies provide an explanation that positions the heterocyclic ring in the same region of the ligand-binding pocket as the A and B rings of conventional steroids. For optimal interactions to the receptor, the heteroatom of the heterocyclic ring should mimic the 3-keto oxygen of the steroid to pick up the key Arg611, Glu570 interactions, and a conserved water molecule.[7] These interactions between GR helices 3 and 5 have been shown to be critical drivers for functional agonism.[43a]

To determine the impact of the sulphonamide substituent a range of sulphonamides of different size and shape were investigated **30–34** (Table 2). All substituted phenyl sulphonamides, entries **30–33**, showed inferior GR binding compared to the mesityl

Table 2 GR binding and activity in TR reporter gene assay for selected compounds

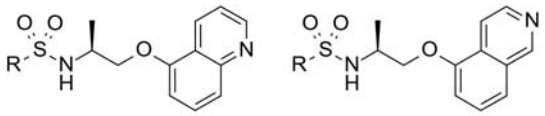

30, 31 **32-34**

Compound	R	GR[a] IC_{50} (nM)	TR[a] IC_{50} (μM)	TR[a] Eff. (%)[b]
30	2,4-Dimethylphenyl	1600	NT	–
31	2,4,6-Trichlorophenyl	80	2.4	64
32	Phenyl	>10,000	NT	–
33	2,4-Dimethylphenyl	410	NT	–
34	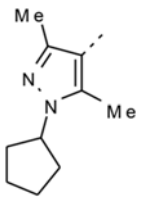	32	NA	–

[a]Values are means of at least two experiments.
[b]% of dexamethasone 10^{-6} M.

sulphonamides. Modeling indicates that the sulphonamide substituent binds in the same region as the steroid D-ring 17α position, and the data confirm the critical role of this pocket for binding affinity. The fact that the potent 1,2-diazole (**34**) is much larger than the original mesityl group also illustrates the flexibility in this region of the receptor, as previously reported.[46a] Since the 1,2-diazole used in compound **34** contributes favorably to decrease the lipophilicity, this motif was selected for further investigations together with the more potent mesityl congeners.

In an effort to mimic the phenyl-pyrazole A-ring substituents in steroid derivatives, e.g., cortivazole (**Fig. 8**), a series of 1-aryl indazoles were investigated (**Table 3**).[46c]

Many compounds from this series showed excellent potency in the binding and TR assays. The activity of compounds in primary cells was studied in hPBMCs, where the release of TNF-α in response to LPS stimulation was used to test the antiinflammatory effects. As can be seen from data in **Table 3**, several of the compounds were confirmed to be potent agonists in this assay.

Functional agonism is driven by a well-defined structural state of the receptor, where coactivators are recruited to the binding surface outlined by helix 3, 4, and 12 (**Fig. 3A**).[42,46e]

While the position of helix 12 is instrumental for achieving receptor activation,[46g] helix 3 also plays an important role spanning the full length of the receptor and provides interaction surfaces that are key for the structural integrity of the receptor. It also has several direct interactions with both ligand and coactivator peptide. As such, helix 3 could be considered the spine of the LBD; both provides a framework that enables productive positioning of helices 5 and 12 and has sensory neurons that read the ligand information and helps transmit this information to the AF-2 surface. Ultimately, the ligand-induced structural state of the LBD drives the intermolecular (in between LBD, DBD, and NTD) and intramolecular (in between GR, coregulators, and DNA) interactions providing the functional response.

To better understand the molecular details of the conformations induced by the sulphonamides, the X-ray structure of the LBD in complex with compound **36** was determined.[46c]

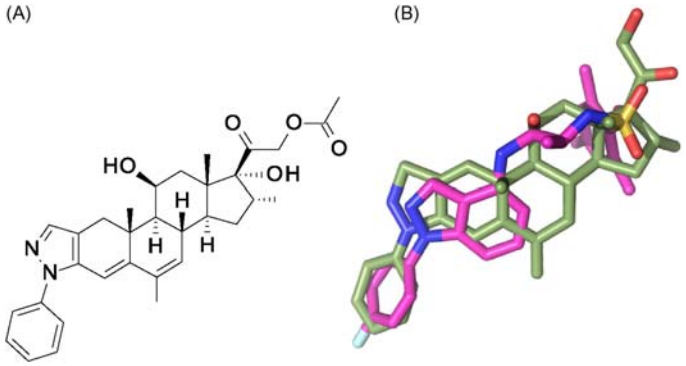

Fig. 8 (A) Structure of cortivazole and (B) Overlay of cortivazole (*green*) and **36** (*magenta*), ligands extracted from the X-ray structures of the GR-LBD ligand complexes.

Table 3 GR binding, activity in TR reporter gene assay and in PBMCs for selected compounds

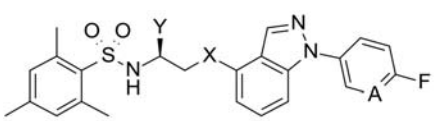

35, 36, and 37

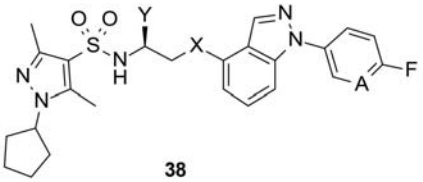

38

					TR[a]		*hPBMC*[a]	
Compound	*X*	*Y*	*A*	*GR IC_{50}*[a] *(nM)*	*IC_{50} (nM)*	*Eff. (%)*[b]	*IC_{50} (nM)*	*Eff. (%)*
35	O	Me	C	5.2	60	93	NA	–
36	NH	Me	C	4.9	1.5	89	14	73
37[c]	O	CF_3	C	3.8	14	73	36	76
38	NH	Me	N	3.0	7.2	88	14	60

[a]Values are means of at least two experiments.
[b]% of dexamethasone 10^{-6} M.
[c]Racemic mixture.

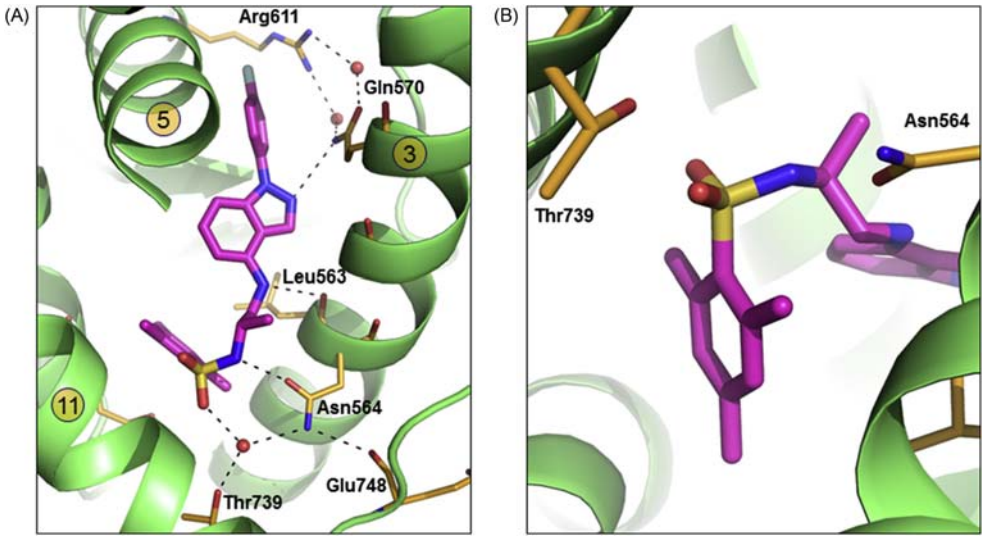

Fig. 9 (A) Refined 2mFo-DFc electron density of GR LBD in complex with the sulphonamide **36**. The dotted lines represent putative hydrogen bonds. The structure shows that **36** make extensive interactions with residues on helix 3. (B) Detailed view of the mesitylene tail.

The compound **36** complex structure confirms the formation of multiple interactions between the ligand and helix 3, stabilizing an agonistic conformation (Fig. 9A). Specifically the nitrogen of the sulphonamide linker makes a direct interaction to the O_δ atom of Asn564 corresponding to Asn705 in AR. In addition, one of the sulphone oxygens is located within hydrogen-bonding distance to a putative water molecule, optimally positioned to make interactions with both Thr739 and the N_δ atom of Asn564. As mentioned previously, interactions to Asn564 are of particular importance as the N_δ atom makes a hydrogen bond to the backbone carbonyl group of Glu748, in the loop between helices 11 and 12, thus stabilizing this region.[44]

Adjacent to Asn564, the backbone carbonyl of Leu563 is within hydrogen-bonding distance of the amino group in the indazole 4-position (Fig. 9). The importance of this interaction highlighted by the ether congener **35**, which lacks a donor at this position and shows no activity in the hPBMC assay (compared to 14 nM for **36**). Interestingly, compound **37** illustrates that the hPBMC activity is restored if a trifluoromethyl group is introduced adjacent to the sulphonamide nitrogen. It is reasonable to argue that the introduction of the electron-withdrawing group strengthens the ability of the sulphonamide nitrogen to donate its hydrogen to Asn564.

Beyond the sulphonamide, the mesitylene group enters the hydrophobic volume created at the intersection of helices 3, 7, and 11 (Fig. 9B). This volume overlaps with the 17α substituent that found in most high potency steroid-based ligands. Compounds like **38**, having a large 17α substituent, highlight the significant flexibility of this region. It is interesting to note that none of the endogenous steroid receptors ligands extends into this volume. In a series of unbiased ligand-binding simulations, it was shown that the plasticity of this region is likely coupled to the ligand entry and exits trajectories into and out of the ligand-binding pocket.[45]

The indazole fragment of **36** makes an interaction to the N_ε atom of Gln570 (Fig. 9A). The gatekeeper residues, Gln570 and Arg611, arranged in the open conformation to accommodate the *p*-fluorophenyl substituent.[46i] The *p*-fluorophenyl acts as a hydrophobic link between helices 3 and 5 at the core of the receptor and contributes significantly to the functional agonism observed for compounds with this and similar moieties.[43b] Mutation studies confirm that the interaction strength in between these helices is a powerful agonist trigger across the steroid receptor family.[22b,43a]

The structural analysis of compound **36** shows that the sulphonamide template exhibits a differentiated binding mode relative to steroid-based ligands. Taken together with the fact that steroids are based upon a more rigid scaffold, we hypothesized the sulphonamides induces a distinct structural state leading to a unique protein–protein interaction pattern. To test this hypothesis, we measured the binding of the GR LBD to various coregulator peptides in the presence of compounds **36** and **38** using surface plasma resonance measurements.[46c] In essence, this is a biophysical measurement of how the structural state of the AF-2 interface varies dependent on the ligand structure (Fig. 10). The result indicates that the sulphonamides **36** and **38** have a different cofactor recruitment profile relative to the glucocorticosteroids dexamethasone and fluticasone propionate; the full pharmacological impact of this observation is yet to be understood.

Both compounds **36** and **38** displayed excellent receptor selectivity against a panel of steroid hormone receptors, in comparison the receptor selectivity for key reference-inhaled steroidal glucocorticoids is less pronounced (Table 4).[52] The antiinflammatory effect measuring TNF-α from LPS-stimulated rat PBMCs (rPBMCs) was used to determine the rat–human crossover preceding the in vivo studies. The physicochemical and in vitro PK properties (Table 4) indicate that both compounds as suitable for inhaled delivery and with property profiles similar to reference IGCs. This includes high hepatic clearance to minimize systemic exposure.

The in vitro metabolite profiles were determined in human liver microsomes and human hepatocytes. For both compounds, oxidative *N*-dealkylation was identified as the major metabolic pathway leading to the release of 4-aminoindazoles. Generally, compounds in this series showed little CYP P450 inhibition.

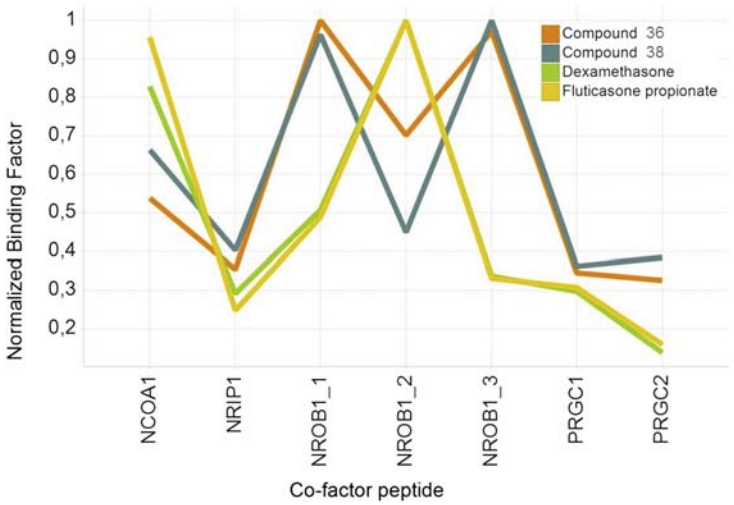

Fig. 10 The binding of various coregulator peptides to the GR LBD in complex with compounds **36**, and **38**, dexamethasone, and fluticasone propionate.

Table 4 Physico-chemical properties and in vitro/vivo profile of **36** and **38**

Assay	*36*	*38*
GR FP binding (μM)	0.0049	0.0030
MR/PR/AR IC_{50} (μM)	>1/0.77/>1	>5/4.5/>1
ERα/ERβ IC_{50} (μM)	>5/>5	>5/>5
Rat PBMC IC_{50} (nM/% efficacy)	0.9/87	4.5/83
logD7.4	4.1	3.7
Solubility (μM)[a]	<0.2/<0.43	1.5/22
Hu PPB (% free)	<0.3	0.5
Rat Mics[b]/Heps CL_{int}[c]	>200/13	>200/33
Hu Mics[b]/Hu Heps CL_{int}[c]	78/18	>200/47
hERG (μM)	NA	8.7
Rat (*iv*) PK Cl/$t_{½}$/Vds[d]	NT	78/6.4/15

[a]Thermodynamic solubility of crystalline/amorphous compound in 0.1 M phosphate buffer pH 7.4 at 25°C for 24 h.
[b]Microsome metabolism intrinsic clearance CL_{int} (μL min^{-1} mg^{-1}).
[c]Hepatocyte metabolism intrinsic clearance CL_{int} (μL min^{-1} 10^{-6} cells).
[d]Blood PK after iv administration; Cl (mL min^{-1} Kg^{-1}), $t_{½}$ (h), Vss (L Kg^{-1})
NA: not active (<25% inhibition) at 50 μM.

The lung and blood concentrations after i.t. instillation were determined for compounds **36** and **38** (Fig. 11). A key driver for lung retention of neutral compounds is the rate of dissolution, often linked to solubility. Compound **36** is less soluble than compound **38**, the lower solubility of compound **36** leading to higher degree of lung tissue retention, with ~50% of the dose remaining in the lung 24 h after dosing compared to only minor amounts remaining in the lung 4 h after dosing for the more polar compound **38**. In a separate study, the blood concentration-time curves after i.t. instillation were determined. The data are in line with the results from the study of lung tissue levels, showing more rapid systemic absorption for compound **38** resulting in higher C_{max} as compared to compound **36**.

The in vivo efficacy of compound **36** was studied in the rat LPS model of acute inflammation.[53] In this model compound **36** was instilled intratracheally 2 h prior to LPS challenge. The total number of leukocytes in the broncho-alveolar lavage (BAL) fluids and increase in lung weight (edema) determined 4 h after challenge. Compound **36** significantly inhibited cell influx at doses of 30 and 100 μg kg^{-1} by 90% and 85%, respectively. The compound also inhibited lung edema, as measured by total lung weight, in a dose-dependent manner. Fluticasone propionate dosed at same doses as compound **36** was used as reference (Figs. 12 and 14).

Cigarette smoke is the main risk factor for developing COPD in humans. Using a mouse model of inflammation, female Balb/C mice were exposed to cigarette smoke for 50 min twice daily for 4 days to induce a local, smoke-induced, inflammatory response in the lung reflected by an increase in the number of neutrophils in BAL fluid.[22] Animals were pretreated with compound **36**, 30 min prior to the first cigarette smoke exposure on each day (4 days treatment in total). Twenty-four hours after last exposure mice were terminated, and the number of neutrophils in the BAL fluids is determined.

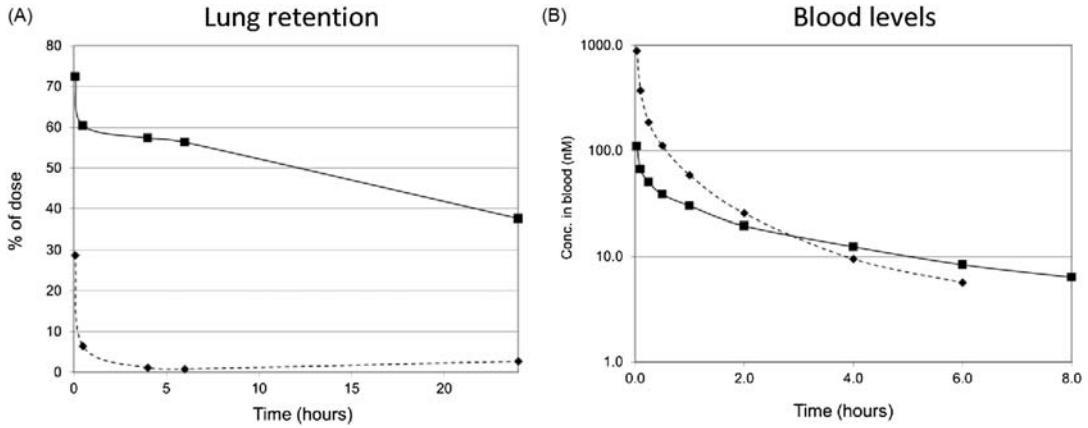

Fig. 11 (A) Lung tissue levels and (B) blood levels of compounds **36** (*dashed line*) and compound **38** (*solid line*) after i.t. administration to the lung (2 μg kg^{-1}).

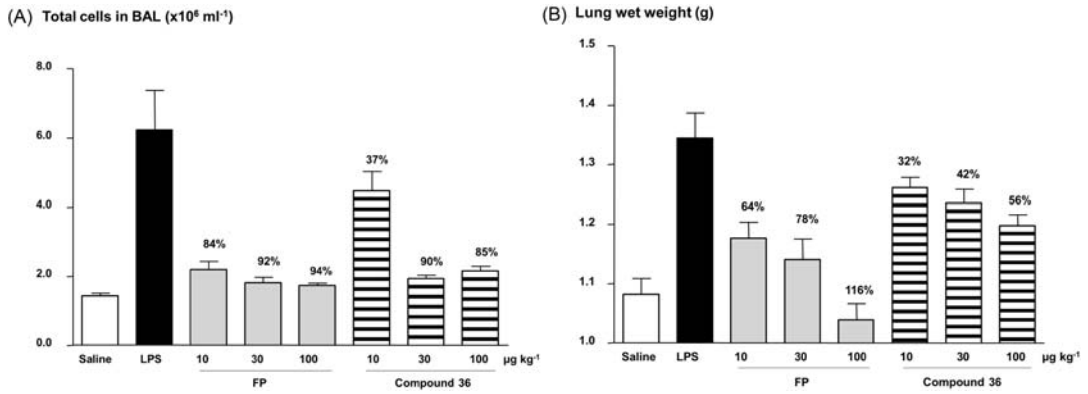

Fig. 12 (A) Inhibition of leukocyte influx. (B) Inhibition of lung edema following *i.t.* administration of compound **36** and fluticasone propionate in the acute LPS model.

In this model **36** significantly inhibited neutrophil influx into BAL fluid of mice exposed to cigarette smoke for 4 days at a dose of 30 μg kg^{-1} (Fig. 13). Fluticasone propionate and budesonide were used as references in this study.

With the identification of potent sulphonamides such as **36** and **38** a series of highly potent and selective nonsteroidal GR modulators had been identified that were suitable for progression into lead optimization.

8.18.5 Lead Optimization Leading to AZD5423, Inhaled SGRM CD1

The initial data generated for compounds belonging to the sulphonamides had shown that this series could provide the project with potent and selective ligands. Selected compounds were shown active in pharmacodynamic models including the acute tobacco smoke model. Structure studies of the receptor–ligand binding provided insight into functional drivers of agonism and cofactor affinity profiles that revealed a differentiated binding mode compared to reference steroidal glucocorticoids. The ligands showed PK properties such as high clearance and a solubility range suitable for further optimization as inhaled GR modulators. *N*-dealkylation via oxidation of the α-methylene position was identified as the major metabolic pathway for this series, leading to compound cleavage and formation of several fragments, including 4-aminoindazoles. However, while the cleavage of the ligand into two discrete parts ensured effective deactivation of GR activity, the formation of 4-aminoindazoles posed an issue due to the potential genotoxicity risk. The lead compound **36**, together with its aniline fragment 4-amino-1-phenylindazol, was subjected to a full Ames test also including metabolizing enzymes. Parent compound **36** came out as inactive from the Ames testing and showed no activity in mutagenic strains of *Salmonella typhimurium* LT2 TA98 and TA100. However, the aniline fragment 4-amino-1-phenylindazol showed a positive response in the Ames test in the presence of lung S9 fraction. Considering that metabolite profiling of **36** had shown that this fragment was formed, it clearly pointed to a genotoxicity risk within the series that needed to be addressed.

Therefore, the primary objective at the initiation of the lead optimization program was to identify GR ligands that were Ames-negative, not forming Ames positive metabolites that retained the overall favorable properties of the lead compound.

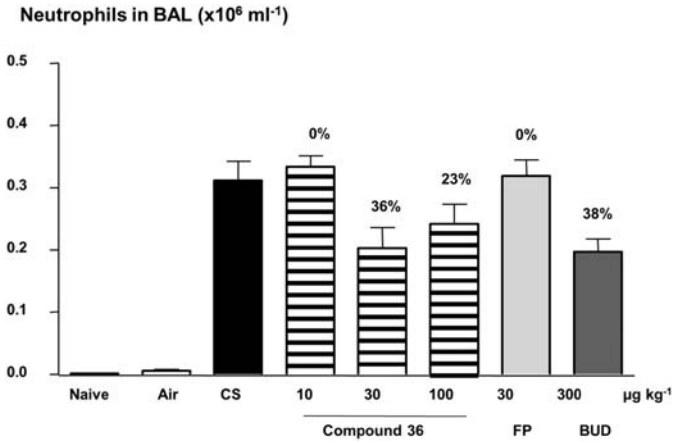

Fig. 13 Inhibition of neutrophil influx in bronchio alveolar lavage (BAL) following *i.t.* administration of compound **36**, fluticasone propionate and budesonide (BUD) in the acute cigarette smoke mice model.

Multiple approaches to resolve the potential Ames issue were investigated in parallel. A particular concern was the fact that crystallography studies of the GR–ligand complexes revealed the formation of a hydrogen bond interaction of the 4-aminoindazole with the backbone carbonyl of Leu563 in helix 3 (Fig. 9A). The importance of this interaction was emphasized by a set of congeners lacking the proton donating capability at this position as exemplified by compound **35**. This compound displayed no activity in cellular functional assays, while the corresponding 4-aminoinazole congener **36** showed excellent functional activity in the cell assays. Interestingly, compound **36** illustrates that the hPBMC activity may be partly recovered if a trifluoromethyl is introduced adjacent to the sulphonamide nitrogen. It is believed that the introduction of the electron-withdrawing group strengthens the ability of the sulphonamide nitrogen to donate its hydrogen to Asn564. However, it is clear that the hydrogen bond formed by the aromatic amine is an integral part of the agonistic pharmacophore by stabilizing GR LBD helix 3 and initially believed to be very difficult to replace.

The first attempt to prevent the metabolic cleavage leading to the formation of aromatic amines focused on the synthesis of compounds **39**–**43** where the secondary amine was made metabolically stable to oxidative cleavage, either by incorporation aromatic amine as a part of a pyrrolidine or a piperidine unit. A second, alternative approach was to block oxidation of the α-position by introduction of a α-methyl or gem-dimethyl substitution next to the aromatic amine. However, both approaches resulted in reduced binding and cellular potency compared to lead compound **36** (Table 5). In the case of the pyrrolidine and piperidine congeners, the loss of functional activity can partly be understood considering that these ligands lack the ability to form a hydrogen bond with Leu563. Compound **43** illustrates an attempt to improve the potency of ether congeners, by moving the ether oxygen away from a potential clash with the Leu563 carbonyl by shifting the ether connection point from 4- to 5-position of the indazole, but again cellular potency was compromised.

Another strategy tried was to identify aromatic amines that were free of genotoxicity, while retaining GR affinity and functional activity in cellular assays for the nonmetabolized sulphonamide ligand. Although aromatic amines have an increased risk, it is far from automatically linked to genotoxicity as has been concluded in several recent articles and reviews.[54] Close aniline congeners such as 5-aminoindazoles or 5-chloro-4-aminoindazoles remained Ames positive. However, the electron-deficient bicyclic aromatic amine, pyrazolopyridin-4-amine showed no activity in the Ames assay, and the corresponding sulphonamide **44** incorporating this amine showed an encouraging PBMC IC_{50} of 15 nM. However, this track to remove the genotoxicity liability was downprioritized in favor of the indazole ether series that was explored in parallel and making significant progress.

As part of the collaboration with Bayer Pharma AG, several series was worked upon in parallel. One compound (**45**) belonging to a series of tetrahydronaphtalenes that showed cellular activity in the TRE assay and in the PBMCs was cocrystallized with the GR-LBD (Fig. 14A).[55] The X-ray structure revealed a binding mode different to the sulphonamide **36**. From the structure it was noted that the aromatic amine in **45** is located 4.5 Å away from the Leu563 carbonyl and, as such, did not appear to make a direct interaction with the helix 3 backbone. Thus, the geometry of the core of **45** offered an option to connect the aromatic amine through an ether linkage instead of an amino group while retaining functional cellular agonistic activity. Furthermore, the structure of compound **45** in complex with GR LBD allowed compounds belonging to a third series part of the collaboration, exemplified by compound **46**, to be confidently modeled into the ligand-binding pocket (Fig. 14B).[56] All key interactions are maintained, but as the tetrahydronaphtalene ring has been opened up resulting in a perpendicular rotation of the phenyl substituent in the minimized conformation. The orientation of the phenyl now allows for the ligand to better exploit the shape and plasticity of the 17α-pocket, which is reflected in a significant improvement of the cellular potency for **46** over **45**.

The GR-LBD ligand complex structure of **46** inspired the design and synthesis of a new series of indazole ether-based GR ligands. Key motifs of the sulphonamide lead **36** were preserved, indazole moiety and the sulphonamide linker, but the connectivity was rearranged (Fig. 15). The secondary amino group was replaced by an ether linkage, and the connection point was moved from 4- to 5-position on the indazole moiety. The terminal aryl group (mesityl in compound **36**) was attached as a branch from the linker unit

Table 5 Compounds explored to investigate potential for reduced metabolic cleavage avoiding release of Ames positive metabolites

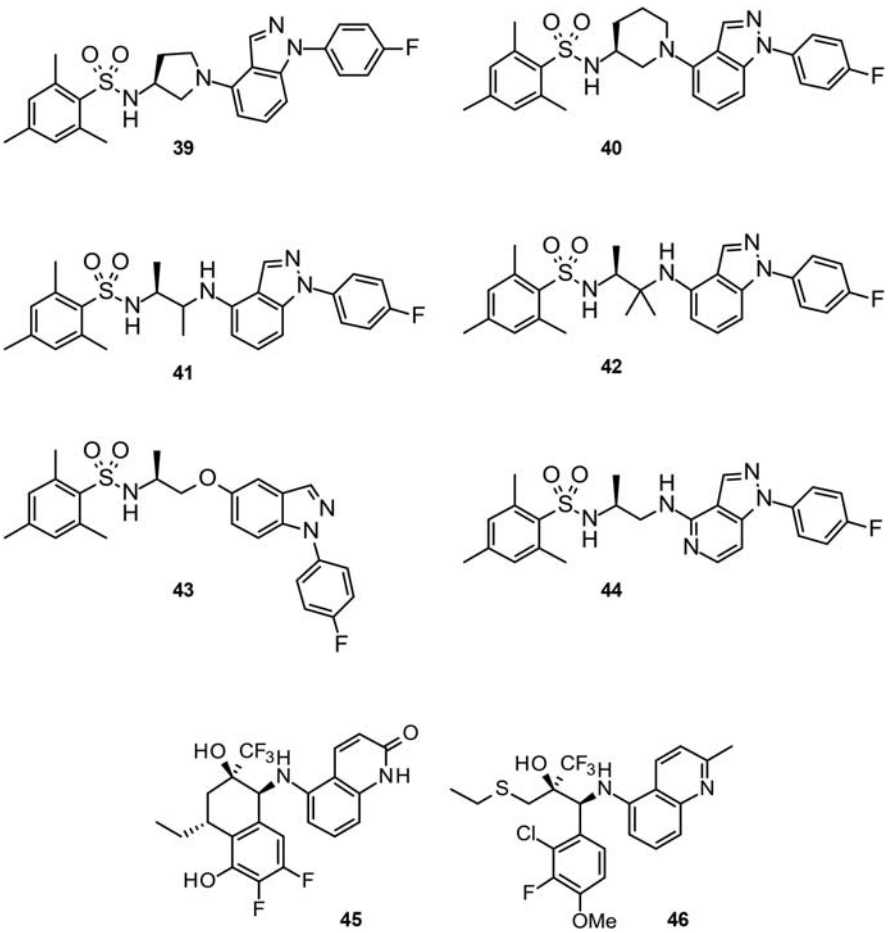

Compound	GR[a] IC_{50} (nM)	TR[a] IC_{50} (nM)	TR[a] Eff. (%)[b]	hPBMC[a] IC_{50} (nM)	hPBMC[a] Eff. (%)[b]
39	41	NV	71	NT	
40	32	NV	27	NT	
41	18	NV	-	NT	
42	20	NV	54	NT	
43	6.8	98	47	NT	
44	20	8.9	72	15	56
45	2.7	1.1	75	37	30
46	3.1	0.32	100	0.65	80

[a]Values are means of at least two experiments.
[b]% of dexamethasone at 10^{-6} M.

and directed into the 17α-pocket. The sulphonamide group is now pointing toward a pocket between helices 7 and 11 to enable a new interaction with the binding pocket, not utilized by lead **36**. Furthermore an additional lipophilic moiety was attached to the sulphone group to compensate for the loss of an H-bonding interaction to helix 3 as a consequence replacing the aromatic amine with an ether linker. Thus the cyclopropyl substituent enables an additional interaction with helix 11, a protein region to which **36** made no interactions, compare **Fig. 9**.

The first compound to be synthesized in this series was compound **47** formed by reacting norephedrine with 1-(4-fluorophenyl)-5-iodoindazole (**I1**) using Ullmann conditions as the key synthetic step (**Scheme 1**). The compound **47** showed excellent cellular potency and did, importantly, not show any Ames activity as the compound lacks the possibility to form Ames positive metabolites. Thus meeting the primary objective for the initial phase of the Lead optimization phase. Compound **47** was selected for further characterization in vitro and in vivo. The compound retained the steroid hormone receptor selectivity previously observed for

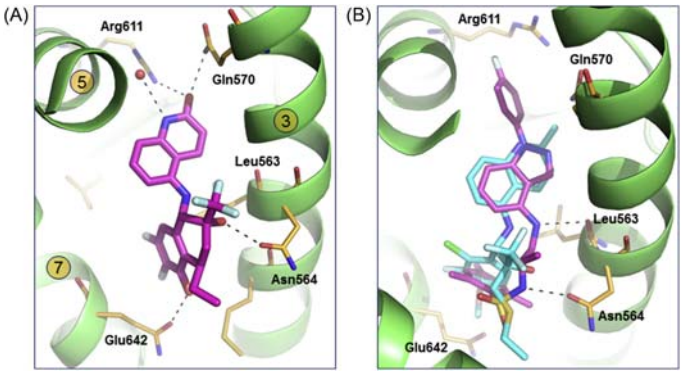

Fig. 14 (A) X-ray structure of the GR-LBD in complex with *tetrahydro*-naphthalene **45** in complex with GR-LBD (B) superimposition of the docked **46** onto the X-ray structure of GR-LBD in complex with **36**.

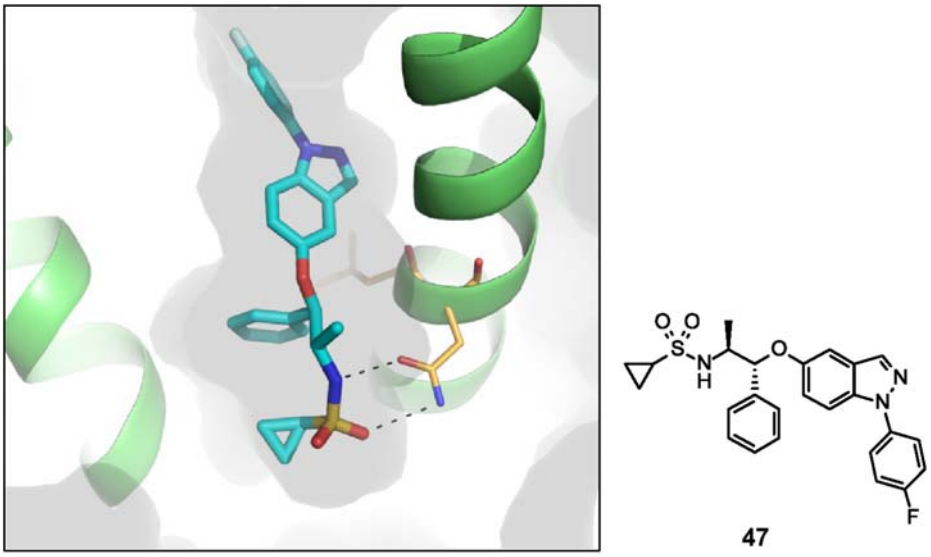

Fig. 15 Docking of hybrid **47** docked into GR-LBD structure obtained from complex with lead **36**.

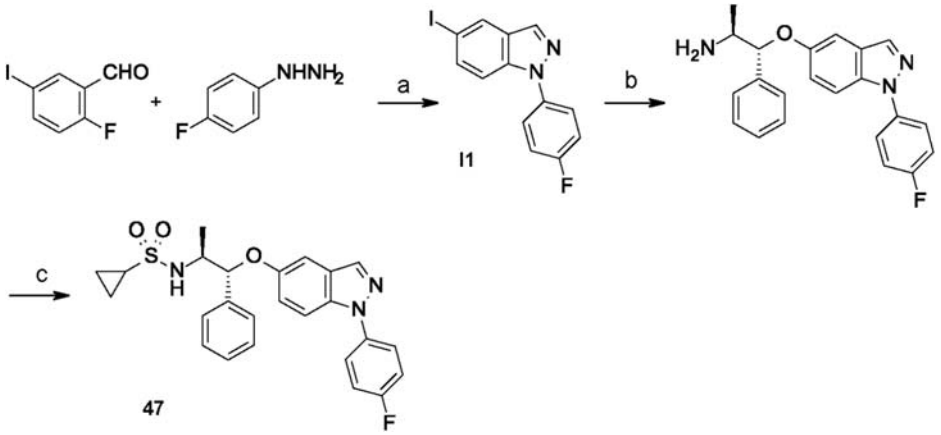

Scheme 1 Synthesis of compound **47**, reagents and conditions: (a) Cs_2CO_3 (3.0 equiv.) NMP, r.t. to 150°C; (b) 1*R*,2*S*-(−)-norephedrine, CuI (0.05 equiv.) Cs_2CO_3 (2.2 equiv.) PrCN, 125°C; (c) cyclopropylsulfonyl chloride (3.0 equiv.) triethylamine (1.4 equiv.), DCM.

Table 6 Physico-chemical properties and in vitro/vivo profile of **47**

MR/PR/AR IC_{50} (μM)	>5/1.2/>10
ERα/ERβ IC_{50} (μM)	>10/>10
Rat PBMC IC_{50} (nM/% efficacy)	2.1/78
logD7.4	4.1
Solubility (μM)[a]	0.3
Hu PPB (% free)	<0.3
Rat Mics[b]/Heps CL_{int}[c]	>23/13
Hu Mics[b]/Hu Heps CL_{int}[c]	16/11
hERG (μM)	>50
Rat (*iv*) PK Cl/$t_{½}$/Vds[d]	57/10/37

[a]Thermodynamic solubility of amorphous compound in 0.1 M phosphate buffer pH 7.4 at 25°C for 24 h.
[b]Microsome metabolism intrinsic clearance CL_{int} (μL min^{-1} mg^{-1}).
[c]Hepatocyte metabolism intrinsic clearance CL_{int} (μL min^{-1} 10^{-6} cells).
[d]Blood PK after iv administration; Cl (mL min^{-1} Kg), $t_{½}$ (h), Vss (L Kg^{-1}).

the lead compound **36**. Inhibition of TNF-α release from LPS-stimulated rPBMCs was used to establish antiinflammatory effects of compounds in rat and to ensure species cross over to in vivo pharmacodynamic models. Analysis of physicochemical and in vitro PK properties (Table 6) indicated that the compound could be regarded as suitable for inhalation and with properties similar to reference IGCs.

Although **47** displayed an excellent profile several properties had to be improved in order to generate a clinical drug candidate. The cellular potency was still too low to meet the dose limitations for a dry powder inhaler for once daily administration. Another property that needed to be improved was metabolic deactivation as measured by its stability in human hepatocytes. A set of analogues was synthesized and profiled (Table 7). Of the arylindazoles synthesized, *p*-fluorophenylindazole was found to be the most potent, and only compounds containing this group will be further discussed. Small alkyl sulphonamides were clearly preferred, as the introduction of larger substituents such as pentyl (**51**) and benzyl (**53**) lost most of the functional cellular activity. This may be rationalized from the X-ray structures indicating that the introduction of a large group would lead to a steric clash with helix 11. The cyclopropyl substituent, as seen in compound **47**, appeared to be the optimal size allowing for a productive interaction with helix 11 when bound to the receptor. It was also observed that the core motif appeared to be inert to oxidative hepatic metabolism, and the metabolism observed was confined to the sulphonyl substituent. Groups such as methyl (**48**) and trifluoromethyl (**49**) were found to be metabolically stable, while compounds containing groups such as benzyl (**55**) and isobutyl (**50**) showed attenuated metabolic stability. A first attempt to introduce metabolic lability was made through the synthesis of the compound **52** demonstrating that metabolic lability could be built in to the norephedrine aryl moiety. However, the postulated oxidation products, **53** and **54**, displayed limited, or no deactivation as compared to compound **52**.

Table 7 Indazole ether sulphonamides

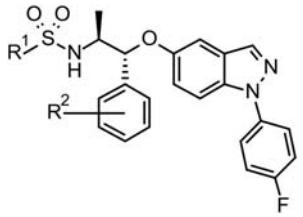

				TR[a]		*hPBMC*[a]		
Compound	R^1	R^2	*GR*[a] IC_{50} (nM)	IC_{50} (nM)	*Eff. (%)*[b]	IC_{50} (nM)	*Eff. (%)*[b]	*HLM (μL min^{-1} mg^{-1})*
47	cPr	H	6.0	0.91	97	3.1	79	16
48	Me	H	2.3	7.4	83	NT		<10
49	CF_3	H	4.6	37	75	NT		<10
50	iBu	H	6.4	44	81	NT		>200
51	1-Pentyl	H	5.7	100	66	NT		180
52	cPr	4-SMe	21	0.75	110	0.67	77	78
53	cPr	4-SOMe	6.4	5.1	99	16	82	57
54	cPr	4-SO_2Me	2.5	1.4	110	0.56	83	<3
55	Bn	H	5.9	51	69	NT		140

[a]Values are means of at least two experiments.
[b]% of dexamethasone at 10^{-6} M.

During the work with the initial sulphonamide hit **9**, it was noted that replacing the sulphonamide with carboxamide congeners, such as **10**, led to complete loss of GR-binding affinity. This was explained by X-ray structure data and modeling indicating that the sulphonamide aryl group enters the hydrophobic volume formed at the intersection of helices 3, 7, and 11 (Fig. 3A). As predicted, this volume of the receptor overlaps with the volume occupied by the steroid 17α substituent, a key structural feature of highly potent steroid GR ligands. Modeling studies indicate that the geometry of corresponding aryl carboxamide is prevented from reaching 17α-binding pocket, as seen for the matched pair **9** and **10**. For the indazole ether series, corresponding alkyl or aryl group no longer serves to occupy the 17α-pocket (Fig. 16). Thus, it was possible to exchange the sulphonamide by a carboxamide group to generate the indazole ether carboxamides **56–63** (Table 8). As the geometry of sulphonamide and carboxamide groups differs significantly in their bonding angles, a diverging SAR for the residue R^1 (Tables 7 and 8) could be expected for the two subclasses. For the most potent sulphonamide residue cyclopropyl, similar cellular potency was found for the corresponding carboxamide, as

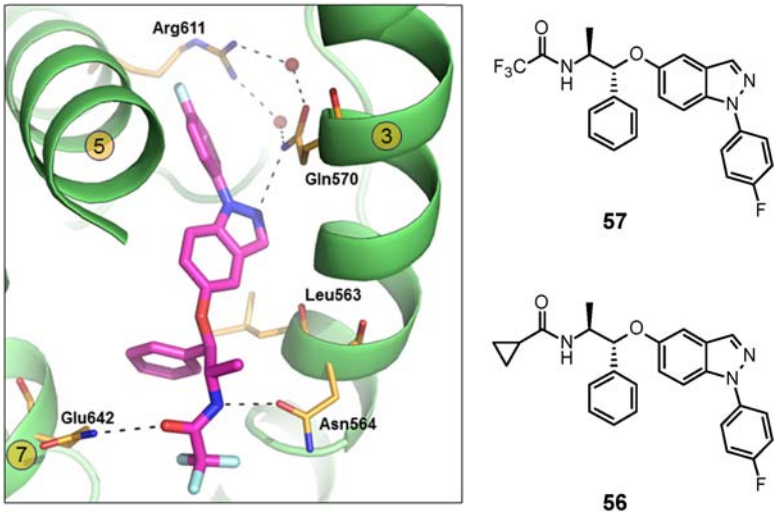

Fig. 16 The X-ray structure of GR-LBD in complex with hybrid **57**.

Table 8 Indazole ether amides

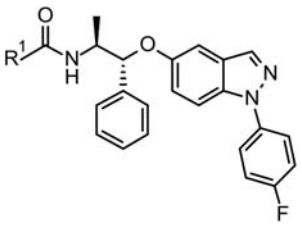

Compound	R^1	GR[a] IC_{50} (nM)	TR[a] IC_{50} (nM)[b]	hPBMC IC_{50}[a] IC_{50} (nM)	hPBMC IC_{50}[a] Eff. (%)[c]	HLM (μL min^{-1} mg^{-1})	c Log P
56	cPr	4.9	0.62	6.0	78	<10	5.4
57	CF_3	2.7	0.13	0.50	83	<10	5.9
58	Me	7.1	3.1	NT		<10	4.8
59	$MeOC_2H_4$	5.2	5.1	64.1	77	>200	5.2
60	Ph	40	1.4	NT		<10	6.5
61	5-Me-1,3,4-oxadiazol-2-yl	6.8	0.095	0.16	79	<10	4.4
62	5-Me-1,2,4-oxadiazol-3-yl	6.0	0.085	0.27	71	NT	5.4
63	tBu	7.0	0.66	1.2	84	62	6.0
64	Bn	18	29	NT		>200	6.5
65	(*R*)-$CHOHCH_3$	2.9	0.36	1.2	74	42	5.0
66	CO_2H	10	NA	NT		98	4.1

[a]Values are means of at least two experiments.
[b]All compounds showed efficacy in range of 87–121% of dexamethasone at 10^{-6} M.
[c]% of dexamethasone at 10^{-6} M.

demonstrated by the matched pair **47** and **56**. However, while the trifluoromethyl sulphonamide showed poor cellular potency (**49**), the corresponding trifluoromethyl carboxamide **57** showed excellent, picomolar cellular potency. Similar level of cellular potency was also obtained for 5-membered ring heterocyclic amide residues, exemplified by compounds **61** and **62**. A loss of potency was observed when alkyl substituents (**58**, **59**) or larger lipophilic phenyl or benzyl substituents (**60**, **64**) were introduced. The compact *tert*-butyl substituent (**63**) was tolerated and showed a similar potency as cyclopropyl. The corresponding amide of lactic acid displayed reasonable potency and provided an opportunity to introduce polar groups. Finally, introduction of an oxalic acid moiety led to pharmacologically inactive compound (**66**). This was expected from SAR of steroids, where formation of acids is known deactivate GR ligands, for example, as seen for fluticasone propionate.

In summary, by the introduction of small electron-withdrawing carboxamides, indazole ethers with excellent cellular potency in range of the project CD target profile had been identified. The compounds tested were lipophilic, with a calculated log *P* ranging from 4 and upwards. Since the objective of the project was to provide compounds for inhaled delivery, issues normally associated with high lipophilicity were not regarded as significant as it would have been for an oral project. However, although several compounds displayed excellent potency in the primary cell assays, they were not suited for further studies in vivo for two reasons. First, the metabolic stability in the in vitro hepatocyte assay of the indazole ether core motif, exemplified by compound **57**. Highlighting the need for introduction of a metabolic soft spot able to generate inactive metabolites to be designed into new compounds. This was in contrast to lead compound **36**, where the core motif had an in-built cleavage point at the aromatic amine α-methylene position and by that, providing means for deactivation of GR activity. The second hurdle to overcome was the need to use crystalline material for appropriate in vivo evaluation on new compounds and ultimately to be used in a dry powder inhaler for clinical use. Most carboxamide analogues synthesized so far in the series were amorphous, probably due to the low number of H-donors and acceptors. Of the 11 compounds **56–66** only **57** was crystalline with a melting point of 123°C. The assumption was that this amide was among the strongest electron withdrawing in the set and with increased electron accepting and donating properties of the amide bond. The chemistry program was therefore guided by two overarching goals: the expansion of the SAR toward crystalline motives and identification of substituents that provided potency, crystalline compounds, and metabolic deactivation via hepatic clearance.

To address these issues a set of compounds were designed and synthesized, key examples are highlighted in **Table 9**. Several of the examples demonstrate that substitution in the 3- and 4-positions of the norephedrine aryl group significantly improved the cellular potency into the low digit picomolar range. Methoxy substitution was accepted and led to rapid oxidative metabolism, as exemplified by entries **67**, **68**, and **72**. The high potency of compounds **70**, **73**, and **75** illustrates the plasticity of the receptor in the 17α-pocket also being able to accommodate larger substituents. The set also generated compounds such as the ether **73** that combined potency with fast clearance in human microsomes. Still morphology was a problem in series. As previously noted crystallinity was sporadically observed for compounds belonging to the trifluoroacetamides sub series, such as **72**, but most compounds remained amorphous even after significant efforts made to crystallize. In order to increase the probability to introduce crystallinity more polar amides, such as oxamides, as well as other electron-withdrawing groups such as 2,2-difluoropropionamides were examined. The oxamides, such as **75**, provided compounds with significant lower lipophilicity but did not yield crystalline compounds. Most often, potency was compromised and metabolic clearance was reduced when lowering log *D*. The examples shown in **Table 9** demonstrate that demethylation of the anisole moiety, which constituted the soft spot in **68**, was reduced and prevented progression as seen for matched pair **68** and **74**. However, 2,2-difluoropropionamides, exemplified by **77** and **78**, provided crystalline and highly potent ligands. Finally, the importance of the stereochemistry of the two chiral centers is highlighted for compound **69**. The depicted compound with absolute stereo configuration (1S,2R) had a GR-binding affinity of IC_{50} 3.6 nM, as expected its enantiomer (1R,2S) had significant weaker-inding IC_{50} of 25 nM. The corresponding diasteromers (1R,2S) and (1R,2R) had GR-binding affinities of IC_{50} 49 and 79 nM, as could be expected from modeling that indicated a less optimal fit.

The structure–activity for variations in other positions was also studied but did not lead to any improvements of properties and is only discussed briefly (**Table 10**). It was previously noted that the *S*-stereochemistry the methyl was clearly preferred over *R*-configuration. Removal of this methyl led to significant loss of activity (**79**). Substitution of the methyl by substituents lager than ethyl (**84**) led to loss of activity (**85**). This may be rationalized from the structural data, where larger substituents collide with helix 11 of the receptor. Variation of the *p*-fluorophenyl moiety by halogen and heteroatom replacements was also investigated, with some compounds showing excellent potency as exemplified by **82**, **87**, and **88**. Introduction of small alkyl ether and amines in the *meta* and *para* positions led to significant loss of potency. As expected, introduction of a carboxylic group (**86**) led to complete loss of activity, similar to what was seen with compound **66**. Use of small saturated alkyl rings led to loss of activity (**80**), and the use pyridyl groups **87** and **88** showed some loss of activity. Finally, substitution of 6-H for Cl or methyl on the indazole was tolerated (matched pairs **81–57** and **83–72**).

From the set of compounds evaluated, compounds **72**, **77**, and **78** were selected for in-depth profiling in vitro and in vivo. This led to the selection of compound **72**, with the development code AZD5423, as the first inhaled SGRM Candidate Drug for progression into clinical studies. Properties will be further described below. Both compounds **77** and **78** showed excellent potency at 18 hours pretreatment in the rat Sephadex model. But neither of the two compounds was considered to provide an improvement over **72** and was therefore parked.

8.18.6 Lead Optimization Leading to AZD7594, Inhaled SGRM CD2

With compound **72** being progressed into clinical studies a follow-up program was initiated. Several properties of AZD5423 needed to be retained, such as the picomolar potency in PBMCs as well as blood flow controlled human hepatic metabolic clearance. While

Table 9 Expansion of carboxamide indazole ethers

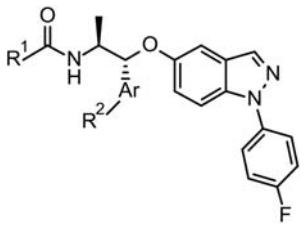

Compd	Ar	R^2	R^1	GR[a] IC_{50} (nM)	TR[a] IC_{50} (pM)[b]	hPBMC IC_{50}[a] (pM)[c]	HLM (μL min^{-1} mg^{-1})	c Log P
67	Ph	4-MeO	tBu	2.4	250	890	>200	6.0
68	Ph	3-MeO	tBu	4.6	80	430	130	6.0
69	Ph	4-F	cPr	3.6	1100	5500	<10	5.2
70	3-quinolinyl	H	CF_3	2.8	44	150	<10	5.8
71	Ph	3-OH	CF_3	2.7	8000	4600	42	5.3
72[e]	Ph	3-MeO	CF_3	1.9	49	161	>192	5.8
73	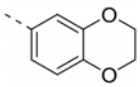		CF_3	5.2	30	73	>200	5.8
74	Ph	3-MeO	$CONH_2$	2.2	138	NT	11	3.6
75	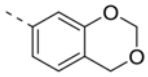		$CONH_2$	2.2	71	154	53	2.6
76	Ph	3-MeO	2-oxazole	2.3	290	355	28	5.2
77[e]	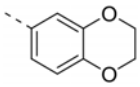		$MeCF_2$	4.0	20	80	>200	5.7
78[d]	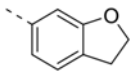		$MeCF_2$	4.8	47	234	>200	6.0

[a]Values are means of at least two experiments.
[b]All compounds showed efficacy in range of 78–120% of dexamethasone at 10^{-6} M.
[c]All compounds showed efficacy in range of 82–101% of dexamethasone at 10^{-6} M.
[d]Crystalline.

clearance of AZD5423 showed the desired profile in human and dog, the clearance profile in rat had two weaknesses: first, the hepatic clearance rate was low, leading to a significant systemic exposure in vivo. Second, metabolism in rat also leads to a significant systemic exposure levels of the GR active metabolite (**71**, rPBMC IC_{50} 0.5 nM), in hPBMCs activity was significantly lower (hPBMC IC_{50} 4.6 nM). However since this metabolite is only present in low concentration in human, **71** was not considered to contribute to any GR-related systemic side effects. Since all PD studies were performed in rodents, this led to a more complex situation estimating the TI for this compound versus reference GR ligands, such as budesonide or fluticasone propionate. Thus a hepatic clearance profile, liver blood flow controlled and without formation of any GR active metabolites was targeted in the back-up program. Furthermore, the deactivation of AZD5423 is dependent on both phase 1 and phase 2 metabolic processes. It was envisioned that the direct deactivation dependent merely on phase 1 metabolism alone would lead to a more efficient reduction of the GR activity. Other properties that could be envisioned to improve the overall properties of a back-up compound were improved solid-state properties, reduced oral absorption to <5%, and a lower volume of distribution.

The initial efforts focused on compounds having a two atom spacer connecting the amino alcohol core chain and the aryl substituent as shown for **90**, introducing a new metabolic soft spot into the core scaffold that would enable complete deactivation by metabolic fragmentation of the molecule (Table 11). The compound **90** showed a rapid clearance in hepatocytes. Furthermore, development led to the identification of **91**, fulfilling the CDTP with regard to cellular potency; this compound was crystalline with a melting point of 160°C associated with rapid metabolism in human hepatocytes. Since the lipophilicity was significantly lower compared to CD1, the volume of distribution was also expected to be reduced. Metabolite ID studies suggested that the main metabolism route was cleavage of the phenol moiety, thus eliminating GR agonism activity.

Table 10 Structure activity exploration of indazole ether carboxamide series

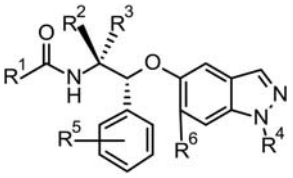

Compound	*R*[1]	*R*[2]	*R*[3]	*R*[4]	*R*[5]	*R*[6]	*GR*[a] *IC*$_{50}$ *(nM)*	*TR*[a] *IC*$_{50}$ *(nM)*[b]
79	CF_3	H	H	4-FPh	H	H	9.1	19
80	CF_3	Me	H	cPentyl	H	H	2.5	1.7
81	CF_3	Me	H	4-FPh	4-F	Cl	2.1	0.34
82	CF_3	Me	H	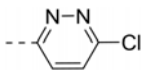	H	H	3.1	NV
83	CF_3	Me	H	4-FPh	3-OMe	Me	3.7	0.042
84	tBu	Et	H	4-FPh	H	H	3.5	0.56
85	CF_3	iPr	H	4-FPh	3-F	H	29	NT
86	$MeCF_2$	Me	H	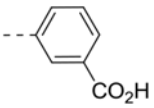	H	H	10	NT
87	CF_3	Me	H	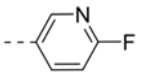	H	H	0.6	0.7
88	CF_3	Me	H	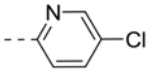	H	H	0.9	2.1
89	$MeCF_2$	Me	Me	4-FPh	H	H	1.6	9

[a]Values are means of at least two experiments.
[b]All compounds showed efficacy in range of 83–111% of Dexamethasone at 10^{-6} M.

Table 11 Phenylindazole ethers having a two atom spacer introducing a metabolic soft spot

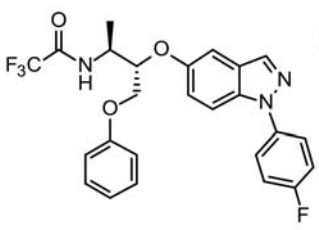

90

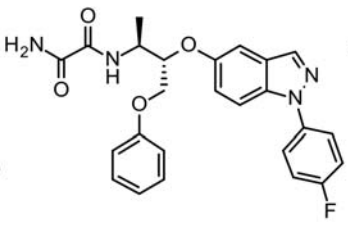

91

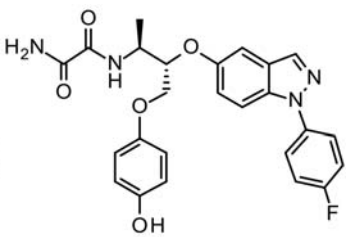

92

Compound	*GR*[a] *IC*$_{50}$ *(nM)*	*TR*[a] *IC*$_{50}$ *(nM)*[b]	*hPBMC IC*$_{50}$[a] *(nM)*[c]	*HLM* ($\mu L\ min^{-1}\ mg^{-1}$)	*hHeps* ($\mu L\ min^{-1}\ 10^6\ cells^{-1}$)	*c Log* P
90	1.7	0.36	2.0	183	26.7	6.0
91	0.9	0.59	0.34	120	21.7	3.7
92	4.8	15.4	32	48	12	3.2

[a]Values are means of at least two experiments.
[b]All compounds showed efficacy in range of 36–107% of dexamethasone at 10^{-6} M.
[c]All compounds showed efficacy in range of 30–72% of dexamethasone at 10^{-6} M.

Compound **91** was investigated in a range of assays as a potential back-up CD, and the compound generally behaved well, including initial safety studies such as being clean in 5-strain Ames. Also, the compound showed excellent efficacy in the tobacco smoke model as well as increased duration of action when compared with fluticasone propionate. However compound repeatedly showed relatively poor potency in the 4-day inhalation Sephadex model with an ED_{50} of 10 μg kg^{-1}. This should be compared to AZD5423 having an ED_{50} of 1 μg kg^{-1} in the same model. Considering that PBMC potency of AZD5423 was approximately twice that of **91** meaning that an unexpected fivefold loss of potency was observed. It should be noted that a similar pattern was also observed in the corresponding studies made using intratracheal administration in the Sephadex model. This unexpected loss of potency eroded the margins with regard to several of the targeted CDTP properties, and the compound was consequently parked.

A breakthrough in the development of a back-up compound came by an integrated crystallography and computational chemistry approach that prompted the exploration of a relatively large and polar cavity adjacent to the position binding to the *p*-fluorophenyl moiety, named by the project as the "water pocket" (Fig. 17). Exploration of this pocket by elongation of the ligands from the *meta*-position of the phenyl group on the phenylindazole moiety provided high clearance compounds with optimized morphological properties preserving both the potency and selectivity profiles. The water pocket is not accessed by current steroid-based ligands. Since this cavity is relatively polar with lattice-bound water molecules in crystal structure this elongation provided decreased lipophilicity as compared to the AZD5423-based series. One property that was significantly influenced was crystallinity. Compounds with an additional amide group were often crystalline and with melting points in the 200°C range.

The first set of compounds represented by compounds **93–95** (Table 12), all showing significantly lower logD compared to AZD5423, still with retained potency as compared to the carboxylic acid matched pair compound **86**. A general issue is that the unsubstituted norephedrine core in this series shows slow hepatic clearance, and it became clear that further optimization was needed to introduce substituents that would be rapidly metabolized into molecules with low affinity to the GR receptor. This was a similar situation as with the original indazole ether lead **57**. Two norephedrine derivatives showing rapid metabolism was identified exemplified by compounds **96–98** and **99** (Table 12). Compound **96–98** and **99** were all crystalline and fulfilled expectation with regard to potency in hPBMCs, hepatic clearance, and improved morphology to be investigated further by profiling in vivo. The compounds were also less lipophilic than AZD5423 with the potential to have lower volume of distribution. Finally, since melting point was higher, solubility was lower than AZD5423 and likely leading to longer lung retention as well as reduced oral bioavailability.

The compounds were profiled in a set of in vitro and in vivo models. Inhaled administration of the compounds in the 4-day Sephadex model was used as primary model in vivo to evaluate potency and mechanistic side effects in the rat. This model was shown to be a good predictor of human efficacy of inhaled steroids in the clinical use, Table 13.

The pyridyl-based ligands **98** and **99** both showed inferior potency compared to compounds **96** and **97** in the Sephadex model, and this was one reason why they were deselected for further progression in clinical studies. Finally compound **97** was prioritized over **96**; one important reason for selecting this compound was that this compound was considered to have a better balanced lung retention profile with a rat lung half-life of 15 h while **96** showed significantly longer retention to the lung (Table 14). Properties such as solubility and optimization of lung retention will be further discussed below. Compound **97** was finally selected as candidate drug for the inhaled treatment of respiratory diseases such as Asthma and COPD, was given AstraZeneca development code AZD7594, and is currently undergoing clinical studies.

8.18.6.1 Synthesis of AZD5423 and AZD7594

The discovery route for the synthesis of both AZD5423 and AZD7494 followed the same overall scheme. The key synthetic step in the synthesis of both compounds was an Ullmann coupling generating the aryl ether linkage. AZD5423 was synthesized in five

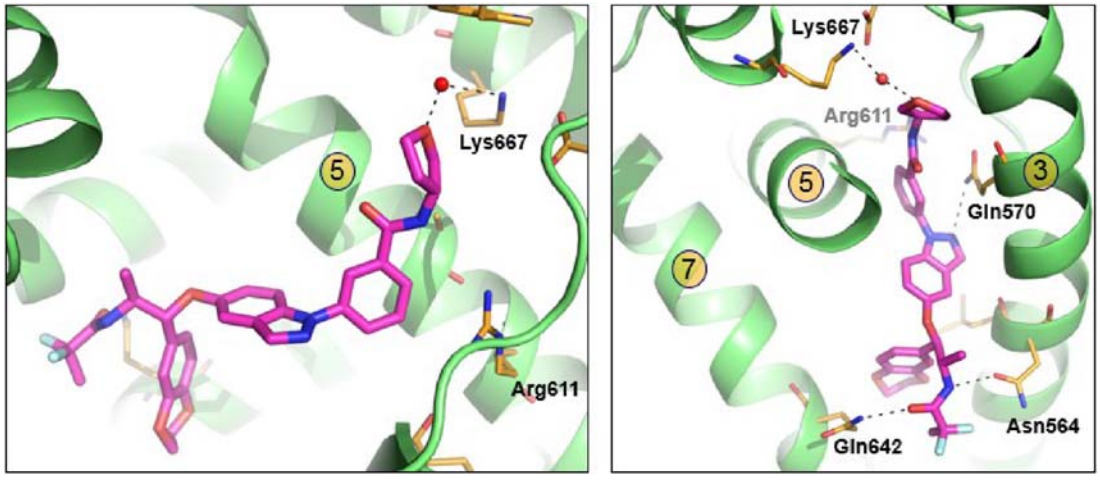

Fig. 17 X-ray structure of the phenylindazole ether carboxamide **97** extending into the water pocket.

Table 12 Phenylindazole ethers exploring the water pocket

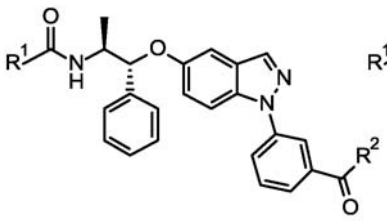

93-95

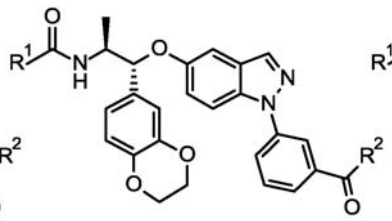

96-98

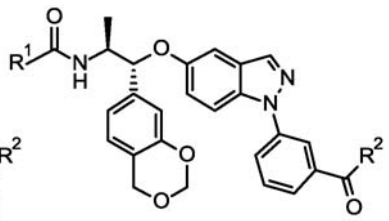

99

Compound	R^1	R^2	*GR*[a] IC_{50} *(nM)*	*TR*[a] IC_{50} *(nM)*[b]	*hPBMC*[a] IC_{50} *(nM)*[c]	*HLM/HHep* ($\mu L\ min^{-1}\ mg^{-1}$)/ ($\mu L\ min^{-1}\ 10^6\ cells^{-1}$)	*c Log* P
93	CH_3CF_2	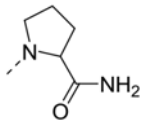	2.8	0.21	1.1	25/<2.7	3.9
94	CH_3CF_2	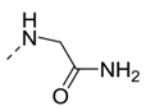	1.6	0.13	0.41	<10/<2.7	3.4
95	CH_3CF_2	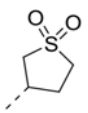	1.7	2.4	5.0	<10/<2.7	3.4
96	CH_3CF_2	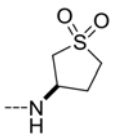	1.5	0.17	0.54	>200/22	3.3
97	CH_3CF_2	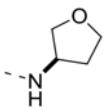	0.9	0.055	0.42	>200/29	4.5
98	CH_3CF_2	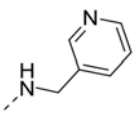	1.0	0.06	0.38	>200/20	4.0
99	CH_3CF_2	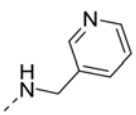	1.0	0.06	0.38	>200/20	4.0

[a]Values are means of at least two experiments.
[b]All compounds showed efficacy in range of 100–119% of dexamethasone at 10^{-6} M.
[c]All compounds showed efficacy in range of 58–75% of dexamethasone at 10^{-6} M.

linear steps leading to a pure enantiomer with an overall yield of 28% as depicted in **Scheme 2**. The key step was the coupling reaction between the linker alcohol and the 5-iodoindazole fragment. The norephedrine moiety was synthesized applying a variant of a Weinreb–Nahm α-aminoketone synthesis, and bromo-(3-methoxyphenyl)magnesium was added to the deprotonated Weinreb amide to yield the arylketone **I2**.[57] The subsequent Meerwein–Ponndorf–Verley reduction proceeded with a high degree of diastereoselectivity to afford the protected *anti*-amino alcohol **I3** (de >99%) which was deprotected to yield the norephedrine analogue **I4** (ee >99%).[58] 1-(4-fluorophenyl)-5-iodoindazol (**I1**) is readily accessible from a condensation reaction of the *ortho*-fluorinated

Table 13 In vivo data for CD2 short list phenylindazole ethers

Compound	*AUC_{0-24} (nM × h) total/free*[a]	*Efficacy (ED_{50} inhibition of lung edema, μg kg^{-1} day^{-1})*	*Side effects (ED_{25} for thymus weight involution, μg kg^{-1} day^{-1})*	*Therapeutic ratio*
96	7.5/0.06	2.4	>130	>54
97	14/0.07	0.8	40	50
98	38/0.03	3.8	27	7
99	28/0.014	8.7	14	<2

[a]Systemic kinetics in rats after inhalation (nose only exposure, lung dose: 0.1 μmol kg^{-1}).

Table 14 Physiochemical properties of lead iSRGM candidate compounds AZD5423 and AZD7594, short list compounds **96** and **99** and key reference compounds

	AZD5423 (form A/B)	*AZD7594*	*96*	*99*	*Fluticasone propionate*	*Budesonide*
C log *P*	5.8	3.4	3.4	4.9	3.8	2.9
Mp (°C)	82/109	177	218	155	280	226
PSA (A^2)	64	115	143	116	86	99
Solubility in aq. buffer pH 7.4 (μM)[a]	<0.05/>0.05	0.02	<0.01	0.02	<0.1	42
Solubility in HIF (μM)[a]	13/6.0	0.6	0.3	1.4	0.6	60
h/r PPB (%free)	0.008/0.007	0.43/0.48	0.7/1.5	0.08	1.6/1.6	14/8

[a]Solubility measured for crystalline compound.

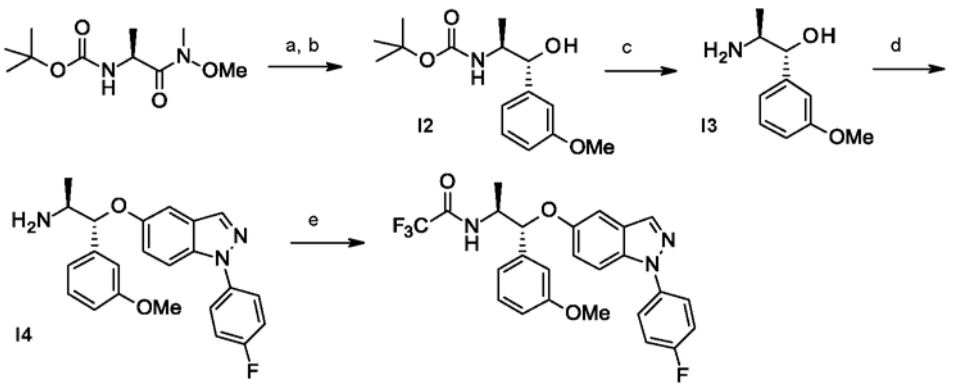

Scheme 2 Discovery route for the synthesis of AZD5324 (**72**), Reagents and conditions: (a) bromo(3-methoxyphenyl)magnesium, THF, r.t.; (b) $Al(OiPr)_3$, ^iPrOH, toluene, 50°C; (c) aq. TFA, DCM, r.t.; (d) 1-(4-fluorophenyl)-5-iodoindazole (**I1**), CuI, Cs_2CO_3, BuCN, 125°C; (e) $(CF_3CO)_2O$, NEt_3, DCM; (f) *p*-fluorophenylhydrazine, Cs_2CO_3 (3.0 equiv.) NMP, r.t. to 150°C.

benzaldehyde with *p*-fluorophenylhydrazine under basic conditions at elevated temperatures. The primary amine of indazole ether scaffold was synthesized in a Ullmann coupling reaction with the iodoindazole **I1**, along with *N*-coupled byproducts limiting the yields in this step.[59]

The synthesis depicted in Scheme 2 leads to a polymorph (form A), with a melting point of 82°C. However in the continued process optimization efforts the synthesis was modified at several steps, leading to the discovery of a new polymorph (form B) with a melting point of 109°C. The different melting points lead to different solubility and as a result different pharmacokinetic properties, both in the lung and in the blood will be discussed in below.

AZD7594 was synthesized in seven linear steps with an overall yield of 13–26%. The 5-iodoindazole intermediate, **I5** was obtained quantitatively in four synthetic steps (Scheme 3).

8.18.6.2 Physical Chemical Properties of Drug Candidates

The physical chemical properties for AZD5423 and AZD7594 are shown in Table 14 as well as properties for fluticasone propionate, budesonide, and compounds **96** and **99**. These properties are important to understand the lung and systemic pharmacokinetic properties. They also illustrate some of the principles of dissolution rate-driven lung pharmacokinetics used to control the duration of effect.

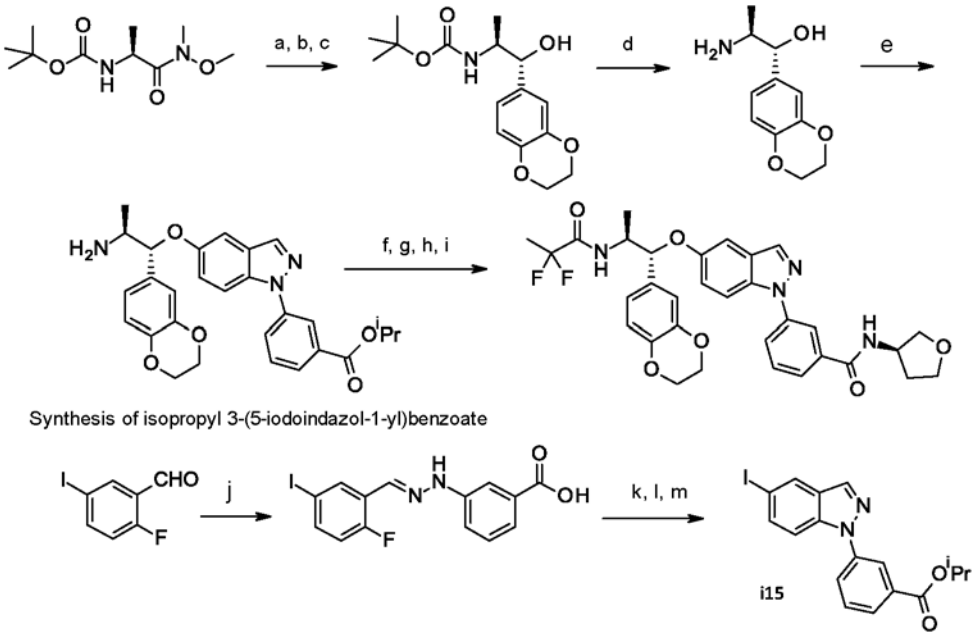

Scheme 3 Discovery route for the synthesis of AZD7594 (**97**), reagents and conditions: (a) ^{i}PrMgBr, THF, −15°C to 0°C; (b) ^{i}PrMgCl, (2,3-dihydrobenz[b](1,4)dioxin-6-yl)magnesium bromide, THF, −15°C to r.t.; (c) Al(O^{i}Pr)$_3$ (0.2 equiv.), ^{i}PrOH (11 equiv.), toluene, 50°C (d) 6 M aq. HCl, EtOAc 40°C; (e) (**i2**), CuI, Cs_2CO_3, dimethylglycine, PrCN, 110°C; (f) 2,2-difluoropropionic acid, HBTU, DIPEA, DCM, r.t.; (g) 0.25 M NaOH, THF/MeCN (5/2); (h) HBTU, DIPEA, DMF, r.t.; (i) (3R)-Tetrahydro-3-furanamine, MeCN; (j) 3-hydrazinylbenzoic acid, Cs_2CO_3, DMF, r.t.; (k) KOtBu/^{i}PrOH, toluene, 50°C,; (l) $NaCO_3$, NMP, 40°C; (m) ^{i}PrBr.

The set of inhaled GR ligands in Table 14 display a range of lipophilicities and melting points. AZD5423 is the more lipophilic, but the low melting point makes it the most soluble compound in the set. It should be noted that solubility in human biological fluids such as human intestinal fluid (HIF) or epithelial lining fluid is more relevant measure to understand properties in the pharmacological setting. Solubility is significantly higher in these fluids and provides a better prediction of in vivo properties. Since epithelial lining fluid is difficult to obtain, HIF was used as surrogate for screening purpose in the project. As predicted from comparator data the lung retention of AZD5423 is expected to be between that of budesonide and fluticasone propionate, while AZD7594 is predicted to have lung retention similar to fluticasone propionate.

8.18.6.3 Metabolism, Major Deactivation Pathways

Rat and dog liver clearances were studied in microsomes and hepatocytes followed by determination of in vivo clearance. As predicted, AZD5423 had high turnover when incubated with hepatocytes and liver microsomes from dog and man. Rat hepatocyte clearance was somewhat lower, the hepatocyte hepatic extraction for male rats was 0.50, compared to 0.77 and 0.68 in dog and human hepatocytes respectively, this difference was even more pronounced using hepatocytes from female rats. AZD5423 was found to be stable when incubated with the S9 sub cellular fraction isolated from human and rat lung, indicating stability in lung tissue. High permeability in combination with the relatively high solubility in HIF indicates full absorption following oral administration. Bioavailability after oral administration was 35% in rat and dog, which is in line with the observed in vivo clearance of 70% and 60% of liver blood flow in rat and dog, respectively.

The in vivo pharmacokinetics for AZD7594 was studied in rat (p.o. and i.v) and dog (i.v.) with data summarized in Table 15. In general, AZD7594 in rats has a high clearance (CL) and low volume of distribution (Vss) and a relatively long half-life. In dog, CL and Vss were lower, and the corresponding half-life was 16 h. The intrinsic clearance (CL_{int}) in rat liver microsomes and hepatocytes predicts in vivo CL relatively well while dog hepatocytes over predict the in vivo CL. The oral bioavailability in rat was low at doses tested.

The pharmacokinetic kinetic profiles of AZD5423, AZD7594, and fluticasone propionate in rats after dry powder inhalation are shown in Table 16. As expected from the solubility differences, AZD5423 has a shorter retention to the lung compared to AZD7594 and fluticasone propionate. However the lung retention is considerably longer than for budesonide (data not shown) as predicted by its lower solubility (Table 14). For AZD7594 lung retention is longer than for fluticasone propionate. Blood PK mirrors the lung PK properties. For AZD5423 higher solubility leads to a higher peak blood C_{max}, it is especially interesting to note the difference between the two polymorphs of AZD5423. Form B with higher melting point has lower solubility and as a consequence longer lung retention and lower blood C_{max}. AZD7594 and fluticasone propionate have similar blood area under curve (AUC); this is what can be expected since both compounds have blood flow controlled hepatic clearance and very limited oral bioavailability.

Table 15 Intravenous and oral pharmacokinetics of AZD5423, AZD7594 and fluticasone propionate in male rats (male Wistar, $n=3$) and dogs (female Beagle, $n=3$). Comparison to scaled CL from liver microsomes and hepatocytes

Compound	*Species*	*Scaled CL (liver mics) (mL min^{-1} kg^{-1})*	*Scaled CL (heps) (mL min^{-1} kg^{-1})*	*CL (mL min^{-1} kg^{-1})*	*Vss (L kg^{-1})*	*F (%)*
AZD5423	Rat	>60	49	31–64	8.6–9.3	35[a]
	Dog	–	30	22	24	35[a]
AZD7594	Rat	>60	49	43–97	0.34–0.58	<1
	Dog	–	30	7.5	0.43	–
Fluticasone propionate	Rat	>60	45	149	4.0	–
	Dog	–	29	40	8.9	–

[a]AZD5423 crystal form A used.

Table 16 Kinetic profile in female Wistar rat after dry powder inhalation (DPI) in nose-only exposure inhalation chamber at 0.1 nmol kg^{-1} (lung dose). Lung levels and corresponding systemic exposure (area under curve, AUC)

Compound	*Lung half-life (h)*	*Lung level at 24 h (% of lung dose)*	*Lung AUC$_{0-24}$ (nM × h)*	*Blood AUC$_{0-24}$ (nM × h)*	*Blood free AUC$_{0-24}$ (nM × h)*	*C$_{max}$ (nM)*
AZD5423 (form A)	<1	<1	9100	288	0.02	83
AZD5423 (form B)	1	<1	21,300	246	0.017	55
AZD7594	15	45	500,000	28	0.13	2.3
Fluticasone propionate	4	3	66,000	29	0.4	ND

Thus, similar dose should lead to similar blood exposure. For AZD5423, due to the low hepatic clearance observed in rat, the blood AUC is significantly higher in rat compared to AZD7594. In dog and human similarly high AUC levels are not expected due to the high hepatic clearance.

Furthermore, inhalation experiments have low lung deposition of ~10%, compared to 35% in human delivered to the lung via inhalation. It can be estimated that ~50% of systemic exposure in the rat experiment will originate from the intestine. In the human about 20% will be originate from the fraction swallowed. Considering these factors, the project expected that systemic exposure at similar doses for AZD5423 and AZD7594 should be similar in the human setting.

8.18.6.3.1 AZD5423 metabolic profile

Identification of the metabolites formed in rat, dog, and human hepatocytes was performed using radiolabeled compounds (Figs. 18 and 20). For AZD5423, the dominating metabolic pathway and deactivation route are O-demethylation providing the phenolic alcohol (**71**) found in rat (44%), human (1.2%), and dog (5.2%) hepatocytes. This metabolite is subjected to phase II

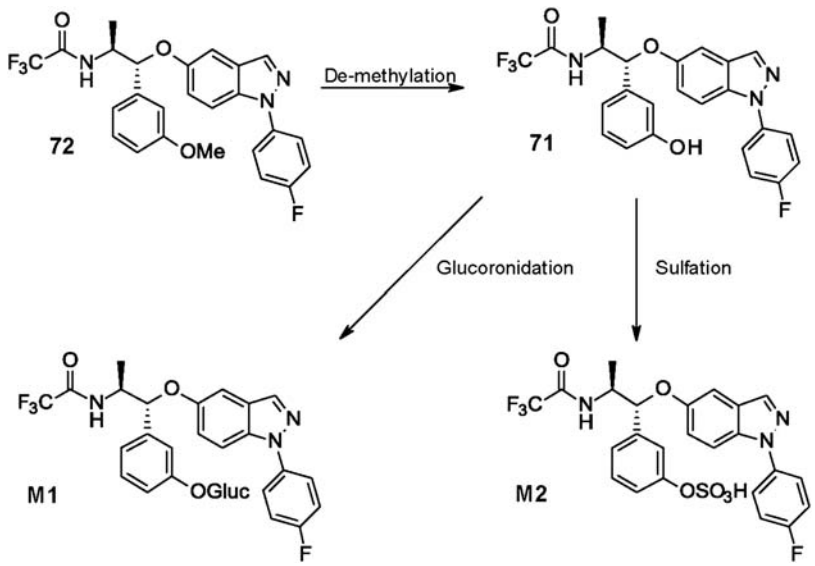

Fig. 18 Major pathways identified leading to metabolic deactivation of AZD5423 (**72**).

Table 17 Amount of metabolites formed following incubation in hepatocytes using ^{14}C-labeled AZD5423 (**72**), expressed as amount of total radioactivity

	71	*M1*	*M2*
Human heps (%)	1	1	97
Dog heps (%)	5	10	65
Rat heps (%)	44	22	19

conjugation, and in human hepatocytes the sulfate was found to be the main metabolite (97%). The sulfate metabolite was also formed, but to a somewhat lesser extent in dog hepatocytes (64%) and in rat hepatocytes (19%). Glucuronide adducts were also identified, including a metabolite with a glucuronic acid in conjugation with the O-demethylated metabolite. In rat hepatocytes these glucuronides represent 22% of the identified metabolites and in human hepatocytes 1.2% (Table 17). The major sulfate metabolite **M2** in man was also detected in vivo in the tox species rat and dog; thus no human specific metabolites was identified. The main metabolites **71** and **M2** were synthesized and tested for PBMC activity. While the polar compound **M2** was inactive in PBMCs, as expected, the phenolic ligand **71** showed significant activity in rPBMCs (Table 18).

The in vivo PK studies in rat and dog with AZD5423 confirmed the presence of the demethylated metabolite **71**. Following oral administration, the blood levels (AUC) of **71** were 85% and 7% of parent in rats and dogs, respectively. In summary, the profiling showed that effective deactivation of GR activity should be expected in man as well as in dogs. Minor contribution of metabolite **71** to systemic GR activity should be expected in rat. Still this contribution is small, compared to the relatively high systemic exposure in rat of AZD5423 due to not full blood flow controlled clearance and absorption from intestine.

8.18.6.3.2 AZD7594 metabolic profile

AZD7594 was metabolized in a similar way in man, dog, and rat hepatocytes (Table 19). The major metabolic pathway was oxidation in the 1,4-dioxane ring giving the hemiacetals **M10** and **M11**. These metabolites were further oxidized to the catechol **M8** that underwent glucuronidation, forming glucuronides **M5** and **M6**. The formation of the 5-hydroxyindazole **M4** as an oxidative cleavage product and its sulfate conjugate **M3** was detected in all three species and represents another pathway of metabolism. Metabolism was also found to occur in the 3-aminotetrahydrofurane ring leading to the carboxylic acid **M9** (Fig. 19).

The project was confident in a significant loss of GR activity for most of the metabolites identified, as they were only fragments, **M3** and **M4**, or highly polar structures such as **M5**, **M6**, **M7**, and **M8**. **M10** and **M11** could potentially have some GR activity. However, as part of evaluating compounds **96**, **97**, **98**, and **99**, the corresponding **M10** and **M11** metabolites for AZD7594 congener **96** were synthesized, and both compounds were found to lose one order of magnitude or more in potency in both hPBMCs and rPBMCs. This in combination with the fact that **M10** and **M11** represent only about 10% of metabolites formed makes it highly unlikely that they would lead to any measurable systemic GR levels of activity. Finally since metabolite **M9** contains a carboxylic acid group located in the very polar part of the GR receptor, it could not be ruled out that some residual activity remained. As expected, activity was largely lost, and the compound showed no activity in rPBMCs and 29 nM in hPBMCs. This should be compared to parent AZD7594 activity in rPBMCs and hPBMCs of 0.30 and 0.42 nM, respectively. This result in combination with the fact that this metabolite was formed in $<10\%$ led to the conclusion that this metabolite should not contribute to any measurable systemic levels of GR activity.

Table 18 Potency of AZD5423 (**72**) primary metabolites in peripheral blood mononuclear cells

	AZD5423	***71***	***M2***
hPBMC (nM)	0.16	4.6	NA
rPBMC (nM)	0.14	0.56	9.0

Table 19 Amount AZD7594 (**97**) metabolites identified in hepatocytes, expressed as percent of total radioactivity

	AZD7594	***M3***	***M4***	***M5***	***M6***	***M7***	***M8***	***M9, M10***	***M11***
Human	15	22	2	15	9	2	18	8	5
Rat	17	11	1	29	3	14	8	3	4
Dog	22	13	1	11	17	6	14	10	3

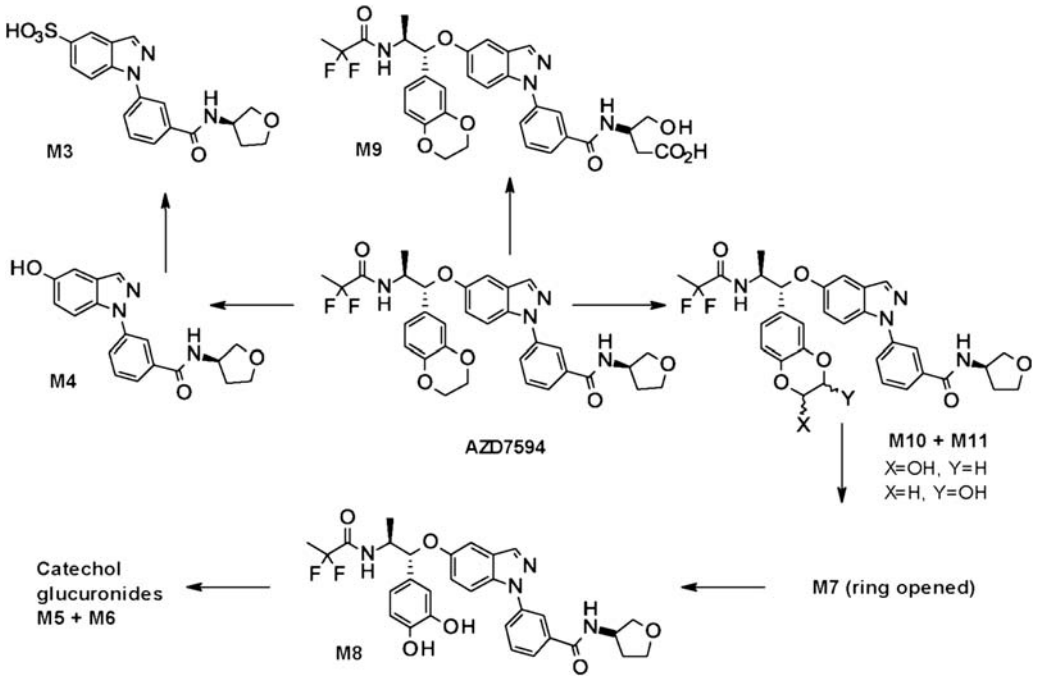

Fig. 19 AZD7594 (**97**) metabolites identified in rat, dog, human, hepatocytes, and in rat bile. All structure identifications are based on MS/MS data.

In bile-cannulated rats, only minor amounts of parent AZD7594 were detected in bile and urine. The metabolites formed in rat hepatocytes were also detected in vivo. It was concluded that the major route of clearance for AZD7594 in rat is by metabolism. The metabolites formed were predominately excreted in bile.

8.18.6.3.3 Assessment of PK based drug–drug interaction potential

The potential of AZD5423 and AZD7594 to inhibit cytochrome P450 was assessed using fluorescent-based in vitro assays and prototypic fluorogenic P450 substrates for CYP 1A2, 2C9, 2C19, 3A4, and 2D6. IC_{50} was >1 μM for all isoforms except 2C9 and where the IC_{50} was determined to 0.9 and 0.45 μM, respectively (Table 20). For both compounds having low predicted doses, low predicted systemic exposure and high plasma protein binding ($<1\%$ fu) ensure that the margins to free C_{max} concentrations are high (100,000-fold).

8.18.6.3.4 Prediction of human pharmacokinetics

The predicted dose to man (PDtM) is based on the efficacious lung-deposited dose levels in the rat Sephadex 4-days model. The PDtM (lung-deposited dose) for AZD5423 and AZD7594 is 1.2 and 0.8 μg kg^{-1}, respectively. This also takes into account the full cross-over potency in rat and human in vitro PBMC models.

The predicted pharmacokinetic profile of AZD5423 in man was based on in vitro to in vivo scaling from liver microsomes and hepatocytes and on allometric scaling of CL and Vss from rat and dog. Furthermore the predicted human absorption profile was based on absorption profile in rats after dry powder inhalation (Table 21).

For AZD7594, the human AUC at PDtM is based on the predicted CL range and assuming that 100% of the lung-deposited dose will be systemically available, according to the formula AUC = Lung Dose/CL (Table 21). Systemic exposure (Free AUC) in man at the therapeutic dose is predicted to be 120 times less than budesonide and at least 9 times less than and fluticasone propionate.

Taking into account in vitro potency the GR-mediated systemic side effects are predicted to be significantly less (>10 times) than for budesonide and fluticasone propionate.

Table 20 CYP inhibition (IC_{50}, μM) for AZD5423 (**72**) and AZD7594 (**97**) compared to fluticasone propionate in relation to predicted C_{max} in man at therapeutic dose

Compound	*1A2*	*2C9*	*2C19*	*3A4*	*2D6*	*3A5, 2C8, 2B6*	*Predicted C_{max} (μM)*
AZD5423	>10	0.88	>1	>10	>10		0.002
AZD7594	>50	0.45	7	9	>50	>50, >50, >50	0.0002
Fluticasone propionate	>50	<0.15	30	<0.15	1.6		0.0004

Table 21 Predicted human PK profile of AZD5423 and AZD7594 at therapeutic dose based on in vitro/in vivo scaling of human hepatocytes. Compared to meassure values for fluticasone proprionate (1000 μg twice daily with Discus)

Compound	*Clearance (mL min^{-1} kg^{-1})*	*PPB (% fu)*	*C_{max} (nM)*	*Free C_{max} (nM)*	*AUC (nM × h)*	*Free AUC (nM × h)*
AZD5423[a]	16	0.4	2.0	<0.006	3.5	<0.01
AZD7594[a]	15	0.4	0.2	0.001	2	0.008
Fluticasone propionate[b]	17	1.6	0.4	0.006	3.3	0.05

[a]Predicted.
[b]Measured.

8.18.6.4 In Vitro Pharmacology Assessment

8.18.6.4.1 Receptor binding and steroid NHR selectivity

In vitro potencies of AZD5423 and AZD7594 were measured in a competitive receptor-binding FP assay using the full-length human GR and radiolabeled dexamethasone. As it is common that GR ligands show crossover to other steroid hormone receptors the binding potency was assessed against the PR, MR, AR, and estrogen receptor α and β (ER α/ER β) in competitive receptor-binding assays using FP-based assay technology. Selectivity was determined as the ratio between receptor potencies.

Both AZD5423 and AZD7594 bound potently to GR, with mean IC_{50} values of 0.9 nM and also demonstrate excellent selectivity over other steroid NHRs (>1000-fold) for all the steroid NHRs. It can be concluded that both compounds showed an excellent level of potency and a better selectivity profile compared to the reference IGCs tested (Table 22).

8.18.6.4.1.1 Cell-based assays

The potency of AZD5423 and AZD7594 was determined in several cell assays. Both compounds demonstrated excellent level of potency in the reporter gene assay measuring gene transrepression(TRE) assay with mean EC_{50} values of 49 and 55 pM, respectively. In hPBMCs, the release of TNF-α in response to LPS stimulation was used to determine the antiinflammatory effects in human primary cells. AZD5423 and AZD7594 were highly potent inhibitors of LPS-induced TNF-α release, with mean IC_{50} values of 161 and 420 pM, respectively. In rPBMCs, the potency was in a comparable range demonstrating good species cross-over to rodents. To test the compound in a physiologically relevant environment mimicking the systemic exposure of free drug, human whole blood was stimulated with LPS and following determination of TNF-α release. In this assay AZD5423 and AZD7594 displayed mean IC_{50} values of 8.0 and 12 nM, respectively. Finally, cross over to rat was confirmed also in the rat whole blood assay (Table 23).

Overall both inhaled SGRM compounds show excellent level of cell potency with good cross over to rat. It has been claimed in the literature that high protein binding leads to a relative lower whole blood activity due to a potency drop off that is beneficial for systemic side effects.[60] This has been claimed, for example, for ciclesonide and fluticasone furoate; however in our hands fluticasone furoate does not have a better in vivo profile compared to fluticasone propionate.

Table 22 Receptor binding potencies for the iSGRM candidate compounds AZD5423 and AZD7594 compared to key IGCs in clinical use

Compound	*GR[a] IC_{50} (μM)*	*PR IC_{50} (μM)*	*MR IC_{50} (μM)*	*AR IC_{50} (μM)*	*ERα IC_{50} (μM)*	*ERβ IC_{50} (μM)*
AZD5423	0.0009	1.76	>5	>10	>10	>10
AZD7594	0.0009	>10	>10	>10	>10	>10
Fluticasone propionate	0.0009	0.02	0.15	>10	>10	>10
Budesonide	0.0038	0.03	0.01	0.71	>10	>10
Mometasone furoate	0.0008	0.01	0.02	0.58	>10	>10

[a]Radioligand assay, except for budesonide where fluorescence polarization assay was used.

Table 23 Potency and efficacy for AZD5423 and AZD7594 in cellular assays compared to key IGCs in clinical use

Assay	*AZD5423*	*AZD7594*	*Fluticasone propionate*	*Budesonide*
Cell TRE (pM)	49	55	40	496
hPBMC (pM)	161	423	44	1570
rPBMC (pM)	138	299	144	412
Hu whole blood (nM)	8.0	12	1.5	5.9
Rat whole blood (nM)	3.4	2.6	2.3	4.2

8.18.6.5 In Vivo Pharmacology Assessment

To evaluate compound potency, duration, functional parameters, mechanistic side effects, and the effects in respiratory animal models in vivo, a variety of animal models was utilized. In the studies described below, AZD5423 and AZD7594 have been delivered to the lung via the intratracheal (it) or inhaled route, and all doses stated refer to the lung-deposited dose.

8.18.6.5.1 Potency and mechanistic side effects in the rat Sephadex model

Male Sprague–Dawley rats were challenged via *it* instillation of Sephadex beads, and due to the inborn hypersensitivity of the rats towards dextran, an eosinophilic-driven inflammation develops in the lungs over time. The inflammatory response can be monitored as an increase in the lung weight (edema), which peaks at 24–48 h and is maintained for more than 7 days after provocation. AZD5423 and AZD7594 were administered to rats as a nose-only inhaled dry powder, where the first administration was given 2 h prior to challenge with Sephadex and was followed by 4 once daily treatments prior to termination.

AZD5423 and AZD7594 demonstrated a potent dose-dependent inhibition of lung edema, with ED_{50} of 1.2 μg kg^{-1} day^{-1} and 0.8 μg kg^{-1} day^{-1}, respectively. Fluticasone propionate dosed within the range 0.4–73.5 μg kg^{-1} day^{-1} resulted in a dose-dependent inhibition of lung edema with a combined ED_{50} of 6.0 μg kg^{-1} day^{-1} (Fig. 20).

8.18.6.6 Predicted Therapeutic Dose

The human dose (DtM) estimates for AZD5423 and AZD7594 were based on the mean efficacious lung-deposited dose levels (ED_{50}) in the rat Sephadex 4-day model (Table 24). The predicted human lung-deposited doses are 1.2 and 0.8 μg kg^{-1}, which is equivalent to predicted daily total doses of 200 and 120 μg for AZD5423 and AZD7594, respectively. When comparing the lung ED_{50} values obtained from the Sephadex model with the clinical effective nominal doses reported in the Swedish PDR (FASS) for a range of registered IGCs, the preclinical in vivo model was shown to be predictive. This evidence from well-known comparators further supports the predicted effective nominal dose to man.

8.18.6.7 Mechanistic Side Effects

To determine mechanistic systemic side effects of ligand models thymic involution was measured in parallel in the 4-day Sephadex model. Thymus involution was chosen as readout due to the high sensitivity of this organ to glucocorticoids (thymus weight decrease compared to vehicle-treated animals), expressed as ED_{25}. This value was then used to determine the therapeutic ratio for the compounds (the ratio between mechanistic side effects [ED_{25} thymus involution] and potency [ED_{50} lung edema]).

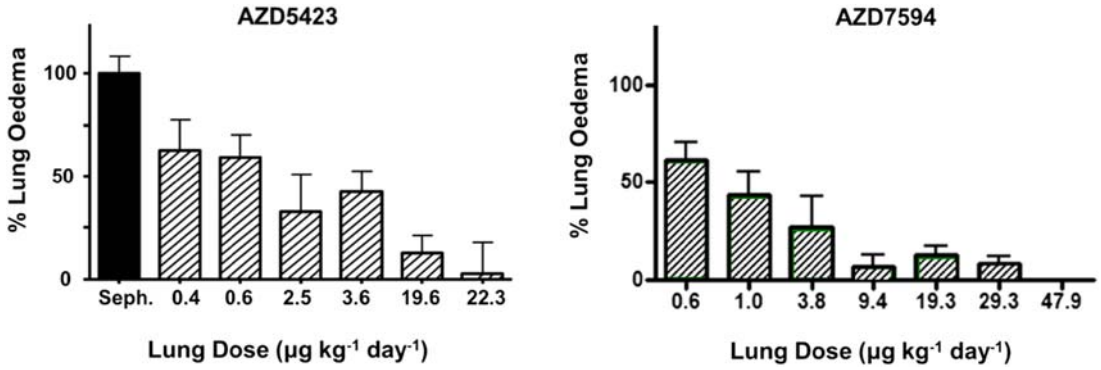

Fig. 20 Effects of repeated dry powder inhalation of AZD5423 and AZD7594 on lung edema reduction in the 4-day Sephadex model.

Table 24 Comparison of lung ED_{50} values from Sephadex model with reported clinical effective nominal doses for IGCs

Compound	*Efficacy in Sephadex model (Lung ED_{50} μg kg^{-1} day^{-1})*	*Clinically effective nominal dose PDR (μg)*
AZD5423	1.25	200[a]
AZD7594	0.8	120[a]
Fluticasone propionate	6.0	500 (50–500)
Budesonide	9.6	800 (200–800)

[a]Predicted.

AZD5423 showed a dose-dependent effect on thymus involution, with an ED_{25} of 4.6 μg kg^{-1} day^{-1} and an estimated therapeutic ratio of 3.7. However, as earlier pointed out, this compound has a significantly higher relative systemic exposure in rat, relative to what's expected in man. For this reason there was reason to believe that the therapeutic ratio would be better in man. AZD7594 demonstrated a weak effect on thymus involution, resulting in ED_{25} of 40 μg kg^{-1} day^{-1}, and estimated therapeutic ratios of 50. Fluticasone propionate had a thymus ED_{25} of 3.9 μg kg^{-1} day^{-1} and an estimated therapeutic ratio of 0.7 (Fig. 21 and Table 25).

8.18.6.8 Duration of Effect

Both AZD5423 and AZD7594 were studied in in vivo models for their potential to be used as a once daily treatment (i.e., 24-h duration of effect). The studies were set up somewhat differently between the two compounds. AZD5423 was administered 6 h prior to Sephadex challenge at time zero, animals were terminated 18 h later, and reduction of lung edema was determined. Administration of AZD5423 at lung doses of 28 and 30 μg kg^{-1} via inhalation resulted in a significant inhibition (69% and 87%, respectively) of lung edema after 24 h. Administration of AZD7594 at lung doses of 39 and 23 μg kg^{-1}, 9 and 24 h prior to Sephadex challenge via inhalation resulted in significant inhibition (107% and 76%, respectively) of lung edema. These data, supported by PK lung retention data, suggest that once daily treatment is feasible with both compounds. Fluticasone propionate was used as reference in the AZD7594 duration study (Fig. 22).

8.18.6.9 Functional Measurements in the Rat Sephadex Model

To investigate the effect of AZD5423 on Sephadex-induced changes in lung function, male Sprague–Dawley rats were treated with AZD5423 (100 μg kg^{-1}) via *it* instillation 30 min prior to challenge with Sephadex. Eighteen hours after Sephadex challenge animals were anesthetized and connected to a ventilator (FlexiVent system) for lung function measurements.

AZD5423 dosed at *it* 100 μg kg^{-1} reduced the Sephadex-induced increase in dynamic lung resistance (lung constriction) (dyn R) and reversed the decline in dynamic lung compliance (lung stiffness) (dyn C) similar to what is observed for budesonide dosed at 1000 μg kg^{-1} (Fig. 23).

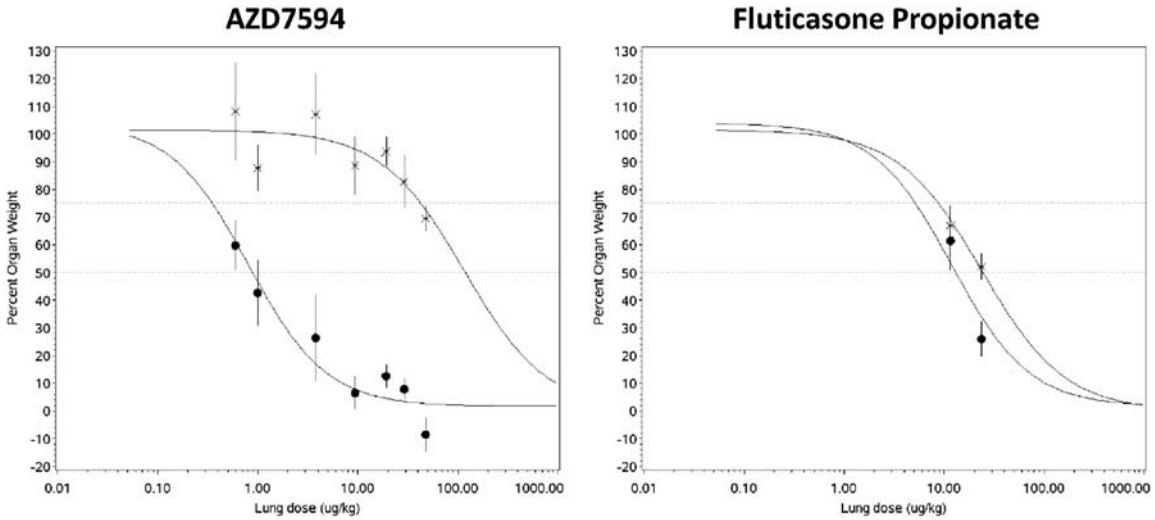

Fig. 21 Effects of repeated dry powder inhalation of AZD7594 and fluticasone propionate on lung edema (●) and thymus weight observed (**X**) reduction in the 4-day rat Sephadex model.

Table 25 Potency, thymus involution and calculation of therapeutic ratio in 4 day rat Sephadex model

Read-out	*AZD5423*	*AZD7594*	*Fluticasone propionate*
ED_{50} inhibition of lung oedema (μg kg^{-1})	1.2	0.8	6.0
ED_{25} for thymus involution (μg kg^{-1})	4.6	40	3.9
Therapeutic ratio, rat (ED_{25}/ED_{50})	3.7	50	0.7
Therapeutic ratio, rat (vs. *fluticasone propionate*)	~5	>10	–

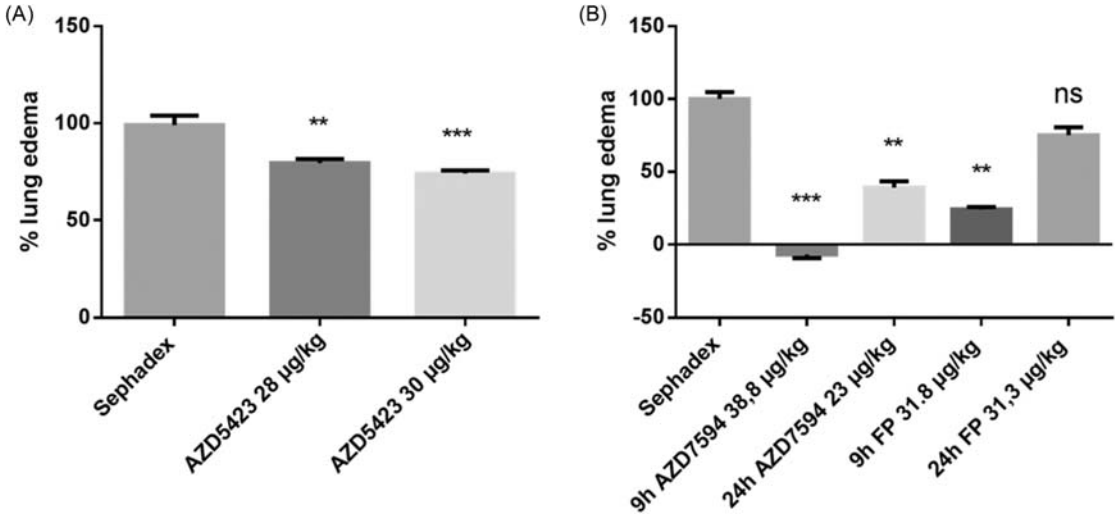

Fig. 22 Duration of effect for (A) AZD5423, (6 h pretreatment, two doses 28 and 30 μg kg^{-1} lung dose) and (B) AZD7594 (9 and 24 h pretreatment, 39 and 23 μg kg^{-1} lung dose respectively) after inhaled administration in the Sephadex rat model.

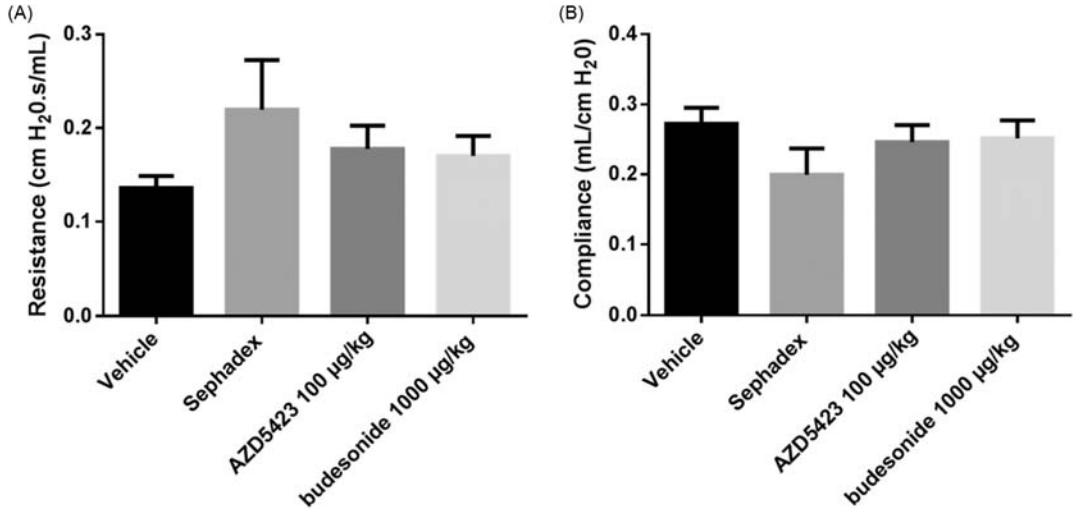

Fig. 23 AZD5423 reduces lung resistance (A) and improves compliance (B) in the rat Sephadex model.

8.18.6.10 Efficacy in a "Disease-Like" Setting (Ovalbumin Model)

AZD5423 and fluticasone propionate were dosed at 100 μg kg^{-1} intratracheally (i.t.) to ovalbumin (OVA) challenged rats (2 week rat model for "asthma") 24 and 1 h prior to, and 24 h after challenge. This resulted in a significant reduction in total cells, eosinophils and neutrophils in lung lavage fluids for AZD5423 and to a lesser degree fluticasone propionate (Table 26).

8.18.6.11 Acute Mouse LPS Model

Exposure to significant levels of LPS is reported to be associated with the development and/or progression of many types of lung disease. In addition, human LPS studies have been used in several programs as the proof of principle model to progress compounds for further studies in COPD patients. The acute effects of LPS can be characterized by inflammatory processes in the lung, including neutrophilic infiltration and the increase in levels of cytokines.

Mice were treated *it* with AZD5423 and AZD7594, one hour before challenge with nebulized LPS (1 mg mL^{-1}) of *Pseudomonas aeruginosa* LPS. Twenty-four hours after the LPS challenged animals were terminated and inflammatory cell numbers in BAL were counted. At a dose of 0.3 mg kg^{-1} AZD5423 significantly inhibited by 78%, the influx of neutrophils recovered from lavage fluids. AZD7594 inhibited the LPS-induced influx in the number of neutrophils in BAL by 66% at a dose of 1 mg kg^{-1}. In the latter study

Table 26 Inhibition of the numbers of total cells, eosinophils and neutrophils in the lung lavage fluids of AZD5423 and fluticasone propionate on OVA-induced eosinophilia in Brown Norway rats

	AZD5423 100 μg kg^{-1}	*Fluticasone propionate 100 μg kg^{-1}*
Total cells (%)	77	55
Eosinophils (%)	80	58
Neutrophils (%)	100	84

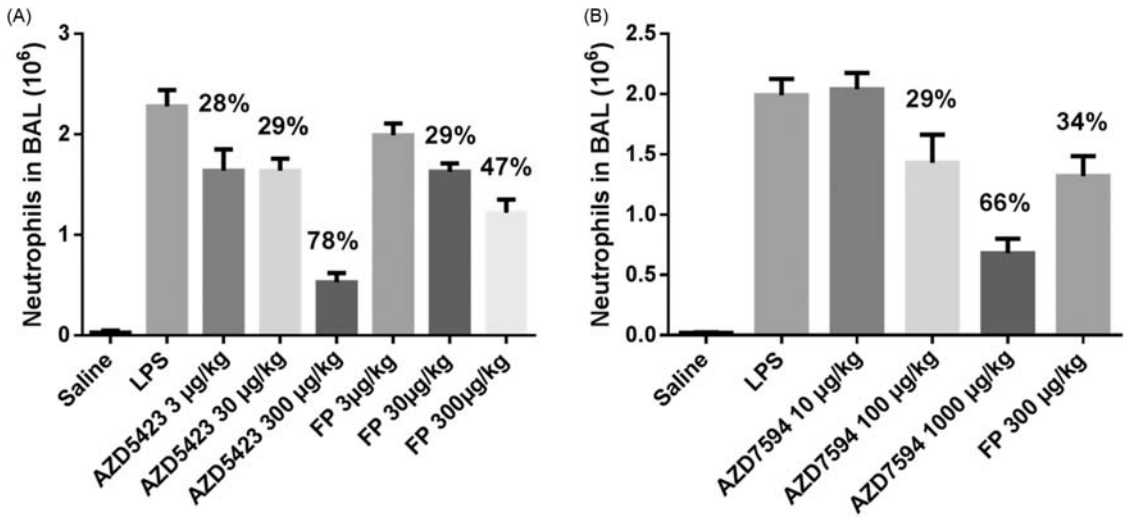

Fig. 24 Effects of (A) AZD5423 and (B) AZD7594 on neutrophil influx in the LPS model compared to fluticasone propionate.

fluticasone propionate was used as reference to benchmark compound efficacy. Fluticasone propionate inhibited the number of neutrophils accumulating in BAL by 47% and 31%, respectively, dosed at 0.3 mg kg^{-1} (Fig. 24).

8.18.6.12 Acute LPS Model—Lung Function Changes and MRI Imaging

LPS-induced effects on lung function change can be investigated using magnetic resonance imaging (MRI) and measuring cell influx in lung. Female Balb/c mice were treated with AZD5423 (0.3 mg kg^{-1}) via *it* instillation 1 h prior to, and 24 and 47 h after challenge with inhaled LPS. Budesonide-dosed 0.3 mg kg^{-1} twice daily was used as reference.

AZD5423 (0.3 mg kg^{-1}) inhibited the inflammatory response to LPS, assessed by the reduction in total number of cells (84% inhibition), neutrophils (85% inhibition), and macrophages (86% inhibition) when compared to vehicle and LPS challenged mice. Budesonide reduced the inflammatory response by the reduction in total number of cells (49% inhibition) and neutrophils (55% inhibition) without effect on macrophages.

Hyperpolarized ^{3}He-MRI which detects ventilation defects and ^{1}H-MRI which primarily detects fluid in the lungs (edema) were used to study the effects of AZD5423 and budesonide in mice. After 24 h both AZD5423 and budesonide showed efficacy by improving ventilation and reducing edema in this model. The two compounds inhibited the number of LPS-induced lung lesions determined by 100% and 86%, and the LPS-induced increase in unventilated lung volume by 100% and 96%, assessed by ^{1}H-MRI and ^{3}He-MRI, respectively (Fig. 25).

8.18.6.13 Acute Cigarette Smoke Model

Cigarette smoke is the main risk factor for developing COPD in humans. By using a mouse model of inflammation, female Balb/C mice the effect of twice daily cigarette smoke exposure for 4 days were studied. The effects on local inflammatory response in the lung are reflected by an increase in the number of neutrophils.

AZD5423 dosed *it* at 0.3 mg kg^{-1} day^{-1} inhibited the cigarette smoke-induced influx of neutrophils into BAL by 29%. Fluticasone propionate dosed at 0.03 and 0.3 mg kg^{-1} day^{-1} had no effect on the number of neutrophils in BAL. In a separate study, AZD7594 at a dose of 0.3 mg kg^{-1} day^{-1} significantly inhibited influx of neutrophils into BAL by 58%. Kineret, a biological that inhibits the IL-1β pathway, was used as a positive control in his study and was administered at 48 mg kg^{-1} day^{-1} via an

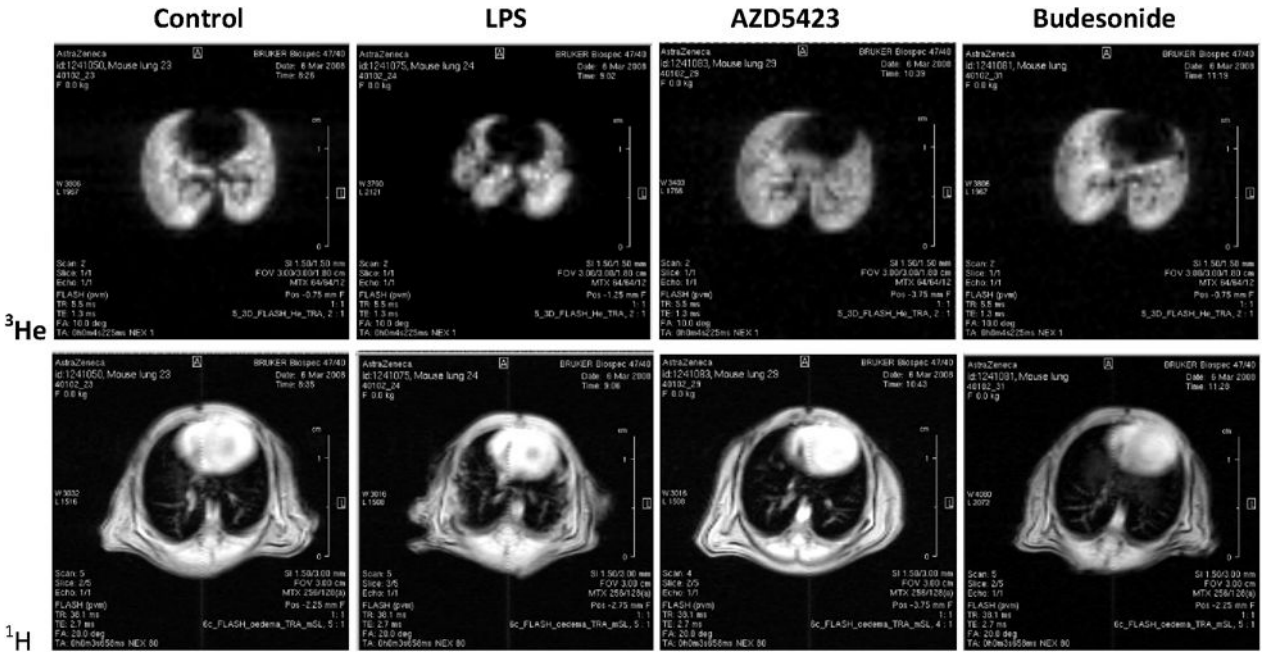

Fig. 25 Effects of AZD5423 (0.3 g kg^{-1}, o.d.) and budesonide (0.3 μg kg^{-1}, bid) improving ventilation and reducing edema in mice 24 h after first administration. The first row images show the free airspace using hyperpolarized ^{3}He-MRI, and the second row images show fluid in the lung using ^{1}H-MRI.

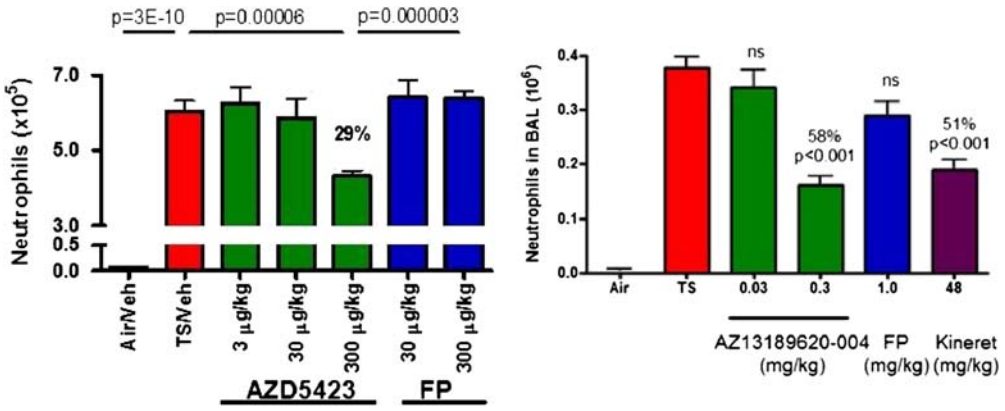

Fig. 26 Effects of AZD5423 and AZD7594 on neutrophil influx in the cigarette smoke model.

osmotic mini-pump placed under the skin of the animal inhibited neutrophil influx into BAL by 51%. In contrast, fluticasone propionate dosed at 1.0 mg kg^{-1} day^{-1} had no significant effect on the number of neutrophils in BAL in both studies (Fig. 26).

8.18.7 Progression of AZD5423 and AZD7594 Into Development

The progression of AZD5423 and AZD7594 into development will only be described briefly, and further details may be found in reference here or will be disclosed in future reports.

8.18.7.1 Progression of AZD5423

AZD5423 was nominated as CD in Dec. 2007. After safety pharmacology studies were completed the compound was approved for human clinical studies. Safety pharmacology data will not be described here, but it is interesting to note that predicted PK profile was confirmed in the larger set of studies that followed in the assessment of the compound. AZD5423 was rapidly absorbed in rat and dog after inhalation. Plasma AZD5423 profile after absorption phase showed rapid distribution kinetics with multiphasic plasma decay.

Data from repeated dose studies in both the rat and dog showed approximate dose linear plasma exposure of AZD5423, and no significant accumulation was observed. In contrast to the dog, a sex difference was indicated for the rat with females having an about twofold higher plasma exposure. A significant plasma exposure of a metabolite **71** was observed in the rat but not in the dog.

An early clinical program was undertaken across several studies to define the safety profile and characterize the pharmacokinetics and pharmacodynamics of AZD5423 following single and multiple ascending doses in healthy subjects, prior to testing in patients with asthma and COPD.[61] AZD5423 was submitted to single and repeat dose-escalating studies in healthy male subjects, including one cohort of male Japanese subjects, up to 1248 μg single doses and 499 μg as once daily lung delivered doses for 14 days. Inhaled, nebulized AZD5423 was safe and well tolerated up to and including the highest doses tested for up to 2 weeks of once daily treatment. Plasma exposure suggested dose-proportional pharmacokinetics and dose-related effects on 24-h plasma and urine cortisol.

Effects on HPA function appeared to increase with dose of inhaled AZD5423: Maximal suppression of 24-h plasma cortisol was 49% attained after the single 1248 μg dose and 40% after the 499 μg daily dose for 14 days. There were no or marginal effects on other biomarkers tested (Osteocalcin, TRAP5b, DHEA-S, and 4βOH-cholesterol). No clinically relevant differences in safety or PK could be distinguished between the two study populations although HPA effects appeared to be marginally greater in the Japanese versus the Caucasian dominant study population. It was concluded that AZD5423, inhaled via nebulization, could be safely used in healthy subjects at doses of at least 300 μg for 2 weeks.

AZD5423 was then evaluated for the effect on allergen-induced responses patients with mild allergic asthma. A study design including 7 days of treatment with nebulized AZD5423 (75 or 300 μg) once daily, budesonide 200 μg twice daily via Turbuhaler, or placebo in a double-blind, four-period, crossover design study.[62] AZD5423 significantly attenuated the drop in FEV1 during the late asthmatic response (both doses led to an 8.7% drop) versus placebo (14% drop) with no effect of budesonide (12.5% drop) versus placebo. There was no effect on the drop in FEV1 during early asthmatic response. AZD5423, 300 and 75 μg significantly attenuated allergen-induced sputum eosinophilia by 63% and 61% at 7 h, respectively, and by 46% and 34% at 24 h after allergen challenge, versus placebo. Budesonide did not reduce allergen-induced sputum eosinophilia versus placebo. AZD5423 at 300 μg significantly attenuated allergen-induced airway hyper responsiveness at 24 h after allergen challenge versus placebo. The efficacy data, taken together with HPA-axis data from phase I studies, indicate that the benefit-risk ratio may be improved relative to conventional inhaled steroids, since effects on markers of adrenal capacity and HPA-axis function were qualitatively similar for AZD5423 as to what has been previously shown for inhaled steroidal GR agonists like budesonide, fluticasone propionate, and fluticasone furoate.[63]

Clinical program for AZD5423 continued with a study to evaluate the efficacy and tolerability of inhaled AZD5423 compared with placebo or budesonide in patients with COPD receiving the LABA formoterol. Patients were randomly assigned (in a ratio of 1:1:1) to a 12-week double-blind treatment to receive one of the following: AZD5423 via Turbuhaler (75 μg lung-deposited dose once daily for 4 weeks followed by 300 μg lung-deposited dose once daily for 8 weeks) or budesonide via Turbuhaler (320 μg delivered dose, 2 doses twice daily), or placebo via Turbuhaler (2 doses twice daily).[61a]

8.18.7.2 Progression of AZD7594

AZD7594 was nominated as CD in Dec. 2009. After safety pharmacology studies were completed the compound was approved for human clinical studies.[64] Safety pharmacology data will not be described here, but it is interesting to note that in a similar way as for AZD5423 the predicted PK profile for AZD7594 was confirmed in the larger set of studies that followed in the safety assessment. AZD7594 was absorbed into systemic circulation in rat and dog after inhalation with C_{max} in plasma generally observed within 30 min after inhalation. There were no significant differences in AZD7594 exposure between genders. Data from the repeated dose studies showed, taken together, a dose-proportional increase in exposure. In general limited accumulation was observed (about two- to threefold or less). An apparent terminal half-life was calculated after single dosing in rat and ranged between 9 and 13 h.

An early clinical program was undertaken to define the safety profile and characterize the pharmacokinetics and pharmacodynamics of AZD7594 following single and multiple ascending doses in healthy subjects, prior to testing in patients with asthma. AZD5423 was submitted to single and repeat dose-escalating studies in healthy male subjects, up to 1872 μg single doses on day 1 and multiple doses days 5–16. The systemic exposure of AZD7594 increased in proportion to dose, and the relatively long half-life of 27.2 and 31.4 h supports that it is potentially suitable for once-daily dosing. At doses up of 7–1248 mg, the plasma cortisol suppression was comparable to placebo. Suppression of the HPA-axis based on plasma cortisol was observed at the highest dose of 1872 mg.[65]

AZD7594 was then studied in a 14-day randomized, double-blind, multiple dosing, placebo-controlled, asthma study to assess efficacy and safety of three dose levels of AZD7594 (58, 250, and 800 μg) given once daily using a commercially available dry powder inhaler, in patients with mild-to-moderate asthma.[66]

8.18.8 Summary

IGCs used either alone or in combination with bronchodilators provide the basis for current treatments of respiratory diseases such as asthma and COPD affecting the life of millions of patients. There is currently a need to develop novel GR modulator-based treatments offering improved therapeutic margins and the possibility for once daily treatment regimens to further improve disease control. AZD5423 and AZD7594 are two novel-inhaled selective, nonsteroidal, GR modulators optimized for the inhaled route of delivery now progressed into clinical development for the treatment of asthma. Data from preclinical in vivo models indicate that these compounds may offer a significant advantages compared to current steroid-based GR modulators.

The identification of the chemical starting point leading up to the candidate compounds AZD5423 and AZD7594 was based on the output from a HTS campaign that identified a series of sulfonamide-based compounds suitable for further optimization. The hit series, represented by compound **9**, showed functional antagonism when tested in the GR TR assay. By applying structural understanding of key GR agonist triggers the desired functional agonistic profile where obtained through the design and synthesis of a series of heterocycle containing analogues. These efforts lead to the identification of the lead series represented by compound **36**.

Compound **36**, and its structural analogues, comprised several of the key features viewed as necessary for successful progression towards an inhaled clinical candidate, including promising level of GR potency, in vitro DMPK profile, and significant level in vivo efficacy when tested in the rat Sephadex model following local administration to the lung. However the continued profiling of the series identified the formation of potentially genotoxic metabolites linked to core pharmacophore motifs requiring a significant redesign of the lead series to allow further progression.

Throughout the duration of the project the design of new SGRM ligands and understanding of their functional behavior benefited significantly from the access to high-quality X-ray structures. In particular this became evident during the redesign of the lead series to remove the potential genotox liabilities associated with compound **36** metabolites. By integration of structural information from multiple GR–ligand complexes a novel series of norephedrine-based GR modulators were discovered. Key motifs of the sulphonamide lead **36** were preserved in the new series, e.g., the indazole moiety and the sulphonamide linker, but their connectivity was rearranged.

The new series, represented by compounds **47** and **56**, offered a significant scope for further optimization of the GR potency as well as other key properties e.g., metabolic soft spots, morphology that ultimately lead to identification of the two clinical candidates AZD5423 and AZD7594.

Key for the final prioritization was the in-depth in vivo evaluation of the short-listed compounds in a panel of pharmacokinetic and pharmacodynamic inhalation in vivo models to fully understand the potential of each individual compound compared to the leading inhaled glucocorticosteroids. So far the clinical data obtained at this point in time confirms the pharmacokinetic and efficacy predictions made from the animal models.

References

1. Flammer, J. R.; Rogatsky, I. Minireview: Glucocorticoids in Autoimmunity: Unexpected Targets and Mechanisms. *Mol. Endocrinol.* **2011,** *25* (7), 1075–1086.
2. Donohue, J. F.; Ohar, J. A. Effects of Corticosteroids on Lung Function in Asthma and Chronic Obstructive Pulmonary Disease. *Proc. Am. Thorac. Soc.* **2004,** *1* (3), 152–160.
3. (a) Greening, A. P.; Ind, P. W.; Northfield, M.; Shaw, G. Added Salmeterol Versus Higher-Dose Corticosteroid in Asthma Patients with Symptoms on Existing Inhaled Corticosteroid. *Lancet* **1994,** *344* (8917), 219–224; (b) Pauwels, R. A.; Löfdahl, C.-G.; Postma, D. S.; Tattersfield, A. E.; O'Byrne, P.; Barnes, P. J.; Ullman, A. Effect of Inhaled Formoterol and Budesonide on Exacerbations of Asthma. *N. Engl. J. Med.* **1997,** *337* (20), 1405–1411; (c) Goldsmith, D. R.; Keating, G. M. Budesonide/Formoterol: A Review of Its Use in Asthma. *Drugs* **2004,** *64* (14), 1597–1618.
4. Ford, E. S.; Murphy, L. B.; Khavjou, O.; Giles, W. H.; Holt, J. B.; Croft, J. B. Total and State-Specific Medical and Absenteeism Costs of Copd Among Adults Aged $\geq$18 Years in the United States for 2010 and Projections Through 2020. *Chest* **2015,** *147* (1), 31–45.
5. Rabe, K. F.; Hurd, S.; Anzueto, A.; Barnes, P. J.; Buist, S. A.; Calverley, P.; Fukuchi, Y.; Jenkins, C.; Rodriguez-Roisin, R.; van Weel, C.; Zielinski, J. Global Strategy for the Diagnosis, Management, and Prevention of Chronic Obstructive Pulmonary Disease. *Am. J. Respir. Crit. Care Med.* **2007,** *176* (6), 532–555.
6. Fitzgerald, M. F.; Fox, J. C. Emerging Trends in the Therapy of COPD: Bronchodilators as Mono- and Combination Therapies. *Drug Discov. Today* **2007,** *12* (11–12), 472–478.
7. Sin, D. D.; Wu, L.; Anderson, J. A.; Anthonisen, N. R.; Buist, A. S.; Burge, P. S.; Calverley, P. M.; Connett, J. E.; Lindmark, B.; Pauwels, R. A.; Postma, D. S.; Soriano, J. B.; Szafranski, W.; Vestbo, J. Inhaled Corticosteroids and Mortality in Chronic Obstructive Pulmonary Disease. *Thorax* **2005,** *60* (12), 992–997.
8. Bourbeau, J.; Christodoulopoulos, P.; Maltais, F.; Yamauchi, Y.; Olivenstein, R.; Hamid, Q. Effect of Salmeterol/Fluticasone Propionate on Airway Inflammation in COPD: A Randomised Controlled Trial. *Thorax* **2007,** *62* (11), 938–943.
9. Welte, T. Optimising Treatment for COPD—New Strategies for Combination Therapy. *Int. J. Clin. Pract.* **2009,** *63* (8), 1136–1149.
10. Zhang, L.; Prietsch, S. O. M.; Ducharme, F. M. Inhaled Corticosteroids in Children With Persistent Asthma: Effects on Growth. *Cochrane Database Syst. Rev.* **2014,** *7*.
11. Mitra, R. Adverse Effects of Corticosteroids on Bone Metabolism: A Review. *PM R* **2011,** *3* (5), 466–471.
12. Smith, S. M.; Vale, W. W. The Role of the Hypothalamic-Pituitary-Adrenal Axis in Neuroendocrine Responses to Stress. *Dialogues Clin. Neurosci.* **2006,** *8* (4), 383–395.
13. Egbuonu, F.; Antonio, F. A.; Edavalath, M. Effect of Inhaled Corticosteroids on Glycemic Status. *Open Respir. Med. J.* **2014,** *8,* 101–105.
14. Dubus, J. C.; Marguet, C.; Deschildre, A.; Mely, L.; Le Roux, P.; Brouard, J.; Huiart, L.; Réseau de Recherche Clinique en Pneumologie Pediatrique. Local Side-Effects of Inhaled Corticosteroids in Asthmatic Children: Influence of Drug, Dose, Age, and Device. *Allergy* **2001,** *56* (10), 944–948.
15. (a) Bourbeau, J.; Bartlett, S. J. Patient Adherence in COPD. *Thorax* **2008,** *63* (9), 831–838; (b) Leflein, J. Once-Daily Use of Inhaled Corticosteroids: A New Regimen in the Treatment of Persistent Asthma. *Allergol. Int.* **2000,** *49* (1), 7–17.
16. (a) Gershon, A. S.; Campitelli, M. A.; Croxford, R.; et al. Combination Long-Acting β-Agonists and Inhaled Corticosteroids Compared With Long-Acting β-Agonists Alone in Older Adults With Chronic Obstructive Pulmonary Disease. *JAMA* **2014,** *312* (11), 1114–1121; (b) Toy, E. L.; Beaulieu, N. U.; McHale, J. M.; Welland, T. R.; Plauschinat, C. A.; Swensen, A.; Duh, M. S. Treatment of COPD: Relationships Between Daily Dosing Frequency, Adherence, Resource Use, and Costs. *Respir. Med.* **2011,** *105* (3), 435–441.
17. Evans, R. The Steroid and Thyroid Hormone Receptor Superfamily. *Science* **1988,** *240* (4854), 889–895.
18. Nuclear Receptors Nomenclature Committee. A Unified Nomenclature System for the Nuclear Receptor Superfamily. *Cell* **1999,** *97* (2), 161–163.
19. Chung, S.; Son, G. H.; Kim, K. Circadian Rhythm of Adrenal Glucocorticoid: Its Regulation and Clinical Implications. *Biochim. Biophys. Acta (BBA) - Mol. Basis Dis.* **2011,** *1812* (5), 581–591.
20. (a) Lorenz, O. R.; Freiburger, L.; Rutz, D. A.; Krause, M.; Zierer, B. K.; Alvira, S.; Cuéllar, J.; Valpuesta, J. M.; Madl, T.; Sattler, M.; Buchner, J. Modulation of the Hsp90 Chaperone Cycle by a Stringent Client Protein. *Mol. Cell* **2014,** *53* (6), 941–953; (b) Kirschke, E.; Goswami, D.; Southworth, D.; Griffin, P. R.; Agard, D. Glucocorticoid Receptor Function Regulated by Coordinated Action of the Hsp90 and Hsp70 Chaperone Cycles. *Cell* **2014,** *157* (7), 1685–1697; (c) Pratt, W. B.; Toft, D. O. Steroid Receptor Interactions With Heat Shock Protein and Immunophilin Chaperones. *Endocr. Rev.* **1997,** *18* (3), 306–360.
21. (a) Vandevyver, S.; Dejager, L.; Libert, C. On the Trail of the Glucocorticoid Receptor: Into the Nucleus and Back. *Traffic* **2012,** *13* (3), 364–374; (b) Conway-Campbell, B. L.; George, C. L.; Pooley, J. R.; Knight, D. M.; Norman, M. R.; Hager, G. L.; Lightman, S. L. The HSP90 Molecular Chaperone Cycle Regulates Cyclical Transcriptional Dynamics of the Glucocorticoid Receptor and Its Coregulatory Molecules CBP/p300 During Ultradian Ligand Treatment. *Mol. Endocrinol.* **2011,** *25* (6), 944–954.
22. (a) Chen, Z.; Lan, X.; Wu, D.; Sunkel, B.; Ye, Z.; Huang, J.; Liu, Z.; Clinton, S. K.; Jin, V. X.; Wang, Q. Ligand-Dependent Genomic Function of Glucocorticoid Receptor in Triple-Negative Breast Cancer. *Nat. Commun.* **2015,** *6,* 8323; (b) McNally, J. G.; Müller, W. G.; Walker, D.; Wolford, R.; Hager, G. L. The Glucocorticoid Receptor: Rapid Exchange With Regulatory Sites in Living Cells. *Science* **2000,** *287* (5456), 1262–1265.

23. Hollenberg, S. M.; Evans, R. M. Multiple and Cooperative Trans-Activation Domains of the Human Glucocorticoid Receptor. *Cell* **1988,** *55* (5), 899–906.
24. (a) Meijsing, S. H.; Pufall, M. A.; So, A. Y.; Bates, D. L.; Chen, L.; Yamamoto, K. R. DNA Binding Site Sequence Directs Glucocorticoid Receptor Structure and Activity. *Science* **2009,** *324* (5925), 407–410; (b) Strähle, U.; Klock, G.; Schütz, G. A DNA Sequence of 15 Base Pairs is Sufficient to Mediate Both Glucocorticoid and Progesterone Induction of Gene Expression. *Proc. Natl. Acad. Sci.* **1987,** *84* (22), 7871–7875.
25. Ratman, D.; Vanden Berghe, W.; Dejager, L.; Libert, C.; Tavernier, J.; Beck, I. M.; De Bosscher, K. How Glucocorticoid Receptors Modulate the Activity of Other Transcription Factors: A Scope Beyond Tethering. *Mol. Cell. Endocrinol.* **2013,** *380* (1–2), 41–54.
26. Surjit, M.; Ganti, K. P.; Mukherji, A.; Ye, T.; Hua, G.; Metzger, D.; Li, M.; Chambon, P. Widespread Negative Response Elements Mediate Direct Repression by Agonist-Liganded Glucocorticoid Receptor. *Cell* **2011,** *145* (2), 224–241.
27. Hudson, W. H.; Youn, C.; Ortlund, E. A. The Structural Basis of Direct Glucocorticoid-Mediated Transrepression. *Nat. Struct. Mol. Biol.* **2013,** *20* (1), 53–58.
28. Ramamoorthy, S.; Cidlowski, J. A. Corticosteroids: Mechanisms of Action in Health and Disease. *Rheum. Dis. Clin. N. Am.* **2016,** *42* (1), 15–31.
29. Vandevyver, S.; Dejager, L.; Libert, C. Comprehensive Overview of the Structure and Regulation of the Glucocorticoid Receptor. *Endocr. Rev.* **2014,** *35* (4), 671–693.
30. De Bosscher, K. Selective Glucocorticoid Receptor Modulators. *J. Steroid Biochem. Mol. Biol.* **2010,** *120* (2–3), 96–104.
31. (a) Martinkovich, S.; Shah, D.; Planey, S. L.; Arnott, J. A. Selective Estrogen Receptor Modulators: Tissue Specificity and Clinical Utility. *Clin. Interv. Aging* **2014,** *2014* (9), 1437–1452; (b) Bhasin, S.; Jasuja, R. Selective Androgen Receptor Modulators (SARMs) as Function Promoting Therapies. *Curr. Opin. Clin. Nutr. Metab. Care* **2009,** *12* (3), 232–240.
32. Sundahl, N.; Bridelance, J.; Libert, C.; De Bosscher, K.; Beck, I. M. Selective Glucocorticoid Receptor Modulation: New Directions With Non-Steroidal Scaffolds. *Pharmacol. Ther.* **2015,** *152,* 28–41.
33. (a) Elmore, S. W.; Coghlan, M. J.; Anderson, D. D.; Pratt, J. K.; Green, B. E.; Wang, A. X.; Stashko, M. A.; Lin, C. W.; Tyree, C. M.; Miner, J. N.; Jacobson, P. B.; Wilcox, D. M.; Lane, B. C. Nonsteroidal Selective Glucocorticoid Modulators: The Effect of C-5 Alkyl Substitution on the Transcriptional Activation/Repression Profile of 2,5-Dihydro-10-methoxy-2,2,4-trimethyl-1H-[1]benzopyrano[3,4-f]quinolines. *J. Med. Chem.* **2001,** *44* (25), 4481–4491; (b) Owen, H. C.; Miner, J. N.; Ahmed, S. F.; Farquharson, C. The Growth Plate Sparing Effects of the Selective Glucocorticoid Receptor Modulator, AL-438. *Mol. Cell. Endocrinol.* **2007,** *264* (1–2), 164–170.
34. Beck, I. M.; Drebert, Z. J.; Hoya-Arias, R.; Bahar, A. A.; Devos, M.; Clarisse, D.; Desmet, S.; Bougarne, N.; Ruttens, B.; Gossye, V.; Denecker, G.; Lievens, S.; Bracke, M.; Tavernier, J.; Declercq, W.; Gevaert, K.; Berghe, W. V.; Haegeman, G.; De Bosscher, K. Compound A, a Selective Glucocorticoid Receptor Modulator, Enhances Heat Shock Protein Hsp70 Gene Promoter Activation. *PLoS One* **2013,** *8* (7). e69115.
35. Ali, A.; Thompson, C. F.; Balkovec, J. M.; Graham, D. W.; Hammond, M. L.; Quraishi, N.; Tata, J. R.; Einstein, M.; Ge, L.; Harris, G.; Kelly, T. M.; Mazur, P.; Pandit, S.; Santoro, J.; Sitlani, A.; Wang, C.; Williamson, J.; Miller, D. K.; Thompson, C. M.; Zaller, D. M.; Forrest, M. J.; Carballo-Jane, E.; Luell, S. Novel N-Arylpyrazolo[3,2-c]-Based Ligands for the Glucocorticoid Receptor: Receptor Binding and In Vivo Activity. *J. Med. Chem.* **2004,** *47* (10), 2441–2452.
36. (a) Harcken, C.; Riether, D.; Liu, P.; Razavi, H.; Patel, U.; Lee, T.; Bosanac, T.; Ward, Y.; Ralph, M.; Chen, Z.; Souza, D.; Nelson, R. M.; Kukulka, A.; Fadra-Khan, T. N.; Zuvela-Jelaska, L.; Patel, M.; Thomson, D. S.; Nabozny, G. H. Optimization of Drug-Like Properties of Nonsteroidal Glucocorticoid Mimetics and Identification of a Clinical Candidate. *ACS Med. Chem. Lett.* **2014,** *5* (12), 1318–1323; (b) Reeves, J. T.; Fandrick, D. R.; Tan, Z.; Song, J. J.; Rodriguez, S.; Qu, B.; Kim, S.; Niemeier, O.; Li, Z.; Byrne, D.; Campbell, S.; Chitroda, A.; DeCroos, P.; Fachinger, T.; Fuchs, V.; Gonnella, N. C.; Grinberg, N.; Haddad, N.; Jäger, B.; Lee, H.; Lorenz, J. C.; Ma, S.; Narayanan, B. A.; Nummy, L. J.; Premasiri, A.; Roschangar, F.; Sarvestani, M.; Shen, S.; Spinelli, E.; Sun, X.; Varsolona, R. J.; Yee, N.; Brenner, M.; Senanayake, C. H. Development of a Large Scale Asymmetric Synthesis of the Glucocorticoid Agonist BI 653048 BS H3PO4. *J. Org. Chem.* **2013,** *78* (8), 3616–3635.
37. Biggadike, K.; Bledsoe, R. K.; Coe, D. M.; Cooper, T. W. J.; House, D.; Iannone, M. A.; Macdonald, S. J. F.; Madauss, K. P.; McLay, I. M.; Shipley, T. J.; Taylor, S. J.; Tran, T. B.; Uings, I. J.; Weller, V.; Williams, S. P. Design and X-Ray Crystal Structures of High-Potency Nonsteroidal Glucocorticoid Agonists Exploiting a Novel Binding Site on the Receptor. *Proc. Natl. Acad. Sci.* **2009,** *106* (43), 18114–18119.
38. Carson, M. W.; Coghlan, M. J. Preparation of a 6,11-dihydro-10-aza-dibenz[b, e]oxepin Derivative as Glucocorticoid Receptor Modulator. WO2008008882A2, 2008.
39. (a) Monica, B.; Santi, S. Mapracorat, a Novel Non-Steroidal Selective Glucocorticoid Receptor Agonist for the Treatment of Allergic Conjunctivitis. *Inflamm. Allergy-Drug Targets* **2014,** *13* (5), 289–298; (b) Schäcke, H.; Zollner, T. M.; Döcke, W. D.; Rehwinkel, H.; Jaroch, S.; Skuballa, W.; Neuhaus, R.; May, E.; Zügel, U.; Asadullah, K. Characterization of ZK 245186, a Novel, Selective Glucocorticoid Receptor Agonist for the Topical Treatment of Inflammatory Skin Diseases. *Br. J. Pharmacol.* **2009,** *158* (4), 1088–1103.
40. Conrado, D. J.; Krishnaswami, S.; Shoji, S.; Kolluri, S.; Hey-Hadavi, J.; McCabe, D.; Rojo, R.; Tammara, B. K. Predicting the Probability of Successful Efficacy of a Dissociated Agonist of the Glucocorticoid Receptor from Dose–Response Analysis. *J. Pharmacokinet. Pharmacodyn.* **2016,** *43* (3), 325–341.
41. Tucker, H.; Crook, J. W.; Chesterson, G. J. Nonsteroidal Antiandrogens. Synthesis and Structure-Activity Relationships of 3-Substituted Derivatives of 2-Hydroxypropionanilides. *J. Med. Chem.* **1988,** *31* (5), 954–959.
42. Bledsoe, R. K.; Montana, V. G.; Stanley, T. B.; Delves, C. J.; Apolito, C. J.; McKee, D. D.; Consler, T. G.; Parks, D. J.; Stewart, E. L.; Willson, T. M.; Lambert, M. H.; Moore, J. T.; Pearce, K. H.; Xu, H. E. Crystal Structure of the Glucocorticoid Receptor Ligand Binding Domain Reveals a Novel Mode of Receptor Dimerization and Coactivator Recognition. *Cell* **2002,** *110* (1), 93–105.
43. (a) Zhang, J.; Simisky, J.; Tsai, F. T. F.; Geller, D. S. A critical Role of Helix 3–Helix 5 Interaction in Steroid Hormone Receptor Function. *Proc. Natl. Acad. Sci. U. S. A.* **2005,** *102* (8), 2707–2712; (b) Yoshikawa, N.; Yamamoto, K.; Shimizu, N.; Yamada, S.; Morimoto, C.; Tanaka, H. The Distinct Agonistic Properties of the Phenylpyrazolosteroid Cortivazol Reveal Interdomain Communication Within the Glucocorticoid Receptor. *Mol. Endocrinol.* **2005,** *19* (5), 1110–1124.
44. (a) Li, Y.; Suino, K.; Daugherty, J.; Xu, H. E. Structural and Biochemical Mechanisms for the Specificity of Hormone Binding and Coactivator Assembly by Mineralocorticoid Receptor. *Mol. Cell* **2005,** *19* (3), 367–380; (b) Matias, P. M.; Donner, P.; Coelho, R.; Thomaz, M.; Peixoto, C.; Macedo, S.; Otto, N.; Joschko, S.; Scholz, P.; Wegg, A.; Bäsler, S.; Schäfer, M.; Egner, U.; Carrondo, M. A. Structural Evidence for Ligand Specificity in the Binding Domain of the Human Androgen Receptor: Implications for Pathogenic Gene Mutations. *J. Biol. Chem.* **2000,** *275* (34), 26164–26171.
45. Edman, K.; Hosseini, A.; Bjursell, M. K.; Aagaard, A.; Wissler, L.; Gunnarsson, A.; Kaminski, T.; Köhler, C.; Bäckström, S.; Jensen, T. J.; Cavallin, A.; Karlsson, U.; Nilsson, E.; Lecina, D.; Takahashi, R.; Grebner, C.; Geschwindner, S.; Lepistö, M.; Hogner, A. C.; Guallar, V. Ligand Binding Mechanism in Steroid Receptors: From Conserved Plasticity to Differential Evolutionary Constraints. *Structure* **2015,** *23* (12), 2280–2290.
46. (a) Biggadike, K.; Bledsoe, R. K.; Hassell, A. M.; Kirk, B. E.; McLay, I. M.; Shewchuk, L. M.; Stewart, E. L. X-ray Crystal Structure of the Novel Enhanced-Affinity Glucocorticoid Agonist Fluticasone Furoate in the Glucocorticoid Receptor – Ligand Binding Domain. *J. Med. Chem.* **2008,** *51* (12), 3349–3352; (b) Carson, M. W.; Luz, J. G.; Suen, C.; Montrose, C.; Zink, R.; Ruan, X.; Cheng, C.; Cole, H.; Adrian, M. D.; Kohlman, D. T.; Mabry, T.; Snyder, N.; Condon, B.; Maletic, M.; Clawson, D.; Pustilnik, A.; Coghlan, M. J. Glucocorticoid Receptor Modulators Informed by Crystallography Lead to a New Rationale for Receptor Selectivity, Function, and Implications for Structure-Based Design. *J. Med. Chem.* **2014,** *57* (3), 849–860; (c) Edman, K.; Ahlgren, R.; Bengtsson, M.; Bladh, H.; Bäckström, S.; Dahmén, J.; Henriksson, K.; Hillertz, P.; Hulikal, V.; Jerre, A.; Kinchin, L.; Kåse, C.; Lepistö, M.; Mile, I.; Nilsson, S.; Smailagic, A.; Taylor, J.; Tjörnebo, A.; Wissler, L.; Hansson, T. The Discovery of Potent and Selective Non-Steroidal Glucocorticoid Receptor Modulators, Suitable for Inhalation. *Bioorg. Med. Chem. Lett.* **2014,** *24* (11), 2571–2577; (d) He, Y.; Yi, W.; Suino-Powell, K.; Zhou, X. E.; Tolbert, W. D.; Tang, X.; Yang, J.; Yang, H.; Shi, J.; Hou, L.; Jiang, H.; Melcher, K.; Xu, H. E. Structures and Mechanism for the Design of Highly Potent Glucocorticoids. *Cell Res.* **2014,** *24* (6), 713–726; (e) Kauppi, B.; Jakob, C.; Färnegårdh, M.; Yang, J.; Ahola, H.; Alarcon, M.; Calles, K.; Engström, O.; Harlan, J.; Muchmore, S.; Ramqvist, A.-K.; Thorell, S.; Öhman, L.; Greer, J.; Gustafsson, J.-Å.; Carlstedt-Duke, J.; Carlquist, M. The Three-dimensional Structures of Antagonistic and Agonistic Forms of the Glucocorticoid Receptor Ligand-binding Domain: RU-486 Induces a Transformation That Leads to Active Antagonism. *J. Biol. Chem.* **2003,** *278* (25), 22748–22754; (f) Madauss, K. P.; Bledsoe, R. K.; McLay, I.; Stewart, E. L.; Uings, I. J.; Weingarten, G.; Williams, S. P. The First X-ray Crystal Structure of the Glucocorticoid Receptor Bound to a Non-Steroidal Agonist. *Bioorg. Med. Chem. Lett.* **2008,** *18* (23), 6097–6099; (g) Schoch, G. A.; D'Arcy, B.; Stihle, M.; Burger, D.; Bär, D.; Benz, J.; Thoma, R.; Ruf, A. Molecular Switch in the Glucocorticoid Receptor: Active and Passive Antagonist Conformations. *J. Mol. Biol.* **2010,** *395* (3), 568–577; (h) Seitz, T.; Thoma, R.; Schoch, G. A.; Stihle, M.; Benz, J.; D'Arcy, B.; Wiget, A.; Ruf, A.; Hennig, M.; Sterner, R. Enhancing the Stability and Solubility of the Glucocorticoid Receptor Ligand-Binding Domain by High-Throughput Library Screening. *J. Mol. Biol.* **2010,** *403* (4), 562–577; (i) Suino-Powell, K.; Xu, Y.; Zhang, C.; Tao, Y.-g.; Tolbert, W. D.; Simons, S. S.; Xu, H. E. Doubling the Size of the Glucocorticoid Receptor Ligand Binding Pocket by Deacylcortivazol. *Mol. Cell. Biol.* **2008,** *28* (6), 1915–1923.

47. Lin, S.; Bock, C. L.; Gardner, D. B.; Webster, J. C.; Favata, M. F.; Trzaskos, J. M.; Oldenburg, K. R. A High-Throughput Fluorescent Polarization Assay for Nuclear Receptor Binding Utilizing Crude Receptor Extract. *Anal. Biochem.* **2002,** *300* (1), 15–21.
48. Piercy, V.; Arch, J. R. S.; Baker, R. C.; Cook, R. M.; Hatt, P. A.; Spicer, B. A. Effects of Dexamethasone in a Model of Lung Hyperresponsiveness in the Rat. *Agents Actions* **1993,** *39* (3), 118–125.
49. Fitzpatrick, F. T. A.; Greenstein, B. D. Effects of Various Steroids on the Thymus, Spleen, Ventral Prostate and Seminal Vesicles in Old Orchidectomized Rats. *J. Endocrinol.* **1987,** *113* (1), 51–55.
50. Clark, T. J. H. Effect of Beclomethasone Dipropionate Delivered by Aerosol in Patients With Asthma. *Lancet* **1972,** *299* (7765), 1361–1364.
51. Bohl, C. E.; Gao, W.; Miller, D. D.; Bell, C. E.; Dalton, J. T. Structural Basis for Antagonism and Resistance of Bicalutamide in Prostate Cancer. *Proc. Natl. Acad. Sci.* **2005,** *102* (17), 6201–6206.
52. Salter, M.; Biggadike, K.; Matthews, J. L.; West, M. R.; Haase, M. V.; Farrow, S. N.; Uings, I. J.; Gray, D. W. Pharmacological Properties of the Enhanced-Affinity Glucocorticoid Fluticasone Furoate in vitro and in an in vivo Model of Respiratory Inflammatory Disease. *Am. J. Physiol. Lung Cell. Mol. Physiol.* **2007,** *293* (3), L660–L667.
53. Jansson, A.-H.; Eriksson, C.; Wang, X. Effects of Budesonide and N-Acetylcysteine on Acute Lung Hyperinflation, Inflammation and Injury in Rats. *Vasc. Pharmacol.* **2005,** *43* (2), 101–111.
54. Shamovsky, I.; Ripa, L.; Borjesson, L.; Mee, C.; Norden, B.; Hansen, P.; Hasselgren, C.; O'Donovan, M.; Sjo, P. Explanation for Main Features of Structure-Genotoxicity Relationships of Aromatic Amines by Theoretical Studies of Their Activation Pathways in CYP1A2. *J. Am. Chem. Soc.* **2011,** *133* (40), 16168–16185.
55. Berger, M.; Rehwinkel, H.; Schaecke, H.; Baeurle, S.; Schmees, N. Preparation of 1-(hetero)arylamino-1,2,3,4-tetrahydronaphthalenes as Antiinflammatories. EP1834948A1, 2007.
56. Berger, M.; Dahmen, J.; Rehwinkel, H.; Jaroch, S.; Schaecke, H. Preparation of Benzyl Amines Useful as Anti-Inflammatory Agents. WO2008006627A1, 2008.
57. Conrad, K.; Hsiao, Y.; Miller, R. A Practical One-Pot Process for α-Amino Aryl Ketone Synthesis. *Tetrahedron Lett.* **2005,** *46* (49), 8587–8589.
58. Yin, J.; Huffman, M. A.; Conrad, K. M.; Armstrong, J. D. Highly Diastereoselective Catalytic Meerwein-Ponndorf-Verley Reductions. *J. Org. Chem.* **2006,** *71* (2), 840–843.
59. Job, G. E.; Buchwald, S. L. Copper-Catalyzed Arylation of Beta-Amino Alcohols. *Org. Lett.* **2002,** *4* (21), 3703–3706.
60. Nave, R. Clinical Pharmacokinetic and Pharmacodynamic Profile of Inhaled Ciclesonide. *Clin. Pharmacokinet.* **2009,** *48* (4), 243–252.
61. (a) Werkström, V.; Prothon, S.; Ekholm, E.; Jorup, C.; Edsbäcker, S. Safety, Pharmacokinetics and Pharmacodynamics of the Selective Glucocorticoid Receptor Modulator AZD5423 after Inhalation in Healthy Volunteers. *Basic Clin. Pharmacol. Toxicology* **2016**; (b) O'Byrne, P. M.; Gauvreau, G. M.; Boulet, L.-P.; Cockcroft, D. W.; Davis, B. E.; Leigh, R.; Aurivillius, M.; Wessman, P.; Jorup, K. Effect Of An Inhaled Selective Glucocorticoid Receptor Modulator (AZD5423) On Allergen-Induced Airway Responses And Airway Inflammation. In *B32. Advances in Asthma Theraphy;* American Thoracic Society, 2013; p A2614; (c) McWhae, A.; Shah, S.; Kärrman-Mårdh, C.; Miller-Larsson, A.; Giembycz, M.; Newton, R. The Novel Glucocorticoid Receptor Agonist, AZD5423, Shows Super-Agonism Relative to the Conventional Agonists, Dexamethasone and Budesonide. In *A31. The Epithelium in Lung Inflammation;* American Thoracic Society, 2015; p A1293; (d) Kärrman-Mårdh, C.; Gustavsson, M.; Smailagic, A. Pharmacological Characterization of AZD5423, an Inhaled Non-Steroidal Agonist of the Glucocortiocoid Receptor. In *D33. New Basic Science in Asthma: Allergic Inflammation II;* American Thoracic Society, 2015; p A5656.
62. Gauvreau, G. M.; Boulet, L.-P.; Leigh, R.; Cockcroft, D. W.; Killian, K. J.; Davis, B. E.; Deschesnes, F.; Watson, R. M.; Swystun, V.; Mårdh, C. K.; Wessman, P.; Jorup, C.; Aurivillius, M.; O'Byrne, P. M. A Nonsteroidal Glucocorticoid Receptor Agonist Inhibits Allergen-induced Late Asthmatic Responses. *Am. J. Respir. Crit. Care Med.* **2014,** *191* (2), 161–167.
63. (a) Woodcock, A.; Bleecker, E. R.; Busse, W. W.; Lötvall, J.; Snowise, N. G.; Frith, L.; Jacques, L.; Haumann, B.; Bateman, E. D. Fluticasone Furoate: Once-Daily Evening Treatment Versus Twice-Daily Treatment in Moderate Asthma. *Respir. Res.* **2011,** *12* (1), 1–8; (b) Grahnen, A.; Jansson, B.; Brundin, R. M.; Ling-Andersson, A.; Lonnebo, A.; Johansson, M.; Eckernas, S. A. A Dose–Response Study Comparing Suppression of Plasma Cortisol Induced by Fluticasone Propionate from Diskhaler and Budesonide from Turbuhaler. *Eur. J. Clin. Pharmacol.* **1997,** *52* (4), 261–267.
64. Kärrman-Mårdh, C.; Russel, W.; Gustavsson, M.; Kurian, N.; Jansson, A. -H.; Smailagic, A.; Edman, K. A Novel Inhaled Non-Steroidal Modulator of Inflammation for the Control of Asthma; AZD7594. In *A31. Asthma Theraphy: Glucocorticoids and Beyond;* American Thoracic Society, 2016; p A1329.
65. Chen, Y.; Prothon, S.; Aurivillius, M.; Eriksson, U. G.; Aggarwal, A. Safety, Tolerability, Pharmacokinetics (PK), and Pharmacodynamics (PD) of AZD7594 After Single and Multiple Ascending Inhaled Doses in Healthy Male Volunteers. American Society for Clinical Pharmacology and Therapeutics 8–12 March, 2016, San Diego. USA.
66. https://clinicaltrials.gov/ct2/show/NCT02479412.

8.19 The Discovery of the MCH-1 Receptor Antagonist NGD-4715 for the Potential Treatment of Obesity

J Tarrant, Neurogen Corporation, a subsidiary of Ligand Pharmaceuticals, Branford, CT, United States; and Harding University, Searcy, AR, United States
KJ Hodgetts, Neurogen Corporation, a subsidiary of Ligand Pharmaceuticals, Branford, CT, United States; and Brigham and Women's Hospital and Harvard Medical School, Cambridge, MA, United States
BL Chenard, Neurogen Corporation, a subsidiary of Ligand Pharmaceuticals, Branford, CT, United States; and Chenab LLC, Waterford, CT 08385
JE Krause and D Doller, Neurogen Corporation, a subsidiary of Ligand Pharmaceuticals, Branford, CT, United States; and Alcyoneus/ScienceWorks, Sparta, NJ, United States

© 2017 Elsevier Ltd. All rights reserved.
The authors of this article were previously employed by Neurogen Corporation, a subsidiary of Ligand Pharmaceuticals.

8.19.1 Introduction 488
8.19.2 Hit-Finding: The Serendipitous Discovery That Led to NDT 9522320, a Tool Compound for in vivo Target Validation 490
8.19.3 Characterization of NDT 9522320 (10): Absolute Configuration, Physicochemical Attributes, and Large-Scale Synthesis 490
8.19.4 Preclinical Proof-of-Concept in Rat 492
8.19.5 Proof of Concept in Dog, a MCHR1/2 Species 493
8.19.6 A Novel Bicyclic System: NGD 9522330 (31) 494
8.19.7 Process Development and cGMP Delivery 501
8.19.8 Seeking a Superior Backup Compound 506
8.19.9 NDT-4715 Clinical Studies 511
8.19.10 Conclusions 513
Acknowledgments 514
References 514
Relevant Websites 515

Abbreviations

BID Bis in die (twice daily)
BOC Benzyloxycarbonyl
Ca K_i K_i determined in intracellular calcium assay
DIO Diet-induced obesity
GPCR G protein-coupled receptor
GTP K_i K_i determined in a GTPγ^{35}S assay
hERG Human ether-a-go-go related gene
HPLC High-pressure liquid chromatography
ICV Intracerebroventricular
LLB Lysosomal lamellar bodies
MAD Multiple ascending dose
MCH Melanin-concentrating hormone
MCHR1 MCH receptor 1
MCHR2 MCH receptor 2
MC/TA 0.5% methyl cellulose/0.1% triacetin, vehicle used for dosing in vivo
MS Mass spectrometry
PBCS Purina body condition score
PL Phospholipidosis
PK Pharmacokinetics
PXR Pregnane X receptor
Q8h Doses 8 h apart
Qsol Quick kinetic solubility assay
SAD Single ascending dose
SAR Structure–activity relationship
TID Ter in die (three times daily)

8.19.1 Introduction

Obesity is a chronic, relapsing health risk defined by excess body fat. A large volume of research suggests the pathogenesis of obesity involves the complex interaction of genetic, environmental, and behavioral factors. Excess body fat increases significantly the risk of death and the occurrence of major comorbidities such as type 2 diabetes, hypertension, dyslipidemia, cardiovascular disease, osteoarthritis of the knee, sleep apnea, and some cancers.[1] Unfortunately, obesity has reached the global epidemics level, as it is

observed in most developed and developing countries in both adult and pediatric populations. Therefore, obesity prevention and management is a public health priority, and intervention strategies have focused primarily on healthy eating and physical activity in children and adults.[2] Naturally, the challenge to discover drug treatments for obesity has been at the center of major research efforts across the whole life science ecosystem.

Several novel drugs and drug combinations to treat obesity have recently been approved by the FDA. There are now five approved treatments, including orlistat (trade name Xenical), lorcaserin (trade name Belviq), liraglutide (trade name Saxenda), phentermine/topiramate extended release (trade name Qsymia), and naltrexone/bupropion (trade name Contrave).[3,4] There are significant differences in the limited efficacy of these approved treatments, as well as with responder rates and differing side effect profiles. No single drug or drug combination has emerged as a first-line treatment for obesity, and comparative drug trials between any of these agents have not been performed. The results from several ongoing cardiovascular outcome trials will be important in assessing the future market potential of these treatments. Therefore, the current state of obesity drugs and novel drug candidates to treat obesity is in its infancy.

The melanin-concentrating hormone (MCH) system has long been known to be involved in the control of feeding behavior and weight control in mammals.[5,6] The discretely localized lateral hypothalamic area (LHA) neurons synthesize the nonadecapeptide MCH and the neuronal projections synapse in cortical, hippocampal, nucleus accumbens, and intra-hypothalamic nervous system regions. Thus, the MCH system appears to integrate appetite with reward, memory, sleep, and emotion centers in the central nervous system (CNS). In rodent species, there exists one MCH receptor type, melanin-concentrating hormone receptor 1 (MCHR1), a G-protein coupled receptor. In dogs, humans, and other higher mammalian species, there exists a second highly homologous MCH receptor type, termed melanin-concentrating hormone receptor 2 (MCHR2). MCH, when administered intracerebroventricularly, induces food and water intake and body weight gain in several animal species. Multiple genetic rodent models have been generated, and a metaanalysis of MCH and MCHR1 deficiency models has been carried out.[7] This analysis has shown that deletion of MCH signaling suppressed body weight, fat mass, and plasma leptin, while MCH signaling deficiency increased body temperature, oxygen consumption, heart rate, and mean arterial pressure. Additional behavioral studies have shown that deletion of MCH signaling enhanced wakefulness, locomotor activity, aggression, and male sexual behavior, and that MCH signaling deficiency suppressed non-REM sleep, anxiety, responses to novelty, startle responses, and conditioned place preferences.[2] More recently, substantial data has been generated, suggesting a role of the MCH system in REM sleep and in depression-like symptoms in experimental animals.[8] Despite the varied potential pharmacologies that could be explored in man, the rationale and degree of robustness for MCH in food intake and obesity control appear to have the best validation in animal systems. Thus, in spite of the lack of clinical target validation and good-quality tool compounds, we embarked on a program aiming to discover and develop a novel MCHR1 antagonist for the treatment of obesity using reliable preclinical molecular and whole animal pharmacology models.

Our strategy was to discover and qualify a good small-molecule tool to enable the testing of the obesity-related target validity of MCHR1 in an MCHR1-only expressing rodent species first, followed by a canine species expressing both MCH receptor types, to explore both the efficacy and potential compensatory effects taking place when MCHR1 is antagonized. Should these efforts meet with success, we then would engage in the discovery of an antiobesity drug for human.

When our efforts began, no high-quality MCHR1 antagonists tool compounds had been reported that could be used in our planned in vivo studies. Over the years, a number of such compounds were disclosed that reached clinical studies. These include compounds **1**,[9] **2**,[10] **3**,[11] **4**,[12] and **6**.[13] We now, for the first time, disclose the discovery, chemical structure, and early development work on NGD-4715 (**7**).

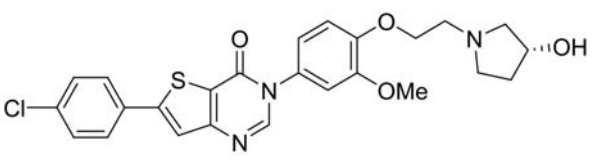

1: GW-856464

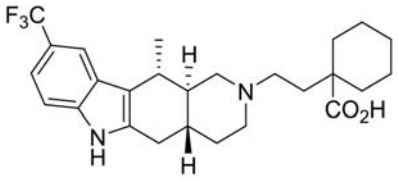

2: AMG 076

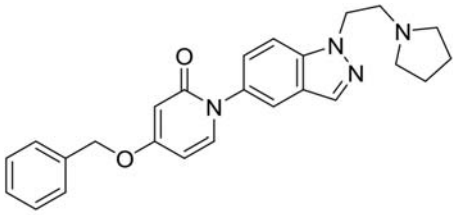

3: ALB-127158

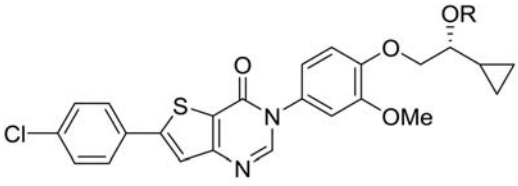

4: BMS-830216 (R=PO_3H_2)
5: BMS-819881 (R=H)

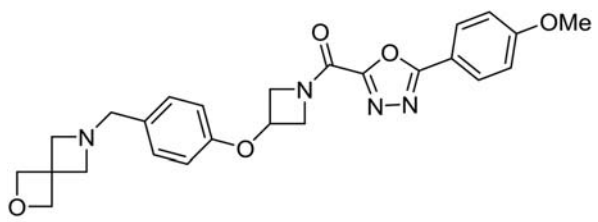

6: AZD1979

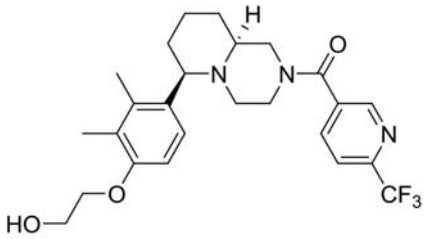

7: NGD-4715

8.19.2 Hit-Finding: The Serendipitous Discovery That Led to NDT 9522320, a Tool Compound for in vivo Target Validation

A high-throughput screening campaign was conducted on the Neurogen proprietary compound library, using a calcium mobilization assay on stably transfected Chinese hamster ovary (CHO) cells overexpressing monkey MCHR1.[14] Among a number of hits considered for confirmatory studies, a compound registered as the arylpiperazine HBr salt (**8**) was shown to have converted under regular vial manipulation and storage conditions (DMSO solution, occasional exposure to air) to bromide **9**. The structure of **9** was confirmed by comparison of spectroscopic (H-1 and C-13 NMR) and chromatographic (high-pressure liquid chromatography–mass spectrometry, HPLC-MS) properties with an authentic specimen synthesized from commercially available starting materials. Compound **9** was an excellent starting point for a CNS drug discovery project, based on its physicochemical attributes ($c\log P = 3.8$; MW = 421.3 amu; polar surface area (PSA) = 34 Å^2, five hydrogen bond acceptors and zero donors, and no violations of the rule of 5, Ro5 = 0), as well as the ease of structure–activity relationship (SAR) development. While compound **9** was a potent inhibitor of MCHR1 in vitro (monkey MCH $K_i = 12$ nM), was stable in microsomal incubations, and showed favorable in vivo pharmacokinetics (PK) in rat, it had significant cross-reactivity with the human ether-a-go-go related gene (hERG) channel (81% inhibition at 3 μM), the α1 adrenergic receptor ($K_i = 400$ nM), and serotonin transporter ($IC_{50} = 460$ nM). Improvements, therefore, were required to generate a suitable tool compound.

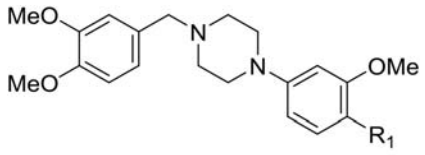

8: R^1=H
9: R^1=Br

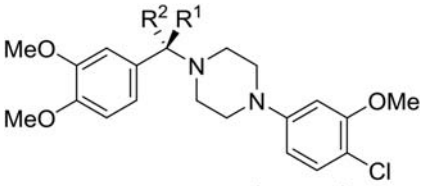

10: NDT 9522320 (R^1=Me; R^2=H)
11: NDT 9522321 (R^1=H; R^2=Me)

The initial objective of the medicinal chemistry program was to discover a tool compound with appropriate attributes to conduct target validation studies in vivo and interrogate the biological hypothesis that central antagonism of MCHR1 leads to observable feeding effects. Some aspects of the SAR of arylpiperazines as MCHR1 antagonists are broadly summarized in Fig. 1. We were encouraged by the highly tractable nature of this SAR. Among a number of productive strategies followed to improve lead compound **9**, the bromine substituent was replaced by chlorine, which reduced lipophilicity and molecular weight, and a methyl group was introduced at the benzylic position. Indeed, the "magic methyl" strategy is well known in medicinal chemistry, and, often times, it results in a favorable trade-off between enhancements to the compound under study (e.g., improvements of in vivo stability, in vitro potency and selectivity, and solubility) and a manageable small increase in molecular weight and lipophilicity.[15] This led to the pair of enantiomers **10** and **11**. As we shall see later on, this SAR tractability was key in the design strategy that led to a novel core and eventually to the clinical compound NGD-4715.

8.19.3 Characterization of NDT 9522320 (10): Absolute Configuration, Physicochemical Attributes, and Large-Scale Synthesis

The two homochiral analogs **10** and **11** were made as exemplified for the former compound in Fig. 2. (1*R*)-1-(3,4-Dimethoxyphenyl)ethan-1-amine (**12**) was obtained by resolution of the racemate using (*R*) mandelic acid. Alkylation with

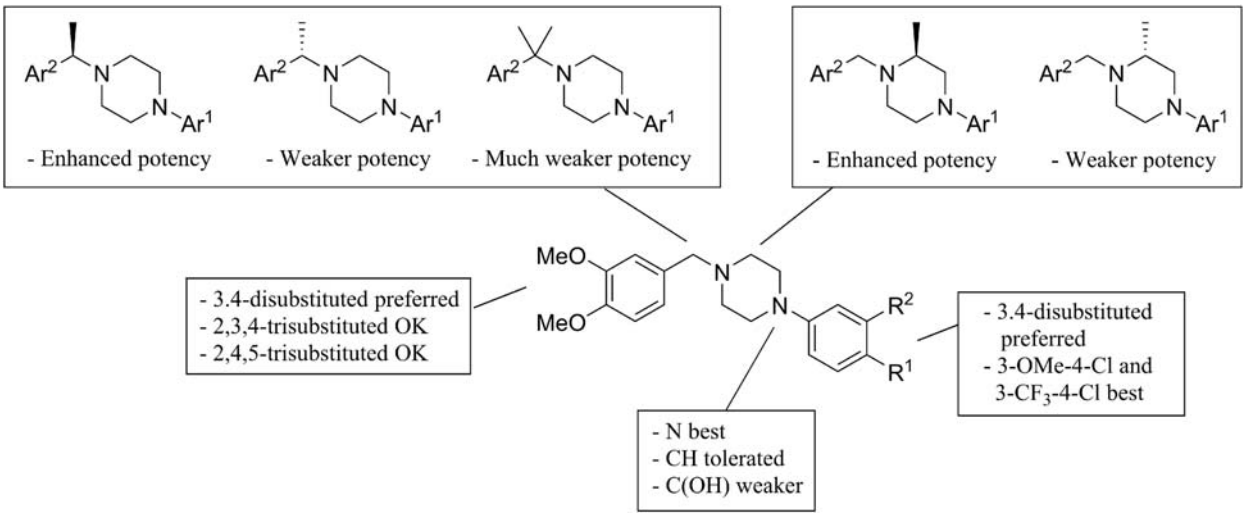

Fig. 1 Some broad aspects of the SAR for in vitro functional activity of arylpiperazines as MCHR1 antagonists.

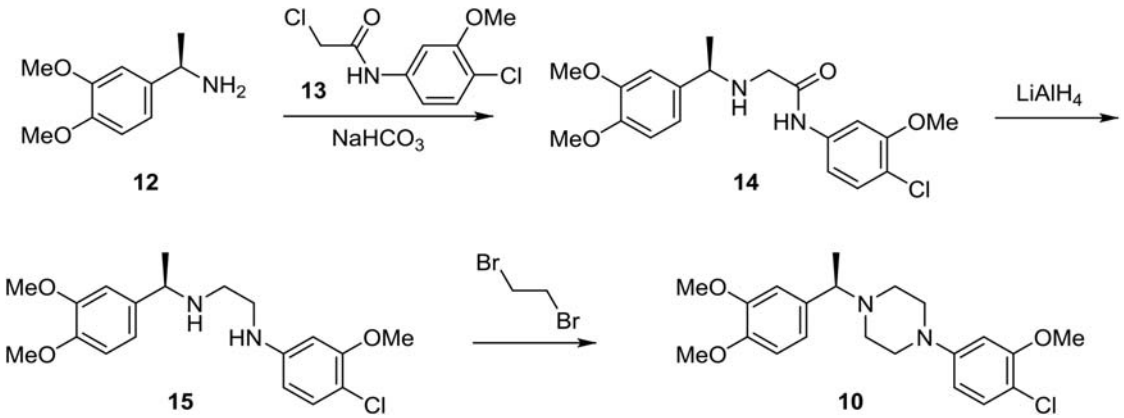

Fig. 2 Reaction sequence used for the enantiospecific preparation and characterization of absolute configuration determination of NDT9522320 (**10**).

chloroacetanilide **13**, followed by amide reduction with $LiAlH_4$, afforded diamine **15**. Alkylation with 1,2-dibromoethane produced compound **10**, also known as NDT 9522320, in 100% enantiomeric excess. The same process, but using (*S*)-mandelic acid, delivered the less-active enantiomer **11**. Since the absolute configuration of the starting material **12** was known, and it remained intact during the synthetic sequence, this scheme enabled the assignment of the absolute configuration of **10**, in spite of a relatively low total yield.

A larger scale synthesis was developed as shown in Fig. 3. Using this protocol enabled the preparation of up to 500 g of compound **10** in a total yield of 14% and enantiomeric excess ee > 99%, as determined by HPLC analysis, which enabled the execution of subchronic studies in rat and dog. 3,4-Dimethoxyacetophenone (**16**) was reacted with piperazine **17** under reductive amination reaction conditions using excess $Ti(OiPr)_4/NaBH_4$, yielding racemic benzylamine **18**. Hydrolysis under strongly basic conditions afforded piperazine **19**, which was resolved with L-tartaric acid (three crystallizations) to produce chiral **20**. Palladium-catalyzed coupling of **20** with 4-bromo-1-chloro-2-methoxybenzene under Buchwald reaction conditions ($Pd_2(dba)_3$, BINAP, KO*t*Bu) delivered after chromatographic purification, compound **10**, which was converted to its bis-HCl salt by treatment with excess HCl in dioxane.

Compound **10** showed high affinity for the MCHR1 receptor, inhibiting the binding of the peptidic agonist [^{125}I]-S36057 in a rat brain membrane assay with $K_i = 15$ nM,[16] and was also a potent inhibitor of the functional effects of MCHR1 in vitro (MCH-stimulated monkey MCHR1 Ca flux $K_i = 4$ nM and GTPγ^{35}S $K_i = 17$ nM). In a monkey MCHR-CHO cell membrane GTPγ^{35}S assay,[17] compound **10** acted as a competitive inhibitor with a $K_d = 12$ nM based on Schild analysis (slope factor 1.14). Compound **10** showed excellent selectivity versus human MCHR2 (no detectable activity at 10 μM) and encouraging improvements in cross-reactivity with hERG (58% inhibition at 3 μM, $IC_{50} = 2.5$ μM), the α1 adrenergic receptor ($K_i = 1933$ nM), and the serotonin transporter ($IC_{50} = 6.5$ μM). A broad panel (40 relevant GPCRs) indicated < 50% inhibition of radioligand binding at 1 μM, with the exception of the histamine H2 receptor, with an $IC_{50} = 470$ nM.

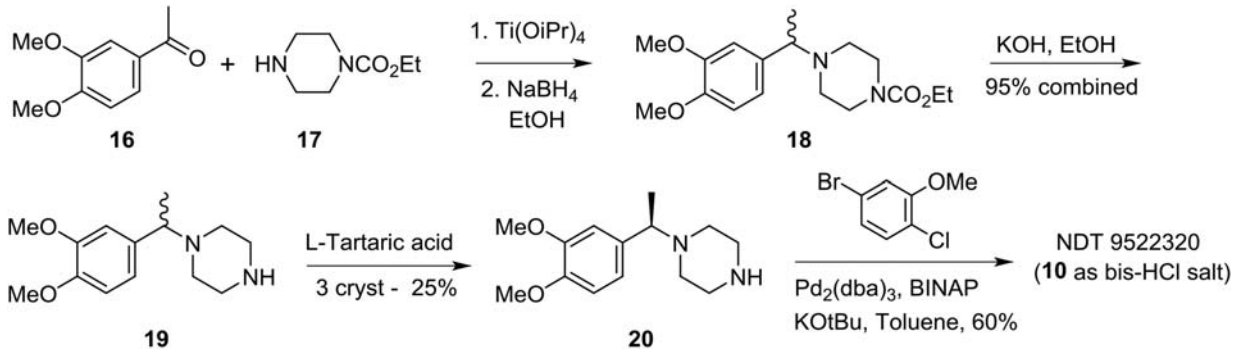

Fig. 3 Reaction sequence used for the scale up of up to 500 g of NDT 9522320 (**10**).

Furthermore, the 100-fold weaker functional in vitro activity at the target of the distomer **11** (mMCH $K_i = 379$ nM) provided a tool compound that could be used as negative control during in vivo efficacy studies, and mechanistically support a link to pharmacodynamic effects of compound **10**.

In terms of physicochemical attributes, **10** has a molecular weight MW = 390.9 amu, calculated $c \log P = 4.2$ and PSA = 34 Å^2, rotatable bonds (RB) = 6, hydrogen bond acceptors and donor are HBA = 5 and HBD = 0, respectively, thus affording no violations of the Lipinski Rule of 5 (Ro5 = 0). It is weakly basic (experimental p$K_a = 7.3$). Aqueous kinetic solubility was moderate (17 μg mL^{-1} or 44 μM at pH 7.4 or 250 μg mL^{-1} or 641 μM at pH 5.4).

Stability in rat, dog, monkey, or human liver microsomes preparations generally was moderate, with predicted hepatic clearance values of CL_H of 60 mL min^{-1} kg^{-1}, 22 mL min^{-1} kg^{-1}, 18 mL min^{-1} kg^{-1}, and 10 mL min^{-1} kg^{-1}, respectively. In vivo rat PK parameters were consistent with expectations set from in vitro values. Compound **10** was dosed as a solution in methylcellulose/triacetin (0.5%/0.1%; 10 mg kg^{-1}, PO or 1.5 mg kg^{-1}, IV). The compound was highly bioavailable ($F = 88\%$), with short $T_{max} = 0.75$ h, high volume of distribution (15 L kg^{-1}), $C_{max} = 268$ ng mL^{-1}, $T_{1/2} = 7.2$ h, and CL = 35 mL min^{-1} kg^{-1}. Compound **10** is highly brain penetrant in rat, showing total brain-to-plasma ratios B/P = 8–10. In a rat brain ex vivo receptor occupancy assay, compound **10** had an $RO_{50} = 4$ mg kg^{-1}. The cerebrospinal fluid levels of **10** were determined at 5 and 20 mg kg^{-1}; dose-proportional concentrations seen were 7 ng mL^{-1} (18 nM) and 31 ng mL^{-1} (80 nM), respectively, commensurate with functional IC_{50} values and in good agreement with the ex vivo RO_{50}.

In dog PK studies, compound **10** was dosed as the bis-HCl salt (IV: 1.5 mg kg^{-1} in 50% PEG; PO: 2 mg kg^{-1} in 2% D-α-tocopheryl polyethyleneglycol succinate). Oral bioavailability was moderate ($F = 54\%$), with short $T_{max} = 0.8$ h, high volume of distribution (9.5 L kg^{-1}), $C_{max} = 393$ ng mL^{-1}, and $T_{1/2} = 19$ h. No differences in drug exposure in fed versus fasted dogs were observed in dog (PO dosing; 10 mg kg^{-1}, capsules; $F = 92\%$ vs. 94%; $C_{max} = 1477$ ng mL^{-1} vs. 1239 ng mL^{-1} for fed and fasted, respectively).

In terms of safety, conjugation with glutathione in vitro was observed (75% vs. 20% for acetaminophen).[18] No reversible or time-dependent inhibition of CYP450 could be determined in vitro.[19] We explored further the potential for cardiovascular liabilities since there was moderate hERG activity, and were pleased to find that **10** had < 10% change in action potential duration at 90% repolarization at 3 μM in rabbit heart Purkinje fiber studies, bolstering its cardiovascular safety profile.[20] Based on these results, we considered that compound **10** was a suitable tool compound to test the biological hypothesis in vivo in both rat (MCHR1-only species) and dog (dual MCHR1/2 species).

8.19.4 Preclinical Proof-of-Concept in Rat

Mechanistic support for the effects of tool compound **10**, being driven by blocking the MCHR1 receptor, came from studies where feeding is elicited by intracerebroventricular (ICV) administration of MCH, and then blocking these effects in the presence of the MCHR1 antagonist. Fig. 4 shows an example of the effects of **10** (dosed at 2 mg kg^{-1}) on MCH-elicited feeding behavior. Similar effects were observed at 5, 10, and 20 mg kg^{-1} doses of compound **10**. On the other hand, the feeding effects elicited by galanin, another orexigenic peptide, were not antagonized by **10**, showing a level of selectivity in its antifeeding effect. These results are consistent with the orexigenic effects of the MCH peptide agonist, and the biological response interrogated with compound **10**.

The diet-induced obesity (DIO) model in rat was chosen to study the effects of MCHR1 antagonism by **10** on the rate of body weight and food intake in drug-treated animals (10 mg kg^{-1}) compared to vehicle-treated control animals on a high-fat diet.[21] In this model, rats are treated with a high-fat diet. Some of them will become obese, some will not. These animals were separated into two groups: obesity-prone and obesity-resistant. Fig. 5 shows that compound **10** had no effect on obesity-resistant animals, while it caused a reduction in the rate of weight gain and food intake in obesity-prone animals.[22] Note that in the experience of Neurogen, the drugs fenfluramine, sibutamine, and rimonabant were active in this DIO model.

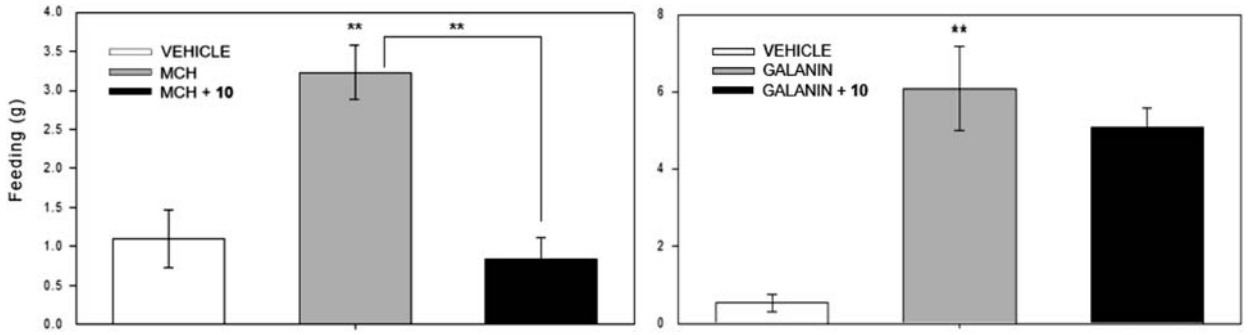

Fig. 4 Effect of **10** (2 mg kg^{-1}, PO) on rat feeding behavior elicited by MCH (*left panel*, 5 μg MCH, ICV) or galanin (*right panel*, 10 μg galanin); 2-h test, $n=7$. Comparisons made against vehicle group. $^{**}p<0.01$.

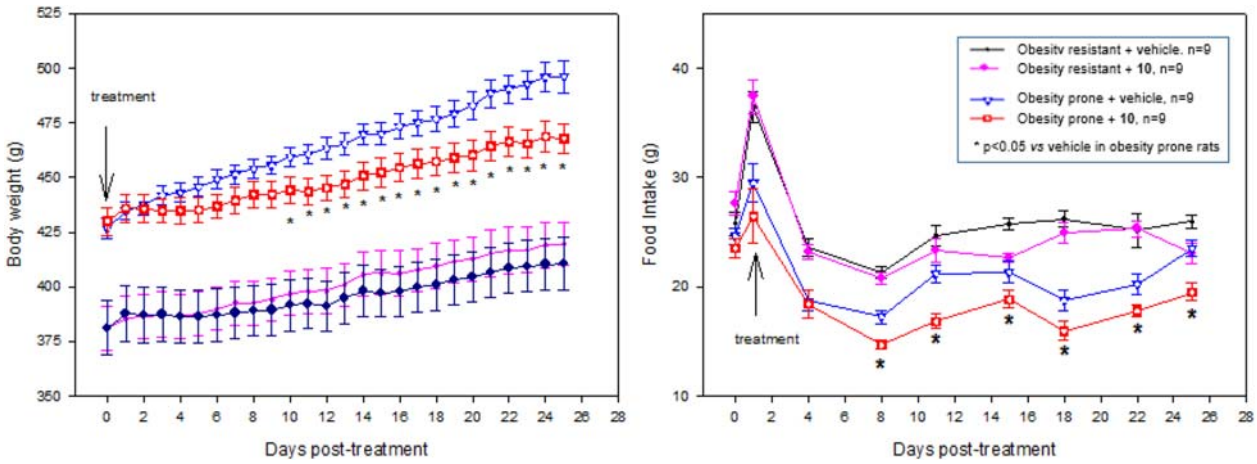

Fig. 5 Effect of **10** (10 mg kg^{-1}, PO) on body weight and feeding behavior in obesity-prone rats. No statistically significant effects of **10** are seen in rats that are not obesity-prone, either on body weight *(left panel)* or food intake *(right panel)*. On the other hand, compound **10** significantly reduces the rate of weight gain and the food intake in obesity-prone rats (*red* vs. *blue squares*).

To rule out the possibility that the feeding behaviors seen were driven by a drug-mediated toxic effect, we evaluated potential changes in a number of behavioral domains. General potential effects of **10** on motor behaviors were explored through their spontaneous locomotor activity, where no evidence of hypo- or hyperactivity was seen. Drug-induced gastrointestinal (GI) malaise may lead to a reduction in food intake, and it is difficult to detect as rats lack the emetic response. However, persistent consumption of nonnutritive substances like kaolin has been considered similar to vomiting in other species. These GI effects were ruled out, as no increase in kaolin consumption was observed versus controls (10 mg kg^{-1} of **10**).[23] Potential anxiogenic effects were investigated in the elevated plus maze, and also were ruled out (2, 5, or 10 mg kg^{-1}). Thus, no effects were seen in any of these tests, suggesting no malaise was caused by **10**, and increasing confidence that the feeding effects could be attributed to central MCHR1 antagonism.

These results support the role of the MCHR1 in weight control in a species only expressing the MCH1 receptor. Would this reduced feeding phenotype be maintained in higher species containing both MCHR1 and MCHR2 receptors? To address this question, we conducted investigations in dog.

8.19.5 Proof of Concept in Dog, a MCHR1/2 Species

As previously discussed, MCH is an orexigenic peptide involved in energy homeostasis expressed in the LHA of the brain. Two MCH receptors are known: MCHR1 and MCHR2, the latter being expressed only in higher species such as dog, monkey, and human.

To explore the effects of MCHR1 antagonism on body weight and food intake in a species expressing both receptors, female spayed beagle dogs were used as subjects and fed 400 g of a high-fat diet daily throughout the study. Three weight-matched groups ($N=6$; vehicle, 3 and 10 mg kg^{-1} bid; capsules) were dosed for 29 days. NGD 9522320 (**10**) significantly prevented body weight gain in the 3 and 10 mg kg^{-1} groups compared with a control group (Fig. 6). The cumulative food intake for the 10 mg kg^{-1} group was reduced significantly from control. Umbilical girth increase was significantly smaller for the 10 mg kg^{-1} group versus control. A Purina body condition score (PBCS) was determined for each dog by veterinary exam.[24] All three treatment groups were scored as

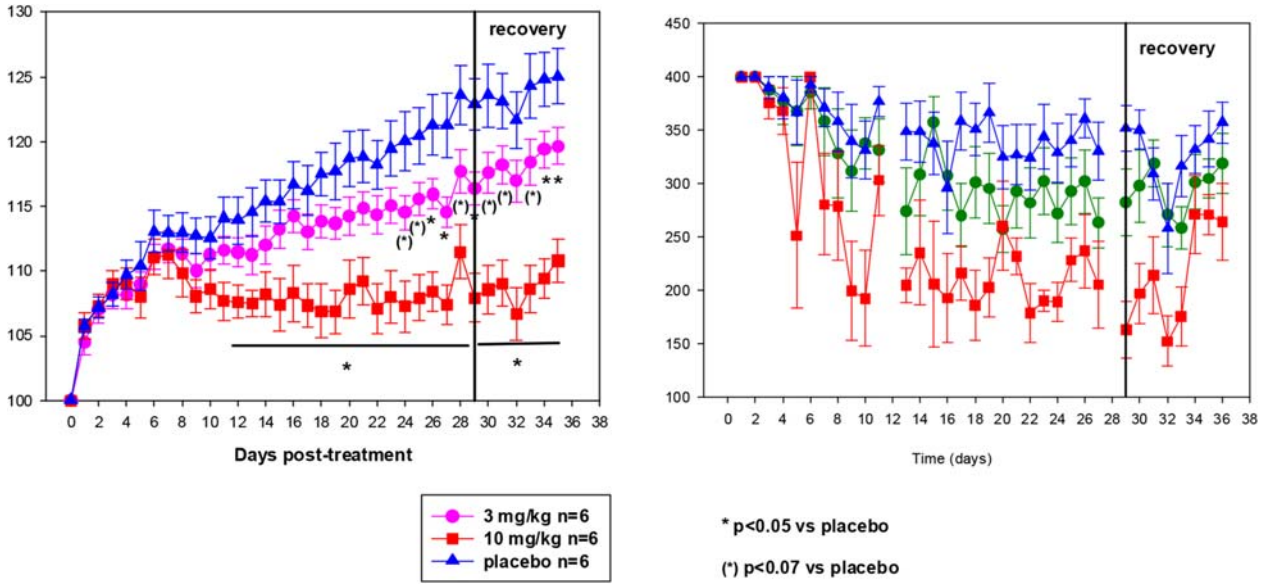

Fig. 6 Effect of NDT 9522320 (**10**, 3 or 10 mg kg^{-1} PO, capsule) on body weight change (left) or food intake (right) in beagle female spayed dogs. Treatment was discontinued after 28 days of dosing.

Table 1 Plasma concentrations for compound **10** at different time points in the dog subchronic study

Dose	*Time (ng mL^{-1})*	*Day 1*	*Day 15*	*Day 29*	*Day 36 (Recovery)*
3 mg kg^{-1}	Peak	410 ± 317	893 ± 323	1101 ± 231	–
	Trough	26 ± 19	199 ± 65	309 ± 129	41 ± 25 ($T_{1/2}$ = 48 h)
10 mg kg^{-1}	Peak	1625 ± 764	2410 ± 962	4412 ± 1051	–
	Trough	196 ± 157	1707 ± 611	2185 ± 912	1009 ± 682 ($T_{1/2}$ = 122 h)

heavy at the start of the study (PBCS = 6.4). By the end of the treatment, the 10 mg kg^{-1} group showed no significant increase in the score (6.7), signifying no increase in adiposity. PBCS for the control group increased to 8.0 (obese). Hormonal measurements revealed that treatment with **10** (3 and 10 mg kg^{-1}) prevented the diet-induced abnormal insulin secretion after the meal as observed in the control group. Neither dose group showed significant alterations in clinical and blood chemistry or any signs of malaise (Kaolin assay). Plasma levels for compound **10** at different time points during the study, including recovery, are shown in Table 1. In agreement with the slow decay in compound **10** plasma concentrations upon ending dosing, both the rate of weight gain and food intake tend to increase toward those for the control group, suggesting a PK–pharmacodynamic relationship.[25]

In summary, this study demonstrated that compound **10**, a selective, brain penetrant, orally active MCHR1 antagonist, was efficacious in an R1/R2 species as evidenced by a dose-related reduction in rate of body weight gain and food intake, reduction in visceral adiposity as measured by girth at the umbilicus, and the PBCS remaining unchanged on Day 29 compared to Day 1 for the 10 mg kg^{-1} group. Treatment with **10** was effective in controlling the hyperinsulinemia associated with the ingestion of a high-fat diet at 3 and 10 mg kg^{-1} (data not shown). Support for MCHR1 antagonism for the treatment of obesity has been obtained in a species that expresses both MCHR1 and MCHR2.

Overall, these data strongly support the efficacy of MCHR1 antagonists in preclinical feeding models of obesity and suggest that MCHR1 antagonists may be useful in the control of multiple complications associated with obesity, diabetes, and metabolic syndrome.

Having gained confidence in the biological hypothesis of MCHR1 antagonism using NDT9522320, we realized that some safety aspects (glutathione conjugation, hERG channel inhibition) of this compound fell short of the very high expectations for an anti-obesity drug.[26] Therefore, our team embarked on a search for a clinical drug candidate with higher safety and efficacy attributes.

8.19.6 A Novel Bicyclic System: NGD 9522330 (31)

Although we could not advance our tool compound, NDT 9522320 (**10**), any further through early development, we nonetheless were encouraged to continue our investigations, this time through the development of additional heterocyclic cores that might provide compounds with superior properties that would further enlarge our patent estate and probability of clinical success. A

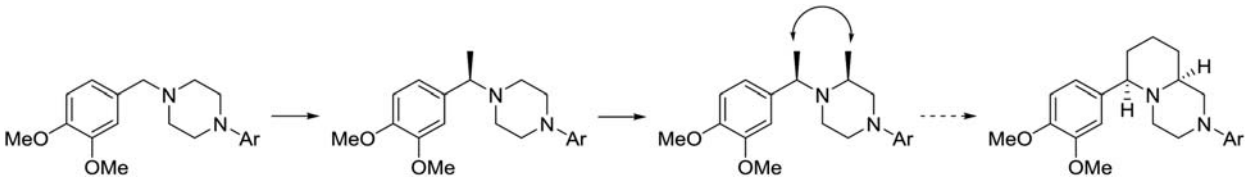

Fig. 7 Proposed pyrido[1,2-*a*]piperazine core.

classic medicinal chemistry strategy is to cyclize portions of a molecule to restrict bond rotation and conformational mobility (Fig. 7). Exploration of this strategy mandated the synthesis of a completely novel bicyclic ring system. It required no small amount of experimentation to devise a successful synthesis of the pyrido[1,2-*a*]piperazine ring system. The preparation methodology finally discovered is presented in the following figures.

Having established the required absolute chirality through our studies on NDT 9522320 (**10**), we turned to the chiral pool for the necessary synthons. Thus, treating L-2-amino-pent-4-enoic acid (**21**) with solid di-*tert*-butyl dicarbonate in 1 N NaOH and dioxane gave L-2-*tert*-butoxycarbonylamino-pent-4-enoic acid (**22**) in quantitative yield. A solution of **22** and 4-chloro-3-methoxyaniline in pyridine was treated with 1-(3-dimethylaminopropyl)-3-ethylcarbodiimide hydrochloride (EDCI) to give (*S*)-[1-(4-chloro-3-methoxy-phenylcarbamoyl)-but-3-enyl]-carbamic acid *tert*-butyl ester (**23**) in 72% yield. Alane-*N*,*N*-dimethylethylamine complex was added to a solution of **23** in toluene. After 25 h, the reaction was quenched and worked up, and the crude product was resubjected to the reduction conditions just described, which provided (*S*)-{1-[(4-chloro-3-methoxy-phenyl-amino)-methyl]-but-3-enyl}-carbamic acid *tert*-butyl ester (**24**) in quantitative yield. A solution of chloroacetylchloride was added to a biphasic mixture of ethyl acetate and saturated sodium bicarbonate to provide (*S*)-1-{[(2-chloro-acetyl)-(4-chloro-3-methoxy-phenyl)-amino]-methyl}-but-3-enyl-carbamic acid *tert*-butyl ester (**25**) in 89% yield. The benzyloxycarbonyl (BOC) group was removed, giving (*S*)-5-allyl-1-(4-chloro-3-methoxy-phenyl)-piperazin-2-one (**26**) in 78% yield. These reactions are summarized in Fig. 8.

To continue the reaction sequence, **26** was subjected to alane-*N*,*N*-dimethylethylamine complex reduction, giving (*S*)-3-allyl-l-(4-chloro-3-methoxy-phenyl)-piperazine (**27**) in quantitative yield. Compound **27** was mixed with di-*tert*-butyldicarbonate in THF to provide (*S*)-2-allyl-4-(4-chloro-3-methoxy-phenyl)-piperazine-1-carboxylic acid *tert*-butyl ester (**28**) in quantitative yield. Wacker oxidation of intermediate **28** gave (*S*)-4-(4-chloro-3-methoxy-phenyl)-2-(2-oxo-propyl)-piperazine-1-carboxylic acid *tert*-butyl ester (**29**) in 63% yield. The BOC group was removed, and the product was treated with 3,4-dimethoxybenzaldehyde and 6 N NaOH in MeOH leading to (6*R*,10*S*)2-(4-chloro-3-methoxy-phenyl)-6-(3,4-dimethoxy-phenyl)-octahydro-pyrido[1,2-*a*]pyrazin-8-one (**30**) in 29% yield. Formation of the tosyl hydrazine followed by reduction with sodium borohydride gave (6*R*,10*S*)2-(4-chloro-3-methoxy-phenyl)-6-(3,4-dimethoxy-phenyl)-octahydro-pyrido[l,2-*a*]pyrazine (NDT9522330, **31**) in 67% yield. These final reactions are presented in Fig. 9.

NDT 9522330 (**31**) exhibited the following physical properties: MW = 416.95 amu, calculated mLogP = 3.1; PSA = 43 Å^2; RB = 6; HBD = 0; and HBA = 6. Thus, only one Lipinski rule was violated, and that only slightly (Ro5 = 1). Compound **21** is weakly basic (calculated pK_a = 7.16). This compound was the first analog made in the pyrido[1,2-*a*]piperazine aniline series. It was a highly potent MCH antagonist in vitro with an IC_{50} = 0.26 nM in a mouse calcium flux assay and K_i = 2.5 nM inhibiting the binding of the peptidic MCHR1 agonist [^{125}I]-S36057 in a rat brain homogenate assay. The half-life in human and rat liver microsomes was

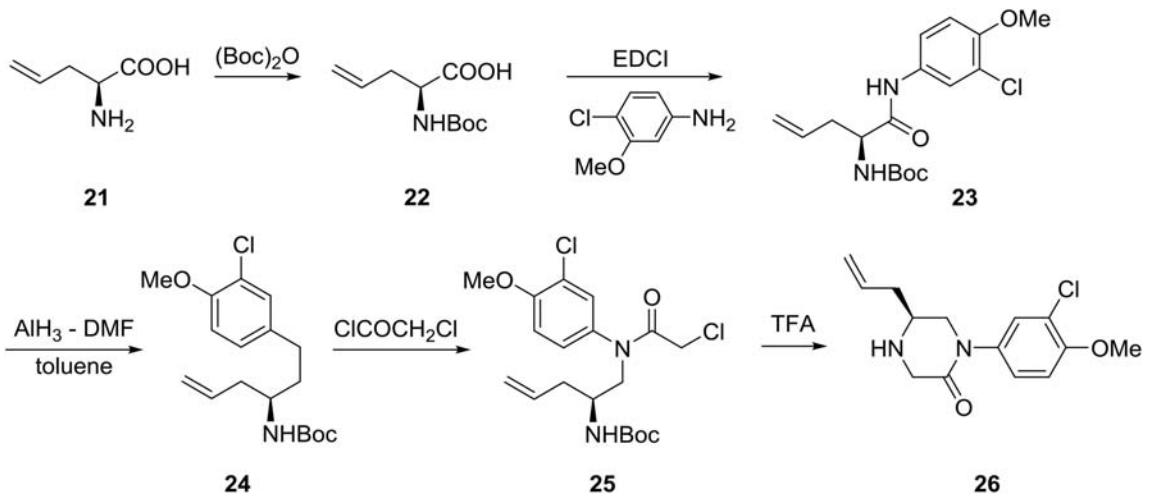

Fig. 8 Preparation of (*S*)-5-allyl-1-(4-chloro-3-methoxy-phenyl)-piperazin-2-one (**26**).

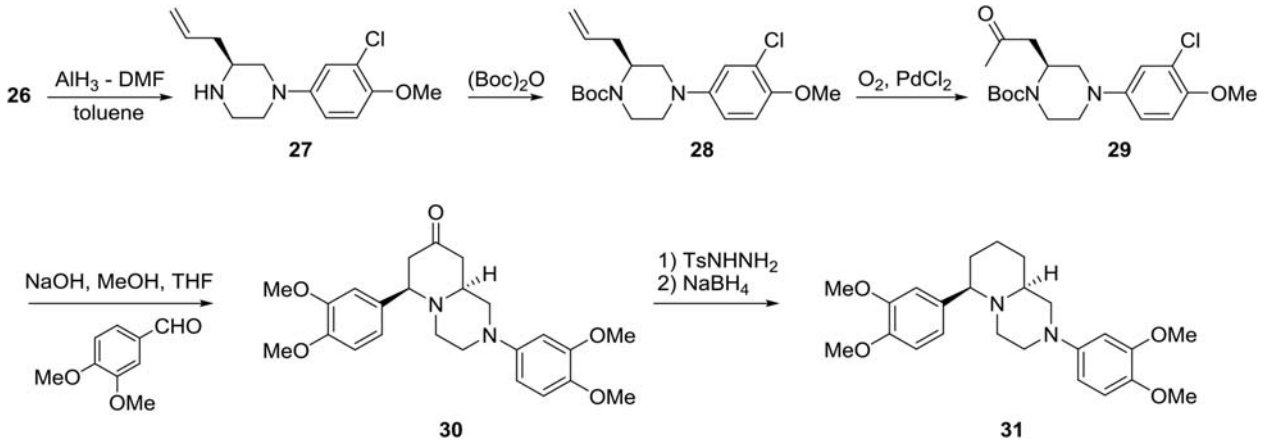

Fig. 9 Preparation of NDT9522330 (**31**).

Fig. 10 Medicinal chemistry strategy seeking MCHR1 antagonists with the right balance of safety and efficacy attributes to become human drugs.

25 min and 43 min, respectively, thereby predicting acceptable metabolic stability. A rigorous analysis of the SAR of this series is beyond the scope of this work, but, despite the compound's excellent in vitro properties, it was found to be a hERG inhibitor with 50% inhibition at a 3 μM concentration in a patch-clamp assay. Indeed, hERG inhibition was a recurring issue with this series and prompted us to continue our exploration.

During the course of our studies in the aryl piperazine series, we discovered that the replacement of the 3,4-dimethoxyphenyl group with a 2,3-dimethyl-4-methoxypheny group resulted in compounds with superior MCH antagonist activity, presumably by restricting rotation about the bond between the phenyl ring and the heterocycle. Furthermore, it is known that reducing the basicity of a compound often reduces the degree of hERG inhibition.[27] Therefore, we thought to accomplish this by replacing the aniline with a carboxamide as shown in Fig. 10.

In order to generate analogs rapidly, we needed a synthesis that would allow facile modification of the western aryl group and modification of the carboxamide. The route utilized by medicinal chemists was designed to allow the exploration of the effects of variable functionality at the head and tail of the bicyclic octahydro-1*H*-pyrido[1,2-*a*]piperazine core. To this end, the sequence of reactions shown in Figs. 10–12 was employed. Benzyl protected L-aspartic acid was coupled to *N*-benzyl glycine ethyl ester using DCC and hydroxybenzotriazole. The resulting dipeptide cyclized spontaneously upon removal of the BOC group with trifluoroacetic acid to give **32**. Reduction with lithium aluminum hydride gave **33**, which was followed by reintroduction of the BOC group,

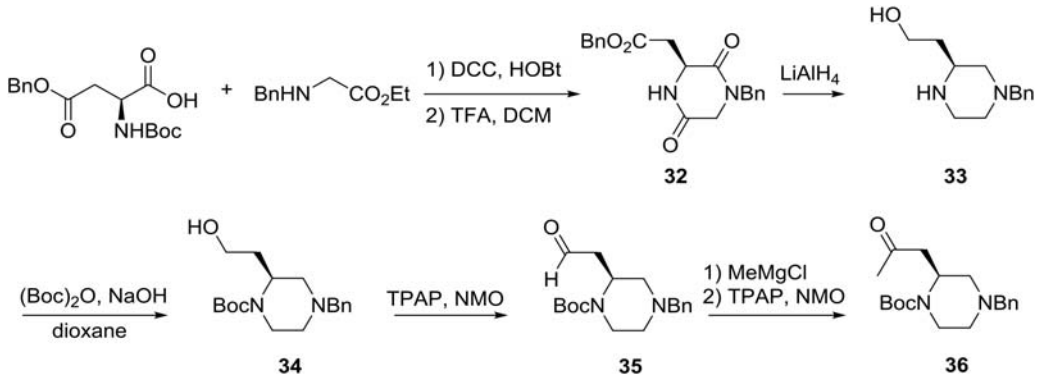

Fig. 11 Preparation of 1-[2*S*-4-benzylpiperazine-2-yl]propan-2-one (**36**).

gave the orthogonally protected piperazine ethyl alcohol **34** in 41% yield for the four steps after column chromatography. This was oxidized to the aldehyde **35** with tetrapropylammonium perruthenate (TPAP) and *N*-methyl morpholine oxide (NMO) in 79% yield after chromatography. After treatment with methyl magnesium chloride, the crude secondary alcohol oxidized using TPAP and NMO to provide the methyl ketone **36** in 73% yield for two steps after chromatography (Fig. 11).

With compound **36** in hand, aldol condensation with 2,3-dimethylanisole (**37**), mediated by DBU and lithium chloride in THF, followed by the removal of the BOC group, gave the enone **38** as a mixture of *cis*/*trans* isomers. The isomeric ratio was not determined, and the mixture was carried on to the next step without additional purification. The bicyclic intermediate **39** was obtained in 50% yield for three steps after chromatography by an intramolecular Michael addition mediated by ammonium acetate. Deoxygenation was accomplished by reduction of the intermediate tosyl hydrazone with sodium cyanoborohydride to give compound **40** in 62% yield for two steps after chromatography. The benzyl group was removed by catalytic transfer hydrogenation using ammonium formate as the hydrogen source in 96% yield, and the deprotected amine then was acylated with a commercially available aroyl chloride, or the acid chloride was prepared using the corresponding aroyl acid using thionyl chloride under standard conditions to give the intermediate (**41**) in good to excellent yields after chromatography. The methyl ether was cleaved with boron tribromide in ~80% yield to give the phenol (**42**), which was used as an intermediate to prepare analogs modified at the 4-position of the (6*R*,9a*S*)-6-(2,3-dimethylphenyl)-octahydro-1*H*-pyrido[1,2-*a*]piperazine ring system (generic structure **43**, Fig. 12).

Selected examples of analogs made are shown in Table 2. As can be seen, the 4-trifluoromethyl group confers optimal activity in this series, although the benzamide **44** still has an unacceptably high level of hERG inhibition. Compound **47**, the 4-trifluoromethyl nicotinamide, exhibits the best in vitro potency with an acceptable level of hERG inhibition—greater than 500-fold its IC_{50} in MCHR1 functional assays. Compound **47** was, therefore, chosen for further optimization.

Compound **47** was demethylated using boron tribromide in good yield, and the resulting phenol (**51**) was alkylated with a variety of agents in poor to good yields depending on the chemistry (Fig. 13). Scores of compounds were prepared and assayed. Table 3 provides a sampling of the data obtained.

The ether analog **53** displayed superior in vitro activity with an acceptable level of hERG inhibition—greater than 1800-fold its IC_{50} in MCHR1 functional assays, and was, therefore, selected for advanced testing. Compound **53** had the following rat PK properties: $T_{1/2}=3.1$ h; CL = 24.8 mL min^{-1} kg^{-1}; $V_{ss}=38.9$ L kg^{-1}; $T_{max}=0.5$ h, $C_{max}=86$ ng mL^{-1}, $F=20\%$; and an $AUC_{0-\infty}=427$ ng h mL^{-1} (10 mg kg^{-1} PO, 1 mg kg^{-1} IV, in 0.5% methyl cellulose/0.1% triacetin as vehicle, as in all studies unless otherwise noted). Brain penetration was good, with a partition B/P = 1.6.

Ether **53** was very active in vivo in our rat DIO model, producing a 3.1% reduction in body weight in male Wistar rats dosed at 5 mg kg^{-1} BID (Fig. 14). Although encouraged as we were by these results, our hopes soon were dashed. We discovered that this compound was retained extensively in adipose tissue in chronically dosed obese rats. We found that invasion into adipose tissue was high, elimination from the adipose was moderate to slow, and the adipose-to-plasma ratio was high (400–500). Since the expected patient population was to be chronically dosed obese humans, this posed an unacceptable potential risk. In retrospect, this high degree of adipose retention might have been indicated by a very large volume of distribution ($V_{ss}=38.9$ L kg^{-1}).

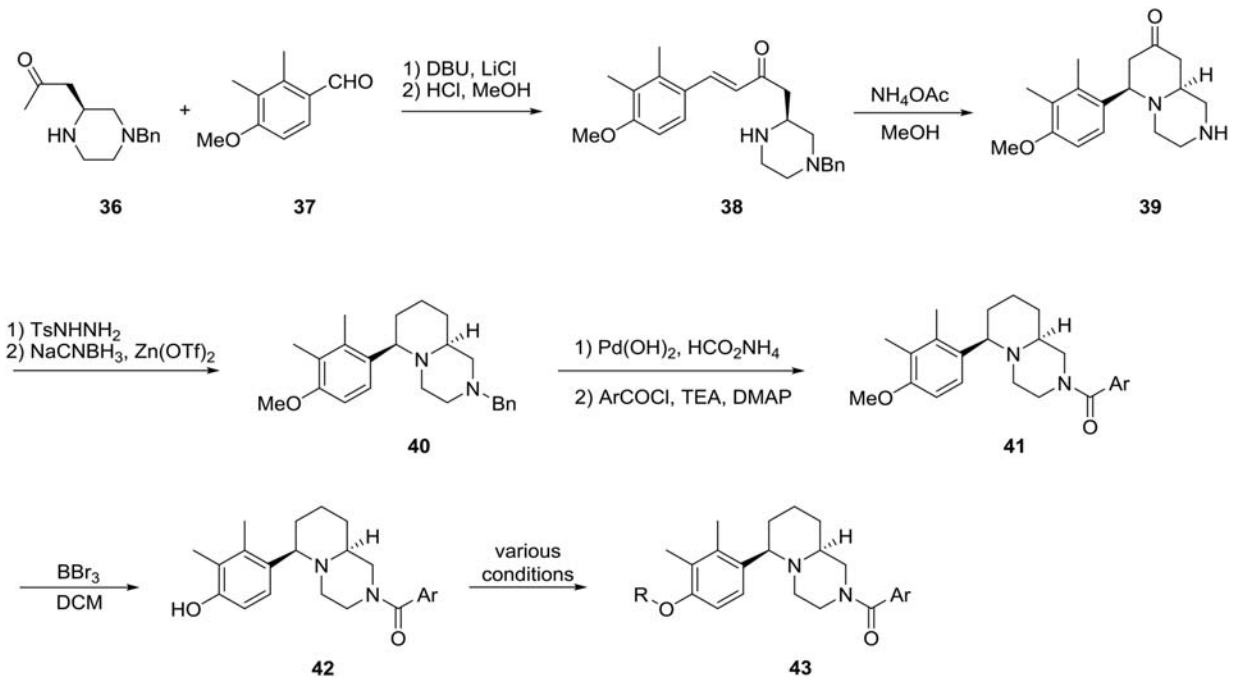

Fig. 12 Synthesis of 5-[(6*R*,9a*S*)-6-(4-methoxy-2,3-dimethylphenyl)-octahydro-1*H*-pyrido[1,2-*a*]piperazine-2-carboxamides (**43**).

Table 2 Selected SAR for the amide series (generic structure **43**, R = Me)[28,29]

Number	*Ar*	*Ca Ki (nM)*	*GTP Ki (nM)*	*Rat striatum Ki (nM)*	*hERG% inh. at 10 μM*
44	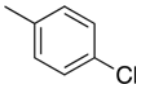	6.6	62	122	87
45	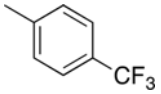	3.4	20	149	87
46	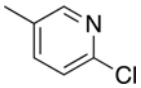	8.5	–	24	37
47	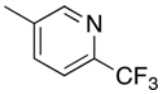	20	8.0	71	41
48	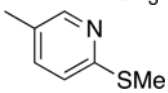	67	30	–	64
49	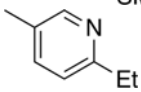	507	150	176	–
50	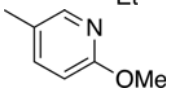	251	190	–	–

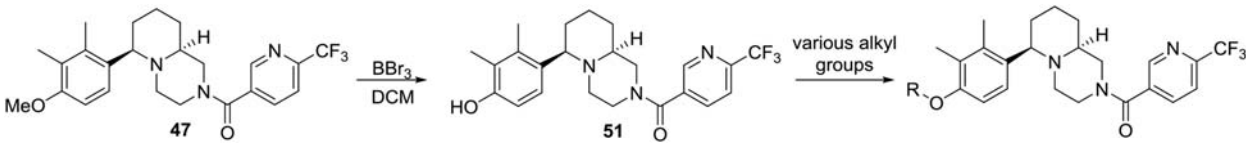

Fig. 13 Preparation of 4-trifluoromethyl nicotinamide analogs.

Table 3 Effect of alkyl groups on the activity of the 4-triflluoromethyl nicotinamide analogs

Number		*R*	*Ca K_i (nM)*	*GTP K_i (nM)*	*Rat striatum K_i (nM)*	*hERG% inh.*
52	Alkyl	Me	20	8.0	71	41%@10 μM
53	Ether	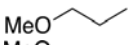	5.5	1.2	6.0	35%@10 μM
54		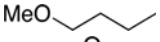	6.2	0.8	17	48%@10 μM
55	Amide	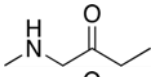	71	146	–	–
56		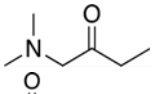	24	47	–	16%@10 μM
57		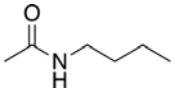	13	13	–	32%@3 μM
58	Heterocycle	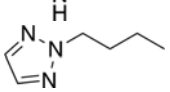	1.3	0.9	2.6	–
59		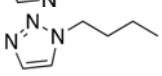	2.2	3.3	3.8	–

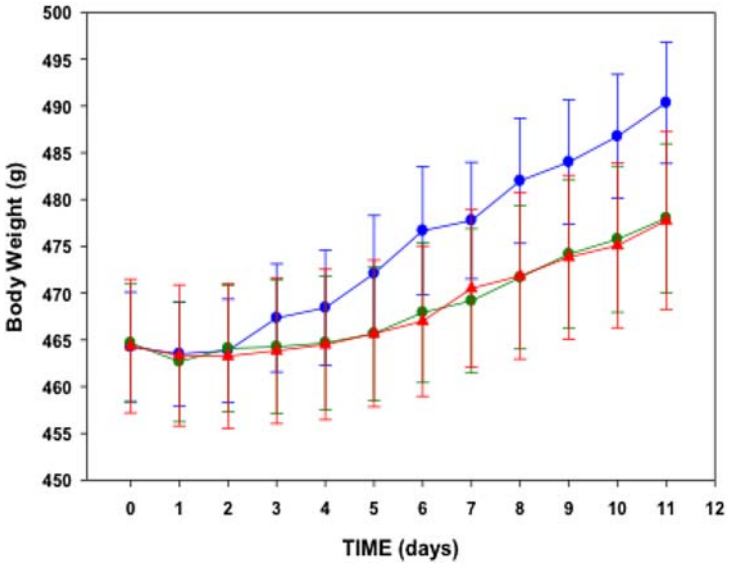

Fig. 14 Effect of **53** on body weight gain in male Wistar rats dosed at 5 mg kg^{-1} BID. *Blue circles* represent vehicle (MCTA); *red triangles* represent treatment with **53**, and *green circles* are the pair-fed group.

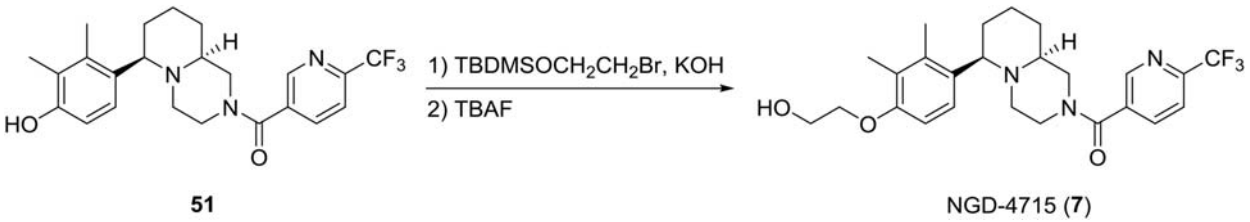

51 NGD-4715 (**7**)

Fig. 15 Final steps to NGD-4715 (**7**) in the medicinal chemistry synthetic route.

In an effort to reduce the lipophilicity and improve the solubility of the series, we undertook the synthesis of several hydroxylated analogs using the sequence shown in Fig. 15; among these was the hydroxyethyl derivative **7**, which would be designated as NGD-4715. Thus, phenol **51** was treated with (2-bromoethoxy)-*tert*-butyldimethylsilane and powder potassium to provide **7**. In summary, the medicinal chemistry synthetic route to NGD-4715 required linear 17 steps, including nine column chromatography purifications with an overall yield of ~9%.

As an interesting footnote, a metabolite identification study of the ether **53** indicated that NGD-4715 was a major circulating metabolite in vivo, suggesting that the efficacy observed in the DIO study with **53** was, at least in part, due to the presence of the primary alcohol **7** (Fig. 16).

NGD-4715 possesses the following physical properties: MW = 477.5 amu; $Qsol_{7.4}$ = 36 μg mL^{-1}; log $D_{7.4}$ = 3.4–3.8; log P = 2.9; RB = 6; PSA = 68 $Å^2$; Rule of Five violations Ro5 = 0. It possesses the following in vitro activity: Ca K_i = 10.6 nM; GTP K_i = 5.9 nM; and rat striatum K_i = 9 nM. The IC_{50} for hERG inhibition was 38.4 μM, which is 6857-fold its IC_{50} in MCHR1 functional assays. In

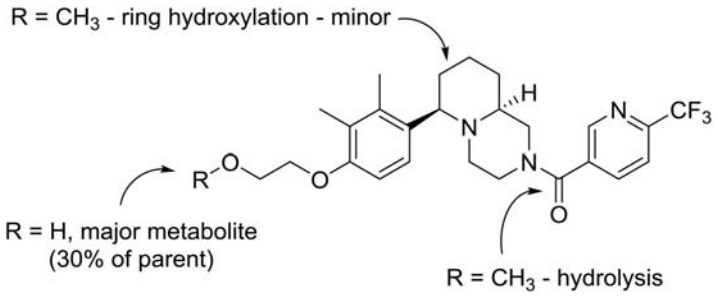

Fig. 16 Metabolites of compound **53** (R = Me).

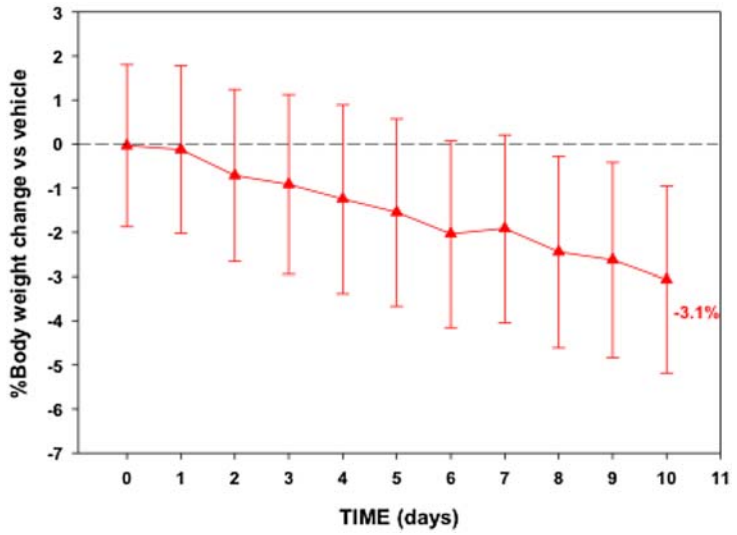

Fig. 17 Effect of NGD-4715 (**7**) on body weight of obesity-prone male Wistar rats dosed orally at 5 mg kg^{-1} BID; % body weight change versus vehicle.

rats, NGD-4715 exhibited the following PK properties: $T_{1/2}=2.1$ h; CL = 27.7 mL min^{-1} kg^{-1}; $V_{ss}=2.8$ L kg^{-1}; $T_{max}=0.5$ h, $C_{max}=212$ ng mL^{-1}, $F=40.0\%$; and $AUC_{0\rightarrow\infty}=765$ ng h mL^{-1} (10 mg kg^{-1} oral in MC/TA). With respect to in vivo activity, the DIO model produced a 3.1% reduction in body weight over 10 days (dosed orally BID at 5 mg kg^{-1}, Fig. 17). NDG-4715 (**7**) had a profound effect on food intake over a 24-h time period in male Wistar DIO rats dosed orally at 5 mg kg^{-1} BID. The animals consumed nearly 12% less food than animals dosed with vehicle (Fig. 18).

In a 26-day study, DIO rats in the control group showed a progressive weight gain during the study. The 5 mg kg^{-1} NGD-4715 treatment group showed less weight gain over the same period, and the 15 mg kg^{-1} group lost body weight compared to the pre-dosing weight. The 15 mg kg^{-1} dose group lost similar body weight compared to a pair-feeding group. A pair-feeding group is one in which food availability is matched to the food intake of a specific drug treatment group. The data obtained from the pair-feeding group allows one to conclude whether the weight loss effect can be attributed to a reduction in food intake alone, or is combined with other effects on metabolic parameters. The pair-feeding data suggest that the weight reduction following NGD 4715 treatment is due to food intake suppression with no apparent contribution from a metabolic effect. Daily food intake also was dose-dependently reduced by NGD-4715. In data not shown, NGD-4715 also lowered blood glucose levels and improved glucose tolerance. Drug treatment also reduced the hyperinsulinemia and hyperleptinemia associated with the ingestion of this high-fat diet. Hyperphagia was not seen in drug-treated groups following discontinuation of drug treatment, and body weight gain in the drug treatment groups paralleled that of the vehicle group during the recovery phase (Fig. 19). It is important to note there

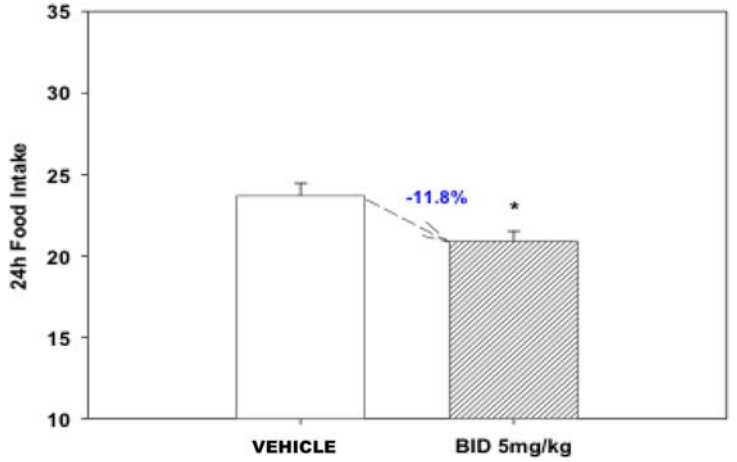

Fig. 18 Effect of NGD-4715 (**7**) on 24-h food consumption of obesity-prone male Wistar rats dosed orally at 5 mg kg^{-1} BID versus rats dosed vehicle (0.5% methyl cellulose/0.1% triacetin) only.

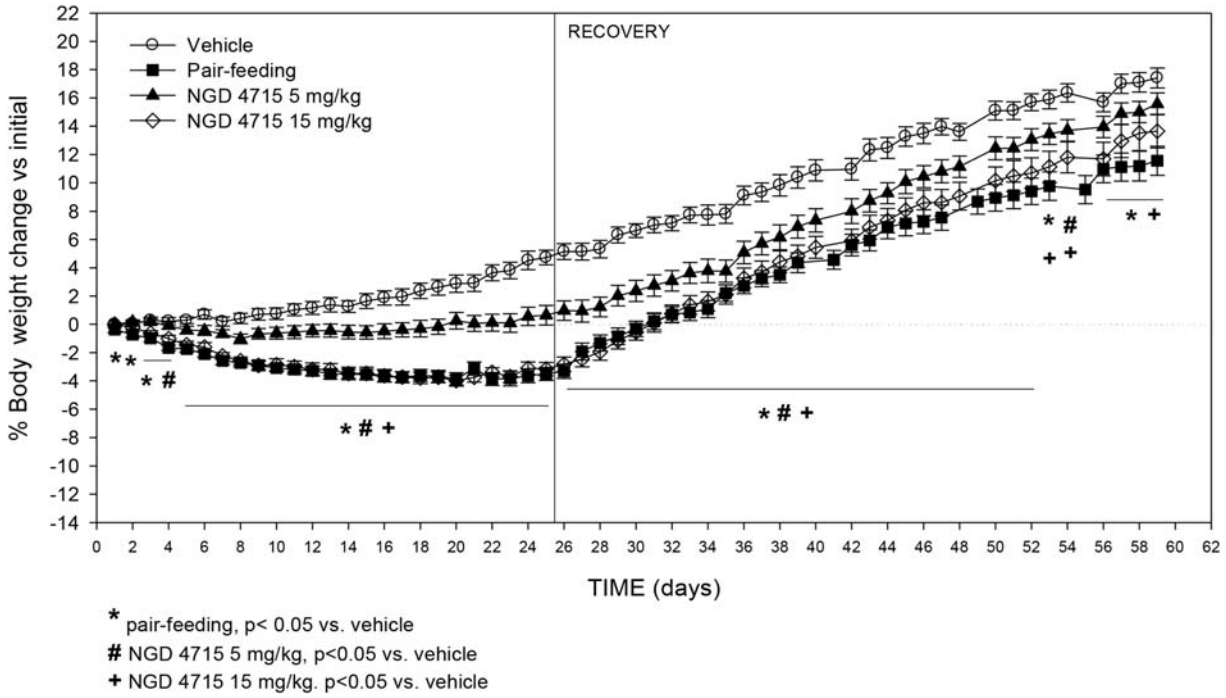

Fig. 19 Effects of orally administered NGD-4715 besylate on body weight gain in a 26-day diet-induced obesity study in rats. Values represent the mean percent body weight change and SEM for each day. All weights were taken before dosing in the afternoon and at the same time during recovery phase. The *n* for each group was 8–9. Rats received vehicle or NGD 4715 besylate 1 h prior to the lights off in the afternoon and 2.5 h after the lights on in the morning. All treatment groups were provided ad libitum access to food without any treatment during the recovery phase. Symbols placed below individual data points denote significant differences from the vehicle group ($p < 0.05$ Fisher's least significant difference test). Vehicle used was methylcellulose (0.5%)/triacetin (0.1%).

was no apparent malaise detected in the kaolin assay, no hypo- or hyperactivity in the locomotion assay, and no apparent anxiogenic effect in elevated plus maze experiment.

8.19.7 Process Development and cGMP Delivery

While useful for the synthesis of compounds to elucidate the SAR of MCH-1 receptor antagonists, the medicinal chemistry route suffered from a number of deficiencies:

1. linear as opposed to convergent;
2. lack of crystalline intermediates, resulting in multiple chromatographic purifications;
3. included a number of "problematic" reagents ($LiAlH_4$, BBr_3, $NaCNBH_3$, $TsNHNH_2$, DCC, TPAP); and
4. too many steps.

One obvious way to make the route more convergent would be to start with a more elaborated 2,3-dimethylanisole. To this end, commercially available and inexpensive 2,3-dimethylphenol (**60**) was alkylated in 83% yield using ethylene carbonate and potassium carbonate in hot DMF to give **61**. Friedel–Crafts acylation of **61**, using two equivalents of acetyl chloride, gave the acetophenone **62** in 97% isolated yield. The *para* isomer was the only product obtained.[30] The terminal acetate group was removed with a catalytic amount of sodium methoxide in methanol in 85% yield after distillation, and the resulting alcohol was protected as the tetrahydropyranyl ether[31] in 87% yield after crystallization to provide **63** (Fig. 20).

An important breakthrough came from the discovery, by Lubell's lab, that enantiopure pipecolate esters could be prepared via catalytic hydrogenation of a suitably protected amino enone (Fig. 21).[32]

Since NGD-4715 could be envisioned as a bicyclic pipecolate derivative, we wondered whether a similar strategy could be used in its preparation (Fig. 22).

Having a suitable route to the acetophenone component (**63**), we turned our attention to preparing an appropriately protected piperazine acetaldehyde, **66**. Our first attempt is outlined in Fig. 22. The reduction of compound **32** was effected with sodium bis(2-methoxyethoxy)aluminum hydride (Red-Al) instead of lithium aluminum hydride. Red-Al is safer (i.e., less pyrophoric), less expensive, and also allows for a simpler work-up when compared to lithium aluminum hydride. The crude product, **33**, then was isolated as the acetate salt, which could be purified from benzyl alcohol and other by-products by simple slurrying with methyl ethyl ketone.

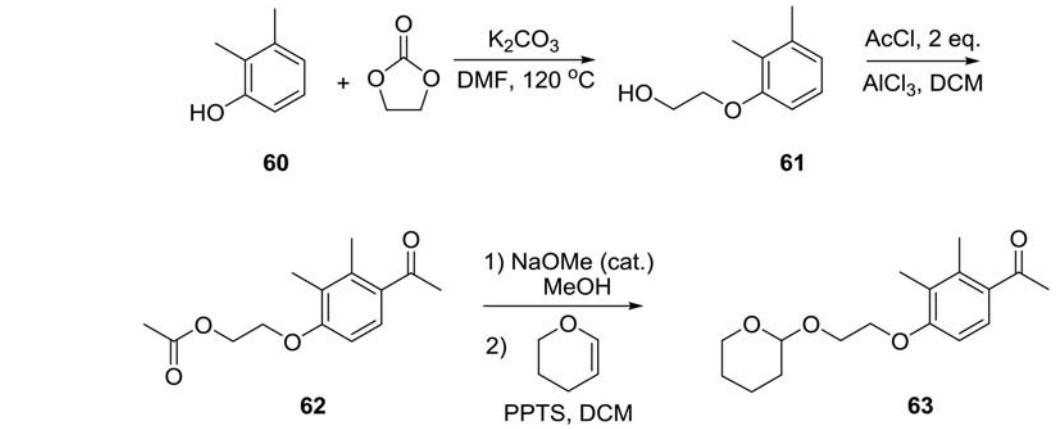

Fig. 20 Preparation of 1-{2,3-dimethyl-4-[2-(oxan-2-yloxy)ethoxy]-phenyl}ethan-1-one (**63**).

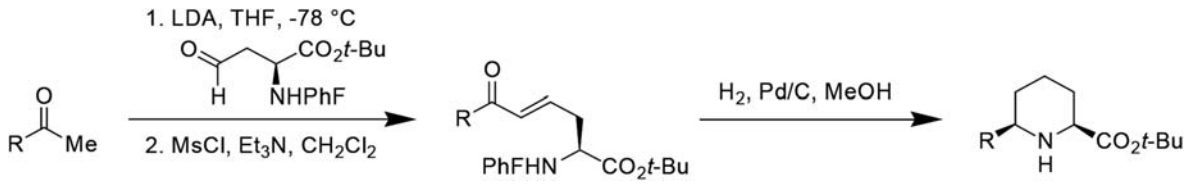

Fig. 21 Lubell's route to enantiopure pipecolic esters (PhF = 9-phenyl fluorene).

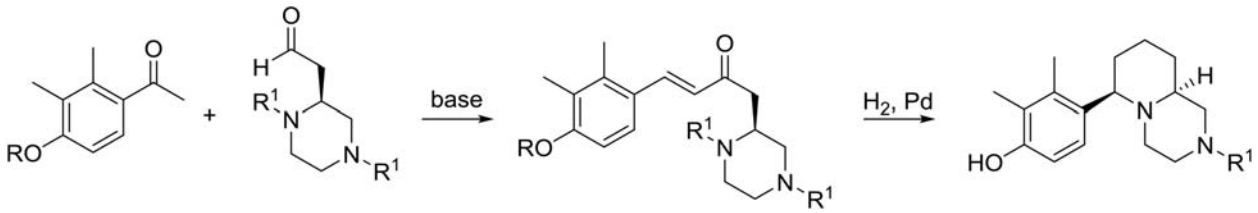

Fig. 22 Catalytic hydrogenation strategy for the synthesis of a key octahydro-1*H*-pyrido[1,2-*a*]piperazine intermediate.

The free base of purified **33** then could be isolated as a solid upon treatment with aqueous sodium hydroxide solution. Removal of the benzyl group by catalytic hydrogenation gave 2-*S*-hydroxethyl piperazine (**2-HEP**, **64**). The carboxybenzyl group (Cbz) was chosen as a protecting group, because it is robust enough to survive various aldol conditions, and because it can be removed by catalytic hydrogenation to facilitate the proposed cyclization.[33] It was installed using classical techniques, and the benzyl alcohol by-product was removed by azeotropic distillation with water (boiling point: 100°C)[34] giving **65**. Finally, oxidation under modified Anelli–Montanari conditions[35], using trichloroisocyanuric acid as the stoichiometric oxidant and a catalytic amount of 1-oxyl-2,2,6,6-tetramethylpiperidine, gave the desired aldehyde (**66**) in 91% yield as a syrup, which was used without further purification (Fig. 23).

With both parts of the target molecule in hand, we now were ready to attempt our new cyclization strategy. Aldol condensation of acetophenone **63** and aldehyde **66** was accomplished using lithium diisopropyl amide in THF at −78°C to give the β-hydroxyketone **67** after quenching the reaction with acetic acid at −78°C (Fig. 24).

Keeping the reaction temperature below −50°C was critical because higher temperatures resulted in the loss of a Cbz group to give the mono-protected enone **68**. At first glance, this would seem to be inconsequential or perhaps advantageous, but attempts to perform the cyclization on compound **68** resulted in a partially racemized product. This was related to a similar result previously observed when an attempt to cyclize the aldol product derived from a bis-benyzl protected aldehyde. We suspect the basicity of the unprotected or benzyl protected nitrogen promoted a retro-Michael reaction that resulted in racemization of the stereocenter. The postulated mechanisms for the Cbz loss and retro-Michael reaction are presented in Fig. 25.

Returning to the reaction sequence, we were delighted to find that the proposed reductive cyclization could be performed directly on β-hydroxyketone **67**. Under the conditions highlighted in Fig. 22, a one-pot sequential hydrogenolysis of both Cbz groups, dehydration, saturation, and reductive amination using hydrogen gas at 50 psi, and Pearlman's catalyst in methanol, with three equivalents of acetic acid in a Parr shaker, resulted in the diastereoselective formation of **68** as a syrup in 90% yield. The crude

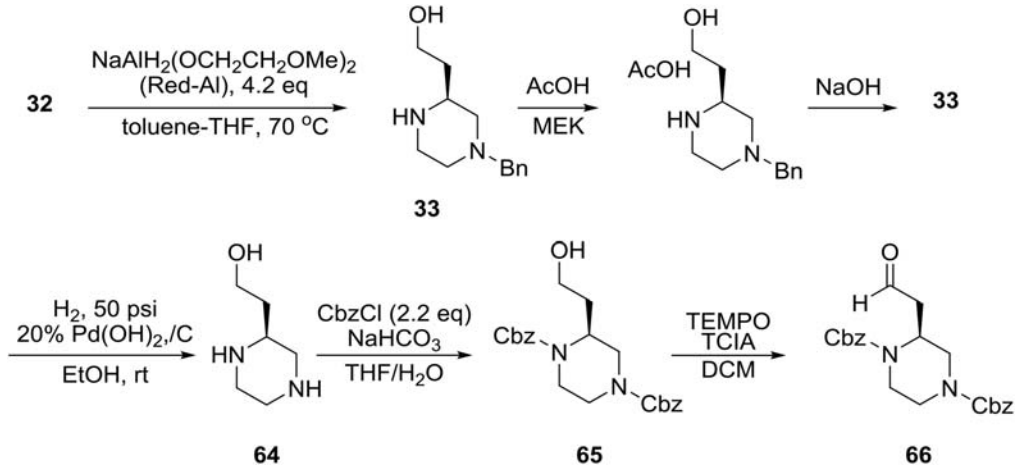

Fig. 23 Preparation of 1,4-dibenzyl (2*S*)-2-(2-oxoethyl)piperazine-1,4-dicarboxylate (**66**).

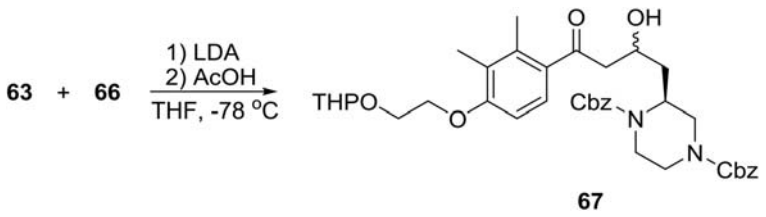

Fig. 24 Aldol reaction yielding 1,4-dibenzyl (2*S*)-2-(4-{2,3-dimethyl-4-[2-(oxan-2-yloxy)ethoxy]phenyl}-2-hydroxy-4-oxobutyl)piperazine-1,4-dicarboxylate **67**.

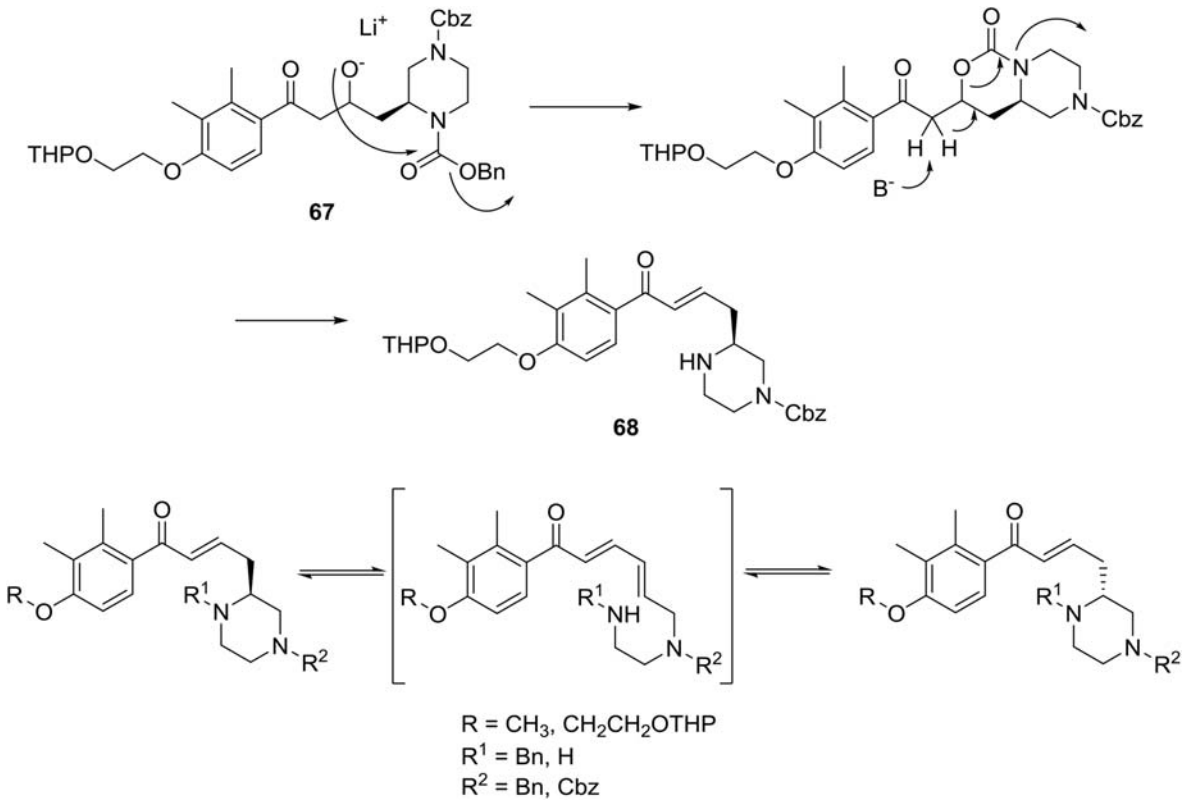

Fig. 25 Proposed mechanisms for Cbz loss above −50°C and retro-Michael reaction.

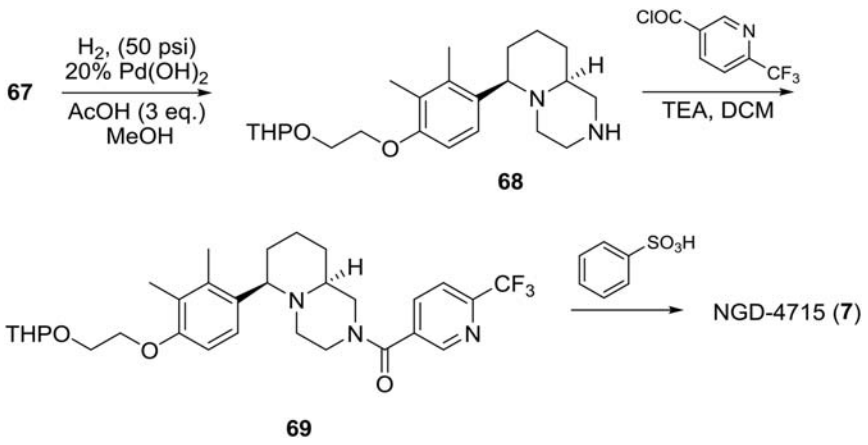

Fig. 26 Reductive cyclization, acylation, and deprotection to form NGD-4715 besylate (**7**).

material could be acylated as before, to give penultimate intermediate **69**, but the presence of diastereoisomers from the THP group made crystallization impossible, and a chromatography was required for purification. Treatment of **69** with benzene sulfonic acid removed the THP group and allowed isolation and crystallization of the desired product as the besylate salt (**7**, Fig. 26).[36]

Clearly, the requirement for a chromatography to purify the penultimate intermediate **69** was disappointing and unsatisfactory. While optimizing the reductive cyclization, we discovered a work-up that allowed us to remove the THP group and isolate the deprotected material (**70**) as a foam in 80% purity. This material then could be converted to the L-tartrate salt and crystallized to a white solid in >95% purity. The L-tartrate salt (**71**) could be used directly in the acylation step, this time using classical Schotten–Bauman conditions, to give **7**. The *iso*-propyl acetate extract then could be used directly to form the besylate salt (Fig. 27).

To summarize, this new route allowed us to prepare in-house 267 g of drug in support of a preclinical toxicology study and was transferred to a contract manufacturer to prepare 6.2 kg of cGMP quality material. NGD-4715 was obtained in 6.6% overall yield in 98.5% chemical purity and >99:1 er. The new route consisted of nine linear steps (13 total) and required no chromatography.

While this route was a significant improvement over the medicinal chemistry route, it still suffered from some deficiencies. The aldol reaction never resulted in the complete consumption of all the acetophenone **63**, and the use of cryogenic reaction conditions was less than ideal. The need for the alcohol to be protected throughout the reaction sequence also was less than desirable. We wondered if a Horner–Wadsworth–Emmons olefination might be employed to give us the reductive cyclization precursor without the requirement of a protecting group.

We were pleased to discover a facile method to prepare a phosphonate from the previously prepared 2,3-dimethyl-hydroxyethoxybenzene (**61**) by treating it with 2-(dimethoxy-phosphoryl)acetic acid in the presence of TFAA and concentrated phosphoric acid to provide ketophosphonate **72** in 66% yield for two steps with >99:1 *para*:*ortho* selectivity (Fig. 28).[37,38] Compound **72** obviated the need for a protecting group, was a crystalline solid, and was soluble in water.

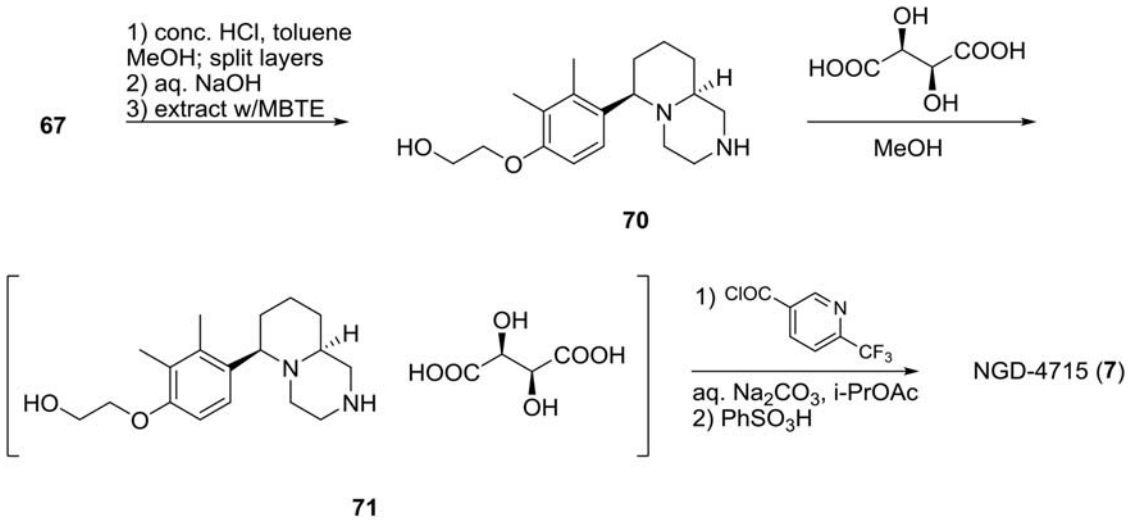

Fig. 27 Formation of crystalline penultimate tartrate **71** and preparation of NGD-4715 (**7**).

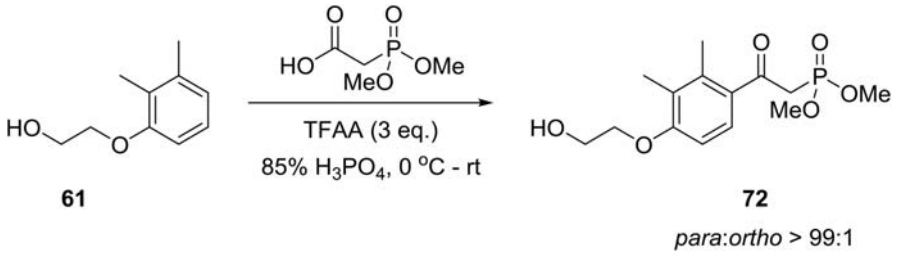

Fig. 28 Preparation of dimethyl {2-[4-(2-hydroxyethoxy)-2,3-dimethylphenyl]-2-oxoethyl}phosphonate (**72**).

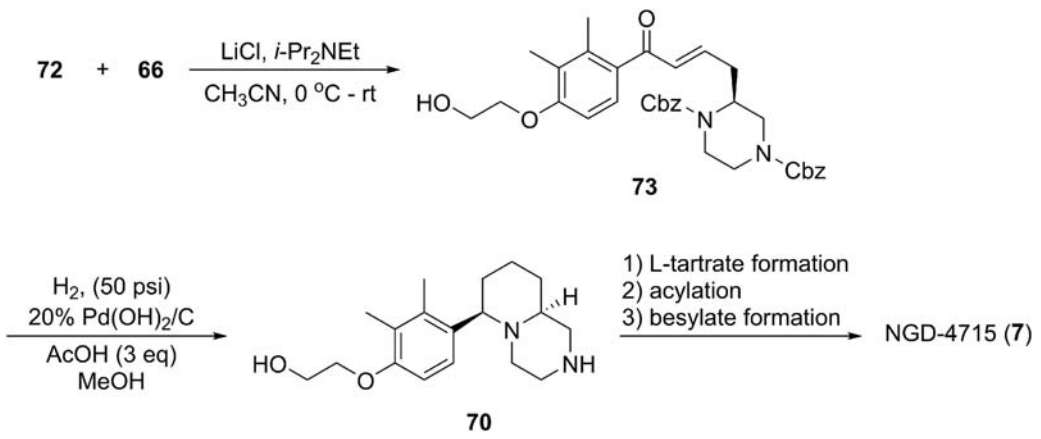

Fig. 29 Ketophosphonate route to NGD-4715 (**7**).

Reaction of ketophosphonate **72** with aldehyde **66** in the presence of lithium chloride and Hunig's base in acetonitrile provided the desired enone (**73**, Fig. 29), which could be reductively cyclized under our standard conditions to give octahydro-1*H*-pyrido [1,2-*a*]piperazine **67** in 80% yield for two steps. Purification of **67** by conversion to the L-tartrate salt proceeded as previously discussed, and this intermediate then was acylated and purified as the besylate salt to give NGD-4715 (**7**, Fig. 29).

Thus, the ketophosphonate route provided NGD-4715 after nine linear steps (11 total) with no chromatographic purifications in 17.9% overall yield. This route was used to prepare a second cGMP batch.

All batches of NGD-4715 besylate that were prepared for nonclinical and clinical use exhibited a single crystalline form, designated as "Form 1." Polymorph screening of NGD-4715 besylate was conducted in 50 solvent systems, including slurries, slow cooling, fast cooling, fast evaporation, sudden cooling, and vapor diffusion. Grinding caused the besylate to revert to an amorphous state. An X-ray crystallographic study on the crystalline besylate salt of NGD-4715 served as the ultimate structural confirmation (Fig. 30).

One last adjustment was required. LC/MS/MS analysis of a batch of NGD-4715 besylate revealed two unexpected impurities (**74** and **75**), shown in Fig. 31. Sulfate impurity **74** probably forms from reaction with sulfuric acid either contaminating the benzene sulfonic acid, or that which arises from sulfuric acid generated during the process of salt formation. Impurity **74** arises from the elimination of the sulfate to give the vinyl ether (Fig. 30). Regardless of the chemistry leading to the formation of these impurities, we thought it necessary to change the NGD-4715 salt to eliminate these impurities from the final drug product.

All batches of NGD 4715 fumarate that were prepared for nonclinical and clinical use exhibited a single crystalline form, designated as "Form 1." Polymorph screening of NGD-4715 fumarate was conducted in 55 solvent systems, including slurries, slow cooling, fast cooling, fast evaporation, sudden cooling, and vapor diffusion. The fumarate was soluble in methanol (42 mg mL^{-1}), sparingly soluble in absolute ethanol (17 mg mL^{-1}), and slightly soluble in *iso*-propanol and acetonitrile (10 mg mL^{-1} and 3 mg mL^{-1}, respectively).

The fumarate salt was formed by reaction of NGD-4715 free base with fumaric acid in *iso*-propyl alcohol followed by recrystallization from acetone and water, as shown in Fig. 32.

In conclusion, to support late-stage development and to supply drug for clinical trials, we were able to substantially improve the medicinal chemistry route to NGD-4715 by reducing the number of steps from 17 linear steps, requiring nine column chromatography purifications with an overall yield of ~9%, to a process requiring nine linear steps (11 total) with no chromatography and a 17.9% overall yield. We were able to eliminate all of the problematic reagents, develop a novel reductive cyclization protocol, and, through the development of a Horner–Wadsworth–Emmons reaction, we were able to eliminate the use of cryogens from the process. We were, thus, successful at conceiving and executing a process for preparing NGD-4715 on a multikilogram scale.

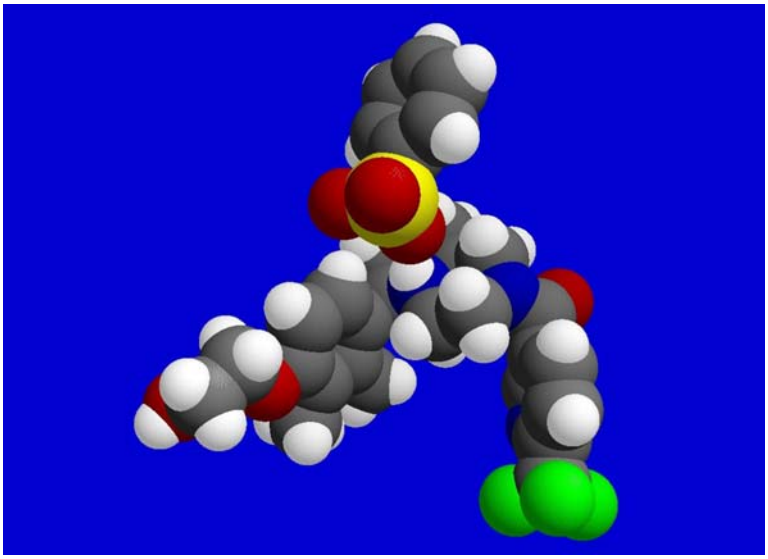

Fig. 30 A view of the crystalline structure of NGD-4715 besylate salt.

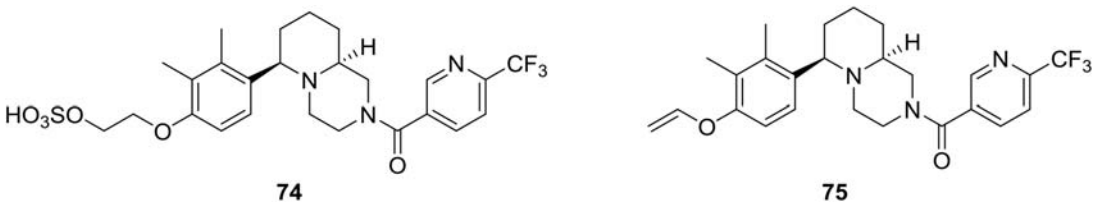

Fig. 31 Impurities found in NGD-4715 besylate.

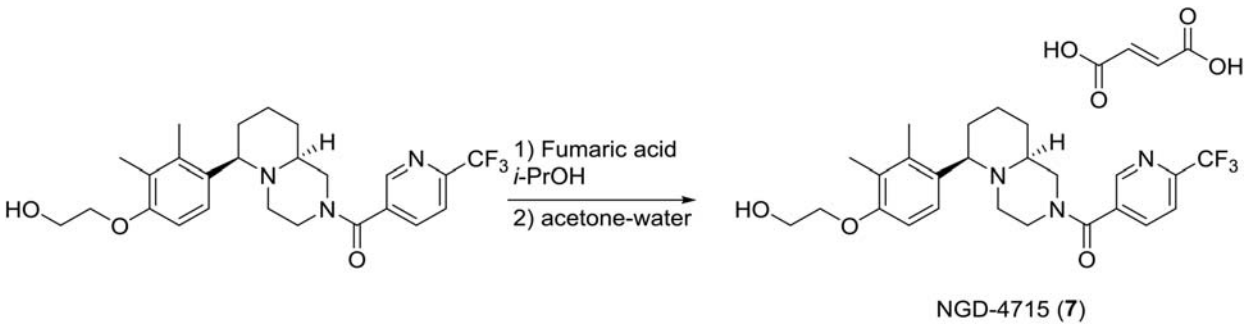

Fig. 32 Formation of NGD-4715 fumarate.

8.19.8 Seeking a Superior Backup Compound

Following the nomination of NGD-4715, the project team identified a number of properties to improve upon in a back-up compound. The properties included improved potency and elimination of CYP3A4 induction, while maintaining the other excellent properties of NGD-4715.

Previously, we demonstrated that the 6-(trifluoromethyl)pyridine-3-carboxyl amide group was a key element to controlling the hERG inhibition that plagued earlier series and competitors' compounds. Replacement of the pyridine in NGD-4715 gave the pyrimidine **76**, which was more potent and had very low hERG inhibition. Unfortunately, **76** demonstrated a similar level of CYP3A4 induction risk as NGD-4715, as measured in the pregnane X receptor (PXR) assay, and was not advanced (Fig. 33). The pyrimidine fragment of **76** was retained in the next series of analogs, as new substituents were introduced to the hydroxyethyl side-chain. This modification was of interest to block oxidation of the primary alcohol, which potentially could form a reactive aldehyde, and as a strategy to lower the clearance and increase half-life observed with NGD-4715. Small alkyl groups (e.g., Me, Et, etc.)

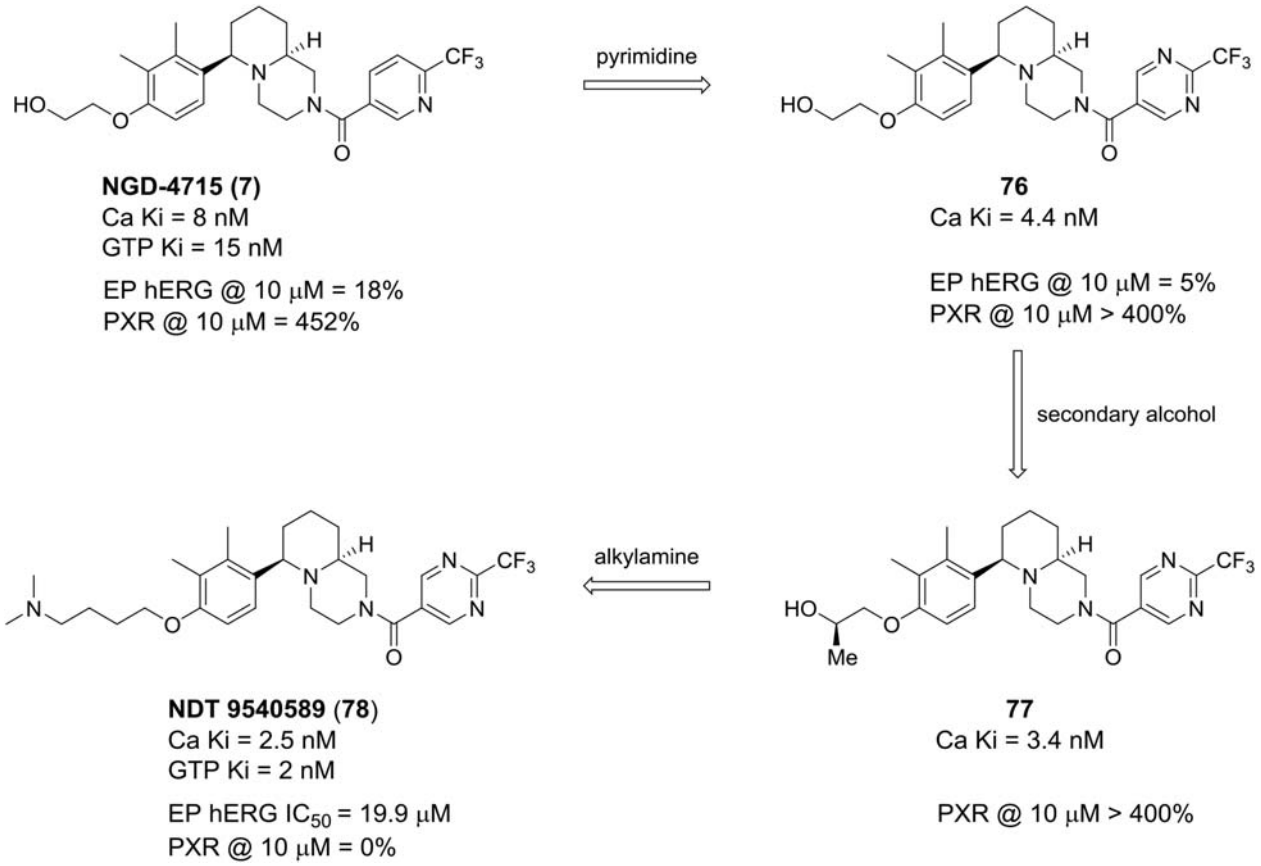

Fig. 33 Discovery of NDT 9540589 (**78**).

were tolerated on the side-chain; for example, the homo-chiral secondary alcohol **77** was of similar activity as **76**, although PXR induction was still high. The strategy that ultimately proved successful in the mitigation of CYP3A4 induction was the incorporation of a basic amine tail. The hydroxyethyl side-chain was replaced by a series of amine and amide groups. It was discovered that a basic amine tail, for example, NDT 9540589 (**78**), gave a modest boost in in vitro potency, but, most significantly, there was no induction in the PXR assay @ 10 μM, and hERG liability was moderate (EP hERG $IC_{50} = 19.9$ μM). NDT 9540589 was advanced as a strong potential back-up to NGD-4715, and it was profiled extensively both in vitro and in vivo.

Physical characteristics: NDT 9540589 (**78**) has many physical chemical characteristics that are consistent with good CNS drugs. The parent molecule has a log $D_{7.4}$ of 2.64 and good solubility (pH 7.4 > 3.0 mg mL^{-1}; pH 5.4 > 500 mg mL^{-1}). This solubility is facilitated by two basic centers with pK_a values of 9.6 and 6.3. The compound has moderate protein binding (82–85%) across species at a concentration of 3 μM. And the molecule conforms to the Rule of Five, except for a molecular weight above 500 (533).

Pharmacology: NDT 9540589 is a potent MCHR1 neutral antagonist in vitro with $IC_{50} = 4$–6 nM in calcium mobilization FLIPR-, GTPγS-, and MCHR1-binding (rat striatum) assays.[39] In an ex vivo receptor occupancy time-course assay, NDT 9540589 (10 mpk) achieved 75% of maximal receptor occupancy over a 6-h test period. An ex vivo ED_{50} was determined to be 0.7 mg kg^{-1} in a dose–response study run with a 3-h compound pretreatment. Single oral doses of compound, ranging from 2.5 to 10 mg kg^{-1}, effectively blocked the orexigenic effect of ICV-administered MCH in the rat, supporting MCH receptor antagonism as the mechanism of action. Additionally, a dose range of 1–10 mg kg^{-1} PO resulted in reduction in overnight food intake from 6% to 18% in DIO rats. Subchronic animal studies in DIO rats (10 days) demonstrated a dose-dependent reduction of food intake and body weight gain versus controls. A persistent, dose-dependent reduction of cumulative food consumption, ranging from 3.6% at 0.75 mg kg^{-1} QD to 21.1% at 10 mg kg^{-1} QD, resulted in a reduction of body weight gain ranging from 1.2% to 5.5%, respectively.

Chronic animal studies in DIO rats (26 days) demonstrated a dose-dependent reduction of food intake and body weight gain versus controls. At 5 mg kg^{-1}, there was a 22.5% reduction in cumulative food intake and a reduction in body weight gain of 9.5% (Fig. 34). Treatment also resulted in decreased blood glucose, basal plasma insulin, and leptin levels, and improvement in glucose tolerance. The reduction in food intake is believed to be mechanism-related, and not due to compound-related general malaise or sedation, since doses up to 20 mg kg^{-1} (20 times the MED) did not increase kaolin consumption or cause changes in locomotor activity.

ADME: NDT 9540589 was well absorbed across species, consistent with its excellent solubility and permeability properties. In addition, high dose PK and 10-day toxicology studies in rats suggest achieving high multiples of therapeutically efficacious plasma

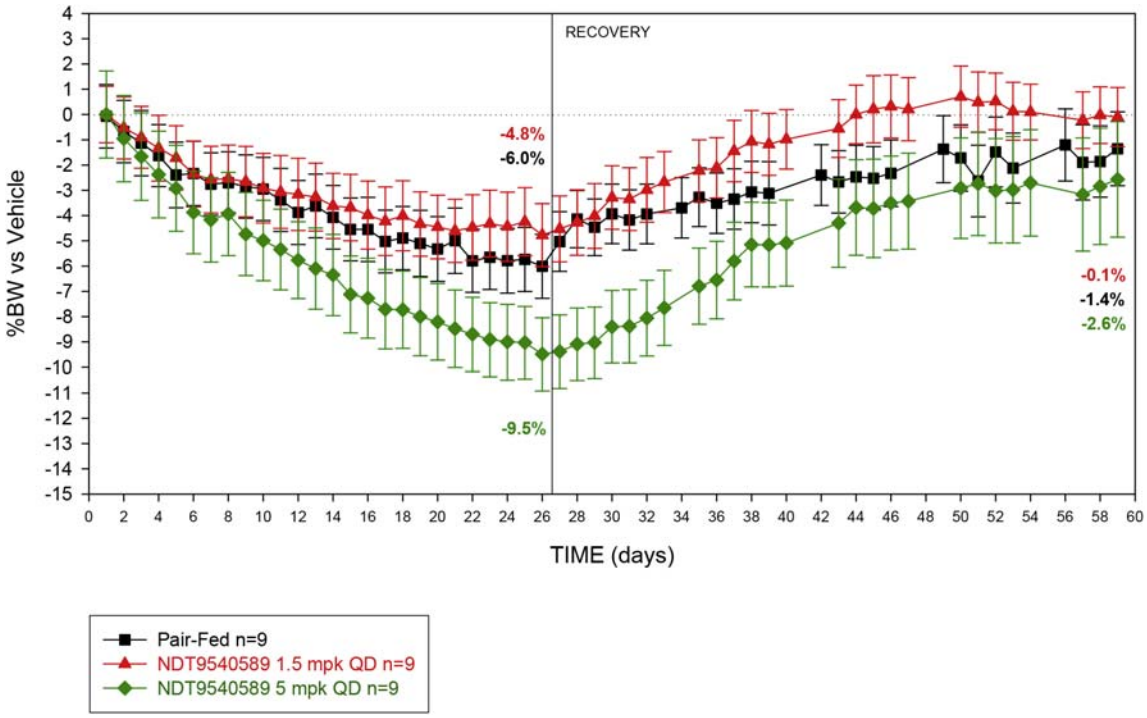

Fig. 34 Obesity-prone rat 26-day DIO study with NDT 9540589 (**78**) with recovery: percent weight loss versus vehicle. Pair-fed group was matched to the 5 mg kg^{-1} day^{-1} dose group.

Table 4 Pharmacokinetic profile of NDT 9540589 (**78**)

	Lean rat	*Obese rat*	*Dog*	*Cyno. monkey*
Dose (IV solution) (mg kg^{-1})	1	1	1	1
Half-life (h)	12	20	45	33
Clearance (mL min^{-1} kg^{-1})	59	31	9.2	17
Volume of distribution (L kg^{-1})	48	47	32	44
Dose (PO) (mg kg^{-1})	3	3	5	5
Oral bioavailability (%)	53	87	56	181[a]
C_{max} (ng mL^{-1})	50	67	111	293
P.O. AUC 0–24 h (ng h mL^{-1})	460	849	5800	4157

[a]Consistent with enterohepatic recirculation.

concentrations. Plasma protein binding appears to be moderate across species, and the compound achieved good brain penetration (B/P 1.6) in rats. NDT 9540589 appeared to have a lower potential to cause induction of CYP450 enzymes compared to NGD-4715. This was evidenced by little to no interaction with PXR, a nuclear receptor responsible for CYP induction, and CYP450 induction in a human hepatocyte assay. These results, along with weak or no CYP inhibition by the compound, suggest a low propensity for drug–drug interactions. NDT 9540589 had moderate to long half-lives, likely driven by its high volumes of distribution across species (Table 4). The predicted human half-life of NDT 9540589, based on allometric scaling, is in excess of 90 h.

NDT 9540589 has properties that favorably differentiate it from NGD-4715 in three distinct areas:

1. the compound has greater in vitro and in vivo potency in decreasing food intake and promoting weight loss compared to NGD-4715;
2. there appears to be a weight loss effect that is greater than that due to decreased food intake alone; and
3. NDT 9540589 appears to have a lower risk of causing CYP450 induction at concentrations substantially higher than the projected efficacy range.

On the basis of these improvements, it was advanced into additional preclinical safety studies.

Safety: NDT 9540589 was assessed in a hERG channel EP assay, where it had an $IC_{50} = 19.9$ μM. This is >1000-fold the IC_{50} in MCHR1 functional assays and >800 times its free efficacious plasma concentration. No changes were observed in QTc interval in a dog CV study at doses as high as 15 mg kg^{-1} IV. A transient decrease in heart rate was observed at 5 and 15 mg kg^{-1}.

In a broad panel of receptors, enzymes, hormones, and ion channels (Neuroscreen and CEREP) no significant interactions (e.g., >50% inhibition of ligand binding) were observed at 10 μM.

A key finding from the exploratory 10-day rat toxicity study was vacuoles and/or foamy macrophages in the liver, lung, and thymus at doses as low as 50 mg kg^{-1} (8–9 times plasma levels), and in the spleen at 150 mg kg^{-1} (16–18 times plasma levels). Electron microscopy study of the spleen revealed the presence of macrophages with lamellar bodies consistent with a finding of phospholipidosis (PL) (**Fig. 35**).

Phospholipidosis: has been associated with "chronic" administration of some small molecule pharmaceuticals, known as cationic amphiphilic drugs (CADs).[40] PL is described as an excessive intracellular accumulation of phospholipids in lysosomes. The accumulation is characterized by formation of lamellar membranous intralysosomal inclusion bodies (LLB) giving a "foamy appearance" in the affected tissues. PL is the result of systemic drug exposure, and can be manifest in many different cell types/tissues (e.g., hepatocytes, kidney, lung, lymphoid cells, and muscle). Some of the postulated mechanisms for induction of PL are the result of inhibition of phospholipid metabolism, inhibition of lysosomal enzyme transport, and/or increased phospholipid or cholesterol biosynthesis. Unfortunately, the pattern of cell type or tissues affected by phospholipigenic agents is not entirely predictable on the basis of structural activity relationships, and may vary according to the species, strain, and age of drug recipient. The toxicological significance of PL is not easy to interpret, as it may (or may not) interfere with cellular function in the affected tissues. It is not known whether drugs that produce PL preclinically also produce PL in humans.[41] Thus, the diagnosis of PL during compounds development raises concerns because of the difficulty in interpreting the outcome of this histopathologic finding.

On the basis of the findings with NDT 9540589, we decided our strategy moving forward would include compound design to *minimize structural elements similar to those in known PL drugs*.

CADs known to cause PL have a combination of both lipophilic and basic functional groups. Prediction of the capacity of drugs to induce PL can be performed by calculation or measurement of their cationic amphiphilic properties. Sophisticated analysis and calculation of the physicochemical interaction of amphiphilic drugs with phospholipids have been reported. Nevertheless, the easily calculated physicochemical parameters pK_a and $c\log P$ proved to be especially helpful in predicating whether a compound may have the potential to induce PL, according to Eq. (1).[42] The "rule of thumb" is that a cationic amphiphilic compound can be suspected to induce PL.

$$\text{PL risk if} (c\log P)^2 + (cpK_a)^2 > 90 \tag{1}$$

For NDT 9540589 ($c\log P = 4.0$ and $cpK_a = 9.6$) the PL risk value >108 indicates a high risk. While compounds that fall into the danger category do not necessarily cause PL, from our experience, there appears to be good correlation between this analysis, the in vitro Nile Red assay using U937 cells, and in vivo observations.

Even though the induction issue could be controlled by a basic amine tail (e.g., NDT 9540589), the basic amine also led to a large volume of distribution, long half-life, and potential for PL. We chose to eliminate any alkylamine ($pK_a > 8$) tails from molecules, and began to consider other SAR on the A-ring (**Fig. 36**). Removal of the hydroxyethyl side-chain itself gave some reduction in PXR activity (e.g., **79**), PXR = 204% @ 10 μM). On analysis of the SAR of the A-ring, it was apparent that 2,3-dimethyl-4-alkoxy substituted A-rings were predominant; indeed, >99% of all analogs in the bicyclic series contained these substituents.

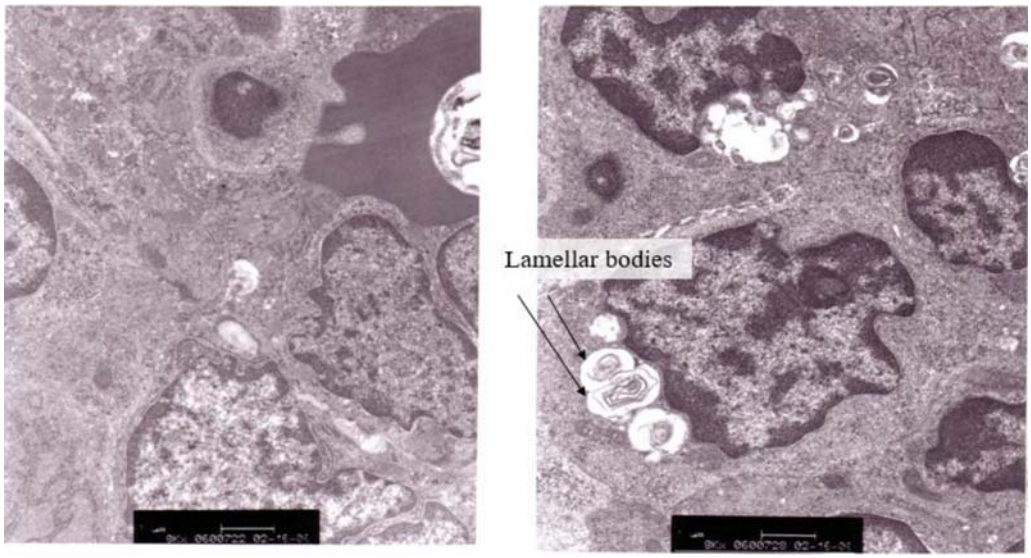

Fig. 35 Rat spleen electron microscopy studies on NDT 9540589 (**78**) confirming a phospholipidosis diagnosis. Left is control (22,400×); right is the spleen from rat following 150 mg kg^{-1} day^{-1} treatment for 10 days.

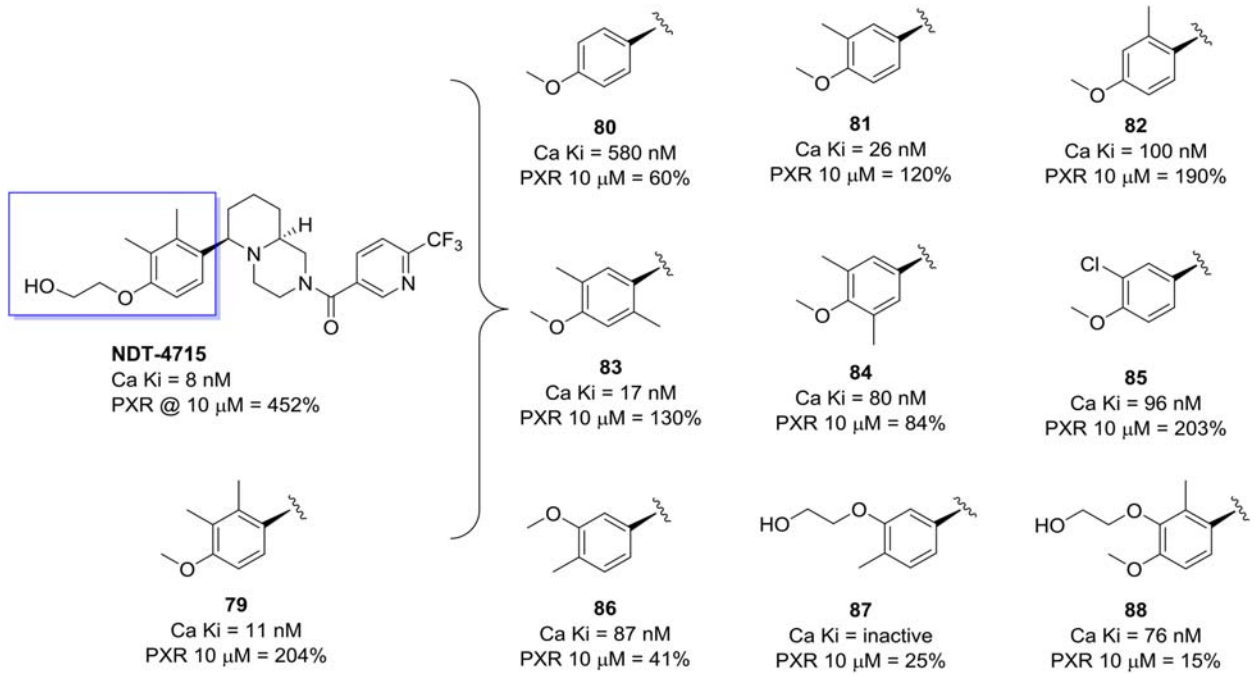

Fig. 36 MCH and PXR activity of non 2,3-dimethyl-4-alkoxy A-rings.

We then reevaluated the nine analogs without the 2,3-dimethyl-4-alkoxy A-ring. We discovered that, although MCHR1 potency generally was reduced, there were compounds with significantly lower induction potential. Deletion of both the 2- and 3-methyl groups gave a significant drop in both MCHR1 and PXR activity (e.g., **80**). Reintroduction of the 3-methyl group (e.g., **81**) restored MCHR1 potency, and there was significant lower PXR activity compared to **83**. The 2-methyl analog (e.g., **79**), however, was less active and had a similar PXR activity as **83**. The three analogs with an alkoxy substituent at the 3-position **84–86** each exhibited significantly lower PXR activity, although MCHR1 inhibition also was reduced. In general, A-rings lacking an *ortho*-substituent had lower levels of PXR induction, as did analogs incorporating a 3-alkoxy substituent.

We considered **81** and **86** to have a promising balance between MCHR1 activity and PXR induction, and that they should be viewed as starting points for the design of new analogs. We chose to incorporate the 3,4-substituents into a heterocyclic ring, and a number of indole, benzimidazole, and indazole isomers were investigated (Fig. 37).

For example, the *N*-methyl indazole (**89**) had very encouraging MCHR1 inhibition (e.g., MCHR1 Ca $K_i = 15$ nM); but of greatest significance was the ablation of PXR induction (PXR = 2% @ 10 μM) along with maintenance of low hERG inhibition (electrophysiology hERG = 6% inhibition @ 10 μM). To increase the MCHR1 inhibition, we introduced a methyl group at each of the three vacant ring positions—aware that this may bring back PXR induction. Indeed, the two *ortho*-methyl analogs (4-methyl indazole (**90**) and 6-methyl indazole (**91**)) both displayed unacceptable levels of PXR induction. However, the 7-methyl indazole (**92**) had excellent MCHR1 inhibition, and there was no induction in the PXR assay @ 10 μM. Next, **92** was evaluated further for CYP3A4 induction potential in cryopreserved cultured human hepatocytes and, gratifyingly, gave only a 0.2-fold induction over control @10 μM. Compound **92** was assessed, in a hERG channel electrophysiology assay, where it had minimal activity at 10 μM. Preliminary oral PK in rat were very encouraging (Fig. 38), and a single 10 mg kg^{-1} PO dose resulted in reduction in overnight food intake of 17% in DIO rats.

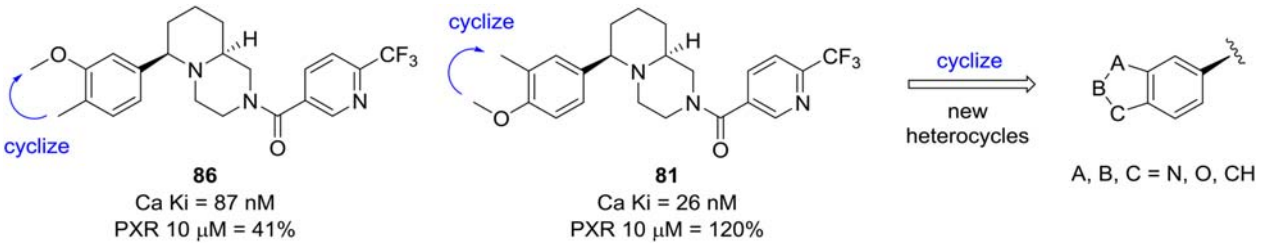

Fig. 37 Design of hetero-bicyclic A-rings.

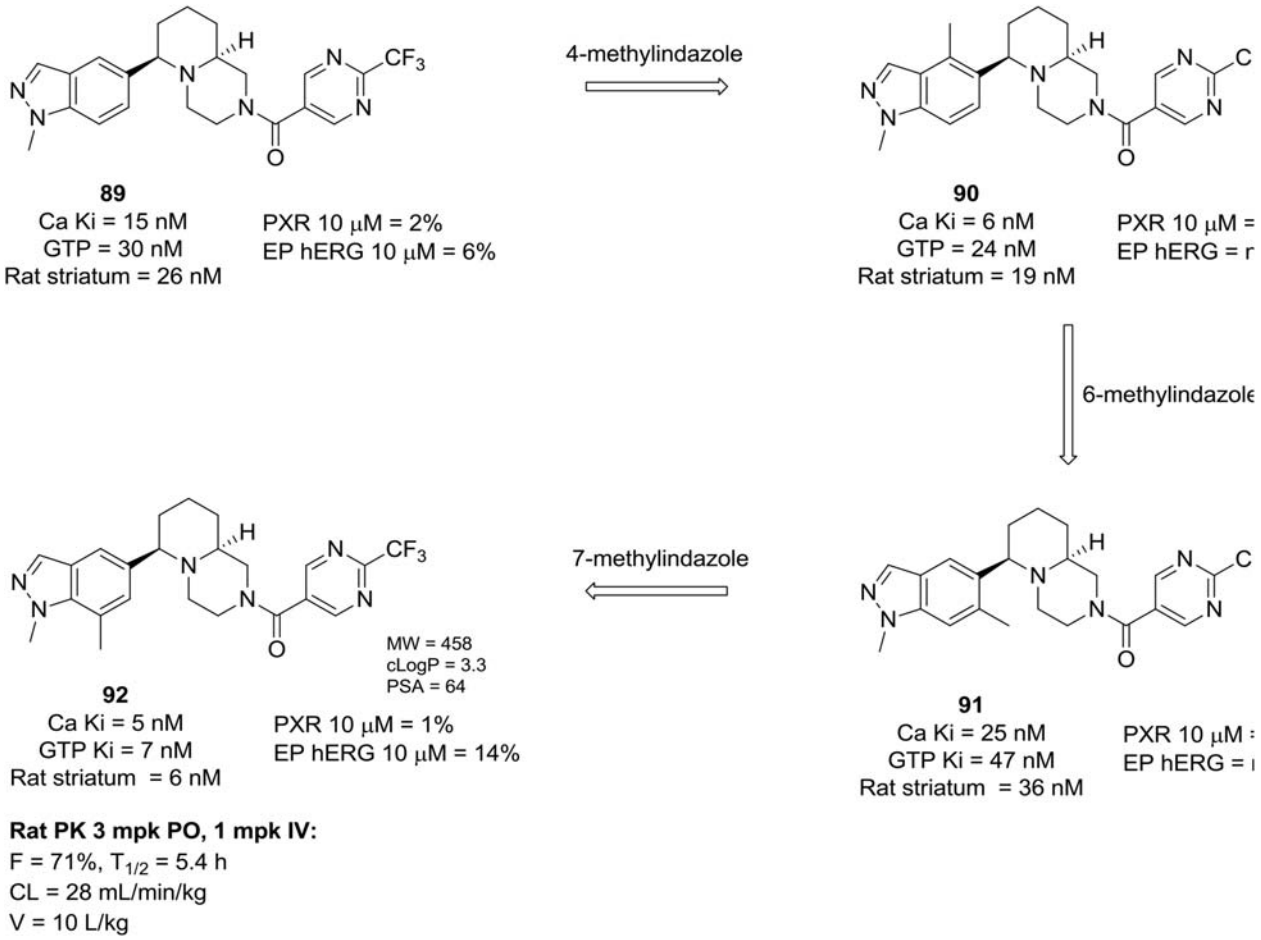

Fig. 38 Indazole A-rings and the effect of the methyl group on PXR induction.

In summary, a back-up program ran in parallel with the advanced preclinical development of NGD-4715 identified NDT 6287241 (**92**) as a development candidate with reduced risk of hepatic CYP450 induction. Compound **92** was efficient in preclinical models of obesity.

8.19.9 NDT-4715 Clinical Studies

NGD-4715, a potent and selective MCHR1 antagonist, was Neurogen's lead drug candidate for the treatment of obesity. While exploration of safety and exposure are the primary goals of phase I clinical studies, we hoped to demonstrate some evidence that blockade of MCHR1 would provide some benefit in the obese population. To achieve these ambitious goals, our approach was to first demonstrate the safety of single ascending doses (SAD) of NGD-4715. We then would progress to multiple ascending doses (MAD) in healthy obese volunteers. In addition, since NGD-4715 was thought to be a moderate inducer of CYP3A4, we included a drug–drug interaction assessment into the MAD portion of the phase I program. Thus, the goals of our phase I clinical study were:

- to evaluate the safety, tolerability, and PK of SAD of NGD-4715 administered to normal healthy volunteers (double blind, placebo controlled);
- to evaluate safety and markers of clinical pharmacology of multiple, escalating oral doses of NGD-4715 in healthy obese (BMI of 30–40 kg m^{-2}) subjects in a 2-week phase I study (double blind, placebo controlled); and
- to characterize the potential for NGD-4715 to induce CYP3A4 activity (midazolam as probe substrate).

During the SAD portion of our clinical program, we evaluated single doses of NGD-4715 from 10 to 900 mg. The compound, generally, was well-tolerated. Exposures (both as C_{max} and AUC) increased with dose, as shown in Fig. 39 and Table 5. With this encouraging data, we progressed into the MAD portion of phase I.

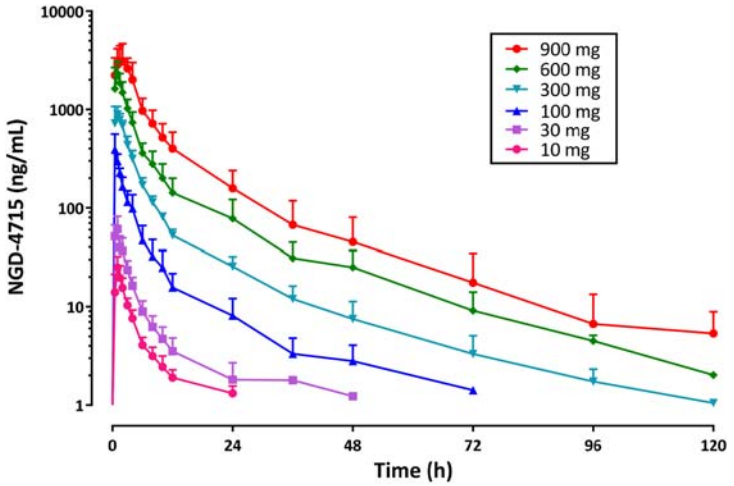

Fig. 39 Exposure-time profile of NGD-4715 in healthy human subjects.

Table 5 Human pharmacokinetic parameters for NGD-4715

		Doses (mg)					
Parameters		*10*	*30*	*100*	*300*	*600*	*900*
C_{max} (ng mL^{-1})	Mean	25.0	61.4	394	984	2484	3481
	SD	7.1	21.0	131	114	812	1318
T_{max} (h)[a]	Mean	1.0	1.0	0.8	1.0	1.0	1.5
	SD	(1–1)	(0.5–1)	(0.5–1.5)	(0.5–1.5)	(0.5–1.0)	(0.5–2.0)
AUC_{0-24} (ng h mL^{-1})	Mean	93.6	224	1289	3816	9160	19,724
	SD	29.8	66.7	358	518	2667	7420
$T_{1/2}$ (h)	Mean	7.83	10.7	15.4	18.2	18.0	16.4
	SD	3.0	3.32	4.29	1.87	2.98	3.02
CL/F (L h^{-1})	Mean	98.4	127	72.2	70.1	62.6	44.2
	SD	30.4	36.3	25.8	10.5	28.3	15.3
V_{ss}/F (L)	Mean	765	1116	746	721	674	462
	SD	42.7	183	116	112	159	85.4
AUC_{0-24}/AUC_{tot} ratio	Mean	0.853	0.887	0.862	0.879	0.862	0.878
	SD	0.026	0.052	0.054	0.037	0.037	0.046

[a]Median and range provided for T_{max}.

The MAD study was a randomized, double blind, placebo controlled investigation of NGD-4715 conducted in four cohorts ($n = 12$ per cohort, 8 drug, 4 placebo) dosed BID on a q8h schedule for 14 days. The sequential dose groups were 30, 100, 200, and 400 mg (total dose per day). Subjects were in the phase I unit for 3 weeks. Unlimited access to food was allowed during the study. Standardized body weights were collected daily prior to morning dosing. Subjects received 5 mg oral midazolam on days 1 and 16. On days 2–15 subjects received their assigned treatment q8h. The projected minimum efficacious plasma concentration was 146 ng mL^{-1}, as determined in the rat model DIO dose–response study.

Steady-state C_{max}, AUC, and C_{min} increased with dose in a less than dose-proportional manner. C_{min} achieved the target efficacious concentration (146 ng mL^{-1}) at 200 mg q8h. Mean steady-state C_{ave} at 100 mg q8h was 123 ng mL^{-1} (Fig. 40).

In terms of efficacy, all treatment groups gained weight. Overall, there was no consistent decrease in body weight gain compared to the placebo group in any of the cohorts tested. This was not surprising, given the low *n* in this study, the short study duration, and the resulting variability. However, there were several hints of efficacy based on an analysis of hormonal and metabolic and metabolic parameters. Nearly all drug treatment groups had lower concentrations of both fasting glucose and insulin compared to placebo on Day 16. NGD-4715 also showed a dose-dependent decrease in total plasma cholesterol levels and low-density lipoprotein (LDL) -cholesterol, and all drug-treated groups showed decreased triglyceride levels relative to placebo. This constellation of biochemical changes in the absence of weight loss represents a highly desirable profile that merits further study. Future experimental design of MCHR1 antagonist clinical trials should consider a standardized reduced caloric diet and exercise paradigm along with behavioral counseling, encompassing a minimum 4-week study duration and 1-week placebo run-in period.

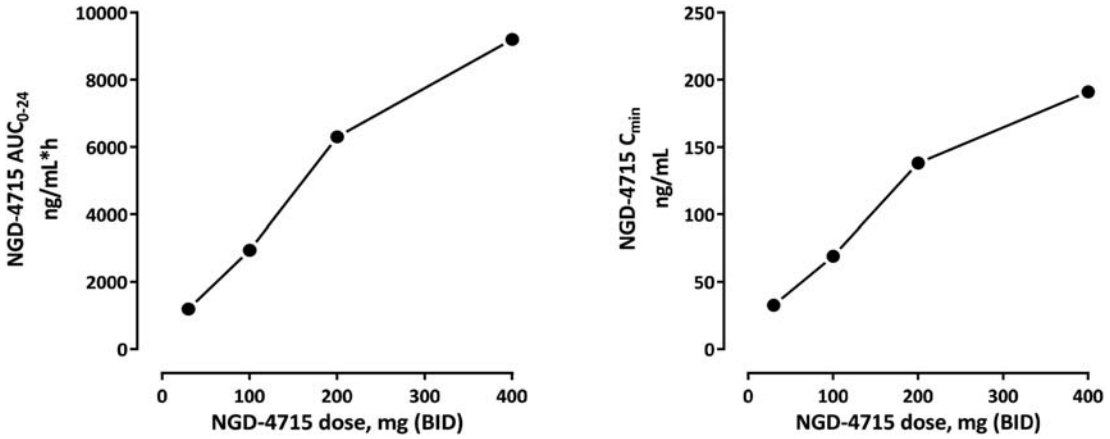

Fig. 40 Multiple ascending dose study with NGD-4715 showing target exposures were achieved at the 200 and 400 mg BID doses, and that increases were less-than-dose-proportional.

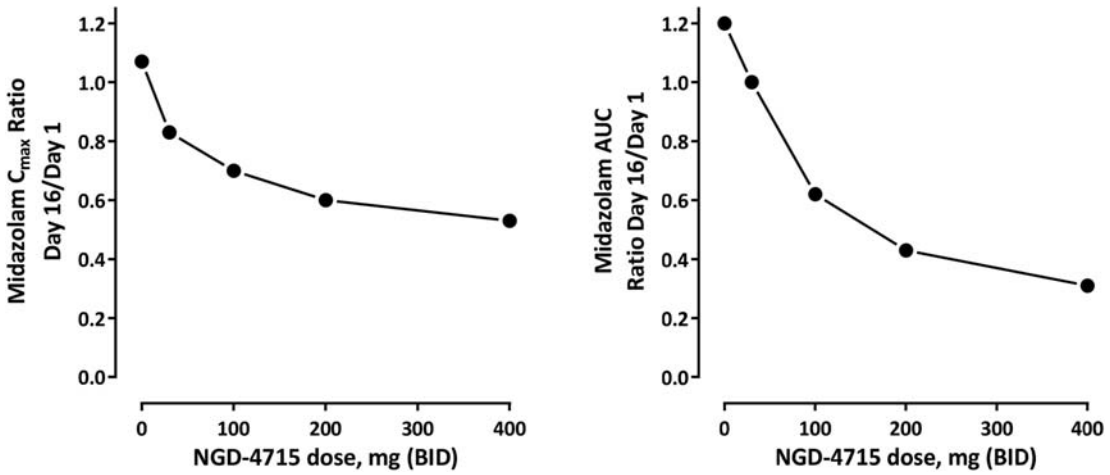

Fig. 41 Multiple ascending dose study with ND-4715 exploring the degree of CYP3A4 induction using midazolam as a substrate.

In terms of safety, unfortunately, NGD-4715 dose-dependently decreased midazolam C_{max} and AUC. The reduction in midazolam exposure was consistent with induction of CYP3A4 (Fig. 41). Thus, NGD-4715 had the potential to cause drug–drug interactions, including with drugs commonly prescribed to the obese population (statins, for example).

Otherwise, NGD-4715, generally, was safe and well-tolerated across the dose range tested. Reported adverse effects include: fatigue from midazolam dosing; GI disturbances (diarrhea, constipation, flatus, nausea); headache; and anorexia. Interestingly, in cohort 3 (200 mg q8h), four subjects reported nightmares and/or vivid dreams and feelings of anxiety, which resolved after study drug discontinuation. In cohort 4 (400 mg q8h), two subjects reported vivid dreams and/or nightmares that resolved within a day of drug discontinuation. All of the above subjects were on NGD-4715.

8.19.10 Conclusions

In summary, we describe, for the first time, the highlights of our efforts at Neurogen Corporation to investigate the potential use of MCHR1 antagonists for the treatment of metabolic diseases including obesity. We discovered an excellent tool compound (NDT 9522320) with which we conducted in vivo proof-of-concept studies both in rat (MCHR1-only species) and dog (MCHR1- and MCHR2-containing species). Encouraged by these positive results, we discovered NDT-4715 and advanced it to clinical testing. Superior compounds were delivered by a back-up program.

Acknowledgments

The authors are grateful to every one of our highly talented former colleagues for their outstanding contributions to the MCH program at Neurogen Corporation.

We thank Dr. Lin Zhi (Ligand Pharmaceuticals) for his help securing approval to publish this work.

References

1. Caterson, I. D.; Hubbard, V.; Bray, G. A.; Grunstein, R.; Hansen, B. C.; Hong, Y.; Labarthe, D.; Seidell, J. C.; Smith, S. C., Jr. Obesity, A Worldwide Epidemic Related to Heart Disease and Stoke. *Circulation* **2004,** *110,* e476–e483.
2. Ross, S. E.; Flynn, J. I.; Pate, R. R. What Is Really Causing the Obesity Epidemic? A Review of Reviews in Children and Adults. *J. Sports Sci.* **2016,** *34,* 1148–1153.
3. Bray, G. A.; Frühbeck, G.; Ryan, D. H.; Wilding, J. P. Management of Obesity. *Lancet* **2016,** *387,* 1947–1956. pii: S0140-6736(16)00271-3.
4. Nuffer, W.; Trujillo, J. M.; Megyeri, J. A Comparison of New Pharmacological Agents for the Treatment of Obesity. *Ann. Pharmacother.* **2016,** *50* (5), 376–388. pii: 1060028016634351.
5. Pissios, P.; Maratos-Flier, E. Melanin-Concentrating Hormone: From Fish Skin to Skinny Mammals. *Trends Endocrinol. Metab.* **2003,** *14,* 243–248.
6. Guyon, A.; Conductier, G.; Rovere, C.; Enfissi, A.; Nahon, J. L. Melanin-Concentrating Hormone Producing Neurons: Activities and Modulations. *Peptides* **2009,** *30,* 2031–2039.
7. Takase, K.; Kikuchi, K.; Tsuneoka, Y.; Oda, S.; Kuroda, M.; Funato, H. Meta-Analysis of Melanin-Concentrating Hormone Signaling-Deficient Mice on Behavioral and Metabolic Phenotypes. *PLoS One* **2014,** *9*, e99961. http://dx.doi.org/10.1371/journal.pone.0099961.
8. Torterolo, P.; Scorza, C.; Lagos, P.; Urbanavicius, J.; Benedetto, L.; Pascovich, C.; López-Hill, X.; Chase, M. H.; Monti, J. M. Melanin-Concentrating Hormone (MCH): Role in REM Sleep and Depression. *Front. Neurosci.* **2015,** *9,* 475.
9. Johansson, A.; Löfberg, C. Novel MCH1 Receptor Antagonists: A Patent Review. *Expert Opin. Ther. Pat.* **2015,** *25,* 193–207.
10. Andersen, D.; Storz, T.; Liu, P.; Wang, X.; Li, L.; Fan, P.; Chen, X.; Allgeier, A.; Burgos, A.; Tedrow, J.; Baum, J.; Chen, Y.; Crockett, R.; Huang, L.; Syed, R.; Larsen, R. D.; Martinelli, M. Stereoselective Synthesis of a MCHr1 Antagonist. *J. Org. Chem.* **2007,** *72,* 9648–9655.
11. Moore, N. A.; Sargent, B. J.; Guzzo, P. R.; Surman, M. D. From Preclinical to Clinical Development: The Example of a Novel Treatment for Obesity. *Neurobiol. Dis.* **2014,** *61,* 47–54.
12. Washburn, W. N.; Manfredi, M.; Devasthale, P.; Zhao, G.; Ahmad, S.; Hernandez, A.; Robl, J. A.; Wang, W.; Mignone, J.; Wang, Z.; Ngu, K.; Pelleymounter, M. A.; Longhi, D.; Zhao, R.; Wang, B.; Huang, N.; Flynn, N.; Azzara, A. V.; Barrish, J. C.; Rohrbach, K.; Devenny, J. J.; Rooney, S.; Thomas, M.; Glick, S.; Godonis, H. E.; Harvey, S. J.; Cullen, M. J.; Zhang, H.; Caporuscio, C.; Stetsko, P.; Grubb, M.; Maxwell, B. D.; Yang, H.; Apedo, A.; Gemzik, B.; Janovitz, E. B.; Huang, C.; Zhang, L.; Freeden, C.; Murphy, B. J. Identification of a Nonbasic Melanin Hormone Receptor 1 Antagonist as an Antiobesity Clinical Candidate. *J. Med. Chem.* **2014,** *57,* 7509–7522.
13. Johansson, A.; Löfberg, C.; Antonsson, M.; von Unge, S.; Hayes, M. A.; Judkins, R.; Ploj, K.; Benthem, L.; Lindén, D.; Brodin, P.; Wennerberg, M.; Fredenwall, M.; Li, L.; Persson, J.; Bergman, R.; Pettersen, A.; Gennemark, P.; Hogner, A. Discovery of (3-(4-(2-Oxa-6-azaspiro[3.3]heptan-6-ylmethyl)phenoxy)azetidin-1-yl)(5-(4-methoxyphenyl)-1,3,4-oxadiazol-2-yl)methanone (AZD1979), a Melanin Concentrating Hormone Receptor 1 (MCHr1) Antagonist With Favorable Physicochemical Properties. *J. Med. Chem.* **2016,** *59,* 2497–2511.
14. Hutchison, A.; Gustavson, L. M.; Peterson, J. M.; Doller, D.; Caldwell, T. M.; Yoon, T.; Pringle, W. C.; Bakthavatchalam, R.; Shen, Y.; Steenstra, C.; Yin, H.; DeSimone, R. W.; He, X.-S. Melanin Concentrating Hormone Receptor Ligands: Substituted 1-Benzyl-4-aryl-piperazine Analogues. US 2006/0229298.
15. Barreiro, E. J.; Kümmerle, A. E.; Fraga, C. A. The Methylation Effect in Medicinal Chemistry. *Chem. Rev.* **2011,** *111,* 5215–5246.
16. Audinot, V.; Lahaye, C.; Suply, T.; Beauverger, P.; Rodriguez, M.; Galizzi, J.-P.; Fauchère, J.-L.; Boutin, J. A. [^{125}I]-S36057: A New and Highly Potent Radioligand for the Melanin-Concentrating Hormone Receptor. *Br. J. Pharmacol.* **2001,** *133,* 371–378.
17. Kinrade, M. B.; Brodbeck, R. M.; Waters, S. M.; Krause, J. E. Monkey and Canine Melanin Concentrating Hormone Receptors. US 2003/0148457.
18. Evans, D. C.; Watt, A. P.; Nicoll-Griffith, D. A.; Baillie, T. A. Drug-Protein Adducts: An Industry Perspective on Minimizing the Potential for Drug Bioactivation in Drug Discovery and Development. *Chem. Res. Toxicol.* **2004,** *17* (1), 3–16.
19. Grimm, S. W.; Einolf, H. J.; Hall, S. D.; He, K.; Lim, H. K.; Ling, K. H.; Lu, C.; Nomeir, A. A.; Seibert, E.; Skordos, K. W.; Tonn, G. R.; Van Horn, R.; Wang, R. W.; Wong, Y. N.; Yang, T. J.; Obach, R. S. The Conduct of in vitro Studies to Address Time-Dependent Inhibition of Drug-Metabolizing Enzymes: A Perspective of the Pharmaceutical Research and Manufacturers of America. *Drug Metab. Dispos.* **2009,** *37* (7), 1355–1370.
20. Lu, H. R.; Vlaminckx, E.; Van Ammel, K.; De Clerck, F. Drug-Induced Long QT in Isolated Rabbit Purkinje Fibers: Importance of Action Potential Duration, Triangulation and Early After Depolarizations. *Eur. J. Pharmacol.* **2002,** *452* (2), 183–192.
21. Hariri, N.; Thibault, L. High-Fat Diet-Induced Obesity in Animal Models. *Nutr. Res. Rev.* **2010,** *23* (2), 270–299.
22. Krause, J. E.; Beretta, E.; Hutchinson, A.; Peterson, J.; Doller, D.; Rajachandran, L. The Effect of the Novel MCHR1 Antagonist NGX-1 on Diet Induced Obesity in Male Sprague Dawley Rats. The Endocrine Society 85th Annual Meeting—ENDO 2003, P1-247, Philadelphia, PA.
23. Vickers, S. P.; Jackson, H. C.; Cheetham, S. C. The Utility of Animal Models to Evaluate Novel Anti-Obesity Agents. *Br. J. Pharmacol.* **2011,** *164,* 1248–1262.
24. https://www.purinaveterinarydiets.com/media/1209/body_condition_chart.pdf.
25. Rajachandran, L.; Beretta, E.; Doller, D.; Brodbeck, R. M.; Kinrade, M. B.; Cheng, C. S.; Fung, L. K.; Shaw, K. R.; Cassella, J. V.; Krause, J. E. Efficacy of a Novel MCHR1 Antagonist in Preventing Weight Gain in Dog. NAASO Annual Meeting, Las Vegas, NV.
26. Guidance for Industry Developing Products for Weight Management. http://www.fda.gov/downloads/Drugs/Guidances/ucm071612.pdf.
27. Jamieson, C.; Moir, E. M.; Zoran, Z.; Wishart, G. Medicinal Chemistry of hERG Optimizations: Highlights and Hang-Ups. *J. Med. Chem.* **2006,** *49* (17), 5029–5046.
28. Hutchinson, A. J.; Chenard, B.; Li, G.; Ghosh, M.; Tarrant, J. G.; Yoon, T.; Luke, G. P.; Lee, K.; O'Donnell, M.-M.; Pringle, W. C.; Peterson, J. M.; Hodgetts, K. J.; Steenstra, C. K.; Doller, D. Aryl-Substitutes Piperazine Derivatives. WO2006/009789.
29. Cheng, Y.-C.; Prusoff, W. H. Relationship Between the Inhibition Constant (KI) and the Concentration of Inhibitor Which Causes 50 Percent Inhibition (IC_{50}) of an Enzymatic Reaction. *Biochem. Pharmacol.* **1973,** *22,* 3099–3108.
30. Cragoe, E. J., Jr.; Woltersdorf, O. W., Jr.; Gould, N. P.; Pietruszkiewicz, A. M.; Ziegler, C.; Sakurai, Y.; Stokker, G. E.; Anderson, P. S.; Bourke, R. S. Agents for the Treatment of Brain Edema. 2. [(2,3,9,9*a*-Tetrahydro-3-oxo-9*a*-substituted-1*H*-fluoren-7-yl)oxy]alkanoic Acids and Some of Their Analogs. *J. Med. Chem.* **1986,** *29,* 825–841.
31. Green, T., Wuts, P. G. M., Eds. *Protective Groups in Organic Synthesis,* 3rd ed.; John Wiley and Sons: New York, 1999; pp 49–54.
32. Swarbrick, M. E.; Gosselin, F.; Lubell, W. D. Alkyl Substituent Effects on Pipecolyl Amide Isomer Equilibrium: Efficient Methodology for Synthesizing Enantiopure 6-Alkylpipecolic Acids and Conformational Analysis of Their *N*-Acetyl *N*′-Methylamides. *J. Org. Chem.* **1999,** *64,* 1993–2002.
33. Green, T., Wuts, P. G. M., Eds. *Protective Groups in Organic Synthesis,* 3rd ed.; John Wiley and Sons: New York, 1999; pp 531–537.
34. Durkee, J. (2000). Binary Organic Azeotropes Useful for Solvent Cleaning. metalfinishing.com (retrieved 29 May 2014).
35. Anelli, P. L.; Biffi, C.; Montanari, F.; Quici, S. Fast and Selective Oxidation of Primary Alcohols to Aldehydes or to Carboxylic Acids and of Secondary Alcohols to Ketones Mediated by Oxoammonium Salts Under Two-Phase Conditions. *J. Org. Chem.* **1987,** *52,* 2559–2562.
36. A rapid salt screen indicated the benzene sulfonic acid salt of NGD-4715 possessed the best combination of crystallinity, stability, and solubility.

37. Luke, G. P.; Seekamp, C. K.; Wang, Z.-Q.; Chenard, B. L. An Efficient Preparation of β-Aryl-β-Ketophosphonates by the TFAA/H_3PO_4-Mediated Acylation of Arenes With Phosphonoacetic Acids. *J. Org. Chem.* **2008,** *73,* 6397–6400.
38. Wilkinson, M. C.; Saez, F.; Hon, W. L. Application of the Catalytic Friedel–Crafts Acylation Reaction and Regioselectivity Correlations. *Synlett* **2006,** *7,* 1063–1066.
39. Chenard, B. L.; Maynard, G. D.; Brodbeck, R. M.; Krause, J. E. G-Protein Coupled Receptor Inverse Agonists: Identification, Pharmacological Relevance and Functional Assays. *Annu. Rep. Med. Chem.* **2005,** *40,* 373–386.
40. Bernstein, P. R.; Morelli, J.; Ciaccio, P. Drug-Induced Phospholipidosis. *Annu. Rep. Med. Chem.* **2011,** *46,* 419–429.
41. Donato, M. T.; Gómez-Lechón, M. J. Drug-Induced Liver Steatosis and Phospholipidosis: Cell-Based Assays for Early Screening of Drug Candidates. *Curr. Drug Metab.* **2012,** *13,* 1160–1173.
42. Ploemen, J. P.; Kelder, J.; Hafmans, T.; van de Sandt, H.; van Burgsteden, J. A.; Saleminki, P. J.; van Esch, E. Use of Physicochemical Calculation of pK_a and *c*log *P* to Predict Phospholipidosis-Inducing Potential: A Case Study With Structurally Related Piperazines. *Exp. Toxicol. Pathol.* **2004,** *55,* 347–355.

Relevant Websites

http://www.cdc.gov/obesity/data/adult.html—Center for Disease Control (CDC) and Obesity.
http://www.cdc.gov/obesity/data/prevalence-maps.html—Obesity Prevalence Maps.
http://www.cdc.gov/obesity/resources/factsheets.html—Obesity Facts.
http://www.criver.com/about-us/eureka/blog/january-2013/models-of-obesity—Animal Models of Obesity: A Crash Course.
http://www.obesity.org/home—The Obesity Society.
https://www.purinaveterinarydiets.com/media/1209/body_condition_chart.pdf—Purina Body Condition Scoring.
http://www.renasci.co.uk/experimental/obesity—Preclinical Models of Obesity.

8.20 Case History: AN5568 (SCYX-7158)

Y-K Zhang, YR Freund, and RT Jacobs, Anacor Pharmaceuticals, Inc., Palo Alto, CA, United States

© 2017 Elsevier Ltd. All rights reserved.

8.20.1	**Introduction**	516
8.20.1.1	Background on Human African Trypanosomiasis	516
8.20.1.2	Progression of Anacor Boron Chemistry Establishing the Benzoxaborole Scaffold for AN5568 (SCYX-7158)	517
8.20.2	**Early Phenotypic Screening of Benzoxaborole Library Against *T. brucei* Parasites**	518
8.20.3	**Lead Optimization Project and Identification of AN5568 (SCYX-7158) as a Preclinical Candidate**	520
8.20.3.1	HAT Screening Cascade for the Discovery of AN5568 (SCYX-7158)	520
8.20.3.2	Early Lead Optimization: Exploration of Linker Groups	521
8.20.3.3	Lead Optimization of the Benzoxaborole-6-Carboxamides	521
8.20.4	**Preclinical Development of AN5568**	523
8.20.5	**Chemical Synthesis**	525
8.20.6	**First-in-Human Clinical Trial of AN5568**	526
8.20.7	**Successful Partnership Model Among DND*i* and Its Research Partners**	526
8.20.8	**Summary and Perspective**	527
References		527

8.20.1 Introduction

8.20.1.1 Background on Human African Trypanosomiasis

Human African trypanosomiasis (HAT), also known as African sleeping sickness, is a disease of sub-Saharan Africa caused by kinetoplastid protozoan parasites of the species *Trypanosoma brucei* and transmitted by the bite of a blood-sucking tsetse fly (*Glossina* spp.). All cases of HAT disproportionally affect the very poor, living in rural areas, and although numbers of new cases have significantly dropped in the last 5 years,[1] unreported cases in rural areas make it difficult to accurately evaluate eradication efforts.

Two main subspecies of *T. brucei* are responsible for human disease, each with distinct geographic areas of habitation and distinct pathologies. *T. b. gambiense*, which is endemic in West and Central Africa, causes a chronic disease and is responsible for 98% of the cases of HAT reported in the last decade.[2] *T. b. rhodesiense*, endemic in eastern and southern Africa, is a zoonotic disease, with animals (livestock and wildlife) as the primary reservoir, thus interruption of transmission is not likely to be feasible.[2a] It is less well adapted to humans and causes an acute and rapidly progressive disease, usually fatal within 6 months.

There are two stages of sleeping sickness, which are commonly referred to as Stage 1 and 2. The initial and acute Stage 1 involves proliferation of the parasites in the bloodstream and lymphatic system (hemolymphatic stage). Clinical symptoms are relatively nonspecific and include fever, pruritus and dermatological problems, arthralgia, enlarged lymph nodes, spleen and liver, fatigue, and headaches. In Stage 2, the meningoencephalitic stage, the parasites have migrated across the blood–brain barrier into the central nervous system (CNS) of the patient, and residence there leads to a multitude of neurological symptoms including sleep disorders, hallucinations, and coma. HAT is a fatal disease with patients progressing from neurological issues to coma, severe organ failure, and death if left untreated.[3]

In sub-Saharan Africa, 97% of all reported cases of HAT occur in only seven countries, with the Democratic Republic of the Congo (DRC) accounting for two-thirds of reported cases.[4] Numbers of cases have dropped dramatically in the last 10 years, but HAT remains a significant problem with over 3000 cases reported in 2014 in DRC.[1] Treatment options for HAT, particularly Stage 2, continue to be complex, with older treatments limited by lack of efficacy, toxicity, and resistance. The current standard of care, nifurtimox–eflornithine combination therapy (NECT) is highly efficacious and nontoxic, but is complex to administer in disease-endemic areas.

For the treatment of Stage 1 HAT where parasites are limited to the blood and lymphatic system, two very old drugs are routinely used. Pentamidine and Suramin (**Fig. 1**), both of which were developed in the early 20th century, are used to treat early stage of *T. b. gambiense* and *T. b. rhodesiense* infections, respectively, and are generally able to cure the patient. For Stage 2 HAT, until 5 years ago the only efficacious drugs are melarsoprol (**Fig. 1**), an arsenic-based derivative that has been used for over 50 years, or eflornithine (α-difluoromethylornithine, DFMO), which was initially developed in the 1970s as an anticancer drug at Merrell Dow Research Institute.[5] In the 1970s, Dr. Cyrus Bacchi at Pace University showed that DFMO cured mice infected with a virulent strain of *T. b. brucei* without any apparent toxic side effects. DFMO was shown to have activity against *T. b. gambiense*, but not *T. b. rhodiesense*, since the target of DFMO, ornithine decarboxylase has a very rapid turnover in *T. b. rhodiesense* ($t_{1/2} = 4.3$ compared to 18–19 h in *T. b. gambiense*).[6] In 1990, DFMO was approved for the treatment of *T. b. gambiense* HAT although it requires lengthy intravenous administration (four infusions per day for 14 days), which is difficult to administer in rural areas. Due to the inactivity of DFMO against *T. rhodesiense*, melarsoprol continues to be the only treatment option for Stage 2 patients

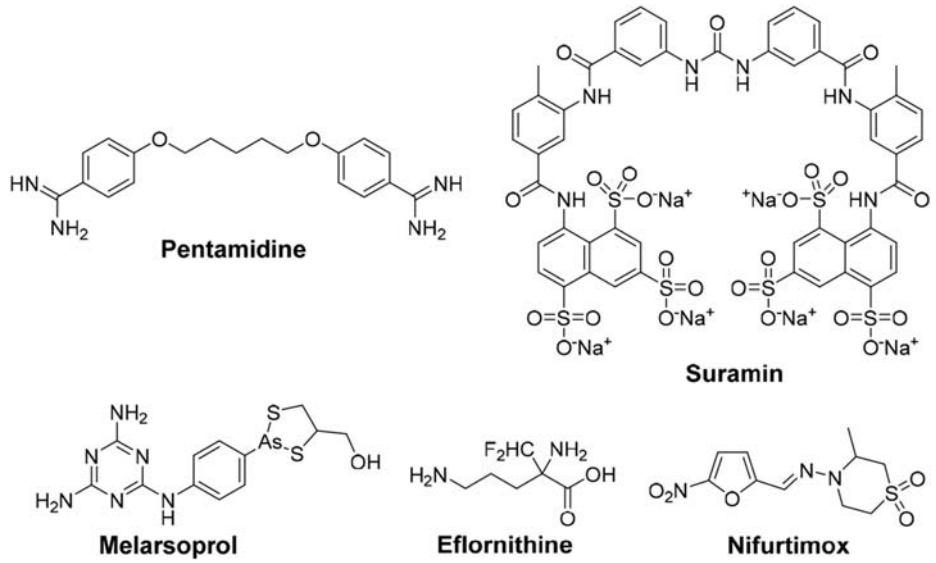

Fig. 1 Drugs approved to treat HAT.

infected with this parasite. While generally effective, melarsoprol treatment is associated with a wide range of adverse effects, the most feared being an encephalopathic syndrome which kills 3–6% of patients.[3b] In addition, treatment failures of up to 25% have been reported for melarsoprol in recent years, due to a combination of resistance to the drug and dosing limitations related to toxicity.[7]

Nifurtimox is an orally active 5-nitrofuran derivative that is used in the treatment of Chagas' disease, caused by the kinetoplastid *Trypanosoma cruzi*, a parasite that is phylogenetically close to the *T. brucei* parasites which cause HAT. In the early 2000s, a combination of eflornithine and nifurtimox (NECT) was explored by the Drugs for Neglected Diseases *initiative* (DND*i*) as an improved treatment option for Stage 2 HAT.[8] NECT was included on the World Health Organization's "Essential Medicines List" in May 2009 and has quickly become the standard of care for the treatment of Stage 2 disease caused by *T. gambiense*.[1,9] This treatment is as effective as melarsoprol, has an improved safety profile, and is easier to administer than eflornithine alone. The NECT protocol consists of an abbreviated course of intravenous eflornithine (two infusions per day for 7 days) accompanied by 10 days of oral nifurtimox (three times daily). The decrease in infusion frequency and duration significantly decreases the burden on health-care providers, reduces the risk of infections for patients in resource-poor settings, and reduces the cost of treatment by 50%.[1,9] This cost reduction is an important factor, as all NECT therapy used for the treatment of HAT is donated by the manufacturers, Sanofi–Aventis and Bayer Schering Pharma AG. Although the NECT therapy is a great improvement, it remains challenging to implement in disease-endemic areas and is not efficacious against *T. b. rhodesiense* HAT.[9] Consequently, there is still an urgent need to discover and develop novel and safe orally active drugs to treat patients with HAT.

8.20.1.2 Progression of Anacor Boron Chemistry Establishing the Benzoxaborole Scaffold for AN5568 (SCYX-7158)

Anacor Pharmaceuticals, Inc. was established in 2002 as a biopharmaceutical company focused on discovering, developing, and commercializing novel small-molecule therapeutics derived from its boron chemistry platform. The primary therapeutic areas that Anacor has focused efforts on include, but are not limited to, inflammatory diseases of the skin such as atopic dermatitis and psoriasis, and infectious diseases caused by bacteria, fungi, viruses, and parasites. In the early days of the company when there were about 15 full-time employees, with tangible excitement and energy surrounding the research projects; there was a weekly, company-wide research meeting chaired by David Perry, then CEO of the company. With tight timelines and a limited research budget, the entire group met to discuss research results, review chemistry strategy, plan next studies, and prioritize resources. The meeting itself was a setting where researchers were challenged with excellent, difficult questions about both the scientific and business aspects of the proposed studies and strategies. The chemistry group was small, and all of the chemists in the group were actively working in the laboratory, synthesizing new boron-containing molecules. In addition to identifying antibacterial and antifungal compounds, it was important that these molecules exhibited attractive chemical stability and pharmacokinetic properties. In 2004, chemists were working on compounds belonging to a B-aryl cyclic borinic ester scaffold, that is depicted in **Fig. 2**.[10] While most substitution patterns on the B-aryl substituent, including 2,6-dialkyl-substituted analogs (**2**) were synthesized without any difficulty, Yong-Kang Zhang observed that during attempted preparation of the 2,6-dimethoxy analog **3** the chromatographic behavior of the product of this reaction was very different from other analogs. Specifically, the new product was much more polar than anticipated. Curious about the apparent failure of the reaction to prepare **3**, he isolated the more polar compound, and characterized it by ^{1}H NMR and LC-MS. These analytical data were consistent with the benzoxaborole structure **4**, which is much more

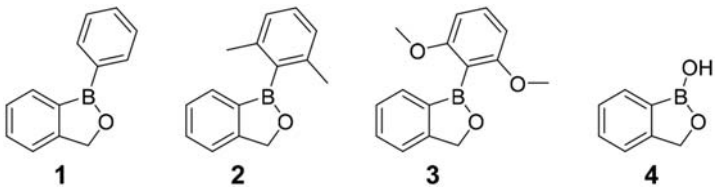

Fig. 2 Structures of three cyclic borinic esters (**1**, **2**, and **3**) and a benzoxaborole (**4**).

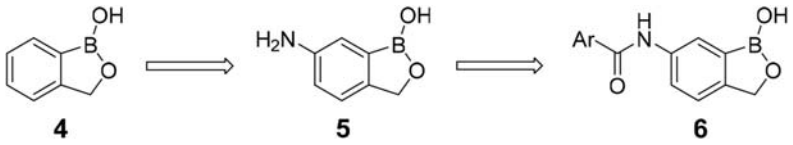

Fig. 3 Structures of small-molecule benzoxaboroles.

polar than the expected product, as TLC analysis had indicated. Considering compound **4** was structurally very different from compounds **1** and **2**, it was submitted to the Anacor library for immediate antifungal testing. As this molecule demonstrated good antifungal activity,[10,11] the chemistry team's focus was expanded to include analogs of this new scaffold.

As part of this effort, the 6-amino analog (**5**) was synthesized by Vincent Hernandez in 2006 (Fig. 3). He demonstrated that the 6-amino group could be further elaborated using traditional methods to make amides, sulfonamides, and ureas. The team recognized the opportunity afforded to generate structurally diverse benzoxaboroles based on these chemistries. With the close involvement of other chemistry team members including Jacob Plattner, Steven Baker, and Tsutomu Akama, Yong-Kang Zhang designed a focused library of 6-carboxamides (**6**) and managed the execution of chemical syntheses in a contract research organization. This focused compound library was later used for screening against a variety of parasites and provided a chemistry foundation for the subsequent discovery of AN5568 (SCYX-7158).[12]

8.20.2 Early Phenotypic Screening of Benzoxaborole Library Against *T. brucei* Parasites

In the early years of Anacor's development, we were interested in exploring all potential activities of the Anacor boron-containing small-molecule library. Some preliminary work to explore the effects of early scaffolds on several parasitic species was initiated with Dr. Reto Brun at the Swiss Tropical Institute (STI) in Basel (now Swiss TPH). Although ~100 compounds were screened in vitro against various parasites, and a few were taken into in vivo efficacy models. These compounds were from early scaffolds such as quinolones, picolinates, and cyclic borinic esters which were deprioritized once the oxaborole scaffold became the primary focus of the chemistry effort. In late 2004, in order to explore the antiparasitic potential of the oxaborole and cyclic borinic esters in the library, Yvonne Freund contacted Drs. Phillip Rosenthal and James McKerrow at the University of California, San Francisco (UCSF) (Fig. 4).

Both had screening capacity and agreed to screen samples from the Anacor library free of charge. Oxaboroles were screened in phenotypic screens against *Plasmodium falciparum* in the Rosenthal laboratory and against *T. cruzi* (Chagas' disease) and *T. brucei* (HAT) in the McKerrow laboratory. Compounds which had been screened at STI and had interest were rescreened at UCSF. Initial screening against *T. brucei* consisted of measuring percent inhibition of parasite growth in triplicate at 1 μM concentrations. From these phenotypic screens, a group of 6-position-linked thioethers (**7**), sulfoxides (**8**), and sulfones (**9**) (Fig. 5) emerged that inhibited *T. b. brucei* growth between 95% and 99% at 1 μM.

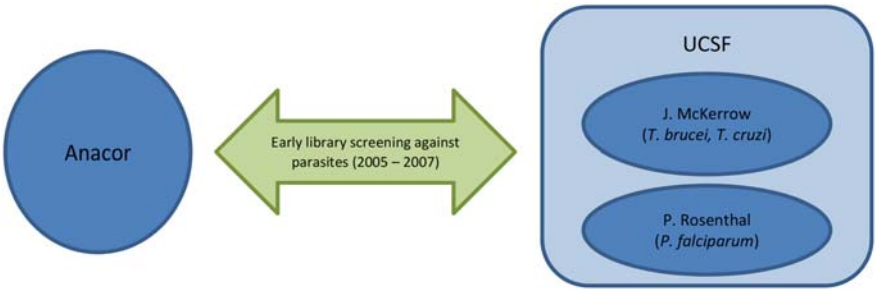

Fig. 4 Initial screening of the Anacor Library at UCSF.

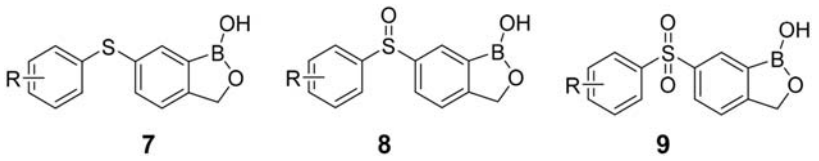

Fig. 5 Screening hits.

Follow-up screening of these analogs, including generation of dose–response data, identified the 4-chlorophenyl sulfoxide benzoxaborole AN2920 as the first lead for inhibition of *T. brucei* growth ($IC_{50} = 1.2$ μg mL^{-1}, 410 nM).[13] Early data for AN2920 suggested it to have acceptable safety, as demonstrated in a 5-day CD-1 mouse study when dosed orally, once daily at 50 and 150 mg kg^{-1}. No gross clinical observations, hematological or clinical chemistry abnormalities were noted with these treatment regimens. When dosed orally once daily at 500 mg $kg^{-1} \times 5$ days, some toxicity was noted, as only 66% survival was observed. Pharmacokinetic parameters were measured in male Sprague-Dawley rats using an IV dose of 25 mg kg^{-1} and oral dose of 100 mg kg^{-1}. Oral bioavailability of 31%, a low volume of distribution (416 mL kg^{-1}) and a $t_{1/2}$ of 1.2 h supported progression to a murine in vivo efficacy model. AN2920 was tested in a murine model of acute *T. b. brucei* infection at 100 mg $kg^{-1} \times 5$ days by intraperitoneal (ip) injection at UCSF and later at 50 mg kg^{-1} BID, ip × 5 days at Pace University.[13,14] In these early days the ip route was used, based on the assumption that this would provide a greater exposure than the oral route, although these experiments were later repeated using oral dosing. Plasma exposure was not measured; however, treatment with 50 mg kg^{-1} resulted in 100% survival and no parasitemia 40 days postinfection. In 2007, with AN2920 and related compounds showing interesting in vitro and in vivo potency, Jake Plattner approached the DND*i* about a potential collaboration to further explore oxaboroles for the treatment of HAT. In December of this year a contract was established between Anacor and DND*i* for this purpose, that provided Anacor with access to the contract research organization Scynexis (Research Triangle Park, North Carolina) for medicinal chemistry, biological screening, and pharmacokinetics (PK) services (Fig. 6).

The first meeting of the DND*i*–Anacor–Scynexis consortium took place on Mar. 14, 2008. Robert Don and Denis Martin attended from DND*i*; Jacob Plattner, Yvonne Freund, Huchen Zhou, and Tsutomu Akama from Anacor; and Robert Jacobs, Bakela Nare, Matthew Orr, Joe Perales, Daitao Chen, and Steven Wring from Scynexis. At this meeting, it was agreed that a set of ~50 compounds would be provided to the Scynexis team for evaluation in the biological and PK assays run in Research Triangle Park, North Carolina. In addition, it was agreed at this meeting that a small number of compounds that exhibited good activity and PK would be evaluated for in vivo efficacy in an acute, blood stage *T. brucei* model that was run at Pace University under the direction of Drs. Cyrus Bacchi and Nigel Yarlett. At Scynexis, Robert Jacobs was the HAT program and medicinal chemistry team leader. Steve Wring was in charge of the PK efforts and Bakela Nare led the activity for the in vitro screening and biology for the project. The final component of the multinational consortium incorporated the expertise of Reto Brun, Marcel Kaiser, and colleagues at the Swiss Tropical and Public Health Institute, and provided the team with access to a broad array of *T. brucei* strains, including *T. b. rhodiense* and *T. b. gambiense* isolates which could be used to test compounds in both in vitro and in vivo assays.

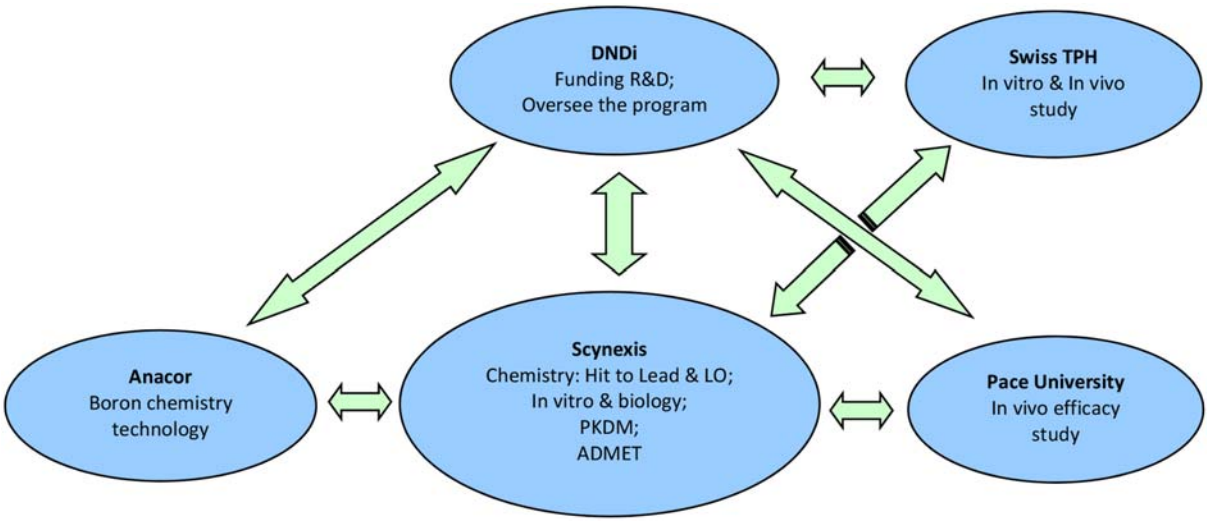

Fig. 6 Consortium structure 2008 to present.

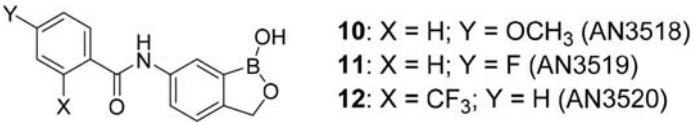

Fig. 7 Structures of benzoxaborole-6-carboxamides which exhibited in vivo activity.

Table 1 Comparison of in vivo efficacies of early leads **AN2920** and **AN3520** in an acute HAT mouse model

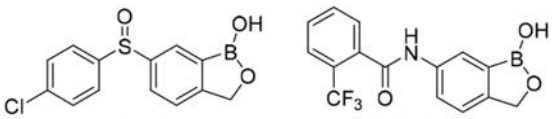

Compound	*Parasites used to infect mice*	*Treatment and dose*	*Result*
AN2920[a]	600 *T. b. brucei*, EATRO 221 strain	50 mg kg^{-1}, b.i.d., ×5 days, *i.p.*	100% cured, 40 days
	10^4 *T. b. rhodesiense*, strain IL1852	Same as above	100% cured, 60 days
	T. b. brucei, EATRO 110 strain	20 mg kg^{-1}, *i.p.*; or 20 mg kg^{-1}, *p.o.*	Effective (*i.p.*); not effective (*p.o.*)
AN3520[b]	2×10^5 *T. b. brucei*, EATRO 110 strain	50 mg kg^{-1}, single dose, 24 h or 48 h postinfection, *i.p.*	Both 100% cured
	2×10^5 *T. b. brucei*, EATRO 110 strain	5 mg kg^{-1}, b.i.d., ×4 days, *p.o.*	100% cured, >30 days
	2×10^5 *T. b. brucei*, EATRO 110 strain	10 mg kg^{-1}, b.i.d., ×4 days, *p.o.*	67% cured (2/3)[c]

[a]Compound **AN2920** efficacy data from Ref. 13.
[b]Compound **AN3520** efficacy data from Ref. 14.
[c]No evidence of compound-related toxicity was found.

The lead 4-chlorophenylsulfoxide benzoxaborole, AN2920, which originated from the McKerrow screening was tested in the mouse model of blood stage *T. brucei* infection at Pace University, as mentioned above. As AN2920 has been tested at UCSF at 100 mg kg^{-1}, b.i.d. ×5 days, the initial assay at Pace was conducted at 50 mg kg^{-1}, b.i.d, for 5 days using the *T. b. brucei* EATRO221 strain. This assay confirmed the previous work, as this dosing paradigm resulted in 100% survival with no detectable parasitemia 40 days after infection, but 20 mg kg^{-1}, b.i.d. for 5 days was not effective, with only 33% survival (at 40 days) observed following ip administration. Treatment of *T. b. rhodesiense* (strain IL18152, 104 parasites)-infected mice at the same dose and route also cleared parasites 60 days after infection.[13] AN2920 was also tested in the *T. b. brucei* EATRO221 assay at Pace at 20 mg kg^{-1}, b.i.d. for 5 days by the oral route, where it was found not to be effective. In these early in vivo efficacy studies at Pace University, a number of other substituted benzoxaboroles, including several 6-carboxamides (**10–12**, Fig. 7), were also evaluated.[13,14]

These studies demonstrated that the 6-carboxamides, and in particular the 2-trifluoromethylbenzamide AN3520, were efficacious following oral administration at doses as low at 5 mg kg^{-1}, b.i.d. for 4 days. The in vivo activities of AN2920 and AN3520 are summarized in Table 1.

8.20.3 Lead Optimization Project and Identification of AN5568 (SCYX-7158) as a Preclinical Candidate

8.20.3.1 HAT Screening Cascade for the Discovery of AN5568 (SCYX-7158)

With these initial results and organizational structure established, the project team initiated a lead optimization program focused on improvement of the benzoxaborole 6-carboxamides with the following specific objectives: (1) improve or maintain the in vitro potency of compounds, (2) improve or maintain the low cytotoxicity of compounds, (3) improve the pharmacokinetic behavior of compounds following oral dosing, (4) demonstrate that compounds in this class could achieve penetration into the CNS, and (5) demonstrate efficacy in models of both Stage 1 and 2 HAT. In order to achieve these goals, a screening cascade was established and is shown in Fig. 8. Compounds from existing libraries or newly synthesized by HAT program chemists were screened in a *T. b. brucei* whole cell assay. Concurrently, in vitro cytotoxicity was evaluated in L929 mouse fibroblasts.[14] Compounds which exhibited good antiparasitic activity ($IC_{50} \leq 1$ μg mL^{-1}) and low cytotoxicity were progressed to a range of in vitro absorption, distribution, metabolism and excretion (ADME) and physicochemical property assays designed to be predictive of potential for good oral pharmacokinetic behavior. Compounds meeting the criteria established for these assays were then progressed to in vivo PK experiments and the Stage 1 HAT mouse model. As experience was gained in the series, evaluation of brain exposure in mice was included as part of the initial PK experiments. Compounds which exhibited good plasma and brain exposure, and were active at doses <10 mg kg^{-1} in the Stage 1 HAT mouse model were progressed to the long duration (180 day)

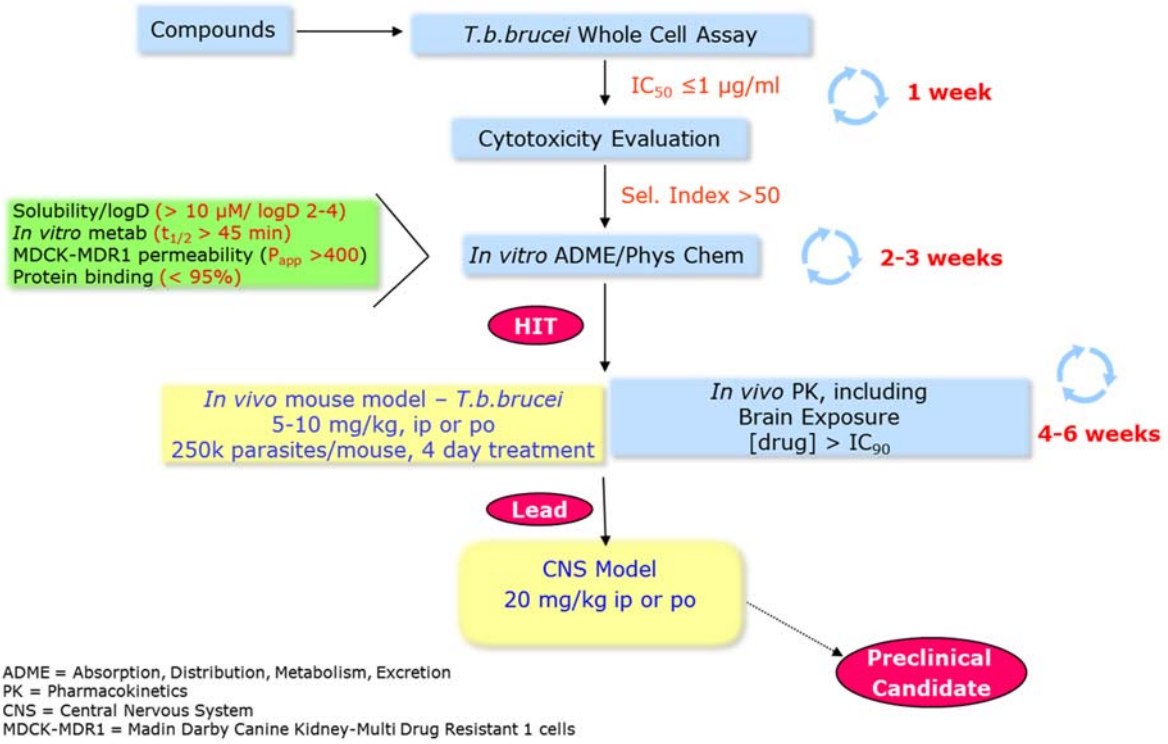

Fig. 8 Screening cascade of the HAT program related to AN5568 (SCYX-7158) discovery.

Stage 2 HAT mouse model. Throughout the program, compounds which represented significant advances in structure-activity relationship (SAR) understanding were also evaluated for a spectrum of activity in other *T. brucei* strains available at both Pace University and STPH.

8.20.3.2 Early Lead Optimization: Exploration of Linker Groups

Given the attractive in vitro profiles (Table 2) of the three carboxamides as shown in Fig. 7, one initial focus of the team was to examine alternative linkers between the benzoxaborole core and the pendant aryl ring including linkers with one, two, or three atoms as summarized in Fig. 9 and Table 3.[13,15]

In addition to the sulfide (**7**), sulfoxide (**8**), sulfone (**9**), and amide (**18**) linkers that were already identified, the ketone (**15**), sulfonamide (**19**), and urea (**24**) groups were found to have good in vitro potency. Synthetic tractability rendered the ketone series less attractive, and in vitro ADME profiling of the sulfonamides and ureas suggested these series would be challenged by permeability, particularly into the CNS. Consequently, the project further refined the chemistry focus to the benzoxaborole 6-carboxamides.

8.20.3.3 Lead Optimization of the Benzoxaborole-6-Carboxamides

The lead optimization chemistry strategy for the benzoxaborole 6-carboxamides was to systematically modify substituents in the amide region and on the benzoxaborole core to improve PK and in vivo efficacy in HAT Stage 2 mouse model (CNS model)[14]

Table 2 Profiles of benzoxaborole 6-carboxamides **10–12**[a]

Compound	T. b. brucei *IC50 (nM)*	*L929 cytotox IC50 (μM)*	*Clint mouse microsomes (μL min^{-1} mg^{-1})*	*Solubility (pH 7.4 PBS, μM)*	*logD*	*Papp (nm s^{-1})*	*Papp + 918 (nm s^{-1})*
10	70	>35	18	>200	2.21	643	647
11	260	>35	17	>200	2.27	625	647
12	120	11.7	2	>200	2.25	471	464

[a]For descriptions of assays summarized in this table, see Ref. 14.

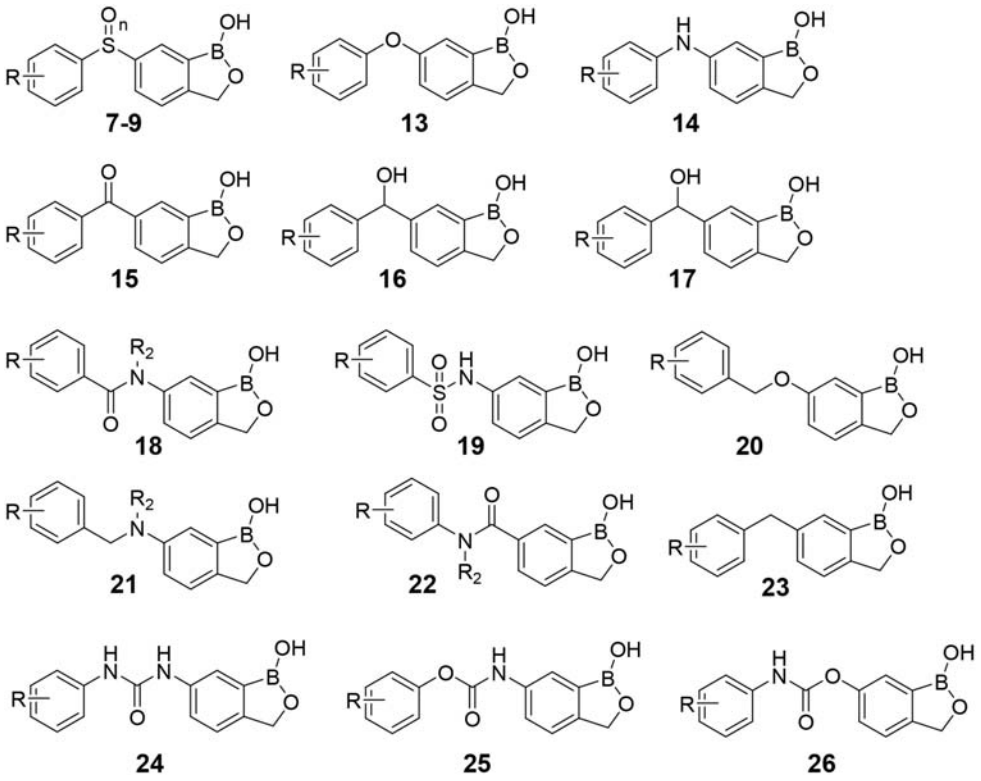

Fig. 9 Linkers explored related to the benzoxaborole-6-carboxamides.

following oral dosing. More specifically, we examined a multitude of substituents on the benzamide ring, substituents at C(3), C(5), and C(7) of the benzoxaborole core.[16] While SAR of the benzamide ring substituents was relatively flat in terms of in vitro potency, we quickly found that addition of a fluorine substituent to C(4′) (Fig. 10) provided a significant improvement in metabolic stability that was reflected in improved plasma and brain exposure following oral dosing. This compound, designated AN4169 (SCYX-6759) exhibited PK and efficacy in the Stage 1 mouse model that viewed as sufficient to warrant evaluation of this compound in the Stage 2 mouse model. In these initial experiments AN3520 was included as well, and it was found to cure 7/9 infected mice when administered intraperitoneally (*ip*) at a dose of 50 mg kg^{-1} twice daily for 14 days (Table 4). AN4169 was able to cure 10/10 infected animals with *ip* administration, and cured 5/6 mice when dosed orally at 50 mg kg^{-1}, BID for 7 days. Lower doses (25, 12.5, or 6 mg kg^{-1}, BID × 7 days) of AN4169 were not effective in the Stage 2 mouse model.[14]

The most significant improvement in the development of the benzoxaborole 6-carboxamide series was when substituents were introduced at the C(3) position of the benzoxaborole ring. Introduction of a single methyl group at C(3) on the 4-fluoro-2-trifluoromethyl benzamide of AN4169 provided (as a racemic mixture) a compound (AN5344) that was essentially equipotent with AN4169, but was significantly more cytotoxic to mouse L929 cells. Interestingly, when the individual enantiomers were prepared, both activities (antitrypanosomal and cytotoxicity) were found to be expressed in the (R) enantiomer, but the (S) enantiomer retained only the antitrypanosomal activity, albeit at a slightly reduced potency. Introduction of larger C(3) substituents (e.g., isobutyl and cyclopentyl) resulted in loss of potency.[16]

This SAR prompted us to prepare several 3,3-disubstituted analogs, and in particular the 3,3-dimethyl analogs. We were pleased to find that the 3,3-dimethyl analogs were only of slightly reduced potency, but this loss of in vitro potency was compensated for by a substantial improvement in PK properties. Of greatest interest was the observation that exposures in the brains of mice increased substantially both in terms of C_{max} and duration of exposure. Of several compounds profiled in the 3,3-dimethyl series, the direct analog of AN4169, AN5568 (SCYX-7158, Fig. 11) stood out as having the best balance of in vitro potency, lack of cytotoxicity, in vitro ADME, and in vivo PK. We initially hypothesized that the improvements in in vivo PK were due to decreased affinity of AN5568 to one or more transporters in the blood–brain barrier as a result of the increased steric bulk around the benzoxaborole core. Data obtained later in the program suggested that a more likely explanation for this behavior was due to different protein binding properties for AN5568 between plasma and brain proteins.[18] We were quite happy to find, therefore, that these properties translated into significantly improved efficacy in both the Stage 1 and 2 mouse models of HAT, with AN5568 exhibiting 100% cure in the Stage 2 model after oral dosing at 25 mg kg^{-1}, qd for 7 days and 80% cure at a dose of 12.5 mg kg^{-1}, qd for 7 days (Table 5). Other 3,3-dimethyl analogs showed similar efficacy, but none surpassed AN5568.

Table 3 Effect of linkage group "L" on *T. brucei* growth inhibition and cytotoxicity[13]

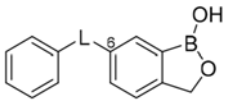

	L	IC_{50} (μg mL^{-1}, T. b. brucei *427 strain)*	IC_{50} (μg mL^{-1}, *L929 cells)*		L	IC_{50} (μg mL^{-1}, T. b. brucei *427 strain)*	IC_{50} (μg mL^{-1}, *L929 cells)*
7		0.51	3.1	**21b**		0.83	>10
8		0.17	>10	**18a**		0.04	>10
9		0.33	>10	**18b**	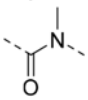	0.32	>10
13		1.11	>10	**22**	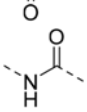	0.44	>10
15		0.15	>10	**26**	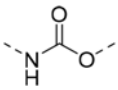	0.35	>10
16		0.16	>10	**19**		0.02	3.48
20		1.62	>10	**14**		0.70	>10
21a		1.21	>10	**23**		0.59	>10
24	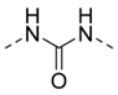	0.05	>10	**26**	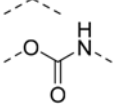	0.57	>10

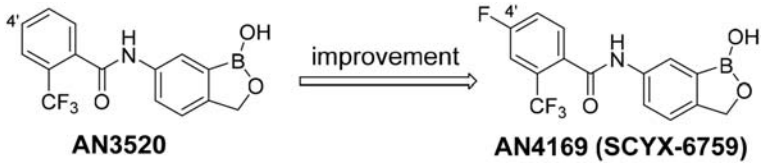

Fig. 10 A fluoro substituent improves in vivo pharmacokinetic and efficacy properties.

8.20.4 Preclinical Development of AN5568

With AN5568 having emerged as a potential preclinical candidate for the treatment of HAT, we next initiated a comprehensive characterization of this compound. We confirmed that AN5568 was potent ($IC_{50} < 0.5$ μg mL^{-1}) against a wide range of *T. brucei* strains, including *T. b. rhodesiense* and *T. b. gambiense* isolates that were resistant to melarsoprol.[17] AN5568 was also fully profiled in a standard battery of non-GLP safety pharmacology and toxicology studies, including AMES, in vitro micronucleus, human Ether-a-go-go Related Gene (hERG), and cytochrome P450 enzyme inhibition studies, where it was found to have properties consistent with those needed for progression.[17] One of the most interesting observations made during the preclinical phase concerned the in vivo PK of AN5568, particularly in dog. In mice, rats, and cynomolgus monkeys, AN5568 exhibited very good and well-behaved PK; plasma concentrations were maintained well above the in vitro minimum inhibitory concentration (MIC) of the compound for at least 24 h, clearance was low across these species, and oral exposure and bioavailability were high. In these species, the plasma half-lives ($T_{1/2}$) of AN5568 following oral administration was 7.7 (m), 15.3 (r), and 20.3 (c) h. When AN5568 was administered to dogs by either the intravenous or oral routes, we were surprised to find that plasma exposures were maintained for several days at concentrations well in excess of the in vitro MIC; a plasma half-life of >63 h was calculated for a 10 mg kg^{-1} oral dose. Furthermore, the shape of the concentration vs. time curve in dogs was suggestive of enterohepatic recirculation, likely a consequence of the

Table 4 Efficacy of 6-amide benzoxaboroles in a mouse CNS HAT model[14,16,17]

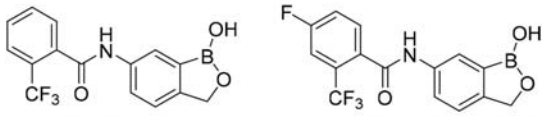

Compound	*Dose (mg kg^{-1})*	*Dose frequency*	*Dose route*	*Relapses*[a]	*Cured*[b]
AN3520	50	BID	*ip*[c]	1D49, 1D56	7/9[d]
AN4169 (SCYX-6759)	50	BID	*ip*[c]	None	10/10
	50	BID	*po*	1D56	5/6[d]
	25	BID	*po*	5D34, 1D41, 2D48	2/10
	12.5	BID	*po*	7D34, 2D41, 1D48	0/10

BID, twice-daily dosing; *ip*, intraperitoneal dosing; *po*, per os (oral) dosing.
[a]Relapses defined as appearance of parasites in blood obtained from a tail snip on day indicated.
[b]Defined as animals that remained parasite free for 180 days postinfection.
[c]Dosed for 14 days, all other groups dosed for 7 days starting on day 21 postinfection.
[d]Each experimental group started with 10 mice. Mice found moribund prior to completion of the dosing period (7 or 14 days) were excluded from the study.

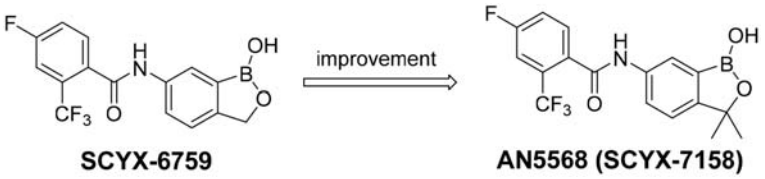

Fig. 11 Additional in vivo efficacy improvement was achieved with 3,3-dimethyl substituents.

Table 5 Activity of AN5568 in the Stage 2 mouse model of HAT[16]

Compound	*Dose (mg kg^{-1})*	*Dose frequency*	*Dose route*	*Relapses*[a]	*Cured*[b]
AN5568 (SCYX-7158)	50	QD	*po*	None	9/9[c]
	25	QD	*po*	None	10/10
	12.5	QD	*po*	1D34, 1D48	8/10
	6	QD	*po*	6D34, 1D41, 3D48	0/10

[a]Relapses defined as appearance of parasites in blood obtained from a tail snip on day indicated.
[b]Defined as animals that remained parasite free for 180 days postinfection.
[c]Each experimental group started with 10 mice. Mice found moribund prior to completion of the dosing period (7 or 14 days) were excluded from the study.
ip, intraperitoneal dosing; *po*, per os (oral) dosing; QD, once-daily dosing.

very high metabolic stability of AN5568. This long half-life was of consequence to our clinical development of AN5568, as in the first human dosing cohort (20 mg), we observed a very long half-life (~400 h, vide infra)—behavior similar to the dog and dissimilar to the rodent and cynomolgus monkey. This observation prompted us to examine whether we could reduce the concentration of the compound in plasma by the administration of activated charcoal.[19] In a series of in vitro experiments, we demonstrated that AN5568 could be removed from phosphate-buffered saline, simulated intestinal fluid (SIF), or SIF containing taurocholic acid by the addition of activated charcoal. In an in vivo experiment, dogs were given a single dose of AN5568, and 24 h later, were administered oral doses (either b.i.d. or t.i.d. for 24 h) of Actidose-Aqua. The results of this experiment demonstrated that the concentration of AN5568 in plasma was reduced more rapidly following the administration of charcoal, and the elimination half-life following charcoal treatment was reduced to 27–29 h, consistent with that predicted by allometric scaling from the mouse, rat, and cynomolgus monkey data.

Concurrent with these experiments to more fully understand the pharmacokinetic behavior of AN5568 in dogs, our colleagues at DND*i* completed all the preclinical toxicology and safety pharmacology studies required to support preparation of an Investigational Medicinal Product Dossier for submission to the European Medicines Agency (EMA) in advance of a first-in-human Phase 1 study.

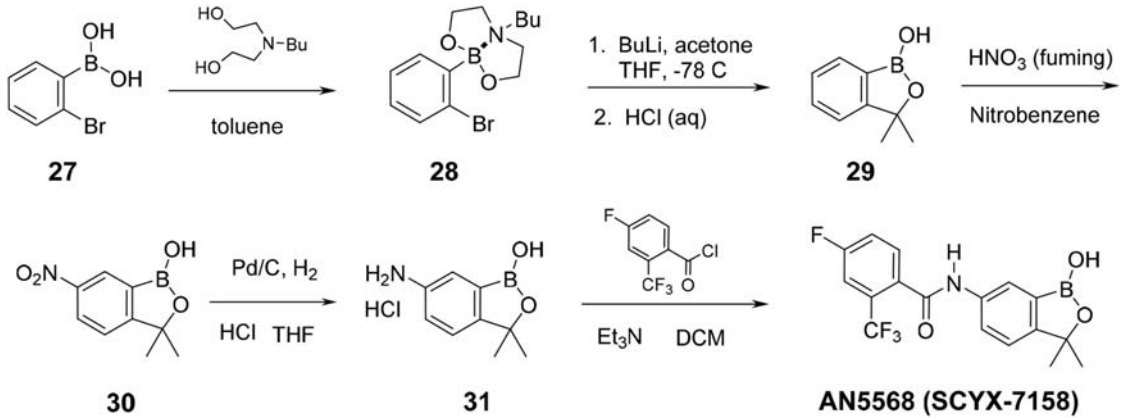

Fig. 12 A synthetic route used for the preparation of AN5568 (SCYX-7158).

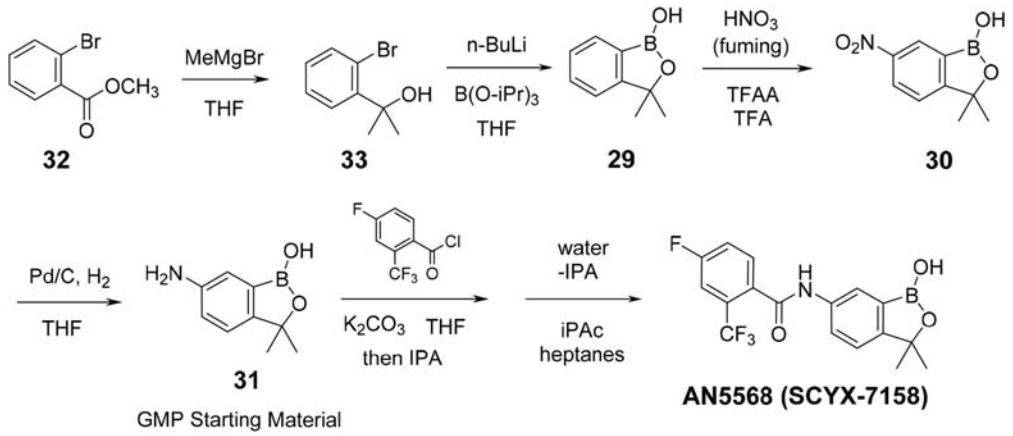

Fig. 13 Process chemistry method used for the preparation of AN5568 (SCYX-7158).

8.20.5 Chemical Synthesis

Two synthetic routes have been used for the preparation of AN5568.[16,20] The method in Fig. 12 was used during the discovery stage of the HAT program and the key common intermediate (**28**) was shared to synthesize the benzoxaboroles with substituent variation at the 3-position. The overall yield was 43% with four isolable solids in the route and no chromatography used. The raw materials are readily available. This route was also used for the first 1 kg synthesis of AN5568 in Mar. 2010.

Following the nomination of AN5568 as a preclinical candidate, development of a more cost effective and efficient process to synthesize the compound was initiated at Scynexis under the supervision of Mark Jensen. The route developed, which has been operated on multikilogram scale including a cGMP manufacture is shown in Fig. 13. Starting from readily available methyl 2-bromobenzoate (**32**), treatment with methyl magnesium bromide provides the 2-bromocumyl alcohol (**33**) in excellent yield. Lithium–halogen exchange followed by boronylation of the incipient aryllithium and benzoxaborole ring closure induced by acid workup afforded the 3,3-dimethylbenzoxaborole (**29**) in modest yield, with cumyl alcohol as a by-product from protonation of the aryllithium reagent. Pure benzoxaborole was isolated following acid–base extraction. Nitration of 3,3-dimethylbenzoxaborole was safely and efficiently accomplished using fuming nitric acid (1.0 eq) in a mixture of trifluoroacetic acid and trifluoroacetic anhydride.[21] Reduction of the nitro group using catalytic hydrogenation gave the 6-amino-3,3-dimethylbenzoxaborole (**31**) a high yield. The final two steps of the synthetic route were operated in a telescoped fashion. Acylation of the 6-amino-3,3-dimethylbenzoxaborole provided crude AN5568, which was converted in situ to the corresponding *O*-isopropyl boronate by azeotropic removal of water. This was then crystallized and isolated to remove colored impurities from the nitration/hydrogenation steps. Resuspension of the boronate in isopropyl acetate, tetrahydrofuran (THF), and water was followed by azeotropic removal of isopropanol affording pure AN5568 upon cooling. No chromatography was required throughout this process, as the isolated intermediates and final active pharmaceutical ingredient (API) were well-behaved crystalline materials. This six-step method has progressed to completion of synthesis of more than 3 kg of AN5568 (SCYX-7158) under chemical good manufacturing process (cGMP) with high purity (>99.5%).

8.20.6 First-in-Human Clinical Trial of AN5568

AN5568 was selected as a preclinical candidate for HAT in late 2009. A reproductive toxicity package was completed in 2014 showing that the drug did not induce any abnormalities. A tablet formulation demonstrated comparable PK to capsules used in a Phase 1 study and was, therefore, suitable for further clinical studies.[22]

The Phase 1 study assessing the safety, tolerability, PK, and pharmacodynamics of AN5568 after single oral ascending doses was a double-blind randomized study which included 128 healthy human volunteers of sub-Saharan origin. This study was completed in France in 2015. In the first volunteer cohort (20 mg), it was determined that the half-life of AN5568 in humans was very long (~400 h per 17 days). This observation, which was suggested by the long half-life observed in dogs, resulted in a protracted withdrawal period for the volunteers, which slowed the rate of dose escalation. In addition, studies were conducted in volunteers to confirm that the reduction of half-life observed following charcoal treatment in dogs could be reproduced in humans. These additional cohorts successfully demonstrated the ability to reduce plasma levels of AN5568 in human volunteers following a 20 mg dose by the activated charcoal method if necessary. Reduction of plasma concentrations of drug was less substantial at higher doses due to limitations in the amount of charcoal that could be administered. A potentially beneficial consequence of this very long half-life in humans is the possibility for AN5568 to be a single-dose cure of Stage 2 disease. Based on the PK–PD relationships established in pre-clinical studies, we hypothesize that maintenance of plasma and brain concentrations in excess of the MIC for trypanocidal activity can be achieved by a single dose of appropriate size.

With this background, and the objective to develop an understanding of the dose required to maintain brain concentrations above the MIC in humans, the Phase 1 study continued until a maximum dose of 1200 mg was reached. During this phase, several cohorts included sampling of CSF, which confirmed that AN5568 crossed the blood–brain barrier and provided CSF concentrations predicted to be sufficient to kill parasites in the brain of infected patients. Based on the PK observed in the Phase 1 trial, it was determined that a single oral dose of 960 mg would be predicted to provide 95% confidence of efficacy in Stage 2 patients.[23] This dosing approach is currently being evaluated for the Phase 2/3 clinical trial design, with implementation of these trials in patients in the DRC anticipated to begin in late 2016.

8.20.7 Successful Partnership Model Among DND*i* and Its Research Partners

As described in this review, the multinational and multipartner consortium, funded by DND*i* and accessing expertise at DND*i*, Anacor, SCYNEXIS, Pace University, Swiss TPH, and many contract research organizations was key to successful completion of this program. The research program delivered AN5568 as a preclinical candidate within 18 months of program initiation, an effort that included hit-to-lead and lead optimization. A reflection about the reasons behind such an excellent achievement may be useful to the tropical diseases research community. It is the view of the authors that each of the following components is necessary for successful delivery of drug candidates for neglected tropical diseases such as HAT in a cost-effective and efficient manner. The components are

(1) *A strong, dedicated, and committed research team*: At Scynexis under the program leadership of Robert Jacobs, the team members included, Bakela Nare, Stephen Wring, Daitao Chen, Eric Gaukel, Matt Orr, Jennifer Owens, Beth Beaudet, Tana Bowling, Matthew Jenks, Luke Mercer, Andy Noe, Robin Parham, Ryan Randolph, Cindy Rewerts, and Jessica Sligar. At Pace University, the team members included Cy Bacchi, Elena Mejia, Ali Hussain, Donna Rattendi, and Nigel Yarlett. At Swiss TPH, the team members included Reto Brun, Marcel Kaiser, Tanja Wenzler, and Monica Cal. At Anacor, the team members included Jacob Plattner, Yvonne Freund, Yong-Kang Zhang, Tsutomu Akama, and Eric Easom. At DND*i*, the team members included Simon Croft, Shing Chang, Graeme Bilbe, Denis Martin, Robert Don, Ivan Scandale, Delphine Launay, and Stephanie Braillard. Many unnamed people in these institutions may have contributed to the success of this research program in various ways. With the tight timeline established for this project, the dedication and commitment of these individuals was critical to success. In addition, it was also critical to have the support of the CEOs of the companies involved in this work (David Perry at Anacor and Yves Ribeill at Scynexis) to permit the teams to be dedicated to developing these drugs, which would have no commercial value to the companies.

(2) *Strong support and leadership from DNDi*: As the sponsor of the HAT research program, DND*i* allocated needed financial resources to ensure the research progressing well. For example, since this program was targeting Stage 2 HAT disease, the active compounds were required to have sufficient CNS exposure. The key to the successful medicinal chemistry strategy was to integrate in vivo pharmacokinetic characterization of lead molecules concurrent with in vivo efficacy studies. These studies were very labor intense and required substantial resources.

(3) *Well-established in vitro assays and in vivo HAT models*: Access to reproducible biological assays and models for HAT research takes special expertise, experience, and time. Therefore, contributions from the biology and pharmacology scientists at Pace University, Scynexis, and Swiss TPH were very critical to the success of the HAT research program. While some of these models were established and had been operated in support of other research programs, the capacity and throughput required to execute an integrated lead optimization project demanded considerable flexibility and adaptation of these models throughout the program.

(4) *Effective communication across different institutions*: Scientists from five organizations participated in the HAT research program. To progress the hit-to-lead (HtL) and lead optimization (LO) projects, as rapidly as, we did required close communication among all of the scientists involved in the research. Fruitful communication and frequent interaction stimulated creative ideas, saved time, and made the program progress well. For example, during the early stage of the research program, chemistry experimental procedures for hit compounds that already existed in the Anacor library were always provided to Scynexis chemists within 24 h of when requested. Biological screening results from both in vitro and in vivo experiments were made available within similar time frames through a web-based data service.[24]

(5) *Privileged benzoxaborole chemistry platform*: Since the discovery of the first benzoxaborole at Anacor in 2004, this class of molecules has been an outstanding source for novel therapeutic product candidates. Twelve new small molecules from the benzoxaborole class have progressed to preclinical evaluation, and six have been tested in humans for antifungal, antibacterial, anti-inflammatory, or antiprotozoal applications. These include Anacor's first drug, KERYDIN (tavaborole) topical solution, 5%, an antifungal LeuRS editing-domain inhibitor that was approved by the US Food and Drug Administration in Jul. 2014 for the topical treatment of onychomycosis of the toenails due to *Trichophyton rubrum* or *Trichophyton mentagrophytes*. Crisaborole topical ointment, 2%, a novel nonsteroidal topical anti-inflammatory PDE-4 inhibitor in development for the potential treatment of mild-to-moderate atopic dermatitis is currently being reviewed by the FDA. In the neglected disease area, several development candidates in addition to AN5568 have been identified, and are currently progressing through preclinical development activities, with the potential to be used as novel antitubercular and antiparasitic agents.[25]

8.20.8 Summary and Perspective

In 1995, a WHO Expert Committee estimated that 60 million people were at risk of being infected with the *T. brucei* parasites that cause HAT, with an estimated 300,000 new cases per year in Africa and fewer than 30,000 cases diagnosed and treated. In 2009, the number of new cases reported dropped below 10,000 (9878) for the first time in 50 years and the actual number of cases at that time was estimated to be ~30,000.[1] This trend has been maintained in 2010, with 7139 new cases reported. HAT caused by *T. b. gambiense* is the most common form of the disease and levels of Gambiense HAT have reached the lowest levels since the disease was targeted for elimination in the WHO's 2012 roadmap on neglected tropical diseases. In Mar. 2016, it was noted that fewer than 3000 new cases were recorded in 2015, the lowest level since the start of systematic global data collection 75 years ago. With the extremely long half-life, potential for a single-dose cure and preliminary safety record of AN5568, this compound has the potential to play a significant role in the elimination of HAT if demonstrated as safe and effective in future clinical trials.

Based on the promising results of preclinical, reproductive toxicity, and Phase 1 studies, AN5568 (SCYX-7158) has been targeted for progression to pivotal Phase 2b/3 clinical trials.[26]

See also: 5.23. Antiparasitic Agents. 8.21. KAE609 (Cipargamin): Discovery of Spiroindolone Antimalarials. 8.22. Medicinal Chemistry Case History: Discovery of the Dihydroorate Dehydrogenase Inhibitor DSM265 as an Antimalarial Drug Candidate.

References

1. World Health Organization. *Trypanosomiasis, Human African (Sleeping Sickness) Fact Sheet.* www.who.int/mediacener/factsheets/fs259/en/ (accessed February 1).
2. (a) Franco, J. R.; Simarro, P. P.; Diarra, A.; Jannin, J. G. Epidemiology of Human African Trypanosomiasis. *Clin. Epidemiol.* **2014,** *6,* 257–275; (b) Franco, J. R.; Simarro, P. P.; Diarra, A.; Ruiz-Postigo, J. A.; Jannin, J. G. The Journey Towards Elimination of Gambiense Human African Trypanosomiasis: Not Far, Nor Easy. *Parasitology* **2014,** *141* (6), 748–760.
3. (a) Barrett, M. P. Potential New Drugs for Human African Trypanosomiasis: Some Progress at Last. *Curr. Opin. Infect. Dis.* **2010,** *23* (6), 603–608; (b) Eperon, G.; Balasegaram, M.; Potet, J.; Mowbray, C.; Valverde, O.; Chappuis, F. Treatment Options for Second-Stage Gambiense Human African Trypanosomiasis. *Expert Rev. Anti-Infect. Ther.* **2014,** *12* (11), 1407–1417.
4. (a) Simarro, P. P.; Cecchi, G.; Franco, J. R.; Paone, M.; Fevre, E. M.; Diarra, A.; Postigo, J. A.; Mattioli, R. C.; Jannin, J. G. Risk for Human African Trypanosomiasis, Central Africa, 2000–2009. *Emerg. Infect. Dis.* **2011,** *17* (12), 2322–2324; (b) Simarro, P. P.; Diarra, A.; Ruiz Postigo, J. A.; Franco, J. R.; Jannin, J. G. The Human African Trypanosomiasis Control and Surveillance Programme of the World Health Organization 2000–2009: The Way Forward. *PLoS Negl. Trop. Dis.* **2011,** *5* (2). e1007.
5. Meyskens, F. L., Jr.; Gerner, E. W. Development of Difluoromethylornithine (DFMO) as a Chemoprevention Agent. *Clin. Cancer Res.* **1999,** *5* (5), 945–951.
6. Steverding, D. The Development of Drugs for Treatment of Sleeping Sickness: A Historical Review. *Parasit. Vectors* **2010,** *3* (1), 15.
7. Brun, R.; Schumacher, R.; Schmid, C.; Kunz, C.; Burri, C. The Phenomenon of Treatment Failures in Human African Trypanosomiasis. *Trop. Med. Int. Health* **2001,** *6* (11), 906–914.
8. (a) Alirol, E.; Schrumpf, D.; Amici Heradi, J.; Riedel, A.; de Patoul, C.; Quere, M.; Chappuis, F. Nifurtimox-Eflornithine Combination Therapy for Second-Stage Gambiense Human African Trypanosomiasis: Medecins Sans Frontieres Experience in the Democratic Republic of the Congo. *Clin. Infect. Dis.* **2013,** *56* (2), 195–203; (b) Priotto, G.; Kasparian, S.; Mutombo, W.; Ngouama, D.; Ghorashian, S.; Arnold, U.; Ghabri, S.; Baudin, E.; Buard, V.; Kazadi-Kyanza, S.; Ilunga, M.; Mutangala, W.; Pohlig, G.; Schmid, C.; Karunakara, U.; Torreele, E.; Kande, V. Nifurtimox-Eflornithine Combination Therapy for Second-Stage African *Trypanosoma brucei* Gambiense Trypanosomiasis: A Multicentre, Randomised, Phase III, Non-Inferiority Trial. *Lancet* **2009,** *374* (9683), 56–64.
9. Drugs for Neglected Diseases *initiative.* NECT: Nifurtimox-Eflornithine Combination Therapy. www.dndi.org/wp-content/uploads/2009/03/nect_dossier_eng.pdf.
10. Baker, S. J.; Zhang, Y. K.; Akama, T.; Lau, A.; Zhou, H.; Hernandez, V.; Mao, W.; Alley, M. R.; Sanders, V.; Plattner, J. J. Discovery of a New Boron-Containing Antifungal Agent, 5-Fluoro-1,3-Dihydro-1-Hydroxy-2,1-Benzoxaborole (AN2690), for the Potential Treatment of Onychomycosis. *J. Med. Chem.* **2006,** *49* (15), 4447–4450.

11. Rock, F. L.; Mao, W.; Yaremchuk, A.; Tukalo, M.; Crepin, T.; Zhou, H.; Zhang, Y. K.; Hernandez, V.; Akama, T.; Baker, S. J.; Plattner, J. J.; Shapiro, L.; Martinis, S. A.; Benkovic, S. J.; Cusack, S.; Alley, M. R. An Antifungal Agent Inhibits an Aminoacyl-tRNA Synthetase by Trapping tRNA in the Editing Site. *Science* **2007,** *316* (5832), 1759–1761.
12. Jacobs, R.; Orr, M.; Wring, S.; Chen, D.; Zhou, H.; Ding, D.; Feng, Y.; Ye, L.; Hernandez, V. S.; Zhang, Y. K.; Plattner, J. J. Boron-Containing Small Molecules as Anti-Protozoal Agents. PCT Int. Appl. WO 2010045503, April 22, 2010.
13. Ding, D.; Zhao, Y.; Meng, Q.; Xie, D.; Nare, B.; Chen, D.; Bacchi, C. J.; Yarlett, N.; Zhang, Y. K.; Hernandez, V.; Xia, Y.; Freund, Y.; Abdulla, M.; Ang, K. H.; Ratnam, J.; McKerrow, J. H.; Jacobs, R. T.; Zhou, H.; Plattner, J. J. Discovery of Novel Benzoxaborole-Based Potent Antitrypanosomal Agents. *ACS Med. Chem. Lett.* **2010,** *1* (4), 165–169.
14. Nare, B.; Wring, S.; Bacchi, C.; Beaudet, B.; Bowling, T.; Brun, R.; Chen, D.; Ding, C.; Freund, Y.; Gaukel, E.; Hussain, A.; Jarnagin, K.; Jenks, M.; Kaiser, M.; Mercer, L.; Mejia, E.; Noe, A.; Orr, M.; Parham, R.; Plattner, J.; Randolph, R.; Rattendi, D.; Rewerts, C.; Sligar, J.; Yarlett, N.; Don, R.; Jacobs, R. Discovery of Novel Orally Bioavailable Oxaborole 6-Carboxamides That Demonstrate Cure in a Murine Model of Late-Stage Central Nervous System African Trypanosomiasis. *Antimicrob. Agents Chemother.* **2010,** *54* (10), 4379–4388.
15. Xie, D.; Zhang, Y. K.; Hernandez, V.; Ding, D.; Xia, A.; Nare, B.; Jacobs, R.; Freund, Y.; Don, R.; McKerrow, J.; Zhou, H.; Plattner, J. A New Class of Benzoxaborole-Based Potent Antitrypanosomal Agents: Probing the Effect of Different Linkage Groups on Trypanosoma brucei Growth Inhibition. 57th Annual Meeting of the American Society of Tropical Medicine and Hygiene, New Orleans, LA.
16. Jacobs, R. T.; Plattner, J. J.; Nare, B.; Wring, S. A.; Chen, D.; Freund, Y.; Gaukel, E. G.; Orr, M. D.; Perales, J. B.; Jenks, M.; Noe, R. A.; Sligar, J. M.; Zhang, Y. K.; Bacchi, C. J.; Yarlett, N.; Don, R. Benzoxaboroles: A New Class of Potential Drugs for Human African Trypanosomiasis. *Future Med. Chem.* **2011,** *3* (10), 1259–1278.
17. Jacobs, R. T.; Nare, B.; Wring, S. A.; Orr, M. D.; Chen, D.; Sligar, J. M.; Jenks, M. X.; Noe, R. A.; Bowling, T. S.; Mercer, L. T.; Rewerts, C.; Gaukel, E.; Owens, J.; Parham, R.; Randolph, R.; Beaudet, B.; Bacchi, C. J.; Yarlett, N.; Plattner, J. J.; Freund, Y.; Ding, C.; Akama, T.; Zhang, Y. K.; Brun, R.; Kaiser, M.; Scandale, I.; Don, R. SCYX-7158, an Orally-Active Benzoxaborole for the Treatment of Stage 2 Human African Trypanosomiasis. *PLoS Negl. Trop. Dis.* **2011,** *5* (6). e1151.
18. Wring, S.; Gaukel, E.; Nare, B.; Jacobs, R.; Beaudet, B.; Bowling, T.; Mercer, L.; Bacchi, C.; Yarlett, N.; Randolph, R.; Parham, R.; Rewerts, C.; Platner, J.; Don, R. Pharmacokinetics and Pharmacodynamics Utilizing Unbound Target Tissue Exposure as Part of a Disposition-Based Rationale for Lead Optimization of Benzoxaboroles in the Treatment of Stage 2 Human African Trypanosomiasis. *Parasitology* **2014,** *141* (1), 104–118.
19. (a) Wong, H.; Theil, F. P.; Cui, Y.; Marsters, J. C., Jr.; Khojasteh, S. C.; Vernillet, L.; La, H.; Song, X.; Wang, H.; Morinello, E. J.; Deng, Y.; Hop, C. E. Interplay of Dissolution, Solubility, and Nonsink Permeation Determines the Oral Absorption of the Hedgehog Pathway Inhibitor GDC-0449 in Dogs: An Investigation Using Preclinical Studies and Physiologically Based Pharmacokinetic Modeling. *Drug Metab. Dispos.* **2010,** *38* (7), 1029–1038; (b) Zhang, D.; Frost, C. E.; He, K.; Rodrigues, A. D.; Wang, X.; Wang, L.; Goosen, T. C.; Humphreys, W. G. Investigating the Enteroenteric Recirculation of Apixaban, a Factor Xa Inhibitor: Administration of Activated Charcoal to Bile Duct-Cannulated Rats and Dogs Receiving an Intravenous Dose and Use of Drug Transporter Knockout Rats. *Drug Metab. Dispos.* **2013,** *41* (4), 906–915.
20. Chen, D.; Orr, M.; Sligar, J.; Jacobs, R.; Plattner, J. Boron-Containing Small Molecules as Antiprotozoal Agents. PCT Int. Appl. WO2011019618, February 17, 2011.
21. (a) Katritzky, A. R.; Scriven, E. F.; Majumder, S.; Akhmedova, R. G.; Vakulenko, A. V.; Akhmedov, N. G.; Murugan, R.; Abboud, K. A. Preparation of Nitropyridines by Nitration of Pyridines With Nitric Acid. *Org. Biomol. Chem.* **2005,** *3* (3), 538–541; (b) Katritzky, A. R.; Vakulenko, A. V.; Sivapackiam, J.; Draghici, B.; Damavarapu, R. Synthesis of Dinitro-Substituted Furans, Thiophenes, and Azoles. *Synthesis* **2008,** *2008* (05), 699–706.
22. Drugs for Neglected Diseases *initiative*. DNDi Launches Phase 1 In-Human Clinical Trial for Promising Oral Drug for Sleeping Sickness. www.dndi.org/2012/media-centre/press-releases/oxa-phasei/ (accessed March 12, 2012).
23. Tarral, A. Human African Trypanosomiasis: First in Man Clinical Trial of a New Medicinal Product, the SCYX-7158. https://clinicaltrials.gov/ct2/show/NCT01533961?term=SCYX-7158&rank=1.
24. Bost, F.; Jacobs, R. T.; Kowalczyk, P. Informatics for Neglected Diseases Collaborations. *Curr. Opin. Drug Discov. Devel.* **2010,** *13* (3), 286–296.
25. (a) Zhang, Y. K.; Plattner, J. J.; Easom, E. E.; Jacobs, R. T.; Guo, D.; Sanders, V.; Freund, Y. R.; Campo, B.; Rosenthal, P. J.; Bu, W.; Gamo, F. J.; Sanz, L. M.; Ge, M.; Li, L.; Ding, J.; Yang, Y. Benzoxaborole Antimalarial Agents. Part 4. Discovery of Potent 6-(2-(Alkoxycarbonyl)Pyrazinyl-5-Oxy)-1,3-Dihydro-1-Hydroxy-2,1-Benzoxaboroles. *J. Med. Chem.* **2015,** *58* (13), 5344–5354; (b) Zhang, Y. K.; Plattner, J. J.; Easom, E. E.; Zhou, Y.; Akama, T.; Bu, W.; White, W. H.; Defauw, J. M.; Winkle, J. R.; Balko, T. W.; Guo, S.; Xue, J.; Cao, J.; Zou, W. Discovery of an Orally Bioavailable Isoxazoline Benzoxaborole (AN8030) as a Long Acting Animal Ectoparasiticide. *Bioorg. Med. Chem. Lett.* **2015,** *25* (23), 5589–5593.
26. Drugs for Neglected Diseases *initiative*. Pivotal Clinical Trial to Begin for First Oral Drug Candidate Specifically Developed for Sleeping Sickness. www.dndi.org/2015/media-centre/press-releases/pr-scyx-7158/ (accessed September 8, 2015).

8.21 KAE609 (Cipargamin): Discovery of Spiroindolone Antimalarials

BKS Yeung, Novartis Institute for Tropical Diseases, Singapore

© 2017 Elsevier Ltd. All rights reserved.

8.21.1	Introduction	529
8.21.2	Important Aspects of Current Antimalarial Drug Discovery	530
8.21.3	Restarting Antimalarial Research and the Search for Next Generation Antimalarial Drugs	530
8.21.3.1	Identification and Triaging Potential Leads From Screening	530
8.21.4	Identification of the Lead	532
8.21.5	The Active Enantiomer of the Lead Compound	532
8.21.6	Asymmetric Synthesis of the Active Enantiomer	534
8.21.7	SAR of the Spiroindolones	535
8.21.8	Surrogate Models of Human Malaria for Drug Discovery	539
8.21.9	In Vivo Efficacy of Spiroindolones in the *P. berghei* Mouse Model	539
8.21.10	The Target and Mechanism of Action of the Spiroindolones	539
8.21.11	Proof of Concept—Rapid Parasite Clearance in Patients	540
8.21.12	Summary and Final Thoughts	541
References		541

8.21.1 Introduction

Malaria caused by *Plasmodium* spp. is a parasitic disease transmitted to humans through the bite of an *Anopheles* mosquito. The earliest descriptions of the periodic fevers associated with malaria can be found in Chinese medical texts dating back to 2700 BCE (http://www.cdc.gov/malaria/about/history/), and by some estimates, the disease is claimed to have killed over half of all the people who have ever lived.[1] Although malaria remains a curable disease, in 2015 there were 214 million reported cases and approximately 438,000 deaths worldwide. Over the past 15 years, incidences of new malaria cases have declined 37% which corresponds to a 60% drop in the overall mortality rate (http://www.who.int/malaria/publications/world-malaria-report-2015/report/en/). Despite the progress in recent years, emerging resistance to current drug therapies threatens to reverse this trend. A disproportionately high number of the global malaria burden is found in Sub-Saharan Africa and was home to 89% of malaria cases and 91% of malaria deaths in 2015. New global health policies which include the widespread deployment of insecticide-treated bed nets have contributed to reducing the prevalence of the disease, however the most significant contribution to reduce the malaria burden over the last two decades has arguably been the development of artemisinin-based combination therapies (ACTs). Among the current list of clinically approved treatments, artemisinin and its derivatives represent the latest (and last) line of approved antimalarial drugs. Their overall success can be traced to the development of this class of drug as a fixed-dose combination, as compared to a single agent therapy, which has resulted in the successful treatment of millions of patients.[2] However as the malaria parasite has shown time and time again, resistance to ACTs, threatens to reverse any progress gained as more cases of artemisinin-resistant malaria are discovered in Southeast Asia.[3–5] Continued efforts are needed to discover and develop classes of antimalarials that work not only though new mechanisms of killing but also have the ability to target more than one developmental stage of the parasite within the human host or mosquito vector.

Among the latest generation of antimalarial drugs currently in clinical development are the spiroindolones, exemplified by KAE609 (cipargamin). KAE609 represents the first antimalarial discovered which works through a previously unknown mechanism of action to enter clinical trials since the artemisinins. The compound was discovered and optimized through a collaborative effort between the Novartis Institute for Tropical Diseases, the Genomics Institute of the Novartis Research Foundation, the Swiss Tropical and Public Health Institute, and the Biomedical Primate Research Center. The work was funded through a public–private partnership between Novartis, the Wellcome Trust, the Medicines of Malaria Venture (MMV), and the Economic Development Board of Singapore. Cipargamin is currently in Phase II development for uncomplicated *Plasmodium falciparum* and *P. vivax* malaria.

This article describes the discovery and optimization of the spiroindolone class of antimalarials. The process from the discovery of the lead to proof of concept in man took little under four and a half years; a remarkably short time span compared to a typical drug discovery program. Along the way some critical findings which in retrospect were rather serendipitous played a large role in continuing to drive the project though lead optimization and development. Although cipargamin has more challenges to overcome before reaching approved drug status, the process of its discovery, chemical, optimization, and impact on the current antimalarial pipeline has changed the way many researchers approach drug discovery for malaria. As much of this work has been previously disclosed I have tried to bridge the various publications to chronologically convey the discovery of this new class of antimalarials.

8.21.2 Important Aspects of Current Antimalarial Drug Discovery

History has shown the malaria parasite to be extremely resilient to chemotherapy with examples of the parasite rapidly developing drug resistance to a new drug, and in some cases within 1 year of the introduction (Table 1).[6] Any new antimalarial drug should have a profile which complements and bolsters the current antimalarial drug arsenal and must include activity against all existing resistant parasite strains and preferably work through a unique, fast acting mechanism of killing.[7] It should have a long half-life to support a single or 3 day dosing regimen for low pill burden and increased patient compliance.

Fixed-dosed combination therapies released over the past decade have proven effective in delaying drug resistance compared to monotherapies and will be a requirement for any next generation drug. These treatments must be formulated for a long shelf life in endemic regions and be orally administrated both for the ease of treatment and keep manufacturing costs low (around $1 per treatment). Finally, the safety profile of the drug needs to be compatible with a target population primarily made up of women of child bearing age and children less than 5 years old but must also be safe for individuals with other indications such as tuberculosis or human immunodeficiency virus (HIV).

In the past, research on malaria drug discovery has largely focused on targeting the asexual blood stage parasites as they are responsible for the symptoms of the disease but also because they are more amenable to manipulate in the laboratory. However, the need for next generation drugs which work through new pathways and targets has lead researchers to broaden their strategy by targeting other life stages of the parasite.[8] For example targeting the parasite liver-stages can result in a drug for prophylactic use while targeting the sexual stages (gametocytes) can result in a drug with transmission blocking properties. Until relatively recent times, few biological tools and assays existed which allowed compound screening outside of asexual blood-stages, however new assays, some of which are amenable to high throughput screening (HTS), can now be leveraged to identify compounds active on blood, liver, and transmission stages of the parasite.[9]

8.21.3 Restarting Antimalarial Research and the Search for Next Generation Antimalarial Drugs

Over the past decade there has been a resurgence in efforts to discover new drugs for neglected diseases facilitated through partnerships between pharmaceutical companies, academic research groups, and funding agencies. This has also coincided with breakthroughs in the pharmaceutical industry in HTS and assay development applied to hit discovery. These advancements have led to the development and implementation of HTS campaigns on *P. falciparum* to identity new chemical starting points for drug discovery.[10–12]

As part of effort to discover new antimalarials we carried out an HTS campaign on *P. falciparum* and against the Novartis natural product (NP) library. At the time this library contained over 12,000 pure natural and NP-like (synthetic) compounds. The screen employed a fluorescence-based assay in 384-well format and active hits were identified as those compounds displaying $>50\%$ inhibition at a single 1.25 μM concentration. The assay monitors parasite proliferation through the fluorescence enhancement of a dye (SYBR green I) upon interacting with *Plasmodium* DNA. As erythrocytes lack both RNA and DNA, changes in the fluorescence intensity directly relates to and monitors parasite growth.[13,14]

Of the 12,000 compounds screened, we identified 275 primary hits that were reconfirmed in a secondary *P. falciparum* in vitro assay of which 49 compounds remained active at <1 μM. The hit list was further refined by testing for toxicity against a mammalian cell-line and for cross resistance on a chloroquine (CQ) resistant (K1) *P. falciparum* strain; leaving 32 compounds remaining out the 275 original hits.

8.21.3.1 Identification and Triaging Potential Leads From Screening

Among the 32 hit compounds selected, several known NPs with antimalarial activity were also identified (Fig. 1). Three different chemotypes were followed up as part of triaging efforts but we were unable to overcome various issues associated with these

Table 1 Emergence of parasite resistance to antimalarial drugs

Drug	*Class/target*	*Discovery/introduction*	*First reported resistance*
Quinine	Quinoline	1632	1910
Chloroquine	4-Aminoquinoline	1934	1957
Proguanil	Antifolate	1947	1948
Sulfadoxine-pyrimethamine	Antifolate	1967	1967
Mefloquine	Quinoline	1977	1982
Atovaquone	Naphthoquinone	1996	1996
Artemisinin and derivatives	Sesquiterpene trioxane	1972	2008

Data adapted from Talisuna, A. O.; Bloland, P.; D'Alessandro, U. History, Dynamics, and Public Health Importance of Malaria Parasite Resistance. *Clin. Microbiol. Rev.* **2004**, *17*, 235–254.

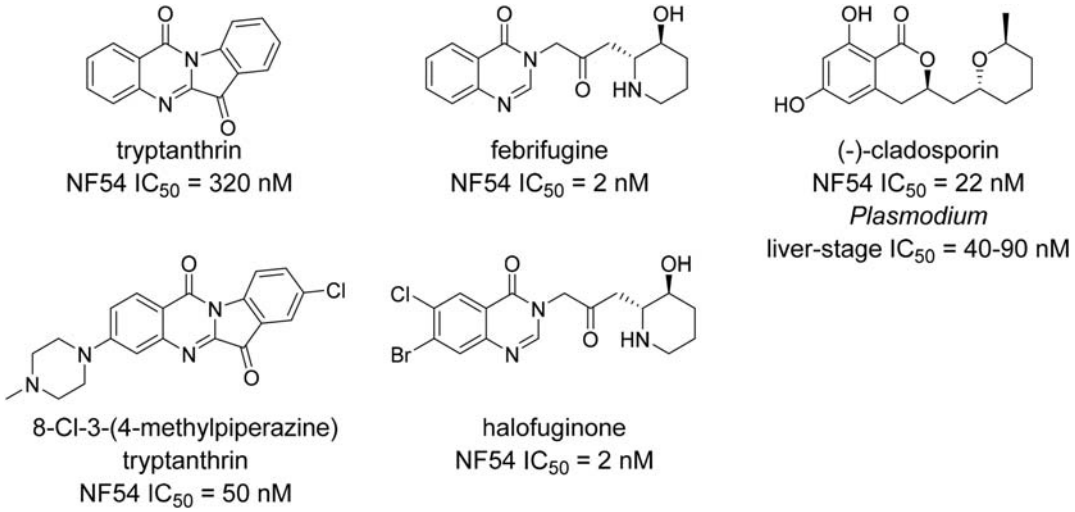

Fig. 1 Examples of known natural product antimalarials and their analogs identified from high throughput screening.

antimalarial scaffolds. Most of the problems encountered centered primarily on improving the drug-like properties and safety profile of the scaffold.

Tryptanthrin is an alkaloid isolated from the medicinal plant, *Strobilanthes cusia* and has been previously described for its potent antimicrobial and antiprotozoal activity.[15] Tryptanthrin and its derivatives display low nanomolar activity on both CQ-sensitive and -resistant malaria and although optimal in terms of their molecular size and synthetic feasibility, their poor drug-like properties (low solubility) has prohibited their development as an oral drug. A number of analogs were prepared and exemplified by the 8-Cl-3-(4-methylpiperazine) derivative of tryptanthrin. Although better potency could be achieved we were unable to improve the solubility of the compound through the introduction of ionizable, polar groups. We attributed the low solubility to the high planarity (sp2 character) of the scaffold and all efforts to reduce the planarity resulted in a loss of potency.[16]

Halofuginone is a halogenated derivative of febrifugine, the active component of a medicinal herb (*Dichroa febrifuga*) long used as a treatment for malaria in traditional Chinese medicine.[17] It displays remarkable in vitro activity against the parasite and is believed to target prolyl-tRNA synthetase (proRS).[18] Although its biological activity also extends to cancer and autoimmune diseases it is believed to operate through an alternative mechanism of action.[19] Similar to tryptanthrin, halofuginone is a chemically tractable scaffold and a potent antimalarial lead; however its polypharmacology and poor tolerability in patients makes it unsuitable for development as a safe antimalarial treatment.[20]

Cladosporin is a fungal secondary metabolite that displays a wide range of biological properties including antibacterial[21] and antifungal[22] activity through an unknown mechanism of action. In addition to its antimalarial activity on *Plasmodium* blood-stages, cladosporin inhibits the development of *P. yoelii* liver-stage parasites as well.[23,24] As opposed to tryptanthrin and halofuginone, cladosporin was not deemed chemically accessible due to its relatively complex structure although there have since been recent reports of the total synthesis of cladosporin and analogs.[25,26] In addition, cladosporin was found to display poor metabolic stability in both mouse plasma and liver S9 fractions which we attributed to Phase II metabolism (glucuronidation of phenol) or hydrolysis of the isocoumarin ring system.

Although unable to explore the structure–activity relationships (SAR) of cladosporin, the liver-stage activity associated with this compound led to an extensive target identification effort. Target identification was carried out using a collection of yeast deletion strains in a haploinsufficiency profiling (HIP) assay.[27] The HIP target discovery assay uses a genome-wide collection of heterozygous knockout yeast strains, each of which contains a marked gene deletion.[28,29] Heterozygous diploid strains bearing a deletion in one copy of a small molecule's target gene will display an increased sensitivity to that small molecule relative to those strains that have two copies of the gene; which is the result of decreased expression of the target in the heterozygous diploid strain.

Using this approach, cladosporin was found to specifically inhibit protein synthesis by directly targeting *P. falciparum* cytosolic lysyl-tRNA synthetase.[23] Furthermore, cladosporin is more than 100-fold potent against *Pf*lysyl-tRNA synthetase relative to the human enzyme, and remarkably conferred by the difference of only two amino acids within the enzyme active site. More recent data supports *Pf*lysyl-tRNA synthetase is an attractive, druggable, antimalarial target that can be selectively inhibited.[30]

Compounds with promising activity from phenotypic cell-based screens, like cladosporin, may not necessarily be good drug leads, however they are still useful in determining their mechanism of action through the identification of specific targets.[31] The successful validation of a target from this approach provides a proof of concept for small molecule inhibition and can support drug discovery based on rational design of the hit compound.

8.21.4 Identification of the Lead

As one of the key profiles for an antimalarial drug is oral route dosing, we prioritized the remaining hit compounds based on their bioavailability in rodents as opposed to in vitro potency alone. Seventeen compounds were selected but only one, a racemic spiroazepineindole **1**, displayed a favorable oral pharmacokinetic (PK) profile in mice (C_{max} = 3.6 μM, bioavailability (F) = 59%) (Fig. 2). Interestingly in our background search it was revealed that compound **1** was not a NP but a synthetic compound previously reported and tested for anticonvulsant activity.[32] The compound was included in our library for its *NP-like* structural properties (i.e., chirality and indole carboline moiety) and purchased as part of the NP library expansion activities. No antimalarial activity had been previously reported for the compound in the original publication.

Spiroindolone **1** displayed moderate activity against both wild type (NF54) and CQ resistant (K1) strains of the parasite when tested in the *P. berghei*-infected mouse model.[33] A single 100 mg kg^{-1} oral dose of the compound resulted in a 96% reduction in parasitemia (activity); although animals survived only up to day 7 post dosing. Nonetheless this was a surprising result for a compound with moderate in vitro activity (~100 nM) and we attributed this to a good oral PK profile. Encouraged by these preliminary results, we surmised that a chemical optimization effort to increase potency and further improve the in vivo PK profile of **1** could deliver a drug candidate.[34]

8.21.5 The Active Enantiomer of the Lead Compound

Resynthesis of **1** was carried out to reconfirm the antimalarial activity. We expected the reported synthetic route to yield a mixture of all four possible stereoisomers based on the reaction conditions (Scheme 1A), however the reaction of the indoleamine and

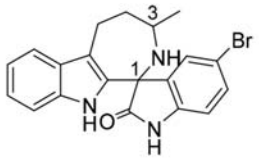

(*rac*)-spiroindolone (**1**)
NF54 IC_{50} = 90 nM
K1IC_{50} = 80 nM

Oral PK parameters (25 mg/kg)

C_{max} (μM)	T_{max} (h)	AUC_{∞} (μM·h)	$t_{1/2}$ (h)	F (%)
3.6	0.25	16.51	3.73	59

Fig. 2 The structure and oral PK properties of the spiroindolone hit.

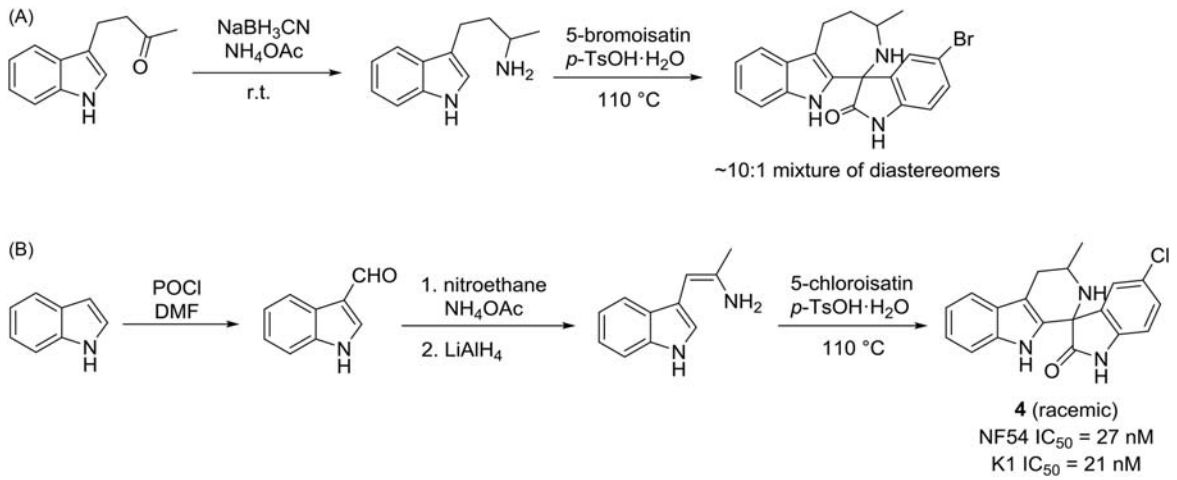

Scheme 1 (A) and (B) Diastereoselectivity in the Pictet–Spengler reaction.

5-bromoisatin provided a 9:1 diastereomeric excess favoring one pair of enantiomers. Diastereoselectivity in the Pictet–Spengler reaction has been widely reported,[35,36] however there have been few examples of reactions involving α-methyl tryptamines and isatin to form the corresponding spirocenter.[37] We extensively investigated the key cyclization step of the spiroindolones to deliver the more favored *trans* product under the thermodynamic conditions of the reaction (Fig. 3).[38] Under reaction conditions, the cyclization step goes through a bis-spiro intermediate independent of the initial imine geometry resulting in **A** and **B**.[39] The formation of the bis-spiro intermediates is fast and reversible but does not influence the stereochemistry of the spirocenter. Instead, bond migration to form the central six-membered ring in intermediates **C** and **D**, is rate determining.[39] The two diastereomeric cations (**C** and **D**) differ only in the configuration of the spirocenter, which places the lactam or the chlorophenyl portion of the isatin in the pseudo-axial position. Of these two possibilities, **C** is favored due to its lower $A^{1,3}$ strain from the *trans* diaxial positioning of the indole and the chlorophenyl of the isatin resulting with the *trans* configuration as the major product formed.

Chiral separation of the mixture of the major product followed by X-ray crystallography provided spiroindoleazepines **2** and **3** and unambiguously identified the active enantiomer as having the 1*R*,3*S* configuration (Fig. 4). Interestingly, its enantiomer (1*S*,3*R*) was completely inactive which possibly implied the presence of a discrete molecular target. This trend was also observed in the spiro-β-carboline series exemplified by **4** (Scheme 1B). In this case all four diastereoisomers were isolated and showed that the major product consisted of the 1*R*,3*S* and 1*S*,3*R* enantiomeric pair (*trans* product) while the 1*R*,3*R* and 1*S*,3*S* enantiomers (*cis* product) made up the minor product (Fig. 5). Ranking the potency of isomers **5**–**8** was useful in rationalizing the SAR between diastereoisomers. The 1*R*-configuration of the spirocenter (C1) is essential as over 100-fold potency is lost with the 1*S*-configuration (**5** and **8** vs. **6** and **7**). The stereochemistry at C3 favors the *S*-configuration as a 50-fold loss in potency is observed for the *R*-configuration (**5** vs. **8**). This trend could also be extended to other spiroindolones analogs where all four diastereoisomers were isolated and profiled. It was completely fortuitous that the active 1*R*,3*S* diastereoisomer was a component of the major *trans* products; had it been a component of the minor products, it would have severely hampered overall progression of the series and likely ended the project if the low yields could not be overcome.

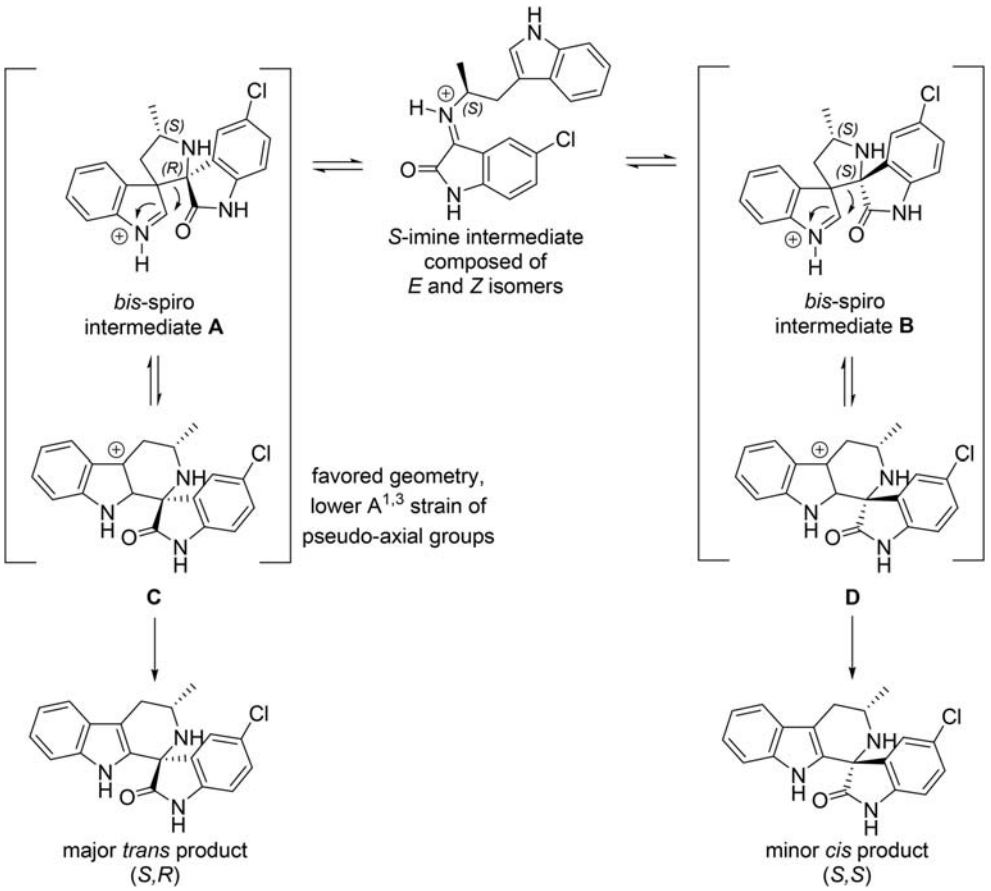

Fig. 3 A proposed mechanism for the cyclization of the *S*-imine under thermodynamic conditions favoring the *trans* product.

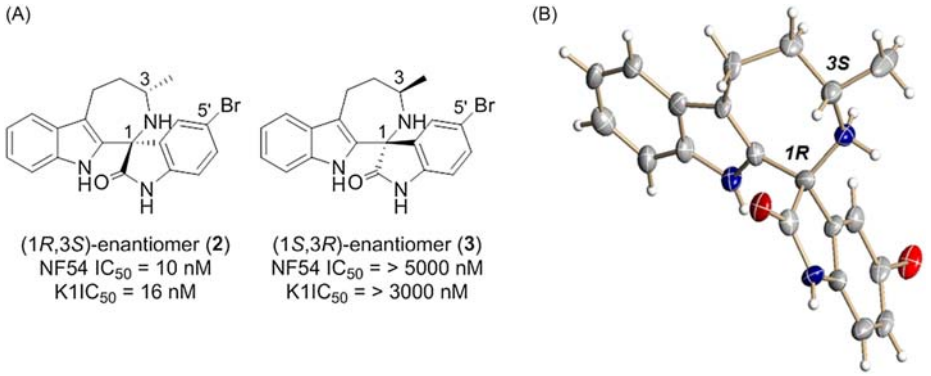

Fig. 4 (A) The activity of the purified enantiomers of the hit. (B) The X-ray crystal structure of the active enantiomer (**2**).

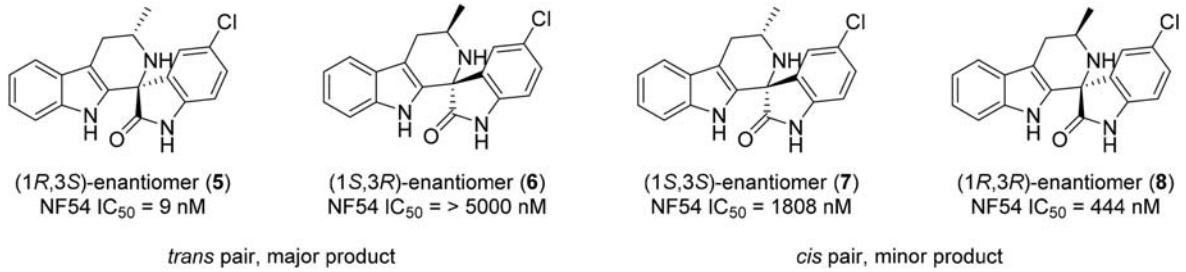

Fig. 5 The four stereoisomers of the spiroindolone products.

8.21.6 Asymmetric Synthesis of the Active Enantiomer

The high diastereoselectivity of the Pictet–Spengler reaction observed in the synthesis of **1** could be exploited to access the active 1*R*,3*S* enantiomers by starting with enantiomerically pure *S*-α-methyl indoleamines (Scheme 2). Starting from D-tryptophanol and following the complete reduction of the hydroxymethyl group to the corresponding methyl, cyclization with 5-chloroisatin in the presence of catalytic acid provided **5** and **6** (Fig. 5) as a 9:1 mixture. Unfortunately, we were unable to capitalize on this route due to the high cost and scarcity of substituted D-tryptophan derivatives. This led us to a significant synthetic effort towards identifying a robust and practical route to substituted *S*-α-methyl indoleamines. Unfortunately, many of the reported or established routes to chiral indoleamine derivatives were not amenable for the substituted or the halogenated indoles we required (Scheme 3). For example, while the acylation reactions generally work well for unsubstituted indoles, the corresponding reaction with 5-fluoroindole and the acid chloride of Fmoc-alanine does not provide the product under any reaction conditions attempted. If the substituted aziridine is used as the alkylating agent, the desired product can be isolated in low yields and poor regioselectivity. Other S_N2-type reactions attempted also resulted in no reaction or poor yields which we were unable to extend to wider array of indole derivatives. One of our final attempts using Fischer indole synthesis not only required a lengthy route to the chiral phenylhydrazone intermediate but also not cyclize under various reaction conditions. We concluded that many of the electron deficient indoleamines we would require for SAR studies could not be easily accessed through an asymmetric route and we ended up reverting to the shorter and more robust racemic synthesis (Scheme 1B). This change in route allowed us to quickly establish the early SAR on racemic mixtures from which the active enantiomer could be obtained through chiral purification.

The two stereogenic centers required for activity for the spiroindolones was deemed a potential liability for the compound as a complex synthetic route would likely result in a high development cost. Simplifying the structure by removing one or both of

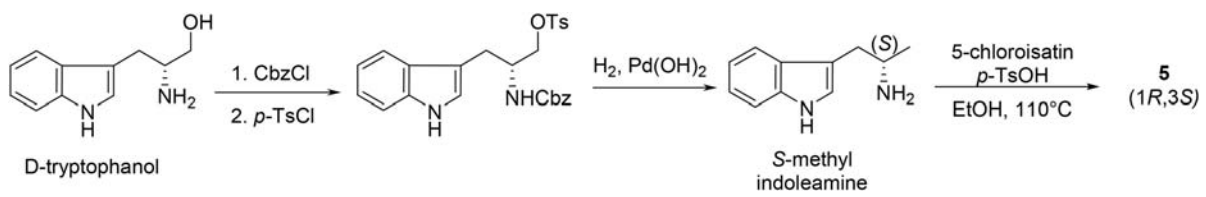

Scheme 2 An asymmetric route to the active enantiomer from D-tryptophanol.

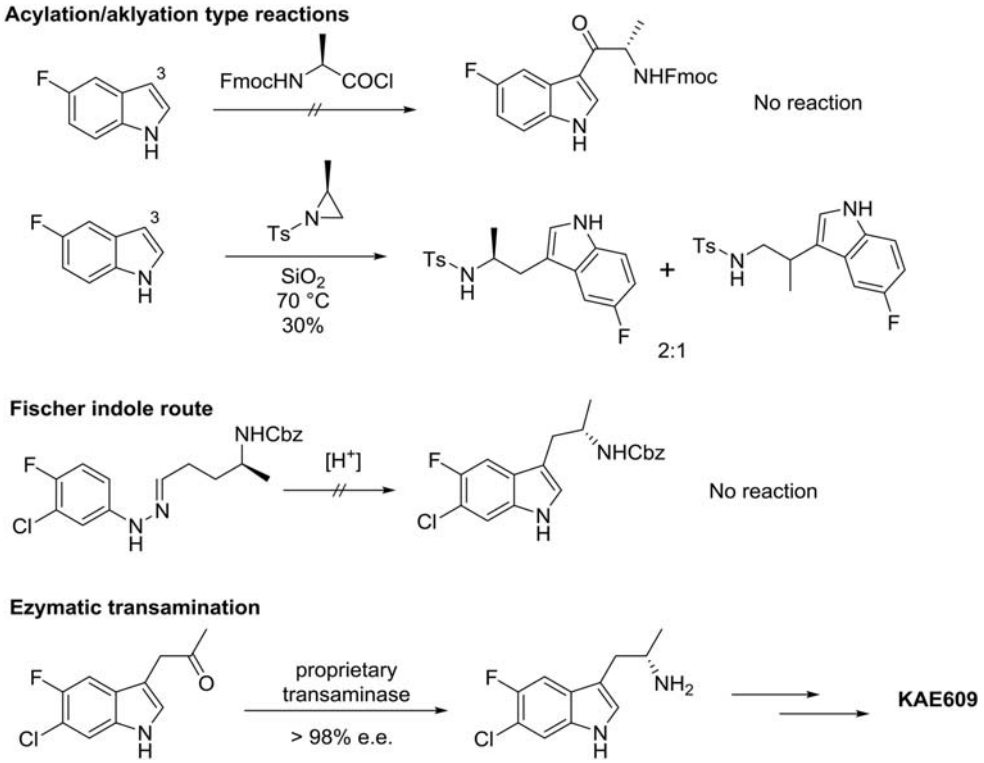

Scheme 3 Attempts to prepare substituted *S*-indoleamine derivatives and the enzymatic route used in the development of KAE609.

the centers resulted in a loss of activity and in the case of the spirocenter, leads to the loss of the pharmacophore as well. Indeed, both centers are required not only for activity but the *S*-configuration methyl group of the indoleamine is needed to set the *R*-configuration of the spirocenter.[38] The racemic route used for lead optimization could not be used as a route for development. Since the active 1*R*,3*S*-enantiomer could be readily obtained from enantiomerically pure *S*-indoleamines, it was necessary to revisit an asymmetric route to the chiral intermediate. The breakthrough came from our colleagues in Novartis Pharma working with a biocatalysis company to identify an efficient enzymatic route to the *S*-indoleamines from achiral starting materials. A proprietary transaminase was developed specifically for the 5-fluoro-6-chloro-indole ketone intermediate that could provide exclusively the *S*-amine with high enantiopurity (Scheme 3).[40] The successful implementation of this process has been critical in overcoming the risk of high development costs associated with an antimalarial drug for widespread distribution.

8.21.7 SAR of the Spiroindolones

A large part of our optimization strategy of **1** was to maintain overall structure of the hit.[34] We believed that the *R*-configuration of the quaternary center was not only important for activity but that the three-dimensionality of the molecule was the source of its favorable physicochemical properties (i.e., high solubility and permeability and low cytotoxicity); and very different from the flat heterocyclic compounds which make up a large part of chemical libraries. The relative compactness and rigidity of the scaffold implied that all the elements representing the complete pharmacophore were present in the molecule. Introducing minute changes to the hit (**1**) such as removing the methyl or bromine substituents markedly impacted the activity. Because of this, much of the optimization focused on the β-carboline ring system as the oxindole moiety was needed to easily access the spirocenter though a Pictet–Spengler cyclization with the corresponding isatin. Halide substituents on the oxindole were needed to maintain activity and the 5′-chloro was found to be equipotent to the 5′-bromo; however, fluorine or hydrogen (**10** and **11**) were not tolerated. Other functional groups and substitution patterns on the oxindole were explored but the 5′-chloro substituent which was identified early, proved to be the optimal balance between potency, synthetic feasibility, and cost (Table 2).

Modifications to the spirocyclic core were directed at optimizing potency by varying the ring size as well as the C3 substituent. The 8-membered ring was inactive (**15**) and deemed too large however 7-membered (azepine) or 6-membered (piperidine) maintained activity around the 100 nM range. The C3 methyl in the azepine series (**9** vs. **16**) had less of an impact on potency than in the piperidine series (**4** vs. **18**) moreover the gem-dimethyl reinforced the importance of the proper stereochemistry at C3; both with respect to potency and diastereoselectivity of the spirocenter at C1. In general, increasing the steric bulk at C3 gave deleterious results as larger groups such as hydroxymethyl, trifluoromethyl, methyl esters, or carboxamide lost activity. Due to the synthetic route

Table 2 The SAR summary of the spiroindolones

Oxindole modifications			*Spirocyclic core modifications*		
Compound	*Structure*	*NF54 IC_{50} (nM)*	*Compound*	*Structure*	*NF54 IC_{50} (nM)*
4 (*rac*)	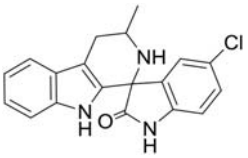	27	**15** (*rac*)	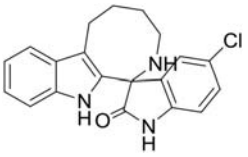	>5000
9 (*rac*)	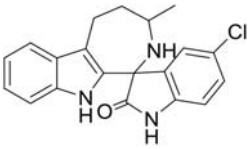	84	**16** (*rac*)	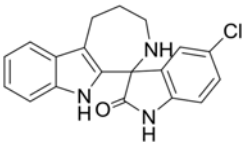	86
10 (*rac*)	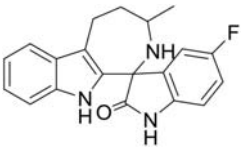	330	**17** (*rac*)	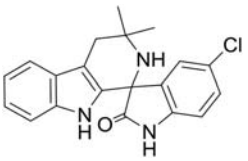	857
11 (*rac*)	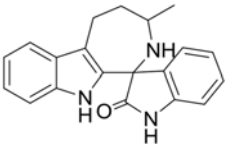	>5000	**18** (*rac*)	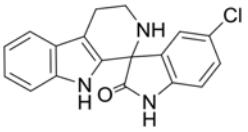	126
12 (*rac*)	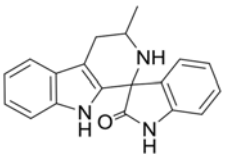	420	**19** (1*R*,3*S*)	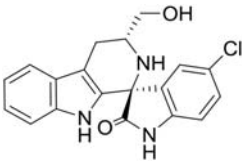	>1000
13 (*rac*)	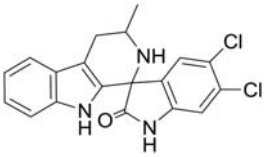	17	**20** (1*R*,3*S*)	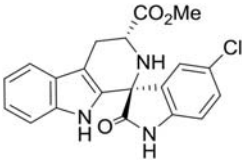	84
14 (*rac*)	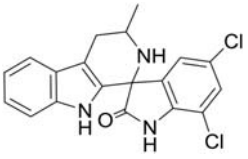	164	**21** (1*R*,3*S*)	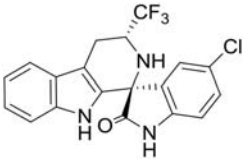	54

(Pictet–Spengler cyclization), we were restricted to tryptamines with limited structural diversity at position C3. The tryptamine $-NH_2$ was optimized for the cyclization step however it was possible to replace it with hydroxyl; albeit with significantly diminished potency and reaction yields. We also briefly explored electron rich phenethylamine derivatives, however these intermediates did not undergo the spiro-cyclization step under various reaction conditions attempted. We concluded that tryptamine derivatives were most amenable to the Pictet–Spengler reaction in terms of yields and diastereoselectivity but it brought an additional chemically-unrelated issue we had up to this point overlooked. During the early days of the project it became apparent that the synthesis of α-methyltryptamine derivatives as spiroindolone intermediates could have led to a potentially serious situation for our chemists given the strict antidrug laws in Singapore. In retrospect many of the substituted α-methyltryptamine derivatives we prepared as racemates or single enantiomers were likely to be highly pharmacologically active (psychedelic and entactogenic properties). As a protective measure we contacted the Central Narcotic Bureau of Singapore to seek approval and establish some guidelines for the synthesis of spiroindolone intermediates that would not result in the incarceration of our medicinal chemists. This was eventually resolved by not preparing any methyltryptamine derivatives on controlled substance list, limiting the quantity of intermediates prepared, and immediately using the intermediates in the cyclization reaction; thereby neutralizing the pharmacological properties of the compound. To date, we are unaware if the pharmacological properties of the 6-Cl-5-F-methyltryptamine intermediate of KAE609 have ever been fully characterized.

To further expand the SAR of the spiroindolones, substitutions to the indole were found to have the largest impact on improving the activity against *P. falciparum* in vitro (Table 3). Chloro-substitutions at C5 (**22**) and C8 (**25**) did not alter the activity compared with the unsubstituted analog (**4**) however low nanomolar potency was reached when the substitution was at C6 or C7 (**23** and **24**, respectively). Combining both C6 and C7 substituents proved to have an additive effect and when incorporated into the active 1*R*,3*S* enantiomer, compounds **28** and **29** achieved subnanomolar inhibitory activity against the parasite.

The enantiomers comprising the racemic mixture of **4** showed markedly different in vitro profiles with respect to metabolic stability and CYP450 inhibition and on the surface seemed like a significant challenge to overcome (Table 4). The moderate stability of the racemate **4** proved to mask the high clearance of eutomer (**5**) versus the low clearance distomer **6**. Both enantiomers proved to represent this trend for all of the pairs of spiroindolone enantiomers. More specifically the distomers exhibited the desired profile that being low clearance in mouse and human liver microsomes and a low propensity for drug–drug interactions (CYP450 inhibition); while in contrast the biologically active 1*R*,3*S* enantiomers displayed high clearance with low microsomal stability and were found to inhibit CYP450 isoforms, 2C9 and 3A4 preferentially. In retrospect this result would not be completely unpredicted based on the marked structural differences between enantiomers of spirocyclic compounds. One might expect significant differences both in the way the individual enantiomers bind within the CYP450 active site and are metabolized. As a result, the optimization

Table 3 Increasing in vitro potency of the spiroindolones

Indole substitutions			*Active enantiomers*		
Compound	*Structure*	*NF54 IC_{50} (nM)*	*Compound*	*Structure*	*NF54 IC_{50} (nM)*
22 (*rac*)	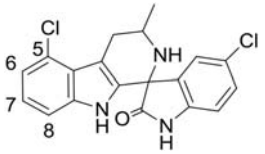	45	**26** (1*R*,3*S*)	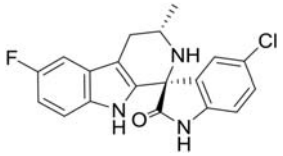	3.4
23 (*rac*)	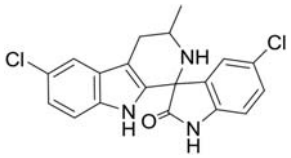	7	**27** (1*R*,3*S*)	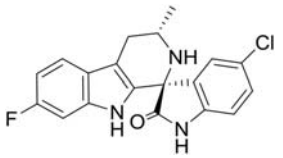	3.5
24 (*rac*)	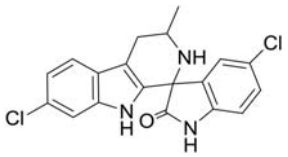	4	**28** (1*R*,3*S*)	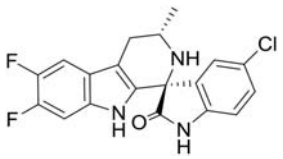	0.2
25 (*rac*)	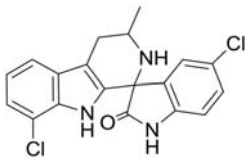	20	**29** (1*R*,3*S*) KAE609	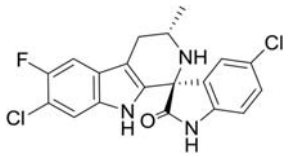	0.7

Table 4 Summary of in vitro and in vivo parameters of spiroindolone analogs

	Microsomal CL_{int}[a]			*CYP450 inhibition (μM)*		
Compound	*Mouse*	*Human*	$t_{1/2}$[b] *(mins)*	*3A4*	*2C9*	*In vivo CL*[c] *(mL min^{-1} kg^{-1})*
4 (*rac*)	Med	Med	9.9	>10	3.9	n.d.
5 (1*R*,3*S*)	High	High	1.2	9.0	1.5	49.7
6 (1*S*,3*R*)	Low	Low	95	>10	>10	n.d.
26 (1*R*,3*S*)	High	Med	10	8.1	3.0	24.0
27 (1*R*,3*S*)	Low	Low	53	>10	6.3	11.8
28 (1*R*,3*S*)	Low	Low	56	>10	7.4	8.5
29 (1*R*,3*S*)	Low	Low	76	>10	5.4	6.7

n.d., not determined.
[a]Intrinsic clearance in liver microsomes, where high clearance corresponds to low stability in the presence of liver enzymes.
[b]$t_{1/2}$ measured in human microsomes.
[c]Measured in mice at a single i.v. dose of 5 mg kg^{-1}.

shifted from addressing potency to incorporating the long lasting and stable profile of the distomer to that of the active (1*R*,3*S*) enantiomer.

We identified the unsubstituted indole moiety on the β-carboline as potentially susceptible to oxidation and high clearance in vivo; and later proven in a follow up metabolite identification study using primary hepatocytes. Electron rich heterocycles like indole are prone to oxidation by CYP450 enzymes and we sought to install electron withdrawing groups (Cl and F) to deactivate the ring.[41] Starting from the active (1*R*,3*S*)-enantiomers, C6-F (**26**), and C7-F (**27**) spiroindolone derivatives exemplified the types of derivatives that were prepared and evaluated in vitro. Both analogs showed marked improvements in potency as predicted by the SAR and although **26** displayed a slightly better in vitro profile to that of compound **5**, the improvements were marginal at best (Table 4). In contrast introducing the C7-F proved to have the desired effect and compound **27** displayed low microsomal clearance and a much improved CYP450 profile across isoforms. Combining both C6 and C7 modifications further improved potency and stability in a profile similar to that of the inactive enantiomers (**28** and **29**). More often than not during the lead phase, chemical optimization of one parameter such as metabolic stability comes at a cost of another—usually potency. This additive effect, where optimizing one parameter on the spiroindolones had a positive influence on another, help to facilitate the lead optimization and resulted in the identification of metabolically stable and highly potent inhibitors of *P. falciparum*. The parallel optimization of two key parameters significantly shortened the lead phase and represented the second occasion where serendipity played a role in delivering a potential drug candidate.

The low in vitro microsomal clearance indicated in vitro was well correlated and highly predictive of the in vivo clearance for compounds **5**, **28**, and **29** (Table 4). Indeed, when evaluated head to head in a mouse PK study there was a marked difference between unsubstituted and substituted spiroindolones with respect to their overall PK parameters (Fig. 6).[42] Following intravenous administration, **5** displayed moderate hepatic clearance on par with what was predicted in vitro and the relatively low oral exposure (3.9 μM h) of the compound resulted in modest bioavailability (13%). In contrast both **28** and **29** displayed significant improvements in C_{max}, area under the curve (AUC), half-life, and bioavailability coupled with a low hepatic clearance rate. Oral exposure was improved 18- and 50-fold for **28** and **29** respectively and when combined with their low nanomolar in vitro potency, the collective data suggested that di-substituted spiroindolones were amenable to a single or low dose treatment regimen for malaria.

The in vitro PK profile of spiroindolones **5**, **28**, and **29** correlated well with their respective in vivo parameters (Table 4 and Fig. 6) which we attributed to the physicochemical properties of the scaffold; namely high solubility and cell permeability. We believed the underlying drivers for this were the presence of sp3 centers and the overall three-dimensionality of the molecule. Unlike other lead optimization programs where compounds possess a high degree of sp2 character, we carried out no efforts to improve the solubility or permeability of the spiroindolones greatly simplifying (and shortening) the overall optimization process.[43]

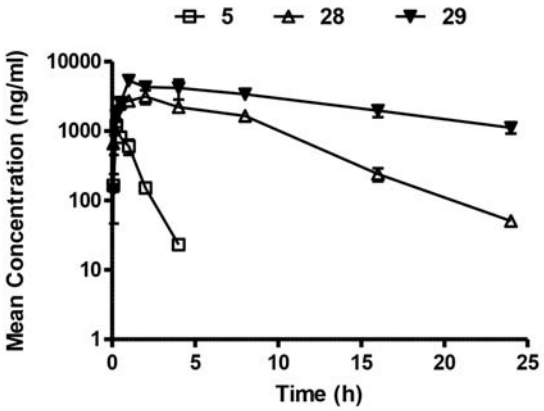

compound	Oral PK parameters					I.V. PK parameters		
	C_{max} (μM)	T_{max} (h)	AUC_{∞} (μM·h)	$t_{1/2}$ (h)	F (%)	Vss (L/kg)	CL (mL/min/kg)	$t_{1/2}$ (h)
5	3.58	0.25	3.88	0.66	13	0.91	49.66	0.42
28	8.32	2.00	71.44	3.18	53	1.60	8.53	2.94
29	13.73	1.0	207.97	10	132	1.42	6.67	3.47

C_{max}, maximum concentration of drug; T_{max}, time to maximum concentration of drug; AUC, area under the curve; V_{ss}, volume of distribution at steady state; CL, clearance; $t_{1/2}$, half-life; F, oral bioavailability.

Fig. 6 The oral PK profile of three spiroindolones depicting their relative exposures following an oral dose of 25 mg kg^{-1} and an i.v. dose at 5 mg kg^{-1} in mouse (see Ref. [42]).

8.21.8 Surrogate Models of Human Malaria for Drug Discovery

In the early days of malaria drug discovery, widespread in vivo screening of the first antimalarial compounds was carried out with *P. gallinaceum* (avian malaria) in chickens because it could easily be maintained and transmitted by mosquitoes.[44] Not until the discovery of the first rodent malaria, *P. berghei*, and the development of a laboratory-adapted *Anopheles* species, *A. stephensi* did the rodent model become the mainstay of malaria research.[45] Since then other rodent species, *P. yoelli*, *P. chabaudi*, and *P. vinckei* have also been used extensively in malaria research and chemotherapeutics to different degrees. The study of the malaria parasite in rodent models has contributed most to our understanding of the life cycle and transmission of human malaria. This is because the *Plasmodium* species that causes disease in humans are unable to infect nonprimate animal models; although an immunocompromised mouse model of *P. falciparum*-infected human erythrocytes has recently been developed for compound screening.[46]

The *P. berghei*-infected mouse remains one of the most widely used efficacy models for antimalarial drug discovery. Compound efficacy is measured by the suppression of parasitemia by a drug as compared to untreated animals.[47] Blood parasitemia levels are monitored postinfection (p.i.) after dosing which provides important preliminary data on the relative potency of a test compound. For the spiroindolones, we employed a 3-day suppressive test in which the effectiveness of three daily oral doses of the compound was measured. In addition to oral dosing, the model also supports alternate routes of administration including intraperitoneal, intravenous, and subcutaneous; generally used for compounds with limited absorption or solubility.

The model can also provide ED_{50} and ED_{90} values for dose ranging as well as useful information on the oral bioavailability of a compound. In parallel to the 3 day test we employed an onset of disease or recrudescence test, where mice were administered a single dose on day 3 p.i. and monitored daily for parasitemia. The results of these tests can be expressed as the rate decrease (or increase) in parasites, the time to the onset of recrudescence, and mouse survival in number of days.[33]

8.21.9 In Vivo Efficacy of Spiroindolones in the *P. berghei* Mouse Model

Average mouse survival results were evaluated at different dose regimens with compound **5**, **28**, and **29** and are shown alongside CQ and artesunate (AS) for comparison (Table 5). Like the standard of care (AS and CQ), the spiroindolones show an excellent initial activity of 99% or greater after a single dose. However, this is not sufficient to completely cure the mice as $<1\%$ parasites remaining can quickly recrudesce in a matter of days. The spiroindolones begin to distinguish themselves in this model only after a multiple dosing regimen (30 mg kg^{-1} q.d. for 3 days). Under these conditions even a high clearance spiroindolone (**5**) with low bioavailability (13%) gives a 60% cure rate. Multiple doses with **28** and **29** have improved the absorption (C_{max}) and exposure (AUC) leading to 29.4 (80% cure) and 29.1 (90% cure) days average mouse survival, respectively, while a single dose of **29** (KAE609) at 100 mg kg^{-1} completely cured infected mice beyond 30 days (end of the study). Optimizing the metabolic stability and improving potency resulted in increased oral absorption, exposure, and efficacy in mice resulting in an in vivo efficacy profile of KAE609 that is consistent with the pharmacokinetic properties required for a single or low dose antimalarial drug.

8.21.10 The Target and Mechanism of Action of the Spiroindolones

The spiroindolones were identified from a phenotypic screen on *P. falciparum* and one of the drawbacks of this approach is that the mechanism of action or molecular target of the compound of interest is usually unknown. However recent advances in parasite biology and biological tools coupled with forward genetic techniques has been successfully leveraged to identify several new antimalarial targets including that of the spiroindolones.

Table 5 In vivo efficacy in the *P. berghei* rodent malaria model of the spiroindolones compared to standard antimalarials

Compound	*Oral dose (mg kg^{-1})*	*% Parasitemia reduction*	*Avg. survival (days)/cure rate (%)*
Artesunate[a]	1×30	99.5	5.8/0
	3×30	99.0	12.2/0
Chloroquine[a]	1×30	99.6	12.5/0
	3×30	99.8	14.3/0
5[a]	1×30	99.9	10.7/0
	3×30	99.9	23.8/60
28[a]	1×30	99.6	12.0/0
	3×30	99.8	29.4/80
29[b] (KAE609)	1×30	99.6	24.1/50
	3×30	99.8	29.1/90
	1×100	99.2	>30/100

Control survival, 6–7 days; cure, parasite free at day 30.
[a]Formulated in 10% ethanol, 30% PEG400, and 6% vitamin E TPGS.
[b]Formulated in methylcellulose 0.5/0.1% solutol HS15.

Plasmodium often acquires mutations in the gene (target) affected by a particular agent as a way of combating drug-induced toxicity. This characteristic of the parasite has been shown to make the in vitro selection of resistance a powerful method for target identification.[31] Changes in the DNA sequence of resistant clones can manifest as small insertions or deletions, copy number variations, and single nucleotide polymorphisms (SNPs) during resistance evolution.[48] The significant genomic changes related to the drug target can then be verified by the reintroduction of the mutant allele into a *P. falciparum* background to validate the conference of resistance.

In order to identify the target of the spiroindolones, drug resistant *Plasmodium* strains were evolved in vitro under sublethal drug pressure in triplicate to yield parasites which displayed a 7–24 fold greater IC_{50} shift compared to wild type strains. The resulting clones were analyzed by whole genome sequencing then compared against the parent strain. Nonsynonymous SNPs, which indicate a change in amino acid sequence, identified mutations in a gene representing a P-type ATPase cation transporter (*Pf*ATP4). These mutations were localized to the putative transmembrane domain of the enzyme and were found to confer low levels of resistance to the spiroindolones.[49]

Upon invasion of *Plasmodium* into the host erythrocyte, merozoites move from a high $[Na^+]$/low $[K^+]$ environment of blood plasma to a low $[Na^+]$/high $[K^+]$ conditions of the host cell cytosol.[50] After establishing an infection, merozoites develop into the ring stage of the parasite which increases the permeability of the erythrocyte to ions such as Na^+ and K^+ among other solutes as part of nutrient uptake within the infected cell. These permeability pathways give rise to an influx of Na^+ effectively raising the $[Na^+]$ in the erythrocyte cytosol close to blood plasma levels.[51] However because the intraerythrocytic parasite requires a low $[Na^+]$ environment it must continuously extrude the influx of sodium ions by continuous efflux through the function *Pf*ATP4.

Plants, fungi, and some protozoa extrude Na^+ through an ENA (*exitus natrus*) P-type Na^+-ATPase which is closely related to sarcoplasmic/endoplasmic reticulum Ca^{2+}-ATPases and plasma membrane Ca^{2+}-ATPases.[52] Although we initially postulated the target of the spiroindolones as a Ca^{2+}-ATPase based on sequence homology, experiments carried out by our collaborators at the Australian National University provided strong evidence that *Pf*ATP4 is in fact a Na^+-ATPase.[53] Live cell assays that monitor the $[Na^+]$ within the parasite have shown that in the presence of spiroindolones, *Pf*ATP4 function is inhibited leading to a rapid increase in the internal $[Na^+]$ resulting in parasite death.

This represents a highly parasite-specific inhibitory mechanism and completely different from the Na^+ transport system used by animals (Na^+/K^+-ATPases). Furthermore it seems unlikely that this unique mechanism of killing would have been discovered by a reverse genetic approach. In other words, in the absence of a tool compound from phenotypic screening, *Pf*ATP4 and is mechanism of action would have likely been overlooked as a potential drug target based on its perceived drugability profile alone (i.e., a membrane-bound transporter and a poorly predicted selectivity index over the host target). Since our disclosure of *Pf*ATP4, at least two other chemotypes have been discovered to work through this mechanism of action and are currently in clinical development for the treatment of malaria.[54,55]

8.21.11 Proof of Concept—Rapid Parasite Clearance in Patients

A Phase II, open-label study was conducted in Thailand to assess the antimalarial efficacy, safety, and adverse event profile of KAE609. A dose of 30 mg day^{-1} for 3 days was chosen for adults with either uncomplicated *P. vivax* malaria (10 patients) or *P. falciparum* malaria (11 patients) with parasite clearance time being the primary endpoint. After treatment, the median parasite clearance time was 12 h in each patient group and the median half-lives for parasite clearance were 0.95 h in the patients with *P. vivax* malaria and 0.90 h in those with *P. falciparum* malaria. Artemisinin and its derivatives are the fastest acting antimalarial agents identified to date; however, the preliminary data from this study suggests that KAE609 may affect an even faster parasite clearance rate. Moreover, some of the patients treated with KAE609 in the study were found to have been infected with artemisinin-resistant *P. falciparum* strains. In general, less than 1% of patients with *P. falciparum* malaria treated with oral AS in Southeast Asia had a parasite clearance half-life of less than 1 h which suggests that the spiroindolones may be highly effective against artemisinin-resistant malaria.[56]

Some adverse events were reported, with nausea being the most common but were generally mild and did not lead to discontinuation of the drug. However more extensive safety studies will be needed to fully assess the adverse event profile of KAE609.

The preliminary clinical findings above support some in vitro and in vivo observations made during the preclinical profiling of KAE609. First, the good pharmacokinetic profile observed in mouse efficacy studies is also present in patients where the mean terminal half-life of elimination of 20.8 h supports a once a day dosing regimen. Secondly, KAE609 displays potent activity on asexual blood-stages but additionally kills ring stage parasites similar to the artemisinin which is believed to translate to the rapidity of symptom resolution. KAE609 also has gametocytocidal activity against *P. falciparum* in vitro and thus may have transmission blocking properties however this will require additional studies to determine its clinical impact.[57]

The remarkable parasite clearance rate in patients dosed with KAE609 has been linked to a particular phenotype that is the result of and specific to *Pf*ATP4 inhibition. In a normal infected red blood cell, parasite development has little effect on the flow of infected blood throughout the body, and in particular the spleen. In the spleen blood is mechanically filtered through splenic sinusoids which are approximately 2 μm in diameter. In the presence of KAE609, infected red blood cells were shown to become more spherical and rigid and thus unable to traverse splenic sinusoids thereby becoming trapped and destroyed by phagocytes. It is believed that the inhibition of *Pf*ATP4 disrupts osmotic regulation in parasite-infected cells leading to parasite death and eryptosis (red blood

cell suicide). By comparison, artemisinins do not have any effect on the rheology of infected red blood cells and lack this dual mechanism of killing which is unique to the spiroindolones and other *Pf*ATP4 inhibitors.[58]

8.21.12 Summary and Final Thoughts

The spiroindolone hit was obtained as part of an effort to expand our chemical libraries and had been through numerous internal HTS campaigns before being identified as a malaria hit. Perhaps the most interesting aspect of the hit compound was that it possessed the essential structural elements required for the desired activity, all of which remain in drug candidate (i.e., the spirocenter, C3-methyl, and oxindole substituents), as well as representing the complete pharmacophore. This simplified and focused our optimization efforts on potency and stability which turned out to have an additive effect; a rarely encountered event in lead optimization. Moreover, the favorable physicochemical properties imparted by the spirocyclic core (three-dimensionality) did not require addressing low solubility or permeability and translated to good oral bioavailability in vivo. Because of these combined factors we were able to identify several potential preclinical candidates after synthesizing around 100 spiroindolone analogs in just over a year.

The discovery of the KAE609 and its path to Phase II clinical trials has also had an impact on the process by which we now approach malaria drug discovery. The HTS approach of large chemical libraries on *Plasmodium* blood-stages has successfully identified other new malaria-specific chemical scaffolds that have been placed in the public domain (www.ebi.ac.uk/chembl). Although the mechanism by which most of these hit compounds inhibit the parasite remains unknown, they in principle represent all potential *Plasmodium* drug targets. By combining forward genetic techniques for target identification through the evolution of drug resistant mutant strains, it is now possible to identify these new targets associated with the active compounds as exemplified by the discovery of *Pf*ATP4. This combined drug discovery approach can lead to new drugs and new drug targets, both of which will be essential to achieve the ultimate goal of malaria eradication.

See also: 5.23. Antiparasitic Agents. 8.20. Case History: AN5568 (SCYX-7158). 8.22. Medicinal Chemistry Case History: Discovery of the Dihydroorate Dehydrogenase Inhibitor DSM265 as an Antimalarial Drug Candidate.

References

1. Whitfield, J. Portrait of a Serial Killer: A Roundup of the History and Biology of the Malaria Parasite. *Nature* **2002**. http://dx.doi.org/10.1038/news021001-6.
2. Bosman, A.; Mendis, K. N. A Major Transition in Malaria Treatment: The Adoption and Deployment of Artemisinin-Based Combination Therapies. *Am. J. Trop. Med. Hyg.* **2007,** *77,* 193–197.
3. Noedl, H.; Se, Y.; Schaecher, K.; Smith, B. L.; Socheat, D.; Fukuda, M. M. Evidence of Artemisinin-Resistant Malaria in Western Cambodia. *N. Engl. J. Med.* **2008,** *359,* 2619–2620.
4. Dondorp, A. M.; Nosten, F.; Yi, P.; Das, D.; Phyo, A. P.; Tarning, J.; Lwin, K. M.; Ariey, F.; Hanpithakpong, W.; Lee, S. J.; Ringwald, P.; Silamut, K.; Imwong, M.; Chotivanich, K.; Lim, P.; Herdman, T.; An, S. S.; Yeung, S.; Singhasivanon, P.; Day, N. P. J.; Lindegardh, N.; Socheat, D.; White, N. J. Artemisinin Resistance in *Plasmodium falciparum* Malaria. *N. Engl. J. Med.* **2009,** *361,* 455–467.
5. Phyo, A. P.; Nkhoma, S.; Stepniewska, K.; Ashley, E. A.; Nair, S.; McGready, R.; Ier Moo, C.; Al-Saai, S.; Dondorp, A. M.; Lwin, K. M.; Singhasivanon, P.; Day, N. P. J.; White, N.; Anderson, T. J. C.; Nosten, F. Emergence of Artemisinin-Resistant Malaria on the Western Border of Thailand: A Longitudinal Study. *Lancet* **2012,** *379,* 1960–1966.
6. Talisuna, A. O.; Bloland, P.; D'Alessandro, U. History, Dynamics, and Public Health Importance of Malaria Parasite Resistance. *Clin. Microbiol. Rev.* **2004,** *17,* 235–254.
7. Burrows, J. N.; van Huijsduijnen, R. H.; Mohrle, J. J.; Oeuvray, C.; Wells, T. N. Designing the Next Generation of Medicines for Malaria Control and Eradication. *Malar. J.* **2013,** *12,* 187–207.
8. Delves, M.; Plouffe, D.; Scheurer, C.; Meister, S.; Wittlin, S.; Winzeler, E. A.; Sinden, R. E.; Leroy, D. The Activities of Current Antimalarial Drugs on the Life Cycle Stages of *Plasmodium*: A Comparative Study With Human and Rodent Parasites. *PLoS Med.* **2012,** *9,* e1001169.
9. Flannery, E. L.; Chatterjee, A. K.; Winzeler, E. A. Antimalarial Drug Discovery—Approaches and Progress Towards New Medicines. *Nat. Rev. Microbiol.* **2013,** *11,* 849–862.
10. Plouffe, D.; Brinker, A.; McNamara, C.; Henson, K.; Kato, N.; Kuhen, K.; Nagle, A.; Adrián, F.; Matzen, J. T.; Anderson, P.; Nam, T.-G.; Gray, N. S.; Chatterjee, A.; Janes, J.; Yan, S. F.; Trager, R.; Caldwell, J. S.; Schultz, P. G.; Zhou, Y.; Winzeler, E. A. In Silico Activity Profiling Reveals the Mechanism of Action of Antimalarials Discovered in a High-Throughput Screen. *Proc. Natl. Acad. Sci. U. S. A.* **2008,** *105,* 9059–9064.
11. Gamo, F.-J.; Sanz, L. M.; Vidal, J.; de Cozar, C.; Alvarez, E.; Lavandera, J.-L.; Vanderwall, D. E.; Green, D. V. S.; Kumar, V.; Hasan, S.; Brown, J. R.; Peishoff, C. E.; Cardon, L. R.; Garcia-Bustos, J. F. Thousands of Chemical Starting Points for Antimalarial Lead Identification. *Nature* **2010,** *465,* 305–310.
12. Guiguemde, W. A.; Shelat, A. A.; Garcia-Bustos, J. F.; Diagana, T. T.; Gamo, F. J.; Guy, R. K. Global Phenotypic Screening for Antimalarials. *Chem. Biol.* **2012,** *19,* 116–129.
13. Smilkstein, M.; Sriwilaijaroen, N.; Kelly, J. X.; Wilairat, P.; Riscoe, M. Simple and Inexpensive Fluorescence-Based Technique for High-Throughput Antimalarial Drug Screening. *Antimicrob. Agents Chemother.* **2004,** *48,* 1803–1806.
14. Bennett, T. N.; Paguio, M.; Gligorijevic, B.; Seudieu, C.; Kosar, A. D.; Davidson, E.; Roepe, P. D. Novel, Rapid, and Inexpensive Cell-Based Quantification of Antimalarial Drug Efficacy. *Antimicrob. Agents Chemother.* **2004,** *48,* 1807–1810.
15. Bhattacharjee, A. K.; Hartell, M. G.; Nichols, D. A.; Hicks, R. P.; Stanton, B.; van Hamont, J. E.; Milhous, W. K. Structure-Activity Relationship Study of Antimalarial Indolo [2,1-b]Quinazoline-6,12-Diones (Tryptanthrins). Three Dimensional Pharmacophore Modeling and Identification of New Antimalarial Candidates. *Eur. J. Med. Chem.* **2004,** *39,* 59–67.
16. Ishikawa, M.; Hashimoto, Y. Improvement in Aqueous Solubility in Small Molecule Drug Discovery Programs by Disruption of Molecular Planarity and Symmetry. *J. Med. Chem.* **2011,** *54,* 1539–1554.
17. Koepfli, J. B.; Mead, J. F.; Brockman, J. A., Jr. An Alkaloid With High Antimalarial Activity From *Dichroa febrifuga*. *J. Am. Chem. Soc.* **1947,** *69,* 1837.
18. Zhou, H.; Sun, L.; Yang, X. L.; Schimmel, P. ATP-Directed Capture of Bioactive Herbal-Based Medicine on Human tRNA Synthetase. *Nature* **2013,** *494,* 121–124.

19. Pines, M.; Spector, I. Halofuginone—The Multifaceted Molecule. *Molecules* **2015,** *20,* 573–594.
20. de Jonge, M. J.; Dumez, H.; Verweij, J.; Yarkoni, S.; Snyder, D.; Lacombe, D.; Marreaud, S.; Yamaguchi, T.; Punt, C. J.; van Oosterom, A.; Group, E. N. D. D. Phase I and Pharmacokinetic Study of Halofuginone, an Oral Quinazolinone Derivative in Patients With Advanced Solid Tumours. *Eur. J. Cancer* **2006,** *42,* 1768–1774.
21. Anke, H. Metabolic Products of Microorganisms. 184. On the Mode of Action of Cladosporin. *J. Antibiot.* **1979,** *32,* 952–958.
22. Scott, P. M.; Van Walbeek, W.; MacLean, W. M. Cladosporin, a New Antifungal Metabolite From *Cladosporium cladosporioides*. *J. Antibiot.* **1971,** *24,* 747–755.
23. Hoepfner, D.; McNamara, C. W.; Lim, C. S.; Studer, C.; Riedl, R.; Aust, T.; McCormack, S. L.; Plouffe, D. M.; Meister, S.; Schuierer, S.; Plikat, U.; Hartmann, N.; Staedtler, F.; Cotesta, S.; Schmitt, E. K.; Petersen, F.; Supek, F.; Glynne, R. J.; Tallarico, J. A.; Porter, J. A.; Fishman, M. C.; Bodenreider, C.; Diagana, T. T.; Movva, N. R.; Winzeler, E. A. Selective and Specific Inhibition of the *Plasmodium falciparum* Lysyl-tRNA Synthetase by the Fungal Secondary Metabolite Cladosporin. *Cell Host Microbe* **2012,** *11,* 654–663.
24. Meister, S.; Plouffe, D. M.; Kuhen, K. L.; Bonamy, G. M.; Wu, T.; Barnes, S. W.; Bopp, S. E.; Borboa, R.; Bright, A. T.; Che, J.; Cohen, S.; Dharia, N. V.; Gagaring, K.; Gettayacamin, M.; Gordon, P.; Groessl, T.; Kato, N.; Lee, M. C.; McNamara, C. W.; Fidock, D. A.; Nagle, A.; Nam, T. G.; Richmond, W.; Roland, J.; Rottmann, M.; Zhou, B.; Froissard, P.; Glynne, R. J.; Mazier, D.; Sattabongkot, J.; Schultz, P. G.; Tuntland, T.; Walker, J. R.; Zhou, Y.; Chatterjee, A.; Diagana, T. T.; Winzeler, E. A. Imaging of Plasmodium Liver Stages to Drive Next-Generation Antimalarial Drug Discovery. *Science* **2011,** *334,* 1372–1377.
25. Zheng, H.; Zhao, C.; Fang, B.; Jing, P.; Yang, J.; Xie, X.; She, X. Asymmetric Total Synthesis of Cladosporin and Isocladosporin. *J. Org. Chem.* **2012,** *77,* 5656–5663.
26. Cochrane, R. V.; Sanichar, R.; Lambkin, G. R.; Reiz, B.; Xu, W.; Tang, Y.; Vederas, J. C. Production of New Cladosporin Analogues by Reconstitution of the Polyketide Synthases Responsible for the Biosynthesis of This Antimalarial Agent. *Angew. Chem. Int. Ed. Engl.* **2016,** *55,* 664–668.
27. Giaever, G.; Shoemaker, D. D.; Jones, T. W.; Liang, H.; Winzeler, E. A.; Astromoff, A.; Davis, R. W. Genomic Profiling of Drug Sensitivities via Induced Haploinsufficiency. *Nat. Genet.* **1999,** *21,* 278–283.
28. Winzeler, E. A.; Shoemaker, D. D.; Astromoff, A.; Liang, H.; Anderson, K.; Andre, B.; Bangham, R.; Benito, R.; Boeke, J. D.; Bussey, H.; Chu, A. M.; Connelly, C.; Davis, K.; Dietrich, F.; Dow, S. W.; El Bakkoury, M.; Foury, F.; Friend, S. H.; Gentalen, E.; Giaever, G.; Hegemann, J. H.; Jones, T.; Laub, M.; Liao, H.; Liebundguth, N.; Lockhart, D. J.; Lucau-Danila, A.; Lussier, M.; M'Rabet, N.; Menard, P.; Mittmann, M.; Pai, C.; Rebischung, C.; Revuelta, J. L.; Riles, L.; Roberts, C. J.; Ross-MacDonald, P.; Scherens, B.; Snyder, M.; Sookhai-Mahadeo, S.; Storms, R. K.; Veronneau, S.; Voet, M.; Volckaert, G.; Ward, T. R.; Wysocki, R.; Yen, G. S.; Yu, K.; Zimmermann, K.; Philippsen, P.; Johnston, M.; Davis, R. W. Functional Characterization of the *S. Cerevisiae* Genome by Gene Deletion and Parallel Analysis. *Science* **1999,** *285,* 901–906.
29. Hegemann, J. H.; Hempel, S.; Herman, Z.; Jaramillo, D. F.; Kelly, D. E.; Kelly, S. L.; Kotter, P.; LaBonte, D.; Lamb, D. C.; Lan, N.; Liang, H.; Liao, H.; Liu, L.; Luo, C.; Lussier, M.; Mao, R.; Menard, P.; Ooi, S. L.; Revuelta, J. L.; Roberts, C. J.; Rose, M.; Ross-Macdonald, P.; Scherens, B.; Schimmack, G.; Shafer, B.; Shoemaker, D. D.; Sookhai-Mahadeo, S.; Storms, R. K.; Strathern, J. N.; Valle, G.; Voet, M.; Volckaert, G.; Wang, C. Y.; Ward, T. R.; Wilhelmy, J.; Winzeler, E. A.; Yang, Y.; Yen, G.; Youngman, E.; Yu, K.; Bussey, H.; Boeke, J. D.; Snyder, M.; Philippsen, P.; Davis, R. W.; Johnston, M. Functional Profiling of the *Saccharomyces cerevisiae* Genome. *Nature* **2002,** *418,* 387–391.
30. Khan, S.; Sharma, A.; Belrhali, H.; Yogavel, M.; Sharma, A. Structural Basis of Malaria Parasite Lysyl-tRNA Synthetase Inhibition by Cladosporin. *J. Struct. Funct. Genom.* **2014,** *15,* 63–71.
31. McNamara, C.; Winzeler, E. A. Target Identification and Validation of Novel Antimalarials. *Future Microbiol* **2011,** *6,* 693–704.
32. Grigoryan, N. P.; Paronikyan, S. A. The Synthesis and Anti-Spasmodic Activity of 2′-oxo-(5′-Bromo)Indoline-3′-Spiro-1-(1,2,3,4-Tetrahydro)-β-Carbolines and 3′-Spiro-1-(1,2,3,4,5,10 Hexahydro)-Indolo(2,3-c)Azepines. *Armenian Chem. J.* **2005,** *58,* 100–104.
33. Fidock, D. A.; Rosenthal, P. J.; Croft, S. L.; Brun, R.; Nwaka, S. Antimalarial Drug Discovery: Efficacy Models for Compound Screening. *Nat. Rev. Drug Discov.* **2004,** *3,* 509–520.
34. Yeung, B. K. S.; Zou, B.; Rottmann, M.; Lakshminarayana, S. B.; Ang, S. H.; Leong, S. Y.; Tan, J.; Wong, J.; Keller-Maerki, S.; Fischli, C.; Goh, A.; Schmitt, E. K.; Krastel, P.; Francotte, E.; Kuhen, K.; Plouffe, D.; Henson, K.; Wagner, T.; Winzeler, E. A.; Petersen, F.; Brun, R.; Dartois, V.; Diagana, T. T.; Keller, T. H. Spirotetrahydro β-Carbolines (Spiroindolones): A New Class of Potent and Orally Efficacious Compounds for the Treatment of Malaria. *J. Med. Chem.* **2010,** *53,* 5155–5164.
35. Bailey, P. D.; Hollinshead, S. P.; McLay, N. R.; Morgan, K.; Palmer, S. J.; Prince, S. N.; Reynolds, C. D.; Wood, S. D. Diastereo- and Enantio-Selectivity in the Pictet–Spengler Reaction. *J. Chem. Soc. Perkin Trans.* **1993,** *1* (4), 431–439.
36. Bailey, P. D.; Beard, M. A.; Phillips, T. R. Unexpected cis Selectivity in the Pictet–Spengler Reaction. *Tetrahedron Lett.* **2009,** *50,* 3645–3647.
37. Pogosyan, S. A.; Grigoryan, N. P.; Paronikyan, R. G. Synthesis and Anticonvulsant Activity of Dihydrochlorides of Indoline-3′Spiro-1-(1,2,3,4-Tetrahydro)-β-Carboline Derivatives. *Pharm. Chem. J.* **2007,** *41,* 527–528.
38. Zou, B.; Yap, P.; Sonntag, L. S.; Leong, S. Y.; Yeung, B. K.; Keller, T. H. Mechanistic Study of the Spiroindolones: A New Class of Antimalarials. *Molecules* **2012,** *17,* 10131–10141.
39. Bailey, P. D. Direct Proof of the Involvement of a Spiro Intermediate in the Pictet–Spengler Reaction. *J. Chem. Res. (S)* **1987,** *6,* 202–203.
40. Crowe, M. F. M.; Francese, G.; Grimler, D.; Kuesters, E.; Laumen, K.; Li, Y.; Lin, C.; Nazor, J.; Ruch, T.; Smith, D.; Song, S.; Teng, S. Chemical Process for Preparing Spiroindolones and Intermediates Thereof. **2013**, WO/2013/139987.
41. Shu, Y. Z.; Johnson, B. M.; Yang, T. J. Role of Biotransformation Studies in Minimizing Metabolism-Related Liabilities in Drug Discovery. *AAPS J.* **2008,** *10,* 178–192.
42. Lakshminarayana, S. B.; Freymond, C.; Fischli, C.; Yu, J.; Weber, S.; Goh, A.; Yeung, B. K.; Ho, P. C.; Dartois, V.; Diagana, T. T.; Rottmann, M.; Blasco, F. Pharmacokinetic-Pharmacodynamic Analysis of Spiroindolone Analogs and KAE609 in a Murine Malaria Model. *Antimicrob. Agents Chemother.* **2015,** *59,* 1200–1210.
43. Lovering, F.; Bikker, J.; Humblet, C. Escape From Flatland: Increasing Saturation as an Approach to Improving Clinical Success. *J. Med. Chem.* **2009,** *52,* 6752–6756.
44. Cox, F. E. History of the Discovery of the Malaria Parasites and Their Vectors. *Parasit. Vectors* **2010,** *3,* 5.
45. Cox, F. Major Animal Models in Malaria Research: Rodent. In *Malaria: Principles and Practice of Malariology,* vol. 2, Wernsdorfer, W., McGregor, I., Eds. **1988,** *vol. 2; pp 1503–1543. Churchill Livingstone.*
46. Moreno, A.; Badell, E.; Van Rooijen, N.; Druilhe, P. Human Malaria in Immunocompromised Mice: New in vivo Model for Chemotherapy Studies. *Antimicrob. Agents Chemother.* **2001,** *45,* 1847–1853.
47. Peters, W.; Robinson, B. L. Malaria. In *Handbook of Animal Models of Infection;* Zak, O., Sande, M., Eds.; Academic Press, 1999; pp 757–773.
48. Dharia, N. V.; Sidhu, A. B.; Cassera, M. B.; Westenberger, S. J.; Bopp, S. E.; Eastman, R. T.; Plouffe, D.; Batalov, S.; Park, D. J.; Volkman, S. K.; Wirth, D. F.; Zhou, Y.; Fidock, D. A.; Winzeler, E. A. Use of High-Density Tiling Microarrays to Identify Mutations Globally and Elucidate Mechanisms of Drug Resistance in *Plasmodium falciparum*. *Genome Biol.* **2009,** *10,* R21.
49. Rottmann, M.; McNamara, C.; Yeung, B. K.; Lee, M. C.; Zou, B.; Russell, B.; Seitz, P.; Plouffe, D. M.; Dharia, N. V.; Tan, J.; Cohen, S. B.; Spencer, K. R.; Gonzalez-Paez, G. E.; Lakshminarayana, S. B.; Goh, A.; Suwanarusk, R.; Jegla, T.; Schmitt, E. K.; Beck, H. P.; Brun, R.; Nosten, F.; Renia, L.; Dartois, V.; Keller, T. H.; Fidock, D. A.; Winzeler, E. A.; Diagana, T. T. Spiroindolones, a Potent Compound Class for the Treatment of Malaria. *Science* **2010,** *329,* 1175–1180.
50. Lee, P.; Ye, Z.; Van Dyke, K.; Kirk, R. G. X-Ray Microanalysis of *Plasmodium falciparum* and Infected Red Blood Cells: Effects of Qinghaosu and Chloroquine on Potassium, Sodium, and Phosphorus Composition. *Am. J. Trop. Med. Hyg.* **1988,** *39,* 157–165.
51. Staines, H. M.; Ellory, J. C.; Kirk, K. Perturbation of the Pump-Leak Balance for Na^+ and K^+ in Malaria-Infected Erythrocytes. *Am. J. Physiol. Cell Physiol.* **2001,** *280,* 1576–1587.
52. Rodriguez-Navarro, A.; Benito, B. Sodium or Potassium Efflux ATPase a Fungal, Bryophyte, and Protozoal ATPase. *Biochim. Biophys. Acta* **1798,** *2010,* 1841–1853.
53. Spillman, N. J.; Allen, R. J.; McNamara, C. W.; Yeung, B. K.; Winzeler, E. A.; Diagana, T. T.; Kirk, K. Na(+) Regulation in the Malaria Parasite *Plasmodium falciparum* Involves the Cation ATPase PfATP4 and Is a Target of the Spiroindolone Antimalarials. *Cell Host Microbe* **2013,** *13,* 227–237.

54. Jimenez-Diaz, M. B.; Ebert, D.; Salinas, Y.; Pradhan, A.; Lehane, A. M.; Myrand-Lapierre, M. E.; O'Loughlin, K. G.; Shackleford, D. M.; Carrillo, A. K.; Clark, J. A.; Dennis, A. S.; Diep, J.; Deng, X.; Duffy, S.; Endsley, A. N.; Fedewa, G.; Guiguemde, W. A.; Gomez, M. G.; Holbrook, G.; Horst, J.; Kim, C. C.; Liu, J.; Lee, M. C.; Matheny, A.; Martinez, M. S.; Miller, G.; Rodriguez-Alejandre, A.; Sanz, L.; Sigal, M.; Spillman, N. J.; Stein, P. D.; Wang, Z.; Zhu, F.; Waterson, D.; Knapp, S.; Shelat, A.; Avery, V. M.; Fidock, D.; Fidock, D. A.; Gamo, F. J.; Charman, S. A.; Mirsalis, J. C.; Ma, H.; Ferrer, S.; Kirk, K.; Angulo-Barturen, I.; Kyle, D. E.; DeRisi, J. L.; Floyd, D. M.; Guy, R. K. (+)-SJ733, a Clinical Candidate for Malaria That Acts Through ATP4 to Induce Rapid Host-Mediated Clearance of Plasmodium. *Proc. Natl. Acad. Sci. U. S. A.* **2014,** *111,* E5455–5462.
55. Vaidya, A. B.; Morrisey, J. M.; Zhang, Z.; Das, S.; Daly, T. M.; Otto, T. D.; Spillman, N. J.; Wyvratt, M.; Siegl, P.; Marfurt, J.; Wirjanata, G.; Sebayang, B. F.; Price, R. N.; Chatterjee, A.; Nagle, A.; Stasiak, M.; Charman, S. A.; Angulo-Barturen, I.; Ferrer, S.; Belen Jimenez-Diaz, M.; Martinez, M. S.; Gamo, F. J.; Avery, V. M.; Ruecker, A.; Delves, M.; Kirk, K.; Berriman, M.; Kortagere, S.; Burrows, J.; Fan, E.; Bergman, L. W. Pyrazoleamide Compounds Are Potent Antimalarials That Target Na^+ Homeostasis in Intraerythrocytic *Plasmodium falciparum*. *Nat. Commun.* **2014,** 5521–5531.
56. White, N. J.; Pukrittayakamee, S.; Phyo, A. P.; Rueangweerayut, R.; Nosten, F.; Jittamala, P.; Jeeyapant, A.; Jain, J. P.; Lefevre, G.; Li, R.; Magnusson, B.; Diagana, T. T.; Leong, F. J. Spiroindolone KAE609 for Falciparum and Vivax Malaria. *N. Engl. J. Med.* **2014,** *371,* 403–410.
57. van Pelt-Koops, J. C.; Pett, H. E.; Graumans, W.; van der Vegte-Bolmer, M.; van Gemert, G. J.; Rottmann, M.; Yeung, B. K.; Diagana, T. T.; Sauerwein, R. W. The Spiroindolone Drug Candidate NITD609 Potently Inhibits Gametocytogenesis and Blocks *Plasmodium falciparum* Transmission to Anopheles Mosquito Vector. *Antimicrob. Agents Chemother.* **2012,** *56,* 3544–3548.
58. Zhang, R.; Suwanarusk, R.; Malleret, B.; Cooke, B. M.; Nosten, F.; Lau, Y. L.; Dao, M.; Lim, C. T.; Renia, L.; Tan, K. S.; Russell, B. A Basis for Rapid Clearance of Circulating Ring-Stage Malaria Parasites by the Spiroindolone KAE609. *J. Infect. Dis.* **2016,** *213,* 100–104.

8.22 Medicinal Chemistry Case History: Discovery of the Dihydroorate Dehydrogenase Inhibitor DSM265 as an Antimalarial Drug Candidate

MA Phillips, University of Texas Southwestern Med Center, Dallas, TX, United States
PK Rathod, University of Washington, Seattle, WA, United States
T Rueckle, D Matthews, and JN Burrows, Medicines for Malaria Venture, Geneva, Switzerland
SA Charman, Monash University, Parkville, VIC, Australia

© 2017 Elsevier Ltd. All rights reserved.

8.22.1	**Malaria Disease and Burden**	544
8.22.2	**Target Candidate Profiles for New Antimalarial Drugs**	545
8.22.3	**Pyrimidine Biosynthesis and DHODH as a Drug Target in Malaria**	546
8.22.4	**Discovery of DSM265**	547
8.22.4.1	High-Throughput Screen	547
8.22.4.2	Early Structure–Activity Relationships and Pharmacokinetic Issues	548
8.22.4.3	X-Ray Structure Determination Informed the Final Step of Lead Optimization	548
8.22.4.4	DSM265 Synthesis	549
8.22.5	**DSM265 Biological Activity**	550
8.22.5.1	Enzyme Activity Including Mammalian DHODH Selectivity	550
8.22.5.2	X-Ray Structure of DSM265 Bound to *Pf*DHODH	550
8.22.5.3	In Vitro Activity Against Parasites	551
8.22.5.4	Efficacy in the *P. falciparum* SCID Mouse Model	552
8.22.5.5	Other Plasmodium Stages	552
8.22.5.6	Mechanism and Frequency of Resistance	552
8.22.6	**DSM265 Pharmacokinetic Properties to Meet the Goal of Single Dose Cure**	553
8.22.6.1	Physicochemical Properties and In Vitro ADME Characteristics	553
8.22.6.2	In Vivo Pharmacokinetic Studies in Preclinical Species	553
8.22.6.3	Human Pharmacokinetic and Dose Predictions	553
8.22.7	**Safety Studies and the Importance of Knowing the Target**	554
8.22.8	**Conclusion and Perspectives**	555
References		555
Relevant Websites		557

8.22.1 Malaria Disease and Burden

Malaria is both a prevalent and a persistent infectious disease with wide global impact. Currently 3.2 billion people in over 97 countries live in malaria endemic regions, and in 2015 there were an estimated 214 million new cases.[1] The disease has its highest impact in Sub-Saharan Africa where 90% of the estimated 438,000 deaths in 2015 occurred mostly in children under the age of 5.[1] The female Anopheles mosquitoes carry the malaria parasite and infect the human host during a blood meal.[2,3] Sporozoites, transmitted through the saliva of the mosquito, travel first to the liver where they invade hepatocytes and propagate into merozoites which are then released to invade red blood cells. This is followed by the erythrocytic stage where parasites undergo repeated rounds of replication, release, and reinfection and it is this cycle that leads to the clinical symptoms of fever, chills, headache, nausea, and eventually death. During the blood stage, a small proportion of the asexual parasites develop into sexual stage male and female gametocytes that are transmitted back to the mosquito during a subsequent blood meal, where they develop into the infective stage ready for transmission to a new host. While five *Plasmodium species* cause malaria, *Plasmodium falciparum* is responsible for almost all mortality and has also been the species for which drug resistance has most impacted treatment options. *P. vivax* is also a significant player as it has a large global distribution and has a dormant form that remains in the liver for years after the primary infection, being released periodically to initiate a relapse infection through mechanisms that are still poorly understood. Disease presentation can vary from uncomplicated malaria to severe infection, with mortality increasing as the percentage of infected erythrocytes rises above about 2%. In severe *P. falciparum* malaria, adherence of infected erythrocytes to blood vessel walls leads to sequestration into key organs including the brain, which can lead to cerebral malaria.[2] Adults living in areas of continual transmission develop temporary protective immunity, which reduces parasite burden and lessens disease severity.[4] As a consequence, young children, pregnant woman, and naive hosts, all of whom lack this immunity are most likely to develop severe disease.

Treatment and prevention of malaria currently relies on a combination of drug therapies and insect control programs.[2] The possibility of developing a vaccine for the prevention of malaria has been pursued vigorously; however, the best candidate vaccine (RTS,S/AS01) developed by GSK has been reported to provide only limited protection (<30% in infants, which are the target

population) and the effects were of short duration.[5,6] Lack of a fully effective vaccine means that malaria control programs will continue to rely on drug therapy for the foreseeable future. A number of safe and effective drugs for the treatment of malaria have been approved for clinical use including the historically important drugs, quinine, chloroquine, and pyrimethamine/sulfadoxine, which provided effective antimalarial therapy for many years.[2] Unfortunately, by the late 1970s both chloroquine and pyrimethamine had become ineffective in many endemic regions due to drug resistance.[7–9] Current treatment therapies are centered on semisynthetic derivatives of the natural product artemisinin, which form the basis of artemisinin combination therapies (ACTs). Wide-spread use of ACTs combined with insecticide-treated bed nets has been largely credited with the significant decline in malaria deaths over the past decade.[2] However, ring stage resistance to the artemisinin derivatives has now been documented in Southeast Asia and threatens to erase the progress that has been made in malaria control and elimination. Kelch13 propeller protein mutations have been linked to delayed parasite clearance times for patients being treated with ACTs, providing a genetic marker to help track the spread of resistance.[10–13] In addition, resistance to the artemisinin combination partners such as dihydroartemisinin and piperaquine (Cuo-cortexin, Euartesim) has been reported in South East Asia.[14,15]

8.22.2 Target Candidate Profiles for New Antimalarial Drugs

The call for malaria eradication by the Bill and Melinda Gates Foundation in 2007 sparked a series of focused reviews that have greatly impacted subsequent drug discovery efforts. The first was an extensive 2 year consultative review involving more than 250 scientists worldwide that defined the scientific knowledge base, strategies and tools required within an eradication agenda.[16] This initiative, called the Malaria Eradication Research Agenda (malERA), identified ideal Target Product Profiles for new drugs being designed for both treatment and chemoprotection.[17] In response to this initiative, the Medicines for Malaria Venture defined a set of target candidate profiles (TCPs, briefly outlined in **Fig. 1**), which describe the key attributes required of candidate molecules to fulfill four different treatment scenarios, in addition to the obvious requirements for safety, low cost of goods, and ease of administration.[8] While a single molecule may well have more than one attribute, new drug products will be developed as fixed dose combinations to reduce the likelihood of developing resistance to a single agent.[18] The concept of Single Exposure Radical Cure and Prophylaxis (SERCaP), a product that would be effective following a single administration against all forms of parasite in a patient as well as providing posttreatment prophylaxis, places enormous demands on any new drug product both in terms of its activity profile and its pharmacokinetic characteristics. Combination products would ideally contain molecules with similar pharmacological durations of cover such that no single agent is left exposed to parasites on its own.[8]

Given the propensity for the malaria parasite to develop drug resistance, a large global effort is underway to deliver new combination therapies that can augment the use of ACTs.[5,7–9] The first novel chemical entities that have advanced to human testing for the treatment of malaria are now in Phase II clinical trials and include a long half-life synthetic peroxide,[19,20] a spiroindolone that targets the P-type cation-transporter ATPase4,[21] an imidazolopiperazine[22,23] and the triazolopyrimidine-based dihydroorotate

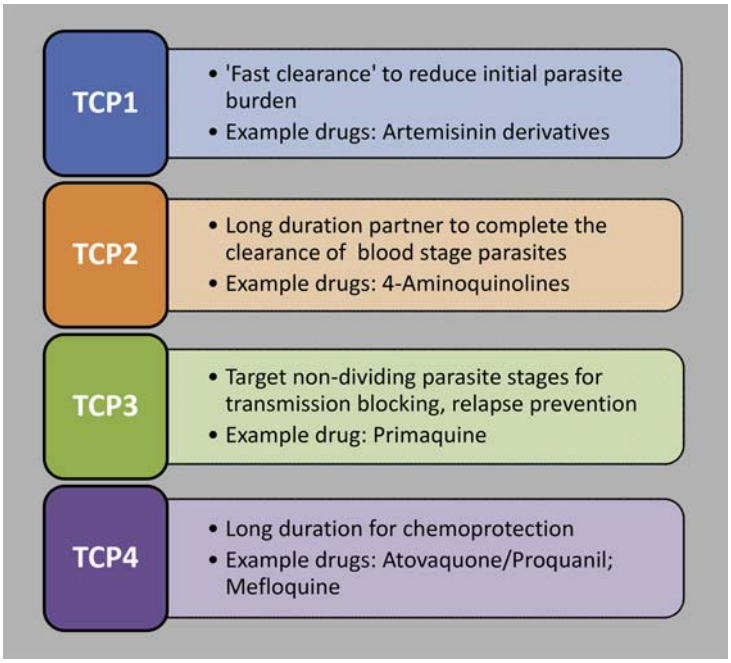

Fig. 1 Target candidate profiles (TCPs) that currently guide antimalarial drug discovery. The reader is referred to the manuscript by Burrows et al. for full details of target profiles.[8]

dehydrogenase (DHODH) inhibitor *DSM265*, which was developed by our group[24] and is the topic of this review. New agents are being developed as combination therapies to combat drug resistance, increasing the number of compounds needed to fill the portfolio. Candidate molecules with activity against all members of the *Plasmodium* genus are desired to simplify treatment in the clinical setting. A broad portfolio of activities covering blood stages for treatment, liver stages for prophylaxis, and sexual stages for transmission-blocking activity are also being pursued, while therapies that are effective with a single dose administration are being prioritized to improve patient compliance.[22,25]

8.22.3 Pyrimidine Biosynthesis and DHODH as a Drug Target in Malaria

Pyrimidine nucleotides are essential for the synthesis of DNA, RNA, and sugar nucleotides, required for glycosylation of proteins and lipids.[26] Pyrimidine nucleosides and bases can be either synthesized de novo from glutamine, aspartic acid, ATP, and bicarbonate, or they can be salvaged from the environment (Fig. 2). Once in the cell they are phosphorylated to yield the final nucleotides. Because of the importance of pyrimidine biosynthesis to cell survival, most cells, including human cells, encode the enzymes necessary for both pathways. However, *Plasmodium* species are atypical and are only able to obtain pyrimidines via the de novo route and thus they are highly vulnerable to inhibition of this pathway.[27] In *Plasmodium*, de novo pyrimidine biosynthesis is accomplished through the action of five enzymes, with the first two steps catalyzed by the same bifunctional enzyme. DHODH catalyzes the fourth step in the pathway, which is the flavin mononucleotide (FMN) dependent conversion of dihydroorotate to orotic acid (Fig. 2). Depending on the species, DHODH can be localized to the mitochondria or the cytoplasm; the distribution of the different enzyme types is spread across evolutionarily diverse organisms.[27] For example, both human and *Plasmodium* species use the mitochondrial-type II enzyme, whereas yeast and Trypanosomatids encode cytoplasmic enzymes. Mitochondrial enzymes (type II) require Coenzyme Q (CoQ) to reoxidize the FMN cofactor, whereas the cytoplasmic enzymes use either fumarate (type 1a) or NAD^+ (type 1b). The mitochondrial enzymes are anchored in the inner mitochondrial membrane and face the inner membrane space. Substrates and products (dihyroorotate and orotate) must diffuse across the outer mitochondrial membrane from and to the cytoplasm.

Prior to our work to develop DHODH as a target for malaria, the usefulness of the pyrimidine biosynthetic pathway as a source for drug targets to treat malaria was already well documented.[27–29] Pyrimethamine, which was a key drug in the antimalarial arsenal until the development of resistance, targets dihydrofolate reductase (DHFR) and prevents formation of thymidine nucleotides. To overcome resistance, recent work has identified a novel *P. falciparum* DHFR inhibitor (P218, currently in preclinical development) that has activity against drug-resistant strains harboring up to four point mutations in the enzyme.[30] In addition to DHFR inhibitors, atovaquone, which targets the cytochrome *bc*1 complex in mitochondria, has also been shown to kill parasites by inhibiting pyrimidine biosynthesis.[28] In elegant work by Vaidya and coworkers,[31] it was shown that blood-stage *P. falciparum* only require mitochondrial electron transport to drive the synthesis of pyrimidines because bc1 is required to reoxidize the CoQ substrate of DHODH (Fig. 2). The authors demonstrated that *P. falciparum* parasites genetically engineered to express yeast DHODH were resistant to atovaquone. This study also served to genetically validate DHODH as an essential target in *P. falciparum*. In subsequent works,

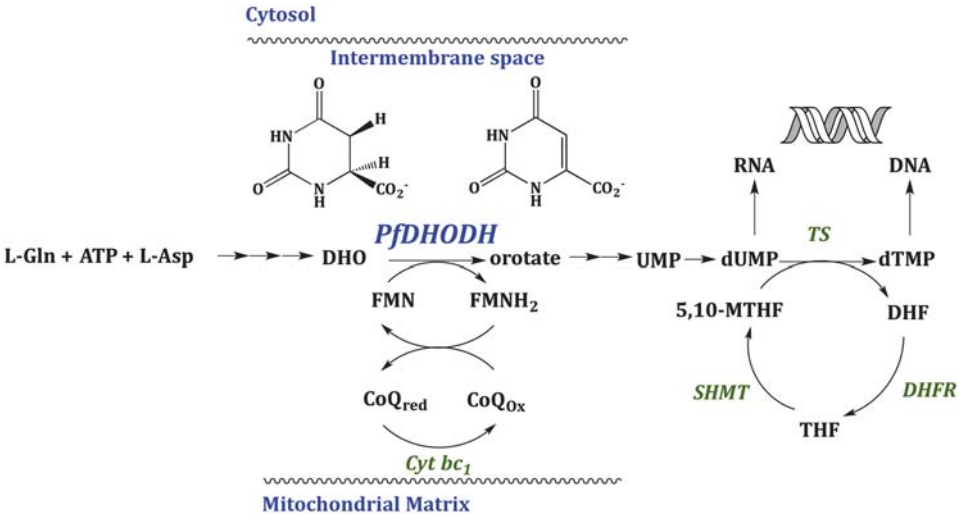

Fig. 2 Pyrimidine biosynthetic pathway in *Plasmodium* species. *Plasmidial* DHODH is a mitochondrial enzyme found anchored in the inner membrane of the mitochondria oriented with the catalytic domain in the intermembrane space.[28] All other enzymes in the pathway are cytoplasmic. *DHODH*, dihydroorotate dehydrogenase; *TS*, thymidylate synthase; *DHFR*, dihydrofolate reductase; *SHMT*, serine hydroxymethyltransferase; *cyt* bc_1, cytochrome bc_1.

this cell line has been used to validate the mechanism of action of DHODH inhibitors, and the yeast DHODH plasmid has been used as a selectable marker for genetic manipulation of *P. falciparum* with DSM1 serving as the selection antibiotic.[32,33]

While the essentiality of the de novo pyrimidine biosynthetic pathway in *Plasmodium* was clear, we sought to first determine if additional enzymes in the pathway would be both druggable and provide the needed species selectivity versus the human enzyme to achieve the necessary safety margin for the treatment of malaria. Our efforts quickly focused on DHODH as the strongest candidate in the pathway. Firstly, there was strong precedence that the mitochondrial-type II DHODH was a druggable target and that small molecule inhibitors that were disease modifying and had "drug-like" properties could be identified. The human DHODH inhibitor leflunomide (Arava) was already marketed for the treatment of rheumatoid arthritis with clear evidence that the mechanism of action occurred via DHODH inhibition by the active metabolite A77 1726 (teriflunomide).[34–37] Teriflunomide has subsequently also been approved for the treatment of multiple sclerosis.[38] While human cells are able to acquire pyrimidines by both de novo synthesis and salvage, proliferation of B and T cells during an immune response requires more nucleotide precursors than can be obtained by the salvage pathway alone and thus inhibition of the de novo pathway dampens the immune response and has proven to be an effective method for managing autoimmune diseases. Additionally, a second class of human DHODH inhibitors, brequinar and its derivatives, had also been described that were potent inhibitors of the enzyme and they were tested as potential anticancer agents and for prevention of graft rejection, eventually failing in Phase II clinical trials.[39–41] A detailed account of reported DHODH inhibitors from a range of eukaryotic and bacterial species can be found in a recent review by Munier-Lehmann et al.[42]

Turning to the question of species selectivity, several cocrystal structures of human DHODH bound to either A77 1726 or brequinar[43] had been reported and our analysis indicated that the inhibitor binding site showed significant species variability at the amino acid sequence level between the human and *Plasmodium* enzymes.[27] This analysis strongly suggested that species selective inhibitors of *Plasmodium* DHODH could be identified that would allow DHODH to be safely targeted for the treatment of malaria. We obtained additional proof for this hypothesis by testing a series of human DHODH inhibitors against recombinant *P. falciparum* DHODH (*Pf*DHODH) and demonstrating that these compounds were poor inhibitors of the *P. falciparum* enzyme.[44] Thus, the available data supported the hypothesis that *Plasmodium* DHODH was essential, druggable, and could be selectively targeted making it a strong candidate for a drug discovery program to identify new compounds for the treatment of malaria.

8.22.4 Discovery of DSM265

8.22.4.1 High-Throughput Screen

To initiate the program to identify *Plasmodium* selective DHODH inhibitors, we performed a high-throughput screen (HTS) of a medium size compound library (220,000 compounds) available from the UT Southwestern HTS core.[45] Recombinant *Pf*DHODH truncated to remove the N-terminal membrane-spanning domain and expressed as a His_6-tag fusion in *E. coli* was used for the screen. A simple end-point colorimetric assay using 2,5-dichloroindophenol as the final oxidant was used to detect enzyme activity. We identified a number of potent ($IC_{50} < 600$ nM) and selective *Pf*DHODH inhibitors in the screen including a series of halogenated phenyl benzamide/naphthamides and urea-based compounds,[45] a singleton called DSM1 that contained a triazolopyrimidine core,[46] and a number of other structural classes which have not yet been disclosed. The triazolopyrimidine series was chosen as the top lead compound series based on superior drug-like properties and the finding that DSM1 inhibited growth of *P. falciparum* in whole cell assays at a similar concentration as observed for inhibition of *Pf*DHODH, while showing no detectable activity against either human DHODH or mammalian cell lines (**Fig. 3**). Genetic rescue studies with the yeast DHODH *P. falciparum*

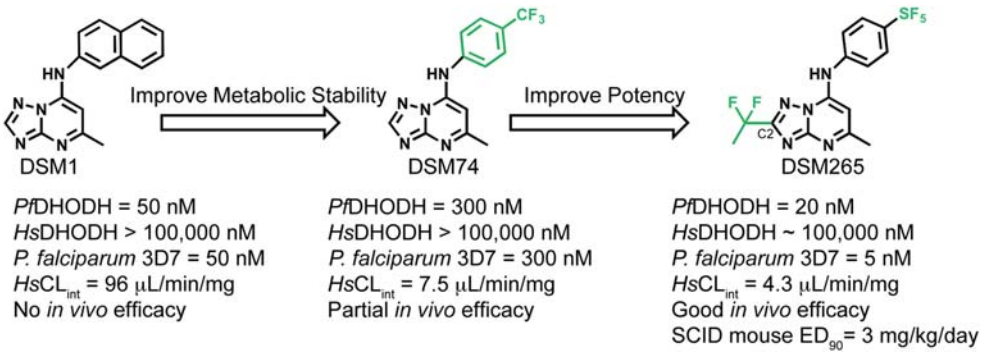

Fig. 3 Key compounds during the lead optimization program that informed the discovery of DSM265. Key compounds along the discovery pathway with relevant activity and ADME properties. *PfDHODH*, *P. falciparum* dihydroorotate dehydrogenase; *HsDHODH*, human dihydroorotate dehydrogenase; *P. falciparum 3D7*, blood-stage *P. falciparum* in vitro growth assay; $HsCL_{int}$, human in vitro intrinsic clearance (μL/min/mg protein) measured using human liver microsomes. Potency data are given in nM to allow comparison between compounds, whereas data in other figures and **Tables 2** and **3** are shown in μg/mL to allow direct comparison to the in vivo pharmacokinetic data.

cell line (described earlier) demonstrated conclusively that DSM1 killed *P. falciparum* parasites by inhibiting *Pf*DHODH.[32] In contrast, the phenyl benzamide series compounds were much less active against the parasite than against the enzyme and thus were not considered as good lead molecules for further medicinal chemistry.

X-ray structure analysis of the most potent benzamide (DSM59)[47] and of DSM1[48] indicated that both compounds bind to a similar conformation of *Pf*DHODH. The observed binding conformation for DSM1 differs to that reported for A77 1726[49] and for the thiophene carboxamide Genz-667348[50] due to the conformational flexibility of F188 which is rotated 180 angles in the pocket between its two conformational states.[48] This conformational flexibility likely accounts for the diversity of chemical scaffolds that can bind potently to *Pf*DHODH and increases the druggability of the target. DSM1 and DSM59 were shown to be specific inhibitors of *Pf*DHODH, and a series of enzymatic studies including pre-steady-state kinetics and mutagenesis analysis showed that they blocked only the second half of the reaction, the reoxidation of the FMN cofactor, and that they were competitive inhibitors of the second substrate CoQ.[46,51]

8.22.4.2 Early Structure–Activity Relationships and Pharmacokinetic Issues

Metabolic and pharmacokinetic studies were performed on DSM1 to profile any liabilities that would need to be addressed in the medicinal chemistry program to advance the series towards lead status. DSM1 was found to have poor metabolic stability based on in vitro studies in liver microsomes and there was a significant reduction in exposure upon repeat dosing to mice over a 4-day period indicative of likely enzyme induction.[52] We suspected that the naphthyl moiety attached to the triazolopyrimidine ring via a bridging nitrogen was associated with these unfavorable metabolism properties and it was replaced by a series of substituted anilines.[52] A total of 39 compounds were synthesized and tested in both enzyme assays and on the parasite in whole cell assays. The most potent compounds contained large bulky substituents at the para position; ortho substituents were not tolerated but fluorine at the meta position could improve the potency of the best para substituents. Metabolism and pharmacokinetic studies showed that compounds that contained fluorinated hydrocarbons in the para position had the best combination of potency and metabolic stability, and from this analysis DSM74 (**Table 1** and **Fig. 3**) was identified. DSM74 had lower potency against *Pf*DHODH and *P. falciparum* 3D7 parasites than DSM1 but it showed good oral bioavailability and prolonged plasma exposure when dosed in mice. Based on these properties, DSM74 was dosed in a *P. berghei* mouse model of malaria infection where doses of 50 mg/kg twice daily for 4 days were shown to suppress parasitemia during the dosing period, but DSM74 was not curative in this model.[52] Importantly, these studies served as a proof of concept that DHODH inhibitors could be disease modifying for the treatment of malaria in vivo and the project progressed to lead optimization status.

While having found a solution to the poor metabolic stability we had reduced the potency of the series necessitating additional lead optimization to improve potency while retaining metabolic stability. One avenue of research led us to explore substitution and heteroatom rearrangement within the triazolopyrimidine ring.[53] We identified imidazole [1,2-*a*]pyrimidine as a core that also gave good binding affinity to *Pf*DHODH, but metabolic stability and pharmacokinetic properties were not as good as with the triazolopyrimidines so this scaffold was not pursued further. Concurrently, additional efforts were also made to further optimize the aniline group in the context of the triazolopyrimidine core leading to the identification of DSM161 (*para*-SF_5 aniline in place of the CF_3 aniline of DSM74) and DSM190 (*meta*-difluoro, *para*-CF_3 aniline) (**Table 1**), both of which had slightly improved potency and improved pharmacokinetic properties when compared to DSM74.[54] These studies led to the identification of the SF_5-aniline as a naphthyl replacement; however, these compounds still lacked the needed potency for a preclinical candidate and so additional lead optimization was required.

8.22.4.3 X-Ray Structure Determination Informed the Final Step of Lead Optimization

In order to improve the potency of the series it was important to gain structural insight into the binding mode of key triazolopyrimidines bound to *Pf*DHODH. To that end, we solved the X-ray structures of *Pf*DHODH bound to both DSM1 and DSM74.[48] These structures showed that most of the molecule formed a good fit into the inhibitor binding site but importantly, allowed us to see that

Table 1 Comparative properties of key compounds in the series contributing to the identification of DSM265

Compound	Pf*DHODH (nM)*	Hs*DHODH (nM)*	Pf*3D7 (nM)*	HsCl_{int} *(μL/min/mg)*	*Kinetic solubility pH 6.5 (μM)*
DSM1	50	>100,000	80	96	50*
DSM74	300	>100,000	300	8	20
DSM161	100	>100,000	200	<5	70
DSM190	200	>30,000	200	<5	9
DSM330	40	20,000	4	<5*	30*
DSM331	20	2000	10	<5*	30*
DSM338	20	2000	2	7*	30*
DSM267	40	>100,000	6	<5	70
DSM265	20	~100,000	5	4	30

Data were taken from Refs. 46, 52, and 54–56, with the exception of the in vitro metabolism and solubility data for * that have not been previously published.

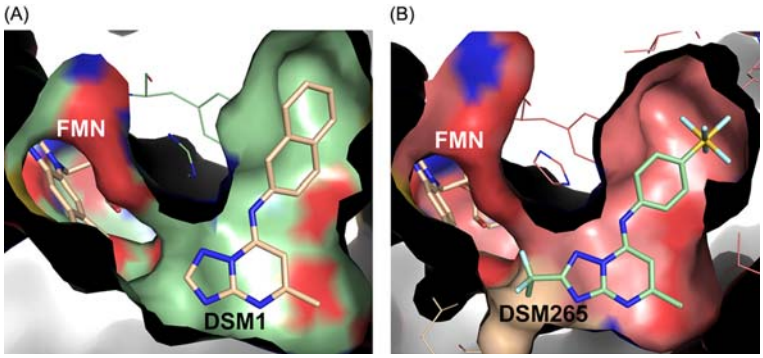

Fig. 4 Comparison of the van der Waals surface between the inhibitor binding site of *Pf*DHODH bound to (A) DSM1 (3I65) and (B) DSM265 (4RX0). The figure shows the van der Waals surface of the triazolopyrimidine binding site to illustrate the channel between the C2 of the inhibitor and FMN. (A) DHODH is shown in *green* and FMN and DSM1 are shown in *tan*. (B) The protein is shown in *salmon* and FMN and DSM265 are shown in *green*. Carbons are colored as indicated, nitrogens are *blue*, oxygens are *red*, fluorine is *light blue* and sulfur is *yellow*. Structures were displayed in PyMol.

there was room to extend into a narrow channel that led from the C2 carbon of the triazolopyrimidine ring towards the FMN cofactor (Fig. 4A). These structural studies provided the insight necessary to improve the potency of the series. Based on this information, we next synthesized a small library of 83 triazolopyrimidine analogs that combined modifications at C2 with several different anilines known to give good binding affinity, including the *para*-CF_3 and *para*-SF_5 anilines found in DSM74 and DSM161, respectively.[55] This work demonstrated that small, halogenated hydrocarbons at C2 (e.g., CF_3, CF_2CH_3, $CF_2CH_2CH_3$) provided the best boast in potency while retaining good metabolic stability. From this effort DSM265, which contains a *para*-SF_5 aniline and a CF_2CH_3 at the C2 position, was discovered (Fig. 3). The X-ray structure of DSM265 bound to *Pf*DHODH was solved demonstrating that it formed good interactions in the channel leading from C2 towards the FMN cofactor as predicted by our design strategy (Fig. 4B).[24] Throughout development of the series we observed very good correlation of activity for *Pf*DHODH versus *P. falciparum* 3D7 in whole cell assays, providing additional evidence that DHODH inhibition was responsible for parasite killing. Several other potent inhibitors with good in vivo properties were also discovered during this final round of lead optimization. These included various combinations of *para*-CF_3-anilines with and without additional *meta*-fluorines and either CF_3 or CF_2CH_3 at the C2 position (Table 1). DSM267 (*para*-CF_3 aniline and CF_2CH_3 at C2) had good properties but was less potent in the SCID mouse in vivo efficacy model than DSM265.[55] Compounds with *meta*-fluorines showed better in vivo potency (e.g., DSM338 (*para*-CF_3, *meta*-difluoro aniline and CF_3 at C2)); however, addition of *meta*-fluorines to the *para*-CF_3 aniline ring led to loss of species selectivity due to inhibition of mammalian DHODHs.[56] Two *meta*-fluorines (DSM331 (CF_2CH_3 at C2) and DSM338 (CF_3 at C2)) led to greater loss of selectivity than one *meta*-fluorine (DSM330 (CF_2CH_3 at C2)), and the rodent DHODHs (mouse and rat) were most vulnerable to inhibition by these compounds. For compounds with two *meta*- fluorines (e.g., DSM338), significant inhibition of the human enzyme was also observed (Table 1). Our X-ray structural and biophysical data for DSM338 suggested that the loss of selectivity was driven by the increasing hydrophobicity of these compounds. Importantly, DSM265 retained selectivity versus human DHODH, although it does inhibit the rodent DHODHs to an extent and these data will be discussed later in the biological activity section. Thus, based on its overall superiority to other potential candidates from the series at the time, DSM265 was nominated as a preclinical development candidate and it has since progressed to clinical development. Subsequently we found that substitution of the SF_5-aniline with halogenated tetrahydro-2-naphthyls led to the identification of compounds that were potent inhibitors of *Pf*DHODH and which showed no activity on human or animal DHODHs.[57] Several compounds from the tetrahydro-2-naphthyl series (most notably DSM426) have the potential to be developed as antimalarial drugs but are less metabolically stable than DSM265 and thus are unlikely to show a long-enough human half-life to support a single dose cure. These analogs have therefore not been progressed as backups to DSM265 but remain as options if needed.

8.22.4.4 DSM265 Synthesis

DSM265 (2-(1,1-difluoroethyl)-5-methyl-[*N*-[4-(pentafluorosulfanyl)phenyl]1,2,4]triazolo[1,5-*a*]pyrimidin-7-amine) is synthesized in four straight-forward steps (Fig. 5). The synthetic method has been well described, including its optimization to generate kilogram quantities of GMP grade material.[24,55] Briefly, the synthetic method starts from aminoguanidine hydrochloride (**1**) and ethyl 3-oxobutanoate (**2**) to generate 2,3-diamino-6-methylpyrimidine-4(3*H*)-one (**3**). Combining **3** with ethyl 2,2-difluoropropionate leads to generation of the triazolopyrimidine ring **4** (2-(1,1-difluoroethyl)-5-methyl-[1,2,4]triazolo[1,5-*a*]pyrimidin-7-ol). Chlorination of **4** followed by addition of 4-(pentafluorosulfanyl)aniline produces the final DSM265 product. All four reactions proceed in good yield. A minor impurity in the final product is DSM430, which contains an additional *meta*-fluorine on the aniline ring and which arises from impurities in the 4-(pentafluorosulfanyl)aniline starting material. The level of this impurity is strictly controlled to remain below 1% in the final product.

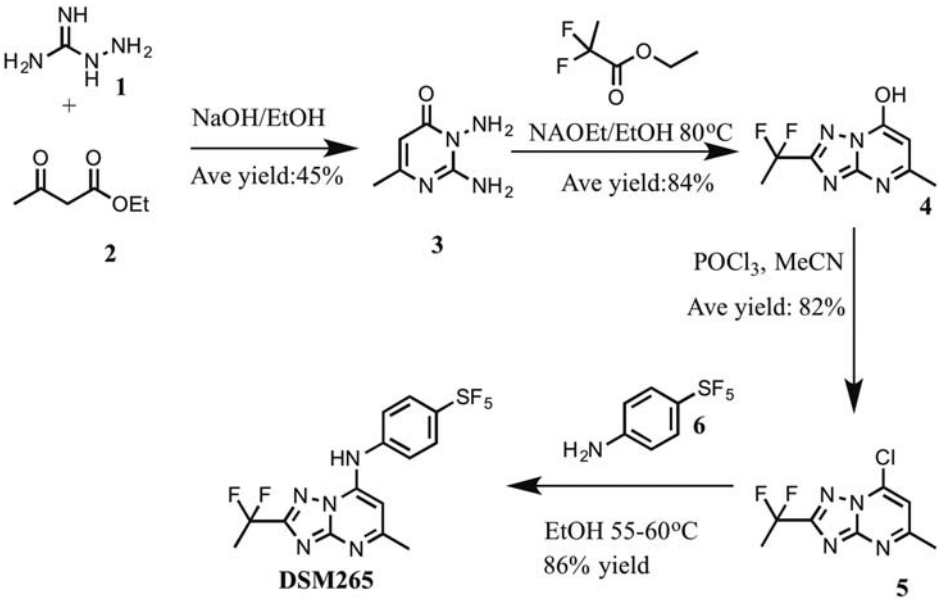

Fig. 5 DSM265 synthetic scheme. The DSM265 synthetic route is displayed with yield values shown for the 12 kg GMP batch.[24]

8.22.5 DSM265 Biological Activity

8.22.5.1 Enzyme Activity Including Mammalian DHODH Selectivity

Recombinant DHODHs, truncated to remove the mitochondrial membrane-spanning domain and any additional sequence to the N-terminus of that region, were expressed as His_6-tagged fusion proteins as described.[24,45,48,54,55] DSM265 was found to be a potent inhibitor of *Pf*DHODH ($IC_{50} = 0.010$ μg/mL).[24,55] The IC_{50} is approximately twofold higher for the *P. vivax* enzyme (Table 2), which may translate to reduced activity on *P. vivax* in the field. Importantly, DSM265 does not show significant inhibition of human DHODH, strongly suggesting that on-target toxicity will not be a concern for clinical use (Table 2). DSM265 was also tested on the enzyme from a range of species potentially important for toxicological studies to support human clinical trials.[24] It showed a range of activities on the rodent and dog enzymes, but like the human enzyme, the rabbit and pig DHODH are not sensitive to DSM265 inhibition (Table 2). It remains much less potent on even the most sensitive mammalian enzyme than on the *Plasmodium* enzymes, but the observation of activity on the rodent and dog enzymes did require careful consideration when selecting species for toxicity studies as described later.

8.22.5.2 X-Ray Structure of DSM265 Bound to *Pf*DHODH

The X-ray structure of DSM265 bound to *Pf*DHODH was solved providing insight into key interactions that drove good binding towards *Pf*DHODH and selectivity against human DHODH.[24] The structure was solved for the N-terminally truncated protein that removes the mitochondrial membrane-spanning domain. DHODH folds into a β/α-barrel with an N-terminal extension that includes two highly hydrophobic α-helices, which presumably pack against the mitochondrial membrane, and which form part of the inhibitor binding site (Fig. 6A). DSM265 sits between these helices and the FMN cofactor, which is bound in the center of the β/α-barrel. Substrate L-orotate is bound on the opposite face of the FMN cofactor compared to DSM265. The DSM265 binding site is likely to overlap the CoQ binding site based on data collected for DSM1 (described earlier). The triazolopyrimidine ring of DSM265 is bound between the only residues in the pocket (R265 and H185) that have side chains that can form hydrogen-bonding interactions. These residues are conserved across all type II DHODH enzymes. DSM265 forms hydrogen bonds with both of these residues (H185 to the bridging nitrogen and R265 to a pyrimidine nitrogen) and these interactions are thought to provide significant binding energy to the interaction of DSM265 with *Pf*DHODH (Fig. 6B). Indeed, in related studies we found by X-ray structure analysis that the inability of human and rat DHODH to form a direct hydrogen

Table 2 DSM265 inhibition data for recombinant *Plasmodium* and mammalian DHODHs

Species	*P. falciparum*	*P. vivax*	*Human*	*Mouse*	*Rat*	*Dog*	*Rabbit*	*Pig*
IC_{50} (μg/mL)	0.010	0.020	~41	1.1	0.82	11	>41	>41

Data were taken from Ref. 24. The molecular weight of DSM265 is 415 g/mol.

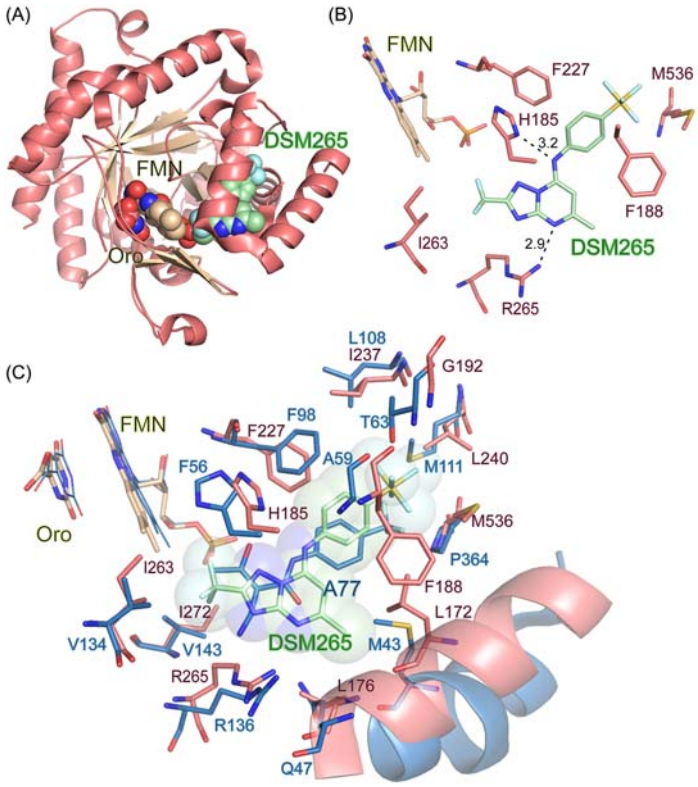

Fig. 6 X-ray structure of *Pf*DHODH bound to DSM265 (4RX0) showing active site ligand/protein contact residues in comparison to the human enzyme. (A) Cartoon diagram showing the overall structure. α-Helices are shown in *salmon*, β-sheets are shown in *tan*, orotate (Oro) (*salmon*), FMN (*tan*), and DSM265 (*green*) are shown as spheres. (B) Inhibitor binding site of DSM265 showing key interactions within the 4 Å shell. Hydrogen bonds are shown by *dashed lines* with indicated distances. *Pf*DHODH is *salmon*, FMN is *tan*, and DSM265 is *green*. (C) Comparison of the DSM265 *Pf*DHODH inhibitor binding site with the human DHODH A77 1726 (1D3H) binding site. Limited residues in the 4 Å shell of DSM265 are shown. Structures were aligned in PyMol using the align command. *Pf*DHODH is in *salmon*, human DHODH is in *blue*, *Pf*DHODH FMN and orotate are shown in *tan*, DSM265 is shown as *green sticks* with transparent spheres. A77 1726 from the human DHODH structure is shown in *blue* and the FMN and orotate from the human structures are shown as *blue lines*. Non-carbon atoms are colored as described in **Fig. 3**.

bond between H56 (H185 equivalent) and analogs from the series contributes to weaker binding to the mammalian enzymes.[47] The remaining DSM265 binding pocket is entirely hydrophobic and the aniline ring of DSM265 forms edge-to-face stacking interactions with F227 and F188, as well as making a number of additional van der Waals contacts with other hydrophobic residues in the binding pocket (primarily leucine and methionine residues) (**Fig. 6B,C**). The CF_2CH_3 group on the C2 carbon of the triazolopyrimidine ring makes close contacts with I263 and I272. These interactions are likely to contribute significant binding energy to the interaction. The structural basis for the species selectivity, which leads to >5000-fold better binding to *Pf*DHODH versus the human enzyme, is also apparent from the structure. A number of amino acid differences are found between the *P. falciparum* and human enzymes within the 4 Å van der Waals radius of DSM265 that change the shape and nature of the binding site (**Fig. 6C**).

8.22.5.3 In Vitro Activity Against Parasites

DSM265 has potent activity against *P. falciparum* blood-stage parasites in phenotypic assays, with similar efficacy observed against both drug-sensitive and drug-resistant strains (EC_{50} in a 72 h assay in albumax media ranged from 0.00066 to 0.0041 μg/mL) with an average of 0.0018 μg/mL.[24] Considering the data from reference strain *P. falciparum* 3D7 (**Table 3**) and assuming that the EC_{99} can be approximated as $9\times$ EC_{50}, these assays show that an unbound concentration of approximately 0.0028 μg/mL is sufficient to completely kill parasites in this test system. In order to assess if the parasite-based activity was cytocidal or cytostatic, washout and regrowth studies were performed after incubation of parasites with DSM265 for 24–120 h. These studies showed that after a 24–48 h lag phase, DSM265 had a kill rate that was similar to that for atovaquone and pyrimethamine, and the time required for >99.9% parasite clearance was ~80 h of drug exposure.[24] Thus, DSM265 does not kill as quickly as the artemisinin derivatives (which provide complete kill in <24 h[58]), but once past the lag phase it demonstrates a medium rate of kill similar to other clinically used antimalarial drugs. The mechanism of cell

Table 3 Activity of DSM265 on *P. falciparum* in blood and liver stages

Assay	*Total conc. (μg/mL)*	*Unbound conc. (μg/mL)*[a]
In vitro blood-stage assays		
P. falciparum 3D7 72 h assay—EC_{50} (EC_{99})	0.0018 (0.016)	0.00031 (0.0028)
P. falciparum 3D7 in vitro washout/regrowth assay—MPC	0.014	0.0020
In vitro liver-stage assays		
P. falciparum schizont 48 h assay—EC_{50}	0.0057	0.0012
In vivo SCID mouse efficacy		
P. falciparum—MPC plasma	1.1	0.0011

[a]Data were corrected for protein binding in the assay media or in plasma.
Data were taken from Ref. 24. *EC_{50}*, concentration required to inhibit 50% of parasite growth. The EC_{99} was estimated as $9\times$ EC_{50}.
MPC, minimum concentration required to achieve the maximum rate of kill.

killing was investigated and as expected, the transgenic *P. falciparum* line expressing yeast DHODH was resistant to DSM265, confirming that its mechanism of parasite killing is DHODH inhibition.[55] Drug synergy studies showed that DSM265 activity was additive with a number of clinically used antimalarial agents and no synergy nor antagonism was observed in these studies.[24]

8.22.5.4 Efficacy in the *P. falciparum* SCID Mouse Model

The gold standard in vivo assay for testing antimalarial drug candidates is currently a SCID (severe combined immune deficiency) mouse model which can be engrafted with human erythrocytes to support infection with *P. falciparum*.[59] When given orally twice daily for 4 days with parasitemia measurements 24 h after the last dose, DSM265 showed potent in vivo activity with an ED_{90} of 3.0 mg/kg/day. The minimum dose that gave the maximum rate of parasite killing was 13 mg/kg/day. The minimum total blood concentration at this dose was 0.53 μg/mL (plasma concentration of 1.1 μg/mL), which corresponds to a minimum unbound plasma concentration of 0.0011 μg/mL (**Table 3**).[24] This concentration represents the minimum concentration that results in the near maximal rate of parasite death and is frequently referred to as the minimum parasiticidal concentration (MPC). The unbound MPC estimated from the in vivo SCID mouse study (0.0011 μg/mL) is very similar to the unbound EC_{99} (0.0028 μg/mL) obtained in the standard in vitro assay as well as the in vitro estimated unbound MPC (0.002 μg/mL) from the washout/regrowth assay, providing confidence in the predictive value of these studies to support human dose predictions (see the following text).

8.22.5.5 Other Plasmodium Stages

From the standpoint of malaria elimination and eradication, assessing the activity of drug candidates on life cycle stages other than the blood stage has become an important priority in an attempt to identify new drugs that not only treat the infection, but that can also be used for prevention and for reducing transmission. DSM265 was tested against *P. falciparum* liver stages where it was found to have potent activity in a cultured hepatocyte model, with similar efficacy to that seen against the blood stage (**Table 3**).[24] These data suggest that DSM265 will be useful not only for treatment of malaria but also for prevention. While DSM265 had activity against liver-stage schizonts, it was not effective against in vitro liver forms most closely related to the dormant hypnozoites present with *P. vivax* infection. DSM265 also did not show activity against the *P. falciparum* sexual stage gametocytes, which is consistent with its mechanism of action. Both blood and liver stages (apart from the dormant stages) undergo many rounds of replication, and DSM265 has been shown to block progression of the life cycle in the early trophozoite immediately before RNA and DNA replication required for cell growth.[24] In contrast, the gametocyte stages in the mammalian host are nonreplicative, and late stage gametocytes are essentially metabolically inactive.[60] Consistently, DSM265 does show activity against the mosquito stage V oocyst, which is also a replicative form, suggesting that DSM265 taken up in the mosquito blood meal could potentially exert some transmission-blocking activity.[24]

8.22.5.6 Mechanism and Frequency of Resistance

The mechanism and frequency of resistance has been evaluated in vitro for both DSM1 and DSM265.[24,61] Resistant parasites were selected in a single step using multidrug-resistant strains (Dd2 and K1) that have a greater propensity to develop resistance. Resistant parasites could be selected using a drug concentration of $3\times$ EC_{50}, but at DSM265 concentrations of $8\times$ EC_{50} and above, resistant parasites were not obtained. Both gene amplification and point mutations in the DHODH gene were observed in these studies, providing additional validation of the target. The frequency of resistance at $3\times$ EC_{50} ranged from 10^5 to 10^7, which is similar to what has been observed for atovaquone. Given the potential for resistant parasites to emerge in vitro, careful monitoring for resistance is an important consideration in the early clinical studies that are underway. These studies also highlight the importance of marketing DSM265 as a combination partner with another antimalarial agent that has similar pharmacokinetic properties to help prevent the development of resistance in the field.

8.22.6 DSM265 Pharmacokinetic Properties to Meet the Goal of Single Dose Cure

8.22.6.1 Physicochemical Properties and In Vitro ADME Characteristics

With the exception of its high log *D* (4.0), DSM265 generally meets accepted "drug-like" criteria in terms of its molecular weight (415 Da), polar surface area (55 Å^2), number of hydrogen bond donors and acceptors (1 and 4, respectively), and freely rotatable bonds (4).[62,63] DSM265 displays high permeability across Caco-2 cell monolayers (P_{app} 50–60 $\times$ 10^{-6} cm/s) with no evidence for efflux. The primary physicochemical liability of DSM265 is its poor aqueous solubility ($\sim$5 μg/mL in simulated fasted state intestinal fluid), leading to it being classified as a BCS Class II molecule (high permeability, low solubility).[24] DSM265 is chemically stable in the solid state but is unstable when solutions are exposed to simulated sunlight.

Consistent with its high log *D*, DSM265 is highly bound to plasma proteins (>99% in human mouse and dog plasma and $\sim$98% in rat plasma).[24] Throughout the program, binding properties were also assessed in various protein-containing media used for in vitro activity testing to enable conversion of total concentrations to unbound concentrations to facilitate comparisons across assays and with the in vivo data. The high binding to plasma proteins resulted in a low blood to plasma partitioning ratio, ranging from 0.7 to 0.8 across species, except in the SCID mouse where the value is 0.5 due to the high hematocrit. When assessed for metabolic stability in vitro using hepatic microsomes or cryopreserved hepatocytes, DSM265 exhibited minimal degradation with an intrinsic clearance of <5 μL/min/mg microsomal protein and <1 μL/min/10^6 hepatocytes for each of the species tested.[24] The major metabolite identified from pooled in vivo plasma samples was DSM450 formed by oxidation of the methyl side chain.[24] This metabolite is approximately 40-fold less active than DSM265 against parasites and so would not be expected to contribute to the efficacy profile.

8.22.6.2 In Vivo Pharmacokinetic Studies in Preclinical Species

Pharmacokinetic studies were conducted in a number of preclinical species to inform the design of preclinical efficacy and toxicology studies, to understand the impact of poor solubility on oral absorption and bioavailability, and to provide a basis for human pharmacokinetic and dose predictions. Across all species tested, clearance following intravenous (IV) administration was low at less than 10% of hepatic blood flow[24] which is qualitatively consistent with the low rate of degradation detected in vitro following incubation with hepatic microsomes and hepatocytes. As would be expected given its log *D*, there was no evidence of renal elimination so hepatic metabolism is likely the main route of elimination. The half-life after IV administration increased from about 3 h in mice, to around 12 h in rats, but could not be determined in dogs due to evidence for enterohepatic recirculation. In monkeys, the half-life was approximately 45 h, providing confidence that there would likely be a further increase in half-life in humans.[24]

As shown in **Fig. 7**, the half-life following oral dosing increased from approximately 3 h in mice to 15 h in rats and more than 20 h in dogs. DSM265 exhibited moderate oral bioavailability following administration of a simple suspension formulation generally ranging from 20% to 50% across species.[24] There was evidence of a food effect in dogs, with area under the curve increasing approximately twofold in the fed state compared to that in fasted dogs (**Fig. 7B**). These initial pharmacokinetic results provided evidence that oral bioavailability was incomplete, most likely due to the poor aqueous solubility of DSM265. Several different formulation approaches were considered to address the low solubility including salt formation, particle size reduction, and an amorphous spray dried dispersion (SDD), with the latter demonstrating the greatest benefit for improving bioavailability.[24] As shown in **Fig. 7C**, exposure in fasted dogs increased approximately eightfold following oral dosing of the SDD formulation compared to a simple suspension formulation. In vitro, the SDD formulation improved the solubility of DSM265 in simulated fasted state intestinal fluids by approximately 20-fold and maintained this level for a period of at least 90 min. Given the high permeability of DSM265, even a short-term increase in solubility would likely be sufficient to improve absorption. These results provided confidence that the solubility-limited absorption could be overcome by disruption of the crystal lattice thereby improving both dissolution and solubility over the timeframe necessary for oral absorption.

8.22.6.3 Human Pharmacokinetic and Dose Predictions

Estimation of the human dose and dosing frequency required an estimate of the target concentration required for efficacy and an estimation of human pharmacokinetic parameters (primarily clearance). In vitro and in vivo activity models all pointed to an unbound concentration of 1–2 ng/mL being needed to achieve the maximum rate of parasite death (**Table 3**). Correcting this unbound concentration to a total plasma concentration, the target efficacious plasma concentration in humans is therefore 1–2 μg/mL. Since DSM265 exhibits a moderate rate of parasite kill, it was estimated that this target concentration would need to be maintained for a minimum period of about four parasite life cycles or 8 days.[64]

To estimate human clearance, we first considered the microsomal and hepatocyte stability data following scaling and application of the well-stirred model of hepatic clearance taking into account binding to both plasma proteins and proteins present in the in vitro incubation media and the blood to plasma ratio.[65] As has been reported previously for drugs that undergo minimal degradation in in vitro test systems,[66] this approach led to an underestimation ($\sim$20-fold) of the measured in vivo clearance in mice, rats, and dogs and we therefore considered this to be an unacceptable approach for predicting human clearance. We instead used allometry of the unbound IV clearance across the available species to estimate a human clearance of 0.25 L/h. To obtain an estimation of the in vivo absorption and distribution properties, measured physiochemical properties (log *D*, solubility of the SDD formulation in simulated intestinal fluids), permeability, plasma protein binding, and blood to plasma partitioning along with the predicted

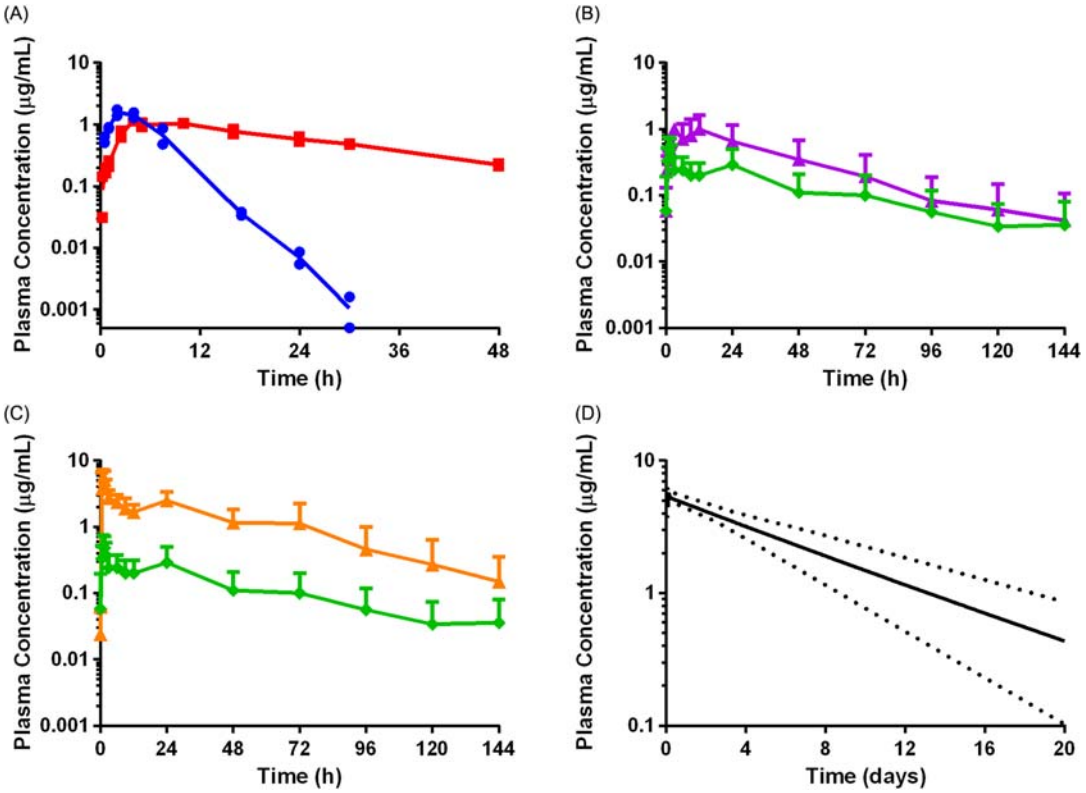

Fig. 7 Pharmacokinetic profiles in preclinical species and predicted human profile. Plasma pharmacokinetic profiles following a 10 mg/kg oral dose of DSM265 as a suspension formulation. (A) Male Swiss outbred mice (*blue*) or male Sprague Dawley rats (*red*); (B) fasted (*green*) or fed (*purple*) male beagle dogs. (C) Administration of a free base suspension (*green*) or spray dried dispersion (*orange*) to fasted male beagle dogs. (D) Predicted human profile following an oral dose of 250 mg along with the predicted 5th and 95th percentiles (*dotted lines*) for the simulated profile (Gastroplus). Data for mice ($n=2$ mice per time point) and rats ($n=2$) are shown as individual data points and data for dogs represent the mean ± SD ($n=6$). Graphs were generated from data reported in our published work.[24]

human clearance were input into a physiologically based pharmacokinetic (PBPK) model (GastroPlus, version 9.0). This software package uses the ACAT model[67] for predicting absorption, and the human physiological fasting condition was selected. A human PBPK model was used with clearance assumed to occur exclusively in the liver. Tissue disposition was simulated using the perfusion rate limited model by Rodgers and Rowland.[68,69] The model provided an estimate of the volume of distribution at steady state (46 L) and the half-life (126 h). We also used the PBPK model to simulate human plasma profiles along with the 5th/95th percentiles for a cohort of 25 males and females aged between 20 and 40 using the population variability data within the software (Fig. 7D). These simulations suggested that a single dose in excess of approximately 250 mg would likely maintain plasma concentrations above the target 1–2 μg/mL for a period of at least 8 days. The Phase I human clinical study has subsequently been completed at single doses (25–1200 mg range) and is currently reporting. Preliminary results for cohorts dosed from 25 to 400 mg confirm that the human half-life is ~104 h (range 60.4–141) and that a dose of 250–400 mg is likely to provide a single dose cure.[70] Thus, the long half-life and acceptable dose estimation, combined with both blood- and liver-stage activity, suggested that DSM265 was a good candidate for both treatment and chemoprotection. For use within a treatment scenario, DSM265 would ideally be combined with a fast-acting compound having a similar pharmacological duration of cover.

8.22.7 Safety Studies and the Importance of Knowing the Target

The safety of DSM265 was evaluated using in vitro safety pharmacology studies and exploratory multi-dose studies in mice and dogs.[24] There were no significant safety pharmacology signals. An initial positive response in the hERG patch clamp study (IC_{50} ranged from 0.7 to 3 μg/mL) was mitigated by completion of both a rabbit wedge study and a dog cardiovascular study, both of which showed that there was no propensity for cardiac risk under the conditions tested. Additionally, because of the high plasma protein binding of DSM265 in humans, the unbound drug concentration at the efficacious dose is expected to be 70–320-fold lower than the IC_{50} in the patch clamp study, suggesting a very low risk. DSM265 was well tolerated in mice and dogs in exploratory 7 and 10 day studies, respectively.[24,61] These studies in addition to subsequent 14-day GLP studies in these same species supported the

advancement of DSM265 into Phase I and II clinical studies. Of note during preliminary exploratory toxicity studies in rats, we found that rats tolerated DSM265 less well than mice and dogs. This result was traced back to the findings that rats suffer from both a low IC_{50} on rat DHODH and higher unbound concentrations compared to other species. As neither of these properties are reflective of the situation in humans, it was determined that rats were an inappropriate species for evaluating the toxicity of DSM265 and mice and dogs were used for the GLP studies to enable the first in man dosing. However importantly, these studies illustrate the value of knowing the protein target of a drug candidate. Knowledge of the target not only assisted the lead optimization, but it was also key to our ability to understand the toxicity that was observed in rats and to mitigate this risk through an understanding of the underlying factors.

8.22.8 Conclusion and Perspectives

DSM265 is a new entity for the treatment of malaria from the triazolopyrimidine structural class that was identified through a target-based screen followed by structure-guided lead optimization. It is the first inhibitor targeting DHODH to be developed for the treatment of malaria. The novel mechanism of action allows it to be active against *Plasmodium* species in the field that are resistant to currently used antimalarial agents. DSM265 has potent blood- and liver-stage activity and thus is expected to be useful for either treatment or chemoprevention of malaria. Its long predicted half-life in humans ($\sim$100 h) has now been confirmed and this supports its use as either a single dose cure or for once weekly prophylaxis. Due to the ability of the malaria parasite to develop resistance to drug therapies, all new drugs will be introduced into the clinic as combinations. Thus, the product development plan for DSM265 is to identify a suitable partner compound for its use in either treatment or prevention of malaria. DSM265 is currently in Phase II clinical development to assess both human safety and efficacy against *P. falciparum* and *P. vivax* malaria (http://www.mmv.org).

See also: 5.23. Antiparasitic Agents. 8.20. Case History: AN5568 (SCYX-7158). 8.21. KAE609 (Cipargamin): Discovery of Spiroindolone Antimalarials.

References

1. WHO. *Malaria;* WHO, 2015. Fact Sheet No 94, 10/2015 ed.
2. White, N. J.; Pukrittayakamee, S.; Hien, T. T.; Faiz, M. A.; Mokuolu, O. A.; Dondorp, A. M. Malaria. *Lancet* **2014,** *383,* 723–735.
3. Miller, L. H.; Ackerman, H. C.; Su, X. Z.; Wellems, T. E. Malaria Biology and Disease Pathogenesis: Insights for New Treatments. *Nat. Med.* **2013,** *19,* 156–167.
4. Cotter, C.; Sturrock, H. J.; Hsiang, M. S.; Liu, J.; Phillips, A. A.; Hwang, J.; Gueye, C. S.; Fullman, N.; Gosling, R. D.; Feachem, R. G. The Changing Epidemiology of Malaria Elimination: New Strategies for New Challenges. *Lancet* **2013,** *382,* 900–911.
5. Hemingway, J.; Shretta, R.; Wells, T. N.; Bell, D.; Djimde, A. A.; Achee, N.; Qi, G. Tools and Strategies for Malaria Control and Elimination: What Do We Need to Achieve a Grand Convergence in Malaria? *PLoS Biol.* **2016,** *14,* e1002380.
6. Tran, T. M.; Portugal, S.; Draper, S. J.; Crompton, P. D. Malaria Vaccines: Moving Forward After Encouraging First Steps. *Curr. Trop. Med. Rep.* **2015,** *2,* 1–3.
7. Wells, T. N.; Hooft van Huijsduijnen, R.; Van Voorhis, W. C. Malaria Medicines: A Glass Half Full? *Nat. Rev. Drug Discov.* **2015,** *14,* 424–442.
8. Burrows, J. N.; Hooft van Huijsduijnen, R.; Mohrle, J. J.; Oeuvray, C.; Wells, T. N. Designing the Next Generation of Medicines for Malaria Control and Eradication. *Malar. J.* **2013,** *12,* 187.
9. Burrows, J. N.; Chibale, K.; Wells, T. N. The State of the Art in Anti-Malarial Drug Discovery and Development. *Curr. Top. Med. Chem.* **2011,** *11,* 1226–1254.
10. Straimer, J.; Gnadig, N. F.; Witkowski, B.; Amaratunga, C.; Duru, V.; Ramadani, A. P.; Dacheux, M.; Khim, N.; Zhang, L.; Lam, S.; Gregory, P. D.; Urnov, F. D.; Mercereau-Puijalon, O.; Benoit-Vical, F.; Fairhurst, R. M.; Menard, D.; Fidock, D. A. Drug Resistance. K13-Propeller Mutations Confer Artemisinin Resistance in *Plasmodium falciparum* Clinical Isolates. *Science* **2015,** *347,* 428–431.
11. Mok, S.; Ashley, E. A.; Ferreira, P. E.; Zhu, L.; Lin, Z.; Yeo, T.; Chotivanich, K.; Imwong, M.; Pukrittayakamee, S.; Dhorda, M.; Nguon, C.; Lim, P.; Amaratunga, C.; Suon, S.; Hien, T. T.; Htut, Y.; Faiz, M. A.; Onyamboko, M. A.; Mayxay, M.; Newton, P. N.; Tripura, R.; Woodrow, C. J.; Miotto, O.; Kwiatkowski, D. P.; Nosten, F.; Day, N. P.; Preiser, P. R.; White, N. J.; Dondorp, A. M.; Fairhurst, R. M.; Bozdech, Z. Drug Resistance. Population Transcriptomics of Human Malaria Parasites Reveals the Mechanism of Artemisinin Resistance. *Science* **2015,** *347,* 431–435.
12. Miotto, O.; Amato, R.; Ashley, E. A.; MacInnis, B.; Almagro-Garcia, J.; Amaratunga, C.; Lim, P.; Mead, D.; Oyola, S. O.; Dhorda, M.; Imwong, M.; Woodrow, C.; Manske, M.; Stalker, J.; Drury, E.; Campino, S.; Amenga-Etego, L.; Thanh, T. N.; Tran, H. T.; Ringwald, P.; Bethell, D.; Nosten, F.; Phyo, A. P.; Pukrittayakamee, S.; Chotivanich, K.; Chuor, C. M.; Nguon, C.; Suon, S.; Sreng, S.; Newton, P. N.; Mayxay, M.; Khanthavong, M.; Hongvanthong, B.; Htut, Y.; Han, K. T.; Kyaw, M. P.; Faiz, M. A.; Fanello, C. I.; Onyamboko, M.; Mokuolu, O. A.; Jacob, C. G.; Takala-Harrison, S.; Plowe, C. V.; Day, N. P.; Dondorp, A. M.; Spencer, C. C.; McVean, G.; Fairhurst, R. M.; White, N. J.; Kwiatkowski, D. P. Genetic Architecture of Artemisinin-Resistant *Plasmodium falciparum*. *Nat. Genet.* **2015,** *47,* 226–234.
13. Menard, D.; Ariey, F. Towards Real-Time Monitoring of Artemisinin Resistance. *Lancet Infect. Dis.* **2015,** *15,* 367–368.
14. Amaratunga, C.; Lim, P.; Suon, S.; Sreng, S.; Mao, S.; Sopha, C.; Sam, B.; Dek, D.; Try, V.; Amato, R.; Blessborn, D.; Song, L.; Tullo, G. S.; Fay, M. P.; Anderson, J. M.; Tarning, J.; Fairhurst, R. M. Dihydroartemisinin-Piperaquine Resistance in *Plasmodium falciparum* Malaria in Cambodia: A Multisite Prospective Cohort Study. *Lancet Infect. Dis.* **2016,** *16,* 357–365.
15. Chaorattanakawee, S.; Saunders, D. L.; Sea, D.; Chanarat, N.; Yingyuen, K.; Sundrakes, S.; Saingam, P.; Buathong, N.; Sriwichai, S.; Chann, S.; Se, Y.; Yom, Y.; Heng, T. K.; Kong, N.; Kuntawunginn, W.; Tangthongchaiwiriya, K.; Jacob, C.; Takala-Harrison, S.; Plowe, C.; Lin, J. T.; Chuor, C. M.; Prom, S.; Tyner, S. D.; Gosi, P.; Teja-Isavadharm, P.; Lon, C.; Lanteri, C. A. Ex Vivo Drug Susceptibility Testing and Molecular Profiling of Clinical *Plasmodium falciparum* Isolates from Cambodia from 2008 to 2013 Suggest Emerging Piperaquine Resistance. *Antimicrob. Agents Chemother.* **2015,** *59,* 4631–4643.
16. Alonso, P. L.; Brown, G.; Arevalo-Herrera, M.; Binka, F.; Chitnis, C.; Collins, F.; Doumbo, O. K.; Greenwood, B.; Hall, B. F.; Levine, M. M.; Mendis, K.; Newman, R. D.; Plowe, C. V.; Rodriguez, M. H.; Sinden, R.; Slutsker, L.; Tanner, M. A Research Agenda to Underpin Malaria Eradication. *PLoS Med.* **2011,** *8,* e1000406.
17. The malEra Consultative Group on Monitoring, Surveillance, and Evaluation. A Research Agenda for Malaria Eradication: Monitoring, Evaluation, and Surveillance. *PLoS Med.* **2011,** *8,* e1000400.

18. Duparc, S.; Lanza, C.; Ubben, D.; Borghini-Fuhrer, I.; Kellam, L. Optimal Dose Finding for Novel Antimalarial Combination Therapy. *Trop. Med. Int. Health* **2012,** *17,* 409–413.
19. Charman, S. A.; Arbe-Barnes, S.; Bathurst, I. C.; Brun, R.; Campbell, M.; Charman, W. N.; Chiu, F. C.; Chollet, J.; Craft, J. C.; Creek, D. J.; Dong, Y.; Matile, H.; Maurer, M.; Morizzi, J.; Nguyen, T.; Papastogiannidis, P.; Scheurer, C.; Shackleford, D. M.; Sriraghavan, K.; Stingelin, L.; Tang, Y.; Urwyler, H.; Wang, X.; White, K. L.; Wittlin, S.; Zhou, L.; Vennerstrom, J. L. Synthetic Ozonide Drug Candidate OZ439 Offers New Hope for a Single-Dose Cure of Uncomplicated Malaria. *Proc. Natl. Acad. Sci. U. S. A.* **2011,** *108,* 4400–4405.
20. Moehrle, J. J.; Duparc, S.; Siethoff, C.; van Giersbergen, P. L.; Craft, J. C.; Arbe-Barnes, S.; Charman, S. A.; Gutierrez, M.; Wittlin, S.; Vennerstrom, J. L. First-in-Man Safety and Pharmacokinetics of Synthetic Ozonide OZ439 Demonstrates an Improved Exposure Profile Relative to Other Peroxide Antimalarials. *Br. J. Clin. Pharmacol.* **2013,** *75,* 524–537.
21. Spillman, N. J.; Allen, R. J.; McNamara, C. W.; Yeung, B. K.; Winzeler, E. A.; Diagana, T. T.; Kirk, K. Na(+) Regulation in the Malaria Parasite *Plasmodium falciparum* Involves the Cation ATPase PfATP4 and Is a Target of the Spiroindolone Antimalarials. *Cell Host Microbe* **2013,** *13,* 227–237.
22. Smith, P. W.; Diagana, T. T.; Yeung, B. K. Progressing the Global Antimalarial Portfolio: Finding Drugs Which Target Multiple Plasmodium Life Stages. *Parasitology* **2014,** *141,* 66–76.
23. Kuhen, K. L.; Chatterjee, A. K.; Rottmann, M.; Gagaring, K.; Borboa, R.; Buenviaje, J.; Chen, Z.; Francek, C.; Wu, T.; Nagle, A.; Barnes, S. W.; Plouffe, D.; Lee, M. C.; Fidock, D. A.; Graumans, W.; van de Vegte-Bolmer, M.; van Gemert, G. J.; Wirjanata, G.; Sebayang, B.; Marfurt, J.; Russell, B.; Suwanarusk, R.; Price, R. N.; Nosten, F.; Tungtaeng, A.; Gettayacamin, M.; Sattabongkot, J.; Taylor, J.; Walker, J. R.; Tully, D.; Patra, K. P.; Flannery, E. L.; Vinetz, J. M.; Renia, L.; Sauerwein, R. W.; Winzeler, E. A.; Glynne, R. J.; Diagana, T. T. KAF156 Is an Antimalarial Clinical Candidate With Potential for Use in Prophylaxis, Treatment, and Prevention of Disease Transmission. *Antimicrob. Agents Chemother.* **2014,** *58,* 5060–5067.
24. Phillips, M. A.; Lotharius, J.; Marsh, K.; White, J.; Dayan, A.; White, K. L.; Njoroge, J. W.; El Mazouni, F.; Lao, Y.; Kokkonda, S.; Tomchick, D. R.; Deng, X.; Laird, T.; Bhatia, S. N.; March, S.; Ng, C. L.; Fidock, D. A.; Wittlin, S.; Lafuente-Monasterio, M.; Benito, F. J.; Alonso, L. M.; Martinez, M. S.; Jimenez-Diaz, M. B.; Bazaga, S. F.; Angulo-Barturen, I.; Haselden, J. N.; Louttit, J.; Cui, Y.; Sridhar, A.; Zeeman, A. M.; Kocken, C.; Sauerwein, R.; Dechering, K.; Avery, V. M.; Duffy, S.; Delves, M.; Sinden, R.; Ruecker, A.; Wickham, K. S.; Rochford, R.; Gahagen, J.; Iyer, L.; Riccio, E.; Mirsalis, J.; Bathhurst, I.; Rueckle, T.; Ding, X.; Campo, B.; Leroy, D.; Rogers, M. J.; Rathod, P. K.; Burrows, J. N.; Charman, S. A. A Long-Duration Dihydroorotate Dehydrogenase Inhibitor (DSM265) for Prevention and Treatment of Malaria. *Sci. Transl. Med.* **2015,** *7,* 296ra111.
25. Burrows, J. N.; Burlot, E.; Campo, B.; Cherbuin, S.; Jeanneret, S.; Leroy, D.; Spangenberg, T.; Waterson, D.; Wells, T. N.; Willis, P. Antimalarial Drug Discovery—The Path Towards Eradication. *Parasitology* **2014,** *141,* 128–139.
26. Garavito, M. F.; Narvaez-Ortiz, H. Y.; Zimmermann, B. H. Pyrimidine Metabolism: Dynamic and Versatile Pathways in Pathogens and Cellular Development. *J. Genet. Genomics* **2015,** *42,* 195–205.
27. Vaidya, A. B.; Mather, M. W. Mitochondrial Evolution and Functions in Malaria Parasites. *Annu. Rev. Microbiol.* **2009,** *63,* 249–267.
28. Phillips, M. A.; Rathod, P. K. Plasmodium Dihydroorotate Dehydrogenase: A Promising Target for Novel Anti-Malarial Chemotherapy. *Infect. Disord. Drug Targets* **2010,** *10,* 226–239.
29. Phillips, M. A. Antimalarial Agents Targeting Nucleotide Synthesis and Electron Transport: Insight From Structural Biology. In *Neglected Diseases and Drug Discovery;* Palmer, M., Wells, T. N. C., Eds.; RCS Publishing: Cambridge, UK, 2011; pp 65–87.
30. Yuthavong, Y.; Tarnchompoo, B.; Vilaivan, T.; Chitnumsub, P.; Kamchonwongpaisan, S.; Charman, S. A.; McLennan, D. N.; White, K. L.; Vivas, L.; Bongard, E.; Thongphanchang, C.; Taweechai, S.; Vanichtanankul, J.; Rattanajak, R.; Arwon, U.; Fantauzzi, P.; Yuvaniyama, J.; Charman, W. N.; Matthews, D. Malarial Dihydrofolate Reductase as a Paradigm for Drug Development Against a Resistance-Compromised Target. *Proc. Natl. Acad. Sci. U. S. A.* **2012,** *109,* 16823–16828.
31. Painter, H. J.; Morrisey, J. M.; Mather, M. W.; Vaidya, A. B. Specific Role of Mitochondrial Electron Transport in Blood-Stage *Plasmodium falciparum*. *Nature* **2007,** *446,* 88–91.
32. Ganesan, S. M.; Morrisey, J. M.; Ke, H.; Painter, H. J.; Laroiya, K.; Phillips, M. A.; Rathod, P. K.; Mather, M. W.; Vaidya, A. B. Yeast Dihydroorotate Dehydrogenase as a New Selectable Marker for *Plasmodium falciparum* Transfection. *Mol. Biochem. Parasitol.* **2011,** *177,* 29–34.
33. Ghorbal, M.; Gorman, M.; Macpherson, C. R.; Martins, R. M.; Scherf, A.; Lopez-Rubio, J. J. Genome Editing in the Human Malaria Parasite *Plasmodium falciparum* Using the CRISPR-Cas9 System. *Nat. Biotechnol.* **2014,** *32,* 819–821.
34. Herrmann, M.; Schleyerbach, R.; Kirschbaum, B. Leflunomide: An Immunomodulatory Drug for the Treatment of Rheumatoid Arthritis and Other Autoimmune Diseases. *Immunopharmacology* **2000,** *47,* 273–289.
35. Kraan, M.; de Koster, B.; Elferink, J.; Post, W.; Breedveld, F.; Tak, P. Inhibition of Neutrophil Migration Soon After Initiation of Treatment With Leflunomide or Methotrexate in Patients With Rheumatoid Arthritis. *Arthritis Rheum.* **2000,** *43,* 1488–1495.
36. Fragoso, Y. D.; Brooks, J. B. Leflunomide and Teriflunomide: Altering the Metabolism of Pyrimidines for the Treatment of Autoimmune Diseases. *Expert. Rev. Clin. Pharmacol.* **2015,** *8,* 315–320.
37. Meier, F. M.; Frerix, M.; Hermann, W.; Muller-Ladner, U. Current Immunotherapy in Rheumatoid Arthritis. *Immunotherapy* **2013,** *5,* 955–974.
38. Miller, A. E. Teriflunomide: A Once-Daily Oral Medication for the Treatment of Relapsing Forms of Multiple Sclerosis. *Clin. Ther.* **2015,** *37,* 2366–2380.
39. Cody, R.; Stewart, D.; DeForni, M.; Moore, M.; Dallaire, B.; Azarnia, N.; Gyves, J. Multicenter Phase II Study of Brequinar Sodium in Patients With Advanced Breast Cancer. *Am. J. Clin. Oncol.* **1993,** *16,* 526–528.
40. Cramer, D. V. Brequinar Sodium. *Transplant. Proc.* **1996,** *28,* 960–963.
41. Dodion, P. F.; Wagener, T.; Stoter, G.; Drozd, A.; Lev, L. M.; Skovsgaard, T.; Renard, J.; Cavalli, F. Phase II Trial With Brequinar (DUP-785, NSC 368390) in Patients With Metastatic Colorectal Cancer: A Study of the Early Clinical Trials Group of the EORTC. *Ann. Oncol.* **1990,** *1,* 79–80.
42. Munier-Lehmann, H.; Vidalain, P. O.; Tangy, F.; Janin, Y. L. On Dihydroorotate Dehydrogenases and Their Inhibitors and Uses. *J. Med. Chem.* **2013,** *56,* 3148–3167.
43. Liu, S.; Neidhardt, E. A.; Grossman, T. H.; Ocain, T.; Clardy, J. Structures of Human Dihydroorotate Dehydrogenase in Complex With Antiproliferative Agents. *Structure* **2000,** *8,* 25–33.
44. Baldwin, J.; Farajallah, A. M.; Malmquist, N. A.; Rathod, P. K.; Phillips, M. A. Malarial Dihydroorotate Dehydrogenase. Substrate and Inhibitor Specificity. *J. Biol. Chem.* **2002,** *277,* 41827–41834.
45. Baldwin, J.; Michnoff, C. H.; Malmquist, N. A.; White, J.; Roth, M. G.; Rathod, P. K.; Phillips, M. A. High-Throughput Screening for Potent and Selective Inhibitors of *Plasmodium falciparum* Dihydroorotate Dehydrogenase. *J. Biol. Chem.* **2005,** *280,* 21847–21853.
46. Phillips, M. A.; Gujjar, R.; Malmquist, N. A.; White, J.; El Mazouni, F.; Baldwin, J.; Rathod, P. K. Triazolopyrimidine-Based Dihydroorotate Dehydrogenase Inhibitors With Potent and Selective Activity Against the Malaria Parasite, *Plasmodium falciparum*. *J. Med. Chem.* **2008,** *51,* 3649–3653.
47. Deng, X.; Matthews, D.; Rathod, P. K.; Phillips, M. A. The X-Ray Structure of *Plasmodium falciparum* Dihydroorotate Dehydrogenase Bound to a Potent and Selective *N*-Phenylbenzamide Inhibitor Reveals Novel Binding-Site Interactions. *Acta Crystallogr. F Struct. Biol. Commun.* **2015,** *71,* 553–559.
48. Deng, X.; Gujjar, R.; El Mazouni, F.; Kaminsky, W.; Malmquist, N. A.; Goldsmith, E. J.; Rathod, P. K.; Phillips, M. A. Structural Plasticity of Malaria Dihydroorotate Dehydrogenase Allows Selective Binding of Diverse Chemical Scaffolds. *J. Biol. Chem.* **2009,** *284,* 26999–27009.
49. Hurt, D. E.; Widom, J.; Clardy, J. Structure of *Plasmodium falciparum* Dihydroorotate Dehydrogenase With a Bound Inhibitor. *Acta Crystallogr. D Biol. Crystallogr.* **2006,** *62,* 312–323.
50. Booker, M. L.; Bastos, C. M.; Kramer, M. L.; Barker, R. H., jr.; Skerlj, R.; Bir Sdhu, A.; Deng, X.; Celatka, C.; Cortese, J. F.; Guerrero Bravo, J. E.; Krespo Llado, K. N.; Serrano, A. E.; Angulo-Barturen, I.; Belén Jiménez-Díaz, M.; Viera, S.; Garuti, H.; Wittlin, S.; Papastogiannidis, P.; Lin, J.; Janse, C. J.; Khan, S. M.; Duraisingh, M.; Coleman, B.; Goldsmith, E. J.; Phillips, M. A.; Munoz, B.; Wirth, D. F.; Klinger, J. D.; Wiegand, R.; Sybertz, E. Novel Inhibitors of *Plasmodium falciparum* Dihydroorotate Dehydrogenase With Anti-Malarial Activity in the Mouse Model. *J. Biol. Chem.* **2010,** *285,* 33054–33064.

51. Malmquist, N. A.; Gujjar, R.; Rathod, P. K.; Phillips, M. A. Analysis of Flavin Oxidation and Electron-Transfer Inhibition in *Plasmodium falciparum* Dihydroorotate Dehydrogenase. *Biochemistry* **2008,** *47,* 2466–2475.
52. Gujjar, R.; Marwaha, A.; El Mazouni, F.; White, J.; White, K. L.; Creason, S.; Shackleford, D. M.; Baldwin, J.; Charman, W. N.; Buckner, F. S.; Charman, S.; Rathod, P. K.; Phillips, M. A. Identification of a Metabolically Stable Triazolopyrimidine-Based Dihydroorotate Dehydrogenase Inhibitor With Antimalarial Activity in Mice. *J. Med. Chem.* **2009,** *52,* 1864–1872.
53. Gujjar, R.; El Mazouni, F.; White, K. L.; White, J.; Creason, S.; Shackleford, D. M.; Deng, X.; Charman, W. N.; Bathurst, I.; Burrows, J.; Floyd, D. M.; Matthews, D.; Buckner, F. S.; Charman, S. A.; Phillips, M. A.; Rathod, P. K. Lead-Optimization of Aryl and Aralkyl Amine Based Triazolopyrimidine Inhibitors of *Plasmodium falciparum* Dihydroorotate Dehydrogenase With Anti-Malarial Activity in Mice. *J. Med. Chem.* **2011,** *54,* 3935–3949.
54. Coteron, J. M.; Marco, M.; Esquivias, J.; Deng, X.; White, K. L.; White, J.; Koltun, M.; El Mazouni, F.; Kokkonda, S.; Katneni, K.; Bhamidipati, R.; Shackleford, D. M.; Angulo-Barturen, I.; Ferrer, S. B.; Jimenez-Diaz, M. B.; Gamo, F. J.; Goldsmith, E. J.; Charman, W. N.; Bathurst, I.; Floyd, D.; Matthews, D.; Burrows, J. N.; Rathod, P. K.; Charman, S. A.; Phillips, M. A. Structure-Guided Lead Optimization of Triazolopyrimidine-Ring Substituents Identifies Potent *Plasmodium falciparum* Dihydroorotate Dehydrogenase Inhibitors With Clinical Candidate Potential. *J. Med. Chem.* **2011,** *54,* 5540–5561.
55. Deng, X.; Kokkonda, S.; El Mazouni, F.; White, J.; Burrows, J. N.; Kaminsky, W.; Charman, S. A.; Matthews, D.; Rathod, P. K.; Phillips, M. A. Fluorine Modulates Species Selectivity in the Triazolopyrimidine Class of *Plasmodium falciparum* Dihydroorotate Dehydrogenase Inhibitors. *J. Med. Chem.* **2014,** *57,* 5381–5394.
56. Marwaha, A.; White, J.; El Mazouni, F.; Creason, S. A.; Kokkonda, S.; Buckner, F. S.; Charman, S. A.; Phillips, M. A.; Rathod, P. K. Bioisosteric Transformations and Permutations in the Triazolopyrimidine Scaffold to Identify the Minimum Pharmacophore Required for Inhibitory Activity Against *Plasmodium falciparum* Dihydroorotate Dehydrogenase. *J. Med. Chem.* **2012,** *55,* 7425–7436.
57. Kokkonda, S.; Deng, X.; White, K. L.; Coteron, J. M.; Marco, M.; de Las Heras, L.; White, J.; El Mazouni, F.; Tomchick, D. R.; Manjalanagara, K.; Rudra, K. R.; Chen, G.; Morizzi, J.; Ryan, E.; Kaminsky, W.; Leroy, D.; Martinez-Martinez, M. S.; Jimenez Diaz, M. B.; Bazaga, S. F.; Angulo-Barturen, I.; Waterson, D.; Burrows, J. N.; Matthews, D.; Charman, S. A.; Phillips, M. A.; Rathod, P. K. Tetrahydro-2-Naphthyl and 2-Indanyl Triazolopyrimidines Targeting *Plasmodium falciparum* Dihydroorotate Dehydrogenase Display Potent and Selective Antimalarial Activity. *J. Med. Chem.* **2016;** http://dx.doi.org/10.1021/acs.jmedchem.6b00275.
58. Sanz, L. M.; Crespo, B.; De-Cozar, C.; Ding, X. C.; Llergo, J. L.; Burrows, J. N.; Garcia-Bustos, J. F.; Gamo, F. J. *P. falciparum* In Vitro Killing Rates Allow to Discriminate Between Different Antimalarial Mode-of-Action. *PLoS One* **2012,** *7,* e30949.
59. Jimenez-Diaz, M. B.; Mulet, T.; Viera, S.; Gomez, V.; Garuti, H.; Ibanez, J.; Alvarez-Doval, A.; Shultz, L. D.; Martinez, A.; Gargallo-Viola, D.; Angulo-Barturen, I. Improved Murine Model of Malaria Using *Plasmodium falciparum* Competent Strains and Non-Myelodepleted NOD-Scid IL2Rgammanull Mice Engrafted With Human Erythrocytes. *Antimicrob. Agents Chemother.* **2009,** *53,* 4533–4536.
60. Sinden, R. E.; Smalley, M. E. Gametocytogenesis of *Plasmodium falciparum* In Vitro: The Cell-Cycle. *Parasitology* **1979,** *79,* 277–296.
61. Guler, J. L.; Freeman, D. L.; Ahyong, V.; Patrapuvich, R.; White, J.; Gujjar, R.; Phillips, M. A.; DeRisi, J.; Rathod, P. K. Asexual Populations of the Human Malaria Parasite, *Plasmodium falciparum*, Use a Two-Step Genomic Strategy to Acquire Accurate, Beneficial DNA Amplifications. *PLoS Pathog.* **2013,** *9,* e1003375.
62. Lipinski, C. A.; Lombardo, F.; Dominy, B. W.; Feeney, P. J. Experimental and Computational Approaches to Estimate Solubility and Permeability in Drug Discovery and Development Settings. *Adv. Drug Deliv. Rev.* **2001,** *46,* 3–26.
63. Veber, D. F.; Johnson, S. R.; Cheng, H. Y.; Smith, B. R.; Ward, K. W.; Kopple, K. D. Molecular Properties That Influence the Oral Bioavailability of Drug Candidates. *J. Med. Chem.* **2002,** *45,* 2615–2623.
64. White, N. J. Assessment of the Pharmacodynamic Properties of Antimalarial Drugs In Vivo. *Antimicrob. Agents Chemother.* **1997,** *41,* 1413–1422.
65. Ring, B. J.; Chien, J. Y.; Adkison, K. K.; Jones, H. M.; Rowland, M.; Jones, R. D.; Yates, J. W.; Ku, M. S.; Gibson, C. R.; He, H.; Vuppugalla, R.; Marathe, P.; Fischer, V.; Dutta, S.; Sinha, V. K.; Bjornsson, T.; Lave, T.; Poulin, P. PhRMA CPCDC Initiative on Predictive Models of Human Pharmacokinetics, Part 3: Comparative Assessment of Prediction Methods of Human Clearance. *J. Pharm. Sci.* **2011,** *100,* 4090–4110.
66. Jones, H. M.; Mayawala, K.; Poulin, P. Dose Selection Based on Physiologically Based Pharmacokinetic (PBPK) Approaches. *AAPS J.* **2013,** *15,* 377–387.
67. Agoram, B.; Woltosz, W. S.; Bolger, M. B. Predicting the Impact of Physiological and Biochemical Processes on Oral Drug Bioavailability. *Adv. Drug Deliv. Rev.* **2001,** *50* (Suppl.1), S41–S67.
68. Rodgers, T.; Leahy, D.; Rowland, M. Physiologically Based Pharmacokinetic Modeling 1: Predicting the Tissue Distribution of Moderate-to-Strong Bases. *J. Pharm. Sci.* **2005,** *94,* 1259–1276.
69. Rodgers, T.; Rowland, M. Physiologically Based Pharmacokinetic Modelling 2: Predicting the Tissue Distribution of Acids, Very Weak Bases, Neutrals and Zwitterions. *J. Pharm. Sci.* **2006,** *95,* 1238–1257.
70. McCarthy, J. S.; Lotharius, J.; Dayan, A.; Phillips, M. A.; Marsh, K.; Walker, D.; Baker, M.; Elliott, S.; Griffin, P.; Ng, C.; Fidock, D.; Bebrevska, L.; Duparc, S.; Moehrle, J.; Rueckle, T. A Phase I/Ib Study to Investigate the Safety, Tolerability and Pharmacokinetic Profile of dsm265 in Healthy Subjects and Then Its Antimalarial Activity in Induced Blood Stage *Plasmodium falciparum* Infection. *ASTMH Annual Meeting Abstract 675*; 2014; pp 204–205.

Relevant Websites

http://www.cdc.gov/malaria/—Centers for Disease Control and Prevention.
http://www.dndi.org—Drugs for Neglected Disease Organization.
http://www.gatesfoundation.org—Gates Foundation.
https://www.ghitfund.org—Global Health Innovative Technology Fund.
http://www.mmv.org—Medicines for Malaria Venture.
http://www.niaid.nih.gov—National Institute of Allergy and Infectious Diseases.
http://www.who.int/en/—World Health Organization.

8.23 Harvoni: A Combination Therapy for Curing HCV

MJ Sofia, Arbutus Biopharma, Inc., Doylestown, PA, United States
JO Link, Gilead Sciences, Inc., Foster City, CA, United States

© 2017 Elsevier Ltd. All rights reserved.

8.23.1	**Introduction**	558
8.23.2	**The Discovery of Sofosbuvir**	559
8.23.2.1	Target Rationale: HCV NS5B RNA-Dependent RNA Polymerase	559
8.23.2.2	A 2′-F, 2′-*C*-Methylnucleoside Inhibitor of HCV Replication	559
8.23.2.3	Rationale and Design of a Liver-Targeted Nucleotide Prodrug	561
8.23.2.4	Prodrug Optimization and Preclinical Evaluation	563
8.23.2.5	Clinical Proof of Concept of a Liver-Targeted Nucleotide Prodrug	565
8.23.2.6	The Single Diastereomer: Sofosbuvir	565
8.23.2.7	Sofosbuvir Clinical Studies and the Backbone of Drug Combinations	566
8.23.3	**Ledipasvir**	567
8.23.3.1	Mechanism of Action and Structural Information	568
8.23.3.2	Discovery of Ledipasvir	569
8.23.3.3	The Genotype 1 Resistance Profile of Ledipasvir	572
8.23.3.4	Broad Genotype Activity of Ledipasvir	572
8.23.3.5	Translation to the Clinic: Ledipasvir Phase 1 Human Pharmacokinetics, Monotherapy Antiviral Activity, and Studies on RAVs	573
8.23.3.6	Phase 2 Studies With Ledipasvir and Agents Other Than Sofosbuvir	575
8.23.4	**Phase 3 Registrational Clinical Studies With Ledipasvir and Sofosbuvir**	575
8.23.4.1	Harvoni® Approval	576
8.23.4.2	Harvoni® Postapproval Studies, Label Expansion and Study in Japan	577
8.23.4.3	Harvoni® Real World Results	578
8.23.5	**Conclusion**	579
References		579

8.23.1 Introduction

The hepatitis C virus (HCV) is a heptatrophic virus that chronically infects approximately 150 million individuals worldwide. Chronic HCV infection is known to cause liver cirrhosis and hepatocellular carcinoma (HCC) and is a leading cause of liver transplants worldwide. Approximately 700,000 individuals globally die from HCV-related liver disease.[1]

The HCV, originally known as non-A non-B hepatitis, was identified and its genome was elucidated in 1989.[2,3] This work led to screening of the human blood supply that has prevented transmission of HCV by blood transfusion. However, HCV continued to be spread through the sharing of needles by injection drug users, unprotected sex, and accidental needle sticks.

The HCV is a single-stranded positive-sense RNA virus of the *Flaviviridae* family of viruses in the genus *Hepacivirus*. There are six major HCV genotypes (GT1–6), the distribution of which varies globally with GT1, 2, and 3 viruses being predominant in North America and Europe. In Africa, HCV infections are almost exclusively genotypes 4 and 5 virus, and genotype 6 virus is most prevalent in Asia and other parts of the world.[4] No protective vaccine exists for HCV.

Until 2011 the standard of care for treating HCV infection was the use of injectable interferon (IFN) and oral ribavirin (RBV).[5,6] This therapeutic regimen provided only a modest 40% cure rate after 48 weeks of therapy and an undesirable side effect profile that included flu-like symptoms, severe anemia, and neurological problems. The side effects were so intolerable that the patient discontinuation rate was exceptionally high. In addition the IFN-containing therapies were shown to have limited effectiveness in difficult to treat patient populations that included African-American patients and patients that harbor a TT or TC allele 3 kb upstream of the IL28B gene in a region that encodes the type III interferon, IFN-λ3.[7,8]

The HCV genome encodes three structural and seven nonstructural proteins (**Fig. 1**). The seven nonstructural proteins play a wide variety of roles in enabling the viral life cycle. These include the processing of the genome-derived polypeptide into the individual viral nonstructural proteins (NS2 protease, NS3 protease, and NS4 cofactor) and formation of the viral replication complex associated with the endoplasmic reticulum (NS4B, NS5A, and NS5B). The NS3 protease also plays a role in how the virus controls the host innate immune response.[9] HCV has a very high error-prone rate of replication which does not incorporate a proof-reading function. Therefore, HCV exhibits a high mutation rate.[10,11]

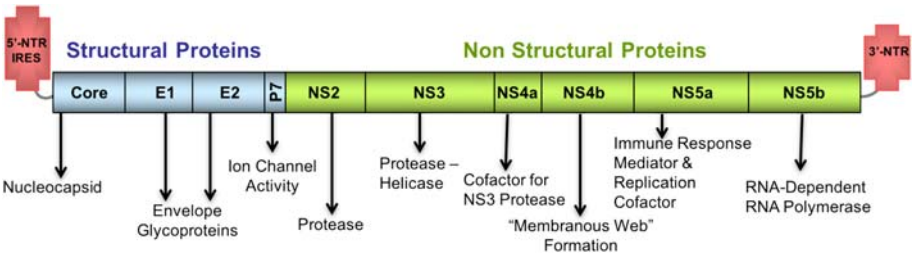

Fig. 1 HCV genome, structural proteins, and nonstructural proteins.

By 1999 with the development of the HCV whole cell replicon assay, the search for direct acting antivirals against HCV became more feasible. However, the search for curative therapies posed many questions which included whether IFN could be eliminated from therapy and whether the duration of therapy could be shortened from 48 weeks. Furthermore, it was not obvious which HCV drug targets were the most relevant for delivering an improved cure rate or what would be the best combination of direct acting antivirals for achieving cures. Other concerns included whether a therapeutic regimen could be identified that covered all viral genotypes and if drug resistance to new therapies would become a major issue. These questions were ultimately answered with the approval of NS5B polymerase inhibitor sofosbuvir (Sovaldi®) **1** plus ribavirin **2** for the treatment of HCV patients infected with genotypes 2 and 3 virus and subsequently with the introduction of Harvoni®, the fixed-dose combination of sofosbuvir **1** and the NS5A inhibitor, ledipasvir **3**, for the treatment of genotype 1 patients.

This article will discuss the discovery and development of sofosbuvir (Sovaldi®) and ledipasvir and the development of the fixed-dose combination agent Harvoni® as a curative therapy for HCV patients.

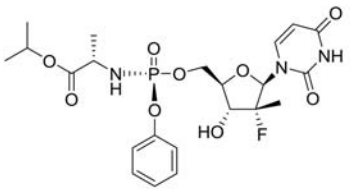

Sofosbuvir
1

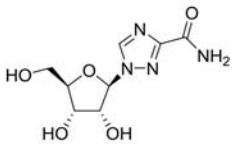

Ribavirin
2

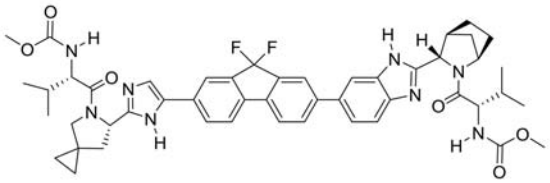

Ledipasvir, GS-5885
3

8.23.2 The Discovery of Sofosbuvir

8.23.2.1 Target Rationale: HCV NS5B RNA-Dependent RNA Polymerase

The HCV NS5B RNA-dependent RNA polymerase (RdRp) is one of seven HCV nonstructural proteins and is a viral specific enzyme that is essential for HCV replication (Fig. 1).[12] The NS5B RdRp is a 66 kDa protein that exhibits the typical palm–finger–thumb structural motif found in many viral polymerases. The Gly317–Asp318–Asp319 (GDD) catalytic motif found in the palm domain of the HCV NS5B RdRp is an invariant element in RNA viral polymerases and is highly conserved across all HCV genotypes.[13] Therefore the HCV RdRp provided an ideal target against which to develop a pan-genotypic, direct-acting-antiviral (DAA) with a high barrier to resistance.

8.23.2.2 A 2′-F, 2′-*C*-Methylnucleoside Inhibitor of HCV Replication

The path forward for the development of a pan-genotypic and high barrier to resistant inhibitor of the HCV NS5B polymerase began with the idea of using a nucleoside analog that resembled the viral polymerase's natural substrate. However, pursuing a nucleoside

drug discovery strategy posed a number of obstacles, one being the complexity of nucleoside metabolism necessary to effect its mechanism of action and the other being selectivity for the viral polymerase over host polymerases. The activity of a nucleoside analog is dependent on the generation of the nucleoside triphosphate in the cell because it is this triphosphate that acts as the alternate substrate for the viral polymerase, and consequently, inhibits viral replication. Early work identified the unique 2′-α-F-2′-β-C-methyl substitution as having anti-HCV activity, leading to the novel nucleoside PSI-6130 **4**, a 2′-F-2′-C-methylcytidine nucleoside.[14] Extensive structure–activity relationship (SAR) work showed that any modification to the ribose or base portion of this nucleoside did not lead to nucleosides with improved potency.[15]

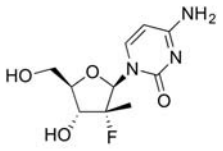

PSI-6130
4

PSI-6130 was shown to be a highly selective inhibitor of HCV replication and functioned as a nonobligate chain terminator.[16] It was also shown to be highly selective for inhibiting HCV over other viruses including human polymerases. The S282T NS5B mutation was identified as the only significant resistant mutation after extended passaging.[17,18] In combination studies with other anti-HCV agents, PSI-6130 showed additive or synergistic activity. The preclinical safety profile supported progression into human clinical studies; however, PSI-6130's pharmacokinetic profile demonstrated modest bioavailability and extensive metabolism into an inactive uridine derivative **5**.[15]

After clinical confirmation of an unfavorable pharmacokinetic profile for PSI-6130, an attempt to overcome this drug's limitations led to the development of a prodrug. This prodrug, RG7128 (mericitabine) **6**, which masked the 3′- and 5′-hydroxyl groups of the nucleoside as their isobutyrate esters did improve oral bioavailability, but formation of significant amounts of the inactive uridine metabolite still persisted.[19,20] However, this prodrug did demonstrate proof of concept for the 2′-F, 2′-methyl nucleosides as inhibitors of HCV replication in humans.[15,21,22] It also showed for the first time that a DAA was effective not only against genotype 1 virus but also against genotypes 2 and 3 virus. Furthermore, within these clinical studies it was observed that no resistant virus emerged when patients were treated with RG7128 and the drug was well tolerated.

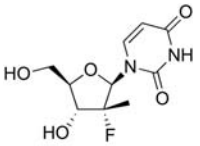

PSI-6206
5

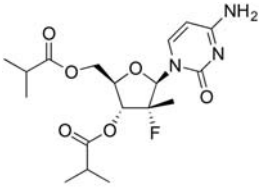

RG7128
(Mericitabine)
6

A seminal study evaluating the all DAA combinations of mericitabine with an HCV protease inhibitor, danoprevir **7**, showed that an IFN-free DAA combination could produce viral load declines (-4.9 to $-5.1\ \log_{10}\ \mathrm{IU\ mL^{-1}}$) on par with regimens containing PEG-IFN/RBV + protease inhibitors.[23] This observation laid the groundwork for future PEG-IFN free all DAA regimens. Unfortunately, because of its modest potency, PK profile, and short intrahepatic triphosphate half-life that required administration of a significant amount of drug, mericitabine lacked the ideal profile for a successful HCV therapy.

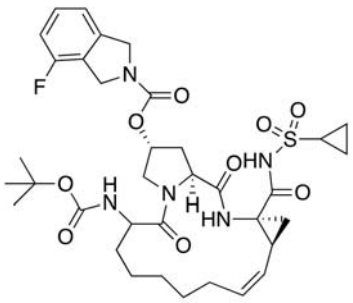

Danoprevir
7

8.23.2.3 Rationale and Design of a Liver-Targeted Nucleotide Prodrug

To overcome the deficiencies with mericitabine, it was determined that a next generation agent would need to demonstrate better intrinsic potency, a PK profile that supported once-daily dosing, a longer intrahepatitic triphosphate half-life, and if possible enable liver targeting while maintaining the clean safety profile, high selectivity for HCV, and a high barrier to resistance exhibited by the 2′-F-2′-*C*-methyl nucleoside substitution. These objectives led to a complete redesign of the nucleoside inhibitor with attention drawn to an unlikely compound, the inactive uridine metabolite of PSI-6130 **4**, PSI-6206 **5**. It had been determined that although the uridine nucleoside PSI-6206 was inactive in the replicon assay, its triphosphate derivative was active as an inhibitor of the HCV polymerase in a biochemical assay (Fig. 2).[19,20] In addition the half-life of the uridine triphosphate in primary hepatocytes was determined to be significantly longer than the triphosphate of the cytidine derivative indicating the potential for increased potency and less frequent dosing in vivo. Ultimately, the inactivity of the uridine nucleoside was attributed to it not being enzymatically

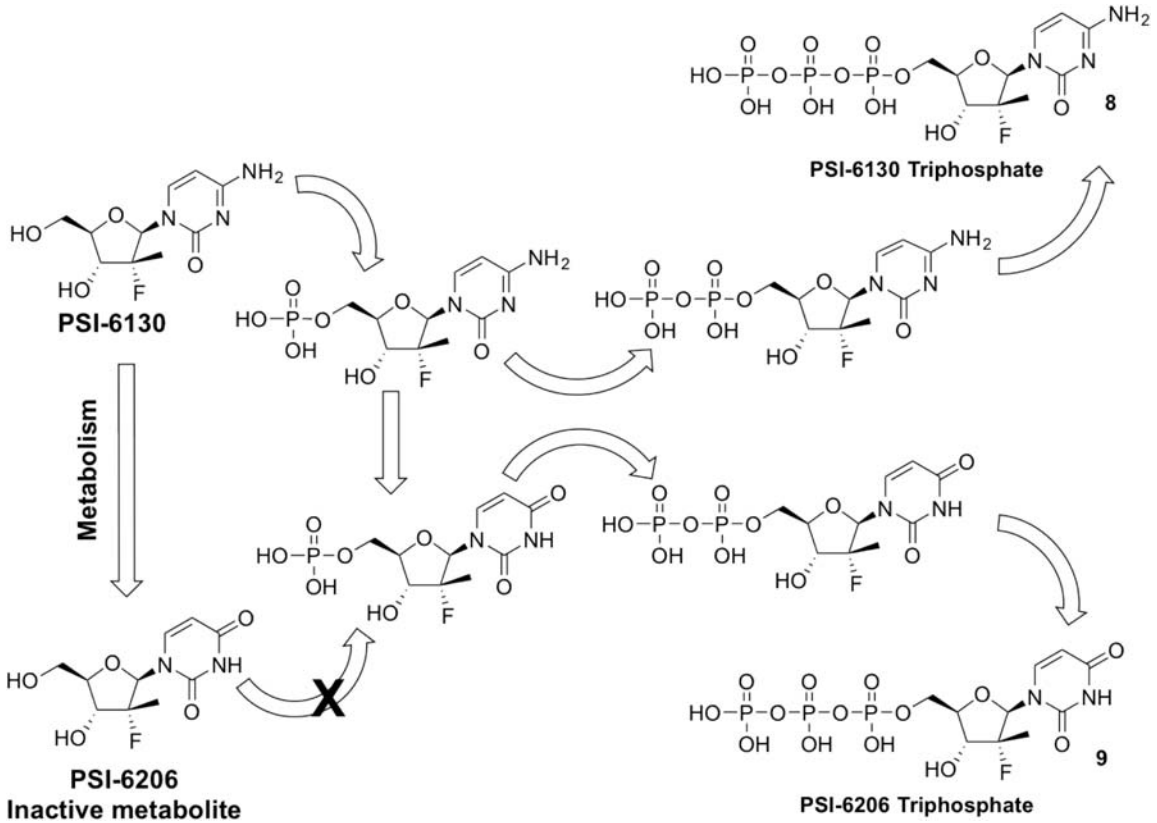

Fig. 2 Metabolism of PSI-6130. Formation of the HCV inactive metabolite PSI-6206 and the formation of the active metabolite triphosphates.

converted to the monophosphate precursor of the triphosphate. The solution to accessing the uridine triphosphate in cells was to find a way of bypassing the blocked phosphorylation step and deliver the monophosphate into hepatocytes (Fig. 2). However, the delivery of a highly charged and chemically and enzymatically unstable molecule was not going to be a simple task.

A possible solution to the delivery of a nucleoside monophosphate into liver cells was to mask the phosphate group such that the molecule is able to traverse biological membranes and is stabilized to chemical and enzymatic degradation. With the eventual loss of the mask in hepatocytes, the nucleoside monophosphate could then be further metabolized to give the active triphosphate. To achieve this objective an appropriate prodrug strategy would need to be implemented.

In considering prodrug options not only did we want to consider the need to mask a phosphate group to impart membrane compatibility and stability but we also introduced the requirement that the prodrug should enable liver targeting (Fig. 3). The concept of designing liver targeting character into a molecule was an aspirational objective and one that had yet to be realized in HCV drug discovery, notwithstanding the fact that a nucleoside phosphate had never been successfully delivered and shown to be effective in a human clinical setting. In contemplating the concept of live targeting, it became apparent that this might be achievable by leveraging liver first pass metabolism. However, the issue became how to build all these requirements into a single molecule.

When considering all of the numerous phosphate prodrug options, the phosphoramidate prodrug construct **10** was thought to potentially provide the best possibility of meeting the requirments.[24] Conceptually, first pass liver metabolism of the terminal ester of the phosphoramidate moiety would initiate a cascade of chemical and enzymatic events that would ultimately result in 2′-F-2′-*C*-methyluridine 5′-monophosphate being trapped within hepatocytes (Fig. 3). However, there still existed the significant hurdle of developing a prodrug that would be stable in the gastrointestinal tract, get sufficiently absorbed through the gut, reach the liver intact, and have an acceptable safety profile (Fig. 3). To predict a priori that the phosphoramidate could deliver on all of these requirements was not possible. There was no literature precedent to support delivery in a human, liver targeting or human safety. Consequently, an extensive structure activity exploration and preclinical assessment was undertaken to determine if we could find the right molecule that could achieve the outcome we desired.[24]

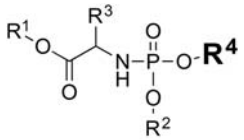

10

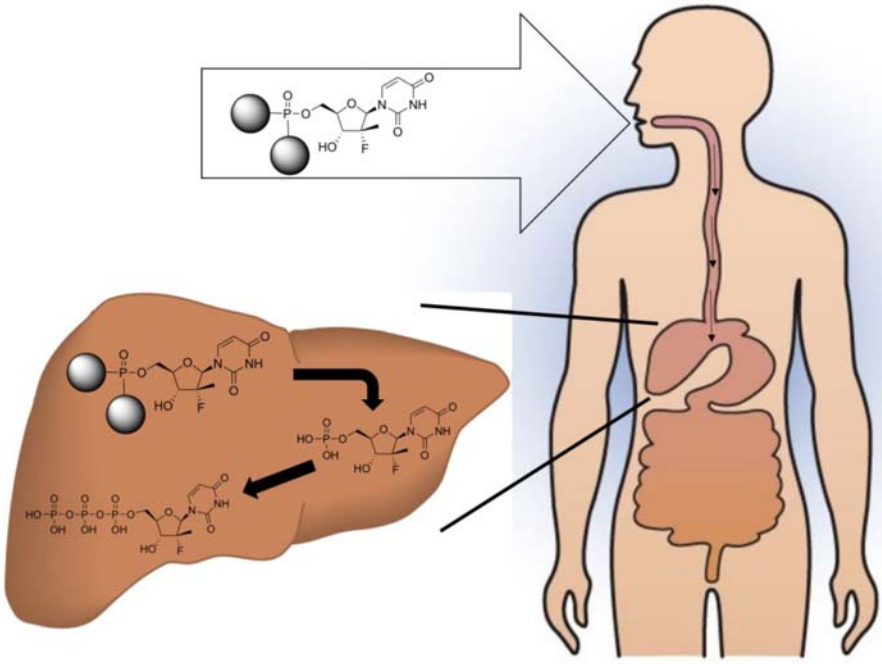

Fig. 3 The concept of a phosphate prodrug and liver first pass metabolism.

8.23.2.4 Prodrug Optimization and Preclinical Evaluation

We concluded that to develop the ideal drug candidate, a preclinical assessment scheme would be needed to consider not only whole cell HCV replicon activity but also cellular toxicity, stability in gastric fluids, and plasma and liver enzyme stability. Other key in vitro studies included assessment of the desired triphosphate levels in primary hepatocytes. Our view was that the ideal drug candidate would demonstrate submicromolar inhibition of HCV replication in the whole cell replicon assay, no cellular toxicity, stability in gastric fluid and plasma, low stability against liver enzymes, and the production of high intracellular triphosphate levels.

Because of historic concerns around nucleoside-based drugs, safety profiling became an important consideration as the preclinical evaluation progressed. This led us to undertake extensive evaluation of cytotoxicity across many different cell lines, and mitochondrial and bone marrow toxicity assessments to address the potential for off-target effects typically seen with nucleosides.

In vivo assessment relied on the development of a surrogate animal model. Chimpanzees were the only HCV animal model available at the time but access to this model was limited. Consequently, we developed an in vivo model that relied on quantitation of nucleoside triphosphate levels in the liver of animals when the drug candidates were administered orally.[24] This animal model was based on the assumption that high liver triphosphate levels correlated with improved efficacy. This model allowed us to assess many compounds and compare pharmacokinetics and efficacy across different species.

With our compound evaluation scheme in place, a structure–activity study of the phosphoramidate moiety was undertaken.[24] The strategy was to evaluate the three variable regions of the phosphoramidate moiety where each compound was first prepared as a diastereomeric mixture at phosphorus. With no available synthetic methods for accessing diastereomerically pure phosphoramidates, the program would have had to develop such methods and slow down progression to proof of concept in humans. Thus this strategy allowed us to more rapidly execute the SAR study and quickly reach a proof of concept for this prodrug approach. It was realized that if the proof of concept was achieved, then we would eventually have to face the task of developing a single isomer approach to this class of molecules.

We were encouraged by the whole cell replicon activity of the first 2′-F-2′-*C*-methyluridine 5′-monophospate phosphoramidate prodrug, PSI-7672 **11**, but to assess whether this prodrug approach would meet all the criteria necessary for a clinical candidate, further development had to be done.[25] As we progressed with the SAR study, there was a constant awareness and concern of potential toxicities that could result from prodrug release products in the liver. This led to a careful selection of prodrug substituents based on known toxicities. The SAR exploration led to the following observations.

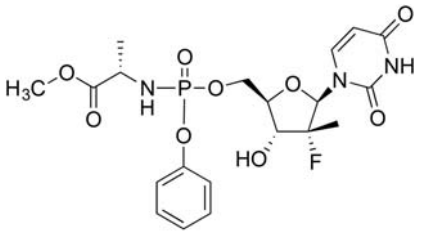

PSI-7672

11

The α-amino acid position of the phosphoramidate only tolerated monosubstitution, and the L-configuration was required (Fig. 4).[24] The preferred substituents at the α-position of the phosphoramidate amino acid moiety were small unsubstituted alkyl groups (Fig. 4). Large alkyl ester groups on the amino acid, such as *n*-butyl, 2-butyl, and *n*-pentyl esters, resulted in molecules with undesired cytotoxicity (Fig. 5). The phosphate ester SAR revealed that aromatic groups were preferred over alkyl esters and that the most potent aryl esters such as 1-naphthyl and halogenated phenyl groups, although superior with respect to potency, generally suffered from unwanted cytotoxicity (Fig. 5).[24]

Further assessment of replicon active compounds looked at gastric fluid stability, plasma stability, and liver enzyme stability and led to the selection of seven key compounds (Fig. 6).[24] This key compound selection set was also chosen because it represented a structurally diverse group since it was not clear to us what structural characteristics were going to control pharmacokinetics and efficacy in vivo.

The seven key compounds were studied first in an in vivo rat model. Each candidate was analyzed for plasma and liver levels of the intact prodrug, the mono-, di-, and triphosphates, and the intermediate prodrug metabolites. This study produced three advanced candidates that were subsequently progressed into in vivo activity and PK evaluation in dogs and cynomolgus monkeys.[24]

In parallel each of the advanced leads, **11**, **12**, and **17**, were incubated with human, rat, dog, and monkey primary hepatocytes to evaluated PSI-6206 triphosphate levels produced.[24] These data would provide a cross species comparison with human hepatocytes and correlation with the in vivo animal studies.

Following in vitro mitochondrial and bone marrow toxicity studies and in vivo whole animal non-GLP 7-day toxicity studies, PSI-7851 **12** was selected as the lead clinical development candidate.[24] PSI-7851 demonstrated submicromolar whole cell replicon activity with no cytotoxicity against a range of primary cell lines and no mitochondrial or bone marrow toxicity. It was metabolically

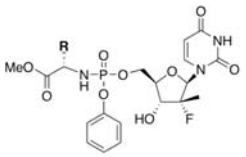

R	Clone A EC_{90} (μM)	Cytotox % Inhib RNA Synth @ 50 μM
H	22.11	0.0
Me	0.91	0.0
Et	1.61	0.0
Me_2CH	>50	0.0
Me_2CHCH_2	5.4	0.0
$MeSCH_2CH_2$	60.13	24.1
$PhCH_2$	57.65	20.6
Indole-2-CH_2	15.6	68.4

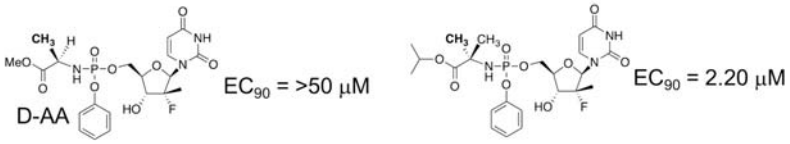

Fig. 4 Structure–activity relationship of the amino acid portion of the phosphoramidate prodrug moiety on the uridine nucleotide PSI-6206.

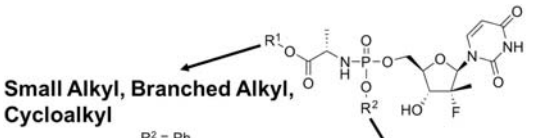

R^2 = Ph

R^1	Clone A EC_{90}	Cytotox % Inhib RNA Synth @ 50 μM
Me	0.91	0
i-Pr	0.52	26
2-Bu	0.06	94
Ph	18	0
Bn	0.13	74

R^1 = Me

R^2	Clone A EC_{90}	Cytotox % Inhib RNA Synth @ 50 μM
Ph	0.91	0
4-Cl-Ph	0.58	63
1-Naphth	0.09	95
Et	>50	17

Fig. 5 Structure–activity relationship overview of the carboxylic acid and phosphate ester portions of the phosphoramidate prodrug portion of the uridine nucleotide PSI-6206.

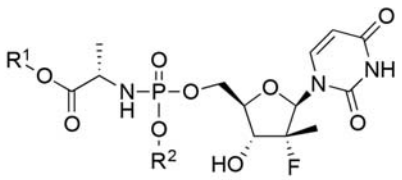

Key Compounds

	R^1	R^2
11	CH_3	Ph
12	iPr	Ph
13	*c*-Hex	Ph
14	Et	4-F-Ph
15	iPr	4-F-Ph
16	iPr	4-Cl-Ph
17	*c*-Hex	4-F-Ph

Advanced Candidates

	R^1	R^2
11	CH_3	Ph
12	iPr	Ph
17	*c*-Hex	4-F-Ph

Fig. 6 Key compounds and advanced candidates of phosphoramidate prodrugs of PSI-6206 monophosphate that were advanced into late preclinical development.

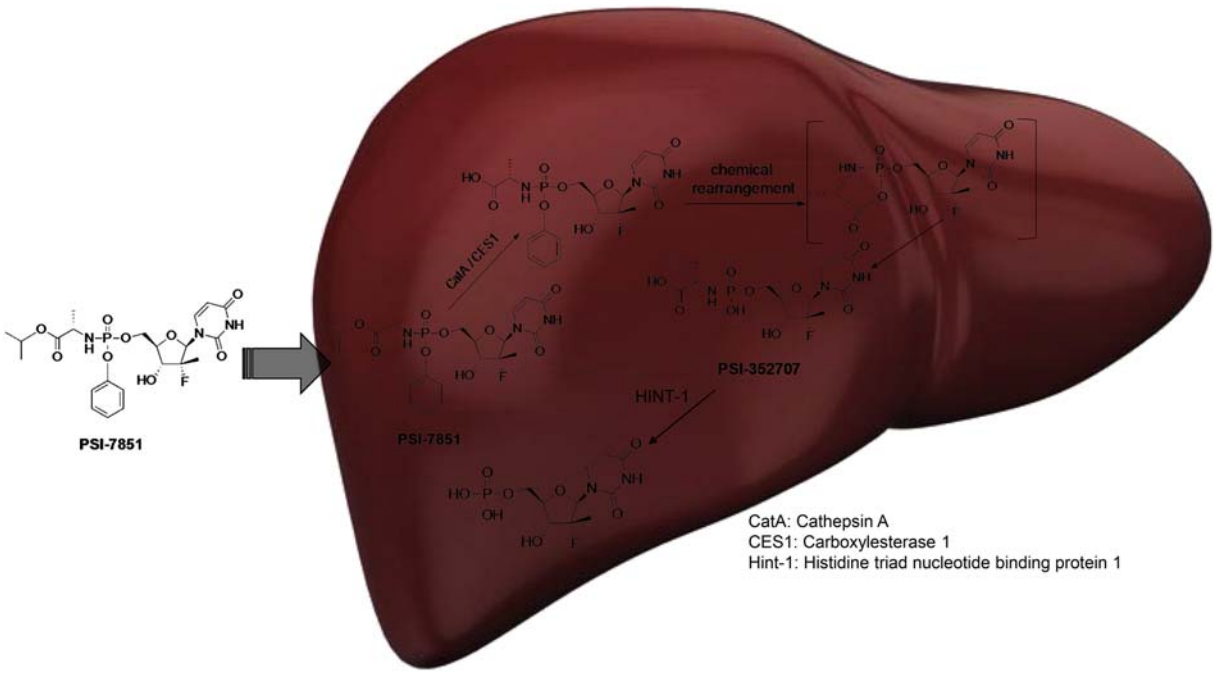

Fig. 7 Detailed picture of the prodrug metabolism of PSI-7851.

stable in plasma and gastric and intestinal fluids. High liver levels of the uridine nucleoside triphosphate were observed in multiple species that were translated into a high liver to plasma ratio. PSI-7851 **12** demonstrated the pan-genotypic activity, and the high barrier to resistance that had been sought in a second generation nucleos(t)ide agent. It was shown that PSI-7851 **12** was sensitive to the S282T amino acid change in the HCV RdRp which had been identified as the resistant variant for 2′-methyl nucleoside HCV inhibitors such as PSI-6130. However, as was observed for the 2′-F, 2′-*C*-methylcytidine nucleoside PSI-6130, the viral phenotype containing the mutated RdRp was shown to have reduced viral replication capacity making the mutant virus very unfit for survival.[26]

A detailed analysis of the metabolism of PSI-7851 that included both in vitro and in vivo radiolabeled whole cell studies and in vivo metabolite profiling provided a complete picture of the prodrug release mechanism and metabolism to the active triphosphate (Fig. 7). These studies showed that carboxylesterase 1 or cathepsin A were responsible for cleavage of the terminal amino acid ester and histidine triad nucleotide binding protein 1 (HINT-1) cleaved the bond between the amino acid and the phosphate group. Isolation and characterization of the putative prodrug cleavage intermediate di-acid, PSI-352707, solidified the prodrug degradation mechanism.[27,28]

8.23.2.5 Clinical Proof of Concept of a Liver-Targeted Nucleotide Prodrug

PSI-7851 was taken into a Phase 1 clinical study to evaluate safety, human pharmacokinetics, and efficacy. The proof of concept for the delivery of a nucleotide prodrug specifically to the liver and its utility as an anti-HCV agent was finally demonstrated when HCV GT1 patients were treated orally with PSI-7851 at doses ranging from 50 to 400 mg once daily over 3 days.[15] HCV RNA declined in these patients in a dose-dependent manner with mean changes from baseline of -0.49 to -1.95 $\log_{10}$ IU mL^{-1}.[29] Analysis of the PK profile showed a systemic profile consistent with rapid uptake by the liver with low plasma exposure of the prodrug PSI-7851 and the 5′-monophosphate prodrug release product, therefore, supporting a liver targeting mechanism. Consistent with earlier work using 2′-F, 2′-methyl nucleosides, patients treated with PSI-7851 exhibited no preexisting nor treatment emergent S282T mutations detected nor evidence of viral resistance following the 3 days of therapy. The proof of concept was achieved.

8.23.2.6 The Single Diastereomer: Sofosbuvir

With the proof of concept that delivery of a nucleotide directly targeted to the liver can reduce HCV levels in patients now in hand, our objective was to access the more potent of the two isomers found in PSI-7851 and complete the clinical development. This was done by first carefully separating the two isomers chromatographically and determining their relative potencies.[24] Following the development of a selective crystallization method to separate the two isomers and then determining by X-ray crystallography the configuration of the preferred isomer a homochiral synthesis of the more potent isomer was designed.[30]

PSI-7977 **1** was determined to be the more potent of the two diastereoisomers found in the mixture PSI-7851 **12** and its configuration at phosphorus was assigned to be Sp (Fig. 8).[24] PSI-7977 **1** was shown to be a potent inhibitor of the HCV RdRp with and

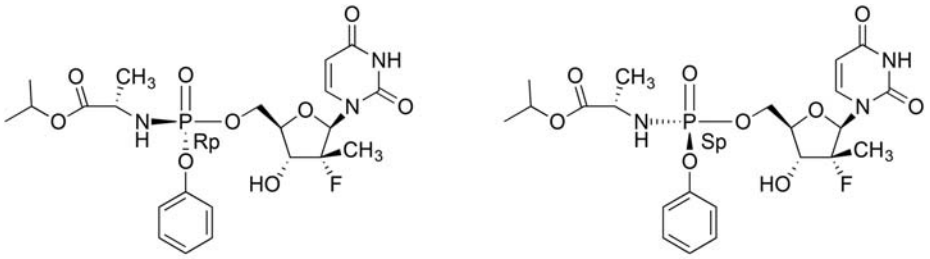

PSI-7976
18

PSI-7977 (sofosbuvir)
1

	Clone A: EC_{90} (μM)		EC_{90} Fold Increase
Compound No.	WT	S282T	S282T/WT
PSI-7976	7.5 ± 3.0	>100	>13
PSI-7977	0.42 ± 0.23	7.8 ± 5.3	18.6

Fig. 8 Structures of each of the two isomers of PSI-7851, PSI-7976, and PSI-7977 (sofosbuvir). The replicon whole cell activities of PSI-7976 and PSI-7977 against the wild-type and S282T mutant replicon.

$EC_{90} = 0.42$ μM in the HCV GT1b replicon assay. It demonstrated pan-genotypic activity and showed additive to synergistic effects when combined with IFN and a wide variety of HCV DAAs including NS5A inhibitors, NS3/4 protease inhibitors, non-nucleoside NS5B inhibitors, and other nucleos(t)ide inhibitors.[31,32] This ability to combine with other DAAs was going to become important in the future development of HCV-cure drug combinations. In vitro, PSI-7977 **1** exhibited no cytotoxicity, mitochondrial toxicity, or bone marrow toxicity.[24] PSI-7977 **1** was shown not to be a substrate for human DNA polymerases, RNA polymerases, or mitochondrial polymerases.[33] Animal toxicology studies and preclinical animal pharmacology studies showed no significant drug-related findings. In addition PSI-7977 **1** was not genotoxic when studied in a battery of in vitro and in vivo tests nor did it show effects on embryo–fetal viability or on fertility when studied in rats.[34] Ultimately, PSI-7977 became known as sofosbuvir (SOF).

A commercially attractive diastereoselective synthesis of sofosbuvir was eventually developed based on new methodology unprecedented in the literature.[30,35]

The synthesis utilized a stable phosphoramidating reagent that incorporated a phenolate leaving group (Fig. 9). When the stable crystalline and isomerically pure phosphoramidating reagent was reacted with the unprotected uridine nucleoside, sofosbuvir was produced in high yield and with high diastereoselectivity (>99.7de).

8.23.2.7 Sofosbuvir Clinical Studies and the Backbone of Drug Combinations

Phase 2 clinical studies with sofosbuvir demonstrated that in combination with IFN at doses of 100, 200, and 400 mg qd over 28 days in GT1 patients, a rapid virological response (RVR) was observed in 88–94% of the patients and viral load declines of 5.1–5.3 $\log_{10}$IU mL^{-1} were observed. Studies also showed that sofosbuvir was significantly more effective at reducing viral load in HCV patients than the single isomer PSI-7851.[36,37]

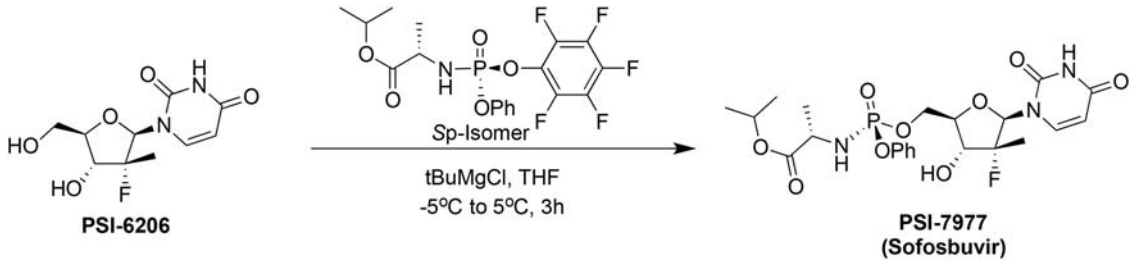

Fig. 9 Diastereoselective synthesis of the phosphoramidate portion of PSI-7977 (sofosbuvir).

A small 50-patient 5-arm Phase 2 clinical study evaluated sofosbuvir as monotherapy, in combination with RBV, or in combination with IFN/RBV for 12 weeks in GT2,3 patients and assessed SVR (sustained viralogic response, or cure—measured as no detectable virus post the last drug dose) rates 12 and 24 weeks after cessation of therapy.[38] The results showed that patients on the IFN-free combination achieved a 100% SVR 12 and 24, identical to patients taking the sofosbuvir + IFN/RBV triple combination.

Subsequently, initial registration studies focused on sofosbuvir in combination with RBV for GT2 and 3 patients and sofosbuvir in combination with Peg-IFN/RBV for GT1 and 4 patients. In a broad GT2 HCV patient population, sofosbuvir + RBV led to high cure rates (SVR12) between 92% and 94% following only 12 or 16 weeks of therapy. This study also showed that GT2 patient status (i.e., treatment naïve, cirrhotics, or treatment experienced) had no impact on cure rates.[39,40]

For GT3 patient the sofosbuvir-based IFN-free regimen containing only RBV was not quite as efficacious as had been seen for GT2 patients. For GT3 patients the best treatment regimens required sofosbuvir + RBV for 24 weeks and achieved an SVR of 86%. GT3 patient status did appear to play some role in outcome where treatment-experienced patients responded less well than treatment-naïve patients, and treatment-experienced cirrhotic patients (SVR12 60%) responded less well than patients without cirrhosis (SVR12 85%).[39,40]

In GT1 or 4 patient populations, sofosbuvir + RBV alone was not sufficient to deliver high cure rates (Fig. 9). In this patient population a sofosbuvir + PEG-IFN/RBV combination therapy for 12 weeks was required to deliver a high overall response rate (SVR12) of 91% (GT1 89%, GT4 96%).[39,40]

Throughout its clinical study history, sofosbuvir resistance never became a concern. Preemergent or on-treatment-emergent resistant variants had never been observed for sofosbuvir-based combination therapies. The HCV polymerase S282T amino acid change, which was identified in the laboratory as the primary sofosbuvir resistance mutation, was shown to be unfit and was not identified as a preemergent variant in the clinic; nor were viral breakthroughs observed on treatment.[26,32,39,41] The less frequent novel double mutation (L159F/L320F) which conferred low level resistance to sofosbuvir was also identified in the laboratory but these single and double mutations were also shown to have a low replication capacity.[41]

On Dec. 6, 2013 sofosbuvir was approved by the US FDA for the treatment of HCV GT1–4 patient populations with regulatory approval for the first IFN-free combination of sofosbuvir + RBV being approved for GT2 and 3 patient populations. However, with all the demonstrated success of sofosbuvir regimens, there still existed the need for an IFN-free regimen for GT1 patients.

From all critical preclinical and clinical data that had been amassed on sofosbuvir, it became clear that sofosbuvir was the ideal backbone therapy for HCV-cure drug combinations. Sofosbuvir demonstrated a high barrier to resistance; it showed pan-genotypic character and exhibited a stellar safety profile.[42,43] Preclinical studies showed that it could be combined with all other DAAs, and drug–drug interaction assessments showed sofosbuvir and its major metabolite, the uridine nucleoside, were not substrates or inducers of CYP450 enzymes, although sofosbuvir was observed to be a substrate for P-glycoprotein and breast cancer resistance protein.[34] Furthermore, in clinical studies no food effects were observed and no accumulation of sofosbuvir or its major metabolite was noted. Finally, clinical drug–drug interaction studies did not identify any limiting combinations that would restrict sofosbuvir's use in a broad patient population.[42,44,45] The question became what other mechanism of action DAA would become the preferred partner with sofosbuvir that would lead to the development of an IFN-free DAA combination to treat HCV GT1 patients?

8.23.3 Ledipasvir

Ledipasvir (LDV, GS-5885) is a highly potent, orally available inhibitor of the HCV nonstructural protein 5A (NS5A) and has a long pharmacokinetic (PK) half-life making it suitable for once-daily dosing (Fig. 10).[46,47] In genotype (GT) 1 HCV-infected patients, monotherapy with LDV results in a rapid ~3 $\log_{10}$ viral load reduction (VLR) for doses from 3 to 90 mg within 24 h from administration of the first dose.[48] The potency, pharmacokinetics, and low efficacious dose make LDV amenable to formulation as a component in a single-tablet regimen (STR).[49] Ledipasvir was selected for development because it met the targeted NS5A program goals: discovery of a once-daily oral molecule that could be coformulated in a complete regimen of drugs efficacious in the

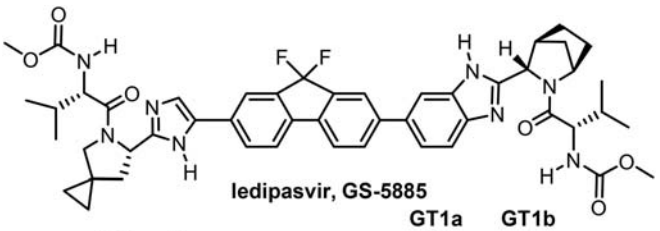

ledipasvir, GS-5885

	GT1a	GT1b
EC_{50}, pM	31	4
Intrinsic EC_{50}, pM	0.31	0.04
Protein-adjusted EC_{50}, pM	208	27
90 mg dose, human $t_{1/2}$, h	49.7	

Fig. 10 Ledipasvir structure, replicon cellular antiviral potency, and human half-life.

treatment and cure of HCV infection. Ledipasvir's picomolar replicon potency, excellent preclinical and clinical safety profile, long PK half-life, favorable drug interaction profile, and rapid and potent antiviral effect in patients are some of the attributes that make LDV an excellent partner for combination with sofosbuvir as Harvoni®. Harvoni® is the first STR approved for treating HCV infection and provides a safe, simple, and efficacious cure.

8.23.3.1 Mechanism of Action and Structural Information

The 56–58 kDa NS5A phosphoprotein is required for replication of the HCV.[50] Although there has been a significant study of this viral protein, a detailed mechanistic understanding of its role in HCV replication remains unclear. NS5A has no known enzymatic activity and has no known homologs in prokaryotes or eukaryotes. NS5A has binding affinity for a number of host cellular proteins, the HCV NS5B RNA-dependent RNA polymerase, and viral RNA, and from the crystal structure of a truncated NS5A dimer, it has been hypothesized to have a viral RNA binding groove.[51–53]

The role of NS5A in HCV replication remains enigmatic, and it is therefore not surprising that the mechanistic basis for the antiviral activity of LDV has not been fully elucidated. A longstanding method of defining the molecular target of antiviral inhibitors has been to treat replicating virus (or replicons) with inhibitor under conditions of incomplete inhibition allowing resistance mutations to develop.[54] Studies of resistance-associated variants (RAVs) provide a connection between LDV and the viral target NS5A. Treatment of the HCV genotype 1a or 1b replicon with LDV results in mutations in the NS5A protein as shown in **Table 1**.[55] In GT1a, Q30E and Y93H are observed along with Y93H in GT1b. These mutations lead to potency shifts for LDV, and are observed in patient isolates (vide infra). The simplest explanation for the association of LDV with mutations in the NS5A protein would be a direct binding of LDV to NS5A. In cases where small molecule inhibitors derive mutations in the active site of a viral enzyme, direct inhibitor/enzyme binding is a reasonable conclusion. Mutational data alone are only suggestive of the direct binding of LDV to NS5A; it is possible that NS5A could act through an independent host protein or proteins to exert its effect on NS5A. Since the molecular details of the role of NS5A in viral replication are unknown, a conclusion on direct binding of LDV based on mutation patterns in NS5A is less clear than for enzyme active-site inhibitors.

Experimental evidence supports direct binding of LDV to NS5A as the basis for LDV's antiviral activity. To help understand the mode of inhibition for LDV, studies of LDV with full-length recombinant GT1b NS5A have been undertaken and demonstrate specific, saturable, and high avidity binding between LDV and NS5A ($K_d = 58.9 \pm 6.6$ nM).[56] Additionally, consistent with its antiviral profile in the GT1b replicon, LDV binding to the Y93H mutant of the full-length recombinant NS5A protein is not measureable up to the solubility limit of LDV in the assay (10 μM). Interestingly, there is a disparity between the nanomolar K_d of LDV for the recombinant wild-type protein and the picomolar EC_{50} of LDV in the GT1b replicon. The shift in K_d has been attributed to a number of possibilities, including the absence of cellular structures (the helices of NS5A are hypothesized to bind to the cellular membrane), or cellular components such as host proteins or RNA that may bind to NS5A during replication. The influence of cellular structures could contribute to the NS5A binding conformation or conformations relevant for NS5A/LDV binding in an infected cell. Further, since the molecular mechanism of NS5A is unknown, the quantitative connection between K_d of binding and inhibition of viral replication is unclear. Indeed, studies have suggested that a stoichiometry of one molecule of an NS5A inhibitor per 10,000 NS5A proteins in the replicon is needed to achieve 50% inhibition of viral replication.[57]

X-ray crystal structures of NS5A where the N-terminal helix domain is removed have been reported. In two GT1b[58,59] and two GT1a[60] structures, truncated NS5A constructs form dimers in the unit cell, although the protein contacts and symmetry in the dimeric forms in the two GT1b reported structures are strikingly different from each other, and the researchers crystallizing the truncated GT1a construct found two additional, distinct dimeric forms. The dimeric forms of the truncated protein, along with the dimer-like structures of inhibitors such as LDV, have prompted some researchers to hypothesize binding modes of NS5A inhibitors to dimeric structures based on modeling studies using reported crystal structures as starting points.

Dynamic imaging during productive infection of Huh-7.5 cells has demonstrated that NS5A undergoes varying multimeric states, where NS5A foci of differing sizes are formed and traffic during the HCV viral life cycle.[61] Further, it has been shown that NS5A can bind to multiple host proteins, and it has been hypothesized that NS5A can bind to viral RNA. With the unknown mode of action of the NS5A protein, multiple states of oligomerization during the HCV viral life cycle, multiple phosphorylated states, and the identification of viral and host binding partners including RNA, it brings into question the biological relevance of static dimeric crystal structures of truncated forms of the NS5A protein, and ultimately their utility in structure-based drug design. Indeed, the existence of multiple dimeric forms of the GT1a and GT1b truncated proteins when crystallized confounds attempts to

Table 1 RAVs observed in GT1 resistance selection with LDV

HCV replicon	*GT1a*			*GT1b*		
LDV concentrations for selection (nM)	10	20	40	0.313	0.625	1.25
NS5A mutations observed	Q30E or Y93H	Q30E ($n=5$) Y93H ($n=1$)	Q30E ($n=4$) Y93H ($n=6$)	Y93H ($n=15$ and the pool)[a]		

Mutations detected only in a single clone not included.
[a]Q54H in two clones in combination with Y93H; mutant replicon didn't replicate.

identify relevant binding modes. The multiple dimeric forms found in apo NS5A crystal structures, and hypothetical binding modes of NS5A inhibitors, present a complex landscape in which to attempt to understand the multiple mechanistic roles of the NS5A protein in HCV replication and the molecular mechanism in which NS5A inhibitors block replication.

8.23.3.2 Discovery of Ledipasvir

The discovery of LDV involved SAR studies where potency and PK enhancing elements were discovered, and their combinations were studied to define optimal properties.[46] Genotype 1a replicon cellular potency (measured as a concentration effective to inhibit by 50%, or EC_{50}) was studied in a range of symmetric *bis*-benzimidazole inhibitors with various aromatic and alkyne-based groups interconnecting the benzimidazoles.[62] Single aromatic groups, such as phenyl in **19**, or naphthyl in **20**, interconnecting the benzimidazoles (Fig. 11) result in potent inhibitors, while biphenyl inhibitor **21** is 7–33-fold less potent. Overall, fused-ring containing core groups were found to be the most potent as exemplified by naphthyl inhibitor **20**, GT1a replicon $EC_{50} = 110$ pM.

Studies with unsymmetric imidazole-X-benzimidazole cores were undertaken and the SAR data is shown in Table 2. The phenyl-based core **22** did not show GT1a activity within the range of the assay (>44,000 pM). It is notable that the phenyl-based core in the unsymmetric series resulted in dramatically lower potency than the phenyl-based core in the symmetric *bis*-benzimidazole series (compound **19**, Fig. 11, 500 pM). The phenyl-alkyne cores **23** and **24** in Table 2 show significant differences in GT1a activity depending on the directionality of their connectivity, where the alkyne connection to the benzimidazole enhances activity by ~sixfold. This potency differential underscores a fundamental property of these unsymmetric-core molecules. The phenyl-alkyne directionality is degenerate in a symmetric *bis*-benzimidazole core, but in the unsymmetric imidazole/benzimidazole core in Table 2, directionality results in strikingly disparate SAR. The theme of directionality relative to an unsymmetric core is important in the discovery of LDV, and is a theme that will be revisited when discussing the SAR of differential modifications to the ends of an unsymmetric series. Biaryl aromatics in **25** and **26** produced potent inhibitors, with the biphenyl inhibitor **26** showing higher potency at 170 pM. In this series, naphthyl inhibitor **27** displays the most potent activity with a GT1a EC_{50} of 71 pM. It is interesting to note that replacement of phenyl in **19** by naphthyl in **20** results in ~fivefold increase in potency, while the phenyl to naphthyl change in compounds **22** and **27** results in a potency difference of >600-fold. The properties of the symmetric and unsymmetric series are clearly different. Nonetheless, in both the earlier *bis*-benzimidazole inhibitors, and in the imidazole/benzimidazole inhibitors, fused-ring core systems produce the most potent compounds within each series, with the naphthyl providing the highest potency overall in the imidazole/benzimidazole series. In the imidazole/benzimidazole system the biphenyl inhibitor **26** is the most potent of the biaryl ring inhibitors. The high potency of biaryl inhibitor **26**, and the finding that ring fusions produce high potency, together led to the design of a series of tricyclic fused-ring inhibitors.

The SAR of tricyclic fused-ring systems (Table 3) were initially studied in a symmetric system to allow rapid synthetic accessibility. The fluorene **28**, although potent, is unstable even to air oxidation, and the oxidation product ketone **29** has decreased

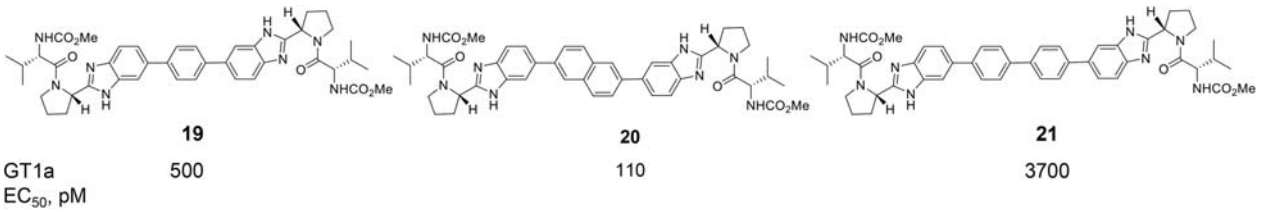

Fig. 11 Symmetric *bis*-benzimidazole inhibitor potency.

Table 2 Effect of core (X group) on potency and PK half-life in unsymmetric series

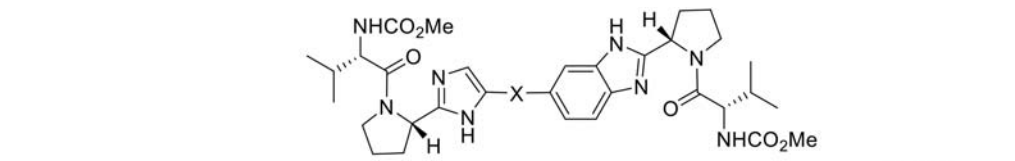

	22	23	24	25	26	27
GT1a EC_{50}, pM	>44,000	2500	380	200	170	71
					Rat	Dog
Pharmacokinetic $t_{1/2}$, h					1.6	2.3

Table 3 Fused tricyclic core inhibitor potency

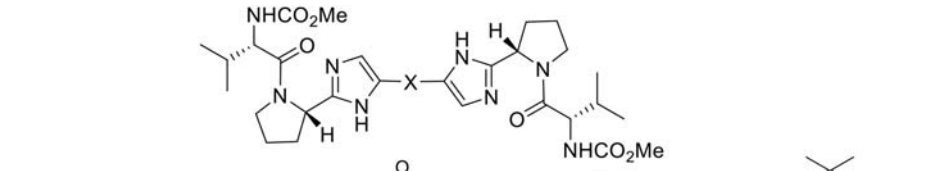

	28	**29**	**30**	**31**
GT1a EC_{50}, pM	94	300	1200	7000

potency, as does the blocked dimethyl fluorene **30**. To avoid the apparent detrimental properties of polarity in **29** and out-of-plane bulk in **30**, the exo-dimethylmethylene compound **31** was synthesized but was the least tolerated of all ring systems with a potency of 7000 pM (unpublished results). From this SAR it was postulated that a small hydrophobic blocking group could be optimal, and difluoro substitution of the fluorene ring system was targeted. Since introduction of fluorine to the fluorene ring system posed synthetic challenges, it was deemed worthwhile to synthesize this important analog directly in the unsymmetric imidazole/benzimidazoles series (inhibitor **32**, Fig. 12). The difluorofluorene indeed introduced stability, and resulted in a highly potent inhibitor with a GT1a potency of 40 pM and PK half-lives of 1.8 and 2.6 h in rat and dog, respectively.

Replacements and modifications of the pyrrolidine ring system were undertaken. It was found that employment of a [2.2.1] azabicyclic ring system imparted a beneficial enhancement in the PK half-life in dog in a biphenyl bisimidazole series,[46] and we sought to further exploit this property. The theme of differential substitution of the unsymmetric benzimidazole/imidazole scaffold was revisited and an intriguing and important SAR emerged. This [2.2.1] azabicyclic pyrrolidine ring system was employed in the unsymmetric scaffold in compounds **33** and **34** (Fig. 13). Compound **34**, with the [2.2.1] azabicyclic ring on the benzimidazole side of the inhibitor is significantly more potent (160 pM) than the corresponding compound **33** with the bicyclic ring system on the imidazole side (660 pM). Attaining such high potency (160 pM) with incorporation of the azabicyclic ring system was important based on the aforementioned PK half-life improvements that this ring system had afforded in the biphenyl bisimidazole series. Importantly, this PK enhancement was successfully translated in the unsymmetric series, where the half-lives for the potent [2.2.1] azabicyclic inhibitor **34** are (1.5 h) in rat and (5.3 h) in dog. The half-life in dog is significantly improved over the corresponding pyrrolidine inhibitor **26** which has a half-life in dog of 2.3 h. Further potency and PK enhancements of **34** were sought.

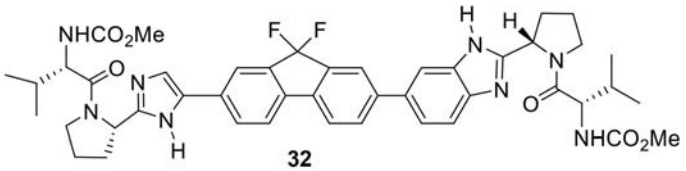

	32	
GT1a EC_{50}, pM	40	
	Rat	**Dog**
Pharmacokinetic $t_{1/2}$, h	1.8	2.6

Fig. 12 Difluorofluorene affords improved potency, and cpd **32** has good PK half-lives.

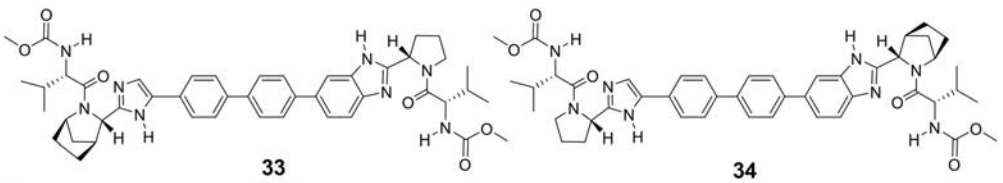

	33	**34**	
GT1a EC_{50}, pM	660	160	
		Rat	**Dog**
Pharmacokinetic $t_{1/2}$, h		1.5	5.3

Fig. 13 Bridged azabicyclic ring system more potent on benzimidazole side, and improves PK half-lives versus pyrrolidine **26**.

Replacement of the biaryl in **34** with the optimized fused tricyclic difluoroflourene afforded **35** (Fig. 14) with a potency enhancement from 160 to 56 pM EC_{50} in the GT1a replicon. Based on a dialysis method to measure plasma protein binding,[63] compound **35** has a protein-adjusted (PA) GT1a EC_{50} of 784 pM, corresponding to a 14-fold protein-binding shift.

In the final stage of optimization, modifications of the remaining pyrrolidine of **35** were investigated. Modification incorporating a spirocyclopropyl pyrrolidine produced ledipasvir (Fig. 10), the most potent compound in the series (GT1a $EC_{50}=31$ pM, GT1b$=4$ pM), which, coupled with its low protein shift of 6.7-fold, results in PA EC_{50} values of 208 pM for GT1a and 27 pM for GT1b. The PK properties of LDV are highly optimized. LDV is stable to oxidative metabolism and no disappearance of LDV is observed in 60 min microsomal incubations resulting in low hepatic extraction values: rat <9.2, dog, <9.5, cyno monkey <12.7, human <12.7% hepatic extraction. Hepatic clearance (CL) predicted from analysis of product formation in human hepatocytes using tritiated LDV is 0.012 L h^{-1} kg^{-1}. The long PK half-lives in rat (4.7 h), dog (7.4 h), and monkey (10.3 h) are apparent in Fig. 15. Bioavailabilities ranging from 32% to 53% and low clearance in all species with volumes of distribution significantly higher than total body water are hallmarks of the favorable PK profile of LDV (Table 4).

Ledipasvir has a free fraction of <1% in rat, dog, cyno, and human based on plasma protein binding. It is interesting that such a highly protein-bound compound can exhibit volumes of distribution in preclinical species significantly higher than the volume of the plasma compartment (V_{ss} from 1.2 to 2.7 L kg^{-1}), since highly protein-bound compounds typically have low volumes of distribution.[64] It is further notable that LDV is highly protein-bound even in the cell-culture medium of the replicon assay at only 1.1% free drug (the replicon cell-culture medium contains 10% bovine serum albumin). Accounting for the low free drug concentration

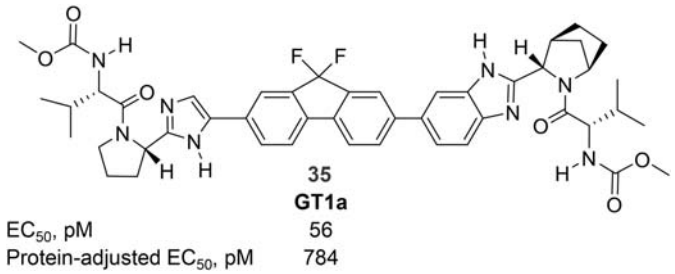

Fig. 14 Difluorofluorene core improves potency in combination with azabicyclic pyrrolidine.

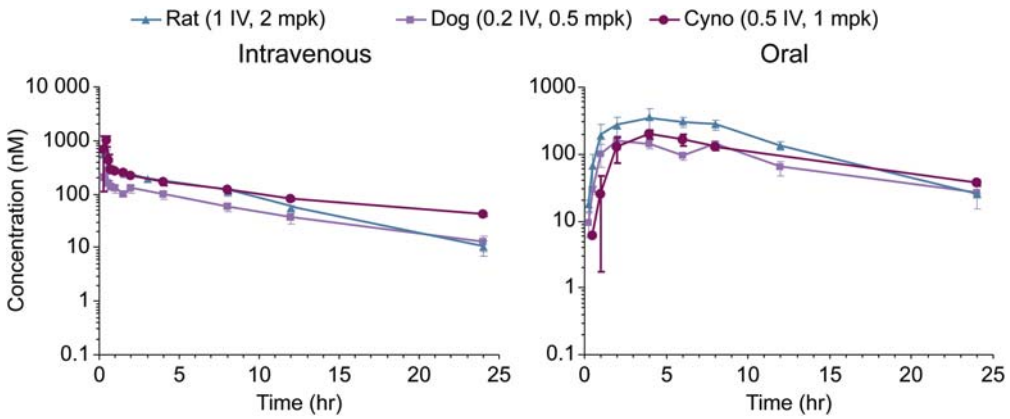

Fig. 15 Preclinical LDV PK curves.

Table 4 Ledipasvir preclinical PK parameters[a]

Species	$t_{1/2}$ *(h)*	*CL (L* h^{-1} kg^{-1}*)*	V_{ss} *(L* kg^{-1}*)*	*MRT*[b] *(h)*	F%
SD rat	4.67 ± 0.56	0.43 ± 0.04	2.66 ± 0.13	6.19 ± 0.28	32.5 ± 6.7
Beagle dog	7.41 ± 0.80	0.13 ± 0.02	1.19 ± 0.13	9.20 ± 1.35	53.0 ± 12.4
Cynomolgus monkey	10.3 ± 1.2	0.17 ± 0.00	2.15 ± 0.42	12.9 ± 2.1	41.1 ± 3.6

[a]All parameters except *F*% are from IV dosing.
[b]Mean residence time.

in the replicon assay, the intrinsic EC_{50} of LDV is 310 femtomolar (fM) for GT1a and 40 fM for GT1b. Ledipasvir's exceptionally high intrinsic potency at the intended viral target, combined with its high level of protein binding, results in a very low free drug concentration in vivo.

8.23.3.3 The Genotype 1 Resistance Profile of Ledipasvir

HCV has a replication rate that is estimated to produce 10^{12} viral particles per day. This high replication rate coupled with the highly error-prone NS5B polymerase leads to production of heterogeneous viral species with a high number of variants, many of which can be detected in circulating virus prior to antiviral treatment.[65] A number of clinically relevant RAVs have been identified in the NS5A region of HCV. The activity of LDV against these RAVs is shown in Fig. 16.[55]

8.23.3.4 Broad Genotype Activity of Ledipasvir

The activity of LDV in genotype 1–6 replicons is shown in Table 5.[55] Ledipasvir has potent activity against genotypes 1a, 1b, 4a, 5a, and 6a replicons with potency ranging from 4 pM to 1.1 nM. Ledipasvir has potent GT1,4,5, and 6 activity and accordingly Harvoni® has been approved for the treatment of patients infected with genotype 1, 4, 5, or 6 HCV. Ledipasvir has weaker antiviral activity against GT2 and 3. Replicon data for NS5A inhibitors are often reported using the JFH-1sequence in the replicon for genotype 2 activity.[66] The JFH-1 sequence includes leucine at position 31 (L31). Baseline sequence differences between genotypes in the NS5A region are the basis for the differing potency of LDV across genotypes. Sequence differences in GT2 are an example: GT2 patients vary significantly at position 31 with the GT2 patients relatively evenly split between leucine and methionine at position 31 (L31 and M31).[67] Thus reporting JFH-1 data for GT2 activity only represents the major viral species for about half of the GT2 infected patients. Table 5 shows that LDV is 12–33-fold less potent in GT2a and GT2b replicons with M31 compared to the L31 replicons. Decreases in antiviral potency when M31 is the dominant amino acid in GT2 have been seen for other NS5A inhibitors both in replicon assays and in suboptimal VLR in the clinic.[68] Despite the weaker potency of LDV in vitro against GT2 and GT3 replicons, clinical efficacy has been observed in several Phase 2 clinical trials with LDV/SOF ± RBV.[69,70]

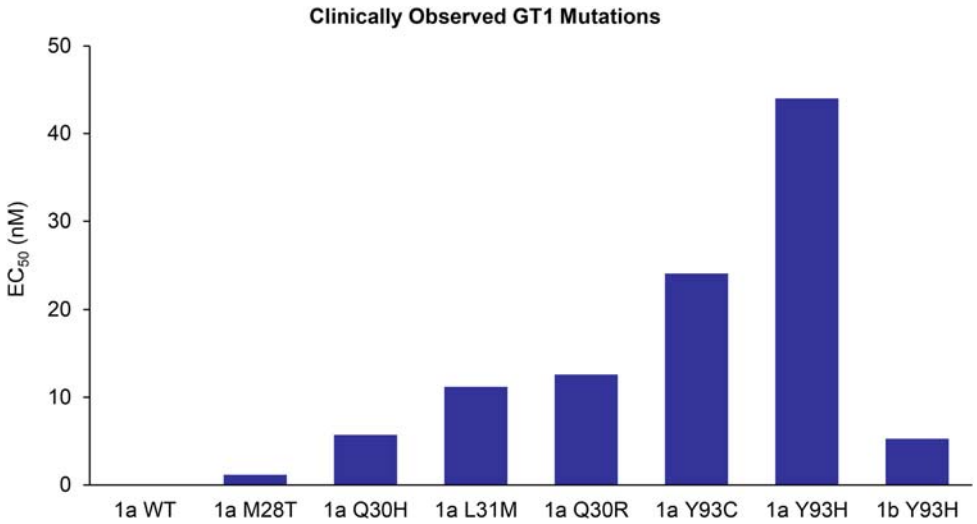

Fig. 16 Ledipasvir potency against clinically observed GT1 RAVs (transient transfection in wild-type replicon).

Table 5 Ledipasvir antiviral activity against GT1–6 HCV

	HCV GT												
	1a	*1b*	*2a*		*2b*		*3a*	*4a*	*4d*	*5a*	*6a*		*6e*
EC_{50} (nM)	0.031[a]	0.004[b]	21[c]	249[d,n]	16[e,n]	530[f,n]	168[g]	0.39[h]	0.29[i]	0.15[j,n]	1.1[k]	0.11[l]	264[m,n]

Stable subgenomic replicon cell lines: [a]H77, [b]Con1, [c]JFH-1 (L31 in NS5A), [h]ED43, [i]QC382, [k]HK6a Consensus. Transiently transfected replicons in 1C cells: [d]J6 (M31 in NS5A), [e]MD2b8-2 (L31 in NS5A), [f]MD2b-1 (M31 in NS5A), [g]S52, [j]SA13, [l]GS16a-1, [m]D88.
[n]NS54 chimeric replicons encoding either full-length NS5A (2a and 2b) or NS5A amino acids 9–184 (5a and 6e).

8.23.3.5 Translation to the Clinic: Ledipasvir Phase 1 Human Pharmacokinetics, Monotherapy Antiviral Activity, and Studies on RAVs

In pharmacokinetic studies, 3, 10, 30, 60, and 100 mg of LDV were dosed in healthy volunteers.[46] The half-life ranged from 37 to 45 h, consistent with the potential for LDV to be used in once-daily dosing (Fig. 17, Table 6). GT1a patients received 1, 3, 10, 30, or 90 mg once daily for 3 days, and 10 mg was dosed to GT1b patients daily for 3 days (Fig. 18, Table 7) in a Phase 1b study. After the third and final dose at 90 mg (LDV dose used in Harvoni®) the half-life of LDV was 49.7 h.[48] An approximately twofold accumulation factor is expected with this long PK half-life. In both healthy volunteers and patients, the AUC increased linearly over the dosing range. In section "Discovery of Ledipasvir" detailing the discovery of LDV, the intensive optimization of PK half-life was discussed. A goal of the preclinical PK optimization was to achieve a long half-life in patients to facilitate efficacy through high drug concentrations over wild-type and resistant virus in real-world settings—that is, to provide consistently high drug exposure outside of the controlled environment of clinical trial settings. The approximate 50-h half-life in patients demonstrates achievement of this goal.

Ledipasvir's protein-adjusted GT1a EC_{50} is 208 pM (dotted red line, Fig. 17), and the GT1b protein-adjusted EC_{50} is 27 pM. The LDV 24 h trough concentration (C24) is 12- and 470-fold over the protein-adjusted GT1a EC_{50} at the 3 and 100 mg doses, respectively (Fig. 17). These C24-fold over PA EC_{50} values would further increase upon reaching steady-state concentrations. The 3 and 100 mg C24 trough concentration are 90- and 3660-fold over the GT1b protein-adjusted EC_{50} after a single dose of LDV.[46] Similar exposures were observed in HCV-infected patients (Fig. 18, Table 7). In patients, the trough concentration (C_{tau}) at 24 h post the third and last LDV dose is 610-fold over the GT1a protein-adjusted EC_{50} at the 90 mg dose used in Harvoni®. The LDV concentration remains multifold above the protein-adjusted EC_{50} at 4 days post the last dose (96 h timepoint in Fig. 18).

Plasma viral RNA measurements in patients treated with 3–90 mg LDV reveal rapid, ≥ 3 $\log_{10}$ median maximal VLRs with three daily doses of 10, 30, or 90 mg of LDV. Approximately 3 $\log_{10}$ VLRs were achieved within 24 h from the first oral dose (Fig. 19).[48] All dose levels were administered in GT1a patients, and a GT1b cohort received the 10 mg dose. This high rate of VLR is a unique feature of NS5A inhibitors. NS5A inhibitors produce the most rapid VLRs among all clinically tested HCV direct-acting antiviral classes including NS3 protease inhibitors, NS5B non-nucleotides, and NS5B nucleosides. The rapid VLR of NS5A inhibitors has been attributed to their interruption of putative roles of the NS5A protein not only in viral RNA replication but also in viral assembly and secretion. Based on viral dynamic modeling, inhibition of several steps in the viral replication cycle is projected to lead to a greater rate of VLR than for inhibitor classes acting by a single mechanism.[46,71]

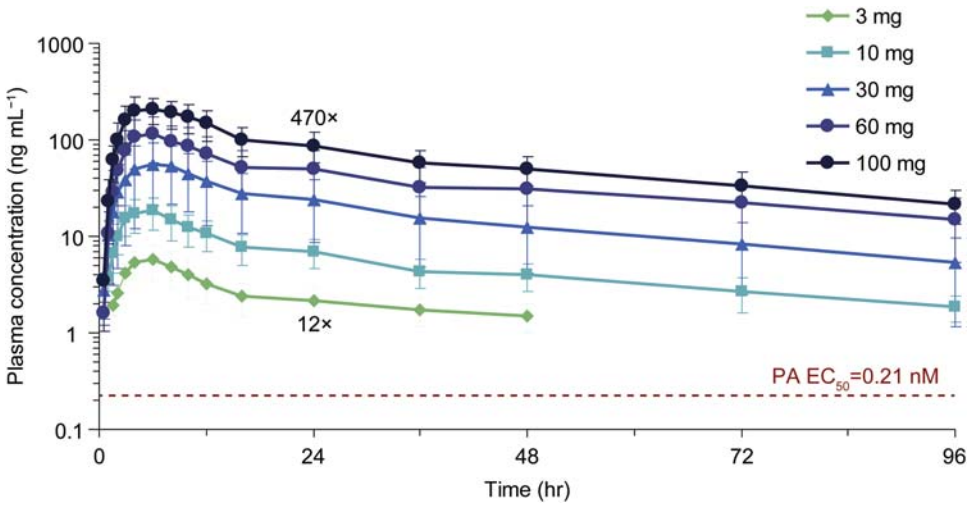

Fig. 17 LDV single oral-dose pharmacokinetics in healthy volunteers.

Table 6 LDV PK parameters after single oral-dose administration, eight healthy volunteers per cohort

	LDV dose (mg)				
Mean parameter (%CV)	*3*	*10*	*30*	*60*	*100*
$t_{1/2}$ (h)	45.2 (51)	42.4 (29)	37.2 (32)	44.2 (22)	39.5 (23)
C_{max} (nM)	6.75 (37)	21.3 (36)	82.2 (51)	133 (50)	242 (35)
AUC_{inf} (nM h)	245 (60.6)	695 (32.3)	2717 (60.3)	5299 (58.2)	8658 (34.3)
$C_{24\ h}$ (nM)	2.45 (37)	7.94 (34)	31.4 (60)	56.4 (57)	98.8 (35)

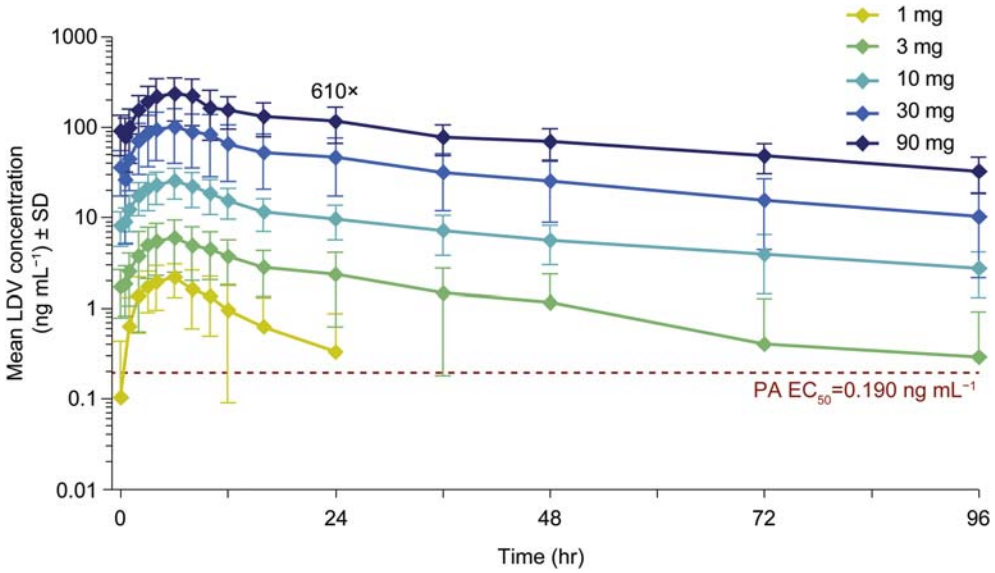

Fig. 18 LDV PK in patients post third (final) dose. Error bars are standard deviation around the mean. Day 3 dose was administered at time zero.

Table 7 Mean LDV PK parameters post third dose in HCV GT1-infected patients

	LDV dose (mg)				
	1	*3*	*10*	*30*	*90*
$t_{1/2}$ (h)	13.0 (7.7, 17.8)	22.8 (13.1, 36.8)	39.9 (28.5, 47.2)	41.7 (25.8, 53.4)	49.7 (37.8, 54.3)
C_{max} (ng mL^{-1})	2.2 (39.7)	6.1 (56.6)	25.3 (40.0)	103.3 (57.5)	247.7 (45.4)
C_{tau} (ng mL^{-1})	0.3 (161.0)	2.4 (73.6)	9.7 (41.5)	46.5 (62.7)	115.9 (42.6)
AUC_{tau} (ng h mL^{-1})	34.0 (29.8)	89.7 (54.6)	368.8 (39.0)	1592.4 (59.5)	3815.5 (42.1)

Tau values are at 24 h postdose.
10 mg cohort ($n=19$) includes GT1a,b patients, others are GT1a ($n=10$).

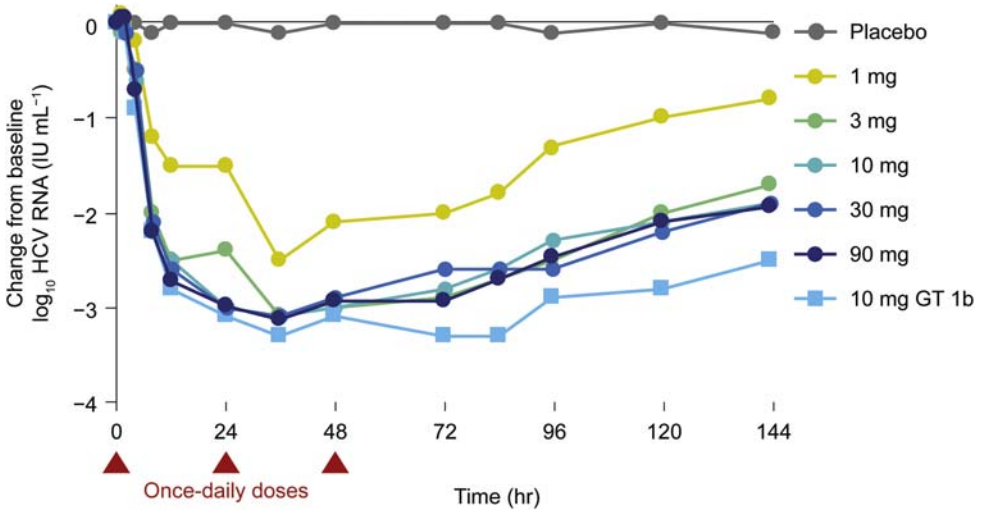

Fig. 19 Viral load reduction, 3-day LDV dosing in monotherapy, GT1a/b patients.

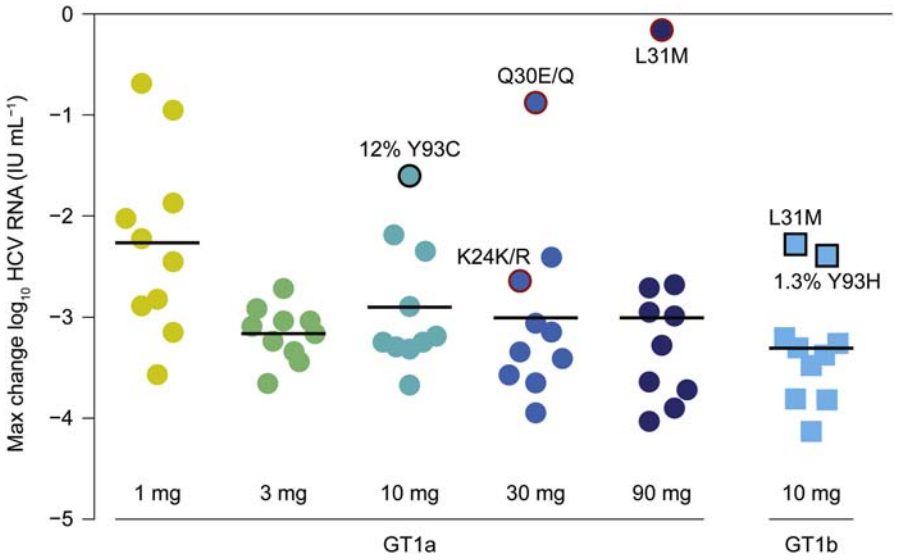

Fig. 20 LDV clinical viral load reduction by patient. Clinical resistance-associated variants (RAVs) found at baseline are noted. RAVs by population sequencing (detectable as >25% of total viral population) are labeled and outlined in *red*. RAVs by deep sequencing (limit of detection ~1% of total population) are labeled and outlined in *black* with the percentage of the resistant population noted. Horizontal lines represent the median viral load reduction.

Fig. 20 depicts the mean maximal VLR for individual patients in the Phase 1 monotherapy dosing of LDV, and also annotates those individual patients who had preexisting RAVs.[72] Of 49 patients that received LDV, six patients had NS5A RAVs prior to dose administration (i.e., at "baseline") either by population sequencing (limit of detection 25% of total viral population, enclosed by square) or by deep sequencing (limit of detection ~1% of total viral population, enclosed by circle). These six baseline RAVs were Y93C (12%, GT1a 10 mg dose), Q30E/Q and K24K/R (GT1a, 30 mg dose), L31M (GT1a, 90 mg dose, and GT1b 10 mg dose), and Y93H (GT1b, 1.3%, 10 mg dose). Only the patient harboring the GT1a L31M RAV at baseline achieved a <0.5 $\log_{10}$ VLR (0.16 $\log_{10}$ from baseline). The other five patients with preexisting RAVs achieved 0.88–2.64 $\log_{10}$ VLRs from baseline. For LDV in combination with sofosbuvir, baseline RAVs have not been associated with statistically significant differences in SVR, and baseline RAV testing is not indicated prior to initiation of LDV/SOF therapy. The Phase 3 clinical section includes a detailed discussion of baseline RAVs in LDV/SOF therapy.

Ledipasvir was well tolerated at all doses and no serious adverse events were reported and no patients discontinued therapy due to adverse events in these early studies.

8.23.3.6 Phase 2 Studies With Ledipasvir and Agents Other Than Sofosbuvir

Prior to its use in combination with sofosbuvir, LDV was studied in interferon-containing and interferon-free regimens in six Phase 2 studies with over 1000 patients in the LDV treatment arms. LDV was studied with GS-9451 (an HCV protease inhibitor) ± ribavirin (RBV) and ± tegobuvir (an HCV NS5B non-nucleoside polymerase inhibitor) in 469 patients.[73] Ledipasvir was also studied with pegylated interferon and RBV ± GS-9451 in 622 patients. These studies demonstrated that LDV was safe and well tolerated in a large number of patients. No patients experienced the same serious adverse event, and no patients had overlapping adverse events that led to discontinuation. Hemoglobin declines were observed but attributed to the presence of ribavirin, and neutrophil declines were associated with the presence of pegylated interferon. Similarly, as discussed in the section "Sofosbuvir Clinical Studies and the Backbone of Drug Combinations," SOF had been studied in a number of Phase 2 clinical trials with a large database supporting its safety in humans. The data from these separate Phase 2 studies formed the extensive safety database supporting the use of LDV in combination with SOF in the ION-1/2/3 registrational Phase 3 studies.

8.23.4 Phase 3 Registrational Clinical Studies With Ledipasvir and Sofosbuvir

Genotype 1 treatment-naïve and treatment-experienced patient populations were the focus of the ION-1, -2, and -3 trials and these results are summarized in Fig. 21.[74–76] In these trials, a STR of LDV (90 mg) and SOF (400 mg) was administered once daily for 8, 12, or 24 weeks with or without RBV (RBV was administered twice daily with its dose adjusted to body weight, 1000 mg daily for patients 75 kg). In ION-1 and -3, treatment durations of 12 and 24 weeks of LDV/SOF with or without RBV in treatment-naïve patients (16% with cirrhosis) were explored. The 12 week arms had SVR rates of 99% without ribavirin and 97% SVR with ribavirin.

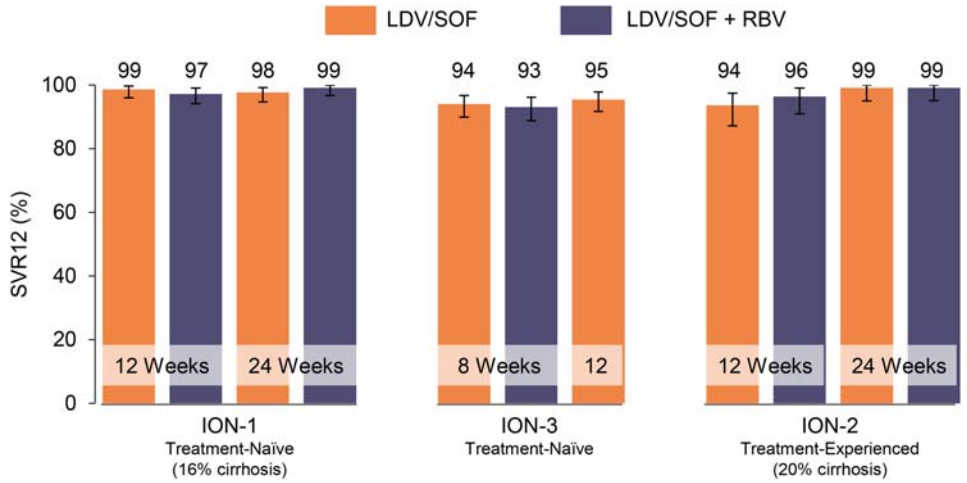

Fig. 21 SVR results from the Phase 3 ION trials of LDV/SOF ± RBV in treatment-naïve and treatment-experienced patients.

The 24-week arm treatment without ribavirin afforded a 98% SVR and 99% with RBV. SVR rates were uniformly high, and differences in SVR in these arms were not statistically significant, demonstrating that addition of RBV or increased treatment duration did not affect outcomes. Shorter treatment was assessed in naïve noncirrhotic patients in ION-3, where 8 weeks of LDV/SOF ± RBV were compared against 12 weeks of SOF/LDV. An SVR rate of 94% in the 8-week arm of LDV/SOF without RBV was comparable to the 8-week arm including RBV (93%) and to the 12-week arm of SOF/LDV alone (95%). These small SVR differences were not statistically significant, demonstrating that 8-week treatment leads to high SVR rates. In ION-2, patients who had previously failed treatment (20% with cirrhosis) with either PEG/RBV alone or the combination of PEG/RBV with a protease inhibitor were treated with LDV/SOF regimens ± RBV. The SVR results in the 12-week arms were 94% (− RBV) and 96% (+ RBV), and in the 24-week arms the SVR was 99% with or without RBV.

In the combined ION-1, -2, and -3 trials the overall SVR rate was 97%. Virologic failure during treatment ("breakthrough" as opposed to virologic failure after treatment, i.e., "relapse") is exceptionally rare during LDV/SOF treatment. Of the 1952 patients treated in ION 1–3, there were only two patients to experience breakthrough, and it was determined that one of these two patients did not adhere to therapy (drug levels were measured at or below the limit of detection at weeks 2, 4, and 6 of treatment). Of the 66 out of 1952 patients who did not achieve SVR, 28 patients were lost to follow-up (patients lost to follow-up are considered treatment failures in the intent-to-treat analysis), and 36 patients relapsed. Therefore, documented virologic failure occurred in 1.9% of the patients in the ION studies.

Analyses of RAVs were completed for the ION studies. In ION-1, deep sequencing showed that 16% of patients (140/861) had NS5A RAVs prior to treatment (baseline RAVs). Approximately 96% of these patients with baseline RAVs achieved SVR. Only three patients had virologic failure; two of the patients with virologic failure had NS5A RAVs at baseline while none had RAVs to SOF. In ION-2 62/439 (14%) had NS5A RAVs at baseline by deep sequencing and 89% of these patients achieved SVR. RAVs associated with NS3/4A protease inhibitors were present in 163/228 patients (71%) in this ION-2 treatment-experienced cohort, and 98% of these patients achieved SVR. No patient had the NS5B polymerase RAV S282T at baseline, during, or after treatment. In ION-3 116/647 patients (18%) had NS5A baseline RAVs by deep sequencing, and 104 (90%) of the patients with RAVs achieved SVR. Baseline RAV testing is not indicated prior to the treatment with LDV/SOF in the United States or European Union (**Fig. 22**).[77,78] In these studies the most common adverse events (AEs) were fatigue, nausea, and headache and were generally mild. In patient arms where ribavirin was added there were higher rates of RBV-associated AEs (headache, fatigue, nausea, insomnia, pruritus, irritability, rash, cough, and anemia). No patient in 12-week arms of ION-1, no patient in ION-2, and no patient in the 8-week LDV/SOF arm of ION-3 discontinued LDV/SOF treatment due to an adverse event.

8.23.4.1 Harvoni® Approval

LDV (90 mg) and SOF (400 mg) are combined in a single tablet that is taken once daily and is branded as Harvoni®. Harvoni® was approved by the Federal Drug Administration (FDA) on Oct. 10, 2014 for the treatment of GT1 infection, and the European Medicines Agency (EMA) on Nov. 18 for GT1 and 4 infection that same year. The US prescribing information (**Fig. 22**) indicates Harvoni once daily for 12 weeks in GT1 treatment-naïve or treatment-experience patients without cirrhosis, and treatment-naïve patients with compensated cirrhosis.[77] Treatment is recommended for 24 weeks in treatment-experienced patients with compensated cirrhosis. Harvoni is the only HCV treatment presently approved for an 8-week duration (considered for treatment-naïve patients without cirrhosis who have HCV RNA < 6 million IU mL^{-1}). Harvoni® is the first STR approved for the treatment and cure of HCV infection and provides a highly effective and a simple treatment option for a broad patient population.

	Patient Population	Treatment Regimen and Duration
Genotype 1	Treatment-naïve without cirrhosis or with compensated cirrhosis (Child-Pugh A)	HARVONI 12 weeks*
	Treatment-experienced** without cirrhosis	HARVONI 12 weeks
	Treatment-experienced** with compensated cirrhosis (Child-Pugh A)	HARVONI 24 weeks*
	Treatment-naïve and treatment-experienced** with decompensated cirrhosis (Child-Pugh B or C)	HARVONI + ribavirin† 12 weeks
Genotype 1 or 4	Treatment-naïve and treatment-experienced** liver transplant recipients without cirrhosis, or with compensated cirrhosis (Child-Pugh A)	HARVONI + ribavirin† 12 weeks
Genotype 4, 5, or 6	Treatment-naïve and treatment-experienced**, without cirrhosis or with compensated cirrhosis (Child-Pugh A)	HARVONI 12 weeks

*HARVONI for 8 weeks can be considered in treatment-naïve genotype 1 patients without cirrhosis who have pre-treatment HCV RNA less than 6 million IU mL^{-1} [see Clinical Studies (14.2)].
**Treatment-experienced patients include those who have failed a peginterferon-alfa + ribavirin based regimen with or without an HCV protease inhibitor.
HARVONI+ribavirin for 12 weeks can be considered in treatment-experienced genotype 1 patients with cirrhosis who are eligible for ribavirin [see Clinical Studies (14.2)]. See footnote for ribavirin dosage recommendations.
In patients with decompensated cirrhosis, the starting dosage of ribavirin is 600 mg and can be titrated up to 1000 mg for patients <75 kg and 1200 mg for those ≥75 kg in two divided doses with food. If the starting dosage of ribavirin is not well tolerated, the dosage should be reduced as clinically indicated based on hemoglobin levels.
†The daily dosage of ribavirin is weight-based (1000 mg for patients >75 kg and 1200 mg for those ≥75 kg) administered orally in two divided doses with food.

Fig. 22 US HARVONI® prescribing information for patients with genotype 1, 4, 5, or 6 HCV (updated 11/13/15).

8.23.4.2 Harvoni® Postapproval Studies, Label Expansion and Study in Japan

FDA approval for the treatment of HIV/HCV coinfected patients is based on the Phase 3 ION-4 trial including 335 patients, where 96% SVR was achieved for GT1 patients, and 100% of GT4 patients achieved SVR (eight patients with GT4 infection were enrolled).[79] Two more studies of LDV–SOF showed high SVR rates in genotypes outside of GT1 in 12-week therapies. These are Study 1119 (GT4, 94% SVR, 65 patients and GT5, 95% SVR, 41 patients)[80,81] and Electron 2 (GT6, 96% SVR, 26 patients) (Fig. 23).[70] 12-week treatment is indicated in the US Harvoni label, Fig. 22 (updated Nov. 13, 2015), for patients with genotype 4, 5, or 6 infection without cirrhosis or with compensated cirrhosis who are treatment naïve or treatment experienced.

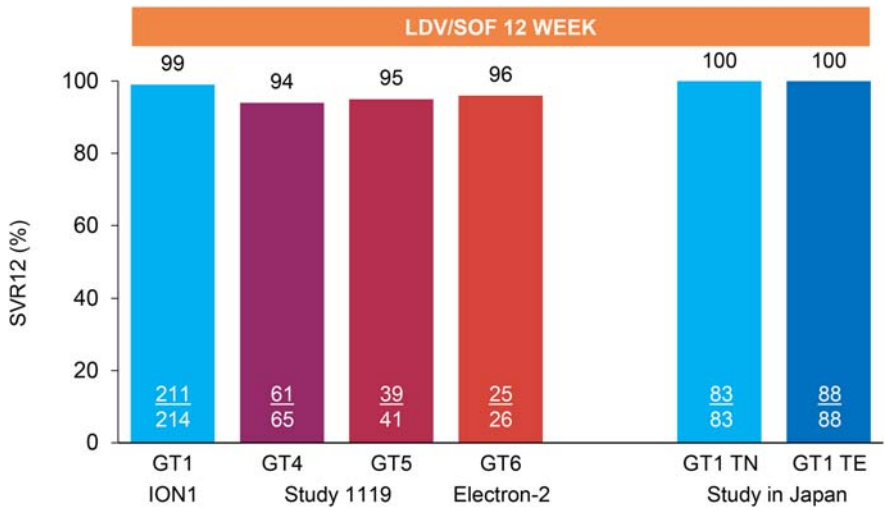

Fig. 23 GT4–6 postapproval studies supporting US label expansion, and study in Japan.

Subsequent to the approval of Harvoni for GT4,5, or 6 HCV-infected patients and for patients with HIV/HCV coinfection, Harvoni was approved for use in combination with RBV for 12 weeks in treatment-naïve and treatment-experienced patients with decompensated cirrhosis. This approval was based on the treatment of patients with decompensated cirrhosis either pre- or postliver transplantation in the SOLAR-1 trial. This 12-week regimen is the first approved HCV therapy for patients with advanced liver disease and represents a major clinical breakthrough with respect to the high efficacy observed in the clinical trials and clinical improvements observed in some patients who achieved SVR.[82]

Treatment of HCV patients in Japan, where GT1b HCV infection is dominant, resulted in 100% SVR in the 170-patient 12-week LDV/SOF arm (Fig. 23). The high SVR rate is notable because this population has increased numbers of patients with characteristics associated with poor outcomes—this population tends to be older, with more advanced liver disease, and many are treatment experienced.[83]

8.23.4.3 Harvoni® Real World Results

It has been long understood that the efficacy or safety results obtained in controlled clinical trials may not translate in "real-world" settings. "Efficacy" (risk benefit in a clinical trial setting) has been contrasted with "effectiveness" (risk benefit in real-world healthcare practice) and differences in outcomes have been described as an "efficacy-effectiveness gap."[84] A number of biological and behavioral factors may contribute to an efficacy-effectiveness gap: contraindications to therapy, drug tolerability, patient compliance, patient demographics, severity of disease, comorbidities, drug interactions, and quality of healthcare. For a disease such as HCV infection where a large population resides in resource-limited settings these factors can be exacerbated.[85] A regimen with high efficacy, safety, and simplicity is of paramount importance for addressing the worldwide HCV burden.

In clinical trial settings, interferon/RBV regimens have achieved approximate SVR rates of 40–50% for GT1, ~80% for GT2, and ~70% for GT3 patients.[86] These relatively high efficacy rates are not recapitulated in studies of effectiveness. A real-world study by the US veteran's administration (VA) underscores the severe shortcomings of interferon-based therapies for the treatment of HCV infection (Fig. 24).[87] For 99,156 veterans with HCV (GT1-4 and "Unknown" HCV GT) assessed in this study, only 36% had no contraindications to treatment. Of the total, 11.6% initiated treatment; low initiation rates for interferon-based therapy are often attributed to patient's unwillingness to undergo this poorly tolerable therapy. Roughly half of those initiating therapy went on to complete therapy, again attributable to poor tolerability. Of the total, the percentage of patients achieving SVR was 3.5%. Since GT1 patients have historically responded with lower SVR rates than GT2 and 3 patients in clinical trials, it might be considered that these real-world results covering combined GT1–4 patients represent an upper limit of response for GT1 patients in the VA.

Recently, the VA also reported a real-world study of the effectiveness of LDV/SOF in GT1 treatment-naïve patients under their care.[88] Fig. 24 shows that the real-world effectiveness of LDV/SOF therapy ($n=4365$) contrasts sharply with the effectiveness of IFN/RBV in the VA patient populations. In the LDV/SOF study, 90% of patients were eligible for treatment, with 92% achieving SVR in 8-week treatment and 94% achieving SVR in 12-week treatment. The authors proposed that the small numerical decrement in effectiveness in their "real world" cohort compared to clinical trial results was based upon patient population differences; the VA study included older male patients, patients with generally higher body mass index, a greater proportion of African Americans, and patients with a greater prevalence of advanced liver disease (fibrosis and cirrhosis including decompensated cirrhosis). These baseline characteristics have historically resulted in lower SVR rates in HCV clinical trials. The advance in therapy represented by the improved real-world effectiveness of LDV/SOF therapy over the prior interferon-based standard of care is striking.

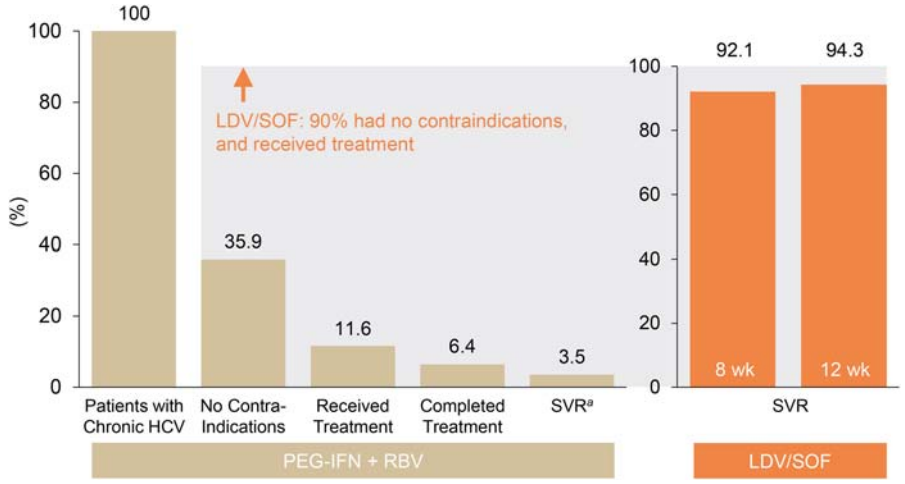

Fig. 24 Real-world SVR rates in the VA: IFN-based effectiveness contrasted with LDV/SOF. Tolerability and simplicity of LDV/SOF therapy present a striking real-world effectiveness advantage. [a]VA calculated IFN-based SVR by including attrition from contraindications, and those who did not receive treatment.

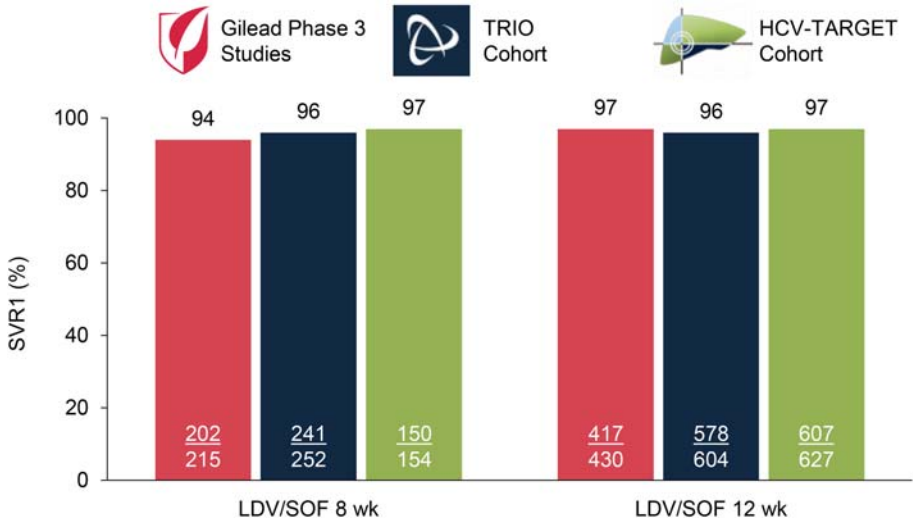

Fig. 25 Comparison of overall SVR rates in Gilead Phase 3 Clinical Studies, to "Real World" SVR reporting from the Trio and HCV-Target Studies (treatment-naïve patients).

Two further real-world studies are compared to ION-1 and ION-3 results in Fig. 25. The Hepatitis C Therapeutic Registry and Research Network (HCV-TARGET) is a multicenter observational study including academic and community medical centers in North America and Europe. Trio Health Innervation Platform (TRIO) is a cloud-based disease-management platform collecting data from specialty pharmacies.[89] In 8-week treatment, TRIO and TARGET reported 96% and 97% SVR rates compared to the 94% reported in ION-3. TRIO and TARGET SVR rates were also 96% and 97% for 12-week therapy, compared to an overall 97% for combined ION-1 and ION-3 12-week arms. The authors noted that unlike prior HCV regimens, the TRIO and TARGET studies suggest that LDV/SOF results in real-world studies provide high rates of SVR similar to those achieved in controlled clinical trials.

8.23.5 Conclusion

Harvoni® is the first STR for HCV treatment, and was approved 25 years after the discovery of the HCV. The 25 years between HCV discovery and the first STR have witnessed therapy that has been interferon-based, with cure rates starting at 10–20% SVR for treatment-naïve noncirrhotic GT1 patients, improving to ~40% for optimized IFN therapy including RBV, and then to ~70% with addition of a protease inhibitor in clinical trials. Severe side effects have been a common in these 24–48-week IFN treatments with examples of "real-world" cure rates at 30%, and most patients unwilling or unable to undergo these difficult treatment regimens.[87] With high SVR rates in real-world settings (Figs. 24 and 25), Harvoni® is a safe, simple, and effective treatment with significant potential to improve human health worldwide. HCV now represents the first prevalent, chronic, life-threatening disease that can be readily cured with simple, finite drug therapy.

See also: 5.18. Direct-Acting Antiviral Agents for the Treatment of Hepatitis C Virus Infection.

References

1. WHO Hepatitis C. http://www.who.int/mediacentre/factsheets/fs164/en/.
2. Alter, H. J.; Purcell, R. H.; Shih, J. W.; Melpolder, J. C.; Houghton, M.; Choo, Q. L.; Kuo, G. Detection of Antibody to Hepatitis C Virus in Prospectively Followed Transfusion Recipients With Acute and Chronic Non-A, Non-B Hepatitis. *N. Engl. J. Med.* **1989,** *321* (22), 1494–1500.
3. Choo, Q. L.; Kuo, G.; Weiner, A. J.; Overby, L. R.; Bradley, D. W.; Houghton, M. Isolation of the cDNA Clone Derived From a Blood-Borne Non-A, Non-B Viral Hepatitis Genome. *J. Hepatol.* **2002,** *36* (1989), 582–585.
4. Simmonds, P. Genetic Diversity and Evolution of Hepatitis C Virus – 15 Years on. *J. Gen. Virol.* **2004,** *85* (Pt 11), 3173–3188.
5. Fried, M. W.; Shiffman, M. L.; Reddy, K. R.; Smith, C.; Marinos, G.; Goncales, F. L., Jr.; Haussinger, D.; Diago, M.; Carosi, G.; Dhumeaux, D.; Craxi, A.; Lin, A.; Hoffman, J.; Yu, J. Peginterferon Alfa-2a Plus Ribavirin for Chronic Hepatitis C Virus Infection. *N. Engl. J. Med.* **2002,** *347* (13), 975–982.
6. Zeuzem, S.; Berg, T.; Moeller, B.; Hinrichsen, H.; Mauss, S.; Wedemeyer, H.; Sarrazin, C.; Hueppe, D.; Zehnter, E.; Manns, M. P. Expert Opinion on the Treatment of Patients With Chronic Hepatitis C. *J. Viral Hepat.* **2009,** *16* (2), 75–90.
7. Ge, D.; Fellay, J.; Thompson, A. J.; Simon, J. S.; Shianna, K. V.; Urban, T. J.; Heinzen, E. L.; Qiu, P.; Bertelsen, A. H.; Muir, A. J.; Sulkowski, M.; McHutchison, J. G.; Goldstein, D. B. Genetic Variation in IL28b Predicts Hepatitis C Treatment-Induced Viral Clearance. *Nature* **2009,** *461* (7262), 399–401.

8. Malet, H.; Egloff, M. P.; Selisko, B.; Butcher, R. E.; Wright, P. J.; Roberts, M.; Gruez, A.; Sulzenbacher, G.; Vonrhein, C.; Bricogne, G.; Mackenzie, J. M.; Khromykh, A. A.; Davidson, A. D.; Canard, B. Crystal Structure of the RNA Polymerase Domain of the West Nile Virus Non-Structural Protein 5. *J. Biol. Chem.* **2007,** *282* (14), 10678–10689.
9. Gale, M., Jr.; Foy, E. M. Evasion of Intracellular Host Defence by Hepatitis C Virus. *Nature* **2005,** *436* (7053), 939–945.
10. Cuevas, J. M.; Gonzalez-Candelas, F.; Moya, A.; Sanjuan, R. Effect of Ribavirin on the Mutation Rate and Spectrum of Hepatitis C Virus In Vivo. *J. Virol.* **2009,** *83* (11), 5760–5764.
11. Ogata, N.; Alter, H. J.; Miller, R. H.; Purcell, R. H. Nucleotide Sequence and Mutation Rate of the H Strain of Hepatitis C Virus. *Proc. Natl. Acad. Sci. U. S. A.* **1991,** *88* (8), 3392–3396.
12. Miller, R. H.; Purcell, R. H. Hepatitis C Virus Shares Amino Acid Sequence Similarity With Pestiviruses and Flaviviruses as Well as Members of Two Plant Virus Supergroups. *Proc. Natl. Acad. Sci. U. S. A.* **1990,** *87,* 2057–2061.
13. Poch, O.; Sauvaget, I.; Delarue, M.; Tordo, N. Identification of Four Conserved Motifs Among the RNA-Dependent Polymerase Encoding Elements. *EMBO J.* **1989,** *8,* 3867–3874.
14. Clark, J. L.; Hollecker, L.; Mason, J. C.; Stuyver, L. J.; Tharnish, P. M.; Lostia, S.; McBrayer, T. R.; Schinazi, R. F.; Watanabe, K. A.; Otto, M. J.; Furman, P. A.; Stec, W. J.; Patterson, S. E.; Pankiewicz, K. W. Design, Synthesis, and Antiviral Activity of 2′-Deoxy-2′-Fluoro-2′-*C*-Methyl-Cytidine, a Potent Inhibitor of Hepatitis C Virus Replication. *J. Med. Chem.* **2005,** *48* (17), 5504–5508.
15. Sofia, M. J.; Furman, P. A.; Symonds, W. T. 2′-F-2′-*C*-Methyl Nucleosides and Nucleotides for the Treatment of Hepatitis C Virus: From Discovery to the Clinic. In *Accounts in Drug Discovery;* Barrish, J. C., Carter, P. H., Cheng, P. T. W., Zahler, R., Eds.; *RSC Drug Discovery Series*; Royal Society of Chemistry: London, 2010; pp 238–266.
16. Stuyver, L. J.; McBrayer, T. R.; Tharnish, P. M.; Clark, J.; Hollecker, L.; Lostia, S.; Nachman, T.; Grier, J.; Bennett, M. A.; Xie, M.-Y.; Schinazi, R. F.; Morrey, J. D.; Julander, J. L.; Furman, P. A.; Otto, M. J. Inhibition of Hepatitis C Replicon RNA Synthesis by Beta-D-2′-Deoxy-2′-Fluoro-2′-*C*-Methylcytidine: A Specific Inhibitor of Hepatitis C Virus Replication. *Antivir. Chem. Chemother.* **2006,** *17* (2), 79–87.
17. Ali, S.; Leveque, V.; Le Pogam, S.; Ma, H.; Philipp, F.; Inocencio, N.; Smith, M.; Alker, A.; Kang, H.; Najera, I.; Klumpp, K.; Symons, J.; Cammack, N.; Jiang, W. R. Selected Replicon Variants With Low-Level In Vitro Resistance to the Hepatitis C Virus NS5b Polymerase Inhibitor PSI-6130 Lack Cross-Resistance With R1479. *Antimicrob. Agents Chemother.* **2008,** *52* (12), 4356–4369.
18. Le Pogam, S.; Yan, J. M.; Kosaka, A.; Ji, Y.; Chin, D. J.; Gonzaludo, N.; Ewing, A.; Klumpp, K.; Najera, I. No Evidence of Drug Resistance or Baseline S282T Resistance Mutation Among GT1 and GT4 HCV Infected Patients on Nucleoside Polymerase Inhibitor RG7128 and PEG-INF/RBV Combination Treatment for up to 12 Weeks: Interim Analysis From the Propel Study. 61st Annual Meeting of the American Association for the Study of Liver Diseases, Boston, MA.
19. Ma, H.; Jiang, W. R.; Robledo, N.; Leveque, V.; Ali, S.; Lara-Jaime, T.; Masjedizadeh, M.; Smith, D. B.; Cammack, N.; Klumpp, K.; Symons, J. Characterization of the Metabolic Activation of Hepatitis C Virus Nucleoside Inhibitor Beta-D-2′-Deoxy-2′-Fluoro-2′-*C*-Methylcytidine (PSI-6130) and Identification of a Novel Active 5′-Triphosphate Species. *J. Biol. Chem.* **2007,** *282* (41), 29812–29820.
20. Murakami, E.; Bao, H.; Ramesh, M.; McBrayer, T. R.; Whitaker, T.; Micolochick, S. H. M.; Schinazi, R. F.; Stuyver, L. J.; Obikhod, A.; Otto, M. J.; Furman, P. A. Mechanism of Activation of β-D-2′-Deoxy-2′-Fluoro-2′-*C*-Methylcytidine and Inhibition of Hepatitis C Virus NS5b RNA Polymerase. *Antimicrob. Agents Chemother.* **2007,** *51* (2), 503–509.
21. Brown, N. A. Progress Towards Improving Antiviral Therapy for Hepatitis C With Hepatitis C Virus Polymerase Inhibitors. Part I: Nucleoside Analogues. *Expert Opin. Investig. Drugs* **2009,** *18* (6), 709–725.
22. Burton, J. R. HCV NS5b Polymerase Inhibitors. *Clin. Liver Dis.* **2009,** *13,* 12.
23. Gane, E. J.; Roberts, S. K.; Stedman, C. A.; Angus, P. W.; Ritchie, B.; Elston, R.; Ipe, D.; Morcos, P. N.; Baher, L.; Najera, I.; Chu, T.; Lopatin, U.; Berrey, M. M.; Bradford, W.; Laughlin, M.; Shulman, N. S.; Smith, P. F. Oral Combination Therapy With a Nucleoside Polymerase Inhibitor (RG7128) and Danoprevir for Chronic Hepatitis C Genotype 1 Infection (INFORM-1): A Randomised, Double-Blind, Placebo-Controlled, Dose-Escalation Trial. *Lancet* **2010,** *376* (9751), 1467–1475.
24. Sofia, M. J.; Bao, D.; Chang, W.; Du, J.; Nagarathnam, D.; Rachakonda, S.; Reddy, P. G.; Ross, B. S.; Wang, P.; Zhang, H. R.; Bansal, S.; Espiritu, C.; Keilman, M.; Lam, A. M.; Steuer, H. M.; Niu, C.; Otto, M. J.; Furman, P. A. Discovery of a Beta-D-2′-Deoxy-2′-Alpha-Fluoro-2′-Beta-C-Methyluridine Nucleotide Prodrug (PSI-7977) for the Treatment of Hepatitis C Virus. *J. Med. Chem.* **2010,** *53* (19), 7202–7218.
25. Murakami, E.; Niu, C.; Bao, H.; Micolochick, S. H. M.; Whitaker, T.; Nachman, T.; Sofia, M. A.; Wang, P.; Otto, M. J.; Furman, P. A. The Mechanism of Action of Beta-D-2′-Deoxy-2′-Fluoro-2′-C-Methylcytidine Involves a Second Metabolic Pathway Leading to Beta-D-2′-Deoxy-2′-Fluoro-2′-C-Methyluridine 5′-Triphosphate, a Potent Inhibitor of the Hepatitis C Virus RNA-Dependent RNA Polymerase. *Antimicrob. Agents Chemother.* **2008,** *52* (2), 458–464.
26. Lam, A. M.; Murakami, E.; Espiritu, C.; Steuer, H. M.; Niu, C.; Keilman, M.; Bao, H.; Zennou, V.; Bourne, N.; Julander, J. G.; Morrey, J. D.; Smee, D. F.; Frick, D. N.; Heck, J. A.; Wang, P.; Nagarathnam, D.; Ross, B. S.; Sofia, M. J.; Otto, M. J.; Furman, P. A. PSI-7851, a Pronucleotide of Beta-D-2′-Deoxy-2′-Fluoro-2′-C-Methyluridine Monophosphate, Is a Potent and pan-Genotype Inhibitor of Hepatitis C Virus Replication. *Antimicrob. Agents Chemother.* **2010,** *54* (8), 3187–3196.
27. Murakami, E.; Tolstykh, T.; Bao, H.; Niu, C.; Steuer, H. M. M.; Bao, D.; Chang, W.; Espiritu, C.; Bansal, S.; Lam, A. M.; Otto, M. J.; Sofia, M. J.; Furman, P. A. Mechanism of Activation of PSI-7851 and Its Diastereoisomer PSI-7977. *J. Biol. Chem.* **2010,** *285* (45), 34337–34347.
28. Niu, C.; Tolstykh, T.; Bao, H.; Park, Y.; Babusis, D.; Lam, A. M.; Bansal, S.; Du, J.; Chang, W.; Reddy, P. G.; Zhang, H. R.; Woolley, J.; Wang, L. Q.; Chao, P. B.; Ray, A. S.; Otto, M. J.; Sofia, M. J.; Furman, P. A.; Murakami, E. Metabolic Activation of the Anti-Hepatitis C Virus Nucleotide Prodrug PSI-352938. *Antimicrob. Agents Chemother.* **2012,** *56* (7), 3767–3775.
29. Lawitz, E.; Rodriguez-Torres, M.; Denning, J.; Albanis, E.; Compropst, M.; Berrey, M. M.; Symonds, W. T. Pharmacokinetics, Pharmacodynamics, and Tolerability of GS-7851 a Nucleotide Analog Polymerase Inhibitor, Following Multiple Ascending Doses in Patients With Chronic Hepatitis C Infection. *Antimicrob. Agents Chemother.* **2013,** *57* (3), 1209–1217.
30. Ross, B. S.; Reddy, G. P.; Zhang, H.-R.; Rachakonda, S.; Sofia, M. J. Synthesis of Diastereomerically Pure Nucleotide Phosphoramidates. *J. Org. Chem.* **2011,** *76* (20), 8311–8319.
31. Hebner, C. M.; Lee, Y.-J.; Han, B.; Chiu, S.; Yian, Y.; Pagratis, N.; Miller, M. D.; Mo, H. In Vitro Pangenotypic and Combination Activity of Sofosbuvir in Stable Replicon Cell Lines. 63rd Meeting of the American Association for the Study of Liver Diseases, Boston, MA.
32. Lam, A. M.; Espiritu, C.; Bansal, S.; Micolochick Steuer, H. M.; Niu, C.; Zennou, V.; Keilman, M.; Zhu, Y.; Lan, S.; Otto, M. J.; Furman, P. A. Genotype and Subtype Profiling of PSI-7977 as a Nucleotide Inhibitor of Hepatitis C Virus. *Antimicrob. Agents Chemother.* **2012,** *56* (6), 3359–3368.
33. Arnold, J. J.; Sharma, S. D.; Feng, J. Y.; Ray, A. S.; Smidansky, E. D.; Kireeva, M. L.; Cho, A.; Perry, J.; Vela, J. E.; Park, Y.; Xu, Y.; Tian, Y.; Babusis, D.; Barauskus, O.; Peterson, B. R.; Gnatt, A.; Kashlev, M.; Zhong, W.; Cameron, C. E. Sensitivity of Mitochondrial Transcription and Resistance of RNA Polymerase II Dependent Nuclear Transcription to Antiviral Ribonucleosides. *PLoS Pathog.* **2012,** *8* (11), e1003030.
34. Gilead Sciences Sovaldi(™)[package insert].
35. Wang, P.; Ching, B.-K.; Rachakonda, S.; Du, J.; Khan, N.; Shi, W.; Stec, D.; Cleary, D.; Sofia, M. J. An Efficient and Diastereoselective Synthesis of PSI-6130: A Clinically Efficacious Inhibitor of HCV NS5b Polymerase. *J. Org. Chem.* **2009,** *74,* 6819–6824.
36. Rodriguez-Torres, M.; Lawitz, E.; Kowdley, K. V.; Nelson, D. R.; Dejesus, E.; McHutchison, J. G.; Cornpropst, M. T.; Mader, M.; Albanis, E.; Jiang, D.; Hebner, C. M.; Symonds, W. T.; Berrey, M. M.; Lalezari, J. Sofosbuvir (GS-7977) Plus Peginterferon/Ribavirin in Treatment-Naive Patients With HCV Genotype 1: A Randomized, 28-Day, Dose-Ranging Trial. *J. Hepatol.* **2013,** *58* (4), 663–668.
37. Lawitz, E.; Rodriguez-Torres, M.; Denning, J. M.; Cornpropst, M. T.; Clemons, D.; McNair, L.; Berrey, M. M.; Symonds, W. T. Once Daily Dual-Nucleotide Combination of PSI-938 and PSI-7977 Provides 94% HCV RNA < log at Day 14: First Purine/Pyrimidine Clinical Combination Data (the Nuclear Study). 46th Annual Meeting of the European Association for the Study of the Liver, Berlin, Germany.

38. Gane, E. J.; Stedman, C. A.; Hyland, R.; Ding, X.; Svarovskaia, E.; Symonds, W. T.; Hindes, R.; Berrey, M. M. Nucleotide Polymerase Inhibitor Sofosbuvir Plus Ribavirin for Hepatitis C. *N. Engl. J. Med.* **2013,** *368,* 34–44.
39. Jacobson, I. M.; Gordon, S. C.; Kowdley, K. V.; Yoshida, E. M.; Rodriguez-Torres, M.; Sulkowski, M. S.; Shiffman, M. L.; Lawitz, E.; Everson, G.; Bennett, M.; Schiff, E.; Al-Assi, M. T.; Subramanian, G. M.; An, D.; Lin, M.; McNally, J.; Brainard, D.; Symonds, W. T.; McHutchison, J. G.; Patel, K.; Feld, J.; Pianko, S.; Nelson, D. R. Sofosbuvir for Hepatitis C Genotype 2 or 3 in Patients Without Treatment Options. *N. Engl. J. Med.* **2013,** *368* (20), 1867–1877.
40. Lawitz, E.; Mangia, A.; Wyles, D.; Rodriguez-Torres, M.; Hassanein, T.; Gordon, S. C.; Schultz, M.; Davis, M. N.; Kayali, Z.; Reddy, K. R.; Jacobson, I. M.; Kowdley, K. V.; Nyberg, L.; Subramanian, G. M.; Hyland, R. H.; Arterburn, S.; Jiang, D.; McNally, J.; Brainard, D.; Symonds, W. T.; McHutchison, J. G.; Sheikh, A. M.; Younossi, Z.; Gane, E. J. Sofosbuvir for Previously Untreated Chronic Hepatitis C Infection. *N. Engl. J. Med.* **2013,** *368* (20), 1878–1887.
41. Tong, X.; Le Pogam, S.; Li, L.; Haines, K.; Piso, K.; Baronas, V.; Yan, J. M.; So, S. S.; Klumpp, K.; Najera, I. In Vivo Emergence of a Novel Mutant L159F/L320F in the NS5b Polymerase Confers Low-Level Resistance to the HCV Polymerase Inhibitors Mericitabine and Sofosbuvir. *J. Infect. Dis.* **2014,** *209* (5), 668–675.
42. Koff, R. S. Review Article: The Efficacy and Safety of Sofosbuvir, a Novel, Oral Nucleotide NS5b Polymerase Inhibitor, in the Treatment of Chronic Hepatitis C Virus Infection. *Aliment. Pharmacol. Ther.* **2014,** *39* (5), 478–487.
43. Sofia, M. J. Beyond Sofosbuvir: What Opportunity Exists for a Better Nucleoside/Nucleotide to Treat Hepatitis C? *Antiviral. Res.* **2014,** *107,* 119–124.
44. Karageorgopoulos, D. E.; El-Sherif, O.; Bhagani, S.; Khoo, S. H. Drug Interactions Between Antivirals and New or Emerging Direct-Acting Antivirals in HIV/Hepatitis C Virus Coinfection. *Curr. Opin. Infect. Dis.* **2014,** *27* (1), 36–45.
45. Mathias, A.; Cornpropst, M. T.; Clemons, D.; Denning, J.; Symonds, W. No Clinically Significant Pharmacokinetic Drug-Drug Interactions Between Sofosbuvir (GS-7977) and the Immunosuppressants Cyclosporine A or Tacrolimus in Healthy Volunteers. 63rd Annual Meeting of the American Association for the Study of Liver Diseases, Boston, MA.
46. Link, J. O.; Taylor, J. G.; Xu, L.; Mitchell, M.; Guo, H.; Liu, H.; Kato, D.; Kirschberg, T.; Sun, J.; Squires, N.; Parrish, J.; Keller, T.; Yang, Z. Y.; Yang, C.; Matles, M.; Wang, Y.; Wang, K.; Cheng, G.; Tian, Y.; Mogalian, E.; Mondou, E.; Cornpropst, M.; Perry, J.; Desai, M. C. The Discovery of Ledipasvir (GS-5885), a Potent Once-Daily Oral NS5A Inhibitor for the Treatment of Hepatitis C Virus Infection. *J. Med. Chem.* **2014,** *57* (5), 2033–2046.
47. Belema, M.; Lopez, O. D.; Bender, J. A.; Romine, J. L.; St. Laurent, D. R.; Langley, D. R.; Lemm, J. A.; O'Boyle, D. R.,. I. I.; Sun, J.-H.; Wang, C.; Fridell, R. A.; Meanwell, N. A. Discovery and Development of Hepatitis C Virus NS5A Replication Complex Inhibitors. *J. Med. Chem.* **2014,** *57* (5), 1643–1672.
48. Lawitz, E. J.; Gruener, D.; Hill, J. M.; Marbury, T.; Moorehead, L.; Mathias, A.; Cheng, G.; Link, J. O.; Wong, K. A.; Mo, H.; McHutchison, J. G.; Brainard, D. M. A Phase 1, Randomized, Placebo-Controlled, 3-Day, Dose-Ranging Study of GS-5885, an NS5A Inhibitor, in Patients With Genotype 1 Hepatitis C. *J. Hepatol.* **2012,** *57* (1), 24–31.
49. Porter, D. P.; Guyer, B. Clinical Benefits of Single-Tablet Regimens. In *Successful Strategies for the Discovery of Antiviral Drugs;* Desai, M. C., Meanwell, N. A., Eds.; Royal Society of Chemistry: Cambridge, 2013; pp 482–508.
50. Huang, Y.; Staschke, K.; De Francesco, R.; Tan, S. L. Phosphorylation of Hepatitis C Virus NS5A Nonstructural Protein: A New Paradigm for Phosphorylation-Dependent Viral RNA Replication? *Virology* **2007,** *364* (1), 1–9.
51. Macdonald, A.; Harris, M. Hepatitis C Virus NS5A: Enigmatic but Still Promiscuous 10 Years on!. *J. Gen. Virol.* **2015,** *96,* 727–738.
52. Hughes, M.; Griffin, S.; Harris, M. Domain III of NS5A Contributes to Both RNA Replication and Assembly of Hepatitis C Virus Particles. *J. Virol.* **2009,** *84,* 1329–1334.
53. Appel, N.; Schaller, T.; Penin, F.; Bartenschlager, R. From Structure to Function: New Insights Into Hepatitis C Virus RNA Replication. *J. Biol. Chem.* **2006,** *281,* 9833–9836.
54. Crumpaker, C., DeClerq, E., Eds.; *Clinical Use of Antiviral Drugs*; Springer: USA, 1988; pp 207–222.
55. Cheng, G.; Tian, Y.; Doehle, B.; Peng, B.; Corsa, A.; Lee, Y. J.; Gong, R.; Yu, M.; Han, B.; Xu, S.; Dvory-Sobol, H.; Perron, M.; Xu, Y.; Mo, H.; Pagratis, N.; Link, J. O.; Delaney, W. In Vitro Antiviral Activity and Resistance Profile Characterization of the Hepatitis C Virus NS5A Inhibitor Ledipasvir. *Antimicrob. Agents Chemother.* **2016,** *60* (3), 1847–1853.
56. Kwon, H. J.; Xing, W.; Chan, K.; Niedziela-Majka, A.; Brendza, K. M.; Kirschberg, T.; Kato, D.; Link, J. O.; Cheng, G.; Liu, X.; Sakowicz, R. Direct Binding of Ledipasvir to HCV NS5A: Mechanism of Resistance to an HCV Antiviral Agent. *PLoS One* **2015,** *10,* 1–14.
57. O'Boyle II, D. R.; Jin-HuaSun, J.-H.; Nower, P. T.; Lemm, J. A.; Fridell, R. A.; Wang, C.; Romine, J. L.; Belema, M.; Nguyen, V. N.; St.Laurent, D,. R.; Serrano-Wu, M.; Snyder, L. B.; Meanwell, N. A.; Langley, D. R.; Gao, M. Characterizations of HCV NS5A Replication Complex Inhibitors. *Virology* **2013,** *444* (1–2), 343–354.
58. Tellinghuisen, T. L.; Marcotrigiano, J.; Rice, C. M. Structure of the Zinc-Binding Domain of an Essential Component of the Hepatitis C Virus Replicase. *Nature* **2005,** *435,* 374–379.
59. Love, R. A.; Brodsky, O.; Hickey, M. J.; Wells, P. A.; Cronin, C. N. Crystal Structure of a Novel Dimeric Form of NS5A Domain I Protein From Hepatitis C Virus. *J. Virol.* **2009,** *83,* 4395–4403.
60. Lambert, S. M.; Langley, D. R.; Garnett, J. A.; Angell, R.; Hedgethorne, K.; Meanwell, N. A.; Matthews, S. J. The Crystal Structure of NS5A Domain 1 From Genotype 1a Reveals New Clues to the Mechanism of Action for Dimeric HCV Inhibitors. *Protein Sci.* **2014,** *23* (6), 723–734.
61. Eyre, N. S.; Fiches, G. N.; Aloia, A. L.; Helbig, K. J.; McCartney, E. M.; McErlean, C. S.; Li, K.; Aggarwal, A.; Turville, S. G.; Beard, M. R. Dynamic Imaging of the Hepatitis C Virus NS5A Protein During a Productive Infection. *J. Virol.* **2014,** *88* (7), 3636–3652.
62. Guo, H.; Kato, D.; Kirschberg, T. A.; Liu, H.; Link, J. O.; Mitchell, M. L.; Parrish, J. P.; Squires, N.; Sun, J.; Taylor, J.; Bacon, E. M.; Canales, E.; Cho, A.; Cottel, J. J.; Desai, M.; Halcomb, R. L.; Krygowski, E. S.; Lazerwith, S. E.; Mackman, R.; Pyun, H. J.; Saugier, J. H.; Trenkle, J.; Tse, W.; Vivian, R. W.; Schroeder, S. D.; Watkins, W. J.; Xu, L.; Yang, Z.-Y.; Kellar, T.; Sheng, X.; Clarke, M.; O'Neil, H.; Chou, C.-H.; Graupe, M.; Jin, H.; McFadden, R.; Mish, M.; Metobo, R.; Phillips, B. W.; Venkataramani, C. A Wide Range of Cores Were Designed, Synthesized and Studied. Antiviral Compounds. WO 2010/132601 A1, November 18, 2010.
63. Mo, H.; Yang, C.; Wang, K.; Wang, Y.; Huang, M.; Murray, B.; Qi, X.; Sun, S. C.; Deshpande, M.; Rhodes, G.; Miller, M. D. Estimation of Inhibitory Quotient Using a Comparative Equilibrium Dialysis Assay for Prediction of Viral Response to Hepatitis C Virus Inhibitors. *J. Viral Hepat.* **2011,** *18* (5), 338–348.
64. Bruno, L. B.; Agrawal, V. K. Prediction of Human Volume of Distribution Values for Drugs Using Linear and Nonlinear Quantitative Structure Pharmacokinetic Relationship Models. *Interdiscip. Sci. Comput. Life Sci.* **2014,** *6,* 71–83.
65. Chatterjee, A.; Smith, P. F.; Perelson, A. S. Hepatitis C Viral Kinetics: The Past, Present, and Future. *Clin. Liver Dis.* **2013,** *17* (1), 13–26.
66. Gao, M.; Nettles, R. E.; Belema, M.; Snyder, L. B.; Nguyen, V. N.; Fridell, R. A.; Serrano-Wu, M. H.; Langley, D. R.; Sun, J. H.; O'Boyle, D. R., 2nd.; Lemm, J. A.; Wang, C.; Knipe, J. O.; Chien, C.; Colonno, R. J.; Grasela, D. M.; Meanwell, N. A.; Hamann, L. G. Chemical Genetics Strategy Identifies an HCV NS5A Inhibitor With a Potent Clinical Effect. *Nature* **2010,** *465* (7294), 96–100.
67. Scheel, T. K.; Gottwein, J. M.; Mikkelson, L. S.; Jensen Bukh, J. Recombinant HCV Variants With NS5A From Genotypes 1–7 Have Different Sensitivities to an NS5A Inhibitor but Not Interferon-α. *Gastroenterology* **2011,** *140,* 1032–1042.
68. Mayers, D.; Vince, B.; Hill, J.; Lawitz, E.; O'Riordan, W.; Webster, L.; Gruener, D.; Mofsen, R. S.; Murillo, A.; Donovan, E.; Chen, J.; McCarville, J. F.; Sullivan-Bólyai, J. Z.; Zhou, X. J. IDX719, HCV NS5A Inhibitor, Demonstrates pan-Genotypic Activity After Three Days of Monotherapy in Genotype 1, 2, 3 or 4 HCV-Infected Subjects [Poster 1774]. *Hepatology* **2012,** *56* (4), 1020A (Suppl AASLD abstracts).
69. Gane, E.; Hyland, R.; Yang, Y.; Svarovskaia, E.; Pang, P.; McHutchison, J.; Stedman, C. Ledipasvir/Sofosbuvir Single Tablet Regimen Is Highly Effective Treatment for Patients With HCV Genotype 2 Infection. *J. Viral Hepat.* **2015,** *22* (S2), 15.
70. Gane, E. J.; Hyland, R. H.; An, D.; Svarovskaia, E.; Pang, P. S.; Brainard, D.; Stedman, C. A. Efficacy of Ledipasvir and Sofosbuvir, With or Without Ribavirin, for 12 Weeks in Patients With HCV Genotype 3 or 6 Infection. *Gastroenterology* **2015,** *149* (6), 1454–1461.
71. Guedj, J.; Dahari, H.; Rong, L.; Sansone, N. D.; Nettles, R. E.; Cotler, S. J.; Layden, T. J.; Uprichard, S. L.; Perelson, A. S. Modeling Shows That the NS5A Inhibitor Daclatasvir Has Two Modes of Action and Yields a Shorter Estimate of the Hepatitis C Virus Half-Life. *Proc. Natl. Acad. Sci. U. S. A.* **2013,** *110* (10), 3991–3996.
72. Wong, K. A.; Worth, A.; Martin, R.; Svarovskaia, E.; Brainard, D. M.; Lawitz, E.; Miller, M. D.; Mo, H. Characterization of Hepatitis C Virus Resistance From a Multiple-Dose Clinical Trial of the Novel NS5A Inhibitor GS-5885. *Antimicrob. Agents Chemother.* **2013,** *57* (12), 6333–6340.

73. Everson, G.; Lawitz, E.; Thompson, A.; Sulkowski, M.; Zhu, Y.; Brainard, D.; Mendelson, L.; McHutchison, J.; Pang, P. S.; Yang, J. C.; Marcellin, P.; Afdhal, N. The NS5A Inhibitor GS-5885 Is Safe and Well Tolerated in Over 1000 Patients Treated in Phase 2 Studies [Poster 783]. 63rd Annual Meeting of the American Association for the Study of Liver Diseases, Boston, MA, November 9–13.
74. Afdhal, N.; Zeuzem, S.; Kwo, P.; Chojkier, M.; Gitlin, N.; Puoti, M.; Romero-Gomez, M.; Zarski, J. P.; Agarwal, K.; Buggisch, P.; Foster, G. R.; Bräu, N.; Buti, M.; Jacobson, I. M.; Subramanian, G. M.; Ding, X.; Mo, H.; Yang, J. C.; Pang, P. S.; Symonds, W. T.; McHutchison, J. G.; Muir, A. J.; Mangia, A.; Marcellin, P. ION-1 Investigators, Ledipasvir and Sofosbuvir for Untreated HCV Genotype 1 Infection. *N. Engl. J. Med.* **2014,** *370* (20), 1889–1898.
75. Afdhal, N.; Reddy, K. R.; Nelson, D. R.; Lawitz, E.; Gordon, S. C.; Schiff, E.; Nahass, R.; Ghalib, R.; Gitlin, N.; Herring, R.; Lalezari, J.; Younes, Z. H.; Pockros, P. J.; Di Bisceglie, A. M.; Arora, S.; Subramanian, G. M.; Zhu, Y.; Dvory-Sobol, H.; Yang, J. C.; Pang, P. S.; Symonds, W. T.; McHutchison, J. G.; Muir, A. J.; Sulkowski, M.; Kwo, P. ION-2 Investigators, Ledipasvir and Sofosbuvir for Previously Treated HCV Genotype 1 Infection. *N. Engl. J. Med.* **2014,** *370* (16), 1483–1493.
76. Kowdley, K. V.; Gordon, S. C.; Reddy, K. R.; Rossaro, L.; Bernstein, D. E.; Lawitz, E.; Shiffman, M. L.; Schiff, E.; Ghalib, R.; Ryan, M.; Rustgi, V.; Chojkier, M.; Herring, R.; Di Bisceglie, A. M.; Pockros, P. J.; Subramanian, G. M.; An, D.; Svarovskaia, E.; Hyland, R. H.; Pang, P. S.; Symonds, W. T.; McHutchison, J. G.; Muir, A. J.; Pound, D.; Fried, M. W. ION-3 Investigators, Ledipasvir and Sofosbuvir for 8 or 12 Weeks for Chronic HCV Without Cirrhosis. *N. Engl. J. Med.* **2014,** *370* (20), 1879–1888.
77. Gilead Sciences Inc. *Harvoni (Ledipasvir and Sofosbuvir) Tablets, for Oral Use. U.S. Prescribing Information;* Gilead Sciences Inc: Foster City, CA, 2014. https://content.govdelivery.com/accounts/USFDA/bulletins/125209b.
78. Website for EU prescribing information: http://www.ema.europa.eu/ema/.
79. Naggie, S.; Cooper, C.; Saag, M.; Workowski, K.; Ruane, P.; Towner, W. J.; Marks, K.; Luetkemeyer, A.; Baden, R. P.; Sax, P. E.; Gane, E.; Santana-Bagur, J.; Stamm, L. M.; Yang, J. C.; German, P.; Dvory-Sobol, H.; Ni, L.; Pang, P. S.; McHutchison, J. G.; Stedman, C. A.; Morales-Ramirez, J. O.; Bräu, N.; Jayaweera, D.; Colson, A. E.; Tebas, P.; Wong, D. K.; Dieterich, D.; Sulkowski, M. ION-4 Investigators, Ledipasvir and Sofosbuvir for HCV in Patients Coinfected With HIV-1. *N. Engl. J. Med.* **2015,** *373* (8), 705–713.
80. Abergel, A.; Loustaud-Ratti, V.; Metivier, S.; Jiang, D.; Kersey, K.; Knox, S. J.; Pang, P. S.; Samuel, D.; Asselah, T. Ledipasvir/Sofosbuvir Treatment Results in High SVR Rates in Patients With Chronic Genotype 4 and 5 HCV Infection. *J. Hepatol.* **2015,** *62,* S219–S220.
81. Abergel, T. A.; Metivier, S.; Kersey, K.; Jiang, D.; Mo, H.; Pang, P. S.; Samuel, D.; Loustaud-Ratti, V. Ledipasvir-Sofosbuvir in Patients With Hepatitis C Virus Genotype 5 Infection: An Open-Label, Multicentre, Single-Arm, Phase 2 Study. *Lancet Infect. Dis.* **2016,** *16* (4), 459–546.
82. Charlton, M.; Everson, G. T.; Flamm, S. L.; Kumar, P.; Landis, C.; Brown, R. S. Jr; Fried, M. W.; Terrault, N. A.; O'Leary, J. G.; Vargas, H. E.; Kuo, A.; Schiff, E.; Sulkowski, M. S.; Gilroy, R.; Watt, K. D.; Brown, K.; Kwo, P.; Pungpapong, S.; Korenblat, K. M.; Muir, A. J.; Teperman, L.; Fontana, R. J.; Denning, J.; Arterburn, S.; Dvory-Sobol, H.; Brandt-Sarif, T.; Pang, P. S.; McHutchison, J. G.; Reddy, K. R.; Afdhal, N. SOLAR-1 Investigators, Ledipasvir and Sofosbuvir Plus Ribavirin for Treatment of HCV Infection in Patients With Advanced Liver Disease. *Gastroenterology* **2015,** *149* (3), 649–659.
83. Mizokami, M.; Yokosuka, O.; Takehara, T.; Sakamoto, N.; Korenaga, M.; Mochizuki, H.; Nakane, K.; Enomoto, H.; Ikeda, F.; Yanase, M.; Toyoda, H.; Genda, T.; Umemura, T.; Yatsuhashi, H.; Ide, T.; Toda, N.; Nirei, K.; Ueno, Y.; Nishigaki, Y.; Betular, J.; Gao, B.; Ishizaki, A.; Omote, M.; Mo, H.; Garrison, K.; Pang, P. S.; Knox, S. J.; Symonds, W. T.; McHutchison, J. G.; Izumi, N.; Omata, M. Ledipasvir and Sofosbuvir Fixed-Dose Combination With and Without Ribavirin for 12 Weeks in Treatment-Naive and Previously Treated Japanese Patients With Genotype 1 Hepatitis C: An Open-Label, Randomised, Phase 3 Trial. *Lancet Infect. Dis.* **2015,** *15* (6), 645–653.
84. Eichler, H. G.; Abadie, E.; Breckenridge, A.; Flamion, B.; Gustafsson, L. L.; Leufkens, H.; Rowland, M.; Schneider, C. K.; Bloechl-Daum, B. Bridging the Efficacy-Effectiveness Gap: A Regulator's Perspective on Addressing Variability of Drug Response. *Nat. Rev. Drug Discov.* **2011,** *10* (7), 495–506.
85. Ford, N.; Singh, K.; Cooke, G. S.; Mills, E. J.; von Schoen-Angerer, T.; Kamarulzaman, A.; du Cros, P. Expanding Access to Treatment for Hepatitis C in Resource-Limited Settings: Lessons From HIV/AIDS. *Clin. Infect. Dis.* **2012,** *54* (10), 1465–1472.
86. Tapper, E. B.; Afdhal, N. H. Is 3 the New 1: Perspectives on Virology, Natural History and Treatment for Hepatitis C Genotype 3. *J. Viral Hepat.* **2013,** *20* (10), 669–677.
87. Kramer, J. R.; Kanwal, F.; Richardson, P.; Mei, M.; El-Serag, H. B. Gaps in the Achievement of Effectiveness of HCV Treatment in National VA Practice. *J. Hepatol.* **2012,** *56* (2), 320–325.
88. Backus, L. I.; Belperio, P. S.; Shahoumian, T. A.; Loomis, T. P.; Mole, L. A. Real-World Effectiveness of Ledipasvir/Sofosbuvir in 4,365 Treatment-Naive, Genotype 1 Hepatitis C-Infected Patients. *Hepatology* **2016,** *64,* 405–414.
89. Younossi, Z. M.; Park, H.; Gordon, S. C.; Ferguson, J. R.; Ahmed, A.; Dieterich, D.; Saab, S. Real-World Outcomes of Ledipasvir/Sofosbuvir in Treatment-Naive Patients With Hepatitis C. *Am. J. Manag. Care* **2016,** *22* (6 Spec No.).

8.24 Discovery of Boceprevir and Narlaprevir: Ketoamide-Derived HCV NS3 Serine Protease Inhibitors for the Treatment of Chronic Hepatitis C

S Venkatraman, Merck Research Laboratories, Kenilworth, NJ, United States

© 2017 Elsevier Ltd. All rights reserved.

8.24.1	Introduction	583
8.24.2	Summary	604
References		606

8.24.1 Introduction

The last 30 years have witnessed an explosive growth in the understanding and treatment of HCV infections. The introduction of direct acting antivirals has caused a paradigm shift in hepatitis C treatment. Prior to this the only treatment option for about 180 million infected with HCV was a regimen of PEG-interferon and ribavirin which had low sustained virologic response (cure) and severe treatment-related side effects.[1,2] Patients infected with HCV were treated for 48 weeks with interferon which resulted in flu-like symptoms and suicidal tendencies for many patients. Patients also suffered from anemia primarily caused by PEG-interferon and ribavirin. Lower sustained virologic response rates particularly in genotype 1-infected patients demanded better treatment options to abate the progression of the disease to liver fibrosis and hepatocellular carcinoma. In fact, the primary cause for liver transplantation in USA is liver failure as a result of chronic hepatitis C infections.[3]

The discovery of the hepatitis C virus as the primary etiological agent for non-A non-B hepatitis resulted in the understanding of the life cycle of the virus.[4,5] The unraveling of HCV genome identified various potential therapeutic targets for drug intervention.[6] Hepatitis C is a positive-strand RNA virus which primarily infects the hepatocytes. Upon entry into the hepatocytes the virus codes for a single polypeptide of approximately 3000 amino acids with the help of host machinery utilizing the IRES site. This polypeptide contains all the structural and nonstructural proteins required for replication, and assembly of new viral particles. HCV virus broadly falls into six genotypes (gt 1–6) and has significant genetic variability resulting in many quasi species. They are widely distributed in the world with gt 1a and 1b prevalent in North America and Western Europe. Until the discovery of direct acting antivirals, the most unmet need in hepatitis patients was the treatment of gt 1 infections. Standard of care was treatment with pegylated interferon which achieved SVR in less than 40% of patients infected with gt-1. The response was much improved in gt-2 and gt-3 patients; however, tolerability and discontinuations to PEG-interferon were high due to severe side effects.

Advances in characterization of HCV biology identified many targets for drug intervention. The single polypeptide encoded by the HCV virus is posttranslationally modified to a number of structural and functional proteins whose functions are well defined.[7] The polypeptide undergoes a *cis* cleavage at the NS2–NS3 junction to release NS3 protease which along with the NS4A cofactor catalyzes the cleavage of the NS3–NS4A, NS4A–NS5A, and NS5A–NS5B junction to form active proteins for viral replication. It was immediately clear from the central role of NS3 protease that inhibition of this enzyme could result in the development of direct acting novel HCV drugs. The success in the development of HIV drugs by inhibition of key viral proteins also increased the confidence in developing HCV therapies adopting similar strategies (Fig. 1).

The X-ray crystal structure of HCV NS3 protease was solved by various groups.[8–10] HCV NS3, a serine protease structurally belonging to the trypsin/chymotrypsin superfamily, shares significant structural similarities to these enzymes.[11] Analysis of the X-ray crystal structure revealed a catalytic site that is shallow, highly solvent, exposed, and located on the surface of the protein. It was immediately clear that any inhibitor that interacts with the enzyme would need to derive a large portion of its binding by only partially interacting with the enzyme. The protease recognizes the natural substrate via an array of hydrogen bond spanning

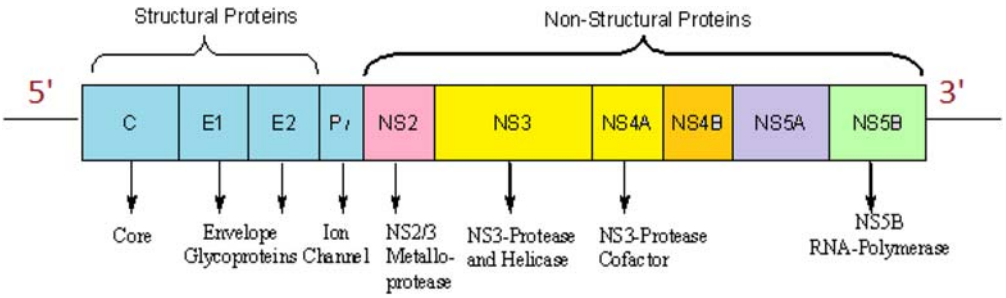

Fig. 1 HCV genome and key structural and nonstructural proteins involved in viral replication.

from P6 to P5′ making these interaction specific. A zinc atom located ~20 Å from the catalytic site is held by four cysteines which impart stability to the tertiary structure. The catalytic triad consisting of His57, Ser139, and Asp81 are located in two subdomains of the enzyme. Binding of NS4A, a 54 amino acid cofactor enhances the catalytic efficiency of the protease. The binding of the NS4A organizes the catalytic triad in a preferred conformation and facilitates His57 to deprotonate Ser139 and hydrogen bond to Asp81. Cysteine is conserved at the P1 position in all *trans* cleavage events, whereas it is replaced with a threonine in the *cis* cleavage process. The P1′, P2, and P3 residues contain hydrophobic amino acids, whereas the P5 and P6 residues contain acidic amino acids such as aspartic or glutamic acid.[12–14]

Advances in biochemical and cell culture assays further augmented the discovery of novel direct acting antiviral to treat HCV. The development of a continuous enzyme binding assay[15] and the replicon-based cell assay[16] by transfection and replication of HCV replicons in hepatocytes allowed rapid triage of chemical compounds to search for potential lead compounds to initiate a drug discovery and optimization program. Screening of libraries containing many diverse compounds did not result in the identification of a lead that inhibited the enzyme even at micromolar levels. Having failed to identify a viable lead to develop structure–activity relationship we resorted to a structure-based design using the natural substrate as the starting point.

Incorporation of a ketoamide at the scissile bond and small modifications of key residues of the NS3 substrate allowed identification of **1** (Fig. 2) which bound to the enzyme with a K_i* [17] of 1.9 nM. Analysis of binding kinetics and X-ray structure of **1** bound to the enzyme revealed a two-step binding mechanism with fast on rates and slow off rates.[17] The hydroxyl group from serine-139 formed a reversible covalent bond at the ketoamide site forming a tetrahedral intermediate. A composite binding efficiency K_i* was measured which allowed rank ordering of compounds for SAR analysis. Compounds were also evaluated for the inhibition of human neutrophil elastase (HNE) as a measure of selectivity for binding to HCV. HNE was chosen because of it close homology to HCV NS3/4A protease.

X-ray crystal structure of **1** bound to the HCV NS3 protease clearly indicated binding to the active site with the nucleophilic serine making a covalent interaction with the enzyme. The ketoamide unlike the natural substrate was attacked from the Re face which placed the oxygen of the amide into the oxyanion hole. This is different from the binding of the natural substrate leading to proteolysis where the serine attacks the substrate from a Si face and the oxygen of the tetrahedral intermediate formed is stabilized by hydrogen bond in the oxyanion hole (Fig. 3).

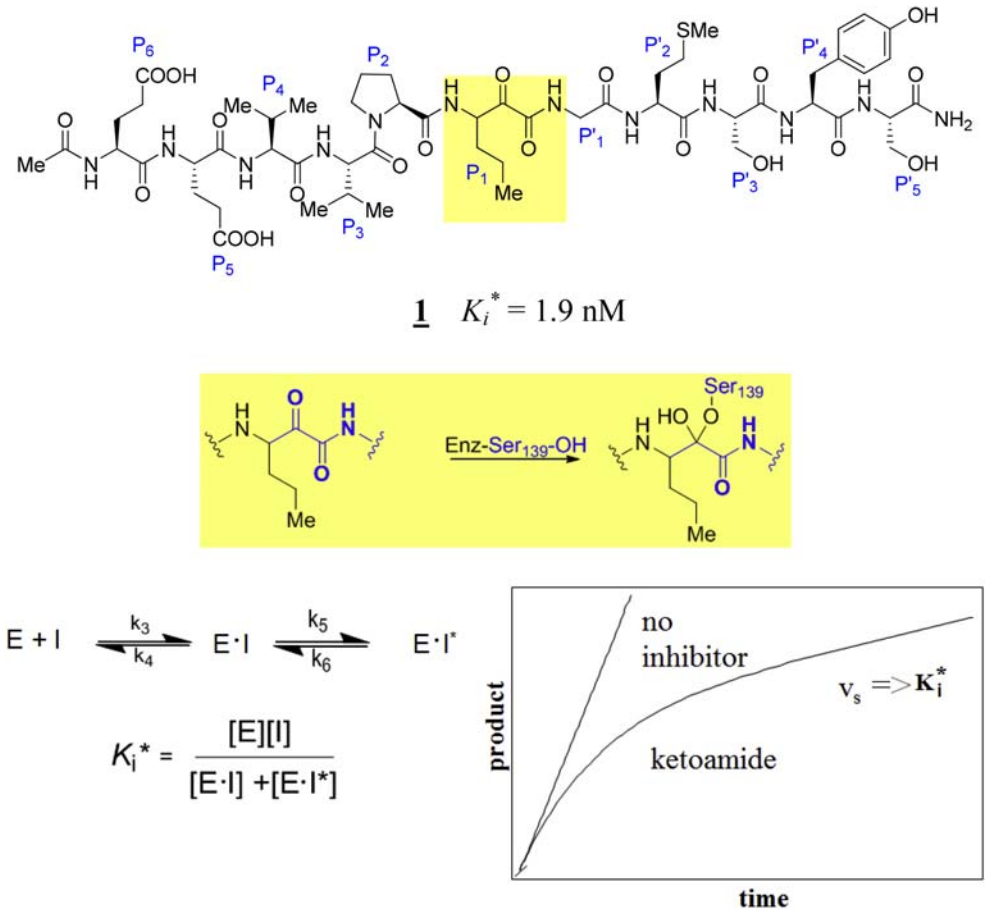

Fig. 2 Kinetics of undecapeptide **1** bound to HCV NS3 protease.

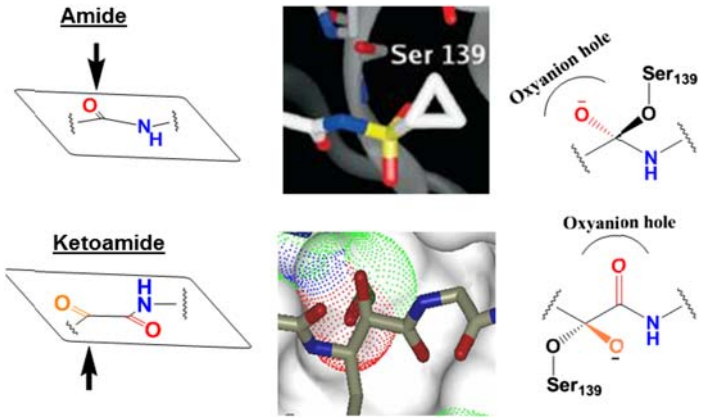

Fig. 3 Mode of attack of serine in ketoamide derived inhibitors.

From the X-ray crystal structure of ketoamide **1** bound to the enzyme it was clear that the inhibitor made several key interactions with the protein. The norvaline at P1 occupied the S1 pocket and the S2 pocket was occupied by the P2 proline moiety. P3 and P4 valines made lipophilic interactions at the shallow S3 and S4 pockets. The acidic groups at P5 and P6 made key interactions with arginines in the backbone. Looking at the structure of **1** with a molecular weight of 1265, it was clear that it could not be developed into an orally bioavailable drug. It was also clear that the peptidic nature of **1** containing all natural amino acids would likely render it unstable in plasma. We therefore decided a strategy to reduce the molecular weight of the inhibitor and replace natural amino acids with nonproteinogenic ones which could render enhanced plasma stability. It was decided to initially truncate the group at P1′ thus eliminating all substitutions from P2′ to P5′. This strategy was taken to understand the extent of loss in potency that would result from the truncation at P1′ position. Table 1 summarizes some of our efforts toward this.

Table 1 Truncation of **1** at P1′ position

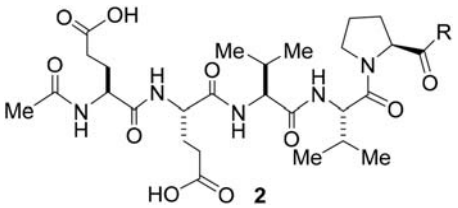

2

Cpd.	*R*	K_i* (μM)
3	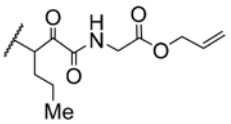	0.057
4	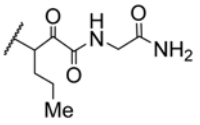	0.043
5	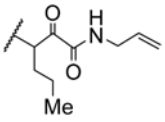	0.270
6	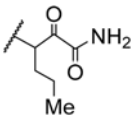	0.760

Replacement of the P1′–P5′ segment in **1** with glycine allyl ester resulted in a loss of 25-fold with analog **3** showing a $K_i^* = 0.057$ μM. Also, modification with glycine amide resulted in compound **4** ($K_i^* = 0.043$ μM) with similar potency. These two analogs indicated that though truncation at the right-hand side resulted in analogs with diminished activity they still retained significant inhibitory activity. However, truncation at the P1 site was less tolerated with analogs **5** ($K_i^* = 0.270$ μM) and **6** ($K_i^* = 0.760$ μM) losing potency by more than 100-fold. From these studies it was clear that the right-hand piece was not required to maintain acceptable potency. The loss in activity may be offset by substituting with a smaller group (at P′) or improving ligand efficiency of P site residues. It was therefore decided that all future SARs would be done with the truncated analogs.

Even though the truncation of **1** at P1′ with glycine and allyl moieties yielded compounds with significantly lower molecular weighs it was clear that the newer analogs **3–6** were still larger with acidic groups at P5 and P6. The team was concerned that the acidic groups could present hurdles to absorption and cellular activity. After significant exploration the team decided to limit the inhibitor at P3 position and eliminate the polar glutamic acid residues at P5 and P6 positions. Analogs were truncated at P3 with a capping group such as isobutyl or *tert*-butyl carbamate where the alkyl group occupied the S4 pocket. Simultaneous SAR studies for replacing different residues with nonproteinogenic amino acids resulted in the discovery of cyclohexyl glycine and *tert*-butyl glycine as suitable replacements at the P3 position that were well tolerated and improved potency. At the same time the SAR at P2 identified a leucine as a potential replacement that was well tolerated and improved potency. Analogs of leucine such as cyclopropyl alanine and cyclobutyl alanine were also well tolerated.

The introduction of P2′ phenyl glycine amide as a replacement for allyl amide had a profound improvement on the potency of P2 leucine-derived analogs of type **7** ($K_i^* = 0.006$ μM). X-ray crystal structure of inhibitor bound to the enzyme revealed P1′–P2′ glycine–phenyl glycine segment wraps around Lys136 forming a "C-shaped clamp" resulting in hydrophobic interaction with the alkyl side chain of the lysine (Fig. 4). Further analogs in this series were synthesized by keeping the P2′ phenyl glycine and modifying the P2 residue with small cyclic alanine-derived amino acids. Table 2 summarizes the inhibitory potencies of these analogs.

Replacement of P2 leucine with homoleucine and pentyl glycine resulted in analogs **9** ($K_i^* = 0.31$ μM) and **10** ($K_i^* = 0.3$ μM) with loss in potency. However, replacement of P2 groups with cyclic amines resulted in marked improvement in potency of resultant analogs. Modification of P2 isoleucine with cyclobutyl alanine resulted in analog **11** with $K_i^* = 0.4$ μM, whereas the replacement with cyclopropyl alanine resulted in a sixfold improvement with $K_i^* = 0.05$ μM. Analysis of X-ray structure of **12** bound to the protease showed the cyclopropyl group making nonbonding interactions with the Arg155 contributing to improved potency (Fig. 5). Having identified a potent inhibitor in the low nM region, we further profiled **12** in the replicon-based cellular assay to determine the cellular potency.

Analog **12** although potent in the enzyme assay was significantly less active in the cellular assay with an $EC_{90} > 5$ μM probably due to the low cell penetration of the compound (Fig. 6). We initially ascribed the poor cellular penetration to the amide moieties. Since analog **12** had 6 hydrogen bond donors and 9 hydrogen bond acceptors, we decided to block some by methylating the nitrogen atoms. It was also recognized that the carboxylic acid would be ionized at physiological pH and would be contributing to low cellular permeability. Previous SAR had shown that the replacement of the P2′ acid with dimethyl amide had retained most of the inhibitory activity. We also decided to explore this strategy to reduce the hydrogen bond donor and avoid acid groups. With this in mind, we initially made the N-methylated analog of P2 cyclopropyl alanine resulting in compound **13**. Methylation of P2 group was well tolerated with analog **13** demonstrating potent enzyme inhibition ($K_i^* = 0.12$ μM); however, the cellular potency was still > 5 μM. We further decided to synthesize the dimethyl amide derivative resulting in compound **14** ($K_i^* = 0.060$ μM). Analysis of this analog in the cellular assay resulted in the first analog to show modest cellular activity with $EC_{90} = 0.95$ μM. We also synthesized dimethyl amide derivative **15** which lacked the P2 methyl group. Even though this analog retained most of the enzyme activity it was not active as analog **14** in the cellular assay. This clearly showed that reducing the number of hydrogen bond donors from six in **12** to four in **14** was required and possibly blocking the P2 amide group was paramount for cellular potency. Having

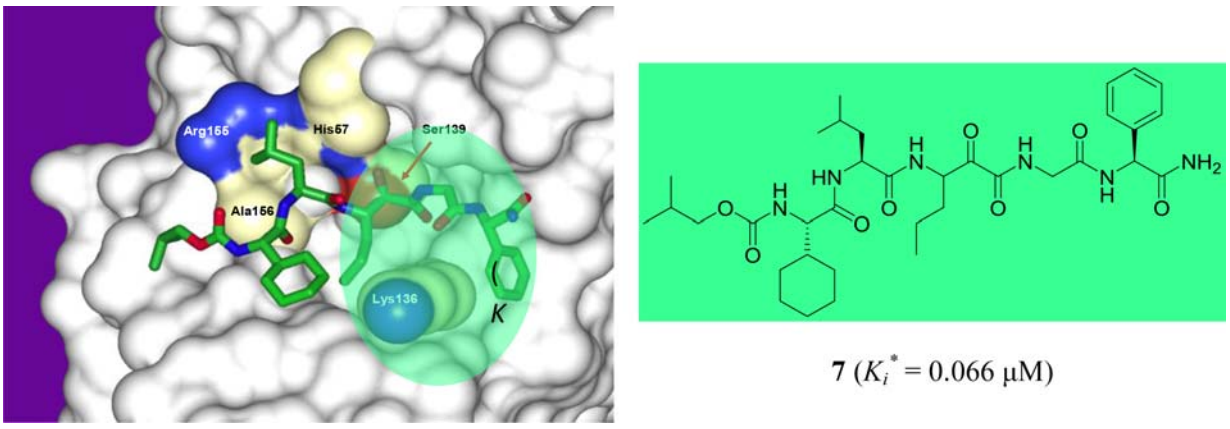

Fig. 4 X-ray structure of leucine derivative **7** bound to the active site of HCV NS3 protease.

Table 2 Replacement of P2 leucine

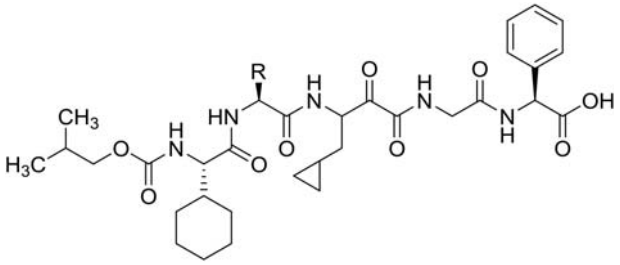

Cpd.	*R*	K_i* (μM)
8	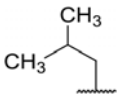	0.12
9	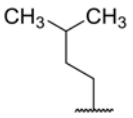	0.31
10	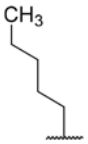	0.3
11		0.4
12		0.05

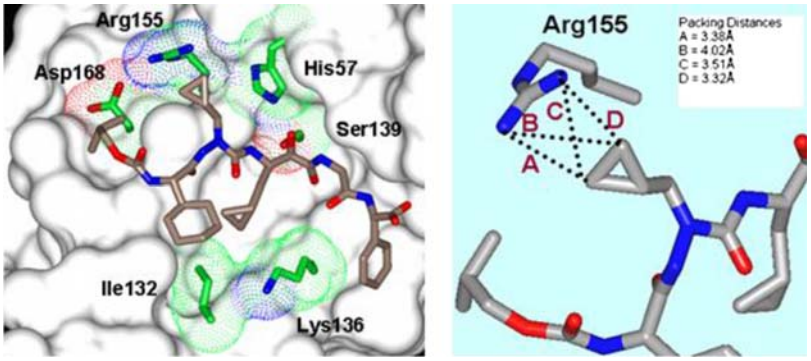

Fig. 5 X-ray structure of P2 cyclopropyl alanine derivative **12** bound to HCV NS3 protease. Interaction of P2 cyclopropyl alanine with the backbone of HCV NS3 enzyme.

discovered that methylation of P2 resulted in analogs with improved cellular potency we envisioned new analogs with cyclic P2 amino acids derived from proline (Table 3).

Introduction of proline at P2 with P1 norvaline resulted in analog **16** with modest inhibitory activity of $K_i^* = 0.36$ μM. This analog was not evaluated in the cellular assay. X-ray structure of proline derivative revealed that the S2 pocket was large and proline did not occupy this pocket efficiently. We therefore decided to investigate substitutions on the proline moiety. Incorporation of

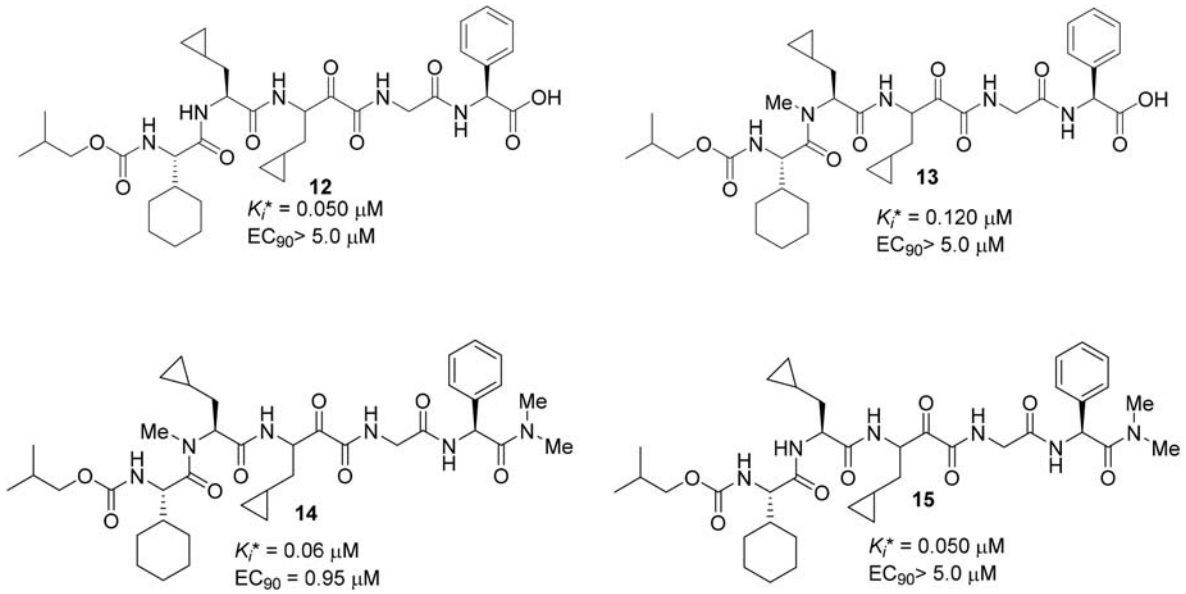

Fig. 6 Effect of P2 N-methylation on potency and cellular activity.

methyl substitution at the 4 position resulted in compound **17** with $K_i^* = 0.14$ μM. It was very encouraging to see the introduction of methyl group having a modest improvement in potency compared to the proline supporting our hypothesis of substituting on the prolines to achieve improvement in potency. We further investigated the introduction of P3 thioacetal modified proline which yielded analog **18** with much improved inhibitory potency of $K_i^* = 0.026$ μM. Concomitant to our efforts of exploring substitutions in the four position of proline we also investigated three, four bicyclic proline analogs. These analogs had a profound influence on potency and cellular activity. Introduction of the bicyclic ether-derived proline (3aR,4S,6aR)-2,2-dimethylhexahydro-2H-furo[2,3-c] pyrrole-4-carboxylic acid resulted in analog **19** ($K_i^* = 0.010$ μM) and a cellular potency of $EC_{90} = 1.9$ μM. Synthesis of the carbon analog **20** ($K_i^* = 0.015$ μM; $EC_{90} = 0.9$ μM) that lacked the oxygen in the proline ring did not change the profile significantly compared to **19**. As we were investigating bicyclic proline derivatives, we became aware of reports from Professor Madalengoitia who had published a novel cyclopropyl proline as a mimic of leucine. Madalengoitia had shown (1R,2S,5S)-6,6-dimethyl-3-azabicyclo[3.1.0]hexane-2-carboxylic acid mimicked leucines in peptide sequences.[18] Since leucine was a P2 moiety that imparted desirable potency in our analogs, we decided to evaluate this moiety. Introduction of (1R,2S,5S)-6,6-dimethyl-3-azabicyclo[3.1.0] hexane-2-carboxylic acid had a profound effect on the activity of the resultant analog **21**. Analog **21** demonstrated improved binding activity of $K_i^* = 0.010$ μM and cellular activity of $EC_{90} = 0.2$ μM. This was a 30-fold improvement compared to unsubstituted proline derivative **16** and a fivefold improvement in cellular activity compared to analog **14**. The strategy of incorporating secondary amino acids was successful in designing derivatives with potent binding and cellular activity. SAR studies around P1 led to the identification of SCH 6 (**22**).[19]

SCH6 (**22**) had an enzyme inhibitory activity of $K_i^* = 0.0038$ μM and a cellular activity of $EC_{90} = 0.10$ μM, our first analog to display potent binding and cellular activity (Fig. 7). We also evaluated the selectivity of this analog against HNE and it had an excellent selectivity of HNE/HCV = 1000. Having accomplished desired potency requirement we next evaluated pharmacokinetics of analog **22**. Administration of SCH6 orally to rats at 10 mg kg^{-1} resulted in poor plasma levels and bioavailability ($AUC_{0-24h} = 0.35$ μM h and $\%\underline{F} = 4$). The same compound when administered subcutaneously resulted in excellent plasma levels ($AUC_{0-24h} = 19.5$ μM h). The same was true for pharmacokinetics in monkeys with subcutaneous administration demonstrating excellent plasma concentration whereas poor blood levels were observed when administered orally.

The poor oral pharmacokinetics of compounds of type **22** was a serious concern and created an additional barrier for further progression of compounds. It was clear from the PK studies that the compound was stable in plasma and the poor oral exposure was primarily due to low drug absorption. We reasoned that the high molecular weights and peptidic nature of these inhibitors made it difficult to be absorbed and significant modifications would be required to achieve absorption. The team devised a strategy to further reduce the molecular weight by increasing ligand efficiency and/or reduce the number of hydrogen bonds by depeptidizing amide bonds. The team explored various strategies to depeptidize analogs such as incorporating peptide isosteres and macrocyclizing these compounds. Fig. 8 outlines some of our efforts in macrocyclization.

Analysis of the X-ray structure of analog **22** bound to the enzyme showed close proximity of P1 and P2 moieties to P3 and P4 groups. We therefore envisioned cyclizing the P2–P4 groups and the P1–P3 groups to form 14- to 17-membered macrocycles (Fig. 8).

Synthesis of P2–P4 biphenyl ether analog **23** resulted in compound with modest inhibitory activity $K_i^* = 0.11$ μM.[20] Replacement of P2 phenyl alanine with proline resulted in analog **24** with much improved potency ($K_i^* = 0.006$ μM and

Table 3 Modified proline derivatives of analog **15**

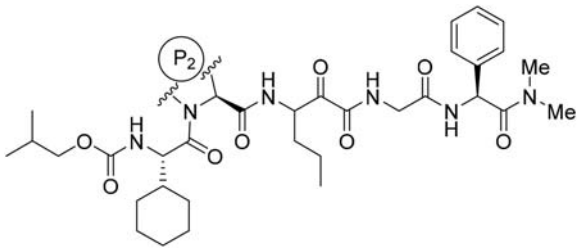

Cpd.	*P_2*	K_i* *(μM)*	EC_{90} *(μM)*
16	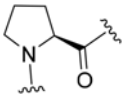	0.36	–
17	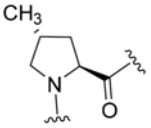	0.14	–
18	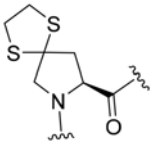	0.026	–
19	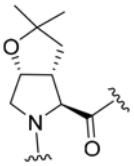	0.010	1.9
20	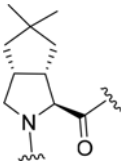	0.015	0.9
21	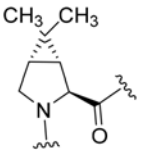	0.010	0.2

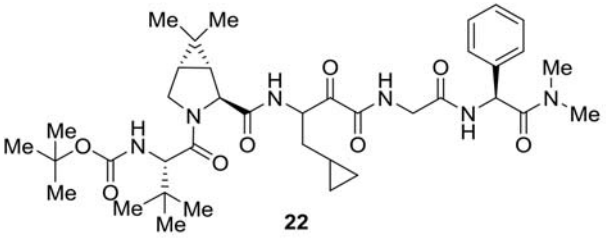

SCH6
K_i* = 0.0038 μM
EC_{90} (Rep) = 0.100 μM
HNE/HCV = 1000

Rat PK:
AUC (SC)= 19.5 μM.hr (%F = 100)
AUC (PO)= 0.35 μM.hr (%F =4)

Monkey PK:
AUC (SC)= 5.6 μM.hr (%F = 100)
AUC (PO)= 0.03 μM.hr (% F = 1)

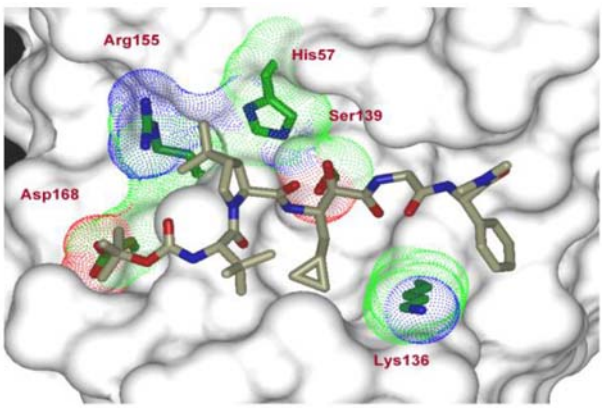

Fig. 7 Profile and X-ray structure of SCH6 bound to HCV NS3 protease.

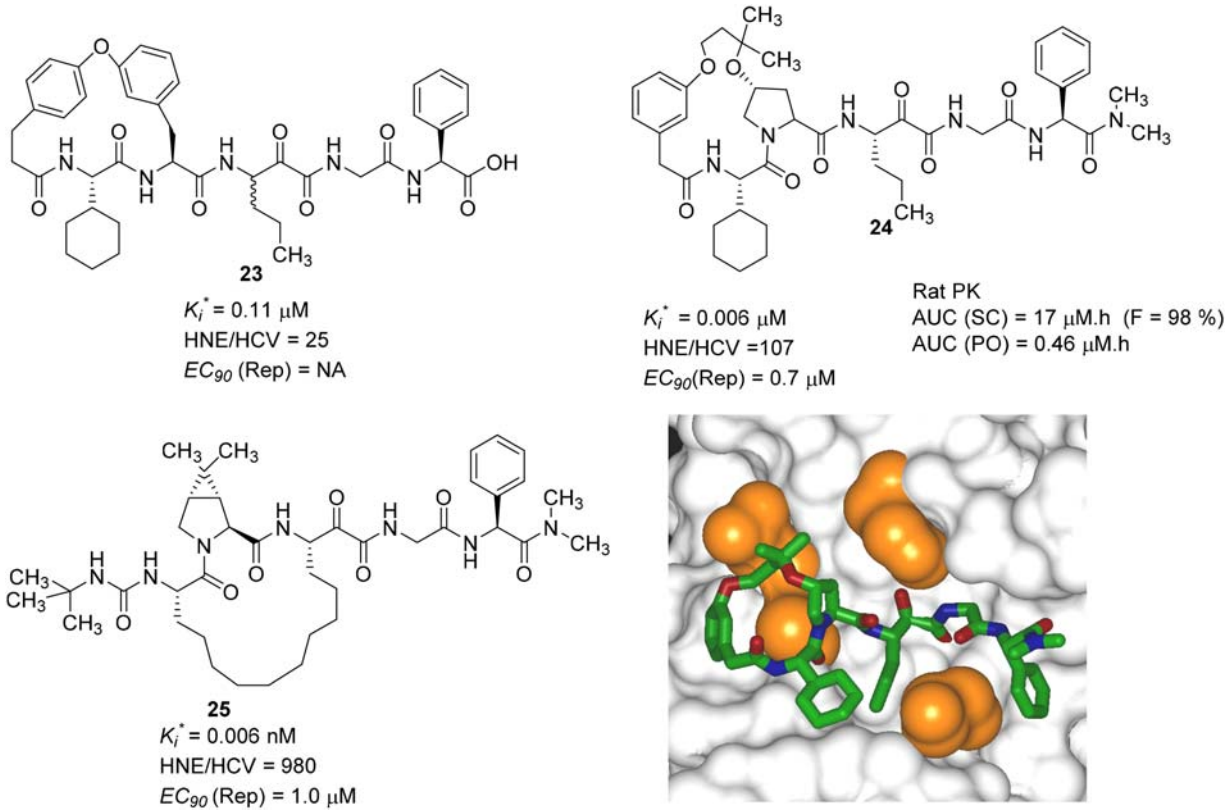

Fig. 8 P2–P4 and P1–P3 macrocyclic analogs.

$EC_{90} = 0.7$ μM).[21,22] With high expectations, analog **24** was evaluated for oral bioavailability in rats. Similar to analog **22**, analog **24** had an excellent exposure when administered subcutaneously with an $AUC_{0-24h} = 17$ μM h. However it was poorly absorbed orally and demonstrated an exposure of 0.46 μM h at 10 mg kg^{-1}. This was no different from the exposure achieved by SCH6. Cyclization to form a P1–P3 macrocycle was tolerated resulting in analog **25** ($K_i^* = 0.006$ μM and $EC_{90} = 1.0$ μM); however, its cellular potency was modest.[23] The X-ray structure of **24** bound to the HCV NS3 protease revealed a doughnut-like structure that encircled Ala156 where majority of the binding efficiency was derived by lipophilic interaction of P2 proline with methyl group of the alanine residue. Since the efforts of macrocyclization did not result in improvement of oral exposures it became necessary to devise other strategies to achieve improved potency and PK.

The lack of oral absorption was once again attributed to the higher molecular weight of the compound and the peptidic nature. It was clear that a reduction in the number of amide bond would overall improve the PK profile of these analogs. We therefore decided to truncate these molecules further and see the effect on potency. We initially explored truncation at P1 glycine position. With the optimized P2 groups we wanted to see the effect of replacement of the (P2′) phenyl glycine amide with smaller alkyl groups (Fig. 9). Replacement of (P2′) glycine–phenylglycine–dimethylamide segment with glycine propyl amide resulted in analog **26** with $K_i^* = 1.0$ μM, a significant loss in potency compared to **22**. However introduction of a cyclopropyl group analog **27** ($K_i^* = 0.090$ μM) and a benzyl amide **28** ($K_i^* = 0.056$ μM) retained significant activity. Analysis of the PK of these analogs in rat at 10 mg kg^{-1} showed improved oral absorption with compound **28** showing an oral $AUC_{0-6h} = 1.27$ μM h. Analog **29**, P3 *tert*-butyl glycine derivative of **28** ($K_i^* = 0.040$ μM and $EC_{90} = 0.8$ μM) was equipotent to the cyclohexyl glycine analog and significantly improved oral exposure ($AUC_{0-6h} = 4.2$ μM h). It was very gratifying to see that the strategy of truncation/depeptidization was on the right track and analogs had potency, cellular activity, and rat PK in desirable range. To further explore this strategy we decided to investigate analogs that were truncated at P1′.

Truncation of P1′–P2′ glycine–phenyl glycine dimethyl amide segment with allyl amide resulted in analog **30** with $K_i^* = 0.48$ μM (Table 4). This was a significant loss in activity compared to analogs of type **22**. However the compound had excellent oral exposure in rats when dosed at 10 mg kg^{-1} ($AUC_{0-24h} = 13.7$ μM h; $\%F = 34$). Replacement of allyl amide with methyl amide also resulted in analog with improved oral exposure. However the potency of both analogs **30** and **31** was suboptimal and needed significant improvement. Replacement of the P1 methyl amide with dimethyl amide resulted in analog **32** ($K_i^* > 13$ μM) with complete loss in potency. This suggested that the NH groups may be involved in hydrogen bonding with the protein backbone. We therefore investigated the synthesis of the primary ketoamide resulting in analog **33**. Introduction of a primary amide was well tolerated with eightfold improvement in potency compared to the methyl amide **31**. The primary amide

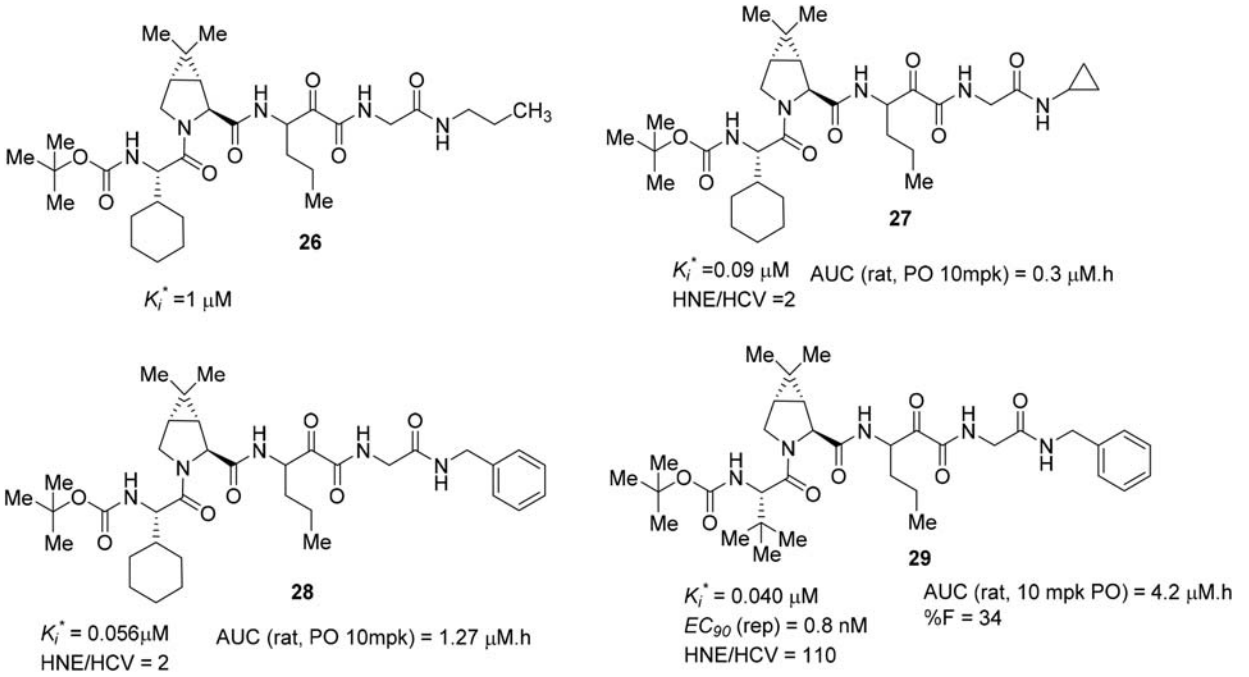

Fig. 9 P2′ truncated analogs

Table 4 P1′ truncated analogs of type 29

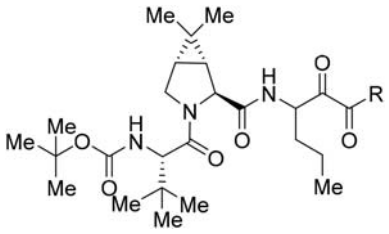

Cpd.	*R*	K_i^* *(μM)*	*AUC (rat) μM h*
30	NH allyl	0.48	13.7 (%*F*=34)
31	NHMe	1.50	13.4
32	NMe_2	>13	–
33	NH_2	0.22	12.8

analog **33** was evaluated for PK in rats dosed at 10 mg kg^{-1}. The compound was well absorbed with an excellent oral exposure of AUC_{0-6h} = 12.8 μM h. Having identified the introduction of primary amide resulted in analogs with acceptable inhibitory activity we next focused our efforts to optimize these analogs by modification of P1 and P3 groups.

X-ray structure of primary ketoamide **33** bound to the enzyme showed that the amide hydrogens making key hydrogen bond interactions with the backbone of the enzyme. This could be an important contributing factor for the improved binding of **33** compared to **31**. With the identification of a primary ketoamide **33** as a key small molecule lead, we next focused our attention in optimizing the potency and cellular activity of this analog. We initially focused our effort toward SAR of the P1 moiety to identify P1 ligands with higher ligand efficiency. Analysis of the X-ray crystal structure of analogs of type **33** showed that the S1 pocket was not completely occupied by the propyl chain of P1 norvaline. We therefore decided to investigate amino acids with small cyclic groups in an effort to fill the S1 pocket. Table 5 summarizes some of the results of our investigation.

Replacement of P3 *tert*-butyl glycine in **32** with P3 cyclohexyl glycine resulted in analog **33** with inhibitory activity of K_i^* = 0.1 μM similar to the *tert*-butyl glycine analog **32**. We therefore investigated P1 SAR with P3 cyclohexyl glycine. Replacement of P1 norvaline with a branching group resulted in leucine analog **34** (K_i^* = 0.40 μM), with significant loss in inhibitory activity. We next evaluated the effect of incorporating small carbocyclic-derived alanines at P1. Introduction of cyclopropyl alanine resulted in

Table 5 Modification at P1 in primary ketoamide series

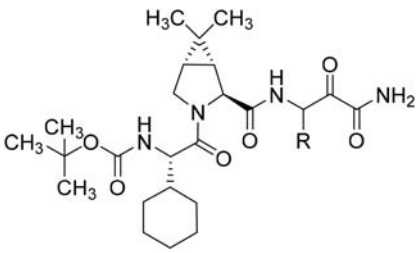

Cpd.	*R*	K_i* (μM)	EC_{90} (μM)	*HNE/HCV*	*Rat AUC (μM h)*
33	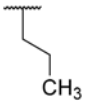	0.10	–	3	–
34	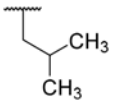	0.40	–	9	–
35		0.025	0.40	23	1.3 (F=3%)
36		0.008	0.40	100	1.5 (F=28%)
37	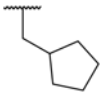	0.15	–	370	–
38	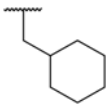	>12.0	–	–	–

analog **35** with K_i* = 0.025 μM and a cellular potency of 0.4 μM. Administration of **35** in rats at 10 mg kg^{-1} resulted in an oral AUC_{0-24h} = 1.3 μM h and a poor bioavailability of F = 3%. It was reassuring to see that introduction of cyclopropyl alanine resulted in improved potency with acceptable cellular activity and oral exposure. Further SAR investigation at P1 identified cyclobutyl alanine as an excellent P1 group that resulted in analog **36** with excellent in vitro activity of K_i* = 0.008 μM and EC_{90} of 0.4 μM. The selectivity of the cyclobutyl analog was much improved compared to the cyclopropyl analog. The cyclobutyl analog was also well absorbed and demonstrated improved oral bioavailability compared to cyclopropyl derivative. Further expansion of the P1 ring to cyclopentyl alanine was less tolerated resulting in **37** with a 15-fold loss in potency compared to **36** but a significantly improved HNE/HCV selectivity. Further expansion of the ring resulted in analogs with K_i* > 12 μM. The introduction of the cyclobutyl P1 resulted in analogs with desirable potency, cellular activity, and PK. We therefore investigated further SAR retaining this moiety. We next decided to investigate the P3 position and P1 group in the primary ketoamide series. Table 6 summarizes the SAR of the P3.

As previously discussed introduction of the cyclobutyl alanine at P1 had a profound effect on the inhibitory activity with analog **36** having a K_i* = 0.008 μM and EC_{90} of 0.4 μM. Replacement of P3 cyclohexyl glycine with *tert*-butyl glycine resulted in analog **39** (K_i* = 0.076 μM and EC_{90} = 0.8 μM) with a 10-fold loss in activity compared to **36** and similar cellular activity. Even though there was a loss in binding efficacy analog **39** had an improved HNE/HCV selectivity. Constraining P3 *tert*-butyl glycine into a ring to form methyl cyclopropylated glycine resulted in loss in the activity with analog **40** having a K_i* = 0.12 μM. We ascribed the loss in potency of **40** to inefficient interaction of the P3 side chain in the S3 pocket. Keeping this in mind we designed methylcyclohexyl glycine to impart characteristics of cyclohexyl glycine for potency and *tert*-butyl glycine for selectivity. The resultant analog **41** had a good binding activity and cellular potency of K_i* = 0.008 μM and EC_{90} of 0.4 μM; however, the HNE/HCV selectivity was suboptimal. Lastly replacement of P3 group with dimethyl-substituted serine to introduce polarity at P3 was not well tolerated. Analog **42** had a significant loss in activity. Structure–activity relationship at the P3 site identified *tert*-butyl glycine **39** as an excellent substitution which retained the cellular activity and improved HNE/HCV selectivity even though it had loss in binding activity. We

Table 6 SAR of P3 modification in primary ketoamide series

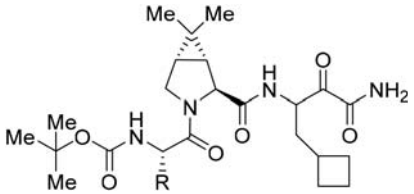

Cpd.	*R*	K_i* (μM)	EC_{90} (μM)	*HNE/HCV*
36		0.008	0.4	100
39	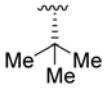	0.076	0.80	684
40		0.12	–	–
41	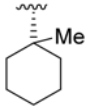	0.08	0.40	100
42	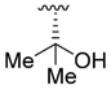	0.22	–	55

therefore decided to retain this along with P3 cyclohexyl glycine as the preferred P3 group and investigate SAR at the P4 region. We also investigated the SAR at P4 region retaining P1 cyclopropyl alanine group and decided to translate key finding to the cyclobutyl glycine series later (Table 7).

Replacement of P4 carbamate in **35** with isopropyl carbamate resulted in analog **43** with K_i* = 0.060 μM whereas the corresponding P3 *tert*-butyl glycine derivative had a K_i* = 0.15 μM. Constraining the isopropyl carbamate into a cyclopropyl ring resulted in twofold loss in potency (P3 Cyg K_i* = 0.12 μM; and P3 *tert*-butyl glycine K_i* = 0.30 μM). Replacement of the P4 group to cyclic cyclohexyl urea yielded analogs with potency of K_i* = 0.054 μM (P_3 cyclohexyl glycine) and K_i* = 0.020 μM (P_3 *tert*-butyl glycine). This replacement of P4 carbamate with urea resulted in improved potency in the case of P3 *tert*-butyl glycine. We next replaced the Boc group with *tert*-butyl urea resulting in analog **46** with K_i* = 0.050 μM and K_i* = 0.013 μM. We next evaluated the synthesis of secondary ureas with the synthesis of isopropyl N-methyl urea P4 cap. This resulted in fivefold loss compared to the *tert*-butyl urea analog. It was clear from these studies that P3 cyclohexyl accommodated a P4 carbamate whereas ureas were preferred when P3 group was a *tert*-butyl glycine. We next evaluated the effect of the potent P4 caps with P1 cyclobutyl alanine groups. This SAR also had a profound effect on the cellular activity and NHE/HCV selectivity of the resultant analogs (Fig. 10).

As previously discussed the introduction of Boc group at P4 with P3 cyclohexyl glycine and P1 cyclobutyl alanine resulted in analog **36** with K_i* = 0.008 μM and EC_{90} of 0.7 μM. The HNE/HCV selectivity of this analog was 140. The corresponding P3 *tert*-butyl glycine analog (**39**) had an enzyme activity of K_i* = 0.076 μM with similar cellular activity of **36** but improved HNE/HCV selectivity. Replacement of P4 Boc in P3 cyclohexyl glycine series with P4 *tert*-butyl urea yielded analog **48** (K_i* = 0.050 μM; EC_{90} = 0.5 μM, HNE/HCV = 90) with a 10-fold loss in binding activity. However, the introduction of *tert*-butyl urea into at P3 *tert*-butyl glycine series analog **49** (K_i* = 0.014 μM; EC_{90} = 0.35 μM, HNE/HCV = 2000) improved enzyme potency cellular activity and selectivity compared to **39** (K_i* = 0.076 μM; EC_{90} = 0.8 μM, HNE/HCV = 580). Since, analog **49** had acceptable binding, cellular activity, and desired selectivity we decided to further profile it for PK (Table 8).[24]

Administration of **49** to rats at 10 mg kg^{-1} resulted in AUC_{0-24h} = 1.52 μM h with an oral bioavailability of 26%. The compound was well absorbed with a mean residence time of 2.1 h. Administration to dogs at 3 mg kg^{-1} resulted in an AUC_{0-24h} = 3.2 μM h with oral bioavailability of F = 30% and a mean residence time of 1.2 h. The compound was poorly absorbed in monkeys with an oral exposure AUC_{0-24h} = 0.12 μM h and bioavailability of 4%. Based on the acceptable oral exposures of the compound in rats and dogs we evaluated the tissue distribution of the drug in rats. Following a 10 mg kg^{-1} administration in rats the concentration of the compound in the liver and plasma was followed (Fig. 11). A significant amount of the compound was distributed into the liver at first pass with a liver/plasma ratio of 30 which was 14 X EC_{90}. This preferential distribution of the compound in the target organ of the disease made it attractive in profiling further.

Table 7 SAR of P4 modifications in P3 cyclohexyl and *tert*-butyl glycine derived primary ketoamides

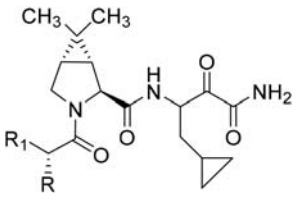

Entry	R_1	*R= Cyg* K_i* (μM)*	R=Tert-*butylglycine* K_i* (μM)*
43	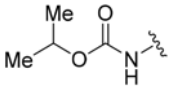	0.060	0.150
44	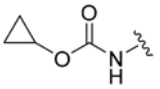	0.120	0.300
45	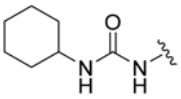	0.054	0.020
46	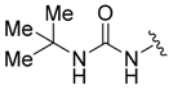	0.050	0.013
47	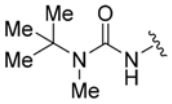	–	0.060

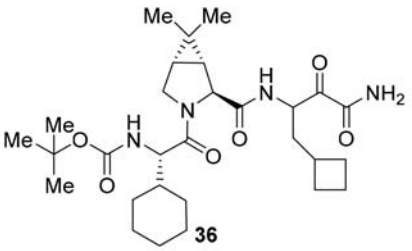

36

K_i^* = 0.008 μM
HNE/HCV =140
EC_{90} = 0.70 μM

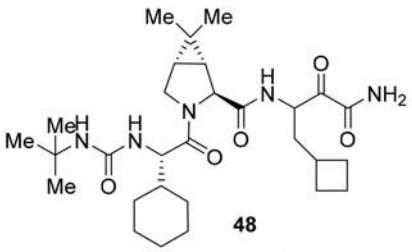

48

K_i^* = 0.05 μM
HNE/HCV =90
EC_{90} = 0.5 μM

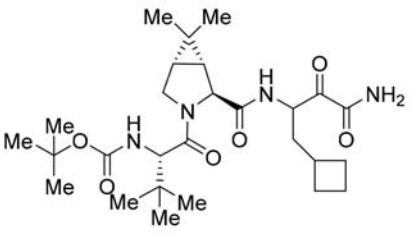

39

K_i^* = 0.076 μM
HNE/HCV =580
EC_{90} = 0.8 μM

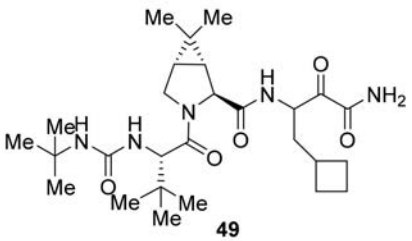

49

K_i^* = 0.014 μM
HNE/HCV =2000
EC_{90} = 0.35 μM

Fig. 10 Effect of P1 cyclobutyl alanine on analogs with optimized P4 groups.

Table 8 Oral PK of compound **49** in different species

Parameter (units)	*Rat*	*Dog*	*Monkey*
Number of individual (*N*)	3	3	3
Dose (mg kg^{-1})	10	3	3
AUC (0–24 h) (μM h)	1.52	3.2	0.12
Bioavailability (%)	26	30	4
Mean residence time (h)	2.1	1.2	2.2
Mean absorption time (h)	1.4	0.5	1.4
Oral C_{max} (μM)	0.65	2.27	0.09
T_{max} (h)	0.9	0.4	0.33
Fraction of oral absorption (%)	37	31	12

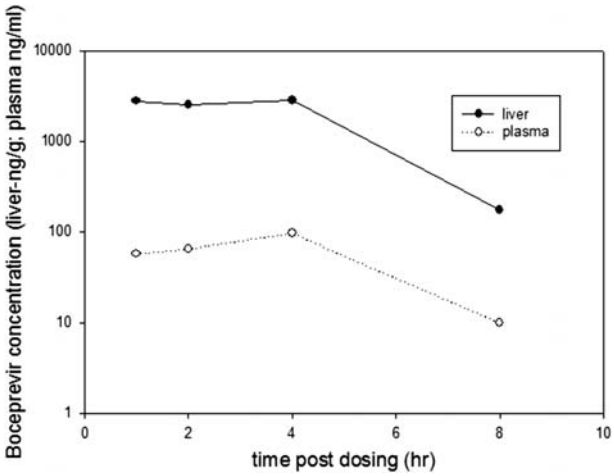

Fig. 11 Liver and plasma concentration of **49** in rats administered orally at 10 mg kg^{-1}.

Analog **49** was evaluated in other studies for progression as a clinical candidate.[25,26] The compound was clean in inhibition of CYP panel with $EC_{90} > 8$ μM against CYP's 3A4, 2D6, 2C9. It was clean in hERG with an $IC_{50} > 30$ μM and clean in Ames test for mutagenicity studies. When dosed in animals the compound showed a linear increase in exposure with rising dose. Based on these characteristics the compound was developed into a clinical candidate for further evaluation in humans.

The X-ray structure of analog **49** bound to HCV NS3 protease was solved and key interaction of the inhibitor was identified (Fig. 12).[27]

The ketoamide moiety at P1 was attacked by serine-139 from the backbone to make a reversible covalent bond. The planar sp2 center of the ketone was transformed into a tetrahedral center with the oxygen of the ketone making a hydrogen bond with His57. The oxygen of the amide moiety was projected toward the oxyanion hole. The primary ketoamide made a key hydrogen bond to the backbone with Gly41 and the oxygen accepted hydrogen bond from the backbone from Ser139 and Gly137. The P1 amide nitrogen was involved in key hydrogen bonding with Arg155 and P3 and P4 groups made key hydrogen bond with Ala 156 and Ala157. This array of hydrogen bond donors and acceptors made the interaction of **49** specific, and P2 proline and the methyl group on the cyclopropyl ring made lipophilic interactions with the methyl group of Ala-156. The P1 cyclobutyl group was deeply buried in the S1 pocket and the P3-*tert*-butylglycine made Van der Waals interactions with the enzyme in the shallow S3 pocket. In combination with the hydrogen bonds the lipophilic interactions contributed to binding and selectivity of **49** to the protease.

A computational analysis revealed the contributions of the various fragment to the overall binding of the inhibitor to the enzyme. As shown in Table 9, the covalent bond with the ketoamide and the P1 cyclobutyl alanine each contributed about two orders of magnitude to affinity. The P2 proline contributed an increase in 16-fold whereas the P3 and the P3 cap contributed to about eightfold in binding. These were in line with the percentage of the surface area that made contact with the protein. It was clear that the P1 ketoamide made significant contribution and the removal of it resulted in significant loss in activity. In addition to binding, the ketoamide group provided additional beneficial effects such as slow off rates from the enzyme.

The ketoamide in **49** is readily hydrated in aqueous medium existing in equilibrium of the keto and hydroxylated form (Fig. 13). The P1 group also readily epimerizes to a ratio of ~1.6:1 and both the P1 *S* and *R* isomers are hydrated. This ready hydration of the ketoamide imparted properties such as improved solubility, potentially contributing to higher free fraction of the compound.

Analog **49** was evaluated in a panel of HCV genotypes and ability to develop resistance. The pan-genotype activity of **49** is shown in Table 10. The compound was active in various genotypes in the enzyme assay with a fourfold loss in activity against genotype 4. It was also tested in replicon-based cellular assay and was found to be potent in most genotypes.

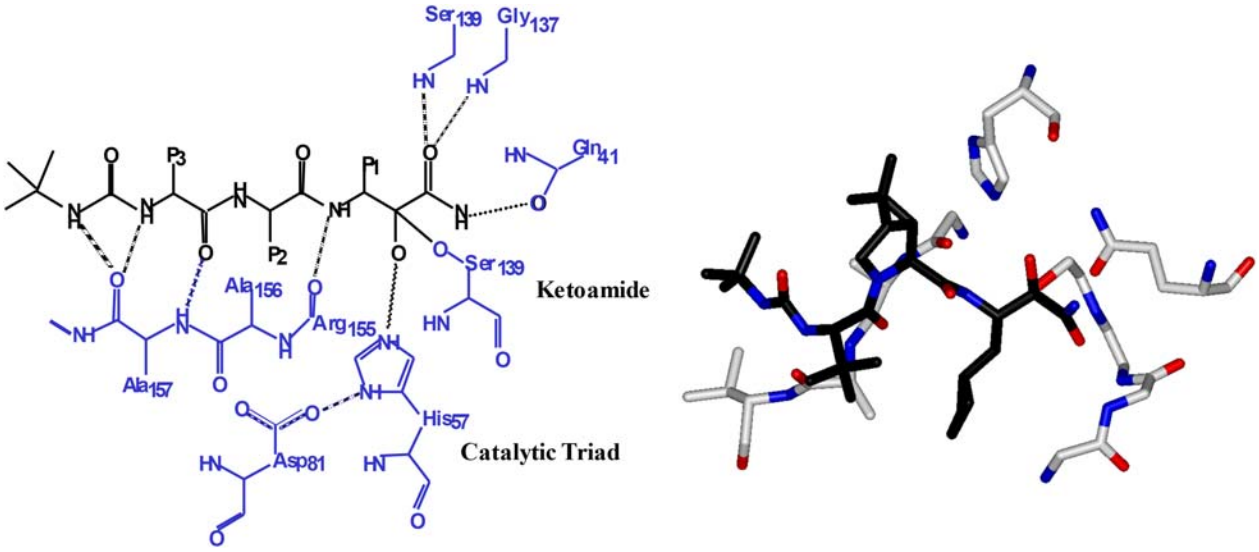

Fig. 12 Key interactions of compound **49** to HCV NS3 protease backbone.

Table 9 Contribution of various groups to the binding of analog **49** to HCV NS3/4A protease

Group	*Contact surface area (A^2)*	*% of Cpd. **49** surface area in contact with protein*	*Fold increase in affinity*
Tert-butyl urea (P3 cap)	26	36	7
Tert-butyl glycine (P3)	27	40	8
Dimethylcyclopropyl proline (P2)	36	40	16
Cyclobutyl alanine (P1)	59	80	93
Sub total	148	49	87,000
H-bonds			30
Covalent bond			100
Total fold increase			2.6×10^8

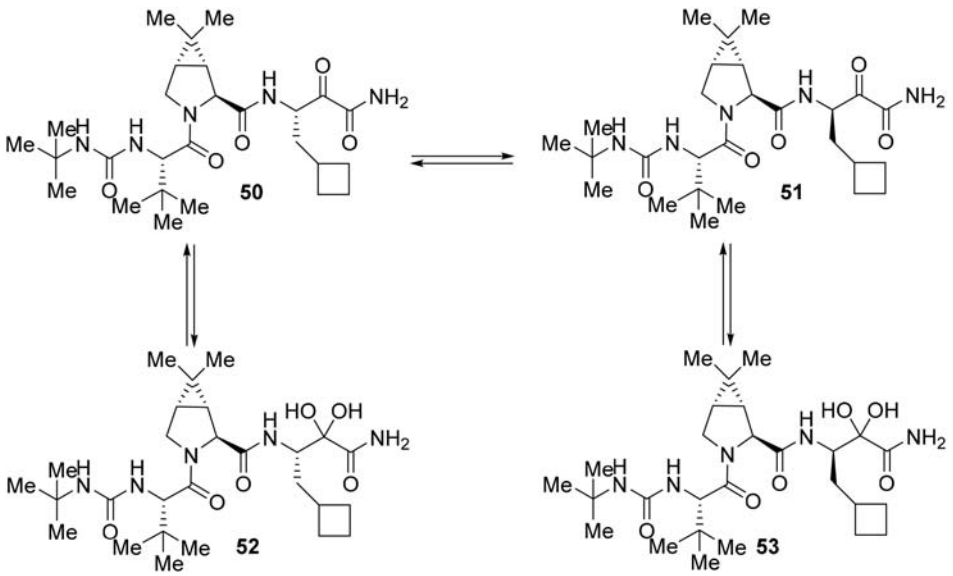

Fig. 13 Keto and hydrated forms of Boceprevir (**49**) in solution.

Table 10 Pan-genotypic activity of analog **49**

	gt1a	*gt1b*	*gt2a*	*gt3a*	*gt4*	*gt5a*
K_i^* (μM)	21	23	11	17	104	53
EC_{50} (μM)	233	220	283	159	–	251

Resistance to **49** was selected against genotype 1b and mutation was mapped by sequencing. In the replicon system, primary resistance was observed at the arginine 155 which was replaced by lysine. Mutation at Ala156 to serine or threonine was also developed that conferred significant loss in potency. Also the mutation of asp168 to glutamic acid resulted in significant loss in potency. Mutations developed in vitro in the replicon system translated well into the clinic with both arg155 mutation and asp168 mutation seen in patients on treatment with **49**.[28–31]

With many desirable properties **49** was evaluated in clinical trials for the treatment of gt1 infections in combination with Peg-interferon and Ribavirin.[32–34] It was well tolerated in SPRINT 2 phase 3 clinical trials. Patients treated with **49** over standard of care demonstrated improved cure rates (SVR) compared to patients on then standard of care (**Fig. 14**). Based on the outcome of these studies **49** (Boceprevir) was approved as first direct acting protease inhibitor for the treatment of HCV for gt1 infections.

In summary, **Fig. 15** describes the transition of undecapeptide **1–49** which resulted in substantial lowering of molecular weights and introduction of all the desired properties for a drug candidate. The molecular weight was reduced from the initial lead of 1265 to 519 retaining most of the inhibitory activity. In this process the selectivity of the analog was improved significantly from HNE/HCV of 7 to 2000 making **49** selective to HCV. Compounds were designed to incorporate cellular activity and desirable pharmacokinetics.

Having identified Boceprevir (**49**) as the first generation compound we decided to initiate a backup program to improve issues faced with its development. A close analysis of PK of **49** revealed it was suboptimal and had to be dosed at 800 mg TID in humans. As a team we decided to address this in the back-up compound with the goal of administering a BID or QD compound at significantly reduced doses. Boceprevir was also administered in an amorphous form as a mixture of isomers at P1 and had significant developmental issues for synthesis, purification, and formulation. We early on decided to develop a back-up compound as a single isomer at P1 which could be also readily purified and administered in a crystalline form. Moreover the oral exposure of the compound in cynomolgus monkeys was poor with a bioavailability of 4–11%. We decided to identify a compound which had acceptable exposures in monkeys for back-up compounds. With these requirements we decided to further improve the PK and potency of **49**.

A review of the metabolism of Boceprevir showed it was primarily metabolized by aldo-keto reductase (AKR) which reduced the ketoamide to the significantly less active hydroxy ketoamide (**Fig. 16**). Our initial efforts were to suppress this reduction by coadministration with AKR inhibitors which did not improve oral exposures significantly. A detailed investigation of various analogs in the ketoamide series revealed that although many primary ketoamides were substrates for AKR reduction, secondary amides were not and the compounds were mostly metabolized by CYPs. This information was vital in devising a strategy for the design of the back-up analogs.

We formulated a back-up strategy for Boceprevir with a target replicon cellular potency of $EC_{90} \leq 0.1$ μM and an improved PK across all preclinical species that could potentially support a BID or a QD dosing in humans. The compound would be a single isomer at P1 and crystalline for development. While investigating the SAR of Boceprevir, we investigated allyl amides at P1′

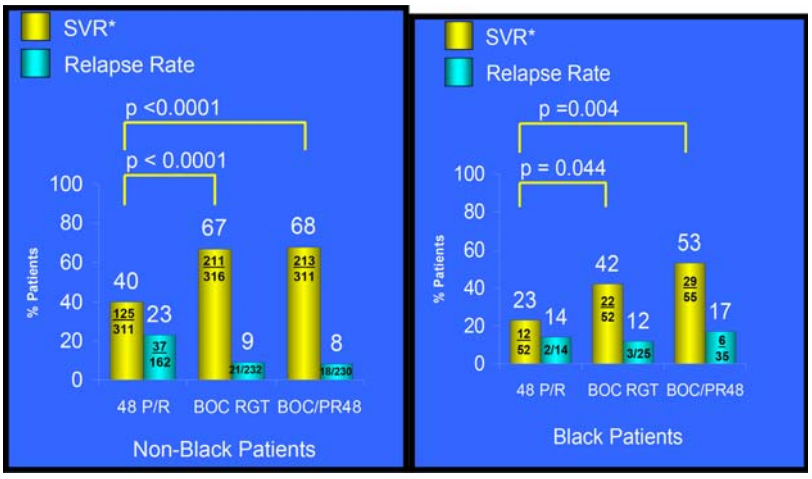

Fig. 14 Response of gt 1 HCV-infected patients treated with **49** in a Phase 3 SPRINT 2 trial.

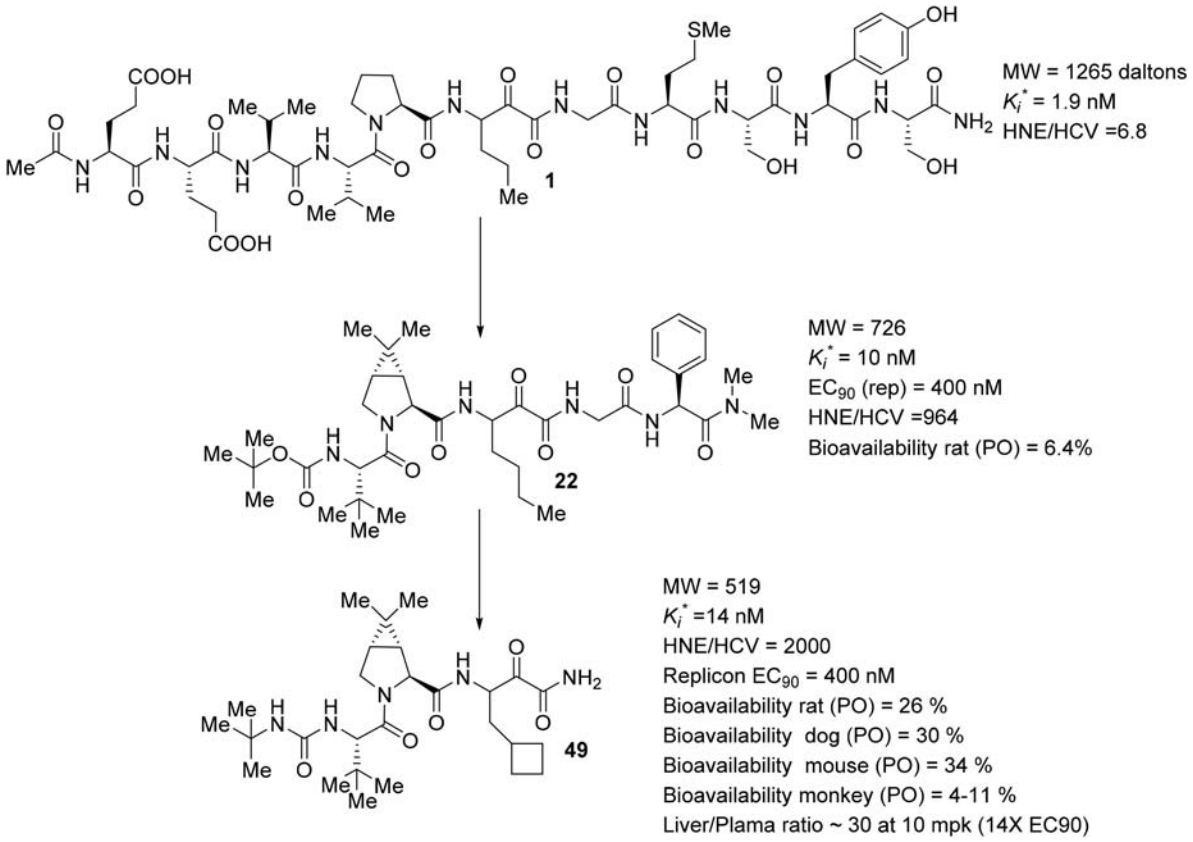

Fig. 15 Summary of optimization of initial lead **1** to Boceprevir (**49**).

Fig. 16 Metabolism of Boceprevir by aldo-keto reductase.

such as compound **30**. Even though the potency of these analogs was suboptimal they were readily absorbed and displayed excellent oral exposure. We thought this could be an excellent starting point. We therefore decided to retain the P1′ allyl group and investigate P4 groups simultaneously modifying P1 and P3 groups. A series of novel P4 substitutions were identified which imparted significantly improved cellular potencies and retained HNE/HCV selectivity. Fig. 17 summarizes some of the classes we identified.

Introduction of P4 urea derived from *tert*-butyl glycinol and capping it with ethyl carbonate resulted in analog **55** with a $K_i^* = 0.009$ μM and a replicon cellular activity of $EC_{90} = 0.150$ μM.[35] It was readily absorbed in rat with an excellent oral $AUC_{0-24h} = 26$ μM h when dosed at 10 mg kg^{-1} and bioavailability of 43%. However it had a modest exposure of AUC = 0.25 μM h in monkeys when dosed at 3 mg kg^{-1}. Similarly capping P4 *tert*-butyl glycine with N-methylated reverse sulfonamide yielded analog **56** with twofold improved cellular activity compared to carbamate analog **55** and much improved HNE/HCV selectivity.[36] However it had a much inferior PK profile compared to **55** with both the rat and rhesus having a significantly poor exposure. We next modified the P4 position by introduction of a lactam and an imide group resulting in analogs **57** and **58** which had excellent inhibitory activity in the replicon system with $EC_{90} = 0.06$ and 0.03 μM and acceptable exposures in rats and dog.[37] Unfortunately oral exposure of the compound **58** was greatly diminished when rats were dosed with crystalline material resulting in reduced interest in this class.

Previously in the process of discovery of Boceprevir **49**, we had designed targets that were functionalized at P4 position with a spirocyclohexyl group. These analogs had significantly improved cellular activity; however, they lacked desirable oral PK in rats. We decided to further investigate this class of analogs and anticipated to engineer desirable PK properties (Fig. 18).

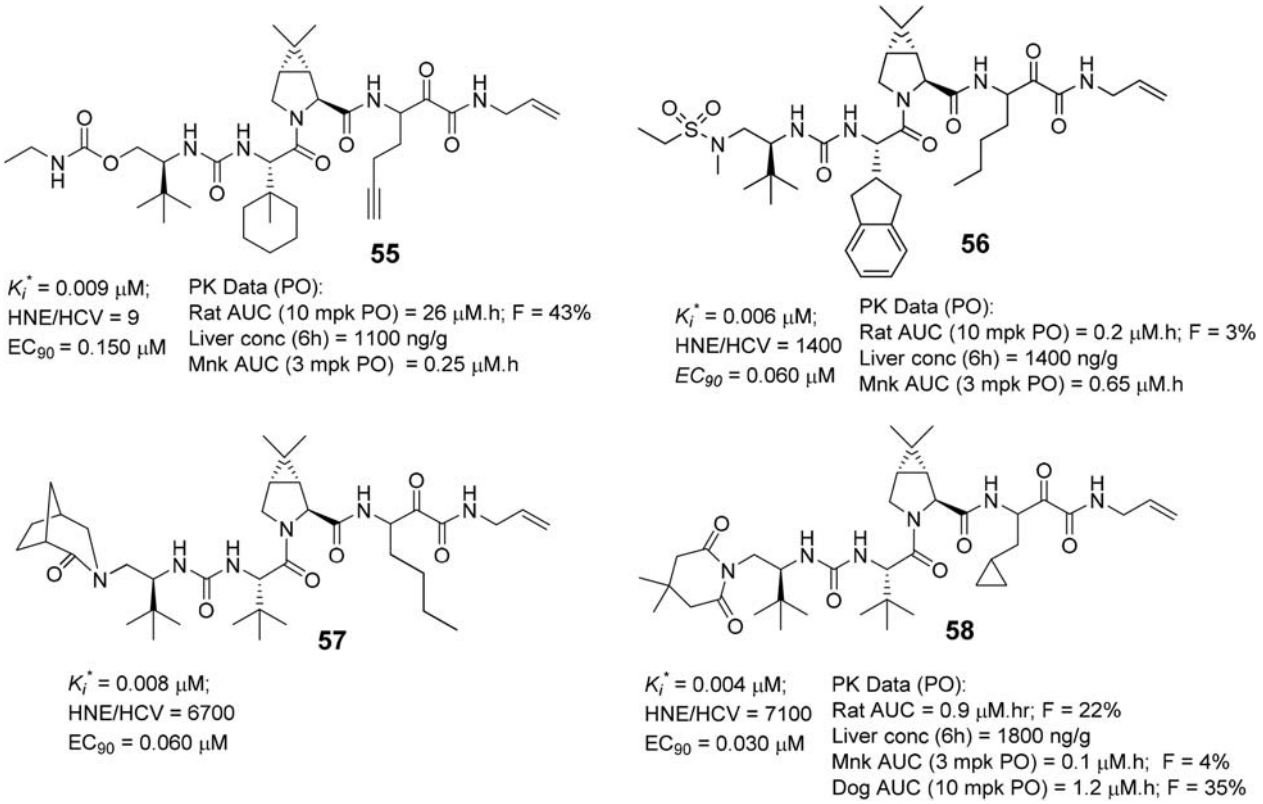

Fig. 17 P1′ allyl amide derivatives with modified P4 groups that imparted improved potency.

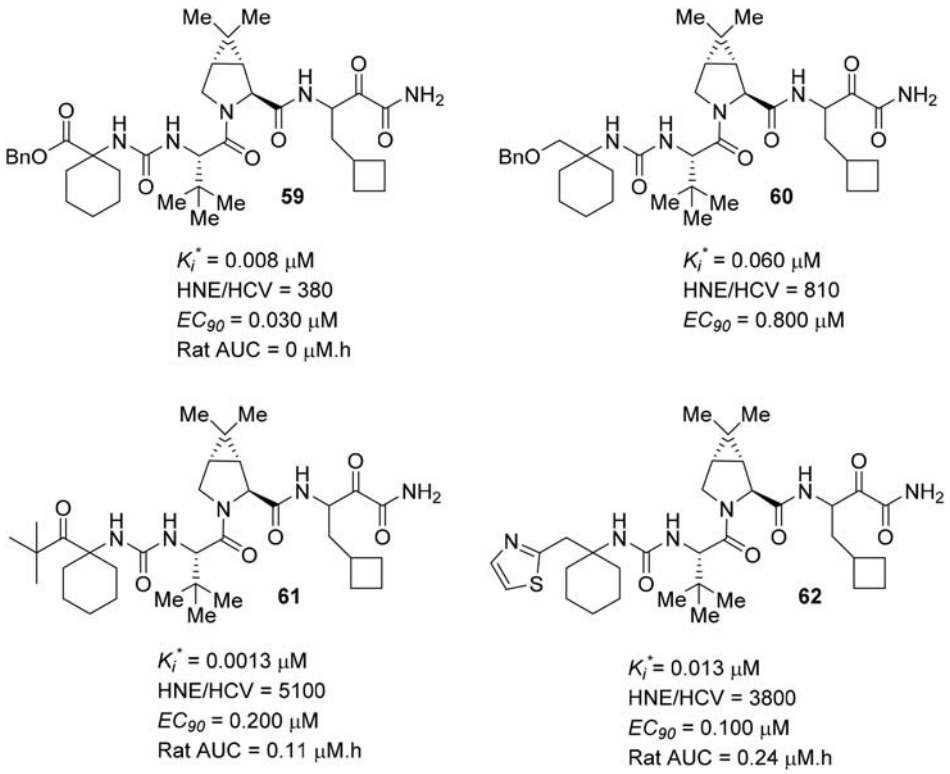

Fig. 18 P4 spirocyclohexyl glycine analogs of Boceprevir.

Introduction of urea derived from benzyl 1-aminocyclohexane-1-carboxylate at P4 resulted in analog **59** with $K_i^* = 0.008$ μM and potent cellular activity of $EC_{90} = 0.030$. However the PK of this analog was poor and no oral exposure was found in rats when orally administered at 10 mg kg^{-1}. Even though the PK of the compound was poor, we learnt that the introduction of a P4 group derived from spirocyclohexane had a potential to yield compounds with much improved cellular activity. The poor oral PK of **59** was probably due to the P4 benzyl ester which was readily hydrolyzed in the gut, resulting in poor absorption and metabolism. We therefore reduced the ester to form P4 benzyl ether exemplified by compound **60** which was significantly less active with $K_i^* = 0.060$ μM and a cellular replicon activity of $EC_{90} = 0.8$ μM. Further SAR analysis also identified analogs **61** and **62** with improved cellular activity. However all these analogs had poor PK and in rats.

In the process of these titrations a series of analogs containing P4 sulfone moiety were synthesized. Many of these analogs were potent in the replicon cellular assay. As shown in **Table 11**, a systematic modification of the alkyl group on the sulfone imparted improved potency. Analogs **64** and **65** containing an ethyl sulfone and *tert*-butyl sulfone are noteworthy.[38] Introduction of these P4 caps yielded analogs with $EC_{90} = 0.100$ μM in the replicon cellular assays and acceptable HNE/HCV selectivities. Further evaluation of these analogs in PK also showed *tert*-butyl analogs to have improved PK in monkeys (**Fig. 19**). This improved monkey PK feature attracted our attention to this series.

Analog **65** derived from P1 cyclobutyl group and analog **69** with P1 cyclopropyl group exhibited poor PK in rats; however, they were very well absorbed in monkeys and dosing these analogs in monkeys showed acceptable oral exposures of 3–4 μM h at 3 mg kg^{-1}. Based on this observation the team decided to focus on this class. Our previous experience had shown the replacement of a primary ketoamide with allyl amide improved rat oral exposure. We therefore wanted to evaluate the effect of incorporating allyl amides in analogs **65** and **66**. The results of this investigation are shown in **Table 12**.

As expected, the introduction of allyl group at P1 in **65** and **69** had a positive effect on rat PK. Allyl amide derivative of analog **65** resulted in analog **70** which had a binding activity of $K_i^* = 0.020$ μM and a cellular activity of $EC_{90} = 0.25$ μM. This modification resulted in a twofold loss in cellular activity; however, it had an oral AUC = 2.8 μM h in rats when dosed at 10 mg kg^{-1}. This was a significant improvement compared to compound **65**. Similarly **71**, ally amide of the P1 cyclopropyl derivative **69**, had an enzyme inhibition activity of $K_i^* = 0.022$ μM and a cellular activity of $EC_{90} = 0.14$ μM. This compound also showed acceptable oral

Table 11 Modification of P4 sulfone group

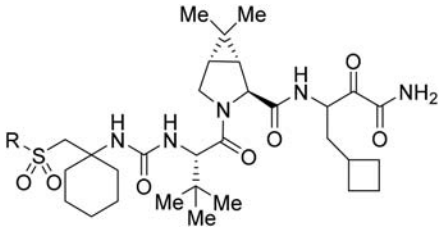

Cpd.	*R*	K_i^* *(μM)*	EC_{90} *(μM)*	*HNE/HCV*
63	Me–	0.005	0.50	2400
64	Et–	0.005	0.10	1200
65	^{t}Bu–	0.004	0.10	715
66	^{i}PrCH$_2$CH$_2$–	0.004	0.25	2800
67	Ph–	0.009	0.20	1100
68	PhCH$_2$–	0.005	0.40	90

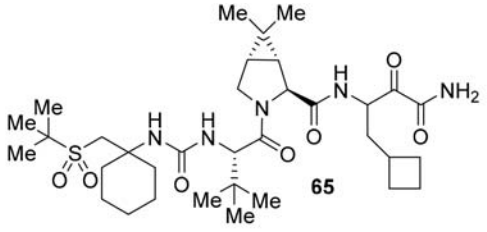

65

K_i^* = 0.004 μM
HNE/HCV = 715
EC_{90} = 0.100 μM
Rat AUC(10 mpk PO) = 0.02 μM.hr
Mnk AUC (3 mpk PO) = 3.2 μM.hr

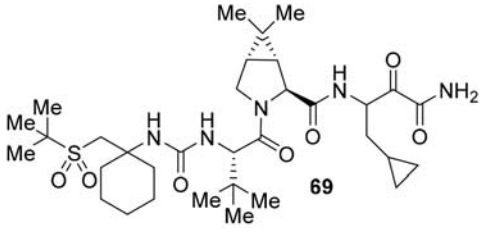

69

K_i^* = 0.009 μM
HNE/HCV = 120
EC_{90} = 0.100 μM
Rat AUC(10 mpk PO) = 0.01 μM.hr
Mnk AUC (3 mpk PO) = 4.1 μM.hr

Fig. 19 P4 sulfone capped analogs with improved monkey PK.

Table 12 Structure–activity relationship of P1 in secondary ketoamide series

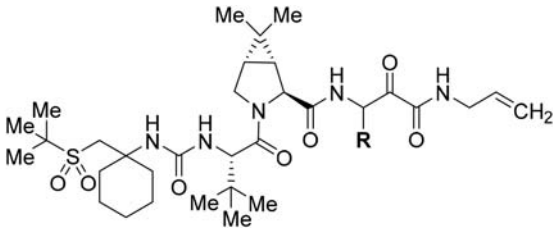

Cpd.	*P_1*	K_i* (μM)	EC_{90} (μM)	*HNE/HCV*	*Rat PK AUC (μM h)*	*Mnk PK AUC (μM h)*
70	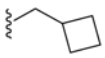	0.020	0.25	1600	2.8	–
71		0.022	0.14	340	1.7 (F=24%)	7.1
72	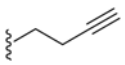	0.002	0.10	60	1.8	0.1
73	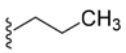	0.011	0.15	85	4	0.3
74	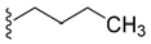	0.011	0.18	1350	5.1 (F=52%)	5.5

Rats were dosed at 10 mg kg^{-1} and monkeys at 3 mg kg^{-1} orally in 0.4% methylcellulose.

exposure in animals with an AUC of 1.7 μM h in rats and 7.1 μM h in monkeys when dosed at 10 and 3 mg kg^{-1}, respectively. With this encouraging finding we next evaluated additional P1 groups to see the effect on potency and PK. Introduction of a butynyl-derived amino acid at P1 resulted in analog **72** which was much potent compared to the cyclobutyl and cyclopropyl analogs. However the selectivity of this analog was modest with HNE/HCV = 60 and the monkey PK was poor. Saturating the triple bond in **72** resulted in norleucine analog **74** with K_i* = 0.011 μM and EC_{90} = 0.180 μM. The compound was well absorbed and had an oral AUC of 5 μM h in both rats and monkeys. It had a good bioavailability in rats (%F = 52%) and good HNE/HCV selectivity of 1350. Even though this compound did not meet the cellular potency cut off of $EC_{90} \leq 0.1$, we felt it was acceptable and we profiled it further. As previously mentioned one of the criteria for identification of a back-up compound to Boceprevir was the development of a crystalline material with single diastereomer at P1. We therefore decided to evaluate future analogs as pure P1 isomers. Secondly the presence of a double bond with allyl group was metabolically concerning. The formation of reactive intermediates had the potential to functionalize proteins and cause liver injury. We therefore decided to investigate new P1′ derivatives of analog **74** that lacked double bond and made new analogs as a single diastereomer at P1 (**Table 13**).

Separation of the P1 isomers of compound **74** resulted in analogs **75** (*S* isomer) and **76** (*R* isomer) at P1. The *S*-isomer was very potent with a K_i* = 0.008 μM and the *R*-diastereomer had a potency of 0.21 μM. Saturation of the double bond of the allyl group at P1′ resulted in loss in potency with analog **77** having a K_i* = 0.014 μM and cellular activity of EC_{90} = 0.100 μM. Replacement of P1′ with ethyl group resulted in analog **78** with similar potency to the propyl group. Further truncation to methyl group resulted in analog **79** with improved potency (K_i* = 0.004 μM and EC_{90} = 0.055 μM). Modifications by replacing P1′ with cyclopropyl methyl or methoxyethyl resulted in significant loss in potency resulting in analogs **80** (K_i* = 0.021 μM) and **81** (K_i* = 0.018 μM). We next investigated introduction of small cyclic moieties at P1′. Introduction of cyclopropyl resulted in analog **82** with K_i* = 0.006 μM and cellular activity of EC_{90} = 0.040 μM. The compound was potent in both the enzyme and cellular assays. It was also selective against HNE with an HNE/HCV selectivity of 600. Further expansion of the ring to cyclobutyl or cyclopentyl amine resulted in loss in activity with K_i* = 0.026 and 0.045 μM. Branching also had a detrimental effect at P1′ with methyl cyclopropyl analog **85** losing a substantial portion of the binding resulting in analog with K_i* = 0.30 μM. The separation of P1 resulted in a marked improvement in activity with the *S*-isomer being more active than the *R*-isomer. Replacements at P1′ were generally well tolerated. The cyclopropyl analog **82** retained most of the enzyme and cellular activity and cyclopropyl group was a good replacement for the allyl group which had a lower potential for formation of reactive intermediate. Having optimized the P1′ we decided to quickly scan the P3 group and P1 group on the optimized core with cyclopropyl group at P1′ and evaluate the pure (*S*)-diastereomer to make sure no difference in SAR was observed (**Fig. 20**).

Replacement of P3 *tert*-butyl glycine with cyclohexyl glycine was well tolerated resulting in analog **87** with K_i* = 0.006 μM and EC_{90} = 0.055 μM. However the HNE/HCV selectivity of the analog was modest with HNE/HCV selectivity of 120. Our previous SAR had indicated that *tert* butyl groups at P3 in general had improved HNE/HCV selectivity. We therefore synthesized analog **88** that contained a P3 methylcyclohexyl glycine group. Though this improved the HNE/HCV to 235 this was still lower than analog **82**. In an effort to improve solubility we next introduced tetrahydropyran-derived glycine analog, which resulted in analog **89** with significant loss in activity. From this scan at P3 it was clear that the *tert*-butyl glycine was still preferred and analog **87** was the optimized analog. We next focused to evaluate the P1 SAR. Analogs with selected P1 group were synthesized and the SAR at P1 was similar to the P1 racemic group.

Table 13 Effect of P1′ residues in P1 chiral norleucine derivative

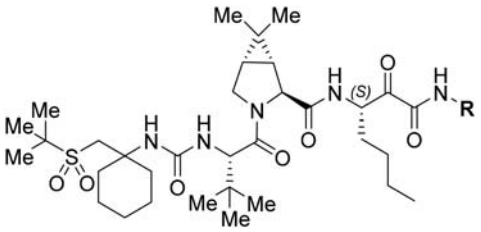

Cpd.	*P_1*	K_i* *(μM)*	EC_{90} *(μM)*	*HNE/HCV*
75	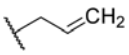	0.008		
	P1 *S* isomer			
76	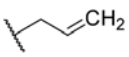	0.201		
	P1 *R* isomer			
77	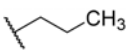	0.014	0.100	340
78	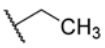	0.009	0.085	800
79		0.004	0.055	1500
80	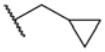	0.021	0.100	130
81	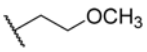	0.018	0.080	340
82		0.006	0.040	600
83		0.026	0.050	170
84		0.045		
85		0.300		
86	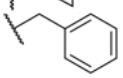	0.006	0.090	250

SAR at P1 still identified the norleucine group as still the most desirable group for overall potency and PK (Table 14). The replacement of P1 norleucine with norvaline resulted in compound **90** which had similar potency and PK profile to analog **82**. However the HNE/HCV selectivity of the norvaline analog was significantly inferior with norvaline analog **90** having HNE/HCV selectivity 8 as compared to 600 for norleucine analog. Introduction of trifluoro norvaline (**91**) and cyclopropyl alanine (**92**) was well tolerated yielding compounds potent in the binding and cellular assays. However these compounds had poor PK in rats and monkeys compared to the norleucine analog **82**. The introduction of a homo cyclopropyl alanine at P1 although well tolerated yielding compound comparable in potency to norleucine derivative had inferior PK in rats and monkeys making the norleucine compound most attractive.[39,40]

From the SAR of the back-up analogs it was clear that the norleucine was still the most preferred and compound **82** had all the desirable properties required in a back-up compound. It satisfied all the key goals that we set out to accomplish in a back-up compound. The compound had a potency of $EC_{90} < 100$ nM in replicon-based cellular assay, a single diastereomer at P1, and good exposure in rats and monkeys with acceptable selectivity. The X-ray structure of the compound **82** was also solved identifying key interactions with the protease (Fig. 21). In addition to the key interactions observed with Boceprevir additional interaction to the backbone contributed to the improved potency. The cyclopropyl amide occupied the lipophilic S1′ pocket and the spirocyclohexyl group occupied the S4 pocket. The oxygen of the sulfone made a hydrogen bond to cysteine 159 on the backbone of the protease.

Sulfone analog **82** was evaluated for oral PK in different species and the parameters were summarized in Table 15. The compound was well absorbed across all species with 43% in rats and 67% in cynomolgus monkeys and good overall oral AUCs. The AUC in rats when dosed at 10 mg kg^{-1} was 0.65 μM h mg^{-1} and 0.3 and 0.45 μM h mg^{-1} in dogs and monkeys. The

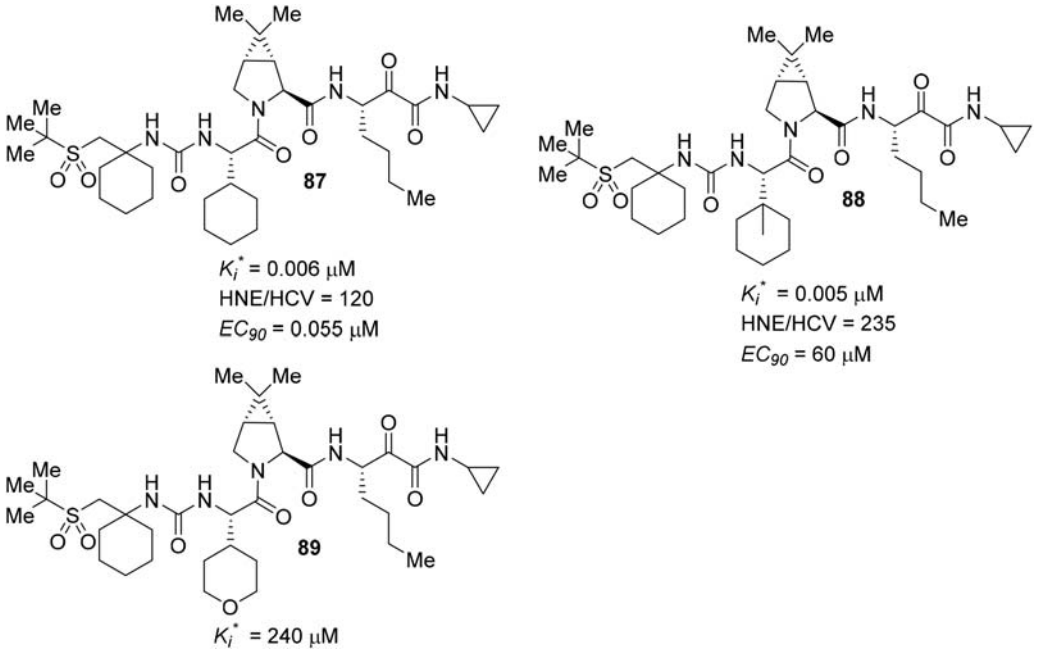

Fig. 20 SAR of P3 analogs in sulfone series.

Table 14 SAR of chiral P1 residue in P1′ cyclopropyl series

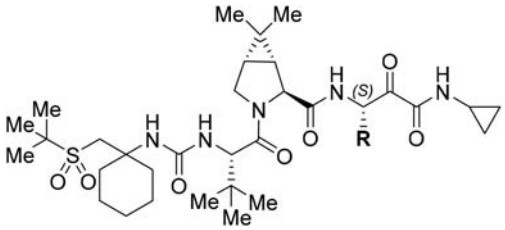

Cpd.	*P_1*	K_i* (μM)	EC_{90} (μM)	*HNE/HCV*	*Rat PK AUC (μM h)*	*Mnk PK AUC (μM h)*
82	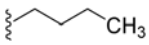	0.006	0.040	600	6.5	1.1
90	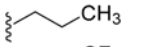	0.008	0.040	8	7.9	1.1
91	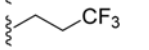	0.008	0.060	930	0.9	–
92		0.009	0.030	110	0.5	–
93	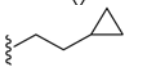	0.006	0.030	820	2.1	0.7

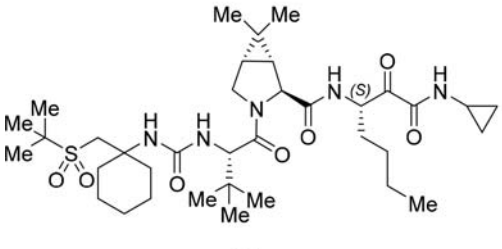

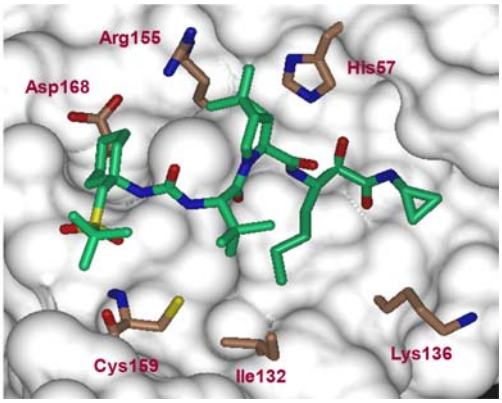

Fig. 21 X-ray structure of **82** bound to HCV NS protease.

Table 15 PK characteristics of **82** in different species

	Dose (PO/IV mg kg^{-1})	*AUC (μM h)*	*Absorption (%)*	F *(%)*	$T_{1/2}$ *(h)*	*Cl (mL min^{-1} kg^{-1})*
Rat	10/4	6.5	43	46	4.8	17
Dog	3/1	0.9	60	29	2	24
Monkey	10/3	4.5	67	39	6.8	21

bioavailability was acceptable, ranging from 30% to 50% and in vivo total clearances were modest in low double digits. Based on the overall exposure, the team decided to further progress this compound. The concentration of the compound in the liver was assessed and the compound had a favorable partition in the rat liver with concentration over the EC_{90} being greater than 400-fold. It was clean in the counterscreens and had no issues of P_{450} inhibition and/or potential for enzyme induction. It was clean in Ames mutagenicity test. Based on these characteristics it was chosen as a potential candidate for toxicology and progression into clinical studies.

Sulfone **82** was evaluated for inhibition of various genotypes and activity against mutant (Fig. 22). The potency of the compound across genotypes is shown. It is interesting to note that the compound is equipotent among all the genotypes and is about 10-fold more potent in genotype 1a compared to 1b. Resistant mutants were developed in replicon cells and the fold loss in potency compared to WT was measured (Table 16). As previously seen with Boceprevir the primary mutations leading to loss in potency were A156S (70-fold) and A158T (>1000-fold). Also Arg155 mutation to lysine conferred a 15-fold loss in activity compared to the wild type. The combination of interferon suppressed the emergence of mutations.

Analog **82** (Narlaprevir) was evaluated in toxicity studies and based on acceptable toxicity profile it was further progressed to phase 1 clinical studies in healthy volunteers and HCV-infected patients. In a clinical study NEXT-1, patients treated with 200 mg QD of Narlaprevir in combination with PEG-interferon, ribavirin, and ritonavir achieved undetectable viral titers in 85% of patients compared to 17% of patients on standard of care (Fig. 23).[41] Based on the positive SVR rates the compound was further progressed to phase 2 studies.

8.24.2 Summary

The identification and characterization of structural and functional proteins that are vital for the replication of hepatitis C virus paved the way for efforts to develop direct acting antivirals for the treatment of HCV. NS3/4A, a central protein required for post-translational modification and replication of the virus, was identified as an excellent target for drug discovery. The lack of starting

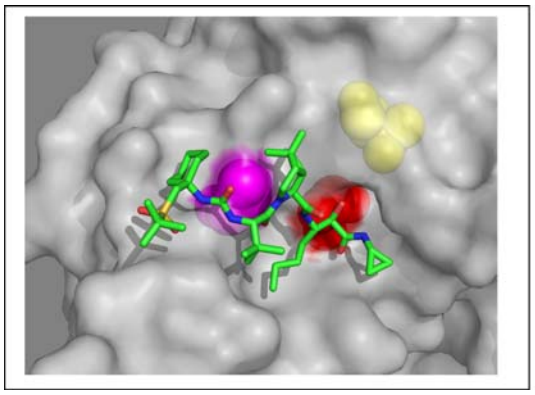

V36M	8
T54A	11
R155K	15
A156S	70
A156T	>1000
D168V	1
V36M	8

V36M 8
T54A 11
R155K 15
A156S 70
A156T >1000
D168V 1
V36M 8

Fig. 22 Mapping of resistance to Narlaprevir in HCV active.

Table 16 Pan-genotypic and mutant profile of inhibitor **82**

	gt1a	*gt1b*	*gt2*	*gt3a*	*gt4*
K_i* (nM)	0.7	6	3	7	16

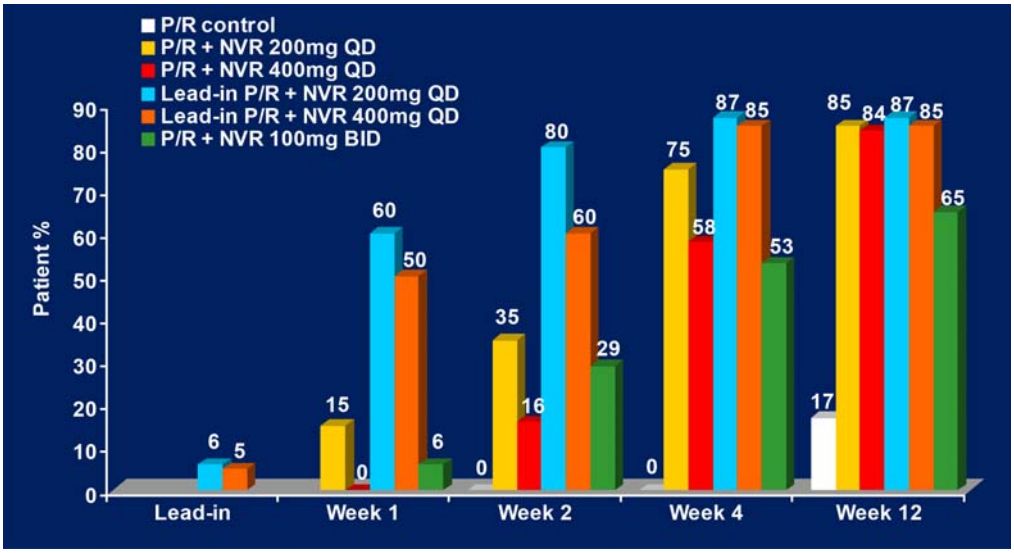

Fig. 23 Response of treatment of Narlaprevir in HCV genotype-infected patients.

points as initial leads for rapid SAR development led to a structure-based approach. An undecapeptide **1** containing a ketoamide electrophilic trap with MW = 1265 was discovered to bind in the active site with a K_i* = 1.9 nM. The catalytic serine made a reversible covalent bond with the inhibitor which attacked the enzyme from the *Re* face. It was clear from the onset that the lead was suboptimal and lacked desirable properties of a potential lead. The initial lead was peptidic with a high molecular weight and was mainly composed of natural amino acids. It was evident that the peptide would not be orally absorbed and would lack the desired pharmacokinetic profiles.

The team initially adopted a strategy to identify a minimum pharmacophore and remove proteinogenic amino acids from the lead. A conscious decision to limit the size of the inhibitor and remove the acidic group at P5 and P6 resulted in truncating analogs at P4. On the P1′ site the team systematically scanned nonnatural amino acids and investigated the effects of truncation on enzyme potency and cellular activity. The identification of P2′ phenyl glycine group and P2 leucine resulted in a series of analogs that were very potent in biochemical assays exemplified by analog **7**. However these analogs did not exhibit the desired cellular potency. To engineer the cellular activity the team went to the drawing board and redesigned the inhibitors by systematically changing the P2′ acid and methylating the amide nitrogens. It was found that methylating the P2 nitrogen had a profound effect on the cellular activity of the inhibitors with analog **15** demonstrating both enzyme potency and cellular activity. This resulted in new analogs derived from modified prolines which led to the identification of the potent inhibitor SCH6 which had both the desirable enzyme activity and cellular potency. Further evaluation of SCH6 and analogs demonstrated that these compounds were poorly absorbed and did not show oral exposure.

The team decided to further reduce the molecular weight and number of amide bonds. Truncation at P1 with a primary ketoamide resulted in analogs such as **35** that retained most of the activity and also was orally absorbed. Modifications at P1, P3, and P4 groups identified cyclobutyl alanine at P1, *tert*-butyl glycine at P3, and a *tert*-butyl urea at P4 as the desirable group that imparted optimal potency, PK, and selectivity. The combination of P3 and P4 capping group had a profound effect on human neutrophil elastase with P1 cyclobutyl alanine in combination with P3 *tert*-butyl glycine imparting high HNE/HCV selectivities. These SAR studies led to the discovery of Boceprevir which was potent with acceptable safety and PK properties and was subsequently progressed to clinical trials. Adding Boceprevir to the then standard of care improved SVR in patients infected with HCV. It was the first direct acting HCV antiviral to be approved for the treatment chronic gt-1 HCV infections.

The team next focused in solving some of the issues faced in the development of Boceprevir in the identification of a back-up compound. The team focused on key issues of improving potency, identifying a single isomer to facilitate development, and improving PK in monkeys. The introduction of a P1′ allyl amide changed the elimination pathway which was now primarily metabolized oxidatively by cytochrome $P_{450's}$. A spirocyclic sulfone-derived P4 moiety, which made a hydrogen bonding with cys-159, was identified that enabled improvement of binding and cellular potencies. Replacement of P1′ from allyl to cyclopropyl group further retained potencies yielding compound with much improved PK in monkey. The separated *S*-isomer at P1 resulted in analog

82 (Narlaprevir) which satisfied all the key requirements of a potential back-up candidate. Adding Narlaprevir to standard of care with ritonavir resulted in a >80% of treatment naive patients achieving undetectable viral titers within 12 weeks of treatments.

From the initial introduction of first-generation direct-acting antivirals Boceprevir and Telaprevir[42,43] targeting the viral protein NS3, many new second-generation drugs have been designed and introduced that vastly improve cure rates in gt1b patients and also exhibit pan genotypic activity. More importantly, other proteins in the life cycle of HCV have been successfully targeted and efficacious drugs have been developed inhibiting HCV NS5B polymerase and HCV NS5A enzymes. From the initial proof of concept demonstrated by BILN-2061[44] various macrocyclic NS3 drugs such as Simeprevir,[45] Vaniprevir,[46] Grazoprevir,[47,48] and Paritaprevir[49] have been approved for the treatment of HCV. The design and development of these compounds is a major accomplishment in medicinal chemistry. Each of these drugs is a testament to ingenious designs and problem solving skills when faced with lack of leads for SAR optimization. Starting from a peptide substrate teams have worked tirelessly to incorporate all the desired properties required for successful drugs. In the processes of introducing novel HCV drugs teams have broken barriers in medicinal chemistry. For example, they have explored novel macrocyclic scaffolds in an undesirable chemical space with molecular weights in ranges >700, depeptidizing them and engineering desirable properties in them and developing excellent synthetic routes for manufacturing and commercialization.

In addition to HCV NS3 protease inhibitors, novel inhibitors to inhibit HCV NS5B have been developed. The identification of nucleoside inhibitors such as Sofosbuvir[50] had a profound impact in the treatment of HCV. It dramatically shortened the treatment times and introduced higher barrier to resistance becoming a backbone for the combination drugs. In addition to NS5B protein the inhibition of NS5A enzyme was a fertile ground which yielded many potent inhibitors. From the initial development of Daclatasvir[51] many imaginative modification to this structures have resulted in the identification of new compounds such as Ombitasvir,[52] Ledipasvir,[53] and Elbasvir[54] with improved potency and activity against key mutants.

The identification of compounds targeting a wide range of mechanisms opened avenues to develop novel combination therapies. Combination therapies allowed not only achievement of very high cure rates >99% but also suppression of resistance and development of regimens to successfully treat different genotypes, null responders, and HIV/HCV coinfected patients. A major positive development of combination therapies is the development of all oral therapies and elimination of PEG intron which was plagued with serious side effects, and significant shortening of treatment durations from initial 48 weeks to around twelve weeks or less with much less side effects.

From the dawn of the century the landscape for HCV treatment has significantly changed with the prognosis for HCV-infected patients being bright. For the first time the vast majority of patients infected with chronic HCV need not progress to liver transplantation or hepatocellular carcinoma. Treatment of patients with a combination of direct acting antiviral will result in complete cure. In combination with blood screening and new drugs for treatments, HCV infections can be hopefully eliminated as a public burden in foreseeable future.

See also: 5.18. Direct-Acting Antiviral Agents for the Treatment of Hepatitis C Virus Infection.

References

1. Zeuzem, S.; Feinman, S. V.; Rasenack, J.; Heathcote, E. J.; Lai, M.-Y.; Gane, E.; O'Grady, J.; Reichen, J.; Diago, M.; Lin, A.; Hoffman, J.; Brunda, M. J. Peginterferon alfa-2a in Patients With Chronic Hepatitis C. *N. Engl. J. Med.* **2000,** *343* (23), 1666–1672.
2. Manns, M. P.; McHutchison, J. G.; Gordon, S. C.; Rustgi, V. K.; Shiffman, M.; Reindollar, R.; Goodman, Z. D.; Koury, K.; Ling, M.-H.; Albrecht, J. K.; International Hepatitis Interventional Therapy Group. Peginterferon alfa-2b Plus Ribavirin Compared With Interferon alfa-2b Plus Ribavirin for Initial Treatment of Chronic Hepatitis C: A Randomized Trial. *Lancet* **2001,** *358,* 958–965.
3. Freeman, A. J.; Dore, G. J.; Law, M. G.; Thorpe, M.; Overbeck, J. V.; Llyods, A. R.; Marinos, G.; Kaldor, J. M. Estimating Progression to Cirrhosis in Chronic Hepatitis C Infection. *Hepatology* **2001,** *4,* 809–816.
4. Choo, Q. L.; Kuo, G.; Weiner, A. J.; Overby, L. R.; Bradley, D. W.; Houghton, M. Isolation of a cDNA Clone Derived from a Blood-Borne Non-A, Non-B Viral Hepatitis Genome. *Science* **1989,** *244,* 359–362.
5. Kuo, G.; Choo, Q. L.; Alter, H. J.; Gitnick, G. L.; Redeker, A. G.; Purcell, R. H.; Miyamura, T.; Dienstag, J. L.; Alter, M. J.; Stevens, C. E.; Tegtmeier, G. E.; Bonino, F.; Colombo, M.; Lee, W.-S.; Kuo, C.; Berger, K.; Shuster, J. R.; Overby, L. R.; Bradley, W.; Houghton, M. An Assay for Circulating Antibodies to a Major Etiologic Virus of Human Non-A, Non-B Hepatitis. *Science* **1989,** *244,* 362–364.
6. Bartenschlager, R. The Ns3/4a Proteinase of the Hepatitis C Virus: Unraveling Structure and Function of an Unusual Enzyme and a Prime Target for Antiviral Therapy. *J. Viral Hepat.* **1999,** *6,* 165–181.
7. Bartenschlager, R.; Ahlborn-Laake, L.; Mous, J.; Jacobsen, H. Nonstructural Protein 3 of the Hepatitis C Virus Encodes a Serine-Type Proteinase Required for Cleavage at the NS3/4 and NS4/5 Junctions. *J. Virol.* **1993,** *67,* 3835–3844.
8. Yan, Y.; Li, Y.; Munshi, S.; Sardana, V.; Cole, J. L.; Sardana, M.; Steinkuehler, C.; Tomei, L.; De-Francesco, R.; Kuo, L. C.; Chen, Z. Complex of NS3 Protease and NS4A Peptide of BK Strain Hepatitis C Virus: A 2.2 Å Resolution Structure in a Hexagonal Crystal Form. *Protein Sci.* **1998,** *7,* 837–847.
9. Love, R. A.; Parge, H. E.; Wickersham, J. A.; Hostomsky, Z.; Habuka, N.; Moomaw, E. W.; Adachi, T.; Hostomska, Z. The Crystal Structure of Hepatitis C Virus NS3 Proteinase Reveals a Trypsin-Like Fold and a Structural Zinc Binding Site. *Cell* **1996,** *87,* 331–342.
10. Kim, J. L.; Morgenstern, K. A.; Griffith, J. P.; Dwever, M. D.; Thomson, J. A.; Murcko, M. A.; Lin, C.; Caron, P. R. Hepatitis C Virus NS3 RNA Helicase Domain With a Bound Oligonucleotide: The Crystal Structure Provides Insights into the Mode of Unwinding. *Structure* **1998,** *6,* 89–100.
11. Kwong, A. D.; Kim, J. L.; Rao, G.; Lipovsek, D.; Raybuck, S. A. Hepatitis C Virus NS3/4A Protease. *Antivir. Res.* **1998,** *40,* 1–18.
12. Steinkuhler, C.; Urbani, A.; Tomei, L.; Biasiol, G.; Sandana, M.; Bianchi, E.; Pessi, A.; DeFrancesco, R. Activity of Purified Hepatitis C Virus Protease NS3 on Peptide Substrates. *J. Virol.* **1996,** *70,* 6694–6700.
13. Urbani, A.; Bianchi, E.; Narjes, F.; Tramontano, A.; De Francesco, R.; Steinkuhler, C.; Pessi, A. Substrate Specificity of the Hepatitis C Virus Serine Protease NS3. *J. Biol. Chem.* **1997,** *272,* 9204–9209.

14. Kolykhalov, A. A.; Agapov, E. V.; Rice, C. M. Specificity of the Hepatitis C Virus NS3 Serine Protease: Effects of Substitutions at the 3/4a, 4a/4b, 4b/5a, and 5a/5b Cleavage Sites on Polyprotein Processing. *J. Virol.* **1994,** *68,* 7525–7533.
15. Zhang, R.; Beyer, B. M.; Durkin, J.; Ingram, R.; Njoroge, F. G.; Windsor, W. T.; Malcolm, B. A. A Continuous Spectrophotometric Assay for the Hepatitis C Virus Serine Protease. *Anal. Biochem.* **1999,** *270,* 268–275.
16. Lohmann, V.; Körner, F.; Koch, J.-O.; Herian, U.; Theilmann, L.; Bartenschlager, R. Replication of Subgenomic Hepatitis C Virus RNAs in a Hepatoma Cell Line. *Science* **1999,** *285,* 110–113.
17. Morrison, J. F.; Walsh, C. The Behavior and Significance of Slow Binding Enzyme Inhibitors. In *Advances in Enzymology,* vol. 61, Meister, A., Ed. **1988,** *vol. 61; pp 201–301.*
18. Mamai, A.; Zhang, R.; Natarajan, A.; Madalengoitia, J. S. Poly-L-Proline Type-II Peptide Mimics Based on the 3-Azabicyclo[3.1.0]hexane System. *J. Org. Chem.* **2001,** *66,* 455–460.
19. Bogen, S. L.; Arasappan, A.; Bennett, F.; Chen, K.; Jao, E.; Liu, Y.-T.; Lovey, R. G.; Venkatraman, S.; Pan, W.; Parekh, T.; Pike, R. E.; Ruan, S.; Liu, R.; Baroudy, B.; Agrawal, S.; Chase, R.; Ingravallo, P.; Pichardo, J.; Prongay, A.; Brisson, J.-M.; Hsieh, T. Y.; Cheng, K.-C.; Kemp, S. J.; Levy, O. E.; Lim-Wilby, M.; Tamura, S. Y.; Saksena, A. K.; Girijavallabhan, V.; Njoroge, F. G. Discovery of SCH446211 (SCH6): A New Ketoamide Inhibitor of the HCV NS3 Serine Protease and HCV Subgenomic RNA Replication. *J. Med. Chem.* **2006,** *49,* 2750–2757.
20. Venkatraman, S.; Njoroge, F. G.; Girijavallabhan, V. M.; Madison, V. S.; Yao, N. H.; Prongay, A. J.; Butkiewicz, N.; Pichardo, J. Design and Synthesis of Depeptidized Macrocyclic Inhibitors of Hepatitis C NS3-4A Protease Using Structure-Based Drug Design. *J. Med. Chem.* **2005,** *48,* 5088–5091.
21. Chen, K. X.; Njoroge, F. G.; Vibulbhan, B.; Prongay, A.; Pichardo, J.; Madison, V.; Buevich, A.; Chan, T.-M. Proline-Based Macrocyclic Inhibitors of the Hepatitis C Virus: Stereoselective Synthesis and Biological Activity. *Angew. Chem. Int. Ed. Engl.* **2005,** *44,* 7024–7028.
22. Chen, K.; Njoroge, F. G.; Arasappan, A.; Venkatraman, S.; Vibulbhan, B.; Yang, W.; Parekh, T. N.; Pichardo, J.; Prongay, A.; Cheng, K.-C.; Butkiewicz, N.; Yao, N.; Madison, V.; Girijavallabhan, V. Novel Potent Hepatitis C Virus NS3 Serine Protease Inhibitors Derived From Proline-Based Macrocycle. *J. Med. Chem.* **2006,** *49,* 995–1005.
23. Venkatraman, S.; Velazquez, F.; Wu, W.; Blackman, M.; Chen, K. X.; Bogen, S.; Nair, L.; Tong, X.; Chase, R.; Hart, A.; Agrawal, S.; Pichardo, J.; Cheng, K.-C.; Girijavallabhan, V.; Piwinski, J.; Shih, N.-Y.; Njoroge, F. G. Discovery and Structure-Activity Relationship of P1-P3 Ketoamide Derived Macrocyclic Inhibitors of Hepatitis C Virus NS3 Protease. *J. Med. Chem.* **2009,** *52,* 336–346.
24. Cheng, K.-C.; Li, C.; Liu, T.; Wang, G.; Hsieh, Y.; Pavlovsky, A.; Broske, L.; Prelusky, D.; Chen, J.; Liu, R.; Uss, A. S.; White, R. E.; Gupta, S.; Njoroge, F. G. Use of Preclinical in vitro and in vivo Pharmacokinetics for Selection of Potent Hepatitis C Protease Inhibitor, Boceprevir for Clinical Development. *Lett. Drug Des. Discov.* **2009,** *6,* 218–312.
25. Venkatraman, S.; Bogen, S. L.; Arasappan, A.; Bennett, F.; Chen, K.; Jao, E.; Liu, Y.-T.; Lovey, R.; Hendrata, S.; Huang, Y.; Pan, W.; Parekh, T.; Pinto, P.; Popov, V.; Pike, R.; Ruan, S.; Santhanam, B.; Vibulbhan, B.; Wu, W.; Yang, W.; Kong, J.; Liang, X.; Wong, J.; Liu, R.; Butkiewicz, N.; Chase, R.; Hart, A.; Agarwal, S.; Ingravallo, P.; Pichardo, J.; Kong, R.; Baroudy, B.; Malcolm, B.; Guo, Z.; Prongay, A.; Madision, B. L.; Cui, X.; Cheng, K.-C.; Hsieh, T. Y.; Brisson, J.-M.; Prelusky, D.; Kormacher, W.; White, R.; Bogonowich-Knipp, S.; Pavlovsky, A.; Prudence, B.; Saksena, A. K.; Ganguly, A.; Piwinski, J.; Girijavallabhan, V.; Njoroge, F. G. Discovery of (1*R*,5*S*)-*N*-[3-amino-1-(cyclobutylmethyl)-2-3-dioxopropyl]-3-[2(*S*)-[[[(1,1-dimethylethyl)-amino]carbonyl]amio]-3,3-dimethyl-1-oxobutyl]-6,6-dimethyl-3-azabicyclo[3.1.0]hexan-2(S)-carboxamide (SCH 503034), a Selective, Potent, Orally Bioavailable, Hepatitis C Virus NS3 Protease Inhibitor: A Potential Therapeutic Agent for the Treatment of Hepatitis C Infection. *J. Med. Chem.* **2006,** *49,* 6074–6086.
26. Malcolm, B. A.; Liu, R.; Lahser, F.; Agrawal, D.; Belanger, B.; Butkiewicz, N.; Chase, R.; Gheyas, F.; Hart, A.; Hesk, D.; Ingravallo, P.; Jiang, C.; Kong, R. L.; Pichardo, J.; Prongay, A.; Skelton, A.; Tong, X.; Venkatraman, S.; Xia, E.; Girijavallabhan, V.; Njoroge, F. G. Sch 503034, a Mechanism-Based Inhibitor of Hepatitis C Virus NS3 Protease, Suppresses Polyprotein Maturation and Enhances the Antiviral Activity of Alpha Interferon in Replicon Cells. *Antimicrob. Agents Chemother.* **2006,** *50,* 1013.
27. Prongay, A. J.; Guo, Z.; Yao, N.; Pichardo, J.; Fischmann, T.; Strickland, C.; Myers, J., Jr.; Weber, P. C.; Beyer, B. M.; Ingram, R.; Hong, Z.; Prosise, W. W.; Ramanathan, L.; Taremi, S. S.; Yarosh-Tomaine, T.; Zhang, R.; Senior, M.; Yang, R. S.; Malcolm, B.; Arasappan, A.; Bennett, F.; Bogen, S. L.; Chen, K.; Jao, E.; Liu, Y.-T.; Lovey, R. G.; Yang, R. S.; Malcolm, B.; Arasappan, A.; Bennett, F.; Bogen, S. L.; Chen, K.; Jao, E.; Liu, Y.-T.; Lovey, R. G.; Saksena, A. K.; Venkatraman, S.; Girijavallabhan, V.; Njoroge, F. G.; Madison, V. Discovery of the HCV NS3/4A Protease Inhibitor (1R,5S)-N-[3-amino-1-(cyclobutylmethyl)-2,3-dioxopropyl]-3-[2(S)-[[[(1,1-dimethylethyl)amino] carbonyl]amino]-3,3-dimethyl-1-oxobutyl]-6,6-dimethyl-3-azabicyclo[3.1.0]hexan-2(s)-carboxamide (Sch 503034). Key Steps in Structure-Based Optimization. *J. Med. Chem.* **2007,** *50,* 2310–2318.
28. Tong, X.; Guo, Z.; Wright-Minogue, J.; Xia, E.; Prongay, A.; Madison, V.; Qiu, P.; Venkatraman, S.; Velazquez, F.; Njoroge, F. G.; Malcolm, B. A. Impact of Naturally Occurring Variants of HCV Protease on the Binding of Different Classes of Protease Inhibitors. *Biochemistry* **2006,** *45,* 1353.
29. Guo, Z.; Prongay, A.; Tong, X.; Thierry, F.; Bogen, S.; Velazquez, F.; Venkatraman, S.; Njoroge, F. G.; Madison, V. Computational Study of the Effects of Mutations A156T, D168V, and D168Q on the Binding of HCV Protease Inhibitors. *J. Comput. Chem.* **2006,** *2,* 1657.
30. Tong, X.; Chase, R.; Skelton, A.; Chen, T.; Wright-Minogue, J.; Malcolm, B. A. Identification and Analysis of Fitness of Resistance Mutations Against the HCV Protease Inhibitor SCH 503034. *Antivir. Res.* **2006,** *70,* 28–38.
31. Barnard, R. J.; Howe, J. A.; Ogert, R. A.; Zeuzem, S.; Poordad, F.; Gordon, S. C.; Ralston, R.; Tong, X.; Sniukiene, V.; Strizki, J.; Ryan, D.; Long, J.; Qiu, P.; Brass, C. A.; Albrecht, J.; Burroughs, M.; Vuocolo, S.; Hazuda, D. J. Analysis of Boceprevir Resistance Associated Amino Acid Variants (RAVs) in Two Phase 3 Boceprevir Clinical Studies. *Virol. J.* **2013,** *444,* 329–336.
32. Kwo, P. Y.; Lawitz, E. J.; McCone, J.; Schiff, E. R.; Vierling, J. M.; Pound, D.; Davis, M. N.; Galati, J. S.; Gordon, S. C.; Ravendhran, N.; Rossaro, L.; Anderson, F. H.; Jacobson, I. M.; Rubin, R.; Koury, K.; Pedicone, L. D.; Brass, C. A.; Chaudhri, E.; Albrecht, J. K.; on behalf of the SPRINT-1 investigators. Efficacy of Boceprevir, an NS3 Protease Inhibitor, in Combination With Peginterferon alfa-2b and Ribavirin in Treatment-Naive Patients with Genotype 1 Hepatitis C Infection (SPRINT-1): An Open-Label, Randomised, Multicentre Phase 2 Trial. *Lancet* **2010,** *376,* 705–716.
33. Poordad, F.; McCone, J., Jr.; Bacon, B. R.; Bruno, S.; Manns, M. P.; Sulkowski, M. S.; Jacobson, I. M.; Reddy, K. R.; Goodman, Z. D.; Boparai, N.; DiNubile, M. J.; Sniukiene, V.; Bacon, B. R.; Bruno, S.; Manns, M. P.; Sulkowski, M. S.; Jacobson, I. M.; Reddy, K. R.; Goodman, Z. D.; Boparai, N.; DiNubile, M. J.; Sniukiene, V.; Brass, C. A.; Albrecht, J. K.; Bronowicki, J.-P.; for the SPRINT-2 investigators. Boceprevir for Untreated Chronic HCV Genotype 1 Infection. *N. Engl. J. Med.* **2011,** *364* (13), 1195–1206.
34. Bacon, B.; Gordon, S. C.; Lawitz, E.; Marcellin, P.; Vierling, J. M.; Zeuzem, S.; Poordad, F.; Goodman, Z. D.; Sings, H. L.; Boparai, N.; Burroughs, M.; Brass, C. A.; Albrecht, J. K.; Poordad, F.; Goodman, Z. D.; Sings, H. L.; Boparai, N.; Burroughs, M.; Brass, C. A.; Albrecht, J. K.; Esteban, R.; for the HCV RESPOND-2 investigators. Boceprevir for Previously Treated Chronic HCV Genotype 1 Infection. *N. Engl. J. Med.* **2011,** *364* (13), 1207–1217.
35. Arasappan, A.; Padilla, A. I.; Jao, E.; Bennett, F.; Bogen, S.; Chen, K. X.; Pike, R. E.; Sannigrahi, M.; Soares, J.; Venkatraman, S.; Vibulbhan, B.; Saksena, A. K.; Girijavallabhan, V.; Tong, X.; Cheng, K. C.; Njoroge, F. G. Discovery of Novel P4 Modified Analogues With Improved Potency and Pharmacokinetic Profile. *J. Med. Chem.* **2009,** *52,* 2806–2817.
36. Venkatraman, S.; Blackman, M.; Wu, W.; Nair, L.; Arasappan, A.; Padilla, A.; Bogen, S.; Bennett, F.; Chen, K.; Pichardo, J.; Tong, X.; Prongay, A.; Cheng, K.-C.; Girijavallabhan, V.; Njoroge, F. G. Discovery of Novel P3 Sulfonamide-Capped Inhibitors of HCV NS3 Protease Inhibitors With Improved Cellular Potencies. *Bioorg. Med. Chem.* **2009,** *17,* 4486–4495.
37. Chen, K. X.; Nair, L.; Vibulbhan, B.; Yang, W.; Arasappan, A.; Bogen, S. L.; Venkatraman, S.; Bennett, F.; Pan, W.; Blackman, M. L.; Padilla, A.; Prongay, A.; Cheng, K.-C.; Tong, X.; Shih, N.-Y.; Njoroge, F. G. Second-Generation Highly Potent and Selective Inhibitors of the Hepatitis C Virus NS3 Serine Protease. *J. Med. Chem.* **2009,** *2009* (52), 1370.
38. Bennett, F.; Huang, . Y.; Hendrata, H.; Lovey, R.; Bogen, S. L.; Pan, W.; Guo, A.; Prongay, A.; Chen, K.-X.; Arasappan, A.; Venkatraman, S.; Velazquez, V.; Nair, L.; Sannigrahi, M.; Tong, X.; Pichardo, J.; Cheng, K.-C.; Girijavallabhan, V.; Saksena, A. K.; Njoroge, F. G. The Introduction of P4 Substituted 1-Methylcyclohexyl Groups Into Boceprevir®: A Change in Direction in the Search for a Second Generation HCV NS3 Protease Inhibitor. *Bioorg. Med. Chem. Lett.* **2010,** *20,* 2617.

39. Arasappan, A.; Bennett, F.; Bogen, S. L.; Venkatraman, S.; Blackman, M.; Chen, K.-C.; Hendrata, S.; Huang, Y.; Huelgas, R. M.; Nair, L.; Padilla, A. L.; Pan, W.; Pike, R.; Pinto, P.; Ruan, S.; Sannigrahi, M.; Velazquez, F.; Vibulbhan, B.; Wu, W.; Yang, W.; Saksena, A. K.; Girijavallabhan, V.; Shih, N.-Y.; Kong, J.; Meng, T.; Jin, Y.; Wong, J.; McNamara, P.; Prongay, A.; Madison, V.; Piwinski, J. J.; Cheng, K.-C.; Morrison, R.; Malcolm, B.; Tong, X.; Ralston, R.; Njoroge, F. G. Discovery of Narlaprevir (SCH 900518): A Potent, Second Generation HCV NS3 Protease Inhibitor. *ACS Med. Chem. Lett.* **2010,** *1,* 64.
40. Tong, X.; Arasappan, A.; Bennett, F.; Chase, R.; Feld, B.; Guo, Z.; Hart, A.; Madison, V.; Malcolm, B.; Pichardo, J.; Prongay, A.; Ralston, R.; Skelton, A.; Xia, E.; Zhang, R.; Njoroge, F. G. Preclinical Characterization of the Antiviral Activity of SCH 900518 (Narlaprevir), a Novel Mechanism-Based Inhibitor of Hepatitis C Virus NS3 Protease. *Antimicob. Agents Chemother.* **2010,** *54,* 2365–2370.
41. Bruijne, J. D.; Bergmann, J. F.; Reesink, H. W.; Weegink, C. J.; Molenkamp, R.; Schinkel, J.; Tong, X.; Li, J.; Treitel, M. A.; Hughes, E. A.; van Lier, J. J.; van Vliet, A. A.; Janssen, H. L. A.; de Knegt, R. J. Antiviral Activity of Narlaprevir Combined With Ritonavir and Pegylated Interferon in Chronic Hepatitis C. *Hepatology* **2010,** *52,* 1590–1599.
42. Kwong, A. D.; Kauffman, R. S.; Hurter, R.; Mueller, P. Discovery and Development of Telaprevir: An NS3-4A Protease Inhibitor for Treating Genotype 1 Chronic Hepatitis C Virus. *Nat. Biotechnol.* **2011,** *29,* 993–1003.
43. Perni, R. B.; Almquist, S. J.; Byrn, R. A.; Chandorkar, G.; Chaturvedi, P. R.; Courtney, L. F.; Decker, C. J.; Dinehart, K.; Gates, C. A.; Harbeson, S. L.; Heiser, A.; Kalkeri, G.; Kolaczkowski, E.; Lin, K.; Luong, Y.-P.; Rao, B. G.; Taylor, W. P.; Thomson, J. A.; Tung, R. D.; Wei, Y.; Kwong, A. D.; Lin, C. *Antimicrob. Agents Chemother.* **2006,** *50,* 899.
44. Tsantrizos, Y. S.; Bolger, G.; Bonneau, P.; Cameron, D. R.; Goudreau, N.; Kukolj, G.; LaPlante, S. R.; Llinas-Brunet, M.; Herber Nar, H.; Lamarre, D. *Angew. Chem. Int. Ed.* **2003,** *42,* 1356.
45. Lin, T. I.; Lenz, O.; Fanning, G.; Verbinnen, T.; Delouvroy, F.; Scholliers, A.; Vermeiren, K.; Rosenquist, A.; Edlund, M.; Samuelsson, B.; Vrang, L.; De Kock, H.; Wigerinck, P.; Raboisson, P.; Simmen, K. In Vitro Activity and Preclinical Profile of TMC435350, a Potent Hepatitis C Virus Protease Inhibitor. *Antimicrob. Agents Chemother.* **2009,** *53,* 1377–1385.
46. McCauley, J. A.; McIntyre, C. J.; Rudd, M. T.; Nguyen, K. T.; Romano, J. J.; Butcher, J. W.; Gilbert, K. F.; Bush, K. J.; Holloway, M. K.; Swestock, J.; Wan, B. L.; Carroll, S. S.; DiMuzio, J. M.; Graham, D. J.; Ludmerer, S. W.; Mao, S. S.; Stahlhut, M. W.; Fandozzi, C. M.; Trainor, N.; Olsen, D. B.; Vacca, J. P.; Liverton, N. J. Discovery of Vaniprevir (MK-7009): A Macrocyclic Hepatitis C Virus NS3/4a Protease Inhibitor. *J. Med. Chem.* **2010,** *53,* 2443–2463.
47. Harper, S.; McCauley, J. A.; Rudd, M. T.; Ferrara, M.; DiFilippo, M.; Crescenzi, B.; Koch, U.; Petrocchi, A.; Holloway, M. K.; Butcher, J. W.; Romano, J. J.; Bush, K. J.; Gilbert, K. F.; McIntyre, C. J.; Nguyen, K. T.; Nizi, E.; Carroll, S. S.; Ludmerer, S. W.; Burlein, C.; DiMuzio, J. M.; Graham, D. J.; McHale, C. M.; Stahlhut, M. W.; Olsen, D. B.; Monteagudo, E.; Cianetti, S.; Giuliano, C.; Pucci, V.; Trainor, N.; Fandozzi, C. M.; Rowley, M.; Coleman, P. J.; Vacca, J. P.; Summa, V.; Liverton, N. J. Discovery of MK-5172: A Macrocyclic Hepatitis C Virus NS3/4a Protease Inhibitor. *ACS Med. Chem. Lett.* **2012,** 332–336.
48. Summa, V.; Ludmerer, S. W.; McCauley, J. A.; Fandozzi, C.; Burlein, C.; Claudio, G.; Coleman, P. J.; Dimuzio, J. M.; Ferrara, M.; Di Filippo, M.; Gates, A. T.; Graham, D. J.; Harper, S.; Hazuda, D. J.; Huang, Q.; McHale, C.; Monteagudo, E.; Pucci, V.; Rowley, M.; Rudd, M. T.; Soriano, A.; Stahlhut, M. W.; Vacca, J. P.; Olsen, D. B.; Liverton, N. J.; Carroll, S. S. MK-5172, a Selective Inhibitor of Hepatitis C Virus NS3/4a Protease With Broad Activity Across Genotypes and Resistant Variants. *Antimicrob. Agents Chemother.* **2012,** *56,* 4161–4167.
49. Kowdley, K. V.; Lawitz, E.; Poordad, F.; Cohen, D. E.; Nelson, D. R.; Zeuzem, S.; Everson, G. T.; Kwo, P.; Foster, G. R.; Sulkowski, M. S.; Xie, W.; Pilot-Matias, T.; Liossis, G.; Larsen, L.; Khatri, A.; Podsadecki, T.; Bernstein, B. Phase 2b Trial of Interferon-Free Therapy for Hepatitis C Virus Genotype 1. *N. Engl. J. Med.* **2014,** *370,* 222–232.
50. Sofia, M. J.; Bao, D.; Chang, W.; Du, J.; Nagarathnam, D.; Rachakonda, S.; Reddy, P. G.; Ross, B. S.; Wang, P.; Zhang, H. R.; Bansal, S.; Espiritu, C.; Keilman, M.; Lam, A. M.; Micolochick, H. M.; Steuer, N. C.; Otto, M. O.; Furman, P. A. *J. Med. Chem.* **2010,** *53,* 7202–7218.
51. Gao, M.; Nettles, R. E.; Belema, M.; Snyder, L. B.; Nguyen, V. N.; Fridell, R. A.; Serrano-Wu, M. H.; Langley, D. R.; Sun, J.-H.; O'Boyle, D. R., II; Lemm, J. A.; Wang, C.; Knipe, J. O.; Chien, C.; Colonno, R. J.; Grasela, D. M.; Meanwell, N. A.; Hamann, L. G. Chemical Genetics Strategy Identifies an HCV NS5A Inhibitor With a Potent Clinical Effect. *Nature* **2010,** *465,* 96–100.
52. Feld, J. J.; Kowdley, K. V.; Coakley, E.; Sigal, S.; Nelson, D. R.; Crawford, D.; Weiland, O.; Agiilar, H.; Xiong, J.; Pilot-Matias, T.; DaSilva-Tillmann, B.; Larsen, L.; Podsadecki, T.; Bernstein, B. Treatment of HCV With ABT-450/r–Ombitasvir and Dasabuvir With Ribavirin. *N. Engl. J. Med.* **2014,** *370,* 1594–1603.
53. Afdhal, N.; Zeuzem, S.; Kwo, P.; Chojkier, M.; Gitlin, N.; Puoti, M.; Romero-Gomez, M.; Zarski, J. P.; Agarwal, K.; Buggisch, P.; Foster, G. R.; Bräu, N.; Buti, M.; Jacobson, I. M.; Subramanian, G. M.; Ding, X.; Mo, H.; Yang, J. C.; Pang, P. S.; Symonds, W. T.; McHutchison, J. G.; Muir, A. J.; Mangia, A.; Marcellin, P.; Ion-1 Investigators. Ledipasvir and Sofosbuvir for Untreated HCV Genotype 1 Infection. *N. Engl. J. Med.* **2014,** *370,* 1889–1898.
54. Coburn, C. A.; Meinke, P. T.; Chang, W.; Fandozzi, C. M.; Graham, D. J.; Hu, B.; Huang, Q.; Kargman, S.; Kozlowski, J.; Liu, R.; McCauley, J. A.; Nomeir, A. A.; Soll, R. M.; Vacca, J. P.; Wang, D.; Wu, H.; Zhong, B.; Olsen, D. B.; Ludmerer, S. W. Discovery of MK-8742, an HCV NS5A Inhibitor With Broad Genotype Activity. *ChemMedChem* **2013,** *8,* 1930–1940.

INDEX

Notes

Cross-reference terms in *italics* are general cross-references, or refer to subentry terms within the main entry (the main entry is not repeated to save space). Readers are also advised to refer to each article for additional cross-references — not all of these cross-references have been included in the index cross-references.

The index is arranged in set-out style with a maximum of three levels of subheading. Major discussion of a subject is indicated by bold page numbers. Page numbers suffixed by t, f, and b refer to Tables, Figures, and Boxes respectively. *vs.* indicates a comparison.

The index entries are presented in word-by-word alphabetical sequence in which a group of letters followed by a space is filed before the same group of letters followed by a letter. For example, entries beginning 'air density' are alphabetized before 'aircraft.' Prefixes and terms in parentheses are excluded from the initial alphabetization.

Where index subentries and sub-subentries pertaining to a subject have the same page number, they have been listed to indicate the comprehensiveness of the text.

A

A-893 **5**:297, **5**:297f
Abandoned assets repurposing, public/private partnerships for **1**:19
Abbott compounds **7**:85–88
Aβ, as AD biomarker **1**:77
Aβ PET tracers
  derived from CR **1**:82–83
  derived from thioflavin T **1**:80–82
Aβ SPECT tracers **1**:84
Abiraterone **5**:142–143, **5**:206f
Abridged guide to hydrogen bonding **3**:73–74
Absorption **4**:61–63
  ADME **4**:34–35
  human PK **4**:54–55
  physicochemical determinants of **4**:104–105
Absorption prediction, BDDCS role in **4**:115–117
  non-transport-mediated interactions affecting drug absorption **4**:117
  processes affecting absorption **4**:115
  requirements of absorption and predicting absorption **4**:115
  transporter effects in the gut **4**:115–116
    apical efflux **4**:116
    apical uptake **4**:115
    basolateral transporters **4**:116
    flip-flop kinetics **4**:116
ABT-199 **2**:219f
  phase III **2**:217–220
ABT-494 **5**:428–430, **5**:429t
  efficacy of **5**:429
  in MTX-IR **5**:429
  safety **5**:429–430
  in TNF IR **5**:429
ABT-639 **7**:71
Academia and market **1**:520–528
  biotechnology
    development and commercialization of **1**:521–523
    industry, recent evolution of **1**:522–523
    upsurge **1**:521
  DBFs **1**:523–527
    and academic institutions, upstream vertical relationships between **1**:523–524
    contribution in drug development and commercialization **1**:521–522
    and pharmaceutical companies, and other organizations, downstream vertical relationships among **1**:524–527
  further research **1**:528
  limitations **1**:528
  overview **1**:520–521
Academic drug discovery centers **1**:1–10
  Bayh–Dole Act of 1980 **1**:2–8
  founder focused **1**:6
  fully integrated **1**:7
  pharmaceutical industry challenges
    cost **1**:2
    patent expirations **1**:2
    politics **1**:2
    productivity **1**:2
  research coordination **1**:6–7
  risks and rewards of **1**:7–8
  role of **1**:3
  structure and function **1**:3
  in US **1**:7
Accelerated metadynamics **3**:43
Acetaminophen **4**:206f, **4**:213
Acetyl choline receptor modulators **1**:242f
Acetyl CoA carboxylase inhibitors **1**:248f
N-Acetylated peptide therapeutics **6**:70, **6**:70t
N-Acetylation **6**:70
N-Acetyl-β-D-glucosaminidase, biomarker of acute kidney injury **4**:274
Acetylgalactosamine **1**:334–335
Acid bioisosteres **7**:119–120
Acoustic membrane microparticle technology on the ViBE platform **6**:192–193
  pros and cons/considerations **6**:193
ACT-128800 **5**:402
Actelion **7**:227–236
  1-acyl-2-benzylpyrrolidines **7**:233–234
  N-glycine-sulfonamides **7**:234–236
  proline sulfonamide ACT-462206 **7**:232–233
  substituted lactams **7**:231–232
  tetrahydroisoquinolines **7**:227–231
Activity cliffs **3**:249
Acturum Life Science, modulators from **7**:284
Acute infections, antiviral drugs for **5**:665–681
Acute kidney injury
  biomarkers **4**:268–275

Acute kidney injury (*continued*)
N-acetyl-β-D-glucosaminidase **4**:274
assays **4**:272
beta-2-microglobulin **4**:273
Clusterin **4**:273
Cystatin-C **4**:273
KIM-1 **4**:274
neutrophil gelatinase-associated lipocalin **4**:274–275
osteopontin **4**:275
pathophysiologic factors **4**:272
postanalysis, interpretation **4**:272
preanalytical factors **4**:269–272
Acute migraine drug classes **7**:178–181
5-$HT_{1B/1D}$ agonists (triptans) **7**:179–181
ergot alkaloids **7**:178–179
Acute neuronal injury **5**:442–443
1-Acyl-2-benzylpyrrolidines **7**:233–234
Adaptive immune system, role in DILI **4**:230–231
overview **4**:230
PBMC from patients with DILI **4**:230–231
Adduct formation by sequencing, identification of **2**:439
Adenine nucleotide-based antagonists **7**:572
Adenosine receptors **5**:368–370, **7**:31
A_{2A} receptors **5**:368–369, **7**:31
A_{2B} receptors **5**:369–370
S-Adenosyl methionine, for chronic inflammatory disorders **1**:131
Adenoviruses **5**:672–673
classes of adenovirus agents **5**:672–673
other targets **5**:673
polymerase inhibitors **5**:672
reasons to develop antiviral drugs for **5**:672
Adenylate cyclase gene therapy **7**:644
ADME (absorption, distribution, metabolism and excretion) **6**:226–227
length of ASOs **6**:227
and safety optimization, screening technologies for **2**:24–27
sugar modifications **6**:226
ADME optimization **4**:34–44
human pharmacokinetic parameters **4**:36–42
human clearance **4**:39–42
oral absorption **4**:36–37
volume of distribution **4**:37–39
overview **4**:34–36
absorption **4**:34–35
distribution **4**:35
excretion **4**:35–36
metabolism **4**:35
ADME prediction **3**:281–286
MetaSite **3**:283–286
MoKa **3**:282–283
VolSurf **3**:282
ADME/PK **4**:1–33
bioavailability **4**:2
continuing need during drug discovery **4**:3–4
distribution **4**:2
excretion **4**:2–3
goal of the medicinal chemist **4**:3
happenings during drug discovery **4**:4–5
biology **4**:4
chemistry **4**:4–5
major characteristics to optimize **4**:5–20
computational approaches to ADME/PK problems **4**:17
distribution **4**:12–14
excretion **4**:16
oral absorption and bioavailability **4**:5–12
persistence **4**:14–16
Right Box analysis **4**:5
screening for DDI potential **4**:17–20
triage of ADME/PK screening assays **4**:20
meaning of **4**:1–2
overview **4**:1–3
persistence **4**:2
in safety assessment **4**:21–23
early toxicity assessment **4**:21
in vivo toxicology assessment **4**:22–23
metabolites in safety testing **4**:23
reactive metabolites **4**:22
safety margin **4**:3
ADME/PK, in clinical development **4**:23–29
clinical ADME/PK studies **4**:25–29
circulating human metabolites **4**:27–28
clinical ^{14}C-ADME study **4**:28–29
clinical pharmacokinetics **4**:25–26
definitive characterization of ddis **4**:26–27
IND-enabling ADME/PK studies **4**:23–25
active circulating metabolites in animals **4**:24–25
animal PK and bioavailability **4**:24
initial in vitro assessment of clinical DDI potential **4**:25
major routes of clearance in animals **4**:24
projection of human PK **4**:25
purpose of **4**:23–24
ADMET **1**:561t
assays **2**:70t
admetSAR **2**:237
β-Adrenergic receptor agonists **7**:644
Adrenocorticotropin hormone (ACTH) for multiple sclerosis **5**:451–452
Adverse drug event (ADE) prediction, systems chemical biology **2**:488–490
Adverse drug reactions
systems biology **2**:461
Adverse outcome pathway (AOP)/MOA framework **4**:250–251
Affinity fingerprints **3**:345
Affinity prediction, in molecular docking **3**:304–310
affinity prediction problem **3**:304–306
overview **3**:309–310
scoring poses in docking **3**:306
validation of docking programs and their associated scores **3**:306–309
AFMoC **3**:289–290
Age, and DILI **4**:208
Agent-based modeling **3**:495–496
Agents targeting epigenetic reader proteins **2**:318–320
Ago2shRNAs **6**:301–302
Akt **5**:91–92
Akt inhibitors **5**:92f
Aladorian **7**:646–647
Alamar blue assay **1**:279
Albaconazole **5**:707f
Albiglutide **7**:486
Albumin-binding **6**:145–146
Alchemical methods **3**:35–38
evolution of **3**:36–38
thermodynamic integration *versus* free energy perturbation **3**:35–36
Alcohol consumption, and DILI **4**:209
ALD403 **7**:216
Aldose reductase
and binding thermodynamics **2**:204
Aldose reductase assay data
of fidarestat **1**:241t
of spirocyclic compounds **1**:240t
of spirocyclic derivatives **1**:240t
Aldose reductase inhibitors **1**:240f
Alemtuzumab, for multiple sclerosis **5**:450
Alipogene tiparvovec **7**:685–686
ALK inhibitors design with potency against mutations **5**:55–58
crizotinib design as effective inhibitor of WT ALK **5**:55
future outlook **5**:57–58
targeting L1196M gatekeeper mutation **5**:56–57
Alkylidene (CH═CH) **6**:84
Alkylsulfanyl triazoles **8**:134–135
All-comers study design **2**:537f
Allosteric GPCR ligands **3**:179–180
Allosteric modulators **2**:276–296
advantages and disadvantages of allosteric protein regulation **2**:276–279
allo-modulator like **2**:284
allosteric protein–ligand interactions **2**:285–290
allo-network modulators **2**:289–290
allosteric and orthosteric collaboration **2**:290
bitopic ligands **2**:288–289
covalent allosteric modulators **2**:285–288
noncovalent allosteric modulators **2**:285
allosteric proteins **2**:279–282
allosteric site properties **2**:280–282
target distribution **2**:279–280
target properties **2**:280
chemical structure and physicochemical properties **2**:283–284
mechanisms of allosteric drug action **2**:290–292
overview **2**:276
privileged scaffolds **2**:284–285
Allostery **2**:277f, **2**:277t
Allylamines **5**:708
ALN-TTR02 **6**:293–294
ALN-TTRSC **6**:294
Alogliptin (SYR-322) **7**:532–533
Alpha 2 delta ligands **7**:114–122
amino acid-derived structures **7**:114–118
gababutins **7**:118–120

nonamino acid structures **7**:120–122
Alpha (α)-4 integrin antagonists, for inflammatory bowel disease **5**:500
Alpha-gluthathione-*S*-transferase **4**:265–266
α-synuclein aggregation **2**:343
Alport syndrome **7**:702
Alternative administration routes **6**:146–147
buccal **6**:147
intranasal **6**:147
pulmonary **6**:147
rectal **6**:147
transdermal **6**:147
vaginal **6**:147
Alternative drug delivery **6**:131–156
Alvespimycin **5**:233f, **5**:234
ALX-0171 translational strategy **2**:519–520
Alzheimer's disease (AD) **1**:74–106, **5**:453–454
and the amyloid hypothesis **7**:327
β-secretase (BACE) for **7**:326–383
donepezil for **5**:455
galanthamine for **5**:456
memantine for **5**:456–457
nutraceuticals for **1**:131–132
overview of therapy and diagnosis **1**:74–75
rivastigmine for **5**:456
select drugs in development for **5**:457–458
targeting γ-secretase, for **7**:280–325
Alzheimer's disease (AD), development of theranostics against **1**:96–101
theranostic nanomedicine **1**:101
theranostic small molecules **1**:97–101
BSB, as theranostic precursors **1**:98
BTA-1 as theranostic precursors **1**:98
CRANAD-28 as **1**:100
G8 as **1**:99–100
PE154 as theranostic precursors **1**:98
PiB-C as **1**:100
SLOH as **1**:98–99
TBT as **1**:100–101
Alzheimer's disease (AD), diagnosis of **1**:75–78
curcumin **1**:94–96
development of PET tracers for **1**:79–87
Aβ PET tracers derived from CR **1**:82–83
Aβ PET tracers derived from thioflavin T **1**:80–82
Aβ SPECT tracers **1**:84
benzoimidazopyrimidine- and pyridoindole-derived tau PET tracers **1**:87
benzothiazole-derived tau PET tracers **1**:86–87
PET tracers approved for Aβ plaque imaging **1**:79–83
PET tracers for Aβ plaque imaging evaluated in human subjects **1**:83–84
PET tracers for NFT imaging **1**:84–87
quinoline- and benzimidazole-derived tau PET tracers **1**:85–86
fluorescent probes **1**:87–94
for amyloid imaging in the retina and olfactory epithelium **1**:94
AOI987 **1**:90
first fluorescent probes, in vivo Aβ plaque imaging **1**:89–90
for in vivo NFT imaging **1**:92–94
NIAD-4 and derivatives **1**:89–90
photoswitchable fluorescent probes **1**:92
recent development **1**:90–92
thioflavin T and CR agents **1**:88–89
THK-265 **1**:90
SPs and NFTs as biomarkers for **1**:76–78
amyloid hypothesis supports Aβ as biomarker **1**:77
background to concept of biomarkers **1**:76
current perspectives **1**:78
tau hypothesis supports tau as an AD biomarker **1**:77–78
Amantadine, for Parkinson's disease **5**:462
α-Amatinin **5**:208f
Ames assay, for genotoxicity evaluation **4**:197–198
AMG 337 **8**:138–160
AMG-334 **7**:216
Amgen
inhibitors reported by **7**:330–333
modulators from **7**:284
Amibegron **7**:723–724
Amide groups, stacking with **3**:77
Amino acid catabolism **5**:362–367
arginine **5**:365–367
tryptophan **5**:362–365
Amino acid modification **6**:77–82
β-amino acids **6**:81–82
bivalirudin **6**:78
C^{α}-tetrasubstitution **6**:81
D-amino acids **6**:77–78
desmopressin **6**:77
GnRH analogs **6**:78
icatibant **6**:78
N-methylation **6**:78–81
octreotide **6**:78
Amino acid-based transporters **6**:141–142
Amino acid-derived structures, alpha 2 delta ligands **7**:114–118
β-Amino acids **6**:81–82
D-Amino acids **6**:77–78
bivalirudin **6**:78
desmopressin **6**:77
GnRH analogs **6**:78
icatibant **6**:78
octreotide **6**:78
β-Amino butanoic acid derivatives **7**:518–524
Amino LNA **5**:188
Aminoacyl tRNA synthetase inhibitors **5**:732–733
3-Aminobenzamide **5**:108f
Aminoglycoside antibiotics **5**:517f
Aminoglycoside resistance **5**:517–518
2-Aminooxazoline beta-site amyloid precursor protein cleaving enzyme (BACE) inhibitors **1**:239f, **1**:239t
AmNA **6**:223
Amoebas **5**:736
AMPA receptor positive allosteric modulators **7**:450–473
chemotypes of AMPAR positive allosteric modulators **7**:451–452
clinical studies with AMPAR potentiators **7**:450
recent medicinal chemistry of AMPAR potentiators **7**:452–473
evolution and optimization of the cortex CX614 series **7**:467–469
HTS and hybridization strategies by Pfizer **7**:459–466
optimization of HTS-derived hit by Organon using SBDD **7**:469–472
two novel templates from GSK **7**:452–459
Work from other pharmaceutical and academic groups **7**:473
AMPA receptors **7**:447–480
antagonists **7**:473–475
conflict of interest **7**:476
effects on food intake **7**:483
inhibition of feeding in rodents and humans **7**:483
function and structure **7**:447–449
glutamate **7**:447–448
future directions **7**:488
future perspective **7**:476
GLP-1R agonists **7**:483–484
interactions with the GLP-1R **7**:483
brief overview of GLP-1 structure **7**:483
mechanism of action **7**:482–483
GLP-1 synthesis and expression **7**:482–483
overview **7**:447, **7**:482
GLP-1 history and background **7**:482
T2D background **7**:482
structure activity relationships of GLP-1 **7**:484–487
albiglutide **7**:486
dulaglutide **7**:486–487
exenatide **7**:485
liraglutide **7**:485
lixienatide **7**:485
semaglutide **7**:486
taspoglutide **7**:485
structure and modulation of **7**:448–449
summary of GLP-1R agonist toxicity **7**:487–488
ADA generations **7**:488
gall bladder events **7**:488
gastrointestinal effects **7**:487
heart rate effects **7**:487
pancreatitis **7**:487–488
thyroid C-cell tumor **7**:487
Amphotericin **5**:705f
AMPK pathway **1**:363–365
metformin **1**:363–365
β-Amyloid **7**:44–45
Amyloid hypothesis supports Aβ as AD biomarker **1**:77
Amyloid imaging in retina and olfactory epithelium, fluorescent probes **1**:94

AN5568 (SCYX-7158) **8**:516–528
  background on human African trypanosomiasis **8**:516–517
  chemical synthesis **8**:525
  early phenotypic screening of benzoxaborole library against *T. brucei* parasites **8**:518–520
  first-in-human clinical trial of **8**:526
  lead optimization project and identification of **8**:520–522
    early lead optimization **8**:521
    HAT screening cascade for the discovery of **8**:520–521
    lead optimization of the benzoxaborole-6-carboxamides **8**:521–522
  overview **8**:516–518
  perspective **8**:527
  preclinical development of **8**:523–524
  progression of anacor boron chemistry establishing the benzoxaborole scaffold for **8**:517–518
  successful partnership model among DND*i* and its research partners **8**:526–527
Anacetrapib **8**:284–307
  adipose distribution studies with **8**:297
  CETP inhibition
    preclinical safety evaluation of **8**:295–296
    torcetrapib termination and the safety analysis of **8**:295
  DEFINE study **8**:296–297
  early clinical evaluation of **8**:292–294
  overview **8**:284–286
    HDL hypothesis and CETP **8**:284–285
    pharmacodynamic validation with early CETP inhibitors **8**:285–286
  preclinical efficacy support for reverse cholesterol transport **8**:298–300
  re-emergent importance of cetp inhibitor-induced lowering of LDL-C **8**:300
  REVEAL study **8**:300–302
  structure activity studies and the discovery of **8**:286–292
Anagliptin (SK-0403) **7**:530–531
Analog-based drug discovery **2**:33–34
Analogs designing **6**:66–115
  amino acid modification **6**:77–82
    β-amino acids **6**:81–82
    bivalirudin **6**:78
    C^{α}-tetrasubstitution **6**:81
    D-amino acids **6**:77–78
    desmopressin **6**:77
    GnRH analogs **6**:78
    icatibant **6**:78
    N-methylation **6**:78–81
    octreotide **6**:78
  combinatorial peptide libraries **6**:104–107
    phage display library **6**:106
    spatially addressable parallel synthesis **6**:105–106
    split and mix synthesis **6**:106
  macrocyclic peptides **6**:88–95
    colistin A **6**:89–90
    conopeptides **6**:92–93
    cyclic melanocortin analogs **6**:94
    cyclic opioid peptides **6**:95
    cyclosporine A **6**:89
    linaclotide **6**:93–94
    octreotide (Sandostatin) **6**:92
    PMX53 (3D53) **6**:91
    tyrocidine A **6**:89
  minimum active sequence **6**:68–69
    annexin A1 **6**:69
    cholecystokinin **6**:68
    enfuvirtide **6**:69
    eptifibatide **6**:69
    glucagon-like peptide-1 **6**:69
    melanin-concentrating hormone **6**:68
    octreotide **6**:69
    P-selectin **6**:68
    sermorelin **6**:69
    teriparatide **6**:69
  modifications at the termini and side chains **6**:70–77
    N-acetylation **6**:70
    C-amidation **6**:71
    glycosylation **6**:75–77
    lipidation **6**:72–75
    PEGylation **6**:71–72
    N-pyroglutamate formation **6**:70–71
  peptide bond replacements and pseudopeptides **6**:82–88
    alkylidene (CH═CH) **6**:84
    azapeptide (CONHNR) **6**:85
    azasulfurylpeptide (AsF, $CONHNRSO_2$) **6**:85
    depsipeptide (CO_2) **6**:84
    endothiopeptide (CSNH) **6**:84
    ketomethylene ($COCH_2$) **6**:84
    methylene ether (CH_2O) **6**:84
    methylene thioether (CH_2S) **6**:83–84
    phosphonamide (PO_2RN) **6**:84–85
    reduced bond (CH_2NH) **6**:83
    retro-inverso (RI, NHCO) **6**:85–88
    thioester (COS) **6**:84
  stabilization of secondary structures **6**:95–104
    stabilized α-helices **6**:98–104
    stabilized β-sheets **6**:97–98
    stabilized β-turns **6**:95–97
Anaplastic lymphoma kinase **7**:431–433
Androgen receptor **5**:331
Androgen receptor signaling axis **5**:134–153
  androgen signaling pathway **5**:135–138
    androgen receptor (AR) **5**:136–138
    androgens **5**:135–136
    mechanism of AR activation **5**:138
  conventional antiandrogens **5**:138–144
    Abiraterone **5**:142–143
    AR ABS **5**:138–140
    ARN509 **5**:141–142
    enzalutamide **5**:141–142
    first-generation antiandrogens **5**:140–141
    gndrogen receptor signaling axis
      galeterone **5**:143–144
      ODM-201 **5**:142
      resistance problem of **5**:144
      second- and next-generation AR inhibitors **5**:141–144
  novel AR inhibitors **5**:144–148
    AR DBD inhibitors **5**:147–148
    AR LBD surface site inhibitors **5**:144–146
    AR NTD inhibitors **5**:146–147
    nonconventional strategies **5**:148
  overview **5**:135
Angiogenesis **5**:6
  and cancer **6**:9
Angiotensin converting enzyme (ACE) **1**:225t
Anidulafungin **5**:709f
Animal models **2**:510–514
  active circulating metabolites in **4**:24–25
  clearance routes in **4**:24
  generalities **2**:510
  implemention into translational strategy **2**:512–514
    back-translate clinical trial findings into animal models **2**:513–514
    designing strategy with high translational value **2**:512–513
  improvement methods **2**:510–512
    designing concurrent with design recommended for pivotal clinical trial **2**:511
    enhance variability and reduce standardization **2**:510–511
    humanize animal models **2**:511–512
    multisite animal model trials **2**:510
    proper validation of animal models **2**:512
    and relevant clinical endpoints **2**:512
  PK and bioavailability **4**:24
  preclinical alternatives to **1**:60–61
  predictive toxicology **2**:102
  reducing the use in toxicology testing **4**:69
Animal research, ethics in drug discovery **1**:542
Anion–π **3**:80–81
Annexin A1 **6**:69
Annexin-V **1**:282
Annexin-V staining **1**:283f
Antagonists **7**:473–475
Antiadrenergics and anti-RAAS **7**:635–638
Anti-aging drugs **1**:349–378
  antioxidants **1**:351–357
    life extension by **1**:352–355
    oxidative damage theory of aging **1**:351–352
    supplementation **1**:355–357
  autophagy **1**:365–367
    pharmacological induction of **1**:366–367
  melatonin **1**:367–368
  overview **1**:349–351
  perspective **1**:368–369
Anti-aging drugs, pharmacological interventions mimicking calorie restriction **1**:357–365
  AMPK pathway **1**:363–365
    metformin **1**:363–365
  GH/IGF-1 pathway inhibitors **1**:359
  glycolytic metabolism inhibitors **1**:358–359

pharmacological inhibition of mTOR pathway **1**:361–363
rapamycin **1**:362–363
sirtuin-activating compounds **1**:359–361
resveratrol **1**:360–361
synthetic activators of sirtuins **1**:361
Antibacterial drug discovery **5**:682–702
cell-wall biosynthesis inhibitors **5**:694
current technical challenges **5**:683–687
physical property determinants of antibacterial chemical space **5**:683–685
siderophore-mediated bacterial cell-wall translocation **5**:686–687
translocation and efflux at molecular level **5**:685–686
DNA synthesis **5**:693–694
economic incentives **5**:683
LptD inhibitors **5**:694
LpxC inhibitors **5**:694–695
new drug approvals **5**:683
protein synthesis inhibitors **5**:691–693
leucine-tRNA synthetase inhibitors and oxaboroles **5**:693
ribosome binders **5**:691–693
Antibacterial drug discovery, β-lactamase inhibitors **5**:687–691
MBL inhibition strategies **5**:687–690
direct MBL inhibitors **5**:689
exploiting monobactam insensitivity to MBLs **5**:690
serine β-lactamase inhibitors **5**:690–691
diazabicyclooctanes **5**:690–691
oxaboroles as β-lactamase inhibitors **5**:690
Antibacterial drug discovery, *Clostridium difficile* infections **5**:695–696
surotomycin from daptomycin **5**:696
cadazolid **5**:696
LFF571 **5**:696
Antibacterial drug discovery, finding new drug leads **5**:697–698
natural products **5**:697–698
new natural products from legacy screening approaches **5**:697
novel screening approaches **5**:697
screening libraries **5**:698
new natural products with new chemistry applied **5**:698
Antibacterial drugs, approved **5**:683t
Antibacterial resistance **5**:512–532
selected drug classes **5**:514–526
aminoglycoside resistance **5**:517–518
colistin resistance **5**:524–525
daptomycin resistance **5**:526
glycopeptide resistance **5**:522–523
β-lactam resistance **5**:514–516
β-lactamase inhibitor resistance **5**:516–517
macrolide resistance **5**:519–520
oxazolidinone resistance **5**:523–524
quinolone resistance **5**:518–519
tetracycline resistance **5**:520–521
trimethoprim resistance **5**:525–526
selected key pathogens **5**:526–532
antibiotic-resistant *N. gonorrhoeae* **5**:527
carbapenem-resistant *Enterobacteriaceae* **5**:526–527
Clostridium difficile **5**:527–529
methicillin-resistant *Staphylococcus aureus* **5**:529–530
multidrug-resistant *Acinetobacter* **5**:529
multidrug-resistant *Pseudomonas aeruginosa* **5**:530
Mycobacterium tuberculosis **5**:530–532
Antibiotic resistance tackling **3**:58–59
Antibiotic-resistant *N. gonorrhoeae* **5**:527
Antibody-dependent cellular cytotoxicity (ADCC) **6**:44
Antibody-dependent cellular phagocytosis (ADCP) **6**:46
Antibody–drug conjugates, tumor targeting **1**:342–343, **6**:42
Antibody-like protein-capture agents **1**:318–319
Anticancer agents, generated via click chemistry reaction **1**:298–304
Anticholinergics, for Parkinson's disease **5**:462
Anticoagulants **7**:600–627
factor IXa inhibitors **7**:617–618
factor VIIa Inhibitors **7**:612–617
agents advanced to clinical development **7**:612–613
preclinical compounds **7**:613–617
target validation and proof of concept **7**:612
factor Xa inhibitors **7**:604–612
additional inhibitors assessed in clinical trials **7**:606
dual thrombin/FXa inhibitors **7**:611–612
marketed inhibitors **7**:605–606
preclinical inhibitors **7**:607–610
reversal agents **7**:610–611
target validation and proof of concept **7**:604–605
factor XIa inhibitors **7**:618–621
preclinical small-molecule FXIa inhibitors **7**:619–621
target validation and proof of concept **7**:618–619
overview **7**:600–601
thrombin inhibitors **7**:601–603
small-molecule direct thrombin inhibitors **7**:601–603
target validation and proof of concept **7**:601
Antidrug antidody (ADA) generations **7**:488
Antiepileptic drugs (AEDs)
next-generation AEDs **7**:15
potential drug targets for **7**:16
preclinical strategies for development of **7**:3–14
recent advances in AED development **7**:15–16
animal models and random phenotypic in vivo screening **7**:15
second-generation **7**:3
third-generation **7**:3
Antifungal chemistry **5**:703–716
current systemic antifungal agents **5**:705–708
allylamines **5**:708
azoles **5**:706–708
echinocandins **5**:708
flucytosine **5**:705
polyenes **5**:705
new antifungals in clinical development **5**:710–714
CD101 **5**:711–712
E1210 **5**:713
F901318 **5**:712–713
SCY-078 **5**:711
VL-2397 **5**:713–714
VT-1161 **5**:710–711
notable others **5**:708–710
nikkomycin Z **5**:708–709
sordarins **5**:710
tavaborole **5**:709
Antifungal resistance **5**:512–514, **5**:532
Anti-hepatitis C virus spirocyclopropane **1**:221t
Antimalarial drug candidate, DSM265 **8**:544–557
Antimalarial drugs **1**:495f
Antimalarial trioxanes **1**:246f
Antioxidant substances **1**:353f
Antioxidants **1**:351–357
life extension by **1**:352–355
oxidative damage theory of aging **1**:351–352
supplementation **1**:355–357
Antiparasitic agents **5**:717–750
overview **5**:717–718
Antiparasitic agents, helminths **5**:737–739
nematodes **5**:737–738
filarial worms **5**:737–738
soil-transmitted helminths **5**:737
trematodes **5**:738–739
Antiparasitic agents, protozoans **5**:718–736
amoebas **5**:736
apicomplexans **5**:718–724
cryptosporidia **5**:723–724
plasmodium **5**:718–722
toxoplasma **5**:722–723
kinetoplastids **5**:724–735
leishmania **5**:725–729
trypanosoma brucei **5**:731–735
trypanosoma cruzi **5**:729–730
Antiplatelet agents **7**:556–599
current treatment and unmet medical need **7**:561–562
clinical use of antiplatelet drugs **7**:561–562
need for novel antiplatelet approaches **7**:562
overview **7**:557–559
epidemiology and antithrombotic market **7**:558–559
hemostasis and thrombosis **7**:557–558
pathology of thrombotic diseases **7**:558
platelet function **7**:559–561
assay systems to monitor platelet inhibition **7**:560–561

Antiplatelet agents (*continued*)
endothelial cell layer and extracellular matrix **7**:559
experimental thrombosis models in vivo **7**:561
inhibition of platelet aggregation **7**:560
platelet adhesion, activation, aggregation, and thrombus stabilization **7**:559–560
platelets formation **7**:559
targets for antiplatelet therapy **7**:562–565
GPCRs as receptors of released signaling molecules **7**:563
mechanism of intracellular signaling and key intracellular enzymes **7**:563–565
platelet adhesion and aggregation receptors **7**:562
Antiplatelet agents, antagonists of GPCRs **7**:565–580
5-HT_{2A} antagonists **7**:579–580
EP_3 antagonists **7**:578–579
IP antagonists **7**:580
protease-activated receptor (PAR) antagonists **7**:574–578
PAR-1 antagonists **7**:574–578
PAR-4 antagonists **7**:578
purinergic receptor antagonists **7**:565–574
$P2X_1$ antagonists **7**:574
$P2Y_1$ antagonists **7**:572–574
$P2Y_{12}$ antagonists **7**:566–572
TP antagonists **7**:580
Antiplatelet agents, inhibition of platelet adhesion and aggregation **7**:580–584
antagonists of adhesion receptors **7**:582–584
$\alpha_2\beta_1$ antagonists **7**:582–583
GPVI antagonists **7**:583
vWF and GPIb receptor antagonists **7**:584
integrin $\alpha_{IIb}\beta_3$ antagonists **7**:580–582
first-generation antagonists **7**:580–581
mechanism of action of integrins and ligand binding mode **7**:581
novel approaches in $\alpha_{IIb}\beta_3$ antagonism **7**:581–582
Antiplatelet agents, inhibitors of intracellular enzymes **7**:584–588
COX inhibitors **7**:584–586
aspirin **7**:584
recent developments **7**:585–586
triflusal **7**:585
kinase inhibitors **7**:587–588
other kinases **7**:588
PI3Kβ inhibitors **7**:587–588
PDE inhibitors **7**:586–587
TXS inhibitors **7**:586
Antiplatelet agents, new frontiers in antiplatelet therapy **7**:588–590
emerging antiplatelet targets **7**:589–590
role of platelets outside hemostasis **7**:588–589
platelets in cancer **7**:589
platelets in inflammation and immunity **7**:588–589
Antiproliferative agents, synthesized using click chemistry **1**:304
Antisense oligonucleotides (ASOs) **6**:281–286
challenges and future perspectives **6**:286
chemical and medicinal chemistry properties **6**:217–218
chemical modification **6**:281–284
class effects of phosphorothioated **6**:227–228
in clinical development **6**:284–286
defined **6**:216
length of **6**:227
pharmacokinetic properties of **6**:284
safety of **6**:227–228
Antiviral drugs **2**:157t
for acute infections **5**:665–681
adenoviruses. *See* Adenoviruses
emerging virus infections. *See* Emerging virus infections
influenza viruses. *See* Influenza viruses
overview **5**:665–666
paramyxoviruses. *See* Paramyxoviruses
respiratory virus targets of research **5**:666
rhinoviruses. *See* Rhinoviruses
Antiviral efficiency, influenza virus mutations effects on **3**:56–57
Antiviral resistance **5**:512–514, **5**:532–542
hepatitis B virus **5**:537–538
new viral targets **5**:538
nucleos(t)ide reverse transcriptase inhibitors **5**:537–538
hepatitis C virus **5**:538–539
drug combinations **5**:539
nonnucleotide NS5B inhibitors **5**:539
NS3/4A protease inhibitors **5**:539
NS5A inhibitors **5**:539
nucleotide analogue NS5B inhibitors **5**:538
human immunodeficiency virus **5**:534–537
drug combinations **5**:537
HIV envelope (ENV) **5**:536–537
HIV integrase **5**:536
HIV protease **5**:535–536
HIV reverse transcriptase **5**:534–535
influenza **5**:540–542
M2 inhibitors (adamantanes) **5**:540
neuraminidase inhibitors **5**:540–541
new influenza antivirals **5**:542
Antiviral synthesis, and click chemistry **1**:305–308
Anti-*Wolbachia* compounds **5**:738
AOI987 **1**:90
Apicomplexans **5**:718–724
cryptosporidia **5**:723–724
plasmodium **5**:718–722
toxoplasma **5**:722–723
Apitolisib (GDC-0980) **5**:217–218
Apomorphine, for Parkinson's disease **5**:462
Apoptosis **5**:16f
induction, targets in **5**:15–16
Apoptosis protein XIAP inhibitors **1**:252t
Apremilast (Otezla) **5**:400
Aptamers **6**:295–299
challenges and future perspectives **6**:299
chemical modifications **6**:295
in clinical development **6**:298
potential therapeutic applications of **6**:296–298
Aqueous solubility of pharmaceuticals, physical–chemical properties **3**:398–399
β_3-AR agonists, for overactive bladder **7**:714–738
β_3-adrenergic receptors (adrenoceptors) **7**:715–716
history of **7**:715–719
medicinal chemistry of human β_3-AR agonists **7**:721–729
amibegron and other cyclic β_3-AR agonists **7**:723–724
BMS-196085 and related analogs **7**:721–722
LY-377604 and related compounds **7**:722–723
mirabegron and a series of biphenyl acid β_3-AR agonists **7**:727–729
MK-0634, vibegron, and related analogs **7**:725–727
ritobegron and related analogs **7**:725
solabegron and related analogs **7**:724–725
overview of, in literature **7**:719–721
pharmacology **7**:717–719
β_3-ARs in overactive bladder **7**:718–719
cardiovascular effects of β_3-ARs **7**:717–718
metabolic effects of β_3-ARs **7**:717
potent rat β_3-AR agonists in early human clinical trials **7**:721
AR LBD **5**:145f
AR NTD **5**:146f
Arachidonic acid turnover **7**:52
Arbidol **5**:670f
ARC-520 **6**:295
Ares Trading/Merck KGAA, modulators from **7**:284
Arginase **5**:365–366
Arginase inhibitors **5**:366, **5**:366f
Arginase-1 **4**:264–265
Arginine **5**:365–367
methyl modifications to **5**:283
Arginine catabolism **5**:365f
Arginine methyltransferases **2**:303t, **5**:287–290
Aristolochic acid injury **7**:702
ARN509 **5**:141–142
Aromatic rings
substituents on **3**:231–232
Aromatic rings, molecular interactions involving **3**:74–82
anion–π **3**:80–81
benzene dimer **3**:74–75
cation–π interactions **3**:78–79
CH π interactions **3**:81–82
hydrogen bond acceptors **3**:79–80
interactions with halogens **3**:77–78
π-stacking **3**:75–77
stacking with amide groups **3**:77
Artemisinins **5**:718f, **5**:719t

N-Aryl imidazoles **2**:145f
N-Aryl-2-phenylcyclopropanecarboxamides **7**:238–239
  E2006 **7**:239
Aryl triazines and derivatives **7**:153–159
Arylated piperidine/piperazine ring systems **2**:128–130
Aryl-linked aminoamides **7**:137–142
Arylimidamides
Aryl-imidazole derivatives
  Forum/EnVivo **7**:295
  GlaxoSmithKline **7**:296–297
  Janssen **7**:299–301
  Merck **7**:304
  Pfizer **7**:305–307
  Roche **7**:307
Aryl-piperazine derivatrives
  Merck **7**:303
Arylthiazolidinediones **7**:79–80
ASD (Allosteric Database) **1**:459
Asialoglycoprotein receptor **1**:334–335
Aspirin **7**:584
Aspirin prodrugs **7**:585–586
Assay development, companion diagnostics **2**:532–534
  assay methodology **2**:533
  assay validation **2**:534
  assay verification **2**:534
  prototype assays **2**:533–534
Assay technology advances for functional screens **2**:43–44
Assays, biomarker of acute kidney injury **4**:272
Assent, in clinical studies **1**:545–546
Association phase, kinetics in drug discovery **2**:183–184
Astellas
  inhibitors reported by **7**:333
  modulators from **7**:285–286
AstraZeneca
  inhibitors reported by **7**:333–335
  modulators from **7**:286–288
Asymmetric tissue distribution, design principles for **2**:23–24
AT-406/SM-406 **5**:255
AT7519 **2**:223f
  phase II **2**:221–222
AT9283 **2**:222f
  phase II **2**:221
AT13387 **2**:220f
  phase II **2**:220–221
Ataxia-telangiectasia and RAD3-related (ATR) **5**:61–64
Ataxia-telangiectasia and RAD3-related (ATR) inhibitors **5**:62–64, **5**:62f, **5**:119–124, **5**:121f
  clinical development of **5**:123–124
Ataxia-telangiectasia mutated (ATM) **5**:59–61
Ataxia-telangiectasia mutated (ATM) inhibitors **5**:60–61, **5**:60f, **5**:117–119, **5**:118f
  clinical development **5**:119
Ataxia-telangiectasia mutated kinase **7**:436
Atom **3**:72
Atom-based 2-D interaction information **1**:454
Atopaxar (E-5555) **7**:576
ATP metabolism **5**:370–371
ATP-competitive mTOR inhibitors **5**:216–227
ATP-sensitive potassium channel **1**:241t
ATP-sensitive potassium channel activator **1**:252f
Attachment inhibitors, HIV **5**:644–645
Augmenting neurogenesis in vivo, regenerative medicine **1**:410–411
Autoantibodies, and DILI **4**:229
AutoDock **3**:290
Autoimmune disorders, epigenetic mechanisms to treat **5**:409–410
Automation of crystallography, challenge of **2**:161–162
Autophagy **1**:365–367, **4**:224, **5**:411
  perturbation **4**:225
  pharmacological induction of **1**:366–367
Autoradiography **1**:276
AZ505 **5**:296f
Azapeptide (CONHNR) **6**:85
Azasulfurylpeptide (AsF, $CONHNRSO_2$) **6**:85
AZD0156 **8**:161–177
  discovery of **8**:169–174
    ATM selectivity with imidazo[5,4-*c*] quinolin-2-one based compounds **8**:170
    basic imidazo[5,4-*c*]quinolin-2-ones optimization **8**:170–171
    scaffold with increased permeability, identification of **8**:169
  importance of predicting dose to man and maximum absorbable dose **8**:167–169
  novel, potent, and selective ATM inhibitors with oral bioavailability **8**:164–167
  overview **8**:161–164
    ataxia-telangiectasia mutated kinase **8**:162
    DNA damage response **8**:161–162
    inhibitors of ATM kinase **8**:162–164
  profile of **8**:171–174
AZD2014 **5**:225–226, **5**:226f
AZD2716 **8**:339–348
  medicinal chemistry strategy **8**:340
  overview **8**:339–340
AZD5423
  acute cigarette smoke model **8**:482–483
  acute lps model **8**:482
  acute mouse LPS model **8**:481–482
  duration of effect **8**:480
  efficacy in disease-like setting (ovalbumin model) **8**:481
  functional measurements in rat sephadex model **8**:480
  in vitro pharmacology assessment **8**:478
  in vivo pharmacology assessment **8**:479
  inhaled drug design and challenges **8**:455–456
  lead identification **8**:456–462
  lead optimization leading to, inhaled SGRM CD1 **8**:462–468
  mechanistic side effects **8**:479–480
  metabolic profile **8**:475–476
  physical chemical properties of drug candidates **8**:473–474
  PK based drug–drug interaction potential assessment **8**:477
  predicted therapeutic dose **8**:479
  prediction of human pharmacokinetics **8**:477
  progression of **8**:483–484
  project objective, screening cascade, and compound target profile **8**:454–455
  synthesis of **8**:471–473
AZD7594
  acute cigarette smoke model **8**:482–483
  acute lps model **8**:482
  acute mouse LPS model **8**:481–482
  duration of effect **8**:480
  efficacy in disease-like setting (ovalbumin model) **8**:481
  functional measurements in rat sephadex model **8**:480
  in vitro pharmacology assessment **8**:478
  in vivo pharmacology assessment **8**:479
  inhaled drug design and challenges **8**:455–456
  lead identification **8**:456–462
  lead optimization leading to, inhaled SGRM CD2 **8**:468–483
  mechanistic side effects **8**:479–480
  metabolic profile **8**:476
  physical chemical properties of drug candidates **8**:473–474
  PK based drug–drug interaction potential assessment **8**:477
  predicted therapeutic dose **8**:479
  prediction of human pharmacokinetics **8**:477
  progression of AZD7594 **8**:484
  project objective, screening cascade, and compound target profile **8**:454–455
  synthesis of **8**:471–473
AZD8055 **5**:225–226
Azides
  continuous flow processing **1**:140–142
Azobenzene linchpin **1**:331f
Azoles **5**:706–708

B

BACE1 inhibitor lead-finding strategies **8**:207–219
  BACE1 and CatD in vitro assays **8**:208
  fragment screening **8**:210–219
    fragment screening and hit triage **8**:210–212
    iminoheterocycle scaffold design and validation **8**:212–214
    iminohydantoin hit-to-lead prosecution **8**:214–219
  hydroxyethylamine-based peptidomimetic inhibitors **8**:208–210
  overview **8**:207–208

Backbone-modified macrocyclic peptides, biological selection of **1**:330–331
Bacterial lectins inhibition, and carbohydrates **1**:585–589
Bacterial resistance concernsa **5**:513t
Banyu **7**:237
  tetrahydroisoquinolines **7**:237
Baricitinib **5**:425–427
  in combination with csDMARDs **5**:425–426
  four pivotal phase 3 clinical trials **5**:425–426
  long-term extension study **5**:426
  phase 2b clinical trial of **5**:425
  safety **5**:426–427
Basic research, rare disease foundations **1**:552–554
Basicity and promiscuity **2**:107
Basket study design **2**:538f
  companion diagnostics **2**:538–539
Basophil degranulation assay **8**:370
Bayesian network models **3**:496
Bayh–Dole Act of 1980 **1**:2–8
BCL-2 **5**:328–330
Bcl-2 family inhibitors **5**:169t–170t
Bcl-2 family PPIs **5**:167–171
Bcl-2/Bcl-x_L–Bak **2**:338
Bcl-x_L-Bak peptides **5**:159
Bcr-Abl inhibitor **5**:41, **5**:47f
BCS class 1
  approval of **4**:113
  BCS class 2a **4**:111
  BCS class 3 **4**:111
Benzene dimer **3**:74–75
  geometries **3**:75f
Benzimidazole analogs **8**:121–122
Benzimidazole-derived tau PET tracers **1**:85–86
Benzimidazolinopiperazinones **2**:135
Benzodiazepine
  and related seven-membered ring systems **2**:130–132
Benzo-fused ring systems
  spiro[4.5] ring systems **1**:215–216
  spiro[5.5] ring systems **1**:218
Benzoimidazopyrimidine-derived tau PET tracers **1**:87
Benzothiazole-derived tau PET tracers **1**:86–87
Benzotropine, for Parkinson's disease **5**:462
Benzoxaboroles **5**:721, **5**:721f, **5**:732
Benzoxazepine-based selective orexin-2 antagonists **7**:272–273
Berberine, for inflammatory bowel disease **5**:504–505
Beta-2-microglobulin, biomarker of acute kidney injury **4**:273
β-cell derivation from stem cells **1**:417–419
β-lactam resistance **5**:514–516
β-lactamase inhibitor resistance **5**:516–517
β-lactams **2**:136–137
β-secretase (BACE) for Alzheimer's Disease **7**:326–383
  Amgen, inhibitors reported by **7**:330–333
  Astellas, inhibitors reported by **7**:333
  AstraZeneca, inhibitors reported by **7**:333–335
  BMS, inhibitors reported by **7**:337–338
  Boehringer Ingelheim/Vitae, inhibitors reported by **7**:335–337
  challenges with early BACE inhibitor discovery **7**:327–330
  Eisai, inhibitors reported by **7**:338–341
  Elan, inhibitors reported by **7**:341
  Genentech/Array BioPharma, inhibitors reported by **7**:342
  Janssen, inhibitors reported by **7**:342–344
  Lilly, inhibitors reported by **7**:344–348
  Lundbeck, inhibitors reported by **7**:349
  Merck Serono/Merck KGAA, inhibitors reported by **7**:349
  Noscira, inhibitors reported by **7**:350
  Novartis, inhibitors reported by **7**:350–353
  overview **7**:327–330
  Pfizer, inhibitors reported by **7**:353–358
    isothioureas and related derivatives **7**:354–358
    spiropiperidine derivatives **7**:353–354
    spiropyrrolidine derivatives **7**:354
  Roche, inhibitors reported by **7**:358–363
  Schering-Plough/Merck, inhibitors reported by **7**:363–367
    amidine and guanidine derivatives **7**:364–367
    early peptidomimetic inhibitors **7**:363
    spiropiperidine derivatives **7**:364
  Shionogi, inhibitors reported by **7**:367–369
  vTv/TransTech/HighPoint, inhibitors reported by **7**:372
  Wyeth, inhibitors reported by **7**:370–372
  Beta-site amyloid precursor protein cleaving enzyme 1 (BACE1) inhibitors **1**:239t
BEZ235 **5**:219–220, **5**:220f
BGT226 **5**:219–220
BI 44370 **7**:188
Biacore **6**:191
  pros and cons/considerations **6**:191
Bias potential methods, metadynamics **3**:25–26
Biased receptor signaling **2**:4–5
BIBN4096 BS **7**:184–188
Bicyclic [5.2.0] and [4.2.0] diamines **7**:269–271
Big data analysis **3**:460–461
Bilastine (Bilaxten) **5**:399
Bile acid toxicity **4**:227–228
  transporters and **4**:228
Bile acid-induced liver injury **4**:225–228
  bile acid toxicity **4**:227–228
  bile acid uptake and excretion **4**:225–226
  cellular and hepatic features of cholestasis **4**:226–227
  model systems for transport evaluation **4**:227
  transporters and bile acid toxicity **4**:228
Biliary elimination of parent drug **4**:109
BIM-23A760 **6**:124f
  profiling **6**:124–127
    metabolite analysis **6**:126–127
    phase 1 clinical studies **6**:125
    phase 2a and b clinical studies **6**:126
BIM-065 **6**:128t
Binary classification, confusion matrix for **1**:482t
Binding affinities of peptides to Bcl-xL **5**:160t
Binding entropy calculations **3**:8
Binding free energies calculations **3**:1–13
  computational strategies **3**:1–5
    rigorous but slowly converging calculations by all-atom models **3**:1–4
    simplified electrostatic models **3**:4–5
  by different strategies **3**:5–8
    binding entropy calculations **3**:8
    FEP approaches **3**:5
    LIE approaches **3**:6
    LRA approaches **3**:6
    protein–protein interactions **3**:6–7
    semimacroscopic and macroscopic calculations of ligand binding **3**:6
  overview **3**:1
  perspectives **3**:8–11
Binding free energies predictions
  GPCRs **3**:160–163
Binding kinetics **3**:45–46
  biochemical methods to determine **2**:186–188
    competition methods **2**:188
    fluorescence approaches **2**:187
    measurement of association rate constant **2**:186–187
    measurement of dissociation rate constant **2**:186
    radioligand binding **2**:186
  biophysical methods for measuring **2**:181
  effect on fractional occupancy and IC_{50} **2**:189–190
  mechanistic aspects to **2**:190–192
  and PK/PD **2**:196–197
Binding kinetics predictions
  GPCRs **3**:160–163
Binding MOAD **1**:456
Binding site flexibility, and pose prediction in docking **3**:302–303
Binding site identification, molecular fields **3**:286–287
  FLAPsite **3**:287
  Q-SiteFinder **3**:286
  SiteHound **3**:286
Binding site of Abl tyrosine kinase, probing **1**:318
Binding site similarity assessment, molecular fields **3**:287–289
  GRID/FLAP **3**:287–288
  IsoMIF **3**:288–289
Binding thermodynamics
  mechanistic aspects to **2**:201–203
    complex role of water **2**:202–203
    enthalpy–entropy compensation **2**:201–202
    enthalpy–entropy transduction **2**:202
  methods for measuring **2**:197

role in fragment-based drug design **2**:205–206
experimental considerations for fragment ITC **2**:206
role in selectivity and efficacy **2**:203–204
aldose reductase **2**:204
HIV-1 protease **2**:203
HMGCoA reductase **2**:204
matrix metalloproteinase 12 **2**:203
thrombin **2**:203–204
BindingDB **1**:455, **3**:470–471
Bioactive compounds, interrogating protein targets with **1**:444–446
Bioactive pose prediction **3**:260–264
Bioactivity data **1**:453
Bioanalysis of biotherapeutics **6**:180–197
differentiating aspects of **6**:180–181
anti-drug antibody **6**:181
ligand binding assays (LBAs) **6**:181
LBAs. *See* Ligand binding assays
Bioanalytical methods **2**:502t
Bioavailability, of ADME/PK **4**:2
Bioavailability predictopm, BDDCS in **4**:119–122
complex considerations, food effects **4**:120–122
Biochemical methods to determine binding kinetics **2**:186–188
competition methods **2**:188
fluorescence approaches **2**:187
measurement of association rate constant **2**:186–187
measurement of dissociation rate constant **2**:186
radioligand binding **2**:186
Biochemically produced RNAs **6**:299–306
CRISPR/Cas9 **6**:303–306
challenges and future perspectives **6**:305–306
potential therapeutic applications of **6**:303–305
RNAi triggers **6**:299–303
Ago2shRNAs **6**:301–302
biochemically produced RNAi in clinical development **6**:302
challenges and future perspectives **6**:302–303
pri-miRNA mimics **6**:299–301
shRNA triggers **6**:301
Bioclipse **2**:237
Biodegradable products **1**:285–286
Biodistribution **1**:272–278
elemental analysis **1**:277
ex vivo fluorescent microscopy **1**:276
autoradiography **1**:276
ex vivo light microscopy **1**:276
in vivo magnetic particles imaging **1**:275
in vivo magnetic resonance imaging **1**:275
in vivo optical imaging **1**:272–274
in vivo positron emission tomography **1**:274–275
magnetometry **1**:277–278
of peptides and small proteins **6**:135
BBB penetration and renal clearance **6**:135
low oral bioavailability of polypeptides, reasons of **6**:135
transmission electron microscopy **1**:276–277
Biogen, modulators from **7**:288–289
Bioinformatics approaches and big data **4**:297–298
Bioinformatics methods
polypharmacology **2**:268
Bioisosteres **3**:249
Bioisosterism **1**:186–210
bioisosterism in nature **1**:187–188
classical bioisosterism **1**:200–202
functional bioisosteres of esters and amides **1**:194–195
functional bioisosterism **1**:188–194
overview **1**:186–187
retroisosterism **1**:195–196
ring bioisosterism **1**:202–207
ring closure or anelation and ring opening **1**:196–200
Biolayer interferometry, kinetics in drug discovery **2**:185–186
BioLip **4**:457
Biologic drugs, endosomal escape of **1**:338–339
Biological and chemical data integration **1**:447–449
Biological data of acetyl CoA carboxylase (ACC) inhibitors **1**:248t
Biologically active compounds identification, privileged scaffolds to **2**:135–137
natural product-inspired chemical synthesis **2**:135–137
benzimidazolinopiperazinones **2**:135
β-lactams **2**:136–137
Biologically active spirocycle **1**:213f
Biologics discovery, high-throughput crystallography **2**:172
Biology and compounds **1**:500–501
Biomarkers **2**:497–503
of acute kidney injury **4**:268–275
N-acetyl-β-D-glucosaminidase **4**:274
assays **4**:272
beta-2-microglobulin **4**:273
Clusterin **4**:273
Cystatin-C **4**:273
KIM-1 **4**:274
neutrophil gelatinase-associated lipocalin **4**:274–275
osteopontin **4**:275
pathophysiologic factors **4**:272
postanalysis, interpretation **4**:272
preanalytical factors **4**:269–272
assays/methods **2**:499–501
enzyme-linked immunosorbent assay **2**:500
mass spectrometry **2**:500–501
multiplex assays **2**:500
of cancer **5**:23–25
challenges and future perspectives **5**:25
in the clinic **5**:24–25
definition **5**:23–24
definition **2**:497
of drug-induced liver injury **4**:263–268
alpha-gluthathione-*S*-transferase **4**:265–266
arginase-1 **4**:264–265
cytokeratin 18 **4**:266
general characteristics of emerging liver safety biomarkers **4**:264
glutamate dehydrogenase **4**:266–267
HMGB1 **4**:267
miR-122 **4**:267–268
of drug-induced phospholipidosis **4**:277–279
qualification and assay validation **4**:256–262
assay validation **4**:260–262
biological qualification **4**:257–258
biomarker evaluation **4**:258–259
molecular classes of biomarkers **4**:256–257
normal range and threshold setting **4**:259–260
regulatory qualification of new toxicity biomarkers **4**:262
statistical approaches **4**:258
for SN30000 **8**:86–88
types **2**:497–499
competitive biomarkers **2**:499
efficacy biomarkers **2**:498
pharmacodynamic biomarkers **2**:497
pharmaco-economic biomarkers **2**:499
safety biomarkers **2**:498–499
stratification and predictive biomarkers **2**:498
use of **2**:499
validation and qualification **2**:501–503
qualification **2**:503
validation **2**:501–503
Biomedical research
clinical data using and reusing for **1**:441
expensiveness **1**:557
Biopharmaceutics classification system (BCS) **4**:109–113, **4**:110f
approval of BCS class 1 classification **4**:113
biowaivers granted by the US Food and Drug Administration **4**:111
BCS class 1 **4**:111
BCS class 2a **4**:111
BCS class 3 **4**:111
comparison with BDDCS **4**:113–115
permeability determination **4**:111–112
in humans **4**:111–112
in vitro **4**:112
in vivo or in situ **4**:112
Biopharmaceutics drug disposition classification system **4**:113–125, **4**:114f
class predictions **4**:125
in silico **4**:125
in vitro **4**:125
comparison with BCS **4**:113–115
development of and dispositional predictions by **4**:113–114
differences in defining permeability **4**:113
interactions, defining methods **4**:114–115

Biopharmaceutics drug disposition classification system (*continued*)
metabolism as surrogate for absorption **4**:113
overview **4**:113–115
predicting bioavailability **4**:119–122
complex considerations, food effects **4**:120–122
primary goals **4**:113
role in predicting absorption **4**:115–117
non-transport-mediated interactions affecting drug absorption **4**:117
processes affecting absorption **4**:115
requirements of absorption and predicting absorption **4**:115
transporter effects in the gut **4**:115–116
role in predicting distribution **4**:122–125
distribution into the brain **4**:122–123
potential extensions to other membranes **4**:124–125
role in predicting metabolism and hepatic elimination **4**:117–119
hepatic apical efflux **4**:118
hepatic basolateral uptake **4**:117–118
metabolism from BDDCS **4**:119
metabolism in the gut **4**:117
value and appropriate uses of **4**:114
Biophysical assays, hit characterization **2**:14–18
Bioreductive drug discovery **8**:63–68
Biotechnology
development and commercialization of **1**:521–523
industry, recent evolution of **1**:522–523
upsurge **1**:521
Biotherapeutics **6**:131–156
alternative administration routes **6**:146–147
intranasal **6**:147
pulmonary, transdermal, buccal, rectal, and vaginal **6**:147
basic formulation principles **6**:132–135
excipients added to solution formulations **6**:134–135
freezing and lyophilization **6**:133–134
nucleic acids, solution behavior of **6**:132
proteins and peptides, solution behavior of **6**:132–133
biodistribution of peptides and small proteins **6**:135
BBB penetration and renal clearance **6**:135
low oral bioavailability of polypeptides, reasons of **6**:135
convenient subcutaneous and intramuscular delivery devices **6**:148
implantable devices for subcutaneous drug delivery **6**:148
improving in vivo circulation time **6**:142–146
albumin-binding **6**:145–146
carbohydrates and nucleic acids **6**:144
conjugation to Fc antibody fragments **6**:144–145
hyperglycosylation and lipidation of large proteins **6**:146
pegylation **6**:143–144
proteins **6**:143–144
overview **6**:131–132
Biotherapeutics, penetration enhancers **6**:136–142
active transport **6**:136–137
carbohydrates **6**:136–137
additional paracellular transport-enhancing additives **6**:141–142
amino acid- and peptide-based transporters **6**:141–142
basic principles **6**:136
competing peptide drug delivery technologies **6**:140
microspheres and lipids in protein drug delivery **6**:140–141
particle delivery **6**:138–140
nanoparticles as modern drug delivery systems **6**:139–140
passive transport **6**:138
cationic antimicrobial peptides as drug delivery vehicles **6**:138
Biotin protein ligase (BPL) inhibitors, screening and identification of **1**:318
Biotransformation studies, of chimeric liver-humanized mice **4**:139–141
Biowaivers granted by the US Food and Drug Administration **4**:111
BCS class 1 **4**:111
BCS class 2a **4**:111
BCS class 3 **4**:111
Biphenyl acid β_3-AR agonists **7**:727–729
Birinapant (TL32711) **5**:257–259
Bis(monoacylglycero)phosphate (BMP) **4**:278–279
Bitopic ligands **2**:288–289
Bival-Bind **1**:458
Bivalent Smac-mimetic IAP antagonists **5**:183–186
Bivalent Smac-XIAP inhibitors **5**:184t–186t
Bivalirudin **6**:78
BIX-01294 **5**:299f
Blood and bone, regenerative medicine **1**:385–392
bone **1**:391–392
bone marrow stem cell niche and signaling pathways **1**:386
chemical manipulation of HSCs **1**:388
current therapies **1**:387–388
diseases involving these cells **1**:387
eltrombopag **1**:389–391
hematopoietic stem cells **1**:385–386
mesenchymal multipotent stromal cells **1**:386
Blood cytokines as safety biomarkers **4**:275–277
biology **4**:275
cytokine biomarkers **4**:276–277
Blood-borne sampling **4**:296
Blood–brain barrier **1**:326
targeting, next-generation therapeutics **1**:340
BMS
inhibitors reported by **7**:337–338
BMS-196085 and related analogs **7**:721–722
BMS-379224 **5**:707f
BMX **5**:92
BMX inhibitors **5**:93f
2′,4′-BNA^{COC} **6**:222
2′,4′-BNA^{NC} **6**:222–223
Boceprevir **8**:583–608
Boehringer Ingelheim **7**:184–188
BI 44370 **7**:188
BIBN4096 BS **7**:184–188
modulators from **7**:292
Boehringer Ingelheim/Vitae
inhibitors reported by **7**:335–337
Bone
regenerative medicine **1**:391–392
Bone marrow stem cell niche and signaling pathways
regenerative medicine **1**:386
Bone marrow-mesenchymal stem cells, regenerative medicine **1**:408
Bone morphogenetic protein (BMP)
regenerative medicine **1**:397
Boolean modeling **3**:494
Boosters and cobicistat, for HIV **5**:647
Bortezomib (MG-341) **5**:263–265, **5**:263f
Botulinum neurotoxin **1**:341
Brain organoids, induced pluripotent stem cell-derived **4**:186–187
BRD4 inhibitors **5**:211–214
Breast cancer **6**:5
Brightfield and widefield microscopy, and live-cell 3D imaging **2**:402–404
Bristol-Myers Squibb **7**:200–213, **7**:572–573
intranasal BMS-694153 **7**:200–204
intranasal BMS-742413 **7**:205–206
modulators from **7**:289–292
orally delivered rimegepant (BMS-927711) **7**:207–213
sulfonamides reported by **7**:102
Bromine–dioxane complex **3**:83f
Bromocriptine, for Parkinson's disease **5**:459
Bromodomain inhibitors **5**:303f–304f
Bromodomain–acetylated histone **2**:341–342
Bromodomains **5**:300–304
and extra c-terminal domain **5**:300–304
Bruton's tyrosine kinase (BTK) **5**:408, **5**:485–486
Bruton's tyrosine kinase inhibitor **2**:223–225, **5**:81–84
covalent BTK inhibitor outlook **5**:84
development of clinical covalent BTK inhibitors **5**:82–83
target biology **5**:81
B-score **2**:395
Btk inhibitors **5**:432–433
BtuCD protein **3**:147f

C

Cabergoline, for Parkinson's disease **5**:459
Caco-2 assay **1**:329
CALAA-01 **6**:294
Calcein acetoxymethyl **1**:281–282
Calcein-AM **1**:281f
Calcineurin/nuclear factor of activated T cells **5**:483
Calcitonin gene-related peptide (CGRP) **7**:181–184
  and migraine **7**:181
  receptor
    antagonist binding **7**:183–184
    structure and function **7**:181–183
Calcitonin gene-related peptide (CGRP) receptor antagonist
  biological data **1**:231t
  structures **1**:231f
Calcium, as nutraceuticals **1**:114
Calcium channel blockers **7**:65–130
  mechanism of action **7**:69–70
  overview **7**:65–66
  target validation **7**:68–69
  voltage-gated calcium channels. *See* Voltage-gated calcium channels
Calcium homeostasis correction **7**:646–648
  aladorian **7**:646–647
  istaroxime **7**:647–648
  mydicar **7**:646
Calcium imbalance, and neurodegeneration **5**:442
Calcium/calmodulin-dependent kinase IV **5**:482–483
C^{α}-tetrasubstitution **6**:81
C-amidation **6**:71
cAMP elevating agents **7**:644
Canagliflozin **8**:349–365
  clinical outcomes **8**:361–363
    24-week phase 3 study in Japanese patients **8**:361–363
    β-cell function improvement **8**:363
    mechanism of action of SGLT2 inhibitors **8**:361
    phase 3 CANTATA trials **8**:363
  concept for novel antidiabetic agents **8**:350
  discovery of **8**:353–361
    exploration of C- and *N*-glucosides bearing a heteroaromatic ring **8**:353–354
    SAR of typical *C*-glucosides with a heteroaromatic ring **8**:355–357
    syntheses of *C*-glucosides bearing a heteroaromatic ring **8**:354–355
  efficacy of **8**:360–361
  first oral SGLT2 inhibitor **8**:350–353
    discovery of T-1095 **8**:350–351
    efficacy and pharmacokinetic issues of T-1095 **8**:351–353
  overview **8**:349
  selective SGLT2 inhibitor **8**:357–358
  synthesis of **8**:357
Cancer **5**:1–38
  biomarkers **5**:23–25
    challenges and future perspectives **5**:25
    in the clinic **5**:24–25
    definition **5**:23–24
  cancer biology and hallmarks of cancer **5**:4–6
    activating invasion and metastasis **5**:6
    avoiding immune destruction **5**:6
    deregulating cellular energetics **5**:6
    enabling replicative immortality **5**:5
    evading growth suppressors **5**:4–5
    genome instability and mutation **5**:6
    inducing angiogenesis **5**:6
    resisting cell death **5**:5
    sustaining proliferative signaling **5**:4
    tumor-promoting inflammation **5**:6
  covalent kinase inhibitors, S). *See* Covalent kinase inhibitors, for cancer
  DNA damage response pathways. *See* DNA damage response pathways. *See* in cancer
  epigenetic regulation inhibitors. *See* Epigenetic regulation inhibitors. *See* in cancer
  overview **5**:4
  polypharmacology in **2**:270–271
  promoter quadruplex nucleic acids. *See* Promoter quadruplex nucleic acids for cancer therapy
  protein–protein interaction inhibitors in. *See* Protein–protein interaction inhibitors in cancer
  protein–protein interactions in **2**:332
  selective kinase inhibitors in **5**:39–75
  stress response and **5**:8–10
    DNA damage and replication stress **5**:9
    hypoxia and nutrient stress **5**:10
    metabolic stress **5**:9–10
    mitotic stress **5**:9
    oxidative stress **5**:10
    proteotoxic stress **5**:10
  targeted cancer therapy, challenges of **5**:25–27
    CSCs **5**:26
    resistance and approaches to overcome resistance **5**:27
    tumor evolution and development of resistances **5**:26
    tumor heterogeneity **5**:25–26
  targets in epigenetics **5**:20–21
    DNA methylation **5**:21
    histone acetylation readers **5**:21
    histone modifications **5**:21
  targets with clinical relevance **5**:11–23
    in cancer epigenetics **5**:20–21
      DNA methylation **5**:21
      histone acetylation readers **5**:21
      histone modifications **5**:21
    in genomic stability **5**:21–23
      PARP inhibitors **5**:22–23
      telomerase inhibitors **5**:21–22
    in immuno-oncology **5**:18–20
      CARs **5**:19–20
      cytokine therapy **5**:19
      immuno-checkpoint inhibitors **5**:19
      tumor-induced immunosuppression **5**:18–19
    in induction of apoptosis **5**:15–16
    kinases and inhibitors **5**:11–15
      approved kinase inhibitors **5**:13
      kinase activation in cancer **5**:12–13
      kinase inhibitor mode of action **5**:13
      kinase mutations and resistance **5**:13
      kinase structure **5**:11–12
      outlook **5**:15
      overview **5**:11
      receptor tyrosine kinases (RTKs) **5**:12
    in neovascularization **5**:23
    in protein folding and degradation **5**:20
      inhibitors of protein degradation **5**:20
      intervention in protein folding **5**:20
    TCA cycle **5**:18
    in tumor metabolism **5**:17–18
      amino acid metabolism **5**:18
      glucose metabolism **5**:17
  TIDVAL **5**:6–8
    target identification **5**:7–8
    target validation **5**:8
Cancer immunity **6**:32–37
  cancer cells
    acquiring resistance to immune cell killing **6**:37
    defending against T-cell frontal assaults **6**:37
    erecting shields to deflect the immune system **6**:36
    hiding from host immune system **6**:35–36
    overwhelming host immune system **6**:35
    subverting immune system **6**:36
Cancer immunotherapy **5**:357–394, **6**:37–58
  cancer immunoediting **6**:39
  concept and history of immuno-oncology **5**:358–359
  future directions **6**:57
  history **6**:38–39
  immunity in the tumor microenvironment (TME) **5**:359–361
    current status of immuno-oncology therapy **5**:361
    modulation of DC function in tumor **5**:361
    modulation of T cell activation and differentiation **5**:360
    myeloid-derived suppressor cells (MDSCs) **5**:360–361
    T regulatory cells (Tregs) **5**:360
    tumor-associated macrophages (TAMs) **5**:361
  limitations of conventional treatments **6**:37–38
  overview **5**:358
  principle of **6**:37
  small molecule targets **5**:361–385
    amino acid catabolism **5**:362–367
      arginine **5**:365–367
      tryptophan **5**:362–365
    checkpoint inhibitors **5**:381–385
      peptide inhibitors **5**:385
      small molecule inhibitors **5**:382–384

Cancer immunotherapy (*continued*)
kinase inhibitors **5**:378–381
CSF-R1 inhibitors **5**:380
PI3K inhibitors **5**:381
RON inhibitors **5**:380
TAM receptor signaling inhibitors **5**:380
TGF-β RI/ALK5 inhibitors **5**:378–379
pattern recognition receptors (PRRs) **5**:372–378
STING **5**:376–377
Targeted delivery of PRR agonists **5**:377–378
TLR agonist in development for IO **5**:375–376
TLR4 **5**:374–375
TLR7/8 **5**:373–374
TLR9 **5**:375
purinergic signaling in immune cells **5**:367–372
adenosine receptors **5**:368–370
ATP metabolism **5**:370–371
COX-2 and EP2/EP4 receptor antagonists **5**:371–372
P2X and P2Y receptor modulators **5**:368
targets for **6**:50–57
targeting cancer cells **6**:50–53
targeting immune cells **6**:55–57
targeting the tumor microenvironment **6**:53–55
types of **6**:39–50
cancer vaccines **6**:48–49
cellular cancer immunotherapy **6**:46–48
cytokines **6**:49–50
monoclonal antibodies **6**:39–46
Cancer prevention, nutraceuticals in **1**:127–129
minerals in cancer management **1**:129
vitamins in cancer management **1**:129
Cancer stem cells (CSCs) **5**:26
Candidate alignments **3**:198–200
algorithms
altering conformations on fly **3**:200
using pregenerated conformers **3**:199
Cannabinoid receptors **7**:31
cannabinoid type 2 (CB2) receptors **7**:31, **7**:52
Caprolactam-based CGRP receptor antagonists **7**:189–195
Capsid binders
rhinoviruses **5**:667–669
Capsid inhibitors, HIV **5**:645
Carbapenem-resistant *Enterobacteriaceae* **5**:526–527
Carbidopa/levodopa, for Parkinson's disease **5**:458–459
Carbohydrate-based diagnostics **1**:601–602
Carbohydrate-mediated drug and gene delivery **1**:598–599
Carbohydrates **1**:578f, **1**:583f, **6**:136–137, **6**:144
in drug discovery **1**:577–610
carbohydrate-based diagnostics **1**:601–602
carbohydrate-mediated drug and gene delivery **1**:598–599
current uses of **1**:578–598
bacterial lectins inhibition **1**:585–589
carbohydrate-based vaccines **1**:596–598
carbohydrates as immune modulators **1**:593–596
DC-SIGN lectin targeting **1**:589–591
galectins inhibition **1**:585
lectin inhibitors **1**:583–591
modulation of enzymes **1**:581–582
selectins inhibition **1**:583–584
in vaccine development **1**:591–598
glycoengineering in therapeutics **1**:602–603
overview **1**:577–578
perspectives **1**:603
and nucleic acids **6**:144
Carbonyl-group interactions **3**:88–89
Carboxylic acid derivatives
Forum/EnVivo **7**:294–295
GlaxoSmithKline **7**:296
Janssen **7**:298–299
Merck **7**:302–303
Pfizer **7**:304
Carcinogenicity testing **4**:239–254
current approaches to **4**:240–245
experience with transgenic carcinogenicity assays **4**:243–245
future approaches of **4**:245–251
adverse outcome pathway (AOP)/MOA framework **4**:250–251
future paradigms for environmental and other carcinogens **4**:247–248
new paradigms in rodent bioassays **4**:246
"-omics" approaches **4**:249–250
pharmaceutical carcinogenicity studies, proposals for **4**:246–247
toxicology testing in the 21st century (Tox21) **4**:248
history of **4**:239–240
overview **4**:239
Carcinogens, classification of **4**:241t
Cardiac late sodium current inhibition **7**:651
Cardiac regeneration, regenerative medicine **1**:393–401
in vitro chemically guided cardiac differentiation **1**:393–400
targeting cardiopoietic signaling pathways **1**:395–400
unspecific mode of action **1**:393–395
in vivo **1**:400–401
murine model **1**:400–401
zebrafish model **1**:401
Cardiac sino-atrial (SA) node pacemaker current inhibition **7**:650–651
Cardiomyocytes, induced pluripotent stem cell-derived **4**:183
Cardiovascular disease
protein–protein interactions in **2**:333
Cardiovascular diseases, nutraceuticals in **1**:125–127
coenzyme Q10 **1**:127
dietary fibers **1**:126
fermented red yeast rice **1**:127
flavonoids **1**:126
plant sterols **1**:126
policosanol **1**:126
polyunsaturated fatty acids **1**:125–126
potassium **1**:127
vegetables in prevention of CVDs **1**:126–127
Carfilzomib **5**:267–269
Carotenoids, as nutraceuticals **1**:118–119
Case studies **4**:72–74
halofantrine concentration-related QTc prolongation **4**:73–74
predicting bioavailability **4**:72–73
CASE Ultra **2**:236
CASE Ultra Expert Rules **2**:235
Casein kinase 1 **7**:415–416
CaseUItra **4**:164–165
Casp experiments, protein model **3**:139
Caspofungin **5**:709f
Catalase (CAT) **1**:352f
Cationic antimicrobial peptides **6**:138
Cation–π interactions **3**:78–79, **3**:79f
Causal biological network models, scoring of **2**:454–456
Cav2.1 inhibitors **7**:72–73
inhibiting compounds **7**:73
nomenclature **7**:72
target validation **7**:72–73
Cav2.2 inhibitors **7**:75–99
arylthiazolidinediones **7**:79–80
diarylmethylpiperazines **7**:81–89
dihydropyridines **7**:80–81
early inhibitors **7**:76
indole-derived structures **7**:96–98
miscellaneous templates **7**:98–99
small-molecule blockers based on peptide toxin structures **7**:76–79
sulfones and sulfonamides **7**:89–96
Cav2.3 blockers **7**:99–100
Cav3 blockers **7**:100–114
dihydropyridine derivatives **7**:113
dihydroquinazolines **7**:113–114
early molecules **7**:100
indoles **7**:113
miscellaneous chemotypes **7**:114
piperazines and homopiperazines **7**:109
piperidine- and piperazine-based structures **7**:103–108
pyridyl amides **7**:110–111
quinazoline derivatives **7**:111–112
sulfonamides **7**:100–102
CB-5083 **8**:119–132
candidate seeking efforts **8**:127–132
further evaluations of **8**:132–134
LipE and cell penetration **8**:132–134
lead development efforts **8**:119–127
alternative synthesis of ML240 **8**:119
benzimidazole analogs **8**:121–122
changes in p97 biochemical assay **8**:119
evidence of p97 inhibition in cellular assays and in vivo **8**:125–127
exploration of other fused pyrimidine cores **8**:123–125
guiding principles used in lead development of 26 (ML240) **8**:120–121

investigation to changes of the *N*-benzyl substituent of ML240 **8**:121
CBS-3595 **8**:439–447
first-use-in-human study of **8**:446–447
pharmacodynamic results **8**:446
pharmacokinetic results **8**:446–447
nonclinical evaluation of **8**:440–446
in complete Freund's adjuvant (CFA) arthritis model **8**:443–444
effect on leukotriene B_4 (LTB_4) release in LPS/fMLP-stimulated human whole blood **8**:441
effect on TNFα release in ex vivo-stimulated whole blood in cynomolgus monkeys **8**:442–443
effect on TNFα release in rat following LPS-challenge **8**:441–442
efficacy in hTNF-transgenic mice **8**:443
IC_{50} determination in in vitro kinase activity assays **8**:440
investigation of kinome selectivity and other potential off-targets **8**:440
metabolism studies **8**:441
Safety pharmacology studies **8**:444–445
toxicological studies **8**:445–446
CBS-3728 **8**:440–446
CCR5 blockers **1**:250t
CCR9 antagonists, for inflammatory bowel disease **5**:499–500
CCX354 **5**:401
CD19 **6**:51
CD20 **6**:50–51
CD30 **6**:51
CD39 inhibitors **5**:370f
CD39 nucleotidases **5**:370–371
CD73 inhibitors **5**:370–371, **5**:371f
CD73 nucleotidases **5**:370–371
CD101 **5**:711–712, **5**:712f, **5**:712t
Cdc2-related kinase 3 inhibitors **5**:726–727
CDC-like kinases inhibitors **5**:351
CDK7 **5**:93
CDK7 inhibitors **5**:93f
CDK9 inhibitors **5**:209–211
CDKI-73 **5**:210f
c[D-Pen2,D-Pen5]-enkephalin (DPDPE) **6**:95f
Cell death
and cancer **5**:5
mechanisms, nanoparticles **1**:282–284
annexin-V **1**:282
cell morphology **1**:284
loss of mitochondrial membrane potential **1**:283–284
ROS generation **1**:283
Cell division assay **1**:280, **1**:280f
Cell membrane permeability, nanoparticles **1**:281–282
calcein acetoxymethyl **1**:281–282
DNA intercalating fluorescent agents **1**:282
fluorescein diacetate **1**:281
lactate dehydrogenaze enzyme **1**:282
trypan blue **1**:281
Cell morphology **1**:284
Cell-based therapies for neurological disorders **1**:409–412
augmenting neurogenesis in vivo **1**:410–411
neural cell migration in vivo **1**:412
NSC differentiation in vivo **1**:411–412
reprogramming in vivo **1**:412
in situ stem cell modulation **1**:410
Cell-penetrating peptides **1**:332
Cell-permeability, molecular determinants of **1**:337–338
Cellular energetics deregulation, and cancer **5**:6
Cellular cancer immunotherapy **6**:46–48
Cellular imaging in drug discovery **2**:362–387
HCS. *See* High-content screening (HCS)
image acquisition and analysis **2**:368–370
image acquisition **2**:368
image analysis algorithm development **2**:368–370
screening compatible image analysis software **2**:368
image technologies and instruments **2**:366–368
confocal imager **2**:366–367
HCS instrument with niches **2**:367–368
laser scanning cytometers **2**:367
wide field imagers **2**:366
overview **2**:362
Cellular models
organoid and three-dimensional (3-D) models **2**:364
validation and quality controls **2**:364–365
Cellular thermal shift assay (CETSA) **1**:571f
Central nervous system (CNS)
disorders
AMPA receptors for **7**:447–480
polypharmacology in **2**:271
protein–protein interactions in **2**:332–333
exposure in drug discovery, assessment **7**:436–439
barriers within CNS System **7**:436–437
in vitro methodology to identify permeability and efflux liability at BBB **7**:437
in vivo methodology to measure the extent of brain penetration **7**:438–439
-focused iPSC drug-discovery screening **1**:61–63
neurodegenerative disorder model screening **1**:62–63
pain and sensory neuron disease model screening **1**:63
psychiatric disorder model screening **1**:61–62
phosphodiesterases **7**:384–407
CETP inhibitors **7**:681–682
CF-101 **5**:400
CGRP receptor antagonists for migraine **7**:176–224
biologics **7**:216–217
monoclonal antibodies **7**:216–217
ALD403 **7**:216
AMG-334 **7**:216
LY2951742 **7**:216
TEV-48125 **7**:216–217
overview **7**:177–181
small-molecule CGRP receptor antagonists. *See* Small-molecule CGRP receptor antagonists
Spiegelmers **7**:217
Chalcogen bonding
and sulfur **3**:90–91
Checkpoint inhibitors **5**:381–385
peptide inhibitors **5**:385
small molecule inhibitors **5**:382–384
ChEMBL **1**:455
Chemical accuracy
in QM/MM calculations **3**:55–56
Chemical and biological data integration **1**:447–449
Chemical category **1**:484f
Chemical file formats and data structures **3**:330–334
line notation formats **3**:331
molecular query language **3**:333–334
international chemical identifier **3**:333–334
simplified molecular-input line-entry system **3**:332
smiles arbitrary target specification **3**:332–333
SMIRKS **3**:333
Chemical manipulation, of pancreatic regeneration **1**:416
Chemical markup language **3**:338
Chemical nature, nutraceuticals classification by **1**:110
Chemical probes for novel therapeutic concepts **2**:52–53
Chemical space considerations **2**:37–40
Chemical stability/degradation
physical–chemical properties **3**:419
statistical methods **3**:419
Chemical structure methods, for drug repurposing **1**:29–30
Chemical table files **3**:335–339
chemical markup language **3**:338
connection table (Ctab)-based file types **3**:335
FASTA **3**:338
other formats **3**:336
Protein Data Bank file format (pdb) **3**:336–338
structure recognition tools **3**:338–339
tripos mol2 format **3**:336
Chemical transformations to create lead-like libraries **2**:139–146
lead-like library synthesis approaches **2**:139–146
Chemistry approaches, for physicochemical property optimization **7**:410–412
Chemistry extraction **3**:469
Chemogenomics **1**:444–446
See also Structural chemogenomics databases
Chemokine receptor 2 (CCR2) antagonists **1**:244f, **1**:244t
Chemokine receptor 2 (CCR2) ligands **1**:249f

Chemokine receptor 5 (CCR5) blockers **1**:249t
Chemokine receptor modulation **5**:404
Chemokines
  and DILI **4**:229
Chemometric/spectral similarity **3**:366
Chimeric antigen receptors (CARs) **5**:19–20
Chimeric liver-humanized mice **4**:138–141
  biotransformation studies **4**:139–141
  examples of studies using **4**:138–141
  inhibition and induction studies **4**:139
Chimeric mice with humanized liver for drug-induced toxicity investigation **4**:48
Chimeric somatostatin–dopamine compounds, for neuroendocrine disease **6**:116–130
  BIM-23A760 profiling **6**:124–127
    metabolite analysis **6**:126–127
    phase 1 clinical studies **6**:125
    phase 2a and b clinical studies **6**:126
  overview **6**:116
  second-generation design and discovery of lead compound BIM-065 **6**:128–129
  second-generation dopastatin
    current status **6**:129
    design concepts **6**:127–128
  somatostatin **6**:117–124
    dopastatin synthesis and structure–activity relationship **6**:122–124
    initial design **6**:119–120
    lanreotide and octreotide **6**:117
    mechanism of action **6**:117–119
CHK1 **5**:66–68
  inhibitors **5**:67–68
CHK1 inhibitors **5**:119–124, **5**:123f
  clinical Development of **5**:123–124
CHK1/2 **5**:67f
CHK2 inhibitors **5**:117–119, **5**:118f
  clinical development **5**:119
Chloramphenicol **5**:530f
Cholecystokinin **6**:68
Cholestasis, cellular and hepatic features of **4**:226–227
Cholesterylester transfer protein (CETP) inhibitors **1**:241t
Chondroitin, for chronic inflammatory disorders **1**:130
CH π interactions **3**:81–82
Chromatin, modifiers of **5**:486–487
Chromatin modifications in cancer **5**:282
Chromium, as nutraceuticals **1**:117
Chromone-derived privileged structures **2**:125
Chromosomal aberrations assay, for genotoxicity evaluation **4**:199
Chronic inflammatory disorders, nutraceuticals in **1**:130–131
  chondroitin **1**:130
  glucosamine **1**:130
  methylsulfonylmethane **1**:130
  pomegranate **1**:131
  S-adenosyl methionine **1**:131
Chronic kidney disease (CKD) **4**:124, **7**:701–705
  animal models of fibrotic renal disease **7**:702
    5/6th nephrectomy **7**:702
    AA injury **7**:702
    Alport syndrome **7**:702
    puromycin aminonucleoside **7**:702
    unilateral ureteral obstruction **7**:702
  current treatment **7**:702–703
  emerging biology and therapeutic treatment **7**:704–705
  epidemiology **7**:701
  ongoing clinical trials **7**:703
  overview **7**:701
  pathophysiology **7**:701
    evidence for role of fibrosis in CKD progression **7**:701
    features of renal fibrosis **7**:701
  perspectives **7**:705
Chronic neurodegeneration **5**:443–444
Ciclesonide (Omnaris/Alvesco) **5**:397
Circular economy **1**:285
Circular fingerprints **3**:342–344
  topological subsets **3**:343–344
Citrullination, and neurodegeneration **5**:442
c-Jun *N*-terminal kinase **7**:415
c-*KIT* **5**:326–328
Cladribine, for multiple sclerosis **5**:452–453
Class A GPCR aminergic **3**:164–170
Class A GPCR chemokine **3**:176–179
Class A GPCR lipid receptors **3**:176
Class A GPCR peptidergic **3**:170
Class A GPCR purinergic **3**:171–175
Classical bioisosterism **1**:200–202
Classification modelds (CMs) **1**:483f
Clearance
  human PK **4**:53–54
  prediction **4**:64–66
Click chemistry **1**:296–325, **1**:306f–308f, **1**:310f
  anticancer agents **1**:298–304
  antiproliferative agents synthesis **1**:304
  antiviral and other lead small molecules synthesis **1**:305–308
  overview **1**:296–298
  in receptor–ligand-binding studies **1**:309–317
    agonist **1**:309–311
    antagonist **1**:311–314
    selective binding ligands **1**:314–317
  in situ click chemistry **1**:317–319
    antibody-like protein-capture agents **1**:318–319
    binding site of Abl tyrosine kinase, probing **1**:318
    biotin protein ligase (BPL) inhibitors, screening and identification of **1**:318
Clinical compounds **7**:318–320
Clinical data
  integrating with biomedical evidence in pharmacovigilance **1**:441
  publicly available sequence, structural, and activity data **1**:446–447
  using and reusing for biomedical research **1**:441
  See also Data integration and sharing supporting drug R&D
Clinical development
  ADME/PK in **4**:23–29
    clinical ADME/PK studies **4**:25–29
    circulating human metabolites **4**:27–28
    clinical ^{14}C-ADME study **4**:28–29
    clinical pharmacokinetics **4**:25–26
    definitive characterization of ddis **4**:26–27
    IND-enabling ADME/PK studies **4**:23–25
      active circulating metabolites in animals **4**:24–25
      animal PK and bioavailability **4**:24
      initial in vitro assessment of clinical DDI potential **4**:25
      major routes of clearance in animals **4**:24
      projection of human PK **4**:25
      purpose of **4**:23–24
  companion diagnostics **2**:535–539
    basket and umbrella studies **2**:538–539
    clinical study design **2**:536–538
    clinical validation **2**:535–539
    cutoff selection **2**:535
Clinical drug candidates, and FBDD **2**:215–217
  fragment elaboration **2**:215–217
  ligand efficiency **2**:215
  medicinal & synthetic chemistry rules **2**:217
Clinical studies **7**:165–167
  ethics in drug discovery **1**:542–546
    benefits to participation in clinical studies of potential medicines **1**:542–543
    consent and assent **1**:545–546
    reporting of clinical study results **1**:546
    role of the independent review board **1**:546
    study design **1**:543–545
Clinical study design, companion diagnostics **2**:536–538
Clinical trials, rare disease foundations **1**:556
Clinical validation, companion diagnostics **2**:535–539
Clinicopathological data **1**:59–60
Clonogenic assay **1**:279–280
Clostridium difficile **5**:527–529
Clotrimazole **5**:706f
Cloud and distributed computing, for molecular simulation **3**:16
Clusterin, biomarker of acute kidney injury **4**:273
Clustering algorithms **3**:362–363
c-*MYC* **5**:316–321
CNV2197944 **7**:70
Coarse-grained force fields **3**:21–22
Cobalt, as nutraceuticals **1**:117
Cobicistat, for HIV **5**:647
Cocrystallization **2**:158–159

Coenzyme Q10, and CVDs **1**:127
Colistin A **6**:89–90
Colistin resistance **5**:524–525
Collaboration tools **3**:461–463
  workflow **3**:461–463
Collaborative models, for partnerships and for building teams **1**:497–498
Collective variables (CVs)
  -based methods **3**:39
  optimal choice of **3**:39–40
Combination therapy
  and polypharmacology, compared **2**:261–262
Combinatorial peptide libraries **6**:104–107
  phage display library **6**:106
  spatially addressable parallel synthesis **6**:105–106
  split and mix synthesis **6**:106
Comet assay, for genotoxicity evaluation **4**:199–201
CoMFA **3**:271–272
Command line/programming tools **3**:440–448
Companion diagnostics **2**:530–546
  assay development **2**:532–534
    assay methodology **2**:533
    assay validation **2**:534
    assay verification **2**:534
    prototype assays **2**:533–534
  biomarker discovery **2**:532
  clinical development **2**:535–539
    basket and umbrella studies **2**:538–539
    clinical study design **2**:536–538
    clinical validation **2**:535–539
    cutoff selection **2**:535
  described **2**:531–532
  future trends **2**:542–543
  historical aspects **2**:531–532
  impact of the drug–diagnostic codevelopment model **2**:540–542
  overview **2**:530
  regulatory aspects **2**:539–540
    EU regulatory requirements **2**:540
    US regulatory requirements **2**:540
  terminology and definitions **2**:531
Competitive biomarkers **2**:499
Complement-dependent cytotoxicity **6**:44–46
Complement system targeting for inflammatory disorders **5**:411–412
Complex cellular models, predictive toxicology **2**:100–101
Complex diseases targeting
  polypharmacology **2**:270–271
    in cancer **2**:270–271
    in CNS disorders **2**:271
Complex genetic disorders, disease mechanisms assessment in **1**:56–57
Complex toxicity endpoints **2**:250–254
  data integration of in vivo toxicity studies **2**:253
  development of prediction models **2**:253–254
  drug-induced liver injury **2**:251–253
  in vivo safety studies **2**:250–251
Compounds and biology **1**:500–501
Computational approaches
  to ADME/PK problems **4**:17
Computational drug discovery criteria **3**:433–436
Computational methodologies
  in systems chemical biology **2**:483–485
    data integration **2**:485
    data mining and machine learning **2**:484
    dynamic modeling **2**:484–485
    network analysis and graph theory **2**:485
Computational modeling
  of protein–ligand interactions **3**:321
  of protein–protein interactions **3**:321
Computational toxicology **4**:297
Computers, information leak through **1**:532
CoMSIA **3**:273
COMT inhibitors, for Parkinson's disease **5**:462
Concentration-dependent DILI **4**:206–207
Condensed-phase and gaseous phase, physical–chemical properties **3**:397
Confocal imager **2**:366–367
Confocal microscopy **2**:404–405
Conformational analysis, of spirocyclic scaffolds **1**:213–218
  overview **1**:213
  spiro[2.*n*] ring systems **1**:214
  spiro[3.*n*] ring systems **1**:214
  spiro[4.4] ring systems **1**:214–215
  spiro[4.5] ring systems **1**:215–216
    benzo-fused ring systems **1**:215–216
    isolated ring systems **1**:215
  spiro[5.5] ring systems **1**:216–218
    benzo-fused spiro[5.5] ring systems **1**:218
    isolated ring systems **1**:216–218
  spiro[*m*.6] ring systems **1**:218
Conformational-selection model **3**:320f
Confusion matrix for binary classification **1**:482t
Conjugation enzymes **4**:136
Conjugation to Fc antibody fragments **6**:144–145
Connection table (Ctab)-based file types **3**:335
Conopeptides **6**:92–93
Consensus scoring **3**:361–362
Consent, in clinical studies **1**:545–546
Constrained nucleic acids (CNAs) **6**:223
Continuous flow processing **1**:135–185
  fragments and heterocycles **1**:136–157
    azides **1**:140–142
    cross-coupling reactions **1**:150
    cycloaddition **1**:151–153
    cyclocondensation **1**:148–149
    diazonium salts **1**:139–140
    hazardous gases **1**:136–139
    miscellaneous **1**:154–157
    nitration **1**:142
    nucleophilic substitution **1**:151
    organometallic reagents **1**:145–147
    oxidation **1**:143
    photochemistry **1**:153–154
    reduction **1**:143–144
  library preparation and automated processes **1**:157–162
  multistep flow processes **1**:166–180
  overview **1**:135–136
  reaction monitoring and self-optimizing systems **1**:162–165
Control-based normalization methods **2**:394
Convenient subcutaneous and intramuscular delivery devices **6**:148
Corneal disease, regenerative drugs **1**:422
Coronary artery disease, secreted phospholipase A2 (sPLA2) inhibitor for **8**:339–348
Coronaviruses
  antiviral drugs for **5**:677
COSMO-RS **3**:402–403
COSMO*sar3D* **3**:274–276
COSMO*sim3D* **3**:255–256
Cost
  of drug repurposing **1**:16
  pharmaceutical industry challenge **1**:2
Coumarin-derived privileged structures **2**:125
Counterscreening and target identification **3**:212–213
Coupling methods **2**:182–183
Covalent allosteric modulators **2**:285–288
Covalent inhibitors **2**:21–22
Covalent inhibitors design, and QM/MM **3**:57–58
Covalent kinase inhibitors, for cancer **5**:76–103
  advantages of **5**:78
    achieving highly selective kinase inhibitors **5**:78
    prolonged residence time via covalency **5**:78
  assessment and optimization **5**:78–81
    on-target in vitro activity **5**:78–79
    pharmacodynamics of covalent inhibitors **5**:81
    safety concerns **5**:80–81
    structure and reactivity of covalent electrophiles **5**:80
  BTK inhibitors **5**:81–84
    covalent BTK inhibitor outlook **5**:84
    development of clinical covalent BTK inhibitors **5**:82–83
    target biology **5**:81
  covalent inhibitors of FGFR family kinases **5**:88–91
    BLU9931 (40)/BLU-554 (41) **5**:90–91
    FIIN-1 (35) **5**:90
    FIIN-2 (36)/FIIN-3 (37) **5**:90
    target biology **5**:88
    TAS-120 (38)/PRN1371 (39) **5**:90
  covalent inhibitors of HER family kinases **5**:84–88

Covalent kinase inhibitors, for cancer (*continued*)
acquired resistance to third-generation covalent EGFR inhibitors **5**:88
covalent HER family kinase inhibitors **5**:84–86
development of rociletinib **5**:87
osimertinib **5**:87–88
second-generation irreversible HER family inhibitors **5**:86
target biology **5**:84
third-generation irreversible mutant-selective EGFR inhibitors **5**:86–88
emerging strategies and technologies **5**:98–100
covalent reversible cysteine inhibition of kinases **5**:98–99
non-cysteine-targeting covalent inhibitors **5**:99
screening approaches to discover covalent inhibitor leads **5**:100
virtual screening of covalent inhibitors **5**:100
kinase targets for covalent inhibition **5**:91–97
Akt **5**:91–92
BMX **5**:92
CDK7 **5**:93
ERK1/2 **5**:93–94
ITK **5**:94
JAK3 **5**:95–96
miscellaneous kinases **5**:97
PI3Kα **5**:96
overview **5**:77
Covalent reversible cysteine inhibition of kinases **5**:98–99
COX inhibitors **7**:584–586
aspirin **7**:584
recent developments **7**:585–586
triflusal **7**:585
COX2 and EP2/EP4 receptor antagonists **5**:371–372
COX2 inhibitors **5**:403–404
CPPs as delivery vectors **1**:336–339
cellular uptake pathways for drug delivery with CPPs **1**:336–337
enhancing endosomal escape of biologic drugs **1**:338–339
molecular determinants of cell-permeability **1**:337–338
CR Agents **1**:88–89
CREDO **1**:457–458
CRISPR single-guide RNA **2**:3f
CRISPR/Cas9 **6**:303–306
challenges and future perspectives **6**:305–306
potential therapeutic applications of **6**:303–305
Critical sequence-structure alignment generation **3**:133
Crohn's disease (CD) **5**:498f
tocilizumab translation in **2**:520
Cross-coupling reactions
continuous flow processing **1**:150
Cross-species translation **2**:464
Cryptosporidia **5**:723–724
Crystal form stability
and hydrogen bonding **3**:92–93
Crystal harvesting **2**:159–160
Crystal-structure interactions, impact on physical properties **3**:94
csDMARDs, combined with baricitinib **5**:425–426
CSF-R1 inhibitors **5**:380
c-SRC **5**:332
Curcumin **1**:94–96
for inflammatory bowel disease **5**:504
Cutoff selection, companion diagnostics **2**:535
Cyclic β_3-AR agonists **7**:723–724
Cyclic melanocortin analogs **6**:94
Cyclic opioid peptides **6**:95
Cyclin-dependent kinase 5 **7**:414
Cycloaddition
continuous flow processing **1**:151–153
Cyclocondensation
continuous flow processing **1**:148–149
Cyclodextrins (CDs) **1**:600f
2-(Cyclohexylmethylamino)pyrimidines **8**:134
Cyclopentane
low energy conformations of **1**:214f
Cyclophosphamide, for multiple sclerosis **5**:451
Cyclosporin A **1**:329, **6**:89
CYP P450-humanized mice **4**:134–136
Cystatin-C, biomarker of acute kidney injury **4**:273
Cytochrome P450 (CYP) enzymes **4**:9t
functionalization by **4**:134
Cytokeratin 18 **4**:266
Cytokine biomarkers **4**:276–277
Cytokine signaling
small molecule immunosuppressants **5**:421
Cytokine therapy **5**:19
Cytokines **4**:277t, **6**:49–50
and DILI **4**:229

D

D0.11.10 proliferation assay **8**:370
D1 receptors **7**:23
D2/D3 receptors **7**:23–25
D4 receptors **7**:25
Dainippon Sumitomo, modulators from **7**:292
Dalfampridine (Ampyra/Fampyra) **5**:398
Daptomycin **5**:526f
Daptomycin resistance **5**:526
Darunavir, for HIV **5**:642–643
Data analysis and visualization tools **3**:440–463
big data analysis **3**:460–461
collaboration tools **3**:461–463
workflow **3**:461–463
command line/programming tools **3**:440–448
desktop tools **3**:448–454
mobile applications **3**:457–460
mobile apps using a client–server model **3**:459–460
overview **3**:440
web-based tools **3**:454–457
Data integration, of in vivo toxicity studies **2**:253
Data integration and sharing supporting drug R&D **1**:436–443
considerations **1**:442
information supporting
hit identification and drug design and development **1**:438
target identification **1**:437–438
integrating clinical data and biomedical evidence in pharmacovigilance **1**:441
overview **1**:436–437
predictive toxicology **1**:438–441
relevant knowledge for a drug discovery project **1**:437
using and reusing clinical data for biomedical research **1**:441
Data mining approaches, for drug repurposing **1**:27–41
data processing **1**:27–28
data types **1**:27
effects-based data mining **1**:31–38
genome-based **1**:33–34
phenome-based **1**:35–38
proteome-based **1**:34–35
transcriptome-based **1**:34
integrated approaches **1**:38–39
practical considerations **1**:40–41
resources **1**:28–29
structure–target data mining **1**:29–31
chemical structure methods **1**:29–30
drug–target interaction profiles **1**:30–31
molecular docking and binding site similarity **1**:30
protein structure methods **1**:30
validation **1**:29
Data sharing
dealing with fragmentation **1**:500
initiatives and data exchange **2**:254–256
IMI eTox and NextGets initiatives **2**:254–255
SEND data model and electronic submission to FDA **2**:255–256
Database analysis and searching **3**:329–378
case studies **3**:368–370
chemical file formats and data structures **3**:330–334
international chemical identifier **3**:333–334
line notation formats **3**:331
molecular query language **3**:333–334
simplified molecular-input line-entry system **3**:332
smiles arbitrary target specification **3**:332–333
SMIRKS **3**:333
molecular fingerprints **3**:339–346
affinity fingerprints **3**:345
circular fingerprints **3**:342–344
EDPrints **3**:345

fingerprints for ligands and proteins (FLAP) **3**:346
hybrid fingerprint **3**:344
interaction fingerprints **3**:346
path-based fingerprints **3**:342
pharmacophore fingerprints **3**:344
reaction fingerprints **3**:346
substructure key-based fingerprints **3**:340–341
text-based **3**:345
topological fingerprints **3**:341
topological subsets **3**:343–344
online web resources **3**:367–368
other line notation formats **3**:334–339
chemical markup language **3**:338
chemical table files **3**:335–339
connection table (Ctab)-based file types **3**:335
FASTA **3**:338
other formats **3**:336
Protein Data Bank file format (pdb) **3**:336–338
representation of organic structures description arranged linearly **3**:334–335
structure recognition tools **3**:338–339
sybyl line notation **3**:335
tripos mol2 format **3**:336
wiswesser line notation **3**:334
overview **3**:330
Database analysis and searching, numerical descriptors and similar representations **3**:346–355
2D descriptors **3**:347–351
indicator variables **3**:351
molecular identification numbers **3**:351
thermodynamic descriptors **3**:351
topological descriptors **3**:349–350
whole-molecular descriptors **3**:347–348
3D descriptors **3**:351–354
3D descriptor families **3**:353–354
electronic descriptors **3**:351–352
molecular field analysis descriptors **3**:353
molecular shape analysis descriptors **3**:353
receptor surface analysis descriptors **3**:353
shape descriptors **3**:352
size descriptors **3**:352
van der Waals parameters **3**:353
volume descriptors **3**:352
4D and other special descriptors **3**:354–355
4D descriptors **3**:354–355
other special descriptors and approaches **3**:355
Database analysis and searching, similarity–dissimilarity measures **3**:355–367
clustering algorithms **3**:362–363
common measures of (distance) **3**:356–361
similarity fusion, fusion rules, consensus scoring **3**:361–362
similarity measures for special tasks **3**:363–367
chemometric/Spectral similarity **3**:366
fuzzy similarity measures **3**:366–367
graph (tree)-based similarities **3**:364–365
other similarity measures **3**:367
semantic similarity measures **3**:365
similarities of 1D structures **3**:363–364
supervised similarity measures **3**:365–366
symmetric field-based similarity indices **3**:363
Database classification criteria, for structural chemogenomics **1**:450–454
data browse and search functionalities **1**:451
database update frequency **1**:454
ligand data types **1**:451–452
protein data types **1**:452–453
protein–ligand interaction data types **1**:453–454
Data-driven interaction network inference, system biology **2**:452–454
algorithms tailored to time-series data **2**:454
experimental data **2**:453
goal of network inference **2**:452–453
inferring edges using pairwise measures **2**:453–454
DC function in tumor, modulation of **5**:361
DCR-MYC **6**:294
DC-SIGN lectin targeting, and carbohydrates **1**:589–591
Death-associated protein kinase 1 **7**:417
Deconvolution software **2**:408
Dedicated biotechnology firms (DBFs) **1**:523–527
and academic institutions, upstream vertical relationships between **1**:523–524
contribution in drug development and commercialization **1**:521–522
and pharmaceutical companies, and other organizations, downstream vertical relationships among **1**:524–527
Delanzomib (CEP-18770) **5**:266
δ opioid receptor agonists **1**:246t, **1**:247f
Democratization
of molecular docking **3**:310
Denagliptin **7**:536
De-novo structure-based design **2**:34–36
Depsipeptide (CO_2) **6**:84
DEREK **4**:167
Derek Nexus **2**:234–235
Designer foods **1**:110
See also Nutraceuticals
Desktop tools **3**:448–454
Desmopressin **6**:77
Deubiquitylating enzymes in cancer therapy **5**:271
Developability classification system (DCS) **1**:563f
Developing world populations, medical need in **1**:541–542
Diabetes, and nutraceuticals **1**:129
Diacylglycerol O-acyltransferase inhibitors **7**:686–687
Diallyl sulfide, for inflammatory bowel disease **5**:506
Diamidines **5**:725, **5**:731
Diamines/MK-4305 **7**:253–254
Diarylmethylpiperazines **7**:81–89
2,5-Diarylnicotinamides **7**:257
Diarylureas related to SB-334867 **7**:268–269
Diazepanes **7**:260
Diazonium salts
continuous flow processing **1**:139–140
Diclofenac **4**:212–213, **4**:212f
Dietary fibers, and CVDs **1**:126
Dietary supplement **1**:109
See also Nutraceuticals
Different sources of β-cells **1**:419–420
fibroblasts **1**:419–420
mesenchymal stem cells **1**:419
other pancreatic cells **1**:419
Different strategies, binding free energies calculations **3**:5–8
binding entropy calculations **3**:8
FEP approaches **3**:5
LIE approaches **3**:6
LRA approaches **3**:6
protein–protein interactions **3**:6–7
semimacroscopic and macroscopic calculations of ligand binding **3**:6
Diffraction experiment **2**:160–161
Digoxin **7**:643–644
Dihydrofate reductase (DHFR) inhibitors **5**:525f
Dihydrofolate reductase–thymidylate synthase **5**:727
Dihydroorate dehydrogenase inhibitor, DSM265 **5**:721–722, **8**:544–557
Dihydropyridine derivatives **7**:113
Dihydropyridines **7**:80–81
Dihydroquinazolines **7**:113–114
Dimethyl fumarate **5**:399
for multiple sclerosis **5**:447
Dinaciclib **5**:209t
1,7-Dioxaspiro[5.5]undecane **1**:218t
Diphenylmethylpiperazines **7**:88–89
Direct calorimetric methods **2**:198–201
principle of ITC **2**:198–199
thermodynamics of T_m shifting assays **2**:200–201
Van't Hoff analysis **2**:199–200
Direct-acting antivirals
for of hepatitis C virus infection **5**:553–627
drug combinations in clinical trials **5**:605–607
of HCV entry inhibitors **5**:558–561
HCV internal ribosome entry site (IRES) inhibitors **5**:604–605
HCV NS2 protease inhibitors **5**:563
HCV NS3 helicase inhibitors **5**:575
HCV NS3 protease inhibitors **5**:563–575
HCV NS4A inhibitors **5**:576
HCV NS4B inhibitors **5**:577–580
HCV NS5A inhibitors **5**:580–586
HCV NS5B inhibitors **5**:587–604
background **5**:587–588

Direct-acting antivirals (*continued*)
HCV NS5B RdRp activity
nonnucleoside inhibitors of **5**:592
nucleoside inhibitors of **5**:588–592
palm site I nonnucleoside inhibitors of **5**:598–601
palm site II nonnucleoside inhibitors of **5**:601–604
palm site (primer grip) nonnucleoside inhibitors of **5**:598
thumb site I nonnucleoside inhibitors of **5**:592–596
thumb site II nonnucleoside inhibitors of **5**:596–597
inhibitors of HCV core (capsid) protein function **5**:556–558
ion channel activity of p7 inhibitors **5**:561–562
overview **5**:554–605
for HIV **5**:650–651
Direct-acting macrofilaricides **5**:738
Directed differentiation, neuronal system **1**:404–409
bone marrow-mesenchymal stem cells **1**:408
embryonic stem cells **1**:404–406
induced pluripotent stem cells **1**:406–408
NSCs and NPCs in vitro **1**:403–404
transdifferentiation of other cell types **1**:408–409
Disease in cellular- and genomic-relevant contexts, iPSCs models **1**:50–57
disease mechanisms assessment in complex genetic disorders **1**:56–57
patient iPSC differentiation into disease-relevant cell types **1**:51–56
Disease mechanisms assessment in complex genetic disorders **1**:56–57
Disease-relevant cell types, patient iPSC differentiation into **1**:51–56
DisGeNET **1**:439f
Dissociation phase, kinetics in drug discovery **2**:184
Dissolution of pharmaceuticals, physical–chemical properties **3**:397–398
Distribution
ADME **4**:35
ADME/PK **4**:2, **4**:12–14
Distribution prediction **4**:105–106
BDDCS in **4**:122–125
distribution into the brain **4**:122–123
potential extensions to other membranes **4**:124–125
Distribution volume
ADME **4**:37–39
human PK **4**:54
prediction **4**:66–67, **4**:105–106
Disulfuram **5**:649t
Diuretics for decongestion in heart failure **7**:649–650
DMPK, safety, and physical properties **2**:70–71
DNA
chemical structure of **6**:217f
damage and replication stress, and cancer **5**:9
damage response pathways, in cancer
overview **5**:105–107
PARP. *See* Poly(ADP-Ribose) polymerase (PARP)
fragments and micro-RNA **4**:296
gyrase inhibitors **1**:251t
intercalating agent **1**:281f–282f
intercalating fluorescent agents **1**:282
DNA methylation, cancer epigenetics **5**:21
DNA methylation/demethylation, epigenetic modulation via **2**:298–300
DNA-dependent protein kinase **5**:115–116
clinical development of DNA-PK inhibitors **5**:116
DNA-PK inhibitors **5**:115–116
DNA-PK **5**:64–65
DNA-PK inhibitors **5**:64–65, **5**:65f, **5**:116f, **5**:116t
Do it yourself options **1**:533–539
Docking
molecular fields **3**:289–291
AFMoC **3**:289–290
AutoDock **3**:290
FLAPdock **3**:291
Glide **3**:291
GOLD **3**:291
Dolutegravir, for HIV **5**:634–635, **5**:634f
Donepezil, for AD **5**:455
Donor/acceptor feature point positioning tautomers **3**:194
Dopamine transporter (DAT) **7**:40
Dopaminergic receptors **7**:23–25
Doravirine, for HIV **5**:641–642
Doxycycline **5**:529f
DPP-4 **7**:512–555
biology **7**:514–517
chemokine and cytokine substrates **7**:516–517
cleavage of neuropeptide Y and peptide YY **7**:516
gene structure, expression, and related enzymes **7**:514–515
processing of glucagon superfamily peptides **7**:515–516
processing of vasoactive peptides **7**:517
substrate specificity **7**:515
crystal structure of **7**:517
overview **7**:513–514
scientific rationale for, in type 2 diabetes treatment **7**:514
DPP-4 inhibitors **7**:518–544
approved and marketed inhibitors **7**:518–534
β-amino butanoic acid derivatives **7**:518–524
pyrimidinedione/xanthine analogs **7**:531–534
pyrrolidine analogs **7**:524–531
from natural extracts **7**:545
natural products as **7**:544–545
in phase I **7**:540–542
in phase II **7**:538–540
in phase III **7**:534–538
denagliptin **7**:536
dutogliptin **7**:534
gosogliptin **7**:534–536
melogliptin **7**:536–538
retagliptin **7**:538
in preclinical development **7**:542–544
Drug at target **1**:564–569
Drug combination, systems chemical biology **2**:487–488
Drug development pipeline, iPSCs role in **1**:61–64
CNS-focused iPSC drug-discovery screening **1**:61–63
neurodegenerative disorder model screening **1**:62–63
pain and sensory neuron disease model screening **1**:63
psychiatric disorder model screening **1**:61–62
quantitative cellular pharmacology **1**:63
advances enabling novel assay development and target validation **1**:63–64
toxicology and drug metabolism **1**:64
Drug discovery, structural chemogenomics in **1**:461–466
combined bioactivity data mining and chemical similarity search for ligand-based target prediction **1**:461–462
combined navigation of protein–ligand interaction and ligand chemistry space **1**:463–466
integrated structure-based medicinal chemistry toolbox for drug discovery and design **1**:463
protein binding site similarity assessments for ligand repurposing and off-target prediction **1**:462–463
Drug discovery ethics. *See* Ethics in drug discovery
Drug discovery process, risks in **1**:557
Drug discovery project, relevant knowledge for **1**:437
Drug efficiency **2**:79–87
definition of **2**:80–81
drug efficiency index **2**:81–87
Drug metabolism prediction, and QM/MM **3**:61–62
Drug repositioning
and polypharmacology **2**:271–272
systems chemical biology **2**:487–488
Drug repurposing **1**:11–47
advantages and disadvantages **1**:14–18
attritional risk **1**:16
cost **1**:16
disadvantages **1**:16–17
off-label medicine **1**:17–18
time **1**:16
historical perspective **1**:11–12
and polypharmacology **2**:271–272
successes **1**:12–14
tailoring an existing drug for a new use **1**:41
variants **1**:18–21

generic drugs **1**:18–19
off-target *versus* on-target **1**:19–20
public/private partnerships for abandoned assets repurposing **1**:19
rare diseases **1**:20–21
Drug repurposing, candidates identification **1**:21–27
experimental approaches **1**:21–23
ontologies **1**:24
target-association screening **1**:21
knowledge-based approaches **1**:23–24
literature-based **1**:23–24
phenotypic screening **1**:21–23
retrospective analysis **1**:25–27
Drug repurposing, data mining approaches for **1**:27–41
data processing **1**:27–28
data types **1**:27
effects-based data mining **1**:31–38
genome-based **1**:33–34
phenome-based **1**:35–38
proteome-based **1**:34–35
transcriptome-based **1**:34
integrated approaches **1**:38–39
practical considerations **1**:40–41
resources **1**:28–29
structure–target data mining **1**:29–31
chemical structure methods **1**:29–30
drug–target interaction profiles **1**:30–31
molecular docking and binding site similarity **1**:30
protein structure methods **1**:30
validation **1**:29
Drug resistance targeting, polypharmacology **2**:271
Drug targets, protein–protein interactions in **2**:334–336
cancer **2**:338–342
Bcl-2/Bcl-x_L–Bak **2**:338
bromodomain–acetylated histone **2**:341–342
MDM2–p53 **2**:338–339
WDR5–MLL **2**:339–341
cardiovascular disease **2**:344–345
central nervous system disorders **2**:342–343
α-synuclein aggregation **2**:343
PDZ domain interactions **2**:342
future prospects **2**:346
hotspots and allosteric sites **2**:334–335
identification of druggable protein–protein interactions **2**:335
infectious diseases **2**:345–346
inflammation and autoimmune diseases **2**:343–344
Keap1–Nrf2 **2**:343–344
LFA-1–ICAM-1 **2**:343
recent advances in drug discovery **2**:338–346
small molecular protein–protein interaction inhibitors **2**:336
strategies to generate inhibitors **2**:336–338
fragment-based drug design **2**:337
high-throughput screening **2**:336–337
peptides and peptidomimetics **2**:336
virtual screening **2**:337–338
Drug transporters, genetically humanized mouse models **4**:137–138
transporter-humanized mice **4**:137–138
DrugBank **1**:456
Drug–diagnostic codevelopment model **2**:532f
and companion diagnostics **2**:540–542
Drug–drug interactions (DDIs)
consequent to drug-mediated cytokine elevations **2**:508
and DILI **4**:209–210
potential
dcreening for **4**:17–20
in vitro assessment of **4**:25
DRUGeff **2**:81f
Druggability **3**:429–439
Druggable protein–protein interactions **2**:335
Druggable target space **1**:328–335
immune targets and vaccines **1**:332–334
oligonucleotides and oligonucleotide drugs **1**:334–335
PPIs and their modulators **1**:328–332
biological selection of backbone-modified macrocyclic peptides **1**:330–331
macrocycles **1**:329–330
stable peptide frameworks for therapeutic applications **1**:331–332
Drug-induced liver injury (DILI) **2**:251–253, **4**:204–238
adaptive immune system, role in humans **4**:230–231
overview **4**:230
PBMC from patients with DILI **4**:230–231
biomarkers of **4**:263–268
alpha-gluthathione-*S*-transferase **4**:265–266
arginase-1 **4**:264–265
cytokeratin 18 **4**:266
general characteristics of emerging liver safety biomarkers **4**:264
glutamate dehydrogenase **4**:266–267
HMGB1 **4**:267
miR-122 **4**:267–268
clinical aspects **4**:205
phenotypes **4**:205
structure and function of the liver **4**:205
detecting hepatotoxicity during drug development **4**:205–206
animal models **4**:205
cell culture **4**:205–206
in silico approaches **4**:206
future perspectives **4**:233
genetic factors affecting, due to specific drugs **4**:210–213
HLA associations **4**:210–211
non-HLA associations **4**:211–213
overview **4**:210
innate immune system, role in DILI in man **4**:228–230
autoantibodies and DILI **4**:229
cytokines and chemokines **4**:229
HLA associations with DILI **4**:228–229
in vitro liver models to capture **4**:230
overview **4**:228
TNFα **4**:229
lysosomal perturbation and DILI **4**:223–225
autophagy, lysosomes, and DILI **4**:224
autophagy perturbation **4**:225
lysosomal perturbations and cytotoxicity **4**:225
overview **4**:223
physicochemical properties of drugs and lysosomes **4**:223–224
mathematical modeling **4**:233
mechanisms **4**:219f
mitochondrial dysfunction (in vitro and in vivo) **4**:221–223
and hepatic specificity of action for drugs **4**:221–223
inhibition of fatty acid oxidation and lipid transport **4**:221
intracellular signaling pathways **4**:221
JNK signaling **4**:221
mitochondrial adaptation to drugs **4**:223
mitochondrial toxicity **4**:221
overview **4**:221
structural aspects of drugs eliciting mitochondrial damage **4**:223
nature of **4**:206–210
age **4**:208
concentration-dependent DILI **4**:206–207
drug–drug interactions **4**:209–210
gender **4**:208
idiosyncratic DILI **4**:207–208
infection **4**:209
nongenetic risk factors for DILI **4**:208
preexisting liver disease **4**:208–209
smoking and alcohol consumption **4**:209
overview **4**:204, **4**:218
in patients including patient-specific risk factors **4**:206–213
prediction of **4**:231–233
role of reactive drug metabolites in **4**:218–220
drug reactive metabolites **4**:220
imbalance in activation and inactivation of drugs **4**:220
overview **4**:218–219
reactive intermediates **4**:220
selectivity of covalent binding **4**:219–220
signaling pathways and mathematical models **4**:231–233
in silico models, for hepatocyte and NPC perturbation detection **4**:232
lessons learned from **4**:232
overview **4**:231
quantification of physiological response and toxicological perturbation of **4**:233
transporters, role in drug- and bile acid-induced liver injury **4**:225–228
bile acid toxicity **4**:227–228

Drug-induced liver injury (DILI) (*continued*)
bile acid uptake and excretion **4**:225–226
cellular and hepatic features of cholestasis **4**:226–227
drug and bile acid transporters, classification of **4**:225
model systems for transport evaluation **4**:227
transporters and bile acid toxicity **4**:228
Drug-like chemical space **1**:560–564
designing permeable compounds beyond the Lipinski rule of five **2**:22–23
rational design of covalent inhibitors **2**:21–22
Drug-like property space **2**:70
Drug-likeness computation **3**:431
Drug-metabolizing enzyme systems I **4**:45–50
chimeric mice with humanized liver for drug-induced toxicity investigation **4**:48
human P450 probes in experimental animals
age-related and polymorphic pharmacokinetic changes of **4**:47–48
in vivo pharmacokinetics of **4**:45–46
overview **4**:45
Drugs failures, reasons for **2**:94
Drugs properties in solution, physical–chemical properties **3**:399–401
ionization constants **3**:399–400
solution stability **3**:400–401
Drug–target identification and prioritization, systems chemical biology **2**:485–486
Drug–target interaction profiles, for drug repurposing **1**:30–31
DSM265 **8**:544–557
biological activity **8**:550–552
efficacy in the *P. falciparum* SCID mouse model **8**:552
enzyme activity including mammalian DHODH selectivity **8**:550
in vitro activity against parasites **8**:551–552
mechanism and frequency of resistance **8**:552
plasmodium stages **8**:552
X-ray structure of DSM265 bound to P*f*DHODH **8**:550–551
discovery of **8**:547–549
early structure–activity relationships and pharmacokinetic issues **8**:548
high-throughput screen **8**:547–548
X-ray structure determination, and lead optimization **8**:548–549
perspectives **8**:555
pharmacokinetic properties **8**:553–554
physicochemical properties and in vitro ADME Characteristics **8**:553
human pharmacokinetic and dose predictions **8**:553–554
in vivo pharmacokinetic studies in preclinical species **8**:553
safety studies and the importance of knowing the target **8**:554–555
Synthesis **8**:549
Dual leucine zipper kinase **7**:426–427
Dual mTOR and PI3K inhibitors **5**:217
Dual $Na_V1.7$–1.8 inhibitors **7**:160–161
Dual $P2Y_1/P2Y_{12}$ antagonists **7**:573
Dual p38α MAPK/PDE-4 Inhibitors **8**:431–449
CBS-3595. *See* CBS-3595
chemistry **8**:434–437
in vitro and in vivo pharmacodynamics **8**:435–437
discovery of **8**:437–439
chemistry of CBS-3595 **8**:439
profiling of CBS-3595 **8**:439
overview **8**:431–434
selective p38α MAPK inhibition **8**:432–433
Dual p38α MAPK/PDE-4 inhibitors, for TNFα-driven diseases **8**:431–449
Dual pan-RET/VEGFR2 kinase inhibitors **2**:226–227
Dulaglutide **7**:486–487
Dundee quinolone carboxamide antimalarials **5**:721f
Dutogliptin **7**:534
Dyslipidemia management, novel therapeutic approaches in **7**:666–687
targeting plasma cholesterol levels **7**:666–684
targeting plasma TG levels **7**:684–687

E

E1 activating enzymes in cancer therapy **5**:247–259
E2 conjugating enzymes in cancer therapy **5**:250
E3 ligases **5**:250–259
pevonedistat (MLN4924) **5**:247–250
E2 enzyme inhibitors **5**:250f
E1210 **5**:713, **5**:713f
E1211 **5**:713f
Ebola, antiviral drugs for **5**:677–678
Echinocandins **5**:708
ECL Assays **6**:190–191
pros and cons/considerations **6**:191
Econazole **5**:706f
EDPrints **3**:345
EdU proliferation assay **1**:280
Effects-based data mining, for drug repurposing **1**:31–38
genome-based **1**:33–34
phenome-based **1**:35–38
proteome-based **1**:34–35
transcriptome-based **1**:34
Efficacy biomarkers **2**:498
Efficiency measures in drug discovery **2**:206–209
common LEM **2**:207–209
enthalpic efficiency **2**:208
kinetic efficiency **2**:208–209
ligand efficiency **2**:207
ligand lipophilicity efficiency **2**:207–208
other size-based metrics **2**:207
future trends for application of LEM **2**:209
EFPIA-contributed collection, The Joint European Compound Library **1**:506
EGFR **7**:428–431
biology
role in nonsmall cell lung cancer **8**:1–2
EGFR inhibitors **5**:85f
mutant selective **5**:51–55
T790M mutant selective **5**:52–55
targeting activating mutations **5**:51–52
EHMT2 inhibitors **5**:299f–300f, **5**:301t–302t
eIF4F
direct inhibitors of **5**:228
upstream regulators inhibitors **5**:215–228
Eisai **7**:238–239
N-aryl-2-phenylcyclopropanecarboxamides **7**:238–239
E2006 **7**:239
inhibitors reported by **7**:338–341
modulators from **7**:293–294
Elamipretide **7**:652–653
Elan
inhibitors reported by **7**:341
Electric biosensor
label-free screening **2**:420
Electric biosensor to assess compound-induced toxicity **2**:428–429
Electron microscopy **3**:114–115
use and limitations of **3**:114–115
Electronic descriptors **3**:351–352
Electrophilic moieties **5**:80f
Elemental analysis **1**:277
ELF rules **1**:517
Eltrombopag **1**:389–391
Elucidating relationships in 3-D **3**:246–247
Elvitegravir, for HIV **5**:633–634, **5**:634f
E-mail, information leak through **1**:532
Embryonic stem cells, regenerative medicine **1**:404–406
Emerging virus infections **5**:677–679
alternative approach to **5**:679
coronaviruses **5**:677
ebola **5**:677–678
nipah and hendra viruses **5**:678
yellow fever **5**:679
zika virus **5**:678–679
Empirical pharmacokinetic/pharmacodynamic models **2**:504
effect-compartment model **2**:507
Enantiomers **3**:232
Endomorphin-2 mimetics **1**:245t
Endothiopeptide (CSNH) **6**:84
Energy differences
of 1-oxa- and 1,5-dioxaspiro[5.5]undecane conformers **1**:218t
of benzo-fused spiro[4.5]decane conformers **1**:216t

of benzo-fused spiro[5.5] ring systems **1**:219t
of spiro[4.5]decane **1**:215t
in spiro[5.5] ring systems **1**:219t
Enfumafungin **5**:711f
Enfuvirtide **6**:69
Ensemble docking **3**:322–324
molecular docking against a structural ensemble **3**:323–324
preparing the protein structural ensemble **3**:322–323
Entacapone, for Parkinson's disease **5**:462
Entamoeba and giardia species **5**:736
Enthalpic efficiency **2**:208
Enthalpy, optimization **2**:204–205
Enthalpy–entropy compensation **2**:201–202, **3**:71
Enthalpy–entropy transduction **2**:202
ENTPD1/CD39 (NTPDase1) **5**:370
Entry inhibition, HBV **5**:657
Environmental carcinogens, future paradigms for **4**:247–248
Enzalutamide **5**:141–142
Enzyme kinetics **2**:188, **2**:458
Enzyme-linked immunosorbent assay biomarkers **2**:500
EP2/EP4 receptor antagonists **5**:371–372
EP_3 antagonists **7**:578–579
Epidemiological changes in infectious diseases. *See* Antibacterial resistance. *See* Antifungal resistance. *See* Antiviral resistance
Epigenetic control of gene expression **2**:300–320
agents targeting epigenetic reader proteins **2**:318–320
epigenetic erasers **2**:309–318
HDACs **2**:309–312
histone demethylases (KDMs) **2**:312–318
epigenetic writers **2**:301–309
HATs inhibitors **2**:301–304
histone methyltransferases inhibitors **2**:304–309
histones and **2**:300–301
Epigenetic mechanisms **5**:409–410
Epigenetic modulation via DNA methylation/demethylation **2**:298–300
Epigenetic regulation inhibitors in cancer **5**:281–307
approved and clinical stage epigenetic regulators **5**:286
challenges in screening **5**:285–286
assay conditions **5**:286
cellular assays **5**:286
enzyme selection **5**:285–286
hit validation **5**:286
substrate identification **5**:286
comparison to kinases **5**:284–285
overview **5**:282
Epigenetic regulation inhibitors in cancer, case studies **5**:286–304
bromodomains **5**:300–304
and extra c-terminal domain **5**:300–304
histone deacetylases **5**:286–287
histone methyltransferases **5**:287–300
arginine methyltransferases **5**:287–290
lysine methyltransferases **5**:290–300
lysine (K)-specific demethylases **5**:300
lysine (K)-specific demethylase 1A **5**:300
Epigenetic regulation inhibitors in cancer, epigenetic modifications **5**:282–284
eraser enzymes **5**:284
histone deacetylases **5**:284
lysine demethylases **5**:284
histone structure **5**:282
methyl modifications to lysine and arginine **5**:283
reader domains **5**:283–284
role of chromatin modifications in cancer **5**:282
writer enzymes **5**:283
histone acetyl transferases **5**:283
histone methyl transferases **5**:283
Epilepsy
AEDs
second-generation **7**:3
third-generation **7**:3
classification of **7**:2
general introduction to **7**:1
management of **7**:2
Epilepsy, preclinical strategies for AEDs development **7**:3–14
brivaracetam **7**:8–9
carbamazepine **7**:10
eslicarbazepine acetate **7**:11
levetiracetam **7**:8–9
second-generation compounds of **7**:9
next-generation AEDs **7**:15
overview **7**:14
overview of common preclinical strategies **7**:3–8
hypothesis-driven, target-based approach **7**:8
random in vivo phenotypic screening **7**:3–7
structural modification of known antiepileptic **7**:7
oxcarbazepine **7**:10–11
perampanel development **7**:11–14
background **7**:11–12
discovery of **7**:12–14
preclinical profile of **7**:14
potential drug targets for **7**:16
recent advances in AED development **7**:15–16
animal models and random phenotypic in vivo screening **7**:15
seletracetam **7**:8–9
Epithelial to mesenchymal transition (EMT) **2**:372f
Epithelial-mesenchymal transition (EMT), and high-content screening **2**:371
Eplica exchange methods **3**:24–25
α′,β′-Epoxyketones **5**:267
Eptifibatide **6**:69
EPZ007345 **5**:288f
EPZ011989 **5**:292f
EPZ031686 **5**:298f
Eraser enzymes **5**:284
histone deacetylases **5**:284
lysine demethylases **5**:284
ErbB/HER receptors, cross talk among **6**:20–23
Ergosterol biosynthesis (CYP51) inhibitors **5**:729
ERK1/2 **5**:93–94
ERK1/2 inhibitors **5**:94f
ES algorithms **3**:38–43
CVs-based methods **3**:39
metadynamics **3**:41–42
optimal choice of the CVs **3**:39–40
steered MD **3**:42–43
successful applications of **3**:44–45
umbrella sampling **3**:41
Essential macrominerals, as nutraceuticals **1**:114–117
calcium **1**:114
magnesium **1**:116
phosphorus **1**:116
potassium **1**:116
sodium **1**:116–117
sulfur **1**:117
Essential trace minerals/microminerals, as nutraceuticals **1**:117–118
chromium **1**:117
cobalt **1**:117
copper **1**:117
fluoride **1**:117
iodine **1**:117
iron **1**:117
manganese **1**:117
molybdenum **1**:117
selenium **1**:117–118
zinc **1**:118
ETC-1002 **7**:682–684
Eteplirsen **6**:285–286
Ethics in drug discovery **1**:540–548
in animal research **1**:542
in clinical studies **1**:542–546
benefits to participation in clinical studies of potential medicines **1**:542–543
consent and assent **1**:545–546
reporting of clinical study results **1**:546
role of the independent review board **1**:546
study design **1**:543–545
ethical reasons to perform drug discovery **1**:540–542
medical need in developing world populations **1**:541–542
medical need in older age **1**:541
medical need in orphan populations **1**:540–541
overview **1**:540
in sales and marketing **1**:546–547
accurate representation **1**:546
pricing **1**:547
role of regulators **1**:547
Ethosuximide **7**:72
eTOXsys **1**:440f

EU regulatory requirements, for companian diagnostics **2**:540
EU-ADR project **1**:442f
European lead factory **1**:505–519
  European screening center and hit list generation **1**:513–515
    development to IHL, hit characterization **1**:515
    HTS assay requirements and assay development **1**:513
    intricate triaging process **1**:514–515
    screening cascade, triaging to qualified hit list (QHL), and development to improved hit list (IHL) **1**:513–514
  honest data broker **1**:515–517
    intellectual property protection and enforcement of ELF rules **1**:517
    project organization **1**:517
    triage tools **1**:515–517
  The Joint European Compound Library **1**:505–512
    EFPIA-contributed collection **1**:506
    public compound collection **1**:506–512
  overview **1**:505
European Patent Office (EPO) **1**:537
European screening center and hit list generation **1**:513–515
  development to IHL, hit characterization **1**:515
  development to improved hit list (IHL) **1**:513–514
  HTS assay requirements and assay development **1**:513
  intricate triaging process **1**:514–515
  screening cascade **1**:513–514
  triaging to qualified hit list (QHL) **1**:513–514
Everolimus **5**:396–397
Evogliptin (DA-1229) **7**:523
Ex vivo fluorescent microscopy **1**:276
  autoradiography **1**:276
Ex vivo generation of replacement β-cells **1**:416–419
  β-cell derivation from stem cells **1**:417–419
  in vitro β-cell expansion **1**:416–417
Ex vivo light microscopy **1**:276
Excipients added to solution formulations **6**:134–135
Excretion
  ADME **4**:35–36
  ADME/PK **4**:2–3, **4**:16
  and bile acid uptake **4**:225–226
Exenatide **7**:485
Experimental approaches, for drug repurposing **1**:21–23
  ontologies **1**:24
  target-association screening **1**:21
Expert rule-based methodology, in silico tools **4**:165–168
  building an expert alerts system **4**:165–166
  DEREK **4**:167
  Leadscope expert alerts **4**:167
  overview **4**:165
  Toxtree **4**:168
  using expert alerts **4**:166–167
Ezetimibe **7**:666–669
EZH2 inhibitors **5**:282, **5**:291f–294f

F

F901318 **5**:712–713, **5**:712f
Factor IXa inhibitors **7**:617–618
Factor VIIa inhibitors **7**:612–617
  agents advanced to clinical development **7**:612–613
  preclinical compounds **7**:613–617
    amidine-based inhibitors and prodrugs **7**:613–614
    nonamidine inhibitors **7**:615–617
  target validation and proof of concept **7**:612
Factor Xa inhibitors **7**:604–612
  additional inhibitors assessed in clinical trials **7**:606
  dual thrombin/FXa inhibitors **7**:611–612
  marketed inhibitors **7**:605–606
  preclinical inhibitors **7**:607–610
  reversal agents **7**:610–611
  target validation and proof of concept **7**:604–605
Factor XIa inhibitors **7**:618–621
  preclinical small-molecule FXIa inhibitors **7**:619–621
    allosteric FXIa inhibitors **7**:620–621
    irreversible FXIa inhibitors **7**:619
    reversible FXIa inhibitors **7**:619–620
  target validation and proof of concept **7**:618–619
FASTA **3**:338
Fatty acid amide hydrolase (FAAH) **1**:227t
Fatty acid oxidation inhibition and lipid transport **4**:221
Favipiravir **5**:671f
FEP approaches, binding free energies calculations **3**:5
Fermented red yeast rice, and CVDs **1**:127
Ferroquine **1**:496f
FGFR family kinases, covalent inhibitors of **5**:88–91
  BLU9931 (40)/BLU-554 (41) **5**:90–91
  FIIN-1 (35) **5**:90
  FIIN-2 (36)/FIIN-3 (37) **5**:90
  target biology **5**:88
  TAS-120 (38)/PRN1371 (39) **5**:90
FGFR inhibitors **5**:89f
Fibroblasts **1**:419–420
Field-based pharmacophores **3**:197–198
FieldQSAR **3**:276
Fieldscreen/blaze, molecular fields **3**:264
FieldTemplater **3**:261–262
Filarial worms **5**:737–738
Filgotinib **5**:427–428
  in combination with MTX **5**:428
  as monotherapy **5**:427
  safety **5**:428
FimH **1**:586f
Fingerprint types **3**:340t
Fingerprints for ligands and proteins (FLAP) **3**:346
Fingolimod **5**:398–399
  for multiple sclerosis **5**:446
First fluorescent probes, in vivo Aβ plaque imaging **1**:89–90
  AOI987 **1**:90
  NIAD-4 and derivatives **1**:89–90
  THK-265 **1**:90
First-generation antiandrogens **5**:140–141
First-in-class drugs, origin of **2**:53–55
First-in-human prediction and trial design **4**:70
First-pass metabolism modeling **4**:88–90
First-pass removal, and SFM-PBPK modeling **4**:90–94
5/6th nephrectomy **7**:702
FLAP **3**:264–265
FLAPdock **3**:291
FLAPpharm **3**:263–264
FLAPsite **3**:287
Flash-cooling **2**:159–160
Flavonoids, and CVDs **1**:126
Fluconazole **5**:707f
Flucytosine **5**:705–706, **5**:706f
Fluorescein diacetate **1**:281
  staining alive cells **1**:281f
Fluorescent probes
  instrumentation for detection of **1**:284
Fluorescent probes, for AD **1**:87–94
  for amyloid imaging in the retina and olfactory epithelium **1**:94
  first fluorescent probes, in vivo Aβ plaque imaging **1**:89–90
    AOI987 **1**:90
    NIAD-4 and derivatives **1**:89–90
    THK-265 **1**:90
  for in vivo NFT imaging **1**:92–94
  recent development **1**:90–92
    photoswitchable fluorescent probes **1**:92
  thioflavin T and CR agents **1**:88–89
Fluoride, as nutraceuticals **1**:117
Fluorine **3**:87–88
  as halogen-bond donor **3**:84
Fluorouracil **5**:706f
Fluspirilene biological data **1**:236t
fMLP/PMA superoxide release assay in neutrophils **8**:369–370
Force field advances, molecular simulation **3**:17–22
  coarse-grained force fields **3**:21–22
  for lipids **3**:19
  for nucleic acids **3**:19
  organic molecule force fields **3**:18–19
  polarizable force fields **3**:19–21
  protein force fields **3**:18
  for sugars **3**:19
  for water **3**:19
ForteBio **6**:192
  pros and cons/considerations **6**:192
Forum/EnVivo, modulators from **7**:294–295
  aryl-imidazole derivatives **7**:295
  carboxylic acid derivatives **7**:294–295
4D descriptors **3**:354–355
14-3-3 proteins **5**:186
Fragment elaboration **2**:215–217
Fragment libraries, halogen-enriched **3**:86

Fragment screening
PPI inhibitor **5**:166–167
Fragment-based drug design (FBDD) **2**:212–232, **2**:337
and clinical drug candidates **2**:215–217
fragment elaboration **2**:215–217
ligand efficiency **2**:215
medicinal & synthetic chemistry rules **2**:217
drug candidate selection **2**:228
fragment elaboration **2**:228
fragment identification **2**:228
fragment-based screening (FBS) **2**:213–215
combination approaches **2**:215
high concentration screening **2**:214–215
isothermal titration calorimetry **2**:214
mass spectrometry **2**:214
nuclear magnetic resonance **2**:213
surface plasmon resonance **2**:214
thermal shift assay (TSA) **2**:214
virtual screening **2**:215
X-ray crystallography **2**:213–214
overview **2**:213
success stories **2**:217–227
ABT-199 (Venetoclax), phase III **2**:217–220
AT7519, phase II **2**:221–222
AT9283, phase II **2**:221
AT13387, phase II **2**:220–221
Bruton's tyrosine kinase inhibitor **2**:223–225
dual pan-RET/VEGFR2 kinase inhibitors **2**:226–227
HCV NS3 protein modulator **2**:225–226
NVP-AUY922, phase II **2**:222–223
RSK2 inhibitor RMM-46 **2**:225
Vemurafenib (PLX-4032), FDA approved drug **2**:217
and thermodynamics **2**:205–206
experimental considerations for fragment ITC **2**:206
Fragment-based drug discovery **2**:14f, **2**:44–46
Fragment-based screening (FBS) **2**:213–215
combination approaches **2**:215
high concentration screening **2**:214–215
isothermal titration calorimetry **2**:214
mass spectrometry **2**:214
nuclear magnetic resonance **2**:213
surface plasmon resonance **2**:214
thermal shift assay (TSA) **2**:214
virtual screening **2**:215
X-ray crystallography **2**:213–214
Fragment-based screening, high-throughput crystallography **2**:168–169
X-ray crystallography-based FBS implementation **2**:168–169
Fragments and heterocycles, continuous flow processing **1**:136–157
azides **1**:140–142
cross-coupling reactions **1**:150
cycloaddition **1**:151–153
cyclocondensation **1**:148–149
diazonium salts **1**:139–140
hazardous gases **1**:136–139
miscellaneous **1**:154–157
nitration **1**:142
nucleophilic substitution **1**:151
organometallic reagents **1**:145–147
oxidation **1**:143
photochemistry **1**:153–154
reduction **1**:143–144
Free drug hypothesis **2**:79–87
Free energy methods **3**:34–50
accelerated MD **3**:43
alchemical methods **3**:35–38
evolution of **3**:36–38
thermodynamic integration *versus* free energy perturbation **3**:35–36
binding kinetics **3**:45–46
combination of methods **3**:44–45
successful applications of ES techniques **3**:44–45
ES algorithms **3**:38–43
CVs-based methods **3**:39
metadynamics **3**:41–42
optimal choice of the CVs **3**:39–40
steered MD **3**:42–43
umbrella sampling **3**:41
oveview **3**:34–35
replica exchange **3**:43
Free energy perturbation
thermodynamic integration *versus* **3**:35–36
Freezing and lyophilization **6**:133–134
Fumagillin analogs **1**:224f
Functional bioisosteres of esters and amides **1**:194–195
Functional bioisosterism **1**:188–194
Functional foods **1**:109
See also Nutraceuticals
Functional screens, assay technology advances for **2**:43–44
Functionalization by cytochrome P450 enzymes **4**:134
Fungal disease **5**:703–704
antifungal chemistry. *See* Antifungal chemistry
Fusion inhibitors **5**:675t
Fusion rules **3**:361–362
Futile cycling kinetics, PBPK modeling **4**:97
Fuzzy similarity measures **3**:366–367
fXa, lead hopping in **2**:171–172

G

G protein-coupled receptors (GPCRs) **3**:146, **3**:151–155, **3**:162t–163t, **5**:11f
binding site analysis **3**:153–155
computational simulation **3**:156–163
binding free energy and binding kinetics predictions **3**:160–163
molecular dynamics simulations **3**:156–159
ligand design **3**:155
hit finding **3**:155
from structure to function **3**:151–153
as tumor targeting vectors **1**:343
G protein-coupled receptors (GPCRs) antagonists **7**:565–580
5-HT_{2A} antagonists **7**:579–580
EP_3 antagonists **7**:578–579
IP Antagonists **7**:580
protease-activated receptor (PAR) antagonists **7**:574–578
PAR-1 antagonists **7**:574–578
PAR-4 antagonists **7**:578
purinergic receptor antagonists **7**:565–574
$P2X_1$ antagonists **7**:574
$P2Y_1$ antagonists **7**:572–574
$P2Y_{12}$ antagonists **7**:566–572
TP Antagonists **7**:580
G protein-coupled receptors (GPCRs) ligands **1**:238f
Gababutins **7**:118–120
Galactosyl calix[4]arene **1**:589f
Galanthamine, for AD **5**:456
Galectins inhibition, and carbohydrates **1**:585
Galeterone **5**:143–144
Gall bladder events **7**:488
Gallic acid, for inflammatory bowel disease **5**:506
Gambogic acid **5**:238, **5**:238f
γ-aminobutyric acid A–benzodiazepine receptor **7**:38–39
γ-secretase (GS), and Alzheimer's disease **7**:280–325
Acturum Life Science, modulators from **7**:284
Amgen, modulators from **7**:284
Ares Trading/Merck KGAA, modulators from **7**:284
Astellas, modulators from **7**:285–286
AstraZeneca, modulators from **7**:286–288
Biogen, modulators from **7**:288–289
Boehringer-Ingelheim, modulators from **7**:292
Bristol-Myers Squibb, modulators from **7**:289–292
clinical compounds **7**:318–320
Dainippon Sumitomo, modulators from **7**:292
Eisai, modulators from **7**:293–294
Forum/EnVivo, modulators from **7**:294–295
aryl-imidazole derivatives **7**:295
carboxylic acid derivatives **7**:294–295
GlaxoSmithKline, modulators from **7**:296–297
arylimidazole derivatives **7**:296–297
carboxylic acid derivatives **7**:296
Janssen, modulators from **7**:298–301
aryl imidazole derivatives **7**:299–301
carboxylic acid derivativess **7**:298–299
Merck, modulators from **7**:302–304
aryl imidazole derivatives **7**:304
aryl-piperazine derivatrives **7**:303
carboxylic acid derivatives **7**:302–303
overview **7**:281–284
GS as pharmaceutical target for AD **7**:282–284
structural determination of GS **7**:281
Pfizer, modulators from **7**:304–307
aryl-imidazole derivatives **7**:305–307
carboxylic acid derivatives **7**:304

γ-secretase (GS), and Alzheimer's disease (*continued*)
photo-activity ligands **7**:315–318
Roche, modulators from **7**:307–308
aryl imidazole derivatives **7**:307
other derivatives **7**:308
Satori, modulators from **7**:308–311
Schering-Plough, modulators from **7**:311
Shionogi, modulators from **7**:312–313
Takeda, modulators from **7**:313–314
UCSD/Neurogenetics Inc/Torrey Pines Therapeutics, modulators from **7**:314–315
Gastric carcinoma **6**:6
Gastrointestinal effects **7**:487
GastroPlus **4**:61–63
absorption model **4**:61–63
tissue distribution model **4**:63
GDC-0152 **5**:256, **5**:256f
GDC-0980 **5**:219f
GED-0301 **5**:402
Geldanamycin **5**:233–234, **5**:233f
Gemigliptin (LC15-0444) **7**:522
GENA **6**:223
Gender, and DILI **4**:208
Gene editing **2**:2–4
Gene therapy **2**:2–4
Gene transcription **5**:204f
Genentech/Array BioPharma
inhibitors reported by **7**:342
Generating Antibiotic Incentives Now Act **5**:683
Generic drugs, repurposing of **1**:18–19
Genetic rescue *versus* rational approach, rare disease foundations **1**:554–555
Genetic toxicology **4**:195–203
genotoxicity testing paradigm in pharmaceutical industry **4**:202
overview **4**:195–196
predictive **2**:105–106
micronucleus test in vitro **2**:106
standard genotoxicity testing battery **2**:105–106
two-strain ames screen **2**:106
Genetic toxicology, genetic damage (genotoxicity) detection methods **4**:196–201
in silico approaches **4**:196–197
in vitro and in vivo assays for genotoxicity evaluation **4**:197–201
ames assay **4**:197–198
chromosomal aberrations assay **4**:199
comet assay **4**:199–201
micronucleus assay **4**:198–199
mouse lymphoma assay **4**:201
pig-a assay **4**:201
toxicogenomic signatures **4**:201
Genetically humanized animal models **4**:130–149
additional models **4**:142–144
chimeric liver-humanized mice **4**:138–141
biotransformation studies **4**:139–141
examples of studies using **4**:138–141
inhibition and induction studies **4**:139
genetically humanized mice and chimeric liver-humanized mouse models, differences between **4**:141–142
humanized mouse model
in the future **4**:145–146
selection **4**:144–145
mouse models. *See* Mouse models, genectically humanized
overview **4**:130–131
Genome instability and mutation, cancer **5**:6
Genome-based data mining, for drug repurposing **1**:33–34
Genomic stability, targets in **5**:21–23
PARP inhibitors **5**:22–23
telomerase inhibitors **5**:21–22
Genomics
predictive toxicology **2**:102–103
Genotoxic impurities assessment **2**:237–246
ICH M7 Guideline **2**:238
mutagenicity prediction with commercial in silico systems **2**:238–246
regulatory requirements **2**:237–238
Genotoxicity assays **4**:241t
GH/IGF-1 pathway inhibitors **1**:359
6-Gingerol, for inflammatory bowel disease **5**:506–507
GLASS **1**:456
Glatiramer acetate, for multiple sclerosis **5**:450
GlaxoSmithKline **7**:213–214, **7**:239–246, **7**:573
GSK early selective OX1R tool compounds **7**:244–245
modulators from **7**:296–297
aryl-imidazole derivatives **7**:296–297
carboxylic acid derivatives **7**:296
SB-649868 and substituted piperidines **7**:239–244
triazolo-thioamides **7**:246
Glide **3**:291
GLP-1
history and background **7**:482
structure **7**:483
synthesis and expression **7**:482–483
GLP-1R agonist toxicity **7**:487–488
ADA generations **7**:488
gall bladder events **7**:488
gastrointestinal effects **7**:487
heart rate effects **7**:487
pancreatitis **7**:487–488
thyroid C-cell tumor **7**:487
GLP-1R agonists **7**:483–484
GLPG0974 **5**:401
Glucagon-like peptide-1 **6**:69
Glucocorticoid receptor **8**:452
structure of **8**:453–454
Glucosamine, for chronic inflammatory disorders **1**:130
α-Glucosidase inhibitors **1**:581f
Glutamate dehydrogenase **4**:266–267
Glutathione peroxidase (GPx) **1**:352f
Glutathione reductase (GR) **1**:352f
N-Glycine-sulfonamides **7**:234–236
Glycine transporter Type 1 (GlyT-1) **7**:42–43
Glycoengineering in therapeutics **1**:602–603
Glycogen synthase kinase 3 **7**:36, **7**:417–419
Glycolytic metabolism inhibitors **1**:358–359
Glycopeptide antibiotics **5**:522f
Glycopeptide resistance **5**:522–523
Glycopolymer (*S*)-PolyBAIT **1**:588f
Glycoprotein-based drugs **1**:602t
Glycosidic linkages **6**:75f
Glycosylation **6**:75–77
GM-CT-01 **1**:585f
GnRH analogs **6**:78
GOLD **3**:291
Gold nanoparticles **1**:266, **1**:266f
Gosogliptin **7**:534–536
GPCRdb **1**:460
GPCRs. *See* G protein-coupled receptors (GPCRs)
Graph (tree)-based similarities **3**:364–365
Graphics processing units, for molecular simulation **3**:15–16
Green nanoscience **1**:285
GRID/FLAP **3**:257–258, **3**:287–288
GRID/GOLPE/FLAP **3**:277
GRIND **3**:277
Growth hormone-releasing hormone **1**:341
Growth suppressors, and cancer **5**:4–5
GSK early selective OX1R tool compounds **7**:244–245
GSK1324726A **5**:213f
GSK2126458 **5**:223–224, **5**:223f
GSK2879552 **5**:302f
Guiding experiment, modeling **3**:128
GuNA **6**:224
Gyrolab **6**:191
pros and cons/considerations **6**:191

H

H1 receptors **7**:25
H3 receptors **7**:25–26
H4 receptors **7**:26
Half-life, human PK **4**:54
Halogen bonding **3**:83–87
background **3**:83–84
in drug development **3**:86
fluorine as a halogen-bond donor **3**:84
geometries **3**:84
halogen-enriched fragment libraries **3**:86
in protein–ligand complexes **3**:84–86
skeptical chemist's view of **3**:86–87
and sulfur **3**:91
Halogens
aromatic rings interactions with **3**:77–78
tautomers **3**:194
Hanging drop method **2**:401
Harvoni **8**:558–582
ledipasvir **8**:567–575
broad genotype activity of **8**:572
discovery of **8**:569–572
genotype 1 resistance profile of **8**:572

mechanism of action and structural information **8**:568–569
phase 1 studies **8**:573–575
phase 2 studies **8**:575
overview **8**:558–559
phase 3 registrational clinical studies with ledipasvir and sofosbuvir **8**:575–579
Harvoni® approval **8**:576
Harvoni® postapproval studies, label expansion and study in Japan **8**:577–578
Harvoni® real world results **8**:578–579
sofosbuvir, discovery of **8**:559–567
2′-F, 2′-*C*-methylnucleoside inhibitor of HCV replication **8**:559–561
clinical studies and the backbone of drug combinations **8**:566–567
liver-targeted nucleotide prodrug, clinical proof of concept **8**:565
liver-targeted nucleotide prodrug, rationale and design of **8**:561–562
prodrug optimization and preclinical evaluation **8**:563–565
single diastereomer **8**:565–566
target rationale **8**:559
HATs inhibitors **2**:301–304
Hazardous gases
continuous flow processing **1**:136–139
HCS software **2**:407t
HCV NS2 protease inhibitors **5**:563f
HCV NS3 protease inhibitors **5**:564f–570f, **5**:573f
HCV NS3 protein modulator **2**:225–226
HCV NS4B inhibitors **5**:577f
HCV NS5A inhibitors **5**:539f, **5**:581f
HCV NS5B inhibitors **5**:538f, **5**:588f
HCV protease inhibitors **5**:539f
Heart failure **7**:628–662
acute heart failure **7**:632
classifications of chronic heart failure **7**:631–632
based on cardiac ejection fraction **7**:631–632
based on disease severity **7**:631
clinical description **7**:631
epidemiology **7**:632
pathophysiology **7**:633–635
calcium homeostasis **7**:634–635
extracellular matrix **7**:635
mitochondria and metabolism **7**:635
neurohomonal **7**:633–634
prognosis **7**:632–633
Heart failure, approved and future pharmacological therapies **7**:635–654
antiadrenergics and anti-RAAS **7**:635–638
compounds affecting metabolism **7**:652–653
elamipretide **7**:652–653
perhexiline **7**:653
ion channel and ion transport modulators **7**:649–652
cardiac late sodium current inhibition **7**:651
cardiac sino-atrial (SA) node pacemaker current inhibition **7**:650–651
diuretics for decongestion in heart failure **7**:649–650
renal outer medullary potassium (ROMK) channel inhibition **7**:651–652
MGN-9103 **7**:654
natriuretic peptide system-related approaches **7**:638–640
corin modulation of natriuretic peptide formation **7**:639–640
LCZ696 **7**:638–639
natriuretic peptide analogs **7**:639
neuregulin-1 **7**:648–649
phosphodiesterase inhibition, activation of soluble guanylate cyclase, HNO donors **7**:640–641
Heart organoids, induced pluripotent stem cell-derived **4**:187
Heart rate effects **7**:487
Helminths **5**:737–739
nematodes **5**:737–738
filarial worms **5**:737–738
soil-transmitted helminths **5**:737
trematodes **5**:738–739
Hematopoietic stem cells, regenerative medicine **1**:385–386
Hematopoietic stem cells (HSCs), chemical manipulation of **1**:388
Hepatic elimination, BDDCS in **4**:117–119
hepatic apical efflux **4**:118
hepatic basolateral uptake **4**:117–118
Hepatic specificity of action for drugs, and mitochondrial dysfunction **4**:221–223
Hepatitis B virus (HBV) **5**:537–538, **5**:651–657
biologics-based approaches **5**:657
capsid assembly inhibitors **5**:655–656
immunomodulators **5**:656–657
new viral targets **5**:538
nucleoside reverse transcriptase inhibitors **5**:653–655
investigational HBV RT inhibitors **5**:654–655
nucleos(t)ide reverse transcriptase inhibitors **5**:537–538
replication cycle and potential drug targets **5**:651–653
Hepatitis C virus (HCV) **5**:538–539, **5**:555f–556f
drug combinations **5**:539
harvoni for **8**:558–582
nonnucleotide NS5B inhibitors **5**:539
NS3/4A protease inhibitors **5**:539
NS5A inhibitors **5**:539
nucleotide analogue NS5B inhibitors **5**:538
Hepatocyte perturbation detection, in silico models **4**:232
Hepatocytes, induced pluripotent stem cell-derived **4**:180–182
Hepatotoxicity **4**:205–206
animal models **4**:205
cell culture **4**:205–206
in silico approaches **4**:206
Heptares **7**:246–247
2*H*-pyrido[2,3-*e*][1,2,4]thiadiazin-3(4*H*)-one 1,1-dioxides **7**:246–247
HER family kinases, covalent inhibitors of **5**:84–88
acquired resistance to third-generation covalent EGFR inhibitors **5**:88
BLU9931 (40)/BLU-554 (41) **5**:90–91
FIIN-1 (35) **5**:90
FIIN-2 (36)/FIIN-3 (37) **5**:90
TAS-120 (38)/PRN1371 (39) **5**:90
covalent HER family kinase inhibitors **5**:84–86
development of rociletinib **5**:87
osimertinib **5**:87–88
second-generation irreversible HER family inhibitors **5**:86
target biology **5**:84
third-generation irreversible mutant-selective EGFR inhibitors **5**:86–88
HER proteins
structure and signaling of **6**:7–8
HER-1 (EGFR) **6**:20
and cancer **6**:8
HER-2
binding sites **6**:15f
and cancer **6**:8
dimerization inhibitor **6**:15
targeted therapies against **6**:13–15
vaccines **6**:15–17
HER family initiating signal transduction, X-ray crystallographic structural studies **6**:15–17
with HER-2 and pertuzumab **6**:16
with HER-2 and trastuzumab **6**:15–16
novel pertuzumab-binding conformational B-cell epitopes **6**:17
novel trastuzumab/herceptin-binding conformational B-cell epitopes **6**:17
rationale for conformational HER-2 epitopes **6**:16
HER-3 **6**:20–22
and cancer **6**:8–9
peptides **6**:22t
HIFα **5**:330–331
High concentration screening **2**:214–215
High-content screening (HCS) **2**:389–396
3D HCS. *See* 3D high-content screening of organoids
application **2**:371–382
epithelial-mesenchymal transition (EMT) **2**:371
invadopodia and cancer invasion **2**:372–373
leishmanial proliferation in macrophage **2**:379–382
lipid accumulation in adipocytes **2**:376–377
lysosomal storage disease **2**:377
oligodendrocyte progenitor cell (OPC) differentiation and remyelination **2**:373–376
progeroid and abnormal nuclear structures **2**:377–379

High-content screening (HCS) (*continued*)
three-dimensional organotypic culture mimics ovarian cancer microenvironment **2**:371–372
tubulin polymerization and redistribution **2**:382
assay development **2**:390–391
assay plates **2**:390
automation **2**:390
fluorescent probes **2**:391
compatible 3D cell culture platforms **2**:400–402
hanging drop method **2**:401
liquid overlay methods with non-adherent surface plates **2**:401
magnetic levitation **2**:401–402
microfluidic devices **2**:402
micropatterned plates **2**:401
and complex cell biology **2**:363–366
applications for different cellular processes **2**:363
data analysis **2**:393–396
data normalization **2**:394–395
data reduction methods **2**:395–396
data visualization **2**:395
hit selection **2**:395
statistical evaluation **2**:393–394
data workflow management **2**:370–371
hardware **2**:402–406
brightfield and widefield microscopy, and live-cell 3D imaging **2**:402–404
confocal microscopy **2**:404–405
laser scanning cytometers **2**:406
light sheet fluorescence microscopy **2**:405
two-photon microscopy **2**:405
image acquisition **2**:391
image analysis **2**:391–392
feature extraction **2**:392
image correction **2**:391
image segmentation **2**:391
machine learning **2**:392
object tracking **2**:392
instrument with niches **2**:367–368
software **2**:406–410
deconvolution **2**:408
image acquisition software **2**:406
image visualizations and analysis software **2**:408–409
workflow platform **2**:410
High-content screening (HCS), complex cellular models for **2**:363–365
complexity and multiplicity of assay readouts **2**:365–366
complexity of readout *versus* stages of drug discovery **2**:366
multiplicity of HCS **2**:365–366
uniqueness of assays and associated detection reagents **2**:365
pathophysiologically-relevant cell lines **2**:364
cellular models validation and quality controls **2**:364–365
organoid and three-dimensional (3-D) cellular models **2**:364
primary cells from human or rodents **2**:363–364
High-level ab initio QM/MM methods **3**:55–56
High-resolution structures, of membrane protein **3**:146–151
GPCRs **3**:146
ion channels **3**:148–151
membrane transporters **3**:147–148
High-throughput 3D HCS culture technologies **2**:396–402
HCS compatible 3D cell culture platforms **2**:400–402
hanging drop method **2**:401
liquid overlay methods with non-adherent surface plates **2**:401
magnetic levitation **2**:401–402
microfluidic devices **2**:402
micropatterned plates **2**:401
traditional 3D culture techniques **2**:397–400
hydrogel **2**:400
solid scaffolds **2**:397
spinner flask and rotating wall vessel bioreactors **2**:397
High-throughput crystallography **2**:153–179
automation, challenge of **2**:161–162
communication of results **2**:163
complex generation **2**:158–159
cocrystallization **2**:158–159
soaking **2**:159
crystal harvesting **2**:159–160
diffraction experiment **2**:160–161
final structure validation **2**:162
flash-cooling **2**:159–160
historical development **2**:155–156
industrial structural biology of the future **2**:172–174
structural biology of integral membrane proteins (IMP) **2**:174
X-ray free electron lasers and cryo-electron microscopy **2**:172–173
ligand placement **2**:160–161
mounting **2**:159–160
overview **2**:154–155
refinement **2**:160–161
storage **2**:159–160
structure determination **2**:160–161
High-throughput crystallography, applications **2**:163–172
biologics discovery **2**:172
cocrystal structures of chemically diverse set of CDK1 inhibitors **2**:166–168
fragment-based screening **2**:168–169
X-ray crystallography-based FBS implementation **2**:168–169
hit validation **2**:165–168
protein–protein interactions **2**:164–165
structure-based molecular design **2**:169–172
isoform selective PI3Kγ inhibitors **2**:169–171
lead hopping in fXa **2**:171–172
structure-based target assessment **2**:163–165
High-throughput screening **2**:336–337, **2**:423–425
molecular docking for ultra-HTS **2**:424
NMR spectroscopy for fragment screening **2**:424–425
PPI inhibitor **5**:165–166
RWG biosensor for (ultra)HTS **2**:423
5-*N*-(3-(1*H*-indol-2yl)-phenyl-piperidines **8**:135
Histamine (H1) **1**:245t
Histaminergic receptors **7**:25–26
Histone acetyl transferases **5**:283
Histone acetylation readers
cancer epigenetics **5**:21
Histone arginine PTM **2**:300–320
Histone deacetylases (HDACs) **2**:298t, **2**:309–312, **5**:284, **5**:286–287
Histone demethylases (KDMs) **2**:312–318
Histone deacetylases (KDMs) inhibitors **1**:369f
Histone lysine **2**:300–320, **2**:303t
Histone lysine demethylases **2**:312–318
Histone methyltransferases **5**:283, **5**:287–300
arginine methyltransferases **5**:287–290
lysine methyltransferases **5**:290–300
Histone methyltransferases inhibitors **2**:304–309
Histone modifications
cancer epigenetics **5**:21
Histone structure, in cancer therapy **5**:282
Hit and lead generation strategies **2**:33–63
hit-to-lead process **2**:51–53
chemical probes for novel therapeutic concepts **2**:52–53
major approaches **2**:33–51
analog-based drug discovery **2**:33–34
de-novo structure-based design **2**:34–36
valid hits identification **2**:50–51
major approaches, screening **2**:36–50
assay technology advances for functional screens **2**:43–44
chemical space considerations **2**:37–40
fragment-based drug discovery **2**:44–46
phenotypic screening **2**:46–50
screening and its impact in drug discovery **2**:36–37
virtual screening **2**:40–43
origin of first-in-class drugs **2**:53–55
overview **2**:33
Hit characterization using computational approaches and biophysical assays **2**:14–18
Hit identification methods **2**:10–14
new technologies for target-based screening **2**:12–14
phenotypic screening **2**:10–12
Hit list generation, and European screening center **1**:513–515
development to IHL, hit characterization **1**:515
development to improved hit list (IHL) **1**:513–514

HTS assay requirements and assay development **1**:513
intricate triaging process **1**:514–515
screening cascade **1**:513–514
triaging to qualified hit list (QHL) **1**:513–514
Hit validation, high-throughput crystallography **2**:165–168
cocrystal structures of chemically diverse set of CDK1 inhibitors, characterization of **2**:166–168
HIV-1 protease, and binding thermodynamics **2**:203
HMGB1 **4**:267
HMGCoA reductase, and binding thermodynamics **2**:204
Holo-acyl (HA) **1**:580f
Homopiperazines **7**:109
Honest data broker **1**:515–517
intellectual property protection and enforcement of ELF rules **1**:517
project organization **1**:517
triage tools **1**:515–517
Host factors and virulence targets **5**:699
Hotspots and allosteric sites **2**:334–335
HPLC and UPLC method development **6**:202
HPLC methods **6**:203f, **6**:203t
2*H*-pyrido[2,3-*e*][1,2,4]thiadiazin-3(4*H*)-one 1,1-dioxides **7**:246–247
HSP70 inhibitors **5**:229–231
HSP-90 **5**:330
HSP90 family **5**:231–246
HSP90 inhibitors **5**:232–244
isoform selectivity **5**:245–246
5-HT_{2A} antagonists **7**:579–580
h*TERT* **5**:321–322
2-(4-(1*H*-tetrazol-1-yl)phenyl)-1-(piperazin-1-yl)ethan-1-one scaffold **8**:312–314
HTS assay requirements and assay development **1**:513
Human, cellular imaging **2**:363–364
Human colorectal cancer **6**:6
Human disease etiology **1**:57–60
integrative approaches across cell models and patient clinicopathological data **1**:59–60
phenotyping pipelines in preclinical studies **1**:57–59
Human drug-metabolizing enzymes **4**:8t
Human epidermal growth factor receptor 2 **6**:52–53, **7**:433
Human Genome Project **1**:551
Human immunodeficiency virus (HIV) **5**:534–538, **5**:535f–538f, **5**:629–651
adherence and resistance **5**:632
attachment inhibitors **5**:644–645
boosters and cobicistat **5**:647
capsid inhibitors **5**:645
current regimens **5**:630–632
drug combinations **5**:537
envelope (ENV) **5**:536–537
HIV cure **5**:648–651
direct-acting antivirals for functional cure **5**:650–651
kick and kill **5**:648–650
integrase **5**:536
integrase inhibitors **5**:632–636
clinical- and preclinical-stage integrase inhibitors **5**:635–636
dolutegravir **5**:634–635
elvitegravir **5**:633
raltegravir **5**:632–633
life cycle and drug targets **5**:630
maturation inhibitors **5**:645–646
noncatalytic integrase inhibitors **5**:646
nonnucleoside reverse transcriptase inhibitors **5**:640–642
doravirine **5**:641–642
rilpivirine **5**:640–641
nucleoside reverse transcriptase inhibitors **5**:636–640
investigational NRTIs **5**:638–640
tenofovir alafenamide **5**:637–638
preexposure prophylaxis (PreP) **5**:647
protease **5**:535–536
protease inhibitors **5**:642–644
darunavir **5**:642–643
other protease inhibitors **5**:644
reverse transcriptase **5**:534–535
simplified regimens and nonstandard regimen research **5**:646–647
Human iPSC models **1**:48–73
challenges **1**:66
overview **1**:48–49
historical and technological advances **1**:48–49
human biology context **1**:49
patient stratification and disease diagnosis **1**:64–66
clinical diagnosis and prognosis **1**:65–66
drug responders and nonresponders prediction **1**:64–65
Human iPSC models, eoles in drug development pipeline **1**:61–64
CNS-focused iPSC drug-discovery screening **1**:61–63
neurodegenerative disorder model screening **1**:62–63
pain and sensory neuron disease model screening **1**:63
psychiatric disorder model screening **1**:61–62
quantitative cellular pharmacology **1**:63
advances enabling novel assay development and target validation **1**:63–64
toxicology and drug metabolism **1**:64
Human iPSC models, iPSCs ex vivo disease models **1**:49–61
animal models, preclinical alternatives to **1**:60–61
disease in cellular- and genomic-relevant contexts **1**:50–57
disease mechanisms assessment in complex genetic disorders **1**:56–57
patient iPSC differentiation into disease-relevant cell types **1**:51–56
human disease etiology, integrative and translational research of **1**:57–60
integrative approaches across cell models and patient clinicopathological data **1**:59–60
phenotyping pipelines in preclinical studies **1**:57–59
Human leukocyte antigen (HLA) associations with DILI **4**:228–229
Human P450 probes in experimental animals
age-related and polymorphic pharmacokinetic changes of **4**:47–48
in vivo pharmacokinetics of **4**:45–46
Human pharmacokinetic parameters **4**:36–42
human clearance **4**:39–42
oral absorption **4**:36–37
volume of distribution **4**:37–39
Human PK **4**:51–82
case studies **4**:72–74
halofantrine concentration-related QTc prolongation **4**:73–74
predicting bioavailability **4**:72–73
future directions **4**:76–77
cultural challenges **4**:77
scientific challenges **4**:76–77
in silico predictions of physicochemical properties **4**:58–60
brief descriptions of QSAR methodologies **4**:59–60
improving in silico predictions of pK_a (Case Study) **4**:60
pharmacodynamics **4**:55–56
pharmacokinetics **4**:53–55
absorption **4**:54–55
clearance **4**:53–54
half-life **4**:54
volume of distribution **4**:54
physicochemical properties and pharmacokinetics, relationship between **4**:56–58
biopharmaceutics classification system **4**:58
hydrogen bonding **4**:57
hydrophobicity **4**:56
implications of physicochemical properties **4**:58
Lipinski rule of five **4**:58
molecular size **4**:56
permeability **4**:57
pK_a **4**:57
solubility **4**:57
prediction and future of in silico-based research and development **4**:52–53
projection of **4**:25
regulatory implications **4**:74–76
Human PK, physiologically based pharmacokinetic model
applications **4**:68–70
description of **4**:60–61
generalized approach to building and validating **4**:70–71
model building and input data **4**:71

Human PK, physiologically based pharmacokinetic model (*continued*)
model optimization **4**:71
reporting **4**:71
lessons learned from the early applications **4**:69–70
assessing the feasibility and performance of human pharmacokinetics **4**:69–70
first-in-human prediction and trial design **4**:70
reducing the use of animals in toxicology testing **4**:69
predicting in vivo pharmacokinetic parameters **4**:63–68
predicting intestinal and hepatic clearance **4**:64–66
predicting permeability **4**:68
predicting transporter effects **4**:67–68
predicting volume of distribution **4**:66–67
representation in GastroPlus **4**:61–63
absorption model **4**:61–63
tissue distribution model **4**:63
and simulation methodology **4**:60–68
Human sequence quadruplex-small molecule complexes **5**:313t
Human sodium/glucose cotransporter 2 (hSGLT2) inhibitors **1**:237t
Human toxicology
ADME **4**:150–151
Humanization of animal models **2**:511–512
Humanized mAbs and small-molecule inhibitors **6**:13–15
clinical trials of trastuzumab **6**:13–14
development of trastuzumab and treatment **6**:13
pertuzumab **6**:15
possible mechanisms of action and resistance to trastuzumab **6**:14
side effects of trastuzumab treatments **6**:14
trastuzumab-DM1 **6**:15
Hybrid fingerprint **3**:344
Hybrid QM/MM simulations **3**:53–54
Hydrogel **2**:400
Hydrogen bond
abridged guide to **3**:73–74
acceptors, and aromatic rings **3**:79–80
diversification **3**:71–72
Hydrogen bonding
and crystal form stability **3**:92–93
human PK **4**:57
involving sulfur **3**:90
tautomers
acceptor features **3**:194
donor features **3**:193–194
Hydrophobic features, of tautomers **3**:196
Hydrophobicity, human PK **4**:56
Hypercholesterolemia **7**:663–693
overview **7**:664
statins in CV disease prevention **7**:665–666
Hypercholesterolemia, novel therapeutic approaches in dyslipidemia management **7**:666–687
targeting plasma cholesterol levels **7**:666–684
CETP inhibitors **7**:681–682
ETC-1002 **7**:682–684
ezetimibe **7**:666–669
lomitapide **7**:679–681
mipomersen **7**:676–679
PCSK9 inhibitors **7**:669–676
targeting plasma TG levels **7**:684–687
alipogene tiparvovec **7**:685–686
diacylglycerol O-acyltransferase inhibitors **7**:686–687
ISIS-APOCIIIRx **7**:686
omega-3 free fatty acids **7**:684–685
Hyperglycosylation and lipidation of large proteins **6**:146
Hypothetical signaling cascade **2**:506f
Hypoxia and nutrient stress, and cancer **5**:10
Hypoxia-activated prodrug SN30000 **8**:58–94
bioreductive drug discovery **8**:63–68
developing a spatially resolved-PK–PD model **8**:67–68
introductory remarks **8**:63
measuring extravascular drug transport **8**:64–67
structure–activity toolset **8**:63–64
overview **8**:58–63
drug development in the context of hypoxia **8**:60–61
hypoxia **8**:58–59
preamble **8**:58
tirapazamine **8**:61–63
second-generation TPZ analog **8**:68–81
3-alkyl BTOs **8**:74–77
BTOs with improved EVT **8**:71–74
design criteria **8**:68–69
designing novel analogs **8**:77–80
DNA targeting **8**:69–70
SN30000 **8**:81–88
as improved TPZ analog **8**:84–86
mechanism of DNA damage **8**:86
predictive biomarkers and response biomarkers for **8**:86–88
synthesis optimization **8**:81–84

I

I-BET762 **5**:214f
IBIS **1**:457
Icatibant **6**:78
ICH M7 Guideline **2**:238
Idiopathic pulmonary fibrosis **7**:696–700
current treatment **7**:697–698
emerging biology and therapeutic treatment **7**:698–700
epidemiology **7**:696
experimental animal models **7**:697
ongoing clinical trials **7**:698
overview **7**:696
pathophysiology **7**:696–697
Idiosyncratic DILI **4**:207–208
IDO1 inhibitors **5**:362–363, **5**:363f
IDO2 inhibitors **5**:364, **5**:364f
IGF-1R **6**:22–23
and cancer **6**:9
Iguratimod (Iremod) **5**:397
Image acquisition
cellular imaging **2**:368
software **2**:406
Image analysis algorithm development **2**:368–370
Image visualizations and analysis software **2**:408–409
Imaging, translational aspects **2**:514–516
computed tomography **2**:514–515
application **2**:515
magnetic resonance imaging **2**:515
application **2**:516
optical imaging **2**:515
positron emission tomography **2**:515
application **2**:516
radiography **2**:514
application **2**:515
IMI eTox **2**:254–255
Imidazo[5,4-*c*]quinolin-2-one based compounds **8**:170–171
Imidazolopiperazines **5**:720–721, **5**:720f
Imidazolopyrazines **5**:720–721, **5**:720f
Iminohydantoins **8**:219–223
advanced lead optimization **8**:221–223
S3 occupancy **8**:219–220
Iminothiadiazinane dioxides **8**:235–237
Immortalized human cells, cellular imaging **2**:364
Immune destruction, and cancer **5**:6
Immune system
components of **6**:33–35
adaptive immunity **6**:33–34
antibodies **6**:34
antigen presentation **6**:34
B-cell activation **6**:34
complement **6**:35
cytokines **6**:35
innate immunity **6**:33
phagocytosis **6**:34
T-cell activation **6**:34
and survival **6**:32–33
Immune targets and vaccines **1**:332–334
Immuno-checkpoint inhibitors **5**:19
Immunocytokine conjugates **6**:43
Immunomodulator drugs, for inflammatory bowel disease **5**:500–501
Immunomodulatory drugs **5**:272–273
Immuno-oncology
concept and history of **5**:358–359
current status of **5**:361
targets in **5**:18–20
CARs **5**:19–20
cytokine therapy **5**:19
immuno-checkpoint inhibitors **5**:19
tumor-induced immunosuppression **5**:18–19
Immunoproteasome subunit inhibitors, for inflammatory bowel disease **5**:503
Immunotoxins **6**:43

Impatient patients, and rare disease foundations **1**:557–558
Imperacer immuno-polymerase chain reaction (PCR) **6**:194
  pros and cons/considerations **6**:194
Implantable devices, for subcutaneous drug delivery **6**:148
Improved hit list (IHL) **1**:513–514
  development to, hit characterization **1**:515
In silico approaches **2**:108–110, **4**:158t
  to evaluate leads **3**:431–433
  for genotoxicity evaluation **4**:196–197
  and medicinal chemistry **3**:436–438
  for membrane protein targets **3**:163–180
  mutagenicity prediction with **2**:238–246
In silico metabolism and elimination predictions **4**:108–109
In silico models **2**:246–250
  exploratory work **2**:246–247
  for hepatocyte and NPC perturbation detection **4**:232
  lead identification phase **2**:249
  lead optimization (LO) phase **2**:249–250
  phase 0 **2**:250
  target assessment **2**:246–247
  target identification (TI) **2**:246–247
In silico predictions of physicochemical properties **4**:58–60
  brief descriptions of QSAR methodologies **4**:59–60
  improving in silico predictions of pK_a (case study) **4**:60
In silico tools **4**:156–176
  case study **4**:171–173
  expert rule-based methodology **4**:165–168
    building an expert alerts system **4**:165–166
    DEREK **4**:167
    Leadscope expert alerts **4**:167
    overview **4**:165
    Toxtree **4**:168
    using expert alerts **4**:166–167
  overview **4**:156–158
  read-across methodology **4**:168–170
  statistical-based methodology **4**:158–165
    assessing quality and overfitting **4**:160–161
    building statistical-based models **4**:159–160
    CaseUItra **4**:164–165
    Leadscope model applier **4**:162–163
    overview **4**:158–159
    Sarah Nexus **4**:163–164
    TEST **4**:164
    using statistical-based methodologies **4**:161–162
In silico-based research and development **4**:52–53
In situ click chemistry **1**:317–319
  antibody-like protein-capture agents **1**:318–319
  binding site of Abl tyrosine kinase, probing **1**:318
  biotin protein ligase (BPL) inhibitors, screening and identification of **1**:318
In situ stem cell modulation, regenerative medicine **1**:410
In vitro and in vivo assays for genotoxicity evaluation **4**:197–201
  ames assay **4**:197–198
  chromosomal aberrations assay **4**:199
  comet assay **4**:199–201
  micronucleus assay **4**:198–199
  mouse lymphoma assay **4**:201
  pig-a assay **4**:201
  toxicogenomic signatures **4**:201
In vitro assays **2**:97t
In vitro β-cell expansion **1**:416–417
In vitro chemically guided cardiac differentiation, regenerative medicine **1**:393–400
  targeting cardiopoietic signaling pathways **1**:395–400
    bone morphogenetic protein (BMP) **1**:397
    microRNAs **1**:400
    small molecule cocktails **1**:397–400
    TGFβ pathway **1**:395–396
    Wnt pathway **1**:396–397
  unspecific mode of action **1**:393–395
In vitro liver models **4**:230
In vitro metabolism and elimination predictions **4**:107–108
In vitro predictions **4**:105
In vivo chemically guided cardiac differentiation, regenerative medicine **1**:400–401
  murine model **1**:400–401
  zebrafish model **1**:401
In vivo circulation time **6**:142–146
  albumin-binding **6**:145–146
  carbohydrates and nucleic acids **6**:144
  conjugation to Fc antibody fragments **6**:144–145
  hyperglycosylation and lipidation of large proteins **6**:146
  pegylation **6**:143–144
  proteins **6**:143–144
In vivo expansion of β-cells **1**:420–421
In vivo magnetic particles imaging **1**:275
In vivo magnetic resonance imaging **1**:275
In vivo metabolism and elimination predictions **4**:108
In vivo NFT imaging
  fluorescent probes **1**:92–94
In vivo optical imaging **1**:272–274
In vivo pharmacokinetic parameters prediction **4**:63–68
  intestinal and hepatic clearance prediction **4**:64–66
  permeability prediction **4**:68
  transporter effects prediction **4**:67–68
  volume of distribution prediction **4**:66–67
In vivo pharmacokinetics, matched molecular pair analysis **3**:235
In vivo positron emission tomography **1**:274–275
In vivo toxicology
  ADME **4**:150–151
  barrier models **4**:151
  biokinetic modeling **4**:151
  data integration of **2**:253
  emerging role of ADME in **4**:151–153
    ADME contributions to ITS **4**:153
    in vitro biokinetics **4**:152
    lack of metabolism in vitro **4**:152
    quantitative in vitro-to-in vivo extrapolation **4**:152
  for future of in vitro toxicology **4**:151–153
  metabolites prediction **4**:151
In vivo studies in zebrafish **1**:421–422
IND-enabling ADME/PK studies **4**:23–25
  active circulating metabolites in animals **4**:24–25
  animal PK and bioavailability **4**:24
  initial in vitro assessment of clinical DDI potential **4**:25
  major routes of clearance in animals **4**:24
  projection of human PK **4**:25
  purpose of **4**:23–24
Independent review board **1**:546
Individual target screening, predictive toxicology **2**:97–100
Indolamine 2,3-dioxygenase (IDO) inhibitors **5**:363f
Indole-derived structures **7**:96–98
Merck compounds **7**:96–98
Indoles **7**:113
N-5-Indolyl-carboxamides **8**:136
Induced pluripotent stem cell-derived
  brain organoids **4**:186–187
  cardiomyocytes **4**:183
  heart organoids **4**:187
  hepatocytes **4**:180–182
  liver organoids **4**:186
  neuronal cells **4**:182–183
  organoids **4**:183–187
Induced pluripotent stem cells (iPSCs) **4**:180f, **4**:181t–182t, **4**:184t, **4**:187–189
  regenerative medicine **1**:406–408
Induced-fit docking **3**:320f, **3**:322
Industrial structural biology of the future, high-throughput crystallography **2**:172–174
  structural biology of integral membrane proteins (IMP) **2**:174
  X-ray free electron lasers and cryo-electron microscopy **2**:172–173
Infections
  acute, antiviral drugs for **5**:665–681
  and DILI **4**:209
Infectious diseases
  protein–protein interactions in **2**:334
Inflammasome **5**:410–411
Inflammation and autoimmune diseases
  protein–protein interactions in **2**:333
Inflammatory bowel disease (IBD) **6**:157–158
  drugs in clinical trials **5**:496–501
    alpha (α)-4 integrin antagonists **5**:500
    CCR9 antagonists **5**:499–500

Inflammatory bowel disease (IBD) (*continued*)
immunomodulator drugs **5**:500–501
JAK inhibitors **5**:499
mucosal barrier enhancer drug **5**:501
S1P receptor modulators **5**:496–498
general characteristics of **5**:496
natural product-derived approaches **5**:504–507
6-gingerol **5**:506–507
berberine **5**:504–505
curcumin **5**:504
diallyl sulfide **5**:506
gallic acid **5**:506
rutin **5**:507
silibinin **5**:505
triterpene ganoderic acid C1 (GAC1) **5**:505–506
orally delivered peptides, for inflammatory bowel disease **6**:157–170
pathological manifestations of **6**:158
preclinical results **5**:501–504
immunoproteasome subunit inhibitors **5**:503
melanin-concentrating hormone (MCH) receptor 1 antagonists **5**:503
receptor-interacting protein kinase 1 (RIP1 and RIP3) inhibitors **5**:503–504
ROR-γT inhibitors **5**:502
sphingosine kinase inhibitors **5**:502
synthetic triterpenoids **5**:501–502
summary **6**:158
Inflammatory bowel disease (IBD) , orally delivered peptides **6**:157–170
constrained and stable peptides **6**:159–162
disulfide-rich peptides **6**:159
disulfide-rich peptides, examples of **6**:159–161
summary **6**:161–162
impact of food **6**:165
orally delivered and targeted agents **6**:165
permeability **6**:163–164
absorption in the GI tract **6**:164
permeability at the epithelial surface **6**:164
transporters on intestinal epithelial cells **6**:164
protease stability for peptides **6**:162
redox stability **6**:162
stability to microbes **6**:163
Inflammatory diseases **8**:408–409
biological DMARDs **8**:409
seletalisib for **8**:366–407
synthetic DMARDS **8**:409
Inflammatory diseases, small molecule immunosuppressants **5**:420–438
ABT-494 **5**:428–430
efficacy of **5**:429
in MTX-IR **5**:429–430
safety **5**:429–430
in TNF IR **5**:429
baricitinib **5**:425–427
in combination with csDMARDs **5**:425–426
four pivotal phase 3 clinical trials **5**:425–426
long-term extension study **5**:426
phase 2b clinical trial of **5**:425
safety **5**:426–427
Btk inhibitors **5**:432–433
cytokine signaling **5**:421
filgotinib **5**:427–428
in combination with MTX **5**:428
as monotherapy **5**:427
safety **5**:428
jakinibs in RA **5**:422–424
MAP kinases **5**:421–422
MAP kinase inhibitors in RA **5**:421–422
MAP kinase pathway **5**:421
overview **5**:421–422
PDE4 inhibitors **5**:433–434
psoriasis **5**:434
psoriatic arthritis **5**:433–434
peficitinib (ASP015K) **5**:430–431
as monotherapy **5**:430
in MTX-IR **5**:430
ruxolitinib **5**:431–432
Syk inhibitors **5**:432
tofacitinib **5**:422–424
clinical development of **5**:422–423
in combination with csDMARDs **5**:423
long-term efficacy (LTE) of **5**:423
as monotherapy **5**:423
safety **5**:423–424
VX-509 (Decernotinib) oral-selective JAK3 inhibitor **5**:431
as monotherapy **5**:431
in MTX-IR **5**:431
Inflammatory disorders, complement system targeting for **5**:411–412
Influenza **5**:540–542
M2 inhibitors (adamantanes) **5**:540
neuraminidase inhibitors **5**:540–541
new influenza antivirals **5**:542
Influenza inhibitors **5**:540f
Influenza viruses **5**:670–672
classes of influenza agents **5**:670–672
fusion inhibitors **5**:670
ion channel blockers **5**:670
combination therapies **5**:672
mutations effects on antiviral efficiency, and QM/MM **3**:56–57
neuraminidase inhibitors **5**:670–671
polymerase inhibitors **5**:671–672
reasons to develop antiviral drugs for **5**:670
Information, lack of control in open labs **1**:532
e-mail **1**:532
multiple devices **1**:532
publications in scientific congresses **1**:532
smartphones and computers **1**:532
Information supporting
hit identification and drug design and development **1**:438
target identification **1**:437–438
Inhaled glucocorticoids, for respiratory diseases **8**:450–452
Inhaled inhibitors of p38α designing **8**:420–425
design phase I metabolism **8**:423
design phase II metabolism **8**:423–424
design to target DFG-out conformation of p38 **8**:421–422
DFG-out conformation of p38 **8**:421
lead optimization of DFG-out binders **8**:422
PF-3715455 identification **8**:424–425
Inhibiting kinases in the CNS **7**:408–446
ataxia-telangiectasia mutated kinase **7**:436
CNS exposure in drug discovery, assessment **7**:436–439
barriers within CNS System **7**:436–437
in vitro methodology to identify permeability and efflux liability at BBB **7**:437
in vivo methodology to measure the extent of brain penetration **7**:438–439
designing kinase inhibitors for CNS indications **7**:410–412
chemistry approaches for physicochemical property optimization **7**:410–412
developmental challenges **7**:410
kinases implicated in CNS pathology **7**:409
neurodegeneration **7**:409
oncology **7**:409
overview **7**:408–409
small molecule kinase inhibitors for CNS disorders **7**:412–436
anaplastic lymphoma kinase **7**:431–433
casein kinase 1 **7**:415–416
c-Jun *N*-terminal kinase **7**:415
cyclin-dependent kinase 5 **7**:414
death-associated protein kinase 1 **7**:417
dual leucine zipper kinase **7**:426–427
epidermal growth factor receptor **7**:428–431
glycogen synthase kinase 3 **7**:417–419
human epidermal growth factor receptor 2 **7**:433
leucine-rich repeat kinase 2 **7**:412–414
mitogen-activated protein kinase kinase 1/2 **7**:414
mixed-lineage kinase **7**:416–417
p21-activated kinase **7**:425–426
p38 mitogen-activated protein kinase **7**:420–422
phosphoinositide 3-kinase **7**:434–436
polo-like kinase 2 **7**:422–425
rho-associated protein kinase **7**:419–420
tropomyosin receptor kinase **7**:428
Inhibition and induction studies, of chimeric liver-humanized mice **4**:139
Inhibitor of Apoptosis Protein (IAP) **5**:255
Innate immune system, role in DILI **4**:228–230
autoantibodies and DILI **4**:229
cytokines and chemokines **4**:229
HLA associations with DILI **4**:228–229
in vitro liver models to capture **4**:230
overview **4**:228
TNFα **4**:229

Innovative Medicines Initiative **5**:683
Inosine-5′-monophosphate dehydrogenase inhibitors **5**:724
IntAct **1**:455
Integral membrane proteins (IMP), structural biology **2**:174
Integrase inhibitors
  HIV **5**:632–636
    clinical- and preclinical-stage integrase inhibitors **5**:635–636
    dolutegravir **5**:634–635
    elvitegravir **5**:633
    raltegravir **5**:632–633
Integrated approaches
  for drug repurposing **1**:38–39
Integrative approaches
  across cell models and patient clinicopathological data **1**:59–60
Integrative biology
  defintion of **3**:491–492
Integrative thinking **2**:520–523
  bedside back to bench **2**:520–521
  in oncology **2**:521–523
  overview **2**:520
Intellectual property **1**:501–502
  protection, and enforcement of ELF rules **1**:517
Intellectual property, in open landscape
  lack of control over information **1**:532
    e-mail **1**:532
    multiple devices **1**:532
    publications in scientific congresses **1**:532
    smartphones and computers **1**:532
  open laboratories **1**:529–531
    inventorship in **1**:530–531
    maintenance of confidentiality in **1**:529–530
  overview **1**:529
  patents in the Internet **1**:533–539
    available resources, making reasonable use of **1**:538–539
    drafting and prosecution **1**:539
    European Patent Office (EPO) **1**:537
    information resources **1**:533–538
    Japanese Patent Office (JPO) **1**:537–538
    legal status of patents and patent applications **1**:539
    searching **1**:539
    United States Patent and Trademark Office (USPTO) **1**:535–536
    World Intellectual Property Organization (WIPO) **1**:533–534
  perspective **1**:539
Interaction fingerprints **3**:346
Interaction network, and mathematical dynamic model **2**:457
Interferon β-1a, for multiple sclerosis **5**:448–449
Interferon β-1b, for multiple sclerosis **5**:448
Interleukin-1 receptor-associated kinase 4 (IRAK4) **5**:405–406
International Institute for Integrative Sleep Medicine **7**:247–248
  OX2R agonists **7**:247–248
Internet, and open labs. *See* Intellectual property in open landscape
Intestinal and hepatic clearance prediction **4**:64–66
Intestine segmental heterogeneity, PBPK modeling **4**:94–95
Intranasal BMS-694153 **7**:200–204
Intranasal BMS-742413 **7**:205–206
Intricate triaging process **1**:514–515
Invadopodia **2**:374f
  and cancer invasion, and high-content screening **2**:372–373
Invasion and metastasis, and cancer **5**:6
Investigational HBV RT inhibitors **5**:654–655
Investigational NRTIs, for HIV **5**:638–640
Iodine, as nutraceuticals **1**:117
Ion channel and ion transport modulators **7**:649–652
  cardiac late sodium current inhibition **7**:651
  cardiac sino-atrial (SA) node pacemaker current inhibition **7**:650–651
  diuretics for decongestion in heart failure **7**:649–650
  renal outer medullary potassium (ROMK) channel inhibition **7**:651–652
Ion channels, membrane protein **3**:148–151
IONIS-TTR$_{Rx}$ **6**:284–285
Ionix compounds **7**:79–80
Ionization constants **3**:399–400
IP antagonists **7**:580
iPfam **1**:459
IPI-493 **5**:234f
iPSC-derived cells, cellular imaging **2**:364
iPSCs ex vivo disease models **1**:49–61
  animal models, preclinical alternatives to **1**:60–61
  disease in cellular- and genomic-relevant contexts **1**:50–57
    disease mechanisms assessment in complex genetic disorders **1**:56–57
    patient iPSC differentiation into disease-relevant cell types **1**:51–56
  human disease etiology, integrative and translational research of **1**:57–60
    integrative approaches across cell models and patient clinicopathological data **1**:59–60
    phenotyping pipelines in preclinical studies **1**:57–59
Iron, as nutraceuticals **1**:117
Irreversible inhibitors **2**:194
Isavuconazole **5**:707f
Isavuconazonium **5**:707f
Isilico predictions of pK_a (case study) **4**:60
ISIS-APOCIIIRx **7**:686
Isoform selective PI3Kγ inhibitors **2**:169–171
Isolated ring systems
  spiro[4.5] ring systems **1**:215
  spiro[5.5] ring systems **1**:216–218
Isolated tissues and organs, predictive toxicology **2**:101
IsoMIF **3**:288–289
Isoniazid **4**:211–212
Isosorbide dinitrate–hydralazine combination **7**:641–642
  correction of calcium homeostasis **7**:646–648
    aladorian **7**:646–647
    istaroxime **7**:647–648
    mydicar **7**:646
  positive inotropic agents and sarcomere targets **7**:643–646
    cAMP elevating agents **7**:644
    digoxin **7**:643–644
    modulators of sarcomeric proteins **7**:644–646
  relaxin **7**:648
  urocortins **7**:643
  vasopressin antagonists **7**:642–643
Isothermal titration calorimetry **2**:214
  to characterize thermodynamics of lead-like compounds **2**:426–427
Istaroxime **7**:647–648
Istradefylline, for Parkinson's disease **5**:463
ITC
  fragmented
    experimental considerations for **2**:206
  principle of **2**:198–199
ITK **5**:94
ITK inhibitors **5**:95f
Itraconazole **5**:707f
Ivermectin **1**:246f
Ixazomib (MLN9708) **5**:260–271

J

JAK inhibitors, for inflammatory bowel disease **5**:499
JAK3 **5**:95–96
JAK3 inhibitors **5**:95f
Jakinibs in RA **5**:422–424
Janssen
  inhibitors reported by **7**:342–344
  modulators from **7**:298–301
    aryl-imidazole derivatives **7**:299–301
    carboxylic acid derivativess **7**:298–299
Janus kinases/signal transducer and activator of transcription **5**:479–480
Japanese Patent Office (JPO) **1**:537–538
JNK signaling, in DILI **4**:221
Johnson & Johnson/Janssen Pharmaceuticals **7**:250–252
  4-phenyl-[1,3]dioxanes **7**:250
  octahydropyrrolo[3,4-*c*]pyrroles **7**:250–252
    JNJ-42847922 **7**:252
The Joint European Compound Library **1**:505–512
  EFPIA-contributed collection **1**:506
  public compound collection **1**:506–512

K

KAE609 (cipargamin) **8**:529–543
  active enantiomer of the lead compound **8**:532–533

KAE609 (cipargamin) (*continued*)
asymmetric synthesis of the active enantiomer **8**:534–535
current antimalarial drug discovery **8**:530
in vivo efficacy of spiroindolones in *P. berghei* mouse model **8**:539
lead identification **8**:532
overview **8**:529
proof of concept **8**:540–541
restarting antimalarial research and search for next generation antimalarial drugs **8**:530–531
identification and triaging potential leads from screening **8**:530–531
SAR of spiroindolones **8**:535–538
surrogate models of human malaria for drug discovery **8**:539
target and mechanism of action of the spiroindolones **8**:539–540
KcsA tetramer **3**:150f–151f
Keap1–Nrf2 **2**:343–344
Ketoamide-derived HCV NS **8**:583–608
Ketoconazole **5**:706f
Ketomethylene ($COCH_2$) **6**:84
Key players, in pharmaceutical industry future **1**:1–10
Kick and kill strategy, for HIV **5**:648–650
KIM-1, biomarker of acute kidney injury **4**:274
Kinase inhibitors **5**:378–381, **7**:587–588
approved **5**:14t–15t
CSF-R1 inhibitors **5**:380
PI3K inhibitors **5**:381
PI3Kβ inhibitors **7**:587–588
RON inhibitors **5**:380
TAM receptor signaling inhibitors **5**:380
TGF-β RI/ALK5 inhibitors **5**:378–379
Kinase inhibitors in cancer **5**:39–75
kinases and cancer **5**:40–43
activating mutations **5**:41–42
gene amplification **5**:43
kinase fusion proteins **5**:41
protein overexpression **5**:43
upstream pathway activation **5**:42
lessons learned from first-generation inhibitors **5**:43–45
combinability **5**:45
on-target selectivity **5**:44–45
target engagement **5**:44
targeting resistance **5**:45
overview **5**:40
Kinase inhibitors in cancer, Bcr-Abl inhibitors **5**:45–51
addressing the gatekeeper T315I mutation **5**:48–51
allosteric Bcr-Abl inhibitors **5**:49–51
ponatinib **5**:49
chronic myeloid leukemia and the discovery of imatinib **5**:45–46
mechanism of resistance to imatinib **5**:46–47
second-generation therapies **5**:47–48
bosutinib **5**:48
dasatinib **5**:48
nilotinib **5**:47–48
Kinase targets for covalent inhibition **5**:91–97
Akt **5**:91–92
BMX **5**:92
CDK7 **5**:93
ERK1/2 **5**:93–94
ITK **5**:94
JAK3 **5**:95–96
miscellaneous kinases **5**:97
PI3Kα **5**:96
Kinases **5**:479–486
Bruton's tyrosine kinase **5**:485–486
calcineurin/nuclear factor of activated T cells **5**:483
calcium/calmodulin-dependent kinase IV **5**:482–483
janus kinases/signal transducer and activator of transcription **5**:479–480
mammalian target of rapamycin **5**:484
phosphaditylinositol-3 kinase **5**:484–485
rho kinase (ROCK) **5**:482
spleen tyrosine kinase **5**:481
Kinases, in DDR **5**:59–69
ATM **5**:59–61
inhibitors **5**:60–61
ATR **5**:61–64
inhibitors **5**:62–64
CHK1 **5**:66–68
inhibitors **5**:67–68
DNA-PK **5**:64–65
inhibitors **5**:64–65
overview **5**:59
WEE1 **5**:66–68
inhibitors **5**:66–67
Kinases, in lung cancer **5**:51–59
ALK inhibitors design with potency against mutations **5**:55–58
ALK inhibitors design targeting L1196M gatekeeper mutation **5**:56–57
crizotinib design as effective inhibitor of WT ALK **5**:55
future outlook **5**:57–58
mutant selective EGFR inhibitors design **5**:51–55
early inhibitors of EGFR, targeting activating mutations **5**:51–52
future outlook **5**:55
T790M mutant selective EGFR inhibitors design **5**:52–55
overview **5**:51
Kinases and inhibitors, cancer targets **5**:11–15
approved kinase inhibitors **5**:13
kinase activation in cancer **5**:12–13
kinase inhibitor mode of action **5**:13
kinase mutations and resistance **5**:13
kinase structure **5**:11–12
overview **5**:11
receptor tyrosine kinases (RTKs) **5**:12
Kinases implicated in CNS pathology **7**:409
neurodegeneration **7**:409
oncology **7**:409
Kinetic efficiency **2**:208–209
Kinetics in drug discovery **2**:181–197
association phase **2**:183–184
binding kinetics and PK/PD **2**:196–197
biochemical methods to determine binding kinetics **2**:186–188
competition methods **2**:188
fluorescence approaches **2**:187
measurement of association rate constant **2**:186–187
measurement of dissociation rate constant **2**:186
radioligand binding **2**:186
biolayer interferometry **2**:185–186
biophysical methods for measuring binding kinetics **2**:181
choice of coupling methods **2**:182–183
consideration of buffers **2**:183
dissociation phase **2**:184
effect of binding kinetics on fractional occupancy and IC_{50} **2**:189–190
enzyme kinetics **2**:188
experimental considerations **2**:182
future trends for kinetic characterization **2**:197
irreversible inhibitors **2**:194
kinetic selectivity **2**:192
ligand immobilization **2**:182
ligand quality control considerations **2**:183
ligand size/molecular weight considerations **2**:182
mechanistic aspects to binding kinetics **2**:190–192
optical waveguide grating **2**:186
optimizing residence time **2**:194–196
principle of SPR **2**:181–182
regeneration procedures **2**:184–185
residence times **2**:188–189
role of kinetics in selectivity and efficacy **2**:192–194
steady-state phase **2**:184
Kinetoplastids **5**:724–735
leishmania **5**:725–729
trypanosoma brucei **5**:731–735
trypanosoma cruzi **5**:729–730
KLIFS **1**:460
K-Map **1**:457
KMTs **2**:304–309
Knottin peptide–drug conjugate **1**:332–333, **1**:333f
Knowledge-based approaches, drug repurposing **1**:23–24
literature-based **1**:23–24
phenotypic screening **1**:21–23

L

L1196M gatekeeper mutation **5**:56–57
Label-free cell phenotypic profiling for target identification **2**:422
Label-free screening technologies **2**:416–433, **2**:417t, **2**:418f
high-throughput screening **2**:423–425
molecular docking for ultra-HTS **2**:424
NMR spectroscopy for fragment screening **2**:424–425
RWG biosensor for (ultra)HTS **2**:423

lead optimization **2**:425–427
isothermal titration calorimetry to characterize the thermodynamics of lead-like compounds **2**:426–427
LBVS to expand compound library **2**:425
RWG to perform quantitative structure–activity analysis (SAR) **2**:425
SPR to characterize the binding kinetics of lead-like compounds **2**:425–426
lead selection **2**:427–429
electric biosensor to assess compound-induced toxicity **2**:428–429
LC/MS to detect the metabolites of lead molecules **2**:429
microfluidics RWG to elucidate the biochemical moa of lead molecules **2**:427–428
RWG-enabled cell phenotypic profiling to prioritize lead molecules **2**:427
virtual screening techniques to identify potential off-target effects of lead molecules **2**:427
overview **2**:417–418
target identification **2**:420–423
label-free cell phenotypic profiling for **2**:422
MS-based proteomics for **2**:420–422
target prediction
ligand-based virtual screening for **2**:423
techniques **2**:418–420
electric biosensor **2**:420
mass spectrometry **2**:418–419
nuclear magnetic resonance **2**:420
resonant waveguide grating biosensor **2**:419
surface plasmon resonance **2**:419
virtual screening techniques **2**:420
Lactate dehydrogenaze enzyme **1**:282
β-Lactones **5**:270
Laninamivir octanoate **5**:670f
Laquinimod, for multiple sclerosis **5**:447–448
Large molecules, biochemical characterization of. *See* Analogs designing
Laser scanning cytometers **2**:367, **2**:406
Lautenberg Act **4**:287t
LBVS, to expand compound library **2**:425
LC/MS to detect the metabolites of lead molecules **2**:429
LCZ696 **7**:638–639
LDH activity detection in dead cells **1**:282f
Lead hopping in fXa **2**:171–172
Lead optimization **2**:18–27, **2**:425–427
ADME and safety optimization, screening technologies for **2**:24–27
asymmetric tissue distribution, design principles for **2**:23–24
drug-like chemical space expansion
designing permeable compounds beyond the Lipinski rule of five **2**:22–23
rational design of covalent inhibitors **2**:21–22
isothermal titration calorimetry to characterize thermodynamics of lead-like compounds **2**:426–427
LBVS to expand compound library **2**:425
RWG to perform quantitative structure–activity analysis (SAR) **2**:425
SPR to characterize binding kinetics of lead-like compounds **2**:425–426
Lead selection **2**:427–429
electric biosensor to assess compound-induced toxicity **2**:428–429
LC/MS to detect the metabolites of lead molecules **2**:429
microfluidics RWG to elucidate the biochemical moa of lead molecules **2**:427–428
RWG-enabled cell phenotypic profiling to prioritize lead molecules **2**:427
virtual screening techniques to identify potential off-target effects of lead molecules **2**:427
Lead small molecules synthesis, and click chemistry **1**:305–308
Lead-like library synthesis approaches **2**:139–146
Lead-like natural products **2**:137–139
Leadscope Expert Alert System **2**:235, **4**:167
Leadscope Model Applier **2**:236, **4**:162–163
LEAPT strategy **1**:600f
LecA lectin **1**:588f
Lectin inhibitors, and carbohydrates **1**:583–591
bacterial lectins inhibition **1**:585–589
DC-SIGN lectin targeting **1**:589–591
galectins inhibition **1**:585
selectins inhibition **1**:583–584
Leishmania **5**:725–729
Leishmanial proliferation in macrophage, and high-content screening **2**:379–382
LEM **2**:207–209
enthalpic efficiency **2**:208
future trends for application of **2**:209
kinetic efficiency **2**:208–209
ligand efficiency **2**:207
ligand lipophilicity efficiency **2**:207–208
other size-based metrics **2**:207
Leucine-rich repeat kinase 2 **7**:412–414
Leukocyte function associated antigen-1 (LFA-1) antagonists **1**:234t
Levodopa, for Parkinson's diseasemulations, for Parkinson's disease **5**:463–464
LFA-1–ICAM-1 **2**:343
Library design and drug discovery, privileged structures and motifs for **2**:120–135
classes of privileged structure **2**:120–135
arylated piperidine/piperazine ring systems **2**:128–130
benzodiazepine and related seven-membered ring systems **2**:130–132
coumarin-/chromone-/pyran-derived privileged structures **2**:125
miscellanea **2**:126–128
privileged 5,5 heterocyclic ring systems **2**:124–125
privileged 6,5 heterocyclic ring systems **2**:123–124
privileged 6,6 heterocyclic ring systems **2**:120–123
rhodanines (and related) **2**:133–134
single-cycle ring systems **2**:132–133
spirocyclic structures **2**:134–135
Library preparation and automated processes, continuous flow processing **1**:157–162
LIE approaches, binding free energies calculations **3**:6
Life extension by antioxidants **1**:352–355
Ligand binding
semimacroscopic and macroscopic calculations **3**:6
Ligand binding assays (LBAs) **6**:181–190
assay types **6**:182–190
critical value of assay reagents and controls **6**:184–185
LBA method development and qualification requirements **6**:188–190
significance and the nature of matrix interferences in LBA protocols **6**:185–188
variety of analytes measured by LBA **6**:183–184
technologies and regulatory expectations **6**:194–195
Ligand binding assays (LBAs), technology platforms **6**:190–194
acoustic membrane microparticle technology on the ViBE platform **6**:192–193
pros and cons/considerations **6**:193
Biacore **6**:191
pros and cons/considerations **6**:191
ECL Assays **6**:190–191
pros and cons/considerations **6**:191
ForteBio **6**:192
pros and cons/considerations **6**:192
Gyrolab **6**:191
pros and cons/considerations **6**:191
imperacer immuno-polymerase chain reaction (PCR) **6**:194
pros and cons/considerations **6**:194
Luminex **6**:192
pros and cons/considerations **6**:192
Maverick (Genalyte) **6**:193–194
pros and cons/considerations **6**:194
SIMOA **6**:193
pros and cons/considerations **6**:193
Singulex Erenna **6**:193
Pros and cons/considerations **6**:193
SQI Diagnostics **6**:194
pros and cons/considerations **6**:194
Ligand data types **1**:451–452
Ligand efficiency **2**:75–76, **2**:207, **2**:215
Ligand flexibility, and pose prediction in docking **3**:300–301
Ligand hydrophobic groups
nonpolar pockets occupation by **3**:82–83

Ligand immobilization **2**:182
Ligand lipophilicity efficiency **2**:207–208
Ligand placement **2**:160–161
Ligand quality control considerations **2**:183
Ligand similarity assessment **3**:254–260
  bioactive pose prediction **3**:260–264
  COSMO*sim3D* **3**:255–256
  FieldTemplater **3**:261–262
  FLAPpharm **3**:263–264
  GRID/FLAP **3**:257–258
  XED/FieldAlign **3**:258–260
Ligand size/molecular weight considerations **2**:182
Ligand-based applications, of molecular fields **3**:254–286
  3D activity cliff analysis **3**:277–281
    activity miner/activity atlas **3**:278–281
  3D clustering of molecule libraries **3**:270
  3D-QSAR **3**:270–277
    CoMFA **3**:271–272
    CoMSIA **3**:273
    COSMO*sar3D* **3**:274–276
    FieldQSAR **3**:276
    GRID/GOLPE/FLAP **3**:277
    GRIND **3**:277
    Template CoMFA **3**:274
    Topomer CoMFA **3**:273–274
  ADME prediction **3**:281–286
    MetaSite **3**:283–286
    MoKa **3**:282–283
    VolSurf **3**:282
  ligand similarity assessment **3**:254–260
    bioactive pose prediction **3**:260–264
    COSMO*sim3D* **3**:255–256
    FieldTemplater **3**:261–262
    FLAPpharm **3**:263–264
    GRID/FLAP **3**:257–258
    XED/FieldAlign **3**:258–260
  scaffold hopping **3**:266–270
    SHOP **3**:267–268
    Spark **3**:268–270
  virtual screening **3**:264–265
    fieldscreen/blaze **3**:264
    FLAP **3**:264–265
Ligand-based methods
  polypharmacology **2**:263–266
Ligand-based virtual screening for target prediction **2**:423
Ligand-complex quadruplex structures **5**:315f
Ligands, molecular alignment **3**:214
Light sheet fluorescence microscopy **2**:405
Lilly
  inhibitors reported by **7**:344–348
Linaclotide **6**:93–94
Linagliptin (BI-1356) **7**:531–532
Line notation formats **3**:331, **3**:334–339
  chemical table files **3**:335–339
    chemical markup language **3**:338
    connection table (Ctab)-based file types **3**:335
    FASTA **3**:338
    other formats **3**:336
    Protein Data Bank file format (pdb) **3**:336–338
    structure recognition tools **3**:338–339
    tripos mol2 format **3**:336
  representation of organic structures description arranged linearly **3**:334–335
  sybyl line notation **3**:335
  wiswesser line notation **3**:334
Lipid accumulation in adipocytes, and high-content screening **2**:376–377
Lipidated peptides **6**:74f
Lipidation **6**:72–75
Lipids
  force field advances **3**:19
  in protein drug delivery **6**:140–141
Lipinski rule of five **4**:58
  designing permeable compounds beyond **2**:22–23
Lipophilic amines **5**:730
Lipophilic and ionic interactions, incorporation of **2**:107–108
Lipophilicity (logD), matched molecular pair analysis **3**:245
Lipophilicity and promiscuity **2**:107
Liposomes **1**:266, **1**:266f
Liquid overlay methods with non-adherent surface plates **2**:401
Liraglutide **7**:485
Literature-based approaches, drug repurposing **1**:23–24
Literature-driven network model building **2**:451–452
Live-cell 3D imaging **2**:402–404
Liver
  DILI. *See* Drug-induced liver injury (DILI)
  structure and function of **4**:205
  targeting, next-generation therapeutics **1**:341–342
Liver enzyme and transporter zonation, PBPK modeling **4**:95–97
Liver fibrosis **7**:705–709
  drugs evaluated in preclinical and clinical trials **7**:707–708
  emerging biology **7**:708
  epidemiology **7**:705
  experimental animal models **7**:707
  overview **7**:705
  pathophysiology **7**:706
Liver injury, drug-induced **2**:251–253
Liver organoids, induced pluripotent stem cell-derived **4**:186
Liver safety biomarkers **4**:264
Lixienatide **7**:485
LLY-507 **5**:297f
Lock-and-key model **3**:320f
Lomitapide **7**:679–681
Loop modeling, protein model **3**:135–137
Losartan analogs **1**:230t
LpxC inhibitors **5**:694–695, **5**:695f
LRA approaches, binding free energies calculations **3**:6
Lu AF21934 **2**:279f
Luminex **6**:192
  pros and cons/considerations **6**:192
Lumiracoxib (Prexige) **5**:397
Lundbeck
  inhibitors reported by **7**:349
Lupus and lupus overlap diseases **5**:474–494
  clinical presentation of SLE **5**:477–478
  current therapeutic paradigm in SLE **5**:479
  etiology and pathophysiology of SLE **5**:477
  future directions **5**:489
  kinases and phosphatases **5**:479–486
    Bruton's tyrosine kinase **5**:485–486
    calcineurin/nuclear factor of activated T cells **5**:483
    calcium/calmodulin-dependent kinase IV **5**:482–483
    janus kinases/signal transducer and activator of transcription **5**:479–480
    mammalian target of rapamycin **5**:484
    phosphaditylinositol-3 kinase **5**:484–485
    rho kinase (ROCK) **5**:482
    spleen tyrosine kinase **5**:481
  loss of tolerance and development of systemic autoimmunity **5**:475–476
  modifiers of chromatin **5**:486–487
  novel lupus therapeutics **5**:479–489
  overview **5**:474–475
  proteasome inhibitors **5**:487–488
  quinoline derivatives **5**:488–489
LY-377604 and related compounds **7**:722–723
LY2857785 **5**:212f
LY2951742 **7**:216
LY3009104 (INCB028050, Baricitinib) **5**:402
Lyophilized drug product development **6**:211–212
Lysine
  methyl modifications to **5**:283
Lysine demethylases **5**:284
Lysine methyltransferases **5**:290–300
Lysine (K)-specific demethylases **5**:300
  lysine (K)-specific demethylase 1A **5**:300
Lysosomal perturbation and DILI **4**:223–225
  autophagy, lysosomes, and DILI **4**:224
  autophagy perturbation **4**:225
  lysosomal perturbations and cytotoxicity **4**:225
  overview **4**:223
  physicochemical properties of drugs and lysosomes **4**:223–224
Lysosomal storage disease, and high-content screening **2**:377

M

M1 receptors **7**:26–27
M2 inhibitors (adamantanes) **5**:540
mAb downstream process platforms **6**:171–179
  current and evolving downstream process **6**:172–175
    broadly applicable downstream platform **6**:174–175

drivers for mAb platform evolution **6**:172
recent downstream platforms **6**:172–174
new technologies impacting **6**:175–176
next-generation antibody constructs impacting **6**:176–177
overview **6**:171
Macitentan **8**:252–283
in humans **8**:271–276
drug–drug interactions **8**:275–276
liver safety **8**:274–275
metabolism **8**:274
pharmacokinetics **8**:273–274
medicinal chemistry efforts leading to the discovery of **8**:261–267
progress of the project **8**:262–267
selected starting points **8**:261–262
overivew **8**:253–260
biology and pharmacology of ET system **8**:253
competition, structures of known ERAs **8**:255–260
compound profiling and selection cascade **8**:254
identifying starting points for discovery program **8**:254–255
project goals **8**:254
preclinical properties of **8**:267–271
distinct physicochemical and conformational properties **8**:268
distinct receptor interaction forces **8**:268–269
in vivo efficacy and comparison with other ERAs **8**:271
sustained target blockade and higher antagonistic efficacy **8**:269–270
tissue distribution in animal models of PAH **8**:270
for treatment of PAH **8**:276
Macrocycles **1**:329–330
Macrocyclic peptides **6**:88–95
colistin A **6**:89–90
conopeptides **6**:92–93
cyclic melanocortin analogs **6**:94
cyclic opioid peptides **6**:95
cyclosporine A **6**:89
linaclotide **6**:93–94
octreotide (Sandostatin) **6**:92
PMX53 (3D53) **6**:91
tyrocidine A **6**:89
Macrolide antibiotics **5**:520f
Macrolide resistance **5**:519–520
Macrophage
leishmanial proliferation in, and high-content screening **2**:379–382
Macroscopic calculations of ligand binding **3**:6
Magnesium, as nutraceuticals **1**:116
Magnetic levitation **2**:401–402
Magnetic nanoparticles **1**:266–267, **1**:266f
Magnetometry **1**:277–278
Major diseases and large foundations **1**:550
Malaria **8**:544–545
disease burden **8**:544–545
pyrimidine biosynthesis and DHODH as drug target **8**:546–547
target candidate profiles for new antimalarial drugs **8**:545–546
Mammalian target of rapamycin **5**:216, **5**:484
Manganese, as nutraceuticals **1**:117
Mannosylated nanodiamonds **1**:591f
MAO-B inhibitors, for Parkinson's disease **5**:463
MAP kinases **5**:421–422
MAP kinase inhibitors in RA **5**:421–422
MAP kinase pathway **5**:421
Marizomib (salinosporamide A/NPI-0052) **5**:271
Market
and academia. *See* Academia and market
Markov state models **3**:22–24
Masitinib **5**:400
Mass spectrometric platforms for metabolomics **2**:447–448
GC/MS **2**:447
LC/MS **2**:447
spectral processing **2**:447–448
Mass spectrometry **2**:214
biomarkers **2**:500–501
label-free screening **2**:418–419
Mast tryptase inhibitors **1**:244t
Matched molecular pair, methods to find **3**:222–231
available software **3**:229
context dependence, set size *versus* specificity **3**:227–229
dataset selection and preparation **3**:230–231
chemical structure **3**:230–231
measured property data **3**:231
recommendations **3**:229–230
supervised **3**:223
unsupervised **3**:223–227
comparisons **3**:227
fragment and index **3**:223–226
maximum common substructure **3**:226–227
Matched molecular pair analysis **3**:221–252
defined **3**:221–222
elucidating pharmacophores **3**:247–248
elucidating relationships in 3-D **3**:246–247
matched series **3**:248–249
related approaches **3**:249
activity cliffs **3**:249
bioisosteres **3**:249
QSAR **3**:249
sharing data among pharmaceutical companies **3**:245–246
specific properties **3**:232–245
in vivo pharmacokinetics **3**:235
lipophilicity (logD) **3**:245
melting point **3**:244
metabolism **3**:235–238
permeability and efflux **3**:238–239
plasma protein binding **3**:244–245
primary potency **3**:232–235
solubility **3**:241–244
toxicity **3**:239–241
specific structures **3**:231–232
enantiomers **3**:232
oxadiazole regioisomers **3**:232
substituents on aromatic rings **3**:231–232
Matched pairs **3**:228f
Matched series **3**:248–249, **3**:248f
Mathematical formalisms **3**:494–497
agent-based modeling **3**:495–496
Bayesian network models **3**:496
Boolean modeling **3**:494
ODE model **3**:496–497
PDE model **3**:496–497
petri nets **3**:494
Mathematical models
for network biology **2**:456–460
enzyme kinetics **2**:458
from interaction network to mathematical dynamic model **2**:457
model analysis and validation **2**:459
model parameter fitting **2**:458–459
model simplification, *S*-systems **2**:459
model usage in systems research **2**:459–460
stochastic *versus* deterministic models **2**:458
for rheumatoid arthritis **2**:509
Matrix metalloproteinase 12, and binding thermodynamics **2**:203
Matrix metalloproteinases (MMP) inhibitors **1**:242t, **7**:53
Maturation inhibitors, HIV **5**:645–646
Maverick (Genalyte) **6**:193–194
pros and cons/considerations **6**:194
Maximum common substructure approach **3**:226f
MCH-1 receptor antagonist NGD-4715, for obesity **8**:488–515
characterization of NDT 9522320 **8**:491–492
hit-finding **8**:490
NDT-4715 clinical studies **8**:511–514
novel bicyclic system **8**:495–501
overview **8**:488–489
preclinical proof-of-concept in rat **8**:492–493
process development and cGMP delivery **8**:501–506
proof of concept in dog **8**:493–494
seeking a superior backup compound **8**:507–511
MDM2 **5**:251
MDM2-p53 **2**:338–339, **5**:173t–176t, **5**:253–254, **5**:254f
and MDMX–p53 **5**:171–178
dual MDM2–p53, MDMX–p53 antagonists **5**:178
MDM2–p53 antagonists **5**:171–178
MDM2–p53 peptides **5**:159–160
MDM2-p53 protein–protein interaction inhibitors **1**:232f, **1**:233t, **1**:234f
Mean±standard deviations **2**:395
Mechanistic models
to system biology models **2**:505–506
Mechanistic pharmacokinetic/pharmacodynamic models **2**:504

Mechanistic pharmacokinetic/pharmacodynamic models (*continued*)
election of starting dose for first-in-human studies **2**:507
Medical foods **1**:109
See also Nutraceuticals
Medical need
in developing world populations **1**:541–542
in older age **1**:541
in orphan populations **1**:540–541
Medicinal & synthetic chemistry rules **2**:217
Medicinal chemistry
and ADME/PK **4**:3
and in silico technologies **3**:436–438
molecular docking **3**:311–314
considerations **3**:312–313
end-user's choice **3**:313
end-users compatible **3**:314
incorporation **3**:312
input protein structure **3**:312
less susceptible results **3**:314
over-interpretation of scores **3**:313
self-critical software **3**:314
software **3**:311–312
usage methods **3**:311
utilization **3**:311
Medicinal chemistry, of spirocyclic scaffolds **1**:220–253
noncarbon spiro atom **1**:253
polyspirocycles **1**:253
spiro[2.*n*] ring systems **1**:220–225
spiro[2.2] ring systems **1**:220
spiro[2.3] ring systems **1**:220
spiro[2.4] ring systems **1**:221–223
spiro[2.5] ring systems **1**:223–225
spiro[2.≥6] ring systems **1**:225
spiro[3.*n*] ring systems **1**:225–229
spiro[3.3] ring systems **1**:225
spiro[3.4] ring systems **1**:225–226
spiro[3.5] ring systems **1**:226–229
spiro[4.*n*] ring systems **1**:229–245
spiro[4.4] ring systems **1**:229–234
spiro[4.5] ring systems **1**:235–243
spiro[4.6] ring systems **1**:243–245
spiro[5.*n*] ring systems **1**:245–252
spiro[5.5] ring systems **1**:245–250
spiro[5.6] ring systems **1**:252
Medicinal chemistry case history **8**:1–32, **8**:408–430
current progress of EGFR-mutant inhibitors **8**:25–26
EGFR biology, role in nonsmall cell lung cancer **8**:1–2
emerging clinical data of osimertinib **8**:24
future challenges **8**:26–30
highlights of clinical data for PH-797804 and PF-3715455 **8**:426
inflammatory diseases **8**:408–409
biological DMARDs **8**:409
synthetic DMARDS **8**:409
inhaled inhibitors of p38α designing **8**:420–425
design phase I metabolism **8**:423
design phase II metabolism **8**:423–424
design to target DFG-out conformation of p38 **8**:421–422
DFG-out conformation of p38 **8**:421
lead optimization of DFG-out binders **8**:422
PF-3715455 identification **8**:424–425
learnings **8**:26–30
opportunities **8**:26–30
osimertinib (AZD9291), discovery of **8**:2–23
EGFR mutant-selective hypothesis **8**:2–4
identification of a mutant-selective lead series **8**:4–11
lead optimization **8**:11–23
p38 MAPK inhibitors, approaches to the discovery of **8**:413–417
first-generation pyrazole-based inhibitors **8**:414
PH-797804, as more potent atropisomer **8**:416–417
second-generation pyridinone-based inhibitors **8**:414–415
structural hypothesis of human kinome selectivity **8**:415–416
structure-based drug design **8**:413
structure-guided lead optimization **8**:416
p38 MAPK pathway **8**:410–413
small-molecule p38 clinical candidates for inflammatory indications **8**:410–413
PH-797804, characterizations of **8**:418–420
crystal structure of PH-797804 bound in p38α kinase **8**:418–419
in vitro activity **8**:418
in vivo efficacy of PH-797804 **8**:420
kinase selectivity screening **8**:418
pharmacokinetic properties of PH-797804 **8**:419–420
rotational barrier, chemical stability, and pharmaceutical properties **8**:419
Medicinal chemistry of antisense oligonucleotides **6**:216–232
ADME **6**:226–227
length of ASOs **6**:227
sugar modifications **6**:226
medicinal chemistry approaches to improving safety profiles **6**:228–230
gap design **6**:229–230
nucleobase modifications **6**:229
sequence design **6**:228–229
nuclease resistance, improvement in **6**:218–219
backbone modifications **6**:218
bulkiness of the substituent on the bridging moiety **6**:219
ring size **6**:219
sugar modifications **6**:219
overview **6**:216–218
safety of ASOs **6**:227–228
class effects of phosphorothioated ASOs **6**:227–228
target specificity and hepatotoxicity **6**:228
Medicinal chemistry of antisense oligonucleotides, target-binding affinity and potency **6**:220–226
backbone modifications **6**:226
number and/or mode of introduction of sugar modifications **6**:225
affinity and potency **6**:225
gapmers **6**:225
sugar modifications and bridged nucleic acids (BNAs) **6**:220–225
control of torsion angles **6**:223–224
introduction of cation into the bridge **6**:223
introduction of heteroatoms into the bridge **6**:222–223
LNA, alkyl LNAs, and their isomers **6**:220–221
replacement of oxygen with carbon **6**:221–222
Melanin-concentrating hormone **6**:68
Melanin-concentrating hormone (MCH) receptor 1 antagonists, for inflammatory bowel disease **5**:503
Melatonin **1**:367–368
Melogliptin **7**:536–538
Melting (fusion) of crystals
physical–chemical properties **3**:397
Melting point
matched molecular pair analysis **3**:244
physical–chemical properties **3**:411–413
physics-based methods **3**:411
statistical methods **3**:412–413
Memantine, for AD **5**:456–457
Membrane barrier for metabolite, PBPK modeling **4**:97
Membrane protein **3**:145–188
allosteric GPCR Ligands **3**:179–180
classes of **3**:145
emergence of high-resolution structures of **3**:146–151
GPCRs **3**:146
ion channels **3**:148–151
membrane transporters **3**:147–148
GPCR computational simulation **3**:156–163
binding free energy and binding kinetics predictions **3**:160–163
molecular dynamics simulations **3**:156–159
GPCR ligand design **3**:155
hit finding **3**:155
in silico design for membrane protein targets **3**:163–180
novel structural understanding, focused on GPCRs **3**:151–155
binding site analysis **3**:153–155
from structure to function **3**:151–153
orthosteric GPCR ligands **3**:164–179
class A GPCR aminergic **3**:164–170
class A GPCR chemokine **3**:176–179
class A GPCR lipid receptors **3**:176
class A GPCR peptidergic **3**:170
class A GPCR purinergic **3**:171–175
overview **3**:145–151

Membrane transporters, membrane protein **3**:147–148
Merck **7**:189–200, **7**:253–263
  caprolactam-based CGRP receptor antagonists **7**:189–195
  diamines/MK-4305 **7**:253–254
  2,5-diarylnicotinamides **7**:257
  diazepanes **7**:260
  MK-1064 **7**:258
  MK-3697 **7**:258
  MK-4305 **7**:255
  MK-8133 **7**:260–263
  modulators from **7**:302–304
    aryl-imidazole derivatives **7**:304
    aryl-piperazine derivatrives **7**:303
    carboxylic acid derivatives **7**:302–303
  piperidine ethers **7**:260
  piperidines/MK-6096 **7**:255–257
  proline bis-amides **7**:253
  spiroindane-based CGRP receptor antagonists **7**:195–200
Merck Serono/Merck KGAA
  inhibitors reported by **7**:349
Mesenchymal multipotent stromal cells
  regenerative medicine **1**:386
Mesenchymal stem cells **1**:419
MET **5**:332
Metabolic control analysis
  defintion of **3**:491
Metabolic stress, and cancer **5**:9–10
Metabolism
  ADME **4**:35
  matched molecular pair analysis **3**:235–238
  as surrogate for absorption **4**:113
Metabolism and elimination prediction **4**:106–109
  characteristics of metabolism **4**:106–107
  in silico predictions **4**:108–109
  in vitro predictions **4**:107–108
  in vivo predictions **4**:108
Metabolism predicaion
  from BDDCS **4**:119
  in the gut **4**:117
Metabolism-based DDIs **4**:26t–27t
Metabolite
  data, in bioequivalence **4**:97–98
  membrane barrier for, PBPK modeling **4**:97
Metabolite formation
  parameters identifying **4**:84–85
Metabolite kinetics study
  PBPK modeling **4**:85–94
    of intestine **4**:85–87
    intestine-liver **4**:88–90
    of liver **4**:87–88
    of whole body **4**:88–90
  SFM
    for lack of codeine demethylation detection (case study) **4**:94
    for route-dependent intestinal glucuronidation of morphine detection (case study) **4**:90–94
Metabolomics **2**:445–450
  mass spectrometric platforms for **2**:447–448
  metabolomics data evaluation **2**:450
  methods and recent developments **2**:446
  predictive toxicology **2**:104–105
  special considerations and outlook **2**:450
  structure identification **2**:449
Metabolomics, data standards and sharing **2**:466–467
Metabolomics workflows **2**:446f
Metabotropic glutamate receptors **7**:29–30
Metadynamics **3**:25–26, **3**:41–42
  Accelerated MD **3**:43
  steered MD **3**:42–43
MetaSite **3**:283–286
Metformin **1**:363–365
Methicillin-resistant *Staphylococcus aureus* **5**:529–530
Methotrexate, for multiple sclerosis **5**:452
Methyl modifications to lysine and arginine **5**:283
2′-*O*-Methyl-A phosphoramidite analyzed by HPLC **6**:243f
N-Methylated peptide therapeutics **6**:79t
Methylation **3**:243t
N-Methylation **6**:78–81
Methylene ether (CH_2O) **6**:84
Methylene thioether (CH_2S) **6**:83–84
Methylsulfonylmethane, for chronic inflammatory disorders **1**:130
mGLU1 receptors **7**:29
mGLU2 receptors **7**:29
mGLU4 receptors **7**:30
mGLU5 receptors **7**:30
MGN-9103 **7**:654
MI77301 **5**:254f
Micafungin **5**:709f
Miconazole **5**:706f
Microarray technology **2**:436–437
Microbes, as nutraceuticals **1**:123–124
  prebiotics **1**:123–124
  probiotics **1**:123
Microbiome **5**:411
Microfluidic devices **2**:402
Microfluidics RWG to elucidate the biochemical moa of lead molecules **2**:427–428
Microgabalin **7**:72
Micronucleus assay, for genotoxicity evaluation **4**:198–199
Micronucleus test in vitro **2**:106
Micropatterned plates **2**:401
Microphysiological models **4**:297
MicroRNAs
  expression **2**:437–438
  regenerative medicine **1**:400
Microscopy
  brightfield and widefield microscopy **2**:402–404
  confocal microscopy **2**:404–405
  light sheet fluorescence microscopy **2**:405
  two-photon microscopy **2**:405
Microspheres, in protein drug delivery **6**:140–141
Miglustat **1**:582f
Migraine
  5-$HT_{1B/1D}$ agonists (triptans) **7**:179–181
  ergot alkaloids **7**:178–179
  medications for **7**:178
  pathophysiology **7**:177–178
  prevalence and symptoms **7**:177
  See also CGRP receptor antagonists for migraine
Minerals, as nutraceuticals **1**:114–118
  essential macrominerals **1**:114–117
    calcium **1**:114
    magnesium **1**:116
    phosphorus **1**:116
    potassium **1**:116
    sodium **1**:116–117
    sulfur **1**:117
  essential trace minerals/microminerals **1**:117–118
    chromium **1**:117
    cobalt **1**:117
    copper **1**:117
    fluoride **1**:117
    iodine **1**:117
    iron **1**:117
    manganese **1**:117
    molybdenum **1**:117
    selenium **1**:117–118
    zinc **1**:118
Minerals, in cancer management **1**:129
Minimum active sequence, analogs designing **6**:68–69
  annexin A1 **6**:69
  cholecystokinin **6**:68
  enfuvirtide **6**:69
  eptifibatide **6**:69
  glucagon-like peptide-1 **6**:69
  melanin-concentrating hormone **6**:68
  octreotide **6**:69
  P-selectin **6**:68
  sermorelin **6**:69
  teriparatide **6**:69
Mipomersen **6**:284, **7**:676–679
miR-122 **4**:267–268
Mirabegron **7**:727–729
MiravirsendLNA **6**:286
Mitochondrial dysfunction, and DILI **4**:221–223
  and hepatic specificity of action for drugs **4**:221–223
  intracellular signaling pathways **4**:221
    inhibition of fatty acid oxidation and lipid transport **4**:221
    JNK signaling **4**:221
  mitochondrial adaptation to drugs **4**:223
  mitochondrial toxicity **4**:221
  overview **4**:221
  structural aspects of drugs eliciting mitochondrial damage **4**:223
Mitochondrial membrane potential, and nanoparticles **1**:283–284
Mitochondrial potential staining **1**:283f
Mitogen-activated protein kinase kinase 1/2 **7**:414
Mitotic stress, and cancer **5**:9
Mitoxantrone, for multiple sclerosis **5**:450–451
Mixed-lineage kinase **7**:416–417

MK-0634 **7**:725–727
MK-1064 **7**:258
MK-3697 **7**:258
MK-4305 **7**:255
MK-8133 **7**:260–263
MNK inhibition **5**:227–228
Mobile applications **3**:457–460
  using a client–server model **3**:459–460
Model analysis and validation **2**:459
Model parameter fitting **2**:458–459
Model simplification, *S*-systems **2**:459
Model usage in systems research **2**:459–460
Model validation and sources of error, protein model **3**:138–139
Modeling and simulations, translational aspects **2**:503–509
  empirical pharmacokinetic/pharmacodynamic models **2**:504
    deffect-compartment model **2**:507
  mechanistic models to system biology models **2**:505–506
  mechanistic pharmacokinetic/pharmacodynamic models **2**:504
    selection of starting dose for first-in-human studies **2**:507
  overview **2**:503
  PBPK models **2**:508
  system biology models
    combinations of molecular targeted drugs in oncology **2**:508–509
    mathematical model for rheumatoid arthritis **2**:509
Modeling protein flexibility **3**:321–324
  ensemble docking **3**:322–324
    molecular docking against a structural ensemble **3**:323–324
    preparing the protein structural ensemble **3**:322–323
  induced-fit docking **3**:322
  in postdocking stage **3**:325
  in protein–peptide docking **3**:325–326
  soft docking **3**:322
Modulation of enzymes, and carbohydrates **1**:581–582
MoKa **3**:282–283
Molecular alignment challenge, pharmacophores **3**:213–214
  alignment of ligands for 3D QSAR **3**:213
  analysis of hits from a random screen **3**:214
  pharmacophore feature representation **3**:215–216
  shared activity of two different types of ligands **3**:214
  validation standards **3**:215
  variable binding modes **3**:216
Molecular chaperones **5**:229
Molecular docking **3**:297–328
  affinity prediction in **3**:304–310
    affinity prediction problem **3**:304–306
    overview **3**:309–310
    scoring poses in docking **3**:306
    validation of docking programs and their associated scores **3**:306–309
  and binding site similarity, for drug repurposing **1**:30
  defining **3**:298–299
  democratization of **3**:310
  medicinal chemistry **3**:311–314
    considerations **3**:312–313
    end-user's choice **3**:313
    end-users compatible **3**:314
    incorporation **3**:312
    input protein structure **3**:312
    less susceptible results **3**:314
    over-interpretation of scores **3**:313
    self-critical software **3**:314
    software **3**:311–312
    usage methods **3**:311
    utilization **3**:311
  modeling protein flexibility **3**:321–324
    ensemble docking **3**:322–324
    induced-fit docking **3**:322
    postdocking stage **3**:325
    protein–peptide docking **3**:325–326
    soft docking **3**:322
  overview **3**:297–298, **3**:319
  pose prediction in **3**:299–304
    sampling algorithms **3**:299–300
    tackling binding site flexibility **3**:302–303
    tackling ligand flexibility **3**:300–301
    treating solvent during docking **3**:303–304
  protein binding mechanisms, models for **3**:319–321
  protein–ligand interactions, computational modeling of **3**:321
  protein–protein interactions, computational modeling of **3**:321
  for ultra-HTS **2**:424
  unsolved docking problems **3**:310
  usefulness **3**:298
Molecular dynamics and quantum mechanics **3**:51–66
  applications **3**:56–62
    antibiotic resistance tackling **3**:58–59
    covalent inhibitors design **3**:57–58
    drug metabolism prediction **3**:61–62
    influenza virus mutations effects on antiviral efficiency **3**:56–57
    sustainable processes in drug development and manufacturing **3**:59–61
  methods for drug discovery and development **3**:55–56
    chemical accuracy in QM/MM calculations **3**:55–56
    recent advances in MD simulations **3**:55
    thermodynamics properties of protein-ligand association **3**:55
  overview **3**:51–52
  theoretical background **3**:52–54
    hybrid QM/MM simulations **3**:53–54
    molecular dynamics, described **3**:52–53
    overview of foundations of quantum chemistry **3**:53
Molecular dynamics simulations
  GPCRs **3**:156–159
Molecular fields **3**:254
  analysis descriptors **3**:353
Molecular fields, ligand-based applications **3**:254–286
  3D activity cliff analysis **3**:277–281
    activity miner/activity atlas **3**:278–281
  3D clustering of molecule libraries **3**:270
  3D-QSAR **3**:270–277
    CoMFA **3**:271–272
    CoMSIA **3**:273
    COSMO*sar3D* **3**:274–276
    FieldQSAR **3**:276
    GRID/GOLPE/FLAP **3**:277
    GRIND **3**:277
    Template CoMFA **3**:274
    Topomer CoMFA **3**:273–274
  ADME prediction **3**:281–286
    MetaSite **3**:283–286
    MoKa **3**:282–283
    VolSurf **3**:282
  ligand similarity assessment **3**:254–260
    bioactive pose prediction **3**:260–264
    COSMO*sim3D* **3**:255–256
    FieldTemplater **3**:261–262
    FLAPpharm **3**:263–264
    GRID/FLAP **3**:257–258
    XED/FieldAlign **3**:258–260
  scaffold hopping **3**:266–270
    SHOP **3**:267–268
    Spark **3**:268–270
  virtual screening **3**:264–265
    fieldscreen/blaze **3**:264
    FLAP **3**:264–265
Molecular fields, structure-based applications **3**:286–292
  binding site identification **3**:286–287
    FLAPsite **3**:287
    Q-SiteFinder **3**:286
    SiteHound **3**:286
  binding site similarity assessment **3**:287–289
    GRID/FLAP **3**:287–288
    IsoMIF **3**:288–289
  determination of water positions **3**:291–292
    WaterFLAP **3**:291–292
  docking **3**:289–291
    AFMoC **3**:289–290
    AutoDock **3**:290
    FLAPdock **3**:291
    Glide **3**:291
    GOLD **3**:291
Molecular fingerprints **3**:339–346
  circular fingerprints **3**:342–344
    topological subsets **3**:343–344
  hybrid fingerprint **3**:344
  other fingerprint types **3**:344–346
    affinity fingerprints **3**:345
    EDPrints **3**:345
    fingerprints for ligands and proteins (FLAP) **3**:346
    interaction fingerprints **3**:346
    reaction fingerprints **3**:346
    text-based **3**:345
  path-based fingerprints **3**:342
  pharmacophore fingerprints **3**:344

substructure key-based fingerprints **3**:340–341
topological fingerprints **3**:341
Molecular interactions **3**:67–100
abridged guide to hydrogen bonding **3**:73–74
atom **3**:72
background **3**:68–71
carbonyl-group interactions **3**:88–89
components of **3**:70
enthalpy–entropy compensation **3**:71
fluorine **3**:87–88
halogen bonding **3**:83–87
background **3**:83–84
fluorine as a halogen-bond donor **3**:84
halogen bonding in drug development **3**:86
halogen bonds in protein–ligand complexes **3**:84–86
halogen-bond geometries **3**:84
halogen-enriched fragment libraries **3**:86
skeptical chemist's view of halogen bonding **3**:86–87
hydrogen bond diversification **3**:71–72
involving aromatic rings **3**:74–82
anion–π **3**:80–81
aromatic rings as hydrogen bond acceptors **3**:79–80
aromatic-ring interactions with halogens **3**:77–78
cation–π interactions **3**:78–79
CH π interactions **3**:81–82
instructive example of the benzene dimer **3**:74–75
interaction formerly known as π-stacking **3**:75–77
stacking of aromatic rings with amide groups **3**:77
major types **3**:73–91
methods **3**:68–70
nonpolar pockets occupation by ligand hydrophobic groups **3**:82–83
overview **3**:68
and pharmaceutical crystal form **3**:91–94
background **3**:91–92
hydrogen-bond patterns and crystal form stability **3**:92–93
impact of crystal-structure interactions on physical properties **3**:94
relative importance assessment **3**:72–73
sulfur interactions **3**:89–91
chalcogen bonding **3**:90–91
hydrogen bonds involving sulfur **3**:90
to nonpolar groups **3**:89–90
sulfur as a halogen bond acceptor **3**:91
water **3**:70–71
Molecular properties **1**:560–564
Molecular query language **3**:333–334
international chemical identifier **3**:333–334
Molecular shape analysis descriptors **3**:353
Molecular simulation **3**:14–33
force field advances **3**:17–22
coarse-grained force fields **3**:21–22
force fields for other species **3**:19
organic molecule force fields **3**:18–19
polarizable force fields **3**:19–21
protein force fields **3**:18
hardware and software advances **3**:14–17
cloud and distributed computing **3**:16
graphics processing units **3**:15–16
novel algorithms and parallelization **3**:16–17
special-purpose machines **3**:14–15
Molecular simulation, novel simulation approaches and trends **3**:22–27
parallel and enhanced sampling **3**:22–26
bias potential methods **3**:25–26
Markov state models **3**:22–24
replica exchange methods **3**:24–25
simulation of large systems **3**:26–27
Molecular size, human PK **4**:56
Molybdenum, as nutraceuticals **1**:117
Monoamine oxidase B enzyme (MAO-B) **7**:51
Monoclonal antibodies **6**:39–46
cancer therapeutic
chimeric murine–human monoclonal antibodies **6**:42
conjugated monoclonal antibodies **6**:42–43
fab-engineered monoclonal antibodies **6**:43
Fc-engineered monoclonal antibodies
fully human monoclonal antibodies **6**:42
history **6**:41
humanized monoclonal antibodies **6**:42
murine monoclonal antibodies **6**:41
defintion **6**:39–40
structure **6**:41
types **6**:40–41
Monotherapy and polypharmacology, compared **2**:261–262
Monovalent Smac-mimetic IAP antagonists **5**:180
Monovalent Smac-XIAP inhibitors **5**:181t–183t
Morpholino oligonucleotide **6**:218f
Mounting **2**:159–160
Mouse lymphoma assay, for genotoxicity evaluation **4**:201
Mouse models, genectically humanized
drug transporters **4**:137–138
transporter-humanized mice **4**:137–138
functionalization (phase I) and conjugative (phase II) drug-metabolizing enzymes **4**:133–137
conjugation enzymes **4**:136
CYP P450-humanized mice **4**:134–136
functionalization by cytochrome P450 enzymes **4**:134
UGT- and NAT-humanized mice **4**:136–137
genetic modifications of xenobiotic receptors **4**:132–133
receptor-humanized mice **4**:133
MRI applications **4**:295–296
MS-based proteomics for target identification **2**:420–422
MT-1303 **5**:403
mTOR pathway, pharmacological inhibition of **1**:361–363
MTT **1**:278–279
MTX
combined with filgotinib **5**:428
MTX-IR
ABT-494 in **5**:429
peficitinib in **5**:430
safety of **5**:429–430
VX-509 in **5**:431
μ opioid receptor agonists **1**:247f
Mucosal barrier enhancer drug, for inflammatory bowel disease **5**:501
Multidrug-resistant *Acinetobacter* **5**:529
Multidrug-resistant *Pseudomonas aeruginosa* **5**:530
Multiobjective optimization **2**:64–93
defining the project target requirements **2**:66–69
target potency and selectivity requirements **2**:67–69
effect of systematic biases in drug discovery **2**:87–88
effect of personal and organization biases **2**:87–88
overcoming systematic biases **2**:88
generally **2**:65–66
overview **2**:64–69
and physical properties **2**:69–76
DMPK, safety, and physical properties **2**:70–71
drug-like property space **2**:70
ligand efficiency **2**:75–76
target activity and physical properties **2**:71–76
of PK/PD parameters **2**:76–87
achieving a balanced PK/PD profile **2**:78–79
drug efficiency, definition of **2**:80–81
drug efficiency and free drug hypothesis **2**:79–87
drug efficiency index **2**:81–87
PK/PD properties of development compounds **2**:76–78
Multiple sclerosis (MS) **5**:439–473
pathology **2**:375f
therapeutic approaches in **5**:444–453
adrenocorticotropin hormone (ACTH) **5**:451–452
alemtuzumab **5**:450
cladribine **5**:452–453
cyclophosphamide **5**:451
dimethyl fumarate **5**:447
fingolimod **5**:446
glatiramer acetate **5**:450
interferon β-1a **5**:448–449
interferon β-1b **5**:448
laquinimod **5**:447–448
methotrexate **5**:452
mitoxantrone **5**:450–451
natalizumab **5**:449
peginterferon β-1a **5**:449
rituximab **5**:451
teriflunomide **5**:447
See also Neurodegenerative disorders

Multiplex assays
  biomarkers **2**:500
Multiscale modeling
  defintion of **3**:491
Multisite animal model trials **2**:510
Multistep flow processes **1**:166–180
Multitargeted agents
  achieving without becoming nonselective **2**:270
  optimizing potency of **2**:269–270
Multitargeted molecular design **2**:259–275
Murine model, regenerative medicine **1**:400–401
Muscarinic receptors **7**:26–27
Muscle regeneration using small molecules, regenerative drugs **1**:414–416
  muscle-based applications of small molecule stem cell modulators **1**:414–416
Mutagenicity **1**:487–488
  prediction with commercial in silico systems **2**:238–246
Mutant selective EGFR inhibitors design **5**:51–55
  early inhibitors of EGFR, targeting activating mutations **5**:51–52
  future outlook **5**:55
  T790M mutant selective EGFR inhibitors design **5**:52–55
Myc/Max inhibitors **5**:186
Mycobacterium tuberculosis **5**:530–532
Mydicar **7**:646
Myeloid-derived suppressor cells (MDSCs) **5**:360–361
N-Myristoyltransferase inhibitors **5**:733

N

Naftifine **5**:708f
Nanocarriers **1**:267f
Nanolayered siRNA delivery for wound healing **6**:293
Nanomaterials **1**:265–272
  actual research trends **1**:268–272
  advantages, in medicine **1**:267–268
  description **1**:265–267
  gold nanoparticles **1**:266
  liposomes **1**:266
  magnetic nanoparticles **1**:266–267
  polymeric nanoparticles **1**:266
  quantum dots **1**:267
  silica nanoparticles **1**:267
Nanoparticles, as modern drug delivery systems **6**:139–140
Nanotechnology **1**:264–295
  biodistribution **1**:272–278
    autoradiography **1**:276
    elemental analysis **1**:277
    ex vivo fluorescent microscopy **1**:276
    ex vivo light microscopy **1**:276
    in vivo magnetic particles imaging **1**:275
    in vivo magnetic resonance imaging **1**:275
    in vivo optical imaging **1**:272–274
    in vivo positron emission tomography **1**:274–275
    magnetometry **1**:277–278
    transmission electron microscopy **1**:276–277
  future challenges **1**:284–286
    biodegradable products **1**:285–286
    circular economy **1**:285
    development of new applications **1**:286
    development of new materials **1**:285
    green nanoscience **1**:285
    transference to industry **1**:286
  nanomaterials **1**:265–272
    actual research trends **1**:268–272
    advantages of nanomaterials in medicine **1**:267–268
    description **1**:265–267
    gold nanoparticles **1**:266
    liposomes **1**:266
    magnetic nanoparticles **1**:266–267
    polymeric nanoparticles **1**:266
    quantum dots **1**:267
    silica nanoparticles **1**:267
  overview **1**:265
Nanotechnology, toxicity **1**:278–284
  cell death mechanisms **1**:282–284
    annexin-V **1**:282
    cell morphology **1**:284
    loss of mitochondrial membrane potential **1**:283–284
    ROS generation **1**:283
  cell membrane permeability **1**:281–282
    calcein acetoxymethyl **1**:281–282
    DNA intercalating fluorescent agents **1**:282
    fluorescein diacetate **1**:281
    lactate dehydrogenaze enzyme **1**:282
    trypan blue **1**:281
  fluorescent probes, instrumentation for detection **1**:284
  general considerations for NPs presence **1**:284
  proliferation assays **1**:278–280
    alamar blue assay **1**:279
    cell division assay **1**:280
    clonogenic assay **1**:279–280
    EdU proliferation assay **1**:280
    MTT **1**:278–279
Narlaprevir **8**:583–608
Natalizumab, for multiple sclerosis **5**:449
Natamycin **5**:705f
Natriuretic peptide system-related approaches **7**:638–640
  corin modulation of natriuretic peptide formation **7**:639–640
  LCZ696 **7**:638–639
  natriuretic peptide analogs **7**:639
Natural food source, nutraceuticals classification by **1**:110
Natural product-based inhibitors **5**:233
Natural product-inspired chemical synthesis **2**:135–137
  benzimidazolinopiperazinones **2**:135
  β-lactams **2**:136–137
Natural products
  as lead structures **2**:137–139
    lead-like natural products **2**:137–139
  PPI inhibitor **5**:157–159
Natural scaffolds **2**:116–152
Nature, bioisosterism in **1**:187–188
$Na_V1.7$ blockers **7**:136–161
$Na_V1.8$ blockers **7**:161–165
$Na_V1.9$ blockers **7**:165
Nedd8-activating enzyme (NAE) **8**:96–97
  profile of the clinical candidate **8**:109–110
  selection of the development candidate **8**:108
Neglected disease populations **1**:491–504
  back to new targets **1**:498–500
  collaborative models for partnerships and for building teams **1**:497–498
  compounds and biology **1**:500–501
  data sharing—dealing with fragmentation **1**:500
  drug discovery, and negative net present value **1**:492–493
  intellectual property **1**:501–502
  new candidates pipeline **1**:493–497
  parasitic infections **1**:491–492
Nematodes **5**:737–738
  filarial worms **5**:737–738
  soil-transmitted helminths **5**:737
Neovascularization, targets in **5**:23
Nepafenac (Nevanac) **5**:397
Net present value, and drug discovery **1**:492–493
Network biology, mathematical models for **2**:456–460
  enzyme kinetics **2**:458
  from interaction network to mathematical dynamic model **2**:457
  model analysis and validation **2**:459
  model parameter fitting **2**:458–459
  model simplification, *S*-systems **2**:459
  model usage in systems research **2**:459–460
  stochastic *versus* deterministic models **2**:458
Network perturbation amplitude (NPA) methodology **2**:455f
Network-based methods
  polypharmacology **2**:267–268
Neural cell migration in vivo, regenerative medicine **1**:412
Neural stem cell culture **1**:403
Neuraminidase inhibitors **5**:540–541
Neuregulin-1 **7**:648–649
Neurodegenerative disorders **5**:453–464
  Alzheimer's disease **5**:453–454
    donepezil for **5**:455
    galanthamine for **5**:456
    memantine for **5**:456–457
    rivastigmine for **5**:456
    select drugs in development for **5**:457–458
  model screening, iPSC models **1**:62–63
  MS. *See* Multiple sclerosis
  overview **5**:441–444
    acute neuronal injury **5**:442–443
    calcium imbalance **5**:442
    chronic neurodegeneration **5**:443–444

citrullination and neurodegeneration **5**:442
Parkinson's disease **5**:458
amantadine for **5**:462
anticholinergics for **5**:462
apomorphine for **5**:462
bromocriptine for **5**:459
cabergoline for **5**:459
carbidopa/levodopa for **5**:458–459
COMT inhibitors for **5**:462
istradefylline for **5**:463
levodopa formulations for **5**:463–464
MAO-B inhibitors for **5**:463
pergolide for **5**:459
pramipexole for **5**:459
ropinirole for **5**:459
rotigotine for **5**:462
Neurogen **7**:215
Neuromed compound **7**:82–84
Neuronal cells, induced pluripotent stem cell-derived **4**:182–183
Neuronal nAChR
α4β2-nAChR **7**:37
α7-nAChR **7**:38
Neuronal system, regenerative medicine **1**:402–413
cell-based therapies for neurological disorders **1**:409–412
augmenting neurogenesis in vivo **1**:410–411
neural cell migration in vivo **1**:412
NSC differentiation in vivo **1**:411–412
reprogramming in vivo **1**:412
in situ stem cell modulation **1**:410
directed differentiation **1**:404–409
bone marrow-mesenchymal stem cells **1**:408
embryonic stem cells **1**:404–406
induced pluripotent stem cells **1**:406–408
NSCs and NPCs in vitro **1**:403–404
transdifferentiation of other cell types **1**:408–409
disease screening and drug discovery **1**:413
neural stem cell culture **1**:403
neuronal regeneration **1**:402–403
Neutral endopeptidase (NEP) **1**:225t
Neutrophil gelatinase-associated lipocalin, biomarker of acute kidney injury **4**:274–275
New candidates pipeline **1**:493–497
New inhibitor chemotypes **8**:210–219
New modalities for target modulation and validation **2**:2–10
biased receptor signaling **2**:4–5
gene editing and gene therapy **2**:2–4
modulating proteostasis and protein degradation **2**:8–10
modulators of protein transcription, translation, and translocation **2**:5–8
Next generation sequencing technologies **2**:354–361
clinical utility of **2**:357–359
described **2**:354–357
in drug discovery and development **2**:359–360
implementation for clinical applications **2**:357
nonoptical **2**:356–357
semiconductor-based **2**:356–357
optical, pyrosequencing-based **2**:355–356
distinctly labeled fluorescent nucleotide **2**:356
overview **2**:354
third generation genome sequencing technologies **2**:357
Next-generation antiandrogens **5**:143f
Next-generation therapeutics **1**:326–328
Next-generation therapeutics, expanding druggable target space **1**:328–335
immune targets and vaccines **1**:332–334
oligonucleotides and oligonucleotide drugs **1**:334–335
PPIs and their modulators **1**:328–332
biological selection of backbone-modified macrocyclic peptides **1**:330–331
macrocycles **1**:329–330
stable peptide frameworks for therapeutic applications **1**:331–332
Next-generation therapeutics, targeted delivery of **1**:335–343
CPPs as delivery vectors **1**:336–339
cellular uptake pathways for drug delivery with CPPs **1**:336–337
enhancing endosomal escape of biologic drugs **1**:338–339
molecular determinants of cell-permeability **1**:337–338
targeting specific tissues **1**:339–342
delivery of therapeutics across the blood–brain barrier **1**:340
targeted delivery to the liver **1**:341–342
targeting the pancreas **1**:342
targeting the pituitary **1**:341
targeting tumors **1**:342–343
antibody–drug conjugates **1**:342–343
GPCRs as targeting vectors **1**:343
NextGets **2**:254–255
NFkB-inducing kinase (NIK) **5**:409
NFTs as biomarkers, for Alzheimer's disease **1**:76–78
NIAD-4 and derivatives **1**:89–90
Nicotinic acetyl choline receptor (nAChR) modulators **1**:243t
Nikkomycin Z **5**:708–709, **5**:709f
Nipah and hendra viruses
antiviral drugs for **5**:678
Nitration
continuous flow processing **1**:142
Nitric oxide–aspirin hybrids **7**:586
Nitroheterocycles **5**:729–730
NK cell-based cancer immunotherapy **6**:48
NMDA receptor **7**:39
NMR spectroscopy for fragment screening **2**:424–425
NNRTIs **5**:642t
Nociceptin/orphanin FQ peptide (NOP) **1**:247f
Nonamino acid structures, alpha 2 delta ligands **7**:120–122
Merck compounds **7**:120–122
nonamino acid derivatives **7**:122
Noncarbon spiro atom **1**:253
Noncatalytic integrase inhibitors, HIV **5**:646
Noncovalent allosteric modulators **2**:285
Non-cysteine-targeting covalent inhibitors **5**:99
Nongenetic risk factors for DILI **4**:208
Non-nucleotide-based antagonists **7**:572–573
Nonnucleoside reverse transcriptase inhibitors
HIV **5**:640–642
doravirine **5**:641–642
rilpivirine **5**:640–641
Nonoptical next generation sequencing **2**:356–357
semiconductor-based **2**:356–357
Nonpolar groups, sulfur interactions to **3**:89–90
Nonpolar pockets occupation, by ligand hydrophobic groups **3**:82–83
Nonrandomized enrichment study design **2**:537f
Nonribosomal peptide synthetases **1**:329
Nonsmall cell lung cancer
and EGFR biology **8**:1–2
Nonsteroidal glucocorticoid modulators **8**:452
Nontest methods for REACH legislation **1**:472–490
dissemination of REACH data **1**:475
nontest methods **1**:475–487
grouping and read-across **1**:483–485
OECD principles for the validation of (Q)SAR **1**:475–483
(Q)SAR toolbox **1**:485–487
(Q)SAR toolbox, main functionalities **1**:485–487
obligations for pharmaceutical companies under REACH **1**:474
overview **1**:472–475
practical example on the use of (Q)SAR under REACH **1**:487–488
REACH Annex XI requirements for (Q)SAR and read-across **1**:474–475
grouping of substances and read-across approach **1**:474–475
(Q)SAR **1**:474
understanding REACH **1**:472–474
alternative methods promotion **1**:473–474
legal framework **1**:472–473
Nontraditional approaches **5**:699
Norepinephrine transporter **7**:40–41
Noscira
inhibitors reported by **7**:350
Novartis **7**:263–267
inhibitors reported by **7**:350–353
pyrazolopyridines **7**:265–267
spirocyclic amino-amides **7**:263–265
Novel algorithms and parallelization, for molecular simulation **3**:16–17

Novel simulation approaches and trends **3**:22–27
  parallel and enhanced sampling **3**:22–26
    bias potential methods **3**:25–26
    Markov state models **3**:22–24
    replica exchange methods **3**:24–25
  simulation of large systems **3**:26–27
Novel therapeutic approaches, in dyslipidemia management **7**:666–687
  targeting plasma cholesterol levels **7**:666–684
    CETP inhibitors **7**:681–682
    ETC-1002 **7**:682–684
    ezetimibe **7**:666–669
    lomitapide **7**:679–681
    mipomersen **7**:676–679
    PCSK9 inhibitors **7**:669–676
  targeting plasma TG levels **7**:684–687
    alipogene tiparvovec **7**:685–686
    diacylglycerol O-acyltransferase inhibitors **7**:686–687
    ISIS-APOCIIIRx **7**:686
    omega-3 free fatty acids **7**:684–685
Novel therapeutic concepts, chemical probes for **2**:52–53
Novel therapeutics targeting epigenetics **2**:297–328
  epigenetic control of gene expression via histone lysine and histone arginine PTM **2**:300–320
    agents targeting epigenetic reader proteins **2**:318–320
    epigenetic erasers **2**:309–318
    epigenetic writers **2**:301–309
    histones and the epigenetic control of gene expression **2**:300–301
  epigenetic modulation via DNA methylation/demethylation **2**:298–300
  overview **2**:297–298
Novel topoisomerase inhibitors **5**:693–694
Novobiocin-based inhibitors **5**:236–237
NPC perturbation detection, in silico models **4**:232
NRTIs **5**:637t
NS3/4A protease inhibitors **5**:539
NS5A inhibitors **5**:539
NS5B
  nonnucleotide inhibitors **5**:539
  nucleotide inhibitors **5**:538
NSC differentiation in vivo, regenerative medicine **1**:411–412
NSCs and NPCs in vitro, regenerative medicine **1**:403–404
Nuclear magnetic resonance **2**:213
  label-free screening **2**:420
Nucleic acid based therapeutics, biochemically produced RNAs **6**:299–306
  CRISPR/Cas9 **6**:303–306
    challenges and future perspectives **6**:305–306
    potential therapeutic applications of **6**:303–305
  RNAi triggers **6**:299–303
    Ago2shRNAs **6**:301–302
    biochemically produced RNAi in clinical development **6**:302
    challenges and future perspectives **6**:302–303
    pri-miRNA mimics **6**:299–301
    shRNA triggers **6**:301
Nucleic acid based therapeutics, synthetic therapeutic oligonucleotides **6**:281–299
  antisense oligonucleotides (ASOs) **6**:281–286
    challenges and future perspectives **6**:286
    chemical modification **6**:281–284
    in clinical development **6**:284–286
    pharmacokinetic properties of **6**:284
  aptamers **6**:295–299
    challenges and future perspectives **6**:299
    chemical modifications **6**:295
    in clinical development **6**:298
    potential therapeutic applications of **6**:296–298
  RNA interference (RNAi) **6**:286–295
    challenges and future perspectives **6**:295
    in clinical development **6**:293–295
    cytoplasmic processing **6**:287–290
    effective delivery **6**:293
    focus areas for improving potency and safety **6**:292
    potential therapeutic applications of **6**:293
    transcriptional silencing and activation **6**:290
    types of synthetic RNAi substrates **6**:290–292
Nucleic acids **6**:144
  force field advances **3**:19
  solution behavior of **6**:132
Nucleophilic substitution
  continuous flow processing **1**:151
Nucleoside reverse transcriptase inhibitors
  HIV **5**:636–640
    investigational NRTIs **5**:638–640
    tenofovir alafenamide **5**:637–638
Nucleoside-based DNMT inhibitors **2**:300f–301f
Number of protein folds **3**:122–123
Numerical descriptors **3**:346–355
  2D descriptors **3**:347–351
    indicator variables **3**:351
    molecular identification numbers **3**:351
    thermodynamic descriptors **3**:351
    topological descriptors **3**:349–350
    whole-molecular descriptors **3**:347–348
  3D descriptors **3**:351–354
    3D descriptor families **3**:353–354
    electronic descriptors **3**:351–352
    molecular field analysis descriptors **3**:353
    molecular shape analysis descriptors **3**:353
    receptor surface analysis descriptors **3**:353
    shape descriptors **3**:352
    size descriptors **3**:352
    van der Waals parameters **3**:353
    volume descriptors **3**:352
  4D descriptors **3**:354–355
  other special descriptors and approaches **3**:355
Nutlins **5**:251–253
Nutraceuticals **1**:107–134
  for Alzheimer's disease **1**:131–132
  in cancer prevention **1**:127–129
    minerals in cancer management **1**:129
    vitamins in cancer management **1**:129
  in chronic inflammatory disorders **1**:130–131
    chondroitin **1**:130
    glucosamine **1**:130
    methylsulfonylmethane **1**:130
    pomegranate **1**:131
    S-adenosyl methionine **1**:131
  classification **1**:110
    by chemical nature **1**:110
    by natural food source **1**:110
    by pharmacological action **1**:110
  in CVDs **1**:125–127
    coenzyme Q10 **1**:127
    dietary fibers **1**:126
    fermented red yeast rice **1**:127
    flavonoids **1**:126
    plant sterols **1**:126
    policosanol **1**:126
    polyunsaturated fatty acids **1**:125–126
    potassium **1**:127
    vegetables in prevention of CVDs **1**:126–127
  for diabetes **1**:129
  different terminologies **1**:109–110
    designer foods **1**:110
    dietary supplement **1**:109
    functional foods **1**:109
    medical foods **1**:109
    nutraceuticals **1**:109
    phytochemicals **1**:110
  health benefits of **1**:124–132
  microbes as **1**:123–124
    prebiotics **1**:123–124
    probiotics **1**:123
  for obesity **1**:129–130
  overview **1**:108
  for Parkinson's disease **1**:131
  phytochemicals as **1**:118–121
    carotenoids **1**:118–119
    organosulfur compounds **1**:121
    phenolics **1**:119–121
  plants as **1**:121–123
  rationale for use of **1**:109
  vitamins as **1**:110–113
    water insoluble vitamins **1**:110–111
    water soluble vitamins **1**:111–113
Nutraceuticals, minerals as **1**:114–118
  essential macrominerals **1**:114–117
    calcium **1**:114
    magnesium **1**:116
    phosphorus **1**:116
    potassium **1**:116
    sodium **1**:116–117

sulfur **1**:117
essential trace minerals/microminerals **1**:117–118
chromium **1**:117
cobalt **1**:117
copper **1**:117
fluoride **1**:117
iodine **1**:117
iron **1**:117
manganese **1**:117
molybdenum **1**:117
selenium **1**:117–118
zinc **1**:118
Nutraceuticals assessment, systems toxicology **2**:462
NVP-AUY922 **2**:224f, **5**:240
phase II **2**:222–223
Nystatin **5**:705f

O

Obesity
MCH-1 receptor antagonist NGD-4715 for **8**:488–515
nutraceuticals **1**:129–130
Octahydropyrrolo[3,4-*c*]pyrroles **7**:250–252
JNJ-42847922 **7**:252
Octreotide **6**:69, **6**:78, **6**:92, **6**:92f
Ocular disease, regenerative drugs **1**:422–427
corneal disease **1**:422
new assays and assay technologies **1**:426–427
ocular applications of small molecule stem cell modulators **1**:422
retinal disease **1**:422–423
retinal therapies using stem cells **1**:423–424
small molecule modulation of hES and iPS cells to retinal cells **1**:425–426
ODE model **3**:496–497
ODM-201 **5**:142
OECD toolbox **2**:237
Off-label medicine
drug repurposing **1**:17–18
Off-target activity, avoiding **2**:269
Off-target engagement **1**:570–571
Off-target *versus* on-target, drug repurposing **1**:19–20
Older age, medical need in **1**:541
Oligodendrocyte progenitor cell (OPC) differentiation and remyelination, and high-content screening **2**:373–376
Oligonucleotide drugs **1**:334–335
Oligonucleotide therapeutics **6**:268t
Oligonucleotides
analytic techniques **6**:266t–267t
Oligonucleotides manufacturing **6**:233–279
analytic tools to support **6**:265–268
branchmers formation **6**:244–245
HPLC techniques for oligonucleotides analysis **6**:265–268
manufacturing process and equipment **6**:258–261
oligonucleotide chromatography equipment **6**:259–260
oligonucleotide cleavage and deprotection equipment **6**:258–259
oligonucleotide lyophilization process and equipment **6**:261
oligonucleotide synthesis equipment **6**:258
oligonucleotide ultrafiltration & diafiltration equipment **6**:260–261
oligonucleotide synthesis, historical perspective of **6**:238–239
overview **6**:234
raw material-related impurities **6**:239–241
nonreactive and noncritical impurities **6**:240
phosphoramidite-related impurities **6**:239
reactive and critical impurities **6**:240–241
reactive but noncritical impurities **6**:240
reagent-related impurities **6**:247–248
activator **6**:247
capping reagent **6**:248
detritylation reagent **6**:247
thiolation/oxidation **6**:247–248
regulatory aspects of oligonucleotides **6**:268–271
assay **6**:270
oligonucleotides characterization **6**:270–271
setting specifications **6**:269–270
research-scale manufacturing **6**:248–258
oligonucleotide cleavage and deprotection **6**:252–253
oligonucleotide isolation **6**:257–258
oligonucleotide purification **6**:253–257
oligonucleotide solid-phase synthesis cycle **6**:249–252
small-scale modeling for **6**:261–264
solid supports **6**:241–243
nucleoside-loaded supports **6**:242–243
therapeutic oligonucleotides
classes of **6**:234–235
heterocyclic base modification **6**:238
internucleotide linkage modification **6**:235–237
sugar modification **6**:237–238
universal supports **6**:245–246
Omarigliptin (MK-3102) **7**:524
Omega-3 free fatty acids **1**:125, **7**:684–685
Omega-6 fatty acids **1**:126
-Omics approaches, to carcinogenicity testing **4**:249–250
OMICS technologies **2**:102–105
genomics **2**:102–103
metabolomics **2**:104–105
proteomics **2**:103–104
Oncogene expression control by small molecules in cancer cells **5**:316–332
androgen receptor **5**:331
BCL-2 **5**:328–330
c-*KIT* **5**:326–328
c-*MYC* **5**:316–321
c-SRC **5**:332
HIFα **5**:330–331
HSP-90 **5**:330
h*TERT* **5**:321–322
MET **5**:332
RAS family **5**:322–325
RET **5**:331–332
VEGF and VEGFR **5**:325–326
Oncology, combinations of molecular targeted drugs in **2**:508–509
1D structures, similarities of **3**:363–364
Online web resources **3**:367–368
Ontologies, drug repurposing **1**:24
Open laboratories. *See* Intellectual property in open landscape
Opper, as nutraceuticals **1**:117
Oprozomib (ONX0912, PR047) **5**:269–270
Optical next generation sequencing, pyrosequencing-based **2**:355–356
distinctly labeled fluorescent nucleotide **2**:356
Optical waveguide grating, kinetics in drug discovery **2**:186
Optimizing residence time **2**:194–196
Oral absorption
ADME **4**:36–37
and availability prediction **4**:104–105
in vitro predictions **4**:105
physicochemical determinants of absorption **4**:104–105
and bioavailability **4**:5–12
Orally delivered peptides, for inflammatory bowel disease **6**:157–170
constrained and stable peptides **6**:159–162
disulfide-rich peptides **6**:159
disulfide-rich peptides, examples of **6**:159–161
summary **6**:161–162
impact of food **6**:165
orally delivered and targeted agents **6**:165
permeability **6**:163–164
absorption in the GI tract **6**:164
permeability at the epithelial surface **6**:164
transporters on intestinal epithelial cells **6**:164
protease stability for peptides **6**:162
redox stability **6**:162
stability to microbes **6**:163
Orally delivered rimegepant **7**:207–213
Orexin receptor antagonists **1**:250t, **7**:225–279
Actelion **7**:227–236
1-acyl-2-benzylpyrrolidines **7**:233–234
N-glycine-sulfonamides **7**:234–236
proline sulfonamide ACT-462206 **7**:232–233
substituted lactams **7**:231–232
tetrahydroisoquinolines **7**:227–231
Banyu **7**:237
tetrahydroisoquinolines **7**:237
compounds that progressed to clinical trials **7**:274

Orexin receptor antagonists (*continued*)
Eisai **7**:238–239
N-aryl-2-phenylcyclopropanecarboxamides **7**:238–239
GlaxoSmithKline **7**:239–246
GSK early selective OX1R tool compounds **7**:244–245
SB-649868 and substituted piperidines **7**:239–244
triazolo-thioamides **7**:246
Heptares **7**:246–247
2*H*-pyrido[2,3-*e*][1,2,4]thiadiazin-3(4*H*)-one 1,1-dioxides **7**:246–247
International Institute for Integrative Sleep Medicine **7**:247–248
OX2R agonists **7**:247–248
Johnson & Johnson/Janssen Pharmaceuticals **7**:250–252
4-phenyl-[1,3]dioxanes **7**:250
octahydropyrrolo[3,4-*c*]pyrroles **7**:250–252
Merck **7**:253–263
2,5-diarylnicotinamides **7**:257
diamines/MK-4305 **7**:253–254
diazepanes **7**:260
MK-1064 **7**:258
MK-3697 **7**:258
MK-4305 **7**:255
MK-8133 **7**:260–263
piperidine ethers **7**:260
piperidines/MK-6096 **7**:255–257
proline bis-amides **7**:253
Novartis **7**:263–267
pyrazolopyridines **7**:265–267
spirocyclic amino-amides **7**:263–265
overview **7**:226–227
Research Triangle Institute **7**:267–269
diarylureas related to SB-334867 **7**:268–269
tetrahydroisoquinolines **7**:267
Rottapharm **7**:269–271
bicyclic [5.2.0] and [4.2.0] diamines **7**:269–271
The Scripps Research Institute **7**:271
piperidin-2-ylmethanamines **7**:271
Taisho **7**:271
TASP0428980 **7**:271
Takeda **7**:271–273
benzoxazepine-based selective orexin-2 antagonists **7**:272–273
spiropiperidine-based selective orexin-2 antagonists **7**:271–272
Organ chips, predictive toxicology **2**:101
Organic and inorganic nanodrugs **1**:269t
Organic molecule force fields **3**:18–19
Organoid and three-dimensional (3-D) cellular models **2**:364
Organoids **4**:185t
3D high-content screening of **2**:388–415
induced pluripotent stem cell-derived **4**:183–187
brain organoids **4**:186–187
heart organoids **4**:187
liver organoids **4**:186
Organometallic reagents
continuous flow processing **1**:145–147
Organosulfur compounds, as nutraceuticals **1**:121
Orphan populations, medical need in **1**:540–541
Orthosteric GPCR ligands **3**:164–179
class A GPCR aminergic **3**:164–170
class A GPCR chemokine **3**:176–179
class A GPCR lipid receptors **3**:176
class A GPCR peptidergic **3**:170
class A GPCR purinergic **3**:171–175
Oseltamivir **1**:581f, **5**:670f
Osimertinib (AZD9291)
discovery of **8**:2–23
EGFR mutant-selective hypothesis **8**:2–4
identification of a mutant-selective lead series **8**:4–11
lead optimization **8**:11–23
emerging clinical data of **8**:24
Osteopontin, biomarker of acute kidney injury **4**:275
OTX015 **5**:213f
Overactive bladder (OAB) **7**:715
etiology **7**:715
impact **7**:715
prevalence **7**:715
treatment **7**:715
See also β3-AR agonists, for overactive bladder
OX2R agonists **7**:247–248
Oxaborole β-lactamase inhibitor **5**:691f
Oxadiazole regioisomers **3**:232
Oxazolidinone antibiotics **5**:523f
Oxazolidinone resistance **5**:523–524
Oxidation, continuous flow processing **1**:143
Oxidative damage theory of aging **1**:351–352
Oxidative stress, and cancer **5**:10
Oxytocin receptor **7**:32

P

P2X and P2Y receptor modulators **5**:368
$P2X_7$ antagonists **5**:368f, **7**:52
p21-activated kinase **7**:425–426
p38 MAP kinase inhibitors **5**:404
p38 MAPK cascade **8**:432–433
p38 MAPK inhibitors, approaches to the discovery of **8**:413–417
first-generation pyrazole-based inhibitors **8**:414
second-generation pyridinone-based inhibitors **8**:414–415
structural hypothesis of human kinome selectivity **8**:415–416
structure-based drug design **8**:413
structure-guided lead optimization **8**:416
p38 MAPK pathway **8**:410–413
small-molecule p38 clinical candidates for inflammatory indications **8**:410–413
p38 mitogen-activated protein kinase **7**:420–422
p97 inhibitors **8**:113–137
as cancer target, rationale for **8**:113–114
nononcogene addiction pathways **8**:113
p97 and protein homeostasis **8**:113–114
future directions **8**:136
hit to lead investigations **8**:117–118
HTS screen and hit triage **8**:115
overview **8**:113–118
reported from competitors' efforts **8**:134–136
2-(cyclohexylmethylamino)pyrimidines **8**:134
5-*N*-(3-(1*H*-indol-2yl)-phenyl-piperidines **8**:135
alkylsulfanyl triazoles **8**:134–135
compounds discovered by U. Pittsburgh/UCSF collaboration **8**:135–136
N-5-indolyl-carboxamides **8**:136
Pain
calcium channel blockers for **7**:65–130
sodium channel blockers for **7**:131–175
Pain and sensory neuron disease model screening, iPSC models **1**:63
pAKT assay in RAMOS cells **8**:370
Pancreas, regenerative drugs **1**:385–427
chemical manipulation of pancreatic regeneration **1**:416
different sources of β-cells **1**:419–420
fibroblasts **1**:419–420
mesenchymal stem cells **1**:419
other pancreatic cells **1**:419
ex vivo generation of replacement β-cells **1**:416–419
β-cell derivation from stem cells **1**:417–419
in vitro β-cell expansion **1**:416–417
in vivo expansion of β-cells **1**:420–421
in vivo studies in zebrafish **1**:421–422
Pancreas, targeting next-generation therapeutics **1**:342
Pancreatic cancer **6**:6
Pancreatitis **7**:487–488
Pan-mTOR inhibitors **5**:224–227
Parallel artificial membrane permeability assay **1**:329
Paramyxoviruses **5**:673–676
antiviral agents for RSV **5**:673–676
fusion protein inhibitors **5**:673–676
RSV RNA replication **5**:676
combination therapies **5**:676
reasons to develop antiviral drugs for **5**:673
intervention opportunities **5**:673
Parasitic infections **1**:491–492
Parkinson's disease **5**:458
amantadine for **5**:462
anticholinergics for **5**:462
apomorphine for **5**:462
bromocriptine for **5**:459
cabergoline for **5**:459
carbidopa/levodopa for **5**:458–459
COMT inhibitors for **5**:462
istradefylline for **5**:463
levodopa formulations for **5**:463–464
MAO-B inhibitors for **5**:463
nutraceuticals for **1**:131

pergolide for **5**:459
pramipexole for **5**:459
ropinirole for **5**:459
rotigotine for **5**:462
PARP inhibitors **5**:22–23, **5**:108f
Partition coefficients, physical–chemical properties **3**:419–421
physics-based models **3**:419–420
statistical methods **3**:420–421
Passive transport of drugs, physical–chemical properties **3**:401–402
Patent expirations
pharmaceutical industry challenge **1**:2
Patent mining, SAR-centric. *See* SAR
Patent SAR retrieval from BindingDB **3**:470–471
Patents, in the Internet **1**:533–539
available resources, making reasonable use of **1**:538–539
drafting and prosecution **1**:539
legal status of patents and patent applications **1**:539
searching **1**:539
information resources **1**:533–538
European Patent Office (EPO) **1**:537
Japanese Patent Office (JPO) **1**:537–538
United States Patent and Trademark Office (USPTO) **1**:535–536
World Intellectual Property Organization (WIPO) **1**:533–534
Patents and papers via PubChem, connecting between **3**:482–484
Path-based fingerprints **3**:342
Pathophysiologic factors, biomarker of acute kidney injury **4**:272
Pathophysiologically-relevant cell lines **2**:364
cellular models validation and quality controls **2**:364–365
organoid and three-dimensional (3-D) cellular models **2**:364
Pathway modeling, defintion of **3**:491
Patient iPSC differentiation into disease-relevant cell types **1**:51–56
Patient stratification and disease diagnosis, iPSC models **1**:64–66
clinical diagnosis and prognosis **1**:65–66
drug responders and nonresponders prediction **1**:64–65
Pattern recognition receptors (PRRs) **5**:372–378
STING **5**:376–377
targeted delivery of PRR agonists **5**:377–378
TLR agonist in development for IO **5**:375–376
TLR4 **5**:374–375
TLR7/8 **5**:373–374
TLR9 **5**:375
PBMC from patients with DILI **4**:230–231
PBPK modeling **4**:83–101
considerations **4**:94–97
futile cycling kinetics **4**:97
intestine segmental heterogeneity **4**:94–95
liver enzyme and transporter zonation **4**:95–97
membrane barrier for metabolite **4**:97
metabolite data in bioequivalence **4**:97–98
for metabolite kinetics study **4**:85–94
intestine-liver **4**:88–90
PBPK model of whole body **4**:88–90
PBPK modeling of the intestine **4**:85–87
PBPK modeling of the liver **4**:87–88
SFM to detect lack of codeine demethylation (case study) **4**:94
SFM to detect route-dependent intestinal glucuronidation of morphine (case study) **4**:90–94
overview **4**:83–84
parameters identifying metabolite formation **4**:84–85
PBPK models, drug–drug interactions consequent to drug-mediated cytokine elevations **2**:508
PCR
quantitative and digital **2**:439
PCSK9 inhibitors **7**:669–676
PD1/PD-L1 interaction **5**:384f–385f
PDBbind-CN **1**:456
PDE inhibitors **7**:586–587, **7**:644
PDE model **3**:496–497
PDE4 inhibitors **5**:433–434
psoriasis **5**:434
psoriatic arthritis **5**:433–434
PDEStrIAn **1**:460–461, **1**:464f
PDSP K_i database **1**:455–456
PDZ domain inhibitors **5**:186–189
PDZ domain interactions **2**:342
Peficitinib (ASP015K) **5**:430–431
as monotherapy **5**:430
in MTX-IR **5**:430
Peginterferon β-1a, for multiple sclerosis **5**:449
PEGylation **6**:71–72, **6**:143–144
carbohydrates and nucleic acids **6**:144
proteins **6**:143–144
Peptide aldehydes **5**:261
Peptide bond replacements and pseudopeptides **6**:82–88
alkylidene (CH]CH) **6**:84
azapeptide (CONHNR) **6**:85
azasulfurylpeptide (AsF, $CONHNRSO_2$) **6**:85
depsipeptide (CO_2) **6**:84
endothiopeptide (CSNH) **6**:84
ketomethylene ($COCH_2$) **6**:84
methylene ether (CH_2O) **6**:84
methylene thioether (CH_2S) **6**:83–84
phosphonamide (PO_2RN) **6**:84–85
reduced bond (CH_2NH) **6**:83
retro-inverso (RI, NHCO) **6**:85–88
thioester (COS) **6**:84
Peptide boronates **5**:262–266
Peptide frameworks for therapeutic applications **1**:331–332
Peptide immunotherapeutic approaches **6**:9–12
peptide vaccine *versus* peptide therapeutics **6**:9–12
effective peptide vaccine *versus* peptide mimic strategy **6**:12
overall strategy **6**:11
peptide mimic approaches, significance of **6**:10–11
peptide vaccine approaches, significance of **6**:10
Peptide inhibitors **5**:385
of MDM2–p53 interaction **5**:161t
Peptide mimetics **5**:163–165
Peptide vinyl sulfones **5**:261–262, **5**:262f
Peptide-based cancer vaccines and therapeutics **6**:1–31
Peptide-based transporters **6**:141–142
Peptides **2**:336
PPI inhibitor **5**:159–165
Peptidomimetics **2**:336
PPI inhibitor **5**:159–165
Peramivir **5**:670f
Pergolide, for Parkinson's disease **5**:459
Perhexiline **7**:653
Permeability
and BDDCS **4**:113
determination **4**:111–112
in humans **4**:111–112
in vitro **4**:112
in vivo or in situ **4**:112
and efflux, matched molecular pair analysis **3**:238–239
human PK **4**:57
prediction **4**:68
Persistence, ADME/PK **4**:2, **4**:14–16
Personalized medicine
systems biology for **2**:463–464
systems chemical biology for **2**:490
Pertuzumab **6**:15
PET imaging
immuno-PET in neurosciences **7**:48–49
improved radiosynthesis methods **7**:47–48
neuroinflammation imaging beyond translocator protein **7**:49–53
possible future developments **7**:53
recent developments **7**:49–53
selected pet tracers under investigation **7**:49
present and future challenges of **7**:47–54
reimbursement of approved diagnostic PET agents **7**:53–54
PET imaging tracers **7**:22–47
overview **7**:22
targeting aggregated proteins **7**:44–47
future developments **7**:47
recent developments **7**:44–47
tracers in clinical use **7**:44
targeting enzymes **7**:33–36
recent developments **7**:33–36
tracers in clinical use **7**:33
targeting G protein-coupled receptors **7**:22–33
recent developments **7**:23–33
tracers in clinical use **7**:23
targeting ion channels **7**:37–39
recent developments **7**:37–39

PET imaging tracers (*continued*)
tracers in clinical use **7**:37
targeting transporters **7**:39–44
recent developments **7**:40–44
tracers in clinical use **7**:40
PET imaging tracers, for Alzheimer's disease **1**:79–87
PET tracers approved for Aβ plaque imaging **1**:79–83
Aβ PET tracers derived from CR **1**:82–83
Aβ PET tracers derived from thioflavin T **1**:80–82
PET tracers for Aβ plaque imaging evaluated in human subjects **1**:83–84
Aβ SPECT tracers **1**:84
PET tracers for NFT imaging **1**:84–87
benzoimidazopyrimidine- and pyridoindole-derived tau PET tracers **1**:87
benzothiazole-derived tau PET tracers **1**:86–87
quinoline- and benzimidazole-derived tau PET tracers **1**:85–86
PET ligands, and CNS drug discovery **7**:20–64
overview **7**:20–22
PET imaging
and CNS drug discovery **7**:21–22
defined **7**:20
Petri nets **3**:494
Pevonedistat (MLN4924/TAK-924) **5**:247–250
discovery of **8**:97–100
in vitro and in vivo evaluation **8**:100–104
PF-04691502 **5**:222
PF-3715455
highlights of clinical data for **8**:426
identification **8**:424–425
PF-4171327 **5**:401
PF-04691502 **5**:223f
Pfizer **7**:573
inhibitors reported by **7**:353–358
isothioureas and related derivatives **7**:354–358
spiropiperidine derivatives **7**:353–354
spiropyrrolidine derivatives **7**:354
modulators from **7**:304–307
aryl-imidazole derivatives **7**:305–307
carboxylic acid derivatives **7**:304
PH-797804 **8**:418–420
crystal structure of PH-797804 bound in p38α kinase **8**:418–419
highlights of clinical data for **8**:426
in vitro activity **8**:418
in vivo efficacy of **8**:420
kinase selectivity screening **8**:418
as more potent atropisomer **8**:416–417
pharmacokinetic properties of **8**:419–420
rotational barrier, chemical stability, and pharmaceutical properties **8**:419
Phage display library **6**:106
Pharmaceutical carcinogenicity studies, proposals for **4**:246–247
Pharmaceutical crystal form **3**:91–94
background **3**:91–92
hydrogen-bond patterns and crystal form stability **3**:92–93
impact of crystal-structure interactions on physical properties **3**:94
Pharmaceutical industry challenges
cost **1**:2
patent expirations **1**:2
politics **1**:2
productivity **1**:2
Pharmacodynamic biomarkers **2**:497
Pharmacodynamics **1**:571–573, **4**:55–56
Pharmaco-economic biomarkers **2**:499
Pharmacokinetics **1**:571–573, **4**:53–55
absorption **4**:54–55
clearance **4**:53–54
half-life **4**:54
volume of distribution **4**:54
Pharmacokinetics, current issues and challenges in **4**:103–109
distribution prediction **4**:105–106
metabolism and elimination prediction **4**:106–109
characteristics of metabolism **4**:106–107
in silico predictions **4**:108–109
in vitro predictions **4**:107–108
in vivo predictions **4**:108
oral absorption and availability prediction **4**:104–105
in vitro predictions **4**:105
physicochemical determinants of absorption **4**:104–105
volume of distribution prediction **4**:105–106
Pharmacological action, nutraceuticals classification by **1**:110
Pharmacological inhibition, of mTOR pathway **1**:361–363
rapamycin **1**:362–363
Pharmacological interventions mimicking calorie restriction **1**:357–365
AMPK pathway **1**:363–365
metformin **1**:363–365
GH/IGF-1 pathway inhibitors **1**:359
glycolytic metabolism inhibitors **1**:358–359
pharmacological inhibition of mTOR pathway **1**:361–363
rapamycin **1**:362–363
sirtuin-activating compounds **1**:359–361
resveratrol **1**:360–361
synthetic activators of sirtuins **1**:361
Pharmacophore elucidation **3**:191–207
3D database searching **3**:205–207
database generation **3**:205–206
feature matching **3**:206
geometry matching **3**:206–207
post-processing **3**:207
causes of underperformance **3**:203–204
evaluation of methods **3**:201–203
feature definition **3**:193
feature representation **3**:192–193
field-based pharmacophores **3**:197–198
matched molecular pair analysis **3**:247–248
practical aspects and applications **3**:204–205
scoring **3**:200–201
searching for candidate alignments **3**:198–200
algorithms that alter conformations on the fly **3**:200
algorithms using pregenerated conformers **3**:199
tautomers **3**:193–197
customized features **3**:197
donor/acceptor feature point positioning **3**:194
excluded volumes **3**:195
halogens **3**:194
hydrogen-bond acceptor features **3**:194
hydrogen-bond donor features **3**:193–194
hydrophobic features **3**:196
positive and negative features **3**:194–195
Pharmacophore fingerprints **3**:344
Pharmacophore keys **3**:207–208
2D pharmacophores **3**:207
3D pharmacophores **3**:207–208
Pharmacophores **5**:162f
and 3D QSAR methods **3**:210–211
concept **3**:192f
exemplar applications of 3D pharmacophore methods **3**:211–212
maximizing the value of **3**:216
Pharmacovigilance, integrating clinical data and biomedical evidence in **1**:441
Phenolics, as nutraceuticals **1**:119–121
Phenome-based data mining, for drug repurposing **1**:35–38
Phenotypes, of DILI **4**:205
Phenotypic screening **2**:10–12, **2**:46–50
Phenotypic screening, drug repurposing **1**:21–23
Phenotyping pipelines in preclinical studies **1**:57–59
4-Phenyl-[1,3]dioxanes **7**:250
Phenylethylamine **2**:145f
Phosphadityinositol-3 kinase **5**:484–485
Phosphatases **5**:479–486
Phosphodiesterase 4 (PDE-4) **8**:433–434
Phosphodiesterases **7**:384–407
CNS drug-like properties **7**:387–389
overview **7**:384–386
PDE inhibitors **7**:33, **7**:389–404
PDE1 **7**:389–392
PDE2 **7**:392–395
PDE2A **7**:34
PDE4 **7**:395–398
PDE7 **7**:34–35
PDE9 **7**:399–400
PDE10 **7**:400–404
PDE10A **7**:35
structure and binding site topology **7**:386–387
Phosphoinositide 3-kinase **7**:434–436
Phospholipid affinity **2**:107–108
Phospholipidosis **4**:277
Phosphomannopentaose sulfate **1**:582f

Phosphonamide (PO_2RN) **6**:84–85
Phosphorothioate **6**:219f
Phosphorus, as nutraceuticals **1**:116
Photo-activity ligands **7**:315–318
Photochemistry, continuous flow processing **1**:153–154
Photoswitchable fluorescent probes **1**:92
Physical properties, and multiobjectuve optimization **2**:70–76
  DMPK, safety, and physical properties **2**:70–71
  drug-like property space **2**:70
  target activity and physical properties **2**:71–76
    ligand efficiency **2**:75–76
Physical–chemical properties **3**:393–428
  background **3**:396–402
  from condensed-phase to gaseous phase **3**:397
  dissolution and solubility of pharmaceuticals **3**:397–399
    aqueous solubility **3**:398–399
    dissolution **3**:397–398
  in drug design **3**:394
  drugs properties in a solution **3**:399–401
    ionization constants **3**:399–400
    solution stability **3**:400–401
  history **3**:394–395
  main questions in **3**:395–396
  melting (fusion) of crystals **3**:397
  overview **3**:394–396
  passive transport of drugs **3**:401–402
  polymorphism **3**:396
  reasons for predicting **3**:394
Physical–chemical properties, applications and limitations **3**:406–421
  aqueous and nonaqueous solubility **3**:415–417
    physics-based models **3**:415–416
    statistical methods **3**:416–417
  chemical stability/degradation **3**:419
    statistical methods **3**:419
  melting point **3**:411–413
    physics-based methods **3**:411
    statistical methods **3**:412–413
  partition coefficients **3**:419–421
    physics-based models **3**:419–420
    statistical methods **3**:420–421
  pK_a **3**:417–419
    physics-based methods **3**:417–418
    statistical methods **3**:418–419
  polymorphism **3**:406–411
    physics-based models **3**:407–410
    statistical methods **3**:410–411
  vapor pressure **3**:413–415
    physics-based models **3**:413–415
    statistical methods **3**:415
Physical–chemical properties, methods for estimation of **3**:402–406
  physics-based methods **3**:402–405
    3D RISM **3**:405
    COSMO-RS **3**:402–403
    SAFT **3**:404–405
    UNIFAC **3**:404
  statistical methods **3**:405–406
    linear methods **3**:405–406
    nonlinear (machine learning) methods **3**:406
Physicochemical determinants of absorption **4**:104–105
Physicochemical properties **2**:106–108
  basicity and promiscuity **2**:107
  implications of **4**:58
  lipophilicity and promiscuity **2**:107
  phospholipid affinity **2**:107–108
Physics-based methods, physical–chemical properties **3**:402–405
  3D RISM **3**:405
  COSMO-RS **3**:402–403
  SAFT **3**:404–405
  UNIFAC **3**:404
Physics-based models
  COSMO-RS **3**:414
  crystal structure prediction **3**:407
  hydrogen bonding propensity approach **3**:410
  melting point **3**:411
  molecular dynamics and Monte Carlo **3**:411, **3**:413–415
  partition coefficient **3**:419–420
  pK_a **3**:417–418
  polymorphism **3**:407–410
  SAFT **3**:415
  squeous and nonsqueous solubility **3**:415–416
  UNIFAC **3**:414
  vapor pressure **3**:413–415
Physiologically based pharmacokinetic model
  applications **4**:68–70
  description of **4**:60–61
  generalized approach to building and validating **4**:70–71
    model building and input data **4**:71
    model optimization **4**:71
    reporting **4**:71
  lessons learned from the early applications **4**:69–70
    assessing the feasibility and performance of human pharmacokinetics **4**:69–70
    first-in-human prediction and trial design **4**:70
    reducing the use of animals in toxicology testing **4**:69
  predicting in vivo pharmacokinetic parameters **4**:63–68
    predicting intestinal and hepatic clearance **4**:64–66
    predicting permeability **4**:68
    predicting transporter effects **4**:67–68
    predicting volume of distribution **4**:66–67
  representation in GastroPlus **4**:61–63
    absorption model **4**:61–63
    tissue distribution model **4**:63
  and simulation methodology **4**:60–68
Physiologically based pharmacokinetics, defintion of **3**:492
Phytochemicals **1**:110
  as nutraceuticals **1**:118–121
    carotenoids **1**:118–119
    organosulfur compounds **1**:121
    phenolics **1**:119–121
  See also Nutraceuticals
PI3K inhibitors **5**:381
PI3Kα **5**:96–97, **5**:97f
PI3Kγ inhibitors, isoform selective **2**:169–171
Pig-a assay, for genotoxicity evaluation **4**:201
Piopharmaceutics classification system **4**:58
Piperazines **7**:109
Piperidin-2-ylmethanamines **7**:271
Piperidine- and piperazine-based structures, Cav3 blockers **7**:103–108
Piperidine ethers **7**:260
Piperidines/MK-6096 **7**:255–257
π-stacking **3**:75–77
Pituitary, targeting, next-generation therapeutics **1**:341
pK_a **3**:417–419
  human PK **4**:57
  physical–chemical properties
    physics-based methods **3**:417–418
    statistical methods **3**:418–419
PKI-587 **5**:220–221, **5**:221f
PK/PD parameters, multiobjective optimization **2**:76–87
  achieving a balanced PK/PD profile **2**:78–79
  drug efficiency and free drug hypothesis **2**:79–87
    drug efficiency, definition of **2**:80–81
    drug efficiency index **2**:81–87
  PK/PD properties of development compounds **2**:76–78
Plant sterols, and CVDs **1**:126
Plants, as nutraceuticals **1**:121–123
Plasma protein binding, matched molecular pair analysis **3**:244–245
Plasmodium **5**:718–722
  benzoxaboroles **5**:721
  dihydroorotate dehydrogenase inhibitors **5**:721–722
  imidazolopiperazines **5**:720–721
  imidazolopyrazines **5**:720–721
  quinoline carboxamides **5**:721
  spiroindolones **5**:720
  synthetic peroxides **5**:719–720
Platinum (database) **1**:458
PLIC **1**:458
Pluripotent stem cells, in toxicology **4**:178–179
PLX-4032 **2**:218f
PMX53 (3D53) **6**:91
Pocketome **1**:458
Polarizable force fields **3**:19–21
Policosanol, and CVDs **1**:126
Politics, pharmaceutical industry challenge **1**:2
Polo-like kinase 2 **7**:422–425
Poly(ADP-Ribose) polymerase (PARP) **5**:107–115
  ATM inhibitors **5**:117–119

Poly(ADP-Ribose) polymerase (PARP) (*continued*)
clinical development **5**:119
ATR inhibitors **5**:119–124
clinical Development of **5**:123–124
CHK1 inhibitors **5**:119–124
clinical Development of **5**:123–124
CHK2 inhibitors **5**:117–119
clinical development **5**:119
discovery and function **5**:107
DNA-dependent protein kinase **5**:115–116
clinical development of DNA-PK inhibitors **5**:116
DNA-PK inhibitors **5**:115–116
inhibitors **5**:107–111
biomarkers to detect HRR deficiency **5**:114–115
chemosensitization and radiosentitization **5**:109
clinical development of inhibitors **5**:111–115
combination chemotherapy **5**:111–112
in combination with molecularly targeted agents **5**:113
in combination with radiation **5**:113–114
combinations with molecularly targeted agents **5**:110–111
single-agent activity **5**:110
synthetic lethality in HRR-defective cancers **5**:112–113
vasoactivity **5**:109–110
Polyenes **5**:705
Polymer particles **1**:266f
Polymerase inhibitors
rhinoviruses **5**:669
Polymeric nanoparticles **1**:266
Polymorphism
physical–chemical properties **3**:396, **3**:406–411
physics-based models **3**:407–410
statistical methods **3**:410–411
Polymyxin antibiotics **5**:524f
Polypharmacology **2**:259–275
advantages **2**:268–269
concept of **2**:259–260
current status of **2**:260–261
and monotherapy and combination therapy, comparison **2**:261–262
overview **2**:259–262
studies **2**:263t
study methods **2**:262–268
bioinformatics methods **2**:268
ligand-based methods **2**:263–266
network-based methods **2**:267–268
structure-based methods **2**:266–267
Polypharmacology applications **2**:270–272
drug repositioning/repurposing **2**:271–272
targeting complex diseases **2**:270–271
cancer **2**:270–271
CNS disorders **2**:271
targeting drug resistance **2**:271
Polypharmacology design, challenges in **2**:269–270
best multitargeted strategies selection **2**:270
multitargeted agents
achieving without becoming nonselective **2**:270
optimizing potency of **2**:269–270
off-target activity, avoiding **2**:269
Polyspirocycles **1**:253, **1**:253f
Polyunsaturated fatty acids, and CVDs **1**:125–126
omega-3 fatty acids **1**:125
omega-6 fatty acids **1**:126
Pomegranate, for chronic inflammatory disorders **1**:131
Porphyrins **5**:318f
Posaconazole **5**:707f
Pose prediction, in molecular docking **3**:299–304
sampling algorithms **3**:299–300
tackling binding site flexibility **3**:302–303
tackling ligand flexibility **3**:300–301
treating solvent during docking **3**:303–304
Positive inotropic agents and sarcomere targets **7**:643–646
cAMP elevating agents **7**:644
digoxin **7**:643–644
modulators of sarcomeric proteins **7**:644–646
PoSSum **1**:457
Postanalysis interpretation, biomarker of acute kidney injury **4**:272
Postdocking stage, modeling protein flexibility **3**:325
Potassium
and CVDs **1**:127
as nutraceuticals **1**:116
Potential medicines studies, benefits to participation in **1**:542–543
PPIs and their modulators **1**:328–332
backbone-modified macrocyclic peptides, biological selection of **1**:330–331
macrocycles **1**:329–330
peptide frameworks for therapeutic applications **1**:331–332
Pramipexole, for Parkinson's disease **5**:459
Preanalytical factors, biomarker of acute kidney injury **4**:269–272
Prebiotics, as nutraceuticals **1**:123–124
Preclinical research, rare disease foundations **1**:555–556
Preclinical studies
animal models **1**:60–61
phenotyping pipelines **1**:60–61
Predictive ADMET **4**:150–155
advent of systems toxicology **4**:153
for future of in vitro toxicology **4**:151–153
ADME contributions to ITS **4**:153
barrier models **4**:151
biokinetic modeling of the in vivo situation **4**:151
emerging role of ADME in in vitro toxicology **4**:151–153
in vitro biokinetics **4**:152
lack of metabolism in vitro **4**:152
prediction of metabolites **4**:151
quantitative in vitro-to-in vivo extrapolation **4**:152
well-established uses of ADME in in vitro toxicology **4**:151
in in vivo and human toxicology **4**:150–151
overview **4**:150
Predictive toxicology **2**:94–115, **2**:233–258
complex toxicity endpoints **2**:250–254
data integration of in vivo toxicity studies **2**:253
development of prediction models **2**:253–254
drug-induced liver injury **2**:251–253
in vivo safety studies **2**:250–251
data integration and sharing in **1**:438–441
data sharing initiatives and data exchange **2**:254–256
IMI eTox and NextGets initiatives **2**:254–255
SEND data model and electronic submission to FDA **2**:255–256
genotoxic impurities assessment **2**:237–246
ICH M7 Guideline **2**:238
mutagenicity prediction with commercial in silico systems **2**:238–246
regulatory requirements **2**:237–238
in silico approaches to **2**:108–110
in silico models **2**:246–250
exploratory work **2**:246–247
lead identification phase **2**:249
lead optimization (LO) phase **2**:249–250
phase 0 **2**:250
target assessment **2**:246–247
target identification (TI) **2**:246–247
model systems for toxicology **2**:97–102
animal models **2**:102
complex cellular models **2**:100–101
individual target screening **2**:97–100
isolated tissues and organs **2**:101
organ chips **2**:101
simple cellular models **2**:100
OMICS technologies **2**:102–105
genomics **2**:102–103
metabolomics **2**:104–105
proteomics **2**:103–104
overview **2**:94–96, **2**:233–234
3Rs **2**:95
assessment of predictivity **2**:96
drugs failures, reasons for **2**:94
predicting targets **2**:95–96
proportionality and predictability of adverse drug reactions **2**:94–95
regulatory context **2**:95
physicochemical properties **2**:106–108
basicity and promiscuity **2**:107
lipophilicity and promiscuity **2**:107
phospholipid affinity **2**:107–108
predictive genetic toxicology **2**:105–106
micronucleus test in vitro **2**:106
standard genotoxicity testing battery **2**:105–106
two-strain ames screen **2**:106
Predictive toxicology methods **2**:234–237
rule-based systems **2**:234–235

CASE Ultra Expert Rules **2**:235
Derek Nexus **2**:234–235
Leadscope Expert Alert System **2**:235
ToxTree **2**:235
statistical-based systems **2**:235–237
admetSAR **2**:237
Bioclipse **2**:237
CASE Ultra **2**:236
Leadscope Model Applier **2**:236
OECD toolbox **2**:237
Sarah Nexus **2**:236
Symmetry **2**:237
Preexposure prophylaxis (PreP), HIV **5**:647
Pre-mRNA processing, in Cancer **5**:341–356
overview **5**:341–347
circular RNAs **5**:344–345
mutations in pre-mRNA **5**:346–347
mutations in spliceosomal proteins **5**:346
pre-mRNA splicing and the spliceosome **5**:344
recognition of exons **5**:344
spliceosome. *See* Spliceosome, as cancer target
Presatovir **5**:675f
Pricing, ethics in **1**:547
Primary cells from human or rodents, cellular imaging **2**:363–364
Primary potency, matched molecular pair analysis **3**:232–235
Pri-miRNA mimics **6**:299–301
Pri-miRNA scaffold **6**:300f
Privileged 5,5 heterocyclic ring systems **2**:124–125
Privileged 6,5 heterocyclic ring systems **2**:123–124
Privileged 6,6 heterocyclic ring systems **2**:120–123
Privileged structures and motifs **2**:116–152
chemical transformations to create lead-like libraries **2**:139–146
lead-like library synthesis approaches **2**:139–146
concept of **2**:116–120
natural products as lead structures **2**:137–139
lead-like natural products **2**:137–139
outlook **2**:146–147
future directions for privileged structure development **2**:146–147
overview **2**:116–120
Privileged structures and motifs, for library design and drug discovery **2**:120–135
classes of privileged structure **2**:120–135
arylated piperidine/piperazine ring systems **2**:128–130
benzodiazepine and related seven-membered ring systems **2**:130–132
coumarin-/chromone-/pyran-derived privileged structures **2**:125
miscellanea **2**:126–128
privileged 5,5 heterocyclic ring systems **2**:124–125
privileged 6,5 heterocyclic ring systems **2**:123–124
privileged 6,6 heterocyclic ring systems **2**:120–123
rhodanines (and related) as a special class of potentially privileged scaffolds **2**:133–134
single-cycle ring systems **2**:132–133
spirocyclic structures **2**:134–135
Privileged structures and motifs, privileged scaffolds to identify biologically active compounds **2**:135–137
natural product-inspired chemical synthesis **2**:135–137
benzimidazolinopiperazinones **2**:135
β-lactams **2**:136–137
Probiotics, as nutraceuticals **1**:123
ProBIS **1**:457
Productivity
pharmaceutical industry challenge **1**:2
Progeroid and abnormal nuclear structures, and high-content screening **2**:377–379
Project target requirements, multiobjective optimization **2**:66–69
target potency and selectivity requirements **2**:67–69
Proliferation assays, nanoparticles **1**:278–280
alamar blue assay **1**:279
cell division assay **1**:280
clonogenic assay **1**:279–280
EdU proliferation assay **1**:280
MTT **1**:278–279
Proliferative signaling, and cancer **5**:4
Proline bis-amides **7**:253
Proline sulfonamide ACT-462206 **7**:232–233
Promiscuity
and basicity **2**:107
and lipophilicity **2**:107
Promiscuity index **2**:108f
Promoter quadruplex nucleic acids for cancer therapy **5**:308–340
oncogene expression control by small molecules in cancer cells **5**:316–332
androgen receptor **5**:331
BCL-2 **5**:328–330
c-*KIT* **5**:326–328
c-*MYC* **5**:316–321
c-SRC **5**:332
HIFα **5**:330–331
HSP-90 **5**:330
h*TERT* **5**:321–322
MET **5**:332
RAS family **5**:322–325
RET **5**:331–332
VEGF and VEGFR **5**:325–326
overview **5**:308–310
quadruplex native structure overview **5**:310–312
quadruplex occurrence and biological function **5**:309–310
quadruplex-small molecule recognition **5**:313–314
telomeric quadruplexes as therapeutic targets **5**:314–316
Proportionality and predictability of adverse drug reactions **2**:94–95
Protease inhibitors
HIV **5**:642–644
darunavir **5**:642–643
other protease inhibitors **5**:644
rhinoviruses **5**:669
Protease-activated receptor (PAR) antagonists **7**:574–578
PAR-1 antagonists **7**:574–578
PAR-4 antagonists **7**:578
Proteasome in cancer therapy **5**:259–271
immunoproteasome inhibitors **5**:271
proteasome inhibitors **5**:260–271
structure and function of the proteasome **5**:259–260
Proteasome inhibitors **5**:487–488
Protegrin LptD inhibitors **5**:695f
Protein arginine methyltransferases (PRMTs) **2**:304–309
Protein binding mechanisms, molecular bonding **3**:319–321
Protein Data Bank file format (pdb) **3**:336–338
Protein Data Bank United States **1**:449–450
Protein data types **1**:452–453
Protein degradation **2**:8–10
inhibitors of **5**:20
Protein expression profiling **2**:440–442
Protein folding **5**:20
Protein folding and degradation, targets in **5**:20
inhibitors of protein degradation **5**:20
intervention in protein folding **5**:20
Protein force fields **3**:18
Protein function prediction **3**:129
Protein interaction profiling **2**:444–445
Protein kinase C theta (PKCθ) **5**:407–408
Protein models, buidling of **3**:129–139
building and refining the model **3**:133–135
model building directly from template structures **3**:134
modeling using spatial restraints **3**:135
segment matching **3**:134–135
evaluating protein model building methods **3**:139
loop modeling **3**:135–137
model validation and sources of error **3**:138–139
sequence and structural analysis **3**:130–133
critical sequence-structure alignment generation **3**:133
fold identification **3**:130–132
side chain assignment **3**:137
structure refinement methods in protein modeling **3**:137–138
Protein phosphorylation profiling **2**:443
Protein sequence and structure, for structural chemogenomics analyses **1**:449–450
Protein structure
determination, history of **3**:102–103
and docking **3**:312

Protein structure (*continued*)
methods, for drug repurposing **1**:30
Protein structure prediction and homology modeling **3**:120–144
current status and future directions **3**:139–141
overview **3**:120–124
3D protein structures in drug discovery and design **3**:120–121
challenges and considerations **3**:124
number of protein folds **3**:122–123
quantifying the need for **3**:121
timeline **3**:124
uses and limitations of models **3**:123–124
usage in drug discovery **3**:124–129
accuracy level **3**:125–126
design of new protein therapeutics **3**:128–129
modeling guiding experiment **3**:128
protein function prediction **3**:129
small molecule drug discovery **3**:126–127
synthetic biology and synthetic biochemistry **3**:128
target tractability and ligandability **3**:127
Protein structure-annotated biological activity databases **1**:454–457
proteome-wide biological activity databases **1**:454–457
mechanism-specific biological activity databases **1**:457
protein family-customized biological activity databases **1**:456–457
Protein synthesis **5**:204f
Protein targets, interrogating with bioactive compounds **1**:444–446
Protein therapeutics **6**:198–215
analytical method development **6**:200–202
general principles **6**:200–202
HPLC and UPLC method development **6**:202
biochemical and biophysical characterization and comparability **6**:206
comparability **6**:206
formulation development **6**:208
formulation optimization **6**:209–211
lyophilized drug product development **6**:211–212
method qualification and validation **6**:204
overview **6**:198–200
analytical **6**:198
CMC, pitfalls in **6**:199
early product development **6**:199
formulation **6**:199
target product profile (TPP) **6**:200
potency assay development **6**:202–204
preformulation and forced degradation **6**:208–209
reference standard **6**:205
specification **6**:204–205
stability studies and expiration dating **6**:212–215
clinical in-use stability studies **6**:214
extractable and leachable studies **6**:214–215
Protein therapeutics, design of **3**:128–129
Protein transcription, translation, and translocation, modulators of **2**:5–8
Protein–ligand interactions **1**:453f
computational modeling of **3**:321
data types **1**:453–454
halogen bonding in **3**:84–86
thermodynamics properties of **3**:55
Protein–peptide docking **3**:325–326
Protein–protein interaction inhibitors **5**:167f, **5**:187t–190t, **5**:192t–193t
Protein–protein interaction inhibitors, in cancer **5**:154–201
approaches to PPI inhibitor discovery **5**:157–167
fragment screening **5**:166–167
high-throughput screening **5**:165–166
natural products **5**:157–159
peptides and peptidomimetics **5**:159–165
virtual screening **5**:166
Bcl-2 family PPIs **5**:167–171
as drug targets **5**:155–157
advantages of PPIs as drug targets **5**:156–157
druggability/ligandability of PPIs **5**:157
identification and validation of PPI targets **5**:157
structure of PPIs **5**:155–156
14-3-3 proteins **5**:186
MDM2–p53 and MDMX–p53 **5**:171–178
dual MDM2–p53, MDMX–p53 antagonists **5**:178
MDM2–p53 antagonists **5**:171–178
Myc/Max inhibitors **5**:186
other inhibitors **5**:191
overview **5**:155–157
PDZ domain inhibitors **5**:186–189
Ras PPI inhibitors **5**:191
S100 protein inhibitors **5**:186
SH2 and SH3 domain inhibitors **5**:189–191
Smac-IAP PPIs **5**:178–186
bivalent Smac-mimetic IAP antagonists **5**:183–186
monovalent Smac-mimetic IAP antagonists **5**:180
Protein–protein interactions **1**:328, **2**:329–353
binding free energies calculations **3**:6–7
computational modeling of **3**:321
critical role of **2**:332–334
cancer **2**:332
cardiovascular disease **2**:333
central nervous system disorders **2**:332–333
infectious diseases **2**:334
inflammation and autoimmune diseases **2**:333
other diseases **2**:334
as drug targets **2**:334–336
hotspots and allosteric sites **2**:334–335
identification of druggable protein–protein interactions **2**:335
small molecular protein–protein interaction inhibitors **2**:336
future prospects **2**:346
high-throughput crystallography **2**:164–165
overview **2**:331–332
recent advances in drug discovery **2**:338–346
strategies to generate inhibitors **2**:336–338
fragment-based drug design **2**:337
high-throughput screening **2**:336–337
peptides and peptidomimetics **2**:336
virtual screening **2**:337–338
Protein–protein interactions, recent advances in drug discovery
cancer **2**:338–342
Bcl-2/Bcl-x_L–Bak **2**:338
bromodomain–acetylated histone **2**:341–342
MDM2–p53 **2**:338–339
WDR5–MLL **2**:339–341
cardiovascular disease **2**:344–345
central nervous system disorders **2**:342–343
α-synuclein aggregation **2**:343
PDZ domain interactions **2**:342
infectious diseases **2**:345–346
inflammation and autoimmune diseases **2**:343–344
Keap1–Nrf2 **2**:343–344
LFA-1–ICAM-1 **2**:343
Proteins and peptides **6**:143–144
solution behavior of **6**:132–133
Proteome activity profiling **2**:444
Proteome synthesis and degradation **2**:442–443
Proteome-based data mining, for drug repurposing **1**:34–35
Proteomics **2**:440–445
data standards and sharing **2**:466
predictive toxicology **2**:103–104
protein expression profiling **2**:440–442
protein interaction profiling **2**:444–445
protein phosphorylation profiling **2**:443
proteome activity profiling **2**:444
proteome synthesis and degradation **2**:442–443
spatial proteomics **2**:442
special considerations and outlook **2**:445
Proteostasis modulation **2**:8–10
Proteotoxic stress, and cancer **5**:10
Prototype assays, companion diagnostics **2**:533–534
Protozoans **5**:718–736
amoebas **5**:736
apicomplexans **5**:718–724
cryptosporidia **5**:723–724
plasmodium **5**:718–722
toxoplasma **5**:722–723
kinetoplastids **5**:724–735
leishmania **5**:725–729
trypanosoma brucei **5**:731–735
trypanosoma cruzi **5**:729–730

P-selectin **6**:68
Psoriasis
  PDE4 inhibitors **5**:434
Psoriatic arthritis
  PDE4 inhibitors **5**:433–434
Psychiatric disorder model screening, iPSC models **1**:61–62
PubChem **1**:454–455
Public compound collection, The Joint European Compound Library **1**:506–512
Publicly available sequence, structural, and activity data **1**:446–447
Public/private partnerships for abandoned assets repurposing **1**:19
Purine-based inhibitors **5**:238–240
Purinergic receptor antagonists **7**:565–574
  $P2X_1$ antagonists **7**:574
  $P2Y_1$ antagonists **7**:572–574
  $P2Y_{12}$ antagonists **7**:566–572
Purinergic signaling in immune cells **5**:367–372
  adenosine receptors **5**:368–370
  ATP metabolism **5**:370–371
  COX-2 and EP2/EP4 receptor antagonists **5**:371–372
  P2X and P2Y receptor modulators **5**:368
Puromycin aminonucleoside **7**:702
Pyran-derived privileged structures **2**:125
Pyrazolopyridines **7**:265–267
Pyridoindole-derived tau PET tracers **1**:87
Pyridyl amides **7**:110–111
3-Pyridyl *N*-oxides **8**:387–400
Pyrimidinedione/xanthine analogs **7**:531–534
N-Pyroglutamate formation **6**:70–71
Pyronaridine **1**:496f
Pyrosequencing-based optical next generation sequencing **2**:355–356
  distinctly labeled fluorescent nucleotide **2**:356
Pyrrolidine analogs **7**:524–531
PZ-1 **2**:227f
PZ-128 **7**:577

Q

QSAR models **3**:249, **4**:161t–163t
  methodologies descriptions **4**:59–60
(Q)SAR toolbox **1**:474, **1**:485–487
  main functionalities **1**:485–487
  OECD principles for validation **1**:475–483
    principle 1 **1**:475–476
    principle 2 **1**:476
    principle 3 **1**:476–479
    principle 4 **1**:479–483
    principle 5 **1**:483
  under REACH **1**:474–475, **1**:487–488
Q-SiteFinder **3**:286
Quadruplex
  native structure overview **5**:310–312
  occurrence and biological function **5**:309–310
  quadruplex-small molecule recognition **5**:313–314
  telomeric quadruplexes as therapeutic targets **5**:314–316
Quadruplex-binding small molecules **5**:316f
Qualified hit list (QHL) **1**:513–514
Quantitative and digital PCR **2**:439
Quantitative cellular pharmacology, iPSC models **1**:63
  advances enabling novel assay development and target validation **1**:63–64
  toxicology and drug metabolism **1**:64
Quantitative structure–activity relationships (QSAR) **3**:379–392
  current trend **3**:380–381
  in drug design SAR **3**:379
  future of **3**:388–390
  history of **3**:379–380
  influential models **3**:387–388
  QSAR model building **3**:381–387
    appropriate measures of goodness-of-fit **3**:384–385
    dataset exploration **3**:383–384
    dataset preparation **3**:382
    defined domain of applicability **3**:385–387
    descriptors calculation **3**:382
    training and test set generation **3**:382–383
  usage of **3**:390–391
Quantitative systems pharmacology **3**:488–504
  defintion of **3**:492–494
  detailed discussion of **3**:497–499
Quantum chemistry
  foundations of **3**:53
Quantum dots **1**:266f, **1**:267
Quarfloxin **5**:318
Quinazoline derivatives **7**:111–112
Quinoline carboxamides **5**:721
Quinoline derivatives **5**:488–489
Quinoline-derived tau PET tracers **1**:85–86
Quinolone antibiotics **5**:518f
Quinolone resistance **5**:518–519

R

Radicicol **5**:234–236, **5**:234f
Radioimmunoconjugates **6**:43
Rafabegron and related analogs **7**:723
Raltegravir, for HIV **5**:632–633, **5**:633f
Randomized enrichment study design **2**:536f
Rapalogs **5**:216
Rapamycin **1**:362–363, **2**:289f, **5**:215–216
  mammalian target of **5**:216, **5**:484
Rare disease foundations (RDFs) **1**:549–559, **1**:552f, **1**:552t
  basic research **1**:552–554
  biomedical research, expensiveness **1**:557
  clinical trials **1**:556
  drug discovery process, risks in **1**:557
  early days **1**:549–550
  genetic rescue *versus* rational approach **1**:554–555
  Human Genome Project **1**:551
  impatient patients **1**:557–558
  major diseases and large foundations **1**:550
  overview **1**:549
  preclinical research **1**:555–556
  social and economic inputs **1**:551
  therapeutic development stages **1**:551
  translational research **1**:554
  treatments discoveries **1**:549–550
  university-based research, inefficiency **1**:557
Rare diseases, drug repurposing **1**:20–21
RAS family **5**:322–325
Ras PPI inhibitors **5**:191
Rasagiline, for Parkinson's disease **5**:463
Ravuconazole **5**:707f
R&D, data integration and sharing supporting **1**:436–443
REACH legislation **1**:472–490
  alternative methods promotion **1**:473–474
  Annex XI **1**:474–475
    grouping of substances and read-across approach **1**:474–475
    (Q)SAR **1**:474
  dissemination of data **1**:475
  legal framework **1**:472–473
  obligations for pharmaceutical companies under **1**:474
REACH legislation, nontest methods **1**:475–487
  grouping and read-across **1**:483–485
  OECD principles for the validation of (Q)SAR **1**:475–483
    principle 1 **1**:475–476
    principle 2 **1**:476
    principle 3 **1**:476–479
    principle 4 **1**:479–483
    principle 5 **1**:483
  (Q)SAR toolbox **1**:485–487
    main functionalities **1**:485–487
Reaction fingerprints **3**:346
Reaction monitoring, continuous flow processing **1**:162–165
Reactive drug metabolites, role of in DILI **4**:218–220
  drug reactive metabolites **4**:220
  imbalance in activation and inactivation of drugs **4**:220
  overview **4**:218–219
  reactive intermediates **4**:220
  selectivity of covalent binding **4**:219–220
Reactive oxygen species (ROS) **1**:351f, **1**:380f
Read-across approach
  in silico tools **4**:168–170
  REACH legislation **1**:474–475, **1**:483–485
Reader domains **5**:283–284
Receptor surface analysis descriptors **3**:353
Receptor tyrosine kinases (RTKs) **5**:12
Receptor-interacting protein (RIP) **5**:406
Receptor-interacting protein kinase 1 (RIP1 and RIP3) inhibitors, for inflammatory bowel disease **5**:503–504
Receptor–ligand-binding studies, click chemistry in **1**:309–317
  agonist **1**:309–311
  antagonist **1**:311–314

Receptor–ligand-binding studies, click chemistry in (*continued*)
selective binding ligands **1**:314–317
Receptor-mediated transcytosis **1**:335–336
Residue-based interaction fingerprint **1**:454
Reduced bond (CH_2NH) **6**:83
Reduction, continuous flow processing **1**:143–144
Refinement **2**:160–161
Regeneration procedures, kinetics in drug discovery **2**:184–185
Regenerative medicine **1**:379–435
definitions **1**:380–384
literature trends in research **1**:384
muscle regeneration using small molecules **1**:414–416
muscle-based applications of small molecule stem cell modulators **1**:414–416
overview **1**:379–384
Regenerative medicine, blood and bone **1**:385–392
bone **1**:391–392
bone marrow stem cell niche and signaling pathways **1**:386
chemical manipulation of HSCs **1**:388
current therapies **1**:387–388
diseases involving these cells **1**:387
eltrombopag **1**:389–391
hematopoietic stem cells **1**:385–386
mesenchymal multipotent stromal cells **1**:386
Regenerative medicine, cardiac regeneration **1**:393–401
in vitro chemically guided cardiac differentiation **1**:393–400
targeting cardiopoietic signaling pathways **1**:395–400
unspecific mode of action **1**:393–395
in vivo **1**:400–401
murine model **1**:400–401
zebrafish model **1**:401
Regenerative medicine, neuronal system **1**:402–413
cell-based therapies for neurological disorders **1**:409–412
augmenting neurogenesis in vivo **1**:410–411
neural cell migration in vivo **1**:412
NSC differentiation in vivo **1**:411–412
reprogramming in vivo **1**:412
in situ stem cell modulation **1**:410
directed differentiation **1**:404–409
bone marrow-mesenchymal stem cells **1**:408
embryonic stem cells **1**:404–406
induced pluripotent stem cells **1**:406–408
NSCs and NPCs in vitro **1**:403–404
transdifferentiation of other cell types **1**:408–409
disease screening and drug discovery **1**:413
neural stem cell culture **1**:403
neuronal regeneration **1**:402–403
Regenerative medicine, ocular disease **1**:422–427
corneal disease **1**:422
new assays and assay technologies **1**:426–427
ocular applications of small molecule stem cell modulators **1**:422
retinal disease **1**:422–423
retinal therapies using stem cells **1**:423–424
small molecule modulation of hES and iPS cells to retinal cells **1**:425–426
Regenerative medicine, pancreas **1**:385–427
chemical manipulation of pancreatic regeneration **1**:416
different sources of β-cells **1**:419–420
fibroblasts **1**:419–420
mesenchymal stem cells **1**:419
other pancreatic cells **1**:419
ex vivo generation of replacement β-cells **1**:416–419
β-cell derivation from stem cells **1**:417–419
ex vivo generation of replacement β-cells in vitro β-cell expansion **1**:416–417
in vivo expansion of β-cells **1**:420–421
in vivo studies in zebrafish **1**:421–422
Regulators, role in sales and marketing of drugs **1**:547
Regulatory context, predictive toxicology **2**:95
Regulatory implications
of human PK **4**:74–76
Regulatory T cell therapy **5**:412
Relaxin **7**:648
Renal elimination of parent drug **4**:108, **4**:124
Renal impairment **4**:124–125
Renal outer medullary potassium (ROMK) channel inhibition **7**:651–652
Replica exchange **3**:43
Replicative immortality **5**:5
Representation of organic structures description arranged linearly **3**:334–335
Reprogramming in vivo, regenerative medicine **1**:412
Repurposing, drug. *See* Drug repurposing
Research Triangle Institute **7**:267–269
diarylureas related to SB-334867 **7**:268–269
tetrahydroisoquinolines **7**:267
Residence times, kinetics in drug discovery **2**:188–189
Resonant waveguide grating (RWG) biosensor **2**:419f
-enabled cell phenotypic profiling to prioritize lead molecules **2**:427
label-free screening **2**:419
to perform quantitative structure–activity analysis (SAR) **2**:425
for (ultra)HTS **2**:423
Resorcinol-based inhibitors **5**:240–242
Resveratrol **1**:360–361
RET **5**:331–332
Retagliptin **7**:538
Retaspimycin **5**:234f
Retina
disease, regenerative drugs **1**:422–423
therapies using stem cells **1**:423–424
Retinoic acid-related orphan receptor γt (RORγt) **5**:407
Retro-inverso (RI, NHCO) **6**:85–88
Retroisosterism **1**:195–196
Retrospective analysis
, drug repurposing **1**:25–27
Rheumatoid arthritis
dual p38α MAPK/PDE-4 inhibitors for **8**:431–449
mathematical model for **2**:509
Rhinoviruses **5**:667–669
classes of rhinovirus agents **5**:667–669
capsid binders **5**:667–669
polymerase inhibitors **5**:669
protease inhibitors **5**:669
combination therapies **5**:669
reasons to develop antiviral drugs for **5**:667
Rho kinase (ROCK) **5**:482, **7**:36
Rho-associated protein kinase **7**:419–420
Rhodanines **2**:133–134
Right Box analysis **4**:5
Rigorous but slowly converging calculations by all-atom models **3**:1–4
Rilpivirine, for HIV **5**:640–641
Ring bioisosterism **1**:202–207
Ring closure or anelation and ring opening **1**:196–200
Ritobegron and related analogs **7**:725
Rituximab, for multiple sclerosis **5**:451
Rivastigmine, for AD **5**:456
RKT's, targeted therapies with **6**:7–9
human epidermal growth factor receptors and cancer **6**:7–9
angiogenesis and cancer, VEGF **6**:9
HER-1 (EGFR) and cancer **6**:8
HER-2 and cancer **6**:8
HER-3 and cancer **6**:8–9
IGF-1R and cancer **6**:9
structure and signaling of HER proteins **6**:7–8
RMM-46 **2**:225f
RNA interference (RNAi) **6**:286–295
challenges and future perspectives **6**:295
in clinical development **6**:293–295
in clinical trials **6**:288t–289t
cytoplasmic processing **6**:287–290
effective delivery **6**:293
focus areas for improving potency and safety **6**:292
HBV **5**:657
potential therapeutic applications of **6**:293
transcriptional silencing and activation **6**:290
triggers **6**:299–303
Ago2shRNAs **6**:301–302
biochemically produced RNAi in clinical development **6**:302
challenges and future perspectives **6**:302–303
pri-miRNA mimics **6**:299–301

shRNA triggers **6**:301
types of synthetic RNAi substrates **6**:290–292
RNA-sequencing **2**:437
RNPs **5**:342f
Roche
inhibitors reported by **7**:358–363
modulators from **7**:307–308
aryl imidazole derivatives **7**:307
other derivatives **7**:308
Rodents
bioassays, new paradigms in **4**:246
cellular imaging **2**:363–364
Roflumilast (Daxas/Daliresp) **5**:399
ROMK inhibitor MK-7145 **8**:308–338
additive or synergistic blood pressure lowering efficacy in combination with candesartan and HCTZ **8**:330
backup efforts focused on longer preclinical half-lives and structural diversity
dibasic piperazine series **8**:331–333
efforts involving alternative scaffolds **8**:334
clinical trials **8**:335
effects of ROMK inhibitor 61 in dahl salt-sensitive rats **8**:333–334
efforts to enhance ROMK selectivity over the hERG channel **8**:317–318
first proof of biology **8**:315–316
hit identification **8**:309–310
hit to lead **8**:311–312
mechanism of ROMK inhibition by compound 25 **8**:316–317
overview **8**:308–309
parallel discovery of 2-(4-(1*H*-Tetrazol-1-yl) phenyl)-1-(piperazin-1-yl)ethan-1-one scaffold **8**:312–314
parallel SAR evolution of the original piperazine series **8**:322–328
program assays **8**:310–311
ROMK inhibitors, and BP lowering in spontaneously hypertensive rats **8**:321–322
scaffold modification toward improving ROMK inhibitor pharmacokinetic properties **8**:319–321
selection of compound 57 as the clinical compound MK-7145 **8**:328–330
RON inhibitors **5**:380
Ropinirole, for Parkinson's disease **5**:459
ROR-γT inhibitors, for inflammatory bowel disease **5**:502
ROS generation **1**:283
Rotigotine, for Parkinson's disease **5**:462
Rottapharm **7**:269–271
bicyclic [5.2.0] and [4.2.0] diamines **7**:269–271
RPC1063 **5**:403
RSK2 inhibitor RMM-46 **2**:225
Rule-based systems, predictive toxicology **2**:234–235
CASE Ultra Expert Rules **2**:235
Derek Nexus **2**:234–235
Leadscope Expert Alert System **2**:235
ToxTree **2**:235
Ruprintivir **5**:669f
Rutin, for inflammatory bowel disease **5**:507
Ruxolitinib **5**:431–432

S

S1P receptor modulators, for inflammatory bowel disease **5**:496–498
S100 protein inhibitors **5**:186
Safety assessment, ADME/PK in **4**:21–23
early toxicity assessment **4**:21
in vivo toxicology assessment **4**:22–23
metabolites in safety testing **4**:23
reactive metabolites **4**:22
Safety biomarkers **2**:498–499
blood cytokines as **4**:275–277
biology **4**:275
cytokine biomarkers **4**:276–277
Safety margin, of ADME/PK **4**:3
SAFT **3**:404–405
Sales and marketing, ethics in **1**:546–547
accurate representation **1**:546
pricing **1**:547
role of regulators **1**:547
Sansalvamide A **5**:238
SAR **3**:464–487
chemistry extraction **3**:469
connecting between patents and papers via PubChem **3**:482–484
overview **3**:464–465
patent SAR retrieval from BindingDB **3**:470–471
prospects **3**:485–486
note added in proof **3**:486
selecting for **3**:480–481
specific patents identification **3**:468–469
statistics of extractable **3**:465–467
statistics of putative patent **3**:467–468
SureChEMBL
patent chemistry in **3**:471–475
target searching in **3**:476–478
tools for stand-alone extraction **3**:478–480
tracking back to first-filings **3**:484
Sarah Nexus **2**:236, **4**:163–164
Sarcomeric proteins modulators **7**:644–646
Satori, modulators from **7**:308–311
Saxagliptin (BMS-477118) **7**:527–529
SB-649868 and substituted piperidines **7**:239–244
sc-PDB **1**:458
Scaffold hopping, molecular fields **3**:266–270
SHOP **3**:267–268
Spark **3**:268–270
Schering-Plough
inhibitors reported by **7**:363–367
amidine and guanidine derivatives **7**:364–367
early peptidomimetic inhibitors **7**:363
spiropiperidine derivatives **7**:364
modulators from **7**:311
Schistosoma and fasciola **5**:738–739
Scientific congresses, publications in **1**:532
Scoring of causal biological network models **2**:454–456
Scoring poses in docking **3**:306
Screening **2**:36–50
approaches, for covalent inhibitor leads discovery **5**:100
assay technology advances for functional screens **2**:43–44
cascade **1**:513–514
chemical space considerations **2**:37–40
compatible image analysis software **2**:368
for DDI potential **4**:17–20
epigenetic regulation inhibitors **5**:285–286
assay conditions **5**:286
cellular assays **5**:286
enzyme selection **5**:285–286
hit validation **5**:286
substrate identification **5**:286
fragment-based drug discovery **2**:44–46
impact in drug discovery **2**:36–37
phenotypic screening **2**:46–50
virtual screening **2**:40–43
The Scripps Research Institute **7**:271
piperidin-2-ylmethanamines **7**:271
SCY-078 **5**:711, **5**:711f
Sdipocytes
lipid accumulation in, high-content screening **2**:376–377
Second- and next-generation AR inhibitors **5**:141–144
Abiraterone **5**:142–143
ARN509 **5**:141–142
Enzalutamide **5**:141–142
Galeterone **5**:143–144
ODM-201 **5**:142
Secondary structures, stabilization of **6**:95–104
Second-generation design and discovery of lead compound BIM-065 **6**:128–129
Second-generation dopastatin
current status **6**:129
design concepts **6**:127–128
γ-Secretase inhibitors **1**:235t, **1**:251t
Segment matching, protein modeling **3**:134–135
Selectins inhibition, and carbohydrates **1**:583–584
Selective COX-1 inhibitors **7**:585
Selective orexin-2 antagonists
benzoxazepine-based **7**:272–273
spiropiperidine-based **7**:271–272
Selegiline, for Parkinson's disease **5**:463
Selenium, as nutraceuticals **1**:117–118
Seletalisib **8**:366–407
clinical data and status **8**:404–405
identification and characterization of **8**:400–404
impact of the CF_3 group 1 **8**:400–402
impact of the CF_3 group 2 **8**:402–403
metabolic profile of compound 86 **8**:403
pharmacological evaluation of compound 86 **8**:403–404
overview **8**:366–371
screening cascade and description of key assays implementation **8**:368–371

Seletalisib (*continued*)
selectively targeting PI3Kδ to treat inflammatory disease, rationale for **8**:367−368
preclinical development **8**:404
Seletalisib, medicinal chemistry program **8**:371−404
driving improvement of ADMET **8**:379−383
replacement of C2 phenyl with acyclic amines **8**:379−380
replacement of C2 phenyl with cyclic amines **8**:380−383
early SAR development **8**:373−377
first generation PI3Kd inhibitors **8**:378
in vitro genotoxicity screening **8**:387
initial approaches to PI3Kδ selective inhibitors **8**:371−372
second generation inhibitors **8**:387−400
3-pyridyl *N*-oxide identification as an effective bioisostere of a carbonyl group **8**:387−389
compound 67 characterization **8**:389−392
metabolite identification studies with compound 67 **8**:397
PK profile of compound 67 **8**:398−400
quinoline C2 pyridyl *N*-oxides, general metabolic profile of **8**:393−397
structure activity relationship development **8**:372−377
triazinyl-piperazinones **8**:383−387
metabolite ID studies with compound 54 **8**:383
off-target and ancillary profiling of compound 54 **8**:386−387
pharmacological assessment of compound 54 **8**:385−386
potency and admet characterization of **8**:383
Self-critical software, for docking **3**:314
Self-optimizing systems, continuous flow processing **1**:162−165
Semaglutide **7**:486
Semantic similarity measures **3**:365
Semiconductor-based nonoptical next generation sequencing **2**:356−357
Semimacroscopic calculations of ligand binding **3**:6
SEND data model **2**:255−256
Sequence and structural analysis, protein models **3**:130−133
critical sequence-structure alignment generation **3**:133
fold identification **3**:130−132
Sermorelin **6**:69
Serotonine (5-HT_{2A}) **1**:245t
Serotoninergic receptors **7**:27−29
5HT1A receptors **7**:27
5HT2 receptors **7**:27
5HT4 receptors **7**:27
5HT6 receptors **7**:28−29
5HT7 receptors **7**:29
Serotonin transporter **7**:41−42
SF1126 **5**:224
SF3B1
natural products and derivatives targeting **5**:350−351
synthetic natural product analogs targeting **5**:351
SFM-PBPK modeling, and first-pass removal **4**:90−94
SH2 and SH3 domain inhibitors **5**:189−191
Shape descriptors **3**:352
Shared activity of two different types of ligands, molecular alignment **3**:214
Sharing data among pharmaceutical companies **3**:245−246
Shionogi
inhibitors reported by **7**:367−369
modulators from **7**:312−313
SHOP **3**:267−268
descriptors **3**:268f
shRNA triggers **6**:301
Side chain assignment, protein model **3**:137
Side-directed mutagenesis **3**:128
σ receptor ligands. **1**:247f
Sigma-1 receptors **7**:32−33
Signal-to-background ratio **2**:393
Signal-to-noise ratio **2**:393
Signaling pathways and mathematical models, for DILI **4**:231−233
future perspectives **4**:233
in silico models, for hepatocyte and NPC perturbation detection **4**:232
lessons learned from **4**:232
mathematical modeling, and in vitro models **4**:233
overview **4**:231
quantification of physiological response and toxicological perturbation of **4**:233
Silibinin, for inflammatory bowel disease **5**:505
Silica nanoparticles **1**:266f, **1**:267
Silicon containing derivatives **7**:120
Similarity fusion **3**:361−362
Similarity measures for special tasks **3**:363−367
chemometric/Spectral similarity **3**:366
fuzzy similarity measures **3**:366−367
graph (tree)-based similarities **3**:364−365
other similarity measures **3**:367
semantic similarity measures **3**:365
similarities of 1D structures **3**:363−364
supervised similarity measures **3**:365−366
symmetric field-based similarity indices **3**:363
Similarity−dissimilarity measures **3**:355−367
clustering algorithms **3**:362−363
common measures of (distance) **3**:356−361
similarity fusion, fusion rules, consensus scoring **3**:361−362
similarity measures for special tasks **3**:363−367
chemometric/Spectral similarity **3**:366
fuzzy similarity measures **3**:366−367
graph (tree)-based similarities **3**:364−365
other similarity measures **3**:367
semantic similarity measures **3**:365
similarities of 1D structures **3**:363−364
Supervised similarity measures **3**:365−366
symmetric field-based similarity indices **3**:363
SIMOA **6**:193
pros and cons/considerations **6**:193
Simple cellular models, predictive toxicology **2**:100
Simplified electrostatic models, binding free energies calculations **3**:4−5
Simplified molecular-input line-entry system **3**:332
Simulation methodology
physiologically based pharmacokinetic model **4**:60−68
Simulation of large systems **3**:26−27
Simulation *versus* prediction
defintion of **3**:491
Single-cell transcriptomics **2**:438−439
Single-cycle ring systems **2**:132−133
Singulex Erenna **6**:193
Pros and cons/considerations **6**:193
Sirtuin-activating compounds **1**:359−361
resveratrol **1**:360−361
synthetic activators of sirtuins **1**:361
Sirtuins, synthetic activators of **1**:361
Sirtuins activators **1**:361f
Sitagliptin (MK-0431) **7**:518−522
SiteHound **3**:286
Size descriptors **3**:352
Size-based metrics **2**:207
SJ733 **1**:498f
SLE
clinical presentation of **5**:477−478
current therapeutic paradigm in **5**:479
etiology and pathophysiology of **5**:477
SLex **1**:584f
Smac-IAP peptides **5**:160−161
Smac-IAP PPIs **5**:178−186
bivalent Smac-mimetic IAP antagonists **5**:183−186
monovalent Smac-mimetic IAP antagonists **5**:180
Small animal PET imaging (micro-PET) **4**:294−295
[^{18}F]-Annexin V **4**:295
[^{18}F]-DFNSH **4**:295
[^{18}F]-FDG **4**:295
[^{18}F]-FEPPA **4**:295
[^{18}F]-FLT **4**:295
Small molecular protein−protein interaction inhibitors **2**:336
Small molecule cocktails, regenerative medicine **1**:397−400
Small molecule drug discovery, protein structure prediction **3**:126−127
Small molecule immunosuppressants, in inflammatory disease **5**:420−438
ABT-494 **5**:428−430
efficacy of **5**:429

in MTX-IR 5:429–430
safety 5:429–430
in TNF IR 5:429
baricitinib 5:425–427
in combination with csDMARDs 5:425–426
four pivotal phase 3 clinical trials 5:425–426
long-term extension study 5:426
phase 2b clinical trial of 5:425
safety 5:426–427
Btk inhibitors 5:432–433
cytokine signaling 5:421
filgotinib 5:427–428
in combination with MTX 5:428
as monotherapy 5:427
safety 5:428
jakinibs in RA 5:422–424
MAP kinases 5:421–422
MAP kinase inhibitors in RA 5:421–422
MAP kinase pathway 5:421
overview 5:421–422
PDE4 inhibitors 5:433–434
psoriasis 5:434
psoriatic arthritis 5:433–434
peficitinib (ASP015K) 5:430–431
as monotherapy 5:430
in MTX-IR 5:430
ruxolitinib 5:431–432
Syk inhibitors 5:432
tofacitinib 5:422–424
clinical development of 5:422–423
in combination with csDMARDs 5:423
long-term efficacy (LTE) of 5:423
as monotherapy 5:423
safety 5:423–424
VX-509 (Decernotinib) oral-selective JAK3 inhibitor 5:431
as monotherapy 5:431
in MTX-IR 5:431
Small molecule inhibitors 5:382–384
Small molecule kinase inhibitors for CNS disorders 7:412–436
anaplastic lymphoma kinase 7:431–433
casein kinase 1 7:415–416
c-Jun *N*-terminal kinase 7:415
cyclin-dependent kinase 5 7:414
death-associated protein kinase 1 7:417
dual leucine zipper kinase 7:426–427
epidermal growth factor receptor 7:428–431
glycogen synthase kinase 3 7:417–419
human epidermal growth factor receptor 2 7:433
leucine-rich repeat kinase 2 7:412–414
mitogen-activated protein kinase kinase 1/2 7:414
mixed-lineage kinase 7:416–417
p21-activated kinase 7:425–426
p38 mitogen-activated protein kinase 7:420–422
phosphoinositide 3-kinase 7:434–436
polo-like kinase 2 7:422–425
rho-associated protein kinase 7:419–420
tropomyosin receptor kinase 7:428
Small molecule modulation
of hES and iPS cells to retinal cells 1:425–426
Small molecule stem cell modulation, drug discovery of 1:389–391
Small molecule stem cell modulators 1:414–416
ocular applications of 1:422
Small molecule targets, cancer immunotherapy 5:361–385
amino acid catabolism 5:362–367
arginine 5:365–367
tryptophan 5:362–365
checkpoint inhibitors 5:381–385
peptide inhibitors 5:385
small molecule inhibitors 5:382–384
kinase inhibitors 5:378–381
CSF-R1 inhibitors 5:380
PI3K inhibitors 5:381
RON inhibitors 5:380
TAM receptor signaling inhibitors 5:380
TGF-β RI/ALK5 inhibitors 5:378–379
pattern recognition receptors (PRRs) 5:372–378
STING 5:376–377
Targeted delivery of PRR agonists 5:377–378
TLR agonist in development for IO 5:375–376
TLR4 5:374–375
TLR7/8 5:373–374
TLR9 5:375
purinergic signaling in immune cells 5:367–372
adenosine receptors 5:368–370
ATP metabolism 5:370–371
COX-2 and EP2/EP4 receptor antagonists 5:371–372
P2X and P2Y receptor modulators 5:368
Small molecules
lupus therapeutics 5:479–489
muscle regeneration using 1:414–416
muscle-based applications of small molecule stem cell modulators 1:414–416
Small-molecule blockers based on peptide toxin structures 7:76–79
Small-molecule CGRP receptor antagonists 7:184–215
from Boehringer Ingelheim 7:184–188
BI 44370 7:188
BIBN4096 BS 7:184–188
Bristol–Myers Squibb 7:200–213
intranasal BMS-694153 7:200–204
intranasal BMS-742413 7:205–206
orally delivered rimegepant (BMS-927711) 7:207–213
from Merck 7:189–200
caprolactam-based CGRP receptor antagonists 7:189–195
spiroindane-based CGRP receptor antagonists 7:195–200
other antagonists 7:213–215
Neurogen 7:215
SmithKline Beecham and GlaxoSmithKline 7:213–214
Vertex 7:215
Small-molecule drugs, for inflammatory bowel disease 5:495–510
drugs in clinical trials 5:496–501
alpha (α)-4 integrin antagonists 5:500
CCR9 antagonists 5:499–500
immunomodulator drugs 5:500–501
JAK inhibitors 5:499
mucosal barrier enhancer drug 5:501
S1P receptor modulators 5:496–498
natural product-derived approaches 5:504–507
6-gingerol 5:506–507
berberine 5:504–505
curcumin 5:504
diallyl sulfide 5:506
gallic acid 5:506
rutin 5:507
silibinin 5:505
triterpene ganoderic acid C1 (GAC1) 5:505–506
preclinical results 5:501–504
immunoproteasome subunit inhibitors 5:503
melanin-concentrating hormone (MCH) receptor 1 antagonists 5:503
receptor-interacting protein kinase 1 (RIP1 and RIP3) inhibitors 5:503–504
ROR-γT inhibitors 5:502
sphingosine kinase inhibitors 5:502
synthetic triterpenoids 5:501–502
Small-molecule immunology 5:395–419
clinical and preclinical struggles 5:403–405
chemokine receptor modulation 5:404
COX2 inhibitors 5:403–404
p38 MAP kinase inhibitors 5:404
TACE inhibitors 5:404–405
clinical promise 5:400–403
ACT-128800 5:402
CCX354 5:401
CF-101 5:400
GED-0301 5:402
GLPG0974 5:401
LY3009104 (INCB028050, Baricitinib) 5:402
Masitinib 5:400
MT-1303 5:403
PF-4171327 5:401
RPC1063 5:403
TRK-170 5:401
VX-509 5:402
clinical success 5:396–400
apremilast (Otezla) 5:400
bilastine (Bilaxten) 5:399
ciclesonide (Omnaris/Alvesco) 5:397
dalfampridine (Ampyra/Fampyra) 5:398
dimethyl fumarate (Tecfidera) 5:399
everolimus (Certican/Zortress 5:396–397
fingolimod (Gilenya) 5:398–399
iguratimod (Iremod) 5:397
lumiracoxib (Prexige) 5:397

Small-molecule immunology (*continued*)
nepafenac (Nevanac) **5**:397
roflumilast (Daxas/Daliresp) **5**:399
teriflunomide (Aubagio) **5**:399
tofacitinib (Xeljanz) **5**:399
emerging paradigms **5**:409–412
autophagy **5**:411
complement system targeting **5**:411–412
epigenetic mechanisms **5**:409–410
inflammasome **5**:410–411
microbiome **5**:411
regulatory T cell therapy **5**:412
emerging specific targets **5**:405–409
Bruton's tyrosine kinase (BTK) **5**:408
interleukin-1 receptor-associated kinase 4 (IRAK4) **5**:405–406
NFkB-inducing kinase (NIK) **5**:409
protein kinase C theta (PKCθ) **5**:407–408
receptor-interacting protein (RIP) **5**:406
retinoic acid-related orphan receptor γt (RORγt) **5**:407
toll-like receptors (TLRs) **5**:406
tyrosine-kinase 2 (Tyk2) **5**:407
overview **5**:396
Small-molecule inhibitors, humanized mAbs and **6**:13–15
Smartphones, information leak through **1**:532
Smiles arbitrary target specification **3**:332–333
SMIRKS **3**:333
SmithKline Beecham **7**:213–214
SN30000 **8**:81–88
as improved TPZ analog **8**:84–86
mechanism of DNA damage **8**:86
predictive biomarkers and response biomarkers for **8**:86–88
synthesis optimization **8**:81–84
SNS-032 **5**:212f
SNX-5422 **5**:242, **5**:242f
Soaking **2**:159
Sodium, as nutraceuticals **1**:116–117
Sodium channel blockers, for pain **7**:131–175
overview **7**:131–132
sodium channel structure and function **7**:132–133
ligand-gated sodium channels **7**:133
mechanisms of ion channel modulation **7**:133
voltage-gated sodium channels **7**:132–133
voltage-gated sodium channel blocking agents. *See* Voltage-gated sodium channel blocking agents
Sodium–glucose cotransporters **7**:491–511
added beneficial effects **7**:508
added GLP-1 effects **7**:508
effects on blood pressure **7**:508
weight loss **7**:508
expression levels of glucose transporters with disease **7**:497
intestine **7**:497
kidney **7**:497
human SGLT loss-of-function patients **7**:492–493
inhibitor binding characteristics **7**:496
origin of *C*-glucoside **7**:499–506
A-ring replacements **7**:505
nonnucleoside inhibitors **7**:505–506
other SGLTs **7**:494
overview **7**:492
potential safety concerns **7**:507–508
diabetic ketoacidosis (DKA) **7**:507
hypoglycemia **7**:507
SGLT in heart **7**:508
urinary tract infections **7**:507
SGLT inhibitors **7**:497–499
O-glycosides **7**:497–498
SGLT inhibitors, limitations on effects of **7**:506–507
competition with glucose **7**:506
drug metabolism and clearance **7**:506–507
increased glucagon response **7**:507
other transporters **7**:506
patients with kidney damage **7**:506
target engagement **7**:506
SGLT knockout animals **7**:493–494
SGLT structure and glucose-binding motif **7**:494–496
Soft docking **3**:322
Software, for docking **3**:311–312, **3**:314
Soil-transmitted helminths **5**:737
Solabegron and related analogs **7**:724–725
Solid scaffolds **2**:397
Solid tumors **6**:1–31
high-value cancer targets overexpressing RTK'S **6**:5–6
breast cancer **6**:5
gastric carcinoma **6**:6
human colorectal cancer **6**:6
pancreatic cancer **6**:6
immunotherapy **6**:2–5
active immunotherapy **6**:2–3
antibody immunotherapy, disadvantages of **6**:3
chimeric peptides incorporating promiscuous T-cell epitopes **6**:4
enhancing immunogenicity of peptide vaccines **6**:4
mAb therapies **6**:3
peptide therapeutics **6**:5
peptide-based cancer vaccines **6**:3
rational design of B-cell peptide vaccines **6**:4
small-molecule TKIs **6**:3
vaccine studies, and cellular immune response **6**:3–4
overview **6**:2–5
Solid tumors, crucial peptides targeting HER-1, HER-3, and IGF-1R **6**:20–23
extensive cross talk among ErbB/HER receptors **6**:20–23
HER-1 **6**:20
HER-3 **6**:20–22
IGF-1R **6**:22–23
Solid tumors, peptide immunotherapeutic approaches **6**:9–12
peptide vaccine *versus* peptide therapeutics **6**:9–12
effective peptide vaccine *versus* peptide mimic strategy **6**:12
overall strategy **6**:11
peptide mimic approaches, significance of **6**:10–11
peptide vaccine approaches, significance of **6**:10
Solid tumors, rationale for developing HER-2 vaccines **6**:15–17
HER family initiating signal transduction, X-ray crystallographic structural studies **6**:15–17
with HER-2 and pertuzumab **6**:16
with HER-2 and trastuzumab **6**:15–16
novel pertuzumab-binding conformational B-cell epitopes **6**:17
novel trastuzumab/herceptin-binding conformational B-cell epitopes **6**:17
rationale for conformational HER-2 epitopes **6**:16
Solid tumors, targeted therapies against HER-2 **6**:13–15
humanized mAbs and small-molecule inhibitors **6**:13–15
clinical trials of trastuzumab **6**:13–14
development of trastuzumab and treatment **6**:13
pertuzumab **6**:15
possible mechanisms of action and resistance to trastuzumab **6**:14
side effects of trastuzumab treatments **6**:14
trastuzumab-DM1 **6**:15
Solid tumors, targeted therapies with RTK'S **6**:7–9
human epidermal growth factor receptors and cancer **6**:7–9
angiogenesis and cancer, VEGF **6**:9
HER-1 (EGFR) and cancer **6**:8
HER-2 and cancer **6**:8
HER-3 and cancer **6**:8–9
IGF-1R and cancer **6**:9
structure and signaling of HER proteins **6**:7–8
Solid tumors, VEGF peptide strategies **6**:18–19
VEGF peptide mimics **6**:18–19
combination therapy **6**:19
design and synthesis of **6**:18–19
Solubility
human PK **4**:57
matched molecular pair analysis **3**:241–244
Solution stability **3**:400–401
Solvent treatment during docking **3**:303–304
Somatostatin **6**:92f, **6**:117–124
dopastatin synthesis and structure–activity relationship **6**:122–124
initial design **6**:119–120
lanreotide and octreotide **6**:117

mechanism of action **6**:117–119
Sordarins **5**:710, **5**:710f
Spark **3**:268–270
Spark's workflow **3**:269f
Spatial proteomics **2**:442
Spatial restraints, protein modeling using **3**:135
Spatially addressable parallel synthesis **6**:105–106
Special-purpose machines, for molecular simulation **3**:14–15
Specific patents identification **3**:468–469
Sphingosine kinase inhibitors, for inflammatory bowel disease **5**:502
Spiegelmers **7**:217
Spinner flask and rotating wall vessel bioreactors **2**:397
Spiperone **1**:236t
Spiro[2.2]pentane **1**:214f
Spiro[2.3]hexane **1**:214f
Spiro[2.4]heptane **1**:214f
Spiro[2.5]octane **1**:214f
Spiro[2.*n*] ring systems **1**:214, **1**:220–225
spiro[2.2] ring systems **1**:220
spiro[2.3] ring systems **1**:220
spiro[2.4] ring systems **1**:221–223
spiro[2.5] ring systems **1**:223–225
spiro[2._6] ring systems **1**:225
Spiro[3.3] ring systems **1**:226f
Spiro[3.*n*] ring systems **1**:214, **1**:225–229
spiro[3.3] ring systems **1**:225
spiro[3.4] ring systems **1**:225–226
spiro[3.5] ring systems **1**:226–229
Spiro[4.4] ring systems **1**:214–215
Spiro[4.5] ring systems **1**:215–216
benzo-fused ring systems **1**:215–216
isolated ring systems **1**:215
Spiro[4.*n*] ring systems **1**:229–245
spiro[4.4] ring systems **1**:229–234
spiro[4.5] ring systems **1**:235–243
spiro[4.6] ring systems **1**:243–245
Spiro[5.5] ring systems **1**:216–218
benzo-fused ring systems **1**:218
isolated ring systems **1**:216–218
Spiro[5.5]undecane **1**:217f
Spiro[5.*n*] ring systems **1**:245–252
spiro[5.5] ring systems **1**:245–250
spiro[5.6] ring systems **1**:252
Spirocycle synthesis using SnAP chemistry **1**:213f
Spirocycles
nomenclature of **1**:212f
Spirocyclic amino-amides **7**:263–265
Spirocyclic angiotensin converting enzyme (ACE) inhibitors **1**:230t
Spirocyclic central nervous system drugs **1**:235f
Spirocyclic checkpoint kinase 1 (ChK1) inhibitor **1**:229t
Spirocyclic ghrelin agonists
biological data **1**:238t
Spirocyclic ghrelin agonists. **1**:238f
Spirocyclic ghrelin receptor inverse agonists **1**:228t
Spirocyclic mineralocorticoid receptor antagonists and amcinonide **1**:229f
Spirocyclic natural products **1**:212f
Spirocyclic Na_V blockers **7**:142–146
Spirocyclic nucleoside antivirals **1**:227t
Spirocyclic scaffolds **1**:211–213
Spirocyclic scaffolds, conformational analysis **1**:213–218
overview **1**:213
spiro[2.*n*] ring systems **1**:214
spiro[3.*n*] ring systems **1**:214
spiro[4.4] ring systems **1**:214–215
spiro[4.5] ring systems **1**:215–216
benzo-fused ring systems **1**:215–216
isolated ring systems **1**:215
spiro[5.5] ring systems **1**:216–218
benzo-fused ring systems **1**:218
isolated ring systems **1**:216–218
spiro[*m*.6] ring systems **1**:218
Spirocyclic scaffolds, medicinal chemistry **1**:220–253
noncarbon spiro atom **1**:253
polyspirocycles **1**:253
spiro[2.*n*] ring systems **1**:220–225
spiro[2.2] ring systems **1**:220
spiro[2.3] ring systems **1**:220
spiro[2.4] ring systems **1**:221–223
spiro[2.5] ring systems **1**:223–225
spiro[2._6] ring systems **1**:225
spiro[3.*n*] ring systems **1**:225–229
spiro[3.3] ring systems **1**:225
spiro[3.4] ring systems **1**:225–226
spiro[3.5] ring systems **1**:226–229
spiro[4.*n*] ring systems **1**:229–245
spiro[4.4] ring systems **1**:229–234
spiro[4.5] ring systems **1**:235–243
spiro[4.6] ring systems **1**:243–245
spiro[5.*n*] ring systems **1**:245–252
spiro[5.5] ring systems **1**:245–250
spiro[5.6] ring systems **1**:252
Spirocyclic structures **2**:134–135
Spirocyclobutyl beta-site amyloid precursor protein cleaving enzyme 1 (BACE1) inhibitors **1**:228t
Spirocyclopropane agonist of human metabotropic glutamate 2 (hmGlu2) and 3 (hmGlu3) **1**:223t
Spirocyclopropane GPR40 agonists **1**:222f
Spirocyclopropane nociceptin/orphanin FQ (ORL1) receptor antagonist **1**:221t
Spirocyclopropane polo-like kinase 4 (PLK4) inhibitors **1**:222t
Spiroepoxide spliceosome inhibitors **1**:224f
Spiroindane-based CGRP receptor antagonists **7**:195–200
Spiroindolone antimalarials **8**:529–543
Spiroindolones **5**:720, **5**:720f
Spiro[*m*.6] ring systems **1**:218
Spirooxetane **1**:213f
Spiropiperidine-based selective orexin-2 antagonists **7**:271–272
Spleen tyrosine kinase **5**:481
Spliceosome **5**:347t
Spliceosome, as cancer target **5**:345–351
CDC-like kinases inhibitors **5**:351
link with other nuclear processes **5**:346
mechanism of the selective antitumor activity **5**:348–350
synthetic lethal spliceosome pairs **5**:348–349
tumors bearing spliceosome mutations, and splicing modulation **5**:349–350
SF3B1
natural products and derivatives targeting **5**:350–351
synthetic natural product analogs targeting **5**:351
Split and mix synthesis **6**:106
SPR
to characterize binding kinetics of lead-like compounds **2**:425–426
principle of **2**:181–182
SPs and NFTs as biomarkers, for Alzheimer's disease **1**:76–78
amyloid hypothesis supports Aβ as biomarker **1**:77
background to concept of biomarkers **1**:76
current perspectives **1**:78
tau hypothesis supports tau as biomarker **1**:77–78
SQI Diagnostics **6**:194
pros and cons/considerations **6**:194
Squeous and nonaqueous solubility
physical–chemical properties **3**:415–417
physics-based models **3**:415–416
statistical methods **3**:416–417
SR-B1 inhibitors **5**:560f
Stabilization of secondary structures **6**:95–104
stabilized α-helices **6**:98–104
stabilized β-sheets **6**:97–98
stabilized β-turns **6**:95–97
Stabilized peptides **5**:161–163
Standard genotoxicity testing battery **2**:105–106
Statistical methods
chemical stability/degradation **3**:419
melting point **3**:412–413
partition coefficient **3**:420–421
pK_a **3**:418–419
polymorphism **3**:410–411
squeous and nonsqueous solubility **3**:416–417
vapor pressure **3**:415
Statistical methods, physical–chemical properties **3**:405–406
linear methods **3**:405–406
nonlinear (machine learning) methods **3**:406
Statistical-based methodology, in silico tools **4**:158–165
assessing quality and overfitting **4**:160–161
building statistical-based models **4**:159–160
CaseUltra **4**:164–165
Leadscope model applier **4**:162–163
overview **4**:158–159
Sarah Nexus **4**:163–164

Statistical-based methodology, in silico tools (*continued*)
TEST **4**:164
using statistical-based methodologies **4**:161–162
Statistical-based systems, predictive toxicology **2**:235–237
admetSAR **2**:237
Bioclipse **2**:237
CASE Ultra **2**:236
Leadscope Model Applier **2**:236
OECD toolbox **2**:237
Sarah Nexus **2**:236
Symmetry **2**:237
Statistics
of extractable SAR **3**:465–467
of putative patent SAR **3**:467–468
Steady-state phase, kinetics in drug discovery **2**:184
Stearoyl-CoA desaturase-1 (SCD1) inhibitors **1**:251t–252t
Steered metadynamics **3**:42–43
Stem cells, cellular imaging **2**:364
Stem cells, in toxicology **4**:177–194
3Rs **4**:189
induced pluripotent stem cell-derived
brain organoids **4**:186–187
cardiomyocytes **4**:183
heart organoids **4**:187
hepatocytes **4**:180–182
liver organoids **4**:186
neuronal cells **4**:182–183
organoids **4**:183–187
induced pluripotent stem cells **4**:187–189
overview **4**:178
pluripotent stem cells **4**:178–179
Steroidal hormone receptors (SHRs) **5**:135f
STING **5**:376–377
STING ligands **5**:376f
STITCH **1**:455
Stochastic *versus* deterministic models **2**:458
Strategy and integration, translational aspects **2**:517–523
combination of technologies **2**:523
design of translation strategies **2**:517–520
ALX-0171 translational strategy **2**:519–520
overview **2**:517
stroke TM strategies **2**:517–519
tocilizumab translation in Crohn's disease **2**:520
integrative thinking **2**:520–523
bedside back to bench **2**:520–521
in oncology **2**:521–523
overview **2**:520
Stratification and predictive biomarkers **2**:498
Stratified study design **2**:538f
Stress response
and cancer **5**:8–10
DNA damage and replication stress **5**:9
hypoxia and nutrient stress **5**:10
metabolic stress **5**:9–10
mitotic stress **5**:9
oxidative stress **5**:10
proteotoxic stress **5**:10
Strictly standardized mean difference **2**:394–395
Stroke TM strategies **2**:517–519
Structural biology, of integral membrane proteins (IMP) **2**:174
Structural chemogenomics databases **1**:444–471
analyses, protein sequence and structure for **1**:449–450
applications in drug discovery **1**:461–466
combined bioactivity data mining and chemical similarity search for ligand-based target prediction **1**:461–462
combined navigation of protein–ligand interaction and ligand chemistry space **1**:463–466
integrated structure-based medicinal chemistry toolbox for drug discovery and design **1**:463
protein binding site similarity assessments for ligand repurposing and off-target prediction **1**:462–463
chemogenomics **1**:444–446
database classification criteria **1**:450–454
data browse and search functionalities **1**:451
database update frequency **1**:454
ligand data types **1**:451–452
protein data types **1**:452–453
protein–ligand interaction data types **1**:453–454
ontology, for integration of curated chemical and biological data **1**:447–449
outlook **1**:466–467
overview **1**:444–450
protein structure-annotated biological activity databases **1**:454–457
mechanism-specific biological activity databases **1**:457
protein family-customized biological activity databases **1**:456–457
proteome-wide biological activity databases **1**:454–457
publicly available sequence, structural, and activity data **1**:446–447
structural protein–ligand interaction databases **1**:457–461
general structural protein–ligand interaction databases **1**:457–458
mechanism-based structural protein–ligand interaction databases **1**:459
protein family-customized structural chemogenomics databases **1**:460–461
systematic analysis and classification **1**:450–454
Structural protein–ligand interaction databases **1**:457–461
general structural protein–ligand interaction databases **1**:457–458
mechanism-based structural protein–ligand interaction databases **1**:459
protein family-customized structural chemogenomics databases **1**:460–461
Structure determination **2**:160–161
Structure recognition tools **3**:338–339
Structure refinement methods, in protein modeling **3**:137–138
Structure-based applications, of molecular fields **3**:286–292
binding site identification **3**:286–287
FLAPsite **3**:287
Q-SiteFinder **3**:286
SiteHound **3**:286
binding site similarity assessment **3**:287–289
GRID/FLAP **3**:287–288
IsoMIF **3**:288–289
determination of water positions **3**:291–292
WaterFLAP **3**:291–292
docking **3**:289–291
AFMoC **3**:289–290
AutoDock **3**:290
FLAPdock **3**:291
Glide **3**:291
GOLD **3**:291
Structure-based methods, polypharmacology **2**:266–267
Structure-based molecular design, high-throughput crystallography **2**:169–172
isoform selective PI3Kγ inhibitors **2**:169–171
lead hopping in fXa **2**:171–172
Structure-based target assessment, high-throughput crystallography **2**:163–165
protein–protein interactions **2**:164–165
Structure–target data mining, for drug repurposing **1**:29–31
chemical structure methods **1**:29–30
drug–target interaction profiles **1**:30–31
molecular docking and binding site similarity **1**:30
protein structure methods **1**:30
Study design, clinical studies **1**:543–545
Subcutaneous drug delivery, implantable devices for **6**:148
Substituted lactams **7**:231–232
Substructure key-based fingerprints **3**:340–341
Successful medicine discovery, contemporary considerations for **1**:560–576
drug at target **1**:564–569
drug-like chemical space **1**:560–564
molecular properties **1**:560–564
overview **1**:560
pharmacodynamics **1**:571–573
pharmacokinetics **1**:571–573
rules **1**:560–564

target and off-target engagement **1**:570–571
target choices **1**:573–574
Sugars, force field advances **3**:19
Sulfonamides **7**:100–102
Sulfones and sulfonamides **7**:89–96
Merck compounds **7**:89–90
Janssen compounds **7**:90–92
Sulfur, as nutraceuticals **1**:117
Sulfur interactions **3**:89–91
chalcogen bonding **3**:90–91
hydrogen bonds involving sulfur **3**:90
to nonpolar groups **3**:89–90
sulfur as a halogen bond acceptor **3**:91
Sumatriptan **7**:179
Sunflower trypsin inhibitors **1**:331–332
Superoxide dismutase (SOD) **1**:352f
Supervised similarity measures **3**:365–366
SureChEMBL
patent chemistry in **3**:471–475
target searching in **3**:476–478
Surface plasmon resonance **2**:214
label-free screening **2**:419
Sustainable processes in drug development and manufacturing, and QM/MM **3**:59–61
Sybyl line notation **3**:335
Syk inhibitors **5**:432
Symmetric field-based similarity indices **3**:363
Symmetry, predictive toxicology **2**:237
Synaptic vesicle proteins 2 (SV2) **7**:43–44
Synsorb Pk **1**:590f
Synthetic activators of sirtuins **1**:361
Synthetic biochemistry **3**:128
Synthetic biology **3**:128
Synthetic carbohydrate-based vaccines **1**:597f
Synthetic lethality **5**:22f
Synthetic peroxides **5**:719–720
Synthetic scaffolds **2**:116–152
Synthetic therapeutic oligonucleotides **6**:281–299
antisense oligonucleotides (ASOs) **6**:281–286
challenges and future perspectives **6**:286
chemical modification **6**:281–284
in clinical development **6**:284–286
pharmacokinetic properties of **6**:284
aptamers **6**:295–299
challenges and future perspectives **6**:299
chemical modifications **6**:295
in clinical development **6**:298
potential therapeutic applications of **6**:296–298
RNA interference (RNAi) **6**:286–295
challenges and future perspectives **6**:295
in clinical development **6**:293–295
cytoplasmic processing **6**:287–290
effective delivery **6**:293
focus areas for improving potency and safety **6**:292
potential therapeutic applications of **6**:293
transcriptional silencing and activation **6**:290
types of synthetic RNAi substrates **6**:290–292
Synthetic trioxolane peroxides **5**:719f
Synthetic triterpenoids, for inflammatory bowel disease **5**:501–502
Syrbactins **5**:261
Systematic biases, effect in drug discovery **2**:87–88
overcoming **2**:88
personal and organization biases **2**:87–88
Systems biology **2**:436, **3**:488–504
defintion of **3**:490
detailed discussion of **3**:497–499
and echanistic models **2**:505–506
identification of optimal combinations of molecular targeted drugs in oncology **2**:508–509
mathematical model for rheumatoid arthritis **2**:509
Systems biology, applications **2**:460–464
cross-species translation **2**:464
systems medicine, diagnostics **2**:462–464
personalized medicine **2**:463–464
translational systems biology **2**:464
systems pharmacology **2**:461
adverse drug reactions **2**:461
target identification **2**:461
systems toxicology **2**:461–462
assessment of nutraceuticals **2**:462
Systems biology, experimental technologies **2**:436–450
identification of adduct formation by sequencing **2**:439
metabolomics **2**:445–450
mass spectrometric platforms for metabolomics **2**:447–448
metabolomics data evaluation **2**:450
methods and recent developments **2**:446
special considerations and outlook **2**:450
structure identification **2**:449
proteomics **2**:440–445
protein expression profiling **2**:440–442
protein interaction profiling **2**:444–445
protein phosphorylation profiling **2**:443
proteome activity profiling **2**:444
proteome synthesis and degradation **2**:442–443
spatial proteomics **2**:442
special considerations and outlook **2**:445
transcriptomics **2**:436–439
microarray technology **2**:436–437
microRNA expression **2**:437–438
quantitative and digital PCR **2**:439
RNA-sequencing **2**:437
single-cell transcriptomics **2**:438–439
Systems biology, network-based modeling approaches for **2**:450–460
data-driven interaction network inference **2**:452–454
algorithms tailored to time-series data **2**:454
experimental data **2**:453
goal of network inference **2**:452–453
inferring edges using pairwise measures **2**:453–454
literature-driven network model building **2**:451–452
mathematical models for network biology **2**:456–460
enzyme kinetics **2**:458
from interaction network to mathematical dynamic model **2**:457
model analysis and validation **2**:459
model parameter fitting **2**:458–459
model simplification **2**:459
model usage in systems research **2**:459–460
stochastic *versus* deterministic models **2**:458
scoring of causal biological network models **2**:454–456
Systems biology, special considerations **2**:464–469
current status of systems biology in industry **2**:467–469
data evaluation **2**:465
data standards and sharing **2**:465–467
metabolomics **2**:466–467
proteomics **2**:466
transcriptomics **2**:466
education on systems biology **2**:467
experimental design and data production **2**:464–465
systems biology verification **2**:467
Systems chemical biology **2**:481–494
ADE prediction **2**:488–490
computational methodologies in **2**:483–485
data integration **2**:485
data mining and machine learning **2**:484
dynamic modeling **2**:484–485
network analysis and graph theory **2**:485
data integration in **2**:482–483
drug repositioning and drug combination **2**:487–488
drug–target identification and prioritization **2**:485–486
overview **2**:481–482
for personalized medicine **2**:490

T

T cell activation and differentiation, modulation of **5**:360
T cell-based cancer immunotherapy **6**:46–48
T regulatory cells (Tregs) **5**:360
T2D background **7**:482
TACE inhibitors **5**:404–405
Taisho **7**:271
TASP0428980 **7**:271
TAK-243 (MLN7243)
discovery of **8**:104–108
Takeda **7**:271–273
benzoxazepine-based selective orexin-2 antagonists **7**:272–273
spiropiperidine-based selective orexin-2 antagonists **7**:271–272

Takeda, modulators from **7**:313–314
TAM receptor signaling inhibitors **5**:380
Tanespimycin **5**:233f, **5**:234
Target
  choices **1**:573–574
  engagement **1**:570–571
Target activity and physical properties **2**:71–76
  ligand efficiency **2**:75–76
Target and chemical druggability **3**:429–439
  computational drug discovery criteria **3**:433–436
  drug target sources **3**:429–430
  drug-likeness computation **3**:431
  in silico methods to evaluate leads **3**:431–433
  in silico technologies, and medicinal chemists **3**:436–438
  overview **3**:429
  target druggability computation **3**:429–430
Target identification
  counterscreening and **3**:212–213
  label-free screening **2**:420–423
    label-free cell phenotypic profiling for **2**:422
    MS-based proteomics for **2**:420–422
  systems biology **2**:461
Target modulation and validation, new modalities for **2**:2–10
  biased receptor signaling **2**:4–5
  gene editing and gene therapy **2**:2–4
  modulating proteostasis and protein degradation **2**:8–10
  modulators of protein transcription, translation, and translocation **2**:5–8
Target prediction, ligand-based virtual screening for **2**:423
Target product profile (TPP) **6**:200
Target searching in SureChEMBL **3**:476–478
Target tractability and ligandability **3**:127
Target-association screening, drug repurposing **1**:21
Target-based screening, new technologies for **2**:12–14
Targeted cancer therapy, challenges of **5**:25–27
  CSCs **5**:26
  resistance and approaches to overcome resistance **5**:27
  tumor evolution and development of resistances **5**:26
  tumor heterogeneity **5**:25–26
Targeted delivery, of next-generation therapeutics **1**:335–343
  CPPs as delivery vectors **1**:336–339
    cellular uptake pathways for drug delivery with CPPs **1**:336–337
    enhancing endosomal escape of biologic drugs **1**:338–339
    molecular determinants of cell-permeability **1**:337–338
  targeting specific tissues **1**:339–342
    delivery of therapeutics across the blood–brain barrier **1**:340
    targeted delivery to the liver **1**:341–342
    targeting the pancreas **1**:342
    targeting the pituitary **1**:341
  targeting tumors **1**:342–343
    antibody–drug conjugates **1**:342–343
    GPCRs as targeting vectors **1**:343
Targeted secretion inhibitors **1**:341f
Targeted therapies against HER-2 **6**:13–15
  humanized mAbs and small-molecule inhibitors **6**:13–15
    clinical trials of trastuzumab **6**:13–14
    development of trastuzumab and treatment **6**:13
    pertuzumab **6**:15
    possible mechanisms of action and resistance to trastuzumab **6**:14
    side effects of trastuzumab treatments **6**:14
    trastuzumab-DM1 **6**:15
Targeting protein degradation **5**:246–273
  degradation of undruggable targets in cancer therapy **5**:272–273
    thalidomide and immunomodulatory drugs **5**:272–273
  deubiquitylating enzymes in cancer therapy **5**:271
  E1 activating enzymes in cancer therapy **5**:247–259
    E2 conjugating enzymes in cancer therapy **5**:250
    E3 ligases **5**:250–259
    pevonedistat (MLN4924) **5**:247–250
  overview **5**:246
  proteasome in cancer therapy **5**:259–271
    immunoproteasome inhibitors **5**:271
    proteasome inhibitors **5**:260–271
    structure and function of the proteasome **5**:259–260
  ubiquitin–proteasome system **5**:246–247
Targeting protein folding **5**:229–246
  HSP70 inhibitors **5**:229–231
  HSP90 family **5**:231–246
    HSP90 inhibitors **5**:232–244
    isoform selectivity **5**:245–246
  molecular chaperones **5**:229
Targeting protein synthesis **5**:203–228
  overview **5**:203–204
  targeting transcription **5**:204–214
    BRD4 inhibitors **5**:211–214
    targeting a TF **5**:204–207
    targeting RNA polymerases **5**:207–211
  targeting translation **5**:214–228
    direct inhibitors of eIF4F **5**:228
    inhibitors of eIF4F upstream regulators **5**:215–228
    inhibitors of ternary complex formation **5**:228
    translational control in cancer **5**:214–215
TASP0428980 **7**:271
Taspoglutide **7**:485
Tat/rev DsiRNA
  with gp120 aptamer **6**:293
  with PAMAM dendrimers **6**:293
Tau **7**:45–47
  as AD biomarker **1**:77–78
Tautomers **3**:193–197
  customized features **3**:197
  donor/acceptor feature point positioning **3**:194
  excluded volumes **3**:195
  halogens **3**:194
  hydrogen-bond acceptor features **3**:194
  hydrogen-bond donor features **3**:193–194
  hydrophobic features **3**:196
  positive and negative features **3**:194–195
Tavaborole **5**:709, **5**:709f
TCA cycle **5**:18
TD139 **1**:585f
TDO inhibitors **5**:364–365, **5**:365f
Technologies **2**:1–32
  hit characterization using computational approaches and biophysical assays **2**:14–18
  hit identification methods **2**:10–14
    new technologies for target-based screening **2**:12–14
    phenotypic screening **2**:10–12
  lead optimization **2**:18–27
    ADME and safety optimization, screening technologies for **2**:24–27
    asymmetric tissue distribution, design principles for **2**:23–24
  new modalities for target modulation and validation **2**:2–10
    biased receptor signaling **2**:4–5
    gene editing and gene therapy **2**:2–4
    modulating proteostasis and protein degradation **2**:8–10
    modulators of protein transcription, translation, and translocation **2**:5–8
  overview **2**:1–2
  perspective **2**:27–28
Telomerase inhibitors **5**:21–22
Telomeric quadruplexes as therapeutic targets **5**:314–316
Template CoMFA **3**:274
Template structures, protein models **3**:134
Teneligliptin (MP-0513) **7**:529–530
Tenofovir alafenamide (TAF), for HIV **5**:637–638, **5**:637f
Tepotinib **8**:178–203
  aryl substitution pattern optimization **8**:182
  bioisosteric carbamate replacements identification **8**:187
  bioisosteric core replacements identification **8**:182–184
  characterization of **8**:192–195
  final optimization, selection, and characterization of putative clinical candidate **8**:184–187
  identification of **8**:190–192
  overview **8**:178–179
  pharmacodynamic characterization of **8**:195–200
  pharmacokinetic characterization of **8**:195
  phenyl pyridazinone substitution pattern **8**:190
  pyrimidine substituents optimization **8**:187–190

supplementary material **8**:201
Terbinafine **5**:708f
Teriflunomide **5**:399
for multiple sclerosis **5**:447
Teriparatide **6**:69
Termini and side chains, modifications at **6**:70–77
N-acetylation **6**:70
C-amidation **6**:71
glycosylation **6**:75–77
lipidation **6**:72–75
PEGylation **6**:71–72
N-pyroglutamate formation **6**:70–71
Ternary complex formation, inhibitors **5**:228
TEST **4**:164
Tetracycline antibiotics **5**:521f
Tetracycline resistance **5**:520–521
Tetrahydroisoquinolines **7**:227–231, **7**:237, **7**:267
Tetrahydropyrazines **2**:144f
TEV-48125 **7**:216–217
Text-based fingerprint **3**:345
TgCDPK1 **5**:723f
TGFβ pathway, regenerative medicine **1**:395–396
TGFβ RI/ALK5 inhibitors **5**:378–379
Thalidomide **5**:272–273
Therapeutic development stages **1**:551
Thermal proteome profiling (TPP) **1**:571f, **2**:421f
Thermal shift assay (TSA) **2**:214
Thermodynamic integration *versus* free energy perturbation **3**:35–36
Thermodynamics in drug discovery **2**:197–206
direct calorimetric methods **2**:198–201
principle of ITC **2**:198–199
thermodynamics of T_m shifting assays **2**:200–201
Van't Hoff analysis **2**:199–200
future trends for thermodynamic characterization **2**:206
mechanistic aspects to binding thermodynamics **2**:201–203
complex role of water **2**:202–203
enthalpy–entropy compensation **2**:201–202
enthalpy–entropy transduction **2**:202
methods for measuring binding thermodynamics **2**:197
optimizing enthalpy **2**:204–205
role of binding thermodynamics in fragment-based drug design **2**:205–206
experimental considerations for fragment ITC **2**:206
role of binding thermodynamics in selectivity and efficacy **2**:203–204
aldose reductase **2**:204
HIV-1 protease **2**:203
HMGCoA reductase **2**:204
matrix metalloproteinase 12 **2**:203
thrombin **2**:203–204
Thermodynamics properties
of protein-ligand association **3**:55
Thioester (COS) **6**:84
Thioflavin T agents **1**:88–89
Third generation genome sequencing technologies **2**:357
THK-265 **1**:90
Three-dimensional cell culture models **4**:296
Three-dimensional organotypic culture mimics ovarian cancer microenvironment, and high-content screening **2**:371–372
3D activity cliff analysis **3**:277–281
activity miner/activity atlas **3**:278–281
3D clustering of molecule libraries **3**:270
3D database searching, pharmacophore elucidation **3**:205–207
database generation **3**:205–206
feature matching **3**:206
geometry matching **3**:206–207
post-processing **3**:207
3D descriptors **3**:351–354
3D descriptor families **3**:353–354
EigenVAlue descriptors (EVA) descriptors **3**:354
GETAWAY descriptors **3**:353–354
Grid-Independent Descriptors (GRIND) **3**:354
Molecular Electronegativity Distance Vector (MEDV) **3**:354
VolSurf descriptors **3**:354
Weighted Holistic Invariant Molecular (WHIM) descriptors **3**:353
electronic descriptors **3**:351–352
molecular field analysis descriptors **3**:353
molecular shape analysis descriptors **3**:353
receptor surface analysis descriptors **3**:353
shape descriptors **3**:352
size descriptors **3**:352
van der Waals parameters **3**:353
volume descriptors **3**:352
3D high-content screening of organoids **2**:388–415
hardware **2**:402–406
brightfield and widefield microscopy **2**:402–404
confocal microscopy **2**:404–405
laser scanning cytometers **2**:406
light sheet fluorescence microscopy **2**:405
two-photon microscopy **2**:405
HCS compatible 3D cell culture platforms **2**:400–402
hanging drop method **2**:401
liquid overlay methods with non-adherent surface plates **2**:401
magnetic levitation **2**:401–402
microfluidic devices **2**:402
micropatterned plates **2**:401
high-throughput 3D culture technologies **2**:396–402
key limitations **2**:410
overview **2**:388–389
software **2**:406–410
deconvolution **2**:408
image acquisition software **2**:406
image visualizations and analysis software **2**:408–409
workflow platform **2**:410
traditional 3D culture techniques **2**:397–400
hydrogel **2**:400
solid scaffolds **2**:397
spinner flask and rotating wall vessel bioreactors **2**:397
3D pharmacophores and protein structure **3**:208–213
counterscreening and target identification **3**:212–213
exemplar applications of 3D pharmacophore methods **3**:211–212
pharmacophores and 3D QSAR methods **3**:210–211
3D protein structures in drug discovery and design **3**:120–121
3D RISM **3**:405
3D structural information in computational design **1**:454, **3**:101–119
considerations **3**:106
electron microscopy **3**:114–115
use and limitations of **3**:114–115
fitting to coordinate *versus* fitting to electron density **3**:113–114
limitations and lessons in using X-ray crystal structures **3**:105–106
overview **3**:101
protein structure determination, history of **3**:102–103
uncertainties in using X-ray crystal structures **3**:106–109
crystallization conditions, and target biology **3**:108
protein flexibility **3**:108–109
water molecules identification in electron-density maps **3**:108
use of X-ray structures in structure-based drug design, history of **3**:103–105
using X-ray crystal structures in docking and scoring validation studies **3**:109–112
validation of X-ray crystal structures **3**:109
3D-QSAR **3**:270–277
alignment of ligands for **3**:213
CoMFA **3**:271–272
CoMSIA **3**:273
COSMO*sar3D* **3**:274–276
FieldQSAR **3**:276
GRID/GOLPE/FLAP **3**:277
GRIND **3**:277
pharmacophores **3**:210–211
Template CoMFA **3**:274
Topomer CoMFA **3**:273–274
3Rs, predictive toxicology **2**:95
Thrombin
and binding thermodynamics **2**:203–204
inhibitors **7**:601–603
small-molecule direct thrombin inhibitors **7**:601–603
target validation and proof of concept **7**:601

Thyroid C-cell tumor **7**:487
TIDVAL, cancer biology **5**:6–8
  target identification **5**:7–8
  target validation **5**:8
TIMBAL **1**:457
Time, and drug repurposing **1**:16
Tissue distribution model **4**:63
Tissue fibrosis **7**:694–713
  chronic kidney disease **7**:701–705
    animal models of fibrotic renal disease **7**:702
    current treatment **7**:702–703
    emerging biology and therapeutic treatment **7**:704–705
    epidemiology **7**:701
    ongoing clinical trials **7**:703
    overview **7**:701
    pathophysiology **7**:701
    perspectives **7**:705
  generally **7**:695–696
  idiopathic pulmonary fibrosis **7**:696–700
    current treatment **7**:697–698
    emerging biology and therapeutic treatment **7**:698–700
    epidemiology **7**:696
    experimental animal models **7**:697
    ongoing clinical trials **7**:698
    overview **7**:696
    pathophysiology **7**:696–697
  liver fibrosis **7**:705–709
    drugs evaluated in preclinical and clinical trials **7**:707–708
    emerging biology **7**:708
    epidemiology **7**:705
    experimental animal models **7**:707
    overview **7**:705
    pathophysiology **7**:706
Tissues targeting, next-generation therapeutics **1**:339–342
  blood–brain barrier **1**:340
  liver **1**:341–342
  pancreas **1**:342
  pituitary **1**:341
TLR agonist in development for IO **5**:375–376
TLR4 **5**:374–375
TLR4 agonist ligands **5**:375f
TLR7 agonists **5**:649t
TLR7/8 **5**:373–374
TLR9 **5**:375
T_m shifting assays, thermodynamics of **2**:200–201
TNF IR
  ABT-494 in **5**:429
TNFα
  and DILI **4**:229
  -driven diseases
    dual p38α MAPK/PDE-4 inhibitors for **8**:431–449
TNP-470, optimization of **1**:224t
Tocilizumab translation in Crohn's disease **2**:520
Tofacitinib **5**:399, **5**:422–424
  clinical development of **5**:422–423
  in combination with csDMARDs **5**:423
  long-term efficacy (LTE) of **5**:423
  as monotherapy **5**:423
  safety **5**:423–424
Tolcapone, for Parkinson's disease **5**:462
Toll-like receptors (TLRs) **5**:406
Topiramate **1**:582f
Topoisomerase inhibitors **5**:694f
Topological descriptors **3**:349–350
Topological fingerprints **3**:341
Topomer CoMFA **3**:273–274
Torin1 **5**:227
Toxicity, matched molecular pair analysis **3**:239–241
Toxicity, nanoparticles **1**:278–284
  cell death mechanisms **1**:282–284
    annexin-V **1**:282
    cell morphology **1**:284
    loss of mitochondrial membrane potential **1**:283–284
    ROS generation **1**:283
  cell membrane permeability **1**:281–282
    calcein acetoxymethyl **1**:281–282
    DNA intercalating fluorescent agents **1**:282
    fluorescein diacetate **1**:281
    lactate dehydrogenaze enzyme **1**:282
    trypan blue **1**:281
  general considerations for NPs presence **1**:284
  instrumentation for detection of fluorescent probes **1**:284
  proliferation assays **1**:278–280
    alamar blue assay **1**:279
    cell division assay **1**:280
    clonogenic assay **1**:279–280
    EdU proliferation assay **1**:280
    MTT **1**:278–279
Toxicity prediction **4**:285–304
  contemporary critical issues, lessons learned from **4**:298
  future directions **4**:299–300
  historical perspective **4**:286–287
  important documents and programs relating to **4**:287–293
    appraisal of the safety of chemicals in foods, drugs, and cosmetics **4**:287
    classical methods for toxicity evaluation **4**:290
    continuing evolution of global consensus on regulatory toxicology **4**:292–293
    current methods **4**:290
    current views on safety evaluation of drugs **4**:287
    FDA guidances on safety evaluation of drugs **4**:288
    fit-for-purpose cellular models for secondary screening **4**:288
    high-throughput gene expression core facility **4**:288
    life cycle of method development, validation, and adoption **4**:290–292
    Redbook 2000; Revised Jul. 2007 **4**:287
    tests required for safety evaluation of new drugs **4**:288–290
    Toxicologic Testing Handbook **4**:288
    toxicology in the 21st century (Tox21) **4**:288
  overview **4**:285–286
  safety evaluation **4**:299–300
Toxicity prediction, indicators of efficacy and toxicity **4**:294–298
  application of bioinformatics **4**:298
  bioinformatics approaches and big data **4**:297–298
  blood-borne sampling **4**:296
  computational toxicology **4**:297
  emerging imaging biomarkers **4**:294
  microphysiological models **4**:297
  MRI applications **4**:295–296
  preclinical imaging as a translatable biomarker **4**:294
  small animal PET imaging (micro-PET) **4**:294–295
    [^{18}F]-Annexin V **4**:295
    [^{18}F]-DFNSH **4**:295
    [^{18}F]-FDG **4**:295
    [^{18}F]-FEPPA **4**:295
    [^{18}F]-FLT **4**:295
  three-dimensional cell culture models **4**:296
Toxicogenomic signatures, for genotoxicity evaluation **4**:201
Toxicology
  genetic. *See* Genetic toxicology
  model systems for **2**:97–102
    animal models **2**:102
    complex cellular models **2**:100–101
    individual target screening **2**:97–100
    isolated tissues and organs **2**:101
    organ chips **2**:101
    simple cellular models **2**:100
Toxicology, stem cells in, derived **4**:177–194
  3Rs **4**:189
  induced pluripotent stem cell-derived
    brain organoids **4**:186–187
    cardiomyocytes **4**:183
    heart organoids **4**:187
    hepatocytes **4**:180–182
    liver organoids **4**:186
    neuronal cells **4**:182–183
    organoids **4**:183–187
  induced pluripotent stem cells **4**:187–189
  overview **4**:178
  pluripotent stem cells **4**:178–179
Toxicology testing in the 21st century (Tox21) **4**:248
Toxoplasma **5**:722–723
ToxTree **2**:235, **4**:168, **4**:168t
TP antagonists **7**:580
Traditional 3D HCS culture techniques **2**:397–400
  hydrogel **2**:400
  solid scaffolds **2**:397
  spinner flask and rotating wall vessel bioreactors **2**:397
Trametinib **8**:33–57
  concept **8**:34–35
  lead compound identification **8**:35–37

mechanism of action and pharmacological characterization **8**:46–52
MEK inhibitory activity of trametinib **8**:49–50
pharmacological characterization of trametinib **8**:50–52
target identification of trametinib **8**:46–48
overview **8**:33–34
polymorphism study **8**:53
SAR study-1 **8**:38–44
SAR study-2 **8**:44–46
synthetic studies **8**:54–55
Transcriptome-based data mining, for drug repurposing **1**:34
Transcriptomics **2**:436–439
data standards and sharing **2**:466
microarray technology **2**:436–437
microRNA expression **2**:437–438
quantitative and digital PCR **2**:439
RNA-sequencing **2**:437
single-cell transcriptomics **2**:438–439
Transgenic carcinogenicity assays **4**:243–245
Transglutaminase (TG2) inhibitors **7**:36
Translatable safety biomarkers **4**:255–284
bis(monoacylglycero)phosphate (BMP) **4**:278–279
blood cytokines as safety biomarkers **4**:275–277
biology **4**:275
cytokine biomarkers **4**:276–277
description **4**:256
emerging biomarkers of acute kidney injury **4**:268–275
N-acetyl-β-D-glucosaminidase **4**:274
assays **4**:272
beta-2-microglobulin **4**:273
Clusterin **4**:273
Cystatin-C **4**:273
KIM-1 **4**:274
neutrophil gelatinase-associated lipocalin **4**:274–275
osteopontin **4**:275
pathophysiologic factors **4**:272
postanalysis, interpretation **4**:272
preanalytical factors **4**:269–272
emerging biomarkers of drug-induced liver injury **4**:263–268
alpha-gluthathione-*S*-transferase **4**:265–266
arginase-1 **4**:264–265
cytokeratin 18 **4**:266
general characteristics of emerging liver safety biomarkers **4**:264
glutamate dehydrogenase **4**:266–267
HMGB1 **4**:267
miR-122 **4**:267–268
methodology of biomarker qualification and assay validation **4**:256–262
assay validation **4**:260–262
biological qualification **4**:257–258
biomarker evaluation **4**:258–259
molecular classes of biomarkers **4**:256–257
normal range and threshold setting **4**:259–260
regulatory qualification of new toxicity biomarkers **4**:262
statistical approaches **4**:258
overview **4**:255–256
phospholipidosis **4**:277
Translational aspects in drug discovery **2**:495–529
biomarkers **2**:497–503
definition **2**:497
qualification **2**:503
use of **2**:499
validation **2**:501–503
biomarkers assays/methods **2**:499–501
enzyme-linked immunosorbent assay **2**:500
mass spectrometry **2**:500–501
multiplex assays **2**:500
biomarkers types **2**:497–499
competitive biomarkers **2**:499
efficacy biomarkers **2**:498
pharmacodynamic biomarkers **2**:497
pharmaco-economic biomarkers **2**:499
safety biomarkers **2**:498–499
stratification and predictive biomarkers **2**:498
overview **2**:496–497
Translational aspects in drug discovery, animal model **2**:510–514
generalities **2**:510
implemention into translational strategy **2**:512–514
back-translate clinical trial findings into animal models **2**:513–514
designing strategy with high translational value **2**:512–513
improvement methods **2**:510–512
designing concurrent with design recommended for pivotal clinical trial **2**:511
enhance variability and reduce standardization **2**:510–511
humanize animal models **2**:511–512
multisite animal model trials **2**:510
proper validation of animal models **2**:512
and relevant clinical endpoints **2**:512
Translational aspects in drug discovery, imaging **2**:514–516
application
of CT in drug development **2**:515
of MRI in drug development **2**:516
of PET in drug development **2**:516
of radiography in drug development **2**:515
types and technologies **2**:514–515
computed tomography **2**:514–515
magnetic resonance imaging **2**:515
optical imaging **2**:515
positron emission tomography **2**:515
radiography **2**:514
Translational aspects in drug discovery, modeling and simulations **2**:503–509
from empirical to mechanistic pharmacokinetic/pharmacodynamic models **2**:504
examples of applications of empirical, mechanistic, and system biology models **2**:507–509
empirical pharmacokinetic/pharmacodynamic models **2**:507
mechanistic pharmacokinetic/pharmacodynamic models **2**:507
PBPK models, drug–drug interactions consequent to drug-mediated cytokine elevations **2**:508
system biology modelsda mathematical model for rheumatoid arthritis **2**:509
system biology modelsdidentification of optimal combinations of molecular targeted drugs in oncology **2**:508–509
from mechanistic models to system biology models **2**:505–506
overview **2**:503
Translational aspects in drug discovery, strategy and integration **2**:517–523
combination of technologies **2**:523
design of translation strategies **2**:517–520
ALX-0171 translational strategy **2**:519–520
overview **2**:517
stroke TM strategies **2**:517–519
tocilizumab translation in Crohn's disease **2**:520
integrative thinking **2**:520–523
bedside back to bench **2**:520–521
in oncology **2**:521–523
overview **2**:520
Translational research, rare disease foundations **1**:554
Translational systems biology **2**:464
Translocator protein **7**:49–51
Transmission electron microscopy **1**:276–277
Transporter effects prediction **4**:67–68
Transporter-humanized mice **4**:137–138
Transporters, role in drug- and bile acid-induced liver injury **4**:225–228
bile acid toxicity **4**:227–228
bile acid uptake and excretion **4**:225–226
cellular and hepatic features of cholestasis **4**:226–227
drug and bile acid transporters, classification of **4**:225
model systems for transport evaluation **4**:227
transporters and bile acid toxicity **4**:228
Transthyretin (TTR) amyloidosis **6**:284–285
Tranylcypromine **5**:302f
Trastuzumab
clinical trials of **6**:13–14
development of **6**:13
possible mechanisms of action and resistance to **6**:14
side effects of **6**:14

Trastuzumab-DM1 **6**:15
Treatments discoveries **1**:549–550
Trelagliptin (SYR-472) **7**:533–534
Trematodes **5**:738–739
Triage of ADME/PK screening assays **4**:20
Triazole-based analogs **1**:299f–300f, **1**:302f
Triazolopyrimidine DHODH inhibitors **5**:722f
Triazolo-thioamides **7**:246
Tricyclo-DNA **6**:224
Tricomponent synthetic vaccine **1**:598f
Triflusal **7**:585
Trihexyphenidyl, for Parkinson's disease **5**:462
Trimethoprim resistance **5**:525–526
TriNA **6**:224
Tripan blue staining dead cells **1**:281f
Tripos mol2 format **3**:336
Triterpene ganoderic acid C1 (GAC1), for inflammatory bowel disease **5**:505–506
TRK-170 **5**:401
Troglitazone **4**:213
Tropomyosin receptor kinase **7**:428
Trospium **1**:253f
Trypan blue **1**:281
Trypanosoma brucei **5**:731–735
Trypanosoma cruzi **5**:729–730
Trypanosomal phosphodiesterase inhibitors **5**:731–732
Tryptophan **5**:362–365
Tryptophan metabolism **5**:362f
TSCA **4**:287t
Tubulin **2**:383f
  polymerization and redistribution, and high-content screening **2**:382
Tumor-infiltrating lymphocytes (TILs) **6**:46–47
Tumor metabolism **5**:17–18
  amino acid metabolism **5**:18
  glucose metabolism **5**:17
Tumor microenvironment (TME) **5**:359–361
  current status of immuno-oncology therapy **5**:361
  modulation of DC function in tumor **5**:361
  modulation of T cell activation and differentiation **5**:360
  myeloid-derived suppressor cells (MDSCs) **5**:360–361
  T regulatory cells (Tregs) **5**:360
  tumor-associated macrophages (TAMs) **5**:361
Tumor necrosis factor-α-converting enzyme (TACE) inhibitors **1**:232t
Tumor-associated carbohydrate antigens (TACAs) **1**:594f
Tumor-associated macrophages (TAMs) **5**:361
Tumor-induced immunosuppression **5**:18–19
Tumor-promoting inflammation **5**:6
Tumors
  evolution and development of resistances **5**:26
  heterogeneity **5**:25–26
  targeting, with next-generation therapeutics **1**:342–343
    antibody–drug conjugates **1**:342–343
    GPCRs as targeting vectors **1**:343
2/3D pharmacophore **3**:189–220
  3D pharmacophores and protein structure **3**:208–213
  counterscreening and target identification **3**:212–213
  exemplar applications of 3D pharmacophore methods **3**:211–212
  pharmacophores and 3D QSAR methods **3**:210–211
  biological context of **3**:191
  challenge of molecular alignment **3**:213–214
    alignment of ligands for 3D QSAR **3**:213
    analysis of hits from a random screen **3**:214
    future **3**:216
    pharmacophore feature representation **3**:215–216
    rationalization of the shared activity of two different types of ligands **3**:214
    validation standards **3**:215
    variable binding modes **3**:216
  future directions **3**:213–216
  overview **3**:190–191
  pharmacophore keys **3**:207–208
    2D pharmacophores **3**:207
    3D pharmacophores **3**:207–208
2D descriptors **3**:347–351
  indicator variables **3**:351
  molecular identification numbers **3**:351
  thermodynamic descriptors **3**:351
  topological descriptors **3**:349–350
  whole-molecular descriptors **3**:347–348
Two-photon microscopy **2**:405
2P2Idb **1**:459
Two-strain ames screen **2**:106
TXS inhibitors **7**:586
Tyrocidine A **6**:89
Tyrosine-kinase 2 (Tyk2) **5**:407

U

Ubiquitin proteasome system **8**:95
Ubiquitin-activating enzyme (UAE) **8**:96–97
  profile of the clinical candidate **8**:109–110
  selection of the development candidate **8**:108
Ubiquitin–proteasome system **5**:246–247
UCSD/Neurogenetics Inc/Torrey Pines Therapeutics, modulators from **7**:314–315
UGT- and NAT-humanized mice **4**:136–137
Ulcerative colitis (UC) **5**:497f
Umbrella study design **2**:539f, **3**:41
  companion diagnostics **2**:538–539
UNC0638 **5**:300f
UNC0642 **5**:300f
Undruggable targets degradation in cancer therapy **5**:272–273
  thalidomide and immunomodulatory drugs **5**:272–273
UNIFAC **3**:404
Unilateral ureteral obstruction **7**:702
UniProt Knowledgebase **1**:449
United States
  academic drug discovery centers in **1**:7
  Food and Drug Administration (FDA) electronic submission to **2**:255–256
  regulatory requirements, for companian diagnostics **2**:540
  United States Patent and Trademark Office (USPTO) **1**:535–536
University-based research, inefficiency **1**:557
Urocortins **7**:643

V

Vaccine development
  carbohydrate-based vaccines **1**:596–598
  carbohydrates as immune modulators **1**:593–596
Valid hits identification **2**:50–51
  hit-to-lead process **2**:51–53
    chemical probes for novel therapeutic concepts **2**:52–53
  origin of first-in-class drugs **2**:53–55
Van der Waals parameters **3**:353
Van't Hoff analysis **2**:199–200
Vapor pressure
  physical–chemical properties **3**:413–415
    physics-based models **3**:413–415
    statistical methods **3**:415
Variability and standardization, in aimal models **2**:510–511
Variable binding modes, pharmacophores **3**:216
Vascular cell adhesion molecule 1 (VCAM-1 or CD106) **7**:53
Vasopressin antagonists **7**:642–643
Vegetables, and CVDs prevention **1**:126–127
  garlic **1**:126–127
  ginger **1**:127
  onion **1**:127
VEGF **6**:9
  and VEGFR **5**:325–326
VEGF peptide mimics **6**:18–19
  combination therapy **6**:19
  design and synthesis of **6**:18–19
Vemurafenib (PLX-4032), FDA approved drug **2**:217
Vernalis HSP70 inhibitors **5**:230f

Vertex 7:215
Verubecestat 8:204–251
  BACE1 characteristics and drug discovery challenges 8:206–207
  BACE1 inhibitor lead-finding strategies 8:207–219
    BACE1 and CatD in vitro assays 8:208
    fragment screening 8:210–219
    hydroxyethylamine-based peptidomimetic inhibitors 8:208–210
    overview 8:207–208
  clinical evaluation 8:243–245
  discovery of 8:237–242
    human dose and PK/PD projections 8:242
    PK/PD profile 8:241–242
    S1–S3 spanning diaryl amides 8:237–238
    verubecestat cocrystal structure, in vitro profile, and key SAR 8:238–240
    verubecestat synthesis 8:240–241
  lead optimization 8:219–237
    from acyl guanidines to sulfonyl guanidines 8:235–237
    core modification 8:223–226
    iminohydantoins 8:219–223
    iminopyrimidinones 8:229–231
    in vivo validation and high-throughput Rat PD assay development 8:226–229
    structural differentiation 8:231–235
  overview 8:204–206
Vesicular monoamine transporter type 2 (VMAT2) 7:43
V-factor 2:393–394
Vildagliptin (LAF-237) 7:524–526
Virtual screening 2:40–43, 2:215, 2:337–338
  of covalent inhibitors 5:100
  to identify potential off-target effects of lead molecules 2:427
  label-free screening 2:420
  molecular fields 3:264–265
    fieldscreen/blaze 3:264
    FLAP 3:264–265
  PPI inhibitor 5:166
Visualization tools and data analysis 3:440–463
  big data analysis 3:460–461
  collaboration tools 3:461–463
    workflow 3:461–463
  command line/programming tools 3:440–448
  desktop tools 3:448–454
  mobile applications 3:457–460
    mobile apps using a client–server model 3:459–460
  overview 3:440
  web-based tools 3:454–457
Vitamins
  in cancer management 1:129
  as nutraceuticals 1:110–113
    water insoluble vitamins 1:110–111
    water soluble vitamins 1:111–113
VL-2397 5:713–714
VolSurf 3:282
Voltage-gated calcium channels 7:66–68
  channel distribution and function 7:66–68
  channel structure 7:66
  channel subtypes 7:66
Voltage-gated calcium channels inhibitors 7:70–122
  alpha 2 delta ligands 7:114–122
    amino acid-derived structures 7:114–118
    gababutins 7:118–120
    nonamino acid structures 7:120–122
  Cav2.1 inhibitors 7:72–73
    inhibiting compounds 7:73
    nomenclature 7:72
    target validation 7:72–73
  Cav2.2 inhibitors 7:75–99
    arylthiazolidinediones 7:79–80
    diarylmethylpiperazines 7:81–89
    dihydropyridines 7:80–81
    early inhibitors 7:76
    indole-derived structures 7:96–98
    miscellaneous templates 7:98–99
    small-molecule blockers based on peptide toxin structures 7:76–79
    sulfones and sulfonamides 7:89–96
  Cav2.3 blockers 7:99–100
  Cav3 blockers 7:100–114
    dihydropyridine derivatives 7:113
    dihydroquinazolines 7:113–114
    early molecules 7:100
    indoles 7:113
    miscellaneous chemotypes 7:114
    piperazines and homopiperazines 7:109
    piperidine- and piperazine-based structures 7:103–108
    pyridyl amides 7:110–111
    quinazoline derivatives 7:111–112
    sulfonamides 7:100–102
  compounds under clinical evaluation 7:70–72
    ABT-639 7:71
    CNV2197944 7:70
    ethosuximide 7:72
    microgabalin 7:72
    Z160 7:70
    Z944 7:72
Voltage-gated sodium channel blocking agents 7:133–165
  antibodies 7:135–136
  small molecules 7:136–165
    clinical compounds with a sodium channel mode of action 7:136
    $Na_V1.7$ blockers 7:136–161
    $Na_V1.8$ blockers 7:161–165
    $Na_V1.9$ blockers 7:165
    rafabegron and related analogs 7:723
  toxins and peptides 7:133–135
Volume descriptors 3:352
Voriconazole 5:707f
Vorapaxar (SCH-530348) 7:574–576
Voxtalisib (XL765) 5:220
VT-1161 5:710–711, 5:710f
vIv/TransTech/HighPoint
  inhibitors reported by 7:372
VX-509 5:402
VX-509 oral-selective JAK3 inhibitor 5:431
  as monotherapy 5:431
  in MTX-IR 5:431

W

Water 3:70–71
  complex role of 2:202–203
  force field advances 3:19
  positions determination 3:291–292
Water insoluble vitamins as nutraceuticals 1:110–111
Water soluble vitamins as nutraceuticals 1:111–113
WaterFLAP 3:291–292
WDR5–MLL 2:339–341
Web-based tools 3:454–457
WEE1 5:66–68
WEE1 inhibitors 5:66–67, 5:66f
Whole-body physiologically based pharmacokinetic model 2:505f
Whole-molecular descriptors 3:347–348
Wide field imagers 2:366
Wiswesser line notation 3:334
Wnt pathway, regenerative medicine 1:396–397
WNT pathway blockers 1:243t
World Intellectual Property Organization (WIPO) 1:533–534
Writer enzymes 5:283
  histone acetyl transferases 5:283
  histone methyl transferases 5:283
WT ALK inhibitor 5:55
Wyeth 5:227
  inhibitors reported by 7:370–372

X

XED/FieldAlign 3:258–260
Xenobiotic receptors, genetic modifications of (mouse models) 4:132–133
  receptor-humanized mice 4:133
X-ray crystal structures
  in docking and scoring validation studies 3:109–112
  limitations and lessons in using 3:105–106
  in structure-based drug design, history of 3:103–105
  uncertainties in using 3:106–109
    crystallization conditions, and target biology 3:108
    protein flexibility 3:108–109

X-ray crystal structures (*continued*)
water molecules identification in electron-density maps **3**:108
validation of **3**:109
X-ray crystallography **2**:213–214
-based FBS implementation **2**:168–169
X-ray free electron lasers and cryo-electron microscopy **2**:172–173

Y

Yellow fever
antiviral drugs for **5**:679

Z

Z′-factor **2**:393
Z160 **7**:70
Z944 **7**:72
Zanamivir **1**:581f, **5**:670f
Zebrafish model, regenerative medicine **1**:401
Zika virus
antiviral drugs for **5**:678–679
Zinc, as nutraceuticals **1**:118
ZK3044709 **5**:211f
Z-score and robust Z-score **2**:394–395

AUTHOR INDEX

A

Abdulrahman, Ganiy Opeyemi
Targeting DNA Damage Response Pathways in Cancer

Abou-Gharbia, M.
Academic Drug Discovery Centers: Key Players in the Future of the Pharmaceutical Industry

Abramov, Y.A.
Empirical and Physics-Based Calculations of Physical–Chemical Properties

Ackley, K.L.
Manufacturing of Oligonucleotides

Adams, J.L.
Cancer Immunotherapy—An Emerging Field That Bridges Oncology and Immunology Research

Adjaye, J.
Use of Stem Cells in Toxicology

Aduda, V.
Manufacturing of Oligonucleotides

Ahn, J.-M.
Strategy and Tactics for Designing Analogs: Biochemical Characterization of the Large Molecules

Ajina, R.
Cancer Immunotherapy

Albrecht, W.
Are Two Better Than One in Rheumatoid Arthritis? Development of Dual p38α MAPK/PDE-4 Inhibitors for Treatment of TNFα-Driven Diseases

AlDeghaither, D.
Cancer Immunotherapy

Aldeghi, M.
Advances in Molecular Simulation

Alden, C.
The Future of Carcinogenicity Testing

Ali, A.
Case Histories: Anacetrapib

Anderson, D.J.
The Discovery of p97 Inhibitors

Andrews, K.A.
Human PK Prediction and Modeling

Armstrong, D.
Predictive Toxicology: Latest Scientific Developments and Their Application in Safety Assessment

B

Baglieri, D.
Closing Distances Between Academia and Market

Bajusz, D.
Chemical Data Formats, Fingerprints, and Other Molecular Descriptions for Database Analysis and Searching

Barreiro, E.J.
Beyond Bioisosterism: New Concepts in Drug Discovery

Baskin, I.I.
Empirical and Physics-Based Calculations of Physical–Chemical Properties

Bauer, S.M.
Are Two Better Than One in Rheumatoid Arthritis? Development of Dual p38α MAPK/PDE-4 Inhibitors for Treatment of TNFα-Driven Diseases

Bayliss, M.K.
Contemporary Considerations for Discovering a Successful Medicine

Bebernitz, G.
Sodium–Glucose Cotransporters

Beedanagari, Sudheer
Genetic Toxicology

Beilke, L.D.
In Silico Tools and their Application

Bekaii-Saab, T.
Peptide-Based Cancer Vaccines and Therapeutics for Solid Tumors Overexpressing HER-1, HER-2, HER-3, VEGF and IGF-1R

Bell, I.M.
CGRP Receptor Antagonists for the Treatment of Migraine

Bender, A.
Drug Repurposing Review

Benet, L.Z.
Drug Classification and Drug Disposition Prediction

Benningshof, J.
European Lead Factory

Bergner, A.
Hit and Lead Generation Strategies

Beswick, P.
Progress in the Discovery of Ca Channel Blockers for the Treatment of Pain

Beswick, Paul
Modulating AMPA Receptors for the Treatment of CNS Disorders

Bhat, A.
Future of Medicinal Chemistry: Next-Generation Therapeutics

Biftu, T.
DPP-4 Inhibitors

Biggin, P.C.
Advances in Molecular Simulation

Birch, M.
Antifungal Chemistry Review

Blass, B.E.
Academic Drug Discovery Centers: Key Players in the Future of the Pharmaceutical Industry

Blaukat, A.
Tepotinib

Boezio, A.A.
Discovery of AMG 337: Using Structure Guided Scaffold Hybridization to Optimize Physicochemical Properties and Target Coverage of a MET Kinase Inhibitor

Bolger, M.B.
Human PK Prediction and Modeling

Bolli, M.H.
The Discovery of Macitentan—A Standard Medicinal Chemistry Program?

Bolognesi, M.L.
From Imaging Agents to Theranostic Drugs in Alzheimer's Disease

Bortolato, A.
Modeling and Design for Membrane Protein Targets

Boss, C.
The Discovery of Macitentan—A Standard Medicinal Chemistry Program?

Brandon, N.J.
Human iPSC Models in Drug Discovery: Opportunities and Challenges

Brigo, A.
Computational Models to Predict Toxicological Endpoints in Drug Discovery and Strategies for Data Integration

Brookings, D.C.
The Discovery and Development of *Seletalisib*: A Potent and Selective PI3Kδ Inhibitor for Inflammatory Diseases

Brown, G.
Modeling and Design for Membrane Protein Targets

Brown, D.G.
New Drugs and Emerging Leads in Antibacterial Drug Discovery

Browne, D.L.
Continuous Flow Processing as a Tool for Medicinal Chemical Synthesis

Burrows, J.N.
Medicinal Chemistry Case History: Discovery of the Dihydroorate Dehydrogenase Inhibitor DSM265 as an Antimalarial Drug Candidate
New Models of Drug Discovery and Development for Neglected Disease Populations

Bush, K.
Recent Epidemiological Changes in Infectious Diseases

C

Callebaut, C.
Recent Epidemiological Changes in Infectious Diseases

Caroff, E.
Advances in Antiplatelet Agents

Carrington, P.
GLP-1 Receptor Agonists for the Treatment of Diabetes and Obesity

Castillo, C.C.
Targeting Promoter Quadruplex Nucleic Acids for Cancer Therapy

Catapano, A.L.
Advances in Hypercholesterolemia

Cathcart, A.
Recent Epidemiological Changes in Infectious Diseases

Cavalla, D.
Drug Repurposing Review

Cesaroni, F.
Closing Distances Between Academia and Market

Céster Schlaak, H.
Present and Future Challenges and Opportunities for Intellectual Property in an Open Landscape: Open Labs and the Internet

Charman, S.A.
Medicinal Chemistry Case History: Discovery of the Dihydroorate Dehydrogenase Inhibitor DSM265 as an Antimalarial Drug Candidate

Chaudhari, R.
Overview of Drug Polypharmacology and Multitargeted Molecular Design

Cheeseman, M.D.
Targeting Protein Synthesis, Folding, and Degradation Pathways in Cancer

Chen, H.
Fragment-Based Drug Design: Strategic Advances and Lessons Learned
Small-Molecule Inhibitors of Protein–Protein Interactions

Chen, K.
Inhibiting Kinases in the CNS

Chenard, B.L.
The Discovery of the MCH-1 Receptor Antagonist NGD-4715 for the Potential Treatment of Obesity

Cherkasov, A.
Targeting the Androgen Receptor Signaling Axis

Childers, W.E.
Academic Drug Discovery Centers: Key Players in the Future of the Pharmaceutical Industry

Ciavarri, J.
The Discovery of First-in-Class Inhibitors of the Nedd8-Activating Enzyme (NAE) and the Ubiquitin-Activating Enzyme (UAE)

Clark, R.D.
Human PK Prediction and Modeling

Cockerill, G.S.
Antiviral Drugs for Acute Infections

Cole, J.
Molecular Docking—A Solved Problem?

Commandeur, J.
Drug-Induced Liver Injury: Mechanism-Informed Prediction in Drug Development

Congreve, M.
Modeling and Design for Membrane Protein Targets

Cooke, R.M.
Modeling and Design for Membrane Protein Targets

Costet, P.
Drug Discovery in Tissue Fibrosis

Cramer, H.
Manufacturing of Oligonucleotides

Cross, A.
Human iPSC Models in Drug Discovery: Opportunities and Challenges

Cross, K.P.
In Silico Tools and their Application

Crupi, A.
Closing Distances Between Academia and Market

Culler, M.
Chimeric Somatostatin–Dopamine Compounds (Dopastatins) for the Treatment of Neuroendocrine Disease

Cumming, J.N.
Verubecestat

Curtin, N.J.
Targeting DNA Damage Response Pathways in Cancer

Cvijic, M.E.
Cellular Imaging in Drug Discovery: Imaging and Informatics for Complex Cell Biology

D

Daly, A.K.
Drug-Induced Liver Disease

Davies, S.G.
Regenerative Medicine

Davis, A.M.
Quantitative Structure–Activity Relationships
Using 3D Structural Information in Computational Design

Davis, E.
Molecular Docking—A Solved Problem?

de Esch, I.J.P
Structural Chemogenomics Databases to Navigate Protein–Ligand Interaction Space

de Graaf, C.
Structural Chemogenomics Databases to Navigate Protein–Ligand Interaction Space

de la Fuente, J.M.
Nanotechnology in Drug Discovery and Development

Detalle, L.
Translational Aspects in Drug Discovery

Dhar, T.G. Murali
Evolution of Small-Molecule Immunology Research—Changes Since CMC II

Doller, D.
The Discovery of the MCH-1 Receptor Antagonist NGD-4715 for the Potential Treatment of Obesity

Dong, J.Z.
Chimeric Somatostatin–Dopamine Compounds (Dopastatins) for the Treatment of Neuroendocrine Disease

Dossetter, A.G.
Matched Molecular Pair Analysis

D'Alonzo, S.
Cancer Biology and the Principles of Targeted Cancer Drug Discovery

Dubowchik, G.M.
CGRP Receptor Antagonists for the Treatment of Migraine

Duffy, K.J.
Cancer Immunotherapy—An Emerging Field That Bridges Oncology and Immunology Research

Duffy, J.
Case Histories: Anacetrapib

Dyckman, A.J.
Evolution of Small-Molecule Immunology Research—Changes Since CMC II

E

Edge, C.M.
Using 3D Structural Information in Computational Design

Edman, K.
The Discovery of Potent and Selective Nonsteroidal Glucocorticoid Receptor Modulators AZD5423 and AZD7594, for the Inhaled Treatment of Respiratory Diseases

Edmondson, S.D.
β_3-AR Agonists for the Treatment of Overactive Bladder

Elisa Pasqua, A.
Targeting Protein Synthesis, Folding, and Degradation Pathways in Cancer

Estarellas, C.
Recent Progress in Free Energy Methods

Ettmayer, P.
Hit and Lead Generation Strategies

F

Fabbro, D.
Cancer Biology and the Principles of Targeted Cancer Drug Discovery

Fang, Y.
Label-Free Screening Technologies

Faulkner, L.
Drug-Induced Liver Injury: Mechanism-Informed Prediction in Drug Development

Fedorov, M.V.
Empirical and Physics-Based Calculations of Physical−Chemical Properties

Fiegen, D.
High-Throughput Crystallography and Its Applications in Drug Discovery

Finlay, M.R.V
Medicinal Chemistry Case History: Osimertinib (AZD9291)

Fitzpatrick, L.R.
Small-Molecule Drugs for the Treatment of Inflammatory Bowel Disease

Fleischmann, R.
Small Molecule Immunosuppressants in Inflammatory Disease

Foley, M.
Inhibitors of Epigenetic Regulation in Cancer

Foote, K.M.
Selective Kinase Inhibitors in Cancer

French, N.
Drug-Induced Liver Injury: Mechanism-Informed Prediction in Drug Development

Freund, Y.R.
Case History: AN5568 (SCYX-7158)

Frieauff, W.
Predictive Toxicology: Latest Scientific Developments and Their Application in Safety Assessment

G

Gao, Y.
Fragment-Based Drug Design: Strategic Advances and Lessons Learned

Gatfield, J.
The Discovery of Macitentan—A Standard Medicinal Chemistry Program?

Gervasio, F.L.
Recent Progress in Free Energy Methods

Giblin, G.M.P
Sodium Channel Blockers for the Treatment of Pain

Gijsen, H.J.M.
Targeting β-Secretase (BACE) for the Treatment of Alzheimer's Disease

Giordanetto, F.
European Lead Factory
Fragment-Based Discovery of AZD2716: A Novel, Potent Secreted Phospholipase A_2 ($sPLA_2$) Inhibitor for the Treatment of Coronary Artery Disease

Gissi, A.
Nontest Methods for REACH Legislation

Gleeson, M.P.
Multiobjective Optimization of Biological and Physical Properties in Drug Discovery

Glunz, P.W.
Advances in Anticoagulants

Goldberg, F.W.
Selective Kinase Inhibitors in Cancer

Goldring, C.
Drug-Induced Liver Injury: Mechanism-Informed Prediction in Drug Development

Gomes, B.C.
An Introduction to Systems Biology and Quantitative Systems Pharmacology

Gonzalez Suarez, I.
Systems Biology: Methods and Applications

Gorovits, B.
Emerging Bioanalytical Methods for the Bioanalysis of Biotherapeutics

Grasela, T.H.
Human PK Prediction and Modeling

Grazú, V.
Nanotechnology in Drug Discovery and Development

Griffen, E.J.
Matched Molecular Pair Analysis

Grime, K.
ADME Optimization in Drug Discovery

Guillouzo, A.
Drug-Induced Liver Injury: Mechanism-Informed Prediction in Drug Development

Gutiérrez, L.
Nanotechnology in Drug Discovery and Development

H

Haggarty, S.J.
Human iPSC Models in Drug Discovery: Opportunities and Challenges

Hall, A.
Targeting β-Secretase (BACE) for the Treatment of Alzheimer's Disease
Targeting γ-Secretase for the Treatment of Alzheimer's Disease

Halleck, M.
GLP-1 Receptor Agonists for the Treatment of Diabetes and Obesity

Han, S.-p.
Current Progress and Future Prospects in Nucleic Acid Based Therapeutics

Hanig, J.P.
Toxicity Prediction—Regulatory Perspective

Hann, M.M.
Contemporary Considerations for Discovering a Successful Medicine

Hannestad, J.
Progress and Challenges in the Development of PET Ligands to Aid CNS Drug Discovery

Hansson, T.
The Discovery of Potent and Selective Nonsteroidal Glucocorticoid Receptor Modulators AZD5423 and AZD7594, for the Inhaled Treatment of Respiratory Diseases

Hardcastle, I.R.
Protein—Protein Interaction Inhibitors in Cancer

Harmange, J.-C.
Discovery of AMG 337: Using Structure Guided Scaffold Hybridization to Optimize Physicochemical Properties and Target Coverage of a MET Kinase Inhibitor

Hartung, T.
A Comprehensive Overview of the Current Status and Application of Predictive ADMET: Introduction and Overview

Harvey, D.
Inhibitors of Epigenetic Regulation in Cancer

Hasselgren, C.
Predicting Target and Chemical Druggability

Hay, M.P.
Discovery of the Hypoxia-Activated Prodrug SN30000

Héberger, K.
Chemical Data Formats, Fingerprints, and Other Molecular Descriptions for Database Analysis and Searching

Henderson, C.J.
Genetically Humanized Animal Models

Hicks, K.O.
Discovery of the Hypoxia-Activated Prodrug SN30000

Hill, J.
Chimeric Somatostatin—Dopamine Compounds (Dopastatins) for the Treatment of Neuroendocrine Disease

Hillmann, P.
Cancer Biology and the Principles of Targeted Cancer Drug Discovery

Hodgetts, K.J.
The Discovery of the MCH-1 Receptor Antagonist NGD-4715 for the Potential Treatment of Obesity

Hoek, M.
Drug Discovery in Tissue Fibrosis

Hoeng, J.
Systems Biology: Methods and Applications

Holdgate, G.A.
Kinetics, Thermodynamics, and Ligand Efficiency Metrics in Drug Discovery

Hooft van Huijsduijnen, R.
New Models of Drug Discovery and Development for Neglected Disease Populations

Hörer, S.
High-Throughput Crystallography and Its Applications in Drug Discovery

Hosey, C.M.
Drug Classification and Drug Disposition Prediction

Howard, J.L.
Continuous Flow Processing as a Tool for Medicinal Chemical Synthesis

Huang, Y.
Drug Discovery in Tissue Fibrosis

I

Iglarz, M.
The Discovery of Macitentan—A Standard Medicinal Chemistry Program?

Imbriglio, J.E.
Drug Discovery in Tissue Fibrosis

Ingelman-Sundberg, M.
Drug-Induced Liver Injury: Mechanism-Informed Prediction in Drug Development

Ito, K.R.
Recent Advances in Medicinal Chemistry of Antisense Oligonucleotides

Ivanov, N.V.
Systems Biology: Methods and Applications

J

Jablonski, S.
Cancer Immunotherapy

Jacobs, R.T.
Antiparasitic Agents
Case History: AN5568 (SCYX-7158)

Jones, A.M.
Privileged Structures and Motifs (Synthetic and Natural Scaffolds)

Jones, P.
European Lead Factory

Jones, G.
Molecular Docking—A Solved Problem?

Jones, K.
Targeting Protein Synthesis, Folding, and Degradation Pathways in Cancer

Jørgensen, J.T.
Companion Diagnostics: From Biomarkers to Diagnostics

Jozwiak, K.
Click Chemistry in Medicinal Chemistry for Comprehensive Medicinal Chemistry III

K

Kamalian, L.
Drug-Induced Liver Injury: Mechanism-Informed Prediction in Drug Development

Kanev, G.K.
Structural Chemogenomics Databases to Navigate Protein–Ligand Interaction Space

Kassees, K.
Strategy and Tactics for Designing Analogs: Biochemical Characterization of the Large Molecules

Kaumaya, P.T.P.
Peptide-Based Cancer Vaccines and Therapeutics for Solid Tumors Overexpressing HER-1, HER-2, HER-3, VEGF and IGF-1R

Kawala, M.-A.
Use of Stem Cells in Toxicology

Kawasaki, H.
Trametinib

Kazuta, Y.
Recent Advances and Future Directions in the Treatment of Epilepsy

Kehler, J.
Targeting Phosphodiesterases in the CNS

Kennewell, P.D.
Regenerative Medicine

Kettle, J.G.
Selective Kinase Inhibitors in Cancer

Kevin Park, B.
Drug-Induced Liver Injury: Mechanism-Informed Prediction in Drug Development

Kim, S.
Chimeric Somatostatin–Dopamine Compounds (Dopastatins) for the Treatment of Neuroendocrine Disease

Kitteringham, N.
Drug-Induced Liver Injury: Mechanism-Informed Prediction in Drug Development

Klingmueller, U.
Drug-Induced Liver Injury: Mechanism-Informed Prediction in Drug Development

Knolle, P.
Drug-Induced Liver Injury: Mechanism-Informed Prediction in Drug Development

Knorr, A.
Systems Biology: Methods and Applications

Kooistra, A.J.
Structural Chemogenomics Databases to Navigate Protein–Ligand Interaction Space

Kotra, L.P.
Therapeutic Approaches to MS and Other Neurodegenerative Diseases

Kovi, R.
The Future of Carcinogenicity Testing

Kramer, B.
Drug-Induced Liver Injury: Mechanism-Informed Prediction in Drug Development

Krause, J.E.
The Discovery of the MCH-1 Receptor Antagonist NGD-4715 for the Potential Treatment of Obesity

Kurokawa, T.
Recent Advances and Future Directions in the Treatment of Epilepsy

Kyttaris, V.C.
Lupus and Lupus Overlap Diseases: Emerging Therapies

L

LaBarbera, D.V.
3D High-Content Screening of Organoids for Drug Discovery

Lang, E.J.M.
Molecular Dynamics, Quantum Mechanics, and Combined Quantum Mechanics/Molecular Mechanics Methods for Drug Discovery and Development

Langston, S.
The Discovery of First-in-Class Inhibitors of the Nedd8-Activating Enzyme (NAE) and the Ubiquitin-Activating Enzyme (UAE)

Laufer, S.A.
Are Two Better Than One in Rheumatoid Arthritis? Development of Dual p38α MAPK/PDE-4 Inhibitors for Treatment of TNFα-Driven Diseases

Lazerwith, S.E.
New Antiretrovirals for HIV and Antivirals for HBV

Leach, A.R.
Contemporary Considerations for Discovering a Successful Medicine
Protein Structure Prediction and Homology Modeling

Leach, A.G.
Matched Molecular Pair Analysis

Lee, T.-K.
Strategy and Tactics for Designing Analogs: Biochemical Characterization of the Large Molecules

Letavic, M.A.
Orexin Receptor Antagonists

Lewis, R.A.
2/3D Pharmacophore Definitions and Their Application

Li, S.
Predictive Toxicology: Latest Scientific Developments and Their Application in Safety Assessment

Li, Z.
Cellular Imaging in Drug Discovery: Imaging and Informatics for Complex Cell Biology

Li, L.
3D High-Content Screening of Organoids for Drug Discovery

Li, H.
Targeting the Androgen Receptor Signaling Axis

Lima, L.M.
Beyond Bioisosterism: New Concepts in Drug Discovery

Link, J.O.
Harvoni: A Combination Therapy for Curing HCV

Liu, Z.
Small-Molecule Inhibitors of Protein–Protein Interactions

Livingstone, D.J.
Empirical and Physics-Based Calculations of Physical−Chemical Properties

Loscalzo, J.
Systems Chemical Biology: Integrating Medicinal Chemistry and Systems Biology for Drug Discovery

Lou, Yan
Covalent Kinase Inhibitors for Cancer

Lu, S.
Allosteric Modulators

Lukac, I.
Matched Molecular Pair Analysis

Lukacova, V.
Human PK Prediction and Modeling

Lynch, Jr., J.J.
Treatments for Heart Failure

M

Ma, L.
Drug Discovery in Tissue Fibrosis

Mackey, M.
Lessons and Successes in the Use of Molecular Fields

MacPherson, D.T.
Sodium Channel Blockers for the Treatment of Pain

Manandhar, B.
Strategy and Tactics for Designing Analogs: Biochemical Characterization of the Large Molecules

Mangiatordi, G.F.
Nontest Methods for REACH Legislation

Martin, F.
Systems Biology: Methods and Applications

Martus, H.-J.
Predictive Toxicology: Latest Scientific Developments and Their Application in Safety Assessment

Mascaraque, A.
Perspectives of Carbohydrates in Drug Discovery

Mathias, J.
Medicinal Chemistry Case History: Structure-Based Drug Design of Oral and Inhaled p38 MAP Kinase Inhibitors as Clinical Candidates

Matthews, D.
Medicinal Chemistry Case History: Discovery of the Dihydroorate Dehydrogenase Inhibitor DSM265 as an Antimalarial Drug Candidate

Matz, P.
Use of Stem Cells in Toxicology

McFadden, R.M.
New Antiretrovirals for HIV and Antivirals for HBV

McGinnity, D.F.
ADME Optimization in Drug Discovery

Meanwell, N.A.
Direct-Acting Antiviral Agents for the Treatment of Hepatitis C Virus Infection

Mercer, A.
Drug-Induced Liver Injury: Mechanism-Informed Prediction in Drug Development

Mercier, J.
Progress and Challenges in the Development of PET Ligands to Aid CNS Drug Discovery

Mestan, J.
Cancer Biology and the Principles of Targeted Cancer Drug Discovery

Meyer, EA.
Advances in Antiplatelet Agents

Michael Seganish, W.
Treatments for Heart Failure

Mikhailov, D.
Predictive Toxicology: Latest Scientific Developments and Their Application in Safety Assessment

Mish, M.R.
New Antiretrovirals for HIV and Antivirals for HBV

Montanari, D.
Multiobjective Optimization of Biological and Physical Properties in Drug Discovery

Moore, M.L.
Cancer Immunotherapy—An Emerging Field That Bridges Oncology and Immunology Research

Morris, D.N.
Human PK Prediction and Modeling

Mortlock, A.A.
Selective Kinase Inhibitors in Cancer

Mulholland, A.J.
Molecular Dynamics, Quantum Mechanics, and Combined Quantum Mechanics/Molecular Mechanics Methods for Drug Discovery and Development

Müller, G.
European Lead Factory

Muster, W.
Computational Models to Predict Toxicological Endpoints in Drug Discovery and Strategies for Data Integration

Myatt, G.J.
In Silico Tools and their Application

N

Naisbitt, D.
Drug-Induced Liver Injury: Mechanism-Informed Prediction in Drug Development

Nakhle, J.
Future of Medicinal Chemistry: Next-Generation Therapeutics

Nar, H.
High-Throughput Crystallography and Its Applications in Drug Discovery
Hit and Lead Generation Strategies

Neidle, S.
Targeting Promoter Quadruplex Nucleic Acids for Cancer Therapy

Nelson, A.
European Lead Factory

Netzeva, T.
Nontest Methods for REACH Legislation

Nicolotti, O.
Nontest Methods for REACH Legislation

Nielsen, K.B.
Companion Diagnostics: From Biomarkers to Diagnostics

Noe, M.C.
Drug Discovery Technologies: Current and Future Trends

Nomura, S.
Canagliflozin

Norata, G.D.
Advances in Hypercholesterolemia

Norman, C.
Evolution of mAb Downstream Process Platforms

O

Obika, S.
Recent Advances in Medicinal Chemistry of Antisense Oligonucleotides

Oerton, E.
Drug Repurposing Review

Oppelt, A.
Drug-Induced Liver Injury: Mechanism-Informed Prediction in Drug Development

Oprea, T.I.
Predicting Target and Chemical Druggability

Otte, J.
Use of Stem Cells in Toxicology

Otvos, Jr., L.
Basic Principles of Formulation for Biotherapeutics: Approaches to Alternative Drug Delivery

Owens, Timothy D.
Covalent Kinase Inhibitors for Cancer

P

Palani, A.
GLP-1 Receptor Agonists for the Treatment of Diabetes and Obesity

Pandiri, A.
The Future of Carcinogenicity Testing

Pang, K. Sandy
PBPK Modeling to Estimate Metabolite Formation From First-Pass Organs: Intestine and Liver

Pannifer, A.
European Lead Factory

Pardo, J.
Nanotechnology in Drug Discovery and Development

Paredes, E.
Manufacturing of Oligonucleotides

Park, J.
Therapeutic Approaches to MS and Other Neurodegenerative Diseases

Pasternak, Alexander
Discovery of ROMK Inhibitor MK-7145: A Novel Mechanism Diuretic

Paulo, A.
Targeting Promoter Quadruplex Nucleic Acids for Cancer Therapy

Pautsch, A.
High-Throughput Crystallography and Its Applications in Drug Discovery

Peakman, M.-C.
Drug Discovery Technologies: Current and Future Trends

Peitsch, M.C.
Systems Biology: Methods and Applications

Pérez-Hernández, M.
Nanotechnology in Drug Discovery and Development

Peterson, E.A.
Discovery of AMG 337: Using Structure Guided Scaffold Hybridization to Optimize Physicochemical Properties and Target Coverage of a MET Kinase Inhibitor

Pettersen, D.
Fragment-Based Discovery of AZD2716: A Novel, Potent Secreted Phospholipase A_2 ($sPLA_2$) Inhibitor for the Treatment of Coronary Artery Disease

Phillips, M.A.
Medicinal Chemistry Case History: Discovery of the Dihydroorate Dehydrogenase Inhibitor DSM265 as an Antimalarial Drug Candidate

Pieters, R.
Drug-Induced Liver Injury: Mechanism-Informed Prediction in Drug Development

Pike, K.G.
Discovery of AZD0156: The First Potent and Selective Inhibitor of ATM Kinase for Clinical Evaluation

Pillutla, R.
Emerging Bioanalytical Methods for the Bioanalysis of Biotherapeutics

Pinto, S.
Drug Discovery in Tissue Fibrosis

Pirillo, A.
Advances in Hypercholesterolemia

Powell, K.L.
Antiviral Drugs for Acute Infections

Pridgeon, C.
Drug-Induced Liver Injury: Mechanism-Informed Prediction in Drug Development

Provins, L.
Progress and Challenges in the Development of PET Ligands to Aid CNS Drug Discovery

Pucci, M.J.
Recent Epidemiological Changes in Infectious Diseases

Q

Quan, M.L.
Advances in Anticoagulants

R

Rácz, A.
Chemical Data Formats, Fingerprints, and Other Molecular Descriptions for Database Analysis and Searching

Rajasekaran, A.
Nutraceuticals

Rajesh Singh, R.
Next Generation Sequencing Technologies

Ramprasad, M.P.
Analytical and Formulation Development Road Map for Protein Therapeutics

Rathod, P.K.
Medicinal Chemistry Case History: Discovery of the Dihydroorate Dehydrogenase Inhibitor DSM265 as an Antimalarial Drug Candidate

Ratkova, E.L.
Empirical and Physics-Based Calculations of Physical−Chemical Properties

Reilly, J.
Predictive Toxicology: Latest Scientific Developments and Their Application in Safety Assessment

Reinert, D.
High-Throughput Crystallography and Its Applications in Drug Discovery

Rennie, P.
Targeting the Androgen Receptor Signaling Axis

Reuillon, Tristan
Modulating AMPA Receptors for the Treatment of CNS Disorders

Riederer, M.A.
Advances in Antiplatelet Agents

Rojo, J.
Perspectives of Carbohydrates in Drug Discovery

Rolfe, M.
The Discovery of p97 Inhibitors

Rossi, J.J.
Current Progress and Future Prospects in Nucleic Acid Based Therapeutics

Rueckle, T.
Medicinal Chemistry Case History: Discovery of the Dihydroorate Dehydrogenase Inhibitor DSM265 as an Antimalarial Drug Candidate

Russell, A.J.
Regenerative Medicine

S

Sage, C.R.
Molecular Docking—A Solved Problem?

Saladino, G.
Recent Progress in Free Energy Methods

Samuelsson, K.
Genetically Humanized Animal Models

Sanz, F.
Data Integration and Sharing Supporting Drug R&D

Sargentini-Maier, M.L.
Translational Aspects in Drug Discovery

Schadt, O.
Tepotinib

Scheer, N.
Genetically Humanized Animal Models

Scherer, L.J.
Current Progress and Future Prospects in Nucleic Acid Based Therapeutics

Schmitz, D.
Cancer Biology and the Principles of Targeted Cancer Drug Discovery

Schnitzer, R.
Hit and Lead Generation Strategies

Schotten, C.
Continuous Flow Processing as a Tool for Medicinal Chemical Synthesis

Scott, J.D.
Verubecestat

Sewer, A.
Systems Biology: Methods and Applications

Shireman, B.T.
Orexin Receptor Antagonists

Shukla, A.A.
Evolution of mAb Downstream Process Platforms

Sibley, G.
Antifungal Chemistry Review

Sidaway, J.
Drug-Induced Liver Injury: Mechanism-Informed Prediction in Drug Development

Siegel, D.
New Antiretrovirals for HIV and Antivirals for HBV

Sills, R.
The Future of Carcinogenicity Testing

Silpa, L.
Regenerative Medicine

Silva, M.C.
Human iPSC Models in Drug Discovery: Opportunities and Challenges

Singh, S.B.
Spirocyclic Scaffolds in Drug Discovery

SinhaRoy, R.
DPP-4 Inhibitors

Sirockin, F.
2/3D Pharmacophore Definitions and Their Application

Sison-Young, R.
Drug-Induced Liver Injury: Mechanism-Informed Prediction in Drug Development

Sjö, P.
The Discovery of Potent and Selective Nonsteroidal Glucocorticoid Receptor Modulators AZD5423 and AZD7594, for the Inhaled Treatment of Respiratory Diseases

Slikker, W.
Toxicity Prediction—Regulatory Perspective

Smallheer, J.M.
Advances in Anticoagulants

Smythe, M.L.
Orally Delivered Peptides for Treatment of Inflammatory Bowel Disease

Snape, M.
Ethics in Drug Discovery

Sobański, T.
Nontest Methods for REACH Legislation

Sofia, M.J.
Harvoni: A Combination Therapy for Curing HCV

Sorota, S.
Treatments for Heart Failure

Sousa-Herves, A.
Perspectives of Carbohydrates in Drug Discovery

Southan, C.
Examples of SAR-Centric Patent Mining Using Open Resources

Spitzhorn, L.-S.
Use of Stem Cells in Toxicology

Stamford, A.W.
Verubecestat

Stamm, S.
Targeting Pre-mRNA Processing in Cancer

Stepien, G.
Nanotechnology in Drug Discovery and Development

Stöhr, T.
Translational Aspects in Drug Discovery

Strickland, C.O.
Verubecestat

Swain, C.J.
Data Analysis and Visualization Tools

T

Takahashi, M.
Current Progress and Future Prospects in Nucleic Acid Based Therapeutics

Talikka, M.
Systems Biology: Methods and Applications

Tan, Z.
Overview of Drug Polypharmacology and Multitargeted Molecular Design

Tarrant, J.
Emerging Translatable Safety Biomarkers
The Discovery of the MCH-1 Receptor Antagonist NGD-4715 for the Potential Treatment of Obesity

Taylor, Robin
Progress in the Understanding of Traditional and Nontraditional Molecular Interactions

Tetko, I.V.
Empirical and Physics-Based Calculations of Physical—Chemical Properties

Thirumurugan, P.
Click Chemistry in Medicinal Chemistry for Comprehensive Medicinal Chemistry III

Thomas, P.J.
Protein Structure Prediction and Homology Modeling

Thomas, E.
Antiviral Drugs for Acute Infections

Tice, C.M.
Spirocyclic Scaffolds in Drug Discovery

Titz, B.
Systems Biology: Methods and Applications

Tosco, P.
Lessons and Successes in the Use of Molecular Fields

Tranfaglia, M.R.
The Rise of Rare Disease Foundations: How Patient Associations Can Drive the Drug Discovery Process

Treiber, A.
The Discovery of Macitentan—A Standard Medicinal Chemistry Program?

Tse, W.C.
New Antiretrovirals for HIV and Antivirals for HBV

Tsomaia, N.
Chimeric Somatostatin—Dopamine Compounds (Dopastatins) for the Treatment of Neuroendocrine Disease
Future of Medicinal Chemistry: Next-Generation Therapeutics

Tsui, H.
Inhibiting Kinases in the CNS

Tzalis, D.
European Lead Factory

U

Ufret, M.
Future of Medicinal Chemistry: Next-Generation Therapeutics

Urban, L.
Predictive Toxicology: Latest Scientific Developments and Their Application in Safety Assessment

V

Vaiserman, A.M.
Anti-Aging Drugs

van Boeckel, S.
European Lead Factory

Van der Water, B.
Drug-Induced Liver Injury: Mechanism-Informed Prediction in Drug Development

Vanheusden, K.
Translational Aspects in Drug Discovery

Velter, A.I.
Targeting γ-Secretase for the Treatment of Alzheimer's Disease

Venkatraman, S.
Discovery of Boceprevir and Narlaprevir: Ketoamide-Derived HCV NS3 Serine Protease Inhibitors for the Treatment of Chronic Hepatitis C

W

Wang, R.-S.
Systems Chemical Biology: Integrating Medicinal Chemistry and Systems Biology for Drug Discovery

Ward, Simon E.
Modulating AMPA Receptors for the Treatment of CNS Disorders

Ward, R.A.
Medicinal Chemistry Case History: Osimertinib (AZD9291)

Warshel, A.
Perspective on Calculations of Binding Free Energies

Watanabe, T.
Recent Advances and Future Directions in the Treatment of Epilepsy

Weaver, R.
Drug-Induced Liver Injury: Mechanism-Informed Prediction in Drug Development

Webb, T.R.
Targeting Pre-mRNA Processing in Cancer

Weiner, L.M.
Cancer Immunotherapy

Wells, T.N.C.
New Models of Drug Discovery and Development for Neglected Disease Populations

Westwood, R.
Regenerative Medicine

White, R.E.
Role of ADME/PK in Drug Discovery, Safety Assessment, and Clinical Development

Whitebread, S.
Predictive Toxicology: Latest Scientific Developments and Their Application in Safety Assessment

Wilding, B.
Targeting Protein Synthesis, Folding, and Degradation Pathways in Cancer

Wilson, I.
Genetically Humanized Animal Models

Wilson, D.M.
Selective Kinase Inhibitors in Cancer

Wilson, W.R.
Discovery of the Hypoxia-Activated Prodrug SN30000

Withnall, M.
Empirical and Physics-Based Calculations of Physical—Chemical Properties

Witty, D.R.
Sodium Channel Blockers for the Treatment of Pain

Woestmann, J.
Use of Stem Cells in Toxicology

Wold, E.A.
Small-Molecule Inhibitors of Protein–Protein Interactions

Woldemariam, T.
Small-Molecule Drugs for the Treatment of Inflammatory Bowel Disease

Wolf, C.R.
Genetically Humanized Animal Models

Wolfe, L.
Evolution of mAb Downstream Process Platforms

Woster, P.M.
Novel Therapeutics Targeting Epigenetics

Wruck, W.
Use of Stem Cells in Toxicology

Wustrow, D.J.
The Discovery of p97 Inhibitors

Wynne, G.M.
Regenerative Medicine

X

Xing, L.
Medicinal Chemistry Case History: Structure-Based Drug Design of Oral and Inhaled p38 MAP Kinase Inhibitors as Clinical Candidates

Y

Yamaguchi, T.
Trametinib

Yamazaki, H.
Drug-Metabolizing Enzyme Systems I

Yan, C.
Modeling Protein Flexibility in Molecular Docking

Yang, Qi Joy
PBPK Modeling to Estimate Metabolite Formation From First-Pass Organs: Intestine and Liver

Yang, J.
Cancer Immunotherapy—An Emerging Field That Bridges Oncology and Immunology Research

Yeung, B.K.S
KAE609 (Cipargamin): Discovery of Spiroindolone Antimalarials

Yigit, H.
Use of Stem Cells in Toxicology

Yoon, H.
Perspective on Calculations of Binding Free Energies

Yoon, S.
Current Progress and Future Prospects in Nucleic Acid Based Therapeutics

Yousif, A.M.
Strategy and Tactics for Designing Analogs: Biochemical Characterization of the Large Molecules

Z

Zarnecka, J.M.
Matched Molecular Pair Analysis

Zeng, Q.
Inhibiting Kinases in the CNS

Zhang, S.
Overview of Drug Polypharmacology and Multitargeted Molecular Design

Zhang, J.
Allosteric Modulators

Zhang, L.
Cellular Imaging in Drug Discovery: Imaging and Informatics for Complex Cell Biology

Zhang, X.
Inhibiting Kinases in the CNS

Zhang, Y.-K.
Case History: AN5568 (SCYX-7158)

Zheng, Y.
Spirocyclic Scaffolds in Drug Discovery

Zhou, X.
Fragment-Based Drug Design: Strategic Advances and Lessons Learned

Zhou, J.
Fragment-Based Drug Design: Strategic Advances and Lessons Learned
Small-Molecule Inhibitors of Protein–Protein Interactions

Zhou, Y.-Y.
GLP-1 Receptor Agonists for the Treatment of Diabetes and Obesity

Zhou, H.-J.
The Discovery of p97 Inhibitors

Zou, X.
Modeling Protein Flexibility in Molecular Docking